Pergamon

*Talanta*, Vol. 42, No. 1, p. 1, 1995
Elsevier Science Ltd
Printed in Great Britain

# PUBLISHER'S ANNOUNCEMENT

It is with great regret that the Publisher and Editorial Board of *Talanta* announce that Professor Elo Hansen has decided to retire from the role of joint Editor-in-Chief after 3 years during which the journal has flourished under his high standards as an Editor. All concerned with *Talanta* would

Pergamon

*Talanta*, Vol. 42, No. 1, p. 3, 1995
Elsevier Science Ltd
Printed in Great Britain

# Biography on Professor Jean-Michel Kauffmann

Professor Jean-Michel Kaufmann

Professor Jean-Michel Kauffmann was born in Arlon, Belgium, in 1954. He became a pharmacist from the Université Libre de Bruxelles, in 1977 and earned a Ph.D. degree in pharmaceutical sciences under Professor G. J. Patriarche in 1983 from the same University. He became Professor and Head of the laboratory of instrumental analysis and bioelectrochemistry at the Institute of Pharmacy of the Université Libre de Bruxelles, in 1992. His research interests include electroanalysis, modified electrodes and biosensors, as well as molecular fluorescence and detector development for flow injection and HPLC analysis. He has published approximately 100 original papers including several chapters related to electroanalysis and biosensors and given more than 140 lectures at national and international meetings. He acted as invited Professor at the Vrij Universiteit Brussel in 1993 and visiting Professor at the University of Extremadura (Badajoz) in 1994. He has been the Treasurer of the International Bioelectrochemical Society since 1989 and became the Vice-President of the Belgian Society of Pharmaceutical Sciences this year. He acts as national representative at the IUPAC—Commission V on electroanalysis. Professor J.-M. Kauffmann is a member of the scientific steering committee of the programme on Artificial Biosensing Interfaces put forward with the support of the European Science Foundation (ESF). He is a member of the Advisory Boards of *Analytical Letters*, *Electroanalysis*, *Talanta* and the *Journal of Pharmaceutical Sciences of Ankara*.

Pergamon

0039-9140(94)00315-7

*Talanta*, Vol. 42, No. 1, pp. 5–8, 1995

0039-9140/95 $9.50 + 0.00

# FORMATION CONSTANTS AT HIGH IONIC STRENGTH—I. POTENTIOMETRIC DETERMINATION OF PROTONATION CONSTANTS FOR SUCCINIC, PROPIONIC AND MONO-METHYL SUCCINIC ACID IN DIFFERENT IONIC MEDIA

GRAHAM E. JACKSON and LISA F. SEYMOUR

Chemistry Department, University of Cape Town, Private Bag, Rondebosch 7700, South Africa

(*Received* 12 *November* 1993. *Revised* 12 *January* 1994. *Accepted* 12 *January* 1994)

**Summary**—The protonation constants, $K_r$, for the ligands succinic acid (SA), mono-methyl succinate (MS) and propionate (PA) have been determined, at 25°C, by glass electrode potentiometry in 3 mol/dm$^3$ ($M$) $NaNO_3$, $KNO_3$, $NH_4NO_3$, $Ca(NO_3)_2$ and $Et_4NBr$ aqueous media. Results are compared with literature constants determined in $3M$ $NaClO_4$. The order of stability was found to be $K_1(SA) > K_1(PA) > K_1(MS) > K_2(SA)$ and for the ligands in the different media $K_r$ followed the general trend with respect to the background electrolyte $Et_4NBr > NaClO_4 > KNO_3 > NaNO_3 > NH_4NO_3 > Ca(NO_3)_2$.

Speciation modelling has been widely used to explain the bioavailability of metal ions in solution.[1–4] In a similar fashion chemical speciation could play a critical role in the emulsifying ability of ionic surfactants. Recently we have become interested in modelling these surfactants which are often used industrially in aqueous solutions of high ionic strength.

As models of the polar headgroups of ionic surfactants, we have chosen propionic acid (PA), succinic acid (SA) and mono-methyl succinic acid (MS). Daniele *et al.* have extensively studied the effect of ionic strength, in the range $0M < I < 1M$, upon the protonation equilibria of carboxylic acids.[5,6] Belavantsev *et al.* have studied the effect of ionic background upon the dissociation constants of monobasic acids.[7] However, as yet no study has been reported of the effect of high ionic strength and background medium upon protonation equilibria. Since these data are necessary in order to model the effect of pH upon the speciation of our model polar head groups, we have undertaken a potentiometric investigation of the protonation equilibria of the above carboxylic acids at high ionic strength ($3M$) and in different background electrolytes ($KNO_3$, $NaNO_3$, $NH_4NO_3$, $Ca(NO_3)_2$, $Et_4NBr$).

## EXPERIMENTAL

Potentiometric titrations were carried out under an atmosphere of high purity nitrogen which was passed through a series of wash bottles to remove any residual $O_2$, $CO_2$ and to humidify the gas. The 50 ml reaction vessel was maintained at $25.00 \pm 0.05$°C and the entire titration apparatus was kept in a room thermostatted at $23 \pm 1$°C. Titrations were repeated using two glass electrodes and a Ag/AgCl reference electrode, connected to the titration solution via a salt bridge. Volumes were dispensed using a Metrohm automatic burette.

All solutions were made up in glass distilled, deionized water, which had been boiled out to remove dissolved $CO_2$. All volumetric flasks used in preparing the solutions were calibrated before use.[8] The strong base solutions were prepared under $N_2$, using Merck titrisols, and were stored in high density polypropylene bottles under an atmosphere of $N_2$.

$NaNO_3$ and $KNO_3$ (Merck GR) were dried under vacuum for 12 hr, at 140°C and 70°C, respectively.[9] $NH_4NO_3$ solutions were standardized using the hydrogen form of a cation exchange resin (Amberlite IR-120) and $Ca(NO_3)_2$ solutions were standardized against EDTA, using magnesium and solochrome black.[8] $Et_4NBr$ (Aldrich-Chemie) was recrystallized from ethanol, dried under vacuum at 100°C for 12 days and stored over $P_2O_5$.[9] Propionic acid (Riedel-de Haën) was purified by distillation, while succinic acid (Merck GR) and mono-methyl succinate (Aldrich-Chemie) were used without further purification.

All solutions were made up to $3M$ ionic strength with respect to the cation of the background electrolyte. The $Et_4NBr$ system was repeated using a background electrolyte concentration of $2.174M$, which is equimolal with $3M$ $KNO_3$. The $HNO_3$ and strong base solutions were standardized against borax and potassium hydrogen phthalate, respectively. With $Ca(NO_3)_2$ and $NH_4NO_3$ as background electrolyte, however, the $HNO_3$ solutions could not be standardized against borax and so were standardized against the strong base of the corresponding system.

In all the six systems studied the strong acid was $HNO_3$. In the case of the sodium and potassium systems, the strong base was NaOH and KOH, respectively. In the ammonium and calcium systems, $Ca(OH)_2$ and $NH_4OH$, could not be used as the strong base, as $Ca(OH)_2$ has low solubility and aqueous ammonia is volatile and has too low a $pK_b$. Similarly, commercially available $Et_4NOH$ proved to have an unacceptable amount of impurity, probably carbonate and, under strongly basic conditions, hydrolysis of the background salt occurred. In these cases therefore the strong base was $1M$ KOH made up to $3M$ $K^+$ with $KNO_3$. Using the base in such a concentrated form resulted in only 0.07% of the background cation being $K^+$ at the end of a titration. As recommended by the IUPAC commission, a summary of the experimental parameters is given in Table 1.[10]

Data were refined using the ESTA suite of programs optimized on weighted emf values.[11–15] A $pK_w$ of 14.18 compiled from 32 references at $3M$, was used throughout.[16] The electrodes were calibrated *in situ* using the refinement option of ESTA. When using ammonium nitrate as the background electrolyte experimental points near the endpoint of the ligand were deleted from the titration data as they had high residuals due to the effect deprotonation of the ammonium ions had on the emf of the solution.

## RESULTS AND DISCUSSION

All the protonation constants determined are shown in Table 2, and have been plotted in Fig. 1 together with literature protonation constants determined in $3M$ $NaClO_4$.[17,18]

The protonation constants, $K_r$, follow the general trend $K_1(SA) > K_1(PA) > K_1(MS) > K_2(SA)$. The differences in protonation constants are due to the different substituents on the carboxylic groups. Substituents which are electron donating weaken the carboxylic acid and hence increase $K_r$, while electron withdrawing groups strengthen the acid and decrease $K_r$. Therefore we would expect carboxylate groups to increase the protonation constant and carboxylic and ester groups to decrease it. These observations, studied in a wide range of acids, provide the basis for the Taft equations and Taft $\sigma^*$ constants which can be used to predict protonation constants.[19] The acid-strengthening ($-\Delta \log K$) electrostatic and inductive effects of representative substituents attached to the $\alpha$-carbon atoms of aliphatic acids have been calcu-

Table 1. Summary of experimental parameters used in the determination of protonation constants for the ligands succinate, propionate and mono-methyl succinate; $T = 25$ °C

| Ligand | Ligand ($mmol/dm^3$) | Major electrolyte ($mol/dm^3$) | pH range | Data points | Number of titrations |
|---|---|---|---|---|---|
| Succinate | | | | | |
| | 7–9 | 3.00–2.93 $Et_4NBr$ | 2–7 | 295 | 5 |
| | 5–9 | 2.17–2.13 $Et_4NBr$ | 2.0–7.0 | 760 | 7 |
| | 14–16 | 3.00 $KNO_3$ | 2.0–6.4 | 268 | 4 |
| | 4–35 | 3.00 $NaNO_3$ | 2.0–7.4 | 1000 | 9 |
| | 6–10 | 3.00–2.81 $NH_4NO_3$ | 2.0–6.1 | 390 | 6 |
| | 3–10 | 1.00–0.97 $Ca(NO_3)_2$ | 2.1–5.8 | 403 | 5 |
| Propionate | | | | | |
| | 7–24 | 3.00–2.93 $Et_4NBr$ | 2–7 | 166 | 4 |
| | 9–17 | 2.17–2.13 $Et_4NBr$ | 2.0–7.1 | 629 | 6 |
| | 33–37 | 3.00 $KNO_3$ | 2.0–6.7 | 410 | 5 |
| | 37–68 | 3.00 $NaNO_3$ | 2.0–7.3 | 596 | 5 |
| | 27–39 | 3.00–2.93 $NH_4NO_3$ | 2.0–6.2 | 767 | 5 |
| | 7–21 | 1.00–0.97 $Ca(NO_3)_2$ | 2.0–6.2 | 751 | 6 |
| Mono-methyl succinate | 16–18 | 3.00–2.94 $Et_4NBr$ | 2–7 | 302 | 5 |
| | 10–19 | 2.17–2.13 $Et_4NBr$ | 2.0–6.7 | 785 | 7 |
| | 35–38 | 3.00 $KNO_3$ | 2.0–6.0 | 325 | 4 |
| | 41–82 | 3.00 $NaNO_3$ | 2.0–7.1 | 811 | 6 |
| | 19–26 | 3.00–2.88 $NH_4NO_3$ | 2.0–5.8 | 458 | 4 |
| | 11–32 | 1.00–0.96 $Ca(NO_3)_2$ | 2.0–5.9 | 590 | 5 |

Table 2. Protonation constants $K_1$ and $K_2$ for the ligands succinate, propionate and mono-methyl succinate in different ionic media, measured at 25°C; $\sigma$ is the standard deviation, R the crystallographic R factor and $R_{lim}$ the minimum possible $R$ value.[15]

| Ligand | Medium | $R$ | $R_{lim}$ | log $K_1$ | $\sigma$ | log $K_2$ | $\sigma$ |
|---|---|---|---|---|---|---|---|
| Succinate | | | | | | | |
| | 3$M$ $Et_4NBr$ | 0.0020 | 0.0023 | 5.979 | 0.0013 | 4.776 | 0.0017 |
| | 2.17$M$ $Et_4NBr$ | 0.0023 | 0.0031 | 5.649 | 0.0011 | 4.533 | 0.0015 |
| | 3$M$ $NaClO_4$[17] | | | 5.485 | 0.001 | 4.323 | 0.001 |
| | 3$M$ $KNO_3$ | 0.0006 | 0.0025 | 5.313 | 0.0003 | 4.131 | 0.0005 |
| | 3$M$ $NaNO_3$ | 0.0012 | 0.0014 | 5.204 | 0.0004 | 4.077 | 0.0007 |
| | 3$M$ $NH_4NO_3$ | 0.0029 | 0.0015 | 5.145 | 0.0022 | 4.027 | 0.0026 |
| | 1$M$ $Ca(NO_3)_2$ | 0.0067 | 0.0031 | 4.590 | 0.0044 | 3.635 | 0.0065 |
| Propionate | | | | | | | |
| | 3$M$ $Et_4NBr$ | 0.0043 | 0.0037 | 5.767 | 0.0028 | | |
| | 2.17$M$ $Et_4NBr$ | 0.0027 | 0.0033 | 5.232 | 0.0008 | | |
| | 3$M$ $NaClO_4$[18] | | | 5.161 | 0.002 | | |
| | 3$M$ $KNO_3$ | 0.0012 | 0.0023 | 4.929 | 0.0004 | | |
| | 3$M$ $NaNO_3$ | 0.0029 | 0.0013 | 4.859 | 0.0011 | | |
| | 3$M$ $NH_4NO_3$ | 0.0026 | 0.0022 | 4.762 | 0.0007 | | |
| | 1$M$ $Ca(NO_3)_2$ | 0.0035 | 0.0034 | 4.418 | 0.0010 | | |
| Mono-methyl succinate | 3$M$ $Et_4NBr$ | 0.0058 | 0.0052 | 5.403 | 0.0022 | | |
| | 2.17$M$ $Et_4NBr$ | 0.0019 | 0.0029 | 4.915 | 0.0006 | | |
| | 3$M$ $KNO_3$ | 0.0028 | 0.0021 | 4.499 | 0.0012 | | |
| | 3$M$ $NaNO_3$ | 0.0088 | 0.0012 | 4.448 | 0.0038 | | |
| | 3$M$ $NH_4NO_3$ | 0.0066 | 0.0027 | 4.337 | 0.0023 | | |
| | 1$M$ $Ca(NO_3)_2$ | 0.0092 | 0.0024 | 4.113 | 0.0034 | | |

lated as a direct function of Taft $\sigma^*$ constants and have been published for a large number of substituents.[19]

For a dibasic acid such as succinic acid there is also a statistical factor which effects the second protonation constant. When the ligand is completely protonated there are two equivalent ways of losing the first proton, therefore $K_2$ should be twice as large as it would be for a closely related monobasic acid. So in predicting the protonation constants, log $K_2$ should be log 2 ($=0.3$) less.

Using the published $\Delta \log K$ values and including the statistical effect, $\Delta \log K_r^{calc}$ can be predicted for the ligands studied. The differences between the experimental protonation constants obtained between the various ligands, $\Delta \log K_r^{expt}$, was taken as the difference between the average protonation constant obtained for the ligand in all media and the average value obtained for propionic acid. Values obtained for $\Delta \log K_r^{calc}$ and $\Delta \log K_r^{expt}$ are given in Table 3. The good correlation obtained between experimental and calculated values lends confidence to our results.

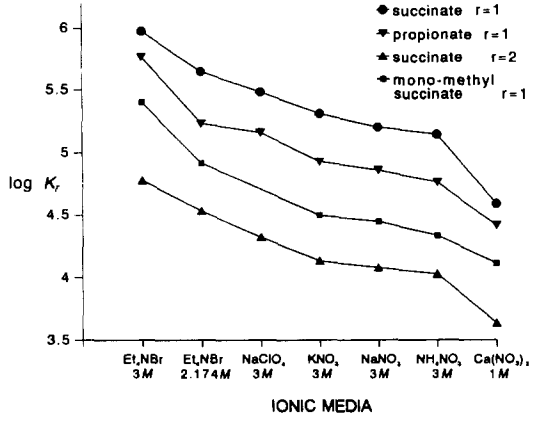


Fig. 1. Protonation constants $K_1$ and $K_2$ plotted for the ligands succinic acid, mono-methyl succinate and propionic acid in different ionic media. The protonation constants determined in 3$M$ $NaClO_4$ were taken from literature.

Figure 1 shows clearly that at high ionic strength, the nature of the background medium has a dramatic effect upon the protonation equilibria of carboxylic acids. De Robertis *et al.* have noted this trend before and have tried to explain it in terms of cation binding to the carboxylate anion, stronger metal binding giving rise to a lower apparent protonation constant.[20–22] This explanation, however, does not account for the consistent difference in protonation constants measured in 3$M$ $NaClO_4$ and 3$M$ $NaNO_3$. Alternatively, in a series of papers, K. S. Pitzer has developed semi-empirical equations for the convenient and accurate description of thermodynamic properties of aqueous electrolytes.[23–26] The Pitzer approach accounts for the change in protonation constant in going from one medium to another in terms of short range interionic forces that are specific

Table 3. Comparison of experimental and calculated $\Delta \log K_r$ for each ligand; where $\Delta \log K_r^{expt} = \log K_r - \log K_l$ (PA)

| Ligand | $r$ | Substituent | $\Delta \log K$ | $\Delta \log K_r^{calc}$ | $\Delta \log K_r^{expt}$ |
|---|---|---|---|---|---|
| Succinate | 1 | $CH_2COO^-$ | 0.244 | 0.244 | 0.318 |
| Propionate | 1 | $CH_3$ | 0.000 | 0.000 | 0.000 |
| Mono-methyl succinate | 1 | $CH_2COOCH_3$ | −0.528 | −0.528 | −0.376 |
| Succinate | 2 | $CH_2COOH$ | −0.548 | −0.848 | −0.800 |

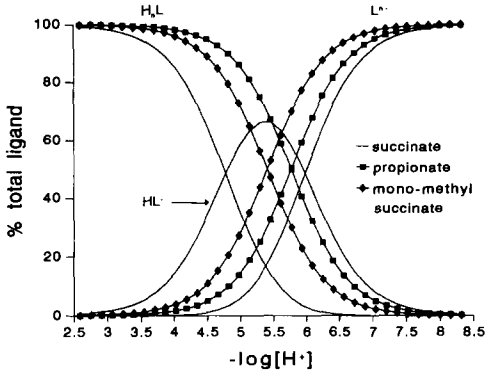


Fig. 2. The speciation of propionate, succinate and mono-methyl succinate plotted over the pH range of 2.5–8.5 in 3*M* $Et_4NBr$. Each species is plotted as a percentage of the total ligand concentration; where $n = 2$ for succinate and $n = 1$ for propionate and mono-methyl succinate.

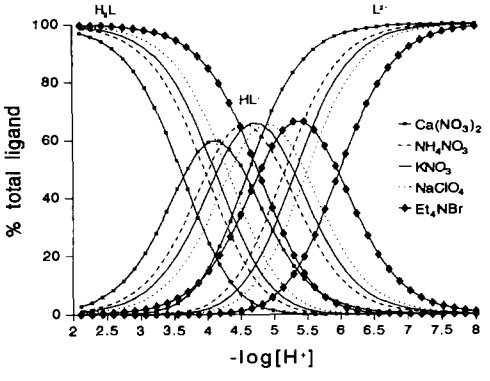


Fig. 3. The speciation of succinate in various 3*M* background electrolytes over the pH range of 2–8. Each species is plotted as a percentage of the total ligand concentration.

to each solute. The Daniele and Pitzer approaches will be examined in more detail in a subsequent paper.

The effect that the nature of the polar head group has on the speciation of model ionic surfactants is shown in Fig. 2. From this we see that in the pH range 4–7 the charge of the carboxylate head groups change from 0 to −1. Similarly, Fig. 3 shows how a change in the background medium affects the speciation of the carboxylic acid. These changes will affect the surface packing of the surfactant and may contribute to the observed pH and medium dependence of emulsion stability.

*Acknowledgements*—The financial support of the University of Cape Town, the Foundation for Research and Development and AECI Ltd is gratefully acknowledged. L.F.S. acknowledges receipt of an AECI Fellowship.

## REFERENCES

1. G. E. Jackson, *Polyhedron*, 1990, **9**, 163.
2. P. M. May, P. W. Linder and D. R. Williams, *J. Chem. Soc. Dalton Trans*, 1977, 588.
3. D. R. Williams, *Chemical Speciation and Bioavailability*, 1989, **1**, 3.
4. J. R. Duffield and D. R. Williams, *Chemistry in Britain*, 1989, 375.
5. V. Cucinotta, P. G. Daniele, C. Rigano and S. Sammartano, *Inorganica Chimica Acta*, 1981, **56**, 45.
6. P. G. Daniele, C. Rigano and S. Sammartano, *Thermochimica Acta*, 1983, **62**, 101.
7. V. I. Belevantsev, I. V. Mironov and B. I. Peschevitskii, *Russ. J. Inorg. Chem.*, 1982, **27**, 29.
8. G. H. Jeffery, J. Bassett, J. Mendham and R. C. Denney, *VOGEL's Textbook of Quantitative Chemical Analysis*, 5th Ed. Longman Scientific & Technical, London, 1989.
9. D. D. Perrin and W. L. F. Armarego, *Purification of Laboratory Chemicals*. Pergamon Press, Oxford, 1988.
10. D. G. Tuck, *Pure & Appl. Chem.*, 1989, **61**, 1161.
11. P. M. May, K. Murray and D. R. Williams, *Talanta*, 1985, **32**, 483.
12. P. M. May, K. Murray and D. R. Williams, *Talanta*, 1988, **35**, 825.
13. P. M. May and K. Murray, *Talanta*, 1988, **35**, 927.
14. P. M. May and K. Murray, *Talanta*, 1988, **35**, 933.
15. K. Murray and P. M. May, *ESTA Users Manual. Ver* 1.0, University of Wales, 1984.
16. A. E. Martell and R. M. Smith, *Critical Stability Constants*, Vols 1–6. Plenum Press, New York, 1989.
17. A. Hamman, A. Olin and P. Svanstrom, *Acta Chem. Scand.*, 1977, **31**, 384.
18. F. J. C. Rossotti and R. J. Whewell, *J. Chem. Soc. Dalton Trans.*, 1977, 1223.
19. D. D. Perrin, B. Dempsey and E. P. Serjeant, *pKa Prediction for Organic Acids and Bases*. Chapman and Hall, London, 1981.
20. A. De Robertis, C. De Stefano, R. Scarcella and C. Rigano, *Thermochimica Acta*, 1984, **80**, 197.
21. A. De Robertis, C. De Stefano, S. Sammartano and C. Rigano, *Talanta*, 1987, **34**, 933.
22. P. G. Daniele, C. Rigano and S. Sammartano, *Talanta*, 1983, **30**, 81.
23. K. S. Pitzer and G. Mayorga, *J. Phys. Chem.*, 1973, **77**, 2300.
24. K. S. Pitzer, *Activity Coefficients in Electrolyte Solns*, R. M. Pytkowicz (Ed.), Vol. 1. CRC Press, Florida, 1979.
25. K. S. Pitzer, *Pure & Appl. Chem.*, 1986, **58**, 1599.
26. J. F. Zemaitis, D. M. Clark, M. Rafal and N. C. Scrivner, *Handbook of Aqueous Electrolyte Thermodynamics—Theory & Appl.*, AIChE, DIPPR. New York, 1986.

Pergamon

0039-9140(94)00316-5

*Talanta*, Vol. 42, No. 1, pp. 9–16, 1995

0039-9140/95 $9.50 + 0.00

# FORMATION CONSTANTS AT HIGH IONIC STRENGTH—II. THE IONIC STRENGTH CORRECTION OF FORMATION CONSTANTS USING A SIMPLIFIED PITZER EQUATION

GRAHAM E. JACKSON and LISA F. SEYMOUR

Chemistry Department, University of Cape Town, Private Bag, Rondebosch 7700, South Africa

(*Received* 12 *November* 1993. *Revised* 12 *January* 1994. *Accepted* 12 *January* 1994)

**Summary**—A simplified approach to the correction of equilibrium constants from one ionic strength and/or medium to another is developed. A computer program capable of performing these calculations is presented together with results of its application to the $NH_3/H^+$, $CH_3COO^-/H^+$, $CH_3CH_2COO^-/H^+$, $-OOCCH_2COO^-/H^+$ and $HOOCCH_2COO^-/H^+$ systems.

In recent years the importance of chemical equilibrium modelling has developed from an empirical qualitative tool to a sophisticated quantitative tool in the armoury of chemists.[1–3] Simultaneous with the development of computer modelling, has grown the realization of chemical speciation as being fundamental to many, if not all, biochemical, and industrial reactions.[4,5] Thus the toxicity of mercury is dependent on its chemical speciation, methyl mercury being highly toxic, but mercury in a gold/mercury amalgam being non-toxic. Fundamental to equilibrium modelling is the availability of a suitable database containing thermodynamic data for all the possible reactions occurring in the model. Several such databases have been constructed.[6,7] However, in order to use these databases, it is necessary to convert the data to the conditions of temperature, pressure and ionic strength applicable to the model. Many attempts have been made to convert equilibrium constants applicable at one ionic strength to another. Most of these methods are based on the Debye–Hückel equation which only shows good accuracy up to 0.1 mol/dm$^3$. At higher ionic strength it is necessary to add terms for short range interionic forces that are specific to each solute. This is the approach of Pitzer.[8] However, because of the large number of virial coefficients needed to evaluate the Pitzer equations, this approach which works well even up to an ionic strength of 6 mol/dm$^3$, has not been generally implemented in equilibrium models. However, under the conditions applicable to most simulation models it is possible to simplify the Pitzer equations, which are then easily built into an equilibrium model. In this paper a computer program for converting equilibrium data from low to high ionic strength and from one background electrolyte to another is presented. The accuracy of this approach is evaluated using data for the protonation of ammonia, acetate, propionate and succinate.

## THEORY

In a solution containing metal ions or cations ($M$), ligands ($L$) and protons or hydroxides ($H$), many complexes may be formed in equilibrium with one another. Each complex has associated with it an equilibrium or stability constant. In general for the reaction

$$pM + qL + rH \rightleftharpoons M_pL_qH_r \qquad (1)$$

the thermodynamic stability constant may be defined as

$${}^T\beta_{pqr} = \frac{a_{M_pL_qH_r}}{a_M^p a_L^q a_H^r} \qquad (2)$$

where $p$, $q$, $r$ are the stoichiometric coefficients and $a$ denotes activity.

When $r$ is negative this refers to the removal or addition of hydrogen or hydroxy ions, respectively.

The basis of many of the variables used in potentiometry vary depending on the composition variable and hence the standard state used. In most potentiometric work the standard

state is taken as unit molarity or 1 mole of solute per $dm^3$ solution. This basis is more convenient as most experimental apparatus is calibrated for the dispensing of volumes. In the more concentrated range molality as the composition variable is more popular where the standard state is defined as unit molality or 1 mole of solute per kg solvent. This basis has an advantage as it does not change with temperature and pressure.

In practice, it is easier to determine the concentration of a species than to determine its activity. The activity of a species can be expressed as a product of its composition variable and its activity coefficient, $\gamma$, so that as the concentration approaches zero the activity coefficient tends to unity. Depending on the basis used the activity of the ion, $i$, in solution can be expressed as follows:

$$a_{c,i} = \gamma_{c,i} c_i \quad \text{or} \quad a_{m,i} = \gamma_{m,i} m_i \tag{3}$$

where $c_i$ and $m_i$ are the molar and molal composition variables of the ion, $i$, in solution and the basis of the activity and activity coefficients is given as a subscript.[9]

Stability constants, activity and activity coefficients are all dimensionless but vary depending on the basis used. To avoid inconsistency in units, the activity should be defined as:

$$a_{c,i} c^0 = \gamma_{c,i} c_i \quad \text{or} \quad a_{m,i} m^0 = \gamma_{m,i} m_i . \tag{4}$$

For convenience, the normal convention is to omit the standard state concentration terms, with the understanding that the activity, activity coefficients and stability constants are dimensionless. To prevent confusion care must be taken to define the composition variable used and not to interchange between different bases.

Following from the definition of activity, the thermodynamic stability constant can be defined as the ratio of its stoichiometric stability "constant", $\beta_{pqr}$, and its activity coefficient quotient, $\Gamma_{pqr}$ defined below

$$^T\beta_{pqr} = \frac{\beta_{pqr}}{\Gamma_{pqr}}, \tag{5}$$

where

$$\beta_{pqr} = \frac{[M_p L_q H_r]}{[M]^p [L]^q [H]^r}, \tag{6}$$

and

$$\Gamma_{pqr} = \frac{\gamma_M^p \gamma_L^q \gamma_H^r}{\gamma_{M_p L_q H_r}}, \tag{7}$$

and the square brackets denote molar concentration.

The mean activity coefficient for a given solution is a function of the ionic strength of the solution and can be determined from experimental measurements. For a solution containing cations, $c$, and anions, $a$, it is defined as follows:

$$\gamma_{\pm} = \sqrt[\nu_a + \nu_c]{\gamma_c^{\nu_c} \gamma_a^{\nu_a}} \tag{8}$$

where $\nu_a$ and $\nu_c$ represent the stoichiometric number of cations and anions in the formula.

Many equations have been proposed to account for the change in activity coefficients with ionic strength and temperature.[10] These ionic strength equations have been used to project stability constants measured at one ionic strength and make them applicable at another ionic strength. The degree of accuracy obtained in these corrections is strongly dependent on the method chosen and the reliability of the original stability constants.

Pitzer has developed semi-empirical equations for the convenient and accurate representation and prediction of the thermodynamic properties of aqueous electrolytes including comples mixtures.[8,11-13] These equations can be extended to high ionic strengths, high temperatures and high pressures.[14-17] The various forms of the Debye–Hückel calculation show good accuracy up to 0.1$M$. At higher concentrations account must be taken of short range interionic forces that are specific to each solute. These terms which take into account the kinetic effect of the hard core have been included by Pitzer without disturbing the basic pattern of the Debye–Hückel equation and are presented as interaction or virial coefficients for each solute. The three virial parameters $\beta^{(0)}$, $\beta^{(1)}$ and $C^{\phi}$ have been evaluated from a wide variety of osmotic or activity coefficient data for pure electrolytes. These parameters take into account any ion pairing or weak association that may take place.

When mixing solutes, the additional combinations of coefficients, $\theta_{MX}$, $\theta'_{MX}$ and $\psi_{MNX}$ were added, however these coefficients were found to be small and frequently negligible.[18] Hence in evaluating activity coefficients in mixtures, it was found that the parameters, determined from the single solutes, are able, in most cases, to define the mixture completely. The Pitzer equations allow the prediction, with considerable accuracy, of the properties of mixtures, if the properties of each pure component are known. This is shown in equation (9). The equation is of the same form as that presented by Guggenheim, with the addition of a third virial coefficient. The second virial coefficient $B$,

is now dependent upon ionic strength and the parameters $\theta$ and $\psi$, which have little effect, have been omitted:[19]

$$\ln \gamma_A \gamma_X = (z_A^2 + z_X^2) f^{\gamma} + \sum_a m_a (2B_{Aa} + ZC_{Aa}) + \sum_c m_c (2B_{cX} + ZC_{cX}) + \sum_c \sum_a m_c m_a [(z_A^2 + z_X^2) B'_{ca} + (|z_A| + |z_X|) C_{ca}] \quad (9)$$

$$Z = \sum_i m_i |z_i| \quad (10)$$

$$f^{\gamma} = -A_\phi \left[ \frac{\sqrt{I_m}}{(1 + 1.2\sqrt{I_m})} + \frac{2\ln(1 + 1.2\sqrt{I_m})}{1.2} \right] \quad (11)$$

$$B' = -2\beta^{(1)} \frac{1 - \left(1 + \alpha\sqrt{I_m} + \frac{\alpha^2 I_m}{2}\right) e^{-\alpha\sqrt{I_m}}}{\alpha^2 I_m^2} \quad (12)$$

$$B = \beta^{(0)} + 2\beta^{(1)} \frac{1 - (1 + \alpha\sqrt{I_m}) e^{-\alpha\sqrt{I_m}}}{\alpha^2 I_m} \quad (13)$$

$$C = \frac{C^\phi}{2|z_+ z_-|^{1/2}} \quad (14)$$

where $f'$ is the general "Debye–Hückel" term for long-range forces; $B$ and $C$ are the second and third virial coefficients; and $B'$ is the derivative of $B$. $\beta^{(0)}$, $\beta^{(1)}$ and $C^\phi$ are empirical parameters, $m_i$ and $z_i$ represent the stoichiometric molality and charge of species $i$ and $I_m$ represents the molal ionic strength $= 0.5\ \Sigma m_i c_i^2$. For 1–1 and 2–1 electrolytes $\alpha = 2.0$ and at 25° $A_\phi = 0.391$. Equations (12) and (13) only apply to 1–1, 2–1 and 3–1 electrolytes.

The Pitzer parameters $\beta^{(0)}$, $\beta^{(1)}$ and $C^\phi$ for over 120 electrolytes have been published by the author and other workers in this field.[8,20] These parameters allow the above equation to be applied to a wide variety of mixed electrolytes at room temperature and at ionic strengths up to 6 molal in many cases and occasionally even higher. If measurements do not extend above 2 molal the third virial coefficient, $C$, can be omitted.

The Pitzer equation was converted by Millero to an individual ion form using the mean salt convention. Single ion activity coefficients in halide salt solutions have been successfully calculated.[21,22] The mean salt method used to obtain absolute values of ionic activity coefficients, has limitations when applied to salts which form ion pairs. The method is also limited to solutions of moderate ionic strength.[21] For these reasons we chose to use Pitzer's equation involving salt parameters.

In the experimental determination of solution equilibrium constants, it is normal practice to keep the ionic strength of the solution constants by using a monovalent background electrolyte, $AX$, at a concentration much higher than that of the reacting species. Under these conditions, as the interaction between species is weighted by their concentration, it is reasonable to assume that the activity coefficient of a species will depend only on its interaction with the background electrolyte, *i.e.* interaction with other species in solution are negligible. Using this approximation, equation (7) becomes:

$$\begin{aligned} \ln \Gamma_{pqr} = {} & \xi f^{\gamma} + \xi m_X^2 B'_{AX} + \sigma m_X^2 C_{AX} \\ & + 2qm_X B_{AL} + \xi m_L m_X B'_{AL} \\ & + \sigma m_X m_L C_{AL} + 2qm_X I C_{AL} \\ & + 2rm_X B_{HX} + \xi m_H m_X B'_{HX} \\ & + \sigma m_H m_X C_{HX} + 2rm_X I C_{HX} \\ & + 2pm_X B_{MX} + \xi m_M m_X B'_{MX} \\ & + \sigma m_X m_M C_{MX} + 2pm_X I C_{MX} \\ & - 2m_X B_J + \xi m_S m_X B'_J \\ & + \sigma m_X m_S C_J - 2m_X I C_J \end{aligned} \quad (15)$$

$$\xi = r + pz_M^2 + qz_L^2 - z_S^2, \quad (16)$$

$$\sigma = r + p|z_M| + q|z_L| - |z_S|, \quad (17)$$

for the reaction $pM + qL + rH \rightleftharpoons M_p L_q H_r$ where $M_p L_q H_r = S$. Depending on the charge of the product, the symbol $J$ refers to the salt parameter of the product, $S$, with either anion, $A$, or cation, $X$, of the background electrolyte, *i.e.* if $z_S > 0$ then $J = SX$, if $z_S < 0$ then $J = AS$ and if either $z_L$, $z_M$ or $z_S = 0$ then their relevant virial coefficients are set to zero.

From the activity coefficient quotient and the thermodynamic stability constant, the stoichiometric stability coefficient at any ionic strength can be calculated (equation (18)):

$$\ln \beta_{pqr} = \ln \Gamma_{pqr} + \ln {}^{T}\beta_{pqr}. \quad (18)$$

Note that the activity coefficient of the species $M_p L_q H_r$ depends on its concentration and the concentration of the free components in solution *i.e.* it depends on the speciation of the

solution. Initial estimates of these concentrations can be estimated from uncorrected $\beta$ values and then refined iteratively.

*Computer program*

A Turbo Pascal 6.0 program has been written to convert stability constants from one ionic strength to other ionic strengths. The Pitzer parameters are stored in binary files associated with the program and can be edited and updated. The program runs interactively and calculates the stability constants at ionic strengths specified as input. The results are plotted on the screen together with a curve showing the variation of the stability constant with ionic strength. Experimental stability constant values can also be plotted simultaneously for an evaluation of the calculated relationship. A copy of the program is available, from the authors, upon request.

## RESULTS AND DISCUSSION

Most experimental stability constants have been measured with molarity as basis, while the Pitzer approach is based on molality. Hence the literature stability constants and ionic strengths had to be converted to molality. This conversion is simple if the density of the solution is known. In potentiometric titrations the concentration of the salt is always in excess and the density of the solution approximates to the density of a solution containing the same concentration of pure salt. Hence molar concentrations were converted to a molal scale using equation (19) and the molar based stability constants were converted to a molal scale using the equation (20).

$$m_{AX} = \frac{[AX]}{\rho_{[AX]} - 0.001[AX]M_{AX}} \qquad (19)$$

$$\log \beta_{m,pqr} = \log \beta_{c,pqr} + (p + q + r - 1) \times \log(\rho_{[AX]} - 0.001 M_{AX}[AX]) \qquad (20)$$

where $M_{AX}$ and $m_{AX}$, are the molar mass and molality, respectively of the salt AX.

Density data for a range of aqueous electrolyte solutions at 25°, were taken from the literature.[23–25] A least squares fit of the density variation with molality for each electrolyte gave the following equations (equation (21)), where the value in brackets is the standard deviation in the last position of each number.

$$\rho_{KNO_3}(0\text{–}2.8M) = 0.99713(4) + 0.06181(7)\,[KNO_3] - 0.00099(3)\,[KNO_3]^2$$

$$\rho_{NH_4NO_3}(0\text{–}7.6M) = 0.9974(1) + 0.03149(7)\,[NH_4NO_3] - 0.000263(9)\,[NH_4NO_3]^2$$

$$\rho_{LiNO_3}(0\text{–}5M) = 0.9975(6) + 0.0395(6)\,[LiNO_3] - 0.0002(1)\,[LiNO_3]^2$$

$$\rho_{NaNO_3}(0\text{–}7.2M) = 0.9977(2) + 0.0545(1)\,[NaNO_3] - 0.00053(2)\,[NaNO_3]^2$$

$$\rho_{LiCl}(0\text{–}14M) = 0.9986(4) + 0.0222(1)\,[LiCl] - 0.00008(1)\,[LiCl]^2$$

$$\rho_{NaCl}(0\text{–}5.3M) = 0.9973(1) + 0.0400(1)\,[NaCl] - 0.00056(2)\,[NaCl]^2$$

Table 1. Literature Pitzer parameters

| Salt | $\beta^{(0)}$ | $\beta^{(1)}$ | $C^{\phi}$ | max ($m$) | $\sigma$ |
|---|---|---|---|---|---|
| HBr | 0.1960 | 0.3564 | 0.00080 | 3 | * |
| $HClO_4$ | 0.1747 | 0.2931 | 0.00819 | 5.5 | 0.002 |
| $HNO_3$ | 0.119 | 0.3206 | 0.0010 | 3 | 0.001 |
| $NaClO_4$ | 0.0554 | 0.2755 | −0.00118 | 6 | 0.001 |
| $LiNO_3$ | 0.1420 | 0.2780 | −0.00551 | 6 | 0.001 |
| $NH_4NO_3$ | −0.0154 | 0.1120 | −0.00003 | 6 | 0.001 |
| $NaNO_3$ | 0.0068 | 0.1783 | −0.00072 | 6 | 0.001 |
| $KNO_3$ | −0.0816 | 0.0494 | 0.00660 | 3.8 | 0.001 |
| $Ca(NO_3)_2$ | 0.2108 | 1.409 | −0.02014 | 2 | 0.002 |
| $Et_4NBr$ | −0.0176 | −0.394 | 0.0156 | 4 | 0.001 |
| Na Acetate | 0.1426 | 0.3237 | −0.00629 | 3.5 | 0.001 |

*High accuracy fit.[8]

A

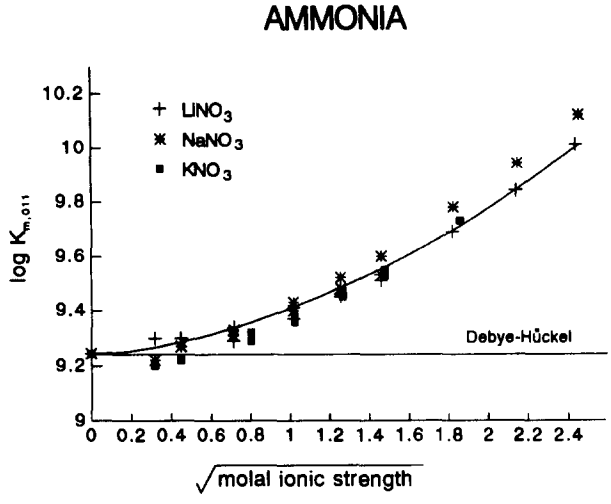


B

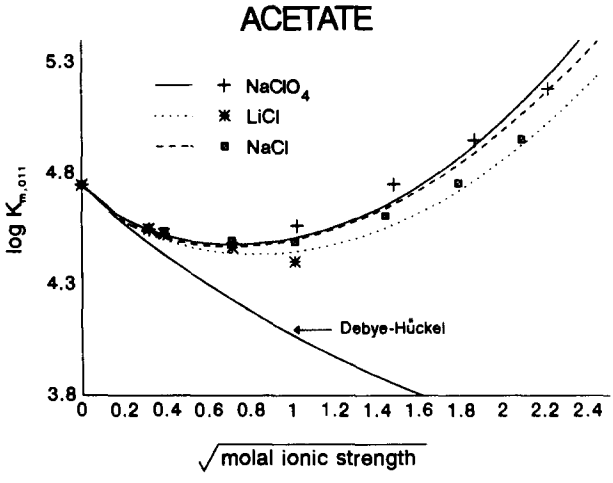


Fig. 1. Protonation constants as a function of ionic strength for various electrolytes. The symbols are experimental data points and the lines were calculated using the simplified Pitzer equation, literature Pitzer parameters and a literature $K^0$. A represents ammonia (log $K^0 = 9.244$) and B acetate (log $K^0 = 4.750$).[6,28]
The Debye–Hückel correction term (equations (11) and (15)), has been included for comparison.

$$\rho_{KCl}(0\text{–}4.1M) = 0.99729(9) + 0.0461(1)\,[KCl] - 0.00068(3)\,[KCl]^2$$

$$\rho_{LiClO_4}(0\text{–}3M) = 0.9973(3) + 0.0631(5)\,[LiClO_4] - 0.0006(2)\,[LiClO_4]^2$$

$$\rho_{NaClO_4}(0\text{–}4M) = 0.9976(8) + 0.078(1)\,[NaClO_4] - 0.0005(2)\,[NaClO_4]^2. \quad (21)$$

The literature Pitzer parameters used in the calculations are given in Table 1.

*Ammonia*

Figure 1(a) shows our simplified Pitzer approach applied to the protonation of ammonia. The symbols are experimental data points while the solid line is the calculated dependence of p*Ka* upon ionic strength. Experimental data were obtained from the literature.[25,26] The Debye–Hückel correction term is shown for comparison. For the uncharged ligand ammonia, the $\xi$ and $\sigma$ terms and hence also the Debye–Hückel term are all zero. As only interactions between ions of opposite sign are included only the *HX* and *SX* interaction

Table 2. Calculated Pitzer parameters

| Salt | $\beta^{(0)}$ | $\beta^{(1)}$ | Salt | $\beta^{(0)}$ | $\beta^{(1)}$ |
|---|---|---|---|---|---|
| Na propionate | 0.1165 | 0.312 | $NH_4$ Propionate | 0.0753 | 0.249 |
| K propionate | 0.1103 | 0.303 | $Et_4N$ Propionate | −0.027 | 1.100 |
| Ca propionate | 0.1061 | 0.921 | $NH_4H$ Succinate | 0.055 | 0.228 |
| NaH succinate | 0.0815 | 0.259 | $Et_4NH$ Succinate | −0.102 | 1.330 |
| KH succinate | 0.0716 | 0.243 | CaH Succinate | 0.0233 | 0.656 |
| Na succinate | 0.250 | 1.417 | $NH_4$ Succinate | 0.218 | 1.105 |
| K succinate | 0.236 | 1.368 | $Et_4N$ Succinate | −0.186 | 3.804 |
| †Ca succinate | 0.527 | 0.527 | | | |

*1–1 electrolyte relationship: $\beta^{(0)} = -0.043 + 0.332\beta^{(1)} + 0.574\beta^{(1)}\beta^{(1)}$. 1–2 electrolyte relationship: $\beta^{(0)} = -0.20(7) + 0.4(1)\beta^{(1)} - 0.03(6)\beta^{(1)}\beta^{(1)}$

†A relationship was not calculated for 2–2 electrolytes. To fit the curve $\beta^{(1)}$ was made equal to $\beta^{(0)}$.

coefficients were used in the ionic strength corrections. The resultant activity coefficient quotient reduces to:

$$\ln \Gamma_{011} = \ln \gamma_{H^+} - \ln \gamma_{NH_4^+}$$

$$= 2m_X(B_{HX} - B_{SX} + IC_{HX} - IC_{SX}). \quad (22)$$

According to the above equation, the cation of the background electrolyte has no affect on the activity coefficient quotient and the same ionic strength relationship was predicted for all nitrate salts. The experimental results for the different nitrates show a similar but not identical trend although the correlation between experimental and calculated results is good for $LiNO_3$ and reasonable for $KNO_3$ and $NaNO_3$.

*Acetate*

Figure 1(b) shows the comparison between the experimental and predicted protonation constants for acetate as a function of $NaClO_4$, LiCl and NaCl concentration.[27–29] Once again the correlation is good over the ionic strength range 0–4 mol/kg. For comparison the results of a Debye–Hückel correction are shown. Clearly the Debye–Hückel equation is not valid above an ionic strength of 0.1 mol/kg.

*Propionate*

For the propionate system not all the necessary Pitzer parameters were available in the literature. However, Pitzer noted a general relationship between the two parameters $\beta^{(0)}$ and $\beta^{(1)}$ for various electrolytes and suggested a

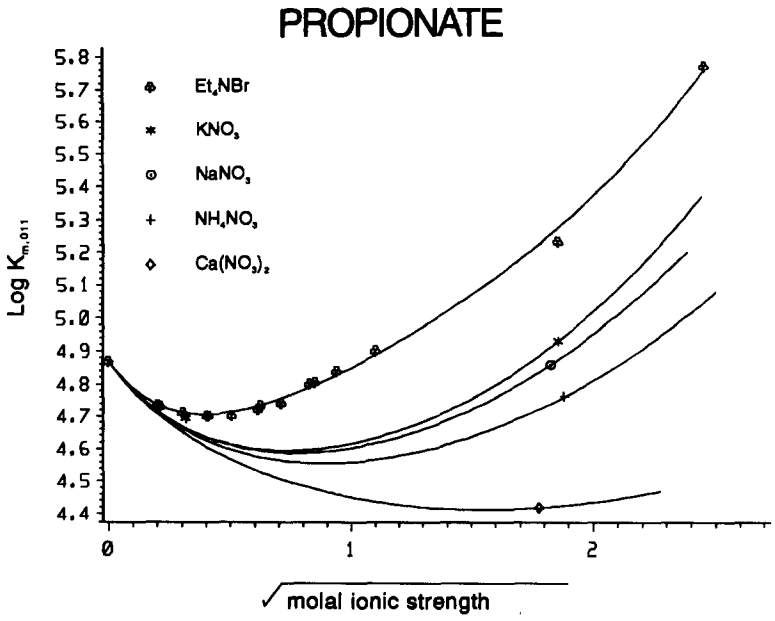


Fig. 2. Propionate's protonation constant as a function of ionic strength for various background electrolytes. The symbols are experimental data points and the solid lines were calculated using the simplified Pitzer equation, literature and calculated Pitzer parameters and a literature $K^0$ ($\log K^0 = 4.868$).

convenient approximation using this relationship to determine $\beta^{(1)}$ and $\beta^{(0)}$ from experimental data, if C is negligible.[30] At the ligand concentrations used to measure protonation constants of propionate, the contribution of terms involving the third virial coefficient to the overall activity coefficient, are small and so may be neglected. Many of the metal–ligand parameters were not available, and when only one protonation constant determined at $3M$ ionic strength, was available, these Pitzer parameters were calculated using the experimental value, the rough approximation method and log $K^0$. When more experimental constants had been determined, or literature values were available, the relevant Pitzer parameters were calculated using a least squares fit of the data. The calculated Pitzer parameters are given in Table 2 and the $\beta$ coefficient relationship used for each electrolyte type is given below the table. For propionic acid, dimerization is also possible but is only apparent at ligand concentrations greater than

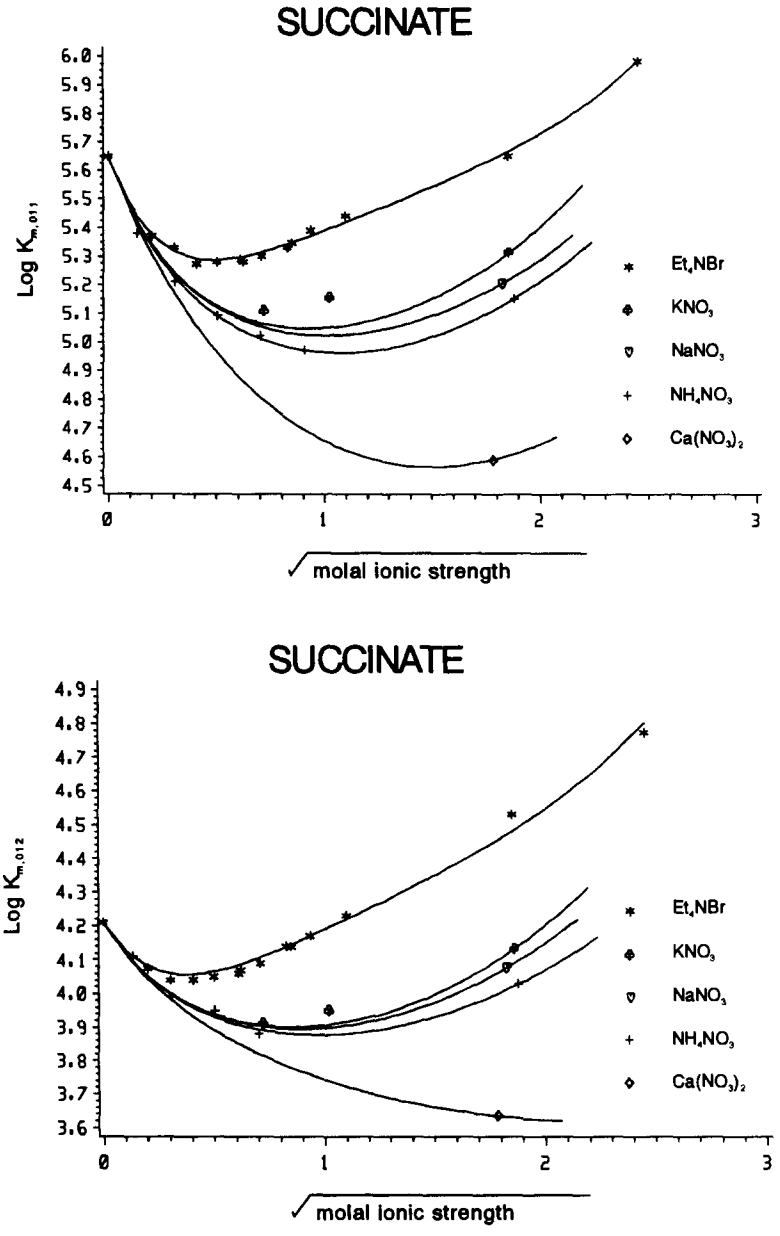


Fig. 3. The first and second protonation constant of succinate as a function of ionic strength for various background electrolytes. The symbols are experimental data points and the solid lines were calculated using the simplified Pitzer equation, literature and calculated Pitzer parameters and a literature $K^0$ ($\log K_1^0 = 5.648$, $\log K_2^0 = 4.209$).

0.05$M$ and so was ignored.[31] Figure 2 shows the experimental protonation constant of propionate measured in different ionic media and at different ionic strengths. Experimental data obtained from the literature have been included in the plot.[32,33] The solid lines in Fig. 2 are the calculated dependence of log $K_{011}$ upon ionic strength and ionic medium based on the parameters listed in Table 2.

### *Succinate*

Succinate presents an interesting example in that the ligand is diprotic and so the solution speciation will depend on the pH of the solution. Once again not all Pitzer parameters were available in the literature and so were estimated from experimental results at 3$M$ ionic strength, using the same procedure as before. The final set of parameters are listed in Table 2. Figures 3(a) and (b) show the experimental data for this system together with the calculated ionic strength dependence. Experimental data obtained from the Jess database and from the literature has been included for comparison.[33–36] These curves show that the simplified Pitzer approach is a good representation of the data.

## CONCLUSIONS

The Pitzer, semi-empirical, method of correcting equilibrium constants from one ionic strength to another or from one ionic medium to another works well for many different electrolytes. However, this method of data correction has not been widely used in equilibrium modelling mainly because of a lack of the necessary parameters for more complex systems. In this paper we have shown that, under the conditions normally used to measure equilibrium constants, that is high background electrolyte concentration relative to reacting species, a simplified Pitzer approach can be used. Using this simplified approach unknown $\beta^{(0)}$ and $\beta^{(1)}$ parameters can be estimated from equilibrium measurements at high ionic strength and then used to predict reliably, equilibrium constants under different modelling conditions. This method should greatly enhance the applicability of chemical equilibrium models.

*Acknowledgements*—The financial support of the University of Cape Town, the Foundation for Research and Development and AECI Ltd is gratefully acknowledged. L.F.S. acknowledges receipt of an AECI Fellowship.

## REFERENCES

1. D. R. Williams, *Chemical Speciation and Bioavailability*, 1989, **1**, 3.
2. Y-H. Li, *Geochim. Cosmochim. Acta*, 1991, **55**, 3223.
3. G. E. Jackson, S. Wynchank and M. Woudenberg, *Magn. Reson. Med*, 1990, **16**, 57.
4. P. W. Linder, A. Voye and S. Cocks, *NATO ASI Series*, 1990, **G23**, 91.
5. J. R. Duffield and D. R. Williams, *Chemistry in Britain*, 1989, 375.
6. A. E. Martell and R. M. Smith, *Critical Stability Constants*, Vols 1–6. Plenum Press, New York, 1989.
7. P. M. May, P. W. Linder and D. R. Williams, *J. Chem. Soc. Dalton Trans*, 1977, 588.
8. K. S. Pitzer, *Activity Coefficients in Electrolyte Solns*, R. M. Pytkowicz (ed.), Vol. 1. CRC Press, Florida, 1979.
9. I. Mills (Ed.), *Quantities, Units and Symbols in Physical Chemistry (IUPAC)*. Blackwell Scientific, Oxford, 1989.
10. M. T. Beck and I. Nagypal, *Chemistry of Complex Equilibria*. Wiley, New York, 1990.
11. K. S. Pitzer, *Acc. Chem. Research*, 1977 **10**, 371.
12. K. S. Pitzer and J. J. Kim, *J. Am. Chem. Soc.*, 1974, 5701.
13. K. S. Pitzer, *J. Phys. Chem.*, 1973, **77**, 268.
14. R. T. Pabalan and K. S. Pitzer, *ACS Symp. Ser.*, 1990, **416**, 44.
15. K. S. Pitzer, *J. Phys. Chem.*, 1984, **88**, 2689.
16. K. S. Pitzer, *Pure & Appl. Chem.*, 1989, **61**, 979.
17. D. J. Bradley and K. S. Pitzer, *J. Phys. Chem.*, 1979, **83**, 1599.
18. K. S. Pitzer, *Pure & Appl. Chem.*, 1986, **58**, 1599.
19. J. F. Zemaitis, D. M. Clark, M. Rafal and N. C. Scrivner, *Handbook of Aqueous Electrolyte Thermodynamics—Theory & Appl. AIChE*, DIPPR, New York, 1986.
20. C. E. Harvie, N. Moller and J. H. Weare, *Geochim. Cosmochim. Acta*, 1984, **48**, 723.
21. F. J. Millero and D. R. Schreiber, *Am. J. Science*, 1982, **282**, 1508.
22. F. J. Millero and D. J. Hawke, *Marine Chemistry*, 1992, **40**, 19.
23. E. W. Washburn (Ed.), *Int. Critical Tables of Numerical Data*, Vol. III. McGraw, London, 1928.
24. R. H. Perry and D. Green, *Perry's Chemical Engineer's Handbook*, 6th ed. McGraw-Hill, Singapore, 1988.
25. M. Maeda, G. Nakagawa and G. Biedermann, *J. Phys. Chem.*, 1983, **87**, 121.
26. K. Szabo, I. Nagypal and I. Fabian, *Talanta*, 1983, **30**, 801.
27. R. K. Cannan and A. Kibrick, *J. Am. Chem. Soc*, 1938, **60**, 2314.
28. A. De Robertis, C. De Stefano, S. Sammartano and R. Scarcella, *J. Chem. Research(M)*, 1985, 629.
29. O. Johansson and W. Wedborg, *J. Soln. Chem.*, 1985, **14**, 431.
30. K. S. Pitzer and G. Mayorga, *J. Phys. Chem.*, 1973, **77**, 2300.
31. D. L. Martin and F. J. C. Rosotti, *Proc. Chem. Soc.*, 1959, 60.
32. E. Dubler, U. Haring, K. Scheller, P. Baltzer and H. Sigel, *Inorg. Chem.*, 1984, **23**, 3785.
33. A. De Robertis, C. De Stefano, C. Rigano and S. Sammartano, *J. Solution Chemistry*, 1990, **19**, 569.
34. P. M. May and K. Murray, *Talanta*, 1991, **38**, 1409.
35. P. M. May and K. Murray, *Talanta*, 1991, **38**, 1419.
36. A. De Robertis, C. De Stefano, S. Sammartano and R. Scarcella, *J. Chem. Research(S)*, 1985, 322.

Pergamon

0039-9140(94)00205-3

*Talanta*, Vol. 42, No. 1, pp. 17–25, 1995

0039-9140/95 $9.50 + 0.00

# PULSED ELECTROCHEMICAL DETECTION OF PENICILLINS USING THREE AND FOUR STEP WAVEFORMS

SELEN ALTUNATA, ROSA L. EARLEY, DANIEL M. MOSSMAN and LAWRENCE E. WELCH*
Department of Chemistry, Knox College, Galesburg, IL 61401, U.S.A.

(*Received* 15 *October* 1993. *Revised* 29 *June* 1994. *Accepted* 8 *July* 1994)

**Summary**—Aided by the construction of a custom potentiostat, a series of different PAD waveforms were compared to find the optimum detector for penicillin oxidation. The waveforms included standard 3-step direct and indirect PAD in addition to reverse-PAD and 4-step PAD. Two new waveforms, the indirect reverse-PAD and the 4-step indirect PAD were examined in the study. Under the solvent conditions of the study (0.01 *M* acetate buffer, pH 4.6) the indirect waveforms yielded the best detectability for penicillin G while the reverse-PAD waveforms yielded the worst performance. The 4-step PAD methods did not improve detectability when compared to the 3-step types, but they did provide output peak profiles with better shapes and less tailing. Although indirect waveforms gave better detectability than direct detection in the 0.01 *M* acetate buffer solution, the limits of detection for each were found to be differing functions of ionic strength. At higher acetate concentrations, direct PAD was more favorable than indirect detection.

The use of amperometric detectors for HPLC offers great selectivity for detection of oxidizable and reducible analytes. Constant potential (DC) amperometry is the simplest form of this detector genre, offering great sensitivity for aromatic organic species and some inorganics.[1,2] The application of DC amperometric detection on noble metal electrodes to aliphatic organic compounds has not proven as fruitful, as both the sensitivity and reproducibility of response are poor.[3–5] This has been attributed to the inability to maintain an active catalytic oxide surface at the working electrode, either by conversion of the oxide to a passive, less catalytic form or by fouling from adsorbates. Adams,[6] noted that electrode ignition, cleaning with chromic or nitric acid, and excursions to potential extremes could all be used in such cases to restore electrode sensitivity. The development of pulsed amperometric detection (PAD) in a sense adapted the potential excursion treatment into one that could be done *in situ* while performing amperometric detection.[7,8] A detection step directly oxidized analytes as in DC amperometry, but was maintained for only a short period of time (typically less than 1 sec). This was followed by a step to a very positive potential to fully oxidize the electrode surface, and then a negative potential step to reduce the surface and provide a clean oxide-free electrode. The entire waveform was repeated at 1–2 Hz, and by use of a lock-in amplifier circuit the current output was sampled only during the detection potential, then held until the next waveform cycle. The use of this original PAD waveform quickly found application for the detection of numerous aliphatic organic compounds.[9–14]

Whereas the original application of PAD oxidized the analyte molecules directly during the detection step, it was found that PAD also would allow some molecules to be monitored indirectly. Using essentially the original PAD waveform, injections into a flowing stream gave "negative" peaks, *i.e.* a decrease in anodic current, for $Cl^-$ in acid, $CN^-$ in base,[15] and for $I^-$ in acid.[3,15] This was attributed to the adsorption of these species, causing a reduction of background current from the formation of electrode surface oxide, with the concurrent absence of any faradaic signal from oxidation of these adsorbates. Indirect PAD was not limited solely to producing "negative" peak response, as $CN^-$ in basic solution can yield enhanced anodic response, *i.e.* "positive" peaks, in an indirect manner.[15] The adsorption of the $CN^-$ causes the kinetics of oxide formation to be altered, creating a potential region where the current from

*Author to whom correspondence should be addressed.

oxide formation is suppressed, and a region where it is enhanced. By selecting a potential in the enhancement region, "positive" response was observed. The absence of $CN^-$ oxidation at this potential led to this method being classified as indirect PAD. Other analytes showing "positive" response were conjectured to be the result of mixed direct and indirect detection.[15]

Early PAD work featured integration of output current for 16.7 msec at the end of the detection potential step, with the original intent being to minimize interference from 60 Hz background signals, but driven in later years by hardware limitations of early generation PAD equipment. An examination of the current integration period found that the use of times longer than 16.7 msec was beneficial for some analytes.[16] The longer integration periods were selected as multiples of 16.7 msec so that the reduction of 60 Hz noise was still effective. Waveforms employing these longer integration periods were originally classified by the title pulsed coulometric detection (PCD), but more recent literature has reclassified them as PAD waveforms.[4]

Polta and Johnson[17] were the first to describe the application of a new PAD waveform with the position of the oxidative and reductive steps following detection inverted. Essentially this eliminated the oxidative cleaning step, as the final oxidative step served to grow the catalytic oxide prior to the detection step in an effort to reduce noise. This waveform yielded better sensitivity than the original PAD method when applied to the detection of thiourea in basic media. The new waveform was not given a title other than PAD in this original work, but a more recent investigation[18] has classified this as a reverse-PAD (R-PAD) waveform to differentiate it from the standard PAD waveform, which was classified as normal-PAD (N-PAD). This recent work studied the R-PAD waveform and concluded that it would be beneficial to use a four step R-PAD waveform. This would insert an anodic cleaning step between the detection step and the cathodic cleaning step while maintaining the final oxidative step to pre-grow surface oxide.

PAD has recently been applied for the detection of penicillins in this laboratory.[5,19,20] Both direct PAD and indirect PAD ("negative" peaks) were found to yield sensitive detection, with the solvent composition determining which of the two gave best results. Direct PAD was best in an aqueous solution of acetate buffer, but when the solvent was altered in preparation for use as an HPLC mobile phase by the addition of organic modifier, the indirect PAD yielded better detectability.[19] It is the goal of this study to examine the use of alternative detection schemes such a R-PAD and 4-step PAD waveforms to determine their practicality for penicillin detection and to understand their function. It should be noted that commerical PAD potentiostats do not allow the use of 4-step waveforms, so their exploration required the construction of a "homemade" potentiostat.

## EXPERIMENTAL

All penicillins were purchased from Sigma (St Louis, MO, USA). All other solutions were made from reagent-grade chemicals from Aldrich (Milwaukee, WI, USA), Baker (Phillipsburg, NJ, USA), or Fisher (Pittsburgh, PA, USA). Water was distilled and deionized before use as a solvent.

Flow injection analysis for the ionic strength variation was done with a Waters 625 LC system (Milford, MA, USA) and a Waters 464 Pulsed Electrochemical Detector. A thin-layer cell was utilized with a single gold working electrode. The counter electrode was a stainless steel block mounted opposing the thin-layer cell, with the flow channel created by a teflon spacer between the two. The reference electrode was a Ag/AgCl. A 50-$\mu$l sample injection loop was employed with this system, and a flow rate of 1 ml/min was standard.

Flow injection analysis for all other experiments described was done using a SSI (State College, PA, USA) Model 300 LC pump with an SSI Model LP-21 pulse dampener and a BAS (West Lafayette, IN, USA) CC-5 flow cell compartment. Potentiostatic control was provided by a Pine Instruments (Grove City, PA, USA) RDE4 potentiostat with external voltage control driven by a Keydata (S. Plainfield, NJ, USA) 486DX2-50 IBM-compatible computer running VIEWDAC 2.1 software from Keithley/MetraByte (Taunton, MA, USA), interfaced with a Keithley DAS-20 interface card and screw terminal board. A dual gold electrode block was used, with the upstream element serving as the working electrode. The counter electrode was a stainless steel block mounted opposing the thin-layer cell, with the flow channel created by a teflon spacer between the two. The reference electrode was a Ag/AgCl. A 50-$\mu$l sample injection loop and a flow

rate of 0.5 ml/min were employed with this system.

A BAS MF-2060 Polishing Kit was used to polish the working electrode; in addition potential cycling to the voltage limits of the system, as defined by the onset of solvent breakdown, was helpful to restore electrode activity following temporary losses of sensitivity. Injected penicillin solutions were all solvent matched with the mobile phase to avoid having a system peak overlapping with the analytical peak. All mobile phases were vacuum filtered through an Alltech (Deerfield, IL, USA) 0.45-$\mu$m nylon filter. Flow injection detector signal polarity was inverted so that increased anodic response would produce peaks rather than troughs on the output plots. All output was filtered through a low-pass frequency filter. Recorded PAD data for quantitative studies was treated with a fourier transform smoothing algorithm to further minimize high frequency noise, and to minimize the impact of regular pump pulsations arising from the lack of back pressure during flow injection trials. Peak heights were used for detection limit and reproducibility calculations. Detection limits ($S/N = 3$) were found by extrapolation from higher concentrations.

## RESULTS AND DISCUSSION

### *Potentiostat development*

The potentiostat used for the waveform optimization work was put together from separate components which are listed above in the Experimental section. The advantage of building this instrument was that it allowed great flexibility in selection of amperometric waveform, which can only be obtained commercially in a very expensive instrument not designed for PAD. The disadvantage of a homemade instrument is that it is likely to suffer from a greater degree of electrochemical noise than a well-made commercial unit. The components that we chose to construct our potentiostat are by no means unique; there are many different options for both software and hardware. One particular concern should be to obtain an interface card that allows both bipolar analog outputs (voltage) and inputs (current); many otherwise very sophisticated and powerful interface cards are only unipolar in nature. Another very important note is that some sample voltage waveforms must be checked with an oscilloscope for validity before the potentiostat can be trusted. We found that some software instructions for a particular potentiostatic function were too cumbersome for the computer to handle in a timely fashion, resulting in slower operation than had been instructed. For example, points to be collected at 1.000 sec intervals may actually be collected at $\sim$1.4 sec intervals if the software is not streamlined. The only way to be certain of the integrity of the user-selected time-dependent operations embedded within a software routine is to check them with an oscilloscope.

Another concern is the need to allow "idle" time to be programmed during the initial phase of an experiment. Whenever an amperometric waveform is initially sent to an electrochemical cell or whenever a significant change in the waveform is made, the current output of the system will change sharply and generally will drift substantially for a number of minutes before the cell reaches an equilibrium state. Any data taken before equilibrium is complete will be suspect; in particular the reproducibility of detector response will be poor. An example of this can be seen in Fig. 1, where the change in output response during equilibration is so acute that the peak polarity inverts for injections of the same solution at differing times following waveform initiation. Although it requires extra programming time, it is essential to produce software that will allow initiation of the desired PAD waveform at the electrochemical cell well before any current data are collected. We found 10 min to be the minimum acceptable idle time with our particular setup.

The potentiostatic software that was developed allowed from one to four potential steps within a waveform, each with a selectable voltage and duration. Current integration always took place during the initial step, although this was not required by the software, and could be done for any length of time desired. Once collected, the raw output data were treated with a low-pass filter and a fourier transform smoothing function as noted in the Experimental section.

### *Waveform optimization*

The names of the waveforms used herein are not completely standardized, so in an effort to clarify the type being used each is illustrated in Table 1 along with a title. 3-step direct PAD (Table 1A) is the standard form of PAD that has been used extensively since the work of Hughes *et al.*[7,8] An oxidative detection step is followed by a step to a more positive potential to provide oxidative cleaning, producing a fully

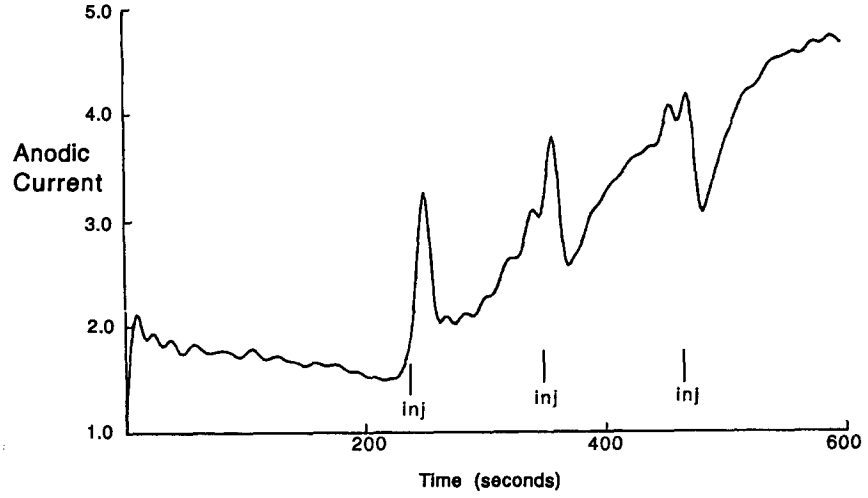


Fig. 1. Detector instability in the absence of a waveform idle period. Flow injection analysis: three injections of $1 \times 10^{-4}M$ penicillin G in a $0.01M$ acetate buffer solvent. Waveform: E1 = 1.1 V for 668 msec, E2 = 1.3 V for 668 msec, E3 = −0.2 V for 835 msec, integrate 17–668 msec.

oxide covered electrode. This is followed by a step to more negative potentials to reduce the surface oxide, providing a clean metal surface which can react with adsorbates. 3-step indirect PAD[5,15] (Table 1B) uses the same basic waveform shape as 3-step direct PAD, although typically the detection step is either less positive, has a shorter duration, or both in comparison to the direct waveform. Indirect PAD results in a change in peak polarity, which is due to suppression of the anodic background signal from the formation of surface oxide at the detection potential. This is suppressed in the presence of an analyte that will adsorb to the electrode surface, resulting in the production of less surface oxide and correspondingly less current from this process. Many adsorbates produce direct PAD response, where the suppression is more than offset by current from oxidation of the adsorbate. However, in indirect PAD the waveform is created to encourage analyte adsorption but to slow its oxidation such that the anodic current produced is not enough to offset the suppressive effect.

Inverse PAD, although not previously used in this lab, has been described by Polta and Johnson,[17] and Roberts and Johnson.[18] The standard form, referred to as direct reverse-PAD (Table 1C) has the anodic and cathodic cleaning steps reversed when compared to 3-step direct PAD. For this to work, the detection potential chosen must be positive enough such that the oxidative cleaning step is not necessary. Following a cathodic cleaning step, a short anodic step is made. This step is designed to "pre-grow" the catalytic oxide necessary for oxidation of the analyte. By forming this oxide prior to the detection step, a reduction in background signal

Table 1

| | A | B | C | D | E | F |
|---|---|---|---|---|---|---|
| **Title** | 3-step direct PAD | 3-step indirect PAD | direct reverse-PAD | indirect reverse-PAD | 4-step direct PAD | 4-step indirect PAD |
| **Polarity** |  |  |  |  |  |  |
| **Waveform Schematic** | 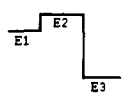 | 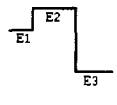 | 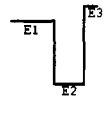 | 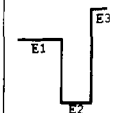 | 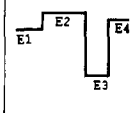 | 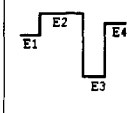 |

(and noise) during detection can be enabled. The short time of this step is critical, as the catalytic "lower oxide" is transient, and at longer times the lower oxide will be converted to the higher oxide, which is not catalytic for most PAD analytes. It was also possible to do indirect reverse-PAD (Table 1D), which has not been described previously in the literature. This waveform has essentially the same structure as direct reverse-PAD, but as in other indirect waveforms the polarity of reponse shifts as the suppression of the anodic background signal predominates. This would seem to be a very unlikely waveform, as a majority of the anodic current from formation of surface oxide would presumably be occurring during the oxide pre-growth phase in step 3, so would not be available for suppression during the detection step. However, this viewpoint only focuses on sensitivity; whereas the oxide pre-growth should result in a much smaller amount of anodic signal than is available for suppression, the degree of uncertainty of this current level should also be smaller. Thus, the background noise should also be less. When evaluating the waveform based on the $S/N$ of response, it can be envisioned that this waveform could be valuable if the reduction in noise was great enough to offset the loss in sensitivity. The construction of an indirect reverse-PAD waveform from direct reverse-PAD generally requires a shift to less positive detection potentials and shorter times for the oxide pre-growth step.

The ability to program waveforms with greater than three potential steps allows the creation of additional PAD waveforms. 4-step direct PAD (Table 1E) has been proposed as advantageous by Roberts and Johnson.[18] During the discussion of direct reverse-PAD, it was noted that this waveform does not have an oxidative cleaning step, relying on the detection potential for this purpose. The availability of a fourth step in the waveform allows the oxidative cleaning step to be retained while still having an oxide pre-growth step just prior to detection. Finally, Table 1F details a 4-step indirect PAD waveform, which also has not been utilized in any published work. The structure of this waveform is basically the same as the previous one, the difference being that the polarity of the output current is inverted, being controlled by suppression of the anodic background signal. As with indirect reverse-PAD, this waveform will theoretically suffer from poor sensitivity, as the fourth potential step for oxide pre-growth will limit the amount of background signal available for suppression during the detection step. Again, as mentioned above, the possible advantage for this type of waveform lies in the fact that noise should be reduced, perhaps to a greater extent than the loss in sensitivity.

Experiments were run to produce the best example of each of the waveforms mentioned above in terms of $S/N$. These waveforms are listed in Table 2 along with their detection limit for penicillin G and the % relative standard deviation (RSD) of response for a set of five consecutive injections of a $1 \times 10^{-4} M$ penicillin G solution. The solvent system chosen was $0.01 M$ acetate buffer (pH 4.6), which was similar to that used for previous flow injection trials for penicillins in this laboratory.[5] The reader should be cautioned that although the performance of the potentiostat was adequate, it does suffer from higher noise levels than its commercial counterparts. As such, slightly better detection limits can be achieved for the 3-step waveforms using a good commercial instrument. However, the absolute values of the detection limits were less important than their comparison for the different waveforms. Although larger than ideal, the noise should impact the different waveforms to the same degree, allowing them to be compared fairly.

From Table 2, it can be seen that all integration times selected were longer than 250 msec. When the traditional 16.7 msec integration time was tested, it was found to yield worse response for all waveforms in terms of both sensitivity and noise. It is interesting to note that in comparison of 3-step direct and 3-step indirect PAD, both optimized waveforms use the same detection potential. Usually, the indirect method will utilize a slightly smaller potential. However, the variations in the other facets of the waveforms are enough to alter the oxidation kinetics to the degree whereby output polarity is inverted. The performance of the indirect method leads to a superior detection limit when comparing the two; a comparison of the output traces can be seen in Fig. 2. The superiority of the indirect PAD method leads to a seeming paradox when comparing this data with that obtained by Koprowski *et al.*[5] In this work, while also using an acetate buffer solvent, a 3-step direct PAD waveform was found to give better detectability than its indirect counterpart. Although the data sets were obtained with different detectors, which would explain some variation in detection limit, this would not

Table 2. Optimized PAD waveforms for penicillin G injections

| Title | Waveform | % Relative standard deviation | Detection limit ($M$) |
|---|---|---|---|
| 3-step direct PAD | E1: 1.3 V for 501 msec<br>E2: 1.6 V for 668 msec<br>E3: −0.3 V for 668 msec<br>Integrate: 17–501 msec | 2.4 | $2 \times 10^{-6}$ |
| 3-step indirect PAD | E1: 1.3 V for 300 msec<br>E2: 1.5 V for 400 msec<br>E3: −0.2 V for 400 msec<br>Integrate: 5–300 msec | 1.7 | $6 \times 10^{-7}$ |
| Direct reverse-PAD | E1: 1.3 V for 501 msec<br>E2: −0.4 V for 224 msec<br>E3: 1.6 V for 334 msec<br>Integrate: 17–501 msec | 20.8 | $3 \times 10^{-6}$ |
| Indirect reverse-PAD | E1: 1.2 V for 668 msec<br>E2: −0.5 V for 334 msec<br>E3: 1.7 V for 68 msec<br>Integrate: 68–668 msec | 4.6 | $5 \times 10^{-6}$ |
| 4-step direct PAD | E1: 1.6 V for 668 msec<br>E2: 1.7 V for 334 msec<br>E3: −0.4 V for 334 msec<br>E4: 1.65 for 17 msec<br>Integrate: 68–668 msec | 3.8 | $3 \times 10^{-6}$ |
| 4-step indirect PAD | E1: 1.3 V for 300 msec<br>E2: 1.5 V for 400 msec<br>E3: −0.2 V for 400 msec<br>E4: 1.4 V for 17 msec<br>Integrate: 5–300 msec | 4.2 | $8 \times 10^{-7}$ |

reasonably explain why direct PAD would be more favorable on one instrument and indirect PAD on the other.

On close examination of the two experiments, it can be found that although both use acetate buffer solvents, the concentrations are slightly differnt ($0.01M$ here *vs.* $0.2M$ in Ref. 5). A set of experiments were run to examine the possibility that this paradox could be explained by the difference in ionic strength of the acetate buffer. Acetate buffer solutions, all at pH 4.6, were made throughout the range of $0.0005$–$0.3M$. For each different solvent, both a 3-step direct PAD and 3-step indirect PAD waveform were optimized. The optimized waveforms were then used to find a detection limit for solvent-

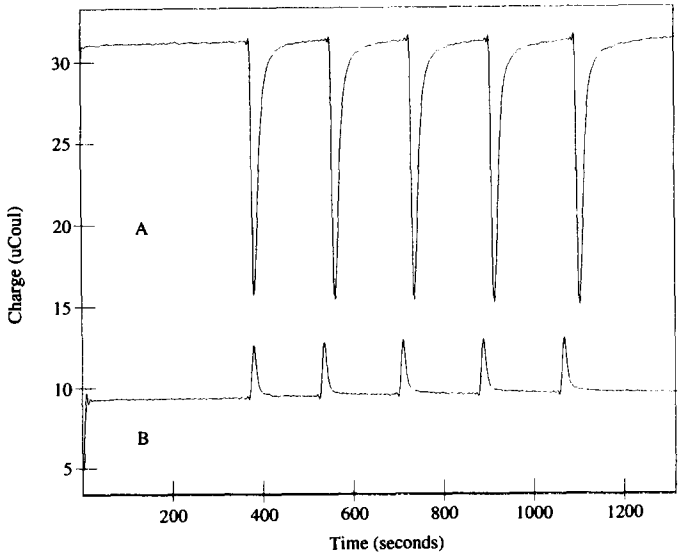


Fig. 2. A comparison of 3-step indirect (A) and 3-step direct (B) PAD. Flow injection analysis: $1 \times 10^{-4}M$ penicillin G in $0.01M$ acetate buffer. Waveforms are given in Table 2.

matched solutions of penicillin G. A plot of the resultant detection limits *vs.* log of acetate concentration is given in Fig. 3. The concentrations were plotted in logarithmic form to allow the variation with concentration to be observed without crowding in the lower region of the concentration scale. At higher concentrations the direct PAD waveform yielded better detection limits, but as acetate concentration is reduced a crossover is observed and the negative PAD produces lower detection limits. This could explain why Koprowski *et al.*,[5] working at high ionic strength, would find positive PAD to be more favorable, while the lower ionic strength used in this work would lead to just the opposite result.

As the electrolyte concentration is reduced, one would expect the oxidation kinetics to be slowed due to the development of an *iR* drop. This problem is noted to be a relatively common occurrence when using a thin-layer electrochemical cell unless a solvent with a high ionic strength is used.[21] The high current requirement for a pulsed waveform and the extreme potentials used to promote penicillin oxidation exacerbate the *iR* drop problem. This has a deleterious effect on direct PAD waveforms, as this tends to attenuate their output response, shifting them toward the crossover to indirect PAD. The application of greater overpotential

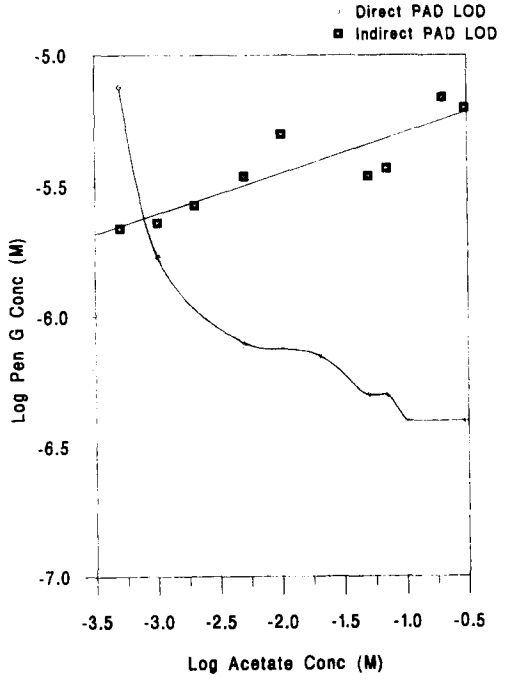


Fig. 3. Penicillin G detectability as a function of acetate concentration in the solvent.

to offset the *iR* drop is not beneficial, as it causes a sharp increase in noise. The *iR* drop caused by the use of a low ionic strength solvent and the resultant slower analyte oxidation kinetics are not a problem for indirect PAD. In fact, it may actually be beneficial since the slowed kinetics are the genesis of the indirect response. High electrolyte concentrations may actually be bad for indirect PAD, as it may be difficult to create a waveform that will produce a slow enough rate of analyte reaction while still forming electrode surface oxide, the growth of which is necessary for indirect PAD. This is illustrated in Fig. 3, as at very high electrolyte concentrations the performance of indirect PAD actually becomes poorer. It is unlikely that the ionic strength effect is a result of a change in analyte adsorption. Adsorption takes place at a separate step in the PAD waveform from detection, and in general the adsorption steps are uniform regardless of waveform type within this work. Since the direct and indirect PAD waveforms feature similar analyte adsorption steps, one would expect that if adsorption was affected by ionic strength it would cause a similar change in both waveforms, rather than the dissimilar one that is observed.

Neither of the reverse-PAD waveforms gave good results. Although the detection limit of the direct reverse-PAD waveform is almost as good as the 3-step direct PAD value, the reproducibility is unacceptable for practical use. The indirect reverse-PAD has a much better RSD, but its detection limit is nowhere close to either of the first two waveforms. It should be noted that reverse-PAD is not universally valuable for all analytes;[22] some analytes respond quite poorly to this type of detection. Most of the analytes that have benefitted from reverse-PAD were sulfur species,[17,22] so it is somewhat of a surprise that the penicillin, with its active sulfide site, was not a better candidate for reverse-PAD.

Neither of the 4-step PAD waveforms offered any gains in detectability. The 4-step direct PAD waveform had virtually the same detection limit as direct reverse-PAD, but this was still three times higher than for 3-step direct PAD. The 4-step indirect PAD, like the 3-step waveforms, gave significantly better output than its direct counterpart. The performance is still slightly poorer than for 3-step indirect PAD, as can be seen in Fig. 4. It can be noted from viewing this figure that the changes in response expected upon moving to a 4-step waveform are indeed present. The added oxide pre-growing

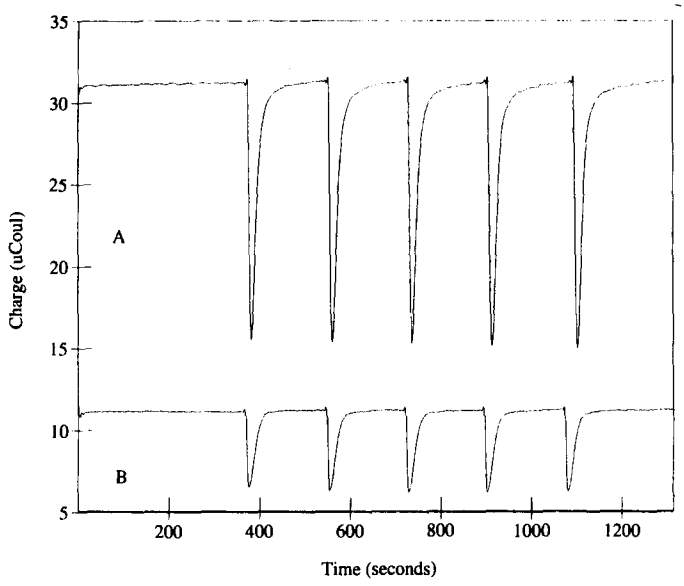


Fig. 4. A comparison of 3-step indirect (A) and 4-step indirect (B) PAD. Flow injection analysis: $1 \times 10^{-4}M$ penicillin G in $0.01M$ acetate buffer. Waveforms are given in Table 2.

step did cause the sensitivity to drop for 4-voltage PAD (16.248 *vs.* 5.080 mean peak heights). The noise level did improve with the addition of the fourth potential step (0.03241 *vs.* 0.01356 standard deviations). Nevertheless, the overall $S/N$ evaluation shows that the 3-step indirect PAD is still superior.

At first glance the data would seem to support the fact that there is no need to produce a potentiostat that can be programmed beyond three potential steps. However, there is a final consideration that does favor the 4-step waveform: peak shape. There is more tailing in the peaks in part A, whereas the 4-step peaks are superior in this regard. The degree of peak distortion can be quantitated by measuring the peak asymmetry factor,[23,24] which gives a value of 4.06 for the 4-step PAD *vs.* 4.24 for 3-step. Although there has been no definitive study detailing the relationship between peak shape and PAD waveform, it has been clearly demonstrated that pulsed electrochemical detection can lead to significant peak tailing,[24] the degree of which is dependent on the waveform design. This is particularly important for indirect PAD, where this has been shown to be more of a problem than for direct PAD.[22] The difference in asymmetry factors is not large, however, it should be noted that the optimization process was based on detectability rather than peak shape. Experience with the two waveforms has shown that the presence of the extra potential step inevitably allows the 4-step waveform to be adjusted to produce better peak shapes than are obtainable with the 3-step. For HPLC experiments where resolution is critical, this new waveform will be a better detector choice than existing 3-step waveforms, as the sacrifice in detectability is small. It should also be noted that although the detectability advantage of the 3-step waveform is clear within the system studied in this project, it is likely that future experimentation with varying solvent systems and sample matrices will uncover conditions for which the 4-step waveform gives the lowest detection limit.

## CONCLUSION

PAD response will vary with ionic strength, even for solutions with the same qualitative composition. This change in electrolyte concentration will change the kinetics of electrochemical response at various PAD waveforms; typically at low ionic strengths the direct PAD response suffers the greatest due to the larger current involved with this process. Indirect PAD waveforms are typically less favorable in the presence of sufficient electrolyte, but at low ionic strengths will become preferable to direct PAD, as the change in oxidation kinetics is less of a problem.

The ability to produce a PAD waveform with four potential steps instead of the traditional three did not result in improved detectability. The detection limit for a 4-step indirect PAD

waveform was only slightly higher than for 3-step indirect PAD, and the obtained peak profiles showed less tailing. The improved peak shapes obtained with the four step waveform will allow improved chromatographic resolution when compared with other forms of PAD.

*Acknowledgements*—This research was supported by an award from Research Corporation. Financial support for RLE was the result of a grant to the college from the U.S. Department of Education's Ronald E. McNair Post-Baccalaureate Achievement Program. Financial support for SA was the result of a grant to the college from the Howard Hughes Medical Institute's Undergraduate Biological Sciences Education Initiative. The generous donation of equipment from the Waters Chromatography Division of the Millipore Corporation is acknowledged with gratitude.

## REFERENCES

1. D. C. Johnson, S. D. Weber, A. M. Bond, R. M. Wightman, R. E. Shoup and I. S. Krull, *Anal. Chim. Acta*, 1986, **132,** 187.
2. L. E. Welch and D. C. Johnson, *J. Liq. Chromatogr.*, 1990, **13,** 1387.
3. D. S. Austin-Harrison and D. C. Johnson, *Electroanalysis*, 1989, **1,** 189.
4. D. C Johnson and W. R. LaCourse, *Anal. Chem.*, 1990, **62,** 589A.
5. L. Koprowski, E. Kirchmann and L. E. Welch, *Electroanalysis*, 1993, **5,** 473.
6. R. N. Adams, *Electrochemistry at Solid Electrodes*. Marcel Dekker, New York, 1969.
7. S. Hughes, P. L. Meschi and D. C. Johnson, *Anal. Chim. Acta*, 1981, **132,** 1.
8. S. Hughes and D. C. Johnson, *Anal. Chim. Acta*, 1981, **132,** 11.
9. D. S. Austin, J. A. Polta, T. Z. Polta, A. P.-C. Tang, T. D. Cabelka and D. C. Johnson, *J. Electroanal. Chem.*, 1984, **168,** 227.
10. S. Hughes and D. C. Johnson, *J. Agric. Food Chem.*, 1982, **30,** 712.
11. J. A. Polta, D. C. Johnson and K. E. Merkel, *J. Chromatogr.*, 1985, **324,** 407.
12. A. Ngoviwatchai and D. C. Johnson, *Anal. Chim. Acta*, 1988, **215,** 1.
13. L. E. Welch, W. R. LaCourse, D. A. Mead Jr and D. C. Johnson, *Anal. Chem.*, 1989, **61,** 555.
14. W. R. LaCourse, W. A. Jackson and D. C. Johnson, *Anal. Chem.*, 1989, **61,** 2466.
15. J. A. Polta and D. C. Johnson, *Anal. Chem.*, 1985, **57,** 1373.
16. G. G. Neuberger and D. C. Johnson, *Anal. Chim. Acta*, 1987, **192,** 205.
17. T. Z. Polta and D. C. Johnson, *J. Electroanal. Chem.*, 1986, **209,** 159.
18. R. Roberts and D. C. Johnson, *Electroanalysis*, 1992, **4,** 741.
19. E. Kirchmann and L. E. Welch, *J. Chromatogr.*, 1993, **633,** 111.
20. E. Kirchmann, R. L. Earley and L. E. Welch, *J. Liq. Chromatogr.*, 1994, **17,** 1755.
21. P. T. Kissinger and W. R. Heineman, *Laboratory Techniques in Electroanalytical Chemistry*. Marcel Dekker, New York, 1984.
22. L. E. Welch, unpublished data, Knox College.
23. L. R. Snyder and J. J. Kirkland, *Introduction to Modern Liquid Chromatography*, 2nd Ed. Wiley-Interscience, New York, 1979.
24. L. E. Welch, Ph.D. Dissertation, Iowa State University, 1988.

Pergamon

0039-9140(94)00211-8

*Talanta*, Vol. 42, No. 1, pp. 27–40, 1995

0039-9140/95 $9.50 + 0.00

# SPECIATION OF IRON AND MANGANESE IN DAM WATER PARTICLES USING ELECTRON SPECTROSCOPY FOR CHEMICAL ANALYSIS (ESCA)

MYINT ZAW[1,*] and BARRY CHISWELL[2]

[1]Environmental Science Programme, Australian Nuclear Science and Technology Organization, Private Mail Bag 1, Menai, NSW 2234, Australia
[2]Department of Chemistry, University of Queensland, St Lucia, Qld 4072, Australia

(*Received* 25 *April* 1994. *Revised* 15 *July* 1994. *Accepted* 19 *July* 1994)

**Summary**—The speciation of iron and manganese compounds retained by membrane filtration of dam water samples was studied by use of electron spectroscopy for chemical analysis (ESCA). Samples were taken at various depths and times of year from North Pine Dam near Brisbane, Australia. Both surface and bulk properties of samples representative of the water column profile were investigated. ESCA results showed that iron(III) compounds were found to predominate in the whole water column in any season of the year while the significance of iron(II) species varied in the hypolimnion (the bottom layer). In summer, although various ratios of manganese(II), manganese(III) and manganese(IV) compounds were found to occur down the water column, manganese(IV) compounds were predominant in the epilimnion (the top layer), while both manganese(II) and (IV) compounds predominated in the metalimnion (the middle layer) and the hypolimnion. The majority of Mn(IV) compounds were found throughout the water column after heavy rain and winter season. The ratios of atomic concentrations of iron and manganese as determined by atomic absorption spectrophotometry and ESCA are also discussed.

In our previous studies[1–3] upon manganese and iron in dam waters, work has been concentrated upon speciating the soluble forms of the metals. However, in the environment of natural waters the speciation of particulate forms of these metals has received little attention. This may be due to the speciation techniques being labor intense and expensive in both capital outlay and maintenance of instruments. This work reviews our results to date on the speciation of iron and manganese in dam water particles using electron spectroscopy for chemical analysis (ESCA) [also known as X-ray photoelectron spectroscopy (XPS)] in order to further understand their behaviour in the dam profiles at different times of the year. This is a new and powerful approach to the study of particulates in natural waters.

Modern surface-sensitive analytical techniques, including secondary ion mass spectrometry (SIMS), Auger electron spectroscopy (AES) and ion scattering spectroscopy (ISS), provide a means for obtaining a chemical analysis of the outer five to 10 atomic layers of the surface of a material, as well as an analysis of the underlying material.[4] Consequently these techniques have found widespread use in many areas of material research and fabrication.[5] Quantitative data can be obtained from the spectra by study of peak heights or areas, and identification of chemical oxidation states often can be made from the exact positions and separations of the peaks, as well as from certain spectral contours.[6]

ESCA is potentially an ideal technique for study of the oxidation states of solid iron and manganese compounds. The core electrons of the molecular bonded atoms in compounds are basically in atomic orbitals with their binding energies being characteristic of the atoms. However, an increase in oxidation state produces a slight increase in binding energy, while a decrease in oxidation state will slightly decrease the binding energy.[7]

The atomic concentration routine calculates relative concentrations of iron and manganese (surface elements), while the atomic per cent values are calculated from the measured signals by applying elemental sensitivity factors and normalizing to 100 atomic per cent. The

*Author to whom correspondence should be addressed.

formula[8] used to calculate the atomic concentration values is given below.

$$\frac{n_1}{n_2} = \frac{I_1/S_1}{I_2/S_2}, \quad (1)$$

where $n$ is the number of atoms per unit volume, $I$ is the number of photoelectrons detected (area under the peak) and $S$ is the atomic sensitivity factor.

In environmental sciences,[9] submicron particles (including inorganic and organic colloids, clay minerals and microorganisms) play an important role in natural waters. Physical and chemical sorption processes result in significant amounts of trace elements (including heavy metals) being associated with these particles in aquatic systems. The physical and chemical behaviour of these metals in the environment and their biophysicochemical properties differ from those of the corresponding dissolved species. Electron microscopy is a powerful tool able to morphologically characterize these submicron particles according to their elemental associations. This technique includes analytical electron microscopy (AEM), scanning electron microscopy (SEM) and transmission electron microscopy (TEM). Although SEM cannot directly speciate iron and manganese compounds, it is a powerful tool in the study of different types of algae and bacteria, some of which are directly related to iron and manganese behaviour in the storage dams.

## EXPERIMENTAL

### *Sample preparation and instrumental settings*

Water samples were collected by a Klemmerer-type depth sampler over almost a full year (11/11/87 to 06/09/88) at various depths of North Pine Dam near Brisbane, Australia (actual dates and depths of samples collected are given in Table 4. Samples of sediments were collected using a cylindrical grab sampler, from the top (1–3 cm depth) of the sediment. Samples were filtered through either a 0.45 $\mu$m filter membrane, or a 0.01 $\mu$m filter membrane after prior passage through a 0.45 $\mu$m filter membrane.

Stratification of North Pine Dam commences in early September and lasts until May. During these warmer months the lake becomes fully stratified whilst in the winter (June to August) destratification results in a fully mixed and aerated profile. In a stratified dam the surface and 3 m samples come from the epilimnion, the 10, 11 and 12 m samples all come from the metalimnion and the 15, 27 and 32 m (bottom sediment) come from the hypolimnion. The variation in the depths of sampling the metalimnion and hypolimnion is related to the date of sampling and the depth of water in the dam at the time of sampling.

The methods of sampling and filtration of dam water samples are described in detail in previous papers.[3,10] Duplicate water samples were shaken thoroughly and then transferred into both 100 ml and 1 l. acid-washed polythene containers to yield a series of like samples. For surface analysis at least 1 l. of the dam water sample was filtered through either a 0.45 $\mu$m filter membrane, or a 0.01 $\mu$m filter membrane after prior passage through a 0.45 $\mu$m filter membrane. The particulate matter remaining on the filter membrane was put into a vacuum desiccator for at least one week for drying, before analysis by ESCA and SEM.

For atomic absorption spectrophotometry (AAS) analysis, the corresponding like sample (100 ml) was filtered through either a 0.45 $\mu$m filter membrane, or a 0.01 $\mu$m filter membrane after prior passage through a 0.45 $\mu$m filter membrane. The particulate matter remaining on the filter membrane was digested in 10 ml concentrated hydrochloric acid (BDH, Analar), gently boiling for 30 min and followed by addition of 1.0 ml concentrated nitric acid (BDH, Analar) with boiling for a further 5 min. After acid treatment the solution was cooled down and then made up to 100 ml in a volumetric flask with Milli-Q water and finally analysed for dissolved iron and manganese concentrations by use of Varian AA 875 spectrophotometer. Blank determinations were carried out for each analysis batch.

With SEM analysis the dry sample was cut out and mounted on a specimen stub, sputtered with argon ion (for a few seconds) and coated with gold in a partial argon atmosphere at 100 m Torr. The samples were then examined in a Phillips model SEM 505 scanning electron microscope. All SEM results indicated that filtrate samples collected on membrane filters were uniformly distributed over the membrane surface and that ESCA could be undertaken on a portion of the membrane to give results representative of the whole sample.

ESCA analyses were carried out on a Perkin Elmer PHI Model 560 Multitechnique System. For these analyses, either Al$K\alpha_{1,2}$ X-rays (1486.6 eV) or Mg$K\alpha_{1,2}$ X-rays (1253.6 eV) were used as

the exciting radiation of the photoelectrons. For the measurement of accurate binding energies and the atomic concentrations, the aluminium anode was used (in preference to the magnesium anode) as it shifted interfering Auger peaks up-scale by 233 eV. Such Auger peaks were found to give iron interference in the manganese 2p photoelectron, and oxygen interference in the iron 2p photoelectron regions, respectively, when the magnesium anode was used.

For ESCA analyses the sample membrane was cut to allow it to be mounted on the sample holder and then inserted into the spectrometer. During the analysis the vacuum inside the ESCA chamber was approximately $2 \times 10^{-7}$ Torr due to argon gas flow for the ion etching procedure. The basic pressure in the analysis chamber was typically about $10^{-9}$ Torr. The instrument was calibrated weekly, and the calibration was checked several times each day during data acquisition. The analyser work function was determined assuming the binding energy of the gold $4f_{7/2}$ peak to be 84.0 eV.[11]

The oxidation states of reference iron and manganese metal sheets, a number of iron and manganese oxides and compounds, and the dam water particulate samples on the millipore filter, were all determined before and after argon ion beam etching. The PHI 04-303 ion gun was operated at a beam energy of 4 keV and a beam current of 1.0 $\mu$A. This beam was incident at an angle of 30° to the sample normal, and was rastered over an area 8 × 6 mm to ensure complete etching of the ESCA analysis area (approximately 5 mm diameter). These conditions gave an etching rate of apporoximately 0.25 nm/min for standard $Ta_2O_5$.[12] The etching rate of the particulate (including carbon, standard iron and manganese compounds) in dam water samples on the 0.45 or 0.01 $\mu$m filter membrane

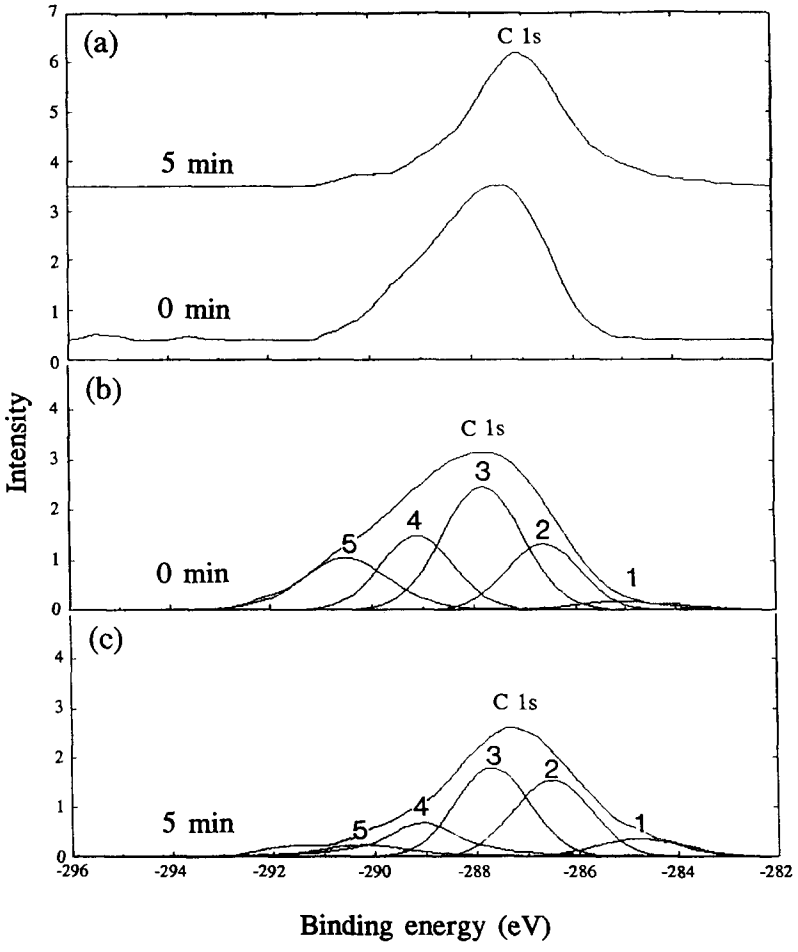


Fig. 1. ESCA high resolution carbon 1s data from North Pine Dam 32 m depth (bottom sediment) sample collected on 06/09/88. (a) Raw data before (0 min) and after (5 min) etch, (b) curve fitted data—unetched surface and (c) curve fitted data—etched surface.

Table 1. Standard iron and manganese compounds for ESCA analysis

| Standard iron compounds | | | Standard manganese compounds | | |
|---|---|---|---|---|---|
| Compound | Purity (%) | Company | Compound | Purity (%) | Company |
| Pure iron sheet | 99.99 | PHI 603965 | Pure Mn sheet | 99.9 | Leico Industry |
| $Fe_2O_3$ | 99.99 | Aldrich | $MnO_2$ | 99.99 | Aldrich |
| $Fe_3O_4$ | 99 | Aldrich | $Mn_3O_4$ | 99.995 | KOH |
| FeS | Technical Grade | Aldrich | $MnCO_3$ | Laboratory reagent | BDH |
| | | | $MnSO_4 \cdot 4H_2O$ | >97% | BDH |
| | | | $Mn(CH_3COO)_2 \cdot 2H_2O$ | >97% | Aldrich |

(after prior passage through a 0.45 $\mu$m filter) relative to $Ta_2O_5$ is unknown, but was assumed to be of similar magnitude.

Iron and manganese $2p_{3/2}$, $2p_{1/2}$ and carbon 1s spectra were recorded, and binding energy measurements were made relative to the carbon 1s spectral peak ($284.8 \pm 0.1$ eV) as a reference value. Carbon is present due to hydrocarbon contamination on the sample surface of the reference material, or is intrinsic to the sample in the case of dam water particulates.

Dam water particulates for the various annual seasons from different depths of North Pine Dam were studied in detail by SEM, while ESCA was used to analyse the oxidation state and binding atoms for iron and manganese present both on the surface and in the bulk of the particulates.

*Data analysis by using curve fitting method*

ESCA measurements involve recording the intensity of emitted electrons as a function of the electron binding energy. The measured spectra consist of peaks at characteristic energies, from which the elemental composition of the sample can be determined. An element is often in several different oxidation states which produces photoelectrons of slightly different binding energies resulting in a composite peak.

Data reduction was carried out using a computer curve fitting program to deconvolute the measured ESCA peaks into the peaks of the individual chemical species.[13] Inputs into the program were the digitized experimental raw data, and the specific peaks shapes (non-Gaussian) for the elements of interest in their various chemical states. The individual peak shapes were obtained from the "Handbook of X-ray Photoelectron Spectroscopy",[14] with the background assumed to vary linearly across each peak. In essence, the computer program calculates an error for each point on the measured curve; such error is the shortest distance between the measured point and the composite curve which is the sum of two or more peaks for particular oxidation states. The program carries out a least squares fit, comparing the measured curve with the sum of the composite curves, systematically varying the intensity and position (within fixed limits) of the composite curves. The final result consists of the raw data, the resolved peaks for the individual oxidation states, the convoluted curve (*i.e.* the sum of the individual peaks) and an error curve which is the difference between the raw data and the convoluted curve.

Each curve-fit was further checked on its suitability with each side of the computer selected error minimum, and each case was further examined to determine if a better fit could be possible using individual peaks with binding energies different from those expected. On the other hand, the slight difference revealed by the rechecking procedures shows that there can be a significant shift in the peak position with ion milling and that this is important when

Table 2. Binding energies for $2p_{3/2}$ line of iron, iron oxides, manganese and manganese oxides as determined by ESCA

| Binding energies (*eV*) | | | | |
|---|---|---|---|---|
| Fe(0) | Fe(II) | Fe(III) | | References |
| 706.2–707.1 | 708.8–710.0 | 710.0–711.6 | | 7, 14, 17–27 |
| $706.8 \pm 0.1$ | $709.8 \pm 0.1$ | $711.0 \pm 0.1$ | | From standard pure iron metal sheet and compounds |
| Mn(0) | Mn(II) | Mn(III) | Mn(IV) | |
| 638.7–639.2 | 640.2–641.3 | 641.4–641.9 | 641.8–642.6 | 14, 15, 28–30 |
| $638.8 \pm 0.1$ | $640.8 \pm 0.1$ | $641.8 \pm 0.1$ | $642.4 \pm 0.1$ | From standard pure manganese metal sheet and compounds |

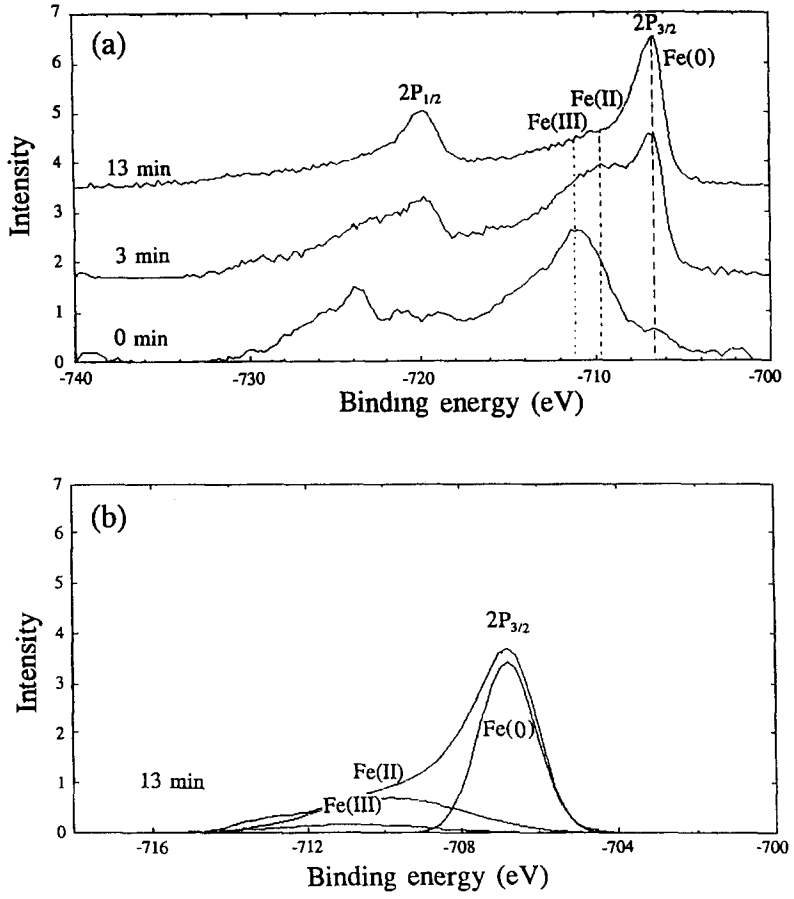


Fig. 2. (a) ESCA spectra of the iron $2p_{3/2}$, $2p_{1/2}$ lines from oxidized iron sheet before (0 min) and after (3 and 13 min) sputtering and (b) curve fitted results of the convoluted iron $2p_{3/2}$ spectra from oxidized iron sheet after 13 min sputtering.

considering the fitting error. Furthermore, the nature of the fit can change depending on the binding energy range chosen. Sometimes these two factors affect each other. The values used are the best fits obtained after these considerations had been taken into account.

## RESULTS AND DISCUSSION

### *Carbon spectrum as a reference peak*

Contamination, which formed on the standard sample surface, consisted mainly of hydrocarbons, water vapour and oxygen, and

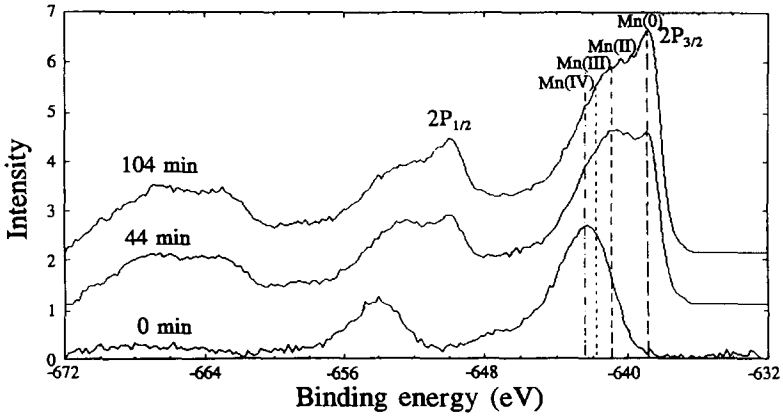


Fig. 3. ESCA spectra of the manganese $2p_{3/2}$, $2p_{1/2}$ lines from oxidized manganese sheet before (0 min) and after (44 and 104 min) sputtering.

originates from exposure to air during the brief period of transfer from the vacuum desiccator to the ESCA apparatus; it can also come from the residual gases within the ESCA chamber.[15] The C 1s peak (284.8 ± 0.1 eV) was observed in all ESCA spectra; however, for the standard samples this peak disappeared after 5 min of ion etching. This was taken to indicate that the carbon contamination on the surface had been removed and any further analysis was representation of the "true" bulk sample. Dam water particulate samples have all the above contaminants; however, most of the carbon in such samples is not contamination but an integral part of the actual sample. The carbon 1s peak for all samples in the unetched state was the most intense spectral peak in comparison with the others, and after ion etching for 5 min, this carbon peak was considerably reduced (Fig. 1). In all the experiments, the carbon 1s spectrum was therefore recorded and used as a reference for charge correction and as a surface contamination removal indicator.[11]

Dilks[16] has claimed that there are five types of bound carbon which can be found from ESCA studies of organic polymer samples, containing carbon and oxygen. These are (1) hydrocarbon ($-CH_x-$), (2) alcohol, ether and peroxide carbon (-C-O-), (3) ketone carbon (>C = O), (4) ester and carboxylic carbon, and (5) carbonate carbon. The binding energies increase from peak 1 to 5 due to the larger dipole difference between carbon and hydrogen or oxygen.

Figure 1(a) shows the ESCA high resolution carbon 1s spectrum both before sputtering and after 5 min sputtering for a 32 m depth sample (bottom sediment) obtained on 06/09/88. Figure 1(b) represents the results of curve fitting for the five differently bound carbon species obtained before sputtering; while Fig. 1(c) is the curve-fitting analysis after 5 min sputtering. These results show that after light sputtering with argon ion on the sample surface, different types of carbon have been removed and their intensity reduced; only the first and second types of carbon have their intensities

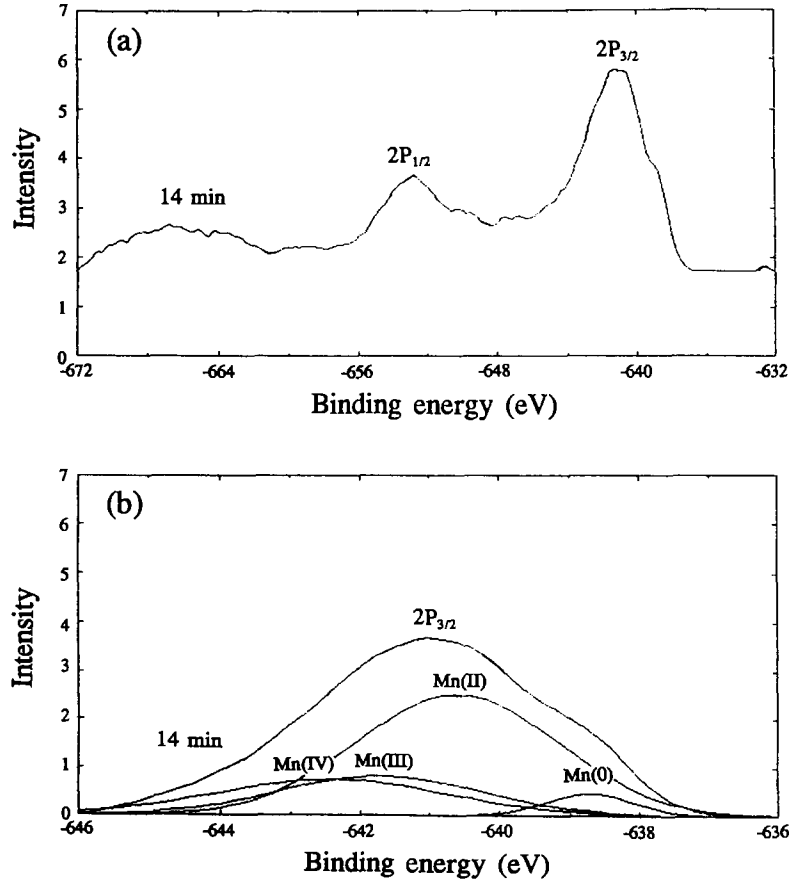


Fig. 4. (a) Raw data and (b) curve fitted results of the convoluted manganese $2p_{3/2}$ spectrum from oxidized manganese sheet.

slightly increased. Also, all the peak positions are slightly shifted to lower binding energies after ion milling by argon ions, which is due to a decrease in sample charging after removal of some of the surface hydrocarbons.

*ESCA measurement on reference iron and manganese metals and compounds*

The iron and manganese oxides and compounds studied by ESCA were commercially obtained high purity powders and crystals (Table 1). Oxide samples were prepared by crushing immediately prior to insertion into the spectrometer. The binding energies for the $2p_{3/2}$ line of standard iron, manganese and their compounds were obtained from a variety of literature sources[7,14,15,17–30] and were confirmed by our own studies as shown in Table 2.

The phenomenon of multiplet splitting associated with photoelectron peaks is due to the presence of unpaired valence electrons, resulting in an exchange interaction which affects differently the remaining spin-up or spin-down core electrons. Another characteristic feature of the oxide spectra, which has been empirically observed for other high spin states of transition metal ions, is the presence of satellite peaks.[31] These shake-up core-level satellites are caused by an incident X-ray photon giving up a discrete portion of its energy to the excitation of a second electron, rather than imparting its entire quantum energy to the primary, photoejected electron. Thus this photoelectron will have lost a small amount of energy and will appear at a slightly higher binding energy than the parent peak. Shake-up peaks are observable for both iron and manganese compounds. These satellite lines have intensities and separations from the parent photoelectron line that are unique to each chemical state. Prominent shake-up patterns typically occur with paramagnetic states including iron(II), iron(III), manganese(II), manganese(III) and manganese(IV) compounds.

An ESCA study on a pure iron metal sheet is shown in Fig. 2(a). After 3 and 13 min heavy sputtering on iron sheet, the iron(III) oxide on the surface can be seen to be almost completely

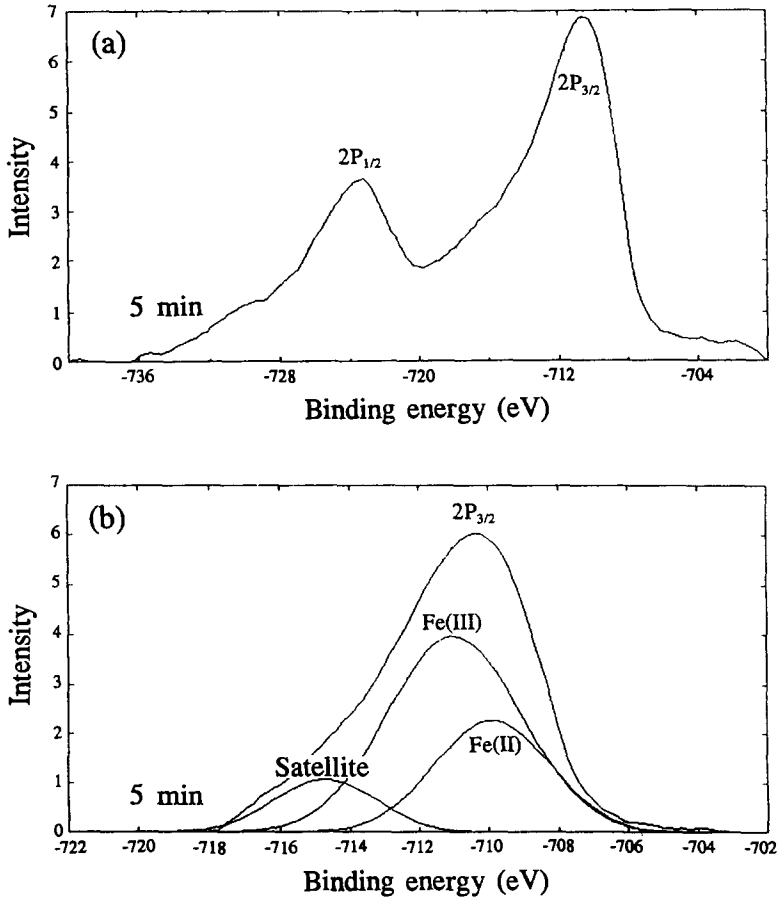


Fig. 5. (a) Raw data and (b) curve fitted results of the convoluted iron $2p_{3/2}$ spectrum from $Fe_3O_4$.

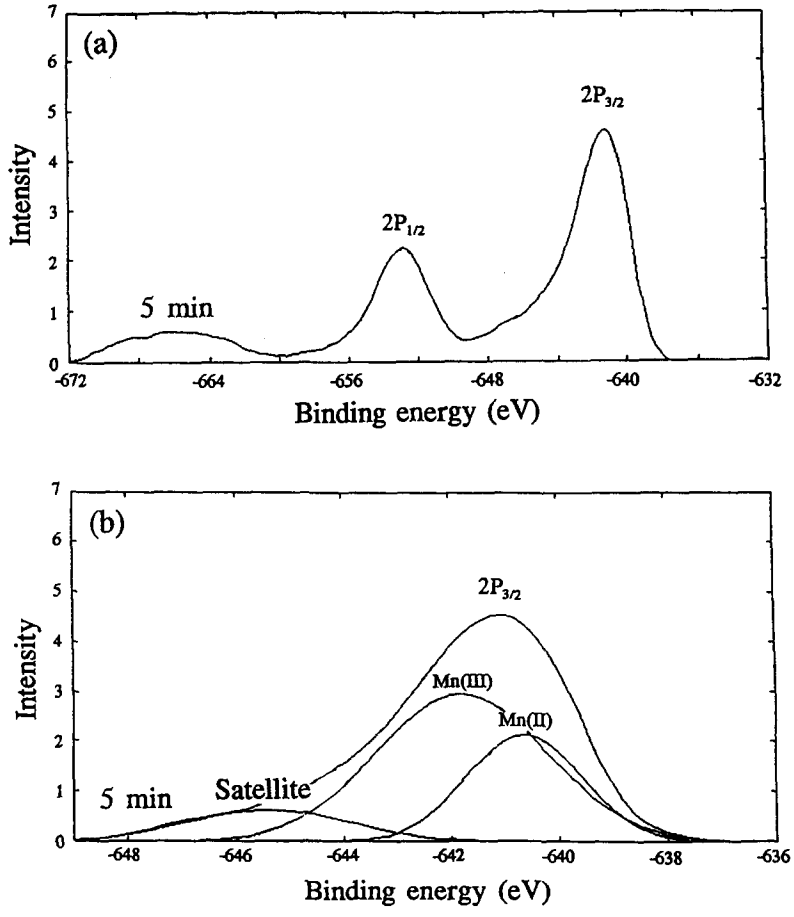


Fig. 6. (a) Raw data and (b) curve fitted results of the convoluted manganese $2p_{3/2}$ spectrum from $Mn_3O_4$.

Table 3. Binding energies for $2p_{3/2}$ line of standard iron, manganese and their compounds as determined by ESCA (B.E. of C 1s = 284.8 ± 0.1 eV as reference)

| Compounds | Before sputtering | | Sputter time (*min*) | After sputtering | |
|---|---|---|---|---|---|
| | B.E.(±0.1)* (*eV*) | FWHM† | | B.E.(±0.1) (*eV*) | FWHM |
| Fe sheet | 706.8 (0)‡ | 2.4 | 3 | 706.8 (0) | 1.9 |
| | 709.8 (II) | | 13§ | 706.8 (0) | 1.8 |
| | 711.0 (III) | | | | |
| FeS | 711.0 (III) | 5.0 | 5 | 709.9 (II) | 4.4 |
| $Fe_3O_4$ | 711.0 (III) | 4.9 | 5 | 709.8 (II) | 4.0 |
| $(FeO \cdot Fe_2O_3)$ | | | | 711.1 (III) | 4.6 |
| $Fe_2O_3$ | 710.8 (III) | 4.8 | 5 | 711.0 (III) | 4.7 |
| Mn sheet | 642.4 (IV) | 3.4 | 44§ | 638.8 (0) | 1.6 |
| | | | 104§ | 38.8 (0) | 1.6 |
| $McCO_3$ | 640.9 (II) | 3.8 | 5 | 640.9 (II) | 3.8 |
| $MnSO_4 \cdot 4\,H_2O$ | 642.4 (IV) | 3.3 | 5 | 640.8 (II) | 3.8 |
| $Mn(CH_3COO)_3$ | 642.4 (IV) | 3.3 | 5 | 641.8 (III) | 4.2 |
| $Mn_3O_4$ | 641.0 (II) | 3.9 | 5 | 640.7 (II) | 2.9 |
| $(MnO \cdot Mn_2O_3$ | 641.8 (III) | 4.3 | | 641.8 (III) | 3.9 |
| $MnO_2$ | 642.6 (IV) | 3.4 | 5 | 642.4 (IV) | 3.5 |

*B.E.: binding energy.

†FWHM: full width half maximum.

‡The number in parentheses indicates the oxidation number of iron or manganese.

§Normally, a light ion dose ($\leq$5 min sputter) was used to remove only the outer few atomic layers (approximately 1.2 nm) exposing an unaltered sample surface. Much longer sputtering (*i.e.* heavier ion dose) was needed to ensure complete removal of the surface oxidized layers and present a clean metal surface for analysis.

eliminated. This conclusion is reinforced by curve fitting as shown in Fig. 2(b), which clearly indicates the presence of mainly iron(0) at the surface following sputtering.

Figure 3 shows the binding energies of manganese before and after (44 and 104 min) sputtering of manganese sheet metals; the removal of manganese oxide is clearly seen in the growth of the manganese(0) peak with increasing sputtering time. Figure 4(a) and (b) shows results after 14 min sputtering, with the curve-fitted peak of Fig. 4(b) indicating the presence, after this sputtering time, of mainly manganese(II).

Figures 5 and 6 show that, after light sputtering (5 min) of pure $Fe_3O_4$ and $Mn_3O_4$ both the ratios of the concentrations of iron(II) to iron(III) and manganese(II) to manganese(III) are 1:2. These experiments strongly indicate that 5 min light sputtering is just sufficient to remove the surface contamination and not result in any oxide reduction,[7,30] this sputter time was used for all samples. The binding energy for $2p_{3/2}$ line of standard iron and manganese and

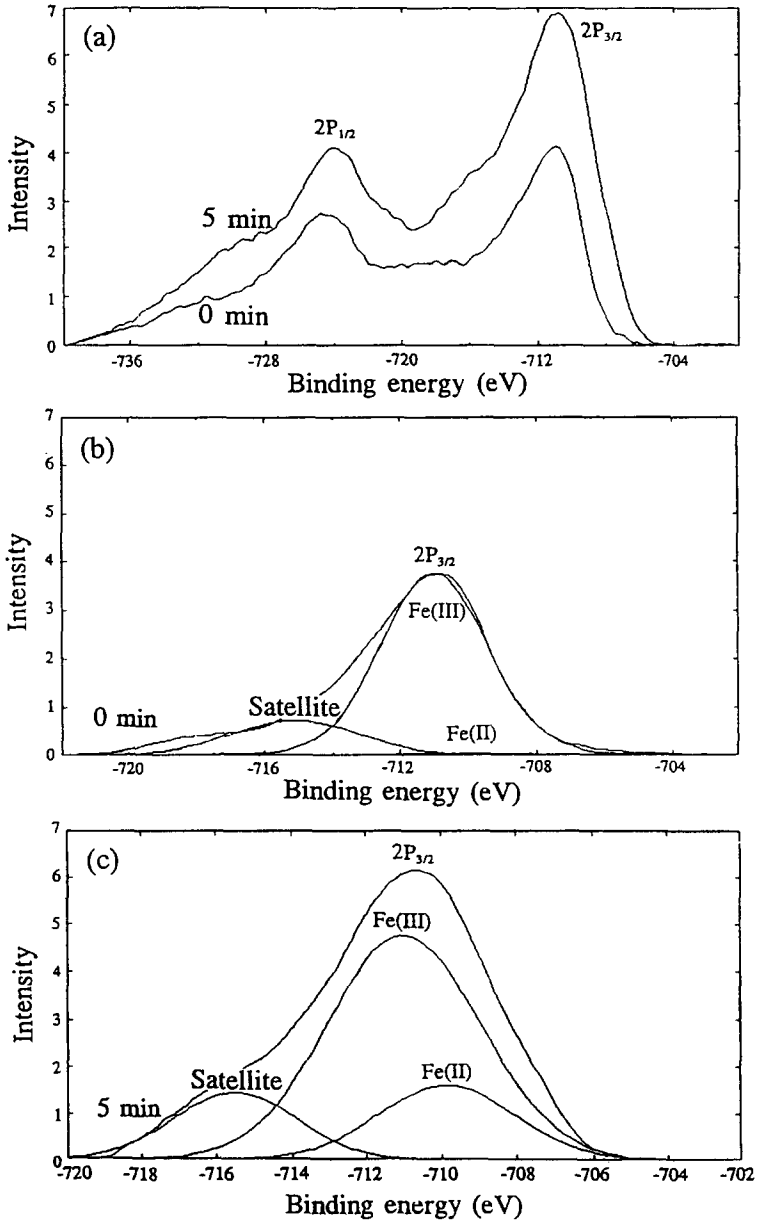


Fig. 7. ESCA high resolution iron 2p data from a North Pine Dam water particulate sample (0.45 $\mu$m membrane filtration) collected on 20/01/88 at a depth of 15 m. (a) Raw data before (0 min) and after etch (5 min); (b) curve fitted data—unetched surface and (c) curve fitted data—etched surface.

its compounds as determined by ESCA are shown in Table 3.

The reference and dam water particulate samples were exposed to the atmosphere when transferred from the vacuum storage desiccator to the ESCA analysis vacuum chamber, therefore, iron(II) compounds might have been oxidized to iron(III) on the outermost surface. However, after light ion beam etching ($\approx$1.25 nm) to remove the normal hydrocarbon surface contamination, any iron(III) surface oxidation layer would also be removed, exposing the true oxidation species present in the bulk. After 5 min of argon ion etching, approximately 1.25 nm (or 2–4 atomic layers) were removed and hydrocarbon, oxygen and other contaminants had been effectively stripped off; as expected the iron(II) concentration was slightly increased. Therefore, the results obtained after etching represent the actual oxidation states of iron and manganese species in the sample. Sullivan and Mills[7] have shown that heavy etching of the bulk iron(III) oxide surface with argon ions leads to a rapid reduction of iron(III) species to iron(II), and, on further reduction finally to iron(0); in heavy etching a large concentration of argon irons are produced with an equal concentration of electrons; these latter will reduce oxidized metal species. A similar situation applies to manganese oxides.[30] For this reason, in all these experiments only a light argon-ion etch was given to each sample surface to prevent

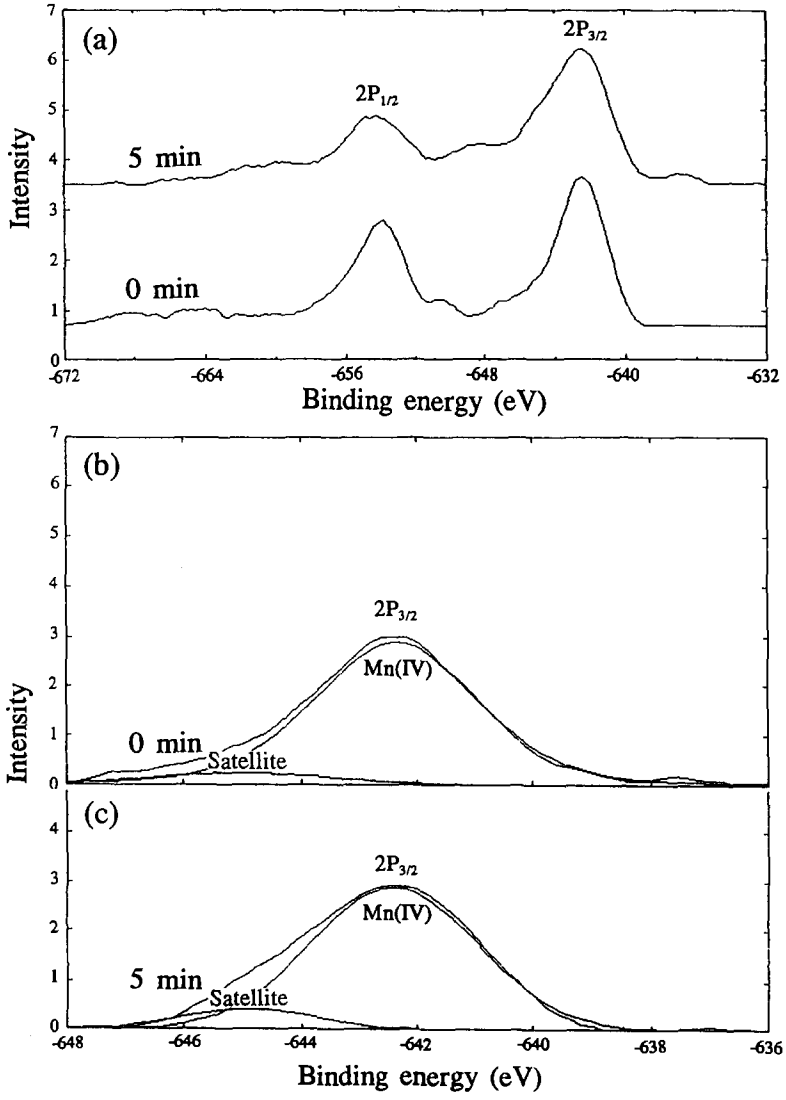


Fig. 8. ESCA high resolution manganese 2p data from a North Pine Dam water particulate sample (0.45 $\mu$m membrane filtration) collected on 13/04/88 at a depth of 21 m. (a) Raw data before (0 min) and after (5 min) etch, (b) curve fitted data—unetched surface and (c) curve fitted data—etched surface.

reduction of iron(III) to iron(II) and manganese(IV) and manganese(III) to manganese(II) species.

*ESCA measurement of iron and manganese compounds in dam water particulate samples*

Figures 7 and 8 show the ESCA high resolution data for iron 2p and manganese 2p, obtained from particulate samples collected on 20/01/88 and 13/04/88, respectively. In each case: (a) represents the raw data for the whole 2p region before and after etching, (b) represents the curve fitted results for the $2p_{3/2}$ peak before etching, and (c) represents the curve fitted results for the $2p_{3/2}$ peak after etching. Iron(III) and manganese(IV) oxidation states are mainly predominant in the dam water particulate both before and after sputtering.

The binding energies, oxidation state assignment, and per cent atomic concentration for iron and manganese compounds in particulates of some 16 dam water samples collected at various depths and dates are shown in Table 4. The ratios of atomic concentrations of iron to manganese as determined by AAS and ESCA are also presented in Table 4.

For the purposes of this work, it was anticipated that the species of iron and manganese found in the dam might be dependent upon the region from which the sample was taken. Discussion of results is, therefore, given in terms of speciation in the epilimnion, the metalimnion, the hypolimnion and the sediment.

*Iron and manganese in the epilimnion*

ESCA results (Table 4) show that iron(III) compounds are found to predominate during the year throughout the water column, however, in the epilimnion the ratio between iron(II) and (III) can vary between an insignificant amount of iron(II) (surface sample on 20/01/88) and an approximately 1:3 ratio for iron(II):(III) (3 m on 13/04/88). This indicates that in April, the iron(II) component is far more significant due to the heavy rain effect and the whole water column mixing together. Under these conditions the concentrations of iron are very similar throughout the water column. After one week of heavy rain (662 mm rainfall in first week of April, 1988) the influx of water and associated debris has altered the nature of the dam water significantly (see Table 4; results from 3 to 32 m bottom sediment) and this can be seen clearly from SEM photomicrograph reported elsewhere.[32] The whole water column including bottom sediment contained nearly equal distributions of clay materials, inorganic and organic mineral compounds and algae debris. Further evidence was given from the temperature, dissolved oxygen, pH, iron and manganese depth profiles which were nearly constant values along the water column.[32]

Table 4 shows that manganese(II), manganese(III) and manganese(IV) compounds occur throughout the whole water column, but that manganese(IV) compounds are predominant in the epilimnion. It is clear that the iron(III) and manganese(IV) compounds are predominant in the epilimnion because of the high dissolved oxygen concentrations (7.4–8.0 mg/l.).[32]

ESCA results (Table 4) show that the ratio of iron to manganese is 1.7 (surface sample on 20/01/88), compared to the results from AAS (1.4). All these results indicate that the concentration of iron is at least as great or greater than manganese in the sample.

*Iron and manganese in the metalimnion*

An ESCA study of the iron compounds (Table 4) in the metalimnion (10 to 12 m on 17/02/88 and 12 m on 13/04/88) shows that the iron in the particulate material is composed mostly of iron(III), with the ratio of iron(III):(II) being approximately 2:1. The exception to this is the 11 m sample collected on the 17/02/88 in which the iron(III):(II) ratio is approximately 1:1 with the iron(II) species being slightly in excess.

For manganese collected at the metalimnion on the 17/02/88, the predominant species are the manganese(II) and manganese(IV) moieties, where these two species are almost at the same concentrations. However, for the 12 m sample collected on the 13/04/88 the situation is quite different, with the manganese(IV) species being the only significant species. This collection followed a long period of very heavy rainfall which may account for the observed difference. This indicates that the rain tends to bring oxidized manganese into the dam. The depth profiles of iron and manganese before and after heavy rain, also supported the notion that the heavy rain brought significant amounts of insoluble iron and manganese into the dam.[32] This is further supported by the high levels of particulate manganese(IV) in all levels of the dam after heavy rain (see Table 4; results of 13/04/88 from 3 to 32 m bottom sediment).

In the metalimnion, the ratio of iron to manganese (see Table 4; results from 17/02/88

Table 4. Binding energies for the $2p_{3/2}$ line of iron and manganese compounds in particulates of North Pine Dam water samples as determined by ESCA and the ratios of iron to manganese as determined by AAS and ESCA

| | | | | | ESCA analysis (after sputtering ≈12Å) | | | | | | |
|---|---|---|---|---|---|---|---|---|---|---|---|
| | | AAS analysis | | | Fe | | | Mn | | | |
| Date | Depth (*m*) | Fe (*mg/l.*) | Mn (*mg/l.*) | Ratio of Fe/Mn | B.E. (*eV*) | Type of species | % atomic conc. | B.E. (*eV*) | Type of species | % atomic conc. | Ratio of Fe/Mn |
| 11/11/87 (early summer) | 27B | 40.880 | 5.300 | 7.7 | 710.0 | Fe(II) | 4.5 | 640.6 | Mn(II) | 14.7 | 18.2 |
| | | | | | 711.0 | Fe(III) | 95.5 | 641.8 | Mn(III) | 37.5 | |
| | | | | | | | | 642.3 | Mn(IV) | 47.8 | |
| 20/01/88 (summer) | Surface | 0.030 | 0.022 | 1.4 | 710.0 | Fe(II) | 3.2 | 640.8 | Mn(II) | 0.2 | 1.7 |
| | | | | | 711.1 | Fe(III) | 96.8 | 641.8 | Mn(III) | 0.2 | |
| | | | | | | | | 642.4 | Mn(IV) | 99.6 | |
| | 15 | 1.213 | 0.022 | 55.1 | 709.7 | Fe(II) | 23.1 | 640.6 | Mn(II) | 30.4 | 124.0 |
| | | | | | 711.0 | Fe(III) | 76.9 | 641.8 | Mn(III) | 0.1 | |
| | | | | | | | | 642.4 | Mn(IV) | 69.5 | |
| 17/02/88 (summer) | 10 | 0.069 | 0.057 | 1.2 | 709.8 | Fe(II) | 29.8 | 640.8 | Mn(II) | 43.9 | 1.4 |
| | | | | | 711.4 | Fe(III) | 70.2 | 641.8 | Mn(III) | 9.5 | |
| | | | | | | | | 642.2 | Mn(IV) | 46.6 | |
| | 11 | 0.100 | 0.044 | 2.3 | 709.8 | Fe(II) | 56.1 | 641.0 | Mn(II) | 55.9 | 6.6 |
| | | | | | 710.8 | Fe(III) | 43.9 | 641.8 | Mn(III) | 0.1 | |
| | | | | | | | | 642.2 | Mn(IV) | 44.0 | |
| | 12 | 0.803 | 0.019 | 42.3 | 709.8 | Fe(II) | 35.0 | 640.8 | Mn(II) | 49.0 | 30.2 |
| | | | | | 710.8 | Fe(III) | 65.0 | 641.6 | Mn(III) | 3.0 | |
| | | | | | | | | 642.2 | Mn(IV) | 48.0 | |
| 13/04/88 (late summer) (after 662 mm rainfall) | 3 | 1.214 | 0.055 | 22.1 | 709.4 | Fe(II) | 28.9 | 640.6 | Mn(II) | 12.5 | 6.6 |
| | | | | | 710.8 | Fe(III) | 71.1 | 641.6 | Mn(III) | 10.6 | |
| | | | | | | | | 642.4 | Mn(IV) | 76.9 | |
| | 12 | 0.878 | 0.092 | 9.5 | 710.0 | Fe(II) | 38.0 | 640.8 | Mn(II) | 1.5 | 3.1 |
| | | | | | 710.8 | Fe(III) | 62.0 | 641.6 | Mn(III) | 2.5 | |
| | | | | | | | | 642.4 | Mn(IV) | 96.0 | |
| | 21 | 1.588 | 0.335 | 4.7 | 710.0 | Fe(II) | 0.1 | 640.6 | Mn(II) | 0.1 | 1.5 |
| | | | | | 711.2 | Fe(III) | 99.9 | 641.7 | Mn(III) | 0.1 | |
| | | | | | | | | 642.4 | Mn(IV) | 99.8 | |
| | 32B | 16.925 | 0.681 | 24.9 | 710.0 | Fe(II) | 24.4 | 640.8 | Mn(II) | 0.5 | 9.7 |
| | | | | | 711.2 | Fe(III) | 75.6 | 641.8 | Mn(III) | 0.5 | |
| | | | | | | | | 642.4 | Mn(IV) | 99.0 | |
| 09/08/88 (winter) | 3 | 0.133 | 0.059 | 2.3 | 709.5 | Fe(II) | 22.0 | 640.7 | Mn(II) | 0.1 | 1.2 |
| | | | | | 710.9 | Fe(III) | 78.0 | 641.7 | Mn(III) | 0.1 | |
| | | | | | | | | 642.5 | Mn(IV) | 99.8 | |
| | 15 | 0.132 | 0.059 | 2.2 | 709.8 | Fe(II) | 19.7 | 640.6 | Mn(II) | 3.6 | 1.2 |
| | | | | | 710.9 | Fe(III) | 80.3 | 641.5 | Mn(III) | <0.1 | |
| | | | | | | | | 642.2 | Mn(IV) | 96.4 | |
| | 32B | 22.278 | 3.357 | 6.6 | 710.0 | Fe(II) | 17.4 | 640.5 | Mn(II) | 10.9 | 7.0 |
| | | | | | 710.9 | Fe(III) | 82.6 | 641.8 | Mn(III) | 10.7 | |
| | | | | | | | | 642.3 | Mn(IV) | 78.4 | |
| 06/09/88 (late winter) | 3 | 0.042 | 0.015 | 2.8 | 709.9 | Fe(II) | 0.1 | 640.7 | Mn(II) | 14.7 | 2.7 |
| | | | | | 710.9 | Fe(III) | 99.9 | 641.8 | Mn(III) | 23.4 | |
| | | | | | | | | 642.4 | Mn(IV) | 61.9 | |
| | 15 | 0.113 | 0.031 | 3.7 | 709.9 | Fe(II) | 34.8 | 640.7 | Mn(II) | 6.9 | 0.9 |
| | | | | | 710.9 | Fe(III) | 65.2 | 641.6 | Mn(III) | 9.6 | |
| | | | | | | | | 642.4 | Mn(IV) | 83.5 | |
| | 32B | 6.005 | 0.941 | 6.4 | 710.0 | Fe(II) | 27.5 | 640.5 | Mn(II) | 14.3 | 5.5 |
| | | | | | 711.1 | Fe(III) | 72.5 | 641.5 | Mn(III) | 0.1 | |
| | | | | | | | | 642.4 | Mn(IV) | 85.6 | |

B, indicates top layer (1 to 3 cm depth) of the bottom sediment sample.

for 10–12 m) increases for all methods of its measurement (AAS and ESCA). ESCA results are different from those of AAS, undoubtedly due to the fact that AAS analyses the total elements in the bulk of the sample, but ESCA gives only the surface concentration.

*Iron and manganese in the hypolimnion*

ESCA results show that the ratio of iron(III) to iron(II) for the 12 and 15 m depths (collected on 17/02/88 and 20/01/88) varies between 2:1 and 3:1. The samples collected from the bottom sediment (27 m, collected on 11/11/87) and 21 m

on 13/04/88 showed a greater variability than this with iron(III) being the only significant species on occasion.

For manganese in the hypolimnic region the predominance of manganese(IV) increases at the expense of manganese(II) compounds (15 m on 20/01/88, 12 m on 17/02/88). This may be due to the adsorbed manganese(II) on the surface of manganese(IV), iron and other particles.[32,33] An anomaly to this trend is found in the 27 m bottom sediment sample collected on 11/11/87 where an unusually large proportion of manganese is present as manganese(III). In previous work,[34] a release of manganese from the sediment has been shown to occur during the spring months, this result may in fact be attributable to this phenomenon.

ESCA results (Table 4) show that the concentrations of iron(III) are slightly greater than iron(II), while for manganese, manganese(IV) compounds predominate in this region, although some manganese(II) compounds are found in the hypolimnion and bottom sediment. The ratios of total iron to total manganese in the hypolimnion (*i.e.* 15 m on 20/01/88; 12 m on 17/02/88) is generally greater than in the epilimnion, due to the significantly increased concentrations of insoluble iron in the hypolimnion.

*Iron and manganese in the sediment*

From the SEM photomicrographs, generally a bottom sediment sample appears to consist of a mixture of algal debris, bacteria, clay materials and inorganic and organic mineral compounds. Concentrations of insoluble iron and manganese are very high, and an ESCA survey gives a strong signal for both iron and manganese.

Table 4 shows that, in general, the bottom sediment samples contain manganese as manganese(IV) (>78%) in winter time (on 09/08/88 and 06/09/88) and after heavy rainfall (on 13/04/88). However various ratios of manganese(II), manganese(III) and manganese(IV) compounds occur in summer time (on 11/11/87). In the case of iron, the majority of material is present as iron(III) (>72%) in the sediment in any season of the year. The ratios of total iron to total manganese in the bottom sediment (Table 4) is significantly greater than in the water column, due to the increased concentrations of insoluble iron compared with insoluble manganese.

*Iron and manganese in winter season*

During the winter destratification, the speciation of iron and manganese takes on a different pattern in the dam. SEM photomicrographs were acquired for samples collected on 0.45 $\mu$m membranes for 09/08/88 and 06/09/88; the general feature of the winter months is the fact that different types of algae bloom down the whole water column depths. There appear to be no colloidal particles.[32]

During this season (Table 4; 09/08/88 and 06/09/88), insoluble manganese(IV) compounds are the predominant form of manganese right down the whole water column. Light sputtering of the ESCA sample to remove surface contamination may be expected to lead to an increase in manganese(II), however, during the destratificated period only manganese(IV) species are observed presumably due to the availability of dissolved oxygen.[32,35] A majority of insoluble iron(III) rather than iron(II) compounds is present consistently over the whole water column. The ratios of iron to manganese (on 09/08/88 and 06/09/88) were very similar over the whole water column (ESCA and AAS values as shown in Table 4). Destratification during this season results in the whole water column becoming homogeneous with respect to temperature, pH and high dissolved oxygen concentrations (3.6–8.2 mg/l.).[32]

## CONCLUSIONS

Surface analysis has been little used for the speciation of particles in natural waters. This may be due to the techniques being labor intense and expensive in both capital outlay and maintenance of equipment. However, these submicron particles play an important role in natural waters and water quality engineering. Physical and chemical sorption processes result in significant amounts of trace elements (including heavy metals) being associated with these particles in aquatic systems. The physical and chemical behaviour of these metals in the environment and their bioavailability differ from those of the corresponding dissolved species. There is no doubt that surface analysis can provide insights into the characteristics of these particles and the information may be applied for water quality improvement and pollution control applications. Our work here has established that ESCA can be used to speciate the oxidation states of solid iron and manganese particles

in dam water and to further understand their behaviour in the dam profiles at different times of the year. Experimental results clearly indicated that during any annual season, iron(III) compounds predominated down the whole water column, however, the significance of the iron(II) species varied in the hypolimnion in summer season. Like iron(III), manganese(IV) compounds also predominated in the whole water column, however manganese(II) species increased in the metalimnion and the hypolimnion in summer time.

*Acknowledgements*—The authors acknowledge financial support for this work through joint research grants from the Queensland Government Water Resources Commission and the Australian Government Water Resource Advisory Council. We also thank the staff from North Pine Dam, Brisbane City Council, the Brisbane Surface Analysis Facility and the University of Queensland Electron Microscope Centre for their valuable assistance. Comments by Dr K. O'Halloran and R. Szymczak are gratefully acknowledged.

## REFERENCES

1. B. Chiswell and M. B. Mokhtar, *Talanta*, 1986, **33**, 669.
2. B. Chiswell and M. B. Mokhtar, *Talanta*, 1987, **34**, 307.
3. B. Chiswell and M. Zaw, *Hydrolog. Proc.*, 1989, **3**, 277.
4. B. J. Wood, *Metals Australasia*, 1984, **16**, 6.
5. S. Hofmann, *Surf. Interface Anal.*, 1986, **9**, 3.
6. C. D. Wagner, W. M. Riggs, L. E. Davis and J. F. Moulder, *Hand-book of X-Ray Photoelectron Spectroscopy*, G. E. Muilenberg (ed.), p. 2, Perkin-Elmer, Eden Prairie, Minnesota, 1979.
7. J. L. Sullivan and P. Mills, in *Fifth Australasian Schools and Conference on X-ray Analysis and Surface Analysis*, p. 238, Melbourne, 1983.
8. C. D. Wagner, L. E. Davis, M. V. Zeller, J. A. Tayler, R. H. Raymond and L. H. Gale, *Surface Interface Anal.*, 1981, **3**, 211.
9. T. Nomizu and A. Mizuike, *Mikrochim. Acta.*, 1986I, 65.
10. B. Chiswell and M. Zaw, *Envir. Monitor. Assess*, 1991, **19**, 433.
11. R. J. Bird and P. Swift, *J. Electron Spectrosc. Relat. Phenom.*, 1980, **21**, 227.
12. G. C. Morris and B. J. Wood, *Materials Forum.*, 1991, **15**, 44.
13. Physical Electronics Division, *PHI Multiple Technique Analytical Computer System (MACS)*, pp. 4.1–4.12. Eden Prairie, MN, 1985.
14. C. D. Wagner, W. M. Riggs, L. E. Davis and J. F. Mouldere, *Hand-book of X-Ray Photoelectron Spectroscopy*, G. E. Muilenberg (ed.), p. 74, Perkin-Elmer, Eden Prairie, Minnesota, 1979.
15. N. S. McIntyre, in *Practical Surface Analysis*, O. Briggs and N. P. Seah (eds), p. 397, Wiley, Chichester, 1983.
16. A. Dilks, in *Developments in Polymer Characterization* J. V. Dawkins (ed.), Vol 2, pp. 145–182, Applied Science Publishers Ltd, London, 1980.
17. C. R. Brundle, T. J. Chuang and K. Wandelt, *Surf. Sci.*, 1977, **68**, 459.
18. N. S. McIntyre and D. G. Zetaruk, *Anal. Chem.*, 1977, **49**, 1521.
19. K. Asami and K. Hashimoto, *Corros. Sci.*, 1984, **24**, 83.
20. I. Olefjord, B. Brox and U. Jelvestam, *J. Electrochem. Soc.*, 1985, **132**, 2854.
21. P. Brüesch, K. Müller, A. Atrens and H. Neff, *Appl. Phys.*, 1985, **38**, 1.
22. H. J. Mathieu and D. Landolt, *Corros. Sci.*, 1986, **26**, 547.
23. S. Jin and A. Atrens, *Appl. Phys. (A).*, 1987, **42**, 149.
24. D. D. Hawn and B. M. DeKoven, *Surf. Interface Anal.*, 1987, **10**, 63.
25. S. Mischler, H. J. Mathieu and D. Landolt, *Surf. Interface Anal.*, 1988, **11**, 182.
26. P. Marcus and I. Olefjord, *Surf. Interface Anal.*, 1988, **11**, 569.
27. S. Myhra, J. C. Rivière and L. S. Welch, *Appl. Surf. Sci.*, 1988, **32**, 156.
28. M. Oku and K. Hirokawa, *J. Electron Spectrosc. Relat. Phenom.*, 1975, **7**, 465.
29. J. S. Foord, R. B. Jackman and G. C. Allen, *Philos. Mag. A.*, 1984, **49**, 657.
30. V. Dicastro and G. Polzonetti, *J. Electron Spectrosc. Relat. Phenom.*, 1989, **48**, 117.
31. D. C. Frost, C. A. McDowell and I. S. Woolsey, *Molec. Phy.*, 1974, **27**, 1473.
32. M. Zaw, *Speciation of Iron and Manganese in Freshwater Storage Dams*. PhD Thesis, University of Queensland, 1992.
33. M. B. Mokhtar, *Manganese Speciation in Dam Water*. PhD Thesis, Univesity of Queensland, 1987.
34. B. Chiswell and G. P. Rauchle, *Proc. R. Soc. Qld.*, 1986, **97**, 53.
35. E. Tipping, D. W. Thompson and W. Davison, *Chem. Geol.*, 1984, **44**, 359.

Pergamon

0039-9140(94)00212-6

*Talanta*, Vol. 42, No. 1, pp. 41–43, 1995

0039-9140/95 $9.50 + 0.00

# SPECTROPHOTOMETRIC DETERMINATION OF ZIRAM (DITHIOCARBAMATE FUNGICIDE) BY THIOCYANATE AND RHODAMINE 6G METHOD

LATA MATHEW, T. PRASADA RAO,* C. S. P. IYER and A. D. DAMODARAN
Regional Research Laboratory (CSIR), Trivandrum 695 019, India

(*Received* 4 *March* 1994. *Revised* 8 *July* 1994. *Accepted* 20 *July* 1994)

**Summary**—A sensitive spectrophotometric method has been developed for the determination of ziram in water, vegetables and grains. The method is based on the dissociation of dithiocarbamate complex of zinc with thiocyanate and rhodamine 6G at pH 4 to form a pink coloured complex that is stabilized by gelatin. The method is simple and Beer's law is obeyed over the concentration range of 0.05–1 ppm of ziram. The method is free from interference of similar dithiocarbamate fungicides containing $Mn^{2+}$ and $Fe^{3+}$ ions.

Ziram or cuman L is the common name for zinc dimethyldithiocarbamate which is used as an agricultural fungicide because of its low phytotoxicity and is applied in the rubber industry as a vulcanization accelerator and antioxidant.[1] Ziram is relatively nontoxic to plants and is particularly useful in controlling diseases of vegetable crops, such as anthracnose of tomatoes and cucurbits and early blight of tomatoes and potatoes. The compound can cause irritation to the mucous membranes in dust or powder form.[1]

The Clarke method[2] is widely used for the determination of ziram. The method is based on the destruction of dithiocarbamate in acidic medium to liberate carbon disulphide which is absorbed in methanolic KOH solution to give potassium methylxanthate which is titrated iodometrically. Petrascu[3] modified the method of Clarke *et al.*[2] and Rosenthal *et al.*[4] which requires the removal of hydrogen sulphide and liberation of carbondisulphide at a particular temperature. Verma *et al.*[5] reported a method based on the measurement of liberated $CS_2$ using benzylmercaptan. The method is less sensitive (14–150 ppm) and uses toxic mercaptan for the determination of dithiocarbamates. Other methods reported are based on the replacement of zinc with toxic metallic compounds.[6,7] Malik and Rao reported a spectrophotometric procedure for the determination of ziram using diphenylcarbazone. The method not only involves extraction, but also is less sensitive.

In the present communication, a new method is described for the estimation of ziram based on the determination of zinc by formation of a ternary complex with potassium thiocyanate and rhodamine 6G at pH 4. The method is free from interference from $Cu^{2+}$, $Hg^{2+}$, $Fe^{3+}$, $Mn^{2+}$ and $Pb^{2+}$ and does not require the removal of $H_2S$. Beer's law is obeyed from 0.05 to 1.0 ppm of ziram solution. The method has been successfully applied to the determination of ziram in water, vegetables and grain samples.

## EXPERIMENTAL

### *Apparatus*

A Hitachi Model 220 microprocessor controlled double beam spectrophotometer with 1.0 cm quartz cells was used for all spectral measurements. An ELICO Model LI-120 digital pH meter was used for all pH measurements.

### *Reagents*

Ziram solution (Hindustan Ciba-Geigy Ltd). A solution of 1 mg/ml was prepared in hot 25% (v/v) hydrochloric acid.

Rhodamine 6G solution, 0.005%. The reagent (0.05 g) was dissolved (BDH, U.K.) in water and diluted to 1 l.

Potassium thiocyanate solution, 5%. AR grade potassium thiocyanate (5 g) was dissolved in water and diluted to 100 ml with water.

*Author to whom correspondence should be addressed.

Gelatin solution, 1%. Gelatin (1 g) was dissolved in hot water, cooled and diluted to 100 ml with water.

Acetate buffer, pH 4.0. Equal volumes of 2*M* solutions of sodium acetate and acetic acid were mixed and the pH adjusted to 4.0 using a pH meter.

*Procedure*

Suitable aliquots (up to 10 ml) of the sample solution containing not more than 25 $\mu$g of ziram were transferred to a 25 ml volumetric flask, 1 ml of buffer, 2.5 ml of potassium thiocyanate, 5 ml of rhodamine 6G and 1 ml of gelatin were added with mixing and made up to the mark. The absorbance of the solution was measured at 570 nm against a reagent blank. A calibration graph using similar procedure was prepared with a solution containing 2.5–25 $\mu$g of ziram.

## RESULTS AND DISCUSSION

*Effect of pH*

It was found that the ternary complex was fully formed when the solutions were buffered in the pH range 1–5. At higher pH the absorbance of the colour system decreased. Hence, all the subsequent studies were carried out at pH 4.

*Effect of reagent concentrations*

It was found that at least 2 ml of 5% potassium thiocyanate and 4 ml of 0.005% rhodamine 6G solutions were required for constant and maximum absorbance. One millilitre of 1% gelatin was sufficient to prevent the precipitation of ternary complex. The order of addition of the reagents were not found to be critical provided that the gelatin solution was added after the addition of other reagents. The absorbance of the coloured complex was found to be stable for ~2 hr.

*Calibration graph and precision*

The colour system showed linear absorbance in the range of 0–25 $\mu$g of ziram present in 25 ml and passed through the origin. The molar absorptivity was found to be $9.71 \times 10^4$ l. mol$^{-1}$. cm$^{-1}$ and Sandell's sensitivity was calculated to be 0.004 $\mu$g/cm$^2$. The relative standard deviation was found to be $\pm 2.19\%$ in the determination of 10 $\mu$g of ziram solution in 25 ml for repetitive analysis carried out over 7 days.

Table 1. Effect of foreign species (concentration of ziram = 10 $\mu$g/25 ml)

| Foreign species | Tolerance limit* ($\mu$g) |
|---|---|
| $F^-$, $Cl^-$, $SO_4^{2-}$, $PO_4^{3-}$, tartrate | 10,000 |
| $Bi^{3+}$ | 5000 |
| $Mn^{2+}$, $Ni^{2+}$, $Cd^{2+}$† | 2000 |
| $VO^{2+}$, $As^{3+}$, $MoO_4^{2-}$, $Pb^{2+}$,† $Hg^{2+}$,† $Fe^{3+}$‡ | 1000 |
| Thiram, dibam | 1000 |
| $Cu^{2+}$† | 100 |

*Amount of foreign species that caused $< \pm 2\%$ error.
†In the presence of 1 ml of 5% thiourea.
‡In the presence of 1 ml of 5% NaF.

*Effect of foreign species*

The effect of foreign species which are known to coexist with ziram were studied and the results obtained are shown in Table 1. The method is free from interference due to other dithiocarbamate fungicides like thiram and dibam. Equal amounts of $Cu^{2+}$, $Cd^{2+}$, $Pb^{2+}$, $Hg^{2+}$ and $Fe^{3+}$ interfered in the determination of ziram. However, the interference due to these species could be masked with thiourea and sodium fluoride and the tolerance limits are given in Table 1. Hence, the developed method may find application in real samples containing the above species.

*Comparison with other methods*

The developed method has been compared with other reported methods (Table 2). The benzyl mercaptan method[5] makes use of toxic mercaptan and the Methylene Blue method[9] is cumbersome as it requires generation of hydrogen sulphide. The diphenyl carbazone method[8] is less sensitive and requires an additional extraction step. The present method is simple (as it does not require the generation of

Table 2. Comparison with other spectrophotometric methods

| S. No. | Method/ reagent | Max (*nm*) | Beer's law range | Sensitivity ($l.mol^{-1} \cdot cm^{-1}$) | Reference |
|---|---|---|---|---|---|
| 1. | Diphenylcarbazone | 520 | 0.12–1.9 | 0.08 $\mu g/ml$ (detection limit) | 8 |
| 2. | Methylene Blue method | 655 | 3–22 | $6.8 \times 10^3$ | 9 |
| 3. | Benzyl mercaptan | 430 | 14–150 | — | 5 |
| 4. | $SCN^-$–rhodamine 6G | 570 | 0.05–1.0 | $9.71 \times 10^4$ | Present method |

Table 3. Recovery of ziram in polluted water, vegetable and grain samples

| Sample | Amount of ziram added ($\mu g$) | Amount of ziram found ($\mu g$)* | | % Recovery | |
|---|---|---|---|---|---|
| | | Proposed method | AAS | Proposed method | AAS |
| Polluted water† | 100 | 95.2 | 98.4 | 95.2 | 98.4 |
| Potato‡ | 100 | 96.2 | 98.2 | 96.2 | 98.2 |
| | 50 | 47.9 | 48.4 | 95.8 | 96.8 |
| Cabbage‡ | 100 | 98.4 | 98.0 | 98.4 | 98.0 |
| | 50 | 48.8 | 49.0 | 97.6 | 98.0 |
| Wheat‡ | 100 | 98.8 | 99.1 | 98.8 | 99.1 |
| | 50 | 49.3 | 49.5 | 98.6 | 99.0 |

*Mean of three replicate analyses.
†Amount of sample = 500 ml.
‡Amount of samples = 200 g.

hydrogen sulphide), highly sensitive and can be applied to real samples in the presence of ferbam and maneb.

*Application of the method*

*Determination of ziram in polluted water.* To check the applicability of the method, the determination of ziram in water from agricultural fields was carried out. These samples were found to be free from ziram. Therefore, known amounts of ziram were added to water samples. Aliquots of spiked water samples were taken in a 25 ml beaker and 2 ml of conc HCl was added followed by 1 ml of buffer and the pH adjusted to 4. These samples were analysed by the recommended procedure. The results are shown in Table 3.

*Determination of ziram in vegetables and grains.* About 200 g of potato, cabbage and wheat grains were taken and blended in a mixer. Known amounts of ziram were added and kept for some time. The blended sample was then digested with 100 ml of 1:1 HCl. The mixture was filtered and aliquots were taken for analysis by the recommended procedure and by standard AAS. The recoveries (Table 3) obtained with the proposed method are comparable with the standard AAS procedure.

*Acknowledgement*—One of the authors (LM) is grateful to CSIR (New Delhi) for the award of a Research Associateship.

## REFERENCES

1. E. H. F. Donald, *Chemistry of the Pesticides*, 3rd Ed., pp. 294–297. Van Nostrand, New York, 1955.
2. D. G. Clarke, H. Baum, E. L. Stanley and W. F. Hesta, *Anal. Chem.*, 1951, **23**, 1842.
3. S. Petrascu, *Rev. Chim. Bucharest*, 1986, **17**, 687.
4. J. Rosenthal, R. L. Carson and F. L. Stanley, *J. Assoc. Off. Agric. Chem.*, 1953, **36**, 1170.
5. B. C. Verma, R. V. Sood and M. S. Sindhu, *Talanta*, 1983, **30**, 784.
6. A. K. Malik and A. L. J. Rao, *Talanta*, 1990, **37**, 1205.
7. A. L. J. Rao and N. Verma, *Talanta*, 1989, **36**, 1041.
8. A. K. Malik and A. L. J. Rao, *Talanta*, 1991, **38**, 941.
9. V. Agrawal, P. Shivhare and V. K. Gupta, *Fres. J. Anal. Chem.*, 1992, **344**, 350.

Pergamon

0039-9140(94)00213-4

*Talanta*, Vol. 42, No. 1, pp. 45–47, 1995

0039-9140/95 $9.50 + 0.00

# DIRECT DETERMINATION OF GALLIUM ON POLYURETHANE FOAM BY X-RAY FLUORESCENCE

MARCELO S. CARVALHO, JOÃO ALFREDO MEDEIROS, ARMI W. NÓBREGA, J. LUIZ MANTOVANO and VALESKA P. A. ROCHA

Instituto de Engenharia Nuclear, Comissão Nacional de Energia Nuclear, Cidade Universitária, Ilha do Fundão-Rio de Janeiro-Brasil 21945-970

(*Received* 4 *March* 1994. *Revised* 11 *July* 1994. *Accepted* 22 *July* 1994)

**Summary**—Gallium chloride is easily extracted from 6*M* HCl by comminuted polyether-type polyurethane foam. After the extraction step, the gallium absorbed by the PU foam can be quantitatively determined by X-ray fluorescence. A procedure for the direct determination of gallium absorbed by PU foam by XRFS is thus described. Gallium is determined at levels as low as 60 ng/ml ($C_L$), with a calibration sensitivity of 424 cps·ml/$\mu$g, within a linear range 0.1–2.30 $\mu$g/ml. The procedure investigated was successfully applied to determination of gallium in aluminum alloys, bauxite and industrial residue samples.

The determination of gallium is not an easy task as several elements which are usually associated with it interfere considerably in the analysis. Thus, gallium is commonly determined after its separation from such elements.[1] The use of polyurethane (PU) foams in the extraction, recovery and preconcentration of various inorganic and organic species in aqueous and non-aqueous media has attracted much attention since Bowen's work on this subject.[2] Many authors have used PU foams to preconcentrate, separate and recover metals to be determined by atomic absorption spectrometry or radiochemical analysis.[3–5] Several authors studied physicochemical parameters related to the sorption mechanisms of metals on the foams.[5–9]

The extraction of gallium from hydrochloric acid solution using polyether-type polyurethane foams has been reported.[10,11] Carvalho[12] studying the same system observed a very high distribution coefficient for gallium ($D \geqslant 10^4$, 6–9*M* HCl), and demonstrated that Al, In, Zn, Ni, and Ti(IV) are not extracted ($D \leqslant 4.5$); Fe(II) and Cu ($D \leqslant 30$) are only slightly extracted from the same medium.

The analytical determination of extracted species when still absorbed in the PU foam has seldom been reported. Radioiodine has been extracted from aqueous solutions[13] and from milk[14] using PU foams, the iodine-131 being determined directly by gamma spectrometry. Open-cell PU foams, loaded with various organic reagents, have been used to detect metal ions directly by comparing the color of the samples thus obtained with standards.[15]

Cobalt has been extracted from 3*M* $NH_4Cl$–1*M* $NH_4SCN$ solution by PU foam discs, and determined by X-ray fluorescence spectrometry (XRFS).[16] The XRFS was employed to determine directly metal thiocyanate complexes of iron, cobalt, zinc, platinum and palladium, extracted on polyether-type PU foam discs.[17] Arsenic[18] and phosphate[19] as arsenomolybdate and molybdoantimonylphosphate, respectively, were also extracted on PU foam and determined directly by XRFS.

This paper describes the direct determination of gallium on open-cell polyether-type polyurethane foam by XRFS, after the extraction of the metal from 6*M* hydrochloric acid solution was performed. This method has been employed to determine gallium in bauxite, alumina, aluminum alloy and residues from the aluminum industry.

## EXPERIMENTAL

### *Apparatus*

A Rigaku-B3 wavelength dispersive X-ray fluorescence spectrometer, with a rhodium tube operated at 40 kV and 30 mA, a LiF crystal, and a scintillation counter was used. Such system is equipped with an automatic unit which drives

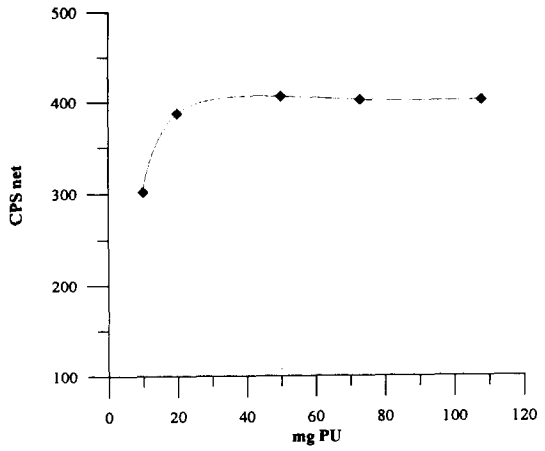


Fig. 1. XRF intensity measured against mass of PU.

the goniometer, sets the discrimination, and acquires the data.

*Reagents*

A gallium stock solution was prepared from its oxide (Johnson Matthey, 99, 99% pure), made 6*M* in hydrochloric acid (Merck, PA), and subsequently standardized with EDTA.[20] Dilute solutions were prepared by appropriated dilution of aliquots from the stock solution with 6*M* hydrochloric acid.

Commercial, open-cell, polyether-type polyurethane foams (Vulcan of Brazil-VCON 202, 42% resilience and 10–12 cells/linear cm) were comminuted in a blender with a large quantity of distilled water. The PU foam was filtered in a vacuum system, squeezed between clean sheets of paper towels and stored in a desiccator.

*General procedures*

A convenient aliquot of the stock solution containing gallium was transferred to stoppered polypropylene flasks. A known amount of comminuted PU foam (previously treated with 6*M* HCl solution for 30 min) was added, and the volume made up to 10.0 ml with 6*M* HCl solution. The system was then shaken mechanically (VKS-100 Mechanical Shaker, 100 cpm) for 1 hr. The PU foam was collected by vacuum filtration (filter paper $\emptyset = 2.0$ cm), covered with a Mylar® film and taken to the XRF spectrometer. The determination of gallium was then made by measuring the gallium $K_\alpha$ line for 40 sec and taking the average of five measurements, after subtracting from each value the measurement corresponding to the blank (CPS net). All experiments were made at $25 \pm 2$°C.

## RESULTS AND DISCUSSION

*Characteristics of the* Ga–*PU*–HCl *system*

As already pointed out,[10–12] gallium can be quantitatively extracted from hydrochloric acid solution by polyether-type polyurethane foams. The efficiency of extraction was found to increase with the hydrochloric acid concentration, reaching a maximum value between 6 and 9*M* HCl, where the system exhibits the highest distribution coefficient ($D \geqslant 10^4$). The extraction is effective after shaking the system for 30 min. In this work the extraction time was always 60 min.

*Effect of the mass of PU on the extraction of gallium from* 6M HCl *media*

The adequate amount of PU foam to be used in the extraction of gallium was found by treating 10.0 ml of 6*M* hydrochloric acid, containing 11.5 $\mu$g of gallium, with masses of comminuted PU foam from 10 to 120 mg. The extraction time was 60 min. A maximal and constant XRF intensity was observed to correspond to masses of PU foam higher than 30 mg (Fig. 1). In this work, $55 \pm 5$ mg of PU foam was selected as optimal mass for the general procedure.

*Analytical characteristics of the method*

For the Ga–PU–6*M* HCl system a linear relationship was found between the gallium concentration and the XRF signal up to 2.3 $\mu$g/ml Ga. The calibration curve was constructed as described under General Procedures. The analytical sensitivity,[21,22] the calibration sensitivity, the limit of detection ($C_L$) and of quantification ($C_Q$),[23] as well as other analytical characteristics of the procedure here described are summarized in Table 1. These analytical characteristics compare favorably with those found on determining gallium by atomic absorption spectrometry, polarography and visual spectrophotometry.[12]

Table 1. Direct determination of gallium by PU–XRFS, analytical characteristics

| Characteristics | Data |
|---|---|
| Calibration sensitivity (*cps ml/μg*) | 424 |
| Analytical sensitivity (*cps ml/μg*) | 8480 |
| Detection limit ($C_L$) (*ng/ml*) | 60 |
| Quantification limit ($C_Q$) (*ng/ml*) | 178 |
| Linear dynamic range (*μg/ml*) | 0.10–2.30 |
| Coefficient of variation (%) | 1.51 |

Table 2. Determination of gallium by PU–XRFS in several samples

| Standard and samples | $N$* | $\mu g/ml$ Ga found | Sd | $\mu g/ml$ Ga | Sd |
|---|---|---|---|---|---|
| Alloy-Al-base NIST 85B | 5 | 192.2 | 5.3 | 190† | 1 |
| Alloy-Al-base NIST 87A | 5 | 195.4 | 8.1 | 200† | 8 |
| Bauxite B4 | 5 | 44.1 | 1.2 | 43.1‡ | 1.3 |
| Alumina I | 5 | 74.5 | 1.9 | 72.1‡ | 2.1 |
| Alumina II | 4 | 97.3 | 3.4 | 98.9‡ | 3.0 |
| Residue 1 | 5 | 399.8 | 6.1 | 398.1‡ | 5.2 |

*Number of determinations.
†NIST Certified Values.
‡Fluorimetry.

*Applications*

The procedure investigated was applied for the determination of gallium in aluminum base alloy standards, a bauxite sample and residues from aluminum production plants. The results are compared with the classical fluorimetric method[1] and are presented in Table 2.

The samples were prepared using a mixture of hydrofluoric acid and hydrochloric acid (3:1). For the bauxite sample, sulfuric acid and some drops of hydrogen peroxide was also used. In all cases, the samples were evaporated to dryness or to $SO_3$ fumes, solubilized in $6M$ hydrochloric acid, treated with a small excess of $0.5M$ titanous chloride solution to reduce Fe(III) and the volume adjusted as desired with $6M$ hydrochloric acid.

The paired $t$-test[23] and least-square analysis[21] were used to compare the two methods, the classical fluorimetric method and the procedure proposed in this work. It was found that the calculated slope (1.001) and the intercept (0.09) do not differ significantly from the ideal values of 1 and 0, respectively. Thus, there is no significant difference between the two methods, at the confidence limit of 95% (Table 2).

## REFERENCES


1. A. M. Dimov, A. P. Savdstin and J. Schmorak, *Analytical Chemistry of Gallium*, Ann Arbor, London, 1970.
2. H. J. M. Bowen, *J. chem. Soc. A.*, 1970, 1082.
3. S. Palágyi and T. Braun, *J. Radioanal. Nucl. Chem. A.*, 1992, **36,** 69.
4. H. D. Gesser and G. A. Horsfall, *J. Chem. Phys.*, 1977, **74,** 1072.
5. R. F. Hamon, A. S. Khan and A. Chow, *Talanta*, 1982, **29,** 313.
6. T. Braun, J. D. Navratil and A. B. Farag, *Polyurethane Foam Sorbents in Separation Science*, CRC Press, 1984.
7. G. S. Schröder and A. Chow, *Talanta*, 1992, **39,** 837.
8. A. S. Khan and A. Chow, *Talanta*, 1986, **33,** 182.
9. M. N. Abbas, A. Verts and T. Braun, *Radiochem. Radioanal. Lett.*, 1982, **54,** 17.
10. H. D. Gesser, E. Bock, W. G. Baldwin, A. Chow, D. W. McBird and W. Lipruski, *Sep. Sci.*, 1975, **11,** 315.
11. H. D. Gesser, G. A. Horsfall, K. M. Gough and B. Krawchuk, *Nature*, 1977, **268,** 323.
12. M. S. Carvalho, *D.Sc Thesis*, Pontfícia Universidade Católica, Rio de Janeiro, 1993.
13. S. Palágyi and T. Braun, *J. Radioanal. Chem.*, 1979, **51,** 267.
14. S. Palágyi and R. Markusova, *Radiochem. Radioanal. Lett.*, 1978, **32,** 103.
15. T. Braun and A. B. Farag, *Anal. Chim. Acta*, 1974, **73,** 301.
16. A. Chow, G. T. Yamashita and R. F. Hamon, *Talanta*, 1981, **28,** 437.
17. A. Chow and S. L. Ginsberg, *Talanta*, 1983, **30,** 620.
18. A. S. Khan and A. Chow, *Talanta*, 1984, **31,** 304.
19. A. S. Khan and A. Chow, *Talanta*, 1985, **32,** 241.
20. G. Schwarzenbach, *Complexometric Titration*, 2nd Ed. F. Enke, Stuttgard,1956.
21. J. Medinilla, F. Ales and F. Garcia Shanchez, *Talanta*, 1986, **33,** 329.
22. K. Laqua, W. H. Meluish and M. Zander, *Pure Appl. Chem.*, 1988, **60,** 1449.
23. D. A. Skoog and J. J. Leary, *Principles of Instrumental Analysis*, Saunders College Publishing, Florida, 1992.

Pergamon

0039-9140(94)00214-2

*Talanta*, Vol. 42, No. 1, pp. 49–53, 1995

0039-9140/95 $9.50 + 0.00

# PRECISE COULOMETRIC TITRATION OF PRECIOUS METALS—II. DETERMINATION OF PLATINUM(IV) WITH ELECTROGENERATED CHLOROCUPROUS ION IN KCl–Cu–EDTA BUFFER MEDIUM

DONG SHOUAN
Institute of Precious Metals, Kunming 650221, China

(*Received* 20 *June* 1994. *Accepted* 25 *July* 1994)

**Summary**—A method for the precise coulometric titration of platinum(IV) with electrogenerated chlorocuprous ion in KCl–Cu–EDTA buffer medium is described. From 2.7 to 18.7 mg of platinum in pure platinum and platinum alloy are determined with standard deviations of less than or equal to 0.034% using potentiometric end point detection. The method has good accuracy and precision, selectivity and rapidity.

Until now, a direct method for the precise determination of platinum purity, its compounds and alloys has not been reported. For the analysis of platinum with 98–99.9% purity, the spectrographic method applicable to the determination of the total impurity content in pure metal is not usable because of the higher impurity concentration and difficult preparation of the standard sample. For the determination of platinum in compounds such as $H_2PtCl_6$ and $PtCl_4$, the gravimetric method based on the precipitation of platinum as ammonium hexachloroplatinate also have insufficient precision and accuracy. The establishment of a coulometric titration method for platinum provides a good approach to precisely and accurately determining large amounts of platinum in platinum materials.[1] However, methods for the coulometric titration of platinum(IV) with electrogenerated tin(II) were not suited to precise analysis owing to the difficulty of obtaining 100% current efficiency of tin(II) electrogeneration.[2–4]. This author[5] has studied coulometric titration of high amounts of platinum with electrogenerated copper(I) in dilute hydrochloric acid medium and obtained good results. However the hydrochloric acid system, the end point potential break in the titration curve is not very pronounced, so it is difficult to improve precision. For this reason, the titration of platinum, in NaOAc–HOAc buffer medium (pH 4), with electrogenerated copper(I) using a EDTA–Cu(II) complex system was studied. The results demonstrate that the system not only decreases the reduction potential of the Cu(II)/Cu(I) couple, but also improves the reaction of Pt(IV) with Cu(I), increases the end point potential break and enhances the selectivity owing to EDTA complexing with impurity. The proposed method is suitable for precise determination of platinum in pure platinum, some platinum alloys and platinum compounds. The method has a high selectivity.

## EXPERIMENTAL

### *Apparatus*

A Gui-III type precision coulometric analyser was used with constant current output of 1, 10 and 100 mA, the current stability and precision for each grade was $5 \times 10^{-6}$. The timer was a six digit display with a precision of 0.002%. The titration assembler was a new type hermetically sealed electrolytic cell system.[6] An XWT-164 desk autobalance recorder (Shanghai, China) was used.

### *Reagents*

Cupric sulfate, hydrochloric acid and nitric acid were of pure grade. Potassium chloride, sodium acetate and disodium EDTA were of analytical-reagent grade. The anolyte was 0.5*M* cadmium chloride in 0.5*M* potassium chloride. The supporting electrolyte was 0.5*M* KCl–0.02*M* EDTA–0.04*M* Cu in 0.2*M* (HOAc–NaOAc) buffer medium (pH 4). A

standard platinum solution was prepared by dissolving pure platinum in aqua regia and evaporating several times with hydrochloric acid to remove oxides of nitrogen. All distilled water used was secondary distilled water (distilled with quartz distillator).

*Titration procedure*

On adding the test solution to the titration cell and the supporting electrolyte in the pre-titration cell, air was removed from both the test solution (including anolyte) and the supporting electrolyte with pure nitrogen. The supporting electrolyte was pre-titrated to the pre-established endpoint potential, then the supporting electrolyte was placed in the titration cell in which has been added the test solution. Finally, the potentiometric endpoint detection, the coulometric titration was run in the usual manner. The results were displayed and printed by the coulometric analyser.

## RESULTS AND DISCUSSION

*Choice of supporting electrolyte and current efficiency for* Cu(I) *generation*

In the HOAc–NaOAc buffer medium (pH 4), Cu(II) complexed with EDTA and formed a stable complex compound, this is shown when the solution becomes deep blue as EDTA is added. When this solution is electrolysed with a platinum cathode, the complex compound $Cu(II)Y_2$ (Y, EDTA) accepts an electron and produces a cuprous ion. It is well known that fresh cuprous ion is a very strong reductant and will rapidly react with oxidizing substances in solution, because the bare cuprous ion is thermodynamically unstable. The following disproportionation reaction occurs: $2Cu(I) \rightarrow Cu + Cu(II)$, so the platinum cathode will be plated with copper metal. Obviously, it is difficult to obtain 100% current efficiency if this electrolyte system is applied.

In order to obtain 100% current efficiency of Cu(I) electrogeneration, the hydrochloric acid medium has always been applied. It is evident that $Cl^-$ is necessary to obtain stable cuprous ion. However, the buffer system will be destroyed if hydrochloric acid is added to above mentioned $Cu(II)Y^{2-}$ solution in HOAc–NaOAc buffer medium, and the Cu(II) complexes of EDTA will also disintegrate. To establish an optimal condition in which not only the $Cu(II)Y^{2-}$ complex system is maintained but also the cuprous ion electrogeneration was stable, KCl–EDTA–Cu(II) in pH 4 NaOAc–HOAc buffer medium was used as supporting electrolyte instead of dilute hydrochloric acid solution used previously and the titration characteristics of platinum studied. Figure 1 shows voltammetric curves of various media in the presence and absence of EDTA or $Cu^{2+}$. It is observed that, when the current density is a certain value (in the presence of EDTA, $I \leqslant 4$ mA/cm$^2$; no EDTA, $I \leqslant 5$ mA/cm$^2$), 100% current efficiency for Cu(I) generation can be ob-

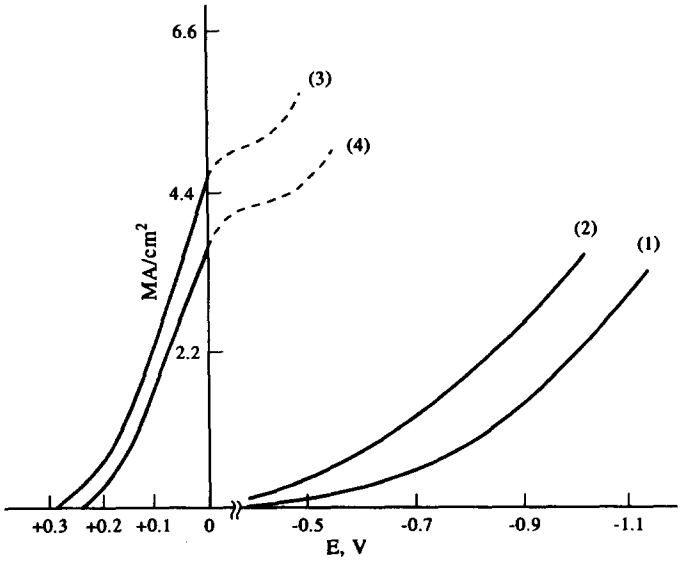


Fig. 1. Platinum cathode voltammetric curves of various media: (1) 0.25*M* KCl + 0.2*M* HOAc–NaOAc, (2) 0.25*M* KCl + 0.02*M* EDTA + 0.2*M* HOAc–NaOAc, (3) (1) + 0.04*M* $CuSO_4 . 5H_2O$, (4) (2) + 0.04*M* $CuSO_4 . 4H_2O$.

tained in either EDTA-containing medium or no EDTA medium. In the presence of EDTA, the density of current allowed became smaller than with no EDTA, and the potential range of curve 4 (electrolyte containing EDTA) in Fig. 1 is more negative than that of curve 3 (no EDTA in the electrolyte), this demonstrates that the reduction potential of the Cu(II)/Cu(I) couple becomes more negative when the electrolyte contains EDTA.

*Mechanism of cuprous chloride generation in the platinum cathode–electrolyte interface and the reaction in solution*

It is well known that the coulometric titrant results from electron transport of ions (or molecules) at the electrode–solution interface when electrolysing. Electron transport in complex systems differs from that in the simple solution, the former usually undergo some intermediate course. In the KCl–Cu(II)–EDTA buffer system, $Cl^-$ is necessary to obtain stable titrant, $CuCl^{2-}$, so it can be deduced that the mechanism of charge exchange in the platinum cathode–solution interface is based on reactions as follows:

$$CuY^{2-} \Rightarrow Cu^{2+} + Y^{4-} \quad (1)$$

$$Cu^{2+} + e \Rightarrow Cu^{+} \quad (2)$$

$$Cu^{+} + nCl^{-} \Rightarrow CuCl_n^{(n-1)-} \quad (3)$$

$$Y^{4-} + 2H^{+} \Rightarrow H_2Y^{2-}. \quad (4)$$

If the electrolyte has no $Cl^-$, above mentioned $Cu^+$ disproportionation reaction will occur instead of reaction (3).

When $CuCl_2$ is produced from the platinum cathode interface in solution, the reactions will occur as follows:

$$PtCl_6^{2-} + 2CuCl_2 \Rightarrow PtCl_4^{2+} + 2Cu^{2+} + 6Cl^{-} \quad (5)$$

$$Cu^{2+} + H_2Y^{2-} \Rightarrow CuY^{2-} + 2H^{+}. \quad (6)$$

It is obvious that coulometric titration of platinum(IV) is based on equation (5).

*Methods of end point detection*

In the above electrolyte solution, the biamperometric method for end point detection is useless with two polarized indicator electrode. However, the potentiometric method for end point detection can obtain good results.

*General potentiometric method* (i = 0). Using a platinum or plated-gold platinum electrode as an indicator electrode (*vs.* SCE), the reduction titration curves of Pt(IV) in various electrolytes were obtained as shown in Fig. 2.

It can be seen from Fig. 2 that the potential break of KCl–$Cu^{2+}$–HOAc–NaOAc system is larger than that of the HCl–$Cu^{2+}$ system. However, the potential break of the EDTA $Cu^{2+}$–KCl–HOAc–NaOAc system is the largest and the potential curve is the most symmetric. Obviously, the concentration of oxidizable Cu(II) decreased owing to formation of $CuY^{2-}$ complex in the electrolyte solution, so the electrode potential of Cu(II)/Cu(I) couple decreased also, and the electrogenerated Cu(I) increased in reducing ability making reaction (5) occur more readily. So the sensitivity and precision for end point detection is improved.

*Bipotentiometer method with two polarized platinum indicator electrodes* ($i \neq 0$). When a small constant current (8.5 $\mu$A) is applied to two identical platinum electrodes (area of either electrode immersed in the electrolyte solution is about 1 $cm^2$), a titration curve graph analogous to that obtained from the classical potentiometric method can be obtained, and the potential break is larger than that of general potentiometric method, so the end point detection is more sensitive. Unfortunately, using this method for end point detection always produced a system negative error, maybe related to reactions on the

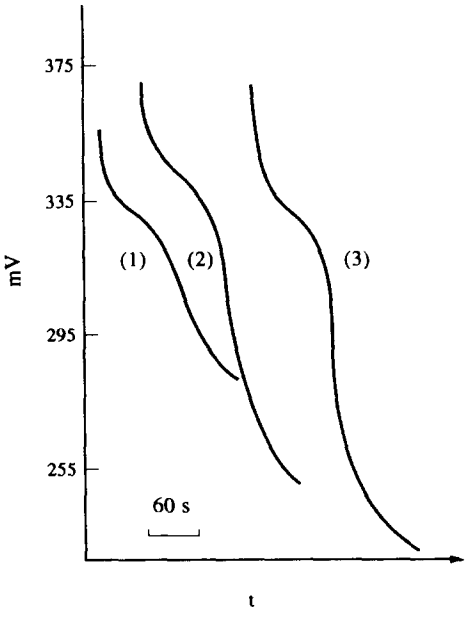


Fig. 2. Potential curves for the coulometric titration of platinum(IV) (about 1.5 mg) with various solutions. (1) 0.25*M* HCl + 0.04*M* $CuSO_4 \cdot 5H_2O$, (2) 0.25*M* KCl + 0.04*M* $CuSO_4 \cdot 5H_2O$ + 0.2*M* HOAc–NaOAc, (3) 0.25*M* KCl + 0.02*M* EDTA + 0.2*M* HOAc–NaOAc + 0.04*M* $CuSO_4 \cdot 5H_2O$.

Table 1. Precise coulometric titration of standard platinum(IV) solution (platinum 99.95%, $I = 9.9824$ mA)

| No. | Platinum taken (*mg*) | Time (*sec*) | Platinum found (*mg*) | Platinum found (%) | Relative SD (%) |
|---|---|---|---|---|---|
| 1 | 5.5016 | 544.9 | 5.4992 | 99.95 | 0.034 |
| 2 | 2.3760 | 235.3 | 2.3746 | 99.94 | |
| 3 | 9.1812 | 901.5 | 9.1789 | 99.96 | |
| 4 | 7.3214 | 725.7 | 7.3238 | 100.03 | |
| 5 | 17.0834 | 1692.5 | 17.0810 | 99.98 | |
| 6 | 18.7220 | 1854.1 | 18.7118 | 99.94 | |

indicator electrodes. For this reason, the general potentiometric method for end point detection was still used.

*Experiments for titration of standard platinum(IV) solution and effect of foreign ions*

In order to improve the precision of titration of platinum(IV) with electrogenerated chlorocuprous ions in the KCl–Cu(II)–EDTA buffer medium, the participation of error resulting from inherent inaccuracy of burette readings was minimized by sampling with a precisely (0.1 mg) weighed platinum(IV) test solution. The titration of platinum(IV) standard solution was carried out as mentioned above; the results are shown in Table 1.

Table 1 demonstrates that, for determination of platinum in the range of 2.7–18.7 mg, accurate and precise results can be obtained with the proposed method.

The effect of foreign ions is summarized in Table 2. Many base metals and considerably larger amounts of Fe(III) do not interfere owing to complex formation with EDTA, larger quantities of Ru(III), Ag(I) and Pd(II) do not interfere either. Ir(IV) and Ru(IV) produce a larger positive interference. Au(III) causes a serious positive interference owing to conjugated electrochemical reactions.[7] From the investigation for titration of standard platinum(IV) solution and effect of foreign ions, it is evident that the proposed method is applicable to the precise titration of platinum in platinum materials.

## ANALYTICAL APPLICATION

Platinum of some materials are determined using precise coulometric titration with electrogenerated chlorocuprous in the 0.25*M* KCl–0.2*M* EDTA–0.04*M* Cu(II)–0.2*M* (HOAc-NaOAc) medium. For metallic platinum of 98 to 99.9% purity and platinum alloys, the sample solution is prepared by dissolving these materials in aqua regia and evaporating several times with hydrochloric acid to remove oxides of nitrogen. Results are shown in Table 3. The results obtained for the titration of platinum samples indicated that the proposed method has good precision and convenience, and allows a precision titration of platinum in some materials. The method can be applied to routine assay for platinum compounds.

Table 2. Effect of foreign ions on the titration of platinum (platinum 99.95%, $I = 9.9824$ mA)

| Foreign ions added (*mg*) | Platinum(IV) added (*mg*) | $M^{n+}$:Pt(IV) | Platinum found (*mg*) | Platinum found (%) | Error (%) |
|---|---|---|---|---|---|
| Fe(III) | | | | | |
| 2.0 | 4.3856 | 0.46:1 | 4.3830 | 99.94 | −0.01 |
| 4.0 | 4.7558 | 0.83:1 | 4.7534 | 99.95 | 0 |
| 10.0 | 5.4479 | 1.83:1 | 5.5416 | 101.72 | +1.77 |
| Pd(II) | | | | | |
| 0.38 | 4.4728 | 0.09:1 | 4.4741 | 99.97 | +0.02 |
| 0.76 | 4.2146 | 0.18:1 | 4.2111 | 100.08 | +0.13 |
| 1.53 | 4.0630 | 0.38:1 | 4.0651 | 100.05 | +0.10 |
| 2.29 | 4.9996 | 0.46:1 | 5.0157 | 100.32 | +0.37 |
| Rh(III) | | | | | |
| 0.93 | 4.1332 | 0.23:1 | 4.1367 | 100.08 | +0.13 |
| 1.23 | 4.3442 | 0.28:1 | 4.3426 | 99.96 | +0.01 |
| 1.54 | 4.0856 | 0.38:1 | 4.0873 | 100.02 | +0.07 |
| Ag(I) | | | | | |
| 2.0 | 4.2952 | 0.47:1 | 4.2992 | 100.08 | +0.13 |
| 2.0 | 7.8067 | 0.26:1 | 7.8022 | 99.94 | −0.01 |

Table 3. Application of proposed method to platinum materials ($I = 9.9824$ mA)

| Sample | Platinum taken (*mg*) | Platinum found (*mg*) | (%) | Relative SD (%) |
|---|---|---|---|---|
| Metallic platinum | 5.3939 | 5.3337 | 98.88 | 0.030 |
| | 5.2842 | 5.2277 | 98.93 | |
| | 6.8648 | 6.7900 | 98.91 | |
| | 5.9816 | 5.9190 | 98.95 | |
| | 5.3037 | 5.2479 | 98.95 | |
| $Pt–Rh_6$ alloy | 6.8005 | 6.3681 | 93.64 | 0.029 |
| | 6.1360 | 5.7485 | 93.69 | |
| | 7.2179 | 6.7577 | 93.62 | |
| | 7.0977 | 6.6487 | 93.67 | |
| | 7.2823 | 6.8202 | 93.66 | |

## REFERENCES


1. Dong Shouan, *Fenxi Shi Yan Shi*, 1987, **6** (11), 41.
2. A. J. Bard, *Anal. Chem.*, 1960, **32,** 623.
3. O. Ginstrip, *Anal. Chim. Acta*, 1976, **63,** 153.
4. A. Hulanicki and W. Jedral, *Talanta*, 1976, **23,** 259.
5. Dong Shouan, *Gui Jin Shu*, 1982, **3** (2), 29.
6. Shiyong Xinxing and Thuanli Gongbao, *CN 2090060U(Cl.G01N27/42)*, 1991, 7 (49), 126.
7. Dong Shouan and Zhang Wei, *Hua Xue Xue Bao*, 1986, **44,** 719.

Pergamon

0039-9140(94)00215-0

*Talanta*, Vol. 42, No. 1, pp. 55–57, 1995

0039-9140/95 $9.50 + 0.00

# REDOX REACTIONS OF HYDROGEN ADDUCTS OF THYMINE: COMPARISONS WITH THE REACTIONS OF HYDROXYL ADDUCTS

S. CHAKRABARTI,* P. C. MANDAL and S. N. BHATTACHARYYA

Nuclear Chemistry Division, Saha Institute of Nuclear Physics, 1/AF, Bidhannagar, Calcutta-700 064, India

(*Received* 29 *March* 1994. *Revised* 25 *July* 1994. *Accepted* 25 *July* 1994)

**Summary**—Hydrogen atoms form two kinds of adducts with thymine (oxidizing and reducing). Redox reactions of these two kinds, popularly known as 5-hydrogenated-6-thyminyl (reducing) and 6-hydrogenated-5-thyminyl (oxidizing), were investigated where ferric ions (oxidizing) and ferrous ions (reducing) were used as the corresponding redox partners. A steady-state gamma radiolytic system was chosen where hydroxyl radicals were scavenged using *t*-butyl alcohol in acidic (pH 1.8) solution. It is inferred that the redox potential of oxidizing hydrogenated thyminyl radicals lies between 0.77 and 1.4 V *vs.* NHE. The reducing hydrogenated thyminyl radical has a redox value less than 0.8 V because it efficiently undergoes electron transfer reaction with Fe(III). A probable range of redox values for hydroxyl adduct of thymine is included for comparison.

Radiolysis of thymine is important in the context of radiation damage of DNA.[1] The radical adducts of thymine as probed by pulse radiolytic study are well known.[2,3] The redox properties of radical adducts of thymine have application for a model study on radiosensitization phenomenon where electron affinity (organic compounds)[4] and redox potentials (metal compounds)[5] are important indices of the capability of the respective compounds using as radiosensitizer. The pulse radiolytic study of thymine has clearly established the dual nature (oxidative and reductive) of the hydroxyl and hydrogen adducts of thymine.[2] However, the electron adduct of thymine is converted only to 6-hydrogenated thymine adduct which is oxidizing in nature and this has been proven by ESR study.[6,7] The 5-hydrogen or hydroxyl adducts of thymine are reducing in nature,[2] yet, little work has been carried out to determine their range of redox potential values. Recently work by Steenken *et al.*[8] has shown that the redox potential of electron adduct of thymine, $T^-$, is of the order of $-1$ V *vs.* NHE. In the present investigation we indicate the redox potential range of hydrogen and hydroxyl adducts of thymine.

*Author to whom correspondence should be addressed.

## EXPERIMENTAL

Thymine (Koch Light) was recrystallized three times from triply distilled water before use. Solutions were prepared in triply distilled water and the experiments were carried out at acidic pH(1.8) (adjusting by $H_2SO_4$). All the reagents used were of analytical reagent grade. Pure argon gas was used throughout the investigation.

### *γ-Irradiation*

The sample were irradiated in a $^{60}Co$ γ-source following purging with argon gas. The dose rate of the source (9 Gy/min) was determined in a Fricke Dosimeter taking $G(Fe^{3+}) = 15.5$.

### *Procedure*

Thymine solutions ($10^{-3}M$) containing either $5 \times 10^{-4}M$ Fe(III) alum or $10^{-4}M$ Fe(III) alum in the presence of $0.4M$ *t*-butyl alcohol in acidic pH were irradiated at different doses. The formation of Fe(II) was followed spectrophotometrically by its complexation with *o*-phenanthroline and measuring the absorption at 510 nm. The formation of Fe(III) was followed in a spectrophotometer by measuring the absorption at 305 nm. In addition to these, some experiments with dihydrothymine(DHT)($10^{-3}M$) containing $5 \times 10^{-4}M$ Fe(III) alum were

carried out, where formation of Fe(II) was followed spectrophotometrically as above. Blank experiments containing only Fe(II) alum and 0.4$M$ $t$-butyl alcohol were done and the formation of Fe(III) was similarly followed spectrophotometrically at 305 nm.

## RESULTS AND DISCUSSION

### *Reactions of 6-hydrogenated 5-yl thymine*

Figure 1 shows the formation of $Fe^{3+}$ in the presence and in the absence of thymine ($10^{-3}M$) following irradiation of solutions containing $10^{-4}M$ ferrous sulphate and 0.4$M$ $t$-butyl alcohol in an argon saturated condition. It may be noted that the formation of Fe(III) significantly increases with dose and then reaches a plateau in both cases. The yield of the corresponding formation of Fe(III) was calculated from the yield dose plot which shows that $G(Fe^{3+})$ in the absence of thymine is much larger than that in the presence of thymine. The $G(Fe^{3+}) = 6.0$, in the absence of thymine, indicates that the $t$-butyl alcohol radical formed also oxidizes quantitatively ferrous ion and thus the yield of Fe(III) (calculated from the initial slope) becomes the sum of the total yield of OH and H radicals at the experimental pH, *i.e.* $G_{OH} + G_H = 2.7 + 3.6 = 6.3$; which is close to our observed value of 6.0. The corresponding reactions are as follows:

$$R_3COH + H/OH \rightarrow R_2(CH_2)COH + H_2/H_2O$$

(R = $CH_3$ and $R_3COH$ = $t$-butyl alcohol)

$$R_2(CH_2)COH + Fe^{2+} \rightarrow R_2(CH_2)COH^- + Fe^{3+}.$$

But when thymine is present at a concentration of $10^{-3}M$ then because of the higher values of rate constants of thymine with H atom, most of the H will react with thymine forming TH radical ($k_{T+H} = 5.7 \times 10^8 M^{-1}$ sec$^{-1}$).[9] It has been well established that 59.5% of the H atom add to the position 6 of the thymine ring, hence the yield of C(6)-TH should be 2.14.[10] Hence, the initial yield of $G(Fe^{3+})$ in the presence of thymine should be 2.14 + 2.7 = 4.84. In fact, the experimentally observed value of $G(Fe^{3+})$ as obtained from the initial slope was 4.8. It should be pointed out that 37% of $G_H$ is converted to the reducing thymine adduct which will certainly reduce the accumulated Fe(III) formed in the radiolytic system. This is actually corroborated by the results shown in Fig. 1.

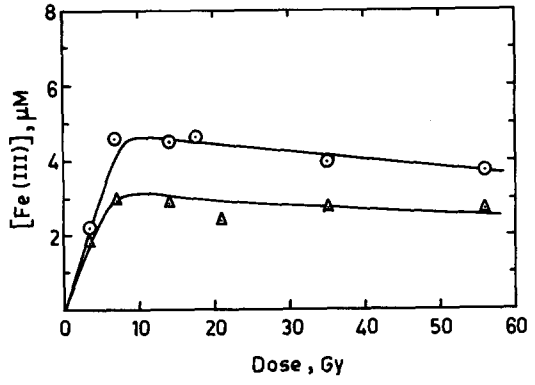


Fig. 1. Formation of Fe(III) at different absorbed doses when radiolysis was carried out with $10^{-4}M$ Fe(II) alum and 0.4$M$ $t$-butanol in presence (△) and absence (○) of thymine ($10^{-3}M$) under argon saturation at pH 1.8.

It is clear from the above that the 6-hydrogenated-5-thyminyl adduct oxidizes ferrous ions. Hence, its redox potential is more positive than the redox potential of the $Fe^{2+}/Fe^{3+}$ couple, *i.e.* 0.77 V *vs.* NHE. However, in our earlier studies we have shown that this oxidizing adduct cannot oxidize $Ni^{2+}$, which has a redox potential value of 1.4 V (for the couple Ni(II)/Ni(III)).[11-13] Hence, the redox potential of C(6)-TH$^{\cdot}$/C(6)-TH$^-$ should lie between these two values, *i.e.* 0.77–1.4 V.

### *Reactions of 5-hydrogenated-6-thyminyl adduct*

In order to follow the reactions of reducing radicals two kinds of experiments were carried out: (i) thymine was radiolysed in the presence of $Fe^{3+}$ and the formation of $Fe^{2+}$ was measured spectrophotometrically at 510 nm by its complexation with $o$-phenanthroline. The yield of $Fe^{2+}$ formation during the radiolysis of thymine in the presence of $Fe^{3+}$ and $t$-butyl alcohol is shown in Table 1. Under the experimental conditions, the concentrations used are such that all the H atoms react with thymine(T) forming TH adduct. It has been reported earlier[10] that only 37% of these TH radicals are reducing and hence the expected yield of $Fe^{2+}$ should be equivalent to the reducing radical yield, *i.e.* 37% of 3.6 = 1.3. This value is very close to the experimental value, 1.4 (Table 1). This experiment clearly indicates that C(5)-TH radical quantitatively reduces $Fe^{3+}$.

$$C(5)\text{-}TH^{\cdot} + Fe^{3+} \rightarrow C(5)\text{-}TH^+ + Fe^{2+}.$$

(ii) The reduction of $Fe^{3+}$ was further evident from an experiment using dihydrothymine(DHT) where only reducing C(5)-TH$^{\cdot}$ radical is formed.[14] Under the experimental concentrations of DHT, $Fe^{3+}$ and $t$-butanol, 81% of the H atom will react with

Table 1. Radiolytic yields of $Fe^{3+}/Fe^{2+}$ formed when solutions containing $10^{-3}M$ thymine or dihydrothymine were radiolysed (in presence and absence of $10^{-4}M$ $Fe^{2+}/5 \times 10^{-4}M$ $Fe^{3+}$) and $0.4M$ *t*-butanol under argon saturated condition at acidic pH (1.8)

| Constituents | $G(Fe^{3+})$* | $G(Fe^{2+})$* |
|---|---|---|
| $10^{-4}M$ $Fe^{2+}$ | 6.0 | — |
| $10^{-4}M$ $Fe^{2+}$ + $10^{-3}M$ thymine | 4.8 | — |
| $5 \times 10^{-4}M$ $Fe^{3+}$ + $10^{-3}M$ thymine | — | 1.4 |
| $5 \times 10^{-4}M$ $Fe^{3+}$ + $10^{-3}M$ dihydrothymine | — | 2.7 |

*1$G$ unit = No. of molecules formed or decomposed/100 eV of energy absorbed = 0.1036 $\mu$mol/J.

thymine forming C(5)-TH$^{\cdot}$. Hence $G(Fe^{2+})$ should be equivalent, *i.e.* 81% of 3.6 = 2.9. The experimental yield of $G(Fe^{2+})$ was 2.7 (Table 1).

From these two reducing radical experiments it can be concluded that the reducing hydrogen adduct of thymine undergoes very efficient electron transfer reaction with $Fe^{3+}$. Hence it can also be concluded that the reducing $TH^{\cdot}/TH^{+}$ couple has a redox potential lower than that of the $Fe^{2+}/Fe^{3+}$ couple, *i.e.* 0.77 V *vs.* NHE.

*Reactions of reducing hydroxyl adduct of thymine*

The electron transfer reaction of the reducing hydroxyl adduct of thymine has been carried out by many workers. The electron transfer from the reducing C(5)-TOH$^{\cdot}$ adduct to electron attracting compounds has been carried out by Kagiya and coworkers.[15] However, the maximum redox values used in their experiment were for the drug 2-methyl-1,4-naphthoquinone, having a redox potential of −0.203 V. However, in our earlier experiments we have shown that the C(5)-TOH adduct can reduce Cu(II)($E_0 = 0.16$ V),[16,17] iron(III)($E_0 = 0.77$ V),[18] but cannot reduce Ni(II) [$E_0 = -2.7$ V for Ni(II)/Ni(I)].[11] It has been reported by Busi *et al.*[19] that the lower domain of the redox value of C(5)-TOH adduct is $< -0.06$ V. Hence the domain of redox potential of this reducing adduct should be $-0.6$ V $< E^0$ C(5)-$TOH^{+}$/C(5)-TOH$^{\cdot}$) $< -0.203$ V.

*Reactions of oxidizing hydroxyl adduct of thymine*

The C(6)-TOH adduct was found to be oxidizing as was evident[2] from the oxidation of TMPD to $TMPD^{+}$. Nishimoto and other coworkers[20] have shown that C(6)-TOH can oxidize transition metal ions such as $FeSO_4$ ($E_0 = 0.77$ V), CuCl ($E_0 = 0.54$ V), $K_2[Fe(CN)_6]$ ($E_0 = 0.36$ V), but cannot oxidize metal ions having $E_0$ values $> 1$ V. Furthermore, we have shown[11] that C(6)-TOH$^{\cdot}$ cannot oxidize Ni(II) to Ni(III) having $E_0 = 1.4$ V. Hence it can be inferred that the C(6)-TOH radical has a redox value of $< 1$ V.

## REFERENCES


1. L. Grossman and A. C. Upton, *Mechanisms of DNA Damage and Repair*, p. 39. Plenum Press, New York, 1985.
2. S. Fujita and S. Steenken, *J. Am. Chem. Soc.*, 1981, **103**, 2540.
3. C. von Sonntag, *Radiat. Phys. Chem.*, 1987, **30**, 313.
4. P. Wardman, *Curr. Topics Radiat. Res.*, 1977, **11**, 347.
5. K. A. Skov, *Radiat Res.*, 1987, **112**, 217.
6. Z. Kabiljo, K. Sankovic and J. N. Herak, *Int. J. Radiat Biol.*, 1990, **58**, 439.
7. M. Yan, D. Becker, S. Summerfield, P. Renke and M. D. Sevilla, *J. Phys. Chem*, 1992, **96**, 1983.
8. S. Steenken, J. P. Telo, H. M. Novais and L. P. Candeias, *J. Am. Chem. Soc.*, 1992, **114**, 4701.
9. G. V. Buxton, C. L. Greenstock, W. P. Helman and A. B. Ross, *J. Phys. Chem. Ref. Data.*, 1988, **17**, 513.
10. C. von Sonntag and H. P. Schuchmann, *Int. J. Radiat. Biol.*, 1986, **49**, 1.
11. S. Chakrabarti, P. C. Mandal and S. N. Bhattacharyya, *Can. J. Chem.*, 1993, **71**, 307.
12. P. C. Mandal, D. K. Bardhan, S. Sarkar and S. N. Bhattacharyya, *J. Chem. Soc., Dalton. Trans.*, 1991, 1451.
13. R. E. Huie, C. L. Clifton and P. Neta, *Radiat. Phys. Chem.*, 1991, **38**, 477.
14. M. N. Schuchmann, S. Steenken, J. Wroblewski and C. von Sonntag, *Int. J. Radiat. Biol.*, 1984, **46**, 225.
15. S. Nishimoto, H. Ide, T. Wada and T. Kagiya, *Int. J. Radiat. Biol.*, 1983, **44**, 585.
16. S. N. Bhattacharyya, P. C. Mandal and S. Chakrabarti, *Anticancer Res.*, 1989, **9**, 1181.
17. S. N. Bhattacharyya, P. C. Mandal and S. Chakrabarti, *Radiat. Phys. Chem.*, 1991, **37**, 347.
18. S. N. Bhattacharyya, P. C. Mandal and S. Chakrabarti, *Bull. Chem. Soc. Jpn*, 1990, **63**, 3001.
19. F. Busi, V. Concialini, O. Tubertini and M. D'Angelantonio, *Radiat. Phys. Chem.*, 1989, **34**, 857.
20. S. Nishimoto, H. Ide, K. Nakamichi, N. Otsuki and T. Kagiya, *Chem. Lett.*, 1983, 1441.

Pergamon

0039-9140(94)00216-9

*Talanta*, Vol. 42, No. 1, pp. 59–64, 1995

0039-9140/95 $9.50 + 0.00

# SEPARATION AND CHARACTERIZATION OF TETROL METABOLITES OF BENZO[a]PYRENE-DNA ADDUCTS USING HPLC AND SOLID-MATRIX ROOM TEMPERATURE LUMINESCENCE

S. W. TJIOE and ROBERT J. HURTUBISE*

Department of Chemistry, University of Wyoming, Laramie, WY 82071-3838, U.S.A.

(*Received* 30 *June* 1994. *Accepted* 27 *July* 1994)

**Summary**—Four tetrols of benzo[a]pyrene-DNA adducts were separated using reversed-phase high performance liquid chromatography. Chromatographic fractions containing a given tetrol were readily characterized with solid-matrix room temperature luminescence techniques. Solid-matrix fluorescence and phosphorescence spectra at picogram amounts of a tetrol were easily obtained. Tetrol fractions collected based on retention times, but with no response from the ultraviolet detector, were characterized by solid-matrix luminescence spectra at very small quantities.

Polycyclic aromatic hydrocarbons are distributed widely in the environment and are known to be associated with the occurrence of cancer in humans and animals.[1] Selkirk *et al.*[2] separated eight metabolites of benzo[a]pyrene (B[a]P) formed by rat liver microsomes via high-performance liquid chromatography (HPLC). They reported that HPLC is an efficient, rapid, and reproducible method for the separation of the metabolites of B[a]P. Rozbeh and Hurtubise[3] reported the reversed-phase chromatographic separation of 14 metabolites of B[a]P using mobile-phase optimization methods. A fluorometric-HPLC assay to quantitate B[a]P metabolites was developed by Rahn *et al.*[4] In their study, isomeric tetrols of B[a]P were liberated by the acid hydrolysis of B[a]P-DNA adducts, separated by HPLC, and the fluorescence of the tetrols was detected in deoxygenated solutions at room temperature. Since the tetrols have high fluorescence quantum yields in deoxygenated solution at room temperature, they can be detected at low levels after separation by HPLC. One B[a]P residue per $10^7$ nucleic bases could be detected as tetrols in 100 $\mu$g of DNA.[4] When applied to B[a]P-DNA adducts, formed under controlled laboratory conditions in the liver and hemoglobin of erythrocyte of the bluegill sunfish, 126 pg of tetrol I-1 could be detected from 195 $\mu$g of isolated DNA.[5] Tromberg *et al.*[6] developed an antibody-based fiber-optic sensor to detect the tetrols. The typical limit of detection for this method was $5 \times 10^{-10} M$ (picomolar range). A fiber-optic antibody-based fluoroimmunosensor for tetrols from B[a]P-DNA adducts in human placenta samples gave a detection limit of 14 amol.[7] However, the characteristic fluorescence spectra of tetrols were not resolvable from these samples at the quantity studied. Tetrols obtained from human lung samples[8] and human urine samples[9] can be quantitated using a combination of immunoaffinity chromatography, HPLC, synchronous fluorescence spectroscopy, and second derivative synchronous fluorescence spectroscopy.

To increase the sensitivity of luminescence detection, after separation of the tetrols, solid-matrices can be used.[10] Solid-matrix room temperature fluorescence (SMRTF) and phosphorescence (SMRTP) are very useful analytical techniques for trace organic analysis.[11–13] In fact, solid-matrix luminescence can give greater fluorescence and phosphorescence quantum yields, in many cases, at room temperature, than the corresponding solution quantum yields at low temperature.[14] Femtomole quantities of tetrols can be detected using various solid-matrices.[15–19]

Corley and Hurtubise[20] reported that the detection limit of a tetrol by SMRTP was 0.38 femtomole/mg using 1:1:8 $\alpha$-cyclodex-

*Author to whom correspondence should be addressed.

trin:$TlNO_3$:$NaNO_3$ as the solid matrix. Tjioe and Hurtubise[19] detected 19 femtomoles of tetrol I-1 by SMRTP on Whatman No. 1 filter paper using thallium acetate as the external heavy atom. The SMRTF dectection limit of tetrol I-1 was 23 femtomoles without the presence of thallium acetate on Whatman No. 1 filter paper.[19] Furthermore, they introduced Whatman 1PS filter paper as a new solid matrix to obtain SMRTP as an alternative to the use of thallium salts which are toxic. The tetrols spotted on 1PS filter paper can be detected at 0.56 and 10.2 femtomoles by SMRTF and SMRTP, respectively.[19] These are among the lowest detection limits reported for a tetrol.

In this work, solid-matrix luminescence was used for the characterization of tetrols after HPLC separation. Whatman No. 1 filter paper was employed for both the SMRTF and the thallium acetate-enhanced SMRTP of tetrol I-1. Whatman 1PS filter paper was also employed to obtain both the SMRTF and SMRTP data for tetrol I-1 without the addition of a heavy atom. There have been very few reports on the use of solid-matrix luminescence for the characterization of HPLC fractions.

## EXPERIMENTAL

### *Chemicals and reagents*

The four tetrols were purchased from the Midwest Research Institute (Kansas City, MO, U.S.A.). Their chemical names and abbreviations are B[a]P-r-7,t-8,9,c-10-tetrahydrotetrol (I-1), B[a]P-r-7,t-8,9,10-tetrahydrotetrol (I-2), B[a]P-r-7,t-8,c-9,t-10-tetrahydrotetrol (II-1), and B[a]P-r-7,t-8,c-9,10-tetrahydrotetrol (II-2). A stock solution for each tetrol was prepared by dissolving 2 mg of a tetrol in 10 ml of absolute methanol (HPLC, Baker, Phillipsburg, NJ, U.S.A.). A standard solution was prepared for each tetrol by adding 100 $\mu$l water (HPLC grade, Baker, Phillipsburg, NJ, U.S.A.) to 100 $\mu$l of the stock tetrol solution in a 1 ml volumetric flask. The contents of the flask were then diluted to 1 ml with methanol:water (55:45, HPLC grade, Baker). A solution which contained the four tetrols was prepared in a similar fashion by adding 250 $\mu$l of each standard tetrol solution to a 1 ml volumetric flask. The concentration for each standard tetrol solution was 20 ng/$\mu$l. The concentration for each tetrol in the four-component solution was 5 ng/$\mu$l. A 500 pg/$\mu$l solution of I-1 was prepared in methanol:water (55:45). Thallium acetate (99.9% pure, Aldrich) solution was prepared by adding thallium acetate and 12 N glacial acid to HPLC grade methanol:water (55:45). This solution was 0.5*M* in thallium acetate and 0.3*M* in acetic acid.

Whatman No. 1 and Whatman 1PS filter paper samples (Whatman Co., Cliffton, NJ, U.S.A.) were developed three times in absolute methanol (Reagent grade, Baker), and dried at 110°C for 30 min. Small circular discs of filter paper were made with a paper punch.

### *Instrumentation*

A Water's Model M-45 or 6000A solvent system was used in conjunction with a U6K universal injector and a Water's Model 440 UV absorbance detector (Milford, MA, U.S.A.). The stationary phase for the reversed-phase chromatographic separation was a Baxter (Burdick and Jackson) octadecyl column (25 cm × 4.6 mm i.d., 5 $\mu$m). The column was kept at ambient temperature during the chromatographic experiments. A Linear Model 1201 (Linear, Reno, NE, U.S.A.) recorder was used to record the chromatograms.

Spectroscopic measurements were performed with a Perkin-Elmer LS-5 fluorescence spectrophotometer. The source employed was a pulsed xenon lamp. The detector was a R777 PMT, and the data were processed with a Perkin Elmer 3600 Data Station.

### *Procedures*

Three chromatographic experiments were performed: (1) To study the retention time of each tetrol, 20 $\mu$l aliquots of each standard tetrol solution were injected into the liquid chromatograph. (2) To study the separation of the four tetrol isomers, 40 $\mu$l aliquots of the four-component tetrol solution were injected into the liquid chromatograph. (3) To study the sensitivity of the solid-matrix room-temperature luminescence techniques, a 1 $\mu$l aliquot of I-1 (500 pg/$\mu$l) solution was injected into the liquid chromatograph and the tetrol fractions were collected.

For the above experiments, injections were repeated three times to ensure reproducibility. Methanol:water (55:45) was used as the mobile phase. The flow rate of the mobile phase was set at 1 ml/min, and the UV detector measured the absorbance of the eluent at 254 nm.

Each chromatographic fraction corresponding to a given tetrol was collected in a test tube. The mobile phase fractions were evaporated to

near dryness by placing the test tubes in a Multi-Block Heater (Model No. 2050, Lab-Line Instrument Inc., Melrose Park, IL, U.S.A.). The temperature at the center of the block heater was set at 110°C. A commercial hot-air dryer was employed to blow a stream of warm air across the openings of the test tubes to assist the evaporation of the solvent. After evaporation, the test tubes were removed from the block heater, cooled to ambient temperature, and diluted with either methanol:water (55:45), or the thallium acetate–acetic acid solution to a specific volume.

The amount of tetrol I-1 recovered in chromatographic experiment 1 (see above) was diluted to 2 ml with methanol:water (55:45), and the quantity of I-1 was calculated from a solution fluorescence calibration curve of I-1. The amount of tetrol I-1 recovered in chromatographic experiment 3 was diluted to 2 ml with the same solvent, and the quantity of I-1 was estimated via comparison of solution fluorescence intensities with a standard solution of I-1 (500 pg/$\mu$l in methanol:water, 55:45). The solution fluorescence of I-1 recovered from chromatographic experiment 3 was examined after the fraction was diluted to 2 ml with methanol:water (55:45). After the solution fluorescence data were obtained, the previous 2 ml solution was evaporated and the residue was dissolved in 30 $\mu$l with methanol:water (55:45). The methanol:water solutions from chromatographic experiments 1 (2 ml) and 3 (30 $\mu$l) were used for SMRTF studies. Samples of I-1 recovered from chromatographic experiment 1 and diluted to 2 ml with thallium acetate–acetic acid were used for SMRTP studies.

To study the solid-matrix room temperature fluorescence and phosphorescence, 1 $\mu$l of I-1 solution (200 pg/$\mu$l) recovered from chromatographic experiment 1 was deposited onto the surface of a Whatman No. 1 filter paper disc which was fitted on top of 4 other pieces of filter paper in a circular depression of a custom-made delrin sample holder. Five microliters of I-1 solution from chromatographic experiment 3 was transferred to the surface of a Whatman 1PS filter paper disc in a separate experiment. The Whatman No. 1 or 1PS filter paper samples in these experiments were dried in the sample holder at 110°C for 30 min and then cooled to room temperature inside the sample compartment of the fluorescence spectrophotometer. A constant stream of dry nitrogen gas was directed into the sample compartment to minimize oxygen and moisture quenching. The sample holder was protected from light during the cooling period which generally required 10 min. The luminescence intensities of tetrol on filter paper were measured by setting the excitation and emission monochromator at the appropriate excitation and emission wavelengths.[19] To measure SMRTF, the excitation and emission wavelengths were set at 346 and 398 nm, respectively. To measure SMRTP, the monochromators were set at 346 and 606 nm, respectively. The SMRTF and SMRTP spectra were obtained in the usual fashion. The limit of detection was obtained as discussed previously.[21]

## RESULTS AND DISCUSSION

### *Retention times of four tetrols*

The four tetrols are stereoisomers and differ from each other in the orientation of the hydroxyl groups covalently bonded to the carbon atoms at the 7, 8, 9, 10 positions.[19] In this work, they gave very good baseline resolution with the HPLC experimental conditions. The separation profile resembled the ones reported in literature.[4,5] The average retention times for the tetrols were: I-1, $11.53 \pm 0.058$ min; II-1, $13.78 \pm 0.058$ min; I-2, $15.97 \pm 0.13$ min; and II-2, $22.37 \pm 0.029$ min. Figure 1 shows a chromatogram for a solution of the four tetrols. Tetrol I-1 and II-1 eluted earlier than I-2 and II-2, indicating less hydrophobic interaction of these two tetrols with the stationary phase. This implied that tetrol I-1 and II-1 are somewhat more polar than I-2. Because tetrol II-2 eluted last, it would be the least polar of the four tetrols. Each peak in Fig. 1 represents an equal quantity of tetrol. Since the peak heights under each chromatographic band were different, the molar absorptivities of the tetrol isomer at 254 nm were not the same. However, the shapes of the chromatographic bands would also contribute to the differences in peak heights. With the experimental conditions presented in Fig. 1, the four tetrol isomers could be completely separated within 24 min.

### *Recovery of I-1*

Fractions of I-1 were collected from the HPLC system with either a M-45 or 6000A pump in the system. The fractions were evaporated to dryness, and then diluted to 2 ml in methanol:water (55:45) as described in the experimental section. The quantity recovered

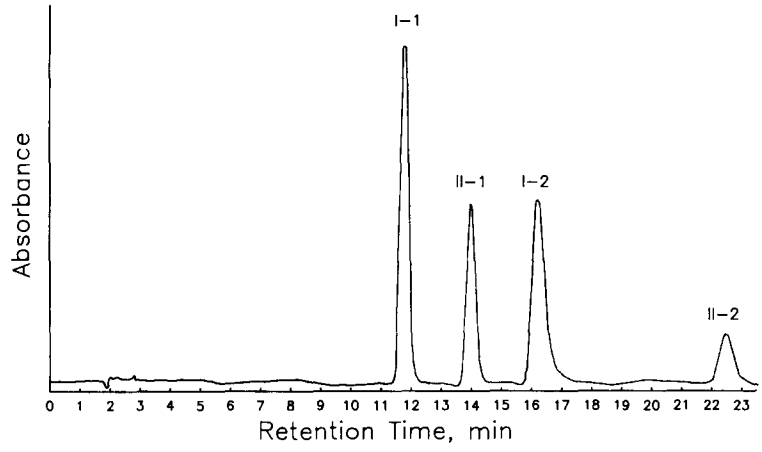


Fig. 1. Chromatogram for the four tetrols. Retention times: I-1 = 11.7 min; II-1 = 13.9 min; I-2 = 16.1 min; II-2 = 22.4 min.

from the liquid chromatograph was calculated using data from a fluorescence calibration curve of I-1. Ninety-one percent of I-1 was recovered. It is assumed that the other tetrols recovered would have similar percent recoveries because identical instrumental conditions were used. The quantity of I-1 recovered from a 20 $\mu$l injection of 20 ng/$\mu$l solution (chromatographic experiment 1) was equal to 0.91 × 400 ng, or 364 ng. The quantity of I-1 recovered from a 1 $\mu$l injection of 500 pg/$\mu$l solution (chromatographic experiment 3) was estimated by comparing the fluorescence intensity of the collected fractions with a standard solution of I-1. Because of the small quantity injected, only 64%, or 0.64 × 500 pg = 320 pg of I-1 was recovered. The solid-matrix luminescence spectra in Figs 2 and 3 were obtained from I-1 (182 pg) recovered from the 20 $\mu$l injections of a 1 ml standard I-1 solution. These figures illustrate that both SMRTF and SMRTP spectra can be obtained easily from picogram levels of I-1 isolated in HPLC fractions.

*Detection limits and smallest quantity for solid-matrix spectra*

The lowest quantity of I-1 detectable by ultraviolet absorbance with the liquid chromatograph was 172 pg. A detection limit of 2.3 pg for I-1 has been reported using a fluorescence detector in conjunction with HPLC.[22] However, the detection limit can be lowered to 0.18 pg, or 0.56 femtomoles, using solid-matrix luminescence techniques reported earlier.[19] This implies that the characterization of tetrols is possible even though no signal would be detected from

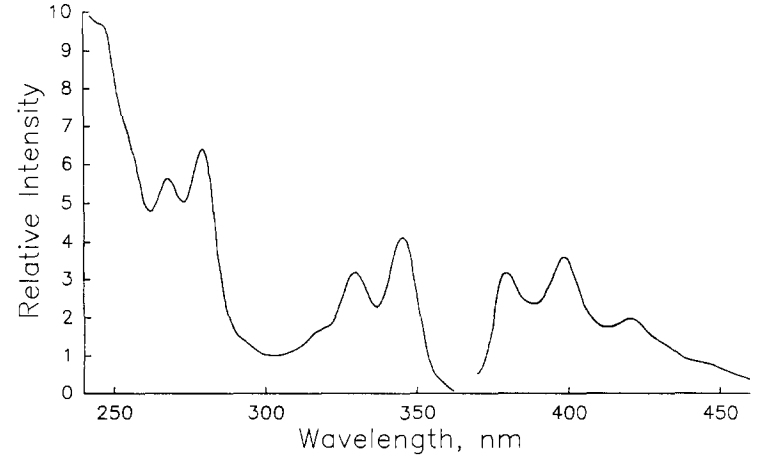


Fig. 2. SMRTF spectra of I-1. One microliter (182 pg) of I-1 spotted on a Whatman 1PS filter paper disc. This solution was recovered from an injection of a 20 $\mu$l aliquot of standard I-1 solution, evaporated, and diluted to 1 ml with methanol:water (55:45).

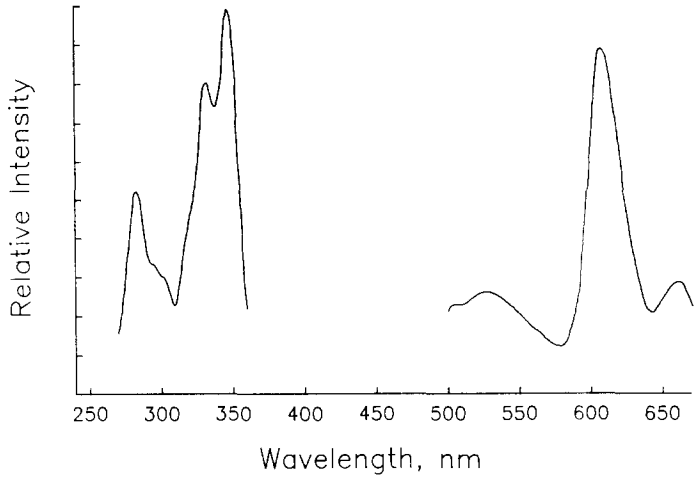


Fig. 3. SMRTP spectra of I-1. One microliter (182 pg) of I-1 spotted on a Whatman No. 1 filter paper disc. This solution was recovered from an injection of a 20 $\mu$l aliquot of standard I-1 solution, evaporated, and diluted to 1 ml with thallium acetate–acetic acid solution.

conventional UV or fluorescence detector. For example, it would be feasible to isolate a tetrol fraction based on the retention time of the tetrol even though the detector did not respond to the tetrol. The isolated fraction could then be characterized by solid-matrix luminescence techniques. In this work, a fraction of I-1 was collected based on its retention time. The fraction gave no response from the UV detector. Poor solution excitation and fluorescence emission spectra of the isolated HPLC fraction were obtained (Fig. 4). However, when the fraction was evaporated and then diluted to 30 $\mu$l (0.16 pg/$\mu$l) in methanol:water (55:45), I-1 could be readily identified by its SMRTF excitation and emission spectra from 53 pg of I-1 adsorbed onto the surface of 1PS filter paper (Fig. 5). As mentioned in reference 19, I-1 deposited on filter paper with thallium acetate solution gave analytically useful SMRTP spectra with only 100 pg on the paper. However, SMRTF gives the lowest limits of detection when 1PS filter paper is used as a solid matrix.[19] For example, SMRTF spectra of I-1 can be obtained with as little as 5 pg on Whatman 1PS filter paper.

## CONCLUSIONS

It was shown that tetrols that were separated by reversed-phase HPLC can be characterized at very low levels by solid-matrix luminescence with Whatman No. 1 or 1PS filter paper. For example, the SMRTF spectra from 53 pg of a recovered tetrol fraction was readily obtained.

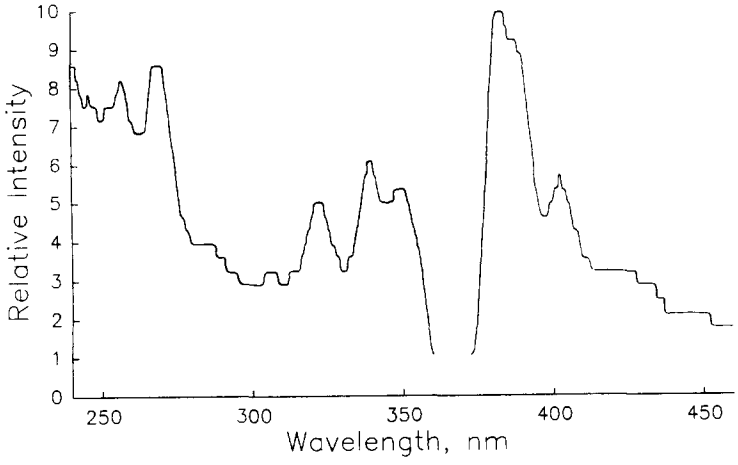


Fig. 4. Solution fluorescence spectra of I-1 (0.16 ng/ml). This solution was recovered from an injection of a 1 $\mu$l aliquot containing 500 pg of I-1.

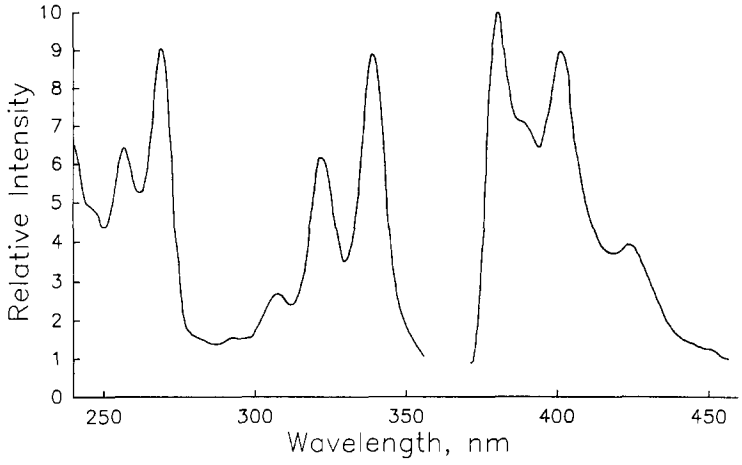


Fig. 5. SMRTF spectra of I-1. The solution in Fig. 4 was evaporated to near dryness. The contents were diluted to 30 $\mu$l with methanol:water (55:45). Five microliters (53 pg) was spotted on a Whatman 1PS filter paper disc.

Solid-matrix luminescence with Whatman 1PS filter paper as the solid matrix was shown to be a very sensitive and convenient method in the trace analysis of tetrol fractions separated by HPLC. The SMRTP of the tetrols on Whatman No. 1 filter paper was also an extremely sensitive approach for the trace characterization of I-1 (and other tetrols) when thallium acetate was used as an external heavy atom. Fractions containing a tetrol can be detected and characterized using solid-matrix room-temperature techniques at a level where conventional solution methods fail.

*Acknowledgement*—Financial support for this project was provided by the United States Environmental Protection Agency, Grant No. R817678.

## REFERENCES

1. A. Bjoreth and G. Becher (eds), *PAH in Work Atmospheres: Occurrence and Determination*. CRC Press, Boca Raton, FL, 1986.
2. J. K. Selkirk, R. G. Croy and H. V. Gelboin, *Science*, 1974, **184,** 169.
3. M. Rozbeh and R. J. Hurtubise, *J. Liq. Chromatogr.*, 1994, **17,** 3351.
4. R. O. Rahn, S. S. Chang, J. M. Holland and L. R. Shugart, *Biochem. Biophys. Res. Commun.*, 1982, **109,** 262.
5. L. Shugart, J. McCarthy, B. Jimenez and J. Daniels, *Aquat. Toxicol.*, 1987, **9,** 319.
6. B. J. Tromberg, M. J. Sepaniak, J. P. Alarie, T. Vo-Dinh and R. M. Santella, *Anal. Chem.*, 1988, **60,** 1901.
7. T. Vo-Dinh, J. P. Alarie, R. W. Johnson, M. J. Sepaniak and R. M. Santella, *Clin. Chem.*, 1991, **37,** 532.
8. A. Weston and E. D. Bowman, *Carcinogenesis*, 1991, **12,** 1445.
9. A. Weston, E. D. Bowman, P. Carr, N. Rothman and P. T. Strickland, *Carcinogenesis*, 1993, **14,** 1053.
10. R. J. Hurtubise, *Solid Surface Luminescence Analysis: Theory, Instrumentation, Application*. Marcel Dekker, New York, 1981.
11. T. Vo-Dinh, *Room Temperature Phosphorimetry for Chemical Analysis*. Wiley, New York, 1984.
12. R. J. Hurtubise, *Phosphorimetry: Theory, Instrumentaion, and Application*. VCH, 1990.
13. S. W. Tjioe and R. J. Hurtubise, *Talanta*, 1994, **41,** 595.
14. R. J. Hurtubise and S. M. Ramasamy, *Appl. Spectrosc.*, 1993, **47,** 116.
15. T. Vo-Dinh and M. Uziel, *Anal. Chem.*, 1987, **59,** 1093.
16. R. W. Johnson and T. Vo-Dinh, *Anal. Chem.*, 1989, **61,** 2766.
17. M. D. Richmond and R. J. Hurtubise, *Anal. Chim. Acta*, 1991, **255,** 341.
18. J. S. Corley and R. J. Hurtubise, *Anal. Lett.*, 1992, **25,** 1559.
19. S. W. Tjioe and R. J. Hurtubise, *Anal. Lett.*, 1993, **26,** 557.
20. J. S. Corley and R. J. Hurtubise, *Appl. Spectrosc.*, 1994, **48,** 747.
21. G. L. Long and J. D. Winefordner, *Anal. Chem.*, 1983, **55,** 712A.
22. E. H. J. M. Jansen, R. H. van den Berg and E. D. Kroese, *Anal. Chim. Acta*, 1994, **290,** 86.

Pergamon

0039-9140(94)00217-7

*Talanta*, Vol. 42, No. 1, pp. 65–72, 1995

0039-9140/95 $9.50 + 0.00

# SIMULTANEOUS DETERMINATION OF LEAD AND CADMIUM IN VARIOUS ENVIRONMENTAL AND BIOLOGICAL SAMPLES BY DIFFERENTIAL PULSE POLAROGRAPHY AFTER ADSORPTION OF THEIR MORPHOLINE-4-CARBODITHIOATES ONTO MICROCRYSTALLINE NAPHTHALENE OR MORPHOLINE-4-DITHIOCARBAMATE–CTMAB–NAPHTHALENE ADSORBENT

RAJESH KUMAR DUBEY and BAL KRISHAN PURI*

Department of Chemistry, Indian Institute of Technology, Hauz Khas, New Delhi-110 016, India

(*Received* 11 *April* 1994. *Revised* 25 *July* 1994. *Accepted* 26 *July* 1994)

**Summary**—A highly selective, sensitive and rapid differential pulse polarographic method (DPP) has been developed for the simultaneous estimation of trace amounts of lead and cadmium in standard alloys, biological and environmental samples. The morpholine-4-carbodithioates of the samples were absorbed on microcrystalline naphthalene in the pH range of 5–10 for lead and 3.4–11 for cadmium. The metal complexes were desorbed with 10 ml of 1*M* HCl and determined simultaneously with a differential pulse polarograph. These metals can alternatively be quantitatively adsorbed on morpholine-4-dithiocarbamate–cetyltrimethylammonium bromide–naphthalene adsorbent packed in a column and determined similarly. The detection limits are 0.14 ppm for Pb and 0.014 ppm for Cd at minimum instrumental settings (signal-to-noise ratio = 2). The linearity is maintained in the concentration ranges of Pb, 0.7–15 ppm and Cd, 0.07–10 ppm with a correlation factor of 0.9997 and relative standard deviations of 0.95 and 0.81%, respectively. Various parameters such as the effect of pH, volume of aqueous phase, and interference of a number of metal ions on the estimation of lead and cadmium have been studied in detail to optimize the conditions for their simultaneous estimation in various biological and environmental samples.

A survey of the literature reveals that lead may be determined in environmental samples using graphite furnace atomic absorption spectrometry;[1,2] however, chloride, copper and nickel interfere seriously and the method has limited applications in a few environmental and biological samples owing to matrix effect. Differential pulse anodic stripping voltammetry (DPASV) is another technique which may be employed for the determination of metal ions. This technique is sensitive, but less selective for complex materials such as biological and environmental samples having complicated matrix.[3] The anodic stripping voltammetric (ASV) method developed by Aualiitia and Pickering[4] is satisfactory for the simultaneous determination of lead and cadmium, but it involves rigid control of conditions like the constant surface area of the hanging mercury drop electrode (HMDE).

Earlier, much attention was given to the direct polarographic estimation of metals after extraction of their metal complexes into organic solvents.[5–9] Unfortunately, electrochemical methods for the direct determination of reducible substances require that the solvent should have a fairly high dielectric constant so a well defined polarogram can be obtained. In this regard, various workers have mixed the organic phase after extraction with a solvent of high dielectric constant to obtain well defined polarograms.[10,11] The main disadvantages of these methods are that the sensitivity and preconcentration factor are considerably lowered. Thus the aim of the preconcentration and direct determination of a metal is not achieved. A similar situation is observed in the determination of a metal ion after extraction of its metal complex into molten naphthalene.[12]

*Author to whom correspondence should be addressed.

In the present communication, we have developed a simple, rapid, sensitive and economical method for the direct differential pulse polarographic determination of lead and cadmium simultaneously after adsorption of their morpholine-4-carbodithioates on microcrystalline naphthalene. The preconcentration of these metal ions is also possible by passing their aqueous solutions over morpholine-4-dithiocarbamate–cetyltrimethylammonium bromide–naphthalene adsorbent taken in a column. The microcrystalline naphthalene method is rapid but the column method gives a better preconcentration factor (8–10 times). Diethyldithiocarbamates and xanthates normally give anodic wave at $\sim -0.2$ V *vs.* SCE on the DME.[13] However, these are decomposed in the mineral acids below pH 4. Therefore, they do not give any wave under these conditions in the range of 0.0 to $-1.7$ V *vs.* SCE. Thus, a wide range of potential is available. Various parameters such as pH, volume of aqueous phase, reagent concentration, amount of naphthalene and interference of several metal ions on the estimation for lead and cadmium have been evaluated. The procedure developed has been successfully employed for the simultaneous estimation of trace and ultratrace amounts of lead and cadmium in various standard alloys, biological and environmental samples.

## EXPERIMENTAL

### *Apparatus*

Polarograms were recorded with a three-electrode Elico Model CL-90 polarographic analyser outfitted with an X-Y recorder (model LR-108). The glass column used for the preconcentration (Fig. 1) was 60 mm long and had an i.d. of 7 mm. All atomic absorption measurements were made with an atomic absorption spectrometer (Varian AA model 475). An Elico Model L1-120 pH meter was used for pH measurements.

### *Reagents*

Lead and cadmium nitrate solutions were prepared by dissolving analytical grade samples in double-distilled water. These metals were standardized complexometrically using Xylenol Orange as an indicator[14] and were further standardized by the AAS method using AAS standard solutions. Potassium morpholine-4-dithiocarbamate (MCDT) was prepared by the method of Macrotrigiano[15] and a 0.2% solution in distilled water was used. A 10% solution of potassium sodium tartrate in distilled water was used to prevent the hydrolysis of lead. Naphthalene and cetyltrimethylammonium bromide (CTMAB) were of analytical grade. Solutions of alkali metal salts (1%) and various metal salts (0.1%) were used to study the interference of anions and cations, respectively. A 4% solution of $NaBH_4$ (Ubichem. Ltd, Analytical grade) was prepared in 0.2*M* NaOH solution. Sodium acetate–acetic acid (0.2*M*) and aqueous ammonia–ammonium ion (0.1*M*) buffers were used for pH adjustment. Twice-distilled water was used wherever required.

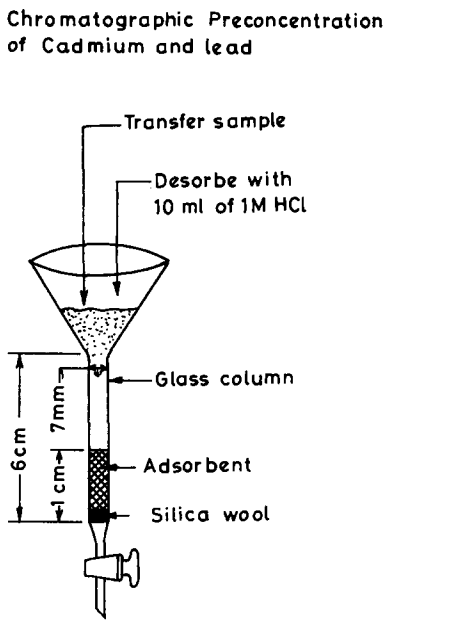


Fig. 1. Separatory column for preconcentration of trace metals.

### *Preparation of MCDT–CTMAB-naphthalene adsorbent*

A naphthalene solution was prepared by dissolving a 10-g sample in 100 ml of acetone followed by 1 l. of distilled water containing 0.050 g cetyltrimethyl ammonium bromide. It was stirred at 25–30°C on a hot plate/stirrer, followed by 100 ml of 0.2% MCDT solution in distilled water. The mixture was stirred for 3 hr and kept for 5 hr at room temperature. The supernatant ligand was aspirated with a siphon and the residue was washed twice with double-distilled water. The final adsorbent was a slurry of MCDT–CTMAB–naphthalene and stored in a bottle for subsequent use.

*Pre-treatment of standard alloys, environmental and biological samples*

The solution of standard alloys was prepared as described in the literature.[16] A 0.01-g sample of each of the standard alloy was dissolved in 50–60 ml of 6*M* HCl by heating on a hot plate, then 3–5 ml of 30% hydrogen peroxide was added. The excess of the peroxide was decomposed by heating. The solution was cooled, filtered if needed, and diluted to 100 ml with distilled water in a calibrated volumetric flask.

Solid environmental samples were dried in an oven at 200°C for 2 hr. A 1.0-g sample of each was decomposed with 50–60 ml of 6*M* HCl,[17] then 3–5 ml of 30% hydrogen peroxide was added. The mixture was heated on a hot plate almost to dryness. The residue was then dissolved in 10 ml of 1*M* HCl and diluted with 10 ml of distilled water and filtered if needed. Finally the solution was made up to 100 ml with distilled water in a calibrated volumetric flask.

A 100-ml sample of each liquid environmental sample was taken and to it added 5 ml of conc $HNO_3$. The solution was heated almost to dryness on a hot plate. The residue was dissolved in 5 ml of 1*M* HCl and finally the solution was made up to 100 ml with distilled water in a calibrated volumetric flask.[18]

A 0.1-g sample of each of the biological samples was dissolved by heating with concentrated nitric and perchloric acids. The solution was cooled and diluted up to a volume of 100 ml with distilled water in a calibrated volumetric flask.[18] In the case of samples of unknown composition cadmium and lead were determined by the AAS method after preconcentration by the proposed method. In this case the naphthalene has to be removed by filtration before aspirating the sample in a flame. In addition, the metals in the unknown samples were also estimated by standard methods reported in the literature.[19]

*General procedures*

An aliquot of lead or cadmium solution (0.5–140 $\mu$g for Cd and 5–200 $\mu$g for Pb) was taken in a 100-ml Erlenmeyer flask with a tightly fitting stopper. To this solution, 2 ml of 10% potassium sodium tartrate and 2 ml of 0.2% reagent solution were added and the mixture diluted to 30–40 ml. The pH of this solution was adjusted by 2 ml of aqueous ammonia–ammonium ion buffer of pH 8.0. The solution was mixed well and allowed to stand for a few seconds. Then, 2 ml of a 20% solution of naphthalene in acetone was added to it with continuous shaking. The solid mass so formed consisting of naphthalene and metal complex was separated by filtration on a Whatman filter paper (No. 1041). The residue was shaken vigorously with 10 ml of 1*M* hydrochloric acid and transferred to the polarographic cell. In the column method, the adsorbent was conditioned to pH 8.0 by passing 5–7 ml of buffer through the column, before the test solution was passed through it at a flow rate of 1–2 ml/min. The column was finally washed with water. Desorption of metal was carried out by passing 10 ml of 1*M* of HCl at flow rate of 1–2 ml/min and the solution was transferred to the polarographic cell. After the addition of 3 ml of 4% $NaBH_4$ solution, the differential pulse polarogram was recorded.

## RESULTS AND DISCUSSION

Preliminary observations indicated that $NaBH_4$ is quite effective for the removal of dissolved oxygen from the solution in a few seconds. Highly purified $N_2$ in contrast takes 5–10 min for the complete removal of $O_2$. Another advantage of using $NaBH_4$ is that it provides $OH^-$ ions and brings the pH in the desired range. Thus, it is helpful for adjusting the pH of a solution (the solution is prepared in 0.2*M* NaOH). There is no need to add extra NaCl as the supporting electrolyte because sufficient quantity is formed in the reaction. Many other supporting electrolytes were also tried without any effect.

*Effect of pH on differential pulse polarograms*

We studied the effect of pH by adding 4% $NaBH_4$ solution, while keeping other variables constant. The shape of the differential pulse polarograms and peak heights were found to be almost constant over the pH range of 0.6–5.0 for both metals (the pH may also be adjusted using NaOH solution). The peak potential ($E_p$) shifted towards more negative values as the pH increased in the range of 5–8, but a plot of $E_p$ *vs.* pH was not linear, indicating that protonation is not taking part in the overall electrode process. The peak heights were considerably decreased above pH 8 in both cases, probably owing to hydroxides formation. Therefore, all studies were carried out at pH $\sim$ 2 since it was conveniently achieved simply by mixing the solutions.

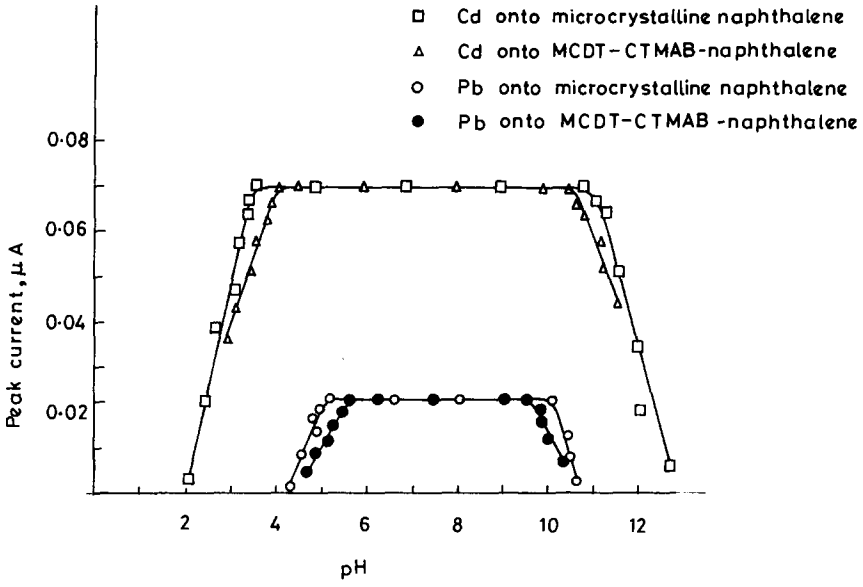


Fig. 2. Effect of pH on adsorption/retention of lead and cadmium complex: lead, 103.5 μg; cadmium, 112 μg; reagent, 2.0 ml; (0.2%) naphthalene, 2.0 ml (20%); reference, reagent blank. Instrumental settings: (a) scan rate = 12 mV/sec; (b) modulation amplitude = 50 mV; (c) drop time = 0.5 sec.

*Effect of pH and buffer on adsorption*

We carried out adsorptions at different pH values, keeping other variables constant. It was found that lead– and cadmium–morpholine-4-carbodithioates were quantitatively retained on naphthalene in the pH ranges of 5–10 and 3.4–11, respectively but in case of column method, lead and cadmium were quantitatively retained on MCDT–CTMAB–naphthalene in the pH ranges of 5.2–9.5 and 4–10.8, respectively (Fig. 2). Addition of 1–5 ml of buffer for adsorption of the complex on microcrystalline naphthalene and 5–15 ml of buffer in the case of the column method did not cause any effect on the adsorption. Therefore, 2.0 ml and 7.0 ml of the aqueous ammonia–ammonium ion buffer were employed in the subsequent determinations in both the cases, respectively.

*Retention characteristics of MCDT*

The chelating agent has the functional group

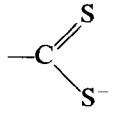

of the dithiocarbamate molecule which is co-ordinated with the metal. Hence, both the cadmium and lead form the chelate with 2 moles of dithiocarbamate molecule on the surface of microcrystalline naphthalene after passing through the column.

*Retention capacity of MCDT supported on naphthalene*

The retention capacity of morpholine-4-dithiocarbamate supported on naphthalene was determined by the batch method. This experiment was carried out by taking 3 mg of metal ion, 2.0 ml of buffer and a suitable amount of the absorbent in a 100 ml separatory funnel. This mixture was diluted to 30 ml, shaken with a mechanical shaker for 15 min and then filtered through a filter paper. The amount of metal ion in the filtrate was determined by AAS. The naphthalene chelating agent material was dried on a filter paper and the solid mass weighed on a balance. The retention capacity of both the metal ions for this adsorbent depends on the amount of adsorbent. The maximum amount of retention was 4.5 mg for cadmium and 4.1 mg for lead per g of the adsorbent.

*Reaction conditions*

Reaction conditions were established using 103.5 μg of lead and 112 μg of cadmium taken individually.

Preliminary observations indicated that lead and cadmium complexes could be desorbed completely with 10 ml of 0.1–5.0*M* hydrochloric acid, but 1*M* of hydrochloric acid was used instead. The reagent concentration was varied over a range of 0.1–7 ml. It was found that adsorptions were quantitative for 0.5–4.0 ml

of 0.2% reagent of lead and cadmium. Consequently, 2.0 ml of the reagent was used in subsequent studies (2 ml of 0.2% reagent corresponds to $\sim$0.02m$M$, while the metal cadmium 112 $\mu$g and lead 103.5 $\mu$g correspond to 0.001 and 0.0005m$M$, roughly more than 10 and 20 times, respectively. The stoichiometric ratio of the metal:ligand is 1:2. Therefore, the calibration curve can be safely constructed as Cd, 0.9–130 $\mu$g; Pb, 9.1–195 $\mu$g in 13 ml of the final solution.) We added various amounts of naphthalene to sample solutions, keeping other variables constant. It was observed that the peak height remained constant with the addition of 0.4–4.5 ml of 20% naphthalene solution. Therefore, 2 ml of 20% naphthalene was used in subsequent studies. The effect of shaking time on the adsorption indicated that the peak height remained constant over a range of 0.5–7 min. Therefore, 1 min of shaking time was maintained in the present work. While in the case of column method, the flow rate was varied from 0.5 to 8 ml/min. It was found that a flow rate of 0.5–5.0 ml/min did not affect adsorption. A flow rate of 1–2 ml/min was recommended in all experiments. The volume of the aqueous phase was varied in the range of 10–800 ml under the optimum conditions. It was observed that the peak height was almost constant up to 100 ml of the aqueous phase (preconcentration factor of $\sim$6) in case of lead and up to 300 ml of the aqueous phase (preconcentration factor of $\sim$20) in the case of cadmium and then decreased gradually in both the cases. Whereas, in the case of column method, peak height was almost constant up to an aqueous phase volume of 600 ml, for both the metals. Therefore, a preconcentration factor $\sim$40 can be achieved by the column method. However, in all the experiments, 40 ml of the aqueous phase was maintained for convenience.

*Calibration*

A calibration curve (Fig. 3) for the determination of lead and cadmium was prepared according to the general procedure for the optimum conditions developed above. The detection limits were 0.14 ppm for lead and 0.014 ppm for cadmium, at the minimum instrumental settings (signal-to-noise ratio = 2). The linearities were maintained in the concentration ranges of Pb, 0.7–15 ppm and Cd, 0.07–10 ppm (9.1–195 $\mu$g for Pb and 0.91–130 $\mu$g for Cd in 13 ml of the final solution) with a

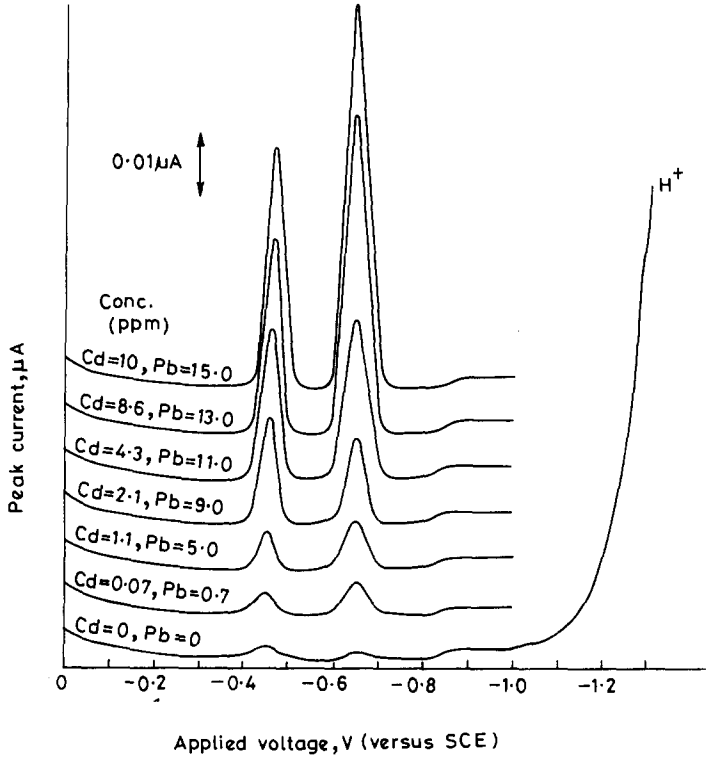


Fig. 3. Typical differential pulse polarograms for a series of lead and cadmium concentrations; conditions as Fig. 2.

Table 1. Determination of lead and cadmium in standard alloys

| Pb/Cd sample | Certified composition (%) | Lead found by present method* (%) | Cadmium found by present method* (%) |
|---|---|---|---|
| N.B.S., SRM-629 Zn-base die-casting alloy E | Cu: 1.50, Mg: 0.094 Fe: 0.017, Sn: 0.012 Cr: 0.0008, Mn: 0.0017 Ni: 0.0075, Al: 5.15 Si: 0.078, Pb: 0.006 Cd: 0.002 | 0.0063 ± 0.0002† | 0.0022 ± 0.0003‡ |
| N.B.S., SRM-94C Zn alloy | Sn: 0.006, Ni: 0.006 Mn: 0.014, Fe: 0.018 Mg: 0.042, Cu: 1.01 Al: 4.13, Pb: 0.0135 Cd: 0.0155 | 0.0137 ± 0.0005‡ | 0.0160 ± 0.0004‡ |

*Average of 10 determinations, ±SD.
†Column method.
‡Microcrystalline naphthalene method.

correlation factor of 0.9997 and relative standard deviations of ±0.95 and 0.81%, respectively.

*Effect of diverse ions*

The effect of various salts of anions and cations on the adsorption and subsequently on the differential pulse polarographic determination of 103.5 μg of lead or 112 μg of cadmium were studied individually. The following anions and cations (the amount shown in parentheses) did not interfere: tartrate, citrate, oxalate, monohydrogen phosphate, carbonate, and nitrate (100 mg each), sulphate, acetate, bromide, and iodide (100 mg of each) in the case of cadmium, but in the case of lead (5 mg of each) could be tolerated. U(VI), Se(VI), Mo(VI), Ti(IV),

Table 2. Determination of lead and cadmium in biological samples

| Sample | Certified composition (μg/g) | Pb determined by present method* (μg/g) | Cd determined by present method* (μg/g) |
|---|---|---|---|
| NIES No. 5 Human hair | Al, 240; Sb, 0.07; Ba, 3.2; Ca, 728; Cr, 1.4; Co, 0.10; Cu, 16.3; Fe, 225; Mg, 208; Hg, 4.4; Ni, 1.8; K, 34; Rb, 0.19; Sc, 0.05; Se, 1.4; Na, 26; Sr, 2.3; Ti, 22. Mn, 5.2; Zn, 169 Pb, 6.0; Cd, 0.20 | 5.876 ± 0.005‡ | 0.214 ± 0.003‡ |
| NIES No. 3 Chlorella | Ca, 4900; Mn, 69; Co, 0.87; Cu, 3.5; Fe, 1850; Zn, 20.5; Mg, 3300; K, 12,400; Sc, 0.013; Sr, 40. Pb, 0.60; Cd, 0.026 | 0.621 ± 0.004† | 0.024 ± 0.002† |
| NIES No. 7 Tea leaves | Al, 775; Sb, 0.014; Ba, 5.7; Mn, 700; Ca, 3200; Cs, 0.022; Cr, 0.15; Co, 0.12; Cu, 7.0; Zn; 33; Mg, 1530; Ni, 6.5; K, 18,600; Sc, 0.011; Na, 15.5; Sr, 3.7. Pb, 0.80; Cd, 0.030 | 0.786 ± 0.003‡ | 0.034 ± 0.005† |

*Average of five determinations, ±SD.
†Column method.
‡Microcrystalline naphthalene method.

Table 3. Determination of lead and cadmium in environmental samples

| Sample | Pb/Cd found by AAS*† ($\mu g/g$) | Pb/Cd found by present method* ($\mu g/g$) |
|---|---|---|
| Fly ash near IP power station, New Delhi, India | Cd = 35 ± 4<br>Pb = 60 ± 5 | Cd = 35 ± 2§<br>Pb = 60 ± 3‡ |
| Soil near Wazirpur industrial area, New Delhi, India | Cd = 0.120 ± 0.005<br>Pb = 24.70 ± 0.07 | Cd = 0.121 ± 0.003‡<br>Pb = 24.71 ± 0.04§ |
| Sediment of Yamuna river, near Wazirpur waste disposal point, New Delhi, India | Cd = 100 ± 2<br>Pb = 50 ± 5 | Cd = 100 ± 4§<br>Pb = 50 ± 4‡ |
| Tapwater from the laboratory of Institute of Technology, New Delhi, India | Cd = 0.720 ± 0.005<br>Pb = 0.971 ± 0.004 | Cd = 0.725 ± 0.002‡<br>Pb = 0.968 ± 0.005§ |

*Average of five determinations, ±SD.
†After preconcentration by the present method.
‡Column method.
§Microcrystalline naphthalene method.

Cr(III), Zn(II), Mn(II), Ni(II) (50 mg each), V(V), Te(IV), Bi(III), Al(III), As(III), Sn(II), Co(II) and Cu(II) (10 mg each), Os(VIII), Cr(VI), Sb(III), Rh(III), Ru(III) and Pd(II) (5 mg each). Fifteen milligrammes of lead in the case of cadmium and 10 mg of cadmium in the case of lead did not interfere. Only Fe(III), Ir(III) and Tl(I) interfered in both the cases, however, 5 mg of Fe(III) could be tolerated after Fe(III) was masked with triethanolamine while in case of Ir(III), the adsorption was carried out at pH 9.0 since Ir(III) did not absorb above pH 9.0. In addition, EDTA interfered seriously in both cases. Adsorption was almost nil in the presence of EDTA (< 1 mg) undoubtedly owing to the high stability of the lead– and cadmium–EDTA complexes.

*Application to the analysis of alloys, biological and environmental samples*

The accuracy and applicability of the proposed method was evaluated by its application on various alloys, biological and environmental samples. An aliquot of the pretreated standard alloys, biological and environmental sample solution was analyzed by the general procedure after iron was masked with triethanolamine. Tap water from the Department of Chemistry, I.I.T. Delhi, was analysed directly by the general procedure after iron was masked with triethanolamine. The results were also compared with atomic absorption spectrophotometrically after the general procedure had been applied. The data are given in Tables 1, 2 and 3. In the case of samples of unknown composition (Table 3), these metals were also estimated by standard methods reported in the literature.[19]

## CONCLUSIONS

It is difficult to obtain a well defined polarogram in traditional analysis of metals after extraction of their complexes into an organic solvent owing to the low dielectric constant of the organic phase. Sensitivity is lost if it is mixed with another solvent of high dielectric constant. Sometimes a maximum suppressor is also required. Another major disadvantage is the removal of dissolved oxygen which is a tedious and time consuming process and affects the reproducibility of the method owing to partial evaporation of the organic solvent. The reported method has solved most of these problems and tested successfully for the simultaneous estimation of lead and cadmium contents in real samples, *viz.*, biological and environmental samples. Although adsorption onto microcrystalline naphthalene is more rapid, the preconcentration factor is comparatively lower than the column method.

## REFERENCES

1. D. C. Manning and W. Slavin, *Atom. Absorpt. News*, 1978, **17**, 43.
2. P. N. Vijan and G. R. Wood, *Analyst*, 1976, **101**, 966.
3. K. Stulik and K. Marik, *Talanta*, 1976, **23**, 131.
4. T. U. Aualiitia and W. F. Pickering, *Talanta*, 1987, **34**, 231.
5. Y. Nagaosa and N. Sato, *Bunseki Kagaku*, 1987, **36**, 877.
6. T. Odshima, Y. Kawate and H. Ishii, *Bunseki Kagaku*, 1988, **37**, 439.
7. Y. Nagaosa and T. Sona, *Anal. Lett.*, 1984, **17**, 243.
8. Y. Nagaosa, *Fresenius Z. Anal. Chem.*, 1983, **316**, 794.

9. Y. Nagaosa and K. Kobayashi, *Talanta*, 1984, **31**, 593.
10. T. Fujinaga and M. Fujita, *Bunseki Kagaku*, 1981, **30**, 148.
11. T. Fujinaga and Y. Nagaosa, *Chem. Lett.*, 1978, **6**, 587.
12. B. K. Puri, M. Gautam and T. Fujinaga, *Bull. Chem. Soc., Jpn*, 1979, **52**, 3415.
13. A. L. J. Rao, B. S. Brar and B. K. Puri, *Bull. Chem. Soc., Jpn*, 1982, **55**, 598.
14. A. I. Vogel, *Textbook of Quantitative Inorganic Analysis*, 5th Edn. Longmans Green & Co., London, 1991.
15. G. Macrotrigiano, G. C. Pallacani, C. Preti and G. Tosi, *Bull. Chem. Soc., Jpn*, 1975, **48**, 1018.
16. M. Satake, B. K. Puri, S. Usami and K. Ishida, *Anal. Chem.*, 1986, **58**, 2502.
17. P. D. Goulden, *Environmental Pollution Analysis*, pp. 2–5. Heyden & Son Ltd, London, 1978.
18. S. Usami, S. Yamada, B. K. Puri and M. Satake, *Mikrochim. Acta*, 1989, **I**, 263.
19. A. K. De, S. M. Khopkar and R. A. Chalmers, *Solvent Extraction of Metals*, pp. 129–131. Van Nostrand Reinhold, London, 1970.

Pergamon

0039-9140(94)00218-5

*Talanta*, Vol. 42, No. 1, pp. 73–76, 1995

0039-9140/95 $9.50 + 0.00

# SENSITIVE SPECTROPHOTOMETRIC METHOD FOR THE DETERMINATION OF PROPOXUR USING 4-AMINOANTIPYRINE

B. VENKATESWARLU and K. SESHAIAH*

Department of Chemistry, Sri Venkateswara University, Tirupati—517502, India

(*Received* 7 *March* 1994. *Revised* 8 *July* 1994. *Accepted* 26 *July* 1994)

**Summary**—The use of 4-aminoantipyrine for the colorimetric determination of propoxur in pesticide formulations and water samples is described. The method is based on the alkaline hydrolysis of the pesticide and the resultant phenol is reacted with 4-aminoantipyrine in the presence of an oxidizing agent. The resultant colored dye is extracted into chloroform and the absorbance measured at 472 nm.

Propoxur (isopropoxyphenyl methyl carbamate) is a carbamate insecticide which has wide applications in controlling numerous species of household and public health pests. It provides control of insects which are resistant to chlorinated hydrocarbons and organophosphates. In view of its wide application there is a need for the development of sensitive and reliable methods for the assessment of quality of insecticide formulations and to quantify the insecticide residues in water. There are spectrophotometric and chromatographic methods for the determination of propoxur. The spectrophotometric methods are based on the alkaline hydrolysis of the insecticide followed by coupling the resultant phenol with reagents such as diazotized 3-nitroaniline-4-sulphonic acid,[1,2] sulphanilic acid,[3] 4-aminoantipyrine,[4] 3,5-dibromo-*p*-benzoquinon chlorimine,[5] 4,4-diaminodiphenyl sulphone,[6] *p*-dimethylamino benzaldehyde and *p*-dimethylamino cinnamaldehyde,[7] 3-methyl-2-benzothia zolinone hydrozone hydrochloride,[8] *p*-dimethylphenylenediamine dihydrochloride[9] and 2-aminobenzophenone.[10] In the above spectrophotometric methods hydrolysed phonolic product is diazotized in aqueous solution as shown in Fig. 1, and the color of the aqueous solution measured. Hence, the sensitivity was less and also there was a possibility of the colored product reacting with other reagents present in the aqueous phase which leads to instability of the compound. We now report a spectrophotometric method based on the reaction of hydrolysed phonolic product with 4-aminoantipyrine in the presence of an oxidizing agent to produce an orange colored dye as shown in Fig. 2. The dye is extracted into organic solvent. Extraction of the dye from aqueous solution into small quantity of organic solvent increased the sensitivity of the method by several-fold compared with the reported methods and also the stability of the colored dye in organic solvents is more when compared with the aqueous phase. The method is extended to the determination of propoxur in commercial formulations and water samples.

*Author to whom correspondence should be addressed.

## EXPERIMENTAL

### *Reagents*

All chemicals used were of analytical grade.

*Propoxur stock solution* (1000 μg/ml)

Insecticide (0.10 g) was dissolved in 100 ml of carbonyl free methanol. The stock solution was progressively diluted with the solvent to obtain standard solution of desired concentration (0.1 μg/ml).

4-*Aminoantipyrine* (2%)

4-Aminoantipyrine (2 g) was dissolved in distilled water and diluted to 100 ml.

*Sodium hydroxide* (2%)

Sodium hydroxide (2 g) was dissolved in 100 ml of distilled water.

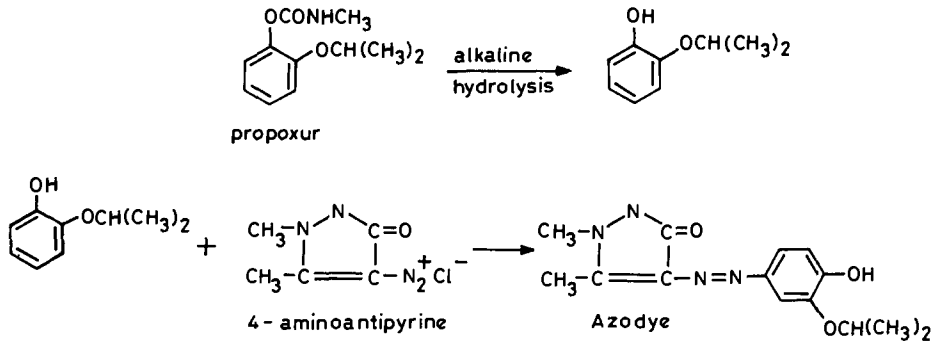


Fig. 1. Coupling reaction of 4-aminoantipyrine with propoxur.

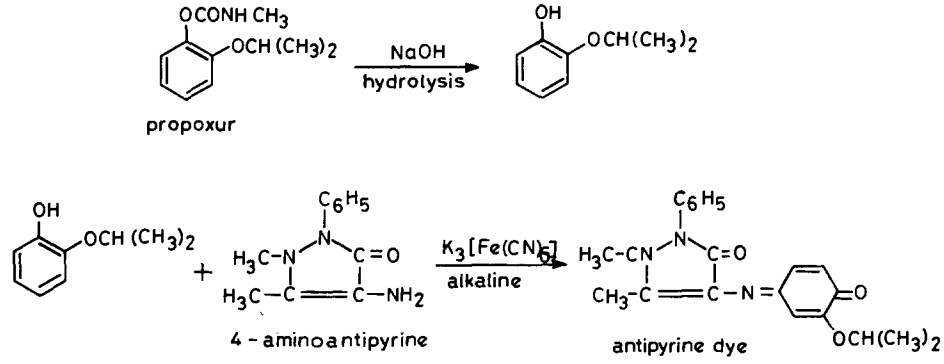


Fig. 2. Reaction mechanism of the antipyrine dye formed with propoxur.

*Buffer solution*

Dipotassium hydrogen phosphate (10.5 g) and 7.3 g of potassium dihydrogen phosphate were dissolved in distilled water and diluted to 100 ml.

*Potassium ferricyanide solution*

Potassium ferricyanide (8 g) was dissolved in distilled water and diluted to 100 ml.

A Shimadzu UV-240 recording spectrophotometer was employed in the studies.

*Procedure*

Insecticide solution (20 ml) was taken in a clean dry 100 ml beaker. Two per cent sodium hydroxide solution (5 ml) was added and allowed to stand for 5 min for complete hydrolysis, the pH of the solution is adjusted to 9.5 by adding 5 ml buffer solution and the requisite amount of HCl and ammonia solution. The solution was transferred to a 50 ml separating funnel and allowed to stand for 2 min and then 3 ml of 4-aminoantipyrine and 3 ml of potassium ferricyanide added and mixed well. The orange colored dye formed was extracted into 10 ml chloroform. The absorbance of the chloroform solution was measured at 472 nm, against a reagent blank.

*Formulations*

Well mixed formulation (equivalent to about 100 $\mu$g of the active insecticide) was shaken with 25 ml of methanol for 5–10 min. The supernatant solution was filtered by decantation into a 100 ml standard flask. The residue was washed twice with 10 ml portions of methanol. The filtrate and washings were diluted to 100 ml with methanol. Analysis was carried out using the above procedure.

Water samples (100 ml) spiked with 2.0, 3.0, 4.0, 5.0 and 6.0 $\mu$g of insecticide were taken, the pH of these samples adjusted to 3–4 with 2% sulphuric acid and 2 g of anhydrous sodium sulphate. The mixture was transferred into a separating funnel and insecticide extracted using approximately 15 ml of chloroform for each extraction by shaking 5–10 min. Combined extracts were washed with 2 ml of 0.1 *M* potassium carbonate to break any emulsion formed during the extraction, then dried over anhydrous sodium sulphate. Finally, chloroform was evaporated and residue dissolved in methanol. Determination was carried out by developing color using the above procedure.

## RESULTS AND DISCUSSION

Propoxur pesticide was hydrolysed and the resultant phenol converted into orange colored dye by reacting with 4-aminoantipyrine in the presence of an alkaline oxidizing agent, potassium ferricyanide.

### *Effect of pH on the formation of colored dye*

The reaction of the phenolic product with antipyrine was carried out in the pH range 6–11. The results are shown in Fig. 3. The absorbance of the colored dye was greater in the pH range 8.5–10. Hence, pH 9.5 was selected for the extraction of dye into organic layer.

### *Effect of solvent*

Extraction of colored dye was carried out in benzene, chloroform, methyl isobutyl ketone and carbon tetrachloride and their absorption spectra are shown in Fig. 4. Absorbance for the benzene extractant was more than the other solvents. The extraction with carbon tetrachloride was less efficient. Though absorbance with the chloroform extraction was slightly less than benzene, chloroform was selected for further extractions because of convenience of extraction.

### *Stability of colored dye*

The stability of the colored dye was studied in different solvents. It was stable for more than 12 hr in chloroform, benzene and methyl isobutyl ketone, but faded quickly in carbon tetrachloride.

Beer's law was obeyed over the concentration range of 0.1 to 1.0 $\mu$g/ml of propoxur and the respective calibration plot is shown in Fig. 5. The molar absorption coefficient of the colored dye was $3.09 \times 10^5$ cm$^{-1}$. The method was applied for the determination of propoxur in commercial formulations, 1% oil-based spray (Baygon spray) and 2% bait (Baygon) and spiked water samples. Results are shown in Table 1. The results indicate that the active insecticide obtained in formulations was in good agreement with the reported results by the manufacturers and the recovery of propoxur from spiked water samples was quite satisfactory. The results further demonstrate that the method is suitable for the analysis of formulations and field water samples.

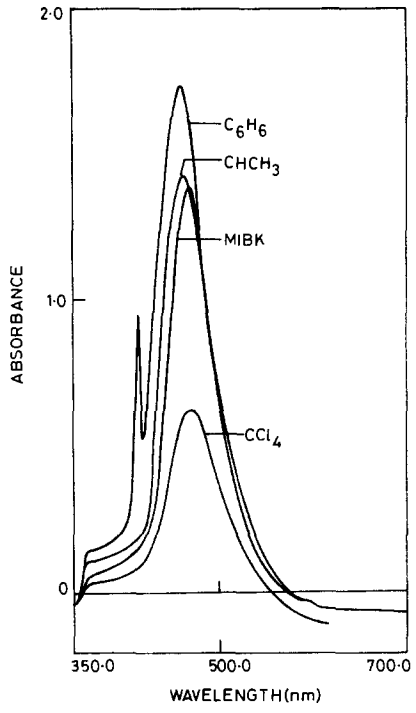


Fig. 4. Extraction of colored dye in different solvents.

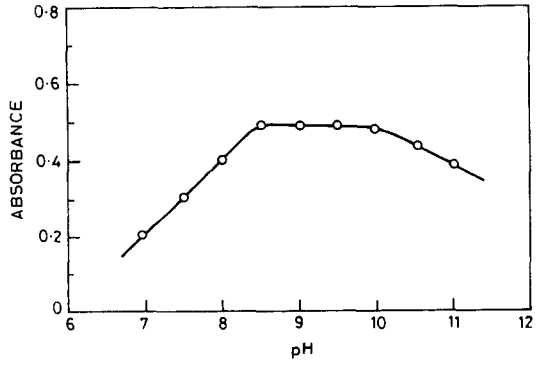


Fig. 3. Effect of pH on color formation.

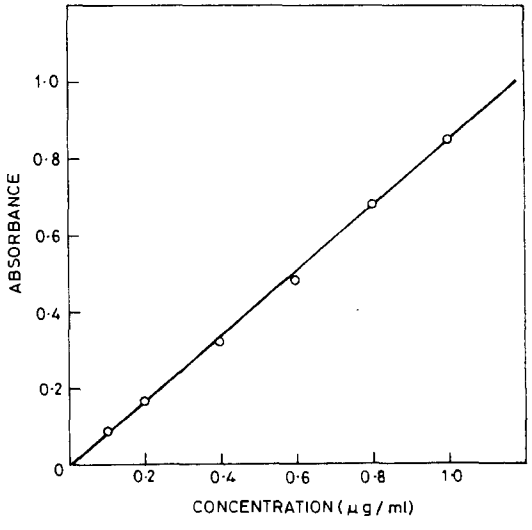


Fig. 5. Verification of Beer's law.

Table 1. Analysis of commercial formulations and spiked water samples

| S. No. | Baygon spray (1% oil-based spray) Taken (μg) | Found (μg) | RSD | Baygon (2% bait) Taken (μg) | Found (μg) | RSD |
|---|---|---|---|---|---|---|
| 1. | 20.0 | 19.6 | 0.51 | 20.0 | 19.4 | 0.48 |
| 2. | 30.0 | 29.4 | 0.48 | 30.0 | 29.2 | 0.53 |
| 3. | 40.0 | 39.2 | 0.50 | 40.0 | 39.1 | 0.49 |
| 4. | 50.0 | 49.2 | 0.51 | 50.0 | 48.7 | 0.47 |
| 5. | 60.0 | 58.9 | 0.57 | 60.0 | 58.3 | 0.51 |
| 6. | 70.0 | 69.0 | 0.45 | 70.0 | 68.3 | 0.50 |

| | Spiked water | | | |
|---|---|---|---|---|
| | Added (*ppb*) | Found (*ppb*) | % Recovery | RSD |
| 1. | 20.0 | 19.7 | 98.5 | 0.62 |
| 2. | 30.0 | 29.3 | 97.6 | 0.57 |
| 3. | 40.0 | 38.9 | 97.2 | 0.53 |
| 4. | 50.0 | 48.7 | 97.4 | 0.56 |
| 5. | 60.0 | 59.2 | 98.6 | 0.52 |

% Recovery and RSD are for five independent determinations.

*Acknowledgement*—The authors are grateful to Bayer (India) Ltd, Bombay, for the supply of technical grade propoxur.

## REFERENCES

1. P. Bracha, *J. Agric. Food Chem.*, 1964, **12,** 461.
2. M. Ramaswamy, *Pestic. Sci.*, 1974, **5,** 383.
3. G. Mukherjee, A. K. Mukherjee and B. R. Roy, *J. Food Sci., Technol.*, 1975, **12,** 96.
4. J. Piechocka, *Rocz. Panstw. Zakl. Hig.*, 1975, **26,** 503–508 (in Polish); *CA* 1976, **84,** 3369X.
5. W. F. Vangils, *Analyst*, 1979, **104,** 1185.
6. K. M. Appaiah, O. P. Kapur and K. V. Nagaraja, *J. Assoc. Offic. Anal. Chem.*, 1983, **66,** 105.
7. C. S. P. Sastry, D. Vijaya and K. E. Rao, *Food Chem.*, **20,** 157 (1986).
8. C. S. P. Sastry and D. Vijaya, *Talanta*, 1987, **34,** 372.
9. C. S. P. Sastry, D. Vijaya and D. S. Mangala, *Analyst*, 1987, **112,** 75.
10. D. Venkaiah and P. R. Naidu, *Talanta*, 1990, **37,** 629.

Pergamon

0039-9140(94)00219-3

*Talanta*, Vol. 42, No. 1, pp. 77–81, 1995

0039-9140/95 $9.50 + 0.00

# SELECTIVE AND SENSITIVE SPECTROPHOTOMETRIC DETERMINATION OF COPPER(II) AND BENZOYLPEROXIDE WITH *N*-ETHYL-2-NAPHTHYLAMINE*

ITSUO MORI,† TSUYOSHI FUJIMOTO, YOSHIKAZU FUJITA and TAKAKO MATSUO
Osaka University of Pharmaceutical Sciences, 2-10-65, Kawai, Matsubara, 580 Osaka, Japan

(*Received* 4 *May* 1994. *Revised* 11 *July* 1994. *Accepted* 26 *July* 1994)

**Summary**—Spectrophotometric determinations of benzoylperoxide (BPO) and copper(II) were, respectively, investigated by using the colour reaction for *N*-ethyl-2-naphthylamine (NENA), BPO and copper(II) as a metal ion in various concentrations of acetonitrile–water mixed solution as acidic media. The calibration graphs were linear in the range of 0–200 $\mu$g BPO with apparent molecular coefficient ($\varepsilon$) of $8.5 \times 10^3 M^{-1}$ cm$^{-1}$ at 530 nm, and 0–2.4 $\mu$g per 10 ml copper(II) with $\varepsilon = 1.72 \times 10^5 M^{-1}$ cm$^{-1}$ at 533 nm, respectively. Additionally, the FIA method for copper(II) was proposed with NENA–BPO. The calibration graph for FIA was linear in the range of 0–7.9 ng copper(II) per 5 $\mu$l at 533 nm. These proposed methods were selective and simple in comparison with previous methods such as cuproin kinetic reactions, especially the spectrophotometry for copper(II) with NENA–BPO was very specific, and the effect of foreign ions was negligible.

Generally, benzoylperoxide (BPO) has been used as a polymerization agent, flour improver, oxidizing and bleaching agent for fats and oils, an organic compound starting material or confirmation agent for hydroxypropylmethyl cellulose, and epispostic pharmaceuticals, *etc.* Various methods for the assay of BPO have been reported; gas chromatography,[1] liquid chromatography,[2] chemiluminescence[3] and spectrophotometry.[4,5] Additionally, many kinetic spectrophotometries of copper(II) with various organic agents such as rhodamine B, eosine and hydrogen peroxide have been reported.[6–9] However, these methods for the assay of copper(II) or BPO lack sensitivity and selectivity. In this paper, with a view to obtaining a more selective and sensitive spectrophotometric method for BPO and copper(II), we have investigated the systematical colour reaction of *N*-ethyl-2-naphthylamine (NENA), BPO and copper(II) in the test tube. The sensitive and selective spectrophotometric determinations for BPO and copper(II) with NENA–BPO in the test tube, and the FIA method for copper(II) were proposed, respectively.

*The application of aromatic amines in analytical chemistry. Part 2.

†To whom correspondence should be addressed.

## EXPERIMENTAL

### *Apparatus and reagents*

The absorption spectrum was recorded on a Shimadzu UV 3100 spectrophotometer with 1.0-cm quartz cells, Hitachi-Horiba Model F-8 and F-11 pHmeters were used. A Shimadzu Model LC-6AD and LC-6A HPLC, and Hitachi 056 recorder were used for the recording of FIA. FIA detection was carried out by a Shimadzu Model SPD-6AV detector. $^1$H NMR spectra were determined with a Varian X1-300 spectrometer in acetone-$d_6$, and mass spectra with a Hitachi M-80 instrument.

All materials and reagents were of analytical grade and were used without further purification. Solutions of $1.0 \times 10^{-1} M$ NENA and $1.0 \times 10^{-3} M$ (NENA–BPO) were prepared by dissolving NENA or (NENA–BPO) in acetonitrile previously synthesized by the Edward method.[10,11] Copper(II) solution was prepared by dissolving copper sulphate in water, and corrected by EDTA titration. Deionized water was used throughout.

### *Standard procedures*

*Determination of BPO.* To a sample solution (0.3 ml) containing 0–200 $\mu$g (0–$8.0 \times 10^{-5} M$)

BPO in a 10-ml calibrated flask, 2.0 ml of pH 5.0 buffer solution (Walpole buffer, acetic acid–sodium acetate mixture) and 0.5 ml of $1.0 \times 10^{-2}M$ copper(II) solution were added. The mixture was diluted to the mark with acetonitrile (final 75% acetonitrile solution) kept at 40°C for 40 min together with a reference solution, and cooled to room temperature or 10–30°C for 5 min. The total amount of BPO was calculated by measuring the absorbance of NENA–BPO–copper(II) solution at 530 nm against a blank [NENA–copper(II) solution] prepared without BPO.

*Determination of copper*(II). (1) Manual method (in test tube). To a solution containing 2.4 $\mu$g copper(II) in a 10-ml calibrated flask, 2.0 ml of pH 5.0 buffer solution and 4.0 ml of $1.0 \times 10^{-3}M$ NENA–BPO acetonitrile solution were added. The mixture was diluted to the mark with water and kept at 25°C for 3 min. The absorbance at 533 nm was measured against water. (2) FIA method. The reaction coil (0.3 mm × 2 m) and the flow rate (1.6 ml/min of $5.0 \times 10^{-4}M$ NENA–BPO acetonitrile solution (carrier 1), and 0.8 ml/min of pH 5.0 acetic acid–sodium acetate buffer solution (carrier 2) were used. The sample solution of 5 $\mu$l containing 0–7.9 ng copper(II) was injected into two mixed carrier streams (carriers 1 and 2), the absorbance at 533 nm monitered, and the output (peak height and area) of the spectrophotometer registered on the chart recorder for the calculation. The amount of copper(II) was found from the calibration graph.

## RESULTS AND DISCUSSION

### *Colouring reaction between naphthylamine derivatives and BPO*

The colour reaction between a secondary naphthylamine such as NENA and BPO as an oxidizing agent were systematically investigated in acetonitrile as weakly acidic media in the presence of copper(II) as a metal ion. As shown in Fig. 1, by heating NENA–BPO and NENA solutions, the difference of absorbances at 530 nm between NENA–BPO and NENA solutions in 75% acetonitrile was proportional to BPO concentration, and its value was stable for 30 min. On the other hand, the reaction products between NENA and BPO, or NENA alone in the absence of copper(II) did not give a coloured product under the conditions investigated.

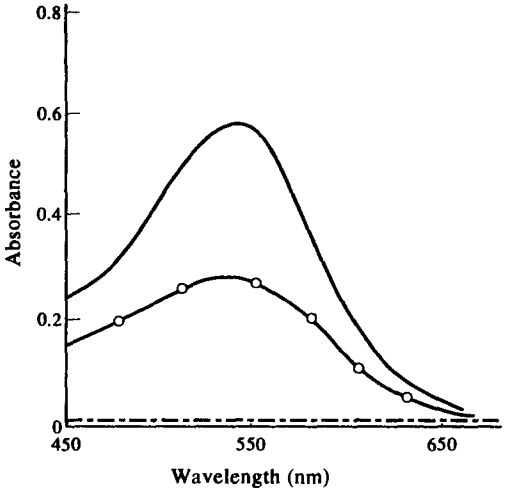


Fig. 1. Absorption spectra of (NENA–BPO–copper(II)) (NENA–copper (II)) and NENA solutions in 75% acetonitrile at pH 5.0. NENA $5.0 \times 10^{-3}M$; copper(II) $2.0 \times 10^{-4}M$; reference, water ——, NENA–BPO–copper(II) solution, BPO (180 $\mu$g); —○— NENA–BPO–copper(II) solution, BPO (90 $\mu$g); – – – – –, NENA–copper(II), NENA solutions.

### *Determination of BPO*

*Effects of solvent and concentration.* The colour reaction among NENA, BPO and copper(II) in acetic acid–sodium acetate medium (apparent pH 5) proceeded readily in acetonitrile, methylalcohol, propylalcohol, dimethylsulphoxide (DMSO), *etc.*, as solvent (mixable solvent with water). Acetonitrile was found to be the optimum solvent for the reaction. In this case, the NENA–BPO colour reaction in large amounts of water was unstable, and

Table 1. Colour reactions among naphthylamine derivatives, BPO and copper(II) in 75% acetonitrile solution

| | Absorbance ($\lambda_{max}$) | | |
|---|---|---|---|
| Naphthylamines (NA) | NA–Cu(II) | NA–BPO | NA–BPO–Cu(II) |
| *N*-Ethyl-1-naphthylamine | None | None | None |
| NENA | None | 0.267 (530) | 1.56 (530) |
| *N*-Phenyl-2-naphthylamine | None | 0.065 (463) | 0.154 (486) |
| *N*-Ethylaniline | None | 0.021 (502) | 0.021 (502) |

Naphthylamines and BPO, $5.0 \times 10^{-4}M$; copper(II), $2.0 \times 10^{-4}M$; reaction time and temperature, at 40°C for 40 min; reference, water.

its absorbance decreased with increasing water concentrations in acetonitrile. Accordingly, the water–acetonitrile (1:3, 75% acetonitrile–water mixture) was used in this colour reaction by considering the amounts of sample (contain water in sample) and reproducibility of absorbance.

*Effects of temperature, heating time and p*H. The colour reaction for NENA, BPO and copper(II) at 50°C for 5–60 min resulted in small absorbance. On the other hand, the colour reaction at 25°C for 120 min exhibited maximum absorbance, but it lacked stability and reproducibility. From these results, the reaction from standing at 40°C for 40 min was used because of the stable and reproducible colour obtained. The absorbance at 530 nm on NENA–BPO in 75% acetonitrile was almost constant at apparent pH 4.5–5.5. In this case, the ionic strength and species of buffer solution did not affect the intensity and stability of the colour reaction.

*Effects of concentration of NENA and copper*(II). From the effect of NENA concentration in the assay of 4.0 or $8.0 \times 10^{-5}M$ BPO, the recommended final concentration of NENA was more than $5.0 \times 10^{-3}M$. In the subsequent procedure, $5.0 \times 10^{-3}M$ NENA was used for the assay of BPO. As the colour reaction between NENA and BPO was catalysed by the coexistence of copper(II) as a metal ion, the coexisting effect of metal ion such as copper(II) was systematically investigated. As shown in Table 2, the coexisting effect of copper(II) as a metal ion was most striking and specific. The optimum copper(II) concentration was $2.0 \times 10^{-4}M$ for the assay of $4.0–8.0 \times 10^{-5}M$ BPO.

*Calibration graph and reproducibility for BPO.* The calibration graph was linear over the wide range from 0 to 200 $\mu$g (0–$8.0 \times 10^{-5}M$) BPO per 10 ml, and the relative standard deviation (RSD, $n = 6$) was 0.6% for 40 $\mu$g BPO in 75% acetonitrile.

Table 2. Effect of metal ions in the colour reaction between NENA and BPO in 75% acetonitrile solution

| Metal ions | Absorbance at 530 nm |
|---|---|
| None | 0.160 |
| Cu(II) | 1.065 |
| Zn(II) | 0.165 |
| Co(II) | 0.205 |
| Ni(II) | 0.145 |
| Pd(II) | 0.003 |
| Fe(III) | 0.131 |
| Mn(II) | 0.163 |

NENA, $5.0 \times 10^{-3}M$; BPO, 400 $\mu$g; pH, 5.0; reference, water.

Table 3. Colour reaction among NENA, BPO and various organic compounds in 75% acetonitrile solution

| Organic substances | Max (*nm*) | Absorbance |
|---|---|---|
| BPO | 530 | 0.418 |
| *m*-Chloroperbenzoic acid | 397 | 0.045 |
| Lauroyl peroxide | 505 | 0.041 |
| *t*-Butylperbenzoic acid | None | None |
| Cumenhydroperoxide | None | None |
| Hydrogen peroxide | None | None |
| Chloramine B | None | None |
| Potassium bromate | None | None |
| Benzoic acid | None | None |
| Benzoyl chloride | None | None |

Organic substances, $5.0 \times 10^{-5}M$; NENA, $5.0 \times 10^{-3}M$; copper(II), $2.0 \times 10^{-4}M$; pH, 5.0; reaction time and temperature, at 40°C for 40 min; reference, water.

*Colour reaction between NENA and other BPO analogues, and effect of foreign substances.* As shown in Table 3, although the colour reaction between NENA, lauroylperoxide and *m*-chloroperbenzoic acid as an oxidizing agent were also recognized, this colour reaction was only one-tenth that of NENA–BPO. On the other hand, other oxidizing agents such as hydrogen peroxide and chloramine B gave no colour reaction.

In this method, the coexistence of various other organic substances scarcely affected the BPO assay.

*Application.* Although further investigation is necessary for the applications for flour samples, *etc.*, the proposed method was applied to a recovery test of BPO in flour; the results were satisfactory, 96.8–98.4% ($n = 3$).

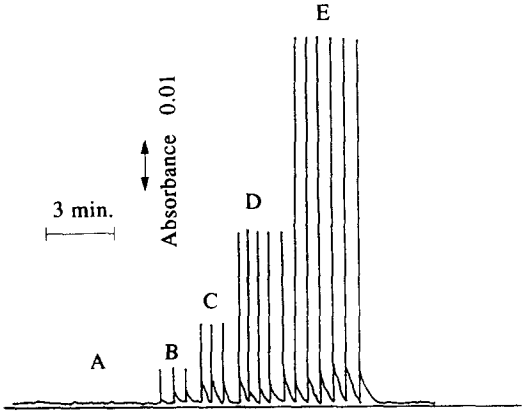


Fig. 2. Calibration peak signal for determination of copper(II) on FIA. Conditions, (NENA–BPO), $5 \times 10^{-4}$ *M*; flow rate of (NENA–BPO) solution 1.6 ml/min; flow rate of buffer solution (pH 5.0) 0.8 ml/min; copper(II) concentrations, A, 0 ng; B, 0.50 ng; C, 0.99 ng; D, 1.99 ng; E, 3.97 ng.

*Reaction between NENA and BPO, and estimation of NENA–BPO*

In previous reports,[10–12] the colour reaction between NENA and BPO was presumed to be *N*-benzolylation and *O*-hydroxylation of NENA; the reaction product (NENA–BPO) was assumed to be 2-*N*-ethylbenzamide-1-naphthol, by the oxidation process shown in Scheme 1. This chemical formula was supported by I mass and $^1$H NMR spectra: $\delta$ 1.17 (3H, *t*, $J = 7.081$ Hz, —$CH_2$—$CH_3$), 3.49 and 4.26 (2H, *dq*, $J = 13.3$, 7.08 Hz, —$CH_2$—$CH_3$), 7.88–8.27 (11H, *m*, arom.H), 8.99 (1H, *br s*, OH).

*Determination of copper*(II)

*(1) Test tube method.* As mentioned above, in the formation of colour reaction product between NENA and BPO in the presence of copper(II), the use of NENA–BPO for measurement was most effective. Accordingly, for the assay of copper(II), NENA–BPO was used.

*Effects of coil length and flow rate.* The peak height lowered and broadened with coil length. Almost constant and reproducible results were obtained with a coil length of 1.5–2.0 m (0.3 mm diameter) and an optimum flow rate of 1.6 ml/min of $5.0 \times 10^{-4} M$

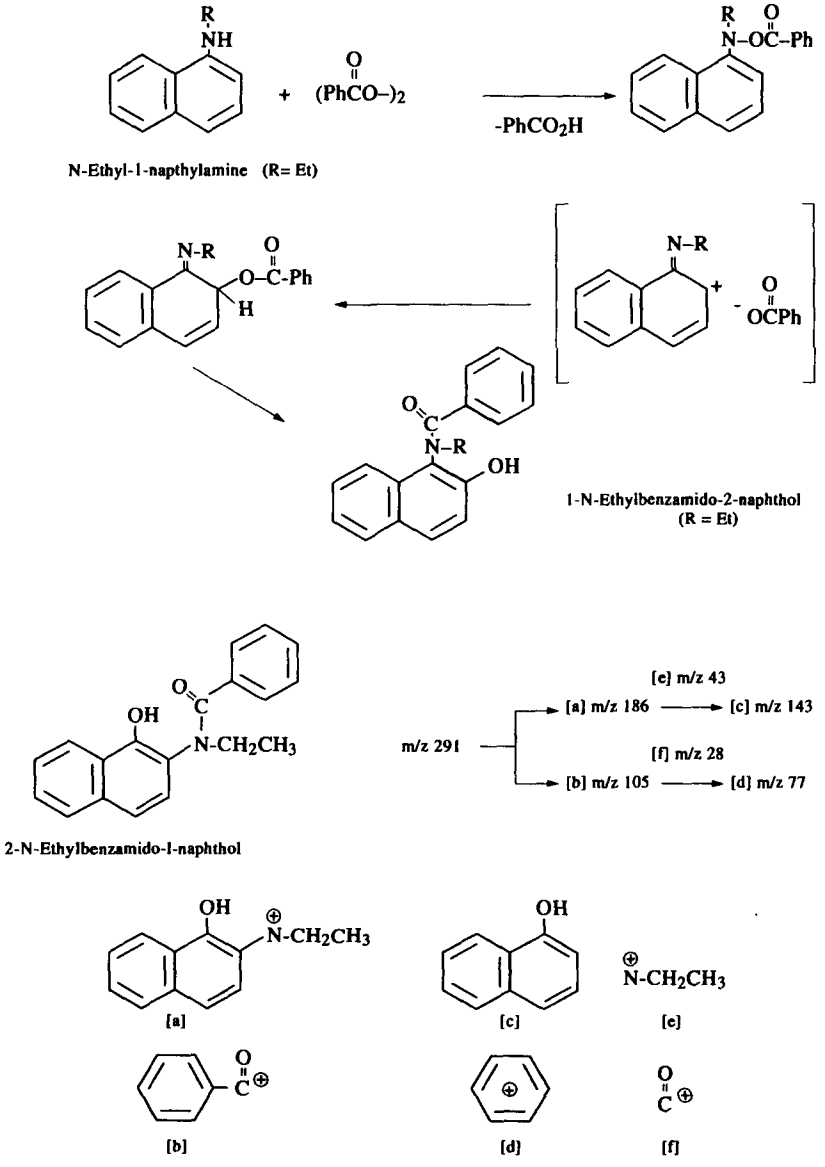


Scheme 1. Reaction between *N*-ethyl-1-naphthylamine and BPO, and mass fragment ions of (NENA–BPO) and (2-*N*-ethylbenzamido-1-naphthol).

Table 4. Effect of foreign ions

| Foreign ions | Added as | Molar ratio | Recovery (%) |
|---|---|---|---|
| None | None | None | 100.0 |
| Fe(III) | Sulphate | 15 | 100.0 |
| Co(II) | Nitrate | 120 | 100.0 |
| Ni(II) | Nitrate | 150 | 100.0 |
| Zn(II) | Chloride | 300 | 100.0 |
| Pb(II) | Nitrate | 1000 | 100.0 |
| Hg(II) | Nitrate | 200 | 100.0 |
| Al(III) | Chloride | 1500 | 100.0 |
| $S_2O_3^{2-}$ | Sodium | 10 | 100.0 |
| | | 100 | 98.0 |
| $F^-$ | Sodium | 20,000 | 100.0 |
| $NO_3^-$ | Potassium | 20,000 | 100.0 |

Copper(II) taken, 0.79 $\mu$g; NENA–BPO, $4.0 \times 10^{-4}M$; pH, 5.0; reaction time and temperature, at 45°C for 40 min; reference, water.

NENA–BPO acetonitrile solution (carrier 1), and 0.8 ml/min of acetic acid–sodium acetate buffer solution (pH 5.0).

*Effects of reaction temperature and concentration of NENA–BPO.* Referring to the above method, the FIA conditions were investigated by changing the flow rate or heating temperature. Optimum and effective temperature and concentration of NENA–BPO solution were respectively 30°C and $5.0 \times 10^{-4}M$ NENA–BPO solution.

*Calibration graph and reproducibility for copper(II) by FIA.* The calibration graph in FIA system showed a good linear relationship over the range 0.5–7.9 ng/5 $\mu$l copper(II) gave a RSD of 1.8% ($n = 5$) (Fig. 2).

*Effect of foreign ions.* The effect of foreign ions was investigated in comparison with the above method. The results were approximately similar to that of the above method.

## CONCLUSIONS

The colour reactions among naphthylamines such as NENA, BPO and various metal ions such as copper(II) were systematically investigated, and a procedure for the assay of BPO was established. By using the selective catalytic action of copper(II) in the colour reaction between NENA and BPO, the selective and sensitive spectrophotometric determination of copper(II) was proposed in 75% acetonitrile. Moreover, the chemical reaction between NENA and BPO (colour reaction) was estimated by $^1$H NMR and mass spectra. The FIA method for the assay of copper(II) was established using the colour reaction of NENA–BPO–copper(II) in 40% acetonitrile solution. The proposed FIA method has the advantages of simplicity, sensitivity and reproducibility; the analytical requirement time was 3 min, and it was little affected by other metal ions.

*Acknowledgements*—The authors would like to thank Mr K. Minoura for NMR measurement, and Mrs M. Fujitake of our University for measurement of mass spectra.

## REFERENCES

1. R. M. Silverstein, *Anal. Chem.*, 1963, **35**, 154.
2. C. K. Chou and D. C. Locke, *J. Assoc. Offic. Anal. Chem.*, 1984, **67**, 913.
3. C. Faven, M. Debacker, and D. Barbly, *Anal. Sci.*, 1993, **9**, 371.
4. L. Dulog, *Fresenius Z. Anal. Chem.*, 1964, **202**, 192.
5. P. R. Dugan and R. D. O'Neil, *Anal. Chem.*, 1963, **35**, 414.
6. Z. Zhang and X. Ma, *Fenxi Huaxue*, 1990, **18**, 520.
7. J. Gao and L. Yao, *Lihua Jianyan Huaxue Fence*, 1991, **27**, 48: *Anal. Chem.*, 1992, **64**, 413R.
8. Z. Jiang, A. Liung and G. Dai, *Fenxi Huaxue*, 1989, **17**, 447.
9. M. Kamaya, I. Ohuri, K. Kaga, E. Ishii and T. Murakami, *Fresenius Z. Anal. Chem.*, 1994, **338**, 918.
10. J. T. Edward, *J. Chem. Soc.*, 1954, **222**, 1464.
11. J. T. Edward and S. A. Sand, *Can. J. Chem.*, 1963, **41**, 1027.
12. Y. Ogata (ed.), *Yukikasankabutu no Kagaku*. Nankodo, 1971.

Pergamon

0039-9140(94)00220-7

*Talanta*, Vol. 42, No. 1, pp. 83–88, 1995

0039-9140/95 $9.50 + 0.00

# DECONTAMINATION OF OIL-POLLUTED SOIL BY CLOUD POINT EXTRACTION

GÁBOR KOMÁROMY-HILLER and RAY VON WANDRUSZKA*
Department of Chemistry, University of Idaho, Moscow, ID 83844-2343, U.S.A.

(*Received* 31 *May* 1994. *Revised* 26 *July* 1994. *Accepted* 26 *July* 1994)

**Summary**—An extraction procedure based on cloud point phase separation of nonionic surfactants was used to remove oil contamination from soils. The detergent employed was Triton X-114, and its clouding behavior was monitored by means of a fluorescence probe. Changes in the $I_1/I_3$ ratio of pyrene indicated gradual dehydration of the detergent micelles upon heating. The rate of phase separation, and the volume and water content of the micellar phase were determined. In the practical clean-up, 85–98% of the oil present in the soil was found to enter the micellar phase of the separated washing liquid. A 15-min washing time with 3–5% detergent was found to be sufficient for this degree of contaminant removal from soil containing 0.009–0.017% oil, using a liquid:solid ratio of 5:2. The extraction efficiency decreased with increasing carbon content of the soil. The process holds promise for large-scale treatment of oil-polluted soils.

The solubility of most solutes in water increases with temperature. Aqueous solutions of nonionic surfactants, however, have a lower consolute temperature and become turbid when heated to their characteristic cloud point. At this and higher temperatures, phase separation takes place—the smaller detergent phase contains most of the surfactant and usually sinks to the bottom, while the more voluminous aqueous supernatant has a surfactant content approximately equal to the critical micelle concentration (CMC). Cloud points vary widely among detergents, generally in the range 20°C–90°C.

Clouding is believed to be due to an increase in micellar size and intermicellar attraction.[1-7] It can be explained by the dehydration of the "wet" outer layer of the micelles of nonionic detergents with increasing temperature.[8] The dielectric constant of water decreases rapidly with increasing temperature, making it a poorer solvent for the hydrophilic portion of the detergent molecule.[2] Clouding can be affected by the addition of other substances to the solution of nonionic surfactants. Small amounts of hydrophobic compounds lower the cloud point of detergents by penetrating the micellar interior and thus swelling the micelle. Excessive addition, however, may increase the cloud point.[6,9] Salts can promote or inhibit the dehydration process and therefore either decrease or increase the cloud point. This behavior is believed to be related to the salting-in and salting-out phenomena encountered in protein denaturation.[10,11]

Surfactant clouding has seen limited use in analytical separations.[5,12-19] In most instances, detergents with a polyoxyethylene hydrophilic group, such as the members of the PEO, Brij, and Triton series, were employed. Mostly extractions from aqueous solutions were investigated, but some attempts were made to extract PAHs from solid matrices.[18,19] The goal of the present investigation was to use the extraction capability of nonionic surfactant solutions to clean oil-contaminated soil, and to survey the possibility for large-scale treatment. The impetus for this work was provided by the widely recognized pollution problems presented by leaking underground fuel storage tanks.[20] Hazards and expense associated with large-scale organic solvent extraction, has provided the rationale for exploring this alternative procedure.

Surfactants suitable for decontamination of natural systems should be soluble in water; have a low cloud point (to reduce heating requirement and keep fuel costs low); solubilize pollutants (especially oil); form an easily separable phase; be readily disposable; be

*Author to whom correspondence should be addressed.

inexpensive; have low toxicity; and be biodegradable. So far no single detergent has met all these requirements. However, we have found that Triton X-114 (TX-114), a polyoxyethylene isooctyl-phenyl ether with an average polyoxyethylene chain of eight units, is a promising candidate. It is relatively inexpensive, has low toxicity, and its solutions have a cloud point around 20°C.[13-16] These features and its low volatility make it an attractive extraction medium.

The work described here addresses both the nature of the clouding process and its application to soil decontamination. Pyrene was used as a fluorescent probe to monitor the kinetics and extent of micellar dehydration as the temperature of detergent solutions was slowly increased. For decontamination trials, characterized soil was amended with old engine oil and then washed in a detergent solution. After draining the washing liquid from the soil, cloud point separation was carried out to isolate the contaminant in the detergent phase.

## EXPERIMENTAL

Pyrene (98%) was purchased from Sigma (St Louis, MO, U.S.A.), recrystallized twice from absolute ethanol, and sublimed onto a cold finger. Triton X-114 (Sigma) was used as received. Deionized water, treated with a 0.22-$\mu$m Millipore filter system to 13 M$\Omega$ cm resistivity, was used in all solutions. Pyrene solutions were made by adding an appropriate aliqot of a $5.0 \times 10^{-3}M$ ethanolic solution to a dry 100-ml volumetric flask. The solvent was evaporated, and the residue redissolved in 0.01$M$ TX-114. After sonicating for 3 hr, the flask was filled to the mark, making a $2.0 \times 10^{-6}M$ pyrene solution. It was left to stand overnight before use.

The water content of the micellar phase produced after clouding was determined by drying a known amount to constant weight at $85 \pm 2$°C. Fluorescence measurements were taken with a Perkin–Elmer MPF-66 fluorescence spectrophotometer equipped with a thermostated cell housing. The instrument produces corrected excitation and emission spectra. The solutions were equilibrated at each new temperature level for 10–15 min before measuring the fluorescence intensity. Each data point is the average of three parallel measurements.

Polarity changes in the micellar phase were monitored by means of a fluorescent probe. The variation of the ratio of the first and third emission peaks of the pyrene ($I_1/I_3$) with the polarity of its surroundings is well established.[21,22] It is large ($>1.4$) in polar, and small ($<1.2$) in nonpolar environments. The hydrophobic pyrene molecule is located inside the Triton X micelle, but in close proximity to the phase boundary with the hydrophilic portion.[23-25] We can, therefore, expect that the dehydration of the micelles will change the $I_1/I_3$ ratio of the fluorescent probe.

Two soils, surface collected (0–15 cm), air-dried, and sieved (2 mm), were used in the study: (i) Latahco silt loam, subgroup Argiaquic Xeric Argialboll, pH 6.1, with the following composition (g/kg): organic carbon 41.0; total carbon 41.0; total nitrogen 3.9; clay 159; sand 122; (ii) Portneuf silt loam, subgroup Durixerollic Calciorthid, pH 7.3, with the following composition (g/kg): total carbon 15.6; total nitrogen 1.7; clay 157; sand 48. Soils (10-g samples) were amended with old engine oil by diluting 0.20, 0.40, 1.00 ml aliquots of a stock solution (0.44111 g/ml oil in $CH_2Cl_2$) to 10 ml with methylene chloride, introducing the soil into this solution of the oil, and evaporating the solvent. In the washing procedure, the contaminated soil was agitated for 15 min with the detergent solution by means of a mechanical shaker. The washing liquid was then separated from the soil by centrifugation at 5000 rpm for 20 min, and the volume of the supernatant was adjusted to 25.0 ml with surfactant solution. Phase separation was carried out above the cloud point (at $50 \pm 1$°C), and the solution was kept at this temperature for 2 hr. The separated micellar phase was run off using a separatory funnel and adjusted to 5.0 or 10.0 ml. Standards were made from the stock solution by evaporating the solvent and redissolving the oil in the surfactant solution.

The oil contents of the washing liquid and the micellar phase were determined by thin-layer chromatography using silica plates and a Programmed Multiple Development instrument (Regis Chemical Company). In a typical separation run, eight to 10 development/heating cycles were used, operating in the linear mode. The usual procedure involved an initial development time of 90 sec, extending to 2.5 min in the last cycle, with each elution followed by a 30-sec drying period. The eluent was a 5:3 mixture of hexanes (Fisher Scientific, Class 1B) and absolute ethanol (Midwest Grain Products Co.). The separated oil spots of samples and standards

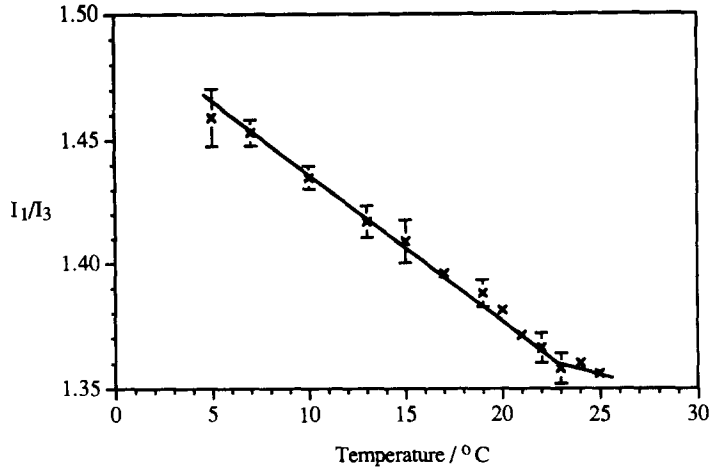


Fig. 1. $I_1/I_3$ ratio of $2.0 \times 10^{-6}M$ pyrene *vs.* temperature in $0.01M$ Triton X-114. Excitation wavelength 336 nm.

were quantified using a polychromatic TLC densitometer (Hoefer Scientific Laboratory). This method was found to give results superior to those obtained with other chromatographic methods, since soil components such as humic materials and mineral colloids did not interfere. All measurements were carried out in duplicate.

## RESULTS AND DISCUSSION

Dong and Winnik[22] have published the Py scale of solvent polarities, based on the ratio of the first and third vibronic band ratio of the pyrene emission ($I_1/I_3$). In our present work with $2.0 \times 10^{-6}M$ pyrene in $0.01M$ TX-114, this parameter showed the polarity of the probe environment at 5°C to be equal to that of 1,2-dichloroethane (1.46). An increase of the temperature to 25°C decreased this polarity to the value of 1,5-pentanediol (1.36). This indicates that the probe molecule, which is known to be located near the hydrated outer layer of the micelle,[23–25] experienced decreasing polarity with increasing temperature. As shown in Fig. 1, the $I_1/I_3$ decrease with temperature was relatively smooth and lacked abrupt changes, suggesting a gradual dehydration process leading up to the cloud point. A similar $I_1/I_3$ change was found when the system was cooled down, indicating that the dehydration and hydration of the polyoxyethylene chains is completely reversible and does not suffer a hysteresis effect.

After the cloud point had been reached, the rate of formation of a separate detergent phase (lower layer) was found to depend on the temperature and the detergent concentration in

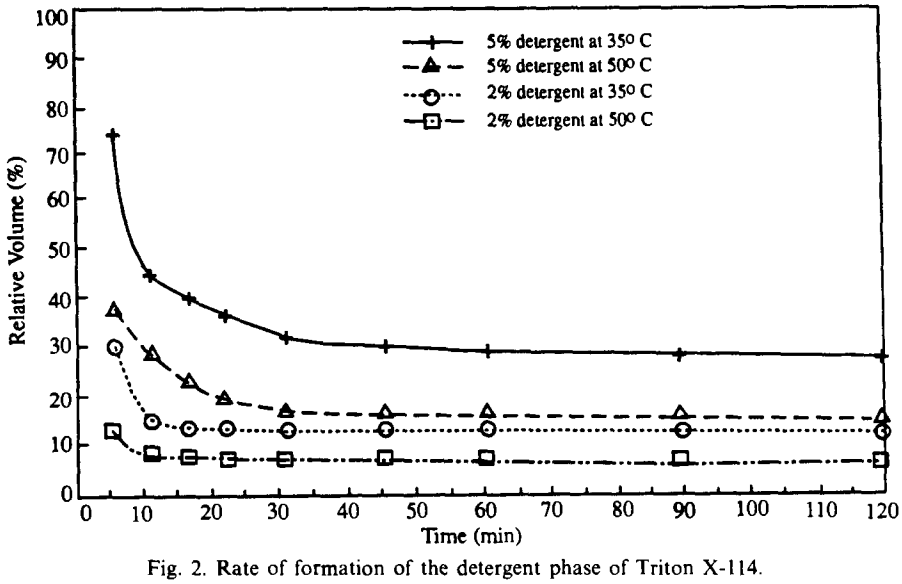


Fig. 2. Rate of formation of the detergent phase of Triton X-114.

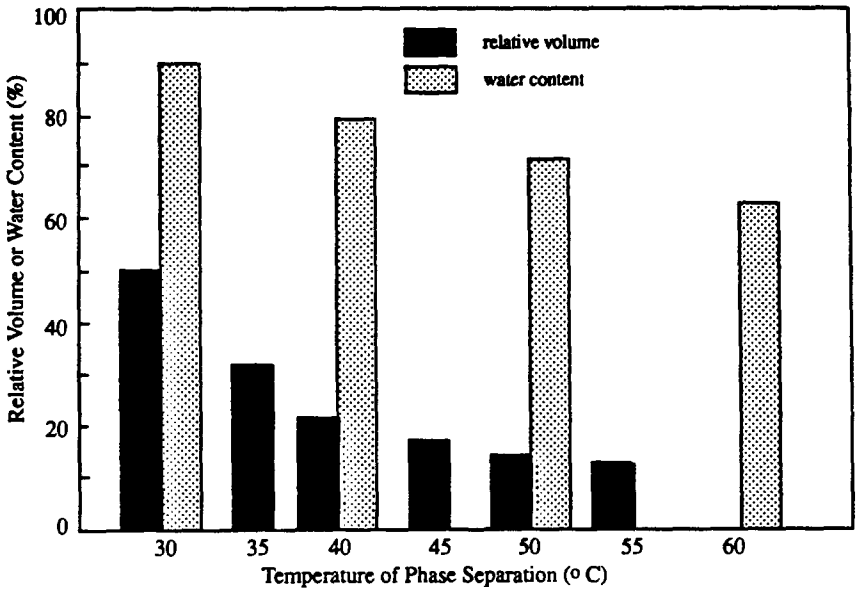


Fig. 3. Relative volume and water content of the detergent phase of 5% Triton X-114 separated at different temperatures. Separation time: 4 hr.

the original aqueous solution. Figure 2 shows the progression of this phase separation. When the detergent-rich layer first became distinct, it had a relatively large volume and water content. As it matured, it shrank through dehydration, reaching a final volume after about 20 min. This was observed by other authors,[13] and seems to be a general trend. The volume decreased with increasing temperature in an exponential fashion (Fig. 3), while the decrease in water content was linear. The water content of the detergent phase was found to be 64% when the phase separation was carried out at 60°C. For practical applications, a small detergent phase would be preferable (*vide infra*), since this minimizes disposal problems. It could be obtained by using low detergent concentrations and high temperatures. At this juncture, both the minimum detergent concentration and the maximum temperature need to be established empirically, depending on the oil concentration in the polluted soil and the admissible energy cost, respectively.

*Treatment of polluted soil*

The effect of agitation time on extraction efficiency of oil from soil is shown in Table 1. With samples of the size indicated, a washing time of approximately 15 min was required. Extending the washing time to 30 min did not significantly improve the extraction efficiency.

The extraction efficiency was found to depend on detergent concentration, washing liquid volume, and oil concentration in the soil (Table 2). As this concentration was increased, the efficiencies of both the extraction into the washing liquid, and the oil migration from the aqueous phase to the detergent phase, decreased. This effect can be ascribed to the detergency of the washing solution—sufficient micelles must be present to solubilize all the oil. To treat soil with high oil concentrations, higher detergent concentrations and/or washing solution volumes must be used (Table 2). With 8900 ppm oil, a 3% Triton X-114 concentration was found to be effective, but at higher oil contamination 5% Triton X-114 was required. With all oil concentrations used (8900–44,300 ppm), a 25 ml volume of washing liquid extracted significantly more oil from 10 g of soil than a 15 ml volume. This suggests that a liquid:solid ratio of 5:2 (w/w) is called for. The organic carbon content of polluted soil did not significantly affect the extraction of oil, but it did have a slightly detrimental effect on the migration of pollutant to the detergent phase (Table 3). Although it is known that surfactant

Table 1. Effect of washing time on extraction efficiency. Latahco soil (10 g) contaminated with 17.7 ppt old engine oil, washed with 25 ml of 3% Triton X-114

| Agitation time (*min*) | Oil extracted into washing liquid (%) |
|---|---|
| 5 | 73 |
| 15 | 82 |
| 30 | 84 |

Table 2. Extraction efficiency of oil. Portneuf soil (10 g) contaminated with old engine oil, washed with Triton X-114 for 15 min

| Volume of washing liquid (*ml*) | Triton X-114 concentration (%) | Oil in soil (*ppt*) | Oil extracted into washing liquid (%) | Oil extracted into detergent phase (%) |
|---|---|---|---|---|
| 25 | 3 | 8.9 | 104 | 105 |
| | | 17.7 | 86 | 106 |
| | | 44.3 | 66 | 86 |
| | 5 | 8.9 | 91 | 100 |
| | | 17.7 | 91 | 95 |
| | | 44.3 | 74 | 76 |
| 15 | 3 | 8.9 | 89 | 50 |
| | | 17.7 | 80 | 42 |
| | 5 | 8.9 | 79 | 88 |

Table 3. Effect of organic carbon content on extraction efficiency of oil. Soil (10 g) contaminated with old engine oil, washed for 15 min with Triton X-114

| Organic carbon (*g/kg*) | TX-114 concentration (%) | Oil in soil (*ppt*) | Oil extracted into washing liquid (%) | Oil extracted into detergent phase (%) |
|---|---|---|---|---|
| ≤15.6 | 3 | 8.9 | 104 | 105 |
| | | 17.7 | 86 | 106 |
| | 5 | 8.9 | 91 | 100 |
| | | 17.7 | 91 | 95 |
| 41.0 | 3 | 8.9 | 102 | 104 |
| | | 17.7 | 82 | 77 |
| | 5 | 8.9 | 93 | 82 |

will be lost due to adsorption to the soil,[19] no attempt was made to quantify this factor in our extraction.

A qualitative study was carried out with uncharacterized soil from a local tanker transfer site which had been subjected to oil spillage for about 40 years. The soil contained approximately 5% (w/w) of weathered oil and showed evidence of extensive pollution by polymerized and oxidized breakdown products. It appeared dark in color, heavily clumped, and of characteristic odor. Treatment with 5% detergent as described above removed these symptoms. The resulting soil was free-flowing, light in colour, and without odor. The age and complexity of the samples precluded quantitative determination of the decontamination efficiency.

## CONCLUSIONS

Cloud point extraction offers an interesting possibility for decontamination of oil-polluted soil. The process is not, as may be expected, unduly impeded by co-extraction of organic matter present in the soil. Likewise, colloidal materials do not appear to constitute a serious problem. The possibility for upscaling to bulk dimensions in which tons of soil can be treated is, therefore, promising. Under no circumstances can a process of this nature be "cheap", but the aqueous character of the washing liquid should make it considerably less expensive than a comparable organic extraction. The low volatility, toxicity, and high biodegradability[26] of the materials are also noted advantages. The detergent phase separated in the clouding process is combustible, despite its relatively high water content. This makes disposal by incineration possible, a process that can be facilitated by the addition of small amounts of low grade ethanol or acetone.[12] The aqueous bulk left after phase separation lends itself to re-use after addition of more detergent. The application of the procedure to other soils and to large-scale pollution remediation is presently under investigation in this laboratory.

*Acknowledgement*—The authors wish to thank Dr M. J. Morra of the University of Idaho Soil Science Division for the characterization of the soils.

## REFERENCES


1. E. D. Siebert and C. M. Knobler, *Phys. Rev. Lett.*, 1985, **54,** 819.
2. P. Nilsson, H. Wennerström and B. Lindman, *J. Phys. Chem.*, 1983, **87,** 1377.
3. B. S. Valaulikar and C. Manohar, *J. Colloid Interface Sci.*, 1985, **108,** 403.
4. M. Corti, C. Minero and V. Degiorgio, *J. Phys. Chem.*, 1984, **88,** 309.
5. T. Saitoh and W. L. Hinze, *Anal. Chem.*, 1991, **63,** 2520.
6. R. Aveyard, B. P. Binks, S. Clark and P. D. I. Fletcher, *J. Chem. Tech. Biotech.*, 1990, **48,** 161.
7. W. Binana-Limbelé and R. Zana, *J. Colloid Interface Sci.*, 1988, **121,** 81.
8. E. Florin, R. Kjellander and J. C. Eriksson, *J. Chem. Soc., Faraday Trans*, 1984, **80,** 2889.
9. H. Saito and K. Shinoda, *J. Colloid Interface Sci.*, 1967, **24,** 10.
10. H. A. Schott, E. Royce and S. K. Han, *J. Colloid Interface Sci.*, 1984, **98,** 196.
11. S. K. Han, S. M. Lee and H. Schott, *J. Colloid Interface Sci.*, 1988, **126,** 393.
12. H. Watanabe and H. Tanaka, *Talanta*, 1978, **25,** 585.
13. B. R. Ganong and J. P. Delmore, *Anal. Biochem.*, 1991, **193,** 35.
14. J. G. Pryde, *Trends Biochem. Sci.*, 1986, **11,** 160.
15. C. J. Bordier, *Biol. Chem.*, 1981, **256,** 1604.
16. C. G. Pinto, J. L. P. Pavón and B. M. Cordero, *Anal Chem.*, 1992, **64,** 2334.
17. W. L. Hinze and E. Pramuaro, *Crit. Rev. Anal. Chem.*, 1993, **24,** 133.
18. C. G. Pinto, J. L. P. Pavón and B. M. Cordero, *Anal. Chem.*, 1994, **66,** 874.
19. A. Bockelen and R. Niessner, *Fresenius J. Anal. Chem.*, 1993, **346,** 435.
20. G. M. Cole, *Assessment and Remediation of Petroleum Contaminated Sites*. Lewis, Boca Raton, FL, 1994.
21. K. Kalyanasundaram and J. K. Thomas, *J. Am. Chem. Soc.*, 1977, **99,** 2039.
22. D. C. Dong and M. A. Winnik, *Can. J. Chem.*, 1984, **62,** 2560.
23. N. J. Turro and P. Kuo, *Langmuir*, 1985, **1,** 170.
24. T. T. Ndou and R. von Wandruszka, *Anal. Lett.*, 1989, **22,** 1997.
25. C. P. Loran and R. von Wandruszka, *Anal. Chim. Acta*, 1992, **258,** 335.
26. B. Baleux and P. Caumette, *Revue de l'Institute Pasteur de Lyon*, 1974, **7,** 279.

Pergamon

0039-9140(94)00221-5

*Talanta*, Vol. 42, No. 1, pp. 89–92, 1995

0039-9140/95 $9.50 + 0.00

# REVERSED-PHASE HPLC DETERMINATION OF Co(II), Ni(II) AND Fe(III) AS THEIR 2-(2-THIAZOLYLAZO)-5-DIMETHYLAMINOPHENOL CHELATES

LI LING YING,* GUI MING-DE and ZHAO YA-QIU
Department of Chemistry, Nankai University, Tianjin, 300071, China

(*Received* 13 *July* 1992. *Revised* 11 *July* 1994. *Accepted* 22 *July* 1994)

**Summary**—The optimum chromatographic separation conditions for Co(II), Ni(II), and Fe(III) chelates with 2-(2-thiazolylazo)-5-dimethylaminophenol (TAM) were investigated. The compositions of chelates were also determined by the HPLC method and thus the possible structure of chelates was given. A precolumn derivatization method was used, followed by separation on an octyl-bonded silica stationary phase with a methanol–tetrahydrofuran–water (40:9:51, v/v/v) mobile phase containing pH 5.8 acetate buffer and $1 \times 10^{-4}M$ TAM. The detection limits of Co(II), Ni(II), and Fe(III) at 560 nm are 0.03, 0.02 and 0.1 ng ($S/N = 2$), respectively. They can be determined by means of the proposed method without interference from other common metal ions and have been determined in five standard alloys with satisfactory results.

The development of HPLC for inorganic compounds has increased rapidly in recent years, because it is not only a sensitive but also a selective and rapid method for separation and determination of metal ions. Many organic chelating reagents have been used widely in HPLC, such as PAN,[1] PAR,[2] dithiocarbamate,[3] $\beta$-diketones,[4] dithizone,[5] 8-hydroxy quinoline,[6] porphyrin,[7] *etc.* However, the use of thiazolylazo reagents is seldom reported in HPLC separations.[8]

2-(2-thiazolylazo)-5-Dimethylaminophenal (TAM) is one of the sensitive reagents used in the spectrophotometric determination of metal ions,[9–12] but its selectivity is very poor. If its chelates can be separated and detected spectrophotometrically by means of HPLC, the reagent would give a highly sensitive and selective HPLC method for the simultaneous determination of some metal ions. We described here the first use of TAM as the chelating reagent in HPLC, and successfully separate the TAM chelates of Co(II), Ni(II), and Fe(III). Among foreign metal ions, only Cu(II) interferes with the determination of Ni(II). By passing $H_2S$ in $0.3M$ HCl to precipitate Cu(II) as CuS, the interference can be avoided.

This method compares to other reverse-phase HPLC by precolum chelating with the similar reagent PAR[2] or 5-Br-PADAP[14] for the separation and determination of heavy metals. This approach has the advantages of high sensitivity (*i.e.* low detection limits), good resolution in a short analytical time and good column efficiency.

## EXPERIMENTAL

### *Apparatus*

LC-4A HPLC equipment (Shimadzu, Japan) was used with a Zorbax-C8 column (5 $\mu$m particle, 150 × 4.6 mm) and an SPD-1 UV-VIS detector. A R-112M registor, C-RIB data processing system, UV-240 type UV-VIS spectrophotometer (Shimadzu, Japan) were used. Stock solutions of Co(II), Ni(II) and Fe(III) in $1M$ $HNO_3$ were prepared from their pure metals (99.99%). A $1 \times 10^{-3}M$ TAM (ICN Pharmaceuticals, U.S.A.) solution was prepared in absolute methanol. The mobile phase was a 40:9:51 (v/v/v methanol–tetrahydrofuran–water ($CH_3OH$–THF–$H_2O$) mixture containing $1 \times 10^{-4}M$ TAM and $0.05M$ acetate buffer (pH 5.8). All reagents used were of A.R. grade. Double-distilled water was used for all solution preparation.

*Author to whom correspondence should be addressed.

*Procedure*

A 3.0 ml portion of 0.05*M* acetate buffer (pH 5.8) and 3.0 ml of $1 \times 10^{-3}M$ TAM solution were mixed with a known volume of the sample solution containing Co(II), Ni(II) and Fe(III), and the mixture was diluted to 10.0 ml with absolute methanol, allowed to stand for 20 min and filtered through a 0.45-$\mu$m filter membrane. For the HPLC analysis, the Zorbax-C8 column was first equilibrated with the mobile phase. A 20-$\mu$l aliquot of the prepared test solution was injected onto the column and the complexes were eluted at a flow-rate of 1.0 ml/min. The peak areas were measured at the detection wavelength of 560 nm.

## RESULTS AND DISCUSSION

*Precolumn derivatization conditions and detection wavelength*

We found by experiment that Co(II), Ni(II) and Fe(III) can be complexed with TAM at pH 4.8–6.1 in 0.05*M* acetate buffer. AT room temperature, all three complexes form rapidly and are stable for 24 hr. The concentration of TAM should be greater than $4.5 \times 10^{-4}M$ for a solution containing 10 $\mu$g/10 ml of each of Co(II), Ni(II) and Fe(III). The wavelengths of the absorption maxma of the CO, Ni and Fe complexes range from 558 to 570 nm (Co 570, Ni 558 and Fe 560 nm). A wavelength of 560 nm was chosen for the determination.

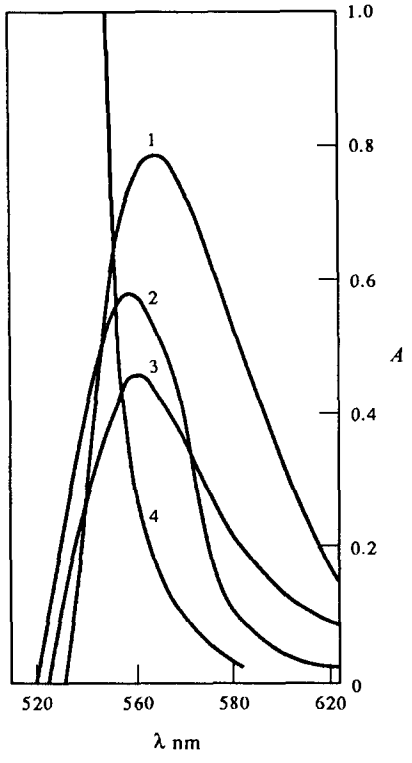


Fig. 1. Absorption spectra: (1) 5.9 $\mu$g/10 ml Co(II) with $3 \times 10^{-4}M$ TAM; (2) 5.8 $\mu$g/10 ml Ni(II) with $3 \times 10^{-4}M$ TAM; (3) 5.6 $\mu$g/10 ml Fe(III) with $3 \times 10^{-4}M$ TAM; (4) $3 \times 10^{-4}M$ TAM. Spectra 1–3 measured *vs.* reagent blank, spectrum 4 measured *vs.* water blank.

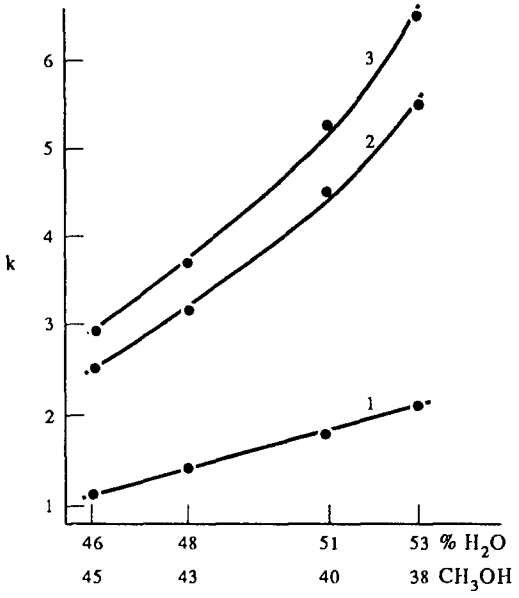


Fig. 2. Effect of the ratio of methanol to water on $K'$ (THF was fixed at 9%). (1) Co–TAM, (2) Ni–TAM, (3) Fe–TAM, pH 5.8 buffer, $1 \times 10^{-4}M$ TAM, concentration of Co(II), Ni(II) and Fe(III) = 10 $\mu$g/10 ml.

*Selection of mobile phase*

The effects of methanol–water, tetrahydrofuran–water and acetonitrile–water used as the mobile phase on the separation of Co, Ni and Fe were investigated. It was found that $CH_3OH$–THF–$H_2O$ was the most suitable mobile phase. To prevent the three complexes from decomposing on the column, the mobile phase had to contain 0.05*M* acetate buffer (pH 5.8) and at least $1 \times 10^{-4}M$ TAM ($1–2 \times 10^{-4}M$ was suitable), otherwise no peak emerged. If there was no excess of TAM in the mobile phase during the elution process, the complex formation equilibrium would shift to the left, and complexes with low stability would decompose. In order to determine the optimum ratio of the three components in the elution for separation, the composition of THF was fixed at 9% and the ratio of methanol to water was varied as shown in Fig. 2. When the ratio of methanol to water was 40:51, *i.e.* the ratio of $CH_3OH$:THF:$H_2O$ was 40:9:51, Co, Ni and Fe complexes were well separated in the least time.

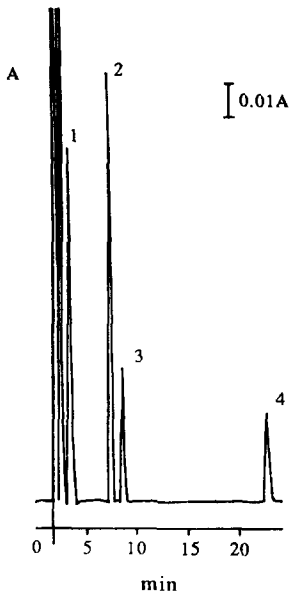


Fig. 3. Separation of Co, Ni and Fe TAM complexes by HPLC. $CH_3OH:THF:H_2O = 40:9:51$ (v/v/v), 0.05*M* pH 5.8 buffer, $1 \times 10^{-4}M$ TAM, concentration of Co, Ni and Fe = 10 μg/10 ml. (1) Co–TAM, (2) Ni–TAM, (3) Fe–TAM, (4) TAM.

*Separation of the* Co, Ni *and* Fe *complexes*

This procedure gave excellent resolution with sharp and symmetrical peaks of the Co, Ni and Fe complexes as shown in Fig. 3. The retention times ($t_R$) were 3.3, 7.3, 8.5, and 22.5 min for TAM, respectively. Linear calibration plots were obtained for Co, Ni and Fe in the ranges of 0–2.0, 0–2.0 and 0–4.0 μg/ml, respectively. Their linear regression equations were as follows:

$$y_{Co} = 0.0946x - 0.004$$

$$y_{Ni} = 0.1180x - 0.0038$$

$$y_{Fe} = 0.0320x - 0.0007.$$

Their regression coefficients were 0.9989, 0.9990 and 0.9995, respectively. The detection limits were 0.03, 0.02 and 0.1 ng ($S/N = 2$) for Co(II), Ni(II) Fe(III), respectively.

Table 1. Effect of foreign ions

| Foreign ions added | Amount of foreign ions tolerated (μg) |
|---|---|
| Al(III), Ca(II), Cd(II), Cr(VI), Ga(III), Hg(II), Mn(II), Pb(II), V(V), W(VI), Ti(IV), Zn(II) | 200 |
| Fe(II), Pd(II) | 100 |
| Cu(II) | 100 [for Co(II)]<br>20 [for Ni(II)]<br>100 [for Fe(III)] |

The effective column efficiency expressed by the number of theoretical plates *N* was calculated for each complex. Using an unretained $KNO_3$ solution, we found that $t_0 = 1.32$ min. According to the formula $N = 5.54 \times ((t_R - t_0)/W_{1/2})^2$ and the chart rate = 2 mm/min, we obtained:

$$N_{eff} = 1595 \text{ for Co–TAM}$$

$$N_{eff} = 17576 \text{ for Ni–TAM}$$

$$N_{eff} = 21309 \text{ for Fe–TAM.}$$

*Effect of foreign ions*

The potential interference of numerous ions was examined by the determination of 10 μg of Co, Ni or Fe in the presence of each foreign ion. The amounts (μg) found to be tolerable (±5% error) as given in Table 1. In fact, all of the foreign ions in Table 1 except Cu(II) did not give a peak at 560 nm, but they consumed the TAM reagent. Their interference can thus be prevented by using excess TAM. Cu(II) interference can be eliminated by passing $H_2S$ into the test solution in advance. Thus only one ion actually interferes with the separation, *i.e.* Cu(II). The $t_R$ of the Cu(II)–TAM complex was 5.6 min, so that the peak of the Cu complex overlaps the peak of the Ni complex.

The use of HPLC to determine the composition of metal complexes has been reported.[13] First, the different TAM peak areas were obtained from different concentrations of TAM

Table 2. Determination of compositions of Co, Ni, and Fe TAM complexes

| Metal ions | Moles of metal ions | Moles of TAM consumed | Mole ratio of metal ion to TAM | Average of mole ratio |
|---|---|---|---|---|
| Co(II) | $3.4 \times 10^{-8}$ | $6.8 \times 10^{-8}$ | 1:2.0 | 1:2 |
| | $3.4 \times 10^{-8}$ | $6.8 \times 10^{-8}$ | 1:2.0 | |
| Ni(II) | $3.4 \times 10^{-8}$ | $6.8 \times 10^{-8}$ | 1:2.0 | 1:2 |
| | $3.4 \times 10^{-8}$ | $6.8 \times 10^{-8}$ | 1:2.0 | |
| Fe(III) | $4.0 \times 10^{-8}$ | $7.9 \times 10^{-8}$ | 1:1.98 | 1:2 |
| | $4.0 \times 10^{-8}$ | $8.0 \times 10^{-8}$ | 1:2.0 | |

Table 3. Results of alloy sample analyses

| Samples | Alloy (μg/ml) | | | Added (μg/ml) | | | Found (μg), $n = 3$ | | | Total recovery(%) | | |
|---|---|---|---|---|---|---|---|---|---|---|---|---|
| | Co | Ni | Fe | Co | Ni | Fe | Co | Ni | Fe | Co | Ni | Fe |
| 4J32 | 0.10 | 1.00 | 1.85 | 1.00 | — | — | 1.09 | 1.00 | 1.86 | 99.1 | 100.0 | 100.5 |
| 224 | — | 0.07 | 1.00 | 1.00 | 1.00 | — | 1.01 | 1.08 | 1.02 | 101.0 | 100.9 | 102.0 |
| 167-2 | — | — | 1.00 | 1.00 | 1.00 | — | 1.00 | 0.99 | 0.98 | 100.0 | 99.0 | 98.0 |
| BH1311-1A | — | — | 1.00 | 1.00 | 1.00 | — | 1.01 | 1.01 | 1.00 | 101.0 | 101.0 | 100.0 |
| BY1912-1 | — | 1.00 | 0.17 | 1.00 | — | 1.00 | 1.00 | 0.98 | 1.16 | 100.0 | 98.0 | 99.1 |

reagent under chromatographic conditions and a plot of TAM peak area *vs.* the concentration of TAM was made. Then a fixed amount of Co(II) or Ni(II) or Fe(III) was mixed with excess amounts of TAM solution, the peak area of the TAM which did not react with Co(II) was measured, and converted to its corresponding concentration from the calibration plot. From these measurements the number of moles of TAM consumed by Co(II) and the mole ratio of Co(II) to TAM could be calculated as shown in Table 2.

The mole ratios of metal ions to TAM in the three complexes were determinated spectrophotometrically by the Job method and the mole ratio method. Results were entirely coincident with those from the above HPLC method.

According to the mole ratios of Co, Ni and Fe to TAM, Co(II) and Ni(II) combine TAM to form a neutral complex, and Fe(III) forms a cation complex first, which then associates with $Ac^-$ to form a neutral association complex. The structures of the three complexes were assumed as follows:

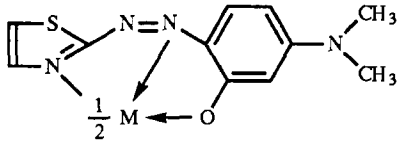


M = Co, Ni

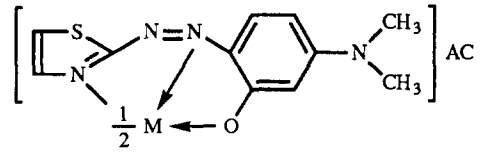


M = Fe

*Analyses of some standard samples*

All the alloy samples used have standard values. They were prepared by the China Steel and Iron Research Institute.

Alloy steel 4j32 (3.32% Co, 33.66% Ni, 0.39% Cu, 62.40% Fe, *etc.*), Cr–Ni–Mn steel 224 (0.031% Cu, 4.86% Ni, 71.40% Fe, etc.), alloy steel 167-2 (0.077% Ni, 0.035% Cu, 99.74% Fe, *etc.*), and low alloy steel BH1311-1A (0.045% Ni, 0.14% Cu, 97.3% Fe, *etc.*) were separately dissolved in 5% $H_2SO_4$, oxidized with 37.5% $HNO_3$ and the excess of $HNO_3$ removed by heating. The solution was transferred to a 100 ml volumetric flask and diluted to the mark with water.

Al–Cu alloy BY1912-1 (57.66% Cu, 3.46% Al, 2.50% Ni, 0.43% Fe, *etc.*) was dissolved in aqua regia, and $HNO_3$ removed by evaporation. The solution was transferred to a 250 ml volumetric flask and diluted to the mark with water. An aliquot of solution was taken to remove Cu(II) by precipitating with $H_2S$ in 0.3*M* HCl, and the precipitate was filtered.

The test solution prepared, following the experimental procedure, were used to determine Co(II), Ni(II), and Fe(III), respectively. Results are shown in Table 3.

## REFERENCES

1. Yu. S. Nikitin, N. B. Morozova, S. N. Lanin, T. A. Bolshova, V. M. Ivanov and E. M. Basova, *Talanta*, 1987, **34**, 223.
2. D. Roston, *Anal. Chem.*, 1984, **56**, 241.
3. A. M. Bond, R. W. Knight, J. B. Beust, D. J. Tucker and G. G. Wallace, *Anal. Chim. Acta*. 1986, **182**, 47.
4. J. F. K. Huber, J. C. Kraak and H. Veening, *Anal. Chem.* 1972, **44**, 1554.
5. M. Lohmiiller, P. Heizmann and K. Ballschmiter, *J. Chromatogr.* 1977, **137**, 165.
6. B. Wenclawiak, *Fresenius' Z.Anal. Chem.*, 1981, **308**, 120.
7. M. Kobayachi, K. Saitoh and N. Susuki, *Chromatographia*. 1985, **20**, 72.
8. Q. Liu, H. Zhang and J. Cheng, *Talanta* 1991, **38**, 669.
9. C. Tsurumi and K. Furuya, *Bunseki Kagaku*, 1975, **80**, 566.
10. J. Minczewki and K. Kasiura, *Chem. Anal. Warsaw*, 1965, **10**, 719.
11. H. Ishii and H. Watanabe, *Bunseki Kagaku*, 1977, **26**, 86.
12. C. Tsurumi and K. Furuya, *Bunseki Kagaku*, 1977, **26**, 149.
13. J. Huang and W. Liu, *Fenxi Huaxue*, 1989, **17**, 55.
14. X. Zhang and C. Lin, *Fenxi Huaxue*, 1988, **16**, 122.

Pergamon

0039-9140(94)00222-3

*Talanta*, Vol. 42, No. 1, pp. 93–100, 1995

0039-9140/95 $9.50 + 0.00

# SYNERGIC SOLVENT EXTRACTION STUDIES OF GADOLINIUM USING A COMBINATION OF THE DI(2-ETHYLHEXYL)PHOSPHORIC ACID AND THREE ADDUCTANTS INTO KEROSINE/CHLOROFORM

YOSHITAKA MASUDA* and MD. HASAN ZAHIR

Division of Science of Materials, The Graduate School of Science and Technology, Kobe University, Rokkodai Nada-ku, Kobe 657, Japan

(*Received* 2 *May* 1994. *Revised* 2 *August* 1994. *Accepted* 4 *August* 1994)

**Summary**—The equilibrium extraction behaviour of Gd(III) using a chloroform/kerosine solution containing di(2-ethylhexyl)phosphoric acid (HDEHP), either alone or combined with one of three adductants, 1,10-phenanthroline monohydrate (phen), α,α′-dipyridyl(2,2′-bipyridine) (bipy) or trioctylphosphine oxide (TOPO) is described. The enhancement of the extraction by addition of such neutral adductants is explained in terms of adduct formation of the metal chelate in the organic phase. Among the three synergistic mixtures, 1,10-phenanthroline is the most promising for the extraction of the last member of light lanthanoids, gadolinium. Gadolinium ions are found to be extracted in the absence of phen, bipy or TOPO; the species was $M(HA_2)_3$ but $M(HA_2)_3(phen)_2$ was found when phen was added and $M(HA_2)_3(bipy)$, $M(HA_2)_3(bipy)_2$ was found when bipy was added and $M(HA_2)_3(TOPO)$ was found when TOPO was added. The compositions of the extracted species are obtained from the slope analysis method. $pH_{1/2}$ values were also obtained. The stoichiometry, extraction constants and stability constants of these systems were determined. Synergistic extraction can be carried out at lower pH.

Solvent extraction undoubtedly represents the best of all the various separation techniques because of its simplicity, rapidity, applicability to various concentration ranges and purity of products.[1] Moreover, in synergistic system the extracting power of the mixture exceeds the sum of the extracting powers of its components. This phenomenon of greatly enhanced extraction or synergism owing to a mixture of extractants has attracted considerable attention in recent years. HDEHP is well-known as a powerful extractant, particularly for the 'hard' metal ions such as lanthanides and alkaline earth metals. Numerous studies of its extractant properties with various metal ions are reported in the literature.[2–4]

Handley examined HDEHPDT [di-(2-ethylhexyl)phosphorodithioic acid] as a metal extractant. According to his results, americium and europium could be extracted into dodecane fairly well with HDEHPDT.[5,6] That a 'hard' metal such as $Eu^{3+}$ can be extracted with a 'soft' ligand such as (DEHPDT), was reminiscent of our findings that a nitrogen ligand such as phen seemed to bond with lanthanide chelates at least as readily as with the hydrated lanthanide ions. TOPO is a monodentate phosphine oxide ligand whose basicity is strong enough to form stable adducts with metal chelates.[7] Recently, Komatsu and Freiser have reported extensive investigations on solvent extraction of tervalent lanthanide (Ln) metal ions with mixed ligands. They described the adduct formation of La(III), Pr(III), Eu(III), Ho(III) and Yb(III) with bis(2,4,4-trimethylpentyl) phosphinic acid (HBTMPP) and TOPO, octyl(phenyl)-*N*,*N*-diisosbutylcarbamoylmethyl phosphine oxide (CMPO) or methylenebis(diphenylphosphine) oxide (MBDPO) into chloroform.[8] The solvent extraction of several divalent metal ions with benzoyltrifluoroacetone into chloroform in the presence of tetrabutylammonium and 2-thenoyltrifluoroacetone ions has been studied in detail.[9] In this paper it was observed that the number of the auxiliary reagent molecules ($n$) that attach to the extracted species in time of adduct formation could be evaluated by a $\log D/D_0$ *vs.* log[adductant] plot analysis.

*Author to whom correspondence should be addressed.

Suzuki *et al.*[10] also examined the number of the auxiliary reagent molecules ($n$) by the above slope analysis.

In the present work it was observed that the synergic effect in extraction increases with increasing basicity of the adduct formation, *i.e.* in the order phen > bipy > TOPO. Oxygen bases such as TOPO, a monodentate phosphine oxide ligand are not strongly effective adductants for metal chelates extracted at the low pH ranges, being characteristic of the cation extractants. Instead, the nitrogen bases 1,10-phenanthroline, which have high proton affinity, are appropriate auxiliary ligands. At low pH ranges one molecule of bipy is included in the extracted species. This work gives fundamental information about the adduct formation affinity and enhancement of extraction rate. The role of diluent was also observed for the evaluation of the association constant.

## EXPERIMENTAL

### *Apparatus*

Extraction was done in a Taiyo M incubator at 25 ± 0.1°C. Ultraviolet and visible absorption spectra were measured with a Shimadzu self-recording spectrophotometer (model 240-UV-Vis) with 10 mm optical path glass cells. The pH of an aqueous phase was measured with a Hitachi Horiba M-7II pH-meter. A Kokusan H-200 centrifuge was used for rapid and complete separation of the phases.

### *Materials*

A standard solution of gadolinium nitrate $1 \times 10^{-2}M$ was prepared by dissolution of a suitable amount of the pure oxide (99.99%) (Santoku Chemicals Ltd) in a small volume of concentrated nitric acid, followed by dilution with distilled water. The solution was then heated in order to remove any excess acid. The solution was diluted to 100 ml with distilled water and the concentration, determined as $1 \times 10^{-3}M$. The solution was standardized complexometrically at pH 5.1–5.6 with Xylenol Orange as the indicator.[11] The prepared solution was then stored in a polyethylene bottle.

### *Preparation of di(2-ethylhexyl)phosphoric acid stock solution*

For the preparation of the stock solution of HDEHP, 348 $cm^3$ of chemically pure HDEHP (DP-8R Daihachi Chemicals Ltd) was taken in a clean 1 $dm^3$ volumetric flask and was made up to the mark with chloroform/kerosine so that the solution was 1$M$. This solution was washed three times with 500 $cm^3$ of 6$M$ HCl and three times with 500 $cm^3$ distilled water, after which the solution was left overnight. Since water is slightly soluble in HDEHP, the final HDEHP contains a small amount (1–2%) of water which may be removed using a rotating evaporator at 50°C and 15 mm Hg pressure. A 0.01$M$ phen, bipy, TOPO solution was prepared by dissolving 1.9823 g 1,10-phenanthroline monohydrate, 0.3867 g trioctyl phosphin oxide and 0.156 g 2,2′-bipyridine (Nakarai Chemicals Ltd) in chloroform and diluting it to 100 ml with the same solvent. A 0.001$M$ arsenazoIII solution was prepared by dissolving 0.0776 g of the reagent (Dojin Chemicals Ltd) in 100 ml of distilled water. This solution was freshly prepared each week. Chloroform was used after distillation. All other chemicals used were of analytical grade.

### *pH determination*

The pH was adjusted with hydrochloric acid or sodium hydroxide solution. After equilibration of the two phases the pH was measured precisely in the aqueous solution with a glass electrode pH-meter. Before taking each reading, the pH-meter was standardized by using standard buffers having pH nearly equal to the test solutions. After standardization of the pH-meter, the electrodes were rinsed with distilled water, the residual water present on the surfaces of the electrode was removed by a filter paper. It was then placed in the test solution and kept in such a way for at least 2 min before taking the reading. Higher pH values could not be used as the equilibration led to turbid aqueous solutions probably owing to microemulsion formation that did not clear up even after centrifugation or on prolonged standing. The pH of the aqueous phase was adjusted by the addition of succinic buffer ($2 \times 10^{-3}M$) in conjunction with HCl for lower pH values.

## RESULTS AND DISCUSSION

### *Dependence of extraction on shaking time to reach equilibrium*

The variation of extraction with shaking time was studied at pH 3.5. The data obtained from the shaking time study of gadolinium(III) is plotted in Fig. 1. Figure 1 shows that more than 7 min is required to reach the equilibrium for the Gd(III) under the experimental conditions

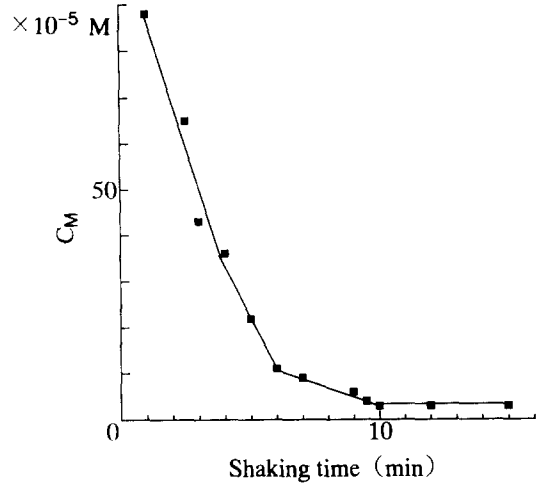


Fig. 1. Determination of the time required to reach equilibrium. Aqueous phase: $[Gd^{3+}] = 1 \times 10^{-4}M$; succinic acid $2 \times 10^{-3}M$. Organic phase: $[(HX)_2] = 2 \times 10^{-3}M$ and $2 \times 10^{-3}M$ phen into $CHCl_3$. Concentration of metal ions in the aqueous phase after extraction as ordinates have been plotted graphically.

stated, at which the $C_M$ *vs.* time plot becomes horizontal, indicating there will be no transfer of Gd(III) from the aqueous phase to organic phase on further shaking.

*Liquid–liquid extraction of metal ions*

The distribution experiments were done at room temperature. An aliquot (10 ml) of the aqueous solution containing the metal ion $1 \times 10^{-4}M$ was taken in a stoppered 50 ml glass tube and that of succinic acid as buffer was $2.00 \times 10^{-3}M$. The ionic strength of the aqueous phase was controlled at $0.1M$ with sodium perchlorate and the extraction was made with HDEHP in the absence of adductants. The extraction of gadolinium–HDEHP alone and with adductants was done in the absence of perchlorate. After the addition of 10 ml of synergistic mixture containing the extractant solution $2 \times 10^{-3}M$ and neutral adductant solution $2 \times 10^{-3}M$ the mixture was shaken for 10 min at 200 strokes/min at $25 \pm 0.1$°C, which was sufficient for equilibration. The mixture was then centrifuged at 2000 r.p.m. for 5 min, the pH of the aqueous phase was measured. The metal content in the aqueous phase was determined spectrophotometrically by the arsenazo III method[12] as was the concentration of gadolinium in the organic phase following back extraction into hydrochloric acid. The concentration of metal ion in the organic phase was determined after back extraction into $6M$ hydrochloric acid for 30 min, 5 ml of strip liquor thus obtained was transferred to a separatory funnel and washed once with 5 ml of pure chloroform to remove the free ligand completely, then the strip liquor was allowed to evaporate. The residue was decomposed and diluted after that the pH was adjusted with 2.5. The solution was transferred into a 10 ml volumetric flask, 0.5 ml of the arsenazo III solution was added and made up to the mark with distilled water. The absorbance was measured at 650 nm. Neither the extractant nor it's complexes in chloroform showed appreciable absorption in the visible region and hence arsenazo III was used in the dual role of calorimetric reagent and scavenger for gadolinium.

*Stripping test*

Stripping tests were carried out with various mineral acids, *viz.* hydrochloric acid, sulphuric acid and nitric acid. The relations between acid concentration and recovery(%) of metal ion are listed in Table 1. These results show that hydrochloric acid with concentrations higher than $4M$ was found to be effective for stripping, while sulphuric acid did not appear to be suitable. Hydrochloric acid was suitable for almost complete stripping.

*Effect of HDEHP concentration*

The effect of HDEHP concentration on the absorbance was studied. This experiment was done in the presence of TOPO, bipy or phen $2 \times 10^{-3}M$, respectively. The effect of neutral adductant concentration on the extraction was also studied. The recommended amount is $2 \times 10^{-3}M$ as shown in Fig. 2.

*Effect of pH on gadolinium(III) extraction systems containing HDEHP and adductant into chloroform/kerosine*

The effective extraction of gadolinium with HDEHP in the presence of phen, bipy or TOPO occurs at the pH of the aqueous phase ranging

Table 1. Relation between the acid concentration and recovery percentage of metal

| Acid | Concentration, $M$ | Recovery percentage |
|---|---|---|
| HCl | 2 | 90 |
| | 3 | 93 |
| | 5 | 98.99 |
| $HNO_3$ | 2 | 85 |
| | 3 | 92 |
| | 5 | 96 |
| $H_2SO_4$ | 2 | 81 |
| | 3 | 88 |
| | 5 | 90 |

from 2.77 to 3.00, 3.45 to 3.79 and 3.45 to 3.70 respectively. Each extraction was kept constant at the log $D$ value of 1.84 for HDEHP(phen), 1.60 for HDEHP(bipy) and 1.30 for HDEHP-(TOPO) synergic extraction systems, respectively, in the pH range from 3.5 to 4.0. It is interesting that the extractability of the gadolinium(III) with HDEHP(phen) synergic extraction process is higher than those of HDEHP(bipy) and HDEHP(TOPO). The optimum pH value to obtain 98% extractability was 2.60 to 3.70 in the case of HDEHP(phen), 97% extraction in the case of HDEHP(bipy) and 95% in the case of HDEHP(TOPO) synergic extraction process, respectively.

The logarithmic distribution coefficients diminished monotonically with increasing aqueous acidities (in the region of pH $>6.0$), implying that the extractions were dominated by the ion-exchange reaction in which hydrogen is liberated. Gaikwad and Damodaran[13] studied the extraction behaviour of Ho(III) with EHPNA(2-ethylhexyl phosphoric acid mono-2-ethylhexyl ester) and they concluded that there is no clear cut separation of phases at higher pH values. The extraction percentage of $Gd^{3+}$ reached a maximum in the case of phen, bipy and TOPO adduct formation at pH 3.00, 3.79 and 3.70, respectively.

*Slope analysis*

A traditional and effective means of obtaining both stoichiometric and equilibrium constant information about extraction processes, called 'slope analysis', is based on an examination of the logarithmic variation of $D$, the distribution ratio, with relevant experimental variables. The log–log plots of the extraction in the form of $D$ vs. a concentration variable indicate the stoichiometry of the formation of the extractable complex and thus lead to the derivation of a suitable equilibrium expression and then to the calculation of equilibrium constants.

*Extraction with HDEHP alone*

The extraction percentage of $Gd^{3+}$ reached a maximum in the case of kerosine and chloroform diluent when extractants were alone at pH 1.95 and 3.00, respectively. Beyond these values the extraction percentage decreased gradually. The plots of log $D$ *vs.* variables such as the pH of the aqueous phase and the logarithm of the concentration of $[(HX)_2]$ were constructed (Figs 3 and 4). Straight lines with a slope of 3 for gadolinium were obtained at the lower levels

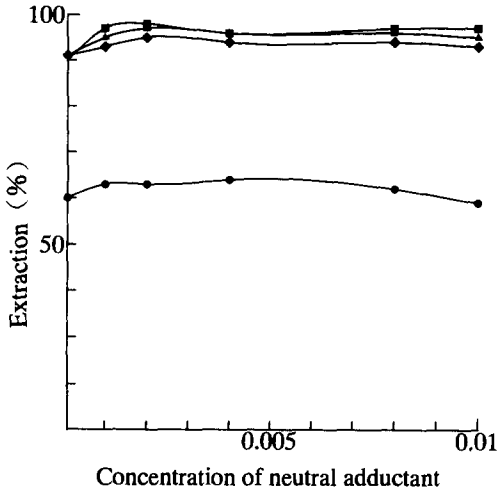


Fig. 2. The effect of HDEHP concentration on extraction in the presence of TOPO, bipy or phen. Organic phase: chloroform containing $1 \times 10^{-2} \sim 1 \times 10^{-4} M$ of di(2-ethylhexyl)phosphoric acid and constant [neutral additive], ● TOPO(kerosine), ◆ TOPO(chloroform), ▲ bipy, ■ phen. The aqueous solution containing gadolinium(III) ion $1 \times 10^{-4} M$, succinic buffer $2 \times 10^{-3} M$; perchlorate absent.

of metal extracted. Thus, the extraction reaction can be written as:

$$M_{aq}^{m+} + m(HX)_{2(O)} \rightleftharpoons M(HX_2)_{m(O)} + mH_{aq}^{+} \quad (1)$$

$$Gd^{3+} + 3(HX)_{2(O)} \rightleftharpoons Gd(HX_2)_{3(O)} + 3H^{+}. \quad (2)$$

Examination of equation (2) leads to the conclusion that the slope of a log $D$ *vs.* pH plot should be 3, indicating that three hydrogen ions are released in the extraction of the metal ion. As seen in Fig. 4, the behaviour of all of the

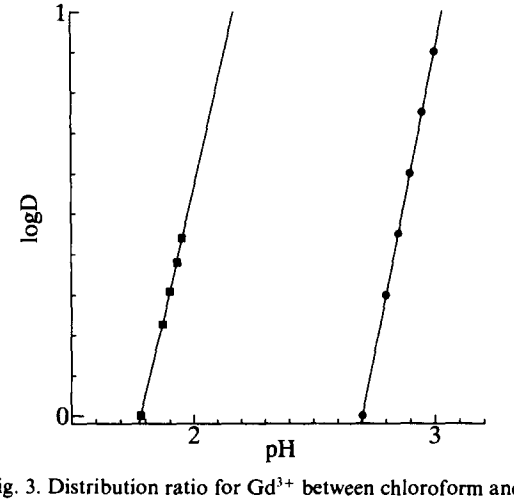


Fig. 3. Distribution ratio for $Gd^{3+}$ between chloroform and aqueous phase as a function of pH in the aqueous phase. Aqueous phase: $[Gd^{3+}] = 1 \times 10^{-4} M$; succinic acid $2 \times 10^{-3} M$. Organic phase: ● chloroform containing $2 \times 10^{-3} M$ HDEHP, ■ kerosine containing $2 \times 10^{-3} M$ HDEHP; perchlorate absent.

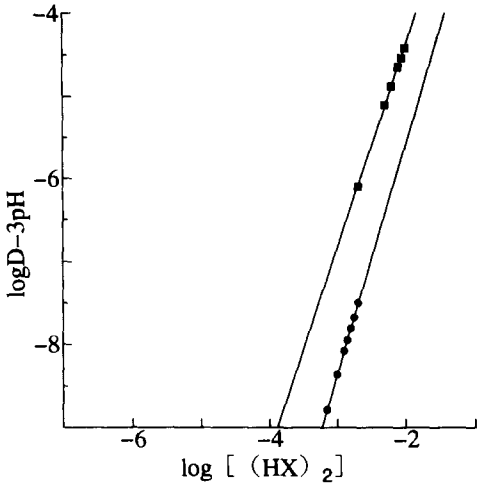


Fig. 4. Distribution ratio of $Gd^{3+}$ as a function of di(2-ethylhexyl)phosphoric acid concentration. Aqueous phase: $1 \times 10^{-4}M$ gadolinium containing no adductants, succinic acid $2 \times 10^{-3}M$. Organic phase as shown in HDEHP into ● chloroform, ■ kerosine.

$Gd^{3+}$ conformed to this simple formulation. In equations (1) and (2) $(HX)_2$ represents the HDEHP dimer. (The subscript O designates concentration in the organic phase.) For the extraction constant, $K_{ex}$, for this reaction refer to equation (3):

$$K_{ex} = [Gd^{3+}(HX_2)_3][H^+]^3/[Gd^{3+}][(HX)_2]^3 \quad (3)$$

or

$$\log K_{ex} = \log D_O - 3pH - 3\log[(HX)_2]. \quad (4)$$

Plots of $(\log D_O - 3pH)$ *vs.* $\log[(HX)_2]_O$ are also linear with slopes of almost +3 in the higher HDEHP concentration range (Fig. 3). +3 indicates the number of molecules of HDEHP combined in the extracted species.

For the kerosine system, the slopes of $\log D_O$ *vs.* pH plots decreased gradually with increasing pH. This type of behaviour was also encountered in the case of the chloroform system, then it was realised that the dependence of HDEHP may be obtained at lower pH values of the aqueous phase.

Thus, from the HDEHP dependence, it can be anticipated that the equation for the extraction reaction for both the chloroform and kerosine systems may be represented by equation (2) at higher acidities or by equation (6) at lower acidities, or by the combination of the two equations

$$Gd^{3+} + 3(HX)_{(O)} \rightleftharpoons [GdX_3]_{(O)} + 3H^+. \quad (6)$$

The applicability of the equations (2) and (6) depends on the assumption that the suppression of ionization of dimeric acid is less than that of the monomeric acid on increasing acidity. Equations (2) and (6) indicate the pH dependence to be +3, but the value obtained were somewhat lower in the case of the kerosine system. The value of $\log K_{ex}$ with chloroform was, unfortunately, smaller than that with kerosine, and this probably reflects the greater HDEHP extractability into chloroform than into kerosine.

*Extraction with a mixture of HDEHP and phen, bipy or TOPO*

As mentioned above the adduct formation of tris-DEHP complexes of $Gd^{3+}$ with oxygen containing monodentate ligand TOPO and bidentate ligand nitrogen containing the chelating agent phen or bipy as representatives of P=O,

$$=N-\overset{\|}{C}-\overset{\|}{C}-N=$$

donor groups, respectively, was studied. It was found that HDEHP complexes showed an exceptionally large tendency to form adducts with nitrogen containing the chelating agent 1,10-phenanthroline. When an auxiliary reagent, such as phen, bipy or TOPO (B), was added to the extraction system, enhanced extraction resulted because of the adduct formation. A per cent extraction (%$E$) pattern of 98.99%(phen) > 97%(bipy) > 95%(TOPO) was obtained into chloroform solvent.

The overall extraction equilibrium and the extraction constant, $K_{ex(B)}$, can be expressed as

$$Gd^{3+} + 3(HX)_{2(O)} + nB_{(O)} \rightleftharpoons Gd(HX_2)_3B_{n(O)} + 3H^+. \quad (7)$$

By subtracting equation (2) from equation (7), the adduct formation in the organic phase can be isolated:

$$Gd(HX_2)_{3(O)} + nB_{(O)} \overset{K_{AD(B)}}{\rightleftharpoons} Gd(HX_2)_3B_{n(O)}. \quad (8)$$

The effect of adduct formation is to increase the extraction equilibrium constant, $K_{ex(B)}$ by a factor given by the adduct formation constants $K_{AD(B)}$.

The adduct formation reaction in the organic phase and the complex stability constant, $\beta_n$ are given by

$$\beta_n = K_{ex(B)}/K_{ex}. \quad (9)$$

In equation (8), $n$ denotes the number of the auxiliary reagent molecules that attach to the

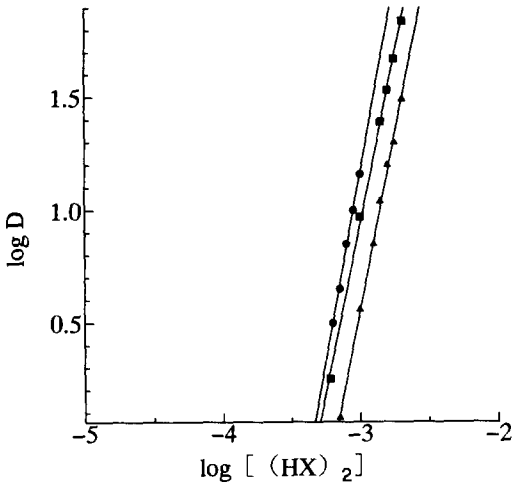


Fig. 5. Distribution ratio for $Gd^{3+}$ as a function of di(2-ethylhexyl) phosphoric acid concentration in the presence of constant adductants ($2 \times 10^{-3}M$) in the organic phase. ■ Phen, ▲ bipy, ● TOPO. Log $D$ *vs.* log[$(HX)_2$] has been plotted graphically according to the condition of Fig. 3.

extracted species. In this paper $n$ was evaluated by the following equation[10,11]

$$\log D/D_O = \log K_{ex(B)}/K_{ex} + n \log[B]_O, \quad (10)$$

where $D$ represents the distribution ratio in time of adduct formation, whereas $D_O$ represents the distribution ratio when HDEHP is alone.

In Figs 5 and 6 the plots of log $D$ *vs.* log$[(HX)_2]_O$ exhibits a slope of +3 and the plots of log $D$ *vs.* pH also have a slope of +3 in the case of the three kinds of synergistic mixture. The results of the extraction of gadolinium using a mixture of HDEHP and phen, bipy or TOPO are shown in Table 2, where it is seen

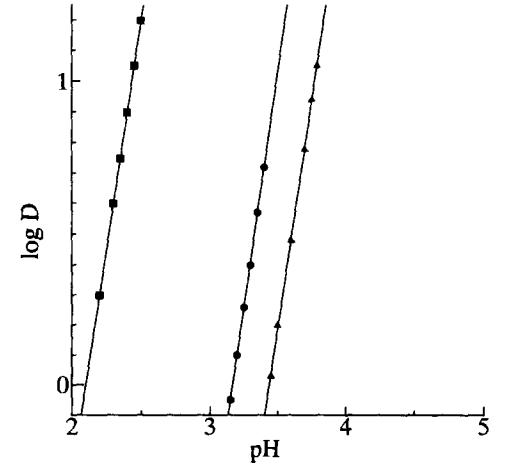


Fig. 6. Distribution ratio for $Gd^{3+}$ as a function of pH in the aqueous phase in presence of ■ phen, ▲ bipy, ● TOPO adductants ($2 \times 10^{-3}M$) in the organic phase.

Table 2. Summary of the results on the extraction of gadolinium with HDEPH and phen, bipy or TOPO

| No | Equation[log $D(y)$] *vs.* pH($x$) | $pH_{1/2}$ |
|---|---|---|
| 1[a] | $y = (3.00 \pm 0.31)x - (6.30 \pm 0.84)$ | 2.1 |
| 1[p] | $y = (2.06 \pm 0.09)x - (2.06 \pm 0.20)$ | 1.9 |
| 2[a] | $y = (2.99 \pm 0.23)x - (1.03 \pm 0.71)$ | 3.4 |
| 2[p] | $y = (1.99 \pm 0.21)x - (2.01 \pm 0.71)$ | 2.0 |
| 3[a] | $y = (3.08 \pm 0.04)x - (9.77 \pm 0.13)$ | 3.1 |
| 3[p] | $y = (2.10 \pm 0.01)x - (8.55 \pm 0.20)$ | 1.9 |
| 4[p] | $y = (3.20 \pm 0.08)x - (8.10 \pm 0.19)$ | 3.0 |
| 4[a] | $y = (2.13 \pm 0.24)x - (10.64 \pm 0.84)$ | 2.1 |
| 5[p] | $y = (2.10 \pm 0.17)x - (4.58 \pm 0.33)$ | 1.7 |
| 5[a] | $y = (2.62 \pm 0.24)x - (7.28 \pm 0.10)$ | 2.2 |

1 = HDEHP (0.002$M$ dimer) with phen, 2 = HDEPH (0.002$M$ dimer) with bipy, 3 = HDEPH (0.002$M$ dimer) with TOPO, 4 = HDEPH (0.002$M$ dimer) alone into $CHCl_3$, 5 = HDEPH (0.002$M$ dimer) alone into kerosine, [a] = ($ClO_4^-$ absent), [p] = ($ClO_4^-$ present).
All experiments were carried out three times.

from the lower $pH_{1/2}$ (pH of 50% extraction) values that highly enhanced extractions were achieved in the presence of as little as $10^{-3}M$ auxiliary reagent.

Figure 5 shows the distribution ratio of the metal ions as a function of HDEHP concentration when $2 \times 10^{-3}M$ phen, bipy or TOPO was added into the organic phase. In the presence of TOPO the plot is almost similar to that of HDEHP alone in chloroform at the above concentration. As can be seen from Figs 4 and 5, the extraction was enhanced by the addition of phen or bipy. The data in Figs 4 and 5 were calculated on the basis of equations (4) and (8), respectively, by a successive approximation method using a least square computer program. It is very interesting that the values of log $K_{ex(B)}$ with HDEHP are very large compared to those with HDEHP alone into chloroform. This is because the steric hindrance of the synergistic mixture is low. We can easily understand that the effect of phen is much larger in the HDEHP system by comparing values of log($K_{ex}/K_{ex(B)}$). In Table 2, values of $pH_{1/2}$ show that gadolinium can be extracted at slightly lower pH in the HDEHP alone system than in the mixed system under the same extraction conditions, it may be influenced by the distribution constant of the $Gd(HX_2)_3$ complex, and the adduct formation constant $K_{AD(B)}$. In order to clarify the composition of the extracted species, the dependencies of log $D/D_O$ on $[B]_O$ were examined. The plot of log $D/D_O$ *vs.* log$(phen)_O$ (Fig. 7) is linear with a slope of 2, indicating that two molecules of phen are included in the extracted species.

In the case of HDEHP and bipy mixture, the corresponding plot is also linear with a slope of

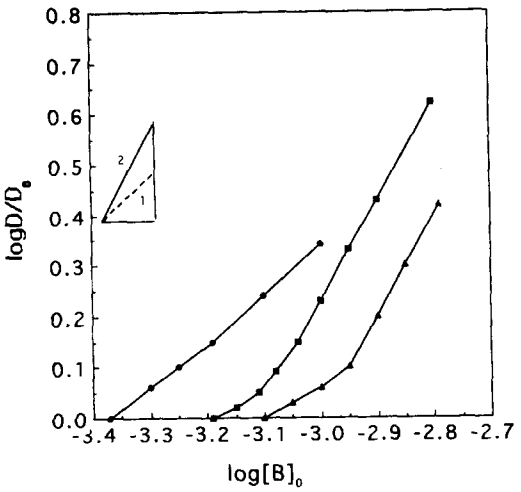


Fig. 7. Plots of $\log D/D_O$ *vs.* concentration of the adductants. From equation (7), $\log K_{AD} = \log D - 3\text{pH} - 3\log(HX_2)_3 - n \log B$. By subtracting $\log K_{ex}$ (equation 4) from $\log K_{AD}$ the following equation was obtained, $\log D/D_O = \log K_{AD}/\log K_{ex} + n \log[B]_O$. The slope of the plot of $\log D/D_O$ *vs.* $[B]_O$ at constant $[(HX)_2]$ and pH gives $n$. The effect of neutral additive concentration to HDEHP on the extraction of $Gd^{3+}$ was observed. Aqueous phase: $[Gd^{3+}] = 1 \times 10^{-4}M$, succinic acid $2 \times 10^{-3}M$. Organic phase: $[(HX)_2] = 2 \times 10^{-3}M$, $B = 2 \times 10^{-3}M$. ■ Phen, ▲ bipy, ● TOPO.

+2 at the higher bipy concentration region, but deviates from the straight line at low bipy concentrations (Fig. 7). This deviation can be explained by considering the extraction of $M(HX_2)_3B$, which takes place in the lower bipy concentration range (dotted lines in Fig. 7). The extraction constant and the stability constant $\beta_n$ are obtained from the linear position of the plot of $\log D/D_O$ *vs.* $\log[\text{phen}]_O$ using equations (8) and (9).

Our data supports the conclusion that TOPO forms a mono adduct extractable species, $Gd(HX_2)_3(TOPO)$, include the finding that the plot of $\log D/D_O$ *vs.* $\log[\text{TOPO}]_O$ have slopes of +1. Thus, it would seem that TOPO reacts as a monodentate ligand.

Generally, in the mixed ligand extraction system of the lanthanides, the decrease of the adduct formation constant may be explained by a diminution of the coordinating power of the lanthanide ion resulting from a stable chelate formation, with a consequently lower stable adduct formation. In addition, the lanthanide ion, to which three molecules of chelating reagent have already coordinated, allows space for the adduct forming reagent, so that steric hindrance for adduct formation increases with atomic number.

For extraction with a mixture of HPMTFP [1-phenyl-3-methyl-4-(trifluoroacetyl)-5-pyrazolone] and MBDPO[methylenebis(diphenylphosphineoxide)], the perchlorate ion was found to have a significant influence.[7] In the absence of the perchlorate ion the slope of the $\log D$ *vs.* pH lines were found to be 2.97 but when the perchlorate ion was present the slope of the $\log D$ *vs.* pH lines was found to be 1.98 for the case of La ion extraction.[7] Table 3 shows the values of the extraction parameters ($\log K_{ex}$) of gadolinium metal ions with HDEHP either alone or combined with phen, bipy or TOPO. Thus the following reaction can be written on the basis of the above findings. In the presence of phen, bipy or TOPO the following extraction may occur:

$$Gd^{3+} + 3(HX)_{2(O)} + 2\text{phen} \rightleftharpoons Gd(HX_2)_{3(O)}(\text{phen})_2 + 3H^+ \quad (11)$$

$$Gd^{3+} + 3(HX)_{2(O)} + 2\text{bipy} \rightleftharpoons Gd(HX_2)_{3(O)}(\text{bipy})_2 + 3H^+ \quad (12)$$

Table 3. Table of equilibrium constants and stability constants at 25°C determined by UV spectrophotometer

| Extractant | Organic phase | $\log K_{ex}$ | $\log K_{ex(B)}$ | $\log \beta_n$ |
|---|---|---|---|---|
| HDEHP alone[p] | $CHCl_3$ | $-0.03 \pm 0.10$ | — | — |
| HDEHP alone[a] | $CHCl_3$ | $0.10 \pm 0.05$ | — | — |
| HDEHP alone[p] | Kerosine | $2.70 \pm 0.03$ | — | — |
| HDEHP alone[a] | Kerosine | $3.05 \pm 0.03$ | — | — |
| HDEHP with phen[a] | $CHCl_3$ | — | $6.22 \pm 0.01$ | $6.25 \pm 0.10$ ($n = 2$) |
| HDEHP with phen[p] | $CHCl_3$ | — | $6.09 \pm 0.05$ | $6.12 \pm 0.11$ ($n = 2$) |
| HDEHP with bipy[a] | $CHCl_3$ | — | $5.75 \pm 0.01$ | $5.78 \pm 0.02$ ($n = 2$) |
| HDEHP with bipy[p] | $CHCl_3$ | — | $5.00 \pm 0.06$ | $5.03 \pm 0.03$ ($n = 2$) |
| HDEHP with TOPO[a] | $CHCl_3$ | — | $3.31 \pm 0.03$ | $3.34 \pm 0.02$ ($n = 1$) |
| HDEHP with TOPO[p] | $CHCl_3$ | — | $2.89 \pm 0.02$ | $2.92 \pm 0.05$ ($n = 1$) |

[p] = [($ClO_4^-$) present]. [a] = [($ClO_4^-$) absent]. Equation: $\log K_{ex} = \log D_O - 3\text{pH} - 3\log[(HX)_2]$ for HDEHP alone; $Gd^{3+} + 3(HX)_{2(O)} + nB_{(O)} \rightleftharpoons Gd(HX_2)_3B_{n(O)} + 3H^+$ for HDEHP with adductants. $\beta_n = K_{ex(B)}/K_{ex}$ for $\log \beta_n$.

$$Gd^{3+} + 3(HX)_{2(O)} + bipy \rightleftharpoons Gd(HX_2)_{3(O)}(bipy) + 3H^+ \quad (13)$$

$$Gd^{3+} + 3(HX)_{2(O)} + TOPO \rightleftharpoons Gd(HX_2)_{3(O)}(TOPO) + 3H^+. \quad (14)$$

Equations (11)–(14) represent the reactions in the absence of sodium perchlorate.

The values were obtained for $\log K_{ex(phen)} = 6.22 \pm 0.01$ and $\log K_{ex(bipy)} = 5.75 \pm 0.01$, respectively. These results indicate that the ligand 1,10-phen forms complexes that are more stable than those formed by bipy with the same metal ion, as was assumed. It seems reasonable to suggest that this effect is because of phen is more effectively pre-organized for coordination relative to bipy. Bipy is highly strained in the conformer with the nitrogens *cis* to each other, as required for coordination of metal ions,[14] because of the steric hinderance between the hydrogens in the 3- and 3′- positions. However, in phen this problem is overcome by fusing the two rings and forcing the ligand to remain in the correct conformation for coordination to a metal ion.

When sodium perchlorate is present, however, a different extractable species is found.

$$Gd^{3+} + 2(HX)_2 + ClO_4^- + 2(phen) \rightleftharpoons Gd(HX_2)_2(ClO_4^-)(phen)_2 + 2H^+ \quad (15)$$

$$Gd^{3+} + 2(HX)_2 + ClO_4^- + 2(bipy) \rightleftharpoons Gd(HX_2)_2(ClO_4^-)(bipy)_2 + 2H^+ \quad (16)$$

$$Gd^{3+} + 2(HX)_2 + ClO_4^- + (bipy) \rightleftharpoons Gd(HX_2)_2(ClO_4^-)(bipy) + 2H^+ \quad (17)$$

$$Gd^{3+} + 2(HX)_2 + ClO_4^- + (TOPO) \rightleftharpoons Gd(HX_2)_2(ClO_4^-)(TOPO) + 2H^+. \quad (18)$$

When these metals are extracted under increasing concentrations of $NaClO_4$ and adductants, a slope of 2 could be obtained in a plot of $\log D$ *vs.* pH, when $[adductants]_{(O)}$ and $[ClO_4^-]$ were $5 \times 10^{-3}$ and $0.2M$, respectively (Tables 2 and 3). As seen in Table 3, the enhancement was much greater when phen was used than with TOPO or bipy. Thus it would seem than phen forms a diadduct extractable species. In the case of bipy a monoadduct was observed when the concentration range was $<0.1M$. Bipy also formed a biadduct in its higher concentration range.

## CONCLUSIONS

In the mixed complex system containing HDEHP, the donating ability of $(HX)_2$ is insufficient to form an adduct. The effect of three adductants on the extraction of Gd(III) with HDEHP mixtures was examined. From these results, it would appear that the formation of mixed complexes with a mixture of two chelating extractants and adduct formation to mixed complexes like quaternary compound formation successfully enhanced the metal chelate extraction. This is, to some extent, similar to the enhancement of metal chelate extraction by adduct formation in the organic phase through dimer extractant. From these results, it would appear that the adduct formation to mixed complexes may further enhance separation capability in the lanthanide series.

## REFERENCES

1. D. F. Peppard, *Adv. Inorg. Chem. Radiochem.*, 1966, **9**, 1.
2. H. Freiser, *Anal. Chem.*, 1966, **38**, 131 R.
3. H. Freiser, *Anal. Chem.*, 1968, **40**, 522 R.
4. Proceedings of an International Conference on Solvent Extraction Chemistry, Gothenberg 1966. North Holland, Amsterdam 1967.
5. T. H. Handley, *Nuclear Sci. Engng*, 1963, **16**, 440.
6. T. H. Handley and J. A. Dean, *Anal. Chem.* 1963, **34**, 440.
7. S. Umetani and H. Freiser, *Inorg. Chem.*, 1987, **26**, 3179.
8. Y. Komatsu and H. Freiser, *Anal. Chim. Acta*, 1989, **227**, 397.
9. T. Sekine, N. T. K. Dung and J. Noro, *Bull. Chem. Soc. Jpn*, 1994, **67**, 432.
10. S. Nakamura and N. Suzuki, *Bull. Chem. Soc. Jpn*, 1993, **66**, 98.
11. K. Marczenko, *Spectrophotometric Determination of Elements*, p. 441. John Wiley, New York, 1976.
12. Z. Marczenko, *Spectrophotometric Determination of Elements*, p. 442. Wiley, New York, 1976.
13. A. G. Gaikwad and A. D. Damodaran, *Sepn Sci. Technol.*, 1993, **28**, 1019.
14. G. Nord, *Comments Inorg. Chem.*, 1985, **4**, 193.

Pergamon

0039-9140(94)00223-1

*Talanta*, Vol. 42, No. 1, pp. 101–103, 1995

0039-9140/95 $9.50 + 0.00

# DETECTION AND SPECTROPHOTOMETRIC DETERMINATION OF COPPER(III) WITH *p*-ANISIDINE

N. KRISHNA MURTHY and B. SREERAMA MURTHY

Department of Engineering Chemistry, Andhra University College of Engineering, Visakhapatnam-530 003, India

(*Received* 4 *April* 1994. *Revised* 2 *August* 1994)

**Summary**—Copper(III) solutions are found to give an instantaneous stable pink-coloured product with 0.2% aqueous *p*-anisidine in the presence of 0.03*N* acetic acid. The wavelength of maximum absorption is 533 nm and obeys Beer's law up to 0.89408 g copper(III). It is also recommended as a spot test for copper(III).

During the course of experiments in search of specific colour reagents for copper(III), we noticed that solutions of copper(III) give an instantaneous stable pink-coloured product with 0.2% aqueous *p*-anisidine in the presence of 0.03*N* acetic acid. The addition of copper(III) solution in 2*M* KOH contributes alkalinity and the effective pH was found to be more than 7, when a stable pink colour was observed. A study of the spectrum of the pink-coloured product and comparison revealed that the pink-coloured product is the oxidized form of *p*-anisidine.[1] Copper(I) and copper(II) and other reagents used did not respond similarly and a survey of the literature indicated that this specific colour reaction between copper(III) and *p*-anisidine has not been previously reported. In view of the importance of the micro determination of copper(III) in non-stoichiometric and super-conducting substances, the above method which is rapid, accurate, simple and specific, will find a wide range of application.

## EXPERIMENTAL

### *Reagents*

*Copper*(III) *solution* (0.02*M*). The solution was prepared from an AnalaR BDH sample of cupric sulphate pentahydrate, by oxidation with potassium persulphate in 2*M* potassium hydroxide media and standardized.[2]

p-*Anisidine* (0.2% *aqueous*). Prepared by dissolving an adequate amount of an AnalaR BDH sample, in double distilled water, standardized against cerium (IV)[3] and stored in amber coloured bottles. All other reagents used were of AnalaR grade only.

### *Apparatus*

A Shimadzu-UV-260 double beam spectrophotometer with recording unit was used for recording the spectra. An ELICO photoelectric colorimeter with filter No.625 (green filter, range 510–590 nm, peak at 540 nm) was used for other experiments.

Preliminary experiments carried out in various acid and alkali media revealed that the pink coloured product obtained by the reaction between copper(III) and *p*-anisidine was instantaneous and stable in the presence of 0.03*N* acetic acid. In view of such experiments the following procedures are recommended.

### *Recommended procedure for the detection of copper*(III) *with* p-*anisidine*

Copper(III) solution (0.05 ml) was mixed with 0.05 ml of 0.1*N* acetic acid and 0.05 ml of 0.2% aqueous *p*-anisidine in the cavity of a white porcelain spot plate, to give an instantaneous pale pink colour. By a systematic quantitative dilution procedure, we found the limits of detection of copper(III) with aqueous *p*-anisidine in the presence of 0.03*N* acetic acid: limit of identification: $0.2 \times 10^{-6}$ g or 0.2 $\mu$g of copper as copper(III); limit of dilution: $1:0.75 \times 10^{6}$.

### *Spectrophotometric estimation of copper*(III) *with* 0.2% p-*anisidine*

Copper(III) solution (1.0 ml) was mixed with 8 ml of 0.1*N* acetic acid and 0.5 ml of 0.2%

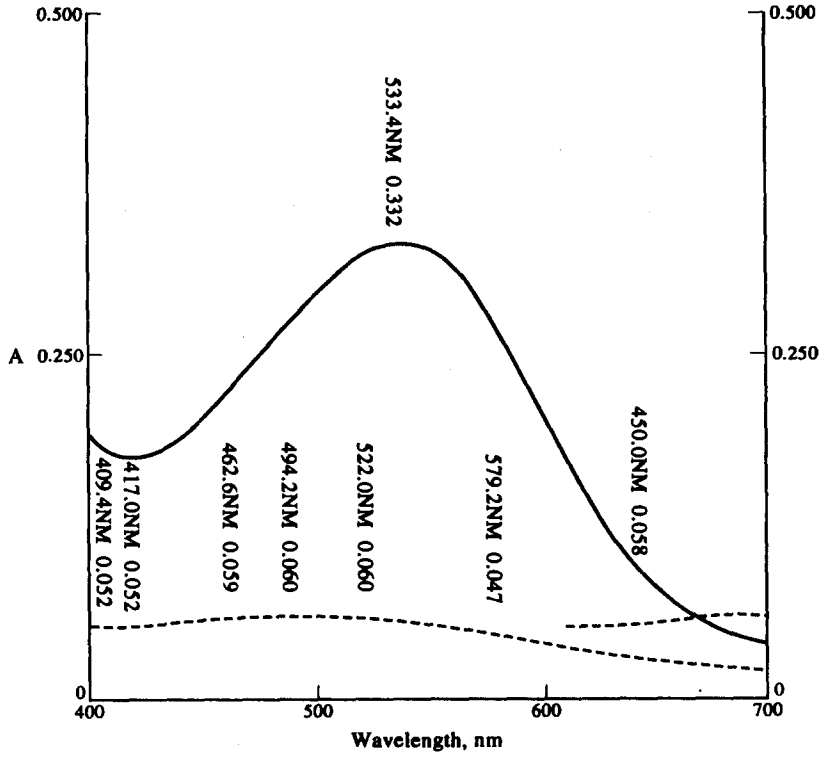


Fig. 1.

aqueous *p*-anisidine to give a stable instantaneous pink-coloured product. The mixture was made up to 25 ml in a volumetric flask and the spectra taken for an aliquot of the solution showed $\lambda_{max}$ at 533 nm (Fig. 1). Solutions of copper(III) and *p*-anisidine have $\lambda_{max}$ as 416 nm

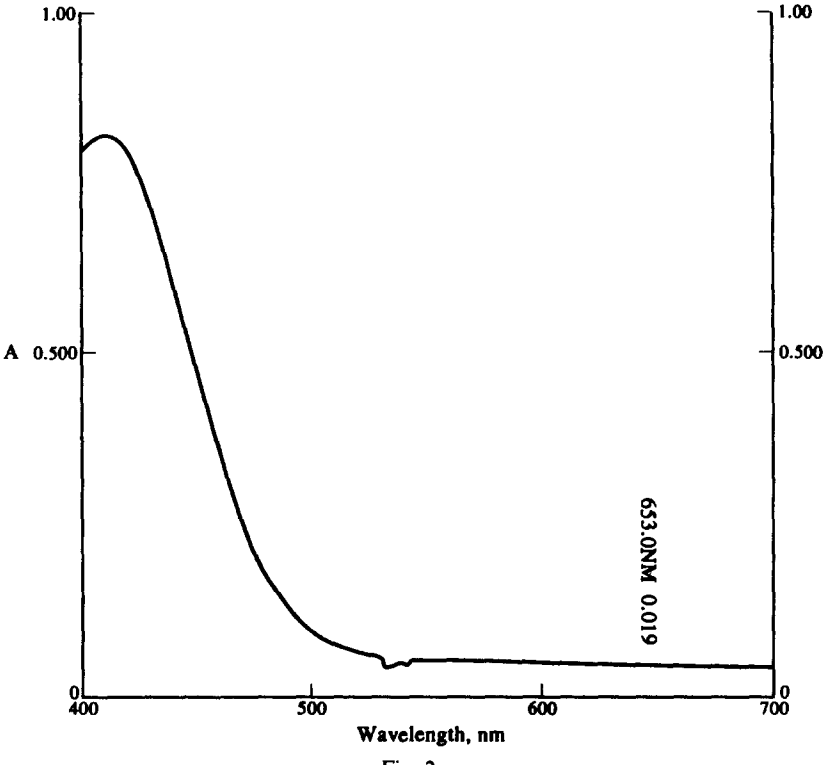


Fig. 2.

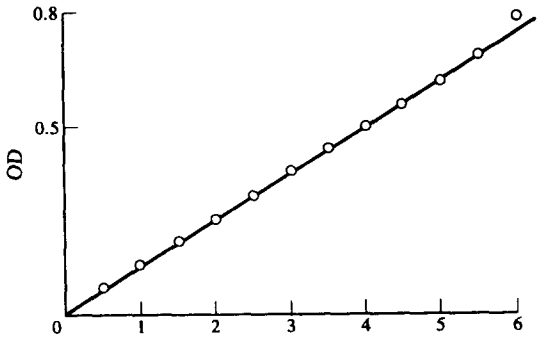

Fig. 3.

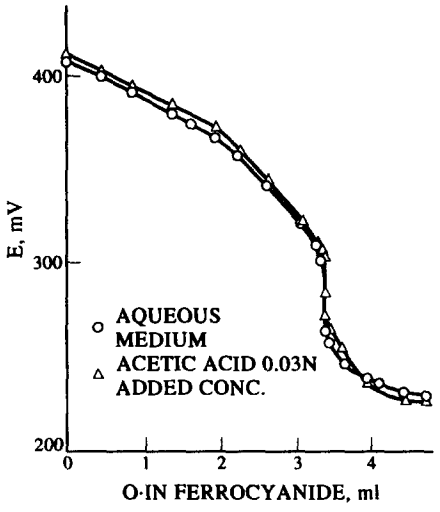

Fig. 4.

(Fig. 2) and 533 nm, respectively, and thus found to have no overlapping.

For the estimation of copper(III), an aliquot volume of copper(III) was mixed with 8 ml of 0.1*N* acetic acid and 2 ml reagent in a 25 volumetric flask to give a stable instantaneous pink-coloured product and the mixture made up to the mark. The solution was taken in an optically matched test tube of an ELICO colorimeter and the optical density measured using filter No. 625 (green filter). The optical density was compared with a standard curve (Fig. 3) and the estimation carried out. Beer's law was found to be obeyed up to 0.89408 g of copper(III).

## DISCUSSION

The specific colour reaction between copper(III) and *p*-anisidine was studied in various acid and alkali media. Copper(III) oxidizes *p*-anisidine to the pink-coloured product [while it is being reduced to copper(II)]. In very low acid concentrations such as 0.1*N* $H_2SO_4$, 0.05*N* HCl, 0.05*N* $H_3PO_4$, an instantaneous pale pink colour was produced, slowly fading away in 5–10 min. It was found that the colour of the product was stable for carrying out further experiments in 0.03*N* acetic acid media. However, even when the concentration of acetic acid was increased over and above 0.06*N*, the intensity of the pink colour and the corresponding optical density were found to decrease. Hence, we used 0.03*N* acetic acid as the optimum condition for the production of oxidized product of *p*-anisidine with copper(III) solution. The $\lambda_{max}$ for the pink-coloured product was 533 nm (Fig. 1) with molar absorptivity, $\varepsilon = 415M^{-1}$ cm$^{-1}$ at 533 nm. There was no overlapping of the spectra of the pink coloured product of *p*-anisidine with other species present in the solution. Beer's law was found to be obeyed up to 0.89408 mg of copper as copper(III).

## CONCLUSION

Copper(III) solutions gave an instantaneous stable pink-coloured product with 0.2% aqueous *p*-anisidine in 0.03*N* acetic acid. The $\lambda_{max}$ was 533 nm for the pink-coloured product with molar absorptivity $\varepsilon = 415M^{-1}$ cm$^{-1}$ at 533 nm. Beer's law was obeyed up to 0.89408 mg of copper and copper(III). This can be used as a spot test for copper(III) with an identification limit of $0.2 \times 10^{-6}$ g and dilution limit of $1:0.75 \times 10^6$. The test and estimation are rapid, easy and accurate.

*Acknowledgement*—One of the authors, BSRM thanks UGC for their financial assistance.

## REFERENCES

1. L. Pepuhado, J. Bacon and R. N. Adams, *J. Electroanal. Chem. Interfacial ElectroChem.*, **24**, App 1–5, 1970.
2. A. Berka, J. Vulterine and J. Zyka, *Newer Redox Titrants* 1st Edn, p. 15. Pergamon Press, London, 1965.
3. R. B. Korupolu, Ph.D. Thesis, p. 29. Andhra Unversity India, 1992.

Pergamon

0039-9140(94)00224-X

*Talanta*, Vol. 42, No. 1, pp. 105–108, 1995

0039-9140/95 $9.50 + 0.00

# SPECTROPHOTOMETRIC DETERMINATION OF DICLOFENAC SODIUM WITH METHYLENE BLUE

JULIO C. BOTELLO and GUADALUPE PÉREZ-CABALLERO*

Facultad de Estudios Superiores Cuautitlán U.N.A.M., Sección de Química Analítica, Campo Uno. Av. Primero de Mayo, s/N Cuautitlán Izcalli, C.P. 54740, Estado de México, México

(*Received* 4 *May* 1994. *Revised* 2 *August* 1994. *Accepted* 4 *August* 1994)

**Summary**—A sensitive spectrophotometric method was established for the determination of Diclofenac sodium (DS) with Methylene Blue (MB) as analytical reagent. It was found that DS reacts with an excess of MB in the pH range 9.2–9.4, to form a chloroform-extractable blue ion-association complex. Good agreement with Beer's law was found in the range of DS concentrations of 0.8–6.4 μg/ml with a detection limit of 0.37 μg/ml. The method was applied for the determination of DS in various tableted forms with a good precision.

2-(2,6-dichloroanilino)Phenyl acetate (Diclofenac sodium) (Fig. 1a) is a nonsteroidal anti-inflammatory agent with potent activity and outstanding tolerability in the treatment of rheumatic diseases.[1,2] It has been measured by a variety of analytical techniques such as ultraviolet[3] and visible spectrophotometry,[4,5] gas[6–8] and liquid chromatography[9–12] and nuclear magnetic resonance spectroscopy.[13]

Spectrophotometric methods provide sensitive, precise and accurate measurements of suitable analytes and they offer practical and economical advantages over other methods. Diclofenac sodium (DS) has been analyzed by spectrophotometric methods using complexation with copper acetate[4] or Methylene Violet[5] followed by extraction, the latter being a more sensitive method than the former. The aim of the present work was to establish an improved extraction and spectrophotometric method with greater sensitivity for the determination of DS using Methylene Blue (MB) (Fig. 1b) in different tableted dosage.

## EXPERIMENTAL

### *Apparatus*

A Beckman DU-65 single beam spectrophotometer with 10 mm glass cells was used for the absorbance measurements. The pH measurements were made with a Corning Model 12 Research pH-meter, calibrated with buffer solution (pH $10 \pm 0.05$).

### *Reagents*

DS (standard drug), 99.46% purity, Voltaren Retard and Flenaken tablets containing 100 mg DS, and Voltaren tablets containing 50 mg DS were analyzed. All other chemicals used were analytical-reagent grade. Deionized water was used to prepare all solutions and in all experiments.

### *Solutions*

A freshly prepared aqueous solution of the pure drug (40 mcg/ml; $1.2573 \times 10^{-4}M$) was used as the standard solution for analytical purposes. A 0.032% w/v ($1.04 \times 10^{-3}M$) aqueous Methylene Blue solution was prepared for these experiments. Ammonium/ammonia buffer solutions covering the pH range from 8 to 11 were made by mixing equal volumes of $1.0M$ ammonia and $1.0M$ ammonium chloride solutions and adjusting the pH with sodium hydroxide or hydrochloric acid.

### *Procedure*

Aliquots of DS solution were transferred into a series of 125 ml separating funnels; then 5 ml of MB solution and 1 ml of buffer (pH 9.4) was added. The total volume of the aqueous phase was adjusted to 10 ml with water. Chloroform (10 ml) was added and the contents shook for exactly 5 min, the separated chloroform layer was collected in a 25 ml volumetric flask. A new

*Author to whom the correspondence should be addressed.

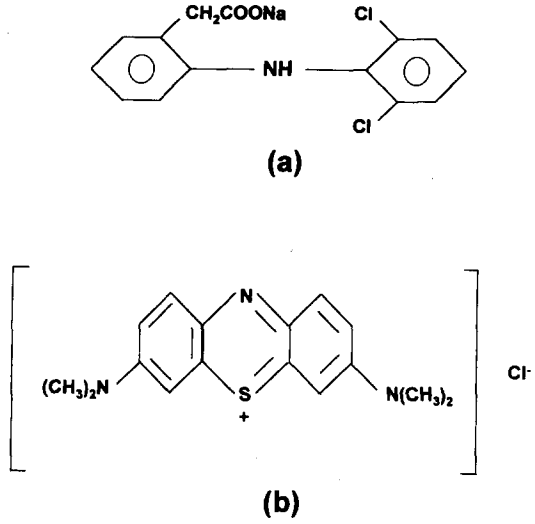


Fig. 1. Structure of (a) Diclofenac sodium and (b) Methylene Blue.

10 ml volume of chloroform volume was added and shook for 5 min, this second extract was combined with the first and this solution diluted to the mark with chloroform. The absorbance of the organic phase was measured against a reagent blank. The reagent blank was prepared exactly like the procedure described above, but in absence of DS.

*Procedure of the assay of tableted dosage*

An amount of tablet powder equivalent to 80 mg of anti-inflammatory agent was weighed accurately and dissolved in water by magnetic stirring. Filtration through a filter paper (Whatman 40) was performed to remove insoluble matter remaining. The solution was diluted to 50 ml with deionized water and treated as described above for the standard drug solution.

## RESULTS AND DISCUSSION

*Absorption spectra*

Diclofenac sodium reacted with MB in aqueous solution in alkaline medium to form a blue ion-association complex which was extracted into chloroform. Figure 2 shows the absorption spectra of this complex and the reagent blank. This complex has an absorption maximum at 653 nm against reagent blank, hence this wavelength was used for all subsequent measurements. Under the same experimental conditions the reagent blank gave a maximum absorption at 642 nm.

*Optimum conditions for complex formation*

In order to establish the optimum pH range, DS was mixed with MB in aqueous solution from pH 8 to 11, and the ion-associated complex absorbance measured. Figure 3 shows that the absorbance increases and reaches a maximum and constant value at 9.2–9.5 pH range. At pH values above 9.5 the absorbance decrease was probably due to the formation of a new ion-associated complex between MB and hydroxyl anion in alkaline medium since experimentally, the reagent blank absorbance increases. Hence, a pH of 9.4 was used in all the subsequent experimental work. The shape of the spectra and maximum position did not vary with pH, so it was concluded that only one complex was formed at this pH range.

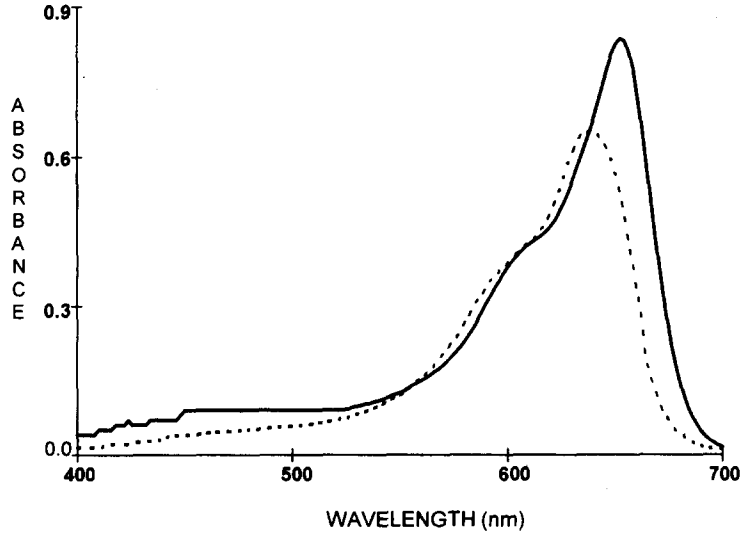


Fig. 2. The absorption spectra of the blank reagent (---), and DS–MB (——) complex formed in the aqueous 0.05$M$ $NH_4^+/NH_3$ buffer containing $5 \times 10^{-4}M$ MB and extracted with chloroform.

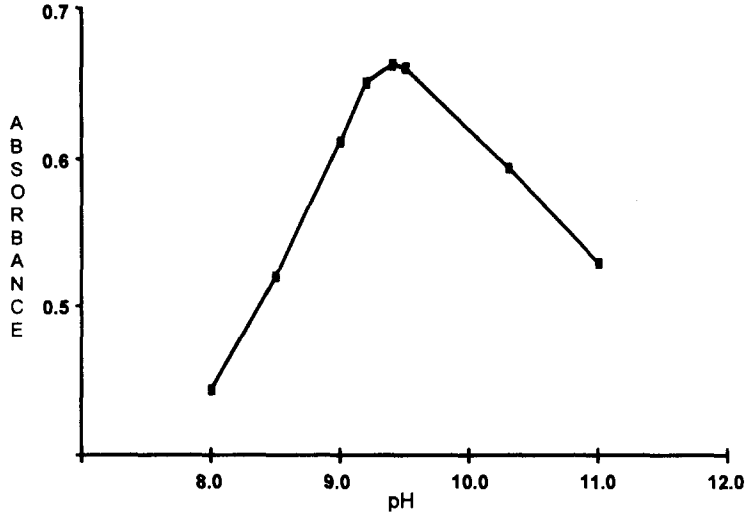


Fig. 3. Variation in absorbance of the DS–MB complex, formed in aqueous 0.05$M$ $NH_4^+/NH_3$ buffer containing $5 \times 10^{-4}M$ MB at different pH values (aborbances were obtained at $\lambda_{653\,nm}$).

The extent of the extraction of the ion-associated complex was found to be affected by the MB concentration. To establish the optimum MB concentration the solution absorbances were plotted as a function of MB concentration (Fig. 4). The absorbance of the system increased in the range of $1–3.5 \times 10^{-4}M$ MB and the absorbance was practically constant in a range of $4–6 \times 10^{-4}M$ MB, hence a concentration of $5.0 \times 10^{-4}M$ MB was used as the optimum concentration. The excess of MB in this system was 25–200 times the concentration of DS.

Two extractions were necessary to achieve a quantitative recovery of the complex. Absorbances of the separated extracts were stable for at least 1 hr. A shaking time of 5 min produced a constant absorbance. An ionic strength of 0.025$M$ was produced by the buffer.

*Linearity*

A calibration curve was obtained under optimum conditions (pH 9.4; $5 \times 10^{-4}M$ MB; ionic strength 0.025$M$), absorbance responses were linear in relation to the calculated concentration of DS over the range 0.8–6.4 mcg/ml ($2.5 \times 10^{-6}–2.5 \times 10^{-5}M$). The equation for one representative calibration curve is:

$$A = (-0.0191 \pm 0.0423) + (0.1789 \pm 0.0105)C,$$

where $A$ and $C$ correspond to absorbance and DS calculated concentration ($\mu$g/ml),

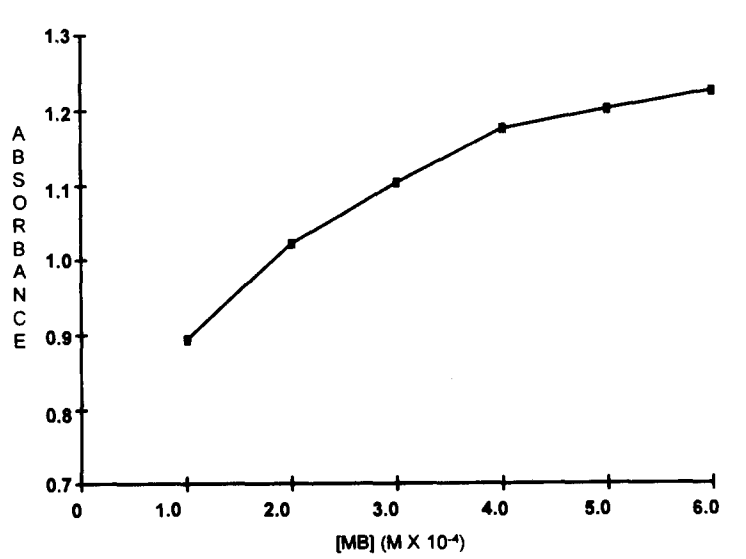


Fig. 4. Variation in absorbance of the DS–MB complex, formed in aqueous 0.05$M$ $NH_4^+/NH_3$ buffer containing different concentrations of MB (absorbances were obtained at $\lambda_{653\,nm}$).

Table 1. Comparison of sensitivity parameters of the different spectrophotometric methods for the determination of Diclofenac sodium

| Analytical reagent | Sandell sensitivity ($mg/cm^2$) | Detection limit ($mcg/ml$) |
|---|---|---|
| Copper acetate | 0.01026 | 1.00 |
| Methylene Violet | — | 72.00 |
| Methylene Blue | 0.006 | 0.37 |

Table 2. Determination of Diclofenac sodium in different tableted dosage

| Drug | Labeled amount ($mg$) | Amount found ($mg$) |
|---|---|---|
| Flenaken | 100.00 | $101.45 \pm 0.42$ |
| Voltaren Retard | 100.00 | $101.35 \pm 0.13$ |
| Voltaren | 50.00 | $49.97 \pm 0.15$ |

Each drug was analyzed eight times.

respectively. The correlation coefficient $(r) = 0.998$ $(n = 8)$, indicating excellent linearity. The molar absorptivity coefficient was $5.7 \times 10^4 M^{-1}$ cm$^{-1}$, and the Sandell sensitivity 0.006 mg/cm$^2$ with a detection limit of 0.37 mcg/ml ($1.2 \times 10^{-6} M$). Table 1 shows that the Table 1 shows that the method reported here has higher sensitivity than other similar methods, in which copper acetate[4] and Methylene Violet[5] are employed as analytical reagents.

*Application*

The applicability of the method to the assay of simple dosage forms was examined by analyzing Flenaken, Voltaren and Voltaren Retard tablets. Table 2 shows the quantities obtained by proposed method and labeled amount. The relative standard deviations are lower than 1% indicating good precision and the independence of the matrix effect over the absorbances measurements.

## CONCLUSIONS

The proposed method is economical, simple, rapid, precise and sensitive. The use of MB as analytical reagent provides a fairly higher sensitivity compared with other similar reagents such as Methylene Violet.

*Acknowledgements*—We thank Dr Ignacio González for his collaboration in this project. J. C. Botello acknowledges the scholarship from CONACYT.

## REFERENCES

1. R. Sallman, *Am. J. Med.*, 1986, **80**, 29.
2. W. Scholer, I. Boettcher and A. Schweizer, *Am. J. Med.*, 1986, **80**, 34.
3. K. Arrawal, V. P. Upayay and S. K. Menon, *Indian J. Pharm. Sci.*, 1988, **50**, 58.
4. A. N. Other. A. N. Other, Agatanovic-Kustrin, L. J. Zivanovic, D. Radulivic and M. Vasiljevic, *Analyst*, 1991, **166**, 753.
5. S. P. Sastry, A. S. R. Prasad Tirpeneni and M. V. Suryanarayama, *Analyst*, 1989, **114**, 513.
6. A. Schweizer, J. V. Willis, D. B. Jack and M. J. Kendall, *J. Chromatogr.*, 1980, **195**, 421.
7. W. Schneider and P. H. Degen, *J. Chromatogr.*, 1981, **217**, 263.
8. B. Henning, A. Steup and R. Benecke, *Pharmazie*, 1987, **13**, 1307.
9. T. Sane, R. S. Samant and V. G. Nayak, *Drug Dev. Ind. Pharm.*, 1987, **13**, 1307.
10. D. Grandjean, J. C. Beolor, M. T. Quincon and E. Savel, *J. Pharm. Sci.*, 1989, **78**, 247.
11. H. Chan, K. H. Vyas and K. Wnuck, *Anal. Lett.*, 1982, **15**, 1649.
12. A. N. Other. Godbilon, S. Gauron and J. P. Metayer, *J. Chromatogr.*, 1985, **338**, 151.
13. A. Abdel Fattah, J. P. El-Khateeb, S. A. Abdel Raxeg and M. S. Tawakkol, *Spectrosc. Lett.*, 1988, **21**, 533.

Pergamon

0039-9140(94)00225-8

*Talanta*, Vol. 42, No. 1, pp. 109–117, 1995

0039-9140/95 $9.50 + 0.00

# THE USE OF MACROCYCLES AS ELECTROOSMOTIC FLOW MODIFIERS IN THE SEPARATION OF INORGANIC ANIONS BY CAPILLARY ELECTROPHORESIS

JOHN D. LAMB,* BRAD R. EDWARDS, ROBERT G. SMITH and RICHARD GARRICK
Department of Chemistry, Brigham Young University, Provo, UT 84602, U.S.A.

(*Received* 11 *May* 1994. *Revised* 1 *August* 1994. *Accepted* 2 *August* 1994)

**Summary**—In a novel approach to the use of macrocycles in separation systems, we report the use of macrocyclic ligands as electroosmotic flow modifiers for the separation of inorganic anions by capillary electrophoresis (CE). Inorganic anions were successfully separated through the use of 18-crown-6 or cryptand 2.2.2. as electroosmotic flow modifiers. We found that for our CE system, use of a macrocycle as the modifier resulted in better baseline stability and better efficiency than the commonly used modifier DETA. In our system, the separation efficiency and electroosmotic flow varied according to the pH of the buffer and the affinity of the macrocycle for the buffer metal cation. Results for sodium- and potassium-based buffers show that for the cryptand, pH plays a role in determining the amount of macrocycle–metal complex formed. Separations of a 12 anion standard illustrate these results. In addition, we report the effect of concentration of both macrocycle and metal ion on complex formation and resultant electroosmotic flow modification. Relationships between the macrocycle–metal complex, the buffer medium, the efficiency of separation, and the migration times of the analytes are discussed, and theoretical interpretations presented.

Traditionally, ion chromatography (IC) has been used for the analysis of inorganic ions. However, in recent years capillary electrophoresis (CE) has been explored as an alternate method of inorganic anion and cation separations because it provides several advantages with regard to sample size and separation efficiency. CE separations have resulted in theoretical plate numbers a hundred times greater than those achieved by IC separations.[1]

CE separations are performed by introducing a sample into a buffer-filled capillary by gravity/siphoning or electromigration, then allowing sample ions to migrate based on their respective charge-to-mass ratios in the presence of an electric field. Various separation systems have been developed that take advantage of the high efficiency of CE.[2] Normally buffer flows toward the negative electrode (cathode). This net flow of liquid towards the cathode, called the electroosmotic flow (EOF), is caused by a dielectric layer which forms between the negatively charged silanol groups on the surface of the capillary and the highly mobile cations in the buffer. The motion of the mobile cations results in a net flow of liquid toward the cathode as the buffer solvent is dragged along by the solvated cations.

The migration order, resolution and migration times of sample ions are optimized by the addition of EOF modifiers in the case of anion separations, or complexing agents in the case of cation separations. EOF modifiers are additives that influence the flow of buffer by modifying the dielectric layer at the surface of the capillary wall, slowing or reversing the direction of the bulk flow of liquid in the capillary. This reversal or slowing of the EOF results in shorter anion analysis times and an increase in peak efficiencies over conventional IC separations.[2]

The focus of the research reported herein is the use of crown ethers or cryptands as EOF modifiers in inorganic anion separations by CE. Many applications of macrocyclic molecules have been explored with excellent results.[3–8] Previous articles have described the incorporation of macrocycles as complexing agents, rather than as EOF modifiers, in CE buffer systems for separating cations.[9–13] The well understood ability of macrocyclic ligands to bind alkali metal cations catalyzed our interest in

*Author to whom correspondence should be addressed.

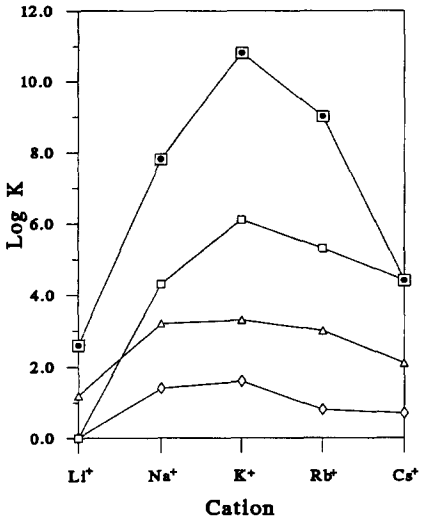


Fig. 1. Equilibrium binding constants (in methanol) of alkali metal cations with various macrocyclic ligands explored in this study. ⊡ cryptand 2.2.2; □ 18-crown-6; △ 15-crown-5; ◇ 12-crown-4.

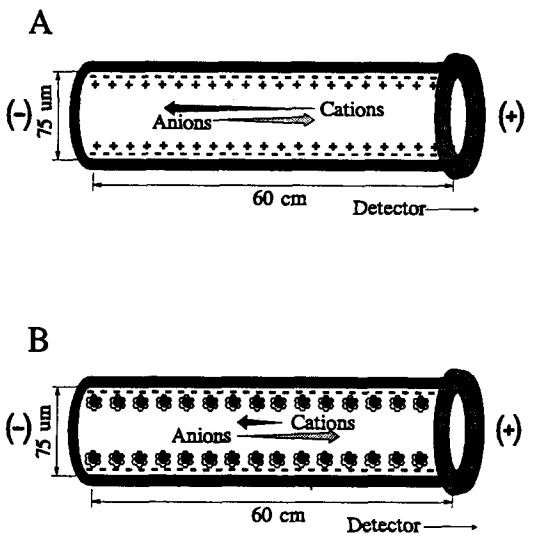


Fig. 2. Direction of electroosmotic flow in (A) an unmodified system and (B) a system in which the flow has been modified by the addition of a macrocycle.

their potential for use in EOF modification.[14,15] High binding constants between alkali metals and macrocycles[14] (Fig. 1) promote the formation in the buffer of cationic complexes, which can act as EOF modifiers by forming a dielectric layer coupled to the negatively charged silanol groups on the wall of the capillary (Fig. 2). Because of the weakly hydrophobic, cationic nature of the macrocycle-metal complex, the bulk flow of solution is slowed to permit the detection of anions at the anode. The binding strength of a particular buffer metal ion with the macrocycle is a determining factor in the rate of EOF.

## EXPERIMENTAL

### *Apparatus*

Analyses were performed on a Dionex capillary electrophoresis system (CES-1). The CES has five main components: an autosampler for sample selection as well as for injection; a fused silica capillary in which sample separations take place; positive and negative polarity high voltage power supplies capable of 30,000 V; a detector where the anion signal can be measured by direct or indirect UV/Vis detection; and a computer which controls voltage, injection method, injection time, number of samples run, the autosampler, time of analysis and rinses of the capillary. All samples in our analysis were introduced from the autosampler by gravity/siphoning injection into the capillary.

### *Materials*

Reagent-grade macrocycles 12-crown-4, 15-crown-5, 18-crown-6 and kryptofix (cryptand) 2.2.2. were obtained from Aldrich Chemicals (Milwaukee, WI) and reagent grade chemicals were used in preparing all buffers and standards. The structures of these ligands are shown in diagram 1. Water used in the preparation of all buffers and standards was purified to 18 MΩ resistivity using a Millipore Milli-Q water purification system (Waters, Bedford, MA, U.S.A.). Buffers were filtered using 0.45 $\mu$m filters, to remove any particulate matter in the solution, and then degassed by sonication and evacuation.

An ion exchange column packed with cation exchange resin (Dowex MSC-1, 20-50 mesh, Sigma Chemical, St. Louis, MO, U.S.A.) was used to prepare buffers containing different cations. The column was packed in water to

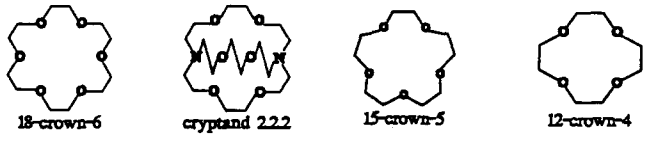


Diagram 1

avoid channeling, and solutions containing the replacement cation were prepared using the nitrate salts of the alkali metals.

The mobility and peak efficiencies of inorganic anions are controlled by matching the background analyte with the species being analyzed. Chromate ion was found to be the most useful in our system, as most of the anions in our standards had high electrophoretic mobilities.[17]

## RESULTS AND DISCUSSION

### *Theoretical*

The relationship between the cation and macrocycle in a chromatographic separation system has been described by Lamb and Smith.[16] The concept behind macrocycle–metal complex formation in a CE system is similar to that described for such an IC system. However, differences arise because the macrocycle incorporated in a CE system is not adsorbed onto a stationary phase, but rather exists in dynamic equilibrium with the metal cation as a solute component of the buffer phase. In an effort to effectively describe the relationships that exist between the various macrocyclic ligands and the metal ions in the buffer system, theoretical calculations were performed for cryptand 2.2.2. and 18-crown-6.

*Cryptand* 2.2.2. The concentration of metal–macrocycle complex in the CE buffer system can be determined for the cryptand 2.2.2. ligand by the following:

$$[L_F] = [L_0] - [ML] - [HL^+] - [H_2L^{2+}], \quad (1)$$

where $[L_F]$ is the concentration of free ligand in the system, $[L_0]$ is the original concentration of ligand, [ML] is the amount of metal–ligand complex formed, and the terms $[HL]^+$ and $[H_2L]^{2+}$ correspond to the first and second protonation steps of the cryptand ligand. Assuming 1:1 stoichiometry, the equilibrium constant for the macrocycle–metal ion complexation is given by the following:

$$L + M^+ \rightleftharpoons ML^+. \quad (2)$$

A combination of equations (1) and (2) yields the equilibrium constant expression:

$$K_m = \frac{[ML^+]}{[L_F][M^+]} \rightarrow \frac{[ML^+]}{([L_0] - [ML^+] - [HL^+] - [H_2L^{2+}])([M_0^+][ML^+])}, \quad (3)$$

where the new $[M_0^+]$ term is defined as the original metal ion concentration. Since the binding of metal ions by the macrocycle occurs in competition with the protonation reaction, we consider the degree to which protonation occurs by incorporating equations (4) and (6) into our overall expression for metal–ligand complex formation. The first expression denotes the protonation of the macrocyclic nitrogens:

$$H^+ + L_F \rightleftharpoons HL^+, \quad (4)$$

which when combined with expression (1) becomes:

$$K_1 = \frac{[HL^+]}{[H^+][L_F]} \rightarrow \frac{[HL^+]}{([L_0] - [ML^+] - [HL^+] - [H_2L^{2+}])([H^+])}. \quad (5)$$

The second protonation constant expression is given by:

$$HL^+ + H^+ \rightleftharpoons H_2L^{2+}, \quad (6)$$

which yields the following expression:

$$K_2 = \frac{[H_2L^{2+}]}{[HL^+][H^+]}. \quad (7)$$

The value of $[H^+]$ was determined by measurement of the pH at equilibrium. The final theoretical solution for $[ML^+]$, the amount of metal–ligand complex in the buffer, is given by a quadratic equation which was used to determine the effect of cation identity, ligand concentration, metal concentration, and pH on the ability of cryptand 2.2.2. to form the metal–ligand complex which would regulate the electroosmotic flow. The theoretical plot of pH *vs.* metal–ligand complex formation is given in Fig. 3, and the effect of ligand concentration on metal–ligand formation is shown in Fig. 4. Each of these factors will be discussed in detail in a later section.

18-*Crown*-6. Macrocycles which cannot be protonated, like 18-crown-6, interact with buffer cations according to the following:

$$L + M^+ \rightleftharpoons ML^+ \quad (8)$$

$$K_m = \frac{[ML^+]}{[L_F][M^+]} \rightarrow \frac{[ML^+]}{([L_0] - [ML^+])([M_0^+] - [ML^+])}. \quad (9)$$

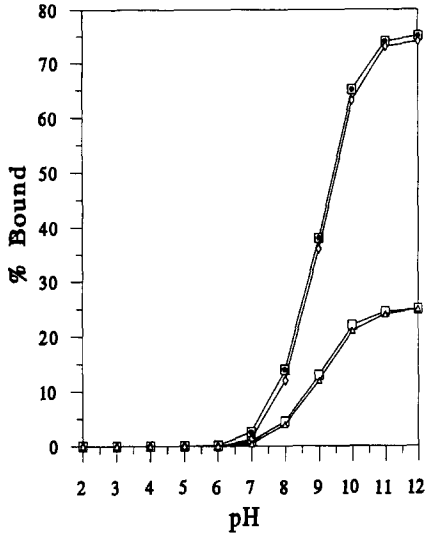


Fig. 3. Theoretical plot of the effect of pH on the binding of cryptand 2.2.2 (2.0 m$M$) to metal ion (6.0 m$M$). ◙ % 2.2.2 bound to $K^+$; ◇ % 2.2.2 bound to $Na^+$; □ % $K^+$ bound to 2.2.2; △ % $Na^+$ bound to 2.2.2.

From these expressions it can be seen that the amount of metal–macrocycle complex formed is not dependent on the pH as was the case for the cryptand 2.2.2. The predicted values for percent ligand and percent metal ion bound under different conditions are shown in Fig. 5. Conditions are given in the figure caption and these results will be discussed in a later section.

Initially four different macrocycles were incorporated into our buffer system as electroosmotic flow modifiers. However, only separations involving 18-crown-6 and cryptand 2.2.2 were extensively explored. The buffers incorporating 15-crown-5 and 12-crown-4 were not pursued after preliminary results (Fig. 6) indicated that analysis times were no longer with these buffers. These results can be compared to those with the 18-crown-6 (Fig. 7) and

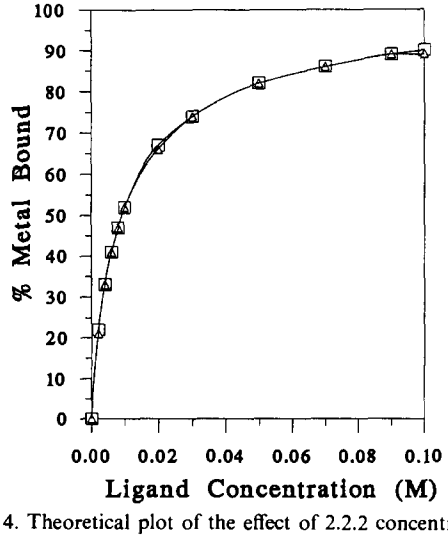


Fig. 4. Theoretical plot of the effect of 2.2.2 concentration on % metal bound at a pH of 10 with a metal ion concentration of 6.1 m$M$. □ % $K^+$ bound; △ % $Na^+$ bound.

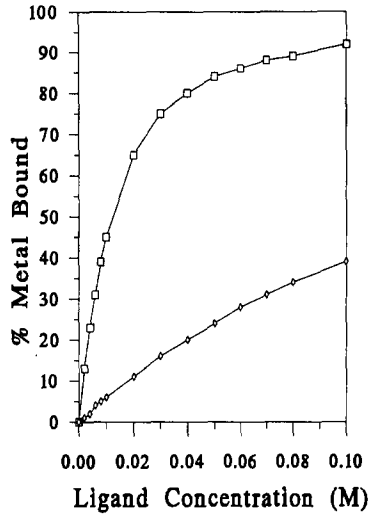


Fig. 5. Theoretical plot of the effect of 18-crown-6 concentration on % metal bound (metal ion concentration = 6.1 m$M$). □ % $K^+$ bound; ◇ % $Na^+$ bound.

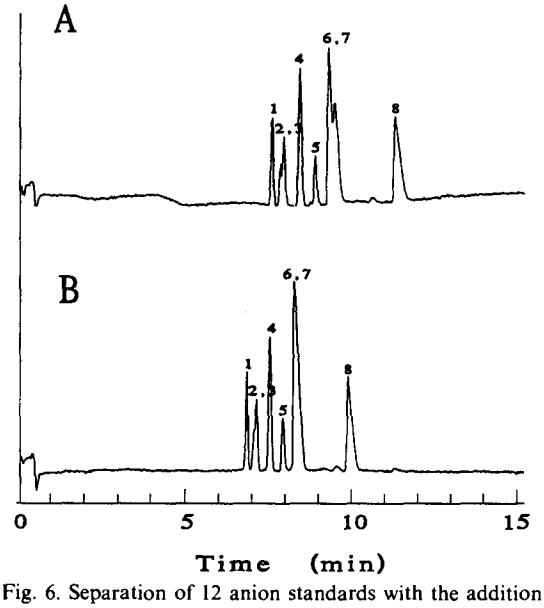


Fig. 6. Separation of 12 anion standards with the addition of (A) 12-crown-4 and (B) 15-crown-5 as the electroosmotic flow modifiers. The conditions are 2.0 m$M$ sodium tetraborate, 1.8 m$M$ sodium dichromate, 43 m$M$ boric acid, and 2.0 m$M$ 18-crown-6 at pH 7.2. Separation conditions: capillary, 75 $\mu$m i.d. × 375 $\mu$m o.d. × 60 cm; injection, gravity, 100 mm for 30 sec at 25 kV, indirect detection at 254 nm. Peak identities: (1) bromide, (2) chloride, (3) iodide, (4) sulfate, (5) nitrite, (6, 7) nitrate and oxalate, (8) thiocyanate. All analyte concentrations are 10 ppm with the exception of chloride which is 3 ppm.

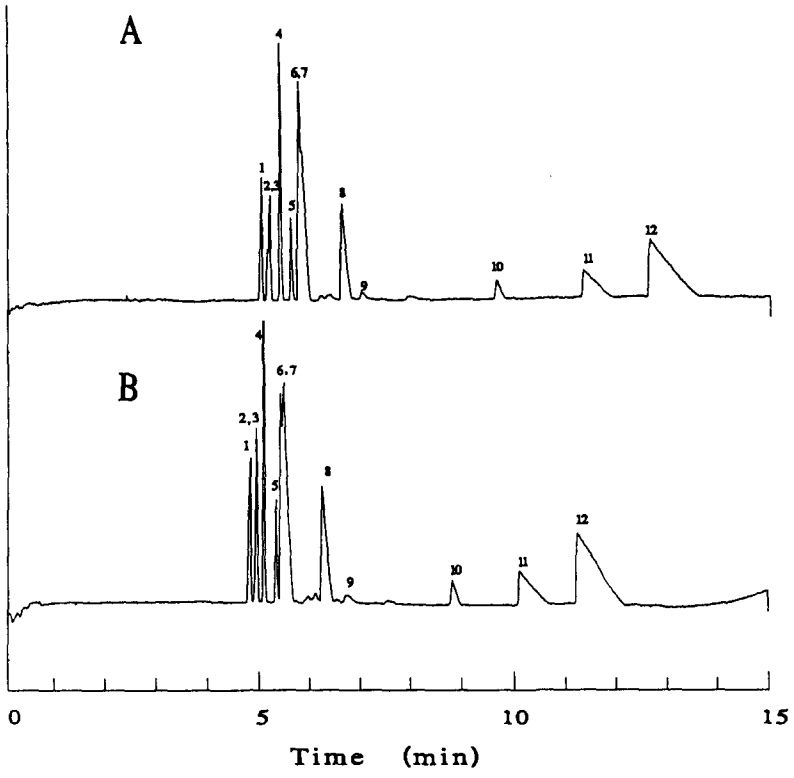


Fig. 7. Separation of a 12 anion standard with (A) 2.0 m*M* sodium tetraborate, 1.8 m*M* sodium dichromate, 43 m*M* boric acid, and 4.0 m*M* 18-crown-6, pH 7.2; and (B) 2.0 m*M* potassium tetraborate (prepared by ion exchange), 1.8 m*M* potassium dichromate, 43 m*M* boric acid, and 4.0 m*M* 18-crown-6, pH 7.2. Separation conditions: capillary, 75 $\mu$m i.d. × 375 $\mu$m o.d. × 60 cm; injection, gravity, 100 mm for 30 sec at 25 kV, indirect detection at 254 nm. Peak identities: (1) bromide, (2) chloride, (3) iodide, (4) sulfate, (5) nitrite, (6, 7) nitrate and oxalate, (8) thiocyanate, (9) citrate, (10) phosphate, (11) phthalate, (12) acetate. All analyte concentrations are 10 ppm with the exception of chloride which is 3 ppm.

cryptand 2.2.2 (Fig. 8), which are superior in terms of overall speed of analysis.

*Effect of buffer cation on separation and complex formation*

The variation in binding constants for the alkali metal cations with both 18-crown-6 and cryptand 2.2.2 are shown in Fig.1.[15] From these binding constants and from effects seen in macrocycle-based IC separation systems,[16] we anticipated changes in EOF according to the order of buffer cation $K^+ > Rb^+ > Na^+ > Cs^+$ and $Li^+$, regardless of which of the two macrocycles was used. This expected order follows the descending order of affinity of these cations for both macrocyclic ligands.

To the extent possible, buffers were prepared using commercially available chemicals. However, the required $Li^+$, $Rb^+$ and $Cs^+$ salts were not commercially available. A cation exchange system was used to replace the sodium ion in buffers made from sodium salts with each of the other three. However, owing to the availability of the different salts, our research focused on $Na^+$ and $K^+$ buffers only.

18-*Crown*-6. To determine the effect of changing the cation in the buffer system, analyses of an anion standard were performed using 18-crown-6 as the EOF modifier with both $Na^+$ and $K^+$ borate/tetraborate buffers. Comparison of the electropherograms in Fig. 7 shows that significant variation in EOF occurs when the cation in the buffer is changed from $Na^+$ (Fig. 7A) to $K^+$ (Fig. 7B). When $K^+$ is the cation in the buffer (Fig. 7B), the migration times and separation show improvement over the system in which the $Na^+$ is the cation in the buffer. Specifically, the migration times of 12 common anions were longer with the $Na^+$-based buffer than with the $K^+$-based buffer and not all peaks were resolved with the $Na^+$-based buffer. These experimental results correspond to theory, which predicts that $K^+$ binds 18-crown-6 more strongly than $Na^+$ (Fig. 5).[16] This conclusion is in keeping with our stated hypothesis concerning the mechanism of EOF modification by

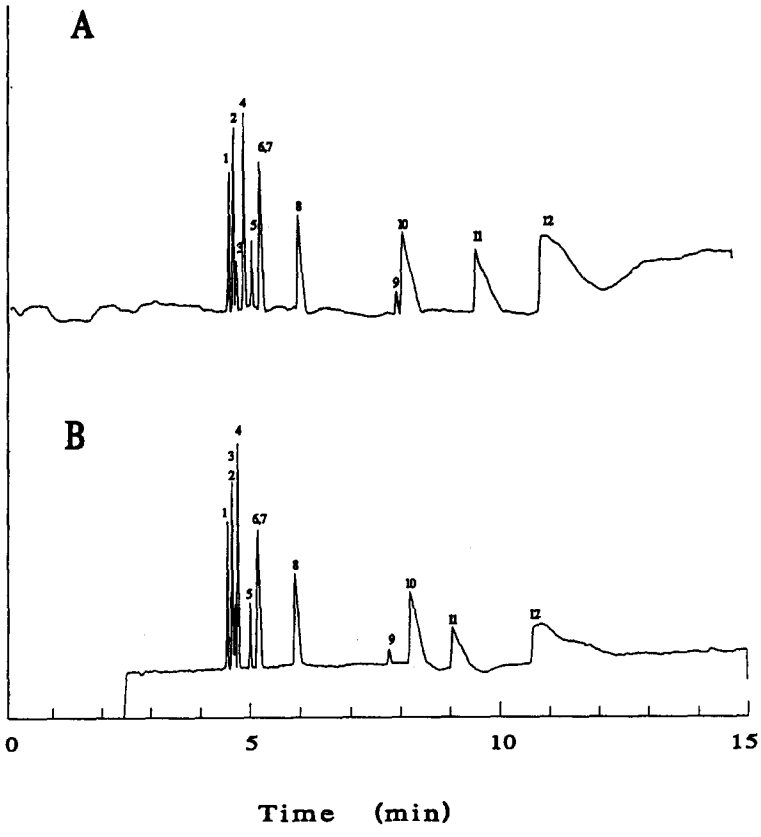


Fig. 8. Separation of a 12 anion standard with (A) 2.0 m*M* sodium tetraborate, 1.8 m*M* sodium dichromate, 43 m*M* boric acid, and 8.0 m*M* cryptand 2.2.2, pH 7.2; and (B) 2.0 m*M* potassium tetraborate (prepared by ion exchange), 1.8 m*M* potassium dichromate, 43 m*M* boric acid, and 8.0 m*M* cryptand 2.2.2, pH 7.2. Separation conditions: capillary, 75 $\mu$m i.d. × 375 $\mu$m o.d. × 60 cm; injection, gravity, 100 mm for 30 sec at 25 kV, indirect detection at 254 nm. Peak identities: (1) bromide, (2) chloride, (3) iodide, (4) sulfate, (5) nitrite, (6, 7) nitrate and oxalate, (8) thiocyanate, (9) citrate, (10) phosphate, (11) phthalate, (12) acetate. All analyte concentrations are 10 ppm with the exception of chloride which is 3 ppm.

macrocyclic complexes. We conclude that the higher population of macrocycle complexes in the presence of $K^+$ is responsible for the superior modification of EOF over the $Na^+$-based buffer.

*Cryptand* 2.2.2. Only above pH of 10 is the cryptand 2.2.2 sufficiently deprotonated for formation of the metal–ligand complex to become important. Above this pH, cation identity and concentration become significant contributors to the degree of EOF modification.

The effect of specific cations on complex formation with the cryptand can be seen in the theoretical plots of Figs 3 and 4. The amount of metal–ligand complex is expected to increase once the second $pK_a$ has been reached for both the $Na^+$-based and $K^+$-based buffers (Fig. 3). It is interesting to note that cation identity does not influence metal–cryptand complex formation (Fig. 4) to the extent seen with the 18-crown-6 system (Fig. 5), even at pH 10. Thus, the modification of EOF expected with the substitution of $K^+$ for $Na^+$ in the buffer system was not as pronounced for the cryptand 2.2.2 as it was for the 18-crown-6. However, the complex formation that occurs with either the $Na^+$ or $K^+$ still results in the expected dielectric layer formation and modification of the EOF.

*Effect of pH on proton ionizable macrocycles*

A plot of pH *vs.* percent cryptand 2.2.2 bound to $Na^+$ or $K^+$ (Fig. 3) illustrates that at pH < 10 the amount of metal–ligand complex is negligible compared to the amount of protonated macrocycle. The modification of the EOF by 2.2.2 in this pH range is based entirely on protonation of the macrocycle rather than the degree of metal ion complexation. At the pH we used in our experiment (pH ≈ 7.2), EOF modification was due to protonation of the nitrogen groups in the macrocyclic ring, and not to the actual binding of the macrocycle with the metal ion.

Table 1. Efficiency and migration times of 3 ppm $Cl^-$ in a borate/tetraborate buffer system

| Ligand concentration (*mM*) | 2.2.2-$Na^+$ | 2.2.2-$K^+$ | 18-crown-6-$Na^+$ | 18-crown-6-$K^+$ | DETA |
|---|---|---|---|---|---|
| | Plates | Plates | Plates | Plates | Plates |
| 2.0 | 81542 | 67154 | 57589 | 53569 | 44713 |
| 4.0 | 71244 | 57795 | 25115 | 59481 | — |
| 8.0 | 76065 | 99929 | 37618 | 61832 | — |
| 16.0 | 100787 | 96529 | 55400 | 55400 | — |
| | Time (*min*) | Time (*min*) | Time (*min*) | Time (*min*) | Time (*min*) |
| 2.0 | 4.48 | 4.58 | 4.92 | 4.92 | 4.27 |
| 4.0 | 4.73 | 4.58 | 4.74 | 4.74 | — |
| 8.0 | 4.51 | 4.48 | 5.49 | 4.82 | — |
| 16.0 | 4.50 | 4.40 | 4.98 | 4.98 | — |

Support of this conclusion can be seen in a comparison of the two cryptand 2.2.2 electropherograms seen in Fig. 8. The two are not significantly different even though Fig. 8A was obtained using a $Na^+$-based buffer and Fig. 8B a $K^+$-based buffer, both at a pH of $\approx$7.2. The large difference in the binding constants between $Na^+$ and $K^+$ with this macrocycle causes one to expect a greater modification of EOF evidenced by shorter retention times of the analytes in Fig. 8B. These results conform to the hypothesis that pH, not metal–macrocycle complex formation, was the predominant factor in EOF modification. The protonated, positively charged cryptand 2.2.2 formed a dielectric layer with the walls of the capillary and resulted in a modification of the EOF that was equal or better in many aspects to modifying agents we had previously used in our buffer systems. A comparison of the electropherogram in Fig. 8B with the electropherogram in Fig. 9 shows the baseline improvement and improved efficiency seen with the protonated macrocycle system over a system employing DETA (diethylenetriamine) as the modifying agent.

An experiment was designed in which phosphate buffers, containing either the $Na^+$ or $K^+$ coupled with the cryptand 2.2.2, were adjusted to higher pH in an attempt to correct for this pH dependency. However, when these buffers were used the current became inordinantly high, resulting in a low resistance error in the system.

*Effect of the modifier on migration times, efficiency and resolution*

Table 1 shows the efficiencies and migration times of $Cl^-$ using the borate/tetraborate buffer system, pH 7.2, using different electroosmotic flow modifiers, including both macrocycles and DETA. The $Cl^-$ migration time and its dependence on the modifier is representative of all sample anions. The migration time of $Cl^-$ follows the order DETA < 2.2.2-$K^+$ $\approx$ 2.2.2-$Na^+$ < 18-Crown-6-$K^+$ $\ll$ 18-crown-6-$Na^+$. Table 2 shows the results of efficiency and migration times for $Cl^-$ in a phosphate buffer system, pH 5.0. The migration order for the phosphate system with the various modifiers followed the order 2.2.2-$Na^+$ $\approx$ 2.2.2-$K^+$ < DETA < 18-crown-6-$K^+$ < 18-crown-6-$Na^+$. Migration times for the two buffers are quite different. However, results for either buffer system support the conclusion that the effect on the electroosmotic flow using cryptand 2.2.2 is independent of buffer cation as described above. Based on these $Cl^-$ results, the borate/tetraborate buffer with cryptand 2.2.2 as the modifying agent resulted in the best efficiencies and migration times in our system.

When 18-crown-6 was used as the modifying agent the borate/tetraborate system yielded better efficiency and resolution than the phosphate buffer system. Results for the $K^+$- phosphate/18-crown-6 buffer system are not included in the

Table 2. Efficiency and migration times of 3 ppm $Cl^-$ in a phosphate buffer system

| Ligand concentration (*mM*) | 2.2.2-$Na^+$ | 2.2.2-$K^+$ | 18-crown-6-$Na^+$ | 18-crown-6-$K^+$ | DETA |
|---|---|---|---|---|---|
| | Plates | Plates | Plates | Plates | Plates |
| 2.0 | 34942 | 34452 | 13234 | — | 48779 |
| 4.0 | 60114 | 47743 | 15063 | — | — |
| 10.0 | 62104 | 65821 | 11300 | — | — |
| | Time (*min*) | Time (*min*) | Time (*min*) | Time (*min*) | Time (*min*) |
| 2.0 | 2.65 | 2.75 | 3.28 | — | 3.13 |
| 4.0 | 2.61 | 2.63 | 3.10 | — | — |
| 10.0 | 3.00 | 2.70 | 2.60 | — | — |

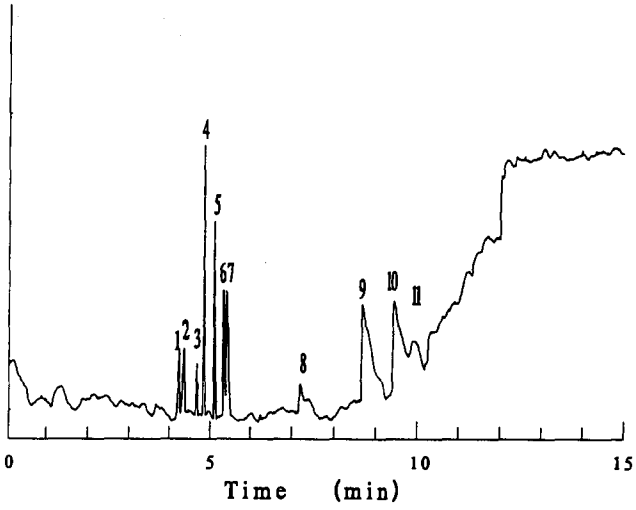


Fig. 9. Separation of a 11 anion standard with (A) 2.0 m*M* potassium tetraborate, 1.8 m*M* sodium dichromate, 43 m*M* boric acid, and 2.0 m*M* DETA, pH 7.2. Separation conditions: capillary, 75 $\mu$m i.d. × 375 $\mu$m o.d. × 60 cm; injection, gravity, 100 mm for 30 sec at 25 kV, indirect detection at 254 nm. Peak identities: (1) bromide, (2) chloride, (3) sulfate, (4) nitrite, (5) nitrate, (6) oxalate, (7) thiocyanate, (8) citrate, (9) phosphate, (10) phthalate, (11) acetate. All analyte concentrations are 10 ppm with the exception of chloride which is 3 ppm.

table as the separation for this system was poor and there was a constant fluctuation in current when this system was employed. A comparison of results for the $Na^+$-borate/18-crown-6 and $K^+$-borate/18-crown-6 buffers for $Cl^-$ ion separation clearly support earlier conclusions that $K^+$, the metal with the higher binding constant, results in the greatest modification of EOF.

As seen in Tables 1 and 2, the efficiency of $Cl^-$ using the macrocycle-based buffers is higher than when using the DETA–borate–tetraborate based buffer. However, the opposite is true when using the phosphate buffer. The migration time results in Table 1 indicate that the DETA–borate–tetraborate buffer yields slightly faster migration times, although higher efficiencies and better baseline stability are observed with a macrocycle as the modifier. The opposite was seen for the phosphate system. The migration times with the phosphate–macrocycle system were faster than with the DETA system, but the efficiency was lower.

In addition to the effects on efficiency and migration times, higher concentrations of the macrocycle resulted in efficiency and resolution improvement when using both the borate and phosphate buffers. The resolution of two peaks as the concentration of cryptand 2.2.2 is increased illustrates this point (Fig. 10).

## CONCLUSIONS

One possible disadvantage of using cryptands as electroosmotic flow modifiers is the expense involved with cryptands. While the current market price of the cryptand 2.2.2 discourages its use in analyses where it is difficult to recover, our results do show that use of macrocycles as electroosmotic flow modifiers in CE buffer systems yields better separations and higher efficiencies than use of DETA. Macrocycles can function as EOF modifiers because the metal–macrocycle complex forms a dielectric layer with the charges on the capillary surface. Theoretical calculations of complexation reactions conform to our experimental results.

One advantage of a macrocycle-based CE system we found is the improved efficiency that can be achieved with the cryptand 2.2.2 over DETA. We also observed an improvement in baseline stability over many analyses we have performed with DETA. Finally, we found that there exists a relationship between the quality of separations and the buffer–macrocycle system used. With phosphate buffer, the migration times of the anions were fast but the efficiencies were poor. With borate–tetraborate buffer the migration times were somewhat slower but efficiencies were much better.

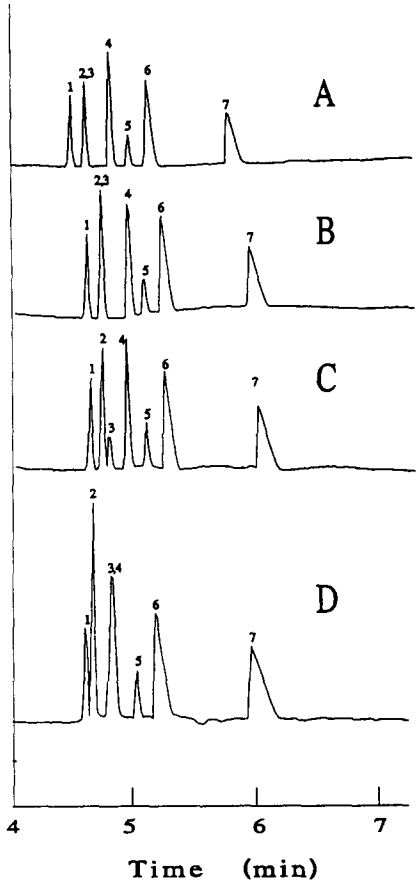


Fig. 10. The effect of changing the modifier concentration is illustrated as the resolution of peaks 2 and 3 is seen as the concentration of the cryptand 2.2.2 changes from: (A, B) 2.0, 4.0 m$M$; peak identities: (1) bromide, (2,3) chloride and iodide, (4) sulfate, (5) nitrite, (6) nitrate, (7) thiocyanate; (C) 8.0 m$M$; peak identities (2) chloride, (3) iodide; (D) 16 m$M$, peak identities: (2) chloride, (3, 4) iodide and sulfate. All analyte concentrations are 10 ppm with the exception of chloride which is 3 ppm.

*Acknowledgements*—The authors would like to thank undergraduate assistants Max Mortensen, Danny Spencer, and Greg Hart for help in the experimental work.

## REFERENCES

1. J. W. Jorgenson and K. D. Lukacs, *Anal. Chem.*, 1981 **53,** 1298.
2. W. R. Jones, P. Jandik and R. Pfeifer, *Am. Lab.*, 1991, **23**(8), 40.
3. K. Kimura, H. Harino, E. Hayata and T. Shono, *Anal. Chem.*, 1986, **58,** 2233.
4. E. Blasius and K. P. Janzen, *Top. Curr. Chem., 1981*, **98,** 163.
5. E. Blasius, K. P. Janzen, W. Klein, H. Klotz, V. B. Nguyen, T. Nguyen-Tien, R. Pfeiffer, G. Scholten, H. Simon, H. Stockemer and A. Toussaint, *J. Chromatogr.*, 1980, **201,** 147.
6. M. Nakajima, K. Kimura and T. Shono, *Bull. Chem. Soc. Jpn.*, 1983, **56,** 3052.
7. T. Iwachido, H. Naito, F. Samukawa, K. Ishimaru and K. Toei, *Bull. Chem. Soc. Jpn.*, 1986, **59,** 1475.
8. M. Lauth and P. Gramain, *J. Chromatogr.*, 1987, **395,** 153.
9. F. S. Stover, *J. Chromatogr.*, 1984, **298,** 203.
10. F. S. Stover, *J. Chromatogr.*, 1986, **368,** 476.
11. K. Fukushi and K. Hiiro, *Talanta*, 1988, **35,** 55.
12. S. Fanali, M. Cristalli and M. G. Quaglia, *J. Chromatogr.*, 1989, **472,** 441.
13. K. Fukushi and K. Hiiro, *J. Chromatogr.*, 1990, **523,** 281.
14. R. M. Izatt, J. S. Bradshaw, S. A. Nielsen, J. D. Lamb and J. J. Christensen, *Chem. Rev.*, 1985, **85,** 271.
15. R. M. Izatt, K. Pawlak, J. S. Bradshaw and R. L. Bruening, *Chem. Rev.*, 1991, **91,** 1721.
16. J. D. Lamb and R. G. Smith, *J. Chromatogr.*, 1993, **640,** 33.
17. P. Jandik, W. R. Jones, A. Weston and P. R. Brown, *LC.GC*, 1991, **9,** 634.

Pergamon

0039-9140(94)00227-4

*Talanta*, Vol. 42, No. 1, pp. 119–127, 1995

0039-9140/95 $9.50 + 0.00

# USE OF SURFACTANT-MEDIATED PHASE SEPARATION (CLOUD POINT EXTRACTION) WITH AFFINITY LIGANDS FOR THE EXTRACTION OF HYDROPHILIC PROTEINS

TOHRU SAITOH* and WILLIE L. HINZE†

Department of Chemistry, Laboratory for Analytical Micellar Chemistry, Wake Forest University, P.O. Box 7486, Winston-Salem, NC 27109-7486, U.S.A.

(*Received* 15 *June* 1994. *Revised* 29 *July* 1994. *Accepted* 2 *August* 1994)

**Summary**—The feasibility of utilizing a zwitterionic surfactant, 3-(nonyldimethylammonio)propylsulfate, or nonionic surfactant, Triton X-114, mediated phase separation in conjunction with affinity ligands was studied for hydrophilic protein extractions. Below (or above) its critical temperature (so-called cloud point), aqueous solutions of zwitterionic (or nonionic) surfactants separate into two immiscible phases, a surfactant-rich phase and an aqueous phase. Avidin was successfully extracted into the zwitterionic surfactant-rich phase when a small amount of the affinity ligand, *N*-(biotinoyl)dipalmitoyl-L-α-phosphatidyl ethanolamine, was added to the system. It was not possible to extract hexokinase into the surfactant-rich phase of the nonionic surfactant, Triton X-114, even if a considerable amount of octyl-β-D-glucoside was added to the solution as an affinity ligand. In contrast, the use of the zwitterionic surfactant and octyl-β-D-glucoside as an affinity ligand proved to be effective for the extraction of hexokinase. The hexokinase extraction efficiency was found to depend upon the solution pH and the concentration of the affinity ligand in the system. The results clearly indicate that hydrophilic proteins can be successfully extracted with surfactant mediated phase separations (cloud point extractions) via use of the zwitterionic surfactant, 3-(nonyldimethylammonio)propylsulfate, and appropriate affinity ligands. Some advantages of zwitterionic surfactants in such extractive processes relative to that of nonionic surfactants are delineated.

Aqueous solutions of many neutral (nonionic and zwitterionic) surfactant micellar systems, when subjected to temperature alterations, exhibit critical phenomenon.[1,2] That is, nonionic surfactant solutions, when heated, became turbid at the cloud point.[1] Above the cloud point temperature, such solutions separate into two isotropic phases, *i.e.* a surfactant-rich phase (also referred to as micellar-rich or coacervate phases in the literature[1–3]) and an essentially bulk aqueous phase. In contrast, aqueous solutions of certain zwitterionic surfactants display an upper consolute boundary. Thus, their isotropic two-phase region exists at temperatures below (rather than above) their critical temperature.[2]

Normally, the surfactant-rich phase has a very small volume element and hydrophobic species are efficiently concentrated into this phase allowing for their extraction and concentration. This phase separation behavior of nonionic surfactant micellar solutions (so-called cloud point extraction) was first utilized by Watanabe for the extraction and preconcentration of metal ions (as their metal chelates).[4,5] Subsequently, Bordier applied such phase separation behavior of solutions of the nonionic surfactant, Triton X-114, for the extraction and purification of hydrophobic membrane proteins.[6] An important advantage of the latter method is that membrane proteins can be easily separated from hydrophilic peripheral proteins. Since nonionic surfactant solutions are relatively mild, the hydrophobic proteins typically do not undergo any denaturation during the process. As a result, this general technique has experienced increasing popularity since Bordier's initial report.[7,8]

Recently, it has been reported that zwitterionic surfactants can be utilized in an analogous manner for the separation of hydrophobic from

*Present address: Hokkaido University, Faculty of Engineering, Analytical Chemistry Laboratory, Sapporo, 060, Japan.

†Author to whom correspondence should be addressed.

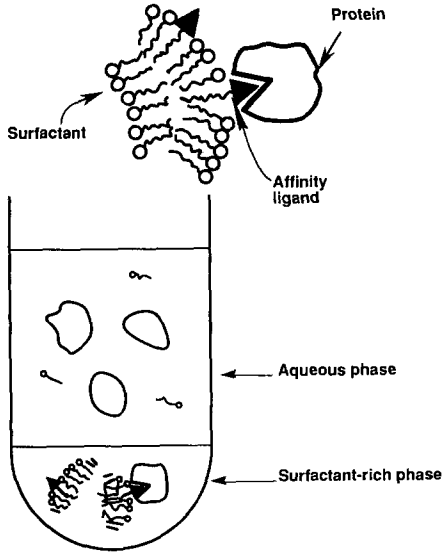


Fig. 1. Schematic representation of the surfactant-mediated phase separation process and affinity ligand partitioning in neutral micellar systems. Note: the surfactant-rich phase in the final phase separated system is not necessarily a micellar aggregate.[1,3,10]

hydrophilic proteins.[9] More important, the general use of zwitterionic (rather than nonionic) surfactants in such an extraction technique appears to offer significant advantages in terms of purer, homogenous surfactant preparation, minimum background absorbance at UV detection wavelengths, the two-phase region occurring at lower temperatures, more rapid phase separation, greater extraction efficiencies and concentration factors among others. A comprehensive review of the theory and applications of surfactant-mediated phase separations in analytical chemistry is available.[10] It should be noted that the phase separation behavior exhibited by aqueous solutions of other molecules, such as derivatized cyclodextrins[11] and polymeric systems,[12] has also been successfully exploited in extractive separations.

As yet, there appear to be no reports in the literature concerning the use of appropriate affinity ligands in conjunction with surfactant mediated cloud point extractions for the subsequent selective extraction and purification of hydrophilic proteins. The idea would be to use a relatively hydrophobic affinity ligand which would be specific for and strongly interact with the desired hydrophilic protein so that the resulting affinity ligand:protein complex would partition to the surfactant micellar aggregate and thus become concentrated in the surfactant-rich phase following phase separation. Figure 1 depicts the affinity cloud point extraction process. The use of affinity ligands in conjunction with the cloud point extraction would thus extend the scope of Bordier's original technique[6] to include selective extraction of hydrophilic proteins. It is rather surprising that this approach has not been previously reported in view of the fact that other extractive separation methods have been developed which employ the affinity interaction between proteins and substrates for efficient protein purification.[13] For example, aqueous polymeric phase separation systems with affinity polymers[12,14,15] as well as reversed micellar solvent extractions with affinity ligands[16] have been examined and developed for large scale protein purifications.

In this paper, we report the preliminary results of a feasibility study concerning the use of affinity ligands in conjunction with the zwitterionic and nonionic surfactant mediated phase separation technique for the extraction of relatively hydrophilic proteins. Avidin and hexokinase were extracted employing alkyl-biotin and octyl-$\beta$-D-glucoside, respectively as the affinity ligands in such cloud point extraction with the zwitterionic surfactant, 3-(nonyldimethylammonio)propyl sulfate (C9-APSO$_4$). In addition, the use of the nonionic surfactant, Triton X-114 in such affinity cloud point extractions was examined.

## EXPERIMENTAL

### *Apparatus*

All absorbance spectra and intensity measurements were made on a Varian Cary 219 UV-visible spectrophotometer. The pH measurements were made on a Corning Model 135 pH/ion meter.

### *Chemicals*

The zwitterionic surfactant, 3-(nonyldimethylammonio)propyl sulfate, (C9-APSO$_4$) was synthesized using a modified literature procedure[2] as recently reported.[9] The corresponding decyl analog (C10-APSO$_4$) is commercially available from Aldrich Chemical Co. (Milwaukee, WI, U.S.A.). The nonionic surfactants, polyethylene(7-8)-*p*-*t*-isooctylphenylether (Triton X-114) and polyoxyethylene(23)dodecanol (Brij-35) were obtained from Sigma Chemical Co. (St Louis, MO, U.S.A.) as 20 and 30 wt% solutions, respectively. The proteins and enzymes, *i.e.* avidin, from egg white; hexokinase, from baker's yeast, type III; concanavalin A, from

*Canavalia ensiformis*, type V; and ribonuclease B, from bovine pancreas, type III-B, were all also purchased from Sigma Chemical Co. and used as received. The affinity ligands *N*(biotinoyl)dipalmitoyl-L-α-phosphatidyl ethanolamine triethylammonium salt (R-biotin) and octyl-β-D-glucoside (octyl-glucoside) were obtained from Molecular Probes (Eugene, OR, U.S.A.) and Boehringer-Mannheim (Indianapolis, IN, U.S.A.), respectively. The water employed in this work was in-house distilled water which was further purified by passage through a Milli-Q System (Millipore Corp.). All other chemicals, reagents, and solvents were of the best commercial grade available.

*Procedures*

*Determination of phase diagrams and phase ratios.* The phase behavior of the zwitterionic surfactant, C9-$APSO_4$, in the presence of different amounts of the affinity ligand, octyl-glucoside, was determined by monitoring the temperature required for clarification of the solution mixture upon heating (or the onset of turbidity upon subsequent cooling). Typically, a 1.00 ml aqueous solution and 0.2000 g total of the surfactant and affinity ligand were thoroughly mixed in a 2.0 ml vial subsequent to being placed in a controlled temperature water bath (Haake, Berlin, Germany). The slope of the temperature change was less than 1°C per 15 min.

In the case of the nonionic surfactant system, a 0.20 ml portion of a 10 g/dl Triton X-114 aqueous solution and varying amounts of a 1.00 g/dl octyl-glucoside solution and methylene chloride were added to a 2.0 ml vial. Enough water was added to this mixture so that the final volume was 1.00 ml. The vial was placed in the controlled temperature water bath and the onset of turbidity (or clarification) temperature determined as described for the zwitterionic system.

The phase ratio (*i.e.* ratio of the volume of the surfactant-rich phase to that of the aqueous phase following phase separation) of the different surfactant micellar aqueous solutions was determined using a calibrated glass tube. The appropriate aqueous surfactant solution was placed into the tube and kept at 4°C for one week in the case of C9-$APSO_4$ (or at 30°C for four days in the case of Triton X-114) prior to measurement of the respective phase volumes. The results reported are the average of triplicate measurements. [Note: this procedure for determination of the phase ratio under different experimental conditions was far more accurate than that determined using centrifuge tubes and direct centrifugation. No detectable effect of centrifugation at 1500 rpm (or even 10,000 rpm) was observed on the determined volume fractions of the aqueous and surfactant-rich phases.]

*Affinity cloud point extraction of avidin with zwitterionic C9-$APSO_4$ and R-biotin as affinity ligand.* A mass (0.00–10.0 mg) of the R-biotin affinity ligand and C9-$APSO_4$ surfactant (190.0–200.0 mg) were placed into a 2.0 ml vial. The total mass of the mixture was kept at 0.2000 g. A 0.950 ml portion of an appropriately buffered aqueous solution was next added to the vial. This solution was sonicated until two clear liquid phases resulted. The vial was placed into an ice water bath in order to maintain a temperature of 0°C. Next, 0.050 ml of an avidin solution (containing 5.0 mg avidin/ml) was added to the vial, the vial mildly stirred for 5 min at 4°C, and then centrifuged at 3000 rpm for 10.0 min. A 0.500 ml aliquot of the bulk aqueous phase of the phase separated system was withdrawn from the vial using a Hamilton microsyringe and mixed well with an equivolume portion of a 1.0 wt% Brij-35 buffered aqueous solution which had been adjusted to the same pH as the extraction solution under study. The concentration of avidin and R-biotin present in the aqueous phase were calculated from absorbance measurements at 282 and 260 nm, respectively. The extraction percentage of avidin as a function of pH was calculated on the basis of the mass balance of avidin and the volume of the aqueous and the surfactant-rich phases.

*Affinity cloud point extraction of proteins with nonionic Triton X-114 and octyl-glucoside as the affinity ligand.* A 0.200 ml aliquot of 10.0 g/dl Triton X-114 aqueous solution (or 10.0 g/dl Triton X-114 solution containing 2.50 g/dl of ocytl-glucoside aqueous solution) was pipetted into a 2.00 ml sample vial. Next, 0.100 ml of 0.05*M* Tris-HCl buffer and 0.600 ml distilled water were added to the vial. After the solution was cooled to 4.0°C, a 0.100 ml portion of an appropriate protein solution (containing 5.0 mg protein per ml) was also added to the vial. The resulting solution was gently stirred for 5 min while the temperature was maintained at *ca.* 4°C. A small amount of methylene chloride was next added in order to promote the phase separation (2 μl in the case of the Triton X-114 only system and 4.3 μl for the Triton X-114-octyl-glucoside affinity system). After the vial

was placed into a constant temperature water bath (30°C) for 5 min, it was centrifuged (at 3000 rpm) for 10 min at room temperature (*ca.* 23°C). An aliquot of the aqueous phase of the phase separated system was withdrawn and the protein concentration determined via use of Lowry's method[17] following appropriate dilution. [Note: The concentration of the surfactants, C9-$APSO_4$ and octyl-glucoside, in the aqueous phase is roughly equal to their critical micelle concentration (CMC). At this concentration level, the surfactants' presence did not interfere with Lowry's method. Some interference was noted due to the buffer components. However, after dilution of the sample, this presented no difficulty.] The protein extraction percentage was calculated on the basis of the material balance and phase ratio of the extraction system.

*Affinity cloud point extraction of hexokinase with C9-$APSO_4$ and octyl-glucoside as affinity ligand.* Portions of octyl-glucoside (0.000–0.0600 g) and C9-$APSO_4$ (0.1400–0.2000 g) were placed in a 2.00 ml vial. The total amount of both materials present was always 0.2000 g. Next, 0.900 ml of buffer solution was added to the vial. The vial was shaken to mix its contents and after a clear homogenous solution (or clear two phase solution) was obtained, the vial was placed into an ice water bath. A 0.100 ml portion of hexokinase (7.5 mg/ml) was added to the system. The contents of the vial were then mildly stirred for 5 min at 4°C after which it was centrifuged (at 3000 rpm) for 10 min at 4°C. A 0.500 ml aliquot of the aqueous phase was collected by use of a microsyringe and mixed with an equivolume buffered 1.0 wt% Brij-35 aqueous solution which was adjusted to the same pH value as that of the original sample solution. The estimation of the extraction percentage of hexokinase was the same as that previously described.

## RESULTS AND DISCUSSION

### *Phase ratios and diagrams*

The phase diagram for the zwitterionic surfactant, C9-$APSO_4$, in the absence of any affinity ligand additives has previously been reported in the literature.[2,9] Figure 2 shows the volumes of the surfactant-rich extractant and aqueous phases as a function of the concentration of the affinity ligand, octyl-glucoside, for the zwitterionic C9-$APSO_4$, surfactant system.

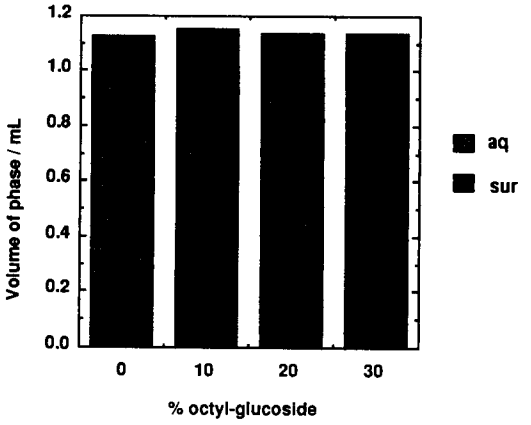


Fig. 2. Volume of aqueous and surfactant-rich phases following phase separation of aqueous mixtures containing C9-$APSO_4$ and octyl-glucoside as a function of the % octyl-glucoside present (*i.e.* [octyl-glucoside]/[octyl-glucoside] + [C9-$APSO_4$]). Conditions: 1.00 ml aqueous solution volume mixed with 0.2000 g total amount of the octyl-glucoside and C9-$APSO_4$ surfactants.

As the amount of the octyl-glucoside increased, the volume of the surfactant-rich extractant phase slightly increased. Additionally, as seen in Fig. 3, the critical temperature for the phase separation of aqueous solutions of C9-$APSO_4$ decreased as the amount of octyl-glucoside present was increased. For example, the critical temperature of an aqueous solution composed of 0.1500 g of C9-$APSO_4$ and 0.1000 g octyl-glucoside was approximately 0°C whereas in the absence of any octyl-glucoside, it was *ca.* 65°C. It may be noted that the critical micelle concen-

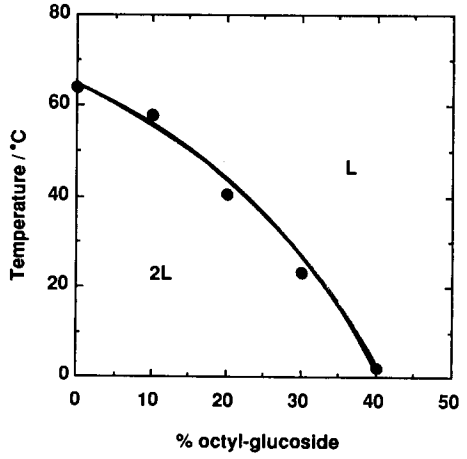


Fig. 3. Cloud point (upper critical temperature) of an aqueous mixed solution of zwitterionic C9-$APSO_4$ surfactant and octyl-glucoside affinity ligand as a function of the % octyl-glucoside present (*i.e.* % concentration ratio of octyl-glucoside [octyl-glucoside]/[octyl-glucoside] + [C9-$APSO_4$]). L refers to the single isotropic solution region, whereas 2L indicates the region where two isotropic phases coexist.

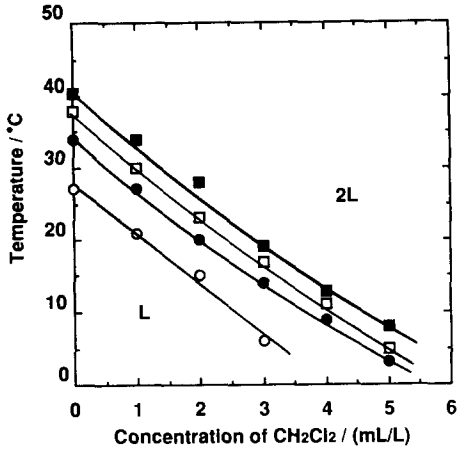


Fig. 4. Cloud point curves for aqueous solutions containing Triton X-114, octyl-glucoside, and methylene chloride as a function of the amount of added methylene chloride. Conditions: [Triton X-114] = 2.0 g/dl with [octyl-glucoside]: (○) 0, (●) 0.20, (□) 0.30, and (■) 0.40 g/dl.

tration (CMC) of C9-APSO$_4$ is 45.0m$M$ in water in the absence of any additives.[9,10]

The cloud point of a 2.00 g/dl Triton X-114 aqueous solution in the absence of any additives is 27°C. This value is in fairly good agreement with literature reports which range from 20 to 30°C for the cloud point of Triton X-114 solutions depending upon the exact surfactant concentration employed.[10] As can be seen from the data presented in Fig. 4, which illustrates the influence of methylene chloride upon the cloud point of Triton X-114 in the presence and absence of different amounts of the affinity ligand, octyl-glucoside, the cloud point temperature of Triton X-114 is drastically altered by additives. If increasing amounts of octyl-glucoside are added to aqueous solutions of Triton X-114, the cloud point increases and higher temperatures are required for the phase separation. This could be detrimental in protein extractions since the activity of many enzymes is known to decrease in the presence of surfactant solutions at or above room temperature.[18,19] However, it is well known that the addition of very small amounts of some relatively hydrophobic organic solvents can cause significant decreases in the cloud point of nonionic surfactant solutions. Thus, as can be observed from Fig. 4, the addition of small amounts of methylene chloride was found to be very effective in that it decreased the cloud point temperature of the Triton X-114/octyl-glucoside affinity system so that protein extractions can be carried out well below room temperature. In addition, its use resulted in the formation of a rigid, surfactant-rich extractant phase. Recently, there was a report in the literature concerning the use of glycerol to decrease the cloud point of Triton X-114 solutions in an analogous manner.[8] In most of our extraction studies the cloud point of the aqueous solutions of Triton X-114 and octyl-glucoside were adjusted to be approximately 7°C by the addition of appropriate amounts of methylene chloride.

The volume of the surfactant-rich phase following phase separation of 1000 ml of an aqueous 2.0 g/dl Triton X-114 solution containing 2 ml/l. methylene chloride was found to be 0.149 ml while that containing 4.3 ml/l. methylene chloride plus 0.50 g/dl octyl-glucoside was 0.178 ml. The CMC value for Triton X-114 in water in the absence of any additives is 0.35m$M$.[10]

*Affinity cloud point extraction of avidin using C9-APSO$_4$ with R-biotin as the affinity ligand*

Figure 5 illustrates the extent of extraction of avidin into the C9-APSO$_4$ surfactant-rich phase as a function of the concentration of the affinity ligand, *N*-(biotinoyl)dipalmitoyl-L-α-phosphatidylethanolamine triethylammonium salt (R-biotin), present. In the absence of any added affinity ligand or at very low R-biotin concentrations, the extraction percentage of avidin was low (*ca.* 10%) and did not significantly increase. However, in the higher concentration region of the R-biotin affinity ligand, the extraction of avidin increased. Thus, the overall shape of the curve for the extraction efficiency of avidin versus concentration of R-biotin is sigmoidal. Although avidin is considered to be a relatively hydrophilic protein, approximately

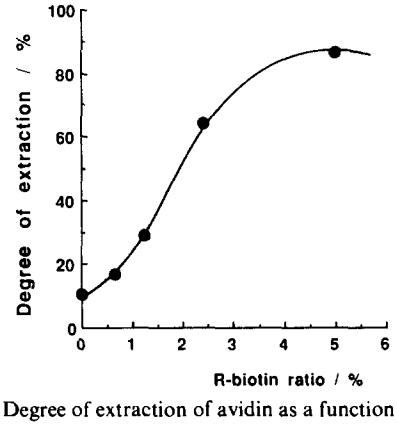


Fig. 5. Degree of extraction of avidin as a function of added affinity ligand, *N*-(biotinoyl)dipalmitoyl-L-α-phosphatidyl ethanolamine (R-biotin) present (*i.e.* [R-biotin]/[R-biotin] + [C9-APSO$_4$]) for the cloud point extraction with the zwitterionic surfactant, C9-APSO$_4$, at 4 C.

88% of the avidin was extracted from the aqueous solution into the C9-$APSO_4$ surfactant phase with only 10.0 mg of the R-biotin affinity ligand being required. The distribution coefficient for avidin (*i.e.* $[avidin]_{surf}/[avidin]_{aq}$) following cloud point extraction with C9-$APSO_4$ was found to be 0.41 in the absence of and 22.5 in the presence of 5.0% of the biotin affinity ligand.

It is well known that the avidin–biotin interaction is very strong. For instance, the avidin:biotin complex reportedly has a dissociation constant ($K_m$) of approximately $10^{-15}M$.[20] The efficient cloud point extraction of avidin can be regarded as resulting from this strong interaction which allows the hydrophobic affinity R-biotin ligand to "drag" the bound avidin into the C9-$APSO_4$ surfactant micellar phase (as illustrated in Fig. 1). The strong avidin–biotin interaction had previously been utilized for several applications in membrane chemistry and molecular biology.[21,22] The developed R-biotin ligand affinity cloud point extraction using C9-$APSO_4$ might also prove to be a useful alternative method in these type of applications.

The described cloud point affinity extraction procedure may not prove to be as useful for the large-scale purification of avidin or avidin-combined protein materials due to the requirements for its subsequent recovery from the extractant phase. In the biotin affinity chromatographic purification procedure for avidin, the conditions required for the subsequent elution of avidin from its biotin-bound state were a combination of low pH (pH 1.5) and a high concentration ($6.0M$) of guanidine hydrogen chloride. However, Orr *et al.*[23,24] have reported that while the free base form of 2-imminobiotin also strongly interacts with avidin ($K_m = 3.5 \times 10^{-11}M$), the cationic form (in the region below pH 4) only interacts weakly ($K_m < 10^{-3}M$). Thus, the use of such alkyl-2-imminobiotin affinity ligand instead of the R-biotin ligand described should prove to be superior for the large scale purification of avidin using the described affinity cloud point extraction method. This is due to the subsequent ease with which the avidin could then be recovered from the extractant surfactant-rich phase.

Under the optimal experimental conditions, the extraction per cent of avidin (*ca.* 88%) was not quite quantitative. This is probably the consequence of the fact that the avidin–biotin interaction is altered by the presence of the C9-$APSO_4$ surfactant present and/or that some of this surfactant still present (after phase separation) in the bulk aqueous phase could solubilize some of the R-biotin affinity ligand (and thus some of the bound avidin). Based on phase diagrams reported by Nilsson *et al.*,[2] the concentration of C9-$APSO_4$ originally present in the extraction system is above 60 wt%. Thus, it would not be surprising if the avidin–biotin binding interaction were affected by this concentrated surfactant solution. Additionally, UV absorbance data show that a small amount of the R-biotin affinity ligand is present in the aqueous phase following the extraction. As some of the zwitterionic C9-$APSO_4$ surfactant is also present in this aqueous phase, its presence may solubilize some of the affinity ligand and thus cause some of the R-biotin to remain in the aqueous phase. Despite the fact that the extraction is not quantitative, the developed cloud point extraction of avidin with R-biotin as the affinity ligand may prove to be a useful method because the preparation of the aqueous–surfactant phase separation system and the extraction procedure are very easy and simple. Additionally, the 88% extraction efficiency achieved is quite good and comparable with other reported extraction schemes for avidin.

*Attempted affinity cloud point extraction of proteins with nonionic Triton X-114 and octyl-glucoside*

Figure 6 illustrates the extent of extraction of the hydrophilic proteins, concanavalin A, ribonuclease B, hexokinase, and cytochrome *c* and the hydrophobic protein, bacteriorhodopsin using the nonionic surfactant, Triton X-114, with octyl-glucoside as the affinity ligand. No apparent extraction was achieved in the case of hexokinase and ribonuclease B and only a very small amount of cytochrome *c* was extracted. As previously reported by Bordier,[6] nearly 100% of the hydrophobic bacteriorhodopsin was extracted with the Triton X-114 in the absence of the octyl-glucoside (as well as in its presence).

Concanavalin A was slightly extracted (*ca.* 12%) by Triton X-114 alone. If the affinity ligand, octyl-glucoside (5 g/l.), was added to the extraction system, then the extent of extraction for concanavalin A increased (Fig. 6). However, the extraction per cent for concanavalin A is still fairly low (*ca.* 28%). This low affinity cloud point extraction efficiency was surprising in view

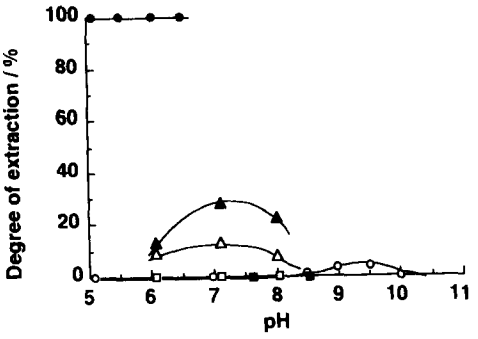


Fig. 6. Degree of extraction for different proteins into the nonionic Triton X-114 surfactant-rich phase using octyl-glucoside as the affinity ligand as a function of pH at 30°C: bacteriorhodopsin (●), cytochrome *c* (○), hexokinase (□), ribonuclease B (■), and concanavaline A in absence (△) and presence (▲) of the affinity ligand. Conditions: for extraction of bacteriorhodopsin and cytochrome [Triton X-114] = 2 g/dl, [octyl-glucoside] = 0.10 g/dl, and 3.0 ml/l. methylene chloride; for extraction of concanavaline A, hexokinase, and ribonuclease B [Triton X-114] = 2.0 g/dl, [octyl-glucoside] 0.50 g/dl, and 4.3 ml/l. methylene chloride; and for extraction of concanavaline A in absence of the affinity ligand [Triton X-114] = 2.0 g/dl and 2.0 ml/l. methylene chloride.

of the fact that it had been reported that the affinity interaction between concanavalin A and octyl-glucoside had been successfully employed for the extraction of concanavalin A into an organic reversed micellar phase at room temperature.[16] Sheu *et al.* found that such reversed micellar aqueous (and thus polar) core region was suitable for the incorporation of proteins (including hydrophilic ones).[25] In contrast, in the case of cloud point extractions, hydrophilic proteins do not appreciably distribute or bind to the relatively hydrophobic surfactant micellar entity.[6] The low extraction efficiency could be due in part to the temperature at which the extraction was conducted (30°C) as it has been reported that the affinity interaction between proteins and substrates decreases as the temperature increases.[26–28] Furthermore, there is the added possibility of denaturation of proteins in such highly concentrated surfactant solutions at high temperature as described previously.[18,28] For instance, solutions of hexokinase, especially type III, were found to be very unstable even if in the presence of suitable stabilizers.[29] Thus, it is thought that successful affinity cloud point extraction systems using nonionic surfactants will require suitable phase separation conditions, *i.e.* a nonionic surfactant–affinity ligand system in which the cloud point is below 0°C and the phases separate well at about 0°C. In this regard, the recent reports on the use of glycerol or Triton X-45 to allow for the low-temperature phase separation of Triton X-114 may prove useful.[8,30]

*Affinity cloud point extraction of hexokinase with zwitterionic C9-$APSO_4$ as surfactant and octyl-glucoside as the affinity ligand*

Figure 7 shows the extent of hexokinase extracted as a function of the solution pH by C9-$APSO_4$ both in the absence and presence of the affinity ligand, octyl-glucoside. In the absence of the affinity ligand, only 4–12% hexokinase was extracted by the C9-$APSO_4$ depending upon the pH employed. As can be seen, at each pH level examined, the presence of the affinity ligand in the zwitterionic surfactant medium led to an appreciable increase in the amount of hexokinase extracted (to over 50%). This fact suggests that the octyl-glucoside was distributed in the surfactant micellar phase and that it acted as an affinity ligand for the hydrophilic protein, hexokinase. A dissociation constant ($K_m = 1 \times 10^{-4} M$) has been reported in the literature for the D-glucose–hexokinase complex.[31] These successful results with the zwitterionic C9-$APSO_4$ surfactant are in sharp contrast with that previously mentioned for the attempted affinity cloud point extraction of hexokinase with the nonionic surfactant Triton X-114 and octyl-glucoside in which no hexokinase was extracted. That a small amount of hexokinase was extracted using just the zwitterionic C9-$APSO_4$ surfactant in the absence of the affinity ligand suggests that the charged head groups of this surfactant might interact with this hydrophilic protein and enhance its extraction efficiency vis-à-vis that

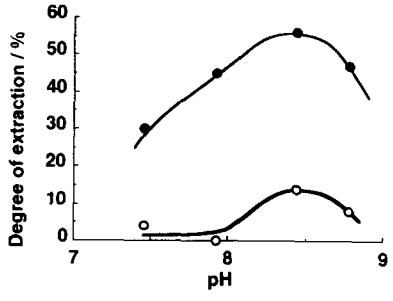


Fig. 7. Dependence of the extraction percentage of hexokinase upon pH for the cloud point extraction using the zwitterionic surfactant C9-$APSO_4$ in the absence (○) and presence (●) of the affinity ligand, octyl-glucoside, at 4°C. Conditions: (○) 0.2000 g C9-$APSO_4$ in 1.00 ml aqueous solution; (●) 0.1600 g C9-$APSO_4$ plus 0.0400 g octyl-glucoside in 1.00 ml aqueous solution.

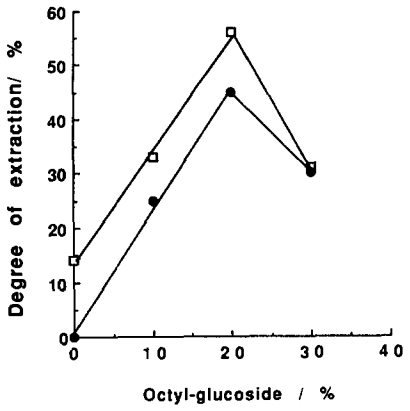


Fig. 8. The effect of the octyl-glucoside affinity ligand concentration ratio (*i.e.* [octyl-glucoside]/[octyl-glucoside] + [C9-$APSO_4$]) upon the extent of extraction of hexokinase at pH 7.92 (●) and 8.44 (□) using the zwitterionic surfactant, C9-$APSO_4$, at 4.0°C.

possible with the uncharged Triton X-114 surfactant system.

Based upon the data in Fig. 7, it appears that the most suitable pH for the affinity extraction of hexokinase with C9-$APSO_4$ is about 8.5. At each pH level between 7 and 9 examined, the maximum extraction efficiency of hexokinase was observed when the concentration ratio of the octyl-glucoside per total surfactant ratio was 20 wt% (see Fig. 8). Strangely, when the concentration ratio of octyl-glucoside was increased to 30 wt%, the extraction efficiency decreased. Bordier has reported that the amount of octyl-glucoside displaced from the surfactant-rich phase of Triton X-114 to the aqueous phase increased as the concentration of octyl-glucoside increased.[6] If the same situation occurs for the zwitterionic C9-$APSO_4$ system, then this might explain the decreased hexokinase extraction efficiency at the highest octyl-glucoside concentration level. It might be noted that under our experimental conditions for the C9-$APSO_4$–octyl-glucoside system, the clear aqueous phase after centrifugation at 4°C turned turbid again if the temperature was lowered to 0°C. This suggests that the aqueous phase still contained both C9-$APSO_4$ and octyl-glucoside. The fact that some of the affinity ligand was still present in the aqueous phase probably explains why the optimum extraction efficiency was only around 58% for hexokinase. Thus, the use of a more hydrophobic alkyl-glucoside affinity ligand possessing a longer alkyl group should be more effective in such affinity cloud point extraction of hexokinase since less of the ligand would be present in the aqueous phase and a clearer phase separation should result.

A significant advantage of the affinity cloud point extraction technique using the zwitterionic surfactant, C9-$APSO_4$, and octyl-glucoside (or other alkyl-glucosides) as affinity ligand is that all procedures, including the extraction of the proteins, can be conducted at low temperature. This is particularly important in the extraction of thermally labile proteins. A more important advantage of this system is that both the extractant surfactant and affinity ligand can be easily removed from the protein sample by subsequent dialysis.[32] This is a consequence of the relatively high CMC values of both of these surfactants (0.045*M* for C9-$APSO_4$[9] and 0.025*M* for octyl-glucoside[33]). In contrast, the CMC of Triton X-114, 0.35m*M*, is too low for the subsequent use of the dialysis technique for its removal from the extracted protein sample. Furthermore, the phase separation occurs much faster for the systems incorporating a zwitterionic surfactant compared to those involving a nonionic surfactant.[9] This quicker phase separation is important not only for handling convenience but also for the potential application of the technique to continuous systems such as a counter-current extraction or a flow injection analysis.

These preliminary results indicate that the affinity cloud point extraction technique is feasible for the purification of hexokinase. This extraction method might also prove useful in those studies concerning determination of the biodistribution of this protein.[34]

## CONCLUSIONS

The preliminary results presented demonstrate the feasibility of employing affinity ligands to extend the scope of Bordier's cloud point extraction technique to include hydrophilic biomaterials in analytical separations. Potential advantages of the approach include experimental convenience, lower cost, and enhanced analytical sensitivity due to the fact that the hydrophilic proteins can be easily extracted from the bulk aqueous solution into the much smaller volume element of the surfactant-rich phase following phase separation. Since zwitterionic and nonionic surfactants are routinely employed in the initial solubilization and fractionation steps of many protein isolation schemes[35,36] means that by judicious selection of that surfactant, the aforementioned affinity

ligand:cloud point extraction procedures can be subsequently employed by mere addition of the proper affinity ligand. Thus, this approach is compatible with the first step in many existing biomaterial separation and purification schemes. The general approach may also prove feasible for the large scale selective separation of some hydrophilic proteins although much more work is required to demonstrate this aspect. A particular advantage in this latter application when employing zwitterionic surfactants will be the ease and rapidness with which its solutions phase separate and the ability to conveniently remove the zwitterionic surfactant from the protein by dialysis as previously mentioned.

*Acknowledgements*—We thank Professor Fawzy S. Sadek (Winston-Salem State University) for providing laboratory space for conducting a portion of this work during which time our building was closed due to an asbestos crisis and Dr Yasuzo Suzuki (Research Institute for Polymers and Textiles, Japan) for helpful discussions. In addition, we thank several anonymous referees for their helpful suggestions. Support of this research by the National Institute of General Medical Sciences through Grant BBCA (AHR-A) 1 R15 GM42076-01 is gratefully acknowledged.

## REFERENCES

1. V. Degiorgia, in *Physics of Amphiphiles: Micelles, Vesicles, and Microemulsions*, V. DeGiorgia and M. Corti (eds), pp. 303–335, North Holland, Amsterdam, 1985.
2. P. G. Nilsson, B. Lindman and R. G. Laughlin, *J. Phys. Chem.*, 1984, **88,** 6357.
3. K. Kenjo, *Bull. Chem. Soc. Jpn*, 1966, **39,** 685.
4. H. Watanabe and H. Tanaka, *Talanta*, 1978, **25,** 585.
5. W. L. Hinze, in *Ordered Media in Chemical Separations*, W. L. Hinze and D. W. Armstrong (eds), pp. 48–55. American Chemical Society, Washington, DC, 1987.
6. C. Bordier, *J. Biol. Chem.*, 1981, **256,** 1604.
7. J. G. Pryde, *Trends Biochem. Sci.*, 1986, **11,** 160.
8. D. Werck-Reichhart, I. Benveniste, H. Teutsch, F. Durst and B. Gabriac, *Anal. Biochem.*, 1991, **197,** 125.
9. T. Saitoh and W. L. Hinze, *Anal. Chem.*, 1991, **63,** 2520.
10. W. L. Hinze and E. Pramauro, *CRC Crit. Rev. Anal. Chem.*, 1993, **24,** 133.
11. D. Warner-Schmid, S. Hoshi and D. W. Armstrong, *Sepn Sci. Technol.*, 1993, **28,** 1009.
12. G. Johansson, in *Partition in Aqueous Two-Phase Systems: Theory, Methods, Uses, and Applications to Biotechnology*, H. Water, D. E. Brooks and D. Fisher (eds), p. 161. Academic Press, New York, 1985.
13. J. Carlsson, J. C. Janson and M. Sparrman, in *Protein Purification: Principles, High Resolution Methods, and Applications*, J. C. Janson and L. Ryden (eds), pp. 275–329. VCH, New York, 1989.
14. G. Johansson, in *Protein Purification: Principles, High Resolution Methods, and Applications*, J. C. Janson and L. Ryden (eds), pp. 330–345. VCH, New York, 1989.
15. G. Johansson, G. Birkenmeier, P. A. Albertsson and G. Kipperschlager, in *Separations Using Aqueous Phase Systems: Applications in Cell Biology and Biotechnology*, D. Fisher and I. A. Sutherland (eds), pp. 7–23. Plenum Press, New York, 1989.
16. J. M. Woll, T. A. Hatton and M. L. Yarmuch, *Biotech. Prog.*, 1989, **5,** 57.
17. O. H. Lowry, *J. Biol. Chem.*, 1951, **193,** 265.
18. H. U. Schulze, R. Kannler and B. Junker, *Biochim. Biophys. Acta*, 1985, **814,** 85.
19. Y. K. Rao, P. Bahadur, A. Bahadur and S. Ghosh, *Indian J. Biochem. Biophys.*, 1989, **26,** 390.
20. N. M. Green, *Adv. Protein Chem.*, 1975, **29,** 85.
21. E. A. Bayer and M. Wilchek, *Trends Biochem. Sci.*, 1978, **3,** N257.
22. E. A. Bayer, E. Skutelsky and M. Wilchek, *Methods Enzymol.*, 1979, **62,** 308.
23. G. A. Orr, *J. Biol. Chem.*, 1980, **256,** 761.
24. G. A. Orr, G. C. Heney and R. Zoheb, *Methods Enzymol.*, 1986, **122,** 83.
25. E. Sheu, K. E. Coklen, T. A. Hatton and S. H. Chen, *Biotech. Prog.*, 1986, **2,** 175.
26. G. Johansson and M. Andersson, *J. Chromatogr.*, 1984, **303,** 39.
27. C. R. Lowe and P. D. G. Dean, *Biochem. J.*, 1973, **133,** 515.
28. R. Lotan, G. Beattie, W. Hubbell and G. L. Nicolson, *Biochemistry*, 1977, **16,** 1787.
29. M. J. Holroyde, M. B. Allen, A. C. Storer, A. S. Warsy, J. Chesher, I. P. Trayer, A. Cornish-Bowden and D. C. Walker, *Biochem. J.*, 1976, **153,** 363.
30. B. R. Ganong and J. P. Delmore, *Anal. Biochem.*, 1991, **193,** 33.
31. E. A. Barnardo, *Methods Enzymol.*, 1975, **42,** 6.
32. C. B. Baron and T. E. Tompson, *Biochim. Biophys. Acta*, 1975, **382,** 276.
33. K. Shinoda, T. Tamaguchi and R. Hori, *Bull. Chem. Soc. Jpn*, 1961, **34,** 237.
34. D. L. Purich, H. J. Fromm and F. B. Rudolph, *Adv. Enzymol.*, 1973, **38,** 249.
35. C. Tiruppathi, D. H. Alpers and B. Seetharam, *Anal. Biochem.*, 1986, **153,** 330.
36. A. Helenius and K. Simons, *Biochim. Biophys. Acta*, 1975, **415,** 29.

Pergamon

0039-9140(94)00228-2

*Talanta*, Vol. 42, No. 1, pp. 129–136, 1995

0039-9140/95 $9.50 + 0.00

# SIMULTANEOUS DETERMINATION OF PYRIDOXAL AND PYRIDOXAMINE BY DIFFERENT SPECTROFLUORIMETRIC TECHNIQUES

J. J. BERZAS NEVADO, J. A. MURILLO PULGARÍN and M. A. GÓMEZ LAGUNA

Department of Analytical Chemistry and Food Technology, University of Castilla-La Mancha, 13071 Ciudad Real, Spain

(*Received* 8 *February* 1994. *Revised* 1 *August* 1994. *Accepted* 2 *August* 1994)

**Summary**—Binary mixtures of pyridoxal and pyridoxamine can be resolved by using zero-crossing first derivative spectrofluorimetry, first derivative constant wavelength synchronous luminescence spectrometry and first derivative constant energy synchronous luminescence spectrometry. These methods do not require any previous separation steps. The lowest quantization limit is obtained with first derivative constant energy synchronous fluorescence (13.0 and 9.0 $\mu$g/l. for pyridoxal and pyridoxamine, respectively). The measurements were performed in aqueous medium at pH 7.0 provided by adding 0.05*M* phosphate buffer solution. In order to demonstrate the validity of these methods a complete and exhaustive statistical analysis of the experimental data was performed. Pyridoxal and pyridoxamine were determined by these methods in synthetic and real mixtures with good results.

The determination of vitamin $B_6$ and its derivatives is of great interest, but this determination is quite complicated owing to the multiple forms and similar structures of these compounds. Different methods have been reported of characterizing and resolving mixtures of these compounds by microbiological,[1] enzymatic,[2] polarographic,[3] spectrophotometric[4] and fluorimetric methods.[5] However, some prior separation steps are necessary in all of them. Petidier *et al.* reported[6] a method for the simultaneous determination of some derivatives of vitamin $B_6$ by using second derivative fluorescence spectroscopy of these compounds, but it is necessary to use reactions of these compounds with beryllium in ammoniacal medium.

The sensitivity and selectivity of fluorescence is quite useful in analyses, but many spectra of several fluorescence compounds are often impossible to resolve satisfactorily without separation techniques, although each fluorescence compound can be characterized by two wavelengths. Therefore, the development of a technique which is able to improve the selectivity of fluorescence for multicomponent analysis and which does not involve separation steps and is less time-consuming, is of great interest.

In this paper we combined synchronous fluorescence spectroscopy introduced by John and Soutar,[7] with derivative fluorescence technique (described by Green and O'Haver[8]), to resolve binary mixtures of pyridoxal and pyridoxamine, since they showed highly overlapping spectra. Constant wavelength synchronous luminescence spectroscopy implied the simultaneous scanning of both the excitation and emission monochromator at the same scan speed. By using this technique, a reduction in Rayleigh scattering can be obtained.

Inman and Winefordner[9] describe constant energy synchronous luminescence spectroscopy, where a constant energy difference is maintained between the monochromators. This technique avoids interference in Raman scattering.

Synchronous spectra are simpler, narrower, and hence more distinctive than conventional spectra. The combination of derivative and spectrofluorimetric techniques improved the selectivity of the analysis. Thus, the derivative synchronous fluorescence method has been described for the resolution of compound mixtures with spectra of similar characteristics such as those provided by motor oil,[10] or polycycle aromatic.[11] A first study appeared in which constant energy synchronous luminescence was combined with derivative fluorescence technique to determine four polynuclear hydrocarbons.[11] Another work appeared recently on the resolution of binary mixtures of nafcillin and methicillin[12] using these techniques.

This paper describes four methods to resolve the mixture of pyridoxal and pyridoxamine by employing first derivative excitation and emission spectra; and first derivative synchronous fluorimetry (constant wavelength and constant energy). In all cases, the mixtures were resolved by scanning only one spectrum.

## EXPERIMENTAL

### *Reagents*

Pyridoxal and pyridoxamine were purchased from Merck and Sigma, respectively. Stock solutions of 50.0 mg/l. of each one were prepared by dissolving in Milli-Q water. A 0.05*M* buffer solution of pH 7.0 was prepared by mixing suitable amounts of dihydrogen phosphate solution with sodium hydroxide. Stock solutions were stored at 4°C and protected from the light. Under these conditions they showed no sign of decomposition for at least eight days.

### *Apparatus*

Fluorescence measurements were performed on a Perkin–Elmer LS-50 equipped with Xenon Lamp, connected to an Attaio S 3000 ST 386 computer, fitted with Perkin-Elmer F. L. Data Manager (FLDM) software and Epson FX-850 printer. 'FTOTAL'[13] software was used for processing the total luminescence spectra.

Thermostatic equipment and a Crison mod 2001, pHmeter with glass-satured calomel combination electrode were also used.

### *Procedures*

*Determination of pyridoxal and pyridoxamine by first derivative of excitation spectra.* A known volume of stock solution containing 24.0–1000 μg/l. of pyridoxal and 22.0–1000 μg/l. of pyridoxamine was placed in a 25-ml volumetric flask. Immediately afterwards, 2.5 ml of pH 7.0 buffer solution were added to every volumetric flask and diluted to the mark with Milli-Q water. Reagent blank was not necessary.

The excitation spectra were recorded with an emission wavelength at 388 nm to determine pyridoxal in the presence of pyridoxamine and pyridoxamine in the presence of pyridoxal. First derivatives were calculated and the absolute value of the first derivatives were measured at 316 and 325 nm for the determination of pyridoxal and pyridoxamine, respectively.

*Determination of pyridoxal and pyridoxamine by first derivative of emission spectra.* By using this technique both vitamins can be determined when they are found in the range 68.0–1000 μg/l. for pyridoxal and 36.0–1000 μg/l. for pyridoxamine.

The samples were prepared as in the first method. The emission spectra were recorded with excitation at 324 nm for the simultaneous determination of pyridoxal and pyridoxamine. First derivatives were calculated and the absolute values of the first derivative were measured at 376 and 391 nm for the determination of pyridoxal and pyridoxamine respectively.

*Determination of pyridoxal and pyridoxamine by first derivative of constant wavelength synchronous spectra.* This technique allows us to determine pyridoxal and pyridoxamine simultaneously by recording only one synchronous spectrum when these vitamins are found in the range 18.0–1000 μg/l. for pyridoxal and 16.0–1000 g/l. for pyridoxamine.

The sample preparations were thermostatically controlled at 20°C, and the synchronous spectra were recorded by scanning both monochromators together, while maintaining a constant of 56 nm difference between both wavelengths. First derivatives were calculated, and the absolute values of the first derivatives were measured at 316 nm for pyridoxal and 328 nm for pyridoxamine.

*Determination of pyridoxal and pyridoxamine by first derivative of constant energy synchronous spectra.* The synchronous spectra must be recorded maintaining a constant difference of $-4900\ cm^{-1}$ between their wave numbers. The first derivative was calculated and the absolute value was measured at 316 and 325 nm for the determination of pyridoxal and pyridoxamine respectively. Samples were prepared as in the previous methods with pyridoxal and pyridoxamine concentrations varying from 13.0 to 1000 μg/l. for pyridoxal and 9.0 to 1000 μg/l. for pyridoxamine.

## RESULTS AND DISCUSSION

### *Spectra characteristics*

Total luminescence spectra show the best characterization of the fluorescence compound. They were generated by a suitable computer program.[13] These spectra can be plotted as an isometric projection, where excitation spectra, at stepped increments of emission wavelength, are recorded and drawn. Total luminescence spectra can be transformed to a two-dimensional plot of excitation and emission wavelengths by linking points of equal intensity to

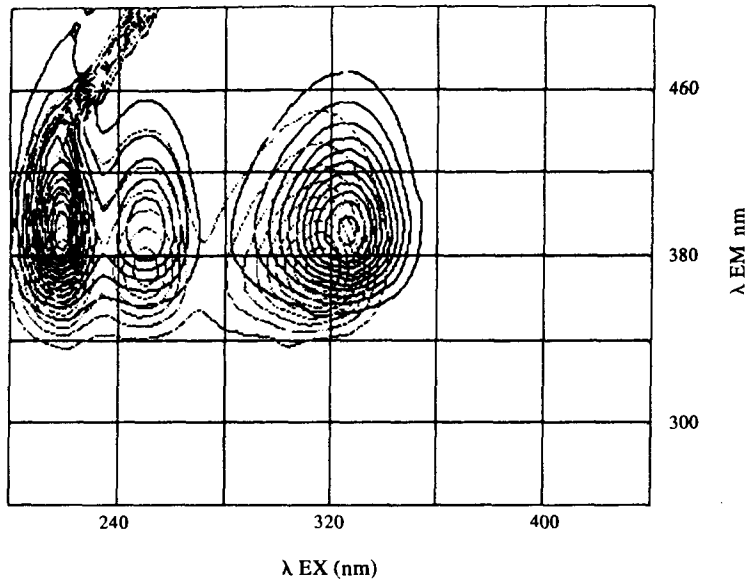


Fig. 1. Contour plots spectra of pyridoxal (---) and pyridoxamine (——).

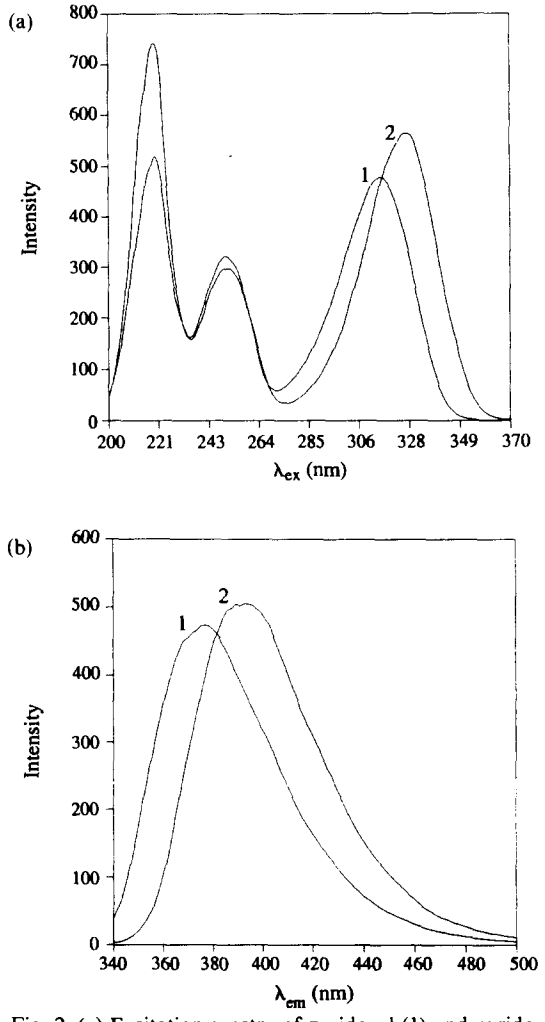


Fig. 2. (a) Excitation spectra of pyridoxal (1) and pyridoxamine (2). (b) Emission spectra of pyridoxal (1) and pyridoxamine (2).

form contours. Contour presentation is more useful than isometric projection due to the presence of hidden excitation peaks shown up by the former. Thus, Fig. 1 presents pyridoxal and pyridoxamine spectra as contour maps.

Pyridoxal exhibits three excitation maxima at 220, 250 and 315 nm, and one emission maximum at 378 nm (Fig. 2A). Pyridoxamine showed excitation maxima at 220, 245 and 327 nm and its emission maximum was at 393 nm (Fig. 2B). For pyridoxal, the wavelengths chosen to work with were 315 and 378 nm for excitation and emission, respectively. For pyridoxamine, 327 and 393 nm were selected for excitation and emission, respectively. In spite of the fact that we do not obtain maximum sensitivity with these, the inner filter effect, which occurs at wavelengths close to 200 nm due to certain inorganic ions, is avoided.

As can be seen in Fig. 3, pyridoxal and pyridoxamine showed highly overlapping fluorescence spectra, so it is not possible to resolve this mixture by conventional fluorescence, and other techniques must be applied.

*Factors affecting fluorescence intensity*

Chemical variables were studied to obtain the best measurement conditions and maximum fluorescence signals. The dielectric constant can modify the fluorescence characteristics of the compound. Thus, the effect of ethanol content in the medium was investigated by preparing samples of both vitamins and varying the ethanol percentage between 0 and 80%. Rela-

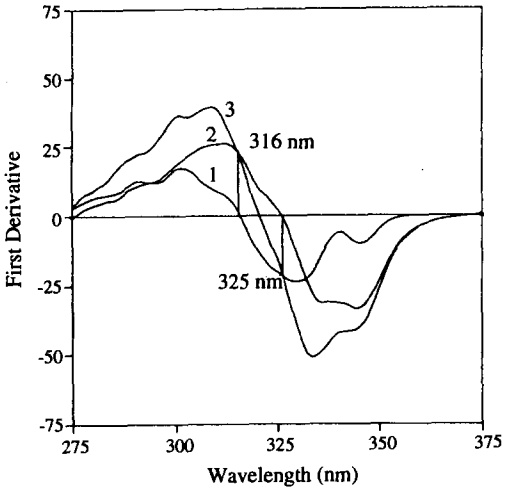


Fig. 3. First derivative excitation spectra of pyridoxal (1), pyridoxamine (2) and their mixture (3).

tive fluorescence intensity decreases as ethanol content in the medium increases, so the final assay samples were made in aqueous solutions as this provided maximum fluorescence intensity.

The influence of pH on the fluorescence intensity was studied by adding different amounts of $HClO_4$ or NaOH solutions. Fluorescence intensities of pyridoxal and pyridoxamine were maximum and constant between pH 5.5 and 9.5, and pH 7.0 was selected as most suitable. pH 7.0 was obtained by adding phosphate buffer solutions. The fluorescence intensities of pyridoxal and pyridoxamine were not affected by the concentration of the buffer. A 0.05*M* concentration of buffer was selected to obtain suitable buffering capacity.

Another factor that affects fluorescence intensity is temperature. Thus, fluorescence intensities show a decrease as temperature increases from 3 to 50°C. Temperature coefficient was of the order of 1.05%°C$^{-1}$ for pyridoxal; this effect can be explained by the higher internal conversion when temperature increased, facilitating non-radiative deactivation of the excited single state.[14] Pyridoxamine showed a temperature coefficient of the order of 1.51%°C$^{-1}$; in this case, the rate of intersystem crossing tends to be highly temperature dependent.[14] Therefore, the use of a thermostat is recommended, choosing a measurement temperature of 20°C, an intermediate room temperature.

In these conditions, the influence of both vitamin concentrations on fluorescence intensity was studied. A linear relation between fluorescence intensity and pyridoxal concentration in the range from 0.05 to 3.0 mg/l. can be observed. For pyridoxal concentration higher than 3.0 mg/l. the intensity decreases due to fluorescence inversion phenomena. Pyridoxamine showed a linear relation fluorescence intensity from 0.05 to 1.5 mg/l.

*Resolution of the mixture of pyridoxal and pyridoxamine*

Contour plots showed highly overlapping spectra, and there are no excitation or emission spectra where the bands were separated (Fig. 1), so when they are together in the same mixture, they cannot be determined by conventional fluorescence. For this reason it is necessary to use another technique.

The first partial derivative of tridimensional spectra in respect of excitation wavelength was calculated. But as it is not possible to resolve the strong overlapping spectra, the zero-crossing technique was applied to them. In order to discover the best instrumental conditions, scan speed and width factor were studied in order to ascertain the most suitable signal-noise ratio. The first derivative was calculated with 60, 240, 720 and 1500 nm/min as scan speed, 240 nm/min was chosen as the most suitable scan speed. The width factor was varied from 2 to 9 (equivalent to 19 points convoluting according to Savitzky and Golay algorithm)[15,16] and 4 was selected as providing the most suitable signal-noise ratio. Although the maximum fluorescence intensities were obtained when the excitation spectra were recorded at 378 and 393 nm as emission wavelengths for pyridoxal and pyridoxamine, respectively, 388 nm was the wavelength chosen because it was possible to determine pyridoxal in the presence of pyridoxamine and pyridoxamine in the presence of pyridoxal by scanning only one spectrum with similar fluorescence intensity and without loss of sensitivity in respect of the maximum for each one. Figure 3 shows the first derivative excitation spectra of pyridoxal, pyridoxamine and their mixture. We selected zero-crossing wavelength 316 and 325 nm for pyridoxal and pyridoxamine.

When first partial derivative of total luminescence spectra in respect of emission wavelength was performed, it was not possible to obtain separate bands in order to determine both compounds simultaneously. By applying the zero-crossing technique to the first derivative emission spectra pyridoxal and pyridoxamine

can be determined by scanning only one emission spectrum at $\lambda_{ex} = 324$ nm.

Although the maximum signal can be obtained when the emission spectra are recorded at $\lambda_{ex} = 315$ nm for pyridoxal and $\lambda_{ex} = 327$ nm for pyridoxamine, 324 nm was chosen as the most suitable excitation wavelength because it was possible to determine pyridoxal and pyridoxamine by scanning one emission spectrum without a significative loss in sensitivity.

The first derivative was calculated with a scan speed of 240 nm/min and a width factor of 4 to provide a suitable signal-noise ratio. The zero-crossings selected were 376 and 391 nm for pyridoxal and pyridoxamine respectively (Fig. 4).

Other fluorescence techniques were used to improve the results: conventional synchronous spectra were used to determine these vitamins by direct measurement of intensity. Figure 5 shows a tridimensional spectra plot of a mixture of pyridoxal and pyridoxamine when scanned at different wavelength intervals (from 5 to 200 nm). The first derivative of these spectra cannot resolve the overlapping spectra, so it was necessary to use the zero-crossing technique to resolve the mixture. The best sensitivity and maximum signal were obtained for pyridoxal when a wavelength interval of 51 nm was used, and 57 nm was used for pyridoxamine. But a wavelength interval of 56 nm was used to determine pyridoxal and pyridoxamine by first derivative of synchronous spectra by scanning only one synchronous spectrum without loss of sensitivity.

Figure 6 shows the first derivative synchronous spectra of pyridoxal, pyridoxamine

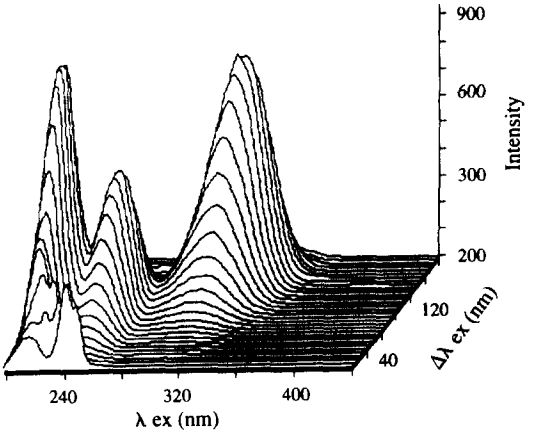


Fig. 5. Tridimensional plots of constant wavelength spectrum of pyridoxal and pyridoxamine mixture.

and their mixture. The selected zero-crossing wavelengths were 316 and 328 nm for pyridoxal and pyridoxamine respectively. Instrumental conditions were the same as described above.

The last method that we used to try to improve the results was constant energy synchronous spectra, where 61 scans of samples of pyridoxal and pyridoxamine were recorded between 200 and 440 nm at different wave number intervals ranging from $-2200$ to $-8300$ cm$^{-1}$. Maximum fluorescence intensity was obtained when the wave numbers $-5300$ and $-5100$ cm$^{-1}$ were used for pyridoxal and pyridoxamine. But $-4900$ cm$^{-1}$ was the most suitable wave number for resolving the mixture of pyridoxal and pyridoxamine by recording only one constant energy synchronous spectrum since suitable fluorescence intensity was obtained without loss of sensitivity. The first derivative

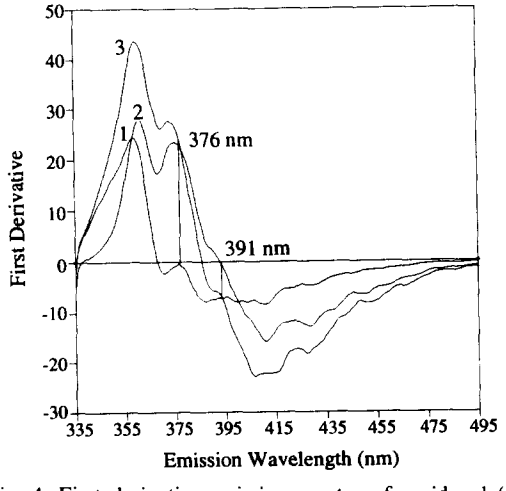


Fig. 4. First derivative emission spectra of pyridoxal (1), pyridoxamine (2) and their mixture (3).

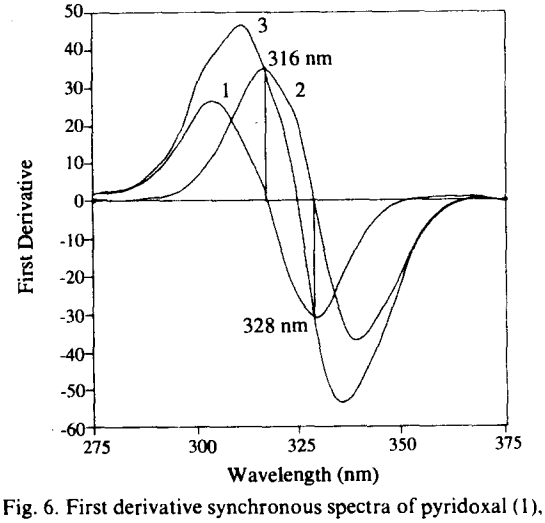


Fig. 6. First derivative synchronous spectra of pyridoxal (1), pyridoxamine (2) and their mixture (3).

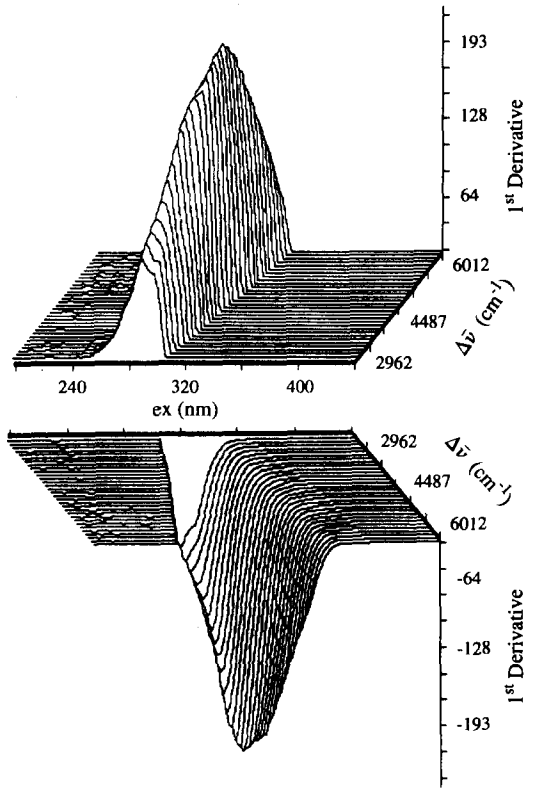


Fig. 7. Tridimensional plots of first derivative constant energy synchronous of pyridoxal and pyridoxamine mixture.

(Fig. 7) was calculated and the zero-crossing technique was also used; in this way, both vitamins were resolved with the greatest sensitivity. Pyridoxal and pyridoxamine concentration were proportional to the signal measured at 316 and 328 nm, respectively.

To provide a suitable signal-noise ratio a scan speed of 240 nm/min and a width factor of 4 were selected.

*Statistical analysis of results*

In order to demonstrate the mutual independence of the analytical signals of pyridoxal and pyridoxamine, we performed an exhaustive statistical analysis of the results in order to test them. We checked whether the zero-crossing wavelengths selected in every method were the most suitable ones or not.

Calibration graphs were constructed from the first derivative signals for standards containing between 20.0 and 1000 $\mu$g/l. of pyridoxal in the absence of pyridoxamine and in the presence of 200, 500 and 800 $\mu$g/l. of pyridoxamine. Similarly, four calibration graphs were prepared for standards containing between 20.0 and 1000 $\mu$g/l. of pyridoxamine in the absence of pyri-

Table 1.

| 1st derivative | Compound | Slope | Intercept | Correlation coefficient | Standard deviation | | Detection limit ($\mu$g/l.) | Quantitation limit ($\mu$g/l.) | Calibration range ($\mu$g/l.) |
|---|---|---|---|---|---|---|---|---|---|
| | | | | | Slope | Intercept | | | |
| Excitation | Pa | 102.2 | 1.39 | 0.9992 | 1.5 | 0.81 | 7.1 | 24.0 | 24.0–1000 |
| | Pm | 95.7 | 1.74 | 0.9994 | 1.4 | 0.72 | 6.2 | 22.0 | 22.0–1000 |
| Emission | Pa | 36.03 | 0.41 | 0.9981 | 0.8 | 0.41 | 20.0 | 68.0 | 68.0–1000 |
| | Pm | 110.12 | 1.26 | 0.9994 | 1.6 | 0.83 | 11.0 | 36.0 | 36.0–1000 |
| Constant wavelength | Pa | 139.8 | 1.98 | 0.9996 | 1.6 | 0.84 | 6.0 | 18.0 | 18.0–1000 |
| Synchronous | Pm | 164.8 | 1.51 | 0.9998 | 1.2 | 0.64 | 5.0 | 16.0 | 16.0–1000 |
| Constant energy | Pa | 141.8 | 1.95 | 0.9994 | 1.9 | 1.0 | 4.0 | 13.0 | 13.0–1000 |
| Synchronous | Pm | 210.3 | 1.96 | 0.9996 | 1.6 | 0.86 | 3.0 | 9.0 | 9.0–1000 |

Pa = Pyridoxal; Pm = Pyridoxamine.

doxal and in the presence of 200, 500 and 800 $\mu$g/l. of pyridoxal.

Linear regression equations ($y = a + mx$) for pyridoxal and pyridoxamine were obtained. The slopes, intercepts, correlation coefficients, standard deviations, detection limits, quantization limits and calibration range obtained for determination of pyridoxal and pyridoxamine by first derivative of excitation, emission, constant wavelength synchronous and constant energy synchronous spectra are summarized in Table 1. The significance of the intercept on the $y$ axis of the obtained regression line was evaluated by applying the Student $t$-test at 95% confidence level. In all the calibration graphs the intercept on the ordinate is negligible, since the experimental $t$-value is smaller than the critical $t$-value. The accuracy of the method can be tested by the use of a statistical technique such as "analysis of variance". Analysis of variance assumes that residual error variance does not change from one sample to another or from one calibration graph to another. The variance ratio (experimental $F$) must be calculated and compared to a theoretical value of $F$, for adequate degrees of freedom at 95% confidence level.

For four series of five standard samples containing 500 $\mu$g/l. of pyridoxal and 500 $\mu$g/l. of pyridoxamine the relative error and standard deviation were calculated for pyridoxal and pyridoxamine, in order to ascertain the reproducibility of the proposed methods. Finally the detection and quantization limits[17,18] were calculated.

To test the accuracy of the method, analysis of variance was applied. The experimental value of $F$, relative errors and standard deviations obtained for determination of pyridoxal and pyridoxamine by first derivative of excitation, emission, constant wavelength synchronous and constant energy synchronous spectra are summarized in Table 2.

## APPLICATIONS

In order to study the validity of the method, and since there are no medicines commercially available which contain these two vitamins, the methods proposed were applied to their determination in physiological serum and glucosed physiological serum, since intravenous injections are usually used for alcohol and pharmacology poisoning. The determination of these vitamins was carried out in commercial preparations of the following companies: "Apiroserum" (Inst. de Biología y Sueroterapia, S.A.) "Pérez Jiménez" (Lab. Pérez Jiménez) and "Grifols" (Lab. Grifols). Three determinations were carried out for each of these sera using pyridoxal and pyridoxamine medicines ("Nervobion" Merck and "Astenolit" Elmu S.A.) Recoveries achieved by means of all the methods proposed are in accordance with the real content of pyridoxal and pyridoxamine in both the physiological serum and the glucosed physiological serum. Recovery percentages achieved in all cases vary between 95.5 and 100.6% for pyridoxal and between 95.3 and 100.9% for pyridoxamine.

## CONCLUSIONS

Molecular fluorescence techniques in combination with derivative techniques resolve binary mixtures of pyridoxal and pyridoxamine without the need for prior separation steps. The use of synchronous fluorescence and constant energy synchronous fluorescence are not sufficient in themselves to separate the bands of these compounds due to the heavy overlap shown by the fluorescence spectra, although, as is to be expected from theory, the spectra are simplified and the bands narrowed. Better separation of the compounds is achieved by applying the first derivative to the different types of fluorescence spectra, but it is still not enough to obtain independent bands.

Table 2.

| 1st derivative | Compound | Experimental $F$ | Theoretical $F$ | Relative error (%) | Standard deviation ($\mu$g/l.) |
|---|---|---|---|---|---|
| Excitation | Pa | 2.01 | 3.07 | 2.81 | 5.1 |
| | Pm | 0.33 | 3.07 | 1.35 | 2.5 |
| Emission | Pa | 3.06 | 3.07 | 2.07 | 8.9 |
| | Pm | 1.56 | 3.07 | 1.11 | 7.1 |
| Constant wavelength | Pa | 0.55 | 3.07 | 2.19 | 8.9 |
| Synchronous | Pm | 2.62 | 3.07 | 1.76 | 7.1 |
| Constant wavelength | Pa | 1.92 | 3.07 | 1.76 | 3.2 |
| Synchronous | Pm | 3.05 | 3.07 | 2.19 | 4.0 |

Pa = Pyridoxal; Pm = Pyridoxamine.

By using the zero-crossing technique it is possible to determine pyridoxal and pyridoxamine simultaneously, both with excitation and emission spectra and with synchronous and constant energy synchronous spectra; in these latter cases greater analytical signals are obtained, which result in better detection and quantization limits. In general due to the similar fluorescent characteristics of vitamin $B_6$ and its derivatives, the methods described involve slow and tedious prior separation. The only fluorimetric method described in the literature which does not involve prior separation is that proposed by Petidier *et al.*,[6] but our methods are more sensitive and faster as it is not necessary to use derivatization reactions or mathematical equations.

## REFERENCES

1. C. A. Storvick and J. M. Peters, *Vitam. Horm.*, 1964, **22**, 833.
2. D. I. Haskell and E. E. Snell, *Anal. Biochem.*, 1972, **45**, 567.
3. E. Leparati, *Anal. Chim. Acta*, 1990, **234**, 2.
4. I. A. Solunia, V. A. Devyatnin and T. N. Kuznetsona, *Farmatsia*, 1972, **21**, 2.
5. Y. H. Loo and L. Badger, *Neurochemistry*, 1969, **16**, 801.
6. A. Petidier, S. Rubio, A. Gómez-Hens and M. Valcàrcel. *Anal. Biochem*, 1986, **157**, 212.
7. P. John and I. Soutar, *Anal. Chem.*, 1976, **48**, 520.
8. G. L. Green and T. C. O'Haver, *Anal. Chem.*, 1974, **46**, 2191.
9. C. M. Kanabrocki, *Undergraduate Research*. Post College, New York, 1979.
10. T. A. Kubic and F. X. Schechan, *Forensic Sci.*, 1983, **38**, 345.
11. Y. Li, X. Huang, J. Xu and G. Chen, *Anal. Chim. Acta*, 1992, **256**, 285.
12. J. A. Murillo and A. Alañón, *Talanta*, 1994, **41**, 21.
13. J. A. Murillo and A. Alañón, *Computers Chem.*, 1993, **17**, 341.
14. P. J. Elving and E. J. Koltoff (eds) *Treatise in Analytical Chemistry* 2nd Edn, Vol. 1, pp. 1–51. Wiley, New York, 1981.
15. A. Savitzky and M. J. E. Golay, *Anal. Chem.*, 1964, **36**, 1627.
16. J. Steinier, Y. Termonia and J. Deltour, *Anal. Chem.*, 1972, **44**, 1906.
17. Nomenclature, symbols, units and their usage in spectrochemical analysis II. *Spectrochim. Acta*, 1978, **33B**, 242.
18. Guidelines for data acquisition and data quality evaluation in environmental chemistry, *Anal. Chem.*, 1980, **52**, 2242.

Pergamon

0039-9140(94)00229-0

*Talanta*, Vol. 42, No. 1, pp. 137–142, 1995

0039-9140/95 $9.50 + 0.00

# TWO-PHASE POTENTIOMETRIC METAL EXTRACTION TITRATIONS OF SILVER(I), COPPER(II) AND CADMIUM(II) USING SOME CATION-EXCHANGERS AS EXTRACTANTS

BRIAN K. TAIT*

Mineralogy and Process Chemistry Division, Mintek, Private Bag X 3015, Randburg 2125, South Africa

(*Received* 10 *March* 1994. *Revised* 11 *July* 1994. *Accepted* 1 *August* 1994)

**Summary**—The use of two-phase potentiometric metal extraction titrations to study solvent extraction equilibria is described. The method provides a highly reproducible and convenient manner by which to determine extraction behaviour. The system was tested on a number of acidic extractants, namely D2EHPA, Ionquest 801, Cyanex 272, naphthenic acid and Versatic 10 acid. The extraction from an aqueous nitrate medium of silver(I), copper(II) and cadmium(II) was studied. The potentiometric data were used to obtain extraction curves and elucidate the nature of the extracted complexes by slope analysis and non-linear least squares treatment. In general, the following extraction order was obtained: D2EHPA > Ionquest 801 > Cyanex 272 and naphthenic > Versatic 10 for copper(II) and cadmium(II). Organophosphorus acids were shown to form complexes of the nature of $Cu(HA_2)_2$ with copper(II) and carboxylic acids formed dimeric complexes $(CuA_2(HA))_2$. With cadmium octahedral complexes of the form $CdA_2(HA)_4$ occurred. The extraction of silver(I) by Versatic 10 gave a dimeric complex $(AgA(HA))_2$. HA denotes the extractant in the acid form.

Batch-wise extractions require a complete set of mixing, separating, sampling and analyses, which often leads to scattered results. Because the batch technique is laborious, semicontinuous and continuous techniques have been proposed.

The stirred cell semicontinuous technique involves either intermittent vigorous stirring, in which case samples are withdrawn after each complete phase separation, or very mild stirring, allowing samples to be withdrawn continuously.

With the AKUFVE technique,[1,2] mixing and separation are achieved in a mixing vessel and at the inflow into a centrifugal separator. The separated phases pass over on-line detectors for pH measurement and metal ion determination by radiometric techniques.

This investigation sets out to adapt the well-known two-phase potentiometric acid–base titration technique developed by Högfeldt,[3,4] which utilizes a pH electrode to determine the acid or base constants of an extractant. The technique is fully automated, using an automatic titrator for additions of base to vary the pH and two electrode systems, one to measure the pH value, and one to measure the concentration of metal ion in the aqueous phase. Consequently, no samples have to be withdrawn for analysis. A similar technique has been used to study the extraction of silver(I) by Cyanex 471X.[5] This work investigates the extraction of silver(I), copper(II) and cadmium(II) by D2EHPA, Ionquest 801, Cyanex 272, Versatic 10 acid and naphthenic acid. The structures of the extractants are given in Table 1.

## EXPERIMENTAL

### *Electrodes*

A cadmium ISE was made by applying a thin layer of $CdS/Ag_2S$ to the bottom of a graphite rod. The sides of the rod were coated with Teflon. Graphite hydrophobized by Teflon is a conductive powder and thus allows electrical contact between the electroactive surface and a connection to a meter. The layer of electroactive material was polished to close the micropores. The electrode exhibited a Nernstein response, and has been described by Ruzicka *et al.*[6,7]

*Present address: Hickson Chemtech, P.O. Box 118, Roodepoort 1725, South Africa.

Table 1. Structure of extractants used

| | |
|---|---|
| D2EHPA | 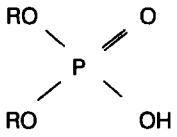 |
| Ionquest 801 | 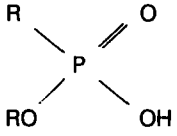 |
| Cyanex 272 | 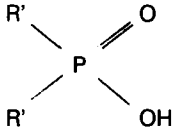 |
| Versatic 10 | 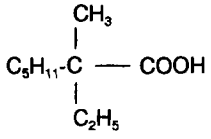 |
| Naphthenic acid | 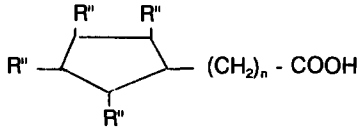 |

R = 2-ethylhexyl
R′ = 2,4,4-trimethylpentyl
R″ = unspecified mixture of alkyl groups

A Metrohm copper ISE was used to detect both copper(II) and silver(I). A double-junction silver/silver chloride reference electrode was used with the same internal electrolyte solution that was used as a constant ionic medium in the extraction experiments (1*M* ammonium nitrate or 1*M* sodium nitrate). The electrode assembly was attached to a Hewlett Packard logging multimeter to record the potential at a set time interval.

A Metrohm combined glass electrode, filled with 3*M* sodium chloride, was used to measure pH values.

*Titration procedure*

The organic and aqueous phases were placed in a water-jacketed vessel at 25°C. The organic-to-aqueous phase volume ratio (O/A) was 1 to 5 initially and decreased during the course of the titration. The organic phase contained 0.5*M* extractant in toluene and the aqueous phase 0.01*M* metal ion in 1*M* sodium nitrate or ammonium nitrate.

The stock organic solutions were analysed by potentiometric titration against sodium hydroxide in ethanolic–water medium. The stock aqueous phases were analysed by potentiometric titration against EDTA.

The pH electrode was calibrated against commercial pH 7.00, pH 4.01 and pH 2.01 buffers at 25°C. The ISE assembly was calibrated against standardized metal ion solutions in 1*M* sodium nitrate or ammonium nitrate in the concentration range $10^{-2}$ to $10^{-4}M$.

The inorganic salts were obtained from Saarchem and were of AR grade. The extractants were supplied by the manufacturers, Daihachi, Akulu Marchon, Cyanamid, Shell Chemicals and BDH for D2EHPA, Ionquest 801, Cyanex 272, Versatic 10 acid and naphthenic acid respectively, and used as supplied. Toluene, Merck pro analysi, was used as the diluent.

The titration was performed using a Metrohm 702SM Titrino. The titrant was 0.1*M* sodium hydroxide in 1*M* sodium nitrate or ammonium nitrate, with 0.5 ml additions at 10 min intervals [silver(I) and copper(II)] or at 18 min intervals [cadmium(II)]. This time was sufficient to ensure equilibration of the phases and the potential of the ISE assembly. The pH was allowed to vary in the range 2–8, in which the effect of pH on the potential of the ISE is negligible. After the elapse of the set time interval the pH and potential of the ISE assembly were recorded automatically, and more base was added to the stirred organic and aqueous phases by the Titrino. The titration stopped automatically when the pH value exceeded 8.

*Data treatment*

A spreadsheet was used to treat the potentiometric data. The logarithm of the metal ion concentration was calculated by linear regression from the calibration graph. The concentration of metal ion in the organic phase was assumed to be the difference between the initial concentration (taking dilution effects into account) and the concentration in the aqueous phase at equilibrium. The distribution ratio, *D*, is the concentration of metal ion in the organic phase divided by the concentration of metal ion

in the aqueous phase. The percentage extraction was calculated from

$$\%E = \frac{100D}{D + \frac{V_{aq}}{V_{org}}}, \quad (1)$$

where $V_{aq}$ is the volume of the aqueous phase and $V_{org}$ the volume of the organic phase.

For the generalized extraction equation

$$x\mathrm{M}^{2+} + x\left(\frac{n}{2}+1\right)\overline{\mathrm{H_2A_2}} \rightleftharpoons \overline{(\mathrm{MA_2(HA)}_n)_x} + 2x\mathrm{H}^+, \quad (2)$$

where the bar denotes a species in the organic phase, the concentration extraction constant, $K$, can be expressed as

$$K = \frac{\overline{[(\mathrm{MA_2(HA)}_n)_x]}[\mathrm{H}^+]^{2x}}{[\mathrm{M}^{2+}]^x\overline{[\mathrm{H_2A_2}]}^{x(\frac{n}{2}+1)}}. \quad (3)$$

The extraction constants were calculated by a non-linear least squares technique,[8,9] which required the input of hydrogen ion concentration, percentage extraction and initial metal ion and extractant concentrations.

## RESULTS AND DISCUSSION

### *Extraction of silver* (II)

Silver nitrate solution was found to be unstable in a sodium nitrate medium. Silver(I) was reduced to metallic silver soon after the preparation of the solution, before contact with the organic phase. Since both silver nitrate and sodium nitrate, when used separately under other experimental conditions, presented no problems, it is unlikely that the problem was caused by impurities. The reason for the instability of this solution is unknown.

Consequently, the extraction was investigated from an ammonium nitrate medium. The system also gave unsatisfactory results when the organophosphorus acid extractants or naphthenic acid were used as the extractants because of third phase problems. This was probably due to the formation of ammonium salts of the extractants.

Thus, only the extraction of silver(I) by Versatic 10 acid was studied. The system was used to determine the reproducibility of the titration technique. Figure 1 shows three extraction curves, which fall very close together. It can be concluded, therefore, that the two-phase potentiometric titration technique provides highly reproducible results.

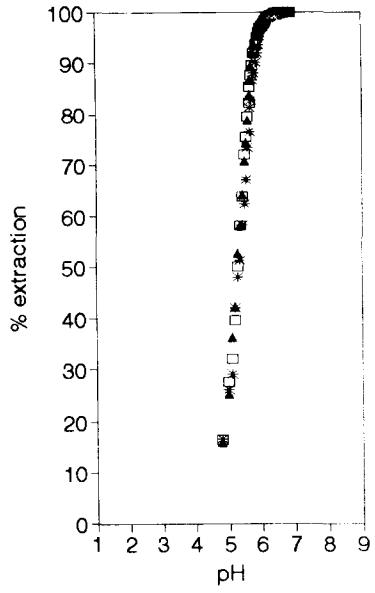


Fig. 1. Extraction of 0.01$M$ silver(I) in 1.0$M$ ammonium nitrate by 0.5$M$ Versatic 10 acid in toluene at 25°C (O/A = 5 initially). The symbols indicate triplicate results.

The $\mathrm{pH}_{0.5}$ value (the pH value at which 50% extraction occurs) for the extraction of 0.01$M$ silver(I) from 1.0$M$ ammonium nitrate by 0.5$M$ Versatic 10 acid in toluene at 25°C is 5.2. An attempt was made to elucidate the extraction stoichiometry by slope analysis. The extraction of silver(I) can be described by

$$x\mathrm{Ag}^+ + \left(\frac{nx}{2}\right)\overline{\mathrm{H_2A_2}} \rightleftharpoons \overline{(\mathrm{AgA(HA)}_{n-1})_x} + x\mathrm{H}^+, \quad (4)$$

where $\mathrm{H_2A_2}$ represents the extractant dimer. It is generally accepted that organophosphorus acids and carboxylic acids form dimers in diluents of low polarity.[10-12]

The extraction constant, $K$, can be expressed as

$$K = \frac{\overline{[(\mathrm{AgA(HA)}_{n-1})_x]}[\mathrm{H}^+]^x}{[\mathrm{Ag}^+]^{x-1}\overline{[\mathrm{H_2A_2}]}^{nx/2}} = \frac{D[\mathrm{H}^+]^x}{[\mathrm{Ag}^+]^{x-1}[\mathrm{H_2A_2}]^{nx/2}}, \quad (5)$$

where

$$D = \frac{\overline{[(\mathrm{AgA(HA)}_{n-1})_x]}}{[\mathrm{Ag}^+]}. \quad (6)$$

By taking logarithms and rearranging, it follows that

$$\log D - \frac{nx}{2}\log[\mathrm{H_2A_2}] - (x-1)\log[\mathrm{Ag}^+] = \log K + x\mathrm{pH}. \quad (7)$$

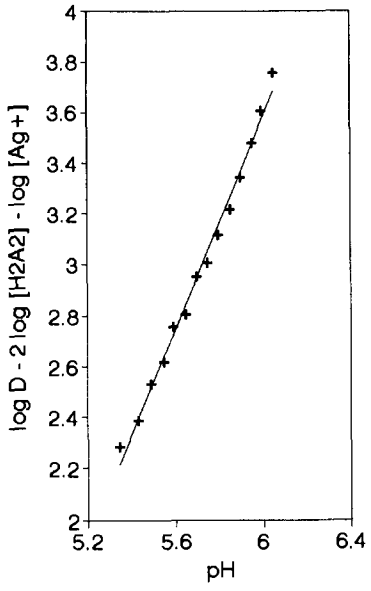


Fig. 2. Slope analysis of silver(I) extraction by Versatic 10 acid. Same conditions as for Fig. 1.

Thus a plot of $\log D - (nx/2)\log[H_2A_2] - (x-1)\log[Ag^+]$ against pH should be a straight line with a slope of $x$ for the correct values of $x$ and $n$. Figure 2 shows such a plot for $x = 2$ and $n = 2$. The slope of the line is 2.07 (correlation coefficient is 0.992) Thus, it can be concluded that the extracted complex is $(AgA(HA))_2$.

*Extraction of copper*(II)

Figure 3 represents the extraction of copper(II) from 1.0*M* sodium nitrate by D2EHPA, Ionquest 801, Cyanex 272, Versatic 10 acid and naphthenic acid in toluene. The $pH_{0.5}$ values under the conditions studied are presented in Table 2. The extraction order is D2EHPA > Ionquest 801 > Cyanex 272 ≈ naphthenic acid > Versatic 10 acid. This order indicates the relative strength of the extractants towards copper(II) extraction.

In general, the extraction of divalent metal ions by organophosphorus acid extractants can be expressed as

$$M^{2+} + n\overline{H_2A_2} \rightleftharpoons \overline{M(HA_2)_2(HA)_{2n-4}} + 2H^+. \quad (8)$$

Thus, a plot of $\log D - n \log[H_2A_2]$ against pH should yield a straight line with a slope of 2 for the correct value of $n$.

In contrast, carboxylic acids often form polymeric extracted complexes with metal ions. For a divalent metal ion

$$xM^{2+} + x\left(\frac{n}{2}+1\right)\overline{H_2A_2} \rightleftharpoons \overline{(MA_2(HA)_n)_x} + 2xH^+ \quad (9)$$

from which it can be deduced that a plot of $\log D - x(n/2+1)\log[H_2A_2] - (x-1)\log[M^{2+}]$ against pH should give a straight line of slope $2x$ for the correct values of $x$ and $n$. The equilibrium dimer concentration was calculated from the initial concentration, taking into account the extractant bound to the metal ion according to the proposed stoichiometry.

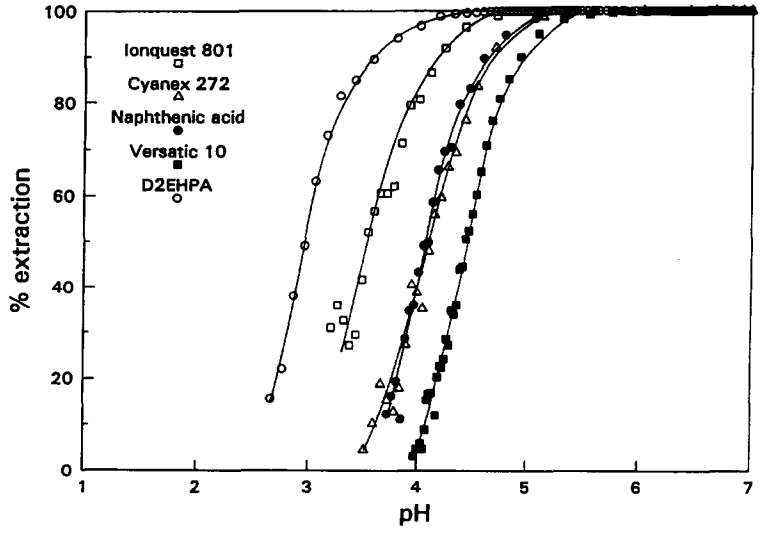


Fig. 3. Extraction of 0.01*M* copper(II) in 1.0*M* sodium nitrate by 0.5*M* extractant in toluene at 25°C (O/A = 5 initially).

Table 2. $pH_{0.5}$ values and results of slope analysis studies for copper(II) and cadmium(II)

| | Copper(II) | | | Cadmium(II) | | |
|---|---|---|---|---|---|---|
| Extractant | $pH_{0.5}$ | slope | $r^2$ | $pH_{0.5}$ | slope | $r^2$ |
| D2EHPA | 3.0 | 1.9 | 0.994 | 3.0 | 1.9 | 0.968 |
| Ionquest 801 | 3.6 | 1.9 | 0.993 | 3.5 | 1.9 | 0.954 |
| Cyanex 272 | 4.1 | 2.0 | 0.998 | 4.3 | 2.2 | 0.972 |
| Versatic 10 | 4.4 | 3.8 | 0.998 | 4.8 | 2.0 | 0.958 |
| Naphthenic | 4.1 | 4.0 | 0.990 | 6.0 | — | — |

The results of the slope analysis studies are consistent with the following extraction equations:

Organophosphorus acids

$$Cu^{2+} + 2\overline{H_2A_2} \rightleftharpoons \overline{Cu(HA_2)_2} + 2H^+, \quad (10)$$

Carboxylic acids

$$2\,Cu^{2+} + 3\overline{H_2A_2} \rightleftharpoons \overline{(CuA_2(HA))_2} + 4H^+. \quad (11)$$

The results are shown in Table 2, and are in agreement with the results of other workers.[10–12] The proposed model was chosen on the basis of the best straight line that gave a slope close to the expected value of 2 or $2x$. Whereas slope analysis was sensitive to the choice of model, the non-linear least squares technique proved relatively insensitive because there was not sufficient variation in the concentration of the extractant. Non-linear least squares treatment of the data was used to calculate the extraction constant, $K$. The results are presented in Table 3. A more rigorous non-linear least squares treatment will require that the extractant concentration is deliberately varied.

The extraction constants confirm the relative extraction order given previously. It should be noted that the constants for organophosphorus acid extractants and carboxylic acid extractants are not comparable because of different stoichiometries (and hence different units). The results of the non-linear least squares treatment show that very good fits of the experimental data were obtained and tend to validate the conclusions drawn from slope analysis studies.

*Extraction of cadmium*(II)

The cadmium ISE built for this set of experiments gave less stable readings than the commercially available copper ISE as it was more sensitive to the presence of organic droplets in the dispersion, and tended to become coated by the organic phase. This problem was solved by stirring the phases slowly. To ensure complete equilibration, measurements were taken at 18 min intervals, as opposed to the 10 min equilibration time used in the previous experiment. The greater instability of the potential measurements resulted in more scatter of the experimental points and this is also reflected in the statistical parameters presented.

The extraction of cadmium(II) from 1.0*M* sodium nitrate by D2EHPA, Ionquest 801, Cyanex 272, naphthenic acid and Versatic 10 acid is presented in Fig. 4. The extraction order D2EHPA > Ionquest > Cyanex 272 and naphthenic > Versatic 10 is the same as obtained with copper(II). The $pH_{0.5}$ values are indicated in Table 2.

Slope analysis studies were consistent with the extraction equation

$$Cd^{2+} + 3\overline{H_2A_2} \rightleftharpoons \overline{CdA_2(HA)_4} + 2H^+ \quad (12)$$

for all extractants except naphthenic acid, for which the stoichiometry could not be determined. The results are shown in Table 2. The same extraction equation for carboxylic acids has been proposed by other workers.[13,14] Grimm[15] has reported the complex $CdA_2(HA)_3$ with D2EHPA and Figuerola[16] proposed the complexes $CdA_2$ and $CdA_2(HA)_3$ with Cyanex 272. Presumably the complexes incorporate water molecules to give a coordination number of four or six.

Non-linear least squares treatment of the data supported the conclusions drawn about the extraction stoichiometry in this work. The extraction constants and related statistics are presented in Table 3.

Table 3. Extraction constants, standard deviation in percentage extraction ($s$) and number of points ($n$) for non-linear least squares treatment of copper(II) and cadmium(II) extraction data

| | Copper(II) | | | Cadmium(II) | | |
|---|---|---|---|---|---|---|
| Extractant | log $K$ | $s$ | $n$ | log $K$ | $s$ | $n$ |
| D2EHPA | $-4.77 \pm 0.01$ | 1.7 | 50 | $-4.48 \pm 0.01$ | 4.4 | 101 |
| Ionquest 801 | $-5.70 \pm 0.01$ | 3.2 | 100 | $-5.27 \pm 0.01$ | 3.9 | 40 |
| Cyanex 272 | $-7.00 \pm 0.01$ | 3.3 | 27 | $-6.83 \pm 0.01$ | 42 | 32 |
| Versatic 10 | $-13.9 \pm 0.01$ | 2.8 | 40 | $-10.3 \pm 0.02$ | 5.9 | 22 |
| Naphthenic | $-12.4 \pm 0.01$ | 2.9 | 40 | — | — | — |

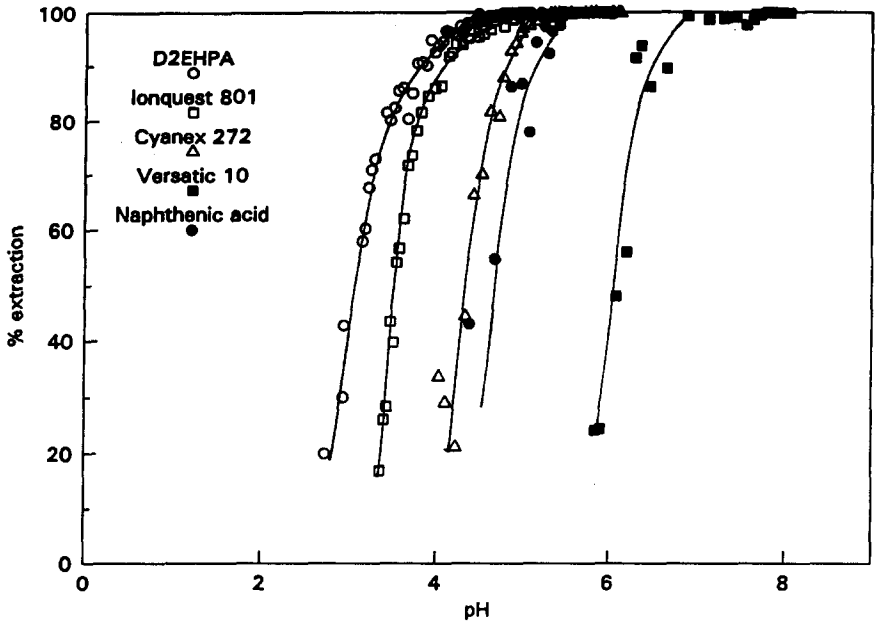


Fig. 4. Extraction of 0.01*M* cadmium(II) in 1.0*M* sodium nitrate by 0.5*M* extractant in toluene at 25°C (O/A = 5 initially).

## CONCLUSIONS

Two-phase potentiometric metal extraction titrations are a convenient and highly reproducible manner in which to obtain extraction–pH curves. Variations can be devised to allow the study of other variables, such as metal ion and extractant concentration. The time taken to produce a curve depends on the number of data points to be collected and the equilibration time chosen.

The method is limited by the number of ISEs available that are sensitive to the metal ion of interest. However, much research is being undertaken to develop new sensors. Although general ion-sensitive electrodes are available, such as the divalent metal ion (water hardness) electrode, these are based on polymer membranes that dissolve in organic solvents. Thus, solid state electrodes or those with a polymer matrix that does not dissolve in the diluent are needed in mixed aqueous–organic systems. Also, because ISEs respond to the activity of the free (aquo) metal ion, investigations must be performed in media in which the metal ion does not complex strongly with the anions in solution.

## REFERENCES

1. H. Reinhardt and J. Rydberg, *Solvent Extr. Met. Processes, Proc. Int. Symp.*, p. 48. Technol. Inst. K.VIV, Antwerp, 1972.
2. J. Rydberg, H. Reinhardt and J. O. Liljenzin, in *Ion Exchange and Solvent Extraction*, J. A. Marinsky and Y. Marcus (eds), Vol. 3, p. 111. Marcel Dekker, New York, 1973.
3. E. Högfeldt, *Acta Chem. Scand.*, 1952, **6**, 610.
4. E. Högfeldt, M. Muhammed and J. Szabon, *Chem. Scr.*, 1974, **6**, 61.
5. M. Munoz, X. Ribas and M. Valiente, *Quim. Anal.*, 1991, **10**, 11.
6. J. Ruzicka, C. G. Lamm and J. C. Tell, *Anal. Chim. Acta*, 1972, **62**, 15.
7. J. Ruzicka and C. G. Lamm, *Anal. Chim. Acta*, 1971, **54**, 1.
8. W. E. Wentworth, *J. Chem. Educ.*, 1965, **42**, 96.
9. B. K. Tait and D. P. Shillington, *S. Afr. J. Chem.*, 1992, **45**, 17.
10. J. S. Preston and A. C. du Preez, *Mintek Report M378*. Randburg, 1988.
11. J. S. Preston, *Hydrometallurgy*, 1985, **14**, 171.
12. K. Inoue, H. Amano and I. Nakamari, *Hydrometallurgy*, 1982, **8**, 309.
13. J. S. Preston, *Solvent Extr. Ion Exch.* 1994, **12**, 667.
14. T. Saito, T. Tanabe, S. Nishimura and Y. Kondo, *Nippon Kogyo Kaishi*, 1972, **88**, 215.
15. R. Grimm and Z. Kolarik, *J. Inorg. Nucl. Chem.*, 1974, **36**, 189.
16. E. Figuerola, N. Miralles, A. Sastre and M. Aguilar, *ISEC '88*, Vol. I, p. 318. Moscow, 1988.

Pergamon

*Talanta*, Vol. 42, No. 1, pp. 143–145, 1995
Elsevier Science Ltd
Printed in Great Britain

# BOOK REVIEWS

**The Kirk-Othmer Encyclopedia of Chemical Technology:** Volume 10, Fourth Edition, Explosives and Propellants to Flame Retardants: J. I. KROSCHWITZ and M. HOWE-GRANT (editors), Wiley, New York, Pages: xxviii + 1022. £185.00. ISBN 0-471-52678-9 (v.10).

Well over 10,000 pages of the 4th edition of this encyclopedia have now been published and only the sixth letter of the alphabet has been reached. This indicates both the wide scope of subject matter and the detail in which it is covered.

Volume 10 contains information under 21 separate headings with the largest entry devoted to Fibers. Both natural fibers (of vegetable, animal or mineral origin) and synthetic fibers (natural organic polymers, synthetic organic polymers or inorganic substances) are mentioned. The characteristics, production, and application of Fibers is well covered and a similar treatment is given to the separate entry on Fiber Optics.

Another major topic dealt with in this volume is Explosives and Propellants which uses the reaction rate to to distinguish between the two categories. Here safety aspects, pollutants, performance, manufacture, properties, and applications of these potentially dangerous chemicals are presented.

The two entries on unit operations: extraction and filtration are dealt with in about the same number of pages. As expected extraction covers liquid-liquid (solvent extraction) and liquid-solid extraction and filtration includes vacuum filters, batch pressure filters, continuous pressure filters and centrifugal filters.

The importance of flame retardants—with particular emphasis on antimony (and other inorganics), halogenated and phosphorus flame retardants—is presented and a separate entry on their use with textiles is included. Another group of chemicals—fat and fatty oils—is covered, as are fat replacers. The various fertilizers in use, *e.g.* nitrogen, phosphate, potash, *etc.*, are surveyed and their environmental and economic impact are covered. Also in relation to aspects of farming there are entries on feeds and feed additives, and on feedstocks.

I found the treatise on fine art examination and conservation by L. van Zelst of the Smithsonian Institution to be the most interesting entry in this volume of the encyclopedia. It covers numerous analytical techniques and shows how these are used in conjunction with technological history to examine works of art. The study of deterioration and conservation of important paintings, metal objects, ceramics, textiles, parchments, *etc.*, is truly an area where the worlds of art and science merge. Indeed, after reading this section I found myself somewhat envious of those who work in this domain.

Completing this volume are short entries of extraterrestrial materials, fans and blowers, fermentation, ferrites, ferroelectrics, film and sheeting materials and fillers.

As with all volumes in this encyclopedia a number of different authors have been used, tables of conversion factors, abbreviations, and unit symbols are given and extensive references are appended to each topic covered. A highly desirable acquisition for all good science libraries.

P. J. Cox

**Analytical Chemistry, 5th Edition:** G. D. CHRISTIAN, Wiley, New York, 1994. Pages: xx + 812. £18.95 (softback), ISBN 047105820. £64.00 (hardback).

This text is aimed at undergraduate (college) students majoring in chemistry and related fields and covers the principles and techniques of quantitative analysis. The 5th edition is over 800 pages long, and contains a wealth of information which reflects the authors lifelong involvement in analytical chemistry. This edition has been reorganised compared to the previous versions, and additions reflect developments in the area over the past few years. These include: the statistics of sampling and of small data sets (which are the norm in many analyses), ultramicroelectrodes and chemically modified electrodes, diode array spectrometers, Fourier infrared spectroscopy and near IR instruments, solid phase extraction, supercritical fluid chromatography, capillary electrophoresis and GC-MS, flow-injection analysis principles and experiments, and laboratory applications of PCs, application software and interfaces.

The organisation of the text helps the student new to the area to quickly identify the core information by means of a summary paragraph introducing each chapter which lists the topics covered and gives a broad overview of the content. In addition, key terms are given in boldface type and important equations and concepts boxed for emphasis. Margin notes are used to expand explanations and reinforce important topics.

After an introduction to analytical chemistry in chapter 1, a series of chapters cover topics which, given the excellent organisation and presentation of the information, make this a very attractive introductory text for physical chemistry course modules. These include; statistics (precision, accuracy, correlation coefficient, range, median, non-linear least squares curve fitting etc.), the mole and stoichiometry, chemical equilibria (Gibb's Free Energy, Le Chatelier's Principle, ionic strength, dissociation etc.), solubility product, recrystallisation, acid-base theory leading to titrations, complexometry, chelates, effect of pH on stability/formation constants, and introduction to electrochemical cells and electrode potentials, the Nernst equation.

Pergamon

*Talanta*, Vol. 42, No. 1, pp. 143–145, 1995
Elsevier Science Ltd
Printed in Great Britain

# BOOK REVIEWS

**The Kirk-Othmer Encyclopedia of Chemical Technology:** Volume 10, Fourth Edition, Explosives and Propellants to Flame Retardants: J. I. KROSCHWITZ and M. HOWE-GRANT (editors), Wiley, New York, Pages: xxviii + 1022. £185.00. ISBN 0-471-52678-9 (v.10).

Well over 10,000 pages of the 4th edition of this encyclopedia have now been published and only the sixth letter of the alphabet has been reached. This indicates both the wide scope of subject matter and the detail in which it is covered.

Volume 10 contains information under 21 separate headings with the largest entry devoted to Fibers. Both natural fibers (of vegetable, animal or mineral origin) and synthetic fibers (natural organic polymers, synthetic organic polymers or inorganic substances) are mentioned. The characteristics, production, and application of Fibers is well covered and a similar treatment is given to the separate entry on Fiber Optics.

Another major topic dealt with in this volume is Explosives and Propellants which uses the reaction rate to to distinguish between the two categories. Here safety aspects, pollutants, performance, manufacture, properties, and applications of these potentially dangerous chemicals are presented.

The two entries on unit operations: extraction and filtration are dealt with in about the same number of pages. As expected extraction covers liquid-liquid (solvent extraction) and liquid-solid extraction and filtration includes vacuum filters, batch pressure filters, continuous pressure filters and centrifugal filters.

The importance of flame retardants—with particular emphasis on antimony (and other inorganics), halogenated and phosphorus flame retardants—is presented and a separate entry on their use with textiles is included. Another group of chemicals—fat and fatty oils—is covered, as are fat replacers. The various fertilizers in use, *e.g.* nitrogen, phosphate, potash, *etc.*, are surveyed and their environmental and economic impact are covered. Also in relation to aspects of farming there are entries on feeds and feed additives, and on feedstocks.

I found the treatise on fine art examination and conservation by L. van Zelst of the Smithsonian Institution to be the most interesting entry in this volume of the encyclopedia. It covers numerous analytical techniques and shows how these are used in conjunction with technological history to examine works of art. The study of deterioration and conservation of important paintings, metal objects, ceramics, textiles, parchments, *etc.*, is truly an area where the worlds of art and science merge. Indeed, after reading this section I found myself somewhat envious of those who work in this domain.

Completing this volume are short entries of extraterrestrial materials, fans and blowers, fermentation, ferrites, ferroelectrics, film and sheeting materials and fillers.

As with all volumes in this encyclopedia a number of different authors have been used, tables of conversion factors, abbreviations, and unit symbols are given and extensive references are appended to each topic covered. A highly desirable acquisition for all good science libraries.

P. J. Cox

**Analytical Chemistry, 5th Edition:** G. D. CHRISTIAN, Wiley, New York, 1994. Pages: xx + 812. £18.95 (softback), ISBN 047105820. £64.00 (hardback).

This text is aimed at undergraduate (college) students majoring in chemistry and related fields and covers the principles and techniques of quantitative analysis. The 5th edition is over 800 pages long, and contains a wealth of information which reflects the authors lifelong involvement in analytical chemistry. This edition has been reorganised compared to the previous versions, and additions reflect developments in the area over the past few years. These include: the statistics of sampling and of small data sets (which are the norm in many analyses), ultramicroelectrodes and chemically modified electrodes, diode array spectrometers, Fourier infrared spectroscopy and near IR instruments, solid phase extraction, supercritical fluid chromatography, capillary electrophoresis and GC-MS, flow-injection analysis principles and experiments, and laboratory applications of PCs, application software and interfaces.

The organisation of the text helps the student new to the area to quickly identify the core information by means of a summary paragraph introducing each chapter which lists the topics covered and gives a broad overview of the content. In addition, key terms are given in boldface type and important equations and concepts boxed for emphasis. Margin notes are used to expand explanations and reinforce important topics.

After an introduction to analytical chemistry in chapter 1, a series of chapters cover topics which, given the excellent organisation and presentation of the information, make this a very attractive introductory text for physical chemistry course modules. These include; statistics (precision, accuracy, correlation coefficient, range, median, non-linear least squares curve fitting etc.), the mole and stoichiometry, chemical equilibria (Gibb's Free Energy, Le Chatelier's Principle, ionic strength, dissociation etc.), solubility product, recrystallisation, acid-base theory leading to titrations, complexometry, chelates, effect of pH on stability/formation constants, and introduction to electrochemical cells and electrode potentials, the Nernst equation.

This provides a sound basis for chapters on acid-base, precipitation, complexometric and redox/potentiometric titrations. The latter half of the book focuses on instrumental methods. All the major electrochemical, spectroscopic and chromatographic techniques are covered in a clear and concise manner. The closing chapters discuss kinetic methods of analysis (mainly the use of enzymes), laboratory automation and two important application areas (clinical and environmental analysis).

A chapter entitled 'Basic Tools and Operations of Analytical Chemistry' serves as an excellent accompaniment to undergraduate practical courses. This is followed by a collection of 44 selected experiments which illustrate techniques, principles and methods discussed in the preceding chapters. The book also contains six appendices which discuss the analytical literature, review mathematical operations, list important constants, give pH transition values for indicators, discuss safety in the lab, and list answers to even numbered questions, respectively. A comprehensive index completes the text.

The book is not really suited for more detailed instrumental courses (a dedicated instrumental analysis text would be more appropriate—voltammetry and computer interfacing/data processing are not covered in any real detail). However, it is an ideal companion for students studying introductory courses in analytical chemistry or physical chemistry, and for faculty staff looking for new experiments or tutorial questions (for which there is a separate solutions manual available). It is worth buying for the anecdotal information alone, which reflects the author's lifetime dedication to research and teaching in analytical chemistry.

D. DIAMOND

**Instrumentation in Analytical Chemistry:** Volume 2, J. ZÝKA (editor), Ellis Horwood, Chichester, 1994. Pages: 336. £69.00. ISBN 0-13-472226-4.

This book completes the 2 volume series 'Instrumentation in Analytical Chemistry' edited by Jaroslav Zýka and contains 16 chapters by selected authors covering a range of analytical methods. Despite the fact that all the authors are from Prague the English is of a high standard throughout. There is a strong analytical community in the Czech Republic which the editor has tapped to produce a volume of consistent quality (often a problem with multi-author books).

The first 6 chapters are devoted to electrochemical techniques, namely, chemically modified electrodes for potentiometry and voltammetry, advances in electrochemical stripping analysis, adsorptive stripping voltammetry, applications of polarography to the study of surface-active substances, amperometric membrane detectors and electrochemical biosensors. The remainder of the book is devoted to topics on spectroscopy (FTIR and Laser Raman spectrometry), chromatography (identification of bacteria by GC and pyrolysis GC of synthetic polymers), radioimmunoassay, the use of surfactants in analytical chemistry and automatic methods of analysis. All chapters are well illustrated with figures and have extensive bibliographies. The two volume series should be useful to the teacher, the researcher and to more advanced undergraduate/postgraduate students.

B. A. MCGAW

**Electroanalytical Stripping Methods:** KH. BRAININA and E. NEYMAN, Wiley, Chichester, 1993. Pages: xxiii + 198. £49.50. ISBN 0-471-59506-3.

This book is the latest addition to the several monographs on electrochemical stripping analysis published over almost three decades. The two Russian authors have been working in the field for many years and the first one is especially well known in the electroanalytical community. The authors state in the preface to the book that one of their principal aims is to fill an information gap on the pertinent Russian literature and, indeed, the list of 546 references cited in the text is heavily biased in favour of papers published in Russian journals, with an ample proportion of articles by the present authors themselves. Generally this is quite useful, however, the information gap is often a two-way one and certain references to non-Russian literature are undoubtedly missing. Moreover, numerous misprints in the references to non-Russian works considerably decrease the informative value of the book.

Another special feature of the book is a great emphasis on electrochemistry of solids. Electrochemical stripping analysis is at present mostly considered as a method useful primarily for determination and speciation of a few metals and certain organics in the environment. The authors point out its usefulness in studying the structure of solid materials, in phase analysis and detection of structural defects, by mixing the test solid material with carbon for the preparation of carbon paste electrodes and following the electrolytic dissolution processes. In doing this, stripping methods transcend the boundaries of common analysis and enter the field of corrosion and materials science. It should, however, be pointed out that interpretation of the results is difficult and that they should be confronted and supplemented with those obtained by the established spectrometric methods of structural analysis. Nevertheless, this is an uncommon, refreshing view of the method.

The book consists of six chapters, supplemented by lists of abbreviations and symbols and a brief subject index. The first chapter deals with the theory of metal deposition on, and stripping from, solid electrodes. In my opinion, the purely thermodynamic approach adopted represents a gross simplification and the results can only be considered as qualitative. There are some unusual symbols, e.g. $\Omega$ for the coverage of the electrode surface, and some poorly defined parameters such as $\gamma$, which is a "proportionality factor reflecting metal-electrode system peculiarities", essentially serving to improve the matching between the calculated and experimental data (see, *e.g.*, Fig. 1.3). Also the use of the terms "strong and weak interactions" (see page 8) is not particularly fortunate, as it evokes the quantum mechanical terms.

This provides a sound basis for chapters on acid-base, precipitation, complexometric and redox/potentiometric titrations. The latter half of the book focuses on instrumental methods. All the major electrochemical, spectroscopic and chromatographic techniques are covered in a clear and concise manner. The closing chapters discuss kinetic methods of analysis (mainly the use of enzymes), laboratory automation and two important application areas (clinical and environmental analysis).

A chapter entitled 'Basic Tools and Operations of Analytical Chemistry' serves as an excellent accompaniment to undergraduate practical courses. This is followed by a collection of 44 selected experiments which illustrate techniques, principles and methods discussed in the preceding chapters. The book also contains six appendices which discuss the analytical literature, review mathematical operations, list important constants, give pH transition values for indicators, discuss safety in the lab, and list answers to even numbered questions, respectively. A comprehensive index completes the text.

The book is not really suited for more detailed instrumental courses (a dedicated instrumental analysis text would be more appropriate—voltammetry and computer interfacing/data processing are not covered in any real detail). However, it is an ideal companion for students studying introductory courses in analytical chemistry or physical chemistry, and for faculty staff looking for new experiments or tutorial questions (for which there is a separate solutions manual available). It is worth buying for the anecdotal information alone, which reflects the author's lifetime dedication to research and teaching in analytical chemistry.

D. DIAMOND

**Instrumentation in Analytical Chemistry:** Volume 2, J. ZÝKA (editor), Ellis Horwood, Chichester, 1994. Pages: 336. £69.00. ISBN 0-13-472226-4.

This book completes the 2 volume series 'Instrumentation in Analytical Chemistry' edited by Jaroslav Zýka and contains 16 chapters by selected authors covering a range of analytical methods. Despite the fact that all the authors are from Prague the English is of a high standard throughout. There is a strong analytical community in the Czech Republic which the editor has tapped to produce a volume of consistent quality (often a problem with multi-author books).

The first 6 chapters are devoted to electrochemical techniques, namely, chemically modified electrodes for potentiometry and voltammetry, advances in electrochemical stripping analysis, adsorptive stripping voltammetry, applications of polarography to the study of surface-active substances, amperometric membrane detectors and electrochemical biosensors. The remainder of the book is devoted to topics on spectroscopy (FTIR and Laser Raman spectrometry), chromatography (identification of bacteria by GC and pyrolysis GC of synthetic polymers), radioimmunoassay, the use of surfactants in analytical chemistry and automatic methods of analysis. All chapters are well illustrated with figures and have extensive bibliographies. The two volume series should be useful to the teacher, the researcher and to more advanced undergraduate/postgraduate students.

B. A. MCGAW

**Electroanalytical Stripping Methods:** KH. BRAININA and E. NEYMAN, Wiley, Chichester, 1993. Pages: xxiii + 198. £49.50. ISBN 0-471-59506-3.

This book is the latest addition to the several monographs on electrochemical stripping analysis published over almost three decades. The two Russian authors have been working in the field for many years and the first one is especially well known in the electroanalytical community. The authors state in the preface to the book that one of their principal aims is to fill an information gap on the pertinent Russian literature and, indeed, the list of 546 references cited in the text is heavily biased in favour of papers published in Russian journals, with an ample proportion of articles by the present authors themselves. Generally this is quite useful, however, the information gap is often a two-way one and certain references to non-Russian literature are undoubtedly missing. Moreover, numerous misprints in the references to non-Russian works considerably decrease the informative value of the book.

Another special feature of the book is a great emphasis on electrochemistry of solids. Electrochemical stripping analysis is at present mostly considered as a method useful primarily for determination and speciation of a few metals and certain organics in the environment. The authors point out its usefulness in studying the structure of solid materials, in phase analysis and detection of structural defects, by mixing the test solid material with carbon for the preparation of carbon paste electrodes and following the electrolytic dissolution processes. In doing this, stripping methods transcend the boundaries of common analysis and enter the field of corrosion and materials science. It should, however, be pointed out that interpretation of the results is difficult and that they should be confronted and supplemented with those obtained by the established spectrometric methods of structural analysis. Nevertheless, this is an uncommon, refreshing view of the method.

The book consists of six chapters, supplemented by lists of abbreviations and symbols and a brief subject index. The first chapter deals with the theory of metal deposition on, and stripping from, solid electrodes. In my opinion, the purely thermodynamic approach adopted represents a gross simplification and the results can only be considered as qualitative. There are some unusual symbols, e.g. $\Omega$ for the coverage of the electrode surface, and some poorly defined parameters such as $\gamma$, which is a "proportionality factor reflecting metal-electrode system peculiarities", essentially serving to improve the matching between the calculated and experimental data (see, *e.g.*, Fig. 1.3). Also the use of the terms "strong and weak interactions" (see page 8) is not particularly fortunate, as it evokes the quantum mechanical terms.

This provides a sound basis for chapters on acid-base, precipitation, complexometric and redox/potentiometric titrations. The latter half of the book focuses on instrumental methods. All the major electrochemical, spectroscopic and chromatographic techniques are covered in a clear and concise manner. The closing chapters discuss kinetic methods of analysis (mainly the use of enzymes), laboratory automation and two important application areas (clinical and environmental analysis).

A chapter entitled 'Basic Tools and Operations of Analytical Chemistry' serves as an excellent accompaniment to undergraduate practical courses. This is followed by a collection of 44 selected experiments which illustrate techniques, principles and methods discussed in the preceding chapters. The book also contains six appendices which discuss the analytical literature, review mathematical operations, list important constants, give pH transition values for indicators, discuss safety in the lab, and list answers to even numbered questions, respectively. A comprehensive index completes the text.

The book is not really suited for more detailed instrumental courses (a dedicated instrumental analysis text would be more appropriate—voltammetry and computer interfacing/data processing are not covered in any real detail). However, it is an ideal companion for students studying introductory courses in analytical chemistry or physical chemistry, and for faculty staff looking for new experiments or tutorial questions (for which there is a separate solutions manual available). It is worth buying for the anecdotal information alone, which reflects the author's lifetime dedication to research and teaching in analytical chemistry.

D. DIAMOND

**Instrumentation in Analytical Chemistry:** Volume 2, J. ZÝKA (editor), Ellis Horwood, Chichester, 1994. Pages: 336. £69.00. ISBN 0-13-472226-4.

This book completes the 2 volume series 'Instrumentation in Analytical Chemistry' edited by Jaroslav Zýka and contains 16 chapters by selected authors covering a range of analytical methods. Despite the fact that all the authors are from Prague the English is of a high standard throughout. There is a strong analytical community in the Czech Republic which the editor has tapped to produce a volume of consistent quality (often a problem with multi-author books).

The first 6 chapters are devoted to electrochemical techniques, namely, chemically modified electrodes for potentiometry and voltammetry, advances in electrochemical stripping analysis, adsorptive stripping voltammetry, applications of polarography to the study of surface-active substances, amperometric membrane detectors and electrochemical biosensors. The remainder of the book is devoted to topics on spectroscopy (FTIR and Laser Raman spectrometry), chromatography (identification of bacteria by GC and pyrolysis GC of synthetic polymers), radioimmunoassay, the use of surfactants in analytical chemistry and automatic methods of analysis. All chapters are well illustrated with figures and have extensive bibliographies. The two volume series should be useful to the teacher, the researcher and to more advanced undergraduate/postgraduate students.

B. A. MCGAW

**Electroanalytical Stripping Methods:** KH. BRAININA and E. NEYMAN, Wiley, Chichester, 1993. Pages: xxiii + 198. £49.50. ISBN 0-471-59506-3.

This book is the latest addition to the several monographs on electrochemical stripping analysis published over almost three decades. The two Russian authors have been working in the field for many years and the first one is especially well known in the electroanalytical community. The authors state in the preface to the book that one of their principal aims is to fill an information gap on the pertinent Russian literature and, indeed, the list of 546 references cited in the text is heavily biased in favour of papers published in Russian journals, with an ample proportion of articles by the present authors themselves. Generally this is quite useful, however, the information gap is often a two-way one and certain references to non-Russian literature are undoubtedly missing. Moreover, numerous misprints in the references to non-Russian works considerably decrease the informative value of the book.

Another special feature of the book is a great emphasis on electrochemistry of solids. Electrochemical stripping analysis is at present mostly considered as a method useful primarily for determination and speciation of a few metals and certain organics in the environment. The authors point out its usefulness in studying the structure of solid materials, in phase analysis and detection of structural defects, by mixing the test solid material with carbon for the preparation of carbon paste electrodes and following the electrolytic dissolution processes. In doing this, stripping methods transcend the boundaries of common analysis and enter the field of corrosion and materials science. It should, however, be pointed out that interpretation of the results is difficult and that they should be confronted and supplemented with those obtained by the established spectrometric methods of structural analysis. Nevertheless, this is an uncommon, refreshing view of the method.

The book consists of six chapters, supplemented by lists of abbreviations and symbols and a brief subject index. The first chapter deals with the theory of metal deposition on, and stripping from, solid electrodes. In my opinion, the purely thermodynamic approach adopted represents a gross simplification and the results can only be considered as qualitative. There are some unusual symbols, e.g. $\Omega$ for the coverage of the electrode surface, and some poorly defined parameters such as $\gamma$, which is a "proportionality factor reflecting metal-electrode system peculiarities", essentially serving to improve the matching between the calculated and experimental data (see, *e.g.*, Fig. 1.3). Also the use of the terms "strong and weak interactions" (see page 8) is not particularly fortunate, as it evokes the quantum mechanical terms.

The second chapter on obtaining an analytical signal is a very brief summary of the measuring methods. Chapter three, equally brief, discusses the electrodes used and electrolysis cells. A great emphasis is placed on solid (especially graphite) electrodes, in accordance with the authors' work. Chapter four surveys stripping analyses in solution, while the last two chapters deal with structural and phase analysis of solids.

The whole book is written more like a journal review than a monograph; therefore, the treatment is rather superficial, non-systematic and appropriate generalizations and conclusions are often missing. In many places the text is not very readable. In my opinion, the book is interesting for specialists because it presents them with an unusual viewpoint and may stimulate them to look beyond the customary boundaries of the method. On the other hand, it would be of little use to the novice in the field.

K. ŠTULÍK

**Flame Chemiluminescence Analysis by Molecular Emission Cavity Detection:** D. A. STILES, A. C. CALOKERINOS and A. TOWNSHEND (editors), Wiley, Chichester, 1994. Pages xiii + 205. £50.00. ISBN 0-471-94340-1.

Molecular emission cavity analysis (M.E.C.A.) shows remarkable sensitivity especially for sulphur, phosphorus and the halides. In addition it is capable of detecting most non-metals and metalloids and can deal with sample types from solid to gaseous. This monograph with contributions from active workers in their respective fields is a welcome coherent summary of this interesting and important field. The topics include the fascinating history of the discovery of M.E.C.A. in Belcher's Birmingham Group in the early 70's (A. Townshend), basic principles (A. C. Calokerinos), instrumentation and automation (N. Grekas) and four chapters on applications. These are grouped under Sulphur, Selenium and Tellurium (E. Henden), Arsenic, Antimony, Boron, Silicon, Germanium and Tin (M. Burguera and J. L. Burguera), Nitrogen, Phosphorus and Carbon (D. A. Stiles and A. Townshend) and Halogens and Metals (D. A. Stiles) and display some interesting aspects of gas phase molecular spectroscopy and selective reaction chemistry in solution or solid phase.

This is a timely and worthy addition to the series "chemical analysis" being produced with the customary attention to layout, quality of diagrams, indexing, *etc.* It is as pleasant to behold as to read. Congratulations to all concerned.

D. THORBURN BURNS

The second chapter on obtaining an analytical signal is a very brief summary of the measuring methods. Chapter three, equally brief, discusses the electrodes used and electrolysis cells. A great emphasis is placed on solid (especially graphite) electrodes, in accordance with the authors' work. Chapter four surveys stripping analyses in solution, while the last two chapters deal with structural and phase analysis of solids.

The whole book is written more like a journal review than a monograph; therefore, the treatment is rather superficial, non-systematic and appropriate generalizations and conclusions are often missing. In many places the text is not very readable. In my opinion, the book is interesting for specialists because it presents them with an unusual viewpoint and may stimulate them to look beyond the customary boundaries of the method. On the other hand, it would be of little use to the novice in the field.

K. ŠTULÍK

**Flame Chemiluminescence Analysis by Molecular Emission Cavity Detection:** D. A. STILES, A. C. CALOKERINOS and A. TOWNSHEND (editors), Wiley, Chichester, 1994. Pages xiii + 205. £50.00. ISBN 0-471-94340-1.

Molecular emission cavity analysis (M.E.C.A.) shows remarkable sensitivity especially for sulphur, phosphorus and the halides. In addition it is capable of detecting most non-metals and metalloids and can deal with sample types from solid to gaseous. This monograph with contributions from active workers in their respective fields is a welcome coherent summary of this interesting and important field. The topics include the fascinating history of the discovery of M.E.C.A. in Belcher's Birmingham Group in the early 70's (A. Townshend), basic principles (A. C. Calokerinos), instrumentation and automation (N. Grekas) and four chapters on applications. These are grouped under Sulphur, Selenium and Tellurium (E. Henden), Arsenic, Antimony, Boron, Silicon, Germanium and Tin (M. Burguera and J. L. Burguera), Nitrogen, Phosphorus and Carbon (D. A. Stiles and A. Townshend) and Halogens and Metals (D. A. Stiles) and display some interesting aspects of gas phase molecular spectroscopy and selective reaction chemistry in solution or solid phase.

This is a timely and worthy addition to the series "chemical analysis" being produced with the customary attention to layout, quality of diagrams, indexing, *etc.* It is as pleasant to behold as to read. Congratulations to all concerned.

D. THORBURN BURNS

Pergamon

*Talanta*, Vol. 42, No. 1, p. 147, 1995
Elsevier Science Ltd
Printed in Great Britain
0039-9140/95 $9.50 + 0.00

# CORRIGENDUM

G. Anderegg and S. Kholeif, The extrapolation of experimental equilibrium constant data to zero ionic strength: critical review and new approach. *Talanta*, **41**, 1507–1522, 1994.

Please note the following list of corrections to this paper:

p. 1509, column 1, equation (9) (last two terms)

$\times[1 - e^{-2\sqrt{I}}(1 + 2\sqrt{I} - 2I)]\}I$ $\times[1 - e^{-2\sqrt{I}}(1 \times 2\sqrt{I} - 2I)]\}I$

Read for

$+\frac{3}{2}\Delta C^{\varphi} I^2$ $+\frac{3}{2}\Delta C\varphi I^2$

p. 1509, column 1, line before last

Read: (m) for ($m$). Read: (c) for ($c$)

p. 1509, column 2, second footnote of Table 1

Read: $DI^{3/2}$ for: $D^{3/2}$

p. 1510, column 1, third line from top

Read: $kt^4)/(1 + ut)$ for: $kt^4)/(1 \times ut)$

p. 1510, column 1, equation 11

Read: m = for: $m =$

p. 1510, column 2, line 15 (end of paragraph)

Delete at $I_i$.

p. 1510, column 2, line 23 (end of paragraph)

Read: $i$ at $I_i$. for: $I_i$.

p. 1511, third footnote, Table 2

Read: $v$ for v

p. 1518, column 1, equation 19

Read: m for $m$

p. 1519 column 2, line 5 from the subtitle "Special cases when . . ."

Read: For for: Four

p. 1521, column 2, reference 4

Read: TDB-2.ı for: TDB-2.$_1$

Pergamon

*Talanta*, Vol. 42, No. 2, p. 149, 1995
Elsevier Science Ltd
Printed in Great Britain

# NEW ADVISORY BOARD MEMBER

The Editorial Board and the Publisher of *Talanta* take pleasure in welcoming the following member of the Advisory Board of the Journal.

JED HARRISON

**Jed Harrison** is a native of Vancouver. He received his B.Sc. in Chemical Physics from Simon Fraser University in 1980, and received the Gordon Shrum Gold Medal upon graduation. He was the recipient of an NSERC Postgraduate Fellowship while undertaking graduate studies in Chemistry at the Massachusetts Institute of Technology. There he worked with Professor Mark Wrighton and graduated with a Ph.D. in 1984. He then joined the Chemistry Department at the University of Alberta, and became a full Professor in 1994. He was the 1993 recipient of the Canadian Society for Chemistry's W.A.E. McBryde Medal, awarded for research in analytical chemistry. In 1994 he received the University of Alberta's first Faculty of Science Research Award.

Harrison is the co-author of over 60 scientific publications, and works with a research group of undergraduate, graduate and Post-doctoral students that numbers about 10. His research interests are generally in electrochemistry, specifically in the development of membranes for chemical and biochemical sensors, and the use of microelectronic fabrication techniques for sensors and sensor systems. This program encompasses the development of new ion-selective electrode membrane matrices suited for use with integrated circuit technology, and the study of transport of ions, neutral molecules and solvents within polymer membrane matrices. Recently his group has begun developing electrophoresis systems on glass "chips". Funding for this research has come from industry and from the Natural Sciences and Engineering Research Council.

Harrison is Associate Editor of a new journal, *Analytical Methods and Instrumentation*. He serves on the program selection committees of the biennial IEEE-sponsored Sensor and Actuator Workshop, and Transducers, the International Conference on Solid-State Sensors and Actuators. He is a member of the Electrochemical Society Sensor Group Executive Committee, and was recently elected a board member of the Society for Electroanalytical Chemistry.

Pergamon

0039-9140(94)00260-6

*Talanta*, Vol. 42, No. 2, pp. 151–169, 1995

0039-9140/95 $29.00 + 0.00

## REVIEW

# HYPHENATED FLOW INJECTION SYSTEMS AND HIGH DISCRIMINATION INSTRUMENTS

M. D. LUQUE DE CASTRO and M. T. TENA

Department of Analytical Chemistry, Faculty of Sciences, University of Córdoba, E-14004 Córdoba, Spain

(*Received* 2 *February* 1994. *Revised* 2 *September* 1994. *Accepted* 2 *September* 1994)

**Summary**—An overview of the state-of-the-art in flow injection analysis (FIA) coupled to instruments capable of providing either multidetection and/or multi-information is reported. The versatility of FIA endows the hyphenated instruments with analytical capabilities which increase from simple sample introduction to more complex sample handling such as automatic dilution and calibration, solvent exchange, derivatization reactions and on-line separation processes, among others. Unexplored aspects of these powerful problem solvers are also discussed.

Unaffordable analytical problems have found proper solutions since the appearance of 'hyphenated techniques', a term coined by Hirschfield at the beginning of the last decade[1] to name the coupling of two or more powerful techniques or instruments to achieve a synergistic effect of their overall performance with respect to their separate use. Liquid,[2,3] gas[4] and supercritical fluid[5] chromatographic techniques interfaced with mass spectrometric or with atomic spectrometric instruments[6] are examples of the excellent performance of these complex systems, as is the mass spectrometry–mass spectrometry tandem.[7] Most of the cases of hyphenated techniques entail powerful, large, expensive units, whose capabilities compensate for both high acquisition and maintenance costs.

Flow injection analysis (FIA)[8–10] is a simple and inexpensive technique the versatility of which affords for developing steps of the analytical process of rather different complexity. The simplest use of FIA is as a way for introducing samples into a detector, which is far from demonstrating the capabilities of this technique. Nevertheless, this simple use enables the sampling frequency to be dramatically increased and reduce the sample and reagent consumption. More interesting is the use of FIA to implement on-line derivatization reactions,[11] separation processes[12,13] as well as a number of sample handling modes to fit the initial sample conditions to the most suitable for single and multidetection[14,15] or implementation of flow-through (bio)chemical sensors,[16–18] among others.

Most of the detectors coupled to FI manifolds, either for sample introduction or for more complex sample handling, have been conventional instruments (e.g. molecular, atomic optical or electrochemical) capable of providing only two dimensional information. As happened with chromatographic techniques,[19] the first attempts to obtain three dimensional information in FIA were performed using either fast scan electrochemical[20] or diode array detectors,[21] thus enlarging the scope of application of FIA to more complex chemical systems. In a parallel but delayed development of hyphenated systems in chromatography, the coupling of FIA with high discrimination instruments pointed out the maturity of this dynamic technique. This last step in FIA started with the FIA–ICP-AES coupling. The capability of ICP-AES for multidetermination has been aided by FIA in different aspects since the earliest 1980's as listed in Table 1[41–103] and has been reviewed by different authors.[22–24] More recent and less numerous have been the arrangements of FI manifolds with instruments which enable three dimensional information and high

Table 1. FIA–ICP coupling

| Technique | FIA contribution | Analyte(s) | Sample(s) | Sample volume ($\mu l$) | Sampling frequency ($hr^{-1}$) | Detection limit | Other aspects | Ref. |
|---|---|---|---|---|---|---|---|---|
| ICP-AES | Sample introduction | Ca | Synthetic, water, cements | 25–300 | 90–320 | 40–400 *ng/ml* | | 41–43 |
| | | B | Water | 300 | 320 | | | 44 |
| | | Organometallic Cd, Pb, Zn | | 50 | | 0.139 *μg/ml* | Interface performance studies | 45 |
| | | Non-metals (Br, C, Cl, S) | Gaseous samples ($SF_6$, $CF_2Cl_2$, $CF_3Br$ in Ar) | 15–500 | | 50, 30, 80, 20 *pg* | | 46 |
| | | Metal Acetylacetone complexes | | 50 *μl* | | | Complex stability studies. Optimization SFC–DAD–ICP system. Supercritical FI system | 47 |
| | | Trace elements (Cu, Fe, Mg) | Fine chemicals | | | | FI slurry atomization | 48 |
| | | Sc | Technological processing solution (containing ~ 30 *mg/ml* Fe and 10 *mg/ml* Ti) | 500 | | 8.4 *ng/ml* | | 49 |
| | | Ca, Mg | Synthetic | 114 | | | Interference studies. Kalman Filter | 50 |
| | | Multielements | Synthetic | 100–500 | | 0.5–6 *ng/ml* | | 43, 51 |
| | | | Used lubricating oils | 500 | 45 | 0.02–1.3 *μg/g* | Robotics | 52 |
| | | | Alloys | | | | On-line electrolytic dissolution | 53 |
| | | | Biological samples | 20–50 | | 10–340 *ng/ml* | Reduced sample volume | 54, 55 |
| | | | Synthetic (aqueous and organic solutions) | 10–300 | 60 | 0.3–500 *ng/ml* | Interface studies | 56–60 |
| | Sample handling | Sc | Synthetic Reference oils | 500 | | | Interference studies | 61, 62 |
| | | Si | 85% phosphoric acid sample | 22.2–88.8 177 | | | FI slurry automization On-line dilution | 63 64 |
| | | Cu | Burt filtrates (from Zn plant) | 150 | 110 | | On-line standard addition On-line matrix matching calibration | 65 66 |
| | | Rare-earth | Metal samples | | | | On-line standard addition. Reverse-FIA | 67 |
| | | Cu, Ni, Zn | Alloys | 500 | | | On-line standard addition | 68 |
| | | Zn, Mn, Ca | Plant digests | 100 | 132 | | On-line standard addition | 69 |
| | | Multielements | Lubricating oils | | 80 | | On-line dilution | 70 |
| | | | Water | | 60 | | Standard salinity matching | 71 |

| | | | | | | | |
|---|---|---|---|---|---|---|---|
| | | Botanical SRM | 15 | | | Time-based injection | |
| | | Botanical SRM | 15 | | | On-line standard | |
| | | | | | | On-line standard addition (computer-guided). Time-based injection | |
| | | Rocks RM | 500 | 120 | | addition (zone sampling) | 73 |
| On-line separation process (I). Liquid–solid interfaces | Au | Refinery effluent water | 10 *ml* (250 eluent) | 6 | 1 *ng/ml* | Amberlyst A-26, mercaptoacetoxy-cellulose | 74 |
| | Mo | Seawater | 10–50 *ml* | | 0.2 *ng/ml* | Activated alumina | 75 |
| | Cr(III) | Human urine | 10 *ml* | | 0.05 *ng/ml* | Activated alumina | 76 |
| | Al | Potable waters and haemodialysis fluids | 1000 (100 eluent) | | 3 *ng/ml* | Chelex 100, Amberlite, Dowex | 77–78 |
| | B | | 250 | | | Amberlite XA-743 resin. Time-based injection | 79 |
| | Cu | Synthetic seawater | 1 *ml* | 30 | 0.16 *ng/ml* | $C_{18}$ bonded silica MIP*–AES | 80 |
| | P | Steels | 200 | 45 | 0.6 *μg/ml* | Activated alumina | 81 |
| | $I^-$, $IO_3^-$ | | 10 *ml* | | 0.75, 31 *ng/ml* | Anion-exchange (AGI-X8 resin). On-line oxidatin to $I_2$ | 82 |
| | $SO_4^{2-}$ | Natural waters, seawater, boiler-feed water | 2 *ml* (200 eluent) | | 2.8 *ng/ml* | Acidic alumina | 83 |
| | Oxyanions | | 200 | | | Activated alumina | 84 |
| | Organotin compounds | River water | 10–50 *ml* (250 eluent) | | 0.15–0.2 *pg* | $C_{18}$ bonded silica. Speciation by chromatography–MIP*–AES | 85 |
| | Multielements | Synthetic | 6–30 *ml* | 30 | 0.008–20 *ng/ml* | Chelex 100. In parallel columns | 86 |
| | | Waters | 7.5–80 *ml* | 12–20 | 0.009–2 *ng/ml* | Chelating resin, basic alumina | 87–89 |
| | | Serum | 0.5–2.5 *ml* | | 0.3–5.1 *ng/ml* | Desolvation device | 90, 91 |
| | | Alkali metal salts Aluminium alloys | 35 *ml* | 20 | 0.0021–0.12 *μg/g* | Chelating-cellulose | 92 |
| | | | | | | Chelating-cellulose Al and Na removal | 93 |

*continued*

Table 1. *continued*

| Technique | FIA contribution | Analyte(s) | Sample(s) | Sample volume ($\mu l$) | Sampling frequency ($hr^{-1}$) | Detection limit | Other aspects | Ref. |
|---|---|---|---|---|---|---|---|---|
| | | Metals | Salts solutions | 350–500 *ml* | 2–8 | *pg/ml* | Donnan dialysis preconcentration | 94 |
| | On-line separation process (II). Liquid–liquid interfaces | $F^-$ | Waters | 200 | 36 | 30 *ng/ml* | Indirect determination liq–liq extraction (La-alizarin complexone fluoride complex) | 95 |
| | | Be | Mg–Al alloys, Cu alloys | 500 | 25 | 50 ng/ml | Liq–liq extraction. Microporous PTFE tubing separator | 96 |
| | | Cu | SRM water | 3 *ml* | 25 | 0.1 *ng/ml* | Liq–Liq extraction (dithizone in $CCl_4$) | 97 |
| | | Cd | SRM (biological) | 5 *ml* | 20 | 0.4 *ng/ml* | Liq–liq extraction. Suction-cup sampling | 98 |
| | On-line separation process (III). Gas–liquid interfaces | Organic C | Water (containing 500 *mg/l* of carbonate carbon) | | | 5 *mg/l* | Evaporation of inorganic C | 99 |
| | | As | Synthetic, SRM, glycerine, geological, NaCl and $AlCl_3$ | 40–374 | 120–200 | 0.025–5.2 *ng/ml* | Hydride generation (with and without microporous PTFE membrane/tubing separator) | 100–105 |
| | | Ge | Single-crystal gallium arsenide (non-, Zn- and Si-dop Al) and poly(ethylene-terephthalate) | 1000 | 150 | 0.4 *ng/ml* | Hydride generation. Microporous PTFE separator | 106 |
| | | Sb(III), Sb(V) | Copper metal, waste water | | | 0.19 *ng/ml* | Hydride generation. Continuous flow system | 107 |
| | | As, Sb, Se | Surface waters | 750 | | 3.5, 7.0, 3.6 *ng/ml* | Hydride generation | 108 |
| | | As, Sb, Bi | Ore rock | | | 0.2, 0.2, 0.1 *μg/g* | Hydride generation | 109 |
| | | Multielements | SRM (steel, coal fly ash, urban particulate, river and seawaters) | | | | Hydride generation | 110 |
| | Speciation | Cr(III), Cr(IV) | Reference waters | 2 *ml* (200 $\mu l$ eluent) | | 1.4, 0.2 *pg/ml* | Acidic alumina column | 111, 88 |
| | | Sb(III), Sb(V) | Waste waters | | | | Hydride generation | 107 |
| | | $PO_4^{3-}$, total P | Waste waters | 200 | 40–80 | 5, 0.6 *μg/ml* | In serial detectors (spectrophotometer UV-visible and ICP-AES) | 112, 113 |

*Microwave plasma torch AES.

Table 2. FIA ICP–MS coupling

| Technique | FIA contribution | Analyte(s) | Sample(s) | Sample volume ($\mu l$) | Sampling frequency ($hr^{-1}$) | Detection limit | Other aspects | Ref. |
|---|---|---|---|---|---|---|---|---|
| ICP/MS | Sample introduction | Mo | Synthetic | 10 | 30 | | | 114 |
| | | U | Nuclear material | | | | | 115 |
| | | Au | Seawater | 120 | 4 | 10 *fM* | Off-line preconcentration $[Au(CN)_2^-]$ | 116 |
| | | In | Synthetic | 100 | 45 | *ng/g* | Ion lens tuning strategies | 117 |
| | | Organomercury | SRM (biological) | 100 | | 2.7 *ng/ml* | Avoidance interface clooging | 118 |
| | | Thimerosal | Biological | | | | | 119 |
| | | Trimethylgallium etherate | Human faeces | | | | Simplex optimization | 120 |
| | | Pt-group metals | Peridotite | | | sub-*ng/g* | Solid content: 5–10% | 121 |
| | | U, Th | Aluminium | 250 | 30 | 0.2 *ng/g* | Comparison with laser-ablation | 122 |
| | | Ba, In | Synthetic seawater | 500 | | | Ion lens tuning strategies | 123 |
| | | Pb, Zn | Powdered, blood plasma | | | | | 124 |
| | | Re, Pb, Ir | Natural water, sediments | 250, 500 | | 5–14 *pg* | Off-line ion-exchange and isotope dilution | 125 |
| | | Tl, Pb, Bi | Nickel-base alloys | 200 | | 1 *ng/ml* | | 126 |
| | | Au, Zn, Cu | Blood plasma, serum | $<1000$ | | 0.2 *ng/ml* | | 127 |
| | | Zn-64/Zn-67 ratio | Human faeces | | | | Feeding experiments | 128 |
| | | Multielement | Synthetic | 10–25 | 60 | 0.01–0.1 *ng* | Optimization study prior to HPLC–ICP-MS coupling | 129, 130 |
| | | | SRM (rock) | 500 | | | Minimized matrix deposition | 131 |
| | | | Organometallic compounds, sediments, alloys | 25, 100 | | 0.52–2.0 *ng/ml* | Special interfaces | 132–136 |
| | | | Trace metals | 50 | | *ng/ml* | Interface introduction volatile organic solvents | 137 |

*continued*

Table 2. *continued*

| Technique | FIA contribution | Analyte(s) | Sample(s) | Sample volume ($\mu l$) | Sampling frequency ($hr^{-1}$) | Detection limit | Other aspects | Ref. |
|---|---|---|---|---|---|---|---|---|
| | Sample handling | Pb (isotopes) | NIS SRM 983 | 1075 | 240 | | Isotopic dilution | 138, 139 |
| | | Multielement | NIS SRM 991<br>Undiluted urine | 500 | 10 | | On-line standard addition method | 140 |
| | | | Highly conc. $H_3PO_4$ and $NH_4NO_3$ | 200 | 10–15 | | On-line standard addition method | 141 |
| | | | High purity Ni | 200 | | *ng/g* | Continuous sample standard mixing, high solid content | 142 |
| | On-line separation process (I). Liquid–solid interfaces | Re | Seawater | 10–50 *ml* | | 0.27 *pg/ml* | Dowex 1-x-8 ($ReO_4^-$) Isotopic dilution | 143 |
| | | Pt | Airborne particulate | 800 | 12 | 0.1 *ng/ml* | Dowex 50 W-X8 (matrix retention) | 144 |
| | | Trace metals | Concentrated brines (30%) | 10 *ml* (0.2 *ml* eluent) | | | On-line proconcentration matrix removal | 145 |
| | | | SRM (seawater) | | | 2 *ng/ml* | In-parallel columns | 146 |
| | | Multielement | Hair, SRM | 50 *ml* | | 27 *pg/ml* (Cu) | On-line anodic stripping voltammetry | 147 |
| | | Cu, Cd | SRM (urine) | 1000 | | 545 *pg/ml* (Cd) | | |
| | On-line separation process (III). Gas–liquid interfaces | Bi | SRM (rock) | 40 | | 1.8 *ng/ml* | Hydride generation | 148 |
| | | Pb | SRM, galene | | | 40 *ng/ml* | Hydride generation Isotopic dilution PTFE tubing separator | 149 |
| | | Hydride-forming elements, Hg | Seawater | 500 | 20 | 4–6 *pg/l* | Hydride generation–vapour generation | 150, 151 |

Table 3. Other FIA/high discrimination detector couplings

| Technique | FIA contribution | Analyte(s) | Sample(s) | Sample volume ($\mu l$) | Sampling frequency ($hr^{-1}$) | Detection limit | Other aspects | Ref. |
|---|---|---|---|---|---|---|---|---|
| FTIR | Sample introduction | Phenyl isocianate | Synthetic | 25 | 60 | 4 $\mu g/ml$ | | 152 |
| | | *o*-Xylene | Xylol | 200 | 20 | 0.02% *v/v* | Comparison flow cells | 153 |
| | | Ibuprafen | Pharmaceuticals | 320 | 20 | 80 $\mu g/ml$ | Partial dissolution in $Cl_4C$ | 154 |
| | | Carbaryl | Pesticide formulations | 300 | 53 | 1.6 $\mu g/ml$ | Flowing or stop-flow modes | 155 |
| | | Allyldiisopropylamine oxide | Synthetic | | 60 | | Carrier: supercritical $CO_2$ | 156 |
| | | Aliphatic esters | Synthetic | 130 | 25 | 14 *mM* | Comparison flowing and stop-flow modes | 157 |
| | | Choline compounds | Pharmaceutical preparations | | 60 | 0.02 $fg/ml$ | $\mu$-CIRCLE cell | 158 |
| | | Xylene compounds | Commercial xylol | 200 | 20 | 0.02% *v/v* | $\mu$-SPEAC cell | 159 |
| | Sampling handling | Benzene | Gasoline | 300 | 18 | 0.02% *v/v* | On-line standard addition | 160 |
| | | tert-Butyl ether | Unleaded gasolines | 320 | 45 | 0.035% *v/v* | First order derivative | 161 |
| MS | Sample introduction | Tributyltin | Sediment, SRM | 500 | 50 | 0.2 $\mu g$ *Sn/g* | Ion spray MS–MS Selected reaction monitoring | 162 |
| | | Acetic acid, acetoin, 2,3-butanediol, ethanol, $CO_2$, $O_2$ | Fermentation broth | 250 | 15 | | MS–MS gas diffusion | 163, 164 |
| | | Toxins | Plankton | | | 2 $\mu g/ml$ | Ion spray MS/MS Selected ion monitoring | 165 |
| | | $\beta$-Blocking drugs | Pharmaceuticals | | | 0.2 *ng* | Study prior to LC-MS coupling | 166 |
| | Sample handling | Acetaminophen, glutathione, cysteine | Synthetic | 100 | | | On-line electrochemical and chemical reactions | 167 |
| | On-line separation process | As, Se, Sb, Sn | Synthetic | 100 | | 0.1–1 $\mu g/ml$ | Hydride generation | 168, 169 |
| | | Chloroform | Synthetic | | | 1 $\mu g/ml$ | Gas diffusion | 169 |
| MECA | Sample introduction | Organophosphorous compounds, insecticides | Synthetic | 2 | 100 | 0.5–50 $\mu g$ *P* | No cavity cooling between injections | 170, 171 |
| | | Sulphide, sulphite, sulphate | Synthetic | 5 | 20 | 1 *ng S* | No cavity cooling between injections | 172 |
| | On-line separation process | Arsenic | SRM (vegetal) | 120 | 100 | 80 $ng/ml$ | Hydride generation | 173 |
| NMR | Sample introduction | Toluene | Acetonitrile | 50 | | 130 $\mu g/ml$ | Evaluation flow-cell | 174 |
| Flame IRES | Sample introduction | Total inorganic carbon, saccharides | Tap water | 25, 250 | 60 | | Design purge-cell FI and continuous modes | 175 |

discrimination capabilities like MS (by direct coupling or through an ICP source), FTIR and NMR, among the most important, which have also been reviewed,[35-40] and whose most significant features are listed in Tables 2[114-151] and 3.[152-175]

Figure 1 shows the dissimilar use of flow injection analysis–high discrimination instrument (FIA–HDI) couplings. For this reason the aim of this work is to give to the analytical community, but particularly FIA users, an overview of the present situation of these hyphenated techniques, emphasizing the advantages involved in them, criticizing their negative aspects and showing the unexplored availabilities of one of the most promising uses of FIA.

## INTERFACES

The connection between a flow injection system and a high resolution detector has a decisive influence on the performance of the hyphenated system, as analytical quality parameters such as reproducibility, accuracy, sensitivity and selectivity are highly dependent on how this coupling is accomplished. The complexity of the interface is very different depending on whether the measurement is performed in solution, plasma or vacuum.

Inexpensive flow-cells (either conventional or demountable micro-flow cells) with KBr windows and different thickness spacers (0.015–0.22 mm, 0.15–9 $\mu$l cell volume) are used in FIA–FTIR coupling when organic solvent carriers are involved.[143-145,159-161] The use of thick spacers yields a higher contribution to the blank measurement from the carrier solvent, so poorer detection limits are obtained. More sophisticated cells are used with uncommon solvents. A 25 $\mu$l-micro-Circle cell equipped with a zinc selenide crystal (0.318 cm diameter) has been used for aqueous samples in FIA–FTIR;[157,158] and a high pressure flow cell (2 $\mu$l, 1 mm optical path length and 2 mm$^2$ cross sectional area) when supercritical $CO_2$ was the carrier.[156]

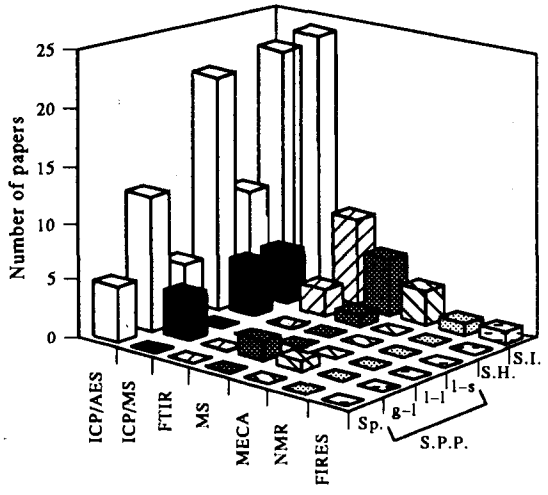


Fig. 1. Tridimensional plot of the main contributions of flow injection analysis coupled to high discrimination detectors. (Sp) Speciation; (g–l) gas–liquid; (l–l) liquid–liquid; (l–s) liquid–solid; (S.P.P.) on-line separation processes; (S.H.) sample handling and (S.I.) sample introduction.

The design of an NMR flow cell should provide rapid sample displacement without significant degradation of resolution. Cells similar to those in Fig. 2, with a 50 $\mu$l observed volume work well at 1 ml/min flow-rate. The FIA injector can be connected directly to the NMR flow cell with 0.01-in i.d., 1/16-in o.d. tubing.[174] Sufficient premagnetization time of the sample can be accomplished by placing the injector and connectors within the magnetic field.

Special attention has been paid to interfacing FI systems and ICP.[42,44-46,56,57,59,60,132,176-179] A general interface to introduce a liquid into a plasma consists of a nebulizer, a spray chamber and a separator. The main shortcomings of using conventional interfaces in FI–ICP and in LC–ICP couplings related to continuous sample aspiration are the large dead volume and the sample loss involved as well as the band broadening. Efforts have been focused on producing interfaces with high analyte transport efficiency and minimal solvent loading and dead volume in order to decrease detection limits. Low analyte transport efficiency of conventional pneumatic nebulizer/spray chamber systems (only 1–2% of the analyte aspirated actually reaches the plasma) limits the ability to analyse small sample volumes. Miniaturized interfaces have been designed[42,44,45] in order to overcome this drawback. The direct injection nebulizer (DIN)[60] is another approach to minimize the dead volume: a microconcentric nebulizer fits into the central aerosol tube of a conventional ICP torch. Solutions are nebulized directly at the base of the plasma and there is no spray chamber or separator. The microconcentric nebulizer[46,59,60] and thermospray nebulizer[57,176,179] have been the most used. In addition, miniaturized glass-frit nebulizers[45] have been reported to couple FIA and ICP. Solvent loading is identified as a major contributor to plasma instability and poor detection limits. A jet separator,[177] a condenser[57,179] or a membrane dryer separator[132,178] can be used to remove the majority of

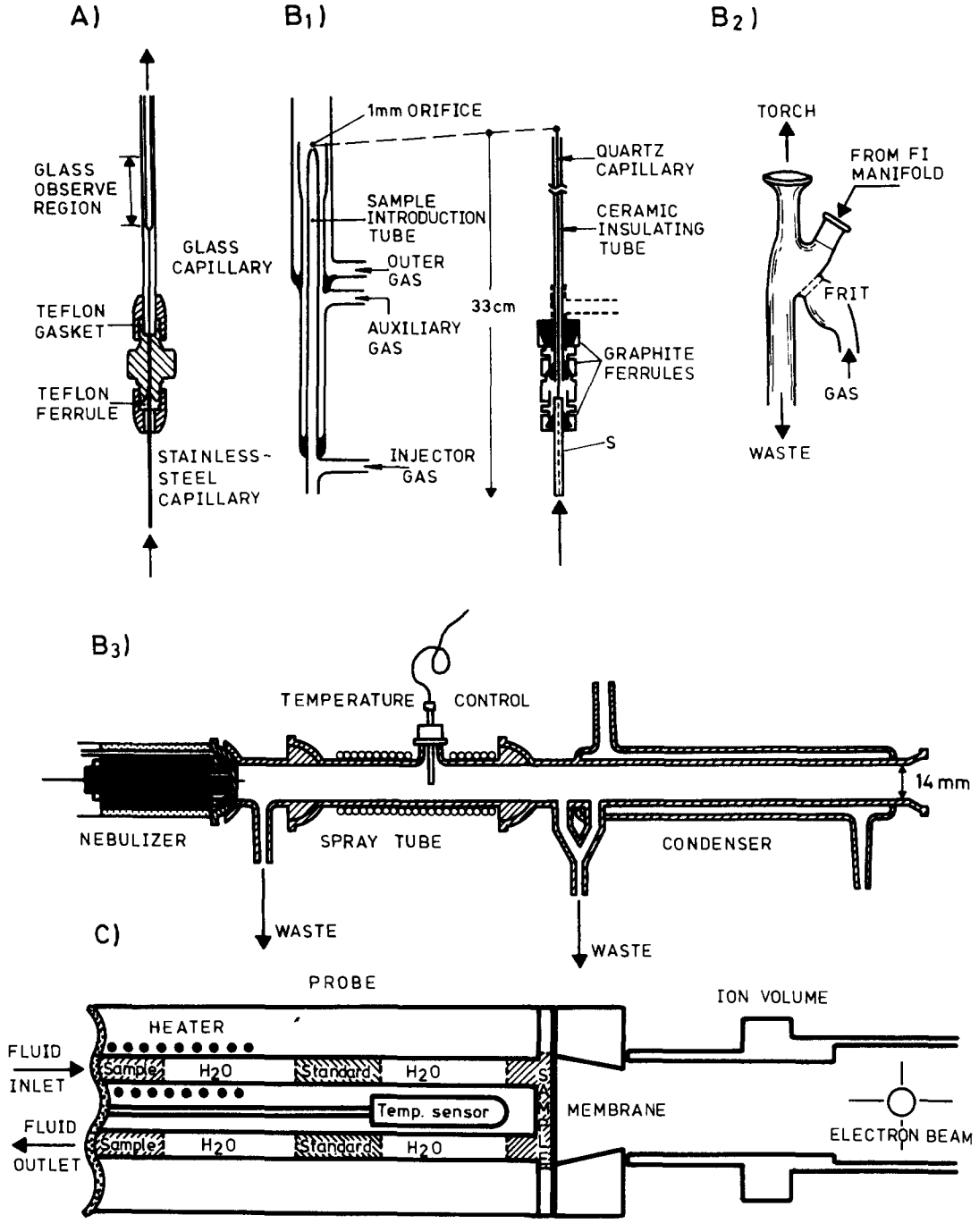


Fig. 2. FIA–HDI interfaces. (A) NMR flow-cell and interface. (B) FIA–ICP interfaces. ($B_1$) Direct insertion of a microconcentric nebulizer (right) into the ICP torch (left). ($B_2$) Miniaturized glass-frit nebulizer. ($B_3$) Thermospray interface consisting of a thermospray nebulizer, a heated spray chamber and a condenser. (C) FIA–MS–MS interface. Sheet membrane probe with membrane temperature control.

the solvent and convert the sample into a dried and desolvated aerosol in a flow of argon. Membrane separators are especially useful for organic solvents.

Flow injection and mass spectrometry have been interfaced either by membrane introduction and ion spray systems. The former consists of a membrane probe directly inserted into the mass spectrometer ion source. The carrier solution flows across the inside surface of the membrane while the outside surface is exposed to the vacuum of the mass spectrometer. This interface is suitable for volatile analytes capable of diffusing through the heated membrane.[163,180]

In ion spray MS the carrier solution is allowed to flow at a rate of 1–500 $\mu$l/min, through a very narrow bore capillary tubing (50–200 $\mu$m) polarized to a high voltage (2–3 kV). Spraying is facilitated by a coaxial flow of nitrogen. The electrically charged droplets found evaporate during their flight to the sampling plate (counter-electrode). The analyte must be present as an ion in solution because there is no ionization process. This injector has been connected to the ionspray interface via a 1 m × 50 $\mu$m i.d. fused-silica tubing.[162]

## SAMPLE INTRODUCTION

Despite the FIA capability to carry out a series of chemical processes, the major use of flow injection-high discrimination instruments (FI–HDI) has been to transport a few $\mu$l of sample to the detector. In addition to this application other more interesting uses are commented on in the following sections.

An extensive use of FIA as a sample introduction tool has been done when coupled to ICP-AES[41–63] and ICP-MS.[114–137] Nevertheless, FIA–ICP hyphenated systems have profited from many other FIA capabilities.

The use of flow injection as a means of sample introduction endows the methods with a number of advantages, namely: reduced sample and reagent consumption, increased sample throughput, higher reproducibility and better detector performance.

The sample saving achievable in FI–ICP is remarkable. Sample volumes in continuous aspiration ICP are usually between 2 and 5 ml, which decreases to 10–500 $\mu$l when coupled to FIA. Continuous aspiration of the sample is too wasteful to be feasible when only a limited sample volume is available (*i.e.* biological, clinical and forensic analysis); so the reduction of sample consumption achievable by FIA is of paramount importance in these fields. By way of example, FIA combined with ICP-AES has been successfully applied to the simultaneous determination of eight elements in 20-$\mu$l serum samples,[54] and acceptable detection limits for the analysis of several metals in biological samples were obtained with the use of *ca.* one-hundreth of the minimum sample volume required for continuous aspiration.[55]

The high sample throughputs achievable by FIA are a consequence of the simple and automatic way of sample introduction, as this can be inserted into the flowing stream and monitored within few seconds, whereas standard NMR methods require at least 45–60 sec before starting monitoring.[174] Flow injection couplings enable near-real time monitoring thus avoiding fraction trapping, which is time-consuming and capable of sample contamination. FI sampling with membrane introduction MS–MS has been used for fully automated monitoring and feedback control of bioreactors.[163] It allows quantification of the major products and metabolites of fermentation and even detection of trace metabolites.

Flow injection is a very reproducible means to introduce a precise volume of sample and also to improve the performance of the detector by minimizing blockage drawbacks in the interface thus favouring the detector stability. The precision of transient signal integration measurements as compared to steady-state integration measurements was found to be at least one of magnitude better for all of the wear metals.[52] The significant improvement in precision is due to reduced carbon build-up (more stable plasma; improved torch stability (no air pockets), constant sample solution flow-rate (use of a pump to avoid problems with viscosity changes) in the coupled FIA–ICP-AES. The ability to use small sample volumes reduces the loading of undesirable matrices on nebulizers and torches, particularly in high salt content samples or organic solvent solutions. An injection volume as low as possible without increasing detection limits must be chosen in order to minimize solid sample deposition on the torch injector tip and on the mass spectrometer sampling interface. Thus, no matrix deposition occurs and therefore reproducibility of a particular measurement is improved. This also provides better long-term stability of the instrument. The flow injection technique enables determinations in samples with total dissolved solid concentration 20–30 times higher than those handled by conventional solution aspiration. The precision of an FIA–ICP-MS approach reported by Vickers *et al.*[114] was found to be *ca.* twice that of a continuous flow mode, whereas Stroh *et al.*[131] have found a mean long-term stability better than 5% RSD for all the elements (10 ng/ml) they have studied in a 3% m/v NaCl matrix.

Memory effects are also minimized in an FIA–HDI coupling as the carrier immediately follows each sample plug, which results in a continuous rinsing effect that dramatically reduces clogging of the interface by deposition of

solid. The rinsing effect of the carrier decreases wash-out times, so the sampling frequency is improved as a result. Since the carrier system is flowing continuously, plasmas which normally extinguish at the air–water interface will no longer do so. In addition, injection of the sample avoids its passage through the flexible tubing of peristaltic pumps, which can adsorb the analyte[116] causing diminished signals and memory effects that severely degrade precision; at the same time, a close control of the flow-rate is accomplished in this way.

The use of FIA–FTIR systems provides simple and rapid sampling and easy cleaning of the flow-cell, and enables the continuous monitoring of the baseline of spectra. Pharmaceuticals[154,158] and pesticide formulations[155] have been determined successfully by FIA–FTIR thus demonstrating the usefulness of this approach.

Detection limits and spectroscopic resolution of FIA–NMR are also better than for static sample measurements.[174] The FI carrier solution provided a suitable medium where stable ion-spray could take place in MS sample introduction.[163]

Solid[181–184] and gaseous[185] samples can also be introduced in FIA–HDI couplings. Despite the capability of FIA for direct introduction of solid and gaseous samples, this potential has not been exploited. Only the direct analysis of solid samples by FIA–ICP-AES has been carried out by electrolytic dissolution[48] and FIA–slurry atomization.[63] Simultaneous determination of Zn, Si, Fe, Mn, Cr, Mg and Cu in aluminium alloys has been accomplished in a few minutes. Gaseous mixtures of compounds containing the elements Br, C, Cl and S were introduced by FIA with various sample loops (15–250 $\mu$l) on the injection valve.[46] Sample gas was added to the loops at *ca.* 10 ml/min, then the sample carrier gas (Ar) was switched through the loops to transport their contents into the ICP.

## SAMPLE HANDLING

This section deals with some simple operations such as automatic mixing of the sample with a dilution, standard or reagent thus completing the step within a short period of time with less sample and diluent, standard or reagent consumption. An additional advantage of the automatic performance of this step is a decrease of sample manipulation and thus of the human errors arose from it.

Dilution is an FIA capability which can be performed in an automatic way, thus achieving dilution factors for samples of standards ranging between 0 and 200. This fact justifies its coupling to HDI instead to other less versatile continuous dilution systems.[70] Different ways have been used to achieve this goal, namely the insertion of a short piece of wide-bore tubing, a delay coil, merging streams, zone sampling approach by using an unstirred or stirred chamber. A dilution step can be mandatory in order to minimize matrix effects in the determination of major components in a complex sample, or to fit the concentration of the analyte(s) within the linear range of determination in concentrated samples. A significant reduction of the mass-dependent interference effects without substantial sacrifice in sensitivity can be achieved by appropriate dispersion in the FI system. Vickers *et al.*[114] have demonstrated the almost complete elimination of signal suppression by using a FI manifold which provides dispersion factors up to 25. Martin and Ihrig[72] have developed an FI–ICP-AES approach for the automatic determination of widely varying elemental composition and concentration in a series of liquid samples without operator intervention. All the samples were appropriately diluted before determination by ICP–AES by using computer-guided sequential dilutions to place all elements within the optimum range. Sample dilution was accomplished by injecting the sample for shorter periods of time (time-based injection). The tandem-injection and merging-streams have also been employed to achieve on-line dilution and steady-state concentrations for ICP-AES and ICP-MS.[64]

### *Automatic calibration*

The ability for on-line development of relatively time-consuming sample pretreatment procedures such as standard additions, internal standard, isotope dilution, and matrix-matching calibration in a simple way, saving both time and sample makes FIA a useful tool for this sample handling.

The standard-addition method has proved to be effective in overcoming matrix effects, one of the main sources of loss in both accuracy and sensitivity in certain types of samples. The FI manifold can be designed either to add the standard to the sample (before, in, or after injection) or to inject the standard into the sample (reversed FIA), among others, thus

avoiding sample and standard contamination and the time-consuming preparation step.

In the reverse-FIA mode the standard-addition method is accomplished by continuous sample pumping to the detector instead of the carrier solution, the detector is zeroed for this baseline value, and the standard solutions are injected in the sample stream. The calibration curve can be run by injecting equal volumes of standards of different concentration; different volumes of the same standard solution, or using any of the FIA alternatives for dilution prior to injection. This method has been proposed to determine benzene in gasoline by FIA–FTIR,[160] and Si in an 85% phosphoric acid sample[65] and rare earth in metal samples[67] by FIA–ICP-AES.

Sample–standard merging before injection is an easy way to implement the standard addition method. A third stream of internal standard can merge after the sample and standard confluence.[141] The standard addition stream is used to add multielement standard solutions of variable concentrations. A complete standard addition can be performed in each sample by changing the standard solution. Unlike the reversed-FIA standard addition method, continuous introduction of the sample matrix into the detector is avoided by the sample standard merging method, which has been successfully used in FIA–ICP-MS[142,113] couplings.

The merging-zone approach has also been used for calibration purposes in the determination of Ni, Cu and Ni in alloys.[68] The system utilized successive injections of the sample, each one accompanied by the injection of a different standard. The limitations of this system include the relatively low sampling rate and the necessity of preparing a series of standards. The latter shortcoming might be overcome by using the zone-sampling mode, which enables controlled dilution of a given standard before its injection into the final standard carrier stream. Standard addition in plant digest samples has been implemented in an FIA–ICP-AES system by merging the sample zone with an aliquot delivered from a trapped standard zone in a modified version of the zone sampling approach. Eleven additions ranging from 3 to 32% of only one standard solution were performed in 5 min.[69] Nine toxic elements in undiluted urine were determined in less than 5 min using an FIA–ICP-MS approach[140] in which the FI manifold, which included a splitter tee, two in-parallel injection valves with different size loops (40 and 500 $\mu$l for standard and sample, respectively) and a mixing tee, was used to inject sequentially three standard solutions into the same sample plug.

Isotope dilution was used by Lasztity, Viczian *et al.* for the determination of lead in various matrices using a merging zones approach with programmable time-based injections.

Matrix matching of sample and standards was implemented in FIA–ICP-AES by Giné *et al.*[71] to minimize the interferences due to easily ionizable elements. Initially the ICP determines the sodium content in the sample and thereafter the computer selects the appropriate sodium addition to match the saline concentration with that of the standards. After having received a suitable amount of sodium, the sample reaches the ICP and the elements are determined.

### *Derivatization*

Flow injection is a suitable tool to carry out on-line chemical reactions in a reproducible and automatic way with a noticeable saving of both sample and reagents. The analyte can be converted into a more suitable form for detection (*e.g.* a volatile species which enhances the selectivity, sensitivity and scope of application of the coupled system). The chemical reactions most widely used in FIA–ICP-AES, FIA–ICP-MS and FIA–MS have been hydride generation and vapour generation.[100–110,148–151,168,169] Getek *et al.*[167] have reported an FIA–MS coupling in which electrochemical and chemical reactions took place. On-line formation and detection of glutathione and cysteine conjugates of acetaminophen were accomplished by interfacing a coulometric cell with a thermospray mass spectrometer in the flow-injection system. The electrochemical information enables the confirmation of *in vivo* reaction mechanisms.

## ON-LINE SEPARATION PROCESSES

One of the more advantageous aspects of FIA is its availability for the development of non-chromatographic continuous separation techniques with minimal complication of the experimental set-up. Flow injection takes advantage of its dynamic nature for an easy, inexpensive implementation of separation techniques involving any of the possible interfaces (liquid–solid, liquid–liquid or gas–liquid). All of them have been implemented in on-line helped by an FI manifold, then hyphenated to a high

capability instrument. The goal of the separation step has been to enhance either the sensitivity of the method by preconcentration of the target analyte(s) or the selectivity by removal of the matrix thus avoiding both its interference on the analytical signal and its passage through the detector, which is of a paramount importance in cases of insufficient or non-discrimination capability. The use of switching valves makes it feasible to lead undesirable species to the waste after separation without passing through the detection point. An additional benefit is an increased reproducibility as distortion of the signal from the analyte is minimized or avoided.

Liquid–solid interfaces have been established in FIA–HDI systems mainly by the use of solid-phase columns packed with either ion-exchange or adsorptive material, particularly with preconcentration purposes. This previous step can improve dramatically the sensitivity of a given method by one or two orders of magnitude. By way of example, the preconcentration FIA–ICP systems described by Hartenstein *et al.* are capable of increasing the signal by 10–15-fold and 20–75-fold per minute of sample loading time for simultaneous multielement integrated and simple element peak height, respectively, giving nearly 100% recovery of spiked analytes in tap and rain run-off waters.[89] Nevertheless, there are two negative aspects of these separation processes, namely: (a) The sample volume used is higher than in the absence of this step (see Tables 1–3). Depending on both the concentration of analyte in the sample and the enrichment factor to be attained the sample volume ranges between 2 and 100 ml, far from the $\mu$l range usual in FIA. (b) The sampling frequency decreases by a factor which depends on the working conditions. In the above example[89] this parameter decreased from 30–60 determinations/hr to 12–20 determinations/hr. This shortcoming can be minimized by using several columns arranged in parallel which work simultaneously and deliver sequentially the eluates to the flow manifold. The location of the column(s) in the dynamic system dramatically affects the overall performance and thus the results obtained. When the column is located in the transport zone of the flow manifold, a switching valve after the column is mandatory in order to waste undesirable sample components, thus avoiding their passage through the detector ($SV_2$ in Fig. 3A) (see Refs 81, 91, 92 and 143 as examples). The main drawback of this arrangement is the continuous

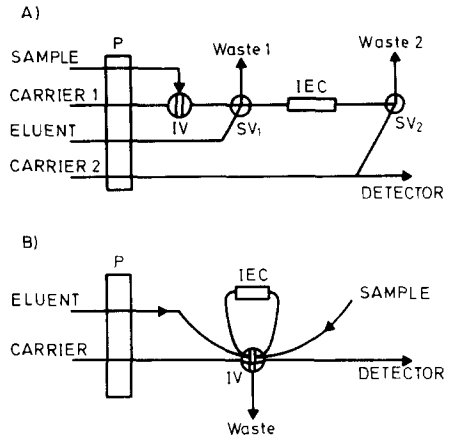


Fig. 3. Schemes of flow injection solid phase separation column coupled to high discrimination detectors. (P) Peristaltic pump; (IV) injection valve; (SV) selecting valve and (IEC) ion-exchange column.

circulation of the liquid in the same direction which tends to compact the packed material in the column and hence increases the pressure within the system. This problem can be overcome by placing the column upright and passing the solution upstream or by carrying out elution in the opposite direction of retention. The implementation of the latter approach is easy if the column is located in the loop of an injection valve (Fig. 3B). (A detailed description of the use of microcolumns in continuous flow systems can be found in Refs 12 and 13.)

In addition to the microcolumn located in any of the commented on above points, other units can be included on-line in the FI manifold to improve the efficiency of the overall process. Such is the case with the desolvation device connected to a microcolumn by Peng *et al.*[91] in the development of a method for the determination of trace elements by FIA–ICP-AES with on-line preconcentration. The authors achieve a desolvation efficiency of 73% at a desolvation temperature of 120 C and apply the method to

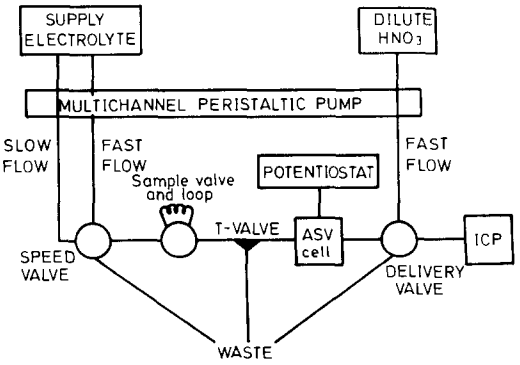


Fig. 4. Scheme of the flow injection-anodic stripping voltammetry inductively coupled plasma (FI-ASV-ICP) approach.

the determination of Al, Cu, Cd, Fe and Mn in serum by separation of the target analytes from various co-existing elements.

A less common liquid–solid interface in FIA–HDI is that created by using an on-line voltammetric stripping cell in the flow manifold such as the arrangement depicted in Fig. 4 which has been used to deposit Cu and Cd at a working electrode, then releasing the analytes for detection by ICP-AES.[147] The deposition step enables the elimination of the sample matrix components that are not electroactive and do not deposit during passage of the sample through the cell, thus being sent to waste by switching the delivery valve. The target analytes were preconcentrated from sample volumes as large as necessary, then stripped for detection into a small volume of liquid of the appropriate characteristics. Detection limits of pg have been achieved for 1-ml urine samples. It must be emphasized that the sampling frequency affordable by a stripping technique is usually higher than by solid columns as both the retention and elution steps are faster. Another additional advantage of stripping is the higher efficiency of the deposition process, which can be 100%.

Liquid–liquid interfaces have seldom been established in FIA–HDI by the use of both extraction and dialysis techniques and in all of the cases the detector has been ICP-AES. In continuous liquid–liquid extraction processes the efficiency of the separation strongly depends on the aqueous–organic flow-rate ratio. One of the earlier papers in this field[98] reported an increase in sensitivity of *ca.* 250-fold in comparison with direct aspiration of an aqueous solution for the determination of Cd by ICP–AES after extraction of its diethyldithiocarbamate into carbon tetrachloride with a detection limit of 4 ng/ml and a sampling frequency of 20 $hr^{-1}$. Indirect methods have also been established in this area, as is the case with the determination of fluoride in water by formation of the lanthanum/alizarin complexone/fluoride ternary complex and its extraction into hexanol containing *N*,*N*-diethylaniline. The introduction of the organic layer into the plasma and measurement of the emission intensity of La III 333.75-nm line enables the determination of the target analyte in a 0.03–1.3 $\mu$g/ml linear range with a sampling rate of 36 samples/hr.[85] Two in-series phase separators are used in order to obtain a pure organic phase to be transferred to the detector.

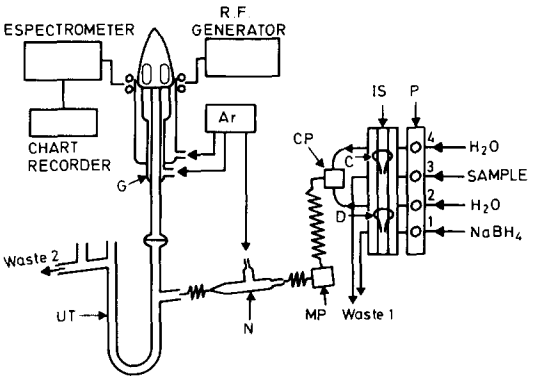


Fig. 5. Scheme of a flow injection–hydride generation–ICP-AES system. (P) Peristaltic pump; (IS) injection system; (CP) confluence point; (MP) mixing point; (N) nebulizer and (UT) U-tube.

A recent combination of flow injection Donnan dialysis with inductively coupled plasma atomic emission spectrometry has proved to yield enrichment factors of over 200 for cations with an 8-min dialysis time, allowing ng/ml level detection limits. These results were obtained for receiver solutions consisting either of Sr(II) or Mg(II), providing complementary free spectral ranges and the applicability of the hyphenated system to trace metal cation analysis for both transition and rare earth elements. The enrichment factors obtained were linear over a wide range of concentrations and limits of detection approximately 100 times lower than for direct aspiration. Additional improvements in enrichment factors were obtained with increases in the dialysis time and/or final sample solution temperature. A signal enhancement factor of 650 with a detection limit of 11 ng/ml for monovalent silver cation was obtained using a 30-min dialysis.[94] These results call for greater attention to be paid to Donnan dialysis as a powerful tool to manipulate the sensitivity of FIA–HDI methods.

Despite the small number of species capable of yielding a gas after reaction, gas–liquid interfaces have gained extensive use in FIA–HDI. Within gas–liquid separation, techniques based on hydride generation are the most common in hyphenated systems, particularly in FIA–ICP-AES and FIA–ICP-MS, where vapour generation has proved considerable enhancement of the analytical capabilities for multielemental determination of volatile vapour-forming elements at ultratrace levels in environmental samples. Very good accuracy and precision in addition to increased sensitivity and avoidance of espectral interferences caused by high salt matrix, as demonstrated in ocean

water samples.[150] An arrangement such as that depicted in Fig. 5 was used in one of the earlier hydride generation–FIA–ICP-AES methods. The determination of arsenic as arsine was performed at a rate of 200 injections/hr with detection limits of 1.4 ng arsenic.[102] Subsequent contributions have been the determination of arsenic in glycerine,[103] that of antimony in waste water,[107] and the simultaneous determination of As, Sb and Se,[108] among others. The simultaneous method,[108] as compared with continuous sample introduction, provides detection limits three times poorer. By contrast, the precision is approximately 150% better with FI due to the reduced pump pulsations. Other advantages of the FI system are the reduced sample size necessary for analysis ($<750$ $\mu$l *vs.* 4–5 ml for the continuous introduction system) and the potential for a greatly increased rate of sample throughput.

One of the scarce contributions on FIA–MS dealing with hydride generation is that reported by Canham and Pacey and consists of preliminary studies of the behaviour of such a system with very promising results.[169] A more complex FIA–ICP-MS arrangement has also been reported for the determination of hydride-generating elements and for the determination of mercury. Several pre-reduction techniques were investigated and applied to the determination of the target analytes (namely, B, Sb, Se, Te, Hg and As) at ultra-trace levels in environmental samples. The detection limits found were in the range 0.5–7.0 pg/ml.

On-line preconcentration and oxidation by hydrogen peroxide were combined to improve the atomic emission limit of detection for iodine. The process was automated by FIA and hyphenated to both ArICP-AES and HeICP-AES for evaluation of the performance of the overall system as a way to circumvent the drawbacks encountered in the batch method, to which $I_2$ is adsorbed onto the peristaltic PVC pump tubing causing a memory effect, and the mixed reagents were only stable for 1 hr. To minimize the memory effect in the batch method, the transfer line was rinsed with a 0.02% solution of sodium thiosulphate in an attempt to reduce $I_2$ (adsorbed on the transfer line) to $I^-$. Although this procedure was effective in reducing the memory effect, its use in routine analysis was limited because of cross-contamination and increased analysis time. To eliminate the cited limitations in the batch method, the reagents were mixed on-line and the formation of $I_2$ took place along the reactor, thus avoiding its passage through the pump tubing. The iodine signal at 183.04 nm was enhanced by a factor of 33 and 100 for ArICP and HeICP, respectively, with detection limits of 5 and 9 ng/ml.[82]

## SPECIATION STUDIES

Speciation has been implemented in FIA–HDI using different capabilities of such arrangements. One of the simpler but more expensive ways to develop speciation is by the use of a detector which allows direct discrimination of the different forms of a given element or compound. This is the case with the FIA–MS–MS tandem, with ion-spray sample introduction and discrimination by selective reaction monitoring of daughter–parent pairs, which has been used for speciation of organotin compounds in sediment and SRM,[162] or the use of molecular emission cavity analysis (MECA) for the speciation of sulphur anions (as sulphide/sulphite/sulphate)[172] and that of phosphorus insecticides[171] and organophosphorus compounds,[170] based on the parameter $t_M$ ($t_M$ is the time elapsed between introduction of the cavity into the flame and analytical achievement of the maximum peak intensity). Speciation can also be implemented in FIA systems coupled to twin in-series detectors with non-capability for speciation. Such is the case with the speciation of phosphorus compounds (as phosphate and total phosphorus) in waste water by FIA and sequential spectrophotometry and ICP-AES. Phosphate was determined as molybdovanadophosphoric acid using a colourimetric method and the solution from the flow cell of the spectrophotometer was directly introduced to an ICP. The determination of total phosphorus was performed by measuring the emission intensity at 177.499 nm. Chromium caused a positive error in the colourimetric determination, but ions commonly existing in waste water did not interfere with the determination of total phosphorus. The sampling throughput was 80 samples/hr. The contributions of FIA to improve the features of the method were the on-line derivatization and the increased sampling frequency.[112]

Discrimination can also be achieved in the FI manifold. Such is the case with speciation of antimony [as Sb(III)/Sb(V)].[107] Antimony was reduced to stibine and determined in 1 *M* malic

acid or 0.5*M* tartaric acid, whereas in either of these media antimony(V) gave little or no signal. Total antimony was separately determined in the presence of 0.1*M* thiourea as pre-reductant.

An on-line separation step can also endow the method with discriminating capability, as in the method proposed for the sequential speciation of chromium [as Cr(III)/Cr(VI)] based on the use of microcolumn of activated alumina in an FIA–ICP-AES arrangement. The column was used to separate and preconcentrate Cr(VI) from Cr(III) before ICP detection at 267.72 nm. Thus, determination limits of 1.4 and 0.20 ng/ml for Cr(III) and Cr(VI), respectively, were obtained.[111]

More complex separation techniques as GC have also been hyphenated to FIA and microwave-induced plasma (MIP) atomic emission spectrometry for organotin speciation analysis. The method was based on the preconcentration of ionic organotin compounds by sorption on bonded silica with octadecyl functional groups followed by on-column ethylation using sodium tetraethylborate. The derivatized species were eluted with 250 $\mu$l of methanol, separated by gas chromatography and detected by MIP–AES. The method was applied to the determination of the target analytes in river samples which were also analysed using a manual liquid–liquid extraction method. The results agreed within 10–15% for concentrations of a few pg/ml.[85]

## CONCLUSIONS

From Tables 1–3 the more extensive use of FI coupled to ICP can be stated. The first of such arrangements exploited the FI manifold only as a means of reproducible transport of the sample into the instrument, with the sole aim of increasing sample frequency. Later it was realized that periodical washing of the nebulizer is beneficial, allowing handling of concentrated samples. These features, together with the feasibility of automated dilution and calibration led to the realization that FIA is the cure of the 'Achilles heel' of ICP. From more recent developments such as FIA preconcentration/separation, FIA speciation and FIA conversion it becomes apparent that FIA can be a more useful problem solver.

The long way ran for full implementation of FIA–ICP coupling seems also to be the way followed by other high discrimination systems, as can be inferred from Tables 2 and 3. In this respect it is noticeable the scarce number of FI–RMN methods proposed so far, despite the fact that interface problems are successfully solved as a result of the previous coupling of RMN with other hydrodynamic systems as is the case with LC-RMN.

Some isolated attempts have been made using these hyphenated systems and should be exploited as they offer interesting perspectives, namely: (a) use of robotic stations for sample pretreatment steps such as weighing and dissolution. The pretreated sample can be introduced directly into the FI manifold,[186,187] thus achieving full automation of the analytical process. (b) Direct introduction of solid samples into the FIA–HDI arrangement. A first attempt has been made in this respect by use of electrical energy for leaching the sample.[181,182] Electrolysis is not the sole way of using solid samples in these dynamic systems, as ultrasounds have also proved their great potential in this context.[183,184] (c) Use of FIA as a 'hyphen' allowing different instrumental techniques to be linked together. The use of a stripping flow-cell for preconcentration purposes is a partial example of this potential, which can also be expanded to its use for preconcentration/determination prior to the high discrimination instrument, thus increasing the information level. Also FIA could be linked to apparatus such as a supercritical fluid extractor and an HDI with accomplishment of the intermediate step (derivatization, separation, *etc.*), which no doubt would improve the overall performance of the method. (d) The scope of non-chromatographic continuous separation techniques coupled to FIA–HDI should be broadened by including prevaporation[188] and continuous precipitation[189] as both have proved their capabilities when coupled to FIA. (e) More attention must be paid to the use of FIA to obtain information in the development of theoretical studies of the dynamics in membrane and membraneless instruments,[180] and to the FIA–HDI coupling interfaced by an autosampler.[190] All these slightly or unexploited aspects of FIA in hyphenated systems can undergo suitable development with the present trend of some manufacturers, which integrate FIA systems in HDI as a means, in principle, of sample handling.

*Acknowledgement*—Comisión Interministerial de Ciencia y Tecnología (CICyT) is thanked for financial support.

## REFERENCES

1. T. Hirschfeld, *Anal. Chem.*, 1980, **52**, 297A.

2. M. A. Brown (Ed.) *Liquid Chromatography/Mass Spectrometry. Applications in Agricultural, Pharmaceutical and Environmental Chemistry.* ACS Symposium Series, 1990.
3. A. L. Yergey, C. G. Edmonds, I. A. S. Lewis and M. L. Vestal, *Liquid Chromatography/Mass Spectrometry. Techniques and Applications.* Plenum Press, New York, 1990.
4. F. W. Karasek and R. E. Clement, *Basic Gas Chromatography-Mass Spectrometry. Principles and Techniques.* Elsevier, Amsterdam, 1988.
5. R. M. Harrison and S. Rapsomanikis, *Environmental Analysis Using Chromatography Interfaced with Atomic Spectroscopy.* Ellis Horwood, Chichester, 1989.
6. K. Jinno (Ed.) *Hyphenated Techniques in Supercritical Fluid Chromatography and Extraction.* Elsevier, Amsterdam, 1992.
7. K. L. Busch, G. L. Glish and S. A. McLuckey, *Mass Spectrometry/Mass Spectrometry. Techniques and Applications in Tandem Mass Spectrometry.* VCH, New York, 1989.
8. M. Valcárcel and M. D. Luque de Castro, *Flow Injection Analysis: Principles and Applications.* Ellis Horwood, Chichester, 1987.
9. J. Ruzicka and E. H. Hansen, *Flow Injection Analysis.* Wiley & Sons, New York, 1988.
10. B. Karlberg and G. E. Pacey, *Flow Injection Analysis. A Practical Guide.* Elsevier, Amsterdam, 1989.
11. T. Yamane, *J. Flow Injection Anal.*, 1991, **8,** 49.
12. M. Valcáracel and M. D. Luque de Castro, *Non-Chromatographic Continuous Separation Techniques.* RSC, Cambridge, 1991.
13. Z. Fang, *Flow Injection Separation and Preconcentration.* VCH, Weinheim, 1993.
14. M. D. Luque de Castro and M. Valcárcel, *Trends Anal. Chem.*, 1986, **5,** 71.
15. M. Valcárcel and M. D. Luque de Castro, *Anal. Chim. Acta*, 1991, **250,** 157.
16. M. D. Luque de Castro and M. Valcárcel, *Lab. Robotics Autom.*, 1991, **3,** 199.
17. M. Valcárcel and M. D. Luque de Castro, *Analyst*, 1993, **118,** 593.
18. M. Valcárcel and M. D. Luque de Castro, *Flow-Through (Bio)Chemical Sensors.* Elsevier, Amsterdam, 1994.
19. L. Huber and S. A. George, *Diode Array Detection in HPLC.* Marcel Dekker, New York, 1993.
20. J. Janata and J. Ruzicka, *Anal. Chim. Acta*, 1982, **139,** 105.
21. F. Lázaro, A. Ríos, M. D. Luque de Castro and M. Valcárcel, *Analysis*, 1986, **14,** 378.
22. J. Ruzicka, *Fresenius J. Anal. Chem.*, 1986, **324,** 745.
23. Z. Fang, S. Xu, X. Wang and S. Zhang, *Anal. Chim. Acta*, 1986, **179,** 325.
24. Z. Fang, S. Xu and S. Zhang, *Anal. Chim. Acta*, 1987, **200,** 35.
25. J. F. Tyson, *Anal. Chim. Acta*, 1988, **214,** 57.
26. J. F. Tyson, *Anal. Chim. Acta*, 1990, **234,** 3.
27. J. A. Koropchak and D. H. Winn, *Trends Anal. Chem.*, 1987, **6,** 171.
28. A. O. Jacintho, E. A. G. Zagatto, H. Bergamin Fo., F. J. Krug, B. F. Reis, R. E. Bruns and B. R. Kowalski, *Anal. Chim. Acta*, 1981, **130,** 243.
29. T. Ito, H. Kawaguchi and A. Mizuike, *Bunseki Kagaku*, 1980, **29,** 332.
30. Z. Fang, *Spectrochim. Acta Rev.*, 1991, **14,** 235.
31. J. F. Tyson, *Spectrochim. Acta Rev.*, 1991. **14,** 169.
32. Z. Fang, *Fenxi Huaxue*, 1986, **14,** 549.
33. S. Xu and Z. Fang, *Huaxue Toghao*, 1984, **8,** 12.
34. L. E. Smythe, *Rev. Anal. Chem.*, 1982, **6,** 1.
35. G. D. Christian and J. Ruzicka, *Spectrochim. Acta*, 1987, **42B,** 157.
36. M. Linscheid, *Chem. Labor. Bert.*, 1990, **41,** 125.
37. T. Shimamura, *Shitsuryo Bunseki*, 1988, **36,** 273.
38. R. M. Barnes, *Spectroscopy*, 1986, **1,** 24.
39. E. G. Bartick and R. G. Messerschmidt, *Int. Lab.*, 1985, **58–64,** 66.
40. O. F. X. Donard and F. M. Martin, *Trends Anal. Chem.*, 1992, **11,** 17.
41. J. A. Koropchak, H. Aryamanya and D. H. Winn, *J. Anal. At. Spectrom.*, 1988, **3,** 799.
42. P. L. Kempster, J. F. van Staden and H. R. van Vliet, *Fresenius J. Anal. Chem.*, 1988, **332,** 153.
43. S. Greenfield, *Spectrochim. Acta*, 1983, **38B,** 93.
44. P. L. Kempster, H. R. van Vliet and J. F. van Staden, *Anal. Chim. Acta*, 1989, **218,** 69.
45. M. Ibrahim, W. Nisamaneepong and J. Caruso, *J. Chromatogr. Sci.*, 1985, **23,** 144.
46. B. R. LaFreniere, R. S. Houk, D. R. Wiederin and V. A. Fassel, *Anal. Chem.*, 1988, **60,** 23.
47. K. Jinno, H. Mae and C. Fujimoto, *J. High Resol. Chromatogr.*, 1990, **13,** 13.
48. A. J. Ambrose, L. Ebdon and P. Jones, *Anal. Proc.*, 1989, **26,** 377.
49. H. Chen, Z. Jiang, Z. Lai and Z. Liao, *Fenxi Huaxue*, 1990, **18,** 1152.
50. J. A. Horner, A. P. Wade and M. W. Blades, *J. Anal. At. Spectrom.*, 1988, **3,** 809.
51. K. R. Brushwyler, L. D. Carter and G. M. Hieftje, *Appl. Spectrosc.*, 1990, **44,** 1438.
52. M. P. Granchi, J. A. Biggerstaff, L. J. Hilliard and P. Grey, *Spectrochim. Acta*, 1987, **42B,** 169.
53. D. Yuan, X. Wang, P. Yang and B. Huang, *Anal. Chim. Acta*, 1991, **251,** 187.
54. C. W. McLeod, P. J. Worsfold and A. G. Cox, *Analyst*, 1984, **109,** 327.5.
55. A. J. Faske, K. R. Snable, A. W. Boorn and R. F. Browner, *Appl. Spectrosc.*, 1985, **39,** 542.
56. K. E. LaFreniere, G. W. Rice and V. A. Fassel, *Spectrochim. Acta*, 1985, **40B,** 1495.5.
57. J. A. Koropchak and D. H. Winn, *Anal. Chem.*, 1986, **58,** 2561.
58. T. J. Brotherton, P. E. Pfannerstill, J. T. Creed, D. T. Heitkemper, J. A. Caruso and S. E. Pratsinis, *J. Anal. At. Spectrom.*, 1989, **4,** 341.5.
59. T. W. Avery, C. Chakrabarty and J. J. Thompson, *Appl. Spectrosc.*, 1990, **44,** 1690.
60. K. E. Lawrence, G. W. Rice and V. A. Fassel, *Anal. Chem.*, 1984, **56,** 289.6.
61. H. Chen, Z. C. Jiang, Y. Zeng and L. Y. Kong, *Guangpuxue Yu Guangpu Fenxi*, 1992, **12,** 49.
62. E. G. Chudinov, I. I. Ostroukhova and G. V. Varvanina, *Fresenius J. Anal. Chem.*, 1989, **335,** 25.
63. A. J. Ambrose, L. Ebdon, M. E. Foulkes and P. Jones, *J. Anal. At. Spectrom.*, 1989, **4,** 219.
64. Y. Israel, A. Lásztity and R. M. Barnes, *Analyst*, 1989, **114,** 1259.
65. Y. Israel and R. M. Barnes, *Anal. Chem.*, 1984, **56,** 1188.
66. D. E. Davey and G. J. H. Metz, *J. Anal. At. Spectrom.*, 1988, **3,** 375.

67. Q. Shen, Z. Jiang and Z. Liao, *Fenxi Shiyanshi*, 1991, **10,** 45.6.
68. E. A. G. Zagatto, A. O. Jacintho, F. J. Krug, B. F. Reis, R. E. Bruns and M. C. U. Araújo, *Anal. Chim. Acta*, 1983, **145,** 169.
69. B. F. Reis, M. F. Giné, F. J. Krug and H. Bergamin Fo., *J. Anal. At. Spectrom.*, 1992, **7,** 865.
70. S. J. Evans and R. J. Klueppel, *Spectrochim. Acta*, 1985, **40B,** 49.
71. M. F. Giné, H. Bergamin Fo., B. F. Reis and R. L. Tuon, *Anal. Chim. Acta*, 1990, **234,** 207.
72. J. M. Martin and P. J. Ihrig, *Appl. Spectrosc.*, 1987, **41,** 986.
73. M. F. Giné, F. J. Krug, H. Bergamin Fo., B. F. Reis, E. a. G. Zagatto and R. E. Burns, *J. Anal. At. Spectrom.*, 1988, **3,** 673.
74. M. M. Gómez and C. W. McLeod, *J. Anal. At. Spectrom.*, 1993, **8,** 461.
75. N. Furuta, K. R. Brushwyler and G. M. Hieftje, *Spectrochim. Acta*, 1989, **44B,** 349.
76. A. G. Cox, C. W. McLeod, *Anal. Chim. Acta*, 1986, **179,** 487.
77. M. R. García-Pereiro, A. López-García, M. E. Diaz-García and A. Sanz-Medel, *J. Anal. At. Spectrom.*, 1990, **5,** 15.
78. M. R. García-Pereiro, M. E. Diaz-García and A. Sanz-Medel, *J. Anal. At. Spectrom.*, 1987, **2,** 699.
79. D. R. Anderson and C. W. McLeod, *Anal. Proc.*, 1988, **25,** 67.
80. Y. Madrid, M. Wu, Q. Jin and G. M. Hieftje, *Anal. Chim. Acta*, 1993, **277,** 1.
81. C. W. McLeod, I. G. Coox, P. J. Worsfold, J. E. Davies and J. Queay, *Spectrochim. Acta*, 1985, **40B,** 57.
82. J. P. Dolan, S. A. Sinex, S. G. Capar, L. Montaser and R. H. Clifford, *Anal. Chem.*, 1991, **63,** 2539.
83. A. G. Cox, C. W. McLeod, D. L. Miles and J. M. Cook, *J. Anal. At. Spectrom.*, 1987, **2,** 553.
84. I. G. Cook, C. W. McLeod and P. J. Worsfold, *Anal. Proc.*, 1986, **23,** 5.
85. J. Szpunar-Lobinska, M. Ceulemans, R. Lobinski and F. C. Adams, *Anal. Chim. Acta*, 1993, **278,** 99.
86. S. D. Hartenstein, J. Ruzicka and G. D. Christian, *Anal. Chem.*, 1985, **57,** 21.
87. S. Caroli, A. Alimonti, F. Petrucci and Zs. Horváth, *Anal. Chim. Acta*, 1991, **248,** 241.
88. C. W. McLeod, Y. Zhang, I. Cook, A. Cox, A. R. Date and Y. Y. Cheung, *J. Res. Nat. Bureau Standards*, 1988, **93,** 462.
89. S. D. Hartenstein, G. D. Christian and J. Ruzicka, *Canad. J. Spectrosc.* 1985, **30,** 144.
90. X. Wang and R. M. Barnes, *J. Anal. At. Spectrom.*, 1989, **4,** 509.
91. X. Peng, Z. Jiang and Y. Zen, *Anal. Chim. Acta*, 1993, **283,** 887.
92. Y. Israel, A. P. Krushevska, H. Foner, L. J. Martines and R. M. Barnes, *J. Anal. At. Spectrom.*, 1993, **8,** 467.
93. J. Dumont, M. Côté and J. Hubert, *Appl. Spectrosc.*, 1989, **43,** 1132.
94. N. Kasthurikrishnan and J. A. Koropchak, *Anal. Chem.*, 1993, **65,** 857.
95. J. L. Marzoori and A. Miyazaki, *Anal. Chem.*, 1990, **62,** 2457.
96. M. Yamamoto, Y. Obata, Y. Nitta, F. Nakata and T. Kumamaru, *J. Anal. At. Spectrom.*, 1988, **3,** 441.
97. X. Wang and R. M. Barnes, *Fenxi Shiyanshi*, 1991, **10,** 7.
98. T. Kumamaru, Y. Nitta, F. Nakata, H. Matsu and M. Ikeda, *Anal. Chim. Acta*, 1985, **174,** 183.
99. O. Emteryd, B. Andersson and H. Wallmark, *Microchem. J.*, 1991, **43,** 87.
100. X. Wang and R. M. Barnes, *J. Anal. At. Spectrom.*, 1988, **3,** 1091.
101. R. M. Barnes and X. Wang, *J. Anal. At. Spectrom.*, 1988, **3,** 1083.
102. R. R. Liversage, J. C. van Loon and J. C. de Andrade, *Anal. Chim. Acta*, 1984, **161,** 275.
103. N. H. Tioh, Y. Israel and R. M. Barnes, *Anal. Chim. Acta*, 1986, **184,** 205.
104. A. Brzezinska-Paudyn, J. van Loon and R. Hancock, *At. Spectrosc.* 1986, **7,** 72.
105. H. Chen, Z. Jiang, L. Kong and Y. Zen, *Fenxi Ceshi Tongbao*, 1990, **9,** 9.
106. F. Nakata, H. Sunahara, H. Fujimoto, M. Yamamoto and T. Kumamaru, *J. Anal. At. Spectrom.*, 1988, **3,** 579.
107. T. Nakahara and N. Nikui, *Anal. Chim. Acta*, 1985, **172,** 127.
108. G. S. Pyen and R. F. Browner, *Appl. Spectrosc.*, 1988, **42,** 508.
109. H. Gao, K. Li, *Fenxi Huaxue*, 1991, **19,** 1285.
110. Z. Li, S. Mcintosh and W. Slavin, *Anal. Proc.*, 1992, **29,** 438.
111. A. G. Cox, I. G. Cook and C. W. McLeod, *Analyst*, 1985, **110,** 331.
112. J. L. Manzoori, A. Miyazaki and H. Tao, *Analyst*, 1990, **115,** 1055.
113. A. Miyazaki and K. Bansho, *Kogai*, 1989, **24,** 87.
114. G. H. Vickers, B. S. Ross and G. M. Hieftje, *Appl. Spectrosc.*, 1989, **43,** 1330.
115. S. Vijayalakshmi, R. K. Prabhu, T. R. Mahalingam and C. K. Mathews, *At. Spectrosc.*, 1992, **13,** 61.
116. K. K. Falkner and J. M. Edmond, *Anal. Chem.*, 1990, **62,** 1477.
117. J. Wang, E. H. Evans and J. A. Caruso, *J. Anal. At. Spectrom.*, 1991, **6,** 605.
118. D. Beauchemin, K. W. Siu and S. S. Berman, *Anal. Chem.*, 1988, **60,** 2587.
119. D. S. Bushee, J. R. Moody and J. C. May, *J. Anal. At. Spectrom.*, 1989, **4,** 773.
120. J. H. D. Hartley, L. Ebdon and S. J. Hill, *Anal. Proc.*, 1992, **29,** 94.
121. A. N. Eaton, R. C. Hutton and J. G. Holland, *Chem. Geol.*, 1992, **95,** 63.
122. P. Van de Weijer, P. J. M. G. Vullings, W. L. H. Baeten and W. J. M. De Laat, *J. Anal. At. Spectrom.*, 1991, **6,** 609.
123. J. Wang, W. L. Shen, B. S. Sheppard, E. H. Evans, J. A. Caruso and F. L. Fricke, *J. Anal. At. Spectrom.*, 1990, **5,** 445.
124. J. R. Dean, L. Ebdon, H. M. Crews and R. C. Massey, *J. Anal. At. Spectrom.*, 1988, **3,** 349.
125. D. C. Colodner, E. A. Boyle and J. M. Edmond, *Anal. Chem.*, 1993, **65,** 1419.
126. T. Mochizuki, A. Sakashita, H. Iwata, Y. Ishibashi and N. Gunji, *Anal. Sci.*, 1990, **6,** 191.
127. S. G. Matz, R. C. Elder and K. Tepperman, *J. Anal. At. Spectrom.*, 1989, **4,** 767.
128. J. Eagles, S. J. Fairweather-Tait, F. A. Mello, D. E. Portwood, R. Self, A. Goetz, K. G. Heumann and H. M. Crews., *Rapid. Commun. Mass. Spectrom.*, 1989, **3,** 203.

129. J. J. Thompson and R. S. Houk, *Anal. Chem.*, 1986, **58,** 2541.
130. H. M. Al-Swaidan, N. Lacy and G. D. Christian, *Anal. Lett.*, 1989, **22,** 2653.
131. A. Stroh, U. Völlkopf and E. R. Denoyer, *J. Anal. At. Spectrom.*, 1992, **7,** 1201.
132. S. J. Hill, J. Hartley and L. Ebdon, *J. Anal. At. Spectrom.*, 1992, **7,** 895.
133. A. N. Eaton and R. C. Hutton, *Lab. Pract.*, 1988, **37,** 61.
134. D. Beauchemin, *Analyst*, 1993, **118,** 815.
135. A. Stroh and U. Völlkopf, *Anal. Proc.*, 1992, **29,** 274.
136. X. Wang, A. Lasztity, M. Viczian, Y. Israel and R. M. Barnes, *J. Anal. At. Spectrom.*, 1989, **4,** 727.
137. S. J. Hill, J. Hartley and L. Ebdon, *J. Anal. At. Spectrom.*, 1992, 723.
138. M. Viczian, A. Lasztity, X. Wang and R. M. Barnes, *J. Anal. At. Spectrom.*, 1990, **5,** 125.
139. A. Lasztity, M. Viczian, X. Wang and R. M. Barnes, *J. Anal. At. Spectrom.*, 1989, **4,** 671.
140. D. R. Wiederin, R. E. Smyczek and R. S. Houk, *Anal. Chem.*, 1991, **63,** 1626.
141. Z. Peng, J. Klingenberg, T. Beeren and W. Van Borm, *Spectrochim. Acta*, 1991, **46B,** 1051.
142. P. Richner, *J. Anal. At. Spectrom.*, 1993, **8,** 927.
143. M. B. Shabani and Akimasa Masuda, *Anal. Chim. Acta*, 1992, **261,** 315.
144. H. Mukai, Y. Ambe and M. Morita, *J. Anal. At. Spectrom.*, 1990, **5,** 75.
145. L. Ebdon, A. Fisher, H. Handley and P. Jones, *J. Anal. At. Spectrom.*, 1993, **8,** 979.
146. E. Liu, W. J. Chen and C. Y. Zhao, *Fenxi Huaxue*, 1993, **21,** 328.
147. J. R. Pretty, E. A. Blubaugh, E. H. Evans, J. A. Caruso and T. M. Davidson, *J. Anal. At. Spectrom.*, 1992, **7,** 1131.
148. T. Akagi, T. Hirata and A. Masuda, *Anal. Sci.*, 1990, **6,** 397.
149. X. Wang, M. Viczian, A. Lasztity and R. M. Barnes, *J. Anal. At. Spectrom.*, 1988, **3,** 821.
150. A. Stroh and U. Völlkopf, *J. Anal. At. Spectrom.*, 1993, **8,** 35.
151. U. Völlkopt, A. Guensel and A. Janssen, *At. Spectrosc.*, 1990, **11,** 135.
152. D. J. Curran and W. G. Collier, *Anal. Chim. Acta*, 1985, **177,** 259.
153. M. de la Guardia, S. Garrigues and M. Gallignani, *Anal. Chim. Acta*, 1992, **261,** 53.
154. S. Garrigues, M. Gallignani and M. de la Guardia, *Talanta*, 1993, **40,** 89.
155. M. Mallignani, S. Garrigues, A. Martínez-Vado and M. de la Guardia, *Analyst*, 1993, **118,** 1043.
156. S. V. Olesik, S. B. French and M. Novotny, *Anal. Chem.*, 1986, **58,** 2256.
157. D. K. Morgan, N. D. Danielson and J. E. Katon, *Anal. Lett.*, 1985, **18,** 1979.
158. B. E. Miller, N. D. Danielson and J. E. Katon, *Appl. Spectrosc.*, 1988, **42,** 401.
159. S. Garrigues, M. Gallignani and M. de la Guardia, *Analyst*, 1992, **117,** 1849.
160. M. Gallignani, S. Garrigues and M. de la Guardia, *Anal. Chim. Acta*, 1993, **274,** 267.
161. M. de la Guardia, M. Gallignani and S. Garrigues, *Anal. Chim. Acta*, 1993, **282,** 543.
162. K. W. Siu, G. J. Gadner and S. S. Berman, *Anal. Chem.*, 1989, **61,** 2320.
163. M. J. Hayward, T. Kotiaho, A. K. Lister, R. G. Cooks, G. D. Austin, R. Narayan and G. T. Tsao, *Anal. Chem.*, 1990, **62,** 1798.
164. M. J. Hayward, D. E. Riederer, T. Kotiaho, R. G. Cooks, G. D. Austin, M. J. Syu and G. T. Tsao, *Process Control Qual.*, 1991, **1,** 105.
165. S. Pleasanse, M. A. Quilliam, A. S. W. De Freitas, J. C. Marr and A. D. Cembella, *Rapid. Commun. Mass Spectrom.*, 1990, **4,** 206.
166. M. S. Leloux, W. M. A. Niessen, R. A. M. Van der Hoeven, *Biol. Mass Spectrom.*, 1991, **20,** 647.
167. T. A. Getek, W. A. Korfmacher, T. A. McRae and J. A. Hinson, *J. Chromatogr.*, 1989, **474,** 245.
168. J. S. Canham and G. E. Pacey, *Anal. Lett.*, 1988, **21,** 1619.
169. J. S. Canham and G. E. Pacey, *Anal. Chim. Acta*, 1988, **214,** 385.
170. J. L. Burguera, M. Burguera and D. Flores, *Anal. Chim. Acta*, 1985, **170,** 331.
171. J. L. Burguera and M. Burguera, *Anal. Chim. Acta*, 1986, **186,** 597.
172. J. L. Burguera and M. Burguera, *Anal. Chim. Acta*, 1984, **157,** 177.
173. J. L. Burguera and M. Burguera, *Analyst*, 1986, **111,** 171.
174. S. A. Curran and D. E. Williams, *Appl. Spectrosc.*, 1987, **41,** 1450.
175. C. K. Y. Lam, Y. Zhang, M. A. Busch and K. W. Busch, *Talanta*, 1993, **40,** 867.
176. J. W. Elgersma and F. J. M. J. Maessen, *Spectrochim. Acta*, 1986, **41B,** 1217.
177. A. Gustavsson, *Spectrochim. Acta*, 1987, **42B,** 111.
178. A. Gustavsson, *Spectrochim. Acta*, 1988, **43B,** 917.
179. J. W. Elgersma, J. Balke and F. J. M. J. Maessen, *Spectrochim. Acta*, 1991, **46B,** 1073.
180. G. J. Tsai, G. D. Austin, M. J. Syu, G. T. Tsao, M. J. Hayward, T. Kotiaho and R. G. Cooks, *Anal. Chem.*, 1991, **63,** 2460.
181. H. Bergamin, F. J. Krug, E. A. G. Zagatto, E. C. Arruda and C. A. Coutinho, *Anal. Chim. Acta*, 1986, **190,** 177.
182. H. Bergamin, F. J. Krug, B. F. Reis, J. A. Nobrega, M. Mesquita and I. G. Souza, *Anal. Chim. Acta*, 1988, **214,** 397.
183. Danhua Chen, F. Lázaro, M. D. Luque de Castro and M. Valcárcel, *Anal. Chim. Acta*, 1989, **226,** 221.
184. F. Lázaro, M. D. Luque de Castro and M. Valcárcel, *Anal. Chim. Acta*, 1991, **242,** 283.
185. F. Cañete, A. Ríos, M. D. Luque de Castro and M. Valcárcel, *Anal. Chim. Acta*, 1989, **224,** 127.
186. J. A. García-Mesa, M. D. Luque de Castro and M. Valcárcel, *Anal. Chem.*, 1993, **65,** 3540.
187. J. A. García-Mesa, M. D. Luque de Castro and M. Valcárcel, *J. Flow Injection Anal.*, 1993, **10,** 262.
188. I. L. de Mattos, M. D. Luque de Castro and M. Valcárcel, *Talanta* (to appear in 1995).
189. V. Kuban, *Fresenius J. Anal. Chem.*, 1993, **346,** 873.
190. P. Moss and E. D. Salin, *Appl. Spectrosc.*, 1991, **45,** 1581.

Pergamon

0039-9140(94)00333-5

*Talanta*, Vol. 42, No. 2, pp. 171–183, 1995

0039-9140/95 $9.50 + 0.00

# DECOMPOSITION OF DIPHENYLAMINE IN NITROCELLULOSE BASED PROPELLANTS—I. OPTIMIZATION OF A NUMERICAL MODEL TO CONCENTRATION–TIME DATA FOR DIPHENYLAMINE AND ITS PRIMARY DEGRADATION PRODUCTS DETERMINED BY LIQUID CHROMATOGRAPHY WITH DUAL-AMPEROMETRIC DETECTION

ARNE BERGENS* and ROLF DANIELSSON

Uppsala University, Institute of Chemistry, Department of Analytical Chemistry, P.O. Box 531, S-751 21 Uppsala, Sweden

(*Received* 5 *November* 1991. *Revised* 2 *April* 1993. *Accepted* 4 *April* 1993)

**Summary**—The consumption of diphenylamine (DPA) in two nitrocellulose (NC) based propellants subjected to a heat storage test at 85° has been studied. A previously developed method based on reversed-phase liquid chromatography with dual-amperometric detection was used to monitor the concentrations of DPA, 2-nitro-DPA and 4-nitro-DPA during the test. A numerical model based on first order rate equations was fitted to the obtained analytical data with the use of a specially written curve fitting program. The model implemented in the program describes the initial nitrosation and nitration steps of DPA in aging NC propellants. The use of matrices in the calculation of concentration–time (CT) curves enables the introduction of a general algorithm which can be readily changed in order to simulate any system of first order reactions. The program can therefore be used in other applications such as mechanistic studies in organic synthesis. The general simulation algorithm allows inclusion of unknown (not analysed) components in the reaction mechanism. In this application, it was possible to simulate the course of *N*-nitroso-DPA which is not detectable by the amperometric principle.

The thermal decomposition of NC is a complex process which is believed to be catalyzed by the decomposition products, especially by reactive nitrogen oxides. A frequently used method for stabilization of NC is therefore to add DPA which reacts with the degradation products such as nitrogen oxides, $HNO_3$ and $HNO_2$. The auto-catalytic decomposition of NC is prevented as long as there is a significant amount of stabilizer present in the NC material. Normally, about 1% is normally added depending upon the intended properties of the propellant. The stabilizer will hence be consumed with time under the formation of different nitro and nitroso derivatives of DPA.[1–3] The danger of self-ignition of the NC will, therefore, increase with time and a good estimate of the safe storage time of a propellant batch is, consequently, a matter of great importance.

A properly stabilized NC-propellant is stable for a relatively long period of time (20–50 years) at normal storage conditions. Stability testing must therfore be carried out by storing propellant samples at higher temperatures in order to obtain degradation within a reasonable time. By raising the storage temperature to 90–110°, about 20 years of storage are compressed into one week in the laboratory. Traditionally, the time elapsed until red fumes appear is used as a measure of stability since it indicates the point at which the DPA is fully consumed by the thermal degradation products of NC. By performing heat storage tests at different temperatures (for example 65–100°), it is possible to estimate the time-to-fume at normal storage temperatures but this procedure usually gives estimates impaired by significant errors since an extrapolation is made over a wide temperature range.

Today, the stabilizer consumption during heat storage tests can be readily monitored by chromatographic techniques. In order to correlate results acquired at elevated temperatures with those obtained under normal storage conditions, the rate of stabilizer consumption in the

*Present address: Pharmacia AB, Pharmaceuticals Uppsala, S-751 82 Uppsala, Sweden.

propellant at different temperatures has been used. Assuming first-order kinetics, the time for the stabilizer to be consumed at lower temperatures can be extrapolated with the use of the calculated activation energy. Practice has, however, shown that this method does not give sufficiently precise estimates. This is not surprising since also this approach involves an extrapolation over a large temperature interval and therefore requires extremely precise experimental data. The use of temperatures above the melting point of the stabilizer compound will also introduce errors, as the diffusion conditions for the reacting species in the propellant sample change in the vicinity of the melting point. A properly manufactured NC propellant is, however, stable for at least 20 years at normal storage temperatures which means that stability testing at lower temperatures would require unrealistically long experiments.

Another problem associated with the monitoring of the stabilizer concentration is that a low stabilizer concentration does not necessarily mean that the propellant is unstable. In the case of DPA, for example, a propellant containing less than 0.1% DPA can for instance show acceptable stability according to weight loss or micro-calorimetric measurements for a long time. The stability after that the DPA has been consumed is largely maintained by the initial degradation products, *e.g.* 2-nitro-DPA and 4-nitro-DPA. 2-nitro-DPA is, in fact, a common stabilizing additive used as an alternative to DPA. During the lifetime of a propellant, one DPA molecule can trap six molecules of $NO_x$ before it decomposes to form picric acid.[1] The ability of the nitro-DPA derivatives to trap nitrogen oxides decreases with increasing number of nitroso and nitro groups. The autocatalytic reactions responsible for the red fumes have already started when di-nitro derivatives are beginning to appear.[4] In stability estimations based on stabilizer consumption it should, therefore, be more appropriate to use the time when also the initial degradation products have been consumed.

The objective of this work is to study the initial stages of DPA degradation in a simple single base propellant by the use of a previously developed analytical method[5] for nitro diphenylamines. A further aim is to try to correlate analytical data with a numerical model describing the early stages in the degradation mechanism of DPA. The nitrosation and nitration of aromatic amines such as DPA has been extensively studied and the reaction is described in many organic chemistry textbooks. The attack of $HNO_3$, $HNO_2$ or nitrous gases on the DPA molecule is most likely to appear at the nitrogen in the amino group with the formation of a nitrosamine.[6–8] The nitrosamine can be further converted to 2-nitro-DPA and 4-nitro-DPA by the Fischer–Hepp rearrangement[9–12] and oxidation of the nitroso group. The initial steps in the DPA-degradation in propellants are therefore well understood, and described as the reaction scheme in Fig. 1. The higher nitrated DPA derivatives with two or more nitro groups

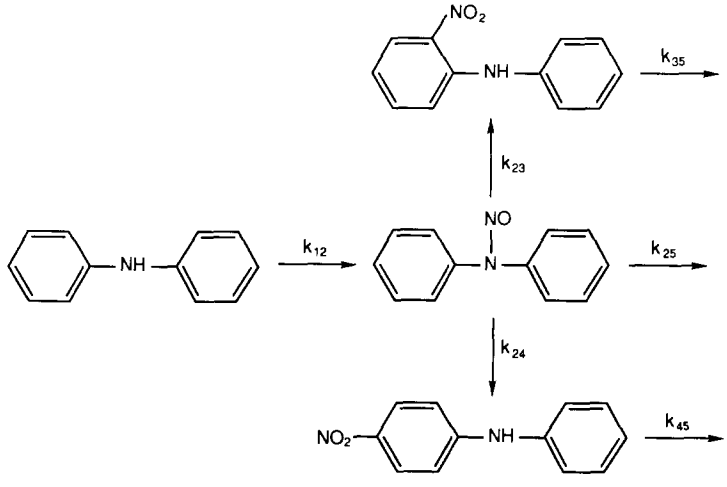


Fig. 1. The dominating reaction routes of the initial DPA degradation in an aging propellant. This reaction mechanism served as a model reaction system for the fitting of CT curves for DPA, 2-nitro-DPA and 4-nitro-DPA. The indexes of the parameters have been chosen on the basis of the numbering of the compounds which is (1) DPA, (2) *N*-nitroso-DPA, (3) 2-nitro-DPA, (4) 4-nitro-DPA and (5) other derivatives with two or more nitro groups.

appear late in the heat storage tests and are therefore only of secondary interest.

A computer program for the simulation of first-order reaction systems has been used to study the degradation mechanism of DPA (Fig. 1). The concentrations of DPA, 2-nitro-DPA and 4-nitro-DPA were monitored during a heat storage test at 85° and the concentraton data obtained were fitted to a model describing the reaction system in Fig. 1. With the dual-amperometric detector used it was, however, not possible to detect and quantify *N*-nitroso-DPA.

## MODELLING AND SIMULATION

The degradation of the stabilizing agent is a complex process, and ideally all components involved should be monitored for a full understanding of the process. In practice only some preselected substances can be analyzed during the experiment, and one has to resort to a model for a more detailed description of the process. Even components of main interest may be unaccessible for analysis, and these must be deduced from what actually can be measured.

This is a situation similar to a complex titration, where a system of equilibrium equations and a set of varying concentrations makes it possible to follow species unaccessible for direct measurements. In our case we need a set of kinetic equations relating the concentration–time (CT) profiles for the different components, when only some of them are experimentally obtained.

A crucial point with this approach is the validity of the model. The fewer components of the proposed reaction scheme that are actually monitored, the higher the demands are put on the precision of the measurements and the degree of fit. There is no simple way of anticipating *a priori* the validity of the results, it is rather a matter of combining chemical reasoning and numerical considerations.

As a tool for this process we have developed a computer program for general use in modelling kinetic reaction schemes described by a set of first-order rate equations. When initial concentrations and rate constants are assigned to the proposed components and selected pathways, the CT curves for all components are simulated. A simplex procedure is then used to make the best least-square fit to the actually measured components.

The simplex method was chosen for optimization of the parameters mainly because the number of calculations required does not increase too rapidly as the number of parameters in the model increases.[13] The simplex algorithm used in the program was based on the modified simplex with variable step length introduced by Nelder and Mead[14] in 1965. No stop criterion for the iterations is included in the program as it is not meant to be operated unattended. When running the program, the progress of the minimization of the square sum is displayed. However, the true progress of the optimization is revealed by visual comparison of the experimental and calculated data.

In the degradation of DPA we are monitoring the origin component and two possible products. The difference between DPA and these two products may be assigned to other products, intermediate as well as final, and to errors of analysis. The simulation makes it possible to separate these contributions, at the expense of the introduction of modelling errors.

The question is then whether the proposed first-order reaction scheme results in assignment of the unexplained amounts to true components or to mere artefacts. In the absence of chemical confirmation we have to rely on sound chemical principles and give preference to simple models. The validity of the model can only be judged by the fit, *i.e.* comparison of the simulated and the recorder CT curves. Attention must also be paid to the uniqueness of the assignment to unmonitored components. If there is insufficient information in the measurements, we should obtain similar degree of fit regardless of the values for the parameters which are related to such components. Inspection of the CT curves for unmonitored components obtained with different starting values for the parameters in the minimization procedure should reveal such problems. Therefore, the development of a fast simulation procedure was an essential step to make such a trial-and-error mode of operation feasible.

It should be emphasised that the optimized parameters are numerically obtained constants. The main purpose of the curve fitting program is to discern which possible reaction mechanisms give the best curve fit to experimentally obtained data. The simulation algorithm uses matrix formalism to calculate the CT curves from the rate equations written in difference

form. For the reaction system given in Fig. 1 these equations are:

$$\frac{\Delta[X_1]}{\Delta t} = -k_{12}[X_1] \quad (1)$$

$$\frac{\Delta[X_2]}{\Delta t} = k_{12}[X_1] - (k_{23} + k_{24} + k_{25})[X_2] \quad (2)$$

$$\frac{\Delta[X_3]}{\Delta t} = k_{23}[k_2] - k_{35}[X_3] \quad (3)$$

$$\frac{\Delta[X_4]}{\Delta t} = k_{24}[X_2] - k_{45}[X_4]. \quad (4)$$

The designations $X_i$ in equations (1)–(4) can be identified from Fig. 1 as: DPA ($i = 1$), *N*-nitroso-DPA ($i = 2$), 2-nitro-DPA ($i = 3$), and 4-nitro-DPA ($i = 4$). The subindex 5 should represent the di-nitro to hexa-nitro derivatives formed later in the storage period. The equation for $X_5$ has been left out since these components were not included in the study.

The concentrations $[X_i]$ are calculated for rather large time intervals $\Delta t$ without loss of accuracy using a novel technique based on matrix exponentiation. This approach enables a computer implementation with short execution time which facilitates the optimization process. The simulation procedure is further described in Appendix 1.

The decomposition of NC is, however, a complicated process with possible unknown steps which might affect the rate of stabilizer degradation. It is, therefore, difficult to obtain CT data with sufficient precision to allow determinations of rate constants since small variations in storage conditions can give rise to large errors in the CT data. The computational approach described here should be more successful for the optimization of coupled rate parameters, for example, in organic synthesis where the surrounding conditions are more easily controlled.

## EXPERIMENTAL

### *Apparatus*

Electrochemical detection at negative potentials suffers from oxygen interferences which therefore have to be minimized. The liquid chromatographic system was, therefore, equipped with a gas tight resevoir for the mobile phase constructed from a 100 ml Merck solvent flask in which the mobile phase could be continuously purged with argon or helium. A small overpressure was maintained inside the reservoir by means of two needle valves regulating the in and outlet gas flows.

The pump used was a Pharmacia LKB, Model 2150 (Pharmacia LKB Biotechnology, Uppsala, Sweden) double-piston pump. The housing of the inlet valves was exchanged with stainless steel housings from two discarded outlet valves in order to allow stainless steel tubing to be used. This was done since the original inlet valves of this pump only allow connection of plastic tubing for the mobile phase supply tube. The walls of the commonly used PTFE tubing are easily penetrated by oxygen which means that stainless steel tubing has to be used exclusively.

The injection of samples were either made with a Millipore Waters Model 712 WISP Sample Processor (Millipore Intertech, Bedford, MA, U.S.A.) or a Carnegie Medicin CMA200 (Carnegie Medicin AB, Stockholm, Sweden) automatic injector. The separations were carried out using a $100 \times 4.6$ mm RP-18 Spheri-5 column obtained from Brownlee labs Inc. (Santa Clara, CA, U.S.A.). The dual electrode amperometric detection system was controlled by two LC-4B potentiostats (Bioanalytical Systems Inc., West Lafayette, IN, U.S.A). The electrochemical cell was used with the electrodes placed in a series arrangement. The reference electrode was an Ag/AgCl electrode and the working electrodes both consisted of glassy carbon. The stainless steel cell body served as counter electrode.

The column, detector cell and waste container were all placed inside a thermostatted shielded box constructed in the laboratory. The temperatures used in this work were 30 and 35°. The temperature was never observed to deviate from the programmed value by more than ±0.1°.

The chromatograms were recorded and processed with a Spectra Physics, Model SP4290 integrator (Spectra Physics, San Jose, CA, U.S.A.). The simulation and simplex optimization algorithms were programmed using the ASYST scientific calculation system (MacMillan Software Company, NY, U.S.A.) and run on an IBM PS/2 model 50 computer equipped with a mathematics co-processor.

### *Chemicals*

The acetonitrile and 2-propanol used in the mobile phase were of Lichrosolv grade (Merck) and could be used without further purification or filtration. *m*-chloroacetic acid was purchased from BDH Chemicals Ltd., Poole, U.K. and

was also used as recieved. The *m*-chloroacetic acid buffer was prepared from a 0.05*M* solution by adjusting the pH to 2.7 with NaOH.

The reference substances DPA (Merck, Darmstadt, Germany, *pro analysi* grade), 4-nitro-DPA (Aldrich-Chemie Gesellschaft GmbH & Co. KG, Steinheim, Germany, specified purity 99%) and 2-nitro-DPA (Aldrich-Chimie, specified purity 98%) were all used as recieved. The internal standard, 4-ethyl-nitrobenzene was also purchased from Aldrich and of 99% specified purity. All standard solutions were prepared weekly and stored in a refrigator.

*Procedures*

*Storage and extraction of propellant samples.* The composition of the two single base NC propellant batches studied in this investigation were 0.5% DPA/99% NC and 0.7% DPA/99% NC. From these two batches, two series consisting of 17 different 4 g samples from each batch were subjected to a heat storage test at 85° according to the Dutch stability test.[15] This test is normally employed for weight loss determinations at temperatures in the interval 95–110°. However, in this investigation the temperature was decreased to 85°, as a lower rate of NC decomposition was desired.

In the Dutch stability test, the samples are placed ungrinded in 160 × 17 mm test tubes with ground glass stoppers. After a predetermined time period, a 1 g portion of the sample is carefully taken out for extraction while the rest is disposed as waste. In this case, the extractions were performed during 4 h using 50 ml of methylene chloride in a Soxhlet extraction unit (Soxtec System 1040 extraction unit, Tecator, Sollentun, Sweden). Methylene chloride was then evaporated at ambient temperature, followed by dissolution and dilution of the residue in acetonitrile to known volume (25–50 ml). It was noticed that the residue needed some time to dissolve and the residue was therefore dissolved using several small portions of solvent. The acetonitrile solutions were then further diluted with mobile phase before transferring them into the automatic injector. Analyses of more than 20 samples were avoided (20 samples correspond to a maximum running time of 6–8 h) because of the unstable 4-nitro-DPA observed in earlier work.[5] With the CMA200 injector the samples were refrigerated to +6°C while stored in the autoinjector.

*Chromatography.* In this investigation two different mobile phase mixtures were used. In the analysis of the nitro derivatives, a mixture consisting of 63% 0.05*M* *m*-chloroacetic acid buffer (pH = 2.7), 13.5% acetonitrile and 23.5% 2-propanol was used at a temperature of 30°. The analysis of DPA was on the other hand performed with a mixture of 60% *m*-chloracetic acid buffer, 13.5% acetonitrile and 26.5% 2-propanol at 35°. In both cases, the mobile phase compositions are given as volumetric percentages. DPA was analysed separately because of the suspected high concentration of DPA and low concentration of nitro derivatives in the beginning of the storage period. The *m*-chloroacetic acid buffer was passed through a 0.45 μm filter (type HVLP, Millipore) before mixing with the organic solvents. As indicated above, the mobile phase was degassed and deoxygenated in its resevoir by purging with helium or argon for 10–15 min before turning the pump on.

All chromatograms were run at flow-rate of 1.1 ml/min and when the chromatographic system was not in use, the mobile phase was left circulating through the system. Since the mobile phase was always kept in an inert atmosphere inside the reservoir flask the start-up time was hereby shortened.

The electrochemical characteristics of 2-nitro-DPA and 4-nitro-DPA have been studied in an earlier report[5] in which the suitable potential settings were found to be W1 = −1.0 V and W2 = +0.4 V *vs.* Ag/AgCl. The potential settings used in the quantification of DPA were on the other hand W1 = 0 V and W2 = +0.9 V. These values were chosen on the basis of literature data[16,17] but were also verified by the recording of hydrodynamic voltammograms.

The injection volumes used were in the range 15–50 μl depending on the concentration level to be analyzed. For the quantification of the nitro diphenylamines, 4-ethyl-nitrobenzene (4-ENB) was chosen as an internal standard since experiments showed that it had similar electrochemical properties as 2-nitro-DPA and 4-nitro-DPA as well as a suitable retention time. In the quantification of DPA an external standard method with a calibration curve was used and the response of the detector was checked at regular intervals by injections of standard solutions. This procedure was employed since oxidation of DPA is suspected to give rise to polymeric products[9] which deactivate the electrode surface by adsorption. Such an effect was, however, never observed during a typical 6–8 hr run including 14–19 samples.

## RESULTS AND DISCUSSION

The electrochemical characterization and evaluation of the analytical conditions for the determinations of 2-nitro-DPA and 4-nitro-DPA have been described in an earlier paper[5] and are therefore only briefly recapitulated. The only reducible substances extracted from the NC-propellants are the different nitro derivatives of DPA. Selective detection of 2-nitro-DPA and 4-nitro-DPA in samples with relatively high amount of DPA present can be achieved with the use of a dual-electrode amperometric detector. In such an arrangement the nitro group is reduced to a hydroxylamine at the first electrode (W1). The latter compound is then oxidized at the second electrode (W2) and it is the current arising form this oxidation that is used as the analytical signal. With the dual-electrode the interference from oxygen in the mobile phase is partly overcome since only some of the hydrogen peroxide formed during the reduction of oxygen is oxidized at the detector electrode.

An example of a chromatogram obtained when analyzing a sample of the 0.7% DPA propellant is shown in Fig. 2(a). The DPA concentration in the injected sample solution was determined to be 19.1 $\mu M$, which corresponds to an injected amount of 0.95 nmol. The concentrations of 2-nitro-DPA and 4-nitro-DPA were determined to be 2.63 $\mu M$ (0.13 nmol injected) and 6.87 $\mu M$ (0.34 nmol), respectively. The oxygen present in the sample solutions gives rise to a peak in the early part of the chromatograms due to oxidation of hydrogen peroxide formed at W1 during the reduction of oxygen. A complete deoxygenation of the samples with any of the two automatic injectors used was found to be difficult. As the hydrogen peroxide peak is not interfering with any analyte peak the problem was, however, left without further attention.

DPA is oxidized at potentials above + 0.7 V at a glassy carbon electrode depending on pH, solvent and the condition of the electrode surface.[16,17] Figure 3 shows a hydrodynamic voltammogram of DPA which reveals that a

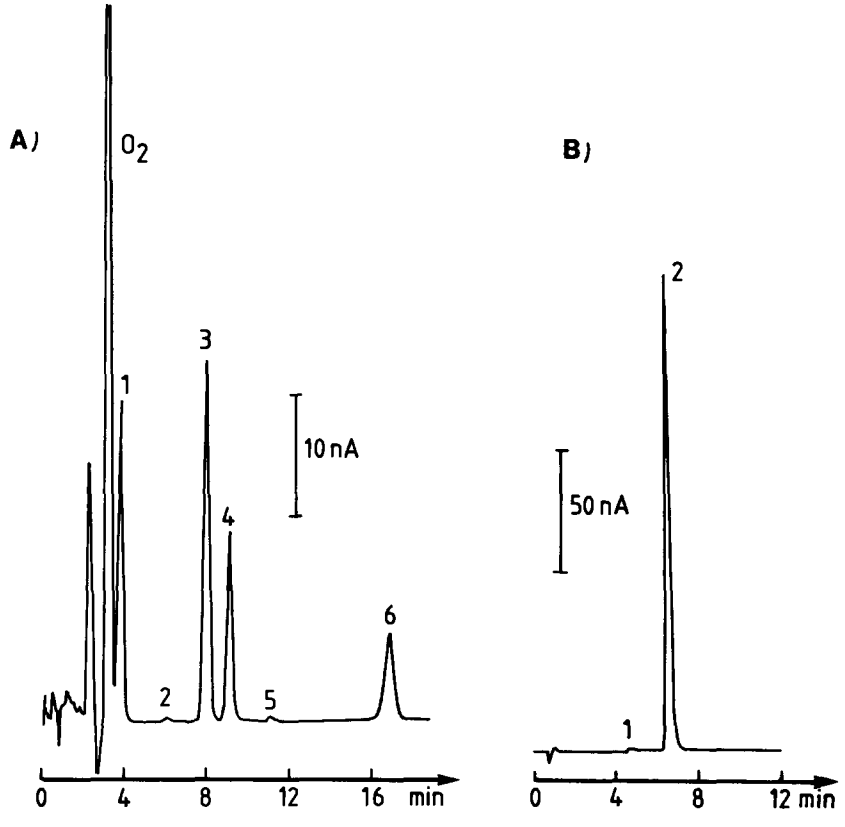


Fig. 2. Chromatograms recorded with dual-electrode amperometric detection with (a) W1 = − 1.0 V, W2 = + 0.4 V *vs.* Ag/AgCl and (b) W1 = 0 V and W2 = + 0.9 V. The sample is a 0.7% DPA propellant stored at 85 for one day. Peak identities in Fig. 1(a): (1, 2) unknown, (3) 4-nitro-DPA, (4) 4-ENB (internal standard), (5) DPA, (6) 2-nitro-DPA. In Fig. 2(b): (1) 4-nitro-DPA and (2) DPA. As explained in the Experimental section, the chromatographic conditions were different in the two cases.

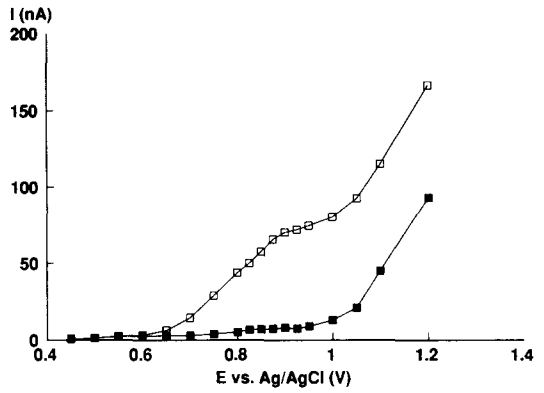


Fig. 3. Hydrodynamic voltammogram for DPA. (□) represents obtained peak currents from injection of 0.2 nmol DPA. (■) represents the background current at the different potentials.

potential of +0.9 V *vs.* Ag/AgCl is necessary in order to obtain a diffusion controlled current. Since the background current rises sharply at potentials more positive than +0.95 V, a detection potential of +0.9 V was chosen. Based on 10 repeated injections, the response for DPA was found to be reproducible within 1%. The calibration graphs were linear in the range of 0.5–11 $\mu M$.

The nitro derivatives of DPA are on the other hand only partly oxidized at +0.9 V *vs.* Ag/AgCl and therefore only give rise to minor peaks. In Fig. 2(b), the oxidation of the eluting 4-nitro-DPA hence only give rise to a small peak at 4.2 min. The different elution times for DPA in Fig. 2(a) and 2(b) stems from the fact that the analyses were carried out with different mobile phases and temperatures.

The results from determinations of DPA, 2-nitro-DPA and 4-nitro-DPA in the two single-base propellants during the heat storage experiment are shown in Fig. 4. As seen in the figure, only a minor part of DPA is converted to 2-nitro-DPA and 4-nitro-DPA, in agreement with previous publications.[1,18] It can further be concluded that the degradation of DPA mainly leads to formation of *N*-nitroso-DPA which in turn is consumed by the NC decomposition products. It can also be seen that 2-nitro-DPA and 4-nitro-DPA are formed simultaneously and that the concentration of 4-nitro-DPA is about twice as high as that of 2-nitro-DPA throughout the whole storage period. At this temperature, the concentrations of 2-nitro-DPA and 4-nitro-DPA reach their maxima after about 15 days of storage.

The solid curves seen in Fig. 4 are those simulated by means of the parameters obtained from the simplex program. Although the assumed first-order kinetics is a simplification, the agreement between the fitted curves and experimental data is good. The theoretical curves for an irreversible first-order reaction system predict asymptotically decreasing concentrations but the measured concentrations decrease more rapidly than the optimized curves predict. This rapid decrease could be caused by an increase of nitrogen oxide formation or indicate that the DPA is involved in other processes.

The three compounds monitored are related to each other as the reaction model implies and the course of one component is dependent on the concentration changes of the others. The concentrations of 2-nitro-DPA and 4-nitro-DPA in the propellant will thus be governed by the change in the *N*-nitroso-DPA concentration through the reactions designated by $k_{23}$ and $k_{24}$. The *N*-nitroso-DPA concentration can, therefore, be simulated by optimizing the parameters in Fig. 1 with respect to the obtained chromatographic data for DPA, 2-nitro-DPA and 4-nitro-DPA. The predicted *N*-nitroso-DPA curve is shown by the dashed curve in Fig. 4.

The guiding principle for the optimizations was to find a reaction system with as few parameters as possible giving a reasonably good curve fit. Parallel routes to 2-nitro-DPA or 4-nitro-DPA with direct nitrosation or nitration at the aromatic rings was considered but did not improve the curve fits. After having tried a number of different mechanisms with parallel reactions, the reaction system originally set up in Fig. 1 was concluded to give the best fits (as shown in Fig. 4) to the experimental data. A general concern in curve-fitting or parameter optimizations based on experimental data is the shape of the response surface. For experimental data in good agreement with a theoretical model the response function (for example the sum of squared residuals) will contain a sharp, well defined, minimum for the parameter set giving the best fit. Complications may, however, arise due to experimental and modelling errors or insufficient data for model validation. Such conditions should give poorly defined parameters of different values depending on the start values used in the optimization of the same data set. The optimization of the parameters $k_{12}$–$k_{45}$ was therefore tested by randomly choosing start values in the interval 0.0001–0.2 day$^{-1}$. In Table 1, the result of 12 such optimizations are presented.

From the min–max ranges of the parameters it can be seen that the optimized parameters $k_{12}$–$k_{45}$ are all relatively well defined by the data sets, with the exception of $[NNODPA]_0$ and $k_{25}$. The latter deviation is, however, not suprising since the parameter $k_{25}$ is related to the *N*-nitroso-DPA component which has not been measured. As already indicated, the optimized parameters in Table 1 can be used to simulate the formation and consumption of *N*-nitroso-DPA during the heat storage test and in Fig. 5, the CT curves for *N*-nitroso-DPA for the 12 different optimizations in Table 1 are shown. The different combinations of parameter values result in different *N*-nitroso-DPA curves which all show realistic shapes according to the assumed reaction mechanism. Whether the curves in Fig. 5 reflect the true course of

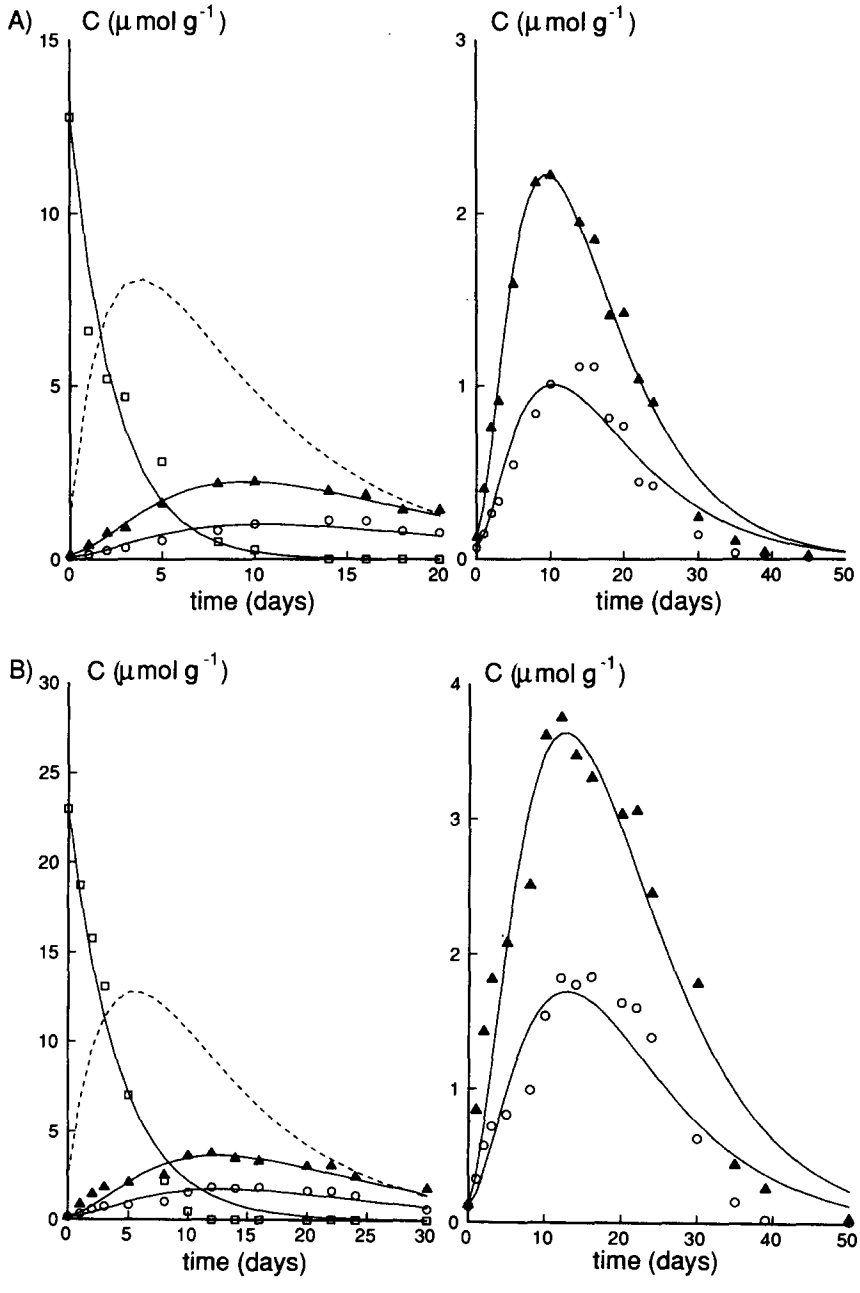


Fig. 4. Resulting curves (solid) for (□) DPA, (▲) 4-nitro-DPA and (○) 2-nitro-DPA from optimizations of the reaction model in Fig. 1 to analytical data of propellants containing (A) 0.5% (30 μmol/g) DPA and (B) 0.7% (41 μmol/g) DPA. To the right the 2-nitro-DPA and 4-nitro-DPA curves are shown with enlarged scales. The data are mean values based on two determinations. The dashed curve is the curve for *N*-nitroso-DPA simulated from the optimized parameters.

Table 1. Ranges of parameter values obtained from different optimizations using a randomly chosen start simplex

| 0.5% DPA | | | | | | | |
|---|---|---|---|---|---|---|---|
| | $k_{12}$ | $k_{23}$ | $k_{24}$ | $k_{25}$ | $k_{35}$ | $k_{45}$ | $[NNODPA]_0$ |
| Min | 0.409 | 0.0260 | 0.0670 | 0.0353 | 0.119 | 0.154 | 0.014 |
| Max | 0.409 | 0.0301 | 0.0770 | 0.0458 | 0.123 | 0.159 | 1.348 |
| 0.7% DPA | | | | | | | |
| | $k_{12}$ | $k_{23}$ | $k_{24}$ | $k_{25}$ | $k_{35}$ | $k_{45}$ | $[NNODPA]_0$ |
| Min | 0.235 | 0.0239 | 0.0573 | 0.0355 | 0.090 | 0.106 | 1.954 |
| Max | 0.239 | 0.0262 | 0.0587 | 0.0665 | 0.113 | 0.135 | 2.366 |

The dimensions of rate parameter day$^{-1}$. $[NNODPA]_0$ is the *N*-nitroso-DPA concentration at $t = 0$ given in $\mu$mol/g.

*N*-nitroso-DPA in the propellant, or not, will be investigated in a continuing study.[19] Table 1 and Fig. 5 do not only show that the simplex algorithm converges from different start values, the sizes of the ranges also show that the assumed reaction model is able to explain the experimental concentration data.

A complication discovered in this investigation was that the initial concentration of DPA at $t = 0$ only corresponded to about 50% of the amount used in the preparation. The low concentration could be due to loss by volatilization of DPA during the preparation process or to losses in the extraction step.

The loss of DPA during the propellant production has also been noticed by other authors such as, for example, Schroeder *et al.*[1] In their study which was undertaken at 71°, samples were stored and continuously swept by a stream of air which then passed through two dry-ice cold traps. The analyses of the traps, however, suggested that evaporation is not responsible for the loss of DPA. This is also in agreement with our results obtained at 85°. After four days at 85°, no visible amounts of DPA could be seen on the inside walls of the glass tubes and loss of DPA through evaporation is therefore considered unlikely.

Losses as high as 50% are neither likely to be due to inefficient extraction as methylene chloride is a very good solvent for DPA and its nitro derivatives. Furthermore, the extractions were carried out by Soxhlet extractions which is a well established procedure for extraction of propellant samples.[1,20]

A third possibility for the losses is coupled to the solvent change after the extraction step and the dissolution of the residue in acetonitrile. This step was therefore tested in an experiment in which five 25 ml portions of standard solutions containing DPA, 2-nitro-DPA and 4-nitro-DPA in methylene chloride

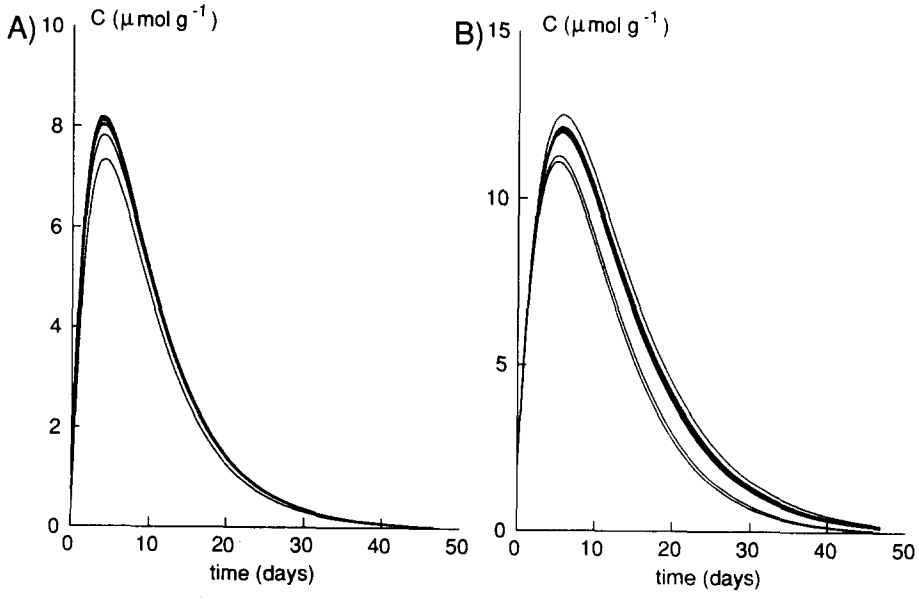


Fig. 5. Simulated curves for *N*-nitroso-DPA based on the optimizations presented in Table 1: (a) 0.5% DPA and (b) 0.7% DPA.

Table 2. Results of the analyses of residues dissolved in methylene chloride solutions

| Sol. no. | DPA(*mg*) | | 2-nitro-DPA(*mg*) | | 4-nitro-DPA(*mg*) | |
|---|---|---|---|---|---|---|
| | A | B | A | B | A | B |
| 1 | 3.63 | 3.64 | 1.31 | 1.30 | 1.72 | 1.72 |
| 2 | 3.62 | 3.61 | 1.31 | 1.29 | 1.71 | 1.70 |
| 3 | 3.62 | 3.62 | 1.31 | 1.32 | 1.71 | 1.71 |
| 4 | 3.65 | 3.64 | 1.32 | 1.32 | 1.73 | 1.74 |
| 5 | 3.63 | 3.61 | 1.31 | 1.31 | 1.72 | 1.73 |

A = Amount in the standard methylene chloride solutions.
B = Amount found in the analysis of the acetonitrile solutions.

were subjected to the same procedure of evaporation and dissolution in acetonitrile as the propellant samples. As seen in Table 2, the results indicate that this step cannot explain the observed loss of DPA. Neither can the losses be explained by a conversion of the DPA into some unknown electroactive compound since there was no unknown peak of the same magnitude as DPA in the chromatograms.

The cause for the significant loss of DPA is presently not fully understood. A remaining possibility is chemical interaction between DPA and NC which could convert DPA into a non-extractable compound or a compound which is not electroactive and therefore not detected. A plausible non-detectable compound is *N*-nitroso-DPA, this compound is namely not reduced within the potential window of the electrochemical detector. By experience from the propellant production, it is known that normally about 5–15% of the DPA is converted into *N*-nitroso-DPA in the preparation process.[20] It is therefore not likely that the observed 50% loss can be fully explained by the formation of *N*-nitroso-DPA.

As other aromatic amines, DPA is known to produce radicals. When heated to about 70° in toluene, the radical diphenylnitrogen ($Ph_2N\cdot$) is formed[7] which readily dimerizes to form tetraphenylhydrazine. Mrzewinski,[21] applied ESR technique to study the transformation of DPA in a NC propellant. According to Mrzewinski, the signal recorded was due to the $Ph_2N\cdot$ radical. In the aging propellant environment the highly reactive $Ph_2N\cdot$ radical could attack the weak nitrate ester bond in the NC.

Several investigations suggest that DPA interacts directly with nitrate esters.[1,2,21–24] The amine nitrogen has two unshared electrons that are easily lost to oxidation agents producting a radical cation, $DPA\cdot^+$ which is quite stable due to the ability for delocalization of the unshared electron to the aromatic rings. The amine functionality together with the delocalized $\pi$-electrons in the aromatic rings make the molecule a very good radical scavenger that could easily react with species having unshared electrons.

Since NC is a widely used material, a number of investigations have been performed concerning its decomposition mechanism. The thermolytic decomposition of NC has been shown to produce radicals in the cellulose polymer. The cleavage of nitrate ester bonds leave alkoxy radicals (RO·) which cause rearrangements and rupture of the cellulose chain.[25–27] The reactivity of DPA towards species with unshared electrons could be regarded as a strong indication that some of the DPA molecules will be incorporated in the NC structure. As already indicated, this could occur either by addition of DPA to the RO· radical sites in the NC structure or by attack of $DPA\cdot^+$ at the nitrate ester bond. The NC-DPA structure formed would probably be equally reactive towards nitrogen oxides as the DPA itself and *N*-nitroso-DPA, 2-nitro-DPA or 4-nitro-DPA could subsequently be released from the NC-DPA structure. A comparable reaction is the reaction between benzoylperoxide and DPA to an O-benzoylhydroxylamine.[28–30] In the latter case, the reaction mixture has been observed to absorb nitrogen oxides from the atmosphere under the formation of *N*-nitroso-DPA.[29,30]

DPA dissolved in acidic media together with an oxidizing agent produces a blue colour and DPA has therefore been widely used as a redox indicator. The blue product is commonly accepted to be a derivative of N, N′-diphenylbenzidine and can also be observed if DPA is oxidized electrochemically. Since nitrous acid is known to be an especially effective oxidizing agent,[8] and also one of the degradation products of NC, it can be expected that the blue oxidation product is formed in the NC-propellant also during storage. An interesting fact in this context is the initial colour change of an aging NC propellant is from yellow to green. The green colour could be produced by a mixture of a

blue DPA oxidation product and the yellow NC polymer. The methylene chloride extracts of green coloured propellant are yellow while the remaining NC-material is green. Most investigations have, however, been focused on the species extracted from the propellant and very little on the remaining NC material after the extraction. Nevertheless, it is known that the amounts of DPA and degradation products never add up to the amount of DPA used in the preparation of the propellant.[20] A study of the material remaining after extraction would therefore be of significant interest.

## CONCLUSIONS

The optimization of rate parameters in a reaction system of pseudo first order can be used as a model for the degradation of DPA in NC based propellants. Surprisingly good agreement between experimental data and theoretical CT curves are obtained, even though NC is a heterogeneous material with different properties depending on the quality of the original cellulose material and the NC preparation procedure. The conditions inside a NC propellant stored at elevated temperatures could provide an environment in which the degradation of DPA follows pseudo first order kinetics. Such an assumption implies that the amount of liberated nitrogen oxides is large compared to the amount of stabilizer added in the propellant. This implication could also be fulfilled because of the large amount of decomposing nitrate ester groups at higher temperatures. The reaction order will, however, change with time as the nitrate ester groups decompose and the formation of nitrogen oxides ceases. In the very early part of the heat storage test, the reaction order would also deviate from first order as the concentration of nitrogen oxides will not exceed that of the DPA. The influence of unknown processes affecting the DPA decomposition hinders the extraction of meaningful rate constant values from the optimizations.

A parallel process which could affect the rate of stabilizer degradation is the oxidation of DPA (*i.e.* oxygen catalyzed radical formation). Such a formation of reactive radicals might further contribute to an increased rate of DPA degradation with time. The influence of oxygen on the formation of reactive radicals is also believed to be the cause for the more rapid consumption of 2-nitro-DPA and 4-nitro-DPA in the later part of the heat storage period.

Although the *N*-nitroso-DPA derivative was not detectable with the amperometric detector used, its CT curve could be simulated from the rate parameter set, given by optimizations based on data for DPA, 2-nitro-DPA and 4-nitro-DPA. In future studies of DPA degradation in NC materials, *N*-nitroso-DPA should also be monitored since most of the DPA is primarily nitrosated at the amine nitrogen and since this compound probably plays an important role for the stability of the NC propellant when the DPA has been consumed. Repeated heat storage tests are needed for a more conclusive interpretation of the ability of the reaction model to predict the course of stabilizer degradation. In part II of this investigation, a study including determination of *N*-nitroso-DPA during a heat storage test at 80°C of the same NC propellants will be presented.

*Acknowledgements*—Acknowledgement is made to Prof. Bengt Nygård for his encouraging support in this work and for reviewing the manuscript. Acknowledgement is also made to the Swedish National Board for Technical Development for the financial support making it possible to complete this work. Finally, the valuable discussions on the mathematics with Professors Svante Jansson and Göran Bergson are gratefully acknowledged.

## REFERENCES

1. E. W. Schroeder, E. W. Malmberg, L. L. Fong, K. N. Trueblood, J. D. Landerl and E. Hoerger, *Ind. Eng. Chem.*, 1949, **41**, 2818.
2. N. J. Curtis and P. E. Rogasch, *Prop. Explos. Pyrotechnics*, 1987, **12**, 158.
3. F. Volk, *Prop. Explos.*, 1976, **1**, 90.
4. A. A. Wickham, *Proc. Int. Symp. Compatibility of Plastics and Other Materials with Explosives, Propellants, Pyrotechnics and Processing of Explosives, Propellants and Ingredients*, Virginia Beach, 1989, 171.
5. A. Bergens, *J. Chromatogr.*, 1987, **410**, 437.
6. C. K. Ingold, *Structure and Mechanism in Organic Chemistry*, pp. 269–288. Bell & Sons, London, 1953.
7. L. F. Fieser and M. Fieser, *Advanced Organic Chemistry*, p. 716. Reinhold, New York, 1961.
8. N. V. Sidgwick, *The Organic Chemistry of Nitrogen*, p. 62, rev. By T. W. J. Taylor, Clarendon Press, Oxford, 1942.
9. B. B. Coldwell and S. R. McLean, *Can. J. Chem.*, 1959, **37**, 1637.
10. D. V. Banthorpe, E. D. Hughes and D. L. Williams, *J. Chem. Soc.*, 1964, 5349.
11. B. T. Baliga, *J. Org. Chem.*, 1970, **35**(6), 2031.
12. D. L. Williams, *Tetrahedron*, 1975, **31**, 1343.
13. L. A. Yarbo and S. N. Deming, *Anal. Chim. Acta*, 1974, **73**, 391.
14. J. A. Nelder and R. Mead, *Computer J.*, 1965, **7**, 308.
15. *Analytical Methods for Powder and Explosives*, p. 59. AB Bofors Nobelkrut, Sweden, 1960.
16. R. N. Adams, *Electrochemistry at Solid Electrodes*, p. 345. Dekker, New York, 1969.

17. A. Bergens, K. Lundström and J. Asplund, *Talanta*, 1985, **32**, 893.
18. T. Lindblom, P. Lagerkvist and L. G. Svensson, *7th Symp. Chem. Probl. Conn. Stab. Explos.* [*Proc.*], Smygehamn, Sweden, 1985.
19. A. Bergens, *Talanta*, 1995, **42**, 185.
20. T. Lindblom, private communications.
21. T. Mrzewinski, *6th Symp. Chem. Probl. Conn. Stab. Explos.* [*Proc.*], p. 317, Sweden, 1982.
22. B. Hetnarski, W. Poludnikiewicz and T. Urbanski, *Tetrahedron Lett.*, 1970, **1**, 3.
23. T. Mrzewinski, *Bull. Acad. Polon. Sci. Ser. Sci. Chim.*, 1970, **18**, 385.
24. N. J. Blay, *3rd Symp. Chem. Probl. Conn. Stab. Explos.* [*Proc.*], p. 61, Ystad, Sweden, 1973.
25. M. L. Wolfrom *et al.*, *J. Am. Chem. Soc.*, 1955, **77**, 6573.
26. R. W. Philips, C. A. Orlick and R. Steinberger, *J. Phys. Chem.*, 1955, **59**, 1034.
27. G. Gelernter, L. C. Browning, S. R. Harris and C. M. Mason, *J. Phys. Chem.*, 1956, **60**, 1260.
28. D. B. Denney and D. Z. Denney, *J. Am. Chem. Soc.*, 1960, **82**, 1389.
29. E. N. Atanesyan and G. A. Marmaryan, *Chemical Abstracts*, 1959, **53**, 1197b.
30. O. A. Chaltykyan, E. N. Atanesyan, N. M. Beileryan and G. A. Marmaryan, *Chemical Abstracts*, 1959, **53**, 13748b.
31. J. Wei and C. D. Prater, *Adv. Catalysis*, 1962, **13**, 203.
32. C. D. Ritchie, *Principal Organic Chemistry, The Fundamental Concepts*. Marcel Dekker, New York, 1990.

## APPENDIX

An optimization of a theoretical model to fit experimental data requires an algorithm that can simulate the model according to given parameter values. Here the optimization program will be described in more detail, with emphasis on the mathematical operations used in the simulation algorithm.

For any reaction mechanism assumed to occur under first order conditions, a system of linear differential equations can be set up. This system of first order rate equations can be expressed in a matrix form that enables rapid and convenient calculations of all concentration changes in the reaction system. The principle for the transformation to matrix operations used in the simulation algorithm will be described below for a reversible reaction system containing three components:

$$X_1 \underset{k_{21}}{\overset{k_{12}}{\rightleftharpoons}} X_2 \underset{k_{32}}{\overset{k_{23}}{\rightleftharpoons}} X_3. \qquad \text{(A1)}$$

The time derivatives of compounds $X_1$, $X_2$ and $X_3$ can be written as equations (A2)–(A4).

$$\frac{d[X_1]}{dt} = -k_{12}[X_1] + k_{21}[X_2] \qquad \text{(A2)}$$

$$\frac{d[X_2]}{dt} = k_{12}[X_1] - (k_{23} + k_{21})[X_2] + k_{32}[X_3] \qquad \text{(A3)}$$

$$\frac{d[X_3]}{dt} = k_{23}[X_2] - k_{32}[X_3]. \qquad \text{(A4)}$$

It is possible to solve this equation system and to calculate the CT curves for the given rate parameter values. This can, however, be a very tedious method for more complex reaction mechanisms since the exact solutions rapidly become complicated as the number of reacting components increases.

A different method for calculating the CT relationships was therefore developed for the simulation algorithm used in this investigation. this method is based on difference approximations of the rate equations (A2)–(A4) and the rates of concentration changes for the components are assumed to be constant over a small period of time, $\Delta t$. This assumption is valid if $\Delta t$ is made sufficiently small, but the calculation error rapidly becomes large with increasing $\Delta t$. Calculation of the CT curves with a very small $\Delta t$ leads to a long execution time and is therefore not a practical solution. The difference approximation, however, has the advantage of being readily transformed to matrix formalism which gives condensed formulas for computer programming. The difference approximations of equations (A2)–(A4) can be written as:

$$\frac{\Delta[X_1]}{\Delta t} = -k_{12}[X_1] + k_{21}[X_2], \qquad \text{(A5)}$$

$$\frac{\Delta[X_2]}{\Delta t} = k_{12}[X_1] - (k_{23} + k_{21})[X_2] + k_{32}[X_3], \qquad \text{(A6)}$$

$$\frac{\Delta[X_3]}{\Delta t} = k_{23}[X_2] - k_{32}[X_3], \qquad \text{(A7)}$$

where $\Delta[X_i] = [X_i]^{(2)} - [X_i]^{(1)}$ and $\Delta t = t_2 - t_1$. $[X_i]^{(1)}$ is the concentration of component $i$ at $t_1$ and $[X_i]^{(2)}$ the concentration of component $i$ at $t_2$. The concentrations $X_1^{(2)}$, $X_2^{(2)}$ and $X_3^{(2)}$ after the time $\Delta t$ are then given by

$$[X_1]^{(2)} = (1 - k_{12}\Delta t)[X_1]^{(1)} + k_{21}\Delta t[X_2]^{(1)}, \qquad \text{(A8)}$$

$$[X_2]^{(2)} = k_{12}\Delta t[X_1]^{(1)} + (1 - (k_{23} + k_{21})\Delta t)[X_2]^{(1)} + k_{32}\Delta t[X_3]^{(1)}, \qquad \text{(A9)}$$

$$[X_3]^{(2)} = k_{23}\Delta t[X_2]^{(1)} + (1 - k_{32}\Delta t)[X_3]^{(1)}. \qquad \text{(A10)}$$

By repeated application of equations (A8)–(A10), the concentrations can be calculated for discrete points of time along the time axis separated by the time interval $\Delta t$. The calculations are most easily performed using matrices and the first step in the matrix reformation is to place the concentrations at $t_1$ and $t_2$ of each component as elements in two column vectors $\mathbf{X}^{(1)}$ and $\mathbf{X}^{(2)}$.

$$\mathbf{X}^{(1)} = \begin{pmatrix} [X_1]^{(1)} \\ [X_2]^{(1)} \\ [X_3]^{(1)} \end{pmatrix}, \qquad \mathbf{X}^{(2)} = \begin{pmatrix} [X_1]^{(2)} \\ [X_2]^{(2)} \\ [X_3]^{(2)} \end{pmatrix}.$$

In order to calculate $\mathbf{X}^{(2)}$ from $\mathbf{X}^{(1)}$ we need to introduce a transition matrix, $\mathbf{T}$, which specifies the flow of mass through the system. The matrix $\mathbf{T}$ should contain the $(1 - \Sigma k_{ij}\Delta t)$ and $k_{ij}\Delta t$ factors in equations (A8)–(A10) and will for our reaction system (A1) have the following shape:

$$\mathbf{T} = \begin{pmatrix} (1 - k_{12}\Delta t) & k_{21}\Delta t & 0 \\ k_{12}\Delta t & (1 - (k_{23} + k_{21})\Delta t) & k_{32}\Delta t \\ 0 & k_{23}\Delta t & (1 - k_{23}\Delta t) \end{pmatrix}.$$

The equation system (A8)–(A10) can finally be written in its matrix form:

$$\mathbf{X}^{(2)} = \mathbf{T} \cdot \mathbf{X}^{(1)}. \qquad \text{(A11)}$$

At this stage, the advantage of using matrix formalism becomes obvious. The matrix $\mathbf{T}$ will give an informative view of how the concentrations (or masses) change during the time step $\Delta t$. The rows of $\mathbf{T}$ tells us how the components are formed from the other components of the system while

the columns describe how the mass from one component is distributed to the other components. The first row of **T**, thus, tells us that $X_1$ is formed from the fraction $k_{21}\Delta t$ of $X_2$. On the other hand, the first column of **T** shows that the fraction $(1 - k_{12}\Delta t)$ of $X_1$ remains as $X_1$ and the fraction $k_{12}\Delta t$ is converted to $X_2$.

In the simulation algorithm a sequence of concentration vectors are calculated by repeated operations of the transition matrix **T** according to equation (A11). The operations are initiated with the concentrations determined at $t = 0$ in an initial concentration vector $\mathbf{X}^{(0)}$.

A problem with the difference approximation method is that the time interval $\Delta t$ must be small to keep the calculation error small. The accuracy of the calculated concentrations, however, can be maintained by a refinement procedure in the calculation of **T**.

For this refinement, the time step $\Delta t$ is divided in a large number of substeps, $n$. Let **T′** be the transition matrix calculated for a substep of length $\Delta t' = \Delta t/n$. For computational convenience, the subdivision is performed as a number of bisections, *i.e.* $n = 2^m$. The matrix **T** for the total interval $\Delta t$ is then given by $(\mathbf{T}')^n$ which is readily computed by squaring **T′** $m$ times. The adjusted transition matrix is then used in the relation between the concentration vectors before and after a time step $\Delta t$ (equation (A11)).

For the general case, the adjusted transition matrix **T** is calculated from all possible rate constants $k_{ij}$ in the following way.

(i) Let **R** be a table of the individual rate constants

$$\mathbf{R} - \{k_{ij}\},$$

*i.e.* a square matrix with zero elements for all non-significant reaction pathways.

(ii) Multiply the transpose $\mathbf{R}^{\mathrm{T}}$ with $\Delta t' = \Delta t/m$, where $m = 2^n$. This results in a matrix that defines the transition between components

$$\mathbf{T}' = \mathbf{R}^{\mathrm{T}} \cdot \Delta t'.$$

(iii) So far, the diagonal elements of **T′** are zero. Now they are calculated by subtracting the sum of the corresponding column from unity. According to the law of conservation of mass, the sum of each column must add up to unity for a closed system.

$$\mathbf{T}'_{ij} = 1 - \sum_{i \neq j} \mathbf{T}_{ij}.$$

(iv) Finally, the adjusted **T** is calculated by squaring **T′** $n$ times.

$$\mathbf{T} = (\mathbf{T}')^{2^n} = (\mathbf{T}')^m.$$

Matrix formalism for the solution of complex first-order reaction systems has been described in the literature.[31,32] The system of rate equations

$$\frac{\mathrm{d}}{\mathrm{d}t}\mathbf{X} = \mathbf{K} \cdot \mathbf{X},$$

has the formal solution

$$\mathbf{X}(t) = \mathrm{e}^{\mathbf{K}t} \cdot \mathbf{X}(0).$$

The matrix **K** is the same as the matrix **T′** from step (ii) above, except for the inclusion of ones in the diagonal elements and the multiplication with $\Delta t'$. The meaning of the exponential function of a matrix can be understood from the series expansion, similar to that for a scalar argument:

$$\mathrm{e}^{\mathbf{A}} = \left(\mathbf{1} + \mathbf{A} + \frac{1}{2}\mathbf{A}^2 + \frac{1}{2 \cdot 3}\mathbf{A}^3 + \ldots\right).$$

To arrive at ordinary time functions for the components of **X**, the exponential function of $\mathbf{K} \cdot t$ can be evaluated by eigenvalue diagonalization of **K**.

$$\mathbf{K} = \mathbf{B} \cdot \mathbf{M} \cdot \mathbf{B}^{-1}$$

where **M** is a diagonal matrix with the eigenvalues $m_1, m_2, \ldots$ as diagonal elements and **B** is composed of the eigenvectors.

Now the powers of **K** can be written

$$\mathbf{K}^n = \mathbf{B} \cdot \mathbf{M}^n \cdot \mathbf{B}^{-1}$$

and the power expansion identified as

$$\mathrm{e}^{\mathbf{K}t} = B \cdot \begin{pmatrix} \mathrm{e}^{m_1 t} & 0 & \cdot & \cdot \\ 0 & \mathrm{e}^{m_2 t} & \cdot & \cdot \\ \cdot & \cdot & \cdot & \cdot \end{pmatrix} \cdot \mathbf{B}^{-1}.$$

This leads to solutions for the components $\mathbf{X}_i$ that are linear combinations of exponential functions with apparent rate constants $m_i$.

Numerical values corresponding to a set of rate constants can thus be obtained by solving the corresponding eigenvalue problem and then evaluating the exponentials for each point of time. However, for regular time intervals $\Delta t$, it is sufficient to calculate the single matrix $\mathrm{e}^{\mathbf{K}\Delta t}$ since

$$\mathbf{X}(t + \Delta t) = \mathrm{e}^{\mathbf{K} \cdot \Delta t} \cdot \mathbf{X}(t).$$

Actually, the transition matrix **T** from step (iv) is a numerical approximation of $\mathrm{e}^{\mathbf{K}\Delta t}$. The validity of our approach is demonstrated by an alternate definition of the exponential function:

$$\mathrm{e}^x = \lim_{m \to \infty}\left(1 + \frac{x}{m}\right)^m,$$

with the matrix version

$$\mathrm{e}^{\mathbf{K} \cdot \Delta t} = \lim_{m \to \infty}\left(1 + \mathbf{K} \cdot \frac{\Delta t}{m}\right)^m.$$

The calculation of **T** is nothing but an evaluation of the latter expression for $m = 2^n$. Another possibility would have been to use a number of terms in the series expansion, but the approach taken is more easily implemented and probably more efficient.

Pergamon

0039-9140(94)00334-3

*Talanta*, Vol. 42, No. 2, pp. 185–196, 1995

0039-9140/95 $9.50 + 0.00

# DECOMPOSITION OF DIPHENYLAMINE IN NITROCELLULOSE BASED PROPELLANTS—II. APPLICATION OF A NUMERICAL MODEL TO CONCENTRATION–TIME DATA DETERMINED BY LIQUID CHROMATOGRAPHY AND DUAL-WAVELENGTH DETECTION

ARNE BERGENS*

Uppsala University, Institute of Chemistry, Department of Analytical Chemistry, P.O. Box 531, S-751 21 Uppsala, Sweden

(*Received* 5 *November* 1991. *Revised* 2 *April* 1993. *Accepted* 7 *April* 1993)

**Summary**—A continued investigation of the primary steps in diphenylamine (DPA) decomposition in nitrocellulose (NC) propellants is presented. The study is based on analytical data obtained by reversed-phase liquid chromatographic separation of the initial degradation products of DPA. Spectrophotometric detection, rather than the amperometric detection used in part I of this work (A. Bergens and R. Danielsson, *Talanta*, 1995, **42**, 171), was employed in order to detect *N*-nitroso-DPA as well as DPA, 2-nitro-DPA and 4-nitro-DPA. The results have been studied with the rate parameter optimization program described in part I and simulations suggest that the decomposition of DPA includes unknown reaction steps. More satisfying curve fits were, for example, obtained when the initial reaction for conversion of DPA into *N*-nitroso-DPA was considered to consist of a two step process with an intermediate. This intermediate could act as a stabilizer as well as DPA and *N*-nitroso-DPA, particularly at lower temperatures.

The decomposition of the stabilizer DPA and the degradation products *N*-nitroso-DPA, 2-nitro-DPA and 4-nitro-DPA can be monitored by reversed-phase liquid chromatography (RPLC) and UV/VIS detection during heat storage tests of NC based propellants. Such tests at elevated temperatures, represent a common strategy for the assessment of propellant stability and the time elapsed until red fumes appear is frequently used as a measure of stability. The time-to-fume value can, however, be regarded as a questionable measure of stability since the stabilizer is then totally exhausted and the dangerous rapid decomposition of NC has already proceeded for some time when visible amounts of nitrogen oxides appear. It has also been shown that the rate of gas evolution from a NC propellant is increased as the nitroso and mono nitro derivatives of DPA are depleted.[1] A more relevant measure of propellant stability would, therefore, be the time at which these primary derivatives of DPA have been consumed, or the time when significant amounts of di-nitro derivatives appear, as suggested by Stine.[2]

In part I of this investigation, a method for optimizing concentration–time (CT) curves to analytical data of DPA, 2-nitro-DPA and 4-nitro-DPA was presented. Data were collected during a heat storage test at 85°C employing a previously described method[3] based on RPLC and dual-amperometric detection. By use of a computer program based on simplex optimization of rate parameters in a reaction system, theoretical curves for DPA, 2-nitro-DPA and 4-nitro-DPA could be fitted to the experimental data. The reaction model used was the commonly accepted mechanism for the initial step in DPA degradation in NC based propellants, seen in Fig. 1.[4,5] The theoretical curve for *N*-nitroso-DPA was also simulated on the basis of the rate parameters which describe the assumed reaction system. The *N*-nitroso-DPA acts as an effective stabilizer in the initial part of the degradation process[6] and the results presented in part I also made it desirable to complete the investigation by including *N*-nitroso-DPA as an analyte. Since *N*-nitroso-DPA is not detectable amperometrically it was favourable to replace the electrochemical detection with UV-visible detection.

*Present address: Pharmacia AB, Pharmaceutical Uppsala, S-751 82 Uppsala, Sweden.

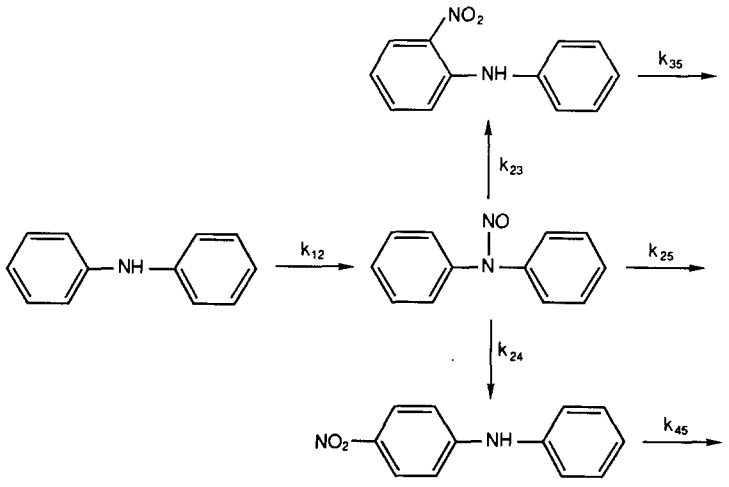


Fig. 1. Reaction scheme for DPA degradation in aging NC propellants. This scheme served as the model system in part I of this investigation.

The present paper is concerned with the results of such a study employing the same mathematical treatment of the experimental data as in part I. The propellant had, however, been subjected to a heat storage test at 80°C rather than at 85°C as in part I.

The reaction mechanisms used in the models of the DPA system have been described with irreversible reaction steps. This was done because the reactions involved in the decomposition of DPA are continuously driven by the excessive formation of nitrogen oxides, and in this sense, the reactions can be described as being irreversible.

## EXPERIMENTAL

### *Apparatus*

The LC-system consisted of a Shimadzu LC-6A pump (Shimadzu Corp., Kyoto, Japan) a Carnegie Medicin CMA200 (Carnegie Medicin AB, Stockholm, Sweden) automatic injector, a home-made column oven and two spectrophotometric detectors placed in series. The first detector was a Kratos Spectroflow, Model 757 (Kratos Analytical Instruments, Ramsey, NJ, USA) while the second was a Shimadzu SPD-6A and the detectors were connected with a 20 cm long piece of PTFE tubing (0.1 mm I.D.) The column used was a 100 × 3.2 mm RP-8 Velosep column (Brownlee labs Inc., Santa Clara, CA, USA).

All chromatograms were recorded and processed with a Spectra Physics, Model SP4290 integrator (Spectra Physics, San Jose, CA, USA) equipped with a dual channel module. The simulation and simplex algorithms were implemented on an IBM PS/2 Model 50 computer using ASYST scientific calculation system (MacMillan Software Company, NY, USA) as described in part I. Spectral characterization of the target compounds was carried out with a Perkin-Elmer Lambda 17 UV/VIS spectrophotometer (Perkin-Elmer Corp., Analytical Instruments, Norwalk, CT, USA) using 1 cm cells and the mobile phase as reference.

### *Chemicals*

The acetonitrile and 2-propanol used as organic modifiers in the mobile phase were obtained from Merck (Lichrosolv grade, Darmstadt, Germany) and used without further purification. The *m*-chloroacetic acid was obtained from BDH Chemicals Ltd., Poole, U.K. and was also used as received. The *m*-chloroacetic acid buffer was prepared from a 0.05*M* solution by adjusting the pH to 2.7 with NaOH.

The reference substances DPA (Merck, pro analysi grade), 4-nitro-DPA (Aldrich Chemie GmbH & Co. KG, Steinheim, Germany, spec. purity 99%) and 2-nitro-DPA (Aldrich Chemie, spec. Purity 98%) were all used as received. *N*-nitroso-DPA was obtained from AB Nobelkrut, Karlskoga, Sweden and found to contain 0.13% DPA.

### *Procedures*

The mobile phase consisted of 71.0% 0.05*M* *m*-chloroacetic acid buffer (pH = 2.7) 19.4% 2-propanol and 9.6% acetonitrile and was filtered and degassed according to the same procedure as in part I. All separations were performed isochratically at a flow rate of

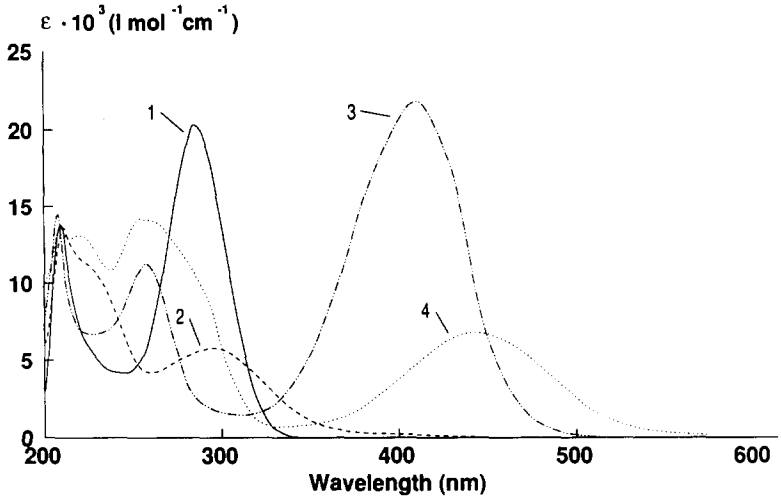


Fig. 2. Spectra of (1) DPA, (2) *N*-nitroso-DPA, (3) 4-nitro-DPA and (4) 2-nitro-DPA. The absorbances have been converted to molar absorptivities for comparison.

0.7 ml/min and at a temperature of 40°C. All compositions are given as volume percentages.

The quantifications were done using calibration curves and injections of external standards were made at regular intervals. The samples were refrigerated at 6°C inside the automatic injector and an injection volume of 15 $\mu$l was used exclusively. The sample solutions were diluted with mobile phase using a dilution factor of 5–10.

*Treatment of propellant samples*

Propellant samples were taken from the two propellant batches investigated in part I having the following specified compositions, 0.5% DPA/99.5% NC and 0.7% DPA/99.3% NC. The compositions correspond to 30 $\mu$mol/g (0.5% DPA) and 41 $\mu$mol/g (0.7% DPA), respectively. The samples were subjected to the Dutch stability test,[7] as described in part I, but the storage temperature was now decreased to 80 C. The DPA and nitro derivatives were extracted during 4 hr in a Soxhlet extraction unit, as also described in part I.

## RESULTS AND DISCUSSION

The results presented in part I of this investigation indicated that *N*-nitroso-DPA may play an important role in the stabilizing function of the DPA system. Spectra for DPA, *N*-nitroso-DPA, 2-nitro-DPA and 4-nitro-DPA obtained with the mobile phase as solvent are shown in Fig. 2. These spectra are in good agreement with published spectra[4] obtained with ethyl alcohol as medium and the choice of mobile phase does, thus, not seem to affect the general spectra characteristics. The spectral differences in Fig. 2 also illustrates the advantage of dual wavelength monitoring. Aromatic nitro compounds absorb in the visible region and 430 nm was therefore chosen as detection wavelength for 2-nitro-DPA and 4-nitro-DPA. *N*-nitroso-DPA on the other hand, shows a maximum at 292 nm which almost coincides with the maximum for DPA and this wavelength was therefore chosen for the detection of these two compounds. Single wavelength detection at, for instance 257 nm, would also have been possible but a better resolution in the chromatographic separation would have been required.

During a heat storage test, the concentrations of stabilizer and degradation products can be expected to change over a wide range. In the early part of the aging process the concentration of nitro derivatives is low compared to that of DPA. Later in the storage period, the DPA concentration is reduced in favour of the nitro derivatives. The situation is illustrated in Figs 3 and 4 in which chromatograms of two samples of the 0.7% DPA propellant are shown prior to and after the heat storage at 80°C. Only small amounts of nitro derivatives and *N*-nitroso-DPA could hence be found for the untreated sample. After 15 days of storage at 80°C (Fig. 4), the concentrations of the nitro derivatives had, however, increased by a factor of about 5 while the DPA concentration had been reduced to about 10% of the value in Fig. 3. As is seen in Fig. 4(b), the dominating derivative at this stage is *N*-nitroso-DPA which is represented by a large peak at 7.5 min in Fig. 4(b).

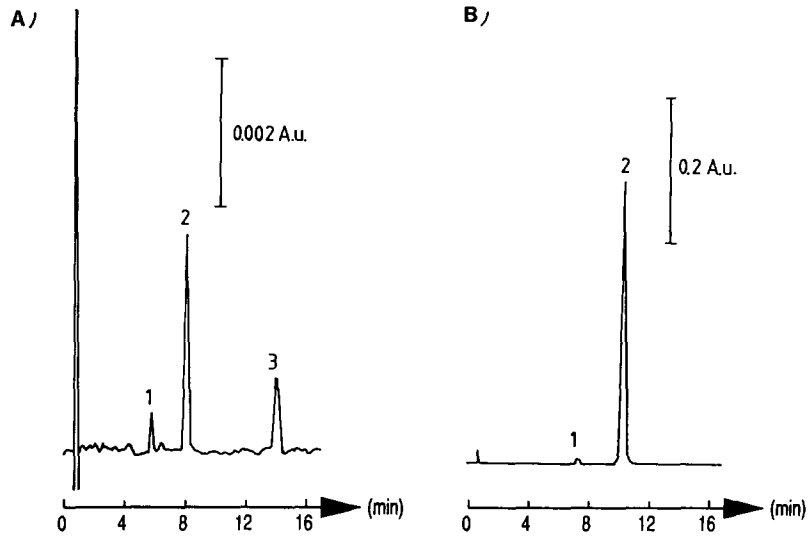


Fig. 3. Chromatograms obtained for an unstored sample with detection at (A) 430 nm and (B) 292 nm. The peaks in (A) correspond to: (1) unknown, (2) 4-nitro-DPA (51 pmol injected which corresponds to 0.14 $\mu$mol/g in the propellant sample), (3) 2-nitro-DPA (59 pmol, 0.15 $\mu$mol/g), in (B): (1) *N*-nitroso-DPA (463 pmol, 1.2 $\mu$mol/g), (2) DPA (9.3 nmol, 24.5 $\mu$mol/g).

The simplex optimization program, described in part I, was then applied to the data obtained from the heat storage test. At first, the proposed scheme for the degradation mechanism used in part I (see Fig. 1) was implemented in the program. The results are shown in Fig. 5(a) and (b) and from the poor agreement between the curves and the experimental data it can be

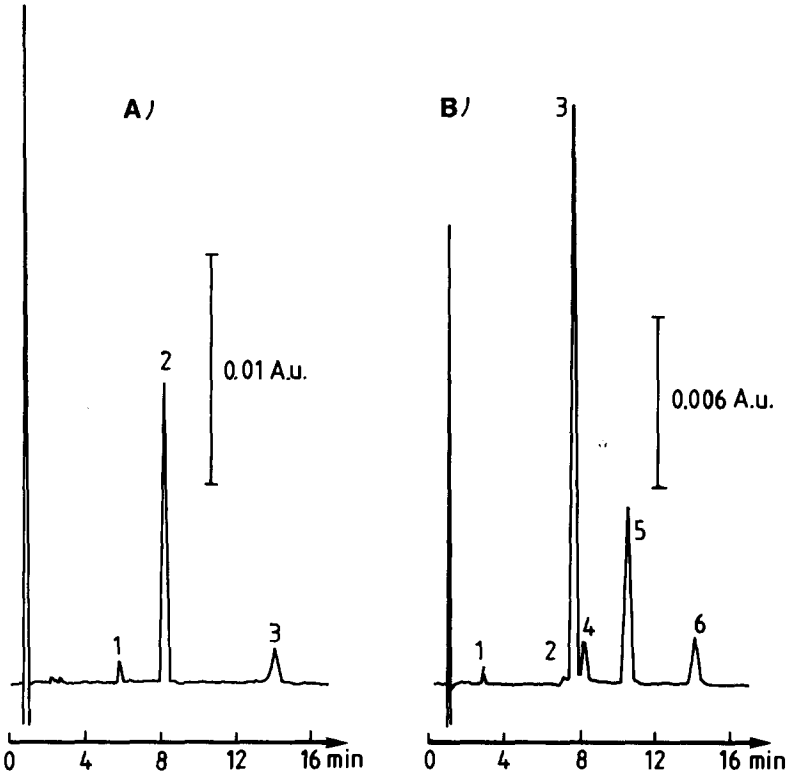


Fig. 4. Chromatograms obtained with detection at (A) 430 nm and (B) 292 nm after 15 days of storage at 80°C. The peaks in (A) correspond to: (1) unknown, (2) 4-nitro-DPA (225 pmol injected which corresponds to 3.0 $\mu$mol/g in the propellant sample), (3) 2-nitro-DPA (88 pmol, 1.2 $\mu$mol/g). In (B): (1) and (2) unknown, (3) *N*-nitroso-DPA (952 pmol, 13.2 $\mu$mol/g), (4) 4-nitro-DPA, (5) DPA (130 pmol, 1.7 $\mu$mol/g), (6) 2-nitro-DPA.

concluded that the assumed reaction mechanism is not applicable for storages at 80°C. The curves in Fig. 5 represent the best possible optimizations obtained after many attempts with different starting values for the initial simplex.

Attempts to optimize CT curves with different values of $k_{12}$ were made but with poor results since it was difficult to find a value for $k_{12}$ compatible with both the rapid decrease in the DPA concentration and the slow increase in the *N*-nitroso-DPA concentration. According to the assumed degradation mechanism, the curve for *N*-nitroso-DPA should also reach a maximum earlier than the 2-nitro-DPA and 4-nitro-DPA curves. Curve fitting experiments with additional parallel routes (*i.e.* direct reactions from DPA to nitro DPAs) did not improve the correlation between the model and the data as all three curves for *N*-nitroso-DPA, 2-nitro-DPA and 4-nitro-DPA passed through their maxima earlier than the experimental data. The fact that the sum of the DPA, *N*-nitroso-DPA, 2-nitro-DPA and 4-nitro-DPA concentrations is decreasing with time indicates that some DPA is lost through an unknown reaction. This reaction could involve thermal radical formation which is common for aromatic amines. The diphenylnitrogen radical is, for example, formed from DPA under influence of heat and oxygen[8,9] and is relatively stable due to the possible electron delocalization. The diphenylnitrogen radical and the radical cation of DPA are also known intermediates in other oxidation reactions of DPA.[8,10–13]

A mechanism that can explain the rapid decrease in the DPA concentration have not yet been elucidated completely. As already stated, the variety of results from different investigations might, however, be explained by competing processes in the aging propellant material. An example of such a side reaction, is oxygen catalyzed oxidation[14,15] by thermally induced radical formation.[8–10,14–17] Opschoor *et al.*[16] have, for instance, shown that the presence of oxygen increases the rate of DPA degradation in NC based propellants significantly and it can therefore be assumed that side reactions of this type will become more pronounced with increasing temperature is increased.

Since this investigation was focused on testing the empirical model presented in part I, we can only speculate on the consumption of DPA in side reactions. As will be shown below, it is, however, possible to modify the degradation scheme in Fig. 1 so that better agreement between the CT data and theoretical curves is achieved at 80°C. The modifications include an intermediate step between DPA and *N*-nitroso-DPA and one additional route for DPA decomposition.

Both chemical[13,18] and electrochemical oxidations[18–24] of DPA are well-known. In acid media, *N*,*N*′-diphenylbenzidine appears to be the major product in electrochemical oxidations of DPA while in neutral to basic media a mixture of tetraphenylhydrazine and *N*,*N*′-diphenylbenzidine is obtained.[21–23] Polymer products resulting from para–para coupling of radicals have also been isolated and characterized after both chemical and electrochemical oxidations.[18–20] The spontaneous thermally induced radical formation of DPA, that could take place in a propellant subjected to high temperatures, must be expected to give a variety of products, not only a straight para–para coupled poly(4-phenylaniline) chain. If the assumed DPA-intermediate is of a polymeric nature the question arises whether this DPA-polymer would degrade into *N*-nitroso-DPA when exposed to nitrogen oxides. Polymerization of DPA would lead to the formation of large aromatic ring systems which probably could trap nitrogen oxides and thereby act as a stabilizer and also result in a decreased rate of *N*-nitroso-DPA formation in accordance with the experimental results. Observations that further support this theory are: the decreasing sum of concentrations in the initial part of aging, and the absence of a peak in the chromatograms which could explain the loss of DPA. For solubility reasons, the polymer could remain in the NC-material even after the extraction with methylene chloride. A large bulky polymer could also be trapped by the NC fibres and therefore not dissolved in the extraction step.

Another suggestion on the stabilizing mechanism of the DPA system made by Urbanski *et al.*[24,25] based on thermal analysis, ESR and IR spectroscopic studies of nitrate esters mixed with aromatic amines and involves the formation of complexes between the aromatic amines and nitrate esters. The complexes could be insoluble in a medium of low dielectric constant such as methylene chloride and probably act as a stabilizer giving nitroso and nitro derivatives of DPA as products.

The reaction model for the optimization program was modified according to the properties of DPA discussed above. The modified reaction

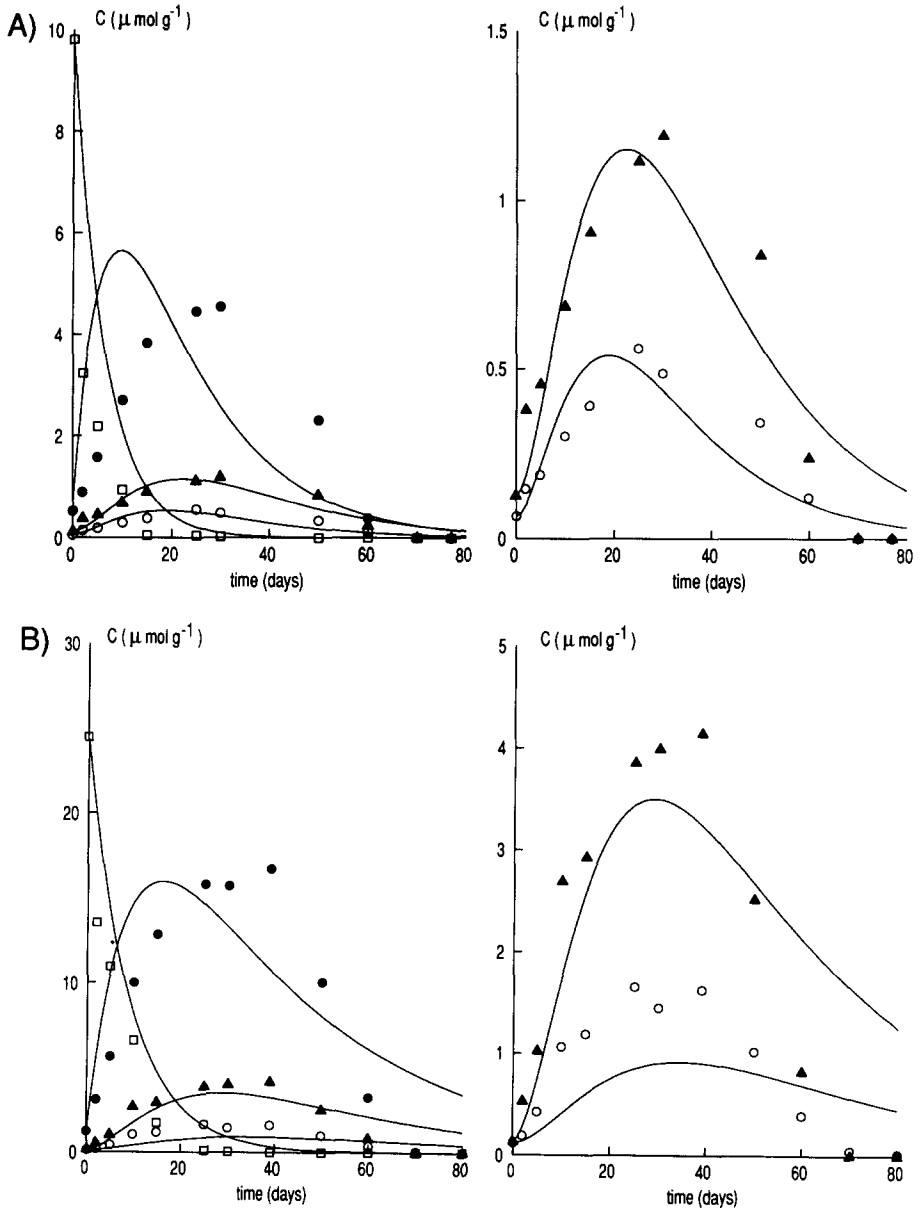


Fig. 5. Resulting CT curves from optimizations of the reaction model in Fig. 1 to data for (□) DPA, (●) *N*-nitroso-DPA, (▲) 4-nitro-DPA and (○) 2-nitro-DPA in (A) 0.5% DPA and (B) 0.7% DPA propellants. The right hand figures show expanded plots for 2-nitro-DPA and 4-nitro-DPA.

scheme is described in Fig. 6 and contains two additional rate parameters when compared with the initial model shown in Fig. 1. If the DPA-intermediate is a resonance stabilized radical it could also give rise to other compounds, not measurable with the analytical procedure used herein. The parameter $k_{27}$ was, therefore, introduced to describe this reaction path. The dashed paths in Fig. 6 were not included in the model since they did not improve the fit. The introduction of an intermediate step in the formation of *N*-nitroso-DPA did, on the other hand, give rise to an improved agreement between the experimental data and the theoretical curves.

In Fig. 7, optimizations of the new model to the data obtained in the heat storage test at 80°C are shown. The poor fits on the consumption side of the curves for *N*-nitroso-DPA, 2-nitro-DPA and 4-nitro-DPA still remain although the overall curve fits for all four analyzed components have been improved. The dashed curves in Fig. 7 represent CT curves for the DPA-intermediate simulated from the optimized parameters. In the optimizations illustrated in Fig. 7, the concentration of DPA-

intermediate at zero time was approximated with the difference between the original DPA content (30 μmol/g for the 0.5% DPA and 41 μmol/g for the 0.7% DPA propellant) and the sum of the DPA, *N*-nitroso-DPA, 4-nitro-DPA and 2-nitro-DPA concentrations at zero time.

The optimization procedure with the new reaction model (Fig. 6) was, therefore, tested with different randomly chosen start values, as in part I. The result is presented in Table 1 and the initial simplex was again defined by start values for $k_{12}$ to $k_{56}$ in the range 0.0001–0.2.

From the width of the ranges given in Table 1 it can be seen that some of the parameters are poorly defined, this applies especially to those parameters which are related to a component lacking in the data sets. The parameter $k_{27}$, thus, exhibits the largest variation since it is only related to the concentration of the DPA-intermediate (*i.e.* component no. 2). The larger variation in $k_{27}$, however, also affects the variation in the other parameters as a result of interaction effects. The parameter $k_{12}$, describing the rate of DPA consumption, is lower for the 0.7% DPA series than for the 0.5% DPA propellant which could indicate that the reaction is not of first order. This could, however, also indicate that the degradation mechanism changes with the DPA concentration but this seems unlikely as the same raw NC material was used in the preparation of both batches. As already stated, the values obtained for the parameters should not be taken as true rate constants since the modified model includes assumed reaction steps.

In spite of the great variations in some of the parameter values, the curve fits were all comparable with those in Fig. 7. Simulations of the CT curves for the DPA-intermediate obtained on the basis of the 12 different parameter sets also showed good agreement with the different optimizations shown in Fig. 8. For the 0.7% DPA propellant, all of the 12 curves coincide even though significant variations in the parameter values between different optimizations were obtained (Fig. 8b). The curves in Fig. 8 indicate that the concentration of the DPA-intermediate increases and goes through a maximum during the first 10 days of the heat storage test. Furthermore, the coinciding curves show that the simplex converges toward solutions that give the same predictions for the DPA-intermediate.

*Optimization to literature data*

There are many reports in the literature where the concentration changes of the stabilizer additive with time have been followed. Only a few of these contain additional data for the subsequently formed nitro derivatives. Curtis and Rogasch[26] published a straight phase LC method for the determination of nitro derivatives formed from DPA during propellant aging. The method was later applied by Curtis[27] in a following study of the DPA degradation in two NC propellants subjected to heat storage at 80°C. The latter report is particularly interesting since it contains data from heat

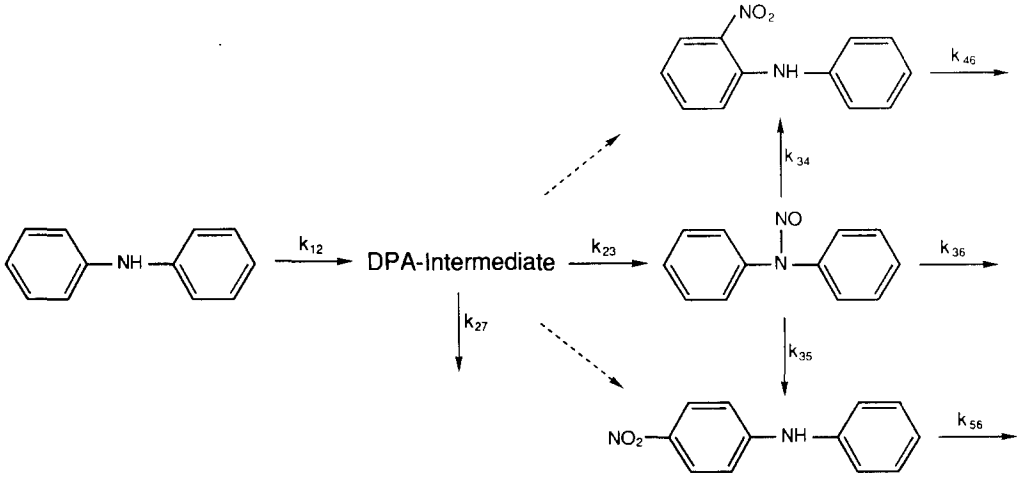


Fig. 6. The modified reaction model used for the optimization to heat storage test data from 80 C. The dashed arrows symbolize the possible reaction paths discussed in the text, but not accounted for in the optimizations for Fig. 7.

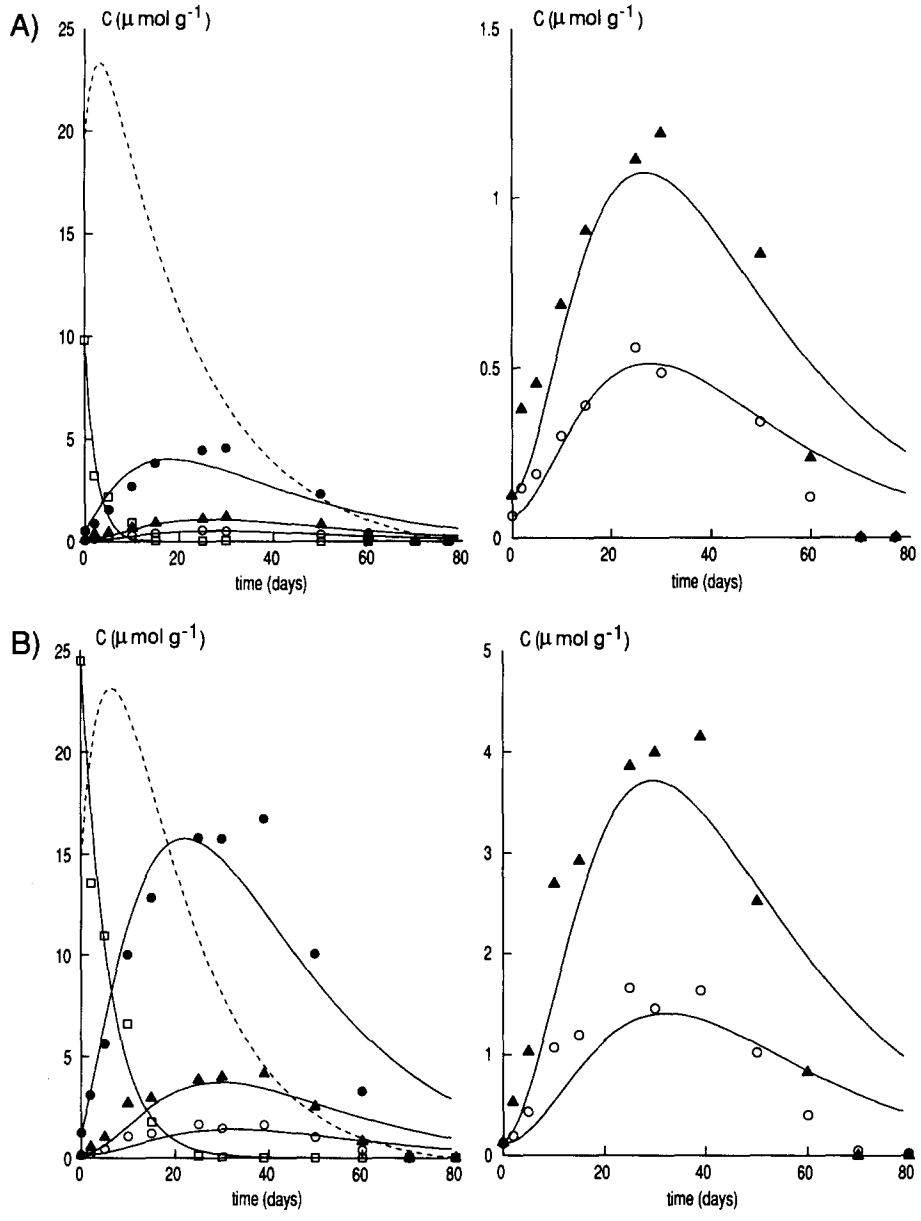


Fig. 7. Resulting curves for the same data sets as in Fig. 5 but for optimizations and curve fittings based on the reaction model described in Fig. 6: (A) 0.5% DPA and (B) 0.7% DPA. The dashed curves are the resulting curves for the DPA-intermediate simulated from the optimizations. The right hand figures show expanded plots for 2-nitro-DPA and 4-nitro-DPA.

storage tests on propellants stored under comparable conditions to this investigation (80°C). It was therefore considered interesting to apply the optimization program on the data reported by Curtis.

In Fig. 9, the optimization of our first assumed model (Fig. 1) to Curtis' set of data is presented. It is noticeable that the decline of DPA concentration does not match the build-up of *N*-nitroso-DPA and the resulting curve shows a poor agreement with the experimental data.

At this stage, it was also interesting to test whether the modification of the reaction scheme from Fig. 6 improves or impairs the curve fit. The inclusion of the intermediate step was found to improve the curve fit for *N*-nitroso-DPA as indicated in Fig. 10.

The improved agreement between the modified reaction model and our CT data can therefore be verified by Curtis' data which have been independently analyzed with no connection at all to our investigation. It is therefore believed that this verification supports the

Table 1. Ranges of parameter values obtained from 12 different optimizations using randomly chosen start simplex

| 0.5% DPA | | | | | | | | |
|---|---|---|---|---|---|---|---|---|
| | $k_{12}$ | $k_{23}$ | $k_{27}$ | $k_{34}$ | $k_{35}$ | $k_{36}$ | $k_{46}$ | $k_{56}$ |
| Min | 0.4190 | 0.0195 | 0.0186 | 0.0058 | 0.0278 | $0.4 \cdot 10^{-6}$ | 0.0543 | 0.1030 |
| Max | 0.4380 | 0.0221 | 0.0389 | 0.0576 | 0.0621 | 0.0076 | 0.6523 | 0.2150 |

DPA-intermediate$_0$ = 19.5 $\mu$mol/g.

| 0.7% DPA | | | | | | | | |
|---|---|---|---|---|---|---|---|---|
| | $k_{12}$ | $k_{23}$ | $k_{27}$ | $k_{34}$ | $k_{35}$ | $k_{36}$ | $k_{46}$ | $k_{56}$ |
| Min | 0.1664 | 0.0631 | $1.0 \cdot 10^{-6}$ | 0.0061 | 0.0282 | $61.8 \cdot 10^{-6}$ | 0.0633 | 0.1131 |
| Max | 0.1697 | 0.0634 | $28.9 \cdot 10^{-6}$ | 0.0109 | 0.0394 | 0.0153 | 0.1104 | 0.1557 |

DPA-intermediate$_0$ = 15.1 $\mu$mol/g. The dimension of parameter values is day$^{-1}$.

indication on the existence of an intermediate step in the degradation mechanism.

The existence of the intermediate has therefore to be verified with other experimental techniques since there is no indication on the existence of an intermediate compound with electrochemical or UV/VIS detection. Future investigations should, therefore, be focused on the remaining NC material after the extraction step. As indicated in part I, this material shows interesting colour changes during the heat test which suggests that an investigation with molecular spectroscopic methods might be able to answer the question whether DPA in any form is incorporated or retained in the NC material. In additional to the two previously mentioned DPA-intermediates suggested in the literature, a reaction between the DPA radicals and the radical formed in the NC polymer is also possible. A hypothetical reaction scheme for such a reaction is presented (Scheme I–III).

The steps I–II represent the formations of the known DPA radical cation[8,10,15] and the alkoxyl radical in the NC chain.[28,29] The incorporation of DPA in the NC chain could occur as described by step III in which the DPA can be bound to the NC in two different ways. It is reasonable to assume that the dominating route would be III(b) as the DPA radical cation is stabilized by delocalization of the unshared electron to the aromatic ring. The hypothetical reactions above would not affect the stabilizing action of DPA since the products (NC-DPA) in step III should be as reactive towards nitrogen oxides as DPA itself. In a reaction with nitrogen oxides, the NC-DPA could decompose to give the various nitro and nitroso derivatives of DPA.

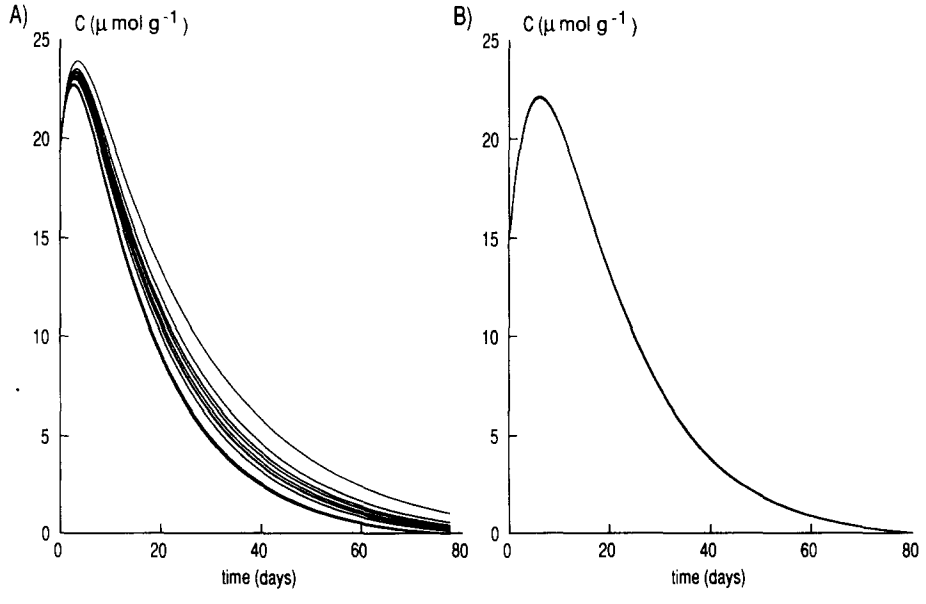


Fig. 8. Simulated curves for the assumed DPA-intermediate obtained on the basis of the 12 repeated optimizations in Table 1: (A) 0.5% DPA and (B) 0.7% DPA.

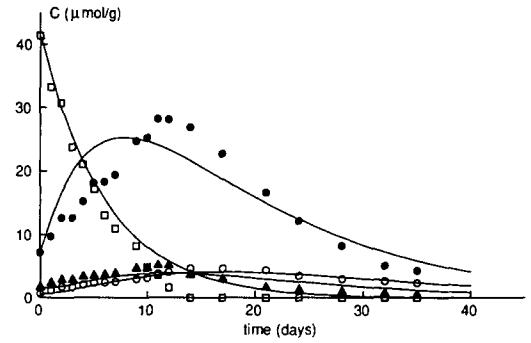


Fig. 9. Optimization of the reaction model in Fig. 1 to data presented by Curtis[27] for (□) DPA, (●) *N*-nitroso-DPA, (▲) 4-nitro-DPA and (○) 2-nitro-DPA. The concentrations were monitored during a heat storage test at 80°C. The optimization is based on data from a similar figure presented by Curtis. The data have been transformed to the unit μmol/g from weight-%.

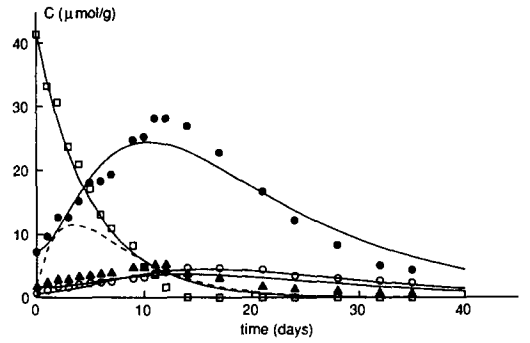


Fig. 10. Optimization of the modified reaction model in Fig. 6 to data from Curtis.[27] Marker identities: (□) DPA, (●) *N*-nitroso-DPA, (▲) 4-nitro-DPA and (○) 2-nitro-DPA. The dashed curve for the DPA-intermediate is calculated from the optimized parameters. The optimization is based on the same data as Fig. 9.

## CONCLUSIONS

The DPA content of a propellant batch usually decreases relatively fast and the stabilizing action after that the DPA has been consumed must, therefore, be attributed to the *N*-nitroso-DPA, 2-nitro-DPA, 4-nitro-DPA and to the possible DPA-intermediate(s). The interesting time to estimate would therefore be the time for consumption of all of these four compounds. However, the curves obtained by the presented optimization procedure fail to predict this time. The reason for this probably lies in the variations in moisture, oxygen and nitrogen oxide concentrations during the course of the heat storage test. In addition, parallel processes involving spontaneous thermal radical formation[17,28] of DPA and nitro derivatives exist. The assumption of first order reactions is therefore not valid over the entire time period for the heat storage test and deviations from the model must therefore be expected. The overall reaction order would be difficult to predict and values in the range 0–1 have been found for the DPA decomposition.[30]

On the basis of the present results it is evident that the mechanism for the initial DPA degradation involves unknown reaction steps which are more significant at lower temperatures. The

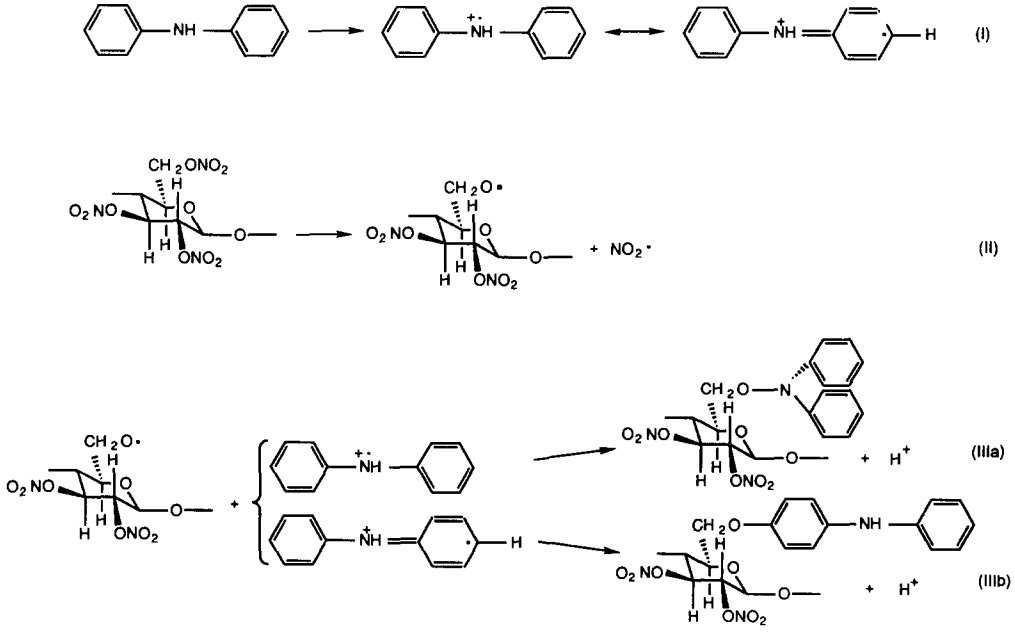


Schemes I–III

experimental data in part II indicate the existence of an intermediate step in the nitrozation of DPA. The high stability of a propellant containing less than 0.1% DPA could be explained by the presence of significant amounts of *N*-nitroso-DPA, 2-nitro-DPA and 4-nitro-DPA. The presence of a DPA-intermediate would further increase the stability of a NC propellant with low DPA content. Since most heat storage tests are performed using high temperatures, the aging of the NC material is accelerated to such a high rate that any intermediate reaction steps are difficult to uncover in the stability tests commonly used. The reasonably good fits obtained in part I at 85°C with the initial mechanism shown in Fig. 1 could be a result of the shorter life time of the intermediate compound. The DPA stabilization of NC is also an extremely temperature dependent process since the time-to-fume at 80°C is approximately 120 days while at 25°C it is in the order of 20–50 years. The strong temperature dependence could be an indication that radical species are involved in the mechanism. Furthermore, the diffusion conditions change around the melting temperature of DPA (53°C). As a consequence of the above mentioned aspects on the reaction mechanism, any extrapolations to room temperatures based on monitoring of stabilizer consumption at these high temperatures will be erroneous. The monitoring of DPA or its degradation products can therefore not compete with for example thermal gravimetry or calorimetry as methods for estimating propellant stabilities.

However, the approach with simultaneous curve fitting has shown itself to be useful in mechanistic studies and could be expected to be applicable to, for example, studies of organic synthesis where the experimental conditions are more easily controlled. The approach for computing CT curves makes the optimization program easy to use and changes of reaction mechanisms can be made quickly.

The loss of DPA from the NC material, observed in part I, and the results in the model optimizations in part II make it appropriate to focus future investigations on the NC material remaining after the extraction of the DPA derivatives and there are, at least, three possibilities for the observed loss of DPA which should be investigated in the future. First, the oxidation of DPA into a compound which is either non-electroactive and non-absorbing at 292 or 430 nm, or completely retained on the column. Secondly, the DPA could react to give rise to a product which is insoluble in methylene chloride. This product could be a polymer, as such polymers are known to be formed in both electrochemical oxidations[19,20] and in oxidation due to the presence of oxygen.[8] Finally, DPA could, according to Urbanski *et al.*[24,25] form a non-soluble complex with NC. A study using molecular spectroscopic methods should most likely be able to answer the question of whether DPA is incorporated in the NC material or not.

*Acknowledgements*—Acknowledgement is made to Dr Rolf Danielsson for introducing me into ASYST programming, supplying the simplex routine and for his invaluable help with the mathematical ideas for the optimization program. The Swedish National Board for Technical Development is also acknowledged for the financial support which made it possible to complete this work.

## REFERENCES

1. A. A. Wickham, *Proc. from Int. Symposium on Compatibility of Plastics and Other Materials with Explosives, Propellants, Pyrotechnics and Processing of Explosives, Propellants and Ingredients*, p. 171, Virginia Beach, 1989.
2. G. Y. Stine, *Anal. Chem.*, 1991, **63**(8), 475 A.
3. A. Bergens, *J. Chromatogr.*, 1987, **410**, 437.
4. W. A. Schroeder, P. E. Wilcox, K. N. Trueblood and A. O. Dekker, *Anal. Chem.* 1951, **23**(12), 1740.
5. J. Tranchant, *6th Symp. Chem. Probl. Stab. Explos.* [*Proc.*], p. 1, 1982.
6. N. J. Blay, *3rd Symp. Chem. Probl. Stab. Explox.* [*Proc.*], p. 61, 1973.
7. *Analytical Methods for Powder and Explosives*, p. 59. AB Bofors Nobelkrut, Sweden, 1960.
8. A. A. Berlin, *Pure Appl. Chem.*, 1973, **36**, 177.
9. L. F. Fieser and M. Fieser, *Advanced Organic Chemistry*, p. 716. Reinhold Publishing Corp., New York, 1961.
10. N. W. Sidgwick, *The Organic Chemistry of Nitrogen*, p. 62, rev. by T. W. J. Taylor (ed.), Clarendon Press, Oxford, 1942.
11. A. N. Pankratov, S. L. Schmakov, S. P. Mushtakova and L. A. Gribov, *J. Anal. Chem. USSR*, 1986, **41**(5), 635.
12. A. N. Pankratov and S. P. Mushtakova, *J. Anal. Chem. USSR*, 1989, **44**(7), 974.
13. E. Bishop, *Indicators, Anal. Chem.*, R. Belcher and H. Frieser (eds), pp. 560–584. Pergamon Press, Oxford, 1972.
14. D. J. Carlsson and D. M. Wiles, *Rubber Chem. Techn.*, 1974, **47**, 991.
15. T. Urbanski, *Chemistry and Technology of Explosives*, Vol. 4, p. 581. Pergamon Press, Oxford, 1983.
16. J. Opschoor, A. H. Heemskerk, J. Verhoeff and H. J. Pasman, *Int. Jahrestag.-Inst. Treib-Explosivst.* [*Proc.*], p. 495, 1983.
17. F. A. Neugebauer and S. Bamberger, *Chem. Ber.*, 1974, **107**, 2362.
18. N. Comisso, S. Daolio, G. Mengoli, R. Salmaso, S. Zecchin and G. Zotti, *J. Electroanal. Chem.*, 1988, **255**, 97.
19. J. Guay and L. H. Dao, *J. Electroanal. Chem.*, 1989, **274**, 135.

20. H. Yang and A. J. Bard, *J. Electroanal. Chem.*, 1991, **306,** 87.
21. C. K. Mann and K. K. Barnes, *Electrochemical Reactions in Nonaqueous Systems*, pp. 260–269. Marcel Dekker, New York, 1970.
22. R. N. Adams, *Electrochemistry at Solid Electrodes*, p. 345. Marcel Dekker, New York, 1969.
23. G. Cauquis, J. Cognard and D. Serve, *Tetrahedron Lett.*, 1971, **48,** 4645.
24. B. Hetnarski, W. Poludnikiewicz and T. Urbanski, *Tetrahedron Lett.*, 1970, **1,** 3.
25. T. Urbanski, B. Hetnarski and W. Poludnikiewicz, *Can. J. Chem.*, 1972, **50,** 3340.
26. N. J. Curtis and P. E. Rogasch, *Prop. Explos. Pyrotech.*, 1987, **12,** 158.
27. N. J. Curtis, *Prop. Expols. Pyrotech.*, 1990, **15,** 222.
28. J. J. Jutier, Y. Harrison, S. Premont and R. E. Prud'homme, *J. Appl. Polym. Sci.*, 1987, **33,** 1359.
29. M. L. Wolfrom, J. H. Frazer, L. P. Kuhn, E. E. Dickey, S. M. Olin, D. O. Hoffman, R. S. Bower, A. Chaney, E. Carpenter and P. McVain, *J. Am. Chem. Soc.*, 1955, **77,** 6573.
30. T. Lindblom, P. Lagerkvist and L. G. Svensson, *7th Symp. Chem. Probl. Conn. Stab. Explos.* [*Proc.*]. Smygehamn, Sweden, 1985.

Pergamon

0039-9140(94)E0122-8

*Talanta*, Vol. 42, No. 2, pp. 197–204, 1995

0039-9140/95 $9.50 + 0.00

# DETERMINATION OF ANTIMONY (III) AND (V) BY DIFFERENTIAL PULSE ANODIC STRIPPING VOLTAMMETRY

PAMELA A. WALLER and WILLIAM F. PICKERING

Chemistry Department, University of Newcastle, N.S.W., Callaghan 2308, Australia

(*Received* 6 *December* 1993. *Revised* 12 *April* 1994. *Accepted* 15 *April* 1994)

**Summary**—Re-evaluation of DPASV procedures for determining low levels of Sb (III) and Sb (V) in solution identified several problem areas, *e.g.* anomalous ASV behaviour, possible formation of an intermediate valency state during the analytical cycle, and chemical interactions in acidified test solutions containing both valency states. Specific determination of Sb (III) can be achieved using base solutions composed of 0.2*M* HCl (detection limit 10 n*M*) or acetic acid/acetate buffer (detection limit 600 n*M*). For the determination of Sb (V), analysis in 2*M* HCl is recommended [with response in 0.2*M* HCl being used to correct for any Sb (III) present].

Antimony species are known to be toxic but monitoring of environmental systems for this element is not a common procedure, possibly because the levels tend to be quite low, for example, the terrestrial abundance level of Sb[1] is around 0.7 $\mu$g/g, and sea-water[2] contains 0.1–0.5 $\mu$g Sb/l. [with 70–94% of the total Sb being present as Sb (V) species]. Much higher Sb levels can be found near non-ferrous smelters, *e.g.* near a lead smelter,[3] soil values ranged between 5 and 260 $\mu$g Sb/g, and up to 10 mg/g were found in soils located near a copper smelter.[4]

The analytical procedure used to determine Sb levels in non-polluted systems thus needs to be highly sensitive, and it should also be capable of distinguishing between Sb (III) and Sb (V) species, because the toxicity threshold for antimony species varies with the valency state of the element. One technique which meets these specifications is atomic absorption spectroscopy,[5–10] where detection limits of 0.5 $\mu$g/l. (4 n*M*) have been achieved using hydride generation. Another promising (but not so fully explored) technique is differential pulse, anodic stripping voltammetry (DPASV).

Application of a DPASV procedure[11] to acidified solutions 200 n*M* in Sb (III) or Sb (V) was found to yield sharp signal peaks when a hanging Hg drop electrode was used. The size of the peaks obtained varied with the molarity of the HCl added and the valency state of the Sb present. It was proposed that one could determine the amount of Sb (III) species present by using dilute acid support solutions, and then determine total Sb content using an acidity level of 4*M* HCl, but no experimental data for mixture analyses was presented.

In another ASV study,[12] an acetate buffer solution was used as the supporting electrolyte. With the experimental conditions adopted, the detection limit for Sb (III) was around 600 n*M* (*i.e.* much less sensitive than HCl based systems). Other limitations of this support medium were not evaluated, nor was the behaviour of Sb (V) in this medium examined. To remedy these omissions, further studies have now been made. The determination of Sb in HCl solutions has also been re-examined in some detail, primarily because the responses obtained using Sb (III)/Sb (V) mixtures differed from the results expected (based on single valency state studies).

## EXPERIMENTAL

### *Standards and base solutions*

(a) *Antimony standards.* Standard stock solutions (25 $\mu$*M*) were prepared by dissolving either Univar A.R. potassium antimonyl tartrate (SbT) or Merck A.R. $KSb(OH)_6$ in pure water (from a reverse osmosis unit). A solution saturated with Aldrich Gold Label $Sb_2O_3$ was also prepared [calibration against KSbT

standards indicated the Sb content (*c.* 13 $\mu M$]. Aliquots of these stock solutions were diluted with base electrolyte solution as required to yield test solutions having Sb levels which ranged from 100 n$M$ to 10 $\mu M$.

(b) *Acetate buffer solution.* The 1$M$ $CH_3COOH$, 0.5$M$ $CH_3COONa$ mixture used was prepared from A.R. grade materials.

(c) *Hydrochloric acid solutions.* Base solutions varying in concentration from 0.08 to 4$M$, were prepared by dilution of Univar A.R. HCl with pure water. For some investigations (*e.g.* identification of baseline noise peaks) higher grade acids (such as B.D.H. 'Aristar' brand HCl and 'Volucon' standard solution ampules) were also utilized.

(d) *Hydrazine dihydrochloride.* Small aliquots (*e.g.* 0.1 ml) of a 0.5$M$ stock solution (prepared daily by dissolving A.R. grade salt (Aldrich brand) in pure water) were added (as required) to Sb test solutions (final hydrazine concentration, 0.01$M$).

(e) *Synthetic mixtures containing* Sb (III) *and* Sb (V). Solutions containing antimony in both valency states were prepared by mixing appropriate volumes of the $Sb_2O_3$ saturated solution and standard $KSb(OH)_6$ solutions. The amount of each solution added was varied, in order to obtain mixtures in which the ratio of Sb (III) to Sb (V) was either 5:1, 2:1, 1:1, 1:2 or 1:5. Different total levels of Sb in solution were obtained by using different aliquot volumes and by diluting more concentrated dual valency mixtures with water. Varying volumes of HCl were added to aliquots of these various mixtures (and to aliquots of standard Sb (III) and Sb (V) solutions), in order to prepare test solutions having final acidity levels which ranged from 0.2 to 3.0$M$.

*Analytical procedure*

Each mixture and standard series solution was analysed (by DPASV) and the peak area plotted as a function of the Sb content. The instrument used for the DPASV analysis was an Amel® Polarographic Analyser (model 473), connected to a hanging drop mercury electrode (PAR model 3038, Ag/AgCl reference electrode). The operating conditions used for the HCl base solutions were: Nitrogen purge time, 2 min; Hg drop size, small; deposition potential, −400 mV; deposition time, 1 sec (extended at times to longer values); pause time 3 sec; anodic scan speed, 5 mV/sec; cut-off potential +50 mV; X, Y recorder speed, 100 mV/cm; FSD current, 10, 20, 50 or 100 nA. Similar operating conditions were used with the acetate buffer solutions except that deposition potentials were varied from −400 to −1400 mV.

## RESULTS AND DISCUSSION

*Irregular behaviour of* Sb *in ASV studies*

Some of the results presented in an earlier DPASV study[11] of Sb systems indicated that responses could deviate from the pattern usually observed in ASV determinations of metals such as Pb, Cd, Zn. For example, it was found that repeated scanning of HCl solutions containing Sb (III) or Sb (V), led to peaks which decreased in size (using a hanging drop mercury electrode and 5 min deposition times). Using a thin Hg film electrode only the first voltage scan of Sb (III) solutions yielded a peak and no stripping peak for Sb (V) was detected. The addition of hydrazine to the test solutions modified this behaviour and determination of Sb (V) was achieved using a supporting electrolyte which was 1.2$M$ in HCl, 1.8$M$ in $H_2SO_4$ and 0.01$M$ in hydrazine sulphate.

In our studies, a fresh mercury drop was used for each scan, and the amount of Sb deposited in (or on) the Hg drop was kept small (*e.g.* by using a 1 sec deposition time). Increasing the loading level (by increasing the deposition time) resulted in a disproportionate increase in the stripping peak size, *e.g.* the area enhancement obtained by using much longer times (*e.g.* 300 secs) was relatively small (*e.g.* less than five-fold, cf. Fig. 1).

Calibration series behaviour was also

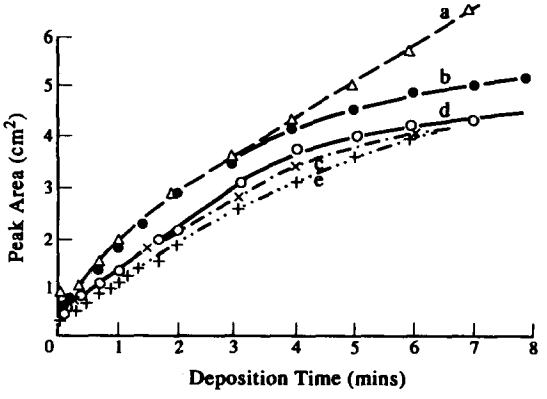


Fig. 1. Effect of deposition time on Sb peak area. (a) 1 $\mu M$ KSbT in acetate buffer; $E_d$ −1.1 V., 20 nA FSD. (b), (c) 5 $\mu$M $Sb(OH)_3$ in 1$M$ HCl; $E_d$ −450 mV, 1 $\mu$A FSD. (d), (e) 50 $\mu M$ $KSb(OH)_6$ in 1$M$ HCl; $E_d$ −500 mV, 200 nA FSD. In systems (b) and (d) hydrazine present.

atypical, because the straight lines which joined the points rarely passed through the origin. For example, the calibration line for Sb (III) in 0.2*M* HCl was defined by the equation: peak area ($mm^2$) = 14 + 63*c*; where *c* is the Sb concentration in $\mu M$ (recorder FSD setting, 50 nA). The magnitude of the intercept value varied with acid molarity and the valency of the Sb salt (*e.g.* in 2*M* HCl, the value for Sb (III) was 25, for Sb (V), 50). Area measurement errors may have contributed to the size of the intercepts, but the marked deviation from zero values suggests that the proportion of analyte reduced at the electrode decreased with increasing concentration. Changing the HCl concentration resulted in small changes in the slope of Sb (III) calibration plots (*e.g.* from 63 in 0.2*M* to 70 in 2*M* HCl), and large changes in the slope of Sb (V) plots (*e.g.* 0.8 in 0.2*M* to 28 in 2*M* HCl).

Abnormal behaviour was most marked in acetate buffer base solutions (discussed in a later section). In this media peak size and shape varied, *inter alia*, with the magnitude of the deposition potential.

The irregular behaviour noted suggests that the processes involved in the ASV deposition stage are more complex than formation of $Sb^0$ (and dissolution in the Hg drop). It appears that some Sb species are adsorbed (or precipitated) on the Hg surface, and during the stripping scan these species influence the size of the current flow.

*Influence of chemical reactions on DPASV responses*

The shape, size and location of the Sb ASV peaks was found to vary with the composition of the base solution, the experimental conditions selected, and the chemical form of the Sb species present. The chemical form of the antimony species introduced into test solutions ranged from being a complex anion (in solutions prepared from potassium antimonyl tartrate), to uncharged molecules or oxycations (in solutions containing dissolved $Sb_2O_3$). Equilibria involved in the dissolution of antimony (III) oxide in water[13] include:

$$Sb_2O_3\ (s) + 3H_2O \leftrightarrow 2Sb(OH)_3 \qquad (1)$$

$$1/2Sb_2O_3 + 1/2H_2O \leftrightarrow SbO^+ + OH^- \qquad (2)$$

$$1/2Sb_2O_3 + 1/2H_2O \leftrightarrow SbO_2^- + H^+ \qquad (3)$$

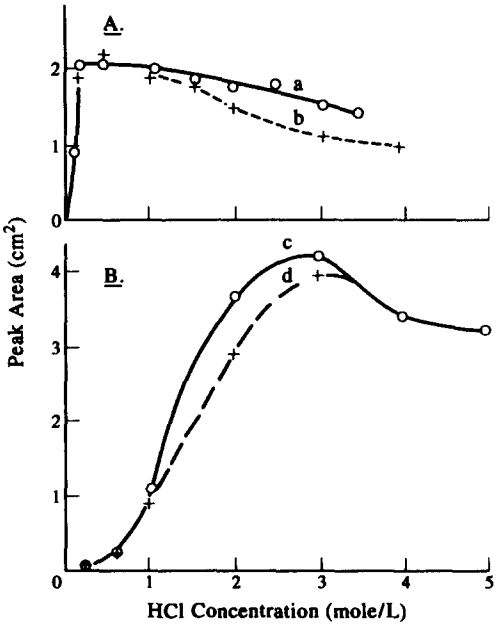


Fig. 2. Effect of HCl concentration and the addition of hydrazine on the DPASV peak areas. $E_d$ −500 mV; deposition time 1 sec; curves (a), (c), symbol o, hydrazine added; curves (b), (d), symbol +, hydrazine absent. (A) Sb (III), 1 $\mu M$ KSbT; recorder setting 20 nA FSD. (B) Sb (V), 50 $\mu M$ $KSb(OH)_6$; recorder setting 500 nA FSD.

The addition of HCl to the $Sb_2O_3$ solutions would have favoured formation of the cation $SbO^+$ (reaction 2), and this transformation was probably near complete at acid levels >0.2*M* (*cf.* plateau region, Fig. 2A). With Sb (V) systems, addition of HCl at levels >0.3*M* was required to achieve a gradual change of the $Sb(OH)_6^-$ ion into a more electro-active species (*cf.* Fig. 2B). The observed differences in Sb (III) and (V) behaviour (*e.g.* HCl concentration effect on peak area, Fig. 2) mainly reflect variations in the deposition stage mechanism, because the stripping peak potential values for Sb (III) and Sb (V) were similar, over a wide range of acid molarity values (*cf.* Fig. 3). It has been concluded that in the stripping cycle, chloro-complexes of similar nature were formed.

The possibility of Sb (IV) species formation during the electro-analytical cycle has been raised in an earlier article.[11] In the deposition stage this could involve processes such as slow oxidation of Sb (III) at the Pt counter electrode and partial (one electron) reduction of Sb (V) compounds. During the anodic stripping stage, oxidation of deposited Sb metal might proceed beyond the Sb (III) state. The Sb (IV) valence state is known[14] to form sparingly soluble compounds, hence formation of this intermediate in the DPASV cycle could result in removal

of some Sb from solution, possibly as partial coatings on the electrodes. It was reported[11] that effects attributed to Sb (IV) could be eliminated by adding hydrazine to the base solutions.

In our investigations, the addition of hydrazine hydrochloride (0.1*M*) to test solutions led to some marginal increases in peak area and slightly sharper peaks, but there were no significant changes in peak potential values. The addition of hydrazine did not promote chemical reduction of Sb (V) [*i.e.* $KSb(OH)_6$] to Sb (III) species. The hydrazine probably acts as a depolarising agent in the electrochemical process, rather than as a chemical reductant.

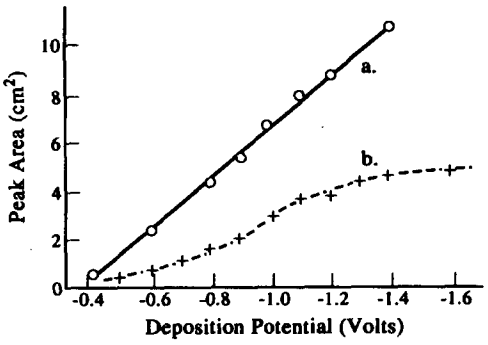


Fig. 4. Graph of effect of deposition potential on peak area values, in acetate buffer solutions. (a) 8 $\mu M$ $Sb(OH)_3$, recorder setting 20 nA FSD; (b) 50 $\mu M$ KSbT, 200 nA FSD.

*Determination of* Sb (III) *in an acetate buffer solution*

No ASV peak assignable to Sb was observed when Sb (V) solutions (50 $\mu M$) were subjected to DPASV analysis, using acetate buffer support solutions. Deposition times ranging from 1 to 360 seconds were examined, and three deposition potentials (−300, −500 and −1100 mV) were used. The scan tracing was the same in the presence, or absence, of hydrazine dihydrochloride. One can, therefore, use an acetate base solution to detect Sb (III) in the presence of pentavalent Sb salts.

For the determination of Sb (III), however, the experimental conditions have to be carefully controlled. It was found, for example, that the area of the Sb peak(s) increased steadily as the negativity of the HMDE was increased from −400 to −1400 mV (as shown on Fig. 4). This suggests that the Sb species present do not dissociate readily under the influence of an applied potential. The shape of the Sb peak also varied. Multiple peaks were found on many of the DPASV traces, *e.g.* applying a potential of −400 mV to buffer solutions containing Sb tartrate yielded two peaks of near equal size (at $E_p$ values of −320 and −270 mV). Using more negative deposition potentials, the −320 mV peak shifted in an anodic direction and the other peak moved in a cathodic direction. Total overlap (*i.e.* a broad symmetrical peak) occurred when deposition potentials of −900 to −1100 mV were used (*cf.* Fig. 5A, curves a–c).

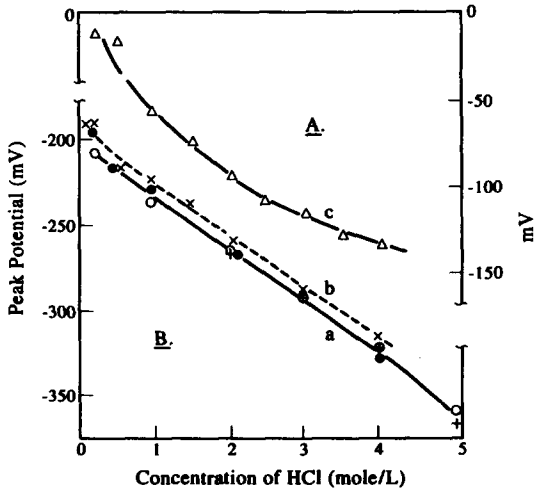


Fig. 3. Effect of HCl concentration on peak potential values. (A) 'acid systems' peaks, curve (c). (B) Antimony peaks. Curve (a) Sb (V): 50 $\mu M$ $KSb(OH)_6$; $E_d$ −500 mV, recorder setting 500 nA FSD, point symbols ○ (closed for hydrazine present). Curve (b) Sb (III): 1 $\mu M$ KSbT; $E_d$ −500 mV, recorder setting, 20 nA FSD; point symbol + (or ×, hydrazine present).

Using longer deposition times did not increase the sensitivity of the procedure proportionally (*cf.* Fig. 5A, curves g–i). Gains in signal size were offset by reduced symmetry of the signals and the appearance of peaks assignable to impurities in the acetate buffer solution (observed when using deposition times >40 secs). One of these impurity peaks ($E_p$ around −300 mV) was not resolved from the Sb peak.

After examining the effect of different variables on the symmetry of Sb peaks (*cf.* Fig. 5A) it was concluded that the optimum operating conditions for quantitative studies would be a deposition potential of −1100 mV applied for one second. Using these conditions, the height (or area) of peaks arising from Sb (III) species was found to be directly related to the concentration present. The detection limit was around 600 n$M$ (10 nA FSD), so the levels of Sb in test solutions should be >1 $\mu M$.

*Determination of* Sb (III) *and* Sb (V) *in* HCl *solutions*

(a) *Effect of* HCl *concentration on DPASV response.* In a previous study[11] of the DPASV responses of Sb (III) and Sb (V) it was found that the size of Sb (III) peaks nearly doubled in size when the level of HCl in the base solution was increased from 0.1 to 1*M*, but little further change in area occurred when the acid level was increased from 1 to 5*M*. Antimony (V) solutions, on the other hand, yielded barely detectable peaks at acidities less than 1*M*; at higher molarities the size of the Sb (V) peaks increased as the level of acid present increased. It was proposed that Sb (III) present in mixtures could be determined using dilute acid (*e.g.* 0.5*M*) support solutions, while for the determination of total Sb contents, a base solution 4*M* in HCl was recommended.

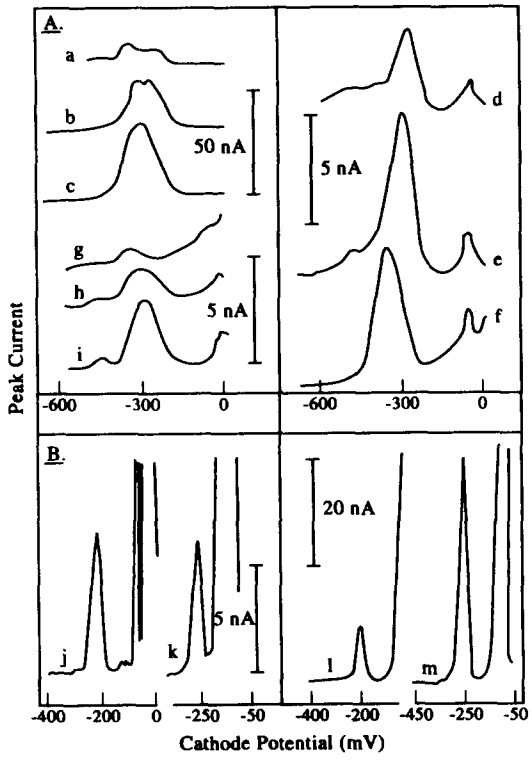


Fig. 5. (A) Typical DPASV curves for Sb (III) in acetate buffer base solution. Effect of deposition potential; Curves (a)–(c), 50 $\mu M$ KSbT; deposition time 1 sec; recorder setting 200 nA FSD. (a) $E_d$ −500 mV, (b) $E_d$ −800 mV, (c) $E_d$ −1.10 V. Curves (d) and (e), 8 $\mu M$ $Sb(OH)_3$; deposition time 1 sec, recorder 20 nA FSD. (d) $E_d$ −600 mV, (e) $E_d$ −900 mV. Curve (f), 10 $\mu M$ KSbT, 0.1*M* in hydrazine; $E_d$ −1.10 V, deposition time 1 sec, recorder 20 nA FSD. Effect of deposition time; curves (g)–(i) 1 $\mu M$ $Sb(OH)_3$, $E_d$ −1.1 V, recorder, 20 nA FSD. (g) 1 sec, (h) 40 sec, (i) 120 sec. (B) Typical DPASV curves for Sb (III) and Sb (V) in hydrochloric acid base solutions. Curves (j) and (k), 1 $\mu M$ Sb (III), $E_d$ −400 mV, deposition time 1 sec, recorder setting 20 nA FSD, in HCl of molarity 0.2 (j) or 1.0. (k) 1.0. Curves (l) and (m), 50 $\mu M$ Sb (V); $E_d$ −500 mV, deposition time 1 sec; recorder setting 50 nA FSD, in acid of molarity 1.0 (l) or 2.0 (m).

Inconsistent responses were obtained when the procedure was applied (in more recent times) to solutions containing the two valency states of Sb. In a bid to identify the problem areas, all aspects of the method were re-examined. Our study, using different instrumental parameters, confirmed that the size of Sb (III) and (V) stripping peaks varied with the molarity of HCl present in the test solutions (*cf.* Fig. 2), but transition point values differed from those previously reported. For example, with Sb (III) solutions, large variations in peak size were restricted to the <0.2*M* HCl region and optimum Sb (III) response occurred in 0.2 to 2*M* acid solutions. The plateau region shown on Fig. 2A had a slight downward slope but this trend had little significance because in calibration plot studies, Sb response in 2*M* acid was marginally larger than in 0.2*M* HCl. In the case of Sb (V) systems, small peaks were observed in 0.5*M* HCl, and size increased with increasing acid molarity until maximum values were reached in solutions 3*M* in acid (*cf.* Fig. 2B). No decline in peak size at higher HCl levels was observed when the Sb (V) concentration was less than 50 $\mu M$. Typical DPASV traces are shown on Fig. 5.

With acid molarities >3*M*, the Sb signal was partially overlapped by the side wing of a large, broad 'system' peak (tentatively attributed to the formation of Hg(II) chlorospecies). Decreasing the molarity of acid present reduced the system peak size (*e.g.* from a peak height of 110 mm in 4*M*, to 5 mm in 0.2*M* HCl), and changed the peak position (*cf.* Fig. 3c). At acid levels less than 3*M*, overlap with the Sb peak became minimal.

Impurities were not a problem when 'Volucon' acid ampules or high purity HCl (*e.g.* B.D.H. 'Aristar' brand) were used to prepare the base solutions, but the A.R. acid used in our study contained a small of impurity (presumably Bi) which had a peak $E_p$ value similar to that of Sb. Correction for this element (via base solution blanks) was most important when analysing solutions containing low levels of Sb (*e.g.* 0.1 $\mu M$). The detection limit for Sb (III) (in 1*M* HCl, using an FSD value of 10 nA) was around 10 nM (*i.e.* 1 $\mu$g/l).

When single valency Sb solutions were repeatedly scanned (or replicates were

analysed), consistent peak area values were usually obtained. The precision of the procedure (expressed as a relative standard deviation) was found to vary with the type of Sb (III) solution being examined. For example, using KSbT standard solutions the RSD value was $\pm 2\%$, with $Sb(OH)_3$ solutions, the RSD value was $\pm 3$–$10\%$.

(b) *Analysis of solutions containing* Sb (III) *and* Sb (V). From the results summarized on Fig. 2 it was concluded that specific determination of the amount of Sb (III) present could be achieved by adjusting aliquots to an acidity level of 0.2 or 0.5*M* HCl. With acid levels $> 1M$, both valency states contribute to the total signal, and for determination of Sb (III) plus Sb (V) values, adjustment of the test solutions to an HCl level of 2.0*M* was selected. [Sb (V) response at this acidity level was less than achieved at higher molarities but the Sb peaks were clearly resolved from any 'acid system' peak]. Since the signal contribution from Sb (III) species varied little with increasing acidity (*cf.* Fig. 2A), any increase in peak area observed using the 2*M* acid solutions could be assigned to the Sb (V) content. Reference to an Sb (V) calibration plot (for the acidity level used) then allows one to convert the difference in peak areas to concentration values.

For this procedure to yield valid results in mixture studies, interaction between the two Sb valency states in acidified solutions must be minimal, and the presence of the second valency state must not alter DPASV response. To test if these conditions were met, synthetic mixtures containing Sb (III) and Sb (V) were prepared, and analysed by DPASV. In the absence of side reactions, the size of the peaks for the various mixtures should match the values obtained by adding together areas which correspond to the concentration of each component in the mixture [as derived from calibration curves prepared for both Sb (III) and Sb (V)].

In one series of studies, the mixtures examined had acid levels adjusted to values ranging from 0.2 to 3.0*M*, and contained equal concentrations of Sb (III) and Sb (V). The concentration of each valency state in the mixtures ranged from 0.8 and 6 $\mu M$. As shown on Fig. 6, the peak sizes varied with acid molarity, and for each level of total Sb content, two plateau regions are discernible on the plots. The first extends from 0.2 to 0.5*M* [contribution of Sb (III) only] and the second embraces the 2 to 3*M* HCl region. These results confirmed that

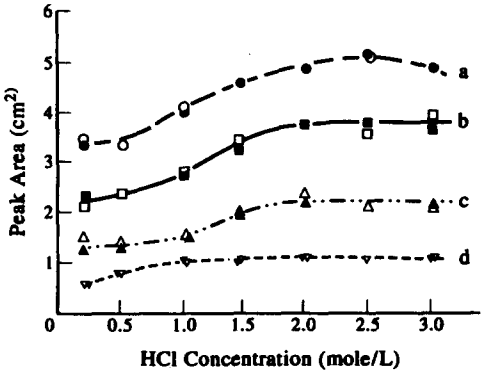


Fig. 6. Effect of acid molarity and amount of antimony present, on the size of the DPASV peak obtained on analysing 1:1 Sb (III), Sb (V) mixtures. Concentration of Sb (III) [and Sb (V)] in the mixtures was (a) 6 $\mu M$, (b) 4 $\mu M$, (c) 2 $\mu M$ (d) 1 $\mu M$. Closed symbol points, mixtures acidified just prior to analysis; Open symbol points, mixtures prepared from antimony standards stored in HCl of different strengths.

analysis in 2*M* HCl was suitable for determining the Sb (V) contribution. Many of the experimental peak area values were higher than 'expected' mixture responses (*i.e.* the sum of calibration curve values for each component), but an equal number were lower. This behaviour suggested that under some conditions the degree of Sb (V) reduction was being enhanced by the presence of Sb (III), while in other conditions Sb was being lost from solution.

In a bid to identify the factors responsible for the varied response, new series of mixtures were prepared. The amount of Sb (III) introduced was again varied between 0.8 and 6 $\mu M$, while the amount of $KSb(OH)_6$ added was adjusted to give mixtures in which the ratios of Sb (III) to Sb (V) were 5:1; 2:1; 1:1; 1:2 and 1:5. These mixtures were analysed by DPASV after adjusting the HCl level to 0.2 or 2.0*M*.

Using test solutions 0.2*M* in HCl [*i.e.* ostensibly determining Sb (III) only] mixture peak areas matched the corresponding points on the Sb (III) calibration plot when the ratio of Sb (III) to Sb (V) in the mixture was 2:1, 1:1 or 1:2. With a marked excess of Sb (III) present (*i.e.* 5:1), the mixture signals were 10% lower (5% if hydrazine added) than the peak areas expected from the Sb (III) calibration plot. This behaviour was attributed to chemical interaction between the valency states, leading to the formation of a small amount of non-reducible (maybe insoluble) Sb species. With excess Sb (V) present [*i.e.* 1:5 mixtures, 4–30 $\mu M$ in

$KSb(OH)_6$], the measured peak areas were about 10% higher than Sb (III) calibration curve values. This behaviour was provisionally attributed to catalysed reduction of some Sb (V) (*e.g.* by Sb/Hg) when the level of this valency state was $>4\ \mu M$. Alternatively, some (or all) of the variance in the mixture analysis results could be assigned to experimental error. The RSD values for the peak area measurements were (on average) larger than those obtained using single valency solutions (with about one fifth having RSD values falling in the 10–15% range).

The results obtained using mixtures $2M$ in HCl are summarized on Fig. 7. One third of the peak area values 'matched' (*i.e.* within $\pm 4\%$)

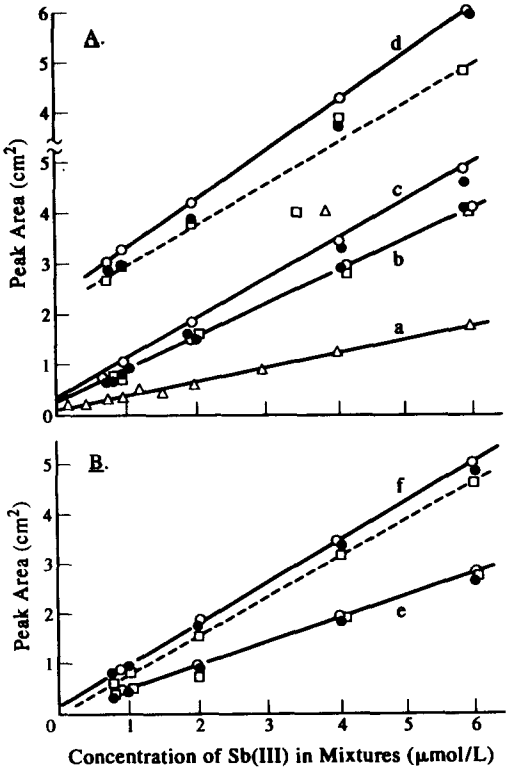


Fig. 7. Effect of Sb concentration on DPASV peak areas, in the presence of $2M$ HCl and differing ratios of Sb (III) and Sb (V). Segment A. Recorder FSD 50 nA; Segment B. FSD 200 nA. System codes: (a) antimony (V) standard solutions, (b) antimony (III) standard solutions, (c) to (e) Sb (III)/Sb (V) mixtures with content ratios of (c) 2:1, (d) 5:1, (e) 1:2 and (f) 1:5. Calibration curves for the different systems are indicated by full lines, and open circle (○) symbols. (For mixtures, calibration point values obtained by adding appropriate areas, drawn from curves (a) and (b), for the concentrations of Sb (III) and Sb (V) present. Experimental peak areas for mixed valency systems which were made $2M$ in HCl just prior to analysis are shown as closed circle (●) points. In another series the mixtures were stored in $2M$ HCl prior to analysis (symbol code □), yielding trends indicated by dashed lines.

the values obtained by addition of $2M$ HCl calibration curve readings [for each specified level of Sb (III) and Sb (V) in the mixture]. Another third of the test solutions yielded results which were 5–10% lower than the calculated value; and the final third [involving mainly mixtures with low Sb (III) contents, *i.e.* 0.8 or 1.0 $\mu M$] had analytical values 15–20% lower than expected (*cf.* closed circles, Fig. 7). The predominance of 'smaller than predicted' peak areas has been attributed to calibration error and/or chemical interactions. The combining of single valency calibration plot points (to yield 'expected' response values) may have led to overestimation of the 'baseline' contribution to mixture signals. [As noted earlier, the intercept value for Sb (V) calibration lines (in $2M$ HCl) was double that found for Sb (III)]. The main cause of smaller DPASV peaks, however, was considered to be formation of an 'ASV inert' Sb species, via a reaction enhanced by the presence of the higher level of acid.

This chemical reaction appears to be a slow process and may only involve one valency state. Peaks 15–30% smaller than expected (*cf.* Fig. 7, dashed lines) were obtained when mixtures (valency ratios 5:1, 2:1 and 1:1) were prepared from Sb (III) and Sb (V) standard solutions which were made $2M$ in HCl several days before being admixed. With an excess of Sb (V) present, the difference between predicted and actual signal size was less (*e.g.* with a valency ratio of 1:5, the values were circa 10% smaller, *cf.* Fig. 7, dashed line f; with mixtures having a valency ratio of 1:2, the analytical results all fell within $\pm 5\%$ of the expected value).

When mixtures were prepared from Sb (III) and Sb (V) standard solutions which were $0.2M$ in HCl, variable DPASV responses were observed. Using 5:1 mixtures, the peaks matched (in size) those obtained using the Sb (III) calibration value. With lower proportions of Sb (III) in the mixture over half of the experimental values deviated from the 'expected' area, with a third being 15–20% higher, and about one fifth lower than expected. The largest deviation (15–20% lower) was found using 1:5 systems.

## CONCLUSIONS

While it is possible to determine both Sb (III) and Sb (V) present in mixtures by control of analyte acidity levels, the speciation data derived from the DPASV studies needs to be

interpreted cautiously, because the accuracy of the analyses can be reduced by secondary chemical processes. For some types of mixtures the values for Sb (III) and Sb (V) may be in error by $\pm 20\%$ of the Sb content, but in most mixture analyses the relative variations should be better than $\pm 10\%$. This error could be reduced by using a two stage calibration procedure (*i.e.* after using single valency calibration plots to obtain the approximate composition of the mixtures, standard mixtures of like composition could be prepared and analysed for both species).

Analytical errors may have less significance when dealing with routine samples (*e.g.* collected from the environment) since preliminary sample treatments can modify the distribution of Sb between valency states. For example, with moist solids, interactions may occur during storage or drying steps. Release of the Sb species from the solids by hot acid extraction, or stabilisation of water samples by adding acid, could also be accompanied by chemical changes (some of which may partially reverse when acid levels are adjusted prior to DPASV analysis).

*Acknowledgements*—This project has received financial support from the Australian Research Committee, and their sponsorship is gratefully acknowledged.

## REFERENCES

1. R. W. Boyle and I. R. Jonasson, *J. Geochem. Explor.* 1973, **2,** 251.
2. S. Ghoda, *Bull. Chem. Soc. Jpn.* 1975, **48,** 1213.
3. R. C. Ragaini, H. R. Ralson, and N. Roberts, *Environ. Sci. Technol.* 1977, **11,** 773.
4. E. A. Crecelius, M. H. Bothner and R. Carpenter, *Environ. Sci. Technol.* 1975, **9,** 325.
5. J. C. Van Loon and E. J. Brooker, *Anal. Letters* 1974, **7,** 505.
6. Y. Yamamoto and T. Kumamaru, *Z. Anal. Chem.* 1976, **281,** 353.
7. S. Nakashima, *Analyst* 1980, **105,** 732.
8. M. Yamamoto, K. Urata and Y. Yamamoto, *Anal. Letters* 1981, **14,** 21.
9. B. Mohammad, A. M. Ure, J. Reglinski and D. Littlejohn, *Chem. Spec. Bioavailabil.* 1990, **3,** 117.
10. N. Ainsworth, J. A. Cooke and M. S. Johnson, *Environ. Pollut.* 1990, **65,** 75.
11. G. E. Batley and T. M. Florence, *Electroanal. Chem. Interfacial Electrochem.* 1974, **55,** 23.
12. P. Thanabalasingam and W. F. Pickering, *Water, Air Soil Pollut.* 1989, **49,** 175.
13. K. H. Gayer and A. B. Garett, *J. Amer. Chem. Soc.* 1952, **74,** 2352.
14. M. G. Tamba and N. Vantini, *Analyst* 1972, **97,** 542.

Pergamon

0039-9140(94)00193-6

*Talanta*, Vol. 42, No. 2, pp. 205–210, 1995

0039-9140/95 $9.50 + 0.00

# THE APPLICATION OF PRINCIPAL COMPONENT REGRESSION ON SIMULTANEOUS MULTICOMPONENT DETERMINATIONS THROUGH A SINGLE CATALYTIC KINETIC RUN

ZHI-CHENG GU* and XIAN DE WANG†

Department of Chemistry, Tongji University, Shanghai 200092, China

(*Received* 27 *January* 1994. *Revised* 3 *June* 1994. *Accepted* 13 *June* 1994)

**Summary**—The kinetic behaviors of Cr(VI) and W(VI), which catalyze a common indicator reaction between $H_2O_2$ and $I^-$, were studied. A new concept, 'Rate Spectrum', is proposed. The two catalysts can be determined simultaneously by analyzing the rate spectra of their mixtures as the rate spectra of each catalyst are linearly independent. Principal Component Regression (PCR) was used to analyze the rate spectra of the mixtures of Cr and W, and in this way the two ions were determined simultaneously through a single kinetic run.

Only a few methods have been proposed to determine catalysts simultaneously through a single kinetic run. Pardue has developed a method for the determination of isoenzymes based on differences in the rate of inhibition.[1] Bromide and iodide were determined simultaneously, using the very large difference in their reaction rate.[2] Nitrite and iodide,[3] Cr(VI) and Fe(III)[4] were determined simultaneously based on their different properties. A method for the simultaneous determination of Ru and Os, based on the difference in the order of the indicator reaction, was carried out recently with multilinear regression.[5] When this method is used, it is necessary that the apparent reaction order for each catalyst is kept constant during the reaction. However, this is not always the case. In order to find a more general method, we studied the application of other chemometrics methods, such as principal component regression (PCR), on the catalytic kinetics. In this paper Cr and W, which catalyze the reaction between $H_2O_2$ and $I^-$,[6,7] were used as an example to investigate the characteristics of applying PCR to simultaneous multicomponent determinations through a single kinetic run. PCR has been used in many cases to resolve spectra of mixtures in chromatography,[8] mass spectrometry[9] and spectrophotometry.[10] The application of PCR in multivariate calibration is more effective than MLR.

## THEORY

A catalyzed indicator reaction can be written as:

$$a\mathrm{A} + b\mathrm{B} \rightarrow x\mathrm{X} + y\mathrm{Y}$$

and its reaction rate equation is:

$$v_i = -\mathrm{d}[\mathrm{A}]/\mathrm{d}t = \mathrm{d}[\mathrm{X}]/\mathrm{d}t = k_i[\mathrm{A}]^{p_i}[\mathrm{B}]^{q_i}[\mathrm{C}_i]. \quad (1)$$

According to stoichiometric relationships:

$$[\mathrm{B}] = [\mathrm{B}]_0 - (b/a)([\mathrm{A}]_0 - [\mathrm{A}]), \quad (2)$$

where $[\mathrm{B}]_0$ and $[\mathrm{A}]_0$ are the initial concentration of B and A, respectively. Substituting equation (2) into equation (1), we have:

$$v_i = k_i[\mathrm{C}_i][\mathrm{A}]^{p_i}\{[\mathrm{B}]_0 - (b/a)([\mathrm{A}]_0 - [\mathrm{A}])\}^{q_i}. \quad (3)$$

For simplification, an approximate equation is used:[11]

$$[\mathrm{B}]^q = \{[\mathrm{B}]_0 - (b/a)([\mathrm{A}]_0 - [\mathrm{A}])\}^q = T[\mathrm{A}]^{p''}$$

and equation (3) becomes:

$$v_i = k_i''[\mathrm{A}]^{p_i'}[\mathrm{C}_i] = f_i[\mathrm{C}_i], \quad (4a)$$

where

$$k_i'' = k_i T,\ p_i' = p_i + p_i',\ \text{and}\ f_i = k_i''[\mathrm{A}]^{p_i'}.$$

Since $k_i''$ is constant under the experimental conditions and $p_i'$ varies with the concentration of A, $f_i$ is the function of concentration of

*Author to whom correspondence should be addressed.

†Present address: Department of Research & Development, Shanghai Jawa Complex, Shanghai 200080, China.

indicator substance A. This is also the case when the product (X or Y) is used as indicator substance, owing to the following relationships:

$$[X] = (x/a)([A]_0 - [A]). \quad (5)$$

A comparison with spectrophotometry is given in the following:
According to Beer's law:

$$A' = \epsilon bC. \quad (6)$$

The absorbance for a mixture of $n$ components is additive. Let $A = A'/b$, we have:

$$A = \Sigma \epsilon_i C_i, \quad (7)$$

where $\epsilon$ can be described as a function of wavelength $\lambda$. While a plot of $A$ *vs.* $\lambda$ is defined as spectrum the simultaneous multicomponent determinations can be carried out when their spectra are linearly independent. Similarly, in catalytic kinetics, when $n$ components behave independently, the reaction rates are additive and equation (4) may be written as:

$$v = \Sigma f_i[c_i]. \quad (8)$$

Compared with equation (7), $f_i$ in equation (8) corresponds to $\epsilon_i$ in equation (7) and concentration of A corresponds to the wavelength. Consequently, the plot of $v$ *vs.* [A] corresponds to the spectrum. We define the plot of $v$ *vs.* [A] as a rate spectrum, and the simultaneous multicomponent determinations by catalytic kinetics can be carried out when the rate spectrum of each component is linearly independent.

When $m$ reaction rate data $v_j$ at $m$ different concentrations of A for each sample are collected, a rate matrix $[v]_{m \times l}$ can be set up, where $j = 1, \ldots, m$, $l$ is the number of samples. And the concentration of the catalysts can be solved from the rate matrix by PCR, as described by Kowalski.[12]

## EXPERIMENTAL

### *Apparatus*

An F7230 spectrophotometer equipped with a thermostat and an IBM personal computer were used.

### *Reagent*

Solutions of 3.0$M$ $H_2O_2$ and 0.1$M$ KI were prepared weekly and diluted freshly before use.

Solutions of 100 $\mu$g/ml Cr and 100 $\mu$g/ml W were prepared and diluted before use.

All the chemicals used were of analytical reagent grade. Redistilled water was used.

### *Procedures*

A suitable portion of KI solution was mixed with sample solution containing Cr and W and diluted to 25 ml with water (solution A).

Solutions of $H_2O_2$, $H_2SO_4$ and starch were mixed to the required concentration (solution B).

After being thermostatted at 20°C for more than half an hour, solutions A and B were mixed in a proportion of 1:2 in a cell as quickly as possible. The absorbance change with time was measured at 580 nm against water. The absorbance at intervals of 10 sec was recorded automatically.

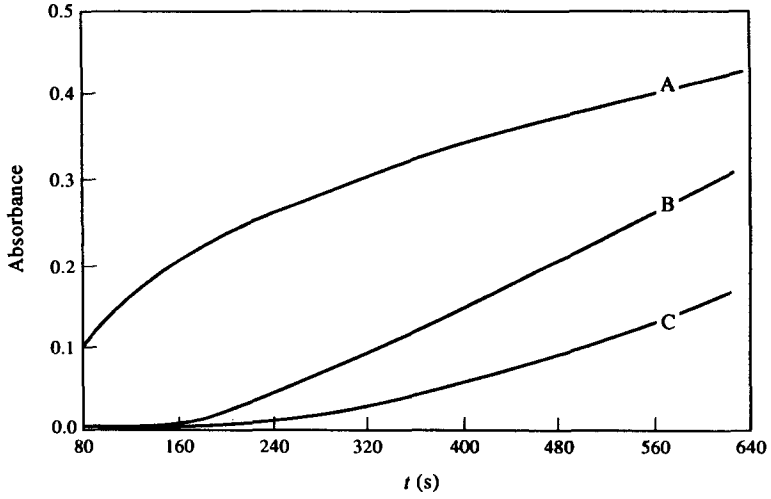


Fig. 1. Absorbance–time curves. $[H_2O_2] = 2.4 \times 10^{-2}$, $[KI] = 6 \times 10^{-4}$, $[H_2SO_4] = 2.7 \times 10^{-2}M$. (A) $[Cr] = 6.41 \times 10^{-6}M$; (B) $[W] = 1.81 \times 10^{-7}M$; (C) blank.

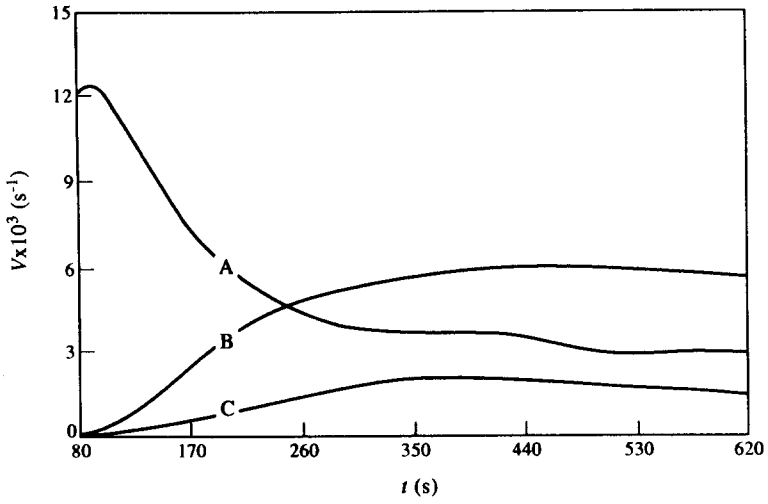


Fig. 2. Reaction rate–time curves. $[H_2O_2] = 2.4 \times 10^{-2}$, $[KI] = 6 \times 10^{-4}$, $[H_2SO_4] = 2.7 \times 10^{-2}M$. (A) $[Cr] = 6.41 \times 10^{-6}M$; (B) $[W] = 1.81 \times 10^{-7}M$; (C) blank.

*Data processing*

The reaction rate $v$ was calculated by the Savitzky–Golay method[13] from the plot of $A$ *vs.* $t$. Based on Beer's law, the absorbance $A$ was used in equation (5) instead of [X]. As described in Ref. 11, the 11 points smooth curve of the second order polynomial were used to derive the first-order derivative, *i.e.* $v$. The rate spectrum was calculated from the plot of $A$ *vs.* $t$ and the plot of $v$ *vs.* $t$. The data of rate matrix was obtained from the plot of $v$ *vs.* $A$ by using the method of linear interpolation. Principal component regression was calculated by PCRRATE program prepared by our laboratory using PASCAL.

## RESULTS AND DISCUSSION

*The possibility of simultaneous determination of Cr and W*

The plot of absorbance $A$ *vs.* time $t$ and reaction rate $v$ *vs.* $t$ are shown in Figs 1 and 2, respectively. The plot of $v$ *vs.* $A$ (the rate spectrum), which is calculated from Figs 1 and 2, is shown in Fig. 3. Obviously the curve B, which is calculated from C and D, is almost overlapped with the experimental one (curve A). It supports the additive assumption, at least under the experimental conditions, and the interaction of the two catalysts can be neglected. The patterns of the curve C and D are quite

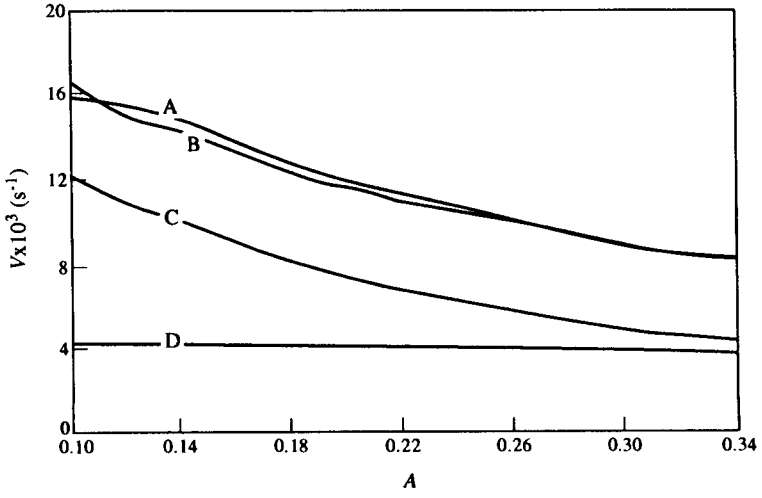


Fig. 3. Rate spectra of the catalyzed reaction. $[H_2O_2] = 2.4 \times 10^{-2}$, $[KI] = 6 \times 10^{-4}$, $[H_2SO_4] = 2.7 \times 10^{-2}M$. (A) $Cr(6.41 \times 10^{-6}M) + W(1.81 \times 10^{-7}M)$; (B) C + D; (C) $[Cr] = 6.41 \times 10^{-6}M$; (D) $[W] = 1.81 \times 10^{-7}M$.

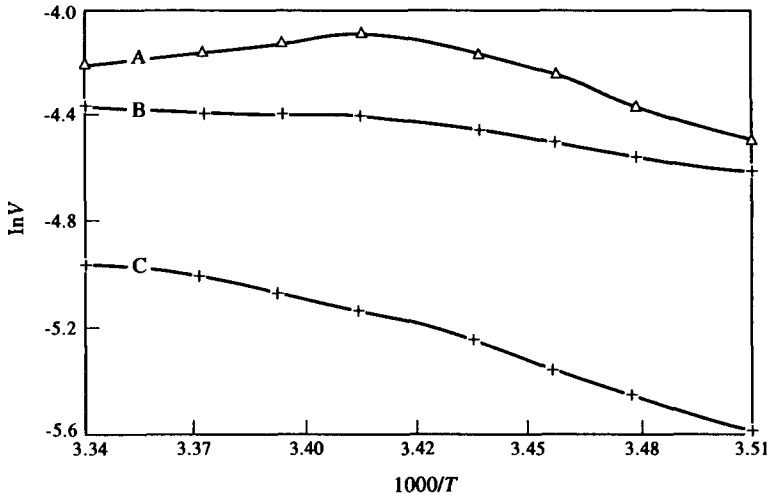


Fig. 4. Active energy curve of the reaction. $[H_2O_2] = 2.4 \times 10^{-2}$, $[KI] = 6 \times 10^{-4}$, $[H_2SO_4] = 2.7 \times 10^{-2}M$. (A) $[Cr] = 6.41 \times 10^{-6}M$; (B) $[W] = 1.81 \times 10^{-7}M$; (C) blank.

different. It suggests that the simultaneous determination of these two catalysts is possible.

*Reaction condition*

The maximum absorption was at 580 nm, so 580 nm is specified as the measuring wavelength in the procedure. The concentration of starch is specified at 0.02%. If the concentration of starch is too high, the blue $I_2$–starch compound will segregate during measuring, and the blank will increase. On the other hand, the sensitivity decreases with decreasing concentration of starch. The effect of temperature on the reaction rate is shown in Fig. 4, 20°C is specified in the procedure.

The rate of W-catalyzed reaction was almost unchanged with $A$ (Fig. 3), while the rate of Cr-catalyzed reaction decreased with the increase of $A$ at the start, and the reaction proceeded with a constant rate after a certain time. This means the kinetic behaviors of W-catalyzed and Cr-catalyzed reaction are different only in the initial period of the reaction. It has also been found that although the rate of the W-catalyzed and the blank reaction varied with the concentration of $H_2SO_4$, $H_2O_2$ and $I^-$, the slope of the plot of $v$ *vs.* $A$ remained unchanged. On the other hand, of the Cr-catalyzed reaction, both the rate and the slope of the plot of $v$ *vs.* $A$ varied with the concentration of $H_2SO_4$, $H_2O_2$ and $I^-$. The plot of $v$ *vs.* $A$ in different reactant ratios is shown in Fig. 5. It shows that the larger $[KI]/[H_2O_2]$ is, the longer the time is in which the reaction rate changed. Obviously the

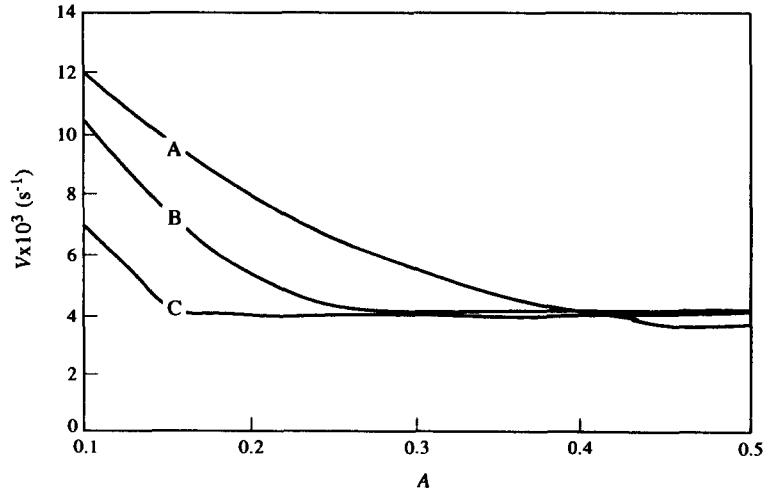


Fig. 5. Rate spectra of Cr-catalyzed reaction at different initial concentration ratios. $[Cr] = 6.41 \times 10^{-6}M$, $[H_2SO_4] = 7 \times 10^{-8}M$. (A) $[H_2O_2]$: $[KI] = 8:15$; (B) $[H_2O_2]$: $[KI] = 8:3$; (C) $[H_2O_2]$: $[KI] = 8:1$.

Table 1. Concentration of simulated catalysts solution

| | | | | | |
|---|---|---|---|---|---|
| $c_1 \times 10^7 (M)$ | 1 | 2 | 3 | 4 | 5 |
| $c_2 \times 10^7 (M)$ | 5 | 4 | 3 | 2 | 1 |

Table 2. Results of PCR on simulated data

| $c_1 \times 10^7 (M)$ | | | $c_2 \times 10^7 (M)$ | | |
|---|---|---|---|---|---|
| Added | Found | %$E$ | Added | Found | %$E$ |
| 5 | 5.045 | 0.9 | 1 | 0.093 | −0.7 |
| 4 | 3.988 | −0.3 | 2 | 2.004 | 0.2 |
| 3 | 2.988 | −0.4 | 3 | 3.009 | 0.3 |
| 2 | 1.996 | −0.2 | 4 | 4.008 | 0.2 |
| 1 | 1.009 | 0.9 | 5 | 4.965 | −0.7 |

behavior of the kinetics of Cr and W are different only in the range of time in which the Cr-catalyzed reaction rate changed. So it is favorable to choose the reactant with high $[I^-]/[H_2O_2]$. The length of time in which the reaction rate changed increased with decreasing concentration of $H_2SO_4$, so a low concentration of $H_2SO_4$ seems feasible. However, it is preferable to choose a suitable reaction rate, neither too fast nor too slow. Thus $7 \times 10^{-8}$, $4 \times 10^{-4}$ and $1.5 \times 10^{-8} M$, $H_2SO_4$, $H_2O_2$ and KI, respectively, are specified in the procedure.

*The rate spectrum range for calculations*

The data from $A = 0.1$–$0.34$ was used for calculations. The kinetic behavior of Cr- and W-catalyzed reaction was not additive in the range $A < 0.1$, because the induction time of W-catalyzed reaction was shortened when Cr was present. The difference in their kinetic behavior decreased with increasing $A$. In the range $A > 0.34$ the difference becomes indistinct.

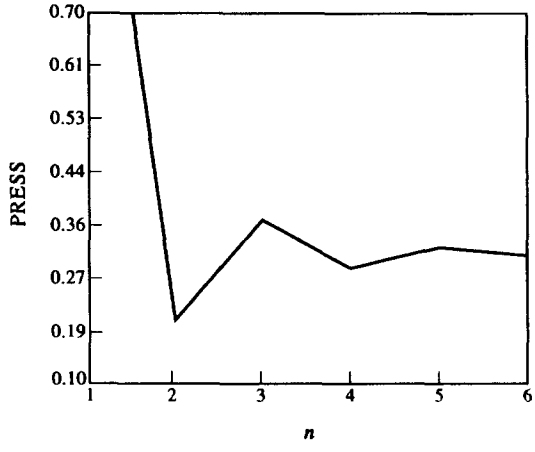


Fig. 6. Dependence of PRESS on number of principal components.

*Error caused by calculation*

The error due to calculation was investigated by computer simulation. Suppose the catalytic effect of the two catalysts $c_1$ and $c_2$ are additive, and the absorbance $A$ is used instead of the concentration of reactant, the rate equation of the mixture can be written as:

$$-dA/dt = k_{11} c_1 A (k_{12} + A) + k_{21} c_2 (A + k_{22}) + k_0, \quad (9)$$

where $k_{11}, k_{12}, k_{21}, k_{22}$ and $k_0$ are constants. After integrating we have $A = f(t, c_1, c_2)$.

Synthetic data sets were obtained using equation (4) and the values of $c_1$, $c_2$ are given in Table 1, $\Delta t = 10$ sec. A set of $A$ at different times was obtained, and the plot of $A$ *vs.* $t$ was set up. Then the rate spectrum and the PCR were calculated by the methods described in data processing. The results are shown in

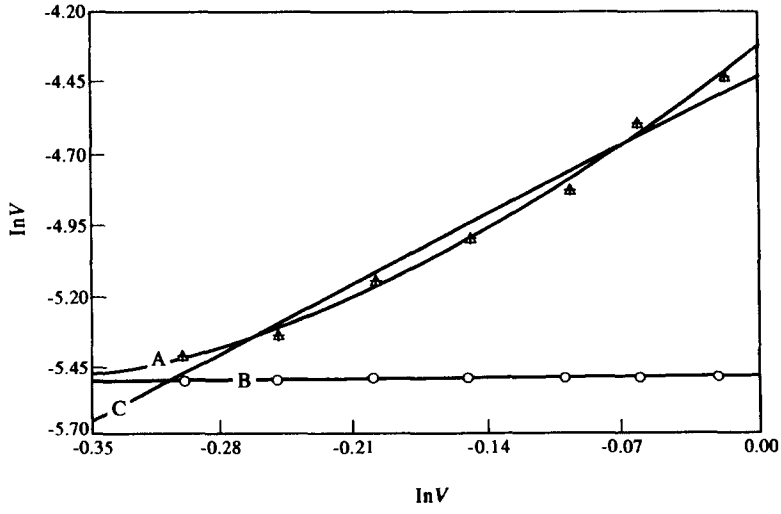


Fig. 7. ln $t$–ln $A$ relationship curves. (A) Cr; (B) W; (C) linear fit of A.

Table 3. Analysis of mixtures of Cr and W with PCR and MLR

| [Cr] × $10^6$ ($M$) | | | | | [W] × $10^7$ ($M$) | | | | |
|---|---|---|---|---|---|---|---|---|---|
| | PCR | | MLR | | | PCR | | MLR | |
| Added | Found | %E | Found | %E | Added | Found | %E | Found | %E |
| 4.17 | 4.58 | 9.8 | 4.86 | 16.5 | 4.53 | 4.30 | −5.1 | 4.08 | −9.9 |
| 5.45 | 5.78 | 6.1 | 6.27 | 15.0 | 4.08 | 3.89 | −4.7 | 3.70 | −8.2 |
| 6.73 | 6.16 | −8.5 | 7.29 | 8.3 | 3.63 | 3.87 | 6.6 | 3.37 | −7.2 |
| 8.01 | 8.40 | 4.9 | 7.95 | −0.7 | 3.17 | 3.09 | −2.5 | 3.28 | 3.5 |
| 9.29 | 9.60 | 3.3 | 8.52 | −8.3 | 2.72 | 2.68 | −1.5 | 3.01 | 10.7 |
| 10.58 | 10.01 | −5.4 | 10.04 | −5.1 | 2.27 | 2.35 | 3.5 | 2.56 | 12.8 |
| 11.86 | 11.15 | −6.0 | 11.47 | −3.3 | 1.81 | 1.67 | −7.7 | 2.02 | 11.6 |
| 13.14 | 13.86 | 5.5 | 12.60 | −4.1 | 1.36 | 1.27 | −6.6 | 1.62 | 19.1 |
| 14.42 | 14.06 | −2.5 | 13.56 | −6.0 | 0.91 | 0.99 | 8.8 | 1.07 | 17.6 |

Table 2. The maximum relative error was 0.9%. Thus the error caused by calculation is small compared with the error derived from the experiment.

*Number of principal components*

The number of the principal component can be obtained by cross-validation. The plot of prediction residual sum of squares (PRESS) *vs.* number of components ($n$) is shown in Fig. 6. $n$ is specified as 2 when PRESS gets to its minimum.

*Comparison of the PCR method with multiple linear regression*

The MLR method was described in detail in Ref. 11. When taking the logarithm, equation (4) becomes:

$$\ln v_i = \ln k_i'' + p_i' \ln[\mathrm{A}] + \ln[\mathrm{C}_i], \qquad (10)$$

$p_i'$ and $k_i''$ can be obtained from the plot of $\ln v_i$ *vs.* ln[A] by calibration with standard solutions of $C_i$. For a two-component mixture,

$$v = \Sigma k_i''[\mathrm{A}]^{p_i'}[\mathrm{C}_i] = \Sigma r_i[\mathrm{A}]^{p_i'}, \qquad (11)$$

$r_1$ and $r_2$ can be obtained by two linear regressions of $v$ *vs.* $[\mathrm{A}]^{p_1}$ and $[\mathrm{A}]^{p_2}$ and $[C_i]$ can be solved from $r_i$ and $k_i''$. The prerequisite condition for using this method (MLR) is that the apparent reaction order for each catalyst should be kept constant during the reaction, because accurate data of the parameters $p_i'$ and $k_i''$ can be obtained only if the plot of $\ln v_i$ *vs.* $\ln A$ is linear. The plot of $\ln v$ *vs.* $\ln A$ of both catalysts is shown in Fig. 7. As shown, the plot of the Cr-catalyzed reaction is nonlinear. The parameters give a large error and, consequently, the error of the simultaneous determination of Cr and W is large. However, this is not the case for PCR. When PCR is used, the concentration of both catalysts can be solved from equation (8) which is based on the rate matrix [V] and can be set up using the reaction rate data $v_j$ at several different concentrations of A for each sample as a vector, just as the absorbance matrix set up by the absorbance data at different $\lambda$ in spectrophotometry. One advantage is that it is not necessary to obtain the exact mathematical form of $v$ as the function of [A] and to obtain the parameters $k_i''$ and $p_i'$ in advance; the other is that it can be used whether the apparent reaction order is kept constant or not. As the apparent reaction order for most catalytic reaction is frequently not constant during the changing of the reactant concentration in the reaction, PCR is more suitable for simultaneous determination in kinetics.

Some synthetic samples were prepared and the data were treated with the PCR and MLR[8] methods. The results of analyses with both methods are listed in Table 3. It can be seen that the error of MLR is larger than that of PCR because the $\ln v/\ln A$ plot of the Cr-catalyzed reaction is not linear.

## REFERENCES


1. W. E. Weiser and H. L. Pardue, *Anal. Chem.*, 1986, **58,** 2523.
2. N. Yonehara, T. Yamane, T. Tomiyasu and H. Sakamoto, *Anal. Sci.*, 1989, **5,** 175.
3. Z. L. Zhu and Z. C. Gu, *Analyst*, 1993, **118,** 105.
4. S. Rubio, A. Gomez-Hens and M. Valcarcel, *Anal. Chem.*, 1984, **56,** 1417.
5. Z. C. Gu, Z. L. Zhu, R. M. Chen, B. L. Lu and C. Q. Han, *Analyst*, 1993, **118,** 1055.
6. K. B. Yatsimirskii and V. I. Rigin, *Zh. Anal. Khim.*, 1956, **11,** 319.
7. T. P. Hadjiioannou, *Talanta*, 1968, **15,** 535.
8. D. Marnaughtan, Jr., L. B. Rogers and G. Wernimont, *Anal. Chem.*, 1972, **44,** 1421.
9. G. L. Ritter, S. R. Lowry, T. L. Isenhour and C. L. Wilkins, *Anal. Chem.*, 1976, **48,** 591.
10. N. Ohta, *Anal. Chem.*, 1973, **45,** 553.
11. Z. L. Zhu, Z. C. Gu and X. D. Wang, *Talanta*, 1993, **40,** 1013.
12. P. Geladi and B. R. Kowalski, *Anal. Chim. Acta*, 1986, **185,** 1.
13. A. Savitzky and M. J. E. Golay, *Anal. Chem.*, 1964, **36,** 1627.

Pergamon

0039-9140(94)00230-4

*Talanta*, Vol. 42, No. 2, pp. 211–218, 1995

0039-9140/95 $9.50 + 0.00

# ON-LINE SORBENT EXTRACTION, PRECONCENTRATION AND DETERMINATION OF LEAD BY ATOMIC ABSORPTION SPECTROMETRY

YANEIRA PETIT DE PEÑA,* MERCEDES GALLEGO and MIGUEL VALCÁRCEL†

Department of Analytical Chemistry, Faculty of Sciences, University of Córdoba, E-14004 Córdoba, Spain

(*Received* 10 *March* 1994. *Revised* 12 *July* 1994. *Accepted* 1 *August* 1994)

**Summary**—A method for the quantitative preconcentration of lead based on an existing batch process was developed for implementation in a flow system including a flame AAS detector. Lead can be quantitatively preconcentrated as pyrrolidinedithiocarbamate or dithizonate on an activated carbon minicolumn. The chelates are eluted in methyl isobutyl ketone and introduced directly into the nebuliser-burner. An enrichment factor of 50 is typically obtained for a preconcentration time of 2 min (lead can be determined at concentrations between 15 and 400 ng/ml), which results in a throughput of *ca.* 25 samples per hr. The sensitivity achieved with the two reagents is similar, but the selectivity provided by APDC exceeds that of dithizone. Based on the results obtained in the determination of lead in reference materials (minerals and skim milk), the proposed APDC method is applicable to real samples.

Analytical separation techniques play a central role in today's analytical chemistry. They are typically used to enrich one of the sample fractions with a given component in trace analyses, as well as to remove complex matrices for enhanced sensitivity or selectivity, respectively, in common place analytical methods. The preconcentration technique has been used to improve the sensitivity and selectivity of trace analyses by replacing the original sample matrix with a new, non-interfering matrix. The enrichment technique has often been used to collect trace elements on solid surfaces;[1] activated carbon can also be used for the preconcentration of trace elements from acid sample solutions provided the trace elements concerned form neutral chelates in the acid medium. Thus, ammonium pyrrolidinedithiocarbamate (APDC),[2] 8-hidroxyquinoline,[3] potassium ethyl xanthate,[4,5] dithizone,[6] Chrome Azurol S[7] and the ammonium salt of the dithiophosphoric acid *o*-*o*-diethylester,[8] have all been used for chelation of trace metals and back-collection on activated carbon following desorption in a small volume of acid for subsequent measurement of the metal concentration by atomic absorption spectrometry (AAS) or ICP-AES.

On-line preconcentration systems have been used in conjunction with AAS for the determination of lead. Thus, lead traces in tap water can be preconcentrated by using a continuous precipitation–dissolution system[9] and a method based on lead precipitation with ammonia and subsequent dissolution of the precipitate (retained on a filter) with a nitric acid stream; preconcentration factors of up to 700 can thus be achieved with a 250-ml volume. Lead can also be coprecipitated with the iron(II)-hexahydroazepinium hexahydroazepin-1-ylformate complex, collected in a knotted reactor, and dissolved in methyl isobutyl ketone; an enrichment factor of 20 can thus be obtained with 2 ml of sample.[10] Various organic reagents have been used in non-immobilized forms for the extraction of lead as a chelate from aqueous samples. The chelate is sorbed on $C_{18}$ bonded silica and then eluted with methanol; the preconcentration factor thus achieved is 5.3 for 1 ml of sample.[11] A sorbent extraction system including a $C_{18}$ column was also used for the determination of traces of lead and other metals by use of diethyldithiocarbamate and ethanol as chelating agent and eluent, respectively;[12] the sensitivity of the graphite furnace technique was enhanced by a factor of *ca.* 20 for a

*Permanent address: University of Los Andes, Faculty of Sciences, Department of Chemistry, Mérida, Venezuela.
†Author to whom correspondence should be addressed.

40-$\mu$l injected volume with only 3 ml of sample. Lead traces were preconcentrated on a column packed with alga immobilized on controlled pore glass, and eluted with nitric acid to obtain a detection limit of 2.5 ng/ml lead with the sole interference of mercury.[13] A cellulose collector containing immobilized triethylenetetraminepentaacetic acid groups was developed for multi-element preconcentration;[14] however, the recoveries obtained were influenced by inorganic and organic substances present in aquatic samples.

Dithizone is one of the few chelating agents that permits the separation of trace metals from acid solutions; on the other hand, APDC is a chelating agent usually employed for preconcentration of metals in FAAS. Both reagents were previously used for trace enrichment of lead by using a flow system similar to that described above for the preconcentration and determination of copper in water.[15] In the proposed method, the lead chelate is quantitatively preconcentrated on a miniature column packed with activated carbon, prior to its determination by FAAS. The analyte is eluted quantitatively from the column with 200 $\mu$l of methyl isobutyl ketone (MIBK); no dispersion occurs during transfer of the eluate because a water stream is used as the carrier. The time-based sampling mode allows the preconcentration factor to be further increased through an increased analyte volume. The accuracy of the results obtained with APDC was checked by using it to analyse reference materials.

## EXPERIMENTAL

### *Apparatus*

A Perkin-Elmer 380 atomic absorption spectrometer equipped with a bead impact system in the burner chamber and a hollow cathode lead lamp was used. The wavelength and lamp current used were 283.3 nm and 10 mA, respectively. Deuterium arc background correction was employed throughout. The acetylene flow rate was 2.0 l./min and an air flow rate of 21.5 l./min was employed to ensure a clean blue flame. The spectrometer output was connected to a Radiometer REC-80 Servograph recorder. The flow manifold comprised a Gilson-Minipuls-2 peristaltic pump furnished with poly (vinyl chloride) tubes, two Rheodyne 5041 injection valves and a laboratory-made adsorption minicolumn packed with 70 mg of activated carbon. The minicolumn (2.5 cm long $\times$ 3 mm i.d.) was made of PTFE capillary and sealed on one end with a small glass wool bed to prevent material losses. The column was initially flushed with 0.1 mol/l. nitric acid and the subsequent use of methyl isobutyl ketone as eluent in each operational cycle was sufficient to make it ready for re-use. A Hetosicc CD 53-1 Freeze Dryer was also employed.

### *Reagents and standards*

A 1000 mg/l. lead stock solution was prepared by dissolving 1.598 g of lead nitrate in $14.4 \times 10^{-2}M$ nitric acid and diluting to 1 l. with $14.4 \times 10^{-2}M$ nitric acid. Freshly prepared 0.1% (w/v) ammonium pyrrolidinedithiocarbamate (Aldrich, Germany) was also used. A saturated solution of dithizone (Riedel, Germany) was prepared as follows: 4 mg of dithizone was shaken electromagnetically in a 100 ml vessel containing 50 ml of $0.4M$ ammonia for 3 min; the solution was then filtered and the filtrate diluted with water in a 100-ml calibrated flask. Methyl isobutyl ketone (Probus, Spain) was also used. Darco 20-40 activated carbon (Aldrich, Germany) and polygosyl bonded silica reversed-phase sorbent containing octadecyl functional groups (RP-$C_{18}$), 60–100 $\mu$m particle size, from Waters (Millipore, Spain), were employed as sorbents. Standard solutions (100 ml) containing 15–400 ng/ml lead were all freshly prepared in $0.1M$ or $0.01M$ nitric acid by appropriate dilution of a stock standard solution (1000 mg/l).

### *Preparation of samples*

Several reference materials were analysed; minerals were supplied by the Bureau of Analysed Samples (BAS, U.K.) and were Standard Reference Materials (SRM) No. 70b, 41dG and 5g, while the skim milk powder was obtained from the Community Bureau of Reference (BCR) and was material No. 150. The reference standards were dried to constant weight by freeze-drying at 6 Pa (0.04 mm Hg) in the case of spiked skim milk powder and by heating in a furnace at 150°C for 24 hr in the case of the mineral reference materials. Once dry, an accurately weighed amount of *ca.* 50–100 mg (minerals) or 4 g (spiked skim milk powder) was mineralized in a glass vessel as follows: zinc concentrate and lead–vanadium concentrate were mixed with 5 ml of $14.4M$ nitric acid and 2.5 ml of $11.2M$ hydrochloric acid; brass and spiked skim milk powder were mixed with 5 and 20 ml of $14.4M$ nitric

acid, respectively. The vessels were heated at *ca.* 180–200°C in a sand bath until the samples were completely dissolved and nitrogen fumes were given off. The vessels were then allowed to cool and the digestion procedure was repeated (about five times) with multiple additions of the acids until a clear solution remained and nitrogen oxide fumes ceased to evolve. Once cold, the solutions were quantitatively transferred into volumetric flasks of 50, 100 or 500 ml capacity and made to volume with ultrapure (Milli Q) water. Reagent blanks were also prepared in parallel. Sub-samples of 0.5–1 ml (for all minerals) were diluted to 100 or 250 ml, adjusted to pH 1.0 with 2*M* nitric acid and immediately analysed by introducing them into the manifold shown in Fig. 1. The spiked skim milk powder required no further dilution.

*Procedure*

The flow manifold depicted in Fig. 1 was employed for the continuous preconcentration and determination of lead. It operated as follows: the standard or sample solution, containing 15–400 ng/ml of Pb(II) in 0.1*M* (for APDC) or 0.01*M* (for dithizone) nitric acid, was continuously pumped through the system for 2 min and thoroughly mixed with the chelating reagent (0.1% APDC or saturated dithizone in 0.2*M* ammonia). The chelate was retained on the activated carbon minicolumn located in the loop of the injection valve and the sample matrix was driven to waste (W). During the preconcentration step, a water carrier was pumped to the instrument in order to flush the nebuliser after each measurement. In the elution step, both injection valves were switched simultaneously, so 200 $\mu$l of MIBK solvent was passed through the adsorbed chelate to desorb it and sweep the lead to the detector. Peak heights were used as analytical measurements and a blank consisting of 200 $\mu$l of MIBK injected prior to sample preconcentration was also used ($A \simeq 0.020$ units).

## RESULTS AND DISCUSSION

The two reagents, *viz.* 0.1% (w/v) APDC and a saturated dithizone solution in ammonia (4 mg in 100 ml of 0.2*M* ammonia), were tested for lead preconcentration in an acid medium. Elution of the adsorbed chelate from the column was assayed with several organic solvents (ethanol, acetone, 1,2-dichloroethane and MIBK) in an automated configuration similar to that depicted in Fig. 1, and 6.0 ml of standard containing 200 ng/ml of Pb(II) in 0.1*M* and 0.01*M* nitric acid for complexation with APDC and dithizone, respectively, was used. The injected eluent volume was 200 $\mu$l in all instances. The best results (difference between sample and blank signals) were provided by MIBK because the chelate was the easiest to dissolve and hence to desorb; in addition, the blank signal (0.020 units) was the lowest and no dispersion was observed during transfer to the detector since MIBK is water-immiscible. Other extractants provided worse results, either because they water-miscible and the plug dispersed to some extent or because the chelate could not be dissolved. Peak height was selected as the analytical measurement because elution with MIBK was quantitative in 200 $\mu$l of solvent.

*Optimization of experimental variables*

The experimental procedure was optimized by using the univariate method. Chemical variables were studied first; for this purpose, a standard solution containing 100 ng/ml lead was continuously introduced into the flow system. A time-based technique equivalent to using only 6.0 ml of sample (sample flow rate, 3.0 ml/min; pumping time, 2 min) was chosen. The effect of the sample pH, adjusted with dilute nitric acid, was studied between 0.5 and 4.0. The maximum chelate adsorption was achieved at

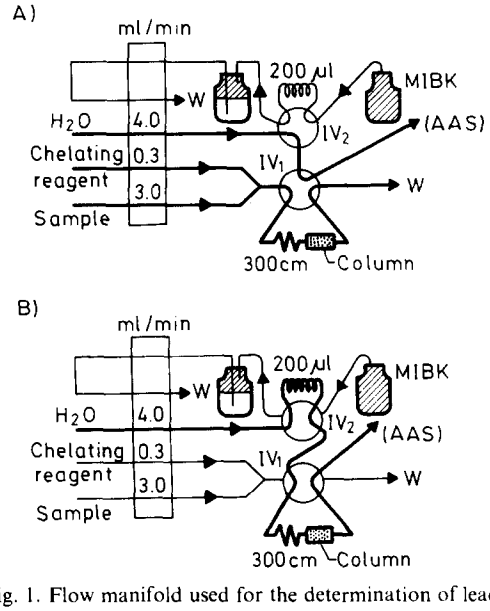


Fig. 1. Flow manifold used for the determination of lead at low concentrations. Bold lines represent channels relevant to the adsorption (A) and elution (B) step. IV, Injection valve; W, waste; MIBK, methyl isobutyl ketone; AAS, atomic absorption spectrometer.

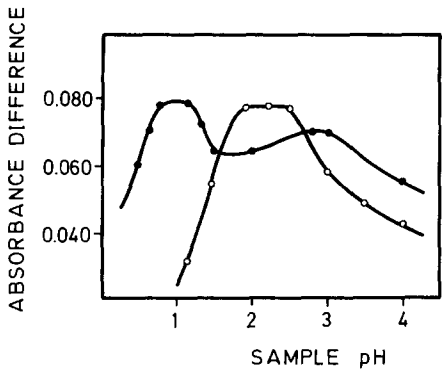


Fig. 2. Effect of pH on lead absorbance following on-line preconcentration with APDC (●) or dithizone (○). Analyte concentration, 100 ng/ml lead.

pH 0.8–1.1 and 1.9–2.5 for APDC and dithizone, respectively (Fig. 2). A further plateau was obtained near pH 3 for APDC that was 10% lower than the first plateau. The influence of various acids used to adjust the sample pH was also studied by using samples containing 100 ng/ml lead at pH 1 and 2 for APDC and dithizone, respectively, adjusted with nitric, hydrochloric and sulphuric acid; the absorbance in hydrochloric and sulphuric acid was 70 and 45% lower, respectively, than that nitric acid, probably because the presence of chloride and sulphate anions hindered the chelate formation by precipitation of their inorganic lead salts. Previous experiments involving a similar flow system[15] had shown the Cu–APDC chelate to be adsorbed as a soluble, precipitated chelate on an activated carbon minicolumn (which acted as a mixing filter/adsorption device); the adsorption increased relative to lead in inorganic salts as a result. Therefore, 0.1 or 0.01*M* nitric acid for APDC or dithizone, respectively, was selected as the optimal medium for sample preparation. The effect of the APDC concentration was studied in the range of 0.001–0.5%; the analytical signal remained constant above 0.05%, so a 0.1% concentration of APDC in water was chosen. The effect of the dithizone concentration was studied in the range $4 \times 10^{-5}$–$4 \times 10^{-4}M$ by dissolving different amounts of the reagent (1–10 mg) in 100 ml of 0.1–0.4*M* ammonia. The signal increased with increasing dithizone concentration up to $1.5 \times 10^{-4}M$ (4 mg of dithizone in 100 ml), above which it remained constant because the solution was saturated; the signal also increased with increasing ammonia concentration up to 0.2*M* at any of the dithizone concentrations tested, but decreased at higher ammonia concentrations through neutralization of the sample. The effect of the dithizone and ammonia concentrations on the lead analytical signal is shown graphically as a three dimensional plot in Fig. 3. Based on the response surface, a dithizone concentration of $1.5 \times 10^{-4}M$ (4 mg in 100 ml) in 0.2*M* ammonia was an experimentally realistic condition, so it was selected for subsequent experiments. Replacing the sample stream with 0.1 or 0.01*M* nitric acid (blanks) or the chelating reagent stream with a water stream (the sample was also circulated) resulted in a similar absorbance in the elution step as that obtained by successively injecting 200 $\mu$l of MIBK solvent before the preconcentration step; no blank was therefore required, and the sample absorbance was obtained by difference from the extractant signal ($A \simeq 0.020$ units).

The flow-rate of sample (6.0 ml of a solution containing 100 ng/ml lead), the effect of which was studied between 0.6 and 4.0 ml/min, resulted in very small variations over the range 1.5–3.0 ml/min. Above 3.0 ml/min, the analytical signal decreased because the residence time also decreased. Increasing the chelating reagent (APDC or dithizone) flow-rate, which was equivalent to increasing the reagent concentration, resulted in concomitant sample dilution and hence in decreased atomic signals. A reagent flow-rate of 0.3 ml/min and a sample flow-rate of 3.0 ml/min were chosen as compromises. The influence of the length of the preconcentration coil (located in the loop of the

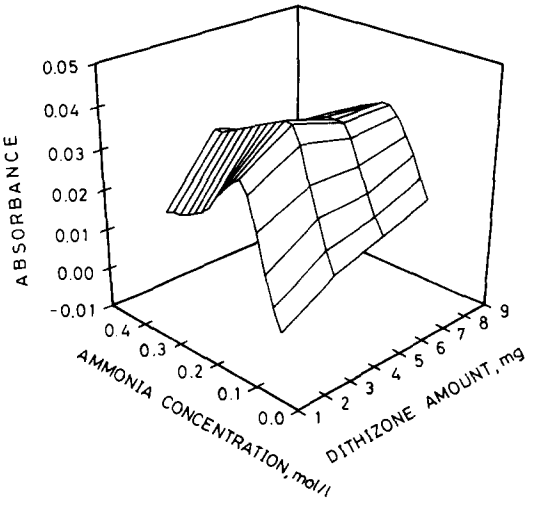


Fig. 3. Response surface for the determination of 50 ng/ml lead at pH 2 and different dithizone and ammonia concentrations.

injection valve before the activated carbon minicolumn) was investigated over the range 50–450 cm (0.5 mm i.d.) by using both chelating reagents. Maximum adsorption was achieved in both instances by using a 300–350 cm preconcentration coil. With coils longer than 350 cm, the chelate formed was carried along the system and probably adsorbed on the inner walls of the PTFE tubing, so it was incompletely dissolved by the injected MIBK, thereby resulting in diminished signals. The effect of the MIBK volume was studied between 25 and 300 $\mu$l. The adsorbed chelate was eluted throughout this range, but some carry-over (incomplete elution) was observed with volumes below 200 $\mu$l. On the other hand, volumes above 200 $\mu$l caused the signal to decrease through dispersion of the analyte in the organic solvent. Based on the above results, flow variables affect the determination of lead to the same extent, whichever chelating agent (APDC or dithizone) is used; therefore, the same flow system can be used for both reagents. A 300 cm long reaction coil (0.5 mm i.d.) and an injected MIBK volume of 200 $\mu$l were selected as optimal for the preconcentration/determination of lead.

*Analytical features*

Several calibration graphs were constructed by introducing the MIBK eluate from the activated carbon minicolumn into the flame using aqueous standard solutions processed along the preconcentration flow system depicted in Fig. 1. Table 1 lists the figures of merit of the graphs and the analytical features of the determination of lead(II) in the range 15–400 ng/ml with a time-based sampling for 2 min, equivalent to a sample volume of 6.0 ml (sample flow-rate, 3.0 ml/min). The detection limit was calculated as three-fold the standard deviation of the peak absorbance for 15 injections of 200 $\mu$l of MIBK (blank). The precision achieved with APDC and dithizone (as relative standard deviation) was checked on 11 standard solutions containing 50 ng/ml lead each.

Automatic preconcentration methods for the determination of lead by AAS are based on sorbent preconcentration by use of minicolumns packed with reversed-phase silica sorbent (RP-$C_{18}$); therefore, a comparative study of the chelate retention on a RP-$C_{18}$ minicolumn was performed. The RP-$C_{18}$ minicolumn was packed with 70 mg, as was the activated carbon minicolumn. The characteristic parameters for the calibration graphs obtained with APDC and dithizone are listed in Table 1. The results allow one to draw the following conclusions: (1) the sensitivity of the method (slope of the calibration graph) does not depend on the chelating reagent used (APDC or dithizone), but only slightly on the minicolumn packing material (thus, it was higher for activated carbon than for RP-$C_{18}$ by a factor of 1.14); (2) the precision was 3.0% or better in all instances; (3) a preconcentration factor of up to 110, calculated as the ratio between the slopes of the calibration graphs obtained with dithizone for a sampling time of 5 min (*i.e.* a sample volume of 15 ml), whether by using the activated carbon minicolumn or by direct aspiration ($A = 0.003 + 1.6 \times 10^{-5}$ [$Pb^{2+}$], lead being given in ng/ml), was achieved.

*Study of interferences*

Under the optimal chemical conditions, the manifold depicted in Fig. 1, an activated carbon minicolumn and a sample volume of 6 ml (sampling time, 2 min) were used to carry out an exhaustive study of potential interferences with both chelating reagents. In previous work,[15] APDC was used for the quantitative preconcentration of copper at pH 1 in the presence of several cations; only $Co^{2+}$ and $Ni^{2+}$ were found to interfere at concentrations 10 times higher than that of Cu. Also, dithizone was found to be less selective than APDC, so it must be subject to a great number of interferences. By using both reagents, the effect of $Zn^{2+}$, $Co^{2+}$,

Table 1. Determination of lead by preconcentration on a sorbent minicolumn (sampling time, 2 min)

| Packing material | Regression equation* | Linear range (*ng/ml*) | Detection limit (*ng/ml*) | RSD (%) | CE ($min^{-1}$)† |
|---|---|---|---|---|---|
| APDC-activated carbon | $A = 0.004 + 0.0008X$ | 15–365 | 10 | 2.3 | 21 |
| APDC-RP-$C_{18}$ | $A = -0.002 + 0.0007X$ | 20–400 | 15 | 2.7 | 19 |
| Dithizone-RP-$C_{18}$ | $A = 0.002 + 0.0007X$ | 20–350 | 10 | 2.9 | 19 |
| Dithizone-activated carbon | $A = -0.005 + 0.0008X$ | 20–400 | 15 | 3.0 | 21 |
| Dithizone-activated carbon‡ | $A = 0.004 + 0.0018X$ | 5–80 | 2 | 2.0 | 18 |

*A, absorbance; X, lead concentration (ng/ml).

†Concentration efficiency = enrichment factor × sampling frequency ($min^{-1}$).

‡Sampling time 5 min.

$Cu^{2+}$, $Cd^{2+}$, $Hg^{2+}$, $Ni^{2+}$, $Sn^{2+}$, $Fe^{3+}$, $Bi^{3+}$, $Al^{3+}$, and $Mn^{2+}$ was checked. Table 2 lists the tolerated levels of foreign cations for APDC and dithizone. APDC is the better choice for preconcentration of lead because of its higher selectivity relative to dithizone. In fact, with APDC, only $Cd^{2+}$, $Bi^{3+}$, $Ni^{2+}$ and $Hg^{2+}$ interfered at low concentrations (tolerated ratio lower than 5). Zinc(II) was the ion causing the most markedly different effect on the two reagents; thus, it interfered at the same concentration as lead with dithizone but did not interfere at concentrations up to 20 $\mu$g/ml with APDC for 100 ng/ml lead (*i.e.* a Zn/Pb ratio of 200:1). The interference decreased the lead signal in all instances. The effect can be ascribed to the chelating reagent concentration being inadequate for the lead and interferent chelates to be formed (that of the species present at the higher concentration would be preferentially formed); otherwise (if the chelating agent concentration were sufficient and both chelates were formed), the eluent volume used (200 $\mu$l of MIBK) may be inadequate to fully elute the chelates from the minicolumn. In conclusion, dithizone is a scarcely selective reagent for lead determination.

*Determination of lead in reference materials*

The accuracy of the proposed method using APDC for the analysis of reference materials with high metals contents was tested in the determination of lead. Each sample was mineralized in duplicate (in triplicate for the skim milk sample) as described under "sample preparation", together with a similarly prepared blank which allowed the contribution of lead ion present in the reagents to the digestion sample used to be assessed. Each dissolved sample was analysed in triplicate. Blank absorbances corresponded to a lead concentration below the detection limit (10 ng/ml). The results are shown in Table 3. Consistency between the results obtained with the proposed APDC method and the certified values was acceptable in all instances.

Table 2. Tolerated concentrations of foreign cations in the determination of 50 or 100 ng/ml lead with dithizone or APDC method, respectively

| Foreign cation | Tolerated amount (*ng/ml*) Dithizone | APDC |
|---|---|---|
| $Al^{3+}$ | 500 | 50,000 |
| $Mn^{2+}$ | 250 | 40,000 |
| $Sn^{2+}$ | 1000 | 20,000 |
| $Fe^{3+}$ | 1000 | 4000 |
| $Hg^{2+}$ | 250 | 400 |
| $Ni^{2+}$ | 250 | 400 |
| $Cu^{2+}$ | 100 | 4000 |
| $Bi^{3+}$ | 100 | 300 |
| $Cd^{2+}$ | 100 | 100 |
| $Co^{2+}$ | 50 | 10,000 |
| $Zn^{2+}$ | <50 | 20,000 |

## CONCLUSIONS

Two classical chelating reagents were tested for the preconcentration of lead by adsorption of their chelates on an activated carbon minicolumn. APDC was found to be more selective than dithizone for the determination of lead, probably because the APDC chelate is formed at a lower pH than is the dithizone chelate. Table 4 summarizes the features of alternative preconcentration flow methods for the determination of lead by atomic spectroscopy. Two types of column packing materials were tested for lead preconcentration and matrix removal, *viz.* ion exchangers and sorbent materials such as silica gel $C_{18}$ (no reference has so far been reported to the use of an activated carbon minicolumn for this purpose). The eluting solvent materials used in all of ion-exchange and sorbent-extraction applications are water-miscible, so they result in higher dispersion of eluted lead during transfer to the detector. The preconcentration factors achieved range from 20 to 500; higher preconcentration factors call for larger sample volumes and hence longer sampling times, to the detriment of sample throughput. The preconcentration limit is seemingly determined by the availability of sample solution and the operator's patience. The precision (as RSD) achieved is quite acceptable in all instances. As regards application, all the methods listed in Table 4 were applied to water samples (there are only three uses for soldering smoke, urine and biological materials). The main differences between the proposed method

Table 3. Results for the determination of lead in reference materials (all values are in % lead)

| Reference material | Certified | Found ($n = 6$) |
|---|---|---|
| BAS N° 70b, lead vanadium concentrate | 42.5 | 41.1 ± 1.3 |
| BAS N° 41dG, zinc concentrate | 0.91 | 0.89 ± 0.03 |
| BAS N° 5g, brass | 2.23 | 2.29 ± 0.08 |
| BCR N° 150, spiked skim milk powder | 1.00 ± 0.04* | 1.02 ± 0.05 |

*Value in $\mu$g/g lead.

Table 4. Features of automatic preconcentration methods for the determination of lead by atomic spectroscopic techniques

| Detection | Preconcentration method | Eluent | Concentration efficiency ($min^{-1}$) | RSD (%) | Applications | Reference |
|---|---|---|---|---|---|---|
| FAAS | I-E (Chelex-100) | 2*M* $HNO_3$ | 15 | | Seawater | 16 |
| FAAS | I-E (Resin-122) | 2*M* $HNO_3$ | 16 | 1.5–4.1 | Water | 17 |
| FAAS | I-E (8-Quinolinol) (a) | (1 HCl + 0.1 $HNO_3$)*M* | 17 | | Tap water | 18 |
| FAAS | I-E (Chelex-100, 8-Quinolinol Resin-122) | 2*M* $HNO_3$ | 50 | 1.2–3.2 | | 19 |
| FAAS | I-E (TriPEN) (a) | 6*M* $HNO_3$ | 22 | | | 20 |
| FAAS | I-E (Dowex A-1) | 1*M* HCl | | 2.0 | Soldering smoke | 21 |
| ICP-AES | I-E (Chelex-100) | 2*M* $HNO_3$ | 10 | 6.0 | | 22 |
| FAAS | I-E (Muromac A-1) | 2*M* $HNO_3$ | 29 | 1.28 | | 23 |
| FAAS | I-E (8-Quinolinol) (a) | 2*M* HCl | 60 | 1.8 | Seawater | 24 |
| ICP-AES | I-E (IDAEC) | 2*M* $HNO_3$ | 8 | 1.5–3.0 | Seawater, urine | 25 |
| FAAS | Sorbent-extraction ($C_{18}$) ($b_1$) | Methanol | | | | 11 |
| ETAAS | Sorbent-extraction ($C_{18}$) ($b_1$) | Ethanol | 7 | 2.0 | Sea- and drinking water SRM | 12 |
| ETAAS | Sorbent-extraction ($C_{18}$) ($b_1$) | Ethanol | 10 | 1.9 | Sea- and riverine water SRM | 26 |
| ETAAS | Sorbent-extraction ($C_{18}$) ($b_2$) | Acetonitrile | | 5.0 | Antarctic seawater | 27 |
| FAAS | Sorbent-extraction (activated alumina) | 2*M* $HNO_3$ | 42 | 5.0 | Drinking water | 28 |
| FAAS | Sorbent-extraction (cellulose) (c) | 2*M* $HNO_3$ | | 2.0 | River and seawater | 14 |
| FAAS | Continuous precipitation (d) | 2*M* $HNO_3$ | 11 | 2.8 | Tap water | 9 |
| FAAS | Co-precipitation (e) | Methyl isobutyl ketone | 30 | 2.7 | Biological materials | 10 |
| FAAS | Biosorption (f) | 0.5*M* $HNO_3$ | 27 | 1.1 | | 13 |

FAAS, flame atomic absorption spectrometry; ETAAS, electrothermal atomic absorption spectrometry; ICP-AES, inductively coupled plasma atomic emission spectrometry; I-E, ion exchange; TriPEN, *N,N,N'*-tri (2-pyridylmethyl)ethylene diamine; IDAEC, iminodiacetic acid/ethylcellulose; (a) immobilized on CPG (b) 1 and 2, chelation by diethyldithiocarbamate and pyrrolidine dithiocarbamate, respectively, with subsequent adsorption; (c) triethylenetetraaminepentaacetic immobilized on cellulose; (d) lead precipitation with ammonia and collection on a filter; (e) co-precipitation with the iron(II)-hexahydroazepinium hexahydroazepine-1-ylformate (hexamethyleneammonium hexamethylenedithiocarbamate) complex, collected without a filter; (f) *Selenestrum capricornutum* algae immobilized on CPG.

and existing alternatives using $C_{18}$ minicolumns lie in the preconcentration step, during which both the sample matrix and the eluent are sent to waste in our method; also, the eluent (MIBK) is water-immiscible, so the analyte is not dispersed on transfer to the instrument nebuliser. Finally, the methods listed in Table 4 are generally used for preconcentration and determination of heavy metal (none was investigated in relation to the potential interference of lead).

*Acknowledgements*—The Spanish CICyT is gratefully acknowledged for financial support (Grant No. PB 93-0717). Y. Petit de Peña is also grateful to the University of Córdoba, the University of Los Andes, and BID-CONICIT (Venezuela) for additional financial support.

## REFERENCES

1. A. Mizuike, *Enrichment Techniques for Inorganic Trace Analysis*. Springer, Berlin, 1983.
2. M. Kimura and K. Kawanami, *Talanta*, 1979, **26**, 901.
3. B. M. Vanderborght and R. E. Van Grieken, *Anal. Chem.*, 1977, **49**, 311.
4. M. Kimura, *Talanta*, 1977, **24**, 194.
5. P. R. Devi and G. R. K. Naidu, *Analyst*, 1990, **115**, 1469.
6. E. Beinrohr, J. Rojcek and J. Garaj, *Analyst*, 1988, **113**, 1831.
7. A. J. Ambrose, L. Ebdon and P. Jones, *Anal. Proc.*, 1989, **26**, 377.
8. V. L. A. Monte and A. J. Curtius, *J. Anal. Atom. Spectrom.*, 1990, **5**, 21.
9. P. Martínez-Jiménez, M. Gallego and M. Valcárcel, *Analyst*, 1987, **112**, 1233.
10. Z. Fang, M. Sperling and B. Welz, *J. Anal. Atom. Spectrom.*, 1991, **6**, 301.
11. J. Ruzicka and A. Arndal, *Anal. Chim. Acta*, **216**, 243.
12. M. Sperling, X. Yin and B. Welz, *Anal. Atom. Spectrom.*, 1991, **6**, 295.
13. H. A. M. Elmahadi and G. M. Greenway, *J. Anal. Atom. Spectrom.*, 1991, **6**, 643.
14. P. Burba, J. C. Rocha and A. Schulte, *Fresenius J. Anal. Chem.*, 1993, **346**, 414.
15. R. Santelli, M. Gallego and M. Valcárcel, *Talanta*, 1993, 1994, **41**, 817.
16. S. Olsen, L. C. R. Pessenda, J. Ruzicka and E. H. Hansen, *Analyst*, 1983, **108**, 905.
17. Z. Fang, S. Xu and S. Zhang, *Anal. Chim. Acta*, 1984, **164**, 41.
18. F. Malamas, M. Begtsson and G. Johansson, *Anal. Chim. Acta*, 1984, **160**, 1.
19. Z. Fang, J. Ruzicka and E. H. Hansen, *Anal. Chim. Acta*, 1984, **164**, 23.
20. M. Bengtsson, F. Malamas, A. Torstensson, O. Regnell and G. Johansson, *Mikrochim. Acta*, 1985, **3**, 209.
21. P. Hernández, L. Hernández, J. Vicente and M. T. Sevilla, *An. Quím.*, 1985, **81B**, 117.
22. S. D. Hartenstein, J. Ruzicka and G. D. Christian, *Anal. Chem.*, 1985, **57**, 21.
23. S. Hirata, K. Honda and T. Kumamaru, *Anal. Chim. Acta*, 1989, **221**, 65.
24. Z. Fang and B. Welz, *J. Anal. Atom. Spectrom.*, 1989, **4**, 543.
25. S. Caroli, A. Alimonti, F. Petrucci and Z. Horvath, *Anal. Chim. Acta*, 1991, **248**, 241.
26. Z. Fang, M. Sperling and B. Welz, *J. Anal. Atom. Spectrom.*, 1990, **5**, 639.
27. V. Porta, O. Abollino, E. Mentasti and C. Sarzanini, *J. Anal. Atom. Spectrom.*, 1991, **6**, 119.
28. Y. Zhang, P. Riby, A. G. Cox, C. W. McLeod, A. R. Date and Y. Y. Cheung, *Analyst*, 1988, **113**, 125.

Pergamon

0039-9140(94)00231-2

*Talanta*, Vol. 42, No. 2, pp. 219–226, 1995

0039-9140/95 $9.50 + 0.00

# MECHANISTIC STUDIES OF METAL ION BINDING TO WATER-SOLUBLE POLYMERS USING POTENTIOMETRY

NEIL V. JARVIS and JUDITH M. WAGENER

Department of Process Technology, Atomic Energy Corporation of South Africa Ltd, P.O. Box 582, Pretoria, 0001, South Africa

(*Received* 15 *March* 1994. *Revised* 20 *June* 1994. *Accepted* 7 *July* 1994)

**Summary**—A method for elucidating metal ion binding mechanisms with water-soluble polymers has been developed in which the polymer is treated as a collection of monomeric units. Data obtained from potentiometric titrations are analysed by the ESTA library of programs and apparent formation constants may be calculated. From this information, predictions may be made as to metal ion separation using complexation–ultrafiltration techniques. The polymer used in this study was Polymin Water-Free and its complexation with Hg(II), Cd(II), Pb(II), Co(II) and Ni(II) was successfully modelled.

Interest in the use of water-soluble polymers in conjuction with ultrafiltration membranes to separate metal ions from aqueous solutions has steadily grown since the work of Geckeler *et al.* was published in the early eighties.[1] The possibility of synthesizing derivatives of commercially available water-soluble polymers such as polyethyleneimine, in order to achieve selective metal ion complexation, was recognized early on. A wide range of applications have been investigated[2] including the nuclear industry[3] and the removal of toxic heavy metal ions such as Pb(II), Cd(II) and Hg(II).[4] As the field of ligand design produces more complicated and selective complexing agents, it has become an attractive option to attach these reagents to polymer backbones in order to minimize losses of expensive compounds.

At this time, little effort has gone into the understanding of metal ion complexation mechanisms of water-soluble polymers in aqueous solution. Recent work by Rumeau *et al.*[2] used potentiometry to calculate stability constants of these polymers with metal ions. We have developed a method to elucidate metal ion bonding mechanisms to chelating resins using two-phase potentiometry.[5] In this paper, we extend this method to water-soluble polymers (although the term "two-phase" may not be entirely applicable here). The repeating unit of the polymer is considered to be the ligand and potentiometric data are submitted to the ESTA library of programs.[6] Apparent formation constants may be accurately calculated and this allows predictions to be made on metal ion separation.

The complexation of Hg(II), Cd(II) and Pb(II) were studied and comparisons could be made with previous ultrafiltration studies.[4] The complexation of Co(II) and Ni(II) were also studied in order to make predictions as to the possible use of complexation–ultrafiltration as a method to separate these two metal ions.

## EXPERIMENTAL

### *Reagents*

Polymin* Water-Free, a polyethyleneimine product in which the ratio of primary, secondary and tertiary amine groups is 1:1:1, was obtained from BASF and used as received. The repeating unit is as follows:[1]

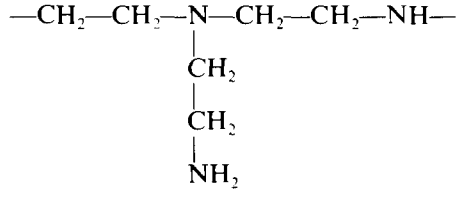

All other reagents used were of analytical grade. Where necessary, metal ion solutions were acidified to prevent hydrolysis and standardized by ICP. Standardized sodium hydroxide solutions were obtained by using Merck Titrisol ampoules.

*Polymin is a registered trademark of the BASF company.

*Potentiometry and computing*

Titrations were performed by a Metrohm Titroprocessor 670 using a Metrohm 665 dosimat and a Metrohm combination glass electrode. The titration solutions were contained in a jacketed vessel through which water at $25 \pm 0.1°C$ was circulated from a Grant W14 thermostatted bath. The compositions of the titration solutions are listed in Table 1. These were performed beginning at low and ending at high pH by the addition of $0.050M$ NaOH in $0.95M$ $NaNO_3$. All titration solutions were held at a constant ionic strength of $1.0M$ $NaNO_3$ and vigorously stirred. Nitrogen gas was bubbled through the solutions during the titrations. Under these conditions, it appeared as though equilibrium was attained within a number of minutes (stable EMF readings were obtained). The Titroprocessor was programmed not to add titrant until the electrode drift was less than 0.5 mV/min or a time of 10 min had elapsed. Most data points were obtained using the former criterion. The remaining points were given low weights by the program ESTA2A. Data were submitted to ESTA which was loaded on a mainframe computer. The above repeating unit of Polymin Water-Free was considered to be the ligand. The module ESTA0 was used to calculate the experimental protonation formation function, $\bar{Z}_H$ = the average number of protons bound per ligand; and the deprotonation function, $\bar{Q}$ = the average number of protons released on complexation per metal ion. Where these were insensible, the data points were rejected for refinement. All optimization was done using ESTA2A with the data weighted.[7] Apparent $pK_a$ values obtained in the titrations without metal ions were fixed during optimization of metal ion titrations. Hydrolysis constants and $pK_w$ were obtained from Smith and Martell[8] and also held constant. The electrode constant ($E_0$) was calculated regularly using a strong acid–base titration. Once a model had been obtained, ESTA2A was allowed to refine $E_0$ resulting in small changes with improved standard deviations for $\beta$ values and the Hamilton $R$-factor.

## RESULTS AND DISCUSSION

*Equilibrium modelling*

The results of modelling are given in Table 2. The low standard deviations of the $\beta$ values and Hamilton $R$-factors indicate the applicability of the method. Calculated and experimental formation and deprotonation curves were all in good agreement indicating that the chosen models were plausible.

*Protonation of Polymin Water-Free*

The protonation formation curves (Fig. 1) show no marked inflections indicating that the ligand's deprotonation reactions overlap in the pH region studied. From the species

Table 1. Compositions of experimental solutions

| Cation | Titration | $1M$ $NaNO_3$ (*ml*) | Metal ion solution* (*ml*) | $0.010M$ Polymin (*ml*) | $2M$ $NaNO_2$ (*ml*) | $0.050M$ $HNO_3$ in $0.95M$ $NaNO_3$ (*ml*) |
|---|---|---|---|---|---|---|
| $H^+$ | 1 | 35.0 | | 5.0 | | 10.0 |
| | 2 | 33.0 | | 7.0 | | 10.0 |
| | 3 | 30.0 | | 10.0 | | 10.0 |
| | 4 | 40.0 | | 5.0 | | 5.0 |
| Pb(II) | 1 | 30.0 | 5.0 | 5.0 | 5.0 | 5.0 |
| | 2 | 28.0 | 5.0 | 7.0 | 5.0 | 5.0 |
| | 3 | 25.0 | 5.0 | 10.0 | 5.0 | 5.0 |
| Cd(II) | 1 | 30.0 | 5.0 | 5.0 | 5.0 | 5.0 |
| | 2 | 28.0 | 5.0 | 7.0 | 5.0 | 5.0 |
| | 3 | 25.0 | 5.0 | 10.0 | 5.0 | 5.0 |
| Hg(II) | 1 | 36.0 | 2.0 | 5.0 | 2.0 | 5.0 |
| | 2 | 34.0 | 2.0 | 7.0 | 2.0 | 5.0 |
| | 3 | 31.0 | 2.0 | 10.0 | 2.0 | 5.0 |
| Co(II) | 1 | 18.0 | 5.0 | 12.0 | 5.0 | 10.0 |
| | 2 | 15.0 | 5.0 | 15.0 | 5.0 | 10.0 |
| | 3 | 10.0 | 5.0 | 20.0 | 5.0 | 10.0 |
| Ni(II) | 1 | 18.0 | 5.0 | 12.0 | 5.0 | 10.0 |
| | 2 | 15.0 | 5.0 | 15.0 | 5.0 | 10.0 |
| | 3 | 10.0 | 5.0 | 20.0 | 5.0 | 10.0 |

*Solutions made up as follows: $0.00941M$ $Pb(NO_3)_2$ in $0.050M$ $HNO_3$, $0.00955M$ $Cd(NO_3)_2 \cdot 4H_2O$ in $0.050M$ $HNO_3$, $0.00911M$ $Hg(NO_3)_2$ in $0.050M$ $HNO_3$, $0.00999M$ $Co(NO_3)_2 \cdot 6H_2O$ and $0.00980M$ $Ni(NO_3)_2 \cdot 6H_2O$.

Table 2. Apparent protonation and formation constants for Polymin Water-Free*

| Cation | Equilibrium† | log$K$ | Hamilton $R$-factor ($R$-limit) | Number of data points |
|---|---|---|---|---|
| $H^+$ | $H + L = HL$ | $9.71 \pm 0.005$ | | |
| | $HL + H = H_2L$ | $7.70 \pm 0.006$ | | |
| | $H_2L + H = H_3L$ | $2.64 \pm 0.04$ | | |
| | $2L + 3H = H_3L_2$ | $30.87 \pm 0.01$ | | |
| | $2L + 5H = H_5L_2$ | $41.58 \pm 0.02$ | 0.00850 | |
| | | | (0.00116) | 436 |
| Pb(II) | $M + OH = MOH$ | 6.4‡ | | |
| | $MOH + OH = M(OH)_2$ | 4.5‡ | | |
| | $M(OH)_2 + OH = M(OH)_3$ | 3.0‡ | | |
| | $MOH + M = M_2OH$ | 1.2‡ | | |
| | $3M + 4OH = M_3(OH)_4$ | 32.1‡ | | |
| | $M_3(OH)_4 + M = M_4(OH)_4$ | 3.9‡ | | |
| | $M + 2L = ML_2$ | $12.53 \pm 0.02$ | | |
| | $ML_2 + H = ML_2H$ | $8.64 \pm 0.02$ | | |
| | $2M + 3L = M_2L_3$ | $23.06 \pm 0.06$ | 0.0256 | |
| | | | (0.00184) | 183 |
| Cd(II) | $M + OH = MOH$ | 3.4‡ | | |
| | $MOH + OH = M(OH)_2$ | 3.6‡ | | |
| | $M(OH)_2 + OH = M(OH)_3$ | 2.6‡ | | |
| | $M(OH)_3 + OH = M(OH)_4$ | 1.7‡ | | |
| | $MOH + M = M_2OH$ | 1.0‡ | | |
| | $4M + 4OH = M_4(OH)_4$ | 24.2‡ | | |
| | $M + L = ML$ | $8.57 \pm 0.03$ | | |
| | $ML + OH = MLOH$ | $4.91 \pm 0.04$ | | |
| | $MLOH + OH = ML(OH)_2$ | $4.42 \pm 0.04$ | | |
| | $ML + L = ML_2$ | $7.84 \pm 0.03$ | | |
| | $ML_2 + H = ML_2H$ | $6.66 \pm 0.04$ | | |
| | $ML_2 + OH = ML_2OH$ | $4.22 \pm 0.03$ | 0.0230 | |
| | | | (0.00163) | 227 |
| Hg(II) | $M + OH = MOH$ | 10.0‡ | | |
| | $MOH + OH = M(OH)_2$ | 11.1‡ | | |
| | $MOH + M = M_2OH$ | 14.6‡ | | |
| | $3M + 3OH = M_3(OH)_3$ | 35.4‡ | | |
| | $M + L = ML$ | $16.06 \pm 0.03$ | | |
| | $ML + L = ML_2$ | $13.46 \pm 0.04$ | | |
| | $ML_2 + H = ML_2H$ | $4.35 \pm 0.04$ | | |
| | $ML_2 + OH = ML_2OH$ | $2.64 \pm 0.05$ | 0.00370 | |
| | | | (0.00176) | 244 |
| Co(II) | $M + OH = MOH$ | 4.0‡ | | |
| | $MOH + OH = M(OH)_2$ | 4.7‡ | | |
| | $M(OH)_2 + OH = M(OH)_3$ | 1.2‡ | | |
| | $M + 4OH = M(OH)_4$ | 9.2‡ | | |
| | $2M + OH = M_2OH$ | 2.5‡ | | |
| | $4M + 4OH = M_4(OH)_4$ | 25.0‡ | | |
| | $M + 2L = ML_2$ | $16.62 \pm 0.03$ | | |
| | $ML_2 + H = ML_2H$ | $6.75 \pm 0.03$ | 0.0256 | |
| | | | (0.00347) | 240 |
| Ni(II) | $M + OH = MOH$ | 3.7‡ | | |
| | $M(OH) + OH = M(OH)_2$ | 5.0‡ | | |
| | $M(OH)_2 + OH = M(OH)_3$ | 3.0‡ | | |
| | $2M + 2OH = M_2(OH)_2$ | 4.7‡ | | |
| | $4M + 4OH = M_4(OH)_4$ | 27.9‡ | | |
| | $M + 2L = ML_2$ | $19.00 \pm 0.02$ | | |
| | $ML_2 + H = ML_2H$ | $6.04 \pm 0.02$ | 0.0130 | |
| | | | (0.00281) | 299 |

*All data at 25°C in 1.0$M$ $NaNO_3$. p$K_w$ was fixed at 13.79 under these conditions.[8]
†In these equilibria, charges on metal ions, the ligand and complexes have been omitted for simplicity. L = Monomeric unit of Polymin Water-Free, M = metal ion, H = proton and OH = hydroxide ion.
‡Estimated from Ref. 8.

distribution plot (Fig. 2), it is clear that complete protonation of Polymin Water-Free does not occur in this pH region. This phenomenon has been previously reported.[9] Evidence for possible nearest neighbour interaction in which intramolecular hydrogen bonding is taking place, is given by the presence of species involving two repeating units. Alternatively, when

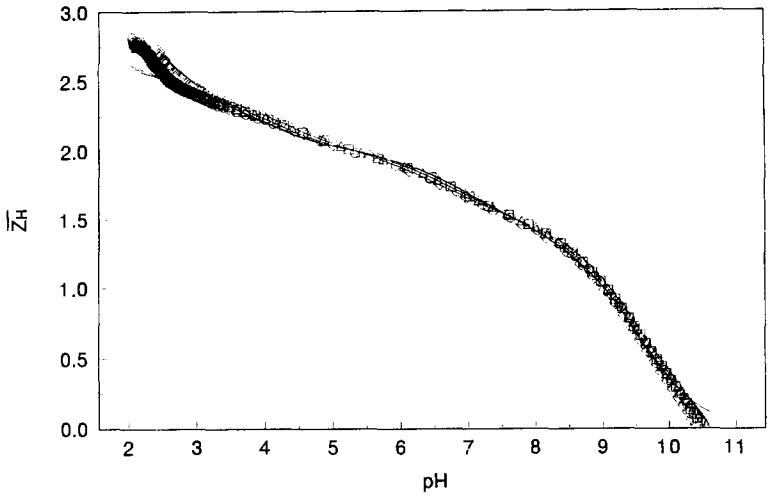


Fig. 1. Experimental (points) and modelled (lines) protonation formation curves for Polymin Water-Free. $\bar{Z}_H$ is the protonation formation function (the average number of protons bound per ligand) and pH is the negative logarithm of the free hydrogen ion concentration. The compositions of the solutions are in Table 1. The titrations are represented by (○) titration 1, (△) titration 2 and (□) titration 3. All solutions were at 25°C and 1.0*M* with respect to $NaNO_3$.

going from low to high pH, the sequence of deprotonation gives some insight as to what is happening at the molecular level. Species involving two repeating units are found between those involving one. This means that, when going from $H_3L$ to $H_2L$ or from $H_2L$ to HL, every second repeating unit becomes deprotonated in preference to each unit giving rise to the intermediate species $H_5L_2$ and $H_3L_2$, respectively. The species $H_6L_2$, $H_4L_2$ and $H_2L_2$, were also submitted to the model but were rejected with ESTA2A preferring to retain species with the same stoichiometric ratios but containing one repeating unit (i.e. $H_3L$, $H_2L$ and HL). Evidence for the species $HL_2$ could not be found.

## Hg(II), Cd(II) *and* Pb(II) *complexation by Polymin Water-Free*

The deprotonation curves (Figs 3–5) show good agreement between observed and calculated values. $\bar{Q}$ values for Hg(II) rise above zero, indicating complexation, at low pH. This is in contrast with Cd(II) and Pb(II) where $\bar{Q}$ becomes sensible above pH 5 and 6, respectively. Thus it may be seen that Hg(II) is more strongly complexed by Polymin Water-Free.

Interpretation of the $\bar{Q}$ curves is difficult—as is often the case. However, with the Hg(II) system, some prediction of complexes for the model is possible. It can be seen (Fig. 5) that at

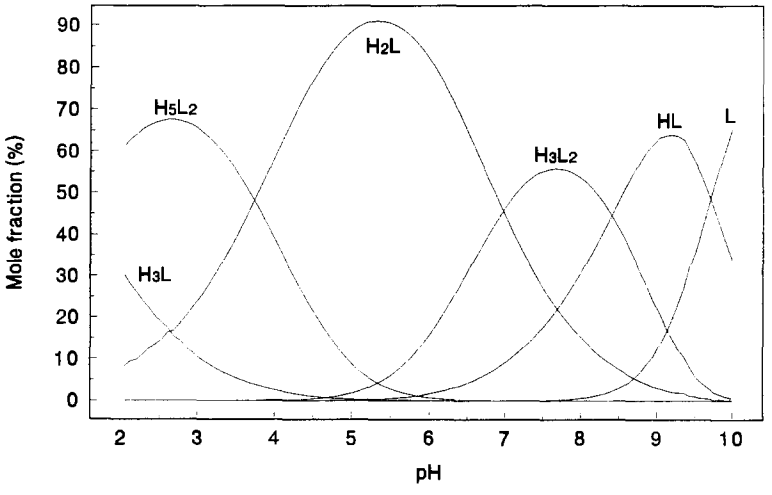


Fig. 2. Species distribution curves for the protonation of Polymin Water-Free at 25 C and 1.0*M* $NaNO_3$, as calculated from the apparent formation constants in Table 2.

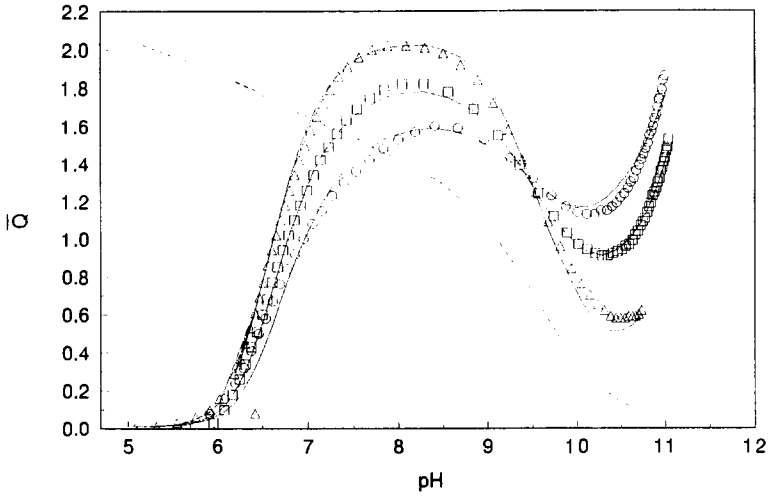


Fig. 3. Experimental (points) and modelled (lines) deprotonation curves for Pb(II) complexation by Polymin Water-Free. $\bar{Q}$ is the deprotonation function (the average number of protons released on complexation per metal ion). The dashed line is the $\bar{n}$ curve, where $\bar{n}$ is the protonation state of the ligand in the absence of the metal ion. The compositions of the solutions are in Table 1. The titrations are represented by (○) titration 1, (△) titration 2 and (□) titration 3. All solutions were at 25 °C and 1.0*M* with respect to $NaNO_3$.

pH 6, the dashed curve which represents $\bar{n}$, the protonation state of the ligand in the absence of the metal ion, is at a value of 2. At this point, $\bar{Q}$ has an inflection at 4. Therefore, the existence of a complex in which a total of five protons have been lost from the ligands in the complex per metal ion is possible. This corresponds to an $ML_2H$ species which was indeed found during modelling.

The $M_2L_3$ species in the Pb(II) system was essential for obtaining a good $\bar{Q}$ fit. The existence of this complex may be due to the large ionic radius of Pb(II) with a repeating unit preferring to bridge two Pb(II) ions.

Species involving one repeating unit in the Pb(II) system were not accepted into the model by ESTA2A. A possible explanation for this may be advanced from comparing the pH values in the deprotonation curves where $\bar{Q}$ rises above zero. It may be seen that Pb(II) is not as well complexed by Polymin Water-Free as Cd(II) or Hg(II). Complexation begins for Pb(II) at pH 6

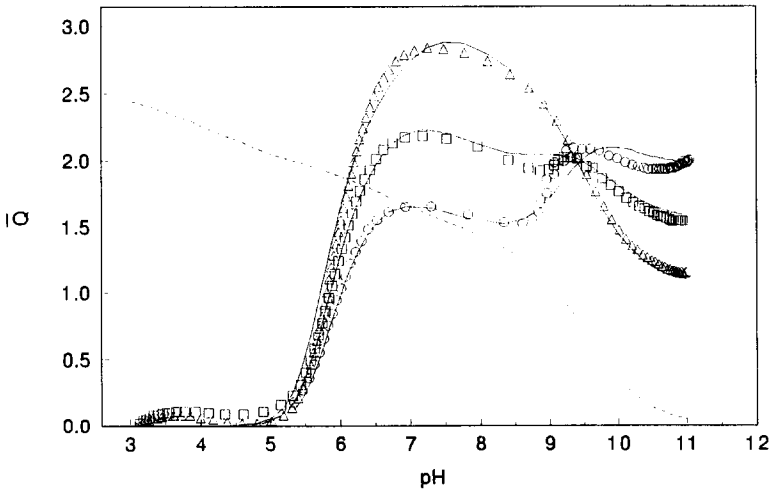


Fig. 4. Experimental (points) and modelled (lines) deprotonation curves for Cd(II) complexation by Polymin Water-Free. The compositions of the solutions are in Table 1. The titrations are represented by (○) titration 1, (△) titration 2 and (□) titration 3. All solutions were at 25 C and 1.0*M* with respect to $NaNO_3$.

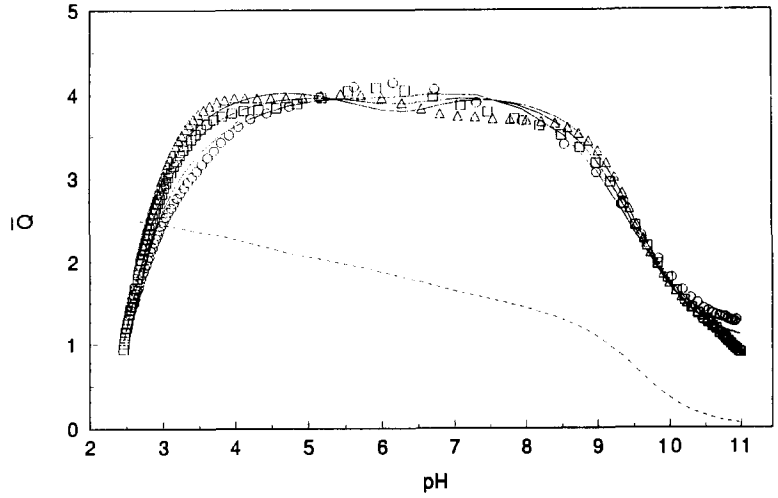


Fig. 5. Experimental (points) and modelled (lines) deprotonation curves for Hg(II) complexation by Polymin Water-Free. The compositions of the solutions are in Table 1. The titrations are represented by (○) titration 1, (△) titration 2 and (□) titration 3. All solutions were at 25°C and 1.0*M* with respect to $NaNO_3$.

where each repeating unit has already lost a proton hence making species involving two repeating units more possible. For Cd(II) and Hg(II) where complexation begins at pH 5 and below pH 2 respectively, species also involving only one repeating unit are possible.

The three metal ions are complexed over a wide pH range. Cd(II) and Pb(II) would be best removed at high pH by ultrafiltration. The pH dependence of Hg(II) removal would not be so critical. These observations are in complete agreement with the complexation–ultrafiltration work performed by Buckley and co-workers.[4]

### Co(II) *and* Ni(II) *complexation by Polymin Water-Free*

Ni(II) is somewhat better complexed by Polymin Water-Free than Co(II). This may be seen by comparing the deprotonation curves (Figs 6 and 7). This is a source of optimism that separation between these two metal ions may be achieved using complexation–ultrafiltration by carefully fixing the pH of the feed stream. However, a more complete picture is obtained by comparing species distribution curves generated by task SPEC in ESTA1. The Co(II)

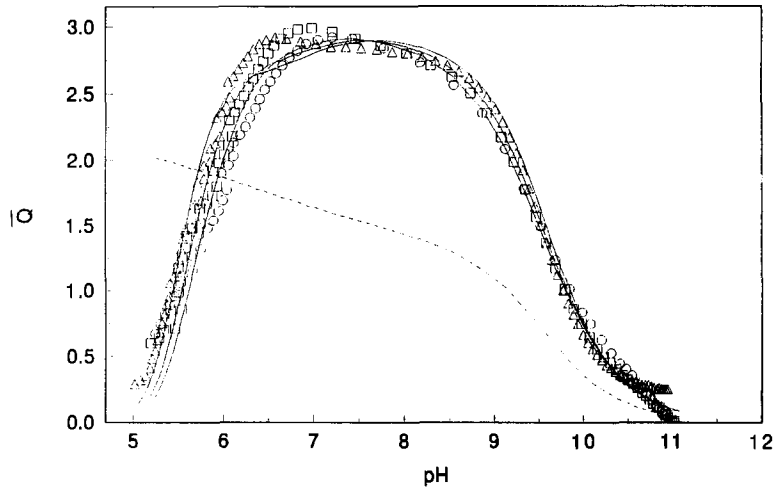


Fig. 6. Experimental (points) and modelled (lines) deprotonation curves for Co(II) complexation by Polymin Water-Free. The compositions of the solutions are in Table 1. The titrations are represented by (○) titration 1, (△) titration 2 and (□) titration 3. All solutions were at 25 C and 1.0*M* with respect to $NaNO_3$.

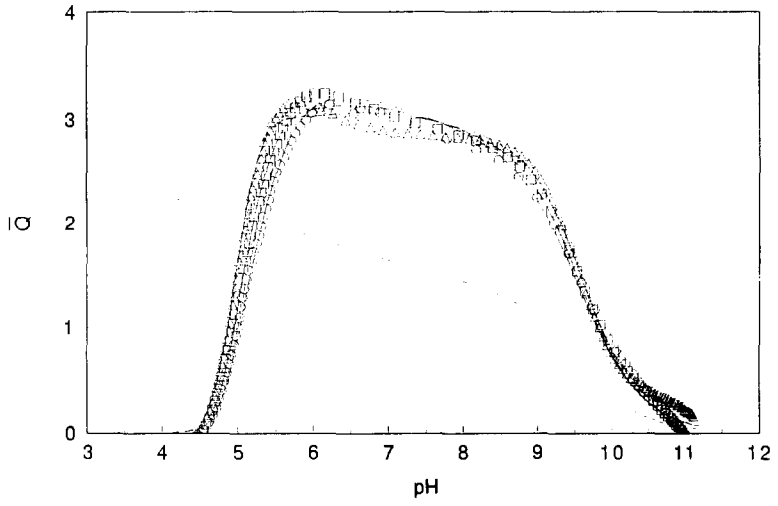


Fig. 7. Experimental (points) and modelled (lines) deprotonation curves for Ni(II) complexation by Polymin Water-Free. The compositions of the solutions are in Table 1. The titrations are represented by (○) titration 1, (△) titration 2 and (□) titration 3. All solutions were at 25 C and 1.0*M* with respect to $NaNO_3$.

system is shown as an example in Fig. 8. If only the curves representing the free metal ions are shown, then plots such as Fig. 9 may be obtained. Here it may be seen that these are close together, making separation difficult. It is, however, hoped that such plots may be used to predict the separation of other metal ions from one another using complexation–ultrafiltration.

For both Ni(II) and Co(II), the $ML_2$ and $ML_2H$ species retained by ESTA2A during modelling are consistent with the deprotonation curve information. It may be seen that $\bar{Q}$ reaches an inflection at roughly a value of three indicating that three protons have been lost on complexation per metal ion. At pH values around 7–8, $\bar{n}$ is close to 1.5. Thus for two repeating units, three protons are lost in the absence of the metal ions. The total number of protons lost for an $ML_2$ species is six which is consistent with the addition of $\bar{Q}$ plus 2 $x$ (total protons on completely protonated repeating unit, $\bar{n}$) which gives a value of six. At lower pH values, where $\bar{n}$ equals two, the same argument may be used to arrive at the $ML_2H$ species. This confirms the best-fitting model reported in Table 2. Species involving one repeating

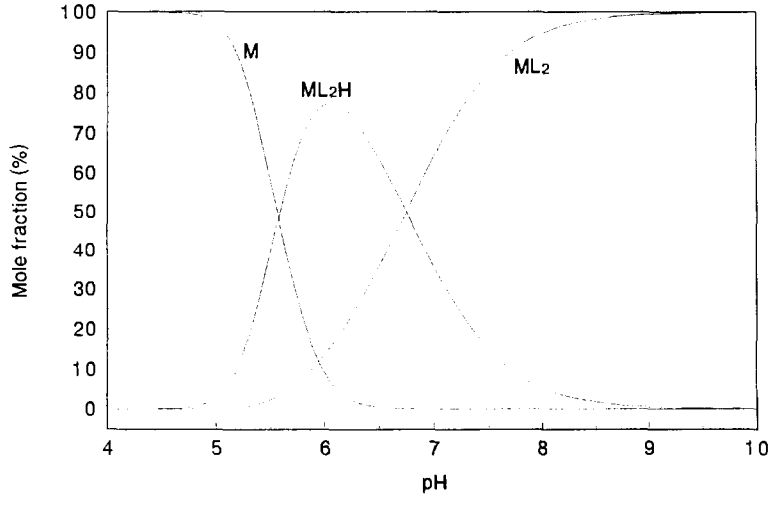


Fig. 8. Species distribution curves for the complexation of Co(II) at 25 C and 1.0*M* $NaNO_3$ (titration 3), as calculated from the apparent formation constants in Table 2.

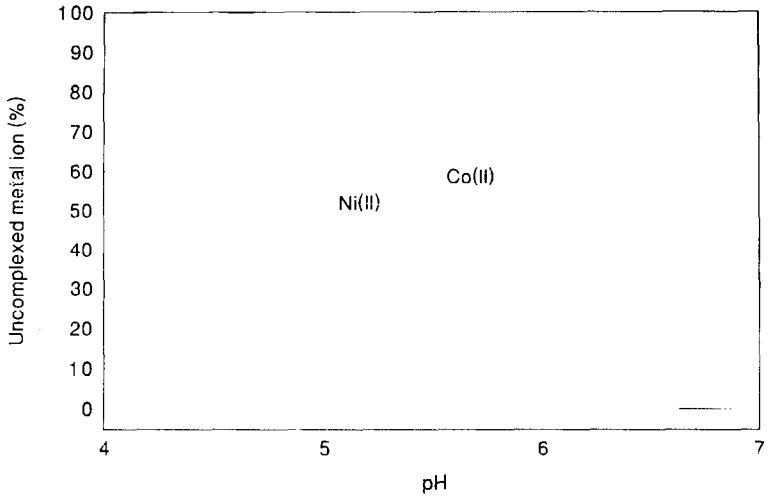


Fig. 9. Species distribution curves for the complexation of Co(II) and Ni(II) at 25 C and 1.0*M* $NaNO_3$ (titration 3), as calculated from the apparent formation constants in Table 2. Only the uncomplexed metal ion plots are shown.

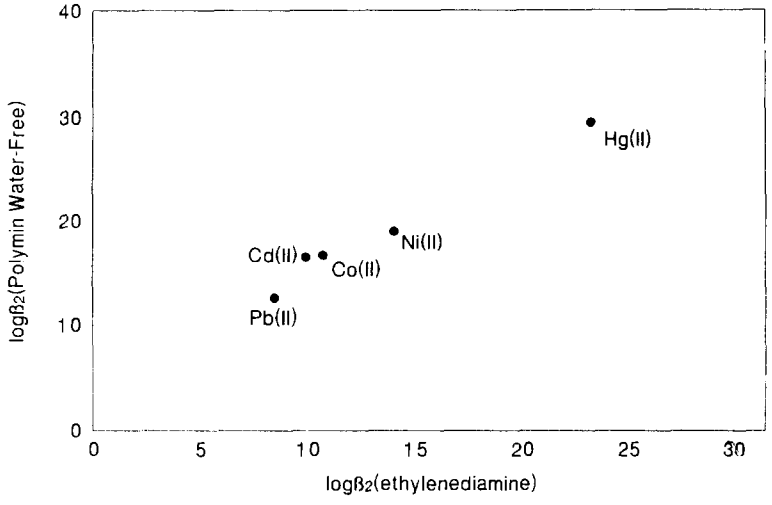


Fig. 10. Plot of $\log\beta_2$(Polymin Water-Free) *vs.* $\log\beta_2$ (ethylenediamine) for the metal ions studied in this paper.

unit were not accepted by ESTA2A into the model.

### *Linear free energy correlations*

A plot of $\log\beta_2$ (Polymin Water-Free) obtained in this study *vs.* $\log\beta_2$ (ethylenediamine)[8] shows a linear correlation (Fig. 10) for the metal ions studied. Such a correlation may be expected. The fact that this was indeed obtained is gratifying and lends credibility to the method of treating the polymer as a collection of monomeric units for modelling purposes.

*Acknowledgements*—The authors wish to thank the Atomic Energy Corporation for permission to publish this work and Annah Rangoaga for performing some of the potentiometric titrations.

## REFERENCES

1. K. Geckeler, G. Lange, H. Eberhardt and E. Bayer, *Pure Appl. Chem.*, 1980, **52**, 1883.
2. M. Rumeau, F. Persin, V. Sciers, M. Persin and J. Sarrazin, *J. Membr. Sci.*, 1992, **73**, 313.
3. A. P. Novikov, V. M. Shkinev, B. Ya. Spivakov, B. F. Myasoedov, K. E. Geckeler and E. Bayer, *Radiochim. Acta*, 1989, **46**, 35.
4. L. P. Buckley, V. T. Le, G. J. McConeghy and J. F. Martin, *Selective Removal of Dissolved Toxic Metals from Groundwater by Ultrafiltration in Combination with Chemical Treatment*, AECL-10030, 1989.
5. N. V. Jarvis and J. M. Wagener, *Talanta*, 1994 (in press).
6. P. M. May, K. Murray and D. R. Williams, *Talanta*, 1985, **32**, 483.
7. P. M. May and K. Murray, *Talanta*, 1988, **35**, 927.
8. A. E. Martell and R. M. Smith, *Critical Stability Constants*, Vols 1–6, Plenum, New York, 1974–1988.
9. D. Horn, in *Polymeric Amines and Ammonium Salts*, E. J. Goethals (ed.), p. 335, Pergamon Press, London, 1980.

Pergamon

0039-9140(94)00232-0

*Talanta*, Vol. 42, No. 2, pp. 227–234, 1995

0039-9140/95 $9.50 + 0.00

# CATALYTIC CATHODIC STRIPPING VOLTAMMETRY OF OXIDIZED GLUTATHIONE AT A HANGING MERCURY DROP ELECTRODE IN THE PRESENCE OF NICKEL ION

FLORINEL G. BĂNICĂ,[1] ARNOLD G. FOGG[2] and JOSINO C. MOREIRA[2]

[1]Department of Analytical Chemistry, The University Politehnica of Bucharest, Spl Independentei 313, Bucharest, Romania

[2]Chemistry Department, Loughborough University of Technology, Loughborough, Leicestershire LE11 3TU, U.K.

(*Received* 22 *April* 1994. *Revised* 11 *July* 1994. *Accepted* 1 *August* 1994)

**Summary**—Oxidized glutathione (GSSG) can be determined after previous accumulation on the HMDE at $E > -0.2$ V (*vs.* the Ag/AgCl reference electrode). GSH is formed during the accumulation, possibly by a mercury-ion-assisted hydrolytic disproportionation of GSSG. In the subsequent cathodic scan GSH is released and catalyses the reduction of nickel ion, giving a peak located at $-0.6$ V. This enables the determination of GSSG by differential-pulse cathodic stripping voltammetry at pH 7.0 in the phosphate acetate or MOPS buffer containing 0.5–1.0 m*M* Ni(II). The detection limit is 10 n*M*. The calibration graph is linear even in the presence of small amounts of human serum albumin, HSA. However, HSA increases the detection limit (20 n*M* for $3 \times 10^{-4}$% HSA). Acetyl-cysteine in small excess or Cu(II) present as reagent impurity do not interfere. Glutathione, cysteine and similar compounds, which accumulate as mercury salts and form stable nickel complexes, will interfere. The method is put forward as a novel alternative stripping voltammetric method to those involving accumulation and determination as mercury or copper salts and complexes, in the knowledge that it may have advantages in particular analytical situations. In particular the method discriminates against compounds which accumulate as mercury salts but which do not form stable nickel complexes.

Oxidized glutathione (GSSG, formula I) is an important component of biological media, in close connection with its reduced form, GSH.[1] Owing to their outstanding biological importance, this couple has been extensively studied from both the biochemical and physico-chemical standpoints. The redox reaction (1) makes the electrochemical methods very useful for the investigation of its reactivity, as well as for the analytical determination.

$$GSSG + 2e^- + 2H^+ \rightarrow 2GSH. \qquad (1)$$

The results of early polarographic investigations on GSSG are summarized in Ref. 2. Accordingly, GSSG gives a single reduction wave with a pH-dependent half-wave potential ($E_{1/2} = -0.56$ V at pH 7). The shape of the wave, however, is not in accord with the equation derived under the assumption of a reversible reduction.

The advent of the new polarographic techniques renewed the interest in the polarography of this compound.[3] Particularly, cathodic stripping voltammetry (CSV) of GSSG appeared very promising. The best results are obtained if traces of Cu(II) are present.[4] From this point of view, GSSG mostly behaves as cystine (Cys, formula II).[5] The main characteristic is the breaking of the disulphide bridge during the accumulation step. The plated compound is a metal thiolate, the metal being either Hg(II) or Cu(I) [provided Cu(II) is present at the 50$\mu M$ level]. As in the case of GSH, the stripping peak is due to the reduction of the metal ion in the plated compound. The Cu(I) thiolate is reduced at more negative potentials as compared with the Hg analogue.[4-6]

Although very sensitive, the CSV of thiols and disulphides is less selective, because the accumulation step is based on the general property of cysteine-like compounds to act as monofunctional ligands (through the sulphydryl group) in the complexes with soft metals.[7] It was recently shown that a better selectivity could be achieved by CSV in the presence of nickel ion.[8,9] The analyte (CysH, Cys[8] or GSH[9] is accumulated on the mercury electrode at $E > -0.3$ V. During the subsequent cathodic scan, the thiol

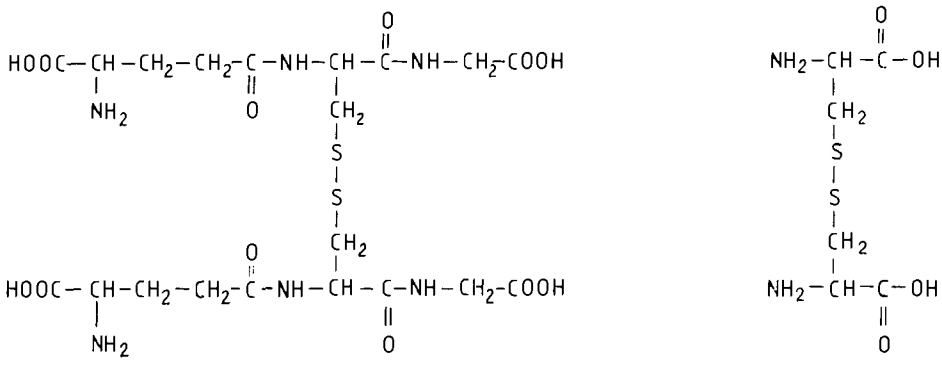

I II

Formulas I and II

catalyses the reduction of Ni(II) giving a characteristic peak in differential-pulse cathodic stripping voltammetry (DPCSV). The same principles are applied in this paper aiming to find the best conditions for the determination of GSSG.

## EXPERIMENTAL

GSSG, GSH, Cys, *N*-acetylcysteine (AcCysH) and human serum albumin (HSA) were Sigma products. Two different buffer systems were used as supporting electrolyte: (1) the phosphate–acetate buffer (PA), which consists of $Na_2HPO4$ and $CH_3COONa$, 0.025*M* each. The pH was adjusted by proper additions of 10% $H_2SO_4$. (2) 0.05*M* 3-(*N*-morpholino)-propanesulphonic acid (MOPS), with the pH adjusted by 10% NaOH.

The Metrohm 663 VA stand in conjunction to the Metrohm 626 Polarecord were employed in the DPCSV experiments. Linear-sweep and cyclic voltammograms were recorded on a PAR 174 instrument. The working electrode was an HMDE (larger size available for the device employed). The cell also included an Ag/AgCl (3M KCl) reference electrode and a glassy carbon rod as auxiliary electrode. The working parameters were as follows: pulse height, 50 mV; pulse interval, 0.5 sec; scan rate, 10 mV/sec. During the pre-concentration step the test-solution was stirred by a Teflon rod usually at the medium speed. Oxygen was expelled by pure nitrogen. Other experimental details are given in Ref. 8.

## RESULTS

### *Behaviour of GSSG in the absence of nickel ion*

Since no previous data on the CSV of GSSG in the buffers here employed are available, its behaviour was tested by several preliminary experiments. Thus, the linear-sweep cathodic stripping voltammograms in Fig. 1 show that after accumulation for 1–2 min at −0.20 V, a cathodic peak forms at −0.47 V. The cyclic voltammogram recorded under similar conditions (Fig. 2) demonstrates that the height of the cathodic peak decreases for successive cycles. On the anodic side, a very small peak appears only during the first scan. It lies in the same potential range as the cathodic one.

The data in Figs 1 and 2 suggest that GSSG is accumulated on the HMDE at potentials close to 0.0 V. In accord with Ref. 4 it may be assumed that the disulphide splits during the plating step and the product of the anodic reaction is a mercury thiolate in the adsorbed state. At more negative potentials this product is reduced and simultaneously the free ligand thus produced desorbs and diffuses back into the bulk of the solution.

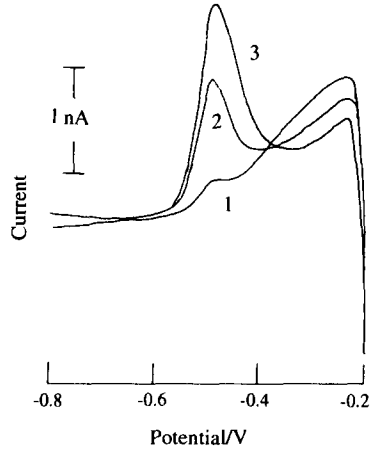


Fig. 1. Linear-sweep cathodic stripping voltammograms (scan-rate, 25 mV/sec) of GSSG (50 n*M*) in the PA buffer (pH 7). Accumulation time (at −0.20 V): (1) 0, (2) 1, (3) 2 min.

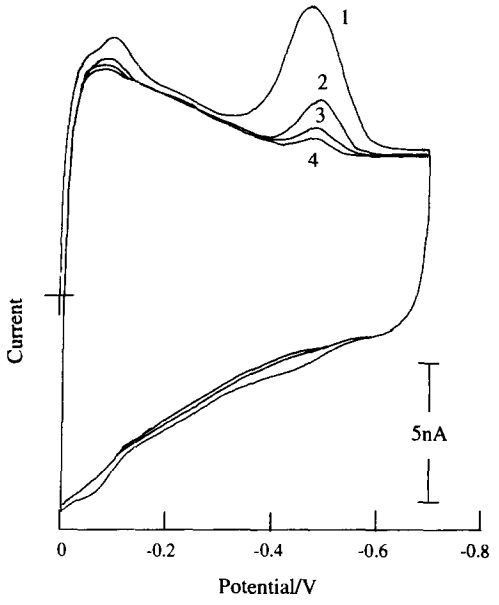


Fig. 2. Cyclic voltammogram of GSSG (50 n$M$) in the PA buffer (pH 7). Start potential, 0.0 V; scan rate, 20 mV/sec. First scan: after 3 min of accumulation at 0.0 V.

DPCS voltammograms recorded under the same conditions also display a symmetrical peak located at $-0.47$ V; as in the case of GSH[9] this will be termed the cathodic stripping peak (CSP). The height of this peak (recorded in the PA buffer) is dependent on the accumulation potential ($E_{acc}$), being slightly larger for $E_{acc} = -0.30$ V, followed by a sharp decrease at more negative values of $E_{acc}$. It vanishes at $E_{acc} \leq -0.45$ V.

*Influence of nickel ion*

As in the case of GSH,[9] the DP cathodic stripping voltammograms recorded in the presence of both GSSG and Ni(II) display a new peak at $-0.60$ V (Fig. 3). It shows a striking analogy with the peak produced under similar conditions by GSH,[9] CysH and Cys.[8] That is why this peak is ascribed to the reduction of $Ni^{2+}$ catalysed by GSH which forms by the splitting of GSSG and will be termed the catalytic cathodic stripping peak (CCSP).

The peak potential is not dependent on Ni(II) concentration. However, as shown in Fig. 4, the DP peak current increases with the rise of NI(II) content, both in the MOPS (curve 1) or PA buffer (curve 2). As usual[8,9] a high excess of Ni(II) is required to achieve good sensitivity. Nevertheless, Ni(II) concentrations higher than 1m$M$ were avoided, because the current due to the diffusion-controlled Ni(II) reduction may overlap the CCSP.

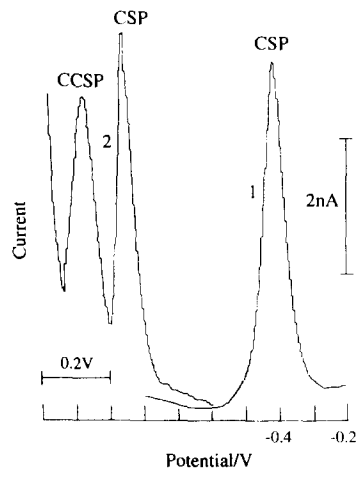


Fig. 3. Effect of nickel ion on GSSG behaviour in DP cathodic stripping voltammetry. MOPS buffer, pH 7.0. GSSG, 50 n$M$. Accumulation: at $-0.20$ V for 2 min. $Ni^{2+}$ (m$M$): (1) 0, (2) 1.

As in the case of GSH[9] the base-line for the measurement of the CCSP current is defined by the lowest level of the voltammogram at the foot of the peak. Tests under various conditions proved that this gives the best relationship between the peak current and GSSG concentration.

The CSP of GSSG is only slightly influenced by Ni(II) (Fig. 3). This behaviour is similar to that of GSH,[9] but strongly contrasts with that of Cys and CysH,[8] whose CSP peaks are suppressed by Ni(II) in high excess.

*Effect of* pH *and buffer composition*

Owing to the competition between proton and Ni(II) for the binding sites in the glutathione molecule, the pH is a very important parameter. In addition, the pH may influence the conversion of GSSG into GSH. Consequently, the effect of pH in the GSSG–Ni(II)

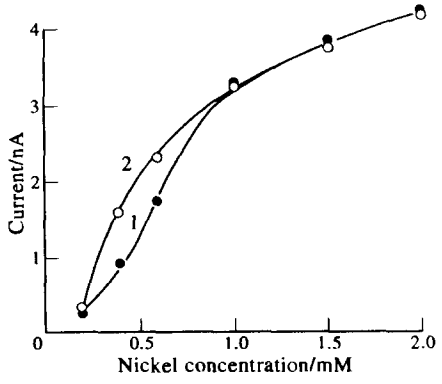


Fig. 4. The dependence of the CCSP DP current on nickel ion concentration. pH 7.0; GSSG 50 n$M$. Accumulation: at $-0.20$ V for 2 min (1) MOPS, (2) PA buffer.

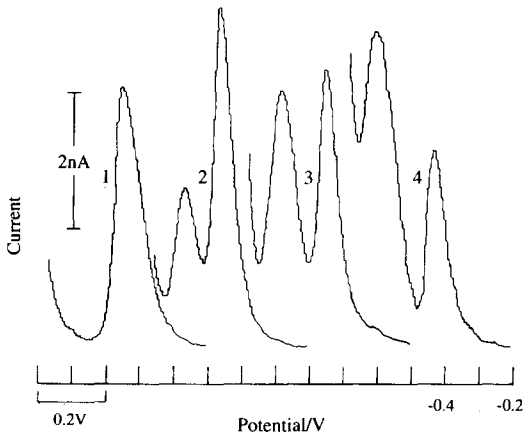


Fig. 5. DP cathodic stripping voltammograms of GSSG (50 n$M$) at various pH-values (MOPS buffer) in the presence of nickel ion (1m$M$). Accumulation: at −0.20 V for 2 min. Potential scale: −0.10 V/div. pH: (1) 6.40, (2) 6.72, (3) 7.00, (4) 7.36.

system was investigated in both the PA and MOPS buffers. Typical DP voltammograms recorded at various pH-values are presented in Fig. 5. Curve 1 in this figure shows that at pH 6.40 only the CSP forms ($E_{peak} = 0.45$ V). The occurrence of the CCSP at −0.60 V requires higher pH-values (curves 2–4). The rise of pH produces a negligible shift in the CCSP potential, but an appreciable increase in the peak height. However, at pH > 7 (curve 4) the catalytic process is partly overlapped by the diffusion-controlled Ni(II) reduction, which slightly shifts towards less negative potentials. This trend was noted in both the PA and MOPS buffer.

The dependence of the CCSP DP current on pH is presented in Fig. 6 for both the MOPS (curve 1) and PA buffer (curve 2). Although pH values higher than 7 seem to offer a better sensitivity, this pH-range was avoided owing to the overlapping effect depicted by curve 4 in Fig. 5. Typically, the pH was adjusted to 7.0 in both buffers. At this pH value, the PA buffer gives a higher peak current, but a better separation of the CCSP from the main nickel peak was noted for MOPS.

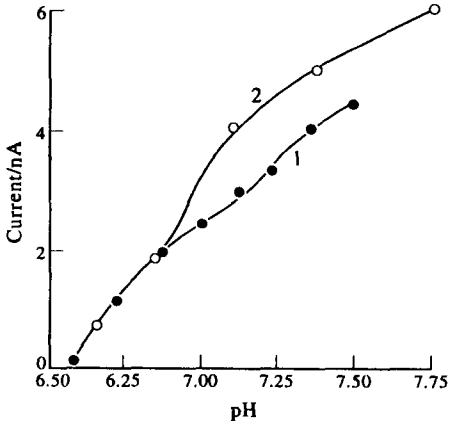


Fig. 6. Dependence of the CCSP DP current on pH in the MOPS (curve 1) or PA buffer (curve 2). Same conditions as in Fig. 5.

*Influence of accumulation conditions*

The effect of $E_{acc}$ in the MOPS buffer on the DP current is presented in Fig. 7a for both the CSP (curve 2) and the CCSP (curve 3). For

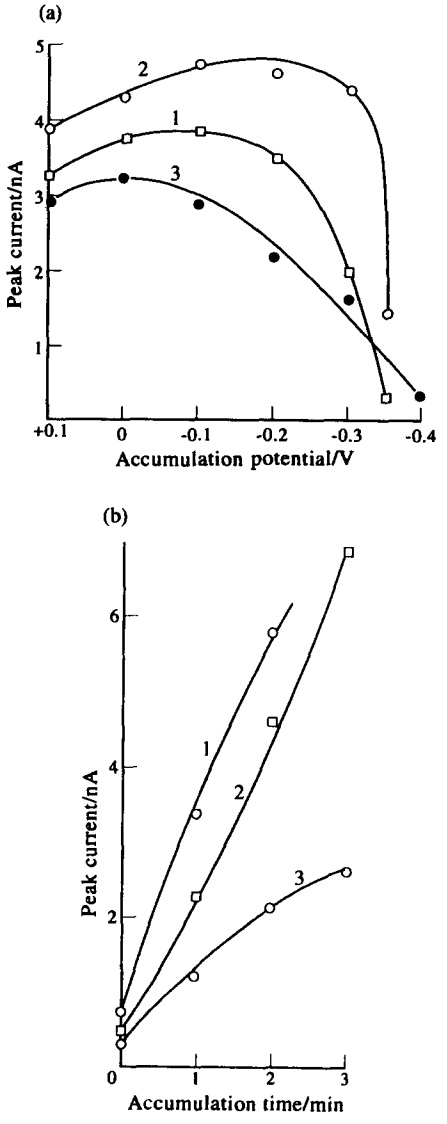


Fig. 7. Effect of accumulation potential (a) and accumulation time (b) on the DP cathodic stripping behaviour of GSSG (50 n$M$) in the MOPS buffer (pH 7.1), in the absence of $Ni^{2+}$ (curve 1) or in the presence of 0.5 m$M$ $Ni^{2+}$ (curves 2 and 3). Curve 2: CSP, curve 3: CCSP. (a) $t_{acc} = 1$ min (curve 1); 2 min (curves 2 and 3). (b) $E_{acc} = -0.20$ V.

comparison, curve 1 in the same figure shows the variation of the CSP in the absence of Ni(II). The CSP sharply decreases for $E_{acc} < -0.25$ V, no matter whether Ni(II) is present or not. Conversely, the CCSP decreased gradually for $E_{acc} < -0.1$ V.

Figure 7b shows the effect of the accumulation time in the MOPS buffer on the DP current. It is seen that the CSP recorded either in the absence (curve 1) or in the presence of Ni(II) (curve 2) strongly increases with the accumulation time. The CCSP current tends to level off after a few minutes' accumulation. The effects of the accumulation conditions in the PA buffer are analogous to those found with MOPS.

*Calibration graph, sensitivity and detection limit*

The CCSP current depends linearly on GSSG concentration. The results of data processing by the least-squares method are summarized in Table 1. From the table it is seen that the intercept of the regression line (peak current *vs.* GSSG concentration, in the form $i = a + bc$) is very small. That is why the parameters of the regression line were also calculated by assuming the direct proportionality (*i.e.* $i = b'c$). These lines were compared by means of the $F$ test, as described in Ref. 9. For all the three sets of data included in Table 1, $F[99\%, 1, (n-2)] > F_{calc}$, proving that the direct proportionality relationship can be accepted.

The values of the slope $b'$ in Table 1 show the influence of some experimental factors on the sensitivity of the method. For instance, the accumulation at 0.00 V (3rd column) brings about a slight improvement in sensitivity as compared with that found for $E_{acc} = -0.20$ V (1st column). As expected, the decrease of the pulse-height from 50 to 10 mV (2nd column) produces a strong decrease in sensitivity, but simultaneously the standard deviation of the fit is much improved. The detection limit in Table 1 is the concentration corresponding to the peak current equal to $3\,s'_0$. The higher value in the 3rd column results from the unfavourable effect of the higher stirring rate on $s'_0$. It is obvious, however, that GSSG may be quantitated even at the level of 10 n$M$, as shown by the data in the 1st and 2nd columns.

Table 1. Parameters of the linear calibration graph for GSSG [$t_{acc} = 2$ min, $E_{acc} = -0.2$ V (1 and 2), 0.0 V (3)]

| | 1 | 2 | 3 |
|---|---|---|---|
| Concn range (n$M$) | 10–200 | 10–130 | 10–200 |
| Buffer and pH | PA, 7.10 | PA, 7.10 | MOPS, 7.10 |
| [$Ni^{2+}$] (m$M$) | 1.0 | 1.0 | 0.5 |
| No. of points ($n$) | 13 | 8 | 13 |
| Line $i = a + bc$ | | | |
| $a$ (nA) | −0.31 | −1.19 | −0.67 |
| b (nA/n$M$) | 0.084 | 0.019 | 0.102 |
| $s_0$ (nA) | 0.22 | 0.05 | 0.40 |
| $r$ | 0.999 | 0.998 | 0.999 |
| Line $i = b'c$ | | | |
| $b'$ (nA/n$M$) | 0.082 | 0.019 | 0.098 |
| $s'_0$ (nA) | 0.27 | 0.05 | 0.59 |
| $F_{calc}$ | 6.61 | 0.29 | 5.38 |
| $F$ (99%, 1, ($n$-2)) | 9.65 | 13.7 | 9.65 |
| Detection limit (n$M$) | 10 | 8 | 18 |

$r$ = Regression coefficient, $s_0$, $s'$ = Standard deviations of the fit; $i$ = peak current (nA), $c$ = analyte concentration (n$M$).

(2): Pulse height = 10 mV; calibration graph bent downward for [GSG] > 130 n$M$.

(3): Maximum stirring speed.

*Interference of some related compound*

Since the CCSP is also produced in the presence of Cys,[8] the effect of this compound on the GSSG–Ni(II) system was investigated. If the CCSP current in the absence of Cys is taken as reference, the peak current increases about two times for a [Cys]/[GSSG] ratio of 0.5 and about three times for this ratio equal to 1. Certainly, this increase is due to CysH which forms by the splitting of Cys.

The mutual interference of GSH and GSSG was also studied. In the presence of each of these compounds the CCSP appears at the same potential. However, under similar conditions, the slopes of the calibration graphs are different, even if it is taken into account that two molecules of GSH could result from one molecule of GSSG.

As in the case of CysH[8] or GSH[9] Ac-CysH has only a minor effect on the CCSP recorded in the presence of GSSG, although, under the same conditions the CSP is strongly enhanced. Thus the CCSP is diminished only by 8% in the presence of a 10 times excess of Ac-CysH.

*Effect of HSA*

The effect of HSA may be typical for some proteins that are present in biological samples. That is why its effect was studied in Ni(II)-containing solutions, both in the presence or in the absence of GSSG.

In the absence of GSSG, after the accumulation at −0.20 V (2 min), HSA gives a shoulder on the DP voltammogram at about −0.6 V (Fig. 8, curve 2). This shoulder is hardly observable for $10^{-4}$% HSA, but sharply increases for higher concentrations. Its height tends to level off for HSA concentrations above $5 \times 10^{-4}$%.

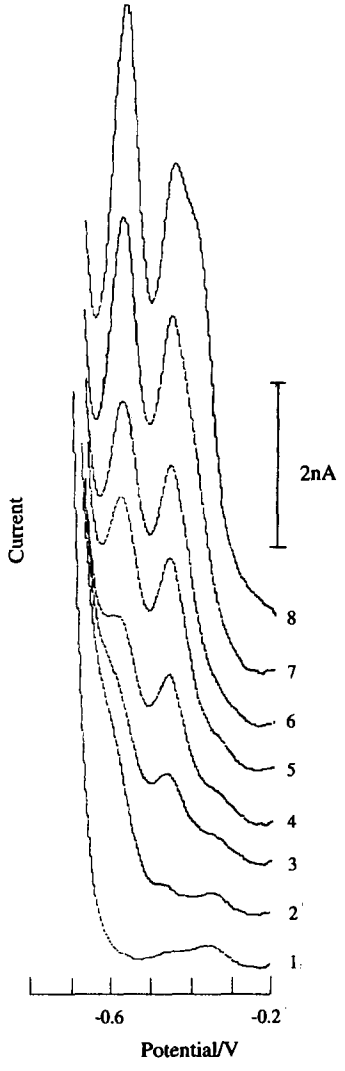


Fig. 8. Effect of HSA on the DP cathodic stripping behaviour of GSSG. pH 7.0 (PA buffer); $Ni^{2+}$, 0.5 m$M$; HSA, $3 \times 10^{-4}$%. Accumulation: at $-0.2$ V, for 2 min. (1) Buffer + $Ni^{2+}$, (2–9) $3 \times 10^{-4}$% HSA added. GSSG, n$M$: (1 and 2) 0, (3) 10, (4) 20, (5) 30, (6) 40, (7) 60, (8) 80.

In the absence of the accumulation step in the stirred solution (but after 30 sec of contact of the quiescent solution with the HMDE), the shoulder is hardly observable. This shoulder may be ascribed to the reduction of Ni(II) catalysed by HSA. Its increase after the accumulation at $-0.20$ V in the stirred solution proves the adsorption of HSA on the HMDE.

At constant concentrations of GSSG (50 n$M$) and $Ni^{2+}$ (0.5 m$M$) the increase of HSA concentration from zero to $6 \times 10^{-4}$% produces a two-fold effect: (1) the CSP is slightly depressed and (2) the CCSP is lifted on the current scale and also its height is increased. By comparing these effects it is observed that the accumulation of GSSG at $-0.2$ V suffers only minor interference from HSA. The main interference occurs in the catalytic reduction of $Ni^{2+}$, in accord with the above-described effect of HSA in the absence of GSSG.

Another experiment was aimed to detect the influence of HSA on the calibration graph. To this end, cathodic stripping voltammograms were recorded at constant concentrations of Ni(II) and HSA and various concentrations of GSSG (curves 2–8 in Fig. 8). Curve 3 in Fig. 8 shows that for 10 n$M$ GSSG the CCSP does not develop properly. However, for higher GSSG concentrations (curves 4–8) the peak assumes the usual shape, enabling the study of the current-concentration relationship. By the same procedure as that described in section, "calibration graph, sensitivity and detection limit" it was found that the peak current is directly proportional to GSSG concentration within the range 20–100 n$M$. The slope is $0.047_1$ nA/nM (standard deviation of the slope, 0.001), and the standard deviation of the fit is 0.20 nA (under the conditions of Fig. 8).

The above data suggest that there is competition for Ni(II) binding between GSH (formed by the cleavage of GSSG) and HSA. This explains the removal of the disturbing effect of HSA at higher values of the [GSSG]/[HSA] ratio.

On the same basis it can be concluded that in the presence of HSA the statistically defined detection limit is unrealistic, the actual one being higher. For example, under the conditions of Fig. 8 the statistical treatment of data gives a detection limit close to 10 n$M$, but at this level HSA strongly disturbs the signal and the actual detection limit (suggested by the examination of voltammograms) seems to be about 20 n$M$.

Despite these disadvantages, it is seen that GSSG can be determined in the presence of a moderate amount of HSA. Moreover, the direct proportionality between the CCSP current and GSSG concentration permits the use of the standard addition method for the analysis of HSA-containing samples.

*Effect of copper ion*

The influence of Cu(II) is similar to that noted in the case of GSH.[9] Thus, for 40 n$M$ GSSG and accumulation at $-0.20$ V, the addition of 0.1$\mu M$ Cu(II) shifts the CSP to $-0.50$ V, partly overlapping the CCSP. For 0.2$\mu M$ Cu(II) the CCSP is almost completely overlapped. The accumulation at more positive potentials (0.0 or $+0.1$ V) diminishes the effect on Cu(II), but its

interference cannot be completely removed in this way. Also, the accumulation at a more negative potential (−0.4 V) does not improve the shape of the voltammogram. Under such conditions, the catalytic reduction of $Ni^{2+}$ gives only a small shoulder, although the peak due to the copper complex is well developed. The interference of Cu(II) is not removed by EDTA even in excess over Cu(II). Nevertheless, traces of Cu(II) present as an impurity in the reagents will not interfere.

## DISCUSSION

A common feature in the CSV of disulphides is that the stripping peak lies at the same potential as that of the corresponding reduced form. This behaviour was noted both in the absence[10,11] or in the presence of Cu(II)[4,5,12] and is explained by the formation of the thiol during the accumulation step of disulphide. In this connection, the occurrence of the CCSP in systems containing either Cys[8] or GSSG (this work) is an additional proof for disulphide cleavage. Usually, the accumulation is effected at a potential too positive to allow the occurrence of disulphide reduction, according to equation (1). The absence of a characteristic peak on the stripping voltammogram demonstrates the absence of such a reaction during the redissolution step. An alternative explanation is founded on the reduction of disulphide by the reaction with mercury[10] or copper amalgam:[5]

$$RSSR + 2M = 2MRS_{ads}, \qquad (2)$$

where M = Hg or Cu. The occurrence of such a reaction has been rejected for both thermodynamic and experimental reasons, at least for mercury.[13]

A more reliable explanation is given in Refs 14, 15, where it is demonstrated that the hydrolytic disproportionation of the disulphide is promoted by Cu(II) ion, according to the reactions:

$$2RSSR + 2OH^- = 2RS^- + 2RSOH \qquad (3)$$

$$2RSOH = RSH + RSO_2H. \qquad (4)$$

In the absence of Cu(II) these reactions occur only at high pH (0.2*M* NaOH).[16] The above reactions occur at pH < 9 for 1m*M* Cu(II) and offer an explanation for the decrease of the cathodic stripping peak of Cys recorded in the presence of Cu(II) when the pH changes from 9.2 to 4.6.[5] Under the typical conditions of CSV (no Cu(II)), the above reactions might be assisted by mercury ions resulting from the anodic oxidation of the mercury electrode. The reaction rate could be sufficiently fast even at pH < 9 owing to the high concentration in the adsorbed state. Another pathway for disulphide degradation leads to *S*-sulphocysteine.[17] This reaction involves an oxidative step with the participation of dioxygen which would not be applicable in CSV.

In conclusion, it may be inferred that both in the case of Cys[8] or GSSG (this work), the disulphide turns into thiol by the mercury ion-assisted mechanism represented by reactions (3) and (4). The plated compound is always a mercury thiol further represented as HgSR (or HgSG).

In connection with the accumulation mechanism it is worth recalling the main difference between glutathione (either reduced or oxidized) on the one hand, and CysH (or Cys) on the other hand. This consists in the effect of Ni(II) on the CSP of the mercury thiolate. The CSP is suppressed by a large excess of Ni(II) in the cases of CysH or Cys[8], but only slight effects are observed for GSH[9] and GSSG (this work). This difference is a consequence of the different kind of Ni(II) binding. Very strong chelates form in the case of CysH, involving both the amino and sulphydryl groups, but much less stable complexes are formed by GSH, which mainly binds by the terminal groups.[18] It can be assumed, therefore, that Ni(II) strongly interferes in the accumulation process involving CysH, no matter whether CysH is initially present in the solution or forms by the cleavage of Cys. Conversely, in the case of GSH the formation of chelates involving the sulfur site is less probable at medium pH.[19] Consequently, as in the case of Ac-CysH, GSH gives a well developed CSP even in the presence of Ni(II). This remark also applies to GSSG in view of reactions (3) and (4).

As shown, even in the case of GSSG, the actual catalyst is GSH produced by reactions (3) and (4), giving only three molecules of GSH from two molecules of GSSG. This characteristic, as well as the sluggishness of reactions (3) and (4), accounts for the difference in sensitivity noted when GSSG is replaced by a two-times higher concentration of GSH.

During the cathodic scan GSH is released according to the reaction

$$GSHg + H^+ + e^- \rightarrow GSH + Hg. \qquad (5)$$

Its catalytic effect must be produced in the same way as previously described.[9] Studies by DC

polarography[20,21] have already proved that GSH is less catalytically active than CysH owing to the differences in the complexing properties. Nevertheless, the CCSP enables the determination of GSSG at the level of 10 n*M* with good accuracy. Only slight interference is produced by Ac-CysH and the determination can be performed even in the presence of small amounts of protein (HSA for example).

The method is not able to distinguish between GSSG and GSH. However, the overall amount of glutathione in the sample could be evaluated after the conversion of one form into the other one by an appropriate reaction. Other compounds which accumulate as mercury salts, and which form stable complexes with nickel, will interfere, and the method presented here does not have a particularly low detection limit, as the catalysis is simply on a one to one basis and does not increase the sensitivity. The method is put forward as a novel alternative stripping voltammetric method to those involving accumulation and determination as mercury or copper salts and complexes, in the knowledge that it may have advantages in particular analytical situations. In particular the method discriminates against compounds which accumulate as mercury salts but which do not form stable nickel complexes. Voltammetric methods, including stripping methods, are being applied increasingly in disposable sensor devices, and accumulation and reduction of nickel complexes might prove advantageous here too.

*Acknowledgements*—FGB thanks the Commission of European Communities for financial support (PECO award), Loughborough University of Technology for research facilities and the University Politechnica of Bucharest for leave of absence. JCM thanks CESTEH (Oswaldo Cruz Foundation) and the Departamento de Quimica (UFRRJ), Brazil, for leave of absence.

## REFERENCES

1. H. Sies, *Naturwissenschaften*, 1989, **76,** 57.
2. M. Brezina and P. Zuman, *Polarography in Medicine, Biochemistry and Pharmacy*, p. 522. Interscience, New York, 1958.
3. C. A. Mairesse-Ducarmois, G. J. Patriarche and J. L. Vanderbalck, *Anal. Chim. Acta*, 1975, **76,** 299.
4. U. Forsman, *Anal. Chim. Acta*, 1984, **166,** 141.
5. U. Forsman, *J. Electroanal. Chem.*, 1981, **122,** 215.
6. A.-C. Le Gall and C. M. G. van den Berg, *Analyst*, 1993, **118,** 1411.
7. I. Sovago and A. Gergely, in *Trace Elements in the Pathogenesis and Treatment of Inflammation*, K. D. Rainsford, K. Brune and M. W. Whitehouse (eds), p. 291. Birkhäuser, Basel, 1981.
8. F. G. Banica, J. C. Moreira and A. G. Fogg, *Analyst*, 1994, **119,** 309.
9. F. G. Banica, A. G. Fogg, and J. C. Moreira, *Analyst* (in press).
10. T. M. Florence, *J. Electroanal. Chem.*, 1979, **97,** 219.
11. R. von Wandruszka, X. Yuan and M. J. Morra, *Talanta*, 1993, **40,** 37.
12. C. M. G. van den Berg, B. C. Household and J. P. Riley, *J. Electroanal. Chem.*, 1988, **239,** 137.
13. M. T. Stankovich and A. J. Bard, *J. Electroanal. Chem.*, 1977, **75,** 487.
14. M. Ostern, J. Pelczar, H. Kozlowski and B. Jezowska-Trzebiatoska, *Inorg. Nucl. Chem. Lett.*, 1980, **16,** 251.
15. W. Stricks and I. M. Kolthoff, *Anal. Chem.*, 1953, **25,** 1050.
16. W. Stricks and I. M. Kolthoff, *J. Am. Chem. Soc.*, 1952, **74,** 4646.
17. P. Mader, J. Volke and J. Kuta, *Collect Czech. Chem. Commun.*, 1970, **35,** 552.
18. K. Varnagy and I. Sovago, *Inorg. Chim. Acta*, 1988, **151,** 117.
19. I. Sovago and R. B. Martin, *J. Inorg. Nucl. Chem.*, 1981, **43,** 425.
20. E. Diacu, F. G. Banica and I. Ion, *Rev. Roum. Chim.*, 1992, **37,** 1389.
21. E. Diacu, F. G. Banica and I. Ion, *Rev. Roum. Chim.*, 1993, **38,** 1397.

Pergamon

0039-9140(94)00233-9

*Talanta*, Vol. 42, No. 2, pp. 235–242, 1995

0039-9140/95 $9.50 + 0.00

# DETERMINATION OF GENTIAN VIOLET IN HUMAN URINE AND POULTRY FEED BY HIGH PERFORMANCE LIQUID CHROMATOGRAPHY WITH ELECTROCHEMICAL DETECTION USING A CARBON FIBRE MICROELECTRODE FLOW CELL

KAMAL A. SAGAR,[1] MALCOLM R. SMYTH,*[1] MARGARITA RODRIGUEZ[2] and PAULINO TUNON BLANCO[2]

[1]School of Chemical Sciences, Dublin City University, Dublin 9, Ireland; [2]Department of Analytical Chemistry, University of Oviedo, Asturias, Spain

(*Received* 26 *April* 1994. *Revised* 27 *June* 1994. *Accepted* 1 *August* 1994)

**Summary**—A sensitive and relatively selective high performance liquid chromatographic method for the determination of Gentian Violet (GV) in human urine and chicken feed is described. The method is based on solid-phase extraction, with subsequent reversed-phase chromatographic separation on a cyano column and amperometric detection using a carbon fibre microelectrode flow cell operated at +1.3 V. The peak currents were directly proportional to GV concentration over the concentration range 1–30 ppb (for urine samples analysis) and 1–20 ppm for poultry feed analysis. Using this method, the minimum detectable concentration was estimated to be 0.5 ppb. The method was applied successfully to the determination of GV in human urine and in chicken feed, and it was concluded that the method could be applied to the quantitative analysis of GV in the presence of its major metabolite, leuco GV. In the proposed procedure, the occurrence of matrix effects during urine analysis was significant. The electrochemical pretreatment regime described in this paper was used to overcome these effects. Recovery studies were performed on both the human urine and chicken feed samples. The recovery of GV ranged from 92 to 96% in both matrices, with a relative standard deviation of less than 5.5%.

Gentian Violet (GV; hexamethyl pararosaniline; also known as Crystal Violet) is classified as a triphenylmethane dye, and has been marketed since 1951 for a variety of uses. It has anthelmintic properties and has been used in the treatment of strongyloid infestation.[1] The compound has also been used in humans, as an antimicrobial agent in the treatment of burn victims, to treat umbilical cords of infants as a vaginal cream, for various purposes in veterinary medicine, and as a pH indicator substance. At present, the U.S. Food and Drug Administration (FDA) permits the use of GV (8 ppm) in poultry feeds as a mould inhibitor. GV has however been determined to be mutagenic to *Bacillus subtilis*, *Escherichia coli*, and *Salmonella typhimurium*,[2] and cytotoxic to mammalian cells.[3] Au *et al.*[4,5] demonstrated its genetic cytotoxicity to Chinese hamsterovary (CHO) cells. Concern about the health risks and carcinogenicity associated with the use of GV requires that a routine laboratory method be developed to monitor the drug and its metabolite.

Typical approaches for determining GV have involved the use of potentiometry,[6] spectrophotometry[7] and mass spectrometry,[8] and lately by HPLC with amperometric detection using macroelectrodes such as the glassy carbon electrode.[9] The virtues of microelectrodes are well known,[10–12] and the advantages of studying their steady-state voltammograms are well documented.[13,14] Use of microelectrodes (typically micron to submicron sizes) has recently made inroads into the use of LC-EC in clinical applications. The main advantage is the ability to construct extremely low volume cells (as low as a few picolitres for a carbon-fibre microcylinder electrode).[15] Other advantages include: (1) detection limit improvements, as reported in the determination of norepinephrine (sub-pmol) using a carbon fibre electrode;[16] (2) a lower dependency on flow rate, and thus lower noise associated with flow-rate fluctuations;[16,17] (3) higher current densities, time-independent

*Author to whom all correspondence should be addressed.

currents and better signal-to-noise ratios; (4) the possibility of using very high scan rates or simpler instrumentation, and (5) the capability of carrying out measurements in solutions with very low conductivity.[18,19] The major drawback with microelectrodes is that fabrication difficulties increase as the size of the microelectrode decreases,[20] and so far they have relatively limited commercial availability. Hence, most workers normally prepare their own microelectrodes by sealing thin wires or fibres in glass capillaries, either by melting the glass or by using an epoxy resin.[21–23] Sealing wires or fibres into glass is technically demanding, and there is always a risk that the relatively high temperatures needed to melt the glass might change the characteristics of the electrode material. It has been reported that carbon fibres which had been in contact with a flame were more fragile and needed longer electrochemical conditioning.[24] It is necessary, therefore, to ensure the highest possible activity of the electrode surface, by establishing the most suitable and convenient pretreatment procedures for the electrochemical detector, following studies relating to the features of the analyte and sample matrix to be dealt with.

This paper describes the development of a LC-EC method using a microelectrode flow cell based on a carbon fibre working electrode, for the determination of GV at concentration ranges of 1–30 ppb in human urine, and at 1–20 ppm in poultry feed. The method could also determine GV in the presence of its major pharmacologically active metabolite (leuco Gentian Violet).

## EXPERIMENTAL

### *Reagents and materials*

Carbon fibres, 14 $\mu$m in diameter, were obtained from Avco (Lowell, MA, U.S.A.). Chemicals were used without further purification. All chemicals were of analytical-reagent grade, unless otherwise indicated. Gentian Violet (USP,[25] Crystal Violet 96%) and leuco Crystal Violet were obtained from Sigma and were used to prepare reference standards.

Chicken basal diet containing GV at 0 ppm and fortified feed containing GV at 2.5, 5.0 and 10.0 ppm were kindly supplied by the National Food Centre (Dublin, Ireland). Human urine for control and recovery analyses were provided by healthy volunteers. The urine specimens were collected in polycarbonate bottles and were stored at −4°C until analysis. Stock standard solutions equivalent to 0.20 mg/ml GV were freshly prepared in LC grade methanol, mixed and then stored in a cool place (*ca.* 4°C) and protected from light. These were diluted and added to GV-free urine aliquots to generate spiked urine standards in the concentration range 1–30 ppb. The "spiked" samples were left for at least 1 hr before they were analysed to

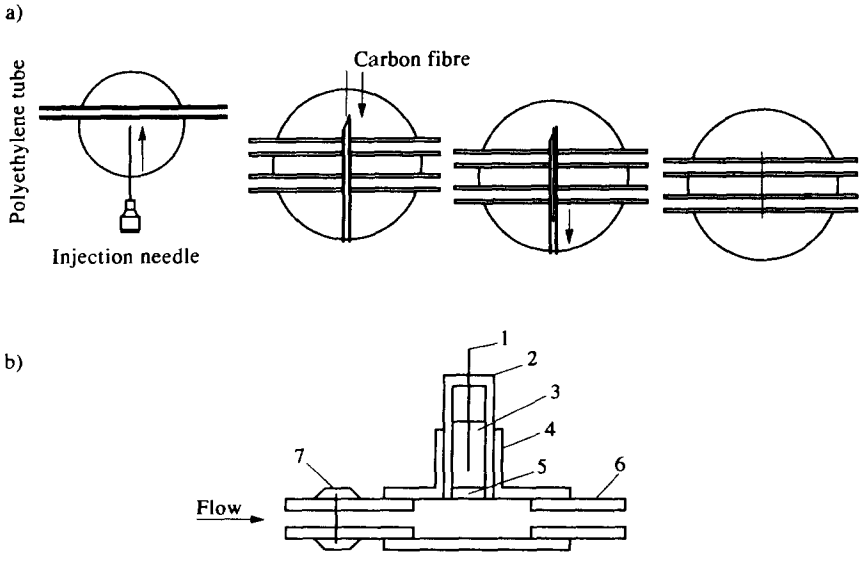


Fig. 1. (a) Method of fixing a carbon fibre into polyethylene tube. (b) The structure of the carbon fibre microelectrode flow cell consisting of: 1, silver wire coated with $Ag_3PO_4$; 2, reference electrode body; 3, internal reference solution; 4, T-tube; 5, ceramic rod; 6, stainless steel counter electrode; 7, carbon fibre flow electrode.

permit any possible interactions between the drug and urine constituents.

*Fabrication of microelectrode flow cell*

The method of inserting the carbon fibre into a polyethylene tube is shown in Fig. 1. An injection needle (o.d. 0.4 mm, i.d. 0.2 mm) was inserted through the centre of a 15-mm piece of polyethylene tube (o.d. 2 mm, i.d. 0.5 mm). A carbon fibre (diameter 14 $\mu$m) was inserted into the injection needle, which was then removed from the tube, leaving the fibre behind. The needle holes were sealed by gentle heating with an electric iron. A copper wire of 0.5 mm diameter was wound around the sealed area for a few turns. The area was then covered with a layer of silver epoxy resin. The resin was diluted with ethyl acetate to a suitable viscosity before application to the tube. After 1 hr the electrode was ready for use. The copper wire was used as a lead for electrical connection. The silver phosphate reference electrode was prepared by connecting a silver wire (0.1 mm in diameter) to the anode and a platinum electrode to the cathode of a 1.5 V battery, while immersing the assembly for 2 min in a solution of 1*M* phosphoric acid. The wire was then inserted into a polyethylene tube, which was 15 mm long and 1 mm in diameter, and a porous rod (2 mm long and 1 mm in diameter) was fitted to one end of the polyethylene tube. The reference electrode tube was then filled with an internal reference solution containing 1*M* phosphoric acid, and this end was closed by heating. A length (2 cm) of stainless steel tubing (1 mm × 0.2 mm i.d.) served as the counter electrode. The working, reference, and counter electrodes were mounted in a T-tube arrangement, and the working electrode was connected to the outlet of the HPLC column (downstream of the working electrode). Hence the mobile phase eluent passed first through the working electrode and then via the counter electrode to waste.

*Cyclic voltammetry*

Cyclic voltammetric experiments were initially recorded on blank solutions of 0.05*M* acetate buffer, followed by solutions containing $1 \times 10^{-3}M$ GV dissolved in 0.05 acetate buffer solution (pH 5.5) at a glassy carbon electrode. Voltammetric conditions were as follows: initial potential 0 V; final potential 1.6 V and scan rate 50 mV/sec. Prior to scanning, the electrode was cleaned by washing with distilled water, polishing the surface with aluminium oxide powder (0.3 $\mu$m), rinsing again with distilled water followed by acetone and finally drying with a tissue-paper. The glass cell and the counter electrode were soaked in $HNO_3$ solution, and then rinsed thoroughly with triply-distilled water. The presence of any adsorption process was investigated by multiple CV scanning without pretreatment of the glassy carbon electrode.

*Extraction and clean-up procedures*

*Poultry feed.* The sample preparation and clean-up procedures were reported previously by Roybal *et al.*[9] Blank chicken feed and sample feed were ground to pass through a 1 mm sieve (Pascal Engng Co. Ltd, Crawley, U.K.), stored in a quart glass jar, and kept in a cool, dry place. Ground feed (20 g) was then accurately weighed into a 500 ml centrifuge bottle, 200 ml methanol/1*M* HCl (99:1) was added and the mixture was shaken vigorously for 1 hr on a mechanical shaker, then left to stand overnight. An appropriate aliquot of the supernatant was then pipetted into a 15 ml centrifuge tube according to the following schedule: GV (ppm), aliquot (ml): 10 ppm, 1 ml; 5 ppm, 2 ml and 2.5 ppm, 4 ml. The aliquot was then diluted to 10 ml with mobile phase and mixed. The solution was then filtered through a disposable, 5 $\mu$m polytetrafluoroethylene (PTFE) membrane (Millipore Corp., Bedford, MA, U.S.A.) into a 25 ml Erlenmeyer flask. Then 20 $\mu$l of filtered solution was injected into the liquid chromatograph. The concentration of GV (ppm) in feed was calculated as follows:

$$\text{ppm} = (P/S) \times (C/W) \times (D),$$

where $P$ = peak height (mm) obtained from injection of filtered solution, $S$ = average peak height (mm) obtained from injection of standard, $C$ = concentration (ppm) of injected standard, $D$ = final volume (ml) of filtered solution, and $W$ = initial weight of feed sample taken for analysis.

*Human urine.* The procedures for extracting GV from urine specimens were based on the work of Rushing and Bowman.[26] A 100 ml portion of spiked human urine in a 165 ml culture tube was adjusted to pH 7.0 with 6*M* NaOH. After the addition of 50 ml of dichloromethane the tube was gently shaken by hand for 3 min with care taken to prevent emulsification of the contents. The tube was then centrifuged for 5 min at 500 rpm and the dichloromethane layer removed by syringe,

percolated through 20 g of sodium sulphate in a glass funnel (3.0 cm diameter), and collected in a 250 ml round-bottom flask. The extraction process was repeated with two additional 20 ml portions of dichloromethane, the sodium sulphate washed with 5 ml of dichloromethane, and the combined extracts evaporated to dryness on a 30°C water bath using water pump vacuum. The dry residue was transferred to a 50 ml round-bottom flask by using four successive 1 ml rinses of the dichloromethane which were then evaporated to dryness as described. The residue was finally dissolved in 1.0 ml of methanol and 100 $\mu$l were injected for analysis.

The stability of the urine samples at room temperature was tested by making 10 consecutive injections of the same urine sample over a period of approximately 5 hr. There were no significant changes in the peak current between the first five and the last five samples. In addition, urine samples spiked with the test compound were stable for more than 5 days at $-4$°C.

*HPLC*

The HPLC separation used in this study for the chromatographic separation of the triphenylmethane dye is similar to those reported by Roybal *et al.*[9] The system consisted of a stainless steel column (250 × 4.6 mm i.d.) packed with cyano packing material (particle size 5 $\mu$m) (Hichrom Ltd, Reading, U.K.). The mobile phase was acetonitrile–acetate buffer (60:40); the acetate buffer was prepared by adjusting 0.1*M* sodium acetate solution (8.2 g sodium acetate/1 l. deionized water) to pH 4.5 with glacial acetic acid (*ca.* 8 ml). Sample injections to the column were introduced via a syringe-loading Rheodyne valve (Cotai, CA, U.S.A.). The analytical column was protected by a 20 mm direct-connect guard column, (LC-18-DB, Supelco, Inc., Bellefonte, PA, U.S.A.) packed with CN packing material (Lichrosorb 10 CN, HPLC Technology, Macclesfield, U.K.). All solvents used in the HPLC system were filtered through a disposable 0.5 $\mu$m fluoropore filter (No. FHLP 04700, Millipore, Bedford, MA, U.S.A.). Oxidative amperometric measurements were performed using an EG&G Princeton Applied Research Model 400 EC potentiostat connected to the flow cell by crocodile pins. GV was detected amperometrically by employing a potential of +1.3 V at the working electrode. The resultant signals were recorded on a Philips Model PM8261 X-t recorder (Eindhoven, The Netherlands) at a chart speed of 300 mm/hr.

The peak currents as a function of concentration were then measured for quantitative analysis. Operating conditions: LC mobile phase at room temperature; the mobile phase flow rate was maintained at 1.0 ml/min through the analytical column: column temperature, ambient; column pressure, *ca.* 1500 psi; the normal operating current range was set at 2 and 20 nA for full-scale deflection for the analysis of GV in human urine and poultry feed respectively.

## RESULTS AND DISCUSSION

*Cyclic voltammetric behaviour*

A typical cyclic voltammogram for a $1 \times 10^{-3}M$ solution of GV obtained using a glassy carbon working electrode in 0.05*M* acetate buffer (pH 5.5) supporting electrolyte is shown in Fig. 2. The voltammogram showed one peak on anodic scanning between 0 and +1.4 V, with no peak on the reverse scan. The appearance of a single anodic peak in the first cycle only, with no cathodic peak on the reverse scan, is indicative of the irreversible nature of the oxidation process. Further cycling without reactivation of the electrode (scan B) showed complete suppression of the anodic peak indicating that the reaction product is strongly adsorbed on the electrode surface.

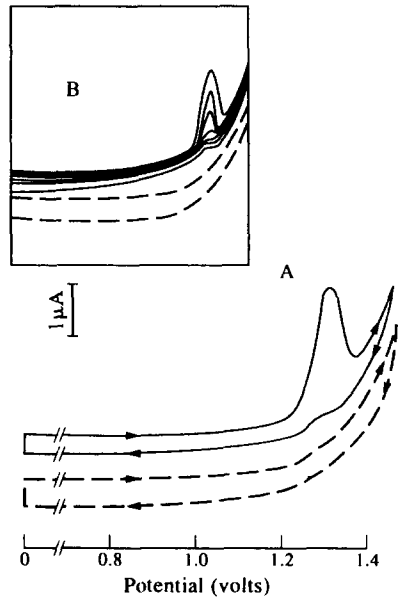


Fig. 2. Cyclic voltammogram of $1 \times 10^{-3}M$ GV in 0.05*M* acetate buffer (pH 5.5) at a stationary glassy carbon electrode (A). The inset in (B) shows the cyclic voltammograms obtained after recycling without intervening activation of the electrode.

*Optimization of LC-EC conditions*

In order to determine the optimum applied potential for amperometric detection following liquid chromatography, a hydrodynamic voltammogram was constructed for GV (Fig. 3) by injecting 100 $\mu$l of 30 ppb GV standard solutions of the compound and recording the detector response at intervals of 0.10 V over the range +0.40 V to 1.40 V. The voltammogram verifies that GV undergoes a single oxidation within this potential range. The maximum currents were achieved at a potential of +1.40 V; however, the magnitude of the background current was about 0.004 nA at this applied voltage. It was found that reducing the potential to +1.30 V afforded a significant reduction in background current, which resulted in better signal-to-noise ratios; therefore, an applied potential of +1.30 V was selected for the remainder of the LC-EC studies. Using cyclic voltammetric data, existing HPLC information and the hydrodynamic voltammogram, the chromatographic system was developed to meet the requirement of both separation and detection of GV in poultry feed and in human urine.

*Pretreatment of the carbon fibre working electrode*

The electrode response is usually affected by the features of the sample matrix. Urine is a complex medium that contains many complex biological materials that can interfere with the performance of the analysis. In the proposed procedure, the occurrence of matrix effects (defined as the relative sensitivity in the presence of a matrix to that in the absence of a matrix)

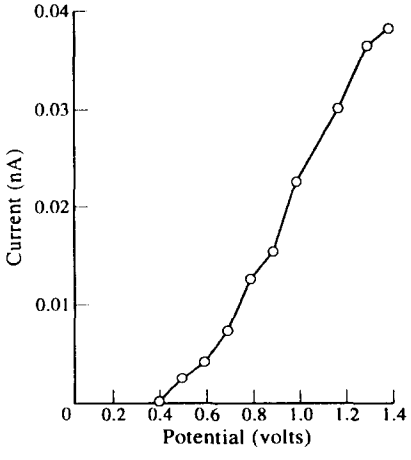


Fig. 3. Hydrodynamic voltammogram obtained for 30 ng/ml GV standard solution. Mobile phase: acetonitrile–acetate buffer (60:40), pH 5.5; working electrode: 14 $\mu$m carbon fibre.

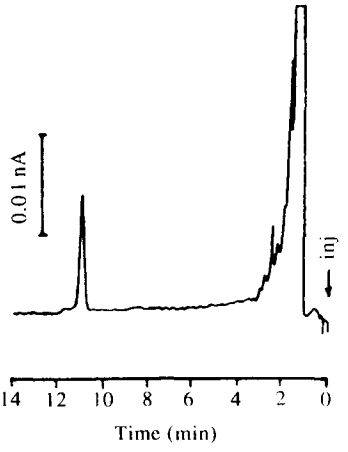


Fig. 4. Chromatogram obtained by analysis of human urine extract spiked with 5 ppb GV. Chromatographic conditions (see text).

during urine analysis was significant. It was necessary to counteract the matrix effect when the carbon fibre electrode surface became contaminated. Electrochemical pretreatment was used to solve this problem. The working electrode was treated by applying −1.40 V for 40 sec and then +1.40 V for 40 sec (*vs.* $Ag/Ag_3PO_4$) followed by equilibration for 3 min. When the upper potential limit was extended to +1.5 V, many fibres were either broken or provided noisy and erratic oxidation peaks. When this pretreatment procedure was applied to the analysis of the urine specimens obtained from healthy volunteers, the interferences from other urinary constituents were effectively eliminated. The pretreatment regime also improved the correlation coefficient for the calibration graph and the sensitivity of the method; making the pretreatment of the electrode an essential step for the determination of GV using the microelectrode flow cell. A similar improvement was observed when the pretreatment procedure was applied during the analysis of the animal feed. One explanation of this behaviour is the increase of the effective rates of electron transfer by generating electrocatalytic functional groups at the surface of the electrode due to pretreatment.

Chemical pretreatment of the carbon fibre electrode were also tried. The working electrode was immersed for 20 min in $HNO_3$, $H_2SO_4$, $H_2O_2$ and concentrated acid dichromate solution. In all these cases the resulting test voltammograms showed poor defined peak shapes. The flow system used provides short contact between the sample and the active surface allows minimal contamination of the electrode surface.

Table 1. Precision of the assay in (a) urine and (b) chicken feed

| Concentration spiked (*ppb*) | Mean concentration found* (*ppb*) | RSD (%) |
|---|---|---|
| (a) | | |
| 4.0 | 3.6 | 3.5 |
| 7.5 | 7.1 | 2.3 |
| 10.0 | 9.4 | 5.1 |
| (b) | | |
| 2.5 | 2.4 | 4.2 |
| 5.0 | 4.7 | 2.5 |
| 10.0 | 9.6 | 1.7 |

*$n = 5$.

*Determination of Gentian Violet in human urine and poultry feed*

The analytical procedure was then applied to control human urine and poultry feed samples to establish the limit of detection and recovery of the method.

*Linear range.* A series of external GV standards were prepared in a mixture consisted of methanol:water (95:5), and a calibration graph based on the mean ($n = 5$) detector response values was constructed by injecting between 1 and 30 ppb of GV for standard solutions for urine samples analysis and between 1 and 20 ppm for poultry feed analysis. Peak currents were measured and graphs of peak current *vs.* amount injected were constructed. The linear calibration curves indicated that the oxidation of GV at the carbon fibre working electrode is reproducible over these ranges using the micro-electrode flow cell and the chromatographic conditions, with correlation coefficients of greater than 0.996 for both studies. The characteristics of these curves were slope: $2.1 \times 10^{-3}$ nA/ppb and $9.1 \times 10^{-2}$ nA/ppm, and intercept $1 \times 10^{-3}$ and $2 \times 10^{-3}$ nA for human urine and poultry feed analysis, respectively. These calibration ranges were considered suitable for the applications being undertaken in this study. The limit of detection was taken to be the concentration at which the signal was three times greater than the noise of the base line. The minimum detectable concentration was found to be 0.5 ppb.

Table 2. Recovery of (a) GV from spiked urine specimens and (b) chicken feed

| Sample | GV concentration (*ppb*) | | |
|---|---|---|---|
| | Present | Mean amount found* | Mean recovery (%) |
| (a) | | | |
| A | 2.0 | 1.8 | 90 |
| B | 5.0 | 4.6 | 92 |
| C | 15.0 | 14.1 | 94 |
| (b) | | | |
| A | 2.5 | 2.4 | 96 |
| B | 5.0 | 4.7 | 95 |
| C | 10.0 | 9.6 | 95 |

*$n = 5$.

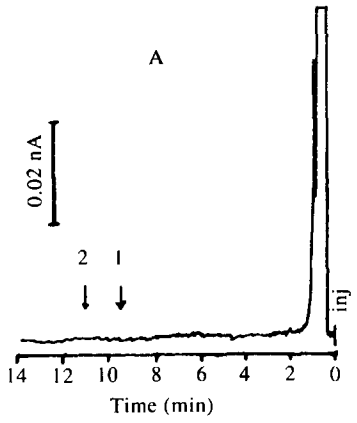


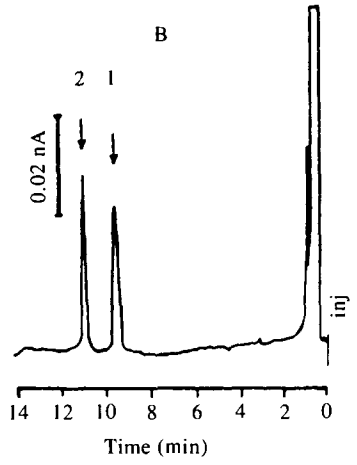


Fig. 5. Typical chromatogram of the separation of leuco Gentian Violet and Gentian Violet at +1.3 V for (A) blank urine extract and (B) spiked human urine containing 15 ppb of (1) leuco and (2) chromatic form of Gentian Violet.

*Precision.* The method described has been applied to a number of samples of human urine and poultry feed. The LC-EC chromatograms obtained for GV extracted from human urine and chicken feed as described earlier, showed a well defined peak for GV with a retention time of 11.0 min (Fig. 4). The precision was measured as the relative standard deviation of a repeated injection of the same quantity of a sample at 4, 7.5, and 10 ppb urine samples and at 2.5, 5, and 10 ppm feed samples. The results summarized in

Table 1(a) and (b) display an acceptable level of accuracy and precision, with the RSD ranging between 1.9 and 4.2%. These results are in good agreement with those published by other authors.

*Recovery studies.* The extraction procedures produced a "clean" extract and consequently good recoveries of GV. Table 2(a) and (b) show the overall recovery of GV, which was assessed by comparing the representative peak currents for spiked urine specimens and poultry feed sample taken through the study with the peak current for corresponding standards. The recoveries of GV from spiked urine blanks and from chicken feed ranged from 91.69 to 94.09% at ppb levels and from 94.85 to 95.70% at ppm levels and averaged 94.06%. These recovery levels are satisfactory, and the concentration of the "spiked samples" did not appear to influence the recovery of GV residues in urine specimens.

*Interference study.* In many cases quantitation of metabolites in addition to the parent drug will be required if these metabolites are pharmacologically active. Intestinal microflora, under anaerobic conditions, are capable of metabolizing GV by reduction to its leuco (colourless) form.[27] According to the U.S.A. National Centre for Toxicological Research,[28] this leuco derivative (LGV) is then "structurally similar to the classical aromatic carcinogens". The possible potential interference of the leuco derivative in the determination of GV was tested using the proposed method.

Figure 5 shows the chromatogram observed for simultaneous determination of spiked human urine containing 15 ppb of GV and LGV. It can be seen from this figure that both forms are well resolved and there were no significant effects due to the added interferent. This metabolic product would not be expected to interfere in real samples as the level of spiking was considerably higher than that normally found in human urine.

## CONCLUSION

This research describes a sensitive LC-EC method for quantitative analysis of GV in human urine and chicken feed using an electrochemical microelectrode flow cell. The detector has been found to exhibit a considerable improvement in the limit of detection over a previously reported method which involved amperometric detection using a glassy carbon macroelectrode.[9] The use of the carbon fibre overcame many problems associated with the use of glassy carbon electrodes. The method eliminates interferences from other urinary constituents and provided a reliable and fairly precise tool for biological monitoring of GV. The ability of simultaneous determination of the parent drug (GV) in presence of its major demethylated metabolite (LGV) could be of great importance in studying the biotransformation of GV into its leuco form. It is considered that the method will be useful for both clinical and pharmacokinetic studies.

## REFERENCES


1. *Martindale, The Extra Pharmacopoeia*, 27th Edn, A. Wade (ed.), p. 516. The Pharmaceutical Press, London, 1977.
2. H. Fujita, A. Mizuo and K. Hiraga, *Tokyo Toristu Eisei Kenkyusho Kenkyu Nempo*, 1976, **27,** 153.
3. K. Norrby and H. Mobacken, *Acta Derm. Venereol.*, 1972, **52,** 476.
4. W. Au, S. Pathak, C. Collie and T. Hsu, *Mutat. Res.*, 1978, **58,** 269.
5. W. Au, M. Butler, S. Bloom and T. Matney, *Mutat. Res.*, 1979, **66,** 103.
6. F. Hao, D. Li and Q. Zhang, *Daxue Xuebao Ziran Kexueban.*, 1984, **25,** 65.
7. S. Chattopadhyay and A. Das, *J. Indian Chem. Soc.*, 1985, **62,** 632.
8. L. Rushing and M. Bowman, *J. Chromatogr. Sci.*, 1980, **18,** 224.
9. J. Roybal, R. Munns, D. Holland, R. Burkepile and A. Hurlbut, *J. Assoc. Off. Anal. Chem.*, 1992, **75,** 433.
10. M. Fleisch, S. Pans, D. Rolison and P. Schmidt (eds), *Ultramicroelectrodes*, Datatech Systems Inc., Morganton, NC, 1987.
11. R. Wightman and D. Wipf, in *Electroanalytical Chemistry*, A. J. Bard (ed.), Vol. 15, p. 268, Marcel Dekker, New York, 1989.
12. M. Montenegro, M. Queiros and J. Daschbach (eds), *Microelectrodes: Theory and Applications*, Kluwer, Dordrecht, 1991.
13. M. Dayton, K. Brown, K. Stutts and R. Wightman, *Anal. Chem.*, 1980, **52,** 946.
14. R. Lafleur, J. Myland and K. Oldham, *Electroanalysis*, 1990, **2,** 223.
15. J. Baur and R. Wightman, *J. Chromatogr.*, 1989, **482,** 65.
16. W. Caudill, J. Howell and R. Wightman, *Anal. Chem.*, 1982, **54,** 2532.
17. F. Matysik and H. Emons, *Electroanalysis*, 1992, **4,** 501.
18. B. Sharifker and G. Hills, *J. Electroanal. Chem.*, 1981, **130,** 81.
19. D. Wong and A. Ewing, *Anal. Chem.*, 1990, **62,** 2697.
20. R. Penner, M. Heben, T. Longin and N. Lewis, *Science*, 1990, **250,** 1118.
21. T. Edmonds, *Anal. Chim. Acta*, 1985, **175,** 1.
22. J. Bixer, A. Bond, P. Lay, W. Thormann, Van de Bosch, M. Fleischmann and S. Pons, *Anal. Chim. Acta*, 1986, **187,** 67.

23. W. Thormann and A. Bond, *J. Electroanal. Chem.*, 1987, **218**, 187.
24. J. Golas and J. G. Osteryoung, *Anal. Chim. Acta*, 1986, **181**, 211.
25. *U.S. Pharmacopeia XXI—National Formulary XVI*, p. 459. U.S. Pharmacopeial Convention, Rockville, MD, 1985.
26. L. Rushing and M. Bowman, *J. Chromatogr. Sci.*, 1980, **18**, 224.
27. J. McDonald and C. Cerniglia, *Drug Metab. Dispos.*, 1984, **12**, 330.
28. National Center for Toxicological Research, Final Report—Metabolism of Gentian Violet, NCTR Technical Report for experiment No. 6040, May, 1985.

Pergamon

0039-9140(94)00234-7

*Talanta*, Vol. 42, No. 2, pp. 243–248, 1995

0039-9140/95 $9.50 + 0.00

# POTENTIOMETRIC DETERMINATION OF AMINAL STABILITY CONSTANTS

P. D. TAYLOR

Department of Chemistry and Biological Chemistry, University of Essex, Wivenhoe Park, Colchester, Essex CO4 3SQ, U.K.

(*Received* 7 *June* 1994. *Accepted* 1 *August* 1994)

**Summary**—Potentiometric titration was used to determine the logarithms of the stepwise equilibrium constants for the species formed between morpholine and formaldehyde in aqueous solution, ionic strength 0.5 and 2.5*M* (KCl) at 25°C. The instrumental and computational techniques developed for metal–ligand stability constant determination were applied. Formaldehyde is equivalent to the metal-ion and is represented by M while neutral morpholine is equivalent to the ligand and is represented by L. The stability constants of the following equilibria were determined by non-linear regression (figures in parentheses are at ionic strength 2.5*M* KCl): $M + L \rightleftharpoons ML$ (hemi-aminal) $\log K_1 = 2.90 \pm 0.02$ ($2.980 \pm 0.004$); $ML + L \rightleftharpoons ML_2$ (bis-aminal); $\log K_2 = 1.3 \pm 0.2$ ($1.41 \pm 0.07$); $MLH \rightleftharpoons ML + H^+$ (protonated hemi-aminal) $pK_a = 5.87 \pm 0.01$ ($6.411 \pm 0.005$); $ML_2H \rightleftharpoons ML_2 + H^+$ (protonated bis-aminal) $pK_a = (7.6 \pm 0.2)$. The $pK_a$ of the protonated bis-aminal could only be determined at the higher ionic strength. The results are in good agreement with reported values determined using the classic formol titration. The automated titration system acquired the full time course of the pH change upon each titrant addition allowing a kinetic analysis to be performed as well as an equilibrium analysis. The forward and reverse rate constants for $M + L \rightleftharpoons ML$ were $0.77M^{-1}$ sec$^{-1}$ and $8.1 \times 10^{-4}$ sec$^{-1}$, respectively.

The species known to form when formaldehyde and a secondary amine are mixed in aqueous solution are shown in Scheme 1. The equilibrium constants of this system have been determined by Kallen *et al.* using the formol titration.[1] This involves measurement of the change in pH of amine/aminium compositions as a function of formaldehyde concentration. The analysis of data in that work involved a number of elegant graphical extrapolations and linearisations. The high pH at which formaldehyde–morpholine solutions undergo changes in speciation simplifies the algebra because the free proton concentration can be neglected in conservation equations. However, it is useful to recognise that the multi-component formaldehyde–morpholine equilibrium system is described by a set of conservation equations and equilibrium equations in an identical fashion to metal–ligand equilibrium systems. Multi-parametric non-linear regression of potentiometric titrations has been widely used to determine metal–ligand stability constants and a number of sophisticated algorithms and computer programs have been developed to handle this type of data analysis.[2] This work examines the application of the experimental and computational techniques developed for metal–ligand stability constant determination to the entirely organic formaldehyde–morpholine system. (See over for Scheme 1).

The set of conservation equations 1–3 and the equilibrium equations 4 describe the system. $M_t$, $L_t$ and $H_t$ are the total analytical concentrations of formaldehyde, morpholine and proton; $m$, $l$ and $h$ are the free concentrations of formaldehyde, morpholine and proton at equilibrium and $p_j$, $q_j$ and $r_j$ are the stoichiometries of formaldehyde, morpholine and proton in the $j$th complex species $S_j$ with formation constant $\beta_j$ and $K_w$ is the ion product of water. The notation is consistent with most metal–ligand titration studies if formaldehyde is considered to be the metal-ion ligated by morpholine.

$$M_t = m + \Sigma p_j S_j \quad (1)$$

$$L_t = l + \Sigma q_j S_j \quad (2)$$

$$H_t = h + \Sigma r_j S_j - K_w/h \quad (3)$$

$$S_j = \beta_j m^p l^q h^r. \quad (4)$$

The set of equations can be solved by Gauss–Newton iteration in the three variables $m$, $l$ and $h$ as described in many previous publications on potentiometric

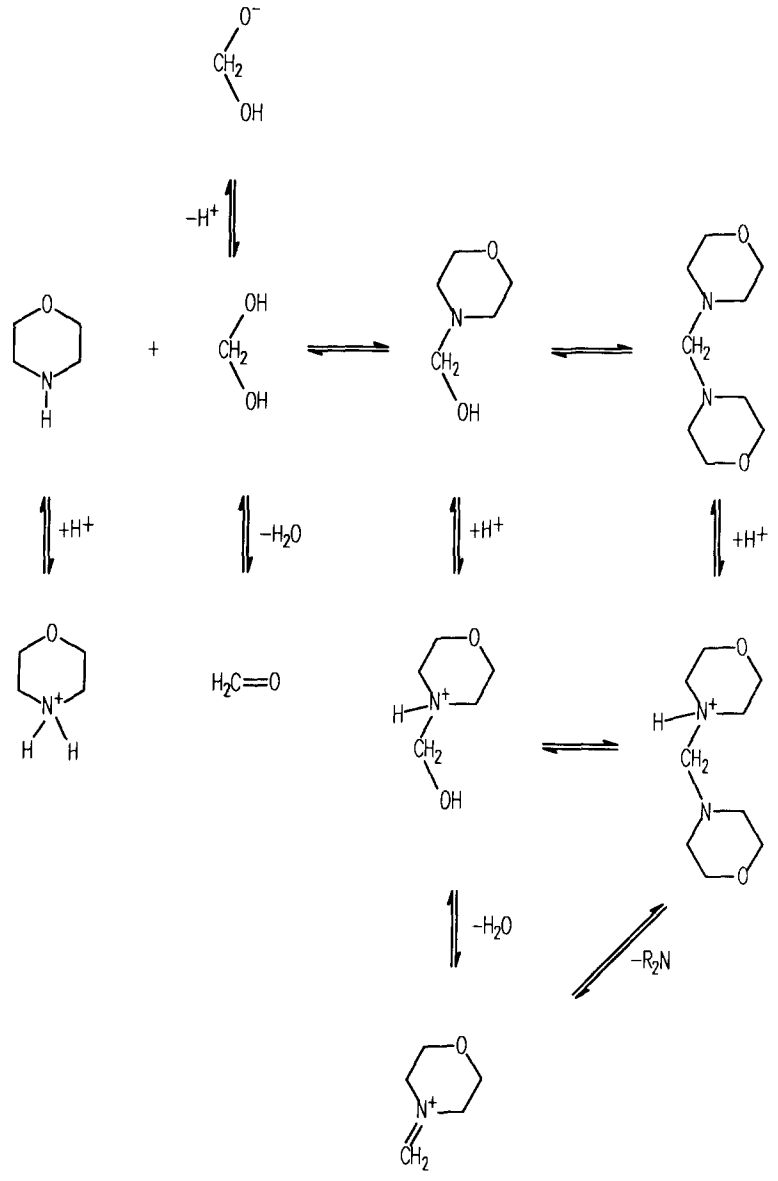

Scheme 1

titrations of metal–ligand equilibria.[3,4] The stability constants and other parameters describing the model system may then be optimized non-linearly by least squares regression analysis of the potentiometric data. The use of these equations in the non-linear regression program NONLIN15 (QuickBasic 4.5) has been described previously.[3]

The only potential difficulty is the slow kinetics of the formaldehyde morpholine system compared with many metal–ligand systems. An automated potentiometric titration system developed for metal–ligand titrations was modified to allow acquisition of pH *vs* time after each titrant addition to ensure that equilibrium had been achieved. The glass electrode response is relatively rapid (about 5 sec to reach a stable reading in calibration titrations of HCl with KOH) so the pH variation after 5 sec reflects the kinetics of hemi-aminal and bis-aminal formation. This slower change is experimentally found to be exponential as expected for a small amplitude perturbation from equilibrium. Fortunately, the half-times of the exponentials obtained in the formaldehyde–morpholine system are short enough to make the titrimetric technique practical. The time course, together with the speciation determined from the equilibrium pH titration permitted the determination of some of the rate constants involved.

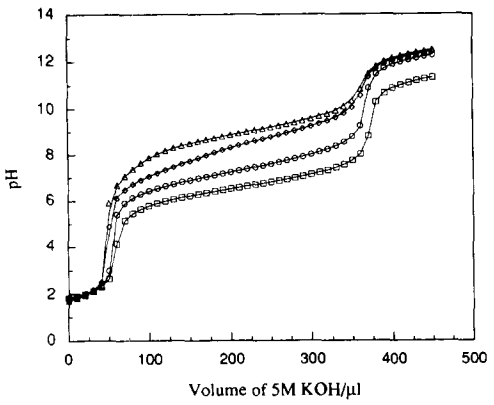


Fig. 1. Titrations of morpholine in the presence of formaldehyde at increasing concentrations giving morpholine:formaldehyde ratios of: curve 1 △, 7.87:1; curve 2 ◇, 2.62:1; curve 3 ○, 0.784:1 and curve 4 □, 0.0784:1. The solid lines are titrations simulated with the parameters optimized by non-linear regression.

## EXPERIMENTAL

Data were collected by an automated titration system operated by a PC and software developed to permit pH to be recorded with time for each titrant addition. The instrument comprises a stepper motor driven, micrometer mounted 1 ml syringe (Agla) and a Corning Δ250 pH meter. The computer program which controls the titrator continues to acquire values of pH until the slope of pH against time, plus twice the standard error of the slope is less than 0.0002 pH units per second. The water jacketed titration vessel was maintained at 25.0°C ± 0.01 by a Grant-Barrington thermocirculator. Stock solutions of formaldehyde and morpholine were all maintained at the same ionic strength (0.5 or 2.5*M* KCl). Formaldehyde solutions were prepared from 37% w/w solution containing 10% methanol stabilizer (Aldrich); morpholine from the free base (Aldrich). A glass electrode and calomel reference electrode were used. Acid was HCl (1.022 or 5.00*M*) base was KOH (0.984 or 5.00*M*) both Aldrich standard solutions. Water was distilled and deionized (18 MΩ/cm).

### *Typical titration procedure*

KCl (10 ml) was acidified with 100 μl of 1.022*M* HCl and titrated with 200 μl of 0.984*M* KOH to calibrate the electrodes. Then 400 μl of HCl and 1 ml of the morpholine solution were added and titrated with 470 μl of KOH in 10 μl aliquots. Thereafter, acidification and titration were repeated after additions of 30, 170 and 1800 μl of formaldehyde solution. Thus all titrations were performed by additions to the same solution without removing the glass electrode.

## RESULTS

### *Stability constants*

Titrations with fixed morpholine and increasing concentrations of formaldehyde are shown in Fig. 1. Introduction of formaldehyde leads to a decrease in pH in the buffer region because the hemi-aminal (ML) and bis-aminal ($ML_2$) are weaker bases than the free morpholine. The $pK_a$ of the hemi-aminal (5.87) is 2.7 units below that of morpholine itself (8.545) while the $pK_a$ of the bis-aminal is only 1.5 units below morpholine so the decrease in pH that results from formation of bis-aminal is less dramatic than that resulting from hemi-aminal formation. Increasing the formaldehyde concentration gives a buffer region of progressively lower pH with the limiting buffer region of $pK_a$ 5.87 corresponding to quantitative formation of the hemi-aminal. The $pK_a$ of formaldehyde hydrate (12.78) becomes significant at high formaldehyde concentrations (Fig. 1, curve 4). This ionization is entirely analogous mathematically with the hydrolysis of metal-ions to metal-hydroxides and is dealt with as such by the computational analysis. Speciation for the titration curve 2 is shown in Fig. 2. High concentrations of formaldehyde and morpholine were required to give concentrations of bis-aminal and the protonated aminals ($ML + H^+$, $ML_2 + H^+$) which could be detected. A correspondingly high concentration of KCl was required in these titrations to keep the ionic strength constant. The parameters optimized by non-linear regression are summarized in Table 1. The sequence of analysis was as

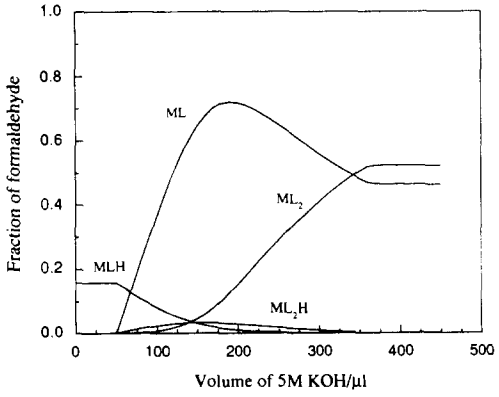


Fig. 2. Speciation of formaldehyde morpholine solution during titration curve 2 (◇) of Fig. 1. Species are shown as the mole fraction of formaldehyde involved.

Table 1. Globally optimized parameters and comparison with values determined by Kallen *et al.*[1] (calculated from Kallen *et al.*[1] Table I)

| | | | | log $\beta$ (25.0°C) | | |
|---|---|---|---|---|---|---|
| | | | | This work | | |
| | $m$ | $l$ | $h$ | 0.5$M$ KCl | 2.5$M$ KCl | Kallen *et al.*[1] 1.0$M$ KCl |
| Morpholinium | 0 | 1 | 1 | 8.545 (0.003) | 9.116 (0.009) | 8.88 |
| Hemi-aminal | 1 | 1 | 0 | 2.90 (0.02) | 2.98 (0.004) | 2.97 |
| Protonated hemi-aminal | 1 | 1 | 1 | 8.77<br>p$K_a$ = 5.87 (0.01) | 9.391<br>p$K_a$ = 6.411 (0.005) | 9.06<br>p$K_a$ = 6.09 |
| Bis-aminal | 1 | 2 | 0 | 4.2<br>log $K_2$ = 1.3 (0.2) | 4.389<br>log $K_2$ = 1.410 (0.07) | 4.23<br>log $K_2$ = 1.26 |
| Protonated bis-aminal | 1 | 2 | 1 | indeterminate | 11.973<br>p$K_a$ = 7.6 (0.2) | 11.61<br>p$K_a$ = 7.38 |
| Formaldehyde p$K_a$ | 1 | 0 | −1 | 12.78 (0.05) | 13.04 (0.05) | — |

Numbers in parentheses are standard errors.

follows. The calibration titration and the morpholine titration were optimized globally to determine the electrode zero, the p$K_a$ of morpholine, the concentration of morpholine, the value of p$K_w$ and the initial acid concentration. Two titrations containing formaldehyde (30 and 200 $\mu$l) were than analysed holding the parameters above constant and globally optimizing only the values of log $K_1$ and log $K_2$, the p$K_a$ value of the protonated bis-aminal, the initial acid concentration, the added acid concentration. Finally the two titrations containing 200 $\mu$l and 2 ml of formaldehyde were analysed optimizing the p$K_a$ of the protonated hemi-aminal, initial acid concentration and added acid concentration. At the lower formaldehyde–morpholine concentration (titration conducted in 0.5$M$ KCl) the concentration of the bis-aminal was too low to determine its p$K_a$.

*Kinetics*

The ability of the instrumentation to record the full time course of the change in pH after each titrant addition (Fig. 3) allows some kinetic analysis. The time course is well modelled by a single exponential (Fig. 4). For a small perturbation of the system shown in Scheme 1, assuming that all proton exchanges are rapid, a two exponential relaxation is expected, one for each equilibrium that is not a proton transfer reaction. Under conditions where [ML] far exceeds [$ML_2$], the amplitude of the second exponential

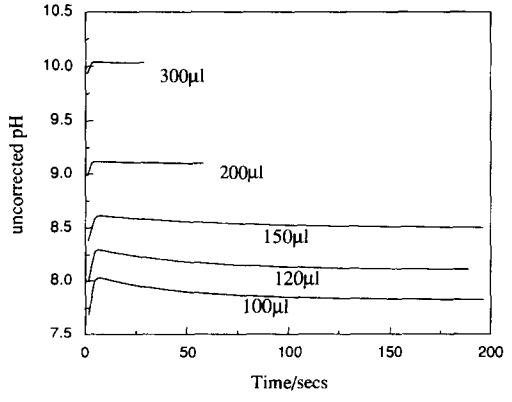


Fig. 3. Variation of pH with time at the titrant volume indicated. The data corresponds to curve 2 (◇) in Fig. 1. The rapid pH change completed in the first 5 sec is the equilibration of the glass electrode with the solution. The slower change is the equilibration of formaldehyde and morpholine with aminal. The slower change is an exponential relaxation with a half-time which varies with pH. The pH is uncorrected and includes an electrode zero of 0.782.

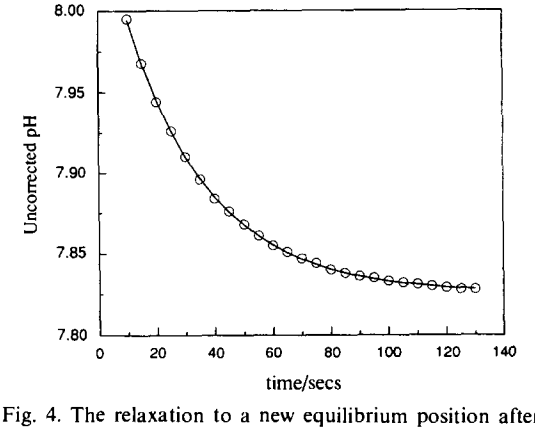


Fig. 4. The relaxation to a new equilibrium position after each titrant addition is a single exponential under conditions where [ML]≫[$ML_2$]. The solid line is simulated from the value of $k_{obs}$ optimized by non-linear regression using a single exponential function. The data corresponds to the addition of 10 $\mu$l of 0.2$M$ KOH to give the 100 $\mu$l titration point of curve 2 (◇) in Fig. 1. The first 10 sec have been truncated to remove the initial response of the glass electrode to the changed pH.

will be negligible and the single remaining exponential should have a rate constant that is dependent on the concentration of free formaldehyde ([M]) and morpholine ([L]) as shown by equation 7.

$$M + L \underset{k_2}{\overset{k_1}{\rightleftharpoons}} ML \quad K_1 = 954$$

$$k_{obs} = k_2 + k_1([M] + [L]) \tag{5}$$

$$K_1 = [ML]/[M][L] = k_1/k_2 \tag{6}$$

$$k_{obs} = k_1(1/K_1 + [M] + [L]). \tag{7}$$

The concentrations, $[M]$ and $[L]$, for each relaxation, were obtained from the speciation calculated from stability constants determined in the previous section. A plot of $k_{obs}$ against $1/K_1 + [M] + [L]$ should then give a straight line through the origin with a gradient of $k_1$ (Fig. 5). Linear regression to this model gives a value of $k_1 = 0.77M^{-1}\text{sec}^{-1}$. Since $k_1/k_2 = 954M/\text{sec}$, $k_2$ must be $k_1/K_1 = 8.1 \times 10^{-4}$ sec$^{-1}$. In principle the same approach could be used to determine the rate constants comprising $K_2$.

## DISCUSSION

The results are generally in agreement with Kallen and Jencks but are likely to be of greater accuracy mainly because analysis of full pH titration curves allows the use of internal calibration of the glass electrode zero, total morpholine concentration and total acid concentration. The introduction of the protonated bis-aminal, led to a significant improvement in the fit, although the standard error of this parameter is large.

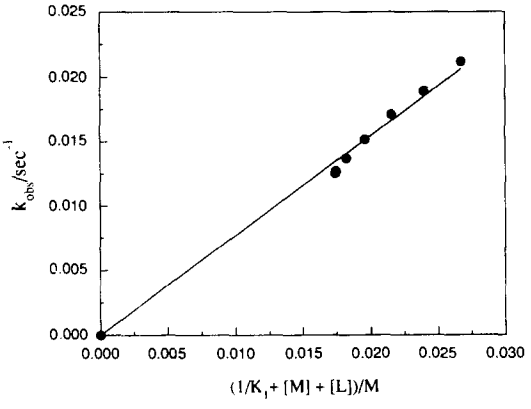


Fig. 5. The value of $k_{obs}$ at each titration point from 120–180 $\mu$l, curve 2 (◇) in Fig. 1, against $1/K_1 + [L] + [M]$ where [L] is the concentration of free neutral morpholine and [M] that of free formaldehyde calculated from the speciation at each point. The solid line is drawn from the slope optimized by linear regression to equation (7). This gives a value for $k_1$ of $0.77M^{-1}$ sec$^{-1}$.

The stability constants of the hemi-aminal and bis-aminal are not altered greatly by a five-fold increase in ionic strength. This is to be expected since both species have no net charge. However the p$K_a$ of the morpholinium ion and of the protonated hemi-aminal increase by 0.57 and 0.54 respectively. Because the p$K_a$ of the protonated bis-aminal could only be determined at the higher ionic strength, the effect of ionic strength on its value is not known. It presumably increases by a similar amount to the hemi-aminal. The result of increased ionic strength is thus to decrease the concentration of hemi-aminal and bis-aminal while the concentration of morpholinium, protonated hemi-aminal, and probably also the protonated bis-aminal, should increase slightly in concentration.

The kinetics of approach to equilibrium at each titration point provides valuable additional information from which rate constants can be readily determined.

Metal–ligand potentiometric studies have led to a large number of computer oriented algorithms and programs which exploit them. The majority of these should be applicable without any modification to the analysis of formaldehyde–amine equilibria if formaldehyde is recognized as playing the role of the metal-ion while the amine is the ligand. Examples are the non-linear regression programs NONLIN15,[3,4] TITFIT[5] and BEST.[6] Most of these programs can also be used to generate simulated speciation.

The stability constants reported in this work and the effect of ionic strength on them, are important in the analysis of reaction rates involving hemi-aminals and bis-aminals as a function of pH and ionic strength. For example, the bimolecular aromatic Mannich reaction in aqueous media probably proceeds via electrophilic attack of hemi-aminals and bis-aminals on phenols. The determination of equilibrium speciation has recently enabled the author to determine, for the first time, the rate constants for the individual species in the Mannich reaction of the 3-hydroxy-4-pyrone, kojic acid.

## REFERENCES

1. R. G. Kallen, R. O. Viale and L. K. Smith, *J. Am. Chem. Soc.* 1972, **94**, 576.

2. A. E. Martell and R. J. Motekaitis, *Determination and Use of Stability Constants*. VCH, New York, 1992.
3. P. D. Taylor, I. E. Morrison and R. C. Hider, *Talanta*, 1988, **35**, 507.
4. J. Miller and P. D. Taylor, *Talanta*, 1989, **36**, 879.
5. A. D. Zuberbühler and A. T. Kaden, *Talanta*, 1982, **29**, 2.
6. R. J. Motekaitis and A. E. Martell, *Can. J. Chem.* 1982, **60**, 168.

Pergamon

00639-9140(94)00246-0

*Talanta*, Vol. 42, No. 2, pp. 249–255, 1995

0039-9140/95 $9.50 + 0.00

# AN ION-EXCHANGE METHOD FOR SELECTIVE SEPARATION OF PALLADIUM, PLATINUM AND RHODIUM FROM SOLUTIONS OBTAINED BY LEACHING AUTOMOTIVE CATALYTIC CONVERTERS

ROMULUS GAITA* and SARGON J. AL-BAZI†

Department of Chemistry, Northeastern Illinois University, Chicago, IL 60625, U.S.A.

(*Received* 17 *May* 1994. *Revised* 15 *August* 1994. *Accepted* 16 *August* 1994)

**Summary**—An ion-exchange method has been developed for the separation of palladium, platinum and rhodium from a solution that is highly acidic and contains a considerable amount of lead, aluminum, iron and cerium, obtained by leaching a used honeycomb type automotive catalytic converter. A column of Amberlite IRA-93 anion-exchange resin was found appropriate to recover platinum metals from the pregnant solution. Selective stripping of these metals from the resin was achieved by eluting rhodium first with 6.0*M* hydrochloric acid, then palladium with a 1% ammonia solution at ambient temperature, and platinum with 5% of the reagent at elevated temperatures. Optimum conditions for leaching these metals from the catalyst were 5.0*M* hydrochloric acid and 0.4*M* sodium chlorate at 70°C. This method can be applied to both analytical as well as large scale operations. It is simple, economical, and relatively safe for human exposure and the environment.

There are two common automotive catalytic converter catalysts in use.[1] The so-called 'low-loading' form contains about 370 ppm of platinum and about 160 ppm of palladium, and the 'high-loading' form contains approximately 60% more of each of these elements. There is also an 'extra high-loading' catalyst which contains about 850 ppm of platinum and 350 ppm of palladium and even some varieties which contain more palladium than platinum. These palladium–platinum catalysts are usually referred to as 'two-way' catalysts since they cause the oxidation of both carbon monoxide and hydrocarbons.

Rhodium has been introduced into catalytic converters. Since then, approximately 73% of the world production of rhodium is consumed in the production of autocatalysts.[2] These monolithic automotive catalysts are typically Cordierite type honeycombs with platinum, palladium and rhodium. These catalysts are called 'three-way' catalysts, since they not only oxidize carbon monoxide and hydrocarbons but also various nitrous oxides.

The average loading of platinum group metals per catalytic converter has been 0.05 troy ounces of platinum, 0.02 troy ounces of palladium and 0.005 troy ounces of rhodium.[3] Each year, approximately 10 million automobiles are scrapped in the United States. Based on an equivalent number of converters, it is estimated that 500,000 troy ounces of platinum and 200,000 troy ounces of palladium and 50,000 troy ounces of rhodium will be wasted annually just in the United States. The annual world consumption of these metals for autocatalyst use could double or triple the above numbers. Since these metals are in limited supply, a successful process for their recovery from catalytic converters will play an important part in their future availability and prices.

Dissolution of palladium, platinum and rhodium presents special problems owing to their generally high ionization potential (the first ionization potential of Pd = 8.3 eV, Pt = 9.0 eV and Rh = 7.5 eV). This coupled with the complex variety of elements in the used catalytic converter makes it difficult to leach these metals from the catalyst, and to isolate them from the pregnant solution. Furthermore, the increasing variety of catalysts produced, the apprehension over industrial pollution, and

*Present address: Allied Signal Research & Technology, Des Plaines, IL 60017, U.S.A.

†Author to whom correspondence should be addressed.

concern with human exposure to chemicals is making the development of new processes to recover these metals from the catalysts more difficult.

The method commonly employed for a selective separation of palladium, platinum and rhodium from the solution obtained by leaching catalytic converters is based on 'wet chemical' procedures.[1,4] Platinum is precipitated as ammonium hexachloroplatinate(IV) and rhodium as ammonium hexachlororhodate(III) by saturating the decomposed mother liquor with ammonium chloride. Palladium is precipitated as ammonium hexachloropalladate(IV) after oxidation to palladium(IV). This method is considered inefficient by today's standards in terms of the degree of separation achieved, the yields obtained, and the complexity of the operation. Solvent extraction methods[5–7] have ben developed to overcome the problems related to traditional practice. However, this technique is characterized by very slow kinetics[8] and selective back-extraction does not appear to be easily achieved.[9–12] Furthermore, the utilized organic solvents tend to be volatile, flammable and toxic which may introduce pollution to the environment.

The purpose of this study was to develop an ion-exchange method for the selective separation of palladium, platinum and rhodium from the solution obtained by leaching them from the honeycomb type catalytic converter. The optimum conditions for leaching these metals from the catalyst were also investigated.

## EXPERIMENTAL

### *Reagents*

Anion-exchange resins Amberlite IRA-68 (20–30 mesh particle size) and Amberlite IRA-93 (20–30 mesh particle size) both from Alfa Products, and Amberlite IRA-400 (16–50 mesh particle size) of Aldrich Chemical Company, were used in their chloride forms. These resins were equilibrated with 10% hydrochloric acid before use. Palladium, platinum and rhodium stock solutions of 1000 ppm were prepared by dissolving a weighed amount of palladium(II) chloride (Aldrich Chemical Company), platinum(II) chloride (Johnson Matthey) and rhodium(III) chloride (Aldrich Chemical Company) in 10% hydrochloric acid solution. A stock solution of 10.0*M* lithium chloride and 0.45*M* lanthanum nitrate hexahydrate (Li/La) was prepared in deionized water. All other reagents were of analytical grade. A used honeycomb type automotive catalytic converter ground to minus 60 mesh particle size was obtained from Catalytic Converter Refining Co., Northlake, IL.

### *Apparatus*

A glass chromatographic column (18 cm long and 4.8 mm inner diameter) was used. Palladium, platinum and rhodium were determined with a Spectraspan IV (Beckman Instruments) direct coupled plasma atomic emission spectrometer. The flow rate was controlled by an Econo peristaltic pump (Bio-Rad, California). An ATC autosampler (Techni Lab, NJ) was used to collect 2 ml fractions.

### *Leaching procedure*

The schematic diagram for leaching palladium, platinum and rhodium from the catalytic converter is shown in Fig. 1. A 20.0 g sample in a 250 ml beaker was treated with 95.0 ml of the desired concentration of hydrochloric acid. With continued stirring, the heterogeneous mixture was heated (see discussion for details) and then a small amount of sodium chlorate was added slowly from a 50.0 ml buret. After cooling to room temperature in an ice bath, the solution was filtered into a 100 ml volumetric flask and distilled water added to the mark. This

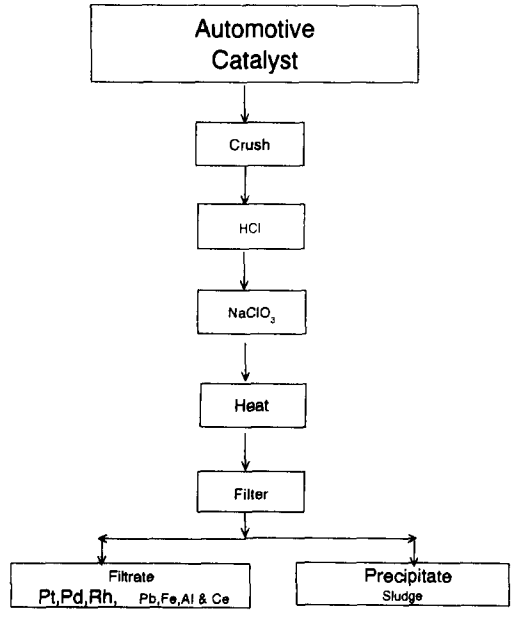


Fig. 1. Flow diagram for leaching palladium, platinum and rhodium from automotive catalyst.

solution was then divided into two 50.0 ml portions. To one portion, 2.50 ml of the Li/La solution was added to suppress interferences and improve detection limits. This portion was then used for the analysis of palladium, platinum and rhodium. The other portion was used to determine the acidic content.

*Recovery and stripping procedure*

*Batch ion-exchange procedure.* Resin (1.0 g) and 10.0 ml solution of palladium, platinum and rhodium were stirred moderately for 2.5 hr at room temperature in a 25 ml beaker. After equilibration the solution was filtered through a Whatman # 2 filter paper. The loaded resin was then washed for 5 min with 10.0 ml deionized water, filtered and mixed with 10.0 ml of the stripping solution for 1.5 hr at room temperature. To the filtrate from the recovery and stripping experiments, 0.50 ml of the Li/La solution was added and the filtrate solution then analyzed for palladium, platinum and rhodium.

*Column ion-exchange procedure.* The column was filled with a slurry of the resin until the settled resin bed reached the top of the column (2.0 g of dry resin). A 25.0 ml portion of the pregnant solution was passed through the column at a flow rate of 1 ml/min controlled by the peristaltic pump. The platinum metals were then selectively eluted from the column with the stripping solution. In both studies, 2 ml fractions of the eluate were collected with auto sampler, treated with 0.10 ml of the Li/La solution, and analyzed for palladium, platinum and rhodium.

## RESULTS AND DISCUSSION

The optimum conditions for leaching palladium, platinum and rhodium from the used catalytic converter were established by investigating the effects of various parameters.

*Effect of sodium chlorate concentration*

Varying the concentration of sodium chlorate from zero to 1.1*M* (Fig. 2) indicating that at zero sodium chlorate, less than 5.0 ppm of palladium, 0.5 ppm of platinum and 1.1 ppm of rhodium were recovered. Leaching increased sharply with increasing sodium chlorate to a maximum of 32.5 ppm palladium, 290 ppm platinum and 7.0 ppm rhodium at 0.4*M* sodium chlorate and then decreased slowly. The effect of sodium chlorate on the concentration of hydrochloric acid of the leached solution was linear; acid concentration decreased with increasing sodium chlorate (fits the least-squares equation $[HCl]_{final} = -1.878\ [NaClO_3]_{initial} + 3.624$). The decrease in acid concentration may explain the decrease in palladium, platinum and rhodium leached beyond 0.4*M* sodium chlorate concentration.

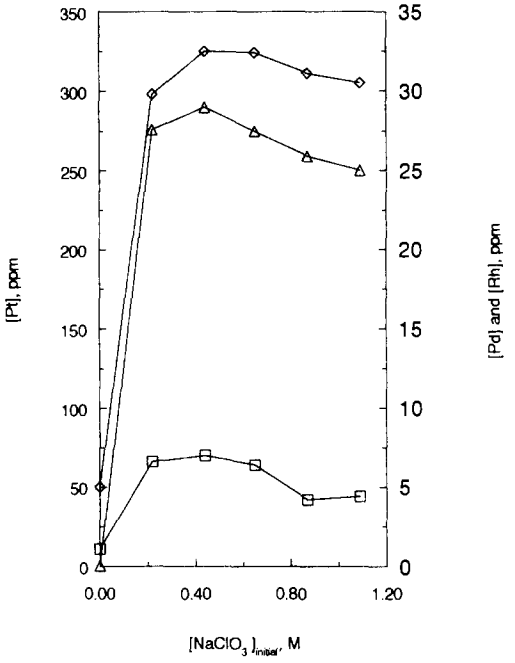


Fig. 2. Effect of sodium chlorate concentration on leaching palladium, platinum and rhodium: autocatalyst weight = 20.0 g, $[HCl]_{initial} = 4.8M$, temperature = 70°C, heating period = 1 hr: (◇) Pd, (△) Pt, (□) Rh.

*Effect of hydrochloric acid concentration*

Leaching palladium, platinum and rhodium from 0.4*M* sodium chlorate solutions increased from 2.0 ppm at zero concentration to a maximum of 31.4 ppm at 1.8*M* hydrochloric acid (Fig. 3). The amount of platinum leached increased sharply from 0.8 ppm at zero concentration to 327 ppm at 7.2*M* and then remained constant at higher concentrations of acid. About 0.1 ppm rhodium was leached in the absence of hydrochloric acid and 5.5 ppm at 1.8*M* which further increased to a maximum of 8.1 ppm from a 5.4*M* solution. The increase in the amount of palladium, platinum and rhodium leached with increasing acid concentration may be related to the formation of chlorocomplexes of these metals [$PdCl_4^{2-}$, $PtCl_6^{2-}$ and $RhCl_6^{3-}$] which are much more stable than their aquocomplexes [$Pd(H_2O)_4^{2+}$, $Pt(H_2O)_6^{4+}$ and $Rh(H_2O)_6^{3+}$].

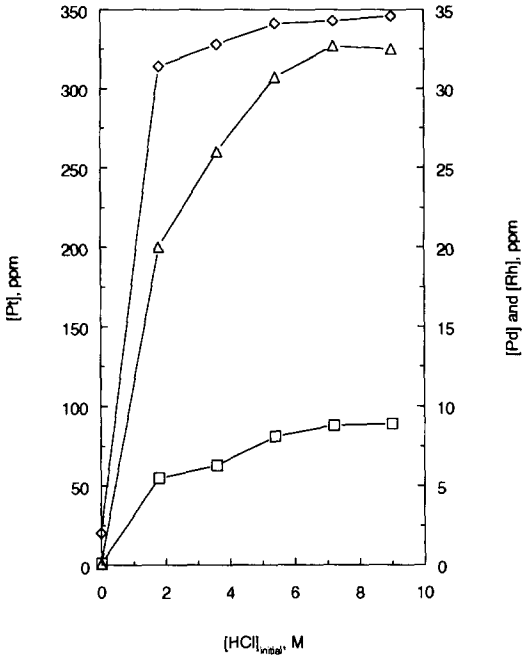


Fig. 3. Effect of hydrochloric acid concentration on leaching palladium, platinum and rhodium: autocatalyst weight = 20.0 g, $[NaClO_3] = 0.4M$, temperature = 70°C, heating period = 1 hr: (◇) Pd, (△) Pt, (□) Rh.

*Effect of temperature*

Palladium leaching was independent of the temperature (Fig. 4), while platinum leaching increased from 176 ppm at room temperature to a maximum of 325 ppm at 95°C. Rhodium leaching increased from 3.3 ppm at room temperature to a maximum of 9.5 ppm at 95°C. The effect of temperature on the hydrochloric acid content of the leached solutions showed a linear decrease in acid concentration with temperature which can be expressed by the following regression equation $[HCl]_{final} = -0.043\ t + 5.104$ over the temperature range of 32° to 95°C studied. Because hydrochloric acid evaporates at elevated temperatures, a temperature of 70°C was recommended for optimal leaching.

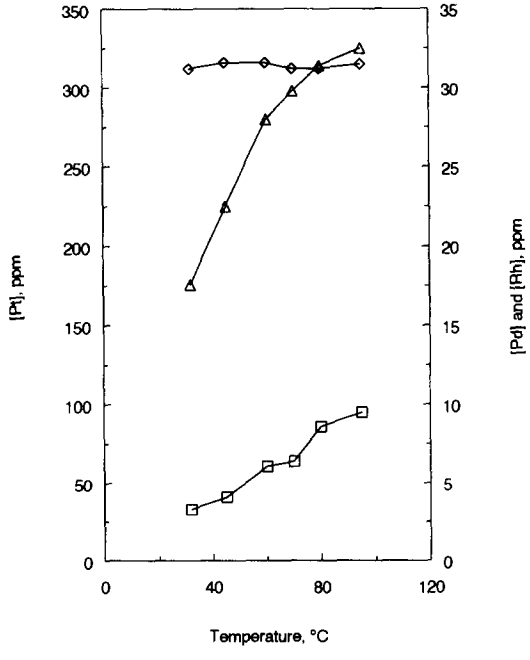


Fig. 4. Temperature effect on leaching palladium, platinum and rhodium: autocatalyst weight = 20.0 g, $[HCl]_{initial} = 4.8M$, $[NaClO_3] = 0.4M$, heating period = 1 hr: (◇) Pd, (△) Pt, (□) Rh.

*Separation of palladium, platinum and rhodium*

*Evaluation of anion-exchange resins.* Three anion-exchange resins, Amberlite IRA-400, Amberlite IRA-93 and Amberlite IRA-68 were tested using a batch procedure to select a resin that is efficient in both recovery and stripping of palladium, platinum and rhodium. Recovery of these metals from a $4.0M$ hydrochloric acid solution containing a synthetic mixture of 25 ppm of each metal, and stripping with 5% $NH_3$ solution were investigated. Although the quantitative recovery of palladium and platinum could be achieved with both Amberlite IRA-400 and Amberlite IRA-93 resins, the latter exhibited more favorable results in the recovery of rhodium and its stripping with platinum (Table 1).

*Recovery of* Pd, Pt *and* Rh. The recovery of palladium, platinum and rhodium from a pregnant solution that was made 280 ppm platinum, 340 ppm palladium, 380 ppm rhodium and which contained 6450 ppm aluminum, 1610 ppm iron, 947 ppm cerium and 397 ppm lead showed a recovery of 99% palladium, 97% platinum and 61% rhodium (Table 2). The results also indicated that 13% aluminum, 32% iron, 18% cerium and 80% lead were retained by the resin. The decomposition of $RhCl_6^{3-}$ in

Table 1. Recovery and stripping efficiencies of palladium, platinum and rhodium using Amberlite IRA-400, Amberlite IRA-93 and Amberlite IRA-68 resins

| | % Recovery* | | | % Stripping† | | |
|---|---|---|---|---|---|---|
| Resin | Pd | Pt | Rh | Pd | Pt | Rh |
| IRA-400 | 95 | 99 | 25 | 100 | 69 | 92 |
| IRA-93 | 95 | 99 | 30 | 100 | 75 | 100 |
| IRA-68 | 74 | 83 | 45 | 68 | 63 | 60 |

*Solution volumes 10 ml; resin weight 1.0 g; initial concentrations of palladium = platinum = rhodium = 20 ppm; $4.0M$ hydrochloric acid

†5% $NH_3$ solution (v/v)

Table 2. Separation of palladium, platinum and rhodium from the pregnant solution by Amberlite IRA-93 resin

| Metal* | % Recovery | %Stripping | |
|---|---|---|---|
| | | 6*M* HCl | 5% $NH_3$ solution |
| Pd | 99 | 0.9 | 98 |
| Pt | 97 | 0.7 | 7 |
| Rh | 61 | 80 | n.d.† |

*Solution volume 25 ml; initial concentrations of palladium 340 ppm, platinum 280 ppm and rhodium 380 ppm; resin weight 2.0 g; flow rate 1 ml/min.
†n.d.: Not determined.

aqueous solution to $[RhCl_{6-x}(H_2O)_x]^{x-3}$ types may be the major problem in its recovery.[13]

*Elution of rhodium.* In an attempt to strip rhodium selectively, the resin was treated with 25.0 ml of 6.0*M* hydrochloric acid solution at 1 ml/min at room temperature. Palladium and platinum remained on the resin whereas 80% of the rhodium was eluted (Table 2). Therefore, a complete elution of rhodium can be achieved by controlling the volume of hydrochloric acid. When the stripping solution was tested for aluminum, cerium, iron and lead, both aluminum and cerium were quantitatively eluted while 84% of the lead and 44% of the iron were eluted under these conditions. These two metals were removed completely with 25.0 ml deionized water at 1 ml/min.

*Elution of palladium.* When the resin from previous investigation was treated with 25.0 ml of 5% $NH_3$ solution (flow rate 1 ml/min), 98% palladium was eluted with only 7% platinum (Table 2).

Elution of palladium and platinum from the resin with different volumes of 5% $NH_3$ solution was studied by passing the eluent through the column loaded with these metals and treated with 25.0 ml each of 6.0*M* hydrochloric acid and deionized water (Fig. 5). A 4.0 ml of 5% $NH_3$ solution was sufficient to strip palladium completely with only a small amount of contaminating platinum. To improve the selectivity of eluting palladium, different percentages of ammonia solution from 1 to 10% (25.0 ml volume) were studied. Less than 2% of ammonia solution was sufficient to strip palladium selectively (Fig. 6). Furthermore, concentrations below the limits of analytical detection were obtained when the eluted solution was tested for iron, lead, aluminum and cerium.

*Elution of platinum.* The stripping of small amounts of platinum from the resin (Figs 5, 6) may be related to the slow rate of formation of $Pt(NH_3)_6^{4+}$ in comparison to $Pd(NH_3)_4^{2+}$ com-

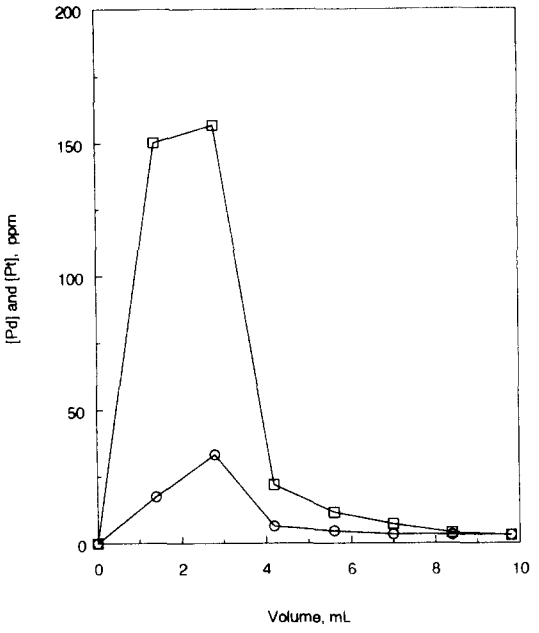


Fig. 5. Elution curves for palladium and platinum: 5% $NH_3$ solution (v/v), flow rate = 1 ml/min (□) Pd, (○) Pt.

plex.[14] In an attempt to improve the stripping efficiency for platinum, the effect of column temperature was studied. The column was packed with resin and loaded with platinum, then immersed completely in a water bath maintained at 65°C. An aliquot of 25.0 ml solution of 5% $NH_3$ (heated to 65°C) was passed through at a flow rate of 1 ml/min. The percentage of platinum recovered increased from 7% at room

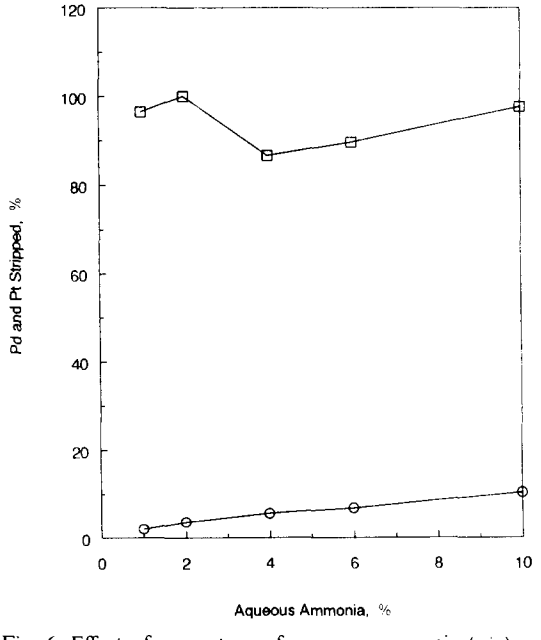


Fig. 6. Effect of percentage of aqueous ammonia (v/v) on stripping palladium and platinum: solution volumes = 25.0 ml, flow rate = 1 ml/min: (□) Pd, (○) Pt.

temperature to 42% at 65°C. When this experiment was repeated at a flow rate of 0.5 ml/min, the per-cent of platinum eluted further improved to 65%. This indicates that a complete recovery of platinum from the resin can be accomplished by controlling the percentage of ammonia solution, its flow rate and the column temperature.

*Capacity of Amberlite IRA-93 for* Pd *and* Pt *uptake*

The capacity of the resin to retain palladium and platinum was estimated from a breakthrough study: 275 ml of 4.0*M* hydrochloric acid containing 350 ppm platinum and 275 ppm palladium were passed through the column (packed with 2.0 g of the resin) at a flow rate of 1 ml/min. From the plot of concentration of the metal unretained versus volume of the solution collected (Fig. 7), capacities of 0.44 mol platinum/kg resin and 0.85 mol palladium/kg resin were calculated. Owing to these high resin capacities, Amberlite IRA-93 may be of practical value in recovering palladium and platinum from a solution obtained by leaching these metals from automotive catalytic converters.

*Recommended process for macro scale recovery of* Pd, Pt *and* Rh

A recommended process for leaching palladium, platinum and rhodium from the automotive catalytic converter and their selective recovery from the leached solution using Amberlite IRA-93 is summarized in Fig. 8. A 5.0*M* hydrochloric acid solution is mixed with the catalyst sample and then heated to 70°C. At this temperature, a 0.4*M* sodium chlorate solution is added slowly and the mixture is filtered. The pregnant solution is then passed through the resin. The column is washed with 6.0*M* hydrochloric acid solution followed by deionized water. The hydrochloric acid solution (containing non-saturating amount of rhodium) is saved for reuse. The resin is then treated at room temperature with 1% $NH_3$ solution to strip palladium followed by 5% of the reagent at elevated temperatures and a slow flow rate to elute platinum. The separation of palladium and platinum from the eluted solution could then be processed either by reduction to metal or precipitation as $(NH_4)_2PdCl_4$ and $(NH_4)_2PtCl_6$ by hydrochloric acid.[15] The original leaching solution is then adjusted to 5.0*M* hydrochloric acid, heated to 70°C and reused several times to leach platinum metals from a new batch of the catalytic converters and passed through the resin again. After several recycling processes, the leaching solution becomes rich in rhodium. This recycled solution can then be passed through the resin many times to recover rhodium. After each cycle, the resin is washed with the saved hydrochloric acid solution to strip rhodium which then can be recovered by a selective reduction to metal.[2]

## CONCLUSIONS

The described ion-exchange method, using Amberlite IRA-93, for selective separation of palladium, platinum and rhodium from acidic solutions obtained by leaching honeycomb type catalytic converter can be considered an efficient technique for the separation of these metals on

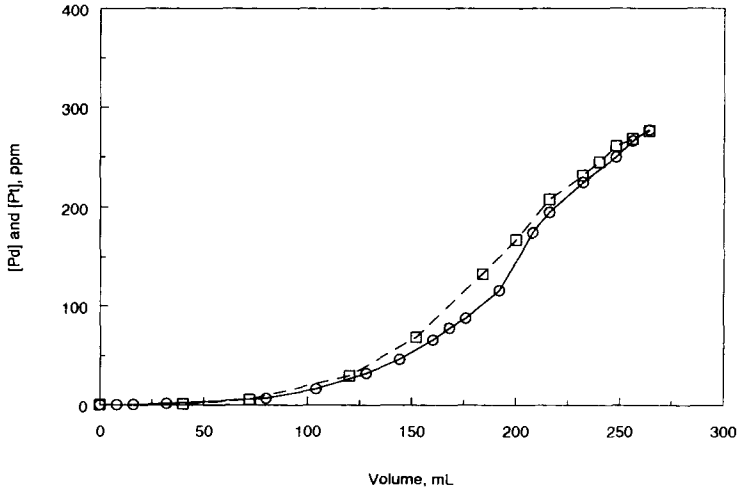


Fig. 7. Breakthrough curves for palladium and platinum: [Pd] = 275 ppm, [Pt] = 350 ppm, [HCl] = 4*M*, solution volume = 275 ml, flow rate 1 ml/min: (□) Pd, (○) Pt.

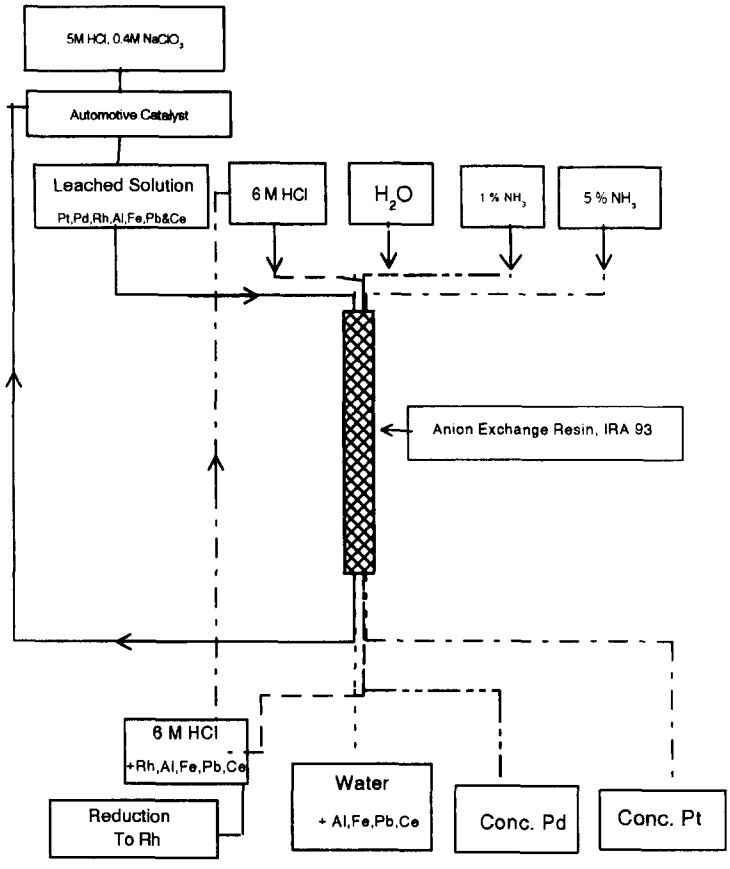


Fig. 8. Simplified flow diagram for leaching, recovery and stripping processes.

an analytical scale and could be applied to large scale operations. This method is not restricted solely to automotive catalysts but is also applicable to petrochemical catalysts, ores, and industrial wastes. It is noteworthy that owing to the nontoxicity, nonvolatility, and nonflammability of the ion-exchange resin, this method may present fewer environmental hazards than the currently adopted solvent extraction and precipitation techniques.

*Acknowledgements*—The authors would like to thank Mr Raymond Sloan from the Catalytic Converter Refining Co., for providing a catalytic converter. This research was supported by a grant from the Northeastern Illinois University Committee on Organized Research.

## REFERENCES

1. M. E. Browning, G. I. Edson and I. S. Bubes, *The Third Conference on Precious Metals*, p. 270. Illinois, 1989.
2. L. Manziek, *Precious Metals Recovery and Refining*, p. 7. Historical Publication, Texas, 1990.
3. E. D. Zysk, *Platinum Group Metals Seminar 1985*, p. 49. Washington D.C. 1986.
4. C. W. Ammen, *Recovery and Refining of Precious Metals*, p. 242. Van Nostrand Reinhold, New York, 1984.
5. J. E. Barnes and J. D. Edwards, *Chem. Ind.*, 1982, **5**, 151.
6. R. I. Edwards, *Proc. Int. Solvent Extr. Conf.*, 1979, **1**, 24.
7. L. R. Reavill and P. Charlesworth, *Proc. Int. Solvent Extr. Conf.*, 1980, **3**, 80.
8. S. J. Al-Bazi and A. Chow, *Talanta*, 1984, **31**, 815.
9. S. J. Al-Bazi and H. Freiser, *Anal. Chim. Acta*, 1991, **245**, 225.
10. S. J. Al-Bazi and H. Freiser, *Inorg. Chem.*, 1989, **28**, 417.
11. S. J. Al-Bazi and H. Freiser, *Solvent Extr. Ion Exch.*, 1987, **5**, 265.
12. S. J. Al-Bazi and H. Freiser, *Solvent Extr. Ion Exch.*, 1986, **4**, 1121.
13. R. E. Connick and D. A. Fine, *J. Am. Chem. Soc.*, 1961, **83**, 3414.
14. F. V. S. Toerien and M. Levin, *J. S. Afr. Chem. Inst.*, 1974, **27**, 87.
15. G. Foo and M. E. Browning, *Symposium on Recovery, Reclamation and Refining of Precious Metals*, presentation no. 13, California, 1981.

Pergamon

0039-9140(94)00247-9

*Talanta*, Vol. 42, No. 2, pp. 257–261, 1995
Elsevier Science Ltd
Printed in Great Britain
0039-9140/95 $9.50 + 0.00

# A FLOW INJECTION ANALYSIS TECHNIQUE FOR THE DETERMINATION OF CHLORIDE USING REFLECTANCE DETECTION

RICHARD H. TAYLOR and JAY W. GRATE
Pacific Northwest Laboratory, K2-12, P.O. Box 999, Richland, WA 99352, U.S.A.

(*Received* 5 *May* 1994; *Revised* 12 *August* 1994. *Accepted* 16 *August* 1994)

**Summary**—A flow injection (FI) determination for chloride has been developed using the light reflectance of the precipitate formed by the reaction of chloride with silver(I) as the method of detection rather than turbidimetry, as in the previous FI method using this reaction. The dynamic range of the analysis is increased to 0–10 m*M* chloride with a 10 m*M* silver(I) reagent and to 0–50 m*M* chloride with a 50 m*M* silver(I) reagent by using this mode of detection. The ability to select the injected reagent from an option of two concentrations via the control program is incorporated into the FI system, enhancing the versatility of the analysis.The dynamic range is further extended to 100 m*M* chloride by measuring the signal levels at the trailing portion of the response curve. The consumption of reagent is kept to a minimum by merging injected zones of sample and reagent instead of using a constant reagent stream.

The determination of chloride concentration was one of the earliest applications of flow injection analysis (FIA) to the analysis of environmental waters.[1,2] These analyses used the formation of an iron(III) thiocyanate complex to determine the chloride spectrophotometrically, after the reaction of chloride with mercury thiocyanate.[1–5] These reports state an initial range up to 75 mg/l.,[3,4] which, through the application of stream splitting[1,2] or pre-injection dilution,[5] was extended up to 800 mg/l. Another method employing photometric detection used the formation of a silver chloride precipitant, by the reaction of chloride with the silver(I) ion, as a method of chloride analysis by FIA.[6] In this study, turbidimetry was used as the method of detection, and a range of 0–14 mg/l. was given.

This report describes the development of a flow injection (FI) method for the determination of chloride. The method has five main features. First, the previously mentioned silver(I)–chloride chemistry, which forms a white precipitate, is used. Second, reflectance rather than turbidimetry is used as the detection method. Reflectance is measured by using a flow cell with a bifurcated optical fiber bundle. The system flow and cell geometry forces the particulate to remain suspended while passing through the flow cell. Third, the ability to select, through the control program, from two silver(I) reagent solutions of differing concentrations is provided. This extends the dynamic range of the analysis when sample concentrations are determined from the maximum reflectance peak height. Fourth, the dynamic range of the analysis is further extended by measuring the signal levels at the trailing portion of the response curve. Concentrations up to 3500 mg/l. were measured by this method, far higher than the previous method using this chemistry. Moreover, this measurement can be done in spite of the increasing solubility of silver chloride at high chloride concentrations. Fifth, the method was developed in such a manner as to minimize the amount of silver reagent used by co-injecting reagent and sample rather than injecting sample into a continuous reagent stream. The advantages of this new method include the extended dynamic range, the avoidance of a mercury-containing reagent, and the minimization of the silver reagent.

## EXPERIMENTAL

### *Reagents*

All solutions were prepared in deionized water. Chloride samples in the range of 2–100 m*M* were prepared with potassium chloride (Mattheson Coleman and Bell) and the reagents were 0.010 and 0.050*M* silver nitrate (Cascade Silver Co.). The carrier for both sample and reagent streams in the determination of chloride

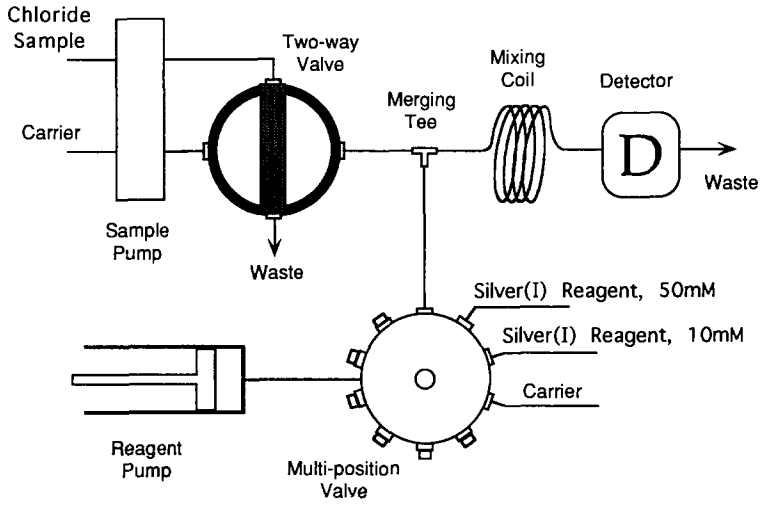


Fig. 1. Schematic of the chloride system.

was deionized water, which was also used as the blank solution for the analysis. When determining the overlap of the sample and reagent zones 0.01*M* borate solution (Aldrich) was used as carrier, and 0.004% Bromothymol Blue (BTB) (Aldrich) was injected in place of sample and reagent.

*Apparatus*

A schematic of the FI system for the determination of chloride is shown in Fig. 1. The system was assembled using an Alitea Modular Injection System Type MIS-1B (housing the peristaltic sample pump and the multi-position reagent stream valve); an Alitea Model S2-V piston pump for the reagent stream; a Valco 10-port 2-way sample injection valve; and an Alitea ODS-1 detection system, which used a Brinkman PC 701 colorimeter. The colorimeter was used without an interference filter installed and was connected to the flow cell (Fig. 2) by a bifurcated fiber optical bundle. The flow cell was modified by the removal of the internal reflecting plate. The direction of flow through the cell was vertical with the lower opening as the inlet. This, along with the force of the flow prevented the accumulation of the precipitate within the flow cell light path. All components were controlled and data collected using the FIALab control program (Alitea) running on a Northgate® 486ZXP computer equipped with a Real Time Device ADA1100 data acquisition board.

Tygon® tubing of 1.02 mm inside diameter was used in the peristaltic pump for both the sample and the sample stream carrier, and a 5 ml syringe was used in the reagent stream pump. The sample injection valve had a 24$\mu$l sample loop. Tubing upstream of the PEEK merging tee was 0.82 mm inside diameter PTFE (Upchurch). The tubing downstream of the tee, which formed the mixing coil, was a 45 cm length of 0.5 mm inside diameter Tygon® tubing.

*General procedure*

Prior to performing the analysis the control program was selected which directed the multi-purpose valve to the port of the reagent with the desired concentration. The selected silver(I) reagent, using the piston pump and the multi-position valve, and the chloride sample, using the peristaltic pump and the 2-way valve, were injected into separate deionized water carrier streams. These two zones were propelled to a tee where they were merged and then sent through the mixing coil to the detector flow cell, where

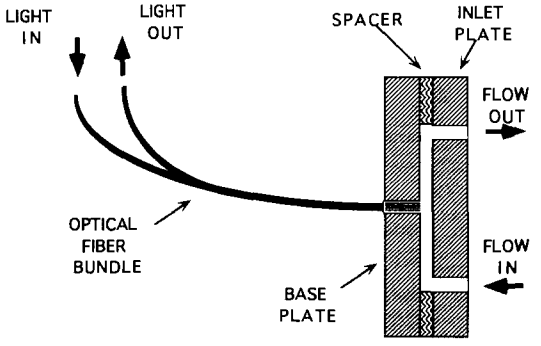


Fig. 2. Cut-away schematic of the detector flow cell. The reflector plate, normally located between the spacer and the inlet plate for absorbance measurements, was removed.

the reflectance of the silver chloride precipitate was measured.

The analysis was initiated by filling the syringe of the piston pump with 0.62 ml of deionized water. The multi-position valve was then directed to the selected reagent line, and 67$\mu$l of the silver(I) reagent of the desired concentration was drawn into the system. At this point the multi-position valve was redirected, and the direction of the piston pump reversed, sending the isolated volume of silver(I) reagent toward the merging tee. At the same time, the peristaltic pump started, and the sample loop of the 2-way injection valve was flushed with the chloride-containing sample for 6 sec before 24 $\mu$l of the chloride sample were injected into the sample stream. Both reagent and sample streams had a flow rate of 1.0 ml/min, creating a flow of 2.0 ml/min downstream of the merging tee, through the mixing coil and the detector flow cell.

*Adjustment of the reagent zone*

In order to form the maximum amount of precipitate possible it is necessary that the entire chloride sample zone come in contact with the silver(I) reagent. The volume of the chloride sample zone was physically fixed by the sample loop on the injection valve. The volume of the silver(I) reagent zone, however, was determined by the length of time the multi-position valve was directed to the reagent line and the flow rate of the piston pump during that time. Varying these parameters involved only software commands, requiring no physical alteration of the system. The silver(I) reagent volume and the time of injection were adjusted such that the silver(I) reagent zone was larger than and completely overlapped the chloride sample zone when the two streams merged. This was determined by injecting BTB dye in lieu of each solution in turn and observing the detector response. This approach provides information on both the timing and dispersion of the zones. The degree of overlap and comparative dispersion of the two zones as determined by this method are illustrated in Fig. 3.

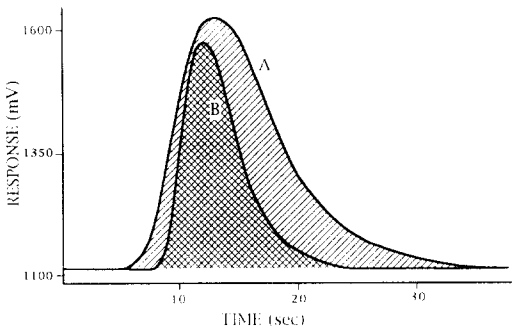


Fig. 3. Representation of the overlap of the reagent zone (A) of the sample zone (B), determined by the injection of 0.004% BTB dye for each zone individually and then combining the two data sets.

## RESULTS AND DISCUSSION

Chloride solutions of varying concentration were injected into the sample stream, and a 0.010 or 0.050$M$ silver nitrate solution was used as reagent. The separate streams merged to mix the two solutions, forming a zone of silver chloride precipitate. This zone passed through the detector flow cell and the reflectance of the white precipitate was measured.

The intensity of the light source was adjusted such that the baseline response corresponded to the reflected light intensity giving a reading of 80% T on the detector meter. The increase of the intensity of the reflected light as the reaction precipitate moved through the flow cell resulted in an increase in the detector response output voltage, and could be viewed on the detector meter as an apparent increase in transmittance. This increase in the detector output voltage was compared with the chloride concentration of the injected sample.

In the range from 0–10 m$M$ (0–354 mg/l.) a linear proportionality between maximum response peak height and the chloride concentration of the sample was obtained using the 0.010$M$ silver(I) reagent. The found line had a slope of 0.0255 m$M$/mV and an intercept of $-0.065$ m$M$, giving a correlation coefficient of 0.998. The non-zero intercept is due to the refractive index change which occurs when the silver(I) reagent zone passes through the flow cell.

Using the 0.050$M$ silver(I) reagent a linear proportionality between maximum response peak height and the chloride concentration of the sample was obtained in the range from 0–50 m$M$ (0–1770 mg/l.). The found line had a slope of 0.0303 m$M$/mV and an intercept of 0.66 m$M$, giving a correlation coefficient of 0.998.

Although the sample undergoes greater dispersion than the reagent (Fig. 3) due to less volume being injected, above a certain chloride concentration (approximately 12 and 60 m$M$ when using the 0.010 and the 0.050$M$ silver(I) reagent, respectively) the silver(I) reagent

becomes the limiting reactant. This is expected to produce a maximum response level which would not be exceeded, forming peaks which had a level plateau on the top, with an increase in peak width with increasing chloride concentration. It was observed, however, that along with the increase in width, the peaks began to 'invert' at the top and that the maximum height decreased as the chloride concentration increased (Fig. 4). Two factors may contribute to the observed effect. First, the solubility of silver chloride increases with the chloride concentration above chloride concentrations of approximately 10 m$M$ [7] due to the formation of soluble silver complexes such as $AgCl_2^-$ and $AgCl_3^{2-}$.[8,9] Second, it is possible that the aggregation and reflectance properties of the precipitate vary depending on which species, silver(I) or chloride, is in excess. The surface charge of the precipitate particles, and hence any particle/particle repulsions, depend on the ions adsorbed on the particle surfaces.

Nevertheless, the varying chloride concentration of the dispersed sample zone creates an area of the merged reactants in which the chloride concentration is less than that of the silver reagent, and signal levels are still proportional to the chloride concentration. Using the detector response after the inverted portion of the response, where the desired sample to reagent ratio is achieved, a convenient correlation between detector response and chloride concentration can still be found. The response levels using the 0.010$M$ silver(I) reagent at delay times of 22 and 24 sec after injection were examined (Fig. 4). These times were determined by observation of the detector response to the injected sample of highest concentration (100 m$M$ $Cl^-$). At a delay time of 22 sec a linear relationship was found with a slope of 0.765 m$M$/mV, an intercept of −0.843 m$M$, with a correlation coefficient of 0.998. At a delay time of 24 sec a linear relationship was found with a slope of 1.77 m$M$/mV, an intercept of −2.10 m$M$, with a correlation coefficient of 0.999.

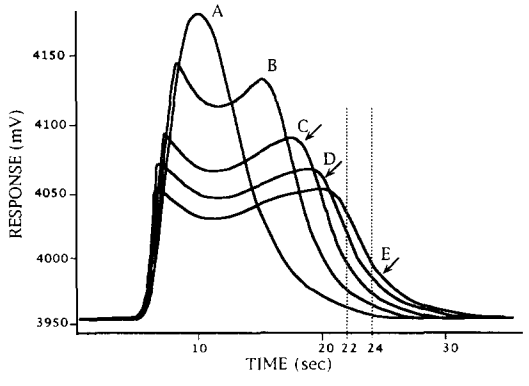


Fig. 4. Representation of the response curves of an injected sample of 10–100 m$M$ chloride reacted with 0.010$M$ silver(I), showing the reduction of response which occurred at higher concentrations. The signal level at delay times of 22 and 24 sec were used to extend the dynamic range of the analysis. (A = 10 m$M$, B = 20 m$M$, C = 50 m$M$, D = 75 m$M$, E = 100 m$M$).

The time required to perform a single analysis was 82 sec, which includes the time to fill the syringe. This gives an analysis frequency slightly greater than 40 $h^{-1}$. Multiple analyses ($\geq 3$) were performed for each sample, with a relative standard deviation (RSD) of less than 1.5% for samples in the range of 0–10 m$M$ $Cl^-$ and less than 3% for samples 10–100 m$M$ $Cl^-$ with the 0.010$M$ silver(I) reagent and an RSD of less than 3.5% for all analyses using the 0.050$M$ silver(I) reagent. This precision is comparable with FI methods using the mercury thiocyanate–iron chemistry which have reported RSD values of 1.2 and 1.3%.[2,5] The automated method introduced here compares favorably with manual titrimetric methods which have reported RSD values of 4.2% by Mohr's method (titration with silver nitrate with a potassium chromate indicator) and 3.3% by mercuric nitrate titration.[10]

## CONCLUSIONS

A flow injection method for the analysis of chloride, with a dynamic range of 0–100 m$M$ (0–3500 mg/l.), using the reaction with Ag(I), and performing detection by reflectance, was devised. This approach greatly increases the dynamic range of the former FIA method using this chemistry, which used turbidimetry as the method of detection. It also avoids the use of mercury containing reagent, which has formerly been used in other FIA photometric determinations of chloride. The silver reagent, although less of a hazard than the mercury reagent, is a controlled waste, and the method is designed such that its use is minimized, thus reducing its consumption and its concentration in the waste generated.

The dynamic range of the analysis can be adjusted in two ways. First, for analyses where the sample concentration is determined from the reflectance peak height, the silver reagent must be present in excess. This can be achieved by

selecting a silver reagent solution of appropriate concentration using the multi-position valve, as we have demonstrated. The possible choices of silver reagent concentration are limited only by the number of valve ports available. Alternatively, when chloride concentrations exceed silver reagent concentrations, the chloride concentration can be determined from trailing portion of the response curve. In this case, the dynamic range is limited by the width of the silver reagent zone that the chloride sample is merged into. The silver reagent zone width can be increased simply by increasing the volume of the silver reagent injected, which can be easily achieved through the manipulation of the flow program. The ability to either select the concentration of the analytical reagent and/or the width of the reagent zone through the control program enhances the overall versatility of the assay. Although the described method was developed to analyze samples with a chlorine concentration up to 100 m*M*, which satisfied the needs of this laboratory, it can be seen that either of these two techniques could allow for further expansion of the dynamic range.

*Acknowledgements*—This research was supported under Grant DE-FG06-89ER-75522 or DE-FG06-92RL-12451 with the U.S. Department of Energy. Pacific Northwest Laboratory is a multiprogram national laboratory operated for the U.S. Department of Energy by Battelle Memorial Institute under Contract DE-AC06-76RLO 1830.

## REFERENCES

1. J. Ruzicka, J. W. B. Stewart and E. A. G. Zagatto, *Anal. Chim. Acta*, 1976, **81**, 387.
2. W.D. Basson and J. F. Van Staden, *Water Res.*, 1981, **15**, 333.
3. J. Ruzicka, E.H. Hansen, H. Mosbaek and F. J. Krug, *Anal. Chem.*, 1977, **49**, 1858.
4. E. H. Hansen and J. Ruzicka, *J. Chem. Ed.*, 1979, **56**, 677.
5. J. F. Van Staden, *Fresenius Z. Anal. Chem.*, 1985, **322**, 36.
6. T. Zaitsu, M. Maehara and K. Toei, *Bunseki Kagaku*, 1984, **33**(3), 149.
7. J. S. Fritz and G. H. Schenk, *Quantitative Analytical Chemistry*, p.148. Allyn and Bacon, Boston, 1974.
8. G. S. Forbes, *J. Am. Chem. Soc.*, 1911, **33**, 1937.
9. G. S. Forbes, *J. Am. Chem. Soc.*, 1921, **43**, 2492.
10. M. J. Taras, A. E. Greenberg, R. D. Hoak and M. C. Rand, *Standard Methods for the Examination of Water and Wastewater*, 13th Ed., p.96. American Public Health Association, Washington, 1971.

Pergamon

0039-9140(94)00253-3

*Talanta*, Vol. 42, No. 2, pp. 263–267, 1995

0039-9140/95 $9.50 + 0.00

# DETERMINATION OF GOLD IN BIOLOGICAL MATERIALS BY ELECTROTHERMAL ATOMIC ABSORPTION SPECTROMETRY WITH A MOLYBDENUM TUBE ATOMIZER

KIYOHISA OHTA,* TIKARA ISIYAMA, MASAYOSI YOKOYAMA and TAKAYUKI MIZUNO
Department of Chemistry for Materials, Faculty of Engineering, Mie University, Tsu, Mie 514, Japan

(*Received* 3 *June* 1994. *Revised* 16 *August* 1994. *Accepted* 19 *August* 1994)

**Summary**—Electrothermal atomic absorption spectrometry (ETA-ASS) of gold with a molybdenum tube atomizer has been investigated. A sensitive ETA-AAS method was developed. The gold absorption signal became higher with the heating rate of the tube atomizer and as the ratio of hydrogen in the argon purge gas decreased. The optimal heating rate and the optimal gas flow rate were 5.5°C/msec and Ar 480 ml/min + $H_2$ 20 ml/min, respectively. The absolute characteristic mass (the mass of element giving 0.0044 abs.) of gold by the atomizer was 1.8 pg and the detection limit was 130 pg/ml ($3S/N$). These values were > 10 times better than those obtained with graphite atomizers, ICP and ICP-MS. The interferences caused by large amounts of interferents were evaluated. The addition of thiourea served to eliminate severe interferences. The recovery of spiked gold in biological materials was in the range of 101–106%.

Gold compounds have been used in the treatment of rheumatoid arthritis.[1] However, they are fundamentally toxic for a living body. The determination of gold in biological materials is, therefore, of interest. Several methods have been used to determine gold concentrations including graphite furnace atomic absorption spectrometry (GFAAS),[2–9] inductively coupled plasma emission spectrometry (ICP)[9,10] and flame AAS.[11,12] Although ICP has high sensitivity, the method has severe optical and chemical interferences.[9,11] Flame AAS has poor sensitivity for measuring trace levels of gold in biological materials.[12] GFAAS is in much more general use throughout the world. There is, however, a problem of chemical interference. In order to eliminate the interferences from biological matrices, electrophoretic separation,[2] standard addition method,[5] chemical modification,[6,8] co-precipitation,[13] liquid–liquid extraction[14] and silica gel adsorption of chelate[15] have been used for gold determination in biological and geological materials.

Electrothermal atomization AAS (ETA-AAS) with metal tube atomizers, developed recently,[16–18] has better sensitivity for most metal elements than other analytical instruments, the ability to use smaller sample sizes, and relatively low power and low cost. Despite the advantages, there is a little information on the application of the metal tube atomizer to ETA-AAS.

In the present work, we report a determination of gold in biological materials by ETA-AAS with a molybdenum tube atomizer. Atomization characteristics for gold in the atomizer were evaluated. Interference studies for the gold absorption signal were also performed.

## EXPERIMENTAL

### *Apparatus*

An atomizer consisting of a molybdenum tube (20 mm long and 2.0 mm i.d.) and two supporters (5 mm wide and 20 mm long) was made from a molybdenum foil (0.05 mm thick and 99.95% purity, Rembar Co.). A 0.3 mm diameter hole was drilled at the midpoint of the tube to inject sample solution. Gold AA signals were measured at 242.80 nm (Au-hollow cathode lamp, Hamamatsu photonics Co.) using a monochromator (Nippon Jarrell-Ash 0.5 m Ebert-type), an amplifier, a storage oscilloscope (Iwatsu MS-5021), and a microcomputer (Sord M223). The electric power for heating the atomizer was supplied with two

*Author to whom correspondence should be addressed.

transformers (Yamabishi volt-slider, S-130-30, Cap. 3 k VA). Two pinhole apertures were placed in front of and in the rear of the atomizer, in order to collimate the light beam and eliminate the radiation from the atomizer surface. Background absorption was checked with a deuterium lamp (Original Hanau D200F). The absorption signal from the amplifier and the output signal from a photodiode for the measurement of atomizer temperature were simultaneously fed into the microcomputer. Calibration of the temperature of the atomizer was done against the photodiode voltage using an optical pyrometer (Chino Works) with microcomputer programming.

*Reagents*

A standard stock solution (1 mg/ml, 1*M* HCl solution) of gold (spectroscopic purity) was obtained from Nacalai Tesque Inc. (Kyoto, Japan). Solutions of the matrix elements for the interference study were prepared as chlorides in 0.1–6*M* hydrochloric acid. Standard solutions with concentrations appropriate to the atomic absorption measurements were diluted from the stock solutions with water immediately before use. All other chemicals used here were of analytical grade purity.

*Procedures*

An accurately weighed biological sample (about 0.1 g) was treated with 3 ml of nitric acid (14*M*) and 1 ml of hydrogen peroxide (30%) in a Uni-seal decomposition vessel and heated for 3 hr in an electric oven at 120°C. After the decomposition, the solution was transferred into a Teflon beaker and evaporated by heating in a polyethylene glycol bath (110°C). Then the residue was dissolved in 5 ml of 6*M* hydrochloric acid on the bath. The evaporation was repeated twice more with addition of hydrochloric acid in between. The solution, in which the residue was dissolved, was diluted to 5 ml with 6*M* hydrochloric acid. The resultant solution was diluted to adequate volume (10–20 ml) with a 10 mg/ml thiourea solution for AA measurements.

For the atomization characteristics, the interference study and the determination of gold in biological materials, a 1 $\mu$l portion of the sample solution containing Au (250 pg) was pipetted into the molybdenum tube atomizer. The sample was dried at 80°C for 20 sec, 720°C (410°C for the atomization characteristics) for 10 sec and heated to atomize at 2240°C for 3 sec. The atomizing temperature corresponded to a heating rate of 5.5°C/msec.

## RESULTS AND DISCUSSION

*Effect of heating rate*

Atomic absorption is related to the density of the atomic vapour. The atomization rate of an atomizer affects the density as reported in previous papers[16–18] and hence the effect of the atomization rate, 1.5–5.5°C/msec, on the gold AA-profile was investigated. At more than 5.5°C/msec, the lifetime of the metal atomizer was very short (< 100 firings).

The absorption profile of gold was characterized by a sharper and narrower peak with the increase of the heating rate, as shown in Fig. 1. The appearance temperature of the gold signal (1150°C), which is defined as the temperature of atomizer giving an absorbance of 0.0044, was independent of the heating rate. However, the temperature at the maximum AA signal (peak temperature) was 1910°C at 5.5°C/msec, 1860°C at 4.2°C/msec, 1700°C at 3.0°C/msec, 1630°C at 2.5°C/msec and 1350°C at 1.5°C/msec, and thus, the peak temperature of the signal was found to be dependent on the heating rate. These phenomena are the same as those observed for the absorptions of silver.[17] Gold in the stock solution is in the form of the tetrachloroaurate ion. The chloride ($AuCl_3$) dissociates to give AuCl and $Cl_2$ at high temperature (254°C) and converts to gold metal during the dry stage.[19,20]

The appearance temperature of gold in the molybdenum atomizer is close to the melting point of gold metal (1064°C), but far from the

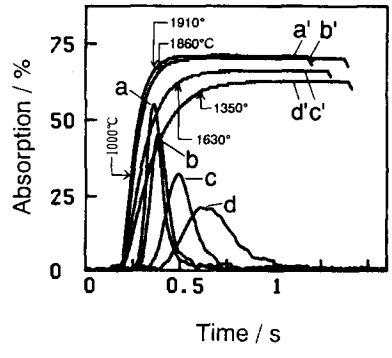


Fig. 1. Effect of heating rate of the molybdenum atomizer on atomic absorption of gold. (a and a') 5.5 C/msec; (b and b') 4.2 C/msec; (c and c') 3.0 C/msec; (d and d') 1.5 C/msec; (a–d) atomization profiles; (a'–d') temperature increasing; Au 250 pg. Purge gas was 480 ml/min Ar + 20 ml/min $H_2$. Pyrolysis temperature: 410 C.

boiling point (2808°C).[19] The vapor pressure for gold metal is $1.47 \times 10^{-7}$ atm, corresponding to $5.20 \times 10^{10}$ atoms in the metal tube atomizer, at 1150°C.[19]

Consequently, 5.5°C/msec heating rate was recommended, in view of the highest peak and the lifetime of the metal atomizer.

*Effect of hydrogen*

Hydrogen added to the argon purge gas is necessary to protect the metal atomizer from oxidation by residual traces of oxygen in the atomizer chamber or in the argon gas cylinder. Therefore, the absorption signal for gold (250 pg) was evaluated in argon–hydrogen purge gas at the heating rate of 5.5°C/msec. In pure argon gas, the highest AA signal for gold was obtained, as shown in Fig. 2. A small addition of hydrogen to the argon purge gas provided the low AA peak. The peak height of the gold signal decreased with increasing ratio of hydrogen. In pure hydrogen, the AA signal became extremely small and shifted to the lower temperature region. The peak temperature for the AA signal was 1610°C in pure argon, 1910°C in Ar 480 ml/min and $H_2$ 20 ml/min, 2000°C in Ar 400 ml/min and $H_2$ 100 ml/min, and 1900°C in pure hydrogen. Thus, the peak temperature of the signal was dependent on the hydrogen ratio in the purge gas. These phenomena are specific for gold and the reason could not be seen clearly, though we discussed it on the grounds of the literature values.

Since gold hydride does not exist at room and high temperatures,[20] the lower peaks of gold given by the addition of hydrogen are a result of the large specific heat of hydrogen.

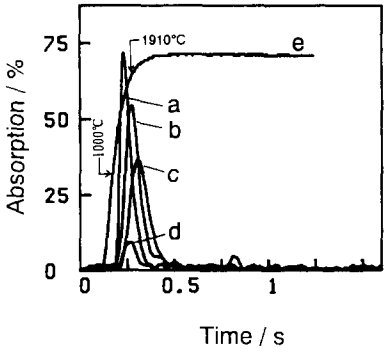


Fig. 2. Effect of hydrogen on atomic absorption of gold. (a) 500 ml/min Ar; (b) 480 ml/min Ar and 20 ml/min $H_2$; (c) 400 ml/min Ar and 100 ml/min $H_2$; (d) 500 ml/min $H_2$; (e) temperature increasing; Au 250 pg; heating rate was 5.5°C/msec. Pyrolysis temperature: 410 C.

The optimal purge gas flow rate for the absorption signal was Ar 480 ml/min and $H_2$ 20 ml/min, considering the lifetime of the molybdenum atomizer.

*Effect of pyrolysis temperature*

It has been reported that the pyrolysis temperature on ETA-AAS sometimes affects the AA peak height in the determination of some element.[16-18] Therefore, the effect of pyrolysis temperature on the absorbance of gold in the molybdenum tube atomizer was investigated. The results are shown in Fig. 3. The highest absorbance for gold in the metal atomizer was obtained at a pyrolysis temperature of about 410°C. Over 410°C, the absorbance decreased significantly. Though the shape of the pyrolysis temperature curve in the presence of thiourea is similar to that obtained without thiourea, the curve shifted to a lower temperature region. This phenomenon is presumably related to the lower decomposition temperature of the sulfide rather than that of the chloride.

On GFAAS, the sensitive pyrolysis temperatures for gold are 780°C,[2] 450°C,[3] 600°C,[5] 1200–1300°C,[6] and 1300°C.[7] The temperature (410°C) in the metal atomizer was very different from those, except one, of the graphite furnace atomizers. The difference may result from the lack of formation of gold carbide in the metal tube. Consequently, 410°C was selected as an optimal pyrolysis temperature for atomization characteristics. For the interference study and the determination of gold in biological materials, 720°C was selected considering the matrix interferences.

*Detection limit, characteristic mass and reproducibility*

The characteristic mass of gold, which was defined as the mass of element giving an

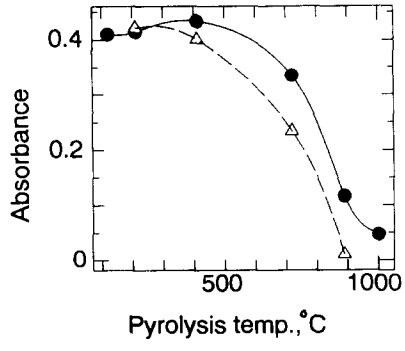


Fig. 3. Effect of pyrolysis temperature on atomic absorption signal of gold. Solid line: Au 250 pg; broken line: Au 250 pg + thiourea.

absorbance of 0.0044, by the atomizer was 1.8 pg. The detection limit, which was the weight of analyte which gave an atomic absorption signal equal to three times the standard deviation of the background, obtained from the measurement of a solution blank, was calculated from the height of gold absorption signal. The detection limit of gold by use of the molybdenum tube atomizer was 1.3 pg, corresponding to 130 pg/ml, given at 10 $\mu$l sample. These values were several times better than the characteristic mass (4.782 pg[7]) and the detection limit (400 pg/ml[6]) obtained with a graphite atomizer, and those with ICP (10 ng/ml[11]) and ICP-MS (200 pg/ml[11]).

A reason for the better sensitivity in the molybdenum atomizer may be the nonporous atomizer wall differing from a graphite furnace and the formation of the Mo-alloy with a low bonding energy.

The reproducibility of the use of the molybdenum atomizer was investigated. The relative standard deviation for 250 pg of gold was 2.9% for 10 measurements. In the case of thiourea addition, the RSD was 2.5%.

*Interference study*

Interferences by some matrix elements in the determination of gold in biological materials by GFAAS have been observed.[2-8] In particular, the interference problems from chloride salts were important.[4] Therefore, the influences of Ca, Cu, Fe, K, Mg, Pb and Zn (0.25–2.5 mg metal/ml), which are included as major elements in biological materials, on a gold absorption signal were investigated in the molybdenum tube atomizer. These coexisting elements were naturally used as chloride salts.

Despite the sensitivity not being optimal, the gold samples were pyrolyzed at 720°C because of the molecular absorption formed from the matrix at the time of atomization after the low temperature pyrolysis. The gold signal in the presence of these elements was measured in terms of both the peak height and the peak area. The peak area measurement method was more unsuitable than the peak height method because of the larger interfering tendency and the inconvenience. The gold signal (250 pg) was influenced by Ca, Cu, Fe, K, Pb and Zn. The interference of potassium was especially severe. Royal[21] found serious depression of the gold signal in the presence of alkali on the determination of gold by GFAAS. In flame AAS, interference owing to copper, iron and sodium was reported.[22] In the metal tube atomizer, interference phenomena observed were similar to those obtained in GFAAS. The effect of copper on the determination of gold by ETA-AAS with a GF has been found to be troublesome, with suppression of the absorbance signal for gold.[13] However, in the molybdenum atomizer, copper enhanced the gold signal.

Matthew and McGaham[8] reported that cysteine served as a matrix modifier for gold determination in biological fluids and tissues. Cysteine is a sulfur compound and hence, in order to eliminate the interferences, thiourea being a sulfur compound was tried as a matrix modifier for gold. A typical effect of thiourea on the gold signal in the presence of calcium is shown in Fig. 4. By the addition of thiourea, the gold signal was little affected by the coexistences of 2.5 mg/l of Mg, 0.25 mg/ml of Ca, Cu, Fe, K, Pb and Zn. The interference reducing effect by thiourea may result from sulfide formation of gold and the coexisting elements.

*Determination of gold*

Since it was found that thiourea was useful for the recovery of gold AA signal in the presence of interferent, a matrix modifier method was applied to the determination of gold in biological materials. The samples were spiked with 200–400 ng Au/g. Following the digestion of biological samples, the samples with thiourea were analyzed by ETA-AAS with the metal atomizer under optimal conditions. Table 1 shows the results obtained for some biological materials (NIST). The recovery of spiked gold in biological materials was in the range of 101–106%. The relative standard

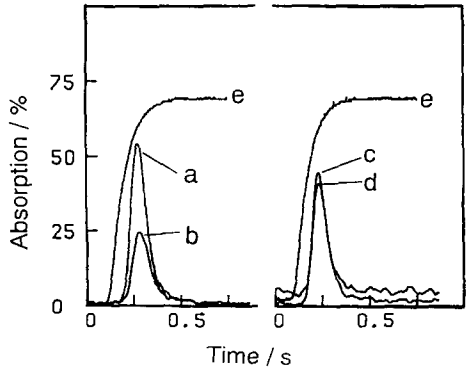


Fig. 4. Interference of calcium and effect of thiourea on the gold signal. (a) Au 250 pg along; (b) Au + Ca 250 ng; (c) Au + thiourea 10 $\mu$g; (d) Au + Ca 250 ng + thiourea 10 $\mu$g; (e) temperature increasing. Pyrolysis temperature: 720 C.

Table 1. Determination of gold in biological materials

| Sample | Amount of gold ($\mu g/g$) | | | |
|---|---|---|---|---|
| | Added | Found | Certified value | Recovery (%) |
| Bovine liver* | 0.00 | — | — | |
| (SRM 1577a) | 0.200 | $0.209 \pm 0.024$ | | 105 |
| | 0.400 | $0.405 \pm 0.046$ | | 101 |
| Non-fat milk* | 0.00 | — | — | |
| powder (SRM 1549) | 0.200 | $0.211 \pm 0.024$ | | 105 |
| | 0.400 | $0.425 \pm 0.015$ | | 106 |
| Orchard leaves* | 0.00 | — | — | |
| (SRM 1571) | 0.200 | $0.202 \pm 0.029$ | | 101 |
| | 0.400 | $0.402 \pm 0.025$ | | 101 |

*NIST standard.
Five analyses were carried out.

deviations were better than 14% at five replicate analyses. The analytical results obtained with the addition of thiourea can be considered satisfactory for the determination of gold in biological materials.

As described above, for the determination of gold in biological materials the addition of thiourea served to eliminate severe interferences. Moreover, the use of molybdenum tube atomizer and an argon–hydrogen atmosphere has large benefits such as high sensitivity and longer lifetime (more than 5000 firings) over a graphite furnace (200–250 firings). Therefore, the performance characteristics of the molybdenum tube atomizer will serve to provide accurate and sensitive determinations of gold in complex samples.

*Acknowledgement*—This work was supported financially by the Ministry of Education, Science and Culture of Japan.

## REFERENCES

1. J. D. Jessop and R. G. S. Johns, *Ann. Rheum. Dis.*, 1973, **32,** 228.
2. H. Kamel, D. H. Brown, J. M. Ottaway and W. E. Smith, *Analyst*, 1977, **102,** 645.
3. R. P. Sharma, *Ther. Drug Monit.*, 1982, **4,** 219.
4. A. I. A. Rodgers, D. H. Brown, W. E. Smith, D. Lewis and H. A. Capell, *Anal. Proc. (Lond.)*, 1982, **19,** 87.
5. J. Lang, O. Wawschinek, F. Rainer and G. Lanzer, *Mikrochim. Acta*, 1983, **3,** 53.
6. X. Shan, J. Egila, D. Littlejohn and J. M. Ottaway, *J. Anal. Atom. Spectrom.*, 1987, **2,** 293.
7. L. Thunus and J. F. Dauphin, *Anal. Chim. Acta*, 1990, **235,** 393.
8. D. O. Matthews and M. C. McGaham, *Spectrochim. Acta*, 1987, **42B,** 909.
9. L. H. J. Lajunen, *Spectrochemical Analysis by Atomic Absorption and Emission, Royal Society of Chemistry, Cambridge, 1992.* pp. 186–189, 230.
10. H. Matusiewicz and R. M. Barnes, *Acta Chim. Hung.*, 1988, **125,** 777.
11. M. N. Rashed, *Int. J. Environ. Anal. Chem.*, 1992, **48,** 41.
12. G. S. Reddi, S. Ganesh, C. R. M. Rao and V. Ramanan, *Anal. Chim. Acta*, 1992, **260,** 131.
13. P. Chattopadhyay and B. N. Sahoo, *Analyst*, 1992, **117,** 1481.
14. S. Hara, H. Matsuo and T. Kumamaru, *Bunseki Kagaku*, 1986, **35,** 503.
15. M. Aihara, H. Watanabe and M. Kiboku, *Anal. Sci.*, 1991, **7**(Suppl.), 87.
16. K. Ohta, S. Y. Su and T. Mizuno, *Anal. Lett.*, 1987, **20,** 1399.
17. K. Ohta, S. Kaneco, S. Itoh and T. Mizuno, *Anal. Chim. Acta*, 1992, **267,** 131.
18. K. Ohta, S. Itoh and T. Mizuno, *Anal. Sci.*, 1991, **7**(Suppl.), 457.
19. D. R. Lide (ed.), *Handbook of Chemistry and Physics*, 72nd Ed., pp. 4-61, 5-70. CRC Press, Boston, 1991.
20. B. F. G. Johnson and R. Davis, in *Comprehensive Inorganic Chemistry*, Vol. 3, J. C. Bailar, H. J. Emeleus, R. Nyholm and A. F. Trotman-Diekeson (eds), pp. 139–143. Pergamon Press, Oxford, 1973.
21. S. J. Royal, *Nat. Inst. Metall., Repub. S. Afr.*, Rep. 2063, April 1980.
22. D. S. Brooks and J. R. Flatt, *Anal. Chim. Acta*, 1992, **264,** 107.

Pergamon

0039-9140(94)00256-8

*Talanta*, Vol. 42, No. 2, pp. 269–281, 1995
Elsevier Science Ltd
Printed in Great Britain

# DIRECT DETERMINATION OF TRACES OF Ag, Cd, Pb, Bi, Cr, Mn, Co, Ni, Li, Be, Cu AND Sb IN ENVIRONMENTAL WATERS AND GEOLOGICAL MATERIALS BY SIMULTANEOUS MULTI-ELEMENT GRAPHITE FURNACE ATOMIC ABSORPTION SPECTROMETRY WITH ZEEMAN-EFFECT BACKGROUND CORRECTION*

J. G. SEN GUPTA† and J. L. BOUVIER

Geological Survey of Canada, Ottawa, Ontario, Canada K1A OE8

(*Received* 16 *May* 1994. *Revised* 30 *August* 1994. *Accepted* 31 *August* 1994)

**Summary**—A method was developed for direct determination of minor and trace amounts of Cr, Mn, Cu, Ni, Co, Li, Pb, Cd, Bi, Sb, Be and Ag in silicate rock, lake and stream sediments using a microwave oven dissolution method and a multi-element graphite furnace atomic absorption spectrometer equipped with a Zeeman-effect background correction device. The measurement technique was also suitable for direct determination of trace and ultra-trace amounts of these elements in drinking and seawater samples. A rock or sediment sample was brought into solution in a Teflon vessel by heating in a microwave oven with a mixture of hydrofluoric acid and aqua regia, followed by a further heating with a mixture of boric acid and ethylenediaminetetraacetic acid. The specified elements were directly determined in a group of four elements in one firing and eight elements in two firings from this solution or from a diluted solution using the optimum operating parameters developed in this work. The method, tested with 23 international reference rocks and sediments and seven international quality control and reference water samples, showed good to excellent agreement with the recommended values.

There is a great demand from scientists of the Geological Survey of Canada (GSC) for determination of minor and trace elements in silicate rocks, rock-forming minerals, and lake and stream sediments for ore genesis studies, and for geochemical prospecting. Determination of trace and ultra-trace elements in environmental water samples is also required by geochemists and others for ascertaining their toxicity levels for drinking purposes, industrial pollution levels and for searching for ore deposits.

The classical colorimetric[1] and titrimetric[2] methods used previously in the GSC for trace analysis have now been replaced by modern spectrometric techniques. Among these, flame atomic absorption spectrometry (FAAS) suffers from lack of sufficient sensitivities and good precision for certain elements such as Ag, Cd, Pb, Bi, Li, Be, Sb and Co in the ng/g and low $\mu$g/g levels present in most rocks, sediments and environmental water samples.

To improve the detection limits for trace elements and eliminate interferences from associated major elements, extraction of suitable complexes of the analytes into organic solvents before FAAS determination was previously favoured by analysts.[3,4] A widely used method for Pb, Cd, Bi and Zn was chelation with ammonium pyrrolidine dithiocarbamate (APDC) and extraction of the complexes with methyl isobutyl ketone (MIBK), followed by back-extraction with an acid into the aqueous phase before determination by graphite furnace atomic absorption spectrometry (GFAAS).[5,6]

Because of the interference from major quantity of iron, the first author used isopropyl ether to separate it from a silicate rock digest in $HF$–$HNO_3$–$HClO_4$. From the remaining solution, Pb and Cd were extracted along with some other trace elements such as Mn, Ni, Co, Bi and Zn with APDC–oxine–MIBK system.

*Paper presented at 39th Canadian Spectroscopy Conference, University of Laval, Quebec City, 16–18 August 1993. Geological Survey of Canada Contribution No. 33892.

†Author to whom correspondence should be addressed.

After back-extraction with an acid into the aqueous phase, these elements were determined by single-element GFAAS.[7]

Attempts to determine Pb and Cd in geological materials by single-element GFAAS were found in the works of Bettinelli *et al.*[8] who used $HCl$–$HNO_3$–$HClO_4$ to decompose samples, and Alvarado and Petrole[9] who employed boric acid to complex excess HF after decompostion by $HCl$–$HF$–$HNO_3$. However, it is our experience that the use of $HClO_4$ is detrimental to the life expectancy of a graphite cuvette used in GFAAS determination.

Deuterium background correction device used with a single-element GFAAS failed to eliminate emission and molecular interferences in direct determination of trace elements in rock sample solutions decomposed by conventional methods with acids and fusion. This was due to the presence of associated major elements and high concentration of salts in solutions.

Neutron activation, and more recently inductively coupled plasma atomic emission spectrometry (ICP-AES) and inductively coupled plasma mass spectrometry (ICP-MS) have been used for trace analysis in geological materials. However, neutron activation and ICP-MS instrumentations are very expensive, and ICP-AES suffers from lack of sufficient sensitivities and interference effects in the determination of some trace elements such as Ag, Pb, Cd, Bi, Sb and Li in silicate rocks and environmental water samples.

The reasons for choosing multi-element GFAAS in the authors' laboratories were: (1) high sensitivities for trace elements present in silicate rocks and environmental water samples, (2) freedom from interference effects from the associated major elements because of the use of Zeeman-effect background correction technique, (3) elimination of the spectral complexity associated with ICP-AES, and (4) the limitations which molecular Cl species impose through isobaric interferences in selecting a decomposition scheme for ICP-MS analysis. Many schemes use HCl and/or $HClO_4$ to dissolve samples and, therefore, require extensive correction for isobaric interferences, if the concentration ratios between the interferent and the analyte permit making the correction at all.

Since a single-element graphite furnace even with the capability of sequential determination and Zeeman background correction would be too slow to be used for routine determination of 12 elements as presented in this work, it was decided to use a relatively inexpensive multi-element graphite furnace atomic absorption spectrometer equipped with a Zeeman-effect background correction device for simultaneous determination of four elements. This instrument, which could be programmed for automatic determination of eight elements in two firings, was successfully used by the first author for multi-element determination of scandium, yttrium, eight rare-earth elements,[10] and seven noble metals[11] in rocks and several candidate reference materials of Canadian Certified Reference Materials Project (CCRMP) after preconcentration by ion-exchange.

A microwave digestion procedure found effective for decomposition of most silicate rocks and naturally occurring sediments in our laboratories was used in this work. This involved heating the sample in a Teflon bomb (in a microwave oven) first with a mixture of HF and aqua regia, followed by second heating with a mixture of boric acid and ethylenediaminetetraacetic acid (EDTA). Compared to the regular method of sample decomposition in the GSC,[10] which uses $HF + HNO_3 + HClO_4 + HCl +$ EDTA (ammonium salt) plus fusion of any insoluble residue with $Na_2CO_3$ and $Na_2O_2$, this method does not use $HClO_4$ which needs to be evaporated in a special fume hood and whose presence even in trace amounts is harmful in GFAAS determination. Since the time of decomposition and steps are shorter in the microwave oven digestion method, it is much faster for routine use. The method is also economical since less acid consumption is required and environmentally friendly because no evaporation of acids is involved.

Table 1. Instrumental parameters (slitwidth fixed at 0.8 nm in an Hitachi Z-9000 instrument).

| Group | Element | Wavelength (*nm*) | Hollow cathode lamp current (*mA*) |
|---|---|---|---|
| 1 | Ag | 328.1 | 3.0 |
| | Cd | 228.8 | 3.0 |
| | Pb | 217.0 or 283.3 | 5.0 |
| | Bi | 223.1 | 8.0 |
| 2 | Mn | 279.5 or 403.1 | 5.0 |
| | Co | 240.7 | 10.0 |
| | Ni | 232.0 | 10.0 |
| | Cr | 357.5 or 425.4 | 5.0 |
| 3 | Li | 670.8 | 5.0 |
| | Be | 234.9 | 10.0 |
| | Cu | 324.7 | 3.0 |
| | Sb | 217.6 | 10.0 |

Table 2. Temperature programmes for simultaneous determination of four elements

| | | Temperature (°C) | | | | | | |
|---|---|---|---|---|---|---|---|---|
| | | Group 1 | | Group 2 | | Group 3 | | |
| | | Ag, Cd, Pb, Bi | | Mn, Co, Ni, Cr | | Li, Be, Cu, Sb | | |
| No. | Stage | Start | End | Start | End | Start | End | Time (*sec*) |
| 1 | Dry | 75 | 75 | 75 | 75 | 75 | 75 | 10 |
| 2 | Dry | 90 | 90 | 90 | 90 | 90 | 90 | 60 |
| 3 | Dry | 120 | 130 | 120 | 130 | 120 | 130 | 20 |
| 4 | Ash | 420 | 420 | 500 | 500 | 800 | 800 | 30 |
| 5 | Atom | 2200 | 2200 | 2400 | 2400 | 2300 | 2300 | 10 |
| 6 | Clean | 2300 | 2300 | 2500 | 2500 | 2400 | 2400 | 5 |

Monitoring stage: 1–6.
Check stage: 1–6.
Carrier gas: 200 *ml/min.*
Interrupted gas: 0 *ml/min.*

In the microwave digestion method, boric acid was used to complex the excess HF, and EDTA to dissolve any insoluble material not completely attacked by the HF + aqua regia mixture. The suitability of EDTA to dissolve insoluble materials of silicate rocks such as barite and strontianite was established in two earlier papers.[12,13]

After microwave digestion and dilution with $HNO_3$, an aliquot of the sample solution was directly injected into the graphite tube furnace of the multi-element atomic absorption spectrometer and atomized for simultaneous determination of up to four elements. The elements were chosen in groups of four primarily for their compatible ash and atomization temperatures; however, their expected abundances in samples also played a role in this choice. The results of these investigations carried out with a variety of international geochemical reference materials and several reference water samples showed good agreement with the recommended values.

After sample solution preparation, concentration of four elements in about 100 samples could be simultaneously determined in one day.

## EXPERIMENTAL

### *Apparatus*

A Hitachi Z-9000 simultaneous multi-element atomic absorption spectrometer equipped with a Zeeman-effect background correction device, built-in autosampler (72 samples holding capacity), plotter and data recorder was used. The instrument was cooled during heating by water maintained at 17°C employing a Neslab Model CFT-33 refrigerated recirculator. Pyrolytic graphite coated graphite tube (part No. 190-6003) and argon gas (UHP, 99.999%, predried by passing through a Matheson Model 6406 gas purifier and pressure maintained at 44 psi) were used throughout this work.

A Milestone microwave oven Model MLS-1200, equipped with six Milestone pressure decomposition Teflon vessels of capacity 100 ml each, a microwave digestion rotor (HPR 1000/6) and a remote control panel, were used for decomposition of samples.

### *Reagents and standard solutions*

Ultra-pure water (ASTM Type 1) made by reverse osmosis with a Millipore apparatus, and

Table 3. Autosampler programme

| | |
|---|---|
| Signal mode | Bkg corrected |
| Measurement mode | Working curve |
| Sample blank | No |
| Standard replicate | 2 |
| Sample replicate | 2 |
| Statistics | No or Yes (as necessary) |
| Sample volume | 40 $\mu l$ (or less*) |
| Dilution | Off or On† |
| Conc. times | 1 |
| Modif. add | Yes or No (as necessary‡) |
| Cup position | 1-*X*§ |
| Reslope | |
| -Standard | Number 3 |
| -Interval | 20 |
| Cuvette | Pyro. |
| Firings | 0 |
| Result on record | Yes (conc. + Abs.) |
| Chart speed | 1 |
| Data communi. | Off or On (as necessary) |
| Calculation | Peak height for each element |
| Carrier gas int. | Yes |
| Opt. temp. contr. | On |

*The instrument allows 10, 20, 30 or 40 $\mu l$ volume automatic pipetting.
†The instrument allows automatic 100 × dilution of sample solutions.
‡"Yes" for Group 1 elements (Ag, Cd, Pb and Bi); "No" for other elements.
§*X* = up to a maximum number of 72.

Table 4. Concentration of elements (*ng/ml* each) in synthetic standard solutions for preparation of calibration graphs

| Group | Elements | Standard 1* | Standard 2 | Standard 3 | Standard 4 | Standard 5 |
|---|---|---|---|---|---|---|
| 1 | Ag | 0 | 5 | 10 | 15 | 20 |
| | Cd | 0 | 1 | 2 | 3 | 4 |
| | Pb | 0 | 25 | 50 | 75 | 100 |
| | Bi | 0 | 5 | 10 | 15 | 20 |
| 2 | Mn | 0 | 10 | 20 | 30 | 40 |
| | Co | 0 | 20 | 40 | 60 | 80 |
| | Ni | 0 | 30 | 60 | 90 | 120 |
| | Cr | 0 | 10 | 20 | 30 | 40 |
| 3 | Li | 0 | 25 | 50 | 75 | 100 |
| | Be | 0 | 4 | 8 | 12 | 16 |
| | Cu | 0 | 10 | 15 | 20 | 25 |
| | Sb | 0 | 10 | 20 | 30 | 40 |

*High purity 2% nitric acid.

ACS grade reagents (unless stated otherwise) were used throughout the work.

*Standard solutions.* A 100 $\mu$g/ml standard solution of each element was prepared by diluting 1000 $\mu$g/ml Plasma Chem ICP standard solutions (Cd, Pb, Bi, Mn, Co, Ni, Cr, Li, Be, Cu and Sb) and Fisher Scientific standard solution (Ag) with 2% nitric acid (Seastar High purity). The above standard solutions were mixed in appropriate amounts and diluted to volumes with the high purity 2% nitric acid to obtain synthetic standard mixtures to be used for preparation of calibration curves (see under Procedure for further details). All standard solutions were stored in tightly stoppered nalgene bottles.

*Mixed solution of boric acid (2.2%) and EDTA (0.165%).* 1.65 g EDTA was dissolved in concentrated ammonia solution, 22 g boric acid was added, and stirred to dissolve and diluted with water to 1 l. It was stored in a nalgene bottle.

*Palladium–magnesium modifier.* A 15 ml solution of 1000 $\mu$g/ml Pd solution was mixed with 50 ml of 1000 $\mu$g/ml Mg solution (both as nitrates) and diluted to 100 ml with 2% nitric acid (Pd:Mg = 0.3). This solution (16.7 ml) was diluted to 100 ml with 2% nitric acid and stored in a nalgene bottle. The diluted solution ($\sim$10 $\mu$l) was used during determination of Pb and Cd (along with Ag and Bi) by the autosampler programme.

## *Recommended procedure*

*Silicate rock, lake or stream sediment sample decomposition.* The finely powdered sample (0.5 g) (−200 mesh) was transferred to a

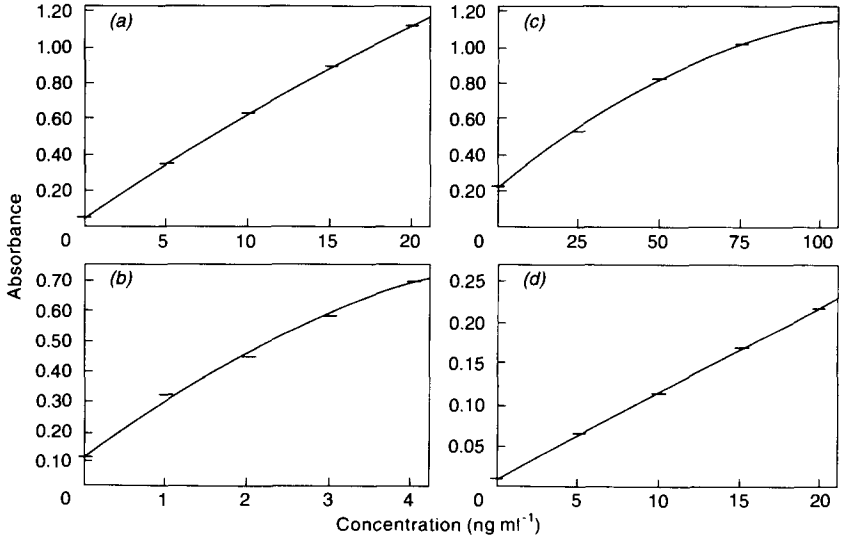


Fig. 1. Calibration graphs for (a) Ag; (b) Cd; (c) Pb (wavelength 283.3 nm) and (d) Bi at atomization temperature of 2200 C (40 $\mu$l soln. of each standard of Group 1 of Table 4). Quadratic correlation: Ag, 0.9998; Cd, 0.9909; Pb, 0.9849; and Bi, 0.9996.

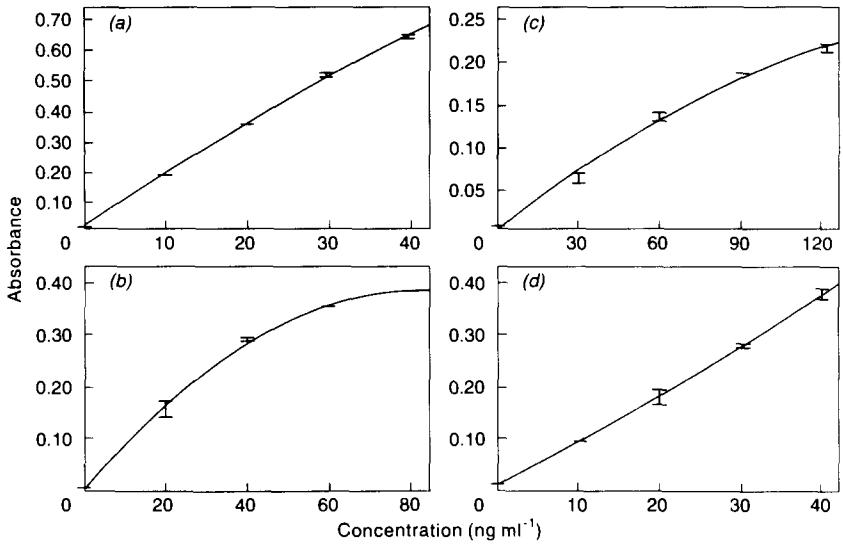


Fig. 2. Calibration graphs for (a) Mn (wavelength 403.1 nm); (b) Co; (c) Ni; and (d) Cr (wavelength 425.4 nm) at atomization temperature of 2400°C (40 $\mu$l soln. of each standard of Group 2 of Table 4). Quadratic correlation: Mn, 0.9991; Co, 0.9616; Ni, 0.9886; and Cr, 0.9993.

Milestone Teflon decomposition vessel (note 1). A total of 2.5 ml 40% hydrofluoric acid was added dropwise while shaking the vessel to allow a smooth reaction to take place and prevent excessive local overheating and loss by sputtering. Concentrated nitric acid (3 ml) was added and stirred thoroughly with a Teflon rod, breaking the lump to a slurry. A total of 9 ml concentrated hydrochloric acid was slowly added while stirring the solution, and finally rinsing the outer side of the Teflon rod into the vessel. The Teflon rod was set aside and the vessel was covered with the lid and the spring assembly. The vessel was then placed inside the protection shield and after six sample vessels had been assembled in the rotor, the screw caps were tightened with the T bar using two $\frac{1}{4}$ rotations towards the end (care was taken not to overtighten to prevent cracking of the Teflon spring cover).

Placing the rotor with the assembled sample vessels inside the microwave oven, the door was closed and it was heated gradually (3 min.) to maximum power (1000 W). It was then further heated at 600 W for 2 min. and 250 W for 10 min. It was allowed to vent until the program was ready and the power shut off automatically.

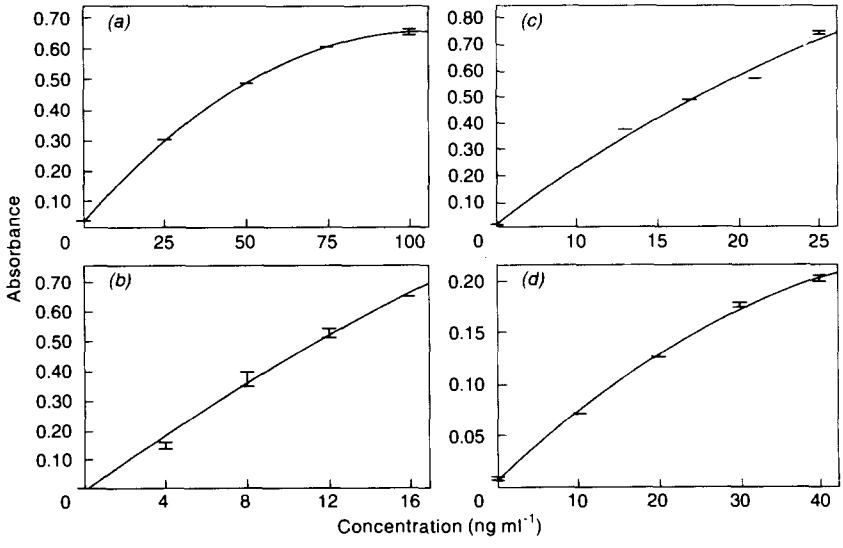


Fig. 3. Calibration graphs for (a) Li; (b) Be; (c) Cu; and (d) Sb at atomization temperature of 2300 C (40 $\mu$l soln. of each standard of Group 3 of Table 4). Quadratic correlation: Li, 0.9648; Be, 0.9947; Cu 0.9915; and Sb, 0.9896.

Table 5. Sensitivities of elements as obtained with a pyrolytic graphite coated graphite tube furnace using the Hitachi Z-9000 simultaneous multi-element atomic absorption spectrophotometer

| Element | Wavelength (*nm*) | Atomization temperature (°C) | Sensitivity* (*pg*) |
|---|---|---|---|
| Ag | 328.1 | 2200 | 3 |
| Cd | 228.8 | 2200 | 0.9† |
| Pb | 217.0 | 2200 | 4.6 |
| | 283.3 | 2200 | 13† |
| Bi | 223.1 | 2200 | 16 |
| Mn | 279.5 | 2400 | 1.5 |
| | 403.1 | 2400 | 10 |
| Co | 240.7 | 2400 | 22 |
| Ni | 232.0 | 2400 | 65 |
| Cr | 357.9 | 2400 | 13 |
| | 425.4 | 2400 | 19 |
| Li | 670.8 | 2300 | 19 |
| Be | 234.9 | 2300 | 4 |
| Cu | 324.7 | 2300 | 5 |
| Sb | 217.6 | 2300 | 29 |

*Defined as the mass of the element in picograms that produces a change in absorbance, compared with a pure solvent or blank, of 0.0044.
†In the presence of a palladium–magnesium modifier (see under Reagents in the text for concentration).

The rotor assembly was removed from the oven, placed on the stand and allowed to cool to room temperature (note 2). Carefully unscrewing the spring cap with the T bar, with $\frac{1}{4}$ rotation at a time until some gas was vented and the top screw was loose, the vessel was removed from the rotor and the lid opened cautiously.

A mixture (30 ml) containing 2.2% boric acid and 0.165% EDTA (note 3) was added, the cover and inner upper side of the vessel were rinsed. The vessel with the cover was inserted

Table 6. Determination of trace elements in quality control and reference water samples by simultaneous multi-element graphite furnace atomic absorption spectrometry (results in *ng/ml*)

| | | Ag | | Cd | | Pb | | Cr | |
|---|---|---|---|---|---|---|---|---|---|
| Source | Sample | This work* | Expected values† | This work* | Expected values† | This work* | Expected values† | This work* | Expected values† |
| NIST | 1643c | 2 ± 0 | 2.2 ± 0.3 | 12 ± 0 | 12.2 ± 1 | 34.0 ± 1.3 | 35.3 ± 0.9 | 28 ± 4 | 19.0 ± 0.6 |
| USEPA | QC1 | 10 ± 0 | 10.0 ± 0.9 | 4.9 ± 0 | 4.6 ± 0.6 | 50 ± 3 | 50.4 ± 5 | 50 ± 2 | 49.7 ± 4.4 |
| USEPA | QC6 | 25 ± 1 | 26.0 ± 2.1 | 4 ± 0 | 3.7 ± 0.3 | 22.6 ± 0.6 | 21.9 ± 2.2 | 31 ± 2 | 31.1 ± 2.5 |
| USEPA | ICAP19 | | | 20 ± 0 | 20 | | | 24 ± 1 | 20 |
| NRC | SLRS-2 | | | | | | | 1 ± 0 | 0.5 ± 0.1 |

| | | Mn | | Co | | Ni | | Li | |
|---|---|---|---|---|---|---|---|---|---|
| Source | Sample | This work* | Expected values† | This work* | Expected values† | This work* | Expected values† | This work* | Expected values† |
| NIST | 1643c | 36 ± 1 | 35.1 ± 2.2 | 27 ± 2 | 23.5 ± 0.8 | 56 ± 5 | 60.6 ± 7.3 | 17 ± 1 | 16.5 ± 1.0 |
| USEPA | QC2 | 9 ± 0 | 9.3 ± 2.0 | 51 ± 1 | 49.7 ± 3.9 | 36 ± 1 | 30.5 ± 3.2 | | |
| USEPA | ICAP19 | 19 ± 1 | 20 | 21 ± 0 | 20 | 21 ± 1 | 20 | | |
| NRC | SLRS-2 | 10 ± 0 | 10.1 ± 0.3 | | | 1 ± 0 | 1.0 ± 0.1 | | |
| NRC | CASS-1 | 2.4 ± 0.6 | 2.3 ± 0.2 | | | | | | |

| | | Be | | Cu | | Sb | |
|---|---|---|---|---|---|---|---|
| Source | Sample | This work* | Expected values† | This work* | Expected values† | This work* | Expected values† |
| NIST | 1643c | 24 ± 0 | 23.2 ± 2.2 | 25 ± 1 | 22.3 ± 2.8 | | |
| USEPA | QC1 | | | 50 ± 0 | 49.6 ± 3.3 | | |
| USEPA | QC2 | 10 ± 0 | 10.1 ± 1.2 | | | 100 ± 0 | 103.7 ± 12.7 |
| USEPA | ICAP19 | 20 ± 0 | 20 | 24 ± 1 | 20 | 20 ± 0 | 20 |

*Mean of 5 values and the standard deviation.
†Quoted from the certificate of analysis sheets (mean and the standard deviation; solution diluted before measurement to suitable concentrations with 2% high purity nitric acid in order that measurement could be made within maximum absorbance values of calibration curves).

Table 7. Determination of Ag, Cd, Pb and Bi in international reference samples of silicate rocks by simultaneous multi-element graphite furnace atomic absorption spectrometry

| | | Ag (ng/g) | | Cd (ng/g) | | Pb (μg/g) | | Bi (μg/g) | |
|---|---|---|---|---|---|---|---|---|---|
| Source | Sample | This work* | Other values | This work* | Other values | This work* | Other values | This work* | Other values |
| USGS | BIR-1 | 50 | 36 (2)† | 150 | 114 ± 38† | 2 | 3.2 ± 0.8† | <0.05 | 0.02 (1)† |
| USGS | DNC-1 | <50 | 27 (2)† | 200 | 182 ± 108† | 6 | 6.3 ± 1† | 0.05 | 0.02 (1)† |
| USGS | W-2 | 50 | 46 (2)† | 100 | 104 ± 27† | 6 | 9.3 ± 3.1† | 0.05 | 0.03 (1)† |
| USGS | MAG-1 | 100 | 80‡ | 200 | 202‡ | 26 | 24‡ | 0.30 | 0.33§ |
| USGS | AGV-1 | 100 | 104 ± 30¶ | 54 | 61 ± 8¶ | 34 | 36 ± 5¶ | 0.05 | 0.054¶ |
| USGS | BCR-1 | <50 | 27 ± 4¶ | 129 | 127 ± 8¶ | 13 | 13.6‡ | <0.05 | 0.047¶ |
| USGS | GSP-1 | 50 | 86 ± 14¶ | 50 | 56 ± 7¶ | 53 | 54 ± 7¶ | <0.05 | 0.04¶ |
| USGS | DTS-1 | <50 | 14 ± 7¶ | <50 | 9¶ | 6 | 12 ± 3¶ | <0.05 | 0.005¶ |
| USGS | G-2 | <50 | 45 ± 6¶ | <50 | 25 ± 11¶ | 34 | 31 ± 4¶ | <0.05 | 0.041¶ |
| NIM | NIM-G | 100 | 42–120‖ | 200 | —‡‡ | 40 | 40‖ | 0.4 | 0.4‖ |
| IWG | BE-N | <50 | 44** | 100 | 100–210‡ | 4 | 4‡ | <0.05 | 0.042‡ |
| CCRMP | MRG-1 | 100 | 110 ± 27†† | 200 | 168 ± 31†† | 9 | 10 ± 4†† | 0.20 | 0.13†† |
| CCRMP | SY-2 | 120 | —‡‡ | 230 | 208 ± 36†† | 80 | 85 ± 8†† | 0.3 | —‡‡ |
| IGGE | GSD-5 | 369 | 360‡ | 900 | 820‡ | 110 | 112‡ | 2 | 2.4‡ |
| IGGE | GSD-6 | 357 | 360‡ | 430 | 430‡ | 27 | 27‡ | 5 | 5‡ |

*Mean of two values.
†'Consensus value' reported in a compilation of data in Ref. 16.
‡'Working value' reported in a compilation of data in Ref. 17.
§'Reported in a compilation of data in Ref. 18.
¶'Consensus value' reported in a compilation of data in Ref. 19.
‖Reported in a compilation of data in Ref. 20.
**See Ref. 21.
††'Recommended concentration' reported in a compilation of data in Ref. 22.
‡‡'Consensus value' not available in the literature.

into the protection shield and placed inside the rotor. The screws were tightened as usual, and the assembled rotor was heated in the microwave oven at 1000 W for 2 min and 250 W for 4 min. After venting was completed and the power automatically shut off, the rotor was removed from the oven, placed in the stand and allowed to cool to room temperature.

The lid was unscrewed with usual caution and the cover opened. The content of the vessel was transferred to a 50 ml graduated polypropylene tube fitted with a screw cap, and rinsed with 2%

Table 8. Determination of Ag, Cd, Pb and Bi in CCRMP reference samples of lake and stream sediments by simultaneous multi-element graphite furnace atomic absorption spectrometry (results in μg/g)

| | Ag | | Cd | | Pb | | Bi | |
|---|---|---|---|---|---|---|---|---|
| Sample | This work* | Other values† | This work* | Other values† | This work* | Other values† | This work* | Other values |
| LKSD-1 | 0.6 | 0.6 ± 0.05‡<br>0.6 ± 0.2§ | 1.0 | 1.2 ± 0.3§ | 72 | 82 ± 5‡<br>84 ± 10§ | 1.0 | —¶ |
| LKSD-2 | 0.9 | 0.8 ± 0.06‡<br>0.8 ± 0.2§ | 1.0 | 0.8 ± 0.2§ | 45 | 44 ± 4‡<br>40 ± 7§ | 1.0 | —¶ |
| LKSD-3 | 2.6 | 2.7 ± 0.11‡<br>2.4 ± 0.4§ | 0.6 | 0.6 ± 0.3§ | 29 | 29 ± 3‡<br>26 ± 5§ | 2.2 | —¶ |
| LKSD-4 | 0.2 | <0.5‡<br>0.2 ± 0.1§ | 2.0 | 1.9 ± 0.5§ | 90 | 91 ± 6‡<br>93 ± 8§ | 0.3 | —¶ |
| STSD-1 | 0.3 | <0.5‡<br>0.3 ± 0.1§ | 1.0 | 0.8 ± 0.2§ | 32 | 35 ± 3‡<br>34 ± 4§ | 0.3 | —¶ |
| STSD-2 | 0.4 | 0.5 ± 0.08‡<br>0.5 ± 0.2§ | 1.0 | 0.8 ± 0.3§ | 67 | 66 ± 4‡<br>66 ± 7§ | 1.7 | —¶ |
| STSD-3 | 0.3 | <0.5‡<br>0.4 ± 0.1§ | 1.0 | 1.0 ± 0.2§ | 41 | 40 ± 3‡<br>39 ± 5§ | 2.0 | —¶ |
| STSD-4 | 0.3 | <0.5‡<br>0.3 ± 0.1§ | 0.6 | 0.6 ± 0.3§ | 17 | 16 ± 3‡<br>13 ± 4§ | 0.2 | —¶ |

*Mean of two values.
†Reported in a compilation of data in Ref. 23.
‡'Total element' as reported in Ref. 23.
§'Partial extraction element in concentrated $HNO_3$ + concentrated HCl' as reported in Ref. 23.
¶Not available.

Table 9. Determination of Cr, Mn, Co and Ni in international reference samples of silicate rocks by simultaneous multi-element graphite furnace atomic absorption spectrometry

| | | Cr (μg/g) | | Mn (%) | | Co (μg/g) | | Ni (μg/g) | |
|---|---|---|---|---|---|---|---|---|---|
| Source | Sample | This work* | Other values | This work* | Other values | This work* | Other values | This work* | Other values |
| USGS | BIR-1 | 365 | 382 ± 38† | 0.12 | 0.13 ± 0.01† | 50 | 51.4 ± 3.4† | 154 | 166 ± 16† |
| USGS | DNC-1 | 296 | 285 ± 32† | 0.10 | 0.12 ± 0.02† | 53 | 54 ± 4† | 264 | 247 ± 18† |
| USGS | W-2 | 107 | 93 ± 6† | 0.16 | 0.13 ± 0.02† | 38 | 43 ± 3† | 70 | 70 ± 8† |
| USGS | MAG-1 | 100 | 97‡ | 0.079 | 0.076‡ | 20 | 20§ | 50 | 54§ |
| USGS | AGV-1 | 10 | 10§ | 0.06 | 0.07 ± 0.01¶ | 15 | 15.1 ± 1.2¶ | 17 | 17 ± 4¶ |
| USGS | BCR-1 | 14 | 16 ± 4¶ | 0.14 | 0.14 ± 0.09¶ | 32 | 36§ | 15 | 13 ± 4¶ |
| USGS | GSP-1 | 13 | 13 ± 2.6¶ | 0.034 | 0.031 ± 0.004¶ | 7 | 6.5 ± 0.8¶ | 9 | 9§ |
| USGS | DTS-1 | 1700 | 4200§ | 0.10 | 0.094 ± 0.008¶ | 128 | 134 ± 17§ | 2500 | 2350 ± 180¶ |
| USGS | G-2 | 14 | 8.7 ± 2.4¶ | 0.026 | 0.025 ± 0.003¶ | 6 | 5§ | 6 | 3.5§ |
| NIM | NIM-G | 12 | 12§ | 0.016 | 0.016§ | 2 | 4?§ | 9 | 8?§ |
| IWG | BE-N | 333 | 360‡ | 0.16 | 0.16‡ | 61 | 61‡ | 260 | 267‡ |
| CCRMP | MRG-1 | 430 | 430 ± 80‖ | 0.14 | 0.13 ± 0.01‖ | 89 | 87 ± 7‖ | 212 | 193 ± 18‖ |
| CCRMP | SY-2 | 26 | 12§ | 0.24 | 0.25 ± 0.01‖ | 6 | 8 ± 1‖ | 12 | 10§ |
| CCRMP | GSD-5 | 108 | 70‡ | 0.12 | 0.12‡ | 18 | 18.9‡ | 43 | 34‡ |
| CCRMP | GSD-6 | 200 | 190‡ | 0.10 | 0.10‡ | 24 | 24.4‡ | 79 | 78‡ |

*Mean of two values.
†'Consensus value' reported in a compilation of data in Ref. 16.
‡'Working value' reported in a compilation of data in Ref. 17.
§'Usable value' reported in a compilation of data in Ref. 24.
¶'Consensus value' reported in a compilation of data in Ref. 19.
‖'Recommended concentration' reported in a compilation of data in Ref. 22.

nitric acid. If some black suspended particles (owing to separation of free carbon particles from a sediment or mud sample) were visible, it was filtered through a glass fiber filter paper and rinsed with 2% nitric acid. The volume was made up to 50 ml with the rinsings, the cap tightly screwed and shaken well to mix. A reagent blank was run throughout the procedure.

*Simultaneous multi-element GFAAS determination*

*Instrumental set up.* The instrument was set up for simultaneous GFAAS determination of a

Table 10. Determination of Cr, Mn, Co and Ni in CCRMP reference samples of lake and stream sediments by simultaneous multi-element graphite furnace atomic absorption spectrometry

| | Cr (μg/g) | | Mn (%) | | Co (μg/g) | | Ni (μg/g) | |
|---|---|---|---|---|---|---|---|---|
| Sample | This work* | Other values† | This work* | Other values† | This work* | Other values† | This work* | Other values† |
| LKSD-1 | 32 | 31 ± 3‡ | 0.06 | 0.07‡ | 11 | 11 ± 1‡ | 26 | 16 ± 3‡ |
| | | 12 ± 2§ | | 0.05 ± 0.01§ | | 9 ± 1§ | | 11 ± 1§ |
| LKSD-2 | 64 | 57 ± 8‡ | 0.17 | 0.20 ± 0.01‡ | 17 | 17 ± 1‡ | 26 | 26 ± 4‡ |
| | | 29 ± 3§ | | 0.18 ± 0.02§ | | 17 ± 1§ | | 23 ± 3§ |
| LKSD-3 | 106 | 87 ± 8‡ | 0.13 | 0.14 ± 0.01‡ | 29 | 30 ± 2‡ | 49 | 47 ± 5‡ |
| | | 51 ± 5§ | | 0.12 ± 0.02§ | | 30 ± 2§ | | 44 ± 4§ |
| LKSD-4 | 32 | 33 ± 6‡ | 0.04 | 0.05‡ | 10 | 11 ± 1‡ | 34 | 31 ± 5‡ |
| | | 21 ± 2§ | | 0.04§ | | 11 ± 1§ | | 32 ± 5§ |
| STSD-1 | 70 | 67 ± 9‡ | 0.32 | 0.40 ± 0.03‡ | 16 | 17 ± 1‡ | 25 | 24 ± 5‡ |
| | | 28 ± 3§ | | 0.37 ± 0.04§ | | 14 ± 2§ | | 18 ± 3§ |
| STSD-2 | 110 | 116 ± 13‡ | 0.08 | 0.11 ± 0.01‡ | 16 | 19 ± 2‡ | 47 | 53 ± 6‡ |
| | | 50 ± 9§ | | 0.07 ± 0.01§ | | 17 ± 1§ | | 47 ± 4§ |
| STSD-3 | 77 | 80 ± 10‡ | 0.26 | 0.27 ± 0.02‡ | 16 | 16 ± 1‡ | 37 | 30 ± 6‡ |
| | | 34 ± 6§ | | 0.26 ± 0.01§ | | 14 ± 1§ | | 25 ± 3§ |
| STSD-4 | 97 | 93 ± 14‡ | 0.12 | 0.15 ± 0.01‡ | 13 | 13 ± 1‡ | 39 | 30 ± 5‡ |
| | | 30 ± 6§ | | 0.12 ± 0.01§ | | 11 ± 1§ | | 23 ± 2§ |

*Mean of two values.
†Reported in a compilation of data in Ref. 23.
‡'Total element' as reported in Ref. 23.
§'Partial extraction element in concentrated $HNO_3$ + concentrated HCl' as reported in Ref. 23.

Table 11. Determination of Li, Be, Cu and Sb in international reference samples of silicate rocks by simultaneous multi-element graphite furnace atomic absorption spectrometry (results in $\mu g/g$)

| | | Li | | Be | | Cu | | Sb | |
|---|---|---|---|---|---|---|---|---|---|
| Source | Sample | This work* | Other values | This work* | Other values | This work* | Other values | This work* | Other values |
| USGS | BIR-1 | 3 | 3.4 ± 0.4† | <2 | 0.58 ± 0.07† | 123 | 126 ± 5† | 0.6 | 0.58 ± 0.15† |
| USGS | DNC-1 | 5 | 5.1 ± 0.5† | <2 | 1.3 ± 0.2† | 104 | 96 ± 9† | 1 | 0.96 ± 0.15† |
| USGS | W-2 | 10 | 9.3 ± 0.7† | <2 | 1.3 ± 0.2† | 109 | 103 ± 12† | 1 | 0.79 ± 0.17† |
| USGS | MAG-1 | 69 | 76 ± 4‡ | 3 | 2.7–3.6‡ | 38 | 25.6–49‡<br>30§ | 1 | 0.91 ± 0.01‡ |
| USGS | AGV-1 | 10 | 12 ± 2¶ | 2 | 2 ± 0.4¶ | 60 | 60 ± 6¶ | 4 | 4.4 ± 0.4¶ |
| USGS | BCR-1 | 12 | 12.9 ± 0.4¶ | 2 | 1.73 ± 0.37¶ | 20 | 19 ± 4¶,19§ | 1 | 0.62 ± 0.10¶ |
| USGS | GSP-1 | 29 | 31 ± 4¶ | 2 | 1.38 ± 0.27¶ | 35 | 34 ± 5¶,33§ | 3.5 | 3.2 ± 0.4¶ |
| USGS | DTS-1 | 2 | 2.1 ± 0.5¶ | <2 | 2.1 ± 0.5¶ | 10 | 7.5 ± 2.4¶ | 0.4 | 0.5§ |
| USGS | G-2 | 34 | 36 ± 5¶ | 2 | 2.4 ± 0.5¶ | 12 | 11 ± 3¶ | 0.1 | 0.08 ± 0.03¶ |
| NIM | NIM-G | 12 | 12§ | 8 | 7§ | 12 | 12§ | 0.5 | 0.41–0.97‖ |
| IWG | BE-N | 8 | 12§ | <2 | 2§ | 82 | 72§ | 0.2 | 0.22§ |
| CCRMP | MRG-1 | 5 | 4.2 ± 1** | <2 | 0.61 ± 0.24** | 122 | 134 ± 14** | 0.9 | 0.86 ± 0.16** |
| CCRMP | SY-2 | 99 | 95 ± 7** | 23 | 22 ± 5** | 3 | 5.2 ± 2.2** | 0.2 | 0.25 ± 0.10** |
| IGGE | GSD-5 | 43 | 45§ | 2 | 2.3§ | 140 | 137§ | 4 | 3.9§ |
| IGGE | GSD-6 | 35 | 40§ | <2 | 1.7§ | 400 | 383§ | 1 | 1.25§ |

*Mean of two values.
†'Consensus value' reported in a compilation of data in Ref. 16.
‡Reported in a compilation of data in Ref. 18.
§'Working value' reported in a compilation of data in Ref. 17.
¶'Consensus value' reported in a compilation of data in Ref. 19.
‖Reported in a compilation of data in Ref. 20.
**'Recommended concentration' reported in a compilation of data in Ref. 22.

group of four elements using the operating parameters of Table 1 and automatic peak adjustments performed.

*Calibration curves.* Calibration curves (peak height measurement) were prepared for a group of four elements using the operating parameters of Tables 1–3 and 40 $\mu$l each of standard solutions of Table 4. Typical calibration curves obtained for the three groups are shown in Figs 1–3.

Table 12. Determination of Li, Be, Cu and Sb in CCRMP samples of lake and stream sediments by simultaneous multi-element graphite furnace atomic absorption spectrometry (results in $\mu g/g$)

| | Li | | Be | | Cu | | Sb | |
|---|---|---|---|---|---|---|---|---|
| Sample | This work* | Other values† | This work* | Other values† | This work* | Other values† | This work* | Other values† |
| LKSD-1 | 6 | 7 ± 2‡ | <2 | 1.1 ± 0.1‡ | 56 | 44 ± 5‡<br>44 ± 5§ | 1 | 1.2 ± 0.1‡<br>1.2 ± 0.4§ |
| LKSD-2 | 20 | 20 ± 2‡ | 2 | 2.5 ± 0.6‡ | 38 | 37 ± 4‡<br>36 ± 3§ | 1 | 1.1 ± 0.1‡<br>1.2 ± 0.5§ |
| LKSD-3 | 26 | 25 ± 2‡ | 2 | 1.9 ± 0.2‡ | 40 | 35 ± 3‡<br>34 ± 3§ | 1 | 1.3 ± 0.1‡<br>1.4 ± 0.5§ |
| LKSD-4 | 12 | 12 ± 2‡ | 2 | 1.0 ± 0.03‡ | 34 | 31 ± 4‡<br>30 ± 3§ | 2 | 1.7 ± 0.1‡<br>1.5 ± 0.6§ |
| STSD-1 | 11 | 11 ± 1‡ | <2 | 1.6 ± 0.6‡ | 34 | 36 ± 4‡<br>36 ± 2§ | 2 | 3.3 ± 0.3‡<br>2.0 ± 1.0§ |
| STSD-2 | 65 | 65 ± 8‡ | 6 | 5.2 ± 0.7‡ | 48 | 47 ± 5‡<br>43 ± 3§ | 4 | 4.8 ± 0.4‡<br>2.6 ± 1.5§ |
| STSD-3 | 29 | 28 ± 2‡ | 2 | 2.6 ± 0.3‡ | 44 | 39 ± 4‡<br>38 ± 2§ | 4 | 4.0 ± 0.4‡<br>2.4 ± 1.2§ |
| STSD-4 | 14 | 14 ± 2‡ | <2 | 1.7 ± 0.3‡ | 68 | 65 ± 6‡<br>66 ± 5§ | 6 | 7.3 ± 0.7‡<br>3.6 ± 2.5§ |

*Mean of two values.
†Reported in a compilation of data in Ref. 23.
‡'Total element' as reported in Ref. 23.
§'Partial extraction element in concentrated $HNO_3$ + concentrated HCl' as reported in Ref. 23.

*Determination of elements in sample solutions.* Using 10–40 $\mu$l of a sample solution (rock, sediment or water sample), or from a diluted solution, as necessary to bring the absorbance values within the limits of calibration curves, the concentration of the unknown was determined using the appropriate operating parameters and calibration curves (note 4). Blank values, if any, were corrected for (note 5).

*Notes*

1. Six samples were always run simultaneously in one batch to prevent excessive pressure build up within each vessel.
2. If necessary, quick cooling can be effected by inserting the whole rotor assembly inside a bath of cold water, or running cold tap water on the outer tube.
3. An automatic dispenser was used in the authors' laboratory to expedite this process.
4. Dilutions were necessary for some sample solutions containing high Pb, Cr, Mn, Ni, Cu, Cd and Li. Also, alternative absorption lines for Pb (283.3 nm), Cr (425.4 nm) and Mn (403.1 nm) were used to reduce sensitivities where needed, particularly for some rock and sediment sample solutions containing high amounts of these elements.
5. Blank reagent values were negligible if appropriate care was taken to clean the decomposition vessels thoroughly with acids, alconox soap and water before use.

## RESULTS AND DISCUSSION

*Sensitivities*

The sensitivities for the 12 elements studied in this work are given in Table 5. Alternative less sensitive lines for Pb (283.3 nm), Cr (425.4 nm) and Mn (403.1 nm) were chosen

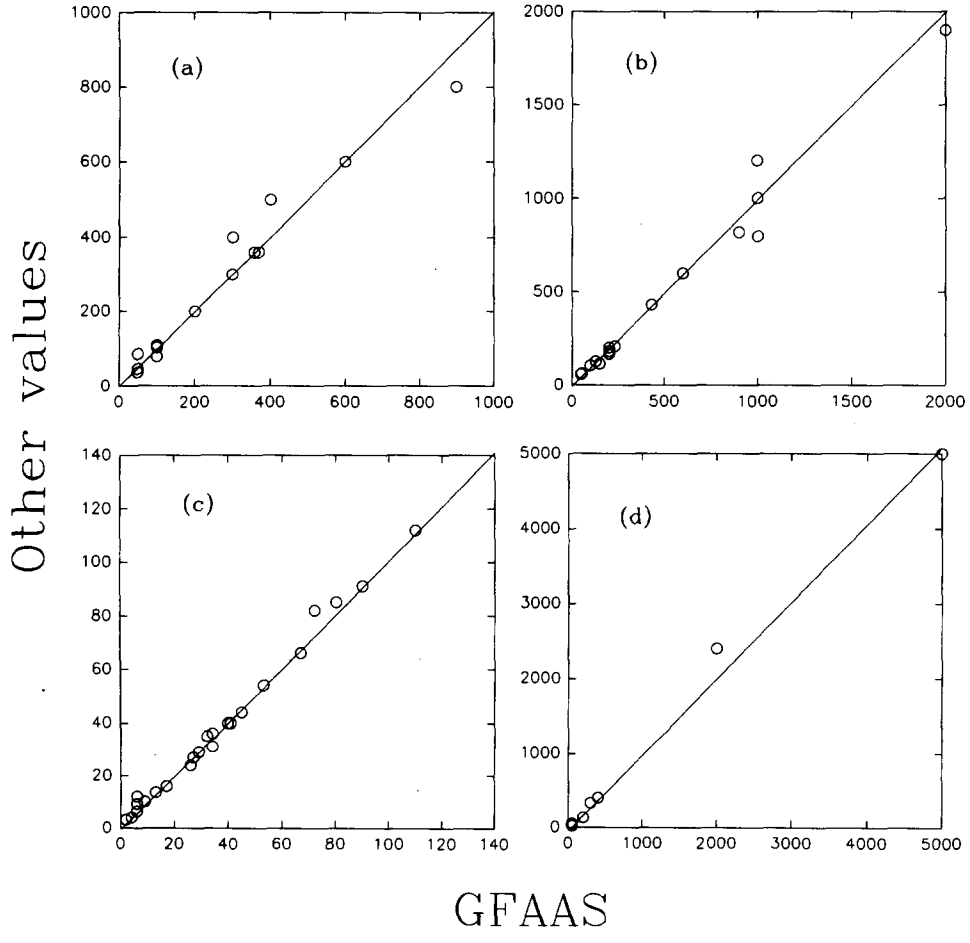


Fig. 4. Correlation plots for multi-element GFAAS *vs.* other values for some international reference rocks and sediments: (a) Ag; (b) Cd; (c) Pb; and (d) Bi. Analyte concentrations for Ag, Cd and Bi in ng/g and for Pb in $\mu$g/g.

for determination in rock and sediment samples since these elements were normally present in higher concentrations than other trace elements. The sensitivities of the primary wavelengths for Pb (217.00 nm), Cr (357.9 nm) and Mn (279.5 nm) are also included in Table 5; these lines were used where high sensitivities were needed for determination of ultra-trace amounts of these elements, *e.g.* in water samples.

*The use of palladium–magnesium modifier for* Pb *and* Cd

Palladium and magnesium chlorides have been used as matrix modifiers to prevent losses of lead in the presence of alkali and alkaline halides during charring.[14] Stabilization of cadmium by addition of magnesium nitrate or phosphate has also been reported by Slavin *et al.*[15] However, in order to lower the blank absorbance values, a lower concentration of palladium–magnesium modifier than reported by these authors[14,15] was used in this work to increase the atomization temperature for Pb and Cd to 2200°C without losses. It was found that in the presence of the specified amount of the modifier (see under Reagents and standard solutions) the ash and the atomization temperatures for Pb and Cd could be increased to 800° and 2700°C, respectively, without any losses. Therefore, using this modifier, Pb and Cd could be simultaneously determined with two other elements (*e.g.* Li and Sb) which required higher atomization temperatures than 2200°C. In this work, Pb and Cd were determined simultaneously with Ag and Bi; however, the modifier did not have any effect on the blank or absorbance values for the latter two elements.

*Analyses of reference materials for trace elements*

The validity of the proposed simultaneous multi-element GFAAS method for trace elements was tested with National Institute of Standards & Technology (NIST) reference water

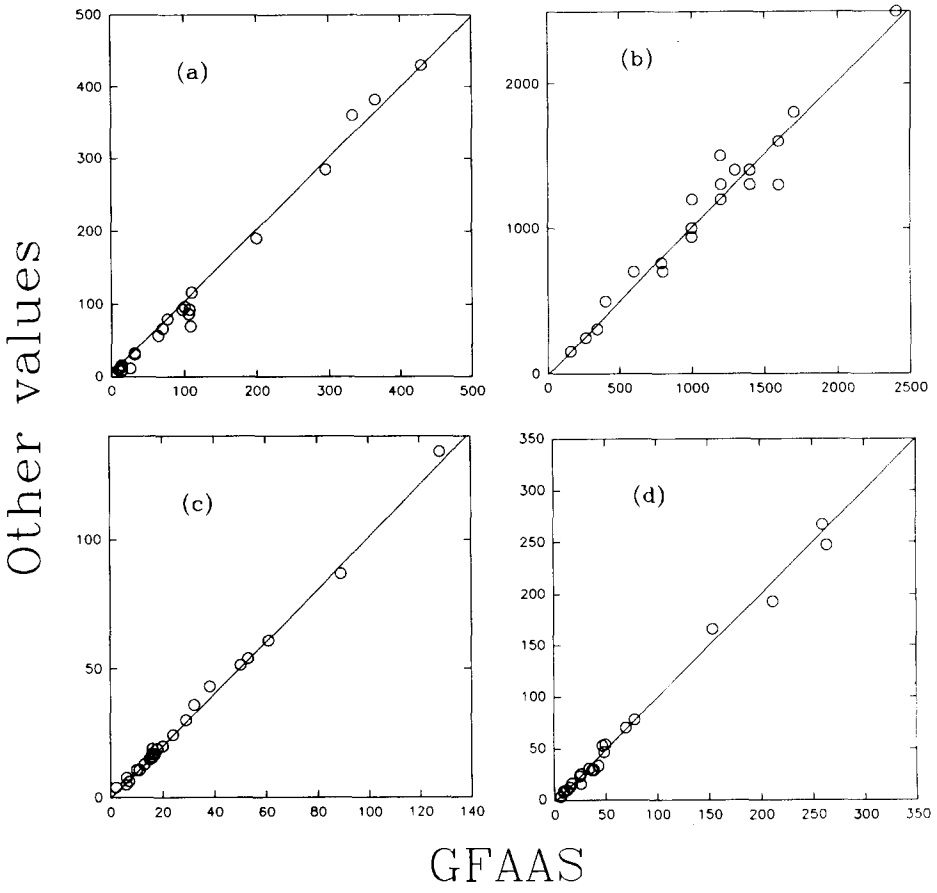


Fig. 5. Correlation plots for multi-element GFAAS *vs.* other values for some international reference rocks and sediments: (a) Cr; (b) Mn; (c) Co; and (d) Ni. Analyte concentrations in $\mu$g/g.

sample 1643c, U.S. Environmental Protection Agency (USEPA) quality control (QC) water samples (concentrates 1, 2, 6 and ICAP 19), National Research Council (NRC) of Canada reference water samples SLRS-2 (riverine water) and CASS-1 (near shore seawater), and a variety of international geochemical reference rocks and sediments issued by Canadian Certified Reference Materials Project (CCRMP), United States Geological Survey (USGS), National Institute for Metallurgy (NIM) (South Africa), International Working Group (IWG) (France) and Institute of Geophysical and Geochemical Exploration (IGGE) (China).

The results for replicate determinations of trace elements in NIST, USEPA and NRC reference water samples, given in Table 6, show good precision and excellent agreement with the expected values in most cases.

Twenty-three international reference rock and sediment samples were decomposed by the Recommended procedure and the specified elements were determined directly either from the solutions thus prepared (sample concentration 0.01 g/ml in each) or from further diluted solutions in groups of four as described above. The averages of two values for Ag, Cd, Pb, Bi, Cr, Mn, Co, Ni, Li, Be, Cu and Sb of this work in these samples are given in Tables 7–12 and compared with other values ('consensus', 'working', 'usable', 'recommended' and 'provisional') quoted from the literature.[16–24]

For each of Ag, Cd and Bi the determination limit (lowest possible amount that could be detected with certainty) of this work was 50 ng/g; it was 2 $\mu$g/g for Be.

In the case of minor and trace elements (*e.g.* Cr, Mn, Pb, Cu, Co, Ni, Cd, Be and Li) of the reference rocks and sediments, the average values of duplicate determinations of this work either agree with or fall within the limits of 'accepted values' (*cf.* Tables 7–12).

For ultra-trace elements (*e.g.* Ag, Bi and Sb) in these samples, the other values are near the determination limits of the GFAAS method, and in some cases (*cf.* Table 7) only one or two other values available in the literature are not even certified. Also, other Ag and Bi values in

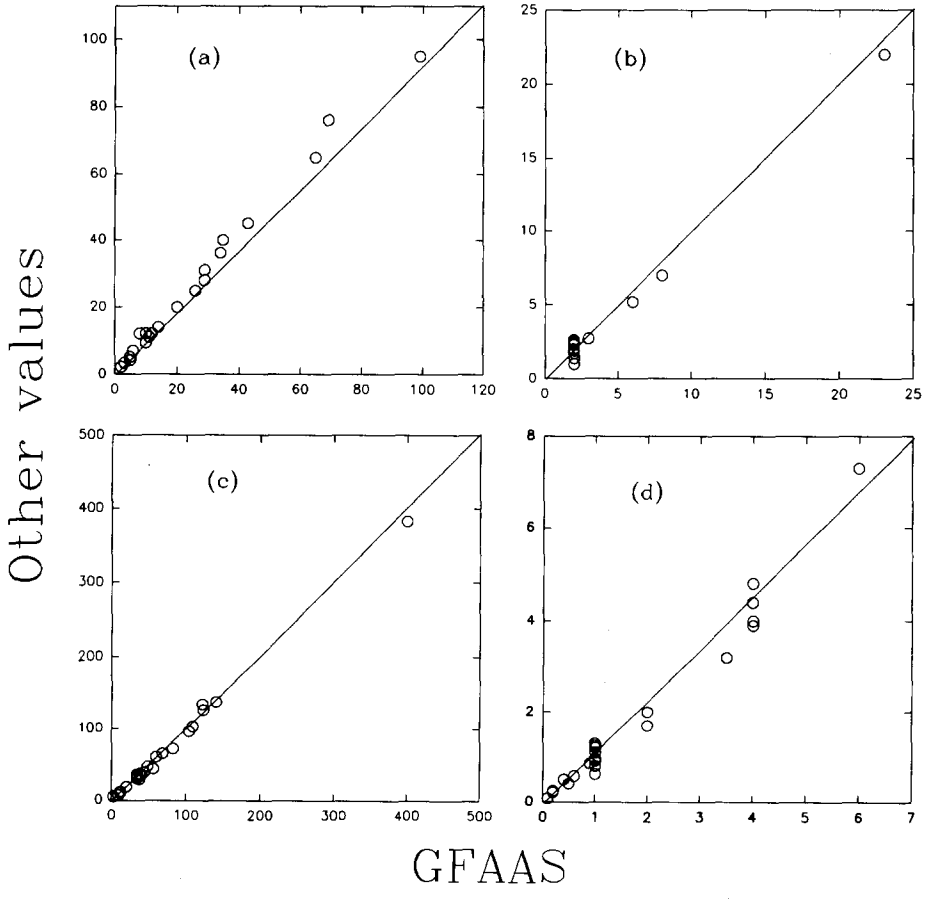


Fig. 6. Correlation plots for multi-element GFAAS *vs.* other values for some international reference rocks and sediments: (a) Li; (b) Be; (c) Cu; and (d) Sb. Analyte concentrations in $\mu$g/g.

SY-2, and Bi value in LKSD-1 to LKSD-4 and STSD-1 to STSD-4 are not available in the literature. Therefore, more data on these elements in the specified samples by other methods are needed for a valid comparison with the GFAAS values.

Where possible, the results of this work are also compared graphically with other recommended values (without standard deviation) in Figs 4–6. With the exceptions for few samples, the data points for these elements in these figures fall reasonably close to the 45° line, demonstrating fair agreement between multi-element GFAAS and other values.

Chromium in DTS-1 (dunite) was found to be lower than the 'consensus value' probably owing to the presence of a significant amount of chromite which was not completely attacked by the decomposition method. A fusion of this partially insoluble chromite residue with $Na_2O_2$ would be required to obtain better results. However, the results for other elements in this sample showed good agreement in most cases with the 'consensus values' and hence justified their inclusion in this work.

## CONCLUSIONS

The direct simultaneous multi-element GFAAS determination of trace and ultra-trace amounts of Ag, Cd, Pb, Bi, Cr, Mn, Co, Ni, Li, Be, Cu and Sb from environmental waters and geochemical sample solutions is relatively rapid and results are of acceptable quality. Low operating and virtually nil maintenance costs make the instrument ideally suited for a laboratory with a small budget. At a lower cost, the multi-element GFAAS results on the common trace and ultra-trace elements in water, rocks and related materials are comparable in quality with those of other more costly instrumental techniques such as ICP-AES and ICP-MS. Therefore, this technique is ideally suited not only for internal routine production work, but also useful for certification of trace elements in international reference samples of water, rocks and related materials.

*Acknowledgement*—The authors are indebted to K. N. De Silva for critical reading of the manuscript.

## REFERENCES

1. E. B. Sandell, *Colorimetric Determination of Traces of Metals*, 3rd Ed. Interscience, New York, 1959.
2. J. A. Maxwell, *Rock and Mineral Analysis*, Interscience, New York, 1968.
3. J. Aznarez, F. Palacios and J. C. Vidal, *Atom. Spectrosc.*, 1982, **3**, 192.
4. G. E. M. Hall and J. L. Bouvier, *Geol. Surv. Can.*, Paper 87-27, 1988.
5. R. E. Sturgeon, S. S. Berman, A. Desaulniers and D. S. Russell, *Talanta*, 1980, **27**, 85.
6. K. L. Cheng, K. Ueno and T. Imamura, *Handbook of Organic Analytical Reagents*, p. 398. CRC Press, Boca Raton, Florida, 1982.
7. J. G. Sen Gupta, Unpublished work.
8. M. Bettinelli, N. Pastorelli and U. Baroni, *Anal. Chim. Acta*, 1986, **185**, 109.
9. J. Alvarado and A. Petrola, *J. Anal. Atom. Spectrom.*, 1989, **4**, 411.
10. J. G. Sen Gupta, *J. Anal. Atom. Spectrom.*, 1993, **8**, 93.
11. J. G. Sen Gupta, *Talanta*, 1993, **40**, 791.
12. J. G. Sen Gupta, *Talanta*, 1987, **34**, 427.
13. J. G. Sen Gupta, *Talanta*, 1991, **38**, 1083.
14. N. Zhe-Ming and S. Xiao-Quan, *Spectrochim. Acta*, 1987, **42B**, 937.
15. W. Slavin, G. R. Carnrick, D. C. Manning and E. Pruszkowska, *Atom. Spectrosc.*, 1983, **4**, 69.
16. E. S. Gladney and I. Roelandts, *Geostand. Newslett.*, 1988, **12**, 63.
17. K. Govindaraju, *Geostand. Newslett.*, 1989, **13**, Special issue, July, 1.
18. E. S. Gladney and W. E. Goode, *Geostand. Newslett.*, 1981, **5**, 31.
19. E. S. Gladney and C. E. Burns, *Geostand. Newslett.*, 1983, **7**, 3.
20. T. W. Steele, A. Wilson, R. Goudvis, P. J. Ellis and A. J. Radford, *Geostand. Newslett.*, 1978, **2**, 71.
21. S. Terashima, *Geostand. Newslett.*, 1991, **15**, 195.
22. E. S. Gladney and I. Roelandts, *Geostand. Newslett.*, 1990, **14**, 373.
23. J. Lynch, *Geostand. Newslett.*, 1990, **14**, 153.
24. S. Abbey, *Geol. Surv. Can.*, Paper 83-15, 1983.

Pergamon

0039-9140(94)00265-7

*Talanta*, Vol. 42, No. 2, pp. 283–289, 1995

0039-9140/95 $9.50 + 0.00

# THE COMPARISON OF CAPILLARY ZONE ELECTROPHORESIS AND ATOMIC SPECTROSCOPY FOR THE DETERMINATION OF THE CATION CONTENT OF A STANDARD REFERENCE MATERIAL IAEA-A-11 MILK POWDER

EMMA L. PRETSWELL,* BRIAN A. MCGAW and ANDREW R. MORRISSON
School of Applied Sciences, The Robert Gordon University, St Andrew Street, Aberdeen AB1 1HG, U.K.

(*Received* 25 *February* 1994. *Revised* 12 *September* 1994. *Accepted* 12 *September* 1994)

**Summary**—Alkali and alkaline earth metals were separated and quantified by Capillary Zone Electrophoresis using a previously developed method. CZE combined with indirect detection has received considerable attention over the last few years. Methods for the determination of inorganic and organic cations and anions have been reported although few of these include quantitative application to real samples. All of these methods are characterized by high efficiencies and high capacity. Application of the method to the determination of the major cation content of an International Atomic Energy Agency (IAEA) standard reference material is described. Complete resolution and quantitation of the ions ($Na^+$, $K^+$, $Ca^{2+}$, $Mg^{2+}$) was achieved with calibration curves, for the individual components, having correlation coefficients ($r^2$) ranging from 0.996 to 0.999 and detection limits (two times the baseline noise) of 10 ppb for potassium and magnesium and of 2.5 ppb for sodium and 2 ppb for calcium were achieved. Comparable results were achieved when employing analysis by Atomic Spectroscopy. The accuracy of this method was tested by comparison with standard flame Atomic Absorption cation analysis. Statistical analysis of the instrumental results indicate that there is no evidence suggesting systematic differences between the methods. In addition, a number of potential advantages of CZE for cation analysis are discussed.

Capillary zone electrophoresis (CZE), a form of CE where separation is mainly based on differences in solute size and charge at a given pH, offers a rapid, high resolution method for the determination of inorganic and organic ions. Ions are separated according to their relative ionic mobilities in an electric field. CE is characterized by the use of narrow bore capillaries (10–100 $\mu$m) operated at high applied potentials (10–30 kV) and is fast becoming a technique complementary to High Performance Liquid Chromatography (HPLC) and Ion Chromatography (IC).

The origins of the use of CE for ion analysis can be traced to 1967[1] but more recently CZE has been demonstrated to be a high efficiency technique for the separation, with indirect detection, of inorganic anions,[2–6] amino acids,[7] organic acids,[8] cations[9] and alkali metals.[10] In 1981 Nukatsuka *et al.*[11] described the use of α-hydroxyisobutyric acid (HIBA) as a complexing agent in an isotachophoretic separation of lanthanides. The use of HIBA and acetic acid were reported by Hirokawa.[12] In 1990 Foret *et al.*[13] reported separation of rare earth metals and lithium, sodium, potassium and magnesium by CZE. In this method, indirect detection was utilized using HIBA and creatinine–acetate buffer. More recently several papers were published by Jandik, Jones *et al.* of Waters Ion Analysis Department[14–17] relating to similar principles of separation of alkali and alkaline earth cations. Although many method development and optimisation papers have been published few applications have been discussed.

This paper describes a comparison of CE cation analysis with standard Flame Atomic Spectroscopy. Using the system reported by Foret *et al.*[13] the simultaneous quantitation of Na, Mg, K and Ca in an International Atomic Energy Agency (IAEA) standard reference material (powdered milk) was performed.

This CE technique relies on indirect photometric detection which can be used for the detection of compounds that have no optical absorbance. When using indirect detection

*Author to whom correspondence should be addressed.

methods with CZE, an absorbing ion, in this instance creatinine, is incorporated in the electrolyte to produce a background signal. Cations present in the sample displace the absorbing cation in the electrolyte and produce a negative peak.

The IAEA standard reference powdered milk sample contains a number of major cations which are routinely determined, the standard analytical methods employed include spectroscopy, XRF and possibly ICP-MS. The IAEA-A-11 powdered milk sample was chosen as it represented a matrix rich in four major cations at varying concentrations. Powdered milk is a major source of cations for formula fed infants and it is, therefore, important for the availability of rapid methods to quantify the cation content in such matrices, with new improved methodology being continually sought. In addition this paper reports the potential advantages of CE for the multi-component analysis of major cations in real samples.

## EXPERIMENTAL

### *Apparatus*

Quantitative and qualitative work was performed with polyimide coated fused-silica capillary tubes (Dionex UK) with an effective length of 65 cm to the detector window. A Dionex CES-1 (Dionex UK, Camberley, Surrey, U.K.) with indirect detection at 220 nm was used for all of the analyses. The instrument was operated at 10 kV with the detector at the cathodic side. The sample solution was loaded onto the capillary under gravity (elevated at 100 mm for 30 sec). Data acquisition was carried out on the CES-1 with a Waters Maxima 820 Chromatography Workstation (Waters Chromatography Division, Watford, U.K.). The AA system employed was the Perkin Elmer PE3100 (Perkin Elmer, Post Office Lane, Beaconsfield, Berks, U.K.).

### *Materials and reagents*

CE electrolyte solutions were prepared from AnalaR-grade chemicals (Merck, Poole, Dorset, U.K.). When preparing the electrolyte, 4.5240 g of creatinine and 1.014 g of HIBA (α-hydroxyisobutyric acid) were added to a beaker containing 500 ml water, the pH was then adjusted to 3.5 by the addition of Aristar grade acetic acid and made up to 1000 ml with 18 MΩ water (Elga Ltd, High Street Lane End, High Wycombe, U.K.). This operating buffer was then vacuum filtered through a 0.45 μm cellulose nitrate filter which also degasses the solution. Glassware for all the analysis was soaked overnight in 2% Decon and thoroughly washed in 18 MΩ water.

The standard reference material milk powder IAEA-A-11 was obtained from the International Atomic Energy Agency (Vienna, Austria).

### *Preparation of standards and samples*

All standard solutions were prepared by a dilution of 1000 ppm stock solutions (BDH AA Standards Poole, Dorset, U.K.) containing a single ion, freshly prepared every month and stored in 500 ml plastic flasks. All mixed ion standards were freshly prepared for each experiment. Elga 18 mΩ water and plastic flasks were used throughout. A standard addition method was employed for the spectroscopic analysis as shown in Table 1a.

Calibration curves for the CE analysis for each of the cations of interest were prepared as mixed standards (BDH AA Standards). Six replicates were performed and the reproducibility of the response factors were expressed as a

Table 1a. Standard and sample preparation for analysis by AA

| Element | Standard | Sample |
|---|---|---|
| Calcium | 0,1,2,3,4,5 *ml* AA standard 1 *ml* stock sample solution* | 0.01% stock sample* |
| Sodium | 0,2,4,6,8,10 *ml* AA standard 1 *ml* stock sample solution† | 0.01% stock sample† |
| Magnesium | 0,2,4,6,8,10 *ml* AA standard 1 *ml* stock sample solution* | 0.1% stock sample* |
| Potassium | 0,2,4,6,8,10 *ml* AA standard 1 *ml* stock sample solution‡ | 0.1% stock sample‡ |

*0.1% KCl and 0.5% lanthanum chloride added.
†0.1% KCl added.
‡0.1% lanthanum chloride added.

Table 1b. AA operating conditions

| Element | Conditions |
|---|---|
| Calcium | Absorbance 422.7 *nm*, air–acetylene flame, oxidizing (lean blue) slit width 0.7 *nm* |
| Potassium | Emission 766.5 *nm*, air–acetylene flame, oxidizing (lean blue) slit width 1.4 *nm* |
| Magnesium | Emission 285.2 *nm*, air–acetylene flame, slit width 0.2 *nm* |
| Sodium | Emission 589.5 *nm*, nitrous oxide–acetylene flame, slit width 0.7 *nm* |

function of concentration and the correlation coefficient of the lines obtained with accuracy and precision stated.

Six weighings of 200 mg of IAEA standard reference sample were prepared. After weighing, one of the six samples was dried in an oven at 80°C for 48 hr to drive off any associated water. This was used as a blank for weight correction. The process used for the dry-ashing is a standard technique[18] as used in all methods for cation analysis and is the rate determining step common to all instrumental procedures. Reduction of the dry-ashing stage may be possible by the implementation of microwave digestion techniques.[19] The samples were then taken up in concentrated nitric acid and made up to volume with deionized water in 10 ml standard flasks to give a 7% nitric acid solution. Subsequent dilutions were carried out prior to injection.

A blank was prepared by analysing the 7% mineral acid identically to the sample analysis. Atomic spectroscopic sample solutions were prepared from dilutions of the digested samples made up in mineral acid. As the analysis is single component, samples were prepared for analysis of individual components as shown in Table 1a.

*Procedure for capillary preparation and handling*

Prior to extended use, the capillary was filled with 1*M* sodium hydroxide and allowed to stand for 1 hr. This solution was replaced with 0.1*M* sodium hydroxide, allowed to stand for 30 min, washed with deionized water before filling with running buffer by pressure injection. The capillary was used for a maximum of 12 injections before regeneration by pressure injection of 0.1*M* sodium hydroxide for 5 min and running buffer for 15 min. This was done during unattended operation (overnight) to ensure good baseline stability and to minimise the chance of capillary blockage. During monitored operation many more runs were achieved before regeneration was required. At the end of each operating day the capillary was flushed with running buffer and left filled.

*Calculation method*

The values quoted for the results obtained are the experimental values corrected after weight and background contribution was taken into consideration. Weight correction was performed by scaling the actual result to a value appropriate for an accurate weighing of 200 mg, this value was also background corrected by subtracting the value obtained for the blank, to remove any contribution from the acid.

*Instrumental operation*

The CES-1 system incorporates three modes of injection into the capillary: hydrostatic, pressure and electromigration. All injections for this study were performed in the hydrostatic mode as non-preferential loading was required. Pressure injection was performed as part of the rinse cycle where buffer was pressure injected onto the capillary. Gravity injection was utilized and the sample was elevated at 100 mm for 30 sec and a running voltage of 10 kV (positive potential) applied. A 40-sample carousel was used with Dionex 2 ml microvials. Indirect UV-detection at 220 nm was employed for the CE work.

The spectrometer was used in both modes of operation, emission and absorption. The conditions employed for the spectroscopic analysis are shown in Table 1b.

## RESULTS AND DISCUSSION

CE calibration graphs for $Na^+$, $K^+$, $Mg^{2+}$, $Ca^{2+}$ showed a linear dependence of the response factor measured in terms of peak area as a function of the concentration of the individual cations, with correlation coefficients ($r^2$) of 0.998, 0.996, 0.999 and 0.998, respectively, and LODs calculated (as two times baseline noise) as 10 ppb for potassium and magnesium, as 2.5 ppb for magnesium and as 2 ppb for calcium (Fig. 1). Correlation coefficients for the spectroscopic analysis were also calculated being 0.997, 0.996, 0.998 and 0.996, respectively.

Figure 2 shows the electropherogram of a standard mixture containing 20 ppm of sodium, potassium, calcium and magnesium with an elution order of $K^+$, $Na^+$, $Ca^{2+}$ and $Mg^{2+}$. It can be seen that complete resolution and detection were achieved within 16 min. Much lower migration times have been demonstrated,[14,16,17] however in this instance the fluctuating baseline and more pronounced baseline noise was accentuated at high applied field strength. This was possibly due to Joule heating in the capillary hence a low operating voltage of 10 kV was applied leading to increased migration times. Manipulation of the control voltage does allow a decrease in the elution time resulting from a faster Electroosmotic Flow (EOF). A compromise is necessary to achieve well defined chromatography and speed of analysis.

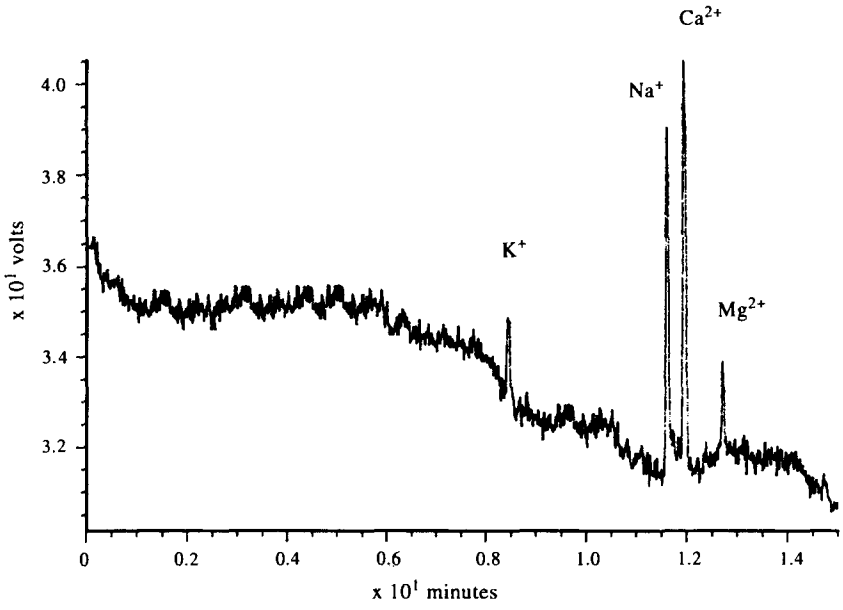


Fig. 1. Electropherogram showing the response factor for a 10 ppb standard solution of the major cations found in the milk powder matrix.

Optimization of the electrolyte system used in the CE analysis was achieved by altering the concentration of the complexing agent (HIBA). This was measured in terms of baseline resolution of the peaks. The stability of the chelant–cation complex formed varies depending on the cations present and the concentration of the chelant itself. The greater the stability of the complex, the more retarded the ion is in the capillary allowing greater separation of components. When analysing samples with disparate concentrations it may be necessary to use a stronger more specific chelant, for example a crown ether (E. Pretswell and K. Cook, personal communication). The crown ether, being highly specific, will strongly complex a specific ion, retarding it and hence changing the elution order of the solutes.

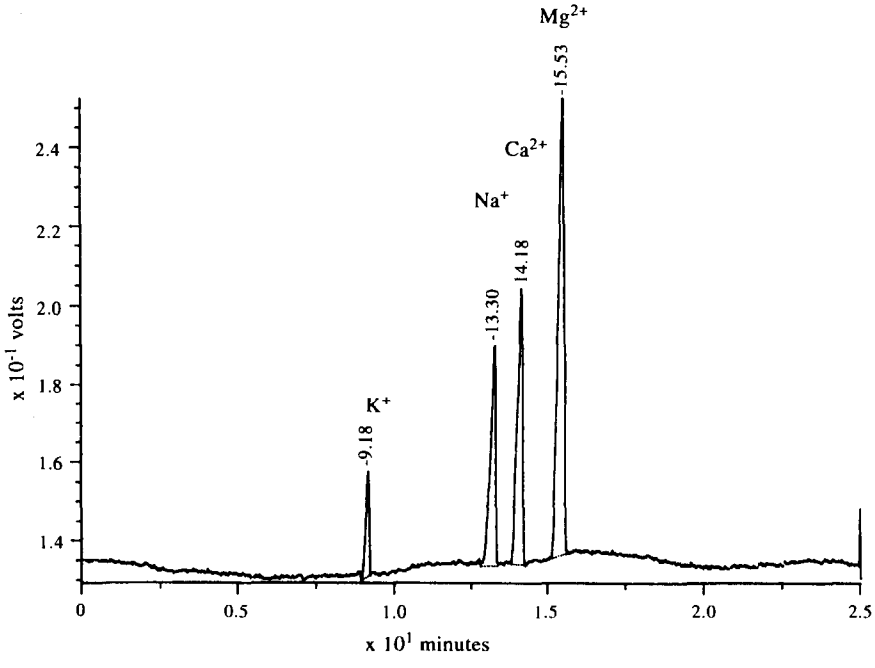


Fig. 2. Electropherogram of the major cations found in a 20 ppm standard solution.

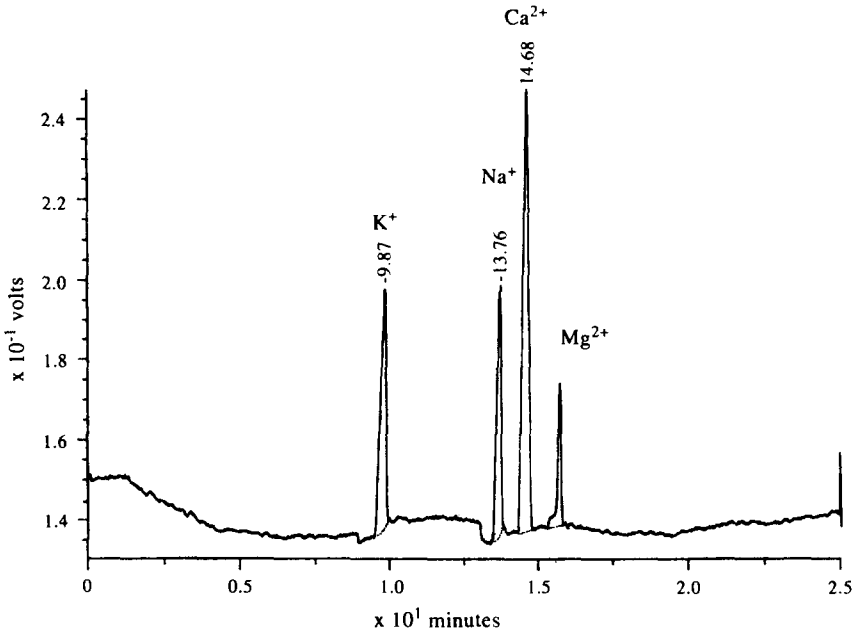


Fig. 3. Electropherogram of the major cations found in the IAEA standard reference sample.

Figure 3 illustrates the optimized separation for the analysis of the IAEA A-11 standard reference milk sample by CE. From the electropherogram the mobility of the last eluting ion varies significantly from the mobility of the buffer ions as peak fronting is observed. This is possibly due to the interference of the sample matrix on the separation pattern (real samples *vs.* laboratory standards) or the presence of nitric acid in the sample on the complex formation between the cation and HIBA. This may cause a shift in the equilibrium and hence alter the mobility of the cation. A shift in the retention time of the standard reference analytes is also observed, one explanation for this may be due to the higher pH of the sample compared to that of the standards. The sample pH may also be responsible for the dips seen in the baseline prior to the sample peaks. The plug flow characteristics of CE and the minimum EOF in the capillary prohibit sample mixing. At the sample-buffer interface a pH gradient exists causing changes in the absorbance of the zone passing the detection window resulting in the characteristic dips in the baseline. It is also possible that the presence of nitric acid may give a positive UV absorbance when passing the detection window resulting in dips in the baseline. This effect was not apparent when analysing the standard cation solutions, but was apparent when the blank nitric acid sample was analysed indicating further evidence that the presence of the nitric acid may be the cause of the undulating baseline.

There was no requirement for trace enrichment of the samples so gravity injections were used throughout because this mode of injection has the high precision of electromigration, but is nondiscriminatory, *i.e.* gives non-preferential loading of individual cation species.

The concentration of $Na^+$, $K^+$, $Mg^{2+}$ and $Ca^{2+}$ were calculated by both instrumental methods for the IAEA A-11 with instrumental

Table 2. Concentrations obtained by Instrumental analysis and those cited by IAEA for the cations analysed (statistical instrumental error quoted)

| | IAEA | CE | AA |
|---|---|---|---|
| Component | (*mg/kg*, error %)* | (*mg/kg*, $r^2$) | (*mg/kg*, $r^2$) |
| Calcium | 12,900 (6.2) | 13,000 (1.27) | 13,020 (1.67) |
| Potassium | 17,200 (5.8) | 17,300 (1.45) | 17,290 (1.56) |
| Sodium | 4420 (7.5) | 4390 (1.86) | 4410 (1.91) |
| Magnesium | 1100 (7.3) | 1090 (1.63) | 1090 (1.74) |

*95% confidence interval for the mean.

Table 3. Table showing the calculated results from the statistical comparison of the methods

| | Method tested | |
|---|---|---|
| Method compared | Spectroscopy | IAEA |
| Capillary electrophoresis | Slope, 0.999<br>Intercept, −0.06<br>$r^2$ −0.995 | Slope, 0.995<br>Intercept, 0.033<br>$r^2$, 0.998 |
| Spectroscopy | | Slope, 0.996<br>Intercept, −0.08<br>$r^2$, 0.999 |

and analytical precision tested and shown in Table 2.

Regression lines were used to compare analytical methods.[20] A statistical comparison was performed between AA and the IAEA cited values and between the CE and the cited values. Statistical analysis of the results is shown in Table 3. From Table 3 it is apparent that there is no evidence for systematic differences between the methods as the calculated slope and intercept do not differ significantly from 1 and 0, respectively.

## CONCLUSIONS

CE offers a rapid and reproducible method for the determination of alkali and alkaline earth metals by capillary zone electrophoresis (CZE) with indirect UV detection. The method gives excellent agreement for four major cations in a certified reference material (IAEA A-11). CE has advantages over spectroscopic analysis namely, simple calibration standards, sample preparation, simpleness of operation, fully automated, multi component analysis, easy operation and implementation. Disadvantages include poor sensitivity for trace element analysis, which may be improved with isotachophoretic stacking of the samples,[21] and loss of resolution when analysing mixtures of disparate concentrations. Conductivity detection has been demonstrated[22–25] where narrow bore capillaries attached to specially designed potentiometric detectors have been able to detect traces ($10^{-9}$ mol/l). Unfortunately, these systems are not widely available commercially.

This paper concludes that CZE can be applied to the analysis of cations in complex matrices and give results comparable to standard methods. This indicates that CE may be an optimal extension of classical methods of cation analysis with sensitive detection at low ppm/high ppb range and may be used reliably as a multi component method for quantifying major cations in food matrices. Application of the method to a wide variety of sample matrices is easily attainable suggesting the versatility and reliability of the method.

*Acknowledgements*—We would like to thank Dr K. Cook and Mr K. Divan of Dionex UK for their invaluable help during the work. In addition we would also like to thank Dr J. S. Park of Procter and Gamble Ltd for his continued support and finally Procter and Gamble Ltd for funding the work.

## REFERENCES

1. S. Hjerten, *J. Chromatogr Rev.*, 1967, **9,** 122.
2. L. Gross and E. Yeung, *J. Chromatogr.*, 1989, **480,** 169.
3. E. L. Pretswell, A. R. Morrisson and J. S. Park, *Analyst*, 1993, **118,** 1265.
4. G. W. Tindall, D. R. Wilder and R. L. Perry, *J. Chromatogr.*, 1993, **641,** 163.
5. W. R. Jones and P. Jandik, *J. Chromatogr.*, 1992, **608,** 385.
6. P. Jandik and W. R. Jones, *J. Chromatogr.*, 1991, **546,** 431–443.
7. W. Khur and E. Yeung, *J. Chromatogr.*, 1988, **60,** 1832–1834.
8. F. Foret, S. Fanali, L. Ossicini and P. Bocek, *J. Chromatogr.*, 1989 **470,** 299.
9. L. Gross and E. Yeung, *Anal. Chem.*, 1990, **62,** 427.
10. W. Kuhr and E. Yeung, *Anal. Chem.*, 1988, **60,** 2642.
11. I. Nukatsuka, M. Taga and H. Yoshida, *J. Chromatogr.*, 1981, **205,** 95.
12. T. Hirokawa, N. Aoki and Y. Kiso, *J. Chromatogr.*, 1989, **312,** 11.
13. F. Foret, S. Fanali, A. Nardi and P. Bocek, *Electrophoresis*, 1990, **11,** 780.
14. A. Weston, P. R. Brown, P. Jandik, W. R. Jones and A. L. Heckenberg, *J. Chromatogr.*, 1992, **593,** 289.
15. M. Koberda, M. Konkowski, P. Youngberg and W. R. Jones, *J. Chromatogr.*, 1992, **602,** 235.
16. A. Weston, P. R. Brown, A. L. Hechenberg, P. Jandik and W. R. Jones, *J. Chromatogr.* 1992, **602,** 249.
17. A. Weston, P. R. Brown, P. Jandik, A. L. Heckenberg and W. R. Jones, *J. Chromatogr.*, 1992, **608,** 395.
18. L. Jorhem, *J. AOAC Int.*, 1993, **76,** 798.
19. P. Schramel and S. Hasse, *Fres. J. Anal. Chem.*, 1993, **346,** 794.
20. J. C. Miller and J. N. Miller, *Statistics for Analytical Chemistry*, 1st edn, pp. 52–33. Wiley, New York, 1984.
21. D. S. Burgi and R. L. Chien, *Anal Chem.*, 1992, **64,** 1046.

22. X. Huang, T. Pang, M. Gordo and R. Zare, *Anal Chem.*, *1991*, **63,** 193.
23. X. Huang, T. Pang, M. Gordo and R. Zare, *Anal Chem.*, *1987*, **59,** 2747.
24. N. Avdolovic, C. A. Pohl, D. Rocklin and J. R. Stillian, *Anal Chem.*, *1993*, **65,** 1470.
25. X. Huang, J. A. Luckey, M. J. Gordon and R. N. Zare, *Anal Chem.*, *1989*, **61,** 766.

Pergamon

0039-9140(94)00243-6

*Talanta*, Vol. 42, No. 2, pp. 293–304, 1995

0039-9140/95 $9.50 + 0.00

# DETERMINATION OF ACECLOFENAC USING ADSORPTIVE STRIPPING VOLTAMMETRIC TECHNIQUES ON CONVENTIONAL AND SURFACTANT CHEMICALLY MODIFIED CARBON PASTE ELECTRODES

J. R. POSAC,[1] M. D. VÁZQUEZ,[1] M. L. TASCÓN,[1] J. A. ACUÑA,[1] C. DE LA FUENTE,[1] E. VELASCO[2] and P. SÁNCHEZ-BATANERO[1]*

[1]Department of Analytical Chemistry, Faculty of Sciences, University of Valladolid, Valladolid, Spain
[2]University Clinic Hospital, Valladolid, Spain

(*Received* 6 *October* 1993. *Revised* 28 *March* 1994. *Accepted* 22 *July* 1994)

**Summary**—An electroanalytical method for determination of the anti-inflammatory agent aceclofenac at the ppb level using adsorptive stripping voltammetric techniques on conventional and surfactant chemically modified electrodes is developed. In this electroanalytical study a process of aceclofenac adsorption on carbon particles has been identified. In order to improve the aceclofenac determination, a chemical modification of the carbon paste was carried out employing several hydrophobic substances such as phospholipid and fatty acids, as well as several surfactants such as the non-ionic Triton X-100 and Triton X-405 and anionic sodium dodecyl sulfate. The influence of parameters such as pH, preconcentration time, carbon/Nujol ratio, surfactant/carbon ratio, potential scan rate, *etc.*, on sensitivity of the method were widely studied. The proposed method was applied to the determination of the active compound in tablets.

Aceclofenac (AC), 2-((2,6-dichlorophenyl)-amino) phenylacetoxyacetic acid, is a new non-steroidal anti-inflammatory agent produced by Prodesfarma (Spain). Experimental studies have demonstrated its ability to reduce prostaglandin synthesis in inflamed areas both in animals and humans.[1,2] Experimental pharmacokinetic studies with animals showed rapid adsorption when administered orally, distribution mainly in the gastro-intestinal tract, liver and kidneys and elimination according a biocompartmental model, with no accumulation when administered in repeated doses.[3–5]

AC is scarcely soluble in n-hexane and water and quite soluble in dimethylformamide, acetone, methanol (96%), ethanol (96%), acetonitrile, chloroform, acetic acid, acetyl acetate and alkaline solutions. It is weakly acidic ($pK_a = 4.7$). In experiments with animals, AC demonstrated an important analgesic and anti-inflammatory effect, similar to that of diclofenac (DC) and stronger than other non-steroidal anti-inflammatory agents.

In humans, using $^{14}C$ radioactivity measurements, according to Chassaud *et al.*[6] and Bastida *et al.*[7] the following metabolites were found: *o*-[(2,6-dichlorophenyl)amine]-phenyl acetic acid (4–7%), 4′-hydroxy-*o* [[(2,6-dichlorophenylamine)]phenyl acetic acid] (10–16%), 4′-hydroxyaceclofenac 'lactam' (11%) and the rest as unchanged AC.[6] These metabolites are mainly in a conjugated form with glucoronic acid, which combines with toxic metabolites.[7]

Regarding the analytical aspects of drugs in general, several papers show an important role played by the electrode used. Patriarche[8] reviews electrode modification, concerning all types of electrodes. According to Patriarche and to the literature,[9–14] solid electrode surface modification generally affects the selectivity and the kinetics of eletrochemical reactions, owing to the presence of intermediate catalyst immobilized onto the electrode surface. Moreover, the solid electrode modification can produce an important preconcentration effect of drugs onto the electrode surface with an enhancement of sensitivity.[15–17]

Analytical determination methods for AC are potentiometric using the acidic properties of this drug[7] and chromatographic using of HPLC[7,18] and by thin layer[7] for identification only. Additionally, the use of the carbon paste electrode in electroanalytical chemistry has permitted its

*Author to whom correspondence should be addressed.

easy modification with a wide variety of modifiers.[19,20] The use of phospholipids and fatty acids as modifier was carried out by Patriarche and co-workers[21,22] and the use of surfactants as modifier was first initiated by Mottola *et al.*[23] by dipping carbon paste electrodes in a surfactant solution, and by us[24] by incorporating a solid state modifier into the paste. Recently, several reviews, concerning chemical modifications of carbon-based electrodes[25] as well as their use in liquid chromatography detection,[26] have appeared.

## EXPERIMENTAL

### *Apparatus*

To obtain voltammograms, a Potentiostat Autolab PSTAT 10 and a GPES software ECO-CHEMIE (Holland) were used.

Electrodes were Ag/AgCl, KCl saturated as reference electrode, a Pt wire as auxiliary electrode and a Metrohm 6.1204.000 carbon rotating disc electrode (diameter = 3 mm) as working electrode (in which a hole, by pressing a carbon disc, was made to be readily filled with carbon paste).

An ultrasonic bath Selecta (Spain) was employed as graphite powder mixer.

### *Reagents*

Graphite powder (200 mesh and spectroscopically pure) was from Johnson Matthey (Paris, France). AC, pure product and tablets, named Airtal, were provided by Prodesfarma (Spain). These tablets had the composition given in Table 1.

All surfactants used were supplied by Serva Feinbiochemica (Heidelberg, Germany) and employed without purification.

Nujol oil was a Merck reagent and all other chemical reagents were of analytical grade and furnished by different firms.

The 2,6-dichloro-*p*-aminophenol was supplied by Aldrich-Chemie.

### *Procedures*

We used two types of carbon paste electrodes: (a) the conventional carbon paste electrode (CPE); (b) the modified carbon paste electrode (MCPE). These types of electrodes were previously prepared by us,[24] but in this case the C (g)/nujol (g) ratio was 68:32, and the surfactant (g)/C (g) ratio was 5:95. In both electrodes, carbon powder/Nujol oil, as well as carbon powder/Nujol oil/chloroform surfactant solution (added to facilitate the modifier dispersion and evaporation), were homogenized by an ultrasonic bath.

The preliminary studies on electroactivity of AC were only carried out on CPE.

The adsorption studies were carried out on both types of electrodes at open circuit before stripping, using the following types of solutions: (a) preconcentration solution, formed by the analyte and the pH buffer; (b) stripping solution, formed by pH buffer and the supporting electrolyte.

In order to develop an electroanalytical deter-

Table 1. Composition of aceclofenac tablets

| Ingredients | Formula of aceclofenac tablet 100 *mg** (*mg*) |
|---|---|
| Active ingredient | |
| Aceclofenac† | 100.0 |
| Other ingredients | |
| Microcrystalline cellulose | 89.2 |
| (Avicel PH 101) | (26.3) |
| (Avicel PH 102) | (62.9) |
| Sodium croscarmellose | 6.6 |
| Glyceryl palmitostearate | 2.6 |
| Povidone | 6.6 |
| Tablet core weight | 205 |
| Film coating | |
| Sepifilm 752 white‡ | 9.0 |
| Total tablet weight | 214 |

*Ethanol is used in the manufacture of the tablet core and dichloromethane and ethanol in the film coating stage; levels in the final product are low.

†Average: none.

‡The composition of Sepifilm 752 white is: hydroxylpropyl methylcellulose, 68–70%; polyoxyl-40 stearate, 6–10%; titanium dioxide, 18–22%.

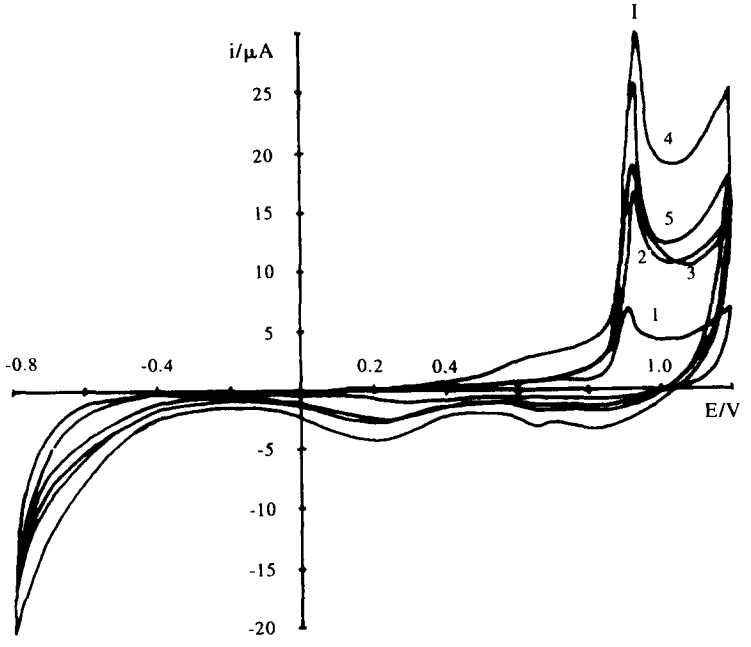


Fig. 1. Voltammogram of $10^{-5}M$ AC at pH 1 ($HClO_4$ $0.1M$) at different scan rate: (1) 1 V/sec; (2) 2 V/sec; (3) 3 V/sec; (4) 4 V/sec; (5) 5 V/sec; starting potential: 0.00 V; first scan forward +1.20 V, reverse up to −0.70 V and reverse up to 0.00 V to complete the cycle; conventional carbon paste electrode.

mination method of AC, the influence of several parameters on voltammetric peak height, such as potential scan rate, pH, preconcentration time, analyte concentration, carbon/Nujol oil (g/g) ratio, surfactant/carbon/Nujol oil (g/g/g) ratio and solution alcohol concentration, were studied. In all the cases, after each experiment, the electrode surface was renewed.

In order to develop an AC electroanalytical method using the conventional CPE, the following experimental conditions were employed. Preconcentration solution: $0.1M$ $HClO_4$ + AC, stripping solution: $0.1M$ $HClO_4 + 0.1M$ $KNO_3$, Nujol oil (g)/carbon (g) ratio: 32/68, preconcentration time: 8 min, potential scan rate: 4 V/sec, solution stirring rate: $10^3$ tpm. In the case of CMCPE the same experimental conditions as above were employed, but in this case a surfactant (g)/carbon (g) ratio of 5/95 was utilized.

## RESULTS AND DISCUSSION

### *Preliminary studies on CPE*

In order to determine if AC was electroactive (no reference about its electrochemical behaviour was found), its electrochemical profiles at different pH (acidic media of $HClO_4$, $AcO^-$/AcOH and $HPO_4^{2-}/H_2PO_4^-$, weakly alkaline medium, $NH_3/NH_4^+$, and strongly alkaline medium, NaOH) were obtained, without and with preconcentration step.

Voltammograms obtained, with a $1 \times 10^{-5}M$ AC solution, at pH 1 ($HClO_4$ $0.1M$) without a preconcentration step, scanning the potential from 0.0 V, up to 1.2 V, and then back to −0.8 V *vs.* Ag/AgCl, KCl satd, at different scan rates (1–5 V/sec), are plotted in Fig. 1. Only one well defined oxidation peak appears at 0.993 V. Its height increases with scan rate up to 4 V/sec, and then decreases at 5 V/sec, probably owing to high cell constant value. The height of this peak increases linearly with AC concentration and with $v^{1/2}$, therefore, it is a diffusion controlled peak. It also appears as a cathodic peak at +0.2 V whose height increases slightly with the scan rate.

Following a preconcentration step, employing the same AC solution but at pH 1.7 ($HClO_4$ $2.10^{-2}M$), the same voltammogram was obtained, in which we observe that the anodic peak is near the electroactivity limit and, therefore, it is difficult to analyse.

In order to obtain a fairly easy to use voltammogram, we proceeded as follows. Without a preconcentration step: with the same AC solution, we completed a whole cyclic voltammetric cycle from +1.00 V to −0.100 V and back to +1.0 V. The voltammogram obtained is plotted in Fig. 2. In this figure, a very suitable analytical peak at +0.5 V and other small peaks (at +0.7, +0.65 and +0.15 V) without analytical significance, are observed. This analytical peak is probably a result of oxidation of a

substance obtained by a series of previous electrochemical and chemical reactions described as follows.

*Analytical peak characterization*

In order to characterize the peak, a series of voltammograms were obtained. These voltammograms have been interpreted according to Adams.[27] Thus, we think that the first step in the electrochemical oxidation of AC is the following reaction (where R is $—CH_2—CO_2—CH_2—CO_2H$, in the aceclofenac formula):

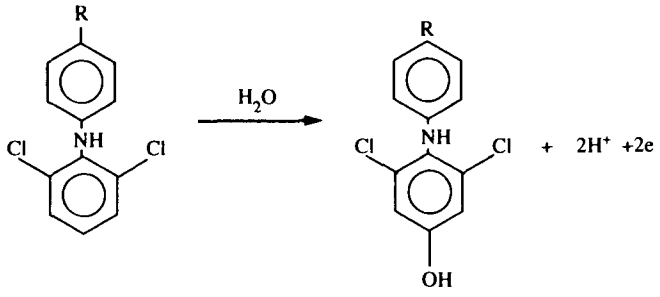


Scheme 1.

obtaining peak I of Fig. 2.

The aminophenol formed is further oxidized in peak I, giving a quinoneimine R derivative:

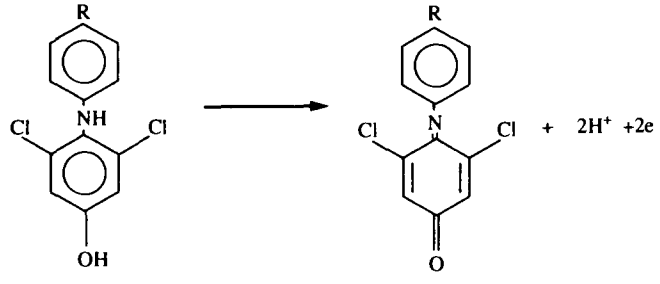


Scheme 2.

This quinoneimine is easily hydrolysed in acidic media according to Adams[27] giving the following compounds:

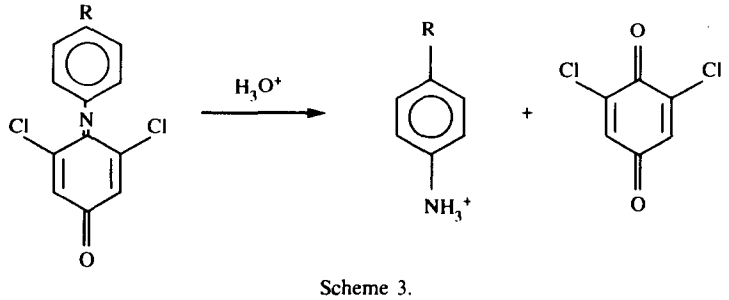


Scheme 3.

The quinoneimine and quinone forms might correspond to the redox peak couple III/III′ and II/II′, respectively.

In order to verify this, we studied the electrochemical behaviour of the commercially available compound 2,6-dichloro-*p*-aminophenol, and the results obtained indicate that its behaviour is similar to that of AC. However, the commercial compound is just slightly adsorbed onto the carbon paste electrode (Fig. 3), corresponding to the case in which a $1 \times 10^{-5}M$ 2,6-dichloro-*p*-aminophenol solution was in contact with a CPE for 8 min.

We also studied $1 \times 10^{-5}M$ 2,6-dichloro-*p*-aminophenol in solution, that is to say without a preconcentration step, by cyclic voltammetry, scanning the potential at 4 V/sec, obtaining the voltammogram plotted in Fig. 4, in which a

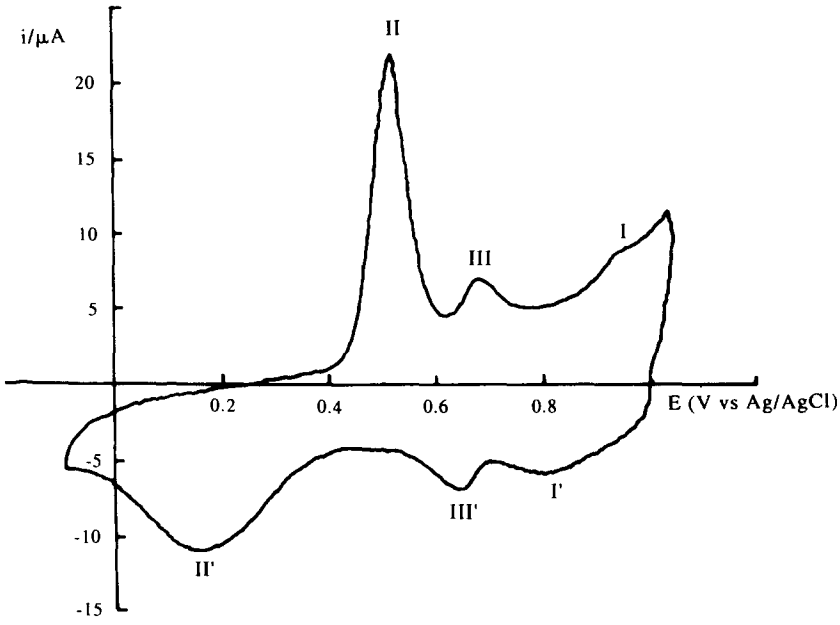


Fig. 2. Voltammogram of $10^{-5}M$ AC at pH 1.7 ($HClO_4$ $10^{-2}M$); starting potential: +1.00 V; first scan up to −0.10 V, reverse up to 1.05 V and finally up to 1.00 V to complete the cycle; scan rate: 4000 mV/sec; conventional carbon paste electrode.

quasi-reversible behaviour of this compound is observed, with an anodic peak developed at about +0.5 V.

We think that the quinone formation is the most probable electrochemical transformation of AC according to Adams.[27] Therefore, we can conclude that the analytical peak of AC obtained must correspond to the anodic oxidation of adsorbed 2,6-dichlorohydroquinone previously produced by electrochemical and chemical processes on AC after its strong adsorption on the carbon paste electrode.

All of the following studies on the electroanalytical behaviour of AC were carried out using

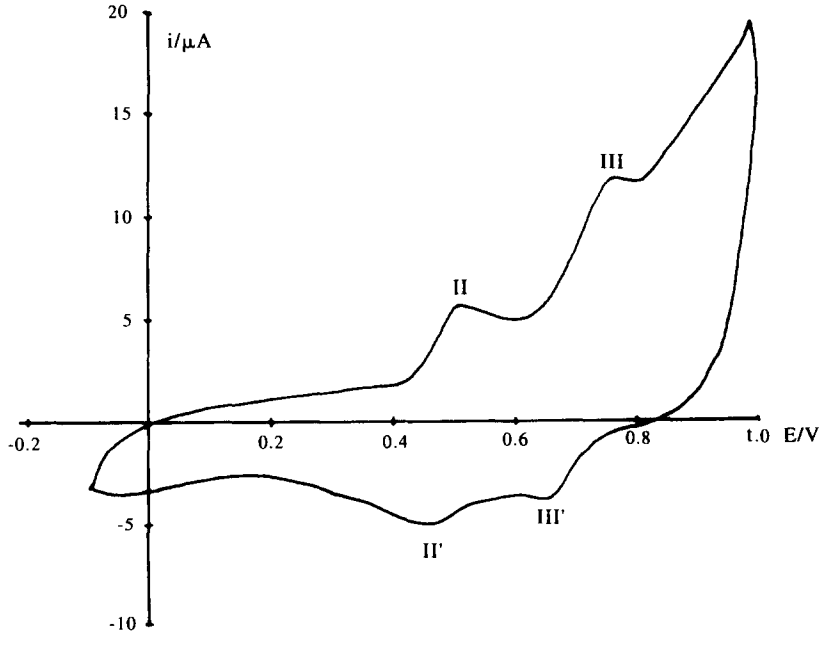


Fig. 3. Voltammogram of 2,6-dichloro-*p*-aminophenol solution after contact with the carbon paste electrode for 8 min; pH 1 both in preconcentration and stripping cells.

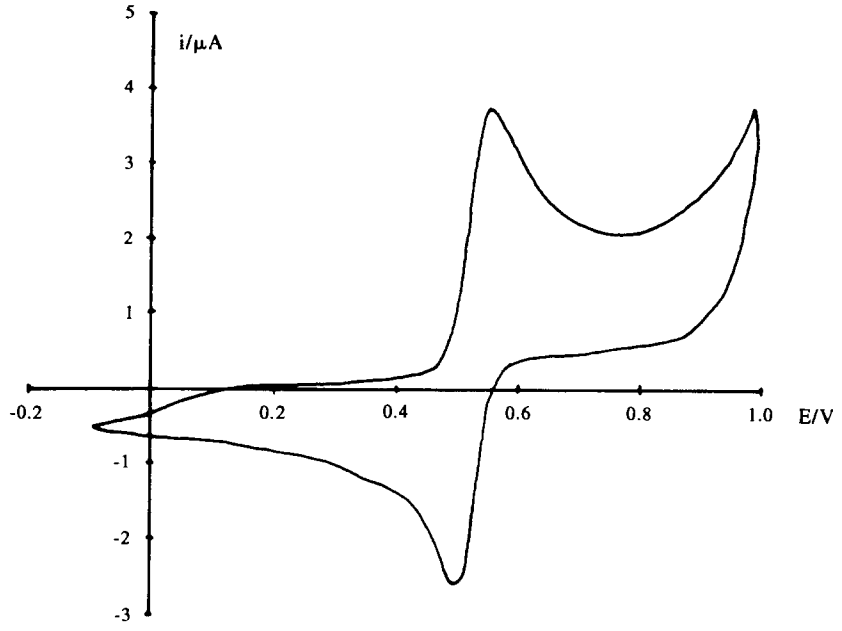


Fig. 4. Voltammogram of a $10^{-5}M$ 2,6-dichloro-*p*-aminophenol solution at pH 1 on a conventional carbon paste electrode; scan rate 4 V/sec (without preconcentration step).

adsorptive voltammetric techniques on CPE and MCPE. For this, two solutions were used: (1) preconcentration solution; (2) stripping solution, as we have previously indicated in Procedures. Several preliminary parameters, such as the water/alcohol ratio of the AC solutions as well as the Nujol oil/carbon ratio of the CPE, were studied.

As AC is sparingly soluble in water we prepared a $1 \times 10^{-2}M$ AC solution in pure ethanol. Nevertheless, according to the AC structure, we think that protons must play an important role

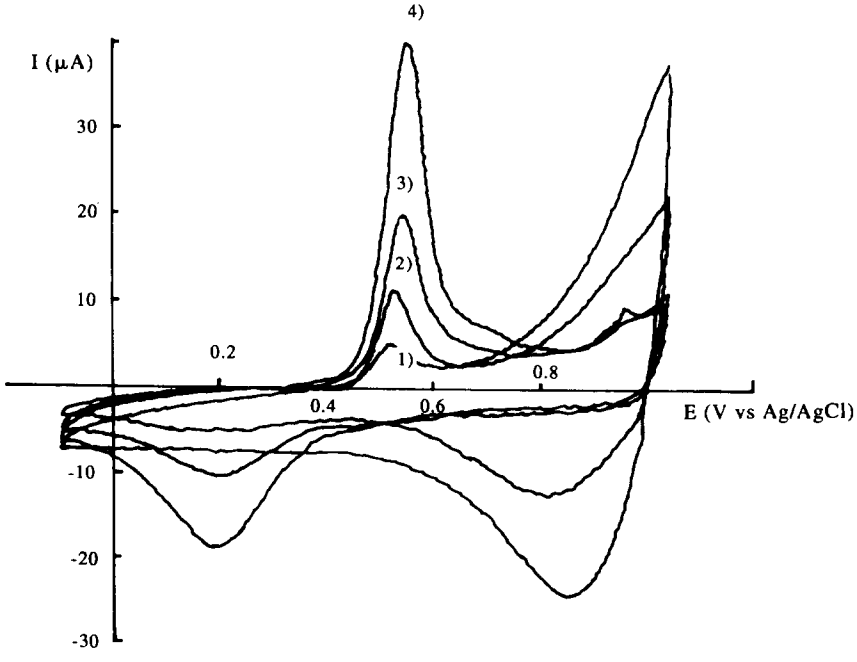


Fig. 5. Voltammograms of $10^{-5}M$ AC at pH 1 ($HClO_4$ $0.1M$). Influence of ethanol/$H_2O$ (v/v) ratio of preconcentration solution on peak height; (1) 3:2; (2) 2:3; (3) 1:4; (4) 0:5; scan rate: 4 V/sec; conventional carbon paste electrode; ad-accumulation time: 8 min.

Table 2. Influence of carbon (g)/Nujol oil (ml) on $I_p$ ($\mu$A), $E_p$, $E_{p/2}$, $E_p - E_{p/2}$ (V) of aceclofenac peak height (ad-accumulation time: 8 min, ad-accumulation pH: 1.0; potential scan rate: 4 V/sec)

| C (g)/Nujol (g) | $I_p$ ($\mu A$) | $E_p$ ($V$) | $E_{p/2}$ | $E_p - E_{p/2}$ |
|---|---|---|---|---|
| 3:1.23 | — | | — | |
| 3:1.32 | 17.04 | 0.548 | 0.548 | 0.035 |
| 3:1.41 | 15.50 | 0.548 | 0.510 | 0.038 |
| 3:1.58 | 4.90 | 0.534 | 0.500 | 0.034 |
| 3:1.76 | 2.60 | 0.539 | 0.503 | 0.036 |

in the reduction mechanism of this drug, therefore, the influence of percentage water and pH must be studied.

*Influence of alcohol/water ratio on peak height.* By varying the ethanol/water ratio, we observe that the lower the ethanol/water ratio, the higher the voltammetric peak height. The influence of ethanol/water ratio on AC peak height is plotted in Fig. 5. These experiments were carried out with a $1 \times 10^{-5}M$ AC solution, at pH 1 into both the preconcentration and stripping solutions, with a preconcentration time of 8 min and a potential scan rate of 4 V/sec. In this figure, we observe that despite the high scan rate, the height of the AC peak can be easily measured.

*Influence of Nujol/carbon ratio on aceclofenac peak height.* This study had a double purpose. Firstly, to obtain a more intense analytical signal, and, secondly, to ascertain if AC is adsorbed on carbon particles or extracted by the Nujol oil used as binder in this type of electrode. The influence of the C (g)/Nujol (g) ratio on $I_p$ ($\mu$A), $E_p$ (V), $E_{p/2}$ and ($E_p - E_{p/2}$) of aceclofenac voltammetric peak height can be seen from Table 2.

The higher the carbon/Nujol (w/w) oil ratio, the higher the peak height, therefore, we can conclude that AC is adsorbed on carbon particles and not extracted by the Nujol oil, as we have found in another work on another substance.[22] By increasing the Nujol oil/carbon (w/w) ratio the CPE electroactive area decreases and so the AC peak height also decreases, that is to say, by decreasing the polarity of the electrode surface the AC adsorption also decreases. We can also observe that both $E_p$, $E_{p/2}$ and $E_p - E_{p/2}$ remain almost invariable with the C (g)/Nujol (g) ratio. As Nujol oil is necessary to bind the carbon particles, an optimal Nujol oil/carbon ratio of 32/68 (w/w) was chosen for all the following experiments.

*Stripping of AC at the CPE*

In this part, a study of several experimental parameters was carried out in order to establish an AC stripping method based on a drug adsorption phenomenon on carbon particles, *i.e.* by using a carbon paste electrode without modification. The studied parameters were scan rate, ad-accumulation time, pH of the preconcentration and stripping solutions, solution stir-

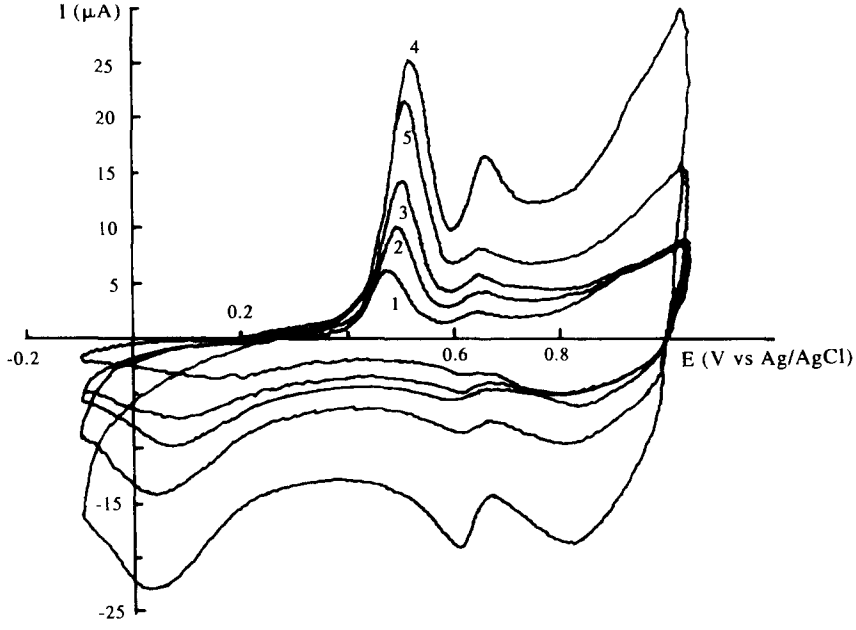


Fig. 6. Voltammograms of $6.10^{-5}M$ AC at pH 4.5 both in preconcentration and stripping cells. Influence of scan rate; (1) 1 V/sec; (2) 2 V/sec; (3) 3 V/sec; (4) 4 V/sec; (5) 5 V/sec; conventional carbon paste electrode; ad-accumulation time: 4 min.

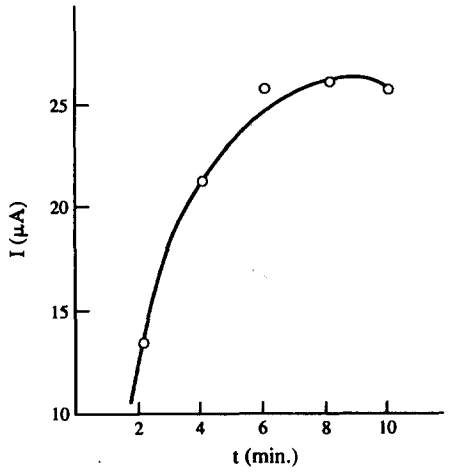


Fig. 7. Influence of ad-accumulation time on peak height of $6 \times 10^{-5}M$ at pH 4.5 ($HAc/Ac^-$ $0.1M$) in preconcentration cell and 1 ($HClO_4$ $0.1M$) in stripping cell; scan rate: 4000 mV/sec; conventional carbon paste electrode.

ring rate, and analyte concentration influence on AC anodic peak height.

*Scan rate influence.* The preconcentration solution was formed by a $6 \times 10^{-5}M$ AC solution and a buffer to give pH 4.5 ($HAc/Ac^-$ $0.1M$), and the stripping solution was formed by $0.1M$ $KNO_3$ solution and a buffer to give pH 4.5 ($HAc/Ac^-$ $0.1M$). Scanning cyclically the potential between 1.05 and $-0.1$ at different scan rates, several voltammograms, plotted in Fig. 6, were obtained, showing that the optimal value was 4 V/sec. In addition, a peak height decrease is observed at 5 V/sec. This 'anomalous result' may be explained by the fact that, at very high scan rate, the percentage of 2,6 dichloro-*p*-hydroquinone formation, from the AC, must decrease.

*Ad-accumulation time influence.* For these experiments the preconcentration solutions and the stripping solutions were the same as above. The scan rate was 4 V/sec and the ad-accumulation time was between 2 and 10 min. The results obtained are plotted in Fig. 7, where optimal values were reached from 8 min of ad-accumulation.

*pH influence.* For these experiments the preconcentration solution pH was firstly varied between 1 and 8.5, whilst the pH stripping solution was constant and equal to 1.7. The scan rate and ad-accumulation time had the optimal values obtained as above, and the AC concentration was also $6 \times 10^{-5}M$. The results obtained are plotted in Fig. 8, where the optimal pH value is 1.0. In this figure we can observe a slight peak potential shift of about 6.6 mV/pH between pH 8.5 and 1.0, whilst the peak height differences are greater, explaining the importance of pH in the ad-accumulation of 2,6-dichloro-*p*-benzohydroquinone according to the AC electrochemical and chemical transformations mentioned above, but especially in the stripping step.

If the pH of the preconcentration solution is maintained at a value of 1, and the pH of the

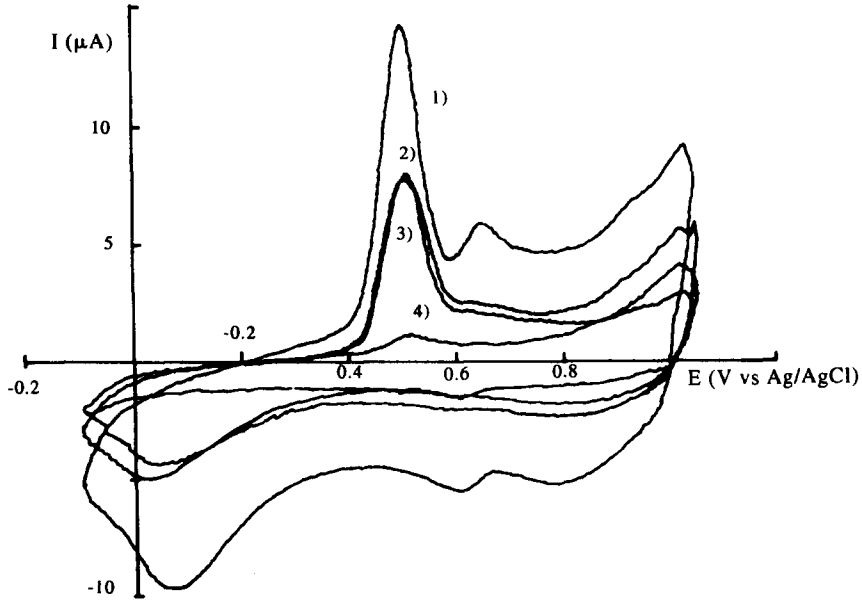


Fig. 8. Influence of the preconcentration cell pH on $6.10^{-5}M$ AC solution peak height; (1) 1.0; (2) 2.3; (3) 5.9; (4) 8.5; stripping cell pH: 1.7; scan rate; 4000 mV/sec; ad-accumulation time: 8 min; conventional carbon paste electrode.

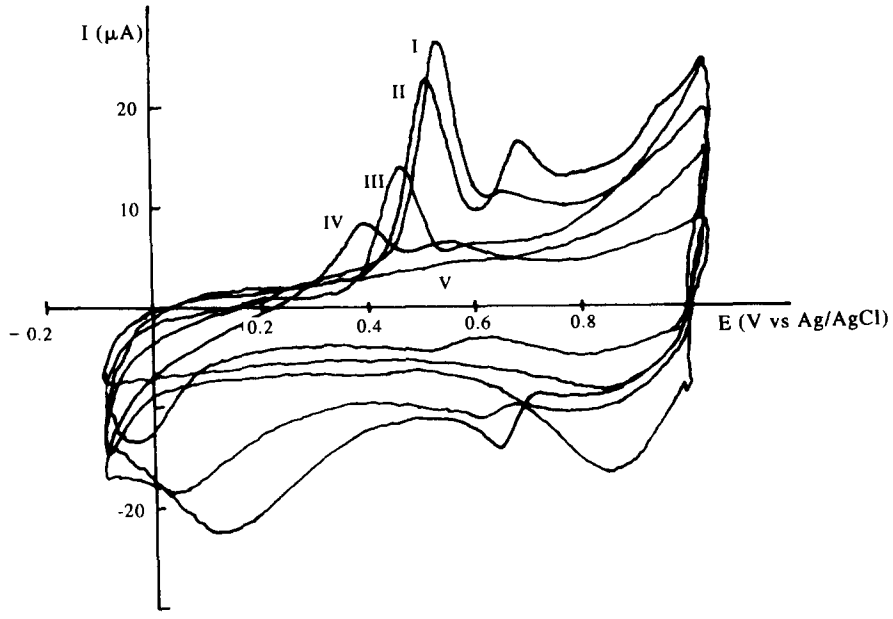


Fig. 9. Influence of the stripping cell pH on $6.10^{-5}M$ AC solution peak height; (I) 1.0; (II) 1.7; (III) 3.0; (IV) 4.7; (V) 6.7; preconcentration cell pH: 1; scan rate: 4000 mV/sec; ad-accumulation time: 8 min; conventional carbon paste electrode.

stripping solution is varied between 1 and 6.7, the higher the pH value, the lower the AC peak height, and the more negative the $E_p$ (Fig. 9).

Although the preconcentration step was carried out at pH 1 in all cases (at open circuit), the oxidation and reduction processes were carried out at different pH (from 1 to 6.7), therefore the formation of electroactive species to give peak II was depleted and the obtained anodic peaks were of different heights, therefore we might affirm that the pH is an important parameter in the mechanism of the AC oxidation on CPE, as we have observed above.

These experimental results confirm our hypothesis that by AC electrochemical oxidation, a molecule of 2,6-dichloro-*p*-benzoquinone is produced. This compound is reduced to 2,6-dichloro-*p*-hydroquinone, causing a higher stripping solution pH, and lower $E_p$ and peak current, because the 2,6-dichloro-*p*-benzoquinone preconcentration depends upon the medium acidity. Also, the lower the pH the higher the $E_p$, according to the electrochemical equilibria shifting laws.

We have also studied the preconcentration solution stirring rate influence on voltammetric peak height, and an optimal value of 1000 rotations/min was obtained.

*Analyte concentration influence.* Finally, in order to apply the proposed AC determination method, by using a stripping voltammetric technique of the CPE, the influence of analyte concentration on voltammetric peak height was studied. For this, the corresponding data are given in the experimental conditions.

After plotting the corresponding voltammetric peak currents *vs.* analyte concentration, a straight line was obtained. By its adjustment by the least square method, the following equation was obtained:

$$I_p(\mu A) = 7.1 \times 10^{-2} + 2.82 \times 10^{6} C\,(M)$$

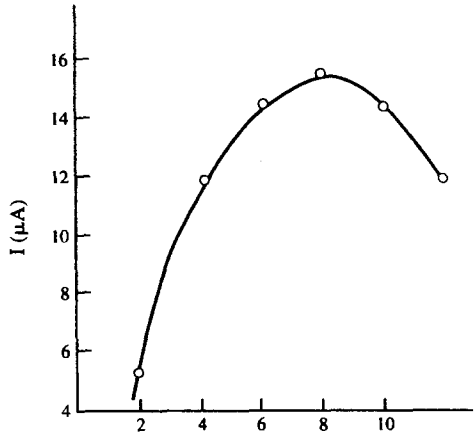


Fig. 10. Influence of preconcentration time of $10^{-6}M$ AC solution peak height; pH 1 in both cells; scan rate: 4000 mV/sec; modified carbon paste electrode with Triton X-405; surfactant/carbon (w/w) ratio of 5/95.

Table 3. Results of AC determination in Airtal R tablets obtained by our adsorptive stripping method and its comparison with a potentiometric one

| Sample | Stripping ($mg \pm s$)* | Potentiometric ($mg \pm s$)* | mg/tablet ($mg$) | $t_m$† |
|---|---|---|---|---|
| 1 | 99.02 ± 1.43 | 98.85 ± 1.85 | 100.00 | 0.22 |
| 2 | 98.63 ± 1.38 | 98.79 ± 1.77 | 100.00 | 0.21 |
| 3 | 98.52 ± 1.54 | 98.78 ± 1.82 | 100.00 | 0.33 |

*These data are the average of nine measurements.

†These data are the Student's $t$ measurements. The Student's $t$ tabulated is 2.12 for $n_1 + n_2 - 2 = 16$ freedom grades for a confidence level of 95%.

with a correlation coefficient of 0.9998 and a detection limit, of $5.4 \times 10^{-8}M$ (19 ppb), according to Miller and Miller.[28]

*Electroanalysis of aceclofenac at the modified CPE*

In order to improve the analytical results obtained at the CPE, a chemical modification of this electrode was carried out. This modification was made by mixing the carbon powder with different surfactants, such as the non-ionic Triton X-100 and X-405, and the anionic sodium dodecyl sulfate (SDS), as well as different hydrophobic substances, such as asolectin (phospholipid) and stearic acid (fatty acid). Interesting improvements were observed only in the case of Triton X-405.

With this type of electrode, prepared as has been indicated in Procedures, we studied the influence of only three parameters: optimal surfactant/carbon (w/w) ratio [obtaining a value of 5/95 (g/g)], optimal preconcentration time and analyte concentration on aceclofenac oxidation peak current. Other parameters, such as Nujor oil/carbon (w/w) ratio, preconcentration time, potential scan rate, *etc.*, are the same as indicated in the case of the CPE.

*Preconcentration time influence.* In Fig. 10, the influence of preconcentration time on peak height has been plotted, in which the maximal preconcentration time was reached at 8 min. From this value, the higher the preconcentration time, the lower the drug reduction peak height as obtained in other works.[24,29]

*Analyte concentration influence.* To study this parameter we employed the conditions given in the Experimental. The AC concentration range studied was between $1 \times 10^{-7}$ and $1 \times 10^{-6}M$. Plotting AC reduction peak current *vs.* analyte concentration a straight line was obtained, whose equation was

$$I_p(\mu A) = 0.95 + 1.2 \times 10^7 C(M)$$

with a correlation coefficient of 0.9997 and a detection limit, according to Miller and Miller,[28] of $1.93 \times 10^{-8}$ (7 ppb), *i.e.* almost one-third of the one obtained in the case of the conventional carbon paste electrode.

From these results, we can confirm that the presence of certain surfactants in the CMCPE improves the AC electroanalytical determination, owing to the increase of chemical affinity between the two types of molecules, as we have found elsewhere by using phospholipids as modifiers.[22]

*Application of our method to drug formulation control.* In order to check our AC determination method, we applied it to determine AC in a drug formulation, Airtal R, which is presented as tablets of about 200 mg, in which, according to the manufacturer, there is 100 mg of pure aceclofenac per tablet and an excipient constituted by several ingredients (Table 1).

To carry out the AC determination we prepared three groups of five tablets, which were well ground and mixed separately in an agate mortar. From each solid sample we took an amount sufficient to prepare a volumetric flask of 25 ml of about $1 \times 10^{-2}M$ aceclofenac* after filtration of the residue. From each solution, a new AC solution of about $1 \times 10^{-4}M$ aceclofenac* was prepared. From each one of these last solutions, three samples of 26 $\mu$l were taken and added to three volumetric flasks of 25 ml, obtaining, after dilution with the appropriate solution, an AC concentration of $1 \times 10^{-7}M$*. With these solutions, a series of voltammograms were obtained according to our proposed method using a surfactant MCPE. In each case, four standard additions of 50, 100, 150 and 225 $\mu$l of $1 \times 10^{-4}M$ AC standard solution† were made, obtaining a series of results, from which an equivalent mean volume is deduced. The results are given in Table 3.

*Certified by the manufacturer.

†Standard prepared by us.

In order to validate our method, a comparison of our results with the one obtained by another method employed by the AC manufacturer to control the AC contents in the tablets, was carried out. The manufacturers normally employ potentiometric or chromatographic techniques. We have chosen the potentiometric technique as a validation method. For this, from each $10^{-2}M$ AC solution, three other solutions 20-fold more diluted ($5 \times 10^{-4}M$) were prepared and then titred with NaOH standardized *vs.* an acid–base standard, the $C_6H_4(COOH)COOK$. The results obtained are given in the third column of Table 3: $t_m$ (measured value) is less than 2.12 (tabulated value), therefore there is no significant difference between the two methods, according to Miller and Miller.[28]

## CONCLUSIONS

The electrochemical behaviour of AC has been studied for the first time in this paper using voltammetric techniques on conventional as well as on surfactant MCPEs, observing a well developed analytical oxidation peak at +0.5 V (Ag/AgCl, KCl satd).

To obtain this peak it was necessary previously to oxidize the compound by starting the potential scan at sufficiently high values, *e.g.* +1.00 V (Ag/AgCl, KCl satd), and then to reduce it at sufficient low potential values, *e.g.* −0.1 V (Ag/AgCl, KCl satd).

An explanation of the AC electrochemical and chemical reactions on CPE and CMCPE is given according to the literature.[27]

AC can be adsorbed on carbon particles of conventional carbon paste electrodes and not extracted by the Nujol oil used as binder, at least in strong acidic media (pH 1). The drug can be also adsorbed on surfactant MCPEs, mainly when the modifier is Triton X-405. On the contrary, this compound does not adsorb on phospholipid chemically modified carbon paste electrode nor on fatty acid chemically modified carbon paste electrode (at least in the case of asolectin).

Adsorptive stripping voltammetric method of AC determination, on conventional and surfactant chemically modified electrodes, is proposed in the present paper, obtaining a very sensitive response (a detection limit of 7 ppb) in the case of surfactant chemically modified electrode, this method being applied to AC control in tablets.

The method is also quite accurate as we have shown by comparing our results with the ones obtained by potentiometry. In this sense our electroanalytical method has been validated *vs.* the potentiometric one based upon a classic acid–base reaction potentiometrically followed by a glass electrode.

*Acknowledgements*—This work has been carried out under the financial support of the Ministerio de Educación y Ciencia of Spain under Project PB 89-0361-C03-01. The authors thank the Prodesfarma Research Center of Barcelona (Spain), especially Dr E. Carrasco, researcher of this Center, for the kind provision of the pure substance, the drug formulations to apply to the proposed method, as well as data about this drug formulation.

## REFERENCES

1. M. Grau, Prodesfarma Research Center, Technical Report. Barcelona.
2. M. Cecchetti, M. Cerea and G. Torri, *Clin. Tri. J.*, **25**, 144, 1988.
3. J. Mestre, Prodesfarma Research Centre, Technical Report. Barcelona, 1990.
4. L. F. Chasseaud, S. G. Wood, P. D. Dalrymple and T. Winwich, Huntington Research Centre, Technical Report. Cambridge, 1988.
5. L. F. Chasseaud, T. Tylor, I. Midgley and A. J. Hood, Huntington Research Centre, Technical Report. Cambridge, 1990.
6. L. F. Chasseaud and S. G. Wood, Huntington Research Centre, Technical Report. Cambridge, 1988.
7. E. Bastida, E. Carrasco, X. Grass and M. Grau, *Drugs Today*, 1991, **27**, Suppl. 10, 39.
8. G. J. Patriarche, III Jornadas Cientiificas de Electroquímica del Grupo de la SEQA y de la RSEQ, Valladolid, Septiembre, 1991.
9. R. W. Murray, Chemically modified electrodes, in *Electroanalytical Chemistry*, Vol. 13, A. J. Bard (ed.), M. Dekker, New York, 1983.
10. A. J. Bard, *J. Chem. Ed.*, 1983, **60**, 4.
11. R. W. Murray, A. G. Ewing and A. Durst, *Anal. Chem.*, 1987, **59**, 397A.
12. S. Dong and Y. Wang, *Electroanalysis*, 1989, **1**, 99.
13. L. Gorton, A. Tortensson, H. Jaegfeldt and G. Johansson, *J. Electroanal. Chem.*, 1984, **161**, 103.
14. D. Leech, J. Wang and M. R. Smyth, *Anal. Proc.*, 1992, **29**, 25.
15. K. N. Thomsen, L. Kryger and R. P. Baldwin, *Anal. Chem.*, 1980, **60**, 151.
16. J. F. Price and R. P. Baldwin, *Anal. Chem.*, 1980, **52**, 1940.
17. G. A. Gerhardt, A. F. Oke, G. Nagy, B. Moghagddam and R. N. Adams, *Brain Res.*, 1983, **290**, 390.
18. J. Honorato, R. Caballero, G. Giordani, P. G. Movilia and R. Tapounet, *Curr. Therap. Res.*, 1990, **47**, 605.
19. K. Kalcher, *Electroanalysis*, 1990, **2**, 419.
20. A. R. Paniagua, M. D. Vázquez, M. L. Tascón and P. Sánchez-Batanero, *Electroanalysis*, 1993, **5**, 155.
21. M. Khodari, J. M. Kauffman, G. J. Patriarche and M. A. Ghandour, *Electroanalysis*, 1990, **1**, 299.

22. J. Arcos, J. M. Kauffmann, G. J. Patriarche and P. Sánchez-Batanero, *Anal. Chim. Acta*, 1990, **236**, 299.
23. F. N. Albahadily, and H. A. Mottola, *Anal. Chem.*, 1987, **59**, 958.
24. J. A. Acuña, C. de la Fuente, M. D. Vázquez, M. L. Tascón and P. Sánchez-Batanero, *Talanta*, 1993, **40**, 1637.
25. S. A. Wring and J. P. Hart, *Analyst*, 1992, **117**, 1215.
26. R. P. Baldwin and K. N. Thomsen, *Talanta*, 1991, **38**, 1.
27. R. N. Adams, *Electrochemistry at Solid Electrodes*, p. 348. Marcel Dekker, New York, 1969.
28. J. C. Miller and J. N. Miller, *Statistics for Analytical Chemistry*. Ellis Horwood, New York, 1984.
29. J. R. Posac, Tesis de Licenciaciatura. Universidad de Valladolid, Valladolid, Spain, 1993.

Pergamon

0039-9140(94)00248-7

*Talanta*, Vol. 42, No. 2, pp. 305–310, 1995
Elsevier Science Ltd
Printed in Great Britain
0039-9140/95 $9.50 + 0.00

# DEVELOPMENT OF A HIGHLY SENSITIVE GALVANIC CELL OXYGEN SENSOR

HIROSHI OGINO* and KIYOTAKA ASAKURA

Toyo Sanso Co. Ltd., Technical Research Laboratory, 3-3, Mizue-cho, Kawasaki, Kanagawa 210, Japan

(*Received* 10 *January* 1994. *Revised* 16 *March* 1994. *Accepted* 1 *August* 1994)

**Summary**—A highly sensitive galvanic cell oxygen sensor was successfully developed for determining parts per billion of oxygen in high purity gases such as nitrogen, argon, *etc.* The response of this improved sensor was proportional in the range of oxygen concentrations from 10.0 ppm to the detection limit. The response speed in this study was improved to within 90 sec for a 90% response. The detection limit was tentatively found to be less than 0.4 ppb corresponding to $S/N = 2$.

In high technology industries such as the manufacture of semi-conductors, the requirement for quality control of gases used as inert and atmospheric gases is becoming more important. The requirement for a highly sensitive oxygen analyzer has increased for gas suppliers and users. There are many types of commercially available oxygen analyzers for the determination of oxygen in gases: (1) galvanic cell type,[1–8] (2) zirconia type,[9] (3) luminescence type,[10] (4) others.[11] However, based on sensitivity and accuracy of the sensor and handling safety, as well as ease of calibration, the galvanic cell oxygen sensor could be considered the most sensitive and reliable sensor for accomplishing the continuous determination of trace levels of oxygen in hydrogen, nitrogen, argon, helium, *etc.*[1–8]

Recently, the purity control management of high purity inert gases such as nitrogen and argon has become more important. It is required to continuously determine and control the concentration of impurities at levels of several parts per billion (ppb, v/v) in high purity gases.

The authors have previously developed and reported a trace oxygen analyzer with a detection limit of 10 ppb.[8] In this paper, the characteristics of an improved galvanic cell oxygen sensor (GOS), which has the capability of a detection limit in the sub-ppb level for the determination of trace levels of oxygen in nitrogen, argon, helium, and hydrogen, are described.

*Author to whom correspondence should be addressed.

## EXPERIMENTAL

### *Apparatus and reagents*

The cross-sectional view of the GOS is shown in Fig. 1. The GOS consists of lead rod (anode) and silver screen mesh (cathode) electrodes as follows,

Pb/Zeolite (KOH sol.)/PE/POF/Ag

When oxygen contacts with the cathode, the GOS produces an electric current via the following reactions: at the cathode (Ag), $O_2 + H_2O + 2e^- \rightarrow 4OH^-$; at the anode (Pb), $Pb + 4OH^- \rightarrow 2Pb(OH)_2 + 2e^-$. The anodic electrode (Pb) was 5 mm diameter × 65 mm long and the cathodic electrode (Ag) was a screen mesh of 0.5 mm thickness. The PE was an 8 mm i.d. × 10 mm o.d. × 70 mm long tube made from sintered porous polyethylene with the pore size of $< 100\ \mu m$ and the POF was a

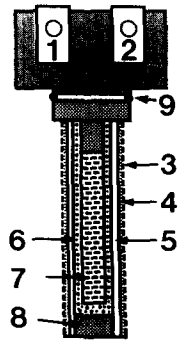


Fig. 1. Cross-sectional view of the GOS. (1) Cathode terminal, (2) anode terminal, (3) silver mesh sheet, (4) porous POF sheet, (5) porous PE sheet, (6) electrolyte, (7) lead rod, (8) cap, (9) O-ring.

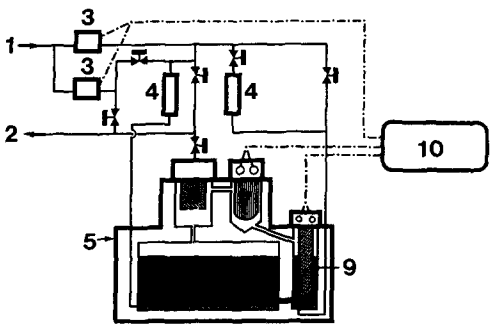


Fig. 2. Brief construction of the detector. (1) Sample gas inlet, (2) gas outlet, (3) mass flow controller, (4) oxygen absorber, (5) detector box, (6) alkaline solution, (7) GOS, (8) mist trap, (9) electrode for oxygen generation, (10) electric control module (microcomputer).

20 $\mu$m thick polyolefin film with *ca.* 0.1 mm diameter holes (50 holes/cm$^2$). The zeolite (*e.g.* MS-5A, 60/80 mesh), which was admixed with agarose, was used to retain 5*M* KOH alkaline solution.

Assembled GOSs were impregnated with 5*M* KOH solution for an adequate time after assembly in order to retain much more alkaline solution. The GOS is installed in a detector box which was made from a polymethacrylate-based resin. The detector box has a humidifier, which can hold *ca.* 350 ml of alkaline solution. The alkaline solution is required as the source of the water for humidifying the GOS and also as the electrolyte solution for the oxygen generator. The GOS requires moisture at a constant level to avoid sensor dryness. For both requirements as described above, the detection system was designed as shown in Fig. 2.

The water content in the electrolyte was reduced by evaporation of water during the sample flow and gas purges. Therefore, refilling with deionized (or distilled) water was required every 4 weeks.

The detection system including the detector box and gas pipeline was heated to 35°C to prevent condensation of water in the pipelines. The coulombic yield of this type sensor can be related to the flow rate of the gas sample, the spacing between the internal surface of the sensor holder and the silver mesh of the GOS, the wetting of the GOS, *etc.*

Stainless steel tubing with a 1/8 inch diameter and stainless steel diaphragmed valves with 1/8 inch VCR fitting (Advanced Pressure Technology, AP-2600, CA, USA) were used: they were very effective for obtaining a faster response and reducing the purge time of oxygen that remained in the analytical system. The alkaline solution was continuously purged with oxygen-free nitrogen (100 ml/min) to completely remove any dissolved oxygen.

The alkaline solution in the humidifier was prepared by mixing 34.5 g KOH (Kanto Chemical, guaranteed purity >85 wt %, Tokyo, Japan) and one l. of deionized water: an alkalinity of 3 wt % KOH was required for stable oxygen generation by water electrolysis.

Nitrogen gas evaporated from liquid nitrogen was used as the sample gas in order to evaluate sensor responses such as sensitivity, stability, zero and span calibration, *etc.* The sample gas was divided into two gas lines: one line was used to produce oxygen-free nitrogen (zero gas), which was purified by passing it through an oxygen absorber to remove trace amounts of oxygen in the nitrogen gas, and the other was used as a sample gas without purification. Both flow rates were controlled using mass flow controllers. The flow rates of the sample and purge gases were regulated at 100 ml/min by the mass flow controllers within $\pm 1\%$ deviation. Oxygen-free nitrogen was prepared by passing nitrogen through an oxygen absorber (Gasclean, Nikka Seikou, Tokyo, Japan), which could remove oxygen to at least the 2–3 ppb level or below: the concentration of residual oxygen in the purified nitrogen was separately and previously confirmed using an atmospheric pressure ionization mass spectromer[11] (API-MS, UG-240 APN, Hitachi, Tokyo, Japan) in the Technical Research Laboratory (Toyo Sanso).

For the experiments at ppb levels of oxygen, a getter type purifier (Saes PureGas, Inc., Model, MonoToor, phase-II, CA, U.S.A.) was used: this getter could remove oxygen to less than 0.1 ppb. The sample gases containing low levels of oxygen in nitrogen were prepared with a standard gas generator (STEC, SGGU-6000, Kyoto, Japan), which has the capability of dilution rates between 1/10 and 1/10,000. The desired oxygen concentration in a sample gas could be provided in the range of ppb to ppm. An amplifier and microcomputer system, which had been installed in a trace oxygen analyzer (GOT-20, Toyo Sanso),[8] was used in this experiment.

## RESULTS AND DISCUSSION

### *Calibration system*

The accurate calibration of the sensor is one of the most important factors for obtaining reliable analytical values: an accurate determi-

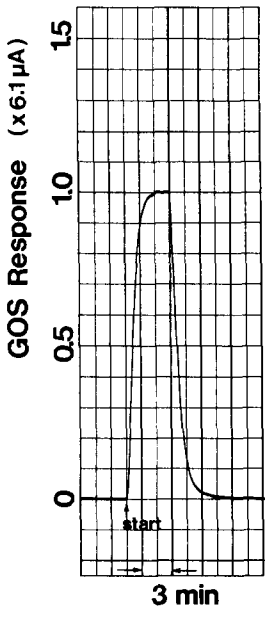


Fig. 3. Typical recording profile of 1 ppm oxygen gas generated by the water electrolysis.

nation depends on how the sensor can be precisely calibrated. The detector box has an internal oxygen generation system[1,4] for the calibration of the GOS: the constant current method was used for water electrolysis in order to generate a small amount of oxygen. In these experiments, the calibration of the GOS was carried out using an oxygen standard gas generated by water electrolysis as described above. The evolution of oxygen is proportional to the amount of electric current based on the Faraday's law.[1] The generated oxygen is mixed with 100 ml/min of oxygen-free nitrogen (zero gas). The oxygen concentration is inversely proportional to the flow rates of the diluting gas. The amount of current is calculated from the following equation.

$$I = 0.263 \,.\, V \,.\, C,$$

where $I$, $V$ and $C$ are the electric current ($\mu$A), the flow rate of the zero gas (ml/min) and the concentration of oxygen (ppm), respectively. The cathodic and anodic electrodes for the water electrolysis were 1 mm diameter × 10 mm long and 0.5 mm diameter × 1 mm long platinum wires, respectively. The cathodic electrode was covered with an anion exchange resin tube to prevent the electrochemical deposition of impurity metals from the electrolyte alkaline solution.[8] The lifetime of the electrode, therefore, could be prolonged so that the electrode could be used for at least several months without cleaning, if the calibration was done once a week. With these improvements, a standard oxygen gas could be accurately provided at the level of ppm in inert gases such as nitrogen and argon using this method. In the experiment to be described, the GOS could be calibrated with 1 or 5 ppm oxygen standard gases in nitrogen. If necessary, an oxygen standard gas from a cylinder could be used for the calibration of the sensor. A typical sensing profile of the GOS for the generation of 1 ppm span gas is given in Fig. 3.

*Stabilization of the GOS*

For stabilizing the GOS response, the electrolyte medium must be in a stable and homogeneous state. As one possibility, agar could be expected to make the zeolite powders homogeneously disperse. However, agar could not be used for this purpose because it was unstable in the strong alkaline solution. On the other hand, agarose was not only stable in the alkaline solution, but also its gelatin was slightly soluble in this solution. Thus, agarose was chosen as the dispersing material of the zeolite and retaining alkaline solution; when admixed with the zeolite powder, it formed a stable gel in the strong alkaline solution to avoid a heterogeneous reaction between the surface of the lead electrode and the zeolite powder.

To demonstrate the effect of agarose addition, a set of experiments for the evaluation of these electrolyte media were separately carried out with two electrolyte media; one (A) was zeolite saturated with 5*M* KOH solution and the other (B) was zeolite–agarose saturated with 5*M* KOH solution. Galvanic cells were constructed with a piece of lead plate, 5 mm width × 20 mm long × 1 mm thickness, as the anodic electrode and a 10 mm width × 35 mm long silver screen mesh as the cathodic electrode. The anodic electrode was dipped into the electrolyte medium. The cathodic electrode was placed on the surface of electrolyte medium and could be exposed to atmospheric air.

The two galvanic cells were allowed to stand under atmospheric air at room temperature for a week. When the galvanic cell was constructed without the agarose, the zeolite was in direct contact with the lead and was deposited on and in the surface of the lead electrode as shown in photograph (A) of Fig. 4. The result from the galvanic cell (A) suggests that the lead plate reacted with the zeolite so that the reaction should take place inside the lead and part of the zeolite could directly react with the lead elec-

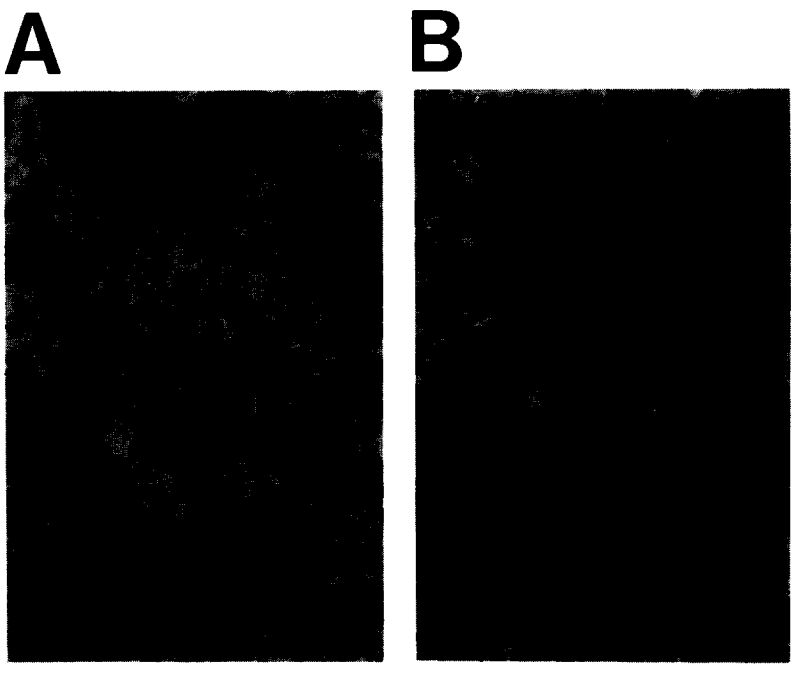


Fig. 4. Photograms of lead plate reacted with the zeolite. (A) Electrolyte medium without agarose, (B) with agarose. Both plates were sonicated for approximate 15 min and rinsed with distilled water.

trode. Its instability and undesirable capability might be largely a result of such a phenomenon: a homogeneous gel could make the electrochemical reaction more stable. On the other hand, if the agarose was used as a gelling reagent, it is clear that the surface would be kept clean as shown in the photogram (B). On the basis of these results, it could be expected that the zeolite was covered with the agarose and the electrolyte medium could retain much more alkaline solution and that the dead volume inside the sensor could be reduced or eliminated.

*Characteristics of the GOS*

In order to evaluate the characteristics of the GOS, several GOSs were made in the same way as previously described. They were fully submerged in 5*M* KOH solution overnight in order to provide enough alkaline solution in the sensor. The measurements were started after the GOS was installed in the detector box. The air remaining inside the GOS and dissolved oxygen in the alkaline solution could be purged with oxygen-free nitrogen for a couple of hours. If the GOS was operated after adequate purging and the response of the GOS was in the stable state, the GOS signal output should be less than 0.1 $\mu$A for oxygen-free nitrogen. It is very difficult for the response of the GOS to reach zero current owing to the residual current of the GOS and the residual oxygen in the zero gas. It takes several hours until the determination of trace oxygen at the ppb level can be done. In order to quantitatively evaluate the response time for the improved and ordinary (without the addition of agarose) GOSs, three GOSs were tested using oxygen-free nitrogen and nitrogen containing 0.63 ppm oxygen. Two GOSs were made by the use of agarose and the other without agarose. Figure 5 is a typical profile for the response change in the GOS (A) between zero gas and reference gases (nitrogen containing 0.63 ppm oxygen). The response profiles were obtained by alternately turning the six port rotary valve from the zero gas line to the sample gas line. The obtained results are summarized in Table 1. The GOSs (A, B) admixed with agarose had a response time of 90 sec for a 90% response and the other (R) without agarose had a response time of 120 sec: the response of the improved GOSs was faster and more stable than that prepared without the agarose.

In order to demonstrate the capability of sensor installed in the prototype oxygen analyzer, the sensor response was recorded stepwise for different oxygen concentrations in nitrogen, which were provided by the use of the standard gas generator. After the GOS was calibrated with the 1 or 5 ppm span gas, the working curves were obtained in the concentration range

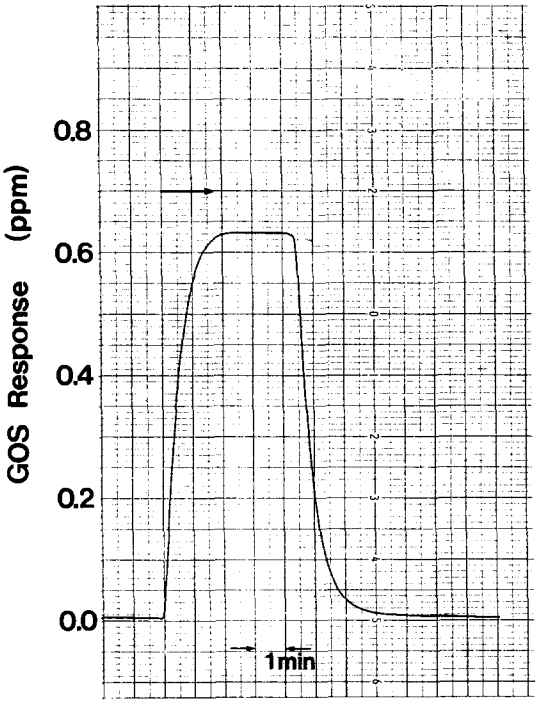


Fig. 5. Typical profile of GOS response speed. The response profile was obtained from sample gases having 0 and 0.63 ppm $O_2$ in nitrogen.

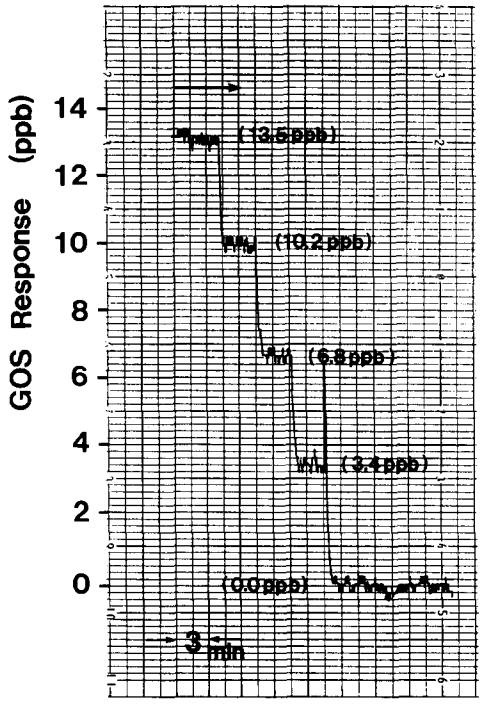


Fig. 6. Typical profile of GOS response ranging from 0 to 13.5 ppb $O_2$ in nitrogen.

of 0–10 ppm. The results showed that the GOS response is linear within experimental error in the range examined.

The typical performance of the GOS response is shown in Fig. 6. The response profile indicated that the GOS could be used for practical monitoring even in the range of 0–20 ppb of oxygen with an accuracy of $\pm 2\%$ deviation to full scale.

*Typical profile of continuous monitoring*

The profile of the continuous monitoring of oxygen in nitrogen, which was supplied from a cold evaporator charged with liquid nitrogen, is shown in Fig. 7. In Fig. 7, several small variations found in the period from 12 to 7 p.m. were a result of pressure changes in the gas supply pipeline. The result shows that when large amounts of nitrogen were used elsewhere for other purposes such as line purging, the GOS could monitor a few ppb of oxygen concentration fluctuations owing to small pressure changes and so on. The obtained profile indicates that the GOS would be reliable and suitable as an oxygen sensor for determining trace levels of oxygen in high purity industrial gases because the GOS has a high sensitivity and long term stability.

## CONCLUSIONS

The results obtained from the prototype trace oxygen analyzer showed that the GOS could have the capability to determine trace levels of oxygen in the sub-ppb and several ppm range. At present, a highly sensitive oxygen analyzer

Table 1. Comparison of the response of GOS constructed with and without agarose

| Sensor | Time at 90% response | | Average (*sec*) | Rel. response (%, $R = 100$) |
|---|---|---|---|---|
| | Up (*sec*) | Down (*sec*) | | |
| A | 80 | 88 | 84 | 63.6 |
| B | 84 | 87 | 85 | 64.4 |
| R | 138 | 126 | 132 | 100.0 |

These data were obtained from sample gases containing 50–70 ppb oxygen in nitrogen.

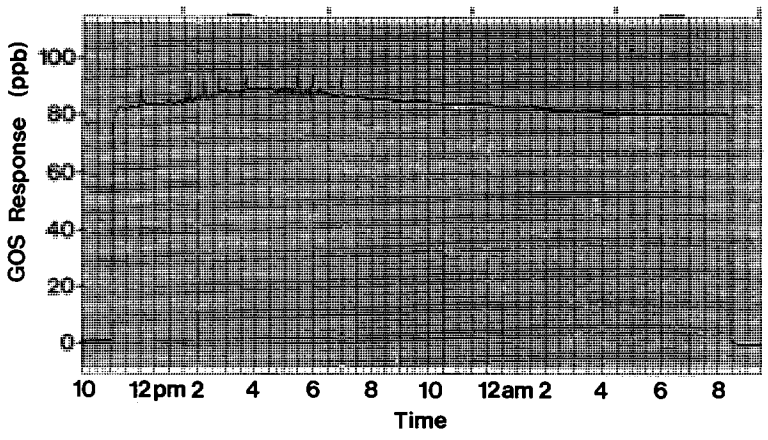


Fig. 7. Continuous monitoring profile for trace oxygen in nitrogen.

(Toyo Sanso, GOT-30, Tokyo, Japan), which was installed in the GOS, has been successfully developed in cooperation with Toyo Sanso Co. Ltd and DKK Corp. (Tokyo, Japan): the full range of determination, 0–10 ppm; detection limit, $\pm 1$ digit corresponding to 1 ppb oxygen concentration. These highly sensitive oxygen analyzers have been used for determining and monitoring ppb levels of oxygen in gas mixtures and for quality control of ultra high purity gases such as nitrogen, argon and helium in Toyo Sanso's manufacturing facility for the past several years.

*Acknowledgements*—The authors are grateful to Mr M. Goto of DKK Corporation and the staff of the Technical Research Laboratory, Toyo Sanso Co. Ltd. for their valuable contribution.

## REFERENCES

1. P. A. Hersch, *Nature*, 1952, **169,** 792.
2. W. J. Baker, J. F. Combs, T. L. Zinn, A. W. Wotring and R. F. Wall, *Ind. Eng. Chem.*, 1959, **51,** 727.
3. P. A. Hersch, *Anal. Chem.*, 1960, **32,** 1030.
4. F. A. Keidel, *Ind. Engng Chem.*, 1960, **32,** 490.
5. J. M. Ives, E. E. Hughes and J. K. Taylor, *Anal. Chem.*, 1968, **40,** 1853.
6. D. R. Kendall, *Anal. Chem.*, 1971, **43,** 944.
7. W. Bahmet and P. A. Hersch, *Anal. Chem.*, 1971, **43,** 803.
8. H. Ogino, O. Maruyama and N. Sakai, *Kouatsu Gasu*, 1990, **27,** 20.
9. D. M. Haaland, *Anal. Chem.*, 1977, **49,** 1813.
10. E. R. Carraway and J. N. Demas, *Anal. Chem.*, 1991, **63,** 337.
11. Y. Mitsui, H. Kambara, M. Kojima, H. Tomita, K. Kato and K. Satoh, *Anal. Chem.*, 1983, **55,** 477.

Pergamon

0039-9140(95)01380-6

*Talanta*, Vol. 42, No. 3, pp. 311–316, 1995

0039-9140/95 $9.50 + 0.00

# EXTRACTIVE SPECTROPHOTOMETRIC DETERMINATION OF SOME FLUOROQUINOLONE DERIVATIVES IN PURE AND DOSAGE FORMS

C. S. P. SASTRY,[1]* KOLLI RAMA RAO[1] and D. SIVA PRASAD[2]

[1]Foods and Drugs Analysis Laboratories, School of Chemistry, Andhra University, Visakhapatnam 530 003, India; [2]Department of Biochemistry, Andhra University, Visakhapatnam 530 003, India

(*Received* 12 *April* 1994. *Revised* 29 *July* 1994. *Accepted* 2 *August* 1994)

**Summary**—Two simple and sensitive extractive spectrophotometric methods for the determination of some fluoroquinolone derivatives (norfloxacin, NRF; ciprofloxacin, CPF; ofloxacin, OFL; and enrofloxacin, ERF) with Supracene Violet 3B (SV 3B, method A) and tropaeolin 000 (TP 000, method B) are described. The methods are based on the formation of ion-association complexes of fluoroquinolones with these dyes, which are extracted into chloroform and have absorption maxima at 575 nm (SV 3B) and 485 nm (TP 000). The methods obey Beer's law and the precision and accuracy of the methods were checked by UV reference methods. The detection limits were 5.0 μg/ml for NRF and 2.5 μg/ml for CPF in method A and 2.5 μg/ml for OFL and ERF in methods A and B.

The fluoroquinolone derivatives norfloxacin [1-ethyl-6-fluoro-1,4-dihydro-4-oxo-7-(1-piperazinyl)-3-quinoline carboxylic acid], ciprofloxacin [1-cyclopropyl-6-fluoro-1,4-dihydro-4-oxo-7-(1-piperazinyl)-3-quinoline carboxylic acid], ofloxacin [9-fluoro-2,3-dihydro-3-methyl-10-(4-methyl-1-piperazinyl)-7-oxo-7H pyrido(1,2,3 de)-1,4-benzoxazine-6-carboxylic acid] and enrofloxacin [1-cyclopropyl-7-(4-ethyl-1-piperazinyl)-6-fluoro-1,4-dihydro-4-oxo-3-quinoline carboxylic acid] are used as broad spectrum antibacterial agents. Norfloxacin and ciprofloxacin are official in the U.S.P.,[1] whilst ofloxacin and enrofloxacin are not official on any pharmacopoeia. A number of visible spectrophotometric methods for the determination of fluoroquinolones such as norfloxacin (NRF),[2–8] ciprofloxacin (CPF)[7,9–13] and ofloxacin (OFL)[8,14,15] are reported in the literature. No spectrophotometric method for the determination of enrofloxacin (ERF) has been reported. Even though extraction spectrophotometric procedures are popular for their sensitivity in the assay of drugs,[16] there is only one report [13] for the determination of ciprofloxacin using the acid dyes, Bromocresol Purple and Bromophenol Blue. The aim of the present work is to provide simple and sensitive methods for the estimation of fluoroquinolones which are basic, in pure and dosage forms. In preliminary experiments, in view of developing methods of analysis suitable for assaying small quantities of fluoroquinolones, we tried seven anionic dyes namely, SV 3B, TP 000, Alizarin red S, Nigrocin water soluble, Fast Green FCF, Congo Red and Bromopyrogallol Red as the colour producing agents at various pH ranges, by a dye salt partition technique. Two visible spectrophotometric estimations using SV 3B (CI No. 60730) for all fluoroquinolones and TP 000 (CI No. 14600) for OFL and ERF were selected as being the most suitable and are described herein.

The proposed extractive spectrophotometric methods are based on the formation of ion-association complexes with SV 3B ($\lambda_{max}$ 575 nm) and TP 000 ($\lambda_{max}$ 485 nm) and their complexes are quantitatively extracted into chloroform. Structures of SV 3B, TP 000 and their chloroform soluble complexes with fluoroquinolones (*e.g.* Enrofloxacin) are shown in Fig. 1.

## EXPERIMENTAL

### *Apparatus*

A Milton Roy spectronic 1201 UV-visible spectrophotometer with 1 cm matched quartz cells was used for all the absorbance measurements. An Elico model LI-120 digital pH meter was used for pH measurements.

*To whom correspondence should be addressed.

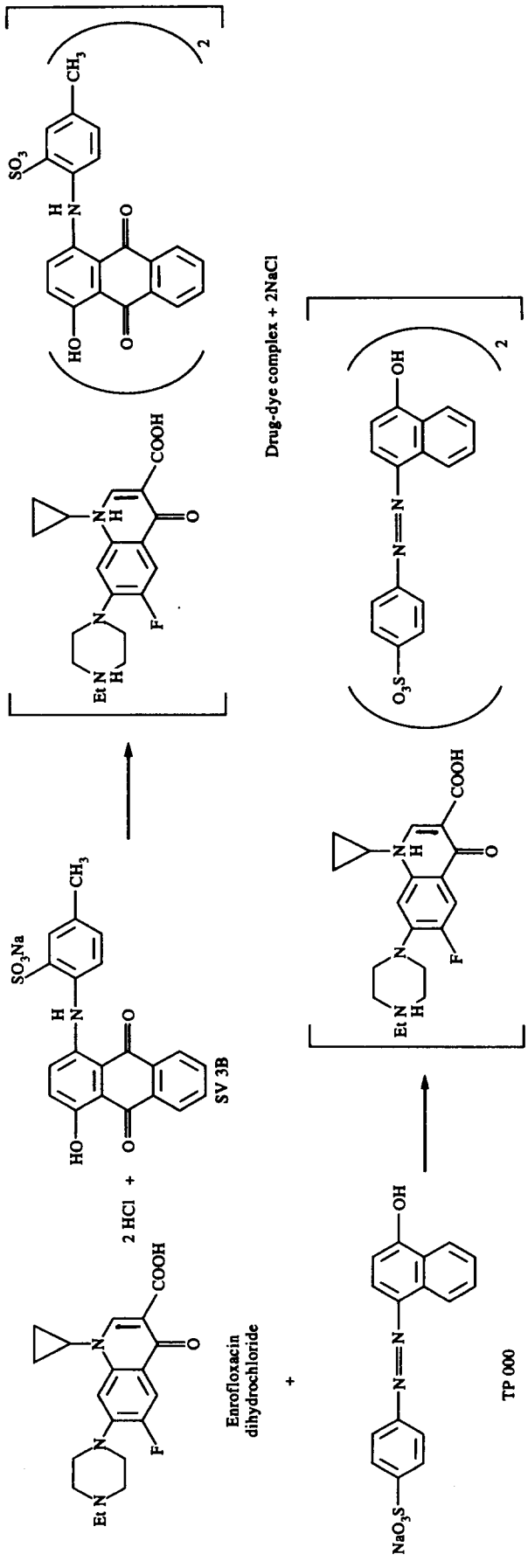


Fig. 1. Structures of Supracen Violet 3B, tropaeolin 000 and their respective complexes with enrofloxacin dihydrochloride.

*Reagents*

Chemicals of analytical grade were used. All solutions were prepared in double distilled water. Aqueous solutions of SV 3B (0.2%, chroma), TP 000 (0.2%, Fluka) and 0.1*M* HCl were prepared.

A buffer solution of pH 1.3 was prepared by mixing 226 ml of 0.1*M* glycine (Loba, 7.507 g of glycine + 5.85 g of NaCl, dissolved in 1 l. of distilled water) and 774 ml of 0.1*M* HCl.

*Standard drug solutions*

Stock solutions of (1 mg/ml) NRF, CPF, OFL and ERF were prepared in 0.01*M* HCl. The working standard solutions were prepared by suitable dilution of the stock solutions with distilled water.

*Analysis of bulk samples*

*Method A.* Drug aliquots of NRF (0.5–4.0 ml, 100 μg/ml), CPF (0.5–6.0 ml, 50 μg/ml), OFL (0.5–5.0 ml, 50 μg/ml) and ERF (0.5–5.0 ml, 50 μg/ml) were placed in a series of 125 ml separating funnels. Then 6.0 ml of buffer (pH 1.3) and 2.0 ml of SV 3B solution were added to each separating funnel. The total volume of aqueous layer in each separating funnel was brought to 15 ml with distilled water. A 10 ml portion of chloroform was added to each and the contents were shaken for 2 min. The two phases were allowed to separate and the absorbance of the separated chloroform layer was measured at 575 nm against a reagent blank within the stability period (1 min–10 hr) at laboratory temperature (28 ± 5°C). The amount of drugs was computed from their calibration graphs.

*Method B.* Aliquots of aqueous OFL (0.5–6.0 ml, 50 μg/ml), ERF (0.5–4.0 ml, 50 μg/ml) were transferred into a series of 125 ml separating funnels. Then 6.0 ml of 0.1*M* HCl and 2.0 ml of TP 000 were added to each separating funnel. The total volume of aqueous phase was adjusted to 15 ml in each separating funnel with distilled water. Then 10 ml of chloroform was added to each and the contents were shaken for 2 min and the two phases were allowed to separate and the absorbance of the separated chloroform layer was measured at 485 nm against a reagent blank within the stability period (1 min–10 hr) at laboratory temperature (28 ± 5°C). The amounts of OFL and ERF were computed from their respective calibration graphs. Method B is not suitable for the determination of NRF and CPF, as they do not form chloroform soluble complexes with TP 000.

*Analysis of formulations*

Twenty tablets were weighed and powdered. The powder equivalent to 100 mg of active ingredient was treated with 100 ml of 0.01*M* HCl and the insoluble residue filtered to obtain a solution of 1 mg/ml. The stock solutions were further diluted with distilled water to obtain working standard solutions and were analysed as described under the procedure for bulk samples.

For the determination of drugs in intravenous (i.v.) fluid and eye/ear drops, the weight of the drug per ml was determined. A quantity of i.v. fluid or eye/ear drops equivalent to 10 mg of the drug was transferred to 100 ml of volumetric flask and diluted to the mark with distilled water to obtain a concentration of 100 μg/ml. This solution was further diluted to the requisite concentration.

As the dosage forms were not available in the local market for ERF, we prepared our own according to the literature methods.[17,18] The results for NRF, CPF, OFL and ERF were compared with their respective UV spectrophotometric procedure as under NRF.[19]

A quantity of cream equivalent to 25 mg of CPF HCl was dissolved in about 50 ml of chloroform and transferred to a separating funnel. The chloroform solution was extracted with 0.01*M* HCl (3 × 25 ml). The aqueous phase in the separating funnel was collected into a 100 ml volumetric flask. The chloroform solution was then washed with 0.01*M* HCl and the washings were collected into the flask and made up to the mark with 0.01*M* HCl to obtain a solution of 250 μg/ml of CPF. This stock solution was diluted stepwise with distilled water to 50 μg/ml working standard solution and analysed by the procedure of method A.

## RESULTS AND DISCUSSION

The absorption spectra of the reaction products in methods A and B showed characteristic $\lambda_{max}$ values (Figs 2 and 3). The experimental conditions were established by varying one parameter at a time and observing its effect on the absorbance of the coloured species.

In method A, in order to establish optimum pH range, the drugs were allowed to react with SV 3B in aqueous solution buffered to pH 1.0–1.5 and the complex formed was extracted

into chloroform for measurement. Constant absorbances were obtained over the pH range 1.1–1.5 in glycine–HCl buffer, hence a pH of 1.3 was used. A 2.0 ml portion of SV 3B solution was found to be optimal. Constant absorbance was obtained for shaking periods between 1 and 5 min, hence a shaking time of 2 min was selected for use. Chloroform was preferred for its selective extraction of the drug–dye complex from the aqueous phase. A ratio of 3:2 of aqueous to chloroform phases was required for efficient extraction of the coloured species.

In method B also, to establish the experimental conditions, the drugs were allowed to react with TP 000 in dilute HCl ranging from 0.05 to 1.5*M* and the complex was extracted into chloroform layer. Constant absorbances were obtained with 0.08–0.12*M* HCl, hence 0.1*M* HCl was used. A 2 ml portion of TP 000 solution was found to be optimal. Shaking times of 0.5–4 min produced constant absorbance, hence a shaking time of 2 min was chosen for use. A ratio of 3:2 of aqueous to organic phases was required for efficient extraction of the coloured species.

*Analytical data*

The Beer's law limits, molar absorptivity, Sandell's sensitivity, regression equation and correlation coefficient obtained by linear least squares treatment of the results are given in Table 1. The precision and accuracy of the two methods were tested by estimating six replicates of the drugs within the Beer's law limits. The per cent standard deviation and the per cent range of error at 95% confidence level are given in Table 1.

The values obtained by the proposed and reference methods for dosage forms are compared in Table 2 and are in good agreement. The results of the recovery experiments by the proposed methods are listed in Table 2. The fluoroquinolones, being basic in nature, forms an ion-association complex with the acidic dye, SV 3B (for NRF, CPF, OFL and ERF) or TP 000 (for OFL and ERF) which are extractable

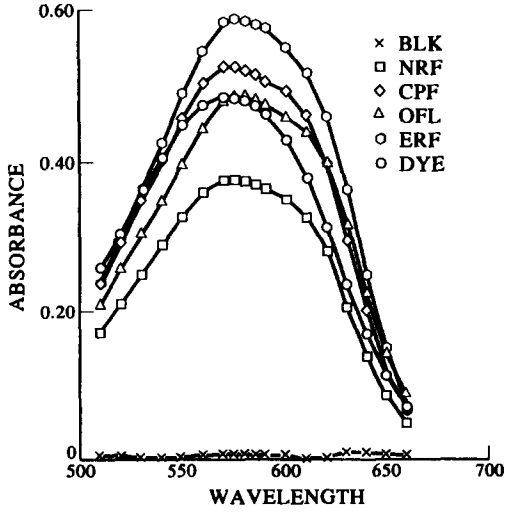


Fig. 2. Absorption spectra of NRF—SV 3B system, CPF—SV 3B system, OFL—SV 3B system, ERF—SV 3B system, aqueous SV 3B (DYE) *vs.* distilled water and Blank (BLK) *vs.* chloroform. NRF: $6.26 \times 10^{-5}M$, CPF: $6.03 \times 10^{-5}M$, OFL: $4.15 \times 10^{-5}M$, ERF: $5.56 \times 10^{-5}M$, SV 3B: $6.17 \times 10^{-4}M$ and aqueous SV 3B: $2.10 \times 10^{-4}M$.

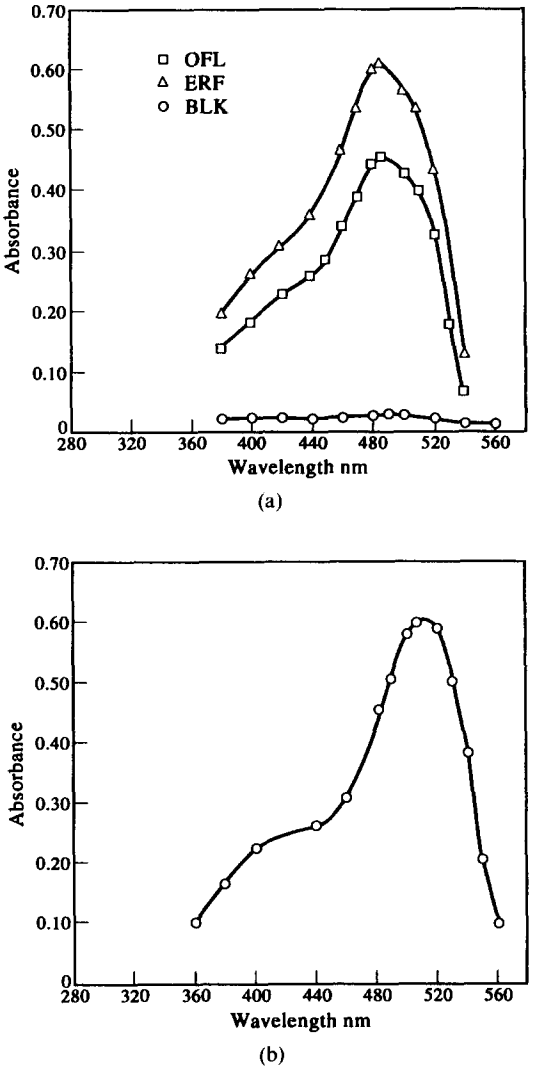


Fig. 3. (a) Absorption spectra of OFL—TP 000 system, ERF—TP 000 system, and blank (BLK) *vs.* chloroform. OFL: $5.53 \times 10^{-5}M$, ERF: $4.17 \times 10^{-5}M$, TP 000: $7.61 \times 10^{-4}M$. (b) Absorption spectrum of aqueous TP 000 (DYE) *vs.* distilled water system. Aqueous TP 000: $2.59 \times 10^{-4}M$.

Table 1. Optical characteristics, precision and accuracy

| | NRF | CPF | OFL | | ERF | |
|---|---|---|---|---|---|---|
| Parameters | A | A | A | B | A | B |
| Beer's law limits ($\mu$g/ml) | 5.0–40 | 2.5–30 | 2.5–25 | 2.5–30 | 2.5–25 | 2.5–20 |
| Molar absorptivity ($M^{-1}$ cm$^{-1}$) | $5.88 \times 10^3$ | $8.62 \times 10^3$ | $1.09 \times 10^4$ | $8.24 \times 10^3$ | $1.04 \times 10^4$ | $1.38 \times 10^4$ |
| Sandell's sensitivity ($\mu$g/cm$^2$/0.001 absorbance unit) | 0.054 | 0.038 | 0.032 | 0.043 | 0.034 | 0.025 |
| Regression equation ($Y$)* | | | | | | |
| Slope ($n$) | $1.84 \times 10^{-2}$ | $2.54 \times 10^{-2}$ | $3.08 \times 10^{-2}$ | $2.35 \times 10^{-2}$ | $2.98 \times 10^{-2}$ | $4.04 \times 10^{-2}$ |
| Intercept ($m$) | $-0.053 \times 10^{-2}$ | $0.34 \times 10^{-2}$ | $-0.25 \times 10^{-2}$ | $-0.72 \times 10^{-2}$ | $-0.20 \times 10^{-2}$ | $0.73 \times 10^{-2}$ |
| Correlation coefficient ($r$) | 0.9999 | 0.9998 | 0.9999 | 0.9998 | 0.9998 | 0.9998 |
| Relative standard deviation† (%) | 0.39 | 0.28 | 0.24 | 0.48 | 0.38 | 0.33 |
| Range of error† (%, 95% confidence limit) | 0.41 | 0.30 | 0.25 | 0.50 | 0.40 | 0.35 |

*$Y = m + nC$, where $C$ is the concentration.
†Six replicate samples.

Table 2. Assayof fluoroquinolone derivatives in dosage forms

| | Labelled amount | Amount found proposed method* | | Reference | % Recovery by proposed method‡ | |
|---|---|---|---|---|---|---|
| Sample | (*mg/tab or ml*) | A | B | method† | A | B |
| NRF | | | | | | |
| Tablets | 400 | 398.9 | — | 393.2 | 100.1 | — |
| Eye/ear drops | 3 | 2.97 | — | 2.87 | 100.5 | — |
| CPF | | | | | | |
| Tablets | 250 | 251.5 | — | 246.4 | 99.5 | — |
| Eye/ear drops | 3 | 2.97 | — | 2.99 | 98.9 | — |
| i.v. fluid | 2 | 1.98 | — | 1.97 | 99.8 | — |
| Cream | 3 | 3.00 | — | 3.02 | 98.6 | — |
| OFL | | | | | | |
| Tablets | 200 | 199.3 | 198.3 | 194.2 | 99.5 | 100.1 |
| i.v. fluid | 2 | 1.98 | 1.99 | 1.95 | 99.5 | 99.6 |
| ERF | | | | | | |
| Tablets I | 50 | 50.3 | 50.1 | 49.7 | 99.9 | 100.5 |
| Tablets II | 100 | 100.2 | 100.3 | 99.1 | 99.9 | 99.4 |

*Average of six determinations.
†UV reference method.
‡Per cent recovery of 10 mg added to the dosage forms.

into chloroform from the aqueous phase. The stoichiometric ratio of the fluoroquinolones to SV 3B or TP 000 was determined with the slope ratio method and found to be 1:2.

The quantitative measure of the effect of complexation on acid–base equilibrium is most likely to be interpretable in terms of electronic, steric and other effects of complexing. The fluoroquinolone (1 mole) and oppositely charged form of the dye (2 moles) behave as a single unit being held together by electrostatic attraction.

The proposed methods are advantageous when compared to many of the reported methods in having higher $\lambda_{max}$ values and sensitivity. This is a decisive advantage since the interference from the associated ingredients shall be generally far less at higher wavelengths than at lower wavelengths. The methods are sensitive enough to permit the determination even up to 2.5 $\mu$g/ml. A significant advantage of an extractive spectrophotometric determination is that it offers distinct possibilities in the assay of a particular component in a complex dosage formulation. In the present study, some fluoroquinolone derivatives were estimated successfully as pure compounds as well as components in representative dosage formulations. The commonly used additives and excipients in the dosage forms of fluoroquinolones such as starch, lactose, talc, stearic acid, hydroxy propyl methyl cellulose, glycerine, titanium dioxide, tartrazine, white soft paraffin, liquid paraffin, sodium chloride, lactic acid and EDTA were found not to interfere in the analysis. Thus the proposed methods are simple, rapid with reasonable precision and accuracy when compared to many of the reported

methods. They offer the advantage that individual compounds can be determined in a multicomponent mixture.

*Acknowledgements*—The authors are grateful to NATCO fine pharmaceuticals Pvt. Ltd, Hyderabad for generously providing gift samples of fluoroquinolones and also to the university grants commission for providing financial assistance to one of us (KRR).

## REFERENCES

1. *United States Pharmacopoeia*, Vol. XXII, p. 963. U.S.P. Convention Inc., 1990.
2. G. Ramana Rao, A. B. Avadhanulu, R. Sridhar and C. K. Kokati, *Indian Drugs*, 1989, **26**, 580.
3. Y. K. Rathore Singh, P. K. Chatterjee, S. C. Mathur, S. Lal and P. D. Sethi, *Indian Drugs*, 1990, **27**, 326.
4. F. Jianzhang, T. Shenyang and Z. Xuguang, *Zhan. Kang Zazhi*, 1992, **17**, 359.
5. M. Pradeep and J. Sandeep, *Indian J. Pharm. Sci.*, 1992, **54**, 114.
6. K. P. R. Chowdary and A. Annapurna, *Indian Drugs*, 1990, **29**, 612.
7. S. K. Bhowal and T. K. Das, *Anal. Lett.*, 1991, **24**, 25.
8. F. Yoshikazu, M. Itsuo, F. Kinukoi and T. Takeshi, *Chem. Pharm. Bull.*, 1987, **35**, 865.
9. G. Ramana Rao, A. B. Avadhanulu and D. K. Vatsa, *Indian Drugs*, 1990, **27**, 532.
10. S. C. Mathur, S. Lal, N. Murugesan, Y. K. S. Rathore and P. D. Sethi, *Indian Drugs*, 1990, **27**, 398.
11. G. S. Suvarna, P. P. Thampi and T. C. Sarala, *Indian Drugs*, 1991, **28**, 279.
12. G. S. Suvarna, P. P. Thampi and T. C. Sarala, *J. Inst. Chem. (India)*, 1991, **63**, 223.
13. T. Sedai and S. Nihal, *Acta Pharm. Turc.*, 1993, **35**, 1.
14. S. C. Mathur, Y. Kumar, N. Murugesan, Y. K. S. Rathore and P. D. Sethi, *Indian Drugs*, 1992, **29**, 376.
15. F. Kinuko, N. Yoshihiro and T. Takeshi, *Chem. Pharm. Bull.*, 1987, **35**, 5004.
16. R. Foster, *J. Phys. Chem.*, 1980, **84**, 2135.
17. H. A. Liberman and L. Lachman (eds), *Pharmaceutical Dosage Forms: Tablets*, Vol. I. Dekker, New York, 1980.
18. L. Lachman, H. A. Liberman and J. L. Kanig (eds), *The Theory and Practice of Industrial Pharmacy*, 2nd Edn. Henry Kimpton, London, 1976.
19. *U.S. Pharmacopoeia XXII*. Mack Printing Co., Easton, 1990.

Pergamon

0039-9140(95)01394-6

*Talanta*, Vol. 42, No. 3, pp. 317–321, 1995

0039-9140/95 $9.50 + 0.00

# DETERMINATION OF STABILITY CONSTANTS OF COPPER(II) COMPLEX OF GLYCINE IN WATER + ALCOHOL MIXED SOLVENTS WITH ION SELECTIVE ELECTRODE TECHNIQUE

JING FAN

Department of Chemistry, Henan Normal University, Xinxiang, Henan 453002, P.R. China

(*Received* 24 *February* 1994. *Revised* 8 *August* 1994. *Accepted* 12 *August* 1994)

**Summary**—The first stability constants ($\log \beta_1$) of the copper(II) complex of glycine in water and in 13 water + alcohol (isopropanol, tert-butanol, 1,2-propylene glycol and glycerol) solvents have been determined at 25°C and an ionic strength of 0.10, from pH and pCu measurements of cells containing copper(II) ion selective electrode. It has been shown that as the proportion of the alcohol increases, the stability constants become increasing positive in all of the mixed solvents examined. An almost linear relation between $\log \beta_1$ and the mole fraction of alcohol was found for the complex in aqueous solutions of isopropanol, tert-butanol and glycerol. The response of the copper(II) ion selective electrode in water and in water + alcohol mixed solvents was also investigated. The advantages of using an ion selective electrode to determine the stability constants in mixed solvents are discussed.

The stability constant of a complex is one of the important basic datum in analytical chemistry. In many analytical methods it may be used to prejudge the interfering elements and to choose the optimum analytical conditions.[1,2] For example, if a complexing agent is used as precipitant in gravimetric analysis, the optimum conditions of precipitation (pH, concentrations, etc.) can be found by equilibrium calculations. It may be predicted whether quantitative precipitation or separation can or cannot be obtained under given conditions.

In recent years, non-aqueous and mixed solvents have been widely used in analytical chemistry with the rapid development of non-aqueous analytical techniques and methods. Although a considerable amount of data on stability constant of complexes in water are available in the literature,[3–5] data in non-aqueous or mixed solvents are limited. In particular, few studies have been reported on the determination of stability constants in non-aqueous or mixed solvents using the ion selective electrode (ISE) method.[6] As a part of the continuing studies on the use of ISE in mixed solvents,[7–10] we report here the first stability constants of the copper(II) complex of glycine in water and in water + alcohol mixed solvents. The alcohols used in this work were isopropanol (IPA), tert-butanol (TBA), 1,2-propylene glycol (PG) and glycerol (GL). The stability constants were determined from pH and pCu measurements of cells containing copper(II) ion solid membrane electrode at 25°C and ionic strength $I = 0.1$. The variation of $\log \beta_1$ with concentrations of the alcohol in a given mixed solvent is illustrated. In addition, the response of the copper(II) ion selective electrode in water and in mixed solvents is discussed.

## EXPERIMENTAL

### *Materials*

IPA, TBA, PG and GL (A.R., all from Shanghai Chem. Co., China) were used after drying over 4 Å type molecular sieves. Glycine (A.R., Beijing Chem. Co., China) was purified by recrystallization from aqueous solution of ethanol and dried under vacuum. Pure copper (99.99%, Shanghai Chem. Co.) and purified glycine were used to prepare the stock solutions of copper(II) nitrate ($0.1182M$) and those of glycine ($0.0100M$) in appropriate solvents, respectively. Water + alcohol mixed solvents were prepared by weight with twice distilled water. The ionic strength in all solutions was supported with $0.1M$ potassium nitrate.

*Apparatus*

The potentiometric titrations were performed at $25 \pm 0.05$°C in a water jacketed glass cell. A copper(II) ion solid membrane electrode (Jiangsu, type 306) was used together with a saturated calomel reference electrode (Jiangsu, type 801) for measurements of the copper(II) ion activity in solution; the pH was measured with a pH glass electrode (Shanghai, type 231) against the same reference electrode. The cell potential and the pH values were recorded by means of a precise pH meter (pH S-2D, Chengdu). Before measurements, the glass electrode was calibrated against standard buffers in water. The Nernstian response of the copper(II) ion selective electrode was checked in aqueous copper(II) nitrate solutions at $I = 0.1$.

*Procedure*

A series of standard solutions of copper(II) nitrate ($10^{-2}$ to $10^{-6}M$) in a given solvent was prepared by successive dilution of the respective stock solution with $0.1M$ potassium nitrate solution. Potentials of copper(II) ion electrode in the standard cooper(II) nitrate solutions were measured. Readings were taken when potential was constant within 0.5 mV for at least 5 min. Then, a standard curve of pCu *vs.* $E$ (potential) was constructed for each given solvent.

A 30.00 ml glycine solution ($0.0010M$) and a 15.00 ml copper(II) nitrate solution ($0.0010M$) were added to the cell. After thermal equilibrium was reached, the cell solution was titrated with small additions of $0.10M$ potassium hydroxide up to pH > 6.4. During titrations, the reaction solution was stirred magnetically. After each titration, the pH value and potential of the copper(II) ion electrode were recorded. Using potential values of the copper(II) ion electrode obtained, values of pCu in reaction solution can be easily found from the standard pCu *vs.* $E$ curves.

In order to reduce the influence of the liquid junction, $0.1M$ potassium nitrate in the same solvent as the reaction solution was used as filling solution for the external salt bridge of the saturated calomel electrode. For example, if the reaction medium is an aqueous solution of 16.3 wt% TBA, a $0.1M$ potassium nitrate solution in this mixed solvent would be the correct filling solution. Otherwise, it is difficult to obtain a stable cell potential.

The response of the copper(II) ion electrode was measured over a range of concentrations of copper(II) ion extending typically from $10^{-1}$ to $10^{-6}M$. The procedure used was similar to that described by Coetzee and Istone.[11]

## RESULTS AND DISCUSSION

The stability constants for the copper(II)-glycine complex in water have been investigated by Hansen and Ruzicka.[12] According to these authors, there are only two possible equilibriums in the reaction solution in the case of pH ≪ 6.9.

$$\underset{(HL)}{H_3N^+CH_2COO^-} \overset{K_2}{\rightleftharpoons} \underset{(L^-)}{H_2NCH_2COO^-} + H^+$$

and

$$Cu^{2+} + L^- \overset{\beta_1}{\rightleftharpoons} CuL^+.$$

Therefore, the first stability constant for the copper(II)-glycine complex can be expressed by equation (1):

$$\beta_1 = [CuL^+]/([Cu^{2+}][L^-]), \tag{1}$$

where

$$[L^-] = (C_L^0 - [CuL^+])/\alpha_{L(H)} \tag{2}$$

and

$$\alpha_{L(H)} = 1 + [H^+]/K_2, \tag{3}$$

here $C_L^0$ is the initial concentration of glycine in the reaction solution, $\alpha_{L(H)}$ the side reaction function of glycine in reaction with hydrogen ion, and $K_2$ the second dissociation constant of glycine under given conditions.

Inserting equations (2) and (3) into equation (1) and taking logarithms, it follows that

$$\log \beta_1 = pCu + \log(1 + [H^+]/K_2) - \log(C_L^0 - [CuL^+])/[CuL^+]. \tag{4}$$

Since $C_L^0$ was known exactly in a given experiment and $[Cu^{2+}]$ was determinable experimentally, the value of $[CuL^+]$ in equation (4) can be calculated from the initial and free concentrations of copper(II). However, the measured pH values in the mixed solvents have to be transformed to hydrogen ion concentrations in order to calculate $\log \beta_1$ using equation (4). In doing so, the procedure proposed by Van Vitert and Haas[13] was closely followed.

Because the ionic strength was kept to be 0.1 in the present work, $K_2$ values involved in equation (4) should be those at $I = 0.1$. Therefore, the thermodynamic second dissociation

Table 1. pH and pCu values for the determination of the first stability constant of the Cu(II) complex of glycine in aqueous solution of 16.3 wt% TBA (25°C, $I = 0.1$)

| $pH_{obs}$ | $pH_{cor}$ | $E$/mV | pCu | $\log \beta_1$ |
|---|---|---|---|---|
| 5.01 | 4.83 | −181.7 | 4.05 | 8.37 |
| 5.22 | 5.04 | −177.2 | 4.20 | 8.38 |
| 5.36 | 5.18 | −173.5 | 4.31 | 8.39 |
| 5.48 | 5.30 | −171.0 | 4.40 | 8.39 |
| 5.64 | 5.46 | −166.5 | 4.53 | 8.38 |
| 5.78 | 5.60 | −163.0 | 4.66 | 8.39 |
| 5.91 | 5.73 | −159.9 | 4.77 | 8.39 |
| Logarithm of arithmetic mean value | | | | 8.38 |
| Standard deviation | | | | 0.01 |
| Coefficient of variation | | | | 0.11% |

constants ($K_{a2}$) of glycine in water and in water + alcohol mixed solvents reported in the literature[14–19] have been corrected to the values at $I = 0.1$ in the solvents concerned, using equation (5) or (6)

$$K_{x2} = K_2 \gamma_{\pm}^2 \quad (K_2 = c_{H^+} c_{L^-}/c_{HL},\ \gamma_{\pm}^2 = \gamma_{H^+}\gamma_{L^-}) \qquad (5)$$

$$K'_{x2} = K'_2 \gamma_{\pm}^2 \quad (K'_2 = m_{H^+} m_{L^-}/m_{HL},\ K_2 = K'_2 \rho) \qquad (6)$$

and mean activity coefficients ($\gamma_{\pm}$) of electrolyte $H^+L^+$ calculated from Davies equation[20]

$$\log \gamma_{\pm} = -A I^{1/2}/(1 + I^{1/2}) + 0.3 A I, \qquad (7)$$

where $\gamma_i$ is the activity coefficient of ion. The activity coefficient of glycine (HL) is assumed to be equal to unity. $m_i$ is the molality of species defined per kg of (water + alcohol) solvent. $A$ is the Debye-Hückel constant given by

$$A = 1.8246 \times 10^6/(DT)^{3/2}. \qquad (8)$$

The required values of the dielectric constant $D$ and density $\rho$ for the mixed solvents are taken from previous studies.[15–18,21,22]

The potentiometric titrations were carried out in the range of pH 4–6.5 for each experiment. It was found that in the case of pH < 5 and >6, the determined $\log \beta_1$ values are not constant and changed greatly with pH. The same experimental phenomena for the same reaction in water was observed by Hansen and Ruzicka.[12] This is a result of the limited stability of the 1:1 ($CuL^+$) complex in acid solutions when pH < 5. When pH > 6, there is a possible formation of a 1:2 ($CuL_2$) complex. In view of this fact, only the experimental data in the range of pH 5–6 were used to calculate the stability constants in all cases. The final result is the average of all the determinations in this pH range. Table 1 lists the observed potentials of the copper(II) ion electrode, pCu, pH and calculated $\log \beta_1$ values for the complexation in aqueous solution of 16.3 wt% TBA, along with the standard deviation and coefficient of variation for $\log \beta_1$. Values of $\log \beta_1$ for the complex in water and in water + alcohol mixed solvents are given in Table 2. For all other systems, the standard deviation and coefficient of variation in $\log \beta_1$ were not greater than 0.03 and 0.4%, respectively. In addition, some critical experiments were repeated several times, reproducible results were obtained in all cases.

The value for $\log \beta_1$ in water obtained in this work was 8.19, which is in excellent agreement with the values 8.07, 8.15 and 8.36 reported previously.[5,12,23] No stability constant data on the complex in aqueous solutions of alcohols has been reported in the literature to the best of our knowledge.

It is evident from the table that the first stability constant of the copper(II) complex of glycine increases with the concentration of alcohols in all the mixed solvents investigated. This experimental fact can be partially explained

Table 2. The first stability constants ($\log \beta_1$) of the Cu(II)-glycine complex in aqueous solutions of alcohols (25°C, $I = 0.1$)

| | $\log \beta_1$ | | | |
|---|---|---|---|---|
| Alcohol wt% | $H_2O$ + TBA | $H_2O$ + IPA | $H_2O$ + PG | $H_2O$ + GL |
| 0.0 | 8.19 | 8.19 | 8.19 | 8.19 |
| 8.0 | 8.26 | 8.25 | — | — |
| 10.0 | — | — | — | 8.21 |
| 16.3 | 8.38 | 8.35 | — | — |
| 18.2 | — | — | 8.44 | — |
| 25.0 | 8.55 | 8.54 | — | — |
| 30.0 | — | — | — | 8.24 |
| 31.9 | — | — | 8.57 | — |
| 34.2 | 8.77 | 8.73 | — | — |
| 43.8 | 8.86 | — | — | — |
| 50.0 | — | — | — | 8.31 |

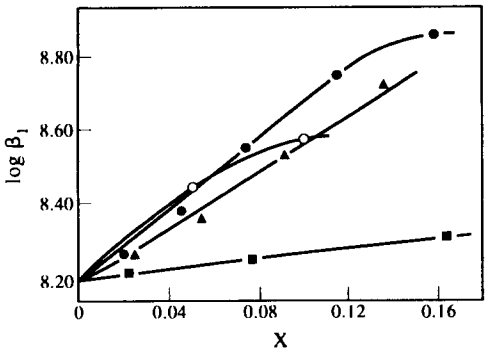


Fig. 1. Variation of the stability constants (log $\beta_1$) with mole fraction (X) of alcohols in mixed solvents. (●) TBA; (△) IPA; (○) PG; (■) GL.

from the decreasing dielectric constant of the mixed solvents,[21] because the lower dielectric constant of the mixed solvents in comparison with that of water would cause the electrostatic contributions to the bond formation to increase with increasing percentage of alcohol in the solvent mixtures. A further analysis of the results reveals that in aqueous solutions of IPA, TBA and GL, $\log \beta_1$ changes almost linearly with the mole fraction of alcohols (Fig. 1). However, this is not true for the complex in aqueous solutions of PG, as illustrated in the same figure.

The response of the copper(II) ion selective electrode was investigated at constant ionic strength of 0.1 in water and in water + alcohol mixtures. In all solvents, at copper(II) ion concentration extending from $10^{-5}$ to between $10^{-2}$ and $10^{-1}M$, the response was linear and Nernstian (slope of response was $29.6 \pm 0.6$ mV/decade). The lower detection limit was about $10^{-6}M$. At higher concentrations, the response became increasingly sub-Nernstian with increasing concentration. At lower concentrations, the response became increasingly sub-Nernstian with decreasing concentration. Very similar results have been reported by Coetzee and Istone[11] from copper(II) ion selective electrode in a variety of organic solvents and their mixtures with water.

In most of the solvents, the slope of response decreases slightly with increasing concentration of alcohol in mixed solvents. For example, the slope of response determined in water was 30.2 mV/decade. It decreases gradually to 29.0 mV/decade when 8.0, 16.3, 25.0 and 34.2 wt% IPA were added to water. Furthermore, we have examined whether the lower detection limit for copper(II) ion in water could be extended by adding alcohols. However, no obvious changes were observed for the lower detection limit in different mixed solvents compared with that in water. This observation is generally in agreement with those previously reported by Rechnitz for methanol and acetone as solvents[24] and Coetzee and Istone[11] in a variety of organic solvents and their mixtures with water.

Finally, a small comment can be made on the applicability of ISE in the determination of stability constants in mixed solvents. The present investigation suggests that ISE can be used successfully for the determination of stability constants of complexes in water + organic solvents under given conditions. This method is characterized by good accuracy, reproducibility and simplicity of the measurement techniques. By using ISE, two parameters, pH and pM (M refer to metal ion), can be measured. Therefore, the determination of stability constants is greatly simplified and the results obtained are more reliable compared with the pH-titration technique.

*Acknowledgement*—The author wishes to thank the referees for their valuable suggestions.

## REFERENCES

1. J. Inczédy, *Analytical Applications of Complex Equilibrium*, J. Tyson (translation ed.) Ellis Horwood, 1976.
2. A. Ringbom, *Complexation in Analytical Chemistry*. Wiley, New York, 1963.
3. L. G. Sillén and A. E. Martell, *Stability Constants of Metal–Ion Complexes*. The Chemical Society, London, 1964.
4. L. G. Sillén and A. E. Martell, *Stability Constants of Metal–Ion Complexes*, Supplement No. 1. The Chemical Society, London, 1971.
5. A. E. Martell and R. M. Smith, *Critical Stability Constants*. Plenum Press, New York, 1974.
6. E. Pungor, K. Toth, P. G. Klatsmanyi and K. Izutsu, *Pure. Appl. Chem.*, 1983, **55**, 2029.
7. J. Wang, J. Fan, W. Liu and J. Lu, *Chem. Sensors (China)*, 1991, **11**, 46.
8. J. Fan, Y. Huang and C. Hao, *Chem. Res. (China)*, 1993, **1**, 17.
9. J. Fan, *Chem. Sensors (China)*, 1993, **13**, 39.
10. J. Fan, S. Gao and H. Huang, *J. Henan Normal Univ. (Nat. Sci. Ed.)*, 1994, **22**, 52.
11. J. F. Coetzee and W. K. Istone, *Anal. Chem.*, 1980, **52**, 53.
12. E. H. Hansen and J. Ruzicka, *Talanta*, 1973, **20**, 1105.
13. L. G. Van Vitert and C. C. Haas, *J. Am. Chem. Soc.*, 1953, **75**, 451.
14. E. J. King, *J. Am. Chem. Soc.*, 1951, **73**, 155.
15. A. Pal, B. P. Dey and S. C. Lahiri, *Indian J. Chem.*, 1986, **25A**, 322.
16. B. P. Dey, S. Dutta and S. C. Lahiri, *Indian J. Chem.*, 1982, **21A**, 886.

17. J. Yang and L. Zhang *et al.*, *Chem. J. Chinese Univ.*, 1990, **11**, 180.
18. J. Yang and D. Men *et al.*, *J. Phys. Chem.*, 1989, **93**, 7248.
19. H. Talukdar, S. Rudra and K. K. Kundu, *Can. J. Chem.*, 1989, **67**, 315.
20. C. W. Davies, *Ion Association*, Butterworths, London, 1962.
21. Y. Y. Akhadov, *Dielectric Properties of Binary Solutions*. Pergamon Press, New York, 1981.
22. E. W. Washburn, *International Critical Tables of Numerical Data, Physics, Chemistry and Technical Tables*. Vol. III. McGraw-Hill, 1928.
23. G. A. Rechnitz and Z. F. Lin, *Anal. Lett.*, 1967, **1**, 23.
24. G. A. Rechnitz and N. Kenny, *Anal. Lett.*, 1969, **2**, 395.

Pergamon

0039-9140(95)01395-4

*Talanta*, Vol. 42, No. 3, pp. 323–329, 1995

0039-9140/95 $9.50 + 0.00

# SPECIATION OF ARSENIC IN A CONTAMINATED SOIL BY SOLVENT EXTRACTION

J. CHAPPELL,[1] B. CHISWELL[1]* and H. OLSZOWY[2]

[1]Department of Chemistry, University of Queensland, Australia
[2]Queensland Government Chemical Laboratory, Australia

(*Received* 12 *May* 1994. *Revised* 8 *August* 1994. *Accepted* 12 *August* 1994)

**Summary**—Soil collected from a disused cattle dip in northern New South Wales was studied with the aim of developing an inexpensive, yet effective method for quantitative determination of arsenic(III), arsenic(V) and total organic arsenic in a contaminated soil. Hydrochloric acid extractions were used as a method for removal of the arsenic from the soil in a form suitable for speciation. It was found that the extraction efficiency varied with the ratio of soil to acid, and the concentration of the acid. Arsenic(III), as arsenic trichloride, was selectively extracted into chloroform from a solution highly concentrated in hydrochloric acid. This was followed by back-extraction of the arsenic into water. Total inorganic arsenic was determined in a similar manner after the reduction of arsenic(V) to the trivalent state with potassium iodide. Arsenic(V) was determined by the difference between the results for arsenic(III) and total inorganic arsenic. All analyses for the various arsenic species were performed by hydride generation–atomic absorption spectroscopy; concentrations of total arsenic in the soil were confirmed using X-ray fluorescence spectrometry. It was found that all the arsenic in the soil was present as inorganic arsenic in the pentavalent state. This reflects the ability of arsenic to interchange between species, since the original species in cattle dipping solution is arsenic(III).

As a result of the injudicious use of arsenic in herbicides, pesticides, tanning solutions and timber preservatives, there are in excess of a thousand arsenic contaminated soil sites in the state of Queensland, Australia alone. Owing to the increases of urbanization, many of these sites are now being used for residential, community and recreational purposes.[1] Because of the toxic nature of arsenic, it is desirable to develop a cost effective method for remediation of such contaminated sites. Before this is possible, it is necessary to have an understanding of which species of arsenic are present in a given soil and how these will be affected by certain conditions.

Probably the most significant work in speciation of arsenic in a soil has been done by Takamatsu *et al.*[2] By use of high performance liquid chromatography anion exchange and an extraction process using 1*M* hydrochloric acid, the so-called bioavailable portion of the arsenic was speciated. However, for the work of this project it was desirable to speciate all of the arsenic present in a soil. For this reason, it was decided to extract the arsenic from the soil with concentrated hydrochloric acid and to speciate using solvent extractions.

The proposed method utilizes the observation that arsenic(III) can be selectively extracted into an organic phase from a strongly acidic phase. This can then be back-extracted into water for analysis.[2–4] It would appear that inorganic arsenic in solution, is most stable in its hydrolysed form.[5] However, in the presence of an excess of hydrochloric acid, chlorination of the arsenic will occur, yielding arsenic trichloride and arsenic pentachloride. It has been shown that arsenic trichloride is a covalent molecule while arsenic pentachloride probably exists as the complex ions, $[AsCl_4]^+[AsCl_6]^-$.[5] If this is the case, then it is quite obvious that the trivalent arsenic can be extracted into an organic phase such as chloroform or benzene, while arsenic pentachloride is excluded owing to its ionic properties. The arsenic contained in the organic phase can be easily recovered by back-extraction with water. As previously stated, inorganic arsenic is most stable in solution in its hydrolysed form. Therefore, when the arsenic comes into contact with water, hydrolysis occurs, excluding the arsenic from the organic phase.

*Author to whom correspondence should be addressed.

## EXPERIMENTAL

### *Reagents and glassware*

Stock solutions for arsenic compounds were prepared from arsenic trioxide ($As_2O_3$, 99.8%, BDH Chemicals Ltd) and arsenic pentoxide ($As_2O_5 . 5H_2O$, 99.9%, Aldrich Chemicals). Concentrations of arsenic(V) solutions were confirmed by calibration against arsenic trichloride standard solution (BDH Chemicals Ltd). All other chemicals were of analytical grade and dilutions were performed with distilled water.

All glassware was soaked for at least 24 hr in 4*M* nitric acid after cleaning in X-tran (BDH Chemicals Ltd), a phosphate-free detergent. Final rinsing was performed with milli-Q water.

### *Preparation of soil*

All soil samples were prepared according to the procedure outlined in AS1289.1(1991).[6] In summary, the soil was dried at 50°C for at least 24 hr. The dried material was ground lightly with a mortar and pestle and sieved through a 2.36 mm sieve, removing foreign bodies such as twigs and stones. In addition to the requirements of AS1289, the fraction which passed the sieve was ground to a fine powder in a tungsten-carbide swing mill. The resulting powder was homogenized by shaking for approximately 30 min.

### *Determination of total arsenic concentration in soil*

Prior to speciation work, the total concentration of arsenic in the soil was determined by X-ray fluorescence spectrometry (XRF) on loose powders. The conversion of an XRF intensity to a concentration is subject to errors due to matrix effects, principally by absorption of the fluorescent (secondary) radiation by the matrix elements. Therefore, it was necessary to initially determine the major and minor components in the soils studied so that a matrix correction factor ($\mu$) could be calculated for each soil. The major and minor components of silicate matrices such as soils consist of the following elements, expressed as oxides: $SiO_2$, $Al_2O_3$, $Fe_2O_3$, MgO, CaO, $Na_2O$, $K_2O$, $TiO_2$, $P_2O_5$, MnO, $SO_3$, SrO and loss on ignition (LOI). These were determined by XRF according to the method of Norrish and Hutton.[7] In summary, a portion of the finely ground sample is fused with a borate based flux containing lanthanum oxide ($La_2O_3$), a heavy absorber, and the resultant melt is pressed to yield a glass bead. XRF intensities are collected from the bead and concentrations are calculated from the Norrish/Hutton algorithm as follows:[8]

$$C_i = D + ER(1 + \Sigma\mu_{ij}C_j),$$

where $C_i$ = concentration of element $i$, $D$ = intercept expressed as a percentage, $E$ = slope, $R$ = intensity of element $i$ (from XRF spectrometer), $\mu$ = matrix correction factors and $C_j$ = concentration of interfering element.

Once the major and minor elements are determined, the matrix correction factor for any analyte radiation, in this case arsenic K-$\alpha$ radiation, can be calculated as shown below:

$$\mu_i = \Sigma M_j W_j,$$

where $\mu_i$ = matrix correction factor for element $i$, $M_j$ = mass absorption coefficient for element $j$ and $W_j$ = weight fraction of element $j$. Having obtained $\mu_{As}$, it is now possible to accurately determine, with full matrix correction, arsenic in the soils under scrutiny. Table 1 outlines the operating parameters of the XRF spectrometer and it should be noted that background intensities are also collected.

Table 1. XRF operating parameters

| | Arsenic | Lead |
|---|---|---|
| Analyte line | *K*-$\alpha$ | *L*-$\beta$ |
| X-ray tube | Rhodium | Rhodium |
| Power | 60 kV; 40 mA | 60 kV; 40 mA |
| Detector | F + S | F + S |
| Crystal | LIF 200 | LIF 200 |
| Peak 2-$\theta$ angle | 33.96 | 28.22 |
| Backgrounds | +0.6; −0.5 | +0.4; −1.2 |
| Counting time (sec)* | 100 | 100 |
| Pulse height discrimination | UL75; LL25 | UL70; LL30 |
| Collimation | Fine | Fine |
| Mask | Small | Small |

*Counting time refers to the time expended on each line, *i.e.* 100 sec for each background and peak.

One complication in the XRF determination of arsenic is that lead overlaps with the arsenic $K$-$\alpha$ analyte line and it is therefore necessary to correct for the lead interference. The calculation for the conversion of the intensity of arsenic $K$-$\alpha$ radiation into a concentration is outlined as follows:

$$C_{Pb} = K_1 R_{Pb} \mu_{Pb}$$

$$C_{As} = (K_2 R_{As} \mu_{As} - (LC_{Pb})),$$

where $C_{Pb}$, $C_{As}$ = concentrations of lead and arsenic, respectively (mg/kg), $K_1$, $K_2$ = calibration slope constants for lead and arsenic, respectively, $R_{Pb}$, $R_{As}$ = net intensities for lead and arsenic, respectively (background corrected), $\mu_{Pb}$, $\mu_{As}$ = matrix correction factors for lead and arsenic analyte lines, respectively, and $L$ = lead line overlap correction factor. It will be noted that the concentration of lead needs to be pre-determined.

As with most forms of modern analysis, XRF requires a calibration procedure to be undertaken before meaningful results can be obtained. This is effected by the use of international standard reference materials (SRM's), containing known amounts of arsenic and lead. The accuracy of the method employed is approximately $\pm 5\%$ with a precision in the order of 1–2%. The lower limit of detection is approximately 1 mg/kg.[1]

*Extraction of arsenic from soil*

Arsenic was removed from the soil by treatment with concentrated hydrochloric acid. A 5 g sample of soil was accurately weighed into a centrifuge tube and 20 ml of 10$M$ hydrochloric acid was added. The extraction was assisted by shaking vigorously for about 30 min. The resulting slurry was centrifuged at 3000 r.p.m. for approximately 5 min and the supernatant was gravity filtered (Whatman 44) into a 100 ml volumetric flask. This procedure was repeated a further two times on the same 5 g sample of soil. When the extraction was complete, the soil was washed into the filter paper with water and the solution diluted.

*Speciation of trivalent arsenic*

A 10 ml aliquot of the arsenic extract was transferred to a 100 ml separating funnel and 80 ml of 10$M$ hydrochloric acid was added, adjusting the acid concentration to greater than 9$M$. This was followed by extraction of arsenic(III) into chloroform with $4 \times 10$ ml washings. At this stage the strongly acidic aqueous phase was discarded. The arsenic was then back-extracted from the organic phase into $2 \times 20$ ml aliquots of water and diluted to 100 ml.

*Speciation of total inorganic arsenic*

A separate 10 ml aliquot of arsenic extract was transferred to a large test tube and 10 ml of 50% potassium iodide was added. The tube was then covered and immersed in a water bath at 60°C for about 30 min. After the solution had cooled, it was diluted to 50 ml, 10 ml of which was transferred to a 100 ml separating funnel. After adjusting the acid concentration to greater than 9$M$, extraction for inorganic arsenic was performed as for arsenic(III).

## RESULTS AND DISCUSSION

*Extraction of arsenic from soil*

Initially, the arsenic was extracted from 1 g of cattle dip soil with 20 ml of hydrochloric acid. The mixture was shaken for about 30 min and the resulting slurry gravity filtered. Consequent analysis revealed that this method yielded 85% of the total arsenic present. In order to achieve a higher extraction efficiency, it was decided to try a multiple extraction. When performing liquid–liquid extractions, it is common practice to extract two or three times to ensure a complete transition between the phases. This same principle was applied to the extraction of arsenic from soil with acid. A three-fold extraction procedure on 1 g of cattle dip soil yielded 97% of the total arsenic present.

The ratio of acid to soil and the concentration of the acid also affects the extraction efficiency. In the first instance, it was found that when applying the extraction technique to 5 g of soil, 86% of the arsenic was removed compared with 97% when extracting 1 g of soil. It is not surprising then that the concentration of hydrochloric acid should also affect the extraction efficiency. During the developmental stages of the process, extractions were attempted using water and 1$M$ hydrochloric acid as well as concentrated hydrochloric acid. Extraction with water yielded less than 5% of the total arsenic while the 1$M$ hydrochloric acid extraction yielded 56% of the total arsenic. Such an effect has also been noted by other workers.[9,10]

Table 2. Reduction of $As^{5+}$ to $As^{3+}$ *vs.* HCl strength[13]

| Normality of HCl | Reduction (%)* |
|---|---|
| 4.0 | 96.29 |
| 5.0 | 96.98 |
| 6.0 | 97.49 |
| 7.0 | 95.68 |
| 7.5 | 31.90 |
| 8.0 | 11.26 |
| 9.0 | 11.98 |

*Reduction performed as follows: (i) adjust the acid strength to approximately 6*N* with HCl, (ii) add 4 ml of 50% $SnCl_2$ solution, (iii) add 5 ml of 15% KI solution and (iv) leave to stand at room temperature for 15 min.

*Importance of acid concentration*

The success of the proposed method is highly dependent upon careful monitoring of the concentration of hydrochloric acid. Trivalent arsenic will only be completely extracted into an organic solvent from a solution which is highly concentrated in hydrochloric acid. Beard and Lyerly[11] employed a similar solvent extraction technique to separate arsenic from antimony and bismuth using benzene as the extracting solvent. It is claimed that the extraction of arsenic(III) into benzene was almost non-existent until the hydrochloric acid concentration reached 4*M*. The efficiency of extraction then rose sharply with increasing acid concentration, yielding a 100% extraction at acid concentrations of 9*M* or greater. Other researchers observed similar results using chloroform as the extracting solvent.[3,12]

The concentration of hydrochloric acid also has a significant effect on the reduction of arsenate to arsenite. This method utilized potassium iodide as a reducing agent. Literature suggests that reduction by this method requires the concentration of hydrochloric acid to be at least 1*M*.[13,14] However, it was found that at acid concentrations above 7*M*, the reduction efficiency decreases significantly. Hydrochloric acid concentrations of 1, 6 and 9*M* were used in the reduction of a 100 mg/l. arsenic(V) solution with potassium iodide. Reduction efficiencies of 93, 95 and 15% were obtained, respectively. Forehand *et al.*[13] performed a more comprehensive study of the dependence of reduction upon concentration of hydrochloric acid when using a potassium iodide/stannous chloride mixture as the reducing agent. Their results clearly show a dramatic decrease in reduction at an acid concentration above 7*M* (Table 2).

*Efficiency of solvent extraction*

Prior to investigation of soil samples, the solvent extraction technique was applied to 100 mg/l. solutions of arsenic(III) and arsenic(V) to ascertain the efficiency of the method. The mean and standard deviation results from eight determinations demonstrated that the method was accurate and precise for both trivalent and pentavalent arsenic (Table 3).

*Fate of organic arsenic during speciation*

The two major forms of organic arsenic are monomethylarsonic acid (MMA) and dimethylarsinic acid (DMA). Neither of these compounds will be extracted into chloroform under the conditions described in this paper.[2] However, one must also consider the fate of these two compounds during reduction of inorganic arsenic(V) with potassium iodide. It is possible that MMA and DMA will be reduced by potassium iodide to $CH_3AsI_2$ and $(CH_3)_2AsI$, respectively.[15] If these compounds are formed and can be extracted into chloroform, then the results for the total inorganic arsenic and hence the inorganic arsenic(V) will be erroneous. However, it would seem that the reduction of DMA to $(CH_3)_2AsI$ is very slow and will not occur to any significant level during the time scale of this experiment.[15] The reduction of MMA to $CH_3AsI_2$ is much faster but the organic arsenic(III) product is not likely to be soluble in chloroform to any appreciable extent.[16] Therefore, it was concluded that only inorganic arsenic(III) would be extracted into the chloroform.

*Results for speciation of arsenic in cattle dip soil*

X-Ray fluorescence spectrometry, based on triplicate analyses, revealed that the cattle dip soil contained $1145 \pm 57$ mg/kg total arsenic. Experiments were then conducted to determine the quantity of soil required to yield meaningful speciation results. The speciation procedure was applied to both 1 and 5 g masses of soils and it was found that the mean results for both masses

Table 3. Solvent extraction of arsenic species in solution

| Arsenic species | Extraction efficiency (%) | Standard deviation (%) |
|---|---|---|
| Arsenite | 97 | 3.4 |
| Arsenate | 95 | 3.6 |

Table 4. Speciation results for cattle dip soil*

| | 5 g of soil | 1 g of soil |
|---|---|---|
| Concentration of arsenic obtained from XRF (*mg/kg*) | 1145 ± 57 | 1145 ± 70 |
| Average concentration of arsenic determined by HCl extraction (*mg/kg*) | 985 ± 70 | 978 ± 70 |
| Extraction percentage | 86% | 85% |
| Concentration of inorganic arsenic (*mg/kg*) | 945 ± 94 | 921 ± 270 |
| Concentration of arsenic(III) (*mg/kg*) | 3 ± 0.3† | 3 ± 1 |
| Concentration of arsenic(V) (*mg/kg*) | 942 ± 94 | 918 ± 270 |
| Concentration of organic arsenic (*mg/kg*) | 40 ± 4 | 64 ± 13 |

*Means and their associated errors are calculated from at least six determinations.
†Calculated but not statistically meaningful standard error.

of soils were similar, but the precision for the lower mass was poor (Table 4). Therefore, it could be generalized that for soils with arsenic concentrations of 1000 mg/kg or greater, at least 5 g aliquots must be used, as it would appear that precision increases with the amount of arsenic being speciated. It follows that for concentrations of less than 1000 mg/kg of arsenic, even larger aliquots would be required. Speciation of arsenic in 5 g of cattle dip soil revealed that all or nearly all the arsenic is present in the inorganic, pentavalent state.

Based on the observation that arsenite and arsenate are more than 99.9% soluble in hydrochloric acid at the concentrations encountered in the method, it was assumed that As(III) and As(V) are extracted from the soil with equal efficiency. On this basis, it can be claimed that 96% of the arsenic is in the pentavalent state and about 0.3% is present as As(III). Therefore, while only 86% of the arsenic was extracted from the soil, nearly 100% of the extracted arsenic was speciated; thereby forming a representative view of the species present in the soil. The results for both organic arsenic and arsenic(III) fall within experimental error and can, therefore, be approximated to zero concentrations. This infers that all or nearly all of the arsenic present in the soil is inorganic and pentavalent. Of course, the above assumption will not hold for all soils. For instance, under reducing conditions, sulfur rich soils can contain arsenic(III) as an acid insoluble sulfide.[17] Therefore, it is necessary to consider each soil sample separately before making such extrapolatory calculations.

Aliquots of the cattle dip soil were spiked with known quantities of arsenite and arsenate (Table 5). The speciation procedure was performed on these spikes. If the method is valid, the results for each of the species present should increase by the amount of the relevant arsenic species added. Table 6 lists the results for speciation of the arsenic extracted from the soil with hydrochloric acid. If it is assumed that the extracted arsenic for the cattle dip soil forms a representative sample of the total arsenic in the soil, then theoretical values can be calculated for the speciation of the total amount of arsenic present (Table 7).

In preparing CDS(III), arsenite was added so that the total concentration of arsenic in the soil increased 83 mg/kg (Table 5). Speciation of CDS(III) yielded an arsenic(III) concentration of 84 mg/kg, an increase of 81 mg/kg when compared with the cattle dip soil (Table 7). This provides strong evidence that the amount of arsenic(III) found in the cattle dip soil is valid. Similarly, preparation of CDS(V) involved the addition of arsenate so that the total concentration of arsenic in the soil increased by 84 mg/kg (Table 5). Speciation of CDS(V) resulted in an arsenic(V) concentration of 1178 mg/kg; an increase of 79 mg/kg when compared with the unspiked cattle dip soil (Table 7). This provides strong evidence that the amounts of arsenite and arsenate determined for the cattle dip soil are valid.

Table 5. Spiked samples of cattle dip soil*

| Soil code | Spike material | Concentration of arsenic (*mg/kg*) |
|---|---|---|
| CDS† | — | 1145 ± 57 |
| CDS(III) | arsenic(III) | 1228 ± 61 |
| CDS(V) | arsenic(V) | 1229 ± 61 |

*Means and their associated errors are calculated from three determinations by XRF.
†CDS: Cattle dip soil.

Table 6. Speciation results for cattle dip spikes*

| Soil code | Total arsenic extracted (mg/kg) | Concentration of arsenic(III) (mg/kg) | Concentration of arsenic(V) (mg/kg) |
|---|---|---|---|
| CDS | 985 ± 70 | 3 ± 0.3† | 945 ± 94 |
| CDS(III) | 1032 ± 72 | 71 ± 7 | 942 ± 94 |
| CDS(V) | 1045 ± 73 | 3 ± 0.3† | 1002 ± 100 |

*Means and their associated errors are calculated from at least six determinations.
†Calculated but not statistically meaningful standard errors.

Table 7. Calculated values for speciation of total amount of arsenic in cattle dip soil*

| Soil code | Total arsenic extracted (mg/kg) | Concentration of arsenic(III) (mg/kg) | Concentration of arsenic(V) (mg/kg) |
|---|---|---|---|
| CDS | 1145 ± 80 | 3 ± 0.3† | 1099 ± 109 |
| CDS(III) | 1228 ± 86 | 84 ± 8 | 1121 ± 112 |
| CDS(V) | 1229 ± 86 | 4 ± 0.4† | 1178 ± 117 |

*Means and their associated errors are calculated from at least six determinations.
†Calculated but not statistically meaningful standard errors.

Since the data in Table 7 are similar to the expected results, yet are calculated from the percentage of arsenic(III) and arsenic(V) in the soil extract, it can be claimed that the extract provides a representative sample of the arsenic present in the soil.

## CONCLUSIONS

The aim of this research project was to develop an inexpensive, efficient method for quantitative determination of arsenic species in a contaminated soil. In order to achieve this, a soil from an abandoned cattle dip site in northern New South Wales was investigated. Satisfactory results were obtained, revealing that nearly all of the arsenic present was in the pentavalent state. Validation of this result was achieved by spiking the cattle dip soil with known amounts of arsenite and arsenate.

Speciation of the cattle dip soil indicated that all of the arsenic was in inorganic forms, within experimental error. However, the method for speciation should also be applicable to organic forms of arsenic, although in this work, validation of the results was focused on the determinations of arsenic(III) and arsenic(V). Speciation of the cattle dip soil after spiking with known amounts of organic arsenic should result in a total arsenic concentration greater than the inorganic arsenic concentration; thus yielding the amount of organic arsenic by difference.

Determination of total arsenic and its species, in a 5 g aliquot of soil, requires the use of about 230 ml of hydrochloric acid. This equates to a cost of slightly less than $1(A) for the acid per sample. The cost of other chemicals, such as potassium iodide and chloroform, is no more than $1(A) per sample. Therefore, at a total reagent cost of approximately $2(A) per sample, this method is inexpensive even on large scale investigations. A major advantage of the proposed method over other techniques lies in the amount of arsenic extracted from the soil. As stated previously, Takamatsu *et al.*[2] speciated the arsenic which they extracted from soil using 1*M* hydrochloric acid. However, of the 12 soils analysed by them, between 3.6 and 53.2% of the total arsenic present was extracted. The method here described yields a similar quality of results, but has a total arsenic extraction of between 80 and 100%.

## REFERENCES

1. R. Sadler, H. Olszowy, G. Shaw, R. Biltoft and D. W. Connell, Report on Arsenic Contamination at Craigslea School, GCL Report Series: No. 4, Queensland Government Chemical Laboratory, Brisbane, 1990.
2. T. Takamatsu, H. Aoki and T. Yoshida, *Soil Sci.*, 1982, **133**, 239.
3. W. Holak and J. J. Specchio, *Atom. Spectrosc.*, 1991, **12**, 105.
4. W. A. Maher, *Anal. Chim. Acta*, 1981, **126**, 157.
5. N. N. Greenwood and A. Earnshaw, *Chemistry of the Elements*, pp. 650–665. Pergamon Press, Oxford, 1984.
6. Australian Standard, AS1289.1(1991)4.6(b)(iii).
7. K. Norrish and J. T. Hutton, *Geochim. Cosmochim. Acta*, 1969, **33**, 431.
8. W. K. de Jongh, *X-Ray Spectrometry*, 1973, **2**, 151.
9. T. Takamatsu, R. Nakata and T. Yoshida, *Bunseki Kaguka*, 1982, **31**, 541.

10. T. Takamatsu, R. Nakata, T. Yoshida and M. Kawashima, *Jap. J. Limnol.*, 1985, **46,** 93.
11. H. C. Beard and L. A. Lyerly, *Analyt. Chem.*, 1961, **33,** 1781.
12. F. Puttemans and D. L. Massart, *Anal. Chim. Acta*, 1982, **141,** 225.
13. T. J. Forehand, A. E. Dupuy and H. Tai, *Analy. Chem.*, 1976, **48,** 999.
14. C. R. Parker, *Water Analysis by Atomic Absorption Spectroscopy*, p. 32. Varian Techtron, Melbourne, 1976.
15. N. Suzuki, K. Sotoh, H. Shoji and H. Imura, *Anal. Chim. Acta*, 1986, **185,** 239.
16. I. T. Miller, H. Heaney, D. M. Heinekey and W. C. Fernelius, *Inorganic Syntheses*, E. G. Rochow (ed.), Vol. 6, p. 113. McGraw-Hill, New York, 1960.
17. G. O. Doak, G. G. Long and L. D. Freedman, *Encyclopedia of Chemical Technology*, R. E. Kirk and D. F. Othmer (eds), Vol. 3, pp. 225–257. John Wiley and Sons, New York, 1978.

Pergamon

0039-9140(95)01396-2

*Talanta*, Vol. 42, No. 3, pp. 331–335, 1995

0039-9140/95 $9.50 + 0.00

# ADSORPTIVE STRIPPING VOLTAMMETRY OF TRACE MANGANESE IN THE PRESENCE OF 2-(5′-BROMO-2′-PYRIDYLAZO)-5-DIETHYLAMINOPHENOL (5-Br-PADAP)

JOSEPH WANG* and JIANMIN LU

Department of Chemistry and Biochemistry, New Mexico State University, Las Cruces, NM 88003, U.S.A.

(*Received* 28 *June* 1994. *Revised* 9 *August* 1994. *Accepted* 9 *August* 1994)

**Summary**—Trace levels of manganese can be determined by voltammetry after controlled adsorptive accumulation of the manganese-2-(5′-bromo-2′-pyridylazo)-5-diethylaminophenol (5-Br-PADAP) complex on a hanging mercury drop electrode. Optimal conditions include an ammonia buffer solution (pH 8.8) containing $1 \times 10^{-5}M$ 5-Br-PADAP and an accumulation potential of $-1.20$ V. The technique offers enhanced sensitivity over analogous measurements of the manganese-Eriochrome Black T chelate. The detection limit is 0.2 $\mu$g/l with 1 min accumulation. The new adsorptive approach is characterized with new selectivity dimensions (compared to the Eriochrome Black T scheme), and is not affected by large excess of commonly coexisting calcium and magnesium cations (which severely interfere in the Eriochrome Black T procedure).

Because of the importance of manganese, highly sensitive analytical methods are required for its determination in biological and environmental matrices. Neutron activation and atomic absorption spectroscopic measurements of trace levels of manganese usually require tedious enrichment steps (such as co-precipitation and extraction).[1,2] The highly sensitive electroanalytical technique, stripping analysis, can also be employed for trace measurements of manganese.[3,4] However, conventional stripping measurements of manganese suffer from difficulties associated with the low solubility of manganese in mercury, large hydrogen evolution background current, the formation of intermetallic compounds, and an irreversible redox process. Such problems may be addressed using an alternative stripping mode based on non-electrolytic preconcentration. Yet, only one adsorptive stripping voltammetric procedure, involving the adsorptive accumulation of the manganese/Eriochrome Black T complex, has been reported.[5]

This article describes an extremely sensitive adsorptive stripping voltammetric method for the quantitation of trace amounts of manganese, in which preconcentration is accomplished by adsorption of the manganese chelate with 2-(5′-bromo-2′-pyridylazo)-5-diethylaminophenol (5-Br-PADAP). The formation of surface active chelates of 5-Br-PADAP with vanadium, iron, or chromium has been utilized recently for measuring low levels of these metal ions.[6–8] The characterization, optimization, and advantages of the manganese–Br-PADAP adsorptive stripping procedure are elucidated in the following sections.

*Author to whom correspondence should be addressed.

## EXPERIMENTAL

### *Apparatus and reagents*

An EG&G PAR Model 264A voltammetric analyzer, a PAR 303A static mercury drop electrode, and a PAR 0073 X-Y recorder were used to obtain the voltammograms. A medium-size hanging mercury drop electrode, with an area of 0.016 cm$^2$ was employed in connection with the 10 ml cell.

All solutions were prepared with doubly distilled water. A 1000 ppm stock manganese solution (atomic adsorption standard, Aldrich) was diluted as required. Stock solutions ($10^{-2}M$) of 5-Br-PADAP (Aldrich) were prepared in ethanol (Quantum Chemical Co.). A $1 \times 10^{-2}M$ ammonia/ammonium chloride buffer (pH 8.8) served as supporting electrolyte.

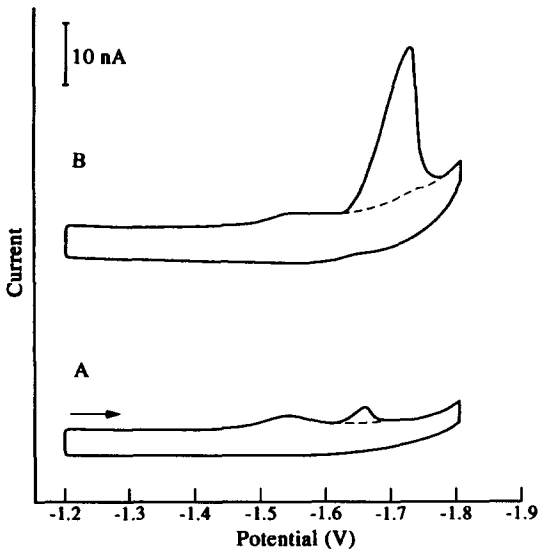


Fig. 1. Cyclic voltammograms for 20 $\mu$g/l. manganese without (A) and with (B) 60 sec prior stirring at $-1.2$ V. Dotted lines are the corresponding curves for the blank solution (0.01 M ammonia buffer, containing $5 \times 10^{-6}M$ 5-Br-PADAP, and 10% ethanol). Scan rate, 50 mV/sec.

### *Procedure*

The supporting electrolyte solution (10 ml), containing $1 \times 10^{-5}M$ 5-Br-PADAP and 10% ethanol was pipetted into the cell and deaerated with nitrogen for 8 min. The preconcentration potential (usually $-1.20$ V) was applied to a fresh mercury drop while the solution was stirred. Following the preconcentration step, the stirring was stopped and after 15 sec the voltammogram was recorded by applying a negative-going differential pulse scan (with 10 mV/sec scan rate and 25 mV amplitude). The scan was terminated at $-1.80$ V. Aliquots of the manganese standard solution were introduced after recording the background voltammograms, and the cycle was repeated using a new mercury drop. Throughout this operation, nitrogen was passed over the solution. All data were obtained at room temperature.

## RESULTS AND DISCUSSION

Figure 1B displays a cyclic voltammogram for 20$\mu$g/l. manganese, in the presence of $5 \times 10^{-6}M$ 5-Br-PADAP, recorded after 1 min preconcentration at $-1.20$ V. A large and well defined cathodic peak is observed at *ca.* $-1.72$ V. No peaks are observed in the anodic branch. Subsequent scans exhibit a rapid diminution of the peak (to a stable value with 15 runs), indicating rapid desorption from the surface (not shown). Voltammogram A displays the analogous response without accumulation. A substantially lower (*ca.* 10-fold) peak, representing the solution species, is observed. The latter is similar to that observed following the desorption. The effect of potential scan rate (v) was evaluated for the surface-confined Mn-5-Br-PADAP complex. A plot of log $i_p$ *vs.* log $v$ was linear over the 5–100 mV/sec range, with a slope of 0.81, indicating deviation for an ideal behavior of adsorbed reactants. Unlike the manganese/Eriochrome Black T voltammetric measurements, which involve the reduction of the ligand electroactive (azo) moiety,[5] the manganese/5-Br-PADAP reduction process

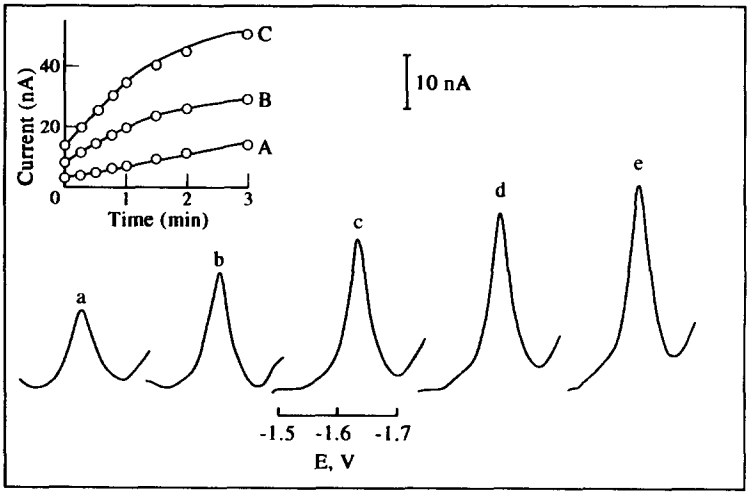


Fig. 2. Differential pulse voltammograms for 10 $\mu$g/l. manganese after different preconcentration times: 0 (a), 15 (b), 30 (c), 45 (d) and 60 (e) sec, with 300 rpm stirring. Inset shows current *vs.* preconcentration plots for 2 (A), 5 (B) and 10 (C) $\mu$g/l. manganese. Accumulation at $-1.2$ V; scan rate, 10 mV/sec; pulse amplitude, 25 mV; solution, as in Fig. 1.

involves the metal center in the complex. This is supported by the fact that measurements without the ligand yielded a small manganese peak, at a similar potential; the peak was greatly (20-fold) enhanced upon adding the 5-Br-PADAP (not shown). Analogous vanadium measurements also involved reduction of the metal center.[9]

Highly sensitive adsorptive stripping voltammetric measurements can be realized utilizing the effective interfacial accumulation of the Mn–5-Br-PADAP complex. For example, Fig. 2 displays differential pulse voltammograms for 10 $\mu$g/l. after different preconcentration periods from 0 to 60 sec (a–e). Larger peak currents are observed for longer accumulation periods. Yet, even without a preceding preconcentration, a well-defined peak is observed (reflecting the strong chelate adsorption during the slow differential pulse scan). Also shown in Fig. 2 (inset) are plots of peak current *vs.* preconcentration time at three manganese levels: 2 (A), 5 (B) and 10 (C) $\mu$g/l. While the 2 $\mu$g/l. experiment yields a linear increase of the peak current, a curvature (above 1 min period) is observed using the 5 and 10 $\mu$g/l. manganese solutions.

Figure 3 examines the influence of various experimental variables upon the stripping response of the Mn–5-Br-PADAP complex. Increasing the pH from 8 to 8.8 results in a gradual increase in the peak height; a sharp decrease in the response is observed as the pH is raised further (A). The optimal pH (8.8) is much lower than that for the eriochrome procedure,[5] which is advantageous considering the higher stability of the dissolved form of the metal. A similar pH was employed in the Fe-5-Br-PADAP procedure,[7] while acetate buffer solutions (of lower pH) were used for the quantitation of vanadium and chromium.[6,8] The peak increases rapidly upon raising the ligand concentration from $2 \times 10^{-6}$ to $8 \times 10^{-6} M$, above which it starts to level off (B). Similar (micromolar) 5-Br-PADAP levels were employed in analogous schemes for iron, vanadium and chromium.[6-8] The dependence of the current on the preconcentration potential was examined over the range from $-0.9$ to $-1.50$ V (C). An optimal behavior was observed around $-1.20$ V. Substantially lower potentials were used in earlier procedures using 5-Br-PADAP.[6-8] The chelate peak also increased upon increasing the ethanol content to 10% (v/v), and then it levelled off (not shown). Such a profile reflects the increased solubility of 5-Br-PADAP. Because of

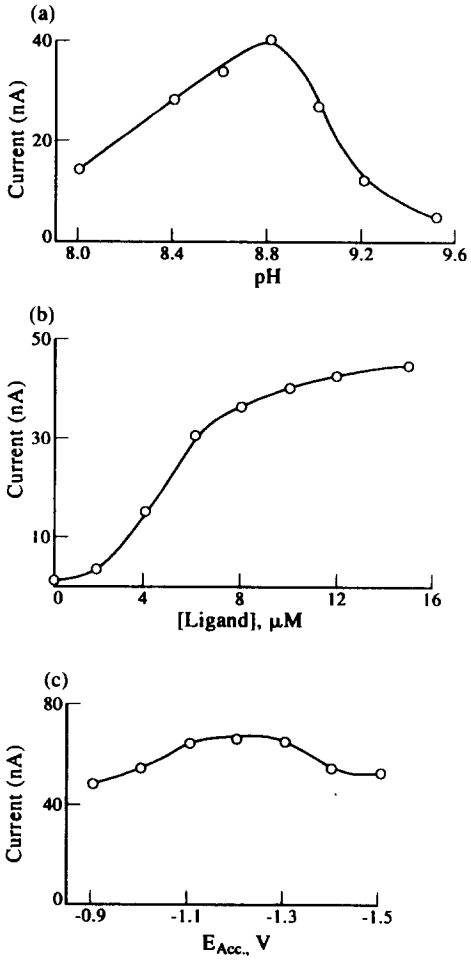


Fig. 3. Effect of pH (A), ligand concentration (B), and accumulation potential (C) on the adsorptive stripping peak current for manganese [10 $\mu$g/l. (A, B), 20 $\mu$g/l. (C)]. Accumulation for 30 (A, C) and 60 (B) sec. Other conditions, as in Fig. 2.

the long desorption time, a new drop was used in each cycle. Both the linear scan and differential pulse modes yielded a well defined stripping response with the latter offering slightly improved signal-to-background characteristics. Best results were obtained with a 25 mV pulse amplitude and 10 mV/sec scan rate.

Figure 4 shows stripping voltammograms obtained for manganese solutions of increasing concentration in 2 $\mu$g/l. steps after a 60-sec preconcentration time. Well-defined peaks, which increase linearly with the manganese concentration, are observed. Also shown in Fig. 4 (insets) are calibration plots over wider concentration ranges [2–14 (A) and 10–90 (B) $\mu$g/l.] following 60 and 30 sec accumulation, respectively. A curvature is observed above 50 $\mu$g/l. with a leveling off above 80 $\mu$g/l. The linear portions are characterized with slopes of 4.3 (A)

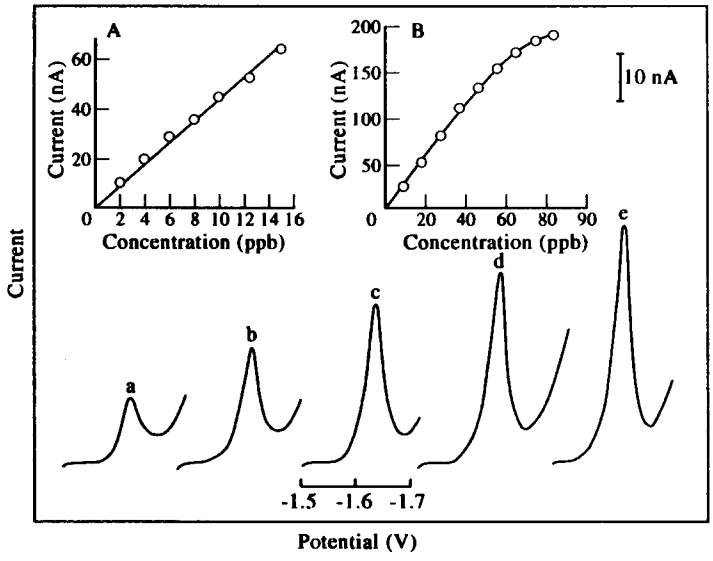


Fig. 4. Stripping voltammograms for solutions of increasing manganese concentration, 2–10 $\mu$g/l. (a–e). Preconcentration for 60 sec; conditions, as in Fig. 2e. Also shown (inset) are calibration plots over the 2–14 (A) and 10–90 (B) $\mu$g/l. ranges, following 60 and 30 sec accumulations, respectively.

and 2.7 (B) nA l./$\mu$g. The detection limit was estimated (from curve a) to be 0.2 $\mu$g/l. ($3 \times 10^{-9} M$). The precision was estimated from 15 successive measurements of the 2 $\mu$g/l. manganese solution (60-sec accumulation); the mean peak current was 9.8 nA (range 9.5–10.3 nA and relative standard deviation of 4.0%).

The inherent sensitivity of the method is apparent from comparison with the earlier procedure based on the manganese/dihydroxyazo-dyes complexes.[5] Figure 5 compares voltammograms for 10 $\mu$g/l. manganese in the presence of 5-Br-PADAP (A) to those obtained in the presence of the azo dye Eriochrome Black T (B) and Solochrome Violet RS (C). Both dihydroxyazo dyes yield a defined manganese peak, superimposed on a decaying background peak (associated with the reduction of the free ligand). A sharper and larger peak, and a lower baseline response, are observed in the presence of 5-Br-PADAP. Even more profound sensitivity improvements were observed using a differential pulse excitation waveform, for which the manganese–azo dyes peaks were obscured by those of the ligand while that of the

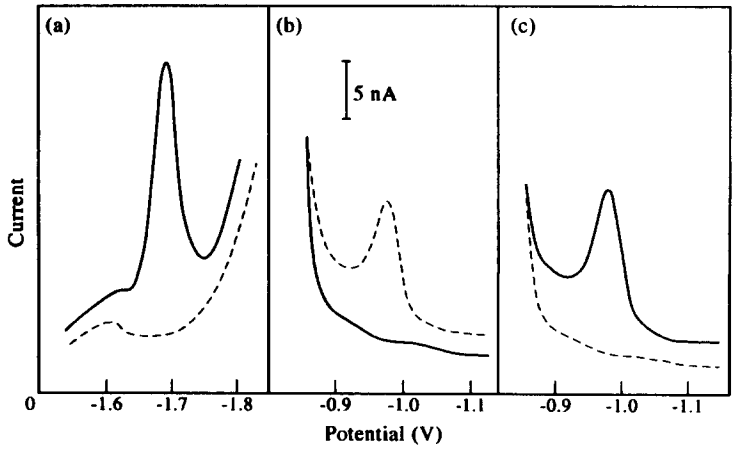


Fig. 5. Stripping voltammograms for 10 $\mu$g/l. manganese in the presence of 5-Br-PADAP (A), Eriochrome Black T (B), and Solochrome Violet RS (C). Conditions, (A) as in Fig. 2e, with $1 \times 10^{-5} M$ 5-Br-PADAP; (B, C), 0.02$M$ PIPES (pH 12) solution, containing $5 \times 10^{-6} M$ of the azo dye, using 60 sec accumulation at $-1.2$ V.

Mn–5-Br-PADAP complex was well defined (as in Fig. 4e).

The following metal ions (20 $\mu$g/l.) were tested and found not to affect the 2 $\mu$g/l. manganese response: Al(III), Bi(IIII), Sb(III), Ni(II), Cu(II), Zn(II), Cd(II), Pb(II), In(III), Ca(II), Mg(II), Ir(III) or Tl(I). It should be pointed out that analogous manganese measurements in the presence of Eriochrome Black T suffer from severe Cu(II), Zn(II), Ca(II) and Mg(II) interferences.[5] The lack of calcium and magnesium interference is of great significance because of their common presence in biological and environmental matrices (*e.g.* mg/l. level in natural waters). Even larger (500-fold) excess of these ions did not affect the manganese response. The insensitivity to copper is also significant considering severe copper–manganese intermetallic problems in conventional stripping measurements.[4] Depressions of the 2 $\mu$g/l. manganese peak were observed in the presence of 20 $\mu$g/l. uranium(VI), Fe(III), Ti(IV), V(V), Cr(III) and La(III). A separation step would be required in the presence of an excess of these metals. Organic surfactants that compete with the chelate on the surface sites represent another source of interference. While 1 mg/l. gelatin or sodium dodecyl sulphate did not affect the 10 $\mu$g/l. manganese peak (60 sec accumulation), 4 mg/l. of these surfactants caused 30 and 70% diminutions of the response, respectively.

In conclusion, the present study describes an effective means for the measurement of trace levels of manganese. Quantitation at the $\mu$g/l. level is feasible with short preconcentration times. The 5-Br-PADAP based approach offers a new selectivity dimension and enhances the signal-to-background characteristics, compared to an early adsorptive stripping procedure. Yet, an even more selective ligand is desired to address remaining selectivity problems. The attractive performance of the 5-Br-PADAP–Mn system should lead to various environmental or clinical applications, and may offer new information related to the speciation of manganese.

*Acknowledgement*—This work was supported by the Waste Management Education and Research Consortium (WERC).

## REFERENCES

1. J. Resing and M. Mottl, *Anal. Chem.*, 1992, **64**, 2682.
2. A. Miyazaki and H. Tao, *J. Anal. Atomic Spectrosc.*, 1991, **6**, 173.
3. J. O'Halloran, *Anal. Chim. Acta*, 1982, **140**, 51.
4. H. Eskilsson and D. R. Turner, *Anal. Chim. Acta*, 1984, **161**, 293.
5. J. Wang and J. Mahmoud, *Anal. Chim. Acta*, 1986, **182**, 147.
6. W. Jin, S. Shi and J. Wang, *J. Electroanal. Chem.*, 1990, **291**, 41.
7. J. Zhao and W. Jin, *J. Electroanal. Chem.*, 1989, **267**, 271.
8. J. Lu, W. Jin, S. Wang and T. Sun, *J. Electroanal. Chem.*, 1990, **291**, 49.

Pergamon

0039-9140(95)01399-7

*Talanta*, Vol. 42, No. 3, pp. 337–344, 1995

0039-9140/95 $9.50 + 0.00

# PRECONCENTRATION OF IRON (III), COBALT (II) AND COPPER (II) NITROSO-R COMPLEXES ON TETRADECYLDIMETHYLBENZYLAMMONIUM IODIDE–NAPHTHALENE ADSORBENT

BAL K. PURI and SANJAY BALANI

Department of Chemistry, Indian Institute of Technology, Hauz Khas New Delhi—110016, India

(*Received* 6 *December* 1993. *Revised* 8 *August* 1994. *Accepted* 16 *August* 1994)

**Summary**—Iron, cobalt and copper form coloured water soluble anionic complexes with disodium 1-nitroso-2-naphthol-3-6-disulphonate (nitroso R-salt). The anionic complex is retained quantitatively as a water insoluble neutral ion associated complex (M-nitroso R-TDBA) on tetradecyldimethylbenzylammonium iodide on naphthalene ($TDBA^+I^-$-naphthalene) packed column in the pH range of: Fe(III): 3.1–6.5, Co: 3.4–8.5 and Cu 5.9–8.0 when their solutions are passed individually over this adsorbent at a flow rate of 0.5–5.0 ml/min. The solid mass consisting of an ion associated metal complex along with naphthalene is dissolved out of the column with 5 ml dimethylformamide/chloroform and metals are determined spectrophotometrically. The absorbance is measured at 710 nm for iron, 425 nm for cobalt and 480 nm for copper. Beers law is obeyed in the concentration range 9.2–82 $\mu$g of iron, 4.2–7.2 $\mu$g of cobalt and 3.0–62 $\mu$g of copper in 5 ml of final $DMF/CHCl_3$ solution. The molar absorptivities are calculated to be Fe: $7.58 \times 10^3$, Co: $1.33 \times 10^4$ and Cu: $4.92 \times 10^4 M^{-1}$ cm$^{-1}$. Ten replicate determinations containing 25 $\mu$g of iron, 9.96 $\mu$g of cobalt and 3.17 $\mu$g of copper gave mean absorbances 0.677, 0.450 and 0.490 with relative standard deviations of 0.88, 0.98 and 0.92%, respectively. The interference of large number of metals and anions on the estimations of these metals has been studied. The optimized conditions so developed have been employed for the trace determination of these metals in standard alloys, waste water and fly ash samples.

Disodium 1-nitroso-2-naphthol-3,6-disulphonate (nitroso R-salt) was introduced in 1921 by Van Klooster for the detection of cobalt[1] and then subsequently used by various investigators for the determination of small quantities of this metal in plant and animal tissues,[2–7] soils,[8–10] grasses,[11,12] steels and carbides.[13] Preliminary experiments indicated that metalions like $Fe^{3+}$, $Co^{2+}$ and $Cu^{2+}$ also react with this reagent and form coloured water soluble anionic complexes. These anionic complexes in the presence of tetradecyldimethylbenzylammonium cation form coloured water insoluble ion associated complexes which can be easily adsorbed on microcrystalline naphthalene.

In the present communication we have synthesized tetradecyldimethylbenzylammonium iodide–naphthalene as an adsorbent and used it for the preconcentration of iron (III), cobalt (II) and copper (II) using nitroso R-salt as the chelating agent. This adsorbent is very easy to synthesize (simply by mixing the solutions) and is highly economical and gives a preconcentration factor $\sim 100$ for these metals. The interference of a large number of metal ions and anions has been studied in detail and the optimized conditions so developed have been employed for the preconcentration and determination of iron, cobalt and copper from the large volume of their aqueous solutions in alloys, waste water and fly ash samples. After preconcentration by this method, these metals may also be determined by atomic absorption spectrometrically by aspirating their DMF solution in a flame. However, the spectrophotometric method is much more economical (since it is cheaper than AAS and does not require any gas or maintenance), sensitive and free from matrix effect. The sensitivity and the selectivity of the developed method has been compared with recent methods reported in the literature (Tables 1 and 2). Except iron, the method is fairly sensitive for cobalt and copper but the preconcentration factor $\sim 100$ is a highly favourable factor for the trace estimation of these metals from a large volume of their aqueous solutions. The selectivity of the method is much better than most of the recent methods.

Table 1. Comparison of sensitivities of various methods

| Metal | Reagent | $M^{-1}\ cm^{-1}$ | Ref. |
|---|---|---|---|
| Fe | 3-Thiobenzoyl-1-*p*-tolythiocarbamide | $4.00 \times 10^3$ | 14 |
| | Mandelohydroxamic acid | $1.15 \times 10^4$ | 15 |
| | Thocyanate and cetyltrimethylammonium bromide | $3.59 \times 10^4$ | 16 |
| | Di-2-pyridylmethanone-2(5-nitro)pyridylhydrazone | $5.83 \times 10^4$ | 17 |
| | 2-Nitroso-5-(*N*-propyl-*N*-sulphopropylamino)phenol | $1.23 \times 10^4$ | 18 |
| | Present method ($TDBA^+I^-$ naphthalene) | $7.58 \times 10^3$ | |
| Cu | 3-Thiobenzoyl-1-*p*-tolylthiocarbamide | $1.00 \times 10^4$ | 14 |
| | 4-(2-quinolylazo)-1,3-Dihydroxy-naphthalene | $6.40 \times 10^3$ | 19 |
| | 1,2-Cyclohexanedione-2-oxime-1-guanylyhydrazone | $5.20 \times 10^3$ | 20 |
| | N(α-pyridyl)2-Thioquinaldinamide | $5.20 \times 10^3$ | 21 |
| | Cyclopentane-spiro-2-(1-phenyl-4-dithio)-*s*-triazine | $1.08 \times 10^4$ | 22 |
| | Present method ($TDBA^+I^-$ naphthalene) | $4.92 \times 10^4$ | |
| Co | 4-Bromodibenzoylmethane | $6.00 \times 10^3$ | 23 |
| | 3-Hydroxy-3-propyl-1-phenyltriazine | $1.00 \times 10^4$ | 24 |
| | 1,5-Bis(2-arsonophenyl) formazan | $5.70 \times 10^3$ | 25 |
| | Thiocyanate and ephederine | $4.30 \times 10^3$ | 26 |
| | 2-(5-bromo-2-pyridyazol)-5-Diethylaminophenol | $9.80 \times 10^4$ | 27 |
| | Present method ($TDBA^+I^-$ naphthalene) | $1.33 \times 10^4$ | |

Table 2. Comparison of selectivity of various methods

| Metal to be determined | Method | Tolerance limit | | | Tolerance limit | |
|---|---|---|---|---|---|---|
| | | Metal | Amount | | Metal | Amount |
| Fe(III) | Using PAN-Fe (III) | Co | 5 μg | Present method | Co | 200 μg |
| | CAPRIOUAT on a | Ni | 5 μg | | Ni | 500 μg |
| | membrane | Cu | 10 μg | | Cu | 700 μg |
| | | Al | 100 μg | | Al | 2.0 mg |
| | Ref. 28 | F | 500 μg | | F | 2.0 mg |
| Fe(III) | Tiron and $TDBA^+$ | Al(III) | 1.0 mg | Present method | Al(III) | 2.0 mg |
| | AAS | Ag | 1.0 mg | | Ag | 1.2 mg |
| | | Cd | 1.0 mg | | Cd | 1.2 mg |
| | | Pb | 1.0 mg | | Pb | 1.2 mg |
| | | Hg | 1.0 mg | | Hg | 1.2 mg |
| | | Bi | 1.0 mg | | Bi | 1.2 mg |
| | | Mn | 1.0 mg | | Mn | 1.2 mg |
| | | Pt | 50 μg | | Pt | 150 μg |
| | | Zn | 700 μg | | Zn | 1.5 mg |
| | | Mo | 500 μg | | Mo | 1.5 mg |
| | Ref. 29 | Cr | 500 μg | | Cr | 1.5 mg |
| Co | Cyanex 272 uv/vis | Al | <0.5 mg | Present method | Al | 2.0 mg |
| | | Cr | <0.5 mg | | Cr | 1.5 mg |
| | | Zn | <0.5 mg | | Zn | 1.5 mg |
| | | Mn | <0.5 mg | | Mn | 1.5 mg |
| | | V | <0.5 mg | | V | 0.7 mg |
| | Ref. 30 | Sn | <1.0 mg | | Sn | 1.5 mg |
| Co | Br PADAP with | Zn | 500 μg | Present method | Zn | 1.5 mg |
| | $NH_4^+$ $TPB^-$ as | Ni | 500 μg | | Cr | 1.5 mg |
| | adsorbent | V | 100 μg | | V | 700 μg |
| | AAS | Cu | 100 μg | | Cu | 700 μg |
| | Ref. 31 | | | | | |
| Cu | 2-Nitroso-1-naphthol | Cr | 100 μg | Present method | Cr | 1.5 mg |
| | 4-sulfonic acid | Co | 100 μg | | Co | 200 μg |
| | | Ni | 100 μg | | Ni | 500 μg |
| | | Pb | 300 μg | | Pb | 1.5 mg |
| | | Al | 200 μg | | Al | 2.0 mg |
| | | Hg, Bi, Zn | 1.0 mg | | Hg, Bi, Zn | 1.5 mg |
| | | Mn | 1.0 mg | | Mn | 1.5 mg |
| | Ref. 32 | Mo | 1.0 mg | | Mo | 1.5 mg |
| Cu | PQM | Os | 450 μg | Present method | Os | 1.0 mg |
| | | Cr | 1.0 mg | | Cr | 1.5 mg |
| | | Zn | 1.0 mg | | Zn | 1.5 mg |
| | | Pb | 1.0 mg | | Pb | 1.5 mg |
| | | F-, Cl-, $NO_3$-, $CH_3COO$-, $SO_4^{2-}$ | 10 mg each | | F-, Cl-, $NO_3$-, $CH_3COO$-, $SO_4^{2-}$ | 30 mg each |
| | Ref. 33 | | | | | |

## EXPERIMENTAL

### *Reagents*

Standard iron, cobalt and copper solutions were prepared from analytical grade ferric ammonium sulphate, cobalt (II) chloride and copper (II) sulphate in double distilled water and standardized by known methods. Sodium acetate/acetic acid and ammonia/ammonium acetate solutions were used to adjust the pH. Naphthalene, chloroform and dimethylformamide were checked spectrophotometrically before use. Double distilled water was used wherever needed. To study the interferences of various ions, a solution containing 25–30 mg of anion or 1 mg of cation were prepared in distilled water.

### *Preparation of tetradecyldimethylbenzyl-ammonium iodide–naphthalene*

A solution of naphthalene was prepared by dissolving 10 g in 100 ml of acetone. This solution was transferred to a beaker containing 0.8 g KI in 1000 ml of distilled water in a fast stream with continuous stirring. An aqueous solution of tetradecyldimethylbenzylammonium chloride ($TDBA^+Cl^-$) was prepared by dissolving 0.4 g in 250 ml of distilled water. This solution was transferred to the beaker containing the above solutions and stirred for 5 h. The supernatant solution was drained off by decantation. The residue was washed twice with distilled water. The final adsorbent $TDBA^+I^-$ supported on naphthalene was stored in a bottle for subsequent use.

### *Apparatus*

An Elico pH meter, Lambda 3b UV/VIS spectrophotometer and a Pye Unicam 191 atomic absorption spectrometer were used.

### *General procedure*

An aliquot of a metal ion solution, Fe: 9.2–8.2 μg, Co: 4.2–72 μg, and Cu: 3.0–62 μg was taken in a 100 ml beaker and to it, 0.2–4.0 ml of 0.20% solution of nitroso-R salt was added. The pH of these solutions was adjusted by adding a suitable volume of buffer solution (sodium acetate/acetic acid, ammonia/ammonium acetate) or dilute solutions of hydrochloric acid or sodium hydroxide (3–5 ml) to adjust the pH; Fe: 3.1–6.5, Co(II): 3.4–8.5 and Cu(II): 5.9–8.0. The metal complex solution was passed over the adsorbent (tetradecyldimethylbenzylammonium iodide–naphthalene, 0.2 g placed to height of 1.2 cm in a column) at a flow rate of 0.5–5.0 ml/min. Metal–nitroso R-TDBA complex along with naphthalene was dissolved out of the column with 5 ml of chloroform in the case of Fe(III) and 5 ml of DMF in the case of Co(II) and Cu(II). The absorbances were measured in a 1 cm cell at 710 nm for iron, 425 nm for cobalt and 480 nm of copper against the reagent blank prepared similarly.

## RESULTS AND DISCUSSION

### *Absorption spectra*

The absorption spectra of metal complexes were recorded in chloroform/dimethyl-

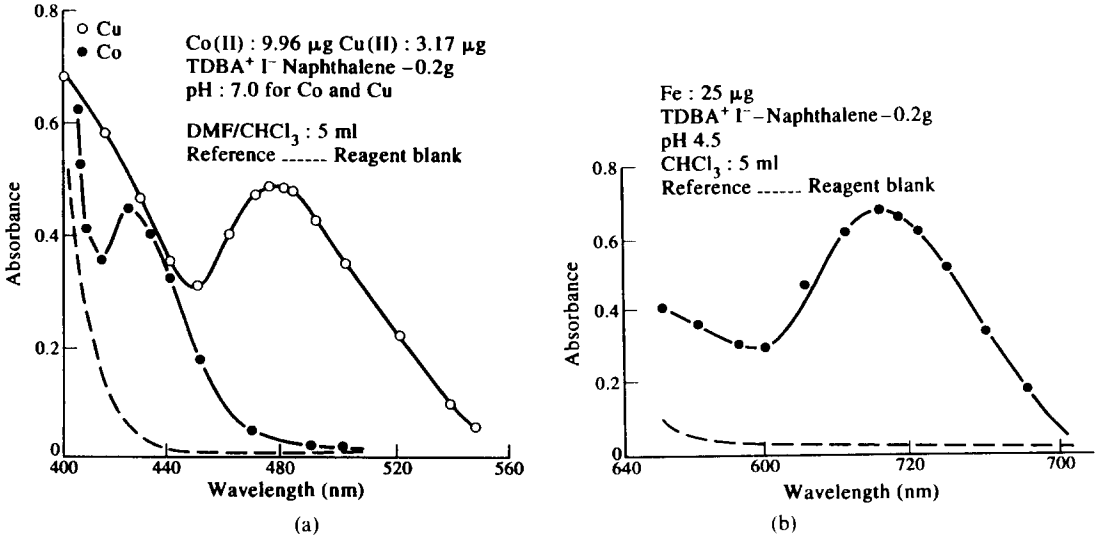


Fig. 1.

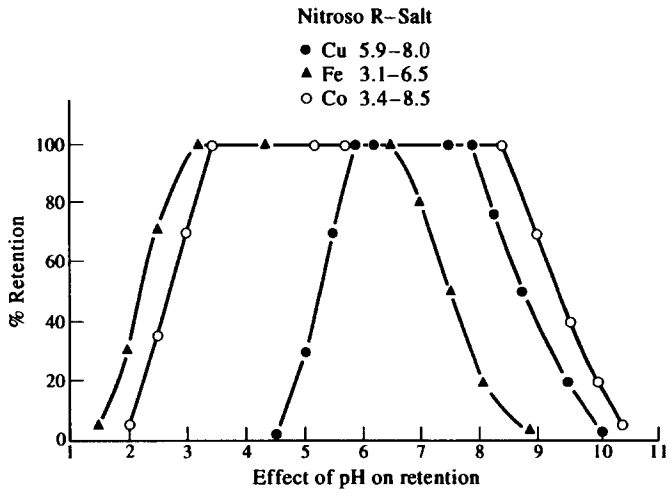


Fig. 2.

formamide against the reagent blank and the reagent blank against water (Fig. 1a, b). These complexes show absorption maxima, iron at 710 nm, cobalt at 425 nm and copper at 480 nm.

*Effect of pH*

Adsorption was carried out at different pH keeping other conditions constant. Adsorption was found to be maximum and constant in the pH range Fe(III): 3.1–6.5, Co(II) 3.4–8.5 and Cu(II): 5.9–8.0 (Fig. 2). Adsorption for each metal chelate anion was carried out by adding different volumes of buffer solutions. It was found that 1.0–5.0 ml of a buffer solution did not affect the percentage of retention of the metal complex on the adsorbent.

*Reaction conditions*

The reaction conditions were established taking 25.00 $\mu$g of iron, 9.96 $\mu$g of cobalt and 3.17 $\mu$g of copper.

Adsorption was maximum and constant when 0.1–1.2 g of tetradecyldimethylbenzylammonium iodide–naphthalene (adsorbent) and 0.2–4.0 ml of 0.20% (w/v) of the reagent (nitroso-R salt) were used. The volume of the aqueous phase containing the metal ion was varied from 20 to 500 ml. It was observed that the adsorbance was constant when the aqueous phase did not exceed 400–500 ml in all the cases (preconcentration factor of ~80–100).

Absorbance of metal–nitroso-R TDBA complex in chloroform/dimethylformamide was constant for 24 hr in all the cases.

Sodium chloride, sodium nitrate and sodium perchlorate when added in the concentration range of 0.01–0.1$M$ had no effect on the adsorption.

The affect of flow rate on adsorption was examined in the range of 0.5–10 ml/min. Adsorption was maximum and constant when the flow rate was between 0.5 and 5.0 ml/min. Above 5 ml/min, the percentage retention of the metal complexes decreased gradually. The percentage retention was decreased by 14% for iron, 8.8% for cobalt and 5% for copper at a flow rate of 10 ml/min.

A flow rate of 1 ml/min, was chosen for subsequent studies for convenience. In cases of larger aqueous phase volume, a flow rate of 5 ml/min may be maintained.

*Beer's law*

Beer's law was obeyed in the concentration range, Fe: 9.2–82 $\mu$g, Co: 4.2–72 $\mu$g and Cu: 3.0–62 $\mu$g, in 5 ml of final solution. The concentration range as given by a Ringbom plot (in ppm) was Fe: 1.84–6.0, Co: 0.8–3.6 and Cu: 0.2–1.27. The molar absorptivities for these complexes were calculated to be ($M^{-1}$ cm$^{-1}$) Fe: $7.58 \times 10^3$, Co: $1.33 \times 10^4$ and Cu $4.92 \times 10^4$. The sensitivity of the developed method is better than many of the recent methods reported in Table 1. Ten replicate determinations containing Fe: 25.00 $\mu$g, Co: 9.96 $\mu$g and Cu: 3.17 $\mu$g gave mean absorbances of 0.677, 0.450 and 0.492 with relative standard deviations of 0.88, 0.98 and 0.92%, respectively. The accuracy of this method was checked by the determination of these metal ions in standard alloys, waste water and fly ash samples.

*Composition of the metal complex*

The composition of the metal–nitroso R complex was studied by Job's method and mole ratio method. Peaks at 0.50 mole fraction for iron, 0.25 for cobalt and 0.33 for copper and a break at 1:1 for iron, 1:3 for cobalt and 1:2 for copper suggested the formation of $Fe(C_{10}H_5O_8NS_2)_2$, $Co(C_{10}H_5O_8NS_2)_3$ and $Cu(C_{10}H_5O_8NS_2)_2$. The structure of the metal–nitroso R-TDBA complex was confirmed by infrared analysis in which $-OH$ stretching was prominent at 3100–3450 $cm^{-1}$ in the free ligand but disappeared completely after the metal complex formation.

*Retention capacity of chelating agent supported on naphthalene*

The retention capacity of the chelating agent supported on naphthalene was determined for each metal ion by a batch method. This experiment was carried out by taking 350 $\mu$g of metal ion, 3–5 ml of buffer, 0.5–4.0 ml of 0.20% reagent (nitroso-R salt) and a suitable amount of the adsorbent in a 100 ml separatory funnel. This mixture was diluted to 30 ml. It was shaken with a mechanical shaker for 15 min and then filtered through a filter paper. The amount of the metal ion in the filtrate was determined by AAS. The retention capacity of metal ion was found to be proportional to the amount of TDBA on naphthalene and also on nitroso R-salt. The maximum capacity was found to be Fe: 1.2 mg, Co: 1.4 mg and Cu: 1.8 mg per g of adsorbent.

*Effect of diverse ions*

The interference of various ions on the estimation of these metal ions has been studied in detail. Generally, 30 mg of the alkali metal salts of anions and 1.5 mg salt of cations were added individually to the solution containing 25 $\mu$g of iron, 9.96 $\mu$g of cobalt and 3.17 $\mu$g of copper, respectively and the general procedure applied. Among the anions examined (Tables 3 and 4) large amounts of chloride, bromide, nitrate, acetate, carbonate and sulphate could be tolerated (30 mg each). Citrate, oxalate, orthophosphate, tartrate and EDTA interfered in all the cases. Except EDTA, a relatively low amount of these anions could be tolerated (Table 3). Obviously the stability constants of these metal–EDTA complexes must be higher than their metal nitroso R-salt complexes. Of the metal ions examined (Table 4), many did not interfere up to mg levels. $Rh^{3+}$, $Ru^{3+}$, $Pd^{2+}$ Os and V interfered, however relatively low amounts could be tolerated. The interference of copper in the determination of iron and cobalt was eliminated by adding 1 mg of thiourea during adsorption. Iron was masked with 3 ml of 5% NaF solution in the determination of copper and cobalt. $Ag^+$ was masked with 3 ml of 1% $Na_2S_2O_3$ in all cases. Interference of cobalt and nickel in the estimation of iron was

Table 3. Effect of diverse anions

| Alkali salt added | Salt of anion added (*mg*) | Fe 710 *nm* | Co Absorbance at 425 *nm* | Cu 480 *nm* |
|---|---|---|---|---|
| | — | 0.677 | 0.450 | 0.492 |
| Sodium chloride | 30 | 0.675 | 0.450 | 0.492 |
| Sodium sulphate | 30 | 0.677 | 0.448 | 0.491 |
| Sodium nitrate | 30 | 0.678 | 0.449 | 0.492 |
| Sodium acetate | 30 | 0.677 | 0.450 | 0.490 |
| Thiourea | 20 | 0.677 | 0.449 | 0.215 |
| | 2.0 | 0.677 | 0.450 | 0.492 |
| Amonium fluoride | 10 | 0.374b | 0.450 | 0.492 |
| | 2.5 | 0.677 | 0.451 | 0.491 |
| Potassium iodide | 25 | 0.677 | 0.451 | 0.491 |
| Sodium thiosulphates | 20 | 0.677 | 0.452 | 0.091 |
| | 2.0 | 0.677 | 0.452 | 0.492 |
| Potassium sodium tartrate | 10 | 0.400 | 0.201 | 0.201 |
| | 7.5 | 0.450 | 0.412 | 0.252 |
| | 6.0 | 0.650 | 0.432 | 0.475 |
| | 5.0 | 0.677 | 0.452 | 0.492 |
| EDTA | 0.08 | 0.092 | 0.221 | 0.101 |
| | 0.04 | 0.677 | 0.452 | 0.492 |

Fe: 25.00 $\mu$g, pH: 6.0.
Cu: 3.17 $\mu$g, pH: 7.5.
Co: 9.96 $\mu$g, pH: 6.5.
Nitroso R-Salt 2–4 ml (0.2%).

Table 4. Effective of diverse cations

| Metal salt added | Salt of metal added (*mg*) | Fe(III) 710 *nm* 0.677 | Co Absorbance at 425 *nm* 0.450 | Cu 480 *nm* 0.492 |
|---|---|---|---|---|
| Zinc (II) sulphate | 1.5 | 0.675 | 0.449 | 0.491 |
| Lead (II) nitrate | 1.5 | 0.677 | 0.450 | 0.490 |
| Manganese (II) sulphate | 1.5 | 0.674 | 0.450 | 0.491 |
| Silver (I) nitrate | 1.2 | 0.677 | 0.450 | 0.492 |
| Tin (II) chloride | 1.5 | 0.675 | 0.450 | 0.493 |
| Cadium (II) chloride | 1.5 | 0.675 | 0.450 | 0.493 |
| Aluminium (II) nitrate | 2.0 | 0.677 | 0.449 | 0.498 |
| Rhodium (III) chloride | 0.5 | 0.675 | 0.450 | 0.491 |
| Platinum (IV) chloride | 0.15 | 0.677 | 0.450 | 0.491 |
| Ruthenium (III) chloride | 0.07 | 0.677 | 0.450 | 0.492 |
| Palladium (II) chloride | 0.05 | 0.675 | 0.449 | 0.491 |
| Iridium (II) chloride | 1.5 | 0.677 | 0.450 | 0.492 |
| Bismuth (III) nitrate | 1.5 | 0.675 | 0.450 | 0.491 |
| Ammonium molybdate (VI) | 1.5 | 0.667 | 0.450 | 0.491 |
| Osmium tetraxoide (VIII) | 1.0 | 0.667 | 0.450 | 0.492 |
| Mercury (II) nitrate | 1.5 | 0.675 | 0.449 | 0.492 |
| Chromium (III) chloride | 1.5 | 0.677 | 0.450 | 0.491 |
| Iron (III) chloride | 0.20* | — | 0.450 | 0.490 |
| Nickel (II) sulphate | 0.500 | 0.677 | 0.450 | 0.492 |
| Copper (II) sulphate | 0.200† | 0.671 | 0.450 | — |
| | 0.700 | 0.677 | 0.449 | — |
| Cobalt (II) sulphate | 0.200 | 0.677 | — | 0.491 |
| Vanadium (V) sulphate | 0.700 | 0.677 | 0.450 | 0.490 |
| Tungsten (IV) chloride | 0.150 | 0.677 | 0.450 | 0.492 |

Conditions same as in Table 1

*Iron was masked with 3.0 ml of 5% sodium fluoride.

†Copper was masked with 1 *mg* of thiourea.

eliminated by pre-adsorption of cobalt and nickel at pH 8.4 where iron did not adsorb on the adsorbent and then after the removal of nickel and cobalt, iron was determined. At pH 8.4 iron does not interfere in the determination of cobalt.

*Determination of cobalt and copper in alloys*

A sample of an alloy (0.1–1.0 g) was dissolved in 10–15 ml of aqua regia on a water bath. After cooling, 3–5 ml of hydrogen peroxide (30%) was added. The excess of peroxide was decomposed by heating the solution on a water bath. The mixture was cooled and filtered if needed and then diluted to 250 ml with distilled water in a calibrated flask. An appropriate volume of this solution was taken, copper and cobalt were determined by the general procedure. The results are given in Table 5.

*Determination of iron and copper in fly ash and waste water sample*

A sample of fly ash (460–600 mg) was taken in a platinum crucible and 250 mg of $Li_3Bo_3$ was added. The crucible was heated at 700°C for an hour and then cooled. The contents of the crucible were transferred to a beaker containing 2.2*M* hydrochloric acid and diluted to 300 ml in a calibrated flask. An aliquot of this solution was taken and iron and copper were determined by the general procedure. Similarly, a waste water sample (100 ml) was treated with 2*M* HCl and heated to 200°C, it was allowed to cool, filtered and diluted to 50 ml in a calibrated flask and iron and copper were determined by general procedure. The relative standard deviation for five determinations in each case did not exceed ±1.3%. The results obtained by this method were found to be in good agreement with those obtained by standard methods reported in the literature.

## CONCLUSION

A solid ion pair produced from tetradecyldimethylbenzylammonium iodide on naphthalene provides a simple, rapid and economical method for column preconcentration of iron, cobalt and copper in alloys, waste water and fly ash sample using nitroso R-salt as the complexing agent. The proposed adsorbent is highly effective for the trace determination of these metal ions from a large volume of their aqueous phase (preconcentration factor 80–100). The method is relatively sensitive and selective as compared to recent methods re-

Table 5. Determination of iron, copper and cobalt in alloys

| Alloy | Composition (%) | Amount of copper found by present method (%) | Amount of iron found by present method (%) | Amount of cobalt found by present method (%) |
|---|---|---|---|---|
| NBS, SRM-85b Aluminium alloy | Cu: 3.99, Mg: 1.49 Mn: 0.61, Cr: 0.21 Si: 0.18, Fe: 0.24 An: 0.03, Ti: 0.02 Pb: 0.021, Ga: 0.019, V: 0.066, Ni: 0.084 | 3.92 ± 0.42 | 0.23 ± 0.020 | — |
| NBS, SRM-94c Die casting Alloy | Cu: 1.01, Al: 4.13 Sn: 0.06, Fe: 0.018 Cd: 0.002, Pb: 0.002 Mg: 0.042, Ni: 0.006 | 0.98 ± 0.017 | 0.017 ± 0.002 | — |
| JSS, 645-7 Stainless steel | Cu: 0.28, C: 0.060 Si: 1.29, Co: 0.45 Mn: 1.69, Cr: 24.84 Ni: 20.30, P: 0.031 Mo: 0.016, N: 0.025 | 0.27 ± 0.021 | — | 0.43 ± 0.042 |
| JSS, 6554-4 Stainless steel | Co: 0.29, C: 0.055 P: 0.33, S: 0.06 Ni: 11.48, Cr: 18.54 Mo: 0.051, Nb: 0.60 Si: 0.060, P: 0.033 N: 0.024, Cu: 0.29 | 0.28 ± 0.021 | — | 0.28 ± 0.029 |
| JSS, 654-7 Stainless steel | Co: 0.45, C: 0.060 P: 0.031, Ni: 20.33 Cr: 24.84, Cu: Mo: 0.016 Si: 1.29, Mn: 1.69 Cu: 0.028, N: 0.025 | 0.027 ± 0.002 | — | 0.44 ± 0.040 |

Average of five determinations, ±standard deviation.

ported in the literature. This adsorbent may also be employed for any metal ion which forms an anionic complex with a complexing agent. Instead of using spectrophotometry as a tool for the estimation of metals, atomic absorption or pulse polarography may also be employed after the preconcentration step. The sensitivity and selectivity of this method may be further improved by using derivative spectrophotometry.

## REFERENCES


1. H. S. Van Klooster, *J. Am. Chem. Soc.*, 1921, **43,** 746.
2. H. R. Marston and D. W. Dewey, *Aust. J. Exp. Biol. Med. Sci.*, 1940, **18,** 343.
3. K. J. McNaught, *Analyst*, 1942, **67,** 97.
4. K. J. McNaught, *Analyst*, 1939, **64,** 23.
5. J. W. H. Lugg and S. W. Josland, *Aust. J. Exp. Biol. Med. Sci.*, 1936, **14,** 319.
6. F. J. Stare and C. A. Elvehjem, *J. Biol. Chem.*, 1933, **99,** 473.
7. R. Q. Parks, S. L. Hood, C. Hurwitz and G. H. Ellis, *Ind. Engng Chem., Anal. Ed.*, 1943, **15,** 527.
8. E. B. Kidson, H. Q. Askew and J. K. Dixon, *N.Z. J. Sci. Technol.*, 1936, **18,** 601.
9. H. T. Macpherson and J. Sttewart, *Biochem. J.*, 1938, **32,** 763.
10. K. J. McNaught, *N.Z., J. Sci. Technol.*, 1936, **18,** 601.
11. E. B. Kidson and H. O. Askew, *N.Z. J. Sci. Technol.*, 1940, **21B,** 178.
12. L. I. Butler and H. D. Allen, *J. Assoc. Off. Agric. Chem.*, 1942, **25,** 567.
13. F. W. Haywood and A. A. R. Wood, *J. Soc. Chem. Ind.*, 1942, **62,** 37.
14. D. M. Ambhore and A. P. Joshi, *J. Indian Chem. Soc.*, 1991, **68,** 175.
15. F. Salinas, J. L. Martinez-Vidal, A. R. Fernandez-Alba, *Anal. Lett.*, 1989, **22,** 187.
16. T. K. Thokdar, P. K. Paria and S. K. Majumdar, *J. Indian Chem. Soc.*, 1989, **66,** 456.
17. T. Takaoka, M. Otomo and T. Taya, *Talanta*, 1992, **39,** 37.
18. N. Ohno and T. Sakai, *Analyst*, 1987, **112,** 1127.
19. Z. Zhengqi and Y. Rugin, *Sci. China, Ser. B*, 1989, **32,** 278.
20. F. Salinas, N. Berzas, J. Juan, V. Acedo and I. Maria, *Ann. Chim. (Rome)*, 1989, **79,** 405.
21. A. K. Chakrabarti, *Indian J. Chem.*, 1986, **25A,** 886.
22. J. D. Chavan and V. P. Joshi, *J. Indian Chem. Soc.*, 1990, **67,** 935.
23. S. C. Sharma and M. P. Tyagi, *Sci. Phy. Sci.*, 1990, **2,** 7.
24. D. N. Purohit and R. Bhatnagar, *J. Sci. Res.*, 1988, **10,** 7.
25. Z. Baowen, H. Wei, M. Grote and A. Kettrup, *Yejin Fenxi*, 1989, **9,** 13.
26. L. Fereria, R. A. Ensanety Berea, M. L. Bermajo, F. Martinez, *Anal. Lett.*, 1989, **22,** 1819.
27. Y. Sun and S. Qian, *Yejin Fenxi*, 1987, **7,** 27.

28. I. Mori, M. Toyoda, Y. Fujik, T. Matsuo and K. Taguchi, *Talanta*, 1994, **41,** 251.
29. M. Satake, T. Nagahiro and B. K. Puri, *J. Anal. Atom. Spectrom.*, 1992, **7,** 183.
30. M. N. Gandhi, N. V. Dorkar and S. M. Khopkar, *Talanta*, 1993, **40,** 1535.
31. M. Satake, T. Nagahiro and B. K. Puri, *Analyst*, 1993, **118,** 85.
32. M. Satake, J. R. Lee, B. K. Puri and M. Katyal, *Analysis*, 1992, **20,** 49.
33. S. Balani and B. K. Puri, *Anal. Lett.*, 1992, **25,** 593.

Pergamon

0039-9140(95)01406-3

*Talanta*, Vol. 42, No. 3, pp. 345–352, 1995

0039-9140/95 $9.50 + 0.00

# POTENTIOMETRIC STUDY OF REACTION BETWEEN PERIODATE AND IODIDE AS THEIR TETRABUTYLAMMONIUM SALTS IN CHLOROFORM. APPLICATION TO THE DETERMINATION OF IODIDE AND POTENTIOMETRIC DETECTION OF END POINTS IN ACID–BASE TITRATIONS IN CHLOROFORM

M. H. POURNAGHI-AZAR* and KH. FARHADI
Faculty of Chemistry, University of Tabriz, Tabriz, Iran

(*Received* 22 *March* 1994. *Revised* 22 *August* 1994. *Accepted* 22 *August* 1994)

**Summary**—A potentiometric method for the titration of tetrabutylammonium iodide (TBAI) in chloroform using tetrabutylammonium periodate (TBAPI) as a strong and suitable oxidizing reagent is described. The potentiometric conditions were optimized and the equilibrium constants of the reactions occurring during the titration were determined. The method was used for the determination of iodide both in chloroform and aqueous solutions after extraction into chloroform as ion-association with tetraphenylarsonium. The reaction between TBAPI and TBAI was also used as acid indicator for the potentiometric detection of end points of acid–base titrations in chloroform.

The high dissolving power and extracting property of chloroform against natural products, organic, organometallic and pharmaceutical compounds make it an excellent solvent and the study of electrochemical behaviour of these compounds in chloroform is interesting in order to develop new electroanalytical methods.

Peover was the first worker who employed polarography for the study of organic molecular complexes in chloroform.[1] In our previous works we have studied the electrochemical behaviour of quinones, anthraquinones and phenothiazines at a Hg electrode,[2–5] ferrocene at bare solid electrodes[6] and hydroquinone at polypyrrole-coated Pt electrode.[7] On the basis of results obtained from these studies, polarography was used for the determination of K group vitamins, anthracycline group anticancer and phenothiazinic drugs in pharmaceutical preparations,[5,8,9] 9,10-anthraquinone in paper samples, black liquors[4] and some naturally occurring hydroxy derivatives of 9,10-anthraquinone in medicinal plants.[10]

In aprotic solvents of low permittivity like chloroform ($\epsilon = 4.8$) all chemical reactions, including proton-transfer, electron-transfer and complex formation are greatly complicated by ion-association leading to ion-pairs of various types. Therefore, incomplete dissociation of electrolytes should be taken into account in potentiometric and, particularly, conductimetric measurements. Rumeau was the first worker to use potentiometry for studying the redox and complex formation reactions in chloroform and developed redox molecular scales in this solvent.[11] Golabi *et al.*[12] applied potentiometry for the detection of equivalence points in oxidimetric titrations of phenothiazinic drugs by bromine solution in chloroform. Recently we have developed the quinhydrone electrode in chloroform and used this electrode as acid indicator for the potentiometric detection of end points in acid–base titrations. A method for the calculation of the equilibrium constants of acid–base reactions in this solvent was proposed.[13]

The aim of this work was to study the reaction between tetrabutylammonium periodate and iodide in chloroform in order to develop a potentiometric titration method for iodide and use the redox system $IO_4^-/I_2$ as an acid indicator for the potentiometric detection of end points of acid–base titrations in this medium.

*Author to whom correspondence should be addressed.

## EXPERIMENTAL

### *Reagents*

The solvent used was chloroform G.R. from E. Merck or Janssen, tetrabutylammonium periodate (TBAPI), iodide (TBAI) and perchlorate (TBAP) were from Janssen or Fluka. (TBAI) was purified from a mixture of etheracetone. Other chemicals were P.A. grade from E. Merck or Fluka. A 0.001*M* solution of periodate was used. Chloroform solutions of perchloric and sulfuric acids were prepared by shaking a 10 ml portion of each concentrated acid and 20 ml chloroform in a separatory funnel for 30 min. The concentration of acids in the extracts was determined potentiometrically using a quinhydrone electrode as acid indicator and a standard solution of $(But)_3N$ in chloroform.[13] The other acid solutions were prepared by direct dissolving of required amount of pure acids in chloroform.

### *Apparatus*

Potentiograph E 536 equipped with an E 578 titration stand (Metrohm) or a Video titrator Vit 90 (Radiometer) coupled with a Toshiba P321SL printer were used to plot the normal and differential forms of the titration curves. The potentiometric cell was thermostated at $25 \pm 0.1°$ using a double membrane cell (Metrohm) and an Eyela UA-10 (Japan) thermostat.

The reference electrode Ag/AgCl (satd) 0.05*M* TBACl and 0.50*M* TBAP in chloroform prepared in a separated compartment with a dense ceramic plug in the bottom was used, the indicator electrode was Pt wire.

### *Procedure*

Tetrabutylammonium iodide 0.005 M (10 ml) was pipetted into the reaction cell, a suitable strong acid added up to 0.2*M*, and titrated by 0.001*M* tetrabutylammonium periodate at 0.5 ml/min.

## THEORETICAL

### *Equations of the potentiometric titration curves*

By gradual addition of periodate to iodide solution in chloroform, the reaction pathway between periodate and iodide may be two successive electron transfer steps forming $AI_3$ and $I_2$, respectively. In strongly acidic medium as 0.2*M* *p*-toluenesulfonic acid ($TSO_3H$) the first step of reaction can be shown as follows:

$$11AI + AIO_4 + 8TSO_3H \rightleftharpoons 4AI_3 + 8ATSO_3 + 4H_2O, \quad (1)$$

where A is the tetrabutylammonium cation. Assuming that the chloroform is saturated with $H_2O$ the equilibrium constant of reaction (1) is:

$$K_1 = \frac{[AI_3]^4[ATSO_3]^8}{[AI]^{11}[AIO_4][TSO_3H]^8}. \quad (2)$$

Before the equivalence point of reaction 1, the half cell reaction at the Pt electrode at 25°C can be shown as:

$$AI_3 + 2e + 2A^+ \rightleftharpoons 3AI$$

$$E = E_1^\circ + \frac{0.059}{2}\log\left(\frac{[AI_3][A^+]^2}{[AI]^3}\right). \quad (3)$$

Because of the ion-pair formation in chloroform the dissociation equilibria for $A^+I^-$, $A^+I_3^-$, $A^+TSO_3^-$ and $A^+IO_4^-$ should be considered.

$$AI \rightleftharpoons I^- + A^+ \quad K_{d_1} = \frac{[A^+][I^-]}{[AI]} \quad (4)$$

$$AI_3 \rightleftharpoons I_3^- + A^+ \quad K_{d_2} = \frac{[A^+][I_3^-]}{[AI_3]} \quad (5)$$

$$ATSO_3 \rightleftharpoons TSO_3^- + A^+ \quad K_{d_3} = \frac{[A^+][TSO_3^-]}{[ATSO_3]} \quad (6)$$

$$AIO_4 \rightleftharpoons IO_4^- + A^+ \quad K_{d_4} = \frac{[A^+][IO_4^-]}{[AIO_4]}, \quad (7)$$

from equations (4)–(6) we have:

$$[A^+] = [I^-] + [I_3^-] + [TSO_3^-]$$

$$= \frac{K_{d_1}[AI]}{[A^+]} + \frac{K_{d_2}[AI_3]}{[A^+]} + \frac{K_{d_3}[ATSO_3]}{[A^+]}. \quad (8)$$

According to the following equation:

$$-\log K_d = C^{te} + \frac{0.43Z_1Z_2Ne^2}{(r^+ + r^-)RT} \times \frac{1}{\epsilon},$$

in which the cation radii ($r^+$) is constant and large for ion-pairs $A^+B^-$, the influence of the anion radii ($r^-$) change upon the log $K_d$ can be neglected and in a first approximation we can assume that:

$$K_{d_1} = K_{d_2} = K_{d_3} = K_{d_4} = K_d.$$

Thus equation (8) can be written as:

$$[A^+]^2 = K_d([AI] + [AI_3] + [ATSO_3]). \quad (9)$$

Considering:

$$x = \frac{\text{added amount of } AIO_4}{\text{required amount of } AIO_4 \text{ until the first equivalence point}} = \frac{\text{added } AIO_4}{C_0/11},$$

where $C_0$ is initial concentration of AI solution. At any point of the titration, we have:

$$F = V/(V+v);$$

$$[AI] = FC_0(1-x);$$

$$[AI_3] = 4FxC_0/11$$

$[ATSO_3] = 8FxC_0/11$ and equation (3) can be shown as:

$$E = E_1^0 + \frac{0.059}{2} \times \log\left[\frac{K_d[FC_0(1-x) + 4FxC_0/11 + 8FxC_0/11](4FxC_0/11)}{[FC_0(1-x)]^3}\right], \quad (10)$$

where $V$ is initial volume of AI and $v$ is added volume of $AIO_4$ or:

$$E = a_1 + \frac{0.059}{2}\log\left(\frac{x(x+11)}{F(1-x)^3}\right), \quad (11)$$

where:

$$a_1 = E_1^0 + \frac{0.059}{2}\log K_d + \frac{0.059}{2}\log(4/121C_0). \quad (12)$$

For a Nerstian behaviour of potential variation, the plot of $E$ *vs.* $\log[x(x+11)/F(1-x)^3]$ should be a straight line with a slope of $0.059/2V$.

The second step of the oxidation reaction is attributed to the oxidation of $AI_3$ formed in the first step to $I_2$ as:

$$7AI_3 + AIO_4 + 8TSO_3H \rightleftharpoons 11I_2 + 8ATSO_3 + 4H_2O \quad (13)$$

$$K_2 = \frac{[I_2]^{11}[ATSO_3]^8}{[AI_3]^7[AIO_4][TSO_3H]^8}. \quad (14)$$

Before the second equivalence point the half cell reaction at the Pt electrode in this step will be:

$$3I_2 + 2e + 2A^+ \rightleftharpoons 2AI_3$$

$$E = E_2^0 + \frac{0.059}{2}\log\left(\frac{[I_2]^3[A^+]^2}{[AI_3]^2}\right). \quad (15)$$

Considering the dissociation equilibrium of $AI_3$ (equation 5) and $ATSO_3$ (equation 6), equation (15) can be written as:

$$E = E_2^0 + \frac{0.059}{2}\log\left(\frac{K_d([ATSO_3] + [AI_3])[I_2]^3}{[AI_3]^2}\right). \quad (16)$$

According to reaction (13) in the interval of $1 < x < 11/7$, ($x = 11/7$ corresponds to second equivalence point) and considering that the concentration of produced AI in first step is $4FC_0/11$, we have:

$[AIO_4]$ added in this step $= F(xC_0/11 - C_0/11)$

$$[AI_3] = FC_0(1 - 7x/11)$$

$$[I_2] = FC_0(x-1)$$

$$[ATSO_3] = 8xC_0F/11.$$

Therefore, equation (16) can be rewritten as:

$$E = E_2^0 + \frac{0.059}{2} \times \log\left(\frac{11F^2C_0^2K_d(x-1)^3(11+x)}{(11-7x)^2}\right) \quad (17)$$

or

$$E = a_2 + \frac{0.059}{2}\log\left(\frac{F^2(x-1)^3(11+x)}{(11-7x)^2}\right), \quad (18)$$

where

$$a_2 = E_2^0 + \frac{0.059}{2}\log K_d + \frac{0.059}{2}\log 11C_0^2. \quad (19)$$

A plot of $E$ *vs.* $\log(F^2(11+x)(x-1)^3/(11-7x)^2)$ must be a straight line with a slope of $0.059/2$ $V$.

After the second equivalence point the half cell reaction in this interval is:

$$2AIO_4 + 14e^- + 16TSO_3H \rightleftharpoons I_2 + 2ATSO_3 + 14TSO_3^- + 8H_2O$$

$$E = E_3^0 + \frac{0.059}{14}\log\frac{[AIO_4]^2[TSO_3H]^{16}}{[I_2][ATSO_3]^2[TSO_3^-]^{14}}. \quad (20)$$

From equation (6)

$$[TSO_3^-]^2 = K_{d_3}^2[ATSO_3]^2/[A^+]^2, \quad (21)$$

since

$$[A^+] = K_{d_3}[ATSO_3] + K_{d_4}[AIO_4] = K_d([ATSO_3] + [AIO_4]). \quad (22)$$

Therefore,

$$[TSO_3^-]^2 = K_d[ATSO_3]^2/([ATSO_3] + [AIO_4]), \quad (23)$$

considering

$$[AIO_4] = (FxC_0/11 - FC_0/7),$$
$$[I_2] = 4FC_0/7,$$
$$[ATSO_3] = 8FC_0/7$$
$$[A^+]^2 = K_d FC_0(11 + x)/11$$

we can write

$$E = a_3 + \frac{0.059}{14}\log(7x - 11)^2(11 + x)^7/F^8, \quad (24)$$

where

$$a_3 = E_3^0 - \frac{0.059}{14}\log C_0^8 - \frac{0.059}{2}\log K_d + 0.0671 \log[TSO_3H] + 0.049. \quad (25)$$

A plot of $E$ *vs.* $\log(7x - 11)^2(11 + x)^7/F^8$ should be a straight line with a slope of $0.059/14$ $V$.

*Potentiometric determination of equilibrium constants*

During the gradual addition of $AIO_4$ to the AI in chloroform the redox reactions of (1), (13) and complex formation reaction of (26) can simultaneously occur as follows:

$$I_2 + AI \rightleftharpoons AI_3 \quad (26)$$

$$K_c = \frac{[AI_3]}{[I_2][AI]} \quad (27)$$

and their equilibrium constants may be determined potentiometrically.

*Determination of* $K_c$

This constant may be obtained as follows: subtracting equations (12) and (19) leads us to:

$$a_2 - a_1 = E_2^0 - E_1^0 + \frac{0.059}{2}\log(332.75C_0^3). \quad (28)$$

Since the potentials of the half cell at the Pt electrode in this interval $(0 < x < 1)$ given by equations (3) and (15) are the same, one can conclude that:

$$E_2^0 + \frac{0.059}{2}\log\frac{[I_2]^3[A^+]^2}{[I_3A]^2} = E_1^0 + \frac{0.059}{2}\log\frac{[AI_3][A^+]^2}{[AI]^3}$$

or

$$E_2^0 - E_1^0 = 0.0885 \log K_c. \quad (29)$$

Inserting equation (29) into equation (28) leads us to:

$$a_2 - a_1 = \frac{0.059}{2}\log(332.75C_0^3) + 0.088 \log K_c. \quad (30)$$

$a_1$ and $a_2$ are determined by means of plots of $E$ *vs.* $\log(x(11 + x)/F(1 - x)^3)$ for $0 < x < 1$ and $E$ *vs.* $\log(F^2(x + 11)(x - 1)^3/(11 - 7x)^2)$ for $1 < x < 11/7$ using the experimental potentiometric titration curves of the known solutions of AI by $AIO_4$.

*Determination of* $K_1$

$K_1$ is accessible from the experimental measurement of $a_1$ and $a_3$: subtraction of equations (25) and (12) leads us to:

$$a_3 - a_1 = E_3^0 - E_1^0 - \frac{0.059}{14}\log C_0 + 0.0591 \log K_d = +0.067 \log[TSO_3H] + 0.093 \quad (31)$$

and according to the equations (2), (3), (20) and (6)

$$E_3^0 - E_1^0 = 0.059 \log K_d - \frac{0.059}{14}\log K_c + \frac{0.059}{7}\log K_1. \quad (32)$$

By inserting equation (32) in equation (31)

$$a_3 - a_1 = -\frac{0.059}{14}\log C_0 + \frac{0.059}{7}\log K_1 - \frac{0.059}{14}\log K_c + 0.067 \log[TSO_3H] + 0.093. \quad (33)$$

$a_3$ can be obtained from the plot of $E$ *vs.* $\log(7x - 11)^2(x + 11)^7/F^8$ for the last segment of the titration curve $(x > 11/7)$ and $\log K_1$ may be calculated from equation (33).

*Determination of* $K_2$

This may be calculated by subtraction of equations (19) and (25)

$$a_3 - a_2 = E_3^0 - E_2^0 - \frac{0.059}{14}\log C_0^{22} - 0.059 \log K_d + 0.067 \log[TSO_3H]. \quad (34)$$

According to equations (15), (20), (5) and (6) we have:

$$E_3^0 - E_2^0 = 0.059 \log K_d + \frac{0.059}{7} \log K_2. \quad (35)$$

Inserting equation (35) in equation (34) gives equation (36) and $\log K_2$ can be determined:

$$a_3 - a_2 = -\frac{0.059}{14} \log C_0^{22} + \frac{0.059}{7} \log K_2 + 0.067 \log[TSO_3H] + 0.018. \quad (36)$$

## RESULTS AND DISCUSSION

The potentiometric curve for the titration of 10 ml 0.005*M* TBAI by a 0.001*M* solution of TBAPI in the presence of a suitable strong acid such as $TSO_3H$ in chloroform is shown in Fig. 1. Two equivalence points corresponding to reactions (1) and (13), are discernible. The color of the titrating solution before the first equivalence point ($0 < x < 1$) was yellowish ($AI_3$ formation) which tended to orange ($AI_3$ and $I_2$ mixture) between the first and second equivalence points ($1 < x < 11/7$). Finally its color changed to violet ($I_2$) after the second equivalence point.

*Influence of acid*

The potentiometric titration plots for a 0.005*M* solution of TBAI were recorded in the presence of various organic and inorganic strong acids. During the titration, $HClO_4$ reacts as an oxidizing agent and the stoichiometry of the reactions according to (1) and (13) was not verified. On the other hand methanesulfonic acid with a moderate concentration, is not strong enough for a quantitative proceeding of reaction (13). The titration curve in the presence of trichloroacetic acid was not reproducible, the electrode potential suffers from a loss of stability during its measurement and the first equivalence point is a poor one. A well defined and reproducible curve was recorded in the presence of *p*-toluenesulfonic and sulfuric acids. Two illustrative curves are shown in Fig. 2. On the other hand the precision and accuracy of the titrations were influenced by the titration speed. More precise and accurate results were obtained with a speed of 0.5 ml/min. The detection of equivalence points is more precise by inflection mode potentiometry.

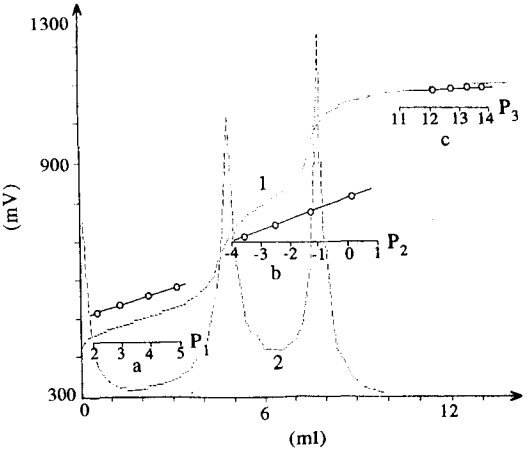


Fig. 1. Potentiometric titration of 10 ml 0.005*M* TBAI + 0.2*M* $TSO_3H$ with 0.001*M* TBAPI solution. (1) Plot of *E vs.* $V_{IO_4}$, (2) plot of $\Delta E/\Delta V$ *vs.* $V_{IO_4}$. (a) Plot of *E vs.* $P_1 = \log[x(11+x)/F(1-x)^3]$, (b) plot of *E vs.* $P_2 = \log[F^2(x-1)^3(11+x)^2/(11+7x)]$, (c) plot of *E vs.* $P_3 = \log[(7x-11)^2(x+11)^7/F^8]$.

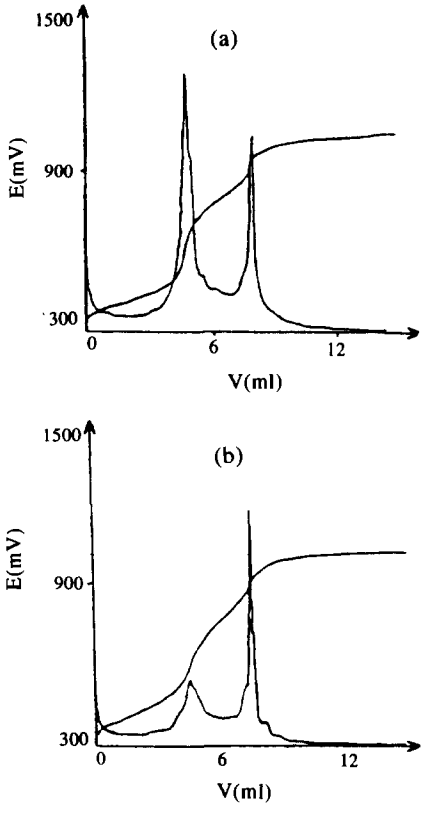


Fig. 2. Titration curves of 10 ml TBAI 0.005*M* by 0.001*M* solution of TBAPI, in the presence of 0.2*M* (a) toluenesulfonic acid, (b) methanesulfonic acid.

*Influence of water*

The addition of a few drops of water to the sample solution (IA) or using an aqueous concentrated solution of $HClO_4$ and $H_2SO_4$ gives rise to second phase formation and the extraction of $I_3^-$, produced during the first step (1), into the aqueous phase. The potential measured

in this condition did not agree with the relationships developed in chloroform (see Theoretical section). In addition, the curves obtained were not verified.

*Influence of the tetrabutylammonium salts*

Potentiometry in the presence of 0.5*M* TBAP shows that the electrode potential is more stable and two well defined equivalence points were observed. But in the presence of $TSO_3H$–$ATSO_3$ and $H_2SO_4$–$AHSO_4$, the solution was buffered, the oxidation reactions became less quantitative and the second step of AI oxidation cannot proceed.

*Determination of the equilibrium constants of reactions*

To prevent intervening of ion-pairs dissociation equilibrium of TBAP, with unknown equilibrium constants, in a thermodynamic analysis of the electrode potential changes, we used potentiometric titration curves recorded in the absence of this salt in spite of its influence on the stability of the potentials measured. The plots of $E$ *vs.* $\log[x(11+x)/F(1-x)^3]$ for the first segment of the titration curve ($0 < x < 1$), $E$ *vs.* $\log[F^2(x-1)^3(11+x)/(11-7x)^2$ for the second segment ($1 < 11/7$) and $E$ *vs.* $\log[(7x-11)^2(x+11)^7/F^8]$ for the last segment were straight lines with slopes of 0.030, 0.031 and 0.005 (Fig. 1a–c), respectively. These agree with the proposed stoichiometry for the titration reactions and equations (30), (33) and (36) allowed the calculation of $K_c$, $K_1$ and $K_2$, respectively. The results obtained are shown in Table 1.

*Analytical applications*

*Determination of iodide concentration.* Since the tetrabutylammonium iodide is used as a phase-transfer catalyst for some organic syntheses in the water–chloroform system,[14,15] the proposed potentiometric method was conveniently used for the determination of this catalyst in chloroform. In addition at pH 1–12 the iodide was extracted from aqueous solutions into chloroform as ion association with tetrabutylammonium chloride,[16] tetraphenylarsonium chloride[17] or tetraphenylphosphonium chloride[18] and then titrated potentiometrically. The method is selective in the presence of bromide and the relative standard deviation for three determination at 0.005*M* concentration level was 1.5%. A typical example of the titration curve for iodide, after its extraction from a 0.005*M* aqueous solution of $I^-$ and $Br^-$ with tetraphenylarsonium chloride into chloroform is shown in Fig. 3. The titration curve exhibits one equivalence point and the concentration of iodide can be determined.

Table 1. Calculated equilibrium constants

| | | | |
|---|---|---|---|
| Intercepts* of $y$-axis | $a_1 = 312.7$ | $a_2 = 671.8$ | $a_3 = 870.4$ |
| Equilibrium* constants | $\log K_c = 5.5$ | $\log K_1 = 62.2$ | $\log K_2 = 1.1$ |
| SD | 0.08 | 0.78 | 0.06 |

*Mean of three determinations.

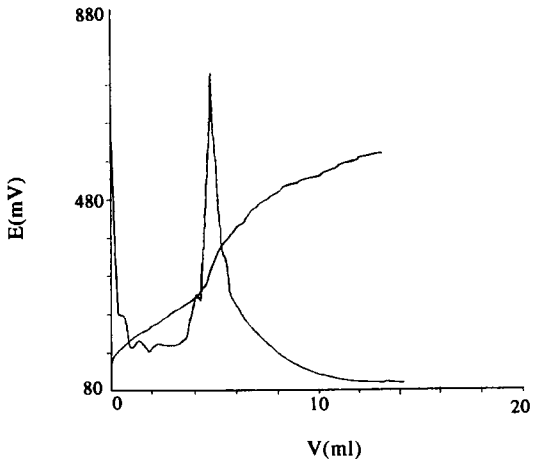


Fig. 3. Potentiometric titration curve for 10 ml chloroform solution of iodide (extracted from an aqueous solution of $I^-$ and $Br^-$ each 0.025*M* as ion association with tetraphenylarsonium into 25 ml chloroform). The titrant solution was a 0.001*M* TBAPI.

*Potentiometric detection of end points in acid–base titrations.* The reaction between periodate (TBAPI) and iodide (TBAI) may be utilized (i) for the potentiometric titration of strong acids and (ii) as a potentiometric indicator for the detection of end points of acid–base titrations in chloroform.

*Titration of Strong Acids*

On the basis of results obtained from potentiometric titration of TBAI with TBAPI, only strong acids seem to be titrated by this way. This can be carried out according to three different procedures as follows: (i) titration of a known solution of TBAI in the presence of TBAPI (excess amount) by the sample acid solution. (ii) Titration of TBAI solution in the presence of the acid sample by TBAPI. (iii) Titration of TBAPI solution in the presence of the acid sample by TBAI. Of the three proposed pro-

cedures only (i) gives a precise and accurate result. A typical example of the titration curve for *p*-toluenesulfonic acid solution is presented in Fig. 4. These behaviors are predictable from the values obtained for $K_c$, $K_1$ and $K_2$ and competition between the various chemical reactions occurring in the titration process.

*Detection of End Points of Acid–base Titrations*

This can be carried out only in the case of the acidimetric mode. The titration plots for 10 ml 0.01*M* solution of various organic bases, by 0.01*M* solution of some organic acid having a different strength are recorded in the presence of $5 \times 10^{-5}M$ TBAI and $2 \times 10^{-2}M$ TBAPI in chloroform. The potential ranges from 0.300 to 1.100 *V vs.* reference electrode with a large rise in the region of the equivalence point for strong acids and bases. The relative standard deviation for three assays of $10^{-2}M$ of the acids or bases was 1–2% depending on the strength of the analyte. Note that the precision and accuracy of the method depend on the concentration of TBAI and titration speed. The most reliable results were obtained with $5 \times 10^{-5}M$ of TBAI and 0.5 ml/min. Typical examples of the titration plots are shown in Fig. 5.

## CONCLUSIONS

On the basis of the results obtained, the chloroform solution of TBAPI in the presence of a suitable strong acid can be used as a powerful and stable reagent for oxidimetric titration in chloroform. The titration reactions were rapid in acidic medium and among the various strong organic and inorganic acids, *p*-toluenesulfonic was convenient for this purpose. The equilibrium constants of the titration reactions may be determined potentiometrically and the reaction between TBAPI and TBAI may be used as a potentiometric indicator for the detection of acid–bases titrations in chloroform.

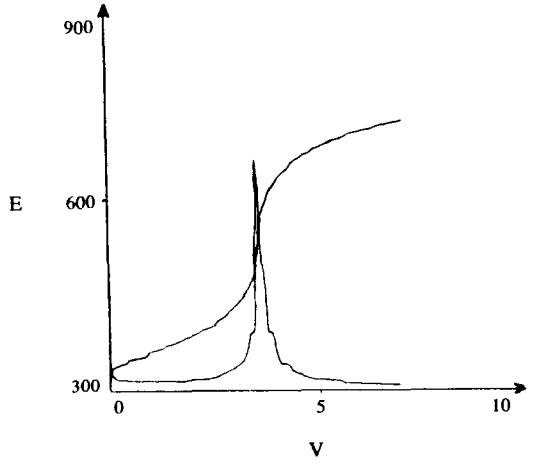


Fig. 4. Titration curve of 10 ml TBAI 0.005*M* + TBAPI (excess amount) by a chloroform solution of *p*-toluenesulfonic acid.

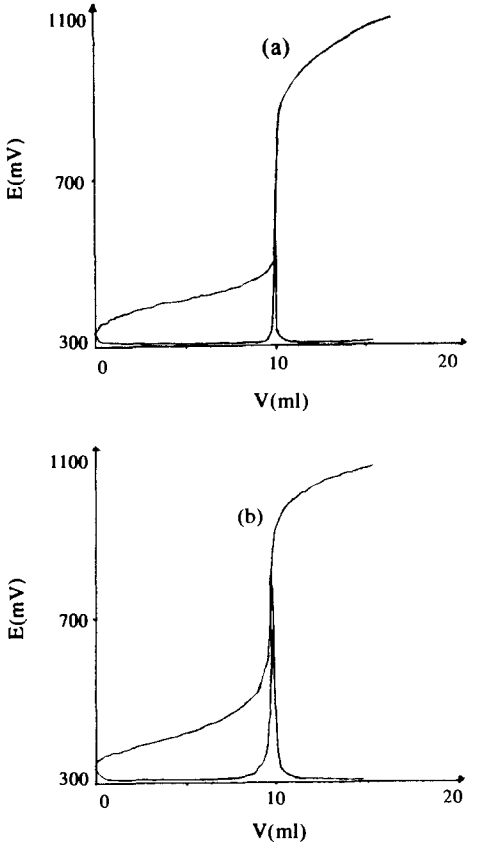


Fig. 5. Typical example of acidimetric titration of 10 ml 0.01*M*. (a) $(Bu)_3N$, by a 0.01*M* methanesulfonic acid, (b) $(C_3H_7)_2HN$ by 0.01*M* *p*-toluenesulfonic acid in the presence of $5 \times 10^{-5}M$ TBAI and $2 \times 10^{-2}M$ TBAPI.

## REFERENCES

1. M. E. Peover, *J. Chem. Soc. Trans. Faraday Soc.*, 1964, **60**, 417.
2. S. M. Golabi and M. H. Pournaghi-Azar, *Electrochim. Acta*, 1987, 32.
3. M. H. Pournaghi-Azar and S. M. Golabi, *Iran. J. Sci. Technol.*, 1987, **13**, 37.
4. M. H. Pournaghi-Azar and S. M. Golabi, *Talanta*, 1988, **35**, 959.
5. S. M. Golabi, M. H. Pournaghi-Azar and M. B. Shabani, *J. Pharm. Belg.*, 1988, **43**, 19.
6. M. H. Pournaghi-Azar and R. Ojani, *Electrochim. Acta*, 1994, **39**, 953.
7. M. H. Pournaghi-Azar and R. Ojani, *Talanta*, in press.

8. M. H. Pournaghi-Azar and S. M. Golabi, *J. Pharm. Belg.*, 1987, **42,** 315.
9. S. M. Golabi and D. Nematollahi, *J. Pharm. Bio. Anal.*, 1992, **10,** 1053.
10. M. H. Pournaghi-Azar, F. Shemirani and S. Pourtork, *Talanta*, in press.
11. M. Rumeau. In *Chemistry of Nonaqueous Solvent*, J. J. Lagowski (ed.) Vol. IV, p. 87. Academic Press, New York, 1976.
12. S. M. Golabi and M. Showkati-Shishvan, *Talanta*, 1991, **38,** 1253.
13. M. H. Pournaghi-Azar and J. Ordokhanian, *Talanta*, 1994, **41,** 611.
14. Review, *Angew. Chem.* 1987, **89,** 521.
15. E. V. Dehmlow. In *Encyclopedia of Chemical Technology*, Kirk-Othmer (ed.) Vol 5, p. 62. John Wiley & Sons, New York
16. K. Gustavii, *Acta Pharm. Suec*, 1967, **4,** 233.
17. R. Bock and G. M. Z. Beilstein, *Anal. Chem.*, 1963, **192,** 44.
18. R. Bock and J. Z. Jainz, *Anal. Chem.*, 1963, **198,** 315.

Pergamon

0039-9140(95)01409-8

*Talanta*, Vol. 42, No. 3, pp. 353–360, 1994

0039-9140/95 $9.50 + 0.00

# SIMULTANEOUS REDUCTION OF ARSENIC AND LEAD TO HYDRIDES BY SODIUM TETRAHYDROBORATE(III) FOR INDUCTIVELY COUPLED PLASMA-ATOMIC EMISSION SPECTROMETRY: AN INVESTIGATION INTO THE REACTION MEDIUM

HENGWU CHEN[1], JIANZHI WU[2] and IAN D. BRINDLE[3]*

[1]Department of Chemistry, Hangzhou University, Hangzhou, Zhejiang 310028, China
[2]Laboratory Centre, Hangzhou University, Hangzhou, Zhejiang 310028, China
[3]Chemistry Department, Brock University, St. Catharines, Ontario L2S 3A1, Canada

(*Received* 16 *June* 1994. *Revised* 30 *August* 1994. *Accepted* 31 *August* 1994)

**Summary**—Nitroso R salt and potassium ferricyanide, in hydrochloric acid, have been used as the reaction medium for simultaneous generation of arsine and plumbane, combined with inductively coupled plasma-atomic emission spectrometric detection. Both of the reagents enhance the lead signal and neither reagent inhibits the arsenic signal, provided that the potassium ferricyanide is mixed on-line with the analyte solution. Potassium iodide, which is used to prereduce As(V) to As(III), does not interfere with plumbane generation in both reaction systems. Various parameters affecting the signals have been studied, and the hydrochloric acid–potassium ferricyanide system has proved to be a better reaction medium. Detection limits of lead and arsenic are 1.1 and 2.8 ng/ml, respectively, have been obtained in the HCl–$K_3Fe(CN)_6$ system at a sample uptake rate of 1.5 ml/min.

The contents of arsenic and lead in the environment is of great concern because both of them are recognized as cumulative poisons to animals and people. In addition, arsenic has been identified as a potential human carcinogen. Therefore, determination of trace arsenic and lead in various samples is of great interest of analysts and environmental chemists.

Among the various techniques, inductively coupled plasma-atomic emission spectrometry (ICP-AES) is favored because of its capability for multi-element analysis. However, the sensitivity of ICP-AES by solution nebulization cannot meet the needs of determining As and Pb at low trace and ultra-trace concentrations. The combination of ICP with mass spectrometry does provide excellent detection limits for arsenic and lead of less than 1 ng/ml,[1] but the expense of such equipment has prevented their being commonplace in analytical laboratories.

Since Thompson and co-workers combined ICP-AES with hydride generation[2] in 1978, this technique has received considerable attention by analysts because the sensitivity and detection limit could be greatly improved, compared to those obtained by conventional solution nebulization into an ICP source. Thus, methods of sequential or simultaneous determination of hydride forming elements,[3] and simultaneous determination both hydride forming elements and non hydride forming elements[4,5] have been developed. Nevertheless, it is difficult to find reasonable compromise conditions required for the simultaneous determination of all eight of the hydride forming elements because of their different requirements for hydride formation. Thompson *et al.* reported that germanium and tin could not be reduced satisfactorily by sodium tetrahydroborate(III) under the high acid conditions necessary for the reduction of arsenic, antimony, bismuth, selenium and tellurium and hence had to be separately reduced in a low acid medium.[6]

Oxidation state of the analytes is another important factor affecting the hydride formation. Trivalent arsenic and antimony, quadrivalent selenium and tellurium are more easily reduced to hydrides in comparison to the corresponding species of higher oxidation state.[7] Therefore, prereduction reagents, such as potassium iodide,[8] potassium iodide plus ascorbic acid,[9] and L-cysteine,[10] have been used to

*Author to whom correspondence should be addressed.

convert arsenic(V) to arsenic(III) before hydride generation. On the other hand, efficient generation of plumbane from lead(II) requires the presence of strong oxidizing reagent such as potassium dichromate,[11,12] hydrogen peroxide[12,13] and ammonium peroxodisulfate.[12] It has been assumed that the lead(II) was converted to metastable lead(IV) by the oxidant before it was reduced to plumbane.[13] The introduction of strong oxidizing reagents into the reaction medium prevented simultaneous reduction of other hydride forming elements, as reported by Zen and his co-workers:[5] the enhancement of lead signal, owing to the presence of $H_2O_2$ and $(NH_4)S_2O_8$, was obtained at the sacrifice of 99, 98, 70 and 32% decrease in the signals from selenium, tellurium, arsenic, and antimony, respectively. The conflicting requirements for the reaction medium lead to difficulties in the simultaneous and efficient generation of arsine and plumbane for ICP-AES determination.

Recently, chelating reagents such as nitroso R salt[14] and 1-(2-pyridylazo)-2-naphthol-6-sulphonic acid (PAN-S), *etc.*[15] were found effective in enhancing the lead signal of hydride generation-atomic absorption spectrometry (HG-AAS) Potassium ferricyanide, a mild oxidizing agent, was also found to be an excellent reagent to enhance efficiency of plumbane generation. (H. Chen, R. Zhu and J. Wu, unpublished results).[16,17] It was assumed that the chelation[14,15] or coordination[17] of lead by these reagents might exert a critical influence in the enhancement of lead signal. Because the conditions for the generation are so mild, it seemed likely that a method could be developed which would enhance the lead signal without depressing the arsenic signal. This paper reports the main results of a detailed investigation into the determination of lead and arsenic using reaction media containing nitroso R salt or $K_3Fe(CN)_6$ for the simultaneous generation of arsine and plumbane, followed by determination with ICP-AES.

## EXPERIMENTAL

### *Apparatus*

A Leeman Labs PLASMA-SPEC inductively coupled plasma-atomic emission spectrometer was use to obtain emission signals.

The continuous hydride generation system, shown schematically in Fig. 1, was constructed by modification of the liquid sample introduction assembly of the plasma source. The pneumatic nebulizer was removed from the Teflon cap of the spray chamber, and was replaced by a rubber septum with the similar dimensions containing two 1 mm i.d. × 30 mm glass tubes. The upper glass tube was connected to the argon carrier, and the lower tube which was positioned above the drain port of the spray chamber, was connected to the reaction tubing (1 mm i.d. × 10 cm) where hydride formation occurred. A PTFE tube (1 mm i.d. × 150 mm) was used to mix the acidic test solution and $K_3Fe(CN)_6$ solution. The three channel peristaltic pump originally attached on the ICP machine was used to propel the analyte, reductant and $K_3Fe(CN)_6$. A second peristaltic pump was used to drain the waste.

### *Reagents*

Arsenic(III) standard solution (1000 μg/ml) was prepared by dissolving 0.1320 g of $As_2O_3$

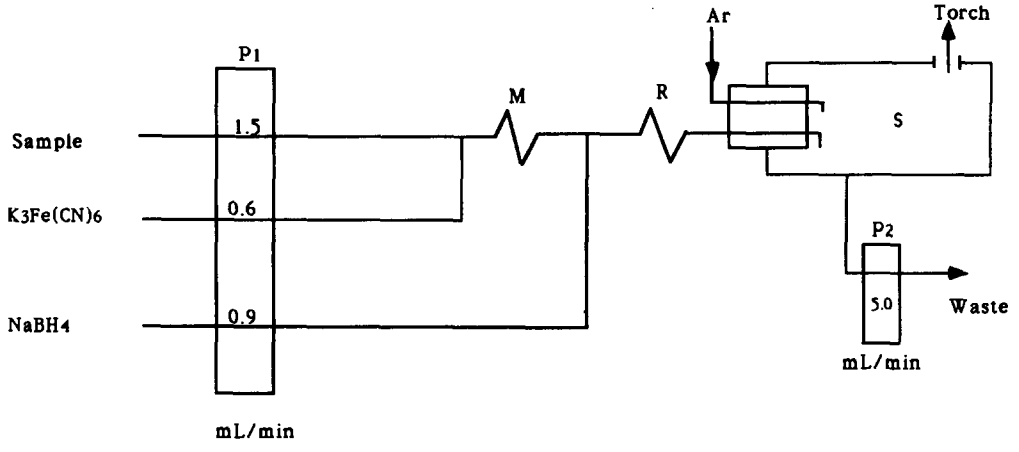


Fig. 1. Manifold of the continuous hydride generation–separation system. M: Mixing tube, $P_1$, $P_2$: peristaltic pumps, R: reaction tube, S: spray chamber.

(analytical grade, The Second Chemical Factory, Tianjin, P. R. China) in 4 ml of 2 mol/l. NaOH solution followed by the addition of 50 ml water and 5 ml of 2*M* HCl. The solution was diluted to 100 ml with deionized distilled water.

Arsenic(V) standard solution (1000 $\mu$g/ml) was prepared by dissolving 0.4179 g of $Na_2HAsO_4 . 7H_2O$ (AnalaR, BDH, Poole, U.K.) in 100 ml deionized distilled water, and was standardized against As(III) standard solution by conventional aspiration into the plasma.

Lead(II) standard solution (1000 $\mu$g/ml) was prepared by dissolving 0.1000 g granular lead (analytical grade, The Third Chemical Factory, Tianjin, China) in nitric acid and was diluted in 100 ml with deionized distilled water.

Sodium tetrahydroborate(III) solution (2.5% m/V) was prepared daily from powder (Merck) by dissolution in 0.2% m/V sodium hydroxide solution and filtered through a filter paper before use.

Nitroso R salt solution (1.6% m/V) was made by dissolution of the reagent (Analytical grade, Beijing Chemical Factory, Beijing, China) in hot deionized distilled water, the solution was cooled to room temperature before use.

Potassium ferricyanide (5% m/V) was made by dissolving 10 g of the salt (Analytical grade, Cuihau Chemical Co., Shanghai, China) in 200 ml deionized distilled water and was kept in a brown bottle.

All other reagents used are analytical grade or better.

*Operating parameters, Plasma-Spec*

Operating conditions for the Plasma Spec were as follows: coolant flow rate, 14 l. Ar/min; carrier gas, 0.6 l Ar/min (optimized); applied powder (measured as oscillator current), 0.52 A ($\approx$1.1 kW); viewing height was aligned on the zone where the best signal to background ratio for lead is obtained. Wavelengths for the determinations were: Pb 220.35 nm, As 234.98 nm (except where stated). Sample flow rate, 1.5 ml/min; $NaBH_4$ flow rate, 0.9 ml/min; $K_3Fe(CN)_6$ flow rate, 0.6 ml/min. Integration tine: 3 sec.

## RESULTS AND DISCUSSION

The sample introduction system of the Leeman Labs Plasma-Spec was equipped with a dual platinum grid nebulizer, which was used for on-line hydride generation by Watling and Collier.[18] Using this device, the spent solution, together with the hydride and by-product gas, was aspirated into the plasma. This created problems for the present work. When nitroso R salt was used as reagent, the introduction of aerosol containing the organic compound into the torch caused the deposition of carbon particles at the tip of the torch injector, which resulted in deterioration of the plasma stability. Therefore, the dual platinum grid nebulizer was simply replaced by a rubber septum with two inlet ports, as described in the Experimental section. With this arrangement, the spray chamber acted as a gas–liquid separator with a large dead volume. Although it is evident that the continuous hydride generation–separation system would be significantly improved by the use of a gas–liquid separator, this device allows rapid conversion of the sample introduction mode from conventional solution nebulization to hydride generation and vice versa.

According to the manual, the spectrometer can undertake a search for the best zone in which to view the plasma. For multi-element analysis by solution nebulization, the manufacturer recommends that the optimal viewing zone be aligned on the area where the most intense signal from nickel is obtained. For the present study, however, since lead and arsenic were the only analytes, the alignment was performed during simultaneous generation of plumbane and arsine. Thus, the viewing zone must be aligned on either lead or arsenic. Tests indicated that the viewing zone for lead was a better compromise condition with respect to signal-to-noise characteristics.

*Hydrochloric acid–nitroso R salt system*

The hydrochloric acid–nitroso R salt system was first chosen as a reaction medium for the simultaneous generation of arsine and plumbane because no oxidizing reagent existed in the system. In the tests, nitroso R salt solution was directly added to the acidic sample solution, and the pump line for $K_3Fe(CN)_6$ solution in the manifold (Fig. 1) was omitted. Figure 2 shows the influence of the nitroso R salt on the arsenic and lead signal. With the increase of the reagent concentration up to 1.0% m/V, the final concentration in the test solution, the lead signal increased steadily while the arsenic signal was not affected. After an initial sharp rise between 0 and 0.4% m/V, the lead signal climbs relatively slowly. Further

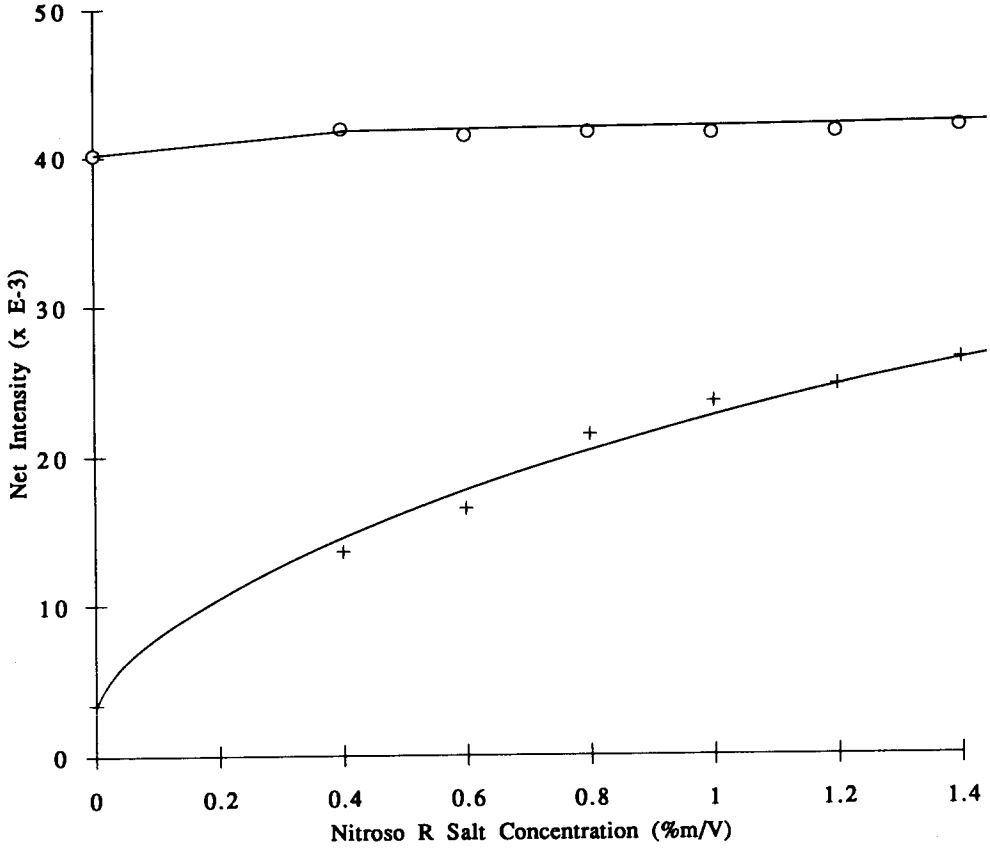


Fig. 2. Influence of nitroso R salt concentration on arsenic and lead signals. 1 $\mu$g/ml Pb ( + ) and 0.5 $\mu$g/ml As(III) (○) in 0.25*M* HCl. 2% m/V $NaBH_4$ as reductant.

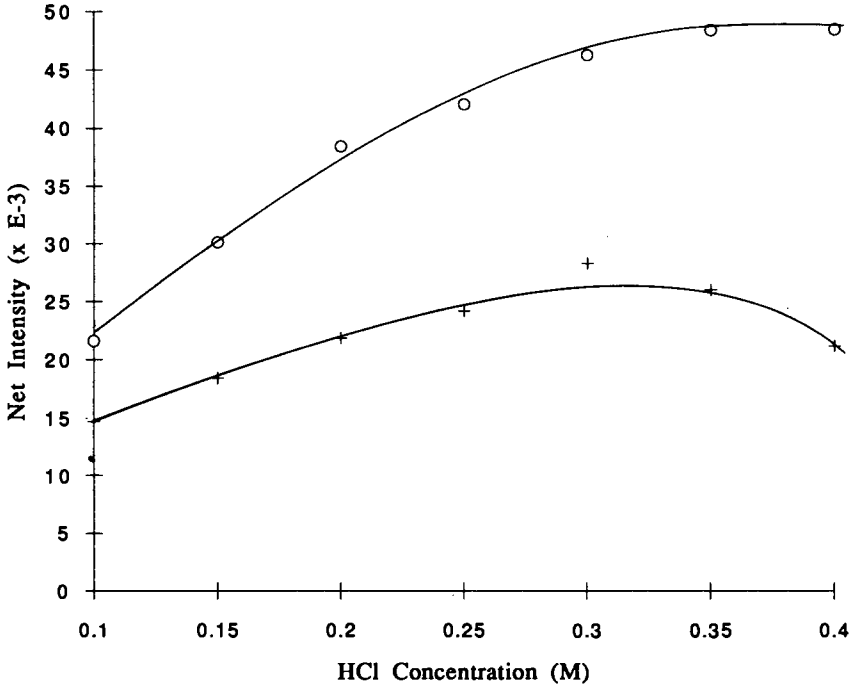


Fig. 3. Influence of HCl concentration on arsenic and lead signals in the HCl–nitroso R salt system. 1 $\mu$m/ml Pb ( + ) and 0.5 $\mu$m/ml As(III) (○) in 1% m/V nitroso R salt. 2% m/V $NaBH_4$ as reductant.

Table 1. The influence of reagents on the signals* of Pb(II), As(III) and As(V) in the medium of HCl–nitroso R salt

| Reagent concentration (%) | | | Relative signals | | |
|---|---|---|---|---|---|
| R† | KI | Ascorbic acid | Pb(II) | As(III) | As(V)/As(III) |
| 1.0 | 0 | 0 | 1.00 | 1.00 | 0.39 |
| 1.0 | 1.0 | 0 | 0.99 | 1.06 | 0.99 |
| 1.0 | 1.0 | 1.0 | 0.80 | 1.13 | 1.06 |

*1 μg/ml Pb(II) and 0.5 μg/ml As(III) [or 0.5 μg/ml As(V)] made 0.24*M* in HCl.
†R: Nitroso R salt.

increase of the reagent beyond 1.4% was restricted by its solubility (approximately 1.5% m/V). Considering both sensitivity and the expense of the reagent, 1% m/V nitroso R salt was chosen for the following study.

Figure 3 shows the effect of acidity on the signal. As can be seen, the lead signal reached a maximum at the HCl concentration of 0.3 mol/l, beyond which it decreased. The optimum acid concentration for plumbane formation was also suitable for arsine formation, since the change in arsenic signal was small after the acid concentration exceeded 0.2*M*. Tests also revealed that changing the length of the reaction tubing in the range of 10–35 cm and changing the $NaBH_4$ concentration over the range of 2–6% m/V had no significant effect on either arsenic or lead signals.

The reagents used for prereduction of As(V) to As(III) were examined to determine whether they had any harmful impact on plumbane generation. Anderson *et al.* reported that reduction of As(V) to As(III) by potassium iodide was incomplete if the acid concentration was less than 0.3 mol/l. Therefore, prereduction of As(V) was carried out in 3 ml of 2*M* HCl, into which 0.25 g KI (or 0.25 g KI plus 0.25 g ascorbic acid) had been added, for 1 hr. The solution containing both Pb(II) and prereduced As(V) was diluted to 25 ml with a solution of 1.2% m/V nitroso R salt for the following hydride generation. The influence of prereducing reagents on the signals from lead, As(III) and As(V) are summarized in Table 1. Thus, without any prereducing reagent, As(V) could not produce the same signal as did As(III). When KI was used, both As(V) and As(III) produced almost the same signal while the lead signal did not change. If the test solution, which had been diluted with nitroso R salt to the acidity required for hydride generation, stood for 1 hr, no change was observed in either the lead or the arsenic signals. Introduction of ascorbic acid, which is recommended to eliminate the formation of free iodine, owing to the oxidation of iodide by dissolved oxygen,[9] caused partial depression of the lead signal. Therefore, potassium iodide was selected as the prereducing reagent for the study.

Despite the fact that the nitroso R salt interfered with neither generation of arsine nor prereduction of As(V) to As(III), its enhancing effect on the lead signal was limited, as can been seen in Fig. 2. As a result, the detection limit for lead, defined as three times the standard deviation of the signals from a blank solution, is high (see Table 2). The poor sensitivity for lead in the present system was not a result of arsenic interference, since the lead signal obtained in the presence of arsenic was the same as that in its absence. Zhang *et al.* obtained a satisfactory sensitivity of atomic absorption spectrometric determination of lead by using batch-wise plumbane generation in the medium of HCl–

Table 2. Comparison of detection limits obtained in various reaction media

| Element | Wavelength (*nm*) | Detection limit (ng/ml) in the reaction medium of | | | | |
|---|---|---|---|---|---|---|
| | | HCl* | HCl–$H_2O_2$† | HCl–$(NH_4)_2S_2O_8$–$H_2O_2$‡ | HCl–Nitroso R salt§ | HCl $K_3Fe(CN)_6$§ |
| Pb | 220.35 | — | 1.0 | 1.4 | 21.4 | 1.1 |
| As | 193.76 | — | — | 7.6 | — | 2.8 |
| | 228.8 | 0.8 | — | — | — | — |
| | 234.98 | — | — | — | 5.7 | 6.0 |

*Sample flow rate 9.2 ml/min.[1]
†Sample flow rate 3.8 ml/min.[19]
‡Sample flow rate 2.0 ml/min.[4]
§Sample flow rate 1.5 ml/min, this work.

nitroso R salt.[14] Thus, the poor sensitivity for lead in the present work was assumed to be related to the continuous flow generation mode that might be kinetically unfavourable for the generation of plumbane in the nitroso R salt medium.

*Hydrochloric acid–potassium ferricyanide system*

When potassium ferricyanide is used, its redox behaviour should be considered. It is a mild oxidant with a standard electrode potential of +0.36 V that is much lower than those of As(V)/As(III) (+0.559 V) and $I_2/I^-$ (+0.5355 V).[19] However, in 1 mol/l. HCl, the formal electrode potential of $K_3Fe(CN)_6$ rises to +0.700 V. Therefore, $K_3Fe(CN)_6$ may be able to oxidize As(III) to As(V) and iodide to iodine in strongly acidic media. This was verified by tests. If $K_3Fe(CN)_6$ was added to the test solution containing Pb(II), As(III) and KI, the arsenic signal steadily decreased as the solution was allowed to stand. Therefore, on-line addition of $K_3Fe(CN)_6$ was adopted for the determinations, which would minimize the contact time between the reagent and the arsenic(III). With the manifold shown in Fig. 1, $K_3Fe(CN)_6$ solution (5% m/V) was mixed on-line with the test solution, resulting in no influence on the As(III) signal, whether KI was added to the test solution or not. Changing the length of the mixing tube from 10 to 80 cm caused no change in either lead and arsenic signals. Therefore, the following tests were made with this manifold.

The influence of $K_3Fe(CN)_6$ concentration on lead and arsenic signals is shown in Fig. 4. From the figure, one can see that $K_3Fe(CN)_6$ greatly enhanced the lead signal while having no impact on the arsenic signal. It should be noted that the lead concentration used in this work was 0.5 μg/ml compared with 1 μg/ml lead used when nitroso R salt was investigated. Moreover, in a wide range of $K_3Fe(CN)_6$ concentration (1.25–10% m/V), both lead and arsenic signals remained constant. Therefore, it is an ideal reagent for simultaneous generation of plumbane and arsine. Figures 5 and 6 show the influence of HCl concentration and that of $NaBH_4$ concentration, respectively. From these figures, one can concluded that 0.3 mol/l. HCl, 2% m/V $NaBH_4$ and 5% m/V $K_3Fe(CN)_6$ are the best compromise conditions for the determination of arsenic and lead.

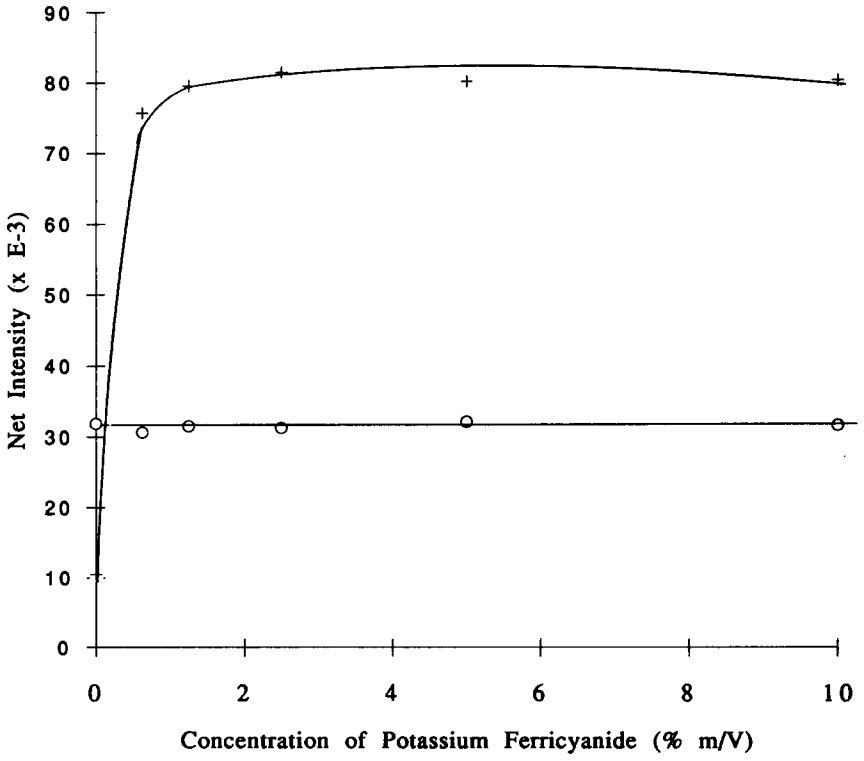


Fig. 4. Influence of $K_3Fe(CN)_6$ concentration on arsenic and lead signals. 0.5 μg/ml Pb (+) and 0.5 μg/ml As(III) (○) in 0.30*M* HCl. 2% m/V $NaBH_4$ as reductant.

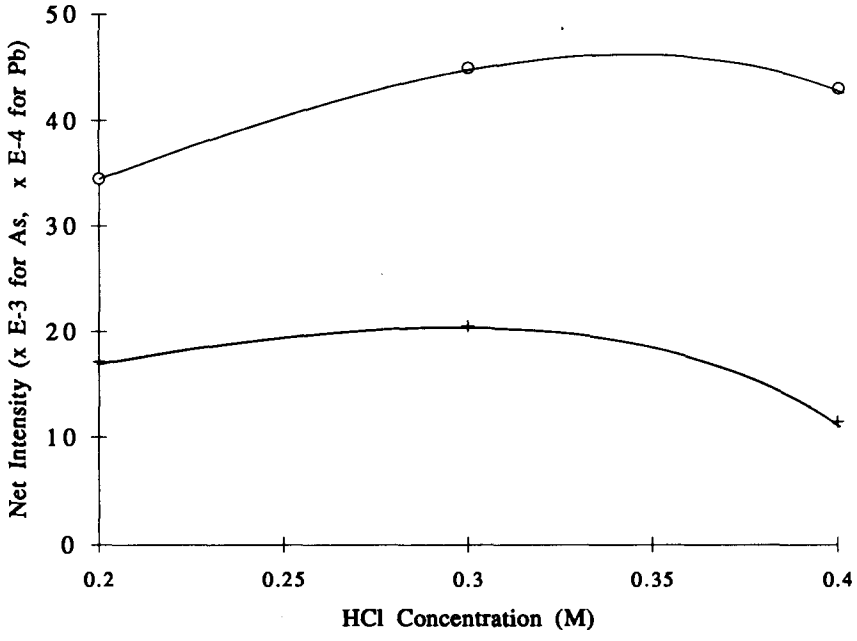


Fig. 5. Influence of HCl concentration on arsenic and lead signals in the HCl–$K_3Fe(CN)_6$ system. 1 μg/ml Pb (+) and 0.5 μg/ml As(III) (○) in 5% m/V $K_3Fe(CN)_6$. 2% m/V $NaBH_4$ as reductant.

Prereduction of As(V) to As(III) was carried out in the same way as with the nitroso R salt system. After prereduction, the test solution was diluted with deionized water to volume, and pumped to mix with $K_3Fe(CN)_6$ solution for hydride generation. The data listed in Table 3 show the influence of the relevant reagents on signals. Ascorbic acid could not be used because it severely inhibited the lead signal. When 1.3% m/V KI was used alone, As(V) could be

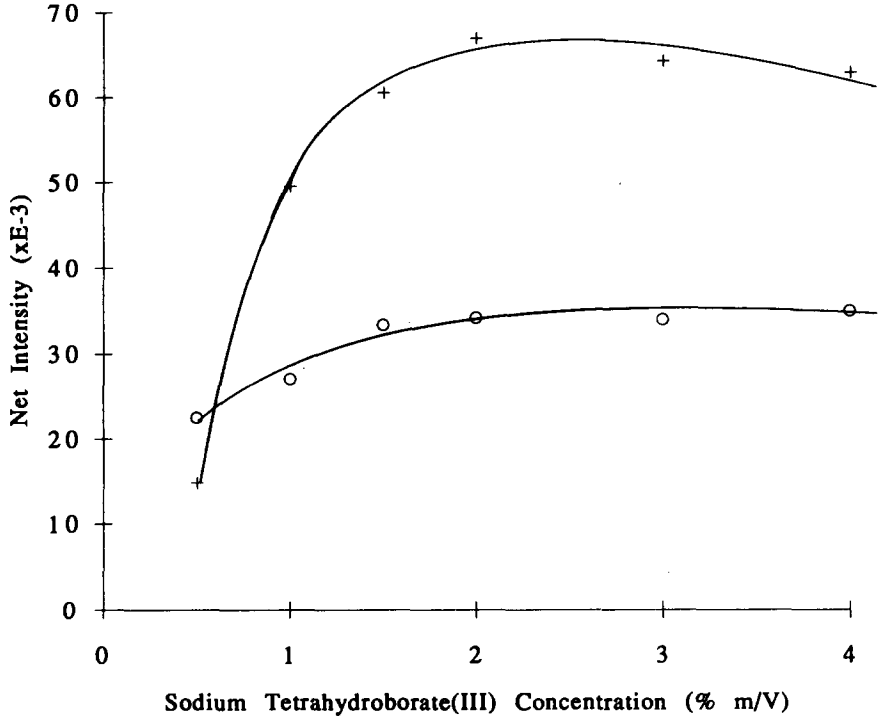


Fig. 6. Influence of $NaBH_4$ concentration on arsenic and lead signals. 0.5 μg/ml Pb (+) and 0.5 μg/ml As (III) (○) in 0.3*M* HCl, mixed on-line with 5% m/V $K_3Fe(CN)_6$.

Table 3. The influence of reagents on the signals* of Pb(II), As(III) and As(V) in $HCl$–$K_3Fe(CN)_6$ medium

| Reagent concentration | | | Relative signals | | |
|---|---|---|---|---|---|
| $K_3Fe(CN)_6$ | KI | Ascorbic acid | Pb(II) | As(III) | As(V)/As(III) |
| 5.0 | 0 | 0 | 1.00 | 1.00 | 0.11 |
| 5.0 | 1.3 | 0 | 1.00 | 0.99 | 0.96 |
| 5.0 | 1.3 | 1.3 | 0.31 | 1.05 | 1.00 |

*0.5 μg/ml Pb(II) and 0.5 μg/ml As(III) [or 0.5 μg/ml As(V)] made 0.3*M* in HCl.

completely reduced to As(III), while the lead signal was not affected. Hence, the $HCl$–$K_3Fe(CN)_6$ system, coupled with KI for prereduction of As(V), is an ideal reaction medium for the simultaneous generation of arsine and plumbane.

The detection limits obtained in the $K_3Fe(CN)_6$ system are listed in Table 2. For comparison, we have compared values for the detection limit, obtained by other groups, in various reaction media. Thus, the detection limits for arsenic and lead obtained in the $K_3Fe(CN)_6$ system are comparable, not only to those obtained in multi-element determination,[1,4] but also to that obtained in determination of lead alone.[20] Since it is well know that faster sample uptake rate usually results in higher sensitivity, it may be possible to improve further the detection limits of the $HCl$–$K_3Fe(CN)_6$ system if a higher sample uptake rate in conjunction with a higher input power for ICP source is applied.

## CONCLUSION

Arsenic and lead can be simultaneously reduced to the hydrides in hydrochloric acid–nitroso R salt and hydrochloric acid–potassium ferricyanide media by means of sodium tetrahydroborate(III) reduction. The latter is preferable owing to the fact that lower detection limits for both arsenic and lead can be obtained by inductively coupled plasma-atomic emission spectrometry in combination with hydride generation. It is well known that hydride generation, especially plumbane generation, is subject to interferences from transition metals and hydride forming elements. Further work on developing an understanding of these interferences occurring in the recommended media and on the way to eliminate these interferences will be necessary before the technique can be applied to analyze real samples with complex matrices. It is very likely that better detection limits would be obtained if a superior gas–liquid separator were used, or, as a reviewer has suggested, an axially viewed ICP system.

*Acknowledgement*—The Educational Commission of Zhejiang Province is thanked for funding this work.

## REFERENCES

1. A. L. Gray, in *Applications of Inductively Coupled Plasma Mass Spectrometry* A. R. Date and A. L. Gray (eds) p. 25, Chapman and Hall, New York, 1989.
2. M. Thompson, B. Pahlavanpour, S. J. Walton and G. F. Kirkbright, *Analyst*, 1978, **103**, 568.
3. T. Nakahara, *Prog. Anal. Atom. Spectrosc.*, 1985, **6**, 163.
4. B. Huang, Z. Zhang and X. Zeng, *Spectrochim. Acta.*, 1987, **42B**, 129.
5. J. Zhang, X. Zeng and Z. Zhang, *Guangpuxue Yu Guangpufenxi*, 1990, **10**(5), 36–40. C.A. **114**, 156205d.
6. M. Thompson and B. Pahlavanpour, *Anal. Chim. Acta.*, 1979, **109**, 251.
7. H. W. Sinemus, M. Melcher and B. Welz, *Atom. Spectrosc.*, 1981, **2**, 81.
8. R. K. Anderson, M. Thompson and E. Culbard, *Analyst*, 1986, **111**, 1143.
9. B. J. A. Haring, W. Van Delft and C. M. Bom, *Fresenius' Z. Anal. Chem.*, 1982, **310**, 217.
10. H. Chen, I. D. Brindle and X.-C. Le, *Anal. Chem.*, 1992, **64**, 667.
11. H. D. Fleming and R. G. Ide, *Anal. Chim. Acta.*, 1976, **83**, 67.
12. K. Jin and M. Taga, *Anal. Chim. Acta.*, 1982, **143**, 229.
13. P. N. Vijan and G. R. Wood, *Analyst*, 1976, **101**, 996.
14. S. Zhang, H. Han and Z. Ni, *Anal. Chim. Acta.*, 1989, **221**, 85.
15. H. Chen, F. Tang, C. Gu and I. D Brindle, *Talanta*, 1993, **40**, 1147.
16. R. Tao and H. Zhou, *Fenxi Huaxue*, 1985, **13**, 283–235. C.A. **103**, 140428r.
17. P. Zhang and Z. Hu, *Fenxi Huaxue*, 1987, **15**, 404–408. C.A. **107**, 189886k.
18. R. J. Watling and A. R. Collier, *Analyst*, 1988, **113**, 345–346.
19. D. A. Skoog and D. M. West, *Fundamentals of Analytical Chemistry*, 4th Ed., p. 829. Saunders and College, 1982.
20. M. Ikeda and J. Nishibe, *Anal. Chim. Acta.*, 1981, **125**, 109.

Pergamon

0039-9140(95)01411-X

*Talanta*, Vol. 42, No. 3, pp. 361–364, 1995

0039-9140/95 $9.50 + 0.00

# APPLICATION OF ANALYSES ON THE BASIS OF CHARACTERISTIC MASS: DETERMINATIONS OF INDIUM, SILVER AND THALLIUM IN DRAINAGE SEDIMENT AND GEOCHEMICAL SAMPLES

YANSHENG ZHENG* and YUQI WANG

Department of Chemistry, Jilin University, Changchun 130023, China

(*Received* 23 *March* 1994. *Revised* 24 *August* 1994. *Accepted* 31 *August* 1994)

**Summary**—When Pd and EDTA ammonium salt are used as a common matrix modifier, the establishment of a common furnace programme for the determinations of indium, silver and thallium would greatly simplify routine analysis. The continuous determination of indium, silver and thallium by the analyses on the basis of characteristic mass and the graphite furnace with the V-shaped boat is described. The possibility of the proposed method for application to continuous determination of indium, silver and thallium in real sample is discussed. The continuous determination of indium, silver and thallium in drainage sediment and geochemical samples by the analyses on the basis of characteristic mass is carried out and the results of sample analyses are in good agreement with the expected values.

Theoretical characteristic masses $m_0$ (cal) were calculated and compared with experimental values $m_0$ (exp) by L'vov *et al.*[1,2] for 32 elements measured under STPF conditions, the mean value of $m_0$ (cal)/$m_0$ (exp) was found to be 0.85 with a SD of 0.10. For the other elements vaporized from the furnace wall or the platform $m_0$ (cal)/$m_0$ (exp) deviated from the ideal value of 1 by a factor of 2–10. The discrepancies may be accounted for by the formation of thermostable gaseous carbides and monocyanides or partial ionization of the atoms. Baxter and Frech[3] have pointed out that temperature gradients over the length of tube may be a limiting factor for absolute analysis by GFAAS. They[4] defined $m_0$ (cal)/$m_0$ (exp) as the calculated atomization efficiency and studied the temperature dependence of calculated atomization efficiencies of some elements in a two-step atomizer, and showed that the calculated atomization efficiency for most elements reaches a plateau, often in the higher temperature region.

There are only a few reports about the absolute analysis applying to the determination of an element in a real sample. Slavin *et al.*[5] reported the possibility of standardless analysis applied to determinations of the elements in real samples. They showed that the stabilized temperature platform furnace (STPF) equipped with Zeeman background correction satisfied the requirements for standardless analysis in GFAAS, and this method was based on the stability of characteristic mass. As the characteristic masses must be determined using standard solutions, the method of Slavin *et al.* is not quite a standardless analysis. However, the analysis on the basis of characteristic mass is simpler and more convenient than applying a calibration curve and the method of Slavin *et al.* accelerates the development of absolute analysis. Recently, Zheng *et al.*[6–8] and Ma *et al.*[9,10] reported the determinations of Ag, Cd, Cr and In in real samples with analyses on the basis of characteristic mass. At the same time, Zheng *et al.*[6] showed that it was an important condition to use a matrix modifier to eliminate interferences for application of analysis on the basis of characteristic mass in real sample. Shan *et al.*[11–13] have reported that the addition of some metal salts result in improved sensitivity for the determinations of indium and thallium, and they found Pd to be the best matrix modifier. Moreover, when ammonium salt of EDTA was used as a matrix modifier, the interference of perchloric acid, which was used for decomposition of sample, was suppressed completely.[14]

In graphite furnace atomic absorption spectrometry, the establishment of a common

*Author to whom correspondence should be addressed.

furnace programme suitable for most elements would greatly simplify operating procedure and reduce test time. Welz *et al.*[15–17] reported use of $Pd(NO_3)_2$–$Mg(NO_3)_2$ as matrix modifier and a uniform furnace programme for determinations of some elements in real samples. Berglund *et al.*[18] have studied the feasibility of using a single set of atomizer conditions for a suite of elements covering a wide range of volatilities using a platform-equipped, integrated-contact furnace and a palladium modifier. Moreover, Harnly *et al.*[19,20] pointed out that simultaneous multielement furnace conditions were accomplished using compromise atomization parameters in multielement GFAAS.

This work aims to establish a common furnace programme suitable for the determinations of indium, silver and thallium. The feasibility of the continuous determination of indium, silver and thallium in real sample using analysis on the basis of characteristic mass is discussed. The proposed method was applied to the continuous determination of indium, silver and thallium in drainage sediment and geochemical samples and satisfactory results were obtained.

## EXPERIMENTAL

### *Apparatus*

A Hitachi 180-50 atomic absorption spectrometer with a GA-3 graphite furnace and a XWT-164 (made in China) strip chart recorder was used. Pyrocoated graphite tubes (made in China) and a V-shaped boat (made in our laboratory)[21] were used. The spectral band width was 1.3 nm. Hollow cathode lamps (made in China) of Ag, In and Tl were used as a light source and operated at 7.5, 7.0 and 6.0 mA, respectively. A deuterium arc background system was used throughout. $N_2$ was used as the purge gas at a flow rate of 150 ml/min and the purge gas was stopped at atomization step. The 328.1, 303.9 and 276.8 nm lines of Ag, In and Tl respectively, were employed for all measurements and read out as peak area, respectively. Sample solution was injected into graphite tube with a 20$\mu$l Eppendorf micropipette. The temperature of the furnace was corrected with a MT-2 optical pyrometer (made in China). The common graphite furnace operating parameters for indium, silver and thallium were: drying 80–120°C, 30 sec; ashing 500°C, 30 sec; atomization 2200°C, 7 sec; cleaning 2600°C, 3 sec.

### *Reagents*

Stock solutions (1 mg/ml) of indium, silver and thallium were prepared by dissolving a suitable amount of metal indium (S.P. grade), $AgNO_3$ (analytical reagent grade) and $Tl_2(SO_4)_3$ (analytical reagent grade) in water obtained from a quartz flask in a sub-boiling still, with metal indium in 10 ml of 6 mol/dm$^3$ nitric acid. It was boiled to expel nitrogen oxide and diluted with sub-boiling distilled water. Working solutions were prepared by appropriate dilution with sub-boiling distilled water.

A 5% (w/v) solution of EDTA ammonium salt was prepared by dissolving 5.00 g EDTA (analytical reagent grade) in sub-boiling distilled water and added 15 ml of 25% aqueous ammonia (analytical reagent grade) to dilute to 100 ml with sub-boiling distilled water.

A solution of palladium (10 mg/ml) was prepared by dissolving a suitable amount of $PdCl_2$ (analytical reagent grade) in concentrated nitric acid, with the addition of several drops of concentrated hydrochloric acid, and diluting with sub-boiling water.

### *Procedures and sample decompositions*

In each case the blank signal was subtracted from the experimental result. The peak area absorbance values of each measurement were the mean of five measurements. The experimental values of characteristic mass were calculated from the average value of peak area absorbance obtained from the aqueous standard solution of the determined element using the formula

$$m_o = (0.0044/A_i)m_a, \qquad (1)$$

where $A_i$ is the average peak area absorbance, and $m_a$ is the mass of analyte in picograms for a particular element. The experimental values of $m_o$ for indium, silver and thallium determined under the operating conditions of the common furnace programme above are listed in the footnote of Table 1.

Standard drainage sediment and geochemical reference samples (made in China) were used in this study. A weighed amount of sample was transferred into a polyfluorotetraethylene crucible, usually 0.1–0.2 g, and 5, 3 and 5 ml of 67% $HNO_3$, 72% $HClO_4$ and 35% HF, respectively were carefully added. The mixture was then heated on a sand bath until it was nearly dry. The residue was dissolved in 0.02*M* solution of nitric acid, and 0.5 ml of 5% (w/v) EDTA ammonium salt and 1.25 mg Pd as a

matrix modifier were added. The solution was made up to the final volume of 25 ml, and the continuous determination of indium, silver and thallium under the operating conditions of the common furnace programme above by GFAAS with the V-shaped boat was carried out.

## RESULTS AND DISCUSSION

### *Establishment of a common furnace programme*

It is an important task to establish a common furnace programme suitable for determining indium, silver and thallium. It is reported[21] that the characteristic masses of some elements in a furnace with a V-shaped boat were lower than that in a furnace with a platform. Palladium is the best matrix modifier for determinations of indium and thallium and EDTA ammonium salt can completely suppress the effect of perchloric acid.[11–14] The experimental results show that use of 50 μg/ml Pd and 2% (v/v) EDTA ammonium salt as a common matrix modifier for determination of indium, silver and thallium was the best choices. Ashing temperature tests for indium, silver and thallium in the presence of Pd and EDTA ammonium salt were carried out. The experimental results show that the highest allowable ashing temperatures of thallium, silver and indium were 500°, 700° and 900°C, respectively. In order to prevent loss of thallium at the ashing step, a common ashing temperature for the continuous determination of indium, silver and thallium was chose to be 500°C.

It was reported[22] that the experimental values of characteristic mass of indium and silver were stable in the ranges of 2200–2400° and 1600–2500°C, respectively. Moreover, the experimental results of atomization temperature show that in the range of 1600–2300°C, not only the experimental value of characteristic mass for thallium was stable, but also its calculated atomization efficiency value [$m_0$ (cal)/$m_0$ (exp)] was close to 100%. The detailed results will be given separately. It must be emphasized that the establishment of a common atomization temperature did not have a negative effect on sensitivity and is regarded as greatly facilitating routine analysis. The calculated atomization efficiency values of indium, silver and thallium at 2200°C were larger than 80% on the basis of the above tests. Therefore, a common atomization temperature was chosen to 2200°C.

After a lapse of over two years we checked the experimental values of the characteristic mass for indium and silver with aqueous standards of the corresponding element once again. The characteristic mass of silver at 2200°C was 0.67 pg and it was in good agreement with 0.68 pg reported in Ref. 22. However, the characteristic mass of indium at 2200°C was 9.6 pg, slightly larger than 6.5 pg reported in Ref. 22. It must be noted that it is possible that the expected characteristic mass of indium is slightly different from the value previously reported because the amount of Pd and ashing temperature used in this study are different from Ref. 22. As shown in Ref. 6 a frequent check of characteristic mass will be a key to assuring accurate analytical results for the application of analysis on the basis of characteristic mass in a practical sample. Moreover, the experimental value of characteristic mass for thallium has appeared to be basically stable for three months.

### *Interference studies*

It has been shown that the use of a matrix modifier to eliminate interference is a necessary condition for application of analysis on the basis of characteristic mass in a practical sample. In order to examine the applicability of the proposed method of analysis on the basis of

Table 1. Determinations of indium, silver and thallium in samples

| | Calculated method of $m_0$ | | | | | | Calibration curve method | | | | Expected value (μg/g) | | |
|---|---|---|---|---|---|---|---|---|---|---|---|---|---|
| | Content† (μg/g) | | | RSD (%) | | | Content† (μg/g) | | RSD (%) | | | | |
| Sample* | Ag | In | Tl | Ag | In | Tl | Ag | In | Ag | In | Ag | In | Tl |
| GSD-2 | 0.065 | 0.042 | 1.87 | 1.5 | 1.7 | 0.8 | 0.065 | 0.041 | 0.6 | 2.2 | 0.066 | 0.043 | 1.90 |
| GSD-8 | 0.064 | 0.042 | 0.79 | 4.7 | 2.0 | 2.4 | 0.061 | 0.047 | 3.5 | 2.8 | 0.062 | 0.046 | 0.78 |
| GSR-3 | 0.041 | 0.063 | 0.11 | 2.4 | 1.6 | 5.5 | 0.039 | 0.062 | 5.1 | 4.7 | 0.040 | 0.063 | 0.12 |
| GSS-4 | 0.070 | 0.11 | 0.86 | 4.3 | 6.5 | 2.3 | 0.070 | 0.12 | 2.4 | 3.6 | 0.070 | 0.12 | 0.90 |

Characteristic mass ($m_0$) of Ag, In and Tl was 0.67, 9.6 and 9.4 pg, respectively. *GSD-2 and GSD-8 are drainage sediment samples (China). GSr-3 and GSS-4 are geochemical reference samples (China). †This value is the average values of four separate determinations.

characteristic mass for continuous determination of indium, silver and thallium in a real sample, a series of experiments was undertaken to test the interference effects of a variety of foreign ions. The interference effect of each foreign ion was estimated by reference to the peak area absorbance obtained by the same amount of corresponding analytical element standard. It was found that there were no interferences in the presence of 0.2*M* $HClO_4$ and $HNO_3$, a 1000-fold excess of K, Na, Ca, Cd, Co, Ba, Mg, Ni, Pb, Si, Ze, Al and Fe when Pd and ammonium salt of EDTA was used as a common matrix modifier. It would appear that the Pd–EDTA ammonium salt is the best choice and it can fulfil the above condition.[6]

*Determinations of indium, silver and thallium*

The continuous determination of indium, silver and thallium in the standard drainage sediment and geochemical reference samples by a graphite furnace with V-shaped boat and the use of 50 μg/ml Pd and 2% (v/v) EDTA ammonium salt as a matrix modifier was carried out. The graphite furnace operating conditions and sample decomposition were described in the Experimental section. Analyses on the basis of characteristic mass, *i.e.* the mass of indium, silver and thallium in the sample were calculated from equation (1) on the basis of characteristic mass value of the corresponding element which was determined by use of the aqueous standard and listed in the footnote of Table 1. In order to examine the accuracy of analysis on the basis of characteristic mass, the calibration curve method for indium and silver was also carried out. The analytical results of samples are listed in Table 1. The calibration curve method is a calibration prepared with the aqueous standard of the corresponding element, It indicated that the continuous determination of indium, silver and thallium in the drainage sediment and geochemical reference samples by analyses on the basis of characteristic mass produces satisfactory results. In conclusion, the proposed Pd and EDTA ammonium salt as modifier makes continuous determination of Ag, In and Tl by analyses on the basis of characteristic mass under study possible, not only with a common modifier, but also using a common furnace programme. Our current experiment indicates that the method can simplify operating procedure and reduce time. It is favourable to routine analysis.

## REFERENCES


1. B. V. L'vov, V. G. Nikolaev, E. A. Norman, L. K. Polzik and M. Mojica, *Spectrochim. Acta*, 1986, **41B,** 1043.
2. B. V. L'vov, *Spectrochim. Acta*, 1990, **45B** 633.
3. D. C. Baxter and W. Frech, *Spectrochim. Acta*, 1987, **42B,** 1005.
4. W. Frech and D. C. Baxter, *Spectrochim. Acta*, 1990, **45B,** 867.
5. W. Slavin and G. R. Carnrick, *Spectrochim. Acta*, 1984, **39B,** 271.
6. Y. S. Zheng and X. G. Su, *Talanta* 1993, **40,** 347.
7. Y. S. Zheng and X. G. Su, *J. Can. Appl. Spectrosc.* 1993, **38,** 109.
8. Y. S. Zheng and X. G. Su, *Mikrochim. Acta*, 1994, 112 (4–6), 237.
9. Y. Z. Ma, J. Bai, J. Z. Wang, Z. K. Li, L. Zhu, Y. G. Li, H. Zheng and B. W. Li, *J. Anal. Atom. Spectrom.* 1992, **7,** 365.
10. Y. Z. Ma, B. W. Li, Z. K. Li, J. Z. Wang and Y. G. Li, *Fenxi Huaxue* 1993, **21,** 745.
11. X. Q. Shan, Z. M. Ni and Z. N. Yuan, *Anal. Chim. Acta*, 1985, **171,** 269.
12. X. Q. Shan, Z. M. Ni and L. Zheng, *Talanta*, 1984, **31,** 150.
13. X. Q. Shan, Z. N. Yuan and Z. M. Ni, *J. Can. Spectrosc.* 1986, **31,** 35.
14. Y. S. Zheng and Y. Xiang, *Fexi Huaxue* 1990, **18,** 676.
15. G. Schlemmer and B. Welz, *Spectrochim. Acta*, 1986, **41B,** 1157.
16. B. Welz, G. Schlemmer and J. R. Mudakavi, *J. Anal. Atom. Spectrom.* 1988, **3,** 93.
17. B. Welz, G. Schlemmer and J. R. Mudakavi, *J. Anal. Atom. Spectrom.* 1988, **3,** 695.
18. M. Berglund, W. Frech and D. C. Baxter, *Spectrochim. Acta*, 1991, **46B,** 1767.
19. J. M. Harnly, T. C. O'Haver, W. R. Wolf and B. M. Golden, *Anal. Chem.* 1979, **51,** 2007.
20. J. M. Harnly, N. J. Miller-Ihli and T. C. O'Haver, *Spectrochim. Acta*, 1984, **39B,** 305.
21. Y. S. Zheng and F. Zhu, *Jilin Daxue Ziran Kexue* 1987, **1,** 103.
22. Y. S. Zheng, X. G. Su and Z. Quan, *Appl. Spectrosc.* 1993, **47,** 1222.

Pergamon

0039-9140(95)01412-8

*Talanta*, Vol. 42, No. 3, pp. 365–373, 1995

0039-9140/95 $9.50 + 0.00

# A RAPID AND HIGHLY SELECTIVE METHOD FOR THE ESTIMATION OF PYRO-, TRI- AND ORTHOPHOSPHATES

D. R. KAMAT,[1] V. V. SAVANT[1] and D. N. SATHYANARAYANA[2]*

[1]Research and Development Laboratory, Ballarpur Industries Limited, Karwar 581 364, India
[2]Department of Inorganic and Physical Chemistry, Indian Institute of Science, Bangalore 560 012, India

(*Received* 5 *May* 1994. *Revised* 24 *August* 1994. *Accepted* 31 *August* 1994)

**Summary**—A rapid, highly selective and simple method has been developed for the quantitative determination of pyro-, tri- and orthophosphates. The method is based on the formation of a solid complex of bis(ethylenediamine)cobalt(III) species with pyrophosphate at pH 4.2–4.3, with triphosphate at pH 2.0–2.1 and with orthophosphate at pH 8.2–8.6. The proposed method for pyro- and triphosphates differs from the available method, which is based on the formation of an adduct with tris(ethylenediamine)cobalt(III) species. The complexes have the composition $[Co(en)_2HP_2O_7]4H_2O$ and $[Co(en)_2H_2P_3O_{10}]2H_2O$, respectively. The precipitation is instantaneous and quantitative under the recommended optimum conditions giving 99.5% gravimetric yield in both cases. There is no interferences from orthophosphate, trimetaphosphate and pyrophosphate species in the triphosphate estimation up to 5% of each component. The efficacy of the method has been established by determining pyrophosphate and triphosphate contents in various matrices. In the case of orthophosphate, the proposed method differs from the available methods such as ammonium phosphomolybdate, vanadophosphomolybdate and quinoline phosphomolybdate, which are based on the formation of a precipitate, followed by either titrimetry or gravimetry. The precipitation is instantaneous and the method is simple. Under the recommended pH and other reaction conditions, gravimetric yields of 99.6–100% are obtainable. The method is applicable to orthophosphoric acid and a variety of phosphate salts.

Of all the condensed phosphates, sodium triphosphate (STP) (also known commercially as sodium tripolyphosphate) and tetrasodium pyrophosphate are of industrial importance. Owing to its extensive use in the manufacture of detergents, anhydrous triphosphate is also of great commercial importance. Because of complexities in controlling the conditions for thermal condensation of orthophosphate to triphosphate, the commercially available anhydrous triphosphate is always contaminated with other phosphates, *viz.* orthophosphate, trimetaphosphate and pyrophosphate.[1]

Chromatographic[2] and infrared spectroscopic techniques[3–5] have been employed for the identification and for the estimation of phosphate compounds. A method based on tris(ethylenediamine)cobalt(III) species forming a solid adduct with pyrophosphate and triphosphate at pH about 6.5 and 3.5, respectively, is widely used for the quantitative estimation of these two compounds gravimetrically.[6] Hexamminecobalt(III) chloride has also been suggested as precipitant for use in the determination of pyrophosphate and triphosphate,[6] but this reagent suffers from nonselectivity when employed to estimate an admixture of pyrophosphate and triphosphate, and is hence not a very valuable reagent. In this paper, a rapid and simple method for the determination of pyrophosphate and triphosphate by forming a coordination complex with aqueous bis(ethylenediamine)cobalt(III) species at pH 4.2–4.3 and 2.0–2.1, respectively, is described. By physicochemical studies, it was found that the solid complexes formed correspond to $[Co(en)_2HP_2O_7]4H_2O$ and $[Co(en)_2H_2P_3O_{10}]2H_2O$, respectively.[7] Gravimetric yields of 99.5% were obtained in the case of pure pyro- and triphosphates.

Various analytical methods for the determination of orthophosphoric acid and phosphate salts have been reported.[8] They include direct titrimetric,[9–11] complexo titrimetric,[12] potentiometric,[13–16] complexo gravimetric,[11,17] colorimetric,[11,18–21] chromatographic[22–27] and atomic absorption spectroscopic techniques.[28] Orthophosphates are also known to form complexes

*Author to whom correspondence should be addressed.

with Co(III), Cr(III), *etc.*, containing other ligands such as ethylenediamine and ammonia. It was found that bis(ethylenediamine)cobalt(III) species also forms complex with orthophosphate anion under specific pH and other reaction conditions. Several phosphato complexes of cobalt(III) of the type $[Co(NH_3)_4PO_4]$, $[Co(NH_3)_5PO_4]$, $[Co(NH_3)_4H_2O \cdot HPO_4]^+$, $[Co(en)_2PO_4]$, $[Co(en)_2H_2O \cdot HPO_4]^+$, $[Co(en)_2OH \cdot HPO_4]$, $[Co(en)_2OH \cdot PO_4]^-$, $[Co(en)_2H_2O \cdot H_2PO_4]^{2+}$ and $[Co(en)_2H_2O \cdot H_3PO_4]^{3+}$ have been reported and characterized. Their hydrolytic properties have also been studied.[29] Although the synthesis of $[Co(en)_2PO_4]$ was reported starting from transdichloro bis(ethylenediamine)cobalt(III) perchlorate,[30] it has not been exploited for the quantitative estimation of orthophosphates.

The above method for the estimation of pyro- and triphosphates is extended for the quantitative estimation of orthophosphate based on the complex formation of orthophosphate anion with acidified solution of (carbonato)-bis(ethylenediamine)cobalt(III) chloride. The precipitation is quantitative between pH 8.2 and 8.6 under the recommended reaction conditions. The solid complex formed corresponds to $[Co(en)_2PO_4]$.[7] The method is also applicable to salts such as $NaH_2PO_4$, $Na_2HPO_4$, $Na_3PO_4$, $(NH_4)_2HPO_4$, $KH_2PO_4$ and other similar salts of orthophosphoric acid. Gravimetric yields of 99.6–100% are obtainable in the case of orthophosphoric acid and its salts. The method was employed for the phosphate estimation of commercial matrices such as tricalcium phosphate, dicalciumphosphate, *etc.* The *cis*- and *trans*-dichlorobis(ethylenediamine)cobalt(III) chloride were also tried as alternative reagents for the quantitative determination of orthophosphate anion. The results were not encouraging.

## EXPERIMENTAL

### *Reagents and instruments*

(Carbonato)bis(ethylenediamine)cobalt(III) chloride was prepared by a known method.[31] It was recrystallized and air-dried. The purity of the compound was checked by chemical analysis. This complex (75 mg) was acidified with 1*M* hydrochloric acid (1 ml) to decompose the carbonate and obtain the aqueous bis(ethylenediamine)cobalt(III) species which was used as the reagent for the precipitation reaction. Tris(ethylenediamine)cobalt(III) chloride was prepared by a known method.[32] It was recrystallized and dried at 110°C before use. A 4% aqueous solution was used for all the experiments. One drop of toluene was added to inhibit mold growth. *cis*- and *trans*-Dichlorobis(ethylenediamine)cobalt(III) chloride were prepared by a known method.[27] These complexes are water soluble and 7% aqueous solutions were used as reagents. Sodium pyrophosphate, analytical reagent tetrasodium pyrophosphate, $Na_4P_2O_7 \cdot 10H_2O$ (Koch-Light, U.K.) was used as a standard pyrophosphate. Sodium triphosphate, from the commercially available anhydrous sodium triphosphate (Ballarpur Industries Ltd, Karwar, India), its hexahydrate was prepared.[34] Sodium trimetaphosphate was prepared by thermal dehydration of $NaH_2PO_4$ under controlled conditions. The condensation polymerization was carried out between 500 and 600°C for about 5 hr, followed by slow cooling.[35] From this product, the monohydrate was prepared by precipitating it from aqueous solution with ethanol at 40°C and then air-dried. Orthophosphoric acid, analytical reagent grade orthophosphoric acid (E. Merck) was used. Orthophosphates, analytical reagent grade $NaH_2PO_4 \cdot 2H_2O$, $Na_2HPO_4$, $Na_3PO_4 \cdot 12H_2O$, $KH_2PO_4$ and $(NH_4)_2HPO_4$ of BDH and Sarabhai chemicals were used. Sodium acid pyrophosphate ($Na_2H_2P_2O_7$) was prepared by a known method[36] by heating $NaH_2PO_4$ to 250°C for 5 hr. It was recrystallized from ethanol. Detergent powders, commercially available spray-dried premier detergent powders of Indian origin were employed.

Model 3B Perkin Elmer double beam electronic spectrophotometer, model 2380 Perkin Elmer atomic absorption spectrophotometer and a model 361 microprocessor pHmeter (Systronics) were used.

### *Procedure*

A known amount of pure tetrasodium pyrophosphate (about 150 mg) in a 100 ml beaker was taken. Distilled water (15 ml) followed by 15 ml of propanol was added, 2–3 ml of bis(ethylenediamine)cobalt(III) reagent was then added and precipitation occurred immediately. The pH of the solution was adjusted to between 4.2 and 4.3 using 1*M* sodium hydroxide and the contents of beaker were stirred for 10–15 min. The precipitate was filtered quantitatively through a G-3 sintered crucible. The filtrate was used for the complete transfer of the precipitate

to the crucible. The precipitate was washed with 1:1 ethanol. It was dried at 110°C for 1 hr and weighed. The same procedure was used for the precipitation of triphosphate except that in this case, the pH was adjusted to between 2.0 and 2.1. In the case of orthophosphate, the reagent requirement was 8 ml and the pH was adjusted to between 8.2 and 8.6. The precipitate was washed with absolute ethanol instead of 1:1 ethanol. Since this complex is hygroscopic, immediately after drying the crucible is kept in a vacuum desiccator and weighed as soon as it attains ambient temperature.

Using the same procedure, *cis*- and *trans*-dichlorobis(ethylenediamine)cobalt(III) chloride were used as precipitating agents for orthophosphates instead of the acidified solution of (carbonato)bis(ethylenediamine)-cobalt(III) chloride. The use of the aquo complex of *trans*-dichlorobis(ethylenediamine)cobalt(III) chloride, obtained by the overnight aquation of the *trans*-dichloro bis(ethylenediamine)cobalt(III) chloride was also attempted.

## RESULTS AND DISCUSSION

The electronic spectra of acidified solution of $[Co(en)_2CO_3]Cl$ and the filtrates of the precipitation experiments showed an absorption maximum at 494 nm. Stoichiometrically for each mole of pyro-, tri- and orthophosphates, one mole of bis(ethylenediamine)cobalt(III) species is required. It was also confirmed by the ratio of Co:P obtained by the analysis of the respective precipitates.

### *Effect of pH*

In a series of beakers, the same amount of pure pyrophosphate (about 150 mg) was taken and the precipitations were carried out at different pH. Similarly, the effect of pH on the precipitation of triphosphate and orthophosphate were also studied. The plots of pH *vs.* mean yield values of pyro-, tri- and orthophosphates are shown in Figs 1–3, respectively. The results indicate that pH 4.2–4.3, 2.0–2.1 and 8.2–8.6 are optimum for the quantitative determination of pyro-, tri- and orthophosphates, respectively, and maximum yields of 99.5–100% are obtainable under these optimum conditions. The advantages of the present method are that it is simple, rapid and more accurate than the available method. The available method requires buffering and seeding for initiation of precipitation and takes 30 min for the precipitation to go to completion in the case of pyro- and triphosphates. However, the addition of a non-aqueous solvent, preferably propanol, is needed in the described method. A few precipitations were carried out by adding excess water during precipitation and without adding propanol before precipitation, to study the effect of dilution and absence of propanol on the quantitative estimations. Precipitations were also carried out using methanol and ethanol instead of propanol. Dilution with water and absence of propanol in the reaction mixture during the precipitation gave lower yields. Although methanol and ethanol could be used, propanol is preferred for the best results. The completeness of the precipitation was confirmed by the absence of phosphate in the mother liquor.

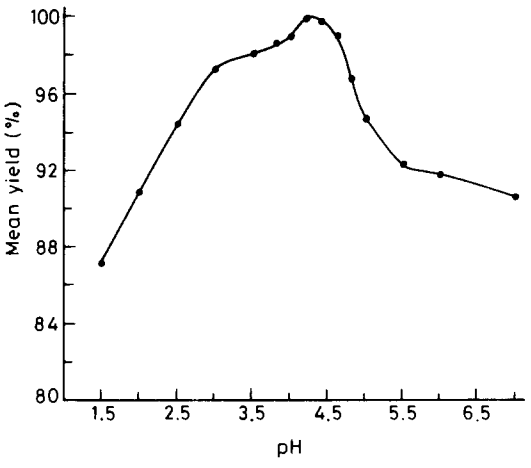


Fig. 1. Effect of pH on the estimation of pyrophosphate.

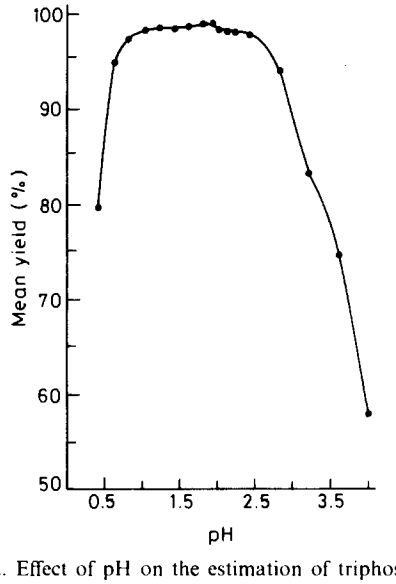


Fig. 2. Effect of pH on the estimation of triphosphate.

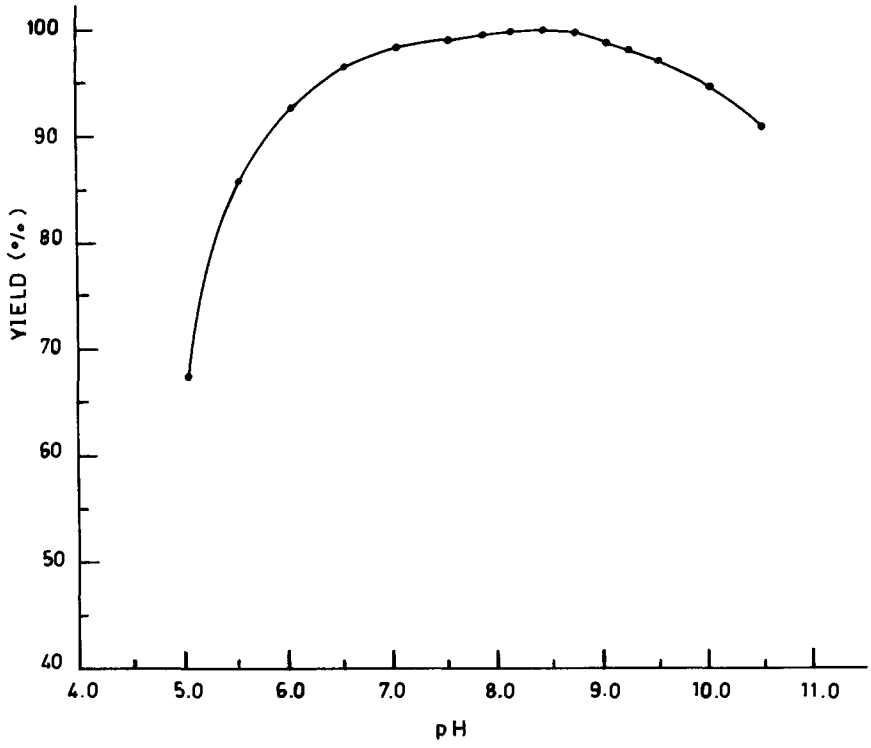


Fig. 3. Effect of pH on the estimation of orthophosphate.

*Determination of excess reagent*

Since the reagent, bis(ethylenediamine)-cobalt(III) is coloured, pyrophosphate and triphosphate were precipitated using a known amount of the reagent and then the excess reagent was measured spectrophotometrically. A calibration curve was made by diluting a known amount of the acidified solution of $[Co(en)_2CO_3]Cl$ and measuring the absorbance. Similarly, the filtrates of pyrophosphate and triphosphate precipitations were collected and diluted to a known volume with water. Absorbances of all these solutions were measured at 494 nm using cells of 1 cm path length. From the calibration curve, the quantity of excess reagent in the filtrate and hence the net amount of the reagent consumed for complexation was determined. From the reagent consumption, condensed phosphate present in a given aliquot was calculated.

The results of the spectrophotometric determination of excess reagent are presented in Table 1. Although the quantity of pyro- and triphosphates could be calculated by determining spectroscopically the quantity of the reagent consumed, the accuracy of the results obtained would depend upon the quantitative collection of filtrate. However, the yield was calculated based on the quantity of precipitate in all further experiments.

*Effect of ortho-, trimeta- and pyrophosphates in triphosphate estimation*

Phosphate solutions of known concentrations were prepared and a known amount of it was added to a known quantity of triphosphate (for fractional volumes, microburette was used) so that the total phosphate in the aliquot was 150 mg. A series of precipitation experiments were carried out using the proposed procedure on binary and quaternary mixtures containing varying amounts of ortho-, trimeta-, pyro- and triphosphates to determine the interference of these components and their effect on the estimation of triphosphate. Similarly, the effect of varying amounts of sodium sulphate in triphosphate estimation was investigated.

The results of interference of ortho-, trimeta- and pyrophosphates in the binary mixtures of each with triphosphate are shown in Tables 2–4. The results indicate that there is no interference up to 10% of orthophosphate in the mixture. However, as noted above, orthophosphate also forms a complex with the new reagent, the precipitation starts at pH 6.5, and it is quantitative between pH 8.2 and 8.6.

Table 1. Determination of tri- and pyrophosphates by excess reagent method

| Sample number | STP/pyrophosphate taken (*mg*) | Reagent added (*mg*) | Reagent in filtrate from absorbance (*mg*) | Reagent consumed for complexation (*mg*) | STP/pyrophosphate found (*mg*) | Deviation (%) |
|---|---|---|---|---|---|---|
| 1 | 150.00 (STP) | 120.00 | 9.00 | 110.00 | 149.00 | −0.66 |
| 2 | 120.00 (STP) | 120.00 | 27.00 | 93.00 | 124.00 | +3.30 |
| 3 | 90.90 (pyro) | 150.00 | 57.00 | 93.00 | 90.10 | −0.88 |
| 4 | 87.20 (pyro) | 150.00 | 58.00 | 92.00 | 89.10 | +2.10 |

Table 2. Effect of orthophosphate in the estimation of triphosphate

| Sample number | Triphosphate taken (*mg*) | Orthophosphate added (*mg*) | In the mixture | | Found* | | |
|---|---|---|---|---|---|---|---|
| | | | Triphosphate (%) | Orthophosphate (%) | I (%) | II (%) | Mean (%) |
| 1 | 150.00 | Nil | 100.0 | Nil | 99.4 | 99.8 | 99.6 |
| 2 | 148.50 | 1.50 | 99.0 | 1.0 | 99.4 | 99.6 | 99.5 |
| 3 | 147.00 | 3.00 | 98.0 | 2.0 | 99.3 | 99.7 | 99.5 |
| 4 | 144.00 | 6.00 | 96.0 | 4.0 | 99.4 | 99.9 | 99.6 |
| 5 | 141.00 | 9.00 | 94.0 | 6.0 | 99.7 | 99.5 | 99.6 |
| 6 | 135.00 | 15.00 | 90.0 | 10.0 | 99.8 | 100.0 | 99.9 |

*Calculated as $[Co(en)_2H_2P_3O_{10}]2H_2O$.

Trimetaphosphate also does not interfere in the precipitation of triphosphate. It is interesting to note that trimetaphosphate does not precipitate as a complex with an acidified solution of bis(ethylenediamine)cobalt(III) species at all pHs. The yields of triphosphate are quantitative, if pyrophosphate present in the mixture is less than 5%. When the pyrophosphate present in the mixture is higher than 5%, owing to the co-precipitation of pyrophosphate complex, the yields were unrealistic, over 100%. This is contrary to the observations made in the literature method, wherein the precipitation is said to be incomplete at increased levels of pyrophosphate.[6]

The results of the studies on the interference of sodium sulphate in triphosphate estimation are presented in Table 5. It was found that sodium sulphate does not interfere up to 10% in the binary mixture with triphosphate.

The results of the determination of triphosphate in the quaternary mixtures containing ortho-, trimeta- and pyrophosphates are presented in Table 6. The results indicate that there is no interference from these up to 5% each of the components in the triphosphate estimation. This study of the multicomponent system was carried out keeping in view the composition of the commercially available sodium triphosphate.

*Accuracy*

The reproducibility of the results by the described method was determined by carrying out five replicate determinations of five different commercial triphosphate samples and a standard sample. Five replicate determinations of triphosphate in all the six samples were also made using the known method.[6] Based on the results, mean and standard deviations have been calculated (Table 7). From the results, it is observed that standard deviations of the present method are lower than those of the available method, showing that more accurate and precise results are obtainable from the present method.

Table 3. Effect of trimetaphosphate in the estimation of triphosphate

| Sample number | Triphosphate taken (*mg*) | Trimetaphosphate added (*mg*) | In the mixture | | Found* | | |
|---|---|---|---|---|---|---|---|
| | | | Triphosphate (%) | Trimetaphosphate (%) | I (%) | II (%) | Mean (%) |
| 1 | 150.00 | Nil | 100.0 | Nil | 99.7 | 99.3 | 99.5 |
| 2 | 149.25 | 0.75 | 99.5 | 0.5 | 99.6 | 99.4 | 99.5 |
| 3 | 148.50 | 1.50 | 99.0 | 1.0 | 99.4 | 99.4 | 99.4 |
| 4 | 147.00 | 3.00 | 98.0 | 2.0 | 99.4 | 99.6 | 99.5 |
| 5 | 145.50 | 4.50 | 97.0 | 3.0 | 99.5 | 99.5 | 99.5 |
| 6 | 142.50 | 7.50 | 95.0 | 5.0 | 99.6 | 99.2 | 99.4 |

*Calculated as $[Co(en)_2H_2P_3O_{10}]2H_2O$.

Table 4. Effect of pyrophosphate in the estimation of triphosphate

| Sample number | Triphosphate taken (*mg*) | Pyrophosphate added (*mg*) | In the mixture | | Found* | | |
|---|---|---|---|---|---|---|---|
| | | | Triphosphate (%) | Pyrophosphate (%) | I (%) | II (%) | Mean (%) |
| 1 | 150.00 | Nil | 100.0 | Nil | 99.4 | 99.6 | 99.5 |
| 2 | 147.50 | 2.50 | 98.4 | 1.6 | 99.6 | 99.6 | 99.6 |
| 3 | 145.00 | 5.00 | 96.6 | 3.4 | 99.6 | 99.8 | 99.7 |
| 4 | 142.50 | 7.50 | 95.0 | 5.0 | 99.9 | 100.1 | 100.0 |
| 5 | 140.00 | 10.00 | 93.3 | 6.7 | 102.0 | 102.3 | 102.1 |
| 6 | 135.00 | 15.00 | 90.0 | 10.0 | 103.0 | 103.9 | 103.4 |
| 7 | 120.00 | 30.00 | 80.0 | 20.0 | 107.4 | 107.6 | 107.5 |
| 8 | 105.00 | 45.00 | 70.0 | 30.0 | 110.4 | 109.5 | 110.0 |

*Calculated as $[Co(en)_2H_2P_3O_{10}]2H_2O$.

Table 5. Effect of sodium sulphate in the estimation of triphosphate

| Sample number | Triphosphate taken (*mg*) | Sodium sulphate added (*mg*) | In the mixture | | Found* | | |
|---|---|---|---|---|---|---|---|
| | | | Triphosphate (%) | Sodium sulphate (%) | I (%) | II (%) | Mean (%) |
| 1 | 150.00 | Nil | 100.0 | Nil | 99.6 | 99.8 | 99.7 |
| 2 | 150.00 | 3.10 | 98.0 | 2.0 | 99.5 | 99.9 | 99.7 |
| 3 | 150.00 | 7.90 | 95.0 | 5.0 | 99.8 | 100.0 | 99.9 |
| 4 | 150.00 | 16.60 | 90.0 | 10.0 | 99.7 | 99.9 | 99.8 |

*Calculated as $[Co(en)_2H_2P_3O_{10}]2H_2O$.

In the case of orthophosphates, the reproducibility of the results by the described method was determined by carrying out six replicate determinations on six samples of analytical reagent grade orthophosphate salts. The mean and standard deviations have been calculated and the results are given in Table 8. It shows that the standard deviations of the present method are low, demonstrating the precision and accuracy of the results obtainable by the described method.

Since the total $PO_4^{3-}$ content present in the aliquot is complexed, it is difficult to distinguish between various types of orthophosphates present in the admixture. However, in the case of a single component pure orthophosphate system, such as $NaH_2PO_4$, $Na_2HPO_4$, *etc.*, it can be distinguished by the weight of the complex, since different orthophosphates contain different weight percentage of $PO_4^{3-}$.

In the case of *trans*-dichlorobis(ethylenediamine)cobalt(III) chloride and also its aquo form as complexing agent, the yields were about 98% for $PO_4^{3-}$ ion. The adjustment of pH was rather difficult owing to the gradual decrease of the pH of the solution with time. The precipitates obtained in these cases were amorphous in nature and the filtration was extremely slow. The same situation was observed in the case of *cis*-dichlorobis(ethylenediamine)cobalt(III) chloride. Hence, these reagents are not suitable for the quantitative estimation of orthophosphates.

Table 6. Effect of ortho-, trimeta- and pyrophosphates in the estimation of triphosphate

| Sample number | Triphosphate taken (*mg*) | Orthophosphate added (*mg*) | Trimetaphosphate added (*mg*) | Pyrophosphate added (*mg*) | In the mixture | | | | Found* mean (%) |
|---|---|---|---|---|---|---|---|---|---|
| | | | | | Tri (%) | Ortho (%) | Trimeta (%) | Pyro (%) | |
| 1 | 150.00 | Nil | Nil | Nil | 100.0 | Nil | Nil | Nil | 99.6 |
| 2 | 147.70 | 0.75 | 0.75 | 0.75 | 98.5 | 0.5 | 0.5 | 0.5 | 99.5 |
| 3 | 145.50 | 1.50 | 1.50 | 1.50 | 97.0 | 1.0 | 1.0 | 1.0 | 99.9 |
| 4 | 141.00 | 3.00 | 3.00 | 3.00 | 94.0 | 2.0 | 2.0 | 2.0 | 99.7 |
| 5 | 136.50 | 4.50 | 4.50 | 4.50 | 91.0 | 3.0 | 3.0 | 3.0 | 99.8 |
| 6 | 127.50 | 7.50 | 7.50 | 7.50 | 85.0 | 5.0 | 5.0 | 5.0 | 99.8 |
| 7 | 123.00 | 9.00 | 9.00 | 9.00 | 82.0 | 6.0 | 6.0 | 6.0 | 100.1 |

*Calculated as $[Co(en)_2H_2P_3O_{10}]2H_2O$.

Table 7. Comparison of the present method with the available method for the determination of triphosphate

| Manufacturer's code number | Triphosphate content by Reported method I (%) | II (%) | III (%) | IV (%) | V (%) | Mean (%) | This method I (%) | II (%) | III (%) | IV (%) | V (%) | Mean (%) | Reported method[6] Mean (dev.%) | Standard (dev.%) | This method Mean (dev.%) | Standard (dev.%) |
|---|---|---|---|---|---|---|---|---|---|---|---|---|---|---|---|---|
| I | 86.5 | 86.2 | 89.1 | 86.9 | 87.5 | 87.2 | 87.4 | 88.0 | 87.7 | 87.4 | 88.0 | 87.7 | 0.84 | 1.10 | 0.24 | 0.30 |
| II | 92.3 | 93.2 | 93.9 | 93.5 | 92.7 | 93.1 | 94.9 | 94.3 | 95.2 | 94.3 | 95.3 | 94.8 | 0.50 | 0.63 | 0.40 | 0.48 |
| III | 88.9 | 91.2 | 92.9 | 90.0 | 92.0 | 91.0 | 93.2 | 92.7 | 92.9 | 92.5 | 93.3 | 92.9 | 1.24 | 1.58 | 0.26 | 0.33 |
| IV | 87.7 | 89.9 | 89.9 | 88.6 | 89.6 | 89.1 | 90.0 | 89.4 | 90.0 | 89.5 | 90.1 | 89.8 | 0.80 | 0.96 | 0.28 | 0.32 |
| V | 92.0 | 93.6 | 94.5 | 93.2 | 93.6 | 93.4 | 95.8 | 95.0 | 94.0 | 95.8 | 94.8 | 95.3 | 0.62 | 0.91 | 0.42 | 0.48 |
| VI* | 76.6 | 76.0 | 76.9 | 76.2 | 76.8 | 76.5 | 77.2 | 76.9 | 77.0 | 76.9 | 76.7 | 76.9 | 0.30 | 0.39 | 0.12 | 0.19 |

*Standard triphosphate namely $Na_5P_3O_{10}6H_2O$ (77.3% $Na_5P_3O_{10}$).

*Application of the method for pyro-, tri- and orthophosphates in commercial matrices*

*Estimation of triphosphate in commercial samples.* The present method was employed for the estimation of triphosphate samples obtained from four different manufacturers spread over four different countries. The estimations were carried out in replicate using both the present and the reported methods. The results are given in Table 7. There are some differences in the results for the triphosphate content in the samples and they can be accounted for by the variations in the raw materials used and conditions for thermal condensation of orthophosphate during the manufacture of triphosphate by different manufacturers. In all the determinations, the results obtained by the known method[6] are lower than the results obtained by the described method. This is also in agreement with the yield obtainable (98–99.5%) by the reported method.[6]

*Estimation of pyrophosphate.* Under the optimum conditions recommended for the precipitation of pyrophosphate, it was found that the present method gives a yield of 99.5% which is in contrast to a maximum yield of 93% obtainable by the known method. The absence of phosphate in the filtrate in all the precipitation experiments by the present method confirmed the completion of precipitation. Generally, commercial samples of pyrophosphate do not contain triphosphate or any other polyphosphates. However, a series of experiments were conducted to study the effect of triphosphate up to 30%, in the determination of pyrophosphate by the described method (Table 9). It is observed that with up to 5% of triphosphate, the yields were as expected. Furthermore, it was found that in the presence of 10, 20 and 30% of triphosphate, the yields were unrealistic, over 100%. Above 30% of triphosphate, the precipitate was sticky in nature at room temperature, which upon cooling to 10 °C turned solid. The present method was also applied to the determination of pyrophosphate in sodium acidpyrophosphate ($Na_2H_2P_2O_7$) prepared by a standard method.[36] The results were found to be good. The replicate experiments showed the purity to be 99.4–99.8%.

*Determination of triphosphate in commercial detergent powders.* The present method was utilized for the determination of triphosphate in premier detergent powders of Indian origin. Detergent powders, in general, are complex and multicomponent systems. The samples for the analysis were prepared by dissolving the detergent powder in 95% ethanol to remove anionic detergent. The alcohol insoluble phosphates were then dissolved in water and used for the estimation.[1] Determinations were made in triplicate for each sample, employing the known and the described methods (Table 10). It is observed that the results of both the methods are in good agreement.

Table 8. Analysis of orthophosphoric acid and its salts by the present method

| Sample | Purity of sample obtained (in wt%) 1 | 2 | 3 | 4 | 5 | 6 | Mean dev. (%) | Standard dev. (%) |
|---|---|---|---|---|---|---|---|---|
| $H_3PO_4$ (85.0%) | 84.8 | 84.8 | 84.9 | 85.3 | 84.6 | 84.9 | 0.15 | 0.25 |
| $NaH_2PO_4 2H_2O$ | 99.9 | 99.8 | 99.6 | 99.6 | 100.0 | 100.1 | 0.16 | 0.21 |
| $Na_2HPO_4$ | 100.1 | 99.7 | 99.5 | 99.9 | 100.0 | 99.6 | 0.20 | 0.24 |
| $Na_3PO_4 12H_2O$ | 100.1 | 100.2 | 100.0 | 99.9 | 99.8 | 100.1 | 0.11 | 0.15 |
| $KH_2PO_4$ | 100.0 | 100.5 | 100.3 | 100.3 | 100.4 | 100.2 | 0.15 | 0.19 |
| $(NH_4)_2HPO_4$ | 99.7 | 99.9 | 99.5 | 100.2 | 99.9 | 100.0 | 0.17 | 0.25 |

Table 9. Effect of triphosphate in the estimation of pyrophosphate

| Sample number | Pyrophosphate taken (mg) | Triphosphate added (mg) | In the mixture | | Found* Mean (%) |
|---|---|---|---|---|---|
| | | | Pyrophosphate (%) | Triphosphate (%) | |
| 1 | 125.00 | Nil | 100.0 | 0.0 | 99.4 |
| 2 | 121.87 | 3.12 | 97.5 | 2.5 | 99.8 |
| 3 | 118.75 | 6.25 | 95.0 | 5.0 | 99.8 |
| 4 | 112.50 | 12.50 | 90.0 | 10.0 | 100.9 |
| 5 | 100.00 | 25.00 | 80.0 | 20.0 | 102.3 |
| 6 | 87.50 | 37.50 | 70.0 | 30.0 | † |

*Calculated as $[Co(en)_2HP_2O_7]4H_2O$.

†The yield could not be accurately determined owing to the sticky nature of the precipitate.

Table 10. Comparison of the present method with the known method for the determination of triphosphate in commercial detergent powders

| Manufacturer's code number | Triphosphate content | | | | | | | |
|---|---|---|---|---|---|---|---|---|
| | Reported method[6] | | | | This method | | | |
| | I (%) | II (%) | III (%) | Mean (%) | I (%) | II (%) | III (%) | Mean (%) |
| A | 19.9 | 20.9 | 20.1 | 20.3 | 20.6 | 21.3 | 20.2 | 20.7 |
| B | 27.9 | 27.9 | 27.0 | 27.6 | 28.5 | 27.5 | 27.3 | 27.8 |
| C | 16.8 | 18.9 | 18.0 | 17.9 | 18.2 | 16.9 | 17.0 | 17.4 |

*Determination of orthophosphate in commercial matrices.* For this purpose, some commercial tricalcium and dicalcium phosphates were taken. Since these are water insoluble, acid extract of these samples were used for the estimation. It was found that calcium severely interferes. At the optimum pH, precipitation of calcium phosphate occurs preferentially over the precipitation of $[Co(en)_2PO_4]$, resulting in a mixture of both the precipitates. Masking of calcium by EDTA followed by precipitation of the phosphate complex by acidified solution of (carbonato)bis(ethylenediamine)cobalt(III) chloride did not give the desired results.

*Acknowledgements*—Authors wish to thank Ballarpur Industries Limited, Karwar, India, for the facilities to carry out this work. The useful advice and assistance of Dr K. S. Ramachandra is gratefully acknowledged. One of the authors (D.R.K.) is grateful to the Indian Institute of Science, for accepting him as an external registrant for the Ph.D. degree.

## REFERENCES

1. H. J. Weiser Jr., *Anal. Chem.*, 1956, **28,** 477.
2. E. Karl-Kroupa, *Anal. Chem.*, 1956, **28,** 1091.
3. G. E. B. Y. Ahlijah and E. F. Mooney, *Spectrochim. Acta*, 1966, **22,** 547.
4. D. E. C. Corbridge, *J. Appl. Chem.*, 1956, **6,** 456.
5. D. E. C. Corbridge and E. J. Love, *Anal. Chem.*, 1955, **27,** 1383.
6. H. W. Mccune and G. J. Arquatte, *Anal. Chem.*, 1955, **27,** 401.
7. D. R. Kamat, V. V. Savant and D. N. Sathyanarayana, *Inorg. Chim. Acta* (1994) (submitted).
8. M. Halmann (Ed.), *Analytical Chemistry of Phosphorous Compounds.* Wiley-Interscience, New York, 1972.
9. B. Paschkes and B. Berman, *Anal. Chim. Acta*, 1961, **24,** 5.
10. IS 567-1969, IS 571-1969, IS 798-1986, Bureau of Indian Standards, New Delhi.
11. A. I. Vogel, *A Textbook of Quantitative Inorganic Analysis.* ELBS, Longmans, London, 1978.
12. R. Bennewitz and I. Taenzer, *Mikro Chim. Acta*, 1959, 853.
13. W. S. Selig, *J. Chem. Educ.*, 1985, **62,** 431.
14. L. S. Rumyantseva and I. L. Jeodovovich, *Dokl. Akad. Nauk. Uzb, SSR*, 1967, **24,** 35.
15. V. Kantere, I. E. Krasnova and G. M. Muskheli, *Otkrytiya, Izobret, Prom. Obraztsy, Tovarnye Znaki*, 1970, **47,** 131.
16. M. L. Marion, *Diss. Abstr. Int. B*, 1973, **33** (Part 1), 5706.
17. S. K. Susic, V. N. Njegovan and B. Solaja, *Z. Anal. Chem.*, 1961, **183,** 412.
18. S. R. Trivedi and G. S. Johar, *Labdev*, 1970, Part A, **8,** 19.
19. T. Takashi, H. Kazuo and K. Akinori, *Bunseki Kagaku*, 1979, **28,** 43.
20. K. Murthy, N. Krishnan and A. V. Suryanarayana, *Fresenius' Z. Anal. Chem.*, 1982, **312,** 546.
21. F. Ruf and C. R. Sem, *Geol. Commun. Nat. Malgache Geol.*, 1966, 70.
22. M. Muto, *Nippon Kagaku Zasshi*, 1964, **85,** 782.
23. J. P. Ebel, *Bull. Soc. Chim. Fr.*, 1968, 1663.
24. D. Lairon, J. Amic and H. Lafont, *J. Chromatogr.*, 1974, **88,** 183.
25. R. K. Ghatuary and A. K. Sen, *J. Indian Chem. Soc.*, 1978, **55,** 337.
26. A. Laurent and R. Bourdon, *Ann. Pharm. Fr.*, 1978, **36** (9–10), 453.

27. T. P. Mawhinney, *Anal. Lett.*, 1983, **16** (A2), 159.
28. G. D. Christian and F. J. Feldman, *Anal. Chim. Acta*, 1968, **40,** 173.
29. S. F. Lincoln and D. R. Stranks, *Aust. J. Chem.*, 1968, **21,** 37.
30. M. Linhard and G. Stim, *Z. Anorg. Chem.*, 1952, **268,** 105.
31. A. Wold and J. K. Ruff, *Inorg. Synth.*, 1973, **14,** 64.
32. W. C. Fernelius, *Inorg. Synth.*, 1946, **2,** 221.
33. J. C. Bailar, *Inorg. Synth.*, 1946, **2,** 222.
34. IS 6100-1986, Bureau of Indian Standards, New Delhi.
35. L. F. Audrieth, *Inorg. Synth.*, 1950, **3,** 103.
36. J. R. Van Wazer, *Phosphorus and Its Compounds*, Vol. 1, p. 607. Interscience, New York, 1958.

Pergamon

0039-9140(95)01413-6

*Talanta*, Vol. 42, No. 3, pp. 375–383, 1995

0039-9140/95 $9.50 + 0.00

# ELECTROTHERMAL ATOMIC ABSORPTION SPECTROMETRIC DETERMINATION OF ULTRA-TRACE AMOUNTS OF TIN BY *IN SITU* PRECONCENTRATION IN A GRAPHITE TUBE USING FLOW INJECTION HYDRIDE GENERATION WITH ON-LINE ION-EXCHANGE SEPARATION

GUANHONG TAO* and ZHAOLUN FANG†

Flow Injection Analysis Research Centre, Institute of Applied Ecology, Chinese Academy of Sciences, Box 417, 110015 Shenyang, China

(*Received* 17 *January* 1994. *Revised* 11 *July* 1994. *Accepted* 17 *August* 1994)

**Summary**—A method was developed for the ultra-trace determination of tin by *in situ* preconcentration in a graphite tube using a flow injection hydride generation technique with on-line ion-exchange separation. The sample was prepared in 2*M* hydrochloric acid before being passed through an incorporated micro-column packed with a strongly basic anion-exchanger D-201. The tin was retained as its chlorostannate complex and subsequently eluted by de-ionized water into the hydride generation system. The hydride and hydrogen gases evolved were separated from the liquid phase in a gas–liquid separator and transferred into a palladium-coated graphite tube pre-heated to 300°C to collect the analyte, which was later atomized at 2300°C. With the reported system, tin was determined at a sampling frequency of 30/hr with a detection limit ($3\sigma$) of 0.01 μg/l. using 10.7 ml sample. The precision was 1.5% RSD at the 0.5 μg/l. level. The proposed method was applied to the determination of tin in tap water, hair, serum samples and geological reference samples.

Recently the *in situ* preconcentration of vapour-forming analytes in a graphite furnace following vapour generation reactions has aroused considerable interest as a new technique for ultra-trace analysis using electrothermal atomic absorption spectrometry (ETAAS). Originally developed for the preconcentration of hydride-forming elements, most recently the technique has been extended also to the preconcentration of mercury.[1,2] Several attempts were made to automate the preconcentration procedure under batch or continuous flow configurations to improve the efficiency as well as to decrease human intervention. The latter is helpful in minimizing contamination risks in the ultra-trace determinations. The implementation of flow injection (FI) techniques in the automation of on-line preconcentration systems for atomic absorption spectrometry (AAS) was frequently shown to provide significant advantages over other approaches.[3] This is also true for *in situ* preconcentration with hydride generation. In a recent application of the FI technique to the determination of germanium in environmental samples in our group using *in situ* preconcentration ETAAS,[4] apart from automation of the system and decreases in contamination, the system featured large improvements in the tolerance to interferences, in comparison to batch procedures. Hitherto, FI *in situ* preconcentration has been applied successfully to germanium,[4] arsenic[5] and tin.[6]

The determination of tin in environmental samples is of importance owing to its biological interest.[7–9] Hydride generation AAS is one of the most commonly used methods owing to its high sensitivity and selectivity,[10–15] but the methods suffer strong influences from acidity in the sample matrix.[10–12] Recently, Fang *et al.*[16] described an on-line modification of the acid matrix of sample digest by incorporation of an anion-exchanger column in an FI system prior to the hydride generation reaction. The analyte was initially converted into its chlorostannate complex, retained on an ion-exchange column and subsequently eluted by diluted nitric acid

*On leave from the Research Centre for Eco-Environmental Sciences, Chinese Academy of Sciences, Beijing, China.
†Author to whom correspondence should be addressed.

under strictly controlled conditions. Reproducible conditions for hydride generation reaction were achieved, with 3.5-fold gain in sensitivity.

Although detection limits as low as 0.08 $\mu$g/l. for tin were reported using hydride generation approaches,[16] the sensitivity is often insufficient for the precise determination of tin at ultra-trace levels in some samples, such as natural waters. More recently, *in situ* preconcentration of tin in a graphite furnace by FI hydride generation was used successfully by Zhang *et al.*[6] to improve the performance of ETAAS procedures. A detection limit of 7 ng/l. was achieved with a precision of 3–5% RSD at the 1.0 $\mu$g/l. level. However, no systematic studies on the influence of acidity were given. In order to enhance the sensitivity, 10 ml sample were used, resulting in a long collection (preconcentration) step of 145 sec at 300°C in the graphite furnace programme.

In this work, an attempt was made to apply the FI on-line ion-exchange sample matrix modification technique to the *in situ* preconcentration of tin in a graphite tube to create robust conditions for hydride generation, with the aim of providing a reliable and sensitive method for the determination of tin. The feasibility of this approach was illustrated by its application to the determination of trace amounts of tin in biological samples and geological reference samples.

## EXPERIMENTAL

### *Apparatus*

A Perkin-Elmer Model 2100 atomic absorption spectrometer with a deuterium lamp background corrector was used with a Perkin-Elmer Model HGA-700 graphite furnace. A wavelength of 286.4 nm was used with a spectral band pass of 0.7 nm. A tin hollow cathode lamp was operated at 30 mA. Pyrolytic graphite coated polycrystalline graphite tubes were used with similarly coated L'vov platforms. The graphite furnace temperature programme is given in Table 1. Integrated absorbance (peak area) was used for evaluating the results throughout this work. The analyte absorption peaks were recorded by a PC computer, presented on a high-resolution screen, and printed out using an Epson EX-800 printer.

A Perkin-Elmer Model FIAS-200 system with a 5-port FI-valve was used with the hydride generation accessories.[17] The rotation speed of the two multichannel peristaltic pumps, their stop and go intervals and the actuation of the injector were programmed and automatically controlled by a separate PC computer, independent of the spectrometer. The outlet of the gas-liquid separator, consisting of a 50 cm length of PTFE tubing, was connected to a 5 cm long × 1.5 mm o.d. × 0.5 mm i.d. quartz capillary with a short piece of silicone-rubber tubing. The quartz capillary was loaded on a laboratory-made rotating arm that could be used to swing the tip of the capillary into the sample introduction port of the graphite tube and functioned as a hydride introduction probe during the *in situ* collection (preconcentration) stage.

The ion-exchange column used for separation was made by packing a strongly basic macroporous anion exchanger D-201, 60–100 mesh (Shenyang Organic Chemicals Co.) into a 3 mm i.d. × 30 mm long column whose construction was described previously.[18] The column was connected to the FI-valve via threaded fittings.

Tygon pump tubing was used to deliver all solutions. All reaction coils and connections were made with 0.7 mm i.d. poly(tetrafluoroethylene) (PTFE) tubing. A chemifold plastic connector block (Perkin-Elmer) furnished with W-configuration conduits was used for merging of the reagent and carrier streams.

Plastic containers were used for the samples.

### *Reagents*

A 1000 mg/l. tin stock standard solution was prepared by dissolving the appropriate amount of $SnCl_2 . 2H_2O$ in 2*M* hydrochloric acid. A series of working standard solutions were

Table 1. Furnace programme for *in situ* preconcentration and atomization

| Step | Temperature (°C) | Ramp time (*sec*) | Hold time (*sec*) | Inner argon flow-rate (*ml/min*) |
|---|---|---|---|---|
| 1. Drying | 90 | 5 | 20 | 300 |
| | 120 | 15 | 20 | 300 |
| 2. Pyrolysis/pre-treatment | 300 | 1 | 20 | 300 |
| 3. Collection | 300 | 1 | 30 | 300 |
| 4. Atomization | 2300 | 0 | 5 | 0 |
| 5. Cleaning | 2650 | 1 | 3 | 300 |

prepared by three-stage dilutions of the stock standard solution with 2*M* HCl.

Ultra-pure reagent grade hydrochloric acid (Beijing Chemical Factory) was further purified by iso-thermal diffusion, as described in the Procedures.

Sodium tetrahydroborate solution (0.1–0.5%, v/v) was prepared using purified $NaBH_4$ (Merck, Schuchardt, Germany) and purified as described under *Reagent purification*. The concentration of sodium hydroxide in the reagent solution was 0.05*M*.

De-ionized water was used throughout. Nitric acid was of ultra-pure reagent grade (Beijing Chemical Factory, Beijing, China). Palladium solution 500 mg/l. was prepared by dissolving 0.166 g of palladium chloride in 10 ml of nitric acid and diluting to 100 ml with de-ionized water. All other chemicals were of analytical, or ultra-pure reagent grade.

*Procedures*

*On line ion-exchange preconcentration.* The FI manifold used for on-line ion-exchange separation hydride generation ETAAS is shown in Fig. 1, together with the optimized operating parameters. The manifold was almost the same as that for hydride generation AAS applications described previously,[16] except the stannane formed (Fig. 1b) was introduced into the graphite furnace for collection instead of the heated quartz tube for atomization. The graphite furnace temperature programme in Table 1 also shows the various stages of operation for the *in situ* collection.

Before each hydride generation and collection cycle, 20 $\mu$l of 500 mg/l. Pd was pipetted into the furnace. Then the furnace programme and FI system were initiated simultaneously. The Pd solution was dried and the furnace was heated to 300°C and held constant at that temperature for 20 sec to complete the pre-treatment. The sample loading procedure of the FI system was performed in parallel with the drying and pyrolysis/pre-treatment steps. In the loading step (Fig. 1a), pump 1 was stopped, and pump 2 actuated to propel the sample in 2*M* hydrochloric acid through the ion-exchange column at 8 ml/min. The chlorostannate complex was sorbed on the column and the effluent emerging from the column was discarded. This step lasted 80 sec which coincided with the drying and pyrolysis/pre-treatment steps of the furnace programme.

At the end of the loading period, which was also the end of the pyrolysis/pre-treatment step, the tip of the quartz capillary probe was inserted through the sample introduction port at the centre of the graphite tube by manually swinging over the arm on which the probe was fixed, and was kept in contact with the graphite platform throughout the collection period. The valve was then actuated automatically, directing the eluent flow into the column. The sorbed chlorostannate complex was eluted by de-ionized water into the hydride generation manifold and merged with the tetrahydroborate reductant solution. The residual acidified sample solution remaining in the column provided the acid conditions for the hydride generation reaction.

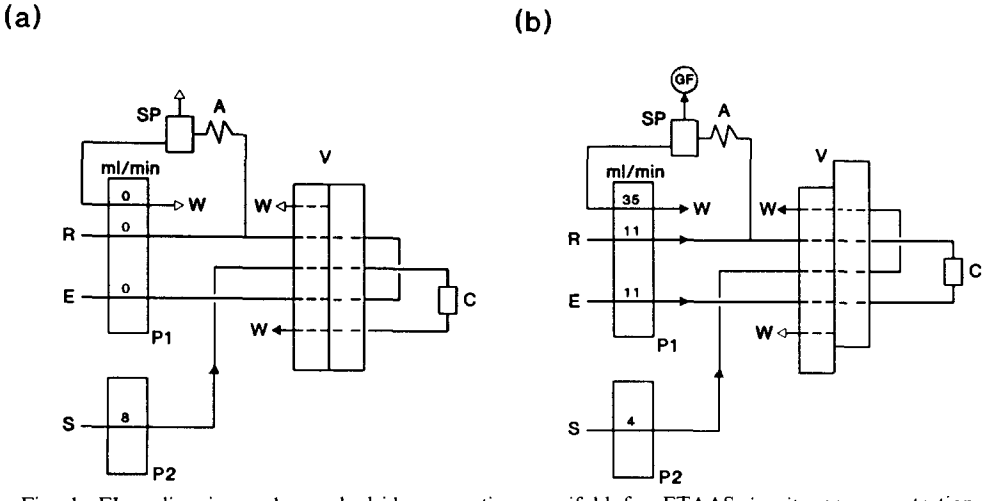


Fig. 1. FI on-line ion-exchange hydride generation manifold for ETAAS *in situ* preconcentration determination of tin: (a) sample loading; and (b) eluting and collecting. (A) Reaction coil; (C) ion-exchange column; (E) de-ionized water; (GF) graphite furnace; (P1,P2) peristaltic pumps; (R) 0.5% $NaBH_4$; (S) sample; (SP) gas–liquid separator; (V) injector valve; (W) waste.

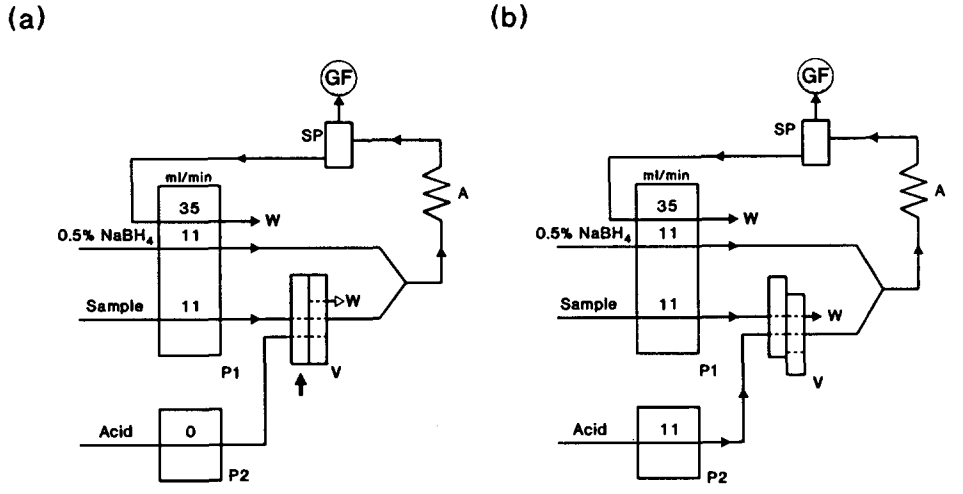


Fig. 2. FI manifold for investigation on effects of the hydride generation media for the *in situ* preconcentration determination of tin: (a) collection; and (b) washing and sample changing. (A) Reaction coil; (GF) graphite furnace; (P1,P2) peristaltic pumps; (SP) gas–liquid separator; (V) injector valve; (W) waste.

After passing through a 30 cm length of reaction coil (A), the gas–liquid mixture was guided into the gas–liquid separator where the waste was pumped out at a flow-rate of 35 ml/min. The stannane generated was separated and transferred by the evolved hydrogen gas into the Pd-coated graphite tube and tin was collected in the furnace following decomposition. The elution procedure was 20 sec. During this stage the next sample was introduced into the uptake line at a reduced rotation speed and ready for the next determination. The FI system was stopped automatically at this point. After an interval of 10 sec for the withdrawal of the quartz capillary probe from the graphite tube, giving a total of 30 sec at the 300°C collection temperature, the graphite furnace was heated to the atomization temperature at 2300°C, using maximum power with interrupted internal argon flow, and the absorbance signals were recorded. Finally, the furnace temperature was increased to 2650°C for 3 sec to clean the furnace.

*Studies on the effects of acidity.* For the studies on the effects of the hydride generation media, the FI manifold shown in Fig. 2 was used. It is very similar to that reported previously[4] for the *in situ* preconcentration determination of germanium. The procedures were also similar to those in the previous system. After the drying and pyrolysis/pre-treatment steps were completed, the tip of the quartz probe was inserted into the graphite furnace and the FI system was actuated immediately. This initiated the collection sequence. The acidified sample was merged with the tetrahydroborate reductant, both propelled by pump P1 at 11 ml/min. The stannane formed was separated and transferred into the Pd-coated graphite tube. After a 30 sec generation (collection) period, the valve was automatically actuated to the washing and sample change position. An acid rinsing solution, propelled by pump 2, was run for 10 sec to expel the residual sample in the reaction coil to the separator in order to prepare the system for the next sample and collect the remaining fraction of stannane evolved from the residual sample after the termination of the sampling period. Meanwhile the next sample was introduced into the sample uptake lines. After the withdrawal of the quartz probe from the graphite tube, the analyte was atomized. The furnace temperature programme was the same as that used in the FI on-line ion-exchange separation hydride generation ETAAS system.

*Reagent purification.* For purification of HCl, 3000 ml HCl were introduced into a 30 cm i.d. desiccator. A 500 ml PTFE beaker containing

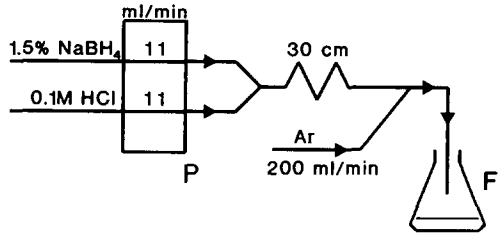


Fig. 3. Schematic diagram for purification of $NaBH_4$. (P) Peristaltic pump; (F) flask.

300 ml de-ionized water was placed on the porcelain shelf of the desiccator. The desiccator was kept sealed at room temperature for 10 days. The final concentration of the purified HCl in the beaker was obtained by titration.

The schematic diagram for the purification of $NaBH_4$ is shown in Fig. 3. The manipulation was conducted in a ventilated hood. Both 1.5% (v/v) $NaBH_4$ solution and 0.1*M* HCl were delivered by a peristaltic pump at flow rates of 11 ml/min. The two solutions merged and reacted in a 30 cm long reaction coil. Analyte contaminant in $NaBH_4$ was transformed to stannane and released from the solution with the aid of an argon stream. The concentration of $NaBH_4$ was about 0.5% after purification.

*Sample pre-treatment.* Geological samples: 0.5 g samples were treated with 5 ml of a nitric acid–hydrofluoric acid mixture (7 + 3 v/v) in PTFE beakers. The vessels were heated on a hot plate at 140°C and gently boiled nearly to dryness. A further 2 ml of acid mixture were added and the solutions were again taken nearly to dryness. After cooling, the digests were diluted to 50 ml. A 1 ml volume was taken and diluted further to 100 ml with 2*M* HCl.

Hair and serum samples: 0.2 g hair or 1 ml serum sample was digested gently in PTFE beakers with 5 ml of a nitric acid–perchloric acid mixture (3 + 1 v/v) on a hot-plate at 140°C until near dryness. A further 1 ml of acid mixture was added and the solution was taken nearly to dryness again. After cooling, the digest was diluted to 50 ml with 2*M* HCl.

Tap water samples were filtered and acidified to 2*M* HCl with concentrated HCl.

## RESULTS AND DISCUSSION

### *Effect of hydride generation reaction medium on* in situ *preconcentration ETAAS signal response for tin*

It has been demonstrated by several authors that the stannane generation efficiency is strongly dependent on the acidity at which the reaction is performed and also on the acid species. Various acidity conditions for the hydride generation determination of tin have been proposed.[10–12,19–21] Thompson and Pahlavanpour[19] observed a distinct maximum of the analytical signal at approximately 0.1*M* HCl. De Doncker *et al.*[11] found that 0.09*M* of $H_2SO_4$ gave optimum sensitivity for the generation of stannane. A mixed reaction medium of 0.4*M* nitric acid and 0.2*M* tartaric acid was used by Legret *et al.*[10] as the optimal condition. By means of radio tracers, Petrick and Krivan[20] showed that the stannane efficiency was close to 100% for 0.5*M* HCl. A model for hydride generation was proposed by Wang and Barnes[21] and they concluded that stannane could be generated only within a critical range in the vicinity of pH 1.0, referring to the final acidity. In the above studies, batch-wise or continuous-flow approaches were used for hydride generation. However recently Fang *et al.*[16] pointed out that influences from acidity were more pronounced in FI approaches than in the batch mode. In their FI application, Welz *et al.*[12] used 0.1*M* HCl in saturated boric acid as reaction medium and observed that sensitivity increased significantly with decreasing HCl concentration in saturated boric acid solution down to 0.1*M* and no reliable signals could be obtained for the concentrations lower than 0.1*M* owing to hydrolysis of tin. In the recent FI hydride generation *in situ* preconcentration application, Zhang *et al.*[6] used 0.5 or 2.0% HCl as the hydride generation medium; but no detailed effects of the acidities and acid species were reported. In their previous work,[13] they reported the efficiency of stannane generation for 0.5% HCl (0.17*M*) was higher than 2.0%.

Therefore, an attempt was made in this work to investigate the effect of hydride generation medium on the sensitivity for the *in situ* preconcentration ETAAS system. Hydrochloric, nitric, and sulphuric acids were studied using the FI manifold shown in Fig. 2. The influence of varying acid concentrations on the signal is shown in Fig. 4. The sensitivity depended strongly on the concentration, but the maximum signals were quite similar for all three

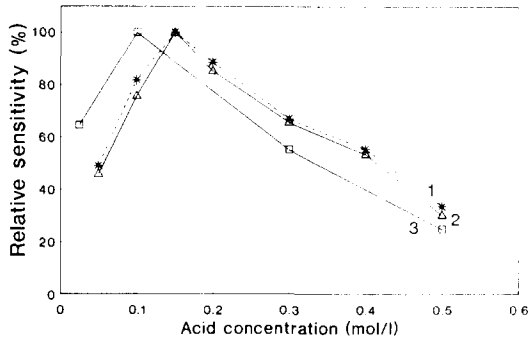


Fig. 4. Effect of acid concentrations on the tin signal expressed in % integrated absorbance, using the manifold shown in Fig. 2 and taking the maximum absorbance as 100% for all the acids studied. (1) Nitric acid; (2) Hydrochloric acid; (3) Sulphuric acid. The concentration of tin was 0.5 μg/l. Other conditions are as shown in Fig. 2.

acids. This observation was quite similar to that reported by Thompson *et al.*[19] and de Doncker *et al.*[11] Although it is not difficult to adjust the sample acidity to 0.15*M* to produce maximum sensitivity, no stable region of influence on sensitivity could be found, which would imply lack of robustness for the method. Therefore, the on-line modification of the acid matrix of sample solutions using an incorporated ion-exchange column proposed by Fang *et al.*[16] was adopted in this work, in order to create more reliable conditions for the hydride generation.

*Optimization of experimental parameters for FI on-line ion-exchange separation* in situ *hydride preconcentration system*

FI hydride generation AAS coupled with on-line ion-exchange separation and preconcentration system has been used successfully in the determination of tin in canned food.[16] The manifold was adapted to the *in situ* preconcentration ETAAS system, resulting in the FI manifold shown in Fig. 1.

In their previous studies,[16] Fang *et al.* used 0.1*M* nitric acid as the eluent and found its concentration very critical for the system's performance. Therefore, a detailed investigation of the acid concentration under different sodium tetrahydroborate concentrations was carried out. The flow-rates for sample, eluent and reductant solutions were adopted mainly based on previously established experimental conditions for FI on-line ion-exchange separation and preconcentration of tin[16] and other hydride-forming elements.[22,23] The results are shown in Fig. 5. The absorbance remained almost constant in the nitric acid concentration range of 0 (de-ionized water)–0.2*M* at all $NaBH_4$ concentrations tested. This phenomenon was different from that reported in Ref. 16 where the peak height absorbances dropped dramatically with an increase in acid concentration from 0 to 0.4*M*. This is because the readouts for the *in situ* preconcentration system were not based on transient signals produced during the hydride generation reaction but on integrated readings from the electrothermal atomization process. The readouts will remain identical as long as the amount of analyte trapped on the tube during the collection period are identical. This is in agreement with the observation of Fang *et al.*[16] that for the transient eluate signals, when the peak height increased with a decrease in acid concentration, the peak width decreased, producing approximately the same peak area. The explanation for the responses using de-ionized water as eluent is that the residual acidified sample solution remaining in the column following sample loading provided the acid conditions for the hydride generation reaction. The sensitivity increased with an increase in tetrahydroborate concentration (Fig. 5). However the reaction became so violent when the concentration was higher than 0.5% that trouble-free gas–liquid separation could no longer be ensured. Since lower reductant concentration also provides reduced blank values. A de-ionized water eluent and 0.5% $NaBH_4$ were used in subsequent studies.

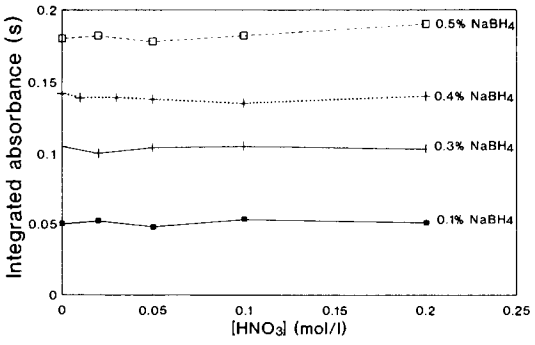


Fig. 5. Effect of nitric acid concentrations on integrated absorbance under different $NaBH_4$ concentrations. The concentration of tin was 0.5 μg/l. Other conditions are as shown in Fig. 1.

In most hydride generation AAS and recently *in situ* preconcentration systems, carrier gases, normally argon, were used to strip and transport the hydrides into the atomizer or graphite tube. However, recent studies by Tao and Fang[4] showed that effects from the carrier gas flow-rate were negligible in the *in situ* preconcentration system. In their system, no carrier gas was used. The hydride was transported into the graphite furnace by the hydrogen generated during the reaction. This produced about 10% higher sensitivity apart from a saving in the argon gas supply. Therefore no argon carrier was used in the present work following this experience. No unfavourable effects were found by doing so. However, no increase in sensitivity was observed either.

The optimum operating conditions for ETAAS are given in Table 1. The catalytic reactivity of palladium was reported to promote low temperature deposition of the hydride by dissociative chemisorption[24–26] and, therefore, palladium was used for coating the furnace tube in the present work. It was found that 20 μl of 500 mg/l. Pd were sufficient for trapping and

Table 2. Effect of co-existing ions on the recovery of Sn

| Interferent | Concentration (*mg/l.*) | Recovery (%) |
|---|---|---|
| Ca(II) | 2000 | 102 |
| Cu(II) | 1 | 101 |
| | 5 | 94 |
| | 10 | 87 |
| Fe(II) | 1000 | 99 |
| Fe(III) | 1000 | 98 |
| Mg(II) | 2000 | 95 |
| Na(I) | 2000 | 100 |
| | 5000 | 110 |
| Ni(II) | 3 | 102 |
| | 10 | 103 |
| As(III) | 20 | 99 |
| | 40 | 105 |
| As(V) | 10 | 100 |
| | 20 | 107 |
| Ge(IV) | 5 | 103 |
| | 16 | 106 |
| Se(IV) | 5 | 98 |
| | 20 | 95 |
| Se(VI) | 10 | 97 |
| | 20 | 93 |
| $C_2O_4^{2-}$ | 100 | 97 |
| $F^-$ | 2000 | 100 |
| $NO_3^-$ | 2000 | 97 |
| | 5000 | 92 |
| OAc | 1000 | 102 |
| | 5000 | 98 |
| $PO_4^{3-}$ | 10 | 95 |
| | 20 | 89 |
| $SO_4^{2-}$ | 20 | 89 |

All samples contained 0.5 μg/l. Sn. All results are averages of three measurements with 2–3% RSD.

stabilizing the collected product on the substrate at a temperature of 300°C. An atomization temperature of 2300°C recommended by the manufacturer for conventional ETAAS,[27] was used in this study.

*Interference studies*

Interferences studies on possible interferents both in the ion-exchange process and in the hydride generation reaction showed considerable high tolerance to a wide range of coexisting ions (Table 2). Cu(II) and Ni(II) were frequently reported to be two of the most significant transition metal interferences in the determination of tin. In their studies,[19] Thompson *et al.* reported that 1 mg/l. Cu(II) and 1 mg/l. Ni(II) could depress responses of tin by 40 and 65%, respectively. In this study, up to 5 mg/l. Cu(II) and 10 mg/l. Ni(II) could be tolerated without any significant adverse effects on the integrated absorbance. Other potential interferents such as Fe(II), Fe(III) did not interfere seriously up to higher levels. Since the stability of the chloro-complexes of these metal ions in 2*M* hydrochloric acid are considerably lower compared to the chlorostannate complex, their introduction into the hydride generation manifold were partially impeded owing to decreased retention on the ion exchanger. The hydride forming elements such as As(III) As (V), Ge(VI) and Se(IV), Se(VI) were also investigated, and neither of these interfered up to at least $2 \times 10^4$-fold excess concentrations. In their FI hydride generation *in situ* preconcentration system,[6] Zhang *et al.* reported that the system could tolerate these hydride forming elements at 200-fold excess. Table 2 also shows that the anions tested exhibit no serious interferences on the determination of tin.

Table 4. Determination of tin in geochemical reference samples ($n = 3$)

| Material | Found (μg/g)* | Recommended (μg/g) |
|---|---|---|
| GSR-1 | 12.8 ± 0.2 | 12.5 |
| GSS-5 | 17.9 ± 0.2 | 17.7 |

*The terms ± are 95% confidence intervals.

*Analytical performance*

Characteristic data for the performance of the FI on-line ion-exchange separation hydride

Table 3. Characteristic performance for the FI on-line ion-exchange separation hydride generation *in situ* preconcentration ETAAS system

| | |
|---|---|
| Sample consumption | 10.7 *ml* |
| Sampling frequency | 30 *sample/hr* |
| Calibration curve | $A = 0.038 + 0.35C_{Sn}$ (0–0.7 μg/l., $r = 0.9996$) |
| %RSD ($n = 11$) | 2.0 (0.3 μg/l.) |
| | 1.5 (0.5 μg/l.) |
| L.o.D. ($3\sigma$) | 0.01 μg/l. |
| Characteristic mass/pg per 0.0044 *sec* | |
| conventional ETAAS* | 75 |
| present method | 127 |
| Overall collection efficiency | 59% |
| Retention efficiency† | 61% |
| Deposition efficiency | 96% |

*The conditions recommended by the manufacturer were used.[27]

†A 0.5 μg/l. solution of tin was used to evaluate the retention efficiency of the ion-exchange procedure.[18, 22]

Table 5. Recoveries of tap water, serum and hair digest samples spiked with 0.2 μg/l. tin ($n = 3$)

| Sample | Concentration* | Recovery (%)* |
|---|---|---|
| Tap water 1 | $0.70 \pm 0.05$ μg/l. | $95 \pm 3$ |
| Tap water 2 | $0.73 \pm 0.05$ μg/l. | $96 \pm 3$ |
| Serum | $32 \pm 2$ μg/l. | $94 \pm 2$ |
| Hair | $89 \pm 1$ μg/kg | $98 \pm 3$ |

*The terms ± are 95% confidence intervals.

generation *in situ* preconcentration ETAAS system are summarized in Table 3. A sampling frequency of 30/hr was achieved owing to the short hydride collection period (30 sec) made possible by the on-line ion-exchange separation system used. With an 80 sec loading period, corresponding to a consumption of 10.7 ml sample solution, and using the proposed conditions, the detection limit ($3\sigma$) was found to be 0.01 μg/l., which was about a factor of eight better than FI hydride generation with ion-exchange separation without collection in a furnace.[16] The detection limit was also similar to that reported in Ref. 6 (0.007 μg/l.), where an electrodeless discharge lamp was used instead of the hollow cathode lamp used in this study. The favourable reproducibility ensured a low detection limit and showed effective control over the conditions for stannane generation through the ion-exchange matrix modification.

Although several purification measures were taken, the high tin blank still remained to be the main obstacle for further improving the detection limit. Iso-thermal diffusion has shown to be an effective method for the purification of HCl. However, it was difficult to purify $NaBH_4$ although several other methods, including filtration,[14] and $BaSO_4$ co-precipitation[28] were tested. Smith[29] and Castillo[14] ascribed the high blank to the contamination of $NaBH_4$ which is usually packed in a plastic bag inside a tin container. Detailed investigations on further reducing tin blank values in $NaBH_4$ are underway.

The characteristic mass of the present method was compared with that of the conventional ETAAS method to evaluate the overall collection efficiency of the ion-exchange separation, hydride generation and *in situ* preconcentration procedures, taking the efficiency of conventional ETAAS as 100%. The overall collection efficiency was 59% since the ion-exchanger could retain only 61% of the analyte (Table 3). The deposition efficiency (overall collection efficiency/retention efficiency) was 96%, which implied complete stannane generation and hydride deposition on the platform. To assess the accuracy of the proposed method, geochemical reference samples were analyzed. The results shown in Table 4 are in good agreement with the recommended values. Determination of tin in tap water, serum and hair samples were also satisfactory (Table 5).

## CONCLUSIONS

The combination of on-line ion-exchange separation with FI hydride generation *in situ* preconcentration was shown to be capable of producing an efficient system for ultra-trace analysis of tin in waters and biological samples. The on-line sample matrix modification technique improved the selectivity and robustness of the method, and significantly reduced the hydride collection time, resulting in higher sample throughput. The detection limit of the system might be further improved by using a tin electrodeless discharge lamp and purer reagents.

*Acknowledgements*—The authors are grateful to Bodenseewerk Perkin-Elmer, Überlingen, Germany, for partial financial support and for the loan of AAS and FI equipment, to Shenyang Organic Chemicals Co. for donating the ion-exchanger.

## REFERENCES

1. X.-P. Yan, Z.-M. Ni and Q.-L. Guo, *Anal. Chim, Acta*, 1993, **272**, 105.
2. H. W. Sinemus, H. H. Stabel, B. Radziuk and J. Kleiner, *Spectrochim. Acta*, 1993, **48B**, 643.
3. Z.-L. Fang, *Flow Injection Separation and Preconcentraion*. VCH, Weinheim, 1993.
4. G.-H. Tao and Z.-L. Fang, *J. Anal. Atom. Spectrom.*, 1993, **8**, 577.
5. Y. An, S. N. Willie and R. E. Sturgeon, *Spectrochim. Acta*, 1992, **47B**, 1403.
6. L. Zhang, S. McIntosh, G. R. Carnrick and W. Slavin, *Spectrochim. Acta*, 1992, **47B**, 701.
7. G. Weber, *Fresenius' Z. Anal. Chem.*, 1985, **321**, 217.
8. World Health Organization, *Technical Report Series No 532*. 1973.
9. World Health Organization, *Technical Report Series No 683*. 1982.
10. M. Legret and L. Divet, *Anal Chim. Acta*, 1986, **189**, 313.
11. K. de Doncker, R. Dumarey, R. Dams and J. Hoste, *Anal Chim. Acta*, 1986, **187**, 163.
12. B. Welz, M. Schubert-Jacobs and T.-Z. Guo, *Talanta*, 1992, **39**, 1097.
13. S. McIntosh, L. Zhang, G. R. Carnrick and W. Slavin, *Spectrochim. Acta*, 1992, **47B**, 897.
14. J. R. Castillo, C. Martinez, R. Tomas and J. M. Mir, *J. Anal. Atom Spectrom.*, 1988, **3**, 595.
15. H. Narasaki and M. Ikeda, *Fresenius' Z. Anal. Chem.*, 1990, **336**, 5.
16. Z.-L. Fang, E. H. Hansen, L.-J. Sun, J. E. Olesen and L. M. Henriksen, *Talanta*, 1992, **39**, 383.

17. Hardware Manual for FIAS 200 Flow Injection Atomic Spectrometry System, Perkin Elmer Publication No: B3502.
18. Z.-L. Fang, S.-K. Xu and S.-C. Zhang, *Anal Chim Acta*, 1987, **200,** 35.
19. M. Thompson and B. Pahlavanpour, *Anal Chim. Acta*, 1979, **109,** 251.
20. K. Petrick and V. Krivan, *Fresenius' Z. Anal. Chem.*, 1987, **327,** 342.
21. X.-R. Wang and R. M. Barnes, *Spectrochim. Acta*, 1987, **42B,** 139.
22. S.-C. Zhang, S.-K. Xu and Z.-L. Fang, *Quim. Anal.*, 1989, **8,** 191.
23. S.-K. Xu and Z.-L. Fang, *Chin. Chem. Lett.*, 1992, **3,** 916.
24. L. Zhang, Z.-M. Ni and X.-Q. Shan, *Spectrochim. Acta*, 1989, **44B,** 339.
25. L. Zhang, Z.-M. Ni and X.-Q. Shan, *Spectrochim. Acta*, 1989, **44B,** 751.
26. R. E. Sturgeon, S. N. Willie, G. I. Sproule, P. T. Robinson and S. S. Berman, *Spectrochim. Acta*, 1989, **44B,** 667.
27. Analytical Techniques for Furnace AAS, Perkin Elmer Publication No: B332.
28. D.-R. Qui, C. Vandecasteele, K. Vermeiren and R. Dams, *Spectrochim. Acta*, 1990, **45B,** 439.
29. A. E. Smith, *Analyst*, 1975, **100,** 300.

Pergamon

0039-9140(95)01420-9

*Talanta*, Vol. 42, No. 3, pp. 385–389, 1995

0039-9140/95 $9.50 + 0.00

# AMPEROMETRIC DETECTION FOR CAPILLARY FLOW INJECTION ANALYSIS

JOSEPH WANG* and LIANG CHEN

Department of Chemistry and Biochemistry, New Mexico State University, Las Cruces, NM 88003, U.S.A.

(*Received* 9 *September* 1994. *Revised* 11 *September* 1994. *Accepted* 11 *September* 1994)

**Summary**—Ultrasmall-volume measurements of oxidizable compounds have been accomplished by coupling a capillary flow injection system with amperometric detection. Remarkably low (femtomole) mass detection limits result from the combination of nanoliter sample volume and the inherent sensitivity of the wall-jet detector. A substantial economy of reagent consumption and disposal accrues from the operation of the nl/min flow regime. Variables influencing the physical dispersion in the capillary flow injection system, including capillary length, sample volume or flow rate, are explored and optimized.

Flow injection analysis (FIA) has proved highly useful in practical applications in fields as varied as environmental monitoring, process analytical chemistry or clinical diagnostics.[1–3] The technique offers distinct advantages in versatility, reproducibility, and sample throughput over conventional (wet-chemistry) methods. Typical sample volumes and flow rates are of the order of 20–50 $\mu$l and 0.5–2.0 ml/min, respectively. Yet, substantial reduction in the carrier consumption and sample volume are highly desired for addressing environmental concerns on reagent/waste disposal or the growing needs for assays of ultrasmall (nanoliter) biological samples. One approach to reduce the flow rate and sample size is to employ miniaturized FIA systems, such as those based on integrated microconduits[4] or micromachined silicon structures.[5] Another promising avenue for ultraflow-volume FIA is to replace the traditional Teflon interconnecting tubing with fused-silica capillary tubes. Liu and Dasgupta[6] reported on a capillary FIA system with calorimetric detection and electroosmotic pumping. Olesik *et al.*[7] employed an infrared-absorption detector for a capillary FIA system with supercritical $CO_2$ as the carrier fluid.

The present note aims at characterizing capillary FIA systems with amperometric detection and elucidating the dispersion phenomena in such systems. Amperometric detection, which has been extremely useful for microscale separations and in other microenvironments,[8] holds great promise for capillary FIA. During the course of this investigation, Matysik and Werner[9] reported on the stripping voltammetric assay of tear samples in connection with capillary FIA. In the following sections we will illustrate how a detailed understanding of the dispersion phenomena and the use of amperometric detection can lead to reliable assays of nanoliter sample volumes, to a million-fold reduction in the flow rate (compared to conventional FIA) and to remarkably low mass detection limits (at the femtomole level).

## EXPERIMENTAL

### *Apparatus*

The capillary FIA system is shown in Fig. 1. It consisted of a sample and carrier reservoirs (D, E), a 52 $\mu$m i.d., 120 cm long, fused-silica capillary (Polymicrotechnologies Inc., F), supported by a glass tube (G), and a large-volume wall-jet detector. Glassy carbon or platinum 2 mm diameter disks (BAS, Models MF-2012 and MF-2013, respectively), placed at a 1 mm distance from the capillary outlet, served as the working electrode (A). The platinum disk was employed in connection with the detection of hydrogen peroxide and hydrazine. The reference electrode (Ag/AgCl, BAS Model RE-1,B) and the platinum wire auxiliary electrode (C) were

*Author to whom correspondence should be addressed.

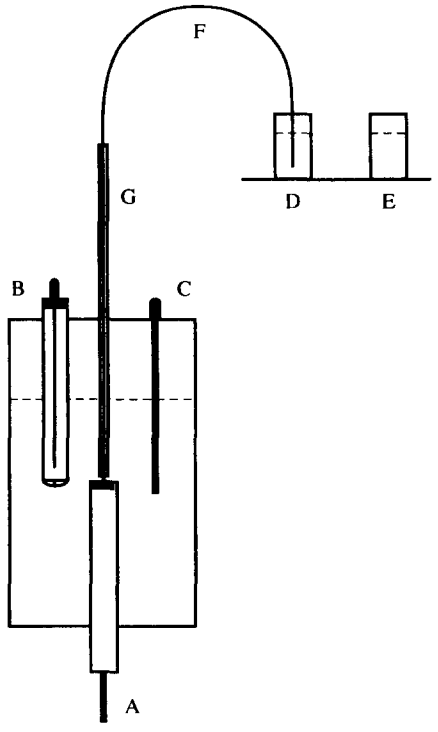


Fig. 1. Capillary FIA system with amperometric detection: A, working electrode; B, reference electrode; C, auxiliary electrode; D and E, sample and carrier reservoirs; F, fused-silica capillary; G, glass-tube support.

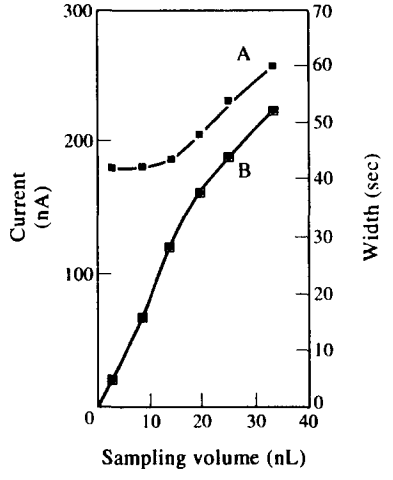


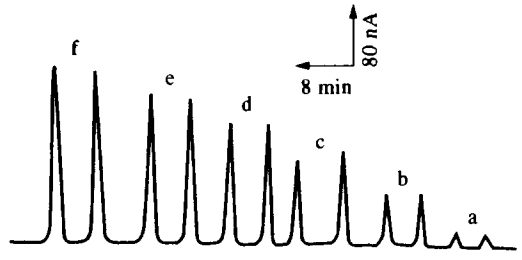


Fig. 2. Capillary-FIA amperometric peaks for different sample volumes: 3(a), 8(b), 14(c), 19(d), 25(e) and 33(f) nl. Analyte, $K_4Fe(CN)_6$ at $1 \times 10^{-3}M$; operating potential, +0.4 V; flow rate, 32 nl/min; capillary length, 120 cm; carrier and electrolyte, 0.05*M* phosphate buffer (pH 7.4). Also shown, the resulting plots of the peak current (B) and width (A) against the volume.

inserted through the cell cover. Amperometric measurements were carried out with an EG&G PAR Model 264A voltammetric analyzer, in conjunction with a Houston Omniscribe strip-chart recorder.

*Reagents*

All chemicals were reagent grade, and solutions were freshly prepared with double-distilled water. Potassium ferrocyanide, hydrazine (Baker), hydrogen peroxide (Aldrich), dopamine and acetaminophen (Sigma) were used without further purification. Phosphate buffer (0.05*M*, pH 7.4) served as the carrier solution.

*Procedure*

Capillary flow injection experiments were performed at room temperature after applying the desired potential and allowing the transient current to decay. The sample introduction was accomplished by switching between the carrier and sample reservoirs under conditions of gravity flow. The sample volume thus varied with the introduction time. Most experiments employed a flow rate of 32 nl/min and a 15 sec sample introduction, *i.e.* a sample volume of 8 nl.

## RESULTS AND DISCUSSION

High-voltage electroosmotic pumping, proposed for capillary FIA with colorimetric detection(6), is not readily compatible with amperometric detection. Gravity flow, in contrast, has been found in the present work to offer a very attractive capillary-FIA/amperometric behavior. Unlike electroosmotic pumping for which flow-induced dispersion is nonexistent[6], the gravity flow induces a significant dispersion of the sample plug. Factors influencing the physical dispersion in capillary FIA systems, and hence the resulting amperometric response, were thus elucidated.

Figure 2 displays flow injection amperometric peaks for different volumes of the ferrocyanide solution, ranging from 3 to 35 nl (a–f). Such volumes are ca. 3 orders of magnitude less than those common in FIA/amperometry. Well-defined peaks are observed inspite of these ultrasmall volumes. The peak current increases rapidly with the volume at first, and then more slowly. Significant dispersion is indicated from

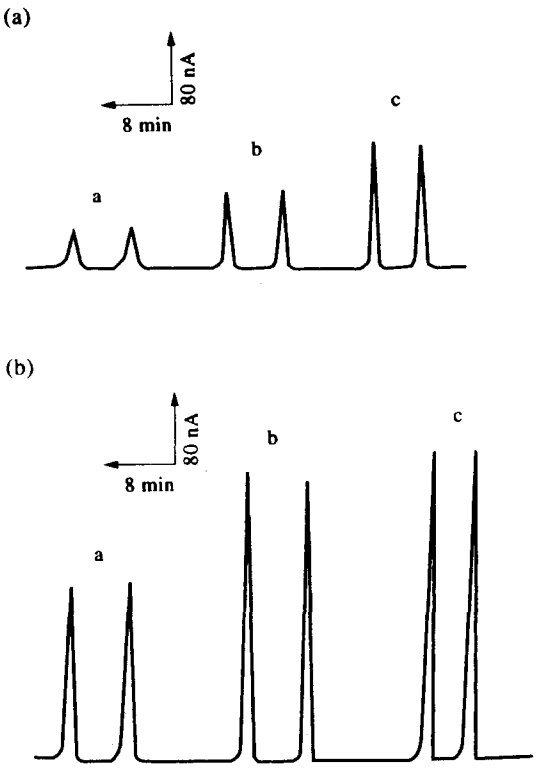


Fig. 3. Effect of capillary length (a) and volume flow rate (b) upon the amperometric response to $1 \times 10^{-3} M$ $K_4Fe(CN)_6$. Sample volume, 8(a) and 22(b) nl; capillary length, 120 (a)a, (b), 95 (a)b and 76 (a)c cm; flow rate, 33 (a), (b)a, 46 (b)b and 66 (b)c nl/min. Other conditions, as in Fig. 2.

the resulting peak widths (43–60 sec). Sample throughputs in the order of 45–75 $hr^{-1}$ can thus be realized. Such frequency, which is similar to that of macro FIA systems, reflects the long residence times of the sample zone. The influence of the capillary length and flow rate is shown in Fig. 3 (a) and (b), respectively. The higher dispersion, expected for longer capillaries, lead to smaller and broader current peaks. Increasing the flow rate not only decreases the dispersion, but also enhances the analyte flux towards the wall-jet detector. The net result is a doubling of the sensitivity between 33 and 66 nl/min. Note that while these flow rates are ca. 5 orders of magnitude lower than those normally employed in FIA/amperometry, the linear flow rate is remarkably high (being inversely proportional to the cross-sectional area of the capillary). The sample plug impinging on the wall-jet detector surface thus leads to remarkable sensitivity despite the ultrasmall volume (22 nl) employed. (Since the jet issuing from the capillary outlet remains intact over larger capillary–electrode separations, there is no apparent advantage to employ an on-capillary detector, a task difficult to implement even with ultramicroelectrodes). Since the wall-jet detector dead volume is effectively the boundary layer, and in the absence of connecting tubing, a detector-induced dispersion is nonexistent. Overall, the influence of the above parameters upon the dispersion of the sample zone is similar to that encountered in conventional FIA systems.

The extremely low flow rates of capillary FIA assure also a highly stable amperometric response. Figure 4(a) displays amperometric

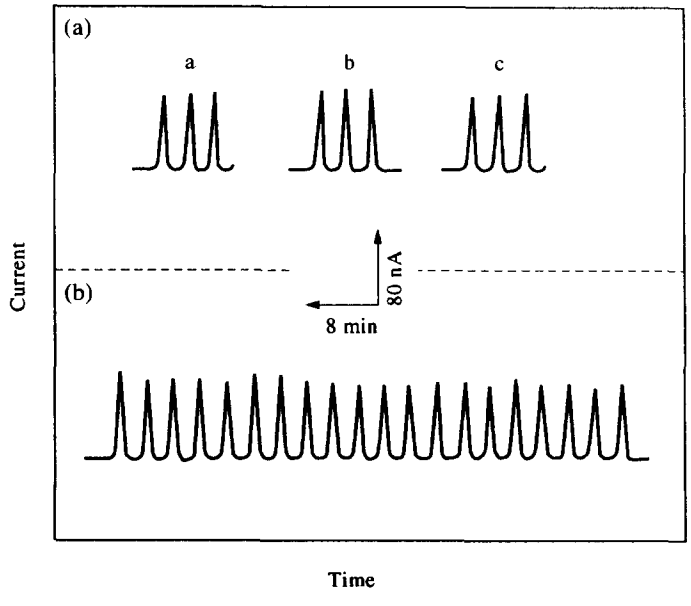


Fig. 4. Flow injection peaks for $1 \times 10^{-3} M$ $K_4Fe(CN)_6$ recorded (a) in 4-day intervals (a, b, c) and (b) during the 10th day of continuous flow. Other conditions, as in Fig. 2(b).

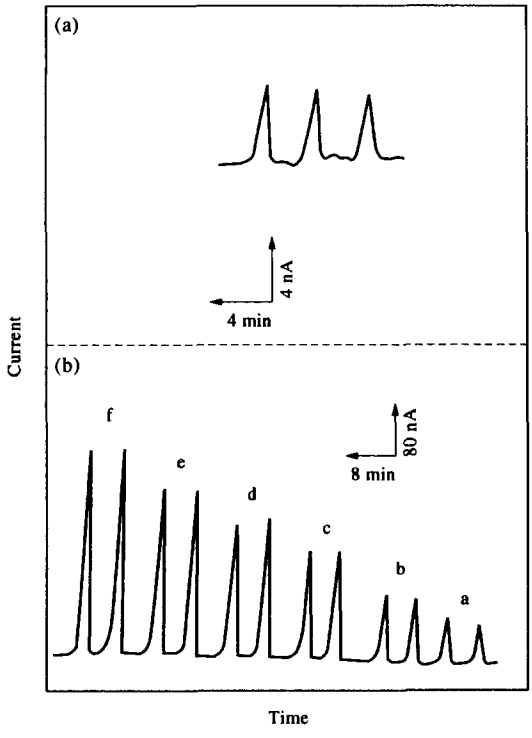


Fig. 5. FIA peaks for $5 \times 10^{-6}M$ hydrogen peroxide (a) and for dopamine solutions of ascending concentration ($2.5 \times 10^{-4}$–$1.25 \times 10^{-3}M$, (b) a–f. Operating potential, +0.75 (a) and +0.70 (b) V. Other conditions, as in Fig. 2(b), except that a platinum working-electrode was used in (a).

peaks recorded during the 1st, 4th and 9th day of a continuous carrier flow. the reproducible response is attributed to the negligible change in the gravity head during this prolonged period. The total volume of the carrier solution consumed during the entire 9 day period corresponds to nearly 500 $\mu$l! Conventional FIA/amperometry, in contrast, would require 20–50 l. over the same period. Also illustrated in Fig. 4(b) is the reproducibility of the data during the 10th day of the operation. This series of 20 successive runs yielded a relative standard deviation of 4.9%.

The coupling of the inherent sensitivity with the ultralow sample volumes of capillary FIA results in remarkably low mass detection limits. Figure 5(a) displays flow injection peaks for an 8 nl sample containing 1.38 pg (i.e. $5 \times 10^{-6}M$) hydrogen peroxide. A detection limit of $2 \times 10^{-6}M$ can be estimated based on the signal-to-noise characteristics ($S/N = 3$) of these readouts. This value corresponds to 540 fg or 16 fmol in the nanoliter sample. Slightly higher detection limits of 0.7, 1.3 and 8.0 pg were estimated from injections of hydrazine, catechol and acetaminophen solutions, respectively. Ordinary FIA/amperometric systems, in contrast, commonly offer detection limits at the low nanogram level. Figure 5(b) illustrates the concentration dependence of the capillary-FIA/amperometric operation. Injections of 8 nl dopamine solutions of increasing concentration ($2.5 \times 10^{-4}$–$1.25 \times 10^{-3}M$, a–f) were used for this purpose. The peak current shows excellent linearity with the injected concentration (slope, 261 nA/m$M$; correlation coefficient, 0.998). Highly linear calibration plots were obtained also for analogous measurements of acetaminophen and ferrocyanide (not shown).

In conclusion, data presented in this article clearly illustrate that the coupling of capillary FIA and amperometric detection provides a powerful analytical tool. The resulting system permits highly sensitive measurements in extremely small sample volume, in connection with ultralow carrier flow rates. The femtomole quantitation is thus coupled with extreme economy in terms of solution consumption. Significantly higher flow rates, at the $\mu$l/min regime, and $\mu$l samples, characterized micromachined FIA systems,[5] as well as the recent capillary-FIA/stripping operation[9]. While the concept is presented in terms of direct amperometry at ordinary electrodes, it could be extended to highly selective amperometric probes based on coverage with biological or chemical recognition layers. For example, the remarkable sensitivity towards hydrogen peroxide holds great promise for many oxidase-based enzymatic assays. Such selective detectors would address the lack of separation power in the FIA system (in comparison with microcolumn separation techniques). There is no fundamental barrier to further downscaling of the FIA/amperometric system to the picoliter sample domain and sub-nl/min flow regime via the use of smaller-diameter capillaries. Such downscaling should push the detection limits even further down to the attomole level. Additional improvements are anticipated by designing more elaborate capillary FIA systems, possessing sample-manipulation and liquid-handling capabilities.

## REFERENCES

1. J. Ruzicka, *Anal. Chem.*, 1983, **55**, 1040A.
2. G. D. Christian, *J. Pharm. Biomed. Anal.*, 1992, **10**, 769.
3. K. K. Stewart, *Anal. Chem.*, 1983, **55**, 931A.
4. J. Ruzicka and E. H. Hansen, *Anal. Chim. Acta*, 1984, **161**, 1.

5. B. H. van der Schoot, S. Jeanneret, A. van den Berg, and N. F. de Rooij, *Anal. Meth. Instrum.*, 1993, **1,** 38.
6. S. Liu and P. Dasgupta, *Anal. Chem.* 1992, **268,** 1.
7. S. V. Olesik, S. D. French and M. Novotny, *Anal. Chem.*, 1986, **58,** 2256.
8. A. G. Ewing, J. M. Mesaros and P. Gavin, *Anal. Chem.*, 1994, **66,** 527.
9. F. M. Matysik; G. Werner, *Analyst*, 1993, **118,** 1523.

Pergamon

0039-9140(95)01421-7

*Talanta*, Vol. 42, No. 3, pp. 391–394, 1995

0039-9140/95 $9.50 + 0.00

# FLOW INJECTION FLUORIMETRIC DETERMINATION OF THIOUREA

TOMÁS PÉREZ-RUIZ,* CARMEN MARTÍNEZ-LOZANO, VIRGINIA TOMÁS and ROCIO CASAJÚS
Department of Analytical Chemistry, Faculty of Chemistry, University of Murcia, Murcia, Spain

(*Received* 10 *June* 1994. *Revised* 23 *September* 1994. *Accepted* 23 *September* 1994)

**Summary**—A flow injection configuration for the fluorimetric determination of thiourea is proposed. The procedure is based on the rapid oxidation of thiourea by thallium(III) with concomitant formation of fluorescent thallium(I). Linear calibration graphs were obtained between $5 \times 10^{-7}$ and $1 \times 10^{-5} M$, with a sampling rate of 90 samples/hr. The usefulness of the method was tested in the determination of thiourea in fruit juices and fruit peels.

Thiourea(TU) and several TU derivatives have various industrial, agricultural and analytical applications. They are widely used in the rubber industry as accelerators, in photography as fixing agents and to remove stains from negatives, and in agriculture as fungicides, herbicides and rodenticides. The use of an aqueous solution of TU as a leaching agent for gold has been widely reported in the literature. TU is also used as a spectrophotometric reagent for the determination of several metals.[1]

The presence of TU in urine was reported to be a non-specific indicator of cancer.[2] TU is toxic owing to its influence on the metabolism of carbohydrates.[3] Moreover, TU has been labelled as having carcinogenic activity[4] and so, all work with this compound should be performed with the greatest of care to prevent direct exposure of researchers and contamination of the environment.

Various methods have been proposed for the determination of TU such as titrimetry with haloamines,[5] *N*-bromosuccinimide,[6] iodine[7] or mercury(II) nitrate,[8] Raman spectrometry,[9] spectrophotometry,[10] polarography,[11] stripping voltammetry,[12,13] high-performance liquid chromatography,[14] kinetic methods,[15,16] ion selective electrode potentiometry[17] and piezoelectric detection.[18]

Despite the large number of manual methods available, there are few automated procedures. In recent years, flow injection analysis has been used in the determination of TU. Flow injection procedures involve the catalyzed iodine–azide reaction using the amperometric[19] and photometric[20] detection of iodine or the electrochemical detection of TU using pulsed amperometry.[21]

In this paper the development of a spectrofluorimetric flow injection method for the determination of TU and its application to routine analysis is presented. The determination is based on the oxidation of TU by thallium(III) and the parameter measured is the fluorescence of the thallium(I) formed. This violet fluorescence has been attributed to the existence of the $TlCl_3^{2-}$ anionic complex[22] and hence the reaction is carried out in the presence of hydrochloric acid. The procedure is very simple, inexpensive and fast and allows the determination of TU in fruit juices and fruit peels.

## EXPERIMENTAL

### *Apparatus*

A SLM-Aminco Bowman Series 2 spectrofluorimeter was used for recording spectra; excitation and emission spectra were corrected. The detector used in the flow system was a Perkin Elmer model 3000 spectrofluorimeter with a Hellma 176.052 QS flow cell (inner volume 25 $\mu$l). A Gilson Minipuls-4 peristaltic pump and an Omnifit rotary valve were also used. Except for the pump tube (Tygon), PTFE tubing (0.5 mm i.d.) was used throughout the manifold.

*Author to whom correspondence should be addressed.

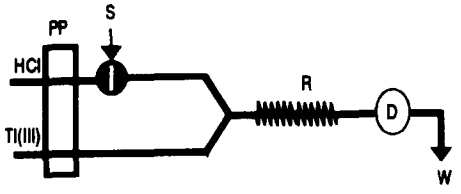


Fig. 1. Schematic diagram of the flow injection system for fluorimetric determination of thiourea. (PP) Peristaltic pump; (S) point of sample injection; (R) reaction coil (30 cm); (D) fluorimeter; (W) waste.

*Reagents*

All reagents were of analytical grade unless otherwise stated. All-glass apparatus was used to produce doubly distilled water, which was used throughout.

Stock thiourea solution ($1 \times 10^{-3}M$) was prepared by dissolving 0.0190 g of thiourea (Merck) in water and diluting to 250 ml in a calibrated flask; this solution remained stable for 1 week if kept refrigerated. Working solutions of lower concentration were prepared daily by appropriate dilution of the stock solution.

Thallium(III) stock solution ($1 \times 10^{-3}M$) in $1M$ hydrochloric acid was prepared from thallium(III) nitrate trihydrate (Merck). Solutions of lower concentration were prepared by dilution with $1M$ hydrochloric acid.

*Manifold*

The schematic diagram of the instrumental set up is shown in Fig. 1 with conditions as stated. The sample is introduced at point S with the aid of the Omnifit rotary valve with a 235-$\mu$l loop. The reagent streams are pumped at the same flow rate in order to achieve effective mixing of both solutions. The reaction is started by injection of the sample and, as the sample zone reaches the flow cell, the fluorescence of thallium(I) formed is measured ($\lambda_{ex} = 227$ nm; $\lambda_{em} = 419$ nm).

## RESULTS AND DISCUSSION

TU is rapidly oxidized by thallium(III) to form fluorescent thallium(I). The fluorescence spectra of a solution containing $1 \times 10^{-4}M$ Tl(III), $1 \times 10^{-5}M$ TU and $1M$ HCl are shown in Fig. 2. The excitation maximum occurs at 227 nm and the fluorescence emission maximum at 419 nm. The fluorescence intensity increases with increasing chloride and ion hydrogen concentrations up to about $0.9M$, above which it remains constant. A $1.0M$ hydrochloric acid was selected for further investigations. Alternatively, TU can be easily oxidized in a flow system by injection into a thallium(III) solution flowing on line. The manifold in Fig. 1 was used to investigate the effect of chemical and flow-injection variables on the peak height.

*Influence of manifold parameters*

The variables studied were flow-rate, volume injected and length of the reaction coil. The reagent concentrations used in these experiments were as follows: thallium(III) line, $2 \times 10^{-4}M$ and hydrochloric acid line, $1M$. The mixing ratio between both streams was always 1:1.

The sample volume was varied between 35 and 285 $\mu$l. The peak heights increased with increasing volumes injected up to 235 $\mu$l, above which they remained virtually constant. A sample volume of 235 $\mu$l was chosen for further experiments.

The peak height obviously depends on the residence time of the sample zone in the system, i.e. on the total flow rate and the tube length. The effect of the flow rate was checked over the range 0.4–2.0 ml/min. The lower flow rates gave higher fluorescence intensities although, up to 0.5 ml/min, peak-height reproducibility was poor and the peaks were so broad that sample throughput was very low. A flow rate of 0.6 ml/min (0.3 for each channel) was selected as the best compromise between reproducibility, sensitivity and throughput.

Reaction coils measuring of 0–150 cm were tested. There was little increase in fluorescence intensity with increased reactor lengths up to 30 cm, above which the signal decreased slightly. The length chosen for the reactor was 30 cm.

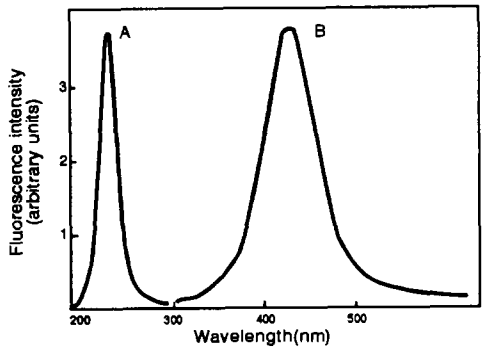


Fig. 2. Excitation (A); and emission spectra (B). [Tl(III)] = $1 \times 10^{-4}M$; [thiourea] = $1 \times 10^{-5}M$; [HCl] = $2M$.

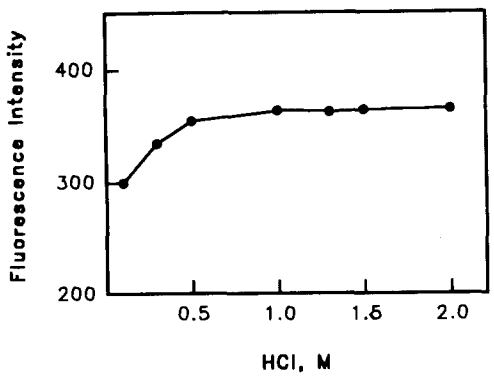


Fig. 3. Effect of hydrochloride acid concentration on the peak height.

*Influence of reagent concentrations*

The effect of varying concentration of thallium(III) and hydrochloric acid were tested in the optimized flow system. The fluorescence intensity increased slightly as the hydrochloric acid concentration was increased from 0.1 to 1.0*M*, above which it remained virtually constant (Fig. 3). The peak height increased steeply with an increase in thallium(III) concentration up to $4 \times 10^{-5}M$, and was constant at higher concentrations (Fig. 4). The reagents used were $1 \times 10^{-4}M$ thallium(III) and 1.0*M* hydrochloric acid.

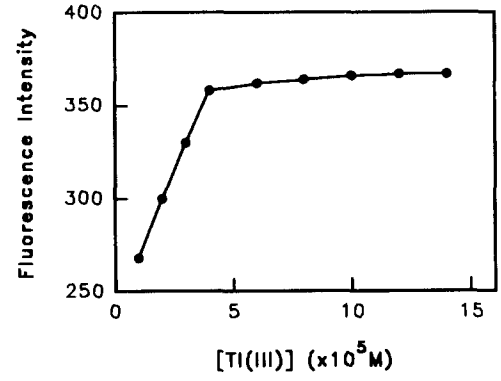


Fig. 4. Effect of thallium(III) concentration on the peak height.

*Calibration graph and reproducibility*

A series of standard solutions of TU were injected into the manifold under the selected conditions to test the linearity of the calibration graph. A linear relationship between TU concentration and fluorescence intensity was obtained over the range $5 \times 10^{-7}$–$1 \times 10^{-5}M$. Regression analysis of the linear portion of the calibration graph gives a standard deviation of 1.6% for the slope and a correlation coefficient of 0.9993. The precision of the method was established by repeated assays ($n = 10$) using $3 \times 10^{-6}$ and $8 \times 10^{-6}M$ solutions of TU. The relative standard deviations were 2.3 and 1.2%, respectively. The sampling rate was about 90 samples/hr.

*Interference studies*

In order to assess the possible analytical applications of the flow injection procedure described above, the effect of concomitant species on the determination of TU in real samples was studied by analysing synthetic sample solutions containing $5 \times 10^{-6}M$ of TU and various excess amounts of the food additives commonly found in fruit juices and fruit peels, inorganic compounds and organic acids. A substance was considered not to interfere if the variation in the peak height of TU was less than 3%. The results are shown in Table 1.

*Analytical applications*

The proposed method was applied to the determination of TU in fruit juices and fruit peels. TU is often added to citrus as a fungicide to assist in its conservation during cold storage. The recoveries from the samples spiked with different amounts of TU are shown in Table 2.

Table 1. Tolerance to different species in the determination of thiourea*

| Species added | Maximum tolerable molar ratio |
|---|---|
| $Cl^-$, $SO_4^{2-}$, $PO_4H_2^-$, acetate, citrate, tartrate, urea, glucose, alanine, $Zn^{2+}$, $Al^{3+}$ | 500† |
| $F^-$, glycine | 100 |
| Hippuric acid, ascorbic acid, $Br^-$, $NO_3^-$, $MoO_4^{2-}$, $Cd^{2+}$ | 10 |
| Uric acid, cystine, $Mn^{2+}$ | 5 |
| $Fe^{3+}$, $Pb^{2+}$, EDTA | 1 |
| $Bi^{3+}$, $Cu^{2+}$, $I^-$, cysteine | 0.1 |

*Thiourea concentration, $5 \times 10^{-6}M$.
†Maximum ratio tested.

Table 2. Recovery of thiourea in fruit juices and fruit peels

| Sample* | Amount added | Amount found† | Average recovery (%) | Found by Reference method[10]‡ |
|---|---|---|---|---|
| Lemon juice | 8.0 | 7.65 ± 0.62 | 95.6 | 7.82 |
| (μg/ml) | 15.0 | 14.43 ± 0.49 | 96.2 | 14.64 |
| | 30.0 | 28.95 ± 0.37 | 96.5 | 29.20 |
| Orange juice | 8.0 | 7.68 ± 0.51 | 96.0 | 7.74 |
| (μg/ml) | 15.0 | 15.04 ± 0.35 | 100.3 | 14.86 |
| | 30.0 | 28.71 ± 0.47 | 95.7 | 29.30 |
| Orange peel | 5.0 | 5.02 ± 0.63 | 100.5 | 4.86 |
| (mg/kg) | 10.0 | 9.58 ± 0.55 | 95.8 | 9.81 |
| | 15.0 | 14.61 ± 0.47 | 97.4 | 15.2 |

*Ascorbic acid was previously eliminated by heating the solution in alkaline medium at 50°C for 30 min.

†Average values of four determinations ± SD.

‡Average of two determinations.

As can be seen, the assay results for all the samples were in good agreement with the values for the nominal contents and with those obtained using the manual photometric method recommended by AOAC.[10]

## CONCLUSIONS

The results obtained demonstrate the utility of measuring the fluorescence of the thallium(I) formed in the reaction between TU and Tl(III) for the determination of TU at trace levels. The proposed method is suitable for determining TU derivatives, which are also oxidized by thallium(III). This scheme would be useful as a postcolumn on-line reaction for the simultaneous determination of several thioureas using high performance liquid chromatography.

*Acknowledgement*—The authors express their gratitude to Dirección General de Investigación Científica y Técnica (projet PB93/1139) and Comunidad de Murcia (projet PIB94-02) for financial support.

## REFERENCES

1. F. D. Snell, *Photometric and Fluorimetric Methods of Analysis*, Parts I and II. Wiley, New York, 1978.
2. K. Okazaki, M. Murakami, H. Kawada and A. Okada, *Jap. Kokay*, 1975, **394**, 7597; *C.A.*, 1975, **83**, 175159z.
3. S. N. Giri and A. B. Combs, *Toxicol. Appl. Pharmacol.*, 1967, **16**, 709.
4. U.S. Department of Health and Human Services, Fourth Annual Report on Carcinogens, p. 423. GPO, Washington, D.C., 1985.
5. C. P. K. Paillai and P. Indrasema, *Talanta*, 1980, **27**, 751.
6. A. Srivastava, *Talanta*, 1979, **26**, 917.
7. D. Amin, *Analyst*, 1985, **110**, 215.
8. K. B. Yatsimirsky and A. A. Artasheva, *Zh. Anal. Khim.*, 1956, **11**, 442.
9. H. J. Bowley, E. A., Crathorne and D. L. Gerrard, *Analyst*, 1986, **111**, 539.
10. Association of Official Analytical Chemists, *Official Methods of Analysis*, 15th Ed., pp. 1160–1163. Arlington, 1990.
11. M. R. Smyth and J. G. Osteryoung, *Anal. Chem.*, 1977, **49**, 2310.
12. M. Fedorenko, O. Manousek and P. Zuman, *Chem. Listy*, 1953, **49**, 1494.
13. V. Stará and M. Kopanica, *Anal. Chim. Acta*, 1984, **159**, 105.
14. A. Trojanek and M. Kopanica, *J. Chromatogr.*, 1985, **328**, 127.
15. J. Richmond, C. Rainey and C. E. Meloan, *Anal. Lett.*, 1976, **19**, 119.
16. H. Weiss, S. Pantel and G. Marquardt, *Anal. Chim. Acta*, 1982, **143**, 177.
17. P. Sharma and M. Singh, *J. Electrochem. Soc. India*, 1985, **34**, 6.
18. S. Z. Yao, F. J. He and L. H. Nie, *Anal. Chim. Acta*, 1992, **268**, 311.
19. J. Kurzawa, *Anal. Chim. Acta*, 1985, **173**, 343.
20. O. F. Kamson, *Anal. Chim. Acta*, 1988, **211**, 299.
21. P. J. Vandeberg, J. D. Kowagoe and D. C. Johnson, *Anal. Chim. Acta*, 1992, **260**, 1.
22. G. F. Kirkbright, T. S. West and C. Woodward, *Talanta*, 1965, **12**, 517.

Pergamon

0039-9140(95)01422-5

*Talanta*, Vol. 42, No. 3, pp. 395–400, 1995

0039-9140/95 $9.50 + 0.00

# CURRENT THEORIES IN THE CALCULATION OF ACTIVITY COEFFICIENTS—II. SPECIFIC INTERACTION THEORIES APPLIED TO SOME EQUILIBRIA STUDIES IN SOLUTION CHEMISTRY

M. P. ELIZALDE and J. L. APARICIO

Departamento de Química Analítica, Universidad del País Vasco, Apartado 644, 48080 Bilbao, Spain

(*Received* 10 *May* 1994. *Revised* 19 *September* 1994. *Accepted* 19 *September* 1994)

**Summary**—The adequation of the current theories for calculating activity coefficients has been studied for a series of ionic equilibria in analytical chemistry: the water ionic product as well as two reactions of complex formation and oxidation–reduction. In all the cases, the specific interaction theory (SIT) has proved to be adequate and simple to apply in a restricted interval (0.5–3*M*), whereas Pitzer's theory is outstanding for its high precision in reproducing experimental behaviour and to correlate values of equilibrium constants for different conditions and media.

Most of the equilibrium constants values reported in analytical chemistry are referred to given ionic medium conditions owing to the dependence of these values on the nature and ionic strength of the ionic medium. Consequently, in most cases a previous selection and extrapolation of these known equilibrium constants values to different experimental conditions is needed. For this purpose, the activity coefficients of the species involved in the reactions should be determined.

The corresponding calculations are often restricted to the use of the Debye–Hückel theory[1,2] or the Davies equation,[3] in spite of their short range of validity. However, some authors have applied the so-called specific interaction theory, SIT,[4–6] to correlate equilibrium constant data and an evaluation of the different theories for calculating mean activity coefficients has been reported.[7]

In a previous publication,[8] the specific interaction and ionic associations theories for calculating mean activity coefficients for 2:1 and 2:2 electrolytes have been applied and criticised. In this work, two representative theories, SIT[9] and Pitzer,[10–13] for calculating single-ion activity coefficients have been compared in terms of their applicability in the prediction and correlation of equilibrium data in different media and ionic strengths. For this purpose, the following examples of general interest in solution chemistry have been selected: the ionic product of water, the formation constant of the diaminsilver complex and the redox potential of the $Hg_2^{2+}/Hg$ pair.

Table 1 shows the general SIT and Pitzer equations for the calculation of single-ion activity coefficients in mixtures of electrolytes. In Table 2 the values of the parameters needed to perform the calculations presented in this work are shown. All the calculations have been carried out by means of the program LETAGROP-MODEL FUNCTION.[14] In this program the function to be minimized is the error square sum, $U$, defined as

$$U = \sum_N (A_{exp} - A_{calc})^2,$$

where $A_{exp}$ is the experimental function and $A_{calc}$ the corresponding magnitude calculated by the program, $N$ is the number of experimental points. The best fit is that which gives the lowest values for both $U$ and the mean standard deviation, $\sigma$. The statistical factor, $R = U/\Sigma A_{exp}^2$ is also given by the program.

## RESULTS

### *The ionic product of water* ($k_w$)

The dependence of $k_w$ on temperature is emphasized in most textbooks whereas the influence of the medium and ionic strength is usually omitted. However, this variation can be appreciable as seen in Fig. 1, where $k_w$ values in LiCl,

Table 1. General expressions of SIT and Pitzer theories for calculating single-ion activity coefficients

SIT

$\log \gamma_M = -z_M^2 D + \Sigma\epsilon\,(M^{z+}, X^-)m_x$

$\epsilon\,(M, X, I) = (|z_M + z_X|^2/4I)(\log \gamma^0_{MX} + |z_M z_X| D)$

$D = A\sqrt{I}/(1 + 1.5\sqrt{I})$, $A = 0.5109$,[7]

$\gamma^0_{MX}$: mean activity coefficient of the pure MX electrolyte.

Pitzer

$\log \gamma_M = z_M^2 f\gamma + 2\Sigma m_a\{B_{Ma} + (\Sigma mz)C_{Ma}\} + 2\Sigma m_c\theta_{Mc} + + \Sigma\Sigma m_c m_a\{z_M^2 B'_{ca} + z_M C_{ca} + \Psi_{Mca}\}$

$\Sigma(mz) = \Sigma m_c z_c = \Sigma m_a |z_a|$

$f\gamma = 0.392\{(\sqrt{I}/1 + 1.2\sqrt{I}) + (2/1.2)\ln(1 + 1.2\sqrt{I})\}$

$B_{MX} = \beta^{(0)}_{MX} + (\beta^{(1)}_{MX}/2I)\{1 - (1 + 2\sqrt{I})\exp(-2\sqrt{I})\}$

$B'_{MX} = (\beta^{(1)}_{MX}/2I^2)\{-1 - (1 + 2\sqrt{I} + 2I)\exp(-2\sqrt{I})\}$

$C_{MX} = C^{\phi}_{MX}/(2|z_M z_X|^{1/2})$.

NaCl and KCl media reported by Harned and Owen[15] have been plotted as a function of the ionic strength. This figure proves that the value $k_w = 10^{-14}$ usually adopted is not adequate and, therefore, extrapolations to given experimental conditions should be carried out, specially when accurate calculations are needed.

The acidity reaction of water was firstly considered with the following relationship between the equilibrium constant at infinite dilution, $k^0_w$ ($10^{-14}$ at 298 K), and the corresponding stoichiometric equilibrium constant, $k_w$:

$$pk_w = pK^0_w + \log \gamma_H + \log \gamma_{OH} - \log a_w, \quad (1)$$

$\gamma_H$ and $\gamma_{OH}$ being the single-ion activity coefficients and $a_w$ the water activity, which can be calculated from:

$$a_w = -0.00784 v\phi m, \quad (2)$$

or taken from literature.[15] In equation (2), $v$ is the stoichiometric index, $\phi$ the osmotic coefficient of the solution and $m$ the molality.

The application of SIT and Pitzer equations shown in Table 1 leads to the following theoretical expressions for $pk_w$ in LiCl, NaCl and KCl media:

SIT:

$$pk^I_w = pK^0_w - 2D + \{\epsilon\,(H^+, Cl^-) + \epsilon\,(OH^-, M^+)\}m_{MCl} - \log a_w \quad (3)$$

PITZER:

$$2.30pk^I_w = 2.30pK^0_w + 2f^{\gamma} + 2m\{B_{HCl} + B_{MOH} + m(C_{HCl} + C_{MOH})\} + m^2(2B'_{MCl} + 2C_{MCl} + \Psi_{HCl-MCl} + \Psi_{MCl-MOH}) + 2m(\theta_{HCl-MCl} + \theta_{MCl-MOH}) - \log a_w, \quad (4)$$

where M refers to $Li^+$, $Na^+$ or $K^+$.

The suitability of SIT and Pitzer theories for calculating single-ion activity coefficients can be evaluated through the comparison of calculated $k_w$ values (using the parameters listed in Table 2) and the corresponding experimental values reported by Harned and Owen.

The results obtained are illustrated in Fig. 1 as $k_w = f$(ionic strength) for the three ionic media. It can be appreciated that at low values of ionic strength both theories approximately predict the experimental behaviour, whereas on increasing the ionic strength the differences are significant. SIT theory qualitatively reproduces the experimental function, whereas Pitzer equation gives rise to an excellent prediction of the experimental behaviour. For comparison, in the same figure, values of $k_w$ derived using the extended Debye–Hückel equation for the value $B \cdot a = 1$ are represented.

Table 2. Values of the known SIT and Pitzer parameters for the calculations

| Interaction coefficient, $\epsilon$[9] | | $\beta^{(0)}$[11] | $\beta^{(1)}$[11] | $C^{\phi}$[11] |
|---|---|---|---|---|
| $\epsilon\,(H^+, Cl^-) = 0.12$ | HCl | 0.1755 | 0.2945 | 0.0008 |
| $\epsilon\,(H^+, NO_3^-) = 0.07$ | LiCl | 0.1494 | 0.3074 | 0.00359 |
| $\epsilon\,(H^+, ClO_4^-) = 0.14$ | NaCl | 0.0765 | 0.2664 | 0.001270 |
| $\epsilon\,(NH_4^+, Cl^-) = -0.01$ | KCl | 0.04835 | 0.2122 | −0.00084 |
| $\epsilon\,(NH_4^+, ClO_4^-) = -0.10 + 0.14 \log I$ | LiOH | 0.015 | 0.14 | — |
| $\epsilon\,(NH_4^+, NO_3^-) = -0.08 + 0.06 \log I$ | NaOH | 0.0864 | 0.253 | 0.0044 |
| $\epsilon\,(Ag^+, NO_3^-) = -0.14 + 0.10 \log I$ | KOH | 0.1298 | 0.320 | 0.0041 |
| $\epsilon\,(Ag^+, ClO_4^-) = 0.0$ | $AgNO_3$ | −0.0856 | 0.0025 | 0.00591 |
| $\epsilon\,(OH^-, Li^+) = -0.04 + 0.071 \log I$ | $HClO_4$ | 0.1747 | 0.2931 | 0.00819 |
| $\epsilon\,(OH^-, Na^+) = 0.04$ | | | | |
| $\epsilon\,(OH^-, K^+) = 0.08$ | | | | |
| | | $\theta$[12] | $\Psi$[12] | |
| | HCl–LiCl | 0.015 | 0.000 | |
| | HCl–NaCl | 0.036 | −0.004 | |
| | HCl–KCl | 0.005 | −0.007 | |
| | LiOH–LiCl | −0.065 | −0.005 | |
| | NaOH–NaCl | −0.050 | −0.006 | |
| | KOH–KCl | −0.050 | −0.008 | |

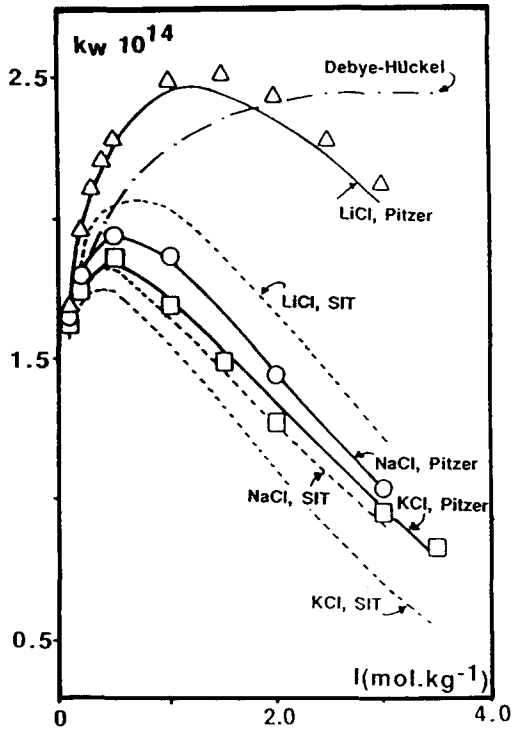


Fig. 1. $k_w$ values in LiCl, NaCl and KCl media as a function of the ionic strength.[14] Lines represent the predicted $k_w$ values using SIT and Pitzer theories.

*The formation constant of the diaminsilver complex*

The diaminsilver formation equilibria has been extensively studied in different media and ionic strengths because of its importance in analytical chemistry. Consequently, there is a significant number of different formation constant values reported for this equilibrium.[16,17]

In this case, the application of SIT and Pitzer theories should allow to correlate the different equilibrium constant values as well as to extrapolate to given experimental conditions. The precision in the correlation will indicate the degree of suitability of both theories.

Besides the stoichiometric equilibrium constant values, $\beta_2^{\mathrm{I}}$, reported in the literature in $NaClO_4$, $KNO_3$, $NaNO_3$ and $LiNO_3$ for the reaction:

$$Ag^+ + 2NH_3 \Leftrightarrow Ag(NH_3)_2^+ \qquad (5)$$

it is necessary to consider the corresponding values, $k_a^{\mathrm{I}}$, reported for the equilibrium:

$$NH_4^+ \Leftrightarrow NH_3 + H^+. \qquad (6)$$

These values can be related to the corresponding at infinite dilution, $\beta_2^0$ and $k_a^0$ by:

$$\log \beta_2^{\mathrm{I}} = \log \beta_2^0 + \log \gamma_{Ag(NH_3)_2} - \log \gamma_{Ag} - 2 \log \gamma_{NH_3} \qquad (7)$$

and

$$\mathrm{p}k_a^{\mathrm{I}} = \mathrm{p}K_a^0 - \log \gamma_{NH_4} + \log \gamma_{NH_3} + \log \gamma_H, \qquad (8)$$

where the calculation of the activity coefficient for the neutral species $NH_3$ is needed. The activity coefficient for this compound can be calculated by means of the Long and McDevit equation:[18]

$$\log \gamma_{NH_3} = s(NH_3, E)m, \qquad (9)$$

where $s(NH_3, E)$ is the so-called salting coefficient of the neutral species $NH_3$ in the ionic medium E, and $m$ is the molality.

Prior to considering the diaminsilver formation equilibrium, $s$ should be evaluated through equations (8) and (9). For the sake of simplicity, the SIT theory has been used to determine the salting coefficients and $\mathrm{p}K_a^0$ values:

$$\mathrm{p}k_a^{\mathrm{I}} + \{\epsilon(NH_4^+, X^-) - \epsilon(H^+, X^-)\}m = \mathrm{p}K_a^0 + sm, \qquad (10)$$

where X refers to $NO_3^-$ or $ClO_4^-$.

The plot of the first member in equation (10) as a function of $m$ is shown in Fig. 2. From the obtained straight line, the value of $\mathrm{p}K_a^0 = 9.25 \pm 0.01$ is concluded and within the experimental error, $s(NH_3, NaNO_3) \approx s(NH_3, NaClO_4) \approx s(NH_3, LiNO_3) \approx 0$ can be derived. These results agree with experimental data reported by Maeda *et al.* indicating that the activity coefficient of ammonia in salt solutions is constant and close to unity.[16]

Therefore, the application of SIT theory to equation (7) leads to:

$$\log \beta_2^{\mathrm{I}} - \epsilon(Ag^+, X^-)m = \log \beta_2^0 - \epsilon(Ag(NH_3)_2^+, X^-)m. \qquad (11)$$

If this equation is valid, the experimental function $\log \beta_2^{\mathrm{I}} - \epsilon(Ag^+, X^-) = f(m)$ should yield two different straight lines, one for the three different nitrate media and another for perchlorate medium, with the same $Y$-axis

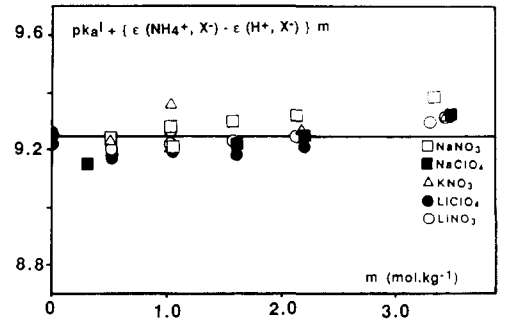


Fig. 2. The application of SIT theory to literature $\mathrm{p}k_a$ ($NH_4^+$) data at different ionic media.

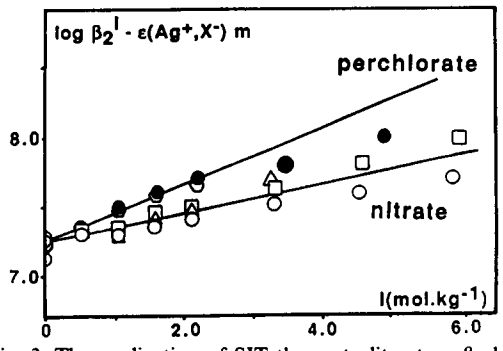


Fig. 3. The application of SIT theory to literature $\beta_2$ data at different ionic strengths and media.

intercept. As seen in Fig. 3, the prediction is fulfilled in the range 0.5–3.0 mol/kg. As the ionic strength increases, deviations between the experimental data and the theoretical functions are higher. From the function expressed in equation (11), the parameters collected in Table 3 were obtained.

On the other hand, the application of Pitzer theory to equation (7) has been restricted to data in nitrate media because the required Pitzer parameters in perchlorate media are not available. The following expression can be derived for the diaminsilver formation constant in nitrate media:

$$\ln \beta_2^I = \ln \beta_2^0 + 2m\{B_{AgNO_3} - B_{Ag(NH_3)_2NO_3} + m(C_{AgNO_3} - C_{Ag(NH_3)_2NO_3}) + \theta_{AgNO_3-MNO_3} - \theta_{Ag(NH_3)_2NO_3-MNO_3})\} + m^2(\Psi_{AgNO_3-MNO_3} - \Psi_{Ag(NH_3)_2NO_3-MNO_3}), \quad (12)$$

where M refers to $Li^+$, $Na^+$ or $K^+$.

In this equation, the function $B_{AgNO_3}$ and the parameter $C_{AgNO_3}$ shown in Table 1 can be evaluated taking into account the values of the parameters $\beta^{(0)}_{AgNO_3}$, $\beta^{(1)}_{AgNO_3}$ and $C^{\phi}_{AgNO_3}$ collected in Table 2. Therefore, in equation (10) there are seven unknown parameters which can be grouped as follows:

$$\ln \beta_2^I - 2m(B_{AgNO_3} + mC_{AgNO_3}) = \ln \beta_2^0 - 2m(\beta^{(0)}_{Ag(NH_3)_2NO_3} + \theta_{Ag(NH_3)_2NO_3-MNO_3} - \theta_{AgNO_3-MNO_3}) - m^2(C^{\phi}_{Ag(NH_3)_2NO_3} + \Psi_{Ag(NH_3)_2NO_3-MNO_3} - \Psi_{AgNO_3-MNO_3}) - \beta^{(1)}_{Ag(NH_3)_2NO_3}\{1-(1+2\sqrt{I})\exp(-2\sqrt{I})\}, \quad (13)$$

where $I \approx m$.

This function has been plotted in Fig. 4 where it can be seen to give a good fit in the range $I = 0$–6 mol/kg. In this case the deviations observed with SIT theory as high ionic strengths do not appear. The value $\log \beta_2^0 = 7.22 \pm 0.01$ can be obtained from the intercept on $Y$-axis as well as the Pitzer parameters collected in Table 3. The similarity of the parameters $\theta$ in $NaNO_3$ and $KNO_3$ media as well as the significant difference with those in $LiNO_3$ medium can be concluded from these results.

As it can be appreciated in all the cases the deviations obtained with Pitzer theory are much lower than those obtained by SIT. However, the application of SIT theory gives rise to acceptable results up to 3 mol/kg, specially if its only parameter involved in comparison with the seven parameters needed in Pitzer equation is considered.

Table 3. Values of the calculated values for SIT and Pitzer parameters, as well as equilibrium constant/potential redox values at infinite dilution, and results of the numerical fits for the data treatment of the formation constant values of the diaminsilver complex (2) and the redox potential data of $Hg_2^{2+}$/Hg pair (3)

| Case | SIT | Pitzer |
|---|---|---|
| 2 | $pK_a^0 = 9.25 \pm 0.01$<br>$s(NH_3,NaNO_3) = 0$<br>$s(NH_3,KNO_3) = 0$<br>$s(NH_3,LiNO_3) = 0$<br>$\sigma = 0.051$, $U = 0.0628$,<br>$R = 5.419 \times 10^{-3}$<br><br>$\log \beta_2^0 = 7.24 \pm 0.02$<br>$\epsilon(Ag(NH_3)_2^+, NO_3^-) = -0.10 \pm 0.06$<br>$\epsilon(Ag(NH_3)_2^+, ClO_4^-) = -0.19 \pm 0.10$<br>$\theta = 0.049$, $U = 0.0620$,<br>$R = 6.225 \times 10^{-3}$ | $\log \beta_2^0 = 7.22 \pm 0.01$<br>$\beta^{(1)}_{Ag(NH_3)_2NO_3} = 0.04 \pm 0.01$<br>$\beta^{(0)}_{Ag(NH_3)_2NO_3} + \theta_{Ag(NH_3)_2NO_3-MNO_3} - \theta_{AgNO_3-MNO_3} =$<br>$-0.049 \pm 0.008$ (Li), $-0.095 \pm 0.005$ (Na,K)<br>$C^{\phi}_{Ag(NH_3)_2NO_3} + \Psi_{Ag(NH_3)_2NO_3} - \Psi_{AgNO_3-MNO_3} =$<br>$0.011 \pm 0.003$ (Li), $0.008 \pm 0.002$ (Na, K)<br>$\sigma = 0.032$, $U = 0.0147$, $R = 1.79 \times 10^{-3}$ (Na, K)<br>$\sigma = 0.041$, $U = 0.0165$, $R = 2.220 \times 10^{-3}$ (Li) |
| 3 | $E^0 = 795.86 \pm 0.09$ mV<br>$\epsilon(Hg_2^{2+}, ClO_4^-) = 0.16 \pm 0.05$<br>$\sigma = 0.222$, $U = 0.394$, $R = 2.51 \times 10^{-4}$ | $E^0 = 796.92 \pm 0.28$ mV<br>$\beta^{(0)}_{Hg_2(ClO_4)_2} + \theta_{Hg_2(ClO_4)_2-HClO_4} = 0.230 \pm 0.03$<br>$\beta^{(0)}_{Hg_2(ClO_4)_2} = 2.136 \pm 0.14$<br>$(1/\sqrt{2})C^{\phi} + \Psi_{Hg_2(ClO_4)_2-HClO_4} = 0.024 \pm 0.09$<br>$\sigma = 0.033$, $U = 0.0089$, $R = 4.284 \times 10^{-4}$ |

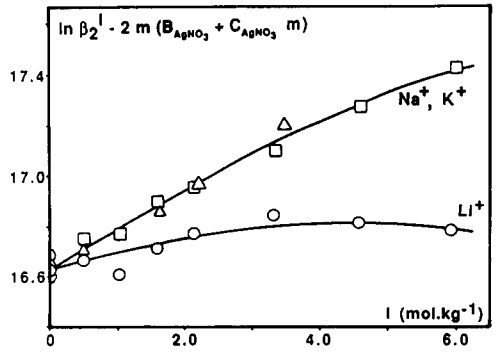


Fig. 4. The application of Pitzer theory to literature $\beta_2$ data at different ionic strengths and media.

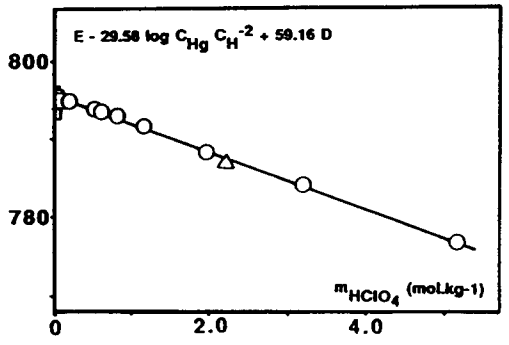


Fig. 5. The application of SIT theory to literature redox potential data of the $Hg_2^{2+}$/Hg pair at different ionic strengths.

*The redox potential of the* $Hg_2^{2+}$/Hg *pair*

Several authors[19–21] have measured the conditional potential values for the $Hg_2^{2+}$/Hg redox couple as a function of $H^+$ concentration by means of potentiometric measurements of the cell:

$$H_2(g)/HClO_4, C_H/HClO_4,$$
$$C_H//Hg_2(ClO_4)_2, C_B/Hg,$$

where $c$ is the molar concentration, and $C_B \cdot C_H \ll 1$.

The measured potential corresponding to the reaction:

$$H_2(g) + Hg_2^{2+} \Leftrightarrow 2H^+ + 2Hg \qquad (14)$$

can be expressed by

$$E = E^0 + 29.58 \log(C_B/C_H^2) + 29.58 \log \gamma_{Hg_2}\gamma_H^2. \qquad (15)$$

The application of SIT theory to this equation leads to the following function:

$$E - 29.58 \log(C_B/C_H^2) + 59.16D = E^0 + 29.58\{\epsilon(Hg_2^{2+}, ClO_4^-) - 2\epsilon(H^+, ClO_4^-)\}m_{HClO_4}. \qquad (16)$$

The linear plot $E - 29.58 \log(C_B/C_H^2) + 59.16D = f(m_{HClO_4})$ is shown in Fig. 5, from which values of $E^0$ and $\epsilon(Hg_2^{2+}, ClO_4^-)$ collected in Table 3 were obtained. On the other hand, the Pitzer theory applied to this system can be expressed by the equation:

$$E - 29.58 \log(C_B/C_H^2) = E^0 - (29.58/2.30)\{-2f^{\cdot\cdot} + 2m_{ClO_4}(2B_{HClO_4} + 2C_{HClO_4}m_{HClO_4} - B_{Hg_2(ClO_4)_2} - C_{Hg_2(ClO_4)_2}m_{HClO_4}) + 2(2m_{Hg} - m_H)\theta_{HClO_4 - Hg_2(ClO_4)_2} + 2m_{Hg}m_{ClO_4}(B'_{Hg_2(ClO_4)_2} + C_{Hg_2(ClO_4)_2} + \Psi_{HClO_4 - Hg_2(ClO_4)_2}) - m_H m_{HClO_4}(4B'_{HClO_4} + 2C_{HClO_4} + \Psi_{HClO_4 - Hg_2(ClO_4)_2}). \qquad (17)$$

Taking into account that $m_H \approx m_{ClO_4} \approx I \approx m$, and $m_{Hg} \ll m_H$, equation (17) can be transformed into:

$$Y = (4.60/59.16)E - 2.30 \log C_B \cdot C_H^{-2} - 2f^{\cdot\cdot} + 4mB_{HClO_4} + m^2C^{\phi}_{HClO_4} - 4m^2B'_{HClO_4} = (4.60/59.16)E^0 + 2m(\beta^{(0)}_{Hg_2(ClO_4)_2} + \theta_{Hg_2(ClO_4)_2 - HClO_4}) + \beta^{(1)}_{Hg_2(ClO_4)_2} + \{1 - (1 + 2\sqrt{I})\exp(-2\sqrt{I})\} + m^2 \times \{(1/\sqrt{2})C^{\phi}_{Hg_2(ClO_4)_2} + \Psi_{HClO_4 - Hg_2(ClO_4)_2}\}, \qquad (18)$$

where the parameters $\beta^{(0)}$ and $\beta^{(1)}$ included in the functions $B_{HClO_4}$ and $B'_{HClO_4}$ as well as the parameter $C^{\phi}_{HClO_4}$ are known (Table 2).

Experimental data $Y = f(m)$ have been plotted in Fig. 6 together with the theoretical function from which the parameter values summarized in Table 3 were derived.

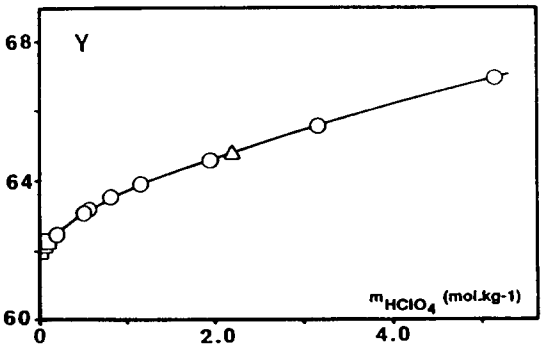


Fig. 6. The application of Pitzer theory to literature redox potential data of the $Hg_2^{2+}$/Hg pair at different ionic strengths.

## DISCUSSION

Values for the determined parameter values derived for the three cases studied are summarized in Table 3 together with the values of the mean standard deviation $\sigma$ and the statistical factor $R$. From the obtained results, the possibility to overcome the difficulty derived from the different equilibrium constant values collected in the literature for a given reaction can be concluded first. In fact, the application of SIT and Pitzer theories allows the selection of the appropriate equilibrium constant values as well as the extrapolation to given experimental conditions with more or less accuracy.

Thus, in the case of the water acidity equilibrium, it should be noted that the use of SIT and Pitzer theories for calculating $H^+$ and $OH^-$ activity coefficients can predict the appreciable variations of experimental $k_w$ values with the ionic media. Especially with the use of Pitzer equations, numerical experimental values for $k_w$ in different media may be deduced with minimum error.

The formation of the diaminsilver complex has been selected as representative of complex formation equilibria. Values of the interaction coefficients ($\epsilon$) of diaminsilver and nitrate or perchlorate agree acceptably with literature values reported for these parameters.[16] The zero mean values of the salting coefficients for $NH_3$ at the different ionic media considered are in agreement with literature values for this parameter.

Although Pitzer parameter values are much more scarce in the literature in relation to complex formation equilibria, it is noteworthy to point out that values obtained for diaminsilver nitrate are within the interval from the upper to the lower values reported by Pitzer for 1:1 electrolytes in nitrate media. Thus, the $\beta^{(0)}$ value varies from 0.1 to $-0.1$, $\beta^{(1)}$ from 0.3 to $-0.4$ and $C^\phi$ from 0.007 to $-0.006$.[11]

The application of SIT theory leads to good results in the range $I = 0.5$–$3.0M$, while with Pitzer theory a good fit is obtained in the range considered (up to $6M$). The deviations observed at the highest ionic strength values can be attributed to the lack of consideration in the SIT theory of the same sign ionic interactions which are appreciable at high values of ionic strength.

The redox potential of the $Hg_2^{2+}/Hg$ couple can be reported as an example of treatment of redox potential data which are scattered and sometimes confused in the literature. Both SIT and Pitzer theories give similar values for $E^0$ magnitude and good fits are obtained, specially in the case of Pitzer equation.

The Pitzer parameter values in perchlorate media for the 2:1 $Hg_2(ClO_4)_2$ electrolyte are within the interval for $\beta^{(0)}$, $\beta^{(1)}$ and $C^\phi$ for this type of electrolyte, 0.8 to $-0.44$ for $\beta^{(0)}$, 2.9 to 2.1 for $\beta^{(1)}$ and 0.04 to $-0.06$ for $C^\phi$, respectively, reported by Pitzer.[11]

The comparison between the results obtained by SIT and Pitzer theories in the prediction or correlation of equilibrium constant and redox potential data in different media clearly indicates the suitability of Pitzer equations for this purpose. On the other hand, the application of SIT theory gives rise to acceptable results up to $3M$, especially if its simplicity, only one parameter ($\epsilon$) is used in the calculations, is taken into account.

## REFERENCES


1. J. N. Brönsted, *J. Am. Chem. Soc.*, 1922, **44,** 938.
2. E. A. Guggenheim, *Philos. Mag.*, 1935, **19,** 588.
3. G. Scatchard, *Chem. Rev.*, 1936, **19,** 309.
4. G. Scatchard, *J. Am. Chem. Soc.*, 1961, **13,** 2636.
5. G. Scatchard, *J. Am. Chem. Soc.*, 1968, **90,** 3124.
6. G. Scatchard, *Equilibrium in Solution, Surface and Colloid Chemistry*, Harvard University Press, Cambridge, 1976.
7. M. Whitfield, *Activity Coefficients in Electrolyte Solutions*, R. M. Pytkowicz (ed.), Vol. 2, Chapter 3, CRC Press, Boca Raton, Florida, 1979.
8. J. L. Aparicio, M. P. Elizalde and J. M. Madariaga, *Quim. Anal.*, 1989, **8,** 41.
9. L. Ciavatta, *Ann. Chim. Ital.*, 1980, **551.**
10. K. S. Pitzer, *J. Phys. Chem.*, 1973, **77,** 268.
11. K. S. Pitzer and G. Mayorga, *J. Phys. Chem.*, 1973, **77,** 2300.
12. K. S. Pitzer and J. J. Kim, *J. Am. Chem. Soc.*, 1974, **96,** 5701.
13. K. S. Pitzer, *Activity Coefficients in Electrolyte Solutions*, R. M. Pytokowicz (ed.), Vol. I, Chapter 7, CRC Press, Boca Raton, Florida 1979.
14. S. Sundstrand, Int. Report Inorganic Chemistry Dept. The Royal Institute of Technology, Stockholm, 1975.
15. H. S. Harned and B. B. Owen, *The Physical Chemistry of Electrolyte Solutions*, 3rd Edn. Reinhold, New York, 1957.
16. M. Maeda, G. Nakagawa and G. Beidermann, *J. Phys. Chem.*, 1983, **87,** 121.
17. E. Högfeldt, *Stability Constants of Metal-Ion Complexes*, Part A: *Inorganic Ligands*. IUPAC Chemical Data Series No. 21, Pergamon Press, Oxford 1982.
18. F. A. Long and W. F. McDevit, *Chem. Rev.*, 1952, **51,** 119.
19. F. Fenwick, *J. Ac. Chem. Soc.*, 1928, **48,** 860.
20. G. A. Linhart, *J. Ac. Chem. Soc.*, 1916, **38,** 2356.
21. A. J. Zielen and J. C. Sullivan, *J. Phys. Chem.*, 1962, **66,** 1065.

Pergamon

0039-9140(95)01423-3

*Talanta*, Vol. 42, No. 3, pp. 401–405, 1995

0039-9140/95 $9.50 + 0.00

# EXTRACTION AND SPECTROPHOTOMETRIC DETERMINATION OF Pd(II) WITH 3,4,4a,5-TETRAHYDRO-3,3,4a-TRIMETHYL-7-(SUBSTITUTED)-PYRIMIDO(1,6-*a*)-BENZIMIDAZOLE-1-THIOL (PBT)

RAJESH SAHU, S. M. SONDHI and BINA GUPTA*

Department of Chemistry, University of Roorkee, Roorkee-247667, India

(*Received* 24 *June* 1994. *Revised* 19 *September* 1994. *Accepted* 19 *September* 1994)

**Summary**—A method for the extraction–spectrophotometric determination of palladium with 3,4,4a,5-tetrahydro-3,3,4a-trimethyl-7-(substituted)-pyrimido(1,6-*a*)benzimidazole-1-thiol (PBT) is described. PBT–Pd(II) complex is extracted from an acidic aqueous solution (0.01–0.5*M* $HClO_4$) into a chloroform layer. The absorbance is measured at 438 nm and the molar absorptivity found to be $1.033 \times 10^4 M^{-1}$ $cm^{-1}$. The complex system conforms to Beer's law over the range 1.9–28.5 $\mu$g/ml palladium(II). The effects of pH (2–6), $HClO_4$ concentration, PBT concentration and shaking time were studied. The ratio of metal ion to ligand molecules in the coloured complex was found to be 1:4. The tolerance limit for many metals have been determined. Finally, the method has been applied successfully to the determination of palladium in synthetic mixtures and in the standard palladium carbon powder (palladium catalyst).

Palladium is one of the platinum group metal. It is a good catalyst and is used widely for hydrogenation and dehydrogenation reactions. Owing to its corrosion resistance nature and alloying ability, palladium and its alloys are used in dental and medicinal devices, and in jewellery manufacture.

Various organic compounds such as 2-hydroxy acetophenone thiosemicarbazone,[1] 1-amino-4hydroxy anthraquinone,[2] 2-hydroxy-4-methoxy-5′-chlorochalcone oxime,[3] di-2-pyridyl methanone-2-(5-nitro)pyridyl hydrazone,[4] 2-carboxy-2′-hydroxy-5-methyl-azobenzene,[5] 5,6-dimethyl-1,3-indanedione-2-oxime,[6] isonitrosomalone dianilide[7] and 3,5-dichloro-2-(2,4-diamino-phenyl) pyridine[8] have been reported as spectrophotometric reagents for the determination of palladium(II). Some organic reagents bearing mercapto group have also been explored for the determination of palladium(II), viz. 2-mercaptobenzoxazole,[9] mercaptoacetic acid-$\beta$-naphthylamide,[10] 8-mercaptoquinoline,[11] $\beta$-mercaptroresorcylic [4-hydroxy-2-mercapto-benzoic] acid,[12] 2-mercaptoacetoacetanilide,[13] 2*N*-(2-mercaptophenyl)-1,2,3-benzothiadiazoline[14,15] and 2-mercaptobenzamide.[16] However, the reported methods suffer from limitations such as longer extraction period,[4,8,9,14,15] less satability,[8] interferences from other commonly associated ions[4,5,12,16] and negligible extraction.[1,2,6,9,12]

Anti-parasitic and anti-inflammatory activity evaluation of pyrimido benzimidazoles[17,18] and their derivatives[19,20] have been reported in the recent literature. The analytical applications of pyrimido benzimidazoles have not been explored so far.

In the present investigation 3,4,4a-5-tetrahydro-3,3,4a-trimethyl-7-(substituted)-pyrimido (1,6-*a*)benzimidazole-1-thiol (**Ia–c**) has been explored as a new reagent for the separation, extraction and determination of palladium. Among the transition metal ions tested the reagent reacts with Pd(II) and Hg(II). But the conditions for the extraction of Hg(II) are different from that of palladium. Hence no interference from Hg(II) is observed during the determination of Pd(II).

## EXPERIMENTAL

### *Reagents*

*Synthesis of* 3,4,4*a*,5-*tetrahydro*-3,3,4*a*-*trimethyl pyrimido*[1,6-a]*benzimidazole*-1-*thiol*(**Ia**) (PBT). o-Phenylene diamine (2.16 g, 0.02 mol) was dissolved in methanol (20 ml) and to it was

*Author to whom correspondence should be addressed.

added 4-methyl-4-isothiocyanato-2-pentanone (3.50 g; 0.022 mol) and 2 drops of conc sulphuric acid (pH ~ 6). The reaction contents were heated under reflux for 8 hr. Solvent was removed under reduced pressure and the residue left behind was basified with sodium carbonate solution. Solid so obtained was filtered, washed with water and air-dried. The crude product was recrystallized[21] from THF to give 3,4,4a,5-tetrahydro-3,3,4a-trimethyl pyrimido[1,6-*a*]benzimidazole-1-thiol (**Ia**), yield 86% mp 223°C, $^1$H NMR (300 MHz; DMSO-$d_6$): $\delta$ 1.2 (*d*, 6H, $CH_3 + CH_3$), 1.35 (*s*, 3H, $-CH_3$), 2.10 (*s*, 1H, $J_{gem.} = 15$ Hz), 2.32 (*d*, 1H. $J_{gem.} = 15$ Hz), 6.5 (*m*, 3H, one H exch. -NH + 2H Ar), 6.80 (*t*, 1H, Ar), 8.3 (*s*, -C-NH, exch.), 8.55 (*d*, 1H, Ar). HR MS *m/z* (rel. int.%), 247.1148 ([M]$^+$, 51.84). Calcd. for $C_{13}H_{17}N_3S$ 247.1143. Elemental analysis found C, 63.00; H, 7.00; N, 17.10; Calcd. for $C_{13}H_{17}N_3S$ C, 63.15; H, 6.88; N 17.00.

Pyrimido[1,6-*a*]benzimidazoles (**Ib** and **c**) were prepared by condensing 4-methyl 1,2-phenylene diamine and 4-methoxy-1,2-phenylene-diamine with 4-isothiocyanato-4-methyl-2-pentanone (Sahu, Guptu and Sondhi, unpublished results).[18] Both these compounds, were purified by recrystallization and purified compounds gave correct $^1$H NMR, HRMS and elemental analysis (within an error of $\pm$0.4%).

### Pd(II) *Standard solution*

A $1.9 \times 10^{-3}M$ stock solution was prepared by dissolving 0.0334 g palladium(II) chloride (Johnson Mathey, London) in a few drops of conc hydrochloric acid and diluting to 100 ml with double distilled water. The stock solution was standardized[22] with dimethyl glyoxime.

All the reagents and chemicals used were of analytical grade. Solutions of other ions were prepared by dissolving the corresponding salts in double distilled water.

### *Apparatus*

Absorbance measurements were carried out with a Shimadzu UV-260 recording spectrophotometer with 1 nm band width and 10 mm matched silica cells. A CL-46 Toshniwal, digital pH meter with a combined glass electrode was used for pH-measurements. For the determination of palladium(II) in aqueous phase, inductively coupled plasma-atomic emission spectrometer, model 8040 Plasma Labtum (Australia) was used.

### *Procedure*

An aliquot of the solution containing 190 $\mu$g palladium(II) was taken in a separatory funnel and mixed with an adequate amount of perchloric acid to have the desired acidity. The aqueous phase was made up to 10 ml with double distilled water. This was shaken for 90 sec with 10 ml of organic phase containing 1.5 ml of PBT-**Ia** (0.01*M*) and 8.5 ml chloroform. The yellow-coloured organic phase was separated and 1 g of anhydrous $Na_2SO_4$ added to remove traces of water. The absorbance of the organic phase was measured at 438 nm against reagent blank.

## RESULTS AND DISCUSSION

### *Spectral characteristics*

Absorption spectra of Pd(II) PBT (**Ia–c**) complexes in chloroform medium against reagent blank were recorded. Maximum absorbance was observed in the case of Pd(II)–PBT-**Ia** complex (Table 1). The absorption spectra of the yellow coloured complex formed between Pd(II) and PBT-**Ia** and the reagent blank are shown in Fig. 1. The palladium complex and reagent have $\lambda_{max}$ at 438 and 340 nm, respectively. In order to minimize the effect of reagent blank, the absorbance of the complex was measured at 438 nm where reagent blank shows negligible absorbance.

### *Choice of acid and effect of acidity*

Choice of acid and its concentration are important in the extraction of Pd(II) with substituted pyrimido[1,6-*a*]benzimidazoles (**Ia–c**). Different acids, viz. $HClO_4$, $HNO_3$, $H_2SO_4$ and HCl, were tried. Nitric acid could not be used because the ligand is oxidized at higher acid concentration (>4*M* $HNO_3$) and up to 4*M* $HNO_3$ extraction is not complete. Amongst the other acids ($H_2SO_4$, $HClO_4$ and HCl) perchloric acid is the most suitable because maximum absorbance is obtained with $HClO_4$ and only a single extraction is required to extract Pd(II) completely from perchloric acid medium. Thus

Table 1. Absorption characteristics of Pd(II)–PBT complexes in chloroform

| Reagent | $\lambda_{max}$ (*nm*) | ($M^{-1}$ $cm^{-1}$) | Acid concentration (*M*) |
|---|---|---|---|
| PBT-**Ia** | 438 | 10,331 | 0.01–0.5 |
| PBT-**Ib** | 438 | 9994 | 0.01 |
| PBT-**Ic** | 434 | 5816 | 0.01–0.1 |

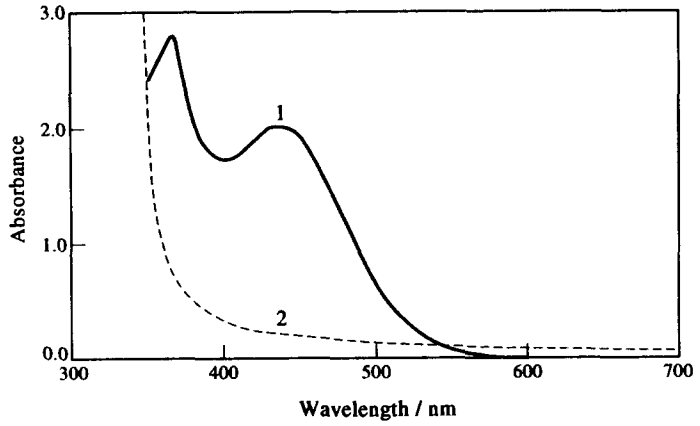


Fig. 1. Absorption spectra of Pd(II)–PBT-**Ia** complex in chloroform. PBT-**Ia** = $1.5 \times 10^{-3}M$; acid concentration $0.1M$; (1) 19 $\mu$g/ml of palladium(II) extracted into chloroform *vs.* reagent blank and (2) reagent blank *vs.* chloroform.

extraction studies were carried out for all the three derivatives from perchloric acid medium.

PBT-**Ia** is the more suitable ligand, as quantitative extraction is obtained with this ligand in the range 0.01–0.5$M$ $HClO_4$. Whereas with PBT-**Ib** quantitative extraction is achieved only at 0.01$M$ $HClO_4$. With PBT-**Ic** the highest percentage extraction obtained is only 52%. Thus PBT-**Ia** was selected for all further studies. Results are illustrated in Fig. 2.

*Calibration, sensitivity and precision*

A calibration curve was drawn for the Pd(II)–PBT-**Ia** complex. The coloured system obeyed Beer's law over the range 1.9–28.5 $\mu$g/ml of palladium(II). The molar absorptivity and Sandell sensitivity for log $I/I_0 = 0.001$ were $1.033 \times 10^4 M^{-1}$ cm$^{-1}$ and 0.009 $\mu$g/cm$^2$, respectively. Coefficient of variation was 0.056% for the determination of 19 $\mu$g of palladium(II).

*Effect of PBT concentration*

The absorbances of a series of solutions containing 190 $\mu$g of palladium(II) and various concentrations of PBT-**Ia** ($1.0 \times 10^{-3}$–$5.0 \times 10^{-3}M$) were measured keeping all other parameters constant. Maximum absorbance was observed at $1.5 \times 10^{-3}M$ PBT-**Ia** concentration. This reveals that the concentration of PBT-**Ia** must be at least 7.5 times greater than that of palladium(II) concentration for full colour development.

*Composition of the extracted species*

The ratio of metal ion to PBT-**Ia** in the extracted species was determined by the log–log plot of distribution ratio *vs.* PBT-**Ia** concentration at a fixed pH. A straight line with a slope of *ca.* 4 was obtained, indicating a 1:4 metal-to-ligand ratio in the extracted complex (Fig. 3).

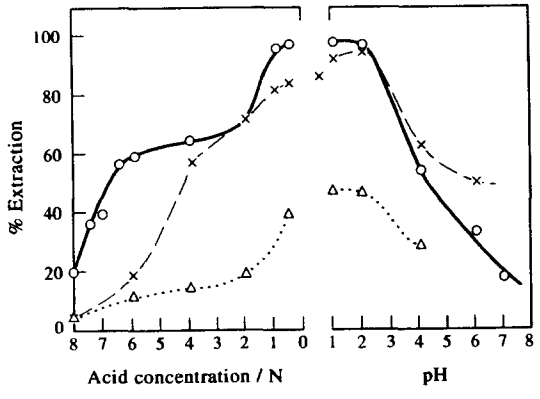


Fig. 2. Effect of pH on the extraction of Pd(II)–PBT complexes. Pd(II), 19 $\mu$g/ml; PBT = $1.5 \times 10^{-3}M$. —○— PBT-**Ia**, — × — PBT-**Ib**, —△— PBT-**Ic**.

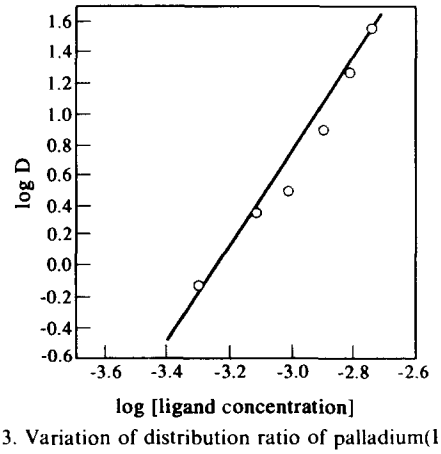


Fig. 3. Variation of distribution ratio of palladium(II) as a function of PBT-**Ia** concentration at constant acid concentration ($0.1M$) and constant metal ion concentration [Pd(II) = 19 $\mu$g/ml].

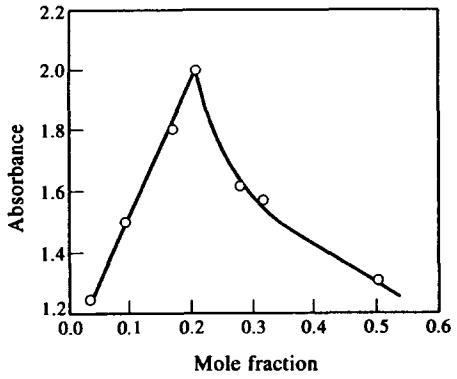


Fig. 4. Plot of composition of the extracted species by Job's continuous variation method. Total concentration of Pd(II) and PBT-**Ia** = $5.0 \times 10^{-4} M$.

The composition was also verified by Job's method of continuous variation (Fig. 4). The results reveal a monodentate behaviour of the ligand. Similar results have also been reported by Singh *et al.*[23]

*Choice of solvent*

Different solvents were tried for the extraction of Pd(II)–PBT-**Ia** complex (Table 2). Out of the eight tested solvents chloroform is the most suitable solvent as maximum absorbance is achieved with this solvent. Thus chloroform was selected for further studies.

*Shaking time and stability*

The shaking time for the extraction was varied from 30 to 300 sec. Minimum shaking time for complete extraction of 19 $\mu$g/ml of palladium(II) with chloroform is 60 sec at $25 \pm 2°C$. Therefore, a 90 sec shaking time was adopted for all further studies. The absorbance of Pd–PBT–**Ia** complex is stable for at least 30 hr at 438 nm.

Table 2. Extraction of Pd(II)–PBT-**Ia** complex with various organic solvents

| | Solvent | $\lambda_{max}$ (nm) | %$E$) | ($M^{-1}$ $cm^{-1}$) |
|---|---|---|---|---|
| (1) | Carbon tetrachloride | — | 0.0 | — |
| (2) | Benzene | — | 0.0 | — |
| (3) | Toluene | — | 0.0 | — |
| (4) | Xylene | — | 0.0 | — |
| (5) | Nitrobenzene | 431 | 95.0 | 8193 |
| (6) | Chloroform | 438 | 100.0 | 10,331 |
| (7) | Butanol | 380 | 67.50 | 4834 |
| (8) | Isoamyl alcohol | 436 | 82.50 | 5856 |
| (9) | Ethyl acetate | 429 | 100.0 | 8872 |

Table 3. Effect of diverse ions on the determination of Pd(II) amount of Pd(II) taken is 19 $\mu$g/ml

| Ion | Added as | Tolerance limit (molar ratio) |
|---|---|---|
| $Na^+$ | $NaNO_3$ | 100 |
| $K^+$ | $KNO_3$ | 100 |
| $Ca^{2+}$ | $Ca(NO_3)_2$ | 100 |
| $Mg^{2+}$ | $MgSO_4$ | 100 |
| $Cu^{2+}$ | $CuSO_4$ | 10 |
| $Co^{2+}$ | $CoSO_4$ | 2 |
| $Ni^{2+}$ | $NiCl_2$ | 100 |
| $Zn^{2+}$ | $ZnCl_2$ | 100 |
| $Ru^{3+}$ | $RuCl_3$ | 50 |
| $Rh^{3+}$ | $RhCl_3$ | 10 |
| $Ir^{3+}$ | $IrCl_3$ | 5 |
| $Au^{3+}$ | $AuCl_3$ | Nil |
| $Hg^{2+}$ | $Hg(NO_3)_2$ | 100 |
| $Fe^{3+}$ | $Fe(NO_3)_3$ | 50 |
| $Cr^{3+}$ | $CrCl_3$ | 50 |
| $Mo^{6+}$ | $(NH_4)_2MoO_4$ | 100 |
| $Pb^{2+}$ | $Pb(NO_3)_2$ | 100 |
| $Mn^{2+}$ | $MnSO_4$ | 100 |
| $Pt^{4+}$ | $H_2PtCl_6$ | 10 |
| $Os^{8+}$ | $OsO_4$ | 25 |
| $V^{5+}$ | $V_2O_5$ | 50 |
| Citrate | Sodium citrate | 2 |
| EDTA | EDTA | 100 |
| $NO_3^-$ | $NaNO_3$ | 100 |
| $Cl^-$ | NaCl | 100 |
| $Br^-$ | NaBr | 100 |
| $I^-$ | KI | 5 |
| $CNS^-$ | KCNS | Nil |

*Effect of diverse ions*

In order to study the effect of various ions on the determination of the Pd(II)–PBT-**Ia** complex, a fixed amount (10 $\mu$g/ml) of palladium(II) was taken with different amounts of foreign ions and the recommended procedure was followed. The results are summarized in Table 3. An error of $\pm 3\%$ in the absorbance was considered tolerable. Cobalt(II), copper(II) and platinum(IV) are tolerated when present in equimolar

Table 4. Determination of palladium(II) in the synthetic mixtures

| Composition of synthetic mixture ($\mu g$) | Pd(II) found by the present method in organic phase* ($\mu g$) | Co(II), Ni(II) and V(V) remaining in the aqueous phase (determined by A.A.S.*) ($\mu g$) |
|---|---|---|
| Pd(100); Co(100); Ni(100) | 97.8 | Ni(88.9); Co(100.2) |
| Pd(200); V(200); Ni(1200) | 199.5 | Ni(1196.5); V(198.6) |
| Pd(100); Pt(200) | 98.9 | Pt(199.2) |

*Triplicate analysis.

Table 5. Determination of Pd(II) in palladium–charcoal

| Sample | Taken ($\mu g$*) (as determined by ICP) | Found ($\mu g$) | Recovery (%) |
|---|---|---|---|
| Pd–Charcoal (E. Merck) | 18.00 | 17.84<br>17.80<br>18.02 | 99.37 |
| Pd–Charcoal (Aldrich) | 28.00 | 27.63<br>27.74<br>27.80 | 99.01 |

*Determined by ICP-AES in aqueous phase.

concentration. The interferences from 10-fold excess of these ions can be masked with 1,10-phenanthroline, EDTA and oxalate, respectively. Iodide and citrate interfere at low concentration Gold(III) and $CNS^-$ interfere seriously in the determination of palladium(II).

*Application of the method to real samples and synthetic mixtures*

In order to confirm the usefulness of the proposed method, it was applied to the determination of palladium(II) in the synthetic mixture and Pd–charcoal. The results of synthetic mixture are given in Table 4. Results indicate a clear separation of Pd(II) from Co(II), Ni(II) and V(V) leaving these metal ions in the aqueous phase. After extraction of Pd(II) concentrations of Ni(II), Co(II) and V(V) were determined in the aqueous phase by A.A.S. (Table 4).

To prepare a solution of Pd–charcoal, 0.1 g of the palladium charcoal was weighed and dissolved in conc $HNO_3$. The solution was evaporated nearly to dryness, extracted with 10 ml of 0.05*M* HCl, filtered and diluted to 100 ml with distilled water. An aliquot of this solution was analysed for palladium(II) by the proposed method. The results were tested by ICP-AES. There was a good agreement between the amount of Pd(II) estimated by this method and that determined by ICP-AES (Table 5).

The palladium(II) in the organic phase can be stripped quantitatively with 10*M* $HClO_4$. Thus the proposed method provides a simple, rapid and selective method for the extraction, separation and spectrophotometric determination of palladium(II).

*Acknowledgements*—The authors gratefully acknowledge the assistance of Dr N. K. Saini and Dr P. P. Kapoor of Wadia, Institute of Geology, Dehradun in some of the I.C.P. measurements.

## REFERENCES

1. G. V. R. Murthy and T. S. Reddy, *Talanta*, 1992, **39**, 697.
2. K. A. Idriss, M. S. Salh, M. M. Selein, F. S. Hassan and S. K. Idriss, *Monatsh. Chem.*, 1990, **121**, 625.
3. B. K. Deshmukh and M. G. Awari, *Chem. Anal. (Warsaw)*, 1987, **32**, 369.
4. T. Kanetake and M. Otomo, *Anal. Sci.*, 1988, **4**, 411.
5. C. Bandyopadhyay, B. C. Roy and M. B. Saha, *J. Indian Chem. Soc.*, 1986, **63**, 707.
6. D. M. Rao, K. H. Reddy and D. V. Reddy, *Talanta*, 1991, **38**, 1047.
7. R. A. Chaudhari and A. D. Sawant, *Indian J. Chem. (Sec. A.)*, 1991, **30**, 643.
8. D. A. Fontan, C. B. Marone and R. Olsina, *Bull. Chem. Soc. Jpn*, 1988, **61**, 412.
9. T. Arita and J. H. Yoe, *Anal. Chim. Acta*, 1963, **29**, 500.
10. R. Berg and W. Roebling, *Angew. Chem.*, 1934, **47**, 404.
11. O. Kammori, I. Taguchi, K. Takahashi and T. Koike, *Bunseki Kagaku*, 1965, **14**, 702.
12. S. P. Bag and B. Bhattacharya, *J. Indian Chem. Soc.*, 1983, **60**, 204.
13. A. K. Das and J. Das, *Indian J. Chem. (Sec. A)*, 1983, **22**, 93.
14. K. Watanabe, M. Hojjatie, S. Imai and S. Kobayashi, *Anal. Sci.*, 1989, **5**, 419.
15. K. Watanabe and K. Tamura, *Bunseki Kagaku*, 1991, **40**, 475.
16. K. Watanabe, M. Hojjatie, T. Nakamure and I. Aoki, *Anal. Chim. Acta*, 1989, **218**, 111.
17. S. M. Sondhi, R. Sahu, A. Magan, D. K. Ghosh, R. M. Mukhopadhya, G. K. Chaterjee, A. K. Das and S. K. Chaudhuri, *Indian Drugs*, 1944, **31**, 317.
18. S. M. Sondhi, A. Magan, R. Sahu, V. K. Mahesh, R. Shukla and G. K. Patnaik, *Synthesis*, 1994, No. 11, 1175.
19. K. Goto, *Jap. Kokai Tokkyo Koho Jpn*, 03, 215, 488 [91, 215, 488]; *Chem. Abstr.*, 1992, **116**, 128962w.
20. K. Goto, K. Hashimoto and K. Kanai, *Jap. Kokai Tokkyo Koho Jpn*, 63, 198, 685 [88, 198, 685]; *Chem. Abstr.*, 1989, **110**, 23911b.
21. R. K. Sahu, A. Magan, B. Gupta, S. M. Sondhi, R. C. Srimal and G. K. Patnaik, *Phosphorus, Sulphur and Silicon*, 1994, **88**, 45.
22. A. I. Vogel, *A Textbook of Quantitative Inorganic Analysis*, 4th Edn, p. 475. Longmans, London, 1978.
23. A. K. Singh, M. Katyal, A. M. Bhatti and N. K. Ralhan, *Talanta*, 1978, **23**, 337.

Pergamon

0039-9140(95)01424-1

*Talanta*, Vol. 42, No. 3, pp. 407–414, 1995

0039-9140/95 $9.50 + 0.00

# PREDOMINANCE-ZONE DIAGRAMS OF Fe(III) AND Fe(II) SULFATE COMPLEXES IN ACIDIC MEDIA. VOLTAMMETRIC AND SPECTROPHOTOMETRIC STUDIES

ADRIÁN F. GIL, LEONARDO SALGADO, LAURA GALICIA and IGNACIO GONZÁLEZ*

Universidad Autónoma Metropolitana-Iztapalapa, Depto de Química, Area de Electroquímica, Apdo. Postal 55-534, 09340 México D.F., Mexico

(*Received* 1 *March* 1994. *Revised* 14 *June* 1994. *Accepted* 23 *September* 1994)

**Summary**—A thermodynamic study based on concepts of generalized species and equilibria, was used to understand the distribution of Fe(III) and Fe(II) species in the Fe(III)/Fe(II)/$H_2SO_4$/$H_2O$ system. The two-dimensional predominance zone diagrams (TDPZ) and Pourbaix type diagrams thus obtained permitted the selection of optimum experimental conditions, to differentiate the chemical species involved in this system. The existence of the different predominant chemical species for Fe(III): $Fe^{3+}$, $FeSO_4^+$ and $Fe(SO_4)_2^-$ was evidenced by spectrophotometrical studies for $pSO_4'$ values from 4 to 0 units in a buffered solution of pH 0.5. Additionally, voltammetric studies performed on Pt, Au and carbon paste electrodes confirmed that the electron exchange between Fe(III)/Fe(II) in $H_2SO_4$ media occurs by an inner Helmholtz layer mechanism. It was also possible to show that the representative couples at $pSO_4' = 0$ (buffered) are: (a) for pH < 0 $FeSO_4^+/FeHSO_4^+$ and (b) for pH > 1.0: $Fe(SO_4)_2^-/FeHSO_4^+$. The last couple presents a coupled chemical reaction in the electrochemical mechanism; this reaction is associated with the different coordination numbers of Fe(III) and Fe(II).

The importance of iron chemistry in geological, environmental, metallurgical, industrial, catalytical and biological contexts makes its understanding of fundamental significance. In connection with applications, it is very important to study the behavior of iron (III) species in weakly acidic solutions. For example, it is well known that the corrosion of metallic iron is strongly accelerated by the presence of sulfate ions.[1–4]

In many of the previous studies on the electrochemical behavior of Fe(II)/Fe(III) couple, two main features have been reported: (a) the dependence of the normal potential values on the supporting electrolyte attributed to the different iron coordination sphere,[2,3,5] and (b) the dependence of the iron redox potential on the solution pH and on the supporting electrolyte anions owing to its complex redox mechanism.[2,4,6]

Despite extensive research on the Fe(II)/Fe(III) couple, few studies have considered the existence of the sulfate–iron complexes in sulfuric acid media in order to explain the electrochemical behavior of this couple. This is a result of the difficult detection of the chemical species involved in the redox equilibria,[7,8] since the formation constants of the iron–sulfates are small.[9,10]

In this work, the Fe(III)/Fe(II)/$H_2SO_4$/$H_2O$ system is studied in several ways: Firstly, a method based on concepts of generalized species and equilibria,[11,12] is used to understand the thermodynamic distribution of Fe(III) and Fe(II) species in sulfuric acid system. This method allows for the construction of two-dimensional predominance zone diagrams and Pourbaix-type diagrams which consider all chemical species present in solution.

From these diagrams, it is possible to explain the spectrophotometric behavior of the solution containing $2 \times 10^{-4} M$ Fe(III) at pH 0.5 with variable sulfate concentration. The Pourbaix diagram constructed by using generalized species allows us to discuss the differences in the electrochemical behavior of Fe(III)/Fe(III) system in sulfuric acid solutions at different pH values (at $pSO_4' = 0$).

## CONSTRUCTION OF THE TWO-DIMENSIONAL PREDOMINANCE ZONE (TDPZ) AND POURBAIX-TYPE DIAGRAMS

The stability of the Fe(III) and Fe(II) species was studied separately by TDPZ diagrams of

*Author to whom correspondence should be addressed.

the corresponding generalized species. The calculations were carried out by analyzing the generalized equilibria[11,12] of the type:

$$Fe(III)' + SO_4' \leftrightarrows Fe(SO_4)' \quad (1)$$

$$Fe(SO_4)' + SO_4' \leftrightarrows Fe(SO_4)_2' \quad (2)$$

as well as the generalized dismutation equilibria:

$$2FeSO_4' \rightleftarrows Fe(SO_4)_2' + Fe(III)', \quad (3)$$

where $Fe(III)'$ represents all the Fe(III) species complexed with ligands other than $SO_4'$: (e.g. $Fe(III)' = \Sigma_i\ Fe(OH)_i$); $SO_4'$ represents all the chemical species containing $SO_4$, except those corresponding to the $FeSO_4$ complexes (e.g. $SO_4' = \Sigma_r\ SO_4(H)_r$), and $FeSO_4$ represents all the chemical species of $FeSO_4$ complexed with species other than $SO_4$ (e.g. $\Sigma_k\ FeSO_4(H)_k$). Where electrical charges are omitted for simplicity.

The definition of generalized species and their relationship with the complexation coefficients ($\alpha$) have been previously discussed in detail.[11,12]

For the system $Fe(III)$–$H_2SO_4$–$H_2O$ the concentrations of the generalized species are defined in such a way that:[11,12]

$$[Fe(III)'] = \sum_{i=0}^{m} Fe(OH)_i = [Fe^{3+}]\alpha_{Fe(H)} \quad (4)$$

$$Fe(SO_4)_j' = \sum_{k=0}^{n} FeH_k(SO_4)_j = [Fe(SO_4)^{3-2j}]\alpha_{(FeSO_4)_j(H)} \quad (5)$$

where $j \in \{0, 1, 2\}$,

$$SO_4' = \sum_{r=0}^{r} H_rSO_4 = [SO_4^{2-}]\alpha_{SO_4(H)}. \quad (6)$$

The generalized species are defined by the same method for the $Fe(II)$–$H_2SO_4$–$H_2O$ system. $\alpha_{FeSO_4j(H)}$ and $\alpha_{SO_4(H)}$ are the complexation coefficients dependent only on the $[H^+]$ buffering[12] (*e.g.* $\alpha_{FeSO_4(H)} = 1 + \Sigma_k K^{FeSO_4.kH}_{Fe(SO_4)_k} H^k$).

The generalized equilibrium is associated with Ringbom-type conditional constants[11,12] (dependent only on the $[H^+]$ buffering) called generalized constants.

$$K^{SO_4'}_{Fe(SO_4)_j'} = K^{SO_4}_{Fe(SO_4)_j} \frac{\alpha_{Fe(SO_4)_{(j+1)}(H)}}{\alpha_{Fe(SO_4)_j(H)}\alpha_{L(H)}} = \frac{[Fe(SO_4)_{(j+1)}]}{[Fe(SO_4)_j'][(SO_4)']}. \quad (7)$$

The method for the construction of predominance-zone diagrams (TDPZ) consists of the following steps.[11-13]

(1) Analysis of the ampholyte's stability: if the generalized dismutation constant of equilibrium (3) is $\geqslant 1$, $Fe(SO_4)'$ cannot predominate in the system, consequently, only the following equilibrium must be considered:

$$Fe(III)' + 2(SO_4)' \leftrightarrows Fe(SO_4)_2'. \quad (8)$$

(2) Study of the predominance of generalized species ($Fe(SO_4)_2'$, ($Fe(SO_4)'$ and $Fe(III)'$) with the following condition: $pSO_4' = -\log K^{(SO_4)'}_{Fe(SO_4)'}$ and $pSO_4' = -\log K^{(SO_4)'}_{Fe(SO_4)_2'}$ where $[Fe(III)'] = [Fe(SO_4)']$ and $[Fe(SO_4)_2'] = [Fe(SO_4)']$, respectively.

(3) Graphical representation in the $pSO_4' = pH$ space with borderlines selected from the conditions just described.

(4) Establishment of the limits for TDPZ imposed by the stabilization of the solid species ($Fe(OH)_3$, $Fe(OH)_2$). The method which considers the condensed phases in TDPZ has been described elsewhere.[14] The stability regions of the $Fe(OH)_2$ and $Fe(OH)_3$ depend upon the Fe(II) and Fe(III) concentrations selected for each case. In the following example, the total Fe(II) and Fe(III) concentrations are $2 \times 10^{-3} M$.

The total sulfates concentration $[SO_4']$ is the sum of $HSO_4^-$ and $SO_4^{2-}$ and is called the generalized sulfate concentration. The values of thermodynamic formation constants for the chemical species employed in this work are reported in Table 1.[9,10]

The TDPZ diagrams for $Fe/H_2SO_4/H_2O$ system are shown in Fig. 1. Figure 1a shows the predominance zones of the $Fe^{III}(SO_4)'$ species (*e.g.* $Fe(SO_4)^+$, $Fe(SO_4)_2^-$, $FeHSO_4^{2+}$) and Fig. 1b shows those of the $Fe^{II}(SO_4)'$ species (*e.g.* $Fe^{2+}$, $FeHSO_4^+$) as a function of $pSO_4'$ and pH, with the same degree of oxidation. Thus, these diagrams do not consider electron exchange. (Fig. 1a only considers the region be-

Table 1. The values of thermodynamic formation constants for iron–sulfate complexes[9,10]

| Ion | Equilibrium | log K |
|---|---|---|
| | $L = SO_4^{2-}$ | |
| $H^+$ | $H + L \rightarrow HL$ | 1.94 |
| $Fe^{3+}$ | $M + HL \rightarrow MHL$ | 1.8 |
| | $M + L \rightarrow ML$ | 4.0 |
| | $M + 2L \rightarrow ML_2$ | 5.8 |
| $Fe^{2+}$ | $M + HL \rightarrow MHL$ | 2.2 |
| | $L = OH^-$ | |
| $Fe^{3+}$ | $M + L \rightarrow ML$ | 11.0 |
| | $M + 2L \rightarrow ML_2$ | 21.9 |
| | $M + 3L \rightarrow ML_3$ | 38.6 |
| $Fe^{2+}$ | $M + 2L \rightarrow ML_2$ | 15.1 |

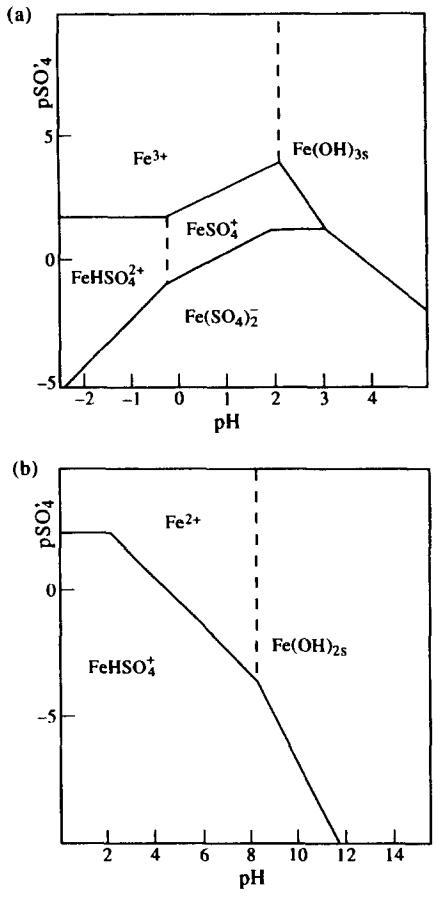


Fig. 1. Two-dimensional predominance zone diagrams ($pSO_4'$/pH) of Fe(II)/Fe(III) chemical species constructed for $C_{Fe(III)} = C_{Fe(II)} = 2 \times 10^{-3} M$, [$SO_4'$] represent the generalized sulfate concentration. (a) Fe(III) chemical species, (b) Fe(II) chemical species.

tween pH $-2$ and 5, since this is the pH range of practical interest.) The solid lines represent the variation of the logarithm of the generalized constants described by equation (7), and the described Fe–$SO_4$ exchange. The dashed lines represent the borderline of the predominance zone of species with the same M–L stoichiometry but different degree of protonation. From this diagram (1a), only $Fe(OH)_3$ and $Fe(SO_4)_2^-$ are present at higher pH values. The region at pH $< 0$ is not useful in our case because it can no longer be considered as dilute. The complete diagram is important for theoretical purposes only.

From the diagram, it can be concluded that in highly acidic media, the Fe(II) and Fe(III) sulfates-complexed species equilibria are predominant. At the conditions of the electrochemical studies previously reported,[2-4] Fe(III) and Fe(II) ions are complexed. For example, at $0 <$ pH $< 4$ and $pSO_4' = 0$ (total sulfate $= 1M$) it may be observed that the Fe(II) ions are the predominant species, mainly as $FeHSO_4^+$, while Fe(III) ions are in the form of $FeSO_4^+$ or $Fe(SO_4)_2^-$. This is a graphical way to analyze the behavior of processes involving only the complexation and hydrolysis reactions (these diagrams may be useful in the study of hydrometallurgical processes such as solvent extraction and ion-exchange). The electron exchange reactions are only considered in Pourbaix type diagrams.

In order to discuss the redox properties of Fe(III)/Fe(II) couple, considering hydrolysis effects on the cations and the formation of sulfate complexes, it would be necessary to construct a three-dimensional Pourbaix type diagram, $E''$–$pSO_4'$–pH. This diagram can be constructed considering the generalized electrochemical equilibria for the $Fe/H_2SO_4/H_2O$ system;[13]

$$Fe(III)'' + 1e^- \leftrightarrows Fe(II)'' \qquad (9)$$

with

$$E'' = E^0_{Fe^{3+}/Fe^{2+}} + \frac{RT}{F} \ln \frac{[Fe(III)'']}{[Fe(II)'']} \qquad (10)$$

where [Fe(III)''] represents the generalized concentration of Fe(III) species complexed with $SO_4$, OH and H.

However, the construction of such diagrams is rather time consuming and complicated. Therefore, to correlate thermodynamic predictions with the experimental results in an adequate manner, two-dimensional Pourbaix type diagrams have been constructed, considering either the $pSO_4'$ or else the pH constant. These diagrams correspond to a slice-cut of the corresponding three dimensional diagrams (as shown in Fig. 2).

The solid lines in Fig. 2 correspond to the variation of the formal potential of Fe(III)/Fe(II) with the $pSO_4'$ buffered at $1M$ or else at buffered pH 0.5. The dashed lines correspond to the border lines of the predominance zones of the different species with the same oxidation degree as a function of pH or $pSO_4'$. In Fig. 2a the potential–pH (or Pourbaix type) diagram for this system at buffered $pSO_4' = 0$ is shown (see below) and the potential–$pSO_4$ (Pourbaix type diagram) for the system buffered at pH 0.5 is shown in Fig. 2b. In Fig. 2b, it is evident that the equilibrium potential of the Fe(III)/Fe(II) couple is practically constant and similar to that of $Fe^{3+}/Fe^{2+}$ couple (0.77 V) even

though the chemical nature of the species involved is not the same (owing to the change in $pSO_4'$). This may be the reason why most authors do not consider the existence of sulfate-complexed Fe(III) ions in their works.[7,8]

The TDPZ diagrams of Fig. 1a and b show that the predominant species of Fe(III) and Fe(II) depend on the pH and $pSO_4'$ values which provoke a change in the redox properties of the system as shown in the Pourbaix-type diagrams of Fig. 2a and b.

In order to verify the chemical changes of the Fe(III) species with pH and $pSO_4'$, electrochemical and spectrophotometrical studies under buffered conditions were performed. The results of these studies prove, as shown below, that the changes in the electrochemical behavior of Fe(III)/Fe(II) system can be associated with modifications in the coordination sphere.

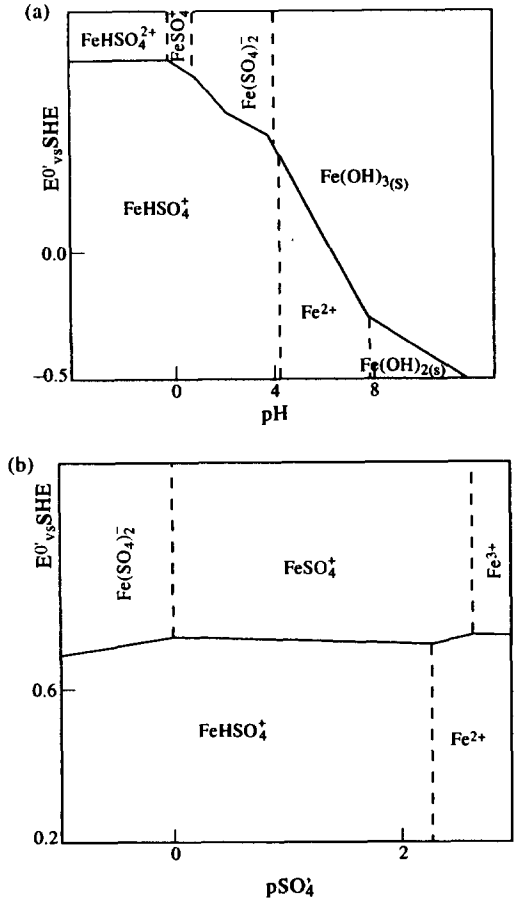


Fig. 2. Pourbaix type diagrams for the Fe(III)/Fe(II)/$SO_4'/H_2O$ system constructed from Fig. 1 and $C_{Fe(III)} = C_{Fe(II)} = 2 \times 10^{-3} M$. The Fe(III), Fe(II) diagrams are constructed for different buffered generalized species. (a) Potential ($E^0$/SHE)–pH diagram under buffered generalized sulfate $[SO_4'] = 1M$. (b) Potential ($E^0$/SHE)–$pSO_4'$ diagram at (buffered) pH 0.5.

## EXPERIMENTAL

The Fe(III) $2 \times 10^{-3} M$ solutions, were prepared by dissolving $Fe_2(SO_4)_3.H_2O$ (Laitz A. R.) in hot $1M$ $H_2SO_4$. The $1M$ $H_2SO_4$ solution was prepared from $H_2SO_4$ (Merck A. R.) and tridistilled water. In all experiments the solutions were previously saturated with $N_2$ and maintained under this atmosphere during each experiment. The pH and $pSO_4'$ were fixed by solid NaOH and $Na_2SO_4$ additions. For the solutions at $pH > 0$, the pH values were measured with a glassy electrode Corning model 240. The $pSO_4'$ were calculated by using the values of the solid $Na_2SO_4$ addition. For the $1M$ $H_2SO_4$ solution, it is not possible to measure the pH with a glassy electrode; in this case we have simply assumed that $pH < 0$.

The electrochemical studies were performed in a three-electrode cell. The working electrodes were Pt, Au and carbon paste (CP) rotating disk electrodes. Carbon paste electrodes were prepared by mixing Aldrich graphite powder with silicone oil, using a carbon rod as the electric contact. A mercury–mercurous sulfate electrode (MSE) was used as the reference, and a high area graphite rod as the counter electrode. All potentials in this work are given with respect to the normal hydrogen electrode (NHE).

The electronic system consisted of a PAR model 173 Potentiostat-Galvanostat, a PAR model 175 Universal Programmer, a Sefram X–Y Plotter and HP 3478A Multimeter. The spectrophotometric experiments were performed using a UV-Visible Hitachi spectrophotometer model 200.

### *Spectrophotometric measurements*

In order to verify the chemical changes in the Fe(III) coordination sphere predicted by the diagram (Fig. 1a), absorbance studies were carried out as a function of $pSO_4'$. It was not possible to perform such studies for the Fe(II) species, owing to the fact that these species easily oxidize in oxygen-containing aqueous solutions[2] and they present small molar extinction coefficients in aqueous solutions in the UV-Visible region.[6,15]

The UV-Visible spectra of the different Fe(III)–sulfate complexes are similar and they present absorption peaks in the 320–350 nm region.[6,15,16] For this reason it is very difficult to differentiate among these complexes by using this technique. However, it is possible to distinguish between Fe(III)–sulfate complexes and

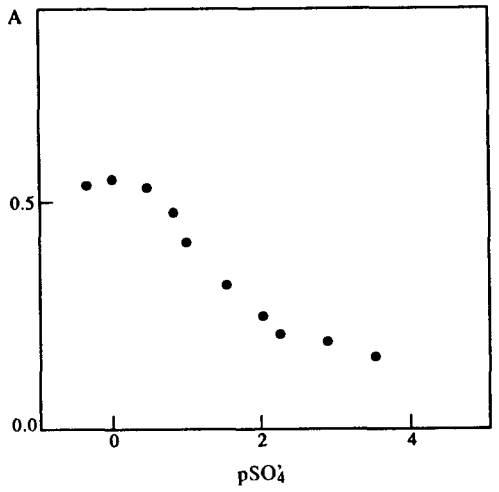


Fig. 3. Variation of absorbance ($\lambda = 318$ nm) as a function of $pSO_4'$, for a solution containing $2 \times 10^{-4} M$ Fe(III) and pH 0.5 (buffered). The sulfate concentration is modified by addition of $Na_2SO_4$.

other Fe(III)–aqueous complexes, because other Fe(III)–aqueous complexes present very small molar extinction coefficients in this region.

The variation of absorbance at $\lambda = 358$ nm as a function of $pSO_4'$ ($pHSO_4$) for pH 0.5 buffered solutions is shown in Fig. 3. The decrease in absorbance with increasing $pSO_4'$ indicates a variation of the coordination sphere of the Fe(III) species even at pH 0.5. Obviously, the absorbance corresponds to the sum of the absorbances of all the Fe(III)–$SO_4$ species in solution. At $pSO_4' < 0.8$, the absorbance is constant and as predicted by the diagrams can be interpreted to be owing to the predominant species $Fe(SO_4)_2^-$.[6,16-18] In the region $0.8 < pSO_4' < 2.2$, the absorbance decreases owing to the decrease in the $Fe(SO_4)_2^-$ molar fraction even though the $FeSO_4^+$ molar fraction increases (predominance of $FeSO_4^+$); this effect is caused by the fact that the $FeSO_4^+$ molar extinction coefficient is lower than that of $Fe(SO_4)_2^-$.[6] For pH > 2.2, the absorbance practically does not change because $Fe^{3+}$ is the predominant chemical species and it absorbs very little at this wavelength (358 nm).[6]

The spectrophotometric behavior of the Fe(III)–sulfate solution is not a definite proof of the presence of the various complexes of Fe(III)–$SO_4$; however, the variation of absorbance with $pSO_4'$ can be predicted by means of the information from Fig. 1a. Figure 1a predicts that $[Fe(SO_4)_2^-] = [FeSO_4^+]$ for pH 0.5 at $pSO_4' = -0.04$, and $[FeSO_4^+] = [Fe^{3+}]$ for pH 0.5 at $pSO_4' = 2.56$. This fact is an indication of the validity of the assumption discussed above, concerning the Fe(III)–$SO_4$ complexes. Unfortunately, the proof of the presence of the different sulfate complexes with iron in aqueous solution is a very difficult task when attempting to use other experimental techniques.

*Voltammetric measurements*

The electrochemical behavior of the Fe(III)/Fe(II) system is predicted by the Pourbaix-type diagram and involves different redox couples of soluble species as a function of pH at buffered $pSO_4'$ (Fig. 2). From the results discussed above, it is clear that pH changes provoke variations in the coordination sphere of Fe(III) but not in that of Fe(II).

According to the selected pH region, four representative electrochemical reactions exist involving soluble species for Fe(II) and Fe(III):

Region I: high acidity
$FeHSO_4^{2+} + 1e^- \rightleftarrows FeHSO_4^+$
Region II: $-0.26 \leqslant pH \leqslant 0.54$
$FeSO_4^+ + H_3O^+ + 1e^- \rightleftarrows FeHSO_4^+ + H_2O$
Region III: $0.54 \leqslant pH \leqslant 1.98$
$Fe(SO_4)_2^- + 2H_3O^+ + 1e^- \rightleftarrows FeHSO_4^+ + HSO_4^+ 2H_2O$
Region IV: $1.98 \leqslant pH \leqslant 4.0$
$Fe(SO_4)_2^- + H_3O^+ + 1e^+ \rightleftarrows FeHSO_4^+ + SO_4^{2-} + H_2O$.

In order to analyze the influence of the change in the coordination sphere of Fe(III) on the electrochemical behavior of the redox couples considered, a voltammetric study of the Fe(III) reduction on stationary disk electrodes was performed at buffered $pSO_4'$ and different values of pH. For this work, two pH regions were chosen: (a) pH < 0 ($1 M$ $H_2SO_4$) and (b) pH > 1. These were selected because they place the system in definite predominance regions of each chemical species (Fe(III): $FeSO_4^+$ and $Fe(SO_4)_2^-$, respectively). Furthermore, since the molar fractions $FeSO_4^+$ and $Fe(SO_4)_2^-$ are similar within the range $0 < pH < 1$, the electrochemical behavior cannot be associated with only one predominant Fe(III) species.

The voltammetric experiments at a stationary electrode (Pt, Au and CP), were carried out at different potential scan rates ($40 < v < 200$ mV/sec) for each pH value. A typical voltammogram obtained for the Fe(III) reduction is shown in Fig. 4. From these curves, cathodic ($E_{pc}$) and anodic ($E_{pa}$) potential peaks and associated currents ($i_c$ and $i_a$) were obtained. The determination of voltammetric parameters was made using stabilized voltammograms (after 3 or 4 cycles). The voltammetric behavior

is similar for different solutions whose pH falls in the same pH region.

Figure 5 shows the variation of $(E_{pa} - E_{pc}) = \Delta E_p$ as a function of $\ln v$ (sweep rate) for the three electrodes used in this work, for the electrochemical process of Fe(III)/Fe(II) in $1M$ $H_2SO_4$.

For both pH regions, $\Delta E_p$ changes with electrode material[19] at the same pH and sweep rate, this means that the heterogeneous rate constant ($\kappa_s$) for Fe(III)/Fe(II) processes is different on each electrode. This fact indicates that the electron transfer of Fe(III)/Fe(II) in sulfuric acid media performed by an "inner Helmholtz layer mechanism"[19] as has been evidenced by other authors.[3,5] The variation of $\Delta E_p$ with the scan rate[20] become more important in solutions at higher pH values. The $\kappa_s$ values could be calculated from the variation of $\Delta E_p$ with scan rate, however it is not possible to attempt this in the scan rate range considered in this work.

On the other hand, the $(E_{pa} + E_{pc})/2$ (generally associated with $E^0$) does not vary with scan rate, and its value is practically independent of the electrode material in solutions with pH < 0. Meanwhile, $(E_{pa} + E_{pc})/2$ varies markedly with the scan rate, and depends on the electrode material in solutions with pH > 1. These facts indicate that the kinetic mechanisms are different in the two pH regions, probably owing to the different predominant species of Fe(III).

Anson[3] reported that the decrease in $\kappa_s$ when the pH increase in sulfate medium is mainly a result of the formation of sulfate complexes with lower exchange current densities. However, Anson has not identified the sulfate complexes involved in the redox mechanism.

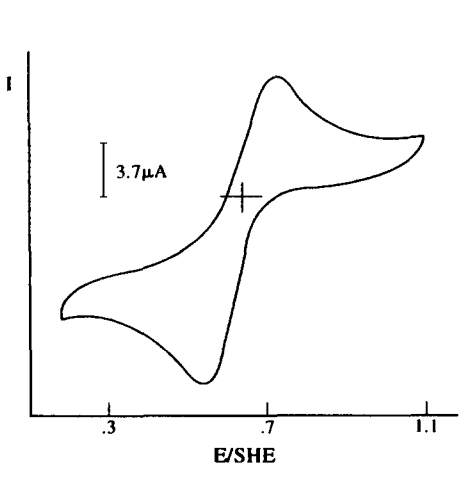


Fig. 4. Typical voltammogram for reduction of Fe(III) in $1M$ $H_2SO_4$ on platinum disk electrode, sweep rate 25 mV/sec.

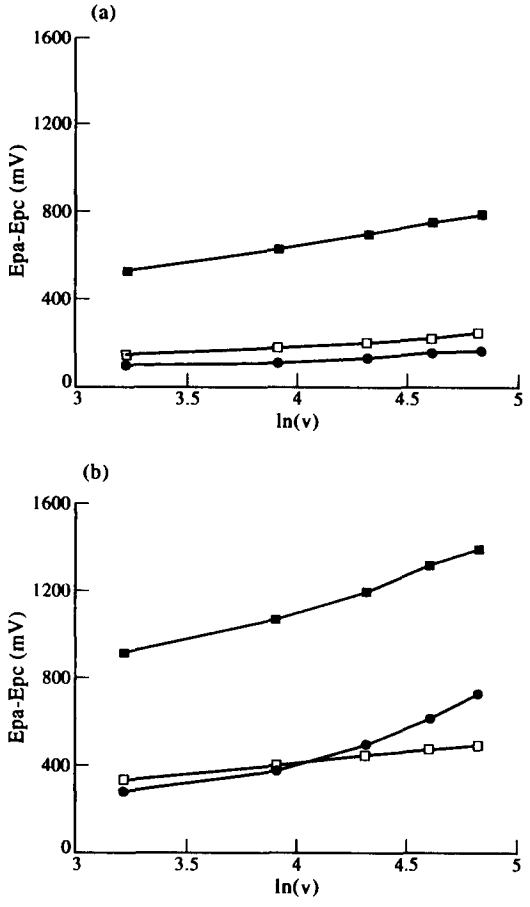


Fig. 5. The variation $E_{pa} - E_{pc}$ as a function of the scan rate potential ($\ln v$) for the Fe(III)/Fe(II) system from voltammetric curves obtained in different disc electrodes: (●) gold, (□) platinum and (■) carbon paste electrode. The electrolytic solution is $1M$ $H_2SO_4$ at different pH: (a) pH < 0, (b) pH > 1.

Figure 6 shows a typical variation of $i_a/i_c$ ratio as a function of $\log v$. For pH < 0 (Fig. 6a) the $i_a/i_c$ ratio varies smoothly with scan rate ($v$), and is essentially equal to unity for the Pt, Au and CP electrodes in the scan rate range considered. However, for pH > 1, the $i_a/i_c$ ratio is different to one, and varies in a distinct manner for Pt, Au and CP electrodes. The electron transfer at pH < 0 is performed between $FeSO_4^+/FeHSO_4^+$; meanwhile, at pH > 1 the couple $Fe(SO_4)_2^-/FeHSO_4^+$ is involved in the process. When the number of sulfate ligands associated with Fe(III) and Fe(II) is the same, the electrochemical behavior is typical of an inner Helmholtz layer mechanism. However, when the number of sulfate ligands is different in Fe(III) and Fe(II), the adsorption processes of Fe(III) inside the inner Helmholtz plane and the rearrangement of Fe(III) complexes are very different to those occurred at pH < 0. These facts are evidenced

by the kinetical complication observed in Fig. 6b.

These differences in electrochemical behavior with pH for the Fe(III) reduction may be attributed to the presence of different chemical species of Fe(III) in solution. The voltammetric results are not complete enough to establish the redox mechanism; however, it is possible to observe the modification in the electron transfer mechanism with the change in the pH of the solution.

Considering that electron transfer between Fe(III) and Fe(II) occurs by an inner Helmholtz layer mechanism, the chemical species involved in the mechanism would have the same coordination sphere; this is the case for the solution at pH < 0 here the predominant species are: ($FeSO_4^+$/$FeHSO_4^+$). Meanwhile, the different coordination numbers of Fe(III) and Fe(II) in the region pH > 1 here, the predominant species are: ($Fe(SO_4)_2^-$/$FeHSO_4^+$) may be related to the chemical complication observed in the voltammetric studies.

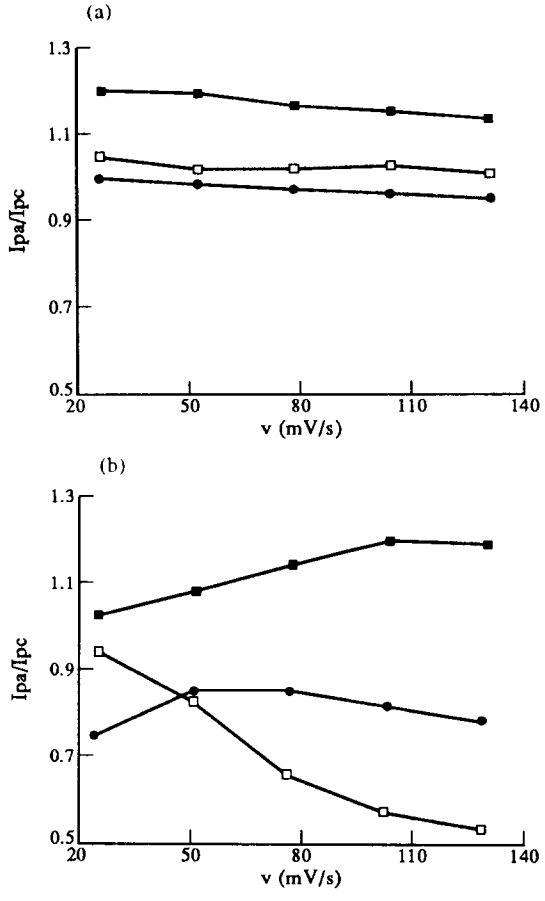


Fig. 6. The variation of the anodic–cathodic peak current ratio ($i_a/i_c$) as a function of the potential scan rate ($v$) for the Fe(III)/Fe(II) system from voltammetric curves obtained in different disc electrodes: (●) gold, (□) platinum and (■) carbon paste electrode. The electrolytic solution is 1*M* $H_2SO_4$ at different pH: (a) pH < 0, (b) pH > 1.

## CONCLUSIONS

A method based on the concept of generalized species and equilibria is used to represent the thermodynamic distribution of Fe(III) and Fe(II) species. The diagrams thus generated facilitate the selection of experimental parameters in order to establish specific equilibrium conditions. On the other hand, this selection permits a more realistic interpretation of the experimental results in complicated systems, similar to the one presented in this work.

This study permitted the selection of optimum experimental conditions since it is possible to identify different chemical species of Fe(III) and Fe(II) and of the redox couples Fe(III)/Fe(II). The spectrophotometric results showed the existence of the different chemical species for Fe(III) in the range of $0 < pSO_4' < 4$. In a similar manner, the electrochemical studies confirmed that the electron exchange transfer occurs by an inner sphere mechanism because the electrochemical behavior is different for the three electrodes used. Other authors have observed this behavior,[5] although to the best of our knowledge none has proposed that the iron–sulfate complexes are involved in the mechanism.

The electrochemical reduction of Fe(III) in $H_2SO_4$ was found to be complicated owing to the presence of different complexes on the electrode surface as a function of pH.

*Acknowledgements*—This work was funded by CONACYT (Mexico), A. F. Gil acknowledges the scholarship (No. GIMA 65022BIL92) granted by SRE (Mexico). We acknowledge Dr J. G. Ibañez for the English corrections.

## REFERENCES

1. C. M. Flyn Jr., *Chem. Rev.*, 1984, **84**, 31.
2. Z. Galus and R. N. Adams, *J. Phys. Chem.*, 1963, **67**, 866.
3. F. C. Anson, *Anal. Chem.*, 1961, **33**, 939.
4. R. S. Sapiesko, R. C. Patel and E. Matijevic, *J. Phys. Chem.*, 1977, **81**, 1061.
5. D. H. Angell and T. Dickinson, *J. Electroanal. Chem.*, 1972, **35**, 55.
6. C. F. Wells and M. A. Salam, *Nature*, 1964, **203**, 751.
7. R. Duo, M. S. Lorenzo, P. Cañas and R. Celdran, *J. Electroanal. Chem.*, 1988, **250**, 321.
8. H. G. Bockman and W. Vielstich, *Electrochim. Acta*, 1988, **33**, 805.
9. R. M. Smith and A. E. Martell, *Critical Stability Constants*, Vol. 4. Plenum Press, New York, 1979.

10. E. Högfeldt, *Stability Constants of Metal–Ion Complexes*, Part A, *Inorganic Ligands*. IUPAC Chemical Data Series, No. 21, Pergamon Press, New York, 1979.
11. A. Rojas and I González, *Anal. Chim. Acta*, 1986, **187,** 279.
12. A. Rojas-Hernández, M. T. Ramírez, J. G. Ibáñez and I. González, *Anal. Chim. Acta*, 1991, **246,** 4351.
13. A. Rojas-Hernández, M. T. Ramírez, J. G. Ibáñez and I. González, *J. Electrochem. Soc.*, 1991, **138,** 365.
14. A. Rojas-Hernández, M. T. Ramírez and I González, *Anal. Chim. Acta*, 1993, **278,** 321.
15. R. L. Willix, *Trans Faraday Soc.*, 1963, **59,** 1315.
16. R. A. Whiteker and N. Davidson, *J. Am. Chem. Soc.*, 1953, **75,** 3081.
17. I.González, L. Galicia, A. Rojas, M. A. Quiroz and Y. Meas, Proceedings of 38th ISE Meeting, Maastricht, Netherlands, p. 354, 1987.
18. L. Galicia, I. González, Y. Meas and J. G. Ibáñez, *Electrochim. Acta*, 1990, **31,** 209.
19. R. S. Nicholson, *Anal. Chem.*, 1985, **11,** 1351.
20. E. J. Calvo, *Comprehensive Chemical Kinetics*, C. H. Bamford and R. G. Compton (eds), Vol. 26, Chap. 1, pp. 1–78. Elsevier, Amsterdam, 1986.

Pergamon

0039-9140(95)01425-X

*Talanta*, Vol. 42, No. 3, pp. 415–422, 1995

0039-9140/95 $9.50 + 0.00

# HIGH PERFORMANCE LIQUID CHROMATOGRAPHIC DETERMINATION OF ALUMINIUM IN NATURAL WATERS IN THE FORM OF ITS LUMOGALLION CHELATE

CHAO YAN ZHOU,[1] JUN WU,[1] HUA CHI,[1] MING KEONG WONG,[1]* LIP LIN KOH[1] and YEOW CHIN WEE[2]

[1]Department of Chemistry, National University of Singapore, Lower Kent Ridge Road, Singapore 0511
[2]Department of Botany, National University of Singapore, Lower Kent Ridge Road, Singapore 0511

(*Received* 1 *June* 1994. *Revised* 16 *September* 1994. *Accepted* 23 *September* 1994)

**Summary**—A high performance liquid chromatographic method for the determination of ultra trace amount of aluminium in natural waters has been developed using lumogallion as a precolumn reagent for fluorimetric detection. The highly fluorescent Al–lumogallion chelate ($\lambda_{ex}$ 500 nm, $\lambda_{em}$ 574 nm) was separated on a LiChrosorb RP 18 column with an eluent containing 3:7 acetonitrile/0.02*M* potassium hydrogen phthalate buffer (pH 4.7) containing $10^{-5}M$ lumogallion. The proposed system provides a simple, quick, selective and sensitive method for the determination of ultra-trace amount of aluminium in water samples. The detection limit defined as three times the standard deviation of the blank signal, was 0.05 $\mu$g/l. in water samples for 100 $\mu$l injection. The tolerance limits were 5 mg/l. for Fe(III) and $F^-$ and over 10 mg/l. for other foreign ions. The sensitivity of the method was independent of salinity. This method had been used for the direct determination of aluminium in both tap and coastal sea-waters without any preconcentration steps.

Aluminium was until recently believed to be relatively harmless, but evidence has grown to implicate it in a variety of potential toxicity in man.[1,2] Al is a minor component of natural water, its typical levels range from 0.5 to 140 $\mu$g/l.[3–5] There is thus an urgent need for the development of sensitive techniques to measure Al in low concentrations. So far, literature values for trace Al in natural waters are relatively scarce. This is mainly owing to analytical difficulties. The most commonly used analytical techniques are graphite furnace atomic absorption spectrometry (GF-AAS) and inductively coupled plasma atomic emission spectrometry (ICP-AES). The detection limits of these methods are about 1 $\mu$g/l., but their precision is poor in this range.[6–8]

The use of high performance liquid chromatographic (HPLC) separation and determination of Al in the form of chelates have been gaining popularity in recent years.[9–13] Spectrophotometric and electrochemical detections are most widely used in HPLC systems for the detection of Al chelates. However, they have poor performance at the $\mu$g/l. level.[9,10,13] Uehara *et al.*[12] recommended salicylaldehydebenzoylhydrazone (SAB) as a precolumn reagent. As SAB forms a chelate with Al, which is sensitive to fluorimetric detection, the detection limit for Al was reported to be 40 pg/ml in a 100 $\mu$l injection. Unfortunately, SAB is not commercially available and the synthesis and purification are inevitable. The success of the SAB method led us to conduct a systematic study on commercially available precolumn reagents for the HPLC analysis of Al with highly sensitive fluorimetric detection.

Fluorimetric analyses of Al with lumogallion as a chelating reagent have gained widespread acceptance.[14–17] Lumogallion has the advantages of high reaction ability, short reaction time, the formation of a stable resolvable chelate with Al at pH 4–5 and the chelate has high sensitivity for fluorimetric detection. However, in those normal fluorimetric analyses of Al using lumogallion as the chelating reagent,[15,17] the interferences from Fe(III) and $F^-$ are appreciable. Thus it was thought that combining HPLC with fluorimetric detection would provide a good solution to the problem. Different metal–lumo-

*Author to whom correspondence should be addressed.

gallion chelates in a sample solution can be separated with HPLC and thus the interferences in Al fluorimetric analyses can be eliminated and the low detection limit of fluorescence method can be achieved.

The aim of the present study is to develop a simple, selective and sensitive HPLC method for the determination of Al using fluorimetric and spectrophotometric detections with lumogallion as a precolumn reagent. The method was applied to the direct determination of Al at sub-ppb level in tap and coastal sea-waters.

## EXPERIMENTAL

### *Reagents and solutions*

The sodium hydroxide pellets from BDH (UK) were of "Aristar" 98.0% grade. All the chemicals used were of analytical reagent grade, unless otherwise indicated. Throughout the study, all glass and polypropylene apparatus were washed with 5% nitric acid and deionized distilled water.

Stock standard aluminium solution containing 1000 mg/l. Al in aluminium nitrate form for atomic absorption spectrometry was bought from BDH. All working standard Al solutions were prepared by serial immediate dilution with 0.2% nitric acid solution. Lumogallion was bought from Tokyo Kasei Kogyo Co. Ltd (Japan) and its solution (0.1 w/v %) was prepared by dissolving 0.1 g of the solid in 100 ml deionized distilled water. Potassium hydrogen phthalate (from BDH) solution (0.2*M*) was obtained by adding 1.02 g of the reagent into 50 ml deionized distilled water. The buffer solution was prepared by dissolving 2.04 g potassium hydrogen phthalate and 0.0017 g lumogallion in 500 ml deionized distilled water and the pH of the solution was adjusted to 4.7 with 1*M* NaOH solution.

### *Apparatus*

HPLC analysis was performed on a Waters Powerline™ HPLC system, including a Waters 600E Multisolvent Delivery System Controller, a Waters 470 Scanning Fluorescence Detector, a Waters 486 Tunable Absorbance Detector, a Waters 700 Satellite WISP™ Autosampler. The Waters Maxima™ 825 HPLC software was used for qualification. A LiChrosorb RP18 10 $\mu$ (25 cm × 4.6 mm i.d.) column from Hichrom Limited (U.K.) was used for the separation.

### *Pretreatment of water sample*

Tap water from the Singapore tap water supply system and coastal sea-water collected from the west coast of Singapore were treated by the following two procedures:[18,19] (A) for the determination of original dissolved Al: after collection, the samples were filtered immediately with cellulose filter (Millipore), pore size 0.45 $\mu$m, and then stored in polypropylene bottle at room temperature and analyzed within one week; (B) for the determination of dissolved Al after acid treatment: after collection, the pH of the sample was immediately adjusted to 1.5 by adding an appropriate amount of hydrochloric acid and the sample filtered with the cellulose filter prior to analysis. The samples were stored in polypropylene container.

### *Analytical procedure*

Pretreated water sample (5 ml) was transferred into a 10 ml polypropylene test tube, and 1 ml of 0.2*M* potassium hydrogen phthalate solution was added. After the pH of the mixture was adjusted to 4.7 by adding an appropriate amount of 1*M* NaOH solution, 0.5 ml of 0.1 w/v % lumogallion solution was added and the volume of the solution made up to 10 ml with deionized distilled water. The mixture was left at room temperature (about 25°C) for 15 min, then a 100 $\mu$l aliquot of the solution was injected into the HPLC.

## RESULTS AND DISCUSSION

### *Detection wavelengths*

Lumogallion reacted readily with Al ion. The UV absorption spectra of lumogallion and its Al chelate in a buffer solution at pH 4.7 are shown in Fig. 1. Lumogallion and its Al chelate gave maximum absorption at around 410 nm. However, the absorption maximum of the chelate was shifted slightly towards longer wavelength. After background subtraction, which was obtained by placing the solution containing lumogallion in the reference cell and the solution containing the chelate in the sample cell, a maximum absorbance related to the chelate appeared at 497 nm. The fluorescence spectra of the chelate and lumogallion are shown in Fig. 2. The optimum excitation and emission wavelengths of the Al-lumogallion chelate were found to be 500 and 574 nm. These wavelengths were used in later experiments.

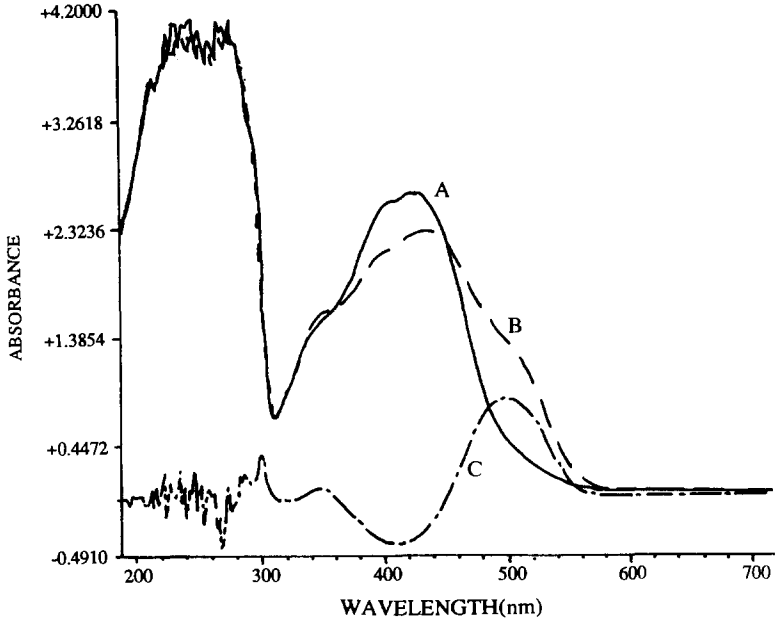


Fig. 1. The UV spectra of: (A) lumogallion; (B) Al–lumogallion chelate; (C) Al–lumogallion chelate with background correction. For A, a buffer solution containing 0.02*M* potassium hydrogen phthalate adjusted to pH 4.7 was used in the reference cell and the buffer solution spiked with 0.005% lumogallion was used in the sample cell; for **B**, the buffer solution in the reference cell and the buffer solution spiked with 0.005% lumogallion and 500 $\mu$g/l. of Al in the sample cell; for C, the buffer solution spiked with 0.005% lumogallion was used in the reference cell and the buffer solution spiked with Al (500 $\mu$g/l.) and lumogallion (0.005%) was used in the sample cell.

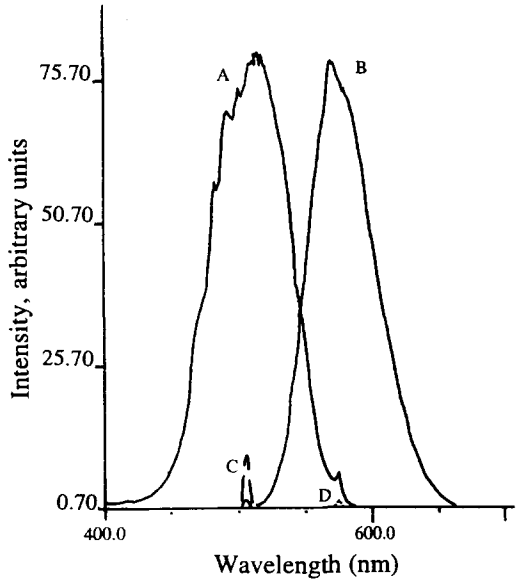


Fig. 2. The fluorescence spectra of 0.005% lumogallion solution containing 0.02*M* potassium hydrogen phthalate at pH 4.7 and the chelate solution containing Al (500 $\mu$g/l.), lumogallion (0.005%) and 0.02*M* potassium hydrogen phthalate at pH 4.7. (A) The excitation spectrum of the chelate solution with emission at 574 nm; (B) the emission spectrum of the chelate solution with excitation at 505 nm; (C) the excitation spectrum of lumogallion solution with emission at 574 nm; (D) the emission spectrum of lumogallion solution with excitation at 505 nm.

*Effects of reaction pH, temperature and time*

For the formation of the Al–lumogallion chelate, optimum pH values were reported to be from 3.8 to 5.0[14-16] Our experimental results were in agreement with the reported pH range. A pH value of 4.7 was chosen in later experiments. The effects of reaction time and temperature in the formation of the chelate were also studied. Following normal analytical procedures, samples containing 20 $\mu$g/l. of Al were prepared, then heated immediately in water bath set at different temperatures for 15 min and then analyzed. Results are shown in Table 1. From Table 1, it is seen that temperature had little effect on the formation of the chelate. For subsequent experiments, 25°C (room temperature) was used. When the temperature was fixed at 25°C, a sample containing 20 $\mu$g/l. of Al was prepared and then analyzed several times within 24 hr. According to the results shown in Table 2, the reaction of Al with lumogallion was completed in 15 min at room temperature and the chelate was stable for at least 24 hr.

*Chromatogram*

The typical chromatograms obtained from a serial injections of the solutions containing

Table 1. Effect of temperature on the formation of the chelate

| $T$ (°C) | 25 | 40 | 50 | 60 | 70 | 80 | 90 |
|---|---|---|---|---|---|---|---|
| Peak height† | 22.7 | 23.4 | 23.8 | 23.9 | 22.1 | 22.8 | 23.2 |

*The water bath temperature.

†The peak height in fluorimetric detection, unit, $10^3$ $\mu$V. Conditions: Al concentration 20 $\mu$g/l., pH 4.7, 0.02$M$ potassium hydrogen phthalate, 0.005% lumogallion; column, Lichrosorb RP 18; mobile phase, 30% acetonitrile and 70% aqueous containing 0.02$M$ potassium hydrogen phthalate, $10^{-5}M$ lumogallion; flow rate, 1.0 ml/min; detection, 500 nm and 574 nm for excitation and emission in fluorimetric detection; injection, 100 $\mu$l.

different Al concentrations are shown in Fig. 3. In the initial study, methanol and acetonitrile were added to the buffer solution as an eluent to separate the chelate and ligand. When methanol was used, poor separation of chelate and ligand was obtained. Addition of acetonitrile to the buffer solution improved the separation. In order to obtain a good separation of the compounds and to save the analysis time, a mobile phase containing 70% buffer and 30% acetonitrile was chosen in the later experiments. Under this condition, potassium hydrogen phthalate, Al–lumogallion chelate and the ligand are well separated as shown in Fig. 4.

*Linear range, precision and detection limit*

In the fluorimetric detection mode, both peak area and peak height of the chelate are increased linearly up to 500 $\mu$g/l. The repeatability (RSD) of the method was 2.43% for six replicate analyses of 50 $\mu$g/l. Al solution. The detection limit (taken as the concentration equivalent to three times the standard deviation of the blank) was 0.05 $\mu$g/l. for fluorimetric detection. Even with UV detection (at 497 nm), the detection limit was 0.3 $\mu$g/l. It was easy to quantify the Al concentration by the peak height method in fluorimetric detection at high concentration level. However, at low concentration level, the peak area method was found to be more accurate. The major sources of extraneous Al were glassware or other containers, reagents and solvents used. It was widely suggested that in the determination of ultra-trace Al, the use of glassware was to be avoided.[3,12,14,15] In our procedure, polypropylene apparatuses were used. Thus the main contamination sources were from reagents, potassium hydrogen phthalate was chosen to prepare the buffer solution. The pH of its solution was 3.9, hence only a small amount of sodium hydroxide solution was needed to adjust the pH to 4.7. In procedure A, the sample solution was filtered without any addition of other chemicals, and the blanks were found to be around 0.02 $\mu$g/l. While in procedure B, higher blank values were obtained around $\mu$g/l. which were caused by extraneous Al from added chemicals.

*Effects of foreign substances*

Iron is known to interfere with the standard lumogallion procedures[15,17] for fluorimetric analysis even at the $\mu$g/l. level. Experiments were, therefore, carried out to assess whether it remained so in the present method. Standard solutions containing 50 $\mu$g/l. of Al were spiked with Fe(III) at levels from 0 to 10 mg/l. and then analyzed. The results are listed in Table 3. When the concentration of Fe(III) reached 0.5 mg/l., the color of the solution changed from light yellow to light brown and the color became deeper with the increase of Fe(III) concentration. As shown in Fig. 5, the chromatogram obtained from UV detection method was influenced strongly and the lumogallion peak was very low, indicating that the Fe(III) in the solution consumed most of the free lumogallion ligand. However, the chromatogram from fluorimetric detection did not change until Fe(III) concentration was over 5 mg/l. The results indicate that Al–lumogallion chelate is more stable than Fe(III)–lumogallion chelate and the two chelates are separated by HPLC.

Table 2. Effect of reaction time on the formation of the chelate

| Reaction time* | 5 min | 15 min | 20 min | 35 min | 50 min | 24 hr |
|---|---|---|---|---|---|---|
| Peak height† | 22.1 | 22.8 | 21.2 | 22.6 | 22.4 | 23.1 |

*At 25 C.

†The peak height in fluorimetric detection, unit, $10^3$ $\mu$V. Other conditions as in Table 1.

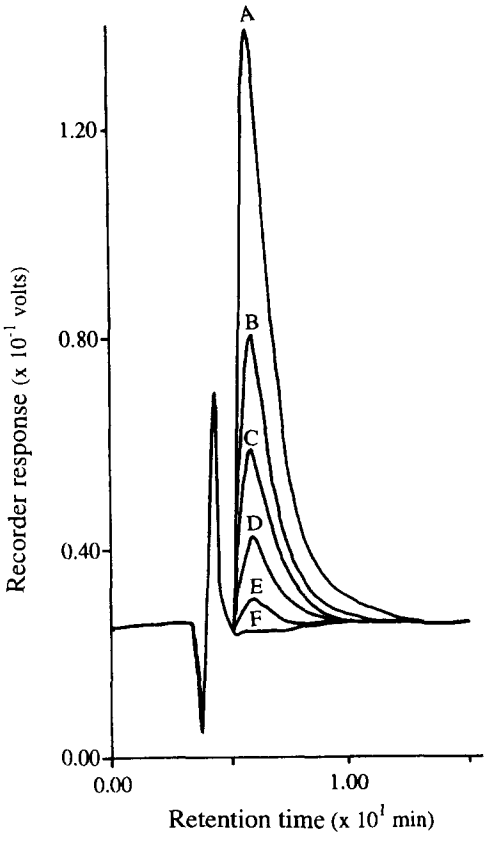


Fig. 3. Typical chromatograms of fluorimetric detection with different Al concentrations: (A) 200 $\mu$g/l.; (B) 100 $\mu$g/l.; (C) 60 $\mu$g/l.; (D) 30 $\mu$g/l.; (E) 10 $\mu$g/l. and (F) 0 $\mu$g/l. The chelate was formed in the solution at pH 4.7 containing 0.02*M* potassium hydrogen phthalate and 0.005% lumogallion; column, Lichrosorb RP 18; mobile phase, 30% acetonitrile and 70% aqueous containing 0.02*M* potassium hydrogen phthalate and $10^{-5}$*M* lumogallion; flow-rate, 1.0 ml/min; detection, 500 nm and 574 nm for excitation and emission in fluorescence detection; injection, 100 $\mu$l.

The second known interference in the conventional fluorimetric assay is that of fluoride.[15,17] Standard solutions of Al (50 $\mu$g/l.) were spiked with fluoride at levels from 0 to 10 mg/l. and analyzed according to the recommended procedure. The results are given in Table 4, which indicated that at below 5 mg/l., fluoride did not interfere with the Al analysis.

Other common metal ions in natural waters such as Ni(II), Co(II), Zn(II), Sn(II), Cu(II), Mo(VI), Pb(II) were also studied. The ions did not interfere in the proposed method at under 10 mg/l. level. Na(I), Mg(II), K(I) and Ca(II) did not interfere with the Al analysis at concentrations present in sea-water. The interferences of foreign ions in the proposed method were 10 times lower than those in fluorimetric methods with lumogallion. Potential interferences from diverse metal ions present in large excess are thought to be caused by the consumption of lumogallion reagent under precolumn derivatization conditions rather than by peak overlap. Such interferences can be overcome by adding sufficient amount of lumogallion, or by diluting the sample prior to derivatization. In the present method, lumogallion was used at a higher concentration than that used in the fluorimetric methods[15,17] in order to eliminate the interference from salts present in natural water samples. The linear range was also increased in the proposed method.

*Practical application*

The proposed method had been successfully applied to the determination of Al in fresh- and sea-water samples. Table 5 summarizes the results obtained by our proposed method and the GF-AAS method for water samples, and samples spiked with the metal standards to ascertain the validity of the analytical data. The good recovery of the spiked Al ion indicates that the procedure is valid.

Sample pretreatment methods would normally influence the final analytical results.[10,18-20] In procedure A, the concentrations of Al in the water samples were at the ppb level, hence the results were obtained by measuring the peak areas and the standard addition method was used. The results are shown in Fig. 6. The concentration values obtained from procedure A represent the original dissolved Al that could form chelate with lumogallion without acid treatment. The Al concentrations obtained from procedure B correspond to the dissolved Al in water after acid treatment. Hence the Al concentrations would include original dissolved Al and Al from particles and colloids which was released during acid treatment. Typical HPLC chromatograms of the tap water, sea-water and their spiked samples from procedure B are

Table 3. Effect of Fe(III) on the aluminium analysis

| [Fe]* | 0 | 0.1 | 0.5 | 2.0 | 5.0 | 10.0 |
|---|---|---|---|---|---|---|
| Peak height† | 48.6 | 47.4 | 46.9 | 47.2 | 48.3 | 33.7 |

*The concentration of Fe(III) added to Al solution, unit, mg/l.
†The peak height in fluorimetric detection, unit, $10^3$ $\mu$V. Al concentration, 50 $\mu$g/l. Other conditions as in Table 1.

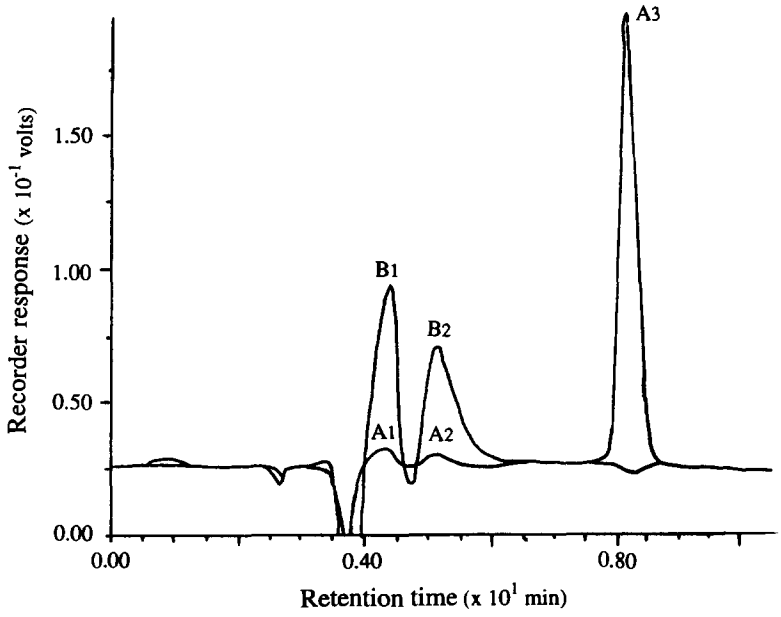


Fig. 4. The chromatograms of UV (at 497 nm) and fluorimetric detections using standard methods for the analysis of Al with Al concentration at 50 μg/l. Other conditions as in Fig. 3. (A1) The peak of potassium hydrogen phthalate; (A2) the peak of Al–lumogallion chelate; (A3) the lumogallion peak in the chromatogram of UV detection at 497 nm. (B1) The peak of potassium hydrogen phthalate; (B2) the peak of Al–lumogallion chelate in the chromatogram of fluorimetric detection.

shown in Fig. 7. Our data (Table 5) show that the proposed HPLC method can be used successfully to determine Al in natural water samples and that there is no interference from matrixes such as alkali and alkaline-earth metals in sea-water. The recoveries of the proposed method were 100 and 96% for tap water and sea-water samples. The results from GF-AAS and the proposed HPLC method were in agreement for tap water and its spiked samples.

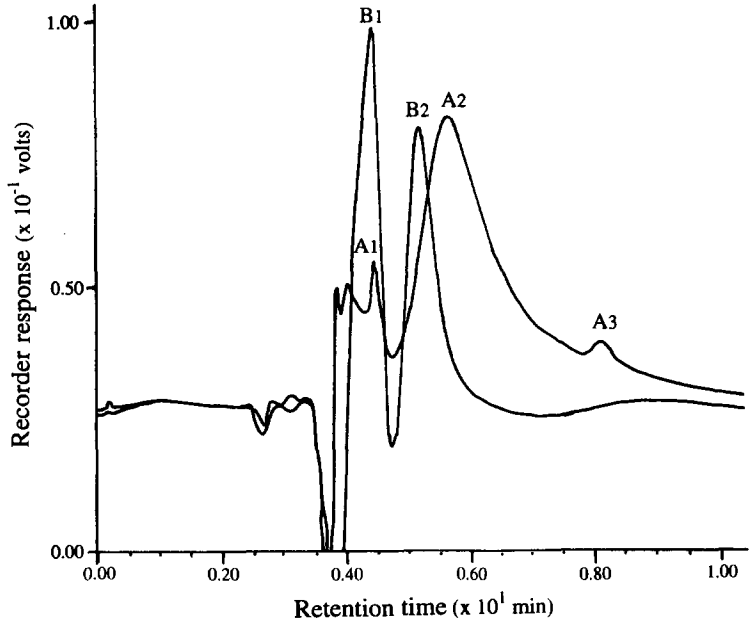


Fig. 5. The chromatograms of UV (at 497 nm) and fluorimetric detections in the presence of Fe(III). These chromatograms were obtained by using a sample containing 50 μg/l. Al and 5 mg/l. Fe(III). Analytical conditions as given in Fig. 3. (A1) The peak of potassium hydrogen phthalate; (A2) the peak of Fe–lumogallion chelate; (A3) the peak of lumogallion in the chromatogram of UV detection at 497 nm. (B1) The peak of potassium hydrogen phthalate; (B2) the peak of Al–lumogallion chelate in the chromatogram of fluorimetric detection.

Table 4. Effect of $F^-$ on the aluminium analysis

| [$F^-$]* | 0.0 | 0.1 | 0.5 | 2.0 | 5.0 | 10.0 |
|---|---|---|---|---|---|---|
| Peak height† | 46.7 | 47.1 | 48.3 | 47.6 | 48.2 | 43.4 |

*The concentration of $F^-$ added to Al solution, unit, mg/l.
The peak height in fluorimetric detection, unit, $10^3$ $\mu$V. Al concentration, 50 $\mu$g/l. Other conditions as in Table 1.

Table 5. Determination of Al in water samples ($\mu$g/l.)

| Procedure | Sample | HPLC | GFAAS |
|---|---|---|---|
| A | Tap water | $5 \pm 0.5$* | |
| A | Sea-water | $0.6 \pm 0.1$* | |
| B† | Tap water | $28 \pm 1.2$ | $28 \pm 1.5$ |
| B† | Tap water + 100 $\mu$g/l. Al(III) | $128 \pm 2.8$ | $130 \pm 3.0$ |
| B† | Sea-water | $210 \pm 4.0$ | $250 \pm 14$ |
| B† | Sea-water + 100 $\mu$g/l. Al(III) | $306 \pm 5.3$ | $320 \pm 16$ |

*The values were obtained from standard addition method.
†The values were obtained from average of four measurements.
The analytical conditions of HPLC method as in Fig. 3.

However, differences were found in sea-water and its spiked samples. Higher values of Al concentration were found in sea-water and its spiked samples by the GF-AAS method compared with that from the HPLC method. Owing to the high salt content in sea-water, the background correction used in GF-AAS may not be able to compensate completely for the background contribution.

## CONCLUSIONS

Lumogallion is a commercially available reagent which reacts cleanly with aluminium, forming a stable and highly fluorescent complex. These characteristics permit the use of lumogallion in the determination of Al in ultra-trace levels. Coupled with HPLC, which functions as a clean-up procedure, interferences from other ions are eliminated. The technique permits trace analysis of aluminium in sub-ppb to 500 ppb level in both fresh and saline waters. The complicated procedures, such as preseparation and matrix-matching that are otherwise needed for the removal of matrix effects are thus eliminated. The proposed method may also be applicable to clinical, environmental and industrial analyses.

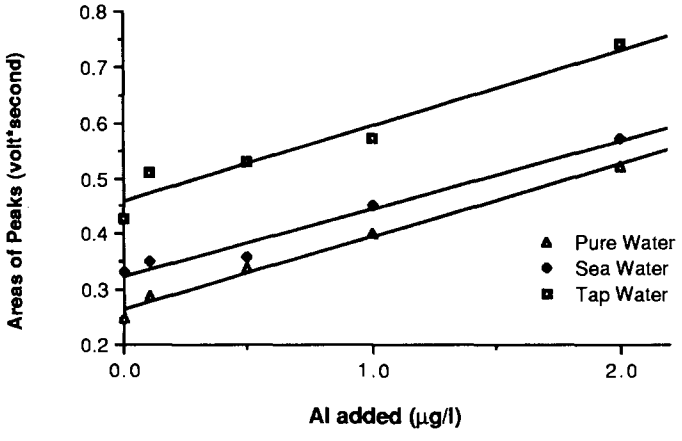


Fig. 6. Standard addition method for Al determination in tap water, sea water and deionized distilled water (pure water) using the sample pretreatment procedure A. Analytical conditions as given in Fig. 3.

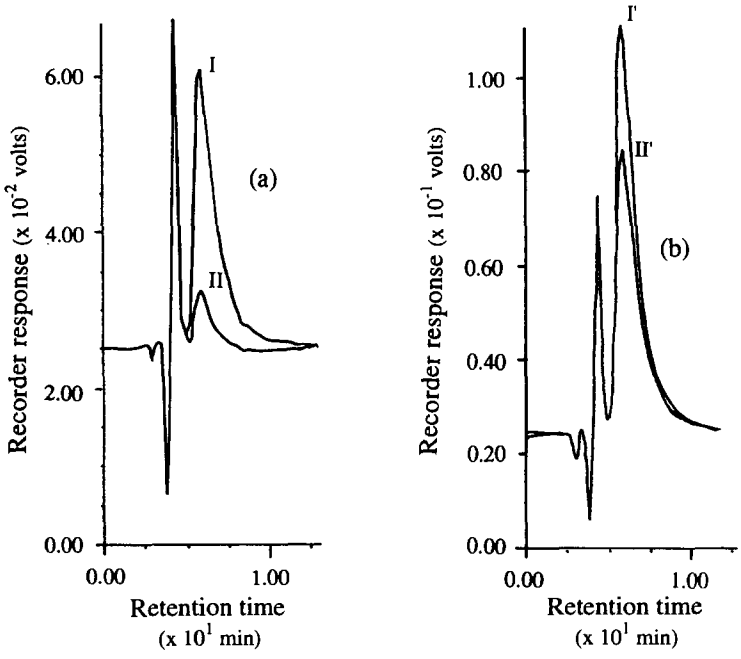


Fig. 7. Typical chromatograms for the determination of Al in (a) tap water samples and (b) coastal sea-water samples. The samples were pretreated by procedure B. In (a): I, the peak of Al–lumogallion chelate in the tap water sample spiked with Al 100 μg/l.; II, the peak of the chelate in the tapwater sample. In (b): I′, the peak of the chelate in the coastal sea-water sample spiked with Al 100 μg/l.: II′, the peak of the chelate in coastal sea-water sample. Other conditions as given in Fig. 3.

*Acknowledgements*—The authors thank the National University of Singapore for financial support and are grateful to Ms Frances Lee for technical assistance.

## REFERENCES

1. H. J. Gitelman, *Aluminum and Health. A Critical Review*. Marcel Dekker, New York, 1988.
2. R. Massey and D. Taylor, *Aluminum in Food and the Environment*, pp. 6–39. Royal Society of Chemistry, London, 1988.
3. D. J. Hydes and P. S. Liss, *Estuar. Coast. Mar. Sci.*, 1977, **5,** 755.
4. J. J. Alberts, D. E. Leyden and T. A. Patterson, *Mar. Chem.*, 1976, **4,** 51.
5. R. J. Gibbs, *Geochim. Cosmochim. Acta*, 1972, **36,** 1061.
6. K. B. Pierson and M. A. Evenson, *Anal. Chem.*, 1986, **58,** 1744.
7. J. R. Andersen and S. Reimert, *Analyst*, 1986, **111,** 657.
8. S. Hirata, Y. Umezaki and M. Ikeda, *Anal. Chem.*, 1986, **58,** 2602.
9. E. Kaneko, H. Hoshino, T. Yotsuyanagi, N. Gunji, M. Sato, T. Kikuta and M. Yuasa, *Anal. Chem.*, 1991, **63,** 2219.
10. Y. Nagaosa, H. Kawabe and A. M. Bond, *Anal. Chem.*, 1991, **63,** 28.
11. Y. Akama and A. Tong, *J. Chromatogr.*, 1993, **633,** 129.
12. N. Uehara, M. Kanbayashi, H. Hoshino and T. Yotsuyanagi, *Talanta*, 1989, **36,** 1031.
13. E. Kaneko, H. Hoshino, T. Yotsuyanagi, R. Watabe and T. Seki, *Bull. Chem. Soc. Jpn*, 1992, **65,** 3192.
14. Y. Suzuki, S. Imai and T. Kamiki, *Analyst*, 1989, **114,** 839.
15. A. G. Howard, A. J. Coxhead, I. A. Potter and A. P. Watt, *Analyst*, 1986, **111,** 1379.
16. D. J. Hydes and P. S. Liss, *Analyst*, 1976, **101,** 922.
17. T. Shigematsu, Y. Nishikawa, K. Hiraki and N. Nagano, *Bunseki Kagaku*, 1970, **19,** 551.
18. A. Ashton and R. Chen, *Analyst*, 1987, **112,** 841.
19. *Methods of Chemical Analysis of Waters and Wastes*. United States Environmental Protection Agency, Cincinnati, OH, 1971.
20. T. Fukasawa, S. Kawakubo and S. Yamamoto, *Nippon Kaisui Gakkaishi*, 1990, **44,** 334.

Pergamon

0039-9140(95)01426-8

*Talanta*, Vol. 42, No. 3, pp. 423–429, 1995

0039-9140/95 $9.50 + 0.00

# OPTIMAL ACIDITY OF COMPLEXES BY SOLUTION OF POLYNOMIALS AND BY ITERATION

B. W. BUDESINSKY*

Department of Chemistry, University of Arizona, Tucson, AZ 85721, U.S.A.

(*Received* 21 *June* 1994. *Revised* 2 *September* 1994. *Accepted* 13 *September* 1994)

**Summary**—The methods for optimal acidity of complexes $M_xL_y(OH)_mH_n$ based on direct iteration or solution of polynomials are described and discussed. Then, by a direct straightforward method of computation (that does not require any iteration) the complexes $M_xL(OH)_mH_n$ and $ML_y(OH)_mH_n$ are treated (where $1 \leqslant x \leqslant 3$ and $1 \leqslant y \leqslant 3$). Finally, the conditions leading to formation of polynuclear complexes are shown and discussed. The importance of study of polynuclear complexes for solving of biochemical problems is pointed out. Practical examples are given for each method.

The optimal acidity of a complex is the acidity for which the concentration of complex formation is reaching its maximum. The optimal acidity of complexes $M_xL_y(OH)_mH_n$ is usually determined by iteration.[1] Among methods of iteration we can even include such methods like regula falsi (or secant *m.*) and the Newton–Raphson method[2] because these methods also require some kind of iteration, just the mechanism of iteration in these methods is different.

Relatively little attention has been paid to polynomial methods like cubic and quartic equations. It is assumed that those methods lead to many complex conjugate roots so that it is difficult to find out the correct result. In this paper I will show that it is not necessarily so. On the contrary, the traditional iteration methods are connected with larger error. However, I do not intend to underrate the iteration methods, whose far reaching universality is of great advantage.

In combination with a sufficiently general method of iteration the optimal acidity of complexes $M_xL_y(OH)_mH_n$ (where $1 \leqslant x \leqslant 4$ and $y$ is any reasonable integer) can be determined. This is particularly useful for problems in biochemistry.

Finally, the conditions are shown that lead to the formation of polynuclear complexes. They are illustrated on the complex formation of chrome azurol S, eriochrome cyanine R, Xylenol Orange and triethylenetetraminehexaacetic acid with ions like $Fe^{3+}$, $Th^{4+}$, $Hg^{2+}$, $La^{3+}$ and $Cu^{2+}$.

*Retired. Present address: 2000 E. Roger Rd., #109-41, Tucson, AZ 85719, U.S.A.

## THEORETICAL

### *Single complex formation* $M_xL_y(OH)_mH_n$

If $[M_xL_y(OH)_mH_n] = c$, then the material balance is

$$c_M = xc + [M]\alpha_{MOH} \quad \text{and} \quad c_L = yc + [L]\alpha_{LH}, \tag{1a, b}$$

where $\alpha_{MOH}$ and $\alpha_{LH}$ are the coefficients of side reactions of the metal with OH ions and of the ligand L with protons H, respectively. We have

$$\alpha_{MOH} = \Sigma\beta_{t'}[OH]^{t'} = \Sigma\beta_{t'}K_w^{t'}[H]^{-t'} = \Sigma\beta_{t'}^{*}[H]^{-t'} \tag{2}$$

$$\alpha_{LH} = \Sigma\beta_t[H]^t, \tag{3}$$

where $K_w$ is the autoprotolytic constant of water ($=[H][OH] = 10^{-14}$ at 25°C). The conditional stability constant $K$ of the complex $M_xL_y(OH)_mH_n$ is given by

$$\begin{aligned} K &= c\,(c_M - xc)^{-x}(c_L - yc)^{-y} \\ &= c\,([M]\alpha_{MOH})^{-x}([L]\alpha_{LH})^{-y} \\ &= \beta_{xynm}\alpha_{MOH}^{-x}\alpha_H^{-y}[OH]^m[H]^n, \end{aligned} \tag{4}$$

where $\beta_{xynm}$ is the overall stability constant of the complex $M_xL_y(OH)_mH_n$. Taking logarithms of equation (4) we obtain

$$\begin{aligned} \log K = \log\beta_{xynm} &- x\log\alpha_{MOH} \\ &- y\log\alpha_{LH} + m\log K_w \\ &- (m-n)\log[H]. \end{aligned} \tag{5}$$

The conditional constant $K$ is reaching its maximum for the optimal acidity of the complex $M_xL_y(OH)_mH_n$. Therefore, we have

$$(\mathrm{d}\log K)/(\mathrm{d}\log[\mathrm{H}]) = 0 \qquad (6)$$

so that if we differentiate equation (5) under the conditions of (6) we obtain

$$x(\mathrm{d}\log\alpha_{\mathrm{MOH}})/(\mathrm{d}\log[\mathrm{H}]) + y(\mathrm{d}\log\alpha_{\mathrm{LH}})/(\mathrm{d}\log[\mathrm{H}]) + m - n = 0. \qquad (7)$$

Furthermore, we have

$$(\mathrm{d}\log\alpha_{\mathrm{MOH}})/(\mathrm{d}\log[\mathrm{H}]) = -(\Sigma t'\beta_t^*[\mathrm{H}]^{-t'})/(\Sigma\beta_t^*[\mathrm{H}]^{-t'}) = -\bar{t}' \qquad (8)$$

$$(\log\alpha_{\mathrm{LH}})/(\mathrm{d}\log[\mathrm{H}]) = (\Sigma t\beta_t[\mathrm{H}]^t)/(\Sigma\beta_t[\mathrm{H}]^t) = \bar{t}. \qquad (9)$$

Combining equations (7)–(9) results in

$$-x\bar{t}' + y\bar{t} + m - n = 0, \qquad (10)$$

which is the final equation for the optimal acidity of a single complex $M_xL_y(OH)_mH_n$. This shows that it is only a function of the composition of the complex and the extent of the side reactions, the metal M with hydroxide anions and the ligand with the protons. It is not a function of the stability of the complex.

If two complexes between M and L are formed, the stabilities of both are required to determine their optimal acidity, or at least one proceeding by the procedure described below.

*Many complexes of* $M_xL_y(OH)_mH_n$

Taking into account the fact that quartic equations can still be solved directly, the system of complexes, the optimal acidity of which we are trying to determine, is described by the material balance equations

$$[\mathrm{M}]^4A + [\mathrm{M}]^3B + [\mathrm{M}]^2C + [\mathrm{M}]D + E = 0 \qquad (11)$$

$$[\mathrm{M}]'^4A' + [\mathrm{M}]'^3B' + [\mathrm{M}]'^2C' + [\mathrm{M}]'D' + E' = 0, \qquad (12)$$

where

$$A = \Sigma\Sigma\Sigma p\beta_{4pef}[L]^p[\mathrm{OH}]^e[\mathrm{H}]^f,$$
$$B = \Sigma\Sigma\Sigma q\beta_{3qgh}[\mathrm{L}]^q[\mathrm{OH}]^g[\mathrm{H}]^h \qquad (13a, b)$$
$$C = \Sigma\Sigma\Sigma r\beta_{2rij}[\mathrm{L}]^r[\mathrm{OH}]^i[\mathrm{H}]^j,$$
$$D = \Sigma\Sigma\Sigma s\beta_{1smn}[\mathrm{L}]^s[\mathrm{OH}]^m[\mathrm{H}]^n \qquad (14a, b)$$
$$E = [\mathrm{L}]\Sigma\beta_t[\mathrm{H}]^t - c_{\mathrm{L}} \qquad (15)$$
$$A' = \Sigma\Sigma\Sigma 4\beta_{4pef}[\mathrm{L}]^p[\mathrm{OH}]^e[\mathrm{H}]^f,$$
$$B' = \Sigma\Sigma\Sigma 3\beta_{3qgh}[\mathrm{L}]^q[\mathrm{OH}]^g[\mathrm{H}]^h \qquad (16a, b)$$
$$C' = \Sigma\Sigma\Sigma 2\beta_{2rij}[\mathrm{L}]^r[\mathrm{OH}]^i[\mathrm{H}]^j,$$
$$D' = \Sigma\Sigma\Sigma\beta_{1smn}[\mathrm{L}]^s[\mathrm{OH}]^m[\mathrm{H}]^n \qquad (17a, b)$$
$$E' = -c_{\mathrm{M}}. \qquad (18)$$

As a measure of the accuracy of iteration, we have introduced

$$A^* = 1 - [\mathrm{M}]/[\mathrm{M}]', \qquad (19)$$

where $|A^*| < 0.001$ throughout.

As a measure of concentration, the molar per cents of the total metal concentration were used:

$$P_{xyur} = 100x\beta_{xyur}[\mathrm{M}]^x[\mathrm{L}]^y[\mathrm{OH}]^u[\mathrm{H}]^r. \qquad (20)$$

Within direct iteration, both material balance equations (11) and (12) are transformed into a form explicit for [M] and [M]′. These two equations are combined with the accuracy equation (19), and the iteration started with the quantity [L] until the condition of accuracy are met. In doing that, another basic rule of iteration is followed, iterating with a quantity which has the most complicated form in the given system.

The mechanism of direct iteration is presented in Fig. 1. It is useful to start the iteration at higher pH since then the interval of permissible [L] values is wider.

There is no need to give the equations for determination of optimal acidity in mono- and binuclear systems. They are evident from equations (11), (12), (14a, b), (15), (17a, b), (18) and (19).

For systems of trinuclear complexes, the equations that hold are

$$P = D/B - (C/B)^2/3 \qquad (21)$$

$$Q = (C/B)^3 2/27 - (CD/B^2)/3 + E/B \qquad (22)$$

$$[\mathrm{M}] = [-Q/2 + (Q^2/4 + P^3/27)^{1/2}]^{1/3} - (C/B)/3 + [-Q/2 - (Q^2/4 + P^3/27)^{1/2}]^{1/3}, \qquad (23)$$

where (23) is the well known Cardano equation.[3] Since that equation has real roots only if

$$Q^2/4 + P^3/27 \geqslant 0, \qquad (24)$$

that does not cover all real roots of cubic equations (11) and (12) ($A = A' = 0$), so that some real roots of (11) and (12) must correspond to (24) even if it is negative. This leads to the equation

$$[\mathrm{M}] = 2(-P/3)^{1/2}\cos\varphi/3 - (C/B)/3 \qquad (25)$$

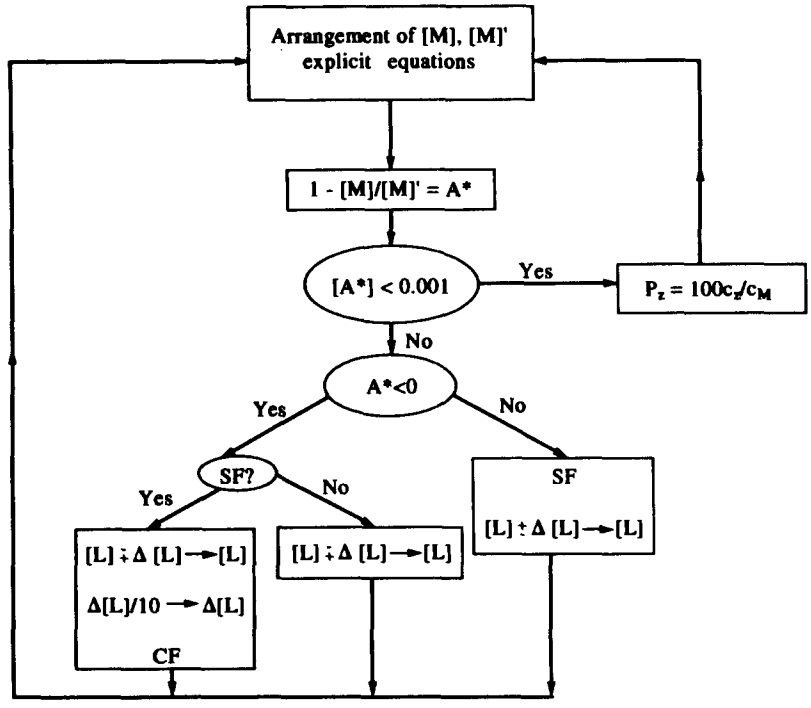


Fig. 1.

where

$$\cos\varphi = -Q/2(-27/P^3)^{1/2}. \quad (26)$$

For derivation of equation (25) see Appendix A.

Under these conditions, equation (23) yields just one real and positive root; if it does not, then (25) takes over. In that way we find the solution of cubic equations (11) and (12).

For systems of tetranuclear complexes, the solution is based on the solution of a quartic equation. We have

$$P^* = BD/A^2 - 4E/A - (C/A)^2/3 \quad (27)$$

$$Q^* = -(C/A)^3 2/27 + (BCD)/A^3 - 4(E/A)/3 - (D/A)^2 - (B/A)^2 E/A + 4CE/A^2 \quad (28)$$

$$y = [-Q^*/2 + (Q^{*2}/4 + P^{*3}/27)^{1/2}]^{1/3} - (C/A)/3 + [-Q^*/2 - (Q^{*2}/4 + P^{*3}/27)^{1/2}]^{1/3}. \quad (29)$$

Because that solution can be rarely found correctly published, it is given in Appendix B.

The condition to obtain positive real roots is again

$$Q^{*2}/4 + P^{*3}/27 \geqslant 0. \quad (30)$$

From Appendix B we have

$$\alpha^2 = (B/A)^2/4 + y - C/A;$$

$$\beta^2 = y^2/4 - E/A \quad (31a, b)$$

so that, for the conditions of complexation, the only acceptable positive real root is given by equation (32). Since the solution of a quartic

$$[M] = (\alpha - B/2A)/2 + [(\alpha - B/2A)^2/4 + \beta - y/2]^{1/2} \quad (32)$$

equation includes the solution of the cubic equation (29), our program must include the selection between (23) and (25), both with asterisk quantities.

Complexes $ML_y(OH)_uH_v$ and $M_xL(OH)_uH_v$. For these complexes no iteration is necessary and the computation of [M] and [L] is a straight operation employing the equations

$$[M]([L]^3U + [L]^2V + [L]W + 1) - c_M = 0 \quad (33)$$

$$[M](3[L]^3U + 2[L]^2V + [L]W) + [L]\alpha_{LH} - c_L = 0. \quad (34)$$

Combination of equations (33) and (34), with elimination of [M], results in

$$[L]^4\alpha_{LH}U + [L]^3(\alpha_{LH}V - c_LU + 3c_MU) + [L]^2(\alpha_{LH}W - c_LV + 2c_MV) + [L](\alpha_{LH} - c_LW + c_MW) - c_L = 0, \quad (35)$$

where $1 \leqslant y \leqslant 3$ and $U = \Sigma\Sigma\beta_{13ef}[OH]^e[H]^f$, $V = \Sigma\Sigma\beta_{12gh}[OH]^g[H]^h$, $W = \Sigma\Sigma\beta_{11ij}[OH]^i[H]^j$.

The situation is similar with complexes $M_xL(OH)_uH_r$. We have again

$$[L]([M]^3U' + [M]^2V' + [M]W' + \alpha_{LH}) - c_L = 0 \quad (36)$$

$$[L](3[M]^3U' + 2[M]^2V' + [M]W') + [M] - c_M = 0. \quad (37)$$

Combining equations (36) and (37) with elimination of [L] we get

$$[M]^4U' + [M]^3(V' - c_MU' + 3c_LU') + [M]^2(W' - c_MV' + 2c_LV') + [M](\alpha_{LH} - c_MW' + c_LW') - c_M\alpha_{LH} = 0, \quad (38)$$

where $1 \leqslant x \leqslant 3$ and $U' = \Sigma\Sigma\beta_{31mn}[OH]^m[H]^n$, $V' = \Sigma\Sigma\beta_{21pq}[OH]^p[H]^q$, $W' = \Sigma\Sigma\beta_{11rs}[OH]^r[H]^s$.

## RESULTS AND DISCUSSION

The conditions of the single complex method are met only seldom in real solutions. Nevertheless, that method gives useful preliminary information about probable behavior of the complex.[4] Some illustrative results and a comparison with the most advanced method as described in this paper are given in Table 1. Similar results, sometimes even more closely related to the facts, can be obtained with buffer ligands described by $\alpha_{MX}$ and $\alpha_{XH}$ (where $X = NH_3$, $CH_3COO^-$, etc.).

The optimal acidities for particular complexes were determined by computing the dependence between the actual concentration of the complex (in Tables the numbers are in parentheses) and the acidity of the coexisting solution. This was done over the whole acidity scale for every complex of the known composition and stability.

Thus Table 2 shows the effect of different total concentration of metal and ligand on the optimal acidity and actual concentration of complexes. Furthermore, Table 2 shows different behavior of the tetradentate ligand (CAS and ECR) and of the octadentate ligand (XO). Thus in the case of XO, only at very low pH, when most of the ligand is blocked by hydrogen complexes and, therefore, the free metal ions are in huge excess, is the binuclear complex $M_2LH_2$ formed. At higher pH (5.8–6.2), when the donors of the ligand are activated and the ligand itself is present in excess, the main complex formed is $M(LH_2)_2$. In between, understandably, there are conditions for the complex $MLH_2$.[5] On the other hand, owing to the presence of two relatively independent chelating systems and the donor deficiency, CAS and ECR form the binuclear complexes $M_2L$ and $M_2L_2$. Only at low pH, when one side of the ligand is blocked by hydrogen, is the complex MLH formed. Ueno *et al.*[6] discussed the conditions of complex formation between $Fe^{3+}$ and CAS. Complexation of CAS and ECR is in good agreement with the theory of binuclear complex formation (see below).

The results of the straightforward method (SFM), employing the quartic equation and cubic equation as a sub-method, are presented in Table 3. The computation shows, that if we have a system of complexes with overall stability constants $\beta_1, \beta_2, \ldots, \beta_z$ then if $\beta_1^z \doteq \beta_z$, the computation runs predominantly via Cardano equation (23). On the other hand, if $\beta_1^z > \beta_z$, it

Table 1. Single complex method (SCM) and advanced method (AM) for determination of optimal acidity of some EDTA complexes

| | $pH_{opt}$* | | | | | |
|---|---|---|---|---|---|---|
| | SCM | | | AM | | |
| Cation | MLH | ML | ML(OH) | MLH | ML | ML(OH) |
| $Al^{3+}$ | 3.2 | 4.6 | 7.8 | 2.2 (59.24) | 4.4 (96.09) | 9.0 (99.92) |
| $Bi^{3+}$ | 2.8 | 4.6 | 7.8 | 1.0 (83.37) | 5.8 (99.99) | 10.0 (92.64) |
| $Cu^{2+}$ | 7.0 | 9.2 | 12.4 | 1.6 (93.52) | 6.0 (99.90) | 11.0 (76.39) |
| $Fe^{2+}$ | 7.8 | 9.8 | 12.4 | 2.6 (46.22) | 6.0 (99.85) | 11.0 (98.70) |
| $Fe^{3+}$ | 3.4 | 5.0 | 7.8 | 0.4 (99.82) | 4.4 (99.82) | 8.5 (82.97)† |
| $Hg^{2+}$ | 3.2 | 4.6 | 7.8 | 1.2 (98.33) | 6.1 (99.80) | 12.0 (99.87) |
| $Mn^{2+}$ | 8.2 | 10.4 | 13.8 | 2.6 (55.48) | 7.0 (99.97) | 12.0 (92.64) |
| $Ni^{2+}$ | 8.0 | 10.4 | 12.8 | 1.8 (94.89) | 7.6 (99.99) | 13.0 (86.32) |
| $Sc^{3+}$ | 4.8 | 5.8 | 8.0 | 0.6 (85.10) | 6.4 (99.99) | 12.0 (88.59) |
| $Th^{4+}$ | 1.0 | 4.0 | 5.0 | 1.4 (91.86) | 4.6 (99.54) | 10.0 (98.21) |

*The numbers in parentheses refer to the per cent of particular complex. The total concentrations are $c_M = c_L = 0.01M$.

†For $FeL(OH)_2$ the corresponding data are 12.0 (SCM) and 13.00 (99.97) (AM).

Table 2. Optimal acidity of iron(III) complexes with chrome azurol S (CAS), with eriochrome cyanine R (ECR) and of thorium with Xylenol Orange (XO)

| System | $c_M$ ($M$) | $c_L$ ($M$) | $pH_{opt}$* MLH | $M_2L$ | $M_2L_2$ |
|---|---|---|---|---|---|
| $Fe^{3+}$–CAS | $3.2 \times 10^{-4}$ | $1.6 \times 10^{-4}$ | 2.2 ($2.40 \times 10^{-2}$) | 2.6 (51.71) | 5.4 (24.96) |
| | $1.6 \times 10^{-4}$ | $1.6 \times 10^{-4}$ | 2.4 ($4.20 \times 10^{-2}$) | 2.4 (44.41) | 6.0 (99.88) |
| | $1.6 \times 10^{-4}$ | $3.2 \times 10^{-4}$ | 2.2 ($6.42 \times 10^{-2}$) | 2.2 (44.52) | 5.6 (99.94) |
| $Fe^{3+}$–ECR | $1.6 \times 10^{-4}$ | $1.6 \times 10^{-4}$ | 2.0 ($4.80 \times 10^{-1}$) | 2.4 (88.19) | 6.0 (99.72) |
| | | | $M_2LH_2$ | $MLH_2$ | $M(LH_2)_2$ |
| $Th^{4+}$–XO | $2.0 \times 10^{-5}$ | $4.0 \times 10^{-5}$ | 1.8 (6.18) | 2.6 (99.39) | 6.0 (83.35) |
| | $2.0 \times 10^{-5}$ | $2.0 \times 10^{-5}$ | 1.6 (15.07) | 5.4 (99.48) | 6.0 (2.75) |
| | $4.0 \times 10^{-5}$ | $2.0 \times 10^{-5}$ | 2.6 (24.07) | 4.6 (37.98) | 5.8 ($1.55 \times 10^{-4}$) |

*The numbers in parentheses refer to the per cent of particular complex; $c_M$ and $c_L$ are the total concentration of the metal and of the ligand, respectively.

runs via the goniometric variant (25). Table 3 also shows the comparison of SFM with the direct iteration method. Both methods give very similar results, but SFM is slightly more accurate. Many times the iteration gives the same concentration of individual complexes in the pH interval 5–6.

Table 4 shows the optimal acidity of metal complexes of TTHA (triethylenetetraminehexaacetic acid). Since it is $y = 1$ throughout, the SFM and direct iteration were used. Again as in Table 3 the SFM gives slightly better results. TTHA forms a wide scale of binuclear complexes.

The conditions of polynuclear complex formation can be summed up as follows: (a) the complexing reagent must contain several relatively independent chelating systems. (b) The primary mononuclear complex is usually a mixed metal–hydrogen–ligand complex. (c) As a

Table 3. Straightforward method (SFM) and method of iteration (ITE) used for computation of optimal acidity of great variety of complexes

| System | $pH_{opt}$* ML | $ML_2$ | $ML_3$ | $10^3 c_M$ ($M$) |
|---|---|---|---|---|
| (a) $Q^{*2}/4 + P^{*3}/27 \geqslant 0$ predominates | | | | |
| $Zn^{2+}$–2,3-dimercapto-1-propanol (BAL) | 3.8 (32.87) | 4.4 ($6.67 \times 10^{-3}$) | 7.0 (99.98) | 1.00 |
| | 3.9 (32.19) | 4.4 ($6.67 \times 10^{-3}$) | 7.0 (99.92) | |
| $Fe^{2+}$–2,2′-bipyridyl | −0.1 (1.69) | 2.2 ($9.60 \times 10^{-3}$) | 6.0 (98.11) | 0.10 |
| | −0.1 (1.70) | 2.2 ($9.00 \times 10^{-3}$) | 6.0 (98.12) | |
| $La^{3+}$–8-hydroxyquinoline | 6.4 (36.68) | 7.2 (32.45) | 8.0 (67.75) | 1.00 |
| | 6.4 (36.68) | 7.2 (32.45) | 8.0 (67.72) | |
| $Fe^{2+}$–1,10-phenanthroline | −0.8 (34.56) | 1.8 ($7.24 \times 10^{-2}$) | 6.0 (99.67) | 0.10 |
| | −0.8 (34.57) | 1.8 ($7.25 \times 10^{-2}$) | 6.0 (99.68) | |
| (b) $Q^{*2}/4 + P^{*3}/27 < 0$ predominates | | | | |
| $Fe^{3+}$–aceto(hydroxamic) acid | 2.6 (78.45) | 5.0 (89.17) | 10.0 (97.35) | 0.10 |
| | 2.4 (77.33) | 5.0 (89.15) | 10.0 (99.98) | |
| $Fe^{3+}$–acetylacetone | 2.2 (55.17) | 3.6 (75.71) | 8.0 (98.31) | 1.00 |
| | 2.2 (55.15) | 3.6 (75.70) | 8.0 (98.72) | |
| $Ni^{2+}$–ethylenediamine | 6.0 (67.63) | 7.0 (80.65) | 11.0 (94.39) | 10.0 |
| | 6.0 (67.62) | 7.0 (80.65) | 11.0 (84.40) | |
| $Ni^{2+}$–glycylglycine | 6.6 (39.35) | 8.0 (84.98) | 10.0 (19.60) | 10.0† |
| | 6.6 (39.40) | 8.0 (85.00) | 10.0 (19.55) | |
| $Ni^{2+}$–2-nitroso-1-napthol-4-sulfonic acid | 3.0 (22.34) | 4.6 (3.47) | 7.0 (94.84) | 0.10 |
| | 3.2 (22.21) | 4.6 (3.46) | 7.0 (94.85) | |
| $Al^{3+}$–oxalic acid | 0.6 (63.69) | 1.4 (59.85) | 5.0 (90.51) | 10.0 |
| | 0.6 (63.71) | 1.4 (59.84) | 5.0 (90.65) | |
| $Al^{3+}$–sulfosalicylic acid | 4.4 (83.05) | 7.2 (93.92) | 10.0 (81.74) | 0.10 |
| | 4.4 (83.03) | 7.2 (93.92) | 10.0 (81.73) | |
| $Fe^{3+}$–sulfosalicylic acid | 2.8 (96.95) | 8.3 (97.48) | 10.6 (90.05) | 0.10 |
| | 2.8 (96.87) | 8.3 (97.45) | 10.6 (90.07) | |
| $Fe^{3+}$–tiron | 3.6 (96.16) | 5.6 (98.39) | 10.0 (99.29) | 0.10‡ |
| | 3.6 (96.15) | 5.6 (98.39) | 10.0 (99.30) | |

*Numbers in the first line of each system are the results of SFM, in the second line the results of ITE. $3c_M = c_L$.
†For MLH, 5.0 (83.74) and 5.0 (83.76).
‡For MLH, 1.6 (45.74) and 1.6 (45.72).

Table 4. Optimal acidity and concentration of some complexes of triethylenetetraminehexaacetic acid (TTHA)

| Cation | $M_2L$ | $M_2LH$ | $M_2LH_2$ | $M_2L(OH)_2$ | ML | MLH |
|---|---|---|---|---|---|---|
| $Al^{3+}$ | 4.4 (99.76) | | | 7.0 (98.73) | 5.8 ($1.86 \times 10^{-2}$) | 3.0 ($6.81 \times 10^{-1}$) |
| | 4.4 (99.79) | | | 7.0 (98.76) | 4.4 ($2.81 \times 10^{-3}$) | 3.0 ($3.75 \times 10^{-1}$) |
| $Cd^{2+}$ | 6.2 (99.09) | | | | 6.2 ($3.43 \times 10^{-3}$) | 3.0 (8.46)* |
| | 6.2 (99.26) | | | | 6.2 ($2.77 \times 10^{-3}$) | 3.0 (8.47) |
| $Co^{2+}$ | 6.0 (99.90) | 2.8 (43.91) | 2.0 (73.77) | | 6.0 ($6.27 \times 10^{-5}$) | 3.4 (2.43) |
| | 6.0 (99.90) | 2.8 (43.92) | 2.0 (73.70) | | 6.0 ($5.60 \times 10^{-6}$) | 3.4 (1.79) |
| $Cu^{2+}$ | 6.0 (99.90) | 2.8 (41.20) | 2.0 (81.75) | | 6.2 ($1.00 \times 10^{-5}$) | 3.0 ($5.50 \times 10^{-2}$) |
| | 6.0 (99.90) | 2.8 (41.16) | 2.0 (81.68) | | 6.2 ($1.00 \times 10^{-5}$) | 3.0 ($1.70 \times 10^{-1}$) |
| $Fe^{3+}$ | 2.0 (99.67) | | | 6.0 (99.99) | 3.6 ($4.11 \times 10^{-7}$) | 1.2 ($1.83 \times 10^{-2}$)† |
| | 1.8 (99.43) | | | 6.0 (99.99) | 5.6 ($7.49 \times 10^{-4}$) | 4.2 ($1.88 \times 10^{-2}$) |
| $Hg^{2+}$ | 6.0 (99.54) | 3.2 (58.32) | 2.0 (82.99) | 6.0 ($6.28 \times 10^{-2}$) | 6.0 ($1.99 \times 10^{-4}$) | 3.6 ($3.84 \times 10^{-3}$)‡ |
| | 6.0 (99.17) | 3.2 (58.10) | 2.0 (82.73) | 6.0 ($6.26 \times 10^{-2}$) | 6.0 ($2.03 \times 10^{-4}$) | 3.2 ($3.74 \times 10^{-3}$) |
| $La^{3+}$ | 8.0 (81.94) | | | | 8.0 (9.03) | 2.6 (12.86) |
| | 8.0 (81.93) | | | | 8.0 (9.00) | 2.6 (12.46) |
| $Mn^{2+}$ | 8.0 (98.63) | | | | 8.0 ($1.05 \times 10^{-1}$) | 3.6 (38.65)§ |
| | 8.0 (98.62) | | | | 8.0 ($1.04 \times 10^{-1}$) | 3.6 (38.71) |
| $Ni^{2+}$ | 6.0 (99.96) | 2.4 (41.16) | 2.0 (61.10) | | 6.0 ($3.52 \times 10^{-6}$) | 3.4 ($1.02 \times 10^{-2}$) |
| | 6.0 (99.96) | 2.4 (41.16) | 2.0 (61.10) | | 6.0 ($3.52 \times 10^{-6}$) | 3.4 ($1.03 \times 10^{-2}$) |
| $Pb^{2+}$ | 6.0 (99.90) | 2.8 (43.51) | 2.0 (70.63) | | 6.0 ($1.25 \times 10^{-4}$) | 3.2 (1.32) |
| | 6.0 (99.90) | 2.8 (43.64) | 2.0 (70.56) | | 6.0 ($1.24 \times 10^{-5}$) | 3.4 $3.80 \times 10^{-1}$) |
| $Zn^{2+}$ | 6.0 (99.90) | 2.8 (43.92) | 2.0 (73.42) | | 6.0 ($3.98 \times 10^{-5}$) | 3.4 ($9.60 \times 10^{-1}$) |
| | 6.0 (99.91) | 2.8 (43.91) | 2.0 (73.32) | | 6.0 ($3.45 \times 10^{-5}$) | 3.4 (1.00) |

*For $CdLH_2$, 2.2 (40.00) and 2.2 (40.00).
†For $FeLH_2$, 1.0 (1.03) and 1.0 (1.11).
‡For $HgLH_2$, 2.0 ($2.01 \times 10^{-2}$) and 2.1 ($1.89 \times 10^{-2}$).
§For $MnLH_2$, 3.0 (7.23) and 3.0 (7.25).
$2c_L = c_M$. See also the footnotes for Table 2: $c_L = 0.01M$.

measure of nuclearity the fraction $F$, equation (39), can be used.

$$F = [M_xL]/[M_{x-1}LH] = \beta_x[M]/(\beta_{x-1}[H]), \quad (39)$$

where $\beta_x$ is the overall stability constant of the complex $M_xL$ and $\beta_{x-1}$ the stability constant of the mixed complex $M_{x-1}LH$. The actual concentrations [M] and [H] should be taken in the conditions of optimal acidity of the complex $M_xL$. The values of $\log F$ for complexes $M_2L$ from Table 4 are listed in Table 5.

Biochemistry is the most fruitful field where polynuclear complexes can occur. One problem is, for example, why rigid and planar polypeptides form only the *trans* configuration of mutual location of nitrogen and oxygen atoms.[7] The presence of a metal ion like $Cu^{2+}$ would favor the *cis* configuration. Tripropylene- or tributylenetetraminohexaacetic acid can be used as model for investigation of tetranuclear complexes.

Table 5. Fraction F in the conditions of optimal acidity

| Metal ion | log F | Metal ion | log F | Metal ion | log F |
|---|---|---|---|---|---|
| $Al^{3+}$ | 2.73 | $Fe^{3+}$ | 3.46 | $Ni^{2+}$ | 5.15 |
| $Cd^{2+}$ | 2.04 | $Hg^{2+}$ | 5.09 | $Pb^{2+}$ | 3.40 |
| $Co^{2+}$ | 3.80 | $La^{3+}$ | 6.18 | $Zn^{2+}$ | 3.95 |
| $Cu^{2+}$ | 4.70 | $Mn^{2+}$ | 2.73 | | |

For equilibrium constants used, see Ref. 8.

## REFERENCES


1. J. F. Traub, *Iterative Methods for the Solution of Equations*. Chelsea, New York, 1982.
2. H. Margenau and G. M. Murphy, *The Mathematics of Physics and Chemistry*, R. E. Krieger (ed.). Huntington, New York, 1976.
3. W. Gellert, H. Küstner, M. Hellwich and H. Kästner (eds), *The VNR Concise Encyclopedia of Mathematics*. Van Nostrand Reinhold, New York, 1977.
4. B. W. Budesinsky, *Anal. Chem.*, 1970, **42**, 928.
5. B. W. Budesinsky, *Anal. Chim. Acta*, 1972, **61**, 465.
6. K. Ueno, T. Imamura and K. L. Cheng, *CRC Handbook of Organic Analytical Reagents*. CRC Press, Boca Raton, Florida, 1992.
7. L. Stryer, *Biochemistry*, 3rd Edn. W. H. Freeman, New York, 1988.
8. J. Kotrly and L. Sucha, *Handbook of Chemical Equilibria in Analytical Chemistry*. J. Wiley, New York, 1985.
9. G. A. Korn and T. M. Korn, *Mathematical Handbook for Scientists and Engineers*. McGraw-Hill, New York, 1968.
10. C. E. Pearson (ed.), *Handbook of Applied Mathematics*. Van Nostrand Reinhold, New York, 1983.


## APPENDIX A

*Goniometric variant of Cardano equation*[9]

The Cardano equation (23) with imaginary components reads

$$[M] = [-Q/2 + i(Q^2/4 + P^3/27)^{1/2}]^{1/3} + [-Q/2 - i(Q^2/4 + P^3/27)^{1/2}]^{1/3} - (C/B)/3. \quad (A1)$$

According to the Moivre theorem we have

$$(\cos x \pm i \sin x)^n = \cos nx \pm i \sin nx \quad \text{(A2)}$$

and introducing

$$\cos x = -Q/2(-27/P^3)^{1/2} \quad \text{(A3)}$$

we obtain

$$[M] = 2(-P/3)^{1/2} \cos x/3 - (C/B)/3, \quad \text{(A4)}$$

where $x = \varphi$. Then (A4) is identical with (25).

## APPENDIX B

*Solution of the quartic equation*[10]

The general equation

$$x^4 + ax^3 + bx^2 + cx + d = 0 \quad \text{(B1)}$$

is squared for its two members by writing

$$(x^2 + ax/2)^2 = x^4 + ax^3 + (a/2)^2x^2 = [(a/2)^2 - b]x^2 - cx - d. \quad \text{(B2)}$$

Furthermore, if we add to each side $(x^2 + ax/2)y + y^2/4$ we get

$$(x^2 + ax/2 + y/2)^2 = x^4 + (a/2)^2x^2 + y^2/4 + ax^3 + x^2y + (a/2)xy. \quad \text{(B3)}$$

That is

$$[(a/2)^2 - b + y]x^2 + (ay/2 - c)x + (y/2)^2 - d = \alpha^2x^2 + 2\alpha\beta x + \beta^2, \quad \text{(B4)}$$

where

$$\alpha^2 = (a/2)^2 - b + y, \quad \beta^2 = (y/2)^2 - d, \quad 2\alpha\beta = ay/2 - c, \quad \text{(B5a, b, c)}$$

so that by mutual combination of (B5, a, b, c) we obtain

$$y^3 - by^2 + (ac - 4d)y - (c^2 + a^2d - 4bd) = 0 \quad \text{(B6)}$$

which is the resolvent of (B1). Since it is a cubic equation, it may be solved by the methods for cubic equations. Thus we get by combination of (B4) and (B5, ab)

$$x^2 + (a/2 - \alpha)x + y/2 - \beta = 0 \quad \text{(B7)}$$

or

$$x = (\alpha - a/2)/2 + [(\alpha - a/2)^2/4 + \beta - y/2]^{1/2} = [M]. \quad \text{(B8)}$$

Pergamon

0039-9140(95)01428-4

*Talanta*, Vol. 42, No. 3, pp. 431–436, 1995

0039-9140/95 $9.50 + 0.00

# DETERMINATION OF EQUILIBRIUM CONSTANTS OF ALKALINE EARTH METAL ION CHELATES WITH DOWEX A-1 CHELATING RESIN

LEO HARJU and TOWE KROOK
Department of Analytical Chemistry, Åbo Akademi, FIN-20500 Åbo, Finland

(*Received* 26 *April* 1994. *Revised* 29 *September* 1994. *Accepted* 29 *September* 1994)

**Summary**—A complexation chemistry model is applied to chelating ion-exchange systems and a method is presented for the determination of equilibrium constants for metal ion chelates with these resins. Protonation constants for the iminodiacetic based chelating resin Dowex A-1 were determined from potentiometric pH-data. Equilibrium constants were determined for 1:1 beryllium, magnesium, calcium, strontium and barium chelates with the resin in a wide pH range by measuring the concentrations of respective metal ions in the aqueous phase with direct current plasma atomic emission spectrometry (DCP-AES). A batch technique was used for the equilibrium experiments. At pH below 7 protonated 1:1 species were also found to be formed with the resin. From the obtained equilibrium constants, theoretical distribution coefficients were calculated as function of pH for respective metal ion resin system.

The synthesis and use of selective chelating resins in chemistry and industry have rapidly increased during the last years. Comprehensive reviews have been written about the synthesis, properties and uses of chelating resins.[1-3] Chelating resins have, for instance, found use for removal of trace metal ions from reagents, biochemical and physiological fluids. The main use in analytical chemistry is for preconcentration and separation, *e.g.* of heavy metal ions from sea-water. In environmental chemistry the resins have been used for speciation studies. One of the present authors has previously utilized Dowex A-1 for separation of Zn-65 isotopes from a large excess of copper ions.[4]

Dowex A-1, the resin studied in this work, has iminodiacetic acid (IDA) as a functional group anchored to the styrene divinylbenzene matrix. Thus the chelating group is tridentate containing one amino and two carboxylate oxygens as donor atoms. Like the monomer aminocarboxylic acids it has a zwitterionic structure. The iminodiacetic acid based resin is also known by several other trade names such as Chelex 100, Diaion CR-10, Duolite ES-466, Lewatit TP-207 and Wofatit MC50.

Equilibrium constants are necessary for the development, theoretical treatment and optimization of, *e.g.* analytical methods and industrial processes. This holds also for ion-exchange systems, like chelating resins. However, in the literature[5-9] equilibrium constants can be found only for a few metal ions. Harju and Perus[7] have reported equilibrium constants for copper(II) chelates with the Dowex A-1 resin.

## EXPERIMENTAL

The chelating resin studied in this work was Dowex A-1 (Fluka, 50-100 mesh). The resin was dried for 1 h at 70°C and stored in an exsiccator until used. A batch technique was used for the determination of equilibrium constants. The measurements were carried out at 25°C (±1°C) and the ionic strength was adjusted to 0.1 *M* by adding potassium nitrate. An inert atmosphere was obtained by outgasing the solutions with nitrogen or argon gases.

The stock solutions of the metal ions studied were prepared from pro analysis reagents and standardized by complexometric titrations against EDTA according to a procedure described earlier.[10] Magnesium ions were titrated at pH 10 with Eriochrome Black T as indicator. Ca, Ba and Sr ions were also titrated at pH 10 with Eriochrome Black T as indicator, but a small amount of Mg-EDTA was added to give a sharp transition. For accurate titrations and standardizations a Metrohm E 457 $\mu$-buret was used.

The cation exchange capacity, $C$, of the resin was determined by two different methods. One

direct method was based on Kjeldahl analysis of the nitrogen content of the dry resin. By assuming that one functional group contains one nitrogen atom, the method gave a capacity of 2.3 mmol/g for the resin in sodium form.

In the second method the resin was allowed to equilibrate with an excess of zinc ions at a pH sufficiently high to guarantee a quantitative sorption of zinc ions. The concentration of zinc in the solution phase was determined by complexometric titrations with a standard EDTA solution at pH 5.3 using Xylenol Orange as indicator. This method gave a capacity of 2.2 mmol/g. The capacity 2.3 mmol/g was used in the calculations in this work.

A Metrohm model 654 pH/mV meter equipped with a Metrohm combined pH electrode was used for the pH measurements. The pH electrode system was calibrated to give hydrogen ion concentrations, [H], according to a procedure described earlier.[11] For very accurate measurements, mV values were recorded and recalculated to $-\log[H]$ values using Nernst's law.

The equilibrium constants were determined using the following procedure: 100 mg of the dry resin was mixed with 100 ml of aqueous phase having an exactly known concentration of the metal ion studied. Appropriate pH values were adjusted with KOH and $HNO_3$, and the mixtures were allowed to equilibrate for 48 hr under constant stirring. No extra buffer agents, which could interfere with the ion-exchange equilibria, were used for adjustment of pH. The final pH of the aqueous phase was measured and the concentration of the metal ion in the filtrate determined. Direct current plasma atomic emission spectrometry (DCP-AES) was used for the determination of the analytical concentrations of metal ions studied in the equilibrium studies. A Spectra span III B spectrometer (Spectrametrics Inc., Andover, MA) was used. Five to seven standards were used for the calibration of the analytical methods for each metal ion studied. $KNO_3$ ($0.1M$) was added to each standard in order to control the matrix effects.

In order to minimize problems with activity calculations and corrections, the determination of equilibrium constants was carried out at constant ionic strength ($\mu = 0.1$) in the solution phase. The ionic strength was adjusted to 0.1 with $KNO_3$. Concentrations of species were determined and calculated and the equilibrium constants are given as concentration constants. The concentrations of the species in the resin phase are expressed as mmol/g and in the aqueous phase as $M$.

## RESULTS AND DISCUSSION

### *Study of time needed for equilibration*

Because of the slow kinetics of Dowex A-1 a test was made to find out the minimum time needed for equilibration with alkaline earth metal ions. In Fig. 1 pCa is plotted as a function of time. The concentration of calcium in the aqueous phase was monitored in suitable time intervals by DCP-AES in presence of an excess of the chelating resin. After about 5 hr of equilibration the pCa values are relatively constant. However, for the determination of equilibriation constants in the present work the mixtures were allowed to equilibrate for 48 hr under constant mixing before the final analytical measurements. According to Sides and Kenner,[12] 6 hr of shaking gave constant distribution coefficients for alkaline earth metals with Dowex A-1. The kinetics of the chelating resin Dowex A-1 has been very thoroughly studied by Schmuckler.[13]

### *Determination of protonation constants*

The experimental data for the determination of the protonation constants of the chelating resin Dowex A-1 are presented as a potentiometric curve in Fig. 2. Each data point in the figure represents a batch experiment where the total volume and total concentration of the resin were kept constant with various volumes of standard acid added. The pH curve exhibits two buffer regions corresponding to the protonation of the amino respective carboxylic group. From these two buffer regions, which are well apart, the protonation constants can be calculated.

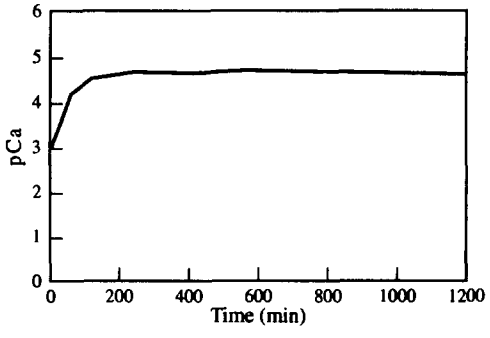


Fig. 1. pCa as function of time for the Ca-Dowex A-1 system at pH 9.51. Volume = 200 ml, $m_R = 200$ mg, $C_{Ca} = 10^{-3.00}M$, $\mu = 0.1$ ($KNO_3$).

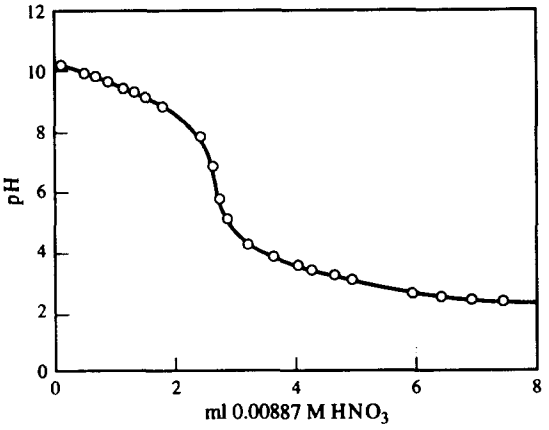


Fig. 2. Potentiometric pH-curve for the chelating resin Dowex A-1. 100.0 mg resin, volume = 50.0 ml, $\mu = 0.1$.

For the protonation of the resin we have the following reactions and stepwise equilibrium constants

$$R + H \rightleftharpoons HR \quad (1)$$

$$HR + H \rightleftharpoons H_2R \quad (2)$$

$$K_{HR}^{H,R} = \frac{[HR]}{[H][R]} \quad (3)$$

$$K_{H_2R}^{HR,H} = \frac{[H_2R]}{[H][HR]}. \quad (4)$$

The ionic charges are omitted for the sake of simplicity. The determination of the first protonation constant, $K_{HR}^{H,R}$, is given in Table 1. The calculation of the concentrations of the protonated and nonprotonated form of the resin is based on the following expressions

$$[R] = \frac{n_R}{m_R} \quad (5)$$

$$n_R = (V_{eq} - V_{HNO_3}) \cdot C_{HNO_3} - V \cdot [OH^-] \quad (6)$$

$$[HR] = C - [R], \quad (7)$$

Table 1. Determination of the first protonation constant, $K_{HR}^{H,R}$, for the resin Dowex A-1 (100.0 mg resin, $\mu = 0.1$, volume = 50.0 ml pH was adjusted with 0.0887$M$ $HNO_3$)

| $-\log[H]$ | $V_{HNO_3}$ ($ml$) | [R] ($mmol/g$) | [HR] ($mmol/g$) | $\log K_{HR}^{H,R}$ |
|---|---|---|---|---|
| 9.71 | 0.80 | 1.56 | 0.74 | 9.38 |
| 9.64 | 0.90 | 1.48 | 0.82 | 9.38 |
| 9.40 | 1.10 | 1.31 | 0.99 | 9.28 |
| 9.33 | 1.30 | 1.13 | 1.17 | 9.35 |
| 9.18 | 1.40 | 1.05 | 1.25 | 9.26 |
| 9.15 | 1.50 | 0.96 | 1.34 | 9.29 |

Mean value of $\log K_{HR}^{H,R} = 9.32$.
Standard deviation 0.05.

where $V_{HNO_3}$ is volume of the standard acid added (ml); $V_{eq}$ the volume of acid added at the first equivalence point (2.59 ml in Fig. 2); $V$ the total volume of the aqueous phase (ml); $C_{HNO_3}$ the concentration of the standard acid ($M$); $m_R$ the mass of the resin (g) and $C$ the capacity of the resin (mmol/g). The concentrations of $H^+$ and $OH^-$ ions at the first equivalence point of the potentiometric curve (Fig. 2) are of no practical significance for the calculations and can be omitted in equation (6).

The following protonation constants were determined in this work: $K_{HR}^{H,R} = 10^{9.32}$ (Table 1) and $K_{H_2R}^{HR,H} = 10^{3.25}$. There are great variations in the values of protonation constants published in the literature for Dowex A-1. Leyden and Underwood[8] have reported $K_{HR}^{H,R} = 10^{8.55}$ and $K_{H_2R}^{HR,R} = 10^{2.95}$. The first protonation constant is clearly below the value obtained in this work. Szabadka[9] has obtained $K_{HR}^{H,R} = 10^{9.12}$, $K_{H_2R}^{HR,R} = 10^{3.12}$ and $K_{H_3R}^{H_2R,H} = 10^{1.44}$, which are in satisfactory agreement with protonation constants obtained by the present authors. From a practical point of view, the first protonation constant is of greatest interest, because most equilibrium constants in this work were determined at pH above 5, where the second protonation constant will not have any influence on the calculations.

*Determination of equilibrium constants of alkaline earth metal ions*

Harju and Perus[7] have shown that copper(II) ions predominantly form 1:1 chelates with the functional group of the Dowex A-1 chelating resin in a large pH region (2.8–9.4). A similar 1:1 model has been reported by Loewenschuss and Schmuckler.[5] The functional groups in the resin are well spaced and it is unlikely that biligands (1:2) are formed with the resin matrix.

The reaction of alkaline earth metal ions with the chelating resin can thus generally be written as

$$M' + R' \rightleftharpoons (MR)', \quad (8)$$

which is defined by the conditional constant

$$K_{(MR)}^{M',R'} = \frac{[(MR)']}{[M'][R']} = K_{MR}^{M,R} \cdot \frac{\alpha_{MR}}{\alpha_M \cdot \alpha_R}. \quad (9)$$

$K_{MR}^{M,R}$ is the usual 1:1 stability constant expressed by

$$K_{MR}^{M,R} = \frac{[MR]}{[M][R]}. \quad (10)$$

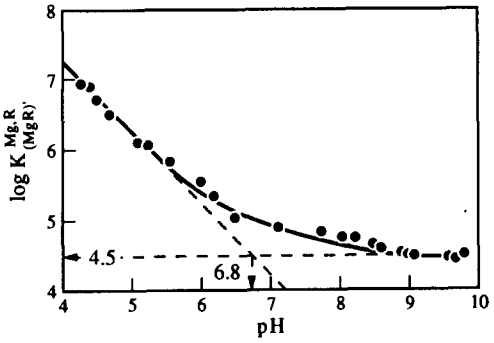


Fig. 3. Log $K^{Mg,R}_{(MgR)'}$ plotted as a function of pH.

The total metal ion concentration in the solution phase, [M′], is determined by direct current plasma atomic emission spectrometry (DCP-AES). The concentration of (MR)′, which also includes the concentrations of protonated 1:1 chelates, can be calculated from the following equation

$$[(MR)'] = \frac{(C_M - [M'])V}{m_R}, \qquad (11)$$

where $C_M$ is total concentration of metal ions added to the solution and $V$ is volume of the solution phase (ml).

For the concentration of resin not bound to metal ions we have the expressions

$$[R'] = C - [(MR)'] \qquad (12)$$

and

$$[R] = \frac{[R']}{\alpha_{R(H)}}. \qquad (13)$$

The α-coefficients are used as defined by Ringbom.[14] $\alpha_{R(H)}$ is defined by the equation

$$\alpha_{R(H)} = 1 + [H]K^{H,R}_{HR} + [H]^2K^{2H,R}_{H_2R}. \qquad (14)$$

The side reactions of metal ions can be considered by the equation

$$[M] = \frac{[M']}{\alpha_M}. \qquad (15)$$

As a demonstration of the theoretical principles used in the present work, Fig. 3 presents log $K^{Mg,R}_{(MgR)'}$ plotted as a function of pH. The almost horizontal course of the curve at pH above 8 indicates that the nonprotonated chelate MgR dominates and $K^{Mg,R}_{MgR}$ equals $K^{Mg,R}_{(MgR)'}$ in this pH region. This region, where the interfering effect from hydrogen ions are still quite small, is optimal for calculation of $K^{Mg,R}_{MgR}$, which is presented in Table 2.

Table 2. Determination of the equilibrium constant for $Mg^{2+}$ with Dowex A-1

| −log[H] | −log[Mg] | [MgR] (*mmol/g*) | [R′] (*mmol/g*) | $\alpha_{R(H)}$ | [R] (*mmol/g*) | log $K^{Mg,R}_{MgR}$ |
|---|---|---|---|---|---|---|
| 9.791 | 4.538 | 0.943 | 1.357 | 1.338 | 1.014 | 4.51 |
| 9.669 | 4.434 | 0.936 | 1.364 | 1.448 | 0.942 | 4.43 |
| 9.569 | 4.424 | 0.938 | 1.365 | 1.564 | 0.873 | 4.45 |
| 9.071 | 4.226 | 0.914 | 1.386 | 2.774 | 0.500 | 4.49 |
| 8.988 | 4.184 | 0.902 | 1.398 | 3.148 | 0.444 | 4.49 |
| 8.914 | 4.160 | 0.905 | 1.395 | 3.547 | 0.393 | 4.52 |
| 8.868 | 4.128 | 0.902 | 1.398 | 3.831 | 0.365 | 4.52 |
| 8.587 | 3.994 | 0.872 | 1.428 | 6.408 | 0.223 | 4.59 |
| 8.496 | 3.981 | 0.870 | 1.430 | 7.668 | 0.169 | 4.65 |

Mean value of log $K^{Mg,R}_{MgR}$ = 4.52.
Standard deviation 0.07.

Table 3. Determination of $K^{H,MgR}_{MgHR}$

| −log[H] | −log[Mg] | [(MgR)′] (*mmol/g*) | [R′] (*mmol/g*) | −log[R] | log $K^{Mg,R}_{(MgR)'}$ | log $\alpha_{MgR(H)}$ | log $K^{H,MgR}_{MgHR}$ |
|---|---|---|---|---|---|---|---|
| 6.49 | 3.135 | 0.243 | 2.057 | 2.514 | 5.034 | 0.518 | 6.85 |
| 6.07 | 3.128 | 0.240 | 2.060 | 2.937 | 5.445 | 0.928 | 6.94 |
| 5.89 | 3.136 | 0.253 | 2.047 | 3.120 | 5.658 | 1.141 | 7.00 |
| 5.43 | 3.098 | 0.187 | 2.113 | 3.568 | 5.939 | 1.421 | 6.83 |
| 5.11 | 3.085 | 0.162 | 2.138 | 3.886 | 6.180 | 1.663 | 6.76 |
| 4.97 | 3.072 | 0.137 | 2.163 | 4.023 | 6.230 | 1.714 | 6.68 |
| 4.57 | 3.071 | 0.136 | 2.164 | 4.435 | 6.640 | 2.123 | 6.69 |
| 4.40 | 3.078 | 0.149 | 2.151 | 4.617 | 6.870 | 2.353 | 6.75 |
| 4.29 | 3.089 | 0.169 | 2.131 | 4.739 | 7.055 | 2.538 | 6.83 |
| 4.18 | 3.077 | 0.146 | 2.154 | 4.855 | 7.097 | 2.580 | 6.76 |
| 4.15 | 3.073 | 0.139 | 2.161 | 4.887 | 7.101 | 2.584 | 6.73 |

Mean value of log $K^{H,MgR}_{MgHR}$ = 6.80.
Standard deviation 0.10.

At pH below 7 there is a rise of the curve in Fig. 3 and this indicates the formation of protonated species. An approximate constant $K_{MgHR}^{MgR,H} = 10^{6.8}$ can be obtained from the figure as the intercept between the horizontal line ($\log K_{MgR}^{Mg,R} = 4.5$) and the tangent of the slope $-1$ to the rising curve, according to a method described earlier by Ringbom and Harju.[15] A more exact calculation of $K_{MgHR}^{MgR,H}$ is given in Table 3, based on the following equations derived from the general expressions for $\alpha_{MR(H)}$

$$K_{MHR}^{MR,H} = \frac{[MHR]}{[MR][H]} = \frac{\alpha_{MR(H)}}{(1+[H])}, \quad (16)$$

where

$$\alpha_{MR(H)} = \frac{K_{(MR)'}^{M,R}}{K_{MR}^{M,R}}. \quad (17)$$

The equilibrium constants determined in this work are summarized in Table 4. For beryllium no constant could be determined for the protonated chelate. The precision obtained for the logarithmic equilibrium constants expressed as standard deviations are mostly about 0.1, which must at least be considered as satisfactorily. In the literature, no equilibrium constants could be found for alkaline earth metal ion complexes with the IDA based chelating resin. In a recent paper Pesavento *et al.*[16] report the formation of a protonated species $Ca(HR)_2$ at pH below 7.

*Calculation of distribution coefficients from the equilibrium constant*

Distribution coefficients are not equilibrium constants because they depend both on pH of the aqueous phase and the load of the resin. The distribution coefficient, $D$, is defined by the equation[14]

$$D = \frac{\text{mmol of metal ion/g dry resin}}{\text{mol/l of metal ions in solution}}. \quad (18)$$

According to the law of mass action the distribution coefficient can at certain pH be calculated from equilibrium constants by the following equation

$$D = \frac{[(MR)']}{[M']} = K_{MR}^{M,R} \cdot \frac{[R'] \cdot \alpha_{MR(H)}}{\alpha_{M(OH)} \cdot \alpha_{R(H)}}, \quad (19)$$

Table 4. Equilibrium constants of alkaline earth metal ion chelates with Dowex A-1 (R)

| | $\log K_{MR}^{M,R}$ | SD | $\log K_{MHR}^{H,MR}$ | SD |
|---|---|---|---|---|
| Be | 6.85 | 0.29 | | |
| Mg | 4.52 | 0.07 | 6.80 | 0.10 |
| Ca | 4.75 | 0.14 | 6.53 | 0.05 |
| Sr | 4.61 | 0.10 | 6.90 | 0.08 |
| Ba | 4.20 | 0.09 | 7.43 | 0.08 |

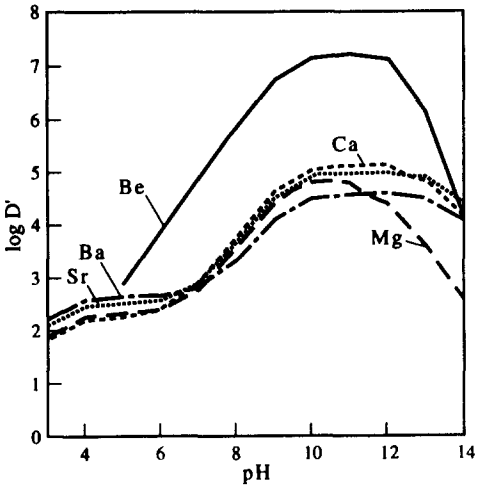


Fig. 4. Theoretically calculated distribution coefficients for alkaline earth metal ions with Dowex A-1.

where

$$\alpha_{MR(H)} = 1 + [H^+] \cdot K_{MHR}^{MR,H}. \quad (20)$$

Figure 4 gives distribution coefficients for the alkaline earth metal ions calculated from equilibrium constants according to the above equation. It is assumed that the metal ions are present in trace quantities and [R′] equals the capacity of the resin. The log $D$ curves plotted for the alkaline earth metal ions show a maximum at pH above 10 and at lower pH a strong pH dependence.

Distribution coefficients for alkaline earth metal ions with Dowex A-1 have been reported by several groups.[8,12,17] The studies have mostly been restricted to pH values below 8 and the results showed large divergences. The formation of protonated chelates in the resin phase explains the unexpected high distribution ratios obtained experimentally by several authors for calcium and other alkaline earth metal ions at lower pH values.

## CONCLUSION

Equilibrium constants for chelating resins are quite difficult to determine, which is reflected by the small number of papers published on the topic in the literature. The slow reactions make the equilibrium studies very time-consuming. The capacity and protonation constants of the resin are not easy to determine. According to Eger *et al.*[6] small amounts of organic material, most likely benzyliminodiacetic acid molecules, are liberated to the aqueous phase due to decomposition of the resin. This will to some

degree affect the equilibria. Potassium, used for the adjustment of the ionic strength will also have a slight diminishing effect on the equilibrium constant. No extra pH buffer, which could affect the equilibria, were used in this work.

The alkaline earth metal ions form relatively weak chelates with the Dowex A-1 resin. Equilibrium constants determined in a wide pH range show that predominantly 1:1 chelates are formed. The optimal region for determination of equilibrium constants for these metal ions is at pH above 8, where the interfering effects of hydrogen ions are small. At pH below 7 the alkaline earth metal ions form protonated 1:1 chelates with the resin. The precision and reliability of the method can be considered as good.

The complexation chemistry model and the equilibrium constants presented in this work for the chelating resin Dowex A-1 can be quite useful for practical purposes, where ion exchange equilibrium data are the basis when developing and optimizing separation procedures. The experimental results showed that the law of mass action and the equilibrium model proposed is valid over a wide pH range for IDA-based chelating resins. As natural ion-exchange resins also can contain carboxylic and amino groups as functional groups, equilibrium studies of this type can contribute to an increased understanding of ion-exchange processes taking place in our environment.

## REFERENCES

1. R. Hering, *Chelatbildende Ionenaustauscher*. Akademie, Berlin, 1967.
2. S. K. Sahni and J. Reedijk, *Coord. Chem. Rev.*, 1984, **59**, 1.
3. G. V. Myasoedova and S. B. Savvin, *CRC Crit. Rev. Analyt. Chem.*, 1986, **17**, 1.
4. L. Harju, *The Åbo Akademi Accelerator Annual Report*, p. 25, 1975.
5. H. Loewenschuss and G. Schmuckler, *Talanta*, 1964, **11**, 1399.
6. C. Eger, W. M. Anspach and J. A. Marinsky, *J. Inorg. Nucl. Chem.*, 1968, **30**, 1899.
7. L. Harju and H. Perus, *Finn. Chem. Lett.*, 1987, **14**, 178.
8. D. E. Leyden and A. L. Underwood, *J. Phys. Chem.*, 1964, **68**, 2093.
9. O. Szabadka, *Talanta*, 1982, **29**, 177.
10. L. Harju and S.-G. Huldén, *Talanta*, 1980, **27**, 815.
11. A. Ivaska and L. Harju, *Talanta*, 1975, **23**, 1051.
12. J. Sides and C. T. Kenner, *Anal. Chem.*, 1966, **38**, 707.
13. G. Schmuckler, in *Essays on Analytical Chemistry in Memory of Anders Ringbom*, E. Wänninen (ed), p. 371. Pergamon Press, Oxford, 1977.
14. A. Ringbom, *Complexation in Analytical Chemistry*. Wiley, New York, 1963.
15. A. Ringbom and L. Harju, *Anal. Chim. Acta*, 1972, **59**, 33.
16. M. Pesavento, R. Biesuz, M. Gallorini and A. Profumo, *Anal. Chem.*, 1993, **65**, 2522.
17. S.-C. Pai, P.-Y. Wung and R.-L. Lai, *Anal. Chim. Acta*, 1988, **211**, 257.

Pergamon

0039-9140(95)01431-4

*Talanta*, Vol. 42, No. 3, pp. 437–440, 1995

0039-9140/95 $9.50 + 0.00

# CHEMILUMINESCENCE DETERMINATION OF NITRATE WITH PHOTOCHEMICAL ACTIVATION IN A FLOW INJECTION SYSTEM

LIU RENMIN, LIU DAOJIE, SUN AILING and LIU GUIHUA

Department of Chemistry, Liaocheng Teachers College, Shandong, P.R. China

(*Received* 17 *May* 1994. *Revised* 19 *September* 1994. *Accepted* 23 *September* 1994)

**Summary**—A chemiluminescence flow injection system is described for the determination of nitrate, involving use of a laboratory-built flow-through photochemical reactor. Optimum analytical conditions were established. The linear range for nitrate is $7 \times 10^{-8}$–$1 \times 10^{-4}M$. The sampling frequency is 60 samples per hour. The relative standard deviation for $1 \times 10^{-7}$, $1 \times 10^{-6}$ and $1 \times 10^{-5}M$ nitrate is 0.97, 0.84 and 0.76%, respectively. The method has been applied to the determination of nitrate in natural water samples, and recoveries of 96–103% have been attained.

## INTRODUCTION

Photochemical analysis is based on the utilization of photochemical reaction in the process of analysis. It has been increasingly used in various fields, owing to its high sensitivity and selectivity. Flow injection analysis (FIA) offers high throughput, cost-effective performance and versatility. The combination of FIA technique with photochemical analysis provides a novel means for studies of photochemical analysis.[1–7] The amperometric determination of oxalate based on the photochemical reaction taking place in the reaction coil of a FIA system that was irradiated with visible light has been reported.[1] A second approach to the photochemical determination of this analyte was based on the use of an amperometric flow cell with several optical fiber, which irradiated the sample only in the flow cell.[2] A similar use of a photochemical reaction in FIA, with unstable compounds such as phenothiazines under ultraviolet radiation was reported.[3] The simultaneous determination of chlorprolazine and promethazine using different configurations for implementation of the photochemical reactions was also reported.[4] Another FIA system involving photochemical reaction is on-line photochemical oxidation of organoarsenicals to inorganic arsenic.[5] In our previous work, a flow-through photochemical reactor was constructed and used in a FIA system for the determination of nitrite based on its inhibitory effect on the photochemical reaction between iodine and ethylenediaminetetraacetic acid.[6] A second approach of our work to photochemical determination in a FIA system was simultaneous determination of iron(II) and iron(III) based on the photochemical reduction of iron(III)-1,10-phenanthroline complex to iron(II)-1,10-phenanthroline complex.[7]

When an acidified nitrate solution is irradiated with ultraviolet light, species like peroxonitrite are formed in the solution, which are the oxidants of luminol. Chemiluminescence was found to appear after mixing an alkaline luminol solution and an acidified nitrate solution initially irradiated with a mercury lamp. A conventional chemiluminescence method was established by Kalinichenko *et al.*[8]

In the present work, a flow-through photochemical reactor was constructed and used for the study of determination of nitrate in a FIA system, based on the photochemical activation and chemiluminescence reactions. The proposed method shows high sensitivity, selectivity and speed.

## EXPERIMENTAL

### *Reagents*

A standard stock solution of nitrate was prepared at $0.1M$ with analytical pure sodium nitrate. The working solution was prepared by diluting the stock solution with a sulfuric acid solution at pH 5.0.

The carrier solution was sulfuric acid solution, pH 5.0.

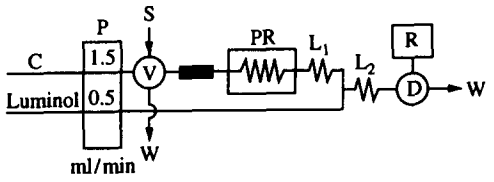


Fig. 1. Schematic diagram of the FIA system. P, Peristaltic pump; S, sample; V, injection valve; PR, photochemical reactor; L1, L2, connection tube; D, detector; R, recorder; C, carrier; W, waste.

The luminol reagent solution was $5 \times 10^{-5}M$ with $0.1M$ potassium hydroxide.

*Apparatus*

The flow injection manifold used is shown in Fig. 1. The peristaltic pump, injection valve and chemiluminescence detector are a FICT-8604 chemiluminescence analyzer (Jiangsu Electroanalytical Instrument Plant). The chemiluminescence signal was recorded with an XWT-S platform recorder (The Third Automatic Instrument Plant of Shanghai). A photochemical reactor (made in this laboratory, Fig. 2) was used in the FIA system. A iminodiacetyl ligand exchange resin column was used in the FIA system to remove the interference of $Fe^{3+}$, $Cu^{2+}$, $Co^{2+}$ and $Ni^{2+}$.

*Procedure*

The FIA system was connected up with PTFE tubing (0.8 mm i.d.) according to the arrangement shown in Fig. 1. The flow-rates of carrier and luminol reagent were adjusted according to the parameters given in Fig. 1. The sampling time was 20 sec and the injection time 40 sec. So the sampling frequency was 60 samples/hr. The chemiluminescence signal was recorded with the recorder. Nitrate was determined according to the peak height.

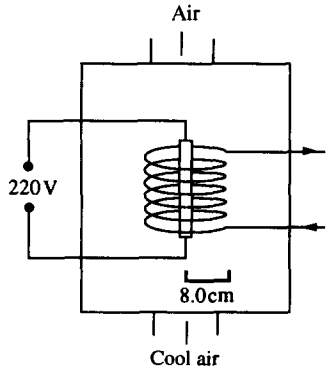


Fig. 2. Schematic diagram of the flow-through photochemical reactor.

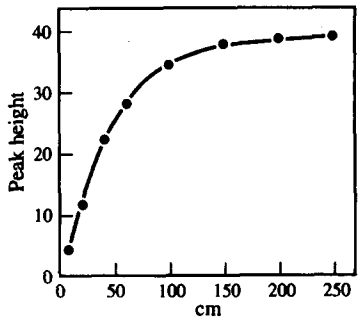


Fig. 3. Influence of the length of reaction tube of the photochemical reactor.

A series of nitrate standard solution was prepared and injected into the carrier before and after the sample runs.

## RESULTS AND DISCUSSION

*Photochemical reactor*

The main parts of the photochemical reactor are the light source and reaction tube. Nitrate has an absorption peak at 202 nm ($\varepsilon = 9500$) and an absorption peak at 304 nm ($\varepsilon = 9$). When the acidified nitrate solution is irradiated with ultraviolet light, species like peroxonitrite are formed, which are oxidants of luminol. A GGZ-125W high-pressure mercury lamp was used as the light source for the photochemical reactor.

An auger-type quartz tube was used as the reaction tube of the photochemical reactor. Its length was found to have a significant effect on the photochemical activation. Higher sensitivity can be obtained when a longer reaction tube is used. Figure 3 shows the influence of the length of reaction tube on the determination of $1.0 \times 10^{-6}M$ nitrate. It can be seen from Fig. 3 that the chemiluminescence intensity basically reached the maximum when a 200 cm long

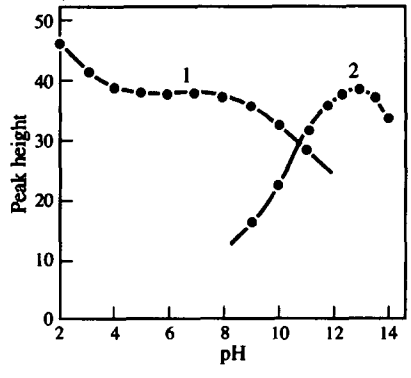


Fig. 4. Influence of pH. (1) Carrier; (2) luminal reagent.

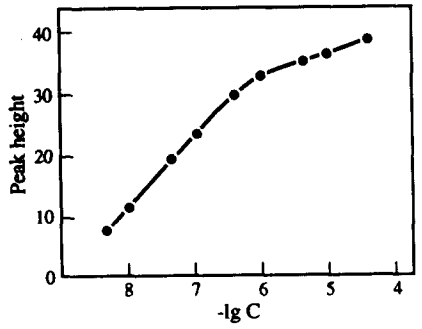


Fig. 5. Influence of the concentration of luminol.

reaction tube was used. In the following experiments, a 200 cm long reaction tube was used.

*Connection tube $L_1$ and $L_2$*

The lifetime of the photochemical product, like peroxonitrite, and the chemiluminescence between the product and luminol is relatively short. Hence, the length of the connection tubes $L_1$ and $L_2$ must be short. In the following experiments, the length of $L_1$ is 15 cm, and $L_2$ is 5 cm.

*Effect of pH*

Keeping the pH of the mixture of carrier and luminol reagent solution constant, the influence of the pH of the carrier on the determination of $1 \times 10^{-6}M$ nitrate was studied. Keeping the pH of the carrier constant, the influence of luminol reagent solution on the determination was studied. All the results are shown in Fig. 4. In the following experiments, the pH of the carrier was controlled at 5.0, and that of luminol reagent solution at 13.0.

*Concentration of luminol*

The influence of the concentration of luminol on the determination of $1.0 \times 10^{-6}M$ nitrate (Fig. 5). Figure 5 shows that high chemiluminescence intensity can be attained when a luminol of high concentration is used. However, a spill-over signal is given out by the chemiluminescence analyzer when the concentration of luminol is higher than $1 \times 10^{-4}M$, and this made the determination impossible. In the following experiments, a $5 \times 10^{-5}M$ luminol solution was used.

Table 1. Effect of foreign ions on the determination of $1.0 \times 10^{-6}M$ nitrate

| Foreign ion | Tolerated molar ratio (ion:nitrate) |
|---|---|
| $Cl^-$, $F^-$, $SO_4^{2-}$, $ClO_4^-$, $PO_4^{3-}$ | 10,000 |
| $Al^{3+}$, $Zn^{2+}$, $Cd^{2+}$, $Fe^{2+}$ | 1000 |
| $Br^-$, $VO_3^-$, $WO_4^{2-}$, $NH_4^+$ | 30 |
| $Mn^{2+}$ | 15 |
| $Fe^{3+}$ | 10 |
| $I^-$, $ClO_3^-$, $CrO_4^{2-}$, $NO_2^-$ | 2 |
| $Cu^{2+}$, $Co^{2+}$, $Ni^{2+}$ | 1 |
| $BrO_3^-$, $IO_3^-$, $MoO_4^{2-}$ | 0.5 |
| $Fe^{3+}$ | 0.1* |
| $Cu^{2+}$, $Co^{2+}$, $Ni^{2+}$ | 0.01* |

*No iminodiacetyl ligand exchange resin column in FIA system.

*Calibration*

According to the proposed procedure, the calibration graph was established with standard solutions of nitrate. The linear range for nitrate is from $7.0 \times 10^{-8}$ to $1.0 \times 10^{-4}M$. The precision for the determination of nitrate was measured by analysing $1.0 \times 10^{-7}$, $1.0 \times 10^{-6}$ and $1.0 \times 10^{-5}M$ nitrate standard solution 11 times. The relative standard deviations were 0.97, 0.84 and 0.76, respectively.

*Interference of foreign ions*

The interference of a number of foreign ions was studied by addition of such ions to $1.0 \times 10^{-6}M$ nitrate. The results listed in Table 1 show the high selectivity of the method (with a relative error of less than 5%).

*Applications*

Natural water samples were determined by the proposed method and the cadmium column

Table 2. Determination of nitrate in natural water samples

| Sample | Data obtained by the proposed method (*mg/l.*) | Data obtained by cadmium reduction method (*mg/l.*) | Relative (%) |
|---|---|---|---|
| Tap water | 0.64 | 0.67 | −4.5 |
| River water | 1.14 | 1.12 | 1.8 |
| Lake water | 2.06 | 2.10 | 1.9 |
| Well water | 0.88 | 0.90 | −2.2 |
| Deep well water | 1.26 | 1.23 | 2.4 |

Table 3. Recovery of nitrate from natural water samples

| Sample | Nitrate found (*mg/l.*) | Total nitrate present after addition (*mg/l.*) | Recovery (%) |
|---|---|---|---|
| Tap water | 0.64 | 1.66 | 102 |
| River water | 1.14 | 2.10 | 96 |
| Lake water | 2.06 | 3.09 | 103 |
| Well water | 0.88 | 1.86 | 98 |
| Deep well water | 1.26 | 2.26 | 100 |

reduction method.[9] The results are listed in Table 2.

Table 3 shows the results obtained with the proposed method for natural water samples to which 1.0 mg/l. nitrate was added. It can be seen from Table 3 that recoveries of 94–103% can be attained.

## REFERENCES

1. L. E. Leon, A. Rios, M. D. Luque de Castro and M. Valcarcel, *Analyst*, 1990, **115,** 1549.
2. L. E. Leon, A. Rios, M. D. Luque de Castro and M. Valcarcel, *Anal. Chim. Acta*, 1990, **234,** 227.
3. D. Chen, A. Rios, M. D. Luque de Castro and M. Valcarcel, *Analyst*, 1991, **116,** 171.
4. D. Chen, A. Rios, M. D. Luque de Castro and M. Valcarcel, *Talanta*, 1991, **38,** 1227.
5. R. H. Atallah and D. A. Kalman, *Talanta*, 1991, **38,** 167.
6. R. Liu and D. Liu, *Analyst*, 1991, **116,** 497.
7. R. Liu, D. Liu and A. Sun, *Analyst*, 1992, **117,** 1767.
8. I. E. Kalinichenko, N. F. Kushchevskaya and A. T. Pilipenko, *Zh. Anal. Khim.*, 1988, **43,** 1051.
9. The Compiling Group of Analytical Methods of Water and Waste Water of Bureau of Environmental Protection, Analytical Method for Water and Waste Water, Third Ed. p. 269. Chinese Environmental Science Press, Beijing, 1989.

Pergamon

0039-9140(95)01433-0

*Talanta*, Vol. 42, No. 3, pp. 441–447, 1995

0039-9140/95 $9.50 + 0.00

# DISSOCIATION PROPERTIES OF LAURENTIDE FULVIC ACID: IDENTIFYING THE PREDOMINANT ACIDIC SITES

ANDREW S. MATHUTHU,[1] JACOB A. MARINSKY[2] and JAMES H. EPHRAIM*[3]

[1]Department of Chemistry, University of Zimbabwe, P.O. Box MP 167, Mount Pleasant, Harare, Zimbabwe

[2]Department of Chemistry, State University of New York, Buffalo, NY 14214, U.S.A.

[3]Department of Water and Environmental Studies, Linköping University, S-581 83 Linköping, Sweden

(*Received* 20 *June* 1994. *Revised* 27 *September* 1994. *Accepted* 5 *October* 1994)

**Summary**—Application of the unified physicochemical approach to the description of the dissociation properties of Laurentide fulvic acid, extracted from peat, has shown that five predominant acidic moieties may account for the observed potentiometric titrations in aqueous medium. Information from non-aqueous titrations and titrations in presence of excess metal ions, *e.g.* $Cu^{2+}$ and $Eu^{3+}$, has shown that three of the acidic moieties are carboxylic in nature while the other two are of alcoholic nature. A comprehensive description of the dissociation properties of natural organic acids, as ligands, is advocated as a pre-requisite step towards understanding their interaction with metal ions in the environment.

The dissociation properties of humic substances have been shown to be complicated by two factors, *i.e.* heterogeneity with respect to molecular size leading to 'ionic strength' effects and functional group heterogeneity.[1] Recent advances have considerably influenced the conceptualization of humic substances in modeling efforts.[2–4] Modeling the role of humic substances in the distribution and mobility of trace metals in the environment, however, requires the identification of the factors that perturb the solution chemistry of these substances. In this paper, methods for the identification of these complicating factors developed earlier[5] have been employed for the Laurentide fulvic acid, a peat-extracted sample obtained from Concordia University, Canada.[6] In the unified physicochemical approach employed here, the humic substances are conceptualized as an assemblage of amphiphilic moieties with varying molecular size and acidic functionalities composed of four to five predominant acidic groups.[7] These sites have varying acidic strengths but they may be averaged. The usefulness of such an approach to identifying the complicating factors in the proton equilibria of humic substances has an analogy in coordination inorganic chemistry where adequate characterisation of the ligand is a pre-requisite for meaningful description of its interaction with metal ions.[8]

*Author to whom correspondence should be addressed.

## EXPERIMENTAL

Details of reagents and extraction procedure are described elsewhere.[5] Potentiometric titrations performed in aqueous medium as function of ionic strength are employed to estimate the ionic strength effects. A combination of titrations in non-aqueous media using an internal reference compound, parahydroxybenzoic acid, and titrations in aqueous media with varying amounts of $Eu^{3+}$ and $Cu^{2+}$ has facilitated an estimation of the relative abundances of the different acid groups present in the fulvic acid.[9,10] Insights into the ionic strength effects and functional group heterogeneity and combination thereof, have made possible the assignment of the predominant acidic moieties determining the dissociation properties of the fulvic acid, as before.[5]

## RESULTS

### *The effect of ionic strength on the measurable acid dissociation properties of Laurentide FA*

The acid dissociation properties measured for the Laurentide FA at three different FA concentration levels (50, 100 and 250 ppm) in sodium nitrate solutions at five different salt

concentration levels (0.0010, 0.010, 0.10, 1.0 and 5.0$M$) are shown in Fig. 1. In this figure, representative data that were compiled at the conditions specified are expressed as plots of $p(K_a^{app})_\alpha$, defined by the equation below

$$p(K_a^{app})_\alpha = pH - \log\left(\frac{\alpha}{(1-\alpha)}\right) \quad (1)$$

*vs.* $\alpha$, the degree of association measured at each step in the titration with standard base. In equation (1) $(K_a^{app})_\alpha$ refers to the overall dissociation constant of the Laurentide FA measured at a particular $\alpha$ value. The overall degree of dissociation, $\alpha$, is obtained from the following expression:

$$\alpha = \frac{\Sigma A_e^-}{\Sigma HA_i} \quad (2)$$

where $\Sigma A_e^-$ is defined as

$$\Sigma A_e^- = bV_b + h_e V_s \quad (3)$$

and $\Sigma HA_i$ is the total titratable acid capacity of the fulvic acid. In equation (3), $V_b$ is the volume in ml of b molar base added and $h_e$ is the proton concentration, while $V_s$ is the total volume of the solution in ml.

The fact that the $p(K_a^{app})_\alpha$ *vs.* $\alpha$ plots obtained at salt concentration levels of 1.0 and 5.0$M$ $NaNO_3$ are almost superimposable in Fig. 1, as they were for the Armadale FA[5] shows once again that a Donnan potential term is no longer operative at these concentrations. At these higher salt concentrations, the concentration of the counter ion in the solution is practically identical to its concentration in the solvent sheat domain of the fulvic acid molecules. The increase in $p(K_a^{app})_\alpha$ with $\alpha$ at these elevated salt concentration levels can, on this basis, be attributed solely to the functional group heterogeneity of the fulvic acid.[5] By subtracting this curve, $p(K_a^{app})_\alpha$ *vs.* $\alpha$ at $NaNO_3$ concentration $\geqslant 1.0M$, from similar separate curves resolved at the lower salt concentration levels ($[NaNO_3] = 0.0010$, 0.01 and 0.1$M$), the unique contribution of the Donnan potential term, $\Delta pK_a^{app}$, to the measurable acid dissociation properties of the Laurentide fulvic acid at the three different salt concentration levels is made accessible (Fig. 2).

The observed response to each 10-fold change in salt concentration is, as it was for the Armadale Horizon Bh fulvic acid,[5] sizeably smaller than the value of unity projected for molecules exhibiting macromolecular properties.[11] This discrepancy has been attributed to the fact that only a fraction of the soil fulvic acid molecules is large enough to develop the separate phase properties operative in the Gibbs–Donnan based model. The molecular size

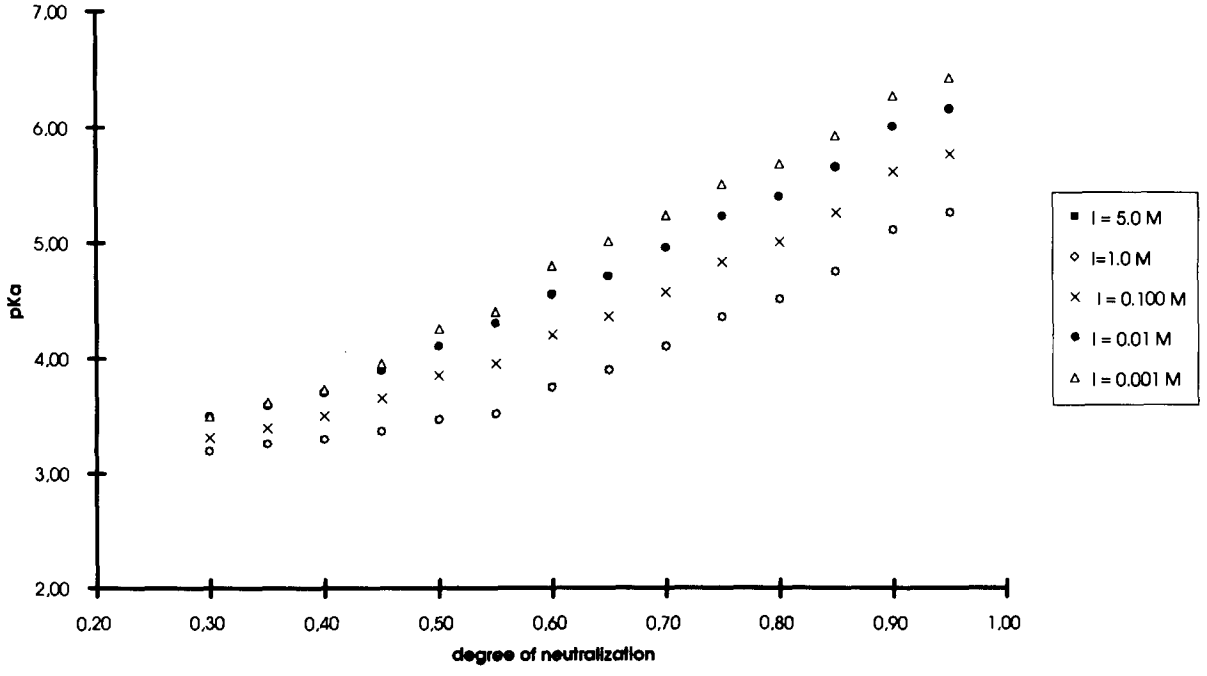


Fig. 1. Plots of $p(K_a^{app})_\alpha$ *vs.* $\alpha$ for Laurentide fulvic acid, LFA, as a function of ionic strength and FA concentration. (Note: $I = 1.0$ and $I = 5.0M$ curves were exactly superimposable.)

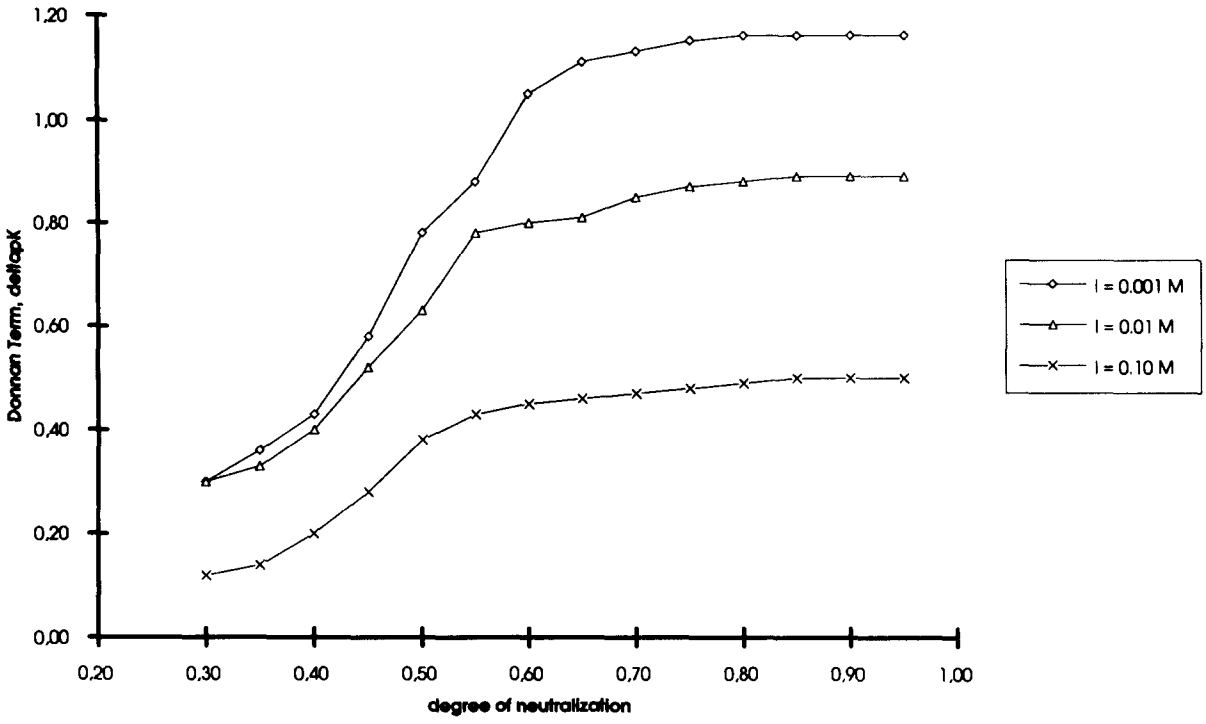


Fig. 2. Variation of the Donnan potential term, $\Delta pK_x$, with degree of dissociation of Laurentide fulvic acid at three different ionic strengths.

heterogeneity existent in humic substances has been exhibited by a number of molecular weight measurements.[12-14]

The $\Delta pK_a^{app}$ values resolved in this research are somewhat smaller than those measured earlier for the Armadale Horizons Bh fulvic acid.[5] On the basis of the Gibbs–Donnan-based interpretation of these changes in the Donnan potential term, one can conclude that the fraction of fulvic acid molecules large enough to exhibit macromolecular properties is smaller in the Laurentide FA over the salt concentration range examined. The fact that the rate of increase in $p(K_a^{app})\alpha$ for each 10-fold increase in salt concentration ($M_{s,2} = 10M_{s,1}$) is larger for the Laurentide FA, however, is believed to show that the Laurentide FA is, on a relative basis, polydispersed to a greater extent than the Armadale FA.[15]

*The employment of acid dissociation studies in non-aqueous media to determine the relative abundances of carboxylic* (R-COOH) *and alcoholic* (R'-$CH_2$-OH) *moieties that constitute the weak acid site heterogeneity of the Laurentide fulvic acid*

The results that were obtained in a representative experiment carried out with *para*-hydroxybenzoic acid, the internal reference standard used in the non-aqueous acid dissociation studies of the Laurentide fulvic acid source, are summarized in Table 1. They show that the measurable acid content in non-aqueous media is identical with the 7.72 mmol/g

Table 1. Functional group analysis of Laurentide fulvic acid in DMF using pHBA as an internal reference standard

| Acid used (*g*) | | Equiv. *ml* of T-nBAH | | Capacities (*meq*/*g* of acid) | | |
|---|---|---|---|---|---|---|
| pHBA | FA | 1st | 2nd | -COOH | -OH | Total |
| 0.032414 | — | 4.950 | 9.900 | 7.24 | 7.24 | — |
| 0.032414 | — | 4.950 | 9.900 | 7.24 | 7.24 | — |
| 0.016207 | — | 2.425 | 4.950 | 7.24 | 7.24 | — |
| 0.032414 | 0.0189 | 7.180 | 12.980 | 5.594* | 2.134* | 7.726* |
| 0.032414 | 0.0209 | 7.41 | 13.306 | 5.594* | 2.130* | 7.730* |
| Average capacities: | | | | 5.597* | 2.131* | 7.728* |

Molarity of T-nBAH = 0.04841.
*After subtraction of pHBA contribution.

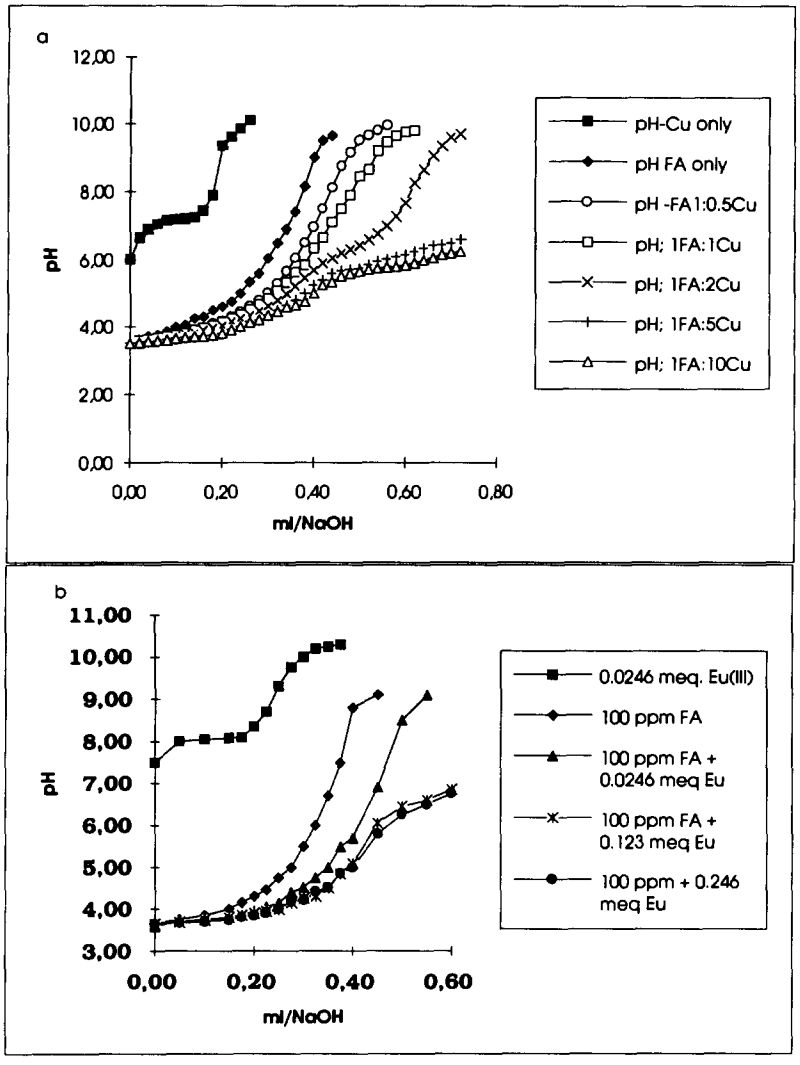


Fig. 3. The enhancement of proton release affected in LFA by increasing amounts of (a) $Cu^{2+}$ and (b) $Eu^{3+}$.

value reached in the aqueous media studies. Slightly more than 73.4% of the acid sites are attributable to carboxylic acid (RCOOH) moieties while the remaining weak acid functionalities are alcoholic ($R'CH_2OH$).

*Studies of proton release enhancement affected in Laurentide fulvic acid samples by the presence of excess* $Cu^{2+}$ *and* $Eu^{3+}$ *ion to provide additional site heterogeneity insights*

The enhancement of proton release affected in Laurentide fulvic acid samples by increasing the presence of $Cu^{+2}$ and/or ($Eu^{+3}$) from zero to greater than a two-fold excess, on a molar charge basis, may be observed by referring to Fig. 3a and b. The plots of p{H} *vs.* aliquots of standard base added that are presented in these figures also include p{H} data compiled during addition of base to the metal ions alone. Referring first to the neutralization studies carried out to study the extra proton release in the presence of Cu(II): when Cu(II) ion alone is titrated with base, the pH immediately rises from 5.5 to 7.0. Further addition of base results in a slow rise in pH. The system remains buffered until the first hydrolysis step $[Cu(II) + nOH = Cu(OH)_n]$ is complete. At this point the pH rises steeply to about 10.5. In systems where FA greatly exceeds the Cu(II), the titration curves resemble those of FA alone but with the equivalence point shifted to higher volumes of NaOH. When FA and Cu(II) are present in equivalent amounts on a millimoles of charge basis, there is a narrow buffered region between pH 6 and 7 owing to the hydrolysis of the small quantity of uncomplexed Cu(II).

In the presence of excess Cu(II), the shape of the titration curve remains unaffected up to a pH of 6.0. At this point the hydrolysis of uncomplexed Cu(II) produces an extended pH-buffered region. From careful extrapolation of the curves which are made to follow the general shape of the FA titration curve, the extra $H^+$ released by chelation of Cu(II) has been estimated to be $45 \pm 3\%$.

In the titration of Eu(III) alone with NaOH, buffering occurs at a pH of about 8; the system remains buffered until inception of the final hydrolysis step where the pH rises sharply to about 10. In titrations of FA where FA exceeds Eu(III) sizeably [5FA:1 Eu(III) in millimoles], the complete removal of Eu(III) by complexation is indicated by the absence of a buffered region. When the ratio is approximately 1FA:1Eu in mmoles, the titration curve exhibits the same shape as the FA titration curve up to a pH of 6.5; a flattened region from pH 7.0 to 7.5 persists until the hydrolysis of Eu(III) is complete. The sharp pH rise to about 10 when this happens is not shown. Analysis of the appropriate curves in this figure indicates that the extra release of $H^+$ ion by chelation of Eu(III) is approximately $26.6 \pm 3\%$. The extra release of protons observed in the presence of excess Cu(II) and Eu(III) arises from the coordination of these multivalent metal ions to ligand combinations that yield complexes of extremely high stability. Such coordination possibilities are facilitated by the close proximity of the very weak phenolic OH acid groups, not otherwise detectable in the FA molecule with standard neutralization procedures, to a fraction of the weak acid functionalities that are detectable in standard neutralization methods.

Since the release from the Laurentide FA of extra protons by Cu(II) is almost a factor of two greater than by Eu(III) just as it was for the Armadale FA, one can deduce as before[5] that, of two bidentate components of the FA molecule accessible to these metal ions, only one complexes both of them strongly enough to affect such a release of extra protons. In the literature the dihydroxyl groups are strongly bound to both Cu(II) and Eu(III)[16] and a dihydroxy moiety has, on this basis, been identified as the likely bidentate functionality in the FA molecule from which the release of extra acidity can be affected by both Cu(II) and Eu(III) ions.[5]

Reference to the literature[16] influences the tentative assignment of the second bidentate group to a salicylic acid-like moiety. The stability constant of the Cu-salicylate chelate is $4.6 \times 10^{10}$, more than six orders of magnitude greater than the analogous Eu-salicylate complex ($3 \times 10^4$). The free energy of formation of the Cu(II) chelate is large enough to promote release of $H^+$ ions from the -OH group ($pK = 13$) *ortho* to the carboxylic acid ($pK = 3$). The extra release of protons in the presence of excess Cu(II) ions is thus compatible with the above assignment of the second bidentate group in the FA molecule as it was for the Armadale Horizons FA.[5]

*Analysis of functional site heterogeneity of the Laurentide fulvic acid via abundance and acid strength assignments*

It has been shown that the acid dissociation feature provided by plots of $p(K_a^{app}{}_{I \geq 1.0})_\alpha$ *vs.* $\alpha$ are completely attributable to the site heterogeneity of the Laurentide fulvic acid.[5] With such information made available, the assignment of acid strengths to functional site possibilities, as well as the selection of suitable abundance for them, become feasible. The quantities of carboxylic and hydroxyl acidity in a particular FA source, accessible from the non-aqueous acid dissociations studies, present a starting point for these estimates. The proton release enhancement studies further facilitate this task.

The additional release of proton ($26 \pm 3\%$) in the presence of excess Eu(III) is about equal to the quantity of weak acid assignable to the OH functionality ($\sim 26.6\%$) in the nonaqueous titrations; much more weakly acidic OH, unaccessible to both the aqueous and non-aqueous studies, can be presumed to be in a position *ortho* to this OH moiety to account for the extra proton release through highly favored chelation reactions with both the Cu(II) and the Eu(III).

The additional proton release of $\sim 17\%$, observed in the presence of excess Cu(II), can be attributed to salicylic acid-like sites whose phenolic OH group, $p(K_a) \sim 13$, would also be expected to escape detection in the aqueous and non-aqueous studies. The fact that the formation constant of Cu(salicylate) is six orders of magnitude larger than the formation constant of Eu(salicylate)$^+$ would account for this result, as pointed out earlier.

On the basis of the above reasoning, the abundance of the acidic alcohol assigned to the FA molecule was assumed to be $\sim 26\%$. The

$pK_a$ of approximately 6 initially assigned to this site facilitated resolution of the abundance and $pK_a$ assignments eventually made. The estimate that a salicylic acid-like group was responsible for the ~17% increase in proton release in the presence of excess Cu(II) led to a $pK_a$ assignment of approximately 3 for the carboxylic acid group presumed to be associated with it. From the acid dissociation studies in aqueous media, it was also noted that approximately 30% of the acidity had to be associated with a fairly strong carboxylic acid ($pK_a \approx 1.7$) moiety. Trial and error estimates of abundances and acid strengths, influenced by the above information, were examined much as they had been in an earlier study.[5] It was found necessary to introduce a third carboxylic acid group with a $pK_a$ of ~4.2 and a second hydroxyl group with a $pK_a$ smaller than the single value of 6 initially assigned to approximate the dissociation properties experimentally measured for the Laurentide fulvic acid in $NaNO_3$ solution at a concentration level of 1.0*M* or higher. The Hendersson-Hasselbalch equation was used to facilitate selection of optimum site parameters. In the program developed for this purpose, the experimental p{H} range encountered in the fulvic, acid dissociation studies at $I \geqslant 1.0M$ was examined in a sequence of steps listed below. First $\alpha_n$, the degree of dissociation of the $n$th acid site at a selected p{H} value was evaluated with equation (1a) employing the dissociation constant assigned to the $n$th site for the series of computations:

$$\log\left(\frac{\alpha_n}{(1-\alpha_n)}\right) = p(K_{a_n}^{intr}) - pH. \qquad (1a)$$

Each of the five $\alpha_n$ values resolved at the selected p{H} value was then multiplied by $A_n$, the fractional abundance assessed for each of the corresponding $n$ sites. To compute the overall degree of dissociation, $\alpha^o_{calc}$, for comparison with the experimental value, $\alpha^o_{exp}$, at each p{H} value selected the $\alpha_n A_n$ values were added together as shown in the following equation

$$\alpha^o_{calc} = \Sigma \alpha_n A_n. \qquad (4)$$

The trial and error adjusted $pK_{a,n}$ and $A_n$ parameters eventually used and the $\alpha^o_{calc}$ values that they resolve are listed in Table 2. The $\alpha^o_{exp}$ values are presented in this table as well, for comparison with the $\alpha^o_{calc}$ values to show the excellent agreement reached between them by the approach that has been described.

## CONCLUSIONS

The dissociation properties of Laurentide FA, isolated from peat, have been studied by following the unified physicochemical approach developed earlier.[1] In such an exercise, it was determined that the observed dissociation properties of the Laurentide fulvic acid may be described by considering five predominant acidic moieties (three of carboxylic nature and

Table 2. Comparison of experimentally based overall degree of dissociation, $\alpha^o_{exp}$, of Laurentide fulvic acid in 1.00*M* $NaNO_3$ with the summation of computed contributions of five different acid sites to overall degree of dissociation, $\alpha^o_{calc}$

| Site identity | $pK^{int}_{a,n}$ | Site abundance ($A_n$) | Acid moiety |
|---|---|---|---|
| 1 | 1.7 | 0.32 | Carboxylic |
| 2 | 3.0 | 0.21 | Carboxylic |
| 3 | 4.0 | 0.204 | Carboxylic |
| 4 | 5.1 | 0.14 | Alcoholic OH |
| 5 | 6.5 | 0.126 | Alcoholic OH |

| $\alpha^o_{calc} = \Sigma \alpha_n A_n$ | | | | | | | |
|---|---|---|---|---|---|---|---|
| p{H} | $\alpha_1 A_1$ | $\alpha_2 A_2$ | $\alpha_3 A_3$ | $\alpha_4 A_4$ | $\alpha_5 A_5$ | $\alpha^o_{calc}$ | $\alpha^o_{exp}$ |
| 3.434 | 0.314 | 0.154 | 0.044 | 0.003 | 0.000 | 0.514 | 0.511 |
| 3.516 | 0.315 | 0.161 | 0.050 | 0.004 | 0.000 | 0.530 | 0.526 |
| 3.607 | 0.316 | 0.168 | 0.059 | 0.004 | 0.000 | 0.548 | 0.549 |
| 3.725 | 0.317 | 0.177 | 0.071 | 0.006 | 0.000 | 0.570 | 0.570 |
| 3.869 | 0.318 | 0.185 | 0.087 | 0.008 | 0.000 | 0.598 | 0.598 |
| 3.953 | 0.318 | 0.189 | 0.097 | 0.009 | 0.000 | 0.613 | 0.616 |
| 4.178 | 0.319 | 0.197 | 0.123 | 0.015 | 0.001 | 0.654 | 0.657 |
| 4.324 | 0.319 | 0.201 | 0.138 | 0.020 | 0.001 | 0.679 | 0.681 |
| 4.725 | 0.320 | 0.206 | 0.172 | 0.042 | 0.002 | 0.741 | 0.744 |
| 5.014 | 0.320 | 0.208 | 0.186 | 0.063 | 0.004 | 0.781 | 0.783 |
| 5.359 | 0.320 | 0.209 | 0.195 | 0.090 | 0.009 | 0.823 | 0.827 |
| 5.833 | 0.320 | 0.210 | 0.201 | 0.118 | 0.022 | 0.871 | 0.874 |
| 6.453 | 0.320 | 0.210 | 0.203 | 0.134 | 0.060 | 0.927 | 0.924 |
| 6.794 | 0.320 | 0.210 | 0.204 | 0.137 | 0.084 | 0.954 | 0.949 |

two of alcoholic OH). The smaller effect of bulk electrolyte on its dissociation properties has permitted the postulation that a smaller fraction of the Laurentide fulvic acid is large enough to exhibit macromolecular properties, as compared to the Armadale Horizons.[1] The approach employed in this study to characterise the acidic properties of Laurentide FA is recommended as an incumbent step towards understanding the interaction between natural organic acids and metal ions. Its compatibility with already existent chemical speciation programs cannot be overemphasized.

*Acknowledgements*—Financial support from NSF-USA for the experimental work is gratefully acknowledged. Support from The Swedish Natural Science Research Council, NFR, during the preparation of manuscript and for travel to one of us (JHE) is additionally acknowledged. We are grateful to an unknown referee for his/her constructive comments.

## REFERENCES

1. J. A. Marinsky and J. Ephraim, *Environ. Sci. Technol*, 1986, **20,** 349.
2. E. Tipping and M. A. Hurley, *Geochim. Cosmochim. Acta*, 1992, **56,** 3627.
3. J. C. M. de Wit, W. H. van Riemsdijk, M. M. Nederlof, D. G. Kinniburgh and L. K. Koopal, *Anal. Chim. Acta*, 1990, **232,** 189.
4. B. M. Bartschat, S. E. Cabaniss and F. M. M. Morel, *Environ. Sci. Technol.*, 1992, **26,** 284.
5. J. Ephraim, S. Alegret, A. Mathuthu, M. Bicking, R. L. Malcolm and J. A. Marinsky, *Environ. Sci Technol.*, 1986, **20,** 357.
6. D. S. Gamble, C. H. Langford and J. P. K. Tong, *Can. J. Chem.*, 1976, **54,** 1239.
7. J. H. Ephraim and B. Allard, in *Ion Exchange and Solvent Extraction*, J. A. Marinsky and Y. Marcus (eds), Vol. 11, Chap. 6. Marcel Dekker, New York, 1993.
8. F. A. Cotton and G. Wilkinson, *Advanced Inorganic Chemistry. A Comprehensive Text*, 4th Edn. Wiley-Interscience, New York, 1980.
9. J. H. Ephraim, *Talanta*, 1989, **36,** 379.
10. J. H. Ephraim, M. M. Reddy and J. A. Marinsky, *Lecture Notes in Earth Sciences*, Vol. 33, p. 263. Springer, Berlin, 1991.
11. J. A. Marinsky, *J. Phys. Chem.*, 1985, **89,** 5294.
12. E. H. Hansen and M. Schnitzer, *Anal. Chim. Acta*, 1967, **46,** 247.
13. J. A. Marinsky and M. M. Reddy, *Anal. Chim. Acta*, 1990, **232,** 123.
14. G. R. Aiken and R. L. Malcolm, *Geochim. Cosmochim. Acta*, 1987, **51,** 2177.
15. M. Nordén, PhD. Thesis. Linköping University, Sweden, 1994.
16. L. G. Sillén and A. E. Martell, *Stability Constants of Metal Ion Complexes*. The Chemical Society, Burlington House, London, 1964.

Pergamon

0039-9140(95)01432-2

*Talanta*, Vol. 42, No. 3, pp. 449–453, 1995

0039-9140/95 $9.50 + 0.00

## SHORT COMMUNICATION

# DEVELOPMENT OF A HIGH-PERFORMANCE LIQUID CHROMATOGRAPHIC SYSTEM WITH ENZYME REACTORS FOR THE DETERMINATION OF *N*-ACETYL BRANCHED-CHAIN AMINO ACIDS

NOBUTOSHI KIBA, YUKIO OYAMA and MOTOHISA FURUSAWA

Department of Applied Chemistry and Biotechnology, Faculty of Engineering, Yamanashi University, Kofu 400, Japan

(*Received* 19 *July* 1994. *Revised* 26 *September* 1994. *Accepted* 27 *September* 1994)

**Summary**—Immobilized enzymes were used as column reactors in a high-performance liquid chromatographic system for the specific detection of *N*-acetyl branched-chain amino acids (AcBCAs) such as *N*-acetyl-L-valine (AcVal), *N*-acetyl-L-leucine (AcLeu) and *N*-acetyl-L-isoleucine (AcIle). Aminoacylase and leucine dehydrogenase were immobilized onto poly(vinyl alcohol) beads. The AcBCAs were separated as three peaks on a Capcell $C_1$ SG120 column with 0.03*M* phosphate buffer (pH 8.0). Aminoacylase was capable of hydrolysing the AcBCAs to amino acids, which react with β-nicotinamide adenine dinucleotide ($NAD^+$) in the presence of leucine dehydrogenase. The reduced nicotinamide adenine dinucleotide (NADH) produced was monitored fluorimetrically. The calibration graphs were linear from 4 to 200μ*M* for AcVal and AcLeu, and from 5 to 300μ*M* for AcIle; detection limits for AcVal, AcLeu and AcIle were 2, 2 and 3μ*M*, respectively. The immobilized aminoacylase reactor should be renewed every 5 days owing to a poor stability of aminoacylase.

## INTRODUCTION

*N*-Acetylation is a reaction of amino acid metabolism, and the increase in the AcBCSs levels in body fluids is known to occur in maple syrup urine disease which is caused by inborn errors of metabolism of branched-chain amino acids (BCAs).

Usually, *N*-acetyl amino acids are determined by gas chromatography–mass spectrometry.[1–3] In a second approach, *N*-acetyl amino acids are hydrolyzed, and the resulting amino acids are quantitated by high-performance liquid chromatography (HPLC) using *o*-phtalaldehyde precolumn derivatization.[4,5] Recently, Kawakami *et al.*[6] developed a HPLC method based on the pre-column derivatization with 9-anthryldiazomethane and fluorimetric monitoring. However, the pre-column techniques are time-consuming.

This paper described the use of immobilized enzymes as post-column reactor in an HPLC system for the selective determination of AcBCAs. The AcBCAs from separation column were hydrolyzed in immobilized aminoacylase reactor and the BCAs formed were mixed with $NAD^+$ solution. The $NAD^+$ was reduced to NADH in the immobilized leucine dehydrogenase reactor and the NADH formed was monitored by fluorescence detection.

Immobilized aminoacylase reactors have been used for the resolution of racemic mixtures of *N*-acetylamino acids and for the preparation of amino acids,[7,8] but there is no paper concerning their application to the determination of the compounds. Leucine dehydrogenase from *Bacillus sphaericus* was immobilized and used in flow-injection systems[9,10] and in HPLC system[11] as reactor for the determination of BCAs. In this work, leucine dehydrogenase from *Bacillus stearothermophilus*[12] that is stable at higher temperature was used.

## EXPERIMENTAL

### *Chemical and reagents*

*N*-acetyl-L-valine, *N*-acetyl-L-leucine and *N*-acetyl-L-isoleucine were purchased from Sigma. Aminoacylase (EC 3.5.1.14, from Porcine kidney, grade III, AA), was obtained from Sigma

with an activity of 110 U/mg with AcLeu as substrate at pH 8.0 at 30°C. Leucine dehydrogenase (EC 1.4.1.9, from *Bacillus stearothermophilus*, LeuDH) was purchased from Unitika (Osaka) with an activity of 42 U/mg with Leu as substrate at pH 10.5 at 30°C. Poly(vinyl alcohol) beads were GS-500 (13 $\mu$m diameter) and were obtained from Showa Denko (Tokyo). $NAD^+$ (98%, free acid) and NADH (disodium salt, 98%) were from Kohjin (Tokyo) and Capcell $C_1$ SG120 was from Shiseido (Tokyo). All other chemicals were of analytical reagent grade.

Phosphate buffer (pH 8.0) consisting of 0.03*M* potassium dihydrogen phosphate–0.03*M* disodium hydrogen phosphate was prepared. $NAD^+$ solution [20m*M* $NAD^+$ in 0.03*M* phosphate buffer (pH 7.0)] and 0.3*M* carbonate buffer (pH 10.0) consisting of 0.3*M* sodium carbonate–sodium hydrogen carbonate were prepared daily.

*Preparation of enzyme reactors*

AA and LeuDH were immobilized onto the poly(vinyl alcohol) beads. The method of amination of the beads was similar to that described by Matsumoto *et al.*.[13] The beads (2 g) were suspended in 50 ml of 50% chloromethyloxirane in 3*M* sodium hydroxide solution at 50°C for 1.5 hr, followed by reaction with concentration aqueous ammonia (50 ml) at 40°C for 3 hr. The attached amine amounted to 3.0 meq./g dry beads. The aminated beads were packed into columns. Glutaraldehyde solution (4%) in 0.1*M* sodium hydrogen carbonate was pumped through the columns at 0.3 ml/min for 3 hr at *ca.* 20°C and the columns were washed with deaerated water at 0.5 ml/min for 30 min. AA solution (20 mg in 10 ml of 0.1*M* phosphate buffer, pH 7.0) was recycled through the column (50 × 4 mm i.d., stainless-steel) for 6 hr at 0.2 ml/min at about 15°C. During the immobilization procedure the enzyme solution was kept at 2–5°C in an ice-box. After the immobilization procedure, AA activity in the solution was measured with AcLeu as substrate at pH 8.0 at 30°C. AA was immobilized with a 46% yield; it was assumed that inactivation of AA during the immobilization process did not occur. LeuDH solution (3 mg in 10 ml of 0.1*M* phosphate buffer, pH 7.0) was circulated through the column (2 cm × 4 mm i.d., stainless-steel) for 3 hr at 0.2 ml/min at about 20°C. LeuDH activity in the solution was measured with Leu as substrate at pH 10.0 at 30°C. LeuDH was immobilized with a 98% yield; it was assumed that inactivation of LeuDH during the immobilization did not occur.

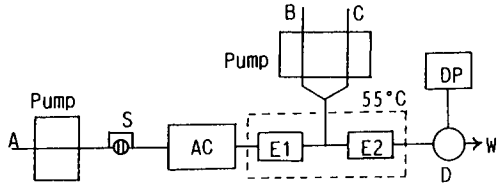


Fig. 1. Flow diagram of liquid chromatographic system for the determination of *N*-acetyl branched-chain amino acids. (A) Mobile phase (0.03*M* phosphate buffer, pH 8.0), 0.4 ml/min, (B) 20 mM $NAD^+$ solution (0.2 ml/min), (C) 0.3*M* carbonate buffer (pH 10.0), 0.2 ml/min, (S) injection valve with a 30 $\mu$l loop, (AC) analytical column (250 × 4 mm i.d.), (E1) immobilized aminoacylase reactor (50 × 4 mm i.d.), (E2) immobilized leucine dehydrogenase reactor (20 × 4 mm i.d.), (D) fluorimeter (*Ex* 340 nm, *Em* 465 nm), (DP) data processor, (W) waste. E1 and E2 were kept at 55 °C.

*HPLC system*

A schematic diagram of the system is shown in Fig. 1. The system consisted of a LC pump (Hitachi L-6000) and a reagent-delivery pump (Kyowa Seimitsu KHU-W-52), an injection valve (Sanuki SVI-6M2) equipped with a 30-$\mu$l loop, an analytical column (250 × 4 mm i.d., stainless-steel column), an immobilized AA reactor, an immobilized LeuDH reactor, a spectrofluorimeter (Jasco FP-210) [*Ex* 340 nm, *Em* 465 nm] equipped with flow-through cell (15 $\mu$l) and a data processor (System Instrument Chromatocorder II). The analytical column was filled with Capcell $C_1$ SG120 (5 $\mu$m). The reactors were kept constant at 55°C in a water bath. The mobile phase was the 0.03*M* phosphate buffer (pH 8.0), which was pumped at 0.4 ml/min and $NAD^+$ solution and the carbonate buffer were pumped at 0.2 ml/min each.

A serum sample was filtered through an ultrafiltration membrane (Advantec 0Q100, nominal molecular weight cut-off 10,000). The filtrate (30 $\mu$l) was injected into the system.

*Reference method*

The AcBCAs content in serum samples was determined for comparison with gradient cation-exchange chromatographic method with post-column derivatization with *o*-phthalaldehyde and fluorimetric detection.[14] The separation column was TSK gel SCX (5 $\mu$m) (30 cm × 7.8 mm i.d.). Serum (200 $\mu$l) was mixed with 0.6*M* ice-cold perchloric acid (400 $\mu$l). The mixture was centrifuged and the clean supernatant was filtered through the ultrafiltration

membrane. For the determination of BCAs a part of the filtrate (10 $\mu$l) was injected into the liquid chromatographic system, and the other portion (300 $\mu$l) was mixed 1.5$M$ tris(hydroxymethyl)aminomethane solution (700 $\mu$l) and 20 $\mu$l of AA solution (10 mg of AA in 1.0 ml of 0.1$M$ phosphate buffer) and was incubated 60 min at 35°C. After the hydrolysis the solution was filtered and for the determination of BCAs plus AcBCAs the filtrate (40 $\mu$l) was injected into the liquid chromatographic system.

## RESULTS AND DISCUSSION

### *Properties of immobilized enzyme reactors*

The properties of immobilized LeuDH were first evaluated without using the analytical column or the immobilized AA reactor. The influence of pH on the enzyme reaction was studied over the pH range 9–11 with carbonate buffer. A standard solution of Leu (20$\mu M$) was injected into the carrier stream (0.03$M$ phosphate buffer, pH 8.0) and mixed with a mixture of $NAD^+$ solution and 0.3$M$ carbonate buffer at various pH values before reaching the reactor. The optimum pH for the enzyme reaction was about 10.0. The reactor was placed in a waterbath and the temperature was varied between 45 and 70°C. The reactor exhibited the highest activity at 60°C. The effect of the concentration of $NAD^+$ in the reactor was examined in the range 1–6m$M$. The peak height was constant at concentrations greater than 4m$M$. The peak height decreased linearly as the flow-rate was increased from 0.6 to 1.2 ml/min. With 4m$M$ $NAD^+$ in carbonate buffer (pH 10.0) at 55°C and at a flow-rate of 0.8 ml/min, 50$\mu M$ Leu was converted by LeuDH with a 89% yield. Under the same conditions, the relative activities of the immobilized LeuDH for Leu, Ile and Val were 100, 100, 95, respectively. The reactor was used for 8 hr/day and was stored at 4°C in 0.1$M$ phosphate buffer (pH 7.0) when not in use. The activity remained at 95% of the initial value for 4 weeks. The peak heights were plotted against the concentrations of the amino acids. The concentration range of linear response was from 1 to 300$\mu M$. The detection limit was 0.7$\mu M$.

The immobilized AA reactor was used in the flow injection mode by omitting the analytical column to evaluate the efficiency of amino acids production from each AcBCA at various temperatures. The reactor was placed in a water bath and the temperature varied from 45 to 70°C in 0.03$M$ phosphate buffer (pH 8.0) at a flow-rate of 0.4 ml/min. The peak height of the liberated amino acid was determined by injecting AcVal, AcLeu and AcIle standards (10$\mu M$). A conversion efficiency of 100% was obtained above 50°C for all AcBCAs. The efficiencies for AcVal, AcLeu and AcIle were maintained at a constant value for 17, 15 and 5 days, respectively, when the reactor was used for 8 hr per day and was stored at 4°C in 0.1$M$ phosphate buffer (pH 7.0) when not in use.

### *Separation of the AcBCAs*

The separation of mixtures of AcVal, AcIle and AcLeu was carried out by reversed phase chromatography on a Develosil ODS-HG-5 (5 $\mu$m) column (150 × 4.6 mm i.d.) with 0.03$M$ phosphate buffer (pH 8.0)–methanol (95:5, v/v) as mobile phase. The use of the mobile phase led to the inactivation of immobilized AA within 2 days, because AA is denatured by methanol. Separation of the AcBCAs was effected on a Capcell $C_1$ SG120 (5 $\mu$m) column (250 × 4 mm i.d.) with 0.03$M$ phosphate buffer (pH 8.0) as mobile phase. By using the mobile phase a stable and reproducible chromatogram was obtained (Fig. 2). The peak height ratio for AcVal,

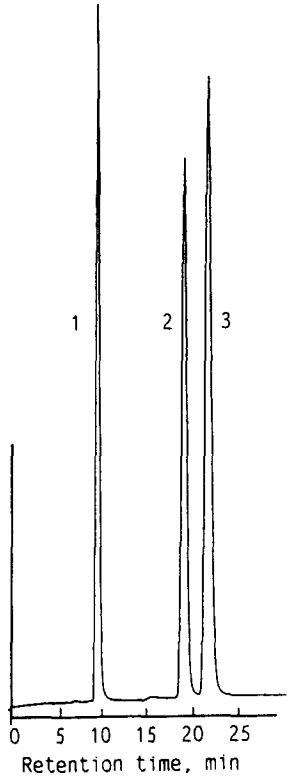


Fig. 2. Chromatogram of standard mixture (each of 20$\mu M$). (1) *N*-Acetyl-L-valine, (2) *N*-acetyl-L-isoleucine, (3) *N*-acetyl-L-leucine.

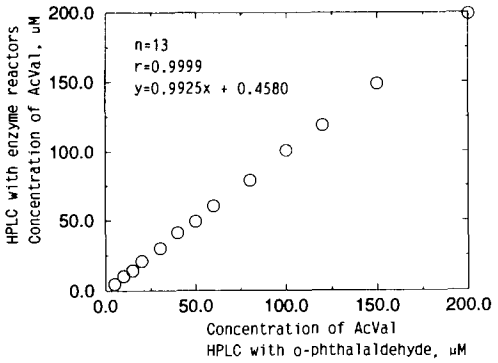


Fig. 3. Comparison of *N*-acetyl-L-valine concentration determined by HPLC with enzyme reactors and by HPLC with *o*-phthalaldehyde.[14]

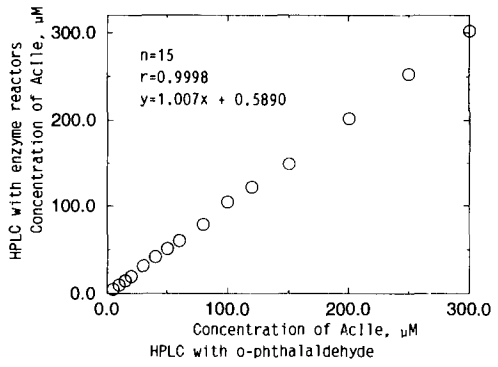


Fig. 5. Comparison of *N*-acetyl-L-leucine concentration determined by HPLC with enzyme reactors and by HPLC with *o*-phthalaldehyde.[14]

AcIle and AcLeu was 100:78:90. The peak height was plotted against the concentration of the compounds. The concentration ranges of linear response were from 4 to 200$\mu M$ for AcVal and AcLeu and from 5 to 300$\mu M$ for AcIle. The detection limits (signal-to-noise ratio = 3) for AcVal, AcIle and AcLeu were 2, 3 and 2$\mu M$, respectively.

*Application*

This system was used to determine the amount of AcVal, AcLeu and AcIle in serum. A sample of normal human serum was filtered on the ultrafiltration membrane. The filtrate (30$\mu$l) was injected into the system. Since no naturally occurring free AcBCAs were found in the serum by this method, the pooled serum was supplemented with AcVal, AcLeu and AcIle to give final concentrations of 5–200$\mu M$ AcVal, 5–300$\mu M$ AcIle and 5–200$\mu M$ AcLeu. Results obtained using this system compared well with a cation-exchange high-performance liquid chromatographic method.[14] The results are summarized in Figs 3–5. The calculated linear regressions and correlation coefficients for AcVal, AcIle and AcLeu were $y = 0.9925x + 0.4580$ and $r = 0.9999$, $y = 1.007x + 0.5890$ and $r = 0.9998$, and $y = 0.9898x + 0.3774$ and $r = 0.9999$, respectively.

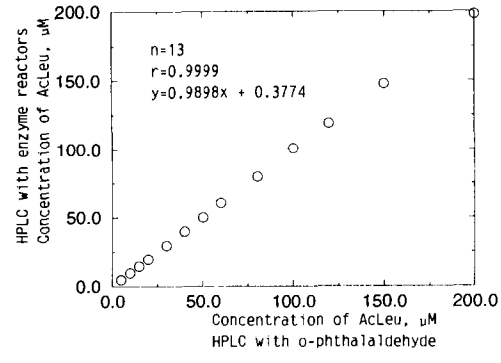


Fig. 4. Comparison of *N*-acetyl-L-isoleucine concentration determined by HPLC with enzyme reactors and by HPLC with *o*-phthalaldehyde.[14]

## CONCLUSIONS

We have shown that immobilized acteylacylase reactor and leucine dehydrogenase reactor are useful for the simultaneous detection of AcVal, AcIle and AcLeu using reversed-phase HPLC and fluorimetric detection. This method proved to be simple and selective for the determination of AcBCAs. However, it should be noted that the immobilized aminoacylase reactor should be renewed every 5 days, and that this is a disadvantage of the proposed technique.

## REFERENCES

1. H. M. Liebich and C. Forst, *J. Chromatogr., Biomed. All.*, 1985, **338**, 187.
2. W. Lehnert and E. Werle, *Clin. Chim. Acta*, 1988, **172**, 123.
3. H. M. Liebich and C. Forst, *J. Chromatogr., Biomed. All.*, 1990, **525**, 1.
4. E. Alonso and V. Rubio, *Anal. Biochem.*, 1985, **146**, 252.
5. B. Gabard and H. Mascher, *Biopharm. Drug Disp.*, 1991, **12**, 343.
6. Y. Kawakami, T. Ohga, C. Shimamoto, N. Satoh and S. Ohmori, *J. Chromatogr., Biomed. Appl.*, 1992, **576**, 63.
7. I. Chibata, T. Tosa, T. Sato and T. Mori, in *Methods in Enzymology*, K. Mosbach (ed.), Vol. 44, pp. 746–759. Academic Press, New York, 1976.
8. I. Chibata and T. Tosa, in *Applied Biochemistry and*

*Bioengineering*, L. B. Wingard, Jr., E. Katchalski-Katzir and L. Goldstein (eds), Vol. 1, pp. 329–357. Academic Press, New York, 1976.
9. S. Girotti, A. Roda, M. A. Angrllotti, S. Ghini, G. Carrea, R. Bovara, S. Piazzi and R. Merighi, *Anal. Chim. Acta*, 1988, **205**, 229.
10. N. Kiba, S. Hori and M. Furusawa, *Anal. Chim. Acta*, 1989, **218**, 161.
11. N. Kiba, S. Hori and M. Furusawa, *J. Chromatogr.*, 1989, **463**, 177.
12. T. Oshima, S. Nagata and K. Soda, *Arch. Microbiol.*, 1985, **141**, 407.
13. I. Matsumoto, Y. Ito and N. Seno, *J. Chromatogr.*, 1982, **239**, 747.
14. S. E. Møller, *J. Chromatogr., Biomed. Appl.*, 1993, **613**, 223.

Pergamon

0039-9140(95)01274-5

*Talanta*, Vol. 42, No. 3, pp. 457–462, 1995
Elsevier Science Ltd
Printed in Great Britain
0039-9140/95 $9.50 + 0.00

# COLORIMETRIC DETERMINATION OF LOW pH WITH MALACHITE GREEN

ELIZABETH W. BAUMANN

Westinghouse Savannah River Company, Savannah River Technology Center, Aiken, SC 29808, U.S.A.

(*Received* 6 *October* 1993. *Revised* 15 *April* 1994. *Accepted* 15 *April* 1994)

**Summary**—A spectrophotometric method was developed for determination of concentration-based pH values from 0 to 2 with Malachite Green indicator. A quadratic model equation was based on the ratio of the absorbances of the peak at 618 nm and the isosbestic point at 518 nm. Normalization to the isosbestic point was used to stabilize the response because the color faded; the useful time interval was within 5 min after indicator addition. Model and verification sets agreed within ±0.02 pH units between pH 0.3 and 1.8. This excellent precision makes the colorimetric method useful for acid determinations with a relative precision of > ±5%. The presence of salts at a salt/acid equivalent ratio >0.1 caused a low pH bias.

Use of color indicators provides a convenient alternative to potentiometric pH measurements for determination of acidity. Modern instrumentation such as diode array spectrophotometry and computerized data reduction has converted this classical technique[1] into one that is practical for field and online applications. Color indicators offer the option of either simple visual estimation or quantitative determination by spectrophotometry, with fiber optics or flow injection interfaces. Mathematical fitting or modeling of the spectral data can provide instant output values. In this work, preparation of models with standard solutions of known hydrogen ion concentrations makes the measured pH one that is based on hydrogen ion concentrations (*i.e.* $-\log[H^+]$), rather than on hydrogen ion activities.

Although many pH indicators are available,[2] only a few have suitable spectra for analytical applications, particularly at the extremes of the pH range. Earlier work described azoviolet indicator for colorimetric pH determinations of solutions such as the concentrated waste solutions with pH > 11 at the Savannah River Site.[3] The present work describes a similar application of Malachite Green to solutions with pH < 2 for other process streams. Normalization of the data to the isosbestic point and development of a quadratic model provides a sensitive method that overcomes the limitations of the indicator due to color fading.

This paper was prepared in connection with work done under Contract No. DE-AC09-89SR18035 with the U.S. Department of Energy. By acceptance of this paper, the publisher and/or recipient acknowledges the U.S. Government's right to retain a nonexclusive, royalty-free license in and to any copyright covering this paper, along with the right to reproduce and to authorize others to reproduce all or part of the copyrighted paper.

## EXPERIMENTAL

The calibration/model was developed by making absorbance measurements with standard solutions of 0.01–1*M* $HNO_3$. These solutions were prepared from a 1*M* stock solution standardized against the primary standard tris(hydroxymethyl)aminomethane.[4] The dilutions were confirmed by nitrate determinations with ion chromatography. Spectra for the acid and base forms of the indicator were established with 2*M* $HNO_3$ and 0.1*M* $KNO_3$, respectively. Samples were prepared and analyzed by the same procedure as the standards. A reference spectrum of the test solution without indicator was used for each measurement.

The Malachite Green solution was 0.1 w/v% of Malachite Green hydrochloride [$(CH_3)_2NC_6H_4C(C_6H_5):C_6H_4:N(CH_3)_2Cl$; CAS No. 569-64-2. Baker P451.03 or equivalent] dissolved in water. The solution was filtered. The pH of the indicator solution was about 3. The usual pH adjustment to midrange (about pH 1) was not made because the indicator is unstable at the lower pH, and the acid

contribution of the indicator to the test system is negligible.

*Procedure*

Four millilitres of solution was pipetted into a vial and 50 $\mu$gl of Malachite Green solution added. The solution was transferred to a 1-cm cuvette and between 0.25 and 5 min after addition of the Malachite Green, the absorbance of solution was measured from 400 to 700 nm (618 nm and 518 nm are the specific wavelengths of interest) with a Hewlett Packard Diode Array Spectrophotometer, or equivalent. The collected data was used to create a model or to determine pH from the established model, as described below.

## RESULTS AND DISCUSSION

*Malachite Green indicator*

Figure 1 shows Malachite Green spectra from pH 0.01 to 2.1. The base form has a strong sharp peak at 618 nm (blue-green), which was used for the analysis. The acid form has a broader, less suitable, peak in the 425–450 nm (yellow) range. The isosbestic point occurs at 518 nm. Kolthoff reported that triphenylmethane dyes, such as Malachite Green, were considered to be of no practical value as pH indicators because of instability and salt errors.[2] Normalization with the isosbestic point absorbance overcame the instability problem; salt error limitations are discussed below. Anionic halide complexes with certain metals (Cd, Co, Ta, Ga, In, Rh, Sn, Zn) are reported to bond with Malachite Green into extractable ion pairs,[5] but this possible interference was not investigated because these metals were not significant in our process streams.

*Collection and interpretation of data*

Spectra were collected at intervals of approximately 0.25, 2.5, and 5 min after the indicator was added. Spectra at the extremes of the indicator pH range were similarly obtained with $2M$ $HNO_3$ and $0.1M$ $KNO_3$. Ratios of absorbances at the peak (618 nm) and at the isosbestic point (518 nm) were used for modeling and for pH determinations from the model.

The color of the Malachite Green faded with time, particularly in more acidic solutions. Normalization to the isosbestic absorbance provided a parameter that was independent of measurement time for the 5 min interval after the indicator was added. Figure 2 shows average values and % relative standard deviations (RSD) for the normalized absorbances taken 0.25, 2.5, and 5 min after addition of indicator. %RSD values were $<1\%$ except at the lowest pH (0.009), where the %RSD rose to 3.5%. The variables $DX_n$, $DA_n$, and $DB_n$ are the ratios of the peak to isosbestic absorbances for the un-

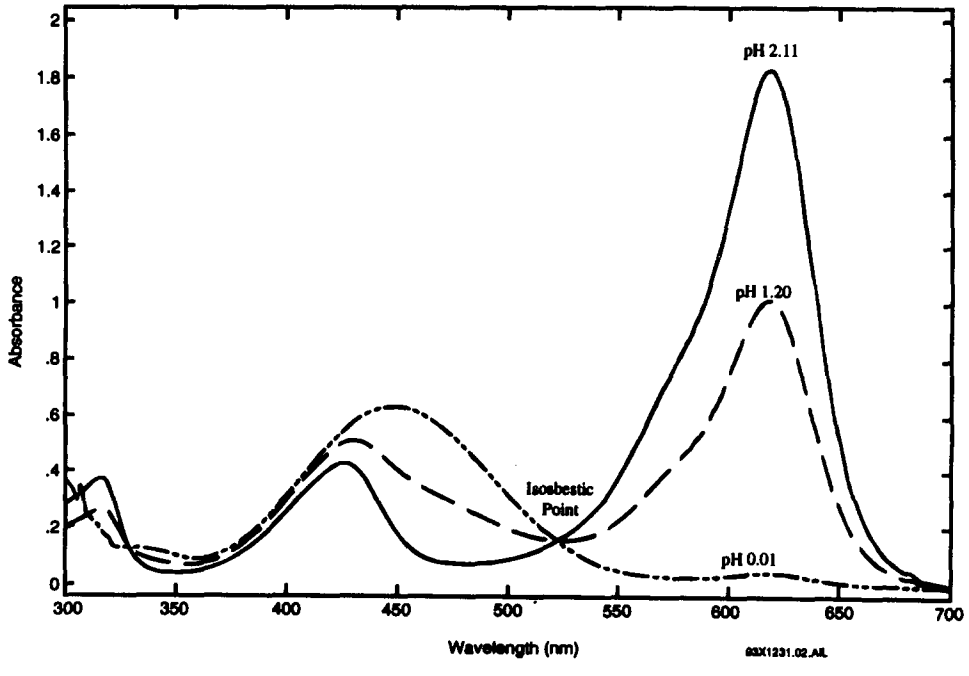


Fig. 1. Effect of pH on the absorption spectrum of Malachite Green. Spectra were taken 0.25 min after addition of indicator. The concentration of Malachite Green was $3.4 \times 10^{-5}M$.

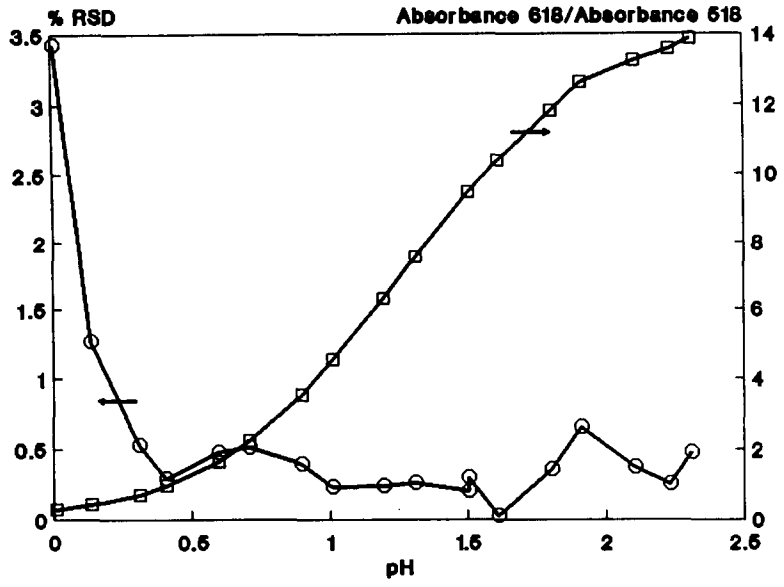


Fig. 2. Average values of $DX_n$, the ratio of absorbances at 618 and 518 nm, for different times. The ratios were averaged for measurements 0.25, 2.5, and 5 min after indicator addition. □ = average $DX_n$; ○ = % relative standard deviation.

known, the acid form and the base form, respectively.

Normalization to the isosbestic point also made the determination nearly independent of indicator concentration. Table 1A shows $DA_n$ and $DB_n$, over a three-fold range of indicator concentrations. The peak absorbance at 618 nm for $DB_n$ with 50 μl of indicator was >3, too high for accurate response.

*Development of model*

The relationships for fitting single peak data were similar to those used earlier.[1,3] $DADB_n$ is defined in equation (1a) in terms of α, the fraction of the indicator in the base form, and in equation (1b) in terms of ($DB_n$), ($DA_n$), and $DX_n$).

$$DADB_n = \alpha/(1-\alpha) \quad (1a)$$

$$=(DX_n - DA_n)/(DB_n - DX_n). \quad (1b)$$

The model was developed with a set of 18 nitric acid standards and was verified with measurements of a newly prepared set of these 18 standards. Three sets of data, collected approximately 0.25, 2.5, and 5 min after the indicator was added, were averaged for the model. $DA_n$ and $DB_n$ values for the model-building (calibration) set and for the verification set were the average of six experimental values (two samples

Table 1. Summary of $DA_n$ and $DB_n$ values

| Malachite Green per 2 ml sample (μl) | $DA_n$ Average | $DA_n$ Standard deviation | $DB_n$ Average | $DB_n$ Standard deviation |
|---|---|---|---|---|
| A. Indicator volume study | | | | |
| 10 | 0.0949 | 0.0079 | 14.67 | 0.05 |
| 20 | 0.0956 | 0.0045 | 14.65 | 0.07 |
| 25 | 0.0960 | 0.0018 | 14.62 | 0.04 |
| 30 | 0.0953 | 0.0005 | 14.42 | 0.04 |
| B. Model development | | | | |
| Model 25 | 0.0944 | 0.0014 | 14.84 | 0.06* |
| Verify 25 | 0.0917 | 0.0082 | 14.90 | 0.08* |

*Pooled Standard Deviations of two sets of timed measurements.

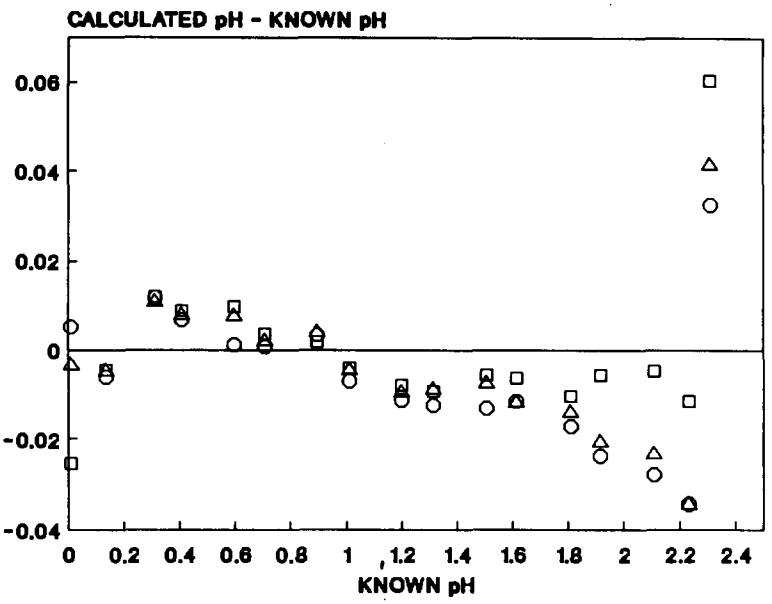


Fig. 3. Agreement of the model and the test set with different development times. Minutes after indicator addition: □ = 0.25; △ = 2.5; ○ = 5.

measured at three different times) for that test. Average $DA_n$ and $DB_n$ and their pooled standard deviations are included in Table 1B.

The model equation, which had an $R$ squared value of 0.999465, was:

$$\text{pH} = 1.298192 + 0.815108\ (\log DADB_n) \\ 0.069844\ (\log DADB_n)^2. \qquad (2)$$

The good agreement of the model with the test set is shown in Figure 3. Between pH 0 and 1.8, differences between calculated and known values were $<0.02$ pH unit. The reason for the trend in the data, with a positive bias at pH $< 1$ and a negative bias at pH $> 1$, is not known.

*Salt error*

The salt error was investigated with solutions that contained hydrolyzable ions or simple salts. In one set of experiments the solutions were standard 0.1$M$ nitric acid containing 0.1$M$ nitrates of aluminum, uranium, iron, thorium, or chromium, cations of interest in our process streams. Limits of the salt effect were investigated with the aluminum–nitric acid system with progressively less aluminum, down to 0.0125$M$ aluminum nitrate. The free acid content of these solutions was determined by standard addition in the presence of KSCN[6] or by titration in the presence of KF. Solutions of 0.1$n$ nitric acid or hydrochloric acid solutions spiked with their respective sodium salts were also analyzed.

The spectra of the solutions with hydrolyzable ions (Fig. 3) showed that, with the exception of iron, the presence of the metals did not affect the shape of the spectra. The results of these studies (Fig. 4) demonstrated that the salt error was related to the number of equivalents of salt present. Equivalent amounts of salt and acid caused a low bias of about 0.06 pH units. To achieve a precision of $\pm 0.02$ pH units the salt/acid equivalent ratio must be $<0.1$.

*Application to determination of acid concentrations*

The model was developed for pH defined in terms of hydrogen ion concentration, not for hydrogen ion activity. The excellent precision of $\pm 0.02$ pH units suggested that this colorimetric method might be useful for determination of acid concentrations in systems where a relative precision of $> \pm 5\%$ is adequate.

Table 2 shows application of the model to determination of the acidity of process solutions that contained up to 0.1$M$ $UO_2(NO_3)_2$. Confirming analyses were performed by titration with NaOH in KF medium and/or by standard additions in KSCN medium.[6] Both these methods determine hydrogen ion concentration. Within the range of the model, the colorimetric method gave comparable results. These determinations also demonstrated that in this low-salt system the method could be extended to more concen-

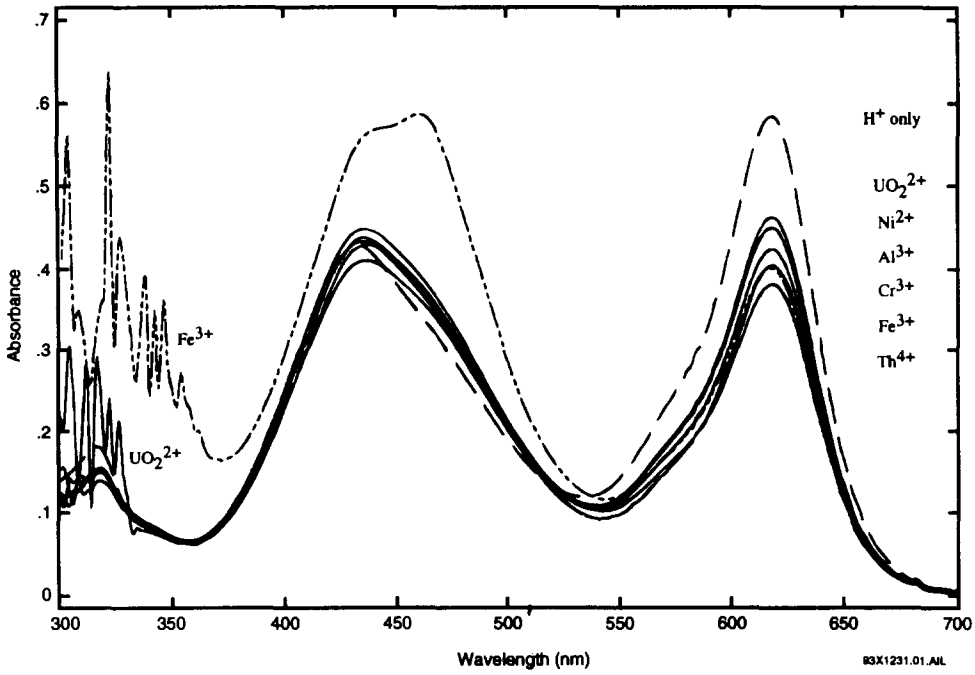


Fig. 4. Effect of hydrolyzable salts on absorption spectrum of Malachite Green. Solutions were 0.1*M* $HNO_3$ + 0.1*M* metal nitrate. Spectra were taken 2.5 min after addition of indicator. Malachite Green concentration was $3.4 \times 10^{-5}M$.

trated acid solutions by making dilutions as large as 10-fold.

*Comments on implementation*

Concentration-based pH determinations are useful for many applications. Sometimes the difference between hydrogen ion activity and acid concentration can be compensated. At the higher pH range of the method, samples may be sufficiently dilute that activity coefficients approach unity. For samples with similar ionic strengths, indicator and electrode pH values will be proportional to one another throughout the range.

The model equation in this paper is intended to serve as a guide for application and performance of the method. For actual implementation, a model for the system of interest should be

Table 2. Determination of acid concentrations

| | Acid concentration (*M*) | | |
|---|---|---|---|
| Solution | Titration in KF | Standard Addition in KSCN | Colorimetric method (dilution) |
| 1 | 0.004 | 0.066 | 0.097 (none) |
| | | | 0.083 (1:10) |
| 2 | nd* | 0.55 | 0.58 (none) |
| 3 | nd | 3.08 | 2.51 (1:10) |
| 4 | 3.45 | 3.58 | 3.59 (1:10) |
| 5 | 5.45 | 5.42 | 5.59 (1:10) |
| 6 | nd | 0.41 | 0.41 (none) |
| | | | 0.43 (1:10) |
| 7 | nd | 2.19 | 1.94 (1:10) |
| 8 | nd | 3.96 | 3.91 (1:10) |
| 9 | nd | 5.11 | 4.88 (1:10) |
| 10 | nd | 5.51 | 5.38 (1:10) |
| 11 | nd | 2.71 | 2.76 (1:10) |
| 12 | nd | 0.006 | 0.008 (none) |
| 13 | nd | 0.62 | 0.62 (1:10) |
| 14 | nd | 2.21 | 1.91 (1:10) |
| 15 | nd | 5.11 | 4.92 (1:10) |

*Nd = not determined.

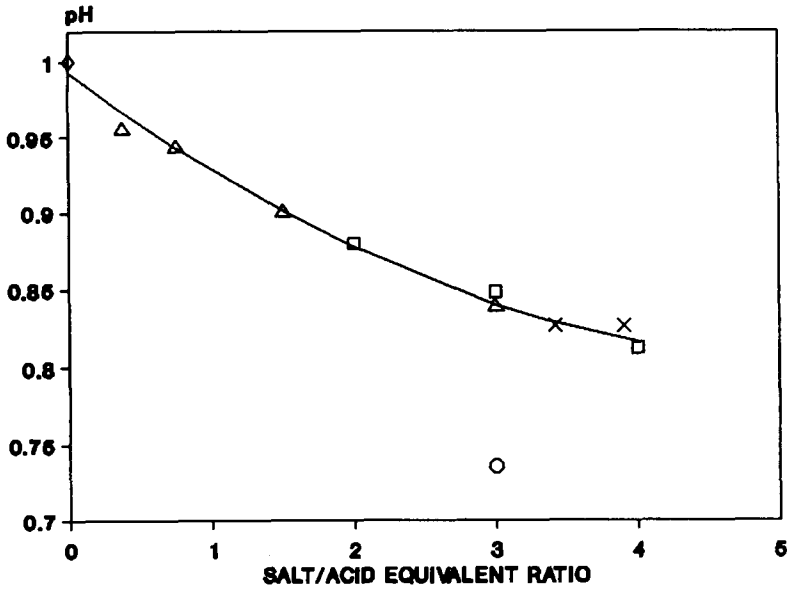


Fig. 5. Salt error in Malachite Green pH determination. ◇ = 0.1*M* $HNO_3$ with pH 1.00; □ = 0.1*M* $HNO_3$ + 0.1*M* nitrate salt of $UO_2^{2+}$, $Ni^{2+}$, $Cr^{3+}$, or $Th^{4+}$; ○ = 0.1*M* $HNO_3$ + 0.1*M* $Fe(NO_3)_3$; △ = 0.1*M* $HNO_3$ + 0.1, 0.05, 0.025 and 0.0125*M* $Al(NO_3)_3$; × = 0.1*M* $HNO_3$ + 0.34*M* $NaNO_3$ or 0.1*M* HCl + 0.39*M* NaCl.

developed. A model that includes the full spectrum can be developed by partial least squares or other techniques, as was done in the previous work with high pH systems and azoviolet indicator.[3] While the full-spectrum model may or may not improve the precision, it most certainly would be useful in flagging inappropriate samples through goodness-of-fit calculations.

*Acknowledgements*—The information in this article was developed during the course of work under Contract No. DE-AC09-89SR18035 with the U.S. Department of Energy.

## REFERENCES

1. R. G. Bates, *Determination of pH Theory and Practice*, 2nd Edn. Wiley, New York, 1973.
2. I. M. Kolthoff and C. Rosenblum, *Acid–Base Indicators*, MacMillan, New York, 1937.
3. E. W. Baumann and B. R. Buchanan, *Applied Spectroscopy*, 1991, **45**, 632.
4. L. Meites (ed.), *Handbook of Analytical Chemistry*, 1st Edn, pp. 3–34. McGraw–Hill, New York, 1963.
5. Z. Marczenko, *Spectrophotometric Determination of Elements*. Halsted Press (Wiley), New York, 1976.
6. E. W. Baumann and B. H. Torrey, *Anal. Chem.*, 1984, **56**, 682.

Pergamon

0039-9140(95)01398-9

*Talanta*, Vol. 42, No. 3, pp. 463–467, 1995

0039-9140/95 $9.50 + 0.00

# DISPOSABLE SCREEN-PRINTED ELECTRODES FOR MONITORING HYDRAZINES

JOSEPH WANG* and PRASAD V. A. PAMIDI

Department of Chemistry and Biochemistry, New Mexico State University, Las Cruces, NM 88003, U.S.A.

(*Received* 10 *May* 1994. *Accepted* 22 *July* 1994)

**Summary**—Disposable amperometric sensors for hydrazines have been fabricated by a judicious tailoring of the surface of screen-printed electrodes. Strong electrocatalytic action towards the oxidation of hydrazines is achieved by incorporating cobalt phthalocyanine within the carbon inks or by covering the printed surface with a mixed valent ruthenium cyanide coating. The electrocatalytic behavior, sensor optimization and analytical performance are reported. The new sensor strips should facilitate on-site environmental and industrial monitoring of hydrazine compounds.

Because of the environmental and toxicological significance of hydrazine compounds, a reliable method is required for their quantitation. Portable instruments, coupled with small sensing probes, are preferred for facilitating environmental field screening or on-site industrial monitoring of hydrazines. Controlled-potential electroanalytical procedures, particularly those relying on electrocatalytic modified electrodes, have been developed for the detection of hydrazine compounds. In particular, glassy carbon electrodes coated with cobalt phthalocyanine (CoPC) or mixed-valent ruthenium (III,II) cyanide (mvRuCN) layers have been shown to catalyze the oxidation of various hydrazines.[1,2] The adaptation of such schemes for mass-producible environmental or industrial sensors is thus a logical extension of their capabilities.

The present work describes disposable modified screen-printed sensors for measurements of hydrazine. The screen-printed (thick film) technology represents an ideal route for large-scale fabrication of highly reproducible and yet inexpensive electrochemical sensors.[3–5] For example, commercial single-use enzyme electrodes are commonly being used for self-testing of blood glucose levels.[6] We have previously used the screen-printing technology as the basis of disposable sensors for metals (such as lead or uranium).[7,8] Cobalt–phthalocyanine based screen-printed electrodes were employed by Wring and Hart[9] for facilitating the determination of biomolecules such as reduced glutathione. In the following sections we will characterize and apply CoPC and mvRuCN modified sensor strips for decentralized testing of hydrazines.

*Author to whom correspondence should be addressed.

## EXPERIMENTAL

### *Apparatus*

Amperometric and voltammetric measurements were carried out with a Bioanalytical Systems (BAS) CV-27 voltammetric analyzer in connection with a BAS Model VC-2 10 ml cell. The screen-printed working-electrode strip, the Ag/AgCl reference electrode (BAS Model RE-1) and platinum wire auxiliary electrodes were introduced to the cell through its Teflon cover.

A semi-automatic screen-printer (Model TF-100, MPM Inc. Franklin, MA, U.S.A.) was used for fabricating the electrode strips. A group of 25 electrodes was thus printed onto the alumina ceramic base (of 10 × 3.4 cm). Each electrode consisted of a 1 × 6 mm working area. The carbon ink was obtained from Gwent Electronic Materials Ltd (No. C10903D14, Gwent, U.K.). The CoPC modified ink was prepared by thoroughly mixing 0.1 g of CoPC with 4.0 g of the carbon ink. The mixing was facilitated by a 15-min sonication period. Coating of the unmodified strip with a mvRuCN layer was accomplished by cycling the potential between 0.4 and 1.0 V (at 50 mV/sec for 30 min) in the

presence of a 0.2*M* $K_2SO_4$ solution (pH 2.0) containing 2.5 m*M* $RuCl_3$ and 2.5 m*M* $K_4Ru(CN)_6$.

*Reagents*

All solutions were prepared with double-distilled water. Hydrazine solutions were prepared from hydrazine sulfate (Baker) and 1,2-dimethylhydrazine (Aldrich). The surface modifiers, CoPC and ruthenium chloride/potassium hexacyanoruthenate, were purchased from Aldrich and Alpha, respectively. The supporting electrolytes were 0.2*M* $K_2SO_4$ and 0.2*M* NaOH in connection with the ruthenium- and CoPC-modified strips, respectively. Ground water and tap water samples were collected at the Hanford Site (Richland, WA, U.S.A.) and the NMSU Chemistry and Biochemistry building (Las Cruces, NM, U.S.A.).

*Procedure*

Quantitation of the hydrazine compounds was accomplished in chronoamperometric experiments (with stepping the potential from open-circuit to +0.1 and 1.0 V for the CoPC- and mvRuCN-based strips, respectively). The current was sampled 210 sec following the potential step. Calibration data were achieved by spiked aliquots of the hydrazine standard solution to the cell.

## RESULTS AND DISCUSSION

Because of the large overvoltage for the electrooxidation of hydrazines at ordinary carbon strip electrodes, modified sensor surfaces are required to catalyze the oxidation process. Two such catalytic surfaces, based on modification with CoPC or mixed-valent ruthenium cyanide (mvRuCN), are known for their catalytic activity toward hydrazines at conventional carbon paste and glassy carbon electrodes,[1,2] and are thus assessed below in connection with the disposable carbon strips. While CoPC can be added to the carbon ink suspension prior to the printing process, the mvRuCN film is grown electrochemically after completing the fabrication.

The electrochemical deposition of the mvRuCN layer on the printed carbon surface is illustrated in Fig. 1. Repetitive cyclic voltammograms reveal two anodic peaks (at $\sim +0.62$ and $\sim +0.88$ V), corresponding to the $Ru^{2+,3+}$ and $Ru(CN)_6^{3-,4-}$ couples, respectively. A cathodic peak, at $\sim +0.66$ V, corresponding to the $Ru(CN)_6^{3-,4-}$ couple, is also observed. Similar peaks, at slightly different potentials, were reported for the analogous modification of glassy carbon electrodes.[10] All peaks gradually increase upon repetitive scanning, reflecting the continuous growth of the mvRuCN film.

Figure 2 displays hydrodynamic voltammograms (HDVs) for $4 \times 10^{-5}M$ dimethylhydrazine (a) and hydrazine (b) at both mvRuCN (A) and CoPC (B) modified strips, as well as the corresponding response at the unmodified sensor (open squares). Different media, $K_2SO_4$ (A) and NaOH (B), as commonly used with mvRuCN[2] and CoPC[1] modified electrodes, were employed. (Owing to its limited anodic potential window of NaOH media and the high potential of the mvRuCN couple, NaOH was not employed in connection with this modifier.) At the mvRuCN-coated strip, the anodic detection of both hydrazines is starting at +0.7 V, reaches a maxima around +1.0 to +1.1 V, and decreases at higher potentials. Similar profiles were reported for mvRuCN-coated glassy carbon electrodes.[2] No response is observed, over the entire potential range, for analogous measurements at the bare strip. At the CoPC-containing strip, the oxidation starts at −0.1 V, with the current increasing slowly up to +0.3 V

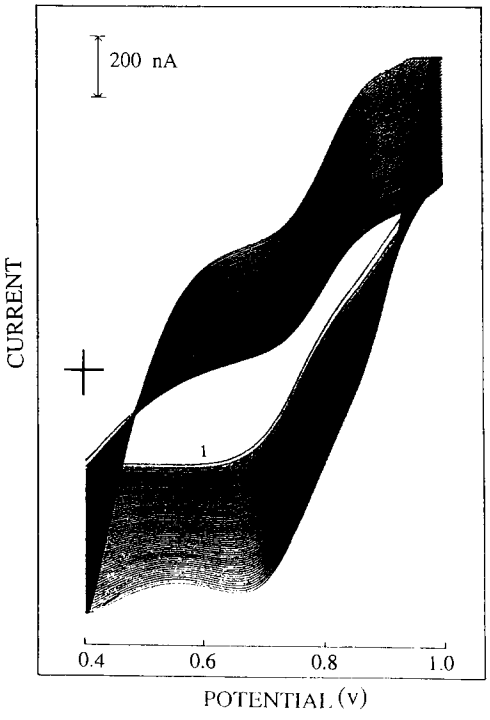


Fig. 1. Repetitive cyclic voltammograms at a screen-printed carbon electrode, dipped in a 0.2*M* $K_2SO_4$ solution (pH 2.0) containing 2.5 m*M* $RuCl_3$ and 2.5 m*M* $K_4Ru(CN)_6$ for 30 min. Scan rate, 50 mV/sec.

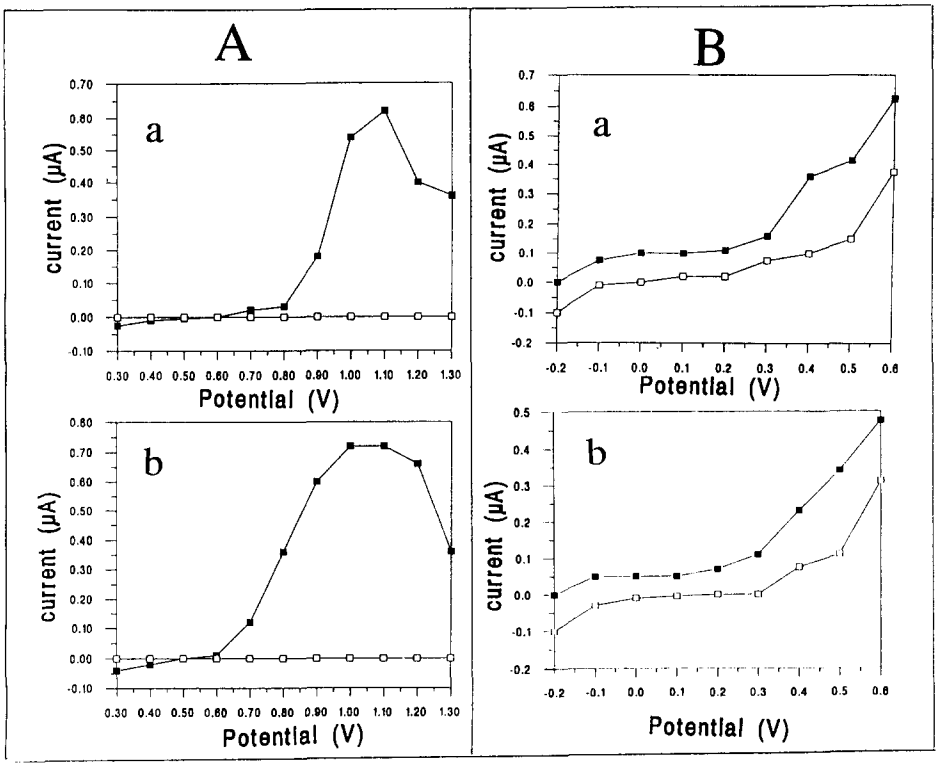


Fig. 2. Hydrodynamic voltammograms for $4 \times 10^{-5}M$ 1,2-dimethylhydrazine (a) and hydrazine (b) at mvRuCN (A) and CoPC (B) modified carbon strips. Electrolytes, $0.2M$ $K_2SO_4$ (A) and $0.2M$ NaOH (B). The individual points were obtained by chronoamperometry.

and then more rapidly. Note that (upon using the NaOH solution) the bare electrode is also responding to these hydrazines, but yields significantly smaller currents. Two oxidation processes (at $-0.2$ and $+0.1$ V) were reported for hydrazine at phthalocyanine-coated glassy carbon electrodes.[1]

The HDVs of Fig. 2 indicate that an optimum strip performance could be achieved around $+0.1$ V (CoPC) and $+1.0$ V (mvRuCN). Considering that quiescent sample droplets are likely to be placed onto the strip surface, chronoamperometry was selected for all subsequent quantitative work. Figure 3 shows chronamperograms for hydrazine solutions of increasing concentration ($4 \times 10^{-5}M$ increments) at the mvRuCN (A(a)) and CoPC (B(a)) modified strips, along with the corresponding response of the naked strip surface (b). Both strips offer convenient quantitation at the micromolar concentration level, as well as an extremely low background response (shown as dotted line). Note also that in accordance with the HDV data of Fig. 2, the unmodified electrodes yield only a negligible response towards the analyte. The resulting calibration plots (not shown) were linear in the case of the mvRuCN-coated strip (slope $8.5 \pm 0.01$

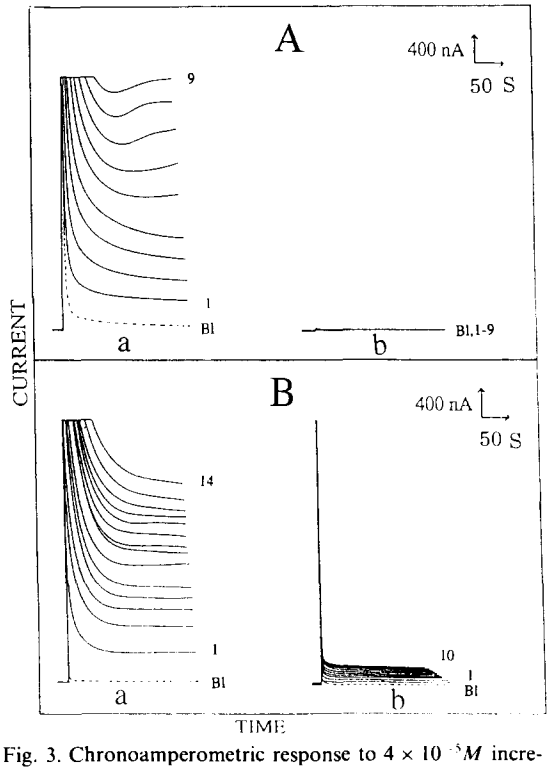


Fig. 3. Chronoamperometric response to $4 \times 10^{-5}M$ increments in the hydrazine concentration, along with the corresponding blank response (dotted line) at the mvRuCN (A(a)) and CoPC (B(a)) modified strips. Also shown (b) the corresponding response at the unmodified strips (b). Potential steps to $+1.0$ V (A) and $+0.1$ V (B). Electrolytes, as in Fig. 2.

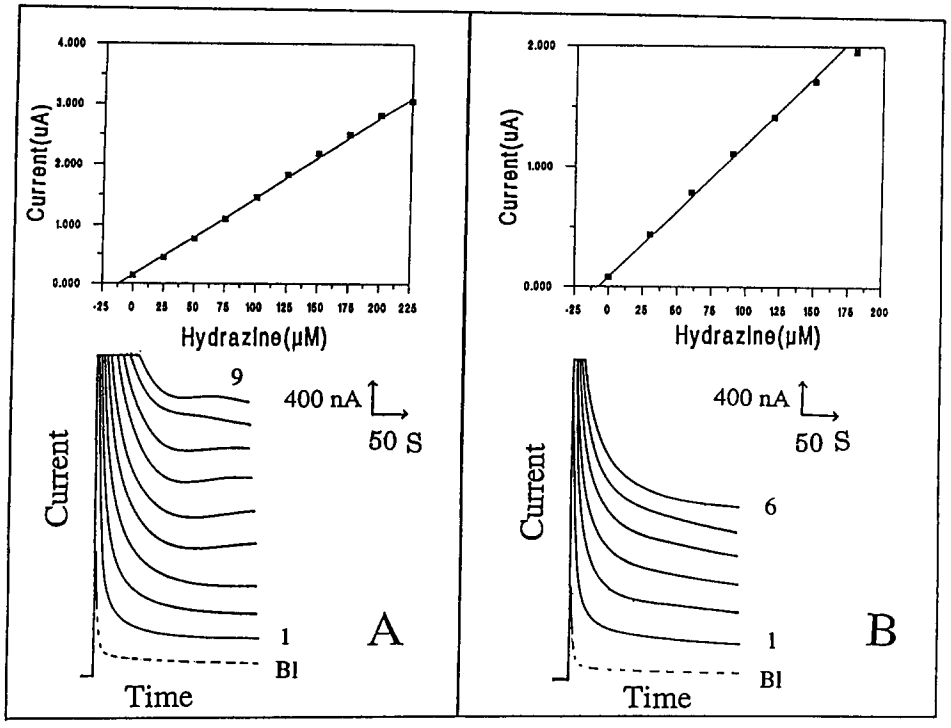


Fig. 4. Chronoamperometric response of the mvRuCN strip to ground water (A) and drinking water (B) samples spiked with increasing hydrazine concentration in $2.5 \times 10^{-5}M$ steps. Also shown (as dotted lines) are the blank sample responses; 8 ml sample +2 ml $0.2M$ $K_2SO_4$. Other conditions, as in Fig. 3A.

mA/$\mu M$, correlation coefficient, 0.997) but displayed a curvature (above $8 \times 10^{-5}M$) for the CoPC-containing sensors (correlation efficient, 0.986). Detection limits of $4 \times 10^{-6}$ and $5 \times 10^{-6}M$ hydrazines can be estimated from the signal-to-noise characteristics ($S/N = 3$) of the response at the CoPC- and mvRuCN strips, respectively. Convenient quantitation was obtained also for analogous measurements of 1,2-dimethylhydrazine, with both sensors displaying nonlinearity, with a leveling off above $1.5 \times 10^{-4}M$ (not shown).

Because of their extremely low cost, the new hydrazine sensors are aimed mainly at single-use applications. Yet, such electrodes hold promise also for use as reusable devices. Long runs of 20 successive runs of $1 \times 10^{-4}M$ hydrazine yielded relative standard deviations of 10 and 12% for the mvRuCN and CoPC modifications, respectively (not shown). A gradual decrease in the response characterized these prolonged series. Electrode-to-electrode reproducibilities of 5% RSD were observed for both modification schemes (conditions: 10 strips of the same batch, using a $1 \times 10^{-4}M$ hydrazine solution; other, as in Fig. 2).

Figure 4 demonstrates the suitability of the mvRuCN sensor strip for direct measurements of hydrazine in ground water (A) and drinking water (B) samples. Small (25 $\mu M$) increments in the hydrazine concentration of both samples yield a well-defined chronoamperometric response, and linear standard additions plots (shown as insets). The extremely low blank response (dotted lines) indicates lack of major interferences in these environmental samples. Whenever needed, improvement in the selectivity can be achieved by covering the strip surface with a size-exclusion coating (permeable mainly to the very small hydrazine species).

In conclusion, this paper demonstrates that effective sensor strips for hydrazines can be fabricated by coupling thick-film and surface modification technologies. Effective electrocatalytic detection of hydrazine compounds can thus be achieved through a judicious tailoring of the strip surface. While requiring different operating conditions (*e.g.* potential, supporting electrolyte), both CoPC- and mvRuCN-based strips offer convenient quantitation of micromolar hydrazine concentrations. The selection of the most appropriate strip for a given analytical task should thus depend primarily on selectivity considerations (based on the different reactivities of these modifiers).

Although the present work deals with printing of the working electrode strip, self-standing hydrazine sensors (suitable for handling small sample volumes) can be easily achieved via coprinting of the reference electrode. Future coupling of such low-cost sensors with portable, battery-operated, instruments should facilitate on-site and real-time environmental and industrial monitoring of hydrazine compounds.

*Acknowledgement*—This work was supported by the Waste Management Education and Research Consortium (WERC).

## REFERENCES

1. J. Zagal, C. Fierro and R. Rozas, *J. Electroanal. Chem.*, 1981, **119,** 403.
2. J. Wang and Z. Lu, *Electroanalysis*, 1989, **1,** 517.
3. M. Alvarez-Icarza and U. Bilitewski, *Anal. Chem.*, 1993, **65,** 525A.
4. D. Craston, C. Jones, D. Williams and N. El Murr, *Talanta*, 1991, **38,** 17.
5. S. Wring and J. Hart, *Electroanalysis*, 1994, **6,** 617.
6. M. Green and P. Hilditch, *Anal. Proc.*, 1991, **28,** 374.
7. J. Wang and B. Tian, *Anal. Chem.*, 1993, **65,** 1529.
8. J. Wang, B. Tian and R. Setiadji, *Electroanalysis*, 1994, **6,** 317.
9. S. Wring and J. P. Hart, *Analyst*, 1992, **117,** 1281.
10. J. Cox and P. Kulseza, *Anal. Chem.*, 1984, **56,** 1021.

Pergamon

0039-9140(95)01434-9

*Talanta*, Vol. 42, No. 3, pp. 469–474, 1995

0039-9140/95 $9.50 + 0.00

# ELECTROPOLYMERIZED *m*-PHENYLENEDIAMINE AS A MEANS TO IMMOBILIZE ACTIVE PROTEIN ON THICKNESS-SHEAR-MODE QUARTZ CRYSTAL

SI SHI-HUI, XU YUAN-JIN, NIE LI-HUA and YAO SHOU-ZHUO*

New Material Research Institute, Hunan University, Changsha, 410082 P.R. China

(*Received* 23 *May* 1994. *Revised* 9 *September* 1994. *Accepted* 12 *September* 1994)

**Summary**—Electropolymerized *m*-phenylenediamine was used as an active coating for immobilizing urease and lectin on a gold-plated thickness-shear-mode (TSM) crystal. To enhance effectiveness of immobilization, a bilayer polymer film composed of polyaniline and poly-*m*-phenylenediamine was proposed. Compared with single poly-*m*-phenylenediamine film, the bilayer polymer film gave better results in terms of immobilizing capacity, stability and reproductivity. On this bilayer-film-coated TSM quartz crystal, the amount of immobilized lectin was estimated about 1.8 $\mu$g/cm$^2$. Detection of purified human erythrocytes is demonstrated as an example of potential application of this lectin-modified TSM biosensor in clinic.

In recent years, applications of thickness-shear-mode (TSM) quartz crystal in solution chemistry have been developing rapidly.[1–3] Because the TSM sensor offers many advantages such as high sensitivity, simplicity of use and cost of effectiveness, some investigators have applied this device to immunosensors.[4] Immunoglobulins were detected with antibody[5,6] or protein A-modified crystal.[7] Microbes,[8] haptens[9,10] or protein antigen[11] were also detected by a similar method. Recently, much attention has been paid to the development of new biological coatings and new film-forming techniques.[12] For the development of a TSM immunosensor, a key step is to immobilize biological species (e.g. enzyme, antibody) effectively on the surface of the TSM crystal. Usually, the surface of the TSM crystal is precoated with functional polymer (e.g. polyethyleneimine[13]) by the dip-coating method. To our knowledge, few electropolymerized films have been used to immobilize biological species on the surface of TSM devices.

Electropolymerized films have been a subject of active investigation owing to their possible utility for a variety of applications including electrocatalyst, selective electrodes and surface modification.[14,15] With electropolymerization it is much easier to control the parameters of film thickness, homogeneity, and reproducibility. Glucose oxidase electrodes have been developed for polyaniline (PAn) or poly-*o*-phenylenediamine coating.[16,17] It is known that PAn can produce adherent and conducting film of uniform thickness on the gold matrix, but no functional group in the PAn structure can be modified with a bifunctional reagent which couples proteins such as antibodies and enzymes.

In this paper, the possibility for immobilizing active protein on the poly-*m*-phenylenediamine-coated TSM crystal is investigated. It was found that the poly-*m*-phenylenediamine (PmPD) coating on PAn matrix gave better results in terms of immobilizing capacity and stability.

## EXPERIMENTAL

### *Apparatus*

AT-cut 6 MHz gold-plated quartz crystal was used (area of electrode, 0.28 cm$^2$). A home-made IC-TTL oscillator was designed to drive the crystal at its resonant frequency,[18] and the frequency of the oscillator was monitored by a universal counter (Iwatsu, Model SC-7201). The experimental data were treated with a Hewlett Packard 9153C computer. The electrochemical quartz crystal microbalance (EQCM) experimental arrangement was similar to Ref. [19]. The QCM electrode facing solution was used as the working electrode, a commercial saturated

*Author to whom correspondence should be addressed.

Table 1. Frequency responses to lectin and urease immobilized on three different coatings (average of five experiments)

| Coating | Urease | Lectin |
|---|---|---|
| $\gamma$-APTES | $-68 \pm 19$ Hz | $-52 \pm 11$ Hz |
| PmPD* | $-45 \pm 6$ Hz | $-42 \pm 8$ Hz |
| PmPD and PAn† | $-137 \pm 7$ Hz | $-118 \pm 9$ Hz |

*The frequency response to PmPD coating is about 400 Hz.
†The frequency responses to PmPD coating and PAn coating are controlled about 300 and 200 Hz, respectively.

calomel electrode (SCE) and a platinum mesh were used as the reference electrode and the auxiliary electrode, respectively. XJP-821 B model polargraph and X-Y recorder were used in EQCM measurements, and all potentials were quoted *vs.* SCE. The admittance measurements of the TSM crystal were performed using a HP 4192A impedance analyser. The temperature was controlled by the thermostat water bath at $15 \pm 0.1$°C except where otherwise stated.

*Materials*

Blood specimen obtained from a healthy man was anti-coagulated with EDTA, and centrifuged at 150 ***g*** for 10 min. The erythrocytes were washed three times with 0.9% NaCl, and suspended in phosphate buffer (pH 7.2, 0.2*M*). Urease (biochemical reagent, BDH Chemical Ltd, Poole, U.K.): 2 mg of urease was dissolved in 1 ml of phosphate buffer (pH 7, 0.2*M*). Lectin (biproducts of WuHan Biological Institute, purified from soybean) was diluted with phosphate buffer (pH 7.2, 0.2*M*), to a concentration of about 2 mg/ml. Glutaraldehyde (GA) was of biochemical reagent grade, from which 3% (pH 7) solution was prepared. $\gamma$-Aminopropyltriethoxysilane ($\gamma$-APTES, Aldrich) was used. *m*-Phenylenediamine was purified by recrystallization from dichloromethane and aniline was distilled under reduced pressure.

*Surface modification*

(a) *Thin silane coating.* After treatment with chloroform and acetone, the TSM crystal was dipped in a 5% solution of $\gamma$-APTES in acetone for 1 hr at 25°C, then air-dried and washed several times with acetone.

(b) *Bilayer polymer coating.* The gold-plated TSM crystal was mounted at the bottom of a well-type cell, and one side of the crystal was kept out of the solution. The TSM crystal electrode facing solution was washed with acetone and distilled water before modification. With steady state scanning from $-0.2$ to 0.8 V in 0.1*M* aniline and 1.2*M* sulfuric acid, the polyaniline coating was deposited on the gold-plated TSM crystal. Then the obtained PAn-coated crystal was washed with distilled water and put into a solution containing 0.12*M* *m*-phenylenediamine and 1.2*M* sulfuric acid, and further treated by electrolysing at 0.70 V to obtain PmPD coating.

*Immobilization*

The polymer-coated TSM crystals were washed thoroughly with distilled water, then treated with 3% GA solution for 2 hr. After washing with phosphate buffer, a steady frequency of GA-treated crystal ($f_1$) was measured in phosphate buffer. Subsequently, the lectin or the urease solution was added into detector cell, and the frequency monitored. When the immobilization completed, the protein-modified crystal was washed with phosphate buffer, and the second steady frequency ($f_2$) was remeasured in phosphate buffer. The values of frequency shift corresponding to immobilized lectin and urease ($f_2$-$f_1$) were obtained (Table 1).

## RESULTS AND DISCUSSION

*Modified gold-plated TSM crystal with PAn and PmPD*

The frequency response for aniline electropolymerization recorded concurrently with the CV sweep is shown in Fig. 1. During CV scanning, the resonant frequency decreases, which means the PAn film is depositing on the surface of gold-plated TSM crystal. When a

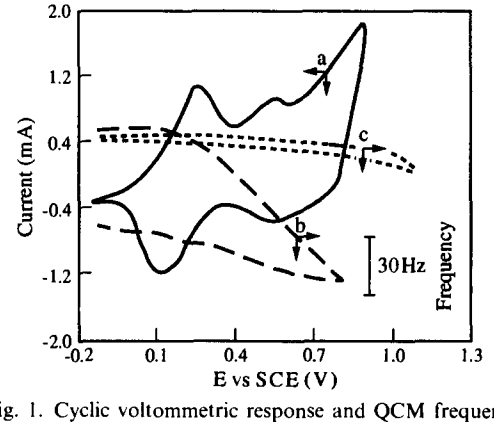


Fig. 1. Cyclic voltammetric response and QCM frequency response during steady state scanning at gold electrode in the solution of 0.1*M* aniline and 1.2*M* sulfuric acid. (a) Cyclic voltammetric response; (b) QCM frequency response. Curve c is the background frequency response in 1.2*M* sulfuric acid medium during cyclic voltammetric sweep (scan rate 40 mV/s).

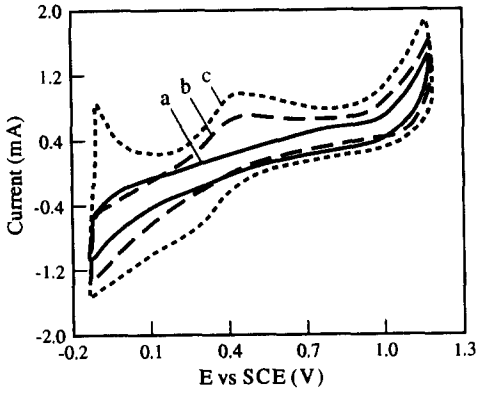


Fig. 2. Cyclic voltammograms for the oxidation of 0.1*M* *m*-phenylenediamine at gold electrode in sulfuric acid solutions of various concentrations. (a) 0.1*M*, (b) 1.2*M* and (c) 3*M*. Curves obtained at the first cycling (scan rate 40 mV/s).

solution containing 1.2*M* sulfuric acid and 0.1*M* aniline was chosen as the polymerizing medium, an excellent cohesive film was obtained on the TSM device. In order to obtain new functional polymer coating, the property of electropolymerized *m*-phenylenediamine coating on gold matrix was investigated. The cyclic voltammograms observed during *m*-phenylenediamine electrolysis reaction in various acidity polymerizing solutions are shown in Fig. 2. It can be seen that the shape of the CV profiles is affected by the change of the medium acidity, and at high potential oxidizing polymerization can occur. The results monitored by the TSM device show that the rate of PmPD depositing on gold matrix is slow during *m*-phenylenediamine electrolysis at constant potential (Fig. 3). However, when the PAn-coated TSM device was used as working electrode, and the electrolysis was carried out in solution containing 1.2*M* sulfuric acid and 0.1*M* *m*-phenylenediamine, a cohesive dark film was easy to obtain on the PAn matrix. As can be seen in Fig. 3, the depositing rate of PmPD is larger on PAn matrix than on gold matrix. Perhaps, it can be attributed to the electrocatalysis property of PAn and the much higher surface area provided by the PAn. With PmPD depositing, the rate of frequency change gradually decreases, which suggests electroinactivation and low conductivity of PmPD film. From the results of CV scanning, it was also found that the electrochemical response of PAn was different in the medium with and without *m*-phenylenediamine, new current peaks show that electrochemical reaction occurred on the PAn matrix (Fig. 4).

On the basis of the electrical equivalent circuit model, it has been demonstrated that the changes of resistance ($R$), inductance ($L$), and capacitance ($C$) components correspond to those of viscosity, mass, and elasticity of the film on the TSM device.[20] Usually, determination of these parameters, especially conductance $G$ ($G = 1/R$), provides useful information about chemical and/or physical properties of the film on the TSM device. While the polymer films are depositing on the surface of the TSM crystal, the $f_{G_{max}}$ decreases, but a very small change is observed in $G_{max}$, which suggests the electropolymerized films are not viscous (if the film were acting as a viscous medium, the $G_{max}$ would decrease[21]) (Fig. 5). It is well known that the width of the half-height of the conductance maximum of the TSM crystal should broaden if the viscoelastic properties of the film affect the resonant frequency. From the conductance spectra of TSM crystal in solution, no detectable difference was found between the bare

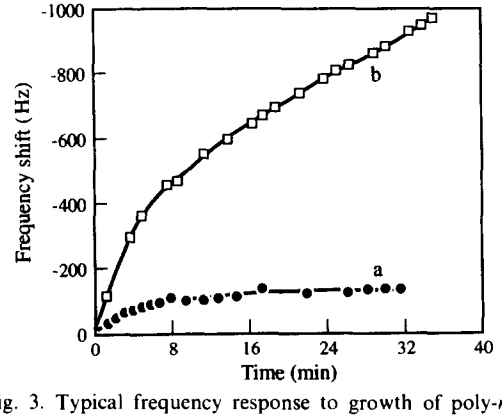


Fig. 3. Typical frequency response to growth of poly-*m*-phenylenediamine film electropolymerized at a constant voltage of 0.7 V (*vs.* SCE) in 1.2*M* sulfuric acid and 0.1*M* *m*-phenylenediamine. (a) On gold matrix, (b) on PAn matrix.

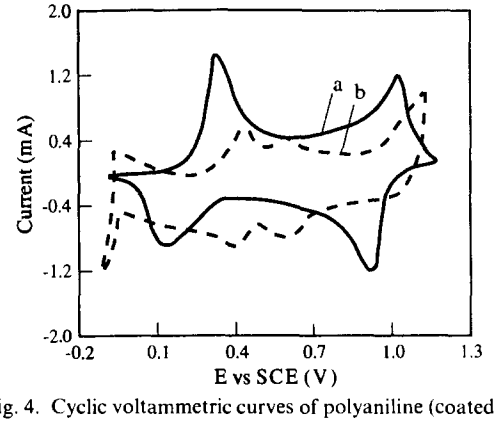


Fig. 4. Cyclic voltammetric curves of polyaniline (coated on gold electrode) in various solution. (a) 1.2*M* sulfuric acid; (b) 1.2*M* sulfuric acid and 0.1*M* *m*-phenylenediamine (scan rate 40 mV/s).

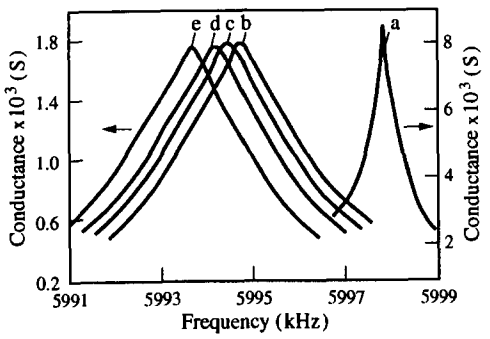


Fig. 5. Comparison of conductance spectra of the TSM crystal with and without the polymer coating. Without polymer coating: (a) in air; (b) in polymerizing solution. With polymer coating in polymerizing solution: (c) PAn coating; (d) PmPD coating; (e) PmPD coating on PAn matrix.

crystal and the polymer-coated crystal. Therefore, those electropolymerized films behaved as a rigid layer under the experimental conditions.

*Comparison of immobilizing capacity*

Owing to the presence of amine groups in the PmPD structure, the polymer-coated piezoelectric crystal can be remodified with GA, and this reaction usually finished within 2 hr at 15°C. To obtain the value of frequency shift corresponding to immobilized protein, the steady frequency of TSM device was measured in the same medium before and after the protein immobilization. The values of frequency shift ($f_2$-$f_1$) are given in Table 1.

It can be seen that the crystal modified with electropolymerized film provided better reproducible results than organic film for the protein immobilization. Compared with single PmPD film or $\gamma$-APTES coating, the bilayer polymer (PAn and PmPD) film dramatically enhanced the amount of immobilized protein. It is known that the electropolymerized aniline usually forms a fibril structure film, in which some enzymes were entrapped,[22] so it can be deduced that the PmPD film deposited on PAn matrix posesses a larger surface area, and provides a rich active site for immobilizing protein. During the growth of film, it was found that the initial depositing rate of the PmPD did not change further if the frequency response to the PAn coating was more than 300 Hz. The immobilizing protein results show that it is not necessary for the PmPD coating to be very thick. Considering the immobilizing capacity and the stability of coating, the thickness of bilayer polymer coating was optimized as: the frequency responses to PAn coating and PmPD coating were controlled about 200 and 250 Hz, respectively. Assuming film density of 1.2 g/cm$^3$,[23] the thickness of bilayer polymer coating was about 11 nm.

In order to test the stability of modification layer, the unreacted aidehyde groups were blocked with 0.1$M$ glycine in phosphate buffer (pH 7, 0.2$M$). Subsequently, the lectin-modified TSM crystal was immersed in phosphate buffer, and the frequency was monitored. The experimental results showed that only at initial time (about 10 min) the frequency of crystal slightly increased (perhaps resulting from the removal of the nonspecifical adsorption), then became steady. The frequency variation of bilayer-polymer-coated TSM device with immobilized lectin was $\pm$4 Hz for observation intervals of 1 h.

Since it was observed that the value of $G_{max}$ decreased when the lectin was immoblized on the surface of TSM device (Fig. 6), the immobilized lectin layer behaved viscoelastically, and the mass of immobilized lectin could not be calculated by Sauerbrey equation. In order to estimate the amount of immobilized lectin on the bilayer polymer-coated TSM device, the experimental relationship between frequency shift and mass of added lectin was obtained as follows: first, the steady frequency ($F_1$) of polymer-coated TSM device (air-dried) was measured. Then, each time 2 $\mu$l of lectin solution (1 mg lectin in 2 ml distilled water) was placed on the surface of polymer layer, and air-dried. Finally, the second steady frequency ($F_2$) was remeasured. The relationship between $F_2$-$F_1$ and the mass of added lectin is shown in Fig. 7.

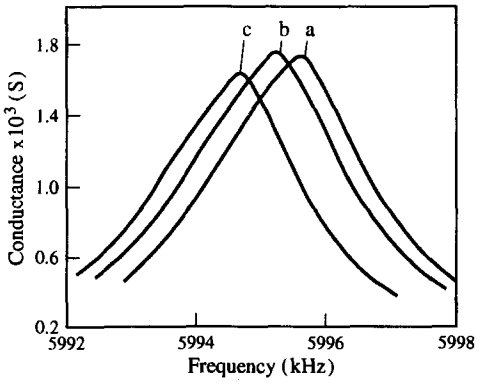


Fig. 6. Conductance spectra of the TSM oscillator in phosphate buffer observed in the course of immobilizing lectin. (a) Polymer-coated TSM crystal; (b) GA-treated TSM crystal; (c) TSM crystal with immobilized lectin.

The frequency response to immobilized lectin was also obtained by a similar method. After the GA-treated crystal was washed with water and air-dried, a steady frequency ($F_1$) was measured. Subsequently, the GA-treated crystal was immersed in the lectin solution. When the immobilization completed (about 3 hr at 15°C), the lectin-modified TSM crystal was washed with water and air-dried. Finally, the second steady frequency ($F_2$) was remeasured. The value of $F_2$-$F_1$ was $-112$ Hz (average of six experiments). According to Fig. 7, the mass of immobilized lectin was estimated about 1.8 $\mu$g/cm$^2$.

*Application of lectin-modified TSM device*

Lectins are very useful for the study of cell-initiated differentiation of cells and the topography of cell surface constituents[24] and, in order to demonstrate the possible utility of this lectin-modified TSM sensor in clinical applications, we have investigated its frequency response to the human erythrocytes. Upon addition of erythrocyte suspension, the frequency of TSM device decreases, which means that erythrocytes combinate to the lectin-coated TSM crystal, and the immobilized lectin is active (Fig. 8). The detection limit is about $10^5$ cells/ml. The experimental result showed that the adsorbed erythrocytes can be removed by 0.2*M* glycine HCl (pH 2.2), and the lectin-modified TSM sensor was reused five times with 8% decreased signal. It was found that over a incubation temperature range from 10° to 35°C, the affinity between the immobilized lectin and the erythrocyte was affected by the temperature. The frequency response to the adsorption of erythrocytes was greater at a higher incubation temperature. But the experimental result also shows that the reusability of this sensor readily dropped off when the temperature was over 35°C. Further studies about the frequency response of lectin-modified TSM sensor are being pursued.

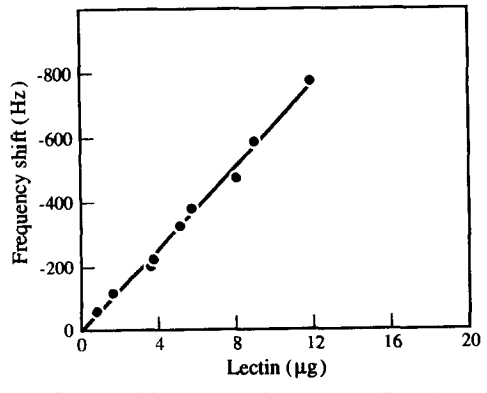


Fig. 7. Relationship between frequency shift and mass of added lectin on polymer-coated TSM quartz crystal.

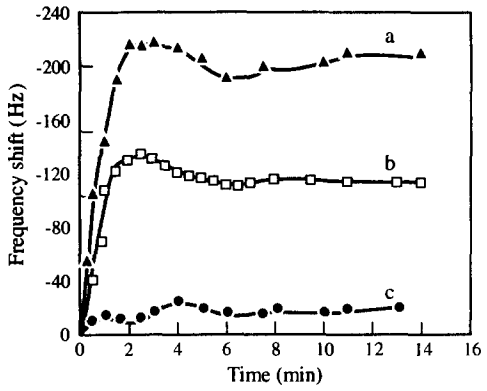


Fig. 8. Frequency change of lectin-modified TSM device with time after addition erythroytes suspension. (a) 3.5 × $10^6$ cells/ml; (b) 1.6 × $10^5$ cells/ml. (c) frequency change of TSM crystal unmodified with lectin upon addition of erythrocyte suspension (3.5 × $10^6$ cells/ml) (25 C).

## CONCLUSIONS

The results described above demonstrate that on the basis of electropolymerized *m*-phenylenediamine coating, lectin and urease can be immobilized on the surface of TSM quartz crystal with glutaraldehyde. Since the regeneration of piezoelectric crystal is easy, the TSM biosensor based on this modification technique becomes economically feasible, it may open up the way to immobilize biological species effectively on the TSM crystal.

*Acknowledgement*—This work was supported by the National Science Foundation and Education Commission of China.

## REFERENCES

1. S-Z. Yao and L-H. Nie, *Anal. Proc.*, 1987, **24**, 336.
2. M. Thompson, A. L. Kipling, W. C. Duncan-Hewitt, L. V. Rajakovic and B. A. Covic-Vlasak, *Analyst*, 1991, **116**, 881.
3. D. A. Buttry and M. D. Ward, *Chem. Rev.*, 1992, **92**, 1355.
4. A. Shons, F. Dorman and J. Najarian, *J. Biomed. Mater. Res.*, 1972, **6**, 565.
5. J. E. Roederer and G. J. Batiaans, *Anal. Chem.*, 1983, **55**, 2333.
6. M. Thompson, C. L. Arthur and G. K. Dhaliwal *Anal. Chem.*, 1986, **58**, 2760.
7. H. Muramatau, J. M. Dicks, E. Tamilya and I. Karube, *Anal. Chem.*, 1987, **59**, 2760.
8. E. Prusak-Sochaczewski, J. H. Luong and G. G. Guilbault, *Enzyme Microb. Technol.*, 1990, **12**, 173.
9. J. Ngeh-Ngwainbi, P. H. Foley, S. S. Kuan and G. G. Guilbault, *J. Am. Chem. Soc.*, 1986, **108**, 5444.

10. L. Rajakovic, V. Chaemmaghami and M. Thompson, *Anal. Chim. Acta.*, 1987, **217,** 111.
11. E. Prusak-Sochaczewski and J. H. T. Luong, *Anal. Lett.*, 1990, **23,** 401.
12. R. Ebersole, R. Foss and M. Ward, *BioTechnology*, 1991, **9,** 450.
13. B. Konig and M. Gratzel, *Anal. Chim. Acta.*, 1993, **280,** 37.
14. K. W. Willman and R. W. Murray, *J. Electroanal. Chem.*, 1982, **129,** 211.
15. J. Yano, A. Kitani, R. E. Vasquez and K. Sasaki, *Bull. Chem. Soc. Jpn*, 1984, **57,** 2254.
16. H. Shinohara, T. Chiba and M. Aizawa, *Sensors Actuators*, 1988, **13,** 79.
17. S. V. Sasso, R. J. Pierce, R. Walla and A. M. Yacynych *Anal. Chem.*, 1990, **62,** 1111.
18. S. Z. Yao, Z. H. Mo, *Anal. Chim. Acta*, 1987, **193,** 97.
19. M. D. Ward, *J. Phys. Chem.*, 1988, **92,** 2049.
20. O. Takeyoshi, S. Hidetaka, O. Noboru, T. Koichi and O. Takeo, Electrochim. Acta, 1993, **36,** 747.
21. M. O'Donnell, L. Busse and J. Millen, in *Methods of Experimental Physics*, L. Marton and C. Merton (eds), Vol. 19, p. 29. Academic Press. New York, 1981.
22. H. Shinohara, T. Chiba and M. Aizawa, *Sensors Actuators*, 1988, **13,** 79.
23. D. Orata and D. A. Buttry, *J. Am. Chem. Soc.*, 1987, **109,** 3574.
24. N. Sharon and H. Lis, *Science*, 1972, **177,** 949.

Pergamon

0039-9140(95)01435-7

*Talanta*, Vol. 42, No. 3, pp. 475–482, 1995

0039-9140/95 $9.50 + 0.00

# APPLICATION OF PATTERN RECOGNITION AND PIEZOELECTRIC SENSOR ARRAY FOR THE DETECTION OF ORGANIC COMPOUNDS

GYÖRGY BARKÓ, BALÁZS PAPP and JÓZSEF HLAVAY*

University of Veszprém, Department of Analytical Chemistry 8201, Veszprém, P.O. Box 158, Hungary

(*Received* 20 *January* 1994. *Revised* 26 *August* 1994. *Accepted* 16 *September* 1994)

**Summary**—Organic vapours were measured by an array of piezoelectric crystal detectors. Quartz crystals were coated by different GC stationary phases. Four coated crystals were placed in an array and pattern recognition was used for identification of the compounds including acetone, benzene, chloroform and pentane. A computer program was developed for the measurement of the frequency changes and data processing. Pattern recognition method using feature extraction was applied for identification of analytes.

The determination of organic compounds can mostly be accomplished by gas chromatography (GC), however, some other chemical sensors have also been used.[1] These sensors could be applied for the monitoring of the organic vapours at trace concentration. Two kinds of chemical sensors have mostly been applied: the metal-oxide semiconductor gas sensors,[2] and the piezoelectric quartz crystal sensors. The quartz crystal might be used as surface acoustic wave (SAW)[3] or as piezoelectric quartz crystal microbalance (PQM).[4] The frequency of the SAW sensor ranges from 30 to 200 MHz, while that of the PQM lies from 8 to 15 MHz.

Owing to the Sauerbrey equation the change of frequency of a quartz crystal is proportional to the change of the mass deposited on the surface of crystals.[5]

$$\Delta F = -2.3 * 10^6 * F^2 * \frac{\Delta M}{A}, \qquad (1)$$

where $\Delta F$ is the change in frequency (Hz), $F$ is the basis frequency of the quartz crystal (MHz), $\Delta M$ is the change in mass (g), $A$ is the area coated ($cm^2$). In the development of the piezoelectric chemical sensors, the first work of King[6] included the investigation of some liquid-coated crystals that can be operated by partition of the analyte between the gas and liquid phases. From equation (1), King estimated a detection limit of $10^{-9}$ g.[7] Guilbault and Tomita[8] developed a piezoelectric device sensitive for the organophosphorus compounds and pesticides. They found a mixture of 3-PAD, Triton X-100 and sodium hydroxide that had excellent selectivity and fast response. Karmarkar and Guilbault[9] used iridium(I) complex as a coating material for aromatic hydrocarbons in air. Hahn and co-workers[10] developed a crystal detector for the determination of the acetoin in air. The quartz crystal was coated with semicarbazide. Ho[11] developed a portable device with the piezoelectric crystal coated by Carbowax-550. This sensor was used for the monitoring of the toluene in ambient air. Edmonds and West[12] built a detector for the determination of the hydrocarbons using Pluronic 64 GC stationary phase as coating material. Two crystals were applied: a coated crystal for measurements and an uncoated reference one. It was found that the coating substance has given poor selectivity for hydrocarbons. Coating such as Pluronic L64, Carbowax 20M and squalane, although sensitive, were not particularly selective, and adsorbed many different organic compounds. An array of detectors was suggested providing that the sensitivity of each detector to each analyte was known, and the signal from each detector could be analysed mathematically and the concentration of each component could be estimated, even in multicomponent mixtures. Fraser and co-workers[13] developed a multisensor piezoelectric crystal detector system for the determination of airborne contaminants such as ammonia. Klinkhachorn and co-workers[14] designed a PQM system that was able to detect

*Author to whom correspondence should be addressed.

nanogram level mass changes of sorbed compounds. Five oscillator modules were used to construct an array of four sensors and pattern recognition was applied for the multi-component analysis. Chang[15] has developed an odour sensing system with PQM using a number of different lipid-coated crystals. The identification of odorant has been found to be dependent on the species of lipids. Schmautz[16] used a quartz sensor array with non-selective but different sensitive coating material for the analysis of the anaesthetic gases. The sensor signals were processed with pattern recognition methods. Carey[17] applied pattern recognition methods for selection of stationary phases. A generally useful procedure was proposed, tested, and the best sensitive coating materials were selected. The major problem using PQM sensors is the interference of water vapour. Most of the sensing compounds are also sensitive to moisture, so it has to be removed from the air without the reduction of the analyte vapours. Among many different solutions, one effective method is the application of the Nafion tubing with a 13X molecular sieve as drying agent packed on the outside of the membrane in a closed container.[20] Others include the use of chromatographic column filled with silica gel or molecular sieves, this has to be set into the sample introduction line.[4,8]

In our work a sensor array has been developed for detection of the organic vapours. It consists of four quartz crystals coated by GC stationary phases. Pattern recognition method using feature extraction has been applied for identification of the analyte. Model experiments were carried out to find the optimal conditions for the analysis of organic contaminants in different workshops.

## EXPERIMENTAL

Analytical grade benzene, *n*-pentane, acetone, chloroform, cyclohexane, toluene and methanol (Reanal, Hungary) were used. Nine MHz AT-cut quartz crystals, resonating in thickness-shear mode, were used. Silver electrodes were deposited to the both sides of the crystals. The crystals were manufactured by Gamma Co., Hungary. Stationary phases of OV1 and OV275 (Supelco), ASI50 (Applied Science Laboratories Inc.), and the polyphenilether (Carlo Erba) were used. The oscillator and data handling system was home-built. The sensor array consisted of four crystals (Fig. 1). The four crystals were coated with stationary phases and the coated area was 0.2 $cm^2$. The thin film of the coating was formed by solvent evaporation. The mass of the coating caused a frequency shift of about 8 kHz. The crystals were placed in a dry nitrogen stream for about 2 hr and then were built into the sensor array. Coatings were purged with dry nitrogen until the resonant frequency of the crystals reached a steady state. Organic vapours of standard compounds were injected into the nitrogen carrier gas. The nitrogen (T 45, supplied by Messer Griesheim, Hungary) contained only 30 ppm water vapour and was dried with $CaCl_2$ to remove the traces of water. The flow rate was measured by rotameter and kept at 20 l./hr (Fig. 2). Thermostatted sample holders were applied and the concentrations of the organic compounds were calculated using the ideal gas law. The vapours of the compounds were injected by a syringe into the flow of the carrier gas and the analytes reached the four crystals simultaneously in the detector. The decrease of the frequency proportional to the change in weight was recorded (equation 1). Frequencies of the crystals were measured with a four channel frequency counter, and compared to the clock of a computer as reference frequency. A computer program was developed for the measurement of the change in frequency and for the application of the pattern recognition method. The pattern recognition uses feature extraction and the K-nearest neighbour method for the processing of the saved frequency files.[18] An IBM AT386 DX2 computer with math coprocessor was used and an AX5216 counter/timer board (AXIOM) was used for the frequency measurement.

## RESULTS AND DISCUSSION

The responses of four quartz crystals coated by different GC stationary phases were investigated as an organic vapour sensor. A characteristic response was given by each sensor placed in the array. Seven different organic vapours were measured. The changes of raw frequency values of a quartz crystal coated by OV1 for 25 $\mu$mol organic compounds as a function of time are listed in Table 1. Adsorption and, consequently desorption, took place in only some hundreds of msec. As can be seen from the data, the recovery rate was the same for all volatile compounds. The reversibility, selectivity and sensitivity of the piezoelectric sensors to vapours rely on the

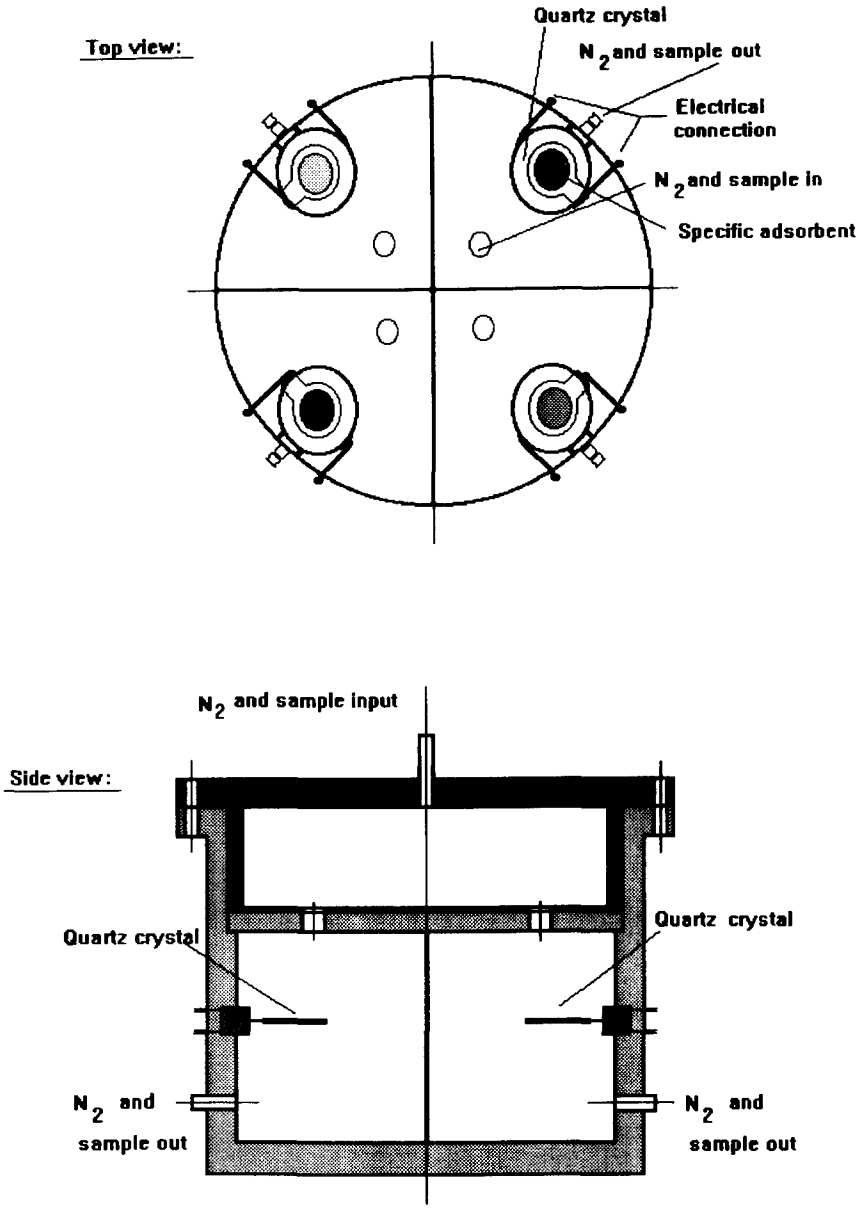


Fig. 1. Piezoelectric sensor array.

coating materials. The recorded frequency change was equilibrium response, and it depends greatly on the flow rate of gas mixture. However, the flow rate was kept constant (20 l./hr) for the reproducible responses. The maximum frequency change of the quartz sensors is listed in Table 2.

The GC stationary phases show different sensitivity to organic vapours. From the results four compounds were chosen for the characterization of the group of the organic materials. Benzene was applied as a representative compound of the aromatic hydrocarbons, acetone for ketones, *n*-pentane for the hydrocarbon groups, and chloroform for the chlorinated hydrocarbons. The frequencies of the compounds have been drawn as a bar chart[19] (Fig. 3). These values were used for the preparation of the data matrices. The frequency was converted to pattern with feature extraction. The feature extraction method consists of signal processing. The PQM sensor signal can be processed by extraction of the most distinctive feature parts of the signal. The lowest and highest frequencies of four crystals were converted into the feature space (see Table 1). Not only the highest frequency change, but also the lowest one contains valuable information concerning the reaction between the coating materials and analytes.

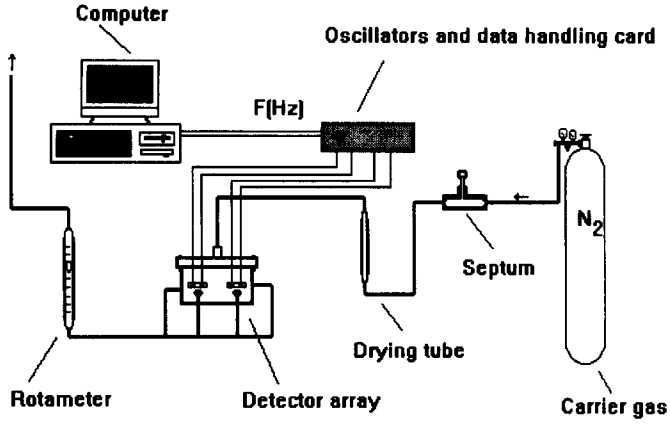


Fig. 2. The experimental set-up.

The feature space presents data files in the computer's memory. In the present case it consists of eight frequency values (two for each sensor). For classification of vapours the signals of the sensor array were transformed into a concentration independent plane. Linear transformation was applied for normalization of the signal. The process is shown by equations 2 and 3.

where $X^+$ is the position of the cluster at the highest value in rows (1 . . . 32); $Y^+$ the position of the cluster at the highest value in columns (1 . . . 4) (OV1 = 1, ASI50 = 2, OV275 = 3 and PPh-ether = 4, see Fig. 4); $\Delta F^+_{\text{OV1}}$ the highest value of the measured frequency on crystal coated by OV1; $\Delta F^+_{\text{ASI50}}$ the highest value of the measured frequency on crystal coated by ASI50;

$$X^+ = \text{INT}\left(\frac{\Delta F^+_{\text{OV1}}}{\Delta F^+_{\text{OV1}} + \Delta F^+_{\text{ASI50}} + \Delta F^+_{\text{OV275}} + \Delta F^+_{\text{PPh-ether}}} \cdot R\right) \tag{2}$$

$$Y^+ = 1,$$

Table 1. The change in frequency (Hz) of a quartz crystal sensor coated by OV1 for 25 $\mu$mol of organic compounds as a function of sampling time

| Time (*msec*) | Benzene | Toluol | Cyclohexane | *n*-Pentane | Acetone | Methanol | Chloroform |
|---|---|---|---|---|---|---|---|
| 0 | 1 | 1 | 1 | 1 | 1 | 0 | 0 |
| 50 | 1 | 1 | 1 | 1 | 0 | 1 | 0 |
| 100 | 1 | −20 | 1 | 0 | 1 | 0 | 1 |
| 150 | 1 | −47 | 2 | −90 | −30 | 1 | 0 |
| 200 | −20 | −30 | 1 | −150 | −90 | −1 | 0 |
| 250 | −70 | −20 | −80 | −177 | −110 | −30 | 1 |
| 300 | −96 | −20 | −160 | −170 | −50 | −32 | −40 |
| 350 | −71 | −10 | −140 | −122 | −30 | −75 | −120 |
| 400 | −61 | −1 | −100 | −80 | −2 | −25 | −150 |
| 450 | −50 | 0 | −80 | −6 | −1 | −20 | −140 |
| 500 | −30 | −1 | −70 | −5 | −1 | −1 | −120 |
| 550 | −4 | 0 | −50 | −3 | −1 | −1 | −100 |
| 600 | −2 | −1 | −5 | −3 | 0 | 1 | −80 |
| 650 | −3 | 0 | −4 | −2 | 0 | 0 | −8 |
| 700 | −2 | 0 | −4 | −1 | 1 | 1 | −6 |
| 750 | −2 | −1 | −2 | −2 | 0 | 1 | 0 |
| 800 | −2 | 0 | −3 | 1 | 1 | 0 | 0 |
| 850 | −1 | 0 | −2 | 0 | 1 | 1 | 1 |
| 900 | −1 | 0 | −2 | 1 | 1 | 0 | 0 |
| 950 | −2 | 0 | −2 | 1 | 0 | 1 | 0 |
| 1000 | −1 | 0 | −2 | 1 | 0 | 1 | 1 |
| 1050 | 0 | 0 | −1 | 1 | 1 | 1 | 0 |
| 1100 | −1 | 0 | −1 | 1 | 1 | 0 | 0 |
| 1150 | −1 | 1 | −1 | 1 | 0 | 1 | 1 |

Table 2. The maximum values of frequency changes (Hz) of quartz crystals coated by GC stationary phases for 25 μmol of organic compounds

| | OV1 | OV275 | ASI50 | PPh-ether |
|---|---|---|---|---|
| 1 Benzene | 96 | 25 | 40 | 125 |
| 2 Toluol | 47 | 10 | 20 | 54 |
| 3 Cyclohexane | 160 | 175 | 0 | 100 |
| 4 *n*-Pentane | 177 | 48 | 30 | 170 |
| 5 Acetone | 110 | 260 | 250 | 390 |
| 6 Methanol | 75 | 30 | 50 | 50 |
| 7 Chloroform | 150 | 120 | 178 | 450 |

$\Delta F^{+}_{OV275}$ the highest value of the measured frequency on crystal coated by OV275; $\Delta F^{+}_{PPh\text{-}ether}$ the highest value of the measured frequency on crystal coated by PPh-ether, $R$ the resolution of the feature extraction ($R = 32$) and

$$X^{-} = \mathrm{INT}\left(\frac{\Delta F^{-}_{OV1}}{\Delta F^{-}_{OV1} + \Delta F^{-}_{ASI50} + \Delta F^{-}_{OV275} + \Delta F^{-}_{PPh\text{-}ether}} \cdot R\right) \qquad (3)$$

$$Y^{-} = 1,$$

where, $X^{-}$ is the position of the cluster at the lowest value in rows (1 . . . 32); $Y^{-}$ the position of the cluster at the lowest value in columns (1 . . . 4) (OV1 = 1, ASI50 = 2, OV275 = 3 and PPh-ether = 4, see Fig. 4); $\Delta F^{-}_{OV1}$ the lowest value of the measured frequency on crystal coated by OV1; $\Delta F^{-}_{ASI50}$ the lowest value of the measured frequency on crystal coated by ASI50; $\Delta F^{-}_{OV275}$ the lowest value of the measured frequency on crystal coated by OV275; $\Delta F^{-}_{PPh\text{-}ether}$ the lowest value of the measured frequency on crystal coated by PPh-ether and $R$ the resolution of the feature extraction ($R = 32$). It can be seen that each transformed response is calculated as the ratio of the summary of the four sensor replies. The patterns of the benzene are shown in Fig. 4.

This method could eliminate the effects of absolute amounts of vapours on pattern recognition. The patterns were stored as binary data set. The data set gives a value of 1 when a cluster has been found in the column of a sensor. In any other case the values are 0. The size of the saved pattern file was about 10% of the file of frequencies recorded. The number of columns of the data set was equal to the number of the sensors (Fig. 4). The number of rows of the data set was proportional to the resolution of the feature extraction. With an increasing resolution the calculation time of pattern recognition should considerably be increased. However, large differences in the frequency changes are not necessary for the distinction of the patterns.[16] The repeatability of the patterns has been found to be the most important criteria of the appropriate recognition.

The pattern recognition approach can be seen in Fig. 5a and b. At first, the computer program was taught. Sample of organic vapours was injected and the changes in the frequencies of

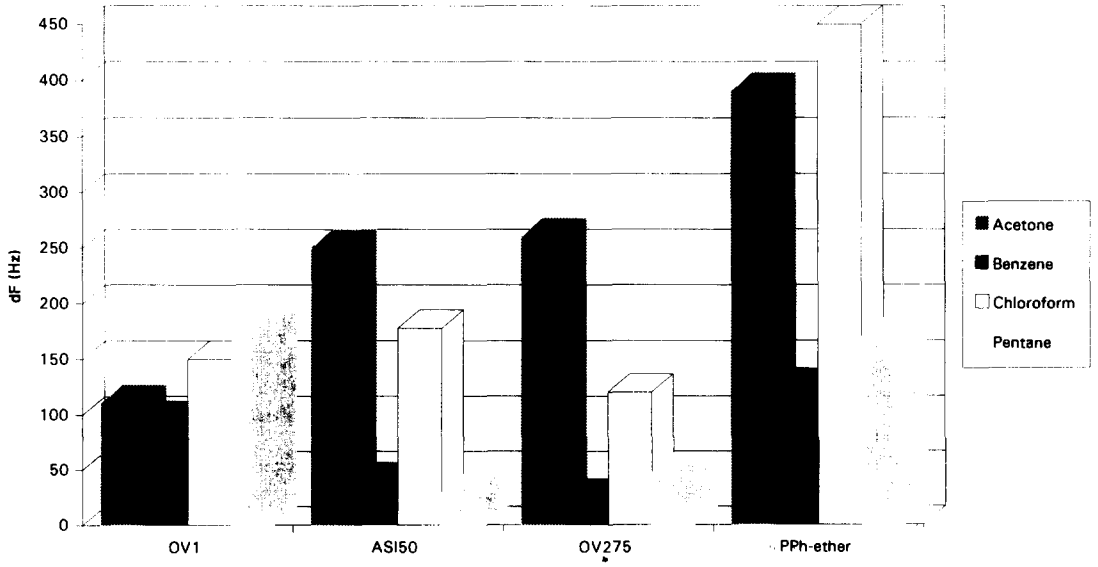


Fig. 3. Frequency changes of piezoelectric quartz crystals for organic vapours coated by different GC stationary phases.

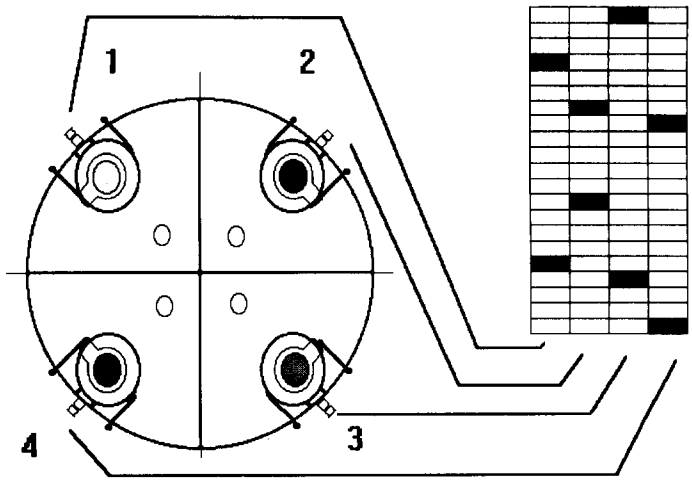


Fig. 4. The piezoelectric sensor array and the pattern for benzene.

the crystals were measured, converted to patterns and saved in the memory (Fig. 5a). After the teaching process, the unknown organic vapour was measured. The pattern of unknown compound was compared with the learned patterns. The two binary data sets were processed by the K-nearest neighbour method. The unknown sample set was grouped to its nearest neighbour learning point. During the learning process the data base of organic compounds can be formed by the given sample set. The maximum score was saved to the matched pattern and the unknown organic compound was identified (Fig. 5b).

The partition of a solute vapour between the surrounding gas phase and the coating material is represented by the adsorption of organic vapour into the sensitive layer.[17] The solubility coefficient, $K$, is a parameter to compare different coating materials referred to the sensitivity of test vapours:

$$\Delta F = k * V_c * C_c = \frac{\Delta F_c}{\rho_c} * C_g * K \tag{4}$$

$$K = \frac{\Delta F * \rho_c}{C_g * \Delta F_c}, \tag{5}$$

where $\Delta F$ is the change in frequency (Hz); $\Delta F_c$ the frequency shift of the coating (Hz); $\rho_c$ the

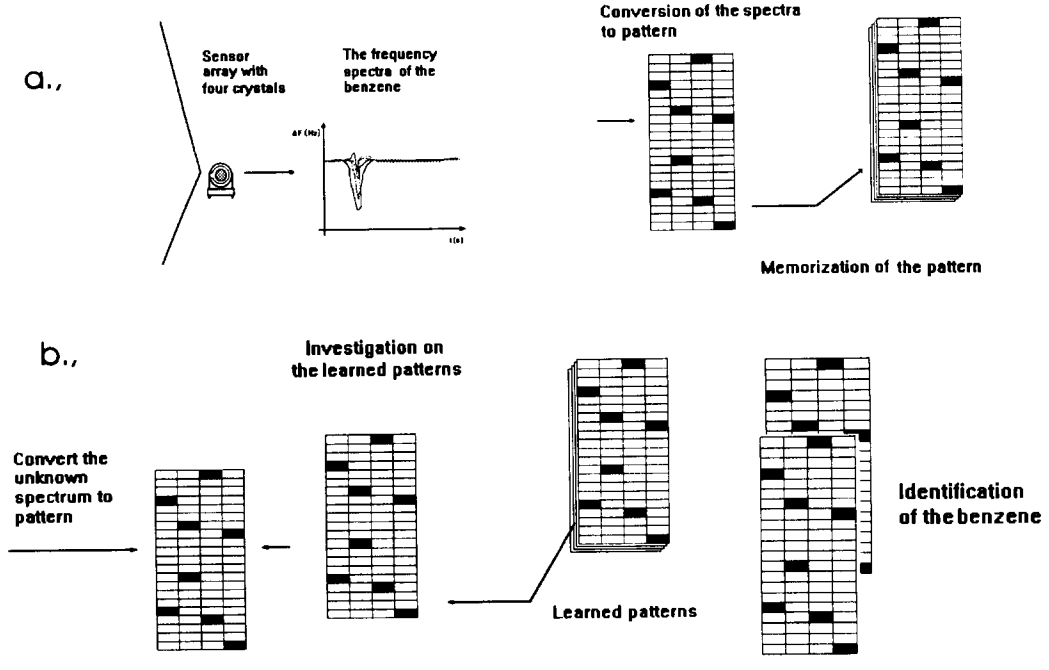


Fig. 5. The process of pattern recognition for identification of benzene.

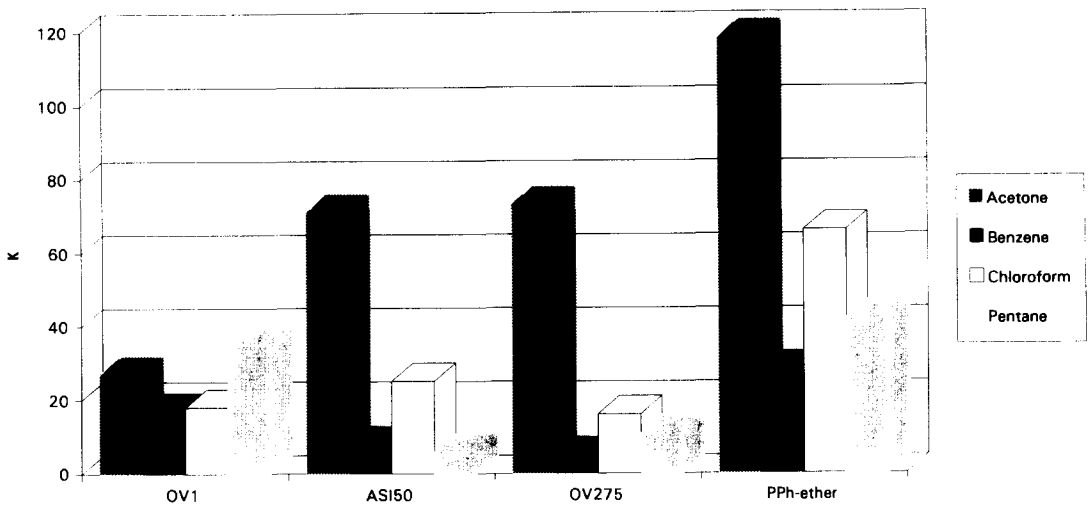


Fig. 6. Solubility coefficients calculated for different GC stationary phases.

density of the coating (g/cm$^3$); $C_c$ the vapour concentration in the coating (g/cm$^3$); $C_g$ the vapour concentration in the gas phase (g/cm$^3$); $k$ is a constant and $V_c$ the gas volume in the coating (cm$^3$). The values of $C_g$ were calculated by the ideal gas law.

The solubility coefficients of the coating materials were compared and the results are shown in Fig. 6. Comparing the values of the $dF$ and $K$ (Figs 3 and 6), it can be seen that only the PPh-ether shows a different pattern. This coating proved to be the most sensitive material for the organic vapours. The ASI50 and the OV275 gave poor sensitivity to the aromatic compounds and the hydrocarbons, but they were found to be sensitive coatings for acetone. The OV1 is generally used in GC for the separation of compounds having different polarity. Therefore, the analytes can appropriately be differentiated by the $K$ values on the four coatings for the pattern recognition.

## CONCLUSIONS

The array of piezoelectric quartz crystals coated with gas chromatographic stationary phases may be a suitable sensor for identifying selected compounds of organic vapours. A computer program was developed for the measurement of the frequency changes and data processing. The array of the chemical sensor consisted of four coated quartz crystals and the model system can be used for detection of different vapours. On the basis of the results of model experiments the identification of several pollutants may be carried out and characterization of a polluted environment may be performed. The application of the chemical sensor developed needs the removal of moisture content of the sample. The sensing elements are usually sensitive to water vapours. The effect of this interference can be overcome by incorporating a drying unit set into the analysis line. Further improvements can be expected by using further crystals coated with different GC stationary phases and applying calibration curves for the determination of the amount of the compounds in air.

*Acknowledgements*—The authors wish to express their gratitude to OTKA 2544 for the financial support.

## REFERENCES

1. S. J. Haswell and A. D. Walmsley, *Anal. Proc.*, 1991, **28,** 115.
2. T. Aishima, *Anal. Chim. Acta*, 1991, **243**, 293.
3. J. T. Wood and J. F. Alder, *Talanta*, 1992, **39,** 1505.
4. M. H. Ho and G. G. Guilbault, *Anal. Chem.*, 1982, **54**, 1998.
5. G. Z. Sauerbrey, *Z. Physik*, 1959, **155**, 206.
6. W. H. King, Jr., *Anal. Chem.*, 1964, **36**, 1735.
7. W. H. King, *Environ. Sci. Technol.*, 1970, **4,** 1136.
8. G. G. Guilbault and Y. Tomita, *Anal. Chem.*, 1980, **52,** 1489.
9. K. H. Karmarkar and G. G. Guilbault, *Environ. Lett.*, 1975, **10,** 237.
10. E. C. Hahn, A. A. Suleiman, J. R. Cavanaugh and G. G. Guilbault, *Anal. Chim. Acta*, 1987, **197,** 195.
11. M. H. Ho, B. Reitz and G. G. Guilbault, *Anal. Chem.*, 1980, **52,** 1489.
12. T. E. Edmonds and T. S. West, *Anal. Chim. Acta*, 1980, **117,** 147.
13. S. M. Fraser, T. E. Edmonds and T. S. West, *Analyst*, 1986, **111,** 1183.
14. P. Klinkhachorn, B. Huner, E. B. Overton, H. P. Dharmasena and D. A. Gustowski, *IEEE Trans. Inst. Meas.*, 1990, **39,** 264.

15. S. M. Chang, Y. Iwasaki, M. Suzuki, E. Tamiya, I. Karube and H. Muramatsu, *Anal. Chim. Acta*, 1991, **249**, 323.
16. W. P. Carey, K. R. Beebe and B. R. Kowalski, *Anal. Chem.*, 1986, **58**, 149.
17. A. Schmautz, *Sensors Actuators B*, 1992, **6**, 38.
18. B. R. Kowalski, Pattern recognition in chemical research, in computers and biochemical research, C. E. Klopfstein (ed.), Vol. 2, p. 74. Academic Press, New York, 1974.
19. A. D. Walmsley, S. J. Haswell and E. Metcalfe, *Anal. Chim. Acta*, 1991, **242**, 31.
20. Y. S. Fung, 83rd Annual Meeting & Exhibition, Pittsburgh, Pennsylvania, Air & Waste Management Association, 1990, 90–170.7.

Pergamon

0039-9140(95)01436-5

*Talanta*, Vol. 42, No. 3, pp. 483–492, 1995

0039-9140/95 $9.50 + 0.00

# A NOVEL OXYGEN AND/OR CARBON DIOXIDE-SENSITIVE OPTICAL TRANSDUCER

MING FAT CHOI* and PETER HAWKINS

Faculty of Applied Sciences, University of the West of England, Coldharbour Lane, Frenchay, Bristol BS16 1QY, U.K.

(*Received* 2 *September* 1994. *Accepted* 12 *September* 1994)

**Summary**—A novel oxygen ($O_2$) and/or carbon dioxide ($CO_2$)-sensitive transducer for the measurement of both gaseous $O_2$ and $CO_2$ over the concentration ranges of $O_2$, 0–100% and $CO_2$, 0–10% has been described employing a solution of 10.6 $\mu M$ fluorescein (FL) and 190 $\mu M$ potassium hydroxide in a solvent mixtures of 1:1 (v/v) *N,N'*-diethylaniline (DEA) and *N,N*-dimethylformamide. Increasing $O_2$ concentrations cause the absorbance of the solution at a wavelength of 400 nm to increase owing to a contact charge transfer reaction existing between $O_2$ and DEA molecules, and increasing $CO_2$ concentrations produce a non-linear fall in absorbance at 520 nm as the colour of FL changes from its orange dianion form to the colourless neutral, lactonic form. Both processes are independent of each other and reversible. The response to changes in $O_2$ concentrations is in good agreement with Beer–Lambert's law and the response to changes in $CO_2$ concentrations in non-linear. A fibre optic sensing system based on this solvent–dye solution has been set up for continuous and reversible determination of both gaseous $O_2$ and $CO_2$. Possible applications include environmental and physiological monitoring of $O_2$ over the ranges of 0–100% and $CO_2$, 0–10%.

Oxygen ($O_2$) can be considered to be one of the most important elements in our nature with an enormous chemical and biochemical reactions involving $O_2$ as reactants or products. Carbon dioxide ($CO_2$) is usually a by-product of many industrial processes and it is believed to aggravate the greenhouse effect of our environment. Medical diagnosis and treatment of critically ill patients in intensive care units and operating theatres often requires monitoring of $CO_2$ and $O_2$ partial pressures of arterial blood. Consequently, the determination of both $O_2$ and $CO_2$ is of considerable importance in environmental, biomedical analysis and analytical chemistry. Considerable effort has been devoted over many years to the development of new techniques for the measurement of $O_2$ and $CO_2$ concentrations. Amperometrical determination of $O_2$ by a Clark-type electrode[1] has been commonly used in the past which suffers from the drawback of $O_2$ consumption. The detection of $CO_2$ is usually based on an infrared detector[2,3] and a Severinghaus electrode[4] with bulky and expensive devices being used. With the advent of fibre optics technology, there is a growing interest in the development of fibre optics $O_2$ and/or $CO_2$ sensors. The attractive features of fibre optics sensors include: immunity to electrical interference; ease of miniaturization; comparatively inexpensive device; remote and *in situ* sensing; and high information carrying capacity (multiwavelength transmission), etc. There have been many publications on single optical fibre $O_2$ sensors[5–8] based on the fluorescent quenching of a dye by molecular $O_2$ and $CO_2$ sensors[9–14] based on the pH modulation accomplishing with the colour change of a dye. Several electrochemical multi-sensors have also been reported for the simultaneously detection of both $O_2$ and $CO_2$. Albery and Barron[15] applied the electroreduction technique for the amperometric determination of $O_2$ and $CO_2$ in which two electrolytes and two applied potentials were used. Arquint *et al.*[16] and Gumbrecht *et al.*[17] employed amperometric and potentiometric techniques for the detection of pH, $pO_2$ and $pCO_2$. Individual pH, $pCO_2$ and $pO_2$ sensors were fabricated and positioned on a miniaturized microchip. Recently, there have been a few combined fibre optic $O_2$ and $CO_2$ sensors described in the literature. Gehrich *et al.*[18] and Miller *et al.*[19] arranged three individual pH, $pCO_2$ and $pO_2$-sensitive optical fibres together in a catheter. Similarly, oxygen-sensitive material

*Author to whom correspondence should be addressed.

and $CO_2$-sensitive material were entrapped in separate gas-permeable membranes and attached to the distal end of a bifurcated optical fibre for sensing gaseous $O_2$ and $CO_2$.[20] In all the above instances, individual sensitive-material was often used for each gas. To the best of our knowledge, not a single sensing medium for both $O_2$ and $CO_2$ have been reported to date.

It has been known that some organic solvents exhibit contact charge transfer absorption (CCTA) bands when in contact with $O_2$.[21] Tsubomura and Mulliken[22] explained that this is caused by the formation of CCT pairs between the organic solvents and molecular $O_2$. The CCTA bands lie in longer wavelength regions if the solvents have lower ionization potentials, like some amine compounds, and usually appear as extensions to the long wavelength edge of the absorption spectra of the deoxygenated solvents. The CCTA intensity of the organic solvents is also related to the partial pressure of $O_2$ in the gas mixtures above the solvents and the reaction between the solvents and $O_2$ is reversible.[23]

Fluorescein (FL) dye immobilized in poly(ethylene glycol) has been successfully applied for fibre optic sensing of $CO_2$.[24] With the combination of organic solvent and dye, a single transducer can possibly be employed for the determination of both $O_2$ and $CO_2$. In this paper, we apply this approach and report here a single $O_2/CO_2$-sensitive transducer in which both gaseous $O_2$ and $CO_2$ can be detected independently based on the CCTA of *N,N'*-diethylaniline (DEA) with $O_2$ and the colour change of FL upon exposure to $CO_2$.

## EXPERIMENTAL

### *Chemicals and reagents*

DEA (>99%), *N,N*-dimethylformamide (DMF > 99.9%, HPLC grade), *n*-heptane (99%, spectrophotometric grade), methanol (>99.9%, HPLC grade) and FL dye (98%) were purchased from Aldrich Chemical Co. Ltd, U.K. Potassium hydroxide (KOH, AnalaR grade) was obtained from BDH Chemical Ltd, U.K. Solutions of 10.6 $\mu M$ FL and 190 $\mu M$ KOH in DMF, and 10.6 $\mu M$ FL and 190 $\mu M$ KOH in 1:1 (v/v) DEA/DMF solvent mixture were prepared by adding 20 $\mu$l of a concentrated methanolic KOH solution (KOH concentration was determined by standard acid–base titration[25]) and 70 $\mu$l of a concentrated FL in DMF solution (concentration of FL solution was determined spectrophotometrically by employing the molar absorptivity of $FL^{2-}$ dianion[26]) into DMF and 1:1 (v/v) DEA/DMF solvent mixture, respectively. Similarly, a solution of 0.10 $\mu M$ FL and 190 $\mu M$ KOH in 1:1 (v/v) DEA/DMF solvent mixture was prepared for fluorescence studies. All reagents were used as received. Nitrogen gas ($N_2$), $O_2$ gas, 10% (v/v) $CO_2$ in $N_2$ gas mixture and $CO_2$ gas were supplied by Distillers MG, U.K.

### *The gas mixing system*

Different $O_2$ (in the range of 0–100%) or $CO_2$ concentrations (in the range of 0–10%) in a gas stream were produced by controlling the flow rates of either $O_2$ gas or 10% $CO_2$ in $N_2$ gas mixture and the diluent $N_2$ gas entering a mixing chamber. The gas mixture was passed through a portable $O_2$ meter (Oxywarn 100I from Draeger Manufacturing, U.K.) or $CO_2$ detector (LFG 10 Landfill Gas Analyser from Analytical Development Company Ltd, U.K.) where the $O_2$ or $CO_2$ concentrations in the gas mixture were determined before bubbling through the investigating solvent or solvent–dye solution contained in a 1 cm path-length quartz cuvette.

### *Instrumentation*

The CCTA spectra were measured on a Perkin-Elmer Lambda 15 Spectrophotometer, fluorescence excitation (EX) and emission (EM) spectra were recorded on a Perkin-Elmer LS-5 Luminescence Spectrometer.

In the fibre optic detecting system of $O_2$ and $CO_2$, a home-made optical arrangement was set up. A modulated beam of light with known wavelength was produced by a 100 W quartz halogen lamp (Bentham Instruments Ltd, U.K.) stabilized by a Bentham 505 current stabilized filament lamp power supply, a Bentham 218 optical chopper at a frequency of 141 Hz and a Bentham M300 monochromator controlled by a Bentham SMD3B stepping motor drive unit before being launched into a plastic optical fibre (1 m long and 2 mm diameter from RS Components, U.K.). The transmitted light from the fibre irradiated the front surface of a 1 cm quartz cuvette containing 1 ml of solvent or solvent–dye solution with gaseous $O_2$ or $CO_2$ standards at a flow rate of about 50 $cm^3$/min continuously passing through it. A second plastic optical fibre (0.5 m long, 2 mm diameter) was positioned on the back surface of the cuvette to collect the transmitted light. The other end of this fibre led directly onto the front surface of a

100 $mm^2$ silicon photovoltaic detector (RS Components, U.K.) and the output signal was amplified by a Bentham 277 current pre-amplifier and a Bentham 223 lock-in amplifier which was synchronized to the modulated light beam by a reference signal provided by the light chopper. The amplified signal was recorded on a Linses 1S chart recorder (Electroplan, U.K.) and displayed on a LED display (Bentham 217 digital unit). To avoid a slight drift caused by a small evaporation of the solvent, the solvent–dye solution was replaced with a fresh one at approximately 2 hr intervals.

## RESULTS AND DISCUSSION

### *Development of $O_2/CO_2$-sensitive transducer*

*N,N'*-Diethylaniline has a strong broad CCTA band lying in the ultraviolet/visible regions and there is an increase in absorbance as the $O_2$ concentration increases (Fig. 1). The CCTA band disappears when the dissolved $O_2$ is removed by purging DEA with $N_2$ or $CO_2$. Note that the reference is air-saturated DEA ($[O_2] = 21\%$ approx.) which explains why DEA has negative absorbances when their $O_2$ concentrations are less than the air-saturated value. A graph of absorbance (abs) at 400 nm against applied $[O_2]$ is plotted where abs = absorbance of DEA saturated with a given applied $[O_2]$ – absorbance of DEA saturated with $N_2$. A linear straight line is obtained which agrees with Beer–Lambert's law having absorbance directly proportional to the applied $[O_2]$. Similarly, the CCTA spectra for different mol percentage (%) mixtures of DEA/*n*-heptane mixture were also recorded (Fig. 2). There is an increase in absorbance as the mol% of DEA in DEA/*n*-heptane mixture increases. *n*-Heptane has no CCTA band at the wavelengths investigated. A graph of abs at 400 nm against mol% of DEA in DEA/*n*-heptane mixture is plotted and a linear straight line is found which indicates that the CCTA is directly proportional to the concentration of DEA in DEA/*n*-heptane mixture. The change of absorbance arises from the CCTA of the DEA and $O_2$ complex and the reaction is reversible.

$$\mathrm{DEA} + \mathrm{O_2} \rightleftarrows \mathrm{DEA}\cdots\mathrm{O_2} \overset{h\nu}{\rightleftarrows} (\mathrm{DEA}\cdots\mathrm{O_2})^*.$$

It is possible that DEA can serve as a sensing medium for $O_2$.

It has also been observed that some pH-sensitive dyes change colour upon exposure to gaseous $CO_2$. The presence of water is crucial for response to $CO_2$ which is based on the following equations:

$$\mathrm{CO_2} + \mathrm{H_2O} \rightleftarrows \mathrm{H_2CO_3}$$

$$\mathrm{H_2CO_3} + \mathrm{H_2O} \rightleftarrows \mathrm{HCO_3^-} + \mathrm{H_3O^+}$$

$$\mathrm{HCO_3^-} + \mathrm{H_2O} \rightleftarrows \mathrm{CO_3^{2-}} + \mathrm{H_3O^+}$$

$$\underset{\text{(colour A)}}{\mathrm{DH}} + \mathrm{H_2O} \rightleftarrows \underset{\text{(colour B)}}{\mathrm{D^-}} + \mathrm{H_3O^+},$$

where DH and $D^-$ are the protonated and deprotonated forms of the dye, respectively. The

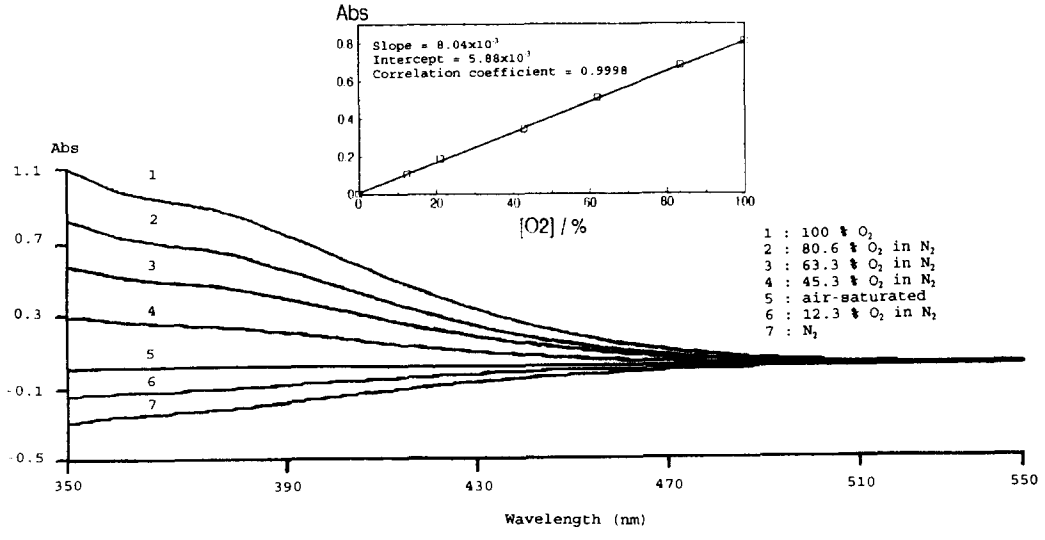


Fig. 1. The effect of different $O_2$ concentration on the CCTA spectrum of DEA. Inset shows the calibration plot of absorbance at 400 nm against $[O_2]$ using the data of the spectra. The optical pathlength is 1 cm and the reference is air-saturated DEA.

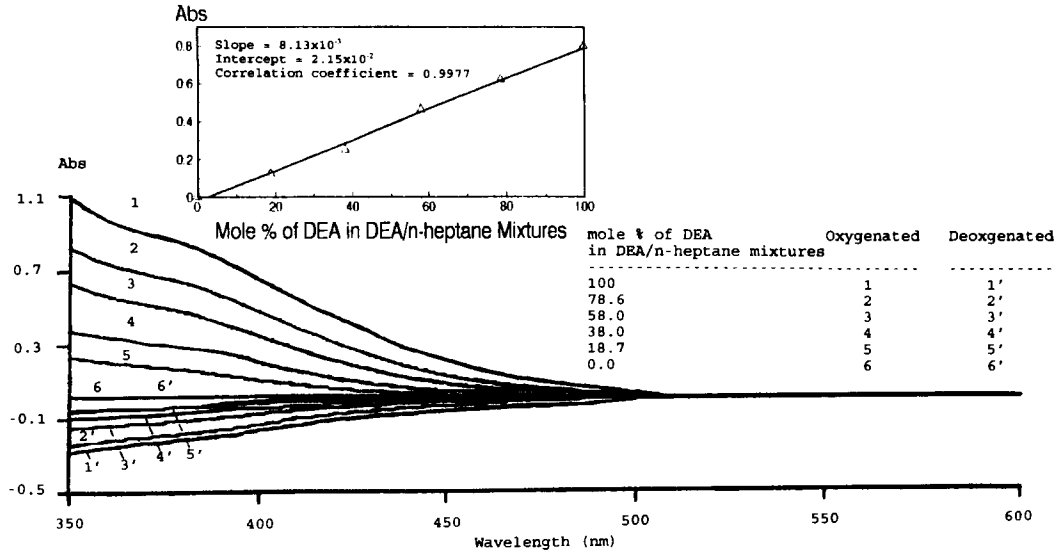


Fig. 2. The CCTA spectra of DEA/*n*-heptane solvent mixtures. Solvent mixtures are in mol%. Inset shows the calibration plot of absorbance at 400 nm against mol% of DEA in DEA/*n*-heptane solvent mixture. The measurement conditions are the same as in Fig. 1.

colour change of the dye is sensitive to pH change of its environment. A solution of 10.6 $\mu M$ FL and 190 $\mu M$ KOH in DMF was tested for its response to $CO_2$ (Fig. 3). It is assumed that FL exists only as $FL^{2-}$ ions in this highly alkaline solvent. Neutral form of FL can occur in three different tautomers, i.e. zwitterion, quinoid and lactone. However, it has been reported that colourless lactonic form is usually the dominant tautomer present in organic solvents.[27] The change of absorbance arises from the conversion of the orange dianion form of FL to the colourless, neutral lactonic form upon exposure to $CO_2$. These changes were brought about from the change of the pH of the solution with the dissolution of $CO_2$ in DMF and can be envisaged in the following reactions:

$$CO_2 + OH^- \rightleftarrows HCO_3^- \quad (1)$$

$$H^+ + OH^- \rightleftarrows H_2O \quad (2)$$

$$2H^+ + FL^{2-} \rightleftarrows H_2FL. \quad (3)$$

Dissolved $CO_2$ removed the $OH^-$ ions in DMF: as a result, the $H^+$ ion concentration is increased which shifts the equilibrium of equation (3) from left to right. A plot of abs at 520 nm against $[CO_2]$ is shown in Fig. 3 and increasing $[CO_2]$ cause a non-linear fall in

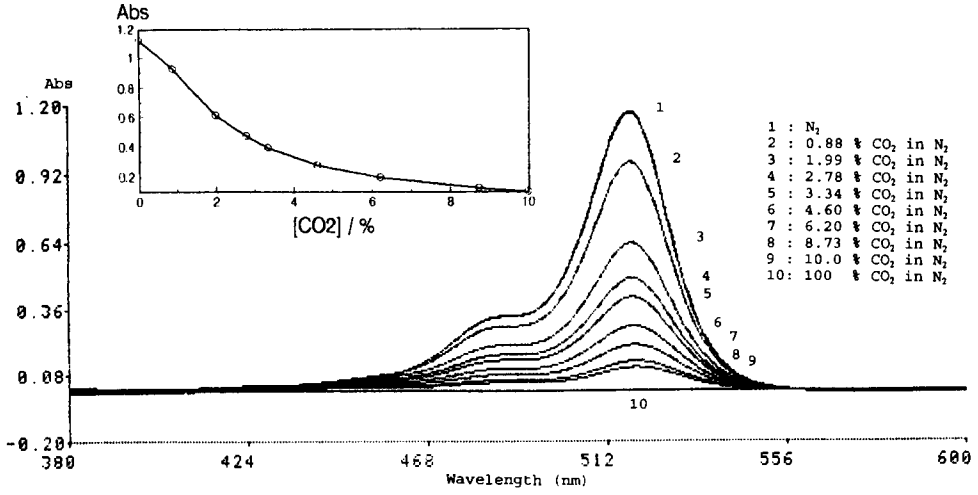


Fig. 3. The effect of different $CO_2$ concentration on the absorption spectrum of a solution of 10.6 $\mu M$ FL and 190 $\mu M$ KOH in DMF. Inset shows the plot of abs against $[CO_2]$ using the data of the spectra. The optical pathlength is 1 cm and the reference is a solution of air-saturated 190 $\mu M$ KOH in DMF.

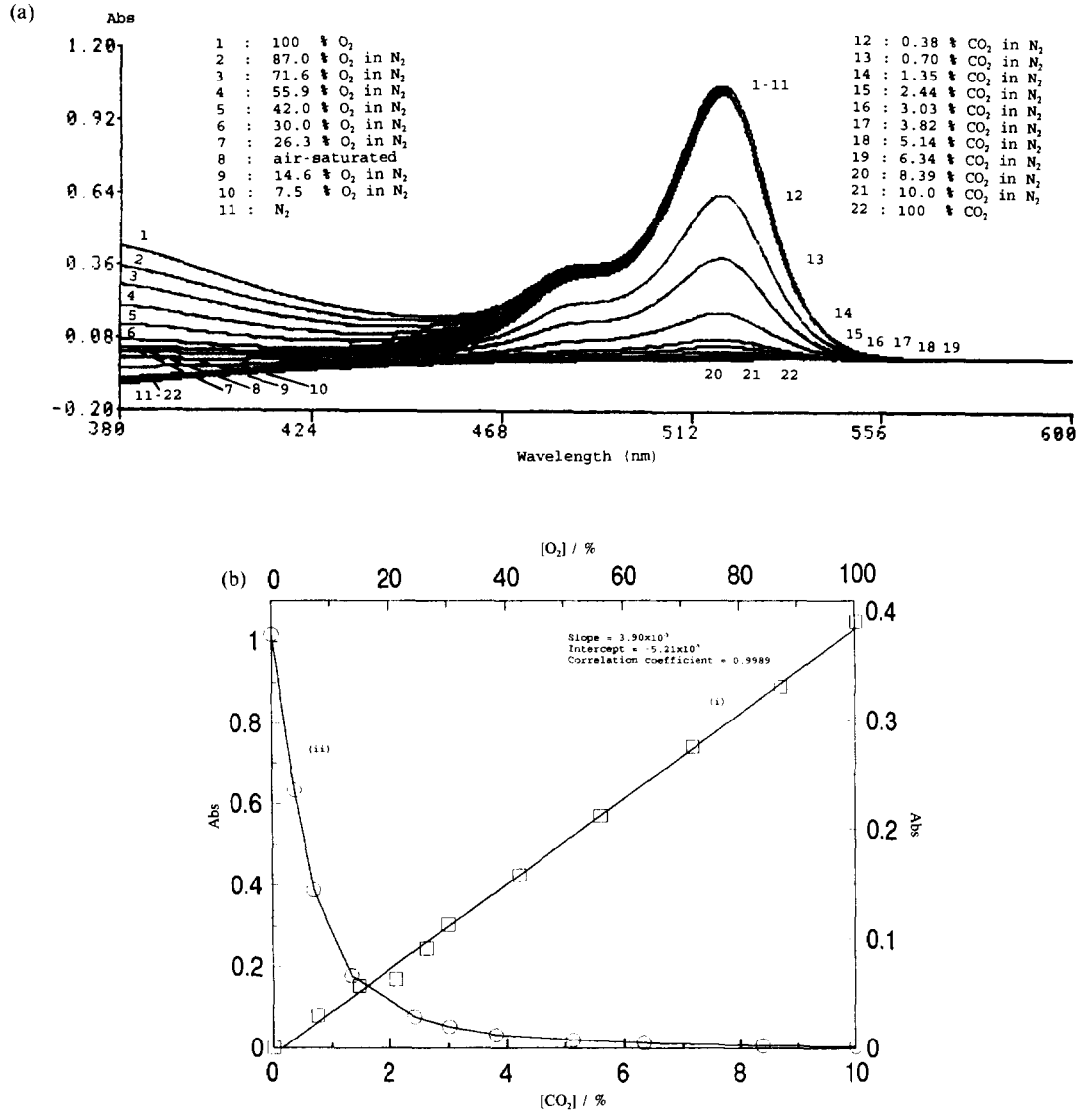


Fig. 4. (a) The effect of $O_2$ and $CO_2$ on the absorption spectrum of a solution of 10.6 $\mu M$ FL and 190 $\mu M$ KOH in 1:1 (v/v) DEA/DMF solvent mixture. Optical pathlength: 1 cm; reference: air-saturated 190 $\mu M$ KOH in 1:1 (v/v) DEA/DMF solvent mixture. (b)(i) Plot of abs against $[O_2]$ at 400 nm using the data in (a). (ii) Plot of abs against $[CO_2]$ at 520 nm using the data in (a).

absorbance with a 91% change in absorbance from 0 to 10% $CO_2$.

We observed that a solution of FL in DEA changes colour on exposure to $CO_2$ but that the change is not entirely reversible which may be probably owing to DEA being an almost completely non-aqueous solvent. As mentioned above, a solution of FL in DMF responds reversibly to gaseous $CO_2$ as DMF contains a small amount of dissolved water (about 0.03%). Unfortunately, DMF has a CCTA spectrum which is too far into the ultraviolet region to be of practical use for future fibre optic sensor development. After further investigation, we devised a way around this problem by using a solution of FL dye and KOH in a 1:1 (v/v) DEA/DMF solvent mixture for the independent and reversible measurements of $CO_2$ (using colour changes of the FL dye) and $O_2$ (using the CCTA of the DEA with $O_2$). The observed changes in absorption spectrum of the solvent-dye solution as a function of $[O_2]$ and $[CO_2]$ are shown in Fig. 4a which demonstrates that there are no cross-interference between the two gases. A graph of abs at 400 nm against applied $[O_2]$ is plotted in Fig. 4b(i). The results agree with Beer–Lambert's law and the absorbance is linearly proportional to the applied $[O_2]$. The

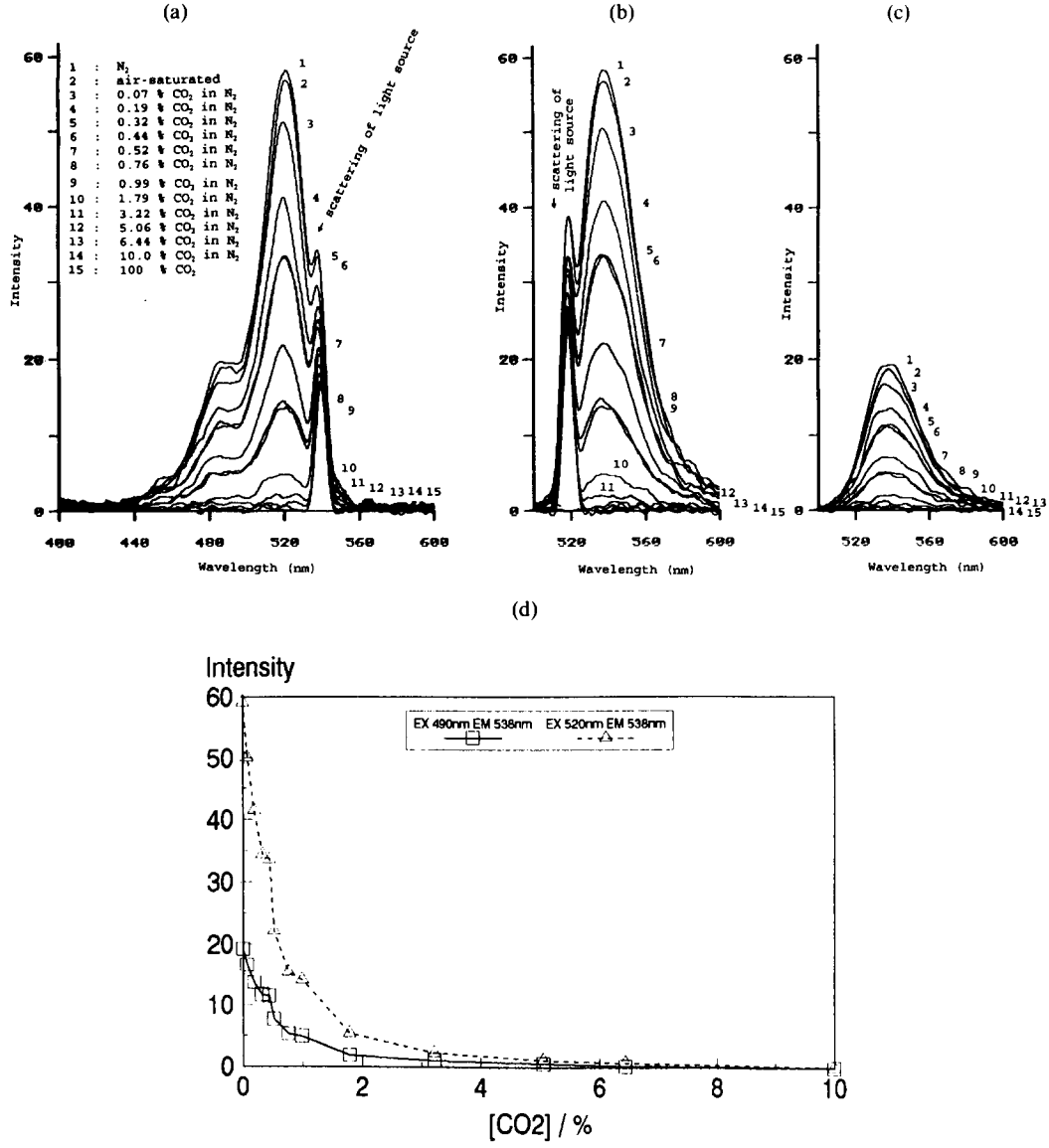


Fig. 5. Fluorescence excitation (EX) and emission (EM) spectra of 0.10 $\mu M$ FL and 190 $\mu M$ KOH in 1:1 (v/v) DEA/DMF solvent mixture. Optical pathlength:1 cm. (a) EX spectra with EM wavelength at 538 nm. (b) EM spectra with EX wavelength at 520 nm. (c) EM spectra with EX wavelength at 490 nm. (d) Plot of intensity against applied [$CO_2$] using the data of the spectra.

change of absorbance is again caused by the CCTA of the DEA and $O_2$ complex. A plot of abs at 520 nm against applied [$CO_2$] is shown in Fig. 4b(ii) and increasing [$CO_2$] produce a non-linear fall in absorbance. The change of absorbance arises from the conversion of the orange dianion form of FL to the colourless, neutral lactonic form upon exposure to $CO_2$.

The fluorescence EX and EM spectra of 0.10 $\mu M$ FL and 190 $\mu M$ KOH in 1:1 (v/v) DEA/DMF solvent mixture is shown in Figs. 5a–c. The fluorescence intensity is decreased when the $CO_2$ concentration is increased. Unlike $FL^{2-}$ ion which is a strongly fluorescent molecule, the neutral lactonic form of FL is non-fluorescent. As explained above, $FL^{2-}$ ions in the solution are probably converted to neutral lactonic form of FL upon exposure to $CO_2$ (equations 1–3). The plot of intensity against applied [$CO_2$] is shown in Fig. 5d which shows that increasing [$CO_2$] generates a non-linear fall in fluorescence intensity.

*Fibre optic sensing system for $O_2$ and $CO_2$*

The experimental results demonstrate that FL dye and KOH in DEA/DMF solvent mixture is a promising $O_2$ and $CO_2$-sensitive transducer to be used for the development of a sensing system

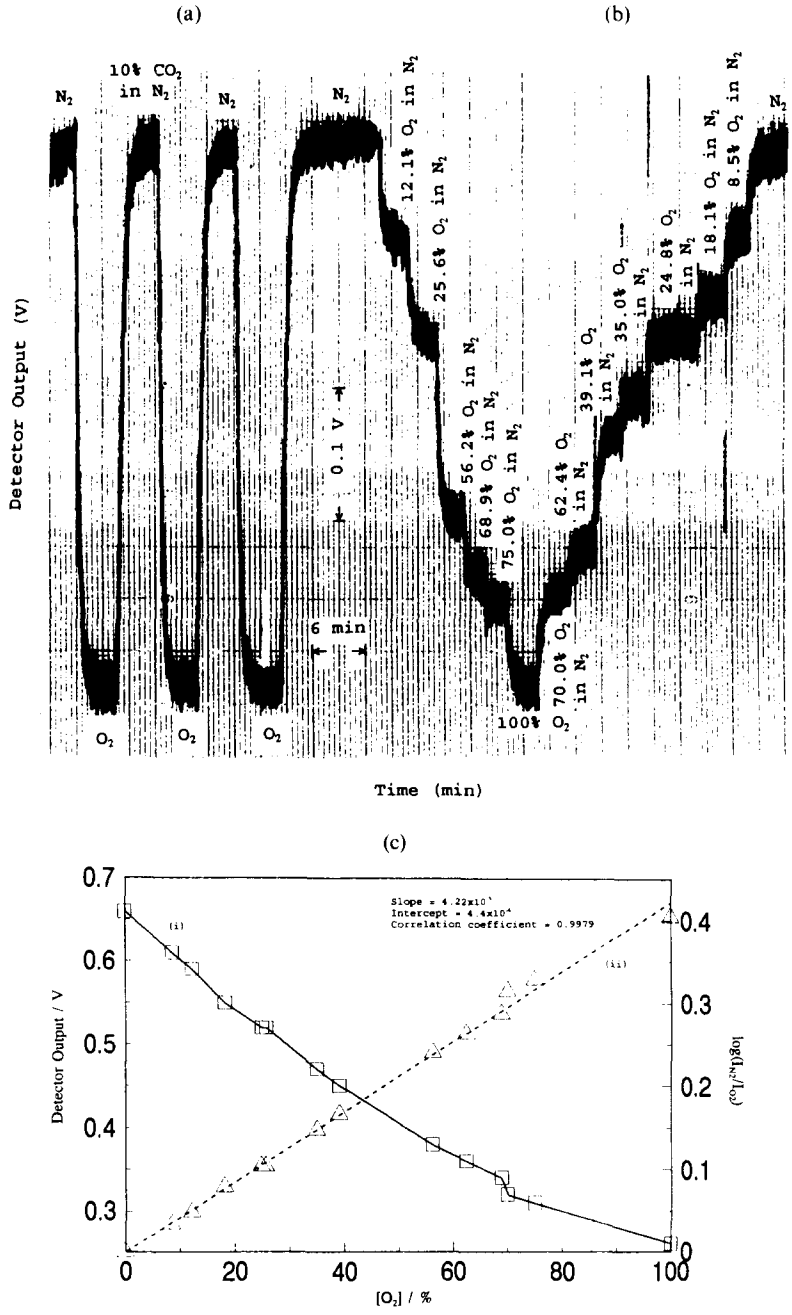


Fig. 6. (a) The response time, reproducibility and total signal change of the fibre optic sensing system when subjected to changes between: $N_2 \rightarrow O_2 \rightarrow$ 10% $CO_2$ in $N_2 \rightarrow O_2 \rightarrow N_2$. 1.0 ml of a solution of 10.6 $\mu M$ FL and 190 $\mu M$ KOH in 1:1 (v/v) DEA/DMF solvent mixture in a 1 cm cuvette was used with a wavelength of 400 nm and a gas flow rate of 50 $cm^3$/min. The amplification is about 10 times that used in Fig. 7. (b) The response of the fibre optic sensing system when subjected to different $O_2$ concentrations. (c) The response of the fibre optic sensing system with $O_2$. (i) Plot of detector output against $[O_2]$. (ii) Plot of $\log(I_{N_2}/I_{O_2})$ against $[O_2]$ using the data in (b).

for both $O_2$ and $CO_2$. The solvent mixture has a CCTA spectrum extending well into the visible region so it can be used with inexpensive plastic optical fibres. Wavelengths at 400 and 520 nm were chosen to monitor the concentrations of $O_2$ and $CO_2$. Although plastic fibres have substantial attenuation around 400 nm, the experimental set-up mentioned above is still sensitive enough for $O_2$ detection. Fluorescence measurement of $FL^{2-}$ ions, in principle, can be adapted to detect $CO_2$. However, we found that there was a cross-interference on $CO_2$ from $O_2$

owing to the fluorescent quenching effect of molecular $O_2$ on $FL^{2-}$ ions. In addition, the determinations of $O_2$ and $CO_2$ can be accomplished easily by only switching between the monitoring wavelengths. Thus, all the measurements were based on the absorption spectroscopic technique. Using the experimental set-up described earlier, the response, reproducibility and total signal change of the sensing system monitoring at 400 nm and a gas flow rate

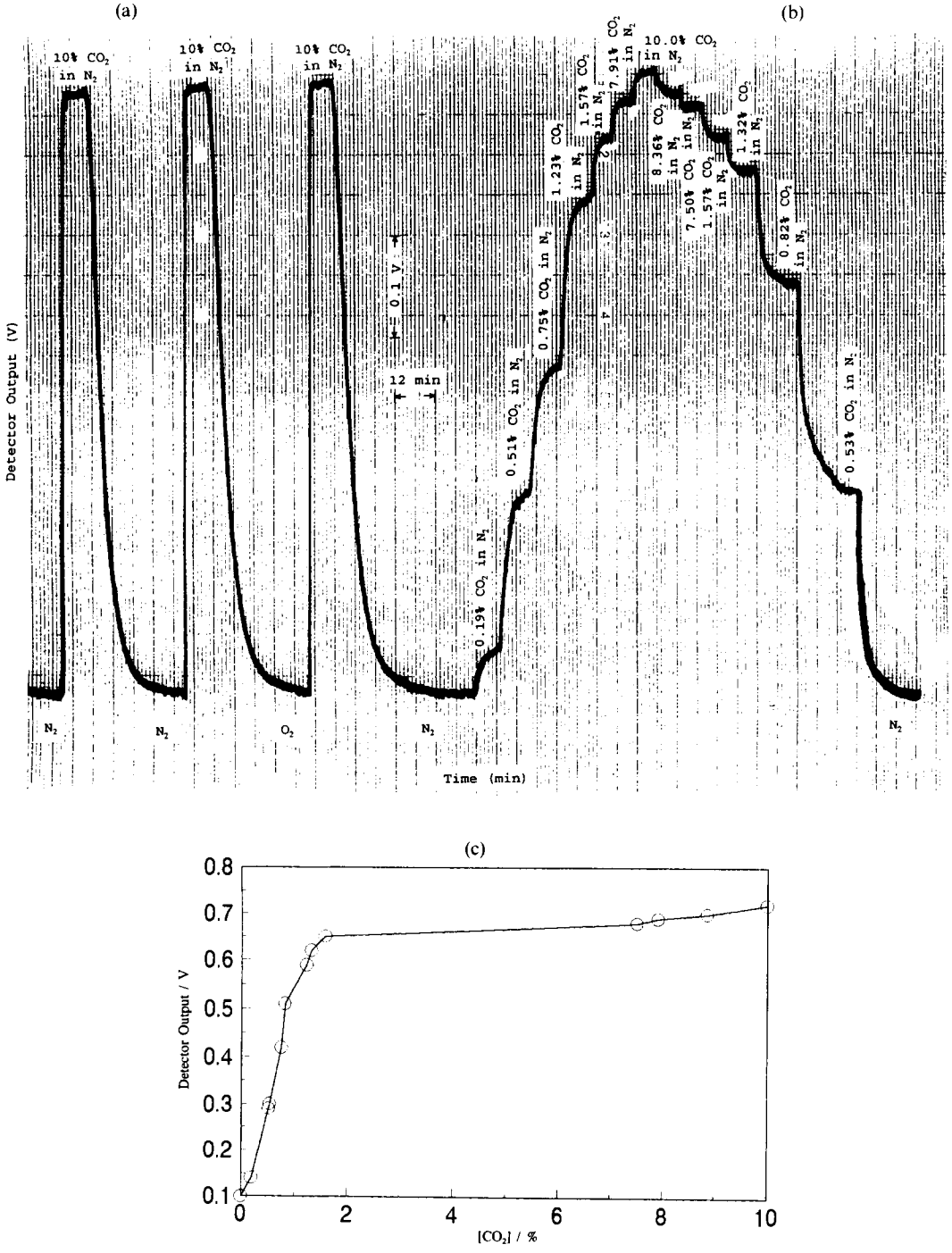


Fig. 7. (a) The response time, reproducibility and total signal change of the fibre optic sensing system when subjected to changes between: $N_2 \rightarrow$ 10% $CO_2$ in $N_2 \rightarrow O_2 \rightarrow$ 10% $CO_2$ in $N_2 \rightarrow N_2$. A solution (1.0 ml) of 10.6 $\mu M$ FL and 190 $\mu M$ KOH in 1:1 (v/v) DEA/DMF solvent mixture in a 1 cm cuvette was used with a wavelength of 520 nm and a gas flow rate of 50 $cm^3$/min. (b) The response of the fibre optic sensing system when subjected to different $CO_2$ concentrations. (c) Plot of detector output against $[CO_2]$.

of 50 $cm^3$/min through the solvent–dye solution in a 1 cm path-length cuvette were investigated. Figure 6a shows the response of the sensing system to step changes in gas concentrations from 100% $N_2$ to 100% $O_2$, from 100% $O_2$ to 10% $CO_2$ in $N_2$, from 10% $CO_2$ in $N_2$ to 100% $O_2$ and again back to 100% $N_2$. The reversibility of the sensing system is good and there is no cross-interference from $CO_2$. The response time is 0.75 and 1.5 min for a 90% signal change from $N_2$ to $O_2$ and from $O_2$ to $N_2$, respectively. The response of the sensing system when subjected to different levels of $O_2$ was investigated (Fig. 6b). The decrease in signal level with increasing $O_2$ concentrations is non-linear [Fig. 6c(i)] and the sensitivity (indicated by the slope of the graph) decreases as the concentration of $O_2$ increases with about a 35% change of signal level from 0 to 25% $O_2$. The sensing system responds over the range of 0–100% $O_2$ with a response which is in agreement with Beer–Lambert's law so that a linear graph [Fig. 6c(ii)] is obtained when $\log(I_{N_2}/I_{O_2})$ is plotted against $[O_2]$ where $I_{N_2}$ is the signal level recorded in $N_2$ only (i.e. $[O_2] = 0$) and $I_{O_2}$ is the level recorded in a gas mixture having an $O_2$ concentration of $[O_2]$. The response, reproducibility and total signal change of the sensing system monitoring at 520 nm were investigated. Figure 7a shows the response of the sensing system to step changes in gas concentrations from 100% $N_2$ to 10% $CO_2$ in $N_2$, from 10% $CO_2$ in $N_2$ to 100% $O_2$, from 100% $O_2$ to 10% $CO_2$ in $N_2$ and again back to 100% $N_2$. The reversibility of the sensing system is good and there is no cross-interference from $O_2$. The response time is 0.41 min and 10.0 min for a 90% signal change from $N_2$ to 10% $CO_2$ in $N_2$ and from 10% $CO_2$ in $N_2$ to $N_2$, respectively. The response of the sensing system when subjected to different concentrations of $CO_2$ was investigated (Fig. 7b) and was shown to be reversible. The increase in signal level with increasing $CO_2$ concentrations is non-linear (Fig. 7c): as a result, a non-linear calibration graph has to be plotted when using the sensing system for $CO_2$ determination over the range of 0–10% $CO_2$.

## CONCLUSIONS

This study demonstrated the use of a single solvent–dye solution as an $O_2$ and $CO_2$-sensitive transducer for the determination of both gaseous $O_2$ and $CO_2$. This detecting system has several advantages: inexpensive plastic optical fibre can be used; DEA and FL are inexpensive and readily available; preparation of solvent–dye solution is simple and fast. Possible applications include environmental and physiological monitoring of $O_2$ over the ranges of 0–100% and $CO_2$, 0–10%. The sensing medium however, still suffers from several drawbacks such as photo-bleaching of the dye, possibly cross-interference from other acidic or alkaline gases and also other electron acceptors like nitric oxide.[28]

Furthermore, we expect the response of the solvent–dye solution to $CO_2$ will be humidity dependent because of the aforementioned reasons. The presence of water is crucial for the response of the solvent–dye solution to $CO_2$ and thus, increasing the water concentration in the solvent–dye solution is likely to shift the equilibrium of equation (2) from right to left and lowering the pH of the solvent–dye solution with a concomittant effect on the equilibrium of equation (3). The water content will certainly vary with the water vapour concentration in an applied gas mixture since DMF is a hydrophilic compound with a propensity to absorb water vapour. Secondly, we have observed that there is a hypsochromic shift of the absorbance band of $FL^{2-}$ in DMF when the water content increases.[29] In order to circumvent this effect, the applied gas mixture can pass through some drying agent such as a molecular sieve before bubbling through the solvent–dye solution.

In addition, the sensing schemes are based on the concentration of dissolved $O_2$ and $CO_2$ in the solvent–dye solution. Any variation of temperature will change the Henry's law constant of these gases and the solvent–dye solution. Although we do not have the gas solubility data of these gases in DMT/DMF solvent mixture, it has been reported that there is a 11.6% decrease in solubility of $CO_2$ in aniline[30] and the solubilities of $O_2$ in carbon tetrachloride, chlorobenzene, benzene and acetone increase by 2.00, 2.79, 4.35 and 4.02%, respectively, from 20 to 30°C.[31] Consequently, we expect the response of the solvent–dye solution to $CO_2$ will be strongly dependent on temperature with a less marked dependence for $O_2$.

Finally, we are now planning to design a $O_2/CO_2$ fibre optic sensor by employing a similar design of Kar and Arnold.[32] Briefly, the solvent–dye solution is entrapped inside a segment of thin-wall poly(tetrafluoroethylene) (PTFE) tubing. A single optical fibre directs the

incident light into the solvent–dye solution through one end of the tubing and the transmitted light is collected by another optical fibre through the other end. Oxygen and $CO_2$ gases can readily diffuse through the thin-wall PTFE tubing into the solvent–dye solution for the reactions.

*Acknowledgements*—The authors would like to express their thanks to Dr A. Tubb for using his oxygen and carbon dioxide detectors and to the University of the West of England, Bristol for providing the financial support.

## REFERENCES

1. M. L. Hitchman, *Measurement of Dissolved Oxygen*, pp. 132–138, John Wiley & Sons, New York, 1978.
2. J. O. Lay, *Metallurgia*, 1955, **51,** 109.
3. R. E. Ellis and B. Schurin, *Appl. Optics*, 1969, **8,** 2265.
4. J. W. Severinghaus, *Ann. N. Y. Acad. Sci.*, 1968, **148,** 115.
5. J. I. Peterson, R. V. Fitzgerald and D. K. Buckhold, *Anal. Chem.*, 1984, **56,** 62.
6. A. Sharma and O. S. Wolfbeis, *Appl. Spectrosc.*, 1988, **42,** 1009.
7. P. Y. F. Li and R. Narayanaswamy, *Analyst*, 1989, **114,** 1191.
8. C. Preininger, I. Klimant and O. S. Wolfbeis, *Anal. Chem.*, 1994, **66,** 1841.
9. G. G. Vurek, P. J. Feustel and J. W. Severinghaus, *Ann. Biomed. Engng*, 1983, **11,** 499.
10. Z. Zhujun and W. R Seitz, *Anal. Chim. Acta*, 1984, **160,** 305.
11. C. Munkholm, D. R. Walt and F. P. Milanovich, *Talanta*, 1988, **35,** 109.
12. C. Goyet, D. R. Walt and P. G. Brewer, *Deep-Sea Res.*, 1992, **39,** 1015.
13. D. R. Walt, G. Gabor and C. Goyet, *Anal. Chim. Acta*, 1993, **274,** 47.
14. M. D. DeGrandpre, *Anal. Chem.*, 1993, **65,** 331.
15. W. J. Albery and P. Barron. *J. Electroanal. Chem. Interfacial Electrochem.*, 1982, **138,** 79.
16. Ph. Arquint, A. van den Berg, B. H. van der Schoot, N. F. de Rooij, H. Bühler, W. E. Morf and L. F. J. Dürselen, *Sens. Actuators B*, 1993, **13–14,** 340.
17. W. Gumbrecht, D. Peters, W. Schelter, W. Erhardt, J. Henke, J. Steil and U. Sykora, *Sens. Actuators B*, 1994, **18–19,** 704.
18. J. L. Gehrich, D. W. Lübbers, N. Opitz, D. R. Hansmann, W. W. Miller, J. K. Tusa and M. Yafuso, *IEEE Trans. Biomed, Engng*, 1986, **33,** 117.
19. W. W. Miller, M. Yafuso, C. F. Yan, H. K. Hui and S Arick, *Clin. Chem. (Winston-Salem, N.C.)*, 1987, **33,** 1538.
20. O. S. Wolfbeis, L. J. Weis, M. J. P. Leiner and W. E. Ziegler, *Anal. Chem.*, 1988, **60,** 2028.
21. D. F. Evans, *J. Chem. Soc.*, 1953, 345.
22. H. Tsubomura and R. S. Mulliken, *J. Am. Chem. Soc.*, 1960, **82,** 5966.
23. A. U. Munck and J. F. Scott, *Nature*, 1956, **177,** 587.
24. Y. Kawabata, T. Kamichika, T. Imasaka and N. Ishibashi, *Anal. Chim. Acta*, 1989, **219,** 223.
25. A. I. Vogel, *Quantitative Inorganic Analysis*, p. 243. Longmans, Green, London, 1961.
26. H. Diehl, *Talanta*, 1989, **36,** 413.
27. N. O. Mchedlov-Petrossyan, M. I. Rubtsov and L. L. Lukatskaya, *Dyes Pigments*, 1992, **18,** 179.
28. J. Jortner and U. Sokolov, *J. Phys. Chem.*, 1961, **65,** 1633.
29. M. F. Choi and P. Hawkins, *Spectrosc. Lett.*, in press.
30. H. Stephen and T. Stephen (eds), *Solubilities of Inorganic Compounds*, Vol. I, Part 2, p. 1068. Pergamon Press, Oxford, 1963.
31. W. F. Linke, *Solubilities: Inorganic and Metal–Organic Compounds*, 4th Ed., Vol. 2, p. 1234. American Chemical Society, Washington, D.C., 1965.
32. S. Kar and M. A. Arnold, *Talanta*, 1994, **41,** 1051.

Pergamon

*Talanta*, Vol. 42, No. 3, pp. 493–495, 1995
Elsevier Science Ltd
Printed in Great Britain

# BOOK REVIEWS

**Chemistry and Physics of Carbon—Volume 24:** P. A. THROWER (editor), Dekker, New York, 1994. Pages: xv + 316. $165.00. ISBN 0-8247-9091-X.

This is the latest volume in a series which has earned a deservedly high reputation in the carbon community. Each volume contains contributions by leading experts and in this book, four quite diverse topics are brought together to form another authoritative account of some currently topical aspects of the chemistry and physics of carbon.

The opening section, comprising some 40 pages, deals with the early stages of pitch carbonization and provides a description of the kinetics of pitch polymerization leading to mesophase formation and development. By focusing on the polymerization process during mesophase formation, the mechanism of the growth of the mesophase spheres from the isotropic phase is also described. Brief descriptions are included of the key analytical methods and procedures used to derive the data on which these descriptions are based, and a good set of references is provided in this very clear expose of recent work of the UCAR Carbon Company in this field. The second chapter deals with the quite different subject of the thermal conductivity of diamond. With the recent advances in the development of diamond films and bearing in mind that diamond has a higher thermal conductivity than copper, this chapter is certainly timely. After an outline of the theoretical background of the thermal conductivity of non-metallic solids, the published data on the thermal conductivity of single crystal diamond and chemically vapour-deposited films follows in successive sections. This provides a thorough review of the available data and leads to a concluding section which highlights the advances made in the past 5 years and indicates where further research is required. The statement that "the thermal conductivity of diamond is one of the most important physical parameters of this fascinating and potentially technologically important forms of carbon" is well justified by this chapter.

The remaining two chapters are of roughly equal length and in total comprise nearly two thirds of the book. "Chemistry in the production and utilization of needle coke" is a contribution from Japanese workers under the leadership of Isao Mochida and is an excellent review covering the properties and structure of needle coke, commercial production procedures and the relevant carbonization chemistry. It is comprehensive, detailed and highly informative and will undoubtedly become essential background reading for anyone starting work in this area. The final chapter examines the role of physical, solid-state analytical and electro-chemistry in the study of carbon surfaces. The authors cited their objective as being to provide a more unified and comprehensive review of carbon surface properties and to illustrate the importance of these properties in some applications such as catalysis and gasification. They must be satisfied with the result of their efforts and they have produced an authoritative account of a topic which has been the subject for a very large number of published papers as evidenced by the extensive references provided.

In keeping with previous books in this series, this one is well produced with clear script and illustrations and is well bound in hard-back form. At $165 it is not cheap but it is an excellent contribution to the subject and will be a valuable acquisition for libraries and indeed for all individual carbon scientists who can afford it.

J. W. PATRICK

**Advances in Steroid Analysis '93:** S. GÖRÖG (editor), Akadémiai Kiadó, Budapest, 1994. Pages: xiii + 623. £85.00.

This book is a record of the fifth in a series of symposia held in Hungary, involving a total of sixty-five papers from contributors in twenty countries. Less than a third of the papers are from the host country. Steroid hormones form the main focus, but analysis of complex mixtures of sterols, bile acids, and the vitamins D, also figure prominently.

The biochemical flavour of these texts increases inexorably, as does the clinical dimension, at the expense of chemical and pharmaceutical aspects of steroid analysis. Accounts of receptor binding studies and immunoassay methods outnumber those concerned with chromatographic methods and spectroscopy (HPLC, HPTLC and GS-MS) and a substantial chapter is devoted to steroid hormone biosynthesis, metabolism and enzymology. In contrast to previous volumes in this series, there is a dearth of novel methodology, testifying no doubt to the success of methods developed in the 1980's for the determination of trace amounts of anabolic steroids.

The final third of the volume is devoted to clinical studies, and a special session entitled "environment, steroids and cancer", in which epidemiology and endocrinology come to the fore. The latter chapter is of the "review-lecture" type and concentrates mainly upon breast cancer and prostatic cancer, and the possible role of dietary habits in influencing the incidence of these diseases.

The book is fairly free of trivial errors and is reasonably uniform in style, in spite of its being reproduced directly from such a large number of authors' manuscripts. It again represents excellent value for money.

A. B. TURNER

**Infrared Characteristic Group Frequencies, Tables and Charts—Second Edition:** G. SOCRATES, Wiley, Chichester, 1994. Pages: xii + 249. $60.00. ISBN 0-471-94230-8.

Infrared spectroscopy is used to identify substances by examining the characteristic absorptions of functional groups. Absorption bands in the region 4000–200 $cm^{-1}$ are normally considered and the technique is used for both qualitative and quantitative analysis. As stated in the introduction to this work, correlation tables and charts, relating frequency intervals to functional groups, have been derived empirically over many years by the careful and painstaking work of very many scientists.

The second edition of this very comprehensive book is in landscape style to facilitate the presentation of charts although some of the tables are printed sideways in portrait format. There is an introduction which includes useful information on spurious bands, 19 chapters on functional groups or classes of compounds, and a chapter on the near infrared region (14,000–4000 $cm^{-1}$). Included in the text are 13 different charts covering 39 pages, numerous tables, 3 figures, an appendix detailing further reading and a useful index.

I found the print size on many of the charts to be very small especially when the characters are superimposed on a 'graph paper' background and I wondered if my days of not wearing spectacles were coming to an end. All the useful charts of a general nature are included in the introduction, these are: regions of strong solvent absorption, negative correlations (absence of band equals absence of group), positions of bands in relation to type of vibration and the main chart (13 pages) of characteristic bands of groups and compounds. The familiar abbreviations are given on the charts; *e.g.*, w—weak, m—medium, s—strong, str—stretch, sym—symmetric, *etc.*, and all such symbols are clearly stated. Similarly the use of thick lines to indicate important band ranges is explained. Most of the remaining charts and tables are more specifically related to functional groups or chemical classes. These are: band positions of alkenes, carbonyl groups, substituted benzenes, ions, hydrides, complexes/ligands/other groups, and transition metal-halides. A chart relating to absorptions in the near infrared region is also included.

The individual chapters are excellent, for example, the chapter on the important carbonyl group covers numerous chemical classes for which a strong absorption band due to the C = O stretching vibration is observed in the 1850–1550 $cm^{-1}$ region. This chapter, at 41 pages the largest in the book, includes 41 tables and 179 references. Other chapters are devoted to alkanes, double-bond compounds, triple-bond compounds, the X = Y = Z group, the O-H group, ethers, and the -O-O- group. Other compounds covered in separate chapters include: amines *etc.*, aromatics, 6-membered heterocyclic compounds, 5-membered heterocyclic compounds, organic nitrogens, organic halogens, sulphur and selenium compounds, organic phosphate compounds, organic silicon compounds, boron compounds and finally inorganic compounds and coordination complexes.

I decided to use the book to examine IR data ($cm^{-1}$) on a couple of compounds that I have been studying. First a FTIR spectrum of a novel organophosphorus carbohydrate with bands at 3213 (OH), 3078-3061 (aryl C-H), 2914-2837 (aliphatic C-H), 1481 (aryl C-H), 1230 (P = O), 1093 and 1041 (C-O), 760 and 717 (monosubstituted aromatic ring). As I also examined the compound by X-ray crystallography, all the groups assigned by IR can be confirmed as present. Next an IR spectrum (lower resolution) of a known compound, gallic acid (3,4,5-trihydroxybenzoic acid), isolated from a herb used in Chinese medicine which gave bands at: 3480 (OH), 1655 (C = O), 1545 and 1440 (aryl C-H), 1270 (C-O) and 728 (aryl C-H). Again all seems to be okay. Many known compounds can, of course, also be identified by comparison with the well-known compilations of standard spectra and brief details of these collections (both book and computer based) are presented in this work.

Overall this book is a welcomed valuable addition to any laboratory engaged in infrared spectroscopy and is highly recommended.

P. J. Cox

**Experimental Mass Spectrometry:** D. H. RUSSELL (editor), Plenum, New York, 1994. Pages: xiii + 311. US$79.50. ISBN 0-306-44457-7.

Mass spectrometry has advanced so rapidly in the last decade that it has become increasingly difficult to keep abreast of developments—especially in the area of biological mass spectrometry. Although technical innovations form a major part of these advances much has also been achieved by the nonspecialist. Indeed many mass spectrometers are now operated routinely by bioscientists, clinicians, *etc*; a situation difficult to imagine 10 years ago. It is in these laboratories where we can arguably expect to see the greatest potential for further development so it is critical for the mass spectrometrists and the bioscientists to interface with one another and learn to communicate across the 'divide'.

The editor, a mass spectrometrist, has done an admirable job in producing a book which he intends as a guide for the nonspecialist in the expanding field of experimental mass spectrometry. The book has eight chapters dealing with diverse areas: negative ion chemistry, organo-alkali metal ions, collision induced dissociation (CID) of ions, Fourier transform ion cyclotron resonance (FTICR) mass spectrometry, protein structure by time-of-light MS, electrospray ionisation and tandem MS of large biomolecules and LC/FAB MS.

This book provides a timely update for both specialist MS operators and for the nonspecialist in some of the most important developments in mass spectrometry. As mentioned in the preface equally important areas have not been covered, notably: in depth coverage of tandem MS, matrix-assisted laser desorption ionisation (MALDI) and, dare I say it, inorganic mass spectrometry. For reasons lost in the mists of time few books on mass spectrometry (and this is no exception) include chapters on inorganic MS which has seen equally important advances in the last decade in terms of applications to the biomedical field.

**Infrared Characteristic Group Frequencies, Tables and Charts—Second Edition:** G. SOCRATES, Wiley, Chichester, 1994. Pages: xii + 249. $60.00. ISBN 0-471-94230-8.

Infrared spectroscopy is used to identify substances by examining the characteristic absorptions of functional groups. Absorption bands in the region 4000–200 $cm^{-1}$ are normally considered and the technique is used for both qualitative and quantitative analysis. As stated in the introduction to this work, correlation tables and charts, relating frequency intervals to functional groups, have been derived empirically over many years by the careful and painstaking work of very many scientists.

The second edition of this very comprehensive book is in landscape style to facilitate the presentation of charts although some of the tables are printed sideways in portrait format. There is an introduction which includes useful information on spurious bands, 19 chapters on functional groups or classes of compounds, and a chapter on the near infrared region (14,000–4000 $cm^{-1}$). Included in the text are 13 different charts covering 39 pages, numerous tables, 3 figures, an appendix detailing further reading and a useful index.

I found the print size on many of the charts to be very small especially when the characters are superimposed on a 'graph paper' background and I wondered if my days of not wearing spectacles were coming to an end. All the useful charts of a general nature are included in the introduction, these are: regions of strong solvent absorption, negative correlations (absence of band equals absence of group), positions of bands in relation to type of vibration and the main chart (13 pages) of characteristic bands of groups and compounds. The familiar abbreviations are given on the charts; *e.g.*, w—weak, m—medium, s—strong, str—stretch, sym—symmetric, *etc.*, and all such symbols are clearly stated. Similarly the use of thick lines to indicate important band ranges is explained. Most of the remaining charts and tables are more specifically related to functional groups or chemical classes. These are: band positions of alkenes, carbonyl groups, substituted benzenes, ions, hydrides, complexes/ligands/other groups, and transition metal-halides. A chart relating to absorptions in the near infrared region is also included.

The individual chapters are excellent, for example, the chapter on the important carbonyl group covers numerous chemical classes for which a strong absorption band due to the C = O stretching vibration is observed in the 1850–1550 $cm^{-1}$ region. This chapter, at 41 pages the largest in the book, includes 41 tables and 179 references. Other chapters are devoted to alkanes, double-bond compounds, triple-bond compounds, the X = Y = Z group, the O-H group, ethers, and the -O-O- group. Other compounds covered in separate chapters include: amines *etc.*, aromatics, 6-membered heterocyclic compounds, 5-membered heterocyclic compounds, organic nitrogens, organic halogens, sulphur and selenium compounds, organic phosphate compounds, organic silicon compounds, boron compounds and finally inorganic compounds and coordination complexes.

I decided to use the book to examine IR data ($cm^{-1}$) on a couple of compounds that I have been studying. First a FTIR spectrum of a novel organophosphorus carbohydrate with bands at 3213 (OH), 3078-3061 (aryl C-H), 2914-2837 (aliphatic C-H), 1481 (aryl C-H), 1230 (P = O), 1093 and 1041 (C-O), 760 and 717 (monosubstituted aromatic ring). As I also examined the compound by X-ray crystallography, all the groups assigned by IR can be confirmed as present. Next an IR spectrum (lower resolution) of a known compound, gallic acid (3,4,5-trihydroxybenzoic acid), isolated from a herb used in Chinese medicine which gave bands at: 3480 (OH), 1655 (C = O), 1545 and 1440 (aryl C-H), 1270 (C-O) and 728 (aryl C-H). Again all seems to be okay. Many known compounds can, of course, also be identified by comparison with the well-known compilations of standard spectra and brief details of these collections (both book and computer based) are presented in this work.

Overall this book is a welcomed valuable addition to any laboratory engaged in infrared spectroscopy and is highly recommended.

P. J. Cox

**Experimental Mass Spectrometry:** D. H. RUSSELL (editor), Plenum, New York, 1994. Pages: xiii + 311. US$79.50. ISBN 0-306-44457-7.

Mass spectrometry has advanced so rapidly in the last decade that it has become increasingly difficult to keep abreast of developments—especially in the area of biological mass spectrometry. Although technical innovations form a major part of these advances much has also been achieved by the nonspecialist. Indeed many mass spectrometers are now operated routinely by bioscientists, clinicians, *etc*; a situation difficult to imagine 10 years ago. It is in these laboratories where we can arguably expect to see the greatest potential for further development so it is critical for the mass spectrometrists and the bioscientists to interface with one another and learn to communicate across the 'divide'.

The editor, a mass spectrometrist, has done an admirable job in producing a book which he intends as a guide for the nonspecialist in the expanding field of experimental mass spectrometry. The book has eight chapters dealing with diverse areas: negative ion chemistry, organo-alkali metal ions, collision induced dissociation (CID) of ions, Fourier transform ion cyclotron resonance (FTICR) mass spectrometry, protein structure by time-of-light MS, electrospray ionisation and tandem MS of large biomolecules and LC/FAB MS.

This book provides a timely update for both specialist MS operators and for the nonspecialist in some of the most important developments in mass spectrometry. As mentioned in the preface equally important areas have not been covered, notably: in depth coverage of tandem MS, matrix-assisted laser desorption ionisation (MALDI) and, dare I say it, inorganic mass spectrometry. For reasons lost in the mists of time few books on mass spectrometry (and this is no exception) include chapters on inorganic MS which has seen equally important advances in the last decade in terms of applications to the biomedical field.

Volume 2, which I eagerly await, is to be devoted to MALDI and I hope Volume 3 will find room for developments in inductively coupled plasma mass spectrometry (ICP/MS), thermal ionisation mass spectrometry (TIMS) and gas isotope ratio mass spectrometry (GIRMS), all of which have made huge contributions to our understanding of mineral metabolism, energy metabolism, amino-acid/carbohydrate/fatty acid metabolism, *etc*.

As a final point, the title of the book will not help it achieve the circulation it deserves within the biological community. Despite this the series should go a long way towards helping mass spectrometrists and bioscientists understand each others needs and limitations.

B. A. McGaw

Pergamon

0039-9140(95)01427-6

*Talanta*, Vol. 42, No. 4, pp. 497–506, 1995

0039-9140/95 $9.50 + 0.00

## REVIEW

# A REVIEW ON THIOCYANATE METHODS FOR THE ESTIMATION OF MOLYBDENUM BY MOLECULAR ABSORPTION SPECTROSCOPY

A. C. BASAK, K. C. GHOSH, A. R. PAUL, S. BHATTACHARJEE* and L. P. PANDEY
Analytical Chemistry Division, National Metallurgical Laboratory, Jamshedpur, 831 007, India

(*Received* 3 *March* 1994. *Revised* 2 *September* 1994. *Accepted* 21 *September* 1994)

**Summary**—A review is presented on thiocyanate methods for the estimation of molybdenum in a wide variety of samples. They include conventional thiocyanate methods in which molybdenum forms an orange red complex with the thiocyanate ions and improved thiocyanate methods where the sensitivity is increased through the formation of ternary ion association complex.

The estimation of molybdenum by thiocyanate method is one of the most commonly used techniques. Molybdenum forms an orange red complex with thiocyanate ions in acid media in the presence of reducing agents. Mo(VI) is reduced to Mo(V) which forms the coloured complex and it has an absorption maximum in the range of 460–470 nm. Normally the complex is extracted into an appropriate solvent for absorbance measurement.

The reaction has been known for a long time; the analytical utility of the molybdenum thiocyanate complex was first shown by Braun who used this technique to detect molybdenum in minerals.[1,2] Its use has grown, though rather slowly, over time.[1–128] The mechanism of the colour reaction is complicated and the system may contain several Mo(V) complexes. The Mo:SCN ratio has been assigned as 1:3, though yellow 1:2 and colourless 1:1 complexes have also been advocated.[11,12] As the reaction involves a number of parameters the reaction conditions must be rigorously maintained for precision and accuracy. Attempts have been continually made to improve the sensitivity and selectivity by judicious choice of solvents, reducing agents and acid concentrations.

The present review aims to assimilate the extensive literature on thiocyanate methods which have been used for the estimation of Mo in a wide variety of samples. A literature search was carried out primarily through *Analytical Abstracts* for the period 1972–1992. While an attempt has been made to be as exhaustive as possible for the period mentioned, the citations before 1971 were collected mostly as cross-references.

The review has been organized in the following manner. It primarily deals with two types of thiocyanate methods, the conventional and the modified type. Section 1 describes the conventional thiocyanate methods which include reducing agent, solvents used for extraction, sensitivity and interference from foreign ions. The modified thiocyanate methods have been listed in a tabular form in Section 2. Section 3 describes the application of both conventional and modified thiocyanate methods followed by conclusions in Section 4.

## 1. CONVENTIONAL THIOCYANATE METHODS

This section describes those methods in which Mo(VI) is first reduced to Mo(V) by using an appropriate reducing agent. The reduced Mo(V) is then allowed to form an orange red complex with the thiocyanate ions under regulated experimental conditions. Subsequently the coloured complex is extracted with a solvent for absorbance measurement at 470 nm.

### 1.1. *Reducing agents*

The role of reducing agent is most important in any thiocyanate method as Mo(VI) must be

*Author to whom correspondence should be addressed.

reduced to Mo(V) to form a complex with the thiocyanate ions. Therefore, the reducing agent should be mild enough not to reduce Mo(VI) below Mo(V). Ascorbic acid has been extensively used for this purpose.[14,27,42,45–48,52,62,63,69,71,73,75,78,81,83,84,86,87,90,94,95,103,104,107,113–115,118,119,122,128] Sn(II) has also been a popular choice.[6,21,44,53,57,61,77,120,121] However, its use has been restricted because of the fact that Sn(II) has a tendency to reduce Mo(VI) below Mo(V) and is not an entirely satisfactory reductant.[4,9,13,52] Also, the sensitivity and precision are poor in the absence of Fe(III). Other reducing agents include, iodide,[5,10,13] hydrazinium sulphate,[55] K-ethyl xanthate,[58] mercaptoacetic acid,[41] ferrocene,[66] CuCl–ascorbic acid,[99] thiourea,[28] titanium,[3] tin and titanium,[34] potassium iodide in the presence of Cu(I)[10] and sulphite.[5] Thiocyanate itself reduces Mo(VI) under the catalytic influence of copper.[18]

### 1.2. *Solvents*

A wide variety of solvents have been used to extract the Mo–SCN complex in the conventional thiocyanate methods. They include butyl acetate,[41] tributyl phosphate in chloroform,[46,47] 4-methyl pentan-2-ol in benzene,[49] amyl alcohol,[52] isoamyl alcohol + carbon tetrachloride,[8] tribenzylamine in chloroform,[55] tributyl phosphate + benzene(1:1),[57] acetophenone,[58] acetic acid,[66] isoamyl alcohol,[77] ethyl acetate,[82] ethyl methyl ketone,[92] butyl acetate,[96] isobutyl methyl ketone,[99] chloroform[110] and hexadecylmethyl ammonium bromide in chloroform.[121] Absorbance measurement in the aqueous medium has also been reported.[9]

### 1.3. *Sensitivity*

The molar extinction coefficient of the conventional thiocyanate complex is $2.0 \times 10^4$ at 470 nm in isoamyl alcohol, $1.45 \times 10^4$ at 465 nm[66] in aqueous acetic acid and $2.0 \times 10^4$ at 470 nm[82] in ethyl acetate.

### 1.4. *Interference*

The conventional thiocyanate methods are prone to interference from many cations and anions. Most common of them is Fe(III). However, under the normal reaction conditions it is reduced to Fe(II) which does not interfere. Interference from niobium may be corrected by measuring the absorbance simultaneously at 390 and 470 nm.[47] Tungsten is masked with oxalic acid,[49] $KHF_2$.[55] Cd, Fe, Cr, Ni, Mn, Cu, Zn, V, U may be tolerated in < 100-fold but Ti and Sn interfere.[41] Fe, V, W and Nb interferences have been overcome in rock samples by acid decomposition and extraction of Mo into xylene with tributylphosphate.[52] Ti, U, Bi, Ru, Mn, Ni, Fe, Co, Cr, V, W, Nb, Ce and Re interferences are overcome by washing the organic phase with $SnCl_2$ solution in acid medium,[55] but Pd, Pt and Os interfere. No interferences have been observed from 1000-fold amount of Zr, Nb, W or Re.[66] Large amounts of Re may be removed by potassium ethyl xanthate.[58] Methods of removing coextracted Fe, Co, Cu and Ti from the organic phase have been discussed but Pd, Hg, fluoride, citrate and oxalate interfere.[92]

## 2. MODIFIED THIOCYANATE METHODS

In this category, in addition to thiocyanate, another reagent is added which forms a ternary ion association complex followed by the solvent extraction of the complex for absorbance measurement. The additional reagent either enhances the efficiency of extraction or it pushes the absorption maximum to higher wavelength thus making it more selective. In both cases, the final objective is to increase the sensitivity and/or selectivity of the conventional thiocyanate methods. In the ternary ion association complex, the metal ion reacts with a ligand to produce a charged binary complex with a second ligand of opposite charge, usually a dyestaff. A ternary complex so formed normally exhibits enhanced selectivity, precision and sensitivity over the equivalent binary complex.

A large number of methods have been reported which adopt this approach.[42,44,48,53,54,56,58,59,60–64,68–75,78–81,83,85–88,90,95,97,102,104–107,110–116,118,119,122–124,126–128] They have been listed in Table 1. The organization of Table 1 is as follows: the second column under the head reagent shows the reagent which is necessary for forming the ternary ion association complex in addition to thiocyanate. In the column headed 'conditions of measurement', informations are given about the absorbance maximum ($\lambda_{max}$), molar extinction coefficient ($\epsilon$) and the metal, thiocyanate and reagent mole ratio ($M:SCN^-:R$), sequentially subject to the availability. The fourth column gives the reducing agent and the fifth and the sixth columns give the solvents and additional reagents and the analytical range, respectively. The column under 'interference' notes a brief summary of foreign ion 'interference' and probable ways to overcome them. The column headed 'matrix' gives the nature of samples where Mo has been estimated by the listed

Table 1. Thiocyanate methods involving ternary ion association complex

| | Reagent | Conditions of measurement $\lambda_{max}/\epsilon$/ M:$SCN^-$:R | Reducing agent | Solvent/ Additional reagent | Analytical range | Interference | Matrix | Ref. |
|---|---|---|---|---|---|---|---|---|
| 1. | Crystal violet | 595 | Ascorbic acid | Toluene +Ethanol | 0.5–4 μg/10 ml | Nb, V, Ti, In, Ga, W, Zr, Co and Zn interfere | | 42 |
| 2. | 1,10-Phenanthroline | 525 | $SnCl_2$ | Dichloroet hane, Methanol | 1–10 μg/ml | 10-fold excess of Fe or V and 100-fold excess of W, P or silicate is tolerated | | 44 |
| 3. | 2-Benzylamino pyridine | 440; 1:3:2 | Ascorbic acid | Chloroform | | | Mo in steel | 48 |
| 4. | 2-Mercaptobenzo-γ-thiopyrone | 470 | $SnCl_2$ | Acetophenone | | Of 40 ions studied only fluoride, thiosulphate, Ni, Cu, Ag and Co interfere | Mo in steel | 53 |
| 5. | Diphenyl guanidine | 470; 21,200 | | Chloroform | 0.7–70 μg/10 ml | 5- to 10-fold of Nb or Bi and 200-fold of Cr, Mn, Ni, Zr, Cu, Ti, W, Re and Co do not interfere | Mo in steel | 54 |
| 6. | 4-Benzylpyridine | 465 | | | | | | 56 |
| 7. | Ethyl xanthate | 470 | | Acetophenone | 1.2–13.8 μg/ml | Na, K, Ba, Ca, Mg, Al, Mn, Cr, Sb, As, Zr, Ti, Pb, Sn, Ce, La and Fe do not interfere in 1000-fold | Mo in steel and Re | 58 |
| 8. | Antipyrene | 440; 19,000 | | Chloroform | 0.1–130 μg/5 ml | Alkali and alkaline earth metals, lanthanoids, Ni, Zn, Cd, Al, Mn, As, Sb and Sn do not interfere. Interference from Fe, Cu, Ti, Nb, Ta, Bi, W, Cr, U, V and Co may be prevented by masking, by reduction or by changing acidity | Mo in steel | 59 |
| 9. | Triethyl amine | 460; 28,000 | | Chloroform | | Alkali, alkaline earth metals, rare earths, Zn, Cd, Ni, Hf, Al, As, Zr, Pb, Bi, Sn, Co, Cu(80-fold), Ta(30-fold), Ti(15-fold), Nb(20-fold), W(40-fold), do not interfere. Thiourea may be used for masking Cu, KF for Ta, Ti, Nb and citric acid for W | Mo in soil | 60 |
| 10. | Quinoline | 470 | $SnCl_2$ | Nitrobenzene | | Cu, Co, Fe, Ti and W interfere. Cu, Co, Fe and Ti are removed by precipitation with NaOH. W is masked with citrate | Mo in steel | 61 |
| 11. | Tetraphenyl arsonium chloride | 470; 17,400 | Ascorbic acid and Ti(III) | Chloroform and quinol | | Cu, Zn, Cd, Al, Sn, Pb, V, Cr, Mn, Co, Ni do not interfere. Oxalic acid can mask 40-fold W and 10-fold Nb | Mo in low alloy steel and tungsten tool steel | 62 |

*continued overleaf*

Table 1—*continued*

| | Reagent | Conditions of measurement $\lambda_{max}/\epsilon$/ M:$SCN^-$:R | Reducing agent | Solvent/ Additional reagent | Analytical range | Interference | Matrix | Ref. |
|---|---|---|---|---|---|---|---|---|
| 12. | Octyl (α-anilino benzyl) phosphate | 470 | Ascorbic acid | Chloroform | 0.7–28 μg/L | Few ions that interfere can be separated or reduced with ascorbic acid | | 63 |
| 13. | Rhodamine B | 600 | Ascorbic acid | | 0.1–10 μg/25 ml | Interference from Fe(III) and tungstate may be masked with ascorbic acid and tartarate, respectively | Mo in soil and plants | 64 |
| 14. | Tetrabutyl ammonium ion | 465; 27,000; 1:4:3 | | Chloroform | 0.2–18 μg/ml | V, Co, Cr, Fe and Cu do not interfere if masked with ascorbic acid | Mo in industrial Cu–$MoS_2$ mixture | 68 |
| 15. | Tetraphenyl phosphonium chloride and tetraphenyl arsonium chloride | 470 | Ascorbic acid | Chloroform | 0.05–0.1 mM | Of 41 species only Ti interferes strongly but it may be masked by the addition of fluoride in the aqueous phase | | 69 |
| 16. | *N*,*N*′-Diethyl aniline perchlorate | 470 | Ascorbic acid | Dichloroethane | 1–10 μg/ml | No interference from 5000-fold Ni, 1000-fold Cu or Mn, 500-fold Fe or V and 300-fold Cr | Mo in steel | 70 |
| 17. | Dialkyl anilinium perchlorate (alkyl = methyl, ethyl, propyl, butyl or octyl) | 470; 15,000 | Ascorbic acid | Dichloroethane | 1–10 μg/ml | Interference by Fe is masked by ascorbic acid | Mo in steel | 71 |
| 18. | Benzoic-α-oxime | 490 | $SnCl_2$ | Isopropyl ether | | Tungsten interferes | | 72 |
| 19. | Crystal violet | 590 | Ascorbic acid | Toluene | | Tungsten interferes | Mo in high purity metallic niobium | 73 |
| 20. | Hexamethyl phosphoramide | 460 | | Chloroform | 0.75–5 μg/ml | Fe is separated by solvent extraction. No interference from 1 mg of U, V, Ta or Zr. 500 mg of Re, Nb and Ta were masked with NaF, Cu with thiourea and W by adding excess ammonium thiocyanate | Mo in alloy steel | 74 |
| 21. | Chlorpromazine hydrochloride | 465; 1:4:1 | Ascorbic acid | Chloroform | 5–50 μg/10 ml | | | 75 |
| 22. | ε-Caprolactum | 475; 20,000; 1:5:4 | Ascorbic acid | Aqueous | 3–18 μg/ml | Mg, Al, Ca(1000-fold), Ba, Mn (500-fold), Ag, Zn, Co, Cr, Fe(100-fold), Ni(50-fold), V, Zr(10-fold), Nb, Cu, Pb, Sn and W interfere | | 78 |
| 23. | $N^1$-(4-chlorophenyl)-$N^2$-(4-chloro-*o*-tolyl)-$N^1$-Hydroxybenzamidine hydrochloride | 470; 4500 | | Benzene | 2–20 μg/ml | No interference from most of the metals normally associated with Mo | | 79 |

| | | | | | | | | |
|---|---|---|---|---|---|---|---|---|
| 24. | $N^1$-(4-chlorophenyl)-$N^1$-hydroxy-$N^2$-(2,3-xylyl)-*p*-(toluamidine)-Hydrochloride | 470; 4000; 1:2:2 | | Benzene | 2.8–14 μg/ml | | | 80 |
| 25. | Mepazine(pecazine)hydrochloride | 465; 17,000 | Ascorbic acid | Chloroform | 0.9–5.4 μg/ml | About 24 cations normally associated with Mo and 8 anions may be tolerated | Mo in alloy steel | 81 |
| 26. | Thiocyanate-hydroxyamidine[$N^1$-hydroxy-$N^1$-*p*-tolyl-$N^2$-3,4-xylylbenzamidine] | 470; 1:2:2 | Ascorbic acid | Benzene | 9–18 μg/ml | No interference from Ni, Co, Cu(II), Mn(II) | Mo in steel and ores | 83 |
| 27. | Rhodamine 6G | 570 | | Aqueous gelatine solution | 0.04–0.24 μg/ml | Interference of 40 foreign ions (except Co and Zn) may be overcome by the addition of thiourea, ascorbic acid and tartarate | | 85 |
| 28. | Nitron | 465 | Ascorbic acid | Chloroform | 1.2–12 μg/ml | Mn, Ti(IV) and peroxide interfere at all concentrations. W(2-fold), Cr, Co, Fe, Pt, U, V(20-fold) and 200-fold amounts of 30 other species do not interfere | Mo in steel | 86 |
| 29. | *NN'*-Diphenyl-*p*-tolyamidine hydrochloride | 470 | Ascorbic acid | Benzene | 0.4–5 μg/ml | Many foreign ions do not interfere | | 87 |
| 30. | (Ethoxy carbonyl pentadecyl) trimethyl ammonium bromide (CPTA) | | | Chloroform, isobutyl alcohol | 0.1–7.0 μg/ml | Interference from several metals can be reduced by the addition of small amounts of citric acid. Interference of 10-fold Fe(III) can be prevented by an appropriate addition of ascorbic acid | Mo in sediments | 88 |
| 31. | *NN'*-Diaryl benzamide | 465; 1:2:1 | Ascorbic acid | Benzene | 0.4–5.4 μg/ml | At least 20,000 ppm of $Cl^-$, $Br^-$, $NO_3^-$, $SO_4^{2-}$, Li, Na, K and 6000 ppm of Be, Mg, Ca, Ba and Sr do not interfere. 12,000 ppm Ni, 1000 ppm Mn, 8000 ppm Cr, 7000 ppm Al may be tolerated. Interference of other ions are also listed | Mo in ores and alloy steels | 90 |
| 32. | Amides (*N*-phenyl acetamide, *N*-*p*-tolyacetamide, *N*-phenyl propionamide and benzamide) | 475; 13,000–18,000; 1:2:1 | Ascorbic acid | Benzene | 0.3–5.2 μg/ml | Nb interferes but may be masked with oxalate. Alkali metals, chloride, bromide, nitrate and sulphate do not interfere at concentration $\leqslant 2M$ | Mo in ores, alloy steel and synthetic mixtures | 95 |
| 33. | Imidoyl derivatives *N*-(*N*-phenylbenzimidoyl)-thiourea, *N*-phenyl-*N*-(*N*-phenyl benzimidoyl)-thiourea and I-(*N*-phenyl benzimidoyl)-thiosemicarbazide | 465 | L-Ascorbic acid | | 0.8–6.5 μg/ml | | Mo in ores and steel | 97 |

*continued overleaf*

Table 1—*continued*

| | Reagent | Conditions of measurement $\lambda_{max}/\epsilon/$ M:$SCN^-$:R | Reducing agent | Solvent/ Additional reagent | Analytical range | Interference | Matrix | Ref. |
|---|---|---|---|---|---|---|---|---|
| 34. | Adogen(methyl trioctyl ammonium chloride) | 467; 21,300 | $SnCl_2$ | Toluene | 2.5–50 μg | | Mo in steel | 102 |
| 35. | Acetone thiosemicarbazone | 472; 19,000; 1:4:2 | Ascorbic acid | Chloroform | 0.1–9.5 μg/ml | 4000 ppm Zn may be tolerated for 3 ppm Mo. Bivalent Pd, Rh show the lowest tolerance of 12 μg/ml | Mo in molybdenum steel | 104 |
| 36. | Perazinedimalonate {10-[3-(4-methyl 1-peparizinyl)propyl]*p* henothiazine dimalonate} | 460; 10,600; 1:1:4 | | Aqueous | 0.1–14 μg/ml | Tl, Fluoride and Zn do not interfere. V, Mn and Cr are eliminated by oxalate, Fe by ascorbic acid. Cu must be removed by extraction with dithiazone | Mo in alloy steel, ores and synthetic mixtures | 105 |
| 37. | Rhodamine B | 580; 150,000 | Ascorbic acid | Aqueous, polyvinyl alcohol, $CuSO_4$, thiourea, citric acid | | | Mo in steel, high speed steel and tungstate | 106 |
| 38. | Ethyl isobutrazine hydrochloride | 460; 38,600 | Ascorbic acid | Chloroform | 0.05–5.6 μg/ml | About 24 cations normally associated with Mo and 8 anions do not interfere | Mo in steel | 107 |
| 39. | Methotrimeprazine | 465; 16,000 | Ascorbic acid | Chloroform | 0.02–6 μg/ml | Tolerance levels of metals usually associated with molybdenum and common anions have been listed. A 100-fold excess of tungsten and a large excess of base metals and anions do not interfere. A large excess of iron may be tolerated in the presence of ascorbic acid. Sodium oxalate may be used to mask interference caused by V and Mn | Mo in steel | 110 |
| 40. | Malachite green | 640; 100,000; 1:5:2 | | | $\leqslant$400 *n*g/ml | | Trace Mo in ore | 111 |
| 41. | Pyrogallol | 465; 100,000; 2:3:2 | | Isobutyl methyl ketone | 0.04–1 μg/ml | | | 112 |
| 42. | 4-Acetyl-2-(acetylamino-5-dimethyl-$\Delta^2$-1,3,4-thiadizole-[5-acetamide-3-acetyl 2,3-dihydro-2,2-dimethyl 1,3,4-thiadiazole] | 470; 20,100 | Ascorbic acid | Chloroform | 0.06–2.5 μg/ml | Ten-fold amounts of Au, Pd and V and slightly higher amounts of Nb, Pt and Ta may be tolerated | Mo in steel | 113 |

| | | | | | | | | |
|---|---|---|---|---|---|---|---|---|
| 43. | 2-Chloro-*NN'*-bis (4-chlorophenyl)-*N*-hydroxybenzamidine | 470; 3300 | Ascorbic acid | Benzene | 3 24 $\mu$g/ml | Chlorine, bromine, nitrate, sulphate, urea, triethanolamine, alakli and alkaline earth metals do not interfere up to 3000 *ppm*. Fe(III), Cd(II) and fluoride (1000 *ppm*), Al(III), Ni(II), Co(II) and Zn(II) (2500 *ppm*), Cr(III) and Mn(II) (1800 *ppm*), Ti(IV) and Zr(IV) (200 *ppm*), Nb(V) and Ta(V) (150 *ppm*), V(V) (50 *ppm*), W(VI) (20 *ppm*) and Cu(II) (3000 *ppm*) do not interfere | Mo in steel ores | 114 |
| 44. | 2-Chloro-*N'*-4-chlorophenyl-*N*-*m*-tolyl benzamidine hydrochloride | 470; 18,000 | Ascorbic acid | Benzene | 0.4–5.4 $\mu$g/ml | 34 foreign ions show no serious interference | Mo in steel and fertilizer dusts | 115 |
| 45. | Ethyl Violet | 580; 900,000 | | Polyvinyl alcohol | $<6$ $\mu$g/50 ml | | Mo in steel and ores | 116 |
| 46. | Vanilline thiosemicarbazone | 470; 19,800 | Ascorbic acid | Chloroform | 0.1–4.6 $\mu$g/ml | | Mo in molybdenum steel | 118 |
| 47. | Rhodamine B | 570; 380,000; 1:6:3 | Ascorbic acid | Polyvinyl alcohol | 12 220 *n*g/ml | Fe and Ni do not interfere | Mo in Fe-Ni-Mo thin film | 119 |
| 48. | Neotetrazolinium chloride | 470; 24,700 | Ascorbic acid | Chloroform, ethanol | $<146$ $\mu$g/ml | | Mo in river water | 122 |
| 49. | Nile Blue | 630; 180,000 | | Polyvinyl alcohol, Arabic gum | $<1.2$ $\mu$g/ml | | Mo in steel | 123 |
| 50. | Butyltriphenyl phosphonium bromide | 470; 12,000 | Ascorbic acid | Chloroform, benzophenone | $<140$ $\mu$g | | Mo in high speed steel | 124 |
| 51. | *N*-Octyl *N'*-phenyl benzamidine | 465; 19,500 | Ascorbic acid | Benzene | | Interference by Nb is masked by oxalate | Mo in rock, alloy steels, ores, ash and fertilizer | 126 |
| 52. | Malachite Green | 652; 380,000 | Ascorbic acid | Aqueous, cyclodextrin, Arabic gum | $<0.2$ $\mu$g/ml | Interference by 18 foreign ions may be tolerated | Mo in minerals | 127 |
| 53. | Thioacetanilide | 470; 19,000 | $SnCl_2$, ascorbic acid | Benzene | | Free from interference by metals normally associated with Mo | Mo in steel, coal ash, ores and waste waters | 128 |

method and the last column gives the reference number.

A number of modified thiocyanate thiocyanate methods have been reported which use ionic[62,68,69,75,81,88,102,107,121,122] nonionic[100,117] surfactants for sensitization.

### 3. APPLICATION

The thiocyanate methods have been applied for estimating Mo in a wide variety of samples, the majority of them being steel samples.[22,23,25,26,48–50,53,54,59,61,62,70,71,74,81,101,102,104,106,107 113–115,118,120,123,124,128] The thiocyanate method has also been used for estimating Mo in rocks,[52] chloroplatinic acid,[46] uranium and uraniferrous compounds,[17,41,51] soil,[7,32,60] alloys containing Nb,[66] concentrated NaCl medium,[72] oxide films,[82] ores and alloy steel,[90,95,105,110,111,116,120] sediment,[88] air,[94] battery grade $MnO_2$,[96] seawater,[31,98] sewage sludge and soil,[99] catalyst,[108] synthetic corrundum and lithium niobate,[121] ash and fertilizers,[126] plant materials,[8,77] soil and plants,[64] rhenium compounds,[14] beryllium,[16] aluminium alloys,[20] copper ores,[27] lead,[24] niobium and tantalum[26] and tungsten and its compounds.[10,14,26]

### 4. CONCLUSIONS

Thiocyanate methods are primarily of two types, the conventional and the modified ones. In the conventional types, Mo(IV) is reduced to Mo(V) by an appropriate reducing agent which forms an orange red complex with the thiocyanate ions. The complex is subsequently extracted by a solvent for absorbance measurement. In the modified type, in addition to thiocyanate, a third reagent is added which forms a ternary ion association complex. The complex either enhances the sensitivity or pushes the absorbance maximum to a higher wavelength thereby enhancing the selectivity. Ascorbic acid and $SnCl_2$ have been the most popular reducing agents. Molar extinction coefficients ($\epsilon$) in the conventional type range from 1.5 to $2.5 \times 10^4$, whereas in the modified type $\epsilon$ value as high as $10^5$ has been reported. Thiocyanate methods have been mostly used for the determination of Mo in steel samples. However, it has also been used for other types of samples ranging from sea-water to rocks, ores and minerals. Thiocyanate methods, though more than 100 years old, will continue to be used for the determination of molybdenum in a wide variety of samples.

*Acknowledgement*—The authors wish to thank the Director, NML for his kind permission to publish this work.

### REFERENCES

1. C. D. Braun, *Z. Analyt. Chem.*, 1863, **2,** 36.
2. C. D. Braun, *Z. Analyt. Chem.*, 1867, **6,** 86.
3. F. A. *Fer'yanchich, Zavod Lab.*, 1937, **6,** 289.
4. A. T. Dick and J. B. Bingley, *Nature*, 1946, **158,** 516.
5. L. B. Ginzburg and Yu. *Lur'e, Zavod. Lab.*, 1948, **14,** 538.
6. F. N. Ward, *Anal. Chem.*, 1951, **23,** 788.
7. J. L. Grigg, *Analyst*, 1953, **78,** 470.
8. C. M. Johnson and T. H. Arkley, *Anal. Chem.*, 1954, **26,** 572.
9. C. E. Crouthamel and C. E. Johnson, *Anal. Chem.*, 1954, **26,** 1284.
10. R. P. Hope, *Anal. Chem.*, 1957, **29,** 1053.
11. A. K. Babko and O. F. Drako, *Zh. Anal. Zhim.*, 1957, **12,** 342.
12. B. I. Nabivanets, *Ukr. Khim. Zh.*, 1958, **24,** 775.
13. D. D. Perrin, *J. Am. Chem. Soc.*, 1958, **80,** 3540.
14. A. I. Lazarev and V. I. Lazareva, *Zavod. Lab.*, 1958, **24,** 798.
15. E. B. Sandell, *Colorimetric Determination of Trace Metals.* Interscience, New York, 1959.
16. J. O. Hibbits, W. F. Davis, M. R. Menke and S. Kallman, *Talanta*, 1960, **4,** 104.
17. P. R. Kuehn, O. H. Howard and C. W. Weber, *Anal. Chem.*, 1961, **33,** 740.
18. B. E. Reznik, G. M. Ganzburg and V. V. Sachko, *Zavod. Lab.*, 1962, **28,** 277.
19. J. O. Hibbits and R. T. Williams, *Anal. Chim. Acta*, 1962, **26,** 363.
20. W. Stross and J. Clark, *Metallurgia*, 1963, **67,** 47.
21. A. M. Wilson and O. K. McFarland, *Anal. Chem.*, 1964, **36,** 2488.
22. A. K. De and M. S. Rahman, *Anal. Chem.*, 1964, **36,** 685.
23. R. Boulin and E. Joudon, *Chim. Anal. (Paris)*, 1965, **47,** 290.
24. A. M. Ustimov and V. P. Gladyshev, Tr. Komos. po Analit. *Khim. Akad. Nauk SSSR*, 1965, **15,** 275.
25. N. Lounamaa, *Anal. Chim. Acta*, 1965, **33,** 21.
26. C. L. Luke, *Anal. Chim. Acta*, 1966, **34,** 302.
27. I. Adamiec, *Chem. Anal.*, 1966, **11,** 1175, 1183.
28. V. K. Potrokhov and L. I. Lebedeva, *Zh. Anal. Khim.*, 1966, **21,** 182.
29. H. Matsuo and S. Chaki, *Bunseki Kagaku*, 1967, **16,** 551.
30. A. I. Busev and T. V. Rodionova, *Zh. Anal. Khim.*, 1968, **23,** 877.
31. Y. S. Kim and H. Zeitlin, *Anal. Chim. Acta*, 1970, **51,** 516.
32. B. Sapek, *Chem. Anal.*, 1970, **15,** 651.
33. Y. S. Kim and H. Zeitlin, *Anal. Chim. Acta*, 1970, **51,** 516.
34. *Determination of Molybdenum*, British Standards Handbook No. 19. British Standards Institution, London, 1970.
35. K. Kawabuchi and R. Kuroda, *Talanta*, 1970, **17,** 67.
36. R. Pribil and J. Adam, *Talanta*, 1971, **18,** 349.
37. A. A. Ponomareva, N. A. Agrinskaya and L. G. Anokhina, *Novye Metody Khim. Anal. Mater.*, 1971, 88.

38. M. M. L. Khosla and S. P. Rao, *Anal. Chim. Acta*, 1971, **57,** 323.
39. C. Rozycki and W. Suszczewski, *Chem. Anal.*, 1972, **17,** 1209.
40. V. Yatirajam and J. Ram, *Anal. Chim. Acta*, 1972, **59,** 381.
41. C. Toussaint and G. Cattin, *Analusis*, 1972, **1,** 347.
42. L. I. Ganago and I. F. Ivanova, *Zh. Anal. Khim.*, 1972, **27,** 713.
43. Z. Kh. Sultanova, L. K. Chuchalin, B. A. Iofa and Yu. A. Zolotov, *Zh. Anal. Khim.*, 1973, **28,** 369.
44. A. K. Bhadra and S. Banerjee, *Talanta*, 1973, **20,** 342.
45. I. F. Ivanova, L. N. Bukhteeva, L. I. Ganago, L. G. Gribkovskaya and L. N. Yurii, *Zavod. Lab.*, 1973, **39,** 388.
46. C. Rozycki and W. Suszczewski, *Chem. Anal.*, 1973, **18,** 621.
47. C. Rozycki and J. Kaminska, *Chem. Anal.*, 1973, **18,** 777.
48. A. T. Pilipenko and Z. G. Solomeina, *Ukr. Khim. Zh.*, 1973, **39,** 1169.
49. S. P. Patil and V. M. Shinde, *Anal. Chim. Acta*, 1973, **67,** 473.
50. R. H. Schunke, *Tech. Note Aust. Def. Stand. Lab.*, 1973, No. 303, 12.
51. J. Korkisch and I. Steffan, *Mikrochim. Acta*, 1973, 545.
52. E. G. Lillie and L. P. Greenland, *Anal. Chim. Acta*, 1974, **69,** 313.
53. C. P. Savariar, M. K. Arunachalam and T. R. Hariharan, *Anal. Chim. Acta*, 1974, **69,** 305.
54. A. V. Dolgorev and I. D. Guschina, *Ind. Lab.*, 1974, **40,** 34.
55. V. Yatirajam and J. Ram, *Mikrochim. Acta*, 1974, 671.
56. A. T. Pilipenko and V. G. Safronova, *Ukr. Khim. Zh.*, 1974, **40,** 971.
57. V. F. Gorlach and L. M. Morchenko, *Ukr. Khim. Zh.*, 1974, **40,** 983.
58. M. K. Arunachalam and M. K. Kumaran, *Talanta*, 1974, **21,** 355.
59. N. A. Verdizade and S. R. Melikov, *Uchebn. Zap. Azerb. gos. Univ. Ser. Khim. Nauk*, 1973, 40; *Referat. Zh. Khim.*, 1974, 19GD, Abstr. No. 11G89.
60. N. A. Verdizade and S. R. Melikov, *Azerb. Khim. Zh.*, 1973, 113; *Referat. Zh. Khim.*, 1974, 19GD, Abstr. No. 18G213.
61. V. P. Rao, Y. Anjeneyulu and A. S. R. Krishnamurthy, *Mikrochim. Acta*, 1975, **I,** 265.
62. A. G. Fogg, J. L. Kumar and D. T. Burns, *Analyst*, 1975, **100,** 311.
63. B. Tamhina, M. J. Herak and V. Jagodic, *Anal. Chim. Acta*, 1975, **76,** 417.
64. P. R. Haddad, P. W. Alexander and L. E. Smythe, *Talanta*, 1975, **22,** 61.
65. M. E. M. S. DeSilva, *Analyst*, 1975, **100,** 517.
66. V. T. Solomatin, P. Ya. Yakovlev, L. A. Lapshina and T. N. Artemova, *Zh. Anal. Khim.*, 1975, **30,** 114.
67. D. A. Wilson, I. J. Holomb and D. F. Boltz, *Anal. Chem.*, 1975, **47,** 2025.
68. Yu. G. Eremin, E. F. Kolpikova and T. V. Rodionova, *Zh. Anal. Khim.*, 1976, **31,** 732.
69. B. Tamhina and M. J. Herak, *Mikrochim. Acta*, 1976, **I,** 553.
70. A. S. Babenko, L. A. Mineeva and K. I. Godovskaya, *Zavod. Lab.*, 1976, **42,** 1035.
71. L. A. Mineeva, A. S. Babenko and K. I. Godovskaya, *Izv. Vyssh. Uchebn. Zaved., Khim. Khim. Tekhnol.*, 1976, **19,** 1671.
72. O. Guertler, *Fr. Z. Anal. Chem.*, 1977, **285,** 259.
73. I. F. Ivanova, L. I. Ganago and I. A. Semenovich, *Izv. Vyssh. Uchebn. Zaved., Khim. Khim. Tekhnol.*, 1977, **20,** 1815.
74. M. Mitra and B. K. Mitra, *Talanta*, 1977, **24,** 698.
75. H. Puzanowska-Tarasiewicz, A. Grundniewska and M. Tarasiewicz, *Anal. Chim. Acta*, 1977, **94,** 435.
76. J. M. Lopez-Fernandez, D. Perez-Bendit and M. Valcarcel, *Analyst*, 1978, **103,** 1210.
77. H. Bergamin Filho, J. X. Medeiros, B. F. Reis and E. A. G. Zagatto, *Anal. Chim. Acta*, 1978, **101,** 9.
78. Yu. G. Eremin, T. V. Rodionova and E. F. Kolpikova, *Zh. Anal. Khim.*, 1979, **34,** 491.
79. R. S. Kharsan, K. S. Patel, K. K. Dev and R. K. Mishra, *Fr. Z. Anal. Chem.*, 1979, **295,** 415.
80. R. S. Kharsan, K. S. Patel and R. K. Mishra, *Mikrochim. Acta*, 1979, **I,** 353.
81. H. Sanke Gowda, P. G. Ramappa and S. Manjappa, *Indian J. Chem., Sect. A*, 1979, **18,** 276.
82. L. B. Tokareva and L. I. Voropaeva, *Khim. prom-st., Ser.: Reakt. Osobo Chist. Veschestva*, 1979, 28.
83. R. S. Kharsan and R. K. Mishra, *Bull. Chem. Soc. Jpn*, 1980, **53,** 1736.
84. K. Hayashi, A. Yamamoto, Y. Fujimura and S. Ito, *Bunseki Kagaku*, 1980, **29,** T39.
85. T. P. Rao and T. V. Ramakrishna, *Bull. Chem. Soc. Jpn*, 1980, **53,** 2380.
86. T. J. Koralewski and G. A. Parker, *Anal. Chim. Acta*, 1980, **113,** 389.
87. R. M. Verma, K. S. Patel and R. K. Mishra, *Fr. Z. Anal. Chem.*, 1981, **307,** 128.
88. M. Rancicova, J. Cuta and M. Malat, *Vodni Hospod., B*, 1981, **31,** 19.
89. K. S. Patel and R. K. Mishra, *Talanta*, 1982, **29,** 791.
90. K. S. Patel, R. M. Verma and R. K. Mishra, *Anal. Chem.*, 1982, **54,** 52.
91. U. Madan and L. R. Kakkar, *Indian J. Chem. Sect. A*, 1982, **21,** 326.
92. U. Madan and L. R. Kakkar, *Indian J. Chem. Sect. A*, 1982, **21,** 661.
93. U. Madan and L. R. Kakkar, *Talanta*, 1982, **29,** 623.
94. B. Xu, Y. Lu and H. Xiao, *Zhonghua Yufangyixue Zazhi*, 1982, **16,** 238.
95. K. S. Patel, H. Khatri and R. K. Mishra, *Anal. Chem.*, 1983, **55,** 1823.
96. H. Suzuki, Y. Nakayama and K. Ishikawa, *New Mater. New Proc.* 1983, **2,** 19.
97. K. S. Patel and R. K. Mishra, *Bull. Chem. Soc. Jpn*, 1983, **56,** 2811.
98. Y. Shizo, K. Ide, K. Sakai, *Bunseki Kagaku*, 1983, **31,** E353.
99. *Methods Exam. Waters Assoc. Mater.*, p. 18. Department of the Environment & National Water Council [U.K.] 1983.
100. L. Ni, *Fenxi Huaxue*, 1983, **11,** 171.
101. F. J. Krug, F. O. Bahia and E. A. G. Zagatto, *Anal. Chim. Acta*, 1984, **161,** 245.
102. F. Salinas, J. J. Berzas-Nevado and M. I. Acedo Valenzuela, *Talanta*, 1985, **32,** 63.
103. W. Lin, *Fenxi Shiyanshi*, 1986, **5,** 58.
104. K. N. Thimmaiah, W. D. Lloyd and G. T. Chandrappa, *Microchem. J.*, 1985, **32,** 281.
105. B. Keshavan and P. Nagaraja, *Mikrochim. Acta*, 1985, **II,** 379.

106. G. Gong and H. Wang, *Fenxi Huaxue*, 1985, **13,** 410.
107. A. T. Gowda and N. M. M. Gowda, *Analyst*, 1985, **110,** 743.
108. H. Li, *Fenxi Shiyanshi*, 1986, **5,** 59.
109. S. K. Menon and Y. K. Agarwal, *Analyst*, 1986, **111,** 911.
110. B. Keshavan, P. Nagaraja and S. Sunderraj, *Analyst*, 1986, **111,** 1397.
111. X. Zhang, *Xiyou Jinshu*, 1987, **6,** 71.
112. B. P. Bermejo, J. F. Vazquez-Gonzalez and M. F. Bermejo, *Microchem. J.*, 1987, **35,** 1.
113. K. N. Thimmaiah, G. T. Chandrappa and V. C. Sekhar, *Mikrochim. Acta*, 1986, **III,** 277.
114. L. P. Chandrakar and R. K. Mishra, *J. Indian Chem. Soc.*, 1986, **63,** 920.
115. L. P. Chandrakar, R. Singh and R. Mishra, *Analyst*, 1987, **112,** 1511.
116. Z. Li and Q. Xu, *Fenxi Huaxue*, 1987, **15,** 870.
117. L. Ni, Lihua Jianyan, *Huaxue Fence*, 1987, **23,** 138.
118. K. N. Thimmaiah, V. C. Sekhar and G. T. Chandrappa, *Acta Chim. Hung.*, 1987, **124,** 491.
119. L. I. Ganago and I. F. Ivanova, *Zh. Anal. Khim.*, 1987, **42,** 1641.
120. I. P. Danilov, A. M. Guzhva and E. A. Molchanova, *Zavod. Lab.*, 1987, **53,** 16.
121. L. A. Egorova and N. T. Sizonenko, *Zavod. Lab.*, 1988, **54,** 35.
122. A. K. Singh and B. K. Ratnam, *Microchem. J.*, 1988, **38,** 408.
123. Z. Li and Q. Xu, *Fenxi Shiyanshi*, 1988, **7,** 13.
124. D. T. Burns and N. Tungkananuruk, *Anal. Chim. Acta*, 1989, **219,** 323.
125. R. Caletka and V. Krivan, *Fr. Z. Anal. Chem.*, 1989, **332,** 866.
126. M. Das, K. S. Patel and R. K. Mishra, *Analusis*, 1989, **17,** 536.
127. C. Huang and W. Qi, *Fenxi Shiyanshi*, 1989, **8,** 20.
128. N. Mishra, A. Ghosh, R. K. Mishra and K. S. Patel, *Anal. Sci.*, 1990, **6,** 407.

Pergamon

0039-9140(95)01448-9

*Talanta*, Vol. 42, No. 4, pp. 507–517, 1995

0039-9140/95 $9.50 + 0.00

## REVIEW

# ALTERNATIVE METHODS FOR TITRATABLE ACIDITY DETERMINATION

O. YU. BEREZIN, YA. I. TUR'YAN, I. KUSELMAN* and A. SHENHAR

The National Physical Laboratory of Israel, Danciger A Build., The Hebrew University, Jerusalem 91904, Israel

(*Received* 20 *April* 1994. *Accepted* 30 *September* 1994)

**Summary**—Methods for determination of titratable acidity, other than traditional titration, *i.e.* methods without titration, are considered. A number of them use analytical acid–base reagents which quickly convert a mixture of strong and weak acids into a new system. This conversion makes it possible to obtain directly the analytical signal (pH, optical density, *etc.*) for titratable acidity calculation. These methods in stationary conditions and in flow injection analysis are discussed. Methods not using acid–base reagent (iodide–iodate, chromatographic, spectroscopic and others) are also described. The advantages of the alternative methods such as the decrease labour-consumption and analysis time, simplicity of automation and others are shown.

Titratable acidity (or acid value) corresponds to the total concentration of titratable acids in a sample. Titratable acidity (TA) is an important characteristic of the quality of numerous products such as vegetable oils, juices, wines, petroleum, motor oils, polyesteric resins, plasticizers and others.

The national and international standards for TA determination are based on acid–base titration techniques.[1] These techniques are time- and labour-consuming, have relatively high detection limits and are difficult for automation, including the Gran technique.[2] These drawbacks are aggravated when TA-control is carried out in non-aqueous solutions and particularly when preliminary acids extraction is necessary.[1]

This review is concerned with alternative methods for TA determination, *i.e.* methods without titration which are free from the drawbacks indicated above. A number of these methods are based on the use of analytical acid–base reagents. After the reagent addition, the measured analytical signal (pH, optical density, *etc.*) permits one to obtain the unknown TA value.

Owing to the reagent, acid extraction from the insoluble material is accelerated. The reagent increases functional capacities of the pH-meter in the case where the pH-analytical signal is used for TA determination, and allows flow injection analysis (FIA) to be used for TA determination without titration.

The methods for TA determination without titration are frequently called 'single point titration'.[3,4] However, as these methods do not actually imply titration of any kind, we have named them 'methods for TA determination without titration'.

The methods using acid–base reagents can be classified on the basis of the type of reagent at the initial state as follows:

(i) one-component acid–base reagent method (OCABR method),
(ii) multi-component acid–base reagent method (MCABR method).

Methods that do not require the use of acid–base reagents for TA determination without titration (such as chromatography, spectroscopy, *etc.*) are also described in the review. These methods are considered in less detail because some of them (for example, chromatographic) have already been analyzed in reviews and others are in the initial stage of being studied.

*Author to whom correspondence should be addressed.

## 1. ONE-COMPONENT ACID–BASE REAGENT METHOD

The OCABR method[5–17] is based on the use of a weak inorganic or organic base as a reagent. In some applications indifferent salt is added into the reagent solution to support the ionic strength ($I$). In spite of this addition the indifferent salt does not become a new component in the solution of the one-component reagent.

### 1.1. *Aqueous systems*

The theory of application of OCABR method in aqueous solutions was suggested by Tur'yan *et al.*.[14] A charged reagent $R^-$ (the anion of the weak acid, for example AcO− from sodium acetate or MR generally)[7,8,12–14] and an uncharged reagent B, for example hexamethylenetetramine[9,11,14] are used. The analytical reactions between the reagent and the sum of the analyzed acids may be expressed by:

$$\Sigma H_z An + \Sigma z R^- \leftrightarrow \Sigma An^{z-} + \Sigma z HR \quad (1)$$

$$\Sigma H_z An + \Sigma z B \leftrightarrow \Sigma An^{z-} + \Sigma z BH^+, \quad (2)$$

where $An^{z-}$ is an anion, $z$ is a stoichiometric coefficient.

The OCABR method is based on the following conditions:

(i) Equilibria (1) and (2) are practically shifted to the right hand side.

(ii) The reagent is in high excess relative to the sum of analyzed acids. In accordance with these conditions the following equations may be obtained for a charged reagent:[7,8,12–14]

$$\lg N_{TA} = -\lg \frac{K_W^\circ}{K_{R^-}^\circ \cdot C_{MR} \cdot f_{R^-}} - pH \quad (3)$$

and for an uncharged reagent[9,11,14]

$$\lg N_{TA} = -\lg \frac{K_W^\circ \cdot f_{BH^+}}{K_B^\circ \cdot C_B} - pH, \quad (4)$$

where $f$ is the activity coefficient (for uncharged particles equal to 1), $K_W^\circ$ is thermodynamic autoprotolysis constant for water, $K_{R^-}^\circ$ and $K_B^\circ$ are thermodynamic constants for the basic dissociation of the reagent (Table 1); $C$ is the total (analytical) reagent concentration.

As can be seen from relations (3) and (4), the dependence $\lg N_{TA}$ *vs.* pH may be expressed in linear form with a slope equal to 1 when $I = \text{const}$ and $C_{MR}$ or $C_B = \text{const}$.[14] In this case the first right hand side item in equations (3) and (4) is a constant value.

The OCABR method is applicable to a great number of both strong and sufficiently weak acids.[14] When $I = 1$ for more complete proceeding of the analytical reaction, hexamethylenetetramine is more preferable than NaOAc as a reagent. But a relative excess of NaOAc ($\gamma = C_{MR}/N_{TA} \approx 200$) provides sufficient completeness of the analytical reaction. Tribasic acids may be analyzed when $I = 1$ and the constant of the third dissociation stage is not below $4 \times 10^{-7}$, which corresponds to citric acid. The dibasic acids may be analyzed when $I = 1$ and the constant of the second dissociation stage is not below $2 \times 10^{-6}$, for example succinic acid.

The upper limit of the acids being determined in the linear interval $\lg N_{TA}$ *vs.* pH is obtained from $(N_{TA})_{max} = C_{MR}/\gamma$ or $(N_{TA})_{max} = C_B/\gamma$. The values $\gamma \geqslant 100$[14] or $\gamma \geqslant 200$[8] are most often chosen and at $C_{MR}$ or $C_B = 1M$, $(N_{TA})_{max} \leqslant 10^{-2}$ eq/l.

The principles of obtaining $(N_{TA})_{min}$ presume[14] that the concentration $(N_{TA})_{min}$ corresponding to the linear plot $\lg N_{TA}$ *vs.* pH must be at least 10-fold greater than the concentration of the hydrolysis products HR (reagent MR) or $BH^+$ (reagent B) in the pure solvents. Hence at $C_{MR}$ or $C_B = 1M$ and $I = 1$ one can observe a linear plot $\lg N_{TA}$ *vs.* pH for NaOAc for $N_{TA} = 2.4 \times 10^{-4} - 1.0 \times 10^{-2}$ eq/l

Table 1. Thermodynamic autoprotolysis constants $K_s^\circ$ for solvents and constants of basic dissociation $K_{R^-}^\circ$ and $K_B^\circ$ for charged and uncharged reagents, accordingly (OCABR method, 25°C)

| Solvents | $H_2O$ | | Complex solvent* |
|---|---|---|---|
| $pK_s^\circ$ | 14.00[18] | | 22.79[15]† |
| Reagents | $pK_B^\circ$ | $pK_{R^-}^\circ$ | $pK_B^\circ$ |
| Triethanolamine | 6.23[19] | — | 11.50[15]† |
| Hexamethylenetetramine | 8.87[18] | — | — |
| Acetate anion | — | 9.24[18] | — |

*Solvent: 80% $Et_2O$ + 19% $C_2H_5OH$ + 1% $H_2O$

†Constants were determined at 20°C.

and for hexamethylenetetramine in the range $N_{TA} = 5.8 \times 10^{-4} - 1.0 \times 10^{-2}$ eq/l.

The decrease of the reagent concentration up to $C_{MR} = 0.01M$ (NaOAc) permits a decrease in the value of $(N_{TA})_{min}$ which allows the reduction of the detection limit, for example in the determination of volatile acids.[13]

The choice of the reagent is determined by its basic properties, that is by its base dissociation constant. From the point of view of completeness of the analytical reaction proceeding, the value of the constant must not be too small. However, an increase in $K^{\circ}_{R^-}$ or $K^{\circ}_{B}$ leads to an undesirable increase in $(N_{TA})_{min}$. The values equal to constant $K^{\circ}_{R^-}$ for NaOAc and to $K^{\circ}_{B}$ for hexamethylenetetramine are optimal.

### 1.2. *Non-aqueous systems*

The theory of the method was developed in detail by Lapshina *et al.*[15]

Uncharged reagent only (triethanolamine) was used in non-aqueous systems.[5,6,10,15–17] Values of $K^{\circ}_{B}$ and the thermodynamic autoprotolysis constant of the non-aqueous solvent $K^{\circ}_{s}$ were established[15] (Table 1). The equation for analytical applications, under conditions similar to those used for aqueous systems, is in principle analogous to equation (4):

$$\lg N_{TA} = A^{\circ}_{s} - \lg \frac{K_s \cdot f_{BH^+}}{K^{\circ}_{B} \cdot C_B} - pH', \qquad (5)$$

where $A^{\circ}_{s}$ is constant at $I = \text{const}$. The value $A^{\circ}_{s}$ follows the change of the glass electrode standard potential (when non-aqueous solvents are used instead of water) and also the value of the interfacial potential on the boundary with the aqueous reference electrode (Ag, AgCl, $KCl_{satd}$). The value pH′ in equation (5) is the conventional pH value. At $I = \text{const}$, one can observe the linear plot $\lg N_{TA}$ *vs.* pH′ with a slope equal to 1.[5,6,10,15]

The OCABR method was theoretically and practically tested for the non-aqueous system:[15] 80% $Et_2O$ + 19%EtOH + 1% $H_2O$ (%V), and for system:[6,16,17] 75% $CHCl_3$ + 24% EtOH + 1% $H_2O$ (%V).

Equation (5) is confirmed in the wide interval of $N_{TA}$.[15] This interval ($4.0 \times 10^{-5}$–$2.0 \times 10^{-2}$ eq/l.) is essentially larger than the one that may be obtained for aqueous solutions. The increase of the linearity interval $\lg N_{TA}$ *vs.* pH′ for the non-aqueous systems in comparison with aqueous systems is a result of the small solvolysis degree of triethanolamine in comparison with the hydrolysis degree of $AcO^-$ or/and hexamethylenetetramine.

### 1.3. *Practical application of the method*

To determine $N_{TA}$ both the calibration plot and the standard addition methods have been used.[5–17] The second method is preferable since it implies a lower probability of changes in the first right hand side item in equations (3) and (4) in the course of the analysis, as well as of changes in the analogous value from equation (5) for non-aqueous systems.

The equation for the final analytical calculation with the use of the standard addition method[14,15,17] is

$$N_{TA} = \frac{N_{st}}{(10^{\Delta pH} - 1)}, \qquad (6)$$

where $N_{st}$ is the concentration of the standard acid in reactive mixture; $\Delta pH = pH_1 - pH_2$; $pH_1$ is the pH of the reagent solution to which the sample was added and $pH_2$ is the pH of the previous (reagent + sample) solution after the addition of the standard acid. For non-aqueous systems the value ΔpH in equation (6) is substituted by ΔpH′.

Equation (6) does not differ in principle from the basic equations of the standard addition method in the ionometric technique which was shown by Tur'yan *et al.*[20] for the glass electrode in the presence of the above OCABR.

Although the precision and the accuracy of titrimetric methods may theoretically be higher than for OCABR method, especially at pH-meter accuracy not higher than pH ±0.01, the possibilities of the OCABR method are sufficient for industrial purposes. At the same time there are a number of advantages of the OCABR method: low labour- and time-consumption, especially in the case of oil-seeds;[6,10,15] simplicity of analysis automation and low detection limit (for example, for volatile acids in wines).[13]

*Aqueous systems.* The method was applied for determination of TA in several materials and products of the wine-making industry. Both total acidity[7,8,11,12] and volatile acidity[13] were determined with the use of pH-meter with accuracy pH ±0.01. Sodium acetate (2.0 *M*) or hexamethylenetetramine (0.2 *M*) were used as the initial reagents for determination of the total acidity. In the first case the calibrated plot was applied; in the second, the standard addition (of oxalic acid) method. The interval of the TA analyzed values, expressed as tartaric

acid, is 0.3–30 g/l. The relative standard deviation is $\leqslant$3.2%. The duration of the analytical determination is 2–3 min. For determination of volatile acids in wines[13] 0.1$M$ NaOAc was used as the initial reagent. Its concentration was 0.01$M$ after water and volatile acids were distilled. For the $N_{TA}$ determination the standard addition method was used. The interval of the determined $N_{TA}$ values, expressed as acetic acid, is 0.22–1.93 g/l. The relative standard deviation is $\leqslant$4–11%. The duration of the analysis is 18–20 min instead of 40–60 min in the standard titrimetric method.

*Non-aqueous systems.* This method was used for determination of TA in vegetable oils[5,6,10,15–17] and in oilseeds.[6,10,15] As the reagent 0.15–0.20$M$ triethanolamine in solvent (80% $Et_2O$ + 19% EtOH + 1% $H_2O$, %V) was used. This reagent accelerates considerably the extraction of acids from solid oilseeds: the extraction time was up to 1 min instead of 4 h in the standard method of oil extraction with pure solvent. The use of the standard addition method appears to be the most efficient one.[15,17] The $N_{TA}$ determination interval in vegetable oils is 0.2–19 mg KOH/g oil and in oilseeds, 0.2–17 mg KOH/g oil.[15] The relative standard deviation is $\leqslant$6% (obtained with the use of a pH-meter with accuracy pH $\pm$0.01). The duration of oil analysis is 2–3 min; of oilseeds, 10–12 min.

## 2. MULTI-COMPONENT ACID–BASE REAGENT METHOD

The MCABR method is often known as the linear buffer method or the linear-response method because of the existence of the simple linear plot $N_{TA}$ *vs.* pH, in contrast to the logarithmic linear plot lg $N_{TA}$ *vs.* pH in the OCABR method. If linearity of $N_{TA}$ *vs.* pH is observed then buffer capacity $\beta = -dN_{TA}/dpH$ is independent from pH.

The MCABR may consist at the initial state of two or more components.[21–23] As in the case of the OCABR method, an indifferent salt added to the system for creation of $I$ = const is not a new component of the reagent. The higher the number of the components in the reagent, the wider the linearity interval of the plot $N_{TA}$ *vs.* pH is.

The MCABR method was first used by Ghosh and Schild,[24] as far as we know, and later by other workers.[25,26] The theoretical analysis of the MCABR method in stationary conditions

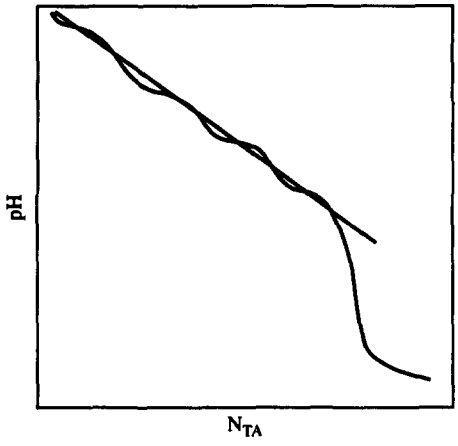


Fig. 1. The titration curve for multi-component acid–base reagent with strong acid (free hand drawing).

was suggested by various authors[21,27,28,30–42] and by others for FIA techniques.[22,23,29,43–48]

In contrast to the OCABR method where only potentiometric detection was used (pH, glass electrode), the MCABR method also utilizes spectrophotometric detection. The MCABR method is usually used in aqueous solutions and only in one case[22] was 10% EtOH 90% $H_2O$ (%v) solvent applied.

### 2.1. *Analysis in stationary conditions*

The most general theory of the MCABR method with the pH-metric detection for bases analysis was suggested by Johansson and Backen.[27] These authors[27] and also Astrom[28] have experimentally confirmed the theory. Astrom[23] applied the MCABR method theory to acid determination.

The titration of a multi-component reagent by a strong acid leads to only one pH break (Fig. 1) because of the proximity of the dissociation constant values for corresponding components. The upper plot of the titration curve is close to the linearity $N_{TA}$ *vs.* pH (Fig. 1). This plot may be expressed by the equation:

$$N_{TA} = L - \beta \,.\, pH, \qquad (7)$$

where $L$ is constant and $\beta$ is buffer capacity. The relation (7) is the basis of the MCABR method.

Johansson and Backen[27] obtained relationships for the description of the above upper plot of the titration curve. In various papers[21,27,28] this relationship was used to describe the reagent consisting of components with two dissociation stages, but it may be easily generalized for components with higher basicity. Determination of the concentration $C_i$

for component $i$ of the reagent was carried out for components of known nature and definite $\beta$ and $L$ values (equation 7). In this case the maximum proximity of the experimental curve to the linear plot $N_{TA}$ *vs.* pH (the upper part, Fig. 1) was to be reached. The following solution was suggested by Olson:[48] firstly, correction is made for the thermodynamic dissociation constants on the basis of the Debye–Hückel equation. Next, the $C_i$ values are calculated by the Johansson and Backen[27] regression method, the obtained dependence $N_{TA}$ *vs.* pH being compared to the experimental titrametric data. The second approximation again involves the calculation of the corrected dissociation constants and a new regression until the linearity dependence $N_{TA}$ *vs.* pH is obtained with the best accuracy. The final results of the determination of the component concentrations in the reagent, as well as the pH range for the linear part of $N_{TA}$ *vs.* pH dependence were suggested by Olson[48] for the FIA, but they may also be used in stationary conditions.

The pH interval of the linear part of the dependence $N_{TA}$ *vs.* pH is sufficiently large and increases with the decrease of the buffer capacity. Therefore, it is possible to determine both strong and relatively weak acids.

The limit of detection for determined acids is approximately the same for strong and weak acids and reaches 0.01–0.02 eq/l.[23] Apparently this limit is affected by the increase of the uncertainty while the $N_{TA}$ value decreases. The decrease of the $\beta$ value leads to reduction of the uncertainty and permits a decrease in the lower limit of the $N_{TA}$ determination up to $N_{TA} = 1 \times 10^{-4}$ eq/l.[48]

Simpler reagents were suggested by Havas,[30] and Damokos and Havas.[36,37,42] These reagents consist of two components: mixtures like phosphate buffer,[30] citric acid and $KH_2PO_4$[36,37,42] *etc.* The intervals of the determined acids are $10^{-2}$–$10^{-1}$ eq/l.[42] and $10^{-3}$–$10^{-1}$ eq/l.[36]

To choose the simplest two-component acid–base reagent (the buffer) it is reasonable to consider the dependence of the buffer capacity *vs.* pH. For buffer MR + HR this dependence may be expressed as[49]

$$\beta = 2.303\left(\frac{K_{H_2O}}{[H^+]} + [H^+] + \frac{C_b \cdot K_a \cdot [H^+]}{(K_a + [H^+])^2}\right), \quad (8)$$

where $K_a$ is the dissociation constant of HR; $C_b$ is the total buffer concentration.

The analysis of relation (8) shows that in the range of pH close to $pK_a$ and under usual conditions ($C_b \cdot K_a \gg K_{H_2O}$ and $C_b \gg K_a$) the buffer capacity is practically independent from the pH-values. The $\beta$ value in this range of pH becomes equal to $\beta_{max} = 0.576 \cdot C_b$ ($pH = pK_a$) and changes slightly when pH values are not far from $pK_a$. This leads to the appearance of a linear plot of $N_{TA}$ *vs.* pH (equation 7). However, the linearity interval of the plot of $N_{TA}$ *vs.* pH for a two-component reagent is usually small: 0.5–1 unit pH.[22,42,43] In spite of this drawback the reagent may be applicable for acid determination.[22,42,43]

It is of interest to compare the OCABR and MCABR methods under stationary conditions for potentiometric detection (pH, glass electrode). Equations (3) or (4) for the OCABR method and equation (7) for the MCABR method yield the following conclusions:

(1) The maximum relative uncertainty of the $N_A$ determination in the OCABR and MCABR methods is approximately the same. But in the MCABR method, in contrast to the OCABR method the uncertainty depends upon the value of $N_{TA}$, and an increase in $N_{TA}$ leads to a decrease in the relative uncertainty.

(2) The detection limit of TA determination is considerably lower in the OCABR method.

(3) The buffer capacity of the reagent in the OCABR method depends upon $N_{TA}$ and may be considerably smaller than for reagents in the MCABR method, but this does not affect the rate of dynamic response of the glass electrode.[14,15]

(4) The sensitivity of the OCABR method depends upon $N_{TA}$ and may be higher or lower than in the MCABR method.[14]

### 2.2. *Flow injection analysis*

The MCABR method was applied to two applications of the FIA technique: (i) the tested sample containing acids reacts with the reagent;[23,29,46] (ii) the tested sample containing the substrate produces an acid or a base as the result of an enzymatic reaction between the immobilized ferment and the substrate in the flow conditions. Finally, products (acid or base) react with the reagent.[21,43–46,48]

In FIA both potentiometric (pH, glass electrode)[22,29,43,45,48] and spectrophotometric[23,44,46,47] detections were used to obtain the analytical signal.

*Potentiometric detection.* For potentiometric detection the following relation may be

obtained on the basis of equation (7) and the known dependence of the glass electrode potential:[21]

$$N_{TA} = (F\beta/2.3RT)\delta E_p, \quad (9)$$

where $\delta E_p$ is the difference between the glass electrode potential for the analytical signal peak and for the flow of the carrier buffer solution (the multi-component reagent); $F$, $R$ and $T$ have their usual meanings.

Paparello *et al.*[21] used immobilized penicillinase to produce penicilloic acid ($H_2$Pen) from penicillin (Pen) under FIA conditions:

$$\text{Pen} \xrightarrow{H_2O,\ \text{penicillinase}} H_2\text{Pen}. \quad (10)$$

The penicilloic acid afterwards reacted with a special multi-component reagent. The reagent consists of $4.0 \times 10^{-4}M$ $K_2HPO_4 + HCl$ (pH 7).[21]

The application of the Michaelis–Menten equation to FIA with enzymatic reaction gives:

$$S = \frac{F}{2.3 \cdot RT} \cdot \frac{K_m \cdot \beta}{V_m \cdot \delta t}\delta E_p, \quad (11)$$

where $S$ is the substrate (penicillin) concentration; $K_m$ is the Michaelis constant ($K_m \gg S$); $V_m$ is the maximum rate of the enzymatic reaction; $\delta t$ is the sample residence time in the reactor (the column).

One can observe from equation (11) that there is a linear plot between the substrate concentration and changes in the glass electrode potential. It was shown[21] that the linear plot may be observed in the interval $S = 8 \times 10^{-5}$–$5 \times 10^{-4}M$.

An analogous determination of the penicillin was made by Gnanasekaran and Mottola,[45] but in contrast to the work[21] they used a more concentrated phosphate buffer ($1 \times 10^{-3}M$) with constant ionic strength and pH 6.4. The interval of the determined penicillin (G and V) concentration is $S = 5 \times 10^{-5}$–$5 \times 10^{-4}M$.

Olsson[48] also investigated the application of FIA with potentiometric detection for penicillin determination based on reaction (10). It should be noted that the author[48] also studied the application of the Michaelis–Mention equation when the condition $K_m \gg S$ is not fulfilled. An interesting point of the work[48] was the research on the influence of the buffer capacity of the reactor upon the analytical signal.

Ruzicka *et al.*[43] elaborated enzymatic determination of urea in serum in FIA conditions. In this case urease was used as the immobilized ferment. The analytical reaction is

$$CO(NH_2)_2 + H_2O + H^+ \xrightarrow{\text{urease}} 2NH_4^+ + HCO_3^-. \quad (12)$$

The multi-component reagent was suggested to detect the product. In this case the base ($HCO_3^-$) but not acid was determined.

For individual acid determinations the multi-component reagent was used by Astrom.[29] The applicability of equation (9) for HCl, formic and acetic acid determination was shown.[29] The interval of the determined acids or bases is 0.01–0.1$M$, which is approximately the same as the one for stationary conditions.[23,28]

*Spectrophotometric detection.* The theoretical and practical approaches to acid determination by FIA with spectrophotometric detection were elaborated by Hansen *et al.*,[44] by Ishilashi and Imato[46] and by Israel.[22] It is common for these approaches to use the acid–base indicators in addition to the above components of MCABR.

The complex reagents approach was suggested by Hansen *et al.*[44] As in the case of pH-metric detection, it is of interest to consider the linear part of the dependence $N_{TA}$ *vs.* $A_p$, where $A_p$ is the absorbance at the peak of the analytical signal. Hansen *et al.*[44] formulated the following conditions for the application of acid–base reagent with indicators:

(1) The dissociation constants of the acid–base components of the reagent must not be far from one another including the acid–base indicators.

(2) The absorptivities of acid–base forms of indicators must be near to one another.

In the mentioned conditions the authors[44] used an equation analogous to (11) to spectrophotometrically indicate the products of the urea enzymatic reaction:[43]

$$S = k\frac{K_m \cdot \beta}{V_m \cdot \delta t}\delta A_p, \quad (13)$$

where $k$ is a constant.

In contrast to the complex reagent,[44] Ishibashi and Imato[46] suggested a simple reagent: $HR + MR + HInd + Ind^-$, consisting of one acid–base buffer pair and one pair of acid–base component indicators. This approach allows one to obtain the simple relation expressing the linear plot $N_{TA}$ *vs.* $A_p$ for acid control by FIA (without sample dilution):

$$N_{TA} = k'\delta A_p, \quad (14)$$

where

$$k' = C_b/C_{Ind} \cdot l \cdot (\epsilon_{HInd} - \epsilon_{Ind^-}), \quad (15)$$

$C_b$ is the total concentration of the buffer components (MR + HR); $C_{Ind}$ is the total concentration of the indicator (HId + $Ind^-$); $l$ is the length of the cell, $\epsilon$ is the absorptivity. It should be noted that equation (14) is true only under the conditions of Hansen *et al.*,[44] *i.e.* when $K_{HR} \approx K_{HInd}$.

Israel[22] used a very simple reagent for acid and base determination by FIA with spectrophotometric detection. The reagent for acid determination is $R^-$ + HInd + $Ind^-$. Under the same conditions[44,46] ($K_{HR} \approx K_{HInd}$) and when $\epsilon\ Ind^- = 0$, $l = 1$ cm an expression analogous to (14) was obtained:[22]

$$N_{TA} = \frac{D \cdot C_R}{C_{Ind} \cdot \epsilon_{HInd}} \delta A_p, \quad (16)$$

where $D$ is the sample dispersion coefficient.

The reagent suggested by Israel[22] is similar to the one-component reagent (NaOAc) considered in Section 1. However, there is a considerable difference between these reagents because the reagent[22] is not used in excess relative to determined acids. Besides, in this reagent an acid–base indicator (a second component) is also present. It should be noted that a one-component base reagent in contrast to this reagent[22] gives a lower detection limit $N_{TA}$: $2 \times 10^{-5}$–$2 \times 10^{-4}$ eq/l.

Ruzicka *et al.*[50–52] suggested the application of FIA for individual strong acid determination by the peak width measured in time units. The authors[51] used Bromothymol Blue as indicator added to the alkaline carrier stream. This interesting idea was developed by Koupparis *et al.*[53] for determination of individual weak acids. Woods *et al.*[54] have shown that in this technique both the peak width and the peak height in the same solution carrier may be used.

*Other kinds of detection.* Polta *et al.*[55] determined strong acids and bases by detecting the time change of the anodic current on the Pt-electrode, *i.e.* by FIA without performing any chemical reaction. Fucsko *et al.*[56] with the same aim used a simpler pH-detector. Weak acids were not considered in these works.[55,56]

### 2.3. *Practical application of the method*

Usually for acid determination by the MCABR method a calibration plot is used. The multi-component reagent was suggested for determination of $N_{TA}$ in gastric juices;[24,42] for determination of sulphuric acid in anodizing electrolytes for aluminium;[26] for determination of metal ions and ligands (complexonometry) without titration;[34,37,57] for determination of ion-exchange capacity[38,40] and also for linearization of the potentiometric acid–base titration curves.[58]

The MCABR method was used for analysis of penicillins after their enzymatic hydrolysis up to penicilloic acid[22,45,48] by FIA. The relative standard deviation was $\leqslant 2\%$[22] in the penicillin concentration interval of $8 \times 10^{-5}$–$5 \times 10^{-4} M$. By the data[48] the relative standard deviation was $\leqslant 1\%$. The sample throughputs were 60 and 150 $h^{-1}$.[45,48]

In previous work[43,44] the MCABR method was used for urea determination in serum after enzymatic conversion of urea into $NH_4HCO_3$. The relative standard deviation was 0.52%. The sample throughput was 60 $h^{-1}$.

## 3. METHODS NOT USING ACID–BASE REAGENTS

### 3.1. *Iodide–iodate method*

The iodide–iodate method has been used for a long time for determination of strong and relatively weak acids generally, owing to its low detection limit.[59] The known reaction

$$IO_3^- + 8I^- + 6H^+ \leftrightarrow 3I_3^- + 3H_2O \quad (17)$$

is the basis of the method. The reaction (17) equilibrium is shifted to the right hand side in analogy to the protolytic reactions considered above. However, in contrast to the latter, reaction (17) proceeds quite slowly when the $H^+$ value is relatively small. The use of excess $Na_2S_2O_3$ leads to acceleration of reaction (17) and shifts its equilibrium to the right hand side. This factor is very important for analytical applications.[59] Both direct and indirect titration are usually used for acid determination by the iodide–iodate method with instrument detection.[60–64] Since this review considers mainly the TA determination alternative to titration, we refer to works[65–67] based on the measurement of the analytical signal connected with produced $I_3^-$, without titration. For this purpose the spectrophotometric absorbance[65,66] or biamperometric indication[67] were used.

Hoppe *et al.*[65] used 1% KI + 0.05% $KIO_3$ under stationary conditions. The concentration of the analyzed acids was: $10^{-5} \div 10^{-3}$ eq/l. The absorbance of $I_3^-$ was measured at wavelength 420 nm. Two intervals of the linear plot $N_{TA}$ *vs.*

$A_p$ with different slope were estimated for $10^{-5} \div 10^{-4}$ and $10^{-4} \div 10^{-3}$ eq/l., respectively. The first interval gives the relative uncertainty of acid determination (HCl, benzoic, salicylic and propionic acids) which is $\leqslant 30\%$ and the second interval $\leqslant 6\%$. But for each of the determined acids it is necessary to obtain the calibrated curve.

Kamson[66] also elaborated spectrophotometric detection for the iodide–iodate method but with the use of the FIA technique. The reagent is $5 \times 10^{-3}M$ KI + $1 \times 10^{-3}M$ $KIO_3$. The absorbance of the $I_3^-$ is measured at wavelength 350 nm, which differs from the one used in the work.[65] Only strong acids ($H_2SO_4$, $HNO_3$, HCl) were determined. The linear calibration plot $N_{TA}$ *vs.* $A_p$ in the concentration interval $4 \times 10^{-4}$–$8 \times 10^{-4}M$ for $H_2SO_4$ and $3 \times 10^{-4}$–$5 \times 10^{-3}M$ for $NHO_3$ and HCl was obtained. Even for strong acids the slopes of the calibration curve were different, probably because of the small concentration of KI.

Matuszewski *et al.*[67] also used FIA for acid determination by the iodide–iodate method. The applied reagent was $2M$ KI + $5.0 \times 10^{-3}M$ $KIO_3$. Biamperometric indication on the polarized Pt electrodes was used for $I_3^-$ determination. For $H_2SO_4$, monochloracetic, formic and acetic acids, the linear interval $N_{TA}$ *vs.* $i_p$ ($i_p$ is the current corresponding to the peak of the analytical signal) was obtained with a slope decreasing with the decrease of the acid strength. Therefore, reaction (17) proceeds incompletely and it is impossible to analyze the sum of acids. Individual acids are determined in the intervals $1 \times 10^{-3}$–$8 \times 10^{-4}$ eq/l. (for $H_2SO_4$) and $2 \times 10^{-3}$–$2 \times 10^{-2}$ eq/l. (for $HNO_3$ and HCl). The relative standard deviation is 0.2%.

The efficiency of potentiometric detection for the system $I_3^-/3I^-$ was shown for $Cu^{2+}$ determination.[68] This detection at the excess of iodide ions permits the control of $I_3^-$ up to $C_{I_3^-} \approx 10^{-7}M$ and may be used under stationary conditions as well as FIA for acid determination.

It should be noted that the iodide–iodate method has been used only for separate acid determination.

### 3.2. *Chromatographic methods*

The chromatographic methods for fatty acids determination have been described recently in Ackman's review[69] and in AOAC book.[70] Below we consider recent publications only (1992–1993). The GC method was used for fatty acids determination in fats and soaps,[71] oilseeds,[72] and fats and oils.[73–76] For analytical purposes the acids were transformed into Me esters[73,75,76] or into acyl pyrolidides as was done by Dasgupta *et al.*[74] In this case[74] the reactions were accelerated by microwave irradiation. FID[72] and MS[72,74,76] were used for detection. The relative standard deviation is 1–8%.[75]

The capillary LC method implying the reversed-phase and laser-induced fluorescence detection was used by Yoo *et al.*[77] for fatty acids determination in fish oil. The accuracy was better than 0.46%.

Jen *et al.*[78] used the HPLC method with UV detection for volatile fatty acids determination in landfill leachates. Olalla Herrera *et al.*[79] used this method for non-volatile acid (non–TA) determination in wines. The relative standard deviation is 1.0–1.1%.[79] Akasaka *et al.*[80] suggested the use of highly sensitive fluorescence reagent for acid detection in HPLC.

May *et al.*[81] automated the GLC method for fatty acids determination in oilseeds. The linear correlation between the results obtained by this method and those obtained by standard titrimetric method was shown.

Chem *et al.*[82] used the ion chromatographic method for determination of organic and inorganic acids in precipitation samples. For more complete determination the gradient and the ion-exclusion techniques were combined.

It should be noted that the chromatographic methods are more suitable for determination of separate acid groups than for TA determination. For example, in some cases,[83,84] the HPLC recovery was only 85–90%.

### 3.3. *Spectroscopic methods*

Sato *et al.*[85] optimized the conditions for the near-IR spectroscopic determination of fatty acids in fats and oils. For these compounds, Fourier transform IR spectroscopy was also successfully applied.[76,86] Ismail *et al.*[86] suggested an indirect method for oxidized oils. Acids were extracted by 1% KOH in MeOH, and carboxylate anions that were formed were determined at 1570 $cm^{-1}$. Determination takes <2 min and the authors believe that method to be suitable for routine TA control.

Sadeghi-Jorabch *et al.*[87] used Fourier transform Raman spectroscopy for determination of fatty acids in oils, margarines and butters. They recommend this method for the food industry

as the most rapid one for TA determination in comparison with conventional methods.

Lin *et al.*[88] suggested the use of atomic absorption spectrometry for free fatty acids determination in biological samples. The method is based on the acid extraction with the help of $CHCl_3$–n–hexane–MeOH in the presence of copper ion which forms copper soaps.

Walde[89] worked out a colorimetric method for free fatty acids determination in oils. The coloured compounds are formed from acids reacting with phenol red in isooctane.

Among the spectroscopic methods Fourier transform IR[86] and Raman[87] spectroscopy are of greatest practical interest. However, unlike the OCABR pH-method (see section 1) the spectroscopic methods were applied only for non-aqueous systems and are considerably more expensive.

### 3.4. *Amperometric methods*

The amperometric monitoring for acid determination in milk was suggested by Baldo *et al.*.[90] In this technique a hydrogen ion discharge current on a Pt-microelectrode was used, value of the current depending on the pH of the milk. However, the correlation of current with the TA was not investigated.

Albery *et al.*[91] studied an amperometric method for bile acids determination. They used an enzyme (3-α-hydroxysteroid dehydrogenase) electrode. Bile acids take part in the electrode reaction as reducers. The method allows only the determination of free bile acids. A detection limit of 1 μM was achieved.

### 3.5. *Gel techniques*

For determination of acidity and alkalinity, Tsionsky and Lev[92] used a capillary detector containing a sol-gel glass doped with acid–base indicators. The concentration of the acid corresponded to the length of the coloured section of the capillary. The method is simple and rapid, but only hydrochloric acid was studied.

Blumenthal *et al.*[93] suggested the determination of TA in oils on the basis of a changing colour indicator in a liquid gel. It is a simple technique of solventless analysis with a non-toxic reagent. The analysis is relatively time-consuming in comparison with the technique,[92] but more studied. Recently a collaborative study of this technique was carried out by AOAC International.[94]

## CONCLUSIONS

For determination of titratable acidity without titration one- or multi-component acid–base reagent can be used.

After reagent addition, potentiometry (with pH-glass electrode) and spectrophotometry were used for detection purposes. The determinations can be carried out both in stationary conditions and by flow injection analysis.

The method of the one-component acid–base reagent is characterized by a lower detection limit. The multi-component reagent may provide higher accuracy, but to control complex acids mixtures over a wide range of strength and concentration the one-component reagent is more efficient. The latter also considerably accelerates acid extraction from insoluble materials, which makes the analysis more rapid.

Determination of titratable acidity may be performed without the use of acid–base reagents, by Fourier transform infrared spectroscopy as well as Raman spectroscopy. Unlike acid–base reagent methods these spectroscopic methods are applied only for non-aqueous systems and are considerably more expensive.

The alternative methods of analysis (without titration) appear to be applicable for standardization and practical usage at the same time as titration methods or instead of them.

*Acknowledgement*—The authors would like to express their gratitude to Prof. E. Schoenberger for his valuable advice.

## REFERENCES

1. J. L. R. Pritchard, *Analysis of Oilseeds, Fats and Fatty Foods*, pp. 69–75. Elsevier, London, 1991.
2. G. D. V. Velinov and N. T. Todorov, *Zh. Anal. Khim.*, 1991, **46**, 274.
3. D. Midgley and K. Torrance, *Potentiometric Water Analysis*, pp. 112–140. Mir, Moscow, 1980.
4. I. M. Korenman, *New Titrimetric Methods*, pp. 18–20. Khimiya, Moscow, 1983.
5. Ya. I. Tur'yan *et al.*, USSR patent No. 989476, Priority 22.03.76.
6. Ya. I. Tur'yan *et al.*, USSR patent No. 749886, Priority 2.06.78.
7. Ya. I. Tur'yan *et al.*, USSR patent No. 1097946, Priority 30.09.80.
8. Ya. I. Tur'yan, O. E. Ruvinski, L. M. Makarova, E. U. Troz and E. O. Gerasimenko, *Izv. Vyssh. Uchebn. Zaved., Pishch. Tekhnol., Krasnodar*, 1984, No. 4, 92.
9. Ya. I. Tur'yan, O. E. Ruvinski, L. M. Makarova and O. E. Gerasimenko, *Elektrokhimiya*, 1985, **21**, 984.
10. S. I. Danilchuk, T. M. Lapshina, T. M. Belova and A. M. Chudnovskaya, *Izv. Vyssh. Uchebn. Zaved., Pishch. Tekhnol., Krasnodar*, 1987, No. 6, 61.

11. Ya. I. Tur'yan *et al.*, USSR patent No. 1605200, Priority 01.09.87.
12. Ya. I. Tur'yan *et al.*, Transactions of XIV Mendeleev Congress on General and Applied Chemistry, Nauka, Moscow, Vol. 2, p. 540, 1989.
13. Ya. I. Tur'yan, V. F. Pokhodzei and D. A. Krukier, *Izv. Vyssh. Uchebn. Zaved., Pishch. Tekhnol., Krasnodar*, 1989, No. 3, 39.
14. Ya. I. Tur'yan, O. E. Ruvinski and S. Ya. Sharudina, *Zh. Anal. Khim.*, 1991, **46,** 917.
15. T. M. Lapshina, Ya. I. Tur'yan and S. I. Danilchuk, *Zh. Anal. Khim.*, 1991, **46,** 1150.
16. Ya. I. Tur'yan *et al.*, USSR patent No. 1688158, Priority 20.04.87.
17. Ya. I. Tur'yan *et al.*, USSR patent No. 1688159, Priority 20.04.87.
18. U. U. Lur'e, *Reference-Book on Analytical Chemistry*, pp. 298–304, Khimiya, Moscow, 1989.
19. R. G. Bates and G. Schwarzenbach, *Helv. Chim. Acta*, 1954, **37,** 1437.
20. Ya. I. Tur'yan, V. F. Pokhodzei and G. I. Ginzburg, *Zh. Anal. Khim.*, 1993, **48,** 1143.
21. J. F. Rusling, G. H. Luttrell, L. F. Cullen and G. J. Papariello, *Anal. Chem.*, 1976, **48,** 1211.
22. Y. Israel, *Anal. Chim. Acta*, 1988, **206,** 313.
23. O. Astrom, *Anal. Chim. Acta*, 1978, **97,** 259.
24. M. N. Ghosh and H. O. Schild, *J. Br. Pharmacol.*, 1958, **13,** 56.
25. W. Leithe, *Chem.-Ing.-Tech. Z.*, 1964, **36,** 112.
26. F. Oehme and L. Dolezalova, *Z. Anal. Chem.*, 1973, **264,** 168.
27. G. Johansson and W. Backen, *Anal. Chim. Acta*, 1974, **69,** 415.
28. O. Astrom, *Anal. Chim. Acta*, 1977, **88,** 17.
29. O. Astrom, *Anal. Chim. Acta*, 1979, **105,** 67.
30. Y. Havas, *Magy. Kem. Foly*, 1975, **81,** 426.
31. T. Damokos, *Magy. Kem. Foly*, 1975, **81,** 427.
32. T. Damokos and J. Havas, *German Patent* 2.546.618, Priority 15.07.76.
33. T. Damokos and J. Havas, *Hung. Sci. Instr.*, 1976, **36,** 7.
34. T. Damokos and J. Havas, *Magy. Kem. Foly*, 1976, **82,** 150.
35. T. Damokos and J. Havas, *Magy. Kem. Foly*, 1976, **82,** 227.
36. T. Damokos and J. Havas, *Magy. Kem. Foly*, 1976, **82,** 453.
37. T. Damokos and J. Havas, *Magy. Kem. Foly*, 1976, **82,** 580.
38. T. Damokos and J. Havas, *Magy. Kem. Foly*, 1977, **83,** 68.
39. J. Havas, M. Kaszas and T. Damokos, *Magy. Kem. Foly*, 1977, **83,** 426.
40. T. Damokos and J. Havas, *Hung. Sci. Instrum.*, 1978, **44,** 19.
41. T. Damokos and J. Havas, *Magy. Kem. Foly*, 1978, **84,** 226, 351.
42. J. Havas, *Ion- and Molecule-Selective Electrodes in Biological Systems*, pp. 109–112. Springer, Berlin, 1985.
43. J. Ruzicka, E. H. Hansen, A. K. Ghose and H. A. Mottola, *Anal. Chem.*, 1979, **51,** 199.
44. A. Ramsing, J. Ruzicka and E. H. Hansen, *Anal. Chim. Acta*, 1980, **114,** 165.
45. R. Gnanasekaran and H. A. Mottola, *Anal. Chem.*, 1985, **57,** 1005.
46. N. Ishibashi and T. Imato, *Fresenius Z. Anal. Chem.*, 1986, **323,** 244.
47. R. S. Vithanage and P. K. Dasgupta, *Anal. Chem.*, 1986, **58,** 326.
48. B. Olsson, *Anal. Chim. Acta*, 1988, **209,** 123.
49. J. N. Butler, *Ionic Equilibrium*, pp. 238–248. Reading, Massachusetts, 1964.
50. J. Ruzicka, E. H. Hansen and H. Mosback, *Anal. Chim. Acta*, 1977, **92,** 235.
51. A. U. Ramsing, J. Ruzicka and E. H. Hansen, *Anal. Chem. Acta*, 1981, **129,** 1.
52. J. Ruzicka and E. H. Hansen, *Flow Injection Analysis*, 2nd Ed. pp. 56, 229. Wiley, 1988.
53. M. A. Koupparis, P. Anagnostopoulou and H. V. Malmstadt, *Talanta*, 1985, **32,** 411.
54. B. W. Woods, J. Ruzicka and G. D. Christian, *Anal. Chem.*, 1987, **59,** 2767.
55. J. Polta, I. Yec and D. C. Johnson, *Anal. Chem.*, 1985, **57,** 563.
56. J. Fucsko, K. Toth, E. Pungor, J. Kunovits and H. Puxbaum, *Anal. Chim. Acta*, 1987, **194,** 163.
57. A. Lewenstam, A. Ivaska and E. Wanninen, *Talanta*, 1986, **33,** 739.
58. T. Damokos and J. Havas, *Magy. Kem. Foly*, 1978, **84,** 187.
59. I. M. Kolthoff, E. J. Sandell, E. Y. Meehan and S. Bruckenstein, *Quantitative Chemical Analysis*, pp. 844–845. MacMillan, New York, 1969.
60. S. N. Nema and R. M. Verma, *Analyst*, 1979 **104,** 691.
61. S. N. Nema, G. P. Soni and R. M. Verma, *J. India. Chem. Soc.*, 1980, **57,** 657.
62. R. Saxena, M. G. Pateria, G. P. Soni and R. M. Verma, *Microchem. J.*, 1981, **26,** 334.
63. M. G. Pateria and R. M. Verma, *J. India. Chem. Soc.*, 1982, **59,** 1203.
64. R. Saxena and R. M. Verma, *J. India. Chem. Soc.*, 1984, **61,** 724.
65. H. Hoppe, B. Wiedemann and F. Winkler, *Z. Chem.*, 1976, **16,** 108.
66. O. F. Kamson, *Anal. Chim. Acta*, 1986, **179,** 475.
67. W. Matuszewski, A. Hulanicki and M. Trojanowicz, *Anal. Chim. Acta*, 1987, **194,** 269.
68. Ya. I. Tur'yan, L. M. Maluka and T. R. Markova, *Zh. Anal. Khim.*, 1992, **47,** 1456.
69. R. G. Ackman, *Food. Sci. Technol. (N.Y.)*, 1992, **53,** 47.
70. K. Helrich (ed.), *Official Methods of Analysis of the Association of Official Analytical Chemists*, 15 Ed., Vol. 2, Methods No. 956.04, 957.13, 963.22, 985.21. Third Suppl., 1992, Method No. 991.39. Arlington, 1990.
71. L. Lin, *Xiamen Daxue Xuebao, Ziram Kexuebon*, 1992, **33,** 103; *Chem. Abstr.*, 1993, **118,** 171388s.
72. L. Lin, Y. Yang, D. Wang, X. Gu and Y. Yu, Fenxi Huaxue, 1993, **21,** 339.
73. L. Hyvanen, A. M. Lampi, P. Varo and P. Koivistoinen, *J. Food Compos. Anal.*, 1993, **6,** 24.
74. A. Dasgupta, P. Banerjee and S. Malik, *Chem. Phys. Lipids*, 1992, **62,** 281.
75. X. Kang, *Sepu*, 1992, **10,** 300; *Chem. Abstr.*, 1993, **118,** 21171b.
76. J. Burhenne and H. Parlar, *Fresenius Environ. Bull.*, 1993, **2,** 119.
77. J. Sh. Yoo and V. L. Mc Gulfin, *J. Chromatogr.*, 1992, **627,** 87.
78. J. F. Jen, Ch. W. Lin, Ch. J. Lin and Ch. T. Yan, *J. Chromatogr.*, 1993, **629,** 394.

79. M. Olalla Herrera, H. Lopez Garcia, M. Villalon Mir and M. C. Lopez Martinez, *J. Liquid Chromat.*, 1993, **16,** 3101.
80. K. Akasaka, H. Ohrui and H. Meguro, *Analyst*, 1993, **118,** 765.
81. W. E. May and D. J. Hume, *J. Am. Oil Chem. Soc.*, 1993, **70,** 229.
82. V. Cheam, *Analyst*, 1992, **117,** 1137.
83. A. E. Berilacqua and A. N. Califano, *J. Food Sci.*, 1989, **54,** 1076, 1079.
84. M. J. Lopez Hernandz, J. Simal Lozano and M. A. Romero Rodriguez, *An. Bromatol.*, 1989, **41,** 65.
85. T. Sato, S. Kawano and M. Iwamoto, *J. Am. Oil Chem. Soc.*, 1991, **68,** 827.
86. A. A. Ismail, F. R. Van de Voot, G. Emo and J. Sedman, *J. Am. Oil Chem. Soc.*, 1993, **70,** 335.
87. H. Sadeghi-Jorabch, R. H. Wilson, P. S. Belton, J. D. Edwards-Webb and D. T. Coxon, *Spectrochim. Acta*, 1991, **47A,** 1449.
88. Z. Liu, X. Hu, Z. Jin and R. An, *Fenxi Huaxue*, 1993, **21,** 446.
89. P. Walde, *J. Am. Oil Chem. Soc.*, 1990, **67,** 110.
90. M. A. Baldo, S. Daniel, G. A. Mazzocchin and M. Donati, *Analyst*, 1991, **116,** 933.
91. W. J. Albery, R. B. Lennox, E. Magner, R. Girish, D. Armstrong, R. H. Dowling and G. M. Murphy, *Anal, Chim. Acta*, 1993, **281,** 655.
92. M. Tsionsky and O. Lev, *Analyst*, 1993, **118,** 557.
93. T. K. Blumenthal, M. M. Blumenthal, R. F. Stier and J. R. Stockler, American Oil Chemists' Society 84th Annual Meeting and Exposition, Anaheim, California, 28 April 1993.
94. AOAC International, *The Referee*, 1993, **17,** 4.

Pergamon

0039-9140(95)01403-9

*Talanta*, Vol. 42, No. 4, pp. 519–526, 1995

0039-9140/95 $9.50 + 0.00

# THE TRIFLUOROACETIC ANHYDRIDE–SODIUM IODIDE SYSTEM AS A REAGENT FOR DETERMINATION AND MICRODETERMINATION OF NITROXIDE RADICALS

WITOLD CIESIELSKI,[1] ZBIGNIEW H. KUDZIN[2,*] and GRZEGORZ GRABOWSKI[2]

[1]Department of Instrumental Analysis
[2]Department of Organic Chemistry, University of Łódź, Narutowicza 68, 90–136, Łódź, Poland

(*Received* 20 *May* 1994. *Revised* 29 *August* 1994. *Accepted* 29 *August* 1994)

**Summary**—A trifluoroacetic anhydride–sodium iodide mixture (TFAA-I) reacts with nitroxide radicals with liberation of iodine. Since stoichiometric amounts of iodine are formed from nitroxides, the TFAA-I reagent can be applied to their analytical determination. Two procedures for the determination of nitroxides (titrimetric on μmol and spectrometric on nmol levels) are described.

Nitroxide radicals belong to the most common classes of stable free radicals. Owing to their EPR activity, nitroxides play a crucial role in the investigations of many chemical, especially bio-organically[1] oriented problems, and are also involved in various industrial applications.[2–4] In spite of such a broad spectrum of applications, their determination still belongs to the problems of analytical chemistry of *N*-oxy compounds,[5] as only a very few reports on this subject are published in the available literature. Nitroxide radicals have been determined iodometrically, after their redox reaction with hydroiodic acid solution.[6] A direct method has been developed for an amperometric titration of free iminoxyl radicals with cerium (IV) sulphate solution by the anodic current of their oxidation.[7] The possibility of the determination of nitroxide radicals by means of their prereduction with ascorbic acid, and subsequent back titration of excess reductant, has also been suggested.[8]

Recently we have published analytical applications of the trifluoracetic anhydride–sodium iodide (TFAA-I) reagent for detection[9–12] and determination[13–16] of various *S*-oxy and *N*-oxy compounds. Among them, we have presented preliminary results on the reaction of the TFAA-I reagent with nitroxide radicals.[15] We have established that this reaction is fast, even under mild conditions (2- to 4-fold excess of TFAA and NaI, room temperature), affording hydroxylamine-*O*-trifluoracetates (**2A**) with simultaneous formation of stoichiometric amounts of iodine according to equation (1).

Since the release of iodine is quantitative in respect to nitroxide radicals **1** in a very broad range of their concentration, the TFAA-I reagent can be considered a prime reagent for iodometric procedures for determination of nitroxide radicals.

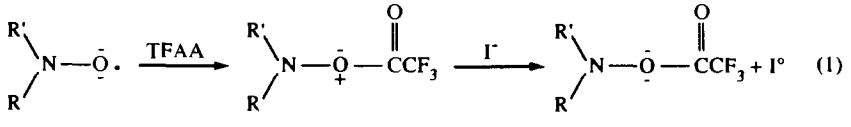


**1** **1A** **2A**

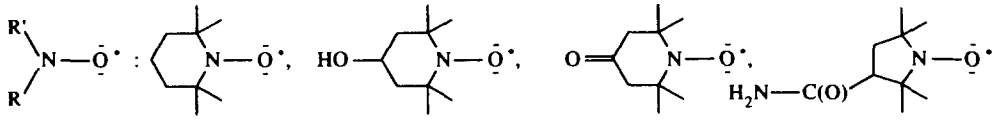

**1** **1a** **1b** **1c** **1d**

*Author to whom correspondence should be addressed.

In this paper we present our results on the application of the TFAA-I reagent for the determination and microdetermination of nitroxide free radicals (**1**) and also their differentiation from nitrones (**3**).

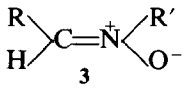

3

## EXPERIMENTAL

### *Materials*

Trifluoracetic anhydride, acetic anhydride, acetyl chloride, benzoyl chloride, methanesulphonyl chloride and *p*-toluenesulphonyl chloride were purchased from Aldrich (Milwaukee, U.S.A.)

Acetone was distilled over phosphorus pentoxide, redistilled over anhydrous potassium carbonate and stored over molecular sieves 3 Å. Sodium iodide (Aldrich) was dried *in vacuo* over phosphorus pentoxide before use.

Nitroxide radicals **1a–d**: 2,2,6,6-tetramethylpiperidinyloxy (TEMPO, **1a**), 4-hydroxy-2,2,6,6-tetramethylpiperidinyloxy (4-hydroxy-TEMPO, **1b**), 4-oxo-2,2,6,6-tetramethylpiperidinyloxy (4-oxo-TEMPO, **1c**) and 3-carbamoyl-2,2,5,5-tetramethylpyrrolidin-1-yloxy (3-carbamoyl-PROXYL, **1d**) free radicals were purchased from Aldrich and purified by two to three crystallizations from pentane. Nitrones: *N*-methyl-α-phenylnitrone (**3a**) and *N*-phenyl-α-phenylnitrone (**3b**) were synthesized according to Refs 18 and 19, respectively. 2,2,6,6-Tetramethylpiperidine (**2a**) and *N*-hydroxy-2,2,6,6-tetramethylpiperidine (**2b**) were synthesized according to Ref. 8.

### *Solutions*

NaI, a 0.5*M* solution of sodium iodide in anhydrous acetone. TFAA, a 0.8*M* solution of trifluoracetic anhydride in anhydrous acetone (the solution was prepared immediately before use). Acetic anhydride (and acid chlorides), 0.8*M* solutions in anhydrous acetone, prepared immediately before use. Nitroxide radicals, 0.1*M* solutions of nitroxide radicals **1a–d** in anhydrous acetone. Working solutions of nitroxide radicals for spectrophotometric determinations had the concentration $1 \times 10^{-3}M$ and were prepared immediately before use by dilution of a 0.1*M* solution with anhydrous acetone. Nitrones, 0.1*M* solutions of nitrones (**3a** and **b**) in anhydrous acetone. Hydroxylamines, 0.1*M* solutions of hydroxylamines (**2a** and **b**) in anhydrous acetone. KI, an aqueous 0.1*M* solution of potassium iodide. Sodium thiosulphate solution, 0.02*M*, standardized by coulometric titration with iodine. Starch, a 0.5% aqueous solution.

### *Instruments*

The absorption spectra were scanned on a Specord UV-VIS instrument, the absorbances were measured on a VSU-2P spectrophotometer (both Zeiss, Jena). EPR spectra were recorded on a SEX-2543 Radiopan Spectrometer at X-band frequencies (*ca.* $9.25 \times 10^9$ Hz) using a 100 kHz modulation unit and 0.1 mT modulation amplitude.

Mass spectra were obtained on a LKB-2091 spectrometer at 70 eV ionization energy. Samples were introduced via a chromatographic column system (OV-17 oil, 3%, 2.7 m of column, at program temperature 100°–260°C, 10°C/min).

### *Procedures*

*Iodometric titration.* A known amount of nitroxide radical (40–200 μmol contained in 0.4–2 ml of 0.1*M* solution) was placed in a 100 ml Erlenmeyer flask and 1 ml of 0.5*M* NaI in acetone added, followed by addition of 1 ml of 0.8*M* TFAA in acetone. The reaction solution was gently mixed for 0.5 min and allowed to stand in a dark place for the time indicated in Table 5, it was then diluted with 20 ml of 0.1*M* KI and titrated at once with sodium thiosulphate. At the end of the titration, starch was added.

Table 1. Reduced mass spectra (GC/EIMS) of derivatives **2Aa–c**

| | Molecular formula (weight) | *m/z* (intensity, %) | | | | | | |
|---|---|---|---|---|---|---|---|---|
| | | [M] | [M − $CH_3$] | [M − $CF_3C(O)$] | [M − $CF_3C(O)O$] | Other ions | | |
| **2Aa** | $C_{11}H_{18}F_3NO_2$ | 253 | 238 | 156 | 140 | 83 | 55 | |
| | (253.3) | (1.2) | (53) | (1.7) | (3.5) | (46) | (100) | |
| **2Ab** | $C_{13}H_{17}F_6NO_4$ | 365 | 350 | 268 | 252 | 236 | 81 | 55 |
| | (365.3) | (1.7) | (27) | (1.7) | (3.8) | (48) | (100) | (34) |
| **2Ac** | $C_{11}H_{18}F_3NO_2$ | 267 | 252 | 170 | 154 | 196 | 83 | 55 |
| | (267.3) | (1.6) | (28) | (9.5) | (2.0) | (6.2) | (100) | (99) |

Table 2. Mass spectrometric investigations of the reaction of nitroxides 1 with the TFAA-I reagent (reaction conditions)

| Exp. | Substrate* | Reagents addition: NaI† (*mmol*) | Time (*min*) | TFAA‡ (*mmol*) | Time (*min*) | Product identified by GCMS |
|---|---|---|---|---|---|---|
| 1 | **1a** | 0.5 | 10 | 0.8 | 60 | **2Aa** |
| 2 | **1a** | — | | 0.8 | 60 | **2Aa** |
| 3 | **1b** | 0.5 | 10 | 0.8 | 60 | **2Ab** |
| 4 | **1b** | — | | 0.8 | 60 | **2Ab** |
| 5 | **1c** | 0.5 | 10 | 0.8 | 60 | **2Ac** |
| 6 | **1c** | — | | 0.8 | 60 | **2Ac** |
| 7 | **2a** | — | | 0.8 | 60 | **2Aa** |
| 8 | **2b** | — | | 0.8 | 60 | **2Ab** |

*1 ml of a 0.1*M* solution of **1** or **2** (0.1 mmol) in acetone. †*ca.* 75 mg of NaI. ‡*ca.* 0.11 ml of TFAA.

*Spectrophotometric determination.* A known amount of nitroxide radical (20–1000 nmol in 20–1000 $\mu$l of an acetone stock solution) was taken in a 10 ml volumetric flask and 1 ml of 0.5*M* NaI in acetone, followed by 100 $\mu$l of 0.8*M* TFAA in acetone added. The reaction mixture was mixed well and diluted with acetone to 10 ml. Part of this solution was placed in a quartz cuvette (for amounts of nitroxide radical 20–100 nmol, - cuvettes with 50 mm light path and for 100–1000 nmol, - cuvettes with 10 mm light path were used) and the absorbance ($A$) was measured after 2 min (after addition of TFAA) against acetone as a reference ($\lambda = 362$ nm). The blank correction measurement ($A_0$) was also performed after 2 min for the reaction mixture of 1 ml of 0.5*M* NaI and 100 $\mu$l of 0.8*M* TFAA, diluted to 10 ml with anhydrous acetone, against acetone as a reference. The relation $A' = A - A_0$ as a function of nitroxide radical quantity constituted the calibration line, which was established from nitroxide **1b** determinations (in the range of 20–1000 nmol of **1b**, linear course) and was applied for determination of other nitroxide radicals.

*Iodometric titration–reverse mode procedure.* A known amount of nitrone or nitroxide radical (100 $\mu$mol contained in a 0.1*M* acetone solution) was taken into a 100 ml Erlenmeyer flask and 1 ml of a 0.8*M* TFAA acetone solution added. After the time indicated in Table 7, 1 ml of 0.5*M* NaI in acetone was added. After gentle mixing for 1 min the contents were diluted with 20 ml of 0.1*M* KI and titrated at once with sodium thiosulphate. At the end of the titration, starch was added.

*Mass spectrometric investigations.* Nitroxide radicals **1** or hydroxylamines **2** (0.1 mmol in 1 ml of a 0.1*M* solution) were placed into a Wheaton 2 ml micro product V-vials, equipped with a spin vane and treated with corresponding components of the TFAA-I reagent (Table 2). The reaction mixtures were stirred at ambient temperature for the time indicated in Table 2 and analyzed by means of GC/EIMS.

These reaction mixtures according to the mass spectrometric analysis exhibited corresponded to 1-trifluoroacetoxy-2,2,6,6-tetramethylpiperidines (**2A**). 1-Trifluoroacetoxy-2,2,6,6-tetramethylpiperidine (**2Aa**, R = R′ = H) was detected in the reaction mixtures in experiments (1), (2) and (7). 1-Trifluoroacetoxy-4-oxo-2,2,6,6-tetramethylpiperidine (**2Ac**, R = R′ = 0) was found in the reaction mixtures of the experiments (5) and (6). 1,4-Di(trifluoroacetoxy)-2,2,6,6-tetramethylpiperidine [**2Ab**, R = H, R′ = $CF_3C(O)O$] was found in the reaction mixtures of the experiments (3), (4) and (8). The partial mass spectra (EIMS) of derivatives **2Aa–c** are presented in Table 1.

Table 3. The results of spectrophotometric determination of nitroxide radicals using TFAA-I reagent ($\lambda_{(I_2)} = 362$ nm, $l = 1$ cm)

| Nitroxide radical **1** | Taken (nmol) | Found (nmol) | Error (%) | RSD ($n = 6$) |
|---|---|---|---|---|
| **1a** | 100.0 | 103.0 | 3 | 0.036 |
| | 400 | 408 | 2 | 0.028 |
| | 1000 | 980 | −2 | 0.022 |
| **1b** | 100.0 | 102.0 | 2 | 0.037 |
| | 200.0 | 196.0 | −2 | 0.018 |
| | 400 | 406 | 1.5 | 0.025 |
| | 600 | 599 | −0.1 | 0.026 |
| | 800 | 799 | −0.9 | 0.018 |
| | 1000 | 1000 | 0.0 | 0.0018 |
| **1b** ($l = 5$ cm) | 20.0 | 19.1 | −4.5 | 0.092 |
| | 40.0 | 39.6 | 2.5 | 0.070 |
| | 60.0 | 62.0 | 3.3 | 0.045 |
| | 100.0 | 101.0 | 1.0 | 0.026 |
| **1c** | 100.0 | 97.0 | −3.0 | 0.036 |
| | 400 | 390 | −2.5 | 0.032 |
| | 1020 | 1020 | 2.0 | 0.036 |

Table 4. Comparison of the reaction course of nitroxide radicals **1** with the various acylating agent–sodium iodide systems

| Acylating agent–NaI reagent (a) | Iodine (μmol) released during reduction of nitroxide radicals **1** (100 μmol) | | | | | | | | |
|---|---|---|---|---|---|---|---|---|---|
| | **1a** | | | **1c** | | | **1d** | | |
| | Exposed time (min) | | | | | | | | |
| | 1 | 10 | 30 | 1 | 10 | 30 | 1 | 10 | 30 |
| 1. $Ac_2O$–NaI | | | 0.0 | | | 0.0 | | | 0.0 |
| 2. AcCl–NaI | 49.8 | 49.8 | | 49.8 | 49.8 | 49.8 | 48.0 | 48.0 | 48.0 |
| 3. TFAA–NaI | 49.6 | 49.7 | 49.7 | 40.0 | 49.8 | 49.8 | 20.0 | 43.5 | 48.8 |
| 4. PhC(O)Cl–NaI | 7.0 | 9.0 | 38.0 | 1.5 | 9.0 | 25.0 | 1.0 | 7.0 | 20.0 |
| 5. TosCl–NaI | 10.0 | 15.0 | 40.0 | 3.0 | 7.0 | 20.0 | 1.0 | 3.0 | 8.0 |
| 6. MesCl–NaI | 0.5 | 1.0 | 1.5 | 0.0 | 0.5 | 1.0 | 0.0 | 0.5 | 1.0 |
| 7. AcOH–NaI (b) | 18.0 | 39.0 | 49.7 | 13.0 | 32.0 | 45.0 | 1.2 | 2.4 | 7.4 |

Nitroxide radicals **1** (100 μmol) were treated with: (a) 800 μmol of acylating agent and 500 μmol of sodium iodide, or (b) 1 ml (17.5 mmol) of glacial acetic acid and 500 μmol of sodium iodide (as above), respectively, and iodine was determined after the indicated exposure time.

## RESULTS AND DISCUSSION

The reaction of the TFAA-I reagent with nitroxide radicals **1** occurs with the formation of *N*-trifluoroacetyloxy-2,2,6,6-tetramethylpiperidines (**2A**) (confirmed by GC-MS measurements of the reaction mixture, see Experimental) and simultaneous release of elemental iodine (equation 1). The results of the titrimetric investigations on the reaction of nitroxide radicals with the TFAA-I reagent and the related systems are presented in Table 4. These results reveal that the rate of iodine formation is strongly influenced by nitroxide radical structure. Thus, the reactivity of TEMPO radical (**1a**) appears to be higher than that 4-oxy-TEMPO (**1c**) which in turn is more reactive than 3-carbamoyl-PROXYL radical (**1d**). The comparison of the activities of various reagents towards nitroxide radicals reveals the distinct differences in the application of the acyl reagent-NaI systems, suggesting the dominating role of the acylation stage on the general course of the reaction.

Consequently, the nitroxide radicals are not reduced by the $Ac_2O$–NaI reagent. The similar 'acylation powers' of acetyl chloride and trifluoroacetic anhydride are reflected by the similar results of nitroxide radicals reductions by means of the TFAA-I and AcCl–NaI systems. The nitroxides reductions occur also when they are carried out in AcOH–NaI acetone solution. In this case the reduction is slower in spite of *ca.* 20-fold excess of acetic acid in comparison with trifluoroacetic anhydride (TFAA) used. The lower reaction rate is also observed for the reagents based on benzoyl chloride, *p*-toluenesulphonyl chloride and methanesulphonyl chloride and sodium iodide. This effect can be explained by the stabilization of the intermediate radical cation **1A** formed, caused by the benzoyl and also the sulphonyl substituents.

These results illustrate superiority of the TFAA-I in comparison with other presented reagents in analytical application, especially that the alternative AcCl-NaI system cannot be applied for the spectrophotometric determination of nitroxide radicals owing to a high blank level (Fig. 1). For reasons analogous to these discussed in our former paper on application of the TFAA-I reagent (Ref. 16), we have used a minimum of a 4-fold molar excess of TFAA and a 2.5-fold molar excess of NaI for the determination of nitroxide radicals on a μmol scale (iodometric titration procedure). The results of the iodometric and spectrophotometric determination of nitroxide radicals **1** are summarized in Tables 2, 5 and 6.

The iodometric titration of the iodine released permits one to determine nitroxide radicals at

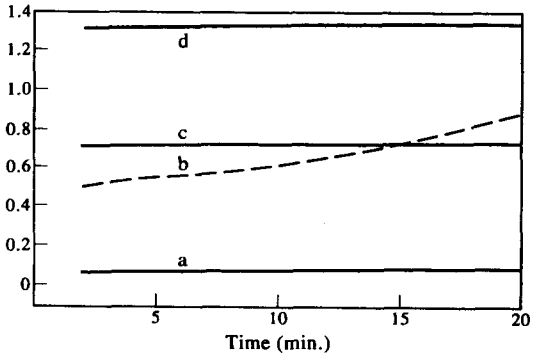


Fig. 1. The dependence of released iodine quantity as a function of time: (a) standard solution of TFAA-I (without nitroxide radical), (b) solution of 1 ml of a 0.5 ml solution of sodium iodide and 0.1 ml of a 0.5*M* solution of acetyl chloride in 10 ml of acetone, (c, d) standard reaction mixtures containing 500 nmol (c) or 1000 nmol (d) of nitroxide radical **1a** in 10 ml of acetonic solutions.

Table 5. The results of iodometric determination of nitroxide radicals **1** using the TFAA-I and AcCl–NaI reagents

| Nitroxide radical **1** | Exposed time (*min*) | Taken (*μmol*) | Found (*μmol*) | Error (%) | RSD ($n = 6$) |
|---|---|---|---|---|---|
| **1a*** | 1 | 40.0 | 39.7 | −0.75 | 0.0062 |
| | 1 | 100.0 | 99.4 | −0.6 | 0.0038 |
| | 1 | 200.0 | 199.0 | −0.5 | 0.0025 |
| **1b*†** | 1 | 40.0 | 39.7 | −0.75 | 0.0055 |
| | 1 | 100.0 | 99.5 | −0.5 | 0.0030 |
| | 1 | 200.0 | 199.2 | −0.4 | 0.0023 |
| | 1 | 600 | 599† | 0.1 | 0.0026 |
| | 1 | 1000 | 1000† | 0.0 | 0.0018 |
| **1c*** | 10 | 40.0 | 39.6 | −1.0 | 0.0084 |
| | 10 | 100.0 | 99.4 | −0.6 | 0.0065 |
| | 10 | 200.0 | 199.0 | −0.5 | 0.0052 |
| **1d‡** | 30 | 40.0 | 39.7* | −2.5 | 0.0094 |
| | 30 | 100.0 | 97.5* | −2.5 | 0.0084 |
| | 30 | 200.0 | 194.5* | −2.75 | 0.0070 |
| | 1 | 40.0 | 39.0‡ | −2.5 | 0.0062 |
| | 1 | 100.0 | 98.0‡ | −2.5 | 0.0067 |
| | 1 | 200.0 | 195.0‡ | −2.5 | 0.0050 |

The determinations of iodine were performed after addition to the nitroxide radical solutions the following amounts of reagents:
*0.8 mmol of TFAA and 0.5 mmol of NaI,
†1.6 mmol of TFAA and 2.0 mmol of NaI,
‡0.8 mmol of AcCl and 0.5 mmol of NaI.

the 40–1000 μmol level with an average deviation up to ±2.8% (RSD 0.0018–0.0094). This method is especially recommended for the fast and accurate determination of nitroxide radicals (*e.g.* determination of purity of **1**, see Table 6).

For kinetic reasons, a 100-fold molar excess of TFAA-I has been applied for the determination of nitroxide radicals on a nmol scale (spectrophotometric procedure). Consequently, the blank correction is only required in the spectrophotometric procedure since the iodine from air oxidation constitutes, in this case, a substantial part of the total released iodine. In fact, examination of the course of iodine release as a function of time (Fig. 1), reveals that the reaction is complete in a short time (dependent on the structure of the nitroxide radical) after mixing of the solutions, with gradual subsequent increase of the iodine level caused by a side oxidation ($A = 0.02$–$0.03$ in 20 min). For this reason the blank reaction is run separately and its absorbance ($A_0$) is subtracted from that for the nitroxide radical determination ($A$). The very low molecular absorbances of nitroxides **1** and hydroxylamine-*O*-trifluoroacetates (**2A**) in the analytical wavelength region (Fig. 2) practically eliminates the requirement of additional correction of absorbance. The results of the spectrophotometric determinations of nitroxide radicals **1** are given in Table 3. This spectrophotometric method permits the determination of nitroxide radicals (equivalent to released iodine) at the 100–1000 nmol level in standard ($l = 1$ cm) and at the 20–100 nmol level using cuvettes with light path $l = 5$ cm. The average deviation of these determinations is ±3% (for the level 20 nmol, 4.5%) and RSD 0.018–0.092. The sensitivity of this method seems comparable with the sensitivities offered by EPR techniques (Fig. 2), additionally presenting better versatility and simplicity of measurements.

Table 6. Determination of purity of nitroxide radicals **1a–c**

| Nitroxide radical **1** (100 *μmol*) | | Number of crystallization I | II | III | Literature[1] m.p. (°C) |
|---|---|---|---|---|---|
| **1a** | m.p. (°C) | 33.5–35.0 | 35.0–36.5 | 36.0–37.0 | 36–38 |
| | purity (%)* | 96.0 | 97.5 | 99.7 | |
| **1b** | m.p. (°C)* | 70.5–72.0 | 71.0–72.0 | 71.5–73.0 | 69–71 |
| | purity (%) | 97.8 | 98.8 | 99.4 | |
| **1c** | m.p. (°C)* | 35.5–36.5 | 36.0–37.0 | 39.0–39.5 | 36–37 |
| | purity (%) | 97.5 | 99.0 | 99.5 | |

*According to the iodometric titration procedure

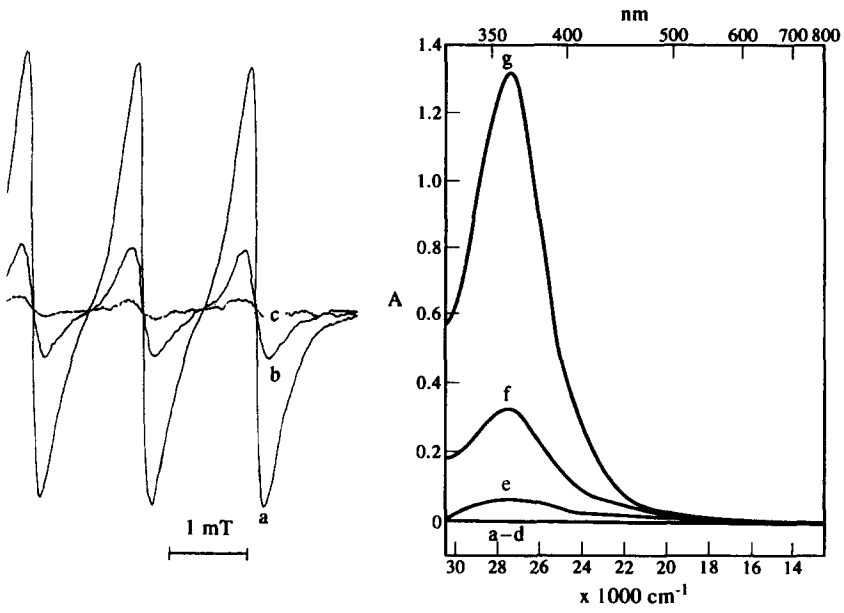


Fig. 2. UV and EPR spectra: (a–c) solutions of nitroxide radical **1a** containing 1000 nmol (a), 200 nmol (b), and/or 8 nmol (c) of **1a** in 10 ml of acetone, (d) $1 \times 10^{-4}M$ solution of *N*-trifluoroacetyloxy-2,2,6,6-tetramethylpiperidine (1000 nmol of hydroxylamine **2a** and 0.1 ml of a $0.5M$ solution of TFAA in 10 ml of acetone). (e) standard solution of TFAA-I (without nitroxide radical), (f, g) standard reaction mixtures containing 200 nmol (f) or 1000 nmol (g) of nitroxide radical **1a** (in 10 ml of acetone), respectively.

This reaction has also been examined in respect to the addition order of sub-components of TFAA-I. Thus, if trifluoroacetic anhydride was added first (reverse mode), and after the exposure time (indicated in Table 7) followed by addition of sodium iodide, the quantities of iodine determined decreased with prolongation of the exposure time (see Table 7).

This effect is in accordance with the mechanism of disproportion of protonated free nitroxide radicals (Ref. 17) and was also confirmed by GC-MS measurements of the reaction mixtures of **1** and TFAA (see Experimental). This slow rearrangement of derivatives **1A** creates a possibility for the differentiation of nitroxide radicals **1** and nitrones **3** (Table 7). Thus, in the reverse

Table 7. Differentiation of nitroxide radicals **1** and nitrones **3** using the reverse order titration procedure

| Structure | Taken (*μmol*) | Determination of iodine (%)* Time (*min*) 1 | 2 | 3 | 4 | 5 |
|---|---|---|---|---|---|---|
| 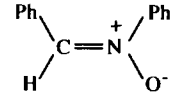 | 100 | 0.2 | 0 | 0 | 0 | 0 |
| 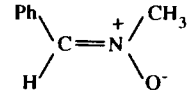 | 100 | 3 | 2 | 0.2 | 0 | 0 |
| 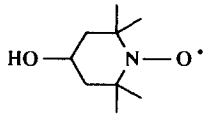 | 100 | 98.7 | 97.2 | 94 | 90 | 82 |

*According to the iodometric titration–reverse order procedure

Table 8. Comparison with other methods of nitroxide radicals **1** determination

| Method | Time (*min*) | Range (*mmol*) | Range (*nmol*) | Accuracy (%) | Standard used |
|---|---|---|---|---|---|
| A. Reduction of **1** with KI in glacial acetic acid. Titration of iodine with 0.1*M* $Na_2S_2O_3$.[6] | 30–45 | 1.6–0.7 | | 0.2–0.9 | **1b** and PhC(O)O-TEMPO |
| B. Amperometric titration of **1** with 0.01–0.1*M* cerium (IV) sulphate[7] | | 0.22–0.001 | | 1.1–4.5 | TEMPO and PROXYL radicals |
| C. Prereduction of **1** with ascorbic acid. Redox back titration with standardized solution of iodine[8] | | | | | |
| D. Acylation-reduction of **1** with the TFAA-I or AcCl-I. Iodometric titration with 0.02*M* $Na_2S_2O_3$ (Table 6) | 1–10 | 1.0–0.040 | | 0.1–2.5 | **1a–d** |
| E. Acylation–reduction of **1** with the TFAA-I. Spectrophotometric determination of iodine (Table 2) | 2 | | 1000–20 | 0.1–4.5 | **1a–c** |

mode of the TFAA-I procedure (TFAA is used in the first stage, followed by addition of NaI) (equations 2 and 3), the corresponding *N-O*-trifluoroacetyl derivatives **1A** and **3A**, formed during the treatment of **1** and **3** by means of TFAA, rearrange at different rates to **2A** and **5**, respectively, which are not able to oxidize the iodide anion.[15,16] (The mechanism of the reaction of nitroxide radicals **1** with the TFAA-I and related reagents is under investigation.)

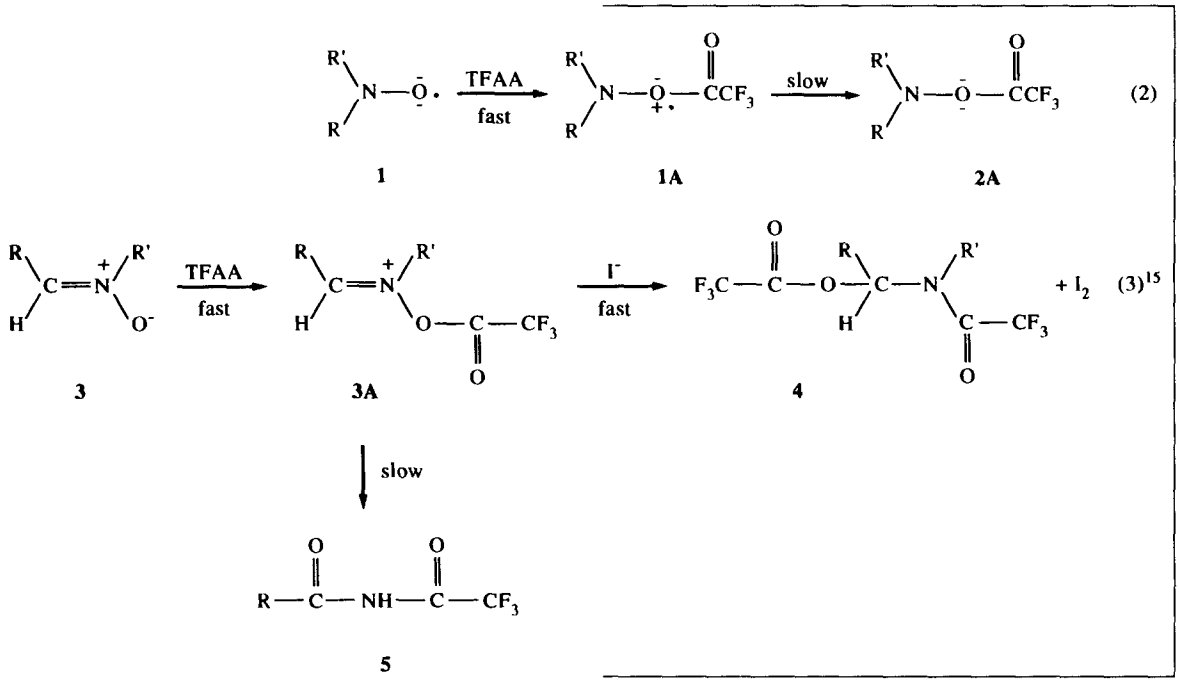


As the reaction **3A** → **5** proceeds much faster than the reaction **1A** → **2A**, the application of this reverse order procedure permits at least the differentiation of these types of *N*-oxy compounds (Ref 12 and Table 7).

A comparison of these methods with other published procedures of determination of nitroxides is presented in Table 8.

## REFERENCES


1. *Aldrich catalogue 1988–9*, pp. 1572–1579
2. M. C. R. Symons in *Chemical and Biochemical Aspects of Electron-Spin Resonance Spectroscopy*. Van Nostrand Reinhold, New York, 1978.
3. J. F. W. Keana, *Chem. Rev.*, 1978, **78**, 37.
4. R. J. Berliner (ed.), *Spin Labeling. Theory and Applications*. Academic Press, New York, 1976.
5. C. A. Streuli and P. R. Averell (eds.), *The Analytical Chemistry of Nitrogen and its Compounds*. Wiley-Interscience, New York, 1970.
6. V. A. Golubev, E. G. Rozantsev and M. B. Neiman, *Izv. Akad. Nauk SSSR, Ser. Khim.*, 1965, 1927.
7. V. T. Solomatin and P. I. Ozhegov, *Zh. Anal. Khim.*, 1973, **28**, 2129.
8. C. M. Paleos and P. Dais, *J. Chem. Soc., Chem. Commun.*, 1977, 345.
9. J. Drabowicz, A. Kotyński and Z. H. Kudzin, *J. Chromatogr.*, 1988, **447**, 225.
10. J. Drabowicz, A. Kotyński, Z. H. Kudzin and R. Skowroński, *J. Chromatogr.*, 1989, **473**, 287.

11. Z. H. Kudzin, A. Kotyński and R. Skowroński, *J. Chromatogr.*, 1990, **516,** 467.
12. A. Kontyński and Z. H. Kudzin, *J. Chromatogr. A*, 1994, **663,** 127.
13. W. Ciesielski, W. Jędrzejewski, Z. H. Kudzin, R. Skowroński and J. Drabowicz, *Talanta*, 1988, **35,** 969.
14. W. Ciesielski, W. Jędrzejewski, Z. H. Kudzin and J. Drabowicz, *Talanta*, 1990, **37,** 435.
15. W. Ciesielski, W. Jędrzejewski, J. Drabowicz, Z. H. Kudzin and R. Skowroński, paper presented at Polish Chemical Society Congress, Poland, Łódź, 1988.
16. W. Ciesielski, Z. H. Kudzin, M. Tasz and J. Drabowicz, *Can. J. Chem.*, 1990, **68,** 679.
17. V. D. Sen, V. A. Golubev and T. M. Koshleva, *Izv. Akad. Nauk SSSR, Ser. Khim.*, 1977, 474.
18. P. De Shong and C. M. Dicken, *J. Org. Chem.*, 1982, **47,** 2047.
19. O. H. Wheeler and P. H. Gore, *J. Am. Chem. Soc.*, 1956, **78,** 3363.

Pergamon

0039-9140(95)01429-2

*Talanta*, Vol. 42, No. 4, pp. 527–533, 1995

0039-9140/95 $9.50 + 0.00

# SLURRY-ELECTROTHERMAL ATOMIC ABSORPTION SPECTROMETRIC DETERMINATION OF ALUMINIUM AND CHROMIUM IN VEGETABLES USING HYDROGEN PEROXIDE AS A MATRIX MODIFIER

P. VIÑAS, N. CAMPILLO, I. LOPEZ GARCIA and M. HERNANDEZ CORDOBA*

Department of Analytical Chemistry, Faculty of Chemistry, University of Murcia, E-30071 Murcia, Spain

(*Received* 14 *June* 1994. *Revised* 30 *September* 1994. *Accepted* 30 *September* 1994)

**Summary**—Fast heating programmes for determining aluminium and chromium in vegetables using electrothermal atomic absorption spectrometry with slurry sampling are developed using wall atomization. The build-up of carbonaceous residues inside the atomizer is avoided by adding 4% hydrogen peroxide and 1% nitric acid to the slurries instead of using an air-ashing stage. In accordance with fast-programme methodology, the conventional drying and charring steps are replaced by a modified drying stage, simplifying the heating programmes. For suspensions containing 0.1% m/V of ground vegetables, the relative standard deviation (RSD) is about ±5% for aluminium. For chromium determination, the use of 0.5–1% m/V suspensions leads to RSDs close to ±4%. Calibration is carried out using aqueous standards. The aluminium and chromium contents of a number of vegetable samples obtained by using the slurry approach agree with those obtained by means of a conventional procedure based on the total dissolution of the samples. The reliability of the procedures is also confirmed by analysing two certified reference materials.

Aluminium is one of the most common elements in the earth and relatively high levels are found in vegetables which could have a potential impact on the environment, animals and man. Chromium is present at low levels and may be toxic if certain limits are exceeded. The dissolution of chromium from stainless steel which is widely used in the food industry, is probably the main source of chromium contamination of food.[1] Electrothermal atomization atomic absorption spectrometry (ETAAS) can be used to determine both elements and a number of papers concerning the determination of aluminium[2–12] and chromium[12–18] in foods and biological samples by ETAAS have been published.

However, the dissolution of samples for analysis in the conventional ETAAS practice is a long and tedious process. When a suitable particle size for solid samples can be attained,[19,20] the use of suspensions has proved useful for ETAAS purpose because, in addition to a considerable saving of time and effort, there is a smaller risk of contamination and loss of analyte. One practical problem associated with the atomization of suspensions prepared from biological materials is the build-up of carbonaceous residues inside the tube, which, in some instances, can even block the light beam. This can be avoided by using an air-ashing step,[17,21,22] although old electrothermal atomizers do not permit this. As has been recently reported,[23–25] the addition to the slurry of a chemical oxidant can also alleviate this problem since the action of the chemical during the heating cycle has a similar effect to that exercised by the air-ashing step. This method of decreasing the accumulation of organic residues can be of practical interest, since it allows a number of low-cost or old instruments to be used in slurry-ETAAS analyses of materials with a high organic content.

This simple approach together with heating programmes based on fast-programme methodology[26–28] are used in this study to develop procedures for the rapid determination of aluminium and chromium in vegetables. The reproducibility and accuracy of the results in a wide variety of vegetable matrices are studied and two reference materials are analysed to confirm the reliability of the proposed methods.

*Author to whom correspondence should be addressed.

## EXPERIMENTAL

### *Instrumentation*

A Perkin-Elmer Model 1100B atomic-absorption spectrometer equipped with deuterium-arc background correction and an HGA-400 electrothermal atomizer were used. The measurements were made using hollow cathode lamps operated at 15 and 10 mA lamp currents, 0.7 nm slits and 309.3 and 357.9 nm wavelengths for aluminium and chromium, respectively. Wall-atomization was used for both elements using Perkin-Elmer pyrolytic graphite coated tubes (Part number B013-5653). Background-corrected integrated absorbance was used as the analytical signal. Argon (purity higher than 99.999% SEO, Spain) was used as the inert gas, the flow-rate being 300 ml/min during all stages except during atomization, when the flow was stopped for chromium. In some instances, a miniflow of 30 or 100 ml/min was maintained during aluminium atomization to decrease sensitivity. A Branson ultrasonic bath of 14 W constant power was used. A Fritsch ball-mill of 80 ml capacity with 20 agate-balls of 1 cm diameter was also used.

### *Reagents*

High quality water obtained using a Milli-Q system (Millipore) was used throughout. All glassware, plasticware, storage bottles and pipette tips used were previously immersed for several hours in a 20% v/v nitric acid solution and then rinsed with water. Aluminium-free paper was used for cleaning pipette tips. Stock solutions of aluminium and chromium (1000 $\mu$g/ml) were obtained from Panreac (Spain) and diluted as necessary to obtain working standards. High quality ethanol (Riedel-deHaër), concentrated (65% m/V) nitric acid (Merck), perchloric acid (Probus, Spain) and 30% m/V hydrogen peroxide (Fluka) were used as received.

### *Analytical procedures*

The vegetables were obtained from a local supermarket, washed repeatedly with pure water, chopped and oven-dried at 90°C. The dried samples were first ground in a domestic grinder for 15 sec and then in a ball mill for 15 min. No sieving was carried out.

Suspensions were prepared by adding 2 ml ethanol, 1 ml hydrogen peroxide and 0.25 ml concentrated nitric acid to the ground sample (typical amounts ranged between 10 and 500 mg, depending on the metal and its level in the sample), the solution being finally diluted up to 25 ml. The use of a high speed tissue homogenizer was discarded because of the high contamination observed for both elements. The suspensions were submitted to ultrasounds for 5 min and then magnetically stirred for another 10 min. The same practical results were obtained by using a manual homogenizer with teflon pestle and glass tube. While the suspensions were being continuously stirred, 20 $\mu$l aliquots were taken and injected into the furnace. The heating programmes given in Table 1 (where the quoted temperatures are values set on the HGA-400 power supply) were run and the background corrected peak areas due to the analytes obtained. Calibration was performed by injecting aqueous standards under the same experimental conditions. Certified reference materials were analysed in the same way.

The samples were previously analysed for comparison purposes. Fractions of 0.2–1 g of the dried, ground vegetables were calcined at 500°C for 8 hr. The ashes were treated with 5 ml nitric acid, heated to dryness and then again treated with 2 ml nitric acid and 2 ml perchloric acid before heating to almost dryness; 2 ml hydrogen peroxide was then added and, after the digestion was complete, the solution was diluted with water and evaporated to reduce acidity, and finally diluted up to 50 or 100 ml with water. Aliquots of 20 $\mu$l were directly injected into the furnace to obtain signals within the linear response range.

## RESULTS AND DISCUSSION

The use of STPF conditions for aluminium determination is widely recommended,[4,11,29] although this is far from being a general rule.[5,30,31] This is not surprising since in those cases where the analyte requires a high atomization temperature, as occurs with aluminium, and depending on the type of sample, the same

Table 1. Fast-furnace programmes for the determination of aluminium and chromium in vegetables

| Step | Temperature (°C) | Ramp (sec) | Hold (sec) |
|---|---|---|---|
| Dry | 200 | 1 | 20 |
| Atomize | 2500*/2300† | 0 | 3 |
| Clean | 2650 | 1 | 3 |

*Aluminium, argon flow, 30 ml/min.
†Chromium, the gas flow was stopped.

practical results can be obtained by using wall atomization or platform atomization.[32,33] For this reason and because of the saving which can be made by using pyrolytic tubes instead of the more expensive platforms for routine purposes, the procedure here studied was optimized by comparing the results obtained with both atomization modes.

Since some of the samples analyzed had too high an aluminium content, it was necessary to reduce the sensitivity. For this purpose, alternative lines or a low-flow of the purge gas during the atomization stage were tried.[34] Wavelengths below 300 nm produced a sufficient decrease in sensitivity; however, the radiation intensity was very low and showed poor signal/background ratios, thus diminishing the reproducibility. The 396.2 nm line permits the calibration range to be extended[31] but the reduction in sensitivity[35] is only about 20%. The sensitivity could also be decreased[34] by about 50% by using the 394.4 nm line, but this was still insufficient for the purpose desired. On the other hand, better results were obtained when, operating at 309.3 nm, the argon flow was not fully stopped at the atomization step. Figure 1 shows the results obtained using alternative lines and the effect of the purge gas flow for a vegetable slurry. A flow ranging from 30 to 300 ml/min was selected. This permitted the analysis of all the samples with their very different aluminium contents without the necessity of preparing extremely diluted suspensions with their inherent problem of poor reproducibility.

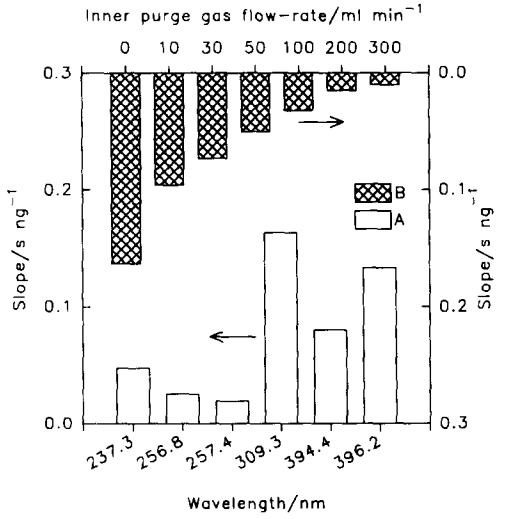


Fig. 1. Effect of different wavelengths (A) and argon flow rate (B) during the atomization step on the slope of aluminium calibration graphs.

*Composition of the suspension medium*

Preliminary experiments concerning aluminium quantification in different samples and reference materials using water as the suspending medium led to standard additions graphs with no reproducible slopes, most of the results being too high for the aluminium content. In addition, the slopes of calibration addition graphs (additions of suspension to a reference solution) were different to those shown by standard additions lines, confirming the unreliability of the results obtained. Similar results were obtained when either wall or platform atomization were used. To overcome these difficulties, the use of several chemical modifiers [$Mg(NO_3)_2$, $Pd(NO_3)_2$, $NH_4H_2PO_4$, $K_2Cr_2O_7$, $NH_4NO_3$] was tried, and again, the results obtained when using both atomization modes differed from the true values and an increase in the absorption background, as has been previously reported,[33] was observed. A number of additional experiments showed that sulphate and halides could be discarded as the cause of the poor results. The non-reproducible slopes are possibly a result of the formation of colloidal aluminium compounds,[31] as is suggested by the fact that only the addition of nitric acid to the suspension medium[2,4,5,30,36,37] led to the correct results being obtained. Apparently, in addition to extracting a fraction of the analyte into the supernatant, nitric acid plays an important role in reproducibility.[36] A detailed study was carried out using a 0.5–5% concentration range of nitric acid in the suspension medium. With concentrations at or above 1% the slopes of standard additions calibration graphs obtained using either of the atomization modes were reproducible and practically identical to those obtained for aqueous standards, leading to correct results for the aluminium content. Other authors[4] used higher percentages of acid (5% of $HNO_3$), which also led to exact results. In our opinion, to enlarge the useful lifetime of the pyrolytic material, it is preferable to maintain the nitric acid concentration as low as possible and so a 1% acid in the suspension medium was selected as adequate.

The direct atomization of suspensions prepared from the ground vegetable samples produced an accumulation of carbonaceous residues inside the atomizer. Thus, a periodic cleaning of the tube was necessary.[2,3] This effect was more marked for concentrated suspensions. Since the only electrothermal atomizer available

did not permit an air-ashing stage to be included in the programme, a recently reported[23–25] simple approach based on the addition of hydrogen peroxide to the suspension medium was used. The combination $H_2O_2$–$HNO_3$ proved an adequate suspension medium for biological materials, thus acting as a true chemical modifier during the drying step. When 4% $H_2O_2$ and 1% $HNO_3$ were used, the carbonaceous residues remaining after the atomization step practically disappeared, the background signals obtained were very low and a mechanical cleaning of the inside of the graphite tube was only needed occasionally. It must be noted that most of the experiments were performed using percentages of solid matter below 1% in the suspension medium. Thus, after 50 injections of 20 $\mu$l of a 0.5% suspension, no carbonaceous residue was observed. When the suspension concentration was higher than 1%, the optimal oxidant concentration had to be reconsidered. Ethanol (8%) was added to the suspensions to aid dispersion of particles, although aliquots were hand-pipetted while solutions were magnetically stirred.[24]

For the determination of chromium, the same suspension medium as was used for aluminium is recommended, thus standardizing both procedures.

*Optimization of furnace programmes*

Since the preliminary experiments showed that the action of hydrogen peroxide together with the use of diluted suspensions led to low background signals, the heating cycles were optimized by means of fast-programme methodology.[26–28] For aluminium, the conventional drying and ashing steps were replaced by a modified drying stage performed at 200°C during 20 sec for wall atomization and 400°C during 30 sec for platform atomization. The atomization temperature was studied in the 1800–2650°C range (Fig. 2). The maximum signal was reached at 2300 and 2600°C for wall (curve A) and platform (curve B) atomization, respectively. Using these temperatures, the appearance time of the signals were 1.4 and 2.6 sec, respectively. Our experience has shown that when using platform atomization at temperatures higher than 2500°C, the useful lifetime of the atomizers was about 200 and 300 firings for standard and fork platforms, respectively, whereas the lifetime of tubes operating at the same temperature was much higher. Since the results obtained were similar as regards sensitivity and precision when

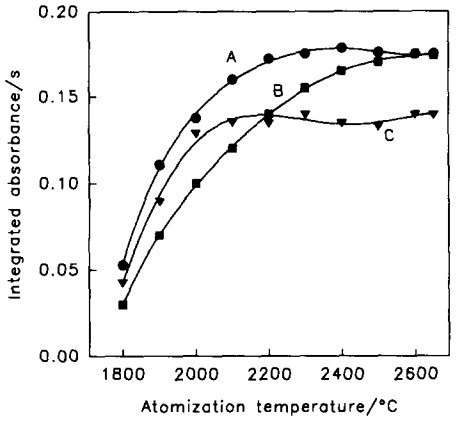


Fig. 2. Influence of the atomization temperature on the peak area signals for Al using wall (A) and platform (B) atomization and Cr using wall atomization (C).

either atomization mode was used, wall atomization was finally selected to cut costs. Although the gas flow was not stopped during atomization, a partial condensation of the analyte in the cold zones of the atomizer might have produced cross-contamination.[38] To avoid this problem, a temperature of 2500°C was selected. By means of a second firing it was verified that the amount of aluminium remaining inside the atomizer was negligible. A cleaning stage at 2650°C was also included in the programme.

In a similar way, the programme for chromium was optimized. In this case, when using a platform, the holding time during the atomization stage had to be at least 7 sec, which shortens the lifetime of the atomizer. In addition, the signal showed a tail, which became more marked with the aging of the platform. Consequently, wall atomization was again selected. Maintaining a drying temperature of 200°C for 20 sec, the atomization temperature was varied from 1800 to 2650°C (Fig. 2, curve C). The peak area increased up to 2100°C and a 2300°C value was selected since higher temperatures distorted the peak profiles. In this case, the argon flow was stopped during the atomization step owing to the lower sensitivity for chromium and the lower content of this element in the samples. A cleaning stage was also included to avoid the carryover of chromium. The final furnace programmes are given in Table 1.

*Extraction of the analyte into the aqueous phase*

As previously described[5,23,24] when dealing with slurries there is generally a partial

Table 2. Extraction of aluminium and chromium from a bean leaves slurry by addition of nitric acid

| Nitric acid (%) | % Extraction | |
|---|---|---|
| | Aluminium | Chromium |
| 0.0 | 34.7 | 45.0 |
| 0.4 | 79.9 | 61.8 |
| 1.0 | 78.0 | 76.0 |
| 2.5 | 81.9 | 81.4 |
| 5.0 | 84.8 | 82.2 |
| 10.0 | 84.6 | 84.7 |

extraction of the analytes into the aqueous phase of the suspension. Table 2 shows the extraction percentages obtained from bean leaves suspensions containing 4% hydrogen peroxide in a 0–10% nitric acid range. The samples were magnetically stirred for 15 min at room temperature and aliquots were centrifuged to allow all the solids to settle out. The supernatant liquid fraction was then injected into the furnace. Values significantly increased in the presence of nitric acid. The high extraction percentage (approximately 75% of the Al and Cr were in the liquid phase for 1% acid) meant that the reproducibility was less dependent on the number of particles sampled in each injection and, consequently, led to a better precision.

Although analyte extraction was also possible with other acids (HCl, HF, $HClO_4$, $H_2SO_4$), interferent effects appeared in the determination of aluminium.[28,38] Chloride and fluoride produced a decrease in the analyte signal in both the suspension and the supernatant due to the formation of volatile halides, which decreased the atomic density in the atomization stage.

*Influence of the slurry concentration*

The precision of the procedure was studied using different slurry concentrations ranging between 0.007 and 0.16% for aluminium and 0.04–2.0% for chromium in cauliflower (80 and 1.9 $\mu$g/g of Al and Cr, respectively). Figure 3 shows the concentration ranges in which a linear response for the Al (Fig. 3a) and Cr signals (Fig. 3b) were obtained. In each case, the mean value and the standard deviation calculated for 10 replicate determinations for each slurry concentration are given. In addition, a bar graph showing the relative standard deviations is also presented. Two successive atomization steps were performed to check that aluminium was

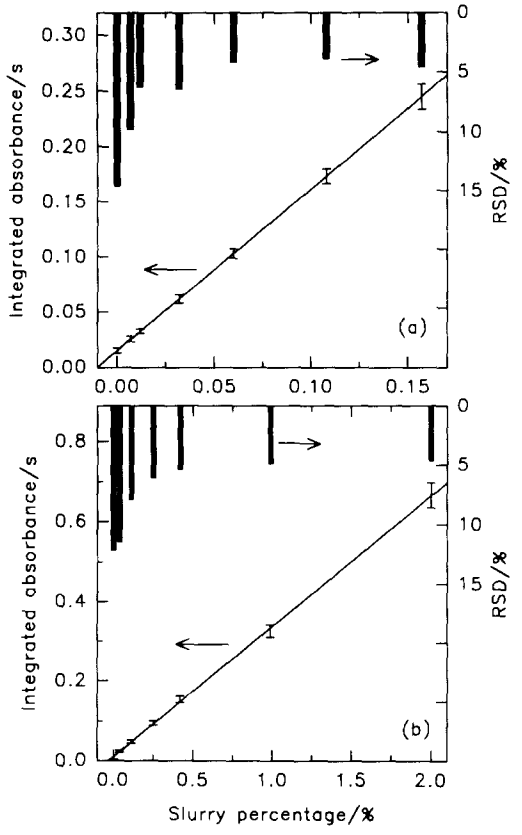


Fig. 3. Effect of the suspension concentration on the signal obtained for (a) Al and (b) Cr. Bar graphs indicate RSD values.

not retained in the tube. RSD values were below ±7%, except for very diluted suspensions, which gave peak area signals lower than 0.05 sec. Optimal slurry percentages ranged from 0.03 to 0.15 and 0.3–2.0% for Al and Cr, respectively.

*Calibration and results*

Figure 4 shows absorbance–time profiles (solid lines) for aluminium and chromium resulting from the analysis of vegetable slurries. These plots were similar to those observed for simple aqueous standards, indicating that the effect of chemical interferences due to the matrix was negligible. The background signals were very low (dotted lines). The standard additions method was also used to investigate the possibility of interference by the matrix. Each graph was constructed from five points and each point was measured three times. The slopes of the aqueous standards and standard additions graphs were similar, confirming the absence of interference from the matrix and showing that the method permitted

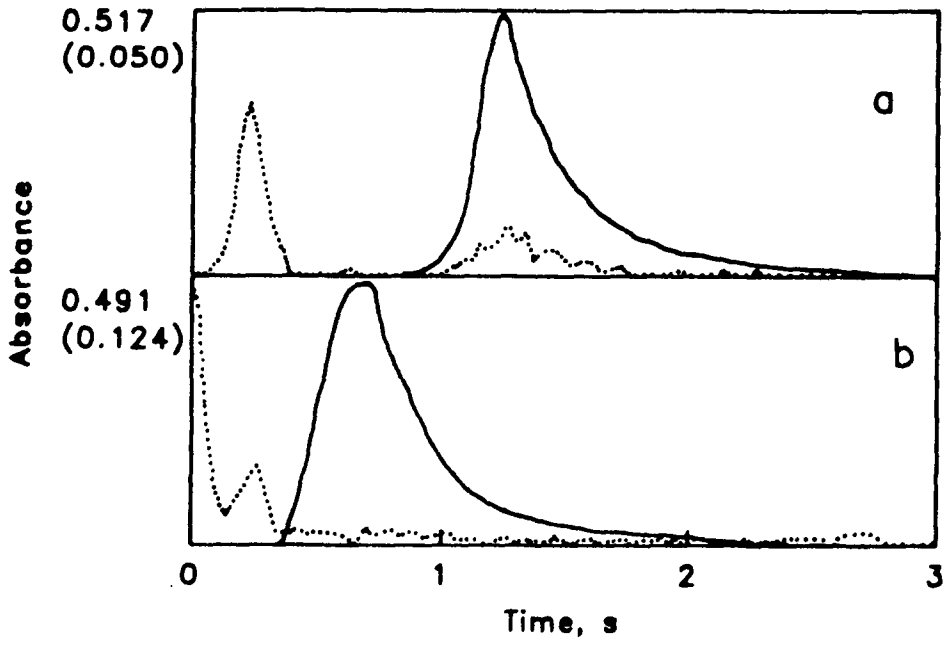


Fig. 4. Atomization profiles (solid lines) of Al obtained from a 0.1% bean leaves slurry (a) and Cr obtained from a 0.92% cauliflower slurry (b). The dotted lines give the background absorbance.

aqueous standards to be used for calibration. The proposed slurry procedures were applied to a wide range of vegetable materials. Results for aluminium and chromium are included in Table 3, showing the comparative results obtained by the slurry methods and those obtained with a conventional procedure based on dry-ashing and acid dissolution. All values are in good statistical agreement. The methods were validated using two certified reference materials and good concordance with the certified values was obtained. To discard the possible effect of contamination due to grinding, these certified materials were analysed both as received and after a grinding stage identical to that applied to the samples, no differences being noted.

A graphic comparison of the results obtained by the proposed procedures and those certified or obtained by mineralization led to correlation graphs which parameters showed no significant differences with the hypothetical values. Results of ordinate $\pm$ confidence interval (CI, 95%) for Al and Cr were $0.015 \pm 1.125$ and $0.037 \pm 0.072$ $\mu$g/g, respectively. Slope $\pm$ CI (95%), were $1.0023 \pm 0.0298$ and $1.0090 \pm 0.0809$ for Al and Cr, respectively.

Table 3. Aluminium and chromium contents in vegetables

| | Aluminium ($\mu g/g$) (mean $\pm$ SD) | | Chromium ($\mu g/g$) (mean $\pm$ SD) | |
|---|---|---|---|---|
| Vegetable | Slurry procedure | Wet-ashing procedure | Slurry procedure | Wet-ashing procedure |
| Potato | $6.5 \pm 2.5$ | $6.4 \pm 0.7$ | $0.59 \pm 0.041$ | $0.64 \pm 0.005$ |
| Celery | $11.9 \pm 1.5$ | $10.4 \pm 0.8$ | $0.15 \pm 0.008$ | $0.15 \pm 0.009$ |
| Carrot | $50.4 \pm 6.7$ | $50.2 \pm 1.5$ | $0.37 \pm 0.023$ | $0.37 \pm 0.013$ |
| Cauliflower | $80.6 \pm 11.8$ | $83.8 \pm 4.9$ | $1.97 \pm 0.114$ | $1.93 \pm 0.098$ |
| Bean leaves | $182.0 \pm 8.2$ | $185.4 \pm 6.7$ | $0.77 \pm 0.020$ | $0.75 \pm 0.022$ |
| Citrus leaves (SRM 1572) | $95.0 \pm 2.0$ | $92.0 \pm 15.0$* | $0.78 \pm 0.072$ | $0.80 \pm 0.200$* |
| Apple leaves (SRM 1515) | $289.0 \pm 7.0$ | $286.0 \pm 9.0$* | $0.38 \pm 0.035$ | 0.3† |

*Certified value.
†Not certified. Value is given by the supplier for informative purposes.

## CONCLUSION

The determination of aluminium and chromium was carried out using the slurry technique for the direct analysis of vegetables, and proved an alternative method to the introduction of solutions in ETAAS for routine analysis. Sample preparation was very simple, thus avoiding any risk of contamination. The use of fast-programme methodology led to a considerable saving of time. No advantages were noted for platform atomization and so, wall atomization was used. Addition of both hydrogen peroxide and nitric acid to the slurry eliminated the build-up of carbonaceous residues inside the tube, and there was no need of an air-ashing step.

*Acknowledgements*—The authors are grateful to the Spanish DGICYT (Project PB93-1138) for financial support. N. Campillo acknowleges a fellowship from Consejería de Cultura y Educación, Comunidad Autónoma de la Región de Murcia (Spain).

## REFERENCES

1. G. A. Smart and J. C. Sherlock, *Food Addit. Contam.*, 1985, **2,** 139.
2. K. B. Pierson and M. A. Evenson, *Anal. Chem.*, 1986, **58,** 1744.
3. W. Frech and D. C. Baxter, *Fresenius Z. Anal. Chem.*, 1987, **328,** 400.
4. N. J. Miller-Ihli, *J. Anal. At. Spectrom.*, 1988, **3,** 73.
5. D. J. Halls, *J. Anal. At. Spectrom.*, 1989, **4,** 149.
6. Y. Wang, C. Lu, Z. Xiao, S. S. Kuan and E. J. Rigsby, *J. Agric. Food Chem.*, 1991, **39,** 724.
7. S. Caroli, *Microchem. J.*, 1992, **45,** 257.
8. J. M. Marchante Gayón, J. Pérez Parajón, A. Sanz-Medel and C. S. Fellows, *J. Anal. At. Spectrom.*, 1992, **7,** 743.
9. N. Xu, V. Majidi, W. D. Ehmann and W. R. Markesbery, *J. Anal. At. Spectrom.*, 1992, **7,** 749.
10. P. Bermejo-Barrera, E. Beceiro-González and A. Bermejo-Barrera, *Microchem. J.*, 1992, **45,** 90.
11. M. A. Z. Arruda, M. Gallego and M. Valcárcel, *Anal. Chem.*, 1993, **65,** 3331.
12. N. J. Miller-Ihli, *Fresenius J. Anal. Chem.*, 1990, **337,** 271.
13. U. Völlkopf, Z. Grobenski, R. Tamm and B. Welz, *Analyst*, 1985, **110,** 573.
14. D. J. Halls, C. Mohl and M. Stoeppler, *Analyst*, 1987, **112,** 185.
15. N. Carrión, Z. A. de Benzo, B. Moreno, A. Fernández, E. J. Eljuri and D. Flores, *J. Anal. At. Spectrom.*, 1988, **3,** 479.
16. D. Wagley, G. Schmiedel, E. Mainka and H. J. Ache, *At. Spectrosc.*, 1989, **10,** 106.
17. L. Ebdon, A. S. Fisher, H. G. M. Parry and A. A. Brown, *J. Anal. At. Spectrom.*, 1990, **5,** 321.
18. R. Rubio, A. Sahuquillo, G. Rauret and Ph. Quevauviller, *Int. J. Environ. Anal. Chem.*, 1992, **47,** 99.
19. C. Bendicho and M. T. C. de Loos-Vollebregt, *J. Anal. At. Spectrom.*, 1991, **6,** 353.
20. N. J. Miller-Ihli, *Fresenius J. Anal. Chem.*, 1993, **345,** 482.
21. S. C. Stephen, D. Littlejohn and J. M. Ottaway, *Analyst*, 1985, **110,** 1147.
22. L. Ebdon and H. G. M. Parry, *J. Anal. At. Spectrom.*, 1988, **3,** 131.
23. P. Viñas, N. Campillo, I. López García and M. Hernández Córdoba, *Fresenius J. Anal. Chem.*, 1994, **349,** 306.
24. P. Viñas, N. Campillo, I. López García and M. Hernández Córdoba, *Food Chem.*, 1994, **50,** 317.
25. P. Viñas, N. Campillo, I. López Garcia and M. Hernández Córdoba, *Analyst*, 1994, **119,** 1119.
26. D. J. Halls, *Analyst*, 1984, **109,** 1081.
27. D. Bradshaw and W. Slavin, *Spectrochim. Acta, Part B*, 1989, **44,** 1245.
28. E. A. Nater, R. G. Burau and M. Akeson, *Anal. Chim. Acta*, 1989, **225,** 233.
29. A. Sanz-Medel, R. Rodriguez Roza, R. González Alonso, A. Noval Vallina and J. Cannata, *J. Anal. At. Spectrom.*, 1987, **2,** 177.
30. D. J. Halls and G. S. Fell, *Analyst*, 1985, **110,** 243.
31. P. E. Gardiner, M. Stoeppler and H. W. Nürnberg, *Analyst*, 1985, **110,** 611.
32. A. Taylor and A. W. Walker, *Ann. Clin. Biochem.*, 1992, **29,** 377.
33. F. Fagioli, L. Scanavini, C. Locatelli and P. Gilli, *Anal. Lett.*, 1984, **17,** 1473.
34. M. Hoenig, P. Regnier and L. Chou, *J. Anal. At. Spectrom.*, 1991, **6,** 273.
35. M. L. Parsons, B. W. Smith and P. M. McElfresh, *Appl. Spectrosc.*, 1973, **27,** 471.
36. P. Allain, Y. Mauras and F. Der Khatchadourian, *Anal. Chem.*, 1984, **56,** 1198.
37. M. J. J. Carrondo, J. N. Lester and R. Perry, *Analyst*, 1979, **104.**
38. D. C. Baxter, W. Frech and E. Lundberg, *Analyst*, 1985, **110,** 475.

Pergamon

0039-9140(95)01437-3

*Talanta*, Vol. 42, No. 4, pp. 535–541, 1995

0039-9140/95 $9.50 + 0.00

# THERMODYNAMICS OF FORMATION OF UREA COMPLEXES WITH MANGANESE(II), NICKEL(II) AND ZINC(II) IONS IN *N,N*-DIMETHYLFORMAMIDE

KAZUHIKO OZUTSUMI*, YOKO TAGUCHI and TAKUJI KAWASHIMA

Laboratory of Analytical Chemistry, Department of Chemistry, University of Tsukuba, Tsukuba 305, Japan

(*Received* 28 *April* 1994. *Revised* 28 *July* 1994. *Accepted* 5 *October* 1994)

**Summary**—The complexation of urea (ur) with manganese(II), nickel(II) and zinc(II) ions has been studied by titration calorimetry in *N,N*-dimethylformamide (DMF) containing 0.4*M* $(C_2H_5)_4NBF_4$ as a constant ionic medium at 25°C. The calorimetric data were well explained in terms of the formation of $[Mn(ur)]^{2+}$, $[Mn(ur)_2]^{2+}$ and $[Mn(ur)_4]^{2+}$ for manganese(II), $[Ni(ur)]^{2+}$ for nickel(II) and $[Zn(ur)]^{2+}$ and $[Zn(ur)_2]^{2+}$ for zinc(II), and their formation constants, reaction enthalpies and entropies were determined. The complexation of the nickel(II)-urea system in DMF has also been studied by means of spectrophotometric titration and electronic spectra of individual nickel(II) complexes were determined. On the basis of the stepwise thermodynamic quantities and the individual electronic spectra of the complexes, it is revealed that the $[Mn(ur)]^{2+}$, $[Mn(ur)_2]^{2+}$, $[Ni(ur)]^{2+}$, $[Zn(ur)]^{2+}$ and $[Zn(ur)_2]^{2+}$ complexes have a six-coordinate octahedral structure, while the $[Mn(ur)_4]^{2+}$ complex has a four-coordinate tetrahedral structure.

Complexation of metal ions with anions is more enhanced in aprotic solvents such as *N,N*-dimethylformamide (DMF), dimethyl sulfoxide, pyridine and acetonitrile than in water, regardless of their different electron-pair donating abilities.[1–4] Large and positive entropies are usually associated with the complexation in the aprotic solvents. These are a result of the enhanced solvation of anions in water, *i.e.* hydrogen bonding of the ions with water molecules, compared with that in aprotic solvents, and also of the hydrogen-bonded water structure in the bulk, *i.e.* entropies of reactions in nonaqueous solvents are closely related with structures of solvents. However, studies on complexation of metal ions with neutral ligands are rather limited in nonaqueous solution. Extended works including various neutral ligands are necessary to elucidate thermodynamics of complexation in aprotic solvent.

First row divalent transition metal ions are relatively hard acceptors and prefer a relatively hard donor atom. Relative affinities among halide ions to these metal(II) ions have been studied in aprotic solvent.[5–13] The affinity decreases in the sequence Cl > Br > I and the metal(II) ions really behave as a hard acceptor in aprotic solvent. Knowledge on affinities of various donor atoms to the metal(II) ions must be important in view of hard and soft acids and bases. However, donor atoms other than halide ions have scarcely been examined in nonaqueous media. In this study we focused our attention on urea (ur) and thiourea (tu) and investigated their complexation with manganese(II), nickel(II) and zinc(II) ions in DMF containing 0.4*M* $(C_2H_5)_4NBF_4$ as a constant ionic medium by precise calorimetry at 25°C. The formation of the nickel(II) complexes was also investigated by spectrophotometry.

## EXPERIMENTAL

### *Reagents*

All chemicals used were of reagent grade. DMF solvates of metal(II) tetrafluoroborate were prepared from relevant hydrates of metal(II) tetrafluoroborate and dried *in vacuo* over $P_2O_5$. Urea and thiourea were used without further purification and dried *in vacuo* at room temperature. Tetraethylammonium tetrafluoroborate was recrystallized once from water and dried in a vacuum oven at 100°C. DMF was purified as described elsewhere.[10] All DMF solutions were prepared and treated under a dry nitrogen atmosphere.

*Author to whom correspondence should be addressed.

*Measurements*

Calorimetric measurements were performed at 25°C on a twin-type calorimeter (Tokyo Riko, Japan) and a PC-9801VM computer (NEC, Japan) was used for the calorimeter control and data acquisition.[14] Two Teflon-coated stainless steel vessels were inserted in an aluminium block thermostated at 25°C within ±0.0001°C. A test solution (40 $cm^3$) containing metal(II) tetrafluoroborate in the vessel was titrated with either 0.2 or 0.4*M* urea DMF solution by using an APB-118 autoburete (Kyoto Electronics, Japan) under a dry nitrogen atmosphere. All test solutions contained 0.4*M* $(C_2H_5)_4NBF_4$ as a constant ionic medium. Heats of complexation ranging from 0.4 to 1.0 J at each titration point were measured with an error of ±0.02 J (three standard deviations). Heats of dilution of titrants were measured by titrating a 0.4*M* $(C_2H_5)_4NBF_4$ DMF solution with either 0.2 or 0.4*M* urea DMF solution.

Spectral changes with varying ligand concentrations for nickel(II) urea DMF solutions were measured on a UV-2100 spectrophotometer (Shimadzu, Japan). The spectrophotometer was controlled with a PC-9801VM computer, which also stored absorbance data in 1 nm interval over the wavelength range 300–850 nm. A nickel(II) tetrafluoroborate DMF solution was placed in a reaction vessel with a thermostated water jacket and titrated with 1*M* urea solution by using an autoburet under a dry nitrogen atmosphere. The reaction vessel was connected to a flow cell with a light path length of 1 cm through Teflon and glass tubes. Absorbances were measured with an error of ±0.006 (three standard deviations). Spectrophotometric data at selected 50 wavelengths were used for a subsequent least-squares calculations.

*Data analysis*

The overall formation of complexes between the divalent metal ion ($M^{2+}$) and ligand (L) can be defined as equations (1) and (2), considering the formation of only mononuclear species.

$$M^{2+} + nL = [ML_n]^{2+} \quad (1)$$

$$\beta_n = [ML_n^{2+}]/[M^{2+}][L]^n. \quad (2)$$

The concentrations of free $M^{2+}$ and L are related to their total concentrations, $C_{M,i}$ and $C_{L,i}$, in a solution $i$ by the following mass-balance equations.

$$C_{M,i} = [M^{2+}]_i + \Sigma\beta_n[M^{2+}]_i[L]_i^n \quad (3)$$

$$C_{L,i} = [L]_i + \Sigma n\beta_n[M^{2+}]_i[L]_i^n. \quad (4)$$

A heat $q_i$ measured at a titration point $i$ is represented by the overall formation constant $\beta_n$ and the enthalpy $\Delta H^0_{\beta n}$ of $[ML_n]^{2+}$ as equation (5),

$$q_i = -(V_i\Sigma\beta_n(\Delta H^0_{\beta n})[M^{2+}]_i[L]_i^n - V_{i-1}\Sigma\beta_n(\Delta H^0_{\beta n})[M^{2+}]_{i-1}[L]_{i-1}^n), \quad (5)$$

where $V_i$ denotes the volume of the test solution.

Similarly, an absorbance $A_{ij}$ measured in a solution $i$ at a given wavelength $\lambda_j$ is expressed by the formation constant $\beta_n$ and the molar absorption coefficient $\epsilon_n(\lambda_j)$ as equation (6).

$$A_{ij} = \Sigma\epsilon_n(\lambda_j)\beta_n[M^{2+}]_i[L]_i^n + \epsilon_M(\lambda_j)[M^{2+}]_i + \epsilon_L(\lambda_j)[L]_i. \quad (6)$$

Formation constants and enthalpies were obtained simultaneously by minimizing the error-square sums $\Sigma(q_{i,obsd} - q_{i,calcd})^2$, and formation constants and molar absorption coefficients by $\Sigma\Sigma(A_{ij,obsd} - A_{ij,calcd})^2$ using nonlinear least-squares programs MQCAL and MQSPEC,[15] respectively, which are based on an algorithm proposed by Marquardt.[16]

## RESULTS AND DISCUSSION

Very small heat of complexation other than heat of dilution of titrant was evolved in the course of the titration of the manganese(II), nickel(II) and zinc(II) ions with thiourea in DMF and thus reliable values of the formation constant and enthalpy were not determined. Also, spectrophotometric titration data for the colored nickel(II) thiourea system slightly changed with varying the $C_{tu}/C_{Ni}$ mole ratios, revealing that the formation constants of nickel(II) thiourea complexes are very small. In the following, we describe the equilibria of the urea system.

*Self-association of urea*

Heats of dilution of urea solutions measured by titrating a 0.4*M* $(C_2H_5)_4NBF_4$ solution are endothermic and relatively large (0.5–1 J) as shown in Fig. 1, where the heat of dilution $q$ measured at each titration point is normalized with the volume of the titrant added $\delta v$ and the concentration of urea in the titrant $C_{L,tit}$, and the term $-q/(\delta v C_{L,tit})$ is plotted against $C_L$, where $C_L$ denotes the total concentration of urea in the test solution. Also, the endothermicity appreciably increases with increasing the concentration of the titrant. The major part of heats

Table 1. The least-squares refinement of overall formation constants, $\log(\beta_n/M^{-(n-1)})$, and enthalpies, $\Delta H^0_{\beta n}$/kJ/mol, of $(ur)_n$ in *N,N*-dimethylformamide containing 0.4*M* $(C_2H_5)_4NBF_4$ at 25°C*†

| | Dimer | Trimer | Dimer + trimer |
|---|---|---|---|
| $\log\beta_2$ | −0.43 (0.05) | — | 0.9 (1.1) |
| $\log\beta_3$ | — | 0.56 (0.08) | 0.7 (0.9) |
| $\Delta H^0_{\beta 2}$ | −15.4 (1.0) | — | 0.2 (2.6) |
| $\Delta H^0_{\beta 3}$ | — | −9.8 (0.4) | −58 (84) |
| $R$‡ | 0.024 | 0.065 | 0.022 |
| $\sigma_{obsd}$§ | 0.014 | 0.037 | 0.013 |

*The number of calorimetric data points is 48.
†Values in parentheses refer to three standard deviations.
‡Hamilton *R* factor.
§Standard deviation of the observed heats.

of dilution (0.2–0.4 J) may usually be a result of the partial self-association of solute molecules in the titrant. The titrant solution is diluted to cause the dissociation of the self-associated molecules to monomers when the formation constants of the self-associated molecules are small and/or the concentration of the solute in the test solution is kept low throughout measurements. Since the concentration of urea in the test solution was low enough (less than 0.2*M*) in the present case, the large and concentration-dependent heats of dilution suggest that the self-associated urea molecules do not completely dissociate to monomers by dilution.

Urea molecules three-dimensionally connect each other by forming hydrogen bonds in crystal[17-20] and thus it is plausible that urea molecules associate by hydrogen bonds to form polymeric species in DMF. The calorimetric data in Fig. 1 were then analyzed by considering the formation of sets of polymeric species and the Hamilton *R* factor and standard deviation of the observed heats $\sigma$ were compared (see Table 1). The data were well explained in terms of the dimer formation but the curves calculated with the best-fit parameters obtained by an assumption of the trimer formation considerably deviate from the experimental points. No significant improvement of the *R* and $\sigma$ values resulted by assuming the formation of both dimer and trimer. The least-squares calculation thus leads to a conclusion that urea associates to form dimers in DMF. The solid lines in Fig. 1, calculated using the parameters under dimer in Table 1, well reproduced the experimental points. The $\Delta G^0$, $\Delta H^0$ and $\Delta S^0$ values for the reaction

$$2\,\mathrm{ur} = (\mathrm{ur})_2$$

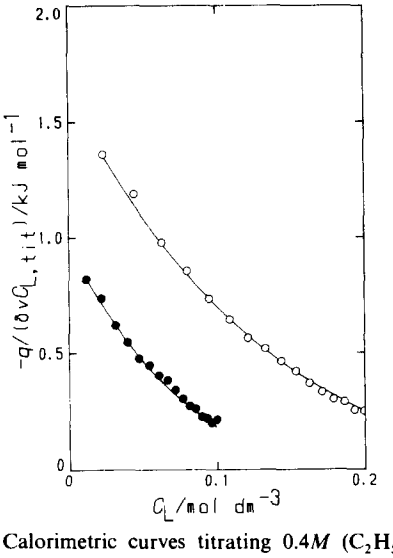


Fig. 1. Calorimetric curves titrating 0.4*M* $(C_2H_5)_4NBF_4$ solutions with urea in DMF at 25°C. Concentrations of urea in titrant solutions, $C_{L,tit}$/m*M*, are 398.7 (○) and 199.4 (●). Solid lines were calculated by using the constants listed under dimer in Table 1.

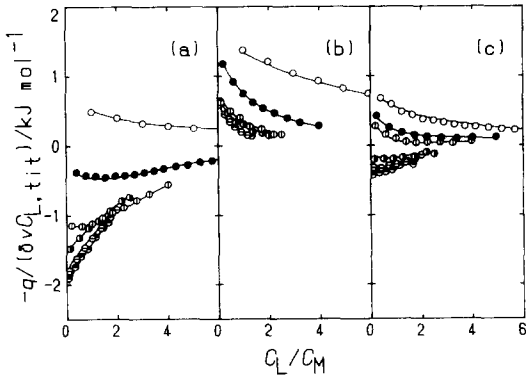


Fig. 2. Calorimetric titration curves for (a) manganese(II), (b) nickel(II) and (c) zinc(II) ions and urea solutions containing 0.4*M* $(C_2H_5)_4NBF_4$ at 25°C. Concentrations of metal ions in initial test solutions, $C_{M,init}$/m*M*, and those of urea in titrant solutions, $C_{L,tit}/M$, are 19.76, 398.7 (○), 52.23, 400.6 (●), 99.36, 400.6 (⦶), 79.96, 199.4 (◑), 100.1, 199.4 (⊖) and 119.8, 199.4 (◓) for manganese(II), 20.21, 398.7 (○), 100.5, 398.7 (●), 79.92, 199.4 (⦶), 100.1, 199.4 (◑) and 150.4, 199.4 (⊖) for nickel(II), 48.45, 400.6 (○), 81.14, 400.6 (●), 100.6, 400.6 (⦶), 79.51, 199.4 (◑), 99.89, 199.4 (⊖) and 119.6, 199.4 (◓) for zinc(II). Solid lines were calculated by using the constants listed in Tables 2–4.

Table 2. The least-squares refinement of overall formation constants, $\log(\beta_n/M^{-n})$, and enthalpies, $\Delta H^0_{\beta n}$/kJ/mol, of $[Mn(ur)_n]^{2+}$ in *N*,*N*-dimethylformamide containing 0.4*M* $(C_2H_5)_4NBF_4$ at 25°C*†

| | (1, 2) | (1, 2, 3) | (1, 2, 3, 4) | (1, 2, 4) |
|---|---|---|---|---|
| $\log \beta_1$ | 1.2 (0.1) | 1.0 (0.1) | 1.1 (0.1) | 1.1 (0.1) |
| $\log \beta_2$ | 1.0 (0.3) | 2.0 (0.1) | 1.9 (0.3) | 1.9 (0.1) |
| $\log \beta_3$ | — | 2.3 (0.2) | 2.6 (0.6) | — |
| $\log \beta_4$ | — | — | 2.7 (1.6) | 3.6 (0.1) |
| $\Delta H^0_{\beta 1}$ | −4.1 (0.5) | −5.2 (0.5) | −4.8 (0.4) | −4.4 (0.3) |
| $\Delta H^0_{\beta 2}$ | −81 (61) | −8.7 (1.1) | −11 (4) | −13.7 (2.4) |
| $\Delta H^0_{\beta 3}$ | — | −36 (13) | −17 (12) | — |
| $\Delta H^0_{\beta 4}$ | — | — | −35 (91) | −18.9 (1.1) |
| $R$‡ | 0.070 | 0.025 | 0.022 | 0.029 |
| $\sigma_{obsd}$§ | 0.039 | 0.014 | 0.013 | 0.016 |

*The number of calorimetric data points is 108.
†Values in parentheses refer to three standard deviations.
‡Hamilton *R* factor.
§Standard deviation of the observed heats.

are $(2.5 \pm 0.3$; three standard deviations) kJ/mol, $(-15.4 \pm 1.0)$ kJ/mol and $(-60 \pm 4)$ J $K^{-1}$ $mol^{-1}$, respectively.

*Manganese(II) complexes*

Calorimetric titration curves for manganese(II)-urea solutions are shown in Fig. 2(a). In the figure, the term $-q/(\delta v C_{L,tit})$ is plotted against $C_L/C_M$, where $q$ is the heat of reaction uncorrected for the heat of dilution of titrant and $C_M$ denotes the total concentration of the metal ion in the test solution.

The calorimetric titration curves were analyzed by assuming the formation of various sets of mononuclear complexes. The dimer formation of urea was taken into account and the formation constant and enthalpy were fixed at the values described above during the least-squares calculations. The results are compared in Table 2. The calorimetric titration curves were not reproducible by an assumption of the formation of two complexes, $[Mn(ur)]^{2+}$ and $[Mn(ur)_2]^{2+}$, owing to large $R$ and $\sigma$ values [see set (1, 2) in Table 2]. Sets (1, 2, 3), (1, 2, 3, 4) and (1, 2, 4), which assume the formation of $[Mn(ur)_3]^{2+}$ and/or $[Mn(ur)_4]^{2+}$ in addition to $[Mn(ur)]^{2+}$ and $[Mn(ur)_2]^{2+}$, gave appreciably smaller $R$ and $\sigma$ values than the set (1, 2). The $R$ and $\sigma$ values for the set (1, 2, 4) are slightly larger than those for the sets (1, 2, 3) and (1, 2, 3, 4), but the difference among the three sets is marginal. Furthermore, the standard deviations of the formation constants for the set (1, 2, 4) are remarkably smaller than those for the sets (1, 2, 3) and (1, 2, 3, 4). This indicates that the formation of $[Mn(ur)_3]^{2+}$ is very much suppressed. We thus propose the formation of the $[Mn(ur)]^{2+}$, $[Mn(ur)_2]^{2+}$ and $[Mn(ur)_4]^{2+}$ complexes in DMF.

*Nickel(II) complexes*

Calorimetric and spectrophotometric titration data of the nickel(II)-urea system are depicted in Figs. 2(b) and 3(a), respectively. The electronic spectra show a monotonous shift with increasing $C_L/C_M$ in solution. Both calorimetric

Table 3. The least-squares refinement of overall formation constants, $\log(\beta_n/M^{-n})$, and enthalpies, $\Delta H^0_{\beta n}$/kJ/mol, of $[Ni(ur)_n]^{2+}$ in *N*,*N*-dimethylformamide containing 0.4*M* $(C_2H_5)_4NBF_4$ at 25°C*

| | Calorimetry | | Spectrophotometry | |
|---|---|---|---|---|
| | (1) | (1, 2) | (1) | (1, 2) |
| $\log \beta_1$ | 0.0 (0.1) | 0.5 (0.7) | 0.15 (0.08) | 0.2 (1.0) |
| $\log \beta_2$ | — | 0.8 (0.5) | — | 0.6 (0.2) |
| $\Delta H^0_{\beta 1}$ | −2.6 (0.4) | −0.9 (1.0) | — | — |
| $\Delta H^0_{\beta 2}$ | — | −6.3 (3.2) | — | — |
| $N$† | 90 | 90 | 2350 | 2350 |
| $R$‡ | 0.032 | 0.027 | 0.019 | 0.010 |
| $\sigma_{obsd}$§ | 0.012 | 0.010 | 0.006 | 0.004 |

*Values in parentheses refer to three standard deviations.
†The number of data points.
‡Hamilton *R* factor.
§Standard deviation of the observed heats and absorbances.

Table 4. The least-squares refinement of overall formation constants, $\log(\beta_n/M^{-n})$, and enthalpies, $\Delta H^0_{\beta n}$/kJ/mol, of $[Zn(ur)_n]^{2+}$ in *N,N*-dimethylformamide containing 0.4*M* $(C_2H_5)_4NBF_4$ at 25°C*†

| | (1, 2) | (1, 2, 3) | (1, 2, 3, 4) | (1, 2, 4) |
|---|---|---|---|---|
| $\log \beta_1$ | 1.0 (0.1) | 0.9 (0.1) | 0.9 (0.2) | 1.0 (0.1) |
| $\log \beta_2$ | 1.3 (0.1) | 1.6 (0.2) | 1.7 (0.3) | 1.6 (0.2) |
| $\log \beta_3$ | — | 2.2 (0.2) | −1.3 (large) | — |
| $\log \beta_4$ | — | — | 3.0 (0.6) | 3.2 (0.2) |
| $\Delta H^0_{\beta 1}$ | −2.2 (0.3) | −2.6 (0.5) | −2.6 (0.6) | −2.4 (0.3) |
| $\Delta H^0_{\beta 2}$ | −14.5 (1.9) | −6.4 (2.7) | −5.8 (3.1) | −8.8 (2.7) |
| $\Delta H^0_{\beta 3}$ | — | −12.0 (2.8) | −large (large) | — |
| $\Delta H^0_{\beta 4}$ | — | — | −8.9 (5.8) | −10.8 (0.7) |
| $R$‡ | 0.078 | 0.059 | 0.058 | 0.058 |
| $\sigma_{obsd}$§ | 0.013 | 0.010 | 0.010 | 0.010 |

*The number of calorimetric data points is 108.
†Values in parentheses refer to three standard deviations.
‡Hamilton *R* factor.
§Standard deviation of the observed heats.

and spectrophotometric data were well explained in terms of the formation of $[Ni(ur)]^{2+}$ only (see Table 3). We further considered the formation of $[Ni(ur)_2]^{2+}$. However, no significant decrease in the *R* and $\sigma$ values achieved, suggesting that the formation of $[Ni(ur)_2]^{2+}$ is practically negligible under the experimental conditions examined. Very similar values of the formation constant of $[Ni(ur)]^{2+}$ are obtained by calorimetry and spectrophotometry. The electronic spectrum of $[Ni(ur)]^{2+}$ in Fig. 3(b) shows a very similar pattern to that of the nickel(II) ion having an octahedral $[Ni(dmf)_6]^{2+}$ structure,[21] indicating the same octahedral geometry of $[Ni(ur)(dmf)_5]^{2+}$.

*Zinc(II) complexes*

Calorimetric curves for the zinc(II)-urea system shown in Fig. 2(c) were analyzed by a similar manner to that employed for the manganese(II)– and nickel(II)–urea systems. The results are summarized in Table 4. The calorimetric data were well explained in terms of the formation of $[Zn(ur)]^{2+}$ and $[Zn(ur)_2]^{2+}$ with appreciably small *R* and $\sigma$ values [see set (1, 2) in Table 4]. Slightly smaller *R* and $\sigma$ values were obtained for sets (1, 2, 3), (1, 2, 3, 4) and (1, 2, 4) considering the formation of $[Zn(ur)_3]^{2+}$ and/or $[Zn(ur)_4]^{2+}$ along with $[Zn(ur)]^{2+}$ and $[Zn(ur)_2]^{2+}$, but the difference is not significant. Thus, complexes higher than $[Zn(ur)_2]^{2+}$ are hardly formed under the experimental conditions examined. It is concluded that the zinc(II) ion forms the $[Zn(ur)]^{2+}$ and $[Zn(ur)_2]^{2+}$ complexes in DMF.

*Stepwise thermodynamic parameters and coordination structure*

The thermodynamic parameters for the stepwise formation of the complexes are summarized in Table 5. The species distribution

Table 5. Thermodynamic quantities, $\log(K_n/M^{-1})$, $\Delta G^0_n$, $\Delta H^0_n$/kJ/mol, and $\Delta S^0_n$/J $K^{-1}$ $mol^{-1}$, for the stepwise formation of $[M(ur)_n]^{2+}$ in *N,N*-dimethylformamide at 25°C*

| | Mn | Ni | Znm |
|---|---|---|---|
| $\log K_1$ | 1.1 (0.1) | 0.0 (0.1) | 1.0 (0.1) |
| $\log K_2$ | 0.8 (0.2) | — | 0.3 (0.1) |
| $\log K_3K_4$ | 1.8 (0.1) | — | — |
| $\Delta G^0_1$ | −6.5 (0.4) | 0.0 (0.6) | −5.9 (0.7) |
| $\Delta G^0_2$ | −4.3 (0.9) | — | −1.7 (0.6) |
| $\Delta G^0_3+\Delta G^0_4$ | −10.0 (0.8) | — | — |
| $\Delta H^0_1$ | −4.4 (0.3) | −2.6 (0.4) | −2.2 (0.3) |
| $\Delta H^0_2$ | −9.2 (2.6) | — | −12.3 (2.1) |
| $\Delta H^0_3+\Delta H^0_4$ | −5.2 (3.2) | — | — |
| $\Delta S^0_1$ | 7 (3) | −9 (3) | 12 (3) |
| $\Delta S^0_2$ | −17 (12) | — | −36 (9) |
| $\Delta S^0_3+\Delta S^0_4$ | 16 (13) | — | — |

*Values in parentheses refer to three standard deviations.

calculated by using the formation constants is depicted in Fig. 4.

The manganese(II), nickel(II) and zinc(II) ions are present as the hexasolvate $[M(dmf)_6]^{2+}$ in DMF.[21] In the nickel(II)-urea system, the $[Ni(ur)]^{2+}$ complex has an octahedral structure because the electronic spectrum of the complex shown in Fig. 3(b) is very similar to that of octahedral $[Ni(dmf)_6]^{2+}$. The $[Mn(ur)]^{2+}$ and $[Zn(ur)]^{2+}$ complexes also have an octahedral structure because of their similar $\Delta H_1^0$ and $\Delta S_1^0$ values to those of nickel(II), although there is no direct spectrophotometric evidence. Both $\Delta H_2^0$ and $\Delta S_2^0$ values for manganese(II) and zinc(II) are more negative than the $\Delta H_1^0$ and $\Delta S_1^0$ values and this is a normal trend when no change in the coordination structure around metal(II) ion occurs. Thus, it is expected that the six-coordination around the manganese(II) and zinc(II) ions is kept in the $[Mn(ur)_2]$ and $[Zn(ur)_2]^+$ complexes. On the other hand, the $(\Delta H_3^0 + \Delta H_4^0)$ and $(\Delta S_3^0 + \Delta S_4^0)$ values for manganese(II) is more positive than the $\Delta H_2^0$ and $\Delta S_2^0$) values. This indicates that the number of solvent molecules liberated on the formation of $[Mn(ur)_4]^{2+}$ is large. The coordination structure around the manganese(II) ion changes from octahedral to tetrahedral at this step. Thus, we conclude that octahedral $[Mn(ur)(dmf)_5]^{2+}$, $[Mn(ur)_2\text{-}(dmf)_4]^{2+}$, $[Ni(ur)(dmf)_5]^{2+}$, $[Zn(ur)(dmf)_5]^{2+}$ and $[Zn(ur)_2(dmf)_4]^{2+}$ and tetrahedral $[Mn(ur)_4]^{2+}$ are formed in DMF.

The enthalpy changes for the formation of $[M(ur)(dmf)_5]^{2+}$ (M = Mn, Ni, Zn) are all negative in DMF (see Table 5). On the other hand, the heats ascribed to the complexation of the metal(II) ions with thiourea were small but evidently endothermic. Although reliable thermodynamic parameters of complexation have not been determined for the thiourea system, it is thus demonstrated that the manganese(II), nickel(II) and zinc(II) ions prefer oxygen atom to sulfur one and behave as a hard acceptor in DMF.

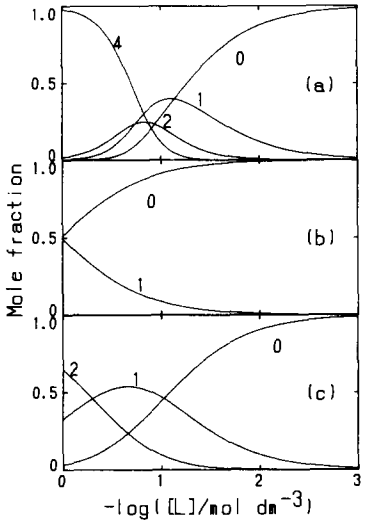


Fig. 4. Species distribution of (a) manganese(II), (b) nickel(II) and (c) zinc(II) urea complexes in DMF. *n* represents $[M(ur)_n]^{2+}$.

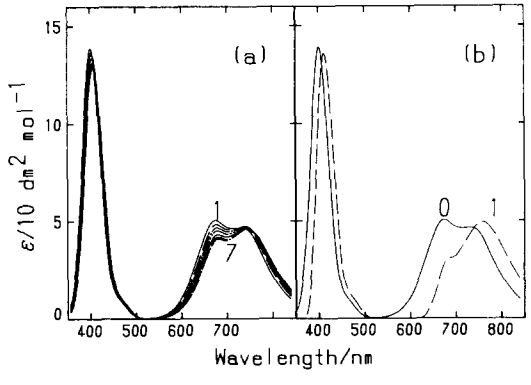


Fig. 3. (a) Typical variation of electronic spectra of nickel(II) urea DMF solutions with varying molar ratios ($C_L/C_{Ni}$) in the range 350–850 nm at 25°C. The total concentrations of nickel(II) and urea, $C_{Ni}$ and $C_L/mM$, in measured solutions are (1) 150.4 and 0, (2) 125.3 and 167.2, (3) 107.4 and 286.6, (4) 93.98 and 376.1, (5) 75.19 and 501.5, (6) 60.15 and 601.8, and (7) 50.12 and 668.7. (b) Electronic spectra of individual nickel(II) urea complexes in DMF. *n* represents $[Ni(ur)_n]^{2+}$.

The entropy changes for the formation of $[M(ur)(dmf)_5]^{2+}$ (M = Mn, Ni, Zn) are nearly zero as seen in Table 5. The DMF molecules in the first coordination sphere within $[M(dmf)_6]^{2+}$ are expected to lose freedom of motion to a considerable extent. The solvating molecules are released from the solvation sphere of the metal(II) ions upon complexation and then enter a structureless bulk solvent to lead to a large entropy gain. In fact, the halogeno complexation of the manganese(II), nickel(II) and zinc(II) ions in DMF is accompanied by a large and positive entropy change,[10–13] as generally seen in aprotic solvent.[1,2] Desolvation of anions also contributes to the positive entropy value of the reaction. Solvation of non-charged molecules is expected to be weaker than that of anions, *i.e.* non-charged molecules may have enough freedom of motion in bulk DMF, and the ligand molecules appreciably lose their freedom of motion upon complexation. Thus, the entropy changes are expected to become a value close to zero as found in the case of the 2,2′-bipyridine complexes with divalent transition metal ions.[22–24]

## REFERENCES


1. S. Ahrland, *Pure Appl. Chem.*, 1979, **51,** 2019.
2. S. Ahrland, *Pure Appl. Chem.*, 1982, **54,** 1451.
3. S. Ishiguro and H. Ohtaki, *J. Coord. Chem.*, 1987, **15,** 237.
4. H. Ohtaki and H. Yamatera (eds), *Structure and Dynamics of Solutions.* Elsevier, Amsterdam, 1992.
5. S. Ahrland and N-O. Björk, *Acta Chem. Scand., Ser. A*, 1976, **30,** 265.
6. S. Ahrland, N-O. Björk and R. Portanova, *Acta Chem. Scand., Ser. A*, 1976, **30,** 270.
7. S. Ahrland and I. Persson, *Acta Chem. Scand., Ser. A*, 1981, **35,** 185.
8. S. Ishiguro, B. G. Jeliazkova and H. Ohtaki, *Bull. Chem. Soc. Jpn*, 1985, **58,** 1143.
9. S. Ishiguro, K. Ozutsumi and H. Ohtaki, *Bull. Chem. Soc. Jpn*, 1987, **60,** 1691.
10. S. Ishiguro, K. Ozutsumi and H. Ohtaki, *Bull. Chem. Soc. Jpn*, 1987, **60,** 531.
11. S. Ishiguro, K. Ozutsumi and H. Ohtaki, *J. Chem. Soc., Faraday Trans. 1*, 1988, **84,** 2409.
12. K. Ozutsumi and S. Ishiguro, *J. Chem. Soc., Faraday Trans.*, 1990, **86,** 271.
13. S. Ishiguro, M. Miyauchi and K. Ozutsumi, *J. Chem. Soc., Dalton Trans.*, 1990, 2035.
14. H. Suzuki and S. Ishiguro, *Netsu Sokutei*, 1988, **15,** 152.
15. H. Suzuki and S. Ishiguro, *Inorg. Chem.*, 1992, **31,** 4178.
16. D. W. Marquardt, *J. Soc. Ind. Appl. Math.*, 1963, **11,** 431.
17. P. Vaughan and J. Donohue, *Acta Crystallogr.*, 1952, **5,** 530.
18. J. E. Worsham, Jr., H. A. Levy and S. W. Peterson, *Acta Crystallogr.*, 1957, **10,** 319.
19. N. Sklar, M. E. Senko and B. Post, *Acta Crystallogr.*, 1961, **14,** 716.
20. A. Caron and J. Donohue, *Acta Crystallogr., Sect. B*, 1969, **25,** 404.
21. K. Ozutsumi, M. Koide, H. Suzuki and S. Ishiguro, *J. Phys. Chem.*, 1993, **97,** 500.
22. S. Ishiguro, L. Nagy and H. Ohtaki, *Bull. Chem. Soc. Jpn*, 1987, **60,** 2053.
23. S. Ishiguro, L. Nagy and H. Ohtaki, *Bull. Chem. Soc. Jpn*, 1987, **60,** 2865.
24. S. Ishiguro, K. Ozutsumi, L. Nagy and H. Ohtaki, *J. Chem. Soc., Dalton Trans.*, 1989, 655.

Pergamon

0039-9140(95)01443-8

*Talanta*, Vol. 42, No. 4, pp. 543–551, 1995
Elsevier Science Ltd
Printed in Great Britain
0039-9140/95 $9.50 + 0.00

# CHEMILUMINESCENCE DETECTION OF HYDRAZINE VAPOR

G. E. COLLINS,[1]* S. LATTURNER[2] and S. L. ROSE-PEHRSSON[1]

[1]Naval Research Laboratory, Chemistry Division, Code 6110, Washington DC, 20375-5342, U.S.A.
[2]University of California, Santa Barbara, Department of Chemistry, Santa Barbara, CA 93106, U.S.A.

(*Received* 23 *May* 1994. *Revised* 13 *September* 1994. *Accepted* 30 *September* 1994)

**Summary**—An efficient, real-time chemiluminescence detector for hydrazine vapor, $N_2H_4(g)$, is described, capable of monitoring sub part-per-billion levels of hydrazine in air. The catalytic oxidation of hydrazine by colloidal platinum forms an intermediate, oxidizing agent (*e.g.* ·OH or ·OOH) which subsequently oxidizes luminol, generating a chemiluminescence signal that is proportional to the hydrazine concentration. Major components of the instrument include a photomultiplier tube (PMT), a short length of glass tubing coiled directly in front of the PMT cathode surface, a vacuum pump for sampling the air, and a peristaltic pump for circulating the liquid reagent. The liquid reagent, a basic solution (pH 13) of luminol and colloidal platinum, is continuously recycled. The detection sequence is initiated by pumping the hydrazine vapor through a short length of teflon tubing that is concurrently transporting the liquid reagent. The liquid is separated from the gas stream in an impinger and quickly pumped to the PMT. We have evaluated the effect of solution pH, luminol and platinum concentrations, and air and liquid flow rates on the analytical characteristics of this system. A linear, dynamic detection range for hydrazine has been obtained from 1 to 2000 ppb in air, with an instrument response that is fully reversible and achieves plateau response in less than 2 min.

Hydrazine is a widely used propellant and a common precursor in the synthesis of a number of polymers, plasticizers, and pesticides. Owing to the toxic nature of hydrazine, there is a growing need in both industrial and government laboratories for the development of a highly sensitive, on-line monitor for low levels of hydrazine in air. This need is spurred by the American Conference of Governmental Hygienists' (ACGIH) proposal to lower the threshold limit value (TLV) for hydrazine from 100 ppb to 10 ppb in air.[1] While other analytical techniques have shown success for the detection of hydrazine, none combines the necessary qualities of an inexpensive, on-line, sensitive and selective monitor for hydrazine that is necessary for protecting the safety of workers in hazardous workplace environments. Examples of other techniques which have been used for the detection of hydrazine include coulometry,[2] potentiometry,[3] mass spectrometry,[4] fluorescence,[5] flow injection analysis,[6] and dosimetry.[7]

Chemiluminescence techniques have been successfully applied to the detection of numerous analytes.[8] These methods typically rely upon the oxidation of a chemically reactive species, *e.g.* luminol or lucigenin, and the subsequent emission of a photon from an electronic, excited-state intermediate. Chemiluminescence sensors are free of Raman and Rayleigh scattering, interferences typically associated with fluorescence techniques, thus permitting the operation of a photomultiplier tube at maximum sensitivity. One of the most widely investigated chemiluminescence reagents is 3-aminophthalhydrazide, or luminol. Luminol has been effectively used for the detection of many different metals and oxidants, due to the catalytic behavior these metals have on the chemiluminescent oxidation of luminol. Examples include the detection of Cr(III),[9] Co(II),[10] Fe(II),[11] $H_2O_2$,[12] $NO_2$,[13] and $ClO^-$.[14]

There have been no reports of chemiluminescence methods for the detection of hydrazine vapor, although Faizullah and Townshend report a flow injection analysis scheme based upon hypochlorite for the chemiluminescence detection of hydrazine in solution.[15] Pilipenko and Terletskaya demonstrated that the detection of trace amounts of platinum (0.02 $\mu$g/ml) is possible in a basic solution of lucigenin and hydrazine.[16] They proposed that hydrazine is

*Author to whom correspondence should be addressed.

catalytically oxidized at the surface of colloidal platinum to form a radical, peroxo intermediate. This reactive intermediate subsequently oxidizes lucigenin, allowing for the detection of platinum. Discussion here will center about the analytical feasibility of employing a basic solution of luminol and colloidal platinum for the detection of hydrazine. Chemiluminescence presents the possibility for the development of an inexpensive, on-line monitor of hydrazine that is rapid, sensitive and reversible over a wide dynamic range.

## EXPERIMENTAL

### *Apparatus*

Initial characterization of the hydrazine/Pt/luminol system was performed using an SLM 8000 spectrofluorometer operating in the chemiluminescence mode of measurement. The injection port consisted of a lid with a septum permitting injection of different levels of hydrazine to a 4 $cm^3$ cuvette, while maintaining complete darkness within the sample compartment. A magnetic stirring bar allowed continuous mixing of the reagents. An EMI (PT9635QA) UV/VIS selected photomultiplier tube was used for these experiments, at a potential of 900–1200 V.

The hydrazine vapor detection system (see Fig. 1) consisted of an Anspec 3-Channel peristaltic pump, a vacuum pump (MSA Flow-Lite Turbo) for controlling the air flow from 0 to 5 l./min, and a photomultiplier tube (PMT). A 1000 V power supply was used to drive the PMT, and a Keithley 485 picoammeter was used to monitor the anodic current. National Instruments' LABView for Windows software was used to control the data acquisition from the analog output of the picoammeter to a National Instruments' analog/digital board (Lab-Pc+). Pharmed tubing (a polypropylene-based material with a plasticizer) was used within the peristaltic pump, while all other tubing within the system was teflon PFTE. Tubing distances used were 60 cm for the gas/liquid sampling line leading to the impinger (1/16″ i.d. PFTE), 40 cm for the tubing leading to the PMT (1/8″ i.d. Pharmed), and 480 cm (3/16″ i.d. PFTE) from the PMT back to the air sampling tee.

The hydrazine vapor generation system, which has been described elsewhere, was used to generate hydrazine concentrations from 0 to 2000 ppb in air.[17] This system consisted of a small ampule containing anhydrous hydrazine (Olin Chemicals), immersed in a temperature controlled, water bath (Neslab exacal). The ampule was plugged with a piece of capillary tubing, around which a continuous flow of nitrogen (0.1 l./min) carried away the hydrazine vapor. The final concentration was adjusted by diluting the hydrazine vapor in a stream of air (0.5–10 l./min). The air stream consisted of house air scrubbed to remove water, $CO_2$, $NO_2$ and organic impurities. All flow rates were controlled using Matheson 8200 mass flow

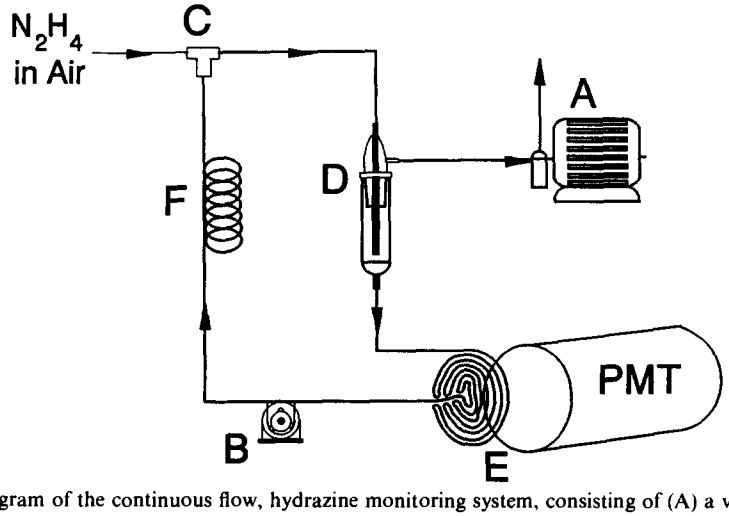


Fig. 1. Diagram of the continuous flow, hydrazine monitoring system, consisting of (A) a vacuum pump for sampling hydrazine in the atmosphere; (B) a peristaltic pump for circulating the luminol/platinum reagent; (C) a sampling tee leading to the liquid/vapor sampling line; (D) an impinger for collecting the liquid prior to transport to (E) a coil of glass tubing positioned in front of a photomultiplier tube; and (F) excess PFTE tubing in order to delay the recycling of the chemiluminescent reagent until the background chemiluminescence has returned to its baseline value.

controllers. Humidity was controlled through the use of bubblers and line mixers, with the humidity being quantitated with a Hygrodynamics hygrometer. The hydrazine concentration was determined using a coulometric method described earlier.[2]

Mixing of all the test gases was obtained within a baffled chamber, containing a port for connection to the vacuum pump of the hydrazine monitoring system. The flow rate to the MSA vacuum pump was determined using an American Meter Model 802.

*Chemicals and stock solutions*

All chemicals were used as received from the suppliers. 3-Aminophthalhydrazide (luminol) (97%) was obtained from Aldrich and a $5 \times 10^{-3}M$ stock solution was prepared in $0.1M$ KOH and stored under dark conditions for a period of several weeks. The stock solution of colloidal platinum was prepared by chemically reducing a $10^{-3}M$ solution of hydrogen hexachloroplatinate (IV) with ascorbic acid at a pH of 3.5, with subsequent dilution to give a $10^{-4}M$ solution of platinum. The chemiluminescent solutions studied were prepared and examined daily by the appropriate dilution of the stock solutions into a buffer solution. Phosphate buffers ($0.1M$) were prepared for all pH studies, using KOH and a calibrated pH meter in order to adjust the pH. The aqueous hydrazine standard solutions were prepared daily by diluting anhydrous hydrazine (Olin Chemicals) in purified water (Millipore) to give the following concentrations: 1, 10, 100 $\mu$g/l., 1, 10, 100 and 1000 mg/l. Stock solutions ($10^{-3}M$) were also prepared for several metal ion catalysts, including $MnSO_4$, $CuCl_2 . 6H_2O$, $FeSO_4 . 7H_2O$, $Fe(NO_3)_3 . 9H_2O$ and $CoSO_4$.

A number of interference gases were tested for chemiluminescence using the hydrazine monitoring system. Gas mixtures were obtained from Matheson and Scott Specialty Gases, and diluted with air to give varying concentration levels. The standards employed include: 99 ppm $NO_2$ in $N_2$; 110 ppm NO in $N_2$; 99.8 ppm $SO_2$ in $N_2$; 10% HCl in Ne; 7.2% $H_2$ in $N_2$; 450 ppm $NH_3$ in $N_2$; 99.99% $CO_2$; Freon 12; multi-component mixture #1 [51.2 ppm Freon 12, 50.7 ppm Freon 11, 49.3 ppm Freon 114, 20.4 ppm $CH_4$, and 9.96 ppm hexane in He]; and, mixture #2 [1.004% CO, 1.098% $CO_2$, 0.9640% $CH_4$, 0.9996% ethane, 1.014% ethylene, and 1.014 acetylene in He].

*Procedure*

For those experiments employing the SLM 8000 spectrofluorometer 2 ml of the appropriate buffer solution was pipetted into a quartz cuvette, along with 10–100 $\mu$l (Eppendorf microburette) of the platinum and luminol stock solutions. The optimal concentrations of luminol and platinum were determined to be $10^{-4}$ and $10^{-6}M$, respectively. Subsequent spiking of these solutions with varying levels of hydrazine was accomplished by injecting 1–100 $\mu$l of solution from the appropriate dilution standard via the injection port of the sample compartment. The final concentration of hydrazine in solution varied from 50 ng/l. to 500 $\mu$g/l. The flow injection analysis experiments were conducted by using a multichannel peristaltic pump in conjunction with a cuvette (Starna Cells) containing three ports: one for injection of the basic, Pt/luminol reagent, one for the hydrazine solution, and one for the exit of the solution from the cuvette.

For those experiments using the continuous flow, hydrazine monitoring system, 150 ml of operating solution were prepared at concentrations of platinum and luminol similar to that described above. Quantitation of the hydrazine vapor concentrations was determined by coulometry, and then sampled by connection of the vacuum pump to the mixing chamber.

## RESULTS AND DISCUSSION

*Chemiluminescence reaction characteristics*

The addition of colloidal platinum to a basic solution of luminol permits the indirect quantitation of hydrazine via a two step process (steps 1 and 2 shown below):

$$2O_2(g) + N_2H_4(aq) \rightleftarrows 2H_2O_2(aq) + N_2(g) \quad (1)$$

$$\text{luminol(aq)} + 2H_2O_2(aq) + 2OH^- \rightleftarrows \text{3-aminophthalate(aq)} + 4H_2O + N_2 + h\nu \quad (2)$$

$$N_2H_4(aq) + 2H_2O_2(aq) \rightleftarrows N_2(g) + 4H_2O \quad \text{(side reaction)}. \quad (3)$$

Both reactions (1) and (2) are catalyzed by colloidal platinum.[16,18] Reaction (1) is the first step in the oxidation of hydrazine at the platinum surface. An important side reaction is

the reaction of hydrogen peroxide with a second molecule of hydrazine, which completes the oxidation of hydrazine to nitrogen and water (reaction 3). Pilipenko *et al.* have indicated that, although hydrogen peroxide is formed in the net reaction of hydrazine with oxygen, it is likely an intermediate, radical peroxo species (and not $H_2O_2$) which is actually responsible for the oxidation and subsequent chemiluminescence of lucigenin.[16] The presence of a radical species was inferred from the immediate inhibition of chemiluminescence following the addition of methyl methacrylate, a free radical acceptor. Regardless of the exact nature of the oxidant formed at the platinum surface, the net result is the oxidation and chemiluminescent response of luminol. Reaction step (2) is a multi-step process giving rise to chemiluminescence, and has been discussed in detail elsewhere.[19]

Initial evaluation of the analytical potential of this system was accomplished by observing the complete, chemiluminescent response obtained following the introduction of 49 $\mu$g/l. of hydrazine to a basic solution (pH 13, NaOH) of platinum (0.25–2.9 $\mu M$) and luminol ($7.4 \times 10^{-5} M$). The concentration of colloidal platinum plays an important role in determining the shape and size of the response curve (see Fig. 2). Note the difference in response obtained for solutions containing 0.25 and 1.0 $\mu M$ colloidal platinum. For the lowest concentration of platinum examined, 0.25 $\mu M$, the time necessary to reach a maximum in signal intensity is longer, the peak height is substantially lower, and the chemiluminescence persists for up to an hour following the injection of hydrazine. As the concentration of colloidal platinum increases

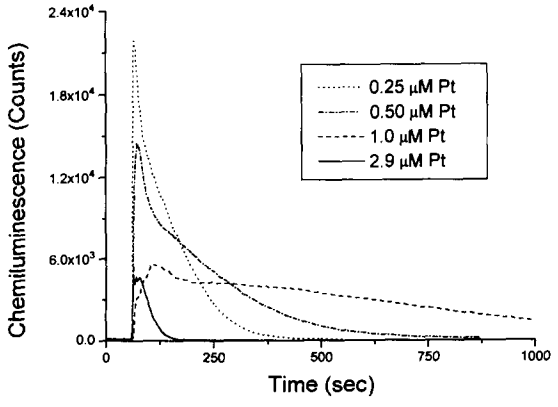


Fig. 2. Time dependence of the chemiluminescence signal following the introduction of 49 $\mu$g/l. hydrazine to a pH 13, $7.4 \times 10^{-5} M$ luminol solution containing 0.25, 0.50, 1.0, and 2.9 $\mu M$ colloidal platinum.

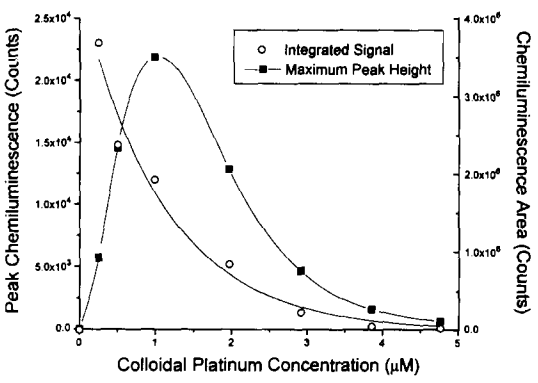


Fig. 3. Peak and integrated chemiluminescence intensities as a function of colloidal platinum concentration.

(up to 1.0 $\mu M$), the decay of the chemiluminescent signal becomes much faster, the maximum in signal intensity is attained in seconds, and the intensity of the chemiluminescent signal is more than four times that obtained for the 0.25 $\mu M$ platinum solution.

These results are summarized in Fig. 3, which is a plot of both the maximum signal intensity and the integrated chemiluminescence acquired for varying concentrations of colloidal platinum. It is evident from Figs 2 and 3 that as the concentration of platinum is increased, the total integrated chemiluminescence signal decreases dramatically. This result is attributed to the catalytic effect platinum has upon the oxidation of hydrazine to water and nitrogen (reactions 1 and 3), a side reaction decreasing the total luminol oxidation possible. Referring to Fig. 3, a maximum in the instantaneous, chemiluminescent intensity is observed for 1.0 $\mu M$ platinum. The signal intensity decreases for either higher or lower concentrations of platinum. The optimal concentration of colloidal platinum requires a compromise between having sufficient metal to promptly catalyze the oxidation of luminol (reaction steps 1 and 2), and having an excess of platinum which catalyzes the oxidation of hydrazine to water and nitrogen (reaction 3). As we shall see in the discussions pertaining to the continuous flow system, the concentration of platinum, the liquid flow rate, and the distance from the vapor/liquid interface to the photomultiplier tube are all important parameters influencing the overall sensitivity of the system.

### *Optimization of parameters in solution*

The pH is an important parameter in determining the magnitude of the chemiluminescence response. A basic solution is required to initiate the reaction sequence. Typically, luminol systems

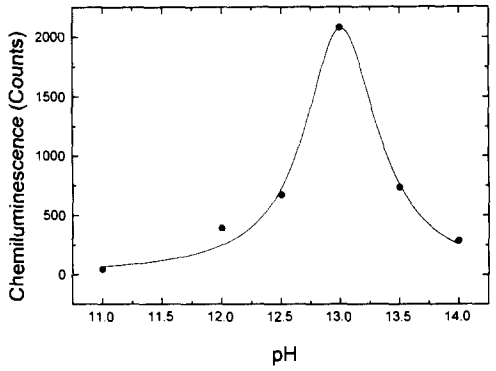


Fig. 4. Effect of pH on the chemiluminescence signal intensity for the introduction of 4.6 $\mu$g/l. of hydrazine to a solution containing $6.1 \times 10^{-5}M$ luminol and $1.2 \times 10^{-6}M$ colloidal platinum.

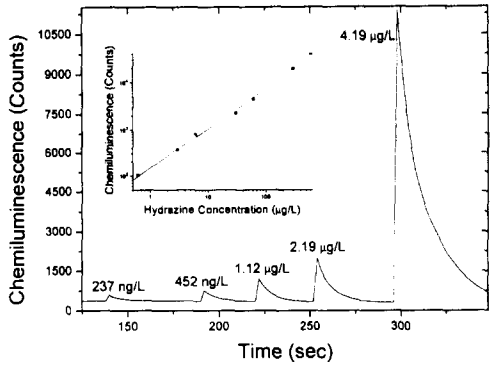


Fig. 6. Chemiluminescent signal intensity following sequential additions of increasing concentrations of hydrazine to a pH 13 (NaOH) solution containing $6.1 \times 10^{-5}M$ luminol and $1.2 \times 10^{-6}M$ platinum. Inset plot is an example of the linear dynamic range obtained for hydrazine detection from the flow injection analysis scheme.

used in the detection of metals or hydrogen peroxide operate optimally at a pH of 10–11.[8] It has been suggested that this is necessary in order to form a reactive diazine by abstraction of the second amino proton from luminol.[20] Figure 4 shows the integrated chemiluminescent response seen with varying pH conditions to the introduction of 4.6 $\mu$g/l. of hydrazine to a luminol/Pt reagent. The optimal pH in the detection of hydrazine is pH 13. Several factors in the reaction sequence are known to be pH dependent. The autoxidation of hydrazine is maximized at a pH of 12–12.5,[18] while the production and lifetime of the intermediate product (peroxide) is highest at a pH of 13–13.5.[16]

Increasing the concentration of luminol results in an increase in the integrated chemiluminescence obtained for a given concentration of hydrazine. Figure 5 demonstrates that the response is non-linear with respect to the concentration of luminol. This may be due to self-absorbance of the chemiluminescence by luminol, or to luminol acting as a bidentate chelate, complexing with platinum, and perhaps

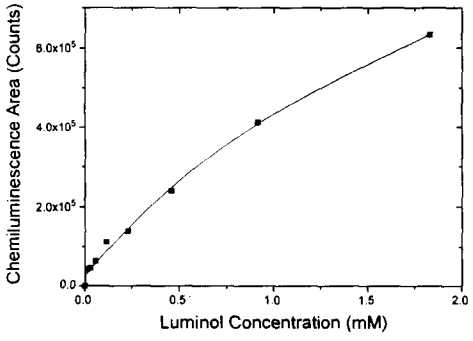


Fig. 5. Integrated chemiluminescence signal dependence on luminol concentration using a pH 13 solution containing $2.3 \times 10^{-6}M$ colloidal platinum and 50 $\mu$g/l. hydrazine.

rendering it inactive. The latter effect has been seen for the cobalt-catalyzed reaction with luminol.[21] The possibility remains, though, that a high concentration of luminol may be used in the hydrazine vapor detection system to improve the lifetime characteristics of the system.

*Analytical characterization of hydrazine detection in solution*

To determine the quantitative potential of the platinum/luminol system for hydrazine detection, a series of increasing concentrations of hydrazine were injected into a cuvette containing the optimum reagent concentrations, while measuring the chemiluminescence. An example of the addition of 0.24, 0.45, 1.1, 2.2 and 4.2 $\mu$g/l. of hydrazine is shown in Fig. 6. A plot of the integrated chemiluminescent response as a function of the hydrazine concentration exhibited excellent linearity over the concentration region examined (50 ng/l.–35 $\mu$g/l.). With the voltage gain on the photomultiplier tube increased to 1275 V, the sensitivity ($m$) was calculated to be $1.05 \times 10^5$ counts/($\mu$g/l.). with an intercept (b) of $1.96 \times 10^4$ counts and a correlation coefficient of $r > 0.9999$ (other regression data include: $n = 5$, $\sigma_m = 4.95 \times 10^3$ counts/($\mu$g/l.), $\sigma_b = 1.07 \times 10^5$ counts, and $\sigma = 2.07 \times 10^5$).

A flow injection analysis scheme for the detection of hydrazine was examined using a modified 4 cm$^3$ cuvette containing three inlet ports. The reagent solution containing luminol and colloidal platinum at pH 13 was mixed directly and continuously with varying concentrations of hydrazine in solution (see the Experimental). The speed of the chemiluminescent reaction makes it feasible to mix the reagents

directly in front of the photomultiplier tube within the cuvette. For this experiment, the chemiluminescent signal came to a plateau response (as opposed to decaying back to the baseline) in less than a minute while using a flow rate of 0.11 ml/min hydrazine solution and 1.8 ml/min platinum/luminol solution. The inset plot in Fig. 6 shows the change in the chemiluminescence response with the concentration of hydrazine in solution ($r > 0.999$). The linear regression data collected for this line are as follows: $n = 8$, $m = 65.0$ counts/($\mu$g/l.), $\sigma_m =$ 0.475 counts/($\mu$g/l.), $b = 189$ counts, $\sigma_b = 115$ counts, and $\sigma = 276$. The detection limit, assuming a signal-to-noise ratio of 3:1, was calculated to be 0.40 ng/l. The limit of detection is ultimately limited by the noise inherent to the PMT, in addition to pumping variability associated with the peristaltic pump.

In addition to colloidal platinum, other metal and metal cation catalysts were evaluated for the detection of hydrazine, *e.g.* $MnSO_4$, $CuCl_2 . 6H_2O$, $FeSO_4 . 7H_2O$, $Fe(NO_3)_3 . 9H_2O$, $CoSO_4$, Pd (colloid) and Ag(colloid). In each case, the sensitivity for hydrazine detection was substantially lower than the response obtained using colloidal platinum. In addition, these other metal catalysts examined resulted in a much higher baseline signal, and a slower return to baseline following the cessation of hydrazine flow. These results are likely due to the catalytic effect these metals have upon the oxidation of luminol by $O_2$.[22] Although there is some oxidation of luminol by $O_2$ in the presence of colloidal platinum, it is not as severe.

*Hydrazine vapor monitor*

The development of a hydrazine vapor monitor employing the Pt/luminol system requires first a means for concentrating hydrazine vapor into solution. A simple method for accomplishing this task is diagrammed in Fig. 1. A peristaltic pump delivers the luminol/platinum/KOH reagent through a short length of teflon tubing which concurrently transports sampled vapor. It is this gas/liquid interface which initiates the oxidation of hydrazine at the Pt surface, and ultimately, the oxidation of luminol. The liquid is efficiently separated in a modified, teflon impinger, and pumped through a short section of glass tubing coiled directly in front of the PMT. The rapid decay of the chemiluminescent signal back to the background level following the addition of hydrazine to the line, allows the reagent to be recirculated.

As demonstrated earlier, the concentration of active platinum in solution determines the magnitude of the chemiluminescence signal seen

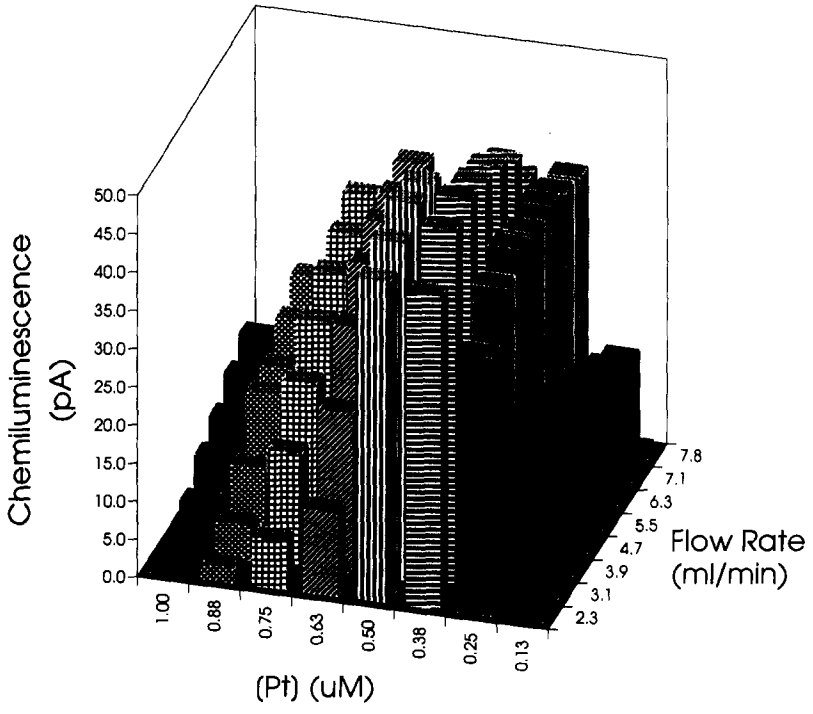


Fig. 7. Plot of the chemiluminescent signal obtained from a $4.9 \times 10^{-5} M$ luminol solution at pH 13, as a function of the concentration of colloidal platinum and the liquid flow rate.

at the photomultiplier tube. The optimum concentration of platinum used for the continuous flow system is closely linked to the liquid flow rate and the length of tubing from the sampling point to the photomultiplier tube. A three-dimensional plot of the chemiluminescence response with respect to the liquid flow rate and the concentration of platinum, while maintaining a constant air pumping rate and luminol, KOH, and hydrazine concentrations is shown in Fig. 7. For the tubing distance used in our experimental setup, low concentrations of platinum ($10^{-7}M$) resulted in a weak, chemiluminescent signal which decreased with increasing liquid flow rate. An examination of Fig. 3 indicates that at these concentrations of platinum, while the signal has a long lifetime, its maximum peak intensity is not very high. The slower the flow rate, then, the longer the liquid remains in view of the PMT, and the larger the chemiluminescent signal will be. In addition, at a constant air flow rate, decreasing the liquid flow rate concentrates more hydrazine vapor into solution, thereby, giving a larger signal at the PMT.

As the concentration of platinum in solution is increased ($5 \times 10^{-7}M$), the chemiluminescent signal becomes larger, and the maximum in peak intensity occurs at higher flow rates. Referring again to Fig. 3, at these platinum concentrations the instantaneous chemiluminescent signal obtained is higher, therefore, giving a larger signal at the PMT. This is providing, of course, that the liquid flow rate is rapid enough to transport the solution to the PMT before the signal decays. If the flow rate is too high, though, the signal will decrease for two reasons: (1) less hydrazine vapor is concentrated into solution; and (2) the solution remains in view of the PMT for a shorter period of time. Ultimately, as the platinum concentration is increased to even higher concentrations ($10^{-6}M$), the signal intensity drops substantially for low flow rates. At these concentration levels, the chemiluminescence signal decays extremely rapidly—long before the solution reaches the PMT. In order to effectively use these higher concentrations of platinum, it is necessary to use extremely rapid flow rates so that the signal is sampled before the chemiluminescence decays away.

Just as the liquid flow rate controls the concentration factor for bringing hydrazine vapor into solution, so too does the air flow rate. As the air flow increases at a constant liquid flow rate, the amount of hydrazine concentrated into solution increases. This is demonstrated in Fig. 8, which is a plot of chemiluminescence intensity *vs.* air flow rate for a pH 13 NaOH solution containing $5 \times 10^{-5}M$ luminol and $10^{-6}M$ platinum (the concentration of hydrazine sampled was 13 ppb in each case). There are several problems associated with operating at high flow rates. Firstly, there is difficulty in preventing air bubbles from entering the tubing leading to the PMT, a result which leads to excessive noise. In addition, at the higher air flow rates, our vacuum pump rate was very uneven, and the level of liquid in the impinger was difficult to maintain constant, both factors leading to inconsistent results. Finally, the efficiency for concentrating hydrazine vapor into solution is expected to decrease at very high flow rates; the hydrazine has less time to interact with the solution within the liquid/gas sampling line. An optimum pumping rate can be determined for a particular platinum concentration that maximizes the trapping efficiency without sacrificing the stability of the measurement.

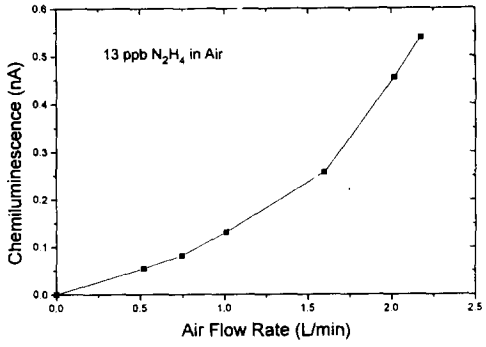


Fig. 8. Effect of air flow rate on the observed chemiluminescence signal intensity to the introduction of 13 ppb hydrazine in air.

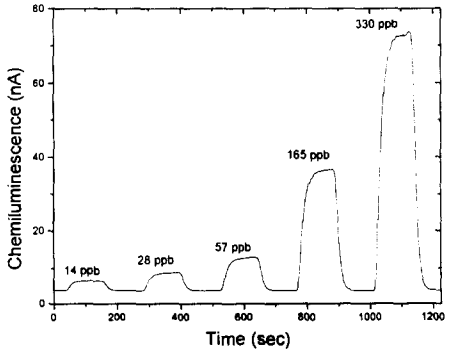


Fig. 9. Time responses obtained using the hydrazine vapor detection system for 14, 28, 57, 165, and 330 ppb hydrazine in air.

Our studies have established the following optimum experimental parameters for the detection of hydrazine: $10^{-6}M$ platinum, $10^{-4}M$ luminol, $0.1M$ KOH, 7 ml/min liquid flow rate, 2 l./min air flow rate. In order to test the analytical response of this system, the chemiluminescent response was monitored for successively higher concentrations of hydrazine in air. An example of the time responses obtained following the introduction and cessation of 14, 28, 57, 165 and 330 ppb hydrazine in air is shown in Fig. 9. A linear relationship was obtained for hydrazine concentrations measured from 10 to 2000 ppb ($r = 0.997$). The linear regression data collected over this concentration regime were as follows: $n = 9$, $m = 1.77$ counts/($\mu$g/l.), $\sigma_m = 0.0516$ counts/($\mu$g/l.), $b = 40.4$ counts, $\sigma_b = 40.6$ counts, and $\sigma = 103$. The time necessary to reach 90% of a plateau response is 1.3 min, and the return to background requires 1.2 min. The detection limit was calculated to be 1.4 ppb, based upon a signal-to-noise ratio of 3:1. The reproducibility of the data is within 5%. The primary disadvantage found for recirculating the chemiluminescent reagent is that the stability of the system will drift slightly over the course of hours of operation (1%/hr). The lifetime of the reagent is ultimately dependent upon the concentration of luminol in solution, and the lifetime of the catalyst. Because of problems associated with the slow oxidation of luminol by $O_2$(g) and/or the gradual change in pH from absorbed $CO_2$(g) in the airstream, it is necessary to change the solution daily to prevent shifts in the sensitivity.

Interference effects were studied by sampling various gases at concentration levels 1 at least twice their regulated exposure levels. A solution of luminol/platinum was prepared at pH 12.6 and exposed to the gases listed in Table 1. For interferents resulting in a measurable chemiluminescence, Table 1 indicates the concentration which gives the same signal intensity as 10 ppb hydrazine in air. The majority of gases examined, with the exception of $NH_3$, $NO_2$, $SO_2$, and HCl, either gave no signal, or actually produced a slight decrease in the baseline signal. This latter effect likely arises from a decrease in the concentration of oxygen. Oxygen results in a small, baseline chemiluminescence signal due to the direct oxidation of luminol. Positive interferences were seen for $NO_2$, $SO_2$, and HCl, but the sensitivities were much lower than for hydrazine. A concentration of 9 ppm $NO_2$ gives a signal comparable to 10 ppb hydrazine in air. Considering that the regulated exposure levels for $NO_2$, $SO_2$, and HCl are 1 ppm (STEL), 2 ppm (TLV), and 5 ppm (TLV), respectively, these interferents are not expected to be a problem for hydrazine vapor detection. The presence of $NH_3$ can give a false positive signal if the sampling line is not constructed correctly. Hydrazine will stick to any portions of tubing on the end of the sampling tee that are not being continually washed by the reagent. Ammonia, a strong Lewis base, competes very well with hydrazine for adsorption to the sides of the tubing leading to the impinger. Any hydrazine which is dislodged will react to give a measurable chemiluminescent response. The signal is spurious, returning to the baseline again after all of the hydrazine coating the tubing has been eliminated. This effect can be mollified by shortening the vapor side of the sampling tee to the point that there are minimal portions which are not continuously being exposed to the reagent. A smaller diameter tubing on the liquid/vapor sampling side (1/16″ i.d. or less) will also help ensure that the tubing does not have trace amounts of hydrazine adsorbed to the sidewalls.

Reports in the literature have demonstrated that the chemiluminescence of luminol systems can be enhanced by the introduction of a high concentration of halide ions.[23] We corroborated

Table 1. Interference vapors tested using the hydrazine vapor monitor, and the concentration required to give an intensity comparable to 10 ppb hydrazine in air

| Interference vapor | Concentration giving a response similar to 10 *ppb* Hydrazine in air |
|---|---|
| $NO_2$ | 9 *ppm* |
| $SO_2$ | 124 *ppm* |
| HCl | 210 *ppm* |
| $NH_3$ (50 *ppm*) | spurious false positive |
| NO, $H_2$, $CO_2$, CO, $CH_4$, $C_2H_6$, $C_2H_5OH$, $(CH_3)_2CHOH$, $C_2H_4$, $C_2H_2$, $C_6H_{14}$, Freon 11, Freon 12, Freon 114 | no effect or a slight decrease in the baseline chemiluminescent signal (see text) |

See text for more detail on the interferents listed in the final section which gave little or no change in the baseline chemiluminescence.

this effect in the detection of hydrazine, via the addition of 0.56*M* KBr to a $5 \times 10^{-5}M$ luminol, and $1 \times 10^{-6}M$ platinum in pH 12.6 solution. These experiments established that the sensitivity to hydrazine can be more than doubled via the introduction of a large concentration of the bromide salt. It is thought that the halide facilitates electron transfer from luminol to the active peroxide.[23]

## CONCLUSIONS

In this paper, we demonstrate the efficacy of colloidal platinum/luminol for detecting trace hydrazine vapor in real-time. The real-time detection limit is 1 ppb hydrazine in air; further improvements in the sensitivity can be accomplished by adding KBr salts, increasing the rate of air flow, or increasing the number of coils in front of the photomultiplier surface. A linear dynamic range was obtained from 10 to 2000 ppb hydrazine, with response times for the detection and return to baseline of less than two minutes. The response time of the system can be improved substantially by increasing the liquid flow rate, although the platinum concentration must also be adjusted to ensure a comparable sensitivity. Selectivity is the biggest potential disadvantage of this system. Our tests indicate that of the gases examined, only $NO_2$ and $NH_3$ gave a positive response, the ammonia response being spurious and the nitrogen dioxide sensitivity being low enough that at the TLV level or below it is undetectable.

We are currently investigating solid-phase chemiluminescence in order to further simplify and improve upon this detection scheme. Some success has been seen in incorporating the colloidal platinum and luminol within a polymer matrix possessing Lewis acid properties. The polymer film itself helps to concentrate the hydrazine within the polymer matrix. Current efforts involve examining different polymer substrates and metal catalysts to obtain optimum response characteristics.

*Acknowledgements*—This research was supported by NASA/ Kennedy Space Center (DL-ESS-24, CC-82360A).

## REFERENCES

1. American Conference of Governmental Industrial Hygienists (ACGIH) report on proposed changes to TLV and BEI lists, 21 May 1989.
2. E. C. Olsen, *Anal. Chem.*, 1960, **32,** 1545.
3. J. R. Stetter, K. F. Blurton, A. M. Valentine and K. A. Tellefsen, *J. Electrochem. Soc.*, 1978, **125,** 1804.
4. B. E. Knox and E. J. McHale, *Anal. Chem.*, 1966, **38,** 487.
5. G. E. Collins and S. L. Rose-Pehrsson, *Anal. Chim. Acta*, 1993, **284,** 207.
6. W. D. Basson and J. F. Van Staden, *Analyst*, 1978, **103,** 998.
7. P. A. Taffe and S. L. Rose-Pehrsson, *U.S. Patent* 4,900,681, 1990.
8. K. Robards and P. J. Worsfold, *Anal. Chim. Acta*, 1992, **266,** 147.
9. R. Escobar, Q. Lin, A. Guiraum and F. F. de la Rosa, *Analyst*, 1993, **118,** 643.
10. J. L. Burguera, A. Townshend and S. Greenfield, *Anal. Chim. Acta*, 1980, **114,** 209.
11. W. R. Seitz and D. M. Hercules, *Anal. Chem.*, 1972, **44,** 2143.
12. F. Shaw, *Analyst*, 1980, **105,** 11.
13. P. Mikuska and Z. Vecera, *Anal. Chem.*, 1992, **64,** 2187.
14. D. Gonzalez-Robledo, M. Silva and D. Perez-Bendito, *Anal. Chim. Acta*, 1990, **228,** 123.
15. A. T. Faizullah and A. Townshend, *Anal. Proc.* 1985, **22,** 15.
16. A. T. Pilipenko and A. V. Terletskaya, *J. Anal. Chem. USSR*, 1973, **28,** 1004.
17. S. L. Rose and J.-R. Holtzclaw, NRL Report 8848, NTIS ADB091299.
18. E. W. Schmidt, *Hydrazine and its Derivatives: Preparations, Properties, Applications.* John Wiley & Sons, New York, 1984.
19. O. S. Federova and V. M. Berdnikov, *Teor. Eksp. Khim.*, 1983, **19,** 334.
20. T. P. Vorob'eva, Yu. N. Kozlov, Yu. V. Koltypin, A. P. Purmal' and B. A. Rusin, *Izv. Akad. Nauk SSSR, Ser. Khim.*, 1978, **9,** 1996.
21. T. G. Burdoad, W. R. Seitz, *Anal. Chem.*, 1975, **47,** 1639.
22. L. L. Klopf and T. A. Nieman, *Anal. Chem.*, 1983, **55,** 1080.
23. D. E. Bause and H. H. Patterson, *Anal. Chem.*, 1979, **51,** 2288.

Pergamon

0039-9140(95)01444-6

*Talanta*, Vol. 42, No. 4, pp. 553–556, 1995

0039-9140/95 $9.50 + 0.00

# ESTIMATION OF CHROMIUM IN ORES AND BENEFICIATED PRODUCTS: AN ULTRASONIC APPROACH

USHARANI PATNAIK and J. MURALIDHAR*

Regional Research Laboratory, Council of Scientific & Industrial Research, Bhubaneswar-751 013, India

(*Received* 24 *June* 1994. *Revised* 13 *September* 1994. *Accepted* 30 *September* 1994)

**Summary**—Cr(III) slowly forms a violet complex with EDTA at pH 3.5 ± 0.2 under normal conditions. The complex formation can be catalyzed by irradiating the reacting mixture with ultrasonic waves. Quantitative formation of the complex was possible with ultrasonic waves of 15 W/cm$^2$ intensity within 7.5 min of sonication. This method may be successfully applied to the determination of chromium in ores and beneficiated products containing 20–60% $Cr_2O_3$ without separating the analyte from the matrix elements.

Colorimetric analysis of chromium involves oxidation of Cr(III) to Cr(VI) followed by complexation.[1–3] Even the methods based on atomic absorption spectrophotometry or ICP also focus on Cr(VI).[4,5] However, colorimetric methods based on Cr(III) are of less importance because of its sluggishness towards any substitution reaction. The reaction between polycarboxylic acids (DCTA, NTA, EDTA) and Cr(III) is very slow.[6] Cr(III) slowly forms a violet complex H[Cr(EDTA)–($H_2O$)] with ethylenediaminetetraacetic acid (EDTA) in the pH range 3–5.2. However, the rate of complexation can be accelerated by the addition of bicarbonate ion,[8] manganese salt[9] or by boiling the solution for 30 min.

The effect of ultrasonic waves on chemical reactions has recently become the focus of research activity.[10–12] High intensity ultrasonic waves may accelerate a chemical reaction which occurs under normal conditions or initiate a reaction which does not take place under ordinary conditions.[13,14] Irving[9] reported that the complexation of Cr(III) with EDTA can be catalysed by the *in situ* generation of chromous ions by the addition of Zn dust to the solution containing an excess of EDTA. However, it has been observed that in the presence of high concentrations of sulphates and phosphates, complexation is not quantitative by the addition of bicarbonate or Zn dust. Hence an attempt has been made to catalyze the complexation of Cr(III) with EDTA by irradiating the reaction mixture with ultrasonic waves and to extend its application to the estimation of chromium in ores and beneficiated products.

## EXPERIMENTAL

A Varian DMS-100S UV-Vis Spectrophotometer equipped with an Epson LX printer and 1.00 cm quartz cells was used for the optical density measurements.

A high intensity ultrasonic liquid processor (Sonics Materials, USA) capable of producing ultrasonic intensity of 50 W/cm$^2$ at 20 KHz frequency was used in these studies. A horn made up of titanium with a tapered micro tip of 3.64 mm diameter was used to sonicate the solutions.

All the chemicals used were of analytical grade. Solutions were prepared in doubly distilled water.

Three chromite ore samples, *viz.* BCS-No. 308 (Grecian chrome ore), CHR-Pt and CHR-Bkg (chromites of CRPT, France, standard) and two beneficiated products, *viz.* SKP-D2 and HG-3 were analysed for chromium content.

### *Procedure*

To 0.5 g of finely ground chromite sample in a 250 ml beaker was added 20 ml each of 50% (v/v) $H_2SO_4$ and 50% (v/v) $H_3PO_4$. The

*Author to whom correspondence should be addressed.

solution was heated on a hot plate at 200°C until the complete disappearance of dark coloured particles. It was cooled, diluted and filtered through a G-4 crucible under suction and made up to 250 ml. A 10 ml aliquot was pipetted into a 100 ml beaker and adjusted to pH 3.5 with 5% (w/v) NaOH solution. A 10 ml 0.3*M* EDTA solution was added and irradiated with ultrasonic waves of 15 W/cm$^2$ intensity for 7.5 min. It was cooled and made up to 100 ml. The solution was taken in a 1.00 cm cell to measure the optical density at 547 nm against reagent blank, drawing the calibration curve using appropriate standards.

*Appropriate standard preparation*

A 0.5 g $K_2Cr_2O_7$ sample was reduced to $Cr_2(SO_4)_3$ in the presence of a 1:1 mixture of $H_2SO_4$ and $H_3PO_4$ (20 ml) and a pinch of $Na_2SO_3$. The volume was made up to 250 ml and diluted to give 1 mg/ml $Cr_2O_3$ solution. A 1 mg/ml $Fe_2O_3$ solution was prepared from $Fe_2(SO_4)_3$ and $Cr_2O_3$ solution taken in 50 ml beakers in quantities equivalent to 10–100 ppm of $Cr_2O_3$. A 3 ml quantity of 1 mg/ml $Fe_2O_3$ was added and boiled for 5 min, cooled and the pH of the solution adjusted to 3.5.

## RESULTS AND DISCUSSION

*Effect of pH*

Owing to protolysis, the absorption spectrum of the Cr(III)–EDTA complex is greatly influenced by the pH of the solution. The pH of the acid decomposed chromite solutions was adjusted at different values starting from 2.5 to 7. A pH of 3.5 $\pm$ 0.2 has been found to be suitable for quantitative formation of complex as well as negligible interference of Fe(III). Beyond pH 5.5, the violet complex transforms into blue Cr(OH)–EDTA$^{2-}$ and $Cr(OH)_2EDTA^{3-}$ hydroxo complexes.[15]

*Effect of ultrasound intensity and sonication time*

The effect of intensity of ultrasound waves and time of sonication on complex formation was investigated and the results are represented graphically in Figs 1 and 2. The reaction mixture containing 100 ppm of $Cr_2O_3$ and 10 ml of 0.3*M* EDTA was irradiated continuously with ultrasonic waves at varying intensities within the range 5–20 W/cm$^2$ for 2 min. Complexation was insignificant at lower intensities, but was maximum at 15 W/cm$^2$. A further increase in the intensity was not beneficial. After sonication, a

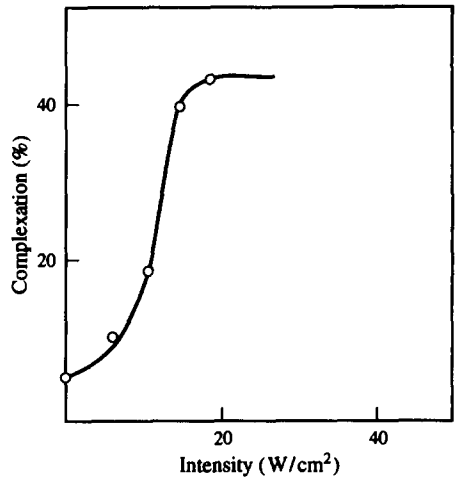


Fig. 1. Effect of intensity of ultrasound waves on rate of complexation.

20°C increase in temperature of the reacting solution from the ambient temperature was observed. The reason may be a result of the rapid generation and collapse of microbubbles within the reacting medium irradiated with ultrasonic waves. This leads to significant pressure and thermal differentials on a microscopic scale resulting in the enhancement of energy transfer and accelerated mass transport.[15]

A comparison of percentage of complexation with respect to time both in the presence and absence of ultrasound waves at 15 W/cm$^2$ intensity reveals that initially a sharp increase in complexation rate was observed in both cases. In the absence of ultrasound where the reacting mixture was heated on a water bath at 60°C for 8.0 min, only 60% complexation was observed with 100% complexaton being achieved after 30 min of further boiling. However, in the presence of ultrasound, quantitative complexation was possible after 7.5 min of sonication.

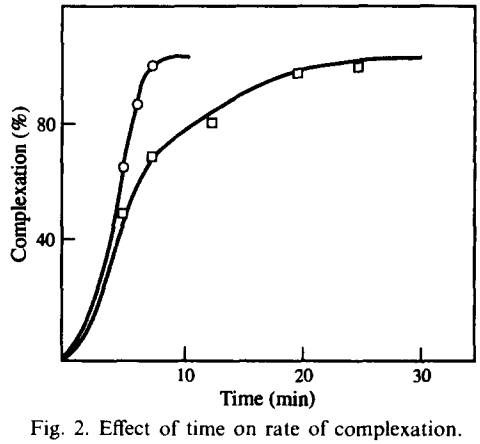


Fig. 2. Effect of time on rate of complexation.

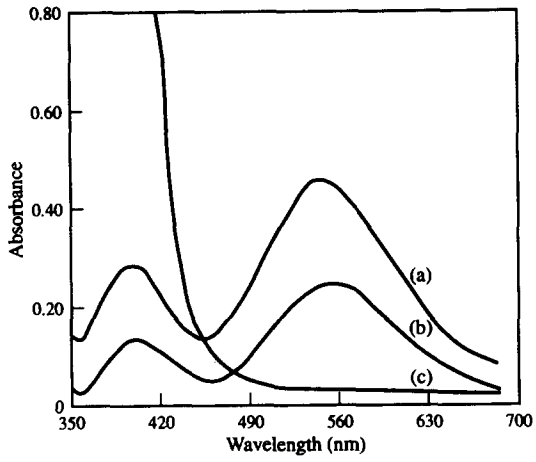


Fig. 3. Absorption spectra of Cr(III)–EDTA in $Cl^-$, $SO_4^{2-}$, $PO_4^{3-}$ and spectra of Fe(III)–EDTA.

*Effect of diverse ions*

In order to assess quantitative determination of chromium by this method, the effect of diverse ions must be taken into consideration. The possible interfering ions in the spectrophotometric determination of Cr(III)–EDTA are $Fe^{3+}$, $Mg^{2+}$, $Al^{3+}$, $Mn^{2+}$, $SO_4^{2-}$ and $PO_4^{3-}$. Spectral interferences owing to colourless cations like $Mg^{2+}$, $Al^{3+}$ and $Mn^{2+}$ in equivalent amounts can be eliminated in the presence of excess EDTA. $Fe^{3+}$ forms a yellow coloured complex with EDTA soon after its addition. The extinction value of Fe(III)–EDTA solution does not change on heating the solution. The molar absorption coefficient of this complex is 4 compared to 180 for Cr(III)–EDTA solution at the measured wavelength (Fig. 3). Therefore, no interference from iron(III) is to be expected during the analysis of Cr(III). However, a calculated amount of $Fe^{3+}$ solution may be added during the standard preparation. Of the anions, the molar absorption coefficient of Cr(III)–EDTA complex in chloride environment ($\epsilon = 202$) decreases significantly in phosphate and sulphate environment ($\epsilon = 180$) (Fig. 3). Hence the use of an appropriate standard is advocated. The absorbance of Cr(III)–EDTA in the presence of these diverse ions is presented in Table 1.

The calibration curve was drawn using the appropriate standards. Beer's law is valid within 5–100 ppm of $Cr_2O_3$ with the correlation coefficient 0.9998.

This method was applied to the determination of chromium in three standard ore samples and two beneficiated products. The results are presented in Table 2. $Cr_2O_3$ values determined by this method are in acceptably close agreement with the certified values. This method has been found to be less time consuming and can be used without separating the analyte from the matrix elements prior to analysis. This method can be conveniently applied to ores and beneficiated products containing 20–60% $Cr_2O_3$.

*Acknowledgements*—The authors thank Dr K. Lakshminarayana for his assistance in conducting the ultrasonic experiments. Thanks are also due to The Director, R.R.L., Bhubaneswar for giving permission to publish the work.

Table 1. Absorbance of Cr(III)–EDTA in the presence of other elements

| $Fe^{3+}$ (*ppm*) | $Mg^{2+}$ (*ppm*) | $Al^{3+}$ (*ppm*) | $SO_4^{2-}$ (*M*) | $PO_4^{3-}$ (*M*) | $Cl^-$ (*M*) | $Cr_2O_3$ (*ppm*) | Optical density |
|---|---|---|---|---|---|---|---|
| | | | | | 0.1 | 100 | 0.265 |
| | | | 0.1 | 0.1 | | 100 | 0.246 |
| | | 100 | 0.1 | 0.1 | | 100 | 0.242 |
| | 100 | | 0.1 | 0.1 | | 100 | 0.241 |
| 50 | | | 0.1 | 0.1 | | 100 | 0.242 |
| 100 | 100 | 100 | 0.1 | 0.1 | | 100 | 0.242 |
| 200 | 100 | 100 | 0.1 | 0.1 | | 100 | 0.240 |

Table 2. Spectrophotometric determination of chromium

| Sample identification | $Cr_2O_3$% (Cert.) | $Cr_2O_3$% (Expt) | SD† (%) | RSD† (%) |
|---|---|---|---|---|
| BCS-No. 308 | 41.59 | 41.05 | 0.21 | 0.51 |
| CHR-Pt | 20.33 | 19.46 | 0.41 | 2.10 |
| CHR-Bkg | 29.04 | 28.94 | 0.16 | 0.55 |
| SKP-D2 | 29.75* | 30.10 | 0.13 | 0.43 |
| HG-3 | 59.70* | 59.60 | 0.06 | 0.11 |

*$Cr_2O_3$ determined by $Na_2O_2$ fusion.
†Mean of five independent experiments.

## REFERENCES


1. F. D. Snell and C. T. Snell, *Colorimetric Methods of Analysis*, Vol. IIA. D. Van Nostrand, 1959.
2. J. B. Raj and H. S. Gowde, *Indian J. Chem. Sci.*, 1988, **2**, 67.
3. C. Guo and Y. Feng, *Fenxi Hauxue*, 1981, **9**, 411.
4. E. Pruszkowaska and P. Barett, *Spectrochim. Acta*, 1984, **39**, 485.
5. C. S. Mayer, C. M. Tineco and I. P. Arraes, *At. Spectrosc.* 1985, **6**, 121.
6. G. Den Boef and B. C. Poeder, *Anal. Chim. Acta*, 1964, **30**, 261.
7. R. Pribil and W. R. Klubalova, *Collec. Czech. Commun.*, 1950, **15**, 42.
8. V. Kameswar Rao, D. S. Sunder and M. N. Sastri, *Chem. Anal.*, 1965, **54**, 86.
9. H. M. N. H. Irving and W. R. Tomlinson, *Chem. Anal.*, 1966, **55**, 14.
10. T. J. Mason and J. P. Lorimer, *Sonochemistry, Theory, Applications and Uses of Ultrasound in Chemistry*, Ellis Horwood, Chichester, 1988.
11. T. J. Mason (ed.), *Chemistry with Ultrasound, Crit. Rep. Appl. Chem.*, No. 28. Society for Chemical Industry, Elsevier, London, 1989.
12. T. J. Mason (ed.), *Advances in Sonochemistry*, Vol. 1. JAI Press London, 1990.
13. T. J. Mason, J. P. Lorimer and B. P. Mistry, *Tetrahedron*, 1985, **41**, 5201.
14. T. J. Mason, J. P. Lorimer and B. P. Mistry, *Ultrasonics*, 1987, **25**, 23.
15. R. Pribil, *Analytical Applications of EDTA and Related Compounds*, p. 139. Pergamon Press, New York, 1972.
16. H. G. Flynn, *Physics of Acoustic Cavitation in Liquids, Physical Acoustics*, Vol. 1, Part B, W. P. Mason (ed.). Academic Press, New York, 1964.

Pergamon

0039-9140(95)01445-4

*Talanta*, Vol. 42, No. 4, pp. 557–560, 1995
Elsevier Science Ltd
Printed in Great Britain
0039-9140/95 $9.50 + 0.00

# DETERMINATION OF LEAD IN PRESERVED EGG BY FLAME ATOMIC ABSORPTION SPECTROMETRY AFTER CHEMICALLY MODIFIED PRECONCENTRATION

LU GUANGHAN, XIA WANG, WAN JIALIANG, SHONG FON and XU HAN YING
Department of Chemistry, Central China Normal University, 430070, Wuhan, People's Republic of China

(*Received* 11 *August* 1993. *Revised* 3 *October* 1994. *Accepted* 10 *October* 1994)

**Summary**—A sensitive method for the determination of lead in preserved egg by flame absorption spectrometry using ammonium pyrrolidine dithiocarbamate–polystyrene chemically modified platinum wire matrix is presented. The modified platinum wire matrix, after preconcentrating the lead, is placed in a flame burner for direct atomization and measurement. The concentration range is linear between 5 and 500 ng/ml lead in solution and the detection limit is 0.65 ng/ml. This new technique is sensitive and convenient.

Atomic absorption spectrometry (AAS), characterized by high sensitivity and considerable accuracy, is an ideal method to determine trace metals. Flame atomic absorption spectrometry is in routine use for the determination of trace amounts of lead. However, this method, like other methods, sometimes requires the metals determined to be accumulated beforehand so that interference can be avoided and the level of analysis and sensitivity raised. In order to increase the detectability of flame atomic absorption spectrometry, lead is often preconcentrated from samples using chelating ion exchange resins,[1] or chelate solvent extraction.[2–6] For example, Chau[7] extracted lead into methyl isobutyl ketone (MIBK) using ammonium pyrrolidine dithiocarbamate (APDC). Belchev *et al.*[8] used APDC–polystyrene as the extraction system in the determination of lead in high purity salts. However, these methods are often time-consuming in the analytic procedure and complicated in application. The aim of the present work is to offer a simple and sensitive method for the analysis of lead.

A new technique for determination of trace lead with a chemically modified platinum wire matrix preconcentration–flame atomic absorption spectrometry was developed. Trace lead was preconcentrated on the ammonium pyrrolidine dithiocarbamate (APDC)–polystyrene modified platinum wire matrix, the platinum wire matrix was then put onto a flame atomizer, and the absorbance measured. The time and labor needed for the analysis is decreased and contamination by impurities contained in the reagent reduced.

## EXPERIMENTAL

### *Apparatus*

A Model WXY-402 atomic absorption spectrophotometer equipped with an air/acetylene flame burner was used. The wavelength was set to 2833 Å and the slit width to 4 nm. A hollow cathode lamp for lead was operated at 4 mA.

### *Reagents*

All reagents used were of analytical reagent grade. A 0.1000 g/ml stock solution of lead was prepared by dissolving metal lead (spectral purity) in a small amount of nitric acid and diluting to 100 ml with water. The standard solutions were obtained by diluting the stock solution. 1.0% APDC and a 1.0% solution of polystyrene in MIBK were prepared for the preconcentrated lead. The solutions were prepared from triply distilled water.

### *Preparation of the modified platinum wire matrix*

The platinum wire (diameter 0.2 mm) was wound into a spiral coil (diameter 0.5 mm) and 10 $\mu$l APDC and MIBK–polystyrene added onto the platinum wire spiral coil (Fig. 1) with a micro-syringe. The modified platinum wire matrix was then dried under an IR lamp, a

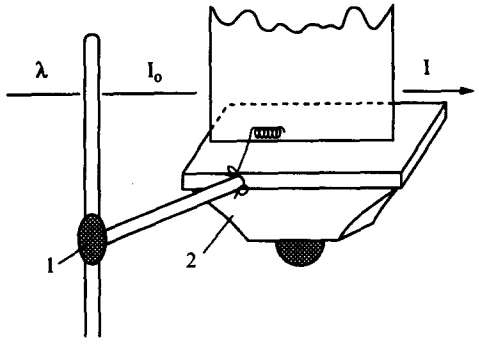


Fig. 1. Position of platinum wire coil in flame. (1) Holder; (2) platinum wire coil.

thin APDC-polymeric film was formed on the platinum wire matrix.

*Procedure*

*Preconcentration and measurement.* The modified platinum wire spiral coil was immersed in a Britton-Robinson (BR) buffer solution (pH 3.0) containing lead[11] (50 ng/ml), which was stirred by a magnetic stirrer, after a given period of time (5 min), the modified platinum wire spiral coil was removed from the preconcentration cell and blotted with filter paper. The modified platinum wire spiral coil was then transferred to the air/acetylene flame burner, positioning the platinum wire spiral coil below the light path (Fig. 1) to measure the absorbance (peak height).

*Effect of pH.* The pH of the solution had a considerable effect on the absorbance. If the pH was higher than 4, the modified reagent fell off from the platinum wire. If the pH was lower than 2, the preconcentration efficiency decreased. Therefore, the optimum is 3, in subsequent experiment, pH was used (Fig. 2).

*Effect of amount of modified reagent.* Polystyrene can adsorb lead, as a result, there is an absorbance from the polystyrene itself. However, the signal was low (Table 1) APDC, when within the range of pH 2 – 4, can form a complex with Pb(II) which can then be extracted. However, APDC cannot be adsorbed

Table 1. Effect of amount of polystyrene

| Polystyrene (1%) (*μl*) | Peak height (*cm*) |
|---|---|
| 0 | 0 |
| 5 | 2.0 |
| 10 | 2.1 |
| 20 | 2.4 |
| 30 | 2.2 |

50 *ng/ml* Pb(II). Preconcentration time: 5 *min.*

Table 2. Effect of amount of APDC

| APDC (1%) (*μl*) | Peak height (*cm*) |
|---|---|
| 0 | 0 |
| 5 | 0.48 |
| 10 | 0.50 |
| 20 | 0.49 |
| 30 | 0.48 |

50 *ng/ml* Pb(II). Preconcentration time: 5 *min.*

very well by the platinum wire as it is slightly soluble in water. Therefore, the absorbance from the APDC is very small (Table 2). The $\pi$ electron of the benzene ring in polystyrene can connect to and share the surface of the platinum wire. Polystyrene, because of its characteristics as a macroporous resins, can function as a carrier of APDC and the fixation APDC–Pb(II) complex is accumulated on the platinum wire (Fig. 3). If both polystyrene and APDC are present at the platinum coil, the absorbance will be significantly enhanced (Table 3).

When the modified platinum wire is put into the solution containing Pb(II), the platinum wire will extract and adsorb the complex formed by Pb(II) and APDC. If there is no modified reagent, Pb(II) cannot be accumulated onto the platinum wire (Table 3). After the modified reagent was applied to the platinum wire, the absorbance gradually increased. Our experiment shows that the absorbance reached a maximum value when 1.0% of APDC and 1.0% of polystyrene were 10 *μl* each (Table 3).

*Effect of preconcentration time.* The dependence of the absorbance on preconcentration time is shown in Fig. 4. The absorbance increased rapidly at first, but after 6 min the quantity of modified platinum wire spiral coil

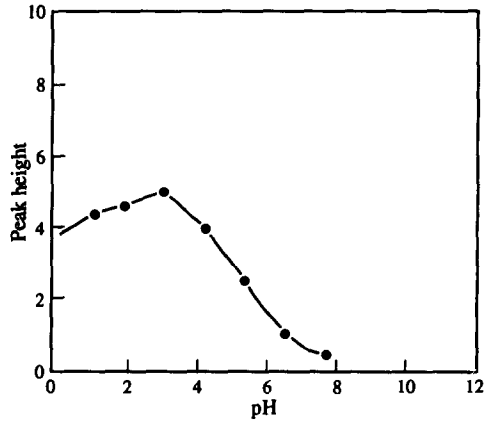


Fig. 2. Effect of pH on the absorbance. 50 ng/ml Pb(II). Preconcentration time, 5 min.

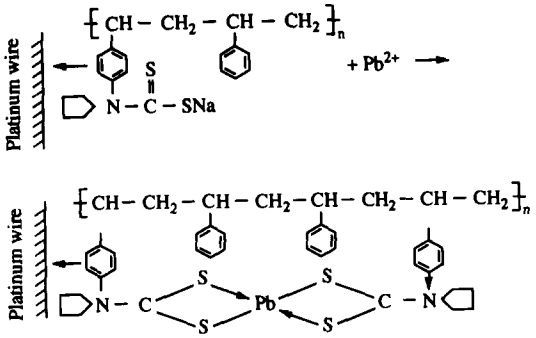


Fig. 3. Adsorption of Pb(II)–APDC complex at platinum wire coil.

surface tended to saturation in the presence of a certain amount of lead, so the absorbance varied little with preconcentration time. It took only 5 min to preconcentrate, because the preconcentration requirements were met.

*Interferences*

The tolerance for various foreign ions was studied for the determination of 50 ng/ml Pb(II). The results show that $SO_4^{2-}$, $Cl^-$ and $NO_3^-$ had no effect, and at least 200-fold amounts of $K^+$, $Na^+$, Ca(II), Mg(II), 100-fold Co(II), Ni(II), Fe(II) Cd(II), Cr(VI), Mo(IV), Zn(II), 50-fold Cr(III). 20-fold Cu(II) and Fe(III) had little effect on the determination. When the contents of Cu(II) and Fe(III) were much higher, the harmful action of those ions were easily removed by addition of 8-hydroxyquinoline.

*Calibration graph, limit of detection and precision*

Under the optimal conditions described above, the absorbance is directly proportional to the lead(II) concentration over the range 5–500 ng/ml. The relative standard deviation was 5.3% ($n = 20$). The detection limit calculated as the concentration corresponding to three times the standard deviation of the blank signal was found to be 0.65 ng/ml. As each amount of the modified reagent is the same, only the modified reagent can adsorb Pb(II), whereas unmodified platinum wire cannot adsorb Pb(II). This accumulation results in a similar amount of Pb(II), and when the absorbance of Pb(II) is determined, the position of the platinum wire in the burner is reproducible. Therefore, the determination can be quite precise.

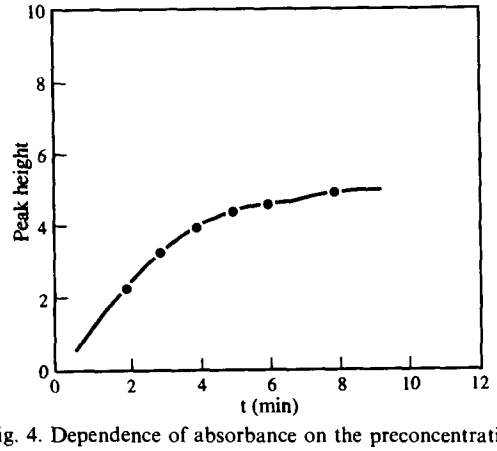


Fig. 4. Dependence of absorbance on the preconcentration time 50 ng/ml Pb(II), pH 3.

Table 3. Effect of amount of modified reagent

| Polystyrene (1%) ($\mu l$) | APDC (1%) ($\mu l$) | Peak height ($cm$) |
|---|---|---|
| 0 | 0 | 0 |
| 5 | 5 | 3.8 |
| 10 | 5 | 4.0 |
| 5 | 10 | 3.9 |
| 10 | 10 | 4.5 |
| 20 | 10 | 4.5 |
| 10 | 20 | 4.4 |

50 *ng/ml* Pb(II). Preconcentration time: 5 *min*.

Table 4. Determination of lead in preserved egg ($n = 6$)

| Sample | Pb(II) added ($\mu g$) | Pb(II) found ($\mu g$) | Recovery (%) | RSD (%) |
|---|---|---|---|---|
| 1 | 0 | 1.68 | 95 | 2.2 |
| | 4.0 | 5.49 | | |
| 2 | 0 | 0.92 | 97 | 2.4 |
| | 4.0 | 4.82 | | |

*Determination of lead in preserved egg*

An appropriate amount of preserved egg was ground. A 0.5000 g sample was put into a beaker (250 ml), 5 ml $H_2SO_4$ and 15 ml $HNO_3$ were added and carefully heated under a cover on a hotplate, and then treated with 1*M* hydrochloric acid evaporated to near dryness. The digested sample was diluted to 100 ml (flask) with R-B buffer solution for analysis. Lead was determined by the above procedure. Table 4 summarizes the results obtained for the determination of lead and recovery studies on preserved eggs. The recovery of lead in preserved eggs was good.

## REFERENCES

1. Z. Wang, S. Luo and Z. Grong, *Fenxi Huaxue*, 1990, **18**, 859.
2. E. Vassileva and S. Arpadjan, *Analyst*, 1990, **115**, 399.

3. Shen Zhentian, Chen Yi and Nie Feng, *Fenxi Huaxue*, 1990, **18,** 61.
4. U. Koklu and S. Akman, *Anal. Lett.*, 1990, **23,** 569.
5. G. Rauret, L. Pineda and R. Compano, *Talanta*, 1989, **36,** 701.
6. R. Saran, T. S. Basu Baul, P. Srinivas and D. T. Khathing, *Anal. Lett.*, 1992, **25,** 1545.
7. Y. K. Chau and K. Lum-Shue-Chan, *Anal. Chim. Acta.*, 1970, **50,** 201.
8. S. T. Belchev, S. Arpadjan, S. Koleva, M. Kostadinova and R. Getcheva, *Anal. Lett.*, 1988, **21,** 529.

Pergamon

0039-9140(95)01446-2

*Talanta*, Vol. 42, No. 4, pp. 561–572, 1995
Elsevier Science Ltd
Printed in Great Britain
0039-9140/95 $9.50 + 0.00

# NON-LINEAR CURVE FITTING USING MICROSOFT EXCEL *SOLVER*

S. WALSH and D. DIAMOND*

School of Chemical Sciences, Dublin City University, Dublin 9, Ireland

(*Received* 8 *September* 1994; *Revised* 12 *October* 1994. *Accepted* 12 *October* 1994)

**Summary**—*Solver*, an analysis tool incorporated into Microsoft Excel V 5.0 for Windows, has been evaluated for solving non-linear equations. Test and experimental data sets have been processed, and the results suggest that *solver* can be successfully used for modelling data obtained in many analytical situations (*e.g.* chromatography and FIA peaks, fluorescence decays and ISE response characteristics). The relatively simple user interface, and the fact that Excel is commonly bundled free with new PCs makes it an ideal tool for those wishing to experiment with solving non-linear equations without having to purchase and learn a completely new package. The dynamic display of the iterative search process enables the user to monitor location of the optimum solution by the search algorithm. This, together with the almost universal availability of Excel, makes *solver* an ideal vehicle for teaching the principles of iterative non-linear curve fitting techniques. In addition, complete control of the modelling process lies with the user, who must present the raw data and enter the equation of the model, in contrast to many commercial packages bundled with instruments which perform these operations with a 'black-box' approach.

Recent trends in data generation, owing in part to the computerization of instrumentation, have led to larger and more complex data sets. Traditional approaches to experimental data processing are largely based on linearization and/or graphical methods. However, this can lead to problems where the model describing the data is inherently non-linear, or where the linearization process introduces data distortion (*e.g.* in standard deviations of data which are logarithmically related to the analyte concentration as with ion-selective electrodes). Hence, with the ready availability of the PCs in laboratories, there is increasing interest in applying non-linear curve fitting techniques to experimental data.

Computers provide an ideal tool to overcome such problems. Although statistical programs have been available for large main-frame computers for many years, these were often cumbersome to use and the computers were not readily available. Many of these statistical packages have now been converted for PCs, but their application to solving analytical data processing problems is still relatively rare as, although scientifically correct and effective, these packages tend to be engineer-orientated, not especially user-friendly and expensive.

In contrast, many analysts are very familiar with spreadsheets such as Microsoft Excel and Lotus 1-2-3, and several books have appeared recently describing their use as sophisticated calculators for processing, displaying and interpreting scientific data, and as tools for teaching calculations in chemistry.[1,2] The familiar Windows user interface, ready availability (often bundled free with new machines or on site-wide licence) and access to desk-top publishing for integrating text and graphics were the main attractions. However, like Lotus 1-2-3, Excel was primarily targeted at the business market, and was frustratingly under-developed for scientific applications, particularly in terms of display and data processing tools (*e.g.* non-linear regression). The balance has been somewhat addressed in recent years, and the appearance of powerful analysis tools such as *solver* makes Excel an important addition to the analyst's armoury for processing experimental data.

Central to the successful application of *solver* is the user's depth of understanding of the problem, in contrast to many analytical data processing packages, in particular those bundled with instruments which often employ a 'black-box' approach. With *solver*, the user

*Author to whom correspondence should be addressed.

must present the raw data in a spreadsheet, enter the model and model parameters correctly, and finally initiate the model building process. Graphical windows enable the dynamics of the model building process to be observed, a feature which can be used to great effect in teaching the principles of data modelling.

## USING *SOLVER*

The following steps describe the general principles of using *solver* which were used in all of the theoretical and practical examples described later. The data set to be modelled must first be obtained. In the case of theoretical studies, the data are generated by means of the equation of interest. A suitable range of values can be quickly obtained by means of the 'edit-fill-down' command. Figures 1 and 2 show the various procedures involved in finding the solution to a Gaussian peak generated using the well known equation;

$$f(X) = H \exp\left[\frac{-(X-\bar{x})^2}{\sigma^2}\right] + B, \qquad (1)$$

where $H$ = peak height above baseline, $X$ = point on $x$-axis, $\bar{x}$ = distance along $x$-axis to peak maximum, $\sigma$ = standard deviation of the peak, $B$ = baseline offset from zero.

Figure 1 shows the layout of a typical Excel spreadsheet prior to using *Solver* using data generated with equation 1. Column A contains the $x$-axis data, and column C Gaussian data generated via equation (1) using column A data and known values for the parameters $H$, $\bar{x}$, $\sigma$ and $B$, which have to be found by *solver*. Column B shows data generated using equation (1) with the initial starting values of $H$, $\bar{x}$, $\sigma$ and $B$ shown in cells G3 to G6. For convenience, these parameters should be entered as named variables in Excel using the 'insert-name' command.

In order to find the solution to the best-fit values of the Gaussian parameters, the user must present a target cell which contains the sum of squared residuals (SSR) between the known data (column C) and the estimated data (column B). The residuals are listed in column D and are obtained by subtracting equivalent cells in columns B and C. Column E contains

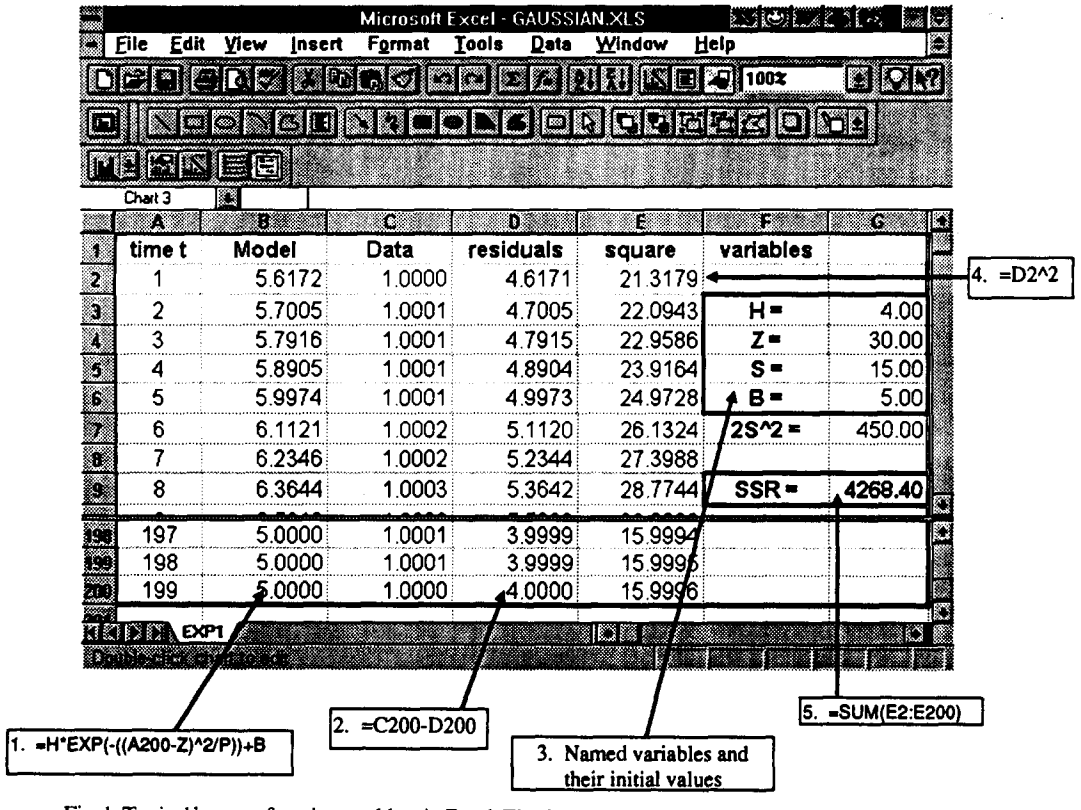


Fig. 1. Typical layout of a *solver* problem in Excel. The data in column C are for the Gaussian peak (generated via equation 1), and the model is entered in column B. Residual errors are in column D and their squares are in column E. The named variables used by *solver* are in cells G3–G6 and the sum of squared residuals (SSR) is in cell G9. Note that $\bar{x}$ is represented by $z$ and $\sigma$ by S in the named variables list.

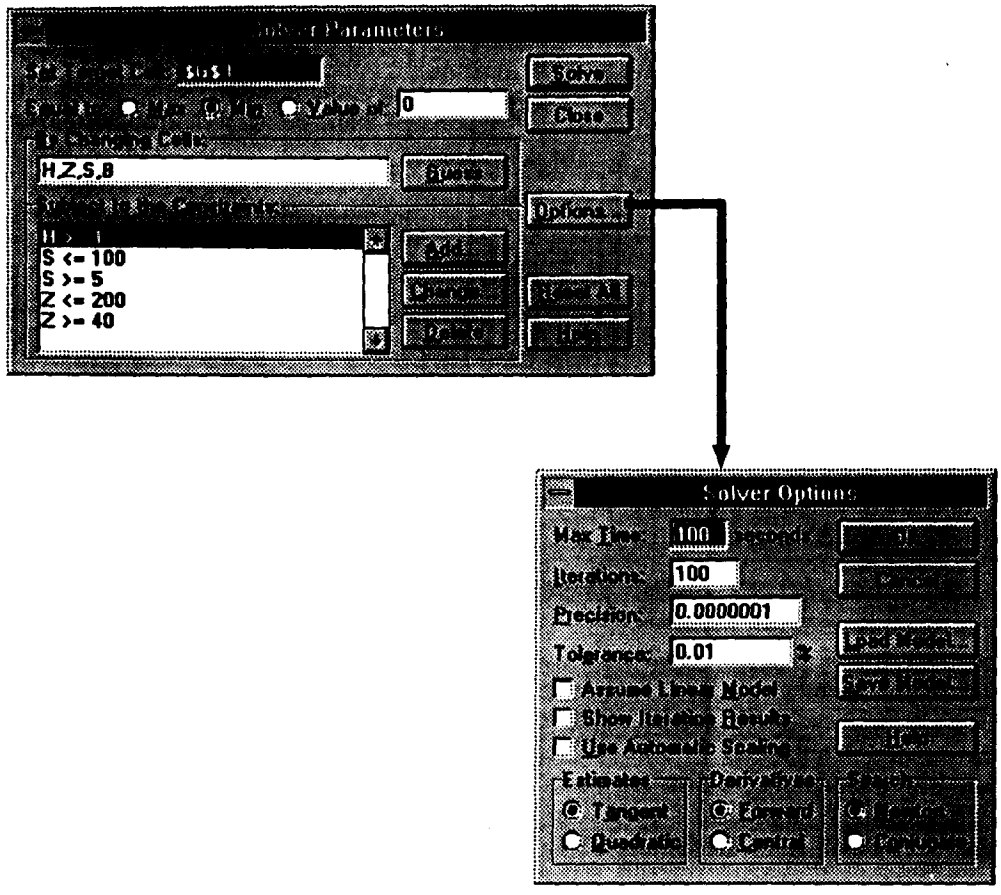


Fig. 2. (a) Initial panel presented to the user when *solver* is activated via the 'tools' menu. (b) The 'options' dialog box which opens when activated by the user. See text for further details.

the squared residuals, and cell G9 the sum of the squared residuals (*i.e.* the sum of cells E2 to E200). This is the quantity which will be minimized by *solver*.

*Solver* is activated via the *tools* menu. On activation, the user is presented with the panel shown in Fig. 2a, which in this case, is set up to solve the Gaussian problem described above. The user options available are:

*Set target cell* specifies the target cell which can be maximized, minimized or set to a certain value. In this case the target cell is *G*9 and it is set to be minimised.

*By changing cells* specifies the cells which will be varied by the search algorithm in order to minimise the number in cell *G*9, *i.e.* cells *G*3 to *G*6 in this example.

*Subject to the constraints*: constraints can be applied by the user to limit the search space explored by the optimization algorithm. As is usual in iterative search procedures based on gradient-type algorithms, efficiency is best if the search is initiated as near the global solution of the problem, and the unknown variables are restricted in value to realistic ranges. This of course implies that the user has considerable knowledge of the problem prior to initiating the search.

*Options* displays the solver options dialogue box (Fig. 2b) in which the user can vary more features of the solution process. These are:

*Max. time* limits the time allowed for the search process.

*Iterations* limits the number of iterations during the search process.

*Precision* sets the precision of the search process. This will determine the minimum change in the target cell which will cause the search process to stop. The best value for precision varies according to how far from the global optimum the initial search position is, and how smooth the error surface is.

*Tolerance* represents a percentage of error allowed in the optimal solution. A higher tolerance would tend to speed up the solution process but at the expense of accuracy in the final solution.

*Assume linear model* will speed up the solution process but obviously should be used only if the relationship is linear.
*Estimates* specifies the approach used to obtain initial estimates of the variables. Briefly, these are

*Tangent* uses linear extrapolation from a tangent vector. That is from a tangent, *solver* extrapolates in different directions to identify which gives a minimum for the target cell. This identifies the next direction of the search process.
*Quadratic* uses quadratic (*i.e.* non-linear) extrapolation which can greatly improve results in very non-linear problems at the expense of speed at arriving at an answer.

*Derivatives* forward and central differentiation options exist for estimates of partial derivatives which give the gradient of the search at that point.
*Search* determines which search algorithm (Newton and Conjugate) is used at each iteration. Both methods are dependent on the calculation of gradient values in the error surface at each stage in the iteration.[3,4]

The Newton method typically requires more memory than the conjugate search but requires fewer iterations. The conjugate search is useful if you have a complex problem (multiple model parameters, large data sets) and memory usage is a concern. We have found little difference in using either algorithm to date.

*Load/save model* is used when more than one solver model is to be used with the worksheet.
*Show iteration results* gives the user a complete update of all data after each complete iteration. If the estimated and known data are graphed, the user can observe a dynamic display of the search process as it proceeds through each iteration. This is very useful in observing visually the progress of the algorithm, but can obviously greatly slow down the process where a large number of iterations are involved. If this option is not exercised, the search process proceeds automatically, reporting only the value of the target cell after each iteration.
*Use automatic scaling* is useful in situations where data may be distorted through gross differences in the magnitude of various parameters in the search algorithm.

Figure 3 shows the results obtained with *solver* for the Gaussian problem. Figure 3a shows the initial position of the search, with the estimated data being well displaced from the required Gaussian curve. Figure 3b shows the final positions of the known and estimated data, illustrating the excellent fit obtained. The values returned by *solver* for the model parameters ($H = 10$, $\bar{x} = 100$, $\sigma = 20$ and $B = 1$) are equal to the values used to generate the test Gaussian curve.

*Modelling two overlapping Gaussian peaks*

A more difficult task is to model two overlapping Gaussian peaks, particularly where one of the peaks appears only as a shoulder on a more dominant peak, a situation which often occurs in spectroscopy and chromatography. Figure 4 illustrates such a situation which has been successfully modelled using *solver*. In this example, both the test data and the model data were generated using the equation;

$$f(x) = H_1 \exp\left[\frac{-(X-\bar{x}_1)^2}{2\sigma_1^2}\right] + H_2 \exp\left[\frac{-(X-\bar{x}_2)^2}{2\sigma_2^2}\right] + B, \qquad (2)$$

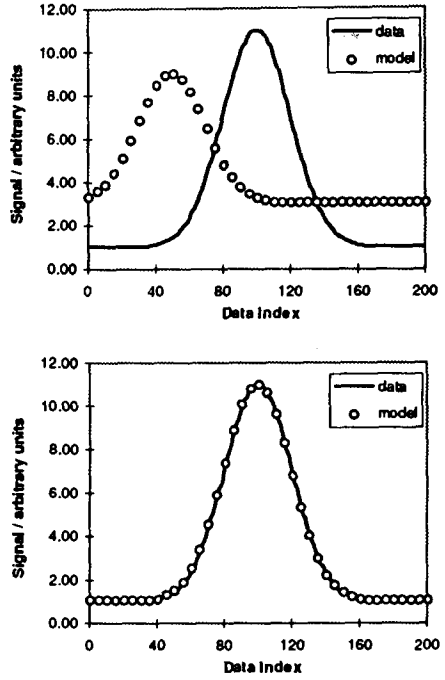


Fig. 3. Results returned by *solver* for the fit to the Gaussian data shown in Fig. 1. (a) The initial positions of the *solver* data and the Gaussian peak. (b) The final fit to the Gaussian peak obtained using *solver*.

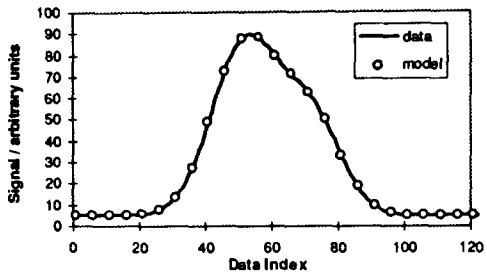


Fig. 4. Fit obtained with *solver* to two overlapping Gaussian peaks where one of the peaks appears only as a shoulder on a more dominant peak.

where $H_1$ = height of peak 1 above baseline, $H_2$ = height of peak 2 above baseline, $\bar{x}_1$ = position of peak 1 maximum along $x$-axis, $\bar{x}_2$ = position of peak 2 maximum along $x$-axis, $\sigma_1$ = standard deviation of peak 1, $\sigma_2$ = standard deviation of peak 2, $B$ = baseline offset from zero on $y$-axis.

Once again, the search returns an exact solution to the problems, with all parameters being successfully returned with the correct values ($H_1 = 80$, $\bar{x}_1 = 52$, $\sigma_1 = 10$, $H_2 = 45$, $\bar{x}_2 = 72$, $\sigma_2 = 9$ and $B = 5$).

Examples like these are very useful for teaching the principles of optimization and non-linear least squares fitting to graduate students, and in particular, in highlighting the need for direction by the user of the process, as initial conditions can easily be set which do not allow the algorithm to locate the desired minimum.

## MODELLING EXPERIMENTAL DATA

In this section, we demonstrate the application of *solver* to modelling experimental data sets which, unlike the theoretical tests discussed previously, will not have exact solutions. However, the validity of the results can be inferred by comparison with results obtained with other optimization algorithms, through knowledge of the system being studied or through examination of the error of the fit.

### *Example (1). Modelling chromatography peaks*

Chromatography (and flow-injection) peaks are characterized by a Gaussian-type shape distorted by tailing which occurs on the falling portion of the peak. Models such as the exponentially modified Gaussian[5-8] and the tanks-in-series[9,10] have been developed in order to allow this distortion of the standard Gaussian peak shape to be described mathematically. This has important applications in the area of data storage (results can be described mathematically rather than stored as relatively large ASCII files), and in the analysis of peak purity (*e.g.* by comparing the shape parameters of experimental peaks to that of a typical peak obtained with the analyte under normal conditions).

*Exponentially modified Gaussian model.*[5-8] The exponentially modified Gaussian function (EMG) is the result of the convolution of a Gaussian function and an exponential decay. In Excel, this is achieved as follows. $Y(n)$ represents an unconvoluted Gaussian data array of $n$ points calculated according to equation (1) above. The difference $\Delta Y(m)$ between a point $Y(m)$ and the previous point $Y(m-1)$ is easily obtained by subtracting the appropriate cells. The convoluted set of points, EMG($m$) is derived from the $Y(m)$ array as follows:

$$\mathrm{EMG}(m) = \mathrm{EMG}(m-1) + \left[\frac{Y(m) - \mathrm{EMG}(m-1)}{A}\right], \quad (3)$$

where

$$A = \left[\frac{1}{1 - \exp(-W_2/\tau)}\right] W_1, \quad (4)$$

where $\tau$ = time constant of the exponential decay (where a time dependent function is being modelled), $W_1$, $W_2$ = weighting factors, with $W_2$ normally set at unity and $m$ is the data index in the array.

On the spreadsheet, the Gaussian equation (1) is first used to create a Gaussian data array over the range of interest. The first point on this array is then set equal to the first convoluted point (EMG(1)). The second EMG point (EMG(2)) can then be calculated via equations (3) and (4) above. This procedure is repeated for the entire Gaussian array using the 'edit-fill-down' command in Excel.

*Tanks-in-series model.*[9,10] In this approach, the flow system is regarded as behaving as a series of mixing chambers which serve to distort the initial ideal square-wave concentration profile of the sample plug as it travels to the detector. The equation used in this instance is;

$$f(t) = H\left[\left(\frac{1}{T_i(t/T_i)^{N-1}}\right) \times \left(\frac{1}{(N-1)!}\right)\exp(-t/T_i)\right], \quad (5)$$

where $T_i$ = mean residence time of an element of fluid in any one mixing tank ($i$). $N$ = number of tanks, $t$ = time ($x$-axis index), $H$ = scaling factor.

Figure 5a–d illustrates the superior performance of the EMG model in describing an experimental HPLC peak. Figure 5a shows the best-fit obtained with the Gaussian model using solver while Fig. 5b and c shows the equivalent best-fit obtained with the EMG and tanks-in-series models, respectively. Figure 5d compares the residual errors obtained with each model expressed as a percentage of the response maximum, and while there is some structure in the

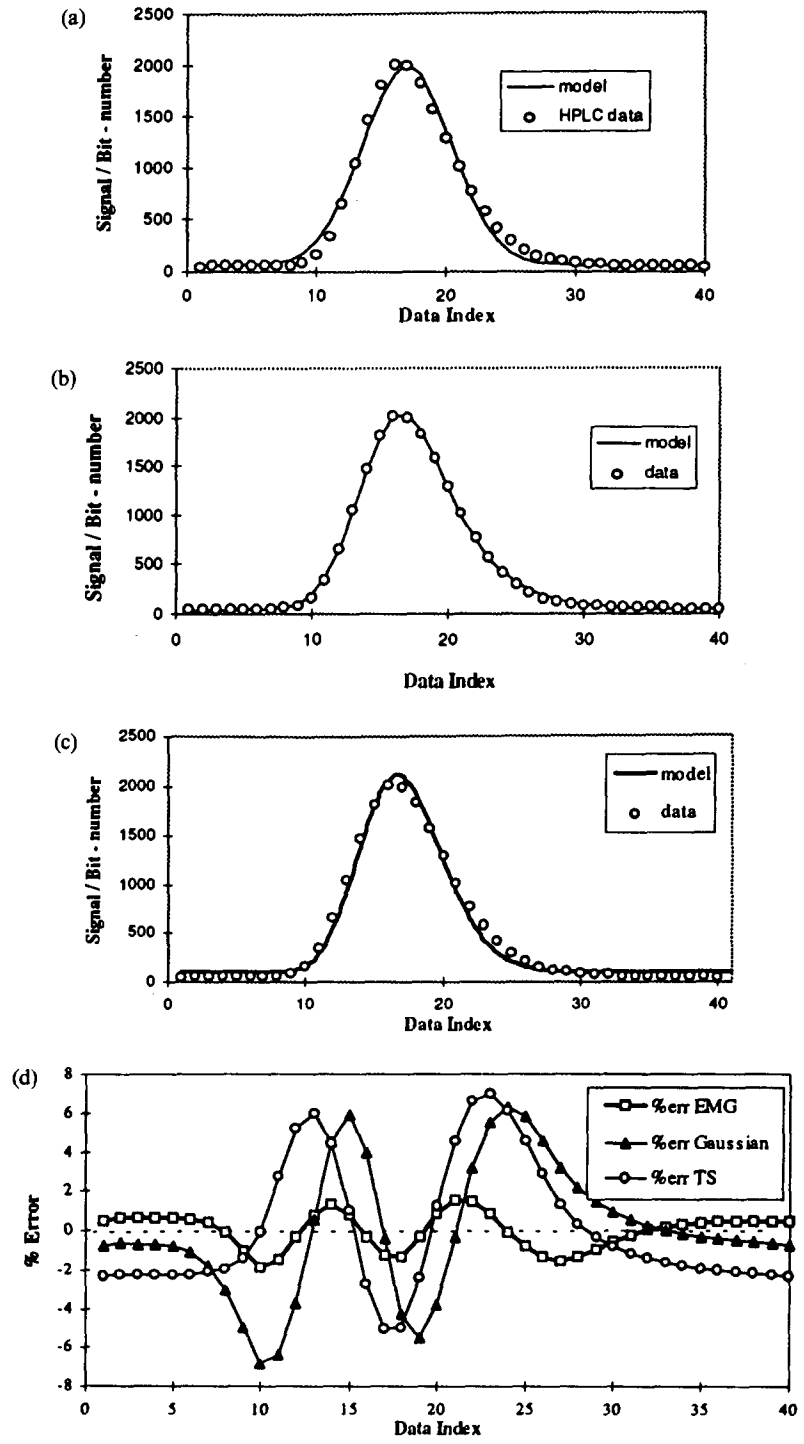


Fig. 5. Comparison of (a) Gaussian, (b) exponentially modified Gaussian (EMG), (c) tanks-in-series models to an experimental HPLC peak and (d) the residuals obtained for each fit (expressed as a % of the peak maximum). The unit 'Bit-number' refers to the number returned by the I/O card on digitization of the detector signal.

EMG residuals, the error is clearly much smaller than that obtained with the other models. The inability of the Gaussian model to cope with the peak tail is demonstrated by the comparatively large residual error for points 22–30 which is much reduced in the EMG residuals.

*Example (2). Modelling fluorescence decay processes*

The data set for the single exponential modelled in this equation refers to fluorescent emission decay lifetime measurements of the compound: ruthenium-bis(2,2′-bipyridyl)(5-isothiocyanate-1,10-phenanthroline) $[Ru(bpy)_2(NCSphen)]^{2+}$ using a Q-switched ND-YAG laser. The samples were aerated and measurements were carried out in 0.1*M* carbonate buffer (pH 9.6). The compound absorbs at 455 nm and is characterized by a fluorescence decay with a single time constant.

The double exponential model has been applied to fluorescent emission decay lifetime measurements of the same compound after attachment of bovine serum albumin via a thio-urea linkage.[11] Once again the samples were aerated and measurements carried out in 0.1*M* carbonate buffer (pH 9.6). Binding of the protein has little effect on the excitation and absorbance wavelengths but lifetimes of fluorescent centres near the binding sites are affected, leading to differing sets of fluorescent emissions emanating from species bound in different environments. The models used in this investigation were general single and double exponential equations of the form:

$$f(t) = [A(1 - \exp(-kt)] + B, \qquad (6)$$

where $A$ = pre-exponential factor, $k$ = rate constant, ($1/k$ = decay lifetime), $t$ = time, $B$ = baseline offset and for the double exponential

$$f(t) = [A_1(1 - \exp(-k_1 t)] + [A_2(1 - \exp(-k_2 t)] + B, \qquad (7)$$

where $A_1$, $A_2$ = pre-exponential factors, $k_1$, $k_2$ = rate constants, $t$ = time, $B$ = baseline offset.

Data obtained from the instrumentation are transformed to suit the above exponential models via in-house software prior to modelling.

Figure 6a and b illustrates the fit obtained using the single exponential model (equation 6) with the NCS compound, and the residuals of the fit, respectively. Clearly the model parameters returned by *solver* fit the data well, with the error (expressed as a percentage of the maximum response) never being greater than ±2%, which is quite acceptable given the noise on the original signal, and the time base of the experiment. The time constant obtained from the fit ($\tau = 450$ nsec) is typical of this material.

Figure 6c and c shows fits obtained with the protein bound ruthenium compound using the double exponential model (equation 7). Again, *solver* returns a good fit to the data, ($\tau_1 = 286$ nsec, $\tau_2 = 833$ nsec) with the error being within about ±3% outside the initial 200 ns of the curve. While, fitting two exponentials to data obtained in these experiments is almost certainly an approximation such an approach can yield important information on the environment of the fluorescent centre through examination of the time constants obtained, while the pre-exponential factors may yield information on the relative populations of centres in the different environments.[11] However, this is a matter of considerable debate amongst specialists in the area. For example, in these experiments it is likely that the fluorescent centres exist in a number of different environments which modify the emission characteristics (*e.g.* the time constants). The fit with the double exponential model is reasonably good, and the time constants obtained are in the range expected. However, the curvature in the residuals suggests that there is some additional structure in the data. This in turn indicates that the fluorescent centres exist in two main environments but this is probably not the complete picture. In addition, careful examination of the residuals suggests an oscillating structure above 1500 nsec, which can also be seen in the original data. It is likely that this is instrumental rather than chemical in origin (*e.g.* environmental noise).

*Example 3. Modelling ion-selective electrode characteristics*

ISEs can be characterized in terms of the well known Nikolskii–Eisenman equation (8) below in terms of the cell constant ($E^\circ$), the slope ($S$), and selectivity coefficients ($K_{ij}^{pot}$) which describe the effect of various interfering ions ($j$) on the response of the electrode to the primary ion ($i$):

$$E = E^\circ + S \log\left(a_i + \sum_j K_{ij}^{pot} a_j^{z_i/z_j}\right), \qquad (8)$$

where $a_i$ and $a_j$ are the activity of the primary and interfering ions, respectively, and $z_i$ and $z_j$ are their charges. We have used a simplified version of the above equation (neglecting the

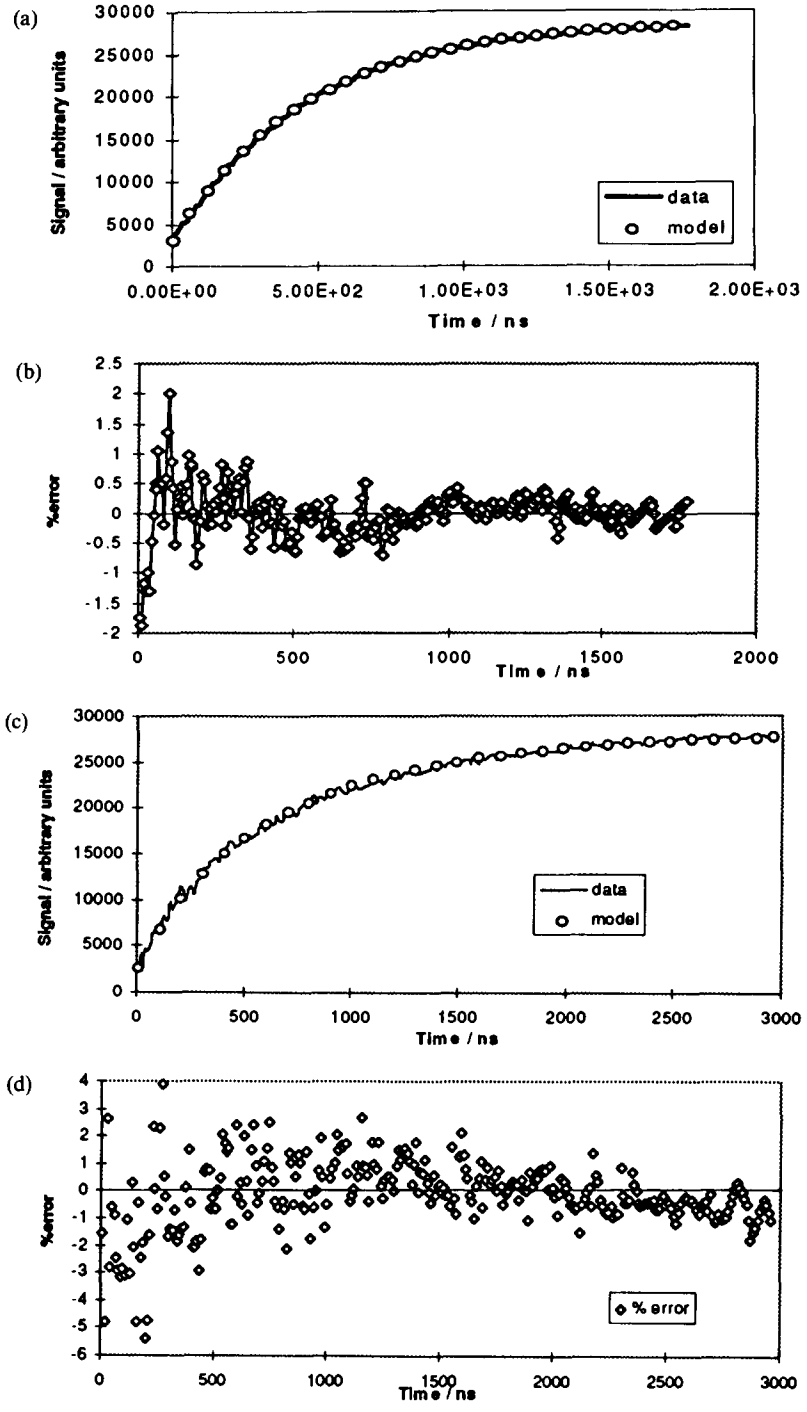


Fig. 6. (a) Fit obtained using a single exponential model for fluorescence decay obtained with ruthenium bipyridyl isothiocyanate phenanthroline using a Q-switched ND-YAG laser,[11] (b) residual errors obtained with the single exponential model. (c) Fit obtained using the double exponential model for the protein bound ruthenium bipyridyl isothiocyanate phenanthroline[11] and (d) the residual errors obtained with the double exponential model.

charge factors on $a_j$) extensively to enable errors on analytical signals arising from interferents to be decoupled and corrected.[12] Approaches such as simplex optimization and genetic algorithms[12,13] have been investigated for estimating the electrode characteristics (selectivity coefficients, slopes, cell constants), which involved extensive programme development. The methodology basically involves generating a matrix of electrode responses to a series of calibration

solutions containing the ions of interest at activity levels set according to a fractional factorial calibration design (see Tables 1 and 2). Thus for a four electrode array, 32 solutions are required, eight of which are targeted at each electrode (*e.g.* solutions 1–8, Table 1 are for the ammonium electrode, solutions 9–16 for the sodium electrode, solutions 17–24 for the potassium electrode and solutions 25–32 for the calcium electrode). We typically model the Nikolskii–Eisenman parameters for a particular electrode using the matrix of potentials obtained from the electrode array with the eight calibration solutions for that electrode, and then estimate the validity of the model by examining the residuals between the predicted array potentials (calculated via the model parameters and the known activities in Table 1) and the observed array potentials (Table 2).

Table 3 show a comparison of fits obtained for the potassium and sodium ISEs by three different approaches, *genetic algorithm with simplex optimization* (uses a genetic algorithm to locate the approximate position of the minimum of the error surface, and then switches to a simplex to fine-tune the position of the minimum), *simplex* (uses the simplex only) and *solver*, results obtained with *solver*.

Table 1. Matrix of ion-activities in calibration solutions[12,13]

| | Activities (*molar*) | | | |
|---|---|---|---|---|
| Solution | $NH_4^+$ | $Na^+$ | $K^+$ | $Ca^{2+}$ |
| 1 | 7.89E-03 | 7.10E-03 | 2.37E-03 | 3.18E-03 |
| 2 | 8.46E-03 | 2.54E-03 | 4.23E-04 | 4.68E-04 |
| 3 | 8.42E-03 | 8.42E-04 | 4.21E-03 | 3.56E-04 |
| 4 | 8.37E-03 | 4.18E-04 | 5.02E-04 | 1.50E-03 |
| 5 | 8.57E-05 | 6.00E-03 | 3.43E-03 | 2.18E-04 |
| 6 | 8.58E-05 | 4.29E-03 | 6.86E-04 | 1.10E-03 |
| 7 | 8.34E-05 | 1.67E-04 | 2.50E-03 | 2.95E-03 |
| 8 | 8.96E-05 | 2.69E-04 | 1.79E-04 | 1.30E-04 |
| 9 | 7.06E-03 | 7.84E-03 | 7.06E-03 | 2.73E-03 |
| 10 | 7.56E-04 | 8.40E-03 | 5.04E-03 | 3.03E-04 |
| 11 | 3.32E-04 | 8.30E-03 | 5.81E-04 | 1.93E-03 |
| 12 | 2.54E-03 | 8.46E-03 | 7.61E-04 | 4.16E-04 |
| 13 | 4.21E-04 | 8.43E-05 | 1.69E-03 | 2.56E-03 |
| 14 | 5.08E-03 | 8.47E-05 | 5.93E-03 | 5.21E-04 |
| 15 | 5.77E-03 | 8.25E-05 | 3.30E-04 | 2.83E-03 |
| 16 | 1.78E-04 | 8.92E-05 | 2.68E-04 | 3.19E-04 |
| 17 | 6.26E-03 | 6.26E-03 | 7.83E-03 | 3.09E-03 |
| 18 | 7.41E-04 | 4.94E-04 | 8.23E-03 | 2.34E-03 |
| 19 | 3.38E-03 | 6.76E-04 | 8.54E-03 | 3.61E-04 |
| 20 | 6.80E-04 | 2.55E-03 | 8.50E-03 | 2.11E-04 |
| 21 | 1.63E-03 | 7.34E-04 | 8.16E-05 | 4.07E-03 |
| 22 | 2.56E-04 | 3.42E-03 | 8.54E-05 | 1.61E-03 |
| 23 | 8.68E-04 | 4.34E-03 | 8.68E-05 | 5.15E-04 |
| 24 | 1.79E-04 | 3.58E-04 | 3.95E-05 | 1.93E-04 |
| 25 | 6.31E-03 | 5.52E-03 | 6.31E-04 | 3.98E-03 |
| 26 | 3.96E-03 | 5.55E-04 | 6.34E-03 | 4.05E-03 |
| 27 | 2.44E-04 | 8.13E-04 | 3.25E-04 | 4.46E-03 |
| 28 | 5.69E-04 | 8.12E-05 | 8.12E-04 | 4.45E-03 |
| 29 | 5.13E-03 | 5.13E-03 | 5.98E-04 | 5.41E-05 |
| 30 | 2.62E-03 | 6.99E-04 | 2.62E-03 | 5.87E-05 |
| 31 | 7.04E-04 | 1.76E-03 | 1.76E-03 | 6.05E-05 |
| 32 | 5.37E-04 | 4.48E-04 | 8.95E-05 | 6.46E-05 |

The results show good agreement on the values of the cell potential and slope for both electrodes with all three approaches. Furthermore, the values for selectivity coefficient for the main interferent are very close for both electrodes (*i.e.* around 0.18 for potassium interference on the ammonium electrode and 0.14 for the value of ammonium interference on the potassium electrode). Even the low-valued selectivity coefficients are modelled to around the same value in each case, which is surprising given their relatively minor effect on the fit. The worst case is for the sodium interference on the potassium electrode ($K^{pot}_{K^+,Na^+}$), for which a value could not be obtained with *solver*. However, examination of the values obtained with the other methods show this to be the smallest coefficient with least effect on the fit. These results show that *solver* can obtain good estimates of electrode parameters using the array-FIA calibration design. However, the genetic algorithm performs better and has the added advantage of being an unsupervised search technique (*i.e.* requires no prior knowledge of the problem). Nevertheless, considering the ease with which *solver* can be used, we feel it performed creditably well in this particular task.

*Example (4). Modelling of ion-selective electrode (ISE) dynamic response in flow-injection analysis*

We have also used *solver* to look at the dynamic responses obtained with PVC membrane electrodes in a flow-injection analysis set-up similar to that used in the calibration experiments.[12] One approach is to use a logistic/sigmoid model to characterize the rising portion of the ISE response peak. The equation used is:

$$E(t) = \left[\frac{a}{(1 + \exp[b(t - c)])^e}\right] + d, \qquad (9)$$

where a = peak height (mV), $b$ = slope coefficient (mV per decade change in $[K^+]$, $c$ = time from beginning of the peak to the inflexion on the rise (sec), $d$ = baseline offset (mV), $e$ = symmetry parameter for the sigmoid, $E(t)$ = electrode response at time $t$ (mV), $t$ = time (sec).

This model can give some indication of the rate of ion-uptake at the membrane surface as the sample plug passes and enable comparisons to be made for different experimental situations (varying concentration of the primary ion, effect

Table 2. Matrix of electrodes responses to calibration solutions[12,13]

| Solution | Measured potentials (*mV*) | | | |
|---|---|---|---|---|
| | $NH_4^+$ | $Na^+$ | $K^+$ | $Ca^{2+}$ |
| 1 | 1.30E + 02 | 1.41E + 02 | 1.43E + 02 | 6.67E + 01 |
| 2 | 1.32E + 02 | 1.18E + 02 | 1.17E + 02 | 4.55E + 01 |
| 3 | 1.32E + 02 | 1.08E + 02 | 1.54E + 02 | 4.01E + 01 |
| 4 | 1.34E + 02 | 7.93E + 01 | 1.22E + 02 | 5.70E + 01 |
| 5 | 8.32E + 01 | 1.49E + 02 | 1.50E + 02 | 3.37E + 01 |
| 6 | 5.99E + 01 | 1.36E + 02 | 1.13E + 02 | 4.92E + 01 |
| 7 | 7.82E + 01 | 7.86E + 01 | 1.41E + 02 | 5.86E + 01 |
| 8 | 4.82E + 01 | 6.89E + 01 | 8.15E + 01 | 2.31E + 01 |
| 9 | 1.30E + 02 | 1.44E + 02 | 1.58E + 02 | 5.92E + 01 |
| 10 | 9.89E + 01 | 1.43E + 02 | 1.54E + 02 | 4.16E + 01 |
| 11 | 7.25E + 01 | 1.44E + 02 | 1.07E + 02 | 5.90E + 01 |
| 12 | 1.12E + 02 | 1.46E + 02 | 1.16E + 02 | 3.49E + 01 |
| 13 | 8.57E + 01 | 6.49E + 01 | 1.32E + 02 | 5.14E + 01 |
| 14 | 1.31E + 02 | 8.49E + 01 | 1.57E + 02 | 4.00E + 01 |
| 15 | 1.29E + 02 | 4.99E + 01 | 1.13E + 02 | 5.93E + 01 |
| 16 | 6.36E + 01 | 4.28E + 01 | 9.74E + 01 | 3.56E + 01 |
| 17 | 1.31E + 02 | 1.42E + 02 | 1.65E + 02 | 6.95E + 01 |
| 18 | 1.06E + 02 | 1.02E + 02 | 1.67E + 02 | 6.28E + 01 |
| 19 | 1.26E + 02 | 9.97E + 01 | 1.61E + 02 | 3.87E + 01 |
| 20 | 1.06E + 02 | 1.25E + 02 | 1.64E + 02 | 3.38E + 01 |
| 21 | 1.02E + 02 | 8.55E + 01 | 9.27E + 01 | 6.15E + 01 |
| 22 | 6.78E + 01 | 1.20E + 02 | 7.00E + 01 | 5.18E + 01 |
| 23 | 9.21E + 01 | 1.26E + 02 | 8.07E + 01 | 4.30E + 01 |
| 24 | 5.85E + 01 | 5.85E + 01 | 6.85E + 01 | 2.81E + 01 |
| 25 | 1.31E + 02 | 1.29E + 02 | 1.22E + 02 | 6.38E + 01 |
| 26 | 1.26E + 02 | 1.00E + 02 | 1.61E + 02 | 6.34E + 01 |
| 27 | 6.57E + 01 | 8.83E + 01 | 9.36E + 01 | 6.36E + 01 |
| 28 | 8.11E + 01 | 5.86E + 01 | 1.18E + 02 | 6.44E + 01 |
| 29 | 1.24E + 02 | 1.48E + 02 | 1.19E + 02 | 2.06E + 01 |
| 30 | 1.14E + 02 | 9.85E + 01 | 1.45E + 02 | 2.11E + 01 |
| 31 | 9.07E + 01 | 1.19E + 02 | 1.34E + 02 | 2.20E + 01 |
| 32 | 7.88E + 01 | 8.56E + 01 | 7.64E + 01 | 2.15E + 01 |

of interferents, injection volume, flow rate, *etc.*). The model parameters in turn can be used as inputs in a further optimization of the instrumental operating conditions (*e.g.* optimize a combination of *a*, *b* and *c* in terms of flow rate and injection volume). Figure 7 shows fits obtained to two valinomycin electrode responses to potassium injections at differing flow rates

Table 3. Comparison of electrode characteristics for valinomycin ($K^+$) and tetramethylacetate *p-t*-butylcalix[4]arene ($Na^+$) based ion-selective electrodes obtained by a (i) genetic algorithm followed by simplex (GA-Simplex), (ii) simplex only, and (iii) *solver*, using the data in Tables 1 and 2

| Electrode parameter | GA-simplex[13] | Simplex[13] | *Solver* |
|---|---|---|---|
| Ammonium ISE | | | |
| $E^\circ$ (mV) | 225.8 | 225.8 | 225.1 |
| $S$ (mV/decade) | 45.4 | 45.5 | 45.2 |
| $K^{pot}_{NH_4^+,K^+}$ | 0.185 | 0.185 | 0.182 |
| $K^{pot}_{NH_4^+,Na^+}$ | $9.36 \times 10^{-4}$ | $2.09 \times 10^{-3}$ | $5.49 \times 10^{-4}$ |
| $K^{pot}_{NH_4^+,Ca^{2+}}$ | $6.46 \times 10^{-3}$ | $4.19 \times 10^{-3}$ | $6.04 \times 10^{-3}$ |
| SSR (8) | 6.313 | 6.507 | 6.405 |
| SSR (32) | 270.2 | 228.29 | 223.3 |
| Potassium ISE | | | |
| $E^\circ$ (mV) | 270.2 | 270.5 | 270.3 |
| $S$ (mV/decade) | 51.4 | 51.5 | 51.5 |
| $K^{pot}_{K^+,NH_4^+}$ | 0.143 | 0.143 | 0.140 |
| $K^{pot}_{K^+,Na^+}$ | $< 1.0 \times 10^{-6}$ | $4.53 \times 10^{-4}$ | 0.00 |
| $K^{pot}_{K^+,Ca^{2+}}$ | $5.36 \times 10^{-3}$ | $5.32 \times 10^{-3}$ | $7.33 \times 10^{-3}$ |
| SSR (8) | 29.17 | 30.04 | 28.97 |
| SSR (32) | 497.7 | 496.3 | 481.8 |

The sum of the squared residuals (SSR) for each method is also shown. SSR (8) refers to the squared residuals for the eight calibration solutions and SSR (32) refers to the squared residuals over the whole situation set.

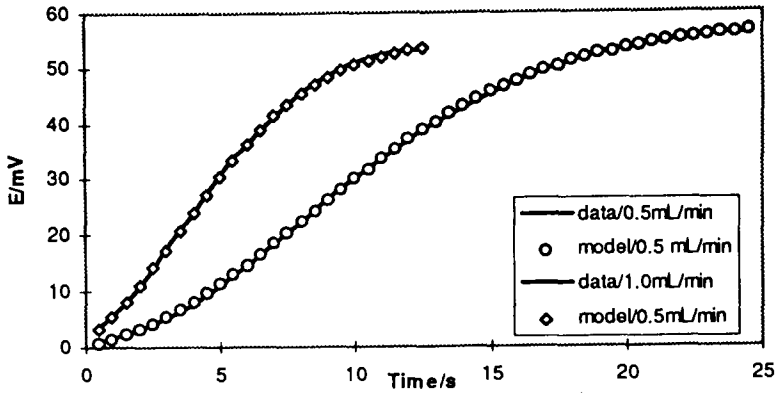


Fig. 7. Fit obtained with sigmoid model for the rising portion of FIA peaks obtained with a potassium PVC membrane electrode at 1.0 and 0.5 mL/min flow rates (see Table 4); Carrier composition: $5 \times 10^{-2}M$ $MgCl_2$, $10^{-6}M$ KCl. Sample composition: $5 \times 10^{-2}M$ $MgCl_2$, $10^{-4}M$ KCl; injection volume: 150 $\mu$l.

(1.0 and 0.5 ml/min). The model parameters returned by *solver* for each flow rate are compared in Table 4.

From these results we can deduce that increasing the flow rate causes a slight reduction in the peak height ($a$), an increase in the slope of the rise (given by the increased magnitude of $b$), a reduced time to the rise inflexion ($c$), and a less symmetrical rise in terms of the sigmoid model (larger value for $e$). Characterizing peaks in this manner can be very useful for instrumental optimization purposes as mentioned above, and for describing peak shapes in terms of a few simple parameters. This characterization can be useful for processing large numbers of peaks and for identifying the possible presence of impurities through the definition of a 'typical' analyte peak as possessing these parameters within certain limits.

## CONCLUSIONS

Using examples from chromatography, spectroscopy and electrochemistry, we have demonstrated the usefulness of *solver* as a tool for mathematical modelling of experimental data.

Table 4. Model parameters for sigmoid model of FIA peak rise obtained with valinomycin ISE in an FIA system at two different flow rates (see Fig. 7)

| Model parameters | 1.0 *ml/min* | 0.5 *ml/min* |
|---|---|---|
| $a$ (mV) | 5.70E + 01 | 5.93E + 01 |
| $b$ (mV per decade change in $[K^+]$) | −1.78E − 01 | −1.03E − 01 |
| $c$ (sec) | 4.84E + 00 | 9.59E + 00 |
| $d$ (mV) | −9.62E + 01 | −1.14E + 00 |
| $e$ | 7.49E + 00 | 4.16E + 00 |

Carrier composition: $5 \times 10^{-2}M$ $MgCl_2$, $10^{-6}M$ KCl. Sample composition: $5 \times 10^{-2}M$ $MgCl_2$, $10^{-4}M$ KCl. Injection volume: 150 $\mu$l.

While it is not on a par with custom-written software packages for this purpose such as Mathlab or Mathcad, or with more complex search methods such as genetic algorithms, it is nevertheless, quite a useful aid to data interpretation and an excellent means for introducing non-linear curve fitting into research and teaching. Given the fact that Excel is readily available, and familiar to most research and undergraduate students, it can be expected to be quickly adopted by many workers for such applications. However, the existence of *solver* appears to be not widely known, a situation which we hope this publication will redress in analytical circles. The fact that the user must import the experimental data, and arrange the spreadsheet in a suitable manner for each problem implies a complete understanding of the mathematics of the model. The ease with which named variables may be varied in Excel enables the user to experiment with equations and become familiarized with their effect on the curve obtained.

In conclusion, we hope the few examples presented in this paper will stimulate other workers unfamiliar with non-linear optimization to experiment with this very useful Excel add-on.

*Acknowledgements*—We wish to thank Maurice Burke (DCU) for providing the chromatography data, Johannes Vos (DCU) for the fluorescence data and useful discussions, and F. J. Sáez de Viteri and Margaret Hartnett (DCU) for the ISE data and useful discussions.

## REFERENCES

1. O. J. Parker and G. L. Brennan, *Spreadsheet Chemistry*. Prentice Hall, Englewood Cliffs, N.J., 1991.

2. H. Freiser, *Concepts and Calculations in Analytical Chemistry—a Spreadsheet Approach*. CRC Press, Boca Raton, 1992.
3. W. H. Press, B. D. Flannery, S. A. Teukolsky and W. T. Vetterling, *Numerical Recipes*. Cambridge University Press, New York, 1990.
4. G. H. Hostetter, M. S. Santina and P. D'Carpio-Montalvo, *Analytical Numerical and Computational Methods for Science and Engineering*. Prentice Hall, Englewood Cliffs, N.J., 1991.
5. E. Grushka, *Anal. Chem.*, 1972, **44**, 1733.
6. J. P. Foley and J. G. Dorsey, *Anal. Chem.*, 1983, **55**, 73.
7. R. Delley, *Anal. Chem.*, 1985, **57**, 388.
8. A. Berthod, *Anal. Chem.*, 1991, **63**, 1879.
9. J. Ruzicka and E. H. Hansen, *Flow Injection Analysis*. Wiley, New York, 1988.
10. O. Lee, G. A. Dumont, P. Tournier and A. P. Wade, *Anal. Chem.*, 1994, **66**, 971.
11. E. Ryan, R. O'Kennedy, M. Feeny, J. Kelly and J. G. Vos, *Bioconjugate Chem.*, 1992, **3**, 285.
12. F. J. Sáez de Viteri and D. Diamond, *Analyst*, 1994, **119**, 749.
13. M. Hartnett, Ph.D. Thesis, Dublin City University, 1994.

Pergamon

0039-9140(95)01449-7

*Talanta*, Vol. 42, No. 4, pp. 573–579, 1995

0039-9140/95 $9.50 + 0.00

# SELECTIVE SPECTROPHOTOMETRIC DETERMINATION OF ASCORBIC ACID IN DRUGS AND FOODS

OSAMA H. ABDELMAGEED, PAKINAZ Y. KHASHABA, HASSAN F. ASKAL, GAMAL A. SALEH and IBRAHIM H. REFAAT

Department of Pharmaceutical Analytical Chemistry, Faculty of Pharmacy, Assiut University, Assiut, Egypt

(*Received* 31 *August* 1994. *Revised* 14 *October* 1994. *Accepted* 14 *October* 1994)

**Summary**—A new analytical method was developed for the determination of ascorbic acid. The method is based on the reaction of ascorbic acid with 4-chloro-7-nitrobenzofurazane (NBD-Cl) in the presence of 0.2*M* sodium hydroxide, where a bluish green colour ($\lambda_{max}$ 582 nm) is developed after dilution with 50% (v/v) aqueous acetone solution. Beer's law was obeyed in a concentration range of 5–20 $\mu$g ascorbic acid/ml with a good correlation coefficient ($r = 0.9990$). The method was found to be highly specific for the determination of ascorbic acid in the presence of dehydro-ascorbic acid, all other vitamins and minerals possibly present in multivitamin preparations, rutin, salicylamide, acetyl salicylic acid, paracetamol, caffeine, phenylephrine hydrochloride and dipyrone. Moreover, the proposed procedure was also successfully applied for the determination of ascorbic acid in some canned and fresh fruit juices, some vegetables and infant milk products without interference from coloured and other substances present in the plant extracts.

Ascorbic acid is an essential vitamin with recommended daily intake of about 70 mg. Continuing interest in the benefits of a well-balanced vitamin intake has resulted in the fortification of many food products with a variety of vitamins, including vitamin C or ascorbic acid. In the case of insufficient uptake the symptoms of scurvy appear.[1] Ascorbic acid occurs naturally in most fresh fruits, fruit juices and is often added during the manufacture of juices or soft drinks. Vitamin C degrades quickly and, therefore, there is special concern regarding the shelf-life of these fortified foods. Consequently, there has been considerable interest in alternative methods of determining the ascorbic acid content of food products.

Since spectrophotometric methods are the instrumental methods of choice commonly used in industrial laboratories; a great number of colourimetric methods have been proposed for the determination of ascorbic acid.[2–11] The majority of these methods are based on its oxidation–reduction properties or its ability to couple with diazotized aniline derivatives. Some of these methods are time consuming and suffer from lack of specificity or good sensitivity especially if they are used for the analysis of beverages, fruits or even some pharmaceutical preparations where colouring matter can interfere with the determination. Tedious pretreatment is often needed to remove possible interferents.[12,13] Therefore, the need for a fast, low cost and selective method is obvious, especially for routine quality control analysis of ascorbic acid-containing products.

In the present work, a facile, sensitive and selective method for the determination of ascorbic acid, based on its reaction with 4-chloro-7-nitrobenzofurazane in alkaline medium, is described.

## EXPERIMENTAL

### *Instrument*

Perkin-Elmer, Lambda 3 B UV/Vis (U.S.A.) and Uvidec-320 (Japan) spectrophotometers with two matched 1-cm quartz cells were used.

### *Reagents and materials*

4-Chloro-7-nitrobenzofurazane (NBD-Cl), (Fluka AG, Switzerland): a 0.1% (w/v) fresh solution in acetone was prepared daily. A 0.2*M* aqueous solution of sodium hydroxide and 25% (w/v) aqueous solution of trichloroacetic acid were prepared, each in distilled water. Ascorbic acid (Sigma, Germany), was used as working standard without further treatment. A stock solution was prepared immediately before use in

cold aqueous solution of 0.5% (w/v) citric acid. This solution was diluted quantitatively with 0.5% citric acid solution in order to obtain 50–200 $\mu$g/ml final concentrations. All other chemicals, reagents and solvents were of analytical grade.

*Dosage forms and food products*

The following commercial ascorbic acid formulations were subjected to analysis by the proposed procedure. Tablets containing only ascorbic acid: vitamin C tablets (Alex. Co., Egypt) and vitacid C effervescent tablets (CID Co., Egypt). Tablets containing ascorbic acid in combination with salicylamide: Cidal C tablets (CID Co., Egypt); in combination with rutin: Ruta C 60 (Kahira Co., Egypt); in combination with paracetamol, caffeine, phenylephrine hydrochloride: Rhino C (CID Co., Egypt). Tablets containing ascorbic acid with vitamins A, B complex, $D_2$, E, nicotinamide and calcium pantothenate together with minerals: Theregran Hematic (Squibb Co., Egypt). Effervescent tablets containing ascorbic acid and calcium carbonate: Vitacal forte and Vitacid Calcium. Tablets containing ascorbic acid and acetylsalicylic acid: Aspocid C. Tablets containing ascorbic acid and multivitamins: Gericid (CID Co., Egypt). Multivitamin capsules containing ascorbic acid and vitamins A, B complex, $D_2$ and E with minerals: Viterra plus (Pfizer, Egypt). Syrups containing ascorbic acid and vitamins A, B complex, $D_2$, E, nicotinamide and calcium pantothenate: Beco C (Misr Co., Egypt), Fruital (CID Co., Egypt) and phosphoplex C (Kahira Co., Egypt). Ampoules containing ascorbic acid only: Cevarol; ascorbic acid in combination with dipyrone: Cevagine (Memphis Co., Egypt). Drops containing ascorbic acid as a single component: Ceviline drops (Kahira Co., Egypt). Canned fruit juices: orange juice (Edfina Co., Egypt), orange juice (Kaha Co., Egypt); apple juice (Foodico Co., Egypt). Fresh fruits and vegetables such as parsley, green pepper, lemon and tomato were purchased from the local market and subjected to the described extraction procedure. Infant milk formula: Dialac-m (N.V. Nutricia, Holland), Neslac® (Nestlé, Holland) and Bebelac® No. 1 (B.V. Lijempf, Holland).

*General procedure*

Into a 10-ml volumetric flask, 1.0 ml of standard or sample preparation was pipetted followed by 1.0 ml of 0.2*M* sodium hydroxide and 1.0 ml of 0.1% (W/V) NBD-Cl solution. The contents of the flask were mixed well and diluted to volume with 50% (v/v) aqueous acetone. The absorbance of the resulting solution was measured at about 582 nm against reagent blank prepared similarly.

*Tablets*

An accurately weighed amount of powder, obtained from 20 tablets, equivalent to about 50 mg of ascorbic acid, was transferred into a 100-ml volumetric flask. 0.5% (w/v) citric acid solution was added to volume and the content of the flask was shaken for about 5 min, filtered and the first portion of the filtrate was rejected. This solution was further diluted with 0.5% (w/v) citric acid to obtain 100 $\mu$g/ml. Then 1.0 ml of this sample preparation was analysed as described under general procedure.

*Capsules*

The contents of 10 capsules were mixed and weighted. Then an amount of the mixed powder equivalent to 50 mg vitamin C was transferred into a 100-ml volumetric flask. The volume was completed with 0.5% (w/v) citric acid solution. The procedure was completed as described for tablet preparation.

*Ampoules, syrups and drops*

An accurately measured volume, equivalent to about 50 mg of ascorbic acid was transferred into a 100-ml volumetric flask. 0.5% (w/v) citric acid solution was added to volume and the contents were mixed well. This solution was further diluted with the same solvent to obtain a sample preparation containing 100 $\mu$g/ml. The procedure was completed as described under general procedure.

*Canned juices*

An accurately weighed amount equivalent to 1.0 g from canned fruit juice was transferred into a 10-ml volumetric flask and diluted to volume with 0.5% (w/v) citric acid. The contents of the flask were mixed well, filtered if necessary and 1.0 ml from this solution was used for the analysis of ascorbic acid as described under general procedure.

*Fruit extracts*

About 50 g portions of each sample was squeezed or homogenized mechanically for about 5 min and then extracted separately with

about 75 ml of 0.5% (w/v) citric acid in divided portions. The extracts obtained were filtered into a 100-ml volumetric flask and the filtrate was made up to volume with the same solution. These solutions were used for the analysis or diluted quantitatively, if necessary, with 0.5% (w/v) citric acid solution to obtain suitable concentrations for the assay. For parsley and green pepper samples a pretreatment step was done before dilution where the extracts were shaken with petroleum ether several times followed by filtration into a 100-ml volumetric flask.

*Infant milk*

About 15 g of the powder milk was accurately weighed in a 250-ml beaker, 80 ml of 0.5% (w/v) citric acid solution was added and the contents were mixed well with continuous stirring in order to obtain a homogenized preparation. A 25% (w/v) aqueous solution of trichloroacetic acid was added dropwise until coagulation of milk started to occur. The mixture was allowed to stand for about 5 min, followed by filtration into a 100-ml volumetric flask. The residue was washed with citric acid solution and the filtrate as well as washing solution, after mixing, was completed to about 95 ml and was treated with 1*N* sodium hydroxide dropwise so as to bring the solution to a final pH of about 6.5. The solution was made up to volume using 0.5% (w/v) citric acid solution and 1.0 ml of this solution was used for the determination of vitamin C content as described under general procedure.

## RESULTS AND DISCUSSION

*Features of the reaction*

4-Chloro-7-nitrobenzofurazane (NBD-Cl), as an activated halide derivative, was first introduced as an analytical fluorigenic reagent for the determination of some amines and amino acids.[14] In a recent report NBD-Cl was further used, for the first time, as a colourimetric reagent for the determination of D-penicillamine in its bulk form and in the presence of other degradation products of penicillin and other possible ingredients that may be present in tablet formulation such as ascorbic acid.[15] Ascorbic acid was found to interfere with the suggested method.[15] Therefore, owing to the fact that no reports could be found in the available literature regarding the use of the cited reagent for the analysis of ascorbic acid in any available dosage forms or in food products, it was decided to extend our previous study to develop a novel approach for the determination of ascorbic acid in bulk drug, dosage forms and some food products.

*Optimization of conditions and absorption spectrum of the reaction product*

Conditions under which the reaction of ascorbic acid with NBD-Cl fulfills the essential analytical requirements were investigated. All conditions studied were optimized at room temperature (25 ± 5°C) and away from direct sun or artificial day light. Because an aqueous solution of ascorbic acid is known to be unstable, 0.5% (w/v) citric acid, was used as an aqueous medium for the cited drug throughout this work as an efficient stabilizer.[16] To generate the nucleophile from ascorbic acid different inorganic aqueous bases were used, such as borax, sodium hydroxide, sodium carbonate or bicarbonate, sodium acetate and sodium dihydrogen phosphate, all 0.1–0.5*M*. The best results were observed with about 1 ml of 0.2*M* sodium hydroxide. The solvents used for NBD-Cl as well as for dilution of the colour formed were carefully studied. A marked red shift was observed with acetone rather than other polar solvents such as alcohols. These results are in good agreement with our previous report.[15] For this reason 0.1% NBD-Cl (w/v), in acetone was recommended and about 1 ml was found to be satisfactory. Because dilution of the colour formed with pure acetone resulted in colloidal solution, probably owing to separation of the excess base, 50% (v/v) aqueous acetone is recommended to avoid any precipitation. Under these conditions the reaction between NBD-Cl and ascorbic acid was found to be instantaneous

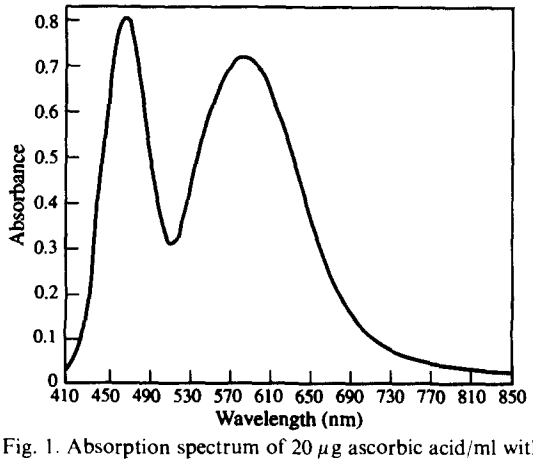


Fig. 1. Absorption spectrum of 20 μg ascorbic acid/ml with NBD-Cl.

Table 1. Determination of ascorbic acid in various types of dosage forms

| Preparation | Ascorbic acid content *mg* | % Recovery* ± SD Proposed | Reported | *t* | *F* |
|---|---|---|---|---|---|
| Tablets | | | | | |
| Vitamin C | 500 | 99.55 ± 1.74 | 98.22 ± 1.03@ | 0.365 | 2.86 |
| Vit C. efferv. | 1000 | 100.00 ± 1.60 | 104.90 ± 1.22@ | 0.423 | 1.72 |
| Theragran | 100 | 99.22 ± 1.26 | 98.54 ± 0.69 | 1.058 | 3.335 |
| Gericid efferv. | 200 | 101.09 ± 1.75 | 99.08 ± 0.78 | 2.343 | 5.034 |
| Vitacal forte efferv. | 50 | 99.59 ± 0.99 | 97.79 ± 1.05@ | 1.087 | 1.125 |
| Aspocid C efferv. | 250 | 98.34 ± 1.40 | 97.93 ± 0.71@ | 0.235 | 3.87 |
| Vitacid calcium efferv. | 1000 | 97.98 ± 2.16 | 97.57 ± 1.50@ | 0.349 | 2.09 |
| Cidal C | 50 | 99.07 ± 0.89 | 98.46 ± 0.79@ | 1.188 | 1.58 |
| Rhino C | 60 | 100.59 ± 1.51 | 102.54 ± 2.07 | 1.701 | 1.880 |
| Ruta C | 160 | 95.39 ± 0.83 | 95.25 ± 0.82@ | 0.219 | 1.025 |
| Capsules | | | | | |
| Viterra plus | 50 | 99.22 ± 1.85 | 98.79 ± 0.90 | 0.467 | 4.225 |
| Ampoules | | | | | |
| Cevagine | 1000 | 95.59 ± 0.92 | 94.51 ± 1.37 | 1.461 | 2.22 |
| Cevarol | 1000 | 98.39 ± 1.10 | 98.15 ± 1.28 | 0.313 | 1.354 |
| Syrups | | | | | |
| Beco C | 50/5 ml | 99.96 ± 1.16 | 99.30 ± 1.55 | 0.287 | 1.785 |
| Fruital | 50/5 ml | 97.51 ± 0.68 | 97.31 ± 1.46 | 0.278 | 4.615 |
| Phosphoplex C | 1500/100 ml | 97.34 ± 0.82 | 96.44 ± 1.82 | 1.003 | 4.926 |
| Drops | | | | | |
| Ceviline | 100/ml | 99.12 ± 1.47 | 98.76 ± 1.46 | 0.389 | 1.01 |

Theoretical value for $t$ is 2.78 ($P = 0.05$) and for $F$ is 6.39 ($P = 0.05$)

*Average of five determinations.

@B.P., 1988, p. 47. (Ref. 23); for other dosage forms, Ref. 10 was used as the reported method.

and stable for at least 30 min as long as it was kept from direct sun or artificial light. Figure 1 represents the bluish-green coloured product with two maxima at about 458 and 582 nm. At 582 nm both the reagent and ascorbic acid have no absorption. In addition, being the more red-shifted one it is expected that measurement at 582 nm should eliminate any interferences which may arise from the presence of colouring matter present in fruits, vegetables or added to liquid pharmaceutical preparations. In our previous report[15] it was proved that reagent blank, prepared under similar conditions, has absorption values in the region of 285–485 nm, with minimum or neglected absorption at 558–612 nm.[15] Therefore, the maximum at about 458 nm probably represents the absorption of the NBD moiety in the reaction product.

Table 2. Determination of ascorbic acid in some canned fruit juices

| Juice | Found* ($\mu g/g \pm$ SD) | Reported† ($\mu g/g$) |
|---|---|---|
| Apple (Foodico) | 8 ± 0.31 | 2–36 |
| Orange (Kaha) | 300 ± 0.50 | 97–700 |
| Orange (Edvina) | 350 ± 0.28 | 97–700 |

*Average of three determinations per sample.

†Ref. 18

*Quantification*

A linear correlation ($r = 0.9990$) was found between the absorbance at 582 nm and the concentration of ascorbic acid in the range of 5–20 $\mu$g/ml. Regression analysis of Beer's plot gave the following linear regression equation:

$$A_{582} = 0.02 + 0.036C \quad (n = 6),$$

where $A_{582}$ is the absorbance at 582 nm and $C$ is the concentration in $\mu$g/ml. This equation has a slope of 0.036 with an intercept of 0.02.

*Application of the proposed method to real samples*

The basic method, as described, was applied for the determination of ascorbic acid in various pharmaceutical preparations (Table 1). Good recoveries were obtained with tablets, capsules and solutions without interference from vitamins A, B complex, D and E, minerals, rutin, acetylsalicylic, salicylamide, paracetamol, caffeine, phenylephrine hydrochloride, dipyrone and tablet excepients.

Results in Tables 2 and 3 give the ascorbic acid contents of some of the seasonally available canned fruit juices or fresh vegetables analysed by the proposed method. The values were found

Table 3. Determination of ascorbic acid in some fresh vegetables

| Vegetable | Ascorbic acid (*mg*/100 *g*) Found* | Reported† | Recovery of the added ascorbic acid Added (*mg*) | Recovered* (*mg*) | % Recovery (±SD) |
|---|---|---|---|---|---|
| Lemon | 48 | 49.7 | 50 | 50.14 | 100.28 ± 2.06 |
| Tomato | 12.3 | 10.2 | 15 | 15.09 | 100.60 ± 0.67 |
| Parsley | 110.2 | 130.6 | 115 | 114.68 | 99.72 ± 1.04 |
| Green pepper | 14.4 | — | 15 | 14.60 | 97.31 ± 1.78 |

*Average of three determinations.
†Ref. 17

to be consistent with the normal concentrations of ascorbic acid reported.[17,18] No interference was observed from the presence of the very complex matrix of the fruit juices or vegetables as indicated by the good recovery of ascorbic acid added to the studied samples. The only recommended pretreatment step was the extraction of chlorophyll with petroleum ether in the case of parsley and green pepper.

Moreover, analysis of different products of dried infant milk for their ascorbic acid content were successfully carried out (Table 4). Trichloroacetic acid, used for milk protein precipitation, being a strong acid can affect the pH of the medium. Therefore, the pH of the studied solution was readjusted to its optimal value, about 6.5, using 1*M* aqueous sodium hydroxide solution, prior to the application of the suggested procedure.

*Possible mechanism*

Being an active halide derivative, NBD-Cl was considered as a likely target for good nucleophile, under basic condition, such as amines, amino acids and thio-compounds.[14,15] This nucleophilic displacement reaction mechanism (SN2) seems obvious in the case of ascorbic acid reaction with the cited reagent. Treatment of ascorbic acid solution with aqueous sodium hydroxide should produce an ascorbate anion (Scheme 1), as reported,[19–21] which in turn can act as nucleophile to displace the $Cl^-$ anion of NBD-Cl to give the corresponding 4-substituted-7-nitro-benzofurazane derivative (Scheme 2). The suggested mechanism is proved by the experimentally negative results obtained upon the interaction of dehydroascorbic acid (Scheme 1), which represents the oxidized form of the enediol group of ascorbic acid, with NBD-Cl under exactly the same described condition. No colour is produced even at concentrations several times more than that recommended for ascorbic acid. Further proof was obtained through the application of Job's method of continuous variation,[22] which revealed a 1:1 ratio of ascorbic acid to NBD-Cl. These findings indicate that the ascorbate anion is the only nucleophile formed during the reaction. Accordingly, the presence of the enediol group makes this reaction highly specific for the determination of ascorbic acid in the presence of other vitamins or/and dehydroascorbic acid.

Another mechanism based on an ion association complex between the two reactants is unlikely owing to the fact that no report(s) could be found in the literature indicating the possible use of NBD-Cl as a basic or acidic dye.

Experimentally, trials have been carried out to extract the colour formed at 582 nm, before and after dilution with 50% (v/v) aqueous acetone, using some water immiscible solvents such as chloroform or toluene. No colour was observed in the immiscible solvents which strongly disagrees with the idea of an ion associ-

Table 4. Determination of ascorbic acid in some infant milk preparations

| Milk product | Ascorbic acid (*mg*/100 *g*) Label claim (*mg*) | Found* (*mg*) | Recovery of the added ascorbic acid to 100 *g* product Added (*mg*) | Recovered* (*mg*) | % Recovery* (±SD) |
|---|---|---|---|---|---|
| Dialac-m | 70 | 68.42 | 70 | 69.66 | 99.52 ± 1.53 |
| Bebelac® No. 1 | 49 | 48.06 | 49 | 48.94 | 99.89 ± 0.36 |
| Neslec® | 41 | 41.07 | 41 | 40.46 | 98.69 ± 0.86 |

*Average of three determinations

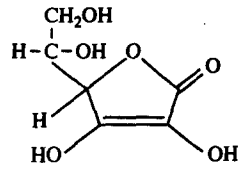

I
Ascorbic acid

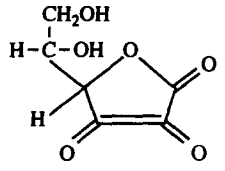

II
Dehydro-ascorbic acid

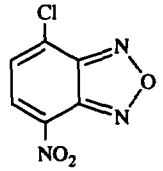

III
NBD-Cl

Scheme 1

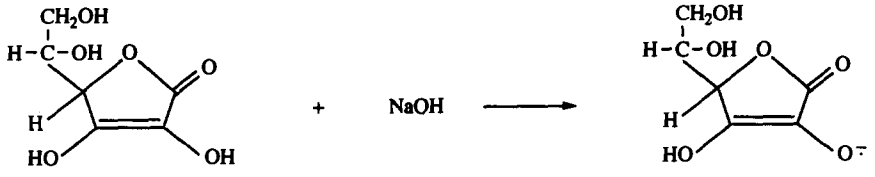

Ascorbic acid

Ascorbate anion

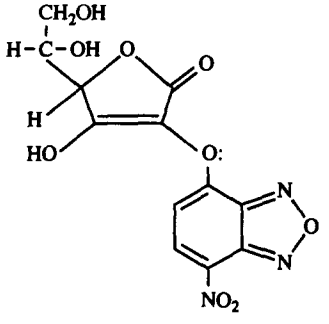

Product

Scheme 2. Possible suggested mechanism.

ation complex under the described experimental condition.

## CONCLUSION

The proposed method offers several advantages over previously used procedures, as it has a high degree of specificity owing to the enediol group of ascorbic acid. With the proposed method, any reducible substances, *e.g.* sugars, should not interfere when present in quantities usually encountered in multivitamin preparations. The method holds good promise for the possible determination of ascorbic acid in biological fluids which will be our target in the future.

## REFERENCES

1. W. H. Sebrell and S. Harris (eds), *The Vitamins*, 2nd Ed, Vol. 1. Academic Press, New York, 1967.
2. S. Morton, W. P. Charles and G. W. Ernest, *Anal. Chem.* 1953, **25**, 1486.
3. B. Jaselskis and S. J. Nelapaty, *Anal. Chem.*, 1972, **44**, 379.
4. M. Hashmi (ed.) *Assay of Vitamins in Pharmaceutical Preparations*, p. 286. Wiley-Interscience, New York, 1972.
5. M. A. Eldawy, A. S. Tawfik and S. R. Elshabouri, *Anal. Chem.*, 1975, **47**, 461.

6. T. Kamangar, A. B. Fawzi and R. H. J. Maghssoudi, *J. Assoc. Off. Anal. Chem.*, 1977, **60,** 528.
7. K. L. Bajaj and G. Kaur, *Analyst*, 1981, **106,** 117.
8. K. Florey (ed.), *Analytical Profiles of Drug Substances*, Vol. 11, p. 76. Academic Press, 1982.
9. J. Augusten, B. P. Klein, D. Becker and P. Venugopal, *Methods of Vitamin Assay*, p. 303. Wiley-Interscience, New York, 1985.
10. E. Y. Backheet, K. M. Emmara, H. F. Askal and G. A. Saleh, *Analyst*, 1991, **116,** 861.
11. M. S. Salah, M. A. Abdella and O. S. F. Eldin, *Talanta*, 1994, **41,** 125.
12. R. C. Williams, D. R. Baker and J. A. Schmidt, *J. Chromatogr. Sci.*, 1973, **11,** 618.
13. M. I. Karayannis and D. I. Farasoglou, *Analyst*, 1987, **112,** 767.
14. P. B. Ghosh and M. W. Whitehouse, *Biochem. J.*, 1968, **108,** 155.
15. H. F. Askal, G. A. Saleh, O. H. Abdelmageed and I. H. Refaat, *Saudi Pharm. J.*, 1994, **2,** 84.
16. J. D. Ponting, *Ind. Engng Chem. Anal. Ed.*, 1943, **15,** 389.
17. R. B. H. Wills, P. Wimalasiri and H. Greenfield, *J. Assoc. Off. Anal. Chem.*, 1983, **66,** 1377.
18. Y. S. Fung and S. F. Luck, *Analyst*, 1985, **110,** 1439.
19. R. R. Grinstead, *J. Am. Chem. Soc.*, 1960, **82,** 3464.
20. Wilson and Gisvold, *Textbook of Organic Medicinal and Pharmaceutical Chemistry*, 8th Ed., p. 804. Philadelphia, London, 1982.
21. S. M. Sultan and E. Bishop. *J. Pharm. Biomed. Anal.*, 1990, **8,** 345.
22. D. T. Sawyer, W. R. Heineman and J. M. Beebe, *Chemistry Experiments for Instrumental Methods*, p. 198. John Wiley, 1984.
23. *British Pharmacopeia*, p. 47. H. M. Stationary Office, London, 1988.

Pergamon

0039-9140(95)01450-0

*Talanta*, Vol. 42, No. 4, pp. 581–589, 1995

0039-9140/95 $9.50 + 0.00

# CHLORDIAZEPOXIDE PHOTOISOMERIZATION KINETICS INTO OXAZIRIDINE. A HPLC STUDY

V. SOENTJENS-WERTS,[1]* J. G. DUBOIS,[1] G. ATASSI[2,3] and M. HANOCQ[1]

[1]Laboratoire de Toxicologie, de Chimie Bioanalytique et de Chimie Physique Appliquée, Institut de Pharmacie, CP 205/1, Université Libre de Bruxelles, Brussels, Belgium

[2]Laboratoire de Pharmacologie Cellulaire, Institut de Pharmacie, Université Libre de Bruxelles, Brussels, Belgium

[3]Division Recherche Cancérologie, IDRS, 11 rue des Moulineaux, 92150 Suresne, France

(*Received* 3 *June* 1994. *Revised* 14 *October* 1994. *Accepted* 14 *October* 1994)

**Summary**—It was proved that the $N_4$-oxide group included in chlordiazepoxide (CDZ) is involved in its phototoxicity. At a wavelength of 350 nm, CDZ photoisomerizes only into oxaziridine (OXA) which is not available as standard. In the course of cytotoxicity investigations, the optimal CDZ irradiation conditions were established as acetonitrile as solvent, 10°C as temperature of the irradiated solutions and 70–90 min as irradiation time for solutions in the range of 12.2–152.0 μg/ml. The kinetic parameters of the CDZ photodegradation reaction order have been calculated using an appropriate algorithm. In all cases, the first order reversible or irreversible was selected by Akaïke's criteria. The percentage of undecomposed CDZ and OXA generated after irradiation were determined by a reversed HPLC method. The latter also permitted the separation of CDZ major impurities in aqueous solutions (demoxepam and 2-amino-5-chlorobenzophenone) as well as the oxaziridine of demoxepam. In this study, the experimental irradiation conditions allowed us to produce 98% pure OXA from CDZ. This HPLC method could be easily extended to the analysis of the molecules in pharmaceutical studies.

Chlordiazepoxide (CDZ) usually used as a tranquillizer, induces undesired side-effects after its consumption and human exposure to sunlight.[1-4] The 1-4 benzodiazepine derivative contains a $N_4$-oxide function involved in the CDZ phototoxicity.[5,6] When exposed to daylight, CDZ, as well as its two major metabolites, desmethylchlordiazepoxide (DES-CDZ) and demoxepam (DEM) respectively, photoisomerize into a photolabile oxaziridine derivative[7,8] (Fig. 1). The epoxy function included in this molecule is unstable. When exposed to UV radiation, it is transformed into quinoxaline and benzoxadiazocine[9,10] and when submitted to high temperature, it is converted back to the parent drug.[7,11]

According to Cornelissen *et al.*,[10,12] 350 nm is the optimal wavelength to photoisomerize CDZ into oxaziridine and avoid its subsequent photodecomposition. In this work, we developed and validated on the one hand a reversed-phase high performance liquid chromatography method in order to quantify the CDZ degradation and the formation of its oxaziridine derivative and on the other we determined the optimal irradiation conditions to quantitatively produce pure OXA as well as to calculate the CDZ photodegradation kinetic parameters. This study is a major step in the investigation of the potential *in vitro* anticancer activity of oxaziridine (unpublished data).

*Author to whom correspondence should be addressed.

## EXPERIMENTAL

### *Reagents and solutions*

Chlordiazepoxide (CDZ) was kindly supplied by Hoffman-La-Roche (Belgium). Chlordiazepoxide hydrochloride (CDZ HCL) was purchased from Federa (Belgium) and 2-amino-5-chlorobenzophenone from Sigma (Belgium). Demoxepam was synthesized according to published methods.[13,14] Disodium hydrogen phosphate . $2H_2O$ and potassium monohydrogen phosphate were of analytical grade (Merck). Acetonitrile was HPLC grade (Labscan analytical science). House-purified, HPLC grade water, was used in all mobile phases and solutions. The mobile phases were filtered through 0.2 μm membranes and sonicated before use.

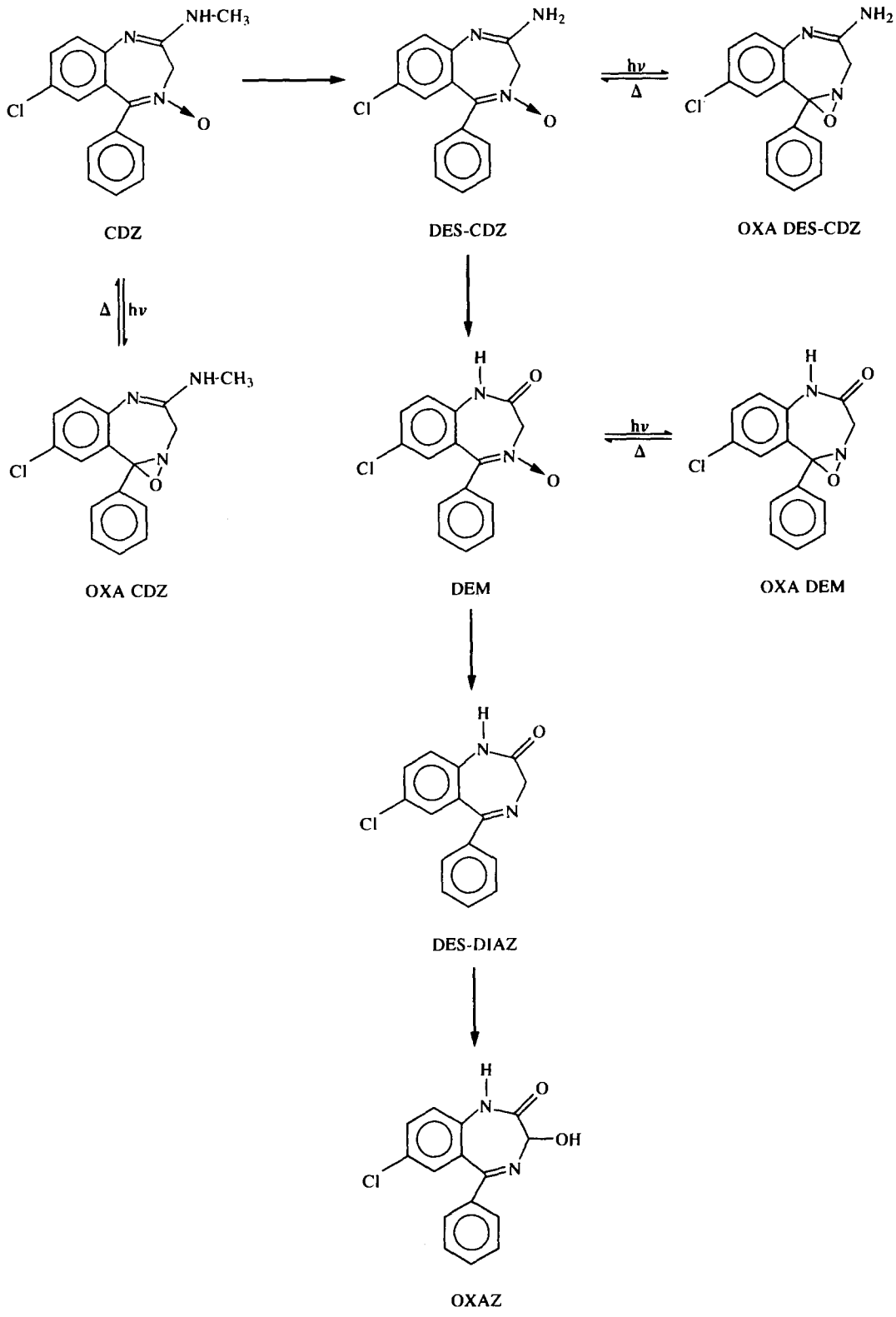


Fig. 1. Structures of chlordiazepoxide (CDZ), its metabolites (DES-CDZ, desmethylchlordiazepoxide; DEM, demoxepam; DES-DIAZ, desmethyldiazepam; OXAZ, oxazepam) and its photoproducts (OXA CDZ, oxaziridine of chlordiazepoxide; OXA DES-CDZ, oxaziridine of desmethylchlordiazepoxide; OXA DEM, oxaziridine of demoxepam).

*The HPLC system*

The HPLC system consisted of a Gilson model 305 pump (Gilson) a model 7125 loop injector (Rheodyne) and a HM holochrome UV monitor (Gilson) connected to a recorder (Kipp and Zonen). The chromatographic column (100 × 4.6 mm i.d.) was packed with 5 $\mu$m particles of $C_{18}$ Nucleosil (Chrompack) and operated at 20°C with a flow rate of 1 ml/min. The mobile phase consisted of a mixture of 0.07*M* phosphate buffer at pH 5.4 and $CH_3CN$ (70:30), 20–70 $\mu$l samples were injected and detection was performed at 280 nm.

*The irradiation system*

The irradiation system was built in our laboratory (Fig. 2). The materials (Oriel, Stratford, U.S.A.) used were: (a) an arc lamp power supply 68806 which operates with a 150 W xenon lamp; (b) a photomax lamp housing 60100 with the xenon lamp in the vertical position, a reflector provided with a demineralized water circulation cooling system, a system of mirror RAL-UV and lens; (c) a monochromator with a band pass of 6 nm and settled at 350 nm; (d) a sample vessel (1 cm i.d., 1 cm height), 0.7 ml volume and thermostatted at a fixed temperature.

*Purity and identification analysis*

The IR spectra were recorded on a Perkin-Elmer 1720 × spectrophotometer equipped with a liquid nitrogen cooled TGA detector, having a resolution of 2 $cm^{-1}$. The oxaziridine was generated after irradiation of a CDZ base solution at a concentration of *ca.* 30 $\mu$g/100 $\mu$l acetonitrile. The CDZ and oxaziridine solutions were deposited on a thallium plate and dried gently under $N_2$ stream before analysis.

The NMR spectra of oxaziridine dissolved in $CDCl_3$ was recorded on a Bruker 2.50 WM; the amount of drug used for NMR spectra was obtained by pooling solutions of six successive CDZ irradiations.

The diode-array analysis [Beckman Instruments: module 168 system gold and system gold chromatography software (ASW-2)] were used for purity determination as well as UV analysis.

*Conditions for the CDZ UV irradiation*

Irradiation was carried out at 350 nm (power supply of the lamp setting at 6.5 A for a tension of 18 V). The energy measured with a OL 730 digital radiometer (Optronic, Orlando, USA), at the surface of the sample, was 0.22 $mW/cm^2$.

Different parameters were investigated: (a) influence of the sample volume (solution volumes between 0.1 and 0.7 ml were tested); (b) influence of the nature of the solvent (organic solvent: acetonitrile and chromatographic mobile phase); (c) influence of the temperature (two different temperatures, 20° and 10°C were considered).

*Kinetic study and data analysis*

Different initial concentrations of CDZ base dissolved in acetonitrile (12.2, 38.0, 60.8, 76.0, 152.0 and 304.0 $\mu$g/ml) were irradiated at 10°C.

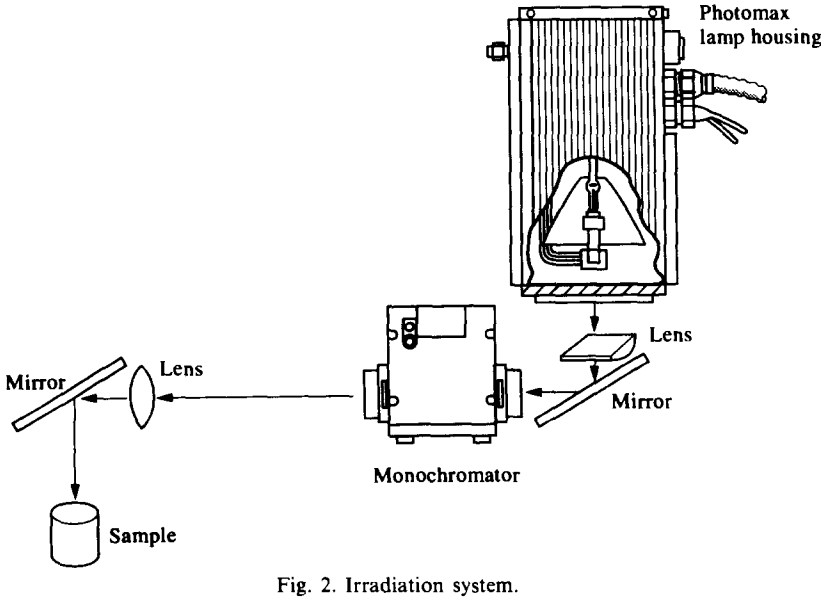


Fig. 2. Irradiation system.

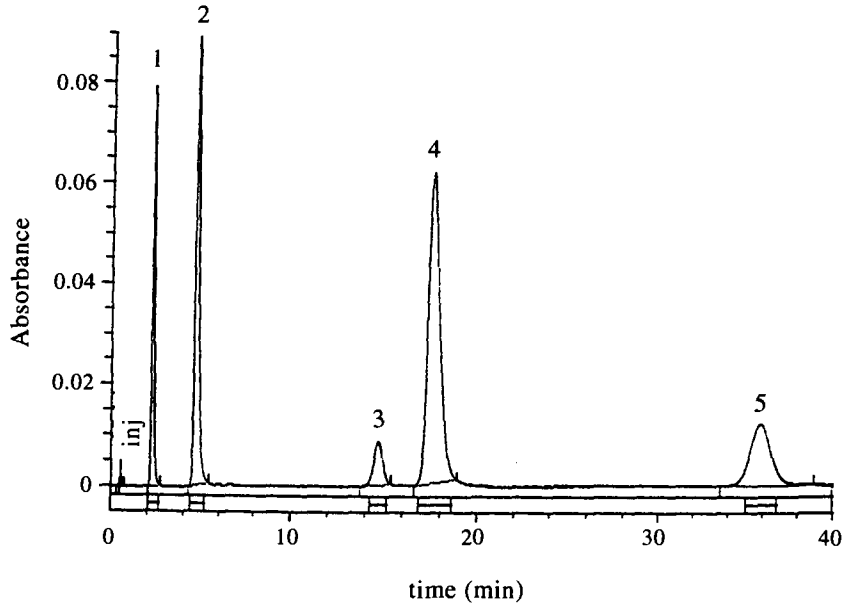


Fig. 3. HPLC separation of chlordiazepoxide (**2**), its photoproduct (**4**) and its decomposition products, namely demoxepam (**1**), as well as its oxaziridine (**3**) and 2-amino-5-chlorobenzophenone (**5**) after irradiation.

Firstly, the data were computed to classical kinetic models namely order O, order 1 reversible or not, order 2. For each concentration studied, the first order reversible or not was selected. Secondly to improve the estimation of CDZ photoizomerization kinetic parameters three software packages were compared: (a) Linreg[15] is based on a least square linear regression analysis. In this regression analysis, data were converted to provide a logarithmic linear transformation. First order reversible equation:

$$\ln(A_t - A_\infty) = \ln(A_o - A_\infty) - Kt, \qquad (1)$$

where $A_t$ is CDZ concentration at time $t$ ($\mu$g/ml), $A_\infty$ is CDZ concentration at time infinity ($\mu$g/ml), $A_o$ is initial CDZ concentration ($\mu$g/ml), $K$ is apparent rate constant ($min^{-1}$), $t$ is time (min). Here, a value for $A_\infty$ is required to allow the logarithmic transformations to $\ln(A_t - A_\infty)$. In the case of first order irreversible, $A_\infty = 0$.

Generally, $A_\infty$ is not known and the usual programs such as Linreg[15] only calculate an approximative concentration at infinity which is then used in the linear regression analysis. In this way, estimations of kinetic rate constants are often erroneous. The best value of $A_\infty$ can only be estimated after non-linear least squares regression analysis by optimization of the parameters in equation (2).

(b) Nonreg[15] and FADHA[16] are based on non-linear least squares regression analysis. Data are fitted to first reversible and irreversible ($A_\infty = 0$) equations (equation 2). First order reversible equation:

$$A_t = A_o e^{-kt} + A_\infty(1 - e^{-kt}). \qquad (2)$$

Nonreg estimations of parameters are based on matrix calculations.[15] In FADHA, we developed an algorithm based on the simplex method which minimizes a non-linear cost function by a sequence of elementary geometric transformations.[16–18]

(c) The Akaïke information criteria (AIC)[19] selected the equation describing the best fit to the data. It is viewed as the sum of a measure of the model fitting criterion and a penalty function proportional to the number of parameters $p$ in the model. In weighted least square analysis with Gaussian errors, the criteria is $AIC = N \ln F + 2p$ in which $F$ is the weighted sum of deviations squared with the $p^{th}$ set of parameters ($F$ = cost function). The lowest value of AIC selects the best model.

## RESULTS AND DISCUSSION

The main objective of this analytical section was to develop a HPLC method suitable to determine the best irradiation conditions to generate OXA-CDZ (peak 4, Fig. 3) and to study the kinetic parameters of this photoisomerization. This method was also used to

Table 1. Unweighted calibration curve of CDZ

| Compounds | Range ($\mu g/ml$) | Slope ($m$) | Intercept ($c$) | $r^*$ |
|---|---|---|---|---|
| CDZ | 1.1–225.4 | 0.4811 | 0.3243 | 0.9996 |
| | | 0.4850 | 0.1908 | 0.9999 |
| | | 0.4832 | 0.8859 | 0.9992 |
| | | 0.5434 | 0.6557 | 0.9997 |
| | | 0.5346 | −0.1677 | 0.9997 |
| | | 0.5225 | 1.1096 | 0.9995 |
| | | 0.5428 | 0.5921 | 0.9991 |
| Mean ± SD | | 0.51 ± 0.03 | 0.5 ± 0.4 | 0.9995 ± 0.0003 |

$r^*$: Regression coefficient.
$y = c + mx$ where $y$ is injected concentration ($\mu$g/ml), $x$ is peak area ($cm^2$).

follow the photoisomerization kinetic of CDZ metabolites (DEM and DES-CDZ) into their oxaziridine derivatives, OXA-DEM and OXA-DES-CDZ (see Fig. 1) (unpublished data). The HPLC methods described in the literature determined the kinetic parameters of the CDZ hydrolysis in aqueous solutions[20,21] and quantified its impurities, namely demoxepam (DEM) and 2-amino-5-chlorobenzophenone (BENZ).[22] Our method permitted the separation of CDZ, DEM and BENZ and the photoproducts of DEM and of CDZ (Fig. 3).

However, the total analysis time is rather high because of the differences in the chromatographic behaviour between CDZ (peak 2), DEM (peak 1) and their oxaziridine derivatives (peaks 4 and 3, respectively). The latter appear to be more lipophilic drugs.

Selectivity of the method and purity of the peaks were controlled by the diode array Gold system.

The linearity of the calibration curve was checked over the range of 1.1–225.4 $\mu$g/ml of CDZ dissolved in acetonitrile. The equation of the mean calibration graphs and the mean regression coefficients as well as standard deviations are given in Table 1 (results of seven successive days). The absolute detection and quantification limits were: 4 ng (for a concentration yielding a signal-to-noise ratio of 2:1) and 20 ng (for concentration yielding a signal-to-noise ratio of 10:1), respectively. Intra- and inter-days determinations of CDZ before irradiation by this HPLC method show a good precision with a mean RSD lower than 4.0%. In order to evaluate the precision of the HPLC assay coupled with the irradiation procedure, three initial CDZ concentrations were irradiated during 70 min (12.2 and 60.8 $\mu$g/ml) or 90 min (304.0 $\mu$g/ml) in $CH_3CN$ before injection. Under these conditions intra-day precisions for CDZ and OXA results were very good since the mean percentage of RSD was below 5%. The inter-day precision for CDZ was maintained under 6% in spite of the low concentration of this drug remaining in solution (0.28 $\mu$g/ml) after a complete as possible isomerization.

This irradiation procedure involves the generation of high concentrations of oxaziridine which can then be measured with an inter-day precision lower than 9%.

Our results showed that the variances were concentration dependent after Fisher–Snedecor's $F$ test ($P < 0.05$). The overall accuracies within the concentration range determined (3.9–175 $\mu$g/ml) were 97–104% with an inter-day RSD less than 5%.

The oxaziridine of CDZ was identified by IR, UV and NMR analysis. UV and NMR spectra were previously published[7,10] and our results have confirmed these works. However, the IR spectra of this drug had not been reported (Fig. 4). The CDZ spectrum showed a characteristical peak of the symmetric stretching of the N—O bond at 1173 $cm^{-1}$, whereas the oxaziridine spectrum indicated two characteristical peaks of the epoxy function: one at 957 $cm^{-1}$ for the asymmetrical ring deformation and the other at 884 $cm^{-1}$ for the symmetrical ring deformation.

One of the main objectives of this study was to produce large amounts of very pure oxaziridine. Experimental conditions which influence CDZ photodegradation were thus particularly investigated, i.e. sample volume, solvent influence, temperature, time of irradiation, sample concentrations.

Several volumes of the sample vessel were investigated. Results showed that 41.3 $\mu$g/ml of CDZ HCl and of CDZ base dissolved in the chromatographic mobile phase (30% acetonitrile) and in pure acetonitrile, respectively, and irradiated for 10 or 34 min at 20°C produce the same percentage of oxaziridine independently of

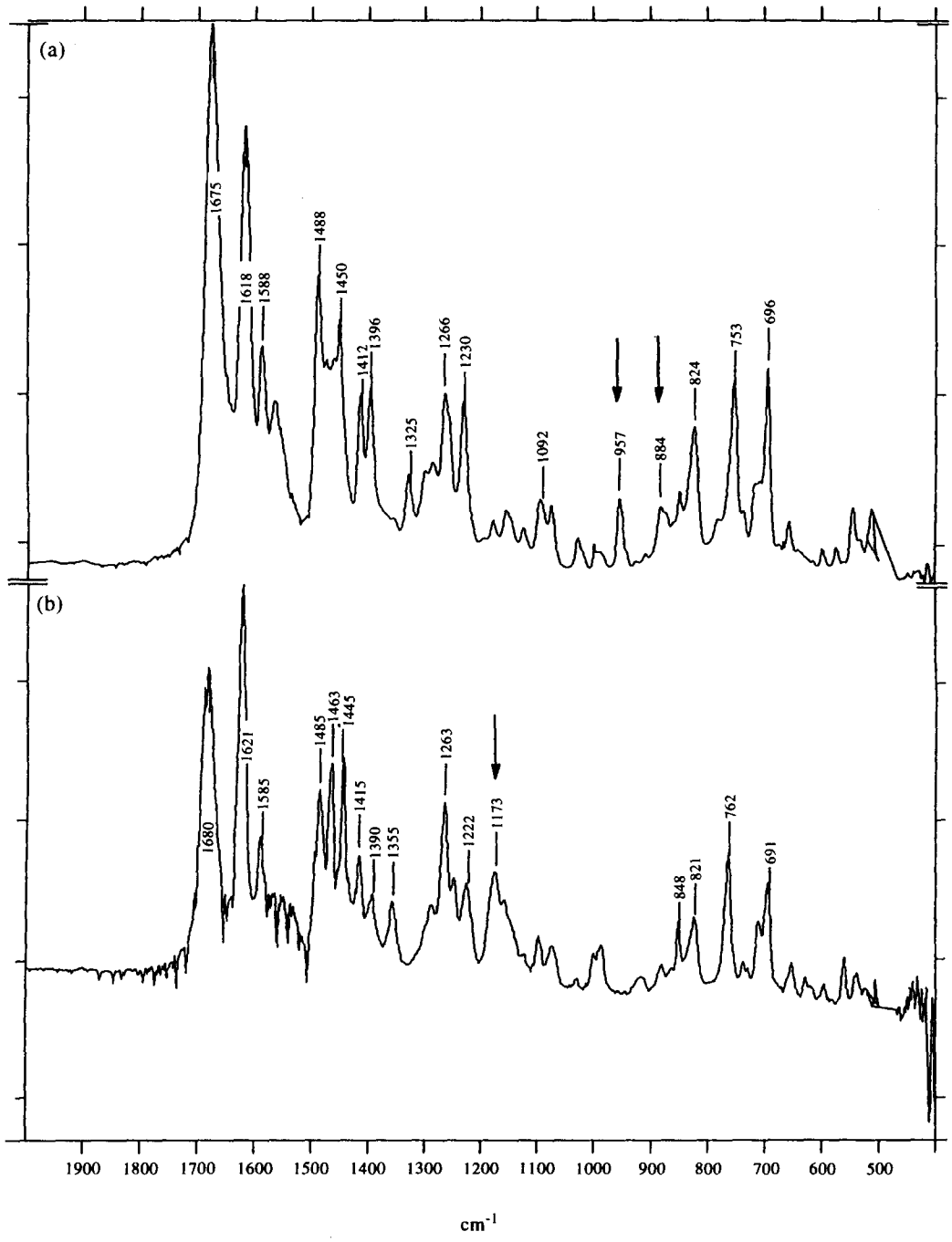


Fig. 4. IR spectra of (a) oxaziridine and (b) chlordiazepoxide in the range of 400–2000 $cm^{-1}$, at a resolution of 2 $cm^{-1}$. (a) Characteristic bands of the epoxy function at 884 and 957 $cm^{-1}$. (b) Characteristic band of the N-oxide at function 1173 $cm^{-1}$.

sample volume within the range of 0.2–0.7 ml (Student's $t$ test $P > 0.05$). Under these conditions, the larger volume was chosen (0.7 ml) and used for all experiments.

The CDZ isomerization time course curves were studied at $20 \pm 1$°C when the drug was dissolved in the chromatographic mobile phase and acetonitrile. Under these experimental conditions and at a concentration of 30.5 $\mu$g/ml, Fig. 5 shows that degradation of CDZ is faster when the drug is dissolved in acetonitrile. After 47 min of irradiation, the percentage of CDZ was still 29% in the mobile phase and only 5% in acetonitrile. The results were confirmed when a concentration 10 times higher was tested. Acetonitrile, which allowed us to obtain high

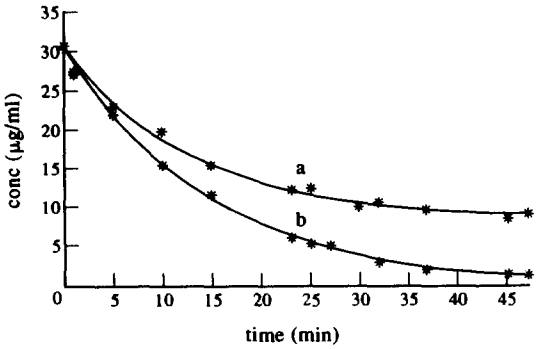


Fig. 5. Influence of solvent composition of CDZ solutions on degraded CDZ fraction during irradiation. (a) CDZ HCl dissolved in chromatographic mobile phase; (b) CDZ base dissolved in acetonitrile. Initial CDZ concentrations = 30.5 μg/ml.

efficiency in producing oxaziridine and to avoid aqueous hydrolysis of CDZ was thus chosen for kinetic studies.

Isomerization of CDZ is faster at 20°C than at 10°C, but the temperature can also influence the stability of the generated oxaziridine and quickly displace the equilibrium to the parent molecule (CDZ) when irradiation is stopped. Therefore, a temperature of 10°C was chosen to quantitatively transform CDZ base into oxaziridine (Fig. 6).

The kinetics of CDZ isomerization was studied at five initial concentrations. Kinetic and fitting parameters were determined by the FADHA algorithm (Table 2). For each concentration, the Akaïke's criteria (AIC) selected the first order reversible or irreversible model but fitting parameters were very similar for both estimation.

At the end of the irradiation period, CDZ concentrations were very low and estimated values of $A_\infty$ in the first order reversible model were close to zero. These observations showed that UV light strongly displaces the

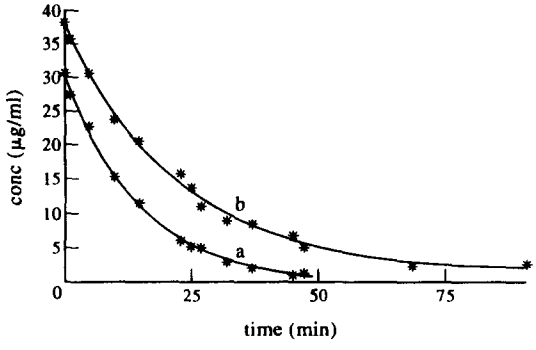


Fig. 6. Influence of irradiation temperature on CDZ photoisomerization kinetic in acetonitrile. (a) 20°C, CDZ (38.0 μg/ml); (b) 10°C, CDZ (30.5 μg/ml).

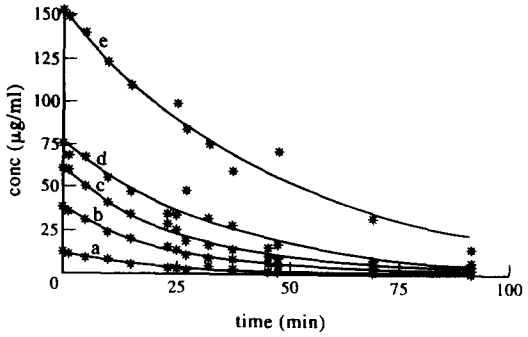


Fig. 7. Evolution of CDZ concentrations as a function of irradiation time. (a) 12.2 μg/ml, (b) 38.0 μg/ml, (c) 60.8 μg/ml (d) 76.0 μg/ml, (e) 152.0 μg/ml.

isomerization equilibrium towards the formation of oxaziridine. As indicated by Fig. 7, synthesis of rather pure oxaziridine from CDZ is thus possible.

A surprising finding is that $K$ is concentration dependent. Actually following a first order kinetic rate constant $K$ should be independent of the initial reactant concentration. Table 2 shows that the apparent kinetic rate constant decreases when CDZ concentration is raised from 12.2 to 152 μg/ml. Percentages of non-transformed CDZ are situated in the range of 2 to 15 after 90 min of irradiation. However, in all cases the first order equations are best fitting to the experimental data. Moreover, the photoisomerization of DEM and DES-CDZ was also a first order reaction (unpublished data). Variation of the rate constant could result because the photoreaction becomes limited by the number of incident quanta of energy and because in concentrated solution quenching of the excited CDZ molecules becomes more efficient.[23]

Data analysis by linear (Linreg) and non-linear (Nonreg and FADHA) least squares regression analysis were compared. Non-linear software has the advantage of estimating values for all parameters of the models. In the linear regression method precise estimation of $A_\infty$ is not possible and users have to approximate its value to calculate other parameters. However, the Nonreg software does not always lead to the absolute minimum or does not assume the convergence. This latter case is illustrated in Table 3, where one can see that appropriate initialization parameters ($K$: 0.05 $min^{-1}$ and $A_0$: 12.2 μg/ml) lead to results. Yet, by selecting 0.2 $min^{-1}$ as the increment of the initial $K$ value, no convergence is observed. Moreover, Nonreg estimations are generally dependent on the initial parameter values. Consequently, kinetic parameters were estimated by FADHA which

Table 2. Kinetic and fitting parameters determined by FADHA software

| | Concentration of CDZ at time zero($\mu g/ml$) | | | | | | | | | |
|---|---|---|---|---|---|---|---|---|---|---|
| | 12.2 | | 38.0 | | 60.8 | | 76.0 | | 152.0 | |
| Parameters | *a* | *b* | *a* | *b* | *a* | *b* | *a* | *b* | *a* | *b* |
| Kinetic | | | | | | | | | | |
| $K$ ($min^{-1}$) | $0.053 \pm 0.006$ | $0.049 \pm 0.004$ | $0.043 \pm 0.004$ | $0.041 \pm 0.004$ | $0.040 \pm 0.003$ | $0.039 \pm 0.001$ | $0.029 \pm 0.003$ | $0.029 \pm 0.003$ | $0.021 \pm 0.002$ | $0.021 \pm 0.002$ |
| $A_\infty$ ($\mu$g/ml) | $0.03 \pm 0.2$ | 0 | $0.9 \pm 0.4$ | 0 | $1 \pm 1$ | 0 | $0.000001 \pm 0.000001$ | 0 | $0.000001 \pm 0.000001$ | 0 |
| $t_{\frac{1}{2}}$ (min) | $14.2 \pm 0.5$ | $14 \pm 1$ | $17 \pm 2$ | $17 \pm 2$ | $17.7 \pm 0.8$ | $17.9 \pm 0.4$ | $24 \pm 3$ | $24 \pm 3$ | $33 \pm 4$ | $33 \pm 4$ |
| $A_0$ ($\mu$g/ml) | $12.1 \pm 0.3$ | $12.0 \pm 0.4$ | $37.6 \pm 0.3$ | $37.5 \pm 0.2$ | $61.7 \pm 0.8$ | $61.5 \pm 0.5$ | $74.6 \pm 0.7$ | $74.6 \pm 0.7$ | $153 \pm 1$ | $153 \pm 1$ |
| Fitting | | | | | | | | | | |
| $R^2$ | 0.9913 | 0.9908 | 0.9984 | 0.9976 | 0.9971 | 0.9963 | 0.9887 | 0.9887 | 0.9947 | 0.9947 |
| AIC | 26.4 | 25.3 | 35.4 | 39.0 | 57.9 | 59.6 | 85.4 | 83.4 | 74.2 | 72.2 |
| $\Sigma r^2$ | 4.3 | 4.6 | 8.2 | 12.2 | 40.8 | 53.2 | 290.0 | 290.0 492.9 | 492.9 | |

*Estimated from mean values.

*a*: first order reversible where $t_{\frac{1}{2}} = \dfrac{\ln\left[\dfrac{A_0 - A_\infty}{A_t - A_\infty}\right]}{k}$.

b: first order irreversible where $t_{\frac{1}{2}} = \dfrac{0.693}{k}$.

Table 3. Comparison of FADHA and Nonreg estimations of kinetic and fitting parameters

| | Softwares | | | |
|---|---|---|---|---|
| | FADHA | | Nonreg | |
| Parameters | First initialization $k = 0.05$ ($min^{-1}$) | Second initialization $k = 0.2$ ($min^{-1}$) | First initialization $k = 0.05$ ($min^{-1}$) | Second initialization $k = 0.2$ ($min^{-1}$) |
| Fitting | | | | |
| $\Sigma r^2$ | 4.6 | 4.6 | 4.6 | overflow |
| $R^2$ | 0.9908 | 0.9908 | 0.9890 | overflow |
| Kinetic | | | | |
| $k$ ($min^{-1}$) | $0.04580 \pm 0.00004$ | $0.04580 \pm 0.00004$ | $0.0458 \pm 0.0003$ | overflow |
| $A_0$ ($\mu$g/ml) | $12.084 \pm 0.002$ | $12.084 \pm 0.002$ | $12.1 \pm 0.4$ | overflow |
| $t_{\frac{1}{2}}$ (min) | 15.1 | 15.1 | 15.1 | overflow |

ensures convergence independently of initial estimations. It proved that the algorithm, based on successive geometric transformations to minimize a cost function, is more efficient than those using matrix calculations.

In conclusion, experimental conditions to generate 98% of pure oxaziridine from CDZ have been established. The determination of the photoisomerization reaction order has permitted us to plan and to quantify the production of OXA from the undegraded CDZ fraction for defined irradiation conditions. Indeed, it is reasonable to consider that at 350 nm each mole of oxaziridine is stoechiometrically generated from 1 mole of the parent benzodiazepine. The HPLC method developed allows the separation of CDZ from its major impurities and photoproducts. The analytical approach is particularly suited to control the synthesis efficiency and its application could be advantageously extended to other pharmaceutical fields. It is interesting to point out that photoproducts are generally not determined in quality control of CDZ. Furthermore, very few assays are suitable to quantify the unstable drugs studied here. The development of the proposed method and the optimal irradiation conditions had been a major step for the investigation of oxaziridines cytotoxicity *in vitro* (unpublished data).

*Acknowledgements*—This study was supported by the "Institut de Recherche Servier" (3 rue de la République, 92150 Suresnes, France). We thank F. Vanhorenbeke for the infrared spectra, G. Verbeeck for the loan of digital radiometer, R. Ottinger for the NMR spectra and Dr R. Collin for helpful scientific discussion. The gift of chlordiazepoxide from Hoffman-La-Roche (Basle) is gratefully acknowledged.

## REFERENCES

1. T. B. Fitzpatrick, M. A. Pathak, L. C. Harber, M. Seiji and A. Kukita, *Sunlight and Man*, p. 3. University of Tokyo Press, Tokyo, 1974.
2. I. A. Magnus, *Dermatological Photobiology*, Chap. 16. Blackwell, London, 1976.
3. O. Widmer, K. Zürcher and A. Krebs, *Dermatologica*, 1976, **152**, 193.
4. A. Bakri, G. M. J. Beijersbergen van Henegouwen and J. L. Chanal, *Photochem. Photobiol.*, 1983, **38**, 177.
5. G. M. J. Beijersbergen van Henegouwen, *Arch. Toxicol. Suppl.*, 1988, **12**, 3.
6. A. Bakri, G. M. J. Beijersbergen van Henegouwen and J. L. Chanal, *Photodermatology*, 1985, **2**, 205.
7. L. H. Sternbach, B. A. Koechlin and E. Reeder, *J. Org. Chem.* 1962, **27**, 4671.
8. P. J. G. Cornelissen, G. M. J. Beijersbergen van Henegouwen and G. R. Mohn, *Photochem. Photobiol.*, 1980a, **32**, 653.
9. G. F. Field and L. H. Sternbach, *J. Org. Chem.*, 1968, **33**, 4438.
10. P. J. G. Cornelissen, G. M. J. Beijersbergen van Henegouwen and K. W. Gerritsma, *Int. J. Pharm.*, 1979, **3**, 205.
11. H. De Vries, G. M. J. Beijersbergen van Henegouwen and P. J. H. H. Wouters, *Pharm. Weekblad Sci. Ed.*, 1983, **5**, 302.
12. P. J. G. Cornelissen, G. M. J. Beijersbergen van Henegouwen, *Pharm. Weekblad Sci. Ed.*, 1980, **2**, 39.
13. L. H. Sternbach, E. Reeder, O. Keller and W. Metlesics, *J. Org. Chem.*, 1961, **26**, 4488.
14. S. C. Bell, T. S. Sulkowski, C. Gochman and S. J. Childress, *J. Org. Chem.*, 1962, **27**, 562.
15. W. J. Irwin, *Kinetics of Drug Composition. Basic Computer Solutions*, p. 1. Elsevier, Amsterdam, 1990.
16. F. Abikhalil, J. Dubois, M. Hanocq, G. Atassi, *Eur. J. Drug Metab. Pharmacokinet.*, 1986, **11**, 51.
17. J. Dubois, F. Abikhalil, M. Hanocq, G. Atassi and R. Arnould, *J. Pharm. Belg.*, 1989, **44**, 181.
18. J. Dubois, M. Hanocq, G. Atassi, R. Arnould and F. Abikhalil, *Eur. J. Drug Metab. Pharmacokinet.*, 1991, **16**, 119.
19. H. Akaïke, *IEEE Trans Autom. Contr., AC 19*, 1974, 716.
20. W. Mayer, S. Erbe und R. Voigt, *Pharmazie*, 1972, **27**, 32.
21. W. W. Han, G. J. Yakatan and D. D. Maness, *J. Pharm. Sci.*, 1976, **65**, 1198.
22. S. L. Ali, *Int. J. Pharm.*, 1980, **5**, 85.
23. K. A. Connors, G. L. Amidon and V. J. Stella, *Chemical Stability of Pharmaceuticals*, p. 105. John Wiley, New York, 1986.

Pergamon

0039-9140(95)01452-7

*Talanta*, Vol. 42, No. 4, pp. 591–596, 1995

0039-9140/95 $9.50 + 0.00

# PREPARATION AND ANALYTICAL PROPERTIES OF A CHELATING RESIN CONTAINING BICINE GROUPS

KAPIL DEV and G. N. RAO*

Department of Chemistry, Indian Institute of Technology, Hauz Khas, New Delhi-110016, India

(*Received* 4 *March* 1994. *Revised* 12 *September* 1994. *Accepted* 18 *October* 1994)

**Summary**—A polystyrene divinyl benzene based resin containing bicine groups has been prepared and its analytical properties investigated. The pH dependence of sorption of metal on the resin has been determined for Cu(II), Fe(II), Ni(II), Co(II), Zn(II), Hg(II) and Pb(II). The important characteristics of the resin are fast equilibrium, high selectivity and small volume change between its hydrogen and metal forms. These enable it to be applied to the rapid concentration of trace amounts of these metal ions. It shows promise for the separation of lead from other metal ions.

Metal chelating resins have found widespread application for the concentration of trace metals from natural waters owing to their selectivity. Use of these resins has allowed field sampling and has eliminated the need for collection and storage of large sample volumes. Many different approaches have been used for the immobilization of metal chelating functional groups on natural and synthetic solid supports for the concentration and/or separation of trace metals.

Muzzarelli and co-workers chemically modified the natural polymer chitosan.[1,2] A number of chelating resins containing aminocarboxylic acid groups (*e.g.* ethylenediamine tetraacetic acid,[3] iminodiacetic acid[4–6]) have been prepared and their analytical properties investigated. Fritz and co-workers synthesized resin containing sulphonic acid, amide and hexylthioglycolate groups.[7–9] Atushi Sughi *et al.* synthesized and applied polystyrene resin containing phenylalanine groups.[10] Schlogl and Fabitschowitz have reported polystyrene resin containing glycine groups.[11]

In the present work, the macroporous resin XAD-4 (polystyrene divinyl benzene) has been functionalized with bicine [*n*,*n*-bis (2-hydroxyethyl) glycine], which contains both alcoholic and carboxylic functionalities. Higher selectivity is expected with bicine ligands over chelating resins having iminodiacetic acid ligand which has only carboxylic groups. The resin has been characterized and sorption behaviour of different metal ions on the resin studied.

*Author to whom correspondence should be addressed.

## EXPERIMENTAL

### *Apparatus*

A Varian AA 475 atomic, absorption spectrometer equipped with a CRA 90 graphite furnace atomizer was used for all metal measurements. An Elico (India) digital pH-meter LI-120 was used for pH measurements. IR spectra were recorded on a Nicolet DX FTIR with KBr pellets. A mechanical shaker (Scientific Instruments, India) with a speed of 200 strokes/min was used for batch equilibration.

### *Reagents*

The stock metal ion solutions were prepared by dissolving the reagent grade nitrates and chlorides in water or the matrix acid. Polystyrene divinyl benzene resin (XAD-4) and bicine were obtained from Fluka. The following buffered solutions were prepared: hydrochloric acid–glycine (pH 1–3); acetic acid–sodium acetate (pH 3–5); disodium hydrogen phosphate–potassium dihydrogen phosphate (pH 5–8); and sodium borate–hydrochloric acid (pH 8–9).

### *Preparation of XAD-4–bicine resin*

Styrene divinyl benzene polymer (XAD-4) was functionalized through an esterification

route. XAD-4 beads (10 g) were refluxed with acetic anhydride (20 ml) and anhydrous aluminium trichloride (1 g) in petroleum ether (60–80°C) at 70°C for 30 hr. The product was filtered off and washed with 50 ml hexane. The intermediate product (II) was then stirred in 500 ml water containing 8.5 g potassium permanganate and 10 g sodium hydroxide at 40°C for 1 hr. The product was filtered off, washed with water and then treated with hydrochloric acid (1:1). It was then refluxed with 50 ml thionyl chloride at 60°C for 30 min. The intermediate resin (IV) was refluxed with bicine (2.5 g) and sodium ethoxide (11.3 m*M*) in toluene at 100°C for 6 hr. A pale yellow resin was obtained. A total of 20 g resin was prepared and the 200–250 mesh fraction of the resin was used for metal sorption studies.

*Optimum pH of metal ion uptake*

The optimum pH of metal ion uptake was determined by batch equilibration technique. Excess metal ion (50 ml, 50 $\mu$g/ml) was shaken with 100 mg of resin for 2 hr. The pH of the metal ion solution was adjusted prior to equilibration over a range of 2–9 with buffer solutions. After the equilibration, the concentration of the metal remaining in the solution was determined by atomic absorption spectrometry (AAS). Adsorption experiments were carried out in duplicate each time.

*Resin capacity*

The capacity of the resin was determined by shaking the excess metal ion (50 ml, 100 $\mu$g/ml) with 100 mg resin (50 mg for mercury and lead) for 6 hr at optimum adsorption pH. Resin was filtered off and concentration of the remaining metal ion in the solution was determined by AAS. The capacity was also checked after soaking the resin in 1*N* HCl/1*N* alkali for 24 hr.

*pH dependence of trace metal ion uptake*

A 50 ml volume of a buffered solution containing 5 $\mu$g/ml of metal ion was shaken with 100 mg of resin for 2 hr in a glass stoppered bottle. The resin was filtered off and the amount of metal ion remaining in the filtrate was determined by atomic absorption spectrometry (AAS). Concentration of the adsorbed metal ion was also determined after eluting with 1*N* hydrochloric acid (10 ml) and diluting the resultant sample solution to 50 ml with distilled water.

*Equilibrium time*

To determine the time of equilibrium for the metal under investigation, the metal ion solution (50 ml, 10 $\mu$g/ml), at a constant pH, was sampled in six bottles. The first bottle was removed from shaker after 5 min and the remaining bottles at intervals of 15 min. The last bottle was removed after 2 hr. The concentration of the metal ion was determined by AAS. The time of equilibrium for all the metal ions was determined in a similar manner. The duplicate values agreed with a precision of $\pm 2\%$.

*Effect of diverse ions*

Standard solutions of 50 ml of Pb, Cu and Ni (1–5 $\mu$g/ml each) containing sodium chloride, Mg and Ca ions as interferents were analysed.

*Concentration and separation of metal ions*

Batch equilibration study was used to concentrate the trace metal ions. Sample solution (250–500 ml) containing 0.1 $\mu$g/ml metal ion was adjusted at optimum pH of adsorption with buffer solution and then shaken with 100 mg of resin for about 10 min. Sorbed metal ions were eluted with 1*N* hydrochloric acid (10 ml) and the concentration of the metal ion in the eluent was determined with AAS.

Based on the sorption behaviour of metal ions on the XAD-4–bicine resin at different pH values, separation of these metals in the binary mixtures were carried out. A 50 ml solution containing lead (5 $\mu$g/ml) and other metal ion was shaken with 100 mg resin at pH 5. Lead retained on the resin was eluted with 1*N* hydrochloric acid (10 ml). Copper, cobalt, nickel and zinc was determined in the effluent and lead in the eluate.

Separation of these metal ions was also carried out by a column method. The dry resin (0.5 g) was loaded into a glass column, immersed in the buffer solution and the metal ion solution was passed through the column at a flow rate of 2.0 ml/min$^{1}$. The adsorbed metal ion was desorbed from the resin with 1*N* HCl.

## RESULTS AND DISCUSSION

The resin was synthesized according to Scheme 1. Spherical macroreticular styrene–divinyl benzene beads were used as starting material.

In the IR spectrum of intermediate IV (Scheme 1, Fig. 1), an absorption band appears

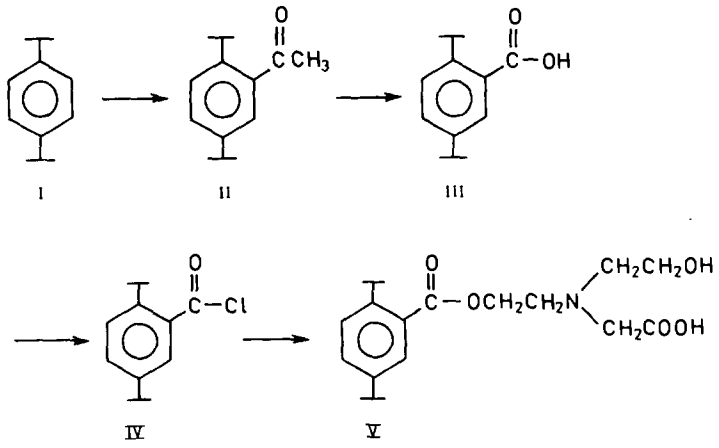


Scheme 1

at 670 $cm^{-1}$ ($\nu_{C-Cl}$) which disappears in the spectrum of resin V. Another feature in the spectrum of IV is the absorption band at 1740–1765 $cm^{-1}$, probably resulting from Fermi resonance between the carbonyl band and the overtone of a longer wavelength band near 875 $cm^{-1}$.[12]

Both the above bands appear in the spectrum of intermediate resin IV and disappear in the final resin V. Comparison of the spectrum of

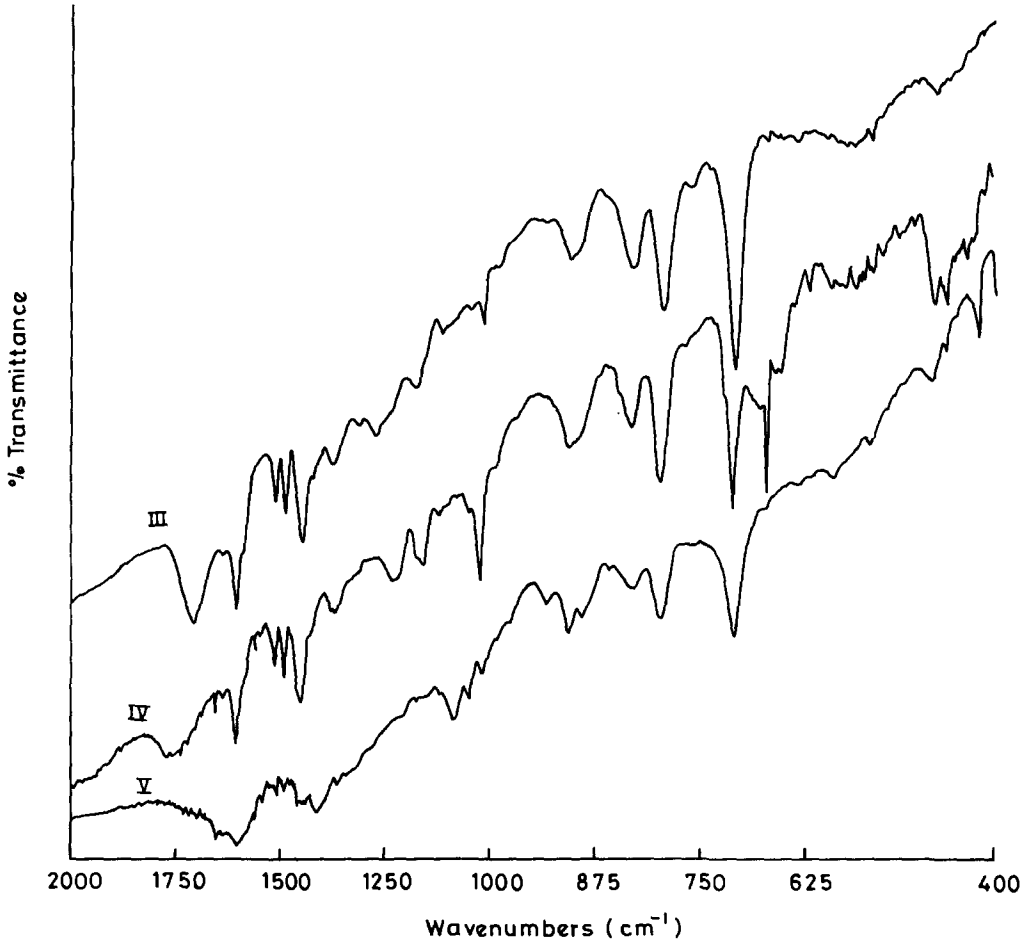


Fig. 1. Infrared spectra of resins (KBr disks). (III) Carboxylated resin, (IV) acid chloride resin, (V) bicine resin.

Table 1. Metal uptake capacities

| Metal | Optimum pH | Capacity (SD) *(mmol/g resin)* |
|---|---|---|
| Cu (II) | 7.06 | 0.38 (0.01) |
| Ni (II) | 8.43 | 0.39 (0.02) |
| Co (II) | 6.55 | 0.42 (0.01) |
| Fe (II) | 5.52 | 0.44 (0.01) |
| Zn (II) | 6.85 | 0.38 (0.01) |
| Pb (II) | 5.58 | 0.40 (0.02) |
| Hg (II) | 5.52 | 0.32 (0.02) |

final resin V with the spectrum of pure bicine also confirms the presence of bicine groups since all the major absorption bands in the spectrum of bicine are present in the spectrum of resin V with reduced intensities.

Nitrogen analysis of the resin gave 0.61% nitrogen. Assuming that all nitrogen is part of intact bicine groups, the capacity for metal ion should be 0.44 mmol/g of resin for the resin. The values actually obtained are reported in Table 1.

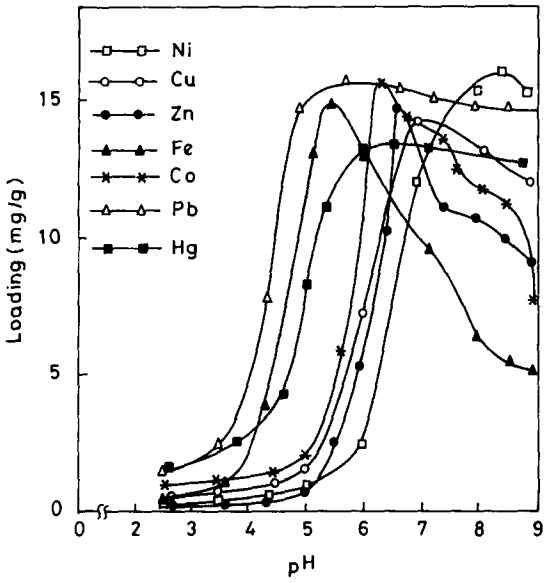


Fig. 2. Effect of pH on metal sorption with bicine resin.

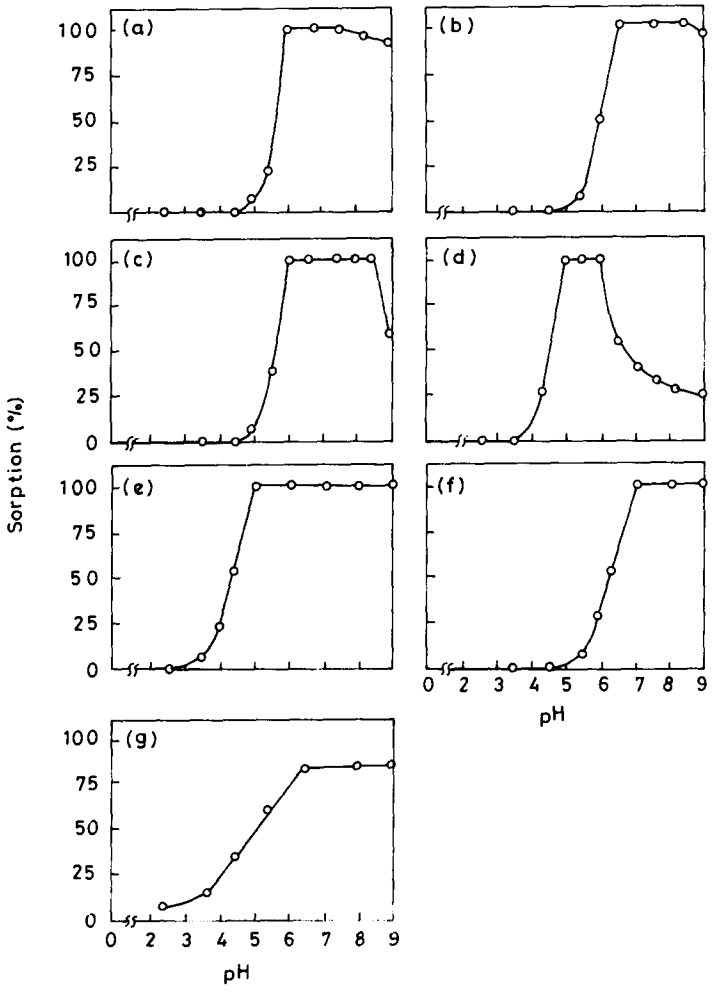


Fig. 3. pH dependence of the uptake of trace metals. (a) Cu(II), (b) Ni(II), (c) Co(II), (d) Fe(II), (e) Pb(II), (f) Zn(II) and (g) Hg(II).

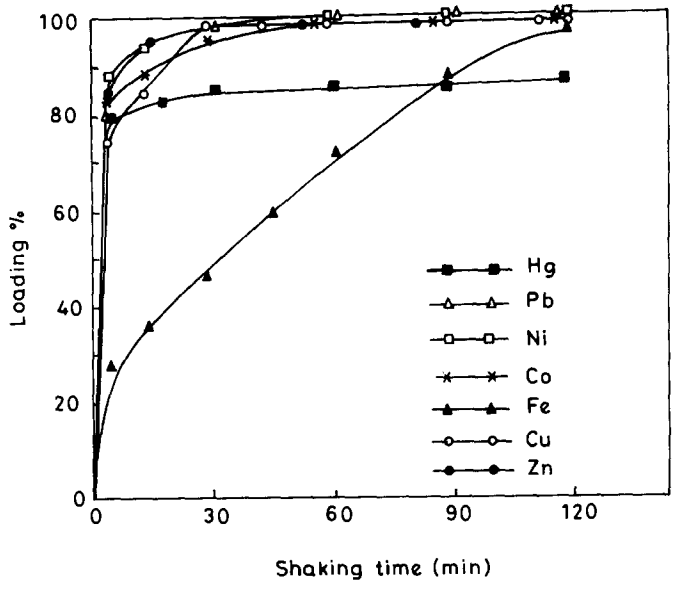


Fig. 4. Rate of uptake of metal ions.

The resin was found to be very stable on successive treatment with dilute acid and alkaline solutions. The stability was checked by change of the hydrogen–metal exchange capacity and the nitrogen content.

In a preliminary experiment, the sorption behaviour of some metal ions on XAD-4–bicine resin at different pH values has been examined by the batch method, and the results are shown in Fig. 2. In general, the adsorption of metal ions increases with increasing pH, reaching a limiting value in each instance, followed by a decrease in adsorption, beyond the limiting value.

The capacity of the resin is an important factor to determine how much resin is required to quantitatively remove a specific metal ion from the solution. The capacity of each metal ion is reported in the Table 1.

Adsorption behaviour of the trace amount of metal ion on the resin is shown in the Fig. 3. The complete adsorption for the trace metal ions are in the region of pH 6–7.5 for Cu(II); 7–8.5 for Ni(II); 6–8.5 for Co(II); 5–6 for Fe(II); 7–9 for Zn(II); 6.5–9 for Hg(II) and 5–9 for Pb(II). A special feature in these breakthrough curves is the complete adsorption of Pb(II) at lower pH, which should enable its separation from other metal ions in this pH region.

The kinetics of the resin–metal interaction are of considerable importance if the resin is to be used in a dynamic system such as a packed column and a flowing stream. If the complexation is not sufficiently rapid for certain metals, then their concentration on a packed column is unlikely owing to the short contact time between the resin and the solution. In those cases a batch extraction with a large excess of resin should be conducted over an extended period.

Kinetic experiments were performed at the optimum pH of adsorption for metal ions and the results are plotted in Fig. 4.

In most cases the kinetics are rapid; Ni(II); Co(II), Pb(II), Hg(II) and Zn(II) are at least 80–90% extracted within 5 min of interaction with the resin. At pH 7.06, Cu(II) is extracted upto 76% after 5 min equilibration with resin. Fe(II) is relatively slower requiring 90 min to reach the 90% extracted level. Considering the

Table 2. Effect of diverse ions

| Interfering ion (*concn*) | Recovery (%) | | |
|---|---|---|---|
| | Pb | Cu | Ni |
| Ca (40 $\mu g/ml$) | 98.8 | 98.7 | 101.0 |
| Mg (40 $\mu g/ml$) | 98.5 | 102.0 | 98.5 |

Table 3. Preconcentration of metal ion (amount of metal ion taken 0.1 $\mu$g/ml)

| Metal | Sample volume (*ml*) | Metal found* ($\mu g/ml$) |
|---|---|---|
| Ni (II) | 250 | 2.42 |
| Ni (II) | 500 | 4.90 |
| Cu (II) | 250 | 2.50 |
| Cu (II) | 500 | 5.02 |
| Co (II) | 250 | 2.48 |
| Co (II) | 500 | 4.98 |
| Zn (II) | 250 | 2.43 |
| Zn (II) | 500 | 4.89 |

*Values agreed with a precision of ±1%.

Table 4. Separation of lead (II) from other metal ions performed at pH 5.0 (amount of lead (II) taken, 5 μg/ml, batch method)

| Metal | Amount of metal added (μg/ml) | Amount of Pb (II)* recovered (μg/ml) | Metal ion* recovered (μg/ml) |
|---|---|---|---|
| Cu (II) | 5 | 4.95 | 4.90 |
| Cu (II) | 10 | 4.92 | 9.85 |
| Ni (II) | 5 | 5.02 | 4.95 |
| Ni (II) | 10 | 5.00 | 10.05 |
| Co (II) | 5 | 4.93 | 4.89 |
| Co (II) | 10 | 4.98 | 9.90 |
| Zn (II) | 5 | 5.04 | 5.01 |
| Zn (II) | 10 | 4.98 | 9.96 |

*Values agreed with a precision of ±1%.

Table 5. Separation of lead (II) from other metal ions performed at pH 5.0 (amount of lead (II) taken, 5 μg/ml, column method)

| Metal | Amount of metal added (μg/ml) | Amount of Pb (II) recovered (μg/ml)* | Metal ion recovered (μg/ml)* |
|---|---|---|---|
| Ni (II) | 10 | 4.88 | 9.82 |
| Co (II) | 10 | 4.94 | 9.91 |
| Zn (II) | 10 | 4.90 | 9.89 |

*Values agreed with a precision of ±1%.

slow reaction kinetics of the Fe(II), separation of small amounts of this metal ion in the presence of some other metal ion by conventional column techniques appeared promising.

Alkali and alkaline earth metals do no effect the recovery of metal ion from the solution. The results in Table 2 show the recovery rates in the presence of excess of these foreign ions. This suggests the use of this resin for trace concentration from natural samples.

Preconcentration of the metal ions on the resin was carried out and results are shown in Table 3. Metal ions could be enriched upto 40–50 times with XAD-4–bicine resin. The separation of trace amounts of lead in the presence of diverse metal ions was examined, both by batch and column methods (Tables 4 and 5). Lead is separable from copper, nickel, cobalt and zinc because they are not retained on the resin at pH 5.0. Lead retained on the resin is eluted with 1*N* hydrochloric acid. Though the elution is easier and complete with column method, but batch method was preferred for the XAD-4–bicine resin as it was found to be less time consuming.

## CONCLUSIONS

These investigations indicate that the XAD-4–bicine resin has good potential for the enrichment of trace metals and their separation from aqueous solutions. Resin can be used for the trace concentration of metal ions from seawater, which has high concentrations of alkali and alkaline earth metals. Enhanced selectivity is observed with XAD-4–bicine resin for lead as compared to Dowex A-1 resin. Equilibration is fast as 80–90% metal ions are sorbed within 5 min of interaction. Resin has high mechanical and chemical strength which makes it useful after recycling.

*Acknowledgement*—The authors thank BRNS (Department of Atomic Energy) for financial assistance.

## REFERENCES

1. R. A. A. Muzzarelli and R. Rocchetti, *Anal. Chim. Acta* 1974, **70**, 283.
2. R. A. A. Muzzarelli and R. Rocchetti, *Anal. Chim. Acta* 1974, **69**, 35.
3. E. M. Moyers and J. S. Fritz, *Anal. Chem.* 1977, **49**, 418.
4. M. Marhol and K. L. Cheng, *Talanta*, 1974, **21**, 751.
5. S. Tomoshige, M. Hirai and H. Ueshima, *Anal. Chim. Acta*, 1980, **115**, 285.
6. P. Figura and B. McDuffie, *Anal. Chem.* 1977, **49**, 1950.
7. M. D. Arguello and J. S. Fritz, *Anal. Chem.* 1977, **49**, 1595.
8. G. M. Orf and J. S. Fritz, *Anal. Chem.*, 1978, **50**, 1328.
9. E. M. Moyers and J. S. Fritz, *Anal. Chem.*, 1976, **48**, 1117.
10. A. Sugii, N. Ogawa, I. Katayama and T. Hida, *Talanta*, 1982, **29**, 263.
11. K. Schlogl and H. Fabitschowitz, *Monatsh*, 1954, **85**, 1223.
12. R. M. Silverstein, G. C. Bassler and T. C. Morrill, *Spectrometric Identification of Organic Compounds*, 5th Ed., p. 120. John Wiley, New York, 1991.

Pergamon

0039-9140(95)01453-5

*Talanta*, Vol. 42, No. 4, pp. 597–603, 1995
Elsevier Science Ltd
Printed in Great Britain
0039-9140/95 $9.50 + 0.00

# BIASES IN SUMMARY STATISTICS OF SLOPES AND INTERCEPTS IN LINEAR REGRESSION WITH ERRORS IN BOTH VARIABLES

A. H. KALANTAR,[1] ROBERT I. GELB[2] and JOSEPH S. ALPER[2]*

[1]Department of Chemistry, University of Alberta, Edmonton, Alberta, Canada T6G 2G2
[2]Department of Chemistry, University of Massachusetts—Boston, Boston, MA 02125, U.S.A.

(*Received* 15 *August* 1994. *Revised* 13 *October* 1994. *Accepted* 18 *October* 1994))

**Summary**—Monte Carlo simulations are employed to investigate the bias in linear regression parameters for cases in which both variables are subject to normally distributed errors. Both homoscedastic and heteroscedastic errors are treated. The results show that, in general, the arithmetic mean, geometric mean, and angle mean (tangent of the mean of the arctangents) of the slopes are biased and non-normally distributed. The arithmetic and geometric means of the intercepts are generally biased and non-normally distributed as well. However, for all the cases considered, the medians of the slopes and of the intercepts are found to be unbiased. In view of the non-normal distributions of the slopes and intercepts, a nonparametric method is used to determine confidence intervals for the slopes and intercepts.

As many previous authors have noted, ordinary least squares regression (OLS) cannot be used to determine slopes and intercepts if there are errors in both the dependent and independent variables.[1–9] This situation arises in a number of chemical applications. In many experiments, the values of the independent as well as the dependent variables are obtained by measurement. In experimental design, calculations performed to determine the optimal choice of the distribution and values of the independent variable must take into account the experimental uncertainties in both variables.

There are several methods for determining the regression parameters for the linear equation $Y^\circ = a^\circ + b^\circ X^\circ$ with errors in both $X^\circ$ and $Y^\circ$.[1–3,5,7,9] We use the superscript '°' in referring to the 'true' values. The Williamson[2] modification of the York[1] method is particularly convenient. Denote the data points by $(X_i, Y_i)$ and their respective uncertainties by $(\sigma_{Xi}, \sigma_{Yi})$. Next, set $x_i = X_i - \langle X \rangle$ and $y_i = Y_i - \langle Y \rangle$, where $\langle X \rangle$ and $\langle Y \rangle$ are the weighted mean values of $X_i$ and $Y_i$, respectively, The York–Williamson (YW) regression slope, $b$, is given by

$$b = \frac{\sum W_i^2 \sigma_{Yi}^2 x_i y_i + b \sum W_i^2 \sigma_{Xi}^2 y_i^2}{\sum W_i^2 \sigma_{Yi}^2 x_i^2 + b \sum W_i^2 \sigma_{Xi}^2 x_i y_i}, \quad (1)$$

where

$$W_i = (\sigma_{Yi}^2 + b^2 \sigma_{Xi}^2)^{-1}. \quad (2)$$

The intercept, $a$, of the regression is given by $a = \langle Y \rangle - b\langle X \rangle$.

In their careful study of the YW regression, Christian and Tucker (CT) used Monte Carlo simulations to study the regression parameters derived from the model equation $Y_i^\circ = X_i^\circ + 1$.[9] They set $X_i^\circ = -2, -1, 0, +1, +2$ and created simulated data sets by assuming $\sigma_{Xi}$ and $\sigma_{Yi}$ to be gaussian deviates each with mean 0 and standard deviation 0.5. They found that the difference between the arithmetic mean of the slopes obtained from 20,000 simulated data sets and the 'true' slope of 1 was statistically significant ($P < 0.01$). However, the geometric mean of the slopes did not exhibit this bias.

In this work, we extend the CT study to more general data sets. We find that for the cases studied, the arithmetic mean, geometric mean (the antilog of the mean of the logs), and angle mean (the tangent of the mean of the arctangents) of the slopes are all biased in the sense described above. To interpret the angle mean, recall that the arctangent of the slope is the angle the regression line forms with the $X$ axis. Unlike these various means, the median of the slopes is consistently unbiased. Similarly, for the general case, only the median of the intercepts is unbiased.

*Author to whom correspondence should be addressed.

The biases in the slopes and intercepts arise from the fact that when there are errors in both variables, the distributions of the slopes and of the intercepts are not normal. This non-normality has the additional consequence that the standard errors of the slopes and intercepts cannot be used to calculate confidence intervals.

## SIMULATIONS AND CALCULATIONS

Following the CT example, we set $X_i^\circ = -2, -1, 0, 1, 2$ and $Y_i^\circ = 1 + X_i^\circ$. Simulated data points, $X_i$ and $Y_i$, were generated from these exact variables by means of the equations

$$X_i = X_i^\circ + \epsilon_{Xi}\sigma_{Xi}; \quad Y_i = Y_i^\circ + \epsilon_{Yi}\sigma_{Yi},$$

where $\epsilon$ is a gaussian random deviate with mean 0 and standard deviation 1, and $\sigma_{Xi}$ and $\sigma_{Yi}$ are the uncertainties in $X_i$ and $Y_i$, respectively. The gaussian deviates were obtained using the method of Box and Muller.[10] The pseudo-random numbers required by the Box–Muller algorithm were calculated from the well established congruential multiplicative generator based on $2^{31} - 1$ and $7^5$.[11–13]

Since several hundred thousand random numbers were used in this study, it was important to check for deviations from randomness and from normality. We examined $\chi^2$, means, standard deviations, skews, run frequencies and lengths, and several autocorrelations.[14–17] These tests were conducted for the entire set of numbers as well as for the subsets added to each $X_i^\circ$ and $Y_i^\circ$. For each test, deviations from randomness or normality were statistically not significant ($P > 0.05$).

For each data set we obtained the regression slope and intercept using the YW method described above. For each group of data sets derived from the same model we calculated the following statistics of the slopes: mean and its standard deviation, skew, kurtosis, and $\chi^2$ per degree of freedom. In addition, we obtained the geometric mean and its standard deviation, the tangent of the mean arctangent and its standard deviation, the median and the nonparametric estimates[18] of its central 68.3 and 90% confidence intervals. The same statistics, with the exception of the tangent, were obtained for the intercepts. All calculations were performed in VS/APL on a mainframe Amdahl 5870, in double precision.

## RESULTS

### *The Christian–Tucker data set*

The CT data set has been described above. Table 1 gives the results of the ordinary least squares (OLS) and the York–Williamson (YW) treatment of 10,000 simulated CT data sets of five points each. These results are in excellent agreement with those reported by CT: CT report $-0.0507$ and 0.029 for the biases in the OLS and YW slopes; we obtain $-0.0498$ and 0.0288. In order to assess the precision of the results, 10 groups of 10,000 data sets were analyzed. Each of the values shown in Table 1 is an average over the 10 groups. Typically, fluctuations in the median and the various means from one group to another were less than $\pm 0.002$.

Standard deviations, $\sigma$, for the slopes and intercepts were calculated using Williamson's expressions.[2] These estimates of $\sigma$ obtained from $\sigma_{Xi}$ and $\sigma_{Yi}$ using propagation-of-variance are approximately 10% too low. For example, $\sigma_{am}$ for the slope obtained using the propagation-of-variance procedure is 0.2236; the observed value is 0.247. The difference arises because the propa-

Table 1. Regression statistics for the Christian and Tucker data sets*†

| | OLS | | | YW | | | |
|---|---|---|---|---|---|---|---|
| | Bias | $\sigma$ | $t$ | Bias | $\sigma$ | $t$ | Counts† |
| Slopes | | | | | | | |
| Arithmetic mean | −0.0498 | 0.217 | −22.9 | 0.0288 | 0.247 | 11.6 | 46.5 |
| Mean of angles | −0.0719 | 0.208 | −34.6 | 0.00058 | 0.233 | 0.3 | 26.0 |
| Geometric mean | −0.0738 | 0.212 | −34.8 | 0.00061 | 0.238 | 0.3 | 26.0 |
| Median | −0.0703 | 0.218 | −32.3 | 0.00083 | 0.249 | 0.3 | 25.6 |
| Intercepts | | | | | | | |
| Arithmetic mean | 0.00016 | 0.313 | 0.5 | 0.00017 | 0.326 | 0.05 | 24.7 |
| Geometric mean | −0.0564 | 0.364 | −15.5 | 0.0616 | 0.388 | −15.9 | 0.4 |
| Median | −0.00002 | 0.313 | −0.01 | −0.00023 | 0.326 | −0.07 | 26.0 |

*All values are averages over 10 runs of 10,000 data sets.

†Based on the division of each run of 10,000 data sets into 50 groups of 200 data sets each. The number of counts is the average number of estimates (out of a total of 50) that lie below the true value.

gation-of-variance procedure, which neglects contributions higher than first-order, is inaccurate when the errors in $X$ and $Y$ are large. For smaller values of the errors (0.05 rather than 0.5), the propagation-of-variance estimates agree more closely with the observed values. Additional calculations confirmed CT's observation that $\sigma$ is essentially proportional to $\sigma_X$ or $\sigma_Y$ and that the bias in the arithmetic mean of the slopes is proportional to $\sigma_X^2$ or $\sigma_Y^2$. In the present context, the bias of an estimator of a parameter is the expectation value of that estimator minus the true value of the parameter calculated from the exact data set. The values of $\sigma$ given in Table 1 are calculated from the means of the variances observed for each of the 10 groups. These values of $\sigma$ are quite stable; their range is no greater than $\pm 2\%$ of the mean.

The statistical significance of a bias is traditionally tested by means of the Student $t$-statistic, the bias divided by the standard error of the mean of the slopes or intercepts. The values of $t$ in the table are averages over the 10 groups. The observed standard deviation of each $t$ over the 10 groups was approximately 1 as expected.[16] If the absolute value of $t$ for a particular estimator is less than 1 or 2, the bias is less than 1 or 2 standard errors from the 'true' value. In this work, we consider such an estimator to be unbiased. This criterion is in accord with the usual threshold of statistical significance, *i.e.* $P = 0.05$.

On the other hand, if the absolute value of $t$ is greater than say, 10, the estimator is almost certainly biased. Assuming that the calculated slopes and intercepts are normally distributed and that the estimator were unbiased, an absolute value of $t$ as large as 10 would occur by chance with a probability of $< 10^{-23}$.[19] Even though, as will be shown below, the actual distributions of the slopes and intercepts are not normal as is required for the application of the $t$-test, we can say with confidence that this extremely small probability indicates a biased estimator.

In contrast, the mean values of the intercepts obtained from either the OLS and YW treatments are unbiased. This result is a consequence of the fact that the mean of the values of $X^\circ$ is 0, and as a result, the intercept ($\langle Y \rangle - b\langle X \rangle$) equals the mean of the values of $Y_i$. The correlation between the slopes and their respective intercepts is 0 for the exact data set. For the actual CT data sets, correlation coefficients averaged 0.006 with an observed range of 0.02. The medians of the intercepts for both regression methods are also observed to be unbiased estimators, but the geometric means are clearly biased and so are not included in the subsequent tables.

As mentioned above, tests of bias using the Student $t$-statistic assume that the parameters are normally distributed. To test this assumption, we calculated $\chi^2$/(degrees of freedom), the skew, and the kurtosis of the parameters for each group of 10,000 data sets. For a normal distribution, these statistics take on the values 1, 0, and 3. For the 10 groups, the means and standard deviations of these statistics for the YW slopes were $34 \pm 3$, $0.90 \pm 0.09$, and $47 \pm 20$, respectively, indicating a decidedly non-normal distribution that is asymmetric and heavy-tailed. However, the corresponding means and standard deviations of these statistics for the intercepts, $0.9 \pm 0.4$, $-0.009 \pm 0.028$ and $3.8 \pm 1.4$, are consistent with a normal distribution.

A more detailed characterization of the distributions of the slopes and intercepts can be obtained by numerically ordering each group of 10,000 slopes. In a normal distribution, 68.3% of the values lie within $\pm\sigma$ of the mean value. To obtain corresponding values for the actual distribution, we select the median, the 8414th and the 1587th entries, which we label $M$, $B_u$, and $B_L$, respectively. If the distribution were normal, both $(B_u - M)$ and $(M - B_L)$ would equal $\sigma$. For the 10 groups of YW slopes, we find $(M - B_L) = 0.828(\pm 0.008)\sigma$ and $(B_u - M) = 1.043(\pm 0.021)\sigma$. The corresponding differences for the 90% interval should, in a normal distribution, be $\pm 1.64\sigma$. For the actual distribution, we find the differences to be $1.30(\pm 0.019)\sigma$ and $1.90(\pm 0.032)\sigma$. Thus, the distribution of slopes is clearly non-normal. For the intercepts, $(B_u - M)$ and $(M - B_L)$ differ on average from $\sigma$ by less than $0.4(\pm 2.9)\%$, consistent with a normal distribution.

The direct examination of the distributions of slopes and intercepts provides a nonparametric method for evaluating the bias. We first partition each group of 10,000 slopes (or intercepts) into 50 bins of 200 each. For each bin, we calculate the following estimators of the slope: the mean, geometric mean, angle-averaged mean (tangent of the mean of the arctangents), and median. For the intercepts, we determine the mean, geometric mean, and median. The Central Limit Theorem states that, in the limit of large $N$, the means of samples drawn from a

population with finite $\sigma$ become normally, and thus, symmetrically distributed. Since each of the estimators obtained from a bin of 200 slopes or intercepts is either a mean, a monotonic function of a mean, or a median, the estimator will have equal probability of being either greater than or less than the mean of the entire population of calculated slopes or intercepts. Consequently, approximately 25 of the 50 values of the estimator will lie above (or below) the value of the estimator obtained from the total population of slopes or intercepts.

We test for bias by counting the number of the 50 values that lie above or below the true value of the slope or intercept. If the estimator is unbiased, this count should also be approximately 25. The values in Table 1 labeled 'counts' are the number of times (out of 50) that the estimators, averaged over the 10 groups were smaller than 1, the true value of both the slope and intercept. For example, on averaging over the 10 groups, we find that 46.5 out of the 50 arithmetic means of 200 slopes lie below the true value of 1. The variation in these 'counts' among the 10 groups ranged from 2 to 4. These results confirm the conclusion suggested by the $t$-tests that the arithmetic mean is a biased estimator of the true slope.

It is natural to ask whether these results for the CT data sets depend on the number of points in each set. To address this question, 10,000 data sets were constructed each with 17 points whose values of $X_i^\circ$ were evenly spaced between $-2$ and $+2$. Setting $\sigma_X = \sigma_Y = 0.5$, the OLS slopes were characterized by $\sigma = 0.121$ and $t = 100$ for the arithmetic mean estimator. A second group of 10,000 consisted of data sets with four points, each with its own value of $X_i$ and $Y_i$, scattered from $X^\circ = -2$, four scattered from $X^\circ = -1$, *etc.*, for a total of 20 points in each set. For OLS regression, $\sigma = 0.100$ and $t = 99$. As expected, in both cases the value of $\sigma$ was smaller than that for the 5 point data set ($\sigma \approx 0.2$, see Table 1). However, the bias of the arithmetic mean of slopes increased markedly, resulting in a much larger value of $t$. For both of these cases, the arithmetic mean OLS slope differs from the true slope by approximately $1.0\sigma$. Thus, increasing the size of the data set does not reduce the bias if an inherently incorrect regression method is used in the analysis.

These two groups of data sets were then analyzed using the YW method. The values of $\sigma$, the bias, and $t$ for each group decreased from the values obtained from the sets with five data points. However, although the magnitude of the bias was reduced, the $t$-statistic showed that the bias remained statistically significant. The median estimators of the slope and intercept of the larger data sets remained unbiased.

We can summarize the analyses of the CT data sets as follows: when there are errors in both coordinates, the arithmetic mean of the slopes obtained by OLS regression is a biased estimator. The arithmetic mean of the slopes obtained using the YW procedure is also biased although considerably less so. However, the geometric mean, angle-averaged mean and median of the YW slopes are unbiased. The arithmetic mean and median provide unbiased estimators of the intercepts. Thus, for the cases studied, only the median is an unbiased estimator for both slope and intercept.

*Other homoscedastic data sets*

We now investigate data sets for which $X_i^\circ = 1, 2, 3, 4$, and 5 and $Y_i^\circ = 1 + bX_i^\circ$, where $b = 1/4$, $1/2$, 1, 2, or 4. $\sigma_X$ and $\sigma_Y$ are chosen from the set 0.125, 0.25, and 0.5. In these examples, determining the intercept involves a short extrapolation. These types of data sets arise in numerous practical situations such as analytical calibrations or dose–response plots where the blank is not determined. In this connection, we emphasize that the present treatment, like that of CT, assumes independent errors in each value of $X_i$ and $Y_i$. This assumption implies that each value of these variables is a measured rather than a preset quantity.

The results shown in Table 2 are based on YW regressions on a single group of 10,000 data sets for each case. The results of the preceding section show that this number of simulations is sufficient. For the sake of clarity, this table includes only a selection of the many possible combinations of slope, $\sigma_X$, and $\sigma_Y$. Since the values of $\sigma$ for the various averaging methods are equal to within a few per cent, only the values of $\sigma$ based on the arithmetic mean are shown.

In general, estimators of the slope based on the arithmetic mean, geometric mean and angle-averaged mean are all biased. For the special case, $\sigma_X = \sigma_Y$, the angle-averaged mean is an unbiased estimator of the slope. If the slope is equal to $\sigma_Y/\sigma_X$, the geometric mean is an unbiased estimator. However, the estimator based on the arithmetic mean is always biased while the estimator based on the median is

Table 2. Regression statistics for selected homoscedastic data sets*†

| Slope | 1 | | 1/4 | | 4 | | 1 | |
|---|---|---|---|---|---|---|---|---|
| $\sigma_X, \sigma_Y$ | 0.5 | 0.5 | 0.5 | 0.125 | 0.5 | 0.5 | 0.5 | 0.125 |
| Slope statistics‡ | | | | | | | | |
| $\sigma_{am}$ | 0.244 | | 0.0612 | | 0.731 | | 0.184 | |
| $t_{am}$, counts | 10.4 | 48 | 12.1 | 47 | 15.5 | 49 | 15.2 | 46 |
| $t_a$, counts | −0.9 | 23 | 10.8 | 47 | 0.6 | 29 | 7.2 | 43 |
| $t_g$, counts | −0.9 | 23 | 0.8 | 25 | 7.8 | 45 | 7.4 | 43 |
| $t_{med}$, counts | 0.9 | 25 | 0.7 | 28 | 0.2 | 27 | −0.6 | 25 |
| Intercept statistics‡ | | | | | | | | |
| $\sigma_{am}$ | 0.803 | | 0.200 | | 0.238 | | 0.597 | |
| $t_{am}$, counts | −10.2 | 5 | −11.1 | 1 | −14.1 | 2 | −14.3 | 1 |
| $t_{med}$, counts | −0.4 | 23 | −1.6 | 20 | −0.8 | 21 | −0.5 | 25 |

*All values are for 10,000 data sets using *YW* regression.
†am = Arithmetic mean, a = angle average, g = geometric mean, med = median.
‡The bias in each case is approximately equal to $t\sigma_{am}/100$ (see text).

always unbiased. Both the parametric and nonparametric methods for detecting bias agree in all cases.

As was the case with the CT data set, the median is also found to be an unbiased estimator of the intercept. However, the arithmetic mean is now significantly biased. Since the mean of the values of $X^\circ$ is no longer 0, the slopes and intercepts are correlated ($\rho = -0.915 \pm 0.001$), resulting in a biased intercept.

Direct examination of the 10,000 intercepts ranked in numerical order shows that their distribution is clearly asymmetric and thus nonnormal. The ratio $(M - B_L)/(B_u - M)$ varied between 1.2 and 1.33. $\chi^2$ per degree of freedom exceeded 25, the kurtosis exceeded 30, and the absolute value of the skew exceeded 0.7 in all cases studied.

As was the case for the CT data sets, increasing the number of points in each data set had no qualitative effect on the results. The bias decreased somewhat, but it remained statistically significant.

In summary, for data sets with homoscedastic errors, if $\sigma_X$ is not equal to $\sigma_Y$ and $\sigma_Y/\sigma_X$ is unequal to the slope, only the medians are found to be unbiased estimators of the slope and intercept.

*Heteroscedastic errors*

In view of the large number of possible combinations of slopes and values of $\sigma_X$ and $\sigma_Y$, we focus, somewhat arbitrarily, on data sets for which the slope is equal to 1, $\sigma_X$ is unequal to $\sigma_Y$, and the mean of the $X_i^\circ$ is not equal to 0. These data sets avoid the special cases in which the angle-average or the geometric means of the slopes are unbiased.

Table 3 shows the results of the analysis of three data sets illustrating heteroscedastic errors in one or both variables. In the first case, $\sigma_{Xi} = 0.5$ and $\sigma_{Yi} = 0.05i$, $i = 1, \ldots 5$. In the second case, $\sigma_{Xi} = 0.2i$ and $\sigma_{Yi} = 0.5i$. Finally, in the third case, $\sigma_{Xi} = 0.2i$ and $\sigma_{Yi} = 0.125i$. In all cases the exact slopes and intercepts were set equal to 1. The YW regression method was used throughout. Table 3 shows that, as in all previous cases, the median of the slopes and intercepts are unbiased. The arithmetic and geometric means of the intercept and the arith-

Table 3. Regression statistics for selected heteroscedastic data sets*

| $\sigma_{X1}, \sigma_{X5}$ | 0.5 | 0.5 | 0.2 | 1 | 0.2 | 1 |
|---|---|---|---|---|---|---|
| $\sigma_{Y1}, \sigma_{Y5}$ | 0.05 | 0.25 | 0.05 | 0.25 | 0.125 | 0.125 |
| Slope statistics | | | | | | |
| $\sigma_{am}$ | 0.187 | | 0.199 | | 0.196 | |
| $t_{am}$, counts | 13.9 | 49 | 17.3 | 50 | 15.1 | 47 |
| $t_a$, counts | 5.7 | 38 | 9.0 | 46 | 6.7 | 43 |
| $t_g$, counts | 5.9 | 38 | 9.3 | 46 | 6.9 | 44 |
| $t_{med}$, counts | −0.9 | 26 | 1.6 | 28 | −1.1 | 21 |
| Intercept statistics | | | | | | |
| $\sigma_{am}$ | 0.600 | | 0.357 | | 0.378 | |
| $t_{am}$, counts | −13.1 | 2 | −14.4 | 3 | −12.2 | 3 |
| $t_{med}$, counts | −0.4 | 27 | −1.1 | 28 | 0.1 | 23 |

*See footnotes of Table 2.

metic, geometric, and angle-averaged means of the slopes all show significant biases. The values of $\chi^2$ per degree of freedom, the skew, kurtosis and $B_u$ and $B_L$ indicate that the distributions of the slopes and intercepts are significantly non-normal.

Calculations with data sets containing a greater number of points show similar results. The bias and the values of $t$ decreased only slightly and not uniformly. The 'count' values were not significantly changed.

To summarize, as was the case with the other types of data sets, for the data sets involving heteroscedastic errors studied here, only the medians provide unbiased estimators of the slopes and intercepts. The magnitude and statistical significance of the bias of the other estimators are not strong functions of the number of data points.

## DISCUSSION

The present results reinforce the conclusion of CT[9] that ordinary least squares regression should not be used when both $X$ and $Y$ are subject to errors because, in general, the slopes and intercepts will be significantly biased. As was shown above for the data sets with 17 and 20 points, the mean OLS values for the slope differ from the true value by approximately $1.0\sigma$. We believe that this bias is sufficiently large to necessitate the use of the YW algorithm in data analysis especially in cases where replicate measurements are used to offset the effects of low precision data. While the YW algorithm significantly reduces the biases of the slope and intercept (based on the arithmetic mean), it does not entirely eliminate the biases. Estimators based on the arithmetic mean, geometric mean and angle-averaged mean all remain biased. Only the median provides unbiased estimators of the slope and intercept for all the cases studied here.

The presence of bias indicates that the distributions of the slopes and intercepts are not normal. As shown by the various statistics discussed above, such as the skew, kurtosis, and the values of $B_u - M$, and $M - B_L$, the deviations from normality are significant. Recall that $M$ is the median, and the interval $[B_L, B_u]$ encompasses 68.3% of the total number of slopes or intercepts. This result implies that the customary parametric estimates of the errors of the slope and intercept will be incorrect. Thus, for the CT data set, the 68.3% confidence interval for the slope is given by $[M - 0.83\sigma, M + 1.04\sigma]$. The symmetric interval, $m \pm \sigma$, where $m$ is the mean, is appropriate only if the calculated slopes are normally distributed.

Although the biases in the parameters obtained by YW regressions are clearly statistically significant, their magnitudes relative to the standard deviations of the slopes and intercepts are small. In most cases, it is unlikely that these biases would lead to serious errors in the analysis of a single set of experimental data. However, these biases may become important in data analyses involving functions of the slopes and/or intercepts. Moreover, they may also become important in the calculations involved in determining the optimal design of an experiment. In such calculations, the analysis of many hypothetical data sets might be required to select the appropriate values of the independent variable. The standard errors of the parameters such as the slope and intercept may become small enough so that the bias becomes important as well as statistically significant. For these cases, the use of biased, and thus incorrect, values of parameters like the slope and intercept may lead to a non-optimal choice of the $X_i^o$'s. In addition, since the distributions of the parameters are non-normal, estimates of confidence intervals for the parameters should be based on (o. at least checked by) nonparametric methods, such as the one outlined above.

The present study is restricted to normally distributed errors in the dependent and independent coordinates and to straight line regressions. For more general situations, the question of whether any averaging procedure, including the median, provides unbiased estimators of the regression parameters remains for future investigations. However, even in these more general situations, the nonparametric method described above will continue to be applicable for the estimation of confidence intervals.

## REFERENCES

1. D. York, *Can. J. Phys.*, 1966, **44**, 1079.
2. J. H. Williamson, *Can. J. Phys.*, 1968, **46**, 1845.
3. M. Lybanon, *Am. J. Phys.*, 1984, **52**, 22.
4. A. H. Kalantar, *Trends Anal. Chem.*, 1990, **9**, 149.
5. J. R. Macdonald and W. J. Thompson, *Am. J. Phys.*, 1992, **60**, 66.
6. P. J. Ogren and J. R. Norton, *J. Chem. Educ.*, 1992, **69**, A130.
7. W. H. Press and S. A. Teukolsky, *Comp. Phys.*, 1992, **6**, 274.

8. D. L. MacTaggart and S. O. Farwell, *J. AOAC Int.*, 1992, **75,** 608.
9. S. D. Christian and E. E. Tucker, *Am. Lab.*, 1986, **18,** 33.
10. G. E. P. Box and M. E. Muller, *Ann. Math Statist.*, 1958, **29,** 610.
11. S. K. Park and K. W. Miller, *Commun. ACM*, 1988, **31,** 1192.
12. R. Y. Rubinstein, *Simulation and the Monte Carlo Method*, Chap. 2. Wiley, New York, 1981.
13. P. Bratley, B. L. Fox, and L. E. Schrage, *A Guide to Simulation*, Chap. 5. Springer, New York, 1983.
14. L. Sachs, *Applied Statistics. A Handbook of Techniques*, 2nd Ed., Chap. 1. Springer, New York, 1984.
15. R. R. Sokal and F. J. Rohlf, *Biometry*. 2nd Ed. Freeman, New York, 1981.
16. J. F. Kenney and E. S. Keeping, *Mathematics of Statistics*, 3rd Ed., Chap. 12. Van Nostrand, Princeton, 1954.
17. E. L. Crow, F. A. Davis, and M. W. Maxfield, *Statistics Manual*, Chap. 1. Dover, New York, 1960.
18. J. S. Alper and R. I. Gelb, *J. Phys. Chem.*, 1990, **94,** 4747.
19. M. Abramowitz and I. A. Stegun (eds), *Handbook of Mathematical Functions*, Table 26.2. Dover, New York, 1965.

Pergamon

0039-9140(95)01455-1

*Talanta*, Vol. 42, No. 4, pp. 605–612, 1995

0039-9140/95 $9.50 + 0.00

# A MULTI-WAVELENGTH PHOTOMETER BASED ON LIGHT-EMITTING DIODES

PETER C. HAUSER,* THUSITHA W. T. RUPASINGHE and NORMAN E. CATES
The University of Auckland, Department of Chemistry, Private Bag 92019, Auckland, New Zealand

(*Received* 14 *July* 1994. *Revised* 25 *October* 1994. *Accepted* 27 *October* 1994)

**Summary**—The light originating from seven light-emitting diodes of different colours is guided, one at a time, into a measuring cell by means of a fibre optic coupler. Detection is carried out with photodiodes which are connected to a log-ratio amplifier yielding direct absorbance readings. Optical filters are used to narrow the emission band from blue light emitting diodes as these bands are relatively wide compared to those of the emitters of other colours. An inexpensive and compact multi-wavelength photometer covering the visible range is thus obtained, which in many cases can replace a conventional spectrophotometer for absorbance measurements. The performance for a range of commonly used photometric analytical procedures is described and compared to conventional measurements with a spectrophotometer.

Light-emitting diodes (LEDs) produce light with bandwidths of typically 25 nm which is comparable to the combination of wideband sources with interference type optical filters. It is, therefore, possible to carry out photometry with LEDs without the use of wavelength discriminating devices. the use of LEDs in photometric detectors has often been reported[1–21] and its application in flow-through methods has been reviewed.[22,23] The LEDs are commonly combined with photodiodes which measure the light intensity after passage through the sample. Geometric arrangements reported include dip-type probes and flow-through cells. The detectors have usually been connected to operational amplifiers in the current follower configuration which yield an output voltage directly proportional to the photo-current and hence light intensity. This signal represents transmittance measurements. A value corresponding to absorbance can be obtained by connection to a logarithmic amplifier. This is more appropriate because it is this value that is directly related to concentration according to Beer–Lambert's law. Such devices have been reported more recently.[17–21] LEDs with colours ranging from the blue to the infrared are available and, therefore, with the exception of the near-UV cover all the wavelength range that is commonly used for analytical spectrophotometry. Absorbance bands for molecular absorption spectroscopy are usually fairly wide, typically 100 nm, and it is therefore almost always possible to find a matching LED. A range of six LEDs of the colours blue, green, yellow, orange, red and near-infrared can thus in many cases replace a conventional visible-range spectrophotometer. However, most LED-photometers described to date have only employed a fixed wavelength for a predetermined purpose. A change of wavelength had to be effected by physically changing the light source. This limitation has been caused by the difficulty in coupling light from more than one source into a single detector cell. Bi-colour LEDs are available which contain two light emitting substrates in one body and have been used for a dual wavelength detector.[13] A tri-colour device has been constructed by using a green/yellow bi-colour LED and a number of red LEDs arranged concentrically around the bi-colour LED in order to pass red light into the cell as well.[14,15] The coupling of the light from two separate LEDs into a single cell with bifurcated optical fibres for the purpose of correction for turbidity has recently been described.[16] Here a multi-LED photometer is described that employs a fibre optic coupler to guide the light from up to seven LEDs into a single measuring cell.

*Author to whom correspondence should be addressed.

## EXPERIMENTAL

### *Electronic and optical components*

The 2 × 7 fibre optic coupler star coupler (15 × 4.5 × 1 cm) was purchased from Luxmatic (PF-SC 2 × 7/1000, Baar, Switzerland) and has cladded plastic fibre pig tails with 1 mm core. LEDs were obtained from Farnell Electronic Components (Auckland, New Zealand) (blue, Part No. 233-511), Radiospares (Auckland, New Zealand) (orange, Part No. 578-200), Hewlett-Packard (Palo Alto, CA) (yellow, HLMA-DLOO) and from Siemens (Wellington, New Zealand) (green, SFH 751; red, SFH 750; infrared, SFH 452). The photodiodes were also obtained from Siemens (SFH 250). The components from Siemens are specifically designed for easy coupling with the 1 mm plastic optical fibres. Conventional LEDs were connected by removing the plastic body close to the active substrate and polishing the surface. Special adaptors made from perspex allowed butting of the fibre end onto the emitter. The log-convertor (LOG100JP) was obtained from Burr-Brown (Tucson, AZ, U.S.A.). The digital panel meter (OEM 33) was from Anders (London, U.K.) and the optical filters were obtained from Eastman Kodak (Wratten Gelatine Filters No 32, 58 and 87, Kodak, Rochester, NY, U.S.A.). Photocurrents were measured by temporarily connecting one of the photodiodes to an operational amplifier in the current follower configuration (OPA121, Burr-Brown).

### *Spectra and conventional absorbance measurements*

Absorbance spectra and conventional absorbance values were obtained with a Shimadzu UV-160A spectrophotometer using 1 cm cuvettes. The emission spectra of the LEDs were acquired on a Hitachi F-2000 spectrofluorometer by mounting them individually in the cell holder. The spectra were redrawn from the scaled numerical output of the instrument. The quoted relative sensitivity values were obtained by comparing the slope of the LED calibration curve (using a mean where this was not constant) with the one obtained on the spectrophotometer.

### *Estimated absorbance values*

The measured emission intensities for the LEDs (for 5 nm intervals from 400 to 600 nm) were corrected for the wavelength dependent sensitivity of the silicon photodiode detector. The sensitivity was taken as 0.327 at 400 nm and to be linearly increasing to 1 at 600 nm.[24] The resulting values were scaled to a peak intensity of unity. Absorbance spectra for the dye representing the different measured concentrations were obtained by scaling (again at intervals of 5 nm from 400 to 600 nm) against the spectrophotometer values for the wavelength of highest absorptivity. The individual values were then transformed into transmittance. A numerical estimate of the light intensities for the different wavelengths measured by the detector was obtained by multiplying the intensity with the transmittance values, since $T = I/I_0$ and $I = T \cdot I_0$, where $T$ is the transmittance, $I_0$ the original intensity (emission intensities of the LED) and $I$ the intensity after passage through the cell. Adding the result for all wavelength intervals gave an estimate for the total intensity over the entire wavelength range. By comparing the total for the different concentrations with the total initial intensity (sum of the values for the LED emission spectrum) an estimate for the integrated overall transmittances was obtained. These values was then transformed back into absorbance according to $A = -\log T$.

### *Solutions*

For the Al determination by the Chrome Azurol S method standards were prepared with an appropriate amount of a stock solution of $KAl(SO_4)_2$, 4 ml of 1% ascorbic acid, 10 ml of 0.1% Chrome Azurol S solution, 4 ml of 20% sodium citrate and this was diluted to 100 ml.[25] The standard solutions for the Cu determination by the Cuprizone method were made up with an appropriate amount of a stock solution of $CuSO_4$, 5 ml of buffer (pH 8–9, 10% citric acid, pH adjusted with ammonia), 12 ml of 0.1% Cuprizone solution and this was diluted to 100 ml.[25] For the $NH_3$ determination by the Indophenol method, standard solutions were prepared from an appropriate amount of a stock solution of $NH_4Cl$, 10 ml of sodium phenolate (70 g of phenol in 15 ml of ethanol plus 20 ml acetone this was diluted with ethanol to 100 ml, then 10 ml of this solution was mixed with 10 ml of 30% aqueous NaOH and diluted with water to 50 ml), 4 ml of 2% sodium hypochlorite and this was diluted to 100 ml.[25] The standard solutions for the Cu determination by complexation with ethylenediaminetetraacetic acid (EDTA) were made up with an appropriate amount of a stock solution of $CuSO_4$, 5 ml of ammonia, 2 ml of 0.05*M* EDTA

and diluted to 100 ml.[26] The standard solution for the Ca determination were made up from an appropriate amount of a stock solution prepared from $CaCO_3$, 10 ml of 0.03% Chlorophosphonazo III, 4 ml of buffer solution (pH 7.5, 50 ml of 0.1*M* $KH_2PO_4$ and 41 ml of 0.1*M* NaOH diluted to 100 ml) and dilution to 100 ml.[25] The standard solutions for the chromium calibration curves were prepared from an appropriate amount of a stock solution of potassium dichromate mixed with 20 ml of $H_2SO_4$ (1:3) and diluted to 100 ml.[25] For the nitrite determination by a modified Griess method, the standards were prepared from an appropriate amount of a stock solution of $NaNO_2$, 2 ml of 0.5% sulphanilamide in 20% (v/v) HCl, 2 ml of 0.3% *N*-(1-naphthyl)-ethylenediamine dihydrochloride in 1% (v/v) HCl and dilution to 100 ml.[27] The standards for phosphate determination were made up with an appropriate amount of a stock solution of $KH_2PO_4$, 10 ml of molybdate ascorbic reagent (10 ml of 1% ammonium molybdate in 0.5*M* nitric acid and 10 ml of 0.7% ascorbic acid diluted to 100 ml) and diluted to 100 ml.[28]

## RESULTS AND DISCUSSION

### *Construction*

The circuit diagram for the multi-LED photometer is shown in Fig. 1. One out of a range of up to seven LEDs is selected with a rotary switch. The LEDs are connected to 1 mm plastic optical fibres leading to the coupler. The 7 × 2-plastic fibre star coupler which is based on the same type of 1 mm plastic fibres is used to merge the light from the seven input channels into two output fibres. One of these is brought to the measuring cell. The cell consists of a black perspex body into which the fibre is inserted and has a 1 cm pathlength and a cell volume of 8 $\mu$l. Details have been given elsewhere.[20] It would of course also be possible to pass the light through a conventional cuvette rather than employing the cell used here. The other fibre leads to the reference photodiode. The amplifier is wired in a log-ratio configuration which emulates absorbance measurements according to $V_o = \log(i_{ref}/i)$, where $V_o$ is the output voltage and $i_{ref}$ and $i$ are the currents from the reference and signal photodiodes, respectively.[29] The arrangement corresponds therefore to a double beam configuration and corrects for drifts in emission intensity of single LEDs and differences in intensity for the individual LEDs. The photocurrents resulting were found to be between about 5 and 18 nA for the green to infrared LEDs. Blue LEDs are presently only available with low intensities and a value of 410 pA was determined for the blue LED used here. This difference in currents for the different LEDs is within the dynamic range of the log-ratio amplifier and does not pose a problem.[29] The output voltage is brought to a digital panel meter for direct display of the measured absorbance. A metal box with dimensions of 20 × 6 × 15 cm (width × height × depth) is used to house the complete circuitry. The measuring

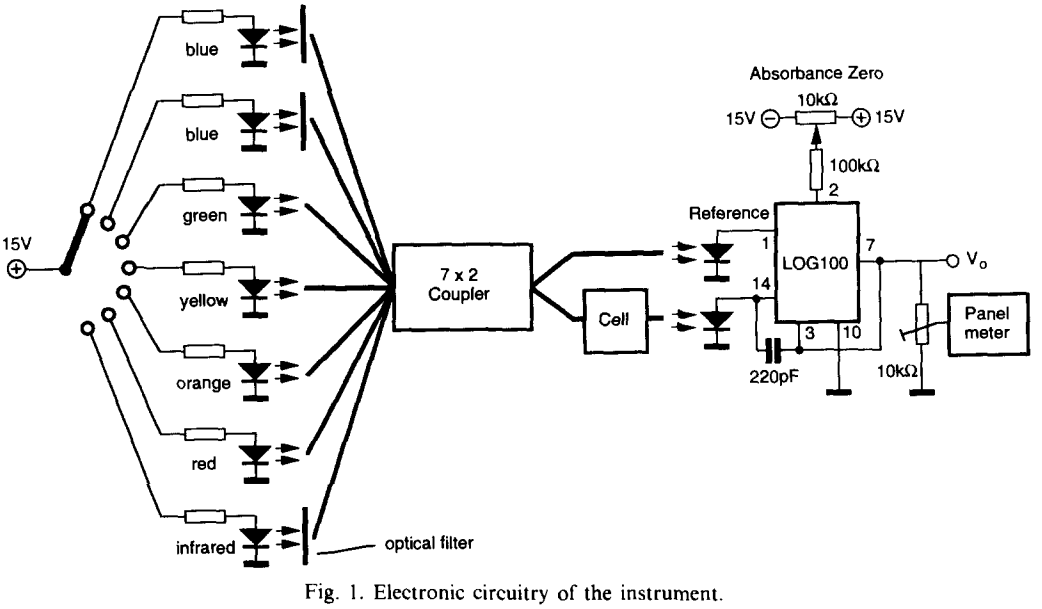


Fig. 1. Electronic circuitry of the instrument.

cell is mounted on the outside of the case for separation of the wet chemistry from the electrical part.

*Spectral considerations*

The emission spectra of the LEDs used for the photometer are given in Fig. 2. Note, that the intensities have been scaled. Incidentally, the spectral window almost exactly covers the visible range of the electromagnetic spectrum (380–780 nm).

The centre range from about 560–660 nm is covered by the widely used LEDs with colours from green to red. A large variety of types with different peak wavelengths, intensities and bodies are available for this range. The particular devices chosen here were picked in order to give a good distribution of peak wavelengths at 563, 590, 620 and 660 nm. The bandwidths for these LEDs are in the order of 20–25 nm (full width at half maximum).

For the longer wavelength range between about 700 and 800 nm few LEDs are available which is the reason for the gap at around 730 nm. Note, that the near-infrared LED with a maximum at 770 nm was combined with an optical filter (Kodak Wratten 87) in order to eliminate low emission intensities which were found at shorter Wavelength for this device.

The wavelength range below 550 nm is covered by blue LEDs. These have only recently become readily available and show an emission band of typically 70 nm bandwidth. This is relatively wide compared to the LED spectra of other colours, as illustrated by the dashed line in Fig. 2. The peak wavelengths of the available types are all between 450 and 480 nm and, therefore, there is also a lack of flexibility in the visible region below 550 nm. To alleviate this situation it was chosen to combine blue LEDs with optical filters. By combination with a long wavelength cut-off filter with appropriate properties (Kodak Wratten 32) it was found possible to obtain a band with a peak at 461 nm (first spectrum from the left in Fig. 2) which is close to the peak of the unfiltered emission, but shows a bandwidth of only 38 nm as compared to the 70 nm of the unfiltered band. The combination with a short wavelength cut-off filter (Kodak Wratten 58) yielded a band at 513 nm with a bandwidth of 40 nm (second spectrum in Fig. 2). These bandwidths do not quite match the values obtained with the conventional LEDs but are a considerable improvement to the unfiltered emission band. The wavelength filters cause a reduction of the photocurrent on the detector from the 410 pA for the unfiltered blue LED to 180 and 80 pA for the shorter and the longer wavelength bands, respectively.

*Performance*

The system was tested with several photometric procedures. The calibration curves obtained with the LEDs in the centre range (560–660 nm) are given in Figs 3–7. Generally the LEDs that gave the highest sensitivity were employed and for comparison conventional measurements with a spectrophotometer using the wavelength of peak absorbance were also carried out. As the pathlength is 1 cm in both cases, it is possible to directly compare the results obtained with the two methods.

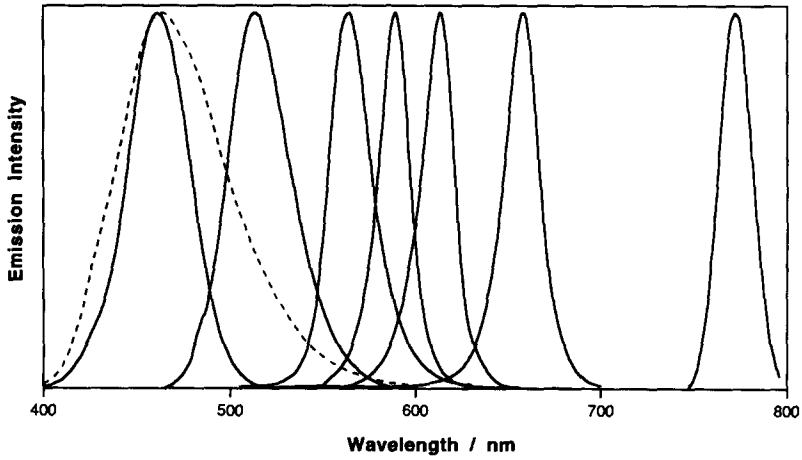


Fig. 2. Emission spectra of the LEDs employed. From left to right: blue without filter (dashed line), blue with long wavelength cut-off filter, blue with short wavelength cut-off filter, green, yellow, orange, red, near-infrared.

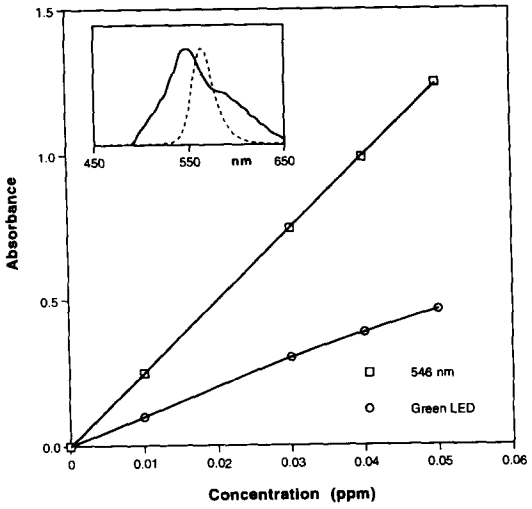


Fig. 3. Calibration curves for the determination of aluminium by the chrome azurol S method obtained for the wavelength of highest sensitivity on a spectrophotometer and for the LED-photometer. The inset shows the absorbance spectrum of the complex (solid line) and the emission band from the LED (dashed line).

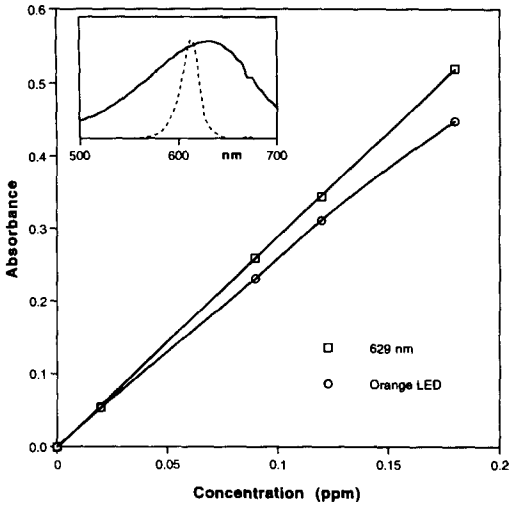


Fig. 5. Calibration curves for the determination of ammonia by the indophenol method.

The calibration curve obtained for the determination of aluminium by the chrome azurol S method is given in Fig. 3. A considerable loss of sensitivity (60%) is observed as it is not possible to match the absorbance peak at 546 nm (see inset of Fig. 3) with an LED having an emission band closer than the one of the green emitter (peak at 563 nm, dashed line inset of Fig. 3). A much closer match of the calibration curves was found for the determination of copper ions by the cuprizone method, see Fig. 4, where the sensitivity of the LED calibration curve is 90% of the spectrophotometer value. This is not surprising since the emission band of the yellow LED comes close to the peak of the wide absorbance band of the complex as illustrated in the inset of Fig. 4. The situation is very similar for the ammonia determination by the indophenol method using an orange LED as illustrated in Fig. 5. Not quite such a good match was possible for the copper determination by measuring the absorbance of its complex with ethylenediaminetetraacetic acid (EDTA), see Fig. 6, were the red LED shows a relative sensitivity of 75%. The match is poorer again for the calcium complex with chlorophosphonazo III using the same LED leading to a 40% loss of sensitivity as shown in Fig. 7.

The red wavelength region between 660 and 770 nm is perhaps not often used and the lack

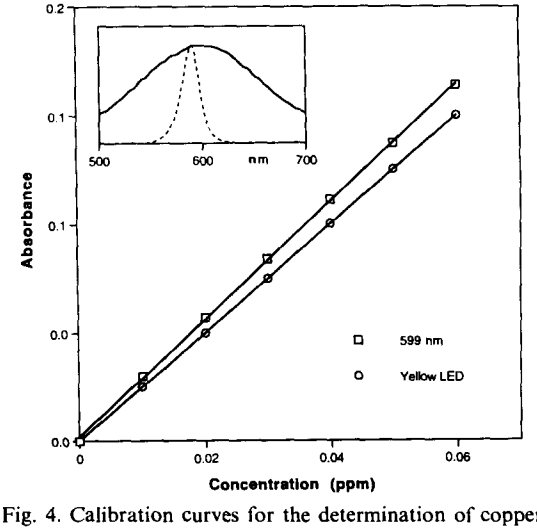


Fig. 4. Calibration curves for the determination of copper by the cuprizone method.

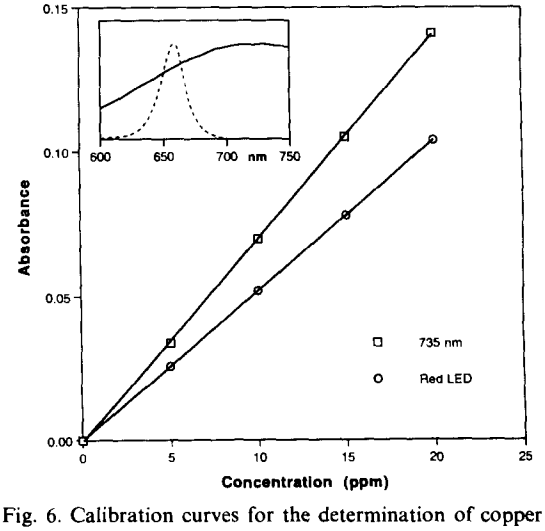


Fig. 6. Calibration curves for the determination of copper by complexation with EDTA.

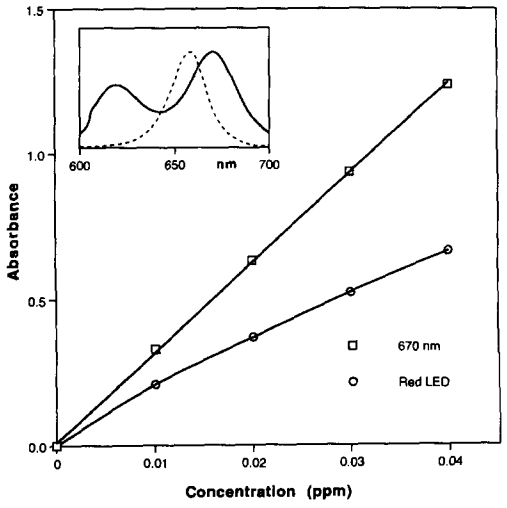


Fig. 7. Calibration curves for the determination of calcium by the chlorophosphonazo III method.

of LEDs with different colours for this range is not a major hindrance. A common analytical procedure employing this wavelength region, however, is the molybdate method for phosphate. As illustrated in Fig. 8, excellent results can be obtained by using the near-infrared LED with a peak-wavelength at 770 nm.

As was reported previously, the light from a blue LED may be used for the determination of absorbing species with peaks in the region of 450–510 nm.[20] It is demonstrated here that the sensitivity with this LED can be improved in certain cases by combination with inexpensive optical filters. The calibration curves for dichromate with a peak absorbance at the low edge of the emission from the blue LED (442 nm) are given in Fig. 9. An improvement of the relative

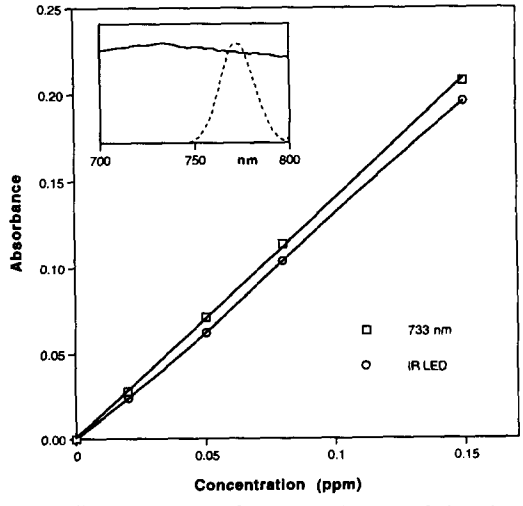


Fig. 8. Calibration curves of the determination of phosphate by the molybdate method.

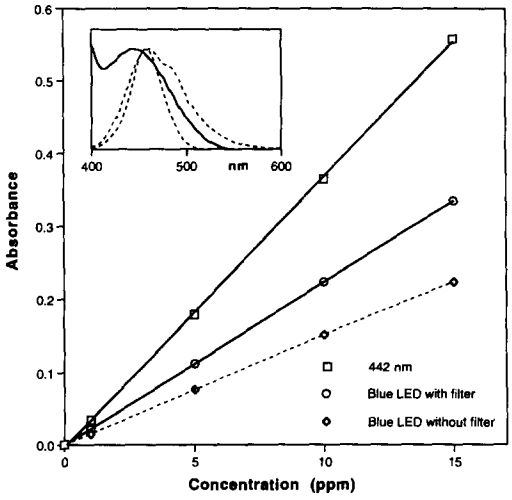


Fig. 9. Calibration curves of the determination of chromium by the dichromate method obtained for the wavelength of highest sensitivity on a spectrophotometer and for the LED-photometer using the blue LED with and without long wavelength cut-off filter. The inset shows the absorbance spectrum for dichromate (solid line) and the emission bands for the blue LED with and without filter (dashed lines).

sensitivity compared to the spectrophotometer from 40 to 60% was found for this system on introducing the optical filter. More pronounced is the effect for the determination of nitrite by a modified Griess method as illustrated in Fig. 10. The dye has an absorbance peak at 535 nm which falls into the relatively wide gap in

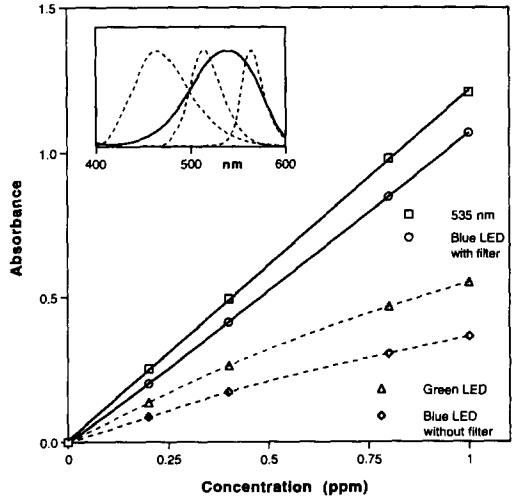


Fig. 10. Calibration curves for the determination of nitrite by the modified Griess method obtained for the wavelength of highest sensitivity on a spectrophotometer and for the LED-photometer using the blue LED with and without short wavelength cut-off filter and the green LED. The inset shows the absorbance spectrum for the dye (solid line) and the emission bands for the blue LED with and without filter and the green LED (dashed lines from left to right, respectively).

emission between the unfiltered blue and the green LEDs as seen in the inset of Fig. 10. Both the blue and the green LEDs led to a sensitivity of less than 50% of the result of the monochromatic wavelength of 535 nm. The use of the optical filter which eliminates low wavelengths from the blue LED emission led to a sensitivity of 90% of the spectrophotometer result for this important photometric procedure.

The relative sensitivity cannot be anticipated from the closeness of the peaks of absorbance and emission bands alone. This for example would predict a lower sensitivity for the copper determination by complexation with EDTA (Fig. 6, $\Delta\lambda = 75$ nm) than for the calcium determination with the chlorophosphonazo III method (Fig. 7, $\Delta\lambda = 10$ nm) when in fact the opposite is observed. Similarly, by considering the spectral match for the nitrite determination (Fig. 10) it is not apparent why the blue LED with filter should give a curve of higher sensitivity than the green LED. It is however possible to fairly closely predict the experimental calibration curves by numerically integrating Lambert–Beer's law over the entire spectra of LEDs and dyes as well as considering the variation of the detector sensitivity with wavelength. When applying this procedure (see Experimental Section) to the data for Fig. 10 a good prediction for the three different LED calibration curves was obtained as is illustrated in Fig. 11. The curvature obtained with some of the LED calibration graphs is also predicted and it can be shown that this is due to the fact that the absorptivities are not constant across the spectral emission bands for the LEDs. The loss of sensitivity of the silicon photodiode detector towards the short wavelength range has the effect of causing a slight apparent skewing of the LED emission spectra towards the high wavelength side of the bands.

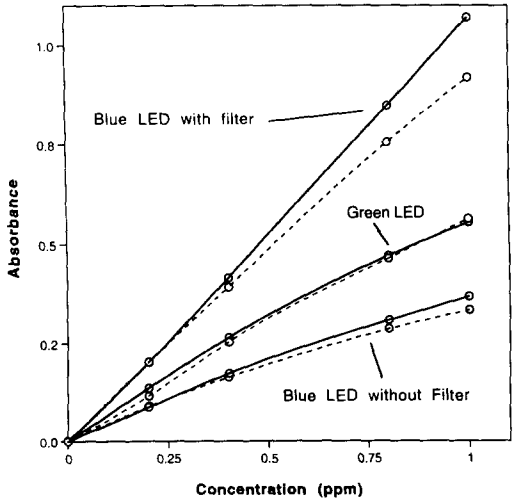


Fig. 11. Calibration curves for the nitrite determination as predicted theoretically from the spectra of the dye and the LEDs (dashed lines) in comparison with the experimental data (solid lines).

The precision obtained with the LEDs was generally 0.002 absorbance units or better (standard deviation, $n = 5$) which is close to the resolution of the instrument (0.001 absorbance units) and comparable with the spectrophotometer results. The relative error in terms of concentration depends on the slope of the calibration curve and varies between about 0.2% in the best case and about 5% for the worst case reported here. Whether the loss of sensitivity encountered with the LEDs is significant depends therefore on the desired relative precision in terms of concentration but should not be a concern in most cases.

## CONCLUSION

It was found that by combining different LEDs covering a wide wavelength range a versatile, inexpensive, compact and portable photometer for absorbance measurements in the visible wavelength range can be obtained. The instrument may also be used in the field as it can be powered by a battery. The lack of strict adherence to Lambert–Beer's law in terms of non-linearity of many of the calibration curves is not a limitation provided the user is aware of this fact and the calibration is carried out appropriately.

*Acknowledgements*—The authors thank Dean Clark from Siemens Wellington for providing samples of some of the optoelectronic components used. Grants from the University of Auckland Research Committee and New Zealand Lottery Science are gratefully acknowledged.

## REFERENCES

1. H. Flaschka, C. McKeithan and R. Barnes, *Anal. Lett.*, 1973, **6**, 585.
2. T. Anfält, A. Granéli and M. Strandberg, *Anal. Chem.*, 1976, **48**, 357.
3. D. Betteridge, E. L. Dagless, B. Fields and N. F. Graves, *Analyst*, 1978, **103**, 897.
4. D. J. Hooley and R. E. Dessy, *Anal. Chem.*, 1983, **55**, 313.
5. M. Trojanowicz, W. Augustyniak and A. Hulanicki, *Mikrochim. Acta*, 1984, 17.
6. G. J. Schmidt and R. P. W. Scott, *Analyst*, 1984, **109**, 997.
7. K. S. Johnson, C. L. Beehler and C. M. Sakamoto-Arnold, *Anal. Chim. Acta*, 1986, **179**, 245.

8. J. A. Sweileh, P. K. Dasgupta and J. L. Lopez, *Mikrochim. Acta*, 1986, III, 175.
9. J. R. Clinch, P. J. Worsfold and H. Casey, *Anal. Chim. Acta*, 1987, **197,** 43.
10. J. R. Clinch, P. J. Worsfold and H. Casey, *Anal. Chim. Acta*, 1987, **200,** 523.
11. P. C. Hauser, S. S. Tan, T. J. Cardwell, R. W. Cattrall and I. C. Hamilton, *Analyst*, 1988, **113,** 1551.
12. P. R. Freeman, I. D. McKelvie, B. T. Hart and T. J. Cardwell, *Anal. Chim. Acta*, 1990, **234,** 409.
13. J. Huang, H. Liu, A. Tan, J. Xu and X. Zhao, *Talanta*, 1992, **39,** 589.
14. M. Trojanowicz and J. Szpunar-Lobinska, *Anal. Chim. Acta*, 1990, **230,** 125.
15. M. Trojanowicz, J. Szpunar-Lobinska and Z. Michalski, *Mikrochim. Acta*, 1991, 159.
16. H. Liu and P. K. Dasgupta, *Anal. Chim. Acta*, 1994, **289,** 347.
17. S. Dong and P. K. Dasgupta, *Talanta*, 1991, **38,** 133.
18. Z. Vecera and P. K. Dasgupta, *Anal, Chem.*, 1991, **63,** 2210.
19. K. Sonne and P. K. Dasgupta, *Anal, Chem.*, 1991, **63,** 427.
20. P. C. Hauser and D. W. L. Chiang, *Talanta*, 1993, **40,** 1193.
21. H. Liu, P. K. Dasgupta and H. J. Zheng, *Talanta*, 1993, **40,** 1331.
22. M. Trojanowicz, P. J. Worsfold and J. R. Clinch, *TrAC*, 1988, **7,** 301.
23. P. K. Dasgupta, H. S. Bellamy, H. Liu, J. L. Lopez, E. L. Loree, K. Morris, K. Petersen and K. A. Mir, *Talanta*, 1993, **40,** 53.
24. J. Wilson and J. F. B. Hawkes, *Optoelectronics*, 2nd Ed. Prentice Hall, New York, 1989.
25. Z. Marczenko, *Separation and Spectrophotometric Determination of Elements*, Ellis Horwood, Chichester, 1986.
26. A. T. Haj-Hussein and G. D. Christian, *Analyst*, 1986, **111,** 65.
27. J. Bassett, R. C. Denney, G. H. Jeffery and J. Mendham, *Vogels's Textbook of Quantitative Inorganic Analysis*, 4th Ed. Longman, London, 1978.
28. E. H. Hansen, F. J. Krug, A. K. Ghose and J. Růžička, *Analyst*, 1977, **102,** 714.
29. *Integrated Circuits Data Book*, Vol. 33. Burr-Brown, 1989.

Pergamon

0039-9140(95)01458-6

*Talanta*, Vol. 42, No. 4, pp. 613–620, 1995

0039-9140/95 $9.50 + 0.00

# COMPARISON OF CALIBRATION METHODS IN QUANTITATIVE DIFFUSE REFLECTANCE INFRARED SPECTROSCOPY

Z. KRIVÁCSY[1] and J. HLAVAY[2]*

[1]Hungarian Academy of Sciences, Research Group of Analytical Chemistry, University of Veszprém, H-8201 Veszprém P.O. Box 158., Hungary

[2]University of Veszprém, Department of Analytical Chemistry, H-8201 Veszprém P.O. Box 158., Hungary

(*Received* 1 *August* 1994. *Revised* 28 *October* 1994. *Accepted* 28 *October* 1994)

**Summary**—Four different calibration methods were used for quantitative analysis of quartz and calcite in atmospheric aerosols by diffuse reflectance infrared Fourier transform spectroscopy (DRIFTS): (A) conventional calibration with one measurement on each standard (single calibration); (B) calibration with an internal standard; (C) calibration with parallel ($n = 4$) measurements on each standard (multiple calibration); (D) multiple calibration followed by reference reflectance correction. The accuracy and the precision of the methods were compared and it was found that by using method D the reliability of the conventional pellet preparation transmission technique can be achieved.

Recently, the number of the quantitative applications of diffuse reflectance infrared Fourier transform spectroscopy (DRIFTS) has been increased. This is owing to the simplicity, speed and the unique potential of the method compared to the time-consuming conventional pellet preparation technique. In DRIFTS, the sample preparation is usually simple, the sample can be investigated in its original physical-chemical state providing the opportunity for *in situ* investigations. Nevertheless, the precision of DRIFTS is usually less that of the transmission IR spectroscopy.

The relationship between the reflectance ($R_\infty$) and the absorbing and scattering properties of the sample can be obtained by the solution of the radiation transfer equation.[1] One of the solutions used most often in DRIFTS is called the Kubelka–Munk (K-M) function ($f(R_\infty)$):

$$f(R_\infty) = \frac{(1 - R_\infty)^2}{2R_\infty} = \frac{k}{s} = \frac{2.303a}{s} \cdot c, \quad (1)$$

where $k$ is the absorption, $s$ is the scattering coefficient of the sample, $a$ and $c$ are the absorptivity and the concentration of the analyte, respectively. The K-M function is linear with the concentration of the analyte if the scattering coefficient is kept constant.

Reinecke *et al.*[2] studied dioctyl phthalate quantitatively as follows. They filled the sample cup with KBr and deposited the analyte on the surface of the KBr from tetrahydrofuran solutions of different concentrations. The quantification of the measurements was based on the K-M function, however, the experimentally obtained K-M function was modified with the absolute reflectance of the reference material. This modification should be performed since the reflectance of the sample ($R_{\infty,s}$) can only be measured against the reflectance of the reference ($R_{\infty,r}$):

$$R_{\infty,\text{exp}} = \frac{R_{\infty,s}}{R_{\infty,r}}, \quad (2)$$

where $R_{\infty,\text{exp}}$ is the experimentally observed reflectance. Kortüm[1] has already pointed out that in the lack of an ideal reference material with $R_{\infty,r} = 1$, the exact value of $R_{\infty,r}$ has to be known to calculate the true value of the K-M function. Reinecke *et al.* developed a method to determine the value of $R_{\infty,r}$ from experimental data. It was found that by this modification the intercept of the calibration curve changed from the unreliable negative value to a positive one close to zero and the linear regression coefficient ($r$) increased from 0.9980 to 0.9992 indicating the improvement in accuracy and the precision of the method.

*Author to whom correspondence should be addressed.

Another possibility to improve the precision of an analytical method is to use an internal standard. Wiberley *et al.*[3] applied potassium thiocyanate (KSCN) in transmission IR technique for quantitative determination of copolymers and free fatty acids. In DRIFTS, the quantitative determination of (3-aminopropyl)triethoxysilane on silica gel surface was carried out using the 1870 $cm^{-1}$ Si-O combination band of the support as a reference absorption band, and $r = 0.9980$ was obtained with linear calibration.[4] Similarly, a normalization against glass absorption bands was made by McKenzie and Koenig[5] for surface analysis of coatings on standard E-glass.

Nevertheless, to obtain reliable quantitative results in DRIFTS is not an easy task. In this work (i) different calibration methods were applied for the quantitative analysis of inorganic crystalline compounds, and (ii) the accuracy and the precision, *i.e.* the reliability of the methods were compared by study of standard samples and environmental aerosols.

## EXPERIMENTAL

### *Materials and sample preparation*

Standard quartz and calcite (Department of Mineralogy, University of Veszprém) and spectroscopic grade KBr (Merck) were used to prepare the calibration mixtures. The concentration of the mixtures ranged between 0.023 and 1 w/w%. The mixtures in the 0.023–0.2 w/w% range and in the 0.2–1 w/w% range were prepared from 1 w/w% and 5 w/w% stock mixtures, respectively. The particle size for quartz and calcite was $<3$ $\mu$m and $<6$ $\mu$m, respectively. The particle size distribution of KBr was determined by Jeol JSM-50A (Japan) scanning electron microscope and was found as $d < 10$ $\mu$m. The aerosol samples were collected in a one-month period at different places in Veszprém county. First, the samples were mechanically removed from the filter, then alcoholic treatment was performed to separate the aggregates and to reduce the particle size. After evaporation of the alcohol the samples were mixed with KBr. For DRIFTS measurements 1 w/w% mixtures of the original samples were prepared. The sample cups in DRIFTS were filled by applying 1 MPa pressure for 1 min using home-made sample filling accessories.[6] The mass of the sample and the depth of the cup were $70 \pm 1.5$ mg and 2 mm, respectively. For the IR transmission measurements, pellets containing 2–3 mg sample and 797–798 mg KBr were prepared.

### *Infrared measurements*

The spectra were recorded by a Digilab FTS 45 and a Digilab FT 60A Fourier transform spectrometer (U.S.A.) with a DTGS detector. A resolution of 4 $cm^{-1}$ was used and 64 scans averaged. The diffuse reflectance spectra were transformed to K-M units. Intensities of the 799 $cm^{-1}$ and 780 $cm^{-1}$ ($\nu_s$ Si-O—Si) and 695 $cm^{-1}$ (deformation) bands of quartz and the 876 $cm^{-1}$ ($\gamma$ $CO_3^{2-}$) as well as 713 $cm^{-1}$ ($\beta$ $CO_3^{2-}$) bands of calcite were determined after a two-point baseline correction. The concentrations of quartz and calcite in the aerosols were calculated from the concentrations of those in the measured 1 w/w% mixtures.

### *Calibration methods*

The calibration curves were prepared by four different methods as follows.

*Method A, single calibration.* One measurement was carried out on each standard sample and the values of the K-M function of the absorption bands were determined.

*Method B, application of an internal standard.* One measurement was done on each standard sample containing 0.2 w/w% $K_2SO_4$ as an internal standard. The K-M values of the absorption bands were normalized against the K-M value of the 621 $cm^{-1}$ $\delta SO_4^{2-}$ absorption band.

*Method C, multiple calibration.* Parallel measurements ($n = 4$) were carried out on each standard sample. The sample cups were reloaded between the parallel measurements. The average value of the K-M functions of the absorption bands was calculated and used as the calibration point at each standard concentration.

*Method D, multiple calibration and reference reflectance correction.* The first step of this calibration was the multiple calibration (method C), then the real value of $R_{\infty,r}$ was determined from the experimental results according to the method of Reinecke *et al.*,[2] and the experimentally measured K-M functions were modified by the calculated value of $R_{\infty,r}$.

## RESULTS AND DISCUSSION

### *Reliability of the methods*

For the investigation of the reliability of the methods, first calibration curves for the different absorption bands of quartz and calcite were

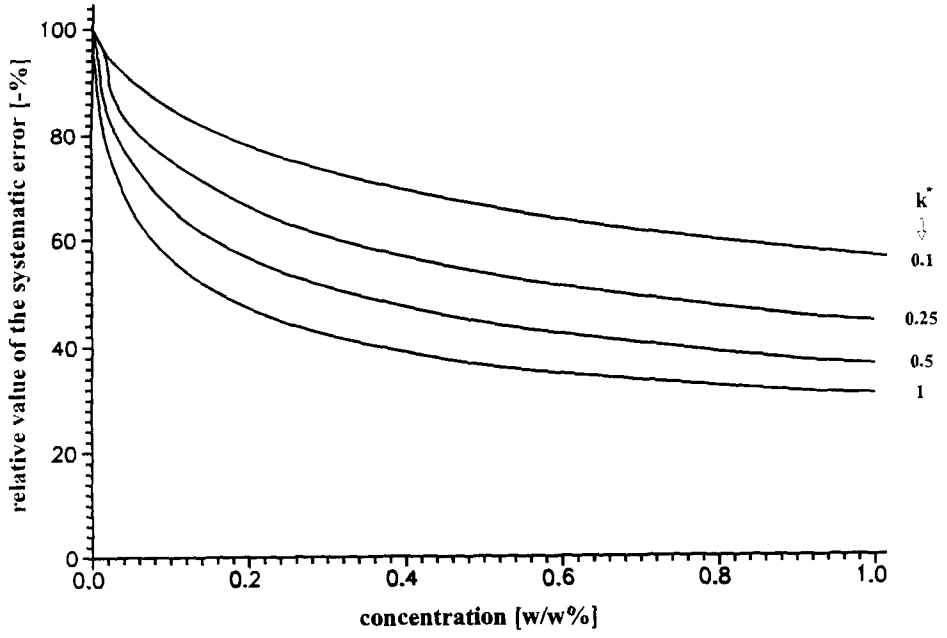


Fig. 1. Theoretical curves for the relative value of the systematic error as a function of the sample concentration for different values of $k^*$ ($R_{\infty,r} = 0.8$).

prepared. It was observed that using the methods A, B, and C for calibration the intercepts of the calibration curves were relatively large negative values in all cases. This is in accordance with the observation of Reinecke *et al.*[2] The negative values for the intercept cannot be explained by the K-M theory. The deviation has been found so large in some cases that the calibration curves have crossed the $x$-axis at the $c = 0.06$–$0.08$ w/w% range. In this case, by the calibration curve, the value of the calibration points at the lowest concentrations should have a negative number. For example, in case of the 799 $cm^{-1}$ band of quartz at $c = 0.023$ w/w% the measured value of the K-M function with method A was 0.0023, however, calculated from the calibration curve it should have been $-0.0112$. This considerable and always negative

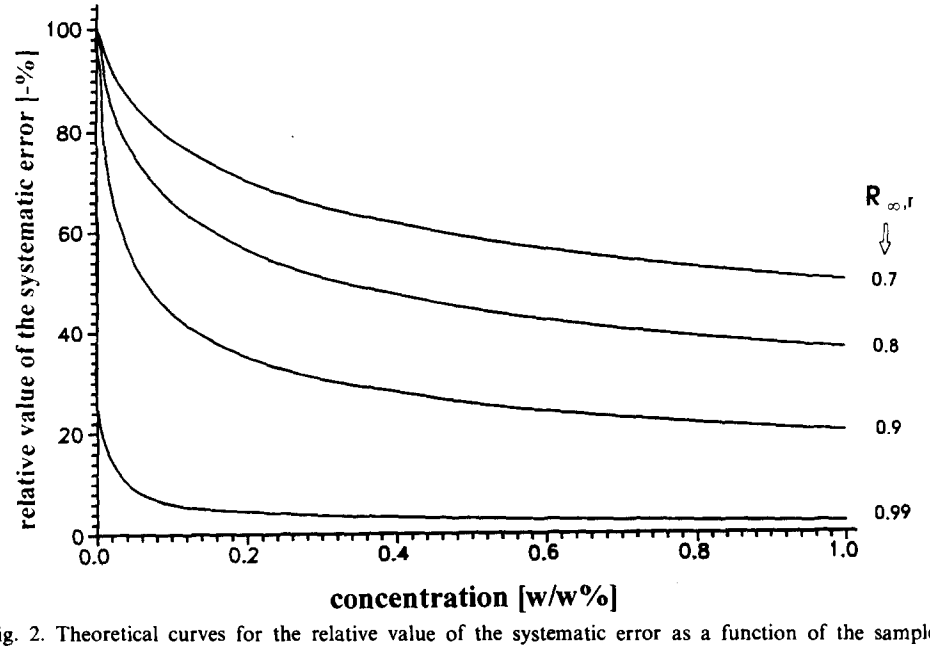


Fig. 2. Theoretical curves for the relative value of the systematic error as a function of the sample concentration for different values of $R_{\infty,r}$ ($k^* = 0.5$).

Table 1. Values of $k^*$ and $R_{\infty,r}$ for the different absorption bands of quartz and calcite

| | Absorption bands of quartz | | | Absorption bands of calcite | |
|---|---|---|---|---|---|
| | 799 $cm^{-1}$ | 780 $cm^{-1}$ | 695 $cm^{-1}$ | 876 $cm^{-1}$ | 713 $cm^{-1}$ |
| $k^*$ | 0.472 | 0.353 | 0.148 | 0.444 | 0.218 |
| $R_{\infty,r}$ | 0.825 | 0.818 | 0.752 | 0.878 | 0.853 |

bias presumably means that the analytical method is distorted by a systematic error.

The systematic error is presumed to exist owing to the incorrect determination of the K-M function assuming $R_{\infty,r} = 1$. In order to study the effect of this type of error on the quantitative analysis theoretical calculations were performed.

The relative value of the systematic error of the K-M function ($\Delta_r$) caused by the absence of the exact value of $R_{\infty,r}$, can be written as

$$\Delta_r = \frac{f(R_\infty)_{exp} - f(R_\infty)_{mod}}{f(R_\infty)_{mod}}, \quad (3)$$

where $f(R_\infty)_{mod}$ is the modified K-M function with $R_\infty = R_{\infty,r}{}^* R_{\infty,exp}$ and $f(R_\infty)_{exp}$ is the experimentally measured K-M function with $R_\infty = R_{\infty,exp}$. If the K-M functions in equation (3) are replaced according to equation (1), the following expression is obtained:

$$\Delta_r = -(1 - R_{\infty,r}) \frac{1 - R_{\infty,r} R^2_{\infty,exp}}{(1 - R_{\infty,r} R_{\infty,exp})^2}. \quad (4)$$

It can be seen from equation (4) that $\Delta_r$ is determined both by $R_{\infty,r}$ and $R_{\infty,exp}$. The sign of $\Delta_r$ is always negative, but if $R_{\infty,r} = 1$, the systematic error is zero. Furthermore, if $R_{\infty,exp} \to 0$ (total absorption) then $\Delta_r \to 1 - R_{\infty,r}$ and if $R_{\infty,exp} \to 1 (c \to 0)$ then $\Delta_r \to -1$ or $-100\%$.

Based on equation (4) theoretical functions between $\Delta_r$ and the sample concentration were also determined for the condition of $c \leqslant 1$ m/m%, where the K-M function is linear with the concentration and $f(R_\infty)_{exp} = k^* . c$. In this case, along with the sample concentration, the value of the systematic error is determined by $R_{\infty,r}$ and $k^*$ (the sensitivity of the analytical method). Theoretical curves for the concentration dependence of $\Delta_r$ at different values of $k^*$ ($R_{\infty,r} = 0.8$) and at different values of $R_{\infty,r}$ ($k^* = 0.5$) are plotted in Figs 1 and 2, respectively. It can be seen that in the 1 w/w% $\geqslant c \geqslant$ 0.2 w/w% range the value of the relative systematic error is only slightly increasing, but in the 0.2 w/w% $> c >$ 0 w/w% range the increase of the error is rather sharp.

After the theoretical calculations, experimental values of $\Delta_r$ as a function of the sample concentration for the different absorption bands of quartz and calcite were determined. The curves for quartz and calcite obtained from the results of method C ($f(R_\infty)_{exp}$) and method D ($f(R_\infty)_{mod}$) are plotted in Fig. 3A, B, respectively. Based upon the shape of the curves it can be concluded that the experimental curves are similar to that of the theoretical ones. The magnitude of $\Delta_r$ was also changed by the theoretical calculations and was increased both by decreasing $R_{\infty,r}$ and $k^*$. The values of $R_{\infty,r}$ and $k^*$ determined from the experimental results of method C are summarized in Table 1. Since $R_{\infty,r}$ is considerably $< 1$ ($R_{\infty,r} = 0.752$–$0.878$) the $-100\%$ limit for the values of $\Delta_r$ is approached if $c = 0.023$ w/w%.

The presence of the systematic error using method A, B, or C was also proved both by the investigation of standard samples and environmental aerosols. The standard samples containing quartz and calcite in known concentration were used to validate the analytical methods. The results for aerosols were compared to those of obtained by the pellet preparation transmission IR technique used as a reference method.

Based on the results of the validation, the relative error of the quantitative determination ($\Delta_c$) was calculated as

Table 2. Relative error and its mean value for the determination of quartz and calcite in standard samples in the different DRIFTS methods

| | Concentration of the analyte [w/w%] | | | Absolute value of the mean error |
|---|---|---|---|---|
| | 1–0.2 | 0.2–0.075 | <0.075 | |
| Method A | −5%–+5% | −10%–+10% | +20%–+222% | 31% |
| Method B | −5%–+5% | −5%–+5% | −20%–+25% | 9% |
| Method C | −4%–+3% | −14%–+9% | +23%–+143% | 21% |
| Method D | −3%–+3% | −5%–+3% | −10%–+3% | 3% |

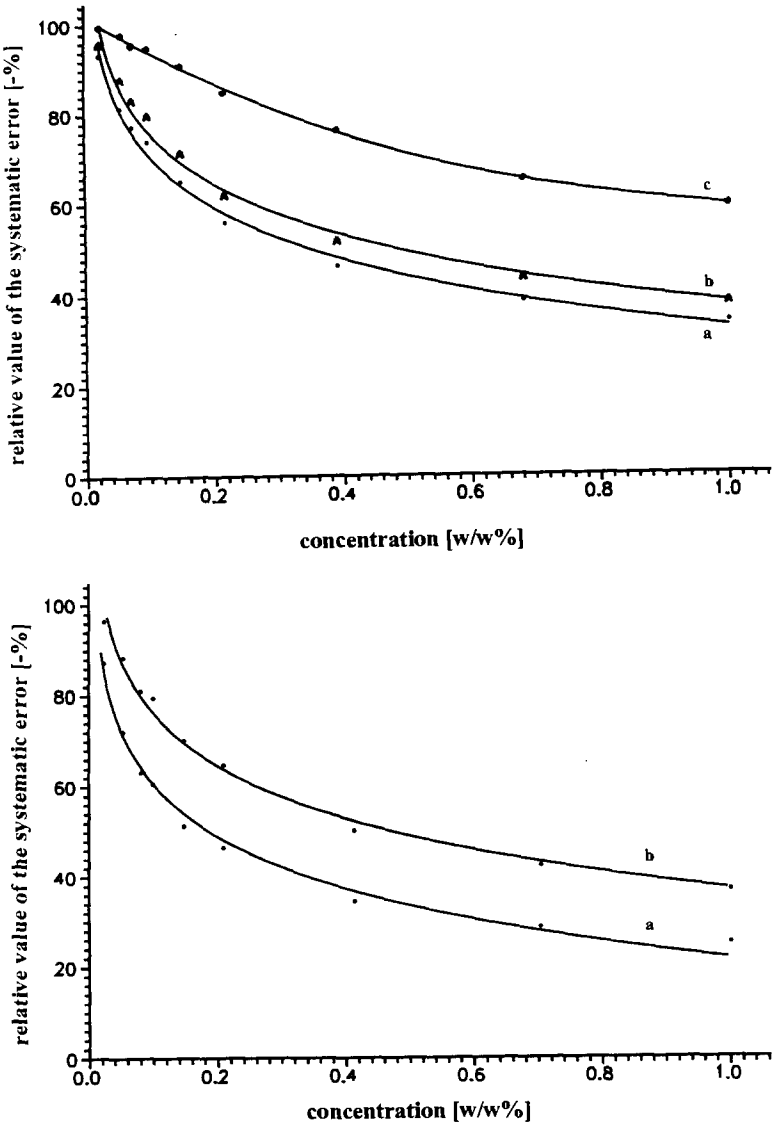


Fig. 3. (A) Experimental curves for the relative vaues of the systematic error ($\Delta_r$) as a function of the sample concentration for the bands of quartz obtained from the results of methods C and D. Absorption bands: (a) 799 $cm^{-1}$, (b) 780 $cm^{-1}$, (c) 695 $cm^{-1}$. (B) Experimental curves for the relative values of the systematic error ($\Delta_r$) as a function of the sample concentration for the bands of calcite obtained from the results of methods C and D. Absorption bands: (a) 876 $cm^{-1}$, (b) 713 $cm^{-1}$.

$$\Delta_c = \frac{c_{meas} - c_{true}}{c_{true}}, \qquad (5)$$

where $c_{meas}$ and $c_{true}$ are the measured and the true concentrations, respectively.

The data for $\Delta_c$ are listed in Table 2. It can be seen that the magnitude of the error is strongly influenced by the sample concentration and the results can be separated into three groups. In the 1 w/w% $\geq c \geq$ 0.2 w/w% range $\Delta_c$ is small independently of the analytical method used which means that in this region the systematic error is still negligible. If 0.2 w/w% $> c \geq$ 0.075 w/w% the errors for method A or C are two to five times higher than those for method B or D. If $c <$ 0.075 w/w% the systematic error can be extremely high resulting even in 150–200% deviation from $c_{true}$. The deviation in this concentration range is positive in all cases in accordance with the negative bias in the calculation of the K-M function. However, in case of the method B, $\Delta_c$ is relatively small having both positive and negative values even if $c <$ 0.075 w/w%. This means that the application of an internal standard partially compensates the effect of the systematic error. The best results were obtained by method D where $-5\% < \Delta_c < 5\%$ was obtained in most cases in the entire concentration range and the average

Table 3A. Concentration of quartz in aerosol samples determined by the different methods of DRIFTS and pellet preparation technique for the 799 $cm^{-1}$ absorption band (w/w%)

| Sample | Method A | Method B | Method C | Method D | Pellet technique |
|---|---|---|---|---|---|
| 1 | 15.0 ± 3.0 | 14.6 ± 1.5 | 15.2 ± 2.0 | 14.6 ± 1.0 | 14.0 ± 1.1 |
| 2 | 12.6 ± 3.0 | 12.4 ± 1.5 | 13.4 ± 2.0 | 11.8 ± 1.0 | 9.5 ± 0.5 |
| 3 | 12.4 ± 2.6 | 12.9 ± 1.3 | 12.1 ± 1.8 | 10.7 ± 0.9 | 10.9 ± 0.6 |
| 4 | 10.1 ± 3.1 | 7.3 ± 1.5 | 10.6 ± 2.0 | 7.3 ± 0.9 | 7.0 ± 0.7 |
| 5 | 9.2 ± 2.7 | 6.3 ± 1.4 | 9.5 ± 1.8 | 6.5 ± 0.9 | 5.0 ± 0.7 |

absolute value of the relative error was found to be 3%.

Based on the results it can be concluded that in cases of the method A, B and C the analysis is influenced by a nonlinear systematic error that is mainly caused by the inadequate calculation of the K-M function assuming $R_{\infty,r} = 1$. However, if the exact value of $R_{\infty,r}$ is determined and the modified value of the K-M function is calculated (method D), the systematic error of the determination can be omitted and the average relative error of the analytical method is ±3%.

The four DRIFTS methods and as a reference, the transmission IR technique were used for the determination of quartz and calcite of aerosol samples and the results are summarized in Table 3A and B, respectively. The effect of the systematic error on the results can most evidently be seen when the quartz concentration has been determined by method A or C and the concentration of quartz has been relatively low (Table 3A, samples 4 and 5). In these cases the measured mean values for quartz concentrations are significantly higher because of the significant systematic error compared to that of either method D or the pellet technique. However, the values obtained for calcite are in a good agreement independently of the method used. This is owing to the relatively high calcite concentration of the samples, when the effect of the systematic error on the analytical result using method A or C is within the magnitude of the random error.

The confidence interval was also calculated as an additional parameter to describe the reliability of the whole analytical procedure. For method D, the magnitude of the confidence limits were found to be three to six times smaller than those for the other DRIFTS methods and about the same compared to the conventional IR transmission technique. This indicates that the reliability of the two different techniques is comparable.

After these general observations the particular features of the modified calibration procedures are discussed in more detail.

*Application of an internal standard*

Potassium sulphate was selected as an internal standard because of its similar refractive index to KBr and relatively simple IR spectrum. The deformation band of $SO_4^{2-}$ at 621 $cm^{-1}$ has been chosen as the reference one because this band is of a well-defined shape and relatively intense absorbance and it does not interfere with the absorption bands of the investigated compounds (Fig. 4). The utility of the internal standard was tested first by carrying out parallel measurements ($n = 5$) on the samples containing 0.5 w/w% analyte and 0.2 w/w% $K_2SO_4$. The RSD of the intensity of the selected absorption bands was decreased from ±4.2% to ±1.5% and from ±3.7% to ±1.3% for quartz and calcite, respectively, proving the effect of the internal standard on the increase of measurement repeatability. However, the application of the internal standard has some disadvantages. One of these is the increase of the detection limit of the method, since the total concentration of the sample for the absorbing substances should not exceed 1 w/w%. Furthermore, the sample must be free of sulphate or other compounds absorbing at the wavelength domain of the reference band. The presence of sulphate or spectral interferences should usually

Table 3B. Concentration of calcite in aerosol samples determined by the different methods of DRIFTS and pellet preparation technique for the 876 $cm^{-1}$ absorption band (w/w%)

| Sample | Method A | Method B | Method C | Method D | Pellet technique |
|---|---|---|---|---|---|
| 1 | 50.8 ± 4.0 | 55.7 ± 1.7 | 49.0 ± 2.1 | 48.9 ± 0.7 | 47.2 ± 1.1 |
| 2 | 29.6 ± 3.6 | 29.7 ± 1.6 | 28.8 ± 1.9 | 25.8 ± 0.6 | 25.1 ± 0.6 |
| 3 | 24.8 ± 3.5 | 22.2 ± 1.5 | 25.3 ± 1.9 | 25.4 ± 0.6 | 26.1 ± 0.7 |
| 4 | 16.9 ± 3.9 | 17.9 ± 1.7 | 18.1 ± 2.1 | 16.2 ± 0.7 | 16.8 ± 0.5 |
| 5 | 15.8 ± 3.7 | 15.6 ± 1.6 | 17.0 ± 2.0 | 14.7 ± 0.6 | 15.3 ± 0.6 |

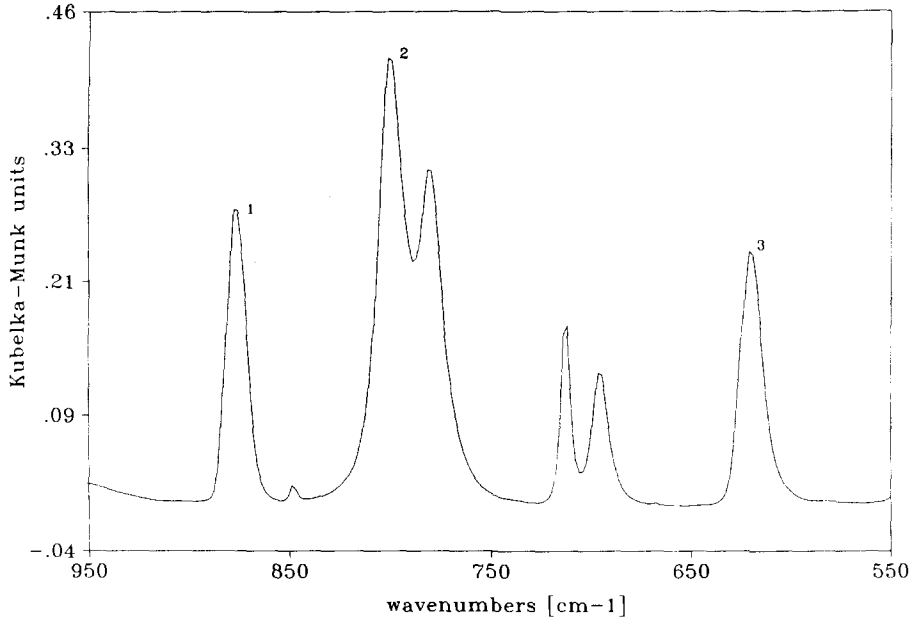


Fig. 4. Diffuse reflectance spectrum of the sample containing 1 w/w% $K_2SO_4$, 1 w/w% quartz and 0.5 w/w% calcite. Absorption bands: (1) $\gamma CO_3^{2-}$ (876 $cm^{-1}$), (2) $\nu_s$ Si-O-Si (799 $cm^{-1}$), (3) $\delta SO_4^{2-}$ (621 $cm^{-1}$).

be checked by preliminary investigation of the sample.

*Multiple calibration*

The performance of parallel measurements on the same sample and averaging the spectra in order to obtain more reliable results is a well-known procedure in DRIFTS. However, the aim of this procedure has been primarily to compensate for the failure of inadequate sample preparation, *e.g.* the irreproducibility of the sample packing. Furthermore, it should be realized that the requirements for a multiple calibration to improve the precision of quantitative DRIFTS also comes from the mathematical behaviour of the relative error of the K-M function. A mathematical model was developed for the concentration dependence of the relative error of DRIFTS measurements and the following equation was obtained:[7]

$$\frac{df(R_\infty)}{f(R_\infty)} = \sqrt{1 + \frac{2}{k^* c}} \cdot \frac{dR_{\infty,s}}{R_{\infty,s}}. \qquad (6)$$

From equation (6) one can see that if both the sample concentration and the sensitivity of the method are small (*e.g.* $c \leqslant 0.1$ w/w% and $k^* < 0.2$), the relative error for a single measurement can be $> \pm 10\%$ even if the sample preparation is appropriately reproducible ($dR_{\infty,s}/R_{\infty,s} = \pm 1\%$). This is a theoretical explanation for the high relative error of a single measurement and the necessity of spectral averaging to determine the reliable position of the calibration points. On the other hand, the disadvantage of the multiple calibration is the time consuming procedure compared to the single calibration methods.

## CONCLUSION

DRIFTS can appropriately be used for quantitative determination of quartz and calcite in aerosol samples diluted in a nonabsorbing matrix. However, keeping the experimental parameters (*e.g.* particle size, packing density, 1 w/w% sample concentration, KBr matrix) constant, accurate and precise quantitative analysis, especially in low analyte concentration range, can only be performed if multiple calibration and subsequently reference reflectance correction is carried out. In this case the reliability of the pellet preparation technique can be achieved.

*Acknowledgements*—The authors thank Mr D. Oravecz for the SEM measurements, Mrs Gy.Bajnóczi, Mrs J. Bakos and Mrs T. Szücs for the help in sample preparation. This research was financially supported by OTKA 2546.

## REFERENCES

1. Kortüm, *Reflectance Spectroscopy*. Springer, Heidelberg, 1969.

2. D. Reinecke, A. Jansen, F. Fister and U. Schernau, *Anal. Chem.*, 1988, **60,** 1221.
3. S. E. Wiberley, J. W. Sprague and J. E. Campbell, *Anal. Chem.*, 1957, **29,** 210.
4. R. S. S. Murthy and D. E. Leyden, *Anal. Chem.*, 1986, **58,** 1228.
5. M. T. McKenzie and J. L. Koenig, *Appl. Spectrosc.*, 1985, **39,** 408.
6. Z. Krivácsy and J. Hlavay, *Spectrochim. Acta A*, 1994, **50,** 49.
7. Z. Krivácsy and J. Hlavay, *Spectrochim. Acta A*, 1994, **50,** 2197.

Pergamon

0039-9146(95)01459-4

*Talanta*, Vol. 42, No. 4, pp. 621–626, 1995

0039-9140/95 $9.50 + 0.00

# APPLICATION OF POTENTIOMETRIC STRIPPING ANALYSIS FOR SPECIATION OF COPPER COMPLEXES WITH A NON-ADSORBABLE LIGAND ON A MERCURY ELECTRODE

HELENA M. V. M. SOARES* and M. TERESA S. D. VASCONCELOS†
LAQUIPAI, Chemistry Department, Faculty of Science, P4000 Porto, Portugal

(*Received* 1 *August* 1994. *Revised* 28 *October* 1994. *Accepted* 28 *October* 1994)

**Summary**—Potentiometric stripping analysis (PSA) was used for determination of conditional stability constants ($\beta'$) of copper(II) complexes. Glycine was used as a model of a non-adsorbable ligand on the mercury electrode that forms well defined 1:1 and 1:2 copper(II)–glycine complexes, which are labile within the time scale of the analytical technique. The calculations were performed by the DeFord–Hume method, which was applied to the shifts in peak potential ($dt/dE$ *vs.* $E$) provoked by the presence of different concentration of the ligand in the metal solution. For comparison purposes, the study was also carried out by differential pulse anodic stripping voltammetry (DPASV). The results obtained by PSA both at pH 6.0, $\log \beta'_1 = 5.0 \pm 0.2$ and $\log \beta'_2 = 7.6 \pm 0.2$, and at pH 6.5, $\log \beta'_1 = 5.7 \pm 0.6$ and $\log \beta'_2 = 8.5 \pm 0.4$ (standard deviations are given), were in agreement with those obtained by DPASV and from the literature, which indicates that PSA is suitable for this type of study.

The main application of potentiometric stripping analysis (PSA) technique has been for determination of the total concentration of heavy metals in diverse types of samples.[1–4] Anodic stripping voltammetry (ASV) techniques have been frequently used for speciation studies, owing to their selectivity and high sensitivity.[5,6] However, the similarity between PSA and ASV suggests PSA may also be used for speciation purposes. The initial step of the analytical techniques is the same: the metal(s) as hydrated form or/and as labile complexes is (are) deposited on the working electrode at a controlled potential. However, instead of applying an anodic potential scan to strip the metal(s) as is used in ASV, in PSA a chemical oxidant from the solution is allowed to diffuse to the working electrode and to oxidize the amalgamated metal(s). In this case, the potential of the working electrode is followed as a function of the stripping time ($t$). The identity of the metal and/or the extension of its complexation (in the case of labile complexes) are given by the peak potential obtained from the curves: current = f[potential ($E$)], in ASV, and $dt/dE = f(E)$, in PSA. In standard solutions, each metal generates a peak whose height is proportional to the metal concentration. Therefore, it can be expected that both techniques give the same type of information. In addition, since redox couples[7] and surface-active substances[8] from the solution do not interfere to the same extent in PSA as they do in ASV methods, PSA may have advantages for studies involving metal speciation. On the other hand, in PSA, an oxidizing agent [mercury(II) in many cases] must be present in the solution, in large excess relatively to the analyte, during the stripping step. Therefore, if the solution also contains ligands and the characteristics of the signal depend on the stripping step, the oxidizing agent might interfere in the metal speciation. Thus, comparative studies of PSA and ASV suitabilities for heavy metal speciation,[9] particularly for determination of conditional stability constants of complexes in natural waters, deserve interest, but are hard to find in the literature.

These facts prompted us to investigate the suitability of PSA for determination of conditional stability constants of copper complexes with organic ligands. Copper was chosen because we are involved in projects whose purpose is the study of the influence of copper speciation on its toxicity for microalgae[10] and bacteria[11] in

*Permanent address: Chemical Engineering Department, Faculty of Engineering, P4099, Porto Codex, Portugal.
†Author to whom correspondence should be addressed.

synthetic culture media. Glycine, an amino acid that is not adsorbed at the mercury electrode, and humic acid, which is marked adsorbed, were selected as model ligands, because both can be considered decomposition products of living organisms in aqueous medium.

For copper(II)–humic acid, the results of the study in progress[12] suggest that, for humic acid concentrations lower than 0.1 m$M$, the adsorption phenomena do not interfere in the determination of the conditional stability constants by PSA, but interfere markedly if DPASV is used.

In this paper, the results obtained for the copper(II)–glycine system are discussed.

## THEORY

In the case of monomeric ligands, L, if there are no adsorption phenomena on the electrode, DeFord–Hume's[13] method has been used for determination of stability constants of metal complexes by voltammetric techniques.[14,15]

For the reaction (the electric charges were omitted for the sake of simplicity, except for the metal ion whose charge is important for equation 3):

$$M^{n+} + jL \leftrightarrow ML_j, \quad (1)$$

whose overall conditional stability constant is:

$$\beta'_j = [ML_j]/([M^{n+}][L]^j). \quad (2)$$

The values of $\beta'_j$ can be obtained by the following equation:[16,17]

$$\Delta E_p = E_p^a - E_p^p = (2.303RT/nF) \times \left[ \log\left( 1 + \sum_{j=0}^{j} \beta'_j [L]^j \right) + \log(i_p^p/i_p^a) \right], \quad (3)$$

where $\Delta E_p$ denotes the difference between the peak potentials measured in metal solutions without and with the ligand. $E_p^p$ and $i_p^p$, and $E_p^a$ and $i_p^a$ are the peak potentials and current for the metal in the presence (p) and in the absence (a) of the ligand, respectively; $n$, $R$, $T$ and $F$ have their usual meaning.

Equation (3) presupposes that: (i) $ML_j$ are labile; (ii) the system is electrochemically reversible; and (iii) the ligand concentration at the electrode surface is equal to the bulk concentration. In addition, if the diffusion coefficient(s) of the complex(es) ($D_{ML_j}$) is (are) similar to those for the free metal ion ($D_M$), $\log(i_p^p/i_p^a) = 0$ (because $i_p^p/i_p^a \cong 1$ since $D_M \cong D_{ML_j}$). The last condition is only valid for small simple ligands such as $Cl^-$, $OH^-$ and amino acids,[18] like glycine. In this case, equation (3) takes the form:

$$\Delta E_p = E_p^a - E_p^p = (2.303RT/nF) \log\left( 1 + \sum_{j=0}^{j} \beta'_j [L]^j \right). \quad (4)$$

Theoretical studies of Chau *et al.*[19] showed that equation (4) is also valid for PSA, but as far as we know, this technique has not been applied for determination of stability constants before.

From equations (3) or (4), it follows that a polynomial fits the experimental data (titrations of metal solutions with a ligand solution). Its degree gives the number of complexes and the coefficients correspond to the overall formation constants.

Buffle *et al.*[20,21] concluded that DeFord–Hume's method can only be applied when the ratio between the total ligand and the total metal concentrations in the analytical solution ($[L]_t/[M]_t$) is higher than 1000 and the deposition time ($t_d$) is low enough to avoid surface effects during the anodic step. In fact, during the stripping step, the metal concentration at the mercury electrode surface ($[M]^0$) is much higher than in the bulk solution, the exact value depending on the $t_d$ and the [M] present in the bulk solution. If the ligand concentration in the solution is not large enough to guarantee excess even at the mercury electrode surface, ligand saturation by the metal at the mercury electrode surface will occur.[22] As a result, the chemical conditions at the electrode surface may change drastically by complex formation at the electrode surface, which are different from those in the bulk solution.[22] This phenomenon gives rise to a non-linear $i_p$ *vs.* $t_d$ function (S-shaped curve) and a decrease of $\Delta E_p$ with $t_d$ ($\Delta E_p$ should be independent of $t_d$).[22]

When $[L]_t/[M]_t$ is lower than 1000, the determination of stability constants by equation (3) requires a previous extrapolation of $\Delta E_p$ *vs.* $t_d$ curve for $t_d = 0$.[20,21]

## EXPERIMENTAL

### *Reagents and material*

For the preparation of solutions, reagent of analytical grade or equivalent without further purification were used, together with deionized water with resistivity $>14$ M$\Omega$ cm. Glycine, from Sigma, ref. G-7126 was used. Copper solutions were prepared from a stock standard solution 0.787 m$M$ $CuCl_2$.

All glass and plastic ware was cleaned by soaking in 20% nitric acid for 24 hr and then rinsing several times with water.

*Apparatus*

PSA and DPASV measurements were performed by using an Eco Chemie Autolab multimode polarograph with an IME module connected to a Metrohm 663 VA device and a MTEK computer. The Metrohm multimode was used in the static mercury drop mode (SMDE).

Alternating current polarography (ACP) measurements were carried out with a dropping mercury electrode (DME) on a Metrohm E506 polarograph combined with a Metrohm 663 VA device.

In all experiments, a conventional three-electrode arrangement, consisting of a glassy carbon electrode, as a counter electrode, an Ag/AgCl(s) 3*M* KCl electrode, as reference, and a multi-mode electrode were used.

*Procedures*

The measurements were performed at 20°C in 0.01*M* potassium nitrate, at pH 6.0 and 6.5, buffered with 0.01*M* piperazine-*N*,*N*-bis[2-ethane-sulfonic acid] (PIPES). Previously, it was verified that PIPES forms no complexes with copper(II). Twenty milliliters of the working solution was used for each experiment. The dissolved oxygen was purged from the solution by using a nitrogen gas stream for 10 min.

Metal losses owing to adsorption on the cell walls[23] were quantified by calibrating the voltammetric system at the same pH and during the same time as the samples but without ligand.

DPASV measurements were carried out using the following instrumental settings: deposition potential, $E_d = -0.3$ V *vs.* Ag/AgCl(s) 3*M* KCl, 50 mV pulse height, 60 msec pulse duration, 1 sec pulse repetition time and 5 mV/sec scan rate. In PSA, the same $t_d$ and $E_d$ were used. In all experiments performed by PSA, 47.2 $\mu$l of 2 m*M* of mercury(II) chloride as the oxidizing agent, which corresponded 4.72 $\mu M$ mercury(II) concentration, were added to the cell solution only just at the end of the deposition period, in order not to disturb the chemical equilibrium in the bulk solution.

PSA and DPASV complexation measurements were carried out by the batch mode on solutions with a concentration of copper(II) of 0.787 $\mu M$ copper(II), which was about four times higher than the limit of detection of both techniques in the experimental conditions ($t_d = 120$ sec and $E_d = -0.3$ V) used.[9] The concentration of glycine was varied between 1.12 and 31.6 m*M*. From the values of $E_p$ obtained in the absence (a) and in the presence (b) of the ligand, $\Delta E_p = E_p^a - E_p^p$ were calculated and used for deriving the conditional complex constants $\beta_1'$ and $\beta_2'$ by equation (4). For this purpose it was assumed that $[L] = [L]_t$, since the ligand concentrations were in very large excess relatively to the metal.

To test the non-occurrence of adsorption phenomena at the mercury electrode, experiments by ACP were performed. For this purpose, an amplitude of the alternating potential of 10 mV, 75 Hz of frequency, a dropping time of 0.8 sec and a scan rate of 5 mV/sec were used. The alternating component of the current ($i_{ac}$) was recorded at a phase angle ($\varphi$) of 90° for solutions with 1.12 or 17.8 m*M* glycine. The total potential range scanned in an experiment was from 0 to −1.2 V.

The occurrence of surface effects at the mercury electrode was tested by DPSAV for $t_d$ between 30 and 1400 sec. Solutions with 0.787 $\mu M$ copper(II) and two different glycine concentrations, 0.55 and 1.12 m*M*, were used.

## RESULTS AND DISCUSSION

*Adsorption and surface effects*

Erroneous stability constants are obtained by the DeFord–Hume method applied to voltammetric data[24-26] when adsorption phenomena take place on the working electrode. Therefore, in a first stage of this work, the absence of glycine adsorption at the Hg electrode was

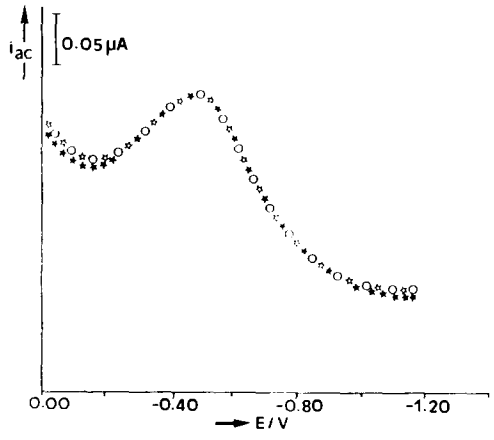


Fig. 1. AC polarograms for glycine solutions: amplitude = 10 mV; frequency = 75 Hz; scan rate = 5 mV/sec; $\varphi = 90°$. [Glycine] = (★) 0.00; (☆) 1.12 m*M*; (○) 17.8 m*M*.

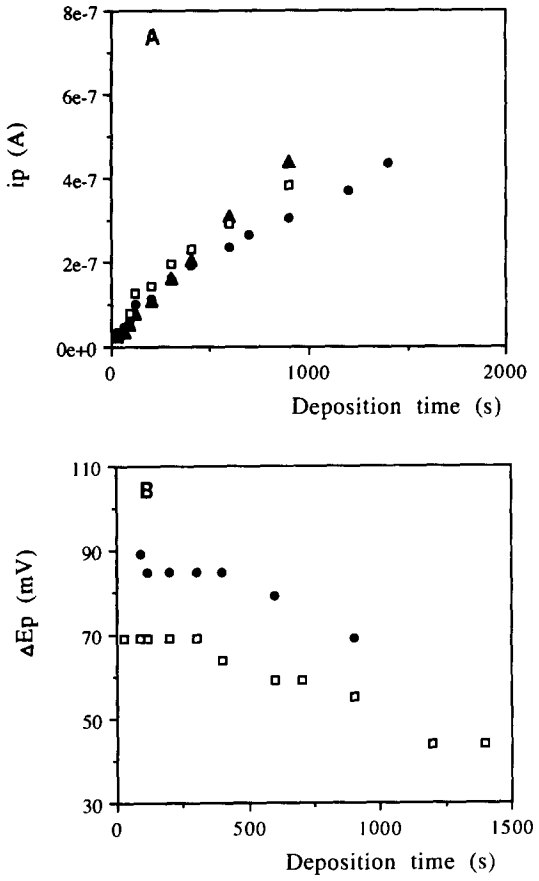


Fig. 2. Influence of glycine (▲ without ligand, □ 0.55 m$M$, and ● 1.12 m$M$) on the DPASV response for a 0.787 $\mu M$ copper(II) solution. $E_d = -0.3$ V *vs.* Ag/AgCl(s), 3$M$ KCl. This is a typical example of an experiment performed twice. (A) $i_p = f(t_d)$; (B) $\Delta E_p = f(t_d)$.

experimentally confirmed. For this purpose, curves of $i_{ac} = f(E)$ by ACP with a phase angle of 90° were recorded. At this phase angle, $i_{ac}$ is capacitive in nature and proportional to the double-layer capacity. Figure 1 shows that $i_{ac} = f(E)$ curves for the two different ligand concentrations are superposed with the curve without ligand, which indicates that no adsorption of glycine occurs.[18]

To evaluate the surface concentration of the oxidized metal during the stripping step, recordings of $i_p = f(t_d)$ and $\Delta E_p = f(t_d)$[18] were performed by DPASV, for two different $[\text{glycine}]_t/[\text{copper}]_t$ ratios. For $[\text{glycine}]_t/[\text{copper}]_t = 699$, an S-shaped curve for $i_p$ *vs.* $t_d$ was obtained (Fig. 2A) as well as a decreasing $\Delta E_p$ with $t_d$ (Fig. 2B). For the higher ratio, 1423, the $i_p$ *vs.* $t_d$ recording was linear and superposed with the curve recorded without glycine until $t_d = 400$ sec (Fig. 2A). This result indicated that no important surface effects occurred when $[\text{glycine}]_t/[\text{copper}]_t = 1423$, and therefore, this or higher values were used in the complexation studies. Furthermore, that result (Fig. 2A) showed that the diffusion coefficient of the metal ion was not significantly influenced by complexation, as expected, because the ligand is a relatively small amino acid.[18]

*Complexation*

Potentiograms and voltamograms carried out for solutions with 0.787 $\mu M$ copper(II) without and with 1.41, 7.94 or 31.6 m$M$ glycine are presented respectively in Fig. 3A and B. This shows that the values of $i_p^p$ obtained for the different glycine concentrations were close and similar to that obtained in the absence of glycine ($i_p^a$), which shows that the copper(II)–glycine complexes were labile within the time scale of these techniques. This figure also shows that the

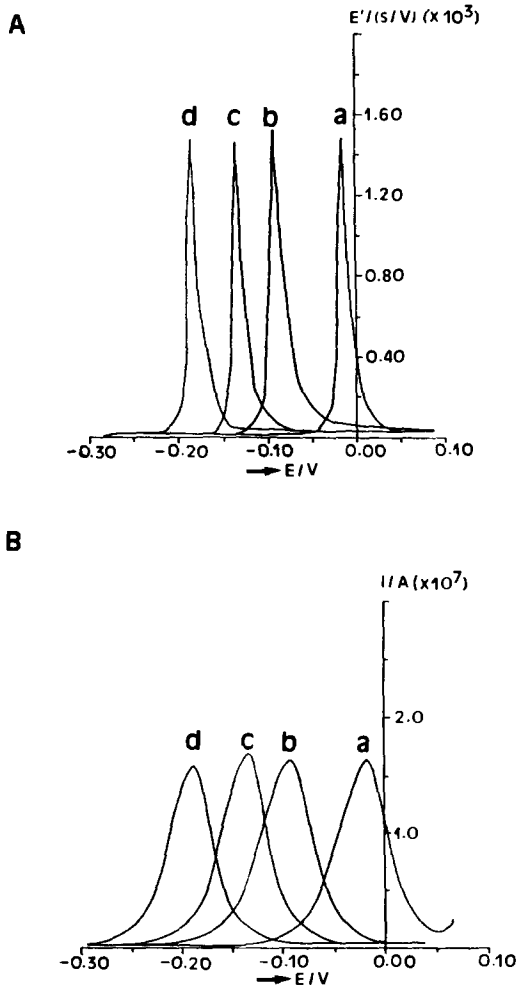


Fig. 3. Potentiograms (dPSA mode) (A) and DPASV voltammograms (B) for 0.787 $\mu M$ copper(II) and different glycine concentrations: (a) 0.0; (b) 1.41; (c) 7.94; and (d) 31.6 m$M$.

Table 1. Values of peak width ($W_{1/2}$) and potential ($E_p$) obtained for solutions with 0.787 $\mu M$ of copper and various glycine concentrations by PSA and DPASV at pH 6.5

| Curves in Fig. 3 | Glycine ($mM$) | DPASV ($mV$) | | PSA ($mV$) |
|---|---|---|---|---|
| | | $W_{1/2}$ | $E_p$ | $E_p$ |
| a | — | 60 | −16 | −15 |
| b | 1.41 | 55 | −94 | −98 |
| c | 7.94 | 54 | −134 | −136 |
| d | 31.6 | 54 | −189 | −185 |

$E_p$ became more cathodic when the glycine concentration increased. Comparable results ($dt/dE$ values) were obtained by PSA (Fig. 3A). The $\Delta E_p = E_p^a - E_p^p$ values were also similar for both techniques (see Table 1). These cathodic shifts resulted from the fast complexation of copper(II) by glycine during the stripping step.[18] Therefore, the cathodic shift depends on the $[L]_t/[M]_t$, but not on $E_d$, which should be only negative enough to allow the reduction of the free metal ion. Figure 3A and B and Table 1 show that, in the absence of ligand, an $E_p \cong -0.015$ V was obtained by both techniques. Therefore, the overpotential selected, *ca.* −0.3 V, can be considered sufficient for the present study purposes.[6]

In addition, results obtained by DPASV (Table 1) indicate that in the absence of glycine, a peak width ($W_{1/2}$) in agreement with theoretical predictions[27] was attained under our experimental conditions. In the presence of glycine, $W_{1/2}$ may still be considered according to theory,[27] although slightly smaller values were obtained (Table 1). Therefore, as no broadening of the peaks was found, the chemical system can be considered reversible.[16] As PSA and DPASV have similar response times ($\log t$(sec) between −0.5 and −1.2[28]), one can also assume that the system has similar electrochemical behaviour in both techniques. Therefore, under the experimental conditions used, the copper(II)–glycine system seems to fulfill the conditions for application of the DeFord–Hume method.[13]

Table 2. Conditional stability constants determined* by PSA and DPASV and calculated from the literature

| $\log \beta'_n$ | PSA | DPASV | Literature† |
|---|---|---|---|
| pH 6.0 | | | |
| $\beta'_1$ | 5.0 ± 0.2 | 4.9 ± 0.6 | 4.58 |
| $\beta'_2$ | 7.6 ± 0.2 | 7.7 ± 0.3 | 7.89 |
| pH 6.5 | | | |
| $\beta'_1$ | 5.7 ± 0.6 | 5.5 ± 0.5 | 5.08 |
| $\beta'_2$ | 8.5 ± 0.4 | 8.6 ± 0.4 | 8.89 |

*Standard deviation ($n \geq 3$) are given.
†Calculated from ref. [29] (see text).

$\Delta E_p = f(\log [\text{glycine}])$ plots, obtained from both PSA and DPASV experimental data at pH 6.0, are present in Fig. 4, which show that curves rather than straight lines were obtained, because of the presence of more than one copper(II)–glycine complex. The data obtained by both techniques fitted a second degree polynomial well, the overall conditional stability constants being obtained from the coefficients of the polynomial (see Table 2):

$$\Delta E_p = (2.303RT/nF) \times \log(1 + \beta'_1[\text{glycine}] + \beta'_2[\text{glycine}]^2). \quad (5)$$

Table 2 shows that PSA and DPASV originate practically identical stability constants. From these results, it can be concluded, that the presence in the solution of mercury(II) during the stripping step, had no significant interference in the analytical signal, probably because the glycine was in large excess.

From stoichiometric stability constants in the literature[29] $\log \beta_1 = 8.5$ and $\log \beta_2 = 15.4$ ($T = 20°C$, $I = 0.01M$), the $\beta'_s$ at values at pH 6.0 and 6.5 were calculated (see Table 2), and were similar to those obtained in this study. In

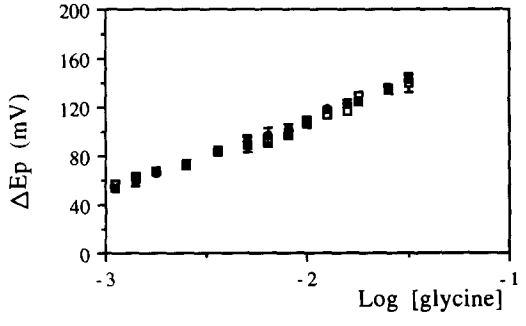


Fig. 4. Mean values and standard deviations ($n = 3$) of $\Delta E_p$ *vs.* [glycine] for 0.787 $\mu M$ copper(II) obtained by PSA (□) and DPASV (●) at pH 6.0.

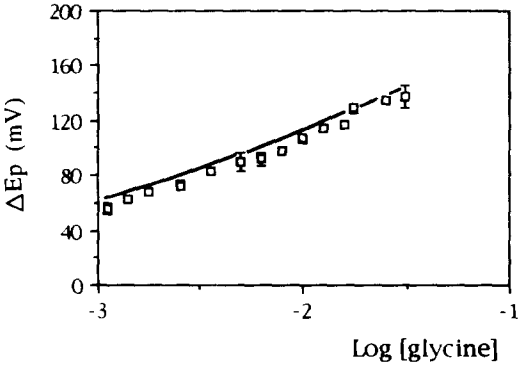


Fig. 5. Mean values and standard deviation ($n = 3$) of $\Delta E_p$ *vs.* [glycine] for 0.787 $\mu M$ copper(II) obtained by PSA (□) and calculated (full line) from known $\beta'$ values from the literature at pH 6.0 (see Table 2).

addition, Fig. 5 shows that the $\Delta E_p$ values estimated from known $\beta'_s$ values (pH 6.0) were similar to the analytical $\Delta E_p$ values obtained by PSA.

The agreement between the experimental results and literature data indicates that copper(II), instead of copper(I) (which is frequently involved in the mechanism of oxidation of copper(0) to copper(II) on stripping of amalgamated copper), is formed directly (*i.e.* by a two-electron process) in the stripping step. This fact corroborates literature information about the electrochemical behaviour of the copper(II)–glycine system,[30] and makes the stripping techniques suitable for determination of the respective stability constants.

Table 2 also shows that, in the pH range studied, the $\beta'_s$ values of the copper(II)–glycine complexes depend markedly on the pH value, as expected since carboxylic groups are involved in the complexation.

## CONCLUSION

The present work showed that PSA is suitable for estimating quantitatively the stability of metal–organic complexes, since the ligand is non-adsorbable at the mercury electrode surface and the conditions for application of the DeFord–Hume method are fulfilled.

*Acknowledgements*—The authors thank Mrs Cidália Botelho and Dr Rui Boaventura who kindly lent the Metrohm polarograph for ACP experiments, and Prof. A. A. S. C. Machado (LAQUIPAI, Chemistry Department, Faculty of Science, University of Oporto, Portugal) for a careful review of the manuscript.

## REFERENCES

1. M. Betti, L. Almestrand, D. Jagner and L. Renman, *An. Chim.*, 1992, **82,** 323.
2. M. Betti, L. Almestrand, D. Jagner and L. Renman, *An. Chim.*, 1992, **82,** 339.
3. M. Froning, C. Mohl and P. Ostapczuk, *Fresenius J. Anal. Chem.*, 1993, **345,** 233.
4. D. Jagner, L. Renman and Y. Wang, *Electroanalysis*, 1993, **5,** 283.
5. T. M. Florence in *Trace Element Speciation: Analytical Methods and Problems*, G. E. Batley (ed.) Chap. 4. CRC Press, Florida, 1989.
6. J. Wang, *Stripping Analysis—Principles, Instrumentation, and Applications*. VCH, Deerfield Beach, Florida, 1985.
7. D. Jagner, M. Josefson and S. Westerlund, *Anal. Chim. Acta*, 1981, **128,** 155.
8. D. Jagner, *Analyst*, 1982, **107,** 593.
9. H. M. V. M. Soares and M. T. S. Vasconcelos, *Anal. Chim. Acta*, 1994 (in press).
10. O. M. Lage, A. M. Parente, H. M. V. M. Soares, M. T. Vasconcelos and R. Salema, *Eur. J. Phycol.*, 1994, **29,** 253.
11. J. P. S. Cabral, M. Azenha and M. T. Vasconcelos, *Environm. Toxicol. Chem.* 1995 (in press).
12. H. M. V. M. Soares and M. T. S. Vasconcelos, submitted for publication.
13. D. R. Crow, *Polarography of Metal Complexes*. Academic Press, New York, 1969.
14. M. Odier and V. Plichon, *Anal. Chim. Acta*, 1971, **55,** 209.
15. M. L. S. Simões Gonçalves, P. Valenta and H. W. Nurenberg, *J. Electroanal. Chem.*, 1983, **149,** 249.
16. R. Ernst, H. E. Allen and K. H. Mancy, *Water Res*, 1975, **9,** 969 and refs therein.
17. D. D. DeFord and D. N. Hume, *J. Am. Chem. Soc.*, 1951, **73,** 5321.
18. J. Buffle, *Complexation Reaction in Aquatic Systems; an Analytical Approach*, Chap. 9 and refs therein. Ellis Horwood, Chichester, 1988.
19. T. C. Chau, D. Y. Li and Y. L. Wu, *Talanta*, 1982, **29,** 1083.
20. A. M. Almeida Mota, J. Buffle, S. P. Kounaves and M. L. S. S. Gonçalves, *Anal. Chim. Acta*, 1985, **172,** 13.
21. J. Buffle, A. M. Mota and M. L. Gonçalves, *Portugaliae Electrochim. Acta*, 1985, **3,** 293.
22. J. Buffle, *J. Electroanal. Chem.*, 1981, **125,** 273.
23. J. M. Diaz-Cruz, M. Esteban, M. A. G. T. Hoop and H. P. van Leewan, *Anal. Chem.*, 1992, **64,** 1769.
24. M. C. Montemayor and E. Fatas, *J. Electroanal. Chem.*, 1988, **246,** 271.
25. M. Lovric, *Anal. Chim. Acta*, 1989, **218,** 7.
26. M. Zelic and M. Branica, *Anal. Chim. Acta*, 1992, **268,** 275.
27. E. P. Parry and R. A. Osteryoung, *Anal. Chem.*, 1965, **37,** 1634.
28. J. Buffle, *Complexation Reaction in Aquatic Systems; an Analytical Approach*, Chap. 6. Ellis Horwood, Chichester, 1988.
29. A. E. Martell and L. G. Sillen, *Stability Constants of Metal–Ion Complexes*, Vol. 17. The Chemical Society, Burlington House, 1964.
30. A. Nelson and R. F. C. Mantoura, *J. Electroanal. Chem.*, 1984, **164,** 237.

Pergamon

0039-9140(95)01464-0

*Talanta*, Vol. 42, No. 4, pp. 627–633, 1995

0039-9140/95 $9.50 + 0.00

# FLOW ANALYSIS-SPECTROPHOTOMETRIC DETERMINATION OF L-DOPA IN PHARMACEUTICAL FORMULATIONS BY REACTION WITH *p*-AMINOPHENOL

BERWEEN A. HASAN,* KARIM D. KHALAF* and MIGUEL DE LA GUARDIA†

Department of Analytical Chemistry, Faculty of Chemistry, University of Valencia, 50 Dr. Moliner, Burjassot 46100, Valencia, Spain

(*Received* 1 *August* 1994. *Revised* 1 *November* 1994. *Accepted* 1 *November* 1994)

**Summary**—A new method has been developed for the spectrophotometric determination of L-dopa in pharmaceutical formulations. The method is based on the reaction between the open-chain quinone of L-dopa, obtained in NaOH, and the benzoqinoneimine form of *p*-aminophenol, in the presence of $KIO_4$. The reaction product is determined at 574 nm by using both alternately procedures, one based on the stopped-flow and another on a flow injection approach. Under the best experimental conditions L-dopa can be determined with a limit of detection of 52 ng/ml and a relative standard deviation of 0.2% for three replicate measurements of a solution containing 4 μg/ml.

L-Dopa or levodopa (3-hydroxy-L-tyrosine) is a catecholamine with the amine group attached to a benzene ring bearing two hydroxyl groups. L-Dopa is a forerunner of dopamine, which is depleted from the brain in Parkinson disease and is commonly employed in the treatment of this disease. L-Dopa is effective in relieving hypokinesia and may also decrease rigidity, oculogyric crises and tremor.[1] The compound is rapidly absorbed through the bowel at the level of the small intestine after oral adminstration and widely distributed in the tissue and metabolized to dopamine by a decarboxylation process. Dopamine is further metabolized to other metabolites and for this reason, carbidopa and benserazide are used as inhibitors for the decarboxylase activity.[2]

Many methods have been developed for the determination of L-dopa and its metabolites in biological and pharmaceutical formulations, such as chromatography techniques and thin-layer chromatography (TLC) has been used for the separation and determination of L-dopa.[3,4] Gas chromatography (GC) has also been employed to study the effect of L-dopa and dopamine in rat brain.[5] High-performance liquid chromatography (HPLC) has been widely used for the determination of L-dopa in brain, plasma, urine, liver, serum, tissues and biological fluids using electrochemical detection,[6–19] or fluorescence detection at 325 nm[20] and 322 nm.[21]

Spectrophotometric methods have also been used for the determination of catecholamines in pharmaceutical formulations and hence, direct measurement of L-dopa in tablets was carried out at 280 and 290 nm,[22] or by derivative spectrophotometry at 276 nm,[23] and in the presence of boric acid,[24] $Na_2B_4O_7$,[25] $Na_2HPO_4$,[26] and germanium dioxide[27] which provide maximum absorbance at 239.5, 287, 292.5 and 292 nm, respectively.

L-Dopa has been determined in the visible region based on the use of several derivative reagents such as $PdCl_2$,[28] metaperiodate,[29] *o*-phenathroline,[30] molybdophosphoric acid,[31] ninhydrine,[32] $NH_4VO_3$[33] and enzymatic incubation with tyrosinase[34] to yield coloured species which show absorption maxima at 392, 520, 510, 825, 582, 430 and 540 nm, respectively. A photokinetic method, based on the photochemical reaction of Rose Bengal with EDTA in the presence of catecholamines has also been proposed[35] for the analysis of pharmaceuticals.

Flow-injection analysis (FIA) was originally designed to carry out several on-line analytical processes, and in spite of the great improvement in the analytical figures of merit provided by the FIA methodology, there are only few

*Permanent address, University of Baghdad, Iraq.
†Author to whom correspondence should be addressed.

papers dealing with the automatization of the L-dopa or other catecholamines. L-Dopa was determined based on FIA-chemiluminometric oxidation with $KMnO_4$,[36] and also by flow injection stopped-flow kinetic spectrophotometry using a micellar-catalyzed reaction with 1-fluoro-2,4-dinitrobenzene to produce a complex which is measured at 340 nm.[37]

L-Dopa has also been determined fluorometrically in pharmaceutical preparations by means of the photochemical inhibition of the reaction between phloxin and EDTA,[38] and a flow system has been developed for the study of the catecholamine secretion from bovine adrenal medulle cells which permits the electrochemical determination of catecholamines.[39]

The purpose of the present investigation is to develop a simple and sensitive method for the determination of L-dopa in pharmaceutical formulations by FIA-spectrophotometry. The proposed method is based on using *p*-aminophenol (PAP) as a derivative reagent which has been successfully employed for the determination of phenolic compounds with a free *para*-position, obtained from the alkaline hydrolysis of carbamate pesticides,[40–43] and also for the direct determination of cresols,[44] and other phenols[45] in natural waters.

## EXPERIMENTAL

### *Apparatus*

A Hewlett-Packard 8452A diode array spectrophotometer, equipped with an HP 89530A MS-DOS software (with a response time of 0.1 sec) was used for the spectrophotometric determination. A flow cell with 50 $\mu$l. internal volume and 1 cm pathlength was used for the absorbance measurements.

Two manifolds of three channels (Fig. 1) were employed to carry out the spectrophotometric determination of L-dopa in the stopped-flow (Fig. 1A) and in the FIA mode (Fig. 1B).

A Gilson $P_2$ minipulse peristaltic pump was used in all cases to transport the carrier solutions. Standard solutions and samples were injected, in the FIA mode, using a Rheodyne type 50 rotary injection valve. As can be seen in Fig. 1A, channel 1 was used to transport *p*-aminophenol and channel 2 to introduce L-dopa in the stopped-flow mode or to inject samples and standards in the FIA mode in a water carrier stream. Channel 3 was employed to transport a sodium hydroxide solution.

The connections between any two channels of both manifolds employed were made by Y-shaped merging zones in order to ensure good mixing between reagents.

Flexible poly(vinyl chloride) tubes of 1.52 mm internal diameter, suitable for peristaltic pump, were used to provide a flow-rate up to 4.2 ml/min in each channel.

A reaction coil of 45 cm ($R_1$) was used to ensure a good mixing between *p*-aminophenol (PAP) and L-dopa. Another reaction coil of 8 m ($R_2$) was employed to provide a good reaction yield between L-dopa and PAP in the presence of sodium hydroxide. The coloured species obtained were measured at 574 nm.

All the reaction coils used in the manifolds were made of Teflon with an internal diameter of 0.8 mm.

### *Reagents*

All reagents were of analytical grade and demineralized distilled water was used throughout.

The L-dopa stock solution (24 $\mu$g/ml) was prepared by dissolving 0.00625 g L-dopa (Fluka) in 250 ml boiled and cooled distilled water. This solution was stored in a refrigerator, being stable for many days.

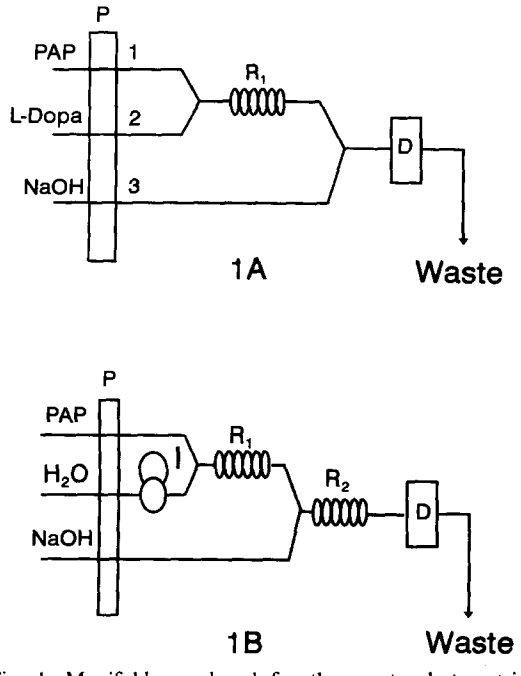


Fig. 1. Manifolds employed for the spectrophotometric determination of L-dopa, (1A) stopped-flow mode and (1B) FIA mode, (P) peristalitic pump, (D) detector, ($R_1$ and $R_2$) reaction coils, (I) injection valve.

The *p*-aminophenol (PAP) standard solution (100 $\mu$g/ml) was prepared daily by dissolving 0.025 g PAP (Fluka) in 250 ml of boiled and cooled distilled water, being stable for more than 8 hr. Stock solution (1*M*) of sodium hydroxide (Probus) was prepared in distilled water and working solutions were prepared by diluting the stock one.

*General procedure*

For the solid formulation of Madopar®, the tablets were ground and, from the final fine powder, 0.0172 g was accurately weighed and dissolved in 250 ml of boiled and cooled distilled water using an ultrasonic water bath for 10 min to ensure complete dissolving of L-dopa in water. The solution was filtered using a Whatmann filter paper No 42 to avoid any suspended excipient. Low concentrated solutions were prepared by diluting the aforementioned filtered solution with boiled and cooled distilled water in order to avoid any oxidation of L-dopa by the dissolved molecular oxygen of water. The spectrophotometric measurements were carried out in stopped-flow mode by introducing sample solutions in channel 2, as indicated in Fig. 1A, using 0.2*M* of sodium hydroxide solution and 100 $\mu$g/ml of PAP, and after mixing all these solutions stopping the flow and carrying out the measurements after 1 min, while in the FIA mode, samples and standards were injected in the manifold indicated in Fig. 1B using 600 $\mu$l. injection volume and distilled water as carrier stream with a flow rate of 3.2 ml/min. In both cases, the spectrophotometric measurements were carried out at 574 nm against a standard calibration graph obtained from standard solutions of L-dopa treated in the same way.

## RESULTS AND DISCUSSION

*Preliminary study of* L-*dopa stability in aqueous solutions*

L-Dopa(levodopa) is slowly soluble in water (66 mg/40 ml $H_2O$)[46] but it undergoes oxidation processes even by the dissolved molecular oxygen, and for these reasons, special attention was taken for the preparation of standard solutions.

In this work, the standard solution of L-dopa was prepared in boiled and cooled distilled water and the UV/Vis spectrum of the prepared solution was daily monitored by using the diode array spectrophotometer for more than 15 days; and results obtained showed that the aqueous solution of L-dopa is highly stable.

On the other hand, it is well known that, L-dopa (**I**) is first oxidized to the open-chain quinone (**II**) which gives a yellow coloured solution[47] which has a very transitory existence[48] and evolves to leucodopachrome (**III**); this substance is in turn oxidized to dopachrome (**IV**) which can be then undergo further transformation by an internal oxidation-reduction mechanism to 5,6-dihydroxyindole-2-carboxylic acid (**V**), or to 5,6-dihydroxyindole (**VI**)[49] according to the following scheme.

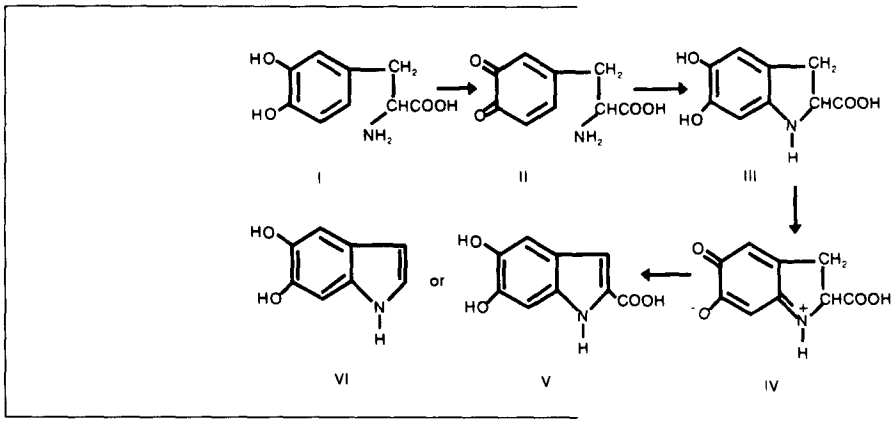


The behaviour of L-dopa in sodium hydroxide 0.2*M* was studied, using the manifold indicated in Fig. 1A, in which distilled water was introduced in channel 1 and 10 $\mu$g/ml of a L-dopa solution was introduced continuously by channel 2 and 0.2*M* NaOH solution by channel 3. Figure 2 shows that the interaction between L-dopa and sodium hydroxide produces a yellow solution which presents two absorption bands at 302 and 440 nm. However, the band at 440 nm decreased gradually and, after 3 min, a new absorption band appeared at 326 nm. This behaviour can be explained by the oxidation of

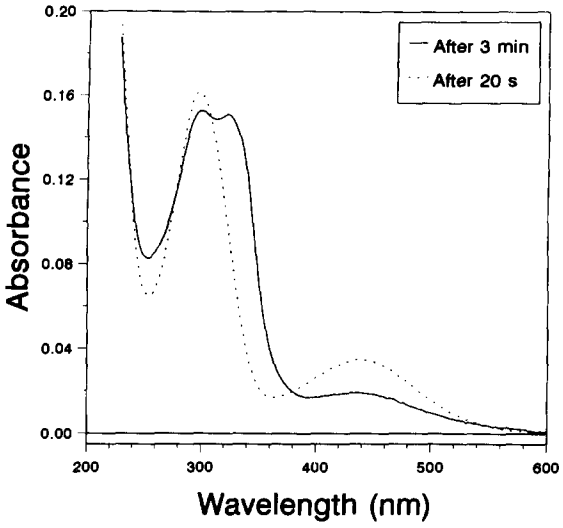


Fig. 2. UV-Vis spectra of 10 mg/ml of L-dopa in 0.2*M* NaOH after 20 sec (· · ·) and after 3 min (——).

L-dopa to the open-chain quinone (**II**) which showed an absorption at 440 nm, and after that evolves to leucodopachrome (**III**).[48]

*Reaction between* L-*dopa and* p-*aminophenol*

It has been mentioned that when PAP (**1**) is oxidized, by the dissolved molecular oxygen or by other oxidizing agents such as $KIO_4$, the benzoquinoneimine form of PAP (**2**) produced readily reacts with the free *para*-position of phenolic compounds by an electrophilic attack which produces complex species which absorb in the visible region.[50] Thus, the aim was to couple benzoquinoneimine (**2**) with the open-chain quinone (**II**) in order to produce a complex compound (**3**). The spectrum in Fig. 3 indicates that the reaction between 100 $\mu$g/ml of PAP and 10 $\mu$g/ml of L-dopa in an alkaline medium of 0.2*M* NaOH carried out in the stopped-flow mode, using the manifold indicated in Fig. 1A, shows a high absorption intensity at 574 nm. The full colour development was achieved after 60 sec, and it remained stable for more than 20 min. On the other hand, when $KIO_4$ was previously mixed with PAP, the colour was formed and decomposed very rapidly.

A possible reaction mechanism is shown in the scheme of the reaction between PAP and L-dopa.

Some evidence about the aforementioned reaction was obtained by additional experiments. When L-dopa is mixed with a NaOH solution and coupled with PAP after 2, 3, 4, and 5 min, results obtained show that there was no reaction between L-dopa and PAP, owing to the formation of leucodopachrome (**III**), in which the *para*-position is blocked.

The reaction between L-dopa and PAP carried out in an alkaline medium of 0.2*M* NaOH provides a higher sensitivity and selectivity than that obtained for the direct spectrophotometric determination of L-dopa prepared in distilled water and measured in the UV-region (see Fig. 3).

*Stopped-flow spectrophotometric determination of* L-*dopa*

The effect of NaOH concentration (from 0.1 to 1*M*) and PAP (from 25 to 300 $\mu$g/ml) on the reaction between L-dopa and PAP was studied using the manifold shown in Fig. 1A.

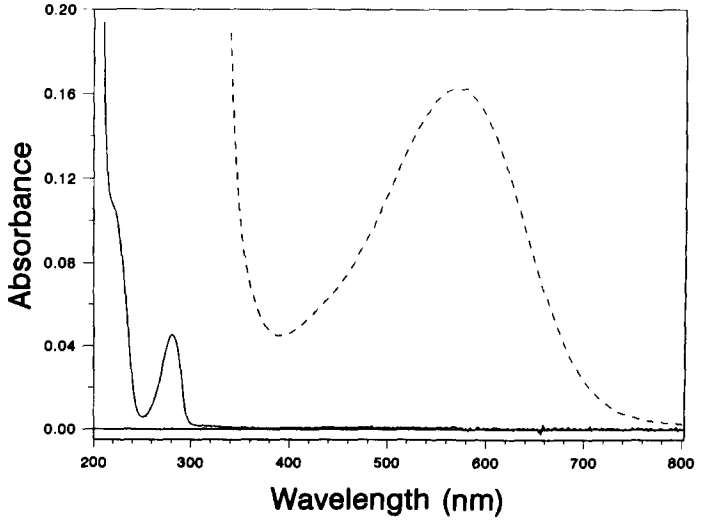


Fig. 3. UV/Vis spectrum of a solution of 10 mg/ml of L-dopa in distilled water (——) and the spectrum of the reaction product between 10 $\mu$g/ml of L-dopa and 100 $\mu$g/ml of PAP in 0.2*M* NaOH (· · ·).

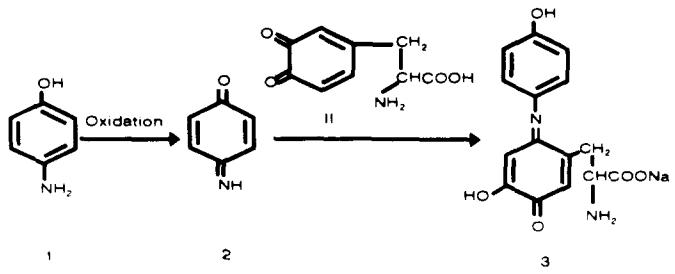


Reaction between PAP and L-dopa.

Results obtained showed that the use of 100 $\mu$g/ml of PAP and 0.2$M$ NaOH provide the highest absorption intensity after a reaction time of 60 sec and hence, a calibration graph was carried out for a series of standard solutions (from 2 to 8 $\mu$g/ml L-dopa) which provided a typical calibration line with the following regression characteristic features:

$$A_{574} = 0.0020 + 0.01495C \ (C \text{ in } \mu\text{g/ml of L-dopa})$$

with the regression coefficient $r$ of 0.9999. The limit of detection obtained was 60 ng/ml and the relative standard deviation of three replicate measurements of a solution containing 4 $\mu$g/ml of L-dopa was 1%.

The stopped-flow method was applied to the determination of L-dopa in real pharmaceutical formulations and hence, Madopar® tablets, which contain 250 mg L-dopa and 50 mg benserazide, was used as a test sample, using the recommended general procedure.

Table 1 shows that the recovery percentages obtained were from 98 to 102% of L-dopa in Madopar® which provided high accurate results and evidence that there is not any effect of benserazide on the final recovery because benserazide does not react with PAP.

In order to verify the validity of the methodology developed, some synthetic samples were prepared by adding known amounts of L-dopa to commonly used excipients, such as starch and lactose, or to pharmaceutical preparations containing other products, such as paracetamol.

Table 1. Determination of L-dopa by stopped-flow spectrophotometry in Madopar® tablets

| Nominal value ($\mu g/ml$) | Found by proposed method ($\mu g/ml$) | Recovery (%) |
|---|---|---|
| 2 | 1.95 ± 0.09* | 98 |
| 4 | 4.05 ± 0.10 | 100.4 |
| 5 | 5.1 ± 0.2 | 101.3 |
| 6 | 6.12 ± 0.06 | 102 |

*Average values found ± SD corresponding to five independent analyses.

Table 2 summarizes the results shown and as can be seen very good recovery values were found, thus indicating that excipients should not provide real problems in the determination of L-dopa by means of its reaction with PAP.

*Study of some possible interferences*

As indicated before all free *para* position phenols can react with PAP to form coloured species, and from our own experience it can concluded that PAP is a general derivative reagent for all these compounds. However, each phenol requires different reaction conditions and reacts with PAP at different rates. Table 3 summarizes the experimental conditions found for the reaction between PAP and *o*-cresol, *m*-cresol, phenol, resorcinol and *m*-aminophenol in the stopped flow mode. As can be seen each compound requires different conditions, and they also provide different absorption maxima, thus indicating the tremendous possibilities offered by this reaction for the simultaneous determination of a series of phenols.

On the other hand, and compared with the reaction between L-dopa and PAP it is shown that simple phenolic compounds need the use of $KIO_4$ and that in the absence of this oxidizing reagent reactions take place very slowly which also contributes to providing a selective method for the determination of L-dopa in pharmaceuticals.

*FIA-spectrophotometric determination of L-dopa*

The effect of flow injection analysis (FIA) parameters were evaluated under the best conditions found for the determination of L-dopa by stopped-flow; such as the reaction coil length $R_2$ (from 1 to 8 m), flow rate (from 1 to 4 ml/min) and the injection volume (from 100 to 800 $\mu$l.). The reaction between L-dopa and PAP was studied using the manifold indicated in Fig. 1B. Results obtained show that a reaction coil of 600 cm, with a flow rate of 3.2 ml/min and an injection volume of 600 $\mu$l. provide the

Table 2. Analysis of L-dopa in synthetic samples in the presence of some commonly used excipients

| Excipients | Concentration added ($\mu g/ml$) | Concentration found ($\mu g/ml$) | Recovery (%) |
|---|---|---|---|
| Starch | 3.94 | $4.00 \pm 0.003$ | 101.5 |
| Lactose | 2.99 | $2.92 \pm 0.02$ | 97.7 |
| Paracetamol | 1.44 | $1.46 \pm 0.04$ | 101.4 |

Table 3. Experimental conditions found for the stopped-flow determination of a series of phenols with PAP

| Experimental conditions | *o*-Cresol | *m*-Cresol | Phenol | Resorcinol | *m*-Aminophenol |
|---|---|---|---|---|---|
| PAP ($\mu g/ml$) | 100 | 300 | 500 | 50 | 115 |
| $IO_4^-$ ($M$) | 0.004 | 0.004 | 0.004 | 0.0002 | 0.004 |
| NaOH ($M$) | 0.06 | 0.06 | 0.005 | 0.006 | 0.05 |
| Reaction time | 35 min | 12 min | 45 min | 45 sec | 10 min |
| $\lambda$ ($nm$) | 614 | 632 | 626 | 540 | 576 |

best absorption intensity. An $R_2$ coil of 45 cm was used only to provide a radial homogenization between PAP and L-dopa. A calibration graph obtained for a series of standard solutions of L-dopa (from 2 to 8 $\mu$g/ml) using the above parameters provided a typical calibration line with the following analytical regression features:

$$A_{574} = -0.0097 + 0.01323C$$

(C in $\mu$g/ml of L-dopa)

with a regression coefficient $r$ of 0.9999. The limit of detection obtained in these conditions was 52 ng/ml and the relative standard deviation for three replicate measurements of 4 $\mu$g/ml of L-dopa was 0.2%. The proposed FIA-method provides high reproducible results and permits the measurement of low concentration levels of L-dopa with a sample throughput of 120 injections/hr. The above FIA-methodology has been applied to the determination of L-dopa in Madopar® tablets using the recommended method and the recovery percentages obtained were from 99.4 to 102.7% (Table 4) which means that there is no significant difference between the results obtained by the proposed method and those reported.

## CONCLUSION

The proposed two procedures (stopped-flow and FIA-methods) offer clear advantages for the fast determination of L-dopa in the presence of related compounds, such as benserazide in pharmaceutical formulations. The method is very simple, does not require any chemical sample pretreatment, is highly economic and very fast and provides highly accurate results with low detection limits.

Table 4. FIA-spectrophotometric determination of L-dopa in Madopar® tablets

| Nominal values ($\mu g/ml$) | Found values ($\mu g/ml$) | Recovery |
|---|---|---|
| 2 | $2.01 \pm 0.06$ | 100.7 |
| 4 | $4.11 \pm 0.06$ | 102.7 |
| 5 | $5.11 \pm 0.01$ | 102.2 |
| 6 | $5.97 \pm 0.04$ | 99.4 |

*Acknowledgements*—Karim D. Khalaf is grateful to the Spanish Institute of International Cooperation with the Arabic World for the fellowship to carry out PhD studies in Spain and to Roche Laboratory in Madrid for supplying the Madopar® samples.

## REFERENCES

1. *British Pharmaceutical Codex*. The Pharmaceutical Press, Bloomsbury, 1973.
2. A. C. Moffat, *Clarke's Isolation and Identification of Drugs*, 2nd Ed. The Pharmaceutical Press, London, 1986.
3. A. G. Milovanovic and A. M. Sekheta, *Glas-Hem-Drus-Beograd*, 1984, **49**, 1.
4. K. Guenther, J. Martens and M. Schickedanz, *Fresenius Z. Anal. Chem.*, 1985, **322**, 513.
5. J. D. Edward and S. P. Doshi, *J. Chromatogr.*, 1981, **210**, 305.
6. S. Sarre, Y. Michotte, P. Herregodts, D. Deleu, N. Deklippel and G. Ebinger, *J. Chromatogr. Biomed. Appl.*, 1992, **113**, 207.
7. D. Deleu, S. Sarre, P. Herregodts, G. Ebinger and Y. Michotte, *J. Pharm. Biomed. Anal.*, 1991, **9**, 159.
8. J. Cummings, M. L. Matheson and F. J. Smyth, *J. Chromatogr.*, 1990, **93**, 43.
9. C. Lucarelli, P. Betto, G. Ricciarello, M. Giabenedetti, C. Corradini, F. Stocchi and F. Belliardo, *J. Chromatogr.*, 1990, **511**, 167.
10. M. J. Cedarbaum, R. Williamson and H. Kutt, *J. Chromatogr.*, 1987, **59**, 393.
11. R. C. Benedict, *J. Chromatogr.*, 1987, **385**, 369.
12. M. Gerlach, N. Klaunzer and H. Przuntek, *J. Chromatogr. Biomed. Appl.*, 1986, **53**, 379.
13. A. Baruzzi, M. Contin, F. Albani and R. Riva, *J. Chromatogr. Biomed. Appl.*, 1986, **48**, 165.
14. T. Ishimitsu and S. Hirose, *Anal. Biochem.*, 1985, **150**, 300.

15. F. Ehrenstron and P. Johannson, *Life Sci.*, 1985, **36,** 867.
16. A. L. Rihbany and F. M. Delaney, *J. Chromatogr.*, 1982, **248,** 125.
17. E. Nissinen and J. Jaskinen, *J. Chromatogr. Biomed. Appl.*, 1982, **20,** 459.
18. C. D. Titus, F. T. August, C. K. Yeh, R. Eisenhandler, F. W. Bayne and G. D. Musson, *J. Chromatogr. Biomed. Appl.*, 1990, **99,** 87.
19. Y. Michotte, M. Moors, D. Deleu, P. Herregodts and G. Ebinger, *J. Pharm. Biomed. Anal.*, 1987, **5,** 659.
20. H. Tsuchiya and T. Hayashi, *J. Chromatogr. Biomed. Appl.*, 1989, **83,** 291.
21. P. Betto, G. Ricciarello, M. Giabenedetti, C. Lucarelli, S. Ruggeri and F. Stocchi, *J. Chromatogr.*, 1988, **459,** 4341.
22. X. Mie and G. Yang, Yaowu. *Fenxi. Zaahi*, 1992, **12,** 172.
23. T. S. Hassib, *Anal. Lett.*, 1990, **23,** 2195.
24. C. Yucesoy, *Gazi. Univ. Ecza Cilik. Fak. Derg.*, 1990, **7,** 43.
25. T. S. Hassib and Z. S. Elkhateeb, *Anal. Lett.*, 1990, **23,** 255.
26. G. A. Davidson, *J. Pharm. Biomed. Anal.*, 1985, **3,** 235.
27. G. A. Davidson, *J. Pharm. Sci.*, 1984, **73,** 1582.
28. L. Zivanovic, M. Vasiljevic, D. Radulovic and S. A. Kustrin, *J. Pharm. Biomed. Anal.*, 1991, **9,** 1157.
29. E. M. El-Kommos, A. E. Mohamed and S. A. Khedr, *J. Assoc. Off. Anal. Chem.*, 1990, **73,** 516.
30. B. P. Issopoulos, *Fresenius J. Anal. Chem.*, 1990, **336,** 124.
31. B. P. Issopoulos, *Pharm. Acta Helv.*, 1989, **64,** 82.
32. A. Steup, J. Metzner and A. Voll, *Pharrmazie*, 1986, **41,** 739.
33. T. R. Sane, J. G. Bhounsule and V. S. Sawant, *Indian Drugs*, 1987, **24,** 207.
34. J. Vachtenheim, J. Duchon and B. Matous, *Anal. Biochem.*, 1985, **146,** 405.
35. C. Martinez-Lozano, T. P. Ruiz, V. Tomas and O. Val, *Analyst*, 1991, **116,** 857.
36. T. N. Deftereos, C. A. Calokerines and E. C. Efstathiou, *Analyst*, 1993, **118,** 627.
37. A. C. Georgiou, A. M. Koupparis and P. T. Hadjiioannou, *Talanta*, 1991, **38,** 689.
38. T. Perez-Ruiz, C. Martinez-lozano, V. Tomas and O. Val, *Talanta*, 1993, **40,** 1625.
39. M. Herrera, L. S. Kao, D. J. Curran and E. W. Westhead, *Anal. Biochem.*, 1985, **144,** 218.
40. K. D. Khalaf, J. Sancenon and M. de la Guardia, *Anal. Chim. Acta*, 1992, **266,** 119.
41. K. D. Khalaf, A. Morales-Rubio and M. de la Guardia, *Anal. Chim. Acta*, 1993, **280,** 231.
42. K. D. Khalaf, J. Sancenon and M. de la Guardia, *Fresenius J. Anal. Chem.*, 1993, **347,** 52.
43. K. D. Khalaf, J. Sancenon and M. de la Guardia, *Talanta*, 1993, **40,** 1173.
44. K. D. Khalaf, B. A. Hasan, A. Morales-Rubio and M. de la Guardia, *Mikrochim. Acta*, 1993, **112,** 99.
45. K. D. Khalaf, B. A. Hasan, A. Morales-Rubio and M. de la Guardia, *Talanta*, 1994, **41,** 547.
46. *Merck Index*, 9th Ed. Rahway, 1976.
47. D. J. Burlock and J. Harley-Mason, *J. Chem. Soc.* 1951, **712.**
48. F. S. Lukovits and L. J. Dombrowski, *J. Assoc. Off. Anal. Chem.*, 1986, **69,** 183.
49. R. A. Heacock, *Chem. Revs*, 1959, **59,** 181.
50. K. C. Brown, J. F. Corbett and R. Babinson, *J. Chem. Soc. Perkin Trans., II*, 1978, 1292.

Pergamon

0039-9140(95)01466-7

*Talanta*, Vol. 42, No. 4, pp. 635–639, 1995

0039-9140/95 $9.50 + 0.00

# EXTRACTIVE SEPARATION OF GROUP IVB ELEMENTS: ANALYSIS OF ALLOY SAMPLES

S. M. KAKADE and V. M. SHINDE*

Analytical Laboratory, Department of Chemistry, The Institute of Science, 15, Madam Cama Road, Bombay 400 032, India

(*Received* 15 *July* 1994. *Revised* 31 *October* 1994. *Accepted* 1 *November* 1994)

**Summary**—A method is proposed for the extraction and mutual separation of quadrivalent titanium, zirconium and hafnium from hydrochloric acid using triphenylphosphine oxide dissolved in toluene as an extractant. The optimum conditions for the extraction and separation have been evaluated from critical study of acid concentration, extractant concentration, period of equilibration and effect of diluent. The effect of foreign ions on the extraction and determination is also discussed. The probable composition of the extracted species has been deduced from log$D$–log$C$ plots. The method affords mutual separation of titanium, zirconium and hafnium and is applicable to the analysis of alloy samples.

Titanium, zirconium and hafnium have increased rapidly in commercial importance. Titanium and its alloys are useful in defence applications, particularly in aircraft, missiles and in rocketry. Zirconium is used in nuclear reactors as a structural and container material. It also finds use in a variety of alloy steels and when added to niobium, forms a superconducting alloy. Hafnium is used as a control material in water cooled nuclear reactors and rectifiers and hence a method is desired for separation and determination of these metal ions.

Several oxygen containing solvents such as dibutyl hydrogen phosphate,[1] bis-(2-ethylhexyl)phosphate,[2,3] tri-*n*-butyl phosphate[4–7] tributylphosphine oxide,[8] tri-isoamylphosphate,[9,10] trioctylphosphine oxide,[11] mesityl oxide,[12] 2,mercaptopyridine-1-oxide,[13] dioctyl methylene diphosphate,[14] 2-ethylhexyl dihydrogen phosphate,[15] petroleum sulphoxide,[16] *N*,*N*-diethyl carbamoylphosphate and *N*,*N*-diethyl carbamoyl methylene phosphate,[17] 4-benzoyl-3-methyl-1-phenyl pyrazolin-5-one[18] and tetraphenyl imidodiphosphate,[19] have been used for extraction studies of quadrivalent titanium, zirconium and hafnium. The methods using high molecular weight amines are also critically discussed in earlier communication.[20] The existing methods have limitations such as longer extraction period,[1,5,7,10,11,14,16,17,19] use of salting out agents,[3,12,18] incomplete extraction,[6,8,9] critical controlling of temperature[10,16,19] and coextractions.[13,15] In our laboratory we have explored the utility of triphenylphosphine oxide for separation of group elements such as gallium, indium and thallium[21] and vanadium, niobium and tantalum.[22] An extension of this study showed that triphenylphosphine oxide dissolved in toluene can also be used for extraction and separation of group IVB elements, namely titanium(IV), zirconium(IV) and hafnium(IV). The proposed method has the following advantages:

1. Extraction time is in seconds.
2. Extraction is possible both at trace and macrolevel.
3. Extraction occurs in single step and recoveries of elements are >99.0%.
4. Provides mutual separation of titanium, zirconium and hafnium.
5. Method is applicable to the analysis of alloy samples.
6. Method is reproducible and accurate.

## EXPERIMENTAL

### *Apparatus*

The absorbance and pH measurements were taken on spectronic 20-D (Milton Roy and Co.) and Control Dynamics digital pH meter with combined glass electrode. ICP-AES was carried out using a Plasmalab 8440 Labtam instrument.

### *Reagents and chemicals*

The stock solutions of titanium(IV), zirconium(IV) and hafnium(IV) were prepared by dis-

*Author to whom correspondence should be addressed.

Table 1. Optimum extraction conditions for titanium(IV), zirconium(IV) and hafnium(IV)

| Metal ion | Acid concentration/ total volume | Organic phase | Extraction period (*sec*) | Stripping solution | Determination procedure |
|---|---|---|---|---|---|
| Titanium(IV) (5–15 μg) | 9.0*M* HCl/10 ml | 2 × 5 ml of 6.5% TPPO in toluene | 60 | 2 × 5 ml water | Spectrophotometry using $H_2O_2$[26] |
| Zirconium(IV) (1–10 μg) | 7.0*M* HCl/10 ml | 5 ml of 6.0% TPPO in toluene | 50 | 2 × 5 ml water | Spectrophotometry using Alizarin Red S as reagent[26] |
| Hafnium(IV) (1–10 μg) | 3.5–5.0*M* HCl/10 ml | 5 ml of 3.5% TPPO in toluene | 35 | 2 × 5 ml water | Spectrophotometry using Xylenol Orange[26] |

solving 1 g potassium titanyl oxalate (together with 2 g of ammonium sulphate in 25 ml concentrated sulphuric acid), 0.1 g zirconium nitrate (in 25 ml concentrated nitric acid) and 0.45 g hafnium dioxide (Koch-light) (in 9 ml of 48% hydrofluoric acid and 1 ml concentrated sulphuric acid), respectively, and diluting to 250 ml with distilled water. The solutions were standardized by known methods[23-25] and diluted as required.

Triphenylphosphine oxide (TPPO) (Fluka grade) dissolved in toluene was used for extraction and separation of titanium(IV), zirconium(IV) and hafnium(IV).

All other chemicals used were of analytical reagent grade.

*General extraction procedure for titanium(IV), zirconium(IV) and hafnium(IV)*

To an aliquot of a solution containing microgram amounts of metal ions, hydrochloric acid was added to give the desired molarity in a total volume of 10 ml (the optimum extraction conditions are reported in Table 1). The solution was transferred into a separating funnel and extracted with TPPO dissolved in toluene for the required shaking time. After removing the aqueous layer, the metal ions were stripped from the organic layer with two 5 ml portions of water and subsequently determined spectrophotometrically.

For titanium(IV), 2 ml of 3% hydrogen peroxide[26] solution were added; made up to the mark with water and the absorbance measured at 410 nm using water as blank. For zirconium(IV), 1 ml of 1% gum arabic solution, 5 ml of 0.05% aqueous solution of Alizarin Red S[26] were added and diluted up to the mark with 0.1*M* hydrochloric acid and the absorbance measured at 520 nm using reagent blank as reference. For hafnium(IV), 2 ml of 1% ascorbic acid and 2 ml of 0.05% aqueous solution of Xylenol Orange[26] were added and diluted up to the mark with water and the absorbance measured at 530 nm using reagent blank prepared analogously.

## RESULTS AND DISCUSSION

Variation in the concentration of acid (HCl/HBr) and TPPO (using toluene as the diluent) show that the quantitative extraction of titanium(IV) occurs from 9.0*M* HCl solution with 6.5% TPPO, whereas extraction of zirconium(IV) is quantitative with 6.0% TPPO from 7.0*M* HCl solution (Figs 1 and 2). Hafnium(IV), extraction is quantitative from 3.5 to 5.0*M* HCl with 3.5% TPPO. Titanium(IV), zirconium(IV) and hafnium(IV) showed no extraction from hydrobromic acid solution.

The suitability of several solvents such as benzene, toluene, xylene, carbon tetrachloride and chloroform for the extraction of titanium(IV), zirconium(IV) and hafnium(IV) using the proposed method was investigated. It was found that TPPO dissolved in toluene or benzene gives quantitative extraction of titanium(IV), zirconium(IV) and hafnium(IV). In all other diluents extraction was incomplete.

Variation of the shaking period showed that the minimum extraction periods for titanium(IV), zirconium(IV) and hafnium(IV) are 60, 50 and 35 sec, respectively. Prolonged shaking leads to emulsion and hinders phase separation.

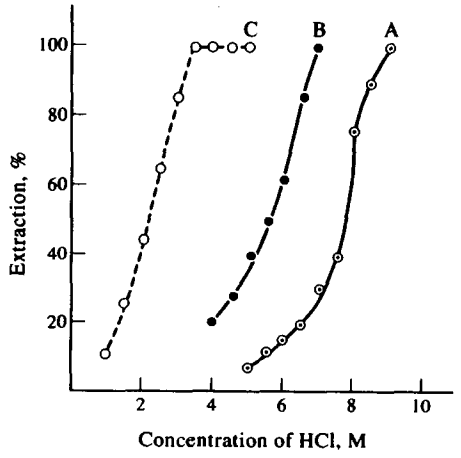


Fig. 1. Extraction behaviour of: Ti(IV), curve A; Zr(IV), curve B; and Hf(IV), curve C all as a function of HCl concentration with 6.5, 6.0 and 3.5% TPPO in toluene, respectively.

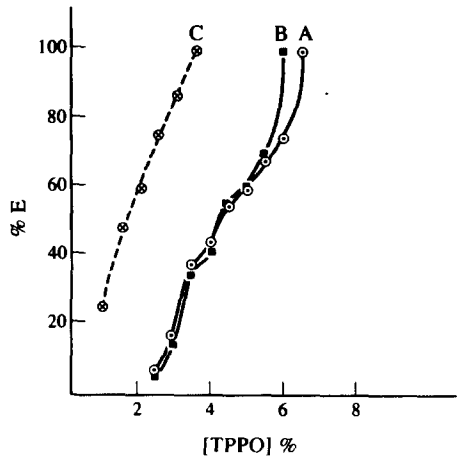


Fig. 2. Extraction behaviour of Ti(IV), curve A; Zr(IV), curve B; and Hf(IV), curve C all as a function of TPPO concentration of 9.0, 7.0 and 3.5*M* HCl concentrations, respectively.

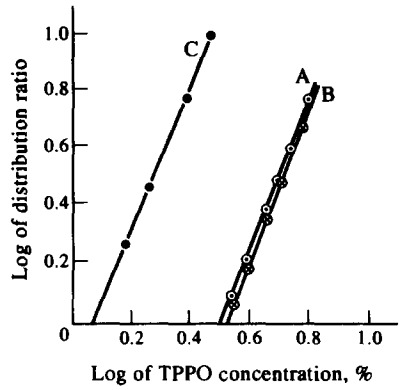


Fig. 3. Plot of the log of the distribution ratio vs log of the TPPO concentration at 9.0, 7.0 and 3.5*M* HCl concentrations for Ti(IV) (A), Zr(IV) (B) and Hf(IV) (C), respectively.

*Nature of extracted species*

The nature of the extracted species was established using log*D*–log*C* plots. A plot of log of distribution ratio *vs.* log of TPPO concentration for titanium(IV), zirconium(IV) and hafnium (IV) at 9.0, 7.0 and 3.5*M* HCl concentration, respectively, gave slopes of 2.3, 2.2 and 2.4, respectively (Fig. 3) indicating a metal to TPPO ratio of 1:2. Since the extraction of titanium(IV), zirconium(IV) and hafnium(IV) are done at reasonably high HCl concentrations, we expect formation of tetrachloro species such as $MCl_4$ [M is titanium(IV), zirconium(IV) or hafnium(IV)] which are further solvated by TPPO. The probable mechanism of solvation is

$$MCl_4 \cdot 2H_2O + 2TPPO \rightleftharpoons MCl_4 \cdot 2TPPO + 2H_2O.$$

TPPO, being more basic, supplants the water molecules and renders the species hydrophobic. A $MCl_4$ type of species was proposed by earlier workers also, for instance $Hf(NO_3)_4 \cdot 2TBP$[27] and $ZrCl_4 \cdot 2TOPO$[28]. At low HCl concentration, however, there is a possibility of species such as $ZrOCl_2 \cdot 2TPPO$ or $HfOCl_2 \cdot 2TPPO$.

*Effect of foreign ions*

Various cations and anions were investigated in an interference study on the extraction and

Table 2. Diverse ion effect

| Tolerance limit, (μg)* | Titanium(IV) | Zirconium(IV) | Hafnium(IV) |
|---|---|---|---|
| None | — | Ga(III), V(V) | — |
| 50 | In(III), V(V) | — | — |
| 100 | Ga(III), Te(IV) | In(III) | Ga(III), V(V) |
| 200 | Au(III), Tl(III), Fe(III),† Nb(V), W(VI) | Tl(III), Fe(III),† Te(IV), Nb(V), W(VI) | In(III), Tl(III), Fe(III),† Te(IV), W(VI) |
| 500 | Hg(II), Ni(II), Sn(II), Ta(V), Mo(VI), $F^-$, $S_2O_3^{2-}$, $PO_4^{3-}$ | Hg(II), Ni(II), Sn(II) Au(III), Mo(VI), $S_2O_3^{2-}$ | Ni(II), Au(III), Nb(V) |
| 1000 | Cu(II), Mn(II), Pd(II), Cd(II), Cr(VI), tartrate, thiourea, oxalate | Se(IV), Ta(V), $F^-$, $PO_4^{3-}$ | Hg(II), Sn(II), Ta(V), Mo(VI), $F^-$, $S_2O_3^{2-}$ |
| 1500 | Bi(III), Ru(III), Th(IV) | Pd(II), Cr(VI), thiourea, oxalate | Se(IV), thiourea, $PO_4^{3-}$ |
| 2000 | Zn(II), Al(III), Se(IV), citrate, EDTA | Zn(II), Mn(II), Bi(III), Ru(III), Al(III), Th(IV), citrate, tartrate, EDTA | Cu(II), Mn(II), Pd(II), Ru(III), Th(IV), Cr(VI), EDTA, oxalate |
| 3000 | Ce(IV) | Ce(IV), Cd(II) | Zn(II), Ce(IV), Cd(II), Bi(III), Al(III), tartrate, $F^-$ |

*Maximum allowable amounts of foreign ions to create ±1% error.
†Iron(III) is masked with 500 μg of EDTA.

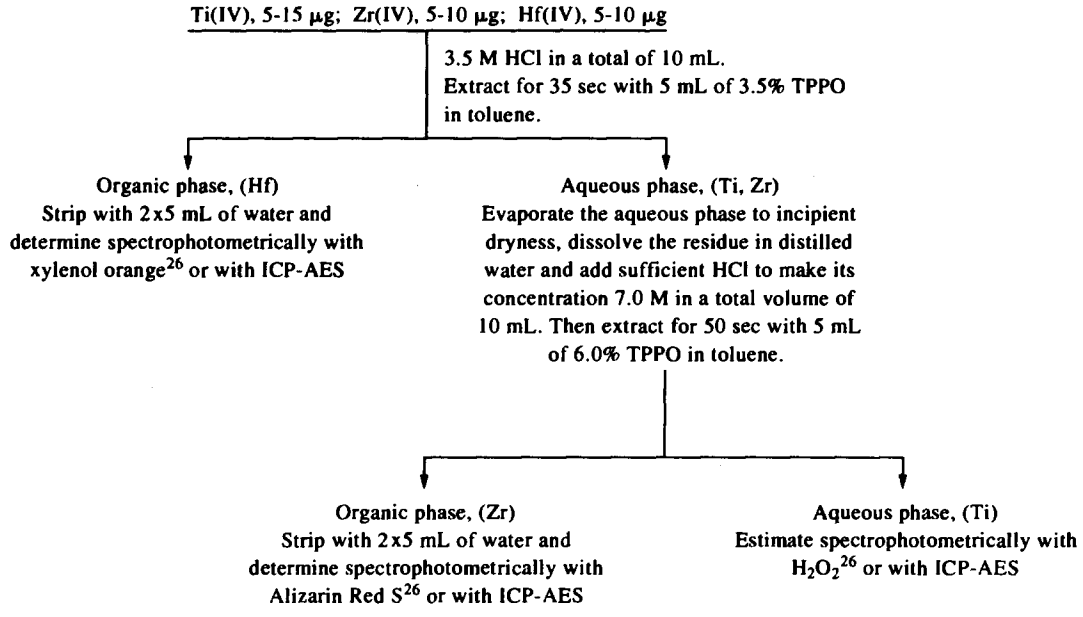


Fig. 4. Flow chart for the mutual separation of Ti(IV), Zr(IV) and Hf(IV) in synthetic mixtures.

determination of titanium(IV), zirconium(IV) and hafnium(IV) by the recommended procedure. The tolerance limit was set at the amount required to cause $\pm 1\%$ error in metal recovery. The results are reported in Table 2.

*Mutual separation of titanium(IV), zirconium(IV) and hafnium(IV)*

Titanium(IV), zirconium(IV) and hafnium(IV) were separated from a ternary mixture by the scheme shown in Fig. 4. The recoveries of titanium, zirconium and hafnium were >99.0% (Table 3).

*Application to the analysis of alloys*

The proposed method was applied to the separation and determination of titanium(IV), zirconium(IV) and hafnium(IV) in alloys such as Ce–Zn–Zr (BCS 307) (0.125 g alloy dissolved in 2 ml concentrated hydrochloric acid and diluted to 25 ml with distilled water), sillimanite (BCS 309) (0.025 g alloy dissolved in 4 ml of aqua regia, evaporated, filtered and diluted to 25 ml with distilled water) and 6% Zn–Al (BCS 300/1) (0.1 g alloy dissolved in 2 ml concentrated hydrochloric acid and diluted to 25 ml with distilled water). We could not procure samples containing hafnium, hence a known amount of hafnium was added to alloy solutions and the procedure was followed for its recovery. The analysis show that the procedure is applicable to alloys which contain all three metals. The recoveries of zirconium and hafnium in Ce–Zn–Zr (Zr, 0.56%; Fe, 0.0021%; Mn, 0.006%; Zn, 2.08%; Cu, 0.005%; Ni, 0.001%; total rare earth 2.84% + 1 mg Hf); that of titanium and hafnium in sillimanite ($SiO_2$, 34.1%; $Fe_2O_3$, 1.51%; CaO, 0.22%; $Na_2O$, 0.34%; $Al_2O_3$, 61.1%; $TiO_2$, 1.92%; MgO, 0.17%; $K_2O$, 0.46% + 1 mg Hf) alloy and recoveries of titanium, zirconium and hafnium in Zn–Al alloy (Ti, 0.09%; Fe, 0.24%; Mg, 2.74%; Zr, 0.18%; Cu, 1.27%; Cr, 0.13%; Si, 0.014%; Mn, 0.33%; Zn, 5.83% + 1 mg Hf) are better than 99%. The recoveries of titanium, zirconium and hafnium were confirmed by ICP-AES before and after extraction.

Table 3. Determination of titanium, zirconium and hafnium in ternary mixtures

| Analysis no. | Mixture (μg) | Recovery (%) | Coefficient of variation (%) |
|---|---|---|---|
| 1 | Ti, 10; Zr, 5; Hf, 5 | Ti, 99.7; Zr, 99.2; Hf, 99.0 | Ti, 0.52; Zr, 0.63; Hf, 1.1 |
| 2 | Ti, 5; Zr, 10; Hf, 5 | Ti, 99.2; Zr, 99.7; Hf, 99.0 | Ti, 1.14; Zr, 0.38; Hf, 1.1 |
| 3 | Ti, 15; Zr, 5; Hf, 10 | Ti, 99.7; Zr, 99.0; Hf, 99.5 | Ti, 0.46; Zr, 0.62; Hf, 0.85 |

*Average of six determinations

*Acknowledgement*—The authors thank the Council of Scientific and Industrial Research (CSIR), New Delhi for financing the project.

## REFERENCES

1. A. Kiss, *Acta Chim.*, 1965, **44,** 357.
2. Yu. B. Kletenie and I. B. Bykhovsky, *Zh Anal. Khim.*, 1966, **4,** 6499.
3. T. Sato, *Anal. Chim. Acta*, 1970, **52,** 183.
4. G. Roland, L. M. Podent and G. Dubeykaerts, *Anal. Chim. Acta*, 1976, **85,** 331.
5. Yu. V. Moracherskii and N. S. Borovaya, *Uch. Zap. Leningrad Gus. Univ.*, 1960, **297,** 99.
6. F. G. Zharovskii, L. M. Vyazovskaya and R. V. Kostova, *Ukr. Khim. II*, 1963, **34,** 181.
7. I. Nario, *Jpn Anal.*, 1971, **20,** 655.
8. H. Umerzawa and R. Kara, *Anal. Chim. Acta*, 1960, **23,** 267.
9. S. H. Hasan and D. G. Rupainwar, *J. Indian. Chem. Soc.*, 1987, **64,** 249.
10. S. H. Hasan and D. G. Rupainwar, *Acta Chim. Hung*, 1990, **127,** 235.
11. J. P. Young and J. C. White, *Talanta*, 1958, **1,** 263.
12. S. M. Khopkar and S. C. Dhara, *Anal. Chem. Acta*, 1965, **37,** 1158.
13. A. I. Buzev, V. N. Byrko Hoang, K. Yen and N. N. Novi Kova, *Vest Mask, Gos Univ. Serkhim.*, 1972, **13,** 319.
14. H. Gorican and C. Djardjeric, *Croat. Chem. Acta*, 1965, **37,** 265.
15. A. Jain, O. V. Singh and S. N. Tondon, *J. Radioanal. Nucl. Chem.*, 1991, **147,** 355.
16. A. I. Nikolaev, A. G. Babkin, L. M. Zalkind and N. I. Kasikova, *Zh. Prikl. Khim.*, 1981, **54,** 506.
17. H. Petrzilova, L. Kuca and J. Binka, *Ustav. Jad. Vysk. UJV*, 1980, **41,** 5093-CH.
18. V. I. Fadeeva, V. S. Putilina and I. P. Alimarin, *Zh. Anal. Khim.*, 1974, **29**(IV), **19,** 1923.
19. O. Navarati and E. Herrmann, *Collec. Czech. Chem. Commun.*, 1992, **57,** 1655.
20. N. M. Sundaramurthi and V. M. Shinde, *Analyst*, 1989, **114,** 201.
21. Sharad M. Kakade and Vijay M. Shinde, *Analyst*, 1993, **118,** 1449.
22. Sharad M. Kakade and Vijay M. Shinde, *Bull. Chem. Soc. Jpn*, 1994, **57,** 1.
23. A. I. Vogel, *A Textbook of Quantitative Inorganic Analysis*, p. 544. Longmans, London, 1962.
24. F. J. Welcher, *Analytical Uses of EDTA*, p. 184. Van Nostrand, Princeton, New Jersey, 1958.
25. A. K. Mukharji, *Analytical Chemistry of Zirconium and Hafnium* p. 36. Pergamon Press, Oxford, 1970.
26. Z. Marczenko, *Spectrophotometric Determination of Elements*, pp. 566, 611, 613. Ellis Harwood, Chichester, 1976.
27. E. N. Lebedeva, S. S. Karovin and A. N. Rozen, *Zh. Neorgan. Khim.*, 1964, **9,** 1744.
28. J. C. White and W. J. Ross, U.S. At. Energy Commis. ORNL, 1958, 2498.

Pergamon

0039-9140(95)01467-5

*Talanta*, Vol. 42, No. 4, pp. 641–645, 1995

0039-9140/95 $9.50 + 0.00

# DEVELOPMENT OF A MONITORING TAPE FOR PHOSGENE IN AIR

NOBUO NAKANO,[1]* AKIHIRO YAMAMOTO, YOSHIO KOBAYASHI[2] and KUNIO NAGASHIMA[3]

[1]Riken Keiki Co., Ltd, 2-7-6, Azusawa, Itabushi-ku, Tokyo 174, Japan
[2]Analysis Center Co., Ltd, Higashimukouzima, Sumida-ku, Tokyo 131, Japan
[3]Faculty of Engineering, Kogakuin University, 1-24-2, Nishishinjuku, Shinjuku-ku, Tokyo 160, Japan

(*Received* 6 *July* 1994. *Revised* 28 *October* 1994. *Accepted* 1 *November* 1994)

**Summary**—A porous cellulose tape impregnated with a processing solution that includes 4-*p*-nitrobenzylpyridine, *N*-benzylaniline and methanol is a highly sensitive means of detecting phosgene and maintains stable sensitivity for at least three months in air in a desiccator. When the sample including phosgene was passed through the tape, the color of tape changed to red. The degree of color change was proportional to the concentration of phosgene at a constant sampling time and flow rate. The degree of color change could be recorded by measuring the intensity of reflecting light (555 nm). The detection limit was 6 ppb for phosgene with a sampling time of 60 sec and a flow rate of 400 ml/min. Reproducibility tests showed that the relative standard deviation of response ($n = 10$) was 2.6% for 0.2 ppm phosgene. No interference was observed from ethanol (1 vol.%), trichloroethylene (1 vol.%), acetone (1 vol.%), carbon dioxide (4.9 vol.%), carbon monoxide (100 ppm), nitrogen dioxide (100 ppm), sulfur dioxide (50 ppm), hydrogen chloride gas (5 ppm), chlorine (3 ppm), acetic acid gas (24 ppm), ammonia (40 ppm), or benzyl chloride (20 ppm).

Phosgene is a highly toxic, colorless, irritating gas. It is important in dye manufacture and in the production of polycarbonate and polyurethane resins, carbamates, organic carbonates, chloroformates, and pesticides. Its occurrence in air is often unpredictable, since many organochlorine compounds thermally and photochemically decompose into phosgenes. Phosgene may also be important in air pollution study, since phosgene is synthesized in the lower troposphere by photochemical smog reactions of halocarbons. The establishment of a threshold limit value of 0.1 ppm of phosgene in air[1] emphasized the need for a sensitive, reliable, and specific method for the determination of phosgene in industrial environments. Several methods have been reported for the detection of phosgene, including colorimetric procedures[2–5] and chromatographic techniques,[6,7] but to achieve widespread routine use, the method should be simple, specific, capable of unattended operation, and also inexpensive. However, few methods exhibit all these desirable performances. Consequently, we chose a tape monitor because of its high sensitivity and selectivity, easy maintenance, continuous monitoring function, small size, low running cost and greater ease of operation in the automatic mode.[8] We investigated a suitable reagent that reacts with phosgene to produce a color stain. Of the investigated colorimetric procedures, the most specific and sensitive reagent used for phosgene was a mixture of 4-*p*-nitrobenzylpyridine (NBP) and *N*-benzylaniline (BA).[4] We studied tape impregnated with these reagents in order to determine phosgene concentrations less than 0.1 ppm in air. In this paper, we described a study to develop a monitoring tape for the determination of phosgene in air in the range 6 ppb to 0.2 ppm. The concentration of NBP and BA in processing solution, gas flow-rate, sampling time, reproducibility, effect of temperature and humidity of sample gas, and stability of the tape and response to other gases were investigated to evaluate the characteristics of the tape for the determination of phosgene in air.

*Author to whom correspondence should be addressed.

## EXPERIMENTAL

### *Reagents and samples*

A processing solution was prepared as follows. To *ca* 100 ml of methanol, 1.5 g of

4-*p*-nitrobenzylpyridine (NBP) and 3 g of *N*-benzylaniline (BA) were added.

Standard phosgene mixtures (0.2–0.03 ppm) were prepared continuously by purging a FEP Teflon permeation tube with various constant flows of purified air (99.9%; Taiyo Sanso).

Humidified phosgene mixtures were prepared by mixing dry air passing through a Gore-Tex (porous Teflon; 4 mm i.d, 6 mm o.d. and 50 mm length) tube immersed in water (25 ± 2°C) with 0.2 ppm phosgene.[9] The relative humidity of the gas mixture was determined by a humidity sensor (Model HMI32; Vaisala) in the gas flow.

*Monitoring tape*

The porous cellulose tape (Whatman 1Chr papers, 20 mm wide, 0.18 mm thick and 25 m length) was immersed in the processing solution for 1 min, oven-dried at 40°C and stored in a desiccator.

*Apparatus*

The experimental apparatus was similar to that previously used.[8] The end (*ca.* 1 cm in diameter) of tube from the suction unit is attached tightly to a tape. The sample gas was sucked through the tape at a constant flow rate (400 ml/min) and a constant sampling time (60 sec). A tape is continuously fed past and exposed to air from a sample draw line. When exposed to phosgene, the NBP-BA reagent on the tape reacted with phosgene to change its homogeneous color. The degree of color change was recorded by measuring the reflected light of 555 nm. Then the pathway of the tape was renewed by moving the tape every 60 sec. The response (reflection absorbance, $A$) is defined by $A = -\log V_1/V_0$, where $V_0$ and $V_1$ are outputs of blank (an atmospheric air) and of the sample, respectively. The 30 min time was required to measure the responses after the tape was set in the tape monitor. All the measurements were carried out at 25 ± 2°C.

## RESULTS AND DISCUSSION

A review of the methods employed to detect trace amounts of phosgene in air disclosed that a few major approaches to the problem had been investigated: (1) determination of chloride ion after hydrolysis, (2) colorimetric analysis. In the first category attention was turned to procedures that depend on the hydrolysis of phosgene to $CO_2$ and HCl: $COCl_2 + H_2O \rightarrow CO_2 + 2HCl$. We studied tape using pH indicator reagents,[10] such as Methyl Yellow, for monitoring tape of acidic gases, which is a highly sensitive means of detecting HCl.[11] In this experiment, we studied tape impregnated with Methyl Yellow for phosgene gas. However, this tape was not successful in detecting 1 ppm phosgene.

In the following sections, we investigate colorimetric analysis; in this experiment, we examined tape using NBP–BA reagents that had obtained good results for phosgene in previous reports.[4] It was concluded that tape impregnated with NBP–BA reagent could serve as a sensitive monitoring tape for phosgene, but the tape impregnated with only NBP was not sensitive for phosgene (1 ppm).

*Reflectance spectra*

After this tape had been exposed to 0.2 ppm phosgene for a sampling time of 60 sec at a flow rate of 400 ml/min, the visible reflectance spectrum of the exposed tapes was recorded with a UV-2200 spectrophotometer (Shimadzu), using a freshly prepared barium sulfate disk as a reference standard (Fig. 1). The solid and broken spectra show the reflectance spectra of the tape exposed to 0.2 ppm phosgene and air (without phosgene), respectively.

*Concentration of NBP-BA reagent*

To obtain the optimum conditions for the detection of phosgene, the response for phosgene was measured with various concentrations

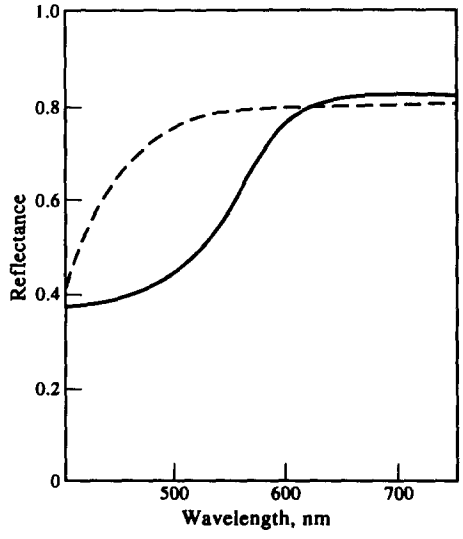


Fig. 1. Reflectance spectra of tapes exposed to $COCl_2$ and air (reference: $BaSO_4$ disk). The solid and broken lines show the reflectance spectrum of the tape exposed to $COCl_2$ in air and air, respectively.

Table 1. Effect of concentration of 4-*p*-nitrobenzylpridine (NBP) and N-benzylaniline (BA) in processing solution on response

| Concentration in processing solution (%) | | |
|---|---|---|
| NBP | BA | Response |
| 0.025 | 0.5 | 0.069 |
| 0.50 | 1.0 | 0.094 |
| 1.5 | 3.0 | 0.105 |
| 2.5 | 5.0 | 0.106 |
| 3.5 | 7.0 | 0.108 |

Concentration of $COCl_2$: 0.2 ppm.
Sampling time: 60 sec.

of NBP–BA reagent (mixture of NBP and BA in the ratio of 1:2, we confirmed it by an analysis of NBP and BA in the mother liquor after the reaction was complete) in the processing solution and various flow-rates of the sample gas. The response for phosgene increased with an increase in concentration of NBP–BA reagent and increased slightly at levels about 1.5 wt% NBP in the processing solution (Table 1). The processing solution used was prepared with 1.5 wt%:NBP–3.0 wt%:BA.

*Gas flow-rate*

Table 2 shows the effect of the sample gas flow-rate on response. The response increased with increase the sample gas flow-rate and slightly above 350 ml/min. The optimum sample gas flow-rate was estimated to be 400 ml/min.

*Sampling time*

The response for fixed concentration of phosgene was plotted against various sampling times. Nonlinear graphs between response and sampling time were obtained in the range 0.05–0.2 ppm and *vs.* sampling time in the range 10–90 sec (Fig. 2).

*Calibration graph*

Typical calibration graphs for phosgene using the optimum experimental condition are shown in Fig. 3. A linear relation was obtained in the region of 0.03–0.2 ppm of phosgene. The response for 0.8 ppm of phosgene was 0.32 which corresponded to 80% for 0.8 ppm. By using optimum conditions, the detection limit (signal-to-noise ratio = 3) was 6 ppb for phosgene with a sampling time of 60 sec. Reproducibility tests ($n = 10$) showed that the relative standard deviation of response was 2.6% for 0.2 ppm phosgene, and the relative standard deviation of the calibration graph was 3.5%.

Table 2. Effect of sample gas flow-rate on response

| Gas flow rate (*ml/min*) | Response |
|---|---|
| 100 | 0.037 |
| 200 | 0.058 |
| 300 | 0.084 |
| 350 | 0.100 |
| 400 | 0.106 |
| 500 | 0.107 |

Concentration of $COCl_2$: 0.2 ppm.
Sampling time: 60 sec.

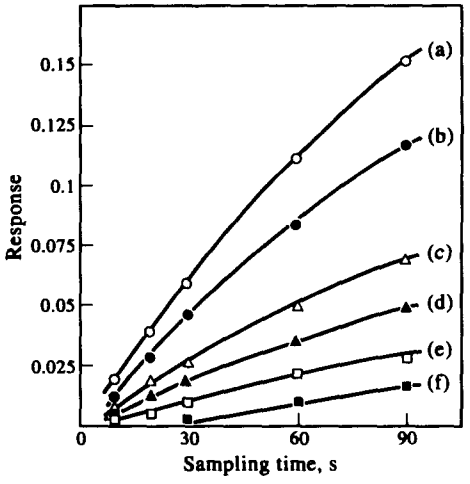


Fig. 2. Relation between sampling time and response at various concentrations of $COCl_2$. Flow rate: 400 ml/min [$COCl_2$]: (a) 0.2 ppm, (b) 0.15 ppm, (c) 0.1 ppm, (d) 0.075 ppm, (e) 0.05 ppm, (f) 0.03 ppm.

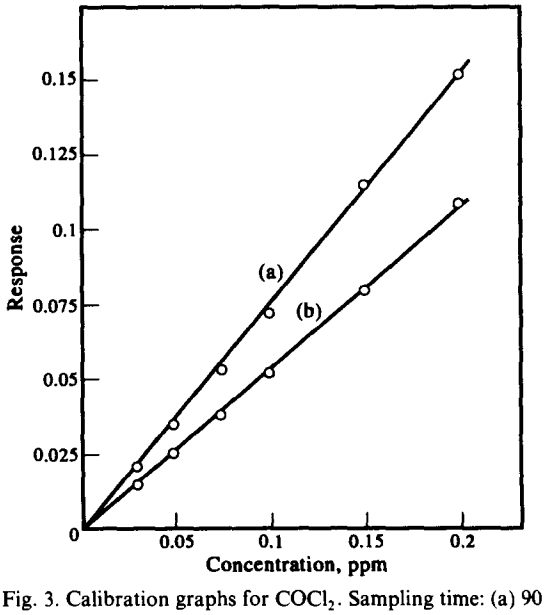


Fig. 3. Calibration graphs for $COCl_2$. Sampling time: (a) 90 sec, (b) 60 sec.

Table 3. Effect of humidity of sample gas on response

| Humidity (%) | Response |
|---|---|
| 10 | 0.084 |
| 30 | 0.097 |
| 40 | 0.105 |
| 50 | 0.105 |
| 60 | 0.110 |
| 80 | 0.110 |

Concentration of $COCl_2$: 0.2 ppm.
Sampling time: 60 sec.

*Humidity of sample gas*

Table 3 shows the effect of humidity of sample gas on the response of the tape. The tape was hardly affected by humidity in the region 30–80%RH used in this experiment, but response decreased gradually at levels below 30%RH. It can be concluded that there is very little effect of humidity on the response of the tape under normal conditions (40–60%RH).

*Temperature of sample gas*

Table 4 shows the effect of the temperature of sample gas variation within the range of 0–40°C on the response of the tape. The tape is hardly affected by temperature in the region 0–30°C used in this experiment, but decreased gradually at levels above 30°C. It can be concluded that there is very little effect of temperature on the response of the tape under normal conditions (10–30°C).

*Selectivity*

The response of the tape for various gases are given in Table 5. The tape is hardly affected by other gases in the concentration ranges used in this experiment, except for acetyl chloride.

*Long-term stability*

As it is very important in the preparation of a reliable tape to use high stable reagents on exposure to air, its stability in a desiccator was studied. The relationship between storage time and response of the tape impregnated with NBP–BA reagent was investigated (Table 6). After storage for about 3 months in a desiccator the response for phosgene was 90% of the original level.

In conclusion, the monitor tape impregnated with NBP–BA reagent is very suitable for the determination of phosgene concentrations in the range 0.006–0.2 ppm. This tape monitor method is simple, specific, capable of unattended operation and is recommended for field operation.

Table 4. Effect of temperature of sample gas on response

| Temperature (°C) | Response |
|---|---|
| 0 | 0.108 |
| 10 | 0.108 |
| 20 | 0.105 |
| 30 | 0.094 |
| 40 | 0.084 |

Concentration of $COCl_2$: 0.2 ppm.
Sampling time: 60 sec.

Table 5. Response for various gases

| Gas examined | Concentration of gas | Response |
|---|---|---|
| Ethanol | 1% | <0.002 |
| Methanol | 1% | <0.002 |
| Isopropanol | 1% | <0.002 |
| Trichloroethylene | 1% | <0.002 |
| Toluene | 1% | <0.002 |
| Acetone | 1% | <0.002 |
| Carbon monoxide | 100 ppm | <0.002 |
| Carbone dioxide | 4.9% | <0.002 |
| Nitrogen dioxide | 100 ppm | <0.002 |
| Hydrogen | 100% | <0.002 |
| Hydrogen sulfide | 30 ppm | <0.002 |
| Hydrogen chloride | 5 ppm | <0.002 |
| Hydrogen fluoride | 9 ppm | <0.002 |
| Sulfur dioxide | 50 ppm | <0.002 |
| Acetic acid | 24 ppm | <0.002 |
| Chlorine | 3 ppm | <0.002 |
| Ethylenediamine | 10 ppm | <0.002 |
| Ammonia | 40 ppm | <0.002 |
| Benzyl chloride | 20 ppm | <0.002 |
| Acetyl chloride | 10 ppm | 0.011 |
| Phosgene | 0.2 ppm | 0.105 |

Table 6. Long-term stability of the monitoring tape

| Day | Response |
|---|---|
| 0 | 0.104 |
| 10 | 0.103 |
| 31 | 0.101 |
| 66 | 0.095 |
| 91 | 0.094 |

Concentration of $COCl_2$: 0.2 ppm.
Sampling time: 60 sec.

## REFERENCES

1. 1992–1993, Threshold Limit Values for Chemical Substances and Biological Exposure Indices, American Conference of Government Industrial Hygienists, Cincinnati, OH, 1992.
2. B. E. Dixon and G. C. Hands, *Analyst*, 1959, **84**, 463.
3. A. L. Linch, S. S. Ford, K. A. Kubitz and M. R. DeBrunner, *Am. Ind. Hyg. Assoc. J.*, 1965, **26**, 465.

4. M. H. Noweir and E. A. Pfitzer, *Am. Ind. Hyg. Assoc. J.*, 1971, **32,** 163.
5. R. N. Matherne, P. L. Lubs and E. J. Kerfoot, *Am. Ind. Hyg. Assoc. J.*, 1981, **42,** 681.
6. G. G. Esposito, Daniel Lillian, G. E. Podolak and R. M. Tuggle, *Anal. Chem.*, 1977, **49,** 1774.
7. W. S. Wu and V. S. Gaind, *Analyst*, 1993, **118,** 1285.
8. N. Nakano, Y. Kobayahi and K. Nagashima, *Bunseki Kagaku*, 1993, **42,** 537.
9. T. Otagawa, S. Zaromb and J. R. Stetter, *J. Electrochem. Soc.*, 1985, **132,** 2951.
10. N. Nakano, Y. Kobayahi and K. Nagashima, *Bunseki Kagaku*, 1994, **43,** 139.
11. N. Nakano, Y. Kobayahi and K. Nagashima, *Analyst*, 1993, **118,** 1539.

Pergamon

0039-9140(95)01405-5

*Talanta*, Vol. 42, No. 4, pp. 649–655, 1995

0039-9140/95 $9.50 + 0.00

# APPLICATION OF A CHOLINESTERASE BIOSENSOR TO SCREEN FOR ORGANOPHOSPHORUS PESTICIDES EXTRACTED FROM SOIL

SATISH KUMARAN and MASATOSHI MORITA*

National Institute for Environmental Studies, 16-2 Onogawa, Yatabe, Tsukuba, Ibaraki 305, Japan

(*Received* 20 *January* 1994. *Accepted* 4 *August* 1994)

**Summary**—Based on the principle of enzyme inactivation, a butyrylcholinesterase (EC 3.1.1.8.) biosensor, to determine some organophosphorus (ORP) pesticides (Fenitrothion, Diazinon, Parathion ethyl, Mevinphos and Heptenophos) in soil extracts, is presented. The enzyme was immobilized on pre-activated Pall Biodyne™ transfer membranes, which were physically attached to the sensitive ends of glass pH electrodes. Contact of the enzyme with pesticide samples results in specific inhibition of enzyme activity. Sensor calibration was possible by correlating the inhibition of enzyme activity (monitored by observing reduction in electrode potential changes with substrate additions) with varying concentrations of pesticide compounds in a buffer solution. A simple procedure was designed to extract ORP pesticides from spiked soil samples using a mixture of dichloromethane and acetone as the extraction solvent mixture. The sensor was successfully used to determine pesticide concentrations ranging from a low of 35 ppb (Diazinon) to 21 ppm (Fenitrothion) in soil, with resultant relative standard deviations of percentage enzyme inactivation less than 12%. The complete extraction and analytical procedure is simple, inexpensive and rapid. Mass production of the enzyme membranes and their easy attachment to the electrodes, render them disposable after a single use. The biosensor is seen as a potential analytical instrument for early warning against pesticide contaminations in soil.

Organophosphorus (ORP) pesticides represent a very large part of agricultural chemicals in widespread use. Owing to their potential mammalian toxicity, the monitoring of pesticide residues in agricultural and food products and in environmental matrices has become a priority field in pesticide research and analysis. The agricultural usage of such chemicals leave residues in soil from fall-out from aerial spraying, in rain or dust or from plant or animal which become incorporated with the soil. Thus, the soil is an environmental reservoir for these residues from which they move into the atmosphere, water or living organisms.

The most common method to analyse organophosphate residues is gas chromatography (GC) with nitrogen–phosphorus or flame-photometric detection, although liquid chromatography is also receiving attention for high detection sensitivity and selectivity.[1] Several extraction procedures and clean-up approaches have been reported for numerous pesticides from soil.[2–5] In most cases, these techniques for extraction and analysis are laborious, time-consuming and expensive.

The toxicity of several ORP pesticides to mammals has been studied quite extensively and is well documented.[6] The inhibition of cholinesterases by these compounds is the result of the formation of stable covalent intermediates such as phosphoryl–enzyme complexes, which hydrolyze very slowly. The reaction scheme below represents the inhibition of the enzyme by an organophosphorus ester.

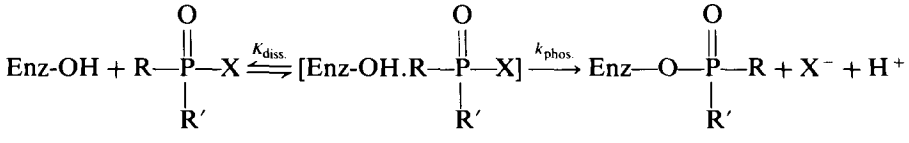


Since the inhibition mechanism is very specific, several analytical techniques have been

*Author to whom correspondence should be addressed.

developed for the determination of such pesticides on the basis of cholinesterase inhibition.[7-10] Recently, a bienzyme sensor[11] has been reported for the determination of organophosphorus pesticides. The biosensor is based on the immobilization of choline oxidase and butyrylcholinesterase on a preactivated nylon membrane attached to a hydrogen peroxide electrode. In yet another study,[12] only butyrylcholinesterase was immobilized onto such preactivated polyamide membranes and used in conjunction with pH glass electrodes to determine organophosphorus and carbamate pesticides. The present work deals with this simple, rapid and inexpensive method to determine ORP pesticides in soil extracts, beginning from sample extraction to the use such butyrylcholinesterase-based biosensors for analysis.

## EXPERIMENTAL

### *Reagents*

Butyrylcholinesterase (EC 3.1.1.8) from horse serum, with a reported specific activity of 18 units/mg protein, was purchased from Sigma Chemical (St. Louis, MO, U.S.A.), and was used as such without any treatment. Butyrylcholine chloride (Sigma Chemical) was used as substrate.

Polyamide pre-activated Pall Biodyne™ general purpose transfer membranes (Type A, porosity 3 $\mu$m), said to present 50% carboxylic and 50% amine groups for protein attachment, were obtained from Nippon Genetics Co., Japan.

The ORP pesticides, Fenitrothion, Diazinon, Parathion Ethyl, Mevinphos and Heptenophos were Pestanal® chemicals, all purchased from Riedel de-Haen AG (D-3016, Seelze, Germany). Stock solutions of the ORP compounds were made in HPLC grade acetonitrile (Cica Merck).

Bromine water (2–3% w/v) from Wako Chemicals, Japan, was used to oxidize the ORP compounds containing P=S moieties to the corresponding P=O esters, thereby making them more reactive as inhibitors.

The composition of the working buffer, used for the preparation of the substrate solution and to conduct the potential measurements, was $2.5 \times 10^{-3}M$ HEPES [4-(2-hydroxyethyl)-piperazine-1-ethane sulfonic acid] from Sigma Chemical, containing $2 \times 10^{-2}M$ $MgCl_2$, $0.1M$ NaCl and 0.01% (m/v) gelatine (Sigma Chemical) from porcine skin. The pH of the buffer was adjusted to 7.55 before use.

Dichloromethane and acetone (both min. 99.5% purity) were purchased from Wako Chemicals, Japan, and used to prepare the extraction solvent mixture.

Toyo Roshi filter paper No. 2 was used to filter the soil samples in the extraction procedure.

Milli-Q® water was used wherever necessary. All other reagents used were of analytical grade.

### *Enzyme immobilization and biosensor preparation*

Butyrylcholinesterase (3.8 mg) was dissolved in 1 ml sodium phosphate buffer ($2.5 \times 10^{-3}M$, pH 6.5). Six pieces of the transfer membrane measuring $15 \times 21$ mm$^2$ were cut and dipped into the enzyme solution one by one, each left immersed in the solution for only 2 min. The membranes were then dried in a stream of nitrogen. A casein blocking solution using phosphate buffered saline (PBS) pH 7.4 ($4 \times 10^{-2}M$ dihydrogen sodium phosphate, $8 \times 10^{-3}M$ in the sodium hydrogen phosphate, $0.15M$ sodium chloride) was freshly prepared. The 0.5% (m/v) solution of casein in PBS was heated to 60°C while stirring. The solution was left to cool to room temperature, before filtering through a 0.45 $\mu$m membrane filter to remove aggregates. The membranes were dipped in the blocking solution one by one, each being left immersed for 2 min. The membranes were completely dried in a stream of nitrogen before being cut into $3 \times 3$ mm$^2$ pieces and stored at 4°C.

The biosensor was prepared by attaching a $3 \times 3$ mm$^2$ piece of enzyme membrane to the bulb of the pH glass electrode (TOA pH combination electrode, Type GST-5425C). The attachment was done using a piece of nylon stocking material and a silicone 'O' ring (Fig. 1a).

### *Soil spiking and extraction*

Soil was collected from the Institute grounds by removing a trowel full down to about 10 cm. The matrix was placed in a tray and left to dry at about 35°C on top of an oven. The dried soil had a particle size distribution of $<0.125$ mm 11.9%, 0.5–0.125 mm 46.2% and $>0.5$ mm 41.9%. Total organic and clay content of the soil were found to be 16.1 and 6%, respectively. The fresh soil had a pH of 6.7 and a moisture content of 14.4%.

Spiking of the soil sample was done by injecting a known amount of the pesticide stock solution to a portion of 1 g ($\pm 0.005$ g) of soil

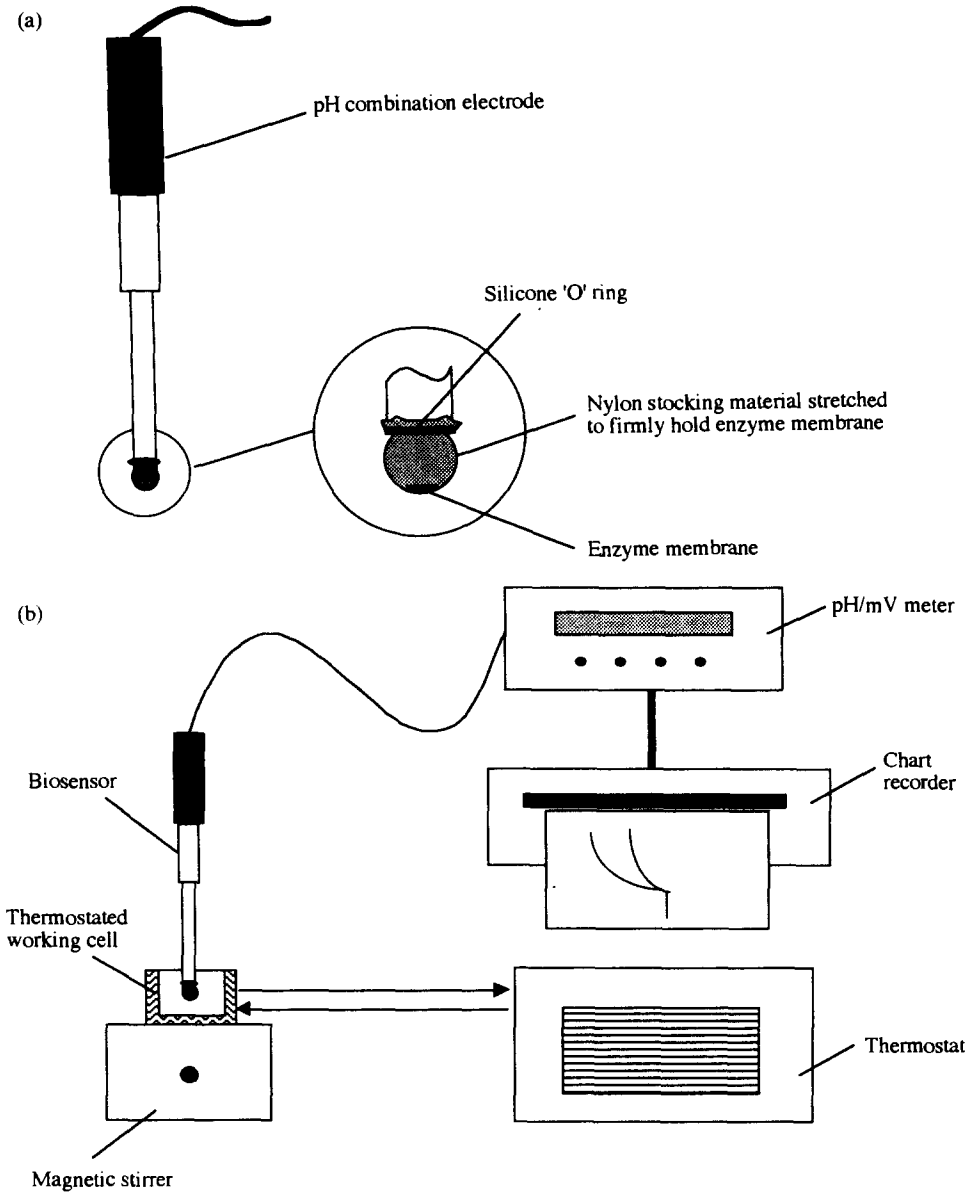


Fig. 1. (a) The biosensor. (b) The experimental set-up.

in a clean 10 ml graduated test tube. The tube was capped and the contents were mixed and left undisturbed overnight at room temperature.

Anhydrous sodium sulfate (100 mg) and 5 ml of a dichloromethane/acetone mixture (2/1 v/v) were added to the spiked soil sample before leaving the tube in a sonicating bath for 2 min. The mixture in the tube was then shaken vigorously by hand for 15 min. The sample was filtered and the cake was washed with an additional 10 ml of solvent mixture. The test tube containing the filterate and washings was placed in a water bath at 35°C with nitrogen bubbling into it till all solvent was completely evaporated.

To the dry residue in the test tube, 100 $\mu$l of acetonitrile was added and mixed, before topping the volume to 10 ml with HEPES working buffer. The tube was left in the sonicator for 2 min to ensure that no residue remained attached to the walls of the test tube. The contents of the tube were then poured into the working cell for analysis.

*Apparatus and analytical procedure*

Figure 1b represents the experimental set-up. The potential measurements were conducted in 25 ml magnetically stirred cells, maintained at 25°C with a thermostat (Endocal RTE 210). The biosensor was linked to a pH meter (TOA

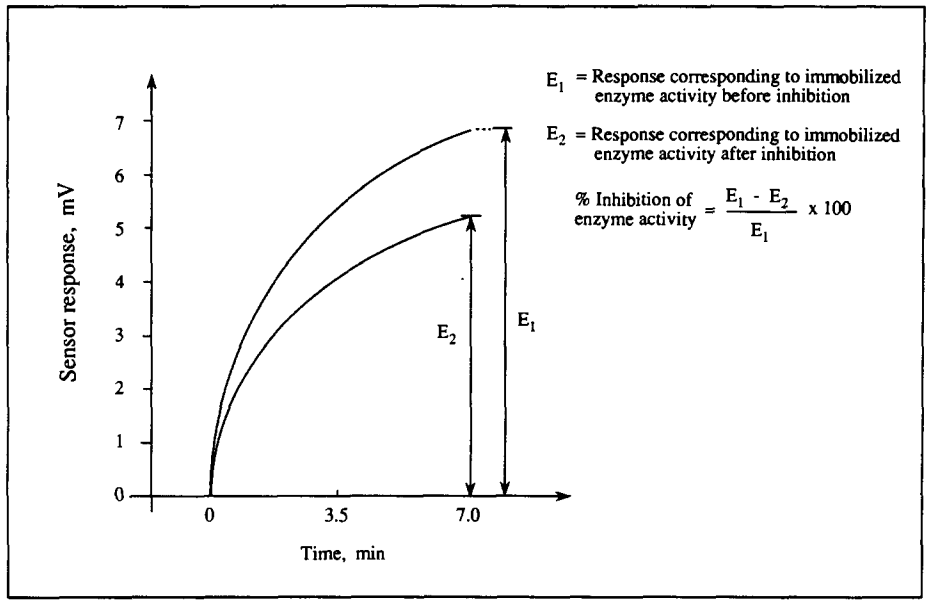


Fig. 2. Typical sensor response and calculation of enzyme inhibition.

Digital pH meter, Type HM-50V), connected to a chart recorder (Rikadenki R50).

The analysis was done by first conducting the blank tests: 20 ml of the HEPES working buffer was pipetted into the working cell and the biosensor placed into it. When a steady baseline was registered, 24 $\mu$l of 1$M$ butyrylcholine chloride was added to the cell. This resulted in a working substrate concentration of $1.2 \times 10^{-3}M$ in the cell.

Butyrylcholinesterase on the membrane catalyzes the hydrolysis of its substrate, butyrycholine, to choline and butyric acid according to the reaction below.

$$\text{Butyrylcholine} + H_2O \xrightarrow{\text{BuChE}} \text{choline} + \text{butyric acid.}$$

The acid dissociates further to release $H^+$ ions, resulting in a local variation of pH. This local variation of pH at the membrane is sensed by the electrode and the response is recorded.

The recording was stopped exactly after 7 min after addition of the substrate. This was done to avoid long waiting times before any steady-state in the electrode response was reached. The working cell was rinsed clean and refilled with the 10 ml HEPES buffer containing the dissolved pesticide residue along with another 10 ml of buffer. Where the pesticide being analysed was the sulfur analog, 4 $\mu$l of bromine water was added to the cell at this stage to transform it to the corresponding oxygen analog. The biosensor was then placed into the cell and the contact time between the enzyme membrane and the pesticide solution was noted. After a contact time of exactly 10 min, the substrate was once again added to the contents of the cell and the above procedure was repeated to note the electrode response. Figure 2 shows typical sensor responses and illustrates the procedure to calculate the percentage inhibition of enzyme activity, based on a diminished sensor response.

Calibration plots were initially made in plain buffer for the biosensor by adding different concentrations of pesticides directly to the working cell. Such plots were later used to determine the efficiency of pesticide extraction from spiked soil.

## RESULTS AND DISCUSSION

### *Choice of working conditions*

The composition of the working buffer, given above, was similar to that used in previous studies.[13] Figure 3 presents a calibration plot of the sensor to butyrylcholine. It was noticed that the response potential change remained below 15 mV, indicating that the number of active sites of the enzyme present in the membrane was suitable for inhibitor determination.[12] A working substrate concentration of $1.2 \times 10^{-3}M$ was chosen, as it was within the linear portion of the curve. The response potential change corresponding to the immobilized enzyme activity for this substrate concentration was about 6.5 mV.

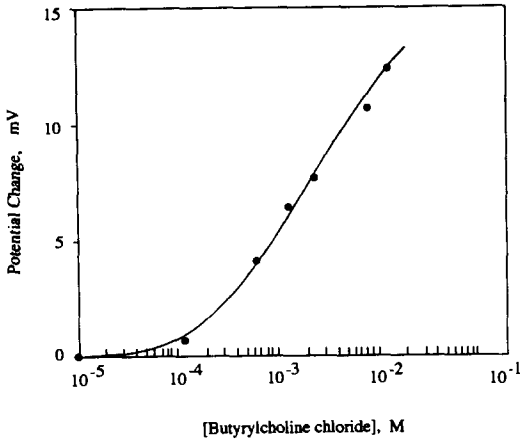


Fig. 3. Calibration plot for butyrylcholine. Working buffer: $2.5 \times 10^{-3}M$ HEPES, containing $2 \times 10^{-2}M$ $MgCl_2$, $0.1M$ NaCl and 0.01% (m/v) gelatin, temperature 25°C.

Earlier studies have demonstrated the high repeatability of measurements using enzyme membranes prepared in lots.[13] However, these membranes were also tested for repeatability in their response to consecutive substrate concentrations of $1.2 \times 10^{-3}M$. For three different membranes the RSD values were less than 5% ($n = 7$).

Figure 4 illustrates the influence of enzyme–pesticide contact time and temperature on the percentage inhibition of enzyme activity. The percentage inhibition was higher with longer contact time periods, indicating that better detection limits could be achieved with extended contact times. However, the experiments were conducted with a contact period of 10 min, in order to maintain a short analysis time. Furthermore, with a 10 min contact, satisfactory detection limits could be achieved with most of the pesticides tested. As expected, the temperature plot indicated a mixed influence on enzyme activity. With higher temperatures, the kinetics of inhibition and thermal deactivation of the enzyme were accelerated. This was seen as a rising curve without any optimum. A temperature of 25°C was chosen to conduct the experiments.

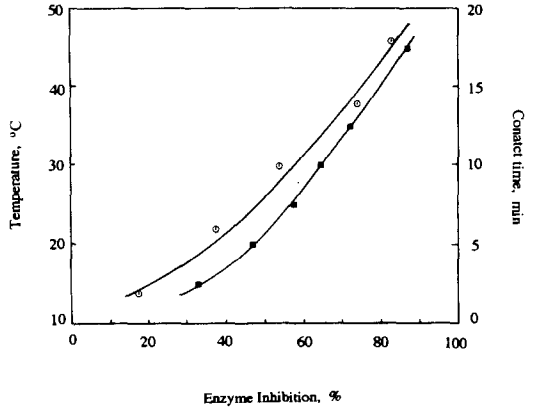


Fig. 4. Influence of enzyme–pesticide contact time (⊙ Heptenophos $3 \times 10^{-7}M$, temperature 25°C) and temperature (■ Mevinphos $8 \times 10^{-7}M$, contact time 10 min) on percentage inhibition of enzyme activity. Working buffer: $2.5 \times 10^{-3}M$ HEPES, containing $2 \times 10^{-2}M$ $MgCl_2$, $0.1M$ NaCl and 0.01% (m/v) gelatin.

Before the experiments were conducted, tests were done to ensure that blank soil extracts or acetonitrile (used to dissolve the pesticides) or bromine water (used for oxidation), did not inhibit the enzyme, individually or combined, at concentrations encountered in the analysis. No effect was observed with 100 $\mu$l acetonitrile in 20 ml buffer in contact with the enzyme up to 25 min. Bromine water, however, inhibited the enzyme and had to be maintained at additions of 4 $\mu$l in 20 ml buffer.

The tests showed that the blank extracts from soil used in this study contained no pH-modifying or other anticholinesterase substances. If pH-modifying substances are co-extracted, the working buffer concentration will have to be correspondingly changed to counter their effect. Other possible interferences in such an analytical method can arise mainly owing to the presence of anticholinesterase compounds such as carbamates, nicotine, $Pb^{2+}$ and $F^-$ ions.[13]

*ORP pesticide analysis*

Calibration plots of the biosensor were made showing extent of enzyme inactivation with varying concentrations of the different pesticides in the working cell, when they were added directly into it. Figure 5a and b are plots for Fenitrothion and Diazinon, respectively. Depending on the inhibitory power of the compound, different limits of detection were observed. Here, the enzyme was more sensitive to Diazinon, (detection limit: $10^{-8}M$) than Fenitrothion (detection limit: $3 \times 10^{-6}M$), both corresponding to a reduction in the response potential change of 1.1–1.7 mV.

Calibration plots showing enzyme inhibition from spiked soil extracts for Fenitrothion and Diazinon are presented in Figure 6a and b. Determination of Fenitrothion was possible in the range from 10 to 320 ppm in soil, while for Diazinon the range was from 10 to 500 ppb.

Since the RSD for the plain substrate injections as reported above was up to 5%, a reduction of about 1.2–1.5 mV in response potential change or 20% in sensor response

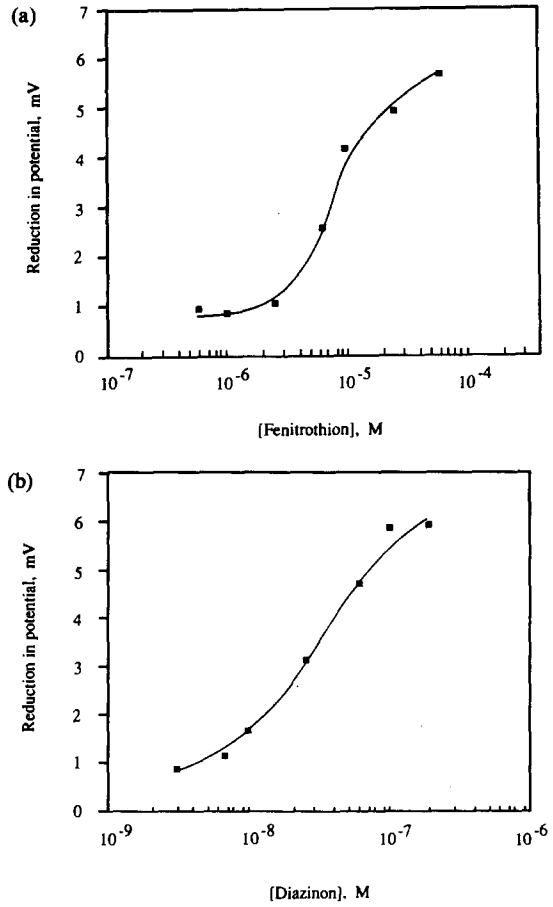


Fig. 5. (a) Calibration plot for Fenitrothion in $2.5 \times 10^{-3}M$ HEPES buffer containing $2 \times 10^{-2}M$ $MgCl_2$, $0.1M$ NaCl and 0.01% (m/v) gelatin, temperature 25°C, contact time 10 min. (b) Calibration plot for Diazinon in $2.5 \times 10^{-3}M$ HEPES buffer containing $2 \times 10^{-2}M$ $MgCl_2$, $0.1M$ NaCl and 0.01% (m/v) gelatin, temperature 25°C, contact time 10 min.

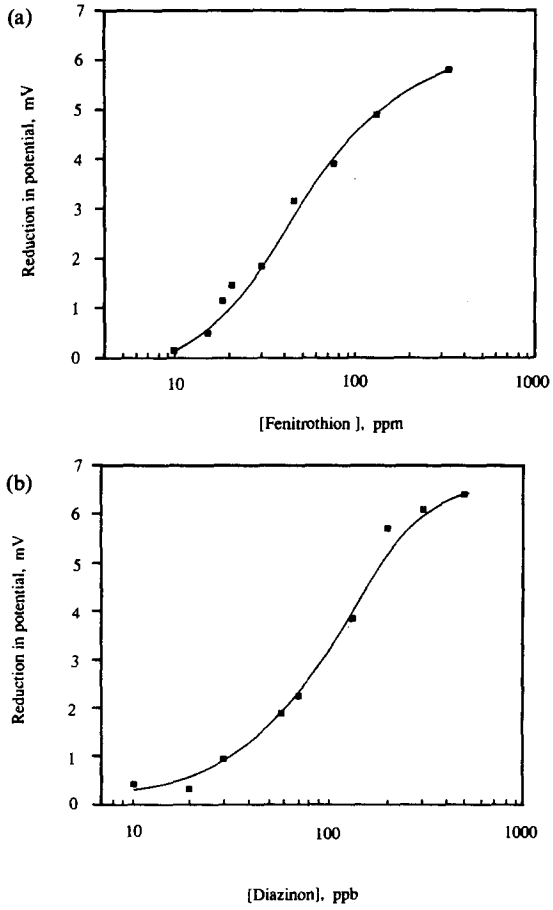


Fig. 6. (a) Calibration plot for Fenitrothion in soil. Working buffer: $2.5 \times 10^{-3}M$ HEPES, containing $2 \times 10^{-2}M$ $MgCl_2$, $0.1M$ NaCl and 0.01% (m/v) gelatin, temperature 25°C, contact time 10 min. (b) Calibration plot for Diazinon in soil. Working buffer: $2.5 \times 10^{-3}M$ HEPES, containing $2 \times 10^{-2}M$ $MgCl_2$, $0.1M$ NaCl and 0.01% (m/v) gelatin, temperature 25°C, contact time 10 min.

(which translates to about 3 times the standard deviation encountered for plain injections) was considered safe to indicate enzyme inactivation owing to the presence of the pesticides. The pesticide concentration leading to a 20% inactivation was, therefore, chosen to represent the detection limit measured by the biosensor.

The detection limits obtained by the sensor (spiked pesticide concentrations) for which the average enzyme inhibitions ranged from 18.6 to 21.1% are presented in Table 1. The corresponding RSD values of the percentage enzyme inhibitions and range of reductions in response potentials are also reported. It was observed that the RSD values remained less than 12%. Data on efficiency of the extraction method as measured from the sensor response is also presented. At concentrations corresponding to the

Table 1. Detection limits of the ORP pesticides tested

| ORP pesticide | Detection limit* | Reduction in potential ($mV$) | Average % inhibition | RSD (%) ($n = 3$) | Average extraction efficiency (%)† | RSD (%) ($n = 3$) |
|---|---|---|---|---|---|---|
| Fenitrothion | 21 ppm | 1.4–1.7 | 20.8 | 7.8 | 75.4 | 9.6 |
| Diazinon | 35 ppb | 1.1–1.4 | 20.3 | 8.8 | 136.2 | 9.4 |
| Parathion ethyl | 3.9 ppm | 1.0–1.4 | 20.5 | 10.7 | 100.0 | 13.6 |
| Mevinphos | 1.4 ppm | 1.2–1.6 | 21.1 | 11.6 | 83.3 | 13.1 |
| Heptonophos | 650 ppb | 1.1–1.4 | 18.6 | 5.4 | 44.8 | 6.2 |

*Corresponds to pesticide concentration spiked in soil (1 ppm = 1 $\mu$g/g, 1 ppb = 1 ng/g).
†As determined from biosensor calibration plots made with pesticide addition into working buffer.

detection limits of the ORP pesticide compounds, the average extraction efficiencies varied from 44.8% (Heptenophos) to 136.2% (Diazinon), with RSD values less than 14%. Such wide variations can only be a result of the low concentrations and possible interactions of the pesticide compounds with organic matter and clay present in soil.

As determined in other studies,[12] the activity of the immobilized enzyme is rapidly lost with continuous use, although when stored dry at 4°C, they have been found to retain their original activities even after a period of 3 years. The membranes prepared in this work showed similar trends. On average, they lost about 65 and 85% of their original activity after 3 and 7 days, respectively. No significant enzyme activity was noticed after 10 days. This rapid loss in activity with continuous use, however, need not be viewed as a disadvantage because the same membrane is not used continuously. Since the enzyme membranes can be mass produced and possess excellent storage stability, they can be discarded after a single use.

## CONCLUSIONS

Determination of ORP pesticides in soil extracts with the butyrylcholinesterase biosensor presents an approach which is cheap, simple and fast. No sophisticated instrumentation nor highly skilled personnel are required to conduct the tests. The pre-activated transfer membranes used for enzyme immobilization are inexpensive and easily available. The enzyme membranes can be mass produced and stored for several years before use. Since the construction of the biosensor involves easy attachment of the membranes to the pH electrode, the need to reactivate or reuse these membranes after enzyme inhibition is precluded, thereby making them disposable after a single use. Beginning from extraction of the pesticide compound by the described procedure, only about an hour is required to obtain the analytical result.

The biosensor demonstrates the possibility of achieving satisfactory detection limits, although these can be improved at the cost of analysis time. Once calibrated, the biosensor can be used as an analytical instrument to screen for ORP pesticides on a routine basis, especially in situations which demand an early warning of soil contamination.

*Acknowledgement*—S. Kumaran takes this opportunity to thank JRDC and JISTEC for his Science & Technology Agency fellowship.

## REFERENCES

1. R. Carabias Martinez, E. Rodriguez Gonzalo, M. J. Amigo Moran and J. Hernandez Mendez, *J. Chromatog.*, 1992, **607,** 37.
2. G. Durand, P. Gille, D. Fraisse and D. Barcelo, *J. Chromatog.*, 1992, **603,** 175.
3. E. G. van der Velde, W. de Haan and A. K. D. Liem, *J. Chromatog.*, 1992, **626,** 135.
4. K. Wuchner, R. T. Ghijsen, U. A. T. Brinkman, R. Grob and J. Mathieu, *Analyst*, 1993, **118,** 11.
5. P. Klaffenbach and T. Holland, *J. Agric. Food Chem.*, 1993, **41,** 396.
6. T. R. Fukuto, *Environ. Hlth Perspectives*, 1990, **87,** 245.
7. S. Kumaran and C. Tran-Minh, *Anal. Biochem.*, 1992, **200,** 187.
8. S. Kumaran, *Engineers. Aust.*, 1992, **64,** (14) 16.
9. P. Skladal, M. Pavlik and M. Fiala, *Anal. Lett.*, 1994, **27,** 29–40.
10. M. Bernabei, C. Cremisini, M. Mascini and G. Palleschi, *Anal. Lett.*, 1991, **24,** 1317–1331.
11. L. Campanella, R. Cocco, M. P. Sammartino and M. Tommasseti, *Sci. Total Environ.*, 1992, **123/124.**
12. S. Kumaran and C. Tran-Minh, *Electroanalysis*, 1992, **4,** 949.
13. S. Kumaran, *Thesis*, p. 49. Univ. de Lyon, France, 1991.

Pergamon

0039-9140(94)01438-1

*Talanta*, Vol. 42, No. 4, pp. 657–662, 1995

0039-9140/95 $9.50 + 0.00

# PREPARATION OF POLYPYRROLE-COATED PLATINUM MODIFIED ELECTRODE IN CHLOROFORM IN THE PRESENCE OF VARIOUS SUPPORTING ELECTROLYTES AND ITS USE FOR THE CATALYTIC OXIDATION OF HYDROQUINONE IN AQUEOUS AND CHLOROFORM SOLUTIONS

M. H. POURNAGHI-AZAR* and R. OJANI
Electroanalytical Chemistry Laboratory, University of Tabriz, Tabriz, Iran

(*Received* 16 *June* 1994. *Accepted* 12 *September* 1994)

**Summary**—Polypyrrole (PPy)-coated platinum modified electrode was prepared electrochemically in chloroform in the presence of tetrabutylammonium perchlorate, tosylate, tetrafluoroborate, periodate, and hydrogen sulphate. Evidence in favour of the occurrence of a redox reaction at the film/solution interface was given by ferrocene oxidation. The electrocatalytic effect of the PPy-coated electrode was revealed by oxidation of hydroquinone on it in water and chloroform. The influence of dopant anion, method of electrosynthesis and operation temperature were demonstrated. The calculated heterogeneous electron transfer rate constant ($k^o$) at the PPy-modified Pt electrode at 25°C was $1.4 \times 10^{-3}$ cm/sec which is 1000-fold greater than the value ($< 10^{-6}$ cm/sec) reported for bare electrode.

One of the important applications of chemically modified electrodes is the electrocatalysis of electrochemical reactions. Among electronically conducting polymers for making modified electrodes, polypyrrole (PPy) has received much attention since 1979 when it was synthesized by Diaz *et al.*[1] The ability of PPy to electrocatalysis some electrochemical reactions has been reported.[2–4] Many investigations have shown the influence of solvent, supporting electrolyte, operation temperature, monomer concentration and method of electropolymerization on the properties of PPy.[5–7] According to previous studies, the polymerization of pyrrole is performed in aprotic solvent[7] and acetonitrile has been the most commonly used solvent. Recently, PPy was prepared on a platinum electrode in acetonitrile and its electrocatalytic effects demonstrated.[8]

The high dissolving power and extracting property of chloroform against organic, organometallic and pharmaceutical compounds, make it as an excellent solvent and the study of electrochemical behaviour of these compounds at bare and chemically modified electrodes is interesting in order to develop new electroanalytical methods.[9–12]

It is the aim of this work to electrosynthesize PPy on a Pt electrode in chloroform as an aprotic solvent, convenient for the electropolymerization which proceeds via a radical mechanism, and used the PPy-coated platinum modified electrode to catalyse some slow oxidation processes in aqueous and particularly in chloroform media for analytical purposes. In this context we report the ability of PPy film prepared in chloroform to oxidize hydroquinone in both media and demonstrate the influence of the type and concentration of dopant anion, electropolymerization method and operation temperature on the electrocatalytic effects.

## EXPERIMENTAL

### *Chemicals*

The solvent was chloroform GR from E. Merck. The supporting electrolytes were tetrabutylammonium perchlorate (TBAP), tetrafluoroborate (TBATFB), periodate (TBAPI) from Janssen; benzoate (TBABz) and tosylate (TBATS) prepared in our laboratory according to the following procedures.

*Author to whom correspondence should be addressed.

*Preparation of TBATS.* A given amount of *p*-toluenesulphonic acid was dissolved in distilled water and the solution neutralized by gradual addition of a required volume of 40% aqueous solution of tetrabutylammonium hydroxide (TBAOH) using a pHmeter. The salt (TBATS) was extracted into chloroform and the white crystalline salt obtained by evaporation of the solvent.

*Preparation of TBABz.* A stoichiometric amount of benzoic acid (insoluble in water) and NaOH (1:1 mol/mol) were introduced in a given volume of water, the soluble sodium benzoate was formed, a required volume of 40% aqueous solution of TBAOH was added and TBABz was extracted into chloroform, the solvent was evaporated and the TBABz was obtained.

The other reagents were of analytical grade, the water was deionized and distilled. The solutions were bubbled with $N_2$ gas (99.99) for 30 min and kept under nitrogen atmosphere during the electrochemical experiments.

*Apparatus*

All voltammograms were recorded with a three electrode system using an EG&G model 273 potentiostat/galvanostat, electrochemical analysis software 3,00 model 270 with an IBM personal computer connected to an Epson model FX-850 printer. Working electrodes were bare and PPy-coated Pt electrodes (area 0.126 $cm^2$ from EG&G). The reference electrodes were SCE in aqueous media and Ag/AgI in chloroform as previously described.[9] A UTU.ZN-68/CZSP-D-98 thermostat from Poland was used for thermostatting the polymerization media.

*Electropolymerization*

The working electrode surface was polished using a thin layer of alumina powder (0.05 $\mu$m), then washed with water and acetone, respectively and used after drying. The PPy films were prepared in 0.5*M* solutions of dopant anion and 0.1*M* pyrrole in chloroform. In the potentiostatic method the applied potential was 1.2 V *vs.* the reference electrode. In the galvanostatic method the current density was 15 $\mu A/cm^2$ (E = 1.1 V) and in the potentiodynamic method the potential was scanned between −0.4 and 1.2 V with a scan rate of 50 mV/sec. Grafting the films onto electrode was stopped when an amount of charge equal to 3 mC had been passed. During the polymerization, the solution were thermostatted.

## RESULTS AND DISCUSSION

*Electrochemical behaviour and properties of the PPy films*

Cyclic voltammograms (CVs) of PPy–$ClO_4^-$ films prepared by different electrochemical methods were recorded in 0.5*M* TBAP–chloroform solution in the absence of the monomer (Fig. 1). The peaks related to doping–undoping cycle were observed at about 0.24 and 0.04 *V*. The corresponding process may be shown as follows:

$$PPy_f^\circ + A_s^- \rightleftharpoons PPy^+A_f^- + e_m$$

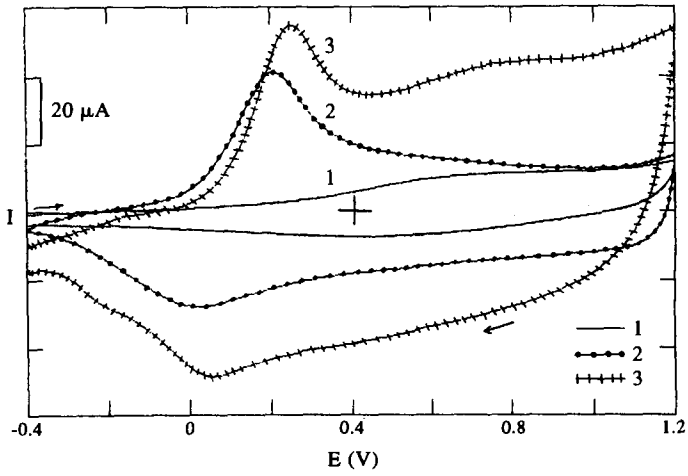


Fig. 1. The CVs of PPy–$ClO_4^-$-coated Pt electrode in 0.5*M* TBAP–$CHCl_3$. PPy films were synthesized (1) potentiodynamically (scanned between −0.4 and 1.2 V), (2) galvanostatically (current density, 15 $\mu A/cm^2$; electrode potential, 1.1 V) and (3) potentiostatically (potential was controlled at 1.2 V). The deposition charges in all cases were approximately 2 mC. The scan rate was 50 mV/sec.

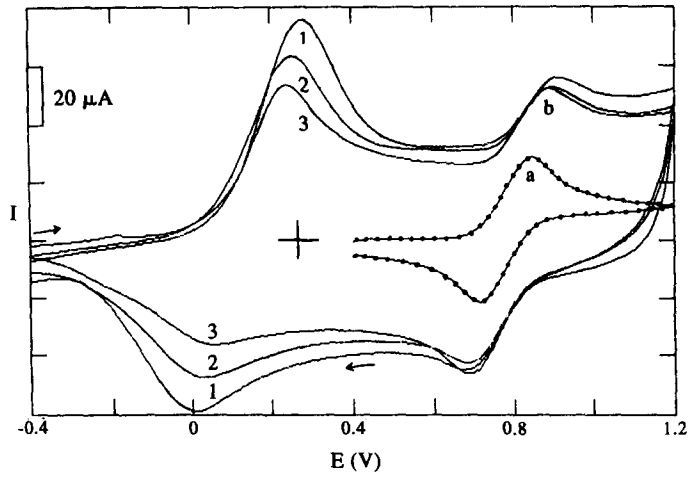


Fig. 2. The CVs of 1 m*M* ferrocene (a) on bare Pt electrode and (b) PPy–$ClO_4^-$-coated Pt electrode with various thickness of the PPy film in 0.5*M* TBAP chloroform solution. The deposition charges were (1) 3 mC, (2) 2.5 mC, (3) 2 mC. The ferrocene peak fell at higher potentials, scan rate was 50 mV/sec.

or

$$PPy\ A^-B_f^+ \rightleftharpoons PPy^+A_f^- + B_s^+ + e_m.$$

Where subscripts s, f and m refer to solution, polymer and metal, respectively. $A^-$ and $B^+$ show the anion or cation intervening in the doping–undoping cycle.

The PPy film prepared by the galvanostatic method was oxidized at a lower potential value than the others and gave redox peaks with a low charging current (Fig. 1). Therefore, we have used this method for the electrochemical experiments in this work.

The PPy films prepared by each method were very stable and quasi-metallic yellowish which changed to brown and dark-green with increasing film thickness. The oxidation of ferrocene at the PPy-coated Pt electrode with various thickness reveals that the redox process was localized at the film/solution interface, because the height of the anodic peaks does not depend on the thickness (Fig. 2), which is typical of the diffusion controlled conditions.

*Oxidation of hydroquinone on the PPy-modified electrode*

The CVs of $H_2Q$ on bare and PPy-coated Pt electrodes in 0.1*M* $LiClO_4$ aqueous solution at pH 2 are shown in Fig. 3. The peak separation potentials $\Delta E_p$ is equal to 550 mV on bare electrode which decreased to 140 and 90 mV at scan rates of 50 and 20 mV/sec, respectively on the

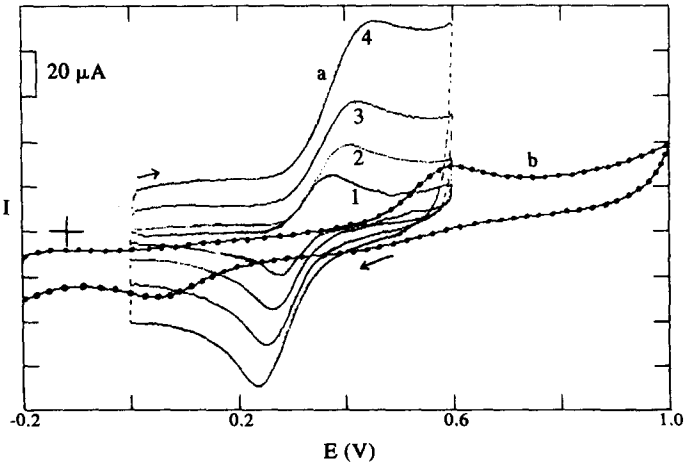


Fig. 3. The CVs of 1 m*M* hydroquinone (a) on PPy–$ClO_4^-$-coated Pt electrode in 0.1*M* $LiClO_4$ aqueous solution, pH 2, at various scan rates: (1) 20, (2) 50, (3) 100, (4) 200 mV/sec and (b) bare Pt electrode with a scan rate of 50 mV/sec. The polymer was prepared by the galvanostatic method and deposition charge was about 3 mC.

Table 1. The voltammetric data of hydroquinone oxidation in chloroform and water on bare and PPy-coated Pt electrodes

| | Aqueous | | | | | Chloroform | | | | |
|---|---|---|---|---|---|---|---|---|---|---|
| | $i_p^c/i_p^a$ | $E_p^a(V)$ | $E_p^c(V)$ | $\Delta E_p(V)$ | $EE_{(mV)}$* | $i_p^c/i_p^a$ | $E_p^a(V)$ | $E_p^c(V)$ | $\Delta E_p(V)$ | $EE_{(mV)}$* |
| Pt | 0.43 | 0.600 | 0.050 | 0.550 | 410 | 0.39 | 1.293 | 0.480 | 0.813 | 233 |
| PPy-Pt | 0.93 | 0.400 | 0.260 | 0.140 | | 0.67 | 1.220 | 0.640 | 0.580 | |

$V = 50$ mV/sec.
*Electrocatalytic effect.

PPy-coated electrodes (Fig. 3). Using the method proposed by Nicholson[13] the heterogeneous electron transfer rate constant ($k^\circ$) value on the PPy-coated Pt was obtained at $1.4 \times 10^{-3}$ cm/sec which is about 1000-fold greater than the value at the bare electrode ($10^{-6}$ cm/sec).[14]

The decrease of $\Delta E_p$ for $H_2Q$ CVs from 813 mV at the bare electrode to 550 mV at the PPy-coated electrode at a scan rate of 50 mV/sec in 0.5$M$ TBAP–chloroform solution also illustrates the electrocatalytic effect of the polymer on the oxidation of hydroquinone in chloroform. The characteristic data for the oxidation of $H_2Q$ on the bare and PPy-modified Pt electrodes in aqueous and chloroform media are given in Table 1.

*Influence of the electropolymerization conditions*

The parameters affecting the electrocatalytic properties of PPy films were the type and concentration of dopant anion, method of electro-

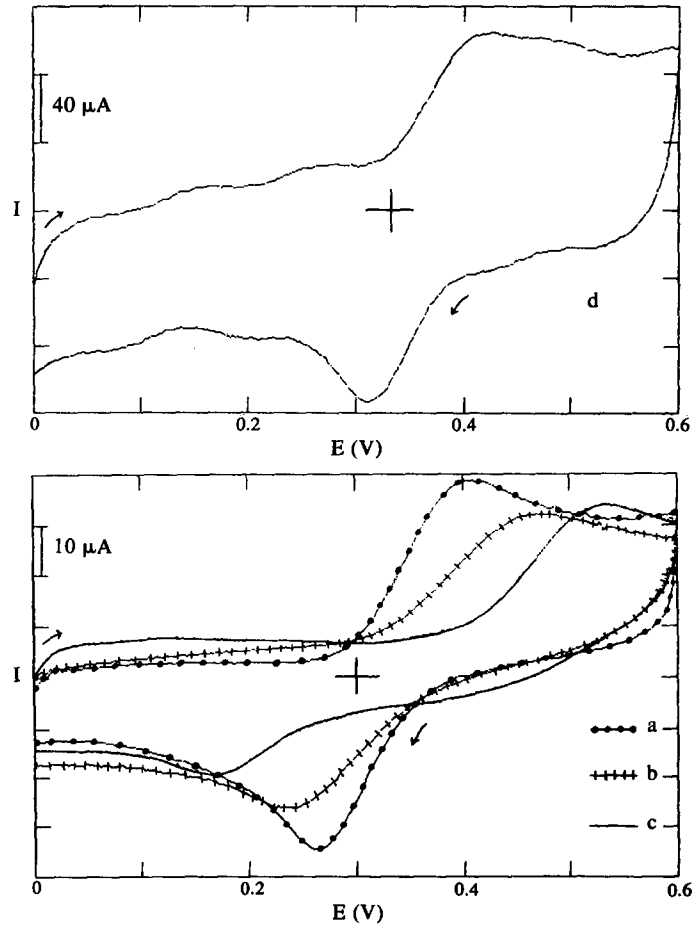


Fig. 4. The CVs of 1 m$M$ hydroquinone on PPy-coated Pt electrode in 0.1$M$ $LiClO_4$ aqueous medium, pH 2, prepared in $CHCl_3$ in the presence of various dopant anions at room temperature. (a) $ClO_4^-$, (b) tosylate (c) $BF_4^-$, (d) $IO_4^-$. The prepared method was galvanostatic and deposition charges in all cases were about 3 mC, scan rate: 50 mV/sec.

Table 2. Characteristic data of $H_2Q$ CVs at PPy-coated Pt electrode prepared in the presence of different dopant anions

| | Water | | | Chloroform | | |
|---|---|---|---|---|---|---|
| Dopant anion | $E_p^a(V)$ | $E_p^c(V)$ | $\Delta E_p$ | $E_p^a(V)$ | $E_p^c(V)$ | $\Delta E_p$ |
| Perchlorate | 0.400 | 0.260 | 0.140 | 1.220 | 0.640 | 0.580 |
| Tetrafluoroborate | 0.535 | 0.171 | 0.364 | 1.267 | 0.530 | 0.737 |
| Periodate | 0.420 | 0.311 | 0.109 | 1.298 | 0.589 | 0.709 |
| p-Toluenesulphonate | 0.470 | 0.244 | 0.226 | 1.382 | — | — |
| Hydrogensulphate | 0.496 | 0.194 | 0.302 | 1.232 | 0.552 | 0.680 |

polymerization and operation temperature. The CVs of 1 m$M$ $H_2Q$ in 0.1$M$ $LiClO_4$ aqueous solution at pH 2, at PPy-coated Pt electrode prepared in chloroform solutions of some dopant anions such as $ClO_4^-$, $BF_4^-$, $IO_4^-$ and tosylate are shown in Fig. 4. The characteristic data are given in Table 2. The greatest electrocatalytic effect was from $ClO_4^-$ and the value of $\Delta E_p$ was minimum for a concentration of 0.5$M$ TBAP (Fig. 4). This may be attributed to (a) high oxidation level as well as high conductivity of PPy–$ClO_4^-$ films,[7] (b) relatively effective doping of PPy–$ClO_4^-$ film compared with the others during the electrochemical oxidation of $H_2Q$ in the presence of 0.1$M$ $ClO_4^-$ solution and (c) preventing release of $ClO_4^-$ ion in PPy–$ClO_4^-$ film placed in $ClO_4^-$ solutions. For $IO_4^-$ the background currents were most pronounced and the stability of PPy–$IO_4^-$ films was considerably lower, probably owing to its high oxidizing power. On the other hand, the chronopotentiogram recorded during the galvanostatic polymerization of pyrrole in $CHCl_3$–benzoate solution, showed that the potential of the working electrode did not remain at 1.1 V (electropolymerization potential of pyrrole) and immediately changed to a very positive value (> 1.8 V), therefore, electropolymerization did not occur. At the same time, the surface of the working electrode was contaminated by forming insoluble oligomers and the conductivity of the electrode fell dramatically. This behaviour is attributed to the basicity of the $Bz^-$ ion preventing the growth of the polymer chain.[15] This was confirmed by the addition of a stoichiometric amount of anhydrous sulphuric acid in order to convert $Bz^-$ to BzH which led to the polymerization of pyrrole in the presence of the $HSO_4^-$ formed.

Similar results were obtained in chloroform solution with 0.5$M$ TBAP + $10^{-3}M$ $H_2Q$. The characteristic data are shown in Table 2.

The influence of temperature on the electrocatalytic effect of PPy was demonstrated using the PPy-coated Pt electrode prepared at various temperatures in chloroform solution of 0.5$M$ TBAP. The CVs of $H_2Q$ at room temperature in water reveal that the electrocatalytic effect of the polymer is increased as the polymerization temperature varies from 0 to 35°C and then decreased when the temperature increased up to 45°C. The same results were obtained in chloroform. This behaviour was explained by the low conductivity of polymer at high temperature[16]

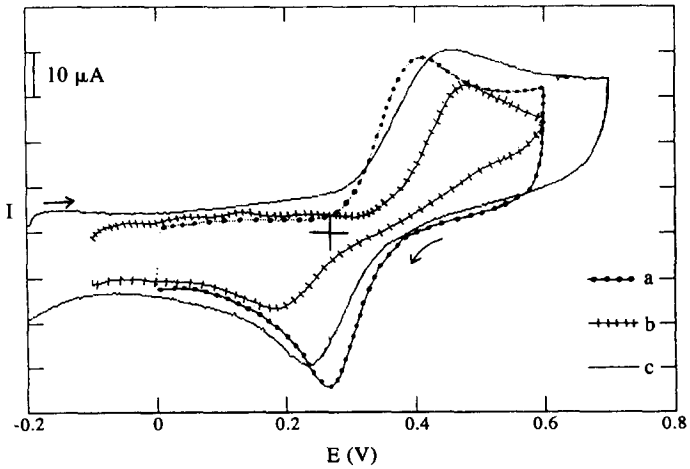


Fig. 5. The CVs of 1 m$M$ $H_2Q$ + 0.1$M$ $LiClO_4$ aqueous solution on PPy-coated Pt electrode prepared by various methods. (a) Galvanostatic, (b) potentiodynamic and (c) potentiostatic. The deposition charges in all three cases were approximately equal, scan rate: 50 mV/sec.

and the poor quality of films at low temperature.[17]

Another affecting parameter was the electrosynthesis method used for the preparation of PPy films. The experimental data obtained from the cyclic voltammetry of $H_2Q$ at PPy-coated Pt electrodes prepared by various methods confirm that the galvanostatic method was the most effective one as well as its electrochemical behaviour (Fig. 5).

## CONCLUSIONS

The results obtained from this study show that the electropolymerization of pyrrole can be performed in chloroform. The PPy film formed on the Pt disk electrode was very stable, quasi-metallic, smooth and coloured from yellowish to dark green depending on its thickness. The electrochemical activity of PPy film is affected by the method of electropolymerization and the best activity is observed for the galvanostatic method. The charge transfer reaction occurs at the film–solution interface. An obvious electrocatalytic effects of PPy film on the oxidation of $H_2Q$ at PPy-coated Pt electrode is observed in aqueous and chloroform solutions. The influence of polymerization conditions such as dopant anion, temperature and method of electrosynthesis on its electrocatalytic effect are evident. These findings suggest the possibility of using PPy-coated platinum electrodes as a chemically modified electrode for the catalysis of some slow oxidation processes in chloroform which are presently under investigation in our laboratory.

## REFERENCES

1. A. F. Diaz and K. K. Kanazawa, *J. Chem. Soc. Chem. Commun.*, 1979, **N14,** 635.
2. R. C. M. Jakobs, L. L. J. Janseen and E. Barendrecht, *Electrochim. Acta*, 1985, **30,** 1313.
3. O. Ikeda, K. Okabayashi, N. Yoshida and H. Tamura, *J. Electroanal. Chem.*, 1985, **191,** 157.
4. R. A. Saraceno, J. G. Pack and A. G. Ewing, *J. Electroanal. Chem.*, 1986, **197,** 265.
5. J. M. Ko, H. W. Rhee, S. M. Park and C. Y. Kim, *J. Electrochem. Soc.*, 1990, **137,** 905.
6. F. T. A. Vork, B. C. A. M. Schuernans and E. Barendrecht, *Electrochim. Acta*, 1990, **35,** 567.
7. A. F. Diaz and J. C. Lacroix, *New Z. J. Chem.*, 1988, **12,** 171.
8. A. Heimerl and A. Merz, *J. Electroanal. Chem.*, 1987, **220,** 55.
9. S. M. Golabi and M. H. Pournaghi-Azar, *Electrochim. Acta*, 1987, **32,** 425.
10. M. H. Pournaghi-Azar and S. M. Golabi, *Talanta*, 1988, **38,** 929.
11. M. H. Pournaghi-Azar and J. Ordokhanian, *Talanta*, 1991, **38,** 1469.
12. M. H. Pournaghi-Azar and R. Ojani, *Electrochim. Acta*, in press.
13. R. S. Nicholson, *Anal. Chem.*, 1965, **37,** 1351.
14. J. H. White, M. P. Soriaga and A. T. Hubbard, *J. Electroanal. Chem.*, 1985, **185,** 331.
15. S. Kuwabata, J. Nakamura and H. Yoneyama, *J. Chem. Soc., Chem. Commun.*, 1988, 779.
16. M. A. Sato, S. Tanako and K. Kaeriyama, *Syn. Metals*, 1986, **14,** 279.
17. M. Satoh, K. Kaneto and K. Yoshino, *Syn. Metals*, 1980, **14,** 289.

Pergamon

0039-9140(95)01465-9

*Talanta*, Vol. 42, No. 4, pp. 663–670, 1995

0039-9140/95 $9.50 + 0.00

# FIBER-OPTIC CHLORINE PROBE BASED ON FLUORESCENCE DECAY OF *N*-(6-METHOXYQUINOLYL)-ACETOETHYL ESTER

SATYAJIT KAR*† and MARK A. ARNOLD

Department of Chemistry, University of Iowa, Iowa City, IA 52242, U.S.A.

(*Received* 6 *September* 1994. *Revised* 14 *October* 1994. *Accepted* 14 *October* 1994)

**Summary**—A fiber-optic probe for measuring chlorine in aqueous solution is evaluated. The probe uses a microporous gas-permeable membrane to trap a small volume of aqueous internal solution made of *N*-(6-methoxyquinolyl)acetoethyl ester (MQAE) in front of a fiber-optic assembly. The working principle of this probe is based on a combination of fluorescence quenching and redox reaction of MQAE by chloride ion and chlorine, respectively. While the magnitude of total fluorescence decay is independent of the sample concentration, the initial rate of decrease in fluorescence intensity is linearly proportional to the chlorine concentration over the range from 8.4 to 418 $\mu M$. Once the probe is exposed to a chlorine sample, the probe tip must be refilled with a fresh aliquot of the internal solution before the next measurement. In this mode, the probe displays excellent reproducibility; the relative standard deviation of the initial rate of fluorescence decay ($n = 3$) is only 1 percent. This probe can also be used for the measurement of hypochlorous acid (HOCl) in aqueous solution. The response properties are identical to those of the chlorine probe.

Chlorine sensing is particularly important because chlorine is used extensively in the chemical industry and in the sterilization of drinking water. The toxicity of chlorine[1] causes problems of overexposure during both manufacturing and use. The danger of pollution demands a sensitive and reliable method for the accurate measurement of chlorine.

The measurement of chlorine in water is complicated by interferences from the combined forms of chlorine (i.e. chloramines) and other potential disinfectants, such as chlorine dioxide and ozone[2]. The currently available methods for the determination of free chlorine are photometric[3], amperometric[4], and chemiluminescence[5]. Narayanaswamy and co-workers[6], have recently reported a number of potential polynuclear aromatic hydrocarbon molecules, which experience fluorescence quenching by chlorine in methanol. However, data are not available regarding the quenching of these compounds in aqueous solution.

This paper describes a fiber-optic probe for measuring free chlorine ($Cl_2$/HOCl) in aqueous solution. The working principle of this probe is based on a combination of fluorescence quenching by chloride and a direct reaction by chlorine with the indicator dye *N*-(6-methoxyquinolyl)-acetoethyl ester (MQAE) in an isolated aqueous-based internal solution. This probe uses a microporous gas-permeable membrane to trap a small volume of internal solution in front of a fiber-optic assembly (FOA). Chlorine from the sample diffuses across the gas-permeable membrane and enters the internal solution. A fraction of this chlorine is converted to chloride ions and the combination of chloride and chlorine diminishes the fluorescence of MQAE. The resulting change in fluorescence intensity is measured as a function of time through the FOA. The rate of change of the fluorescence intensity is related to the concentration of chlorine in the sample.

## EXPERIMENTAL

### *Apparatus and reagents*

Fluorescence quenching measurements from the internal solution were performed with an FOA by using an instrumental arrangement similar to that reported earlier[7] with some modifications. Light from a 100 W tungsten–

*Author to whom correspondence should be addressed.
†Present address: Department of Chemistry and Biochemistry, Texas Tech University, Lubbock, TX 79409-1061, U.S.A.

halogen lamp passed through an IR-blocking filter and then a KV-470 cut-off filter before being focused into a bundle of quartz optical fibers. The exiting radiation was collimated before passing through a mechanical chopper, which was operated at 224 Hz. One of the fused-silica optical fibers carried the chopped light and directed this excitation radiation towards the internal solution at the tip of the FOA. A second set of fused-silica fibers collected a portion of the luminescence from the internal solution and directed this light to a 490 nm bandpass filter. After passing through the filter, the light was focused onto the face of a photomultiplier tube (PMT) which was operated at 650 V.

MQAE was purchased from Molecular Probes (Eugene, OR), and used as received. Chlorine standards were prepared from stock sodium hypochlorite (NaOCl) solutions, whose chlorine concentration was established by iodometric titration. All other reagents were analytical grade quality and were purchased from common suppliers. All solutions were made with distilled-deionized water that was prepared immediately before use by passing the house distilled water through a Milli-Q three house water purification unit.

*Procedures*

*Probe fabrication.* Chlorine probes were constructed by trapping a small volume of internal solution between a gas-permeable membrane and an FOA (Fig. 1). The FOA was fabricated by packing one 600 $\mu$m (FP-600-UHT) and seven 400 $\mu$m (FP-400-UHT) fibers into a 7.0 cm long (2.5 mm i.d. and 3.0 mm o.d.) plastic tubing. Both types of fibers were high-hydroxy fibers designed for UV transmission and were obtained from 3M Specialty Optical Fibers, West Haven, CT. The FP-600-UHT fiber had a numerical aperture of 0.30, core diameter of $600 \pm 10$ $\mu$m, cladding diameter of $830 \pm 30$ $\mu$m, and buffer diameter of $1050 \pm 30$ $\mu$m. The FP-400-UHT fibers had a numerical aperture of 0.30, core diameter of $400 \pm 8$ $\mu$m, cladding diameter of $600 \pm 30$ $\mu$m, and buffer diameter of $750 \pm 30$ $\mu$m. The 600 $\mu$m fiber was positioned in the center of seven 400 $\mu$m fibers. Epoxy was applied to hold the fibers and fill the void volume inside the fiber–tubing assembly. The other end of the

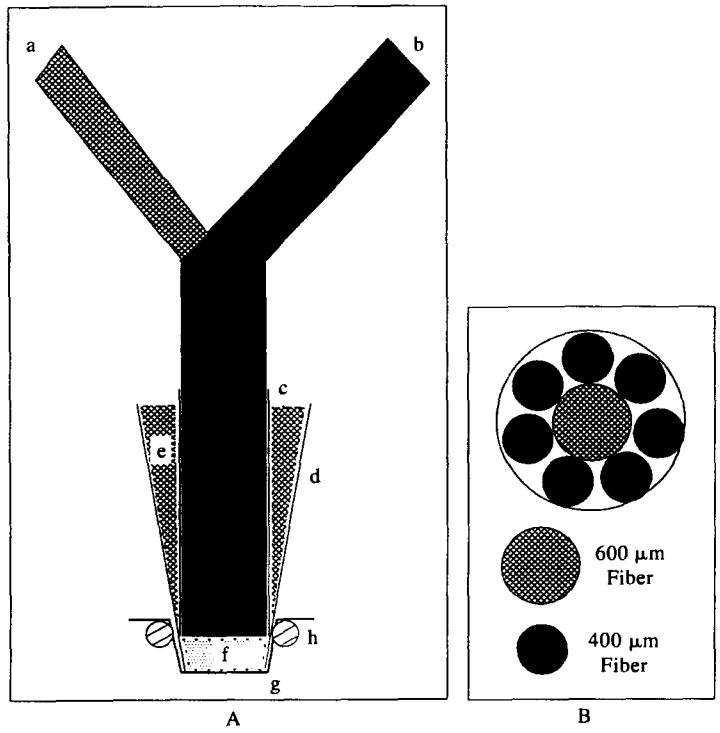


Fig. 1. Schematic diagram of the fiber-optic chlorine probe. Part A: a, 600 $\mu$m excitation fiber; b, seven 400 $\mu$m emission fibers, c, plastic tubing; d, conical plastic pipette tip; e, epoxy, f, internal solution; g, microporous Teflon membrane; and h, plastic spacer ring. Part B: arrangement of fibers at the probe tip (cross-sectional view).

600 $\mu$m and seven 400 $\mu$m fibers were inserted through two plexiglass connectors separately and held in position with epoxy. The fiber ends were polished with 400-grit abrasive paper. The FOA was then inserted into a conical shaped small plastic tube and held in place by an adhesive sealant. A small reservoir was created at the tip by slightly recessing the FOA relative to the outer edge of the tube. The outer diameter of the resulting probe tip was about 5.0 mm and the volume of the reservoir was less than 10 $\mu$l. The internal solution and gas-permeable membrane were added by inverting the probe body, applying approximately 20 $\mu$l of solution into the reservoir, stretching a small square of membrane over the solution and holding the membrane in place with a plastic spacer ring. Unless otherwise mentioned, the internal solution was composed of 0.1 m*M* MQAE in water. Gas-permeable membranes were microporous Teflon from Gore and Associates (Elkton, MD) and had an average pore size of 0.02 $\mu$m.

*Spectral measurements.* Absorbance spectra of aqueous standard MQAE solutions were obtained on an OLIS-modified Cary-14 spectrophotometer (On-Line Instrument Systems, Inc.). Fluorescence measurements were obtained with an SLM AMINCO SPF-500 C spectrofluorimeter. The excitation spectra of 0.10 m*M* MQAE were obtained by measuring the luminescence intensity at 456 nm while varying the excitation wavelength from 250 to 600 nm. Fluorescence spectra, on the other hand, were collected by using a fixed excitation wavelength of 346 nm and recording the emission intensity as a function of wavelength from 350 to 600 nm. Fluorescence intensities of a series of 1 to 100 $\mu M$ aqueous MQAE solutions were measured at 456 nm by using 346 nm as the excitation wavelength. The effect of pH on the fluorescence intensity was examined by measuring the fluorescence spectra (excitation at 346 nm) of 0.17 m*M* MQAE solutions in different buffer solutions over the pH range from 3.58 to 10.27.

*Fluorescence quenching measurements.* The effect of $Cl^-$, $OCl^-$, HOCl, and $Cl_2$ on the fluorescence intensity of MQAE were tested. Microliter aliquots of 1.0*M* stock solution of NaCl were added to 0.1 m*M* aqueous solution of MQAE to study the quenching caused by the $Cl^-$ ion. In order to correct for the dilution due to the addition of the $Cl^-$ standard, an equal volume of 0.2 m*M* MQAE was added. Fluorescence intensities were measured before and after the addition of quencher. Quenching by $OCl^-$ was tested by adding a standard NaOCl solution to a freshly prepared 0.17 m*M* aqueous solution of MQAE in a pH 10.66 buffer. The effect of HOCl on fluorescence intensity was investigated by adding a standard NaOCl solution to a 19 $\mu M$ solution of MQAE in 0.1*M* $H_2SO_4$. Finally, the effect of $Cl_2$ on the fluorescence intensity of MQAE was measured by mixing microliter aliquots of 1.0*M* NaCl and standard NaOCl followed by the addition of 2.0 ml of a 17 $\mu M$ MQAE (in 0.1*M* $H_2SO_4$) solution. The Stern–Volmer quenching constant was calculated from a linear fit to the equation

$$F_0/F = 1 + K_q[Q] \quad (1)$$

where $F_0$ and $F$ are the fluorescence intensities in the absence and presence of quencher, respectively, $[Q]$ is the concentration of quencher, and $K_q$ is the Stern–Volmer constant.

*Probe characterization and chlorine calibration curves.* Unless stated otherwise, measurements were made in thermostatted glass jacketed cells and the temperature was maintained at 25°C with a Fisher model 90 water bath. The probe tip was immersed in a 20.0 ml aliquot of a 0.10*M* hydrochloric acid (blank) solution. A particular chlorine concentration was obtained by making a microliter addition of a sodium hypochlorite (NaOCl) standard to the blank solution. The probe response was recorded for about 30 min. The probe tip was refilled with fresh internal solution and response to a different concentration of chlorine was measured. The rate of decrease in fluorescence intensity was computed as the slope from the linear regression analysis of the linear portion of the intensity–time plot. Finally, a calibration curve was constructed by plotting the slope with respect to the chlorine concentration.

## RESULTS AND DISCUSSIONS

### *Spectroscopic properties of MQAE*

MQAE was considered as a $Cl^-$ sensitive fluorescent compound for the detection of $Cl_2$ with the fiber-optic probe in aqueous solution in an indirect approach. Verkman *et al.*[8] synthesized and characterized MQAE as water soluble (270 g/l. at 23°C) and highly $Cl^-$ sensitive (Stern–Volmer constant $200M^{-1}$) compound with peak excitation and emission wavelengths of 355 and 460 nm, respectively, and molar absortivity of $4850M^{-1}$ $cm^{-1}$.

Fluorescence intensity of this compound was quenched by $Cl^-$, $Br^-$, $I^-$, $SCN^-$, and by organic anions such as citrate. However, MQAE fluorescence was not affected by $NO_3^-$, $SO_4^{-2}$, $HCO_3^-$, $Na^+$, $K^+$, and $Ca^{2+}$, and pH in the range of 4–8.

According to our studies, a plot of fluorescence intensity *vs.* concentration is linear over the concentration range from 1 to 25 $\mu M$ MQAE. The effect of chloride on the absorption spectrum of MQAE was evaluated in order to determine the mode of quenching. The presence of chloride did not significantly perturb the absorption spectrum of MQAE, which indicates the absence of static quenching. From a regression analysis of a plot of $F_0/F$ *vs.* $[Cl^-]$, $199.1 \pm 0.7 M^{-1}$ was obtained as the Stern–Volmer constant for fluorescence quenching of MQAE by $Cl^-$. Interestingly, we have discovered that the fluorescence of MQAE is also quenched by the $OCl^-$ ion. Under the experimental conditions described above, $Cl_2$ and HOCl slowly decreased the fluorescence intensity until the fluorescence diminished completely, indicating a decomposition of MQAE possibly due to oxidation of MQAE by $Cl_2$ and HOCl. MQAE also decomposed in a $0.01 M$ NaOH solution by hydrolysis.

*Principle of probe operation*

To carry out the measurement of gaseous chlorine in aqueous solution by the fiber-optic chlorine probe, the spectroscopic properties of MQAE (as described above) and the following reactions are considered[5]:

$$Cl_2 + H_2O \rightleftharpoons HOCl + H^+ + Cl^- (K_d = 4.0 \times 10^{-4}) \quad (2)$$

$$HOCl + H_2O \rightleftharpoons H_3O^+ + OCl^- (K_a = 3.16 \times 10^{-8}). \quad (3)$$

According to the above equations, the addition of NaOCl in a $Cl^-$-containing acidic solution (such as dilute HCl) provides most of the chlorine species in the form of $Cl_2$. A portion of the chlorine then diffuses through the gas-permeable membrane and reaches the internal MQAE solution. It is evident from the above reactions that a high pH in the internal MQAE solution is desirable. High pH facilitates an immediate dissociation of $Cl_2$ into equimolar quantities of chloride and hypochlorite ions. Thus, no appreciable partial pressure of chlorine gas will build up in the internal solution. As a result, gaseous chlorine will continue to cross the membrane due to the difference in partial pressure between the sample and internal MQAE solutions. The rate of $Cl_2$ influx will depend on its partial pressure in the outside sample solution and will be limited by the concentration of MQAE, volume of internal solution, membrane porosity, and membrane thickness.

*Background and internal solution composition*

A $0.1 M$ HCl solution was chosen as the background solution into which the fiber-optic probe was placed. This solution ensured the formation of $Cl_2$ when standard NaOCl was added. Equations (2) and (3) suggest that the formation of HOCl is thermodynamically unfavorable. Therefore, gaseous $Cl_2$ is the only species that can diffuse through the membrane and enter the internal solution.

Selection of the internal solution composition is a critical issue. Although chloride ion formation is favorable under basic conditions, MQAE hydrolysis limits the pH to values below 12.0. The background fluorescence intensity of MQAE in $0.1 M$ NaOH decreased with time, which resulted in poor reproducibility of the probe response in repeated measurements. An acidic internal solution, on the other hand, restricts the dissociation of $Cl_2$ to form chloride. However, measurements with acidic internal solutions are possible because $Cl_2$ itself diminishes the fluorescence of MQAE. In the current system, the internal MQAE solution was made in water. In this solution, some quantities of all forms of chlorine species are present. In slightly basic solution (pH 9.0), background fluorescence intensity was stable. This pH also ensures almost a complete conversion of $Cl_2$ into $Cl^-$ ion. However, the magnitude and rate of change of probe response due to a $Cl_2$ sample were identical to those obtained when the internal solution was made with plain water.

*Calibration curve*

Figure 2 illustrates six intensity–time curves representing the exposure of the probe to 8.4–835 $\mu M$ $Cl_2$ solutions. The internal solution was composed of 0.1 m$M$ MQAE in water. For each measurement, the probe tip was refilled with a fresh aliquot of internal solution. It is evident from these curves that initially the intensity of fluorescence decreased linearly with time. The initial rate of decrease in fluorescence inten-

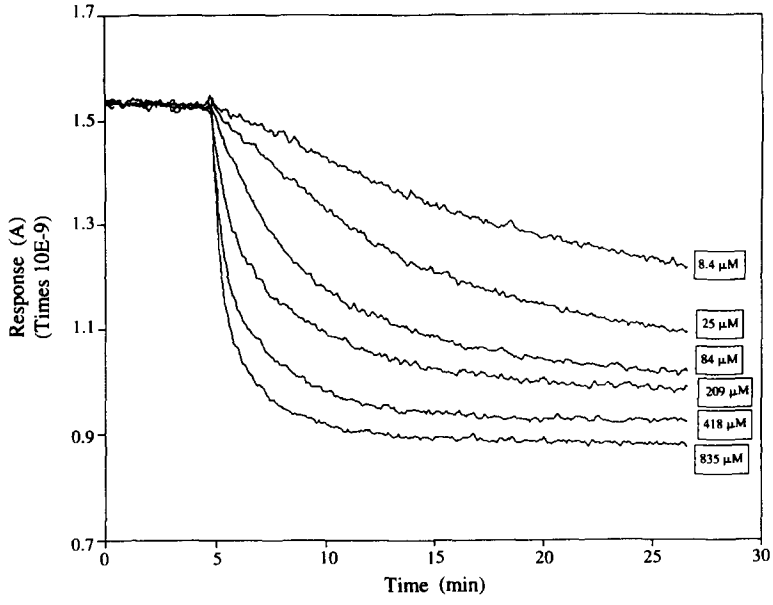


Fig. 2. Intensity–time curves for the chlorine probe obtained from different concentrations of standard chlorine solutions.

sity was proportional to the concentration of $Cl_2$ in the sample. This rate of change in response represents the flux of $Cl_2$ transported through the gas-permeable membrane. If the probe is kept in the sample solution for sufficient time, the final intensity for all sample concentrations is identical. Once the signal became steady, it remained essentially unchanged when the concentration of $Cl_2$ in the sample was increased. The magnitude of the total signal change was not dependent on the concentration of $Cl_2$ in the sample. Therefore, a Stern–Volmer plot could not be used as the calibration method for this probe. The initial rate of decrease in fluorescence intensity was calculated from linear regression analysis of the linear portion of the intensity–time curves. Calibration curves were constructed by plotting these slopes as a function of $Cl_2$ concentration. A typical calibration curve is presented in Fig. 3. The slopes increased linearly as a function of chlorine concentration over the range from 8.4 to 418 $\mu M$. This linearity was not maintained at high $Cl_2$ concentrations because the rate of $Cl_2$ influx became

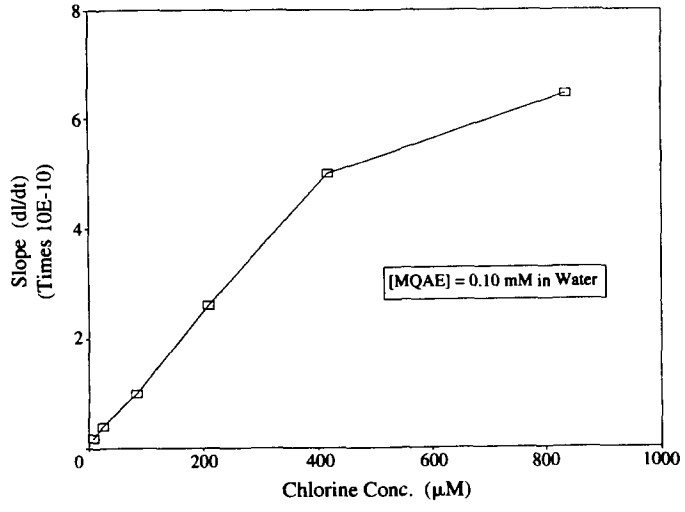


Fig. 3. Calibration curve for the chlorine probe made by plotting the rate of decrease in response as a function of concentration of standard chlorine solutions.

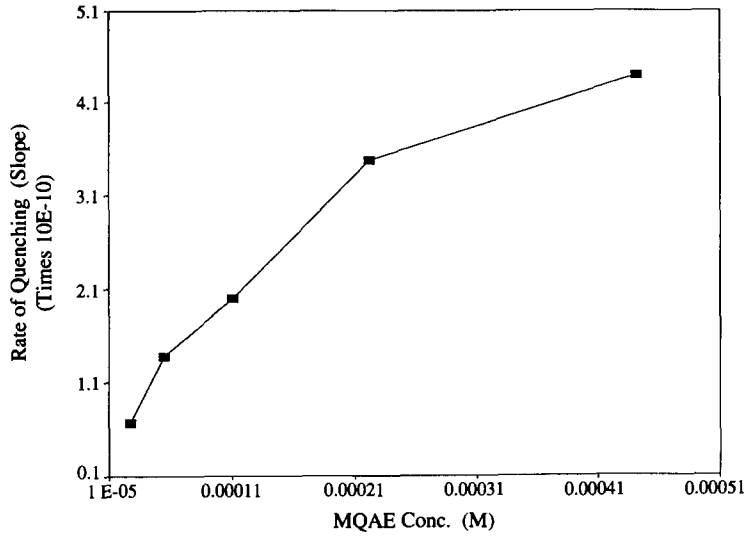


Fig. 4. Effect of the concentration of MQAE on the rate of decrease in the fluorescence signal. The concentration of chlorine in the sample was 168 $\mu M$.

limited by the porosity and thickness of the gas-permeable membrane.

*Reversibility*

The probe response was not reversible. After the probe reached a steady signal in a $Cl_2$ solution, the probe was immersed in 20.0 ml of either 0.1$M$ HCl (background) solution or in 0.1$M$ NaOH solution to extract gaseous chlorine species ($Cl_2$ and HOCl, respectively) from the internal solution. The fluorescence signal remained unchanged even after 30 min indicating that the interaction between MQAE and chlorine species is irreversible. The inability to remove chlorine from the internal solution may be caused by either a high stability constant for the quencher–fluorophore complex or extremely high concentrations of the chlorine species in the internal solution, which causes the decomposition of MQAE due to oxidation by HOCl and $Cl_2$. In either case, once the probe is exposed to a $Cl_2$ sample, the probe cannot be reused and must be refilled with a fresh aliquot of the internal solution before the next measurement.

In an attempt to make the probe reversible, the internal MQAE solution was made with 1.0 m$M$ NaCl in order to drive equation (2) toward the formation of $Cl_2$. The response property of the resulting probe was the same as before with no reversibility. These observations suggest that typical steady-state gas-sensing measurements cannot be obtained with this type of probe.

*MQAE concentration in internal solution*

Probe responses were recorded for a 0–168 $\mu M$ chlorine concentration step while varying the concentration of MQAE in the internal solution from 0.028 to 0.442 m$M$. The rate of change of signal, which represents the sensitivity of the probe, increases with higher MQAE concentrations as shown in Fig. 4. At MQAE concentrations approaching 0.442 m$M$, the response rate began to level off at a maximum value. This leveling off was probably caused by the effectiveness of complex formation between the quenchers and the excited state of MQAE being limited by the bimolecular collision rate responsible for dynamic quenching. Self absorption at high concentration of MQAE could also be a factor.

*Reproducibility*

The probe displayed good reproducibility when a fresh aliquot of internal solution was used for repeated measurements. Figure 5 demonstrates the reproducibility of the probe for consecutive responses for a 0–168 $\mu M$ chlorine concentration step. Each measurement was performed after refilling the probe tip with fresh internal solution. The magnitude of overall signal change is identical in three measurements; the relative standard deviation of the initial rate

of change of fluorescence intensity is about 1 percent.

*Probe calibration*

Once constructed, the probe requires calibration so that it can be used for determination of $Cl_2$ in unknown samples. The baseline response could not be re-established after the first exposure of the probe to a sample solution. Therefore, for analysis of unknown samples, it is necessary to make a calibration curve by following the procedure described earlier where the probe tip is refilled before each measurement. If all the experimental parameters are kept constant, then the concentration of an unknown sample can be measured by comparing the slope of the initial intensity–time curve with the calibration curve. Since the response of the refilled probe is reproducible, multiple analyses can be performed with a single probe unit. The probe tip must be refilled with fresh internal MQAE solution for each determination, which is a relatively simple procedure.

*HOCl gas measurements*

A system was designed where HOCl was the only species present in the sample solution by making microliter additions of a standard solution of NaOCl to the sample cell containing 0.01*M* $H_2SO_4$. The internal MQAE (0.1 m*M* in water) solution was trapped at the probe tip with a gas-permeable membrane. When sufficient partial pressure of HOCl was established in the sample solution, HOCl diffused through the membrane and entered the internal MQAE solution.According to equations (2) and (3), the predominant chlorine species in the internal solution would be HOCl. As was expected, the fluorescence intensity decreased when HOCl entered the internal solution. Unfortunately, the probe did not respond to a second addition of HOCl. Overall, the response properties of the HOCl probe are similar to those of the $Cl_2$ probe.

## CONCLUSION

The aspects of developing a fiber-optic probe based on MQAE-quenching for the measurement of free chlorine in aqueous solution are presented. Compositions of the internal and blank solution were identified as aqueous MQAE and dilute HCl, respectively. Although the total fluorescence decay cannot be used for the calibration purpose, the initial rate of fluorescence decay is proportional to the sample concentration. The probe possesses excellent reproducibility when the probe tip is refilled with fresh internal solution before each measurement.

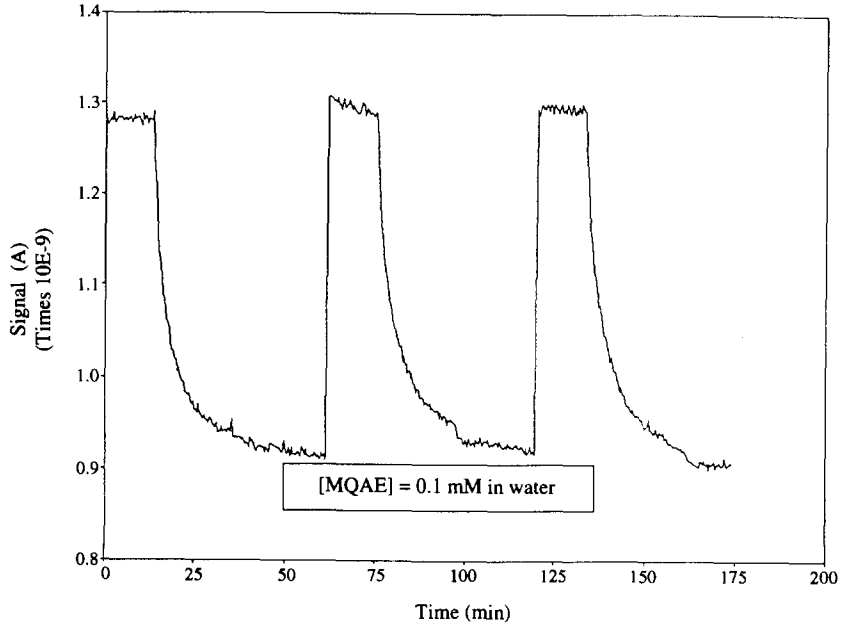


Fig. 5. Reproducibility of the chlorine probe obtained by measuring repeated responses to 168 $\mu M$ $Cl_2$ solutions. The probe tip was refilled with fresh internal MQAE (0.1 m*M* in water) solution before each measurement.

*Acknowledgements*—Financial support by the National Science Foundation (#BNS-8716768) is acknowledged. Very helpful discussions with Dr Purnendu K. Dasgupta are appreciated.

## REFERENCES

1. R. M. Turnaer and S. Fairhurst, *Toxicology of Substances in Relation to Major Hazards. Chlorine.* Health and Safety Executive, HM Stationery Office, London, 1990.
2. G. Gordon, G. E. Pacey, J. Cooper and R. G. Rice, Disinfectant Residual Measurement Methods, Report to *American Water Works Association Research Foundation* (Project 102–85), 1987.
3. R. Bauer and C. O. Rupe, *Anal. Chem.*, 1971, **43,** 421.
4. J. Stanley and R. Nossel, In *Water Chlorination, Environmental Impact and Health Effects*, R. L. Jolley, W. A. Grungs, J. A. Lontruvo, R. B. Cumings, J. S. Mattrice and V. A. Jacobs (eds), Vol. 4, p. 699. Ann Arbor Sci., Ann Arbor, 1983.
5. J. G. Gord, G. Gordon and G. E. Pacey, *Anal. Chem.*, 1988, **60,** 2.
6. S. A. Momin and R. Narayanaswamy, *Analyst*, 1992, **117,** 83.
7. S. Kar and M. A. Arnold, *Anal. Chem.*, 1992, **64,** 2438.
8. A. S. Verkman, M. C. Sellers, A. C. Chao, T. Leung and R. Ketcham, *Anal. Biochem.*, 1989, **178,** 355.

Pergamon

*Talanta*, Vol. 42, No. 4, pp. 671–675, 1995
Elsevier Science Ltd
Printed in Great Britain
0039-9140/95 $9.50 + 0.00

# BOOK REVIEWS

**Chemometrics for Analytical Chemistry, Volume 1—PC-aided statistical data analysis:** M. MELLOUN, J. MILITKY and M. FORINA, Ellis Horwood, 1992. Pages 330. £65.00. ISBN 0-13-126376-5.

This book is the first of a set (it is not clear whether another one or two volumes are intended) designed to provide a fairly comprehensive treatment of chemometrics for analytical scientists at the advanced undergraduate or postgraduate level. There is a matching and extensive suite of software (on 4 high density floppy discs), variously called Adstat or Chemstat, which provides both elementary and advanced statistical calculations and utilises the extensive example data sets described in the book. This software is PC-based (minimum configuration is a 286 processor, 1 Mb RAM, 8.5 Mb hard disk space, maths co-processor recommended), and I have not heard of a Mac version, or of the price of the PC version.

This first volume covers exploratory data analysis, univariate statistics, one- and two-way ANOVA, and exploratory and factor analysis of multivariate data. It does not include (despite the claims on the back cover) regression methods: these must await later volume(s). Adstat/Chemstat has eight modules, five of which deal with regression and calibration. The book's coverage of many topics is exceptionally detailed to the point of intimidation: several variants of box-and-whisker plots are given extended treatment, while Laplace, 1- and 2-parameter exponential, rectangular, and 2- and 3-parameter log-normal distributions are covered in addition to the familiar normal and Poisson ones. Elsewhere the comprehensive coverage is welcome, for example in the good treatment of robust methods, absent from many other texts. The book claims to require little mathematical background, and matrix algebra is summarised in a separate and very condensed appendix, but the reality is that from the very first page integration, partial differentiation, *etc.* are assumed to be absolutely familiar, whereas alas they are not for many students these days. A knowledge of basic statistics would also be useful before starting the book.

The software is probably of value most obviously in its provision and treatment of a number of useful and interesting data sets. The calculation facilities offered are equalled or exceeded by many other established suites of statistics software, and extensive testing would be needed to verify that Adstat/Chemstat is stable and bug-free. It provides good printout options, with presentation standard graphics on Epson- and Hp-compatible printers, but the manual is written in very poor English, in contrast to the book where the translation editing is generally excellent, and which has the rare attribute of a good index.

When the remaining volumes of text are published and when the software has an improved manual this combined book and software will provide a formidable resource for teachers of chemometrics. But it will be hard going for many students, and it is certainly not suitable for beginners.

J. N. MILLER

**Asphaltene Particles in Fossil Fuel Exploration, Recovery, Refining, and Production Processes:** M. K. SHARMA and T. F. YEN (editors), Plenum, New York, 1994. Pages xiii + 244. US$75.00. ISBN 0-306-44709-6.

This well produced book documents the proceedings of the International Symposium on Asphaltene Particles in Fossil Fuel Exploration, Recovery, Refining and Production Processes held in Las Vegas, Nevada, 13–17 July 1992. Eighteen selected papers are presented and these can be divided into four main categories: (1) Bitumen and Coal-Derived Asphaltenes, (2) Asphalt and Asphaltene Conversion, (3) Surface and Colloidal Aspects of Asphaltenes, and (4) Thermodynamic and Molecular Aspects of Asphaltenes. The intended objective of the book is to reflect the current understanding of formulation and process problems related to asphaltenes. Almost all of the contributing authors are from Canada or the USA and several different disciplines are represented, *e.g.* chemical and petroleum engineering, geological engineering, and civil and environmental engineering. Some authors contribute to more than one paper, *e.g.* the editor T. F. Yen is co-author of six of the 18 papers. Both an author index and a subject index are included.

The various papers attempt to define asphaltenes as the heavy ended fraction of petroleum or the bitumen fraction which is insoluble in hot *n*-pentane. Investigations of the molecular properties of the asphaltenes—high molecular weight polyaromatic or polycyclic molecules which may be joined together by links containing heteroatoms such as N, O and S—are presented. One interesting paper discusses the concept of a "single molecule representation" or "average molecule" to interpret the NMR spectra. Physical properties discussed include rheological behaviour, surface activity and thermodynamics.

Asphalt is a very complex mixture that consists of saturates, aromatics, resins and asphaltenes. These four fractions can be separated by column chromatography and the final paper of this book entitled 'Fractionation of asphalt by thin-layer chromatography interfaced with flame ionization detector and subsequent characterization by FTIR' is perhaps the most analytical report presented. Another paper by J. Lian and T. F. Yen classifies asphalts into sol, sol-gel and gel types depending on their physical and chemical properties. The sol and sol-gel types are used for paving while the gel type asphalts are used in roofing.

Pergamon

*Talanta*, Vol. 42, No. 4, pp. 671–675, 1995
Elsevier Science Ltd
Printed in Great Britain
0039-9140/95 $9.50 + 0.00

# BOOK REVIEWS

**Chemometrics for Analytical Chemistry, Volume 1—PC-aided statistical data analysis:** M. MELLOUN, J. MILITKY and M. FORINA, Ellis Horwood, 1992. Pages 330. £65.00. ISBN 0-13-126376-5.

This book is the first of a set (it is not clear whether another one or two volumes are intended) designed to provide a fairly comprehensive treatment of chemometrics for analytical scientists at the advanced undergraduate or postgraduate level. There is a matching and extensive suite of software (on 4 high density floppy discs), variously called Adstat or Chemstat, which provides both elementary and advanced statistical calculations and utilises the extensive example data sets described in the book. This software is PC-based (minimum configuration is a 286 processor, 1 Mb RAM, 8.5 Mb hard disk space, maths co-processor recommended), and I have not heard of a Mac version, or of the price of the PC version.

This first volume covers exploratory data analysis, univariate statistics, one- and two-way ANOVA, and exploratory and factor analysis of multivariate data. It does not include (despite the claims on the back cover) regression methods: these must await later volume(s). Adstat/Chemstat has eight modules, five of which deal with regression and calibration. The book's coverage of many topics is exceptionally detailed to the point of intimidation: several variants of box-and-whisker plots are given extended treatment, while Laplace, 1- and 2-parameter exponential, rectangular, and 2- and 3-parameter log-normal distributions are covered in addition to the familiar normal and Poisson ones. Elsewhere the comprehensive coverage is welcome, for example in the good treatment of robust methods, absent from many other texts. The book claims to require little mathematical background, and matrix algebra is summarised in a separate and very condensed appendix, but the reality is that from the very first page integration, partial differentiation, *etc.* are assumed to be absolutely familiar, whereas alas they are not for many students these days. A knowledge of basic statistics would also be useful before starting the book.

The software is probably of value most obviously in its provision and treatment of a number of useful and interesting data sets. The calculation facilities offered are equalled or exceeded by many other established suites of statistics software, and extensive testing would be needed to verify that Adstat/Chemstat is stable and bug-free. It provides good printout options, with presentation standard graphics on Epson- and Hp-compatible printers, but the manual is written in very poor English, in contrast to the book where the translation editing is generally excellent, and which has the rare attribute of a good index.

When the remaining volumes of text are published and when the software has an improved manual this combined book and software will provide a formidable resource for teachers of chemometrics. But it will be hard going for many students, and it is certainly not suitable for beginners.

J. N. MILLER

**Asphaltene Particles in Fossil Fuel Exploration, Recovery, Refining, and Production Processes:** M. K. SHARMA and T. F. YEN (editors), Plenum, New York, 1994. Pages xiii + 244. US$75.00. ISBN 0-306-44709-6.

This well produced book documents the proceedings of the International Symposium on Asphaltene Particles in Fossil Fuel Exploration, Recovery, Refining and Production Processes held in Las Vegas, Nevada, 13–17 July 1992. Eighteen selected papers are presented and these can be divided into four main categories: (1) Bitumen and Coal-Derived Asphaltenes, (2) Asphalt and Asphaltene Conversion, (3) Surface and Colloidal Aspects of Asphaltenes, and (4) Thermodynamic and Molecular Aspects of Asphaltenes. The intended objective of the book is to reflect the current understanding of formulation and process problems related to asphaltenes. Almost all of the contributing authors are from Canada or the USA and several different disciplines are represented, *e.g.* chemical and petroleum engineering, geological engineering, and civil and environmental engineering. Some authors contribute to more than one paper, *e.g.* the editor T. F. Yen is co-author of six of the 18 papers. Both an author index and a subject index are included.

The various papers attempt to define asphaltenes as the heavy ended fraction of petroleum or the bitumen fraction which is insoluble in hot *n*-pentane. Investigations of the molecular properties of the asphaltenes—high molecular weight polyaromatic or polycyclic molecules which may be joined together by links containing heteroatoms such as N, O and S—are presented. One interesting paper discusses the concept of a "single molecule representation" or "average molecule" to interpret the NMR spectra. Physical properties discussed include rheological behaviour, surface activity and thermodynamics.

Asphalt is a very complex mixture that consists of saturates, aromatics, resins and asphaltenes. These four fractions can be separated by column chromatography and the final paper of this book entitled 'Fractionation of asphalt by thin-layer chromatography interfaced with flame ionization detector and subsequent characterization by FTIR' is perhaps the most analytical report presented. Another paper by J. Lian and T. F. Yen classifies asphalts into sol, sol-gel and gel types depending on their physical and chemical properties. The sol and sol-gel types are used for paving while the gel type asphalts are used in roofing.

Overall some interesting research is presented in this collection of papers. The diagrams and tables are very clear (although one conversion sequence lacks arrows and occasionally the English is abrupt) and the print font and size are consistent throughout. A useful publication, especially for those working in the oil or chemical industries.

P. J. Cox

**Flow-Through (Bio)Chemical Sensors:** M. VALCÁRCEL and M. D. LUQUE DE CASTRO, Elsevier, Amsterdam, 1994. Pages 331. Dfl 355.00 US$202.75. ISBN 0-444-89866-2.

As a result of intense commercial and academic interests, an impressive amount of manpower has been spent at numerous laboratories worldwide on the development of chemi- and biosensors. Yet, considering these vast research efforts, the practical applications of sensor technology have been rather limited. The reasons for this lack of visible success are many, but one of the major factors is undoubtedly owing to the harsh requirements that these devices must fulfil in order to meet the desires of their originators as well as the expectations of the end-users in real-life applications. To be useful, a biosensor must inevitably meet a variety of demands which must be honoured simultaneously. However, considering the diversity of chemical and physical events that can be involved in its function, in addition to satisfying individually dictated reaction parameters, it is not surprising that operational compromises necessarily have to be made for practical synchronization of all the processes required. Therefore, and in order to implement functions such as periodic calibration, conditioning and regeneration, it is, as this reviewer has repeatedly advocated, advantageous to use these devices in a flow-through mode. Or more specifically in the flow injection mode. Only in such a *sensor system*, comprising fluid drives, injectors and flow-through cells, can all experimental conditions be strictly affixed and reproducibly maintained under computer control.

Although principally and conceptually implied by the authors, this is exactly, in my opinion, what this monograph should have been about, as such a broad concept would have been its *raison d'etre*. Yet, Valcárcel and Luque de Castro surprisingly appear to have gone only half the way, by emphasizing the advantages of flow-through sensor construction rather than pointing out that a full transition is necessary from a dip type probe to a sensor system. This is indeed surprising considering that their experience includes authorship of two monographs and numerous papers on flow injection. One can only wonder why they have selected this approach, especially considering that volume 7 in this series from Elsevier is, in fact, focused on, and entitled, 'Biosensors' (by F. Scheller and F. Schubert), while at the same time the text contains a good deal of recycled material from these prolific authors' previous works. This is by no means meant to be a negative comment, but rather a question mark as to whether such a narrow subject area actually can bear an entire monograph *per se*.

The book is divided into five main chapters, where the introductory Chapter 1 provides an overview of (bio)chemical sensors and their place within analytical chemistry as this field has emerged over the last couple of decades. With its emphasis on the practical and mechanistic aspects of these devices (as their operation "requires that the sensor [can] be reliably used by unskilled personnel, who often work under stressing conditions") and its rendition of commercially available sensors (one wonders if they indeed fulfil these requirements), and the accompanying philosophical remarks, this chapter is interesting reading. The second chapter is devoted to essential and fundamental concepts of (bio) sensors, their construction and classification, and their modes of operation (batch and continuous flow mode), while the following three chapters arrange the most relevant types of flow-through (bio)chemical sensors according to the processes taking place at the sensing/recognition microzone, as well as their position in space and time. In this context, the three operational key parameters are *separation*, *reaction* and *detection*, the applicable combinations of which resolve the ensuring structural arrangement of the monograph. Thus, Chapter 3, with well over 100 pages and the largest in the book, is devoted to flow-through sensors based on integrated reaction and detection in the absence of a separation process, *i.e.* describing sensors based on either immobilized species (catalyst, antibody or reagent) or *in situ* produced reagents. Chapter 4 deals with sensors based on integrated separation and detection (separation being accomplished for instance via gas diffusion or liquid–liquid extraction), special emphasis being placed on multi-determination sensors (*e.g.* ISE and ISFETs), while Chapter 5 reviews flow-through sensors relying on the sequential or simultaneous integration of all the three intricate processes involved for their function.

As the reading progresses, it very quickly becomes apparent that the conditions *sine qua non* for successful application of biosensors are the timing of sample introduction into the sensor and data collection. These events must be reproduced from cycle to cycle since the dynamic response of a sensor must be captured in a reproducible fashion. For that reason alone a flow injection-based sensor system is the only viable choice. Unfortunately, this information is not emphasized or systematically organized, but rather scattered throughout the monograph (indeed flow injection is not even mentioned in the otherwise detailed index). What the book offers is essentially an account on the construction and operation of biosensors, a feature which is at the same time its strength as well as its weakness, leaving no room for a critical evaluation or a theoretical treatment (interestingly, the entire book does not contain a single mathematical equation). Yet, the overview of types and configurations of biosensors is comprehensive. The only significant omission is the absence of a discussion of the BIAcor system, which, marketed by Pharmacia, probably is the most successfully applied automated biosensor system known today. However, the book has a pedagogical value (as one would expect from two experienced university professors), the descriptions are painstakingly detailed with many examples, and the text is supplemented with an abundance of figures, from the authors' own works as well as generously selected from the current literature.

It is my belief that the authors have spent a commendable effort compiling this book, which is well documented and gives a wealth of information, to seasoned researchers and novices alike. It is only to be hoped that this publication will advance the field toward real life applications—a development badly needed in this fashionable field of research.

E. H. HANSEN

Overall some interesting research is presented in this collection of papers. The diagrams and tables are very clear (although one conversion sequence lacks arrows and occasionally the English is abrupt) and the print font and size are consistent throughout. A useful publication, especially for those working in the oil or chemical industries.

P. J. Cox

**Flow-Through (Bio)Chemical Sensors:** M. VALCÁRCEL and M. D. LUQUE DE CASTRO, Elsevier, Amsterdam, 1994. Pages 331. Dfl 355.00 US$202.75. ISBN 0-444-89866-2.

As a result of intense commercial and academic interests, an impressive amount of manpower has been spent at numerous laboratories worldwide on the development of chemi- and biosensors. Yet, considering these vast research efforts, the practical applications of sensor technology have been rather limited. The reasons for this lack of visible success are many, but one of the major factors is undoubtedly owing to the harsh requirements that these devices must fulfil in order to meet the desires of their originators as well as the expectations of the end-users in real-life applications. To be useful, a biosensor must inevitably meet a variety of demands which must be honoured simultaneously. However, considering the diversity of chemical and physical events that can be involved in its function, in addition to satisfying individually dictated reaction parameters, it is not surprising that operational compromises necessarily have to be made for practical synchronization of all the processes required. Therefore, and in order to implement functions such as periodic calibration, conditioning and regeneration, it is, as this reviewer has repeatedly advocated, advantageous to use these devices in a flow-through mode. Or more specifically in the flow injection mode. Only in such a *sensor system*, comprising fluid drives, injectors and flow-through cells, can all experimental conditions be strictly affixed and reproducibly maintained under computer control.

Although principally and conceptually implied by the authors, this is exactly, in my opinion, what this monograph should have been about, as such a broad concept would have been its *raison d'etre*. Yet, Valcárcel and Luque de Castro surprisingly appear to have gone only half the way, by emphasizing the advantages of flow-through sensor construction rather than pointing out that a full transition is necessary from a dip type probe to a sensor system. This is indeed surprising considering that their experience includes authorship of two monographs and numerous papers on flow injection. One can only wonder why they have selected this approach, especially considering that volume 7 in this series from Elsevier is, in fact, focused on, and entitled, 'Biosensors' (by F. Scheller and F. Schubert), while at the same time the text contains a good deal of recycled material from these prolific authors' previous works. This is by no means meant to be a negative comment, but rather a question mark as to whether such a narrow subject area actually can bear an entire monograph *per se*.

The book is divided into five main chapters, where the introductory Chapter 1 provides an overview of (bio)chemical sensors and their place within analytical chemistry as this field has emerged over the last couple of decades. With its emphasis on the practical and mechanistic aspects of these devices (as their operation "requires that the sensor [can] be reliably used by unskilled personnel, who often work under stressing conditions") and its rendition of commercially available sensors (one wonders if they indeed fulfil these requirements), and the accompanying philosophical remarks, this chapter is interesting reading. The second chapter is devoted to essential and fundamental concepts of (bio) sensors, their construction and classification, and their modes of operation (batch and continuous flow mode), while the following three chapters arrange the most relevant types of flow-through (bio)chemical sensors according to the processes taking place at the sensing/recognition microzone, as well as their position in space and time. In this context, the three operational key parameters are *separation*, *reaction* and *detection*, the applicable combinations of which resolve the ensuring structural arrangement of the monograph. Thus, Chapter 3, with well over 100 pages and the largest in the book, is devoted to flow-through sensors based on integrated reaction and detection in the absence of a separation process, *i.e.* describing sensors based on either immobilized species (catalyst, antibody or reagent) or *in situ* produced reagents. Chapter 4 deals with sensors based on integrated separation and detection (separation being accomplished for instance via gas diffusion or liquid–liquid extraction), special emphasis being placed on multi-determination sensors (*e.g.* ISE and ISFETs), while Chapter 5 reviews flow-through sensors relying on the sequential or simultaneous integration of all the three intricate processes involved for their function.

As the reading progresses, it very quickly becomes apparent that the conditions *sine qua non* for successful application of biosensors are the timing of sample introduction into the sensor and data collection. These events must be reproduced from cycle to cycle since the dynamic response of a sensor must be captured in a reproducible fashion. For that reason alone a flow injection-based sensor system is the only viable choice. Unfortunately, this information is not emphasized or systematically organized, but rather scattered throughout the monograph (indeed flow injection is not even mentioned in the otherwise detailed index). What the book offers is essentially an account on the construction and operation of biosensors, a feature which is at the same time its strength as well as its weakness, leaving no room for a critical evaluation or a theoretical treatment (interestingly, the entire book does not contain a single mathematical equation). Yet, the overview of types and configurations of biosensors is comprehensive. The only significant omission is the absence of a discussion of the BIAcor system, which, marketed by Pharmacia, probably is the most successfully applied automated biosensor system known today. However, the book has a pedagogical value (as one would expect from two experienced university professors), the descriptions are painstakingly detailed with many examples, and the text is supplemented with an abundance of figures, from the authors' own works as well as generously selected from the current literature.

It is my belief that the authors have spent a commendable effort compiling this book, which is well documented and gives a wealth of information, to seasoned researchers and novices alike. It is only to be hoped that this publication will advance the field toward real life applications—a development badly needed in this fashionable field of research.

E. H. HANSEN

**Instrumental Methods for Determining Elements:** L. TAYLOR, R. B. PAPP and B. D. POLLARD, VCH, Weinheim, 1994. Pages ix + 322. DM128.00 £51.50. ISBN 1-56081-038-6.

Analysts are often faced with the need to qualitatively and/or quantitatively determine elements—single or multi, stand-alone or as the detection component of a bigger system. If you have already chosen a technique and are happy with it, then this book may not be for you. It does not give in-depth treatment of any particular technique although you may find general and useful information and up-to-date references for in-depth treatment. If you do not know which technique to use or you are considering alternatives, then this book is extremely helpful.

The book begins with two 'introductory' chapters giving brief examination of the factors which govern the choice of a technique. It then follows with seven chapters dedicated to atomic absorption, atomic emission, voltametry, potentiometry, chromatography, X-ray fluorescence and combustion techniques. It ends with a chapter on miscellaneous techniques which describes briefly capillary electrophoresis, flow-injection analysis, mass spectrometry, neutron activation analysis and UV/Vis spectrometry. In fact most of the available techniques for elemental analysis have been covered.

Each of the dedicated chapters gives a minimal account of the necessary theory, a simple but adequate description of the instrumentation (with helpful illustrations), a succinct examination of choice factors such as sensitivity, detection limit, automation and operating costs, and also a substantial list of applications. What is particularly useful are the references to applications, lists of suppliers with addresses and the price range (given in American currency).

This book is obviously written by pesons who are in the trade as the information given is usually comprehensive, practical and up-to-date. There are few mistakes, most of them editorial and appear in Chapter 6. As the title suggests, the techniques described will be limited to total determination of elements but some mention has been made on speciation. A slight misgiving is the very brief (half a page) treatment on ICPMS which is a powerful and increasingly popular technique for elemental analysis.

This book is very readable and provides much useful and practical information. I think it deserves a place on the shelves of many analytical laboratories.

S. C. TAM

**Pharmacodynamics and Drug Development—Perspectives in Clinical Pharmacology**: N. R. CUTLER, J. J. SRAMEK and P. K. NARANG (editors), Wiley, Chichester, 1994. Pages: xv + 491. £65.00. ISBN 0-471-950-521.

This textbook may be of particular interest to researchers in the pharmaceutical industry and those in academia who have close links with industry. Users will require a sound knowledge of pharmacokinetics and at least some knowledge of pharmacodynamics. It does not, however, claim to be a basic textbook but rather one which addresses the increasing interest in the use of pharmacodynamic modelling in the design of clinical trials.

The first seven chapters provide an overview of pharmacodynamics and the causes of variation in both pharmacokinetics and pharmacodynamics. Unfortunately there is a certain amount of duplication in the material covered by the authors of different chapters but this permits each chapter to be read in isolation.

The second section of the book addresses the application of pharmacodynamic modelling to areas of the cardiovascular system, central nervous system and the use of antibiotics, antineoplastics and antiviral agents. This section provides ample demonstration of both the utility of pharmacodynamic models and the difficulty of selecting appropriate models and suitable measures of effect.

The final three chapters of this textbook consider molecular approaches to clarifying the mechanisms of drug action. They provide an interesting counterpoint to the rest of the text with consideration of methods for classification and elucidation of $\alpha$-adreno receptors, muscarinic receptors and serotonin receptors.

This textbook is unlikely to appeal to a large readership but provides a valuable overview of recent work in pharmacodynamics.

M. HAWTHORN

**Polymeric Site-Specific Pharmacotherapy**: A. J. DOMB (editor), Wiley, Chichester, 1994. Pages xi + 464. £75.00. ISBN 0-471-93824-6.

This book comprises a review of a most relevant and expanding area of research into efficient drug delivery systems in which drugs may be delivered specifically to their sites of action thereby increasing therapeutic effectiveness and reducing harmful systemic effects. Bio-absorbable polymers, of which there is an ever-increasing array, may be used as ideal drug carrier systems to the target tissue for the treatment of several diseased states. Each chapter, dealing with a specific site of target tissue, has been written by specialist authors active in their respective areas of research. The presentations are extensively detailed and referenced and therefore the book would be aimed largely at postgraduate level rather than the undergraduate student.

The initial chapters review extensively several biocompatable polymers in current use for implantation. These chapters concentrate on the types of polymers, their structure, degradation rates, blending possibilities, and some major concerns such as biocompatability and toxicity (especially tests for cytotoxicity, mutagenicity and teratogenicity). The kinetics of drug release from polymer implants are also thoroughly reviewed. A further chapter deals specifically with the concepts necessary to understand modelling of drug delivery to brain tissue from interstitial sources. There is a chapter with an in-depth account of tumour-specific drug targeting constituting a description of the work done over a period of time on polymer-conjugated

**Instrumental Methods for Determining Elements:** L. TAYLOR, R. B. PAPP and B. D. POLLARD, VCH, Weinheim, 1994. Pages ix + 322. DM128.00 £51.50. ISBN 1-56081-038-6.

Analysts are often faced with the need to qualitatively and/or quantitatively determine elements—single or multi, stand-alone or as the detection component of a bigger system. If you have already chosen a technique and are happy with it, then this book may not be for you. It does not give in-depth treatment of any particular technique although you may find general and useful information and up-to-date references for in-depth treatment. If you do not know which technique to use or you are considering alternatives, then this book is extremely helpful.

The book begins with two 'introductory' chapters giving brief examination of the factors which govern the choice of a technique. It then follows with seven chapters dedicated to atomic absorption, atomic emission, voltametry, potentiometry, chromatography, X-ray fluorescence and combustion techniques. It ends with a chapter on miscellaneous techniques which describes briefly capillary electrophoresis, flow-injection analysis, mass spectrometry, neutron activation analysis and UV/Vis spectrometry. In fact most of the available techniques for elemental analysis have been covered.

Each of the dedicated chapters gives a minimal account of the necessary theory, a simple but adequate description of the instrumentation (with helpful illustrations), a succinct examination of choice factors such as sensitivity, detection limit, automation and operating costs, and also a substantial list of applications. What is particularly useful are the references to applications, lists of suppliers with addresses and the price range (given in American currency).

This book is obviously written by pesons who are in the trade as the information given is usually comprehensive, practical and up-to-date. There are few mistakes, most of them editorial and appear in Chapter 6. As the title suggests, the techniques described will be limited to total determination of elements but some mention has been made on speciation. A slight misgiving is the very brief (half a page) treatment on ICPMS which is a powerful and increasingly popular technique for elemental analysis.

This book is very readable and provides much useful and practical information. I think it deserves a place on the shelves of many analytical laboratories.

S. C. TAM

**Pharmacodynamics and Drug Development—Perspectives in Clinical Pharmacology**: N. R. CUTLER, J. J. SRAMEK and P. K. NARANG (editors), Wiley, Chichester, 1994. Pages: xv + 491. £65.00. ISBN 0-471-950-521.

This textbook may be of particular interest to researchers in the pharmaceutical industry and those in academia who have close links with industry. Users will require a sound knowledge of pharmacokinetics and at least some knowledge of pharmacodynamics. It does not, however, claim to be a basic textbook but rather one which addresses the increasing interest in the use of pharmacodynamic modelling in the design of clinical trials.

The first seven chapters provide an overview of pharmacodynamics and the causes of variation in both pharmacokinetics and pharmacodynamics. Unfortunately there is a certain amount of duplication in the material covered by the authors of different chapters but this permits each chapter to be read in isolation.

The second section of the book addresses the application of pharmacodynamic modelling to areas of the cardiovascular system, central nervous system and the use of antibiotics, antineoplastics and antiviral agents. This section provides ample demonstration of both the utility of pharmacodynamic models and the difficulty of selecting appropriate models and suitable measures of effect.

The final three chapters of this textbook consider molecular approaches to clarifying the mechanisms of drug action. They provide an interesting counterpoint to the rest of the text with consideration of methods for classification and elucidation of $\alpha$-adreno receptors, muscarinic receptors and serotonin receptors.

This textbook is unlikely to appeal to a large readership but provides a valuable overview of recent work in pharmacodynamics.

M. HAWTHORN

**Polymeric Site-Specific Pharmacotherapy**: A. J. DOMB (editor), Wiley, Chichester, 1994. Pages xi + 464. £75.00. ISBN 0-471-93824-6.

This book comprises a review of a most relevant and expanding area of research into efficient drug delivery systems in which drugs may be delivered specifically to their sites of action thereby increasing therapeutic effectiveness and reducing harmful systemic effects. Bio-absorbable polymers, of which there is an ever-increasing array, may be used as ideal drug carrier systems to the target tissue for the treatment of several diseased states. Each chapter, dealing with a specific site of target tissue, has been written by specialist authors active in their respective areas of research. The presentations are extensively detailed and referenced and therefore the book would be aimed largely at postgraduate level rather than the undergraduate student.

The initial chapters review extensively several biocompatable polymers in current use for implantation. These chapters concentrate on the types of polymers, their structure, degradation rates, blending possibilities, and some major concerns such as biocompatability and toxicity (especially tests for cytotoxicity, mutagenicity and teratogenicity). The kinetics of drug release from polymer implants are also thoroughly reviewed. A further chapter deals specifically with the concepts necessary to understand modelling of drug delivery to brain tissue from interstitial sources. There is a chapter with an in-depth account of tumour-specific drug targeting constituting a description of the work done over a period of time on polymer-conjugated

anticancer agents (SMANCS). A chapter is concerned with interstitial drug delivery to the brain using controlled-release polymers, overcoming the problem of the blood–brain barrier. There is also a discussion of the treatment of neurologic diseases by using biodegradable polymers as matrices for controlled delivery of neurotransmitters. There is an interesting review of developments related to the site-specific targeting of drugs to the bone marrow. As the authors point out, the ability to target colloidal drug carriers to bone marrow may hold promise for the improvement of cancer chemotherapy and radiotherapy. The subject of polymeric perivascular delivery systems is also addressed. Studies are described confirming the feasibility of using drug-eluting polymeric matrices placed around the adventitial surface of injured carotid arteries to evaluate the effects of specific drugs. Attention is also paid to techniques of localised cardiac administration of therapeutic agents, *e.g.* antiarrhythmic agents, and their potential for improving cardiovascular pharmacotherapies. Acute osteomyelitis, a serious bone infection, is very difficult to treat, and a chapter deals with drug delivery systems, such as carrier systems, that will ensure high local effects of effective antibiotics. The gastrointestinal tract also comes under scrutiny when physiological parameters crucial for the rational design of specific drug delivery are discussed. Some traditional and novel methods that target and localise drugs in the alimentary tract are reviewed. The description of drug delivery systems used in ophthalmology concentrates on solid erodible or non-erodible polymeric systems including a discussion of solid nano- and micro-particles and capsules. The interesting survey of methods of site-specific drug delivery to the lung discusses the use of carriers as aerosols, liposomes, microspheres, erythrocytes and antibodies. There is a discussion of the use of polymers for the prevention of surgical adhesions, and a chapter containing general information on the regulatory process for a polymer implant from a point of view of a research scientist involved with the approved process of a drug delivery system. However, Quality Assurance and clinical trial processes are not discussed. The final chapter describes methods used to delivery drugs to the peripheral nerves, such as sustained site-specific systems of local anaesthetics constituted of either liquid or solid matrices.

There are not many books covering these topics in such an up-to-date manner by authors with first hand knowledge of their topics. In an age when cost effective medical and pharmaceutical practice is under the spotlight, there would be few health professionals not interested in site-specific pharmacotherapy.

D. L. MUNDAY

**Environmental Analysis**: R. N. REEVE, Wiley, Chichester, 1994. Pages: xx + 263, £19.50. ISBN 0-471-95134-X (hardback); 0-471-93833-5 (softback).

This new volume in the successful *Analytical Chemistry by Open Learning* series departs from the approach of the previous volumes in that it deals with a field of application of analytical techniques, rather than with a particular technique. It is, of course, a most important field these days, and this volume will certainly be of interest to many people who are not primarily chemists, but who nevertheless require to do some analyses in the course of their investigations.

Roger Neeve discusses transport of pollutants in the environment, then goes on to deal with water analysis, first for major, then for trace constituents. This enables him to survey the applicability of both chromatographic and spectroscopic techniques, but the reader is referred to other relevant volumes in the ACOL series for further details of the theory of these techniques. Analysis of solids—in particular of soils and sediments—is covered next, which permits some account of sample handling and pretreatment, both for inorganic and for organic compounds. Indeed, sampling crops up at various points as appropriate to each type of environmental material. The review of methods in air analysis is rather brief, but does cover the question of sampling as it relates to measurements of exposure of people at work. Particulates are dealt with separately, giving an excuse to mention a few more exotic techniques, such as X-ray spectroscopy and neutron activation, but there is a serious omission in that X-ray diffraction is absent. Finally, under ultra-trace analysis, GC-MS gets a balanced and informative discussion—it seems here, as in the other mentions of trace organics generally, that this is where the author is at home.

The ACOL house style necessarily leads to a certain amount of repetition of material to hammer the main points home, but in this case the space so used could have been much better employed giving a few real details: that the scallops for which analyses are reported in Fig. 2.4b (surely a Table, not a Figure) were exposed to spiked or contaminated seawater (p. 30), that the quick permanganate test for oxygen demand takes 10 min boiling (p. 62), that special glass electrodes should be used for low-conductivity river waters (p. 66), that temperature affects electrical conductivity of salt solutions markedly (p. 69), that EDTA, or CDTA, must be added to samples for the potentiometric determination of fluoride, so as to mask the trace metals (p. 83), and that $CS_2$ is the most appropriate solvent for trace organics by GLC when the FID is used (p. 103), to give some examples. So often the reader's appetite is whetted by what looks like becoming interesting but then the reader is left to hunger as the author has to go on to another topic.

There are a number of errors, especially in Chapter 2 such as the formula for DDT (p. 26). The axis in Fig. 3.1a has a wrong concentration scale for ions in seawater, and the method of oxidation of the organics in water does not affect the sensitivity of the TOC determination (p. 63) but the method of detection of the evolved $CO_2$ does. However, the book gets steadily better as it goes on, and I have to say that I enjoyed reading it, and will recommend it for students at a beginner's level who need to be introduced to the fascinating problems of applying analytical chemistry to real samples. This is, however, not a book for someone wanting to *do* some environmental analysis, but rather one for the arm-chair scientist who wants to think about it.

I. L. MARR

anticancer agents (SMANCS). A chapter is concerned with interstitial drug delivery to the brain using controlled-release polymers, overcoming the problem of the blood–brain barrier. There is also a discussion of the treatment of neurologic diseases by using biodegradable polymers as matrices for controlled delivery of neurotransmitters. There is an interesting review of developments related to the site-specific targeting of drugs to the bone marrow. As the authors point out, the ability to target colloidal drug carriers to bone marrow may hold promise for the improvement of cancer chemotherapy and radiotherapy. The subject of polymeric perivascular delivery systems is also addressed. Studies are described confirming the feasibility of using drug-eluting polymeric matrices placed around the adventitial surface of injured carotid arteries to evaluate the effects of specific drugs. Attention is also paid to techniques of localised cardiac administration of therapeutic agents, *e.g.* antiarrhythmic agents, and their potential for improving cardiovascular pharmacotherapies. Acute osteomyelitis, a serious bone infection, is very difficult to treat, and a chapter deals with drug delivery systems, such as carrier systems, that will ensure high local effects of effective antibiotics. The gastrointestinal tract also comes under scrutiny when physiological parameters crucial for the rational design of specific drug delivery are discussed. Some traditional and novel methods that target and localise drugs in the alimentary tract are reviewed. The description of drug delivery systems used in ophthalmology concentrates on solid erodible or non-erodible polymeric systems including a discussion of solid nano- and micro-particles and capsules. The interesting survey of methods of site-specific drug delivery to the lung discusses the use of carriers as aerosols, liposomes, microspheres, erythrocytes and antibodies. There is a discussion of the use of polymers for the prevention of surgical adhesions, and a chapter containing general information on the regulatory process for a polymer implant from a point of view of a research scientist involved with the approved process of a drug delivery system. However, Quality Assurance and clinical trial processes are not discussed. The final chapter describes methods used to delivery drugs to the peripheral nerves, such as sustained site-specific systems of local anaesthetics constituted of either liquid or solid matrices.

There are not many books covering these topics in such an up-to-date manner by authors with first hand knowledge of their topics. In an age when cost effective medical and pharmaceutical practice is under the spotlight, there would be few health professionals not interested in site-specific pharmacotherapy.

D. L. MUNDAY

**Environmental Analysis**: R. N. REEVE, Wiley, Chichester, 1994. Pages: xx + 263, £19.50. ISBN 0-471-95134-X (hardback); 0-471-93833-5 (softback).

This new volume in the successful *Analytical Chemistry by Open Learning* series departs from the approach of the previous volumes in that it deals with a field of application of analytical techniques, rather than with a particular technique. It is, of course, a most important field these days, and this volume will certainly be of interest to many people who are not primarily chemists, but who nevertheless require to do some analyses in the course of their investigations.

Roger Neeve discusses transport of pollutants in the environment, then goes on to deal with water analysis, first for major, then for trace constituents. This enables him to survey the applicability of both chromatographic and spectroscopic techniques, but the reader is referred to other relevant volumes in the ACOL series for further details of the theory of these techniques. Analysis of solids—in particular of soils and sediments—is covered next, which permits some account of sample handling and pretreatment, both for inorganic and for organic compounds. Indeed, sampling crops up at various points as appropriate to each type of environmental material. The review of methods in air analysis is rather brief, but does cover the question of sampling as it relates to measurements of exposure of people at work. Particulates are dealt with separately, giving an excuse to mention a few more exotic techniques, such as X-ray spectroscopy and neutron activation, but there is a serious omission in that X-ray diffraction is absent. Finally, under ultra-trace analysis, GC-MS gets a balanced and informative discussion—it seems here, as in the other mentions of trace organics generally, that this is where the author is at home.

The ACOL house style necessarily leads to a certain amount of repetition of material to hammer the main points home, but in this case the space so used could have been much better employed giving a few real details: that the scallops for which analyses are reported in Fig. 2.4b (surely a Table, not a Figure) were exposed to spiked or contaminated seawater (p. 30), that the quick permanganate test for oxygen demand takes 10 min boiling (p. 62), that special glass electrodes should be used for low-conductivity river waters (p. 66), that temperature affects electrical conductivity of salt solutions markedly (p. 69), that EDTA, or CDTA, must be added to samples for the potentiometric determination of fluoride, so as to mask the trace metals (p. 83), and that $CS_2$ is the most appropriate solvent for trace organics by GLC when the FID is used (p. 103), to give some examples. So often the reader's appetite is whetted by what looks like becoming interesting but then the reader is left to hunger as the author has to go on to another topic.

There are a number of errors, especially in Chapter 2 such as the formula for DDT (p. 26). The axis in Fig. 3.1a has a wrong concentration scale for ions in seawater, and the method of oxidation of the organics in water does not affect the sensitivity of the TOC determination (p. 63) but the method of detection of the evolved $CO_2$ does. However, the book gets steadily better as it goes on, and I have to say that I enjoyed reading it, and will recommend it for students at a beginner's level who need to be introduced to the fascinating problems of applying analytical chemistry to real samples. This is, however, not a book for someone wanting to *do* some environmental analysis, but rather one for the arm-chair scientist who wants to think about it.

I. L. MARR

**The Kirk-Othmer Encyclopedia of Chemical Technology: Volume 11, Fourth Edition, Flavor characterization to Fuel cells**: J. I. KROSCHWITZ and M. HOWE-GRANT (editors), Wiley, New York. 1994. Pages: xxviii + 1121. £185.00. ISBN 0-471-52680-0. (v. 11).

Volume 11 covers 26 topics—all beginning with the letter 'F'. It is dominated by almost 500 pages dealing with fluorine (the most electronegative and reactive element) and its inorganic and organic compounds. Details of the production, economic aspects and uses of fluorine are presented but most detail is reserved for the numerous compounds of this element. Indeed, bibliographies are given after each compound type, *e.g.* 84 references follow the section 'Fluorine compounds, inorganic (boron)' and similarly 124 references are given for the (calcium) section. Physical properties, chemical properties, manufacture, economic aspects, toxicity, uses, *etc.*, are all given. Fluorine polymers are well covered—PTFE, FEP, ETFE, PFA, PVF, PVDF, and PCTFE all have separate entries.

Those working in the food and consumer industries will also find this volume interesting as numerous topics relate to these areas. Chapters on food additives, food packing, food processing, nonconventional foods, and naturally occurring food toxicants are included. There are also related entries on flavor characterization, flavors and spices, and fruit juices. Although all entries are by necessity very factual I enjoyed discovering the names of the chemicals responsible for the flavor characteristics of substances such as caramel, chocolate, coffee, cognac, onion, popcorn, strawberry, *etc.* Details of individual spices were also of interest, *e.g.* the aroma of *Pimenta* berries resembles that of cloves, cinnamon, black pepper, and nutmeg, hence the name allspice or *quatre épices.*

Entries in this volume which are clearly of interest to chemical engineers include flotation, flow measurement, fluidization, fluid mechanics and fracture mechanics. Mathematical expressions, graphs, flow sheets and other diagrams are much in evidence for these entries.

The remaining contents include flocculating agents, fluorescent whitening agents, foamed plastics, foams, forensic chemistry, formaldehyde, fractionation (blood), Friedel-Crafts reactions and fuel cells. The section on forensic science is short, for example, the table of commonly encountered drugs of abuse could be extended, but the reader is directed to other parts of the encyclopedia for additional information and the entry is followed by a comprehensive bibliography.

As with all volumes so far published in this series the editors have produced an excellent collection of topics which is presented in a clear and logical manner. There is something here for chemists of all persuasions.

P. J. Cox

Pergamon

0039-9140(95)01451-9

*Talanta*, Vol. 42, No. 5, pp. 677–684, 1995

0039-9140/95 $9.50 + 0.00

# ELECTROCHEMICAL BEHAVIOUR OF SOME NATURALLY OCCURRING HYDROXY DERIVATIVES OF 9,10-ANTHRAQUINONE IN CHLOROFORM AT MERCURY AND GLASSY CARBON ELECTRODES: APPLICATION OF AC POLAROGRAPHY TO THE ANALYSIS OF RHUBARB ROOTS

M. H. POURNAGHI-AZAR,* F. SHEMIRANI and S. POURTORK

Electroanalytical Chemistry Laboratory, Faculty of Chemistry, University of Tabriz, Tabriz, Iran

(*Received* 25 *May* 1994. *Revised* 14 *October* 1994. *Accepted* 14 *October* 1994)

**Summary**—Electrochemical behaviour of some naturally occurring hydroxy derivatives of 9,10-anthraquinone such as chrysophanic acid (Ch), rhein (Rh) and emodin (Em) at mercury and glassy carbon electrodes using two different supporting electrolytes in chloroform is described. In the presence of piperidinium perchlorate (0.75*M*) + piperidine (0.25*M*) as a suitable acid supporting electrolyte, the reduction of Ch and Rh was a reversible two-electron process without complicating chemical reactions or adsorption phenomena, but the reduction process of these compounds in the presence of tetrabutylammonium perchlorate (TBAP) 0.5*M* + 5% acetic acid (AcOH) in chloroform was quasi-reversible. In both supporting electrolytes the overall reduction process of Em was irreversible. In the AC polarography and DP voltammetry at a GC electrode, the detection limit for Ch, Rh and Em was acceptably low and the relative standard deviation for the determination of $5 \times 10^{-6}M$ level, never exceeded 2%. AC polarography has been used for the determination of Ch and Em in a local rhubarb sample after extraction into chloroform and separation by column chromatography.

The hydroxy derivatives of 9,10-anthraquinone are of great importance in phytochemistry and pharmacy. Dock-flower, senna and rhubarb have all been used as oriental laxative medicaments owing to the presence of anthraquinones. Simultaneous determination of hydroxy derivatives of anthraquinone in some medicinal plants and pharmaceutical preparations has remained a problem in analytical chemistry for years. The earlier methods involved analytical methods, combined with separation procedures as TLC–spectrophotometry,[1] TLC–fluorimetry,[2] TLC–densitometry,[3] extraction–spectrophotometry,[4] and column chromatography–spectrophotometry.[5]

Because of the pronounced oxidation–reduction properties of anthraquinones, electrochemical methods are convenient for their determination. A few polarographic methods have been reported.[6,7] Most of these methods, suffer from a lack of sensitivity or specifity and are time-consuming and complex. Some methods based on HPLC reported recently[8,9] are relatively fast and selective.

On the basis of the results obtained from our previous studies on the electrochemical behaviour of quinones and anthraquinones in chloroform,[10–12] extraction AC and DP polarography in chloroform has been used for the determination of K group vitamins and anthracycline group anticancer drugs in pharmaceutical preparations.[13,14] In this manner, the AC method was used for the determination of 9,10-anthraquinone in paper samples and black liquors after their extraction into chloroform.[12] Extraction polarography for the determination of naturally occurring hydroxy derivatives of 9,10-anthraquinone seems to be fast and simple. On the other hand, in our analytical chemistry department, 1,8-dihydroxy 6,methylanthraquinone or chrysophanic acid (Ch), 1,8-dihydroxy 3,carboxyanthraquinone or rhein (Rh) and 1,3,8-trihydroxy 6,methylanthraquinone or emodin (Em), three principal anthraquinone derivatives in medicinal plants (Scheme 1) were recently separated by HPLC

*Author to whom correspondence should be addressed.

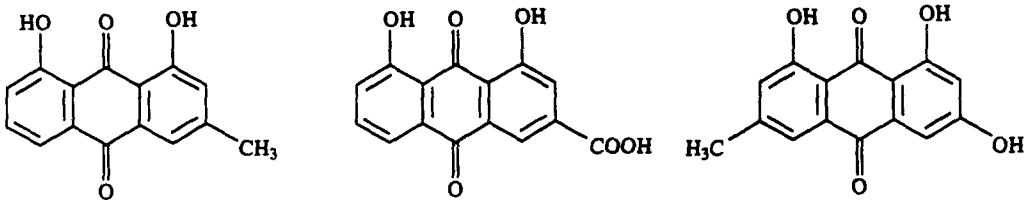

**Chrysophanic Acid** **Rhein** **Emodin**

Scheme 1

using chloroform–acetic acid (95:5) as mobile phase.[15] Therefore, the electrochemical detection of these compounds in HPLC seems to be possible. In this respect, the study of electrochemical behaviour of Ch, Rh and Em in chloroform at mercury and solid electrodes is desirable.

This paper presents the results obtained from polarography of Ch, Rh, and Em in chloroform in the presence of 0.75*M* piperidinium perchlorate (PP) + 0.25*M* piperidine (P) as a suitable supporting electrolyte[12] and voltammetry on a glassy carbon electrode in chloroform–acetic acid (95:5) + 0.5*M* tetrabutylammonium perchlorate (TBAP). An attempt is made to use AC polarography for the determination of Ch, Rh and Em in rhubarb roots.

## EXPERIMENTAL

### *Chemicals and reagents*

The solvent used was chloroform G.R from E. Merck or Fluka. Piperidinium perchlorate (PP) 0.75*M* + piperidine (P) 0.25*M* or tetrabutylammonium perchlorate (TBAP) 0.5*M* were used as supporting electrolytes. PP was prepared by gradual addition of the required amount of perchloric acid to a given volume of piperidine at room temperature. TBAP was purified by recrystallization from a mixture of water–acetone and drying at 60°C *in vacuo* for 24 hr.

Chrysophanic acid (Ch), rhein (Rh) and emodin (Em) were from Aldrich, other chemicals were P.A grade from E. Merck or Fluka.

### *Electrodes*

The reference electrode, Ag/AgI (satd), TBAI 0.05*M* and TBAP 0.50*M* in chloroform in separated compartments, was directly immersed in the reaction cell. It gave stable and reproducible potentials when evaporation was prevented and the solution was protected from light. The working electrode was mercury (DME and HMDE) or glassy carbon (GC) disk (0.062 $cm^2$ area obtained from Metrohm or 0.126 $cm^2$ from EG & G). The auxiliary electrode was a platinum wire.

### *Apparatus*

All voltammograms were recorded with a three electrode system. A multipurpose instrument from EG & G including; potentiostate/galvanostat model 273, Electrochemical Analysis Software 3.00 model 270 coupled with an IBM Personal computer and an Epson FX 850 printer were used. A rotating electrode system model 616 from EG & G was used for the voltammetric measurements at a rotating GC disk electrode A polarecord E 506 with E 663 stand, a function generator V.A. Scanner 610 from Metrohm and a X-Y Hewlett-Packard 3310-A recorder were used for AC polarography at DME and cyclic voltammetry at HMDE.

In all electrochemical experiments the test solution was deaerated by a stream of $N_2$ passing through chloroform.

### *Extraction of free anthraquinones from a local rhubarb sample (procedure I)*

Some free hydroxy derivatives of anthraquinone such as Ch, Rh and Em are soluble in chloroform and, therefore, can be extracted from medicinal plants as follows: about 0.05 g of powdered rhubarb root sample was weighted and placed in a 15 ml test tube. It was extracted with chloroform, shaken three times with 10,10 and 5 ml portions of chloroform (15 min each on a shaker), centrifuged in order to separate and the chloroform layers combined.

### *Extraction of anthraquinonic glycosides (procedure II)*

After extraction of the free anthraquinones (oxidized forms) from the sample, the residue was shaken three times with 10,10 and 5 ml portions of water–methanol (50:50) mixture (15 min each on a mechanical shaker) and the

residue separated by centrifugation. In order to hydrolyse the glycosides, the water–methanol phase was placed in a funnel equipped with a water cooler, 2.5 ml of conc HCl added, boiled for 20 min, cooled and transferred into a 100 ml separatory funnel. The released anthraquinones were extracted three times with 10,10 and 5 ml portions of chloroform, and the extracts combined.

*Extraction of total anthraquinones (procedure III)*

In order to hydrolyse and oxidize the glycosides and the reduced forms of anthraquinones, about 0.05 g of powdered sample was placed in a 15 ml test tube, and the procedure for anthraquinone glycosides followed, replacing 2.5 ml HCl with 2.5 ml HCl–40 ml $FeCl_3$ 10% (as an oxidizing agent). In this process the total anthraquinones were extracted into chloroform as their free oxidized forms.

*Identification of hydroxy derivatives of anthraquinone occurring in the rhubarb root sample (procedure IV)*

Using the chloroform layers obtained from the extraction procedures above for TLC, the sample spot was accompanied by spots of standard solutions of Ch, Rh and Em with a 2 cm interval, using TLC plastic sheets, silica gel 60 F 254 layer thickness 0.2 mm. The plate was developed for 10 cm in a mixture of cyclohexane and ethylacetate (60:40), dried at 100°C and the spots detected under UV light.

*Separation of the extracted hydroxy derivatives of anthraquinone by column chromatography (procedure V)*

Fifteen grammes of silica gel was placed in a beaker containing a mixture of hexane and ethylacetate (60:40) as mobile phase and this suspended silica gel entered in a column 20 cm long and 2 cm diameter with a stopcock and allowed to settle into a wet bed with a little liquid remaining above the surface. The stopcock was opened and the liquid level allowed to fall just to the top of the bed. The chloroform layers obtained from the extraction processes were evaporated on a water bath, and the residues dissolved in 2 ml of mobile phase, this solution was carefully pipetted onto the top of the bed. The mobile solvent reservoir containing about 60 ml of mobile phase was positioned and the flow of this phase started with a flow rate of 0.3 ml/min. The effluent solution was collected in a series of 20 fractions of 3 ml each, using a fraction collector they were grouped into two groups of 10 fractions by TLC. Combining the fractions of each group, the solvent was evaporated and the residues dissolved in 10 ml chloroform and transferred into the polarographic cell. The quantities of Ch and Em were determined by AC polarography using PP ($0.75M$) + P ($0.25M$) as supporting electrolyte.

## RESULTS AND DISCUSSION

*Electrochemical behaviours*

*On the mercury electrode.* In chloroform in the absence of an acid and with a convenient supporting electrolyte such as TBAP, the reduction of Ch, Rh, and Em at the DME gives one cathodic wave related to the semiquinone formation.[10] The wave nearly coalesces with the cathodic limit of the electroactivity range, therefore an accurate and quantitative measurement of this wave could not be made. The results obtained from DC and AC polarography, controlled potential coulometry and cyclic voltammetry showed that the reduction of Ch and Rh in the presence of $0.75M$ PP + $0.25M$ P as a suitable acid electrolyte[12] in chloroform was a two-electron, nearly reversible process. The overall reduction reaction of Em under the same conditions was irreversible, because the cyclic voltammetry of Em at the Hg electrode gave only one cathodic peak and the corresponding anodic peak was not discernable. These may be attributed to the formation of reduction product, dihydroemodin, containing five hydroxyl groups per molecule and insoluble in chloroform (see Introduction). The formulation of insoluble dihydroemodin in this medium has been confirmed during the controlled potential coulometry of Em. Typical example of cyclic voltammograms obtained at a scan rate of 100–800 mV/sec are shown in Fig. 1 and characteristic data of DC and AC polarograms are summarized in Table 1.

*On solid electrodes.* Current–potential curves for the reduction of $5 \times 10^{-4}M$ chrysophanic acid, rhein and emodin in chloroform–acetic acid (95:5) in the presence of TBAP $0.5M$, were recorded at GC, Pt and Au electrodes. Under these conditions, the studied anthraquinones were not reducible at Pt and Au electrodes. At the GC electrode with different rotation speeds, a single two-electron cathodic wave with a well defined limiting current was obtained (Fig. 2a). The height of the waves was linearly dependent

Table 1. Characteristic data of DC, AC polargrams and DC, DP voltammograms at 25 C

| Anthraquinones | $E_{\frac{1}{2}}$ (V) | S* | $E_p$ (V) | $\Delta E_{i_{p/2}}$† (mV) | $E_{\frac{1}{2}}$‡ (V) | $E_p$§ (V) |
|---|---|---|---|---|---|---|
| Ch | −0.175 | 31 | −0.168 | 52 | −0.01 | 0.026 |
| Rh | −0.240 | 29 | −0.232 | 52 | 0.112 | 0.076 |
| Em | −0.240 | 29 | −0.260 | 64 | 0.015 | −0.025 |

*Slope = $dE/d\log[(i_d - i)/i]$.
†AC peak width for $i = i_{p/2}$
‡$E_{\frac{1}{2}}$ of RDE voltammograms at GC electrode.
§$E_p$ of pulse voltammograms at GC electrode.

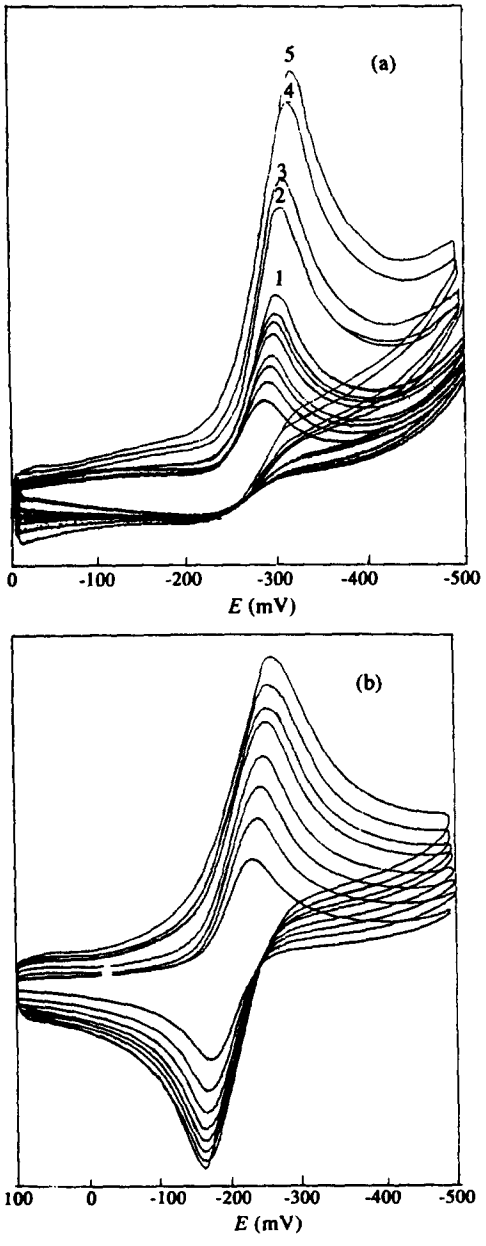


Fig. 1. Cyclic voltammograms of (a) 0.2 m*M* emodin and (b) 0.5 m*M* rhein at HMDE in chloroform solution of 0.75*M* PP + 0.25*M* P. Scan rates: 100–800 mV/sec, for rhein in 100 mV increments, for emodin (1) 100 (2) 400, (3) 500, (4) 700 and (5) 800 mV/sec.

on the concentration of the anthraquinones. This linearity confirms that the electrode process was mass transfer dependent. Plotting of $\log[(i_d - i)/i]$ against $E$, gave a straight line with a slope of 0.048, 0.048 and 0.068 V, respectively. The slopes obtained indicate that the reduction of Ch and Rh in this medium was a two-electron quasi-reversible process, but the reduction process of emodin tended to be irreversible.

Cyclic voltammetry of Ch and Rh at GC electrode produced one cathodic and anodic peak for each, but for emodin the corresponding anodic peak was not discernable. The values of $\Delta E = E_p^a - E_p^c$ for Ch and Rh at a low scan rate (<20 mV/sec) and with IR compensation were 55 and 56 mV, respectively. The $i_p^a/i_p^c$ ratio at a scan rate of 20 mV/sec was 0.75 which increased to unity at a scan rate of 2000 mV/sec. These confirm that an irreversible chemical reaction follows a quasi-reversible electron transfer reaction, note that the following chemical reaction is very fast in the case of emodin.

*Analytical application*

The results obtained from the studies on the electrochemical behaviour of Ch, Rh and Em at mercury and glassy carbon electrodes indicate that the electrochemical reduction of these compounds is quasi-reversible. These findings suggest the possibility of using polarography and voltammetry at a GC electrode for the determination of these compounds in chloroform in the presence of two different supporting electrolytes.

*AC and DP polarography.* AC polarography in the presence of PP (0.75*M*) + P (0.25*M*) gave a well defined two-electron reduction peak for each anthraquinone. The calibration graphs were linear over the range $10^{-6}$–$5 \times 10^{-5}$*M* Ch, Rh and Em. The detection limits with this method were 0.2, 0.1 and 0.8 μg/ml, respectively. The characteristic data of the AC polarograms are summarized in Table 1. From the data in the table it can be concluded that $\Delta E_p$ between Ch and Em, Ch and Rh are not large

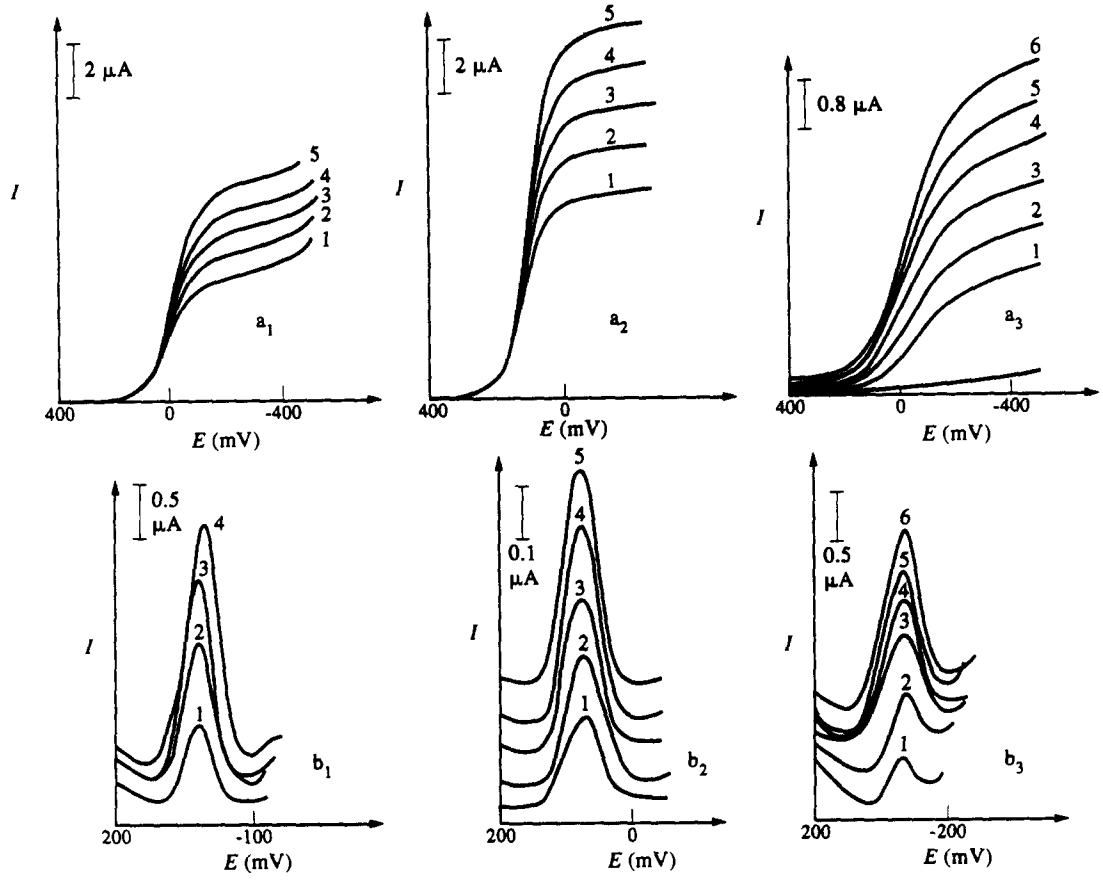


Fig. 2. Voltammetry of the anthraquinones in chloroform–acetic acid (95:5) + 0.5*M* TBAP at GC electrode ($A = 0.026$ cm$^2$). (a) Rotating disk voltammograms with rotation speed of 1000 rp/min. ($a_1$) Ch: 8, 9.1, 10.5, 11.9 and 13.3 × $10^{-5}$*M*, ($a_2$) Rh: 7.9, 9.1, 10.5, 11.9 and 13.3 × $10^{-5}$*M*, ($a_3$) Em: 5.4, 7, 8.6, 10.2, 11.7 and 13.1 × $10^{-5}$*M*. (b) Differential pulse voltammograms with pulse amplitude of 50 mV, pulse width of 60 msec, duration between pulses 1 sec, and scan rate 4 mV/sec: ($b_1$) Ch: 2.37, 4.72, 7.04 and 9.35 μ*M*, ($b_2$) Rh: 2.25, 2.68, 3.09, 3.5 and 3.91 μ*M*, ($b_3$) Em: 1.85, 3.64, 5.36, 7.01, 8.62 and 10.17 μ*M*.

enough to allow simultaneous determination of these compounds in a mixture. The assays in this connection remained unsuccessful.

The pulse polarograms recorded under the same conditions coalesced with the cathodic limit of electroactivity range and quantitative measurement of these peaks could not be made.

*DC and DP voltammetry at a GC electrode.* DC voltammetry at a rotating disk GC electrode revealed that the height of the waves was linear dependent on the concentration of the anthraquinones (Fig. 2a). The correlation coefficient of the calibration graph over the range 5 × $10^{-5}$–$10^{-3}$*M* was 0.999. The relative standard deviation for three determinations of 5 × $10^{-5}$*M* of the anthraquinones was about 1.5%. The detection limit for Ch, Rh and Em was 1.5, 1 and 5.7 × $10^{-5}$*M*, respectively. On the other hand, a well defined DP voltammogram was obtained for different concentrations of Ch, Rh and Em at a GC electrode in chloroform–acetic acid (95:5) + 0.5*M* TBAP (Fig. 2b). The calibration graphs were linear over the range $10^{-6}$–5 × $10^{-5}$*M* and the detection limit obtained at about 5 × $10^{-7}$*M* is acceptably low. The method may thus be used for the determination of anthraquinones in μg/ml concentration level. The relative standard deviation for the determination of $10^{-6}$*M* Ch and Rh was about 3%. The characteristic data of the DC and DP voltammograms are summarized in Table 1. From the data in Table 1 the $E_{\frac{1}{2}}$ and $E_p$ of Ch, Rh and Em are very close to each other and simultaneous determination of these compounds by DP voltammetry was not possible.

*Analysis of a local rhubarb*

*Determination of free anthraquinones.* AC polarography of 10 ml portion of chloroform layer obtained from the extraction of 0.027 g of the rhubarb root into 25 ml chloroform (procedure I) in the presence of PP (0.75*M*) + P (0.25*M*) as

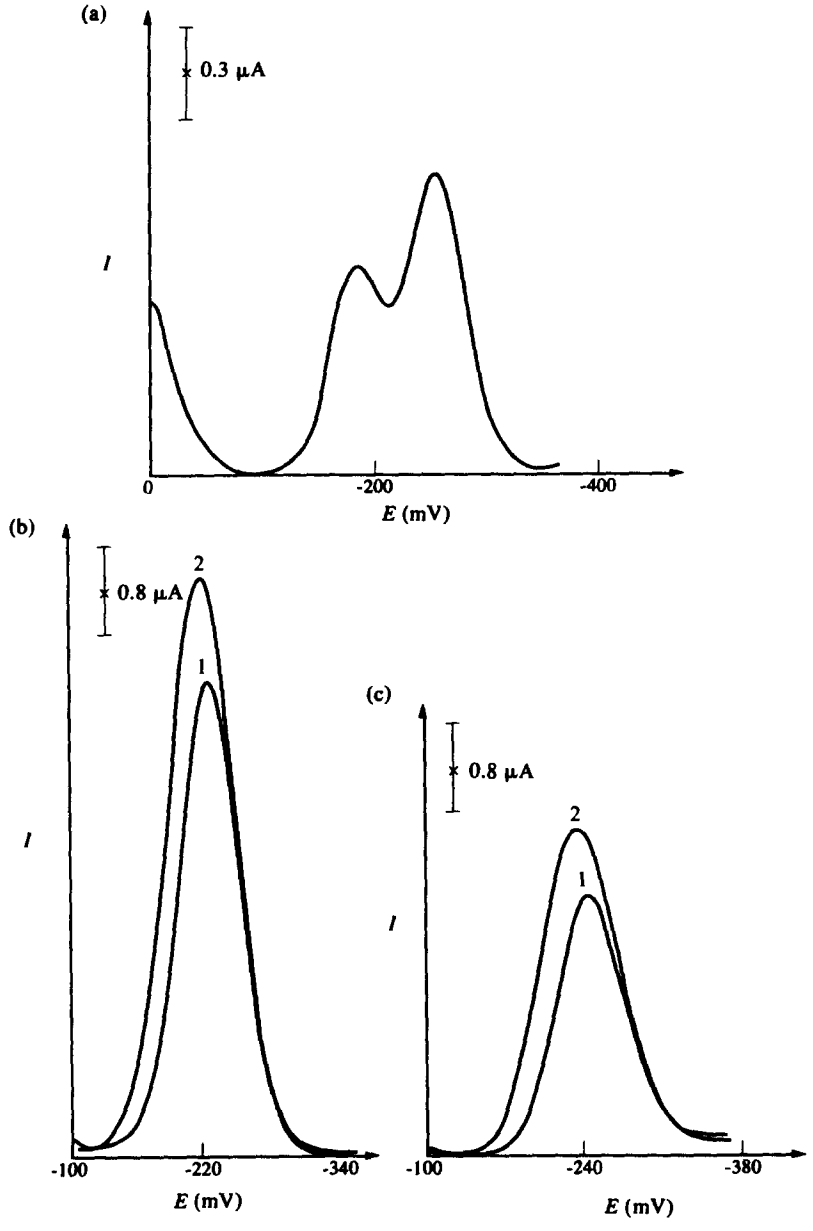


Fig. 3. Alternating current polarograms of (a) chloroform layer containing free anthraquinones obtained according to extraction procedure I for 0.027 g of a local rhubarb root sample into 25 ml chloroform, (b, c) combined fractions obtained from column chromatography (procedure V) for 0.067 g of sample, ($b_1$) Ch, ($c_1$) Em, ($b_2$) $b_1$ + 0.2 ml $5 \times 10^{-4}M$ Ch, ($c_2$) $C_1$ + 0.2 ml $5 \times 10^{-4}M$ Em. Supporting electrolyte was 0.75$M$ PP + 0.25$M$ P. $\underset{\sim}{V}$ = 10 m $V$, $f$ = 1 sec and $f$ = 75 Hz.

supporting electrolyte, presents two peaks with peak potentials very close to $E_p$ of Ch and Em under the same conditions (Fig. 3a). Addition of a standard solution of Ch or Em to the test solution augmented the height of the first or second peak, respectively. TLC of this chloroform layer confirmed that chrysophanic acid and emodin were the unique free anthraquinone

Table 2. Amounts* (percent in dried sample) of different forms of hydroxy derivatives of 9,10-anthraquinone in a local rhubarb root sample

| Anthraquinones | Total | RSD% | Free | RSD% | Glycoside | RSD% | Reduced |
|---|---|---|---|---|---|---|---|
| Ch | 0.57 | 2.5 | 0.14 | 3.1 | 0.04 | 3.8 | 0.39 |
| Em | 0.29 | 2.8 | 0.11 | 2.9 | 0.01 | 4.1 | 0.17 |

*Mean of three determinations.

Table 3. Recovery studies of the anthraquinones

| Spiked compounds | Spiked media | Spiked amounts | Procedure | Mean* recovery | RSD% |
|---|---|---|---|---|---|
| Ch + Em | Powdered rhubarb root | 9.1 mg | I, V | 99.8 | 1.8 |
| | | 25.2 mg | | 99.6 | 2 |
| Ch + Em | Methanol +water† | 9.3 mg | II, V | 99.8 | 2.3 |
| | | 27.1 mg | | 99.4 | 2.6 |
| Anthrone | Methanol +water† | 0.35 ml | III, V | 99.9 | 1.5 |
| | | | of 0.50 $\mu M$ | | |

*Mean of three replicate assays.
†Solvent used in procedures II and III.

components of the sample. A precise and simultaneous determination of Ch and Em was unsuccessful. Therefore, the components of the solution were separated by column chromatography according to procedure (V) and then determined by AC polarography using the standard addition method. Typical example of AC polarograms related to Ch and Em, extracted from 0.067 g of the rhubarb sample and separated by column chromatography are shown in Fig. 3b, c and the quantity obtained for each are summarized in Table 2.

*Determination of glycosides and total anthraquinones.* TLC of the chloroform layer obtained from extraction procedures II and III showed that the anthraquinones released during the acid hydrolysis of glycosides and oxidation of reduced forms were again Ch and Em. The chromatographic separation and AC polarographic measurement of the released anthraquinones were carried out in a similar manner as described for the free anthraquinones. The results are shown in Table 2.

*Recovery studies*

The extraction efficiency of the free anthraquinones into chloroform (procedure I) was investigated as follows: solid residue left from the extraction step was added to a polarographic cell containing a chloroform solution of PP (0.75$M$) + P (0.25$M$), in which the solubility of free anthraquinones is high. The mixture was stirred for about 20 min and allowed to settle. AC polarography of the solution showed that free anthraquinone was absent from the residue. This confirms the exhaustion of the sample during the extraction by chloroform.

In addition, the recovery of spiked powdered rhubarb samples with a known amount of pure Ch + Em was very close to 100%. Nearly 100% recovery of spiked extracting solvent of glycosides (water + methanol) with a known quantity of pure Ch + Em and anthrone (reduced form of anthraquinone) has been confirmed during the extraction by procedures II and III, respectively. We have also shown that the reduced forms of anthraquinones in the samples were not oxidized by dissolved oxygen in the solutions during the extraction steps according to procedures I and II. This study was carried out using anthrone as an available reduced form of anthraquinone. The results obtained from recovery studies are summarized in Table 3.

## CONCLUSION

On the basis of results obtained from DC and AC polarography, controlled potential coulometry and cyclic voltammetry, the reduction of Ch and Rh in the presence of PP (0.75$M$) + P (0.25$M$) in chloroform is a two-electron nearly reversible process, but the overall reduction reaction of Em was irreversible in this medium. The results obtained from rotating disk electrode and cyclic voltammetry at a GC electrode confirm that the reduction of Ch, Rh and Em in 5% AcOH + 0.5$M$ TBAP solution is a two-electron quasi-reversible process following an irreversible chemical reaction.

DC and AC polarography are directly applicable for the determination of Ch, Rh and Em in chloroform. From data in Table 1 it can be concluded that $\Delta E_{\frac{1}{2}}$ or $\Delta E_p$ between Ch and Rh, and Ch and Em are not large enough to allow determination of these compounds in a mixture. Therefore, the analysis of the mixture necessitates a preliminary separation by column chromatography. The AC polarographic method proposed in this work is suitable for the analysis of rhubarb roots.

The results obtained from differential pulse voltammetry reveal that this method may be used for the determination of Ch, Rh and Em at the $\mu$M/l level in chloroform. On the other hand, these findings suggest the possibility of using the amperometric measurement at the GC electrode for the electrochemical detection of the naturally occurring hydroxy derivatives of

9,10-anthraquinone during their analysis by HPLC using chloroform–acetic acid (95:5) as mobile phase (flow rate of 0.6–1 ml/min) and Spherisorb–CN as stationary phase. These are presently under investigation in our laboratory.

## REFERENCES


1. M. Kubiak, *Herba Poland*, 1977, **23**, 217.
2. K. Kobashi, T. Nishimara, M. Kusada, M. Hattori and T. Namba, *Planta Med.*, 1980, **40**, 226.
3. R. Dequeker, J. Lemli and J. Cuveele, *Planta Med.*, 1964, **21**, 51.
4. A. Hassoun and I. Turkovic, *J. Pharm. Belg.*, 1963, **18**, 259.
5. J. H. Zwaving, *Planta Med.*, 1972, **21**, 254.
6. R. Hiltunen and K. Savonius, *Acta Pharm. fenn.*, 1980, **89**, 37.
7. Zhang Xiugin, Xa Lixin and Yaowa, *Fenxi Zazhi*, 1984, **4**, 347.
8. G. Nanaka, M. Nishizawa and T. Yamagish, *Wakan Lyaka Gakkaishi*, 1985, **2**, 89.
9. H. Oshio, and N. Kawamura, *Shoyakugaku Zashi*, 1985, **39**, 131.
10. S. M. Golabi and M. H. Pournaghi-Azar, *Electrochim. Acta*, 1987, **32**, 425.
11. M. H. Pournaghi-Azar and S. M. Golabi, *Iran J. Sci. Technol.*, 1990, **13**, 37.
12. M. H. Pournaghi-Azar and S. M. Golabi, *Talanta*, 1988, **35**, 959.
13. M. H. Pournaghi-Azar and S. M. Golabi, *J. Pharm. Belg.*, 1987, **42**, 1464.
14. S. M. Golabi and D. Nematollahi, *J. Pharm. Biol. Anal.*, 1992, **10**, 1053.
15. D. Djozan and Y. Assadi, *Talanta*, in press.

Pergamon

0039-9140(95)01456-X

*Talanta*, Vol. 42, No. 5, pp. 685–692, 1995

0039-9140/95 $9.50 + 0.00

# ON-LINE PRECONCENTRATION AND SEPARATION OF PALLADIUM, PLATINUM AND IRIDIUM USING α-AMINO PYRIDINE RESIN WITH FLAME ATOMIC ABSORPTION SPECTROMETRY

P. Di and D. E. Davey*

School of Chemical Technology, University of South Australia, The Levels, S.A. 5095, Australia

(*Received* 18 *March* 1994. *Revised* 17 *October* 1994. *Accepted* 21 *October* 1994)

**Summary**—A flow injection on-line microcolumn method has been studied for the separation and preconcentration of noble metals, Pd, Pt and Ir, followed by flame AAS determination. An α-amino pyridine resin was used as preconcentration reagent. Non-noble metals studied could be eliminated by 2*M* HCl solution in the rinsing stage. A group-eluent for all Pd, Pt and Ir was studied. Separation of individual noble metals could also be accomplished using selective eluents. This approach can be used both for the separation and determination of Pd, Pt and Ir in samples. The sensitivities and the sample frequency have been improved. The method has been applied to certified samples.

The separation and determination of trace amounts of noble metals in mineral, metallurgical and environmental samples has been made difficult by the limited concentration of these metals in nature, and various interferences in both separation and determination methods. A preconcentration procedure is, therefore, often needed to increase concentration levels in analysed solutions and remove matrix interference. A number of organic extractants for the concentration and separation of noble metals have been studied by solvent extraction and paper and column chromatography.[1–6] Some chelating resins have been found more effective,[7,8] whilst cationic surfactants have also been investigated.[9] Efforts have also been made to improve determination methods of noble metals. For example, Lu *et al.* modified a tungsten wire with trioctylphosphine oxide (TOPO) to preconcentrate gold in waste water, then placed the wire in a graphite cup for direct atomic absorption spectrometry determination.[10] However, it is true to say that traditional preconcentration methods have been unwieldy, with large sample consumption (50–500 ml) and long preconcentration times (10–100 min per sample).[11,12]

On-line preconcentration techniques offer a way around these hurdles, and atomic absorption spectrometry (AAS) or inductively coupled plasma-optical emission spectrometry (ICP-OES) promise improved sensitive and rapid methods for trace element analysis by such means.[13–16] Recently, Taylor[17] and Qi[18] presented methods for gold analysis with on-line preconcentration AAS, the first by forming supported-liquid membranes, the second linking a functional group of a neutral phosphine oxide extractant to an inert fibre and then packing the fibre into a column. They reported that the sensitivity and analysis frequency were greatly improved using these techniques.

Compared with off-line preconcentration methods, an on-line method requires a fast concentration and elution reaction, which implies that highly selective reagents are needed in a continuous-flow system. In our previous work,[19] an organophosphorus compound, di(methylheptyl)methyl phosphonate (DMHMP), was studied as an on-line preconcentration reagent for gold with AAS analysis, the basis for the selection being the work of Li and coworkers.[20] These authors determined the selectivities of DMHMP for more than 50 metals with paper chromatography, and it was found that only Au and Tl could be fully retained by DMHMP. Following the lead given by Pohlandt and

*Author to whom correspondence should be addressed.

Table 1. AAS parameters used for the determinations of Pd, Pt and Ir

| Element | Wavelength (*nm*) | Slit (*nm*) | Lamp current (*mA*) | Flame type and flow rate (*l./min*) | Burner height (*mm*) | Aspiration rate (*ml/min*) |
|---|---|---|---|---|---|---|
| Pd | 246.7 | 0.2 | 5.0 | air (8.0)–acetylene (2.5) | 5.0 | 4.5 |
| Pt | 266.0 | 0.2 | 10.0 | air (8.0)–acetylene (2.0) | 5.0 | 4.5 |
| Ir | 208.9 | 0.2 | 20.0 | air (8.0)–acetylene (3.0) | 5.0 | 4.5 |

Steele,[21] we then designed a reverse-phase extraction column for an on-line preconcentration system with the DMHMP coated on macroporous resin beads. Both a single column and dual column system were found to give increased sensitivity. A computer program was also developed to control both the FIA preconcentration procedure and simplex optimisation of the system parameters, such as the column dimensions, the flow rates and the aspiration rate of flame AAS.[19]

In fact, as pointed out by Qi,[18] a number of preconcentration reagents are available for noble metals. Some neutral phosphine oxide and nitrogenous extractants have been found so effective for noble metals that their extraction constants are several orders of magnitude higher than those of competing elements.[22,23] However, if the affinity of noble metal with reagent is too strong, elution would become more difficult, a particular problem in an on-line operation. In such cases, to determine the noble metals, the resin containing the analytes has to be decomposed to prepare the analyte solution,[23] or alternatively, some strong acids have to be used in the elution.[8,21] Some reverse-phase extraction columns are not suited to this circumstance as a relatively weak physical adsorption exists between extractants and adsorbent resin beads, and the lifetime of the column would be affected by strong acid.

In the present study, an α-amino pyridine (AP) resin, formed by bonding a functional group of α-amino pyridine to a cross-linked polyphenylethene support, has been selected as the immobilized phase of the column. A similar on-line manifold to that previously designed by us for a Au study[19] has been employed to preconcentrate and separate the other noble metals, namely Pd, Pt and Ir. Eluents, both for the group of elements, and also for the individual metals were studied. The resin has performed well in both the preconcentration and elution stages for the noble metals analysed, flame atomic absorption spectrometry being used as the analysis method.

## EXPERIMENTAL

### *AAS determination*

The atomic absorption spectrometer used for all determinations throughout this work was a GBC 905 flame model instrument (GBC Scientific Equipment Pty Ltd, Australia). GBC hollow cathode lamps for Pd, Pt and Ir were used in the experiments. Peak areas computed by the software in the AA instrument were chosen for the measurements of Pd and Pt and peak height was chosen for the Ir determination. The graphs and data were printed with an Epson RX 80 printer (Epson Corporation, Japan). All backgrounds were corrected by the deuterium lamp. All instrumental parameters are summarized in Table 1.

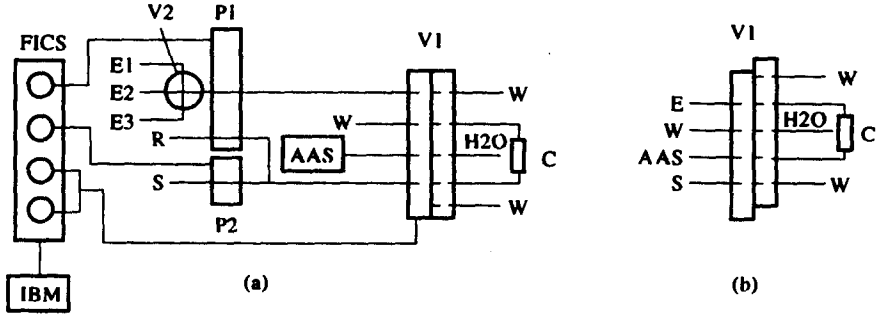


Fig. 1. The manifold used with on-line separation and preconcentration of Pd, Pt and Ir with AAS determination. (a) Preconcentration stage; (b) separation and elution stage. S: Sample; E, E1, E2, E3: eluent; R: rinsing solution; and W: waste.

*On-line preconcentration system*

The manifold of the on-line preconcentration flow injection system is shown in Fig. 1. It consists of two peristaltic pumps (an 8-channel multi-speed pump P1, Gilson, France, and a single speed pump P2, Mini-S 860, Ismatec, Switzerland), a pneumatic valve (V1, home-made) with a glass microcolumn (C), and a flow injection control system (FICS, home made) linked to an IBM computer. A four-way rotary valve (V2, Rheodyne Incorporated, U.S.A.) was also used to change eluent. Tygon pump tubes (2.06 mm i.d.) were used for all solutions and connected by Teflon connectors (Gradko, U.K.) to PTFE fine-bore tubing (0.8 mm i.d.).

A program allowing the time parameters to be entered into the computer prior to the run was developed to control the on-line preconcentration operations. Sixty seconds was chosen for the preconcentrations, and 20–30 sec was selected for the elutions.

*Reagents*

Stock solutions of Pd, Pt and Ir (each 1 mg/ml) were prepared using spectro-grade $(NH_4)_2PdCl_4$, $(NH_4)_2PtCl_6$ and $(NH_4)_3IrCl_6$ (Chemicals Co. Pty. Ltd, Tianjin, China). An α-amino pyridine (AP) resin (60–80 mesh, Institute of Polymer Chemistry, Nankai University, China) was employed as an immobilized phase. Buffer solutions were prepared from $KH_2PO_4$(AR) by NaOH addition. The other chemicals used in this work are all analytical grade.

*Column preparation and regeneration*

The AP resin contained in a beaker was washed repeatedly following the sequence, 6*M* HCl solution, deionized water, 6*M* NaOH solution, and then deionized water. The deionized water wash was continued until the effluent solution became neutral. One end of the glass column was first blocked with a small piece of plastic foam. The column was then filled with the AP resin. The other end of the column was again finally blocked with foam. The column dimensions were 3.5 mm (i.d.) × 10 mm (l); 10 ml 0.5*M* $Mg(ClO_4)_2$–0.5*M* $HClO_4$–0.5*M* HCl solution was used to regenerate the column.

## RESULTS AND DISCUSSION

*Preconcentration reaction*

Separation and concentration reagents most used for platinum metals and gold include organophosphorus,[1-3,18] sulfoxide[24] and thiourea derivatives,[8,25,26] and some nitrogen-containing compounds.[11,12,27] Most of them contain either a lone pair-bearing atom or a group readily protonated in an acidic solution, or both of these. Two mechanisms were proposed by Mojski[1] for the extraction of noble metal chloride complexes:

(a) solvation

$$MeCl_p^{(p-n)-} + m(R)_{(o)} = MeCl_n(R)_{m(o)} + (p-n)Cl^- \quad (1)$$

(b) ion-exchange

$$MeCl_p^{(p-n)-} + (p-n)(RH^+ \cdot Cl^-)_{(o)} = (RH^+)_{p-n}MeCl_{p(o)}^{(p-n)-} + (p-n)Cl^-, \quad (2)$$

where Me is a noble metal, R is an extractant or a resin, and o represents an organic phase or a resin phase.

In the first case, the reagent must have one or more co-ordinate atoms available to replace the chloride ligands from the central ion. In the second, the system requires an acid environment to protonate the organic reagent.

The α-amino pyridine (AP) resin selected in this study, contains a coordinating pyridine N and an amino group which easily associates with $H^+$ in acid solution. The structure of the AP resin with $AuCl_4^-$ has been discussed[28] and is given as follows:

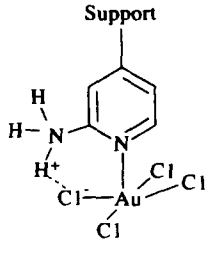


A similar mechanism may apply in the present study for $PdCl_4^{2-}$, $PtCl_6^{2-}$ and $IrCl_6^{3-}$. $[PdCl_4]^{2-}$ is either a planar,[29,30] or a bridged structure. Such bridged species are generally subject to cleavage by donors to give mononuclear species.[31] $PtCl_6^{2-}$ and $IrCl_6^{3-}$ are known to be octahedral complex anions.[31] During the preconcentration stage, the AP resin may form coordinate complexes with these anions by replacing the chloride ions with pyridine N linkages or form ion pair compounds by association through the chloride ions in the complex with the $—NH_3^+$, or both processes may happen at once, as with $AuCl_4^-$.

pH tests show that the recoveries of Pt and Ir are not effected significantly within the pH range 0–5, while the recovery of Pd strongly decreases

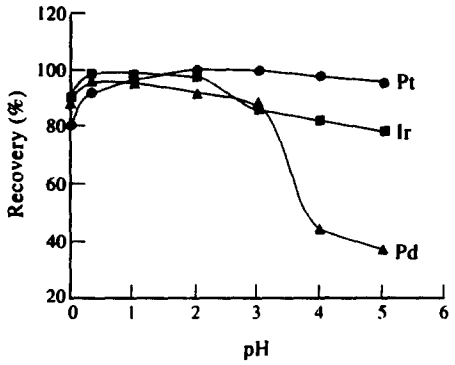


Fig. 2. Effect of pH on the preconcentration of Pd, Pt and Ir. The concentrations of solutions are 0.5 μg/ml for Pd, 1 μg/ml for Pt, and 10 μg/ml for Ir.

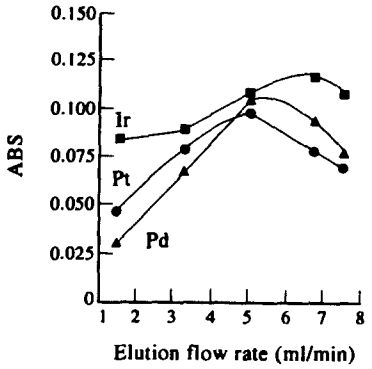


Fig. 4. Effect of elution rate on the determination of Pd, Pt and Ir. The flow rates were changed by altering the pump speed during the elutions. The same eluent, 0.5*M* $Mg(ClO_4)_2$–0.5*M* $HClO_4$–0.5*M* HCl, was used for three elements. Noble metal concentrations as in Fig. 2.

when pH > 2 (Fig. 2). Therefore, the reactions of platinum and iridium with AP resin appear to mainly conform to the solvation mechanism, while ion exchange may be involved in the preconcentration of palladium.

Figure 2 shows that recoveries greater than 90% were achieved for Pd and Ir when the pH was between 0.3 and 2. Pt showed similar recoveries in the pH range 0.3–5. In the experiment, the solutions to be analysed could be prepared in pH 0.3–2 solution for the preconcentration of Pd, Pt and Ir. Of course, the other interesting feature of this experiment is that pH 4–5 can now be chosen to partially eliminate Pd in the Pt and Ir preconcentration steps.

*Flow rates during sample introduction and elution*

Since a time-based sampling mode was used in the preconcentration stage, a faster sample flow rate may provide improved sample throughput through the column. However, analytes may not be efficiently preconcentrated on the column, and partly lost when the flow rate is too high. A sample flow rate of 6.4 ml/min using 2.06 mm (i.d.) pump tube was found optimal for the preconcentrations of all three elements (Fig. 3).

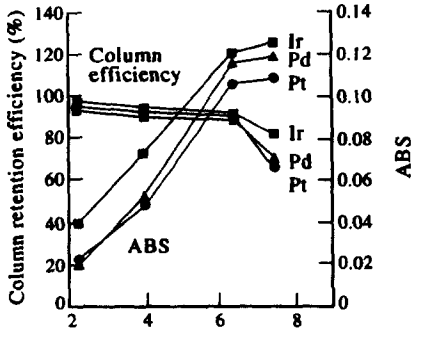


Fig. 3. Effect of sample flow rate on the column retention efficiency and absorbance for Pd, Pt and Ir. The column retention efficiency were obtained by measuring the concentrations of the solutions before and after their passing the column. See Fig. 2 caption for the concentrations of the metals.

The optimal elution rates of Pd, Pt and Ir were then determined, with a constant aspiration rate of 4.0 ml/min into the AAS. As shown in Fig. 4, Ir was relatively easy to elute and gave a higher absorbance at the elution rate of 6.8 ml/min, while the elution of both Pt and Pd was best carried out at the flow rate of 5.0 ml/min.

The fast sample and elution flow rates prove that the AP resin has performed satisfactorily during both the preconcentrations and the elutions. Firstly, a fast sample flow rate implies improved sensitivity, with good sample throughput; secondly, a fast preconcentration reaction provides the column with good retention efficiency for the selected analytes; and thirdly, a good tolerance of the resin for strong acid elution ensures a long lifetime for the column.

*The selection of eluents*

*Group elution.* Perchloric acid and solutions of perchlorate salts have been used to elute noble metals in off-line column preconcentration systems with similar reagents to that studied here.[28,32] In this study, $NaClO_4$ and $Mg(ClO_4)_2$ in HCl solution were investigated for Pd, Pt and Ir elutions. An unsatisfactory elution for Pt and high backgrounds in the three element determinations were, however, observed with $NaClO_4$ solution (Fig. 5a). $Mg(ClO_4)_2$ with 0.5*M* HCl solution was found effective in the elutions and gave a low background in the flame AAS determinations for the chosen noble metals

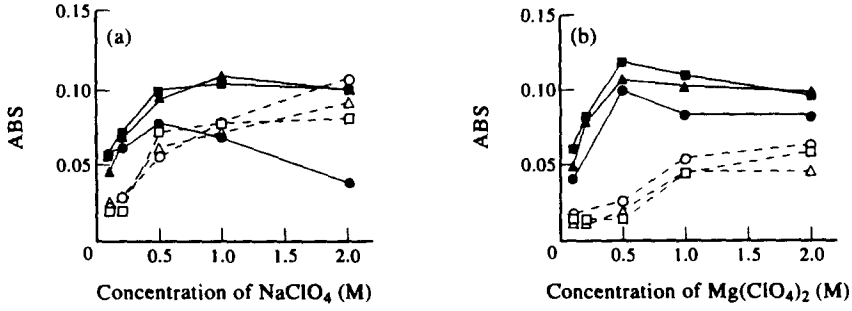


Fig. 5. Selection of the eluent for the Pd, Pt and Ir group. (a) 0.1–2.0*M* $NaClO_4$–0.5*M* HCl solution; (b) 0.1–2.0*M* $Mg(Cl_4)_2$–0.5*M* HCl solution. The dashed lines show the background absorption recorded during the determinations. [—▲— Pd; —●— Pt; —■— Ir; Background values - - - △ - - - Pd; - - - ○ - - - Pt; - - - □ - - - Ir].

(Fig. 5a, b). The better performance of the $Mg(ClO_4)_2$ solution can be attributed to its relatively low background in the flame, and in its ability to provide more $ClO_4^-$ (compared to a solution of $NaClO_4$), improving the overall metal elution. At a $Mg(ClO_4)_2$ concentration of 0.5*M*, even higher absorbances could be obtained but salt deposits occurred on the burner when the concentration of $Mg(ClO_4)_2$ was further increased. Thus, we chose to add 0.5*M* $HClO_4$ to the eluent to increase the $ClO_4^-$ concentration in the solution. A final solution of 0.5*M* HCl–0.5*M* $HClO_4$–0.5*M* $Mg(ClO_4)_2$ performed satisfactorily as the eluent for Pd, Pt and Ir. Figure 6 shows the elution curves of those elements determined individually using the flame AAS method. The procedure described should enable the simultaneous determination of the three noble metals listed using ICP-OES or multi-element AAS detection.

*Selective elutions.* Interferences between noble metals in their determinations by flame AAS may be of crucial importance, and thus efforts have been made to reduce such potential influences in determinations.[33,34] In this section of our work, selective elution for the metals has been studied to avoid any interference in determinations with the group eluent for samples with high concentrations of one or more noble metal.

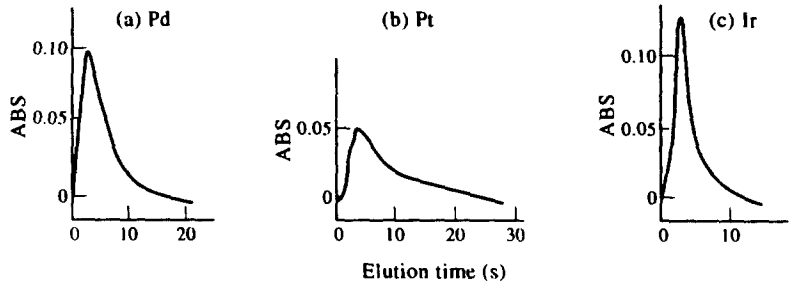


Fig. 6. Elution curves of Pd (a), Pt (b) and Ir (c) determined by FAAS. The eluent used was 0.5*M* HCl–0.5*M* $HClO_4$–0.5*M* $Mg(ClO_4)_2$ solution.

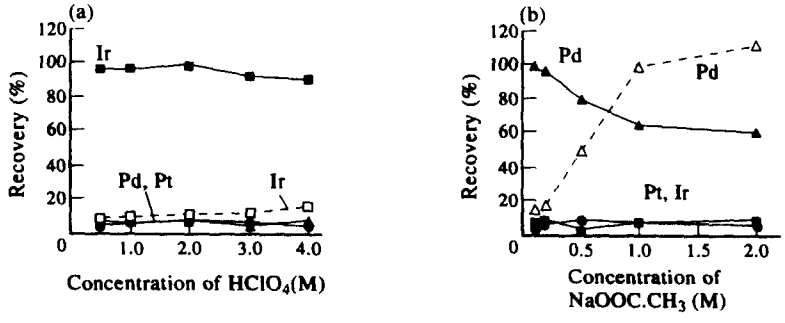


Fig. 7. Selection of the eluent for individual elements. (a) 0.5–4.0*M* $HClO_4$–4*M* HCl solution; and (b) 0.1–2.0*M* $NaOOC.CH_3$–0.5*M* HCl solution. The dashed lines show the relative absorption of the background against the analyte signal.

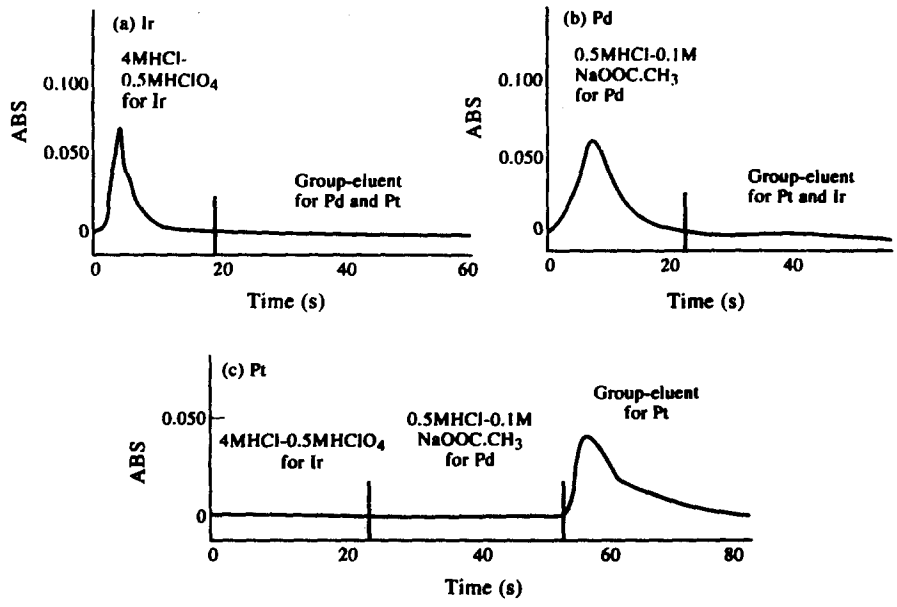


Fig. 8. Separation of Ir (a), Pd (b) and Pt (c) using selective eluents. The group eluent was 0.5*M* HCl–0.5*M* $HClO_4$–0.5*M* $Mg(ClO_4)_2$ solution.

0.5*M* $HClO_4$–4*M* HCl and 0.1*M* $NaOOC.CH_3$–0.5*M* HCl were found efficient for the Ir and Pd elutions, respectively. The performance of these eluents is shown in Fig. 7(a, b). The background absorption of eluents did not influence the determinations at the selected concentration of the eluents. The separation procedures for Pd, Pt and Ir, determined individually by flame AAS, are shown in Fig. 8(a–c).

In the cases of Fig. 8(a, b), Ir and Pd were the specific elements to be determined. They were eluted by their own selective eluents and determined at their characteristic wavelengths. Other metals of interest could be then eluted by the group eluent described earlier. Since no particular eluent had been found to be suitable for the Pt elution, the group eluent was used to elute that element (Fig. 8c). In this case, Ir and Pd had to be removed using the selective eluents prior to the Pt elution. No signal for Pt was detected during the Ir and Pd elutions.

*Separation of Pd, Pt and Ir with non-noble metals*

The influences of co-existing alkali, earth alkali and heavy metal salts in this system were investigated and the results are presented in Table 2. The non-noble elements studied could be washed off the column by 2*M* HCl solution prior to the elution of the noble metals. This separation step could be carried out for 20 sec or more in the rinsing stage of the system operation (Fig. 1a).

The recoveries of the noble metals were strongly influenced by iron in the solution at levels higher than 200 mg Fe/ml. This chemical

Table 2. Effect of the presence of salts on Pt, Pd and Ir recoveries

| Salt added | Concentration of added salt (*mg/l.*) | Recovery of the noble metals (%) Pt (5 *mg/l.*) | Pd (1 *mg/l.*) | Ir (5 *mg/l.*) |
|---|---|---|---|---|
| $KNO_3$ | 4000 | 98.5 | 103 | 97.4 |
| NaCl | 29,000 | 99.2 | 100 | 92.3 |
| $CaCl_2$ | 5000 | 110 | 105 | 101 |
| $MgSO_4$ | 6000 | 101 | 105 | 94.9 |
| $AlCl_3$ | 800 | 102 | 96.0 | 103 |
| $Fe(NO_3)_3$ | 100 | 93.8 | 95.5 | 105 |
| $CrCl_3$ | 480 | 111 | 103 | 103 |
| $NiSO_4$ | 280 | 104 | 101 | 93.6 |
| $Pb(NO_3)_2$ | 200 | 93.4 | 102 | 91.0 |
| $Cu(NO_3)_2$ | 400 | 94.1 | 108 | 106 |

Table 3. Comparison of detection limit (DL, $3\sigma$, μg/ml), relative standard deviation (RSD, %) and sample frequency for the described method with conventional measurement procedures

| | Pt | | Pd | | Ir | |
|---|---|---|---|---|---|---|
| Method | DL | RSD | DL | RSD | DL | RSD |
| Conventional FAAS | 0.51 | 4.5 | 0.062 | 4.8 | 0.97 | 6.4 |
| On-line method (this work) | 0.017 | 2.9 | 0.009 | 1.3 | 0.11 | 3.8 |

| | Sample flow rate (*ml./min*) | Sample frequency ($hr^{-1}$) | Preconcentration method used | Reference |
|---|---|---|---|---|
| On-line method | 6.4 | 36 | Column | This work |
| Off-line method* | 2.0 | 1–2 | Column | [12] |
| | NA | 3 | Static adsorption | [23] |
| | 2.5 | 0.5 | Column | [11] |
| | 1.5 | 4 | Column | [7] |

*The sample frequencies are estimated from preconcentration, desorption and determination procedures reported.
NA: Not applicable.

interference can be eliminated by adding 0.2*M* EDTA solution to complex most of iron in samples prior to the sample preconcentration stage.

*Comparison with conventional methods*

Direct flame AAS possesses low sensitivity for the determination of noble metals. The sensitivity can be improved by combining a preconcentration procedure with the determination.[8] Conventional preconcentration methods are, however, time-consuming since many manual operations are involved in an off-line sample introduction and eluate collection. The on-line preconcentration technique with computer control provides a much quicker and more precise method for noble metal analysis. Table 3 compares the detection limits, relative standard deviations and sample frequencies of the on-line technique and conventional methods.

*Sample analysis*

Pd, Pt and Ir were separately determined using group eluent in mixed composition samples and certified standard samples, containing $K^+$, $Na^+$, $Ca^{2+}$, $Mg^{2+}$, $Al^{3+}$, $Fe^{3+}$, $Cr^{3+}$, $Ni^{2+}$, $Pb^{2+}$ and $Cu^{2+}$, with metal to analyte ratios of 200–60,000. Pd and Pt in a certified ore sample were also determined using the group eluent. Solutions containing different levels of Pd, Pt and Ir were prepared using the certified standard materials and determined separately both with the selective eluents. The results are shown in Table 4. Non-determined noble metals (50 mg/l.)

Table 4. Determination of Pt, Pd and Ir from mixed composition samples and certified samples

| | Pt | | Pd | | Ir | |
|---|---|---|---|---|---|---|
| | Added | Found | Added | Found | Added | Found |
| Sample | (*mg/l.*) | (*mg/l.*) | (*mg/l.*) | (*mg/l.*) | (*mg/l.*) | (*mg/l.*) |
| Group elution | | | | | | |
| 1 | 0.20 | 0.21 ± 0.01 | 0.25 | 0.26 ± 0.03 | 2.00 | 2.1 ± 0.1 |
| 2 | 0.40 | 0.43 ± 0.02 | 0.50 | 0.48 ± 0.02 | 5.00 | 4.8 ± 0.2 |
| 3 | 0.80 | 0.78 ± 0.05 | 1.00 | 0.98 ± 0.04 | 10.0 | 10.5 ± 0.5 |
| 4 | 1.60 | 1.7 ± 0.1 | 1.50 | 1.5 ± 0.1 | 20.0 | 20 ± 1 |
| 5 | 0.22 | 0.19 ± 0.04 | 0.22 | 0.20 ± 0.05 | 2.00 | 2.2 ± 0.2 |
| 6* | 3.74 | 3.56 ± 0.08 | 1.53 | 1.49 ± 0.05 | 0.074 | UD |
| Selective elution | | | | | | |
| 7 | 0.40 | 0.37 ± 0.06 | 50.0 | ND | 50.0 | ND |
| 8 | 50.0 | ND | 0.50 | 0.53 ± 0.05 | 50.0 | ND |
| 9 | 50.0 | ND | 50.0 | ND | 2.00 | 2.3 ± 0.2 |

Samples 1–4 were prepared with the compounds mentioned in the experimental section and for matrices described in the text. Samples 5, 7–9 were prepared with certified standard materials, provided by Johnson Matthey, Materials Technology, U.K., with the same matrices as prepared for samples 1–4. Sample 6 is a certified ore sample, SARM 7, provided by South African Bureau of Standards (SABS), South Africa.
The results listed are the average values of six tests. Error estimates are appropriate standard deviation values.
*The concentration units of this sample were originally given in g/t, rather than mg/l. as given in the table.
UD: Under detection limit.
ND: Not determined.

were added to samples for the selective elution to test the efficiency of the elution process.

## CONCLUSIONS

On-line microcolumn preconcentration techniques have provided simpler, more sensitive and more rapid methods for the analyses of trace elements, being especially successful in heavy metal analysis. The reports concerning rare metal and noble metal analysis by this approach are, however, scarce because of the lack of appropriate preconcentration reagents.

In this study, an α-amino pyridine resin-packed microcolumn has performed satisfactorily for noble metal preconcentration and separation. Pd, Pt and Ir can be simultaneously retained on the column by adjusting the sample solution at pH 0.3–2 in the sampling stage, and then be eluted from the column using the group-eluent. Most non-noble metals studied do not influence the noble metal analysis and could be eliminated by 2*M* HCl during the rinsing stage. Separation of the noble metals could then be done by first adjusting the sample solution to pH 4–5, followed by elution for the individual element.

The use of an on-line flow technique and computer control meant that the analysis frequency was also increased compared to the conventional preconcentration method. The sensitivities and recoveries were satisfactory.

*Acknowledgements*—The authors express their gratitude to Professor L. Li for providing chemical reagents, and to the Department of Employment, Education and Training (Australia) for financial support for P. Di.

## REFERENCES

1. M. Mojski, *Talanta*, 1980, **27**, 7.
2. M. Mojski, *J. Radioanal. Chem.*, 1978, **46**, 239.
3. P. Tarapcik, *Radiochem. Radioanal. Lett.*, 1981, **49**, 353.
4. M. Mojski and K. Kalinowski, *Microchem. J.*, 1980, **25**, 507.
5. J. Rubeska, J. Kroeckova and D. Weiss, *Atom. Absorption Newslett.*, 1977, **16**, 1.
6. J. G. Sen Gupta, *Talanta*, 1993, **40**, 791.
7. X. Chang, X. Luo, G. Zhan and Z. Su, *Talanta*, 1992, **39**, 937.
8. X. Chang, Z. Su and G. Zhan, *Analyst*, 1994, **119**, 1445.
9. V. Otruba, M. Strnadova and B. Skalnikova, *Talanta*, 1993, **40**, 221.
10. G. Lu, J. Xu and T. Xu, *Talanta*, 1992, **39**, 51.
11. L. Li, L. Huang, X. Lin and F. Zhao, *Xiyou Jinshu*, 1986, **5**, 126.
12. L. Li, Y. Yan, X. Lin and Y. Yang, *Fenxi Huaxue*, 1990, **18**, 1035.
13. S. Olsen, L. C. R. Ressenda, J. Ruzicka and E. H. Hansen, *Analyst*, 1983, **108**, 905.
14. F. Malamas, M. Begtsson and G. Johansson, *Anal. Chim. Acta*, 1984, **160**, 1.
15. Z. Fang, S. Xu and S. Zhang, *Anal. Chim. Acta*, 1985, **169**, 321.
16. Z. Fang, J. Ruzicka and E. H. Hansen, *Anal. Chim. Acta*, 1984, **164**, 23.
17. M. J. C. Taylor, D. E. Barnes and G. D. Marshall, *Anal. Chim. Acta*, 1992, **265**, 71.
18. W. Qi, X. Wu, C. Zhou, H. Wu and Y. Gao, *Anal. Chim. Acta*, 1992, **270**, 205.
19. P. Di and D. E. Davey, *Talanta*, 1994, **41**, 565.
20. L. Li and P. Di, *Huaxue Shiji*, 1988, **10**, 8.
21. C. Pohlandt and T. W. Steele, *Talanta*, 1972, **19**, 839.
22. J. C. White and W. J. Ross, US At. Energy Comm. Rep., 1961, NAS-NS 3102.
23. L. Li, Y. Yan, K. Chen, X. Lin and Y. Yang, *Ion Exch. Adsorp.*, 1989, **5**, 426.
24. L. Li, Y. Sun, H. Ren and P. Di, *Chem. J. Chin. Univ. (Eng.)*, 1986, **2**(2), 79.
25. G. Koster and G. Schmuckler, *Anal. Chim. Acta*, 1967, **38**, 179.
26. A. Warshawsky, *Sep. Purif. Meth.*, 1980, **9**, 209.
27. C. Pohlandt and J. S. Fritz, *J. Chromat.*, 1979, **176**, 189.
28. L. Li, Y. Zhou and Z. Yin, *Fenxi Huaxue*, 1987, **15**, 297.
29. A. F. Wells, *Structural Inorganic Chemistry*, 3rd Ed., pp. 920–935. Clarendon Press, Oxford, 1962.
30. C. J. Ballhausen, *Introduction to Ligand Field Theory*, pp. 277–283. McGraw-Hill, New York, 1962.
31. F. A. Cotton and G. Wilkinson, *Advanced Inorganic Chemistry*, 5th Ed., pp. 900–937. John Wiley & Sons, New York, 1988.
32. R. D. Rocklin, *Anal. Chem.*, 1984, **56**, 1959.
33. A. Janssen and F. Umland, *Z. Anal. Chem.*, 1970, **251**, 101.
34. J. G. Sen Gupta, *Anal. Chim. Acta*, 1972, **58**, 23.

Pergamon

0039-9140(95)01457-8

*Talanta*, Vol. 42, No. 5, pp. 693–699, 1995

0039-9140/95 $9.50 + 0.00

# SPECIATION OF Cr(III) AND Cr(VI) AND SEPARATION OF COMMON ANIONS BY ION PAIR CHROMATOGRAPHY WITH *TRANS*-1,2-DIAMINECYCLOHEXANE-*N*,*N*,*N*′,*N*′-TETRAACETIC ACID

A. PADARAUSKAS* and G. SCHWEDT†

Institut für Anorganische und Analytische Chemie, Technische Universität Clausthal, Paul-Ernst Strasse 4, 38670 Clausthal-Zellerfeld, F.R.G.

(*Received* 11 *August* 1994. *Revised* 25 *October* 1994. *Accepted* 25 *October* 1994)

**Summary**—A reversed phase ion pair chromatographic method for the simultaneous determination of Cr species and common anions on a $C_{18}$-bonded stationary phase was developed by using acetonitrile-water (2:98 v/v) containing 1.0 m*M* tetrabutylammonium hydroxide and 0.5 m*M* *trans*-1,2-diaminecyclohexane-*N*,*N*,*N*′,*N*′-tetraacetic acid (DCTA) at pH 6.5 as mobile phase and UV-detection at 210 nm. Chromatographic parameters were optimized for separation of Cr(III)–DCTA complex, chromate and other anions. The detection limits were found as 8 ng/ml for Cr(III) and 35 ng/ml for Cr(VI). Under the optimum conditions, most other ions did not interfere. The method can be applied to separate a number of common anions simultaneously with the separation of Cr(III) and Cr(VI).

Chromium exists in the environment predominantly in two oxidation states, Cr(III) and Cr(VI). The toxicity of their compounds differs widely: the hexavalent state of chromium is more toxic than the trivalent state. Also, the trivalent state is necessary for the maintenance of normal glucose tolerance factor.[1,2] Therefore, it is important to establish an accurate, rapid and simple method for the determination of both chromium species.

Several methods for the speciation of chromium have been proposed, as shown in review articles.[3,4] In most of them only one Cr species is directly determined and the concentration of the other is calculated by substraction from the total Cr content, which is determined separately.

Some possibilities for separation of Cr species are co-precipitation,[5,6] ion-exchange,[7,8] or solvent extraction[9,10] followed by a spectrometric or electrochemical detection of Cr in the separated fractions. Both procedures are complicated and time consuming.

High-performance liquid chromatography (HPLC) is extensively applied to the determination and speciation of a number of metal ions. It provides several advantages over many other methods, as the separation, the identification and the quantitation of the different species down to trace concentration levels can be performed in one procedure. Schwedt[11] described a reversed-phase HPLC system with UV-detection for the separation and determination of Cr(III) and Cr(VI) by using different reaction products of Cr species with ammonium pyrrolidindithiocarbamate. The procedure is applied to the determination of both Cr species in waste water. Andrle and Broekaert[12] optimized this procedure by a modified simplex method.

Several papers have been published on the determination of Cr species using HPLC combined with atomic absorption spectrometric detection[13–15] and ion chromatography (IC) with direct current plasma emission[16] or chemiluminescence[17] detecton. However, when using hyphenated techniques, the interface usually complicates the operation procedure and the eluting condition is restricted by the detection mode.

An alternative to the traditional IC method is reversed-phase ion pair chromatography (IPC).

*Permanent address: Department of Analytical Chemistry, Vilnius University, Naugarduko 24, 2006 Vilnius, Lithuania.

†Author to whom correspondence should be addressed.

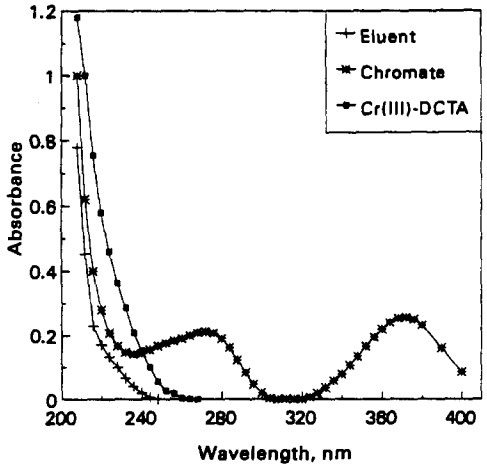


Fig. 1. UV-absorption spectra of Cr(III)–DCTA chelate, chromate and eluent. Chromium(III) and chromate concentrations, 0.1 m*M*.

In this method, a dynamic ion-exchange bed is created by the sorption of a hydrophobic counter ion (from a ion-pairing reagent) in the eluent on the stationary phase of a reversed-phase column.[18] In IPC many different parameters modify the retention of the solute and the selectivity of the separation. So it is more efficient and selective than IC and able to separate and determine inorganic, organic and complex ions.[19]

Usually, Cr(III) exists in a positively charged state and Cr(VI) in a negatively charged state. This can be simplified by converting Cr(III) to a negatively charged complex ion and then separating from Cr(VI). Aminepolycarboxilic acids are known for their ability to form highly stable metal complexes in a negatively charged state.[20] Jen *et al.*[21] used a reversed-phase IPC system with a $C_{18}$ column to determine Cr species based on the formation of a stable Cr(III) complex with ethylendiaminetetraacetic acid (EDTA). The interesting results obtained with this ligand suggest a possibility of using other aminopolycarboxilic acids. It is true that many metal complexes of 1,2-diaminecyclohexane-*N*,*N*,*N*′,*N*′-tetraacetic acid (DCTA) have larger stability than the complexes formed by EDTA.[22]

In this study, a reversed-phase IPC procedure based on the off-line DCTA chelation was developed for the simultaneous separation and determination of Cr(III), Cr(VI) and common anions.

## EXPERIMENTAL

### *Apparatus*

The HPLC instrumentation consisted of a high-performance liquid chromatographic pump L-6000 with a 100-$\mu$l injection loop, an UV/Vis detector L-4200 and a Chromato-Integrator D-2000 (Merck/Hitachi, Darmstadt, F.R.G.). The separation column used was Nucleosil $5C_{18}$ (250 × 4 mm I.D.) (Macherey-Nagel, Düren, F.R.G.). Absorption spectra were obtained by a model Lambda 2 UV/Vis spectrophotometer (Perkin-Elmer).

### *Reagents and solutions*

All chemicals used were of analytical reagent grade. Deionized water was obtained by passing distilled water through a Waters Milli-Q water-purification system. Stock solutions for Cr(III), Cr(VI) and other anions were prepared from inorganic salts in concentrations of 1 mg/ml. Analyte solutions [except Cr(III)] were prepared

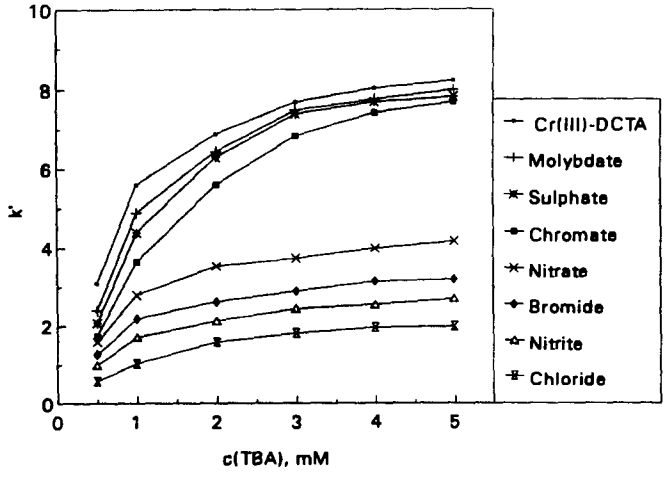


Fig. 2. Effect of TBA concentration on the capacity factor ($k'$). Eluent: acetonitrile–water (2:98 v/v) containing TBA and 0.5 m*M* DCTA, pH 6.5; flow-rate 1.0 ml/min.

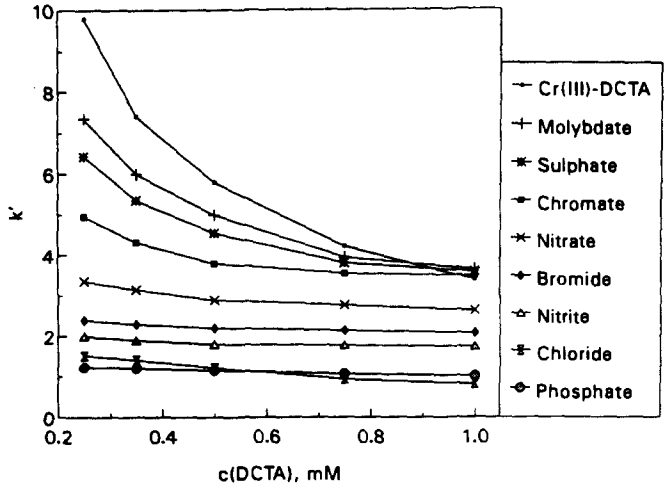


Fig. 3. Effect of DCTA concentration on the capacity factor ($k'$). Eluent: DCTA and 1 m$M$ TBA, other conditions as in Fig. 2.

daily by dilution of appropriate volumes of the stock solutions.

DCTA was obtained from Fluka (Neu-Ulm, F.R.G.), tetrabutylammonium hydroxide (TBA) from Merck (Darmstadt, F.R.G.). The acetonitrile used for mobile phase preparation was of HPLC quality (Merck, Darmstadt, F.R.G.). The mobile phase was prepared from acetonitrile, TBA and DCTA followed by pH adjustment with 0.1$M$ NaOH. All mobile phases were filtered through a 0.45 $\mu$m membrane filter and degased by stirring for 1 h under vacuum before use.

*General procedure*

The analyte solutions of Cr(III)-DCTA chelate were prepared in the following manner. To an aliquot of the solution containing $\leqslant 500$ $\mu$g of Cr(III) in a 25 ml calibrated flask were added appropriate [Cr(III)/DCTA molar ratio 1:5] volume of 5.0 m$M$ DCTA solution (pH 6.5). After heating in a water-bath at 60°C for 10 min, the solution was cooled to room temperature and diluted to the mark with water.

The formation of Cr(III)–DCTA complex was investigated by absorption measurements at 540 nm.[23] In all experiments the flow-rate of the mobile phase was 1.0 ml/min and samples of 100-$\mu$l volumes were analysed.

At least triplicate injections were made for each experiment. The relative standard deviations of capacity factors all of ions were less than 0.5%. The calibration graphs for Cr species were obtained by plotting the peak area against the concentration of the injected ion. The detection limits were obtained based on a signal-to-noise ratio of 3.

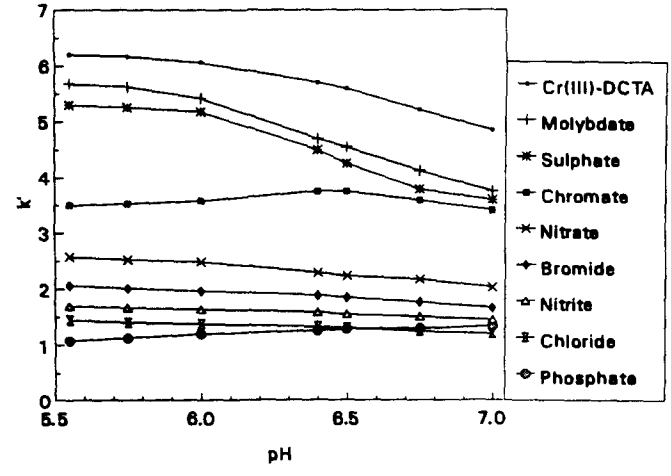


Fig. 4. Effect of eluent pH on the capacity factor ($k'$). Eluent: 1 m$M$ TBA, other conditions as in Fig. 2.

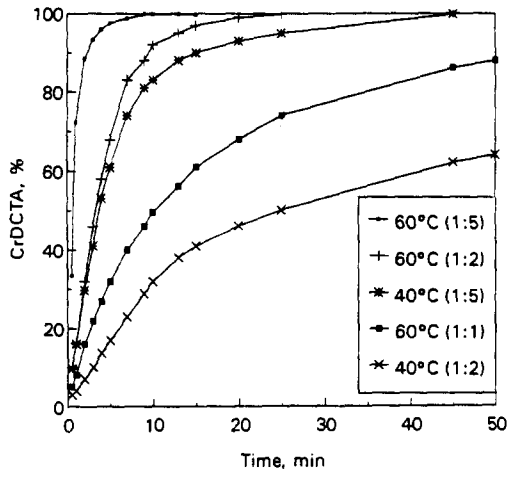


Fig. 5. Effect of temperature and Cr(III)/DCTA molar ratio on the rate of complex formation. All solutions at pH 6.5.

The building materials and leather extracts were prepared by shaking 0.200–0.500 g of the sample crushed with 20 ml of mobile phase or water for 6 hr. After addition of DCTA, heating and dilution as described above, the solutions were filtered through a 0.45 $\mu$m membrane filter and samples of 100-$\mu$l volumes were analyzed.

## RESULTS AND DISCUSSION

### *Absorption spectra of* Cr *species*

The UV absorption spectra of mobile phase containing 1 m*M* TBA, 0.5 m*M* DCTA and 2% acetonitrile (v/v) and both Cr(III) chelate with DCTA and chromate in the mobile phase against water as the blank are shown in Fig. 1. All solutions were at pH 6.8. Three absorption maxima of chromate were observed at wavelengths of 370, 272 and below 220 nm. The Cr(III)–DCTA complex does not absorb UV-light above 250 nm. Both Cr species are detectable at a wavelength range of 200–250 nm and the maximum of detection sensitivity is below 220 nm. In the present studies, a detection wavelength of 210 nm was used. This wavelength is suitable also for the direct detection of a number of anions (e.g. bromide, nitrite and nitrate) and indirect detection of anions, which have no absorption, such as chloride, phosphate and sulphate.

### *Effect of mobile phase composition*

It is important to choose mobile phase in optimizing separation of Cr species and other anions. Selection of the mobile phase concentration was based on not only resolution but also signal response and separation time: Mobile phases containing TBA concentrations ranged from 0.5 to 5.0 m*M* (Fig. 2). The results obtained show that all anions are more strongly retained with increasing amount of TBA in the mobile phase. But the change of the TBA concentrations has greater influence on the retention time in the lower range than in the higher range of the concentrations. The explanation of this fact can be the limited adsorption capacity of the stationary phase and/or the increasing concentration of phosphate with increasing TBA concentration. While the TBA concentration increases (up to 5 mM), the signal responses of all anions decrease.

Figure 3 shows the dependences of the retention on the concentration of DCTA in the mobile phase. For elution of inorganic anions and Cr(III) chelate with DCTA all capacity factors decreased regularly with increasing DCTA concentration. Thus with increasing DCTA concentration selectivity of separations and the signal response of directly detected anions [$NO_2^-$, $Br^-$, $NO_3^-$, $CrO_4^{2-}$, $MoO_4^{2-}$ and Cr(III)–DCTA] decreases. The elution sequence of some anions can be reversed by changing the DCTA concentration. With high concentrations the Cr(III)–DCTA complex was eluted before $MoO_4^{2-}$, $SO_4^{2-}$, $CrO_4^{2-}$ and $Cl^-$ before $HPO_4^{2-}$.

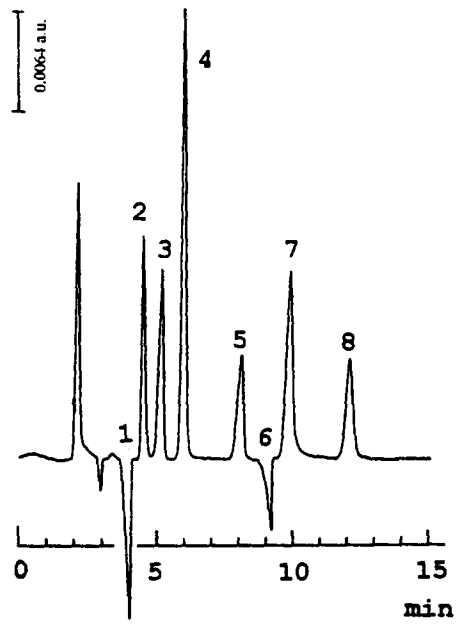


Fig. 6. Chromatogram of Cr species and common anions under the optimum conditions. Eluent: acetonitrile–water (2:98 v/v) containing 1 m*M* TBA, 0.5 m*M* DCTA, pH 6.5; flow-rate 1.0 ml/min. (1) $Cl^-$ (10 ppm); (2) $NO_2^-$ (0.25 ppm); (3) $Br^-$ (5 ppm); (4) $NO_3^-$ (0.5 ppm); (5) $CrO_4^{2-}$ (2 ppm); (6) $SO_4^{2-}$ (10 ppm); (7) $MoO_4^{2-}$ (2 ppm); (8) Cr(III) (0.5 ppm).

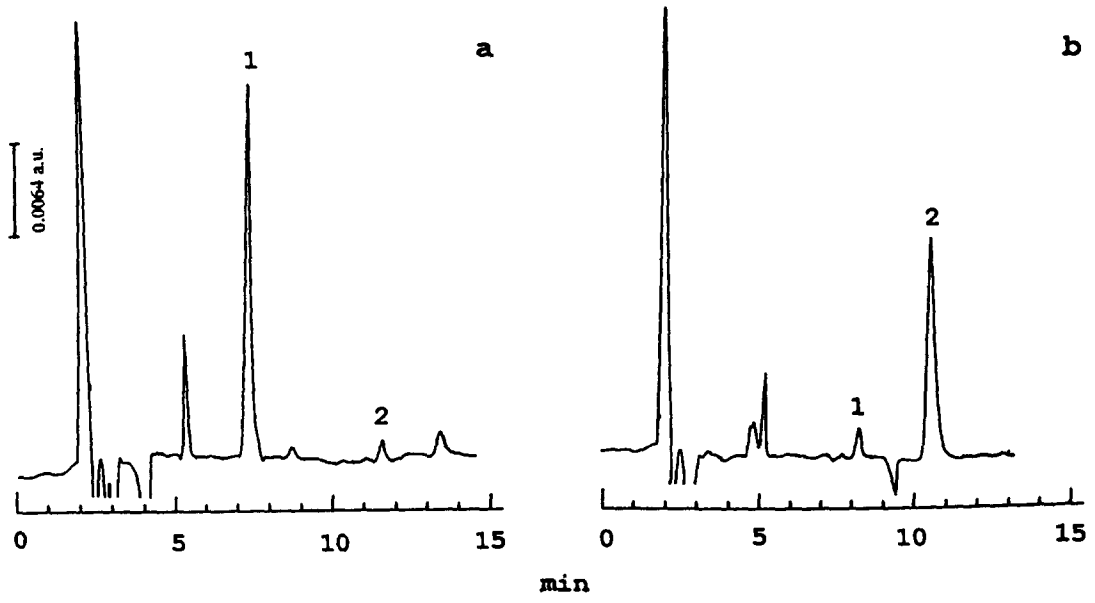


Fig. 7. Chromatograms of mortar (a) and leather (b) extracts with eluent. Condtions as in Fig. 6. (1) $CrO_4^{2-}$; (2) Cr(III).

*Effect of pH*

The active species of aminepolycarbonic acids as eluents are their anions, which depend directly on the pH of the mobile phase. The influence of pH on selectivity and retention of the Cr species and some inorganic anions were therefore systematically investigated. Results are shown in Fig. 4. In consideration of the stability of the silica-based stationary phase and the solubility of DCTA, pH of the mobile phase was adjusted to a certain value between 5.5 and 7. It can be observed that the capacity factors of some anions except $CrO_4^{2-}$ and $HPO_4^{2-}$ increase with decreasing the pH of the mobile phase. This fact can be explained by the decrease elution strength of mobile phase because of the protonation of the DCTA anion with increasing acidity [$pK_1$(DCTA) = 2.4; $pK_2 = 3.5$; $pK_3 = 6.1$ and $pK_4 = 12.4$). There are two species of Cr(VI) in neutral medium: $CrO_4^{2-}$ and $HCrO_4^-$ ($pK_2(H_2CrO_4) = 6.5$). With increasing acidity of mobile phase the equilibrium $CrO_4^{2-} + H^+ = HCrO_4^-$ moves to the right, *i.e.* the quantity of monocharged $HCrO_4^-$ ions increases. Competition of two contrary processes takes place in the system. Protonation of the DCTA anion increases the retention of Cr(VI). On the other hand with protonation of $CrO_4^{2-}$ ions their charge and retention at the same time decreases. In addition, with decrease of mobile phase pH dimerization of $HCrO_4^-$ ions to dichromate takes place because the signal response of Cr(VI) ions begins to decrease at pH < 6.5. The influence of pH has the same effect on the capacity factor $HPO_4^{2-}$.

*Formation of* Cr(III)*–DCTA complex*

Chromium(III) forms kinetically inert complexes and its chelation reactions are very slow.[22] Therefore, for speciation of Cr with DCTA, off-line derivatizing of Cr(III) is required. In addition, it is important for the analytical technique that all procedures last only a short time.

The ratio of complex formation depends on temperature, ligand concentration, pH and other parameters. Figure 5 shows the time necessary for complete formation of Cr(III)–DCTA complex at various temperatures and Cr(III)/DCTA molar ratio. All solutions were at pH 6.5. At room temperature this reaction happened very slowly. If the solution was warmed up to 60°C and Cr(III)/DCTA molar ratio was 1:5, it required only 10 min to complete the chelation.

Under these conditions the following experiments were carried out.

*Characteristics of* Cr *determination*

In order to test the applicability of the method for analysis of Cr species calibration graphs were constructed. Calibration graphs of peak area *vs.* Cr concentration were linear in the concentration ranges 0.1–20 μg/ml for Cr(III) and 0.2–20 μg/ml for Cr(VI) with correlation coefficients both above 0.998 ($n = 3$).

Table 1. Results of building materials and leather extracts analysis ($n = 3$)

| Sample | Element | IPC ($mg/g$) | R.S.D. (%) | Spectophotometry* ($mg/g$) |
|---|---|---|---|---|
| Brick (White) | Cr(VI) | 8.51 | 1.2 | 8.75 |
| | Cr(III) | 0.22 | 2.4 | 0.16 |
| Brick (red) | Cr(VI) | 11.2 | 0.9 | 11.6 |
| | Cr(III) | 0.28 | 2.5 | 0.23 |
| Mortar | Cr(VI) | 52.4 | 0.7 | 50.8 |
| | Cr(III) | 1.16 | 1.8 | 1.25 |
| Leather | Cr(VI) | 0.09 | 2.8 | 3.58† |
| | Cr(III) | 3.61 | 1.2 | |

*Spectrophotometry with diphenylcarbazide.[24]
†Total Cr with atomic-absorption spectrometry.[25]

The repeatability was examined with five injections of 2 $\mu$g/ml of each Cr species. The relative standard deviation for Cr(III) was 1.34 and for Cr(VI) −1.17%.

The detection limits were 8 ng/ml for Cr(III) and 35 ng/ml for Cr(VI), respectively. Because the method developed is to be applied for the speciation of Cr in water and other samples, possible interferences of concomitants were investigated. Moreover, the influence of Cr(III) species present on the determination of Cr(VI) was studied. Solutions containing Cr(III)–DCTA complex and chromate were analysed using the calibration function mentioned previously. It was found that excess of the other Cr species up to 20-fold caused no interferences to each other. The metals Ca, Mg, Ni, Cu, Co, Zn and Fe, which are often present in real samples, were added separately in concentrations of 10 $\mu$g/ml and no influences from them were found in the analysis results. A standard chromatogram of Cr species and other anions is shown in Fig. 6.

*Application examples*

The proposed method was applied to the simultaneous determination of Cr species in real samples. In the leather industry Cr(III) compounds are used as tanning agents. Building materials with a chromate additive have persisted at high temperature and are used for heat storage. Human skin often comes into contact with these materials and, therefore, determination of mobile Cr species in these samples is an important task. Figure 7 shows the chromatograms of mortar (a) and leather (b) extracts. The column used for the leather analysis (Fig. 7b) longer than that used for mortar analysis (Fig. 7a) and for the chromatogram in Fig. 6. Generally, with a longer column the retention times of the analyte ions are shorter. The influence of the column quality appears in the retention time of Cr(III) earlier than in that of other ions, therefore the retention time of Cr(III) in Fig. 7b is different from that in Fig. 7a or Fig. 6. The retention time of Cr(VI) ions differs only a little because of the same reason. The results of the determination of Cr species in building materials and leather extracts are shown in Table 1.

In conclusion, this IPC method is a simple and practical technique for the simultaneous determination of Cr(III), Cr(VI) and other anions in real samples.

*Acknowledgements*—This work was supported by the Stiftung Volkswagen, Hannover, F.R.G.

## REFERENCES

1. A. K. Mathur, S. V. Chandra and S. K. Tandon, *Toxicology*, 1977, **8**, 53.
2. U. Korallus, *Toxicol. Environm. Chem.*, 1986, **12**, 47.
3. C. Harzdorf, *Spurenanalytik des Chroms*, p. 122. Georg Thieme, Stuttgart, 1990.
4. P. MacCarthy and R. W. Klusman, *Anal. Chem.*, 1989, **61**, 269R.
5. R. E. Cranston and J. W. Murray, *Anal. Chim. Acta*, 1978, **99**, 275.
6. H. F. Zhang, J. Holzbecher and D. E. Ryan, *Anal. Chim. Acta*, 1983, **149**, 385.
7. J. F. Pankow and G. E. Janauer, *Anal. Chim. Acta*, 1974, **69**, 97.
8. K. Yoshimura and Sh. Ohashi, *Talanta*, 1978, **25**, 103.
9. K. S. Subrananian, *Anal. Chem.*, 1988, **60**, 11.
10. M. R. Midgett and M. J. Fishman, *At. Absorption Newslett.*, 1967, **6**, 128.
11. G. Schwedt, *Fresenius Z. Anal. Chem.*, 1979, **295**, 382.
12. I. Andrle and J. A. C. Broekaert, *Fresenius Z. Anal. Chem.*, 1993, **346**, 653.
13. I. S. Krull, K. W. Panaro and L. L. Gershman, *J. Chromatogr. Sci.*, 1983, **21**, 460.
14. K. E. Lawrence, G. W. Rice and W. A. Fassel, *Anal. Chem.*, 1984, **56**, 292.

15. A. Syty, R. G. Christensen and T. C. Rains, *At. Spectrosc.*, 1986, **7**, 89.
16. I. T. Urasa and S. H. Nam, *J. Chromatogr. Sci.*, 1989, **27**, 30.
17. H. G. Beere and P. Jones, *Anal. Chim. Acta*, 1994, **293**, 237.
18. R. Modin and G. Shill, *Talanta*, 1975, **22**, 1017.
19. A. V. Padarauskas, I. K. Stulgene, R. M. Kazlauskas and O. M. Petrukhin, *Zh. Anal. Khim.*, 1991, **46**, 1169.
20. R. Pribil, *Komplexone in der chemischen Analyse*, p. 474. VEB Deutscher der Wissenschaften, Berlin, 1961.
21. J. F. Jen, G. L. Ou-Yang, C. S. Chen and S. M. Yang, *Analyst*, 1993, **118**, 1281.
22. A. Ringbom, *Complexation in Analytical Chemistry*, Vol. 16, p. 395. John Wiley & Sons, New York, 1963.
23. A. R. Selmer-Olsen, *Anal. Chim. Acta*, 1962, **26**, 482.
24. L. Chuecas and J. P. Riley, *Anal. Chim. Acta*, 1966, **35**, 240.
25. K. Scot, *Analyst*, 1978, **103**, 754.

Pergamon

0039-9140(95)01468-3

*Talanta*, Vol. 42, No. 5, pp. 701–709, 1995

0039-9140/95 $9.50 + 0.00

# FACTORIAL DESIGN FOR THE RESPONSE EXPLORATION OF A FLOW INJECTION SYSTEM

A. MATOUSEK DE ABEL DE LA CRUZ, J. L. BURGUERA, M. BURGUERA and C. RIVAS

IVAIQUIM (Andean Institute for Chemical Research), Faculty of Sciences, University of Los Andes, P.O. Box 542, Mérida 5101-A, Edo. Mérida, Venezuela

(*Received* 3 *August* 1994. *Revised* 1 *November* 1994. *Accepted* 1 *November* 1994)

**Summary**—A factorial composite design was employed for the exploration of the response as a function of the flow rate and length of the dispersion coil of a flow injection system employed for on-line dilution and determination of copper by flame-AAS. For this purpose, an empirical response function (RF), which takes into account the peak height and the response time, was employed to evaluate the response. This RF was modified using the coefficient of variation in order to discriminate not only for high absorbance and adequate response time, but also for the best precision.

Flow injection (FI) has proved to be a convenient way of sample introduction for spectrometric techniques, owing to the possibility of handling small sample volumes under controlled conditions of dilution. However, often the difficult in controling the variability among the transient signals is one of the principal weaknesses of the technique in this case.[1-3] FI systems are generally characterized by complex interrelations between several factors, for example, the dilution of a plug of sample inserted in a continuous carrier stream is influenced by physical variables such as the injected volume, the flow rate, the geometry (size and orientation) of the mixing coils or dilution chambers employed, and if the analytical method involves other phenomena such as chemical reactions. Other important factors such as reagent concentration, pH, kinetics, etc., make the optimization a very complicated and time-consuming process.[1,3] Furthermore, if the FI system is coupled to the nebulizer of the flame burner, the competing fast aspiration flow introduces an additional source of variation.[4,5]

The optimization of analytical systems is carried out in order to find the combination of factors levels which maximizes the response. The traditional empirical univariate method of optimization involves varying each parameter in turn while keeping the others constant. This method has been applied to improve the behavior of analytical systems with varying degrees of success. However, in complex systems, such as the FI systems, in which the variables involved may not be independent of each other, this method may not be suitable owing to the convergence problems which may appear in some particular situations. In recent years, several methods for response surface modeling and prediction have been applied successfully to the optimization of flow injection systems such as the simplex and the Powell.[6-8] These methods are very useful for the optimization of flow and chemical conditions of flow injection systems, however, they offer little information about the nature of the response surface, and the experimental generation of this surface is needed as an aid to characterize the system.[6] Factorial optimization is a very fast method to find the conditions that maximize the response of system as long as the area of response surface studied presents only one maximum and the same is not located at the border of the surface.[9-13] There are several reasons for employing a factorial design instead of an univariate (one-at-a-time) design for system optimization, particularly when the experiment is carried out to test whether the response depends on a factor level. First, with the factorial design it is possible to detect and estimate any interaction among the factors involved which is not possible with an univariate design. Second, when the effects of the factors are additive, the factorial design requires fewer measurements, in order to obtain the same precision. Third, when the optimization involves more than one variable or factor, and the factors affect the response in an interactive fashion (the variables are not independent of each

other), the univariate method is unsatisfactory for achieving the optimum conditions.[10-13] Box and Wilson[14] added star designs (additional axial and center points) to $2^k$ factorials to form central composite designs which are useful for modeling response surfaces with a reduced number of experimental runs.

In this work we study the usefulness of a totally randomized factorial central composite design (a second factorial design augmented with a star)[10,13] as a tool for the rapid exploration of the response as a function of the flow rate and the length of the dispersion coil of a flow injection system for on-line dilution.

## EXPERIMENTAL

### *Apparatus*

A Varian atomic absorption apparatus model AA-1475 with deuterium lamp background corrector was employed as a detector. A Varian copper hollow cathode lamp was operated at 4 mA at a wavelength set to 324.6 nm and a spectral slit-width of 0.5 nm. Two peristaltic pumps, a Gilson (model Miniplus 2) and a Sage Instruments (model 375 A) were employed. A graduated 50 $\mu$l micro-syringe and a homemade septum injector were used for initial sample introduction. The suction air-pressurized device consists of a bottle with a pressure regulator up to 40 cm Hg and an Iwaki AP-115 air pump which produces the suction pressure. A Gralab 900 digital temporizer was used to control the operation time of a solenoid injector described elsewhere by Burguera *et al.*[15,16] PTFE tubing of 0.8 mm i.d. was employed in all the system, except for the injector valves where resistant and flexible Viton® tubing was employed. The loops of the dispersion coil had an i.d. of 1 cm. All the connections were made as indicated in Fig. 1.

### *Reagents*

A stock solution of Cu (10,000 mg/l.) prepared by dissolving 1 g of copper (Merck, 99.99%), in 15 ml of $HNO_3$ (1:1) (Merck, 65% Pro-Analysis), to a final volume of 100 ml, was employed for the dilutions. Deionized water was used throughout.

### *Manifold*

The flow injection manifold employed is represented in Fig. 1. The graduated dilution chamber with agitation has a maximal volume of 50 ml. The agitation is produced with a small motor at the top of the chamber. Valves (V1–V5) are controlled by the temporized solenoid injector.

### *Operation*

For the present work the flow system has two sets of tubing (set 1: $V_1$, $V_3$ and $V_5$; set 2: $V_2$ and $V_4$), which are used for regulating the flow of sample and carrier through the system. The doubly stopping shutter of the solenoid injector[15] either closed or opened any of these sets of tubing at a fixed time, thus allowing the sequential introduction of sample as described below. The sample volume was assessed by a procedure similar to that used earlier,[15] by the differences in weight over cycles of 50 injections.

The operation of the manifold is as follows: (1) 25 $\mu$l of concentrated copper solution (500–4000 mg/l.) are injected using the sample injection septum (I of Fig. 1); (2) the pump number 1 is operated for 3 min until the 25 ml mark is reached in the dilution chamber (flow rate of 8.3 ml/min), where the solution is constantly agitated; (3) the loading operation is performed by operating the solenoid injector for 2 to open and close the first and second sets of valves, respectively. In this way the sample fills the coil 1 by suction, while the carrier is pumped

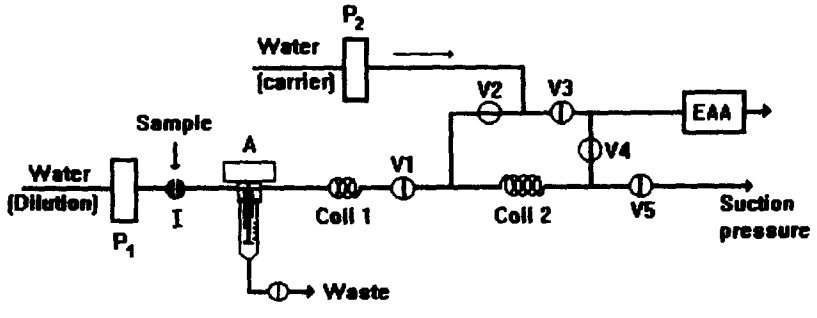


Fig. 1. Representation of the flow-injection manifold employed (A, dilution chamber with agitation; $P_1$ and $P_2$, peristaltic pumps; V1–V5 valves 1–5.

by $P_2$ to the spectrometer's nebulizer; (4) The sample introduction procedure is performed by activating the solenoid to the alternate position for 10 sec in order to pump the solution contained in coil 2 to the spectrometer's nebulizer; (5) The injection cycle is performed by the sequential alternation of both solenoid positions for periods of 0.8 and 10 sec. This allows the repetitive and reproducible intercalation of 120 $\mu$l in coil 2 and its transportation to the nebulizer by the carrier solution. By injecting 120 $\mu$l of sample volumes good precision and sensitivity were obtained. Besides, no overheating of the solenoid valve was observed when the solenoid activation time was of 0.8 sec, which was used to dispense this sample volume.

*Software*

The three-dimensional graph of the experimental surface was plotted with the aid of the Excel program (version 4.0; for Windows 3.1 of Microsoft). The statistical analysis of the factorial model for surface fitting and the plot of the estimated response function was realized with the aid of the Statgraph program (version 5.1, Statistical Graphics).

*Procedures*

*Response surface.* A three dimensional response surface (RS) was constructed from the data obtained by systematically varying the factors levels.[11] In order to elaborate the RS, a fixed volume (120 $\mu$l) of a 20 mg/l. copper solution was injected in the FI system at least 10 times in each set of conditions of carrier flow rate and dispersion coil length. The carrier flow rate was varied from 3.5 to 10 ml/min for each dispersion coils employed of 34, 50, 70, and 140 cm. An aspiration rate of 6.0 ml/min for the spectrometer nebulizer was kept constant throughout the experiment.

Firstly, the RS was constructed taking the average peak height absorbance. Secondly, the response was evaluated as a modified experimental target function similar to the one successfully employed earlier for this purpose. This response function (RF) is a linear combination of the peak height and residence time aimed to achieve the maximum sensitivity and sample throughput.[6,7]

$$\mathrm{RF} = k_1 H_n + k_2(1 - t_n), \qquad (1)$$

were $H_n$ and $t_n$ are the normalized values of the peak height and residence time, and the constants $k_1 = k_2 = 0.5$ give the same signification to both terms.[6]

The modified response function (MRF) employed in this work also takes into account the variability of the peak height absorbance measured in each set of experimental conditions. This is accomplished by dividing the RF calculated by the coefficient of variation (CV) of at least 10 consecutive measurements.

$$\mathrm{MRF} = RF/CV. \qquad (2)$$

This modification favors not only the conditions in which the maximum sensitivity and sample throughput are reached, but also the ones in which the precision is best. This function was employed in the construction of the experimental response surface and in the factorial design for surface fitting to the mathematical model from which the optimum values of the variables were derived.

*Univariate evaluation of the response.* The response was evaluated employing the univariate method. For this purpose, the response was evaluated for varying the coil length at a fixed flow rate. The coil length of maximal response was chosen from the curve obtained. Then the response was evaluated varying the flow rate from 3.5 to 10 ml/min.

*Factorial exploration of the response of the FI system.* The exploration of the response of a flow injection system (carrier flow and dispersion coil length) of the manifold represented in Fig. 1 was carried out using a second factorial design ($2^k$, $k = 2$ factors) augmented with a star design to form a second order composite design.[14] Composites or complete factorial require at least $2^k + 2k + 1$ experimental runs ($k$ = number of factors).[17,18] For the response surface fitting, an orthogonal two-factor central composite design with five center points was employed. The additional center points are used for the evaluation of the internal variation of the method.[10,13] The central composite design employed had four cube points, four axial points and five center points and an axial spacing of $\pm 1.2671$, for a matrix of 13 experimental runs which were carried out in a randomized way. The minimum ($-1$), maximum ($+1$), medium (0) and axial ($\pm 1.2671$) values of the factors codified in this matrix are presented in Table 1. The design expanded the run ranges from 3.5 to 8.5 ml/min for the carrier flow rate and from 34 to 224 cm for the dispersion coil length.

Table 1. Values of the factors codified in the factorial matrix

| | −1 | +1 | 0 | −1.2671 | +1.2671 |
|---|---|---|---|---|---|
| Carrier flow rate (*A*) (*ml/min*) | 4 | 8 | 6 | 3.5 | 8.5 |
| Dispersion coil length (*B*) (*cm*) | 55 | 205 | 130 | 34 | 224 |

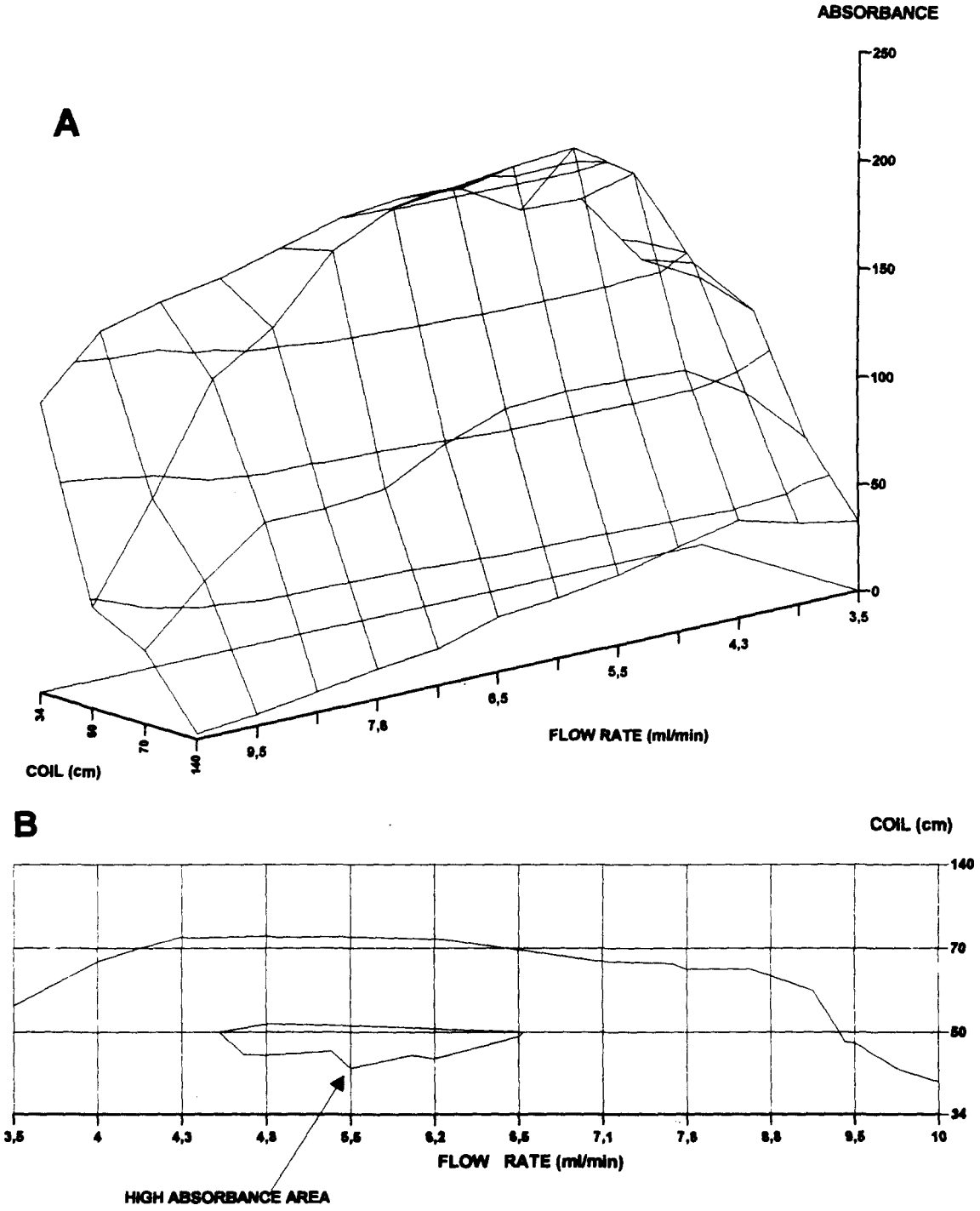


Fig. 2. (A) Three-dimensional plot of the peak height absorbance experimental response produce by the variation of the dispersion coil length *vs.* the flow rate. (B) Peak height absorbance contour surface plot showing the area of maximal response for the dispersion coil of 50 cm and flow rates between 4.5 and 6.5 ml/min.

## RESULTS AND DISCUSSION

### *Description of the experimental response*

The RS for the peak height absorbance surface and its contour surface are projection is presented in Fig. 2. The RS derived from the application of the RF to the absorbance and response time data is shown in Fig. 3, and the plot of the %CV vs. flow rate for the different coil lengths is presented in Fig. 4. The RS obtained from the MRF and its contour surface are shown in Fig. 5.

The RS for the peak absorbance (Fig. 2A) shows a flat maximal absorbance for the 50 cm coil over a wide range (Fig. 2B) of carrier flow rates (~4–6 ml/min) which apparently could indicate the possibility to chose among any of this flow rates without any adverse effects over the quality of the signal. Though the application of the RF (Fig. 3) discriminates the too-long and too-short response times, it did not changed the appearance of the surface in the area of maximal response. However, a study of the distribution of the %CV for the different flow rates and coil lengths (Fig. 4) suggests that the variation gradually increases with the flow rate and that it is very high for all the coil lengths at flow rates over 7.1 ml/min. The lowest variation appears to be related to the shorter coils (34 and 50 cm) and to moderate low flow rates of 4–6 ml/min. In fact, from the MRF surface (RF discriminated by the CV) shown in Fig. 5A, it is evident that the shape of the surface changes drastically, and from the MRF contour surface shown in Fig. 5B, the maximal response appears to be lying at the surface area which corresponds to a flow rate of around 5 ml/min and a dispersion coil of near 50 cm. However, in spite that the MRF yields an RS which gives an apparently better picture of the location of the maximal response (maximal absorbance, minimal variation and adequate response time), a more detailed description of the area of maximal response would be required in order to chose the optimum values of the parameters. This would require a considerable amount of experimentation with no guarantee of the successful location of the real maximal response.

### *Factorial optimization*

The factorial optimization of the FIA system performed gave the estimated regression

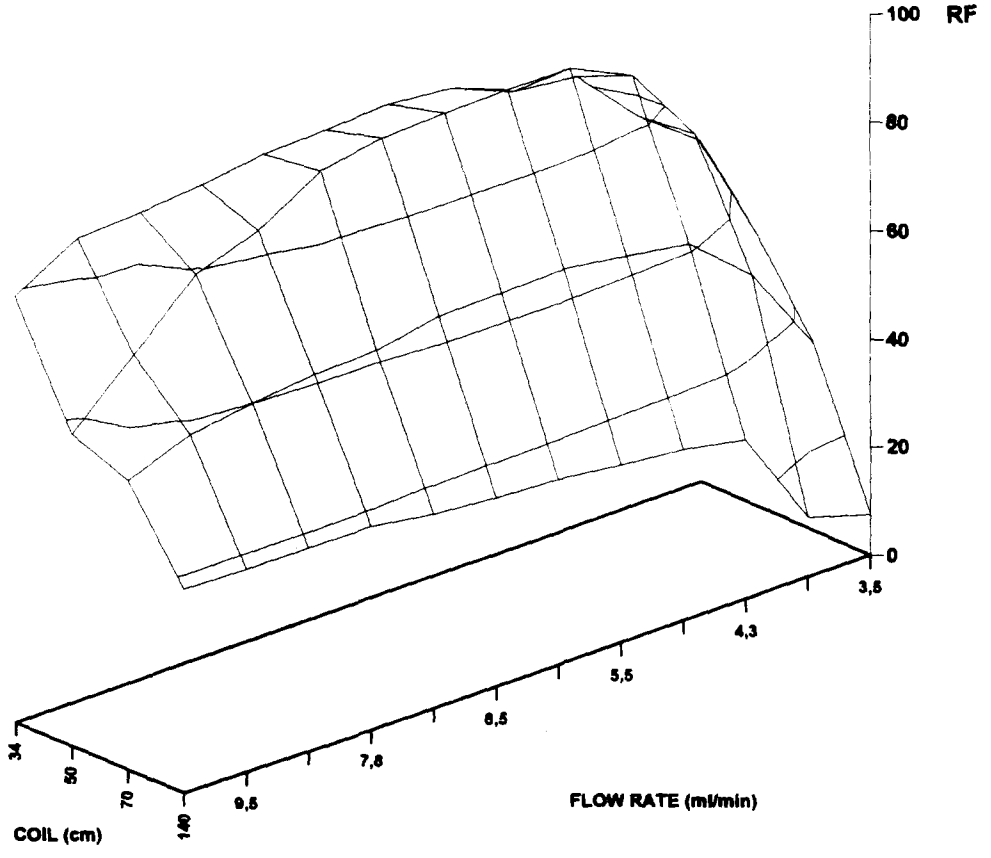


Fig. 3 Experimental response surface obtained from the empirical target function RF.

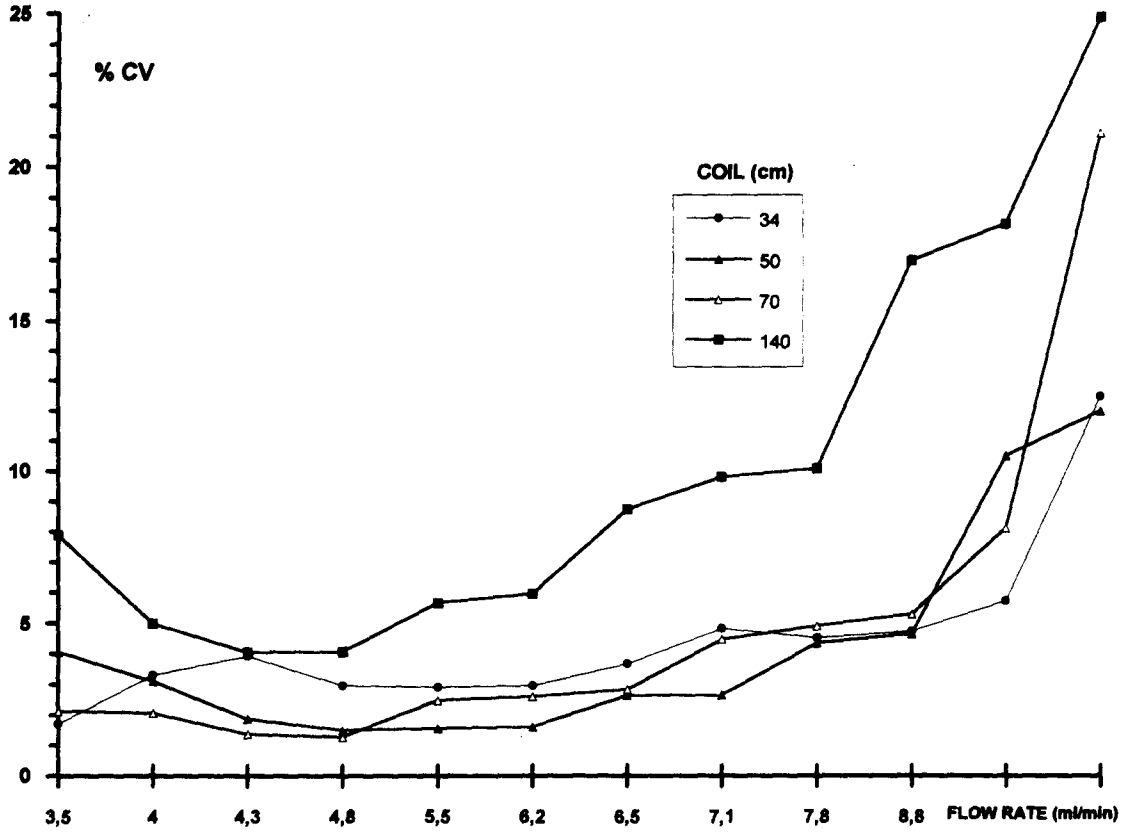


Fig. 4. Plot of % CV *vs.* flow rate. The minimal variation is observed for flow rates between 4.3 and 5.5 ml/min and dispersion coil length of 36 and 50 cm.

coefficients the second-order equation (equation 3) which describes the response as a function of the coded factor levels

$$Y = 53.01 - 11.16A - 15.82B - 22.05A^2 - 9.13B^2 + 8.69AB. \quad (3)$$

The analysis of variance (ANOVA) of the two-factor composite design is presented in Table 2. The sums of squares owing to the regression as a percentage of the total sum of squares was 99.9%, indicating that most of the variance is explained by the regression equation. The ratio of the sum of squares due to lack-of-fit and the sum of squares due to pure error is 0.35 (Table 2), a low value which indicates that the second order model is an adequate approximation to the data. The total error mean square of 0.3897 can be used as an estimate of the error variance. The square root of this value (0.6243) gives the standard deviation about the regression. Three times this value (1.87) indicates that there is a 99.7% probability that any single additional measurement within the region of interest would fall within plus minus 1.87 units of the predicted response. The adequacy of the fit was further evaluated analyzing the coefficients of the regression. First, the estimated variances of the individual coefficients were obtained by multiplying corresponding value of the principal diagonal of the $X'X^{-1}$ matrix by the residual mean square.[17,18] The square root of these variances provide the standard error of the estimates. The regression coefficients were then individually tested in order to determine if they were significantly different from zero. This was achieved by forming ratios of the coefficients to their standard errors to give $t$-values. The probability that the coefficient is not zero is equal to one minus twice the probability that a sample from a $t$-distribution should be at least as large as the observed $t$-value. The probability values observed of $>99.5\%$ in all indicate that all the coefficients would seem to be non-zero. This confirms that an adequate fit has been made.

The plot of the mathematically estimated response surface and its contour, using MRF as the target function, are shown in Figs 6 and 7, respectively. The predicted maximal response according to this model is 64.11, and its correspondent stationary or critical point are of

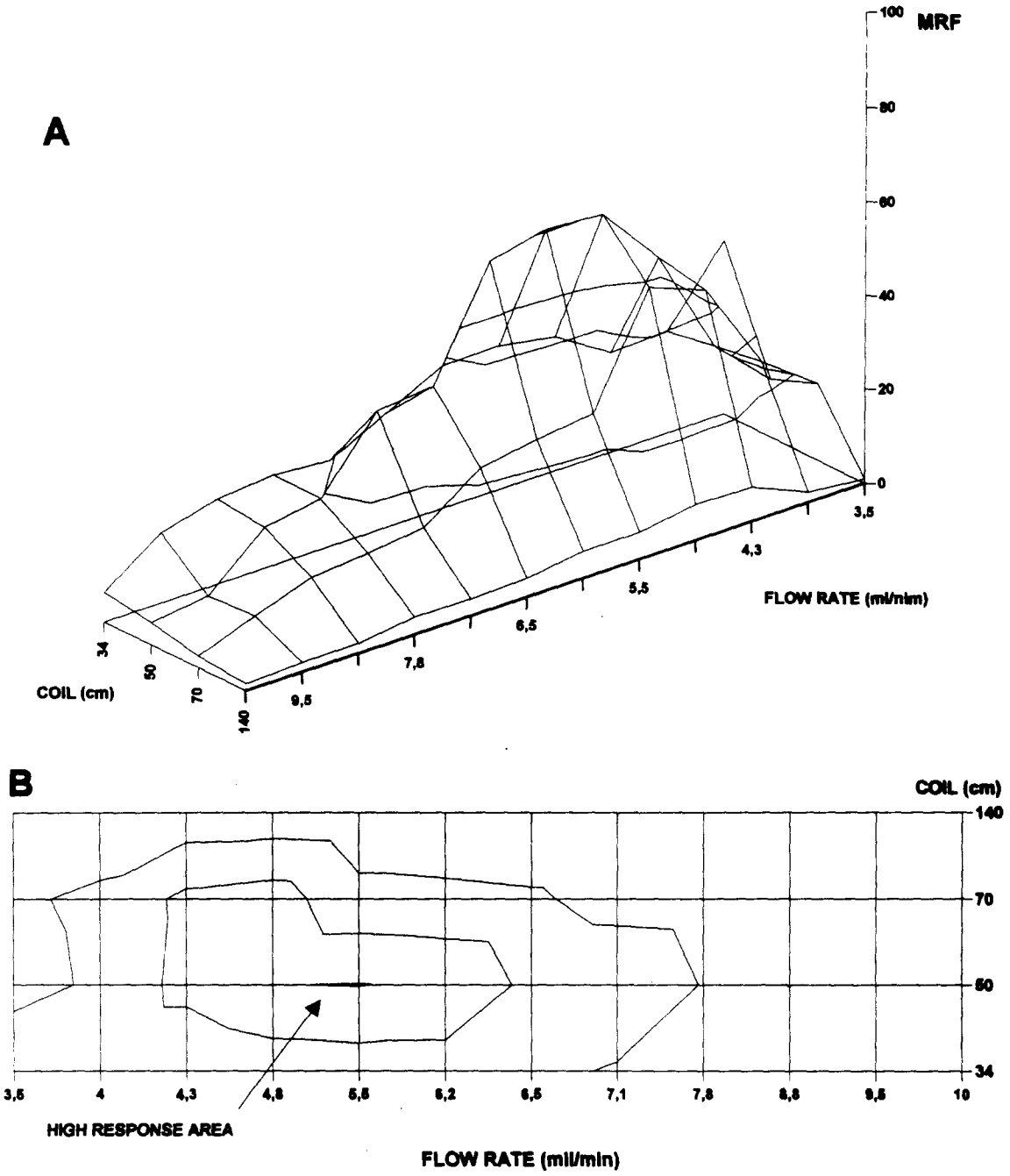


Fig. 5. (A) Response surface calculated with the modified target function MRF; (B) Contour map of the MRF response surface showing a narrower area of maximal response at flow rates between 4.8 and 5.5 ml/min.

$-0.4669$ for $A$ and $-1.0875$ for $B$. This maximal response was found by taking partial derivatives of the prediction equation with respect to each factor. These derivatives were equated to zero and solved for the factor levels. The optimal values of the factors predicted by this model are of 5.07 ml/min for the carrier flow rate and of 48.5 cm for the dispersion coil length. These values agree with the area of maximal response observed in the experimental response surfaces derived from the MRF (Fig. 5A and B). A comparison of the results obtained for the values of the dispersion coil and the flow rate with the factorial and the univariate methods is presented in Table 3.

Fixing the optimal conditions found for the FI system, an experimental response of 63.0 was observed for an injection of 120 $\mu$l of a solution

Table 2. ANOVA for the MRF–carrier flow rate–dispersion coil

| Effect | SS | d.f. | MS | *F*-ratio |
|---|---|---|---|---|
| Flow rate (*A*) | 898.90115 | 1 | 898.9011 | 2306.84 |
| Dispersion coil (*B*) | 1804.38032 | 1 | 1804.3803 | 4630.56 |
| *AB* | 301.88281 | 1 | 301.8828 | 774.72 |
| *AA* | 2507.49514 | 1 | 2507.4951 | 6434.95 |
| *BB* | 429.95485 | 1 | 429.9548 | 1103.39 |
| Total error | 2.72768 | 7 | 0.3897 | |
| Lack-of-fit | 0.7121 | 3 | 0.2374 | 0.35 |
| Pure error | 2.0156 | 4 | 0.5039 | |
| Regression | 5943.0368 | 5 | | |
| Total (coor.) | 5945.34986 | 12 | | |

*R*-squared = 0.9995.
*R*-squared (adj. for d.f.) = 0.9992.

of 20 mg/l. of copper (2.4 $\mu$g/injection), which is a 98.3% of the expected response. The low carrier flow of 5.07 ml/min (lower than the aspiration rate of 6.0 ml/min) agrees with the results reported by Fang and Welz.[8] They studied the effects of carrier flow rate and of the. aspiration rate over the peak height absorbance and found that (for injection volumes $\geqslant 100$ $\mu$l) lower-than-aspiration carrier flow rates improve the precision and the sensitivity in flow injection systems possibly due to an increase in the nebulization efficiency.

The characteristics of the calibration graph equation obtained after setting the conditions found (5 ml/min flow rate of carrier and 48.5 cm dispersion coil length) are described by the equation: $Y = 0.23 + 10.49X$ for an *r*-squared of 0.9999, where $Y$ represents absorbance and $X$ (5–60 mg/l.) represents the copper concentration. A coefficient of variation (CV) of 2.0% (from 1.5 to 2.4%) was obtained for 20 consecutive measurements of 20 mg/l. copper.

## CONCLUSION

The optimization of the carrier flow rate and the dispersion coil length of the FI system studied by the modification of the response surface, employing the MRF as the target function, yields the practical possibility to discriminate not only for the conditions of best sensitivity and residence times but also for the ones that minimize variation an therefore improve the precision. The factorial optimization of the system using this MRF is a tool which allows to find, in a rapid and efficient way, the optimum conditions for the maximal response. However, it must be kept in mind that the factorial method has several important limitations for its application, for example, when the maximal response is located at the border of the surface. In the particular situation studied, the maximum is located near the center of the experimental surface, and the modification of the RS by the MRF gives a roughly parabolic surface.

Table 3. Univariate *vs.* Factorial—Comparison of results

| | Method | |
|---|---|---|
| | Univariate | Factorial |
| No. of experiments | 20 | 13 |
| No. of measurements | 200 | 130 |
| Coil length of maximal response (*cm*) | 50 | 48.5 |
| Flow rate of maximal response (*ml/min*) | 5.5 | 5.07 |
| Maximal response | 60.0 | 64.14 |

## REFERENCES

1. J. L. Burguera (ed.), *Flow Injection Atomic Spectroscopy*. Dekker, New York, 1989.
2. J. F. Tyson, *Anal. Proc.*, 1983, **20**, 488.
3. J. Ruzicka and E. H. Hansen, *Flow Injection Analysis*, 2nd Ed. Wiley, New York, 1988.
4. E. A. Zagatto, F. J. Krug, F. Bergamin, S. S. Jørgensen and B. F. Reis, *Anal. Chim. Acta*, 1979, **104**, 279.
5. Z. Fang and B. Welz, *J. Anal. At. Spectrom.*, 1989, **4**, 83.
6. M. del Valle, M. Poch, J. Alonso and J. Bartroli, *Anal. Chim. Acta*, 1990, **241**, 31.
7. J. Alonso, J. Bartroli, J. Coello and M. del Valle, *Anal. Lett.*, 1987, **28**, 1247.
8. J. L. Montesinos, J. Bartroli, M. Poch, M. del Valle, J. L. F. C. Lima and A. N. Araujo, *Anal. Chim. Acta*, 1990, **234**, 67.
9. V. L. Anderson and R. A. McLean, *Design of Experiments*, p. 225. Dekker, New York, 1974.
10. G. E. P. Box, W. G. Hunter and J. S. Hunter, *Statistics for Experimenters; An Introduction to Design, Data Analysis and Model Building*. Wiley, New York, 1978.
11. J. C. Miller and J. N. Miller, *Statistics for Analytical Chemistry*, p. 175. Wiley, New York.

12. C. Liteneau and I. Rîkâ, *Statistical Theory and Methodology of Trace Analysis*, p. 365, Wiley, New York, 1980.
13. E. Morgan, K. Burton and P. Church, *Chemomet. and Intell. Lab. Syst.*, 1989, **5**, 283.
14. G. E. P. Box and K. B. Wilson, *J. R. Statist. Soc., Series B*, 1951, **13**, 1.
15. J. L. Burguera, M. Burguera, C. Rivas, M. De la Guardia and A. Salvador, *Anal. Chim. Acta*, 1990, **234**, 253.
16. P. Carrero, J. L. Burguera, M. Burguera and C. Rivas, *Talanta*, 1993, **40**, 1967.
17. G. E. P. Box, *Biometrics*, 1954, **10**, 16.
18. A. I. Khuri and J. A. Cornell, *Response Surfaces; Designs and Analyses*, p. 105. Dekker, New York, 1987.

Pergamon

0039-9140(95)01475-6

*Talanta*, Vol. 42, No. 5, pp. 711–715, 1995

0039-9140/95 $9.50 + 0.00

# DETERMINATION OF IRON AT ng/ml LEVEL BY SOLID PHASE SPECTROPHOTOMETRY AFTER PRECONCENTRATION ON CATION EXCHANGE FILTERS

F. CAPITÁN GARCÍA, RAMÓN CHECA, RAMIRO AVIDAD and L. F. CAPITÁN-VALLVEY*

Department of Analytical Chemistry, University of Granada, 18071 Granada, Spain.

(*Received* 11 *July* 1994. *Revised* 28 *September* 1994. *Accepted* 9 *November* 1994)

**Summary**—A cationic exchanger paper is used to retain analytes in solution and, after drying, to analyze directly by measuring the UV-Vis absorbance of the paper. The method was applied to determination of iron using its known 1,10-phenanthroline complex. Using 100 ml of sample the applicable concentration range was between 1.0 and 10.0 ng/ml with a detection limit of 0.2 ng/ml and a RSD around 2%. The method was applied to determination of iron total in snow, human serum and wine.

Preconcentration is not only an alternative to the use of sophisticated instrumentation in trace level analysis, but is also a previous step in the treatment of the sample before the measurement when the analyte to be determined is present in the sample at levels below the detection limits of the method.

The use of filters (cellulose, ion exchange resin loaded paper or PTFE, chelating paper, glass fiber, *etc.*) is a very elegant way to retain analytes and is often used as a preconcentration procedure. When the sample is concentrated by fixation on the filter it is usually desorbed with the aid of a reagent[1] or dissolved together with the filter, before making the measurements.[2] Another way is to make the measurement directly on the filter in order to combine preconcentration and measurement. The use of ion-collecting filters as a preconcentration step for analysis of water by X-ray spectrometric techniques has also been described in the literature.[3]

The direct measurement of luminescence properties allows the direct assay of substances in the solid-phase.[4]

UV-Vis absorption techniques used in connection with filtration systems are related to solid phase spectrophotometry (SPS).[5] Four main groups of applications are described in the literature:

(i) Use of finely divided ion-exchanger resin particles ($d \leqslant 30$ $\mu$m) to collect rapidly coloured analytes or reaction products and back coagulation by addition of suspensions of oppositely charged resin particles. The filtration of the coagulated resin through a filter paper and the measurement of the absorbance allows one to do the analysis.[6–9]

(ii) In some cases the desired coloured complex in the presence of ionic surfactants is collected onto a membrane filter and then determined directly on it.[10–11]

(iii) Separation by a membrane filter of the coloured complex sorbed with a finely dispersed ion exchanger and direct spectrophotometric measurement.[12]

(iv) The direct retention of a complex on a solid support. For instance, the strong retention of the Be(II)–Chromazurol B complex in a cellulose nitrate membrane filter in the presence of hexadecyltrimethylammonium bromide combined with SPS allows the Be analysis.[13]

The aim of this work was to use an ion-exchanger paper to retain a coloured complex by filtration and, after its preconcentration, to analyze it directly on the same filter by SPS. To the best of our knowledge the retention of analytes or reaction products on ion-exchanger paper through filtration and direct determination has not been reported.

As a model system we have selected the well known Fe(II)–1,10-phenanthroline system,

*Author to whom correspondence should be addressed.

applying it to the analysis of both Fe(III) and Fe(II) in samples from several provenances.

## EXPERIMENTAL

### *Apparatus and software*

All spectrophotometric measurements were performed with a UV-Vis Beckman DU-8B spectrophotometer. A pellet holder (ref. MD-OZ) from an IR spectrophotometer Beckman IR 4240 was used as a support for the filter paper disk. A Crison 501 digital pH-meter with a combined glass-saturated calomel electrode and a vacuum pump (Edwards model ED 100) were used.

We used a 47 mm glass filter holder Millipore (ref. XX1004700) taking advantage of a ring-shaped metachrylate plug with an internal diameter of 14 mm to decrease the filtration area contacting a like rubber ring of 1 mm thickness to allow for good adjustment and avoiding lateral diffusion of the solution.

Startgraphics software package[14] was used for regression analysis (linear model).

### *Reagent*

All reagents used were of analytical reagent grade. Reverse osmosis type quality water was used for the dilution of samples and preparation of reagents.

Fe(III) stock solution (1 g/l.) was prepared by dissolution of 1 g of Fe metal (Merck) in 50 ml of $HNO_3$ (1:1) (v/v) and later dilution with high purity water to 1 l. Working solutions were prepared by appropriate dilution maintaining the pH at 2.2 in all instances by addition of $1M$ $HNO_3$.

Buffer solutions of the required pH were prepared from $0.01M$ sodium acetate (Merck) and $0.01M$ acetic acid (Merck).

A stock solution of hydroquinone ($9.0 \times 10^{-4}M$) was prepared by dissolving appropriate amounts of hydroquinone (Merck) in water.

A stock solution of 1,10-phenanthroline ($2.78 \times 10^{-3}M$) was prepared by dissolving 0.1250 g of 1,10-phenanthroline (Merck) in hot water and levelling off to 250 ml.

Cation exchanger paper was Whatman P-81 cellulose phosphate paper, thickness 0.23 mm, linear flow rate (water) 125 mm/30 min and an exchange capacity of 20.34 $\mu$eq/cm$^2$ calculated by us. This paper was cut in a circular shape of 16 mm diameter. In order to compact the filter paper and obtain repeatability in the measured absorbance, immediately before utilization 100 ml of deionized water was filtered through the paper disks.

### *Absorbance measurements*

The paper disk with the retained coloured complex was placed on a 13 mm KBr pellet holder from an IR spectrophotometer and subsequently attached into the sample compartment of a UV-VIS spectrophotometer. The absorbance was measured at 510 nm with a slit width of 5 nm.

The net absorbance of the complex fixed on the paper disk was obtained at 510 nm subtracting from the observed absorbance the absorbance of a paper disk equilibrated with blank solution.

### *General procedure*

To an aliquot of sample containing between 100 and 1000 ng of iron, 10 ml of pH 3.5 acetate buffer solution, 5 ml of $9.0 \times 10^{-4}M$ hydroquinone solution and 2 ml of $2.78 \times 10^{-3}M$ 1,10-phenanthroline solution were added levelling to 100 ml with water. After 10 min the mixture was filtered under suction at 10 ml/min through a 16 mm diameter circular cation exchanger paper, which was dried by blowing hot air for 10 min at 60°C.

The other paper filter disk was prepared using a blank solution containing all the reagents except the analyte and treated in the same way. The absorbance of both paper filters (sample and blank) were measured at 510 nm. The calibration curve was drawn in the same way using Fe(III) solutions of known concentration.

### *Procedure for real samples*

For determination of iron in 2 ml samples wine were previously diluted to 200 ml with water and appropriate volumes were taken for analysis applying the General Procedure. The standard addition method was used for calibration purposes.

For determination of Fe in snow, 10 ml samples were taken and the standard addition method was also used.

In the case of human serum a blood sample was previously centrifuged and 1 ml of serum was taken and diluted to 25 ml with water. Appropriate volumes were taken for analysis applying the General Procedure. For calibration, the standard addition method was used.

*Treatment of the samples*

Wine, serum and melted snow were filtered through filter paper of pore size 0.45 μm (Millipore HAWP04700) and collected into a polyethylene container which had been carefully precleaned with nitric acid and water. The snow samples were preserved at pH 2.2 with nitric acid and stored at 4°C till analysis. Analysis were performed with the least possible delay and the usual general precautions were taken to avoid contamination.

## RESULTS AND DISCUSSION

The simplest system for retention of an analyte on an ion-exchanger filter is its filtration through it. Owing to hindrances caused by the glass filter holder located below the ion-exchanger paper, the use of a vacuum pump was required.

As a small diameter filtration zone increases the sensitivity of the method and a large diameter decreases filtration time, we selected a 16 mm diameter filter as a compromise and a glass filter holder as described under Apparatus.

*Physical variables*

In order to test the influence of the vacuum pressure on the absorbance measurements different values of vacuum pressure, *i.e.* different flow rates, were checked for solutions containing 15.0 ng/ml of iron. The absorbance remained stable at vacuum pressure values higher than 70 mbar (Fig. 1). As a compromise, 75 mbar vacuum pressure (rate of filtration 10 ml/min) and filtration times of around 10 min were used.

On the other hand, as adequate reproducibility requires measurements to be carried out over dry paper, several drying tests indicated the suitability of blowing hot air at 60°C for 10 min.

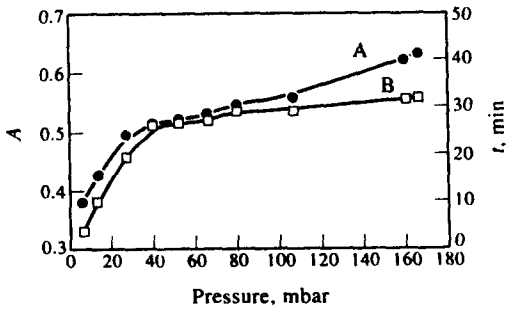


Fig. 1. Absorbance of the Fe(II)–1,10-phenanthroline complex as a function of the pressure and filtration time at $\lambda = 518$ nm. [Fe(III)] = $2.7 \times 10^{-7} M$; [hydroquinone] = $4.5 \times 10^{-5} M$; [1,10-phenanthroline] = $5.56 \times 10^{-5} M$. (A) Absorbance *vs.* pressure; (B) filtration time *vs.* pressure.

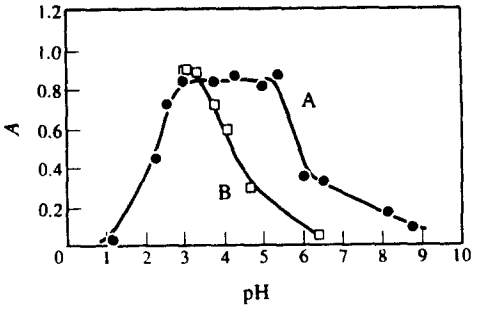


Fig. 2. Influence of the pH on the absorbance of Fe(II)–1,10-phenanthroline complex. [Fe(III)] = $4.1 \times 10^{-7} M$; [hydroquinone] = $4.5 \times 10^{-5} M$; [1,10-phenanthroline] = $5.56 \times 10^{-5} M$; filtration rate = 10 ml/min. (A) Absorbance *vs.* pH adjusted by $H_2SO_4$ (0.1 *M*); (B) absorbance *vs.* pH adjusted by acetate buffers (0.01 *M*).

*Chemical variables*

The cationic Fe–1,10-phenanthroline complex is strongly retained on cellulose cation exchanger paper (Whatman P-81) containing phosphate as functional groups, showing the well known red colour of the complex and an absorption spectrum similar to that of solution ($\lambda_{max} \doteq 510$ nm).

The effect of pH was studied using sodium hydroxide and hydrochloric acid for adjustment.

The optimum pH value for the fixation of the Fe(II)–1,10-phenanthroline complex was within the range 3–5.5 (Fig. 2). At pH values below 3 absorbance of the complex decreases significantly because the fixation process does not take place owing to the protonation of the functional groups. At pH values above 5.5, the $Na^+$ cations compete with the complex in the fixation. This behaviour is different to that showed in solution where the absorbance does not change for pH range between 2 and 9.

Citrate, monochloroacetate, hydrogen phthalate, oxalate and acetate buffer solutions of various concentrations ($1 \times 10^{-1}$, $1 \times 10^{-2}$ and $1 \times 10^{-3} M$) were tested. It was found that acetic acid–sodium acetate ($1 \times 10^{-2} M$) buffer affected the absorbance reading the least.

An acetic/acetate buffer solution pH 3.5 (0.01 *M*) was used to adjust the pH according to the major buffer capacity and the minor decrease in the analytical signal (Fig. 2).

An increase in the concentration of the cationic components of the solution brings about a

competition in the complex retention which reduces the absorbance. From a study carried out with several common electrolytes (NaCl, $KNO_3$ and $NaNO_3$) it was shown that for concentration levels of electrolyte up to $10^{-3}M$ there were no absorbance decreases, while for values such as $10^{-2}M$ decreases of 60% were detected.

It was observed that the proportion of 1,10-phenanthroline necessary for the formation and retention of the complex is higher than in solution, in which proportions near stoichiometric are needed. Here a plateau was observed between $10^{-4}$ and $10^{-5}M$, $5.65 \times 10^{-5}M$ was selected as working concentration.

The most useful reducer for Fe(III) was hydroquinone, ascorbic acid and hydroxylamine also having been assayed. Independence from hydroquinone concentration was observed between $3.0 \times 10^{-4}$ and $1.0 \times 10^{-6}M$. In this work $4.5 \times 10^{-5}M$ hydroquinone solutions were used in all instances.

The stability of the complex fixed on the filter paper is very high. Thus, measurements repeated on samples formerly evaluated up to three years ago showed only a decrease in absorbance of around 5%.

*Analytical parameters*

*Effect of sample volume on sensitivity.* One of the main advantages of the solid-phase spectrophotometry method is the potential increase in sensitivity with an increase in the volume of the sample taken for analysis. This effect can be assessed by measuring the absorbance of ion exchange paper equilibrated with different volumes of solution containing the same concentration of Fe(III) and proportional amounts of the other reagents.

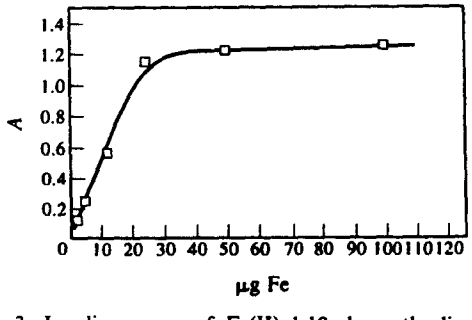


Fig. 3. Loading curve of Fe(II)–1,10-phenanthroline on ion-exchange filters. [Fe(III)] = $4.6 \times 10^{-7}M$; [hydroquinone] = $4.5 \times 10^{-5}M$; pH 3.7 [$CH_3COOH$/$CH_3COONa$] = $0.01M$; [1,10-phenanthroline] = $5.56 \times 10^{-5}M$. Filtration rate = 10 ml/min.

Table 1. Analytical parameters and statistical calculus

| Parameter | Sample volume 100 *ml* |
|---|---|
| Intercept | 0.012 |
| Standard error (intercept) | $2.91 \times 10^{-3}$ |
| Slope | 0.034 |
| Standard error (slope) | $5.51 \times 10^{-4}$ |
| Standard error of estimation | $3.93 \times 10^{-3}$ |
| Linear dynamic range (*ng/ml*) | 1.0–10.0 |
| Correlation coefficient | 0.9998 |
| Detection limit (*ng/ml*) | 0.2 |
| Quantification limit (*ng/ml*) | 1.0 |

Figure 3 show the dependence of absorbance *vs.* increasing amounts of Fe(II)–1,10-phenanthroline. Amounts of Fe greater than 13 μg cannot be retained by the ion exchange papers because they exceed the loading capacity of the filters.

*Analytical features*

A calibration graph for the determination of Fe(III) was prepared as described under Procedure. The regression line equation for the iron concentration was $A = 3.37 \times 10^{-2}C$ (ng/ml) + 0.012 ($r = 0.9998$) in the range 1.0–10.0 ng/ml. In all instances 100 ml of sample volume were used. The analytical parameters are summarized in Table 1.

At iron concentrations higher than 10 ng/ml the calibration graph bends, thus in order to adjust correctly the values a 2nd-order equation is required. The relative standard deviations were 5.3 and 4.9% for 10 replicate determinations of 5.0 and 10.0 ng/ml of Fe(III).

If we define the sensitivity of a method as the analyte concentration giving an absorbance of 0.100 then we have no doubt that the method reported in this paper is quite sensitive when compared to other spectrophotometric methods described in the literature. Using the proposed method, the sensitivity is some $4.6 \times 10^{-8}M$ which is indeed much higher than the $10^{-5}M$ for the common 1,10-phenanthroline spectrophotometric method in solution and nearly one order of magnitude higher than the resin phase method ($5.8 \times 10^{-7}M$).[15]

The detection limit ($k = 3$) according to IUPAC[16] and the quantification limit ($k = 10$)[17] were calculated for 100 ml sample volumes, the results obtained are summarized in Table 1.

*Effect of foreign ions*

A systematic study of the effect of common foreign ions on the determination of iron at the 5.0 ng/ml level was undertaken. The tolerance level was defined as the amount of foreign ions

Table 2. Effect of foreign ions on the determination of 5.0 ng/ml of Fe(III)

| Foreign ions | Tolerance level (*ng/ml*) |
|---|---|
| K (I) | 20,000 |
| Na (I) | 15,000 |
| Mg (II) | 10,000 |
| $SiO_3^{2-}$ | 4000 |
| Ca (II) | 1000 |
| Ni (II) | 400 |
| $SO_4^{2-}$ | 400 |
| $PO_4^{3-}$ | 200 |
| Co (II) | 80 |
| Al (III) | 40 |
| Cu (II) | 30 |
| Cr (III) | 30 |
| $F^-$ | 30 |
| Zn (II) | 10 |
| EDTA | 5 |

producing an error not exceeding $\pm 5.0\%$ in the determination of the analyte (Table 2).

*Applications*

The proposed method was applied to determination of iron in samples of wine (C. B. Alvear and Espinosa brands), snow from Sierra Nevada, Granada (Spain) and human serum from patients of the Ruiz de Alda Hospital (Granada). In all instances the standard addition method was used in order to avoid the matrix effect. As a reference method we used graphite furnace AAS and the 1,10-phenanthroline spectrophotometric method.

Table 3 shows that results are comparable when using the proposed method and the reference methods whenever the detection limits of each of the methods can be compared.

Table 3. Determination of iron in different samples

| Sample | Proposed method | Reference methods |
|---|---|---|
| Wines | | |
| Espinosa | 7.3 *μg/ml* | 6.8* *μg/ml* |
| Alvear | 2.1 *μg/ml* | 2.1* *μg/ml* |
| Human serum | 787 *μg/ml* | 800* *μg/ml* |
| Snow | 17.5 *ng/ml* | 18.3† *ng/ml* |
| Sierra Nevada (Granada) | | |

Data are based on the average obtained from four determinations.

*1,10-Phenanthroline spectrophotometric method in solution.

†Graphite furnace atomic absorption spectrometry.

## CONCLUSIONS

A new application of ion-exchanger paper as a system to collect coloured species that contain the analyte by filtration, followed by drying of the retaining paper and solid phase spectrophotometry is described. It has been used for iron determination using 1,10-phenanthroline as a reagent, revealing several advantages over the solution and resin phase methods.

The increase in sensitivity obtained with the proposed method ($4.6 \times 10^{-8} M$) with respect to the solution method ($8.96 \times 10^{-6} M$) and the resin phase method ($5.8 \times 10^{-7} M$) is substantial. The method is faster and simpler than the resin phase method because no isolation of the ion-exchanger from samples is required. Furthermore, there are no equilibration steps, only the passage of the solution through a filter. Moreover, only measurement at one wavelength is needed and not two as is usual in the SPS methods.

Other advantages are the higher stability of the complex fixed on the filter and the fact that it is possible to retain the iron as a complex and then to be able to measure it at a much later time without apparent loss in detection levels.

## REFERENCES


1. C. Gennaro, C. Baiocchi, E. Campi, E. Mentasti and R. Aruga, *Anal. Chim. Acta*, 1983, **151**, 339.
2. I. Kasahara, R. Terai, Y. Murai, N. Hata, S. Taguchio and K. Goto, *Anal. Chem.*, 1987, **59**, 787.
3. R. Van Grieken, *Anal. Chim. Acta*, 1982, **143**, 3.
4. R. J. Hurtubise, *Solid Surface Luminescence Analysis*. M. Dekker, New York. 1981.
5. K. Yoshimura and H. Waki, *Talanta*, 1985, **32**, 345.
6. K. Ohzeki, T. Sakuma and T. Kambara, *Bull. Chem. Soc. Jpn*, 1980, **53**, 2878.
7. K. Matsuhisa, K. Ohzeki and T. Kambara, *Bull. Chem. Soc. Jpn*, 1981, **54**, 2675.
8. K. Matsuhisa, K. Ohzeki and T. Kambara, *Bull. Chem. Soc. Jpn*, 1982, **55**, 3335.
9. K. Matsuhisa and K. Ohzeki, *Analyst*, 1986, **111**, 685.
10. I. Nakatsuka, K. Takahashi, K. Ohzeki and R. Ishida, *Analyst*, 1989, **114**, 1473.
11. I. Nakatsuka, T. Miura, K. Ohzeki and R. Ishida, *Anal. Chim. Acta*, 1991, **248**, 529.
12. A. T. Pilipenko, A. V. Terletskaya and T. A. Bogoslovskaya, *Zh. Anal. Khim.*, 1990, **45**, 1624.
13. I. Nakatsuka, T. Ohba, H. Ishida, H. Satoh, K. Ohzeki and R. Ishida, *Analyst*, 1992, **117**, 1513.
14. Startgraphics V. 6.0 Manugistics Inc. and Statistical Graphics Corporation, U.S.A. 1992.
15. K. Yoshimura, H. Waki and S. Ohashi, *Talanta*, 1976, **23**, 449.
16. IUPAC, Nomenclature, Symbols Units and Their Usage in Spectrochemical Analysis, *Pure Appl. Chem.*, 1976, **45**, 105.
17. Guidelines for Data Acquisition and Data Quality Evaluation in Environmental Chemistry, *Anal. Chem.*, 1980, **52**, 2242.

Pergamon

0039-9410(95)01476-4

*Talanta*, Vol. 42, No. 5, pp. 717–724, 1995

0039-9140/95 $9.50 + 0.00

# DETERMINATION OF ATRAZINE, ITS DEGRADATION PRODUCTS AND METOLACHLOR IN RUNOFF WATER AND SEDIMENTS USING SOLID-PHASE EXTRACTION

Hassan Sabik,[1] Sam Cooper,[1]* Pierre Lafrance[2] AND Josette Fournier[3]

[1]Institut National de la Recherche Scientifique (INRS-Santé), 245 Boul. Hymus, Pointe-Claire, Québec, Canada H9R 1G6

[2]Institut National de la Recherche Scientifique (INRS-Eau), 2800, rue Einstein, Sainte-Foy, Québec, Canada G1V 4C7

[3]Centre Régional d'Etude des Produits Agropharmaceutiques (CREPA), 8, rue Becquerel, 49070 Beaucouzé, France

(*Received* 5 *August* 1994, *Revised* 1 *November* 1994, *Accepted* 8 *November* 1994)

**Summary**—In order to determine the fate of the herbicides atrazine (as well as some of its degradation products) and metolachlor in water and sediments, a method was developed to extract and analyse these compounds. The two matrices were separated completely by centrifugation followed by filtration using nylon filters (0.45 $\mu$m). Sediments were extracted with a mixture of methanol–0.1*N* hydrochloric acid (50:50, v/v) using a wrist-action shaker. Filtered water and extracts of sediments were adjusted to pH 4, then concentrated and purified onto two solid-phase extraction cartridges using in tandem $C_{18}$ bonded phase column atop sulfonic acid bonded column (SCX). Atrazine, deethylatrazine, deisopropylatrazine and metolachlor retained by the $C_{18}$ column were eluted with ethyl acetate. Chlorodiaminotriazine and hydroxyatrazine retained by the SCX column were eluted with a 50:50 (v/v) acetonitrile–0.1*M* $Na_2HPO_4$ aqueous solution (pH 8.5). The extracts were quantified by high performance liquid chromatography with diode array detector (HPLC-DAD) and by gas chromatography with nitrogen–phosphorus detector (GC-NPD). Overall percent recoveries were about 75% and detection limits were between 0.05 and 0.15 $\mu$g/l., and 0.5 and 1.5 $\mu$g/kg for water and sediments, respectively.

Atrazine [6-chloro-*N*-ethyl-*N*′-(1-methylethyl)-1,3,5-triazine-2,4-diamine] and metolachlor [2-chloro-*N*-(2-ethyl-6-methylphenyl)-*N*-(2-methoxy-1-methylethyl acetamide] are pre- and post-emergent herbicides, used in combination to control weeds in a variety of food crops. Their widespread utilization and their remanence in soil are responsible for their presence in environment.[1–6].

In soil, atrazine is slowly degraded over a period of weeks to months through hydrolytic reactions and microbiological transformations.[7] Its degradation products which have significant toxicity[5] should also be considered for their environmental impact.

In order to reduce the loss of herbicides when used as treatment, and to prevent soil and water contamination, it is essential to assess their residue level, after treatment, in runoff water and sediments which constitute drainage sources towards surface and groundwater.

The aim of the present work was to develop a rapid, inexpensive, quantitative and reproducible method for the determination of atrazine, four of its principal degradation products and metolachlor in water and sediments.

Despite the fact that several studies on the subject have been published[8–11] none of them, with the exception of Schiavon's method,[12] describes extraction of these combined products from water or sediments. However, in some of these works,[13,14] extraction and purification of two or three of these products were exhibited in a chromatogram with other degradation products. The main difficulty consists essentially in extracting and purifying all these products together in different matrices.

Schiavon[12] developed a method to extract all these products from the soil, to concentrate the aqueous extract by lyophilization and to analyse it by high performance liquid chromatography (HPLC). Although this method has yielded good results, it is time consuming and, therefore, cannot be used for routine work.

*Author to whom correspondence should be addressed.

Solid-phase extraction (SPE) is by far the best method for isolating pesticides from water.[8,9,14–21] However, the specificity of adsorbents used for this method makes it impossible to extract all these products together which have different polarities. By using a large volume of water on a $C_{18}$ column, Nash *et al.*[19] recovered 95% of atrazine but only 26% of deethylatrazine, which is relatively more polar than the former compound. To avoid such a low recovery of degradation products, Karlaganis *et al.*[10] divided the water sample into two fractions; $C_{18}$ (non-polar) was used for atrazine and alumina oxide (polar) for deisopropylatrazine and deethylatrazine.

In the majority of articles on this subject, authors only report the efficiency for the recovery of parent products, which are mostly non-polar products, using non-polar adsorbents.[9,15,18,22,23]

On one hand, metolachlor, atrazine and its degradation products can be analyzed without difficulty by HPLC and gas chromatographic (GC) methods.[13,14,24–28] On the other hand, extraction and purification processes represent a real problem for analysts. In order to solve this problem a unique method has been developed to concentrate and purify simultaneously atrazine (AT), deethylatrazine (DEA), deisopropylatrazine (DIA), chlorodiaminotriazine (CDAT), hydroxyatrazine (HA) and metolachlor (M) in water and sediments samples, by using two cartridges in series: $C_{18}$ (non-polar) and SCX (polar and ion exchange).

To our knowledge, this is the first report, which describes the use of two SPE cartridges ($C_{18}$ and SCX) installed vertically in series, for efficient extraction and separation of AT, its four principal degradation products and M from runoff water and extracts of sediments.

## EXPERIMENTAL

### *Chemicals*

All the organic solvents (HPLC grade) were used as received from Caledon Labs (Georgetown, Ont., Canada). *O*-Phosphoric acid, hydrochloric acid, anhydrous sodium phosphate monobasic and acetic acid were purchased from Fisher Scientific (Fairlawn, NJ, U.S.A.). Propylamine hydrochloride sodium salt and sodium carbonate were obtained from Aldrich Chemical Company (Milwaukee, WI, U.S.A.). Water was distilled, deionized and filtered by Milli-Q-4-bowl reagent-grade water system (Continental Water Systems, Oakville, Ontario, Canada).

### *Standards*

The analytical standards of AT, DEA, DIA, CDAT and HA were obtained from Chem Service (West Chester, PA, U.S.A.). M was obtained from Polyscience (Niles, IL, U.S.A.) and the internal standard (IS) diphenylamine from Aldrich Chemical Company. Figure 1 illustrates the chemical structure of the compounds.

### *Preparation of standards*

Stock standard solutions of AT, DEA, DIA, CDAT, and M and diphenylamine used as an internal standard (0.5 mg/25 ml) were prepared either in ethyl acetate (for GC analysis) or in acetonitrile (for HPLC analysis). A standard solution of HA was made by dissolving 0.5 mg of this compound in 10 ml of 0.1*M* HCl solution and adjusting its volume to 50.0 ml with acetonitrile. From these solutions, working standards were prepared at the concentration range of 0.1–5 mg/l.

### *Sampling and fortification of water and sediment samples*

Runoff water and entrained sediments were collected near an agricultural field following rainfall. The plot had a slope of 5% and was located on a Neuboir silty loam having a moderate organic matter content (4%). Samples

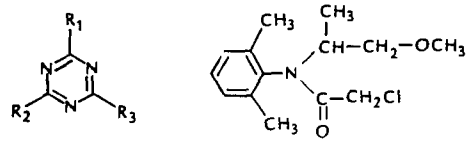


S-Triazine Metolachlor

| Atrazine and its degradation products | $R_1$ | $R_2$ | $R_3$ |
|---|---|---|---|
| AT | Cl | $NHCHC_2H_6$ | $NHC_2H_5$ |
| DIA | Cl | $NH_2$ | $NHC_2H_5$ |
| DEA | Cl | $NHCHC_2H_6$ | $NH_2$ |
| CDAT | Cl | $NH_2$ | $NH_2$ |
| HA | OH | $NHCHC_2H_6$ | $NHC_2H_5$ |

Fig. 1. Chemical structures of atrazine, its degradation products and metolachlor.

were preserved at 4°C until extraction procedure. Being taken in the spring and outside treated fields, the samples did not contain herbicides residue.

Water (100 ml) and sediment (10 g) samples, free of herbicides, were fortified under homogenization with 100–500 ng of each compound. Spiked samples were kept 2 h at room temperature before extraction. Unfortified samples were also analyzed for background comparison.

*Water samples. Liquid–liquid extraction.* Five hundred nanogrammes of each compound was added to 50 ml of a water sample. The extraction was carried out with three successive portions of 20 ml of organic solvent. The following solvents were tested: ethyl acetate, dichloromethane, ethyl acetate–isopropanol (50:50, v/v) and ethyl acetate–hexane (80:20 and 90:10, v/v).

*Solid-phase extraction.* In the preliminary experiments, different cartridges ($C_{18}$, $C_8$, $C_2$, CH, CN, 2OH, SCX) containing 100 mg of the adsorbents were used for the percent recovery of all the compounds. These pilot studies helped:

(i) to study the effect of each type of cartridge on percent recovery of each compound,
(ii) to select $C_{18}$ and SCX cartridges, which yielded the maximum per cent recovery.

In order to increase the concentration factor of the compounds by using higher sample volume (100 ml) compared to lower sample volume (25 ml), cartridges containing higher amount of adsorbent (1000 mg) were used. In addition, the degree of separation and purification is related to the quantity of adsorbent used.

A $C_{18}$ solid-phase cartridge of 6-ml volume size containing 1000 mg of $C_{18}$ octadecyl adsorbent (Lida, Kenosha, WI, U.S.A.) was mounted on top to an aromatic sulfonic acid cartridge filled with 1000 mg of propylbenzenesulfonyl adsorbent (Lida). A 75 ml reservoir was fixed on $C_{18}$ cartridge (Fig. 2). These cartridges were washed in series with 6 ml of methanol, then with 6 ml of distilled water followed by 2 ml of 0.1% acetic acid at a flow-rate of 3 ml/min. A 100 ml aliquot of the sample was centrifuged and filtered through 0.45 μm nylon filter, to which 0.1 ml of concentrated acetic acid was added (final pH 4). The sample was later aspirated through the two cartridges at a flow-rate of 3 ml/min. At no time during this operation were the cartridges allowed to aspirate to dryness. After the sample had been applied, the two

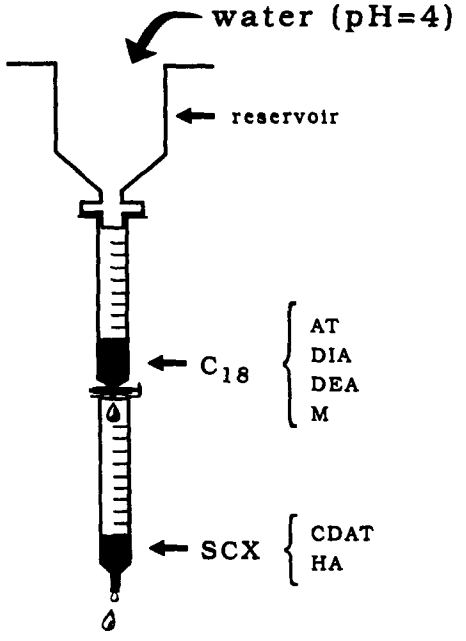


Fig. 2. Scheme for extraction of water samples.

solid-phase cartridges were rinsed in series with 6 ml of distilled water and then separated.

The $C_{18}$ cartridge was aspirated further for 30 min using vacuum to remove any residual water. AT, DEA, DIA and M were then eluted by passing 2 ml of ethyl acetate through the cartridge at a flow-rate of 1 ml/min.

The SCX column was rinsed again with 2 ml of acetonitrile to remove interfering products. The CDAT and HA were eluted from the column by passing a mixture of 2 ml of acetonitrile–aqueous 0.1*M* $Na_2HPO_4$ solution (50:50, v/v) (pH 8.5) through the column at a flow-rate of 1 ml/min. Twenty-five microliters of internal standard equivalent to 500 ng was added to each eluent emerging either from $C_{18}$ or SCX cartridge. These eluents were concentrated separately to 100 μl with nitrogen at 40°C for analysis.

*Sediment samples.* A sample of about 10 g was accurately weighed into a 50 ml centrifuge bottle. Prior to extraction, sediments were saturated with distilled water and a mixture containing 25 ml of methanol–0.1*N* hydrochloric acid (50:50 v/v) was added to it. The heterogeneous mixture was vigorously shaken using a wrist-action shaker for 30 min at 300 rpm. The extracts were centrifuged at 2300 rpm for 10 min, and the supernatant was decanted into a 250 ml bottle. The extraction was repeated twice. The centrifuge bottle was rinsed with 5 ml of organic-free water, which was

combined with the extract. The methanol was evaporated under vacuum and the pH was adjusted to 4 with a few milligrams of sodium carbonate powder. SPEs and elutions were carried out on each sediment extract (total volume of eluate was about 25 ml) using the two cartridges described in the procedure for water samples. Twenty-five microliters of internal standard equivalent to 500 ng was added to each eluent emerging either from $C_{18}$ or SCX cartridge. These eluents were concentrated separately to 100 $\mu$l with nitrogen at 40°C for analysis.

*High pressure liquid chromatography*

The sample extracts emerging from the SCX cartridge were analyzed using a Hewlett Packard 1090 Liquid Chromatograph equipped with a diode array detector. An ODS Hypersil $C_{18}$ guard column (5 $\mu$m, 20 mm × 4.0 mm) and an ODS Hypersil $C_{18}$ column (5 $\mu$m, 20 cm × 4.6 mm) were used with 60:40 (v/v) acetonitrile–water containing 0.017*M* of propylamine hydrochloride and 0.05*M* of sodium phosphate monobasic (pH 4.5) as the mobile phase at a flow-rate of 1.0 ml/min. The sample volume injected for analysis was 20 $\mu$l. CDAT was determined at a wavelength of 223 nm, and HA at 240 nm. Retention times were 2.679, 2.963 and 10.338 min for CDAT, HA and diphenylamine (IS), respectively. Since no traces of CDAT and HA were found in the field extracts, only the chromatogram of authentic standards of these compounds analyzed at 223 nm is presented in Fig. 3.

*Gas chromatography*

The sample extracts emerging from the $C_{18}$ cartridge were analyzed using a Hewlett Packard 5730A gas chromatograph equipped with a nitrogen–phosphorus detector. A DB-5 (5% phenyl–95% methyl) capillary column (30 m × 0.25 mm i.d., 0.25 $\mu$m coating thickness) was used with helium as the carrier gas at a flow-rate of 2 ml/min. The detector was supplied with hydrogen at a flow-rate of 3.4 ml/min and with air at a pressure of 35 psi. The nitrogen make-up flow-rate was 34.4 ml/min. The injector and detector port temperatures were 250 and 300°C, respectively. The temperature of the column was initially programmed at 50°C. It was increased to 160°C at a rate of 20°C/min, then to 185°C at a rate of 5°C/min and finally to 240°C/min at a rate of 20°C/min. The latter temperature was held for 3 min. The split/splitless capillary injector was operated in the splitless mode and the injection volume was 1 $\mu$l. Retention times were 9.225, 9.525, 9.702, 10.967 and 13.100 min for diphenylamine (IS), DIA, DEA, AT and M, respectively. Chromatograms of field extracts are shown in Figs 4 and 5.

## RESULTS AND DISCUSSION

Being aware that extraction and purification are the most critical steps in developing a

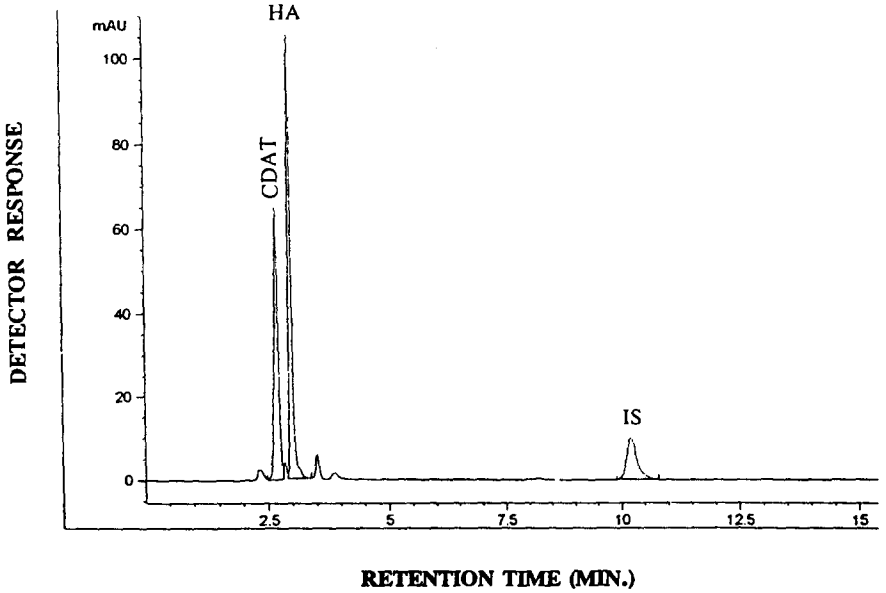


Fig. 3. Chromatogram of CDAT and HA standards by HPLC. CDAT, 1 $\mu$g/ml; HA, 5 $\mu$g/ml; IS, 5 $\mu$g/ml.

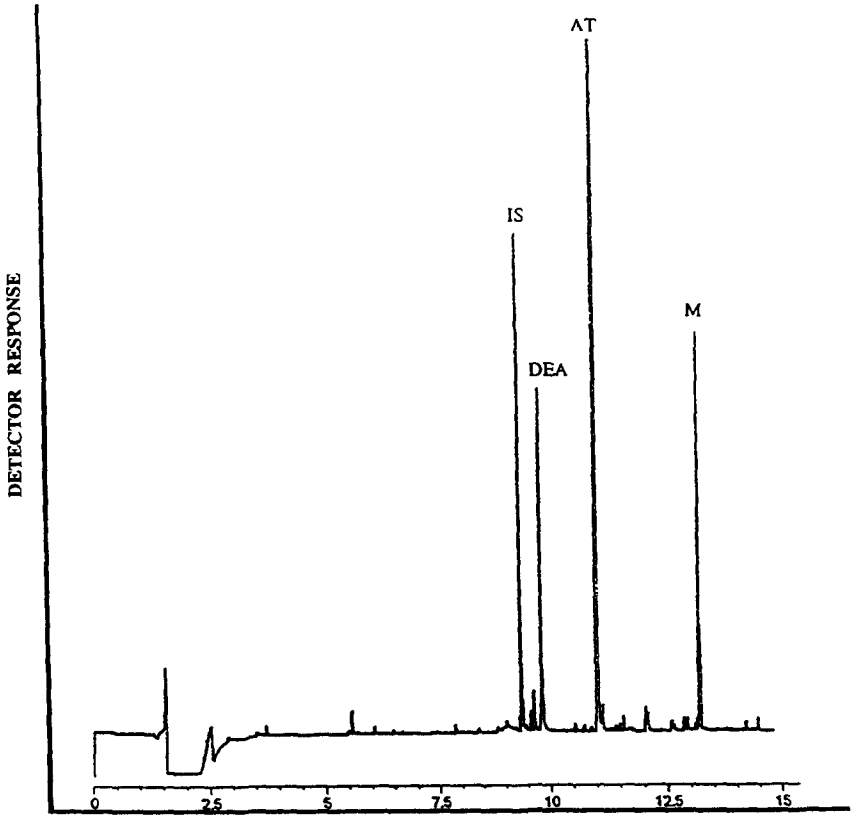


Fig. 4. Chromatogram of an extract of a water sample by GC. IS, 50 μg/l.; DIA, 1.9 μg/l.; DEA, 3.9 μg/l.; AT, 12.2 μg/l.; M, 13.3 μg/l.

method, this investigation was thus oriented towards that objective. The first attempt was made using liquid–liquid extraction methods and later more trials were given to the SPE techniques.

For liquid–liquid extraction methods, various organic solvents were tested by keeping water samples at neutral pH. None of them gave satisfactory results either for CDAT or HA (per cent recovery $<30\%$). For all others products, overall per cent recoveries were more than 80%. As for SPE techniques, three factors which determined the percent recoveries were studied namely the type of adsorbent (Table 1), the sample volume (Table 2) and the type of eluent.

The choice of SPE adsorbent and extraction conditions were driven by the physicochemical properties of the herbicide products. The work of Wenheng *et al.*[13] describing the separation of AT and HA by SCX cartridge was applied first in this study. The results obtained by this method are shown in Table 1. All the compounds studied possess at least one amine function and in addition HA contains an hydroxyl group. This fact leads one to think, that the sulfonic acid group of SCX cartridge will retain the compounds, whose functional groups are protonated by the acidic medium of the samples. The results show, that by using SCX cartridge, all compounds were retained except M (Table 1). This could be due to the presence of tertiary amine in the chemical structure of M. The presence of bulky substituents linked to the nitrogen atom in M (Fig. 1) may hinder the ion-exchange capacity of SCX cartridge. Since SCX cartridge could not separate all the compounds, other cartidges described in Table 1 were tried. The $C_{18}$ cartridge gave better per cent recovery for AT, DEA, DIA and M compared to all other cartridges. This fact was the turning point for the installation of $C_{18}$ and SCX cartridges vertically in series (Fig. 2). The ion-exchange process using SCX cartridge requires acidic pH. This pH did not affect the per cent recovery of the compounds, which were retained by $C_{18}$ cartridge. Therefore, all the field samples were acidified to pH 4 before applying to the two cartridges in series.

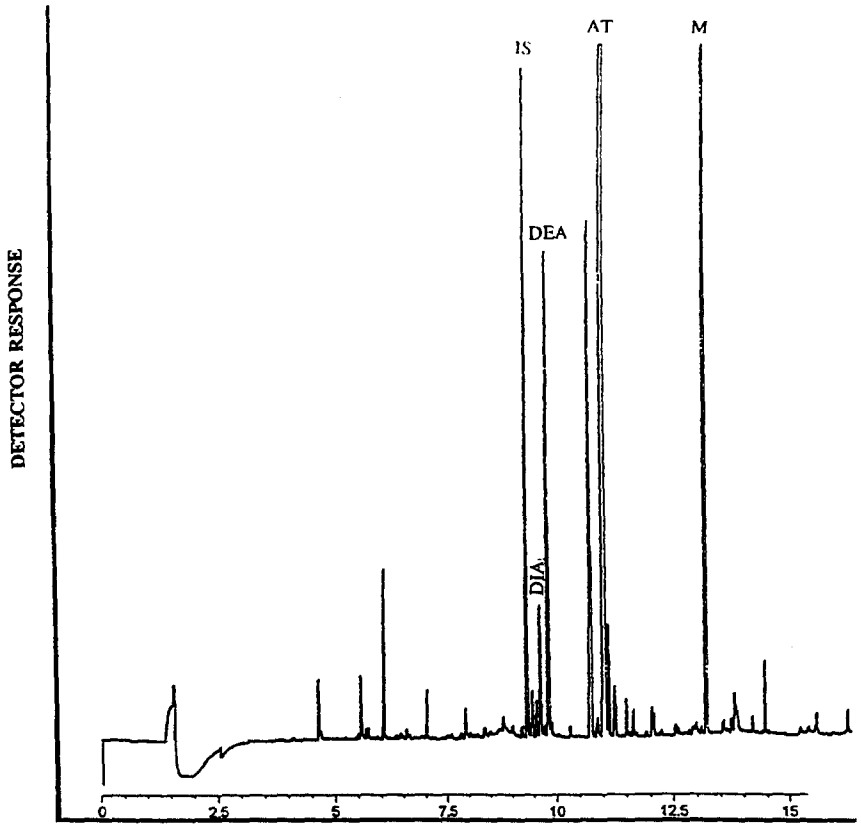


Fig. 5. Chromatogram of an extract of a sediment sample by GC. IS, 5 μg/kg; DIA, 27.2 μg/kg; DEA, 47.2 μg/kg; AT, 629.5 μg/kg; M, 824.3 μg/kg.

The volume of water has no effect on the recovery rate of parent compounds namely AT and M. Contrary, once the volume passes beyond 100 ml, the per cent recovery of DEA and DIA decreases significantly. The optimum sample volume was found to be 100 ml during the per cent recovery experiments of each component using $C_{18}$ cartridge (Table 2). The same volume was used for SCX cartridges as two columns were installed in series. Therefore, the effect of sample volume on SCX cartridge was not studied.

Table 1. Effect of the adsorbents on per cent recoveries of different compounds

| | Adsorbent | | | | | | |
|---|---|---|---|---|---|---|---|
| Compound | $C_{18}$ | $C_8$ | $C_2$ | CH | CN | 2OH | SCX |
| AT | 99 | 98 | 93 | 96 | ND | ND | 70 |
| DEA | 101 | 90 | 24 | 65 | 11 | 2 | 81 |
| DIA | 100 | 70 | 9 | 95 | 3 | 3 | 111 |
| M | 97 | 96 | 95 | 94 | ND | ND | ND |
| CDAT | ND | ND | ND | ND | ND | ND | 101 |
| HA | 41 | 6 | ND | 4 | ND | ND | 80 |

Twenty-five milliliters of water and 100 *mg* of adsorbent were used. Ethyl acetate (2 *ml*) was employed for elution of AT, DEA, DIA and M using $C_{18}$, $C_8$, $C_2$, CH, CN and 2OH cartridges whereas acetonitrile–aqueous 0.1*M* $Na_2HPO_4$ solution (50:50, v/v) (2 *ml*) was employed for elution of CDAT and HA using SCX cartridge.

The elution of HA and CDAT on $C_{18}$, $C_8$, $C_2$, CH, CN and 2OH cartridges was carried out using 2 *ml* of ethyl acetate followed by 2 *ml* of methanol.

Table 2. Effects of sample volume on per cent recoveries on a $C_{18}$ cartridge containing 100 mg of the adsorbent

| | Volume (*ml*) | | | | |
|---|---|---|---|---|---|
| Compound | 25 | 50 | 100 | 150 | 250 |
| AT | 99 | 96 | 97 | 95 | 92 |
| DEA | 101 | 95 | 87 | 41 | 21 |
| DIA | 100 | 87 | 60 | 19 | 9 |
| M | 97 | 95 | 98 | 96 | 95 |
| CDAT | ND | ND | ND | ND | ND |
| HA | 41 | ND | ND | ND | ND |

ND: Non detected.

A fixed quantity (500 *ng*) of each compound was spiked to different volumes of herbicide free-water. The elution of HA and CDAT was carried out using 2 *ml* of ethyl acetate following by 2 *ml* of methanol.

Table 3. Recovery of different products from fortified samples

| Compound | Adsorbent | Water samples | | Sediment samples | |
|---|---|---|---|---|---|
| | | Recovery (%) | C.V. (%) | Recovery (%) | C.V. (%) |
| AT | $C_{18}$ | 99 | 5 | 92 | 5 |
| DEA | $C_{18}$ | 98 | 6 | 89 | 7 |
| DIA | $C_{18}$ | 96 | 6 | 86 | 8 |
| M | $C_{18}$ | 97 | 5 | 91 | 5 |
| CDAT | SCX | 103 | 10 | 82 | 12 |
| HA | SCX | 78 | 10 | 75 | 12 |

The volume of water samples was 100 *ml*; the weights of sediment samples and adsorbents were 10 and 1 *g*, respectively. Values represent the mean of three tests.

Table 4. Detection limits (in ppb) of different compounds in water and sediment samples

| Sample | Compound (values in ppb)/method | | | | | |
|---|---|---|---|---|---|---|
| | AT/GC | DEA/GC | DIA/GC | M/GC | CDAT/HPLC | HA/HPLC |
| Water | 0.05 | 0.05 | 0.05 | 0.15 | 0.15 | 0.15 |
| Sediment | 0.5 | 0.5 | 0.5 | 1.5 | 1.5 | 1.5 |

Generally the use of solid phase cartridges would only be applicable to samples or extracts entirely free of sediments. On one hand, the sediments present in water can adsorb the herbicides. On the other hand, these sediments can affect the per cent recovery and can block the content of the cartridge rendering extraction impossible.

In order to determine the effect of eluents of per cent recoveries using $C_{18}$ cartridges, 1 ml aqueous solutions containing 100–500 ng of AT, its degradation products and M were directly deposited on these columns containing 100 mg of adsorbent and three tests were performed using three different solvents namely methanol, ethyl acetate and acetonitrile. The experiments on per cent recovery using SCX cartridges were performed according to the method already described in the literature.[13] With 2 ml of each solvent the total amount of the products was recovered with the exception of HA. HA could be totally recovered only with methanol. Ethyl acetate and acetonitrile yielded a recovery of about 30% of the latter compound.

The per cent recoveries of all the products are presented in Table 3. The overall coefficient of variation (C.V.) of the compounds extracted with $C_{18}$ is below 10%. The C.V. of those products extracted by SCX cartridge is below 12%.

The concentration factors obtained for water and sediment samples are 1000 and 100, respectively.

The detection limit of each compound was fixed to the minimum response of each detector to the respective compounds with a signal-to-noise ratio of 5. The lowest detection limits of each compound in water and sediment samples are given in Table 4.

## CONCLUSION

The per cent recoveries and detection limits obtained with the present method are satisfactory and, moreover, they correspond to those mentioned in the literature.[12,14,19] Using SPE the water volume is of primary importance for the recovery rate. It is obvious that the use of a large sample volume increases chances of detecting low concentrations. But unfortunately, it also has a negative double-action: the sample passage time in the cartridge is increased and the per cent recovery, for some products, is directly affected.[19]

The type of adsorbents and eluents also play major roles. The utilization of columns in series provides a good solution when one needs to simultaneously extract, purify and concentrate parent products and their degradation products, which otherwise would be highly time consuming. This method could very well be used with a great variety of products which have different polarities.

*Acknowledgements*—The authors would like to thank the Natural Sciences and Engineering Research Council of Canada for financial support. Dr Sabik gratefully acknowledges AUPELF (International Network of French Universities) and INRS (Institut National de la Recherche Scientifique) for fellowships.

## REFERENCES


1. R. Zhang, *J. Environ. Sci.*, 1989, **1**, 98.
2. G. S. Raju, J. A. Millette and S. U. Khan, *Chemosphere*, 1993, **26**, 1429.
3. D. J. Pantone, R. A. Young, D. D. Buhler, C. V. Eberlein, W. C. Koskinen and F. Forcella, *J. Environ. Qual.*, 1992, **21**, 567.
4. R. A. Leonard, in *Environment Chemistry of Herbicides*, R. Grover (ed.), Vol. III, pp. 45–87. CRC Press, Boca Raton, FL, 1988.
5. D. A. Belluck, S. L. Benjamin and T. Dawson, in *Pesticide Transformation Products*, American Chemical Society, ACS Symposium Series, No. 459, Chap. 18, pp. 255–273, 1991.
6. R. Frank, B. S. Clegg and N. K. Patni, *Arch. Environ. Contam. Toxicol.*, 1991, **21**, 41.
7. D. D. Kaufman and P. C. Kearney, *Residue Rev.*, 1970, **32**, 235.
8. L. Q. Huang and J. J. Pignatello, *J. Assoc. Off. Anal. Chem.*, 1990, **73**, 443.
9. M. W. Brooks, J. Jenkins, M. Jimenez, T. Quin and J. M. Clark, *Analyst*, 1989, **114**, 405.
10. G. Karlaganis and R. Von Arx, *J. Chromatogr.*, 1991, **549**, 229.
11. A. D. Lucas, A. D. Jones, M. H. Goodrow, S. G. Saiz, C. Blewett, J. N. Seiber and B. D. Hammock, *Chem. Res. Toxicol.*, 1993, **6**, 107.
12. M. Schiavon, *Ectotoxicology and Environmental Safety*, 1988, **15**, 46.
13. Q. Wenheng, N. A. Schultz, J. D. Stuart, J.-R. Hogan and A. S. Masson, *J. Liquid Chromatography*, 1991, **14**, 1367.
14. T. R. Steinheimer, *J. Agric. Food Chem.*, 1993, **41**, 588.
15. M. J. M. Wells and J. L. Michael, *J. Chromatogr. Sci.*, 1987, **25**, 345.
16. A. Di Corcia, M. Marchetti and R. Samperi, *J. Chromatogr.*, 1987, **405**, 357.
17. R. J. Ozretich and W. P. Schroeder, *Anal. Chem.*, 1986, **58**, 2041.
18. W. E. Johnson, N. J. Fendinger and J. R. Plimmer, *Anal. Chem.*, 1991, **1**, 1510.
19. R. G. Nash, *J. Assoc. Off. Anal. Chem.*, 1990, **73**, 438.
20. N. T. Basta and A. Olness, *J. Environ. Qual.*, 1992, **21**, 497.
21. G. Durand and D. Barcelo, *Talanta*, 1993, **40**, 1665.
22. T. R. Shephered, J. D. Carr, D. Duncan and D. T. Pederson, *J. Assoc. Off. Anal. Chem.*, 1992, **75**, 581.
23. J. C. Molto, Y. Pico, G. Font and J. Manes, *J. Chromatogr.*, 1991, **555**, 137.
24. V. Pacakova, K. Stulik and M. Prihoda, *J. Chromatogr.*, 1988, **442**, 147.
25. N. M. J. Vermeulen, Z. Apostolides, D. J. J. Potgieter, P. C. Nel and N. S. H. Smit, *J. Chromatogr.*, 1982, **240**, 247.
26. S. U. Khan, R. Greehalgh and W. P. Cochrane, *J. Agric. Food Chem.*, 1975, **23**, 430.
27. S. U. Khan and T. S. Foster, *J. Agric. Food Chem.*, 1976, **24**, 768.
28. D. C. C. Muir and B. E. Baker, *J. Agric. Food Chem.*, 1978, **26**, 420.

Pergamon

0039-9140(95)01478-0

*Talanta*, Vol. 42, No. 5, pp. 725–731, 1995

0039-9140/95 $9.50 + 0.00

# EVALUATION OF A β-DIKETONE-IMBEDDED POLYURETHANE FOAM

S. KATRAGADDA, H. D. GESSER and A. CHOW*

Department of Chemistry, University of Manitoba, Winnipeg, MB, R3T 2N2, Canada

(*Received* 16 *August* 1994. *Revised* 3 *November* 1994. *Accepted* 8 *November* 1994)

**Summary**—A β-diketone-imbedded polyurethane foam was made for the sorption of uranium from aqueous solutions. The incorporation of the β-diketone functional group into the polyurethane foam was simple, and relatively inexpensive. The β-diketone foam was ground to facilitate the evaluation of its ability to extract uranium from aqueous solutions with a wide range of temperature and pH values. The β-diketone material showed superior extractability of uranium from solutions with pH 7 ± 3. In general, the β-diketone material showed greater extractability of uranium at all temperatures and pH values tested when compared to a blank polyurethane foam without the β-diketone functional group.

The use of polyurethane foams for the extraction, recovery and preconcentration of various inorganic and organic species from aqueous, non-aqueous and gaseous mixtures has received considerable attention during the past two decades. Reviews of literature devoted to polyurethane-based polymeric sorbents in separation chemistry have been documented by Moody and Thomas[1] and Braun *et al.*[2,3] Polyurethane foams are stable in most acids, bases and organic solvents. The foams will degrade in concentrated nitric or sulphuric acids or when heated above 180–200°C.

The field of reagent-treated polyurethane foam materials is very extensive and has been comprehensively reviewed by Braun *et al.*[2,3] He first published investigations[4,5] in 1972 using tributylphosphate-loaded polymer to sorb several metal complexes from solution and since then many other loaded or coated polyurethane materials have been examined for concentrating various inorganic and organic species and for separations as detailed in the reviews.[2,3] Several chelating agents have been immobilized on polyurethane foam using a plasticizer such as tributylphosphate[6,7] and this material used to selectively sorb metal ions from solution. Liquid ion exchangers can also be used conveniently when they are held on polyurethane foam[8,9] or in a plasticizer on the foam.[10] Polyurethane foams have also been used as supports for various extractants; for example, foams treated with dithiazone or diethyldithiocarbamate or sulphide-treated foams have been used for the sorption of mercury,[11–13] ethanediol-treated foams for antimony,[14] and pyridylazonaphthol-treated foams for the sorption of zinc, copper and mercury.[15] Copper and cadmium were extracted using polyurethane treated with benzoyl-acetone.[16] Braun *et al.*[17] found that foam could be coated with various colour-forming reagents either with or without plasticizer; these 'chromofoams' can be used qualitatively and semi-quantitatively to determine several metal ions. Huang *et al.*[18] and Korkisch *et al.*[19] have extracted uranium from nitrate solutions with polyurethane foam. Korkisch and Steffan[20] and Pearson and Bowen[21] have used polyurethane foam impregnated with trioctylphosphine oxide to sorb uranium from hydrochloric acid solution. Polyurethane foam, when coated with a long chain tertiary amine, was also effective in extracting uranium[22] from acidic solutions with pH values between 1 and 3.

Hypol™ prepolymers, which are derived from toluene diisocyanate, react with active hydrogen-containing compounds (*i.e.* $H_2O$, ROH, *etc.*) to form polyurethane foams that are both elastomeric and hydrophillic in nature. These foams can be prepared by mixing equal weights of Hypol™ prepolymers and water or other active hydrogen-containing compounds. Additives may be suspended or dissolved in either or both of the organic and aqueous layers.[23] Additives that contain a functional group for the

*Author to whom correspondence should be addressed.

sorption of uranium can be dissolved in the organic layer or the aqueous layer to produce a modified polyurethane foam with a functional group imbedded into the foam.

Selective extraction of uranium using sorbents with amidoxime functional groups has been reported extensively by workers in Japan and Europe,[24-32] mainly for the extraction of uranium from seawater. $\beta$-diketone has been shown to be particularly effective in extracting uranium from seawater with good selectivity[24] Other materials for extracting uranium include polystyrene with 1,3-diketone as the anchor group[25], a macrocyclic hexaketone and a cyclic tetraketone[33], and a poly-$\beta$-diketone resin.[34]

The preparation of a $\beta$-diketone-imbedded polyurethane foam using the Hypol™ prepolymer and the evaluation of this material for extracting uranium from aqueous solutions with a wide range of temperature and pH values is described in this paper.

## EXPERIMENTAL

### *Reagents*

1-Benzoylacetone, *N*-(2-thiazolyl)acetoacetamide, 4,4,4-trifluoro-1-phenyl-1,3-butanedione and Arsenazo III were obtained from Aldrich Co. (WI, U.S.A.). Acetylacetone and uranyl acetate were obtained from Fisher Scientific Co. (NJ, U.S.A.) and BDH (U.K.), respectively. The above chemicals were of reagent grade and were used without further purification.

Hypol™ FMP 2002 prepolymer, used in the production of the foam, was a sample provided by W. R. Grace and Co., (MA, U.S.A.). Uranium solutions ranging from 1 to 10 ppm were prepared by successive dilution of a 2000 ppm uranium stock solution which was prepared from uranyl acetate $[UO_2(CH_3COO)_2 . 2H_2O]$. Water was purified by reverse osmosis followed by a Barnstead Nanopure II™ system.

### *Apparatus*

A Fisher Accumet™ (Model 825 MP) pH meter was used to measure pH. Polyurethane foams, with and without $\beta$-diketone functional groups, were first cut into small pieces and were then frozen in liquid nitrogen. The frozen foams were ground to a powder in a stainless steel container on a Waring™ blender (Dynamics Corporation of American CT, U.S.A.).

Sample solutions were shaken either with a Burrell Wrist-Action Shaker (Burrell Corp., PA, U.S.A.) for solutions at 4°C and 22°C or a Dubnoff Metabolic Shaking Incubator (Precision Scientific, IL, U.S.A.) for solutions at 40°C and 70°C. Absorbance measurements were obtained with a Hewlett-Packard (Model 8452A) Diode Array spectrophotometer (Hewlett-Packard Company, CA, U.S.A.).

A quartz flow cell with 0.5 cm path length (Markson Science Inc., CA, U.S.A.) was used for the specrophotometric analysis. Sample solutions were pumped through the flow cell using a Piper Pump™ (Model P10T) peristaltic pump (Dungey Inc., Ontario, Canada).

### *Method*

Solutions containing uranium were analyzed using a continuous flow spectrophotometric method (CFSM).[35] This method consists of simultaneously pumping 0.006% Arsenazo III in 0.12*M* HCl (photometric reagent) and the uranium solution into a flow mixer to form the Arsenazo III–uranium complex. This complex then enters a flow cell where the absorbance is measured with a diode array spectrophotometer. A flow cell requires less time per sample because the tedious process of cleaning and rinsing is avoided and the time for complex formation is always constant.

Arsenazo III, [2,2′-(1,8-dihydroxy-3,6-disulphonaphthylene-2,7-bisazo)-bisbenzenearsonic acid, FW 776.37], reacts with a wide variety of metal ions in weakly acidic to alkaline aqueous solutions, but reacts with only a few metals in strong mineral acid, forming highly coloured complexes (molar absorptivity approximately $10^5$). Arsenazo III has been recommended as a highly sensitive and selective photometric reagent for Mg, Zr, U, Th and rare earths.[36] Arsenazo III is available as either a free acid or the disodium salt and is stable both as a solid and in the dissolved form. The free acid form of Arsenazo III was used for our analysis.

More than 150 papers have been published in the last three decades,[37,38] wherein Arsenazo III is the preferred choice of chromogenic reagent for the spectrophotometric determination of uranium. Uranyl ions form a 1:1 complex[39,40] in moderately acidic media and the stability constant for the complex[40] is $\log \beta_1 = 5.42$. For these analyses the concentration of Arsenazo III was always higher than that of uranium. The flow rates of the Arsenazo III solution and uranium sample solution were each 8 ml/min

with a combined flow rate of 16 ml/min when reaching the flow cell. At this flow rate the air bubbles that often adhered inside the flow cell were forced out.

An internal referencing method was used where the absorbance at a reference wavelength (768 nm) was subtracted from the absorbance at the analytical wavelength (650 nm). This absorbance difference was used to obtain the calibration curve and for sample analysis. Internal referencing was done to improve the precision of the results by minimizing the impact of any changes that cause a baseline shift due to dust or other particles, air bubbles or a drift in lamp intensity. Quantitative analysis was performed by using the 'Quantitation' program which was part of the software menu for the Hewlett-Packard system. Uranium standards ranging from 1 to 10 ppm uranium were used to obtain the calibration curve in Fig. 1 using a second order curve fit. The absorbance obtained was the average reading obtained for a 10 sec scan period.

The 0.006% Arsenazo III (wt/vol.) reagent solution in 0.12*M* HCl was prepared as it was found that acid concentrations higher than 0.12*M* HCl produced larger errors with lower pH uranium solutions and concentrations lower than 0.12*M* HCl resulted in larger errors with higher pH uranium solutions. The choice of 0.12*M* HCl permitted the analysis of uranium solutions whose pH ranged between 1 and 11.

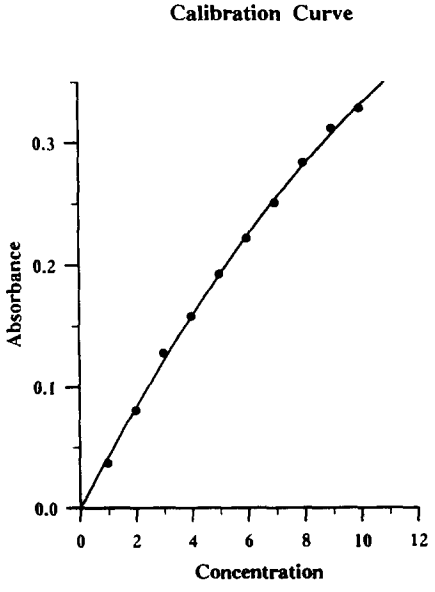


Fig. 1. Calibration graph for uranium standards between 1 and 10 ppm. A 5 mm Markson™ flow cell and 0.006%. Arsenazo III in 0.12*M* HCl was used.

*Procedure*

Hypol™ foams are usually produced by thoroughly mixing approximately equal weights, of Hypol™ prepolymer and water. Additives that contain β-diketones may be suspended or dissolved in either or both of the organic and aqueous layer. In a preliminary study, different β-diketones [acetylacetone, *N*-(2-thiazolyl)acetoacetamide, 1-benzoylacetone and 4,4,4-trifluoro-1-phenyl-1,1-butanedione] were used with varying amounts (1, 5 and 10% by weight) in the prepolymer matrix in an attempt to incorporate them into the Hypol™ foam matrix. Among various β-diketones studied only the foam prepared with 5% (wt/wt) 1-benzoylacetone, 'β-diketone foam', showed good foam formation and also exhibited the ability to extract uranium from aqueous solutions. The incorporation of acetylacetone and 4,4,4-trifluoro-1-phenyl-1,3-butanedione resulted in the formation of a solid plastic instead of a foam. *N*-(2-thiazolyl)Acetoacetamide formed a foam, but it did not extract uranium.

β-Diketone foam was prepared by mixing Hypol™ prepolymer with 1-benzoylacetone solid to form a clear viscous solution. An equal weight of water was then added to the viscous polymer solution followed by rapidly stirring of the mixture for 15 sec by using a glass rod. The mixture initially became cloudy and then rose to 10 times the original volume by releasing small bubbles of carbon dioxide. The resulting β-diketone foam became tack-free within 5 min and was air-dried in a fumehood for at least 8 h. The β-diketone foam was cut into small pieces which were frozen in liquid nitrogen and then the brittle foam was ground to a powder in a stainless steel container on a Waring™ blender. The size of this material was not determined but consisted of various small sizes of foam particles. These do not have the overall physical structure normally associated with the flexible polymer but naturally possess the same chemical composition. The physical form of the polymer should have no significant effect on the sorption since the mechanism is a chemical process. Because this is an evaluation investigation, it is more important that comparative studies be done in a reproducible manner and if possible, that an equilibrium be obtained. Powdered foam reaches equilibrium more quickly with the uranium solutions and also ensures more reproducible results. If the foam was used unground, it would take more time for the

uranium solution to equilibrate but qualitatively, the results would be the same as with the ground material.

The powdered foams were initially soaked in water for 4 h and the resulting slurry was then filtered under vacuum through a Whatman™ No. 541 filter paper using a Buchner funnel. The foam was recovered from the filter paper and the soaking and filtering was repeated twice more. The foam was washed in a similar manner with acetone and then left to dry under vacuum for 4 h to remove traces of acetone vapour. The above cleaning procedure was undertaken to remove any water or acetone soluble impurities. A blank foam was prepared in a similar manner without the addition of 1-benzoylacetone. The colour of the clean, dry $\beta$-diketone foam was cream yellow compared to the blank foam which was white.

The extraction capability was evaluated using 25 ml of 10 ppm uranium solution with $0.200 \pm 0.003$ g of foam in a 60 ml Nalgene™ bottle. The capped bottles were shaken for 5 h in an automatic shaker and the solutions filtered and then analyzed for uranium content using the spectrophotometric method.

*Characterization of the foam*

The extraction characteristics of the $\beta$-diketone foam were studied by equilibrating the foam with uranium solutions at different temperatures and pH values. Uranium solutions were adjusted with 2*M* HCl or 2*M* NaOH solution to pH values between 1.4 and 11.0 and studied at temperatures between 4°C and 70°C with $\beta$-diketone foam.

All solutions were equilibrated to the required temperatures before adding them to the plastic bottles containing the foam. Shaking of solutions at room temperature (22°C) and at cold room temperature (4°C) was done using a Burrell Wrist Action Shaker. Similar experiments at 40°C and 70°C were performed with a Dubnoff Metabolic Shaking Incubator equipped with a variable temperature-controlled water bath. Temperature measurements were within ±2°C.

Per cent extraction was calculated as

$$\%E = 100(I - F)I^{-1},$$

where % *E* is per cent extraction, *F* is the concentration of uranium left in solution after extraction and *I* is the concentration of uranium originally available for extraction. *I* is the concentration of uranium in solution after it was subjected to the identical filtration, pH and temperature conditions as the foam sample solution, but without the presence of any foam.

The concentration of available uranium, rather than the initial concentration (*i.e.* 10.0 ppm), was used to take into account any precipitation of uranium species which is known to occur at pH > 2. This precipitate is not visible to the naked eye, however, Feldman[41] *et al.* observed the precipitation of uranyl nitrate at pH > 4.5 by centrifuging the solution. The values for *I* and *F*, used in the calculation of % *E*, were the averages obtained from experiments that were performed in triplicate at the same pH and temperature.

## RESULTS AND DISCUSSION

The $\beta$-diketone foam exhibits high extraction between pH 3 and 8 with a decrease at either end of the pH ranges as shown in Figs 2–5.. The change in extraction can be explained by the fact that the formation of the various uranium species depends on the pH of the aqueous solutions.

For uranium solutions acidified with 2*M* HCl, the species formed in aqueous medium are $UO_2Cl_2$ and $UO_2Cl^+$ at pH values below 3, and above pH 10 species such as $UO_2(OH)_3^-$ are formed owing to the hydrolysis of the uranyl ion.[42] These species may not be as extractable by this foam.

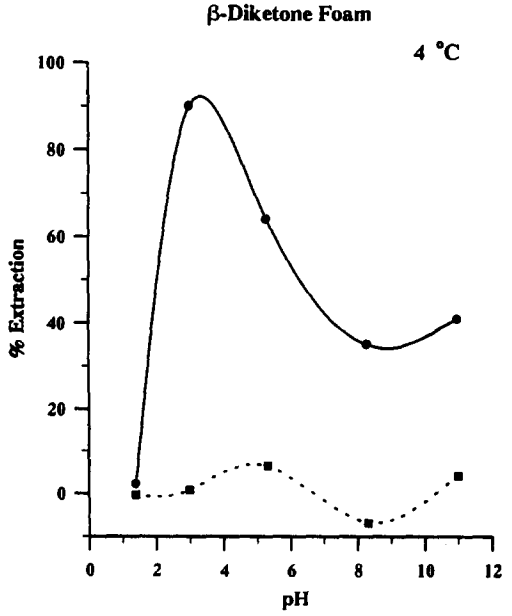


Fig. 2. Comparison for the extraction capability of uranium from solution by the $\beta$-diketone foam and blank foam at 4°C. —●— $\beta$-Diketone foam; - -■- - blank foam.

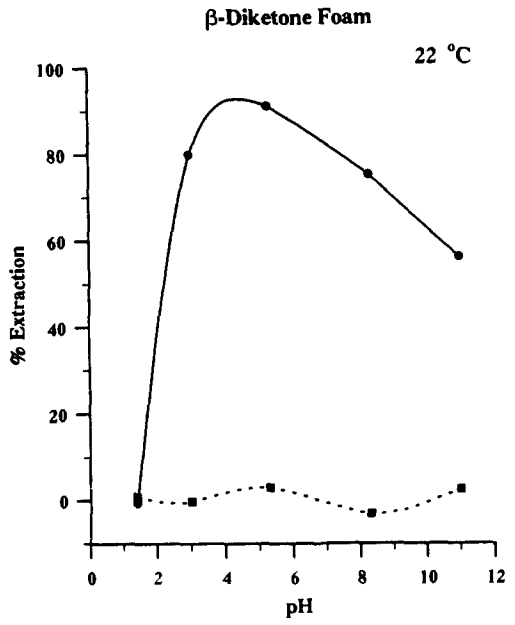


Fig. 3. Comparison of the extraction capability of uranium from aqueous solutions by the β-diketone foam and blank foam at 22°C. —●— β-Diketone foam; --■-- blank foam.

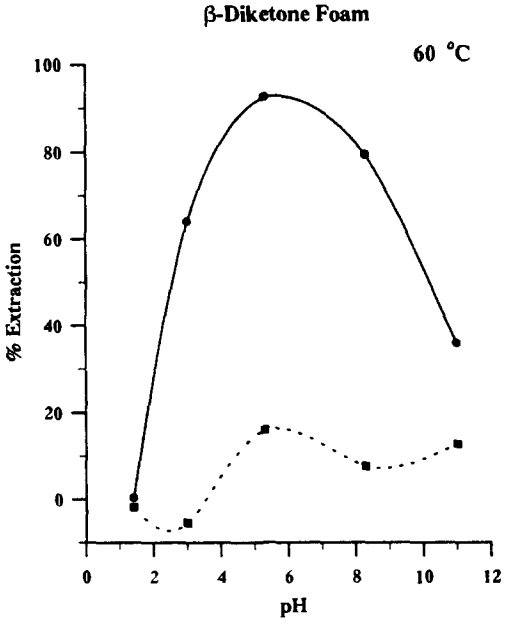


Fig. 5. Comparison of the extraction capability of uranium from aqueous solutions by the β-diketone and the blank foam at 60°C. —●— β-Diketone foam; --■-- blank foam.

Stary and Hladky[43] undertook a systematic investigation of the solvent extraction of 30 metals using various solvents such as acetylacetone, benzoylacetone and dibenzoylmethane in benzene. Included in their study was the extraction of uranium by benzoylacetone and the extraction profile reported by Stary and Hladky[43] is similar to the β-diketone foam profile at 22°C (Fig. 3). This suggests that the β-diketone foam's ability in sorbing uranium involves a solvent extraction type of mechanism.

It can be seen in Table 1 that between pH 3 and 8 the extraction generally increases with an increase in temperature from 4°C to 40°C,

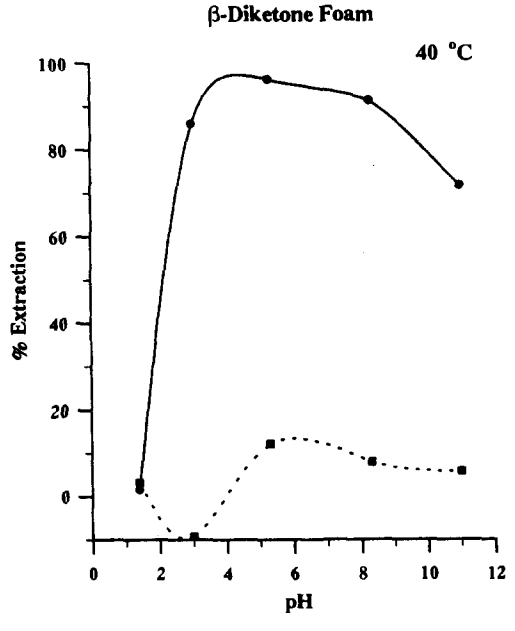


Fig. 4. Comparison of the extraction capability of uranium from aqueous solutions by the β-diketone foam and the blank foam at 40°C. —●— β-Diketone foam; --■-- blank foam.

Table 1. Comparison of the extraction capabilities of β-diketone foam with the blank foam for the extraction of uranium from aqueous solutions at various temperature and pH values

| pH | β-Diketone foam % extraction | Blank foam % extraction | Temperature (°C) |
|---|---|---|---|
| 1.4 | 2.3 ± 3.9 | −0.3 ± 3.4 | 4 |
| 3.0 | 90.0 ± 4.0 | 0.8 ± 9.5 | 4 |
| 5.3 | 63.8 ± 14.1 | 6.5 ± 6.1 | 4 |
| 8.3 | 35.0 ± 14.7 | −6.8 ± 4.1 | 4 |
| 11.0 | 40.8 ± 3.6 | 4.1 ± 5.8 | 4 |
| 1.4 | −0.7 ± 2.7 | 0.8 ± 3.2 | 22 |
| 3.0 | 79.9 ± 3.0 | −0.3 ± 15.5 | 22 |
| 5.3 | 91.1 ± 2.7 | 2.9 ± 4.0 | 22 |
| 8.3 | 75.2 ± 4.2 | −3.1 ± 5.1 | 22 |
| 11.0 | 56.1 ± 3.3 | 2.5 ± 3.0 | 22 |
| 1.4 | 1.6 ± 3.8 | 3.2 ± 3.1 | 40 |
| 3.0 | 86.0 ± 2.9 | −9.3 ± 20.5 | 40 |
| 5.3 | 96.2 ± 0.4 | 12.2 ± 11.1 | 40 |
| 8.3 | 91.3 ± 1.9 | 7.9 ± 9.7 | 40 |
| 11.0 | 71.7 ± 3.0 | 5.8 ± 2.3 | 40 |
| 1.4 | 0.3 ± 6.9 | −1.9 ± 6.8 | 60 |
| 3.0 | 63.9 ± 6.6 | −5.5 ± 22.6 | 60 |
| 5.3 | 92.6 ± 0.2 | 16.1 ± 3.8 | 60 |
| 8.3 | 79.3 ± 10.6 | 7.5 ± 5.0 | 60 |
| 11.0 | 35.6 ± 7.8 | 12.6 ± 10.0 | 60 |

followed by a drop at 60°C which may be attributed to the instability of the β-diketone foam at high temperatures. The decrease in extraction efficiency at the lower end of the pH range is due to a change in the uranium species and suggests using a solution with pH < 1 as a possible eluting solution to desorb uranium from the foam.

Blank foams (*i.e.* without the inclusion of 1-benzoylacetone) showed little capability in extracting uranium from aqueous solutions in comparison to the β-diketone foam. Overall, the β-diketone foams showed superior extractability of uranium over blank foam at all values of pH and temperatures tested as shown in Figs 2–5.

In general it was found that the variation in per cent extraction was higher for the blank foam when compared with the β-diketone foam. The ideal temperature was 40°C for maximum extraction of uranium by β-diketone foam for uranium solutions with pH $7 \pm 3$.

Gesser and Ahmed[22] have reported that Adogen-impregnated polyurethane foam is capable of extracting uranium from acidic solutions whose pH values range from pH 1 to 3. The β-diketone foam synthesized in this work extracts uranium from aqueous solutions whose pH values range from pH 3 to 10. Both foams (*i.e.* Adogen-impregnated and β-diketone foams) complement each other by extending the ability of modified foams to extract uranium from aqueous solutions with a wide range of pH values.

## CONCLUSIONS

1-Benzoylacetone was imbedded into the matrix of the polyurethane foam during the fabrication of the foam. The resulting β-diketone foam is capable of extracting uranium from aqueous solution between pH 3 and 10. The β-diketone foam would be useful for the sorption of uranium from natural waters as the pH of most natural waters is usually in the range of pH $7 \pm 3$. The β-diketone foam is simple to make, relatively inexpensive, has high porosity and has good chemical and mechanical stability. The above qualities make the β-diketone foam a promising sorbent for the separation and preconcentration of uranium for both analytical and large scale industrial applications, including the nuclear industry and in clean-up procedures for spills involving uranium.

*Acknowledgements*—The authors acknowledge the financial assistance provided by the Natural Sciences and Engineering Research Council of Canada. Hypol™ FHP 2002 prepolymer was a sample provided by W. R. Grace and Co. (MA, U.S.A.).

## REFERENCES

1. G. J. Moody and J. D. R. Thomas, *Chromatographic Separation and Extraction with Foamed Plastics and Rubbers*. Marcel Dekker, New York, 1982.
2. T. Braun, J. D. Navratil and A. B. Farag, *Polyurethane Foam Sorbents in Separation Science*. CRC Press, Boca Raton, FL, 1985.
3. S. Palágyi and T. Braun, *Preconcentration Techniques for Trace Elements*, Z. B. Alfassi and C. M. Wai (eds), CRC Press, Chapter 3. Boca Raton, FL, 1992.
4. T. Braun and A. B. Farag, *Talanta*, 1972, **19**, 828.
5. T. Braun, L. Bakos and Zs. Szabó, *Anal. Chim. Acta*, 1973, **66**, 57.
6. T. Braun and A. B. Farag, *Anal. Chim. Acta*, 1974, **69**, 85.
7. T. Braun and A. B. Farag, *Anal. Chim. Acta*, 1975, **76**, 107.
8. T. Braun, É. Huszár and L. Bakos, *Anal. Chim. Acta*, 1973, **64**, 77.
9. M. P. Maloney, G. J. Moody and J. D. R. Thomas, *Proc. Anal. Div. Chem. Soc.*, 1977, **14**, 244.
10. C-S. Xie, *Acta Chim. Sinica*, 1982, **40**, 605.
11. T. Braun and A. B. Farag, *Anal. Chim. Acta*, 1974, **71**, 133.
12. A. Chow and D. Buksak, *Can. J. Chem.*, 1975, **53**, 1373.
13. M. A. J. Mazurski, A. Chow and H. D. Gesser, *Anal. Chem. Acta*, 1973, **65**, 99.
14. T. Valente and H. J. M. Bowen, *Anal. Chim. Acta*, 1977, **90**, 315.
15. K. Srikameswaran and H. D. Gesser, *J. Environ. Sci. Hlth*, 1978, **A15**, 415.
16. G. N. Lypka, H. D. Gesser and A. Chow, *Anal. Chim. Acta*, 1975, **78**, 367.
17. T. Braun and A. B. Farag, *Anal. Chim Acta*, 1974, **73**, 301.
18. T. C. Huang, D. H. Chen, M. C. Shieh and C. T. Huang, *Sepn Sci. Technol.*, 1992, **27**, 1619.
19. J. Korkisch, I. Steffan and J. D. Navratil, *Radioact. Waste Manage.*, 1982, **6**, 349.
20. J. Korkisch and I. Steffan, *Solv. Ext. Ion Exch.*, 1983, **1**, 607.
21. S. Pearson and H. J. M. Bowen, *J. Radioanal. Nucl. Chem. Lett.*, 1985, **96**, 499.
22. H. D. Gesser and S. Ahmed, *J. Radioanal. Nucl. Chem.*, 1990, **140**, 395.
23. Hypol Plus™, *Laboratory Procedures and Foam Formulations*. W. R. Grace, MA, U.S.A., 1987.
24. I. Tabushi, Y. Kobuke and T. Nishiya, *Nature*, 1979, **280**, 665.
25. M. G. Djamali and K. H. Lieser, *Ang. Makromol. Chem.*, 1983, **116**, 195.
26. K. Schwochau, *Top. Curr. Chem.*, 1984, **124**, 91.
27. C. Kantipuly, S. Katragadda, A. Chow and H. D. Gesser, *Talanta*, 1990, **37**, 491.
28. L. Astheimer, H. J. Schenk, E. G. Witte and K. Schwochau, *Sepn Sci. Technol.*, 1983, **18**, 307.
29. P. H. Koske, K. Ohlrogge and K. V. Peinemann, *Sepn Sci. Technol.*, 1988, **23**, 1929.

30. T. Hirotsu, S. Katoh, K. Sugasaka, M. Senō and T. Itagaki, *J. Chem. Soc., Dalton Trans.*, 1986, 1609.
31. H. Omichi, A. Katakai, T. Sugo and J. Okamoto, *Sepn Sci. Technol.*, 1985, **20**, 163.
32. H. Omichi, A. Katakai, T. Sugo and J. Okamoto, *Sepn Sci. Technol.*, 1986, **21**, 299.
33. I. Tabushi, Y. Kobuke and T. Nishiya, *Tetrahedron Lett.*, 1979, **37**, 3515.
34. S. Marmor and G. Kidane, *Polym. Bull. (Berlin)*, 1978, **1**, 239.
35. S. Katragadda, Ph.D. Thesis. University of Manitoba, 1993.
36. S. B. Savvin, *Talanta*, 1961, **8**, 673.
37. A. Bermejo-Barrera, M. C. Yebra-Biurrun and L. M. Fraga-Trillo, *Anal. Chim. Acta*, 1990, **239**, 321.
38. J. A. Perez-Bustamente and F. Palomares-Delgado, *Analyst*, 1971, **96**, 407.
39. K. Sekine and H. Onishi, *Anal. Chim. Acta*, 1972, **62**, 468.
40. M. Suchanek, F. Sipek, L. Kabrt, V. Radil and J. Makovicka, *Sb. Vys. Sk. Chem-Technol. Praze, Anal. Chem.*, 1989, **H23**, 65; *Chem. Abstr.*, 1989, **111** 161517z.
41. I. Feldman, W. F. Neuman and J. R. Havill. Report UR-85, 1949; *Spectroscopy and Photochemistry of Uranyl Compounds*, E. Rabinowitch and R. L. Belford (eds). Pergamon Press, New York, 1964.
42. R. Djogic, L. Sipos and M. Branica, *Limnol Oceanogr.*, 1986, **31**, 1122.
43. J. Stary and E. Hladky, *Anal. Chim. Acta*, 1963, **28**, 227.

Pergamon

0039-9140(95)01479-9

*Talanta*, Vol. 42, No. 5, pp. 733–736, 1995

0039-9140/95 $9.50 + 0.00

# POTENTIOMETRIC AND COULOMETRIC TITRATION OF 2-THIOBARBITURIC ACID

WITOLD CIESIELSKI, JOANNA KOWALSKA and ROBERT ZAKRZEWSKI

Department of Instrumental Analysis, University of Łódź, Lindleya 3, 90-131 Łódź, Poland

(*Received* 22 *April* 1994. *Revised* 11 *November* 1994. *Accepted* 11 *November* 1994)

**Summary**—A new method for the determination of 2-thiobarbituric acid, using its reaction with iodine in an alkaline medium is presented. In the volumetric titration with potentiometric end-point detection, the determinability range is 10–400 μmol (1.4–58 mg). In coulometric titration using the biamperometric end-point detection, 0.1–20 μmol ($1.4 \times 10^{-2}$–2.9 mg) of 2-thiobarbituric acid was successfully determined.

2-Thiobarbituric acid (4,6-dihydroxy-2-mercapto-pyrimidin) is used in chemical analysis for spectrophotometric determination of copper,[1,2] iron,[2,3] bismuth,[4,5] and ruthenium[6] as well as many organic compounds including aldehydes and carbohydrates.

The tested compound has been determined previously by titration methods, using silver(I)[7] and mercury(II)[8] ions, iodine,[9,10] bromine chloride,[11] dichromate ions[12,13] and sodium methylate.[14] Spectrophotometric[15–22] and polarographic[23–26] methods, cathodic inversion voltamperometry[27] and chromatographic[28,29] methods have also been proposed. The determination has also been carried out using the induced iodine–azide reaction.[30–32] Hitherto developed iodometric back-titration methods for the determination of 2-thiobarbituric acid, consisted of introducing excess iodine to the tested sample and titration of the unreacted residue[9] after 10–20 min, or determination of the resultant iodide ions.[10]

In the present paper, the determination of 2-thiobarbituric acid by direct titration with iodine in an alkaline medium based on the apparent stoichiometry:

$$RS^- + 3I_2 + 6OH^- \rightarrow RSO_3^- + 6I^- + 3H_2O$$

is presented. Iodine disproportionates quickly in alkaline medium to give iodide and hypoiodite ions, so hypoiodite is the actual oxidizing agent. Since hypoiodite is a stronger oxidant than iodine in neutral medium the above reaction may be rapid and the proposed determination can be carried out.

In determinations of larger quantities of 2-thiobarbituric acid, volumetric titration with a potentiometric detection of the end-point was used. Lower amounts were determined by coulometric titration using biamperometric detection of the end-point.

## EXPERIMENTAL

### *Reagents*

Twice distilled water in glass apparatus, potassium iodide, sodium hydroxide. 2-Thiobarbituric acid purum (Fluka): a standard solution $2 \times 10^{-3}M$ was taken by dissolving a weighed amount of the reagent in $3M$ sodium hydroxide. Sodium salt of 5-ethyl-5′-(1-methylbutyl)-2-thiobarbituric acid (thiopental) (United Pharmaceutical Works, Praha). Iodine: standard solution $1 \times 10^{-1}M$ and $1 \times 10^{-2}M$.

### *Apparatus*

Universal coulometric analyser 'Radelkis' (Hungary), type OH-404. Electrolysis cell with two platinum electrodes with an area of 5 $cm^2$ each, working in generating circuit and with a OH-9381 double electrode in an amperometric indicator-circuit with two polarized electrodes. Mechanical stirrer. pH-meter type OP-206 'Radelkis' (Hungary) with platinum electrode and saturated calomel electrode.

### *Procedure*

*Volumetric determination.* A sample of 2-thiobarbituric acid (10–400 μmol) was dissolved in 50 ml of 3M NaOH solution and titrated with

iodine, using potentiometric detection of the end-point with a platinum indicator electrode and a saturated calomel electrode.

*Coulometric determination.* The coulometric titration was carried out in the reaction solution containing 1*M* KI and 3*M* NaOH. A sample solution containing 0.1–20 μmol of 2-thiobarbituric acid was introduced into 20 ml of the reaction solution placed in the anode part of the electrolysis cell. The polarization voltage applied to the indicator system electrodes was 200 mV. After starting the mechanical stirrer, stabilized current was passed through the solution. The current applied to the generating circuit (Table 1) depended on the quantity of the compound being determined and was adjusted so as to maintain the titration time from several to a dozen or so minutes. The charge ($Q$) was noted after completing the titration of 2-thiobarbituric acid up to an indicator current of 0.02 μA and a delay time of 5 sec.

The rate of the reaction between 2-thiobarbituric acid and hypoiodite close to the end of the coulometric titration is lower than the rate of hypoiodite generation. Therefore, the appearance of the excess of hypoiodite in the solution and the increase of the indication current cannot be considered to be the equivalence point of titration. Thus adtitration is necessary, which resolves into a renewed connection of current in the generation circuit if during the fixed period of time the indicator current decreases. This time is called the 'delay time'. The coulometric analyser, which was used made it possible to estimate the length of the delay time. The delay time was determined as the shortest time in which the correct results of the coulometric titration were obtained.

The 2-thiobarbituric acid content (μmol) in the tested sample was calculated according to Faraday's law:

Table 1. Results of coulometric determination of 2-thiobarbituric acid ($n = 6$)

| Taken (*μmol*) | Found $\bar{x} \pm t_{0.95} \cdot \bar{s}$ (*μmol*) | Relative standard deviation (%) | Current (*mA*) |
|---|---|---|---|
| 0.1000 | 0.1004 ± 0.0006 | 0.53 | 1 |
| 0.2000 | 0.1998 ± 0.0006 | 0.29 | 1 |
| 0.5000 | 0.5003 ± 0.0017 | 0.33 | 2 |
| 4.000 | 4.004 ± 0.016 | 0.38 | 10 |
| 10.00 | 9.987 ± 0.013 | 0.12 | 20 |
| 20.00 | 19.99 ± 0.023 | 0.11 | 20 |

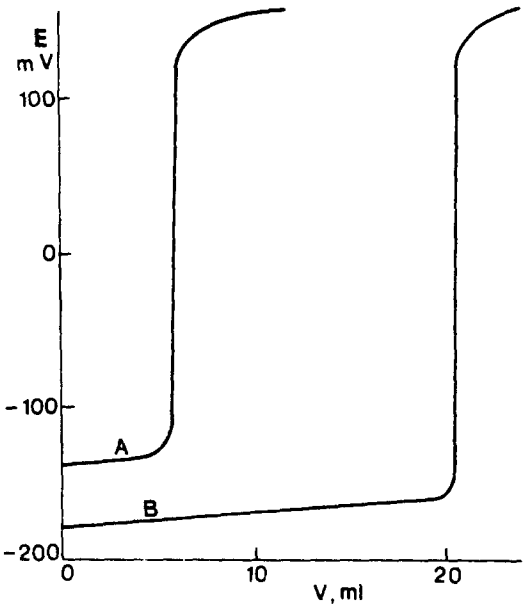


Fig. 1. Curves of potentiometric titration of (A) 10 *μmol* 2-thiobarbituric acid with $10^{-2}M$ iodine solution; (B) 400 *μmol* 2-thiobarbituric acid with $10^{-1}M$ iodine solution.

$$n = \frac{\Delta Q}{z \cdot F} 10^3,$$

where: $\Delta Q = Q - Q_0$ (mC), $Q_0$ is charge corresponding to blank titration, $z$ is number of electrons transferred in the reaction of 1 mol, $F$ is the Faraday constant ($F = 96485$ C/mol).

In order to compute the electric charge $Q_0$, a suitable amount of water instead of 2-thiobarbituric acid was introduced into the reaction solution placed in the anode part of the electrolysis cell.

## RESULTS AND DISCUSSION

It was found experimentally that the reaction rate of 2-thiobarbituric acid with iodine increases with an increase in concentration of sodium hydroxide. A concentration of sodium hydroxide greater than 2*M* provides a sufficiently high reaction rate enabling direct titration with iodine. In neutral and acidic medium, the reaction rate of iodine with 2-thiobarbituric acid was very low and iodometric titration was impossible.

### *Potentiometric titration*

In the volumetric titration of 10–400 μmol of 2-thiobarbituric acid, good results were obtained using the potentiometric detection of the end-point. Potentiometric titration curves are shown in Fig. 1 and the results of determinations are given in Table 2.

Table 2. Results of potentiometric determination of 2-thiobarbituric acid ($n = 6$)

| Taken ($\mu mol$) | Found $\bar{x} \pm t_{0.95} \cdot \bar{s}$ ($\mu mol$) | Relative standard deviation (%) |
|---|---|---|
| 350.0 | $349.7 \pm 0.9$ | 0.25 |
| 35.0 | $35.01 \pm 0.14$ | 0.37 |
| 10.0 | $10.03 \pm 0.11$ | 1.02 |

Direct titration considerably reduced the duration of analysis, and the use of potentiometric end-point detection improved the accuracy of determination in comparison with the methods using visual detection.[9,11,14] The proposed determination provided a higher rise in potential near the end-point (about 200 mV/0.05 ml of the titrant) than the potentiometric titration with mercury(II) ions.[8]

*Coulometric determination*

The use of potentiometric end-point detection in coulometric titration of lower amounts of 2-thiobarbituric acid has turned out to be impossible, owing to the slow settling of the platinum indicator electrode potential at low concentrations of the tested compound. The use of the biamperometric indicator system made it possible to obtain correct results in the coulometric determination of 2-thiobarbituric acid within the range of 0.1–20 $\mu$mol. The results of coulometric determination are given in Table 1. The coulometric method presented is characterized by a high accuracy and short analysis time. The reaction solution containing potassium iodide and sodium hydroxide is stable with time; unlike the acidic solutions, the alkaline one shows no oxidation of iodide ions with oxygen.

*Titration of a derivative of 2-thiobarbituric acid*

It was also examined whether potentiometric titration with iodine in the alkaline medium could be used for the determination of sodium salt of 5-ethyl-5′-(1-methylbutyl)-2-thiobarbituric acid (thiopental).

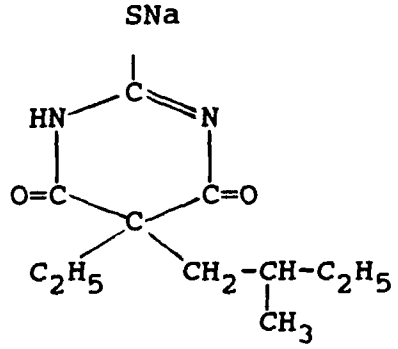


thiopental

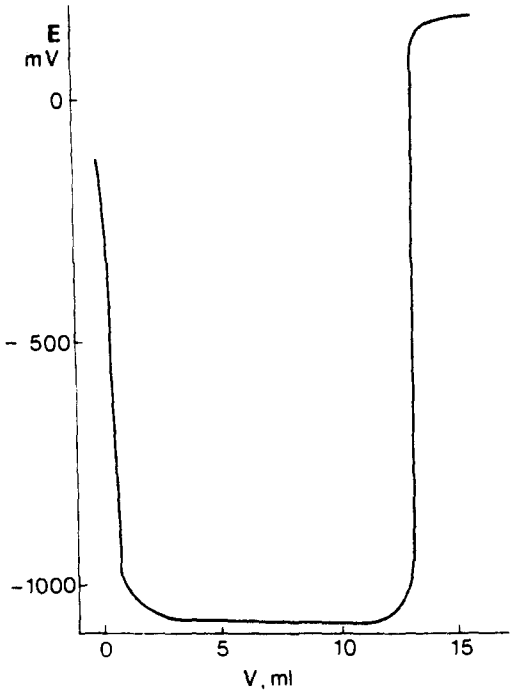


Fig. 2. Curve of potentiometric titration of 0.05 g of thiopental with $10^{-1}M$ iodine solution.

Again, in this case, the reaction rate increased with an increase in concentration of sodium hydroxide. To provide sufficient reaction rate employing the potentiometric titration, the concentration of sodium hydroxide had to be at least $5M$. Titrations of this compound were carried out at 5 and $10M$ NaOH and the identical titration curves obtained are shown in Fig. 2.

The shape of the potentiometric titration curve is noteworthy. A small amount of iodine (oxidizer) added brings about a strong potential drop in the initial part of the curve. The end-point of titration corresponding to the maximum potential increase indicates that the number of electrons transferred in the reaction of 1 mol thiopental is equal to 7.43. The titration results are reproducible, but the titration runs more slowly than that of 2-thiobarbituric acid, owing to the lower reaction rate.

When excess iodine is added to the thiopental solution and the unreacted hypoiodite is back-titrated after 15 min,[9,33] the process proceeds according to the 8-electron apparent stoichiometry:

$$RS^- + 4I_2 + 10OH^- \rightarrow RO^- + SO_4^{2-} + 8I^- + 5H_2O.$$

The coulometric determination of thiopental failed owing to the iodine reaction being too slow. It is interesting to note that 2-thiobarbituric acid behaves differently from thiopental during the titration with iodine in a very strong alkaline medium.

In the potentiometric titration of 2-thiobarbituric acid in 5 and 10*M* NaOH the curve shape (Fig. 1) and the number of electrons transferred in the reaction of 1 mol of compound ($z = 6$) were unchanged.

The only difference in the structure of these compounds is the presence of two alkyl substituents at the fifth carbon atom in the thiopental molecule. This makes the formation of tautomeric forms impossible, unlike in the case of 2-thiobarbituric acid,

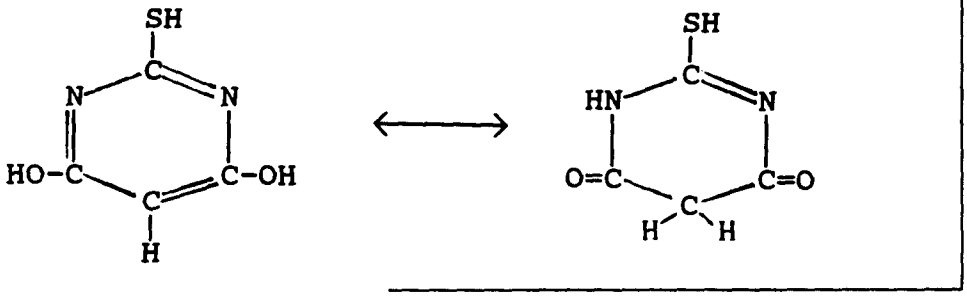


and hence the titration curves are completely different.

## CONCLUSIONS

Comparing the proposed determination of 2-thiobarbituric acid with the methods previously reported[7–32] one may conclude that it is characterized by a short analysis time, a simple procedure, commonly available reagents and determination over a wide order of magnitude (0.1–400 μmol in a sample). The accuracy of coulometric determinations is higher than reported previously.

## REFERENCES


1. H. Sikorska-Tomicka, *Mikrochim. Acta*, 1969, 718.
2. B. Morelli, *Analyst*, 1983, **108**, 870.
3. H. Sikorska-Tomicka, *Fresenius' Z. Anal. Chem.*, 1968, **234**, 414.
4. H. Sikorska-Tomicka, *Mikrochim. Acta*, 1969, 715.
5. B. Morelli, *Analyst*, 1982, **107**, 282.
6. B. Morelli, *Analyst*, 1983, **108**, 386.
7. V. V. Cosofret and A. A. Bunaciu, *Anal. Lett.*, 1979, **12**, 617.
8. S. Pinzauti, V. D. Piaz and E. L. Porta, *J. Pharm. Sci.*, 1973, **62**, 997.
9. H. Wojahn and E. Wempe, *Archiv Pharm*, 1955, **288/60**, 1.
10. S. S. M. Hassan, *Mikrochim. Acta*, 1977, **5–6**,405.
11. K. K. Verma, A. Srivastava, J. Ahmed and S. Bose, *Talanta*, 1978, **25**, 469.
12. P. C. Gritzapis, C. E. Efstathiou and T. P. Hadjiioannou, *Anal. Chim. Acta*, 1985, **171**, 165.
13. H. Sikorska-Tomicka, M. Samsonowicz and R. Świsłocka, *Zesz. Nauk. Polit. Białostockiej*, 1992, **13**, 17.
14. J. S. Fritz, *Anal. Chem.*, 1952, **24**, 674.
15. M. Qureshi, H. S. Rathore, A. Mohammad and V. P. Singh, *Ann. Chim. (Rome)*, 1978, **68**, 763.
16. C. S. P. Sastry, P. Satyanarayana and M. K. Tummuru, *Acta Cienc. Indica, Chem.* 1985, **11**, 26; *Chem. Abstr.* 1987, **107**, 70015k.
17. C. S. P. Sastry, P. Satyanarayana and M. K. Tummuru, *Indian. J. Chem.*, 1985, **24A**, 258.
18. C. S. P. Sastry, P. Satyanarayana and M. K. Tummuru, *Analyst*, 1985, **110**, 189.
19. C. S. P. Sastry, P. Satyanarayana, N. R. P. Singh and A.R. M. Rao, *Acta Cienc. Indica, Chem.* 1988, **14**, 37; *Chem. Abstr*, 1989, **111**, 180870a.
20. C. S. P. Sastry, P. Satyanarayana, A. R. M. Rao, N. R. P. Singh and K. Hemalatha, *Acta Cienc. Indica, Chem.*, 1988, **14**, 227; *Chem. Abstr.* 1990, **112**, 245454k.
21. H. Sikorska-Tomicka and W. Wawrzyńczak, *Chem. Anal.*, 1991, **36**, 41.
22. J. Soriano, F. Jimenez, A. I. Jimenez and J. J. Arias, *Spectros. Lett.*, 1992, **25**, 257.
23. W. F. Smyth, G. Svenhla and P. Zuman, *Anal. Chim. Acta*, 1970, **52**, 129.
24. K. Takamura and M. Sakamoto, *Tokyo Yakka Daigaku Kenkyu Nempo*, 1972, **22**, 177; *Chem. Abstr.*, 1974, **80**, 19653p.
25. C. A. Mairesse-Ducarmois, G. J. Patriarche and J. L. Vandenbalck, *Anal. Chim, Acta*, 1975, **79**, 69.
26. H. Sohr and K. Wienhold, Sitzungsber. *Akad. Wiss, DDR, Math., Naturwiss, Tech.*, 1982, **2N**, 40; *Chem. Abstr.* 1983, **98**, 140023h.
27. T. M. Florence, *J. Electroanal. Chem.*, 1979, **97**, 219.
28. E. Interschick, H. Wuest and H. Wimmer, *GIT Labor-Med.*, 1981, **4**, 412; *Chem. Abstr.* 1982, **96**, 98864y.
29. S. P. Srivastava and Reema, *J. Liq. Chromatogr.*, 1985, **8**, 1265.
30. Z. Kurzawa and A. Dobrzańska-Jajszczyk, *Chem. Anal.*, 1974, **19**, 1071.
31. J. Kurzawa, *Anal. Chim. Acta*, 1985, **173**, 343.
32. J. Kurzawa and Z. Kurzawa, *Chem. Anal.*, 1986, **31**, 45.
33. F. Jancik, J. Korbl and J. Hodonicka, *Ceskoslov. Farm.*, 1964, **13**, 70.

Pergamon

0039-9140(95)01482-9

*Talanta*, Vol. 42, No. 5, pp. 737–745, 1995

0039-9140/95 $9.50 + 0.00

# ENHANCED SPECTROPHOTOMETRIC DETERMINATION OF NICOTINIC ACID IN A SODIUM DODECYL SULPHATE MICELLAR MEDIUM

J. S. ESTEVE-ROMERO,[1] LL. MONFERRER-PONS,[1] G. RAMIS-RAMOS[2] and M. C. GARCÍA-ALVAREZ-COQUE[2]*

[1]Departament de Ciències Experimentals, Escola Superior de Tecnologia i Ciències Experimentals, Universitat Jaume I, 12080 Castelló, Spain

[2]Departament de Química Analítica, Facultat de Química, Universitat de València, 46100 Burjassot, València, Spain

(*Received* 15 *August* 1994. *Revised* 16 *November* 1994. *Accepted* 16 *November* 1994)

**Summary**—The spectrophotometric determination of pyridine and pyridine derivatives by means of the König reaction was studied in micellar media of sodium dodecyl sulphate (SDS), *N*-cetylpyridinium chloride and Triton X-100. The sensitivity was largely increased in SDS micellar medium. The attack of the pyridine ring with cyanogen bromide to produce a glutaconic aldehyde was not affected by the presence of SDS, but the yield of the coupling reaction with an arylamine to produce a polymethine dye was largely increased. In the SDS micellar medium, aniline was superior to other coupling reagents. The limits of detection (LODs) were $6 \times 10^{-7}$, $1 \times 10^{-6}$ and $5 \times 10^{-7}M$ for pyridine, pyrrol-ylmethylpyridine and nicotinic acid, respectively, and the reproducibility for $2 \times 10^{-5}M$ solutions was *ca.* 2%. In the absence of SDS, the LODs were $3 \times 10^{-6}$, $3 \times 10^{-6}$ and $9 \times 10^{-6}M$, respectively, and the reproducibility was *ca.* 3.5%. Application was made to the determination of nicotinic acid in pharmaceuticals.

The spectrophotometric determination of pyridine and pyridine derivatives can be performed previous derivatization with the König reaction[1,2] (Fig. 1). Pyridine derivatives with a hydrogen in at least one of the positions adjacent to the heterocyclic nitrogen react with cyanogen bromide to produce a derivative of glutaconic aldehyde. The stability of this compound is frequently poor, but a stable polymethine dye can be obtained by coupling with an arylamine or a compound containing an active methylene group. Polymethine dyes absorb in the 450–550 nm wavelength range. Coupling agents differ in their toxicity, and in the sensitivity and stability of the final product. Aniline,[3] benzidine,[4] *o*-toluidine,[5] barbituric acid, sulphanilic acid,[6] *p*-phenylenediamine,[7] anthranilic acid,[8] 4,4′-diaminostilbene-2,2′-disulphonic acid,[9] 2,2-dimethyl-1,3-dioxane-4,6-dione,[10] 4-aminosalicylic acid,[11] and 6-amino-1-naphthol-3-sulphonic acid[12] have been recommended.

In the last five years, an extensive investigation has been carried out in our laboratory on the improvement of analytical procedures through the use of micellar media. In the presence of surfactants, equilibrium, kinetic and spectral properties can be modified. Some favourable effects are the inhibition of undesirable reactions, such as hydrolysis and photolysis, stabilization of reaction intermediates, co-solubilization of non-polar and polar derivatization reagents, products and samples, and increase in reaction rates by means of micellar catalysis.[13] In some cases, use is made of the modification of a single parameter to improve an analytical procedure, but most frequently, the simultaneous alteration of various physico-chemical properties of the reagents, intermediates and products, is involved. Spectrophotometric procedures for the determination of organic compounds that have been improved by the use of micellar media are the coupling of the diazotized arylamines with *N*-(1-naphthyl)ethylenediamine,[14] the coupling of phenols with diazotized 2,4,6-trimethylaniline,[15] 4-aminoantipyrine, 2,6-dihalochinone chlorimides and 1-nitroso-2-naphthol,[16] the coupling of pyrroles with 4-(dimethylamino)benzaldehyde,[17] the nitrosation of *N*,*N*-diethylaniline,[18] the oxidation of pyridoxal in the presence of cyanide,[19]

*Author to whom correspondence should be addressed.

and the reduction of 5,5′-dithiobis-(2-nitrobenzoic acid) with sulphur dioxide.[20]

Nicotinic acid is one of the many bioactive substances that can be determined by means of the König reaction. Nicotinic acid or niacin is a vitamin found in minute amounts in liver, yeast, milk, adrenal glands, white meat, legumes, whole cereals and corn. Poor dietary habits produce pellagra and may be corrected by administration of multivitamin preparations containing nicotinic acid. Increased requirements of this vitamin may be associated with hyperthyroidism, diabetes mellitus, cirrhosis, pregnancy, and lactation.

In this work, the effects of the presence of surfactants on the spectrophotometric analytical procedure for the determination of pyridine derivatives, by using the König reaction are studied. Aniline is demonstrated to be superior to other coupling reagents when used in sodium dodecyl sulphate (SDS) micellar solutions. Application is made to the determination of nicotinic acid in pharmaceuticals.

## EXPERIMENTAL

### *Reagents and apparatus*

The substrates were pyridine, nicotinic acid and pyrrol-ylmethylpyridine (Janssen Chimica, New Brunswick, NJ, U.S.A.). Cyanogen bromide (Fluka, Buchs, Switzerland) was used as the hydrolysis reagent. The coupling reagents were: *p*-aminophenol, aniline, *p*-phenylenediamine, *p*-toluidine (Panreac, Barcelona, Spain), sulphanilamide (Sigma, St Louis, MO, U.S.A.), *p*-aminobenzoic acid, sulphanilic acid (Fluka), and *p*-aminoacetophenone (Janssen Chimica). The surfactants were: sodium dodecyl sulphate (Merck, Darmstadt, Germany), *N*-cetylpyridinium chloride (Scharlau, Barcelona) and Triton X-100 (Panreac). Distilled deionized water (Barnstead, Sybron, Boston, MA, U.S.A.) was used throughout. A spectrophotometer UV-Vis-nir Lambda 19 (Perkin Elmer, Norwalk, CT, U.S.A.), and a Crison model micropH 2001 potentiometer (Barcelona, Spain), provided with a combined Ag/AgCl/glass electrode, were used.

### *Procedure*

The derivatives were prepared by mixing in a 25-ml volumetric flask, 5 ml of 0.2*M* acetic acid–sodium acetate buffer (pH 4.5), 5 ml of 0.5*M* SDS or 5 ml of water, 0–5 ml of pyridine, pyrrol-ylmethylpyridine or nicotinic acid, and 5 ml of 0.25*M* BrCN. After 10 min (time required to complete the hydrolysis of the substrate), 2 ml of 0.6*M* aniline was added for pyridine and pyrrol-ylmethylpyridine, and 0.4 ml for nicotinic acid. The mixture was allowed to react for 15 min, and the volume was completed up to the mark to measure the absorbance.

## RESULTS AND DISCUSSION

### *Optimization of the analytical procedure*

The optimization studies were performed using three model compounds: pyridine, pyrrol-ylmethylpyridine and nicotinic acid. Hydrolysis of these compounds to the corresponding glutaconic aldehyde derivatives, and the coupling of the derivatives with aniline to yield the polymethine dyes was studied spectrophotometrically in the presence and absence of SDS at room temperature. The absorbance of a blank solution prepared in the absence of the model compounds was also measured, and was checked to be always negligible. The wavelength of maximum absorption of the dyes changed in the different media studied (Table 1).

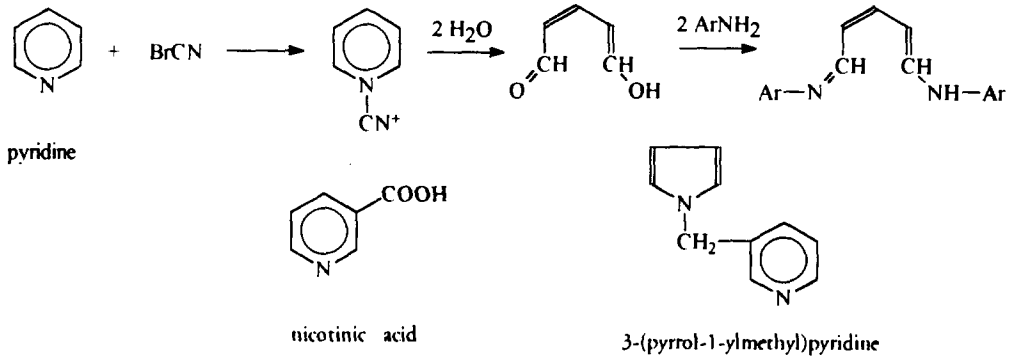


Fig. 1. Scheme of reaction for the hydrolysis of pyridine derivatives with cyanogen bromide, and coupling with an arylamine.

Table 1. Wavelengths of maximum absorption (nm) for the aniline polymethine dyes in the presence of surfactants*

| Compound | Non-micellar | Sodium dodecyl sulphate | *N*-Cetylpyridinium chloride | Triton X-100 |
|---|---|---|---|---|
| Pyridine | 480 | 485 | 480 | 490 |
| Pyrrol-ylmethylpyridine | 440 | 485 | 465 | 480 |
| Nicotinic acid | 430 | 440 | 460 | 470 |

*Wavelengths measured at pH 4.5 and for 0.1*M* surfactant solutions.

The influence of the time of hydrolysis and time of coupling on the final absorbance of the polymethine dyes was studied. First, the reaction time between the addition of BrCN and the addition of aniline was varied. Figure 2a shows the results obtained for nicotinic acid. The hydrolysis reaction was completed after 5 min, the absorbance being constant at least in the 5–45 min range in both SDS micellar and non-micellar media. The reaction rate was similar for both media, however, an important enhancement in the sensitivity of the reaction was observed in the micellar medium. Similar results were obtained for pyridine and pyrrol-ylmethylpyridine in the micellar medium.

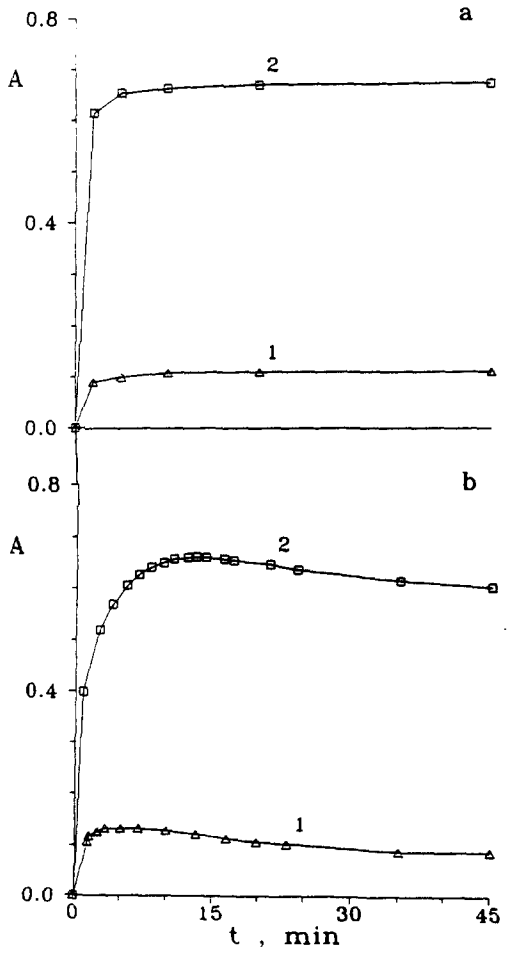


Fig. 2. Influence of the time of hydrolysis (a) and time of coupling (b) for $2 \times 10^{-5}M$ nicotinic acid in: (1) a non-micellar solution, and (2) a 0.05*M* SDS micellar solution.

Secondly, the absorbance was monitored for some time after the addition of aniline. For the three model compounds in an SDS micellar medium, a coupling time of 15 min was required, however, the derivative was not stable, and a slow decomposition began after a flat maximum (Fig. 2b). In the non-micellar solution, the derivatives were formed in less than 3 min, but they also showed a slow decomposition. The derivatives of pyrrol-ylmethylpyridine and nicotinic acid decomposed more rapidly in the absence of surfactant than in the micellar medium.

The concentration of BrCN was optimized by adding different volumes of 1*M* BrCN, to cover the 0–0.25*M* concentration range. In both SDS micellar and non-micellar media, and for the three model compounds, maximum absorbance was observed for concentrations of BrCN close to 0.05*M*. This concentration was used in the next series of experiments.

The aniline concentration was optimized within the 0–0.3*M* range. In the micellar medium, an increase in the absorbance of the pyridine dye was observed at increasing concentrations of aniline up to a concentration of 0.05*M*, the signal being almost constant within the 0.05–0.3*M* aniline concentration range. In the non-micellar medium, the absorbance of the pyridine dye increased up to 0.1*M* aniline, and was constant in the 0.1–0.3*M* range. For nicotinic acid, the absorbance was constant in the 0.005–0.02 and 0.01–0.03*M* aniline concentration ranges in the micellar and non-micellar media, respectively, and decreased slowly at higher aniline concentrations. A 0.05*M* aniline concentration was selected as adequate for the determination of pyridine and the pyridine derivatives, and was used in the recommended procedure.

*Influence of pH*

Both the hydrolysis and coupling reactions can be influenced by the pH of the solutions.

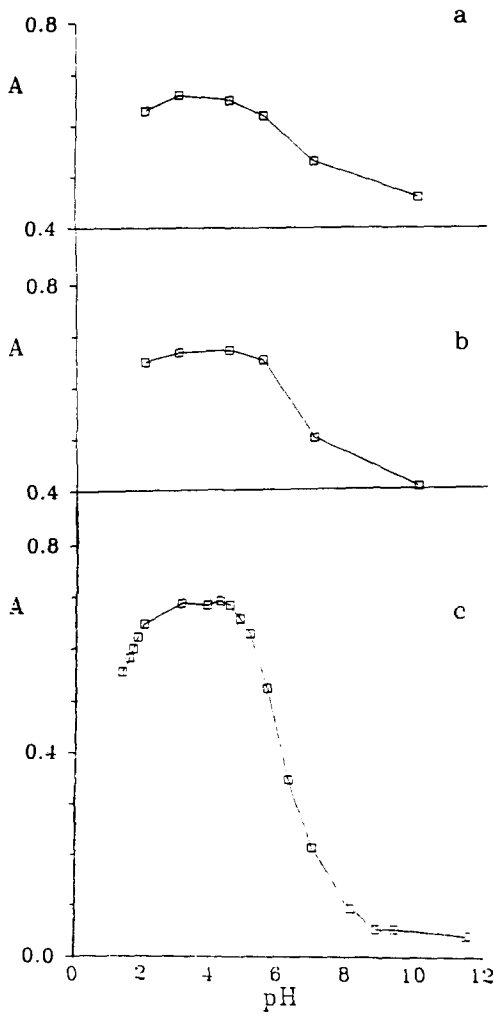


Fig. 3. Dependence of the absorbance of the polymethine dye of nicotinic acid on (a) the pH of the hydrolysis reaction, and (b) the pH of the coupling reaction (for a and b, the pH of measurement was 4.5). (c) Titration of the polymethine dye of nicotinic acid formed at pH 4.5, with NaOH (the absorbance was corrected for dilution). The concentrations of nicotinic acid and SDS were always $2 \times 10^{-5}M$ and $0.05M$ SDS, respectively.

First, the optimum pH for hydrolysis with BrCN was studied in a $0.1M$ SDS medium, by adding to the nicotinic acid solution 5 ml of a universal buffer ($0.1M$ acetic acid–$0.1M$ $NaHCO_3$–$0.1M$ $Na_2B_4O_7$), and HCl or NaOH to achieve a constant pH during hydrolysis in the 2–10 pH range. After 15 min from the addition of BrCN, the pH was adjusted to 4.5, aniline was added, and 10 min later the absorbance was measured. Figure 3a shows that the optimum pH range for hydrolysis was 3–5.

A similar study was performed for the coupling reaction. Nicotinic acid was hydrolyzed at pH 4.5, 5 ml of universal buffer was added, and the pH was adjusted to several values within the 2–10 pH range with HCl or NaOH. Aniline was added, after 15 min the pH of the solution was fixed to 4.5 and the absorbance was measured. The dependence of the absorbance with pH was similar to that observed for the hydrolysis reaction (Fig. 3b).

The polymethine dyes formed by coupling with aniline exhibited a decrease of the molar absorptivity in the pH 4.5–9 range, which was attributed to the deprotonation of the secondary arylamino group, For the nicotinic acid dye this equilibrium coincided with the deprotonation of the carboxylic group. The protonation equilibria were observed by titration with NaOH, by using simultaneous potentiometric and spectrophotometric monitoring. First, after 15 min of addition of aniline to the glutaconic aldehyde formed at pH 4.5, a small volume of HCl was added to lower the pH of the polymethine dye solution to 1. Then, the solution of the dye was titrated in the presence of the universal buffer with $0.25M$ NaOH, and the absorbance was measured at the wavelength of maximum absorbance (see Table 1). Figure 3c shows the absorbance–pH titration curve for the nicotinic acid dye, obtained in the SDS micellar medium. It may be observed that the absorbance was constant in the pH 3–4.5 range, and decreased abruptly outside this range. In the recommended procedure, an acetic acid/acetate buffer was used to regulate the final pH to 4–4.5.

In an acidic SDS micellar medium, the spectrum of the polymethine dye of nicotinic acid showed a maximum at 440 nm, which shifted to longer wavelengths at increasing pH values. Also, in a basic solution a new maximum appeared at 350 nm. The pyridine dye showed a wavelength of maximum absorption at 485 nm in acidic and weakly basic solutions, and a new maximum at 405 nm in a more basic medium. The pyrrol-ylmethylpyridine dye showed a maximum at 485 nm, which shifted to shorter wavelengths at increasing pH values.

For the polymethine dye of pyridine, the protonation constant of the arylamino group was evaluated according to García *et al.*,[21] being $\log K = 9.7 \pm 0.3$ and $7.6 \pm 0.2$ in a $0.1M$ SDS micellar and non-micellar media, respectively. The earlier protonation of the dye in the micellar solution indicated that the protonated cationic species was more strongly associated to the anionic SDS micelles than the basic non-ionic species. In the micellar medium, the protonation constants of the arylamino group of the polymethine dyes of nicotinic acid and pyrrol-

ylmethylpyridine were $\log K = 5.8 \pm 0.2$, and $7.8 \pm 0.1$, respectively. The protonation constant of the nicotinic acid dye should be slightly biased due to the almost simultaneous protonation of the carboxylate group. These constants could not be obtained in the absence of surfactant due to precipitation.

Usually, protonation of alkyl-arylamino groups takes place around pH 5–6. The larger values obtained both in the micellar and non-micellar media can be explained as owing to the large conjugated system of the polymethine dye molecule, where the positive charge of the acidic proton can be easily accepted and stabilized.

*Effect of the surfactant character*

A comparative study of the hydrolysis and coupling reactions, and the enhancement of the absorbance signal of the polymethine dyes was performed in micellar solutions of an anionic (SDS), cationic (*N*-cetylpyridinium chloride, NCPC) and non-ionic surfactant (Triton X-100). The experimental conditions (pH, BrCN and aniline concentrations) were those optimized above, and the concentration of the surfactants was always above the critical micellar concentration (cmc).

The influence of the concentration of the surfactant on the absorbance of the final product was first studied. The results for nicotinic acid can be observed in Fig. 4. The larger enhancement of the signal corresponded to SDS solutions. For this surfactant, a large and constant absorbance was achieved just above the cmc ($8 \times 10^{-3} M$). At the pH of the reaction, both the aniline and the polymethine dyes were protonated, and thus they were strongly bound to the anionic SDS micelles. On the other hand, at pH 4.5 the glutaconic aldehyde derivatives produced by pyridine and pyrrol-ylmethylpyridine are non-ionic, and should be associated to the SDS micelles by hydrophobic interactions. At this pH, the glutaconic aldehyde of nicotinic acid could be anionic, however, protonation of the carboxylate group of this derivative should take place at a higher pH in the SDS micellar medium than in non-micellar medium. The sensitivity enhancement produced by the SDS micelles could be explained in terms of an increase of both the reaction yield and the molar absorptivity of the polymethine dye. The experiments below were addressed to identify the main cause of the enhancement in sensitivity.

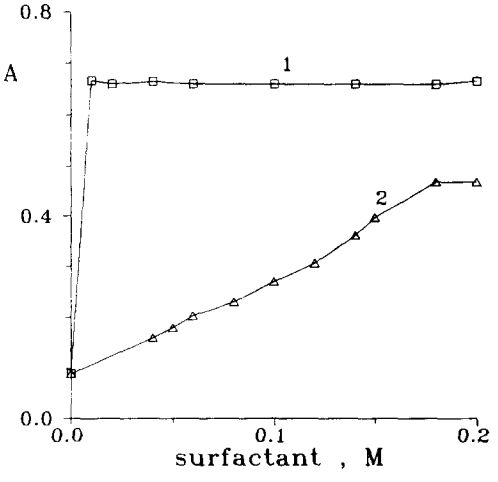


Fig. 4. Influence of the surfactant concentration on the absorbance of the polymethine dye of nicotinic acid for (1) SDS, and (2) NCPC.

For NCPC, the absorbance increased slowly with the concentration of surfactant. At the pH of the reaction, both the aniline and the polymethine dyes should be rejected by the cationic NCPC micelles. Thus, the increase of either the reaction yield or the molar absorptivity of the dye when the NCPC concentration increased was an unexpected result. This suggested that the sensitivity increase was mainly due to the association of the non-ionic glutaconic aldehyde to the surfactant assemblies, which is consistent with the hypothesis of the modification of the reaction pathway. Owing to the hydrophobic interactions, and independently from the charge of the surfactant, the association of the non-ionic form of the glutaconic aldehyde should increase when the concentration of the surfactant increases. It was checked that the polymethine dye of nicotinic acid was formed rapidly in the NCPC micellar solution, and the stability during the first 30 min was similar to that observed with SDS. Finally, a precipitate appeared in Triton X-100 solutions for a concentration of the surfactant larger than $0.02 M$, and no enhancement in the absorbance was observed for lower concentrations.

A series of experiments were performed to investigate the effect of the presence of SDS and NCPC on the hydrolysis and coupling reactions. The study was performed with nicotinic acid, by adding the surfactant at several points of the procedure: (1) before the addition of BrCN, to perform the hydrolysis and coupling reactions in the presence of the surfactant; (2) before the addition of aniline, thus only the coupling reaction occurred in the presence of the surfactant; (3) 10 min after the addition of aniline, to

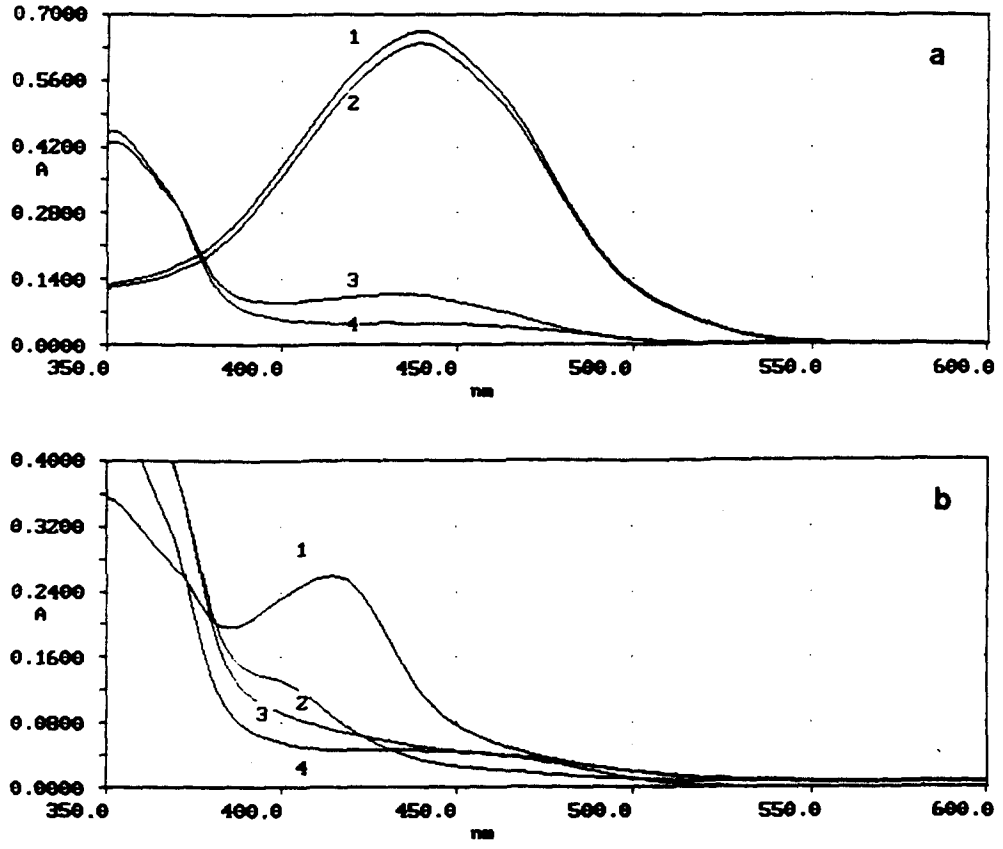


Fig. 5. Modification of the spectrum of the polymethine dye of $2 \times 10^{-5}M$ nicotinic acid in a micellar medium of (a) $0.1M$ SDS, and (b) $0.1M$ NCPC, when the surfactant was added (1) before hydrolysis, (2) before coupling, (3) before the measurement of the absorbance, and (4) no surfactant added.

observe the effect of the surfactant on the absorbance of the polymethine dye formed in a non-micellar medium; (4) the whole experiment was performed in the absence of surfactant.

The effect of the presence of the surfactant can be found out by observing the spectra of the dyes (Fig. 5). The similarity of the spectra obtained with procedures 1 and 2, when SDS was used, indicated that the hydrolysis reaction was not affected by the presence of the anionic surfactant (Fig. 5a). On the other hand, the comparison, in the same figure, of the spectra obtained with procedures 3 and 4 indicated that the absorbance of the polymethine dye formed in a non-micellar medium was only slightly enhanced in the presence of SDS. Therefore, most of the enhancement in the absorbance was produced by an increase in the reaction yield. This enhancement occurred when the surfactant was added before the hydrolysis of the pyridine derivative and also when it was added before the coupling reaction. Once finished the coupling reaction, the addition of the surfactant scarcely affected the absorbance of the solutions. Since no increase in the absorbance was produced by addition of SDS after the addition of aniline, a modification of the reaction pathway rather than an equilibrium shift should take place. Thus, the coupling reaction is in fact a competitive process in which the glutaconic aldehyde forms the polymethine dye and other less coloured or even colourless products.

The behaviour was completely different for NCPC, where the enhancement of the absorbance was mainly achieved when the surfactant was added before the hydrolysis (Fig. 5b). This adds a new evidence about the association of the glutaconic aldehyde derivative to the NCPC micelles.

*Use of other coupling reagents*

A study was performed on the influence of the nature of the coupling reagent on the formation of the polymethine dye in the SDS micellar medium. First, only two arylamines were taken, *i.e.* sulphanilamide and *p*-toluidine, more and less polar than aniline, respectively, to study the

time required for coupling. The results obtained in an SDS micellar and in non-micellar medium with these reagents were compared with those obtained with aniline. The model compound was pyridine.

The *p*-toluidine dye was sparingly soluble in a non-micellar medium, thus for this reagent, the analytical procedure required the presence of SDS. In the micellar medium, the coupling reaction with *p*-toluidine was very slow, being only completed after 40 min. When sulphanilamide was used in a non-micellar solution, 30 min was required to stabilize the absorbance, whereas in the presence of SDS the signal was constant after 20 min. Finally, when aniline was the coupling reagent, 5 and 20 min was required to achieve a constant absorbance, in the absence and presence of SDS, respectively. For the three arylamines, the final product was more stable in the micellar medium.

Secondly, the evaluation of the absorbance enhancement obtained with other arylamines was performed by measuring the signal 45 min after the addition of the coupling agent. The reagents studied were: *p*-aminoacetophenone, *p*-aminobenzoic acid, *p*-aminophenol, aniline, *p*-phenylenediamine, sulphanilamide, sulphanilic acid, and *p*-toluidine. Increasing volumes of the coupling agents were added to the glutaconic aldehyde solution to make a final concentration in the 0–0.3$M$ range.

The results are shown in Table 2. All the reagents gave the coupling reaction in the micellar medium. The micellar medium allowed the use of coupling reagents that formed sparingly soluble dyes in the absence of surfactant (*p*-toluidine and *p*-aminophenol). Most of the reagents studied gave maximum absorbance in the 0.05–0.1$M$ reagent concentration range. It should be remarked that only the use of aniline allowed a wide concentration range of the coupling reagent, giving the same absorbance signal (0.05–0.3$M$). In other cases, the sensitivity depended largely on the concentration of the coupling reagent. For some reagents, a constant absorbance was achieved above a given concentration of the reagent, but for other reagents, the absorbance increased continuously with their concentration (*p*-aminoacetophenone, *p*-aminophenol and sulphanilamide). Also, for some reagents, the polymethine dye or the reagent itself precipitated (sulphanilic acid and sulphanilamide). The sensitivity enhancement was large in all cases (usually 1.7- to 3.7-fold), but it was especially high for the *p*-phenylenediamine dye (13-fold), which could be a result of the very strong association of this reagent to the SDS micelles by both electrostatic and hydrophobic interactions. However, the molar absorptivity of the *p*-phenylenediamine dye in the SDS solution was similar to the aniline dye, and the reagent concentration range was more critical.

In the past, several reagents were proposed to substitute the use of aniline in the König reaction due to its low sensitivity. The results given

Table 2. Influence of different coupling reagents on the formation of polymethine dyes of pyridine (the concentration of pyridine was $2 \times 10^{-5}M$)

| Coupling reagent | Medium | Optimum concentration range ($M$) | Molar absorptivity ($M^{-1}\,cm^{-1}$) (reagent concentration, $M$) |
|---|---|---|---|
| *p*-Aminoacetophenone | SDS | * | 55000 (0.08†) |
| | Non-micellar | * | 31000 (0.08†) |
| *p*-Aminobenzoic acid | SDS | 0.05–0.1† | 52000 (0.1) |
| | Non-micellar | 0.05–0.1† | 31000 (0.1) |
| *p*-Aminophenol | SDS | * | 2600 (0.02‡) |
| | Non-micellar | | |
| Aniline | SDS | 0.05–0.3† | 37000 (0.05) |
| | Non-micellar | 0.1–0.3† | 10000 (0.1) |
| *p*-Phenylenediamine | SDS | 0.02–0.06† | 34000 (0.06‡) |
| | Non-micellar | 0.02–0.06† | 2600 (0.06‡) |
| Sulphanilic acid | SDS | * | 8400 (0.06§) |
| | Non-micellar | 0.06–0.08§ | 2600 (0.06) |
| Sulphanilamide | SDS | * | 43000 (0.1†) |
| | Non-micellar | * | 21000 (0.1†) |
| *p*-Toluidine | SDS | 0.004–0.007† | 63000 (0.02) |
| | Non-micellar | — | |

*There was no coupling reagent concentration range for which a constant absorbance was obtained.
†Maximum coupling reagent concentration studied.
‡The absorbance of the blank solution was excessive at larger concentrations of the coupling reagent.
§A precipitate appeared for larger concentrations of the coupling reagent.

Table 3. Evaluation of nicotinic acid in pharmaceutical formulations

| Formulation (laboratory) | Composition | Recovery* (%) | CV (%) $n = 3$ |
|---|---|---|---|
| Espasmo Digestomen (Menarini, Badalona, Barcelona) | per tablet: 10 *mg* nicotinic acid, 20 *mg* flopropione, 100 *mg* methionine phenylbutyrate, 25 *mg* pepsin (1:2500), 50 *mg* papain, 25 *mg* betaine chlorhydrate, 15 *mg* diastase, 50 *mg* pancreatin, 10 *mg* pancreatic lipase, 25 *mg* liver bile extract, 15 *mg* cellulase, 15 *mg* hemi-cellulase, excipient | 99 | 4.0 |
| Landrina 300 (Landerlan, Madrid) | per pill: 300 *mg* xanthinol nicotinate, excipient | 96 | 3.1 |
| Plasmaclar (Lacer, Barcelona) | per capsule: 100 *mg* xanthinol nicotinate, 35 *mg* pentosan sulphonic ester, excipient | 97 | 3.1 |
| Rulun (Lacer, Barcelona) | per tablet: 100 *mg* xanthinol nicotinate, 20 *mg* hydrochlorothiazide, 3 *mg* trichloromethiazide, 170 *mg* sacarose, 2.3 *mg* selective fraction of Rauwolfia S. Dehra Dun alcaloids, 25 *mg* pentosan sulphonic ester, lactose, excipient | 98 | 2.0 |
| Tensiocomplet (Medea, Barcelona) | per pill: 50 *mg* xanthinol nicotinate, 15 *mg* chlorthalidone, 10 *mg* dihydralazine chlorhydrate, 0.25 *mg* reserpine, 0.20 *mg* protoveratrine A + B, 5 *mg* rutoside, 50 *mg* potassium gluconic acid, 144 *mg* sacarose, excipient | 97 | 2.1 |

*Recovery with respect to the contents declared by the manufacturer.

in this work indicated, however, that in an SDS micellar medium aniline was perhaps the best coupling reagent of those studied, because of the large absorbance enhancements produced, which gave high molar absorptivities. Also, the coupling time (15–20 min) with aniline was not excessive, the optimum reagent concentration range was wide, and the reaction was possible for different substrates.

*Analytical figures*

The recommended procedure with aniline was used to obtain the calibration plots for pyridine, pyrrol-ylmethylpyridine and nicotinic acid. The calibration straight lines fitted by least-squares gave an intercept at 0.002–0.003. The molar absorptivities were $3.7 \times 10^4$, $2.35 \times 10^4$ and $4.25 \times 10^4 M^{-1}$ cm$^{-1}$, in a 0.1$M$ SDS medium, and $1.0 \times 10^4$, $1.0 \times 10^4$ and $3.0 \times 10^3 M^{-1}$ cm$^{-1}$, in the non-micellar solution, for pyridine, pyrrol-ylmethylpyridine and nicotinic acid, respectively.

The limits of detection (LODs) in the SDS micellar medium were obtained by measuring the absorbance of the blank solution in the absence of the analyte (16 replicates, 3s criterion), being $6 \times 10^{-7} M$, $1 \times 10^{-6} M$ and $5 \times 10^{-7} M$ for pyridine, pyrrol-ylmethylpyridine and nicotinic acid, respectively. The reproducibility was obtained from the measurement of the absorbance of 16 aliquots of the analytes, which were hydrolyzed and coupled separately. The coefficients of variation were 2.1% for $2 \times 10^{-5} M$ pyridine, 2.0% for $2 \times 10^{-5} M$ pyrrol-ylmethylpyridine, and 1.7% for $1.5 \times 10^{-5} M$ nicotinic acid. In the absence of SDS, the LODs were $3 \times 10^{-6} M$, $3 \times 10^{-6} M$ and $9 \times 10^{-6} M$, respectively, and the reproducibility *ca.* 3.5%.

*Evaluation of nicotinic acid in formulations*

The optimized procedure was applied to the determination of nicotinic acid in several pharmaceutical preparations. For the analyses, 10 tablets or pills were weighted and pulverized, a portion was taken, weighted, dissolved in 5 ml of ethanol, and diluted with 0.5$M$ SDS. In addition, the contents of 10 capsules were homogenized before a portion was taken, following the same procedure. The results are given in Table 3. The recoveries were always close to 100%, with coefficients of variation of 2.0–4.0%.

*Acknowledgements*—This work was supported by the DGICYT of Spain Project PB91/629 and the BANCAIXA Project PB-54C.

## REFERENCES

1. W. J. König, *J. Prakt. Chem.*, 1904, **70**, 19.
2. R. E. Schirmer, *Modern Methods of Pharmaceutical Analysis*, Vol. I. CRC Press, Boca Raton, FL, 1982.
3. S. B. Tallantyre, *J. Soc. Chem. Ind.*, 1930, **40**, 466.
4. R. C. Kroner, M. B. Ettinger and A. W. Moore, *Anal. Chem.*, 1952, **20**, 1877.
5. F. Feigl, *Spot Tests in Organic Analysis*. Elsevier, Amsterdam, 1966.
6. F. D. Snell and C. T. Snell, *Colorimetric Methods for Analysis*, Vol. 4A. Van Nostrand, Princeton, NJ, 1967.
7. H. G. Higson, R. F. Raimonds and E. N. Tunstall, *Anal. Chem.*, 1969, **20**, 1474.
8. S. Amlathe, S. Upadhyay and V. K. Gupta, *Microchem. J.*, 1988, **37**, 225.

9. E. Cassasas, M. Peydeo and L. Puignou, *Anal. Lett.*, 1989, **22,** 729.
10. S. O'Doherty, M. Cooke and D. J. Roberts, *J. High Resol. Chromatogr.*, 1990, **13,** 74.
11. M Bhattacharjee, S. Amlathe and V. K. Gupta, *Int. J. Environ. Anal. Chem.*, 1991, **45,** 127.
12. K. N. Ramachandran and V. K. Gupta, *Microchem. J.*, 1991, **44,** 272.
13. J. S. Esteve Romero, E. F. Simó Alfonso, M. C. García Alvarez-Coque and G. Ramis-Ramos, *Trends Anal. Chem.*, 1995, **14,** 29.
14. J. S. Esteve Romero, E. F. Simó Alfonso, M. C. García Alvarez-Coque and G. Ramis-Ramos, *Talanta*, 1993, **40,** 1711.
15. J. S. Esteve Romero, L. Alvarez Rodríguez, M. C. Garcia Alvarez-Coque and G. Ramis-Ramos, *Analyst*, 1994, **119,** 1381.
16. M. C. Garcia Alvarez-Coque, G. Ramis-Ramos and J. S. Esteve Romero, *Anal. Lett.*, 1992, **25,** 2059.
17. J. S. Esteve Romero, Ll. Monferrer Pons, M. C. Garcia Alvarez-Coque and G. Ramis-Ramos, *Anal. Lett.*, 1994, **27,** 1557.
18. B. F. Johnson, R. E. Malick, B. Ghearing and J. G. Dorsey, *Analyst*, 1992, **117,** 1833.
19. M. A. Hernández Torres, M. G. Khaledi and J. G. Dorsey, *Anal. Chim. Acta*, 1987, **201,** 67.
20. Abdel-Latif and G. G. Guilbault, *Anal. Lett.*, 1989, **22,** 1355.
21. M. C. García, G. Ramis-Ramos and C. Mongay, *Spectrochim. Acta*, 1982, **38A,** 1005.

Pergamon

0039-9140(95)01483-7

*Talanta*, Vol. 42, No. 5, pp. 747–753, 1995

0039-9140/95 $9.50 + 0.00

# HPLC DETERMINATION OF A NEW MULTIDRUG RESISTANCE MODULATOR (S9788) EXTRACTED FROM CANCER CELLS IN VITRO

J. P. TASSIN,[1,2]* J. DUBOIS,[2] M. HANOCQ[2] and G. ATASSI[1,3]

[1]Université Libre de Bruxelles, Institut de Pharmacie, Laboratoire de Pharmacologie Cellulaire et Animale, cp 206/03, Campus de la Plaine, Bld du Triomphe, 1050 Bruxelles, Belgium
[2]Université Libre de Bruxelles, Institut de Pharmacie, Laboratoire de Chimie Bioanalytique, Toxicologie et chimie physique appliquée, cp 205/01, Campus de la Plaine, Bld du Triomphe, 1050 Bruxelles, Belgium
[3]Institut de Recherches Servier, Division de Cancérologie Expérimentale, 11 rue des Moulineaux, 92150 Suresnes, France

(*Received* 28 *June* 1994. *Revised* 13 *October* 1994. *Accepted* 16 *November* 1994)

**Summary**—S9788 is a novel triazinodiaminopiperidine derivative which reverses the multidrug resistance of tumour cells to anticancer drugs. In this study, a new HPLC method was developed to determine this compound in P388 leukaemia cells. The influence of various parameters (composition and pH of the mobile phase, nature of the column) on the separation of S9788 and derivatives was investigated. Using a microsphere C18 column and the optimal mobile phase (acetonitrile–0.4*M* phosphate buffer containing 0.2% triethylamine, 40:60 v/v, pH 6.5) it was possible to separate S9788 and seven hypothetical metabolites and derivatives in 15 min. The limits of detection and quantification of S9788 are 75 and 250 pg, respectively. This MDR modulator was extracted from biological media by a rapid two-step procedure which removed proteins before direct injection of the sample. Absolute recoveries ranged from 90 to 100% with a mean RSD (%) lower than 5.

The resistance of tumours to anticancer drugs, whether innate or acquired, is a crucial problem in the treatment of cancer diseases. Multidrug resistance (MDR) is a pleiotropic type of resistance which mainly affects anthracyclines, vinca-alkaloids and epipodophyllotoxines[1–4] and may be particularly important. The most important type of MDR is known to be associated with the overexpression of a membrane glycoprotein, Pgp 170. In tumours, Pgp encoded by the mdr-1 gene,[5] has been identified as an energy-transducing transport pump which appears to confer resistance by inducing the efflux of cytotoxic drugs, thereby diminishing their intracellular concentrations.[6] A wide variety of compounds have now been shown to reverse MDR *in vitro*.[7] Among these molecules only verapamil has been extensively tested in clinical studies; however, serious side effects such as hypotension and arrhythmia were observed.[8] S9788, a novel triazinodiaminopiperidine derivative which does not belong to any of the classes of agents known to reverse MDR, was able to increase the accumulation and retention of cytotoxic drugs in rodent and human tumour cell lines displaying the MDR phenotype.[9–13] This drug is currently under clinical investigation as an MDR modulator in cancer diseases.[9–13] However, numerous problems of disposition remain to be solved to understand its mechanism of action.[14] Therefore, the aim of this paper is to develop a selective high performance-liquid chromatography (HPLC)[15] assay suitable to study the intracellular drug accumulation *in vitro* of S9788 and five hypothetical metabolites. The optimisation of the isocratic elution conditions permitted the separation, within 15 min, of compounds which had very different partition coefficients. The protocol was conducted according to the stability and characteristics of the C18 or C8 reversed phase columns. We describe here a rapid method to extract S9788 from cancer cells and discuss for the first time the simultaneous HPLC separation of this drug in the presence of five potential metabolites and two structurally related derivatives.

*Author to whom correspondence should be addressed.

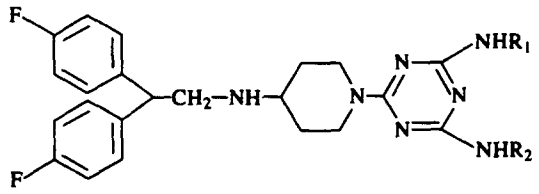

| | $R_1$ | $R_2$ |
|---|---|---|
| S 16636 | $-CH_2-CH=CH_2$ | -H |
| S 16637 | -H | -H |
| S 16638 | $-CH_2-HCOH-H_2COH$ | $-CH_2-HCOH-H_2COH$ |
| S 16639 | $-CH_2-HCOH-H_2COH$ | -H |
| S 16640 | $-CH_2-HCOH-H_2COH$ | $-CH_2-CH=CH_2$ |
| S 9788 | $-CH_2-CH=CH_2$ | $-CH_2-CH=CH_2$ |

Fig. 1. Structures of molecules.

## EXPERIMENTAL

Chemicals: S9788 (Fig. 1) was kindly provided by the Institute of International Research Servier (Courbevoie, France). Its hypothetical metabolites: S16636, S16637, S16638, S16639 and S16640 (Fig. 1) and a derivative S15061 tested as an internal standard (Fig. 2a) were kindly offered by Servier Research and Development Ltd (Fulmer, U.K.). Hexamethylmelamine (HMM) was a generous gift from the National Cancer Institute (Bethesda, MD, U.S.A.) (Fig. 2b).

### *Reagents and instrumentation*

All reagents were of analytical grade (Merck; Overijse, Belgium), except acetonitrile (Lab-Scan Analytical Sciences, Ireland, far UV grade). The HPLC system consisted of: a Rheodyne 71125 injector (Analysis, Belgium) equipped with a 100 $\mu$l injector loop, a Gilson 307 solvent delivery system (Analysis, Belgium) operated at a flow rate of 1.00 ml/min, a precolumn (10 × 4.6 mm) packed with reverse-phase ($R_2$) C18 (Chrompack, Belgium) and a column (100 × 4.6 mm) packed either with 3 $\mu$m reverse phase microsphere C18 or 5 $\mu$m chromspher C8 (Chrompack, Belgium).

Two detectors were used: a HP 1050 variable wavelength detector operated at 220 nm (Hewlett-Packard), linked to a Kipp and Zonen BD40 potentiometer recorder (Ankersmit, Belgium) and a photodiode array detector (Beckman Instruments: module 168 system gold and system gold chromatography software (ASW 2). After optimization of the method, the following mobile phase was chosen: 0.4*M* phosphate buffer containing 0.2% triethylamine and acetonitrile (60:40, v/v) on a C18 column. The pH of a 0.4*M* $KH_2PO_4$ solution was adjusted to 6 with 0.4*M* $K_2HPO_4$; the apparent pH of the mobile phase was 6.5. The flow rate was fixed at 1.00 ml/min, analyses were performed at ambient temperature and the injected volume was 50 $\mu$l.

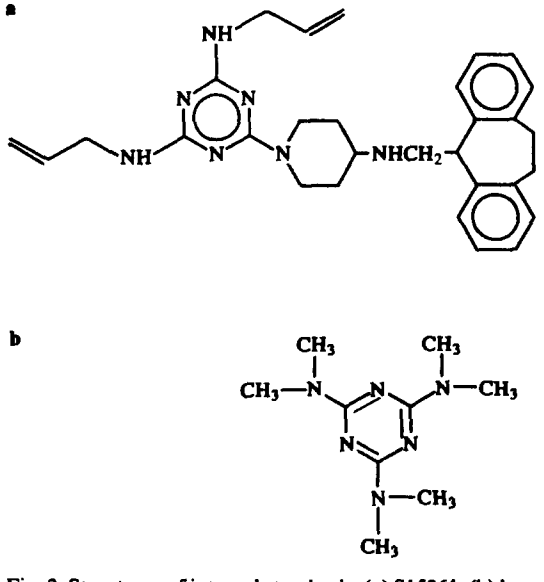

Fig. 2. Structures of internal standards. (a) S15061; (b) hexamethylmelamine (HMM).

### *Cell line and culture medium*

The P388 murine leukaemia cell line[16] was used to study the extraction procedure. These cells, obtained from the institute of Research Servier (Suresnes, France), were maintained in RPMI medium 1640 supplemented with 10% foetal calf serum, 2 m*M* L-glutamine (100 U/ml) 10 m*M* Hepes buffer (pH 7.4) (Gibco, Belgium), 20 $\mu$M $\beta$ mercapto-ethanol (Sigma, Belgium), penicillin (100 U/ml) and streptomycin (100 $\mu$g/ml).

Table 1. Influence of acetonitrile percentage, pH, and packing material (C8, C18) on capacity factor ($k'$), selectivity ($\alpha$) and resolution ($R_s$)

| | | C18 | | | | | | | | C8 | | | | | | | |
|---|---|---|---|---|---|---|---|---|---|---|---|---|---|---|---|---|---|
| | | pH 3.0 | | pH 4.0 | | pH 5.0 | | pH 6.0 | | pH 3.0 | | pH 4.0 | | pH 5.0 | | pH 6.0 | |
| | | S9788 | S15061 | S9788 | S15061 | S9788 | S15061 | S9788 | S15061 | S9788 | S15061 | S9788 | S15061 | S9788 | S15061 | S9788 | S15061 |
| acetonitrile 60% phosphate buffer 40% | $k'$ | 2.5 | 3.0 | 3.0 | 3.2 | 3.5 | 4.5 | 4.7 | 6.2 | 4.0 | 5.0 | 4.2 | 5.2 | 4.0 | 4.5 | 4.0 | 4.5 |
| | $\alpha$ | | 1.2 | | 1.1 | | 1.3 | | 1.3 | | 1.2 | | 1.2 | | 1.1 | | 1.1 |
| | $R_s$ | | 0.4 | | 0.7 | | 0.8 | | 1.0 | | 0.5 | | 0.5 | | 0.6 | | 0.6 |
| acetonitrile 50% phosphate buffer 50% | $k'$ | 4.0 | 5.0 | 5.2 | 7.0 | 7.2 | 9.5 | 11.2 | 14.5 | 7.5 | 8.7 | 7.7 | 9.0 | 9.0 | 10.0 | 9.5 | 10.5 |
| | $\alpha$ | | 1.2 | | 1.3 | | 1.3 | | 1.3 | | 1.2 | | 1.2 | | 1.1 | | 1.1 |
| | $R_s$ | | 0.6 | | 0.8 | | 1.0 | | 1.2 | | 0.5 | | 0.8 | | 0.5 | | 0.6 |
| acetonitrile 40% phosphate buffer 60% | $k'$ | 9.0 | 10.0 | 16.0 | 20.0 | 23.0 | 29.5 | 43.0 | 51.0 | 17.5 | 20.0 | 27.5 | 30.5 | 33.5 | 36.5 | 38.5 | 38.5 |
| | $\alpha$ | | 1.1 | | 1.2 | | 1.3 | | 1.2 | | 1.2 | | 1.1 | | 1.1 | | 1.0 |
| | $R_s$ | | 0.6 | | 0.9 | | 1.2 | | 1.1 | | 0.4 | | 0.5 | | 0.3 | | 0.0 |

### *Extraction of S9788, S15061 and HMM from P388 cells*

Before extraction, the cells were plated in 96 well microtiter plates (Nunc, Gibco, U.K.) (25,000 cells/well). The cells were then further incubated in a drug free medium (250 $\mu$l) for 24 hr at 37°C in humidified air containing 5% $CO_2$. The supernatant was then carefully drawn up and replaced by 100 $\mu$l of culture medium containing the investigated drug. After stirring for 30 sec, the cell suspension was transferred in a glass tube and the cells were disrupted and the proteins precipitated by adding of 0.4 ml acetonitrile. The tube was then stirred for 10 sec, left at 4°C for 10 min and centrifuged 10 min at 600 *g*. An aliquot (50 $\mu$l) of the supernatant was directly injected into the chromatograph. Low intracellular concentrations were determined by pooling cells from several wells.

## RESULTS AND DISCUSSION

The main goal of this work was to develop an HPLC method allowing the analysis of the new reversant drug S9788 in biological media and particularly in cancer cells. In order to identify the optimal separation conditions, the chromatographic behaviour of the analytes was studied as a function of pH and organic modifier concentration. The former was regulated with 0.025*M* phosphoric acid, 0.025*M* potassium dihydrogen and 0.025*M* monohydrogen phosphate. Four pH values (3.0, 4.0, 5.0, 6.0) were studied for each acetonitrile concentration (40, 50 and 60%) and column packing (C18, C8).

### *Influence of* $CH_3CN$ *concentration and pH*

*C18 column.* Table 1 shows that capacity factors were higher and that resolution and selectivity were better when the pH of the mobile phase was increased from 3 to 6. Investigations of buffers with pH above 6 were not conducted to insure an optimum stability of the column. On the other hand the trend showed that pH below 3 would decrease the resolution factor and increase the risk of hydrolysis of the bonded moiety. Furthermore, our data showed that at pH 6 the phosphate buffer system was mostly effective and the solutes were highly stable. Decreasing the acetonitrile concentration to 40% gave better selectivity and resolution at pH 5, the peak width was sharper at pH 6. The selectivity was

generally better when 50% acetonitrile were included into the mobile phase but 40% acetonitrile gave the highest capacity factor and the best resolution of analytes at all pHs. Our results showed that analysis with higher or lower concentrations of $CH_3CN$ would give either bad resolution, or unsatisfactory $k'$. For this reason we did not explore other $CH_3CN$ concentrations. To maintain easy and highly reproductible analysis conditions suitable for the determination of numerous samples, gradient elution was not investigated in this study.

*C8 column.* A complex behaviour was observed during the separation of these drugs on a C8 column. Generally, capacity factors increased as the pH increased but this feature was not systematically observed. No direct correlation, between selectivity and resolution on one hand and pH on the other was found. Capacity factors increased when the concentration of acetonitrile in the mobile phase was lower. Resolution and selectivity were generally poor when the concentration of the organic modifier decreased. These effects were particularly observed when the pH was raised from 3 to 6. Table 1, clearly indicates that an acceptable separation of S9788 and S15061 was reached with a C18 column and a mobile phase constituted of 40% of acetonitrile and 60% of 0.025*M* phosphate buffer containing 0.2% triethylamine. The C18 column was selected for further studies.

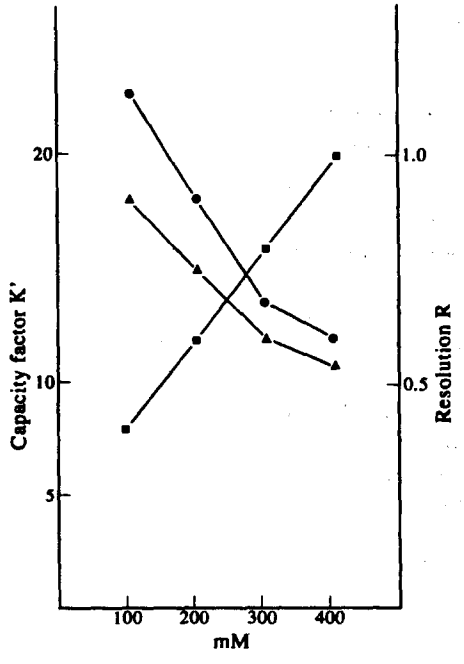


Fig. 3. Effect of phosphate buffer concentration on the resolution $R_s$ (■) and the capacity factors $k'$ of derivatives S9788 (▲) and S15061 (●).

*Tailing suppression*

Triethylamine significantly diminished the tailing of peaks whereas THF had no effect. In the range 0.05–0.2% in the mobile phase, triethylamine did not modify the retention

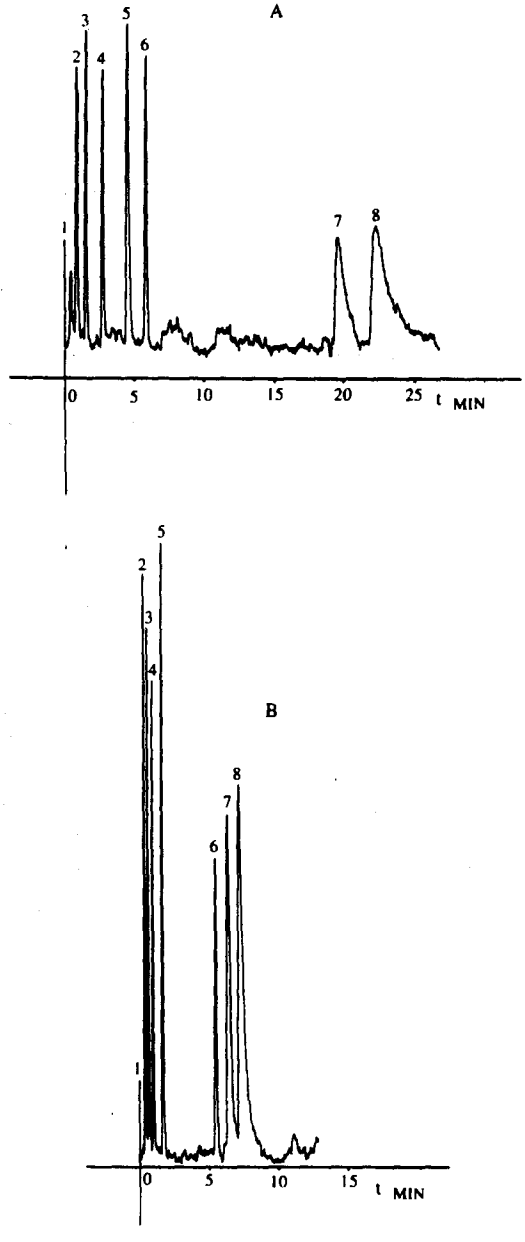


Fig. 4. Influence of buffer concentration on chromatographic separation. Peaks: 1 = injection; 2 = S16636 (2.0 μg); 3 = S16640 (0.5 μg); 4 = S16637 (0.5 μg); 5 = S16638 (0.5 μg); 6 = HMM (0.3 μg injected); 7 = S9788 (1.6 μg injected); 8 = S15061 (1.5 μg injected). Buffer contraction in mobile phase (A) 25 m*M* phosphate; (B) 400 m*M* phosphate.

Table 2. Spectral UV characteristics of S9788 and derivatives

| Compounds | $a$* | $b$* | $r$ | Limit of quantification ($pg$) | Limit of detection ($pg$) |
|---|---|---|---|---|---|
| S16638 | 1.82 | −7.15 | 0.9893 | 62 | 12 |
| S16639 | 1.98 | −0.90 | 0.9974 | 62 | 12 |
| S16637 | 1.14 | 0.94 | 0.9997 | 125 | 37 |
| S16640 | 1.45 | 2.24 | 0.9995 | 83 | 25 |
| S16636 | 0.94 | 2.22 | 0.9968 | 83 | 25 |
| HMM | 0.94 | 2.21 | 0.9968 | 62 | 12 |
| S9788 | 0.26 | −0.35 | 0.9994 | 250 | 75 |
| S15061 | 0.22 | −0.00 | 0.9992 | 250 | 75 |

*Standard curves $y = ax + b$.
$y$ = Absorbance; $x$ = amount of S9788 injected; $r$ = correlation coefficient; $a$ = slope; $b$ = intercept.

times. Choice of optimal conditions required a compromise between maximum resolution for the two analytes and capacity to separate five additional hypothetical metabolites. In order to conduct the optimisation, we selected a mobile phase buffered at pH 6 and containing 0.2% triethylamine. These conditions permitted us to increase the capacity factor without an appreciable degradation of performances ($\alpha = 1.2$ and $R_s = 1.1$).

*Buffer concentration*

The buffer concentration (C18 column) was varied from 0.025 to 0.4$M$ phosphate at pH 6 in the presence of 40% of acetonitrile. Figure 3 shows that lower values of $k'$ were observed when phosphate concentration was increased. The $k'$ values were decreased while the resolution factors were better. Moreover, sensitivity was increased twice (Fig. 3, Fig. 4a, b). The optimum buffer concentration was found to be the highest tested (400 m$M$). At this concentration, no problem of salt precipitation was encountered. The optimum buffer concentration was found to be the highest tested (400 m$M$). This concentration was the maximum admissible limit to prevent salt precipitation which occurred when higher phosphate concentrations were used. The results showed that it was more adequate to increase the phosphate concentration than the percentage of $CH_3CN$ in the mobile phase in order to obtain the highest Rs with the lowest $k'$. At 0.025$M$, the $k'$ were very high and the trend clearly indicated that lower concentration of buffer could not offer acceptable analysis conditions. As a result the final composition of the mobile phase was acetonitrile–0.4$M$ phosphate buffer containing 0.2% triethylamine 40:60 (v/v). To obtain good operatory conditions for this type of column, the flow rate was fixed at 1 ml/min which produced a pressure of approximately 130 bars.

Table 3. Analytical parameters of the investigated compounds standard curves, linearity range 5–6.5 × $10^5$ ng/ml

| Compounds | $\lambda_{nm\ max}$ | $\epsilon_{max}$ $10^6$ |
|---|---|---|
| S9788 | 204 | 0.79 |
| S15061 | 199 | 0.70 |
| HMM | 225 | 0.56 |
| S16636 | 203 | 0.74 |
| S16637 | 203 | 1.13 |
| S16638 | 203 | 1.25 |
| S16640 | 204 | 1.64 |

$\lambda$: Wavelength; $\varepsilon$: molar absorbance coefficient.

*Calibration curve limit of detection and limit quantification*

Each data-item of the calibration curves was the mean of three injections (solvent:mobile phase). Linear regression equation and correlation coefficients are collected in Table 2. All drugs showed a linear relationship between peak height and concentration, over a range of 5 ng/ml–650 $\mu$g/ml. The absolute limits of detection and quantification, calculated as three and 10 times the standard deviation of the baseline signal, respectively were at the picogram level (Table 3).

*UV study*

The detection wavelength was chosen following a UV spectral study of all derivatives dissolved in the chromatographic mobile phase. Even though the optimal wavelength of the derivatives was around 205 nm (Table 3)

Table 4. Intra- and inter-assay validation of the S9788 determination after extraction

| | S9788 | | | | HMM | | | | S15061 | | | |
|---|---|---|---|---|---|---|---|---|---|---|---|---|
| | Intra-assay | | Inter-assay | | Intra-assay | | Inter-assay | | Intra-assay | | Inter-assay | |
| Concentration added (*ng/ml*) | recovery (%) | R.S.D. (%) | recovery (%) | R.S.D (%) | recovery (%) | R.S.D. (%) | recovery (%) | R.S.D. (%) | recovery (%) | R.S.D. (%) | recovery (%) | R.S.D. (%) |
| 8 | 91 | 12 | 94 | 21 | 93 | 10 | 94 | 18 | 94 | 13 | 95 | 23 |
| 40 | 93 | 5.9 | 96 | 15 | 96 | 6.2 | 95 | 16 | 94 | 7.0 | 95 | 18 |
| 200 | 97 | 3.1 | 97 | 12 | 99 | 4.3 | 98 | 10 | 97 | 6.2 | 98 | 15 |
| 1000 | 102 | 2.8 | 99 | 8.0 | 100 | 2.3 | 101 | 7.0 | 100 | 4.4 | 99 | 12 |
| 5000 | 101 | 2.4 | 100 | 5.0 | 102 | 2.1 | 101 | 6.2 | 104 | 3.0 | 101 | 10 |
| 25,000 | 100 | 1.9 | 101 | 3.2 | 101 | 1.7 | 99 | 3.7 | 102 | 2.1 | 102 | 7.3 |
| 125,000 | 102 | 1.7 | 100 | 2.7 | 99 | 1.3 | 100 | 3.1 | 101 | 1.9 | 100 | 4.7 |
| 625,000 | 100 | 1.4 | 100 | 2.5 | 100 | 0.8 | 100 | 2.6 | 102 | 2.1 | 101 | 4.2 |

a working wavelength of 220 nm was chosen in order to minimize unspecified absorbance.

### *Extraction of S9788, HMM and S15061 from cancer cells*

The good linear relationship in the calibration curves calculated after extraction of these three drugs from cancer cells ($r > 0.996$), as well as the excellent recovery results (Table 4) are likely owing to the simplicity of sample treatment prior to analysis. The procedure used for the sample preparation is virtually a dilution in a acetonitrile/water mixture. This provides maximum of accuracy while introducing minimum of artefacts during the preparation. Intra-day variability was assessed with six extraction procedures and the inter-assay reproducibility was determined by pooling the data of three days. As indicated by the RSD (%) values (Table 4), the precision of this method is reasonably good and can be used in a very large range of concentrations. Similar results were found for drugs S16636, S16637, S16638, S166639 and S16640. Specificity of the method was controlled by diode array analysis. The chromatographic behaviour and recovery results showed that HMM and S15061 are possible internal standards (IS) to quantify S9788 in cells. HMM has the advantage of a shorter retention time.

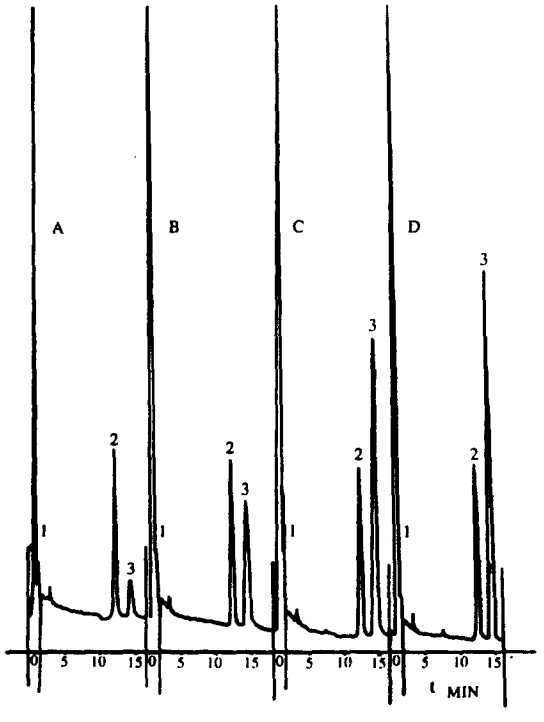


Fig. 5. Uptake of S9788 by P388 cells. Time (A) 1.00 min; (B) 10.00 min; (C) 60.00 min; (D) 120.00 min. Peaks: 1 = injection; 2 = HMM (IS); 3 = S9788. Incubated concentration of S9788:5 $\mu M$.

Preliminary *in vitro* transport studies of S9788, showed that the limit of quantification of the proposed method would allow us to determine the intracellular drug concentration vs. time curves from micro samples. This feature is essential in order to follow the transport kinetics in 96 well micro plates used for parallel cytotoxic tests. Figure 5 shows chromatograms obtained after incubation of S9788 with cells for 1, 10, 60 and 120 min. No metabolite was detected in P388 cells even after 120 min of incubation. Moreover, no interference peak was detected (HMM was used as IS). The results proved a (quick) penetration and accumulation of this new drug in the cells.

In conclusion, the HPLC system developed permitted the separation of S9788, five possible metabolites and two IS, which are molecules comprising a large range of lipophilicity and polarity, in less than 15 min. The selectivity and reproducibility of the method is good, allowing the successful determination of S9788 in P388 leukaemia cells.

*Acknowledgement*—Thanks are expressed to the KISANE foundation for its generous support which greatly contributed to the achievement of this study.

## REFERENCES


1. L. J. Goldstein, H. Galski, A. Fojo, M. Willingham, S. L. Lai, A. Gazdar, R. Pirker, A. Green, W. Grist, G. M. Brodeur, M. Lieber, J. Cossman, M. M. Gottesman and I. Pastman, *J. Natl Cancer Inst.*, 1989, **81**, 116.
2. K. E. Noonan, C. Beck, T. A. Holzmayer, J. E. Chin, J. S. Wander, I. L. Andrulis, A. F. Gazdar, C. L. Willman, B. Griffith, D. D. Hoff and I. B. Roninson, *Proc. Natl Acad. Sci. USA*, 1990, **87**, 7160.
3. G. C. Wishart, J. A. Plumb, J. J. Going, A. M. McNicol, C. S. McArdle, T. Tsuro and S. B. Kaye, *Br. J. Cancer*, 1990, **62**, 758.
4. S. E. Salmon, T. M. Grogan, T. Miller, R. Scheper and W. S. Dalton, *J. Natl Cancer Inst.*, 1983, **81**, 1285.
5. K. Ueda, C. Cardarelli, M. M. Gottesman and I. Pastan, *Proc. Natl Acad. Sci. USA*, 1987, **84**, 3004.
6. M. Inaba, H. Kobayashi, Y. Sakurai and R. K. Johnson, *Cancer Res.*, 1979, **39**, 2200.
7. C. P. J. Vendrick, J. J. Bergers and W. H. De Jong, *Cancer Chem. Pharmacol.*, 1992, **19**, 413.
8. D. J. Stewart and K. Evans, *Cancer Treatment*, 1989, **16**, 1.
9. A. Dhainaut, G. Regnier, G. Atassi, A. Pierré, S. Léonce, L. Kraus-Berthier and J. F. Prost, *J. Med. Chem.*, 1992, **35**, 2481.
10. A. Pierré, T. Dunn, L. Kraus-Berthier, S. Léonce, D. Saint-Dizier, G. Régnier, A. Dhainaut, M. Berlion, J. P. Bizzari and G. Atassi, *Invest. New Drugs*, 1992, **10**, 137.
11. S. Gros, N. Guilbaud, M. Berlion, T. Dunn, G. Atassi and J. P. Bizzari, *Cancer Chem. Pharmacol.*, 1992, **3**, 491.
12. S. Léonce, A. Pierré, M. Anstett, V. Perez, A. Genton, J. P. Bizzari and G. Atassi, *Biochem. Pharmacol.*, 1992, **44**, 1707.
13. G. Atassi, A. Pierré, G. Regnier, A. Dhainaut, S. Léonce, L. Kraus-Berthier, N. Guilbaud and S. Gros, *J. Cancer Res. Clin. Oncol.*, 1991, **117** (3), S 108.
14. G. Atassi and J. P. Tassin, *Int. J. Clin. Pharmacol. Therap. Toxicol.*, 1992, **30**, 526.
15 J. Dubois, M. Hanocq, G. Atassi and L. Molle, *Anal. Letters*, 1987, **20**, 1635.
16. R. I. Geran, N. H. Greenberg, M. M. McDonald, A. M. Schumacher and B. J. Abbot, *Cancer Chemother. Rep.*, 1972, **3**, 11.

Pergamon

0039-9140(95)01491-8

*Talanta*, Vol. 42, No. 5, pp. 755–763, 1995

0039-9140/95 $9.50 + 0.00

# PERVAPORATION: AN INTEGRATED EVAPORATION/GAS-DIFFUSION APPROACH TO ANALYTICAL CONTINUOUS SEPARATION TECHNIQUES

IVANILDO L. DE MATTOS,* M. D. LUQUE DE CASTRO and MIGUEL VALCÁRCEL

Department of Analytical Chemistry, Faculty of Sciences, University of Córdoba, E-14004 Córdoba, Spain

(*Received* 5 *October* 1994. *Revised* 29 *November* 1994. *Accepted* 1 *December* 1994)

**Summary**—A flexible pervaporation module was developed and characterized. The spacers it uses allows the volume of the donor and/or acceptor to be altered as required. The performance of the module was tested as regards both dynamic behaviour and continuous pervaporation in terms of flow-rates, temperature, type of membrane, flow mode, *etc.* A method for the determination of ethanol in different types of wine was developed and applied to various samples in order to validate the proposed continuous separation approach.

Non-chromatographic continuous separation techniques make interesting choices for implementing various preliminary operations of the analytical process[1] in order to accommodate the raw sample to the measuring instrument.[2] Besides the well known advantages of separation techniques, they offer additional assets such as reduced human participation, easy on-line coupling with many instruments, diminished errors and hazards, markedly increased sample throughput and sparing used of sample and reagents. There are a variety of continuous sample treatment techniques that can be classified according to the type of interface involved in the mass transfer process, namely gas–liquid (*e.g.* gas-diffusion, continuous hydride generation, distillation, evaporation), liquid–liquid (*e.g.* dialysis, extraction) and solid–liquid (*e.g.* ion-exchange, precipitation, supercritical fluid extraction).

Indirectly improving the selectivity and sensitivity by interference removal and preconcentration, respectively, are no doubt the two primary targets of separation techniques in many analytical processes involving real samples. Occasionally, the complexity of such techniques entails using more than one separation approach in order to accomplish the desired sensitivity and/or selectivity levels. Coupling two identical or different continuous separation techniques can aid in dealing with complex samples via a synergistic effect. There are three general approaches to this type of coupling, namely (a) parallel; (b) serial; and (c) integrated.[3]

Separation membranes play a crucial role in continuous-flow systems, where they can be used for gas-diffusion or dialysis, as well as for separation of immiscible liquid phases, among others.[4] Continuous gas-diffusion techniques take advantage of the volatility of some analytes or their reaction products. They provide excellent means for enhancing selectivity and sensitivity.[2,5] A serial of parallel combination of gas-diffusion and another separation technique (*e.g.* dialysis,[6,7] ion-exchange[8,9]) in continuous flow systems clearly improves on the individual use of such techniques. On the other hand, continuous distillation and evaporation, both based on the differential volatility of the analyte and other sample components are scarcely used in continuous flow manifolds owing to the inherent difficulty to achieve reproducible results and the high complexity of the associated continuous separation methods.[2]

In this work we developed a relatively new approach to implementing non-chromatographic continuous separation techniques on the analytical scale based on the volatility of an analyte removed from a complex matrix. The proposed approach combines evaporation and

*Permanent address: Institute of Chemistry, State University of Campinas, SP, Brazil (C.P. 6154).

gas-diffusion through a gas-permeable membrane in the same unit. The phenomenon is called 'pervaporation' in order to emphasize the fact that the analyte or its reaction product (whichever the permeate is) undergoes a phase change from liquid to vapor before reaching the gas-diffusion membrane.[10] The new methodology integrates two different analytical separation principles in the same micromodule for simplicity, miniaturizability and minimal human participation in order to enhance analytical quality and productivity.[11]

Pervaporation is a developing membrane technology that is raising great expectations according to the DOE study 'Membrane Separation Systems. A Research Needs Assessment', sponsored by the US Department of Energy, which includes this integrated separation alternative on its top research priority list for organic/organic separations in the chemical industry.[12] Several pervaporation studies have been carried out on a small scale. Toshiro *et al.*[13] developed a new type of membrane based on the plasma-graft co-polymerization of 2-hydroxyethyl methacrylate with acrylic–methacrylic acids on polypropylene films that selectively permeate water from water–ethanol mixtures. Strathman *et al.*[14] used composite hollow-fibre membranes with poly(sulfone) as support, coated with a solvent-selective layer of poly (dimethyl siloxane) for continuous removal of ethanol from fermentation broths by pervaporation. Also, Hickey *et al.*[15] used hydrophobic silicone-based membranes for separation of alcohols such as n-butanol and isopropanol from a bioreactor.

There are few references to the use of pervaporation for analytical purposes. Schmidt *et al.*[16] used a pervaporation module coupled on-line with an enzymatic continuous manifold for the determination of ethanol and diacetyl in simulated brewing mixtures. Recently the same team have developed an improved pervaporation module integrated in a flow injection enzymatic manifold for the determination of ethanol in both beer and baker's yeast cultivation.[17] Determinations based the separation of aqueous–organic mixtures by pervaporation, followed by mass spectrometry or coupled gas-chromatography–mass spectrometry, were reported over 10 years ago.[18]

In this work we constructed a flexible miniature pervaporation module able to work in either a single or a double dynamic mode, that was coupled on-line to a continuous unsegmented flow manifold. After the module was characterized in hydrodynamic and separation terms, a non-enzymatic photometric method for the determination of ethanol in different types of wine was developed in order to test the potential of this integrated separation technique for analytical purposes.

## EXPERIMENTAL

### *Reagents*

All chemicals used were of analytical reagent grade, and solutions were prepared in distilled/deionized water. An aqueous potassium dichromate solution was prepared by dissolving 17.0 g of $K_2Cr_4O_7$ (Merck) in *ca.* 100 ml water, adding 162.5 ml $H_2SO_4$ (96%, Panreac) and making up to 500 ml with water. A $1 \times 10^{-2}M$ $Na_2B_4O_7$ aqueous solution was used as carrier for the Bromocresol Green (BCG) solution, which was also made in this borate medium (50 and 100 $\mu$g/ml). An absolute ethanol standard (Merck) was used at a suitable dilution. Wine samples provided by Official Start of the Montilla-Morilles region (Córdoba, Spain) were also used.

Cellulose, PTFE and PDVF pervaporation membranes (all of 5.0 $\mu$m pore size and 47 mm diameter and supplied by Millipore) were used.

### *Apparatus*

A Unicam 8625 spectrophotometer furnished with a Hellma QS flow-cell (10-mm light path) and connected to a Radiometer REC-80 recorder and a Selecta 382-S recirculating thermostat was used. A four-channel Gilson Minipuls-2 peristaltic pump fitted with a rate selector, a Rheodyne 5041 injection valve, and Teflon tubing of 0.5 mm i.d. was also used.

### *Pervaporation module*

The pervaporation unit was custom-built from machined parts and is shown schematically in Fig. 1. It consisted of the following elements:

(a) An upper chamber with an inlet and outlet through which the acceptor stream is circulated. The acceptor solution collected the gaseous analyte, whether by dissolution or by reaction with a suitable reagent contained in it.
(b) A thin membrane support (1 mm thickness) made of Teflon owing to the difficulty to machine it in methacrylate.

(c) Spacers of different thickness (from 2 to 10 mm) placed below and above the membrane support in order to enlarge the lower and upper chamber, respectively.
(d) A lower, donor stream/sample chamber through which the feed stream for evaporation/diffusion process was circulated.

The whole pervaporation module (membrane support excluded) was made of methacrylate in order to allow continuous checking of its operation during the experiments.
(e)–(g) Additional fastening devices intended to avoid leaking. Firm contact between parts was achieved by screwing the aluminium supports (e) with four cylinders (f). Previously, the different parts of the pervaporation module were aligned by passing (g) through the four cylinder bores.
(h) Connectors for the inlet and outlet stream in both chambers.

The cross-sectional views of Fig. 1(B) show the dimensions and shape of the two chambers.

(A)

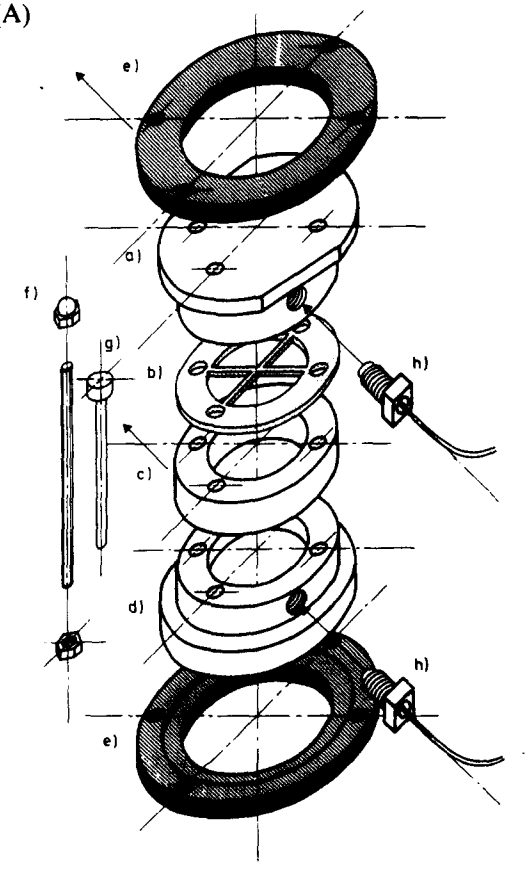


Fig. 1(A). (Caption on following page).

## RESULTS AND DISCUSSION

After the pervaporation module was designed and built, its performance was tested using the univariate experimental approach in order to determine which variables affected its operation. In this case the implementation of the optimization studies using a multivariate experimental design could be highly beneficial taking into account the large number of variables which influence the performance of the module, but these designs are usually 'blind' to the effect of each individual variable. For this reason the module was checked by the univariate method. First, it was checked for hydrodynamic performance, and for continuous pervaporation. Finally, a method for determining ethanol was developed and used to quantify the analyte in various types of wine.

### *Characterization of the pervaporation module*

*Dynamic behaviour.* In order to check the performance of the pervaporation unit (Fig. 1) in a continuous dynamic regime, it was coupled to a flow injection manifold as shown in Fig. 2. For this purpose a volume of 500 $\mu$l of 50 or 100 $\mu$g/ml Bromocresol Green (BCG) in borate buffer was injected into a borate carrier stream and the transient signal obtained on passage through the detector was monitored and used to determine the influence of the incoming and outgoing flow-rates ($q_{in}$ and $q_{out}$, respectively) of the donor and acceptor streams. Both the upper and the lower chamber were checked in turn by connecting the spectrophotometric detector to their outlets.

It should be noted that the detector waste in both the upper and lower chamber must be aspirated in order to aid circulation of the streams through the unit and avoid leakage of the solution through the membrane and the wall-module/membrane in the upper chamber, as well as to raise the donor stream level in the lower chamber.

The operation of the upper chamber was checked by keeping the flow-rate in the lower chamber constant ($q_{in} = q_{out} = 2$ ml/min) and changing at the upper chamber inlet between 0.7 and 3.0 ml/min while keeping both constant at 0.7 ml/min the $q_{out}$ and using the same value as in the inlet. Identical incoming and outgoing flow-rates resulted in no leakage, whatever their value. At $q_{in} > q_{out}$ the dye leaked both through the membrane and (particularly at the latter). Leakage was assessed by keeping $q_{out}$ constant at

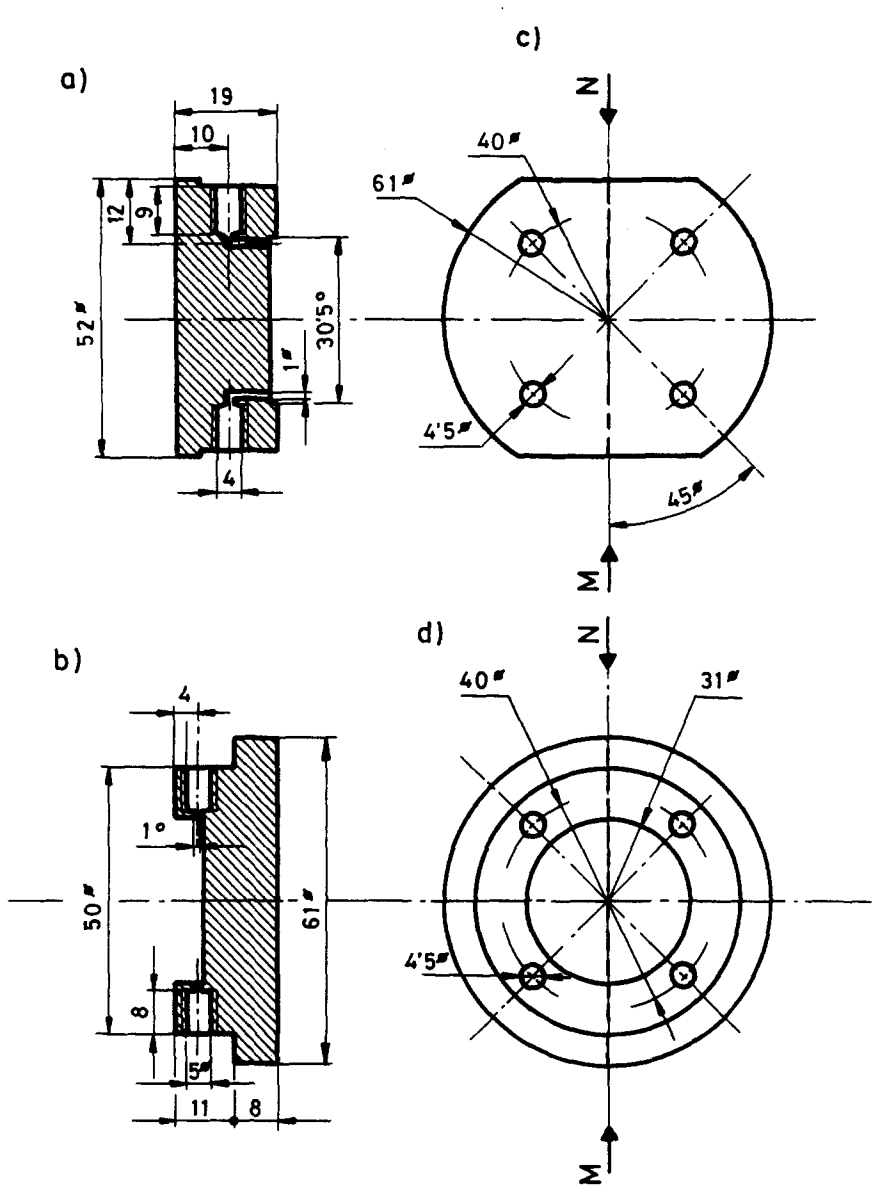


Fig. 1. (A) Parts of the pervaporation module. (a) Receptor chamber, (b) membrane support, (c) spacer, (d) donor/sample chamber, (e) aluminium supports, (f) and (g) rods for screwing and aligning the module, (h) connectors. (B) Cross-sectional (a and b) and plant views (c, d) of the acceptor and sample chambers, respectively.

0.7 ml/min while changing $q_{in}$. The analytical signal decreased by *ca.* 10% at $q_{in} = 1.0$ ml/min, and by as much as *ca.* 50% at $q_{in} = 3.0$ ml/min. The detector response was strongly distorted at $q_{out} > q_{in}$ as a result of air bubbles crossing the membrane and reaching the flow-cell. Thus, correct functioning of the upper chamber required using a flow-rate ratio $q_{in}/q_{out} = 1$.

The operation of the lower chamber was studied in respects: The influence of the $q_{in}/q_{out}$ ratio and the extent of homogenization of the injected dye in the carrier solution, on which reproducibility was found to depend. The different $q_{in}/q_{out}$ ratios were studied by injecting 1 ml of dye into the carrier solution and connecting the spectrophotometer to the chamber outlet. The solution level in the chamber remained virtually constant at $q_{out} > q_{in}$ at the in–out level and the maximum transient signal was obtained which was unstable as air bubbles were pulled to the flow-cell from the chamber liquid surface. Increasing the $q_{in}/q_{out}$ ratio decreased the solution level in the chamber being raised and as a result of dye augmented. A $q_{in}/q_{out}$ ratio of 1 was thus required for optimal functioning of the lower chamber.

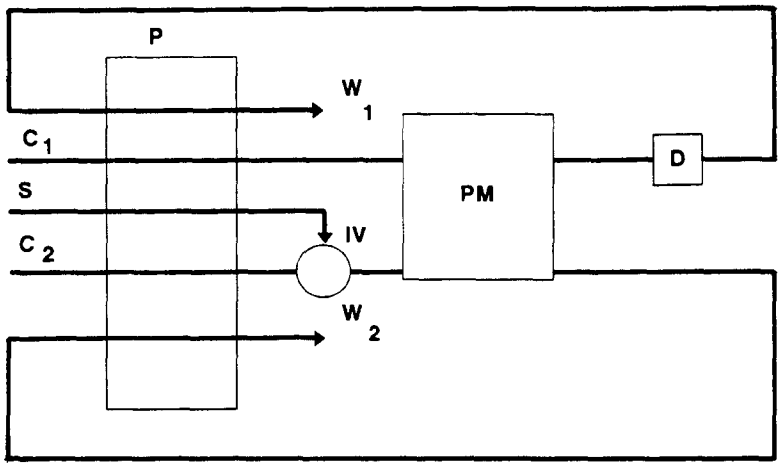


Fig. 2. Flow injection arrangement used to characterize the pervaporation module and develop a method for the determination of ethanol. ($C_1$ and $C_2$) Donor and acceptor stream, respectively; (S) sample; (IV) injection valve; (PM) pervaporation module; (D) detector; (W) waste.

Even if a unity flow-rate ratio was maintained, irreproducible signals were still obtained in successive injections. Dispersion of the dye in the carrier solution held in the chamber was visually observed to be non-uniform and irreproducible. This problem was addressed in two ways were: with magnetic stirring at 60 rpm and by packing the chamber with glass beads (0.3 mm diameter). As shown in Table 1, the reproducibility (as r.s.d.) was improved by using either magnetic stirring or a packed chamber, particularly in the latter case. Also, the signal obtained was higher as the chamber volume occupied by the sample/carrier mixture was smaller (even though the solution level was the same in all the experiments—$q_{in} = q_{out}$—the real volume was smaller as a part of it was occupied by the beads). In addition magnetic stirring would hinder thermostatting of the module, is usually required in pervaporation processes.

Based on the above results, no BCG was pervaporated (*i.e.* no dye passed from the lower chamber to the upper chamber).

*Continuous pervaporation.* The effect of the parameters potentially influencing continuous pervaporation in the proposed module was studied by using the flow system depicted in Fig. 2. Ethanol, the target analyte, was injected into a water-carrier stream that drove it to the lower chamber, where it evaporated and permeated across the membrane into a cold potassium dichromate acid stream where the following reaction took place:

$$2Cr_2O_7^{2-} + 3C_2H_5OH + 16H^+ \rightarrow 4Cr^{3+} 3CH_3COOH + 11H_2O.$$

The $Cr^{3+}$ formed was driven to the spectrophotometer and monitored at 600 nm.

The *flow-rates* of the donor and acceptor stream had a critical effect on the separation efficiency. Their optimal values were found to depend on the module design and the nature of the analyte.

First, the influence of the $q_{in} = q_{out}$ ratio for the acceptor stream was studied by keeping the donor stream conditions constant (2 ml/min and 40°C). A decrease in the analytical signal of *ca.* 50% was observed by changing the flow-rate from 0.5 to 1.0 ml/min (see Fig. 3). However, the decrease was not so marked above 1.0 ml/min. Higher acceptor stream/analyte interaction was achieved by decreasing the flow-rate as a result of the longer contact time.

According to van der Linden,[19] the amount of analyte that diffuses into the acceptor stream depends on the rate of diffusion of the analyte from the bulk solution to the membrane surface, partitioning between donor and separation element, diffusion inside the membrane pores, partitioning between membrane and acceptor, and diffusion from the membrane surface into the bulk acceptor.

Thus, the separation efficiency can be altered by changing the acceptor stream flow-rate.

Table 1. Ways of improving homogenization inside the sample compartiment

| Chamber type | Mean | SD | RSD (%)* |
|---|---|---|---|
| Open | 0.443 | 0.050 | 11.29 |
| Packed with glass beads | 0.548 | 0.004 | 0.79 |
| Magnetically stirred | 0.289 | 0.004 | 1.87 |

*Injection of 1 *ml* of 100 μg BCG/*ml*, $n = 10$.

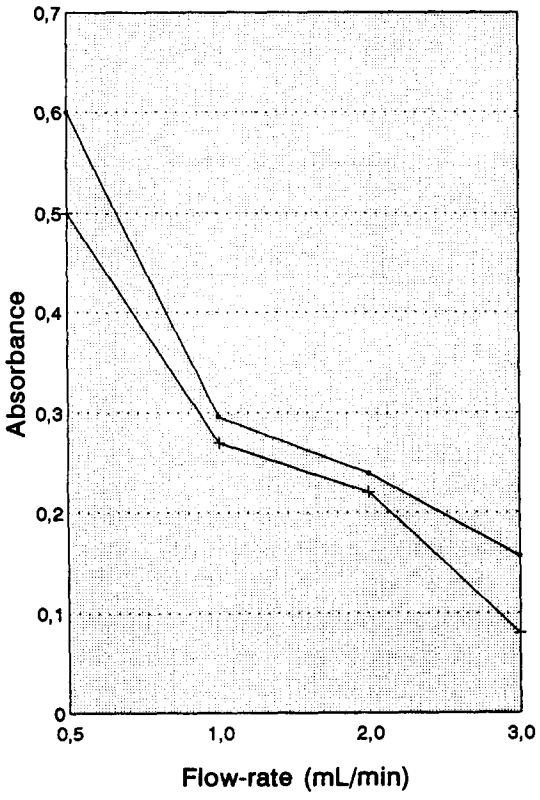


Fig. 3. Influence of the acceptor and donor flow-rate on the pervaporation process (injected volume 2.0 ml/min; 40°C; PTFE membrane, 5 $\mu$m pore size).

However, it should be noted that increasing the analytical signal in this way decreases the sampling frequency. Thus, a compromise must be made; a flow-rate of 2.0 ml/min selected for subsequent experiments as a compromise between sensitivity and throughput.

Second, the donor stream flow-rate was changed from 0.5 to 3.0 ml/min. Figure 3 also shows changes in the analytical signal with changes in this variable. The response was identical with that of the acceptor stream in all instances. Increasing the flow-rate shortened the residence time of the sample in the lower chamber, thereby reducing the time for analyte evaporation and decreasing the separation efficiency. An incoming and outgoing flow-rate of 2 ml/min as a compromise between adequate sensitivity and sampling frequency was also used for the donor stream.

The *separation unit variables* studied included the temperature (through which the pervaporation efficiency can be altered), the type of membrane used for permeating the analyte; and the volume of the sample and collecting chamber.

The effect of temperature was studied by immersing the donor carrier and sample reservoirs, the pervaporation module and the connecting tubes in a thermostatted bath at 30, 40, 50 and 60°C. Various membranes of the same pore diameter (5.0 $\mu$m) were assayed at each temperature. Figure 4 illustrates the influence of temperature and the type of membrane used on the absorbance of the transient signal obtained.

As expected, the separation efficiency increased with increasing temperature for any type of membrane, as the logical result of a higher analyte volatility. There was no a thermal gradient inside the pervaporation module, which would have boosted separation. The different types of membrane provided variable efficiency; PTFE yielded the best results (an analytical signal 30 and 60% higher than those provided by PDVF and cellulose membranes, respectively, at 30°C). An absorbance increase by *ca.* 80% was obtained with the PTFE membrane by raising the temperature from 30 to 60°C. Although the effect of tem-

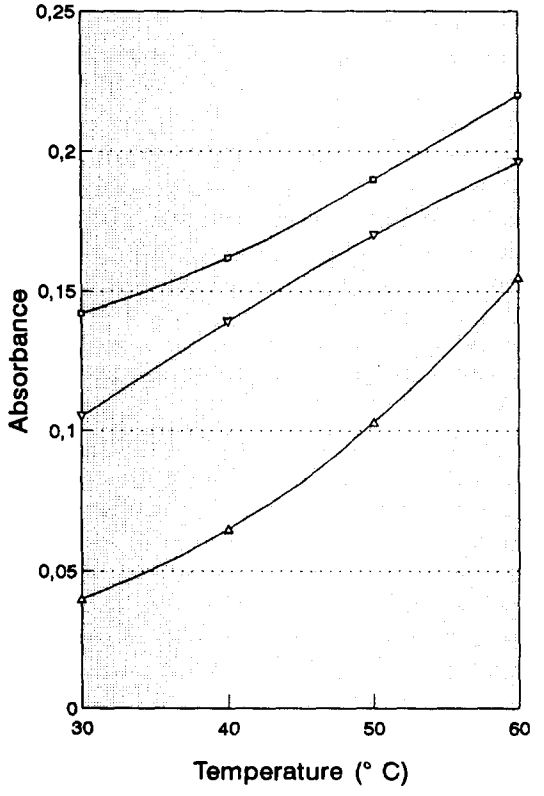


Fig. 4. Influence of temperature and the type of membrane used on the pervaporation process. Working conditions: membrane pore size 5.0 $\mu$m; inlet/outlet flow-rate 2.0 ml/min; sample volume, 2 ml of 10% (v/v) ethanol standard solution (□ PTFE, ▽ PDVF, △ cellulose membranes).

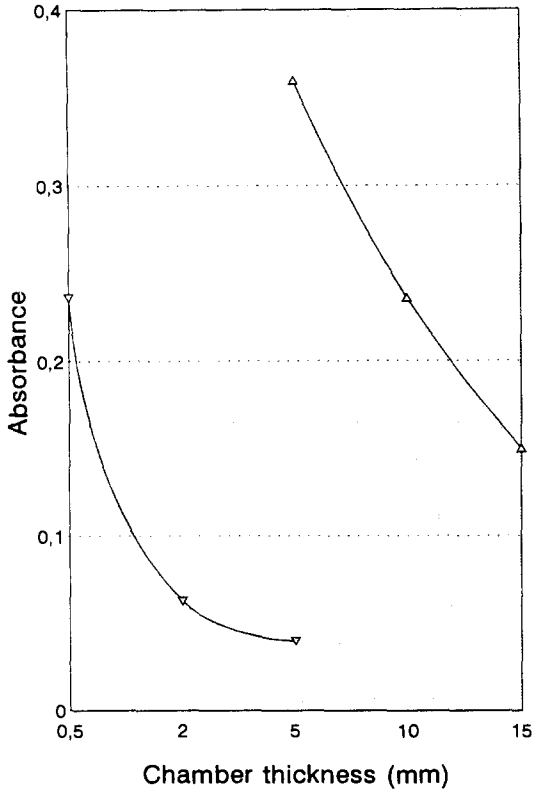


Fig. 5. Influence of the inner volume of the chambers on the pervaporation process. Working conditions: inlet/outlet flow rate = 2.0 ml/min (in both the acceptor and sample chamber); sample volume, 2.0 ml of 10% (v/v) ethanol standard solution and 40°C; PTFE membrane (▽ upper chamber, △ lower chamber).

perature on the performance of the other two membrane materials was more marked than that on PTFE, the absolute absorbance obtained was greater for the latter (see Fig. 4). In addition, the PTFE membrane proved more stable as it remained unaltered for at least one day's worth of work. On the other hand, the PDVF and cellulose membranes allowed leakage of the dichromate solution into the sample chamber after a few minutes. Taking into account the corrosive nature of the acceptor stream, which increased temperature, 40°C was selected in order to avoid rapid deterioration.

The inner volume of the acceptor and/or donor chamber was found to strongly affect the separation efficiency. The effect of this variable was readily studied by placing spacers of variable thickness (*c* in Fig. 1A) in the module as required. As can be seen in Fig. 5, both chambers performed optimally at the minimum volume tested; the spacers caused dilution of the analyte, both in the gas phase and in the acceptor liquid phase.

The effect of *halting the flow* during pervaporation was studied in three modes: by stopping the acceptor stream, the donor stream or both. The stop time was varied from 30 to 180 sec, and each time was tested in two sample introduction modes: continuous insertion and injection. In the latter mode, the flow was halted 10 sec after injection, *i.e.* when most of the injected plug was inside the lower chamber.

Figure 6 shows the effect of both variables. As can be seen, halting the acceptor stream strongly influenced the analytical signal in both sample introduction modes, which showed the membrane to have a restrictive effect.

A higher analytical signal was also obtained by increasing the stop-time. In fact an increase in the analytical signal by *ca.* 130% relative to the continuous working conditions was obtained for a 180 sec stop-time. The effect was even more marked (*ca.* 170%) if both streams were halted. The stopped-flow mode can be of special interest when a high sensitivity is required; however, these working conditions dramatically decrease sample throughput, which hinders application in routine work.

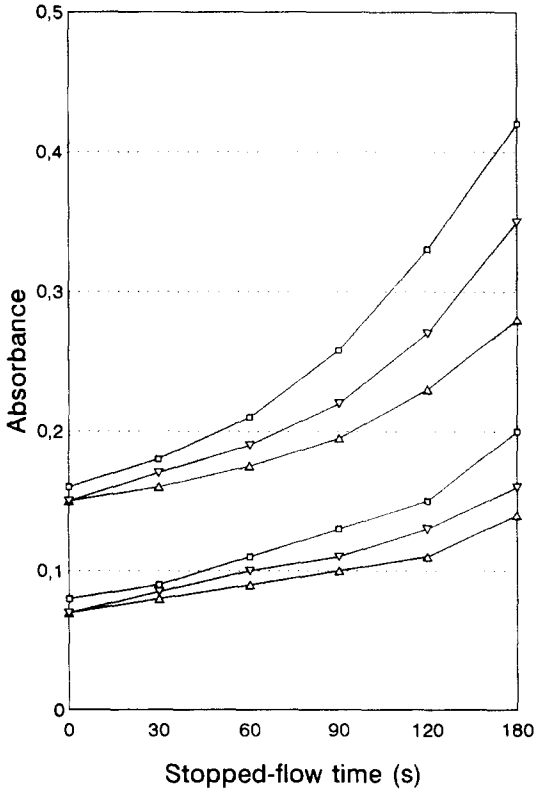


Fig. 6. Effect of stopping the acceptor stream, the donor stream or both on the pervaporation process. The flow was halted for 0 and 180 sec. (1) With continuous sample aspiration; (2) with sample injection, 1.0 ml of 10% (v/v) ethanol standard solution, 40°C (flow stopped in the upper chamber ▽; lower chamber △; both □).

Table 2. Analytical curves obtained under various experimental conditions

| Working condition | | Linear | | | |
|---|---|---|---|---|---|
| Temp. (°C) | Time (sec) | interval (%) | Equation | r | RSD* |
| 40† | 0 | 0.0–40.0 | $A = 0.02(\text{Eth}) - 0.027$ | 0.9985 | 1.5 |
| 40 | 60 | 0.0–40.0 | $A = 0.03(\text{Eth}) - 0.029$ | 0.9982 | 1.7 |
| 40 | 180 | 0.0–15.0 | $A = 0.07(\text{Eth}) + 0.024$ | 0.9982 | 2.0 |
| 60 | 0 | 0.0–20.0 | $A = 0.02(\text{Eth}) + 0.004$ | 0.9993 | 2.0 |
| 60 | 60 | 0.0–20.0 | $A = 0.04(\text{Eth}) + 0.027$ | 0.9950 | 2.3 |
| 60 | 180 | 0.0–10.0 | $A = 0.11(\text{Eth}) + 0.023$ | 0.9970 | 2.4 |
| 40‡ | 0 | 0.0–40.0 | $A = 0.01(\text{Eth}) + 0.005$ | 0.9992 | 1.7 |
| 40 | 60 | 0.0–40.0 | $A = 0.02(\text{Eth}) + 0.014$ | 0.9991 | 2.1 |
| 40 | 180 | 0.0–20.0 | $A = 0.03(\text{Eth}) + 0.020$ | 0.9980 | 2.5 |
| 60 | 0 | 0.0–30.0 | $A = 0.01(\text{Eth}) + 0.016$ | 0.9970 | 2.0 |
| 60 | 60 | 0.0–30.0 | $A = 0.02(\text{Eth}) + 0.020$ | 0.9980 | 2.1 |
| 60 | 180 | 0.0–20.0 | $A = 0.05(\text{Eth}) + 0.020$ | 0.9980 | 2.6 |

*10% (v/v) in ethanol, $n = 10$.
†Sample aspiration.
‡Sample injection (1 ml).
§Both the acceptor and donor stream were halted.

*Determination of ethanol in wine*

The proposed manifold (Fig. 2) is remarkably stable; in fact, no significant change in the baseline absorbance was observed after 8 hr operation. Several calibration graphs were run at various temperature and stoptimes and fitted by least-squares polynomial regression. Their equations and statistical parameter are shown in Table 2. The working conditions can be matched to the linear range and sensitivity required. As noted earlier a flow stopping time of 180 sec provided the best slope for the calibration graph, to the detriment of the sample throughput. The slope was maximal at 60°C; under these conditions the relative standard deviation was increased as a result, however, and the membrane deteriorated more rapidly.

Wider linear ranges and better reproducibility were obtained by shortening or suppressing the flow stopping time. With no flow stopping, the sampling frequency obtained was 10 $hr^{-1}$, with a repeatability of 1.7%, expressed as RSD.

Table 3. Determination of ethanol in wine

| | | Recovery (%)‡ | |
|---|---|---|---|
| Sample* | Ethanol† | 1st addition | 2nd addition |
| 1 | 10.96 | 92.4 | 97.9 |
| 2 | 11.76 | 92.6 | 98.3 |
| 3 | 11.86 | 95.0 | 94.9 |
| 4 | 10.26 | 91.7 | 89.7 |
| 5 | 9.46 | 95.9 | 99.4 |
| 6 | 10.26 | 102.7 | 101.4 |

*Wines from the Montilla-Moriles region.
†Injection of undiluted samples.
‡2.5 and 5% (v/v) for the first and second addition, respectively.

In order to test the performance of the reported approach on real samples, the ethanol content in various wines (white, rosé and red) was determined. Table 3 summarizes the results: the analyte contents found and the recoveries obtained from two standard additions (between 89.7 and 102.7%).

## FINAL REMARKS

Pervaporation enhances the performance of continuous flow systems, as shown in this work by using a pervaporation module to determine ethanol in real samples. The most salient advantage of continuous pervaporation over existing alternatives such as gas diffusion arises from the fact never contacts the separation membrane, thereby avoiding a number of problems (*e.g.* pore clogging) encountered in processing real samples (*e.g.* waste water, fermentation broth). By using appropriate working conditions, a variety of analytical problems can be addressed with the aid of the proposed module. Some potential applications include the direct determination of volatile species such as acetone, biacetil, alcohols, and the indirect determination of analytes forming volatile species such as fluoride and boron. In addition, pervaporation could be used for the determination of such analytes as ammonium, sulphite and carbonate by pH changes, and compared in terms of performance with conventional gas-diffusion methods for these ions.

*Acknowledgements*—The Spanish Dirección General de Investigación Científica y Técnica (DGICyT) is gratefully acknowledged for financial support (Project No. PB93-0827). One of the authors (I.L.M.) wishes to express his

gratitude to Dr G. Oliveira Neto and the Brazilian Conselho National de Desenvolvimento Cientifico y Technològico (CNPq) for funding his stay in Spain.

## REFERENCES

1. M. Valcárcel, M. D. Luque de Castro and M. T. Tena, *Anal. Proc.*, 1993, **30**, 276.
2. M. Valcárcel and M. D. Luque de Castro, *Non-Chromatographic Continuous Separation Techniques*. Royal Society of Chemistry, Cambridge, 1991.
3. M. D. Luque de Castro and M. Valcárcel, *Anal. Chim. Acta*, 1992, **261**, 525.
4. M. D. Luque de Castro, *Lab. Robotics Autom.*, 1992, **5**, 179.
5. F. Lázaro and M. D. Luque de Castro, *Analusis*, 1988, **16**, 216.
6. V. Spohn, R. Everhart, R. Joksch, R. Wichmann, C. Wandrey and H. Vob, *GBF Monographs*, Vol. 13. VCH, 1991.
7. P. K. Dasgupta and H. C. Yang, *Anal. Chem.*, 1986, **58**, 2839.
8. G. Shulze, C. Y. Liu, M. Brodonski, O. Elsholz, W. Frenzel and J. Möller, *Anal. Chim. Acta*, 1988, **214**, 121.
9. C. Pasquini and L. C. Faria, *Anal. Chim. Acta*, 1987, **193**, 19.
10. R. Y. M. Huang (ed.), *Pervaporation Membrane Separation Processes*. Elsevier, Amsterdam, 1991.
11. M. Valcárcel and A. Ríos, *Anal. Chem.*, 1993, **65**, 781A.
12. J. Haggin, *Chem. Engng News (ACS)*, 1990, Oct. 1, 22.
13. H. Toshiro and I. Munetoshi, *J. Membr. Sci.*, 1989, **45**, 137.
14. H. Strathmann and W. Gudernatsch, in *Separation for Biotechnology*, Verrall, M. S. and Hudson, M. J. (eds), Chap. 26. Ellis Horwood, Chichester, 1987.
15. P. Hickey and C. Stewart-Slater, *Sepn Purif. Met.*, 1990, **19**, 93.
16. V. Prinzing, I. Ogbomo, C. Lehn and H. L. Schmidt, *Sens. Actuators*, 1990, **B1**, 542.
17. I. Ogbomo, A. Steffl, W. Schuhmann, U. Prinzing and H. L. Schmidt, *J. Biotechnol.*, 1993, **31**, 317.
18. H. Usthche and G. Histi, *J. Membr. Sci.*, 1981, **8**, 105.
19. W. E. van der Linden, *Anal. Chim. Acta*, 1983, **151**, 359.

Pergamon

0039-9140(95)01481-0

*Talanta*, Vol. 42, No. 5, pp. 767–773, 1995

0039-9140/95 $9.50 + 0.00

# PHASE-INVERSION CELLULOSE ACETATE MEMBRANES FOR SUPPRESSION OF PROTEIN INTERFERENCES IN ANODIC STRIPPING VOLTAMMETRY

BOY HOYER* and NINA JENSEN

Department of Chemistry, Aarhus University, Langelandsgade 140, 8000 Aarhus C, Denmark

(*Received* 22 *July* 1994. *Accepted* 14 *November* 1994)

**Summary**—The phase-inversion (PI) method was used to cast permselective cellulose acetate membranes on glassy carbon electrodes with the aim of suppressing protein interferences in anodic stripping voltammetry (ASV). By using cadmium and lead as test analytes and differential pulse ASV as detection method, it was found that the modification of the electrode greatly reduces the interference from albumin. Cellulose acetate membranes prepared by the PI method give better protection against protein interference and have more reproducible permeability characteristics than membranes of comparable thickness prepared by the base hydrolysis method. An optimization study of the PI coating procedure was undertaken.

The direct determination of trace metals in polluted waters and biological samples by anodic stripping voltammetry (ASV) is often hampered by interference effects from organic constituents of the sample matrix. Adsorption of surface-active compounds onto the working electrode usually causes peak depression,[1] and the adsorption/desorption process as such may yield tensammetric peaks which can interfere with or be mistaken for the metal peaks.[2] Consequently, it is often necessary to mineralize the sample matrix prior to stripping analysis. However, sample decomposition complicates and lengthens the analytical procedure and introduces contamination risks.

Recently, coating of the working electrode with permselective membranes has been introduced as a means of circumventing the organic interferences in ASV. One of the most successful membrane materials for this purpose has proven to be cellulose acetate (CA). The coating of the electrode is done either by mounting a preformed bulk membrane directly in contact with the electrode, or by casting the membrane *in situ* on the electrode surface, usually followed by suitable conditioning. Stewart and Smart[3,4] covered a glassy carbon electrode with a bulk CA membrane (1000 MW cutoff) through which a thin mercury film was plated. For cadmium, excellent resistance toward organic interferences was obtained, although the membrane to some extent interfered with the mass transport of the analyte. Owing to their thickness, bulk membranes suffer from the general drawback that the time required for equilibration with the contacting solution is of the same order of magnitude as the duration of a typical ASV experiment, and the response time of the electrode can become a limiting factor. Moreover, bulk membranes strongly impede the mass transport of the analyte to and from the electrode surface, and cause a reduction of the sensitivity in ASV by a factor as high as 18,[5] which is unacceptable in most applications. In contrast, an *in situ* formed CA membrane can be made much thinner, partly owing to the fact that it is cast directly on a solid support (the electrode) and is not moved herefrom. Therefore, the membrane does not need to be mechanically self-supporting. Wang and coworkers have extensively demonstrated the utility of permselective, *in situ* formed CA coatings on electrodes for protection against surfactant interferences in stripping analysis[6,7] and for selective detection of low molecular weight species in amperometric detectors.[8,9] Electrode modification was carried out by casting a dense CA film which was subsequently subjected to base hydrolysis (BH). This treatment breaks the polymer backbone and increases the

*Author to whom correspondence should be addressed.

permeability of the CA membrane,[8] and the permselectivity can be controlled via the hydrolysis time. However, poor stability and reproducibility of CA coatings prepared in this manner have also been reported,[10] which probably is a result of the degradation of the membrane polymer in the BH step.[11]

An alternative way of controlling the permeability of CA membranes is achieved in the wet phase-inversion (PI) process, in which a pore former or swelling agent is added to the casting solution.[12] When the casting solvent has evaporated, leaving behind a viscous solution of CA and the pore former, the membrane is immersed in a non-solvent gelation bath where the polymer precipitates. The precipitation begins at the surface of the membrane and propagates as pore former is exchanged by non-solvent. The porosity of the resulting membrane depends in a complex manner on the composition of the casting solution, the pore former/swelling agent used, and the experimental conditions in the casting procedure.[12-14] Generally, anisotrophic membranes are produced with a dense skin layer, which accounts for the permselectivity, and a porous sub-layer.[12,14] Kuhn *et al.* concluded that this structure is also found in very thin membranes prepared by the PI process.[11] The PI method has two advantages in comparison with the BH method: firstly, the process does not involve any degradation of the CA polymer. Secondly, the main diffusional barrier in CA membranes prepared by the PI process is the thin skin layer, and the inevitable inhibition of the mass transport of analytes caused by the permselective coating is therefore minimal. In contrast, CA coatings prepared by the BH process are homogenous in depth, and the diffusional resistance of the membrane relative to its permselectivity is higher. In spite of these advantages, only Kuhn *et al.* have used the PI process for preparation of membrane coatings on electrodes.[11,15]

Nafion, a perfluorosulfonate cation-exchange resin, has also proven to be a useful material for preparation of protective electrode coatings in ASV. A Nafion-coated thin mercury film electrode (NCTMFE) is less susceptible to interference from surface-active compounds (including proteins) than the conventional TMFE,[16] and it has been used successfully for the direct determination of trace metals in body fluids.[17] Moreover, signal enhancement is achieved with the NCTMFE when used in conjunction with differential stripping techniques,[16,18] and it offers high signal stability.[18] However, the permselectivity of thin Nafion membranes is complex as it results from a combination of charge and size exclusion effects and hydrophobic interactions between the fluorocarbon polymer backbone and the penetrating species.[19-21] In contrast, the permselectivity of CA membranes is primarily based on size exclusion,[8] and this membrane material is, therefore, to be preferred when interfering species can be discriminated against on the basis of molecular size alone.

The purpose of the present work was to assess the usefulness of the PI process for preparation of CA-coated electrodes for protection against protein interferences in ASV, and to compare the virtues of CA coatings made by the PI and the BH methods. Most of the results and conclusions concerning the usefulness of the PI process for preparation of permselective membrane coatings on electrodes are not limited to ASV but also apply to many other electroanalytical methods where suppression of interferences from surface-active compounds is desirable.

## EXPERIMENTAL

### *Apparatus*

Voltammetric measurements were performed with a programmable electrochemical analyser.[22] The electrochemical cell comprised a Metrohm 628-50 rotating disk electrode unit with a 3-mm diameter glassy carbon electrode. The reference electrode was a Radiometer K401 saturated calomel electrode (SCE), while the counter electrode was a glass-fitted platinum wire (1 cm long, 0.5 mm thick).

### *Reagents*

Buffers and supporting electrolyte media were prepared from Merck Suprapur reagents and triply distilled water, while other reagents were of analytical grade. Cellulose acetate (39.8% acetyl content, 30,000 MW) was obtained from Aldrich. Bovine albumin (fraction V, essentially globulin free, lyophilized, 66,000 MW) was obtained from Sigma. A 0.1 (w/v)% albumin solution in distilled water was prepared daily. The composition of the casting solution for the PI membranes was: 20 ml acetone, 0.5 ml of 0.52*M* $Mg(ClO_4)_2$ in water and 0.05 g CA, while the casting solution for the BH membranes was composed of 10 ml acetone, 10 ml cyclohexanone and 0.05 g CA. The concentration of CA in both solutions was 0.25 (w/v)%. In the

following, the formulations of these casting solutions are referred to as the standard compositions.

*Procedure for preparation of modified electrodes*

Prior to coating, the glassy carbon electrode was polished with 0.25 $\mu$m diamond paste, rinsed with ethanol and dried with lens paper. Coating with CA was done by inverting the rotating disk electrode and applying 2.5 $\mu$l of the casting solution to the glassy carbon surface. Rotation was immediately switched on at 1500 rpm. In the preparation of the PI membranes, the duration of this evaporation step was 30 sec, after which the electrode was immersed in an ice-water gelation bath (0°) for 30 min. For the BH membranes, the evaporation step lasted 20 min, and the electrode was subsequently immersed in a 0.06$M$ KOH solution for 16 min. Mercury was deposited on the glassy carbon/CA substrate by electrolysis for 10 min. at $-1$ V *vs.* SCE in deaerated acetate buffer spiked with $2.5 \times 10^{-5}M$ mercury(II). A conventional thin mercury film electrode (TMFE) was prepared in the same manner apart from the polymer coating.

The procedure for the preparation of the BH membranes was adopted from Ref. 10, while the general guidelines for the preparation of the PI membranes were found in Ref. 11. In the following, a TMFE coated with CA by the BH or the PI process is abbreviated as BH-TMFE and PI-TMFE, respectively.

*Procedure for DPASV measurements*

All measurements were performed in 0.1$M$ acetate buffer spiked with $2.0 \times 10^{-7}M$ Cd(II) and $2.0 \times 10^{-7}M$ Pb(II). Solutions were deaerated with argon for 5 min prior to DPASV measurement. The working electrode was rotated at 750 rpm during deposition, while stripping was carried out in a quiescent solution following a 15 sec rest period. The stripping signals were recorded in differential pulse mode with the following instrumental settings: deposition potential, $-1000$ mV *vs.* SCE; deposition time, 2 min; scan range, $-1000$ to $-50$ mV *vs.* SCE; pulse height, 50 mV; pulse width, 22 msec; sampling time, 2 msec; pulse repetition time, 0.24 sec; effective scan rate, 12.3 mV/sec. Signals were smoothed with a seven-point Savitsky-Golay algorithm, and the background signal was corrected for by subtraction of an interpolated linear baseline. A freshly prepared electrode was preconditioned by performing two deposition/stripping cycles in the acetate buffer. In the stability studies, the repeated DPASV experiments were performed automatically under computer control.

In the protein interference experiments, the albumin concentration in the test solution was raised incrementally in the following sequence: 1, 2, 5, 10 and 20 ppm. Two stripping measurements were carried out after each addition. In this manner, the dependence of the DPASV peak current on the protein concentration could be studied, and the adsorption of protein onto the working electrode was closer to equilibrium.

## RESULTS AND DISCUSSION

The DPASV peak currents for cadmium and lead at the conventional TMFE are strongly depressed by albumin (Fig. 1 and Table 1). Moreover, the functional relationship between the peak current and the albumin concentration is such (*cf.* Fig. 1) that even low concentrations of albumin (1–2 ppm) cause a large peak depression, while further increases of the protein concentration only affect the peak current modestly. Both the BH- and the PI-cellulose acetate coatings suppressed the albumin interference, but the latter was clearly superior (Table 1). A $t$-test showed that the peak depression observed with the two electrode modification schemes is different at a 98% confidence level for cadmium as well as lead. Equally important, the variability of individual electrode preparations with respect to the suppression of the albumin interference is much smaller for the PI-TMFE than for the BH-TMFE. Most likely, this

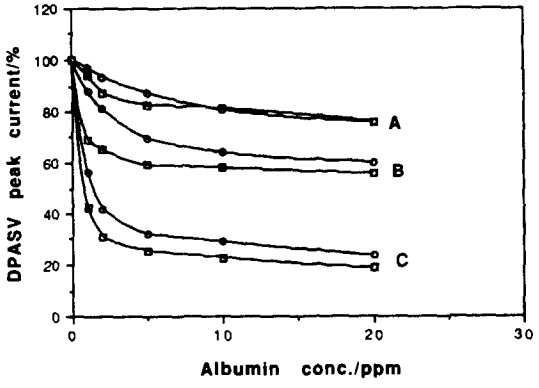


Fig. 1. Effect of albumin on the DPASV peak current of cadmium (□) and lead (○) obtained with (A) PI-TMFE, (B) BH-TMFE and (C) TMFE. The peak currents are given relative to the initial value prior to albumin addition. The measurements were performed with electrodes which were representative for each type of electrode preparation.

Table 1. Effect of albumin on the DPASV peak current for cadmium and lead

| Electrode preparation | Cd | | Pb | | |
|---|---|---|---|---|---|
| | Mean change of peak current* (%) | Standard deviation of change of peak current (%) | Mean change of peak current* (%) | Standard deviation of change of peak current (%) | n† |
| TMFE | −85 | 3 | −75 | 3 | 5 |
| PI-TMFE | −26 | 12 | −28 | 11 | 18 |
| BH-TMFE | −47 | 26 | −44 | 20 | 15 |

*Change in DPASV peak current after addition of 20 ppm albumin (see Experimental).
†No. of individual electrode preparations.

improvement is owing to the fact that no degradation of the cellulose acetate takes place in the PI process. Dam *et al.*[10] also attributed the poor reproducibility of BH-TMFEs to the breakdown of the polymer during the hydrolysis step.

The DPASV peak currents obtained with the PI-TMFE and the BH-TMFE are similar for cadmium as well as lead (Table 2). Thus, the superior resistance of the PI-TMFE over the BH-TMFE towards the albumin interference is not achieved at the expense of sensitivity. The peak currents at the membrane-coated electrodes are reduced by a factor of approximately 2.5 in comparison with the bare TMFE. This effect can be explained by increased diffusional resistance due to the membrane barrier, and possibly also a reduction of the effective electrode area. It was found that the signal suppression caused by albumin and the initial DPASV peak current for individual electrode preparations were weakly correlated. Thus, for the PI-TMFE the correlation coefficient was 0.42 for cadmium and 0.50 for lead, while the corresponding figures for the BH-TMFE were 0.72 and 0.67, respectively. The correlation can be explained by random variations in the distribution of pore sizes between individual membranes because a membrane with a more open pore structure will yield a higher signal but will withhold the interferent less effectively and vice versa.

The signal stabilities of the TMFE and the modified electrodes in the absence of albumin were similar (Table 3). For all electrode preparations, the decrease in the signal during the repeated stripping experiments was larger for lead than for cadmium. The PI-TMFE and the BH-TMFE have lower signal stability than the Nafion-coated TMFE.[18] As explained above, the addition of albumin in the protein interference study was done incrementally during a total of 12 deposition/stripping cycles, and the "natural" fall-off of the signal occurring in the absence of protein will, therefore, contribute to the peak depressions given in Table 1.

The detection limit for a PI-TMFE with typical sensitivity was found to be 9 n$M$ for cadmium and 5 n$M$ for lead ($3\sigma$ level, 2 min deposition time). The linear range for the DPASV peak current measured with a PI-TMFE was evaluated by varying the concentration of cadmium and lead between 40 n$M$ and 1.0 $\mu M$. Again, a 2 min deposition time was employed. For cadmium, the data for the resulting calibration line were: slope, 9.0 $\mu A/\mu M$; intercept, 0.15 $\mu$A; regression coefficient, 0.9990 ($n = 10$), while the corresponding figures for lead were: 19.1 $\mu A/\mu M$, 0.22 $\mu$A and 0.9989 ($n = 10$). Curvature of the calibration plot was observed at metal concentrations higher than 1 $\mu M$. In practice, however, this problem was easily remedied by lowering the deposition time.

The cellulose acetate coatings prepared by the BH as well as the PI method were transparent and somewhat more dull than the bare glassy carbon electrode. No pinholes in the polymer

Table 2. DPASV peak current of cadmium and lead obtained with the PI-TMFE, BH-TMFE and TMFE

| Electrode preparation | Cd | | Pb | | |
|---|---|---|---|---|---|
| | Mean peak current ($\mu A$) | Standard deviation of peak current ($\mu A$) | Mean peak current ($\mu A$) | Standard deviation of peak current ($\mu A$) | n* |
| TMFE | 5.7 | 1.9 | 10 | 1.1 | 10 |
| PI-TMFE | 2.4 | 1.1 | 4.5 | 1.7 | 26 |
| BH-TMFE | 2.3 | 1.4 | 3.9 | 1.8 | 24 |

*No. of individual electrode preparations.

Table 3. Signal stability of PI-TMFE, BH-TMFE and TMFE*

| Electrode preparation | Cd | | Pb | | |
|---|---|---|---|---|---|
| | Mean change of peak current† (%) | Standard deviation of change of peak current (%) | Mean change of peak current† (%) | Standard deviation of change of peak current (%) | $n$‡ |
| TMFE§ | −13 | 8 | −17 | 6 | 5 |
| PI-TMFE | −12 | 5 | −20 | 5 | 6 |
| BH-TMFE | −9 | 7 | −20 | 6 | 5 |

*Each stability experiment commenced with a freshly prepared working electrode. Twenty consecutive DPASV signals were acquired during 72 min.

†Change of the DPASV peak current between first and twentieth signal.

‡No. of individual electrode preparations.

§Data from Ref. 17.

layer could be seen in an optical microscope at 500× magnification. The cellulose acetate coating adhered strongly to the glassy carbon substrate, and withstood gentle wiping with filter paper.

As discussed by Kesting,[12] the properties of PI cellulose acetate membranes are strongly dependent on the formulation of the casting solution as well as the experimental conditions during drying and gelation of the membrane. Therefore, an optimization study was undertaken with the aim of preparing membrane coatings with high permselectivity and high reproducibility of the properties of the resulting electrodes. In order to avoid an excessive number of experiments, an experimental design was chosen in which one parameter at a time in the standard procedure described above was varied. Furthermore, some constraints on the formulation of the casting solution were chosen. Dam *et al.*[10] have previously obtained good protection against protein interference with a BH-TMFE by applying an amount of cellulose acetate corresponding to 0.8 $\mu$g/mm$^2$ on the electrode surface, and this value was initially chosen as reference for the PI membranes as well. The surface tension of the casting solution was such that a maximum of 2.5 $\mu$l could be applied to the glassy carbon surface without spillage during the spin-coating procedure. These considerations in combination dictate the polymer-to-solvent ratio in the casting solution. The composition of the swelling agent [0.52$M$ aqueous $Mg(ClO_4)_2$] was chosen on the basis of the recommendations in Ref. 11 and was not varied.

The influence of the concentrations of cellulose acetate and swelling agent in the casting solution on the properties of the PI-TMFE is given in Table 4. The DPASV peak current and the suppression of the albumin interference vary monotonically with the amount of cellulose acetate applied to the electrode, and the composition of the standard casting solution is an acceptable compromise between suppression of the albumin interference and sensitivity. Surprisingly, a reduction of the amount of swelling agent led to a poorer suppression of the albumin interference. This observation, which was verified in four separate experiments, implies that there is an optimal concentration of swelling agent in the casting solution at which the best rejection of albumin is obtained. For bulk PI membranes, the general rule is that permeability decreases monotonically with decreasing content of swelling agent.[12,14] However, it should be noted that the PI membranes employed in the present study were much thinner than those used in the previous model experiments,[14] and it is, therefore, likely that the explanation of the discrepancy is linked to this difference in the experimental conditions.

A number of variations of the coating procedure for the PI membranes were also attempted. At room temperature, the solvent

Table 4. Effects of variations in the casting solution composition on DPASV response of the PI-TMFE*

| Variation* | Effect |
|---|---|
| Amount of cellulose acetate doubled | substantial decrease in peak currents; little improvement in suppression of albumin interference |
| Amount of cellulose acetate halved | increase in peak currents; poorer suppression of albumin interference |
| Amount of swelling agent doubled | increase in peak currents; poorer suppression of albumin interference |
| Amount of swelling agent halved | substantial decrease in peak currents; poorer suppression of albumin interference |

*The variations are relative to the standard composition of the casting solution given in Experimental. A minimum of three electrode modifications were carried out for each variation.

quickly evaporated when the casting solution was applied to the electrode surface, and the system was, therefore, far from equilibrium during the formation of the cellulose acetate/swelling agent phase. Thus, it was examined whether any advantages accrued from slowing down the evaporation of the solvent. This was accomplished in two different ways: by performing the electrode coating at 4° in a cold room (after equilibrating the equipment and the casting solution to this temperature), or by applying the casting solution in an atmosphere in equilibrium with mixtures of water and acetone in varying ratios. However, neither method led to any improvement in the properties of the resulting membranes and it was, therefore, concluded that the evaporation step in the electrode preparation procedure is not critical.

Spin-coating was found to improve the reproducibility of the characteristics of the PI-TMFE as well as the BH-TMFE in comparison with electrodes where no rotation was applied during the evaporation step. This improvement, which is quite general,[23] is probably a result of a more even spreading of the polymer over the electrode surface. Spin-coating changed the visual appearance of the coating: without rotation, chaotic refraction patterns could be seen, while the electrodes which had been rotated only had diffuse, concentric refraction rings. These observations can also be attributed to the more uniform polymer layer obtained by spin-coating.

The temperature of the gelation bath had a pronounced effect on the performance of the PI-TMFE. Increasing the gelation bath temperature to 22° was accompanied by a decrease in the discriminative power of the membrane towards albumin and an increase in the DPASV peak current for cadmium and lead, and gelation at 40° yielded electrodes which resembled the conventional TMFE. Thus, gelation in ice water is essential in order to obtain good permselectivity. These observations are in agreement with the work of Kesting *et al.*,[14] who explained the loss in permselectivity at higher gelation temperatures by rupture of the skin layer owing to mechanical stress during the rapid precipitation of the polymer.

Annealing of the PI membrane in warm or hot water after the gelation bath is known to decrease the permeability of the membrane,[14] and this procedure was also attempted. It was found that the effect of the treatment was strongly dependent on the temperature of the annealing bath. At 50°, little effect on the performance of the electrode was noted, but raising the annealing temperature to 60° or higher caused a substantial reduction in the DPASV currents without any accompanying improvement in the suppression of the albumin interference. Therefore, further use of the annealing procedure was given up.

In conclusion, the protein interferences in ASV are significantly suppressed at a PI-TMFE, and it offers better protection than a BH-TMFE coated with the same amount of CA. Moreover, the variation in permselectivity between individual coatings prepared by the PI process is smaller than is the case with the BH method. Even so, the reproducibility of the PI method with respect to the properties of the resulting membranes needs to be improved in order to make the PI-TMFE more useful for routine use. At present, the possibility of further optimizing the procedure for casting PI membranes onto electrodes is being investigated.

*Acknowledgements*—The authors are most grateful to Dr K. N. Thomsen, I/S Nordkraft, Aalborg, Denmark and Dr M. E. R. Dam, Aalborg University, Aalborg, Denmark, for valuable discussions and for providing a preprint of Ref. 10.

## REFERENCES

1. P. L. Brezonik, P. A. Brauner and W. Stumm, *Water Res.*, 1976, **10**, 605.
2. G. E. Batley and T. M. Florence, *J. Electroanal. Chem.*, 1976, **72**, 121.
3. E. E. Stewart and R. B. Smart, *Anal. Chem.*, 1984, **56**, 1131.
4. R. B. Smart and E. E. Stewart, *Environ. Sci. Technol.*, 1985, **19**, 137.
5. J. H. Aldstadt and H. D. Dewald, *Anal. Chem.*, 1993, **65**, 922.
6. J. Wang and L. D. Hutchins-Kumar, *Anal. Chem.*, 1986, **58**, 402.
7. J. Wang, M. Bonakdar and M. M. Pack, *Anal. Chim. Acta*, 1987, **192**, 215.
8. J. Wang, and L. D. Hutchins, *Anal. Chem.*, 1985, **57**, 1536.
9. L. D. Hutchins-Kumar, J. Wang, and P. Tuzhi, *Anal. Chem.*, 1986, **58**, 1019.
10. M. E. R. Dam, K. N. Thomsen, P. G. Pickup and K. H. Schrøder *Electroanalysis*, 1995, **7**, 70.
11. L. S. Kuhn, S. G. Weber and K. Z. Ismail, *Anal. Chem.*, 1989, **61**, 303.
12. R. E. Kesting, *Synthetic Polymer Membranes*, 2nd Edn, Chap. 7. Wiley, New York, 1985.
13. R. E. Kesting, *J. Appl. Polym. Sci.*, 1965, **9**, 663.
14. R. E. Kesting, M. K. Barsh and A. L. Vincent, *J. Appl. Polym. Sci.*, 1965, **9**, 1873.
15. L. S. Kuhn and S. G. Weber, *Electroanalysis*, 1991, **3**, 941.
16. B. Hoyer, T. M. Florence and G. E. Batley, *Anal. Chem.*, 1987, **59**, 1608.

17. B. Hoyer and T. M. Florence, *Anal. Chem.*, 1987, **59**, 2839.
18. B. Hoyer and N. Jensen, *Talanta*, 1994, **41**, 449.
19. G. A. Gerhardt, A. F. Oke, G. Nagy, B. Moghaddam and R. N. Adams, *Brain Res.*, 1984, **290**, 390.
20. B. Hoyer and M. Loftager, *Anal. Chem.*, 1988, **60**, 1235.
21. M. W. Espenscheid, A. R. Ghatak-Roy, R. B. Moore, R. M. Penner, M. N. Szentirmay and C. R. Martin, *J. Chem. Soc., Faraday Trans.*, 1986, **82**, 1051–1070.
22. K. N. Thomsen, H. J. Skov and L. Kryger, *Anal. Chim. Acta*, 1989, **219**, 105.
23. J. Labuda, *Selective Electrode Rev.*, 1992, **14**, 33.

Pergamon

0039-9140(95)01430-6

*Talanta*, Vol. 42, No. 6, pp. 775–778, 1995
Elsevier Science Ltd
Printed in Great Britain
0039-9140/95 $9.50 + 0.00

# NEW FLUORIGENIC REAGENTS AND THEIR FLUORESCENT REACTIONS FOR AMINO ACID MEASUREMENTS

M. AMINUDDIN* and J. N. MILLER

Department of Chemistry, Loughborough University of Technology, Loughborough, Leicestershire LE11 3TU, U.K.

(*Received* 10 *April* 1994. *Revised* 19 *September* 1994. *Accepted* 24 *September* 1994)

**Summary**—Naphthalene-2,3-dicarboxaldehyde, 1-phenylnaphthalene-2,3-dicarboxaldehyde and anthracene-2,3-dicarboxladehyde have been characterized for use as fluorigenic reagents for the determination of primary amines and amino acids at the microgram level. The reaction conditions, spectral properties and the stability of the derivatives (isoindoles) have been investigated with standard amino acids. The results have been compared with other fluorigenic reagents such as *ortho*-phthalaldehyde.

## INTRODUCTION

Fluorimetry is a sensitive method for detection of amino acids and there are a number of useful fluorigenic reagents such as *o*-phthalaldehyde (OPA),[1,2] dansyl chloride,[3] fluorescamine,[4] 4-chloro-7-nitrobenzo-2-oxa-1,3-diazole (NBD-Cl)[5] and 3-benzoyl-2-quinoline carboxaldehyde (BQ CA).[6,7] Of these, OPA is widely used for amino functional groups. The reaction product is an isoindole with optimal wavelengths, $E_{ex} = 340$ nm and $E_{em} = 455$ nm. The emission, however, suffers spectral interferences, especially for biological samples in which background emission overlaps the emission of the isoindoles.

New reagents such as 1-phenylnaphthalene-2,3-dicarboxaldehyde ($\phi$NDA), anthracene-2,3-dicarboxaldehyde (ADA) including the published naphthalene-2,3-dicarboxaldehyde (NDA)[8,9] have been synthesized in the author's laboratory according to Cook *et al.*[8] and used for measuring amino acid groups. These reagents from fluorescent isoindoles (Fig. 1, I–III) with compounds containing a primary group. The emission wavelengths of the products obtained by using these reagents are much longer than those for OPA-adducts.

This paper reports reactions of these reagents and their utility for determination of amino acids in trace quantities. Important properties, *e.g.* reaction time, effect of solvent, pH of the medium and stability of the product, are reported.

## EXPERIMENTAL

### *Borate buffer* (pH 10.0)

Borax (4.8 g/l.) and sodium hydroxide (0.80 g/l.) were dissolved in distilled water and stirred well to obtain a clear solution.

### *Fluorigenic reagent solution*

Each fluorigenic reagent was dissolved in a minimum volume of ethanol and made up to the required volume with either distilled water or 0.025*M* sodium borate buffer (pH 10.0) to obtain solutions of known molarity.

*o*-Phthalaldehyde (OPA), ethanethiol (ET), 2-methyl-2-propanethiol (2MPT), 2-mercaptoethanol and 3-mercaptoropionic acid were purchased from Aldrich Chemical Co. Ltd. Amino acids and all other chemicals were of analytical grade.

### *Spectrofluorimetric procedure*

Dilute solutions, $10^{-4}$–$10^{-3}M$, of sample (0.2–0.3 ml) were treated with 1 ml of 10.9m*M* $\beta$-cyclodextrin ($\beta$-CD). A 0.5 ml portion of borax–sodium hydroxide buffer (pH 10.0) and 0.1 ml aqueous thiol solution (0.1% v/v) were then added, followed by the addition of the suitable fluorigenic reagent in slight excess over the sample. The final volume was made up to 5 ml with water. The fluorescence emission was

*Present address for correspondence: Department of Chemistry, Islamia University, Bahawalpur, Pakistan.

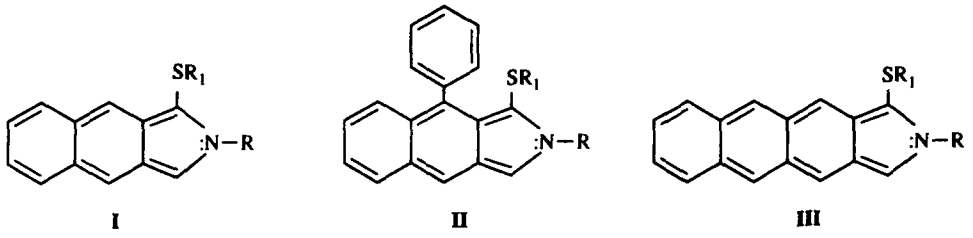


Fig. 1. Fluorescent isoindoles: I, NDA-derivative; II, $\phi$NDA-derivative; and III, ADA-derivative.

then measured at a suitable wavelength with excitation of the fluorescent derivative at an appropriate wavelength. Blanks without amino acid were used to evaluate blank interferences. For the OPA derivatives the labelling procedure was same as above but omitting $\beta$-CD from the reaction solution, unless stated otherwise.

## RESULTS AND DISCUSSION

### *Reaction and fluorescence spectra*

The fluorigenic reagents studied are dialdehydes similar to *o*-phthalaldehyde (OPA). With the use of a thiol as the nucleophilic substitution in derivative formation it may be assumed that the resultant fluorophores are 1-alkylthio-2-alkyl substituted isoindoles.[2,10,11] Decomposition occurs owing to spontaneous intramolecular sulphur-to-oxygen rearrangement leading to non-fluorescent 2,3-dihydro-1H-isoindole-1-one.[2,10] The fluorigenic reaction of the polyaromatic dialdehydes, e.g. NDA, $\phi$NDA and ADA, in the presence of thiol, with amines, amino acids and proteins is useful since it can be conducted in aqueous solution.

Figure 2 shows emission spectra of NDA and OPA-glycine derivatives using 2MPT and ET. The observed fluorescence spectra were obtained by excitation of the molecules at 462 and 350 nm, respectively. The fluorescence emission occurred at 550 and 510 nm for the NDA-adducts by using ET and 2MPT, respectively. A similar trend was observed for the OPA-adducts where the wavelengths of emission shifted from 450 to 410 nm for a corresponding change of thiols.

Similarly, $\phi$NDA and ADA derivatives of glycine were also found to give fluorescence emission at longer wavelengths, 520 and 640 nm, for excitation wavelengths of 462 and 470 nm, respectively.

The derivatization reaction, using all these new fluorigenic reagents, is fast. It takes only 3–5 min for full fluorescence intensities to develop.

### *Fluorescence intensity as a function of* pH

The yield of the derivative is sensitive to pH changes. The fluorescence intensity at 520 nm was measured as a function of pH. Glycine and NDA both at $2 \times 10^{-5}M$ concentration were derivatized in the presence of a thiol, varying the pH of the reaction medium from 5 to 12. Results showed that as the pH increased there was a gradual increase in fluorescence intensity, reaching a maximum around pH 10 followed by a continuous decrease in fluorescence intensity. The fluorescence increase with increasing pH may be ascribed to contributions owing to the unprotonated amino group at high pH. This point of view is supported by the fact that the reaction rates are faster[12] at high pH. The other fluorigenic reagents, $\phi$NDA and ADA, showed

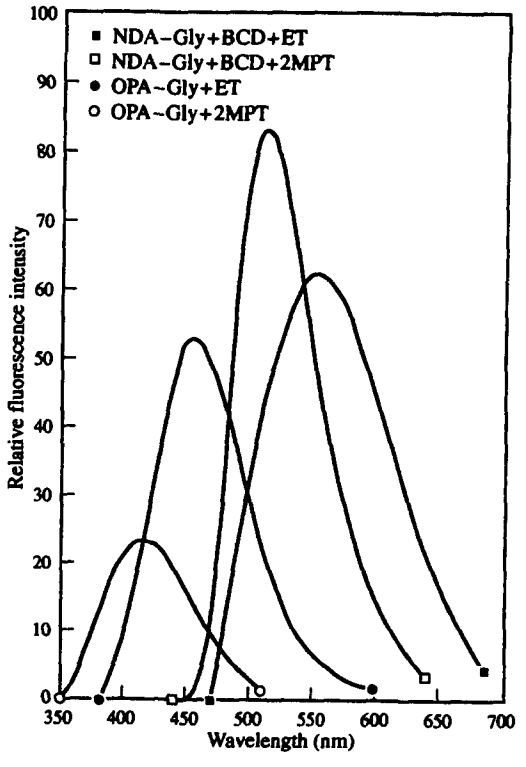


Fig. 2. Emission spectra of NDA- and OPA-glycine derivatives.

similar behaviour to that of the OPA fluorigenic reaction.

*Enhancement of fluorescence intensity by β-cyclodextrin and detergent*

In order to obtain enhanced fluorescence of the derivative, cyclodextrins were incorporated into the fluorigenic reaction of $10^{-4}M$ glycine with NDA of the same molarity as glycine. Cyclodextrin possesses cyclic sugar molecules which form a cavity rich in electron density because of glucosidic oxygens, and has the tendency to physically trap the guest molecules entering the cavity. Cyclodextrins, in fact, form complexes in aqueous solution with various substrates.[13] Experiments have indicated the effects of three cyclodextrins ($\alpha$, $\beta$ and $\gamma$). $\beta$-Cyclodextrin ($\beta$CD), enhances fluorescence intensity of the NDA derivatives by nearly eight times, compared with the NDA-derivative without $\beta$CD. Similar results were obtained using $\phi$NDA and ADA as fluorigenic reagents. However, the fluorescence enhancement was greater for an addition of a little over 2.5 mmol of $\beta$CD to the reaction mixture. The significant increase in fluorescence of the derivatives may be caused by side chain functional groups of the derivative entering the cavity while the rest of the molecule may remain outside.

The effect of the detergent, Brij-35, on fluorescence intensity is noticeable. In the presence of Brij-35, the NDA-glycine derivative formed with 2-methyl-2-propanethiol (2MPT) was found to give enhanced fluorescence. A very small improvement in the fluorescence intensity by the detergent may be a result of: (i) shielding of the NDA–glycine fluorophore from vibrational quenching by the hydrogen bond structure of water, (ii) alteration of the quantum efficiency[14–16] or (iii) increased local viscosity about the fluorophore micelle binding sites not being so effective as the deactivation modes.

*Influence of thiol structure on the stability of the derivatives*

The utility of thiol structure for amino acid analysis is demonstrated by the following observations. The wavelengths of emission are considerably affected by the thiol structure and this has been discussed in the preceding section. Furthermore, the thiol structure seems to alter the stability of the derivatives. The amino acid derivatives formed with the active, NDA, $\phi$NDA or ADA/thiol reagent exhibited not only varying fluorescent responses but also varying degrees of stability. The ADA–gly derivative using 2MPT was found to be very stable. On the other hand, NDA and $\phi$NDA derivatives of glycine with 2MPT were comparatively less stable and decomposed sharply. The stability was, however, found to be much more affected if the 2MPT is replaced by ethanethiol, 2-mercaptoethanol or 3-mercaptopropionic acid (not shown here). These results are in agreement with those for OPA-derivatives which showed similar instability[17,18] in the presence of 2-mercaptoethanol and ethanethiol. A branched thiol provides stability to the molecule through steric hinderance.

*Effect of solvents on the fluorescence properties of the derivatives*

A study of the effects of organic solvents on fluorescence intensity and wavelengths of emission has led to some interesting results. $\phi$NDA–glycine derivatives exhibited emission wavelength shifts from longer to shorter wavelengths as the reaction medium was changed from water to an organic solvent (Fig. 3). The results indicate that the lower the dielectric constants of the solvent, the shorter is the wavelength of emission, suggesting a much reduced dipole–dipole interaction between the fluorescent molecules and the solvent. The interaction is increased in water and the emission

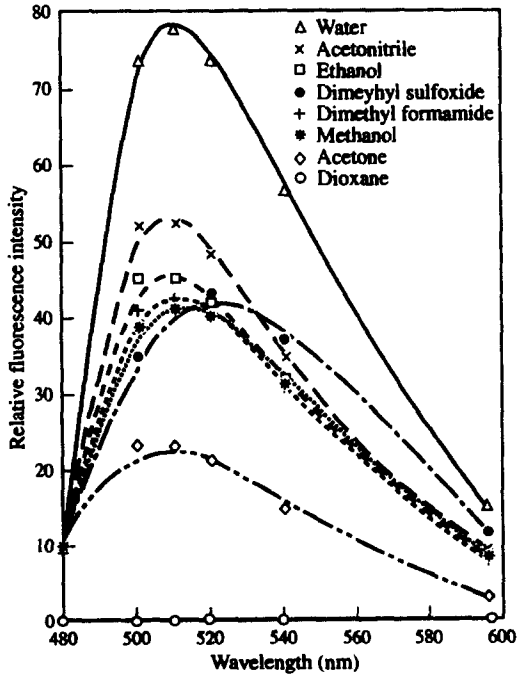


Fig. 3. Spectra of NDA–glycine derivative showing the effect of organic solvents on fluorescence properties.

moves further towards lower energy.[19] An investigation on NDA and OPA–glycine derivatives resulted in similar solvent effects on their spectral properties.

The effects of solvents on the fluorescence intensity of the NDA, $\phi$NDA and OPA-adducts seemed to be moderate. The fluorescence intensity seems to depend very much on the structure of the fluorigenic reagents. A more hydrophobic character associated with $\phi$NDA offers enhanced fluorescence in the solvents having lower dielectric constants. This result is supported by the observation that NDA-derivatives fluoresce more intensely in water as compared to organic solvents.

*Limits of detection*

One of the benefits of using fluorimetric methods of analysis is the ability to identify and determine much smaller quantities of analyte than would be possible using classical techniques.

Limits of detection for the technique are of particular interest. The limit of detection is defined as the quantity or concentration of analyte that produces a signal 2 standard deviations above the blank (i.e. $a + 2SY/X$), where $a$ is the background signal (the intercept) and $SY/X$ is the standard deviation of a single measurement. Such a concentration can be distinguished from the blank with 97.5% confidence.

The limit of detection for glycine using both NDA and $\phi$NDA was found to be $3.6 \times 10^{-7}$m$M$ ($3.2 \times 10^{-5}$ g/ml). This result compares with *o*-phthalaldehyde[20] which has limits of detection of $0.2 \times 10^{-9}$ mol/ml for $NH_4^+$ in sea-water[21] and picograms (55–100) for catechol-amines[22] in urine following prechromatographic derivatization reaction. The newly produced fluorigenic reagents offer a wavelength of emission which is at longer wavelengths (550–620 nm). Although the present study does not include work for real biological samples it is hoped that measurement of emission at the reported longer wavelengths will have little interferences, especially from the background signal[23] which has a direct bearing on the limit of detection in fluorescence spectrophotometry.

The detection limit capabilities[24] are greatly increased using high performance liquid chromatography (HPLC) coupled with laser-induced fluorescence (LIF) detection. The results in that study indicated that NDA is superior to OPA as a labelling reagent. The detections of amino acids using LIF were at the sub-fmol range with NDA-derivatization, lower by over an order of magnitude compared to the results for OPA-amino acids.

## CONCLUSIONS

The newly synthesized reagents have been useful for producing fluorescent derivatives of amino acids. The reaction is rapid and proceeds reproducibly in aqueous medium (pH 10, room temperature). The fluorescence emission of the derivatives at longer wavelengths makes the reagents suitable for use in the analysis of biological samples, minimizing interference.

## REFERENCES

1. M. Roth, *Anal. Chem.*, 1971, **43**, 880.
2. S. S. Simons, Jr. and D. F. Johnson, *J. Org. Chem.*, 1978, **43**, 2886.
3. R. F. Chen, *Arch. Biochem. Biophys.*, 1967, **120**, 607.
4. S. Stein, *Arch. Biochem. Biophys.*, 1974, **163**, 400.
5. P. B. Ghosh and M. W. Whitehouse, *Biochem. J.*, 1968, **108**, 155.
6. S. Beale, J. Savage, D. Wiesler, S. Wietstock and M. Novotny, *Anal. Chem.*, 1988, **60**, 1765.
7. S. C. Beale, Y. Hsieh, J. C. Savage, D. Wiesler and M. Novotny, *Talanta*, 1989, **36**, 321.
8. J. W. Cook, L. Hunter and R. Schoental, *J. Chem. Soc., Suppl.*, 1949, 228.
9. P. de Montigny, J. F. Stobaugh, R. S. Givens, R. G. Garlson, K. Srinivasachar, L. A. Sternson and T. Higuchi, *Anal. Chem.*, 1987, **59**, 1096.
10. S. S. Simons, Jr. and D. F. Johnson, *J. Am. Chem. Soc.*, 1976, **98**, 7098.
11. S. S. Simons, Jr. and D. F. Johnson, *J. Chem. Soc., Chem. Commun.*, 1977, 374.
12. R. F. Chen, C. Scott and E. Trepman, *Biochim. Biophys. Acta*, 1979, **576**, 440.
13. J. Pagington, *Food F.I.P.P.*, 1985.
14. W. I. Heinz, in *Solution Chemistry of Surfactants*, K. L. Mittal (ed.), Vol. 1, p. 79. Plenum Press, New York, 1979.
15. N. J. Turro, M. Gratzel and A. M. Braun, *Angew Chem. Int. Ed. Engl.*, 1980, **19**, 675.
16. L. A. Singer, in *Solution Behaviour of Surfactants*, K. L. Mittal and E. J. Findler (eds), Vol. 1, p. 73. Plenum Press, New York, 1982.
17. S. S. Simons, Jr. and D. F. Johnson, *Anal. Biochem.*, 1977, **82**, 250.
18. S. S. Simons, Jr. and D. F. Johnson, *Anal. Biochem.*, 1978, **90**, 705.
19. E. Lippert, *Z. Electrochem.*, 1957, **61**, 962.
20. W. S. Gardner, *Limnol. Oceanogr.*, 1978, **23**, 1069.
21. W. S. Gardner, *Limnol. Oceanogr.*, 1978, **23**, 1069.
22. J. F. Lawrence, *J. Chromatogr. Sci.*, 1979, **17**, 147.
23. T. G. Mathews and F. E. Lytle, *Anal. Chem.*, 1979, **51**, 583.
24. C. R. Mark and D. H. Marlin, *Anal. Chem.*, 1987, **59**, 412.

Pergamon

0039-9140(95)01477-2

*Talanta*, Vol. 42, No. 6, pp. 779–787, 1995
Elsevier Science Ltd
Printed in Great Britain
0039-9140/95 $9.50 + 0.00

# DETERMINATION OF ASCORBIC ACID IN SOFT DRINKS, PRESERVED FRUIT JUICES AND PHARMACEUTICALS BY FLOW INJECTION SPECTROPHOTOMETRY: MATRIX ABSORBANCE CORRECTION BY TREATMENT WITH SODIUM HYDROXIDE

ARCHANA JAIN, ANUPAMA CHAURASIA and KRISHNA K. VERMA*
Department of Chemistry, Rani Durgavati University, Jabalpur 482001, Madhya Pradesh, India

(*Received* 17 *February* 1994. *Revised* 2 *November* 1994. *Accepted* 8 *November* 1994)

**Summary**—Two flow injection systems for the spectrophotometric determination of ascorbic actid at 245 nm have been described. On treatment with sodium hydroxide a fraction of the ascorbic acid was decomposed into substances, which do not absorb in UV region, and the decrease in signal measured. This was directly related to the amount of ascorbic acid present. The calibration graph was linear over the range 1–25 and 1–50 $\mu$g/ml in the two methods with a correlation coefficient of 0.9981 and 0.9994, respectively. The detection limit ($2\sigma$) was 0.5 and 0.2 $\mu$g/ml, respectively. The RSD for 1 $\mu$g/ml standard was 2.5 and 1.8% ($n = 6$) in the two methods, and the sampling throughput 30/hr. The methods permitted the use of 6 $\mu$g/ml of 2-mercaptoethanol as an anti-oxidant and stabilizer for ascorbic acid, which is difficult to handle at its $\mu$g/ml level. Upon matrix absorbance correction, spiked samples that are known to contain UV-absorbing substances produced an average recovery of 101% with a RSD of 1.2%. The methods were used for the rapid and simple determination of ascorbic acid in soft drinks, preserved fruit juices and pharmaceuticals and the results thus produced compared with those obtained by previously checked methods involving titration with iodine, chloranil 2,6-dichlorophenolindophenol, and HPLC. When there was a disagreement between the results, this was traced to the presence of substances which are known to interfere in comparison methods.

Its simplicity and relatively close correlation with the results of biological assays have led to the extensive use of titration with 2,6-dichlorophenolindophenol for the determination of ascorbic acid in fruit juices, pharmaceuticals and biological samples. However, difficulties are encountered with coloured samples, when the detection of the end point is cumbersome, or in the presence of reducing substances other than ascorbic acid, which can bleach the dye and make analysis non-specific.[1–3] Among these substances some are naturally present in fruit juices and biological fluids, *e.g.* cysteine, reduced glutathione and iron(II), whereas others are added to foodstuffs as preservatives, *e.g.* sulphite, dithionite and sulphide. Dithiothreithol,[4] homocysteine[5] and cysteine[6] are added to reduce concomitant dehydroascorbic acid to ascorbic acid in order to determine a total of two species. Excess thiol reagent can also react with the indophenol dye and vitiate the analysis. Besides achieving higher sensitivity and rapidity, most methods that are reported in literature attempt to circumvent some of these drawbacks.

Titration with *N*-bromosuccinimide in the presence of iodide/starch indicator, giving intense blue colour at the end point, has been reported to tolerate large quantities of iron(II),[7] and found applicable to coloured samples.[8] Interference from sulphur containing reducing substances was still a shortcoming. Many other redox titrants behave analogously.[9–11] Interference of thiol groups and sulphite has been avoided by their masking with acrylonitrile[12–14] and acrylamide,[15] and of sulphite with furan-2-aldehyde.[12]

Owing to the non-equilibrium state of the chemical system, interferences occur at a lower level in flow injection analysis. Manual titrimetric methods[12,16,17] based on redox properties of ascorbic acid have been adapted to flow injection analysis.[18–21] Methods based on reduction of

*Author to whom correspondence should be addressed

iron(III) and measurement of iron(II) by its complex formation with 1,10-phenanthroline,[22] or catalyzed light emission from luminol oxidation with hydrogen peroxide,[23] and photochemical reduction of methylene blue[24,25] have been of late reported. These methods work well for assay in drug formulations and fresh fruit juices, however, the interference of sulphur containing reducing substances is much the same.

A high sensitivity measurement of ascorbic acid has been carried out amperometrically.[26] The detector is not selective, however, when measurements are made without and with reaction with immobilized ascorbate oxidase that is incorporated in a flow injection system, and the difference in detector response is related with the ascorbic acid content, a good correlation with the actual values is obtained.[27] The enzyme activity has been reported to remain unimpaired in the presence of thiols.[28]

HPLC[5,6,29-31] is more selective and sensitive, nevertheless, in most methods ascorbic acid elutes very close to the void volume which may lead to errors.

Ascorbic acid absorbs strongly at 245 nm in acidic media and at 267 nm in neutral solutions, and is electroactive whereas dehydroascorbic acid has no such property. These characteristics form the basis for the determination of ascorbic acid. However, the detector response corresponds to any ascorbic acid present and to that of the sample matrix in case the concomitant substances either also absorb at the wavelength of determination in spectrophotometry, or are electroactive in amperometry. A correction can be made by measuring the matrix contribution on a second aliquot of sample solution in which ascorbic acid is predecomposed to produce materials that are unresponsive to the detector. The difference in detector response observed is related to ascorbic acid present. Since dilute solutions of ascorbic acid are only stable in the presence of reducing agents such as 2-mercaptoethanol, as used in this work, which does not absorb in the UV region of determination but has significant electroactivity, spectrophotometry was considered as a method of choice for matrix correction.

## EXPERIMENTAL

### *Apparatus*

A Shimadzu SPD-2A variable wavelength UV detector (8-$\mu$l flow-through cell), a Shimadzu C-R2AX integrator fitted with a printer-plotter, two Rheodyne 5020 4-way rotary valve sample injectors (Anachem), a Rheodyne 5031 double 3-way switching valve (Anachem) and an Ismatec Mini-S 820 peristaltic pump (Zurich) were used. The manifold and reaction coil tubing was 0.5 mm i.d. PTFE. Flangeless end fittings were made using plastic nuts and Tefzel couplers (Anachem). Home-made T-joints of 0.8 mm bore were employed.

### *Flow injection manifolds and experimental conditions*

*Manifold A.* The system consisted of a two-channel manifold with a carrier stream of 6 mg/l. of 2-mercaptoethanol with a flow rate of 0.36 ml/min and on to which a 4-way injection valve (V1) was placed, another similar valve (V2) was nested on the loop of the first valve (Fig. 1). Two 'a' and 'b' portions of loop on valve V1 were, respectively, 40 and 50-$\mu$l, whereas V2 had a 50-$\mu$l loop. The effluents were passed through a 80-cm reaction coil, merged with 0.2*M* sulphuric acid stream that had a flow rate of 0.13 ml/min, passed through another 30 cm coil and finally monitored at 245 nm. To determine the total absorbance of ascorbic acid and matrix, the sample solution was injected through valve V2 into the carrier stream whilst the valve V1 already in inject position. The matrix absorbance (plus that of any remaining ascorbic acid) was determined by simultaneously injecting 0.2*M* sodium hydroxide through valve V1, and sample solution through valve V2. The difference in peak heights was related to the amount of ascorbic acid present.

*Manifold B.* A single channel manifold was used that consisted of 6 mg/l. of 2-mercaptoethanol as a carrier solution with a flow rate of 0.82 ml/min and valves V1 and V2 were placed on it, valve V2 being nested on the loop of the valve V1 (Fig. 1). The loop sizes were the same as in manifold A. The simultaneously injected 0.02*M* sodium hydroxide and sample solution, through valves V1 and V2, respectively, were allowed to mix in a delay coil of 25 cm and then the plug stopped in the detector 6 sec after injection by diverting the flow of effluents to waste using a double 3-way switching valve (V3) placed between the delay coil and detector. The flow was resumed after 60 sec. The decrease in peak height during this period was owing to the decomposition of ascorbic acid, and related to its concentration.

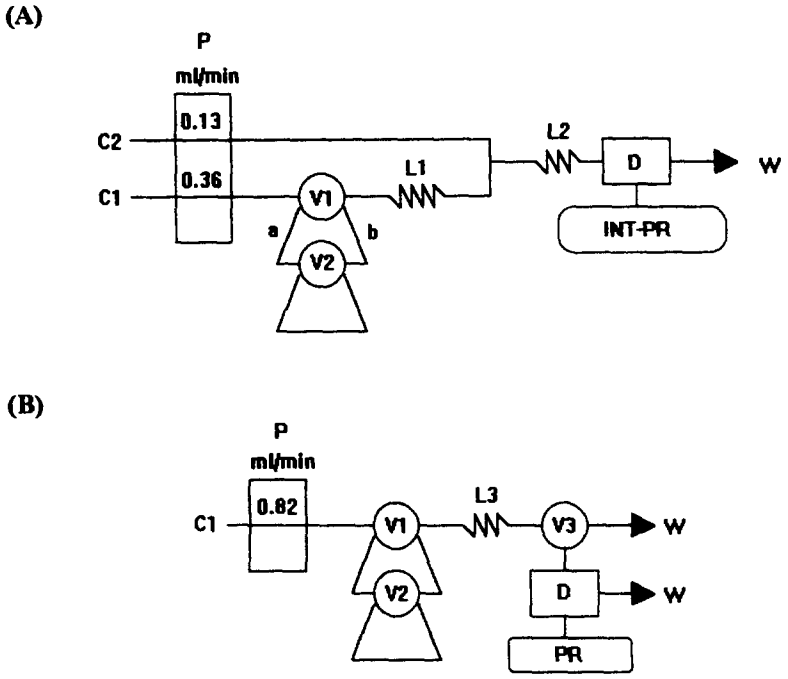


Fig. 1. Schematic diagrams of the flow injection systems used for the determination of ascorbic acid by matrix absorbance correction. Manifold (A) was used for continuous flow injection and (B) for stopped-flow experiments. C1 = water carrier; C2 = 0.2*M* sulphuric acid; V1 = 4-way loop injection valve ('a' = 40-$\mu l$; 'b' = 50-$\mu l$); V2 = 4-way loop injection valve (50-$\mu l$); V3 = double 3-way switching valve; L1 = delay coil of 80 cm; L2 = delay coil of 30 cm; L3 = delay coil of 25 cm; P = peristaltic pump; D = detector (8-$\mu l$) set to 245 nm; INT-PR = integrator and printer; PR = printer; and W = waste. All flow lines were made from 0.5 mm i.d. PTFE tubing.

*Reagents*

All reagents used were of analytical reagent grade. 2-Mercaptoethanol, 6 mg/l. was used as a carrier solution. Sodium hydroxide: 0.2 and 0.02*M*. Sulphuric acid: 0.2*M*. A guaranteed-reagent grade ascorbic acid from Sarabhai M. Chemicals (Baroda, India) was used that had a purity of 99.7% as determined by titration with 2,6-dichlorophenolinophenol,[32] 99.5% as determined by iodimetric titration[33] and 99.8% as determined by titration with chloranil.[15] A standard solution (1000 $\mu$g/ml) was prepared by dissolving 100.00 mg of ascorbic acid in 100 ml of de-ionized water in a calibrated flask. Calibration standards were prepared by sequential dilution of the stock solution with the carrier solution.

*Samples*

All pharmaceutical dosage forms and multivitamin preparations tested were fresh and purchased from the local pharmacy. A known number of capsules were weighed and ground into a fine powder. An accurately weighed aliquot containing about 100 mg of ascorbic acid was shaken with about 25 ml of de-ionized water and filtered through Whatman No. 41 filter-paper. The insoluble mass was washed with three successive 5 ml portions of water, and the filtrate plus washings were diluted to volume in a 100-ml calibrated flask. A known volume was further diluted with the carrier solution for analysis. The contents of a known number of vitamin C injections were mixed together and a suitable portion of the mixture was sampled. The stock solutions were used for analysis by the comparison methods.

Known volumes of thawed soft drinks and juice concentrates were mixed with 10 ml of the carrier solution and filtered through Whatman

Table 1. Calibration data for the determintion of ascorbic acid involving matrix absorbance correction

| Ascorbic ($\mu g/ml$) | Slope | Intercept | AFS | $r$ | $n$ |
|---|---|---|---|---|---|
| *Method using manifold A* | | | | | |
| $\Delta H$ *ml*/$\mu g$ | | $\Delta H$ | | | |
| 1–50 | 22.262 | $0.448_8$ | 0.64 | 0.9994 | 12 |
| *Method using manifold B* | | | | | |
| $\Delta h$ *ml*/$\mu g$ | | $\Delta h$ | | | |
| 1–25 | 9.546 | −1.573 | 0.64 | 0.9981 | 12 |

$\Delta H$ and $\Delta h$ = Difference in peak heights in integrator arbitrary units and in *mm*, respectively.

No. 42 filter-paper. The residue was washed with 2 successive 2 ml portions of the carrier, and the filtrate plus washings were diluted with carrier to known volume in calibrated flasks to give solutions for analysis. Suitable portions of soft drinks and juice concentrates were diluted with water, filtered and analyzed by the comparison methods.

In cases when the sample contained a soluble salt of iron(II), which interfered in the proposed method, an aliquot of the above prepared stock solution was shaken with 5 ml of 25 mg/100 ml of sodium sulphide for 2 min and filtered. The filtrate was diluted with the carrier solution for analysis.

## RESULTS AND DISCUSSION

Ascorbic acid solutions deteriorate rapidly owing to oxidation by the dissolved oxygen. At 25°C, 1–20 $\mu$g/ml solutions have been found in this work to lose their total ascorbic acid content within 20 min. Thus, dilute solutions are very difficult to handle unless a stabilizing agent is used, and the sample pre-treatment, if any, and determination done under rapid flow injection conditions. Commonly used stabilizers are reducing agents, which interfere severely with methods based on the redox property of ascorbic acid, or metaphosphoric acid which has been reported to result in reduced retention of ascorbic acid on anion exchange columns.[29] 2-Mercaptoethanol was found to be transparent in the UV region, especially at 245 nm, and worked as an effective stabilizer. In this work, a 6 mg/l. solution of 2-mercaptoethanol has been used as a carrier and in preparing the working solutions of ascorbic acid.

A number of methods are described in the literature for producing a sample blank, such as enzymatic methods,[27,34,35] thermal decomposition,[36] catalytic decomposition with copper(II),[36–38] and UV irradiation, [36,39] Ascorbic acid is well known to be unstable in alkaline solutions,[36,40] the decomposition products being dehydroascorbic acid and threonic acid which do not appreciably absorb in UV region. Thus, adjustment of the sample pH to the alkaline range was studied as a potential blank correction method in this work. Although rapid, decomposition by alkali is not selective for ascorbic acid, many hydroxy compounds and certain dyestuffs are also unstable in alkaline media. Thus, the study of flow injection parameters aimed at decomposing only a good fraction of ascorbic acid before any side reaction becomes appreciable.

### *Study of flow injection parameters*

Out of several ways possible, nested loop injection was found as a simple means of effectively mixing ascorbic acid and sodium hydroxide. Initial flow injection experiments were carried out using manifold A (Fig. 1) in which the nested loop injectors placed on water carrier stream (C1, flow rate 0.82 ml/min) and the reaction quenching agent was 0.1*M* sulphuric acid (C2, flow rate 0.54 ml/min). The alkaline degradation reaction occurred in a coil (L1) of 100 cm and the neutralization reaction in another coil (L2) of 75 cm. Conditions were studied for the determination of 10 $\mu$g/ml

Table 2. Validation of the matrix absorbance correction method by determination using manifold A of known amounts of ascorbic acid in soft drink cola

| Ascorbic acid added ($\mu g/ml$) | AFS | *Peak height** I | *Peak height** II | $\Delta H$† | $\Delta H$ corrected to AFS 0.64 |
|---|---|---|---|---|---|
| 1 | 0.04 | 698 | 410 | 288 | 18.0 |
| 2 | 0.08 | 676 | 332 | 344 | 43.0 |
| 5 | 0.16 | 750 | 332 | 418 | 104.5 |
| 10 | 0.32 | 750 | 310 | 440 | 220 |
| 20 | 0.64 | 732 | 275 | 457 | 457 |
| 30 | 0.64 | 1078 | 395 | 683 | 683 |
| 40 | 0.64 | 1346 | 458 | 888 | 888 |
| 50 | 1.28 | 948 | 401 | 547 | 1094 |
| | | | | slope = 22.164 $\Delta H$ ml/$\mu g$ | |
| | | | | intercept = 0.7049 $\Delta H$ | |
| | | | | $r(n = 8) = 0.9996$ | |

*Peak height, I = before alkali treatment; II = after alkali treatment.

†$\Delta H$ = Difference in peak heights (I − II) at corresponding AFS in integrator arbitrary units.

ascorbic acid using 0.1*M* sodium hydroxide as a reagent for producing blank absorbance.

Over a flow rate 0.1–1.2 ml/min of each channel studied, maximum peak height difference was observed when flow rate for C1 was 0.36 ml/min and for C2 0.13 ml/min. Other parameters studied were L1 = 80 cm (studied 30–135 cm); L2 = 30 cm (studied 10–135 cm); ascorbic acid loop size (valve V1) = 50 $\mu$l (studied 10–100 $\mu$l); sodium hydroxide loop size (valve V2), side 'a' = 40 $\mu$l (studied 10–100 $\mu$l), and side 'b' = 50 $\mu$l (studied 10–75 $\mu$l). Sodium hydroxide (studied 0.05–0.5*M*) and sulphuric acid (studied 0.025–0.4*M*) were each 0.2*M*.

Table 3. Interference of common ingredients of pharmaceuticals, soft drinks and fruit juices in the determination of 10 $\mu g/ml$ ascorbic acid Manifold A was used and no matrix absorbance correction made

| Additive | Mass ratio (additive:ascorbic acid) | Recovery* (%) |
|---|---|---|
| *Organic acids* | | |
| Citric | 300 | 101 |
| Oxalic | 150 | 99 |
| Tartaric | 250 | 101 |
| Malic | 100 | 99 |
| Maleic | 2 | 130 |
| Benzoic | 1 | 110 |
| Salicylic | 2 | 150 |
| *Amino acids* | | |
| Cysteine | 75 | 100 |
| Glycine | 200 | 99 |
| Serine | 250 | 101 |
| Tryptophan | 3 | 140 |
| Tyrosine | 5 | 125 |
| Histidine | 10 | 110 |
| *Vitamins* | | |
| Thiamine hydrochloride | 1 | 140 |
| Riboflavin | 2 | 160 |
| Pyridoxine hydrochloride | 2 | 135 |
| Folic acid | 1 | 110 |
| *Mineral salt* | | |
| Magnesium sulphate | 800 | 100 |
| Manganese sulphate | 500 | 99 |
| Copper(II) sulphate | 2 | 91 |
| Iron(II) fumarate | 100 | 101 |
| Iron(II) sulphate | 2 | 142 |
| Potassium chloride | 600 | 100 |
| Calcium chloride | 200 | 99 |
| Zinc sulphate | 400 | 101 |
| *Antioxidant* | | |
| Sodium hydrogen sulphite | 800 | 102 |
| Hydroquinone | 2 | 155 |
| Sodium sulphide | 400 | 101 |
| Thiomalic acid | 10 | 102 |
| 2-Mercaptoethanol | 50 | 101 |
| *Colouring matter* | | |
| Amaranth | 2 | 138 |
| Tartrazine | 2 | 165 |
| Caramel | 5 | 110 |
| Ponceau 4R | 12 | 125 |
| *Active drug* | | |
| Paracetamol | 1 | 172 |
| Caffeine | 5 | 115 |
| Salicylamide | 1 | 150 |
| Acetylsalicylic acid | 1 | 180 |
| *Miscellaneous* | | |
| Calcium gluconate | 100 | 101 |
| Glucose | 500 | 102 |
| Starch | 500 | 99 |
| Lactose | 500 | 99 |
| Sucrose | 1000 | 100 |
| EDTA, disodium salt | 600 | 103 |
| Disodium hydrogen phosphate | 500 | 99 |

*The results are the average of two determinations.

Table 4. Determination of ascorbic acid by matrix absorbance correction using manifold A

| Ascorbic acid taken (μg/ml) | Additive* | Ascorbic acid found† (μg/ml) | RSD (%) |
|---|---|---|---|
| 1.00 | Caffeine (5) | 1.02 | 1.3 |
| 2.50 | Caffeine (10) | 2.55 | 0.8 |
| 5.00 | Paracetamol (10) | 4.96 | 1.0 |
| 10.0 | Paracetamol (20) | 10.1 | 1.5 |
| 12.5 | Salicylamide (5) | 12.3 | 1.1 |
| 15.0 | Salicylamide (10) | 15.4 | 1.5 |
| 20.0 | Thiamine hydrochloride (5) | 19.8 | 0.8 |
| 25.0 | Thiamine hydrochloride (10) | 25.3 | 2.0 |
| 30.0 | Acetylsalicylic acid (6) | 30.1 | 1.2 |
| 35.0 | Acetylsalicylic acid (15) | 36.0 | 2.1 |
| 15.0 | Sodium hydrogen sulphite (20) | 14.8 | 0.6 |
| 20.0 | Sodium hydrogen sulphite (50) | 20.4 | 1.1 |
| 5.0 | Sodium saccharin (5) | 5.05 | 0.8 |
| 10.0 | Sodium saccharin (15) | 10.4 | 1.2 |

*Values in parenthesis are amounts added in μg/ml.
†The results are the average of five determinations.

Under these conditions of sample blank determination 76% of ascorbic acid was decomposed.

In stopped-flow experiments using the manifold B (Fig. 1), the nested loops as used above were placed on water carrier stream (flow rate 0.82 ml/min), the mixing was allowed to occur in a reaction coil (L3) of 25 cm and the plug stopped in the detector for a pre-determined period. With this configuration, the peak maximum appeared 6 sec after injection. Sodium hydroxide concentration was found to play a critical role that determined the sensitivity of the method. A 0.02*M* sodium hydroxide solution was optimum over the studied range 0.01–1*M*. Most of the ascorbic acid was decomposed before reaching the detector when a more concentrated reagent was used, thus giving a small

Table 5. Comparison of results for the determination of ascorbic acid in soft drinks and preserved fruit juices. Matrix absorbance correction was applied by using manifold A

| Sample | Present method* | RSD (%) | Comparison method† | Difference‡ (%) |
|---|---|---|---|---|
| Orange juice | 64.1 | 0.8 | 64.9 (CA) | −1.6 |
| | | | 67.1 (IOD) | −4.7 |
| | | | 63.2 (HPLC) | +1.6 |
| Grape juice | 3.8 | 0.6 | 3.7 (CA) | +2.6 |
| | | | 4.0 (IOD) | −5.3 |
| | | | 4.1 (IND) | −7.9 |
| Pineapple juice | 8.5 | 1.0 | 8.4 (CA) | +1.2 |
| | | | 8.9 (IOD) | −4.7 |
| Apple juice | 3.1 | 2.2 | 3.0 (CA) | +3.2 |
| | | | 3.3 (IOD) | −6.4 |
| Lemon juice | 51.0 | 1.1 | 49.3 (CA) | +3.3 |
| | | | 52.8 (IOD) | −3.5 |
| | | | 51.3 (HPLC) | −0.6 |
| Lime drink | 10.3 | 0.5 | 10.6 (CA) | −2.9 |
| | | | 10.8 (IOD) | −4.8 |
| | | | 10.5 (IND) | −1.9 |
| Cola | 0.0 | | 0.0 (CA) | |
| Orange drink | 4.5 | 0.8 | 4.4 (CA) | +2.2 |
| | | | 4.6 (IOD) | −2.2 |
| | | | 4.5 (IND) | 0.0 |

*The results, given as mg/100 ml of ascorbic acid, are the average of five determinations.
†The results are the average of three determinations. IOD = iodine titration:[33] CA = chloranil titration;[15] HPLC = high performance liquid chromatography;[30] and IND = 2,6-dichlorophenolindophenol titration.[32]
‡Present method—comparison method.

Table 6. Recovery test for lime drink and cola by matrix correction using manifold B

| Serial no. | Ascorbic acid added (*mg*/100 *ml*) | Recovery* (%) | RSD (%) |
|---|---|---|---|
| *Lime drink* | | | |
| 1 | 5.0 | 102 | 1.5 |
| 2 | 10.0 | 98 | 0.8 |
| 3 | 15.0 | 97 | 1.0 |
| 4 | 20.0 | 101 | 1.1 |
| 5 | 25.0 | 98 | 2.2 |
| *Cola* | | | |
| 1 | 5.0 | 101 | 0.7 |
| 2 | 10.0 | 103 | 0.6 |
| 3 | 15.0 | 99 | 0.8 |
| 4 | 20.0 | 98 | 1.0 |
| 5 | 25.0 | 104 | 1.5 |

*The results are the average of five determinations.

peak height difference and poor sensitivity. During a stop flow period of 1 min, about 55% of ascorbic acid was decomposed. This period may be suitably altered if the sample matrix behaviour is known.

### *Calibration graph and statistical data*

Calibration graphs were constructed under optimum flow injection conditions using the manifolds A and B, and by using standard solutions of ascorbic acid. The regression data are given in Table 1. In the determination of 1, 5 and 10 $\mu$g/ml ascorbic acid in pure solution, the RSD ($n = 6$) as found by using manifold A (*manifold B*) was, respectively, 1.8% (2.5%), 1.1% (1.5%) and 0.6% (1%). The detection limit[40] was 0.2 $\mu$g/ml (0.5 $\mu g/ml$) with a RSD of 3%(5%).

### *Validation of matrix correction method*

The matrix correction method was validated by determination of ascorbic in soft drink cola that originally contained no ascorbic acid and had strong UV absorbance owing to the colouring matter caramel. Suitable aliquots of cola and of ascorbic acid standards were mixed, diluted to known volume and analyzed using manifold A. The values of actual responses are given in Table 2, and the calibration data are in

Table 7. Comparison of results for the analysis of laboratory made formulations. Matrix absorbance correction was made by using manifold A

| Formulation no. | Nominal* | Present method† | RSD (%) | Comparison method‡ | Difference§ (%) |
|---|---|---|---|---|---|
| 1‖ | 50 | 51.4 | 0.7 | 50.8 (IOD) | +1.2 |
| | | | | 49.6 (CA) | +3.5 |
| | | | | 50.5 (IND) | +1.7 |
| 2¶ | 100 | 99.4 | 0.8 | 99.0 (IOD) | +0.4 |
| | | | | 101.1 (CA) | −1.7 |
| | | | | 99.2 (IND) | +0.2 |
| | | | | 100.9 (HPLC) | −1.5 |
| 3** | 150 | 148.5 | 1.0 | 152.1 (IOD) | −2.4 |
| | | | | 151.6 (CA) | −2.1 |
| | | | | 152.0 (IND) | −2.3 |
| 4†† | 200 | 198.1 | 1.1 | 228.5 (IOD) | −15.3 |
| | | | | 201.8 (CA) | −1.9 |
| | | | | 238.1 (IND) | −20.2 |
| | | | | 198.7 (HPLC) | −0.3 |
| 5‡‡ | 500 | 505.3 | 1.4 | 503.2 (IOD) | +0.4 |
| | | | | 508.8 (IND) | −0.7 |
| | | | | 506.4 (CA) | −0.2 |
| 6§§ | 500 | 497.5 | 2.0 | 508.1 (IOD) | −2.1 |
| | | | | 503.1 (CA) | −1.1 |
| | | | | 501.0 (HPLC) | −0.7 |

*The nominal amount and results are given in *ng* of ascorbic acid.

†The results are the average of five analyses.

‡The results are the average of three determinations. IOD = iodine titration;[33] CA = chloranil titration;[15] HPLC = high performance liquid chromatography;[30] and IND = 2,6-dichlorophenolinophenol titration.[32]

§Present method—comparison method.

‖Also contains acetylsalicylic acid (25 *mg*) and glucose (50 *mg*).

¶Also contains salicylamide (50 *mg*) and lactose (50 *mg*).

**Also contains paracetamol (50 *mg*) and starch (50 *mg*).

††Also contains methionine (50 *mg*) and potassium hydrogen sulphite (20 *mg*).

‡‡Also contains iron(II) sulphate (25 *mg*).

§§Also contains iron(II) fumarate and Indigo Carmine (2 mg).

Table 8. Comparison of results for the analysis of commercial formulations. Matrix absorbance correction was made by using manifold A

| Formulation | Nominal* | Present method† | RSD (%) | Comparison method‡ | | Difference§ (%) |
|---|---|---|---|---|---|---|
| *Tablet* | | | | | | |
| Celin | 500 | 495.5 | 0.6 | 493.9 | (IOD) | +0.3 |
| | | | | 494.0 | (CA) | +0.3 |
| | | | | 497.4 | (HPLC) | −0.4 |
| Sorvicin | 500 | 480.2 | 0.8 | 489.1 | (CA) | −1.8 |
| | | | | 485.0 | (IOD) | −1.0 |
| | | | | 486.8 | (IND) | −1.4 |
| Rutin‖ | 100 | 98.6 | 1.1 | 97.4 | (CA) | +1.2 |
| | | | | 96.9 | (IOD) | −1.7 |
| | | | | 99.0 | (IND) | −0.4 |
| Chromostat¶ | 150 | 152.6 | 1.5 | 150.8 | (IOD) | +1.2 |
| | | | | 154.2 | (IND) | −1.0 |
| | | | | 151.3 | (CA) | +0.8 |
| | | | | 155.0 | (HPLC) | −1.6 |
| *Capsule* | | | | | | |
| Fesovit** | 50 | 45.8 | 2.0 | 46.5 | (IOD) | −1.5 |
| | | | | 47.3 | (CA) | −3.2 |
| Beplex†† | 150 | 141.3 | 2.2 | 140.0 | (IOD) | +0.9 |
| | | | | 143.5 | (CA) | −1.6 |
| *Injection* | | | | | | |
| Redoxon‡‡ | 500 | 502.6 | 1.2 | 500.5 | (CA) | +0.4 |
| | | | | 505.8 | (IOD) | −0.6 |
| | | | | 498.3 | (IND) | +0.8 |

*The nominal amount and results are given in *mg* of ascorbic acid.

†The results are the average of five analyses.

‡The results are the average of three determinations, IOD = iodine titration;[33] CA = chloranil titration;[15] HPLC = high performance liquid chromatography.[30]

§Present method—comparison method.

‖Also contains rutin (100 *mg*), acetaminadione (20 *mg*), adrenochrome monosemicarbazone (1 *mg*) and calcium dibasic phosphate (150 *mg*).

¶Also contains adrenochrome monosemicarbazone (0.5 *mg*), menaphthone sodium hydrogen sulphite (10 *mg*), dibasic calcium phosphate (132 *mg*) and calciferol (300 *U*).

**Also contains iron(II) sulphate (150 *mg*), thiamine mononitrate (2 *mg*), nicotinamide (15 *mg*), pyridoxine hydrochloride (1 *mg*), panthothenic acid (calcium salt) (2.5 *mg*) and Amaranth.

††Also contains thiamine mononitrate (10 *mg*), riboflavin (10 *mg*), nicotinamide (45 *mg*), nicotinic acid (15 *mg*), pyridoxine hydrochloride (25 *mg*), folic acid (1.5 *mg*), vitamin $B_2$ (15 *mg*) and Amaranth.

‡‡Also contains methyl paraben (0.08% m/v) and propyl paraben (0.01% m/v).

close agreement with those obtained using pure ascorbic acid (Table 1).

### *Sample matric interference*

Using manifold A, the determination of 10 μg/ml of ascorbic acid was carried out without any matrix absorbance correction in the presence of known amounts of a large variety of substances which are usually present in soft drinks, fruit juices and pharmaceutical preparations, and include sweeteners, acids, colouring agents, preservatives, mineral salts, amino acids, vitamins and active drugs. Many substances which have a chromophore either a C=C bond or a benzenoid structure interfere severely by absorbing at 245 nm (Table 3). Iron(II) fumarate did not interfere owing to its insolubility in the carrier in which the solutions were prepared. To assess the efficacy of the alkali treatment as a method of sample blank determination, recovery tests were carried out on laboratory made synthetic samples which are known to contain interfering substances (Table 4). The average recovery was 101% (range 98–104%) and average RSD of 1.2% (range 0.6–2.1%) over all spikes. The average RSD on % recovery was 1.7%.

### *Applications*

The flow injection technique was applied to determine ascorbic acid in soft drinks and preserved fruit juices by using manifold A (Table 5), and for recovery studies on a soft drink spiked with known amounts of ascorbic

acid using manifold B (Table 6). Method using manifold A was used to determine ascorbic acid in drug formulations prepared in the laboratory (Table 7) and commercially available pharmaceuticals (Table 8).

Titration with iodine,[33] chloranil[15] and with 2,6-dichlorophenolindophenol titration,[32] and HPLC[30] were used to produce comparison results. In many samples there was a difference between the results obtained by the different methods. This difference was not considered to invalidate the present method as the titration methods are prone to interferences and the end-point was difficult to determine in coloured solutions. Because of the presenece of stabilizers, which are reducing in nature, and colouring matter, preserved fruit juices are believed to be difficult samples to analyze for ascorbic acid by a redox method. HPLC appears to tolerate most interferences and produce similar results.

## CONCLUSION

The present flow injection methods are very simple and rapid (2 min per sample), and have high sensitivity. Using a background correction with sodium hydroxide, the method is made selective for ascorbic acid. This also allows the use of 2-mercaptoethanol as an anti-oxidant in the carrier solution and in preparing the sample solution otherwise ascorbic acid at $\mu$g/ml level concentration are very difficult to keep at ordinary temperatures. The accuracy of the method has been illustrated for various soft drinks, preserved fruit juices and pharmaceuticals but with the good sensitivity attained it would also be suitable for biological samples.

*Acknowledgements*—Sincere thanks are due to the Council of Scientific & Industrial Research, New Delhi, for the award of a Senior Research Associateship to A. J., and to the Department of Atomic Energy, Bombay, for a K. S. Krishnan Fellowship to A. C.

## REFERENCES

1. C. N. Konidari and M. I. Karayannis, *Anal. Chim. Acta*, 1989, **224**, 199.
2. C. N. Konidari and M. I. Karayannis, *Talanta*, 1991, **38**, 1019.
3. C. N. Konidari, S. M. T. Karayanni, L. E. Bowman and M. I. Karayannis, *Talanta*, 1992, **39**, 863.
4. S. Uchiyama, Y. Kobayashi, O. Hamamoto and S. Suzuki, *Anal. Chem.*, 1991, **63**, 2259.
5. W. D. Graham and D. Annette, *J. Chromatog.*, 1992, **594**, 187.
6. H. Iwase and I Ono, *J. Chromatog.* 1993, **654**, 215.
7. M. Z. Barakat, M. F. Abdel Wahab and M. M. El-Sadr, *Anal. Chem.*, 1955, **27**, 536.
8. D. F. Evered, *Analyst*, 1960, **85**, 515.
9. A. Srivastava, R. Abbi, A. Gupta, S. Bindra and S. K. Singh, *Mikrochim. Acta*, 1989, **III**, 81.
10. K. G. Kumar and P. Indrasenan, *Talanta*, 1990, **37**, 269.
11. S. Z. Qureshi, A. Saeed, S. Haque and M. A. Khan, *Talanta*, 1991, **38**, 637.
12. K. K. Verma and A. K. Gulati, *Anal. Chem.*, 1980, **52**, 2336.
13. K. K. Verma, *Talanta*, 1982, **29**, 41.
14. A. Srivastava and S. K. Singh, *Analyst*, 1988, **113**, 259.
15. K. K. Verma, A. Jain and R. Rawat, *J. Assoc. Off. Anal. Chem.*, 1984, **67**, 262,
16. O. A. Bassy and C. C. King, *J. Biol. Chem.*, 1933, **103**, 687.
17. *British Pharmacopoeia*, Vol. II, p. 901, 5th Edn. HM Stationery Office, London, 1988.
18. J. Hernandez-Mandez, A. Alonso Mateos, M. J. Alnendral Parra and C. Garcia de Maria, *Anal. Chim. Acta*, 1986, **184**, 243.
19. F. Lazaro, A. Rios, M. D. Luque de Castro and M. Valcarcel, *Analyst*, 1986, **111**, 163.
20. F. Lazaro, A. Rios, M. D. Luque de Castro and M. Valcarcel, *Analyst*, 1986, **111**, 167.
21. S. M. Sultan, *Talanta*, 1993, **40**, 593.
22. S. M. Sultan, A. M. Abdennabi and F. E. O. Suliman, *Talanta*, 1994, **41**, 125.
23. A. A. Alwarthan, *Analyst*, 1993, **118**, 639.
24. A. Sanz-Martinez, A. Rios and M. Valcarcel, *Analyst*, 1992, **117**, 1761.
25. L. E. Leon and J. Catapano, *Anal. Lett.* 1993, **26**, 1741.
26. A. M. Almuaibed and A. Townshend, *Talanta*, 1992, **39**, 1459.
27. G. M. Greenway and P. Ongomo, *Analyst*, **115**, 1297.
28. S. Uchiyama, *Talanta*, 1992, **39**, 1289.
29. L. A. Pachla and P. T. Kissinger, *Anal. Chem.*, 1976, **48**, 364.
30. I. A. Nicolson, R. Macrae and D. P. Richardson, *Analyst*, 1984, **109**, 267.
31. W. Hou and E. Wang, *Talanta*, 1990, **37**, 841.
32. W. Horwitz, *Official Methods of Analysis of the Association of Official Analytical Chemists*, W. Horwitz (ed), AOAC, 13th Edn, p. 746. Arlington, 1980.
33. O. A. Bassy and C. C. King, *J. Biol.Chem.*, 1933, **103**, 687.
34. T. Tono and S. Fujita, *Agric. Biol. Chem.*, 1981, **45**, 2945.
35. T. Tono and S. Fujita, *Agric. Biol. Chem.*, 1982, **46**, 2953.
36. Y.-S. Fung and S.-F.Luk, *Analyst*, 1985, **110**, 201.
37. O.-W. Lau, S.-F.Luk and K.-S. Wong, *Analyst*, 1986, **111**, 665.
38. O.-W. Lau, S.-F. Luk and K.-S. Wong, *Analyst*, 1987, **112**, 1023.
39. A. F. A. Moussa, *Pharmazie*, 1977, **32**, 724.
40. J. C. Miller and J. N. Miller, *Statistics for Analytical Chemistry*, p. 116. Ellis Horwood, Chichester, 1992.

Pergamon

0039-9140(95)01480-2

*Talanta*, Vol. 42, No. 6, pp. 789–795, 1995

0039-9140/95 $9.50 + 0.00

# EFFECTS OF SOLVATION ON PARTITION AND DIMERIZATION OF BENZOIC ACID IN MIXED SOLVENT SYSTEMS

HIROMICHI YAMADA,[1]* KYOKO YAJIMA,[1] HIROKO WADA[1] and the late GENKICHI NAKAGAWA[2]

[1]Department of Applied Chemistry, Nagoya Institute of Technology, Gokiso-cho, Showa-ku, Nagoya 466, Japan

[2]Department of Industrial Chemistry, School of Science and Technology, Meiji University, Higashimita, Tama-ku, Kawasaki 214, Japan

(*Received* 1 *August* 1994. *Revised* 28 *October* 1994. *Accepted* 1 *December* 1994)

**Summary**—The partition of benzoic acid between 0.1*M* perchloric acid solution and two kinds of mixed solvents has been carried out at 25°C. The partition and dimerization constants of benzoic acid have been determined in the 1-octanol–benzene and 2-octanone–benzene systems. In both the mixed solvent systems, with increasing content of 1-octanol and 2-octanone in each mixed solvent, the partition constant of benzoic acid has been found to increase, and the dimerization constant of benzoic acid in each organic phase to decrease. These phenomena are attributable to solvation of monomeric benzoic acid by 1-octanol and 2-octanone molecules in each mixed solvent.

Halogenated solvents such as chloroform, carbon tetrachloride, 1,2-dichloroethane, *etc.*, have ben extensively used not only in the field of solvent extraction but also in other branches of chemistry. However, environmental concerns have led to voluntary control for the use of these halogenated solvents. The selection of the most appropriate solvent is an important factor in solvent extraction and a new useful solvent is expected to be developed in the place of these halogenated solvents. Such a mixed solvent is anticipated to be useful for solvent extraction, but has not been appreciably investigated for solvent extraction. A mixed solvent which consists of two kinds of solvents may be expected to retain the inherent property of each solvent and to induce a synergistic effect between the two solvents. In a series of investigations on the extraction of some metals with LIX 26 in heptane, 1-octanol was used to avoid third phase formation as phase modifier by Olazabal *et al.*[1-3] In the extraction of aluminum with LIX 26 in heptane containing 5–15% 1-octanol, it was found that the extraction curve of aluminum is independent of the 1-octanol concentration.[1]

In an investigation on solvent extraction of metal ions, it is necessary to have information about the partition equilibrium of the extracting agent itself. The partition constant of benzoic acid and its dimerization constant in the organic phase were presented in 2-heptanone–dodecane–water ($H^+$, $Na^+$, $SO_4^{2-}$) systems by Kalembkevich.[4] However, the values presented by him seem to be unreasonable, judging from the relationship between the partition and dimerization constants of benzoic acid which was not touched upon at all in his work and is referred to in detail in our present work.

The present work deals with the partition equilibrium of benzoic acid, which is known to be useful for metal ions such as copper(II), between aqueous solution and mixed solvents consisting of benzene and 1-octanol or 2-octanone. It has been found that with increasing concentrations of 1-octanol and 2-octanone in each mixed solvent, the partition constant of benzoic acid increases, and the dimerization constant of the acid in each mixed solvent phase decreases in both the mixed solvent systems. Detailed explanation for these phenomena was attempted by considering the solvation of monomeric benzoic acid by 1-octanol and 2-octanone molecules.

*Author to whom correspondence should be addressed.

## EXPERIMENTAL

### *Reagents*

Reagent grade benzene was washed successively with concentrated sulfuric acid, dilute sodium hydroxide solution, dilute perchloric acid solution, and distilled, deionized water. 1-Octanol and 2-octanone of reagent grade solvents were purified in a similar manner as for benzene except for concentrated sulfuric acid. Benzoic acid and perchloric acid were of reagent grade and used without further purification. Aqueous solutions were prepared with distilled, deionized water. Mixed solvents were prepared to a given volume by diluting known amounts (by weight) of 1-octanol or 2-octanone with benzene. Before mixing, each solvent was saturated with water. A trace amount of water which is negligible was released by mixing the two solvents.

### *Procedures*

A volume of 10 ml each of 0.1$M$ perchloric acid aqueous solution and mixed solvent (Tables 1 and 2) containing 0.05–1.4$M$ benzoic acid were added to a 50 ml centrifuge tube. After shaking for 1 hr, which is sufficient for complete equilibration, the tube was centrifuged for 5 min at 3000 rpm. Subsequently the concentration of benzoic acid in the aqueous phase was determined by measuring the absorbance of the aqueous phase diluted 100 times with 0.1$M$ $HClO_4$ aqueous solution, at 229 nm, one of absorption maxima of benzoic acid ($\varepsilon = 1.11 \times 10^4 M^{-1}$ cm$^{-1}$). Trace amounts of benzene in the aqueous phase did not interfere with the measurement of the absorbance at 229 nm, because before measuring the absorbance each aqueous phase was diluted 100 times with 0.1$M$ perchloric acid solution.

Table 1. Partition and dimerization constants of benzoic acid (1-octanol–benzene system)

| No. | Concentration of 1-octanol ($M$) | | $\log K_{D,HA}'$ | $\log K_{2,HA}'$ | Sum |
|---|---|---|---|---|---|
| 0 | 0 | (0) | 0.14 | 2.42 | 2.70 |
| 1 | 0.10 | (1.5) | 0.81 | 1.05 | 2.67 |
| 2 | 0.25 | (3.7) | 1.07 | 0.52 | 2.66 |
| 3 | 0.30 | (4.5) | 1.21 | 0.16 | 2.58 |
| 4 | 0.40 | (6.0) | 1.31 | −0.09 | 2.53 |
| 5 | 0.50 | (7.5) | 1.39 | −0.43 | 2.35 |
| 6 | 1.00 | (15.1) | 1.63 | — | — |
| 7 | 2.00 | (30.5) | 1.75 | — | — |
| 8 | 3.00 | (46.5) | 1.84 | — | — |
| 9 | 4.00 | (62.5) | 1.89 | — | — |
| 10 | 5.00 | (78.6) | 1.88 | — | — |
| 11 | 6.00 | (94.6) | 1.86 | — | — |
| 12 | 6.34 | (100) | 1.84 | — | — |

The values in parentheses denote the concentration of percentage by volume, and sum = $\log K_{2,HA}' + 2 \log K_{D,HA}'$.

Table 2. Partition and dimerization constants of benzoic acid (2-octanone–benzene system)

| No. | Concentration of 2-octanone ($M$) | | $\log K_{D,HA}'$ | $\log K_{2,HA}'$ | Sum |
|---|---|---|---|---|---|
| 0 | 0 | (0) | 0.14 | 2.42 | 2.70 |
| 13 | 0.10 | (1.5) | 0.53 | 1.63 | 2.69 |
| 14 | 0.20 | (3.0) | 0.59 | 1.52 | 2.70 |
| 15 | 0.30 | (4.4) | 0.67 | 1.37 | 2.71 |
| 16 | 0.40 | (6.0) | 0.74 | 1.23 | 2.71 |
| 17 | 0.50 | (7.5) | 0.85 | 1.02 | 2.72 |
| 18 | 1.00 | (15.0) | 1.18 | 0.31 | 2.67 |
| 19 | 2.00 | (30.1) | 1.33 | 0.03 | 2.69 |
| 20 | 3.00 | (45.6) | 1.50 | −0.41 | 2.59 |
| 21 | 4.00 | (61.5) | 1.64 | −0.86 | 2.42 |
| 22 | 5.00 | (77.6) | 1.78 | — | — |
| 23 | 6.00 | (94.3) | 1.85 | — | — |
| 24 | 6.40 | (100) | 1.91 | — | — |

The values in parentheses and sum are the same as in Table 1.

### *Apparatus*

The partition of benzoic acid was performed in a Cool Bath Shaker ML-10 (TAITEC Co., Koshigaya, Japan) thermostatted at 25.0°C. A Table Top Centrifuge Model 5100 (Kubota Seisakusho Ltd, Tokyo, Japan) was used for centrifugation. The solubility of water in each mixed solvent was coulometrically measured using a Karl-Fischer Moisture Titrator MKC-210 (Kyoto Electronics Manufacturing Co., Kyoto, Japan). Spectrophotometric determination was carried out on a UVIDEC-430A Double Beam Spectrophotometer (Jasco, Tokyo, Japan).

## RESULTS AND DISCUSSION

### *Determination of partition and dimerization constants of benzoic acid*

The partition ratio of benzoic acid between the aqueous and organic phases can be represented by the following expression with the use of three kinds of equilibrium constants, *i.e.* the partition constant between the aqueous and organic phases ($K_{D,HA} = [HA]_o/[HA]_w$), the dimerization constant in the organic phase ($K_{2,HA} = [(HA)_2]_o/[HA]_o^2$), and the dissociation constant in the aqueous phase ($K_a = [H^+][A^-]/[HA]_w$):

$$D = \frac{C_{HA,o}}{C_{HA,w}} = \frac{K_{D,HA}(1 + 2K_{D,HA}K_{2,HA}[HA]_w)}{1 + \dfrac{K_a}{[H^+]}}, \quad (1)$$

where the subscripts o and w refer to the organic and aqueous phases, respectively, and $[(HA)_2]_o$ denotes the concentration of the dimeric benzoic acid in the organic phase. As the dissociation of benzoic acid in the aqueous phase is negligible under the present partition conditions, the following equation can be obtained from equation (1):

$$\log D - \log K_{D,HA} = \log(1 + 2K_{D,HA}K_{2,HA}[HA]_w). \quad (2)$$

If $\log D - \log K_{D,HA} = Y$ and $2K_{D,HA}K_{2,HA}[HA]_w = X$, equation (2) is equivalent to $Y = \log(1 + X)$. Then, on the basis of equation (2), by fitting the plots of $\log D$ against $\log[HA]_w$ with the normalized curve, $\log(1 + X)$ *vs.* $\log X$, the partition and dimerization constants can be estimated from the respective deviations of the ordinate and abscissa between the plots and the normalized curve. The results for 0.5 and 6.0*M* 2-octanone–benzene mixtures are shown in Fig. 1. The plots for the former fit well with the normalized curve described above. Then, the monomeric and dimeric species of benzoic acid were found to coexist in the organic phase in such mixed solvent. On the other hand, the plots for the latter are parallel to the horizontal axis, irrespective of the concentration of benzoic acid (Fig. 1). In this system, it has been shown that the dimerization of benzoic acid in the organic phase does not occur to any appreciable extent. The similar results were obtained in the mixed solvent systems containing 1-octanol of more than 1*M* and 2-octanone of more than 5*M*,

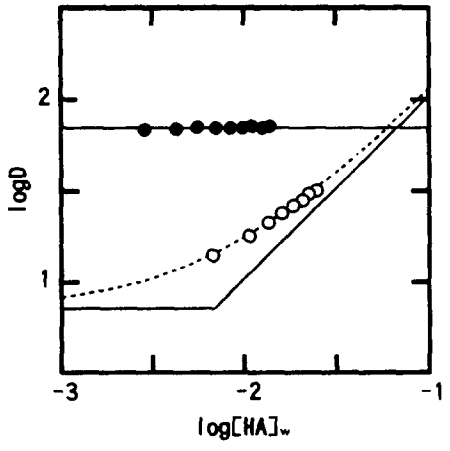


Fig. 1. Determination of the partition and dimerization constants of benzoic acid (2-octanone–benzene system). Open and closed symbols refer to the mixed solvents containing 0.5 and 6.0*M* 2-octanone, respectively. Dotted curve is the normalized curve, $\log(1 + X)$ *vs.* $\log X$. Solid lines are the asymptotes of the normalized curve.

respectively. In these cases the constant distribution ratio of benzoic acid is equal to its partition constant.

The values of the partition and dimerization constants of benzoic acid obtained for the 1-octanol–benzene and 2-octanone–benzene mixtures with various compositions are summarized in Tables 1 and 2, respectively. The values for pure benzene are also listed in the tables, and are in agreement with those presented by Fujii *et al.* within experimental error.[5]

As shown in the tables, with increasing the content of 1-octanol or 2-octanone in the mixed solvents, the partition constant of benzoic acid tends to increase, but the dimerization constant of the acid in each organic phase tends to decrease. These changes in the partition and dimerization constants of benzoic acid may be ascribed to solvation by 1-octanol and 2-octanone molecules.

*The effects of solvation on the partition constant of benzoic acid*

Benzoic acid is solvated with 1-octanol or 2-octanone molecules in the present mixed solvents in the following manner:

$$(HA)_o + n(S)_o \rightleftarrows (HA \cdot S_n)_o$$

with

$$\beta_{sv,n} = \frac{[HA \cdot S_n]_o}{[HA]_o[S]_o^n}, \quad (3)$$

where $S$ and $\beta_{sv,n}$ represent the solvent molecule, and the overall solvation constant of benzoic acid with 1-octanol or 2-octanone molecules, respectively. Then, in the region where the monomeric benzoic acid in the organic phase prevails, and the dissociation of benzoic acid in the aqueous phase is negligible, the distribution ratio of benzoic acid is equal to its conditional partition constant and can be represented as follows:

$$D = K_{D,HA}' = \frac{[HA]_o + \sum_n [HA \cdot S_n]_o}{[HA]_w}$$

$$= K_{D,HA}(1 + \sum_n \beta_{sv,n}[S]_o^n), \quad (4)$$

where $K_{D,HA}'$ and $K_{D,HA}$ denote the partition constants of benzoic acid for the mixed solvent and benzene, respectively. The partition constant of benzoic acid, which was determined in the present work, is this conditional constant, $K_{D,HA}'$ as shown below.

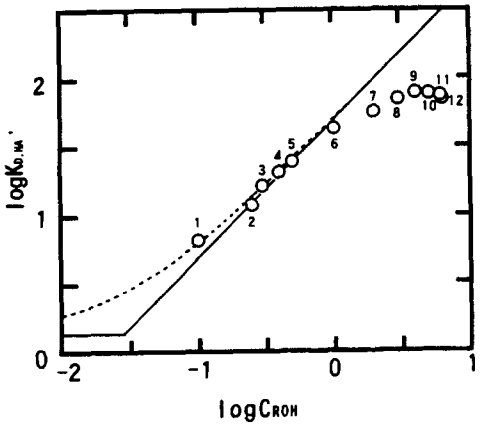


Fig. 2. Effect of solvation on the partition constant of benzoic acid (1-octanol–benzene system). Numbers are the same as in Table 1. Dotted curve and solid lines are the same as in Fig. 1.

If the main solvated species is only $HA \cdot S_n$, the following expression can be obtained from equation (4):

$$\log D = \log K_{D,HA}' = \log K_{D,HA} + \log(1 + \beta_{sv,n}[S]_o^n). \quad (5)$$

Substituting $\log K_{D,HA}' - \log K_{D,HA} = Y$ and $\beta_{sv,n}^{1/n}[S]_o = X$, the above expression is equivalent to $Y = \log(1 + X^n)$. According to equation (5), by fitting the plots of $\log K_{D,HA}'$ against $\log[S]_o$, with the normalized curve, $\log(1 + X^n)$ *vs.* $\log X$ with suitable $n$, the number of solvent molecules solvated to monomeric benzoic acid, and the solvation constant, $\beta_{sv,n}$ may be determined. Such plots are shown in Figs 2 and 3 for the 1-octanol–benzene and 2-octanone–benzene systems, respectively. In Figs 2 and 3, $\log K_{D,HA}'$ from Tables 1 and 2 is plotted against $\log C_S$

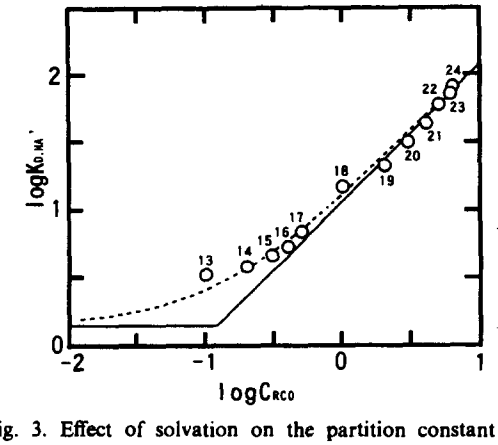


Fig. 3. Effect of solvation on the partition constant of benzoic acid (2-octanone–benzene system). Numbers are the same as in Table 2. Dotted curve and solid lines are the same as in Fig. 1.

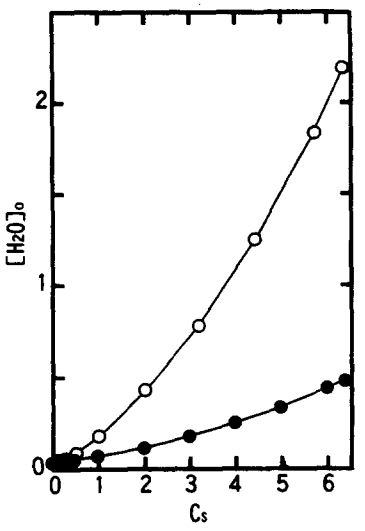


Fig. 4. Solubility of water in the mixed solvents. Open and closed symbols refer to the 1-octanol– and 2-octanone–benzene systems, respectively.

($C_S$: total concentration of 1-octanol or 2-octanone in each mixed solvent) instead of $\log[S]_o$. Under the present experimental conditions, $[S]_o$ can be approximated by the total concentration of 1-octanol or 2-octanone. The plots fit in the normalized curve with $n = 1$, *i.e.* $\log(1 + X)$ *vs.* $\log X$ in both the mixed solvent systems. It is suggested that the main monomeric species are HA and HA·S in each system. In addition, the solvation constant was obtained as follows: $\log \beta_{sv,1} = \log K_{sv,1} = 1.54$ for the 1-octanol–benzene system, and $\log \beta_{sv,1} = \log K_{sv,1} = 0.92$ for the 2-octanone–benzene system, respectively. As can be seen from Fig. 2, the plots deviate downward from the normalized curve, with increasing content of 1-octanol in the mixed solvent in the region where 1-octanol concentration is more than $1M$ in the 1-octanol–benzene mixture. In these regions the observed partition constant, $K_{D,HA}'$ is appreciably smaller than the value which is expected from solvation of benzoic acid by one 1-octanol molecule. The solubility of water in the mixed solvent increased with increasing concentration of 1-octanol in the mixed solvent (Fig. 4). Then, the decrease in the partition constant is attributable to the some effect of water on the mixed solvent and benzoic acid.

*Inhibition of dimerization of benzoic acid by solvation*

On increasing 1-octanol and 2-octanone contents in the respective mixed solvents, the dimerization constant of benzoic acid in the organic

phase decreased (Tables 1 and 2). Beyond 0.5*M* 1-octanol and 4.0*M* 2-octanone contents in each mixed solvent, respectively, the dimerization of benzoic acid did not occur to any appreciable extent in either mixed solvents. This decrease in the dimerization constant can be anticipated to result from the formation of solvated monomeric benzoic acid by 1-octanol or 2-octanone molecules. Taking into account solvation of monomeric benzoic acid by 1-octanol or 2-octanone molecules, the conditional dimerization constant of benzoic acid in each mixed solvent can be represented as follows:

$$K_{2,HA}' = \frac{[(HA)_2]_o}{([HA]_o + [HA \cdot S]_o)^2} = K_{2,HA}(1 + K_{sv,l}[S]_o)^{-2}, \quad (6)$$

taking logarithms of equation (6), the following expression is obtained:

$$0.5 \log K_{2,HA}' = 0.5 \log K_{2,HA} - \log(1 + K_{sv,l}[S]_o), \quad (7)$$

where $K_{2,HA}$ denotes the dimerization constant of benzoic acid in the benzene phase. The dimerization constant of benzoic acid estimated in this work is this conditional constant except for the pure benzene system. Substituting $0.5 \log K_{2,HA'} - 0.5 \log K_{2,HA} = Y$, and $K_{sv,l}[S]_o = X$, expression (7) is equivalent to $Y = -\log(1 + X)$. The plots of $0.5 \log K_{2,HA}'$ against $\log C_S$ on the basis of equation (7) are shown in Figs 5 and 6 for the 1-octanol–benzene and 2-octanone–benzene systems, respectively. As described above, $[S]_o$ can be approximated to the total concentration of 1-octanol or 2-octanone, $C_s$ under the present experimental conditions. The plots for 2-octanone–benzene system fit well with the normalized curve, $-\log(1 + X)$ *vs.* $\log X$ which is depicted on the basis of the values of $K_{2,HA}$ and $K_{sv,l}$ estimated in this work. Then, the decrease in the dimerization constant of benzoic acid is attributable to solvation of monomeric benzoic acid by one 2-octanone molecule as well as in the case of the increase in the partition constant of monomeric benzoic acid. On the other hand, the plots for the 1-octanol–benzene system deviate downward from the normalized curve in the region where the content of 1-octanol is more than 0.3*M*. Therefore, in this system the dimerization of benzoic acid has been suggested to be inhibited by not only solvation of monomeric benzoic acid by 1-octanol molecule but also some effects attributed to hydration by water molecules

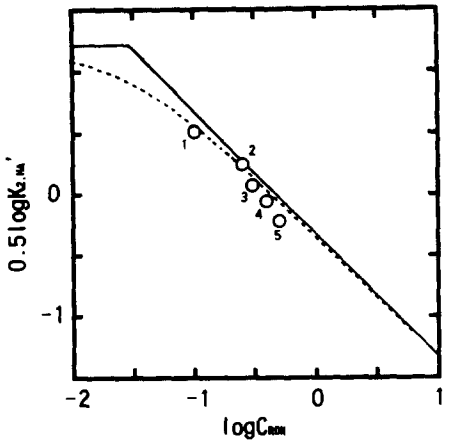


Fig. 5. Inhibition of dimerization of benzoic acid by solvation (1-octanol–benzene system). Numbers are the same as in Table 1. Dotted curve is the normalized curve, $-\log(1 + X)$ *vs.* $\log X$, which was located on the basis of $\log K_{2,HA} = 2.42$ in benzene and $\log K_{sv,l} = 1.54$. Solid lines are the asymptotes of the normalized curve.

whose concentration increases with increasing the 1-octanol content in this mixed solvent, or to the physical property of mixed solvent as a whole such as polarity, solubility parameter *etc.*

*Correlation of dimerization and partition constants of benzoic acid*

The relationship between the dimerization and partition constants of benzoic acid obtained in this work is shown in Fig. 7. The plots of $\log K_{2,HA}'$ *vs.* $\log K_{D,HA}'$ fit a straight line well with a slope of $-2$, which passes through the point for benzene, up to 0.25*M* of 1-octanol

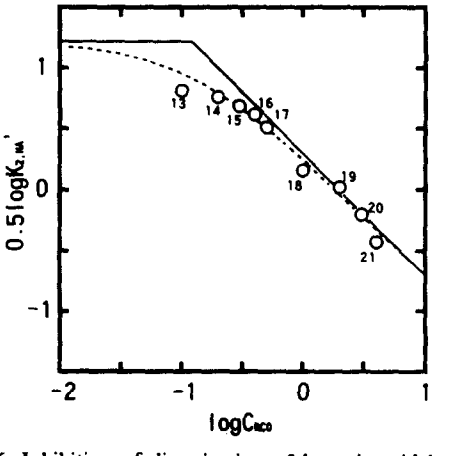


Fig. 6. Inhibition of dimerization of benzoic acid by solvation (2-octanone–benzene system). Dotted curve is the normalized curve, $-\log(1 + X)$ *vs.* $\log X$, which was located on the basis of $\log K_{2,HA} = 2.42$ in benzene and $\log K_{sv,l} = 0.92$. Numbers and solid lines are the same as in Table 2 and in Fig. 5, respectively.

content in the 1-octanol–benzene system and 2.0$M$ of 2-octanone content in the 2-octanone–benzene system, respectively. In other words, the sum of $\log K_{2,HA}'$ and $2\log K_{D,HA}'$ is kept constant up to these contents of 1-octanol and 2-octanone in the respective mixed solvents (*cf.* Tables 1 and 2). In the 2-octanone–benzene system, the sum of $\log K_{2,HA}'$ and $2\log K_{D,HA}'$ is kept constant over the wide concentration region of 2-octanone, in contrast to the 1-octanol–benzene system, in which the sum remains constant only over the very limited concentration region of 1-octanol.

Similar relationships of the partition and dimerization constants of di-n-butyl phosphate[6] and some aliphatic carboxylic acids[7] for some organic solvents have previously been reported. However, the sum of $\log K_{2,HA}'$ and $2\log K_{D,HA}'$ reported by them varies widely from solvent to solvent, especially in the former case.

As the dissociation of benzoic acid in the aqueous phase can be neglected under the present experimental conditions, the partition behaviour of benzoic acid can be represented by the following scheme,

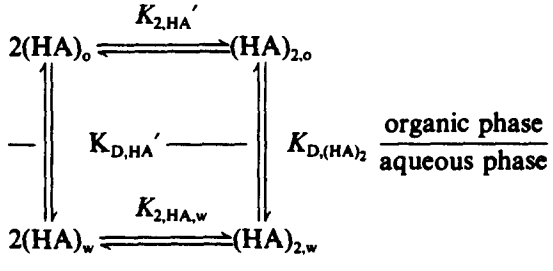


where $K_{2,HA,w}$ and $K_{D,(HA)2}$ denote the dimerization constant of benzoic acid in the aqueous phase, and the partition constant of dimeric benzoic acid, respectively. Then, the following relationship among the four kinds of equilibrium constants may hold:

$$\log K_{2,HA}' + 2\log K_{D,HA}' = \log K_{2,HA,w} + \log K_{D,(HA)2}. \quad (8)$$

From Fig. 7, and Tables 1 and 2, it is found that the value of the left-hand side of equation (8) tends to decrease rapidly from the constant value ($2.69 \pm 0.03$), when the 1-octanol and 2-octanone contents in each mixed solvent rise above 0.25 and 2.0$M$, respectively. As the dimerization constant of benzoic acid in the aqueous phase can be regarded as being constant, irrespective of the composition of the organic phase, the partition constant of dimeric

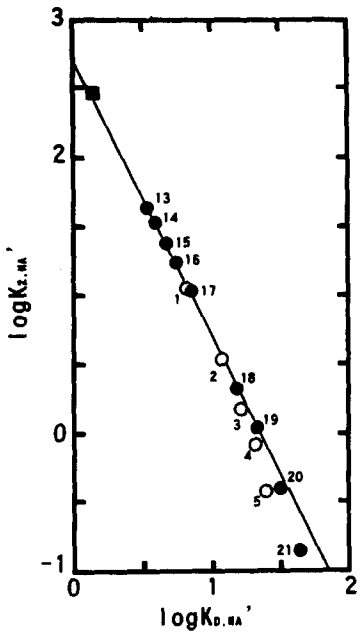


Fig. 7. Relationship between the partition and dimerization constants of benzoic acid. Open and closed symbols refer to the 1-octanol–benzene and 2-octanone–benzene systems, respectively. Closed square refers to benzene. Numbers are the same as in Tables 1 and 2. The solid line is a straight line with a slope of −2.

benzoic acid is also anticipated to remain constant under the region where the sum of $\log K_{2,HA}'$ and $2\log K_{D,HA}'$ remains constant, regardless of the composition of the mixed solvents. Therefore, it has been found that the partition behaviour of dimeric benzoic acid is difficult to be influenced by the solvent, contrary to that of monomeric benzoic acid which is subject to solvent effect. It is suggested that the main dimeric benzoic acid is the cyclic dimer in which two molecules are linked by a hydrogen bond, and because of the cyclic structure, dimeric benzoic acid is hard to be influenced by the solvent.

## CONCLUSIONS

As can be seen from Figs 2, 3, 5 and 6, significant differences in the solvent effect on the partition equilibrium of benzoic acid between 1-octanol–benzene and 2-octanone–benzene systems have been observed. This discrepancy may be attributed to whether the hydroxyl substituent is involved or not in the 1-octanol and 2-octanone which were mixed with benzene. In the 1-octanol–benzene system, the hydroxyl substituent in 1-octanol molecule is anticipated to enhance the solvation ability of the 1-octanol molecule and also to increase the solubility of water in 1-octanol–benzene mixed solvent by

hydrogen bonding. Enhancement of solvation ability is enhanced by the value of the solvation constant of monomeric benzoic acid, which is larger in the 1-octanol–benzene system than in the 2-octanone–benzene system. An increase in solubility of water in 1-octanol–benzene mixtures with increasing content of 1-octanol in the mixed solvents results in an increase in polarity as a whole and of the hydration ability of the mixed solvents. In a higher 1-octanol region of the mixed solvent, consequently, the partition and dimerization constants are anticipated to become smaller than those predicted by solvation of monomeric benzoic acid by the 1-octanol molecule.

In the 2-octanone–benzene systems, on the other hand, as shown in Figs 3 and 6, not only the increase in the conditional partition constant but also the decrease in the conditional dimerization constant may be reasonably explained on the basis of solvation of monomeric benzoic acid by 2-octanone. This suggests that the partition equilibrium of benzoic acid is not influenced to any appreciable extent by water, because of the lower concentration of water in the 2-octanone–benzene systems which can be attributed to the absence of the hydroxyl substituent in the 2-octanone molecule in contrast to the 1-octanol one.

In the 1-octanol–benzene systems, if it were not for the effects of water, the conditional partition constant of monomeric benzoic acid should be estimated to be log $K_{D,HA}' = 2.48$ by extrapolation to pure 1-octanol in Fig. 2.

It has been found that even such a simple equilibrium as the partition of benzoic acid is significantly dependent on kinds and contents of solvating solvents which are mixed with inert solvents. Then, the solvent extraction of a metal ion with an extracting reagent may be complicatedly influenced by kinds and contents of mixed solvents. Therefore, a useful mixed solvent for the solvent extraction of a metal complex can be expected to be developed by an additional investigation on mixed solvent for solvent extraction.

## REFERENCES

1. M. A. Olazabal, L. A. Fernandez and J. M. Madariaga, *Solvent Extr. Ion Exch.*, 1991, **9**, 735.
2. M. A. Olazabal, M. M. Orive, L. A. Fernandez and J. M. Madariaga, *Solvent Extr. Ion Exch.*, 1992, **10**, 623.
3. M. M. Orive, M. A. Olazabal, L. A. Fernandez and J. M. Madariaga, *Solvent Extr. Ion Exch.*, 1992, **10**, 787.
4. Ya. Kalembkevich, *Zh. Ob. Khim.*, 1992, **62**, 1012.
5. Y. Fujii, K. Sobue, and M. Tanaka, *J. Chem. Soc. Faraday Trans. I.*, 1978, **74**, 1467.
6. D. Dyrssen and L. D. Hay, *Acta Chem. Scand.*, 1960, **14**, 1091.
7. I. Kojima, M. Yoshida, and M. Tanaka, *J. Inorg. Nucl. Chem.*, 1970, **32**, 987.

Pergamon

0039-9140(95)01484-5

*Talanta*, Vol. 42, No. 6, pp. 797–801, 1995

0039-9140/95 $9.50 + 0.00

# THE IONIZATION CONSTANTS OF α-ALANINE IN NaCl AT 25°. EFFECT OF THE IONIC STRENGTH BASED ON THREE MODELS

S. FIOL, I. BRANDARIZ and M. SASTRE DE VICENTE*

Departamento de Química Fundamental e Industrial Facultad de Ciencias, Universidad de La Coruña, Campus da Zapateira, s/n 15071 La Coruña, Spain

**Summary**—In the present work we obtained the experimental p*K*s of the amino acid α-alanine in NaCl at 25° and different ionic strengths. The equilibrium constants have been potentiometrically determined with a commerical glass electrode and the results analysed through three models: two directly based on the Pitzer and Scatchard approaches to the ion specific interaction theory and the other based on a simpler modification of the Debye–Hückel equation. The three models fit the data reasonably well and the extrapolated p*K* values obtained show a good agreement. The goodness of the ridge regression method cannot be probed in this case.

The problem of the dependence of the protonation constants on ionic strength is of considerable importance both from theoretical and practical points of view.[1] However, systematic studies are scarce: a clear exception is the work by Sammartano *et al.*,[2–5] who have been using a semiempirical equation obtained by modifying the Debye–Hückel equation in order to find similarities in the behavior of some classes of ligands and for some background salts for several years. More recently, our group has started to study the dependence of the salt composition and ionic strength on the acid–base equilibrium constants of organic molecules both in single electrolytes and mixtures. The dependence mentioned above was assessed by using different models (Pitzer, Scatchard, Guggenheim[6–8]) which account for the specific interaction of any ion in solution. These treatments, mainly Pitzer's equations, have been widely used to determine the dependence of the osmotic and activity coefficients as a function of the ionic strength, particularly in aqueous solution of strong electrolytes. Weak electrolytes have been, however, scarcely dealt with, except for the work by Millero *et al.* on relevant inorganic equilibria in seawater.[9] In this work we report the ionization of α-alanine ($CH_3CHNH_2COOH$) at different ionic strength values in NaCl at 25°.[10] Data were treated in terms of Pitzer and Scatchard's models and the equations used by Sammartano *et al.*[4] Also the results were compared when the ridge regression (RR)[11] is applied instead of the ordinary least squares regression method, in order to overcome the presence of multicolinearity.[12]

## EXPERIMENTAL

The amino acids and NaCl were Merck (reagent and p.a. grade, respectively). Experimental details have been previously described.[13–16] Potentiometric titrations were carried out on a glass cell furnished with a thermostatting jacket and inlets for the electrode, burette and a nitrogen stream intended to remove $O_2$ and $CO_2$ and at the same time, homogenize the solution. Merck p.a. NaOH was added from a Crison microBU 2031 autoburette to the amino-acid solution containing Merck p.a. HCl, both 0.01*M*. The EMF was measured by means of a Crison micropH 2002 pH-meter furnished with Radiometer GK2401C combined glass membrane electrode, using Ag/AgCl as reference.

Stoichiometric equilibrium constants were calculated from data obtained in the potentiometric titrations of α-alanine by using the program MINIQUAD. The electrode was previously calibrated for the proton concentration in order to obtain the reference potential for each experiment. Calibrations were carried out for the pH-range between 2.3 and 2.9,[12] following the procedure described in Ref. 13 in order to minimize the influence of systematic errors. However, the response (nernstian or not)

*Author to whom correspondence should be addressed.

was checked in the whole interval. Known volumes of a 0.1*M* HCl solution of the desired ionic strength were added over a solution of the background electrolyte at the same ionic strength and the solution potential was measured on each addition.

The amino acid solutions were automatically titrated with the aid of the program ALIA,[17] (F. Penedo and F. Arce, unpublished work) which controls titrant additions from the burette, commands potential readings and creates the entry file for the program MINIQUAD. All regression analyses were performed by using the Statgraphics *Standard Statistical Package*.[17] The MINIQUAD provides p$K$ values in the molar scale while Pitzer and Scatchard models apply for molal scale. Conversion can be easily made from molar to molal scale: $pK_m = pK_c + \log(c/m)$, where $pK_m$ is in molal scale, $pK_c$ is in molar scale, $m$ is the concentration in mol/kg water and $c$ in $M$. The molality can be determined through the density. The expressions based on Sammartano *et al.*'s equations can be also used in molal scale since the difference owing to the p$K$ scale lies below the maximum experiment error conventionally admitted (*ca.* 0.06 p$K$ units).[18]

## RESULTS AND DISCUSSION

The protonation equilibria of neutral amino acids can be expressed as follows:

$$AH_2^+ \rightleftarrows AH + H^+, \quad K_1^T = K_1^* \frac{\gamma_{AH}\gamma_{H+}}{\gamma_{AH_2^+}} \quad (1)$$

$$AH \rightleftarrows A^- + H^+, \quad K_2^T = K_2^* \frac{\gamma_{A^-}\gamma_{H^+}}{\gamma_{AH}}. \quad (2)$$

The stoichiometric equilibrium constants of the aminoacid α-alanine are listed in Table 1. The final relationships obtained to show the $pK_i^*$ (in molal scale) dependence on ionic strength are as follows.

*Based on Pitzer's formalism*[19,20]

$$pK_1^* = pK_1^T + A_1 f^{(1)} + B_1 f^{(2)} + C_1 f^{(3)} \quad (3)$$

$$pK_2^* - D_2 f^{(4)} - E_2 f^{(5)} = pK_2^T + A_2 f^{(1)} + B_2 f^{(2)} + C_2 f^{(3)}, \quad (4)$$

where

$$A_1 = -\frac{1}{\ln 10}(\beta^0_{AH_2Cl} - \lambda - \beta^0_{HCl} + \theta_{AH_2Na} - \theta_{HNa}) \quad (5)$$

$$B_1 = \frac{-1}{\ln 10}(\beta^1_{AH_2Cl} - \beta^1_{HCl}) \quad (6)$$

$$C_1 = \frac{-1}{\ln 10}(\psi^\phi_{AH_2Cl} - C^\phi_{HCl} - \psi^\phi_{AH_2NaCl} - \psi_{HNaCl}) \quad (7)$$

$$A_2 = \frac{1}{\ln 10}(\beta^0_{ANa} + \theta_{ACl} + \beta^0_{HCl} + \theta_{HNa} - \lambda) \quad (8)$$

$$B_2 = \frac{1}{\ln 10}(\beta^1_{ANa} + \beta^1_{HCl}) \quad (9)$$

$$C_2 = \frac{1}{\ln 10}(C^\phi_{ANa} + C^\phi_{NaCl} + C^\phi_{HCl} + \psi_{ANaCl} + \psi_{HCaCl}) \quad (10)$$

$$D_2 = \frac{2\beta^1_{NaCl}}{\ln 10} \quad (11)$$

$$E_2 = \frac{2}{\ln 10}. \quad (12)$$

The ionic strength functions in equations (3) and (4) are as follows:

$$f^{(1)} = 2I$$

$$f^{(2)} = 1 - (2\sqrt{I})\exp(-2\sqrt{I})$$

$$f^{(3)} = I^2$$

$$f^{(4)} = -1 + (1 + 2\sqrt{I} + 2I)\exp(-2\sqrt{I})$$

$$f^{(5)} = -0.392\left(\frac{\sqrt{I}}{1 + 1.2\sqrt{I}} + \frac{2}{1.2}\ln(1 + 1.2\sqrt{I})\right). \quad (13)$$

*Based on Scatchard's formalism*[19]

$$pK_1^* = pK_1^T + P_1 I + Q_1 I^2 + R_1 I^3 \quad (14)$$

$$pK_2^* + \left\{\frac{2\sqrt{I}1.17202}{(1 + 1.5\sqrt{I})\ln 10}\right\} = pK_2^T + P_2 I + Q_2 I^2 + R_2 I^3, \quad (15)$$

Table 1. Stoichiometric p$K^*$s (in molal scale) of α-alanine in NaCl at 25°

| | α-Alanine | |
|---|---|---|
| $I$, $m$(NaCl) | $pK_1^*$ | $pK_2^*$ |
| 0.05 | 2.534 | 9.868 |
| 0.17 | 2.521 | 9.780 |
| 0.22 | — | 9.777 |
| 0.39 | 2.478 | 9.704 |
| 0.56 | 2.554 | 9.723 |
| 0.86 | 2.627 | 9.821 |
| 1.25 | 2.700 | 9.892 |
| $\sigma^*$ | (0.003–0.01) | (0.001–0.02) |

*Standard deviation.

Table 2. Interaction parameters obtained by means of the Pitzer (equations 3 and 4), Scatchard (equations 13 and 14) and Sammartano *et al.* (equations 26 and 27)

| | | | Pitzer | | | |
|---|---|---|---|---|---|---|
| $k$† | $i$ | $pK_i^T$ | $A_i$ | $B_i$ | $C_i$ | $\sigma$ |
| 0 | 1 | 2.55(0.05) | 0.678(0.444) | −1.587(0.992) | −0.351(0.200) | 0.028 |
| | 2 | 10.08(0.05) | 0.488(0.383) | 0.676(0.858) | −0.142(0.289) | 0.028 |
| 0.006 | 1 | 2.54(0.04) | 0.091(0.060) | −0.274(0.200) | 0.081(0.071) | 0.039 |
| | 2 | 10.04(0.03) | 0.122(0.044) | 0.141(0.154) | 0.129(0.055) | 0.031 |
| | | | Sammartano *et al.* | | | |
| $k$ | $i$ | $pK_i^T$ | $C_i$ | $D_i$ | $\sigma$ | |
| 0 | 1 | 2.53 ± 0.03 | 0.248 ± 0.209 | −0.350 ± 0.178 | 0.032 | |
| | 2 | 10.04 ± 0.03 | 0.188 ± 0.170 | −0.371 ± 0.145 | 0.026 | |
| 0.025 | 1 | 2.51 ± 0.03 | −0.026 ± 0.081 | 0.159 ± 0.069 | 0.038 | |
| | 2 | 10.01 ± 0.02 | 0.028 ± 0.063 | 0.185 ± 0.054 | 0.031 | |
| | | | Scatchard | | | |
| $k$ | $i$ | $pK_i^T$ | $P_i$ | $Q_i$ | $R_i$ | $\sigma$ |
| 0 | 1 | 2.56 ± 0.03 | −0.521 ± 0.243 | 1.122 ± 0.468 | −0.495 ± 0.240 | 0.024 |
| | 2 | 10.11 ± 0.01 | −3.410 ± 0.203 | 4.272 ± 0.384 | −1.672 ± 0.196 | 0.021 |
| 0.025 | 1 | 2.51 ± 0.04 | 0.007 ± 0.092 | 0.085 ± 0.035 | 0.027 ± 0.047 | 0.045 |
| | 2 | 10.02 ± 0.02 | 0.071 ± 0.068 | 0.096 ± 0.026 | 0.031 ± 0.035 | 0.034 |

*values in parenthesis correspond to the error in the parameters.
†$k$ is the ridge parameter: $k = 0$ applies for Ordinary Least Squares Regression and $k \neq 0$ for Ridge Regression.

where

$$P_1 = \frac{1}{\ln 10}\left(a^{(1)}_{HX} + b^{(0,1)}_{MX,HX} - a^{(1)}_{AH_2X} - b^{(0,1)}_{AH_2X,MX} + h_0\right) \quad (16)$$

$$Q_1 = \frac{1}{2\ln 10}\left(a^{(2)}_{HX} + b^{(0,2)}_{MX,HX} - a^{(2)}_{AH_2X} - b^{(0,2)}_{AH_2X,MX} + h_1\right) \quad (17)$$

$$R_1 = \frac{1}{3\ln 10}\left(a^{(3)}_{HX} + b^{(0,3)}_{MX,HX} - a^{(3)}_{AH_2X} - b^{(0,3)}_{AH_2X,MX}\right) \quad (18)$$

$$P_2 = \frac{1}{\ln 10}\left(a^{(1)}_{AH} + b^{(0,1)}_{MX,AH} + a^{(1)}_{MX} - h_0\right) \quad (19)$$

$$Q_2 = \frac{1}{2\ln 10}\left(a^{(2)}_{AH} + b^{(0,2)}_{MX,AH} + 2a^{(2)}_{MX} - h_1\right) \quad (20)$$

$$R_1 = \frac{1}{3\ln 10}\left(a^{(3)}_{AH} + b^{(0,3)}_{MX,AH} + 3a^{(3)}_{MX}\right). \quad (21)$$

Coefficients $A_i$, $B_i$, $C_i$ and $D_i$ in the Pitzer equations and $P_i$, $Q_i$ and $R_i$ in the Scatchard equations are parameters that result independently from the ionic strength and are related to the ionic interaction between the species involved in the equilibria and the medium.

*Based on a simpler modification of the Debye–Hückel equation*[2–5]

Among the very few systematic studies on ionization constants of organic compounds found in the literature we would like to mention the work carried out by Sammartano *et al.*[2–5] (and references therein). This group has systematically analysed the behaviour of such constants as a function of the ionic strength and the complex formation for a great number of

Table 3. Correlation and VIF matrix for the first $pK$

| Correlation matrix ($k = 0$)* | | | VIF matrix ($k \neq 0$) | | |
|---|---|---|---|---|---|
| 1. Pitzer equations (3) and (4) ($k = 0.006$) | | | | | |
| 1.0000 | 0.9689 | 0.9639 | 9.682353 | −4.922482 | −4.727976 |
| 0.9689 | 1.0000 | 0.8699 | −4.924825 | 6.276455 | −0.843336 |
| 0.9639 | 0.8699 | 1.0000 | −4.727976 | −0.843336 | 6.08551 |
| 2. Scatchard equations (14) and (15) ($k = 0.025$) | | | | | |
| 1.0000 | 0.9639 | 0.9126 | 4.224269 | −0.86069 | −2.97766 |
| 0.9639 | 1.0000 | 0.9874 | −0.86069 | 1.107245 | 0.070510 |
| 0.9126 | 0.9874 | 1.0000 | −2.97766 | 0.070510 | 3.218550 |
| 3. Sammartano *et al.* equations (27) and (28) ($k = 0.025$) | | | | | |
| 1.0000 | | 0.9881 | 4.615115 | | −4.12453 |
| 0.9881 | | 1.0000 | −4.12453 | | 4.615115 |

*$k$ is the ridge parameter: $k = 0$ applies for Ordinary Least Squares Regression and $k \neq 0$ for Ridge Regression

species: carboxylic acids, amines, amino acids, *etc.*

The general equation used by this group to express the stoichiometric equilibrium constants of amino acids is:

$$\log K_i^* = \log K_i^T - z_i^* \frac{\sqrt{I}}{2+3\sqrt{I}} + C_i I + D_i I^{3/2}, \quad (22)$$

where

$$C_i = p_i^* c_0 + z_i^* c_1 \quad (23)$$

$$D_i = p_i^* d_0 + z_i^* d_1 \quad (24)$$

$$p_i^* = \sum (\text{moles}_{\text{reactants}}) - \sum (\text{moles}_{\text{products}}) \quad (25)$$

$$z_i^* = \sum (pz^2)_{\text{reactants}} - \sum (pz^2)_{\text{products}}, \quad (26)$$

$z$ being the charge of the species. For the first equilibrium (1): $z^* = 0$ and $p^* = -1$ and for the second one (2): $z^* = 2$ and $p^* = -1$.

Taking these expressions into account, we can write the stoichiometric p$K^*$s as a function of the ionic strength by means of the following equations:

$$pK_1^* = pK_1^T - C_1 I - D_1 I^{3/2)} \quad (27)$$

$$pK_2^* + z^* \frac{\sqrt{I}}{2+3\sqrt{I}} = pK_2^T - C_2 I - D_2 I^{3/2}. \quad (28)$$

Table 2 shows for the three models the effect of multicolinearity between the explanatory variables in the calculation of highly correlated regression coefficients (close to unity) in the fitting interval used. This phenomenon is also revealed[12] by a value of the VIF (variation inflation factor) greater than 10, which is also shown in Table 3. From the data in Table 2 it follows that any of the assayed models reproduce experimental p$K^*$ *vs* I quite accurately and all the models yield similar curves (Fig. 1) and show an error of the fit within the conventionally admitted range for potentiometry wtih commercial $H^+$ glass electrodes (*ca.* 0.06 p$K$ units).[18]

The ridge parameters that appear in Tables 2 and 3 were obtained by applying the ridge trace method to equations (3), (4); (14), (15) and (27), (28). An analysis of the results also reveals that only for the p$K_2$ value does the application of ridge regression lead to smaller errors in the calculated parameters when using the Pitzer treatment. For the other parameters no improvement is observed.

The only parameter we can compare for the three models is the extrapolated p$K$. From Table 2 it can be concluded that good agreement can be achieved. For p$K_1^T$ the maximum difference between the values obtained is 0.03, which is under the 0.06 accepted as experimental error[18,21] and for p$K_2^T$ the difference become slightly greater that 0.06 p$K$ units, at 0.07. p$K_1^T$ values of $\alpha$-alanine in the literature[22] are very scarce and range from a minimum of 2.34 up to 2.63 while the averaged extrapolated value that we obtained is 2.55. The values found for p$K_2^T$ are 9.87, 9.89 and we obtained 10.08.

It can be concluded that although Scatchard and mainly Pitzer approaches are very useful for fitting data in wide ranges of $I$ and in mixtures of electrolytes, advantages that are not offered by other approaches, in the present case of a single electrolyte and a relatively reduced interval of ionic strength these models do not show remarkable superiority compared to a simpler model.

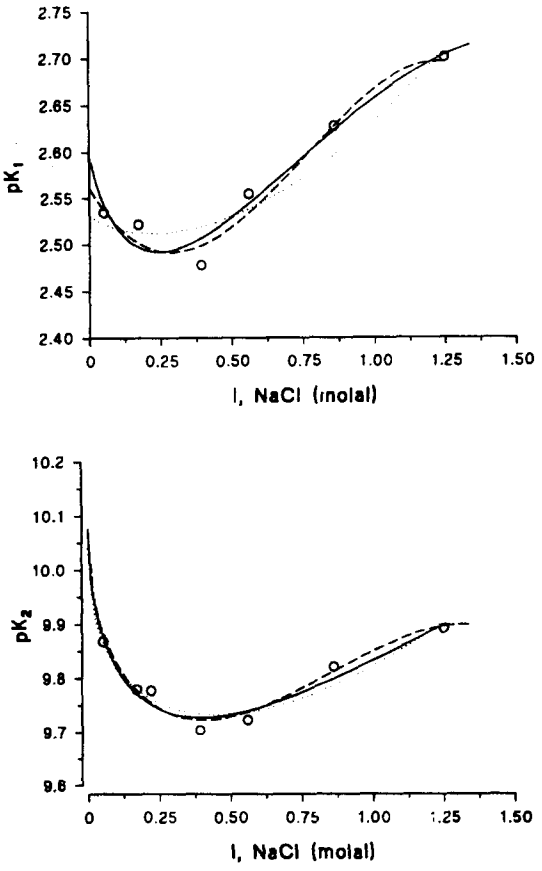


Fig. 1. Fitting curves based on Pitzer, Scatchard and Sammartano *et al.* equations. (○) Experimental data; (——) based on Pitzer's model; (– – –) based on Scatchard's model; (· · ·) based on a more simple modification of the Debye–Hückel equation.

*Acknowledgement*—The authors wish to acknowledge financial support from the Xunta de Galicia. Project XUGA 10303B92.

## REFERENCES

1. A. de Robertis and S. Sammartano, *Talanta*, 1993, **40**, 609.
2. A. de Robertis, C. de Stefano. G. Patane and S. Sammartano, *J. Soln Chem.*, 1993, **22**, 927.
3. P. G. Daniele, C. Rigano and S. Sammartano, *Ann. Chim.*, 1983, **73**, 741.
4. A. Casale, C. de Stefano, S. Sammartano and P. G. Daniele, *Talanta*, 1989, **36**, 903.
5. A. de Robertis, C. de Stefano, C. Rigano and S. Sammartano, *J. Soln Chem.*, 1990, **19**, 569.
6. K. S. Pitzer, *J. Phys. Chem.*, 1973, **77**, 268.
7. K. S Pitzer and G. Mayorga, *J. Soln Chem.*, 1974, **3**, 539.
8. G. Scatchard, *J. Amer. Chem. Soc.*, 1961, **83**, 2636.
9. F. J. Millero, *Limnol. Oceanogr.*, 1986, **31**, 839.
10. R. Herrero, I. Brandariz and M. E. Sastre de Vicente, *Ber. Bunsenges. Phys. Chem.*, 1993, **97**, 59.
11. P. F. M. van Gaans, *J. Soln Chem.*, 1990, **20**, 703.
12. N. R. Draper and H. Smith, *Applied Regression Analysis*, 2nd Edn, John Wiley and Sons, U.S.A. 1981.
13. S. Fiol, F. Arce, X. L. Armesto, F. Penedo and M. Sastre de Vicente, *Fresenius J. Anal. Chem.*, 1992, **343**, 469.
14. R. Herrero, X. L. Armesto, F. Arce and M. Sastre de Vicente, *J. Soln Chem.*, 1992, **21**, 1185.
15. I. Brandariz, F. Arce, X. L. Armesto, F. Penedo and M. Sastre de Vicente, *Monat. Chem.*, 1993, **124**, 249.
16. I. Brandariz, R. Herrero and M. E. Sastre de Vicente, *J. Chim. Phys.*, 1993, **90**, 63.
17. *Statistical Graphics System*, STATGRAPHICS by Statistical Graphics Corporation, Version 4.0, 1989.
18. A. Albert and E. P. Serjeant, *The Determination of Ionization Constants*. Chapman & Hall, 1984.
19. S. Fiol, I. Brandariz, X. L. Armesto, F. Arce and M. Sastre de Vicente, *Ann. Chim. (Rome)*, 1993, **83**, 175.
20. S. Fiol, I. Brandariz, R. Herrero, T. Vilariño and M. Sastre de Vicente, *Ber. Bunsenges. Phys. Chem.*, 1994, **98**, 164.
21. R. Herrero, I. Brandariz, S. Fiol and M. Sastre de Vicente, *Collect. Czech. Commun.*, 1993, **58**, 1269.
22. I. Sovago, T. Kiss and A. Gergely, *Pure Appl. Chem.*, 1993, **65**, 1029.

Pergamon

0039-9140(95)01492-6

*Talanta*, Vol. 42, No. 6, pp. 803–809, 1995

0039-9140/95 $9.50 + 0.00

# THE SEPARATION OF $^{99}$Tc FROM LOW AND MEDIUM-LEVEL RADIOACTIVE WASTES AND ITS DETERMINATION BY INDUCTIVELY COUPLED PLASMA MASS SPECTROMETRY

P. HEPIEGNE[1], D. DALL'AVA[1]*, R. CLEMENT[2] and J. P. DEGROS[2]

[1]Commissariat à l'Energie Atomique, Centre de Valduc, Service Contôle Essais, Is sur Tille 21120, France
[2]Commissariat à l'Energie Atomique, Centre de Saclay, Service de Prestations Nucléaires, Gif sur Yvette 91191, France

(*Received* 12 *October* 1994. *Revised* 5 *December* 1994. *Accepted* 5 *December* 1994)

**Summary**—A chemical separation method has been developed for the determination of $^{99}$Tc in various types of radioactive wastes. Such a method includes (i) fusion with NaOH, (ii) extraction in a column containing methyltrioctylammonium chloride, (iii) extraction by solvent with *N*-benzoyl-*N*-phenylhydroxylamine and, (iv) measurement by inductively-coupled plasma mass spectrometry (ICP-MS). From the performance standpoint, the recovery of $^{99}$Tc, using $^{99m}$Tc as a yield tracer, is higher than 70%. This analytical method, as developed, ensures effective decontamination with respect to the radionuclides, insofar the decontamination factors are greater than $10^{+5}$, whenever the residual activity may be measured. Taking into account a $3\sigma$ counting error, the detection limit obtained with the ICP-MS technique is 1.9 mBq/ml; the method enabling hence to detect activities as low as 0.3 Bq/g, with analysed samples of 0.2 g and a radiochemical yield of 70%. Studies have been dedicated to the $^{99}$Tc measurement, using the electrothermal vaporization ICP-MS technique, which lowers the detection limit by a factor 10, with the standard solution (0.3 pg/ml), compared with the previous ICP-MS technique.

Consideration has to be given to a number of long-lived radionuclides derived from the disposal of radwastes—and especially spent nuclear fuels, while assessing the environmental impact over the long term, of the nuclear power generation. It is thus essential to know the concentrations of long-lived nuclides (such as $^{79}$Se, $^{99}$Tc, $^{126}$Sn, $^{129}$I, $^{135}$Cs, $^{226}$Ra, $^{229}$Th, $^{237}$Np and $^{242}$Pu) as much in the spent nuclear fuels and other radwastes, as in the environment.[1] It is also mandatory to known the chemical behaviour of the radionuclides, to assess their transfer pathway in the environment over the long term, in the vicinity of the disposal sites. It stands to reason that the theoretical estimates to be validated by actual analytical determinations.

Among the whole spectrum of long-lived nuclides derived from nuclear reactors, special concern is given to $^{99}$Tc, on grounds of its long half-life (i.e. $2.2 \times 10^5$ *y*), decay mode ($\beta^-$), and the storage and disposal related problems, insofar $^{99}$Tc is very mobile in surface waters. Various analytical methods for determination of $^{99}$Tc in the environmental samples have been reported.[1] The techniques developed for $^{99}$Tc pre-concentration and/or pretreatment involve evaporation, [2,3] ion-exchange,[4,5] co-precipitation,[3,6,8] fusion,[8,9] and leaching with acidic solutions,[5,7,10,11]. The purification methods consist in co-precipitation with $(Ph)_4AsClO_4$,[12] ion-exchange[2,4,8–11,13,14] and extraction with organic solvents.[5,6,8,9,14,15] Such work does not concern radwaste samples containing radionuclides, which requires small-sized samples.

With respect to the determination of $^{99}$Tc in radwastes, the literature is scarce.[2,3] Compared with the environmental samples, determination of $^{99}$Tc in the radwaste samples differs basically insofar the latter contain several radioactive contaminants. Therefore, it is of the utmost importance to remove the associated ions from the radwaste samples used for the $^{99}$Tc separation.

The conventional method for $^{99}$Tc determination is $\beta$-counting either a low-background

*Author to whom correspondence should be addressed.

Table 1. ICP-MS and ETV-ICP-MS equipment and operating parameters

| | |
|---|---|
| ICP/MS | |
| Instrument | PlasmaQuad II+ (VG elemental) |
| Detector type | Pulse counting |
| Nebulizer type | Meinhard Type C |
| Solution uptake (*ml/min*) | 1.2 |
| Argon gas flows (*ml/min*) | Coolant: 13 Auxiliary: 0.65 Nebulizer: 0.75 |
| Plasma rf power | Incident: 1.3 *kW* Reflected: < 5 *W* |
| Electrothermal vaporization | |
| Ar carrier gas (*l./min*) | 0.75 |
| Drying temp. | 25–120°C for 2 *min* |
| Ashing temp. | 450–800°C for 1 *min* |
| Vaporization temp. | 800–2400°C to 1 *sec* |
| Acquisition | 5 *sec* |
| Sample injection | 50 *μl* |

proportional gas-flow counter, or a liquid-scintillation counter. This method has its drawbacks, as it requires a rather long counting time and a high degree of radiochemical $^{99}$Tc purification, to eliminate the $\beta$-emitting nuclides in the samples.

The inductively-coupled plasma mass spectrometry (ICP-MS) used until recent years,[18] has resulted in a very convenient method featuring low detection limits, which seems to be appropriate to radionuclides with a half-life exceeding 1000 years.[19] Halverson[20] and Rosenberg[1] have reviewed the application of mass spectrometry to the measurement of various low-concentration nuclides such as $^{99}$Tc, $^{129}$I, $^{135}$Cs and Pu isotopes.

This paper presents a method for measuring $^{99}$Tc derived from radwastes, using the ICP-MS technique. The separation method, as developed, enables to separate technetium from a 0.2-g radwaste sample, while using $^{99m}$Tc as a yield tracer (half-life: 6 hr). It also features the elimination from the $^{99}$Tc solution, of Ru—entailing isobaric interferences, and of many other radionuclides. Another advantage of this chemical separation method is that the ICP-MS may be used without a glove-box.

## EXPERIMENTAL

### *Apparatus*

The ICP-MS spectrometer used, was of the VG PlasmaQuad 2$^+$ type (VG Elemental, Winsford, Cheshire, U.K.). The operating parameters are shown in Table 1 The background at $m/z$ 101 was used for background correction at $m/z$ 99, in the absence of Ru. The scintillation spectrometer used, was a 1.K.B., Wallac 1410, with Instagel Packard. The activity of interfering radionuclides was measured with a high-purity germanium type detector (EGPC 18), connected to an appropriate data acquisition system.

### *Reagents*

A calibrated reference source of $^{99}$Tc has been purchased from L.M.R.I.,[21] and diluted in a 0.1*M* ammonia solution, having the appropriate specific activities. The $^{99}$Tc tracer has been derived from a medical $^{99m}$Tc generator (Elumatic III, 1.85 GBq, 50 mCi). Methyltrioctylammonium chloride and *N*-benzoyl-*N*-phenylhydroxylamine (BPHA) have been purchased from Aldrich Chemical Company Inc. All the chemicals were of the analytical-reagent grade.

Table 2. Recoveries of $^{99}$Tc (used as yield tracer) with the developed procedure

| | $^{99}$Tc recovery (%) | |
|---|---|---|
| Chemical procedure | Yield per phase | Cumulative overall yield |
| Pretreatment | | |
| Fusion (NaOH) | 84.4 | 84.4 |
| Extraction column-eluate | 94.0 | 79.4 |
| Purification | | |
| Extraction (BPHA/$CHCl_3$) | 97.5 | 77.4 |
| Cleaning (6*M* $HClO_4$) | 97.5 | 75.4 |
| Back extraction (0.01*M* $HNO_3$) | 97.6 | 73.6 |

Table 3. Initial activities from a low-level waste*

| Radionuclide $\gamma$ | Activity ($Bq/g$) | Radionuclide $\alpha$ $\beta$ X | Activity ($Bq/g$) |
|---|---|---|---|
| $^{54}Mn$ | 140,000 | $^{3}T$ | 88 |
| $^{57}Co$ | 2000 | $^{14}C$ | 2100 |
| $^{58}Co$ | 40,000 | $^{63}Ni$ | 80,000 |
| $^{60}Co$ | 50,000 | $^{90}Sr$ | 980 |
| $^{110m}Ag$ | 100,000 | $^{55}Fe$ | 27,000 |
| $^{124}Sb$ | 2700 | $^{238}Pu$ | 4 |
| $^{125}Sb$ | 6500 | $^{239-240}Pu$ | 3300 |
| $^{134}Cs$ | 260,000 | $^{241}Am$ | 8 |
| $^{137}Cs$ | 300,000 | $^{242}Cm$ | 12 |
| $^{140}Ba$ | 1000 | $^{243-244}Cm$ | 1 |
| $^{140}La$ | 1000 | | |

*Glass filter (0.2 $g$), $^{99}Tc = 8$ $Bq/g$.

*Preparation of the extraction column*

Methyltrioctylammonium chloride (1 g) was dissolved in 10 ml of acetone/pentan (1:1) mixture. Voltalef 300 LDPL Micro (4 g) (Atochem) was added, with stirring, the mixture being further spread out and dried. The column (Wright DC 7/6 Amicon, dia. 8 mm) was filled with 1 g of the mixture. Before use, the column was washed with 50 ml of 0.1$M$ $HNO_3$.

*Chemical separation*

*Pretreatment.* The solid sample (0.2 g) taken from radwastes in a shielded box, was transferred to a nickel crucible, with 0.2 ml of the 12$M$ ammonia solution. An aliquot of $^{99m}Tc$ (5000 Bq)—as a tracer—was added to measure the radiochemical recovery. As regards the liquid waste sample, $^{99m}Tc$ was added to the solution which is adjusted to pH 7, with the 12$M$ ammonia solution. After volume reduction, the concentrated solution was transferred to the crucible. In any case, the resulting solution was dried at 150°C for 10 min prior to adding 4 g of NaOH. Fusion took place on heating to 600°C. After cooling down, 50 ml of 6$M$ $HNO_3$ were placed in the crucible and heated to 80°C. Twenty millilitres of 12$M$ ammonia solution were added and the solution was heated to reflux, and filtered after cooling. The dark blue solution was adjusted to pH 1.5, with 6$M$ $HNO_3$, prior to passing through the extraction column. The column was then washed with 50 ml of 0.1$M$ $HNO_3$ and the technetium was eluted with 20 ml of 6$M$ $HClO_4$.

*Purification.* The eluate was transferred to a separating funnel and was washed with 5 ml of $CHCl_3$; technetium was extracted twice with 10 ml of $CHCl_3$ 1%-BPHA w/v. The organic-phase was sent to another clean separating funnel, and washed with 10 ml of 6$M$ $HClO_4$. After adding 10 ml of 0.01$M$ $HNO_3$, the solution was stirred for 3 min to facilitate the technetium back-extraction to aqueous phase. This was performed twice to recover technetium more efficiently. The volume was then adjusted to 25 ml with 0.01$M$ $HNO_3$, and the $^{99m}Tc$ tracer activity measured by $\gamma$-counting. The final solution may be concentrated up to 2 ml, without dry evaporation.

## RESULTS AND DISCUSSION

The chemical separation method, described herein, has been developed with various kinds of radwaste, the sampling solutions being prepared using glass filters, ion-exchange resins, cellulose paper, textiles, distillation residues and waste-embedding bitumen. The technique developed for $^{99}Tc$ pretreatment involves fusion with NaOH prior to passing through an extraction column containing methyltrioctylammonium chloride, which is an ion-exchange reagent. The purification process used consists in extraction with BPHA (*N*-benzoyl-*N*-phenylhydroxylamine) ligand, dissolved in an organic solvent. BPHA is used extensively for the extraction of metal ions from aqueous solutions. Being an acidic extractant, this reagent generally extracts metal cations into organic solvents as chelates. This chemical separation method has been selected as it features a high percent of $^{99}Tc$

Table 4. Activities retained and decontamination factors (DF) concerning four radionuclides

| | Radionuclides | | | |
|---|---|---|---|---|
| Procedure | $^{54}Mn$ | $^{60}Co$ | $^{110m}Ag$ | $^{137}Cs$ |
| Pretreatment | | | | |
| Fusion ($Bq$) | 10,200 | 777,300 | 78,800 | 9160 |
| Eluate ($Bq$) | 6 | 55 | 132 | 9 |
| DF | $2 \times 10^3$ | $1 \times 10^4$ | $6 \times 10^2$ | $1 \times 10^3$ |
| Purification | | | | |
| Final solution ($Bq$) | <0.2 | <0.3 | <0.3 | <0.4 |
| DF | $>5 \times 10^4$ | $>3 \times 10^6$ | $>3 \times 10^5$ | $>2 \times 10^4$ |

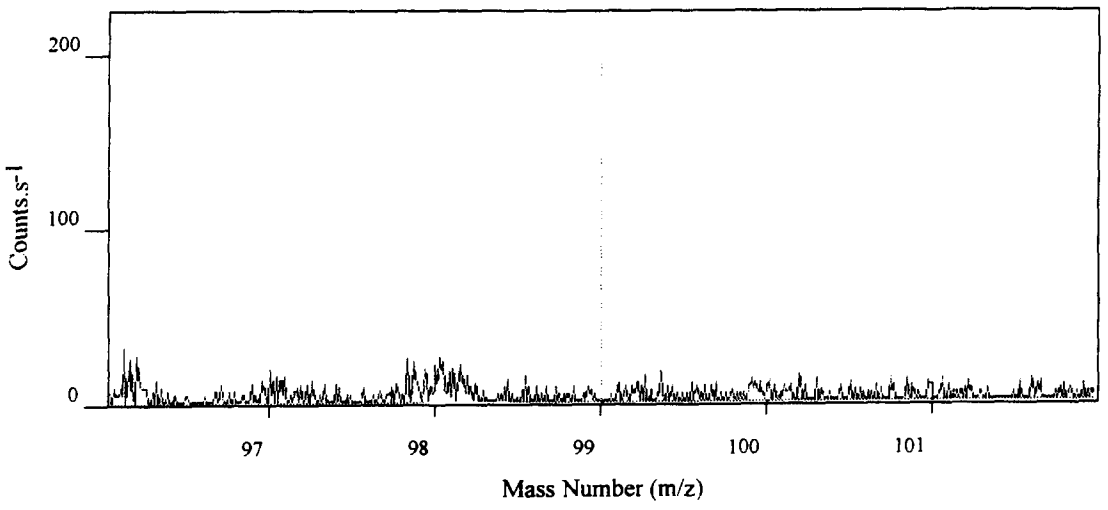


Fig. 1. Mass spectrum of the final solution after chemical processing (initial: Ru = 4 mg/l., Mo = 4 mg/l.; final: $^{99}$Ru < 1 ng/l., $^{98}$Mo = 3 ng/l.)

chemical recovery and an acceptable level of decontamination with respect to the radionuclides, as described below.

It is difficult to determine the chemical recovery of $^{99}$Tc, because technetium has no stable isotope. The $^{95m}$Tc[22], $^{97}$Tc[23] and $^{99m}$Tc[16] radionuclides have been used as yield tracer. As regards the chemical separation method described herein, the radwaste samples have been mixed with a $^{99m}$Tc tracer (half-life: 6 hr) obtained from a medical $^{99m}$Tc generator, the radiochemical recovery being performed by $\gamma$-counting, once the whole chemical separation is over.

*Pretreatment*

The pretreatment method has been developed, first with non-radioactive simulated samples, the solutions being prepared, using clean silica filters, cellulose filters, and ion-exchange resins. $^{99}$Tc is added to determine a specific radiochemical yield, with both $\beta$-counting and ICP-MS techniques. During the fusion process, the sample was completely dissolved whatever might by the matrix used. The loss of $^{99}$Tc observed at 600°C was less than 20%, as shown in Table 2. Technetium results to be more volatile from acidic solutions evaporated to dryness.[24] Most of the constituent elements prevailing in the initial solution were eliminated on passing through the extraction column, and the $^{99}$Tc recovery was then greater than 75%.

*Purification*

The purification method has been developed with radioactive-sample solutions. Table 3 shows the activities of the radionuclides present in the solution prepared from one of the radwastes used. As an instance, $^{99}$Tc activity was 8 Bq/g. Table 4 shows the decontamination factors of the main radionuclides ($^{54}$Mn, $^{60}$Co, $^{110m}$Ag and $^{137}$Cs). One may observe that the developed analytical procedure provides an effective extraction capability with respect to the nuclides. Using the extraction column, more than 99% of the original radioactive elements are separated from the technetium. The purification method complemented the radionuclide decontamination carried out with the chemical separation method. The decontamination fac-

Table 5. Decontamination factors of Ru and Mo in simulated sample and chemical yield of $^{99m}$Tc

| | Chemical separation procedure | | |
|---|---|---|---|
| Element | Initial solution* (*mg/l.*) | Final solution* (*ng/l.*) | Decontamination factor |
| Ru | 4 | <9 | $>4 \times 10^5$ |
| Mo | 4 | 12 | $3 \times 10^5$ |
| $^{99m}$Tc | — | — | chemical recovery: 70.3% |

*25 *ml.*

Table 6. $^{99}$Tc activities in radwaste samples and related $^{99m}$Tc tracer recoveries*

| Radioactive waste | $^{99m}$Tc recovery (%) | $^{99}$Tc (*Bq/g*) |
|---|---|---|
| Cellulose filter | 73 | $1.5 \pm 0.2$ |
| Cellulose filter | 73 | $0.9 \pm 0.3$ |
| Textile | 77 | $(9.1 \pm 0.1) \times 10^{3}$ |
| Ion exchange resin | 70 | $1.6 \pm 0.2$ |
| Ion exchange resin | 64 | $<0.3$ |
| Coating with bitumen | 65 | $30 \pm 1$ |
| Glass filter | 63 | $15.6 \pm 0.8$ |
| Glass filter | 70 | $5.0 \pm 0.5$ |
| Glass filter | 75 | $32.4 \pm 0.9$ |
| Glass filter | 70 | $1.8 \pm 0.2$ |
| Glass filter | 82 | $3.6 \pm 0.4$ |
| Distilling residue | 76 | $1.1 \pm 0.2$ |
| Radioactive water (1 l.) | 54 | $(3.3 \pm 0.9) \times 10^{-4}$ |

*Average of three replicate determinations (ICP-MS) on 0.2 *g* waste samples.

tors were all over $10^{+5}$, when the residual activities can be measured: $^{99m+99}$Tc is extracted selectively in the organic phase (BPHA/$CHCl_3$), and no other radionuclides are found in the final chemical extract. Fouché,[25] in an extensive investigation of the extraction of pertechnetate ions by BPHA from perchloric acid solutions, found that Tc(VII) is extracted and that the extracted compound contains pertechnetate in a 1:1 ratio to BPHA.

### *$^{99}$Tc measurement by ICP-MS*

Determination of $^{99}$Tc by ICP-MS requires that $^{99}$Tc be free of Ru ($^{99}$Ru mass abundance: 12.7%) and free of Mo ($^{98}MoH^{+}$ having the same mass number as $^{99}$Tc). $^{99m}$Tc, as a tracer, was added to a solution prepared with Ru (4 mg/l.), Mo (4 mg/l.) and a silica-filter (0.2 g), to determine the extraction factors of Ru and Mo. After chemical processing, the $^{99m}$Tc chemical recovery was 70%, and a mass spectrum of the final solution was obtained (Fig. 1). As shown in Fig. 1, Ru is eliminated from the $^{99m}$Tc solution. Although the $^{98}$Mo peak is developed, no interferences from $^{98}MoH^{+}$ is reported. Table 5 shows Ru and Mo concentrations and the extraction factors, all greater than $10^{+5}$.

Furthermore, $^{99}$Tc, $^{106}$Ru and $^{99}$Mo were added to a solution prepared with a silica filter (0.2 g), as radiochemical tracers. On completion of the chemical process, the $^{106}$Ru was trapped with $^{99}$Tc, in the extraction column, but not extracted with BPHA ligand. As regards $^{99}$Mo, it was not trapped in the column, hence eliminated. In this case, the decontamination factors were also over $10^{+5}$.

### *Precision and minimum detectable activity*

The data presented in Table 6 serve to illustrate the precision of the technique as well as the levels of $^{99}$Tc present in 0.2 g waste and the overall yield typically obtained. The precision of determination depends on the concentration of $^{99}$Tc in final solutions but not of the initial radwaste used. The overall yield of $^{99m}$Tc recovery is, as a rule, greater than 70%, independently of the original material. The results secured by the ICP-MS technique have been compared with those obtained by the liquid scintillation counting method. The results were in good agreement (Table 7).

The detection limit, 1.9 mBq/ml (3 pg/ml) was lower than that for the liquid scintillation counting method (38 mBq/ml), as shown in Table 8. The detection limit ($3\sigma$ counting error) with respect to the ICP-MS technique was calculated

Table 7. Agreement between the ICP-MS and $\beta$-counting method measurements of $^{99}$Tc

| | $^{99}$Tc (*Bq/g*) | |
|---|---|---|
| Radioactive waste | ICP-MS | $\beta$ counter |
| Textile | $(9.1 \pm 0.1) \times 10^{+3}$ | $(9.3 \pm 0.4) \times 10^{+3}$ |
| Water | $43.0 \pm 1$ | $49 \pm 5$ |
| Water | $19.8 \pm 0.8$ | $20 \pm 10$ |
| Glass filter | $3.6 \pm 0.4$ | $<18$ |

Table 8. Detection limits (DL) in several analytical methods for the determination of $^{99}$Tc and minimum detectable activity (MDA) of the developed procedure*

| Analytical method | DL (*mBq/ml*) | MDA (*Bq/g*) 25 *ml* | 2 *ml* |
|---|---|---|---|
| Liquid scintillation counting | 114 | 18 | — |
| ICP-MS | 1.9 | 0.3 | 0.03 |
| ETV-ICP-MS | 0.2 | — | — |
| HR-ICP-MS† | 0.005 | | |
| Low background gas flow counting[22] | 3 | | |
| Neutron activation analysis (n,n')[22] | 400 | | |

*Waste 0.2 *g*; $^{99m}$Tc yield 70%.
†High resolution ICP-MS.[27]

from the measurements carried out with 10 blank solutions obtained on completion of the chemical process—without using any radioactive sample—and from 10 measurements carried out with a standard $^{99}$Tc solution. The minimum detectable activity of the developed analytical procedure with a radiochemical yield of 70% and an analysed sample of 0.2 g, was found to be 0.3 Bq/g using ICP/MS, and 18 Bq/g with $\beta$-counter.

The chemical separation procedure took approximately one day, providing high chemical recoveries of technetium from limited amounts of radwastes containing many interfering elements. Using the autosampler in conjunction with the ICP-MS technique, up to four samples per hour could be analysed, which was much faster compared with the conventional counting techniques.

### *$^{99}$Tc measurement with ETV technique*

Lower detection limits can be obtained with more radioactive waste sampling. It is also possible to reduce the final solution from 25 to 2 ml and/or use electrothermal vaporization inductively coupled plasma spectrometry (ETV-ICP-MS), ETV as a means of sample introduction into an ICP-MS instrument.[26] Using this method, 50 $\mu$l of solution are placed in a graphite furnace, and by controlling the heating cycle, the samples can typically be dried, ashed, and then vaporized at temperatures up to 2800°C, using argon as the carrier gas. ETV-ICP-MS has been applied, chiefly, to improve the detection limits by a factor of 10 to 100, compared with the pneumatic nebulization methods (ICP-MS). The determination of technetium by ETV-ICP-MS has not been reported in the literature.

Our preliminary analytical results obtained with $^{99}$Tc standard solutions indicate detection limits of 0.3 pg/ml ($^{99}$Tc: 0.015 pg introduced). Unfortunately, it was not possible to obtain good results with solutions containing 0.01*M* $HNO_3$ because of the volatility of technetium from acidic solutions. Standard ammonia solutions of $^{99}$Tc could only be used. We are presently modifying the purification method to be able to use the ETV-ICP-MS technique. Likewise, we are investigating the possibility for using a chemical modifier to be inserted with the sample in the graphite furnace, which would prevent untimely $^{99}$Tc evaporation.

## REFERENCES

1. R. J. Rosenberg, Technical Research Centre of Finland, Espoo 1992, Research Notes 1357.
2. N. Y. Chu and J. Feldstein, *Talanta*, 1984, **31**, 809.
3. N. W. Golchert and J. Sedlet, *Anal. Chem.*, 1969, **41**, 669.
4. J. P. Riley and S. A. Siddioui, *Anal. Chim. Acta*, 1982, **139**, 167.
5. Q. Chen, H. Dahlgaard, H. J. M. Hansen and A. Aarkrog, *Anal. Chim. Acta*, 1990, **228**, 163.
6. E. Holm, J. Rioseco, S. Ballestra and A. Walton, *J. Radioanal. Nucl. Chem.*, 1988, **123**, 167.
7. N. Matsuoka, T. Umata, M. Okamura, N. Shiriaishi, N. Momoshima and Y. Takashima, *J. Radioanal. Nucl. Chem.*, 1990, **140**, 57.
8. M. Koide and E. D. Goldberg, *J. Environ. Radioact.*, 1985, **2**, 261.
9. S. Foti, E. Delucchi and V. Akamian, *Anal. Chim. Acta*, 1972, **60**, 269.
10. J. E. Martin and J. M. Hylko, *Appl. Radiat. Isot.*, 1987, **38**, 447.
11. M. Otsuji, R. Seki and N. Ikeda, *Radioisotopes*, 1987, **36**, 473.
12. S. Cattarin, L. Doretti and U. Mazzi, *Health Phys.*, 1985, **49**, 795.
13. R. J. Silva, R. Evans, J. H. Rego and R. W. Buddemeier, *J. Radionanal. Nucl. Chem.*, 1988, **124**, 397.
14. G. E. Boyd and Q. V. Larson, *J. Phys. Chem.*, 1960, **64**, 988.

15. S. Hirano, M. Matsube and H. Kamada, *Radioisotopes*, 1989, **38**, 186.
16. J. H. Chiu, T. C. Chu and P. S. Weng, *Anal. Chim. Acta*, 1992, **256**, 293.
17. B. J. Mincher and J. D. Baker, *J. Radioanal. Nucl. Chem., Articles*, 1990, **139**, 273.
18. Y. Igarashi, C. K. Kim, Y. Takaku, K. Shiraishi, M. Yamamoto and N. Ikeda, *Anal. Sci.*, 1990, **6**, 157.
19. M. R. Smith, E. J. Wise and D. W. Koppenaal, *J. Radioanal. Nucl. Chem., Articles*, 1992, **160**, 341.
20. J. E. Halverson, *Nucl. Instr. Meth.*, 1984, **223**, 349.
21. DAMRI/LMRI, BP6, F-91191 Gif sur Yvette.
22. S. Moriat, C. K. Kim, Y. Takaku, R. Seki and N. Ikeda, *Appl. Radiat. Isot.*, 1991, **42**, 531.
23. D. M. Beals, Westinghouse Savannah River Company, WSRC-MS-92141.
24. B. R. Harvey, K. J. Williams, M. B. Lovett and R. D. Ibbett, *J. Radioanal. Nucl. Chem.*, 1992, **158**, 417.
25. K. F. Fouché, *J. Inorg. Nucl. Chem.*, 1971, **33**, 857.
26. K. E. Jarvis, A. L. Gray and R. S. Houk, *Handbook of Inductively Coupled Plasma Mass Spectrometry*. Blackie, Glasgow, 1992.
27. C. Kim, R. Seki, S. Morita, S. Yamasaki, A. Tsumura, Y. Takaku, Y. Igarashi and M. Yamamoto, *J. Anal. At. Spectrom.*, 1991, **6**, 205.

Pergamon

0039-9140(95)01493-4

*Talanta*, Vol. 42, No. 6, pp. 811–816, 1995

0039-9140/95 $9.50 + 0.00

# UPTAKE OF CESIUM, STRONTIUM AND EUROPIUM BY A POLY(SODIUM ACRYLATE–ACRYLIC ACID) HYDROGEL

E. H. RIFI, F. RASTEGAR and J. P. BRUNETTE*

Laboratoire de Chimie Minerale et Analytique, E.H.I.C.S., C.N.R.S. URA 405, 1, Rue Blaise Pascal, 67008 Strasbourg Cedex, France

(*Received* 14 *October* 1994. *Revised* 2 *December* 1994. *Accepted* 2 *December* 1994)

**Summary**—The uptake of cesium, strontium and europium from dilute nitric acid solutions by a poly(sodium acrylate–acrylic acid) PAA hydrogel has been investigated. pH variations are consistent with cation exchange processes: $—COO^-$, $Na^+/H^+$, $—COO^-$, $Na^+/M^{m+}$ ($M^{m+} = Cs^+$ and $Sr^{2+}$) and $—COOH/Eu^{3+}$. Saturation of the gel is achieved for metal/carboxylate ratios $R = 0.5$. The swelling ratios of gels loaded with metal cations are those of uncharged, shrunk gels (Sr, Eu) or of charged, swollen gels (Cs) in agreement with the formation of uncharged $(—COO)_2Sr$, $(—COO)_2EuX$ (X = $NO_3$ or OH) type complexes and $(—COO^-, Cs^+)$ ion pairs. The metal cations are extracted in the gels following the order of their affinities with carboxylic groups $Eu^{3+} > Sr^{2+} > Cs^+$. An increase of the ionic strength of the metal aqueous solution up to 0.5*M* $NaNO_3$ leads to slightly decrease the europium uptake by the PAA hydrogel, but 0.1*M* $NaNO_3$ is sufficient to prevent the Sr and Cs extractions.

Swelling polymer (or copolymer) networks (polyethylene, polybutadiene, polystyrene, polyvinylchloride, polyurethane . . .) with solubility-consistent metal extracting solvents leads to lipophilic gels or impregnated resins which can be applied to recovery of precious metals, to removal of toxic or radioactive elements from various effluents and to metal preconcentration for environmental sample analysis.[1–9] Metal coordinating resins have also been extensively studied with the aim of preventing loss of expensive (but selective) ligands in the aqueous phase.[10] Because of the lipophilic character of neutral coordinating resins, the water–resin contact is often weak, thus limiting the ligand accessibility and the extraction rate.[11] Moreover, a number of these materials are expensive and their applications remain very specific. On the contrary, the water 'superabsorbent' property of cheap hydrophilic polymer or copolymer networks (e.g. hydrolysed polyacrylamide, ionized polymethacrylic and polyacrylic acids) has led to important applications in hygiene and agriculture, and also in concentrating macromolecular solutions by selective water absorption.[12] Since only a few of fundamental investigations on the complexation of metal cations with polyelectrolyte hydrogels were available,[13–22] application to metal recovery from dilute effluents have been patented only recently.[23] Water absorption in the hydrophilic polymer network warrants an excellent accessibility of the metal coordinating moieties, but the volume variations of the hydrogel, with pH and metal cation binding, must be considered in liquid–hydrogel extraction processes. Thus, further informations on the hydrogel behaviour immersed in metal cation solutions are needed with particular attention paid to the interdependence of physical and chemical parameters involved: *i.e.* metal valence, pH and ionic strength of the metal feed solution, gel swelling and shrinking, nature of the metal–carboxylate interactions, *etc.* The present paper deals with the uptake of metal cations of different valencies, cesium, strontium and europium, three metal ions which are relevant in radio-

*Author to whom correspondence should be addressed.

*Abbreviations*: *l*, initial parameters before liquid–gel contact; * species in the SAPGel; $M^{m+}$, $Cs^+$ or $Sr^{2+}$ or $Eu^{3+}$; α, ionization ratio = mol $—COO^-$/total mol —COO(H, Na); *r*, cross-linking ratio; *R*, mol metal in the gel/total mol —COO(H, Na); *Q*, $m/m_i$ = swelling ratio; *m*, SAPGel mass at equilibrium; $m_i$, initial mass of SAP network; *D*, [(metal amount/g of dry polymer)]/[(metal amount/ml of liquid phase)]; SAP, poly(sodium acrylate–acrylic acid) network; SAPGel, SAP network after swelling in an aqueous solution.

active waste management, by a poly(sodium acrylate–acrylic acid) polymer network.

## EXPERIMENTAL

### *Reagents*

10SHP Super Absorbent Polymer (SAP), which is a poly(sodium acrylate–acrylic acid) polymer network, was supplied from Norsolor-Atochem Co. This material consists of 'cauliflower' type beads of about 0.5 mm average diameter. It is 1% cross-linked with diethylene glycol diacrylate, 80% ionized and contains 10 mmol —COO(H, Na)/g (residual water contents: 9%). All other chemicals, from Prolabo, Merck or Fluka, were of analytical grade.

### *Gel preparation*

Super absorbent polymer gels (SAPGel) were prepared by immersing 0.1 g of SAP network into 200 ml of bidistilled water. The excess of water was removed by filtration giving (46.8 ± 0.1) g of SAPGel.

### *Metal extraction and analytical procedure*

The following general procedure was used: SAPGel (0.94 g = $2.0 \times 10^{-5}$ mol —COO(H, Na) or 2 mg SAP network) was introduced into a thermostatted vessel (25.0 ± 0.2°C) containing 100 ml of $1 \times 10^{-4}M$ metal ion aqueous solution prepared with nitrate salts (Cs, Sr) or oxide (Eu). The gel samples were suspended in a small cotton gauze bag to avoid breakage during stirring using magnetic bars rotated at about 200 rpm. In order to avoid the erratic presence of $CO_2$, the experiments were run in stoppered vessels. Aliquots of metal ion solution were withdrawn and analysed, after suitable dilution by atomic emission (Cs, Sr) using a 2380 Perkin Elmer or a JY24 Jobin-Yvon ICP spectrophotometer, or by energy dispersive X-ray fluorescence (Eu) using an EDXRF Siemens prototype. Metal inside the gel was determined by mass-balance calculation or analysed after back extraction in $0.1M$ $HNO_3$. pH, measured with a digital pHmeter and a combination glass-reference electrode, was adjusted with concentrated $HNO_3$.

### *Gel swelling*

The gel swelling was measured by weighing the gel before and after contact (4–6 hr) with the aqueous solution.

## RESULTS AND DISCUSSION

### *SAPGel behaviour in aqueous solutions free of metal cations*

*Swelling.* If a SAPGel network is soaked in dilute $HNO_3$ solutions of various concentrations and free of metal cations, an internal acid–base rearrangement of the polymer is observed which is clearly indicated by a slow decrease of the hydrogen ion concentration in the outer solution. The higher the pH, the higher is the SAPGel ionization and, consequently, its swelling. Swelling ratios ($Q$) at various pH measured at equilibrium are given in Table 1.

It is interesting to note that, at pH 2.5, the swelling ratio decreases from 70 to 40 when the quantity of immersed SAP network increases from 2.0 to $7.6 \times 10^{-5}$ mol —COO(H, Na): in both cases, the resulting gel is neutral, *i.e.* entirely protonated and uncharged, and the more the $Na^+$ release in the outer solution, the less is the swelling ratio. An opposite behaviour is observed at pH 7, which probably means that the effective gel ionization, responsible for the swelling, is a little higher in the latter case. The swelling ratio is strongly dependent on the ionic strength of the outer solution: *e.g.* $Q$ = 370, 95, 55 and 45 when 9.4 mg of SAP network is

Table 1. Swelling of the SAP network in dilute $HNO_3$ (100 *ml*)

| | Free of metal cations | | | | | | | |
|---|---|---|---|---|---|---|---|---|
| pH | 2.5 | 3.4 | 3.85 | 4.7 | 5.46 | 6.0 | 7.0 | —COO(H, Na) |
| $Q$ | 70 | 106 | 120 | 164 | 256 | 272 | 286 | $2.0 \times 10^{-5}$ mol |
| $Q$ | 40 | 60 | 84 | 152 | 232 | 288 | 320 | $7.6 \times 10^{-5}$ mol |

| | Containing metal cations, and metal uptake | | | | | |
|---|---|---|---|---|---|---|
| $M^{m+}$ | $Cs^+$ | $Na^+$ | $Sr^{2+}$ | $Sr^{2+}$ | $Eu^{3+}$ | $Eu^{3+}$ |
| —COO(H, Na) mol × $10^5$ | 7.6 | 7.6 | 7.6 | 7.6 | 2.0 | 2.0 |
| $[M^{m+}]_i \times 10^4$ | 31.5 | 31.5 | 1 | 1 | 1 | 1 |
| pH | 7.15 | 7.15 | 2.5 | 5.46 | 2.5 | 3.85 |
| $R$ | 0.20 | >0.8 | 0 | 0.42 | 0 | 0.50 |
| $Q$ | 190 | 210 | 38 | 36 | 70 | 70 |

soaked in 100 ml of water at $pH_i$ 5.4 and containing 0, 5, 25 and 100 g/l. $NaNO_3$, respectively.

*Dissociation.* It is not easy to determine the dissociation constant of carboxylic groups bound to the SAPGel because of the difficulties to measure the hydrogen ion concentration within the gel. One can consider the total gel in equilibrium with the outer solution but its titration leads to important changes of volume (1–500) and, moreover, several hours are needed to reach equilibrium in every step of titration. Nevertheless, it is interesting to note that the ionization ratio of the SAPGel is $\alpha = 0.5$ at pH 6.0 (pH of the outer solution after equilibration of 2 mg of SAP network soaked in 100 ml $HNO_3$ $10^{-4.2}M$). This value is close to the intrinsic $pK_a$ of the linear polyacrylic acid (6.17) at low ionic strength.[13]

*Cesium uptake*

When a SAPGel (*species in SAPGel) is soaked in a cesium nitrate solution, the cesium concentration in the outer solution decreases rapidly to reach a minimum after 20 min, then it slightly increases and reaches a stable value about 30 min later (Fig. 1). During this time, the pH increases and then stabilizes after 50 min. It is likely that during the first 20 min both *—$COO^-$, $Na^+/H^+$ and *—$COO^-$, $Na^+/Cs^+$ exchanges occur (reactions 1 and 2). After 20 min, excess of cesium in the gel is released in the outer solution (*—$COO^-$, $Cs^+/H^+$ exchange) because of the final acid–base rearrangement of the gel.

$$*\text{—}COO^-, Na^+ + H^+ \underset{-1}{\overset{1}{\rightleftarrows}} *\text{—}COOH + Na^+ \quad (1)$$

$$*\text{—}COO^-, Na^+ + Cs^+ \underset{-2}{\overset{2}{\rightleftarrows}} *\text{—}COO^-, Cs^+ + Na^+. \quad (2)$$

The cesium uptake, noticeable above pH 4.5, increases with pH and becomes constant above pH 6.5 with $R = 0.13$ [$R$ = mol metal in gel/total mol —COO(H, Na)] (Fig. 2). It is drastically lowered if $NaNO_3$ is added to the outer solution: no cesium extraction is observed from 0.1 to 0.5$M$ $NaNO_3$ at pH 7. These results agree with a cesium uptake via equilibrium 2.

Increasing the cesium concentration of the outer solution leads to increase the cesium uptake. A maximum occurs at $R = 0.5$ ($[Cs^+]_i > 6 \times 10^{-4}M$, pH 7) (i = initial parameters before liquid–gel contact). This value, far from 1, can be explained by the difficulty encountered by two cesium cations in approaching two neighbouring carboxylate anions because of the large $Cs^+$ size, and electrostatic repulsions. Thus, at saturation, each *—$COO^-$,

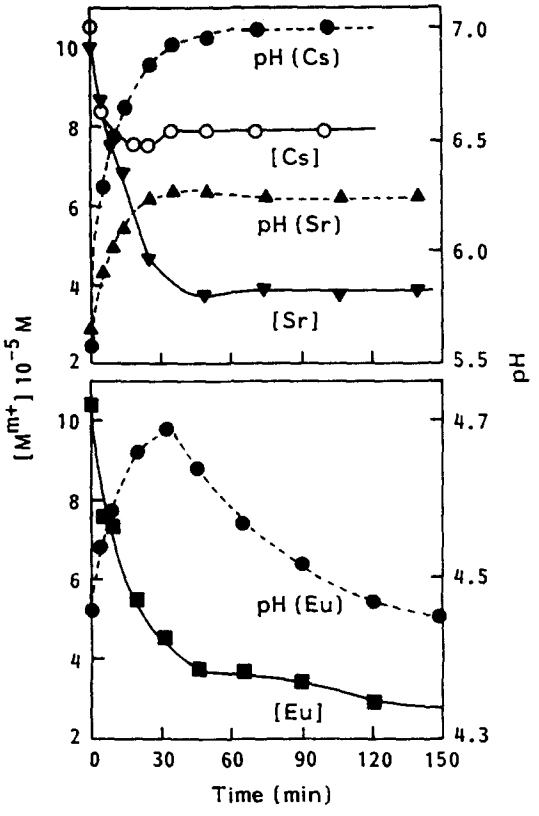


Fig. 1. Variations of the pH and metal ion concentration of an aqueous solution (100 ml) in contact with a SAPGel [—COO(H, Na) $2.05 \times 10^{-5}$ mol; $pH_i = 5.57$ (Cs), 5.66 (Sr), 4.46 (Eu); $[M^{m+}]_i = 1 \times 10^{-4}M$].

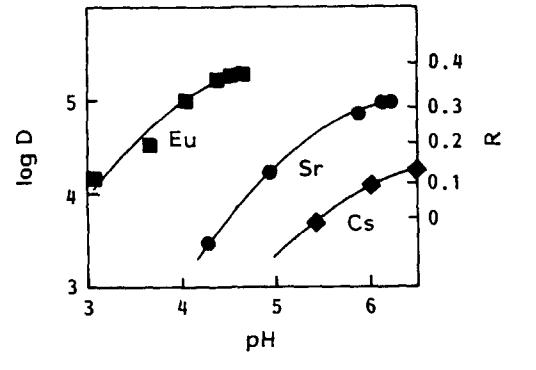


Fig. 2. pH effect on the uptake of cesium, strontium and europium from an aqueous solution (100 ml, $[M^{m+}]_i = 1 \times 10^{-4}M$) by a SAPGel [—COO(H, Na) $2.05 \times 10^{-5}$ mol]. pH measured at equilibrium (only $[HNO_3]_i$ was varied), shaking time > 3 hr. $R$ = mol metal in the gel/total mol —COO(H, Na). $D$ = [(metal amount/g of dry polymer)]/[(metal amount/ml of liquid phase)].

$Cs^+$ is probably surrounded by *—$COO^-$, $Na^+$ moieties.

Attempts to describe quantitatively the uptake of cesium and other cations ($Sr^{2+}$, $Eu^{3+}$) using elementary adsorption functions have failed: indeed, variations of ion concentrations in the outer solution lead to change the gel volume and the ion activities within the gel which are difficult to determine.

It is interesting to note that the swelling ratio of SAPGel loaded with cesium is that of a charged (ionic) gel since $Q = 190$ ($m/m_1$, swelling ratio) at pH 7.15 and $R = 0.2$ ($7.6 \times 10^{-5}$ mol —COO(H, Na) in 100 ml $[Cs^+]_i = 3.15 \times 10^{-3} M$), close to $Q = 210$ measured under the same experimental conditions in the absence of cesium (replace by $[Na^+]_i = 3.15 \times 10^{-3} M$) (Table 1). Thus, the uptake of cesium by the gel as *(—$COO^-$, $Cs^+$) ion pairs can explain the gel behaviour in cesium nitrate solutions.

*Strontium uptake*

The kinetics of strontium removal from a dilute aqueous solution by extraction into a SAPGel are shown in Fig. 1: pH of the outer solution increases whereas the strontium concentration decreases, both stabilizing about 1 hr after immersing the SAPGel into the solution. Both equilibria 3 and 4 could explain the strontium uptake:

$$n\text{*—COOH} + Sr^{2+} \underset{-3}{\overset{3}{\rightleftarrows}} \text{*(—COO)}_n Sr^{(2-n)+} + nH^+ \quad (3)$$

$$n\text{*—COO}^-, Na^+ + Sr^{2+} \underset{-4}{\overset{4}{\rightleftarrows}} \text{*(—COO)}_n Sr^{(2-n)+} + nNa^+, \quad (4)$$

where $n = 1$ or 2 and water molecules are omitted.

Strontium uptake via reaction 3 would have induced a significant pH decrease down to 4–4.5, which is not observed. On the contrary, a pH increase occurs in agreement with a *—$COO^-$, $Na^+/H^+$ exchange (reaction 1). It can be concluded that the strontium uptake mainly proceeds via reaction 4. The kinetics of the metal ion uptake process is relatively slow, but one must remember that fully swollen gels have been used in the present experiments: it follows that the diffusion of ions inside the hydrogel is likely the rate limiting factor. This is supported by a previous work[24] which has shown that increasing the cross-linking ratio of an hydrogel leads to a faster metal uptake because of a weaker polymer swelling and consequently a shorter diffusion distance inside the gel. Of course, the metal uptake becomes faster if the dry and unswollen polymer SAP network is directly soaked in the metal ion solution: in this case, the polymer network first swells but, because of the neutralization of electric charges by metal ion binding to the carboxylate anions, it quickly deswells.[25]

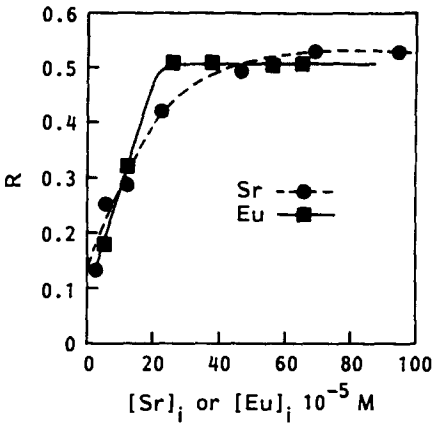


Fig. 3. Effect of the metal ion concentration on its uptake by a SAPGel [—COO(H, Na) 2.05 mol] immersed in 100 ml of aqueous solution. Strontium: $pH_i = 5.5$, europium: $pH_i = 3.9$. $R$ = mol metal in the gel/total mol —COO(H, Na).

The pH dependence of the liquid–gel strontium extraction is shown in Fig. 2: the extraction increases up to pH 6 and remains constant with $R = 0.32$. Increasing $[Sr^{2+}]_i$ (Fig. 3) leads to a saturation effect at $R = 0.53$ which is close to the stoichiometry of *$(—COO)_2Sr$ complexes. Swelling ratio measurements (Table 1) support the formation of such neutral complexes into the gel: indeed, when 7.5 mg SAP network are soaked in 100 ml of a strontium nitrate solution ($[Sr^{2+}]_i = 3.15 \times 10^{-3} M$), the swelling ratios are $Q = 36$ at pH 5.46 with $R = 0.42$, and $Q = 38$ at pH 2.50 with $R = 0$. In the absence of strontium, the swelling ratios are 250 and 40, respectively. At pH 2.50, the gels are uncharged and shrunk. At pH 5.46, it is likely that the formation of neutral (*—$COO)_2Sr$ type complexes explains the gel shrinking from 250 (charged gel) to 36 (uncharged and complexed gel). Similar results were previously found with other divalent cations, notably for $Cu^{2+}$ and $Cd^{2+}$.[25]

As previously observed with cesium, no strontium uptake by SAPGels was observed from 0.1 to $0.5M$ $NaNO_3$ solutions at pH 6.25, an obser-

vation which supports the strontium uptake via equilibrium 4.

Strontium removal from 100 ml of an aqueous solution (4.2 mg/l. Sr, $pH_i$ 5.6) can be achieved by soaking consecutively five SAPGels each containing $2 \times 10^{-5}$ mol —COO(H, Na): 80% Sr are removed by the first gel, whereas the Sr concentration after treatment with the fifth gel drops to less than 0.05 mg/l.

*Europium uptake*

The europium removal from an europium nitrate aqueous solution by a SAPGel is shown in Fig. 1. The pH *vs.* $t$ (current time) and $[Eu^{3+}]$ *vs.* $t$ diagrams deserve some comments: the pH increases from 4.46 to 4.70 where a maximum is reached after 30 min, then it decreases slowly to stabilize at 4.40 several hours later. $[Eu^{3+}]$ decreases rapidly during the first 30–50 min and remains almost constant after about 2 hr. Gel protonation (reaction 1) may explain the pH increase during the first 30 min. In the same time *—$COO^-$, $Na^+/Eu^{3+}$ cationic exchange can occur but after 30 min, the *—COOH form becomes predominant over *—$COO^-$, $Na^+$ and a release of protons is observed because of *—$COOH/Eu^{3+}$ cationic exchange. The very different trends of pH *vs.* time curves in Fig. 1 result from the different pH ranges of the metal liquid–gel extraction: Sr and Cs are extracted in the pH range 5.5–7 where the *—$COO^-$, $Na^+$ form predominates over *—COOH, whereas Eu is extracted in the pH range 4.4–4.7 where the *—COOH form predominates. Accordingly, the Cs and Sr uptakes proceed via *—$COO^-$, $Na^+/M^{m+}$ exchange, whereas Eu extraction proceeds via *—$COOH/Eu^{3+}$ exchange which induces a release of hydrogen ions in the outer solution. Unlike Cs and Sr extractions which are strongly decreased by increasing ionic strength of the outer solution, Eu extraction is only slightly decreased: $-20\%$ from $[NaNO_3] = 0$ to $[NaNO_3] = 0.5M$. This is in agreement with the suggested metal extraction process.

At pH 3.85, the gel saturation with europium occurs at $R = 0.50$ (Fig. 3). The swelling ratio drops from $Q = 120$ (in the absence of $Eu^{3+}$) down to $Q = 70$ because of the europium gel binding: indeed, 70 is the swelling ratio of the uncharged SAPGel measured at pH 2.5 in the absence of $Eu^{3+}$ under the same experimental conditions (Table 1). Thus, the formation of neutral *$(—COO)_2EuX$ complexes (X = $NO_3$ or OH) in the gel could explain the experimental data.

*Selectivity*

In order to check the selectivity of the SAPGel, $\approx 1.9$ g SAPGel ($4.0 \times 10^{-5}$ mol —COO(H, Na)) have been immersed into 100 ml of an equimolar solution ($[M^{m+}] = 8.5 \times 10^{-5}M$) of Eu, Sr and Cs at $pH_i$ 4.5: the extraction yield follows the expected order Eu (87.2%) > Sr (19.5%) > Cs (0) which allows an easy separation (this order is that of the affinities of metal cations with carboxylic sites).

*Metal stripping from the loaded SAPGel*

The is readily achieved in $0.1M$ $HNO_3$ after a few minutes.

## CONCLUSIONS

The uptake of cesium, strontium and europium by poly(acrylic acid–sodium acrylate) hydrogels from dilute aqueous solutions has been investigated. The uptake follows the order of the metal cation affinities towards the carboxylate group: $Eu^{3+} > Sr^{2+} > Cs^+$. The maximum SAPGel loading, $R$ = mol metal in the gel/total mol —COO(H, Na) = 0.5, observed with europium and strontium agrees with the formation of *$(—COO)_2Sr$ and $(—COO)_2Eu^+$ moieties. In both cases, the swelling factors are close to that of an uncharged SAPGel, and thus the formation of neutral *$(—COO)_2EuX$ (X = $NO_3$ or OH) type complexes is likely. The behaviour of the SAPGel in cesium solutions is very different since the swelling ratios are those of charged gels containing (*—$COO^-$, $Cs^+$) ion pairs. The maximum experimental uptake ratio of cesium is only 0.5, and sodium cations counterbalance the rest of carboxylate charges within the gel. Cesium and strontium uptakes decrease strongly with increasing sodium concentration ($NaNO_3$) in the outer solution according to a *—$COO^-$, $Na^+/M^{m+}$ cation exchange process. The europium uptake proceeds via a *—$COOH/Eu^{3+}$ exchange reaction which is characterized by a proton release into the outer solution and only a slight dependence on the $NaNO_3$ concentration. Europium, strontium and cesium stripping from loaded SAPGels is readily achieved by washing with $0.1M$ $HNO_3$. It is possible to remove metal cations from dilute solutions by immersing consecutively several SAPGels, which leads to very low concentrations, *e.g.* less than 0.05 mg/l. of strontium.

The complexation of metal cations by crosslinked sodium polyacrylate type hydrogels fol-

lowed by the gel shrinking gives the possibility of a 'pseudo-precipitation' of metal cations at low concentrations. Thus, they are promised agents for detoxication, or preconcentration of metal cations before analysis, but further experiments are needed which take in account the specific conditions of an application. Indeed, it has been shown here that high ionic strength can greatly limit the strontium and cesium extractions. Of course, synergistic effects or antagonisms may occur because of the presence of other ions in the metal solution: *e.g.* the high concentration of carboxylate groups in PAA hydrogels can favour the formation of mixed-metal carboxylates (previously found in related liquid–liquid extraction systems[26]), which can overthrow the expected selectivities.

*Acknowledgement*—The authors are grateful to Norsolor-Atochem Co. for supplying the superabsorbant polymer network.

## REFERENCES

1. D. K. Hale, Methods or processes of extracting a solute from a solution, British Patent 738,500, 1955.
2. C. W. Babcock, E. M. Tuttle, W. J. Brooke and W. R. Baker, Recovery of ammoniacal copper with novel organogels, U.S. Patent 585,977, 1984.
3. S. Palagyi and T. Braun, *Radioakt. Ziv. Prost.*, 1986, **9**, 137.
4. S. Török, T. Braun, P. Van Dyck and R. Van Grieken, *X-Ray Spectrom.*, 1986, **15**, 7.
5. J. P. Brunette, E. H. Rifi, M. J. F. Leroy, P. Mallo, G. Waton and M. Prévost, *Solvent Extr. Ion Exch.*, 1987, **5**, 1017.
6. J. F. Loret, J. P. Brunette, M. J. F. Leroy, S. J. Candau and M. Prévost, *Solvent Extr. Ion Exch.*, 1988, **6**, 585.
7. J. Rigas, S. Palagyi, G. Holeczyova and Matherny, *Chem. Papers*, 1991, **45**, 509.
8. J. P. Brunette and J. F. Dozol, *New Separation Chemistry Techniques for Radioactive Waste and other Specific Applications*, L. Cecille, M. Casarci and L. Pietrelli (eds), p. 116. Elsevier, Amsterdam, 1991.
9. K. Shakir, M. Aziz and S. G. Beheir, *Hydrometallurgy*, 1992, **31**, 41.
10. S. K. Sahni and J. Reedijk, *Coord. Chem. Rev.*, 1984, **59**, 1.
11. G. Zirnhelt, M. J. F. Leroy, J. P. Brunette, Y. Frère and Ph. Gramain, *Sep. Sci. Technol.*, 1993 **28**, 2419.
12. E. L. Cussler, M. R. Stokar and J. E. Varberg, *AIChE J.*, 1984, **30**, 578.
13. H. P. Gregor, L. B. Luttinger, and E. M. Loebl, *J. Phys. Chem.*, 1955, **59**, 366.
14. W. M. Anspach and J. A. Marinsky, *J. Phys. Chem.*, 1975, **79**, 433.
15. J. A. Marinsky and W. M. Anspach, *J. Phys. Chem.*, 1975, **79**, 439.
16. J. A. Marinsky, *J. Phys. Chem.*, 1982, **86**, 3318.
17. G. C. Rex and S. Schlick, *J. Phys. Chem.*, 1985, **89**, 3598.
18. P. Mallo, S. Candau and C. Cohen, *Polymer Commun.*, 1985, **26**, 232.
19. J. Ricka and T. Tanaka, *Macromolecules*, 1985, **18**, 83.
20. G. Burrafato, S. Carminati, F. Bonaccorsi and T. P. Lockhart, *Macromolecules*, 1990, **23**, 2402.
21. S. Morohashi, S. Akakabe, T. Isobe and T. Sasakura, *J. Chem. Engng Jpn*, 1990, **23**, 275.
22. S. Sakohara, F. Muramoto and M. Asaeda, *J. Chem. Engng Jpn*, 1990, **23**, 119.
23. S. Candau, M. Leroy, J. P. Brunette, P. Mallo, J. F. Loret and G. Waton, Process for the extraction of cations and application thereof to the treatment of aqueous effluents, U.S. Patent 4,876,036, 1989.
24. C. Schloesser-Becker, PhD. Dissertation Thesis, U.L.P. Strasbourg, 1991.
25. E. H. Rifi, M. J. F. Leroy, J. P. Brunette and C. Schloesser-Becker, *Solvent Extr. Ion Exch.*, 1994, **12**, 1003.
26. H. Yamada and M. Tanaka, *Adv. Inorg. Chem. Radiochem.* 1985, **29**, 143.

Pergamon

0039-9140(95)01494-2

*Talanta*, Vol. 42, No. 6, pp. 817–825, 1995

0039-9140/95 $9.50 + 0.00

# DETERMINATION OF SELENIUM IN FRESHWATERS BY CATHODIC STRIPPING VOLTAMMETRY AFTER UV IRRADIATION

GUNNAR MATTSSON, LEIF NYHOLM,* ÅKE OLIN and ULF ÖRNEMARK

Department of Analytical Chemistry, Institute of Chemistry, Uppsala University, P.O. Box 531, S-751 21 Uppsala, Sweden

(*Received* 23 *September* 1994. *Revised* 2 *December* 1994. *Accepted* 2 *December* 1994)

**Summary**—An analytical method was developed for the determination of total dissolved selenium in fresh waters, using linear sweep cathodic stripping voltammetry (CSV) in combination with UV photolytic digestion. Both the CSV method, based on the electrodeposition and stripping of $Cu_2Se$, and the UV irradiation procedure were investigated in detail. In the presence of dissolved organic substances, as in freshwaters, Se(VI) is reduced to Se(IV) by UV irradiation in 0.1*M* hydrochloric acid. Glucose can be used as the carbon source in samples low in natural dissolved organic carbon (DOC). The photolytic yields of Se(IV) were about 90% in both cases. Five freshwater samples were analysed for total selenium by CSV after UV photolysis, and by hydride generation atomic absorption spectrometry (HG-AAS) after oxidative digestion followed by reduction with hydrochloric acid. The results agreed well and the concentrations were in the range 70–190 ng/l., well above the detection limit of the CSV method at 2 ng/l.

Total selenium concentrations in natural waters are often in the ng/l. or low μg/l. range. A number of analytical methods has been applied to the quantitation of total selenium or Se(IV) in such waters.[1,2] Hydride generation-atomic absorption spectrometry (HG-AAS),[3,4] gas chromatography[5,6] and molecular fluorescence spectrometry,[7] each usually combined with a preconcentration technique, are most frequently employed. These methods are specific to Se(IV).

Electrochemical methods, which also respond to Se(IV) only, are not often resorted to, but differential pulse (DPV) and square-wave cathodic stripping voltammetry (CSV) have been used for the determination of total selenium and/or Se(IV) in fresh-,[8] sea-[9–11] and rainwater.[12–14] Attractive features of the CSV method are its efficient combination of the preconcentration and quantitation steps and the small sample volume needed. However, an accurate direct determination of Se(IV) in natural waters does not seem possible owing to interferences from surface active dissolved organic substances, as observed by Zelic and Branica,[14] and van den Berg and Khan.[10,11] Poor sensitivity and an interfering voltammetric peak were encountered in sea-, estuarine- and rainwater. The CSV technique is better suited for the determination of total selenium, as the interfering organic material is removed when the sample is digested in order to transform selenium bound in organic compounds to inorganic selenium.[3,10] After most wet digestion procedures, the selenium is present predominantly in its hexavalent oxidation state. A succeeding reduction step, usually employing a high concentration of hydrochloric acid,[1] is required. Since high concentrations of chloride at low pH interfere with the CSV method[15] and the margin available for dilution is limited in trace analysis, the common reduction procedures cannot be combined with a subsequent CSV determination. Development of an alternative digestion and reduction method is, therefore, essential for the application of CSV to lake- and riverwater samples.

Measures and Burton[5,16] reported that a reproducible distribution of total selenium between Se(IV) and Se(VI) resulted upon UV irradiation of standard solutions, sea-, estuarine- and riverwater. The samples were buffered with borate at pH 9 and hydrogen peroxide was added before irradiation for 5 hr. On the average, 86% of added Se(VI) or Se(IV) was recovered as Se(IV) with a 1250 W mercury lamp. The recovery was found to increase gradually with pH between 7 and 10 but it was not affected by

*Author to whom correspondence should be addressed.

the water salinity. Batley[17] found 89–98% yields of Se(IV) from Se(VI) added to 0.5*M* NaCl, distilled water or sea-water, buffered at pH 10.5 and deaerated during photolysis. A pH dependence of the fractional conversion to Se(IV) similar to that observed by Measures and Burton was reported. Dissolved oxygen, or addition of hydrogen peroxide or alcohols reduced the yields. Van den Berg *et al.*[10,11] were able to determine total selenium in sea- and estuarine-water by CSV after photolysis for 4 hr with a 1000 W high pressure mercury lamp. Complete recovery of Se(IV) was obtained from 4 n*M* Se(VI) added to sea-water at its natural pH 8, whereas the yield decreased rapidly at pH < 7.5. UV irradiation of the sample at pH ≥ 8 thus eliminates the organic interferents and transforms selenium predominantly to the tetravalent state. A pH ≥ 8 is, however, not suitable for natural freshwaters in general, since precipitation might occur of hydroxides or oxides of iron, manganese and other metal ions released from destructed humic and fulvic acid complexes. These precipitates are very efficient scavengers of Se(IV).[1] Modification of the UV irradiation procedure to make it applicable to acid solutions and compatible with the CSV method is reported here.

Co-electrodeposition in acidic solution of Se(IV) and added $Cu^{2+}$ at a mercury electrode, subsequently giving rise to a copper selenide stripping peak, appears to be the most convenient and reliable way to perform CSV determinations of selenium.[8,10,14,15] The deposition of selenium in the presence of $Cu^{2+}$ can be represented by

$$H_2SeO_3 + 2Cu^{2+} + 4H^+ + 8e^- \rightarrow Cu_2Se + 3H_2O. \quad (1)$$

The accumulated copper selenide is reduced in the stripping reaction

$$Cu_2Se + 2H^+ + 2e^- \rightarrow H_2Se + 2Cu(Hg). \quad (2)$$

Se(IV) can also be accumulated as HgSe,[18] but the $Cu_2Se$ stripping peak yields a lower detection limit, a longer linear calibration curve and is less subject to interference from peak splitting and from metal ions present in the sample.[8,10,14,15]

The influence of organic substances dissolved in freshwater on the CSV voltammograms is described. A methodology is presented for the accurate evaluation of the selenium concentration from linear sweep (LSV) voltammograms recorded in UV irradiated samples. The photolytic digestion method and the voltammetric finish were combined to a procedure which is described together with an application to five freshwater samples.

## EXPERIMENTAL

### *Chemicals*

Standard solutions of Se(IV) and Se(VI) were obtained by dilution of 1 g/l. stock solutions, which had been prepared from an ampoule of selenium dioxide in dilute nitric acid (Merck), and from solid sodium selenate (BDH), respectively. The Se(VI) solutions were standardized against Se(IV) standards by HG-AAS after reduction by hydrochloric acid. Dilute standard solutions contained 0.01–0.02*M* HCl. The water used had been deionized, distilled and further purified in a Milli-Q system (Millipore) to 18MΩcm quality. The mercury and the hydrogen peroxide (30%) were of Suprapur® quality (Merck). The other chemicals were of analytical grade. Deaeration of stripping solutions was performed with nitrogen which had passed through an acidic vanadium(II) scrubber solution in contact with zinc amalgam. Argon (99.998%) was employed for deaeration of solutions prior to some of the photolytic experiments.

### *Equipment*

The home-built UV irradiation apparatus was a modified version of that described by Gustavsson and Hansson.[19] It consisted of a TQ 718 high pressure mercury lamp (Heraeus) inserted into a quartz tube, which was mounted in the centre of a circular rack surrounded by an aluminium cage. The lamp was operated at 600 W. Twelve 60 ml stoppered quartz sample tubes surrounded the lamp symmetrically. Sample solutions were placed at the level of the lamp. To increase the radiative flux into the solutions, the aluminium surfaces facing the quartz tubes had been polished to mirror finish. The apparatus was cooled by a small fan and placed in a fume cupboard to dispose of generated ozone. Less than 1% of the sample volume was generally lost by evaporation during irradiation.

The hanging mercury drop electrode and the purging and stirring facilities employed in the CSV experiments all belonged to a Metrohm 647 VA Stand. To improve the performance of the electrode glass capillary, the tip was occasionally silanized *in situ*, *i.e.* without removing

the mercury from the capillary. After rinsing in dilute nitric acid and water, respectively, the capillary tip was soaked in dry methanol for 10–20 min, followed by rinsing with toluene and silanization with 5% dimethyldichlorosilane in toluene for about 30 min. Finally, the tip was rinsed with toluene, methanol and water, respectively. This treatment is important in order to secure reproducible and smooth backgrounds in the voltammograms. All potentials are given with respect to the Ag|AgCl|(3*M* KCl) reference electrode which was placed in a bridge containing 0.1*M* $HNO_3$. A glassy carbon rod served as the auxiliary electrode.

Linear sweep stripping voltammograms were recorded with a PAR 174A Polarographic Analyzer. Current and potential data were sampled by an IBM personal computer equipped with a data acquisition board (Keithley). The voltammograms were evaluated using a computer program written in the ASYST™ environment. This program allowed background subtraction, noise filtering, integration of peak areas and estimation of peak potentials and currents by fitting a third order polynomial to the data in the vicinity of the peak maximum. Baseline subtraction was carried out by fitting a third order polynomial to the data on each side of the peak. A Metrohm 646 VA Processor in combination with the 647 VA Stand was used to register differential pulse stripping voltammograms.

Selenium determinations by HG-AAS after liquid nitrogen cold trap preconcentration were carried out using the system previously described.[3] Digestions and reductions of Se(VI) to Se(IV) were performed in 250 ml beakers on a hot plate.

Determinations of dissolved organic carbon (DOC) were made with a Shimadzu 5000 TOC analyser at Pharmacia Biotech (Uppsala, Sweden). UV spectra were recorded with a Perkin-Elmer Lambda 17 UV/VIS spectrophotometer.

Quartz tubes, glass vessels and polyethylene bottles were soaked in 7*M* nitric acid and repeatedly rinsed with water before use.

*Water samples*

Water samples were collected in June 1994 as surface water from lakes and streams in the vicinity of Uppsala. The samples were filtered through a 0.45 $\mu$m membrane filter (Millipore), acidified to pH 2 with hydrochloric acid and then stored refrigerated in 2 l. polyethylene bottles. Analyses were completed within 3 weeks of collection.

*Analytical procedure for total selenium*

Approximately 40 ml of sample were weighed into each quartz tube. The solution was made 0.1*M* with respect to hydrochloric acid and 40 $\mu$l of 30% hydrogen peroxide were added. Some of the samples were spiked with 0.2 $\mu$g/l. of Se(VI) and used to determine the recovery of Se(VI) as Se(IV) after photolysis. The solutions were exposed to UV light for 60 min, then glucose (dissolved in 0.01*M* HCl) was added to a concentration of 30 mg/l. in order to establish more reducing conditions. Finally, the samples were irradiated for another 45 min. Note that these times will highly depend on the intensity of the UV lamp and other properties of the photolytic equipment such as the reflectance of the aluminium casing and the positions of the tubes relative to the lamp.

About 20 ml of the digested sample, accurately weighed into the electrode vessel, were deaerated with nitrogen for 6–7 min. Five mercury drops (0.13 $mm^2$ area) were extruded and electrodeposition was performed at −300 mV for 180 sec in stirred solution. After a rest period of 20 sec, a voltammogram was recorded from −300 to −850 mV with a scan rate of 200 mV/sec. A second voltammogram on the same sample was registered in a similar way after the addition of 1 mg/l. of $Cu^{2+}$, and a third after a standard addition of 0.4 $\mu$g/l. of Se(IV). The first voltammogram was used as a background and subtracted from the other two, as discussed in more detail below. The concentration of Se(IV) was evaluated using the LSV peak area and the sensitivity obtained from the increase in peak area between the second and third voltammograms brought about by the standard addition. The total concentration of dissolved selenium in the sample was obtained after correction for dilution and photolytic recovery and subtraction of the blank value. Blank solutions were subjected to the same treatment as sample solutions, except that additional 60 mg/l. of glucose were added prior to the first irradiation period.

*The HG-AAS procedure*

The water samples were digested by the addition of 30–50 mg of potassium permanganate per 100 ml of sample at pH 2.[3] The solution was boiled for 30 min, made 4*M* in hydrochloric acid and kept at boiling temperature for another 60 min in order to reduce Se(VI) to Se(IV). After dilution to 250 ml, Se(IV) was determined by

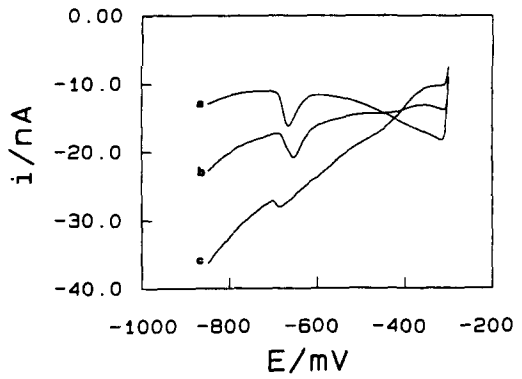


Fig. 1. The effect of dissolved organic substances on the cathodic stripping voltammogram. Dissolved organic matter from a lake water (Lafssjön) was added to a 0.4 μg/l. standard solution of Se(IV), also containing 0.1*M* hydrochloric acid and 1 mg/l. of $Cu^{2+}$. Concentrations of DOC in mg/l.: (a) 0; (b) 0.2; (c) 0.7.

HG-AAS as previously described.[3,4] The selenium concentration was evaluated from a calibration curve using peak heights.

## RESULTS AND DISCUSSION

### *The CSV method*

At the DOC levels of 1–100 mg C/l. normally found in freshwaters,[20] severe interference can be expected in stripping voltammetry.[21,22] The influence of dissolved organic matter on the CSV method was studied by addition of water from a lake (Lafssjön) and a stream (Sävjaån) to standard solutions of Se(IV). The results for the two waters were similar, and some characteristic LSV voltammograms are displayed in Fig. 1. Even DOC concentrations below 0.1 mg C/l. affected the shape of the background. The background current increased with the DOC concentration and the deposition time at potentials more negative than −400 mV. At about 0.5 mg C/l., the shape of the stripping peak also started to change, which caused a decrease in the peak height. At somewhat higher DOC concentrations, the peak became more asymmetric, split or disappeared. Only a very small, scarcely discernible stripping peak situated on a high and sloping background current was obtained from a drinking water sample containing 5–6 mg C/l. and spiked with 0.5 μg/l. of Se(IV). Similar observations were made when the experiments were repeated with DPV as the stripping technique. The change in the background was smaller, whereas the effect of high DOC concentrations on the shape and size of the stripping peak was more pronounced. The DPV peak disappeared almost completely at about 1 mg C/l.

It was found previously that the selenium concentration is best evaluated from the LSV peak area.[15,18] The fact that the LSV peak area was less influenced than the LSV and DPV peak currents by the presence of dissolved organic matter is another reason to use peak area measurements for analytical purposes. However, attempts to determine Se(IV) in freshwaters containing more than about 0.5 mg/l. of DOC are likely to fail. Since the freshwater samples studied contained 3–20 mg C/l. (see Table 1), a direct determination of Se(IV) was precluded. Only total selenium concentrations could thus be determined after destruction of organic material by UV irradiation.

A reliable background subtraction procedure is essential in LSV for accurate evaluation of peak areas and achievement of low detection limits. Most often, background voltammograms are recorded either in pure electrolyte solution or in the sample without a preceding deposition step.[21] Such background curves were, however, found to poorly match stripping voltam-

Table 1. Total dissolved selenium concentrations in fresh water samples determined by CSV and HG-AAS

| | | Total concentration of dissolved Se (*ng/l.*) | | | |
|---|---|---|---|---|---|
| Sample | DOC (*mg/l.*) | Uncorrected | CSV Recovery (%) | Corrected | HG-AAS |
| Blank solution | — | 3 ± 1 | 91 ± 2 | 3 ± 1 | 13 ± 4 |
| Institute drinking water | 3 | 172 ± 2 | 90 ± 4 | 190 ± 10 | 179 ± 9 |
| Ekoln, Skarholmen (lake) | 9 | 115 ± 1 | 86 ± 2 | 133 ± 4 | 118 ± 6 |
| Sävjaån, Falebro (stream) | 12 | 109 ± 1 | 94 ± 6 | 116 ± 8 | 121 ± 5 |
| Trehörningen (lake) | 12 | 70 ± 2 | 91 ± 6 | 77 ± 7 | 74 ± 7 |
| Lafssjön (lake) | 19 | 101 ± 1 | 96 ± 2 | 105 ± 3 | 96 ± 8<br>101 ± 6* |

Each DOC concentration is the mean of two measurements, differing by less than 0.6 mg C/l. Selenium concentrations and recoveries are presented as mean ± SD from three complete analyses.
*Digested with peroxodisulphate.

mograms recorded in incompletely digested water samples or other solutions containing dissolved organic matter. A change in the background current brought about by surface active or reducible substances can, on the other hand, be accounted for by recording stripping voltammograms before and after the addition of $Cu^{2+}$ to the sample. The former voltammogram, containing a fairly low and broad HgSe wave around $-500$ mV, is then subtracted from the latter, which exhibits a $Cu_2Se$ peak at $-660$ mV. By this procedure, demonstrated in Fig. 2, it is possible to check that there are no interfering peaks at the position of the $Cu_2Se$ peak and a blank voltammogram is obtained which will match the background of the $Cu_2Se$ stripping voltammogram well, except in the region of the small HgSe wave. The vertical shift between the two voltammograms seen in Fig. 2(a, b) is caused by the additional current from diffusion limited reduction of $Cu^{2+}$. The procedure was found to work well for the five freshwater samples analysed and no interfering peaks were detected. In fact, the backgrounds in these samples were generally low and smooth, revealing no sign of interference from residual organic substances after digestion.

The Se(IV) concentrations were evaluated by the method of standard additions. One subsample from each water received three consecutive standard additions of Se(IV) to check the linearity of the analytical curve. The plots of peak area *vs.* added Se(IV) concentration all showed good linearity with correlation coefficients $r \geqslant 0.9998$ ($n = 4$). Only one addition was made to the other subsamples, as the precision was satisfactory. The reproducibility of the CSV method was very good considering the concentration level. The within-day relative standard deviation of the sensitivity was 3–4% ($n = 12$), which is only slightly larger than the 2–3% usually encountered from consecutive measurements of the stripping peak area on a standard solution at the 0.1–0.5 $\mu$g/l. level. The sensitivities were not significantly different between the five water samples and between the samples and standard solutions. Therefore, the more convenient evaluation from a calibration curve can be used. This is true only for the peak area, since the peak shape and, hence, the peak current sensitivity varied between samples. Usually, the $Cu_2Se$ stripping peak was somewhat sharper in standard solutions than in digested samples. This indicates that the stripping process was slightly affected by the sample matrix while the efficiency of the deposition process, which is associated with the stripping peak area, was virtually unperturbed.

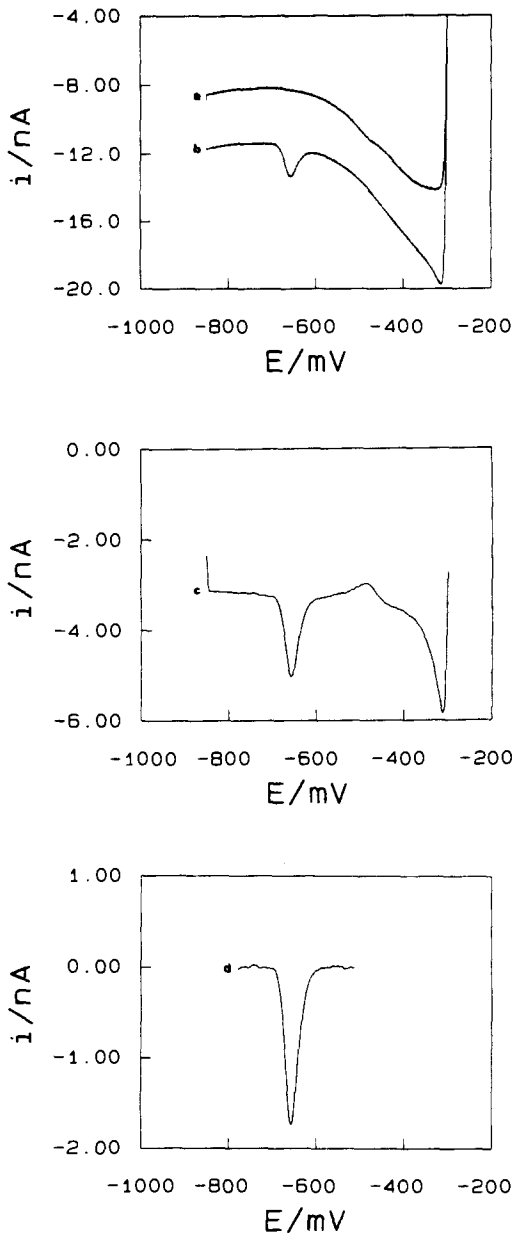


Fig. 2. The evaluation of a representative cathodic stripping voltammogram from a photolysed lake water sample (Lafssjön) containing 0.10 $\mu$g/l. of Se and 0.1*M* hydrochloric acid. (a) Voltammogram recorded in the absence of copper; (b) voltammogram acquired after the addition of 1 mg/l. of $Cu^{2+}$; (c) the resulting background subtracted (b – a) and filtered voltammogram; (d) the $Cu_2Se$ stripping peak at $-660$ mV after subtraction of the fitted baseline. The small negative HgSe wave appearing at $-500$ mV in (a) is reproduced as a positive wave in (c).

The detection limit of the CSV method, using a deposition time of 3 min, has previously been estimated to 2 ng/l. from three times the stan-

dard deviation of the $Cu_2Se$ stripping peak area recorded at 20 ng/l. of Se(IV).[15] In the present work, this low detection limit was further verified by the measurement of the blank level in Table 1.

*UV photolytic experiments*

Irradiation of alkaline standard solutions yielded fractional conversions that agreed with the observations made by Measures and Burton,[5] and by Batley.[17] After irradiation of two freshwater samples (Lafssjön and Sävjaån) for 3 hr at pH 9.8 (0.05*M* $NH_3$ added), the Se(IV) concentrations determined by CSV were, however, not reproducible and ranged from 75 to 100% of the total concentrations of selenium found by HG-AAS after permanganate digestion. These results initiated a study of the photolysis of acidic solutions containing selenium, despite the report of a recovery of only 5% of Se(IV) from sea-water at pH 3.7.[10]

In the presence of 0.1*M* HCl, irradiation of the two freshwater samples yielded fractional conversions to Se(IV) around 90%. The yield was found to be fairly independent of the hydrochloric acid concentration between 0.1 and 0.4*M*. In the presence of 0.3 g/l. of hydrogen peroxide, the recovery decreased to about 70%. The dissolved organic material (about 20 mg C/l.) was sufficiently digested after 1.5 hr also in the absence of hydrogen peroxide. The yellow colour still present after irradiation for 1.5 hr in samples previously deaerated with argon indicated that dissolved oxygen was essential for the photo-oxidation process.

In contrast to the freshwaters, standard solutions of Se(VI) in 0.01–0.4*M* hydrochloric acid yielded low and highly irreproducible recoveries of Se(IV) when irradiated, both in the presence and in the absence of hydrogen peroxide. The recovery was not improved if the solutions were deaerated with argon prior to photolysis. Obviously, some constituent of the freshwater samples facilitated the reduction of Se(VI) to Se(IV). The fairly high content of dissolved organic material suggests that the presence of certain organic substances, or organic material in general, supports the reduction. This hypothesis was tested by addition of various organic compounds to Se(VI) standard solutions prior to photolysis. Among the substances tested, glucose (0.17–0.36 m*M*) and maleic acid (0.25 m*M*) produced the highest yields of Se(IV), in both cases around 90%. With 2 m*M* methanol added alone or together with 0.03 m*M* benzoic acid, 2,5-dihydroxybenzoic acid, gallic acid, hydroquinone, maleic acid, nicotinic acid, phenylalanine, phthalic acid, salicylic acid or tryptophan, yields of 50–80% were obtained. Even though the concentration of the organic additives was rather low, interference in the CSV voltammograms from incompletely digested matter was encountered from most of the aromatic compounds. A few inorganic ions ($Fe^{2+}$, $Br^-$) that might occur in natural waters were also tested, but only negligible concentrations of Se(IV) could be detected after irradiation. No effort was made to optimize the conditions in the screening tests. Thus, higher yields of Se(IV) might have been obtained at other concentrations of the added compound or for other irradiation times.

Glucose was selected for further study as it gave rise to acceptable Se(IV) yields and interference-free solutions after photolysis. Selenium(VI) standard solutions containing glucose at three concentrations were irradiated and the yield of Se(IV) is plotted as a function of irradiation time in Fig. 3. Three time regions can be distinguished in the plots. Initially, the production of Se(IV) is quite fast and the time dependencies for the two lowest concentrations of glucose are similar. The second region is a plateau where the Se(IV) yield is about 90%. The length of this plateau depends on the glucose concentration. Finally, the concentration of Se(IV) drops almost to zero over a short period of time. Solutions from the end of the third region were reduced with 4*M* hydrochloric acid for 1 hr. As virtually all selenium was recovered as Se(IV) after this treatment, it can be concluded that the Se(IV) formed initially must have been re-oxidized to Se(VI). The

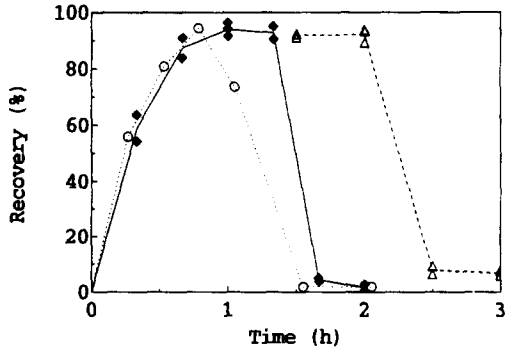


Fig. 3. Recovery of Se(IV) from UV irradiated Se(VI) standard solutions *vs.* irradiation time. The solutions contained 0.4 μg/l. of Se(VI), 0.1*M* hydrochloric acid and glucose/m*M*: (a) 0.056, ○; (b) 0.17, ◆; (c) 0.33, △.

conditions in the solutions apparently change from reducing to oxidizing during the course of the photolysis. Evaluation of the Se(IV) concentrations was not possible at the highest glucose concentration after irradiation times shorter than 1.5 hr owing to serious interferences in the stripping voltammograms. Some change in the shape of the LSV backgrounds was also noted for the lower glucose concentrations at short irradiation times. Since glucose itself does not cause such problems, the interferences must have been brought about by photo-oxidation products of glucose. This conclusion is supported by UV spectra of the irradiated solutions, which showed the generation and disappearance of a broad absorbance band between 210 and 300 nm.

With standard solutions of Se(IV) or Se(VI) containing 0.17 m$M$ glucose, the intermediate concentration in Fig. 3, the following observations were made. The recovery of Se(IV) after 1 hr of irradiation was $92 \pm 1\%$ (mean $\pm$ SD, $n = 4$) for solutions initially containing 0.4 $\mu$g/l. of Se(IV), and $93 \pm 3\%$ ($n = 5$) for solutions of Se(VI). Approximately the same yield was obtained with a 100 times higher concentration of Se(VI), which indicates that the fractional conversion is independent of concentration. Moreover, the yield of Se(IV) did not change for hydrochloric concentrations between 0.1 and 0.4$M$, but decreased somewhat for concentrations below 0.1$M$. In solutions of perchloric and sulphuric acid, on the other hand, the yield of Se(IV) was low. Deaeration with argon before irradiation did not seem to change the recovery, which may imply that dissolved oxygen is not the cause of incomplete conversion.

Hydrogen peroxide may have to be added to samples containing concentrations of DOC higher than about 25 mg C/l. to assist in the photo-oxidation. The effect of hydrogen peroxide on the recoveries is puzzling. A reduction in yield was observed when freshwater samples were irradiated in the presence of hydrogen peroxide, whereas the normal yield of about 90% Se(IV) was obtained from standard solutions containing 0.17 m$M$ glucose. All added hydrogen peroxide is decomposed, as judged from the CSV voltammograms.

A procedure leading to high and equal recoveries irrespective of the initial DOC content of the sample is, of course, desirable. The irradiation scheme finally adopted consists of two steps. In the first step, oxidation of dissolved organic matter is assisted by addition of hydrogen peroxide. With the addition of 0.3 g/l. of hydrogen peroxide, all the freshwater samples in Table 1 were sufficiently digested after 1 hr. DOC was determined in two of the digested water samples (Lafssjön and Sävjaån) and the carbon content was found to be reduced to 10 and 22%, respectively, of the initial concentration. No interference from surface active substances could be detected in the stripping voltammograms and the UV absorbance at 254 nm had decreased to about 3% of its initial value. Hence, an efficient photolytic degradation of the dissolved organic substances, preceding their complete photo-oxidation to carbon dioxide and water, occurs in the first step. Omission of this step or the addition of 60 mg/l. of glucose is recommended for solutions having a very low DOC content, such as blank and standard solutions. Otherwise, $Cl_2$ is likely to form and the conditions during the second step may become too oxidizing. The second irradiation is performed after the addition of 30 mg/l. glucose, which ensures a fractional conversion to Se(IV) of about 90% during a limited period of time. It must be observed that the appropriate lengths of the two steps in the procedure have to be found experimentally for each irradiation apparatus, as the radiative flux experienced by the sample solutions is highly dependent on the lamp and the configuration of the apparatus. Similar yields of Se(IV) were observed with a brand new lamp as with a lamp of the same type that had been operated for several hundred hours, but the irradiation times differed by 30–40%.

The irradiation procedure proposed is empirical and its physico-chemical rationale is unknown. Such knowledge might facilitate further optimization of the method with the objective to achieve 100% yields of Se(IV). An investigation of the wavelength dependence of the fractional conversion and a more extensive screening of photolytic additives beside glucose may be particularly fruitful approaches. The distribution of total selenium between 90% of Se(IV) and 10% of Se(VI) suggests that either a redox equilibrium is set up between the two oxidation states by the redox potential of the solution during irradiation, or a steady state is created by opposing reduction and oxidation reactions. The redox pair Se(VI)/Se(IV) is known to be very sluggish but equilibrium can be mediated by the $Cl_2/Cl^-$ couple. Both selenite and selenate ions absorb light below 230 nm,[23] and directly induced photo-reactions are, thus, poss-

ible and have been studied.[24] On the other hand, various molecules, including reactive radicals, are generated by the photochemical degradation of glucose and natural dissolved organic substances, and some of these might react with Se(IV) or Se(VI). Most of the carbon containing radicals are likely to have reducing properties. The absence of a significant reduction of Se(VI) in deaerated solutions free from organic compounds supports the view that organic radicals are involved. Highly oxidizing chlorine and hydroxyl radicals, which are formed by the action of UV light with wavelengths $<200$ nm,[25] may also be important, especially in the observed reoxidation of Se(IV) after long irradiation times. Perhaps these oxidizing radicals react with the degradation products of glucose and dissolved organic matter until the latter have been totally consumed. Thereafter they start to oxidize Se(IV).

*Determination of total selenium in freshwaters*

Five freshwaters of varying origin were analysed for total dissolved selenium by combining the UV photolysis and CSV procedures outlined above. The waters were also analysed by HG-AAS after permanganate digestion.[3,4] One of the samples (lake Lafssjön) was also digested with peroxodisulphate at pH 2[3] for comparison. The results, including recoveries of added Se(VI) as Se(IV) from the UV irradiation step and the concentrations of DOC, are presented in Table 1. They show reasonably good agreement between the two methods considering the low concentrations involved. The significantly different results for Lake Ekoln may be connected to the somewhat low recovery of added Se(VI) for this sample. The recovery of added Se(VI) as Se(IV) varied between 86 and 96% in the samples. The yields are, thus, similar to the yields of Se(IV) from Se(VI) and Se(IV) standard solutions containing glucose. By analysis of variance, no significant difference at the 95% level was found between the recoveries from the different water samples. Since the chemical constitution of the five water samples, most likely, varied quite a lot, it seems plausible that yields around 90% would be obtained also for other freshwater samples.

A low reagent blank, a low detection limit, fairly good precision and rather simple equipment are the main merits of the UV photolysis-CSV method. Recoveries less than 100% constitute a drawback of the method. Determination of the recovery adds to the analysis time and to the standard deviation of the final result. There is also a risk for an erroneous compensation for incomplete transformation to Se(IV), if added Se(VI) behaves differently than the various selenium species making up the total selenium concentration.

## CONCLUSIONS

Reduction of Se(VI) to Se(IV) by UV irradiation has been demonstrated in acidic solutions containing natural dissolved organic matter or added glucose. The developed irradiation procedure was found to be a digestion method well suited for the CSV determination of total dissolved selenium in fresh waters. Selenium concentrations can be evaluated from a calibration curve if LSV peak areas are measured. Most likely, the irradiation procedure can be adapted to other analytical methods for selenium as an attractive alternative to the more common wet digestion-hydrochloric acid reduction procedures. More detailed investigations are needed to clarify the mechanisms of the photolytic reduction of Se(VI) and to further optimize the irradiation method.

A desirable improvement of the method would be to perform UV irradiation on-line, incorporated in an automated flow system together with the voltammetric cell. Such flow systems, employing quartz coils as photolytic cells, have been constructed and successfully applied to the photo-reduction of nitrate[26] and to the photo-oxidation of dissolved organic matter and Cr(III).[27] Complete destruction of dissolved organic matter was reported to occur within a few minutes, which is a significant reduction in the irradiation time compared to the 1–4 hr normally required for batch-wise digestions.[27]

*Acknowledgements*—The authors greatly appreciate the assistance with computers and ASYST programming given by Alf Eriksson and Rolf Danielsson, and the help on practical matters provided by Lena Hansson and Roland Pettersson. Thanks are also due to Bo-Lennart Johansson for performing the DOC determinations.

## REFERENCES

1. H. Robberecht and R. van Grieken, *Talanta*, 1982, **29**, 823.
2. G. A. Cutter, in *Occurrence and Distribution of Selenium*, M. Ihnat (ed.), Chap. 10. CRC Press, Boca Raton, Florida, 1989.
3. U. Örnemark, J. Pettersson and Å. Olin, *Talanta*, 1992, **39**, 1089.

4. U. Örnemark and Å. Olin, *Talanta*, 1994, **41**, 1675.
5. C. I. Measures and J. D. Burton, *Anal. Chim. Acta*, 1980, **120**, 177.
6. K. Johansson, U. Örnemark and Å. Olin, *Anal. Chim. Acta*, 1993, **274**, 129.
7. D. Wang, G. Alfthan and A. Aro, *Environ. Sci. Technol.*, 1994, **28**, 383.
8. J. H. Lowry, Ph.D. Thesis. University of Michigan, 1978.
9. P. Breyer and B. P. Gilbert, *Anal. Chim. Acta*, 1987, **201**, 33.
10. C. M. G. van den Berg and S. H. Khan, *Anal. Chim. Acta*, 1990, **231**, 221.
11. C. M. G. van den Berg, S. H. Khan, P. J. Daly, J. P. Riley and D. R. Turner, *Estuarine Coastal Shelf Sci.*, 1991, **33**, 309.
12. V. D. Nguyen, P. Valenta and H. W. Nürnberg, *Sci. Total Environ.*, 1979, **12**, 151.
13. L. Vos, Z. Komy, G. Reggers, E. Roekens and R. van Grieken, *Anal. Chim. Acta*, 1986, **184**, 271.
14. M. Zelic and M. Branica, *Electroanalysis*, 1990, **2**, 455.
15. G. Mattsson, L. Nyholm and Å. Olin, *J. Electroanal. Chem.*, 1994, **379**, 49.
16. C. I. Measures and J. D. Burton, *Earth Planet. Sci. Lett.*, 1980, **46**, 385.
17. G. E. Batley, *Anal. Chim. Acta*, 1986, **187**, 109.
18. G. Mattsson, L. Nyholm and Å. Olin, *J. Electroanal. Chem.*, 1994, **377**, 149.
19. I. Gustavsson and L. Hansson, *Int. J. Environ. Anal. Chem.*, 1984, **17**, 57.
20. J. Buffle, *Complexation Reactions in Aquatic Systems*, Chaps 2–3. Ellis Horwood, Chichester, 1988.
21. J. Wang, *Stripping Analysis*. VCH, Deerfield Beach, 1985.
22. G. Scarano and E. Bramanti, *Anal. Chim. Acta*, 1993, **277**, 137.
23. A. Treinin and J. Wilf, *J. Phys. Chem.*, 1970, **74**, 4131.
24. *Gmelin Handbook of Inorganic Chemistry*, No. 10 (Se), B1, pp. 213, 280–281. Springer, Berlin, 1981.
25. J. G. Calvert and J. N. Pitts, *Photochemistry*. John Wiley, New York, 1966.
26. K. Takeda and K. Fujiwara, *Anal. Chim. Acta*, 1993, **276**, 25.
27. E. P. Achterberg and C. M. G. van den Berg, *Anal. Chim. Acta*, 1994, **291**, 213.

Pergamon

0039-9140(95)01495-0

*Talanta*, Vol. 42, No. 6, pp. 827–836, 1995

0039-9140/95 $9.50 + 0.00

# SIMULTANEOUS DETERMINATION OF EQUIVALENCE VOLUMES AND ACID DISSOCIATION CONSTANTS FROM POTENTIOMETRIC TITRATION DATA

G. PAPANASTASIOU* and I. ZIOGAS

Laboratory of Physical Chemistry, Department of Chemistry, Faculty of Sciences, Aristotle University of Thessaloniki, 540 06 Thessaloniki, Greece

(*Received* 7 *September* 1994. *Revised* 22 *November* 1994. *Accepted* 2 *December* 1994)

**Summary**—New iterative methods for analysis of potentiometric titration data of (a) mixtures of weak monoprotic acids with their conjugate bases, (b) solutions of polyprotic (di- and triprotic) acids, and (c) mixtures of two diprotic acids are presented. These methods, using data exclusively resulting from the acidic region of the titration curve permits the accurate determination of the analytical concentration of one or more acids even if the titration is stopped well before the end point of the titration. For the titration of a solution containing a conjugate acid/base pair, the proposed procedure enables the extraction of the initial composition of the mixture, as well as the dissociation constant of the concerned acid. Thus, it is possible by this type of analysis to distinguish whether a weak acid has been contaminated by a strong base and define the extent of the contamination. On the other hand, for the titration of polyprotic acids, the proposed approach enables the extraction of the accurate values of the equivalence volume and the dissociation constants $K_i$ even when the ionization stages overlap. Finally, for the titration of a mixture of two diprotic acids the proposed procedure enables the determination of the composition of the mixture even if the sum of the concentrations of the acids is not known. This method can be used in the analysis of solutions containing two diastereoisomeric forms of a weak diprotic acid. The test of the proposed procedures by means of ideal and Monte Carlo simulated data revealed that these methods are fairly applicable even when the titration data are considerably obscured by 'noise' or contain an important systematic error. The proposed procedures were also successfully applied to experimental titration data.

In a recent paper,[1] we developed new iterative methods for the analysis of potentiometric titrations data of weak monoprotic acids or of mixtures of monoprotic acids. By using these methods it is possible to extract the accurate values of the equivalence volume and simultaneously the acid dissociation constants. These methods are valid even when the titrations are carried out under conditions of varying ionic strength, but there is no reason why the analysis could not be done under conditions of constant ionic strength. Hence the addition of a neutral salt to the titrated solution to keep the ionic strength constant is not necessary. Therefore, the p$K$ values obtained in media of low ionic strength ($I < 0.1M$) are free of any possible 'salt effect'. On the other hand, it has been argued in literature that in media of high ionic strength, even in the absence of a 'salt effect', the theoretical prediction of the activities of the various ionic species become inaccurate; the higher the ionic strength at which measurements are made the more serious the difficulties in obtaining the dissociation constant become.[2]

In this paper, the logic of the above mentioned approaches has been extended to other more complicated titrations. Thus, we have obtained theory and methods for analysis of potentiometric titration data of (a) mixtures of weak acids with their conjugate bases (buffer solutions), (b) solutions of polyprotic (di- and triprotic) acids with overlapping ionization steps, and (c) mixtures of two diprotic acids. In the first case our analysis permits to define the 'prehistory' of the neutralization of the concerned acid and simultaneously to extract its dissociation constant. Therefore, this method is suitable to distinguish if a certain weak acid has been contaminated by a strong base and determine the extent of this contamination.

Over the years, a variety of solutions has been suggested for the analysis of potentiometric

*Author to whom correspondence should be addressed.

titration curves of polyprotic (mainly diprotic) acids or of mixtures of acids with weak bases.[3-9] However, most of these methods are valid under conditions of constant ionic strength or require prior knowledge of accurate values of the dissociation constants of the acids, these constants being determined by a separate titration. To our knowledge, methods for analysing titrations of triprotic acids with overlapping successive ionization steps (without prior knowledge of the $pK_i$ values) are not yet reported in the literature.

With our methods and accurate data it is possible to determine precise concentrations from the buffer region of the titration curve. Therefore, the accurate determination of the analytical concentration of one or more acids is possible even if the titration is stopped well before the complete neutralization of the solution. In addition the suggested methodology enables the determination of the corresponding $pK$ from the same experimental data and only in the case of the titration of a mixture of two diprotic acids the proposed method requires prior knowledge of the values of the corresponding dissociation constants.

It should be noted that the determination of the accurate $pK$'s values, apart from its theoretical significance, is of major analytical interest. Indeed, $pK$ being independent of the concentration could be considered as the 'fingerprint' of the titrated acid. So, from the comparison of the determined $pK$ values with tabulated ones it is possible to identify the titrated acid. It is evident that, the determination of the dissociation constants, especially of the polyprotic acids, require laborious calculations. However, with the opportunities offered today by high-speed personal computers, all the proposed methods can be easily carried out in a time interval from a few seconds to a few minutes.

## EXPERIMENTAL

The potentiometric titrations were carried out as described previously.[1] Conductivity water (conductance = $1.0 \times 10^{-6}\ \Omega^{-1}\ cm^{-1}$) was used throughout. Analytical reagent grade acids (Fluka, puriss p.a. >99.5%) were used without further purification; their purity was checked by potentiometric titrations. All sodium hydroxide solutions were prepared from stock solutions of known concentration (Merck, Titrisol).

## POTENTIOMETRIC TITRATION OF A SOLUTION CONTAINING A CONJUGATE ACID–BASE PAIR

### *Theoretical*

Consider a volume $V_0$ of a solution containing a conjugate acid–base pair, where the initial analytical concentrations (*i.e.* the total concentrations irrespective of form) of the weak acid HA and its conjugate base are respectively equal to $C_0$ and $C_b^0$. This mixture can be considered as being prepared by partial neutralization of a solution of the acid HA, of concentration $C_0'$ and volume $V_0 - Z$, with $Z$ ml of a solution of a strong base MOH of concentration $C_B$. At any point of the titration curve the mass and charge balance is expressed by the equations:

$$[A^-] + [OH^-] = [M^+] + [H^+] \quad (1)$$

$$T_L = [HA] + [A^-], \quad (2)$$

where

$$[M^+] = \frac{C_B \cdot V}{V_0 + V} + \frac{C_b^0 V_0}{V_0 + V} = b_N C_B (Z + V) \quad (3)$$

$$T_L = \frac{T_L^0 V_0}{V_0 + V} = \frac{(Z + V_e) C_B}{V_0 + V} = b_N C_B (Z + V_e) \quad (4)$$

$$C_b = \frac{C_b^0 V_0}{V_0 + V} = \frac{Z C_B}{V_0 + V} = b_N Z C_B, \quad (5)$$

where $V$ is the volume of the added titrant and $b_N = 1/(V_0 + V)$.

Assuming that all singly charged ions ($z_i = 1$) have the same activity coefficient $y_i$ and that the activity coefficients of uncharged species are unity, the acid constant of HA is given by

$$K_a = \frac{\alpha_H \cdot [A^-] \cdot y_i}{[HA]}, \quad (6)$$

$\alpha_H$ being the hydrogen ion activity.

Combining the above equations and rearranging gives

$$y = V_e - \frac{1}{K_a} x, \quad (7)$$

where

$$y = V + \frac{1}{y_i C_B b_N} \left\{ \alpha_H - \frac{K_w}{\alpha_H} \right\} \quad (8)$$

and

$$x = \alpha_H \left( y_i (V + Z) + \frac{\alpha_H}{C_B b_N} - \frac{K_w}{\alpha_H C_B b_N} \right), \quad (9)$$

where $K_w$ is the autoprotolysis constant of the solvent used. For dilute solutions ($I < 0.1M$) the

activity coefficient $y_i$ can be calculated from the Debye–Hückel equation:

$$\log y_i = -\frac{Az_i^2\sqrt{I}}{1 + B\mathring{a}\sqrt{I}}, \quad (10)$$

where $A$ and $B$ are constants, the values of which depend on the physical properties of the medium, [10] $I$ is the ionic strength of the solution, $z_i$ the charge number and $\mathring{a}$ the distance of closest approach of the ions. In principle $\mathring{a}$ is a function of the solvent and electrolyte, but in practice it is traditionally taken to be equal to 5 Å.[11–13] The ionic strength, at any point of the titration curve, is given by:[14,15]

$$I = [M^+] + [H^+] = b_N C_B(Z + V) + [H^+]. \quad (11)$$

To determine $y_i$, it is obviously necessary to know the value of $[H^+] = \alpha_H/y_i$ and vice versa. It is noted that when the electrode system is standardized against the aqueous buffer solutions recommended by the National Bureau of Standards, the measured pH value of a solution is identified very closely with the conventional value of $-\log \alpha_H$ (where $\alpha_H$ is the corresponding hydrogen ion activity). The values of $[H^+]$ and $y_i$ may be obtained from the measured value of $\alpha_H$ by successive approximations.[1,14] Assuming first $y_i = 1$, so that $\alpha_H = [H^+]$, it is possible to calculate $I$ from eqn (11), and hence $y_i$ from eqn (10). This new value of $y_i$ can be used to refine the values of $[H^+]$, $I$ and $y_i$. All these operations are repeated until $y_i$ converges (the criterion here being less than 0.00001 difference in $I$, between two subsequent cycles).

Equation (7) predicts a linear relationship between $y$ and $x$ with a slope equal to $1/K_a$. Alternatively, the experimental confirmation of such a correlation, using $V$ and pH data, supports the assumption that the titrated solution is a mixture of a monoprotic acid with its conjugate base. Then, $V_e$ and the acidity constant $K_a$ can be deduced, by linear regression, from the coefficients of eqn (7). This procedure can be realized by the presently proposed iterative method, which is analogous with previously proposed techniques for the determination of rate constants of various chemical and electrochemical reactions.[16–20]

*Iterative method for the determination of $Z$, $V_e$ and $K_a$*

It is assumed first that the value of $Z$ lies on an interval (a, b). Choosing arbitrarily from this interval a value for $Z$, it is possible to trace, by means of the experimental $V$ and pH data, the curve $y = f(x)$. This curve will approach a straight line to the extent where the chosen value of $Z$ also approaches the exact value of this parameter. Hence, the best linearity that could be obtained, by means of the available experimental data, evidently corresponds to the best approximation to the exact value of $Z$. Therefore, by seeking the $Z$ value within the interval (a, b), it is possible to trace $N$ curves $y = f(x)$, $N$ being the number of $Z$ values taken for these calculations. For each of these curves, the calculation of $R^2$ (square of the correlation coefficient) and $S_{y/x}$ (standard error of the estimate)[1,21] permits a comparison of the linearity of various $y = f(x)$ plots and trace the curves $R^2 = f(Z)$ or $S_{y/x} = f(Z)$. These curves must present respectively a maximum and minimum at a value of $Z$ equal to $Z_m$, which can be considered as the best approximation to the exact value of $Z$. The exact values of $V_e$ and $K_a$ can be deduced respectively from the $y$-intercept and the slope of the corresponding to $Z_m$ straight line.

*Application of the iterative method for the determination of $Z$, $V_e$ and $K_a$ using simulated and experimental data*

*Simulated data.* To establish the reliability of the proposed procedure, first it must be shown that it actually works by comparison to a system where the answer is already known. Experimentally, this implies that the proposed approach, applied to a previously reported system, gives a reasonable (or even better) precision on the extraction of the sought parameters. In this respect, it was considered necessary to test the proposed methods, first with simulated data corresponding to various values of $pK_a$, $Z$ and $V_e$ and second to experimental data resulting from titrations of mixtures of weak acids (of known $pK_a$) with their conjugate bases.

Simulated $V$ and pH ($pH = -\log \alpha_H$) data have been derived by solving eqn (7) using the so-called secant methods.[22] In all these calculations we assumed that $V_0 = 50$, $C_B = 0.1$ M, $V_e = 4.00$ ml ($C_0 = 0.008M$), $Z = 1.00$ ml ($C_b^0 = 0.002M$), $T = 298.15$ K and $pK_w = 14.0$. First, the titration of an acid with $pK_a = 4.80$ was considered. This value represents the mean $pK_a$ value of the lower members of the aliphatic series of monocarboxylic acids.[10,11] The results obtained are reported in Table 1. Taking into account that the NBS buffer solutions used for the standardization of the pH-meters are given at most to three decimal figures, the simulated

Table 1. Ideal and Monte Carlo (M-C) pH values of the titration of a conjugate acid–base pair with a strong base

| | pH | | | pH | | | pH | |
|---|---|---|---|---|---|---|---|---|
| $V$ | Ideal* | M-C† | $V$ | Ideal* | M-C† | $V$ | Ideal* | M-C† |
| 0.0 | 4.194 | 4.188 | 1.1 | 4.635 | 4.631 | 2.2 | 5.017 | 5.013 |
| 0.1 | 4.243 | 4.250 | 1.2 | 4.669 | 4.669 | 2.3 | 5.054 | 5.051 |
| 0.2 | 4.289 | 4.293 | 1.3 | 4.703 | 4.705 | 2.4 | 5.093 | 5.091 |
| 0.3 | 4.333 | 4.329 | 1.4 | 4.737 | 4.749 | 2.5 | 5.133 | 5.120 |
| 0.4 | 4.375 | 4.375 | 1.5 | 4.771 | 4.766 | 2.6 | 5.175 | 5.177 |
| 0.5 | 4.415 | 4.426 | 1.6 | 4.805 | 4.800 | 2.7 | 5.218 | 5.223 |
| 0.6 | 4.454 | 4.452 | 1.7 | 4.840 | 4.839 | 2.8 | 5.264 | 5.269 |
| 0.7 | 4.492 | 4.488 | 1.8 | 4.874 | 4.871 | 2.9 | 5.313 | 5.307 |
| 0.8 | 4.528 | 4.524 | 1.9 | 4.909 | 4.904 | 3.0 | 5.365 | 5.365 |
| 0.9 | 4.564 | 4.566 | 2.0 | 4.944 | 4.941 | | | |
| 1.0 | 4.600 | | 2.1 | 4.980 | 4.978 | | | |

$V_0 = 50$, $C_B = 0.1M$, $V_e = 4.00$ ml ($C_0 = 0.008M$), $Z = 1.00$ ml ($C_b^0 = 0.002M$), $T = 298.15$ K, $pK_a = 4.80$ and $pK_w = 14.0$.

*Values that exactly fit equation (7).

†Mean values of six normally distributed deviates generated from the ideal data with standard deviation equal to 0.01 pH unit.

pH values were rounded to three decimal places. It is now examined whether it is possible, using these data and by means of the proposed method, to extract the values $pK_a = 4.80$, $V_e = 4.00$ ml ($C_0 = 0.008M$) and $Z = 1.00$ ml ($C_b^0 = 0.002M$).

The variations of $R^2$ and $S_{yx}$ with $Z$ are presented graphically in Fig. 1. It can be seen that these curves pass through a maximum and minimum, respectively, corresponding to $Z = 1.00$ ml. Furthermore, in the vicinity of the maximum ($4.9 \leqslant Z \leqslant 5.1$), it was found that the curve $R^2 = f(Z)$ can be perfectly fitted, by a least squares analysis, to the following polynomial (the squared correlation coefficient was very close to unity):

$$R^2 = \sum_{n=0}^{4} A_n Z^n = 0.1082 + 2.9761Z - 3.7216Z^2 + 2.0820Z^3 - 0.4447Z^4. \quad (12)$$

Consequently, the exact value of $Z$ at which $R^2$ reaches a maximum value can be determined from the solution of the following equation:

$$\frac{dR^2}{dZ} = \sum_{n=0}^{4} nA_n Z^{n-1} = A_1 + 2A_2 Z + 3A_3 Z^2 + 4A_4 Z^3 = 0. \quad (13)$$

From eqn (13) one obtains $Z_m = 1.00$ ml. Using this value, the following relationship was found:

$$y = 4.000 - 63091.16x. \quad (14)$$

Comparison of this equation with eqn (7) leads to the values: $V_e = 4.00$ and $pK_a = 4.80$.

In an attempt to generalize the conclusions concerning the applicability of the proposed method, this procedure was also applied to various simulated titration curves corresponding to different $pK_a$ ($3.0 \leqslant pK_a \leqslant 6.5$) and $Z$ values ($0.5 \leqslant Z \leqslant 2.5$). The obtained results showed that the proposed method reaches the desired values of $Z$, $V_e$ and $pK_a$ with a fair accuracy.

The examples studied previously showed that the proposed procedures are able to extract $V_e$ and $pK_a$ values in the particular case where the $V$ and pH data used, resulting from the buffer region of a titration curve, are free of experimental errors.

However, of more experimental interest is the question of how well the new techniques are able to cope with data containing random extraneous contributions, such as annoying

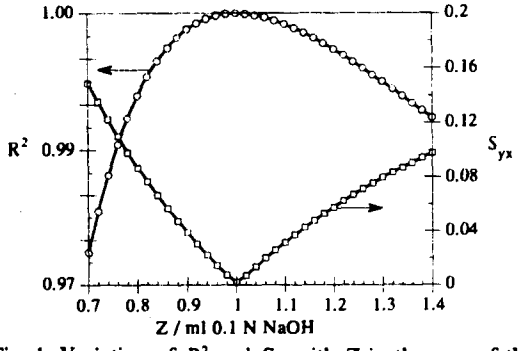


Fig. 1. Variation of $R^2$ and $S_{yx}$ with $Z$ in the case of the simulated titration of 50 ml of a conjugate acid–base pair [$C_0 = 0.008M$ ($V_e = 4.0$ ml), $C_b^0 = 0.002M$ ($Z = 1.00$ ml), $pK_a = 4.80$] with $0.1M$ NaOH at 25°C.

experimental 'noise'. To investigate this, a Monte Carlo technique was used, which has been detailed in a previous paper[18] and need not be repeated here. The main idea of this procedure is based on the observation that, often, random experimental errors closely follow a Gaussian (or normal) distribution. Thus, at each point ($V_i$ and $pH_i$) of the theoretical titration curve $pH = f(V)$, we produced a number $N$ of normally distributed random variables $pH_{i,j}$ with mean $pH_i$ and standard deviation $S_i$. In the experimental level, this implies the realization of N titrations with a precision equal to $S_i$. Using this technique, we treated again, as an example, the titration of an acid with $pK_a = 4.80$. In this treatment we assumed that $S_i$ is equal to 0.01 pH unit. At each volume $V_i$, we created six values of $pH_{i,j}$ and the results were averaged. The mean values $\overline{pH}_{i,j}$ are summarized in Table 1. Evidently, these values would coincide with the corresponding $pH_i$ ones only in the case where the number $N$ of the produced random variables $pH_{i,j}$ tends to infinity. Using these Monte Carlo data $\overline{pH}_{i,j}$, the proposed method gives the values $Z = 1.006$ ml, $V_e = 4.005$ ml and $pK_a = 4.799$. These results are respectively within 0.6, 0.12 and 0.03% ($\delta pK_a = 0.001$) of their true magnitudes. Evidently the proposed techniques are able to extract $Z$, $V_e$ and $pK_a$ values, even when the pH data are obscured by noise.

Finally, the proposed methods were applied to various simulated titration curves, corresponding to different $pK_a$ values, where the pH data contained a systematic error equal to 0.01 pH unit (about 5–10 times greater than the accuracy of a precision instrument). Experimentally such errors are usually introduced by an erroneous standardization of the pH-meter assembly. A systematic error in the pH values gives rise to systematic titration errors $\delta Z$, $\delta V_e$ and $\delta pK_a$ in the values of $Z$, $V_e$ and $pK_a$.

In all instances examined here ($Z = 1$ and $3.5 < pK_a < 6.5$), it was found that the titration errors $\delta Z$, $\delta V_e$ and $\delta pK_a$, at constant $\delta pH$, are dependent upon the strength of the acid that is being titrated. These errors decrease as $pK_a$ increases. For moderately strong acids (with $pK_a < 3.8$) $\delta V_e$ is less than 0.2%, $\delta pK_a < 0.008$ and only $\delta Z$ takes values greater than 1.0%. On the contrary, for acids with $pK_a \approx 4.8$ (such as the lower members of the aliphatic series of monocarboxylic acids) $\delta Z$ takes values less than 0.2%. For such acids the proposed techniques are able to extract the values $Z$, $V_e$ and $pK_a$ with only a modest error ($\delta Z \approx 0.14\%$, $\delta V_e \approx 0.00\%$ and $\delta pK_a \approx 0.01$), even when the pH data contain a systematic error $\delta pH = 0.01$.

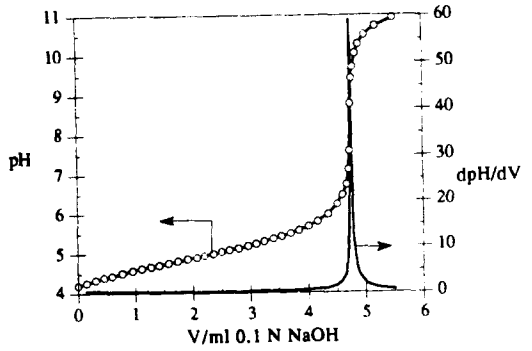


Fig. 2. Titration and differential titration of 50 ml of a mixture of propionic acid ($C_0 = 0.0095M$) with sodium propionate ($C_b^0 = 0.002M$, $Z = 1.00$ ml) with $0.1M$ NaOH at 25°C.

It is noted that in all calculations an unweighted least squares method has been used. However, in some selected examples, the data have been also analysed by means of a weighted least squares method reported in literature.[23] No significant differences have been found.

*Experimental data.* In the attempt to test this methodology on experimental data, a solution was prepared by mixing 5 ml of $0.1151M$ propionic acid with 1 ml of $0.1M$ NaOH and diluting with water until the final volume of 50 ml ($V_0 = 50$ ml, $C_0 = 0.0095M$, $Z = 1$, $C_b^0 = 0.002M$). This solution was titrated with $0.1M$ NaOH. The titration curve presents a pronounced inflection at $V \approx 4.75$ ml. (Fig. 2) The obtained measurements, lying in the 0 to 75% neutralization range of the corresponding titration curve, are given in Table 2. The plots of $R^2 = f(Z)$ and $S_{yx} = f(Z)$ present a maximum and a minimum, respectively, at a value of $Z$, equal to $Z_m$, lying in the vicinity of $Z = 1$ (Fig. 3). The exact value of $Z_m$ has been found

Table 2. Experimental titration of a mixture of propionic acid ($C_0 = 0.0095M$) with sodium propionate ($C_b^0 = 0.002M$, $Z = 1.00$ ml) with $0.1M$ NaOH at 25°C

| $V$ | pH | $V$ | pH |
|---|---|---|---|
| 0.00 | 4.200 | 1.58 | 4.760 |
| 0.15 | 4.266 | 1.74 | 4.807 |
| 0.31 | 4.335 | 1.91 | 4.856 |
| 0.46 | 4.395 | 2.07 | 4.904 |
| 0.60 | 4.445 | 2.20 | 4.943 |
| 0.78 | 4.510 | 2.36 | 4.991 |
| 0.96 | 4.569 | 2.50 | 5.035 |
| 1.12 | 4.620 | 2.64 | 5.080 |
| 1.28 | 4.671 | 2.80 | 5.132 |
| 1.42 | 4.713 | 2.96 | 5.188 |

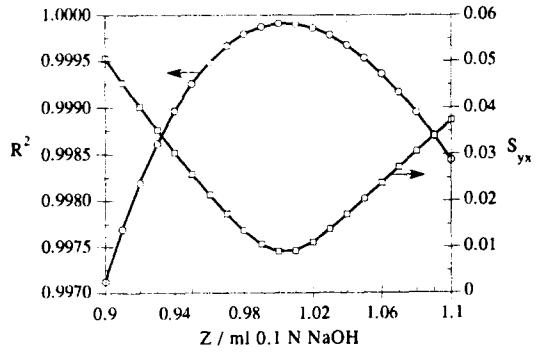


Fig. 3. Variation of $R^2$ and $S_{y.x}$ with $Z$ in the case of the titration of 50 ml of a mixture of propionic acid ($C_0 = 0.0095M$) with sodium propionate ($C_b^0 = 0.002M$, $Z = 1.00$ ml) with $0.1M$ NaOH at 25°C.

equal to 1.004 ml by seeking within the intervals (0.90, 1.10) and (1.000, 1.010) the $Z$ value successively. Furthermore, for $0.90 \leqslant Z \leqslant 1.10$ it was found that the curve $R^2 = f(Z)$ can be perfectly fitted, by least squares, to the following polynomial (where the squared correlation coefficients were very close to unity):

$$R^2 = \sum_{n=0}^{5} A_n Z^n = 0.2778 + 1.9511Z - 1.7374Z^2 - 0.5084Z^3. \quad (15)$$

By combining this equation with eqn (13), one again obtains the root $Z_m = 1.0035 \approx 1.004$ ml ($C_b^0 = 0.00201M$). From the coefficients of the linear regression equation $y = f(x)$ corresponding to this value of $Z$ we obtain $V_e = 4.751$ ml ($C_0 = 0.00950M$) and $pK_a = 4.878$. These values are in excellent agreement with the expected values of the above parameters. It is noted that the p$K$ value of propionic acid, reported in literature, is equal to 4.874 at 25°C.[10,11]

## POTENTIOMETRIC TITRATION OF WEAK POLYPROTIC ACIDS WITH STRONG BASES

Consider a solution of a molecular polyprotic acid $H_nA$ with overlapping ionization steps. A volume $V_0$ of this solution of initial analytical concentration $C_0$ is titrated with a solution of a strong base MOH of concentration $C_B$. The titration is assumed to be carried out in the acidic range. In this range, the analysis of the titration curve leads to the following equation:[24]

$$\hat{h} = \frac{\dfrac{K_1}{\alpha_H y_1} + \dfrac{2K_1K_2}{\alpha_H^2 y_2} + \cdots + \dfrac{nK_1K_2 \ldots K_n}{\alpha_H^n y_n}}{1 + \dfrac{K_1}{\alpha_H y_1} + \dfrac{K_1K_2}{\alpha_H^2 y_2} + \cdots + \dfrac{K_1K_2 \ldots K_n}{\alpha_H^n y_n}}, \quad (16)$$

with

$$\hat{h} = \frac{[M^+] + [H^+] - [OH^-]}{C} \quad (17)$$

and

$$C = \frac{C_0 V_0}{V_0 + V} = b_N C_0 V_0 = \frac{1}{n} b_N C_B V_e, \quad (18)$$

where $y_i$ denotes the activity coefficient of the species $H_{n-i}A^{i-}$ ($i = 0,1,2 \ldots n$) and $K_i$ the dissociation constant of the corresponding ionization step:

$$H_{n-(i-1)}A^{(i-1)-} \rightleftarrows H_{n-i}A^{i-} + H^+. \quad (19)$$

For diprotic acids, assuming that $y_0 = 1$, a combination of eqns (16)–(18) gives:

$$y = -K_1 + K_1K_2x, \quad (20)$$

with

$$y = \frac{Z}{X} \quad \text{and} \quad x = \frac{Y}{X} \quad (21)$$

and

$$X = \frac{y_2\left\{b_N C_b\left(V - \dfrac{V_e}{2}\right)y_1 + \alpha_H - \dfrac{K_w}{\alpha_H}\right\}\alpha_H}{y_1} \quad (22)$$

and

$$Y = b_N C_b (V_e - V) y_1 + \frac{K_w}{\alpha_H} - \alpha_H \quad (23)$$

$$Z = \left(b_N C_b V y_1 + \alpha_H - \frac{K_w}{\alpha_H}\right)\alpha_H^2 y_2. \quad (24)$$

For dilute solutions ($I < 0.1M$), the activity coefficient $y_1$ and $y_2$ can be determined from eqn (10), with the ionic strength $I$ of the solution from the appropriate formula.[15]

The determination of $V_e$, $K_1$ and $K_2$ from eqn (20), using $V$ and pH data, is possible with the iterative method proposed here. It is assumed first that the value of $V_e$ lies on an interval (a, b). Choosing arbitrarily from this interval a value for $V_e$, calculation of $y_1$ and $y_2$, at any point of the titration curve, requires knowledge of the corresponding value of $I$. On the other hand, $I$ is a function of $K_1$, $K_2$, $y_1$ and $y_2$. So, determination of $y_1$ and $y_2$ requires prior knowledge of $y_1$ and $y_2$. It appears that these calculations constitute a typical case of a vicious circle. However, calculation of $y_1$ and $y_2$ may be obtained by successive approximations. Assuming first that $y_1$, $y_2 = 1$, it is possible to determine from the coefficients of eqn (20), by means of the experimental $V$ and pH data, approximate values (apparent constants) of $K_1$, $K_2$.

Starting from these values and assuming

again that $y_1$, $y_2 = 1$, so that $\alpha_H = [H^+]$, it is possible to calculate $I$ at any chosen point of the titration curve, and hence $y_1$ and $y_2$ from eqn (10). These new values of $y_1$ and $y_2$ can be used to refine values of $I$ and repeat until it converges (the criterion being less than 0.00001 difference in $I$, between two subsequent cycles). By repeating these approximations at each point of the titration curve, it is possible to trace the curve $y = f(x)$ and determine by least squares the values of $K_1$ and $K_2$. These new values can be used to refine the values of $K_1$ and $K_2$ and repeat until they converge (the criterion being less than 0.0001 difference in $pK_1$ and $pK_2$ values, between two subsequent cycles). The final curve $y = f(x)$ obtained, by means of these approximation, will approach a straight line to the extent the chosen value of $V_e$ also approaches the exact value of this parameter. Hence, the best linearity that could be obtained, by means of the available experimental data, evidently corresponds to the best approximation to the exact value of the equivalence volume. Therefore, by seeking within the interval (a, b) the $V_e$ value, it is possible to trace $N$ curves $y = f(x)$, $N$ being the number of $V_e$ values taken for these calculations. For each of these curves, the calculation of $R^2$ and $S_{yx}$ permits the comparison of the adequacy of the fit of eqn (20) to the experimental $V$ and pH data. At the true value of $V_e$, these statistics may reach a maximum and minimum value respectively. Then, the exact values of $K_1$ and $K_2$ can be deduced respectively from the coefficients of the corresponding straight line.

An analogous procedure can be used in order to analyse the titration curves of triprotic acids. Assuming again that $y_0 = 1$, a combination of eqns (16)–(18) gives:

$$Y = K_1 + K_1K_2X_1 + K_1K_2K_3X_2, \qquad (25)$$

with

$$Y = \left(\frac{\hat{h}}{1-\hat{h}}\right)\alpha_H y_1,$$

$$X_1 = \left(\frac{2-\hat{h}}{1-\hat{h}}\right)\frac{y_1}{\alpha_H y_2}$$

and

$$X_2 = \left(\frac{3-\hat{h}}{1-\hat{h}}\right)\frac{y_1}{\alpha_H^2 y_3}. \qquad (26)$$

As in the case of diprotic acids, the activity coefficients $y_1$, $y_2$ and $y_3$ introduced in the above relationships can be determined from eqn (10), with the ionic strength $I$ of the solution from the appropriate formula.[26,27] The coefficients $y_1$, $y_2$ and $y_3$ can be calculated by successive approximations as in the case of diprotic acids.

Equation (25) predicts that the relationship $Y = f(X_1, X_2)$ is linear. The determination of $V_e$, $K_1$, $K_2$ and $K_3$ from this equation, using $V$ and pH data, is possible with the iterative method proposed here. As previously, we assume that $V_e$ lies in an interval (a, b). By seeking within this interval the $V_e$ value, it is possible to obtain $N$ relationships $Y = f(X_1, X_2)$, $N$ being the number of $V_e$ values taken for these calculations. For each of these relationships, the calculation of $R^2$ and $S_{yx}$ permits the comparison of the adequacy of the fit of eqn (25) to the experimental $V$ and pH data. At the true value of $V_e$, these statistics may reach a maximum and minimum value, respectively. Then, the exact values of $K_1$, $K_2$ and $K_3$ can be deduced, respectively, from the coefficients of the corresponding multiple linear regression equation.

The proposed procedures were applied to various simulated titration curves corresponding to different $pK_i$ and $V_e$ values of diprotic or triprotic acids. The obtained results showed that the proposed methods reach the desired values of the above parameters with a fair accuracy even when the data are considerably obscured by extraneous 'noise' or contain an important systematic error. For polyprotic acids and $pK_1 > 2.9$, the proposed techniques lead to the exact value of $V_e$ even when the pH data contain an important systematic error $\delta pH = 0.02$. For these acids a rough calibration of the electrode system is sufficient in order to extract the accurate value of the acid concentration.

The proposed methods were also applied on experimental data. Thus, in the titration of a diprotic acid, a solution of 0.00988$M$ succinic acid ($pK_1 = 4.209$, $pK_2 = 5.638$ at 25°C[11,25]) was prepared. A volume of 50 ml of this solution was titrated with 0.2$M$ NaOH. It was found that the graph $S_{yx}$ *vs.* $V_e$ presents a pronounced minimum (Fig. 4). In the vicinity of the minimum ($4.92 \leqslant V_e \leqslant 4.94$), the following polynomial was found:

$$(R^2 = 0.9997) \qquad 10^7 S_{yx} =$$

$$14889.0 - 6049.38V_e + 614.678V_e^2. \qquad (27)$$

From this equation one obtains $V_e^{min} = 4.9208$ ml ($C_0 = 0.00984M$) which is in excellent agreement with the expected value of the equivalence volume ($V_e = 4.94$ ml). Using this value, one

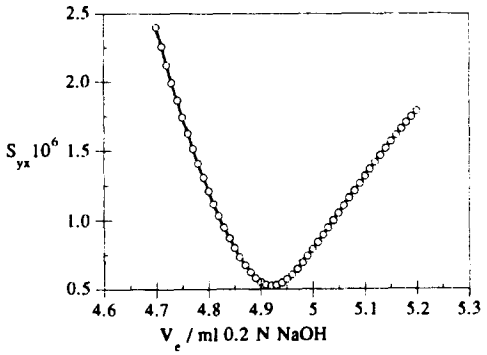


Fig. 4. Variation of $S_{yx}$ with $V_e$ in the case of the titration of 50 ml of 0.00988$M$ succinic acid with 0.2$M$ NaOH at 25°C.

obtains $pK_1 = 4.205$ and $pK_2 = 5.635$ from the coefficients of the corresponding linear regression equation $y = f(x)$. These values virtually coincide with those reported in the literature.

Finally, in the attempt to test this methodology on experimental data of the titration of a triprotic acid, a solution of 0.00968$M$ citric acid was prepared. A volume of 50 ml of this solution was titrated with 0.3$M$ NaOH. As previously, it was found that the plot $S_{yx} = f(V_e)$ presents a very pronounced minimum (Fig. 5). In the vicinity of the minimum ($4.82 \leqslant V_e \leqslant 4.84$), the following polynomial was found:

$$(R^2 = 0.9989)$$

$$10^2 S_{yx} = 109.06 - 45.130 V_e + 4.6689 V_e^2. \quad (28)$$

From this equation one obtains $V_e^{min} = 4.833$ ml ($C_0 = 0.0967M$) which is in excellent agreement with the expected values of the equivalence volume ($V_e = 4.84$ ml). Using this value, one obtains $pK_1 = 3.127$, $pK_2 = 4.776$ and $pK_3 = 6.385$ by fitting equation (25) to the titration data. These values virtually coincide with those suggested by N.B.S. ($pK_1 = 3.128$, $pK_2 = 4.761$ and $pK_3 = 6.396$ at 25°C).[28]

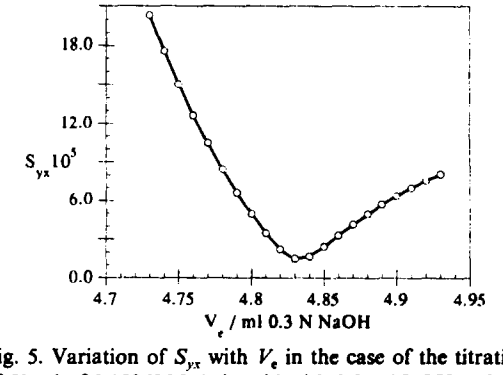


Fig. 5. Variation of $S_{yx}$ with $V_e$ in the case of the titration of 50 ml of 0.00968$M$ citric acid with 0.3$M$ NaOH at 25°C

## POTENTIOMETRIC TITRATION OF MIXTURES OF TWO WEAK DIPROTIC ACIDS WITH STRONG BASES

The titration of mixtures of two weak monoprotic acids has been treated previously.[1] Here, we present a method for analysis of potentiometric titrations of mixtures of two diprotic acids. It is noted that this problem has also been treated by Purdie *et al.* previously.[29] However, Purdie's method requires the knowledge of the sum of the concentrations of the acids; the $pK$'s values being known. On the contrary, in the present method the sum of the concentrations need not be known.

Consider a solution of a mixture of two weak diprotic acids $H_2A_1$ and $H_2A_2$ of initial analytical concentrations $C_1^0$ and $C_2^0$. A volume of $V_0$ of this solution is titrated with a solution of a strong base MOH of concentration $C_B$. Assuming that all equally charged ions have the same activity coefficients, the dissociation constants $K_{i1}$, $K_{i2}$ of the acid $H_2A_i$ (with $i = 1, 2$) are given by:

$$K_{i1} = \frac{\alpha_H \cdot [HA_i^-] \cdot y_1}{[H_2A_i]}$$

and

$$K_{i2} = \frac{\alpha_H \cdot [A_i^{2-}] \cdot y_2}{[HA_i^-] \cdot y_1}, \quad (29)$$

where $y_1$ and $y_2$ are the activity coefficients of the species $HA_i^-$ and $A_i^{2-}$, respectively.

At any point of the buffer region a relatively simple calculation gives:

$$Y = \left(\frac{K_{11}}{K_{21}}\right) C_1^0 + C_2^0 X, \quad (30)$$

where

$$Y = \frac{F \alpha_H^2 y_1 y_2 D_1}{b_N V_0 (\alpha_H y_2 + 2K_{12} y_1) K_{21}}$$

$$X = \frac{D_1 (\alpha_H y_2 + 2K_{22} y_1)}{D_2 (\alpha_H y_2 + 2K_{12} y_1)} \quad (31)$$

$$D_i = 1 + \frac{K_{i1}}{\alpha_H y_1} + \frac{K_{i1} K_{i2}}{\alpha_H^2 y_2}$$

$$F = b_N C_B V + \frac{\alpha_H}{y_1} - \frac{K_w}{\alpha_H y_1}. \quad (32)$$

For dilute solutions ($I < 0.1M$) the activity coefficients $y_1$ and $y_2$ can be determined from

eqn (10). Concerning the ionic strength $I$, a simple calculation gives:

$$I = [M^+] + [H^+] + [A_1^{2-}] + [A_2^{2-}] = b_N C_B V + \frac{\alpha_H}{y_1} + \frac{b_N V_0}{\alpha_H^2 y_2}\left(\frac{K_{11}K_{12}C_1^0}{D_1} + \frac{K_{21}K_{22}C_2^0}{D_2}\right). \quad (33)$$

Equation (30) predicts a linear relationship between $Y$ and $X$ with a $y$-intercept and slope equal to $K_{11}C_1^0/K_{21}$ and $C_2^0$, respectively. So, the composition of the mixture can be deduced, by linear regression, from the coefficients of eqn (30); the acidity constants $K_{i1}$, $K_{i2}$ (with $i = 1, 2$) being known. This procedure can be realized by the presently proposed iterative method.

Assuming first that $I = b_N C_B V + \alpha_H$, so that $\alpha_H \approx [H^+]$ and $[A_1^{2-}], [A_2^{2-}] \approx 0$, it is possible to determine from the coefficients of eqn (30), by means of the experimental $V$ and pH data, approximate values of $C_1^0$ and $C_2^0$. Starting from these values and assuming again that $\alpha_H \approx [H^+]$, it is possible to calculate $I$ from eqn (33) at any chosen point of the titration curve, and hence $y_1$ and $y_2$ from eqn (10). These new values of $y_1$ and $y_2$ can be used to refine values of $I$ and repeat until it converges (the criterion being less than 0.00001 difference in $I$, between two subsequent cycles). By repeating these approximations at each point of the titration curve, it is possible to trace the curve $Y = f(X)$ and determine by least squares the values of $C_1^0$ and $C_2^0$. These new values can be used to refine the values of $C_1^0$ and $C_2^0$ and repeat until they converge (the criterion being less than $10^{-12}$ difference in $C_1^0$ and $C_2^0$ values, between two subsequent cycles).

This procedure was applied to various simulated (ideal and Monte Carlo) titration data corresponding to different $C_1^0$ and $C_2^0$, $pK_{i1}$ and $pK_{i2}$ values. The obtained results showed that the proposed method reaches the desired values of $C_1^0$ and $C_2^0$ with a fair accuracy even when the data are considerably obscured by extraneous 'noise' (about 5–10 times greater than the accuracy of a precision instrument). Finally, in the attempt to test the proposed methodology on experimental data, a mixture was prepared by mixing 20 ml of 0.00988$M$ succinic acid with 30 ml of 0.00982$M$ tartaric acid. This mixture was titrated with 0.20$M$ NaOH. In all the calculations, we used experimental $pK_{i1}$ and $pK_{i2}$ values obtained, as described previously, from separate titrations. Thus, we used the values $pK_{11} = 4.205$, $pK_{12} = 5.635$, $pK_{21} = 3.033$ and $pK_{22} = 4.366$ which are in excellent agreement with the corresponding values suggested by N.B.S. ($pK_{11} = 4.209$, $pK_{12} = 5.638$, $pK_{21} = 3.033$ and $pK_{22} = 4.366$).[11,25,30] Assuming first that $I = b_N C_B V + \alpha_H$, so that $\alpha_H \approx [H^+]$ and $[A_1^{2-}], [A_2^{2-}] \approx 0$, the following approximate values of $C_1^0$ and $C_2^0$ were obtained: $C_1^0 \approx 4.043 \times 10^{-3}M$ and $C_2^0 \approx 5.878 \times 10^{-3}M$. Starting from these values one finally obtains, after four iterations, the following values: $C_1^0 = 3.928 \times 10^{-3}M$ and $C_2^0 = 5.883 \times 10^{-3}M$. These values are in excellent agreement with the expected values of $C_1^0$ ($= 20 \times 0.00988/50 = 3.952 \times 10^{-3}$) and $C_2^0$ ($= 30 \times 0.00982/50 = 5.892 \times 10^{-3}$). Finally, it should be noted that at these values of $C_1^0$ and $C_2^0$, the anticipated by equation (30) linear relationship between $Y$ and $X$ has been perfectly confirmed ($R = 0.99995$).

## CONCLUSIONS

The methods proposed in this investigation, based on equations without approximations, are valid throughout the acidic strength range. These methods, using data resulting from the acidic region of the titration curves, enable the prediction of the accurate value of the equivalence volume and determine simultaneously the acid dissociation constants, even if the titration is stopped well before the complete neutralization of the solution. The proposed procedures are valid even when the titrations are performed under conditions of varying ionic strength, but there is no reason why the analysis would not be carried out in conditions of constant ionic strength. Hence the addition of a neutral salt to the titrated solution to keep the ionic strength constant is not necessary. Therefore, the $pK$ values obtained in media of low ionic strength are free of any possible 'salt effect'.

The main advantage of the proposed techniques, in comparison to other approaches appearing in the literature, is the simultaneous determination of the equivalence volume and the accurate values of the corresponding $pK$. Indeed, $pK$ being independent of the concentration could be considered as the 'fingerprint' of the titrated acid. So, from the comparison of the determined $pK$ values with tabulated ones it is possible to identify the titrated acid.

In the titration of a solution containing initially a monoprotic acid in admixture with its conjugate base, the proposed procedure determines the initial composition of the mixture as well as the accurate values of the dissociation

constant of the concerned acid. Thus, it is possible by this type of analysis to distinguish if an weak acid has been contaminated by a strong base and define the extent of the contamination. This method is fairly applicable even when the titration data are considerably obscured by experimental 'noise' or contain an important systematic error.

In the titration of polyprotic (di- and triprotic) acids, the proposed procedures enable the extraction of the accurate values of the equivalence volume and the dissociation constants $K_i$ even when the ionization stages overlap. This investigation revealed that these methods are fairly applicable even when the titration data are considerably obscured by experimental 'noise' or contain an important systematic error.

Finally, in the titration of a solution containing a mixture of two diprotic acids, the proposed method enables the determination of the composition of the mixture without prior knowledge of the sum of the concentrations of the acids. This method could be applied to the determination of the composition of two-component mixtures of closely related acids such as mixtures containing two diastereoisomeric forms of weak diprotic acids.

## REFERENCES


1. G. Papanastasiou, I. Ziogas and G. Kokkinidis, *Anal. Chim Acta*, 1993, **277**, 119.
2. J. E. Prue, *The International Encyclopedia of Physical Chemistry and Chemical Physics, Ionic Equilibria*, Vol. 3, p. 6. Pergamon Press, Oxford, 1966.
3. D. M. Barry, L. Meites and B. H. Campbell, *Anal. Chim Acta*, 1974, **69**, 143.
4. D. Midgley and C. McCallum, *Talanta*, 1974, **21**, 723.
5. A. Ivaska, *Talanta*, 1974, **21**, 1175.
6. L. Pehrson, F. Ingman and S. Johansson, *Talanta*, 1976, **23**, 781.
7. S. Johansson, *Analyst*, 1979, **104**, 593.
8. J. Stur, M. Bos and W. E. E. Vann der Linden, *Anal. Chim Acta*, 1984, **158**, 93.
9. P. Gans, A. Sabatini and A. Vacca, *J. Chem. Soc., Dalton Trans.*, 1985, 1195.
10. R. A. Robinson and R. H. Stokes, *Electrolyte Solutions*, 2nd Ed., pp. 230, 517. Butterworths, London, 1968.
11. A. Albert and L. P. Serjeant, *The Determination of Ionization Constants*, 2nd Ed., pp. 28, 82. Chapman & Hall, London, 1971.
12. A. L. Bacarella, E. Grunwald, H. P. Marshall and E. L. Purlee, *J. Org. Chem.*, 1955, **20**, 747.
13. C. L. De Ligny, P. F. M. Luykx, M. Rehbah and A. A. Wieneke, *Recl. Trav. Chim. Pay-Bas*, 1960, **79**, 713.
14. H. Rossotti, *The Study of Ionic Equilibria*, pp. 19, 41. Longman, London, 1978.
15. G. Papanastasiou, G. Stalidis and D. Jannakoudakis, *Bul. Soc. Chim. Fr.*, 1984, 255.
16. P. Cayzergues, C. Georgoulis and G. Papanastasiou, *J. Chim. Phys.*, 1977, **74**, 1112.
17. A. Papoutsis, G. Papanastasiou, C. Georgoulis and D. Jannakoudakis, *J. Chim. Phys.*, 1985, **82**, 907.
18. G. Papanastasiou, G. Kokkinidis and N. Papadopoulos, *J. Electroanal. Chem.*, 1991, **305**, 19.
19. G. Kokkinidis, G. Papanastasiou, C. Hasiotis and N. Papadopoulos, *J. Electroanal. Chem.*, 1991, **309**, 263.
20. G. Papanastasiou, G. Kokkinidis and N. Papadopoulos, *J. Electroanal. Chem.*, 1993, **352**, 153.
21. S. Chatterjee and B. Price, *Regression Analysis by Example*, p. 3. J. Wiley, New York, 1977.
22. G. Dahlquist and A. Björck, *Numerical Methods*, p. 227. Prentice-Hall, Englewood Cliffs, NJ, 1969.
23. R. de Levie, *J. Chem. Educ.*, 1986, **63**, 10.
24. E. J. King, *The International Encyclopedia of Physical Chemistry and Chemical Physics, Acid–Base Equilibria*, Vol. 4, p. 227. Pergamon Press, Oxford, 1965.
25. G. Kortüm, M. Vogel and K. Andrussow, *Dissociation Constants of Organic Acids in Aqueous Solutions*, p. 252. Butterworths, London, 1961.
26. G. Papanastasiou and I. Ziogas, *Talanta*, 1989, **36**, 977.
27. G. Papanastasiou and I. Ziogas, *Anal. Chim. Acta*, 1989, **222**, 189.
28. R. G. Bates and C. D. Pinching, *J. Am. Chem. Soc.*, 1949, **71**, 1274.
29. N. Purdie, M. B. Thomson and G. K. Cook, *Anal. Chem.*, 1972, **44**, 1525.
30. R. G. Bates and R. G. Canham, *J. Res. Nat. Bur. Stand.*, 1951, **47**, 343.

Pergamon

0039-9140(95)01497-7

*Talanta*, Vol. 42, No. 6, pp. 837–843, 1995

0039-9140/95 $9.50 + 0.00

# DEVELOPMENT OF A SPECTROPHOTOMETRIC DETERMINATION OF SIDEROPHORES USING FLOW-INJECTION ANALYSIS

R. TRSKOVÁ,[1] P. RYCHLOVSKÝ,[1] I. NĚMCOVÁ[1] and A. JEGOROV[2]

[1]Department of Analytical Chemistry, Charles University, Albertov 2030, 12840 Prague 2, Czech Republic
[2]Galena Co., Research Unit, Branišovská 31, 370 05 České Budějovice, Czech Republic

(*Received* 7 *June* 1994. *Revised* 2 *December* 1994. *Accepted* 2 *December* 1994)

**Summary**—A method has been developed for the spectrophotometric determination of siderophores using flow-injection analysis (FIA) based on the reaction of siderophores with the ternary complex Eriochrome Cyanine R–Fe(III)–cetyltrimethylammonium bromide. 2,3-Dihydroxybenzoic acid, 2,3-dihydroxynaphthalene, and tolypocine were used as the model iron-binding ligands. The calibration curve for one of the siderophores (tolypocine) is linear in the concentration range $2.6 \times 10^{-6}$–$1.5 \times 10^{-4}M$. The determination limit ($10\sigma$) for tolypocine was $2.6 \times 10^{-6}M$. The applicability of the method was demonstrated on the determination of the complexation ability of siderophores produced by some entomopathogenic fungi. Samples can be analysed at a rate of 30 samples per hour.

Siderophores are natural low molecular weight iron-binding ligands containing catechol, hydroxamic, α-hydroxy-carboxylic or oxazoline groups. The extracellular production of siderophores and selective transmembrane withdraw of iron complexes help various microorganisms to obtain iron, an essential element for their growth and multiplication.[1,2] In living organisms siderophores produced by some pathogens are able to compete with iron-binding proteins of their hosts. In some cases, a correlation was found between the production of siderophores and the ability of these pathogens to cause systemic disease.[3] Thus in principle, the development of a suitable method for the determination of siderophores might contribute to the evaluation of the virulence of causative pathogens of immunocompromized, e.g. HIV-positive persons. Since manipulation with the infected material represents a serious health hazard, FIA was chosen as a method permitting fully automated sample handling.[4–6] To avoid such a health hazard in the course of the method development, fungi which are not pathogenic to humans were used as a model in this study.

Tolypocine ($C_{15}H_{21}NO_3$, $M_r$ 263,34) is a siderophore isolated from the fungus *Tolypocladium geodes* and has the structure of hydroxamic acid (1′*S*,2′*R*,4′*S*,6′*R*)-5-(2′-vinyl-4′,6′-dimethyl-cyclohexyl)-1,4-dihydroxy-2(1*H*)-pyridone. The isolation and characterization of tolypocine were described by Jegorov *et al.*, who also described the crystal structure of tolypocine and its Fe(III) complex.[3] Some related fungal genera used in this study also produce hydroxamic acids of similar structure.[7]

Catecholic siderophores can be determined by the Arnow spectrophotometric method based on the nitration of the aromatic ring by sodium nitrite in the presence of sodium molybdenate.[8] This method is selective for aromatic vicinal diols that are not substituted in the 3- or 4-positions.[9] In the presence of triethylamine in ethanol solutions, aromatic vicinal diols also form blue-green chelates with Fe(III) ions.[10] Rioux *et al.*[9] described a method for the spectrophotometric determination of catechol compounds based on the ability of the vicinal aromatic hydroxyl group to reduce Fe(III) to Fe(II) in acidic medium. Our work follows from the work of Schwyn and Neilands,[11] who described a method for the determination of various types of siderophores based on the replacement of a weakly bonded triphenylmethane dye from the Fe(III)–dye–surfactant complex by the siderophore.

## EXPERIMENTAL

### *Apparatus and manifold*

A Pye-Unicam PU 8800 spectrophotometer with 1.0-cm quartz curvettes was used for recording the spectra. A Radiometer PHM 64 pH-meter was used. A scheme of the apparatus for flow-injection analysis constructed in our laboratory is depicted in Fig. 1. The length of reaction coil was $L = 6$ m, the reagent was pumped at a flow rate of $v_2 = 0.4$ ml/min and the carrier stream of deionized water had a flow rate of $v_1 = 1.0$ ml/min.

The equipment for flow-injection analysis was constructed using a peristaltic pump (Cole-Parmer Instrument Co., U.S.A.) with tygon pumping tubing, rotation injection valve (Valco, U.S.A.), Spekol 11 spectrophotometer with accessory EK 5 (K. Zeiss, Germany) and flow-through cell (Hellma, German, internal volume 80 $\mu$l), TZ 4620 x -t recorder (Laboratorní přistroje, Czech Republic), PE tubing 0.5 mm i.d.), polypropylene connectors (Cole-Parmer Instrument Co., U.S.A.).

The HPLC measurements were carried out with a reverse phase C-18, Pico-fag (Waters), particle size 4 $\mu$m. Dimensions of the column were 150 x 3.9 mm. The mobile phase for tolypocine consisted of 60% methanol, 0.2% trichloroacetic acid and water, flow rate 1.5 ml/min. UV photometric detection at 290 nm was used; measurement was carried out at 20°C. Retention time for tolypocine was 5.50 min.

### *Chemicals*

All chemicals were of analytical grade and were used as received. The following aqueous stock solutions were used: Chrome Azurol S (CAS, $2 \times 10^{-3}M$, Merck, Germany), Pyrocatechol Violet (PV, $2 \times 10^{-3}M$, Lachema, Czech Republic), Eriochrome Cyanine R (ECR, $2 \times 10^{-3}M$, Lachema, Czech Republic), cetyltrimethylammonium bromide (CTAB, $5 \times 10^{-2}M$, Lachema, Czech Republic), 1-ethoxycarbonylpentadecyltrimethylammonium bromide (Septonex, $5 \times 10^{-2}M$, Slovakofarma, Slovak Republic), 2,3-dihydroxynaphthalene (2,3-DHN, $5 \times 10^{-3}M$, Fluka, Switzerland), pyrocatechol, pyrogallol and hydroquinone ($5 \times 10^{-3}M$, Lachema, Czech Republik). The purity of ECR was checked using thin-layer chromatography.[12] $1 \times 10^{-3}M$ Fe(III) ion solutions were prepared by dissolving $FeCl_3 . 6H_2O$ (Lachema, Czech Republic) in $1 \times 10^{-3}M$ hydrochloric acid. The iron content was checked by the AAS method. The $5 \times 10^{-4}M$ standard solution of tolypocine was prepared by dissolving tolypocine, $C_{15}H_{21}NO_3$[3] in a 40% (v/v) aqueous methanol solution. The $1.67M$ stock solution of piperazine buffer was prepared by dissolving anhydrous piperazine (Merck, Germany) in deionized water; the pH value was adjusted with hydrochloric acid to pH 7.0. The solution was quantitatively transferred to a 1000 ml volumetric flask and filled with deionized water. All the chemical glass used was prior rinsed with $6M$ hydrochloric acid.

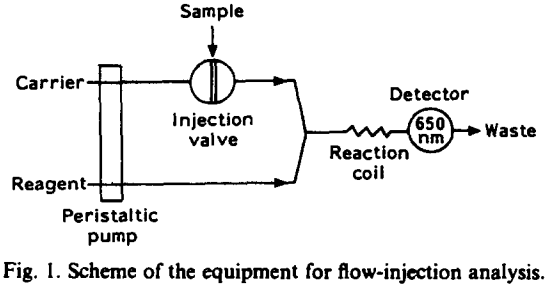


Fig. 1. Scheme of the equipment for flow-injection analysis.

### *Reagent preparation*

A solution of Eriochrome Cyanine R (12.5 ml) with a concentration of $2 \times 10^{-3}M$ and 2.5 ml of a solution of $FeCl_3$ with a concentration of $1 \times 10^{-3}M$ were pipetted into a 250 ml volumetric flask and left to react for 3 min. Then 12.5 ml of $5 \times 10^{-2}M$ CTAB solution was added to 75 ml of the stock solution of piperazine buffer, transferred quantitatively to the volumetric flask with ECR and Fe(III), and filled with deionized water. The reagent can be used for measurement 15 min after mixing the ECR and Fe(III) solutions.

### *Fungal material*

The following entomopathogenic fungal strains were used for the study: *Scopulariopsis bravicaulis* (CB-SR), *Olpitrichum* sp. (CCEB 2061, *Dendrolimus pini*), *Tolypocladium geodes* (CCF 257, *Tolypocladium inflatum* (CCF 1897), *Tolypocladium terricola* (CB-TTR1), *Beauveria bassiana* (CB-BBA5, *Hylobius abietis*), *Trichoderma konigii* (CCEB 2063, Cuba), *Paecilomyces farinosus* (CB-STR, *Hylobius abietis*), *Paecilomyces fumosoroseus* (CCEB 2012), *Beauveria brongniartii* (cceb 2176, *Ibs typographus*, Bulgaria). Strains were cultivated and provided by Dr Z. Kadlec (Galena, České Budějovice). Fungi were cultured either stationary (21 days at 25°C in conical flasks on 100 ml of Sabouraud medium) or in submerged culture

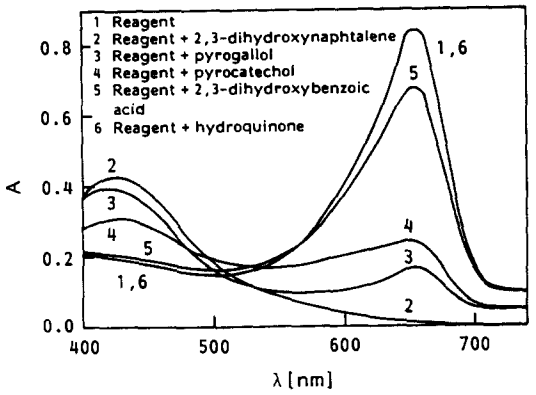


Fig. 2. The absorption spectrum of the reagent in the absence and presence of hydroxy compounds. $c_{ECR} = 3.75 \times 10^{-5}M$; $c_{Fe(III)} = 3.75 \times 10^{-6}M$; $c_{CTAB} = 1.5 \times 10^{-4}M$; $c_{hydroxy\ compound} = 3 \times 10^{-5}M$; pH 7.5; $t = 2$ min.

(10 days at 25°C in conical flasks in 200 ml of Sabourad medium). A 72-hr submerged preculture on Sabouraud medium (18 g glucose (Lachema, Czech Republic), 18 g maltose (Lachema, Czech Republic), 8 g pepton (Fluka, Switzerland), 0.3 g yeast extract (Difco) per 1000 ml) was used as inoculum (1:10, v/v). Samples of the non-sterile media were obtained by filtration of the fermentation broths and were used without stabilizers.

## RESULTS AND DISCUSSION

The described method is based on the fact that the Fe(III) has a high affinity for the siderophores.[3,11] Thus, the following reaction occurs:

$$[Fe^{3+} - B - T] + S \rightarrow [Fe^{3+} - S] + B - T, \quad (1)$$

where B is the triphenylmethane dye, T is the tenside and S is the siderophore.

The reagent is the complex of the triphenylmethane dye with Fe(III) in the presence of the cationogenic tenside (the tensides shift the absorption maximum of complexes to the longer wavelength, increasing the $\lambda_{max}$ difference of complex and dye[13]).

### *Spectrophotometric determination of* 2,3-*dihydroxynaphthalene*

Preliminary experiments were carried out using 2,3-dihydroxybenzoic acid (2,3-DHBA), which has been used in some other methods as a model substance for determining siderophores.[1,9] Its reaction with the following triphenylmethane dyes was studied: Chrome Azurol S, Pyrocatechol Violet and Eriochrome Cyanine R. The most sensitive was found to be Eriochrome Cyanine R[14-16] ($\varepsilon_{650} = 3.2 \times 10^6 M^{-1}$). In the course of reaction of the Fe(III)–dye–tenside complex with a siderophore, the color changes from blue, corresponding to the ternary complex, to an orange, corresponding to the liberated dye–tenside. The decrease of absorbance is monitored at the wavelength of the absorption maximum of the original ternary complex (reagent).

As the reaction of 2,3-DHBA with the reagent was not sufficiently sensitive, a different substance was sought, that would have greater affinity for the Fe(III) ions and retaining complexing properties similar to the siderophores. Comparison was carried out (see the absorption spectra in Fig. 2) using hydroxy compounds with hydroxyl groups in the *ortho* position on the aromatic nucleus. Hydroquinone, with hydroxyl groups in mutually *para* positions, which does not form a complex with Fe(III), was also used for comparison. As follows from Fig. 2, a redox reaction with Fe(III) did not occur even with this substance. On the basis of these reactions, 2,3-dihydroxynaphthalene (2,3-DHN) was chosen for further work; the affinity of this substance for Fe(III) makes it useful for the determination of this element.[15-17] Of the cationogenic tensides CTAB and Septonex were selected for study of the reaction. The effect of the pH (Fig. 3), reagent composition and concentrations of the individual components of the reagent [ECR, Fe(III), CTAB, Septonex] on the sensitivity of the reaction was studied. The sensitivity achieved using CTAB tenside is approximately twice the greatest sensitivity of the reaction using Septonex. The following optimum reagent composition was found: $c_{Fe(III)} = 1 \times 10^{-5}M$, $c_{ECR} = 1 \times 10^{-4}M$, $c_{CTAB} =$

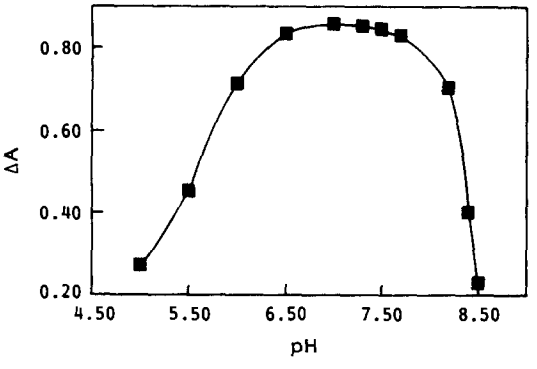


Fig. 3. Dependence of the absorbance change ($A$) at the wavelength of maximum reagent absorbance on the pH. $c_{ECR} = 7.5 \times 10^{-5}M$; $c_{Fe(III)} = 7.5 \times 10^{-6}M$; $c_{CTAB} = 3 \times 10^{-4}M$; $c_{2,3\text{-}DHN} = 3 \times 10^{-5}M$, $t = 60$ s.

$2.5 \times 10^{-3}M$, *i.e.* where the ratio of the concentrations of the components of the reagent is Fe(III):ECR:CTAB = 1:10:250. The maximum decrease in the absorbance was obtained 90 sec after mixing the reagent with the 2,3-DHN solution; the absorbance values were constant for at least 300 sec. In addition, it was found that the reaction rate is practically temperature-independent at all the temperatures tested; the equilibrium state of the reaction was attained 90 sec after mixing the reagent with the test substance.

The reagent with pH 7.0 exhibits maximum absorbance at 650 nm. If stored in a glass volumetric flask, it is stable for 4.5 hr; new reagent must be prepared for a longer series of measurements. In the measurement of a number of series of samples during a single day, it was found useful to store the reagent in a polyethylene bottle, where the absorbance at 650 nm attains maximum value after 2 hr and is constant for at least 10 hr. The lower stability of reagent in a glass volumetric flask than in a polyethylene bottle is probably caused by higher sorption of reagent on the glass wall.

Under the optimum conditions found ($\lambda = 650$ nm, pH 7.0, $c_{Fe(III)} = 1 \times 10^{-5}M$, concentration ratio Fe(III):ECR:CTAB = 1:10:250, $t = 90$ sec), the dependence of the absorbance change ($\Delta A$) on the concentration of 2,3-dihydroxynaphthalene was measured; the calibration curve is linear for the 2,3-DHN concentration range from $5 \times 10^{-7}$ to $8 \times 10^{-6}M$, *i.e.* 0.08–1.28 $\mu$g of 2,3-dihydroxynaphthalene per mil. The reproducibility of the measurement was tested in repeated determinations. The relative standard deviation of the measurement (determined from 5 measurements) varied from 0.7 ($8 \times 10^{-6}M$) to 1.3% ($5 \times 10^{-7}M$). The parameters of the calibration straight line $A = a + b \,.\, c_{2,3\text{-DHN}}$ were $b = 8.83 \times 10^{-4}M$, $a = -0.0178$, and the correlation coefficient $r = 0.9998$. The detection limit ($3\sigma$) was $5 \times 10^{-7}M$ and the determination limit ($10\sigma$) was $1.2 \times 10^{-6}M$. A study was also made of the effect of the presence of methanol on the reaction of reagent with 2,3-dihydroxynaphthalene. It was found that methanol disturbs the reaction above a concentration ratio of 2,3-DHN:methanol = $1:10^5$.

*Spectrophotometric determination of tolypocine*

Using parameters optimized with 2,3-dihydroxynaphthalene, tolypocine was used as an alternative ligand. An appropriate amount of $5 \times 10^{-4}M$ methanol solution of tolypocine was added to the Fe(III):ECR:CTAB (1:10:250) reagent in a volumetric flask and diluted with deionized water. Reagent with deionized water was used as blank. After 90 sec the absorbance was measured at a wavelength of 650 nm, giving the calibration curve. The dependence of the absorbance change ($\Delta A$) on the tolypocine concentration (measured at the same conditions as in the case of 2,3-DHN) was linear from $8 \times 10^{-7}$ to $2 \times 10^{-5}M$, *i.e.* from 0.2 to 5.3 $\mu$g tolypocine per ml. The relative standard deviations (from 5 measurements) varied in the range 0.9% ($2 \times 10^{-5}M$) to 1.9% ($8 \times 10^{-7}M$). The parameters of the calibration straight line were $b = 4.96 \times 10^{4}M^{-1}$, $a = -0.017$, and the correlation coefficient $r = 0.9994$. The detection limit ($3\sigma$) is $7.6 \times 10^{-7}M$ and the determination limit ($10\sigma$) was $1.7 \times 10^{-6}M$.

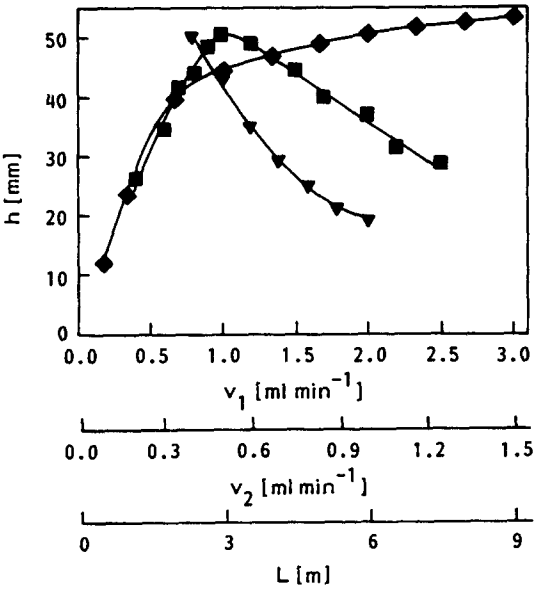


Fig. 4. Dependence of the recorded peak height (h) on the flow rate of the carrier stream $v_1$ (▼, at $v_2 = 0.4$ ml/min, $L = 6$ m) on the flow rate of the reagent $v_2$ (■, at $v_1 = 1.0$ ml/min, $L = 6$ m) and on the length of the reaction coil L (◆, at $v_1 = 1.0$ ml/min, $v_2 = 0.4$ ml/min). pH 7.0, $c_{Fe(III)} = 1 \times 10^{-5}M$, concentration ratio Fe(III):ECR:CTAB = 1:10:250, $c_{2,3\text{-DHN}} = 3.5 \times 10^{-5}M$, volume injected = 100 $\mu$l.

*Optimization of flow-injection analysis*

The parameters of the flow-through apparatus were optimized on the basis of the reaction with 2,3-dihydroxynaphthalene in order to achieve the maximum sensitivity and reproducibility of the determination. Figure 4 depicts the effect of the length of the reaction coil, and the flow rate of the carrier stream and of the reagent

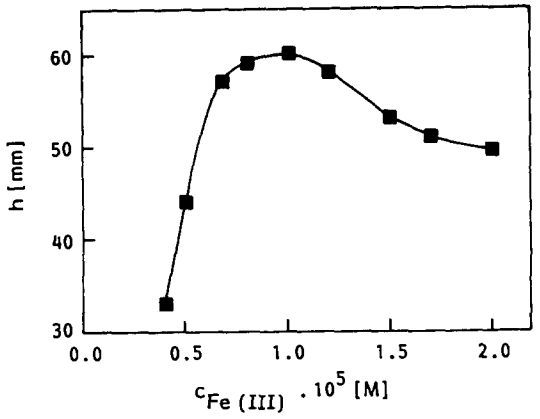


Fig. 5. Dependence of the recorded peak height (h) on the reagent concentration related to the Fe(III) concentration [the concentration ratio Fe(III):ECR:CTAB = 1:10:250]. $L = 6$ m, $v_1 = 1.0$ ml/min, $v_2 = 0.4$ ml/min, pH 7.0, $c_{2,3\text{-}DHN} = 3.5 \times 10^{-5} M$, volume injected = 100 $\mu$l.

on the height of the peaks obtained. It follows from this figure that the optimal FIA parameters were: reaction coil length, $L = 6$ m (chosen as a compromise between the maximum sensitivity of the determination and maximum number of analyses per hour), carrier stream flow rate, $v_1 = 0.10$ ml/min, reagent flow rate, $v_2 = 0.4$ ml/min. The optimal ratio of the reagent components was determined by varying the concentrations of the individual components and was found to be Fe(III):ECR:CTAB = 1:10:250. The optimum reagent concentration (Fig. 5) was related to a Fe(III) concentration of $1 \times 10^{-5} M$.

The effect of the injected volume of sample on the sensitivity of the determination was evaluated in the range 35–1000 $\mu$l, under the selected optimum conditions. The optimum injection volume was selected as 100 $\mu$l. The effect of the injected volume on the linear calibration dependence was also tested (Table 1). It was found that (compared to an injected amount of 35 $\mu$l), the injection of 100 $\mu$l increased the sensitivity of the determination, found from the slope of the calibration curve, by about 2.5-fold. Using an injected amount of 35 $\mu$l, a total of 40 samples per hour could be analysed; the use of an injected amount of 100 $\mu$l decreased this to 30 analyses per hour.

It follows from these results that the constructed apparatus for flow-injection analysis exhibits parameters comparable with equipment used by other authors.[18–21]

*FIA determination of tolypocine*

The dependence of the peak height ($h$) on the tolypocine concentration was linear in the concentration range from $2.6 \times 10^{-6}$ to $1.5 \times 10^{-4} M$, *i.e.* from 0.7 to 39.5 Mg tolypocine per ml. The relative standard deviation (from 5 measurements) varied in the range 1.2% ($1.5 \times 10^{-4} M$) to 3.5% ($2.6 \times 10^{-6} M$). The parameters of the calibration straight line $h = a + b \,.\, c$ were $b = 7.7 \times 10^5$ mm $.\, M^{-1}$, $a = 5.48$ mm and the correlation coefficient $r = 0.9994$. The determination limit ($10\sigma$) was $2.6 \times 10^{-6} M$.

*Determination of siderophores in real samples*

The parameters of simple spectrophotometric and FIA analysis optimized for the model compounds were used to determine the production of siderophores by some entomopathogenic fungi. Conditions and results of this study are summarized in Table 2. In the case of analysed siderophores the duration of reaction was a few minutes; the measurement was carried out in 90 sec after injection of sample. As follows from the table, all fungal strains belonging to genera *Beauveria* and *Paecilomyces* produce relatively large amount of siderophores. Assuming that the fungus *Tolypocladium geodes* produce only tolypocine its concentration was evaluated by the method of standard additio. The value obtained, *i.e.* 17.5 $\mu$g/ml ($6.6 \times 10^{-5} M$) is in good agreement with that found by HPLC (data not shown). In contrast, the production of siderophores was very small with the isolates of *Scopulariopsis* and *Olpitrichum*. The correlations between the results of spectrophotometric and FIA analysis of samples obtained by stationary and submerged cultivation are given

Table 1. Parameters of the calibration straight lines for various injected volumes of the test substances

| Injection volume, $V$ ($\mu l$) | 35 | 100 | 500 |
|---|---|---|---|
| Intercept, $a$ ($mm$) | 2.02 | 5.36 | 5.41 |
| Line slope, $b$ ($mm \,.\, M^{-1}$) | $1.24 \times 10^6$ | $3.00 \times 10^6$ | $4.48 \times 10^6$ |
| Correlation coefficient, $r$ | 0.9998 | 0.9998 | 0.9998 |
| Number of points of calibration line, $n$ | 10 | 10 | 8 |

$L = 6$ $m$, $v_1 = 1.0$ $ml/min$, $v_2 = 0.4$ $ml/min$, pH 7.0, $c_{Fe(III)} = 1 \times 10^{-5} M$, concentration ratio Fe(III):ECR:CTAB = 1:10:250

Table 2. The total complexation ability of siderophores produced by various fungal isolates cultivated by stationary or submerged cultivation (values in table were corrected with blank)

| Fungus | Spectrophotometry* ($\Delta A$) | | FIA† ($h$ in *mm*) | |
|---|---|---|---|---|
| | Submerged c. | Stationary c. | Submerged c. | Stationary c. |
| *Scopulariopsis bravicaulis* | 0.002 | 0.360 | 1 | 27 |
| *Olpitrichum* sp. | 0.008 | 0.075 | 2 | 7 |
| *Tolypocladium geodes* | — | 0.070 | — | 5 |
| *Tolypocladium inflatum* | 0.020 | 0.173 | 3 | 13 |
| *Tolypocladium terricola* | 0.101 | 0.181 | 8 | 18 |
| *Beauveria bassiana* | 0.303 | 0.595 | 20 | 49 |
| *Trichoderma konigii* | 0.425 | 0.584 | 35 | 46 |
| *Paecilomyces farinosus* | 0.502 | 0.593 | 33 | 50 |
| *Paecilomyces fumosoroseus* | 0.830 | 0.700 | 64 | 60 |
| *Beauveria brongniartii* | 0.995 | 0.647 | 79 | 51 |

*$c_{ECR} = 1 \times 10^{-4} M$, $c_{Fe(III)} = 1 \times 10^{-5} M$, $c_{CTAB} = 2.5 \times 10^{-3} M$, pH 7.0, protocol: reagent 5 *ml*, medium 1 *ml*, water to the total volume 10 *ml*, $t = 90$ *sec*.

†$L = 6$ *m*, $v = 1.0$ *ml/min*, $v_2 = 0.4$ *ml/min*, pH 7.0, $c_{Fe(III)}$ $1 \times 10^{-5} M$, Fe(III):ECR:CTAB = 1:10:250, volume injected = 100 *µl*.

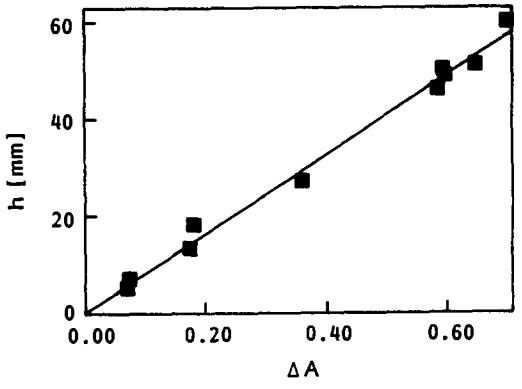


Fig. 6. Correlation graph between the spectrophotometric and FIA results for siderophores produced by various fungal isolates cultivated by stationary cultivation.

in Figs 6 and 7. The parameters of the correlation straight lines $h = a + b \,.\, \Delta A$ were $b = 81.79$ (76.77), $a = 0.0657$ (0.0400) and the correlation coefficient $r = 0.9954$ (0.9955)) for stationary (submerged) cultivation.

Owing to the fact that the different fungal isolates produce various types of siderophores, which also differ in their stability constants with Fe(III), values obtained represent only the relative complexation ability, *e.g.* the sum of contributions of all ligands present in the particular medium. Only in the case, the sole siderophore is produced, the method can be used for the quantification of its production. Whereas the methods like GC or HPLC are usually much better for the determination of the absolute concentration of the particular compound, FIA is the favoured method for the screening of siderophores of unknown structure. Owing to the extremely short time necessary for one analysis, FIA is also a method of choice for the fast comparison of fungal or bacterial isolates even in the case where the structure of the produced siderophores is well known.

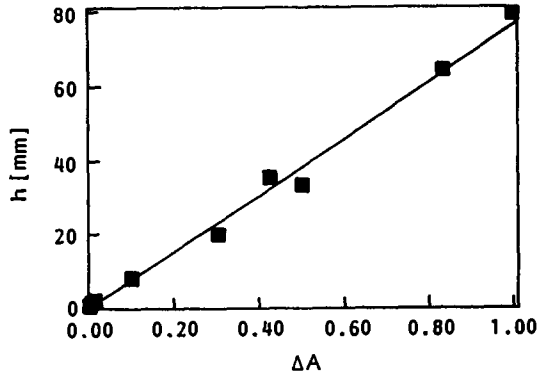


Fig. 7. Correlation graph between the spectrophotometric and FIA results for siderophores produced by various fungal isolates cultivated by submerged cultivation.

## REFERENCES

1. J. B. Neilands (ed.), Iron and its role in microbial physiology. In *Microbial Iron Metabolism*. New York, 1974.
2. G. Winkelmann, Iron complex products. In *Biotechnology* H. Pape and H.-J. Rehm (eds), Vol. 4, VCH, Weinheim, 1986.
3. A. Jegorov, V. Matha, M. Hušák, B. Kratochvíl, J. Stuchlík, P. Sedmera and V. Havlíček, *J. Chem. Soc. Dalton Trans.*, 1993, **8**, 1287.
4. J. Růžička and E. H. Hansen, 'Flow Injection Analysis. Wiley Interscience, New York, 1981.
5. M. Valcarcel and M. D. Lugue de Castro, *Flow Injection Analysis. Principals and Applications*. Ellis Horwood, New York, 1987.
6. L. Sommer, *Analytical Absorption Spectrophotometry in the Visible and Ultraviolet. The Principles*. Akadémiai Kiado, Budapest, 1989.
7. C.-K. Watt, A. G. McInnes, D. G. Smith, J. L. C. Wright and L. C. Vining, *Can. J. Chem.*, 1977, **55**, 4090.
8. L. E. Arnow, *J. Biol. Chem.*, 1937, **118**, 531.

9. C. Rioux, D. C. Jordan and J. B. M. Rattray, *Anal. Biochem.*, 1983, **133**, 163.
10. B. Kakáč, Z. J. Vejdělek, *Handbuch der photometrischen Analyse organischer Verbindungen*. Verlag Chemie, Weinheim, 1977.
11. B. Schwin and J. B. Neilands, *Anal. Biochem.*, 1987, **160**, 47.
12. J. Gasparič and J. Churáček, *The Paper and Thin-layer Chromatography of Organic Compounds* (in Czech). SNTL, Praha, 1981.
13. W. L. Hinze, Use of Surfactant and Micellar Systems in Analytical Chemistry. In *Solution Chemistry of Surfactants*, K. L. Mittal (ed.), Vol. **1**, Plenum Press, New York, 1979.
14. Z. Marczenko and H. Kalowska, *Anal. Chim. Acta*, 1981, **123**, 279.
15. Z. Holzbecher, L. Diviš, M. Král, L. Šůcha and F. Vláčil, *The Organic Reagents in the Inorganic Analysis*. SNTL, Praha, 1983.
16. V. N. Tikhonov and T. M. Anisimova, *Zh. Anal. Khim.*, 1983, **38**, 778.
17. V. Patrovský, *Collec. Czech. Chem. Commun.*, 1970, **35**, 1599.
18. S. Motomizu, M. Oshima and Y. Hosoi, *Microchim. Acta*, 1992, **106**, 67.
19. M. J. M. Hernandez, S. S. Vives and M. C. G. Alvarezcoque, *Microchim. Acta*, 1992, **108**, 293.
20. D. Narinesingh, V. A. Stoute, G. Davis and D. Persad, *Anal. Chim. Acta*, 1992, **258**, 141.
21. N. Chimpalee, D. Chimpalee, R. Jarungpattananon, S. Lawratchavee and D. T. Burns, *Anal. Chim. Acta*, 1993, **271**, 247.

Pergamon

0039-9140(95)01498-5

*Talanta*, Vol. 42, No. 6, pp. 845–850, 1995

0039-9140/95 $9.50 + 0.00

# DETERMINATION OF THE INTRINSIC SITE p$K_a$ VALUE AND COOPERATIVITY OF THE SYMMETRICAL HEXADENTATE CHELATOR *N,N′,N″*-TRIS[2-(3-HYDROXY-2-OXO-1,2-DIHYDROPYRIDIN-1-YL)ACETAMIDO]ETHYLAMINE

PAUL D. TAYLOR

Department of Chemistry and Biological Chemistry, University of Essex, Wivenhoe Park, Colchester, CO4 3SQ, U.K.

(*Received* 7 *June* 1994; *Revised* 29 *November* 1994; *Accepted* 2 *December* 1994)

**Summary**—The three overlapping p$K_a$ values of *N,N′,N″*-tris[2-(3-hydroxy-2-oxo-1,2-dihydropyridin-1-yl)acetamido]ethylamine, a tripodal hexadentate chelator formed from three 3-hydroxy-2(1*H*)-pyridinone moieties amide linked to tris-(2-aminoethyl)amine, were determined by simultaneous spectrophotometric and potentiometric titration. The data was analysed by non-linear regression with constraints to deal with (a) the highly correlated absorptivities and (b) the highly correlated p$K_a$ values. The three p$K_a$ values were optimized first from the spectrophotometric data (absorbance *vs.* pH) by non-linear regression to a model in which the molar absorptivity of the *i*th species ($\epsilon_i$) was constrained by the correlation equation $\epsilon_i = \epsilon_0 + (\epsilon_3 - \epsilon_0)i/3$ with $i = 0, 1, 2, 3$, where $\epsilon_3$ and $\epsilon_0$ represent the molar absorptivities of the most protonated and least protonated species, respectively. The molar absorbitivity of the four species defined by three p$K_a$ values is, therefore, linearly related to proton stoichiometry. The p$K_a$ values were then optimized from the potentiometric data (pH *vs.* titrant volume) by non-linear regression to a model in which the three p$K_a$ values were constrained by the correlation equation $pK_{a_i} = pK_{a_{int}} + b(i-1) + (i-2)\log(3)$ where $i = 1$, 2 or 3. This expresses the three p$K_a$ values in terms of only two optimizable parameters, the intrinsic site p$K_a$ (p$K_{a_{int}}$) and the interaction energy between sites (b). The fixed term $(i-2)\log(3)$ accounts for the statistical effect on the p$K_a$ values of three equivalent ionizable sites. The modified analytical derivatives required for optimization of these parameters by the Gauss–Newton–Marquardt algorithm and the merits of optimizing p$K_a$ values with these two correlation equations are discussed. The optimized p$K_a$ values were $9.31 \pm 0.01$, $8.75 \pm 0.01$ and $8.19 \pm 0.01$. The separation between p$K_a$ values is 0.58 comprising 0.477 for the statistical effect and 0.081 for the interaction energy while the intrinsic site p$K_a$ is $8.672 \pm 0.005$. The tertiary amine at the centre of the tripodal backbone has a p$K_a$ of $5.88 \pm 0.03$.

Braibanti *et al.*[1] have emphasized the inadvisability of optimizing several stepwise p$K_a$ values in molecules with several identical ionizable sites, as independent variables. The hexadentate metal-ion chelator *N,N′,N″*-tris[2-(3-hydroxy-2-oxo-1,2-dihydropyridin-1-yl)acetimido]ethyl-amine (**1**), is of medicinal interest in the treatment of iron-overload.[2] The molecule coordinates iron(III) strongly with its three identical 3-hydroxy-2(1*H*)-pyridinone units, each of which has an ionizable hydroxyl group. The p$K_a$ values of these identical groups are, therefore, highly correlated. This work considers two methods for optimising the three p$K_a$ values by non-linear regression to models which account for this correlation.

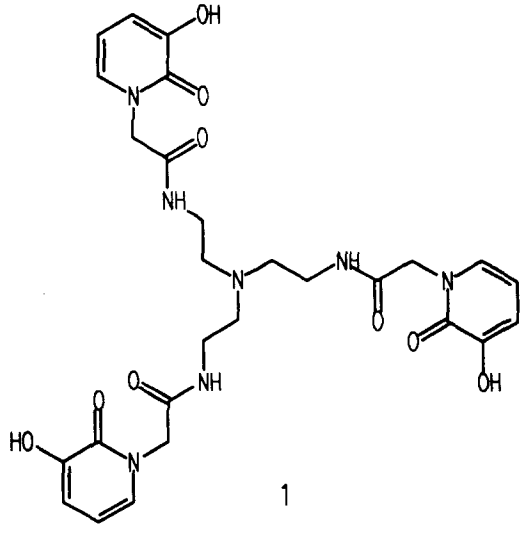


1

The analysis of spectrophotometric data (absorbance vs. pH) was carried out using a correlation equation which linearly relates molar absorptivity to proton stoichiometry. Thus, if the molar absorptivities of the most protonated and the least protonated species are represented by $\epsilon_3$ and $\epsilon_0$, respectively, then the molar absorptivity of the $i$th protonated species is given by eqn (1).

$$\epsilon_i = \epsilon_0 + (\epsilon_3 - \epsilon_0)i/3. \quad i = 0,1,2,3 \qquad (1)$$

The work demonstrates that this simple equation is valid for the particular case examined and suggests the criteria to test its validity in other cases.

The analysis of potentiometric data (pH *vs.* titrant volume) was carried out using a correlation equation which expresses the stepwise $pK_a$ values of identical sites, in terms of an intrinsic site $pK_a$, a statistical term, and a site interaction term (eqn 2). In the case of $n$ identical subunits, purely statistical factors would lead to $n$ $pK_a$ values, with the $i$th $pK_a$ given by $pK_{a_{int}} - \log\{(n - i + 1)/i\}$ where $pK_{a_{int}}$ is the intrinsic $pK_a$ of the site. In this case, $n = 3$ and the three $pK_a$ values of the hexadentate would then be $pK_{a_1} = pK_{a_{int}} - \log(3)$, $pK_{a_2} = pK_{a_{int}} - \log(1)$ and $pK_{a_3} = pK_{a_{int}} - \log(1/3)$ or $pK_{a_i} = pK_{a_{int}} + (i - 2)\log(3)$. Interaction between sites introduces an additional term, largely coulombic, for each $pK_a$ which is assumed in eqn (2) to increase linearly with the charge on the species from which a proton is dissociating.

$$pK_{a_i} = pK_{a_{int}} + b(i - 1) + (i - 2)\log(3). \quad i = 1,2 \text{ or } 3 \qquad (2)$$

The determination of an intrinsic site $pK_a$ and an electrostatic correction, proportional to the net charge, has previously been performed for polymers, using the linear transformation of Tanford[3] eqn (3), which is itself obtained from the Linderstrøm–Lang equation.[4]

$$pH - \log\frac{\alpha}{(1-\alpha)} = pK_{a_{int}} - Cz. \qquad (3)$$

Here, $\alpha$ is the proportion of protonated sites, $z$ is the average net charge and $C$ is electrostatic proportionality factor. The value of $\alpha$ can be determined from the spectrophotometric data [if eqn (1) is valid], or from the potentiometric titration data. The net charge may be calculated from $z = J(\alpha - \alpha_u)$, where $\alpha_u$ is the value of $\alpha$ at which the net charge is zero and $J$ is the maximum number of protons that can be bound.

The author is grateful to one of the referees for suggesting that the interaction term in eqn (2) might not be linear. J. R. Miller, at this Department, has suggested that a coulombic interaction term should be expressed as the sum of pairs of interactions between ions. The number of ways of choosing such pairs increases with the number of ionized sites according to $i!/2!(i-2!)$ or $i(i-1)/2$. The first few terms of this quadratic expression are, therefore, 0, 1, 3 for $i = 1, 2, 3$. The interaction term in eqn (2) would then be $b\{i(i-1)/2.\}$ instead of $b(i-1)$. However, the experimental results are more consistent with a linear effect of charge on $pK_a$. In either case, only two parameters, $pK_{a_{int}}$ and $b$ need to be optimized to determine all three $pK_a$ values.

The reliability of the spectrophotometric and potentiometric methods are compared.

## SPECTROPHOTOMETRIC ANALYSIS

The computer program NONLIN15[5] was used for non-linear, least squares regression analysis of the titration data. The program uses the Gauss–Newton–Marquardt algorithm to optimize the $pK_a$ values from spectrophotometric and potentiometric data.[5,6] New analytical partial derivatives for $\partial A/\partial\epsilon_i$ were calculated to introduce correlation eqn (1). Since the analytical derivatives for absorptivities are simply the species concentrations, the required derivatives are easily calculated from eqn (4).

$$\partial A/\partial\epsilon_i = [L^{-3}] + ([LH_3] - [L^{-3}])i/3. \quad i = 0,1,2,3 \qquad (4)$$

The partial derivatives of the two underlying molar absorptivities, $\epsilon_0$ and $\epsilon_3$, are then given by eqn (5) and (6).

$$\partial A/\partial\epsilon_0 = \Sigma[(\partial A/\partial\epsilon_i)(\partial\epsilon_i/\partial\epsilon_0)] \qquad (5)$$

$$\partial A/\partial\epsilon_3 = \Sigma[(\partial A/\partial\epsilon_i)(\partial\epsilon_i/\partial\epsilon_3)] \qquad (6)$$

The derivatives $\partial\epsilon_i/\partial\epsilon_0$ and $\partial\epsilon_i/\partial\epsilon_3$ required in eqns (5) and (6) are easily calculated from eqn (1) (*e.g.* $\partial\epsilon_i/\partial\epsilon_0 = 2/3$).

## POTENTIOMETRIC ANALYSIS

Equation (2) indicates that only two parameters, $pK_{a_{int}}$ and $b$, define all three $pK_a$ values. Optimization of $pK_{a_{int}}$ and $b$ was again accomplished using NONLIN15. Analytical

partial derivatives for $\partial pH/\partial pK_{a_{int}}$ and $\partial pH/\partial b$ are required. These were obtained from eqns (7) and (8).

$$\frac{\partial pH}{\partial pK_{a_{int}}} = \sum_{i=1}^{3} \frac{\partial pH}{\partial pK_{a_i}} \frac{\partial pK_{a_i}}{\partial pK_{a_{int}}} \quad (7)$$

$$\frac{\partial pH}{\partial b} = \sum_{i=1}^{3} \frac{\partial pH}{\partial pK_{a_i}} \frac{\partial pK_{a_i}}{\partial b} \quad (8)$$

$$\frac{\partial pH}{\partial pK_{a_{int}}} = \sum_{i=1}^{3} \frac{\partial pH}{\partial pK_{a_i}} \quad (9)$$

$$\frac{\partial pH}{\partial b} = \sum_{i=1}^{3} \frac{\partial pH}{\partial pK_{a_i}} (i-1). \quad (10)$$

The evaluation of analytical partial derivatives $\partial pH/\partial pK_{a_i}$ in eqns (7) and (8) has been discussed previously.[5,6] Equations (9) and (10) follow, since, in the case of a linear interaction term, we find from eqn (2) that $\partial pK_{a_i}/\partial pK_{a_{int}}$ is unity while $\partial pK_{a_i}/\delta b$ is simply $i-1$ [or $i(i-1)/2$ for the quadratic interation term]. The statistical terms in eqn (2) were provided and fixed during optimization. Other optimized parameters were the electrode zero, initial acidity and ligand concentration.

## EXPERIMENTAL

Titrations were performed using an automated titrator which has been described previously.[5] This acquires data for the pH, titrant volume, absorbance at a monitor wavelength and full spectra at regular intervals of absorbance change. Hydrochloric acid solution ($0.2M$) and potassium hydroxide ($0.2M$) were prepared from nominally $1M$ Aldrich Volumetric Standards. Ionic strength was maintained at $0.1M$ with potassium chloride (BDH Analar). All solutions were made up with 18MΩ/cm water. Temperature was maintained at $25.0 \pm 0.1$°C with a Grant-Barrington thermocirculator. The hexadentate chelator *N,N′,N″*-tris[2-(3-hydroxy-2-oxo-1,2-dihydropyridin-1-yl) acetamido]ethylamine was synthesized and purified in our laboratory. The calibration titration and all subsequent titrations were performed without removal of the glass electrode. Factor analysis was carried out using a QuickBasic 4.5 program which implements Hotelling's original procedure with Horst's scaling factor and an initial trial vector given by a zero-one vector with one in the position of the largest diagonal entry in the symmetrical matrix being factored, and zero for all other elements.[7]

## RESULTS

### *Spectrophotometric titrations*

Spectra (350–200 nm) taken at intervals during the titration are shown in Fig. 1. Two isosbestic points at 300 and 275 nm and three temporary isosbestic points at 243, 227 and 207 nm are apparent. Factor analysis of the data matrix from 350–250 nm, where only the heterocycle changes in absorbance, gives only two components. This indicates that over this wavelength range the spectra of the four species defined by three $pK_a$ values, are all linear combinations of two spectra but does not necessarily mean that the linear combination coefficients are *linearly* related to proton stoichiometry. However, the additional observation of the isosbestic points at 300 and 275 nm in this conserved titration system *does* require that linear combination coefficients are *linearly* related to proton stoichiometry. The assumption of eqn (1) is, therefore, fully justified.

Factor analysis of the data matrix using the data from 250–200 nm gives the three components shown in Fig. 2. The extra component is required to account for the spectrum of the fifth species resulting from ionisation of the tertiary amine group. The spectra of the four remaining species $LH_3$, $LH_2^-$, $LH^{-2}$ and $L^{-3}$ are, therefore, still constructed from just two principal components. Non-linear regression analysis of these three principal components according to correlation eqn (1), is shown in Fig. 2. The optimized parameters are given in

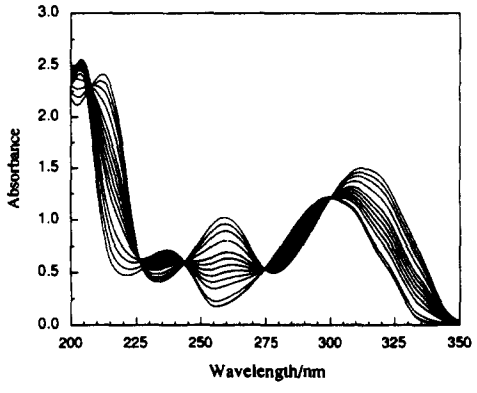


Fig. 1. Spectra of compound 1 from 350 to 200 nm at pH values of 3.310, 5.768, 6.656, 7.520, 8.079, 8.272, 8.439, 8.587, 8.726, 8.862, 9.134, 9.405, 9.678, 10.217. Absorbance increases with increasing pH at 220, 258 and 325 nm.

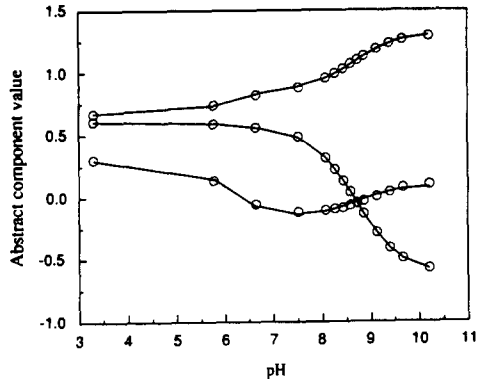


Fig. 2. Factor analysis of the absorbance data from 250 to 220 nm (○). The solid lines are simulated from the parameters in Table 1, optimized by non-linear regression.

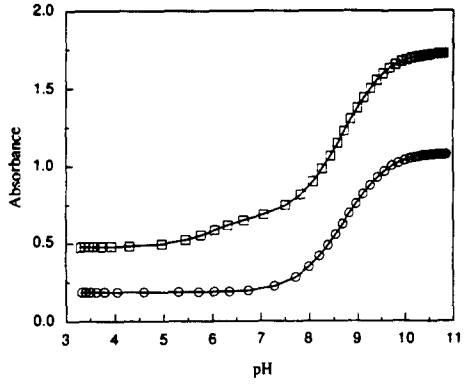


Fig. 3. Single wavelength titration of 1 at 258 nm, (○); and 220 nm (□). The ionization of the tertiary amine group ($pK_a$ 5.88) is only apparent at 220 nm.

Table 1, column 1. The single wavelength titrations at 220 and 250 nm are shown in Fig. 3. At 258 nm only the heterocycle changes in absorbance, while at 220 nm an additional sigmoid for the ionization of the central tertiary amine is apparent. Non-linear regression analysis of the single wavelength spectrophotometric titration data at 220 nm was performed according to correlation eqn (1). The molar absorptivities of $LH_3$ ($\epsilon_3$) and $L^{-3}$ ($\epsilon_0$) were, therefore, optimized as independent variables, while $\epsilon_1$ and $\epsilon_2$ were calculated from eqn (1). The molar absorptivity of the species $LH_4^+$ ($\epsilon_4$) which has the tertiary amine protonated, was also optimized as an independent variable. Optimized parameters are shown in Table 1, column 2.

*Potentiometric titration*

Potentiometric titrations at two ligand concentrations are shown in Fig. 4. The buffer region around pH 6 is the result of ionization of the central tertiary amine of the tripodal backbone. The ionization of the hydroxyl groups of the three heterocycles, produces a buffer region (pH 8–10) which extends for three times the width of the tertiary amine group buffer region. Analysis was performed using the correlation in eqn (2), initially without reference to the spectrophotometric data. Global non-linear regression optimization of the intrinsic site $pK_a$ ($pK_{a_{int}}$) and the interaction term ($b$) from the two potentiometric titrations, gave values of $pK_{a_{int}} = 8.660 \pm 0.008$ and $b = 0.099 \pm 0.006$. The first heterocyclic proton dissociation ($LH_3 = LH_2^- + H^+$) leads to the formation of a mono-anion from a neutral ligand. The coulombic interaction term is therefore zero and only the statistical term $(i-2)\log(3) = -0.0477$ contributes in eqn (2) to give $pK_{a_1} = 8.183 \pm 0.008$. The second and third dissociation constants can similarly be calculated from eqn (2). The fourth $pK_a$ for the

Table 1. The four $pK_a$ values of *N,N′,N″*-tris[2-(3-hydroxy-2-oxo-1,2-dihydropyridin-1-yl)acetamido]ethylamine (1), optimized from spectrophotometric data using correlation eqn (1) and from potentiometric data using correlation eqn (2)

| | | Spectrophotometric data optimized according to eqn (1) | | Potentiometric data optimized according to eqn (2) | |
|---|---|---|---|---|---|
| | | Column 1 Principal components 350–250 *nm* | Column 2 Single wavelength 220 *nm* | Column 3 Both $b$ and $pK_{a_{int}}$ optimized | Column 4 Value of $b$ fixed at 0.081, $pK_{a_{int}}$ optimized |
| $pK_a$* | $LH_4^+ = LH_3 + H^+$ | 6.08 (0.06) | 5.993 (0.005) | 5.87 (0.03) | 5.88 (0.03) |
| $pK_{a_2}$ | $LH_3 = LH_2^- + H^+$ | 8.15 (0.05) | 8.132 (0.008) | 8.183 (0.008) | 8.19 (0.01) |
| $pK_{a_2}$ | $LH_2^- = LH^{-2} + H^+$ | 8.69 (0.04) | 8.686 (0.005) | 8.76 (0.014) | 8.75 (0.01) |
| $pK_{a_3}$ | $LH^{-2} = L^{-3} + H^+$ | 9.23 (0.06) | 9.249 (0.005) | 9.33 (0.022) | 9.31 (0.01) |
| | Intrinsic site $pK_a$ | 8.63 (0.05) | 8.609 (0.005) | 8.660 (0.008) | 8.672 (0.005) |
| | Interaction term ($b$) | 0.064† | 0.081† | 0.099 (0.006) | 0.081†‡ |

*The $pK_a$ of the central tertiary amine group.
†Obtained from the average of $(pK_{a_3} - pK_{a_2})/2 + (pK_{a_2} - pK_{a_1})/2 - \log(3)$.
‡Fixed during optimization.

tertiary amino group was optimized simultaneously as an independent variable to give $5.87 \pm 0.03$.

## DISCUSSION

Correlation eqn (1), which linearly relates absorptivities to proton stoichiometry, has been shown here to be valid on the basis of an isosbestic point *and* the presence of only two principal components for the four species defined by the three heterocycle $pK_a$ values. Application of correlation eqn (1) to the analysis of spectrophotometric data at 220 nm (Table 1, column 2) gives $pK_a$ values with a spacing of $0.563 \pm 0.008$ ($pK_{a_3}$–$pK_{a_2}$) and $0.554 \pm 0.005$ ($pK_{a_2}$–$pK_{a_1}$). The regular spacing of the $pK_a$ values, within experimental error, is independent evidence of the validity of the linear interaction term used in the potentiometric correlation eqn (2), rather than the quadratic interaction term. From eqn (2) the spacing between successive stepwise ionizations $pK_{a_{i+1}}$ and $pK_{a_i}$ is given by eqn (11), from which eqn (12) gives the interaction term $b$.

$$pK_{a_{i+1}} - pK_{a_i} = b + \log(3) \qquad (11)$$

$$b = pK_{a_{i+1}} - pK_{a_i} - \log(3). \qquad (12)$$

The mean spacing between successive $pK_a$ values ($\{pK_{a_3}$–$pK_{a_2}\}/2 + \{pK_{a_2}$–$pK_{a_1}\}/2$) is 0.558. Using this value for $pK_{a_{i+1}} - pK_{a_i}$ in eqn (12), gives the spectrophotometrically determined interaction term $b$ as 0.081.

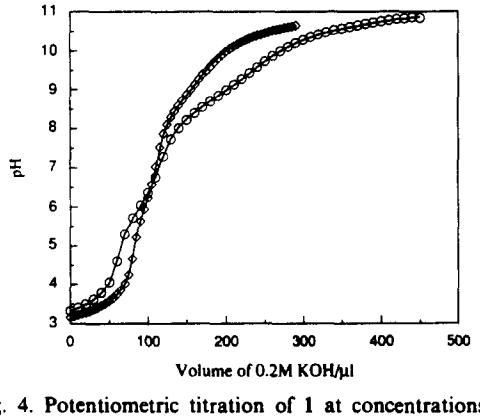


Fig. 4. Potentiometric titration of 1 at concentrations of 0.214 nm, ⟨◇⟩; 0.428 mM, (○), with 0.2*M* KOH. The solid lines are simulated with the optimized parameters. The interaction term $b$ in this plot was fixed at the value determined from the spectrophotometric titration (0.081), and the remaining parameters optimized. When $b$ was optimized simultaneously a value of $0.099 \pm 0.006$ was obtained with no significant improvement in fit.

Optimization of the potentiometric data using eqn (2) gives the results shown in Table 1, column 3. Here the value of $b$ is 0.099 rather than 0.081 determined spectrophotometrically. However, if the value of $b$ is fixed at 0.081 during optimization of the potentiometric data (Table 1, column 4), the goodness of fit is not significantly impaired (solid line in Fig. 4). A satisfactory fit was also obtained using the quadratic interaction term $i(i-1)/2$, however, the separation of the $pK_a$ values obtained in this way ($pK_{a_3}$–$pK_{a_2} = 0.621$ and $pK_{a_2}$–$pK_{a_1} = 0.549$) were not consistent with the values obtained spectrophotometrically.

The best procedure, therefore, is to optimize the spacing between the $pK_a$ values from the spectrophotometric data according to the correlation of eqn (1). This eliminates the effect of several potential sources of systematic error such as errors in the concentration of ligand, initial acidity, contamination by carbonate and $pK_w$. The value of $b$ then calculated from eqn (12), may then be fixed during optimization of the potentiometric data according to eqn (2). The rigorous internal calibration of the glass electrode, which is possible with potentiometric titrations, can then be applied. The values obtained in this way were $pK_{a_1} = 8.19$ ($\pm 0.01$), $pK_{a_2} = 8.75$ ($\pm 0.01$), $pK_{a_3} = 9.31$ ($\pm 0.01$) while the tertiary amine has a $pK_a$ of 5.88 ($\pm 0.03$). This low tertiary amine $pK_a$ is presumably due to the partial positive charge on the three amide functions. It would, of course, be simple to include both correlation eqn (1) and (2) in the analysis of the spectrophotometric titration. In conclusion, correlation eqn (1) is valid if the interaction energy between adjacent ionisable sites is linear with respect to proton stoichiometry and this interaction leads to linear alteration of molar absorptivities. This is true, within experimental error, for molecule 1 although the interaction between sites has been shown to be a minor contribution to the spacing between successive $pK_a$ values compared to the statistical term. Larger interaction energies may lead to shifts in the $\lambda_{max}$ of absorption peaks. The assumption of linear alteration of molar absorptivities will then be only approximately valid for wavelengths over which the first derivative of the spectrum is approximately constant. The presence of an isosbestic point *and* the presence of only two principal components for the $n + 1$ absorbing species in factor analysis of the absorbance data should be used to confirm the validity of eqn (1).

*Acknowledgement*—I wish to acknowledge J. R. Miller at this Department for helpful discussion of the manuscript.

## REFERENCES

1. A. Braibanti, F. Dallavalle and E. Fisicaro, *Ann. Chim.* 1988, **78**, 679.
2. M. Streater, P. D. Taylor, R. C. Hider and J. Porter, *J. Med. Chem*, 1990, **33**, 1749.
3. Y. Nozaki, L. Bunville and C. Tanford, *J. Am. Chem. Soc*, 1959, **81**, 5523.
4. K. Linderstrøm-Lang, *Compt. Rend. Trav. Lab. Carlsberg*. 1924, **15**, (7).
5. P. D. Taylor, I. E. Morrison and R. C. Hider, *Talanta*, 1988, **35**, 507.
6. J. R. Miller and P. D. Taylor, *Talanta*, 1989, **36**, 879.
7. E. E. Cureton and R. B. D'Agostino, *Factor analysis: an Applied Approach*, pp. 146–151. Laurence Erlbaum Associates, U.S.A., 1983.

Pergamon

0039-9140(95)01499-3

*Talanta*, Vol. 42, No. 6, pp. 851–860, 1995

0039-9140/95 $9.50 + 0.00

# FLAME AAS DETERMINATION OF LEAD IN WATER WITH FLOW-INJECTION PRECONCENTRATION AND SPECIATION USING FUNCTIONALIZED CELLULOSE SORBENT

ABDULMAGID M. NAGHMUSH, KRYSTYNA PYRZYŃSKA and MAREK TROJANOWICZ*
Department of Chemistry, University of Warsaw, Pasteura 1, 02-093 Warsaw, Poland

(*Received* 15 *March* 1994. *Revised* 6 *December* 1994. *Accepted* 6 *December* 1994)

**Summary**—The on-line solid phase extraction of trace amount of lead in flow-injection system with flame AAS detection was investigated using cellulose sorbents with phosphonic acid and carboxymethyl groups, $C_{18}$ sorbent non-modified and modified with Pyrocatechol Violet or 8-quinolinol, commercial chelating sorbents Chelex 100 and Spheron Oxin 1000, non-polar sorbent Amberlite XAD-2 modified with Pyrocatechol Violet and several cation-exchange resins. The best dynamic characteristics of retention were observed for functionalized cellulose sorbents. For Cellex P assumed as optimum sorbent, elution with a separate fractions of nitric acid and ethanol allows the differentiation between tetraalkyllead and sum of inorganic lead and organolead species of smaller number of alkyl groups. The detection limit for the determination of inorganic Pb(II) was estimated as 0.17 $\mu$g/l. at preconcentration from 50 ml sample at a flow rate of 7 ml/min.

Solid-phase extraction (SPE) is a preconcentration technique of rapidly growing importance in trace metal determination with atomic absorption spectrometry. The main advantage of this is the possibility of the use of a relatively simple detection system with flame atomization instead of flameless techniques, which require more expensive equipment and are usually much more sensitive to interferences from macrocomponents of various natural matrices. Especially efficient preconcentration can be carried out in flow-injection (FI) systems and this methodology has been discussed in several reviews.[1-3]

Lead is a trace heavy metals of great importance in environmental protection, and the development of a fast and efficient method for its determination has been the subject of numerous studies. In recent years growing attention has been paid not only to the determination of total lead content, but also to its speciation, with particular emphasis to very toxic organolead species, mostly using chromatographic methods interfaced with atomic absorption spectrometry.[4-6]

In SPE of lead species in FI systems, interactions based on chelate formation are generally utilized. The appropriate ligand is immobilized on a stationary support or is dissolved in the carrier solution and sorption of chelates formed on non-polar sorbents is utilized for the preconcentration.

The commercially available chelating resins Chelex 100 with imminodiacetic groups was among the earliest used for that purpose,[7,8] as well as its Japanese analogue Muromac A-1,[9] although their use is troublesome because of swelling of the resin and changes of the microcolumn packing during elution of retained metal ions with solutions of mineral acids.

The most commonly used sorbents for the on-line preconcentration of lead are those containing immobilized 8-quinolinol. They include commercially available Spheron Oxin 1000[10] or the resin synthesized by cross-linking with appropriate aldehyde.[11] Sorbents with oxine immobilized on controlled-pore glass[12,13] or silica gel[14,15] were more frequently used. Sorption of oxine chelates formed in the solution on non-polar resin Amberlite XAD-2 was also reported.[16] In the latter case similar results were obtained for oxine and pyrrolidine dithiocarbamate. A strong influence of the presence of other cations including Ca and Mg was observed for oxine immobilized on silica gel.[14] The selectivity

*Author to whom correspondence should be addressed.

of lead preconcentration can be improved by the use of appropriate masking agent.[15]

The preconcentration of Pb(II) chelates with dithiocarbamate was also carried out with the use of a column with bonded silica reversed-phase sorbent with octadecyl functional groups.[17-19] The sorption on silica and $C_{18}$ bonded silica columns was employed for the speciation of Pb(II) complexes,[20] whereas Amberlite XAD-4 modified with thioglycolate complexing group was applied for efficient Pb(II) preconcentration.[21] Preconcentration of Pb(II) based on ion-exchange in FI-AAS systems was reported only with the use of activated alumina.[22]

The aim of this study was to investigate the possibility of the use of commercial cellulose sorbents for on-line Pb(II) preconcentration in FI-AAS systems. They should be suitable for such an application owing to very fast sorption and desorption properties. A study on the possibility of differentiation between inorganic and organic lead species using different eluents were also carried out. The use of Cellex P for off-line preconcentration of lead and other metals was reported earlier.[23,24]

## EXPERIMENTAL

### *Apparatus*

A Beckman atomic absorption spectrometer model 1272 equipped with an Unilam air/acetylene burner was used for AAS measurements. The measurements were performed at 283.3 nm, using a HCl lamp at 10 mA current and at slit width 0.41 nm. In conventional measurements with an aspiration nebulizer the uptake was 3.5 ml/min. The output absorbance signal was recorded with a potentiometric strip-chart recorder Knauer 1000 (Berlin, Germany).

The flow injection manifold consisted of a peristaltic pump model MS/4 Reglo from Ismatec (Zurich, Switzerland), low pressure rotary injection valve model 5020 from Reodyne (Cotati, CA, U.S.A.) and a home-made rotary injection valve. The manifolds were assembled using teflon tubing of 0.8 mm i.d. The same tubing of 8 cm length was used for the coupling between the flow injection manifold and the flame AAS. The FI carrier flow rate was lower than the nebulizer uptake and the nebulizer was working on starvation mode without any compensation. For elution of tetraethyl lead loaded columns with different solvents a teflon tubing loop was used, without need of the use of solvent resistant pump tubes.

A digital pH meter model OP-211/1 from Radelkis (Budapest, Hungary) was used for pH measurements and plate shaker model 357 from Elpan (Warsaw, Poland) was used for static mode experiments.

### *Reagents*

A 1000 ml/l. Pb(II) standard solution was obtained from the Research and Development Centre for Standard and Reference Materials (Warsaw, Poland) and diluted as required. For preparation of all solutions deionized water from the Waters Milli-Q system was used.

Pyrocatechol Violet (PV) was from BDH chemicals and 8-quinolinol from POCh (Gliwice, Poland). Alkyllead compounds used were a kind gift from Wilhelm University, Munster, Germany and they are abbreviated in the text as follows: DMLCl, dimethyllead chloride; TriMLCl, trimethyllead chloride; DELCl, diethyllead chloride; TriELCl, triethyllead chloride; TEL, tetraethyllead.

The following cationic sorbents were used: Cellex P (CP) and Cellex-CM (CCM) from Bio-Rad (USA) which is highly purified cellulose powder with phosphonic acid or carboxymethyl exchange groups of ion-exchange capacity 0.8 and 0.65 meq/g, respectively; chelating resin Chelex-100 from Bio-Rad; chelating resin Spheron-Oxine 1000 containing 8-quinolinol immobilized on glycol methacrylate from Lachema (Brno, Czechoslovakia); Amberlite XAD-2 from BDH; reversed phase bonded silica gel with octadecyl functional groups, 40–60 $\mu$m diameter, from POCh (Gliwice, Poland); Dowex 50 W × 4 cation exchanger, 50–100 mesh from Serva (Germany); Varion KS cation exchanger from Nitrokemia (Hungary).

### *Preparation of Amberlite XAD-2 loaded with PV*

The dry XAD-2 resin (1 g) was washed with 2*M* HCl, distilled water, 1*M* NaOH and distilled water again to remove traces of soluble species. The resin was put in a stoppered bottle, 50 ml PV solution containing 0.045 g of the reagent was added and the bottle put in a mechanical shaker for 1 hr. The resin was filtered out and washed with distilled water, ethanol and left to be air-dried.

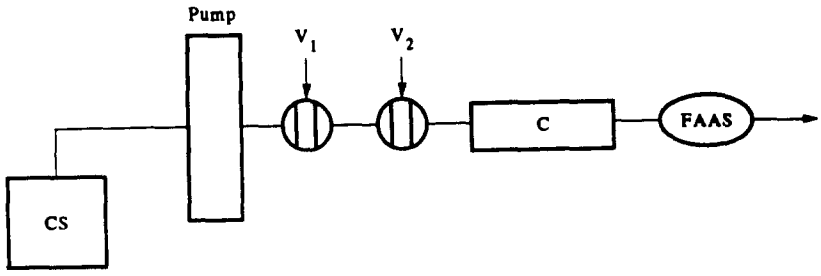


Fig. 1. Schematic diagram of flow-injection system used for the optimization of preconcentration and elution conditions. CS, container with carrier solution; $V_1$, $V_2$, injection valves; C, column with sorbent; FAAS, flame atomic absorption spectrometer.

*Retention of* Pb(II) *on different sorbents in static conditions*

To 0.2 g of the sorbent, 20 ml solution containing 1 mg Pb(II) was added, the pH of the solution was adjusted with nitric acid or sodium hydroxide to the required value, and the mixture shaken for 1 hr on a plate shaker. The mixture was left to settle and the Pb concentration determined by FAAS in conventional mode with aspiration of analyte solution.

*On-line preconcentration of* Pb(II)

The manifold used for the optimization of the conditions for the on-line preconcentration is shown in Fig. 1. Valve $V_1$ is used for the injection of the Pb(II) solution, and $V_2$ for the injection of the eluent. C is a microcolumn made of 1 ml plastic pipette tip, packed with the sorbent. The solid sorbent is held in place inside the column by placing a piece of plastic foam in the outlet of the column. For large volume samples $V_1$ is removed from the manifold and the sample is continuously aspirated.

*Determination of the ion exchange breakthrough capacity*

The breakthrough capacity of the sorbents was determined by pumping 5 mg/l. Pb(II) solution through a column with a packed bed of 20 mm height (400 $\mu$l volume) at flow rate of 6 ml/min until the concentration of the effluent was the same as the feed ($C/C_0 = 1$), 50 ml effluent portions were collected, in which the Pb(II) content was measured by conventional aspiration and flame AAS detection.

*Retention and recovery of* Pb(II) *on Cellex-P*

A column of bed height 20 mm (400 $\mu$l volume) was used. Two hundred milliliters of 0.1 mg/l. Pb(II) solution was pumped at 5 ml/min. The preconcentrated Pb(II) was eluted by two successive portions of 1 ml of 1*M* nitric acid in a 4 ml volumetric flask and then the Pb concentration was determined by conventional FAAS.

*Effect of the presence of common cations on the retention of* Pb(II) *on different sorbents*

The effect of the presence of Na, K, Mg, Ca, Cu, and Fe(III) cations on the retention of Pb(II) on different sorbents was examined.

The microcolumn used was 20 mm bed height (400 $\mu$l volume). Using 25 ml of 0.1 mg/l. Pb(II) solution containing the interfering cation Na, K, Mg, Ca at concentrations up to 200 mg/l., and for Cu, and Fe(III) up to 20 mg/l. were examined. The elution signal obtained was compared to the signal of solution without interferents.

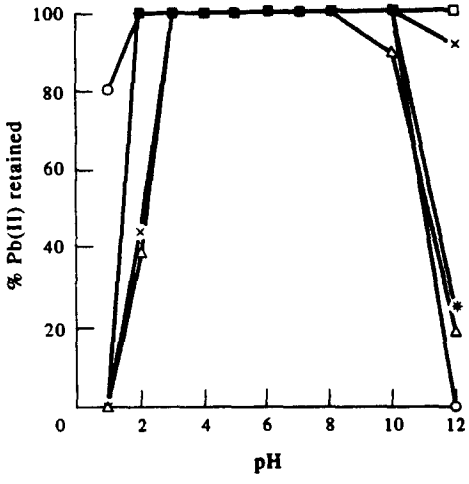


Fig. 2. Effect of pH on retention of Pb(II) in static conditions for Cellex P (*), Cellex-CM (△) Spheron Oxin 1000 (○) Chelex-100 (=) and Varion KS (×).

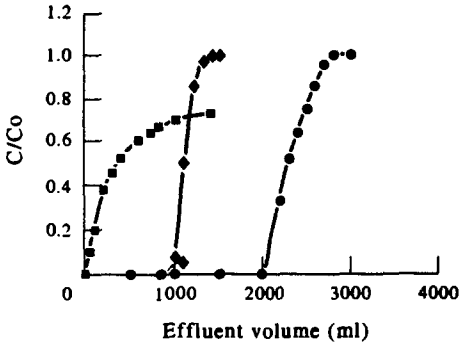


Fig. 3. Breakthrough curves for Cellex P (●), Cellex-CM (◆) and Spheron Oxin 1000 (■) columns for the continuous delivery of 5.0 μg/l. Pb(II) at flow rate 6.0 ml/min.

### *Speciation of lead in natural samples with Cellex P sorbent*

The collected water samples, were filtered, using a 0.45 μm filter, and acidified to pH 2.5 with nitric acid.

Samples (50 ml) were used for preconcentration at flow rate of 5 ml/min, two portions were taken from each sample, one spiked with Pb(II) and TEL, while the other was analyzed as collected for inorganic lead and TEL. The inorganic lead with the organolead compounds except TEL were eluted with 1*M* nitric acid while TEL was eluted with ethanol.

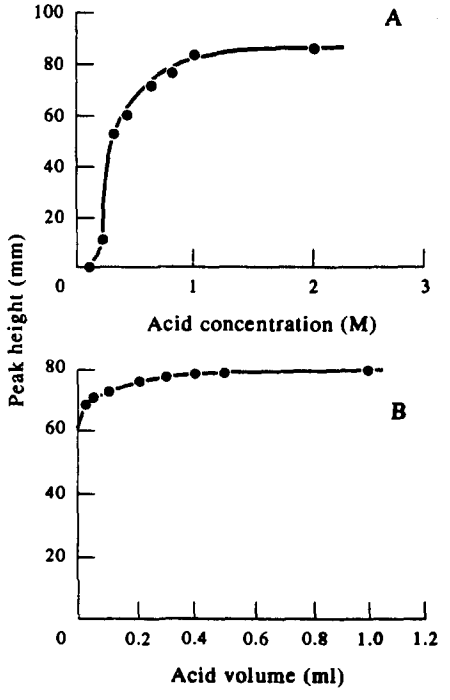


Fig. 4. Effect of nitric acid concentration at injection volume 1 ml (A) and of the injection volume of 1*M* nitric acid (B) on peak height corresponding to the elution of Pb(II) retained on Cellex P sorbent from 1.0 ml of 5.0 mg/l. Pb(II) solution at a flow rate of 3.3 ml/min.

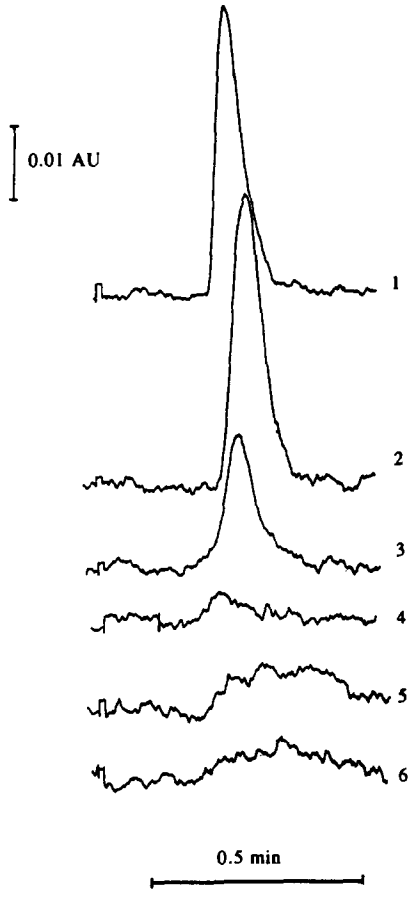


Fig. 5. Elution peaks recorded for Pb(II) with expanded time preconcentrated from 1.0 ml of 5.0 mg/l. Pb(II) solution at (pH 4.5), flow rate 3.3 ml/min and 0.4 ml bed volume for columns with Cellex P (1), Cellex-CM (2), Spheron Oxin 1000 (3), Pyrocatechol Violet loaded XAD-2 (4), Chelex 100 (5), Dowex 50 w × 4 (G) and Varion KS (6). Preconcentration without pH adjustment. Elution with 1.0 ml of 1*M* nitric acid.

## RESULTS AND DISCUSSION

### *Comparison of sorbents for* Pb(II) *preconcentration*

In the preliminary study for the selection of the appropriate sorbent for further study, a number of sorbents was tested for the retention of Pb(II) in batch mode at various pH values (Fig. 2). Pb(II) was completely retained on all sorbents examined in a broad range of pH. For some of the examined sorbents a breakthrough capacity determination was also carried out (Fig. 3). It can be seen that both Cellex P and Cellex CM gave the ideal breakthrough curves, and the capacity was calculated as 0.66 meq/g for CP, and 0.52 meq/g for CCM. In the case of Spheron Oxin 1000 some of Pb(II) was detected in the second portion (50 ml) of effluent and the concentration of Pb(II) in the effluent did not

reach that of the feed Pb solution of 5 mg/l. even after pumping 1400 ml. For Chelex-100 there was no Pb(II) detected even after pumping of more than 7 l. of Pb(II) solution indicating height capacity (2.9 meq/g as stated by the manufacturer).

*Elution of* Pb(II) *retained on Cellex P*

Because of the good properties of cellulose sorbents exhibited in the batch mode, and since CP was successfully used earlier for off-line preconcentration of Pb(II),[23,24] this sorbent was selected for the study of the elution of retained Pb(II). Two acids, hydrochloric and nitric were tested for the elution of Pb(II) retained on CP. Both gave satisfactory results and for further study nitric acid was chosen as it does not precipitate Pb(II). The effect of acid concentration and acid volume is shown in Fig. 4. It was found that 1.0*M* acid completely eluted Pb(II) retained on CP, since when 1 ml of 2*M* nitric acid was injected for the second time, no second peak was observed indicating that the elution was complete and 0.5 ml of 1*M* nitric acid was sufficient for the elution. For further study either 0.5 or 1.0 ml of 1*M* nitric was used for the elution of Pb(II).

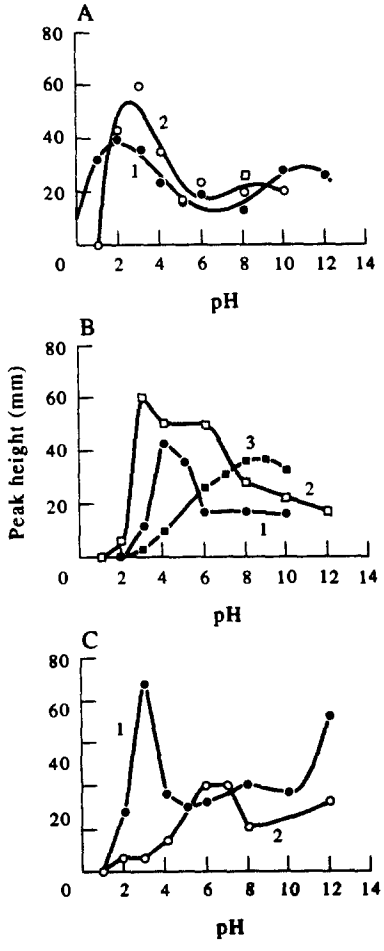


Fig. 6. Effect of pH on flow-injection signal magnitude obtained for preconcentration of Pb(II) from 25 ml 100 μg/l. (Pb(II) solution on 25 mm column with (A) Cellex P (1) and Cellex CM (2); (B) $C_{18}$ silica gel (1), $C_{18}$ loaded with Pyrocatechol Violet (2), $C_{18}$ loaded with oxine (3); (C) Spheron Oxin (1), Pyrocatechol Violet loaded XAD-2 (2). Elution with 1.0 ml of 1*M* nitric acid.

In order to compare different sorbents in dynamic condition the elution signal corresponding to preconcentration of 1 ml 5.0 mg/l. Pb(II) solution of pH 4.5 (without adjustment) on each sorbent of the same bed volume using 1.0 ml 1*M* nitric acid for elution was recorded on an expanded time scale (Fig. 5). The highest peaks were obtained using CP, CCM, and Spheron Oxin 1000, indicating that the elution process of the retained Pb(II) from these sorbents was fast. The elution peaks for two cation exchangers Varion KS and Dowex 50 W × 4 were small and broad indicating that the elution process using this eluent was much slower, while for others, the process was moderate.

*Effect of* pH *and flow rate on the retention of* Pb(II) *on different sorbents*

The effect of pH on the retention of Pb(II) on different sorbents was also studied in dynamic conditions. The column used was 25 mm bed height (500 μl) and 25 ml of 0.1 mg/l. Pb(II) solution was preconcentrated on the sorbent at a flow rate of 6 ml/min. The retained analyte was eluted with 1 ml of 1*M* nitric acid at a flow rate of 3.3 ml/min. It was found that for the sorbents studied the optimum pH was on the acidic side (2–4) except for $C_{18}$ loaded with 8-quinolinol and XAD-2 loaded with PV, in which the optimum pH was in the alkaline range (7–10) (Fig. 6).

The effect of preconcentration flow rate was also studied for the investigated sorbents. It was found that the variation of the flow rate from 3.0 to 10 ml/min had no effect on the signal when CP or CCM were used, while for Spheron Oxin 1000 the signal magnitude was reduced with increasing sampling flow rate.

*Effect of potential interferences*

The obtained results for two Cellex sorbents and oxine sorbent are shown in Table 1. The best selectivity was obtained for Cellex P, where only some positive interference was observed at high Ca concentration. The same effect, however, was found in conventional aspiration of

Table 1. Effect of the presence of other common cations on Pb(II) preconcentrated elution signal for different sorbents (elution with 1 ml of 1*M* nitric acid)

| Sorbent | Interferent concentration (*mg/l.*) | % change in peak height for Pb(II) | | | | | |
|---|---|---|---|---|---|---|---|
| | | Na | K | Ca | Mg | Cu(II) | Fe(III) |
| Cellex P | 5 | — | — | — | — | 0 | 0 |
| | 10 | 0 | 0 | +15 | +5 | 0 | 0 |
| | 20 | — | — | — | — | 0 | 0 |
| | 50 | 0 | 0 | +7.5 | +8 | — | — |
| | 100 | 0 | 0 | +7.5 | +3 | — | — |
| | 200 | 0 | 0 | −32 | +3 | — | — |
| Cellex CM | 5 | — | — | — | — | 0 | −24 |
| | 10 | −4 | 0 | −7 | 0 | 0 | −78 |
| | 20 | — | — | — | — | 0 | −94 |
| | 50 | −13 | −19 | −20 | 0 | — | — |
| | 100 | −36 | −29 | −49 | +11 | — | — |
| | 200 | −68 | −40 | −55 | +11 | — | — |
| Spheron Oxine-1000 | 5 | — | — | — | — | −57 | −36 |
| | 10 | +65 | 0 | 0 | −3 | −61 | −54 |
| | 20 | — | — | — | — | −50 | −64 |
| | 50 | +65 | 0 | 0 | −7 | — | — |
| | 100 | +76 | 0 | 0 | −7 | — | — |
| | 200 | +106 | 0 | 0 | — | — | — |

Pb(II) solution containing calcium. At 100 mg/l. Ca and 10 mg/l. Pb(II) 12% enhancement of signal was observed in comparison to Pb(II) measurement without calcium. This suggests the spectral nature of this interference. A similar effect was also observed for Pb(II) preconcentration on immobilized 8-quinolinol,[14] however, on the contrary preconcentration using Cellex P in the presence of magnesium exhibited a much smaller effect.

For the other tested sorbents much larger interferences were observed. Using $C_{18}$, even in the presence of 50 mg/l. sodium, the Pb signal was reduced by 82% and in the presence of 5 mg/l. Fe(III) no signal was obtained. In the presence of 50 mg/l. Ca or Mg the signal was reduced by 100 and 95%, respectively.

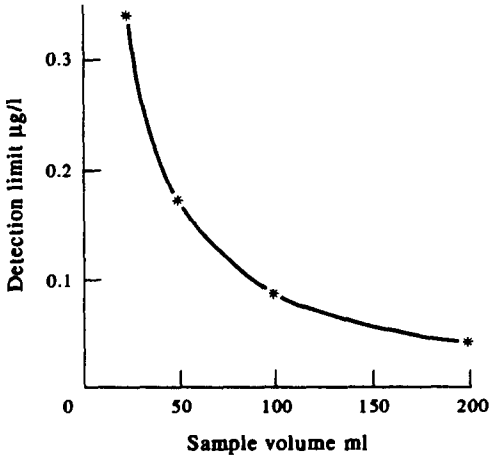


Fig. 7. Effect of the volume of preconcentrated Pb(II) solution on detection limit in flow-injection system with 25 mm column with Cellex P. Preconcentration at flow rate 7.0 ml/min. Elution with 1 ml of 1*M* nitric acid at flow rate 3.0 ml/min.

Using $C_{18}$ loaded with PV (PV was added to the sample), in the presence of 50 mg/l. Na, Ca or Mg the signal was reduced by 55, 82 or 77%, respectively, while in the presence of 5 mg/l. Cu(II) or Fe(III) it was reduced 68 or 81%, respectively.

Using $C_{18}$ loaded with 8-quinolinol, in the presence of 10 mg/l. Mg the Pb signal was reduced by 12%, while in the presence of 5 mg/l. Fe(III) the signal was reduced 11%.

Using XAD-2 loaded with PV, the presence of Na or K at 10 mg/l. the signal was enhanced by 10 or 23%, respectively, and in the presence of Cu(II) or Fe(III) at 5 mg/l. the signal was suppressed by 14 or 75%, respectively.

### *Calibration and detection limit*

For the FIAAS system with C-P column, the linearity of response as a function of preconcentrated sample volume was examined. The sample pH was adjusted to 2.5 with nitric acid. Preconcentration was done at a flow rate of 6 ml/min. In the volume range from 5 to 100 ml, for preconcentrated 10 µg/l. solution the obtained relation was described by the equation: $H = 2.00V + 0.0$, and the correlation coefficient was 1.0 ($n = 10$), where $H$ is the peak height (mm) and $V$ is the sample volume (ml).

For the calibration in the Pb(II) concen-

Table 2. Comparison of the efficiency of Pb(II) preconcentration on solid sorbents in flow injection systems with flame AAS detection

| Sorbent used | Sampling volume (*ml*) | Sampling rate ($hr^{-1}$) | CE value | Reference |
|---|---|---|---|---|
| Activated alumina | 25 | 12 | 50 | 22 |
| Chelex 100 | 10 | 60 | 50–100 | 8 |
| | 10 | 10 | 10–13 | 28 |
| 8-quinolinol on CPG | 100 | 2 | 20 | 12 |
| | 12 | 20 | 13 | 14 |
| Muromac A-1 | 20 | 13 | 20–39 | 9 |
| Cellex P | 50 | 6 | 10–15 | This work |

tration range 10–100 $\mu$g/l. for the sample volume 50 ml, the relation was linear in the range studied. The equation for the plot obtained is: $H = 0.705C + 0.545$, where $H$ is as above and $C$ is the sample concentration in $\mu$g/l., with a correlation coefficient of 0.9989 ($n = 10$).

The detection limit based on the triple value of the standard deviation of the blank for lead (II) determination using a 50 ml sample was estimated as 0.17 $\mu$g/l. The precision at the 10 $\mu$g/l. level was 5.9% RSD ($n = 10$).

The effect of the preconcentrated sample volume on the detection limit was also examined and it was found that the detection limit could be decreased down to 0.04 $\mu$g/l. for sample volume of 200 ml (Fig. 7). The efficiency of the on-line preconcentration is usually given by enrichment factor and concentration efficiency (CE) values. In the system developed for the analyte preconcentration from 50 ml sample containing 10–50 $\mu$g/l. Pb(II), the enrichment factor ranges between 100 to 150. For flow rate 5 ml/min. this corresponds to concentration efficiency value in the range 10–15. As can be seen from the comparison shown in Table 2. This is rather a low value referring to other works reported in the literature, but the developed method, in contrary to previous reports, provides some possibility of speciation.

Some improvement of concentration efficiency can be expected by lowering the sorbent bed dimensions and also the diameter of

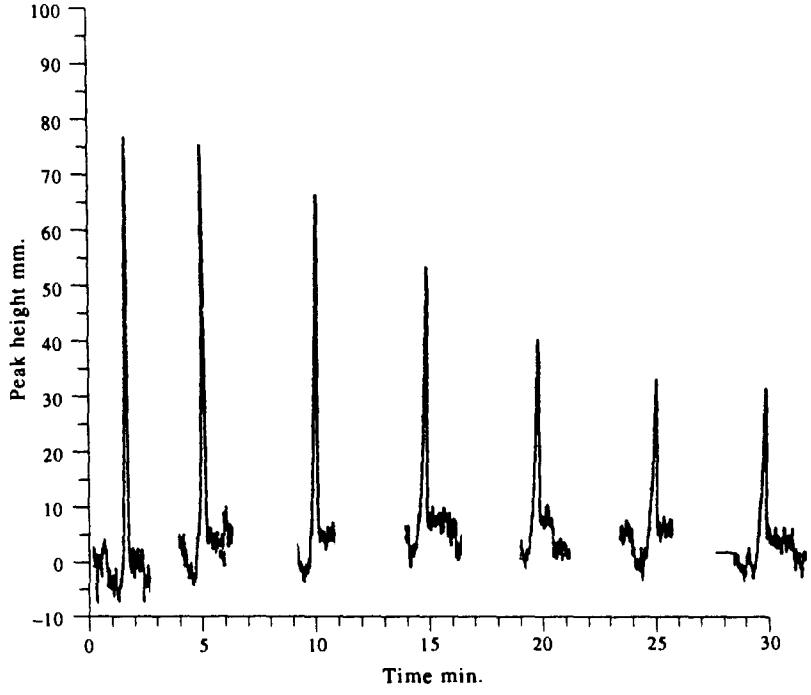


Fig. 8. Variation of elution signal of tetraethyllead preconcentrated on Cellex P with time.

Table 3. Effectiveness of elution of alkyllead compounds and inorganic lead retained on Cellex P 25 mm column of bed volume 0.4 ml (preconcentration from 1 ml of 5 mg/l. Pb solutions, elution with 0.5 ml volume of eluent at flow rate 3 ml/min)

| Preconcentrated lead species | Elution peak height for different eluents (*mm*) | |
|---|---|---|
| | Ethanol | 1*M* nitric acid |
| DML | 0 | 62 |
| TriML | 0 | 70 |
| DEL | 0 | 65 |
| TriEL | 0 | 60 |
| TEL | 60 | 0 |
| Pb(II) | 0 | 60 |

the tubing connecting the FI system with AAS. For a concentration of Pb(II) in the sample larger than 3 $\mu$g/l. a sample volume of 25 ml is sufficient. This will increase the sampling rate up to 10–12 $hr^{-1}$. For the preparation of calibration plot, five different standard solutions are required and it takes about 40 min to perform the calibration procedure. The Cellex P column can be used for months without any significant change of its ion-exchange properties. This corresponds to hundreds of cycles of sorption and elution.

*Sorption of alkyllead compounds on different sorbents*

Using 5 mg/l. tetraethyllead (TEL) solution several sorbents were also tested for the retention of this compound in on-line mode. It was found that using RP $C_{18}$, and Amberlite XAD-2 loaded with PV, most of the analyte passed through the column without retention. Using CP, TEL was completely retained on the column and then it could be completely eluted with ethanol. For the elution of TEL from CP

Table 4. Effectiveness of elution of alkyllead compounds and inorganic lead retained on Cellex P 25 mm, column of bed volume 0.4 ml with consecutive 1 ml portions of 0.1 and 1.0*M* nitric acid (preconcentration from 1 ml of 5 mg/l Pb solutions)

| Preconcentrated lead species | Elution peak height (*mm*) for consecutive elution | |
|---|---|---|
| | 0.1*M* nitric acid | 1.0*M* nitric acid |
| DML | 28 | 68 |
| TriML | 82 | 0 |
| DEL | 20 | 62 |
| TriEL | 20 | 68 |
| TEL | 0 | 0 |
| Pb(II) | 0 | 95 |

Table 5. Parameters of the linear calibration curves obtained in FIAAS measurements of alkyllead compounds retained on Cellex P from 1 ml solutions for the concentration range 1–5 mg/l. (elution with 1 ml of 1*M* nitric acid)

| Alkyllead species | Curve equation* | Correlation coefficient |
|---|---|---|
| DML | $H = -1.08 + 11.08C$ | 0.9983 |
| TriML | $H = -1.24 + 14.03C$ | 0.9991 |
| DEL | $H = -0.43 + 14.34C$ | 0.9993 |
| TriEL | $H = -1.43 + 14.37C$ | 0.9994 |

*$H$ = Peak height in *mm*, $C$ = concentration in *mg/l.*

a number of other solvents were also tested, including methanol, acetone and acetonitrile. However, ethanol was found the best, nitric acid showing no elution of the TEL species.

In the study of TEL retention on CP it was observed that the elution signal was reduced in time without peak broadening (Fig. 8). It can be attributed to several reasons. One of them is the decomposition of TEL by light, which was observed by other authors, too.[25] It can be also caused by the adsorption of the compound on the walls of the container.[26] This may also result from the effect of ethanol on the sorbent since when the column is used the flow rate is reduced owing to the back pressure of the packed resin that became more compact. After about 30 min stabilization, the microcolumn can be used for quantitative determinations.

Several other alkyllead compounds examined (DELCl, DMLCl and TriMLCl) were also completely retained on CP. The ionic alkyllead compounds were found to behave similarly to inorganic Pb(II) in that they were completely eluted by 1*M* nitric acid, while the neutral TEL species was not eluted by the acid as mentioned above. The effectiveness of elution of the different alkyllead compounds is shown in Table 3.

Additionally, it was found that trimethylleadchloride (TriMLCl) was completely eluted by 0.1*M* nitric acid, and since this dilute acid solution did not elute Pb(II), the possibility of

Table 6. Parameters of linear dependence of flow-injection peak height on the volume of preconcentrated 0.1 mg/l. alkyllead solutions for the system with Cellex P column in the volume range from 5 to 50 ml (elution with 1 ml of 1*M* nitric acid)

| Alkyllead species | Curve equation* | Correlation coefficient |
|---|---|---|
| DML | $H = -0.95 + 0.91V$ | 0.9993 |
| TriML | $H = -0.48 + 2.00V$ | 0.9984 |
| DEL | $H = -0.33 + 1.30V$ | 0.9974 |
| TriEL | $H = -0.76 + 1.20V$ | 0.9981 |

$H$ = Peak height in *mm*, $V$ = volume in *ml.*

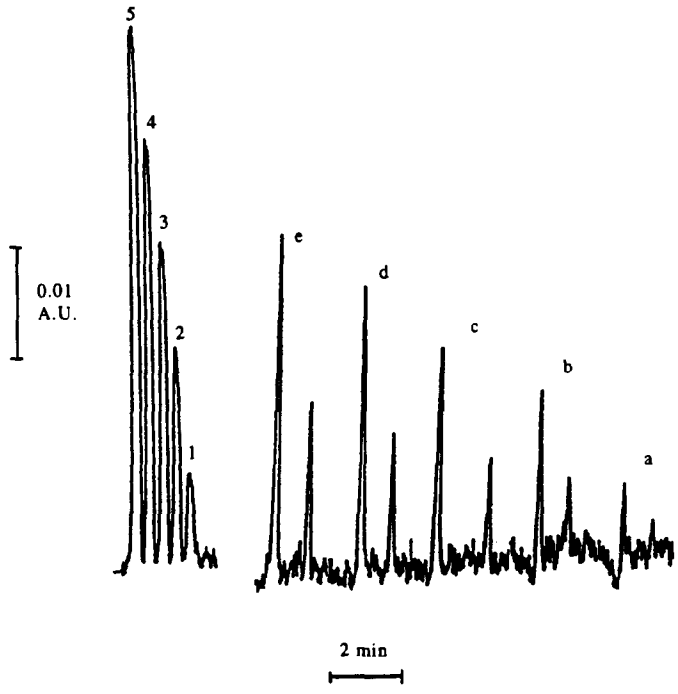


Fig. 9. Examples of recording for flame AAS determination with conventional aspiration (A) obtained for 2 (1), 4 (2), 6 (3), 8 (4) and 10 (5) mg/l. Pb(II) and for flow-injection determination with preconcentration on 20 mm column (B) of solutions containing: (a) 10 $\mu$g/l. Pb(II) and 10 $\mu$g/l. TEL; (b) 20 $\mu$g/l. Pb(II) and 20 $\mu$g/l. TEL; (c) 30 $\mu$g/l. Pb (II) and 30 $\mu$g/l. TEL; (d) 40$\mu$g/l. Pb(II) and 40 $\mu$g/l. TEL and (e) 50 $\mu$g/l. Pb(II) and 50 $\mu$g/l. TEL. Sample volume for preconcentration 50 ml. Elution with 1.0 ml of 1*M* nitric acid for Pb(II) (smaller peak) and 0.5 ml ethanol for TEL (larger peak).

the differentiation of the ionic alkyllead compounds and inorganic lead was tested. It was found, however, that the other ionic alkyllead compounds, dimethylleadchloride, diethylleadchloride and triethylleadchloride (DMLCl, DELCl, and TriELCl) were only partially eluted using the diluted acid (Table 4). So, it can be concluded that the only speciation that can be done is the elution of ionic alkyllead compounds together with inorganic lead by 1*M* nitric acid, then the elution of TEL by ethanol.

The parameters of linear calibration curves obtained in FI-AAS measurements of alkyllead compounds retained on CP from 1 ml solution of concentration range 1–5 and elution with 1 ml of 1*M* nitric acid are shown in Table 5. The parameters of linear dependence on the volume is shown in Table 6.

Table 7. Analysis of natural water samples for lead preconcentrated on Cellex P column of 0.4 ml bed volume for 50 ml sample [Eluent (1) 1.0 ml of 1.0*M* nitric acid for Pb(II); (2) 0.5 ml ethanol for TEL]

| | Lead concentration ($\mu g/l.$) | | | |
|---|---|---|---|---|
| Sample | Pb(II) added | Pb(II) found | TEL added | TEL found |
| Tap water | 0.0 | 8.5 | 0.0 | — |
| | 20.0 | 25.7 | 20.0 | 20.7 |
| G. water I | 0.0 | 4.3 | 0.0 | — |
| | 20.0 | 25.7 | 20.0 | 19.23 |
| G. water II | 0.0 | 8.4 | 0.0 | — |
| | 20.0 | 23.2 | 20.0 | 21.3 |
| G. water III | 0.0 | 2.4 | 0.0 | — |
| | 20.0 | 23.5 | 20.0 | 20.6 |
| River water | 0.0 | 5.9 | 0.0 | — |
| | 20.0 | 27.1 | 20.0 | 19.4 |

The recording of the signal obtained for standard samples containing different Pb(II) and TEL concentrations is shown in Fig. 9.

*Analysis of natural water samples*

The results obtained (Table 7) indicate that the lead level in the water samples analyzed was below the permissible level for drinking water (50 $\mu$g/l.)[27] and the TEL in these samples was below the detection limit of the method which for 50 ml sample was estimated as 1.8 $\mu$g/l. The spiked samples show that the recovery was 81–105% for a spike of 20 $\mu$g/l. of lead from different water samples.

*Acknowledgements*—A.M.N. expresses his gratitude to the Secretary of the Scientific Research of Libya for the scholarship. The authors thank Dr Norbert Buschmann of the Westfalian Wilhelms University, Munster, Germany, for gift of samples of alkyllead compounds. This research was supported by grant No. 2 055 91 01 from the Polish State Committee for Research.

## REFERENCES

1. Z. Fang, S. Xu and S. Zhang, *Anal. Chim. Acta*, 1987, **200**, 35.
2. Z. Fang, *Spectrochim. Acta Rev.*, 1991, **14**, 235.
3. M. Trojanowicz and E. Olbrych-Śleszyniska, *Chem. Anal. (Warsaw)*, 1992, **37**, 111.
4. D. Chakraborti, W. R. A. De Jonghe, W. E. Van Mol, R. Y. A. Van Cleuvenbergen and F. C. Adams, *Anal. Chem.*, 1984, **56**, 2692.
5. L. Ebdon, S. Hill and R. W. Ward, *Analyst*, 1987, **112**, 1.
6. W. M. R. Dirkx, R. J. A. Van Cleuvenbergen and F. C. Adams, *Mikrochim. Acta*, 1992, **109**, 133.
7. S. Olsen, L. C. Pessenda, J. Ruzicka and E. H. Hansen, *Analyst*, 1983, **108**, 905.
8. Z. Fang, J. Ruzicka and E. H. Hansen, *Anal. Chim. Acta*, 1984, **164**, 23.
9. S. Hirata and K. Honda, *Anal. Chim. Acta*, 1989, **221**, 65.
10. V. Kuban and R. Bulava, *Collec Czech. Chem. Commun.*, 1989, **54**, 2674.
11. R. Purohit and S. Devi, *Anal. Chim. Acta*, 1992, **259**, 53.
12. F. Malamas, M. Bengtsson and G. Johansson, *Anal. Chim. Acta*, 1984, **160**, 1.
13. Z. Fang and B. Welz, *J. Anal. At. Spectrom.*, 1989, **4**, 543.
14. S. R. Bysouth, J. F. Tyson and P. B. Stockwell, *Anal. Chim. Acta*, 1988, **214**, 329.
15. S. R. Bysouth, J. F. Tyson and P. B. Stockwell, *Analyst*, 1990, **115**, 571.
16. L. Elei, M. Soylak and M. Dogan, *Fresenius J. Anal. Chem.*, 1992, **342**, 175.
17. J. Ruzicka and A. Arndal, *Anal. Chim. Acta*, 1989, **216**, 243.
18. M. Sperling, X. Yin and B. Welz, *J. Anal. At. Spectrom.*, 1991, **6**, 295.
19. Z. Fang, T. Guo and B. Welz, *Talanta*, 1991, **6**, 613.
20. R. H. Atallah, G. O. Christian and A. E. Nevissi, *Anal. Lett.*, 1991, **24**, 1483.
21. A. G. Howard and R. Danilona-Mizaians, *Anal. Lett.*, 1989, **22**, 257.
22. Y. Zhang, P. Riby, A. G. Cox, W. McLeod, A. R. Date and Y. Y. Cheung, *Analyst*, 1988, **113**, 125.
23. K. Brajter and K. Słonawska, *Anal. Chim. Acta*, 1986, **185**, 271.
24. K. Brajter and K. Słonawska, *Fresenius Z. Anal. Chem.*, 1885, **320**, 142.
25. W. De Jonghe, D. Chakraborti and F. Adams, *Anal. Chim. Acta*, 1980, **115**, 89.
26. R. M. Harrison and M. Radojevc, *Environ. Technol. Lett.*, 1985, **6**, 129.
27. H. H. Rump and H. Krist, *Laboratory Manual for the Examination of Water, Waste Water and Soil*. VCH, F.R.G., 1988.
28. Y. Liu and D. Ingle Jr., *Anal. Chem.*, 1989, **61**, 520.

Pergamon

0039-9140(95)01500-0

*Talanta*, Vol. 42, No. 6, pp. 861–865, 1995

0039-9140/95 $9.50 + 0.00

# DETERMINATION OF ANTHRAQUINONES IN RHUBARB ROOTS, DOCK FLOWERS AND SENNA LEAVES BY NORMAL-PHASE HIGH PERFORMANCE LIQUID CHROMATOGRAPHY

DJ. DJOZAN* and Y. ASSADI

Department of Analytical Chemistry, Faculty of Chemistry, University of Tabriz; Tabriz, Iran

(*Received* 17 *January* 1994. *Revised* 22 *November* 1994. *Accepted* 1 *December* 1994)

**Summary**—A normal-phase high performance liquid chromatography using a 5-$\mu$m Spherisorb-CN column (250 × 4.6 mm i.d.) has been used for determination of the monomeric anthraquinones and their glycosides present in rhubarb roots, senna leaves and dock flower. The effects of various parameters were studied and the conditions for the extraction of the anthraquinones from herbal samples and their chromatographic separation were optimized. The nature and the quantity of anthraquinones and their conjugates were determined with a good precision and accuracy.

## INTRODUCTION

Senna leaves, rhubarb roots and dock flowers are used as oriental laxative medicines. These plants contain a wide variety of compounds including monomeric anthraquinones (as shown below), together with their glycosides and dimeric anthrones glycosides. Sennosides are the purgative principles of these plants[1] and like other glycosides are metabolized by animals and humans into monomeric rhein or other anthraquinones which are the active metabolites.[2,3]

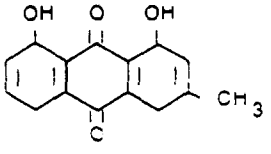

**Chrysophanol**

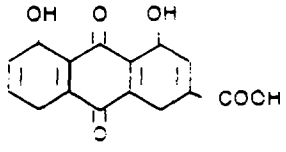

**Rhein**

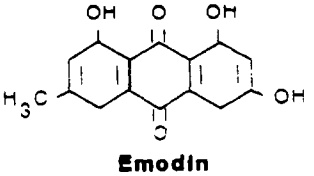

**Emodin**

The natural free anthraquinones are not effective and it has been confirmed that they are reduced into anthrones and anthranoles in the human intestine, and act as laxative compounds.[4] The stimulant laxatives composed of the anthraquinones (*e.g.* senna, rhubarb, *etc.*) are the cause of the greatest side-effects and are often abused by the public,[5–7] therefore the identification and analysis of anthraquinones in herbal samples, pharmaceutical preparations and biological fluids are of great importance.

A few spectrophotometric and electrochemical methods have been reported for the determination of these compounds and their conjugates. An earlier fluorimetric method suffered from a lack of sensitivity and specifity;[7,8] another fluorimetric method involving thin layer chromatographic separation with two solvent systems was somewhat time-consuming and complex.[9] Simultaneous determination of chrysophanol (Ch), rhein (Rh), emodin (Em) and their glycosides in some medicinal plants and pharmaceutical preparations has remained a problem in analytical chemistry for years.[10] Recently, an electrochemical method has been developed for direct analysis of these compounds in chloroform.[11,12] It is still non-selective, but it may be a valuable and new detection system for such compounds in normal-phase liquid chromatography.

The aim of this work was to develop a normal-phase chromatographic method using

*Author to whom all correspondence should be addressed.

chloroform as mobile phase for effective separation and determination of anthraquinones.

## EXPERIMENTAL

### *Chemicals and reagents*

Rhein (Rh), emodin (Em) and chrysophanol (Ch) were from Aldrich-chemie (U.K.). Solvents, acetic acid and all other reagents were purchased from E. Merck (Germany). Chloroform was distilled, poured through the silica column and redistilled.

### *Apparatus*

The HPLC apparatus consisted of Bruker LC-21, equipped with a Bruker UV-Vis detector model LC 313 I, Rheodyne loop injector and Qx–16 Epson personal computer with Epson FX–800 printer. A normal-phase column of Spherisorb-CN (250 × 4.6 mm i.d., particle size 5 $\mu$m) was from Bischoff (Germany).

### *Solutions*

Stock solutions (100 ppm) of Ch, Em and Rh were prepared in chloroform. The standard solutions of 0.01–100 ppm were prepared by dilution of the stock solution with mobile phase, from which a 20 $\mu$l aliquot was injected.

### *Chromatographic procedure*

The column temperature was ambient (25 ± 4°C). For separation of anthraquinones, the isocratic elution with an organic phase of chloroform–concentrated (96%) acetic acid (95:5 v/v) was carried out at a constant flow-rate of 0.7 ml/min. The absorption of the column eluate was monitored at 254 nm.

### *Extraction of anthraquinones from herbal samples*

Rhubarb roots, senna leaves and dock flowers were examined in this work. Dried and powdered herbal samples (0.100 g) were mixed twice with 40 ml water and methanol (50:50). The mixtures were stirred for 15 min, filtered collected and diluted to 100 ml with water (solution A). A 10 ml portion of solution A were extracted three times with 5 ml portions of chloroform. The organic phases were collected into 25 ml conical flasks, 1.25 ml of concentrated acetic acid was added to each flask and then diluted to 25 ml with chloroform (solution B). These solutions were used for determination of monomeric anthraquinones. The impurities were eliminated by a one step pre-extraction of solution A into 5 ml chloroform in alkaline media.

For the determination of glycosides, five 10 ml portions of solutions A, each acidified with 1 ml concentrated HCl and separately refluxed. The refluxing times ranged from 5 to 60 min. The solutions were cooled rapidly and the extraction carried out as in the previous step. The extracts (solution C) were used for the determination of total anthraquinones (free anthraquinones and acid hydrolysed glycosides).

## RESULTS AND DISCUSSION

### *Detection wavelength*

The absorption spectra of Ch, Rh and Em dissolved in mobile phase were studied at 200–700 nm using both batch and stop flow mode. Owing to the remarkable absorption of

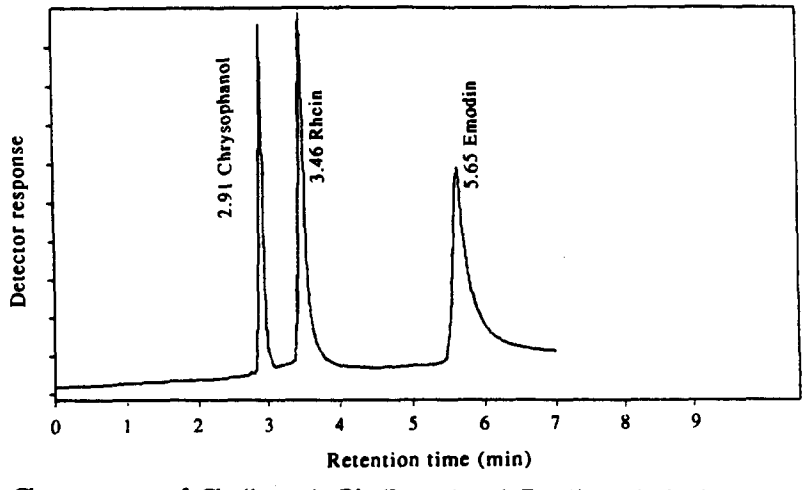


Fig. 1. Chromatogram of Ch (1 ppm), Rh (2 ppm) and Em (4 ppm). Stationary phase: 5-$\mu$m Spherisorb-CN. Mobile phase: chloroform–pure (99.9%) acetic acid (95:5). Flow rate: 1 ml/min.

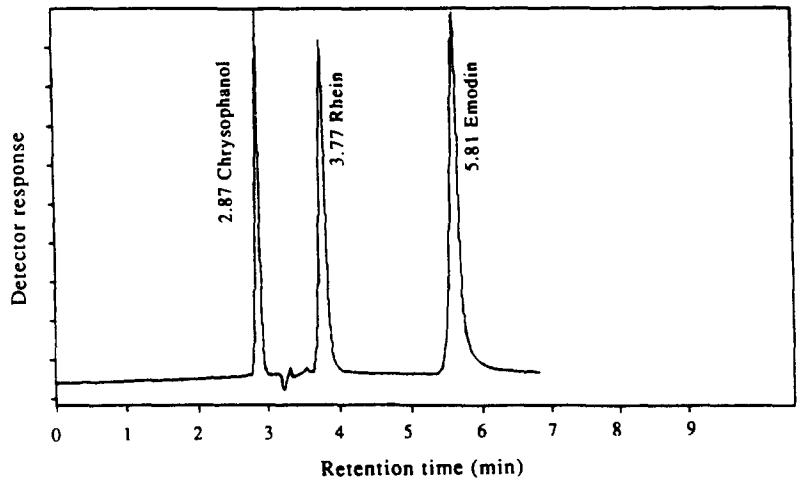


Fig. 2. Chromatogram of Ch (1 ppm), Rh (2 pmm) and Em (4 ppm). Stationary phase: 5-μm Spherisorb-CN. Mobile phase: chloroform–concentrated (96%) acetic acid (95:5). Flow rate: 1 ml/min.

chloroform at $\lambda < 245$ nm, the strong background attenuation increase the noise. Two maxima at about 254 and 430 nm were observed for these compounds. For the sensitive quantitative analysis, the column eluate was monitored at 254 nm.

*Optimization of HPLC parameters*

*Choice of packing material.* One of the best commercially available stationary phases for normal-phase HPLC is the bonded phase with cyano group, therefore we selected 5-μm Spherisorb-CN column (250 × 4.6 mm i.d.).

*Choice of mobile phase.* The pure chloroform was used as mobile phase and the effect of ethanol, methanol and concentrated acetic acid were examined as modifiers. From the obtained chromatograms (Fig. 1), the chromatographic performance characteristic such as plate numbers, $N_1 = 8731$, $N_2 = 5555$ and $N_3 = 3649$ (where 1, 2 and 3 are chromatographic peaks of chrysophanol, rhein and emodin, respectively) and column resolution ($R_s > 1.5$) reveal a good efficiency when 5% v/v pure acetic acid (containing 0.1% water), was added as modifier. It should be noted that the

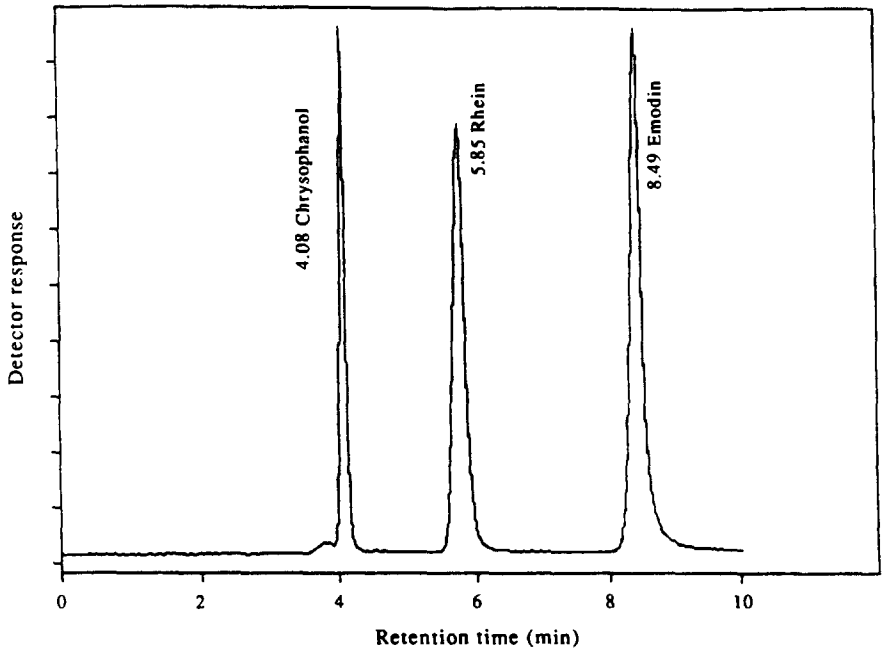


Fig. 3. Chromatogram of Ch (1 ppm), Rh (2 ppm) and Em (4 ppm). Stationary phase; 5-μm Spherisorb-CN. Mobile phase: chloroform–concentrated (96%) acetic acid (95:5). Flow rate: 0.7 ml/min.

Table 1. Quantitative analytical characteristic of the method. Column: Spherisorb-CN (250 × 4.6 mm i.d., particle size 5 μm. Mobile phase: chloroform–concentrated (96%) acetic acid (95:5). Flow rate: 0.7 ml/mn. Injection volume: 20 μl. Detection wavelength: 254 mn

| | Chrysophanol | Rhein | Emodin |
|---|---|---|---|
| Retention time (*min*) | 4.10 ± 0.03 | 5.80 ± 0.08 | 8.50 ± 0.05 |
| Linear calibration range (*mg/l*) | 0.02–30 | 0.06–30 | 0.1–100 |
| Regression equation * | $Y = 9950 + 88800X$ | $Y = -6700 + 58300X$ | $Y = -9270 + 44300X$ |
| Correlation coefficient | 0.99992 | 0.99995 | 0.99997 |
| Limit of detection (*mg/l*)† | 0.01 | 0.005 | 0.02 |
| %RSD ($n = 7$) | 0.72 | 1.24 | 0.79 |

*$Y$ = Peak area, $X$ = concentration (*mg/l*).
†$S/N = 3$.

water content in the mobile phase was only 0.005%. The peak tailing ($T_1 = 1.00$, $T_2 = 1.25$ and $T_3 = 3.15$ for Ch, Rh and Em, respectively) was probably caused by the packing, because it has been shown that the residual silanol group on partially reacted bonded phase can interact with solutes in a mode different from the bonded stationary phase, which often leads to tailing peaks.[13,14]

*Effects of traces of water.* The chromatograms obtained with a mixture of chloroform–acetic acid–water (95:4.8:0.2), prepared by means of pure chloroform and acetic acid (96%), is illustrated in Fig. 2. The comparison of the chromatograms in Figs 1 and 2 reveals that increasing the water amount in the mobile phase (from 0.005 to 0.2%) effectively improves the peaks symmetry ($T_1 = 1.00$, $T_2 = 1.00$, $T_3 = 1.05$) and plate numbers ($N_1 = 9577$, $N_2 = 9090$ and $N_3 = 11904$) without retention times distortion. These phenomena probably are due to the presence of small amounts of water molecules in the mobile phase that cause a decrease in the tendency of the residual silanol group to interact with susceptible solutes.

*Flow rate.* For the investigation of the optimum flow rate the variation of plate height ($H$) *vs.* mobile phase velocity for different monomeric anthraquinones were studied. From the results obtained the optimum flow-rates were in the range 0.3–0.7 ml/min.

The chromatograms obtained for the standard solutions with 0.7 ml/min flow rate of mobile phase are shown in Fig. 3. The plate numbers, peaks resolution and retention times ($N_1 = 13370$, $N_2 = 12315$, $N_3 = 15340$, $R_s > 1.5$) represent a useful resolution and reasonable analysis time.

### *Qualitative analysis*

The standard solutions of analytes (20 μl) were analysed using optimized chromatographic conditions. Owing to the reproducibility of the retention time (RSD% < 1.4) and height resol-

Table 2. Determined amounts of anthraquinones and their glycoside derivatives in herbal samples of senna leaves, rhubarb roots and dock flowers

| | Chrysophanol | | Chrysophanol glycosides | |
|---|---|---|---|---|
| Material | Mean | SD | Mean | SD |
| Senna leaves | 0.0185 | 0.0001 | 0.0089 | 0.0002 |
| Rhubarb roots | 0.428 | 0.003 | 0.182 | 0.004 |
| Dock flowers | 0.0380 | 0.0003 | 0.0326 | 0.0005 |
| | Rhein | | Rhein glycosides | |
| Materials | Mean | SD | Mean | SD |
| Senna leaves | 0.097 | 0.001 | 0.413 | 0.006 |
| Rhubarb roots | N.D. | – | N.D. | – |
| Dock flowers | N.D. | – | N.D. | – |
| | Emodin | | Emodin glycosides | |
| Material | Mean | SD | Mean | SD |
| Senna leaves | 0.0420 | 0.0003 | 0.0431 | 0.0007 |
| Rhubarb roots | 0.297 | 0.002 | 0.141 | 0.003 |
| Dock flowers | 0.150 | 0.001 | 0.09 | 0.01 |

All data are in weight per cent of herbal sample.
N.D. = Not detected.

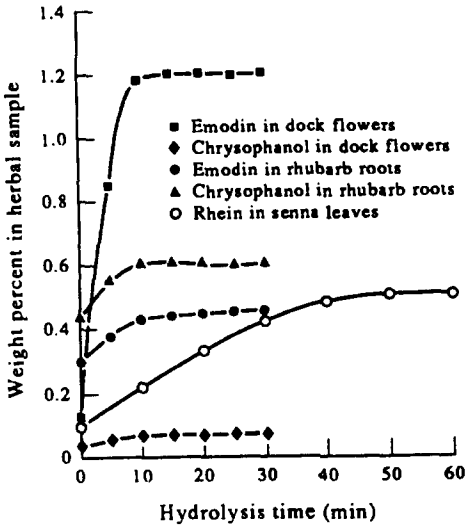


Fig. 4. Total Ch, Em and Rh per cent (w/w) in senna leaves, rhubarb roots and dock flowers *vs.* hydrolysis time.

ution ($R_s \gg 1.5$) in any arbitrary concentration of analytes in two successive peaks, the qualification of each compound can be affected precisely. The signal to analyte concentration proportional in the extract of herbal samples was studied by comparing the absorption of two wavelengths (254 and 430 nm).

*Quantitative analysis*

The standard solutions of Ch, Rh and Em were injected into chromatograph with different concentrations. The amount of each compound were plotted *vs.* peak area. Characteristic data of the calibration curves and the obtained detection limit (L.O.D.) are presented in Table 1. From these results, the quantitative analysis of the anthraquinones can be carried out with a good sensitivity and accuracy.

*Herbal samples*

Rhubarb roots, senna leaves and dock flowers were examined in this work.

*Determination of free anthraquinones.* Solution B (20 $\mu$l) (see Experimental) was injected for the separation and determination of monomeric anthraquinones. The results obtained are presented in Table 2.

*Determination of glycosides.* Solution C (20 $\mu$l) (see Experimental) was injected for the separation and determination of total anthraquinones (free anthraquinones and acid hydrolyzed glycosides). The weight percentage of anthraquinones *vs.* hydrolysing time is plotted in Fig. 4. Since the curve of each sample reaches a plateau in more than 10 min, the total anthraquinone in the herbal samples may be analysed following acid hydrolysis in a convenient time with a good precision. The quantity obtained for glycosides are shown in Table 2.

*Recovery study of extraction procedures.* The original and spiked samples with 100 ppb of each Ch, Em and Rh were treated as mentioned previously and injected. The absence of a chromatographic peak (smaller than L.O.D. or detector threshold) in the third extract proves the complete extraction of accessible anthraquinones in the first and second steps.

## CONCLUSION

From the obtained results the efficiency of the proposed method for the qualitative and quantitative analysis of the free anthraquinones and their conjugates in the cited medicinal plants has been proved. This method can also be utilized for the analysis of these compounds in biological media.

## REFERENCES

1. Y. Ohshima, Y. Ohno, K. Kajiyama and K. Takahashi, *J. Chromatogr.*, 1986, **360**, 303.
2. J. Lemi and L. Lemmens, *Pharmacology*, 1980, **20**, (Suppl. 1), 50.
3. M. Hattori, G. Kim, S. Motoike, K. Kobashi and T. Namba, *Chem. Pharm. Bull.*, 1982, **30**, 1338.
4. M. Hattori, G. Kim, S. Motoike, K. Kobashi and T. Namba, *Chem. Pharm. Bull.*, 1983, **31**, 235.
5. G. R. Annabell and K.J. Mitchell, *Aust. J. Hosp. Pharm.*, 1986, **16**, 29.
6. R. G. Pietrusko, *Am. J. Hosp. Pharm.*, 1977, **34**, 291.
7. K. Ushino, Y. Yamamura, Y. Saitoh and F. Nakagawa, *J. Chromatogr.*, 1986, **380**, 462.
8. A. C. Lane, *Anal. Chem.*, 1973, **45**, 1911.
9. K. Kobashi, T. Nishimura, M. Kusada, M. Hattori and T. Namba, *Planta Med.*, 1980, **40**, 225.
10. R. O. Fullinfaw, R. W. Bury and R. F. W. Moulds, *J. Chromatogr.*, 1988, **443**, 131.
11. M. H. Pournaghi-Azar and S. M. Golabi, *Talanta*, 1988, **35**, 959.
12 M. H. Pournaghi-Azar and S. M. Golabi, 3rd International Symposium of Drugs Analysis, Belgium, 1989, p. 45.
13. B. L. Karger and E. Sibly, *Anal. Chem.*, 1973, **45**, 740.
14. L.R. Snyder and J.J. Kirkland, *Introduction to Modern Liquid Chromatography*. p. 294. John Wiley, New York, 1979.

Pergamon

0039-9140(95)01496-9

*Talanta*, Vol. 42, No. 6, pp. 867–869, 1995

0039-9140/95 $9.50 + 0.00

## Short Communication

# INVESTIGATION OF THE EXTRACTION EQUILIBRIA IN THE SYSTEM HEXACHLORIDORHENATE(IV)–NEOTETRAZOLIUM CHLORIDE–DICHLOROETHANE–WATER

ZH. SIMEONOVA, A. ALEXANDROV* and S. DICHEVA

Department of General and Inorganic Chemistry, Plovdiv University, BG-4000 Plovdiv, Bulgaria

(*Received* 3 *August* 1994. *Revised* 22 *November*. *Accepted* 5 *December* 1994)

**Summary**—The neotetrazolium hexachloridorhenate(IV) ($NTReCl_6$) has been synthesized and its composition checked. The optimum conditions for the extraction of $NTReCl_6$ with dichloroethane have been established. The recovery factor for one-fold extraction is $R = 74\%$. The distribution constant, $K_D$, extraction constant, $K_{ex}$, and ion-association constant, $\beta$, have been determined. Neotetrazolium chloride was found to be suitable reagent for extraction–spectrophotometric determination of rhenium(IV) ($\epsilon_{NTReCl_6} = 3.42 \pm 0.20 \times 10^4 M^{-1}\ cm^{-1}$).

In contrast to rhenium(VII) very little work has been reported on the liquid–liquid extraction of rhenium(IV).[1–5] In a previous article[6] we reported on the formation and extraction of iodo-nitro-tetrazolium hexachloridorhenate. The present paper reports on the extraction of $ReCl_6^{2-}$ with neotetrazolium chloride (NTC). NTC differs from the previously studied iodo-nitro-tetrazolium chloride (INT) by the number of substituents in tetrazolium rings.

## EXPERIMENTAL

### *Reagents and apparatus*

2,2′;5,5′-Tetraphenyl-3,3′-(*p*-biphenyl)-ditetrazolium chloride, neotetrazolium chloride (NTC) from Fluka, $2 \times 10^{-3} M$ aqueous solution. Potassium hexachloridorhenate(IV) was synthesized and recrystallized as described elsewhere.[7] $2 \times 10^{-4} M$ aqueous solution. 1,2-Dichloroethane, Puriss, from Fluka was used without additional purification.

A Carl Zeiss Jena VSU-2P spectrophotometer was used for all absorbance measurements. The samples were shaken on a Thys 2 shaking machine (Germany).

### *Procedures*

*Establishment of optimum extraction conditions.* Dichloroethane (10 ml), an aliquot of the NTC solution to cover the concentration from $4 \times 10^{-5}$ to $8 \times 10^{-5} M$ NTC and an aliquot of the potassium hexachloridorhenate(IV) solution to cover the concentration range from 0.5 to 5.2 $\mu$g/ml $ReCl_6^{2-}$ were introduced into 100-ml separatory funnels. The aqueous phases were brought to 10 ml with water and the funnels shaken on a shaking machine for 60 min. The oganic layer was filtered through a filter paper impregnated with dichloroethane into a 1-cm quartz cell and the absorbance measured at 281 nm against dichloroethane. The absorbance of the blank was also measured.

## RESULTS AND DISCUSSION

On mixing aqueous solution of NTC and $K_2ReCl_6$ an ion-association complex was formed. The absorbance of this aqueous solution of the complex corresponds to the sum of absorbances of the individual components $K_2ReCl_6$ and NTC which is an indication that the resulting compound is an ion-association complex. No frequency shift was observed. In 1,2-dichloroethane, $NTReCl_6$ is soluble, NTC-slightly soluble and $K_2ReCl_6$ not soluble at all. The composition of the complex was

*Author to whom correspondence should be addressed.

determined by the continuous variation method[8] to be 1:1, which corresponds to the formula $NTReCl_6$. The same NTC to $ReCl_6^{2-}$ molar ratio was obtained according to the Likussar and Boltz method[10] (see below). In both methods the absorbance of the complex $NTReCl_6$ was measured in the organic phase.

Hydrochloric acid appeared to be the best medium for the formation of the ion-association complex and its subsequent extraction. The experiments were carried out with a constant concentration of $ReCl_6^{2-}$ in the aqueous phase of $0.5 \times 10^{-5}M$ and $4.0 \times 10^{-4}M$ NTC and varying pH values of the aqueous phase adjusted by means of suitable buffer solutions. The optimum pH range for the formation and extraction of $NTReCl_6$ was established to be within pH 3–7. Maximum extraction of $ReCl_6^{2-}$ was achieved with a 30-fold excess of NTC. The absorbance of $NTReCl_6$ (organic layer) *vs.* original concentration of $ReCl_6^{2-}$ (aqueous phase) plot showed good linearity in the range of $0.13 \times 10^{-5}$ to $1.17 \times 10^{-5}M$ $ReCl_6^{2-}$. The molar absorptivity of $NTReCl_6$ in dichloroethane was found to be $\epsilon = 3.42 \pm 0.20 \times 10^4 M^{-1}\,cm^{-1}$. The molar absorptivity of $(INT)_2ReCl_6$ was $3.9 \times 10^4 M^{-1}\,cm^{-1}$,[6] while the molar absorptivity of $NT(ReO_4)_2$ was $\epsilon = 7.0 \times 10^3 M^{-1}\,cm^{-1}$.[11] Hence, the molar absorptivity of $NTReCl_6$ is higher by a factor of 10 than that of $NTReO_4$.

The effect of diverse ions that usually accompany rhenium in environmental and industrial samples was studied under the optimum extraction conditions. The following amounts are tolerated with the extraction of $2.5 \times 10^{-6}M$ $ReCl_6^{2-}$ with NTC: Ni(II), $1.7 \times 10^{-2}M$; Mo(VI), $8.3 \times 10^{-3}M$, Cd(II), $7.1 \times 10^{-3}M$, Zn(II), $7.6 \times 10^{-3}M$; Cu(II), $4.7 \times 10^{-3}M$; Fe(III), $8.9 \times 10^{-3}M$. $BrO_3^-$, $IO_4^-$ and $ClO_4^-$ interfere.

*Determination of the equilibrium constants $K_{ex}$, $K_D$, $\beta$*

The extraction equilibrium was studied according to the chemical model applied in Ref. 9. The following equilibria were considered:

(i) formation of an ion-associate in the aqueous phase according to the reaction:

$$NT^{2+} + ReCl_6^{2-} \rightleftharpoons NTReCl_6, \qquad (1)$$

with an equilibrium constant (ion-association constant)

$$\beta = [NTReCl_6]/[NT^{2+}][ReCl_6^{2-}].$$

(ii) Distribution of the ion-association complex between the aqueous and the organic phase

$$[NTReCl_6] \rightleftharpoons NTReCl_6]_{org}, \qquad (2)$$

with a distribution constant

$$K_D = [NTReCl_6]_{org}/[NTReCl_6].$$

The overall extraction process is described by the equation:

$$NT^{2+} + ReCl_6^{2-} \rightleftharpoons [NTReCl_6]_{org} \qquad (3)$$

with a corresponding equilibrium constant

$$K_{ex} = [NTReCl_6]_{org}/[NT^{2+}][ReCl_6^{2-}].$$

According to Ref. 9 the constants $K_{ex}$ and $K_D$ can be graphically determined from the experimental $\lg D_{ReCl_6^{2-}}$ *vs.* lg[NTC] plot (Fig. 1). The distribution coefficient $D_{ReCl_6^{2-}}$ was determined with a constant $ReCl_6^{2-}$ concentration in the aqueous phase according to the formula:

$$D_{ReCl_6^{2-}} = [NTReCl_6]_{org}/[NTReCl_6] + [ReCl_6^{2-}].$$

$K_{ex}$ and $K_D$ are read from the plot and $\beta$ calculated from $\beta = K_{ex}/K_D$. The slope of the plot shows the composition of the extracted species. Figure 1 presents an experimental $\lg D_{ReCl_6^{2-}}$ *vs.* lg[NTC]. The slope of the plot confirms the composition of the extracted complex to be $NT^{2+}:ReCl_6^{2-} = 1:1$.

The value of $K_{ex}$ was determined independently by the Likussar and Boltz method[10]

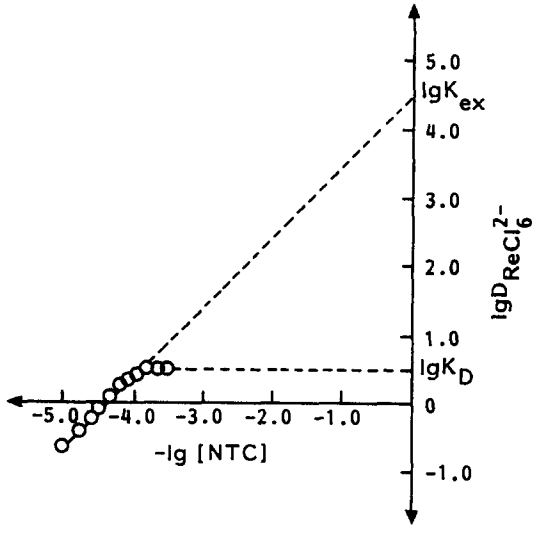


Fig. 1. $\lg D_{ReCl_6^{2-}}$ *vs.* $\lg C_{NTC}$ plot ($C_{ReCl_6^{2-}} = 1.6 \times 10^{-5}M$).

Table 1. Values of $K_{ex}$, $K_D$ and $\beta$ for the extraction system $ReCl_6^{2-}$–neotetrazolium chloride (NTC)–water–dichloroethane

| | | | |
|---|---|---|---|
| 1 | $\lg K_{ex}^* = 4.46 \pm 0.10$ | $K_{ex}^* = (2.99 \pm 0.74) \times 10^4$ | $n = 7$ |
| 2 | $\lg K_{ex}\dagger = 4.41 \pm 0.02$ | $K_{ex}\dagger = (2.70 \pm 0.70) \times 10^4$ | $n = 4$ |
| 3 | $\lg K_D = 0.46 \pm 0.03$ | $K_D = 2.40 \pm 0.22$ | $n = 6$ |
| 4 | $\lg \beta = 3.99 \pm 0.05$ | $\beta = (1.02 \pm 0.12) \times 10^4$ | $n = 10$ |

*Value obtained from the $\lg D_{ReCl_6^{2-}}$ *vs.* $\lg C_{NTC}$ plot.[9]
†Value calculated by the Likussar and Boltz method.[10]

with $C_{NT^{2+}} + C_{ReCl_6^{2-}} = 1.0 \times 10^{-4} M$. Table 1 lists the values of equilibrium constants of the system $ReCl_6^{2-}$–neotetrazolium chloride (NTC)–water–dichloroethane.

## CONCLUSIONS

The extraction constant $K_{ex} = (2.99 \pm 0.74) \times 10^4$ and the recovery factor achieved with one-fold extraction is $R = 74\%$. The extracted species $NTReCl_6$ is an ion-association complex of moderate stability $\beta = (1.02 \pm 0.12) \times 10^4$. The molar absorptivity of the ion-associate $\epsilon = (3.42 \pm 0.20) \times 10^4 M^{-1}$ $cm^{-1}$ competes favourably with the molar absorptivity of neotetrazolium perrhenate NT $(ReO_4)_2$ ion-associate ($\epsilon = 7.0 \times 10^3 M^{-1}$ $cm^{-1}$). The results obtained show that NTC can be successfully applied to the selective extraction of Re(IV).

*Acknowledgement*—The authors would like to thank the National Research Fund for financial support.

## REFERENCES

1. V. Yatirajam, *Z. Anal. Chem.*, 1966, **219**, 128.
2. K. A. Bolshakov, N. M. Sinicin, V. F. Travkin and L. N. Antimova, *Zh. Neorg. Kim.*, 1970, **15**, 2220.
3. K. A. Bolshakov, N. M. Sinicin, V. F. Travkin and L. N. Antimova, *Zh. Neorg. Khim.*, 1973, **18**, 2209.
4. A. I. Busev and M. B. Ogareva, *Zh. Anal. Khim.*, 1965, **10**, 1731.
5. N. Jordanov and M. Pavlova, *Chem. Anal.*, 1972, **17**, 819.
6. Zh. Simeonova, A. Alexandrov and M. Dzarkova, *Fresenius J. Anal. Chem.*, 1994, **348**, 329.
7. M. Pavlova, N. Jordanov and D. Staikov, *Compt. Rend. Acad. Bulg. Sci.*, 1974, **27**, 67.
8. M. I. Bulatov and M. G. Kalinkin. *Practicheskoe rukovodstvo po photometricheskim i spectrophotometricheskim methodom analyza.* Khimia, L. 1976.
9. A. Alexandrov, O. Budevsky and A. Dimitrov, *J. Radioanal. Chem.*, 1976, **29**, 243.
10. W. Likussar and D. Boltz, *Anal. Chem.*, 1971, **43**, 1265.
11. A. Alexandrov and Zh. Simeonova, *Nauch. Tr. Plovdiv. Univ. Bulg.*, 1981, **19**, 27.

Pergamon

0039-9140(95)01404-7

*Talanta*, Vol. 42, No. 6, pp. 873–877, 1995
Elsevier Science Ltd
Printed in Great Britain
0039-9140/95 $9.50 + 0.00

# THE DEVELOPMENT OF A SAMPLER–SENSOR USING A VANADIUM–OXINATE–POLYMER FILM FOR THE SELECTIVE AND DIRECT DETERMINATION OF ATMOSPHERIC ETHANOL

E. T. HAYES, A. GALAL and H. B. MARK, JR.

Department of Chemistry, University of Cincinnati, Cincinnati, OH 45221-0172, U.S.A.

(*Received* 12 *July* 1994. *Revised* 27 *July* 1994. *Accepted* 10 *August* 1994)

**Summary**—The development of a sensor for the direct and selective determination of atmospheric ethanol is in the initial stages. The sensor takes advantage of the selective chemical reaction between ethanol and vanadium oxinate. This reaction occurs in an organic medium where a red colored complex is the product. This reaction is determined spectrophotometrically where the absorbance maxima is 475 nm. The focus of this paper is to discuss the parameters necessary to develop a solid sorbent sampling–sensor which can be used to determine atmospheric ethanol.

Over the course of the past 10 years, this research group has been developing sampler-sensoring devices for trace gas analysis.[1–3] The research involves the use of chemical reagents immobilized on solid sorbents for selective surface reaction with the analyte of interest. In most cases, the reaction between the reagent and analyte on the surface results in the formation of an irreversible complex. The product yields a colored or fluorescent surface where either visual and/or an appropriate spectrochemical technique can be utilized to determine the analyte concentration. The advantages of using solid sorbents for trace gas analysis are low cost, selectivity, simplicity, high sample collection efficiency, suitable storage time, and detection limits in low ppm–ppb range.[4]

In addition to these advantages, the use of an archimedean sampler-sensor adds the dimension of direct *in situ* analysis of air pollutant. An archimedean sampler–sensor has been developed in this laboratory for the direct determination of air pollutants and has been previously described.[2] The novelty of this device is the elimination of instrumentation for analyte determination. The species of interest is quantified by measuring the spiral length of color established by the pollutant reaction.

The use of sorbent material for the determination of atmospheric ethanol is not widely accepted, but there exist detector tubes available for this analysis. Sorption tubes containing activated charcoal are common for ethanol detection.[5] Although suitable for atmospheric ethanol determination, activated charcoal tends to be nonspecific and adsorbs other organic volatiles present. In addition, humidity greater than 60% can reduce the adsorptive capacity of activated charcoal.[6] In general, chemical sorbent chosen for atmospheric ethanol need not be very sensitive since the Federal Permissible Exposure Limits (PEL) is 1000 ppm. However, the surface reagent must be selective to ethanol due to the presence of other organics and high humidity available in environmental and industrial atmospheres.[5]

In this research, the reagent chosen for ethanol selectivity is a compound referred to as vanadium oxinate. 7 Vanadium oxinate, a phenol ester of orthovanadic acid, reacts with ethanol to form a red colored complex (equation 1).

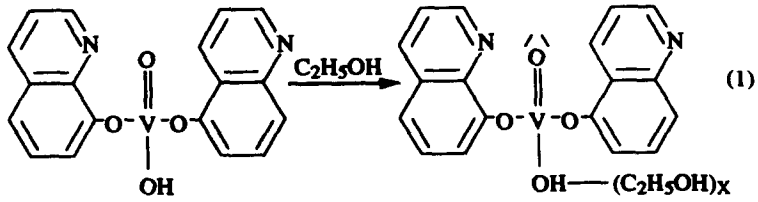


(1)

Vanadium oxinate grey green — Alcoholate complex red

This reaction is characteristic of alcohols over all organic functionalities. As a matter of fact, this reagent, which is sparingly soluble in many organic solvents, has been used to remove low levels of ethanol in mixtures containing other organics.[7] In addition this compound is completely insoluble and non-reactive with water. Because of the selectivity, the vanadium oxinate has been used to determine levels of ethanol in beers, wine, blood samples, and other solvent mixtures.[8-10] The detection occurs with minimum sample preparation and the ethanol levels are quantified with basic UV-Vis spectrophotometry. Thus, because of its selectivity, vanadium oxinate appears to be a prime sorbent reagent for the selective determination of atmospheric ethanol using a sampler–sensor device.

## EXPERIMENTAL

### *Reagent*

The vanadium oxinate was prepared to adding solutions of 0.02*M* ammonium vandate (Fischer) to 2.5% 8-hydroxyquinoline (MCSB) in 5% acetic acid (Fischer). The resulting precipitate was soaked in an acetic acid–sodium acetate (Fischer) solution, pH 4, for 1 hr. All solutions were prepared in analytical grade deionized water. The precipitate was filtered in a sinitered glass filter and allowed to dry overnight in the oven at temperatures ranging from 100 to 120°C. Reagent solutions ranging from $2.0 \times 10^{-4}$ to $4.5 \times 10^{-4}M$ were tested for solubility and ethanol sensitivity in the following solvents: (1) toluene, (2) 2,4-dichlorotoluene, (3) cyclohexane, (4) acetonitrile, (5) benzene, and (6) chloroform. The chloroform had to be washed with analytical grade deionized water to remove residual ethanol. The effectiveness of these reagent solutions were tested in contact with solutions of ethanol at concentrations (V/V) ranging from 0.001 to 10%. The ratio of organic to aqueous phase was 1 to 2, and analyses were carried out in 25 ml test tubes. Reaction times were varied from 20 min to 3 hr depending on concentration and temperature. The colored product in the organic phase was analyzed spectrophotometrically at 475 nm.

In addition to various solvents, several polymers were also investigated as a matrix for vanadium oxinate immobilization. The following polymers were explored: (1) polyvinyl acetate, (2) polymethacrylate, (3) cellulose acetate, (4) polyethylene oxide, and (5) polyvinyl alcohol. The polymer films were formed by dissolving 10 mg of vanadium oxinate and 2 g of polymer in 60 ml of solvent. An aliquot of 2 ml was placed on a polypropylene disk (7.5 cm diameter) where the solvent would evaporate, leaving a caste film. These polymer films were tested for the mechanical stability, capacity to immobilize the reagent, and interaction with atmospheric ethanol.

### *Instrumentation*

UV-Vis spectra of the various solutions were obtained on either a Perkin-Elmer Lambda 5 UV/Vis Spectrophotomer or Hewlett Packard 8452A Diode Array Spectrophotometer. The sample was placed in a 1 cm quartz curvette. These spectrophotometers were also used to analyze atmospheric ethanol collected on the various polymer surfaces. The complex was recovered in an appropriate solvent for analysis. Calibration gas standards were prepared from a VICI Dynacalibrator Model 230-50-2. A 5 mm diffusion vial (VICI metronics) with 100% ethanol was inserted into the instrument chamber and concentration was controlled by adjusting the gas flow rates. The atmospheric ethanol entered a reaction chamber where reaction with the vanadium–oxinate polymer film occurred.

## RESULTS AND DISCUSSION

### *Solvent test*

Initial research was devoted to determining the best solvent for the dissolution of the vanadium compound. Ideally the solvent should meet several criteria. The ideal requirements are as follows: (1) totally immiscible with water, (2) possess a low dielectric constant, (3) be able to dissolve sufficient amounts of the vanadium–oxinate, (4) non-hazardous to users, (5) ability to dissolve a polymer–reagent mixture for the film formation, and (6) have a high volatility. Furthermore, the reaction with ethanol in the aqueous or gas phase has to be rapid, have a large formation constant to yield sensitivity, and must be selective. It is to be noted that none of the solvents tested fulfilled all the criteria. The advantages and limitations of each of the solvents in contact with ethanol solutions is listed below.

*Toluene.* Toluene meets many of the ideal specifications for choosing a solvent. It has a low dielectric constant, immiscible with water, and non-hazardous to potential users. Never-

theless, vanadium–oxinate is sparingly soluble in toluene limiting the effectiveness to determine low levels of ethanol. Reagent solutions ranging from $2.0 \times 10^{-4}$ to $5.0 \times 10^{-3} M$ were tested. Levels of 0.5% (5000 ppm) and 1% (10,000 ppm) were detected at the saturated reagent concentration. This is insufficient for the required PEL (1000 ppm) needed for atmospheric ethanol.

*2,4-Dichlorotoluene.* 2,4-Dichlorotoluene was chosen to investigate possible substituent effects of the chlorine on improved solubility. Results for this solvent, however, had identical detection levels as toluene offering no advantages.

*Cyclohexane.* In terms of the criteria, cyclohexane has similar properties to toluene. However, the vanadium oxinate is completely insoluble in cyclohexane; therefore, no color formation occurred in the organic phase with ethanol solution.

*Acetonitrile.* This was the only water miscible solvent investigated; thus it is in essence undesirable. In addition, acetonitrile is more hazardous than the previous solvents mentioned. Nevertheless, the acetonitrile can dissolve a sufficient amount of vanadium oxinate to determine ethanol levels of 0.1% (1000 ppm).

*Benzene.* Benzene is the solvent most widely used to dissolve the vanadium compound, but it is the most toxic, thus, least preferred. The desirable aspect of using benzene is that ethanol levels as low as 0.05% (500 ppm) can be determined.

*Chloroform.* Chloroform is a compromise solvent, therefore, being the choice solvent for sensor development. It dissolves a sufficient amount of vanadium to determine ethanol at levels of 0.01% (100 ppm) and it is immiscible. The apparent disadvantage is the toxicity of this solvent; although, its toxicity is less severe than benzene and acetonitrile. Figure 1 shows the UV-Vis spectra of the vanadium solution in contact with 1 and 3% ethanol solutions. The absorbance maxima occurs at 475 nm. This maxima agrees closely to reported literature values for this complex.[9] In addition, this solvent is capable of dissolving most of the polymers investigated. Its volatility is suitable for casting polymer films containing the immobilized reagent.

Regardless of the solvent, there was a major problem associated with dissolution of the vanadium compound. Vanadium–oxinate, as mentioned earlier, is sparingly soluble in most solvents. When this compound dissolves in an organic medium, it forms a dark black solution which tends to precipitate in the organic layer on standing. Thus, the reagent solution has a variation in color intensity and absorbance for a particular ethanol concentration which is time dependent. In order to circumvent this particular problem, sieving of particles and filtering of solutions were employed before analysis. However, time dependent changes persisted. This problem is carried into the second stage of polymer film development for atmospheric determination of ethanol. In conclusion, none of the above solvents fulfil all requirements of ideality. Chloroform is the choice solvent due to its ability to determine ethanol at levels of 0.01% (100 ppm).

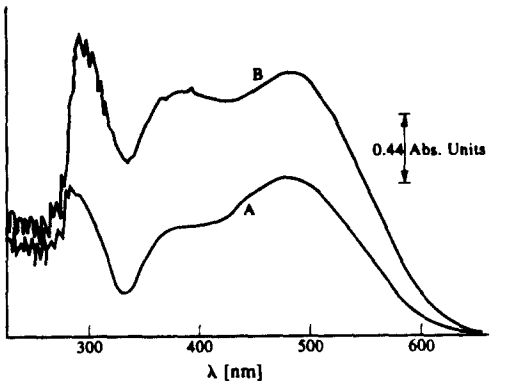


Fig. 1. Absorbance spectra of vanadium–oxinate solution in contact with (A) 1% aqueous ethanol, (B) 3% aqueous ethanol.

*Polymers*

The next stage of sensor development was to find a polymer which can incorporate the vanadium compound in a film. In essence, the ideal polymer should have compatibility with the ethanol promoting adsorption and/or permeability, it should be soluble in organic solvents that dissolve the vanadium oxinate, it needs to be mechanically stable when cast, and the reagents should be homogeneously distributed in the film. Thus, these criteria were explored for identifying the choice polymer.

*Polyethylene oxide.* Polyethylene oxide had many desirable properties for immobilizing the reagent. It exhibited mechanical stability, dissolved well in chloroform, and formed homogeneous films of the immobilized reagent. It also exhibited surface reaction with ethanol solutions of 10% (v/v) and greater. However, no reaction occurred with atmospheric ethanol.

*Polyvinyl alcohol.* Polyvinyl alcohol had many undesirable attributes as a substrate matrix.

This polymer did not have any permeability for the ethanol. In addition, the oxine reagent was formed in non-homogeneous and irreproducible zones on the polymer surfaces. Although the surface vanadium reagent reacted with ethanol solutions, it was impossible to obtain reproducible color changes with ethanol concentration.

*Polymethacrylate.* The polymethacrylate be haved similar to polyethylene oxide in all regards. Surface color change reactions with ethanol solutions greater than 10% (v/v) occurred, but it was non-active to atmospheric ethanol.

*Cellulose acetate.* Cellulose acetate was very ineffective. As a matter of fact, this polymer film was mechanically unstable on incorporating the vanadium reagent. Thus, no further testing were performed.

*Polyvinyl acetate.* Polyvinyl acetate fulfilled all the necessary requirements for formation of a sensor film. It readily permeated with the ethanol and exhibited a rapid color change for both ethanol solutions and gases. Solutions of 1% (V/V) and 1200 ppm of ethanol gases were easily detected. In addition, the films were mechanically stable and uniform in terms of reagent distribution. Figure 2 shows the UV-Vis spectra of films exposed to 8300 ppm and 10,000 ppm of ethanol where the film was dissolved in chloroform. Notice the characteristic absorbance maxima of 475 nm.

In summary, polyvinyl alcohol and cellulose acetate which are hydrophillic in nature tend to precipitate the vanadium compound out as the solvent evaporates on casting the film. Polyethylene oxide and polymethacrylate films distribute the vanadium compound uniformly on film formation. However, the ethanol does not readily permeate these films, thus, forming color changes only with ethanol solutions greater than 10% (v/v). Moreover, this inability to adsorb ethanol produces no color change for atmospheric samples. Polyvinylacetate shows both hydrophobic and hydrophillic characteristics. Thus this polymer promotes the uniform distribution of the vanadium oxinate on casting and has sufficient hydrophillicity to interact with the atmospheric ethanol. This allows the ethanol to react both at the surface and within the matrix with reagent. Response time for color formation varied from 3 to 6 hr for atmospheric samples depending on concentrations.

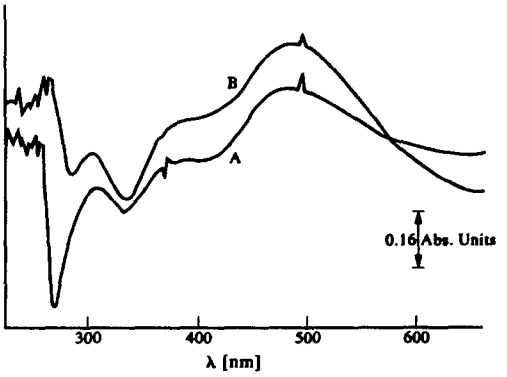


Fig. 2. Absorbance spectra of vanadium–oxinate film in contact with (A) 8300 ppm ethanol–air sample, (B) 10,000 ppm ethanol–air sample.

## CONCLUSIONS

The combination of a reagent, solvent, and polymer for an immobilized surface sensor film for atmospheric ethanol determination was successfully completed. The selectivity of the vanadium–oxinate towards ethanol is excellent in both the solution and gas phase. Ethanol solutions as low as 0.01% (v/v) were determined in chloroform solvent–reagent system, and the immobilized vanadium oxinate–polyvinyl acetate substrate film can detect as little as 1200 ppm of atmospheric ethanol. However, the problem of solvent–vanadium stability gave non-reproducible color formation for each concentration of ethanol tested. This has not yet been solved. Thus, continued work must be performed on establishing stable and homogeneous reagent solutions for improved sensor data reproducibility. Once this problem is solved, the applicability of these films for use in the archimedean sampling–sensor unit can be evaluated.

*Acknowledgements*—This research was supported in part by a grant from Phillip Morris, U.S.A. and the Department of Chemistry at the University of Cincinnati. Eric T. Hayes is grateful of the support offered by the Patricia Robert Harris Fellowship Foundation.

## REFERENCES

1. E. T. Hayes, O. Y. Ataman, A. E. Karagözler, Y. L. Zhang, D. P. Hautman, R. T. Emerich, A. G. Ataman, H. Zimmer and H. B. Mark, Jr., *Microchem. J.*, 1990, **41**, 98.
2. R. LaRue, O. Y. Ataman, G. Gerhardt, H. Zimmer and H. B. Mark, Jr., *Anal. Chem.*, 1987, **59**, 2313.
3. S. Vasiraddy, K. W. Street and H. B. Mark, Jr., *Anal. Chem.*, 1981, **53**, 868.

4. R. Narayanaswamy and S. Fortunato, *Analysis*, 1988, **113**, 661.
5. Annual Book of ASTM Standards published as D3686-89.
6. B. C. Turner and D. E. Glutfelty, *Anal. Chem.*, 1977, **49**, 7.
7. F. Buscarons, J. L. Marins and J. Claver, *Anal. Chim. Acta*, 1949, **3**, 310, 47.
8. M. Stiller, *Anal. Chim. Acta*, 1961, **25**, 85.
9. M. Tanaka, *Talanta*, 1960, **5**, 162.

ELSEVIER

Talanta 42 (1995) 879–880

Talanta

# The Benedetti–Pichler Award

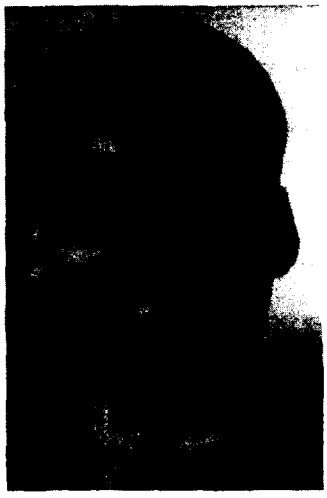

**Leslie Colin Ebdon**

Leslie (Les) Colin Ebdon, Deputy Vice-Chancellor (Academic), at the University of Plymouth in Plymouth, UK, will be presented with the prestigious Benedetti–Pichler Memorial Award by the American Microchemical Society, during a symposium in his honor at the annual meeting of the Eastern Analytical Symposium in Somerset, NJ, USA, November 12–17, 1995. This award is given annually and was established in 1966 to recognize outstanding achievements in microanalytical chemistry.

Les obtained a B.Sc. in chemistry in 1968 and a Ph.D. in 1971 at Imperial College, University of London, UK. His Ph.D. was supervised by Professor Tom West and (the late) Professor Gordon Kirkbright. He was a lecturer in chemistry at Makerere University, Kampala, Uganda for two years before accepting a position as lecturer in analytical chemistry at Sheffield Polytechnic, Sheffield, UK, being promoted to senior lecturer in 1976. In 1981, Les took the newly promoted position of Reader in Analytical Chemistry in the Department of Environmental Sciences at Plymouth Polytechnic, which later became the University of Plymouth. In 1989 he became Deputy Vice-Chancellor (Academic) at the University of Plymouth.

Les's interests are in trace analysis particularly applied to environmental problems. At present he has nearly 200 publications, 4 books, and 5 patents. He has given plenary lectures in over 20 countries and over 200 invited conference contributions. He is the 1986 SAC Silver Medal recipient. He currently serves on the editorial board of 8 journals. In a recent survey (Chemistry & Industry, August 1993, p. 571,) Les was reported as the most cited analytical chemist in the UK and the 14th most cited of all UK chemists.

The following is a list of presentations at the Benedetti–Pichler Award Symposium at Eastern Analytical Symposium:

**Ramon M. Barnes**, Department of Chemistry, University of Massachusetts, Amherst, MA, USA
*Electrophoresis and ICP-MS*

**Kenneth W. Jackson**, Department of Environmental Health and Toxicology, State University of New York at Albany, Albany, NY, USA
*Electrothermal Atomic Absorption Spectrometry: Fundamental Research Leads to Accurate Applied Methods*

**Richard F. Browner**, Department of Chemistry, Georgia Institute of Technology, Atlanta, GA, USA
*Coupling Microflow Chromatography to LC-ICP-MS, LC-MS, and LC-MS-MS*

**Robert G. Michel**, Department of Chemistry, University of Connecticut, Storrs, CT, USA
*New Laser Technologies for Atomic Spectroscopy*

**Les Ebdon**, Department of Environmental Sciences, University of Plymouth, Plymouth, Devon, UK
*New Plasmas for Old Speciation Problems*

## NOMINATIONS FOR THE 1996 BENEDETTI-PICHLER AWARD

The American Microchemical Society is soliciting nominations for the prestigious 1996 Benedetti-Pichler Award. The award, established in 1966, is given annually to recognize outstanding achievements in microanalytical chemistry. The award consists of a plaque and expenses to attend the Eastern Analytical Symposium in Somerset, NJ, USA, in November 1996 to receive the award at a session in honor of the awardee.

Nominations, including at least two supporting letters, should be sent no later than October 30, 1995 to:

Len Klein
Secretary
American Microchemical Society
FMC Corporation
Agricultural Chemical Group
P.O. Box 8
Princeton, NJ 08543, USA

For further information, please contact:

Dr. Joseph Sneddon
Head
Department of Chemistry
McNeese State University
Lake Charles, LA 70609, USA
*Telephone:* (318) 475 5777
*Fax:* (318) 475 5234

ELSEVIER

Talanta 42 (1995) 881–884

Talanta

# Adsorptive stripping measurements of germanium(IV) in the presence of pyrogallol

ChangQing Sun *, Qian Gao, LiLing Liu

*Department of Chemistry, Jilin University, Changchun, 130023, People's Republic of China*

Received 16 June 1994; revised 15 November 1994; accepted 16 December 1994

**Abstract**

The adsorptive stripping voltammetric determination of germanium(IV) based on the adsorptive accumulation of the germanium(IV)–pyrogallol complex on a hanging mercury drop electrode is reported. The reduction current of the adsorbed germanium complex is measured by differential-pulse cathodic stripping voltammetry. The peak potential is at −0.42 V vs. Ag/AgCl (saturated KCL). The effects of various parameters (ligand concentration, supporting electrolytic composition and concentration, accumulation potential and collection time) on the response are discussed. With controlled accumulation for 3 min, the detection limit is $1.2 \times 10^{-9}$ M germanium. The relative standard deviation (at $1.2 \times 10^{-8}$ M germanium) is 3.6%. Possible interferences are evaluated. The applicability of the method to the determination of germanium(IV) in ore samples was also successfully carried out.

## 1. Introduction

Germanium is a rare element in the earth's crust and because of its industrial and biological significance, a highly sensitive method is required for reliable measurement. Germanium(IV) complex with organic ligands such as polyhydroxy compounds [1–4] have been applied in the polarographic determination of germanium, but these methods are not sufficiently sensitive to detect trace germanium. Recently, the adsorptive characteristics of complexes have been used in the determination of traces of inorganic elements [5–7]. The adsorptive stripping measurements of germanium(IV) in the presence of catechol and pyrogallol have been reported [8] and the method has been applied to determination of trace germanium in ginseng and garlic.

In this paper, a sensitive adsorptive stripping voltammetric method is described for the determination of trace amounts of germanium based on differential-pulse cathodic stripping voltammetry (DPCSV) of the accumulated germanium(IV) complex with pyrogallol at a hanging mercury drop electrode. The optimum analytical conditions for germanium(IV) determination are discussed in detail.

## 2. Experimental

### 2.1. Apparatus and reagents

The voltammograms were recorded on a PAR model 384A polarographic analyzer. The working electrode was a PAR model 303 static mercury drop electrode and a medium-sized hanging mercury drop electrode (HMDE) was employed. Ag/AgCl(saturated KCl) and platinum wire served as reference and auxiliary electrode, respectively, A model 79-1 voltammetric analyzer (Jinan Fourth Radio Factory, China) coupled with a model Series 60000 XYt recorder (Gould Electronics, China) was used for cyclic voltammetry.

* Corresponding author. Fax: (86) 431-823-907

Unless specified otherwise, all reagents were of analytical-reagent grade. All solutions were prepared from doubly distilled water. A stock solution of $1.2 \times 10^{-2}$ M germanium(IV) (atomic absorption standard) was used and diluted with water as required. A stock solution of 0.1 M pyrogallol was prepared weekly and was stored at 4 °C in a refrigerator.

### 2.2. Procedure

Voltammetric stripping experiments were performed in the following manner. The supporting electrolyte (10 ml) containing 0.5 M HCl, 0.1 M KCl and $4 \times 10^{-4}$ M was pyrogallol transferred into the voltammetric cell and purged with pure nitrogen for 4 min. The preconcentration potential (usually 0.0 V vs. Ag/AgCl (saturated KCl)) was applied to a fresh mercury drop while the solution was stirred. Stirring was stopped and after 30 s the voltammogram recorded by applying a negative scan (at 4 mV $s^{-1}$) from 0.0 to −0.60 V using the differential-pulse stripping mode. After the ground voltammogram has been obtained, the adsorptive stripping experiment was repeated with a new drop for the addition of the germanium sample. After additions of each sample, nitrogen was passed through the solution for about 1 min.

## 3. Results and discussion

### 3.1. Response characteristics

Fig. 1 shows cyclic voltamperograms for $6 \times 10^{-7}$ M germanium(IV) in a medium containing $4 \times 10^{-4}$ M pyrogallol, 0.1 M KCl and 0.5 M HCl. In the absence of accumulation, only a small peak from the reduction of the germanium–pyrogallol complex was observed at −0.42 V (a). When the above experiment was repeated for a 30 s stirring period at −0.20 V vs. Ag/AgCl (saturated KCl), a significantly larger cathodic peak was observed (b), indicating an interfacial accumulation of the complex. The fact that a well-defined cyclic voltammetric response was observed shows the remarkable sensitivity associated with the interfacial accumulation process.

To check the applicability of the adsorption preconcentration behaviour of the germanium(IV)–pyrogallol complex at the HMDE for the determination of germanium(IV) by

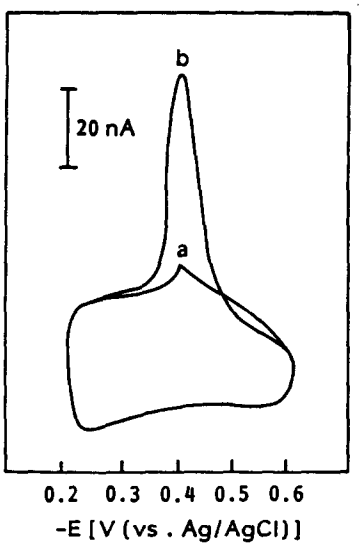


Fig. 1. Cyclic voltamperograms of germanium(IV) after 0 (a) and 30 (b) sec stirring at −0.20 V vs. Ag/AgCl (saturated KCl). Scan rate, 100 mV $s^{-1}$. The solution contained 0.5 M HCl, 0.1 M KCl, $4 \times 10^{-4}$ M pyrogallol and $6.0 \times 10^{-7}$ M Ge(IV).

DPCSV, different parameters (supporting electrolytic composition and concentration, accumulation potential, collection time, ligand concentration and germanium(IV) concentration) were investigated.

By comparing $HClO_4$, HAc–NaAc, $H_2SO_4$, and KCl–HCl solution, we found that the germ-anium(IV)–pyrogallol complex peak was highest and constant in KCl–HCl solution and the optimum concentration was 0.1 M KCl and 0.5 M HCl.

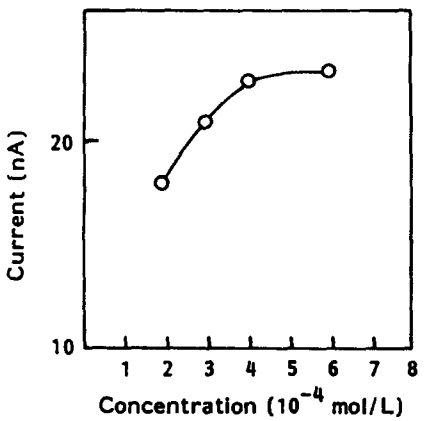


Fig. 2. Dependence of the reduction peak current of the adsorbed Ge(IV) complex with pyrogallol on the concentration of pyrogallol. The solution contained 0.1 M KCl, 0.5 M HCl and $1.2 \times 10^{-7}$ M Ge(IV). Scan rate, 4 mV $s^{-1}$. Preconcentration time, 30 s. Preconcentration potential, 0.0 V vs. Ag/AgCl (saturated KCl).

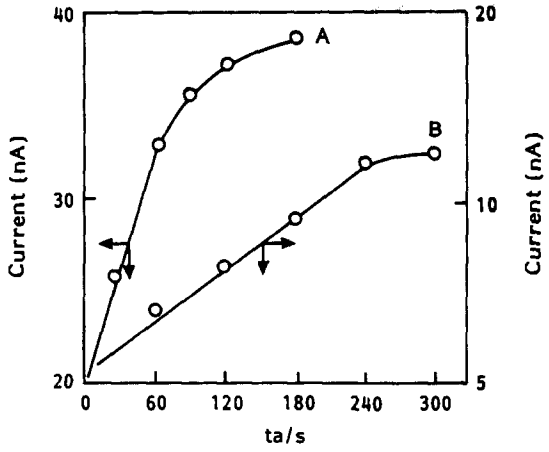


Fig. 3. Dependence of the reduction current of the adsorbed Ge(IV) complex with pyrogallol on the preconcentrated time. The conditions are 0.1 M KCl, 0.5 M HCl, $4 \times 10^{-4}$ M pyrogallol and $1.2 \times 10^{-7}$ M Ge(IV) (A) and $3.6 \times 10^{-8}$ M Ge(IV) (B). Other conditions are the same as those in Fig. 2.

Fig. 2 shows the dependence of the germanium(IV)–pyrogallol complex peak on the ligand concentration. The peak height increases linearly with the pyrogallol concentration at a concentration of less than $4 \times 10^{-4}$ M. The peak height tended to remain constant at a concentration of more than $4 \times 10^{-4}$ M. Therefore, $4 \times 10^{-4}$ M was selected as the optimum concentration of the pyrogallol.

The dependence of the maximum stripping peak current on the collection time was examined for samples containing $1.2 \times 10^{-7}$ M (Fig. 3A) and $3.6 \times 10^{-8}$ M (Fig. 3B) germanium(IV) in the range of 0–300 s. The maximum peak height was observed at 120 and 240 s for $1.2 \times 10^{-7}$ M and $2.6 \times 10^{-8}$ M germanium (IV), respectively, and was constant during the longer time.

The effect of the accumulation potential on the stripping peak current of the germanium(IV)–pyrogallol complex was examined over the potential range from 0.0 to −0.30 V in 0.1 M KCl, 0.5 M HCl, $4 \times 10^{-4}$ M pyrogallol and $1.2 \times 10^{-7}$ M germanium(IV) solution at the optimum collection time. The largest peak current was obtained at a deposition potential of 0.0 V and the current decreased slowly at more negative potentials. Electrostatic exclusion may be responsible for the observed effect. Because the germanium (IV)–pyrogallol complex appears negatively charged, a more positive potential is favorable for its adsorption at HMDE. Therefore, 0.0 V was selected as the accumulation potential in the recommended procedure.

From the results above, we chose the following as the optimum experimental condition: 0.1 M KCl, 0.5 M HCl, $4 \times 10^{-4}$ M pyrogallol. The accumulation potential was 0.0 V vs. Ag/AgCl (saturated KCl).

### 3.2. Analytical application

The greatest advantage of the determination of germanium(IV) by proposed adsorptive stripping voltammetric method is the inherent sensitivity. Under the optimum conditions, a linear relationship between the peak current and the germanium(IV) concentration was obtained in the range of $0–6 \times 10^{-7}$ (Fig. 4A), $0–6 \times 10^{-8}$ (Fig. 4B) and $0–10 \times 10^{-9}$ (Fig. 4C) M when collection time was 60, 90 and 180 s, respectively. When the collection time was 180 s, the detection limit of the method was $1.2 \times 10^{-9}$ M. Reproducibility tests on eight results at $1.2 \times 10^{-8}$ M germanium(IV) showed a relative standard deviation of 3.6%.

The selectivity of the method was tested by studying the effects of foreign ions on the determination of $1.2 \times 10^{-8}$ M germanium(IV). The results showed that 100-fold excess of Cu(II), Cd(II), Fe(III), Fe(II), Co(II), Pb(II), Mg(II), Al(III), Ni(II), Mn(II), Zn(II), Ca(II) and 20-fold exess of As(III) did not interfere with the determination of germanium(IV) under the experimental conditions. In addition, because Tin(IV) can complex with pyrogallol

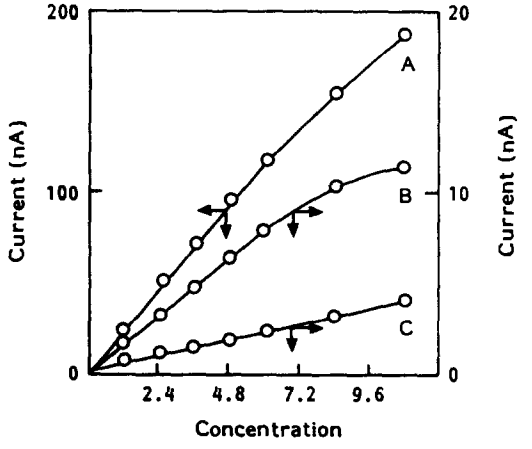


Fig. 4. Dependence of the reduction peak current of the adsorbed Ge(IV) complex with pyrogallol on the concentration of germanium(IV). The conditions are as follows. (A) $0–10.8 \times 10^{-7}$ M Ge(IV), preconcentration time was 60 s. (B) $0–10.8 \times 10^{-8}$ M Ge(IV), preconcentration time was 90 s. (C) 0–10, $8 \times 10^{-9}$ M Ge(IV), preconcentration time was 180 s. Other conditions are the same as those in Fig. 3.

Table 1
Results of the determination of germanium in standard ore samples

| Sample | Stated content ($\mu g\ g^{-1}$) | Content determined ($\mu g\ g^{-1}$) | Average value found ($\mu g\ g^{-1}$) |
|---|---|---|---|
| GSD-2 | 1.70 | 1.65, 1.71, 1.68 | 1.68 |
| GSD-4 | 1.40 | 1.35, 1.40, 1.39 | 1.38 |
| GSD-5 | 1.40 | 1.32, 1.39, 1.41 | 1.37 |

and adsorb at HMDE, a cathodic stripping peak was produced. In experiments it was found that the sensitivity of tin(IV) was low. When the concentration of tin(IV) was 20-fold excess of Ge(IV), the relative response was 5.6%.

The adsorptive stripping voltammetric method can be applied to the determination of germanium(IV) in ore samples. A 0.2 g ore sample was dissolved in 5 ml of nitric acid (1 + 1) and the solution diluted to 25 ml. An appropriate volume of this sample solution was transferred into a 50 ml volumetric flask containing supporting electrolyte and diluted to the required volume with water. After these steps, a certain amount of this solution was added to the cell and tested to the procedure above.

Typical results obtained for standard samples are summarized in Table 1. The results for the determination of germanium(IV) are in agreement with the stated contents.

## 4. Conclusions

The results above demonstrate the feasibility of the method for the determination of trace germanium by cathodic stripping voltammetry. The detection limit is $1.2 \times 10^{-9}$ M. The method is sensitive, simple and relatively rapid.

## References

[1] N. Konopik, Anal. Abstr., 10 (1963) 3638.
[2] R.G. Canham and D.A. Aikens, J. Phys. Chem., 74 (1970) 1082.
[3] A.M. Shafiqul Alam, O. Vittori and M. Porthault, Anal. Chim. Acta, 102 (1978) 113.
[4] H.C. Liu, Phys. Testing Chem. Anal. (Part B: Chem. Anal.), 2 (1983) 20.
[5] J. Wang, Am. Lab., 17(5) (1985) 41.
[6] R. Kalvoda, M. Kopanica, Pure Appl. Chem., 61 (1989) 97.
[7] R. Kalvoda, Anal. Chim. Acta, 11 (1982) 138.
[8] C. Schleich and G. Henze, Fresenius' Z. Anal. Chem., 338 (1990) 145.

ELSEVIER

Talanta 42 (1995) 885–890

Talanta

# Electrocatalytic oxidation and flow detection of cysteine at an aquocobalamin adsorbed glassy carbon electrode

Huimei Li, Tao Li, Erkang Wang *

*Laboratory of Electroanalytical Chemistry, Changchun Institute of Applied Chemistry, Chinese Academy of Sciences, Changchun, Jilin 130022, People's Republic of China*

Received 12 July 1994; revised 15 December 1994; accepted 16 December 1994

**Abstract**

A chemically modified electrode (CME) constructed by adsorption of aquocobalamin (VB12a) onto a glassy carbon electrode surface was demonstrated to catalyze the electro-oxidation of cysteine, a sulfhydryl-containing compound. The sulfhydryl oxidation occured at 0.54–0.88 V vs. Ag/AgCl depending on pH value (3.0–10.0). The electrocatalytic behavior of cysteine is elucidated with respect to solution pH, operating potential and other variables as well as the CME preparation conditions. When used as the sensing electrode in flow injection amperometric detection, the CME permitted detection of the compound at 0.8 V. The detection limit was 1.7 pmol. The linear response range went up to 1.16 nmol. The stability of the CME was shown by RSD (4.2%) over 10 repeated injections.

## 1. Introduction

Numerous methods for the amperometric determination of physiologically important thiols following liquid chromatographic separation have been reported. Unfortunately, those thiols exhibit irreversible oxidation requiring extreme positive overpotential at most conventional electrode surfaces and, consequently, are not ideally suitable for quantification via conventional electrochemical approaches following liquid chromatography [1–3]. Electrochemical detection of those species is usually performed at mercury [4–7] or mercury amalgam [8,9] electrodes at which the formed mercury sulfide species can be oxidized at comparatively modest values of applied potential. Much effort has been made towards decreasing the overpotential and increasing the oxidation current [10–22]. Zagal et al. [10] reported the phthalocyanine tetrasulphonate adsorbed graphite electrode used for the electrocatalytic oxidation of cysteine. Baldwin [11,12] has developed carbon paste electrode containing cobalt phthalocyanine (CoPC) to decrease the overpotential for the oxidation of sulfhydryl compounds. Later, a polymeric CoPC chemically modified electrode was constructed to improve the stability of the electrode in organic solvents [13]. Some other medically important sulfhydryl containing substances such as thiopurines [14] and 2-thiothiazolidine-4-carboxylic acid [15] were also detected ideally on CoPC carbon paste electrode and electropolymerized CoPC glassy carbon electrode, respectively. Hart et al. [16–18] devised a carbon–epoxy resin composite electrode chemically modified with CoPC for catalytic oxidation and determination of glutathione following liquid chromatography. Kulys et al. [19] constructed graphite electrodes modified with tetracyano-*p*-quinodimethene, tetrathiafulvalene and 1,1′-dimethylferrocene for the electrocatalytic

* Corresponding author.


*SSDI* 0039-9140(95)01502-7

oxidation and determination of sulfhydryl compounds. He et al. [20] prepared a Nafion-$Os(bpy)_3^{2+/3+}$ film coated glassy carbon electrode for the determination of trace amounts of thiols via LCEC. Wang [21] and Cox [22] devised mixed-valent inorganic film modified electrodes for electrocatalysis and determination of those thiols.

Aquocobalamin (VB12a) is a Co(III) corrin complex with the structure shown in Fig. 1. It is related to the biologically active adenosylcobalamin, in which adenosine replaces water as an axial ligand. In conjunction with the proper enzyme system, the latter compound catalyzes a variety of group-transfer and other unique reactions in living systems [23]. There is an extensive body of literature on the chemistry of VB12 [24,25], and there has been recent interest in its catalytic properties for organic reduction [26–29], mostly about the alkylhalides [27–29], and also about oxygen [30]. The catalytic utility of VB12a in reduction is due to its facile chemical or electrochemical reduction to B12s [Co(I)alamine], a powerful nucleophile that is readily alkylated to yield alkyl Co(III) alamins. Compared to the wide research on catalytic reduction by VB12a, there has been little study on the catalytic oxidation by vitamin B12 and its analogues [31,32], not least the catalytic mechanism. In view of the well known catalytic activity of VB12a toward a wide variety of redox systems, we have constructed an aquocobalamin modified electrode (VB12a–CME) which not only greatly enhanced the oxidation peak but also decreased the oxidation overpotential of cysteine. We further investigate the use of the VB12a–CME as analytical sensors in voltammetry and flow injection analysis (FIA).

## 2. Experimental

### 2.1. Reagents and apparatus

Vitamin B12 and DL-cysteine (Cys) were of biochemical grade obtained from Shanghai Chemical Corp. (Shanghai, China). A stock solution (0.1 M) of cysteine was prepared with 0.1 M KOH and stored at 4 °C in the dark. Doubly distilled water was used for the preparation of all solutions. Vitamin B12a was obtained by photolysis [33,34]. A $1 \times 10^{-3}$ M solution of vitamin B12 in acetate buffer pH 4.75 was subjected to photolysis for 30 min.

Voltammetric experiments were performed with a laboratory-built voltameter. All experiments were done by using a three-electrode cell configuration with a modified or unmodified glassy carbon working electrode, a saturated Ag/AgCl reference electrode and a platinum wire auxiliary electrode.

Flow injection analysis was performed with a Gilson 306 pump (Gilson Medical Electronics, France), a model 7125 Rheodyne injector (Berkeley, CA, U.S.A.) with a 20 µl sample loop and a model 400 electrochemical detector with MP 1303 GCE for detection. The mobile phase was 0.1 M potassium phosphate buffer (pH 7.0), containing 50 µM EDTA, and was delivered at a constant flow rate of 1.0 ml/min. The mobile phase was filtered through 0.45 µm Type HA filter paper (Millipore Corp., U.S.A.) and was briefly degassed in an ultrasonic bath and a vacuum system about 15 min before use. The experiments were carried out at room temperature. A 125 W mercury lamp was used for photolysis.

### 2.2. Electrodes

Prior to surface modification, the glassy carbon electrode was polished successively using 1, 0.3 and 0.05 µm alumina powder suspension on

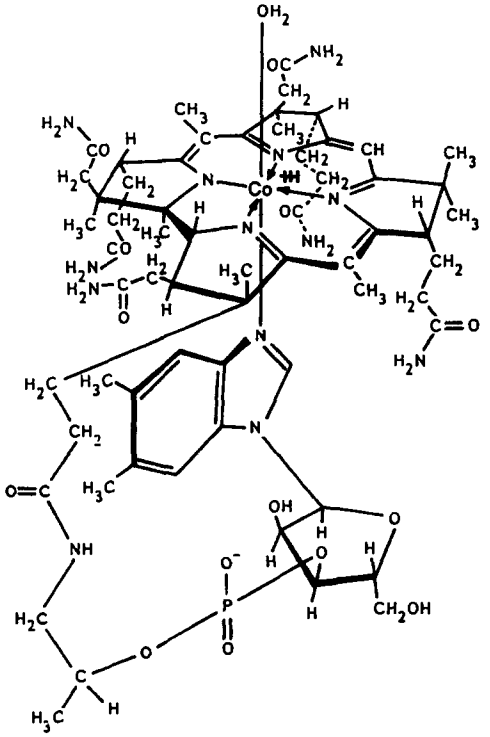

Fig. 1. The structure of aquocobalamin.

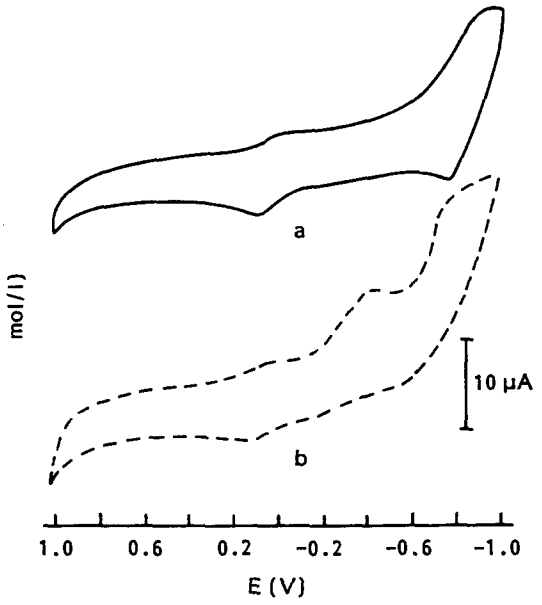


Fig. 2. Cyclic voltammograms of 1 mM vitamin B12a on bare glassy carbon electrode in 0.1 M phosphate buffer (pH 7.0) before (b) and after (a) degassing with nitrogen for 10 min. Scan rate, 100 mV/s.

a smooth cloth and then thoroughly ultrasonicated in a water bath several times, and finally rinsed with water. This electrode is referred to as fresh glassy carbon electrode (GCE). The CME was prepared by applying 10 μl of 1 mM aquocobolamin solution onto the dried GCE surface. The electrode was then left to dry in the air, until a uniform brown reddish film was observed to cover the entire disk. The electrode was rinsed with water and was then ready to use.

## 3. Result and discussion

### 3.1. Cyclic voltammetry of vitamin B12a

Fig. 2 shows cyclic voltammograms of vitamin B12a on the freshly cleaned glassy carbon in a neutral phosphate buffer solution. Fig. 2a was obtained after degassing with oxygen, while Fig. 2b was not degrassed with oxygen. Two cathodic waves, $P_c$ and $P_{c'}$ were observed at cathodic scan, with peak potential of $E_{pc} = 0.01$ V and $E_{pc'} = -0.94$ V which were with two corresponding anodic peaks ($E_{pa} = -0.1$ V and $E_{pa'} = -0.75$ V).

A detailed picture of the redox behavior of vitamin B12a has emerged from the work of Saveant [35–37]. As shown in those reports, VB12a is electroactive and followed two steps of a one-electron transfer redox process at the pH values involved in our experiment. The base-on aquo-B12a and the base-on B12r are the electrochemically reacting species as shown below:

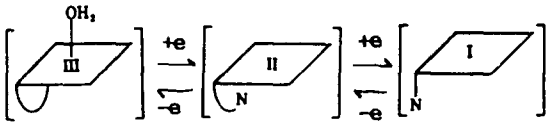


base-on base-on base-off

The first redox couple $P_c$ and $P_a$ features the reversible reduction and oxidation of B12a and B12r through its aquous form, and the second redox pair ($P_{c'}$ and $P_{a'}$) represents the redox process of B12r and B12s couple, the peaks at −0.54 and −1.0 V in Fig. 2b belong to the catalytic reduction of oxygen by VB12a. [37].

### 3.2. Electrocatalysis

Among the compounds whose redox reactions have been shown to be catalyzed by B12a are homocysteine and several other sulfhydryl-containing species [31]. In view of the importance of these compounds in a number of biological, pharmaceutical and environmental areas, we investigated the electrocatalytic oxidation of cysteine on VB12a and applied the VB12a–CME for the determination of cysteine. The CVs obtained for a GCE (a), VB12–CME (b) and VB12a–CME (c) immersed both in 0.1 M phosphate buffer (pH 7.0) blank solution and in the same solution doped with 0.5 and 1 mM cysteine are shown in Fig. 3. The VB12a–CME containing higher modifier concentration were found to yield a slightly higher current level and thus was not investigated further. By itself, the VB12a–CME exhibited anodic and cathodic peaks which matched the adsorption wave observed for a VB12a solution in Fig. 2b (without degassing oxygen by $N_2$). The introduction of a cysteine to this CME/solution system resulted in a marked increase in current and a decrease in overpotential compared with the GCE/solution system. As before, the catalytic currents observed were proportional to the cysteine concentration and no cathodic currents were seen on the reverse scan. Furthermore, the currents due to the cysteine oxidation were diffusion controlled exhibiting a linear dependence on the square root of the scan rate range from 10 to 250 mV/s. Compared to the significantly catalytic oxida-

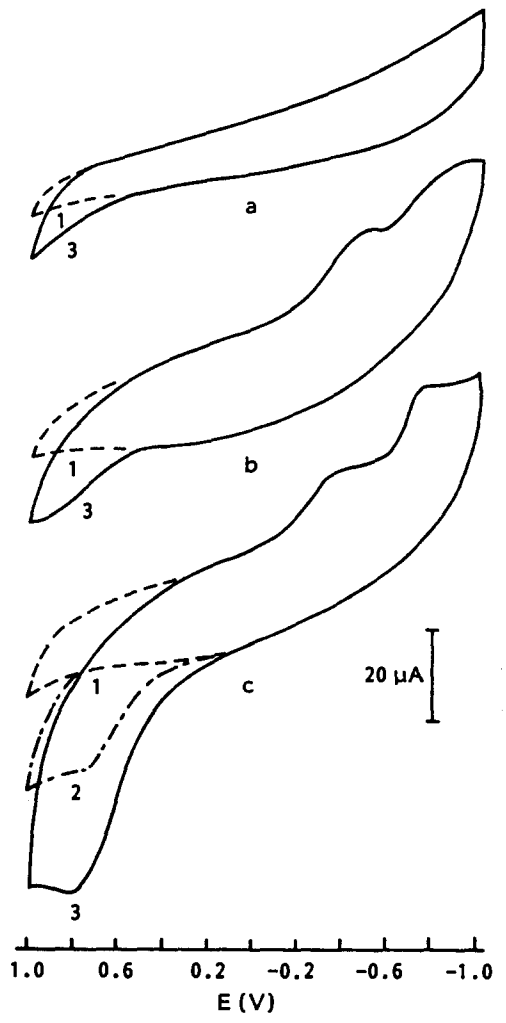


Fig. 3. Cyclic voltammograms of GCE (a), VB12–CME (b) and VB12a–CME (c) in 0.1 M phosphate buffer solution (1) and doped with 0.5 mM (2) and 1 mM (3) cysteine. Scan rate, 100 mV/s.

tion of cysteine on VB12a, there was almost no catalytic effect towards cysteine on VB12 (Fig. 3b), where the current was almost the same as at GCE with the addition of an adequately high concentration of cysteine. The catalytic mechanism was not clear. It is the same phenomenon in the chemically catalytic oxidation homocysteine by VB12a derivatives [31].

The effects of different pH values on catalytic peak current and oxidation wave are illustrated in Fig. 4. In general, increasing the solution pH caused a shift of the catalytic waves to lower potentials, and an identical increasing anodic current. The peak currents in neutral and alkali media were generally larger than those in low pH values.

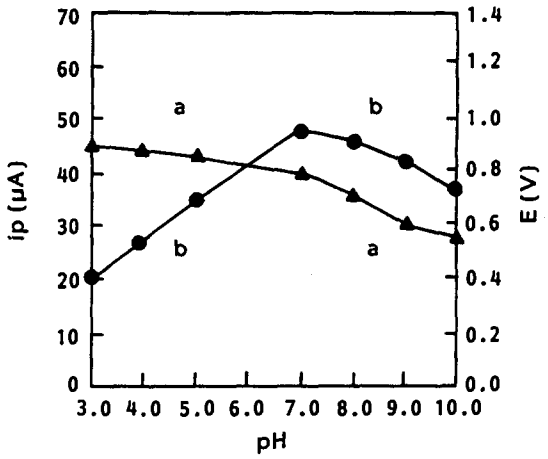


Fig. 4. Media pH effect on the peak potential (a) and peak current (b) on CVs obtained at VB12a–CME for 1 mM cysteine in 0.1 M phosphate buffer. Scan rate, 100 mV/s.

### 3.3. Flow injection amperometry

Despite some uncertainty concerning the catalysis mechanism, it was apparent that the response enhancement produced by the use of VB12a–CME should make its usage attractive in a number of analytical applications. One area where its use could be of particular advantage is as the sensing electrode for the detection of thiols in flow injection analysis and liquid chromatography.

Hydrodynamic voltammograms (HDVs) obtained for cysteine via flow injection on both GCE and VB12a–CME are shown in Fig. 5. A

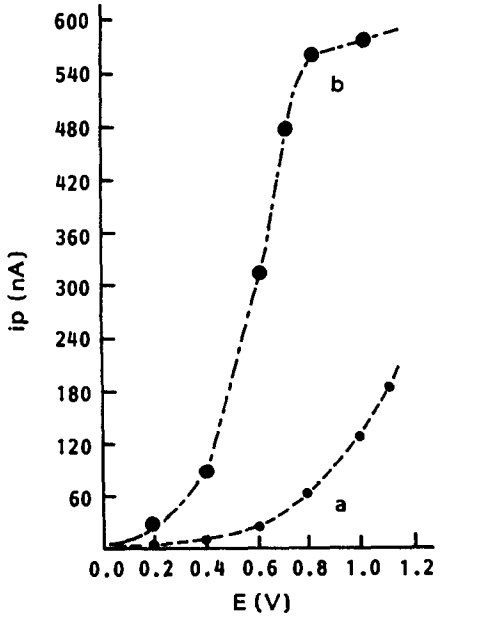


Fig. 5. Hydrodynamic voltammograms of $5.0 \times 10^{-5}$ M cysteine of GCE(a) and VB12a–CME(b). Mobile phase, 0.1 M phosphate buffer (pH 7.0) Flow-rate, 1.0 ml/min. Injection volume, 20 μl.

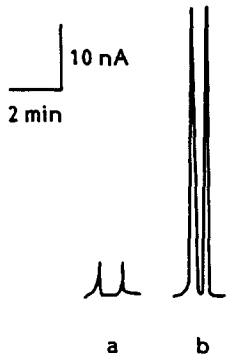


Fig. 6. Flow injection amperometric responses at GCE(a) and VB12a–CME(b) of $4 \times 10^{-6}$ M cysteine. Potential applied at 0.8 V vs. Ag/AgCl. Flow conditions as in Fig. 5.

substantial decrease in the half-wave potentials was observed at the CME and the response to cysteine was greatly enhanced. The optimum response in items of sensitivity, i.e. operation on the plateau region, occurred at 0.8 V. Also provided for comparison is the HDV obtained at an unmodified carbon electrode, which, as in CV, showed little response at potentials lower than 1.0 V. The mobile phase employed in these flow injection experiments consisted of 0.1 M phosphate buffer (pH 7.0) containing 50 μM EDTA.

On the basis of the HDVs, it appeared that the optimum potential for FIA detection of cysteine at VB12a–CME should be larger than 0.8 V vs. Ag/AgCl. As a high detection potential results in a more serious deactivation and high noise, 0.8 V was chosen as the detecting potential. Anodic peaks were obtained at this potential only when the VB12a–CME was employed (Fig. 6). Under those conditions, the calibration curve for cysteine was linear with injected amounts of analyte from 1.16 nmol to 1.7 pmol (Table 1). The regress equation was

Table 1
Dependence of the current response on concentration of cysteine [a]

| Concentration cys. (M) | Current response (nA) |
|---|---|
| $5.8 \times 10^{-5}$ | 596 |
| $1.0 \times 10^{-5}$ | 98 |
| $7.0 \times 10^{-6}$ | 64 |
| $1.5 \times 10^{-6}$ | 17 |
| $5.0 \times 10^{-7}$ | 7 |
| $8.5 \times 10^{-8}$ | 0.9 |

[a] Mobile phase: 0.1 M phosphate buffer, pH 7.0 and 50 μM EDTA, $E = 0.8$ V vs. Ag/AgCl, flow rate 1 ml/min, injection column 20 μl).

Table 2
The current responses of the injection of $5 \times 10^{-6}$ M cysteine

| Injection no. | Current response (nA) |
|---|---|
| 1 | 52 |
| 2 | 53 |
| 3 | 56 |
| 4 | 54 |
| 5 | 50 |
| 6 | 57 |
| 7 | 51 |
| 8 | 53 |
| 9 | 55 |
| 10 | 52 |

RSD = 4.2%.
Experimental conditions as Table 1.

$ip = -0.521 + 1.124C$ (ppm) (the correlation coefficient was 0.996). The detection limit was 1.7 pmol ($S/N = 2$). Typical peak currents obtained in this manner for the injection of $5.0 \times 10^{-6}$ M cysteine solution yielded a relative standard deviation of 4.2% for 10 successive trails (Table 2).

## 4. Conclusion

A VB12a–CME was constructed and showed effective catalysis of the oxidation of cysteine. In general, the performance of the VB12a–CME for cysteine determination seems to be at least comparable to that of other carbon- and mercury-based electrode systems. The detection limit of 1.7 pmol found for VB12a–CME is not less than those of previous reported assays [1–15]. The VB12a–CME was used in the flow injection analysis of cysteine with satisfactory results for high sensitivity and stability.

## References

[1] I. Mefford and R. N. Adams, Life Sci., 23 (1978) 1167.
[2] I.C. Shaw A.E.M. Mcclean and C.H. Boult, J. Chromatogr., 275 (1983) 206.
[3] K. Freuzig and J. Frank, J. Chromatogr., 218 (1981) 615.
[4] R. Saetre and D.L. Rabenstein, Anal. Chem., 50 (1978) 276.
[5] R. Saetre and D.L. Rabenstein, Anal. Biochem., 90 (1978) 276.
[6] D.L. Rabenstein and R. Saetre, Anal. Chem., 49 (1977) 1036.

[7] D.L. Rabenstein and R. Saetre, Clin. Chem., 24 (1978) 1140.
[8] R.F. Bergstrom, D.R. Kay and J.G. Wagner, J. Chromatogr., 222 (1981) 445.
[9] L.A. Alison and R.E. Shoup, Anal. Chem., 55 (1983) 8.
[10] J. Zagal, C. Fierro and R. Rozas, J. Electroanal. Chem., 119 (1981) 403.
[11] M.K. Halberb and R.P. Baldwin, Anal. Chem., 57 (1985) 591.
[12] M.K. Halbert and R.P. Baldwin, J. Chromatogr., 345 (1985) 43.
[13] X. Qi, R.P. Baldwin, H. Li and T.F. Guarr, Electroanalysis, 3 (1991) 119.
[14] M.K. Halbert and R.P. Baldwin, Anal. Chim. Acta, 187 (1986) 89.
[15] A. Ciucu and R.P. Baldwin, Electroanalysis, 4 (1992) 515.
[16] S. A. Wring, J. P. Hard and B. J. Brick, Analyst, 114 (1989) 1536.
[17] S. A. Wring, J. P. Hard and B. J. Brick, Analyst, 114 (1989) 1517.
[18] S. A. Wring and J. P. Hard, Talanta, 38 (1991) 1257.
[19] J. Kulys and A. Drunggiliene, Anal. Chim. Acta, 243 (1991) 287.
[20] X. Chen, B. Xia and P. He, J. Electronal. Chem., 281 (1990) 85.
[21] W. Hou and E. Wang, J. Electroanal. Chem., 316 (1991) 155.
[22] J. A. Cox and T. J. Gray, Electronalysis, 2 (1990) 107.
[23] D. Dolphin (ed.) B12, Vol. II., Wiley, New York 1982.
[24] J. Halpern, in D. Dolphin (ed.), B12, Vol. I. Wiley, New York, 1982, pp. 501–504.
[25] J.H. Grate and G.N. Schrauzer, J. Am. Chem. Soc., 101 (1979) 4601.
[26] R. Scheffold (ed.), Modern Synthetic Methods; Vol. 3. Wiley, New York, 1983, pp. 355–439.
[27] T.F. Connors, J.V. Arena and J.F. Rusling, J. Phys. Chem., 92 (1988) 2810.
[28] J.F. Rusling, T.F. Connors and A. Owlia, Anal. Chem., 59 (1987) 2123.
[29] D. Lexa, J.M. Saveant and J.P. Soufflet, J. Electroanal. Chem., 100 (1979) 159.
[30] J.H. Zagal, M. Paez and C. Paez, J. Electronanal. Chem., 237 (1987) 145.
[31] J. Aronovitch and N. Grossowicz, Biochem. Biophys. Res. Commun., 8(6) (1962) 416.
[32] J. Zhou and E. Wang, Electroanalysis, 4 (1992) 473.
[33] W.L.C. Veer, J.H. Edelhausen, H.G. Wijmenga and J. Lens, Biochim Biophys. Acta, 6 (1950) 225.
[34] J.M. Pratt, J. Chem. Soc., 988 (1964) 5154.
[35] N.R. De Tacconi, D. Lexa and J.M. Saveant, J. Am. Chem. Soc., 101(2) (1979) 467.
[36] D. Lexa and J.M. Saveant and J. Zickler, J. Am. Chem. Soc., 99(8) (1977) 2786.
[37] D. Lexa and J.M. Saveant, J. Am. Chem. Soc., 98(9) (1976) 2652.

ELSEVIER

Talanta 42 (1995) 891–895

Talanta

# Dual-wavelength $\beta$-correction spectrophotometric determination of arsenic in wastewater with ethyl violet

Hong-Wen Gao

*Huaibei Environmetal Monitoring Centre, Anhui Province 235000, People's Republic of China*

Received 4 April 1994; revised 3 October 1994; accepted 7 December 1994

**Abstract**

Arsenic has been determined by $\beta$-correction spectrophotometry with ethyl violet (EV) in the presence of sodium nitrite which is an oxidant and effective for removing absorption spectra and increasing analytical sensitivity. Extraction with benzene can separate most other metals ions and concentrate arsenic in wastewater. The $\beta$-correction method can eliminate completely the effect of excess EV in its As colored solution to give the real absorbance of the chelate produced. Sensitivity, precision and accuracy are all increased. Beer's law is obeyed over the range 0–2.0 mg $l^{-1}$ at 630 nm and the detection limit of arsenic is 0.02 mg $l^{-1}$. The results show that the relative standard deviation was less than 12% with the recovery between 91.0 and 114%.

## 1. Introduction

Arsenic is a poisonous element and often exists in waters, polluted by, for example, the pesticide chemical, paper and other industries. Although spectrophotometry with Ag-DDC [1] is now a usual method for the determination of trace arsenic, the reaction between arsenic(III) and ethyl violet (EV) in the presence of sodium nitrite was developed first. Sodium nitrite is an oxidant for changing trivalent As(III) in a colored solution into As(V), it was also found to be effective in removing the absorption spectra and increasing sensitivity. Both the extraction with benzene and the back-extraction with water may separate other metal ions [2] to increase the selectivity. Because of the serious effect of excess EV in As solution, it is difficult to accurately determine trace As by single wavelength spectrophotometry. The $\beta$-correction method described in this paper is a new dual-wavelength method for the determination of trace metal, which is different from other dual-wavelength spectrophotometries [3–6]. It may completely eliminate the interference of excess complex to give the real absorbance of chelate produced. The sensitivity, precision and accuracy by the dual wavelength $\beta$-correction method are all higher than those for the ordinary one. Recently, such a method has been applied to the analysis of $Be^{2+}$ [7] $Sb^{3+}$ [8] etc. Here, this method is utilized for the determination of trace amounts of arsenic(III) in wastewater using the above reaction. Beer's law is obeyed over the range 0–2.0 mg $l^{-1}$ As at 630 nm and the relative standard deviation is less than 12% and the recovery between 91.0 and 114%. The detection limit of arsenic is 0.02 mg $l^{-1}$. It is suitable for the determination of As(III) in wastewater from the chemical industry.

## 2. Principle

The following reaction of the colorant R and the metal is given to illustrate the $\beta$-correction


*SSDI* 0039-9140(95)01503-5

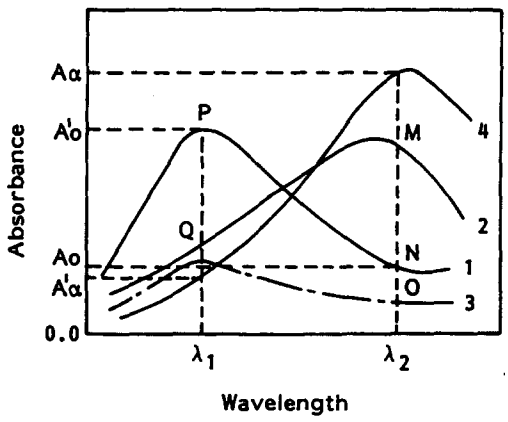


Fig. 1. Absorption spectra of R and its Me colored solution: (1) R ($a$ amount); (2) R($a$) + Me($b$) colored solution; (3) excess R ($c$ amount); (4) MeR$\gamma$ chelate. All against water reference.

principle and its spectrophotometry. The reaction is expressed by

$$a\mathrm{R} + b\mathrm{Me} \rightarrow b\mathrm{MeR}\gamma + c\mathrm{R}$$

where $a$ and $b$ are the starting amounts of R and Me, respectively, and $c$ is the excess R in its colored solution. $\gamma$ is the complex-ratio of R to Me. The absorption spectra sketch is shown in Fig. 1. At the wavelength $\lambda_2$ the real absorbance ($A_c$) of the MeR$\gamma$ chelate should be equal to the interval MO but not MN. The $A_c$ value is expressed by

$$A_c = (\Delta A - \beta\, \Delta A')/(1 - \alpha\beta) \quad (1)$$

where $\alpha$ and $\beta$ are both correction coefficients. They are calculated by, respectively,

$$\alpha = A'\alpha/A\alpha \quad (2)$$

and

$$\beta = A\mathrm{o}/A'\mathrm{o} \quad (3)$$

$\Delta A$, $\Delta A'$ are the absorbances of the colored solution of R ($a$ amount) with Me ($b$ amount) at $\lambda_2$ and $\lambda_1$, respectively, against its reagent blank ($a$R) reference. From Fig. 1 $\Delta A = \mathrm{MN}$ and $-\Delta A' = \mathrm{PQ}$. $A\alpha$, $A'\alpha$ are the absorbance of the chelate MeR$\gamma$ at $\lambda_2$ and $\lambda_1$, respectively, against water. $A$o, $A'$o are that of a reagent blank at $\lambda_2$ and $\lambda_1$ against water, $A\alpha$, $A'\alpha$; $A$o, $A'$o are shown in Fig. 1.

## 3. Experimental

### 3.1. Apparatus and reagents

Visible spectra were recorded with a Model 7230 spectrophotometer (Shanghai Third Analytical Instruments) in a 3 cm cell.

Standard arsenic(III) solution, 1.00 g $l^{-1}$: 0.1320 g $l^{-1}$ of arsenic trioxide (C.P., Beijing Chemical, China) was dissolved in 5 ml of 10% sodium hydroxide then the solution neutralized to pH 6–7 with 10% hydrogen chloride and diluted to 100 ml with distilled water. A 10.0 mg $l^{-1}$ arsenic solution was prepared by dilution. EV (Shanghai Chemical Reagents, China) solution, 0.010%; sodium nitrite (A.R., Beijing Hongxing Chemical, China) solution, 1%; hydrochloric acid solution, 0.125 mol; Benzene (Shanghai Organic Chemical, China).

### 3.2. Recommended procedures

To 50 ml of a wastewater containing less than 50 μg of arsenic(III), sulfuric and hydrochloric acid were added to give the desired 10 mol hydrogen ion molarity in a total volume of 100 ml. The solution was transferred into a separating funnel and extracted with 10 ml benzene. After separating the aqueous layer, As(III) was stripped with two 5 ml portions of water. The water-phase solution was taken in a 25 ml standard flask. Then, 2 ml of hydrochloric acid solution, 0.5 ml of sodium nitrite solution and 1.5 ml of EV solution were added. It was diluted to volume with distilled water and mixed well. After 1–5 min, the absorbances were measured at 560 and 630 nm, respectively, against a reagent blank reference.

## 4. Results and discussion

### 4.1. Absorption spectra

The absorption spectra of EV against water in the presence of sodium nitrite, that of As(III)–EV colored solution against its reagent blank and that of As–EV chelate which was measured from the colored solution as the mole ratio of EV to As(III) nears zero against the water reference, are shown in Fig. 2. From curve 3, two wavelengths may be selected such that the difference in absorbance is maximal: 560 and 630 nm. From curves 3 and 4, we see that sodium nitrite is effective in increasing the sensitivity and removing the absorption spectra. From curve 1,$\beta$ was calculated as 0.657 and from curve 2,$\alpha$ as 0.623.

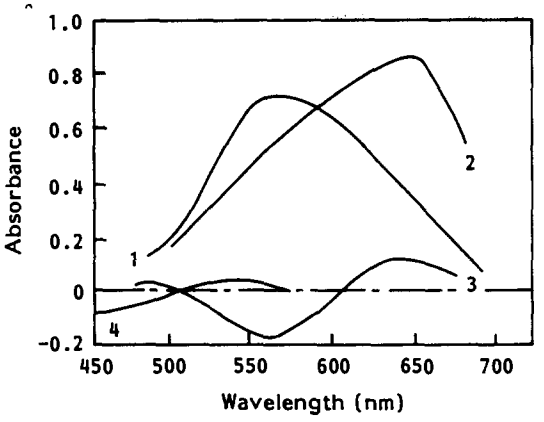


Fig. 2. Absorption spectra of EV and its As(II) colored solution in the presence of sodium nitrite: (1) EV (6.0 mg) with 0.02% sodium nitrite against water reference in 0.01 M HCl; (2) the colored solution of As(III) (500 mg) and EV(6.0 mg) with 0.02% sodium nitrite, regarded as only As–EV chelate not excess EV in the colored solution, against water reference; (3) the colored solution of As(III) (2.0 mg) and EV (6.0 mg) with 0.02% sodium nitrite, against its reagent bland reference; (4) same as (3) with sodium nitrite.

### 4.2. *Effect of EV concentration*

The effect of EV in the presence of sodium nitrite is shown in Fig. 3. Curve 1 is drawn from curves 2 and 3 and formula (1). From curves 1 and 2, $A_c$ is much higher than $\Delta A$, which shows the high sensitivity of the dual-wavelength $\beta$-correction method. From curve 1, $A_c$ reaches a maximal valve remains constant for the addition of more than 1.5 ml of 0.010% EV solution.

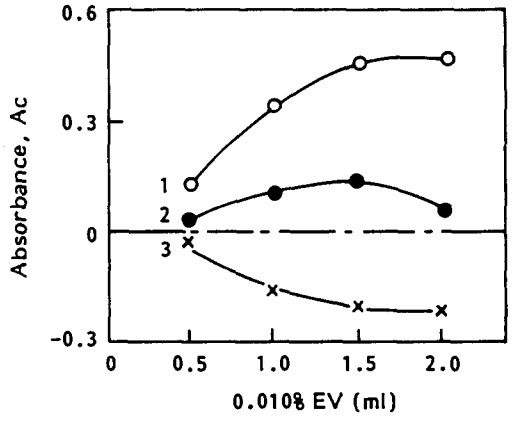


Fig. 3. Effect of EV in the presence of sodium nitrite at 630 nm: (1) the real absorbance ($A_c$) of the As–EV chelate in its colored solution containing 2.00 mg As(III); (2) the absorbance of the colored solution of As(III) (2.00 mg) and EV against its reagent blank reference; (3) same as (2) at 560 nm.

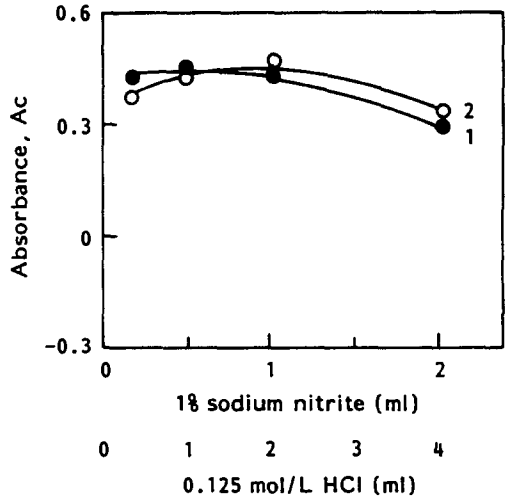


Fig. 4. Effect of HCl and sodium nitrite concentration on $A_c$ of As(III) (2.0 mg) colored solution at 630 nm: (1) 0.125 M HCl; (2) 1% sodium nitrite.

### 4.3. *Effect of acid and sodium nitrite concentration*

Varying molar concentration of HCl in a colored solution was investigated and the effect on the $A_c$ value of the colored solution containing 0.800 mg As has been drawn as Curve 1 in Fig. 4. The use of between 0.3 and 2.0 ml of 0.125 M HCl was found to give maximal colour intensity. Curve 2 in Fig. 4 shows the effect of sodium nitrite concentration. We see $A_c$ reach a maximum and was mostly stable for the addition of 1% sodium nitrite between 0.2 and 1.5 ml.

### 4.4. *Stoichiometry of complex*

A trial to determine As(V)–EV composition in the presence of sodium nitrite for the aqueous binary complex using the continuous variations method showed the As to ligand ratio to be 1:1. On the other hand, attempts to determine the composition of ternary complex were not made, because about 100-fold molar excess of nitrite ($NO_2^-$) was required for complete complex formation.

### 4.5. *Effect of development time*

The effect of reaction time on the real absorbance of 2.0 mg As(III) solution at 630 nm is shown in Fig. 5. We see that the formation of the complex of As(V) with EV in the presence of sodium nitrite is complete in 1 min but the fading of the colors becomes rapid after

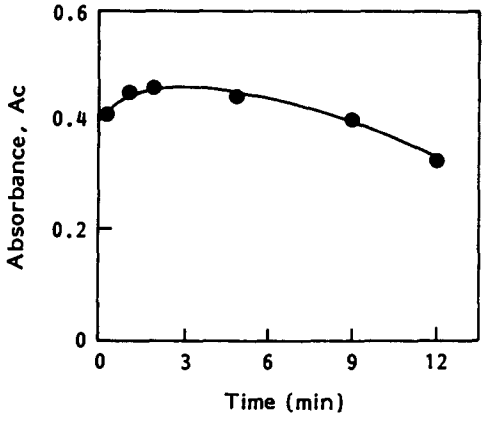


Fig. 5. Effect of development time on $A_c$ of As(III) (2.00 mg) colored solution at 630 nm.

10 min. Therefore, the measurement of absorbance should be completed in 1–5 min.

### 4.6. Calibration graph

A series of standard arsenic solutions were prepared and the absorbance of each was measured and plotted. Curves of $A_c$ and $\Delta A$ with As concentration ($x$) at 630 nm have been drawn in Fig. 6. Curve 1 is more linear than curve 2. It shows that the accuracy of the $\beta$-correction method is higher than that of the single wavelength method. The sensitivity of the recommended procedure is increased as shown by the higher gradient.

### 4.7. Effect of foreign ions

Once both the recommended extraction and back-extraction are carried out, none of the following metal ions affect the determination of 50 μg of As: 10 mg of $Na^+$, $K^+$, $Ca^{2+}$, $Mg^{2+}$, $Ti^{4+}$, $Al^{3+}$, $V^{5+}$, $W^{3+}$; 2 mg of $Zn^{2+}$, $Pb^{2+}$, $Mn^{2+}$, $Sn^{2+}$, $Fe^{2+}$, $Be^{2+}$; 1 mg of $Ni^{2+}$, $Cu^{2+}$, $Hg^{2+}$, $Cd^{2+}$; and 0.1 mg of $Sb^{3+}$, $Ag^+$, $Te^{3+}$.

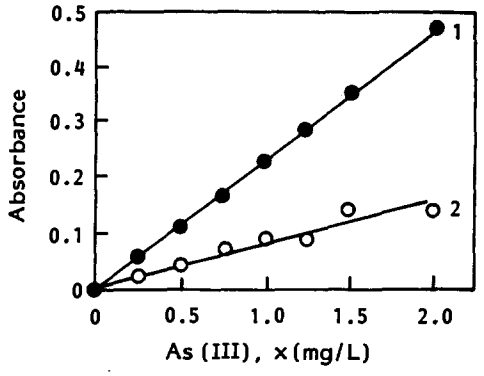


Fig. 6. Standard curves for the determination of As(III) at 630 nm: (1) $A_c$–$x$; (2) $\Delta A$–$x$.

### 4.8. Precision and detection limit

Direct replicate (10) determinations of standard As(III) solutions containing 2.00 mg As(III) were made, the relative standard deviation (RSD) being 2.3%. However, the RSD for the single wavelength method was 7.8%. Therefore, the precision by the dual-wavelength $\beta$-correction spectrophotometry is higher than that of the single wavelength method.

We used a real absorbance of 0.010 to calculate the detection limit of arsenic as 0.02 mg for 50 ml of wastewater.

### 4.9. Samples analysed

As a test of the method, arsenic(III) was determined in wastewater, from sulfuric acid [1] chemical [2], river [3] and Environmental Certified Reference Material: No. 3620106 [4]. The

Table 1
Analytical results of arsenic in wastewater

| Sample | Arsenic (mg $l^{-1}$) | | | RSD (%) | Recovery (%) |
|---|---|---|---|---|---|
| | By Ag–DDC | Added | Found [a] | | |
| 1 [b] | 81.4 | 0 | 76.3 | 2.6 | |
| | | 100 | 169 | | 92.7 |
| 2 | 0.391 | 0 | 0.419 | 7.6 | |
| | | 0.30 | 0.781 | | 114 |
| 3 | 0.094 | 0 | 0.104 | 12 | |
| | | 0.10 | 0.195 | | 91.0 |
| 4 [b] | | Certified value | | | |
| | 0.323 | +uncertainty | 0.346 | 2.7 | 100 |
| | | =0.338 + 0.022 | | | |

[a] Average of six determination.
[b] Direct determination without the extraction.

results are listed in Table 1. There is no obvious difference from that by the Ag–DDC method. The recovery was between 91.10 and 114% with a RSD of less than 12%.

## References

[1] P.K. Gupta and P.K. Gupta, Microchem. J., 33 (1986) 243.
[2] H.C. Beard, Anal. Chem., 33 (1961) 1781.
[3] V.Ma Carmen, S. Boudra and J.M. Bosque-Sendra, Analyst, 118 (1993) 1333.
[4] S.O. Farwell and C.T. Kagel, Anal. Chim. Acta, 178 (1985) 325.
[5] H.W. Gao, 4th Asian Chemical Congress, Chinese Chemical Society, Beijing, 1991, p. 372.
[6] H. Watanabe and H. Ohmori, Talanta, 26 (1979) 959.
[7] H.W. Gao and P.F. Zhang, Anal. Proc., 31 (1994) 85.
[8] H.W. Gao and P.F. Zhang, Analyst, 119 (1994) 2109.

ELSEVIER

Talanta 42 (1995) 897–900

Talanta

# Trace adsorptive voltammetric determination of antimony in hair

Xiaoli Zhang *, Chengsong Ma, Lizeng Wang, Jianguo Zhang

*Department of Chemistry, Shandong University, Jinan, Shandong 250100, People's Republic of China*

Received 12 July 1994; revised 14 November 1994; accepted 9 December 1994

**Abstract**

A very sensitive electrochemical procedure for trace determination of antimony is described. The complex of antimony with *p*-dimethyl-aminophenyl-fluorone (p-DMPF) is adsorbed on a hanging mercury drop electrode (HMDE), and the reduction current of the accumulated complex is measured by voltammetry. In linear sweep voltammetry, the reduction potential of the complex is more positive than that of the free dye. The peak height of the complex is proportional to the concentration of antimony in the range of $4.0 \times 10^{-9}$ to $4.0 \times 10^{-7}$ M, the detection limit is $1.0 \times 10^{-9}$ M Sb(III) for a 5 min preconcentration time. The relative standard error for the determination of $8.0 \times 10^{-8}$ M Sb(III) is 2.9%.

## 1. Introduction

Antimony exists widely in alloy, rock, soil, mineral, air, water and biological samples, China having the largest natural deposits of antimony in the world. Lately, the study of the distribution, excretion and accumulation of antimony in the human body has been widely studied in biological science. Human hair is the excretory organ and storehouse of trace elements in the human body. Thus, sensitive analytical methods to determine trace Sb in human hair are needed.

Many methods for determining trace Sb are available, including spectrometry, fluorometry, etc [1–3]. The polarographic behaviour of antimony has been reported previously. In the early 1960s, Gao [4] observed the Sb–hydrogen catalytic wave in an aqueous $Na_2SO_4$–$CoSO_4$–$(C_4H_9)_4NBr$ medium. This method may be used to determine Sb in semiconductor materials at a level of $2.0 \times 10^{-7}$ M. In succinic acid buffer solution (pH 4), a complex polarographic wave which is formed by $Sb^{3+}$ and cupferron was observed by Donoso. The detection limit of this AC polarographic method is $2 \times 10^{-6}$ M Sb(III) [5]. In recent years, some other methods for Sb analysis have also been reported [6–9], the lower detection limit of Sb with these methods is ca. $10^{-8}$ M.

While studying the Ga–salicyl fluorone complex adsorption wave [10], we found that after Sb had combined with fluorone type reagents, a clear adsorptive complex wave appeared on a Hg electrode. In this paper, the polarographic behaviour of Sb(III)–*p*-dimethylaminophenyl-fluorone (p-DMPF) is reported. The experimental results showed that Sb could give a sensitive complex adsorptive wave in 0.01 M $H_2C_2O_4$ (pH 1.8) which contained a small amount of DMPF. The linear relationship holds between the peak height of the complex and the concentration of Sb in the range from $4.0 \times 10^{-9}$ to $4.0 \times 10^{-7}$ M, the detection limit is $1.0 \times 10^{-9}$ M. This method has been applied to the analysis of trace Sb in human hair and satisfactory results were obtained.

* Corresponding author.

*SSDI* 0039-9140(95)01504-3

## 2. Experimental

### 2.1. Apparatus

A Model (79-1) voltammetric analyser (Jinan Fourth Electronic Factory, China) coupled with an X-Y recorder (Model 3086) (Shanghai Dahua Instrument Factory, China) were used. The three-electrode system consisted of a HMDE as the working electrode, a Pt plate as the counter electrode and a SCE as the reference electrode. A Model pHs-2 pH meter (Shanghai Second Analytical Instrument Factory, China) was used.

### 2.2. Reagents

A $1 \times 10^{-2}$ M stock solution of $Sb^{3+}$ was prepared by dissolving the appropriate amount of antimony metal in concentrated $H_2SO_4$ (GR) with heating. After being cooled, this solution was transferred to a 100 ml volumetric flask and diluted to the mark with 40% $H_2SO_4$. Standard solutions were obtained by diluting this stock solution with water. A $1 \times 10^{-3}$ M stock solution of p-DMF was prepared by dissolving the p-DMPF in ethanol (GR) containing 10 ml of 6 M HCl. A 0.5 M $H_2C_2O_4$ solution was prepared by dissolving reagent grade $H_2C_2O_4$ in water. All of the solutions were prepared from triply distilled water.

## Results and discussion

### 3.1. Voltammetric behaviour of p-dimethylaminophenyl fluorone

The fluorone dye, *p*-dimethylaminophenyl fluorone (p-DMPF) is commonly used as a developer in spectrophotometry. DMPF gives a reduction wave in various acidic or weak acidic electrolytes, such as HAc/NaAc, HCl, $HClO_4$, $H_2SO_4$, $H_2C_2O_4$, $NH_4Cl$ and $(CH_2)_6N_4$. In a solution of pH 2.0, DMPF gives a well-defined wave in DC, normal-pulse polarography (NPP), and differential pulse polarography (DPP). A logarithmic analysis of DMPF DC polarograms indicated that two electrons are involved in the reduction step as is the case for fluorescein. A series of solutions containing 0.01 M $H_2C_2O_4$ and $3.2 \times 10^{-7}$ M DMPF were prepared with different pH values by adding HCl or NaOH. The peak potentials and peak currents of these mixtures were measured by voltammetric analysis. The results are shown in Table 1.

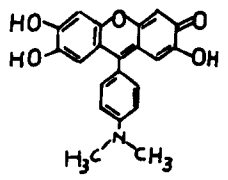

*p*-Dimethylaminophenyl fluorone

From Table 1, one can see that in the range of pH 1–6, a relationship of $E_p$ −0.59–0.06 pH holds. According to the relationship $s = (m/n)59$ mV (25 °C) [11], where $n = 2$ [12] and $m = 2$, every DMPF molecule must consume two $H^+$ during reduction.

### 3.2. Voltammograms of the Sb(III)–DMPF system

Voltammograms for DMPF containing $H_2C_2O_4$ solutions in the absence (a) and presence (b) of Sb(III) are shown in Fig. 1. When the DMPF containing solution was stirred for 1 min while the electrode was held at −0.25 V prior to the scan, a large cathodic peak associated with the reduction of the adsorbed DMPF was observed at −0.68 V. When the same experiment was repeated after the addition of $1.0 \times 10^{-7}$ M Sb(III), two additional peaks associated with the reduction of the Sb–DMPF complex were observed at −0.38 and −0.56 V, a very small peak $P_2$ and a large peak $P_3$, appeared at a position more positive than the reduction peak of DMPF $P_1$. It is reasonable to propose that the two new peaks result from the Sb(III) complex with DMPF.

Table 1
DMPF reduction waves at different pH values

| pH | 1.0 | 2.0 | 2.4 | 2.8 | 3.8 | 4.5 | 5.3 | 5.7 | 6.0 |
|---|---|---|---|---|---|---|---|---|---|
| $-E_p$ (V) | 0.65 | 0.70 | 0.73 | 0.75 | 0.80 | 0.84 | 0.90 | 0.91 | 0.94 |
| $i_p$ (μA) | 0.29 | 0.44 | 0.52 | 0.66 | 0.58 | 0.52 | 0.48 | 0.29 | 0.10 |

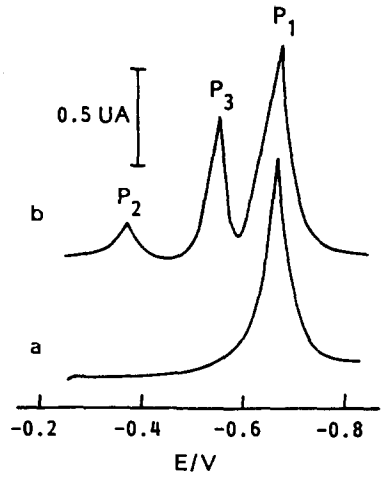


Fig. 1. Typical adsorption reduction voltammograms for DMPF containg solutions in the absence (a) and presence (b) of $1.0 \times 10^{-7}$ M Sb(III). Preconcentration for 60 s at −0.25 V; DMPF concentration $1.0 \times 10^{-6}$ M; scan rate, 100 mV/s; electrolyte, 0.01 M $H_2C_2O_4$ (pH 1.8).

### 3.3. Composition of the Sb-DMPF complex

Voltammograms for the Sb–DMPF complex are shown in Fig. 2. A peak $P_2$ appeared at a more positive potential when the concentration of Sb(III) was lowered. The peak potential of the $P_2$ was −0.38 V (Fig. 2a). When the concentration of Sb(III) was higher, another new peak, $P_3$, appeared at a potential slightly positive compared with that of DMPF. The peak potential of $P_3$, $E_{P_3}$, was −0.56 V (Fig. 2b). With an increase of the concentration of Sb(III), $P_2$ decreased, and $P_3$ gradually increased. These results suggest that Sb(III) reacted with DMPF to form two complexes, i.e. $SbL_3$ and SbL. This conclusion also has been

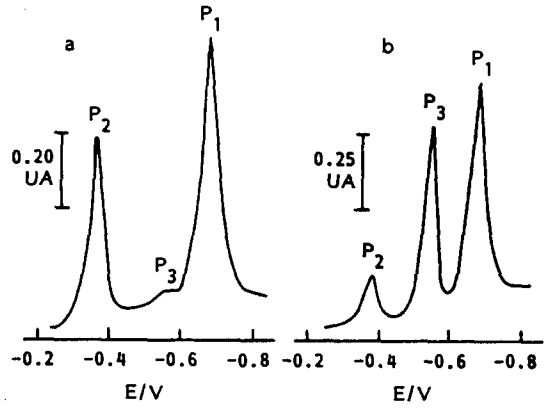


Fig. 2. Adsorption reduction voltammograms of Sb(III)–DMPF complexes at different Sb(III) concentrations. (a) $2.0 \times 10^{-8}$ M; (b) $8.0 \times 10^{-8}$ M. Experimental conditions as in Fig. 1.



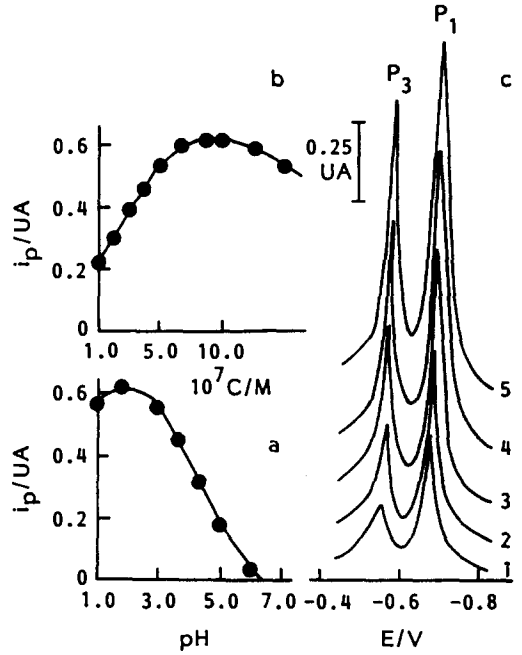


Fig. 3. Effect of pH (a), DMPF concentration (b) and scan rates (c) on the Sb(III)–DMPF adsorptive stripping response. Other conditions as in Fig. 2(b), except for $E_a$ = −0.45 V; pH (a); $C_{DMPF}$ (b); and scan rates (c): scan rate $V$ (mV/s): (1) 40, (2) 60, (3) 80, (4) 100, (5) 120.

proposed by Xia [13] using spectrophotometry. This means that at lower concentrations of Sb(III), the prevailing form of the complex is $SbL_3$ and with increasing concentrations of Sb(III), the concentration of SbL gets larger.

We use the following equation [14]:

$$1/i_p = 1/i_{p_{max}} + 1/\beta i_{p_{max}} C_L^m$$

to obtain the coordination number of the complex adsorbed on the surface of the electrode, where $i_p$ is the measured peak current, $i_{p_{max}}$ is the peak current when all the metal ions form the complex and $C_L$ is the concentration of the ligand. When $m = 3$, a straight line is obtained from a plot of $1/i_p$ vs. $1/C_L^3$. This indicates that the composition of the electroactive complex on the surface of the mercury electrode, which results in peak $P_2$ is Sb:DMPF = 1:3. When the same method is repeated for peak $P_3$, we get Sb:DMPF = 1:1.

### 3.4. Response characteristics and optimization

The effect of various operational parameters on the Sb–DMPF adsorptive stripping response is shown in Fig. 3. The pH dependence of the complex peak was studied in the range from pH 1 to 6 (Fig. 3a). No peaks were observed at pH values higher than 6. The

relationship between the peak current of the reduction of the Sb–DMPF complex, $i_{p_3}$ and pH is shown in Fig. 3a. Maximum peak current was reached at pH 1.8. Therefore, this value was used throughout this study. The DMPF concentration had a pronounced effect on the adsorptive stripping response (Fig. 3b). As the DMPF concentration increased, the peak current rapidly increased at first and then less rapidly. The effect of the scan rate on the peak current was evaluated over the 40 to 120 mV/s range (Fig. 3c), the current of $P_3$ varied linearly with the potential scan rate. The peak current, $i_{p_3}$ increased upon extending the preconcentration time, $t_a$. These phenomena suggest that the reactant is adsorbed on the electrode surface.

### 3.5. Linear range and reproducibility

There are two linear relationships between the Sb(III) concentration and the reduction peak current of the Sb(III)–DMPF complex. Using linear sweep voltammetry, a linear relationship between Sb(III) concentration and peak current of peak $P_2$ in the concentration range of $4.0 \times 10^{-9}$ to $5.0 \times 10^{-8}$ M Sb(III) can be obtained in 0.01 M $H_2C_2O_4$(pH 1.8) and $1.0 \times 10^{-7}$ to $1.0 \times 10^{-6}$ M DMPF. Another linear relationship between the Sb(III) concentration and the peak current of $P_3$ is $2.0 \times 10^{-8}$ to $4.0 \times 10^{-7}$ M Sb(III). The relative standard error for the determination of $8 \times 10^{-8}$ M Sb(III) is 2.9%.

### 3.6. Analytical utility

The experimental results show that a 1000-fold excess of $Cu^{2+}$, $Zn^{2+}$, $Al^{3+}$, $Fe^{3+}$, $Ca^{2+}$, $Mg^{2+}$; a 200-fold excess of $Pb^{2+}$, $Ni^{2+}$, $Nb^{5+}$; a 10-fold excess of $V^{5+}$; 50-fold excess of $Ga^{3+}$; and a two-fold excess of $Mo^{6+}$ and $Sn^{4+}$ did not interfere with the determination of $8.0 \times 10^{-8}$ M Sb(III).

A human hair sample was prepared by placing an exact amount of sample in a 50ml beaker. Approximately 15 ml of a mixed acid ($HNO_3$: HCl:$H_2O$, 1:3:3) was added to the beaker, and it was heated on a hotplate at 80 °C for about 5 h. Then, 1 ml of $HClO_4$ was added to the sample and it was heated until the evolution of white smoke. After cooling, the resulting white deposit was dissolved in water, and transferred to a 50 ml volumetric flask and diluted to volume with water.

Table 2
Results of the determination of Sb(III) in samples of human hair

| Sample | Content determined [a] (ppm) | Added (ppm) | Found [a] (ppm) | Recovery (%) |
|---|---|---|---|---|
| A | 2.40 | 2.50 | 4.88 | 99 |
| B | 2.25 | 2.00 | 4.13 | 94 |
| C | 3.30 | 3.00 | 6.33 | 101 |
| D | 2.65 | 3.00 | 5.74 | 103 |
| E | 3.00 | 3.00 | 5.88 | 96 |

[a] The values are the mean of five determinations.

Typical results determined by linear sweep adsorption voltammetry with two successive standard additions for treated samples, and the analysis of samples spiked with known quantities of Sb(III) are summarized in Table 2.

## References

[1] H.R. Hovind, Analyst, 100 (1975) 769.
[2] V. Stara, Talanta, 18 (1971) 228.
[3] G.Q. Gong, A.P. Wang and H.G. Wang, Fenxi Huaxue (China), 17 (1989) 524.
[4] H. Hua, X.X. Gao and W. Y, Scientia Sinica (China), 12 (1963) 1588.
[5] G. Donoso N. and M.A. Santa Ana V., Anal. Chim. Acta, 42 (1968) 109.
[6] R.D. Jee, Analyst, 113 (1988) 1321.
[7] A. Kumar, R.S. Agarwal and M. Jain, Chim. Acta Turc., 18 (1990) 493.
[8] N.V. Tobolkina and N.D. Fedorova, Zavod. Lab., 59 (1993) 16 (in Russian).
[9] H.L. Huang and D. Jagner, Anal. Chim. Acta, 202 (1987) 123.
[10] R.L. Chen and X.L. Zhang, Chem. J. Chinese Univ., 12 (1989) 1180.
[11] M.P. Zhang and X.X. Gao, Anal. Chem., 56 (1984) 1917.
[12] X.L. Zhang et al., Chin. Chem. Lett., 925 (1993) 4.
[13] X.L. Xia and G.J. Shao, Fenxi Lab. (China), 7 (1988) 41.
[14] N. Li and X.X. Gao, Fenxi Huaxue (China), 1 (1973) 40.

ELSEVIER

Talanta 42 (1995) 901–907

Talanta

# Separation mechanism exploration on metal–MBTAE–salicylic acid mixed ligand complexes by reversed-phase high performance liquid chromatography

Liu Qiping, Wang Yuanchao, Liu Jinchun *, Cheng Jieke

*Department of Chemistry, Wuhan University, Wuhan 430072, People's Republic of China*

Received 15 July 1994; revised 15 November 1994; accepted 28 November 1994

**Abstract**

The separation and determination of platinum metal and co-existing metal complexes by reversed-phase high performance liquid chromatography (HPLC) with 2-(6-methyl-2-benzothiazolylazo)-5-diethylamino phenol (MBTAE) as a precolumn derivatizing reagent is presented. The separation mechanism of these complexes was investigated by combining spectrophotometry with HPLC while salicylic acid was contained in the mobile phase. The results show that most platinum metal ions, Co(II) and Cu(II) can form ternary mixed ligand complexes with MBTAE and salicylic acid. The relationship of the retention behavior of complexes and the surface tension of the mobile phase ($\gamma$), the column temperature ($T$), and the composition and space configuration of complexes was also investigated. Some possible configurations of complexes are also proposed. These may all be illustrated well from the viewpoint of solvophobic theory. These method allowed the prediction of the composition and structure of metal complexes by utilizing HPLC.

## 1. Introduction

Platinum metals are rare and highly dispersed in the earth. They co-exist with large amounts of non-noble metals. Though platinum metals analysis had been a concern of analysts from early times, it is still difficult to preconcentrate, separate and quantitatively determine them owing to their similar physicochemical properties, various valences and existing species in solution. The development of HPLC provided a powerful and practical technique for platinum metals analysis, and the micro and trace analysis of platinum metals by HPLC had been a challenging research topic in inorganic analysis.

In order to avoid possible changes in species or valence during the chromatographic process, platinum metal ions are often detected in the form of stable complexes. The application of inorganic [1,2] or organic [3–5] reagents to platinum metals analysis had been frequently reported. Much attention had been paid to the organic reagents utilized because of their useful properties and wide selection. Therefore, it was our first premise to synthesize and select a group reagent with good stability and high sensitivity for separation and determination of platinum metals by HPLC. Among the organic reagents, pyridylazo compounds owing to high detection sensitivities with platinum metal ions, have been mostly applied, e.g. PAN [6] and various new reagents [7,8]. These reagents remarkably enhance the detection sensitivities of platinum metals. The use of thiazolylazo reagents in platinum metals analysis by HPLC has increased gradually in recent years [9,10]. These reagents contain a sulfur coordination

* Corresponding author.


*SSDI* 0039-9140(95)01510-8

atom and can form stable complexes with platinum metal ions. They can not only enhance the detection sensitivities, but also increase the number of platinum metals separated and detected. They have been applied to complicated real sample analysis [11–13].

Among the reported literature, an overwhelming majority is concerned with the selection and optimization of separation conditions, a few are on mechanism research. Furthermore, there was also a limit to the detection sensitivities and the number of separated platinum and co-existing metals.

2-(6-Methyl-2-benzothiazolylazo)-5-diethylamino phenol (MBTAE) is a new reagent which was synthesized by us [14]. It has been used for the separation and determination of some platinum and co-existing metal ions in the presence of ethylenediaminediacetic acid diethyl acetate (EDDD) [11] and malic acid [13]. Novel use of MBTAE in the presence of salicylic acid (SA) as well as a separation mechanism study of metal mixed ligand complexes is emphasized in this paper. The results showed that Pd(II) and Ni(II) can form binary complexes with MBTAE, while other platinum metal ions, Co(II) and Cu(II) can form ternary mixed ligand complexes with MBTAE and SA. All of the complexes except Rh(III) and Ir(IV) can be separated well at the mobile phase of the methanol–water system. Good correlations were found among the retention values of complexes and the surface tension of the mobile phase ($\gamma$), the column temperature ($T$), and the composition and space configuration of the complexes. All of these can be interpreted by solvophobic theory. It allowed the prediction of the composition and configuration of the metal complexes and had also some reference value for metal complexes analysis.

## 2. Experimental

### 2.1. Apparatus and reagents

A Shimadzu LC-6A high performance liquid chromatograph equipped with a Shimadzu C-R3A recorder was used. A Shimadzu UV-3000 spectrophotometer. Model DF-801 acidimeter from Zhongshan University and a supersonic degasser from Shanghai Int. Corp. were also used. The chromatographic column was Spherisorb C18 (5 μm, 150 × 4.6 mm i.d.) from Dalian Research Institute of Chemistry and Physics of China.

Stock solutions of Os(IV), Ir(IV), Ru(III), Rh(III), Pd(II) and Co(II) were prepared from analytical grade $(NH_4)_2OsCl_6$, $(NH_4)_2IrCl_6$, $RuCl_3$, $RhCl_3$, $PdCl_2$ and $CoSO_4$ dissolved in 1 M HCl, respectively. Ni(II) and Cu(II) standard solutions were obtained by dissolving 99.99% nickel and copper metals in dilute nitric acid, respectively. Pt(II) standard solution was obtained by reducing analytical grade $K_2PtCl_6$ standard solution with $SO_2$. The work solutions were 10.0 or 1.0 μg/ml.

Sodium salicylate from Shanghai Reagent Corp. was prepared as 0.2 M. Buffer solutions were mixed with 1 M acetic acid and 1 M sodium actate by adjusting to the proper pH values with an acidimeter. The synthesis and identification of MBTAE was given previously [14]. It was prepared in 0.02% absolute alcohol solution. Tetrabutylammonium bromide (TBA. Br) solution was prepared as 0.5 M. Methanol and alcohol were of analytical grade and double distilled water was used.

### 2.2. Analytical procedure

A known volume of Ru(III), Rh(III), Pd(II), Os(IV), Ir(IV), Pt(II), Co(II), Ni(II) and Cu(II) standard solutions were added to a 25 ml volumetric flask. Then 4.0 ml of pH 5.0 acetic acid–sodium acetate buffer solution, 2.0 ml of 0.02% MBTAE solution and 5 ml of 95% alcohol were added in order. The mixture was heated in an 80°C water-bath for 40 min, cooled to room temperature and diluted to the mark with 95% alcohol. This solution (20 μl) was injected onto the chromatographic column for analysis.

The composition of the mobile phase was of (v/v) methanol–water (82:18) containing 10.0 mM SA. 10.0 mM of pH 5.0 acetate buffer solution and 5.0 mM TBA. Br. The mixture was filtered through a 0.45 μm Millipore filter and degassed for 10 min before use.

The ODS column was pre-equilibrated with the mobile phase for 30 min. The column temperature was kept at 35°C. The flow rate was 1.0 ml/min. All of the complexes were detected at 575 nm with peak area for quantitative analysis.

## 3. Results and discussion

In reversed-phase HPLC, the interactions among the solute, solvent and stationary phase

are very complicated. Many models and theories have been proposed to interpret it including the solvophobic theory proposed first by Horvath and co-workers [15] which is well regarded. This theory emphasizes the important action of the mobile phase during the chromatographic process. It holds that during the chromatographic process, the polar mobile phase excludes non-polar or weak-polar solutes, and the combination of solute and stationary phase reduces the exclusion action from the solvent. According to Horvath's hypothesis and their mathematical calculations, an equation closely related to the experimental parameters is obtained:

$$\ln k' = \ln \Phi + \frac{[N\,\Delta A + 4.836N^{1/3}(K^e - 1)V^{2/3}]}{RT}\gamma \quad (1)$$

where $\Phi$ is the volume ratio of the stationary and mobile phase, $N$ is the Avogadro constant, $\Delta A$ is the reduction of the surface area as a consequence of the association of the solute with the stationary phase, $K^e$ is a factor for converting the bulk surface to molecular dimensions, $R$ is the universal gas constant, $V$ is the molar volume of the solvent, $T$ is the absolute temperature and $\gamma$ is the surface tension of the bulk solvent.

The importance of Eq. (1) is that it connects the microscopic chromatographic process with the macroscopic parameters of the mobile phase, the column temperature, etc. Therefore, the retention behavior of solutes can be predicted by adjusting and controlling the chromatographic parameters.

It was well known that platinum metal ions can form stable complexes with many ligands containing an oxygen atom. In this paper, salicyclic acid was chosen to investigate the complexes' retention behavior. The results are shown in Fig. 1. An interesting aspect is that the Cu–R complex (where R is MBTAE) was

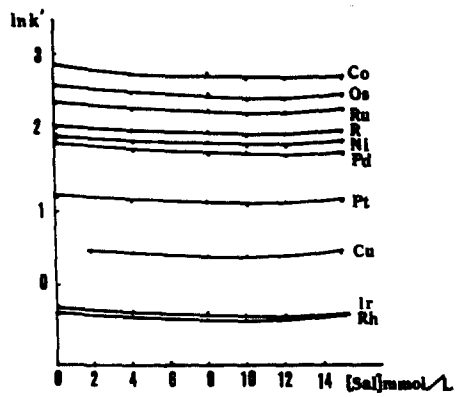


Fig. 1. The effect of SA concentration on ln $k'$. Chromatographic conditions: column, Spherisorb C18 (5 μm, 150 × 4.6 mm i.d.); mobile phase, methanol–water (82:18, v/v), 0 ~ 15 mM SA, 3 mM TBA. Br, 20 mM, pH 5.0 HOAc–NaOAc; flow rate, 1.0 ml/min; column temperature, 35°C; detection wavelength, 575 nm.

retained strongly on the C18 column when SA was absent from the mobile phase, and no peak could be observed for the Cu–R complex even after a long elution time. In contrast a remarkably sharp and symmetric Cu–R peak appeared after SA was added to the mobile phase. Not only the retention time, but also the detection limit, was reduced for platinum metals in the presence of SA (Table 1). The detection limits of platinum metals were raised by three to 33 times. Under optimum conditions, a typical separation chromatogram is shown in Fig. 2.

Now the problem was that the separation mechanism of platinum and their co-existing metals on a C18 column still cannot be explained clearly if only based on the results of Figs. 1, 2, and Table 1. Therefore, it was necessary to explore further the effect of the mobile phase composition, the oven temperature, the composition and the configuration of complexes on retention behavior of platinum and co-existing metals.

Eq. (1) indicated that ln $k'$ is directly proportional to the surface tension of the mobile phase ($\gamma$) and the reciprocal of column temper-

Table 1
The effect of SA concentration on detection limit and analysis speed ($S/N = 3$)

| Complexes | Ru–R | Rh–R | Pd–R | Os–R | Ir–R | Pt–R | Co–R | Ni–R | Cu–R | Elution time (min) (last one, Co) |
|---|---|---|---|---|---|---|---|---|---|---|
| Detection limit (I) [a] (ng/ml) | 26.75 | 0.65 | 1.48 | 36.67 | 4.65 | 7.76 | 0.41 | 0.16 | — | 35 |
| Detection limit (II) [b] (ng/ml) | 2.14 | 0.10 | 0.46 | 1.11 | 1.20 | 2.00 | 0.10 | 0.10 | 0.24 | 23 |

Chromatographic conditions were the same as Fig. 1.
[a] SA was absent.
[b] 10 mM SA in the mobile phase.

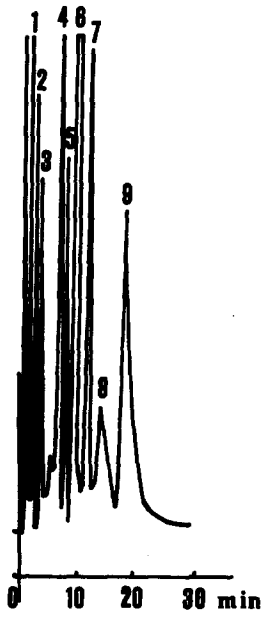


Fig. 2. Separation chromatogram of metal complexes. (1) 0.4 ng Rh + 1, 2 ng Ir; (2) 2.0 ng Cu; (3) 4.0 ng Pt; (4) 0.5 ng Pd; (5) 0.4 ng Ni; (6) MBTAE; (7) 2.0 ng Ru; (8). 7.0 ng Os; (9) 0.4 ng Co.

ature ($1/T$). Strictly speaking, with the mixed solvents as mobile phase, the dependence of $\ln k'$ on surface tension values is strongly non-linear as a consequence primarily of non-linearity between $\gamma$ and the composition in mixed solvents. Moreover, the molar volume of the eluent is a function of its composition, and $K^c$ is also likely to change. At a certain column temperature, if the change of mobile phase composition is comparatively small, $K^c$ and $V$ would be regarded as constants. So $\ln k'$ will be linear with $\gamma$ as shown in $\ln k' = A + B\gamma$ (Table 2). For the same reason, when the mobile phase composition was kept as a constant for a given temperature, $\gamma$ was a fixed value, $\ln k'$

Table 2
The relationship between $\ln k'$ and surface tension [a]

| Complexes | $A$ | $B$ | $r$ |
|---|---|---|---|
| Ru–R | −9.6121 | 0.4633 | 0.9948 |
| Rh–R | −10.801 | 0.4073 | 0.9877 |
| Pd–R | −13.424 | 0.6017 | 0.9978 |
| Os–R | −9.2801 | 0.4605 | 0.9917 |
| Ir–R | −7.3980 | 0.2785 | 0.9993 |
| Pt–R | −6.6345 | 0.3022 | 0.9992 |
| Co–R | −8.5060 | 0.4382 | 0.9999 |
| Ni–R | −13.603 | 0.6034 | 0.9988 |
| Cu–R | −6.5516 | 0.2746 | 0.9990 |

Chromatographic conditions: mobile phase, methanol–water, 20 mM, pH 5.0 HOAc–NaOAc; 10 mM SA; 3 mM TBA. Br; other conditions were the same as Fig. 1.

Table 3
The relationship between $\ln k'$ and $1/T$

| Complexes | $A'$ | $B'$ | $r$ |
|---|---|---|---|
| Ru–R | −5.291 | 2358.5 | 0.9914 |
| Rh–R | −4.529 | 1258.4 | 0.9905 |
| Pd–R | −6.006 | 2404.3 | 0.9985 |
| Os–R | −5.162 | 2371.0 | 0.9958 |
| Ir–R | −3.713 | 1028.5 | 0.9985 |
| Pt–R | −2.425 | 1096.2 | 0.9874 |
| Co–R | −4.332 | 2180.4 | 0.9991 |
| Ni–R | −6.988 | 2763.2 | 0.9994 |
| Cu–R | −3.913 | 1034.3 | 0.9992 |

Chromatographic conditions were the same as Fig. 2.

can also be regarded as linear with $1/T$ as shown by $\ln k' = A' + B'/T$ (Table 3). Good linear relationships between $\ln k'$ and $\gamma$, and $\ln k'$ and $1/T$ were established in the tested range (Tables 2 and 3).

Yet, there was still a question. What was the function of SA in the metal ion–MBTAE–SA system? Can it be regarded as the secondary complexing component to react with metal ions to form ternary mixed ligand complexes? How did it affect the retention behavior of metal complexes? It is generally believed that ternary mixed ligand complexes have three main characteristics as compared with binary complexes. The first is the sensitization action, the second is the solubilization action. Lowering the detection limits and shortening the retention time are the direct results of the above two actions on chromatography. These results are supported by data in Table 1. The third characteristic is the change of maximum absorption wavelength ($\lambda_{max}$) of metal complexes. The change of $\lambda_{max}$ of complexes in the presence of SA is shown in Table 4. It showed that most complexes had different changes in $\lambda_{max}$. The Ru–R complex showed two peaks when SA was absent. However, after SA was added in the mobile phase, the second peak, Ru–R (644 nm), disappeared and the $\lambda_{max}$ of the first

Table 4
The change of absorption wavelength in the presence of SA

| Complexes | $\lambda_{max}$ (nm) [a] | Complexes | $\lambda_{max}$ (nm) [a] |
|---|---|---|---|
| Ru–R | 574 (570, peak 1) | Ir–R | 593 (585) |
| | — (644, peak 2) | Pt–R | 585 (578) |
| Rh–R | 586 (590) | Co–R | 581 (575) |
| Pd–R | 589 (589) | Ni–R | 579 (579) |
| Os–R | 618 (600) | Cu–R | 584 (578) |

[a] $\lambda_{max}$ in the absence of SA in parentheses.

Table 5
Composition of metal complexes

| | Ru | Rh | Pd | Os | Ir | Pt | Co | Ni | Cu |
|---|---|---|---|---|---|---|---|---|---|
| M:R | 1:2 | 1:1 | 1:2 | 1:2 | 1:1 | 1:1 | 1:2 | 1:2 | 1:1 |
| M:R:SA | 1:2:1 | 1:1:2 | — | 1:2:1 | 1:1:1 | 1:1:1 | 1:2:1 | — | 1:1:1 |

R: MBTAE.

peak changed and its absorption increased. All of these are beneficial for the separation and quantitative analysis of Ru(III).

It is reasonable to deduce from the above discussion that SA may take part in coordination with metal ions and MBTAE to form ternary mixed ligand complexes under the given conditions. To verify this deduction, we determined the metal complexes composition by the Asmus [17] and Shi Huiming [18] methods, respectively (Table 5).

In Table 5, the complexes can be divided into four types: (i) Ni(II) and Pd(II) only reacted with R to form 1:2 complexes, and they did not complex with SA; (ii) Cu(II), Pt(II), Ir(IV) can react with R and SA to form ternary mixed ligand complexes of 1:1:1; (iii) Rh(III) formed 1:1:2 complex with R and SA; (iv) Ru(III), Os(IV), Co(II) reacted with R and SA to form ternary mixed ligand complexes of 1:2:1.

Why was the ternary mixed ligand complex more stable than the binary complex? An important factor was the electrostatic effect. It included the charge-neutrality principle and an entropy effect. The net charge of each complex after forming binary complexes is listed in Table 6. According to the charge-neutrality principle, if a complex is neutral, it is more stable than that with charge, and will not try to react with another charged ligand. In contrast, if a binary complex is charged, it is not sufficiently stable and will try to react with other ligands with the opposite charge to form a ternary mixed ligand complex. In Table 6, Pd–R and Ni–R complexes are neutral and thus it would be difficult for them to react with SA to form a ternary mixed ligand complex. The other binary complexes in Table 6 have +1, +2, or +3 charges and had a greater tendency to react with SA. The Co–R complex in Table 6 had an unusual behavior, differing from the others. This may be a result of the oxidation of Co(II), producing Co(III) under the experimental conditions, which would make a Co(III)–R complex with a +1 charge. It would then react with SA to form a ternary mixed ligand complex. Once the ternary mixed ligand complex is formed, both the system disorder tendency and its entropy increase, and this would increase the stability of complexes.

Eq. (1) also indicated that the slope of the $\ln k'$ vs. $\gamma/T$ curve is related to the $\Delta A$ value if the mobile phase composition change relatively slowly at the given temperature. Under these circumstances, $\ln K'$ can be regarded as being proportional to $\Delta A$. The larger the contact area of complexes with the hydrophobic stationary phase, the bigger the $\Delta A$ value and the curve slope. Otherwise, the $\Delta A$ value and the curve slope should be smaller. In our experiment, the volume of the MBTAE molecule was much bigger than that of the SA. Therefore, it would contribute much more to the $\Delta A$ value than the SA molecule does. The results in Tables 2 (B value), 3 (B′ value) and 5 demonstrate this. The sequence of curve slopes was (M:R:SA) 1:2:1 > 1:1:2 > 1:1:1.

An interesting question here was why the binary complex slopes of Ni–R and Pd–R(1:2) were larger than those of Ru–R–SA, Os–R–SA, and Co–R–SA complexes whose composition was 1:2:1? It cannot be explained only by the complex composition.

On the basis of reaction principles, metal complexes may have 12 kinds of configurations. They belong to the plane quadrilateral and regular octahedral structure, respectively. The configuration of the Pd–R and Ni–R complexes was plane quadrilateral and the others were regular octahedral. The typical configurations are shown in Fig. 3. We believe a plane quadrilateral complex would occupy a larger surface area on the stationary phase when adsorbed by the stationary phase, because its molecule is situated in the same plane, it has a larger cross-sectional area. This means that the $\Delta A$ value would increase and the slope of curve would be larger. On the other hand, a regular octahedral structure had eight planes, and its effective cross-sectional area is smaller than that of the plane quadrilateral when ad-

Table 6
Charge of the binary complexes

| | Ru–R | Rh–R | Pd–R | Os–R | Ir–R | Pt–R | Co–R | Ni–R | Cu–R |
|---|---|---|---|---|---|---|---|---|---|
| Charge | +1 | +2 | 0 | +2 | +3 | +1 | 0 | 0 | +1 |

sorbed by the stationary phase. So its contribution for $\Delta A$ and slope of curve would be smaller compared with the plane quadrilateral structure. For these reasons, the slope of the Ni–R and Pd–R complexes (1:2) was larger than that of the (Ru, Os, Co)–R–SA complexes (1:2:1).

## 4. Conclusion

Based on the above discussion we obtain the following conclusions.

(i) SA can react with some binary metal complexes to form ternary mixed ligand complexes under certain chromatographic conditions.

(ii) This method remarkably improved the detection limit of platinum metals, shortened the analytical time and increased the number of separable and determinable elements in the presence of SA in the mobile phase.

(iii) The retention behavior of metal complexes in reversed-phase HPLC was related to the stationary phase, the composition and properties of the mobile phase, the column temperature, and the composition and configuration of complexes.

In this paper, solvophobic theory gives a satisfactory interpretation to the retention mechanism of platinum metals and their coexisting metal complexes on a C18 column with salisylic acid in the mobile phase. This work should be of value in predicting the composition, configuration and retention behavior of metal complexes by the HPLC technique.

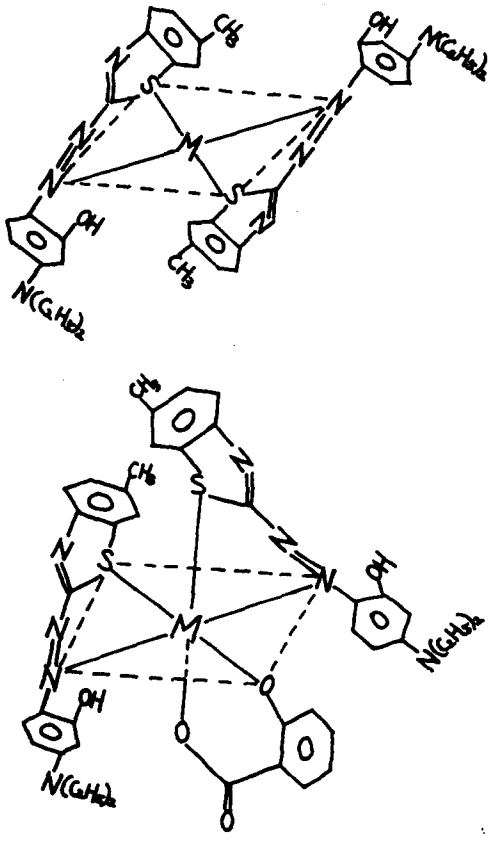

Fig. 3. Typical structures of metal complexes.

## References

[1] K. Hayakawa, T. Takizawa, M. Furuta and M. Miyazaki, Bunseki Kagaku 32 (1983) E243.
[2] P.R. Haddad and N.E. Rochester, Anal. Chem., 60 (1988) 536.
[3] B.J. Muller and R.J. Lovett, Anal. Chem., 59 (1987) 1405.
[4] B.J. Muller and R.J. Lovett, Anal. Chem., 57 (1985) 2693.
[5] I.P. Alimarin, E.M. Basova A.Yu. Malykhin, and T.A. Bol'shova, Talanta, 37 (1990) 485.
[6] E.M. Basova, T.A. Bol'shova, V.M. Ivanov and N.B. Morozova, Zh. Anal. Khim., 44 (1989) 680.
[7] N. Uehara, Y. Annok, T. Shimizu and Y. Shijo, Anal. Sci., 5 (1989) 111.
[8] Cheng Ruizhen, Liu Mancang and Hu Zhide. Sepu, 6 (1988) 34.
[9] Liu Qiping, Zhang Huashan and Cheng Jieke, Talanta, 38 (1991) 669.
[10] N.A. Beketova, E.M. Basova, V.M. Ivanov and T.A. Bol'shova, Zh. Anal. Khim, 45 (1990) 2178.
[11] Liu Qiping, Liu Jinchung, Tong Yan and Cheng Jieke, Anal. Chim. Acta., 269 (1992) 233.
[12] E.N. Shapovalova, I.V. Mishenine, M. Basova, T.A. Bol'shova, and O.A. Shpigun, Zh. Anal. Khim. 46 (1991) 1503.
[13] Liu Qiping, Wang Yuanchao, Liu Jinchun and Cheng Jieke, Anal. Sci., 9 (1993) 523.
[14] Liu Qiping, Zhang Huashan and Cheng Jieke, Chem. Res. Chin. Univ., 9 (1993) 18.
[15] C. Horvath, W. Melander and I. Molnar, J. Chromatogr., 125 (1976) 129.

[16] R.C. Weast and M.J. Astle, CRC Handbook of Chemistry and Physics, CRC Press, Boca Raton, FL, 1982.
[17] E. Asmus, Fresenius' Z. Anal. Chem., 178 (1960) 104.
[18] Shi Huiming and He Xiweng, Fenxi Huaxue, 7 (1979) 228.

ELSEVIER

Talanta 42 (1995) 909–913

Talanta

# FIA-spectrophotometric determination of N-substituted phenothiazine derivatives by oxidation with a solid-phase reactor of manganese dioxide incorporated in polyester resin beads

A. Kojło [a,*], J. Martinez Calatayud [b]

[a] *Institute of Chemistry, Warsaw University Branch at Białystok, 15-443 Białystok, Poland*
[b] *Departamento de Quimica Analitica, Universitat de Valencia, Valencia, Spain*

Received 20 June 1994; revised 3 January 1995; accepted 5 January 1995

**Abstract**

The determination of several *N*-substituted phenothiazine derivatives was carried out by the reaction of the drug with manganese dioxide entrapped in a polymeric material in a packed-bed reactor; the oxidized drug was monitored at $\lambda_{max}$. The calibration graph is linear over the range 5–50 μg/ml of phenothiazine derivatives with a relative standard deviation of 0.5–1% (at 10 μg/ml) and sample throughput of 40–48 $h^{-1}$. The influence of foreign compounds was studied and the method was applied to the determination of six different phenothiazine derivatives in pharmaceutical formulations.

## 1. Introduction

The phenothiazines are one of the most important groups of pharmaceuticals, used as antihistamines, tranquillizers, antiemetics and anti-Parkinson drugs and, therefore, their determination in pharmaceutical formulations is of considerable importance [1]. On the other hand, phenothiazines exhibit certain interesting analytical properties owing to their characteristic structure, the presence of chemically active sulfur and nitrogen atoms and substituents. It is important to point out the liability to oxidation by means of many oxidants with formation of coloured or fluorescent oxidation products. The oxidation involves a series of one-electron steps providing free radicals and cations [2–4]. As a result, there are many published procedures dealing with the determination of different phenothiazines with the aid of strong oxidative reagents. Some FIA procedures which have been published deal with formation of ion-association compounds with liquid–liquid separation [5] or turbidimetric monitorization [6], fluorimetric or spectrophotometric procedures based on the reaction with oxidants in solution [7–11] or immobilized [12–15] or fluorimetric procedures based on photoreactions [16–21]. Other FIA procedures using amperometric [22,23] and voltametric [24,25] detection have also been reported.

On the other hand, the use of solid-phase reactors has become one of the most interesting developments in continuous-flow analytical methodologies, including FIA. The interest is ascribed to their different advantages over reagents in solution; the advantages have been reported earlier [26,27]. This paper deals with the immobilization of reagents based on polymerization of linear unsaturated polyester chains as a type of the broad category of physical entrapment of the reagent. The proposed procedure allows the use in flow-injection manifold of reagents commercially

* Corresponding author.

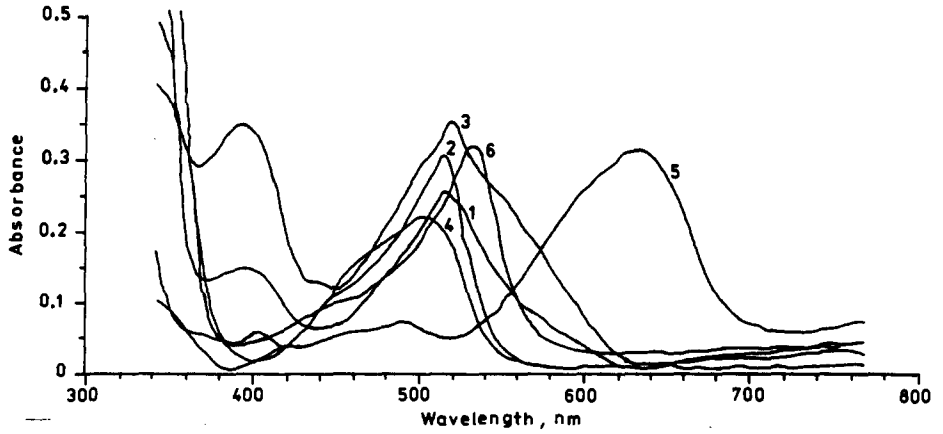


Fig. 1. Absorption spectra of the products from the oxidation of N-substituted phenothiazines. (1) DTZ · ML; (2) PMZ · HCl; (3) PMT · HCl; (4) TFP; (5) TRZ · HCl and (6) CPM · HCl.

available as fine powder without high-pressure FIA manifolds. The analytical procedure is based on the reaction of the drug with manganese dioxide and spectrophotometric monitorization of the oxidized drug which results in a simpler FIA manifold and lower consumption of reagents.

## 2. Experimental

### 2.1. Reagents and apparatus

Promazine (PMZ · HCl), promethazine (PMT · HCl), thioridazine (TRZ · HCl) and chloropromazine (CPM · HCl) hydrochlorides, diethazine maleate (DTZ · ML) and trifluoroperazine (TFP) were obtained from Polfa, Jelenia Góra, Poland and the aqueous solutions were prepared in bidistilled water. Hydrochloride, sulfuric, citric and ascorbic acids, formaldehyde, glucose, lactose calcium and sodium chlorides, sodium sulfite and disodium-EDTA were obtained from POCh, Gliwice, Poland. All reagents used were of analytical-grade unless otherwise stated. The bed-reactor was prepared with $MnO_2$ (A.R., Panreac, Barcelona, Spain), Al-100-A polyester resin solution (Reposa, Valencia, Spain) containing low-molecular weight polyester chains, with a cobalt compound as an activating agent and metyl ethyl ketone as a catalyst (Akco, Valencia, Spain) in the reaction.

*FIA manifold*

Fig. 1 shows the continuous-flow manifold used. A sample injector from Rheodyne, model 5041; and a Gilson Minipuls 2 pump were used. The determination of phenothiazine derivatives was carried out by means of a model 8452A diode array spectrophotometer (Hewlett-Packard, Waldbronn, Germany) at different wavelengths, with a flow-cell of 18-μl and 1 cm path length (Tecator, Hoganas, Sweden). The PTFE tubing was of 1.0 mm i.d. for the solid-phase bed reactor and the rest of the manifold.

*Preparation of the solid-phase reactor*

The bed-reactor was prepared as described previously [28]. A 11.81-g mass of manganese dioxide was added to 15.74 g of the resin solution; after its homogenization by manual stirring the catalyst was added and stirred before it became solid. The obtained solid was reduced to small particles, out of which those measuring 300–400 μm were selected, washed and introduced into the PTFE tubing by suction.

### 2.2. Determination of phenothiazine derivatives

*Tablets*

Five tablets were powdered and a weighed portion, equivalent to one tablet was dissolved in methanol and any remaining residue was

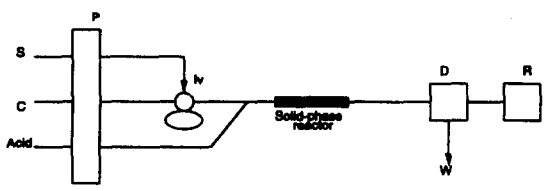


Fig. 2. The flow-injection manifold proposed for the determination of different phenothiazine derivatives. S, sample; C, carrier; $I_v$, injection valve; D, detector; W, waste; and R, recorder.

Table 1
Selected chemical and FIA parameters obtained with the optimization experiments

| Parameter | All drugs | TRZ |
|---|---|---|
| Sample volume (μl) | 612 | 612 |
| Carrier flow-rate (ml/min) | 3.2 | 3.2 |
| Length of the column (cm) | 170 | 120 |
| Distance reactor-flow cell (cm) | 300 | 250 |
| Concentration of HCl (M) | 1.0 | 0.5 |
| Wavelength [a] (nm) | 500–526 | 634 |

[a] Selected wavelengths (nm, drug) were: 514, DTZ; 512, PMZ; 516, PMT; 500, TFP; and 526, CPM.

filtered. The clear solution was made up to 100 ml with methanol. Aliquots of 10 ml of the methanolic solution were taken and evaporated to dryness. Solid residue was dissolved and diluted to 100 ml with bidistilled water. Calibration graphs were constructed from the results obtained with standard solutions of the phenothiazine derivatives.

*Injections*

The content of the drug in vial injections was diluted and levelled with bidistilled water up to 50 ml before introduction into the stream for analysis.

## 3. Results and discussion

Preliminary batch studies were designed to examine the reaction between the immobilized reagent with different N-substituted phenothiazines in aqueous solutions. Different acidic media were tested. Spectra of aqueous solutions were obtained before and after the oxidative treatment; absorption spectra after oxidation are shown in Fig. 1. In further experiments oxidized forms of the drugs were measured spectrophotometrically at the corresponding wavelengths of maximum absorbance. Non-oxidized forms of the drugs were not absorbed at these wavelengths.

Further preliminary tests were carried out with the aid of different flow assemblies to select the best manifold-configuration. The assembly in Fig. 2 was selected as the one producing the best compromise between the peak height and reproducibility of the transient signals. In this assembly the aqueous drug solution is injected into a pure distilled water stream which merges with the acidic solution stream.

The influence of the acidic media was tested with the aid of the selected flow assembly and hydrochloride and sulfuric acids were selected for further studies.

Different concentrations of HCl and $H_2SO_4$ were tested (flow-rate of carrier and acidic solution 3.2 ml/min, column length 170 cm, injector-detector length 270 cm and sample volume 612 μl). Hydrochloride acid was selected for further work in 1.0 M concentration, except the determination of thioridazine hydrochloride in which the selected concentration was 0.5 M.

The influence of the temperature was studied by the introduction the bed-reactor into a water-bath; the influence of this parameter resulted in decreased outputs owing to the increase of the reaction rate; the complete reaction leads to the final oxidation products which are colorless. Room temperature was the suitable choice.

The optimization of FIA parameters was carried out by the univariate method for 10 μg/ml of each phenothiazine derivatives in the order: column length (612 μl sample volume, 3.2 ml/min flow-rate and 1.0 M HCl), sample volume (170 cm column length, 3.2 ml/min flow-rate and 1.0 M HCl) and flow-rate (170 cm column length, 612 μl sample volume and 1.0 M HCl). The optimized response of the measuring system was the flow-injection peak height. The FIA parameter corresponding to the assembly selected as the best ones are given in Table 1.

## 4. Analytical applications

The calibration graphs were obtained by plotting peak-height (in mm) vs. phenothiazines concentration (μg/ml). The corresponding regression coefficients, detection limits (considered as three times the background noise) and the linearity ranges for each tested drug are depicted in Table 2. The reproducibility (15 replicates) calculated for chlorpromazine as %RSD, was (drug amount in μg/ml and RSD as %): 10, 1.3; 20, 1.0; and 30, 0.5. Sample throughput (tested for 25 μg/ml), 40 $h^{-1}$, except for thioridazine hydrochloride which was 48 $h^{-1}$.

The influence of foreign compounds that are commonly found in pharmaceutical formulations containing phenothiazines was investigated for chlorpromazine hydrochloride. Various concentrations of the possible interfer-

Table 2
Analytical parameters on the determination of N-substituted phenothiazines

| Phenothiazine | Calibration equations [a] | Correlation coefficient [b] | Detection limit (μg/ml) |
|---|---|---|---|
| Diethazine maleate | $1.154c + 1.462$ | 0.9997 | 0.7 |
| Promazine hydrochloride | $1.222c + 0.407$ | 0.9999 | 0.8 |
| Promethazine hydrochloride | $0.876c + 2.833$ | 0.9979 | 1.2 |
| Trifluoperazine | $0.563c + 0.707$ | 0.9998 | 0.3 |
| Thioridazine hydrochloride | $0.591c + 0.660$ | 0.9994 | 1.1 |
| Chlorpromazine hydrochloride | $1.170c + 0.081$ | 0.9995 | 0.6 |

[a] Linearity range for all drugs was 5–50 μg/ml.
[b] The correlation coefficients were calculated using 10 different concentrations of each amalyte.

Table 3
Influence of foreign compounds on the chloropromazine determination

| Compound | Concentration (μg/ml) | Relative error (%) |
|---|---|---|
| Ascorbic acid | 0.1 | 5.0 |
| Citric acid | 10.5 | 4.0 |
| Phenol | 2230 | 2.3 |
| Formaldehyde | 214 | 3.7 |
| Glucose | 100 | 2.6 |
| Lactose | 252 | 4.0 |
| NaCl | 451 | 1.8 |
| $CaCl_2$ | 56 | 4.0 |
| $Na_2SO_3$ | 19 | 4.0 |
| $Na_2$-EDTA | 37 | 3.8 |

ing substances were added to the solution containing 10 μg/ml, up to the amounts when the relative error (by comparison with pure chlorpromazine hydrochloride solutions, 10 μg/ml) was about 5%. The results in terms of concentration (μg/ml) and relative error (%) are depicted in Table 3. Phenol, formaldehyde, lactose and NaCl were tolerated in large amounts. Ascorbic acid and sodium sulfite interferred owing to their redox properties.

Promazine, chlorpromazine and thioridazine were determined in Promazine injection, Fenactil injection (Polfa, Jelenia Góra, Poland) and Melleril tablets (Sandoz, Rueil-Malmaison, France), respectively. The relative error was calculated by comparing the results with the content obtained with the aid of the proposed FIA assembly with the official gravimetric method [29] based on reaction with silicotungstic acid or by the Blażek's method [30] based on absorption measurements of phenothiazine derivatives at 254 nm in methanolic solution. Obtained results and calculated relative errors are depicted in Table 4.

## 5. Conclusions

The results show that the procedure based on physical entrapment of the solid reagent ($MnO_2$) by a polymeric resin is quite simple, fast, inexpensive, and can be alternative to procedures utilizing other strong oxidizing reagents. The proposed FIA system is suitable for the control analysis of the phenothiazine derivatives in pharmaceutical preparations.

Table 4
Determination of phenothiazines in pharmaceutical formulations

| Formulation | Source | Drug | Found (mg) [a] | | |
|---|---|---|---|---|---|
| | | | FIA method | Reference method [b] | $E$ (%) |
| Promazin (inj.) | Polfa | Promazine · HCl | 221.5 ± 0.5 | 228.0 ± 1.3 | 3.1 |
| Fenactil (inj.) | Polfa | Chlorpromazine · HCl | 97.4 ± 0.5 | 93.9 ± 0.7 | 3.7 |
| Melleril (tab.) | Sandoz | Thioridazine · HCl | 99.4 ± 0.5 | 100.9 ± 0.4 | 1.5 |

[a] Mean of three determinations ± SD.
[b] Gravimetry according to Polish Pharmacopoeia [29] or Blażek's method [30] (for thioridazine only).

## References


[1] Martindale, The Extra Pharmacopoeia, 30th edn., Pharmaceutical Press, 1992.
[2] G. Duchinski, Pharmazie, 13 (1958) 478.
[3] G.J. Patriarche, Microchim. Acta, 84 (1970) 9750.
[4] G. Clarke, in K. Florey (Ed.), Analytical Profile of Drug Substances, Vol. 9, Academic Press, New York, 1990, p. 284.
[5] S.L. Bhongade and A.V. Kasture, Talanta, 40 (1993) 1525.
[6] J. Martinez Calatayud, S. Navasquillo Sarrion, A. Sanchez Sampedro and C. Gomez Benito, Microchem. J., 45 (1992) 129.
[7] J. Martinez Calatayud and T. Garcia Sancho, J. Pharm. Biomed. Anal., 10 (1992) 37.
[8] J. Martinez Calatayud and T. Garcia Sancho, Pharmazie, 47 (1992) 557.
[9] M.A. Koupparis and A. Barcuchova, Analyst, 111 (1986) 313.
[10] S.M. Sultan, Analyst, 116 (1991) 177.
[11] T. Perez-Ruiz, C. Martinez-Lozano, V. Tomas and C. Sidrach de Cardona, Talanta, 40 (1993) 1361.
[12] J. Martinez Calatayud and V. Garcia Mateo, Anal. Chim. Acta, 264 (1992) 283.
[13] A. Kojło, H. Puzanowska-Tarasiewicz and J. Martinez Calatayud, J. Pharm. Biomed. Anal., 10 (1992) 785.
[14] A. Kojło, H. Puzanowska-Tarasiewicz and J. Martinez Calatayud, Anal. Lett., 26 (1993) 593.
[15] S. Laredo Ortiz, C. Gómez Benito and J. Martinez Calatayud, Anal. Chim. Acta, 276 (1993) 281.
[16] J. Martinez Calatayud and C. Gómez Benito, Anal. Chim. Acta, 256 (1992) 105.
[17] A. Mellado Romero, C. Gómez Benito and J. Martinez Calatayud, Anal. Lett., 25 (1992) 1289.
[18] D. Chen, A. Rios, M.D. Luque de Castro and M. Valcarcel, Analyst, 116 (1991) 171.
[19] D. Chen, A. Rios, M.D. Luque de Castro and M. Valcarcel, Talanta, 38 (1991) 1227.
[20] M.T. Tena, M.D. Luque de Castro and M. Valcarcel, J. Automat. Chem., 13 (1991) 11.
[21] B. Laassis, J.J. Aaron and M.C. Mahedero, Anal. Chim. Acta, 290 (1994) 27.
[22] F. Belal and J.L. Anderson, Analyst, 110 (1985) 1493.
[23] J. Michałowski, A. Kojło, B. Magnuszewska and M. Trojanowicz, Anal. Chim. Acta, 289 (1994) 339.
[24] J. Wang and H.D. Dewald, Anal. Chim. Acta, 153 (1983) 325.
[25] J. Wang and H.D. Dewald, Talanta, 387 (1984) 31.
[26] J. Martinez Calatayud and J.V. Garcia Mateo, Chem. Anal. (Warsaw), 38 (1993) 1.
[27] H.A. Mottola, Quim. Anal., 8 (1989) 119.
[28] L. Lahuerta Zamora, J.V. Garcia Mateo and J. Martinez Calatayud, Anal. Chim. Acta, 81 (1992) 265.
[29] Polish Pharmacopoeia PZWL, Warsaw, 1965.

ELSEVIER

Talanta 42 (1995) 915–920

Talanta

# Determination of aniline by adsorptive stripping voltammetry using an improved diazotization and coupling procedure
## Application to the evaluation of the light degradation of D&C Red No. 33 in the presence of ascorbic acid

J.A. Rodrigues *, A.A. Barros

*Department of Chemistry, Faculty of Sciences, University of Porto, 4000 Porto, Portugal*

Received 25 October 1994; revised 3 January 1995; accepted 4 January 1995

**Abstract**

A method for the determination of aniline was developed, based on the diazotization and coupling of the aromatic amine to form an azo compound capable of being determined by adsorptive stripping voltammetry. A fast derivatization procedure was developed using 1-naftol as the coupling agent. A detection limit of 0.8 μg/l was obtained for aniline, using an accumulation time of 2 min. The method was applied in the determination of the amount of aniline in the colouring matter D&C Red No. 33, after a liquid–liquid extraction with chloroform, before and after submitting the colouring matter to a process of degradation, using accelerated light conditions in the presence of ascorbic acid.

## 1. Introduction

Adsorptive stripping voltammetry (AdSV) has been demonstrated to be a highly sensitive electroanalytical method for the determination of a wide range of electroactive compounds [1]. The use of derivatization reactions in analytical chemistry to improve the characteristics of analytes is widely reported. In the case of AdSV using derivatization reactions prior to making determinations has extended the advantages of the technique to a range of electroinactive or poorly adsorbed compounds and permits the differentiation of the analyte from interferents by providing signals at different potentials from those of unmodified molecules [2].

Aromatic amines are compounds that can be easily absorbed by the skin causing a systematic poisoning [3] and some of them are recognized carcinogenic agents [4]. A method frequently employed for the determination of aromatic amines involves diazotization and coupling, with formation of an intensely coloured azo compound, that can be detected spectrophotometrically [5]. In this work the same method of derivatization was applied in the determination of aniline, but an adsorptive stripping voltammetric method of detection was used instead, that enables a much lower detection limit to be achieved. In fact, the compound formed by diazotization and coupling of aniline, being structurally similar to azo colouring matters, is expected to be electroactive and to adsorb at the surface of a mercury electrode [6]. Using 1-naftol as a convenient coupling agent, conditions were optimized for the adsorptive stripping voltammetric determination of the azo compound

* Corresponding author.


*SSDI* 0039-9140(95)01512-4

formed, with a limit of detection of 0.8 μg/l being obtained for the determination of aniline.

The method was applied in the determination of aniline in the colouring matter D&C Red No. 33, before and after submitting the colouring matter to a process of accelerated light degradation. The method includes a liquid–liquid extraction of the aromatic amine from the azo dye, using chloroform, before the diazotization and coupling process.

## 2. Experimental

### 2.1. Instrumentation and conditions

The adsorptive stripping voltammetric determination was performed by differential-pulse voltammetry using a Metrohm system including a VA stand (E663), a VA scanner (E612), a VA detector (E611) and a VA controller (E608). This equipment was connected with a X-Y recorder (Houston 2000).

A three electrode system was employed, with the multimode electrode of the VA stand in its HMDE configuration, a glassy carbon counter electrode and a silver/silver chloride (3 M KCl) reference electrode.

In the voltammetric analysis, after bubbling $N_2$ for 15 min to deoxygenate the solution, accumulation was performed with stirring (2000 Hz) using a mercury drop area of 0.52 $mm^2$. After a rest period of 10 s, a cathodic potential scan of 10 mV $s^{-1}$ was applied, with cathodic pulses of 50 mV every second.

Measurements of pH were made using a pH 537 microprocessor pH meter, with a combined pH-reference electrode, both from WTW (Germany).

Light degradation studies were carried out in a specially constructed light box containing a 500 W tungsten filament lamp (Philips E40). To dissipate heat produced by the lamp, a fan was placed under the sample container.

### 2.2. Reagents and solutions

All chemicals were of analytical grade. Deionized and distilled water was used for the preparation of solutions.

D&C Red No. 33 (Colour Index No. 17200) is the disodium salt of 8-amino-2-phenylazo-1-naftol-3,6-disulfonic acid; the colouring matter was obtained from HKohnstamm, New York and has a pure dye content of 85% (about 15% of sodium chloride and sodium sulfate are present to match the required colour strength).

The diazotization solution was prepared daily by dissolution of 50 mg of sodium nitrite in 50 ml water. The coupling solution was prepared daily by dissolution of 50 mg of 1-naftol in 50 ml of 1 M sodium hydroxide. Stock standard solutions of aniline (about 200 mg/l) were prepared weekly by weighing about 50 mg of aniline accurately, dissolving it in water and diluting to 250 ml. More dilute standards were prepared daily by convenient dilution with water. Solid ascorbic acid was directly added in the preparation of the solutions for the degradation studies.

### 2.3. Diazotization and coupling of aniline

Solutions containing up to 100 μg of aniline were diluted to 10 ml and acidified with sulfuric acid to a pH of 2.5. Then, 1 ml of 0.1% sodium nitrite was added and the mixture was allowed to react during 5 min with stirring. Finally, 1 ml of 1-naftol 0.1% in 1 M NaOH was added and the solution diluted with 0.2 M ammonium nitrate to 25 ml, obtaining a pH of about 9 ready for the subsequent voltammetric analysis.

### 2.4. Extraction of aniline from D&C Red No. 33

About 50 mg of colouring matter was weighed accurately and dissolved in 100 ml of a solution 0.01 M in NaOH and 1% in NaCl. The solution was transferred to a separation funnel and extracted three times with 20 ml of chloroform. The organic extracts were drained through a washed (25 ml of chloroform) glass wool pledget in the constriction of a funnel into the flask of a rotary evaporator. Sulfuric acid 0.002 M (10 ml) was added to the chloroform extract, and the organic layer was completely removed in the rotary evaporator, using reduced pressure and a temperature of 45 °C. The aqueous solution remaining in the evaporator was diluted to 50 ml with 0.002 M sulfuric acid and 10 ml aliquots were used in the diazotization and coupling procedures previously described, preceding the voltammetric analysis.

### 2.5. Light degradation studies of D&C Red No. 33

In the light degradation box, 100 ml of 0.1% solutions of D&C Red No. 33, containing different amounts of ascorbic acid, were submitted to intense light. The solutions were contained in small, screw capped, glass vials, held at a uniform close distance from the 500 W lamp. After the established degradation time, aniline was extracted, diazotized and coupled with 1-naftol, and the azo compound formed was determined by adsorptive stripping voltammetry, as previously described.

## 3. Results and discussion

### 3.1. Determination of aniline

The spectrophotometric determination of aniline, after diazotization and coupling, is commonly used in the analysis of primary aromatic amines and has been extensively studied, with a large number of methods being proposed and recommended. In spite of the similarity of the methods, with slight differences concerning the nature of the coupling agent or some conditions of analysis, only occasionally efforts have been made to establish standard procedures, as is the case of Norwitz's work [5]. Taking into consideration this situation and the fact that we intend to use a voltammetric method of determination, instead of a spectrophotometric one, it was decided to make a complete investigation of the method of determination of aniline, including all the steps connected with the derivatization procedure. As the voltammetric response of the azo compound formed was used to measure the completeness of the derivatization reaction of aniline, voltammetric variables had to be studied before optimization of the reactions of diazotization and coupling was undertaken.

### 3.2. Selection of the coupling agent

Besides some general conditions that must be fulfilled irrespective of the method of detection (stability of the coupling agent, fastness of the coupling reaction, stability of the azoic product), two more conditions are needed for a coupling agent used with adsorptive voltammetric detection: not to interfere with the determination and to produce an azoic compound that adsorbs on the mercury electrode. The investigation started with H-acid (8-amino-1-hydroxy-3,6-naphthalenedisulfonic acid), the coupling agent selected by Norwitz [5], but the compound was found to interfere slightly in the voltammetric determination, with a marked effect on the detection limit of the method. Two other coupling agents were tried, resorcinol and 1-naftol, both phenols, a group of compounds that is known to react quickly with diazotized aniline. Resorcinol could not be used because it formed an unstable azo compound and resorcinol itself was oxidized, probably by atmospheric oxygen [7], giving a product that interfered in the voltammetric determination. On the contrary, 1-naftol proved to be a suitable coupling agent, being stable in alkaline solution and forming a stable azo derivative that was adsorbed on mercury. The only drawback of 1-natftol is its low solubility in water that forced the preparation of its solutions in 1 M sodium hydroxide.

### 3.3. Selection of pH and accumulation potential for the voltammetric determination

It was decided to use a pH value of 9 because both voltammetric sensitivity and adsorption of derivatized aniline were higher at this pH. The effect of varying the potential of accumulation, necessarily more positive than the reduction potential of the compound, was negligible. So it was fixed at the more negative value allowed, 200 mV more positive than the reduction potential. It was decided to use an accumulation potential about 400 mV more positive than the reduction potential of the compound.

### 3.4. Amount of coupling agent and sodium nitrite

It was found that 1 mg of 1-naftol and 1 mg of sodium nitrite were sufficient for the quantitative diazotization and coupling of up to 100 μg of aniline. This excess of diazotization and coupling agents ensures that the reaction is sufficiently quantitative and fast.

### 3.5. Selection of the coupling conditions

The coupling reaction is considered before the diazotization reaction because it does not impose many restrictions. In fact the only potential problem is the decomposition of the

diazotized aniline before coupling, and this does not happen as the coupling reaction is very fast if the pH of the solution is between 9 and 13. For simplicity, a pH of 9 (ammoniacal buffer) was used for coupling, the same that is used in the subsequent voltammetric analysis. The elimination of excess nitrite prior to the coupling reaction can be obtained, for example, by addition of sulfamic acid, but the need for this elimination is still controversial [5]. In our work it was not undertaken because it was found that the presence of nitrite had no influence on the results.

### 3.6. Selection of the diazotization conditions

In the preparative chemistry of azo compounds it is recommended that diazotization takes place in an ice bath. This low temperature is used to minimize the decomposition of the diazonium ion before the coupling reaction. In our case there was no need of such a precaution, which made the method simpler. In fact, as can be seen in Fig. 1, the same amount of derivatized aniline was formed in an ice bath and at room temperature, probably because the diazotized aniline is quite stable and the coupling reaction is fast. The use of room temperature is even better as it is possible to use a shorter diazotization time.

Another important variable in diazotization is pH. Acid conditions are required, but there is not a simple dependence of diazotization rate on pH [8,9]. Results obtained using solutions with different concentrations of sulfuric acid show that diazotization rate increases with decreasing acidity (Table 1). A sulfuric acid concentration between $10^{-3}$ and $10^{-2}$ M proved to be a good choice.

Using the method of determination of aniline just optimized, and described in the Experimental section, a calibration curve for aniline was obtained. A detection limit less than 1 ppb can be obtained if adsorptive accumulation is used (Fig. 2). Of course, for higher concentrations of aniline the saturation of the mercury electrode must be taken into consideration. For instance, with an accumulation time of 2 min the calibration curve is linear only if the concentration of aniline does not exceed 20 ppb. The proposed method has a detection limit about 50 times lower than the spectrophotometric method, if an accumulation time of 2 min is used.

Table 1
Diazotization of aniline (%)

| Diazotization time | $H_2SO_4$ concentration | | | | |
|---|---|---|---|---|---|
| | 1 M | 0.2 M | 0.1 M | 0.02 M | 0.002 M |
| 1 min | 11 | 20 | 25 | 79 | 100 |
| 5 min | — | — | 69 | 100 | 100 |

### 3.7. Determination of aniline in D&C Red No. 33

One of the applications of some primary aromatic amines is in the production of synthetic colouring matters, using the diazotization/coupling procedure just mentioned. As azoic colouring matters are used in the colouration of foods, drugs and cosmetics, it is important to have methods to verify if the amine used in the production of a colouring matter was completely removed after synthesis. Aniline is the primary aromatic amine used in the synthesis of the colouring matter D&C Red No. 33 (Fig. 3).

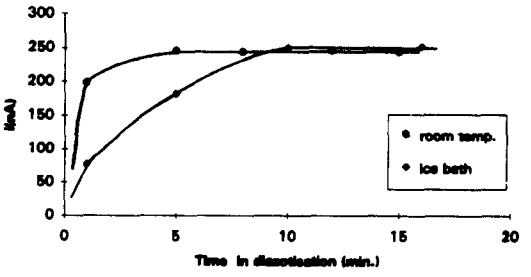


Fig. 1. Effect of temperature on the rate of diazotization of 100 μg of derivatised aniline. Analysis by AdSV: 1 min of accumulation; aniline concentration = 80 ppb; supporting electrolyte, 0.1 M ammonia buffer; pH 10. Diazotization in 0.02 M sulphuric acid.

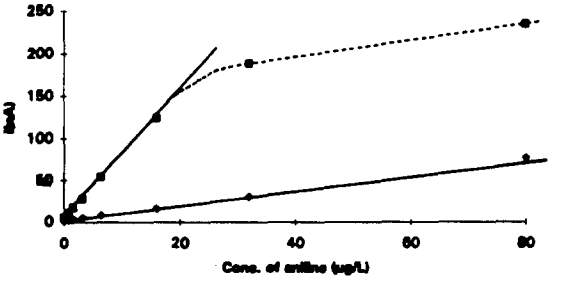


Fig. 2. AdSV calibration curves for derivatized aniline, using different accumulation times. Acc. potential = −240 mV (vs. AgCl/Ag, KCl 3 M); supporting electrolyte, 0.1 M ammonia buffer; pH 10. Acc. time (min): ◆ 0; ■ 2.

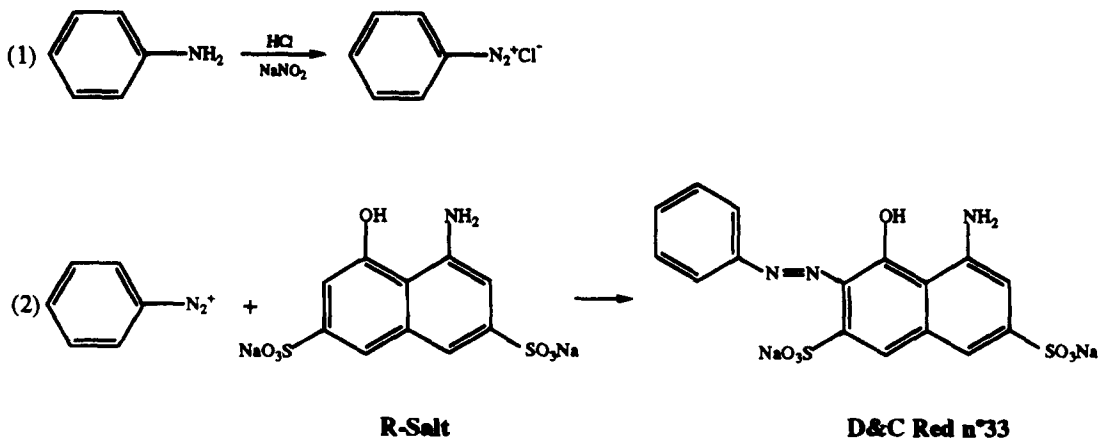


Fig. 3. Synthesis of the colouring matter D&C Red No. 33: (1) diazotization, (2) coupling.

Of course, if the usual method of analysis of amines is employed, involving their conversion into azo compounds, the colouring matter itself, structurally similar to the derivatized amine, will interfere in the determination. Thus, an intermediate step is needed for the separation of the amine from the colouring matter. The spectrophotometric determination of aniline (and other primary aromatic amines) in D&C Red No. 33 was reported by Bailey [10], based on the extraction of the amines from an aqueous solution of the colouring matter into chloroform. In our laboratory we have made a similar determination of aniline, using the adsorptive stripping voltammetric method in the detection step and the results are in good agreement with those reported in Bailey's work. The method of standard additions was used, with standards of aniline being added to the samples before the diazotization and coupling reactions (Fig. 4). Using standards alone, the same result was obtained with and without extraction, proving that extraction was complete. For a set of three replicates, the amount of aniline found in the colouring matter D&C Red No. 33 was $17 \pm 1$ ppm. The amount of aniline found in a commercial sample of D&C Red No. 33 is low considering the fact that this compound is used as an intermediate in the preparation of this colouring matter. As referred to by Bailey [10], this result suggests that the D&C Red No. 33 is thoroughly purified by the manufacturer before its commercialization, which is expected owing to the applications of this colouring matter and the potential health hazards associated with the aniline.

### *3.8. Determination of aniline formed in the degradation of D&C Red No. 33 solutions*

The method was also applied in the determination of aniline formed in studies of degradation of 0.1% solutions of D&C Red No. 33. In fact, besides being intermediates in the synthesis, the presence of amines in colouring matters

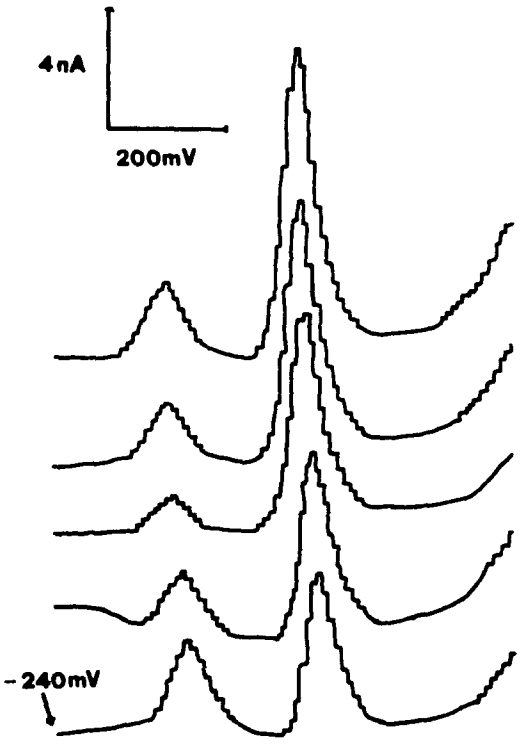


Fig. 4. AdSV determination of aniline in the colouring matter D&C Red No. 33. using the method of standard additions. Accumulation = 2 min. Aniline added (ppb) from bottom to top: 0, 0.8, 1.6, 3.2, 4.8.

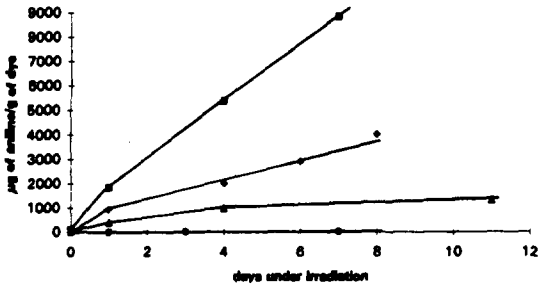


Fig. 5. Effect of the amount of ascorbic acid and of degradation time on the formation of aniline from D&C Red No. 33. Supporting electrolyte 0.1 M phosphate buffer, pH 7. Amount of ascorbic acid (%): ● 0; ▲ 0.02; ◆ 0.2; ■ 2.

can have a different origin, if degradation of the colouring matters occurs by reductive splitting of the azo group [11]. Although solutions of D&C Red No. 33 submitted to intense light conditions to accelerate degradation were found to be quite stable, in the presence of the antioxidant ascorbic acid the colouring matter was degraded to produce aniline, to an extent increasing with the amount of ascorbic acid and with the degradation time (Fig. 5). It was found that the main reason for degradation is the presence of ascorbic acid, as the results obtained with the use of light irradiation are not very different from those obtained in the dark (Table 2). Some preliminary studies indicate that the influence of pH on degradation is not very important, as similar values for degradation were obtained with pH 2 and 7.

Table 2
Degradation of D&C Red No. 33 in the presence of 0.2% ascorbic acid, at pH 2 (μg of aniline found/g of colouring matter).

| | Degradation times (days) | | | | |
|---|---|---|---|---|---|
| | 0[a] | 0.2 | 1 | 2 | 10 |
| In the dark | 17 | 198 | 645 | — | 5159 |
| Light irradiation | 17 | 101 | 888 | 1332 | — |

[a] Without addition of ascorbic acid.

## References

[1] J. Wang, Voltammetry following nonelectrolytic preconcentration, in A.J. Bard (Ed.), Electroanalytic Chemistry, Vol. 16, Marcel Dekker, New York, 1989.
[2] J.C. Moreira and A.G. Fogg, Analyst, 116 (1991) 249.
[3] G.D. Christian, Analytical Chemistry, 4th edn., J. Wiley, New York, 1986, p. 653.
[4] K. Venkataraman, The Analytical Chemistry of Synthetic Dyes, J. Wiley, New York, 1987, p. 571.
[5] G. Norwitz and P.N. Keliher, Anal. Chem., 53 (1981) 56.
[6] A.G. Fogg, A.A. Barros and J.O. Cabral, Analyst, 111 (1986) 831.
[7] Z.E. Zoller, Nitrogen Derivatives of Anilines: Nitrosamines; Diazo, Azo, Azoxy and Hydrazo Compounds, in E.H. Rodd (Ed.), Vol. III, Part A, Aromatic Compounds, Elsevier, Amsterdam, 1954.
[8] J.H. Ridd, J. Soc. Dyers Colourists, 81 (1965) 355.
[9] L.P. Hammett, Physical Organic Chemistry, McGraw-Hill, New York, 1940.
[10] J.E. Bailey Jr, Anal. Chem., 57 (1985) 189.
[11] A.G. Fogg and A.M. Summan, Analyst, 108 (1983) 691.

ELSEVIER

Talanta 42 (1995) 921–926

Talanta

# Determination of palladium by flame atomic absorption spectrometry combined on-line with flow injection preconcentration using a micro-column packed with activated carbon fibre

Soulin Lin *, Chunsong Zheng, Guizhen Yun

*Department of Applied Chemistry, China University of Geosciences, Wuhan 430074, People's Republic of China*

Received 17 August 1994; revised 27 December 1994; accepted 5 January 1995

**Abstract**

The versatility of flow injection as a procedure for enhancing the performance of atomic spectrometry is demonstrated by the on-line separation and preconcentration of analyte ions of interest for methods employing atomic spectrometric measurements. In this paper, a sensitive method for the determination of palladium by flame atomic absorption spectrometry associated on-line with the flow injection technique has been developed. A flow system comprising a micro-column packed with activated carbon fibre was used for the concentration of palladium. In order to further enhance the performance of the analysis a new manifold with an additional column has been designed to increase the sensitivity by doubling the analytical signals. The method is sensitive and easily operating with a sampling rate of 15–20/h. The detection limit of this method is 0.3 ng/ml in standard solution and the precision is 3.9% relative standard deviation at 50 ng/ml. Recoveries of palladium in spiked solutions are 103–107%.

## 1. Introduction

Palladium is an element of medium sensitivity for atomic absorption spectrometry (AAS) and inductively coupled plasma-atomic emission spectrometry (ICP-AES). Enrichment of the element is often needed prior to determination. Palladium is often determined together with Ru, Rh, Pt, Os and Ir in samples for platinum-group element analysis. AAS determinations have been applied to the analysis of platinum group elements (PGEs) by the fire assay method [1–3] in early works. The detection limits reported were 0.06 ppm (20 g sample) [1] and 0.08 ppm [3]. Hoashi et al. [4] described a method for the determination of Pd, Pt and Rh in iron meteorites by procedures involving extraction into organic solvents and subsequent analysis of the extracts by graphite furnace AAS. The reported detection limit was 0.01 μg/g (0.1–0.5 g sample). Since its appearence in 1980 [5], inductively coupled plasma-mass spectrometry(ICP-MS) has become one of the most sensitive techniques for the determination of the PGEs. Methods demonstrating the application of ICP-MS to the determination of these precious metals with and without fire assay preconcentration have been published [6–8]. However, all these procedures require complex chemical manipulation of the samples and the analysis of sample solutions. Totland et al. [9] reported a method for direct determination of the PGEs in solid samples where the PGEs are directly determined by slurry nebulization ICP-MS. Excellent data of limits of quantitative analysis

* Corresponding author.


*SSDI* 0039-9140(95)01513-2

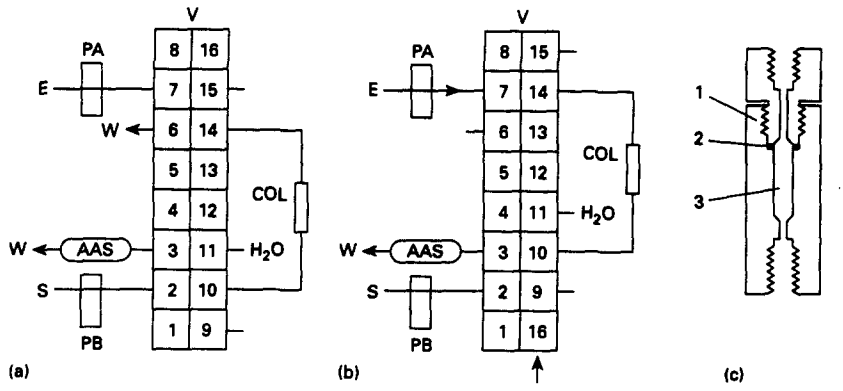


Fig. 1. Manifold using single column for FI preconcentration-flame atomic absorption spectrometry. V, rotary injection valve; PA, PB, peristaltic pump; COL, preconcentration column packed with ACF; AAS, atomic absorption spectrometer; E, 1% thiourea solution in 1 M HCl; S, sample solution (pH 3); W, waste; 1, Perspex jacket; 2, seal ring; 3, cavity; a, preconcentration position; b, elution position; c, diagram of the construction of the preconcentration column.

(0.04–0.2 μg/g) for the method were reported and the analytical reproducibility was in the range 2–30% RSD. The detection limit for palladium was 0.17 ng/ml in HCl blank. However, these procedures require expensive instruments not common in conventional laboratories.

The objective of this work is to develop a method utilizing the combination of the flow injection preconcentration technique and atomic absorption spectrometry for the determination of Pd at a low concentration level. We used a flow system similar to that described by Olsen et al. [10]. The preconcentration column was packed with activated carbon fibre (ACF) to retain Pd and eluted by thiourea. Chemical conditions and manifold parameters were investigated in detail and the potential of ACF as a preconcentrator was demonstrated. In order to increase the concentration factor, we have designed a so-called double column manifold, which will be discussed in detail in the manifold section, to double the concentration of Pd, and thus double the analytical signal. With this manifold scheme, up to 145 times preconcentration of Pd with a sample throughput of 15–20/h can be achieved. It is apparent that the present FIA–FAAS system with online preconcentration might thus challenge the detection limits for graphite furnace AAS [11] and ICP-MS [12].

## 2. Experimental

### 2.1. Apparatus and manifold

The flow injection units used were an IFIS-A intelligent flow injection sampler comprising an eight-channel rotary injection valve and two three-channel peristaltic pumps (Xian Spring Institute, China) for the majority of experiments and a FIA-2400 flow injection analyser (Xintong Scientific Instrument Corp., China) for manual operation. All experiments were conducted with a WFX-1A atomic absorption spectrometer (Beijing Second Optical Instrument Factory, China) and a single pen recorder (PM 8521, Philips, Holland) for measuring and registering the absorption signals. A palladium hollow cathode lamp with an operating current of 6 mA was used. The sensitive Pd 247.64 nm line and a narrow spectral bandpass of 0.2 nm were adopted. A fuel-lean stoichiometric air–acetylene flame was employed for the atomization of palladium.

The manifold comprising a single column for the preconcentration of palladium is shown in Fig. 1. The two positions of the valve rotor (the channels are arranged in a circular pattern) refer to sampling S and elution E. The preconcentration process proceeds when the valve is in position 'a' and the elution process starts by back flushing with eluent stream E when the valve is switched to position 'b'. The preconcentration column with an inner volume of 180 μl (3 mm i.d. × 25 mm) was made of Perspex and was demountable for packing the activated carbon fibre.

The manifold scheme for the double column system is shown in Fig. 2. Note that the double column system differs in principle from the existing dual column system described in the literature [13,14] in that : (i) the two columns are in parallel in the preconcentration mode and the columns are connected in series in the elution mode; (ii) the double column system

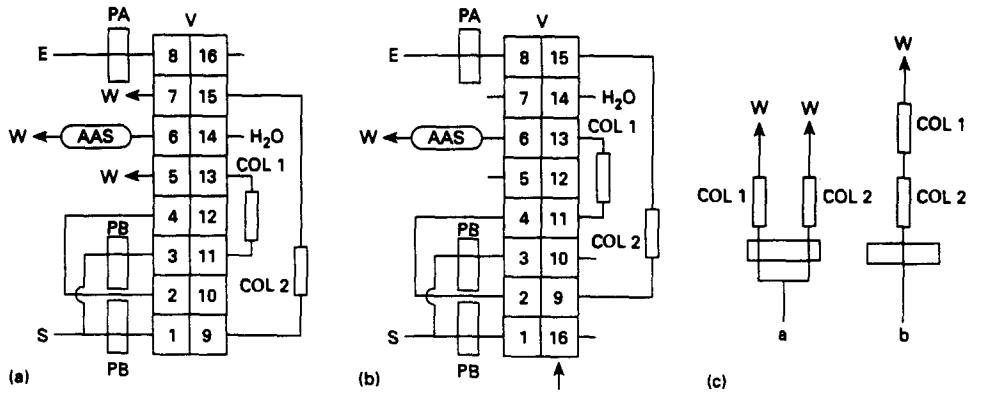


Fig. 2. Manifold scheme of double column system for FI preconcentration-atomic absorption preconcentration. V, rotary injection valve; PA, PB, peristaltic pump; COLI, COL2, preconcentration column packed with ACF; AAS, atomic absorption spectrometer; E, elution solution; S, sample solution; W, waste; a, preconcentration position; b, elution position; c, diagram of the principle of double column system.

doubles the analytical signal without doubling the preconcentration time, and thus the concentration efficiency (CE) can be increased; and (iii) the double column system can easily be reduced to a single column system simply by sampling water instead of sample solutions in the COL 1 channels.

### 2.2. Reagents and procedures

All reagents were of analytical reagent grade. Water from subboiling distillation was used throughout.

A Pd standard solution of 1000 μg/ml was prepared from palladium chloride and was made 2% in hydrochoric acid. This solution may be further diluted to give a series of calibration standards. The elution solution was prepared by dissolving 1 g thiourea in 100 ml water and the solution was made 1 M in hydrochloric acid. the buffer solution (pH 3.0) was prepared according to Clark and Lubs [15]: 50 ml 0.2 M KHphthalate + 20.40 ml 0.2 M HCl, diluted to 200 ml. The activated carbon fibre (High Polymer Institute, Zhongshan University, China) was treated with dilute nitric acid and thouroughly washed with water prior to use.

Most experiments were carried out with the IFIS-A intelligent flow injection sampler. The program and time cycle of operation are shown in Tables 1 and 2.

## 3. Results and discussion

### 3.1. Chemical conditions

*Acidity of the sample solution*

Palladium can be retained onto ACF in slightly acidic solution and the acidity of the solution considerably affected the retention of the metal. Experimental results indicated that the best pH value for the retention of the metal was 3.0. Sample solutions should approximately be adjusted to slightly acidic with dilute hydrochloric acid or sodium hydroxide solution and the solution finally made exactly pH 3 with KHphthalate buffer solution prior to sampling. Nitric acid was not preferred owing to the suppression effect on the absorption of palladium onto the activated carbon fibre.

*Concentration and acidity of thiourea solution*

The absorption signal increased with increasing thiourea concentration and remained unchanged when the concentration of thiourea exceeded 1.5%. In order to shorten the time to wash thiourea out of the column and manifold tubing for the next sample, a compromise thiourea concentration of 1% was used. Although a 10% loss of absorption signal resulted from this concentration, the wash time could be greatly reduced. The thiourea solution was

Table 1
Manifold program, both for the single and double column systems

| | Step | | | |
|---|---|---|---|---|
| | 1 | 2 | 3 | 4 |
| Time (s) | 40 | 2 | 180 | 20 |
| Pump A | stop | stop | stop | go |
| Pump B | go | stop | go | stop |

Table 2
Time cycle of operation

| Time (s) | Function |
|---|---|
| 223–242 | PA and PB stop. Hint for replacing water with |
| 0–40 | PA stops, PB goes, V turns to position 'a'. Wash the column with water. |
| 41–42 | PA and PB stop. Hint for replacing water with sample solution. |
| 43–222 | PA stops, PB goes. Duration of sampling. |
| 223–242 | PA goes, PB stops, V turns to position 'b'. Backflush with thiourea, the eluent is propelled into the AAS. |

made 1 M in hydrochloric acid to achieve maximum sensitivity. Again, nitric acid was not preferred.

*Interferences*

Elements other than palladium of the platinum group, as well as cadmium, copper, and lanthanum were tested for interference effects. The platinum group elements at concentration levels listed in Table 3 did not interfere in the determination of 50 ng/ml of Pd. The three other elements showed no interference effects. Alkali and alkaline earth elements showed no affinity with ACF and did not interfere with the determination of palladium.

### 3.2. Manifold parameters

Manifold parameters were optimized with respect to flow rates and sampling time. The effects of these parameters on the absorption sensitivity are shown in Figs. 3–5. The selected flow rates can be summarized as 5.2 ml/min for sampling and 4.1 ml/min for elution. It can be seen from Fig. 5 that the required concentration factor depends on the sampling time. Since

Table 3
Effects of coexisting ions (me)

| Ion | Added (μg/ml) | Concentration ratio (me/Pd) | Recovery (%) |
|---|---|---|---|
| 0 | 0 | 0 | 100 |
| Ag | 2.5 | 50 | 100 |
| Au | 5 | 100 | 100 |
| Pt | 3.2 | 64 | 103 |
| Cd | 2.5 | 50 | 97 |
| Cu | 5 | 100 | 100 |
| La | 2.5 | 50 | 100 |

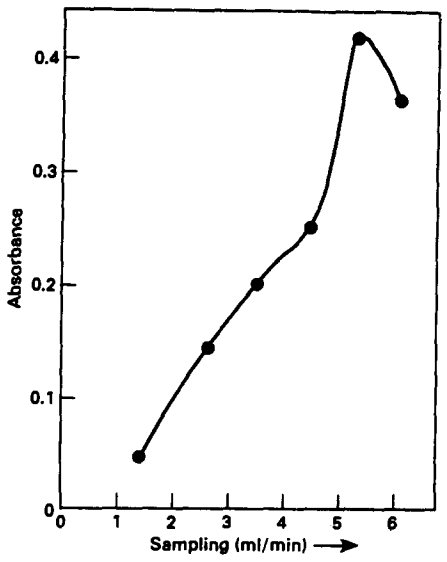


Fig. 3. Effect of the flow rate for sampling on the absorption sensitivity. Pd = 50 ng/ml (pH 3), sampling time = 2 min.

high concentration efficiency (a CE value up to 38 can be achieved) can be obtained by this method, longer sampling time is allowable and a sampling time of 3 min was used for investigation of analytical performance and for real sample analysis throughout unless otherwise stated.

### 3.3. Calibration graphs and analytical performance

Good linearity of the calibration graph of palladium was obtained in the range 0–30 ng/

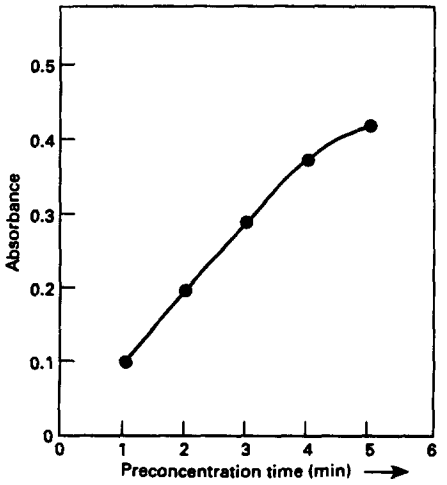


Fig. 4. Effect of sampling time on the absorption sensitivity. Pd 50 ng/ml, sampling flow rate = 5.2 ml/min.

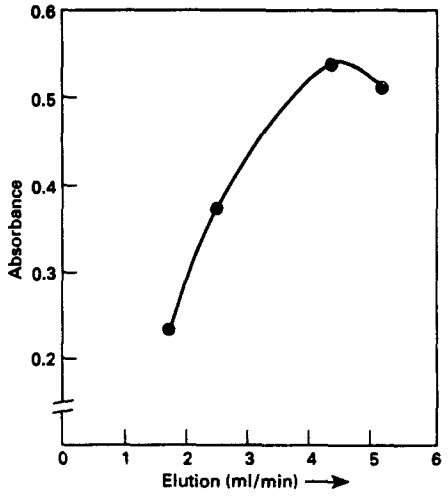


Fig. 5. Effect of the flow rate for elution on the absorption sensitivity. Pd = 200 ng/ml, sampling flow rate = 5.2 ml/min, sampling time = 3 min.

ml. The regression equation for calibration is $y = 0.014x + 0.0043$ with a correlation coefficient of 0.998. Sensitivities, detection limits and precision for direct nebulization and for sampling with preconcentration using single and double systems are listed in Table 4 for comparison. The sensitivities listed are referred to slopes of the calibration curves and the detection limits are calculated based on $3\sigma$.

## 4. Real sample analysis

Three geological samples were analysed for palladium with the suggested procedure to investigate the accuracy of the proposed method. Sample I (standard reference rock sample GSO-Au-2 containing 52.5 ng/g of Au) and sample II(Yangxin copper ore containing 200 ng/g of Au and 6500 ng/g of silver) were used as blank ores and Pd was spiked. Sample III and the analytical result of palladium was provided by the Hubei Geological Bureau.

### 4.1. Procedure

*Calibration series*

Palladium (0, 0.5, 1.0, 1.5, 2.0, 2.5 μg) was pipetted into six 25 ml colorimetric tubes, respectively, and made up to about 10 ml with water, adjusted to approximately pH 3 with pH test paper. KHphthalate buffer solution (2 ml) was added and diluted to the mark with water.

*Sample preparation*

Rock sample (0.1000 g) was weighed into a PTFE crucible, wetted with water, 10 ml of hydrofluoric acid added, heated and evaporated to dryness. Aqua regia (15 ml) was added and it was heated gently to dissolve the residues and evaporate to near dryness. Hydrochloric acid (2 ml) was added to eliminate nitric acid. Then, a few drops of (1 + 1) hydrochloric acid added and the wall of the crucible rinsed with hot water and transferred to a 100 ml volumetric flask and made up to the mark with water. The resulting solution (1 ml) was pipetted to a 25 ml colorimetric tube and subsequently treated the same as the standard series. The analytical data obtained using double column system are listed in Table 5. It can be seen that the analytical results of sample III was in good agreement with the reference value and the recoveries of Pd in all samples were satisfactory.

Table 4
Comparison of analytical performance

| Mode of sampling | Sensitivity (A $ng^{-1}$ $ml^{-1}$) | Detection limit (ng/ml) | Precision (RSD%) | Concentration factor (CF) |
|---|---|---|---|---|
| Direct nebulization | $9.6 \times 10^{-5}$ | 46 | 2.3 (1000 ng/ml) $n = 11$ | |
| With preconcentration (single column) | $6.6 \times 10^{-3}$ | 0.8 | 3.5 (100 ng/ml) $n = 8$ | 69 |
| With preconcentration (double column) | $1.4 \times 10^{-2}$ | 0.3 | 3.9 (50 ng/ml) $n = 8$ | 145 |

Table 5
Analytical results

| Sample | Found (μg/g) | Reference (μg/g) | Spiked (μg) | Recovery (%) |
|---|---|---|---|---|
| I | 0 | — | 1 | 107 |
| II | 0 | — | 1 | 107 |
| III | 580 | 530 | 2 | 103 |

## 5. Conclusion

Flow injection solid phase extraction is a potentially important technique in trace and/or ultra-trace analysis. Through optimizing the wash stage, sample loading rate and manifold design, high CE values are achievable. Data demonstrated in this paper are very encouraging. The main features of the suggested flow system are (i) that it can easily double the analytical signal and (ii) the system is semi-automated with only one manual step of feeding samples.

## Acknowledgements

The authors are grateful to The Foundation for Developing Geology Science and Technology of China for financial aid and to Professor Lu Yun of Zhongshan University for providing the activated carbon fibre.

## References

[1] M.M. Schnepfe and F.S. Grimaldi, Talanta, 16 (1969) 591.
[2] J.C. Van Loon, Z. Anal. Chem., 246 (1969) 112.
[3] S. Kalman and E.W. Hobart, Talanta, 17 (1970) 845.
[4] M. Hoashi, R. R. Brookes and R.D. Reeves, Chem. Geol., 106 (1992) 207.
[5] R.S. Houk, V.A. Fassel, G.D. Flesh, H.J., Svec, A.L. Gray and C.E. Taylor, Anal. Chem., 52 (1980) 2283.
[6] A.F. Dates, A.E. Davis and Y.Y. Cheung, Analyst, 112 (1987) 1217.
[7] D.C. Gregorie, J. Anal. At. Spectrom., 3 (1988) 309.
[8] S.E. Jackson, B.J. Feyer, W. Goose H.P. Longerichh and D.F. Strong, Chem. Geol., 83 (1990) 119.
[9] M. Totland, I. Javis and R.E. Javis, Chem. Geol., 104 (1993) 175.
[10] S. Olsen, L.C.R. Pessenda, J. Ruzicka and E.H. Hansen, Analyst, 108 (1993) 905.
[11] C.W. Fuller, Electrothermal Atomization for Atomic Absorption Spectrometry, Berlington House, London, 1979, p. 76.
[12] VG Plasmaquad Brochure, VG Instrumental, VG Isotopes Ltd., U.K.
[13] Z. Fang, J. Rusicka and E.H. Hansen, Anal. Chim. Acta, 164 (1984), 23.
[14] J. Rusicka and E.H. Hansen, *Flow Injection Analysis*, 2nd edn., John Wiley, New York, p. 206.
[15] A.I. Vogel, Quantitative Inorganic Analysis, Theory and Practice, 2nd edn., Longmans, Green and co., London, 1951, p. 870.

ELSEVIER

Talanta 42 (1995) 927–936

Talanta

# Investigations for the determination of lead by in situ hydride trapping within a graphite electrothermal atomizer for routine analysis

D. Erber *, L. Quick, F. Winter, K. Cammann

*Institut für Chemo- und Biosensorik e.V., Mendelstraße 7, D-48149 Münster, Germany*

Received 11 July 1994; revised 23 December; accepted 3 January 1995

**Abstract**

A new commercial system consisting of a flow injection analysis system for hydride generation coupled with a transversely heated graphite atomizer–atomic absorption spectrometer for the determination of lead is investigated in detail. The hydride generation is optimized by using an ammonium peroxodisulphate–hydrochloric acid system as oxidant and sodium borohydride as reducing reagent. The addition of sodium cumol sulphonate as surface active substance shows advantages considering efficient plumbane production. The hydride trapping and atomization in a graphite electrothermal atomizer is also optimized. The characteristic concentration was 0.74 μg/l, the detection limit was 0.70 μg/l for 500 μl sample volumes. The relative operation standard deviation of this method was smaller than 2%. Further examinations demonstrate the influence of several heavy metals on the determination of lead. Finally, the measurement of standard reference materials shows the efficiency of the method in combination with decomposition with aqua regia solutions.

## 1. Introduction

Since 1975 the determination of lead using hydride techniques has been of great interest and research in trace metal analysis. Plumbane production and following detection investigated for analytical purposes was first described by Thompson and Thomerson [1]. Further applications of this analytical problem have been published with a full range of generation and detection methods [2–13]. Difficulties arose from two facts: the oxidation of lead (II) to lead (IV) followed by plumbane generation and its stability [14,15].

Oxidants like potassium dichromate [3,16], ammonium cerium nitrate [9], potassium permanganate/manganese sulphate [5] or hydrogen peroxide [2,6] made the production possible, but the use of dichromate seemed to be problematic owing to the health hazard and environmental relevance. However, hydrogen peroxide as a substitute showed less sensitivity. Similar results were only obtained with ammonium peroxidisulphate [4,8,12].

Another relevant problem is the efficient atomization of lead. Obviously, the almost exclusively used quartz tube is not well suited to obtain satisfactory sensitivity, e.g. detection limits of 30 μg/l for lead [13]. However, the enrichment and atomization of gaseous products from hydride-forming elements in a graphite furnace has been well known for some time [16–22]. The first use of this technique was reported by Lee [23]. The in situ trapping technique needs the graphite furnace both for hydride trapping and for the atomization. The hydrides purged from the gas–liquid separator decompose in the preheated graphite furnace (ca. 300–600 °C) and are then trapped on the graphite surface. The trapped products are

* Corresponding author.


*SSDI* 0039-9140(95)01517-5

then atomized normally at 1600–2000 °C. This technique is superior to quartz tube atomization. It should be preferred because of its greater sensitivity and its effective elimination of possible influences of hydride generation kinetics. The lastest developments of Perkin-Elmer make it possible to accomplish this process for the first time in a routine way [24].

With the use of a continuous flow or flow injection system, the sensitivity for the determination of lead could be increased and interferences be minimized. The combination of flow injection hydride generation and graphite furnace seems to be advantageous for the detection limits owing to continuous hydride enrichment in the furnace without any loss of reproducibility. However, inconsistent data are given in the literature with regard to interferences on the determination, e.g. the influence of nickel [7,10,11]. Certainly, different observations are dependent on the parameters used. Generally, tolerable concentrations of interfering metallic ions in flow injection procedures are often reported to be one or two orders of magnitude higher than in batch systems [25].

The use of surface active substances such as sodium cumol sulphonate or Triton X-100 [26] increases the sensitivity with great effect. Such micellaric systems influence different analytical systems and have been used in diverse applications [26,27]. The maintenance of more effective hydride formation described for lead and arsenic using several substrates [12,28] was confirmed for lead by the application of several surface active substances in this study.

The technique is applied for the determination of lead in several real samples decomposed with aqua regia extraction. It demonstrates the suitability and the efficiency of the technique by analysing standard reference materials with different organic and inorganic matrices. The results are compared with results obtained by another graphite furnace routine analysis system (ZL 4100 from Perkin-Elmer) and a special new arrangement with a graphite furnace (frequency modulated simultaneous AAS) developed by Cammann et al. [29].

This paper reports the optimization procedure for the hydride generation of lead as a simple and fast method for its determination using the continuous flow system hydride generation atomic absorption spectrometry with enrichment and atomization in a graphite furnace.

## 2. Experimental

### 2.1. Instrumentation

A Perkin-Elmer Model 4100 ZL atomic absorption spectrometer was used in combination with the FIAS 200. The available background correction with longitudinal Zeeman effect was not required for this application. For the hydride trapping and atomization in the graphite furnace a special application software from Perkin-Elmer was used (software version 7.21). The hydride generator was coupled via a Teflon tube to the graphite furnace. A quartz tip was fixed to a pipet arm inside the graphite furnace during the enrichment time. Before atomizing, the pipet arm was moved outside this oven.

The flow injection system scheme is described in Fig. 1. Three tubes with reagents for the hydride generation are connected to the chemifold in which plumbane is formed. An inert gas stream transports the hydride products to the graphite furnace. The parameter for the hydride generation, trapping and atomization are summarized in Table 1. The program for the enrichment step is presented in Table 2. Because of large amounts of reagents, two pump tubes instead of the normal one are used as waste tubes to prevent an overflow of the gas–liquid separator.

For the assessment of the results obtained, a new method in atomic absorption spectrometry was used and it is described in the following. In frequency modulated simultaneous AAS (FremsAAS) [29] the light is provided with additional information by modulation of the light sources with different frequencies (300–700 Hz). By using interference filters the resonance lines are separated from other emission. Lock-in amplifiers selectively amplify the modulated signal of light source in a DC signal.

### 2.2. Gases and substances

Argon (99.996%); (Sauerstoffwerk Westfalen AG, Münster). As(III)-, Bi(III)-, Mn(II)-standard: 0.100 g (all Fixanal; Riedel de Haën AG, Seelze). Sb(III)-, Cr(VI)-standard: 1.000 g (Fixanal). Se(IV)-, Ti(IV)-, Cr(III)-, V(V)-, As(V)-, Sn(IV)-, Pb(II)-, Hg(II)-, Cd(II)-, Cu(II)-, Ni(II)- standard: 1.000 g (all Titrisol; E. Merck, Darmstadt). Fe(III)-, Zn(II)-, Co(II)-standard solution: 1g/l (all E. Merck). Sodium borohydride p.a., sodium hydroxide p.a., sodium per-

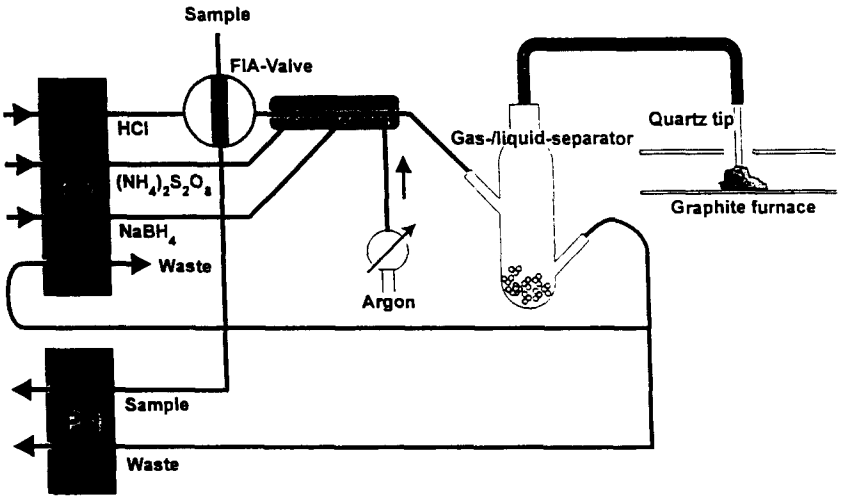


Fig. 1. Schematic diagram of the flow injection system for hydride generation coupled with a transversely heated graphite atomizer.

oxodisulphate p.a., hydrochloric acid 30% suprapure, nitric acid 65% suprapure, hydrochloric acid conc. p.a. (all E. Merck). Triton X-100 (TX-100) (E. Merck), tetrabutylammonium hydrogen sulphate (Fluka AG, CH-Buchs), Sodium cumol sulphonate (Hüls AG, Marl).

### 2.3. Certified substances

Estuarine sediment CRM 277, aquatic moss (*Platihypnidium ripariodes*) BCR 61, rye grass CRM 281 [all Commission of the European Communities, Community Bureau of Reference (BCR), Brussels]; pine needles SRM 1575 (U.S. Department of Commerce, National Institute of Standards and Technology Gaithersburg, MD, U.S.A.).

### 2.4. Optimization of the hydride generation and atomization technique

Several parameters were optimized to reach highest sensitivity for the lead determination. Erber et al. [30] optimized some parameters by using this technique for the sensitive detection of ionic organolead compounds. Because of a large difference between the hydride generation of organolead compounds and lead itself, which is a result of the enormous difference in stabilities of the hydride products, optimization of the parameters, especially for inorganic lead, was necessary to achieve good results. The parameters having influence on the sensitivity of the formation of lead hydride are sodium borohydride as reducing reagent, the oxidization agent ammonium peroxodisulphate, the type and concentration of the acid and the sodium cumol sulphonate (chemical), as well as the flow of the inertia gas and the enrichment temperature and the atomization temperature (apparational). The optimization procedures were carried out by measuring a solution of 50 µg/l lead. Because apparational parameters and chemical parameters are mostly independent from each other, the first mentioned are optimized first.

*Inert gas flow*

Argon as an inert gas transports the hydride products from the gas–liquid separator to the graphite furnace and so the influence of its flow rate on the signal intensity was investigated. The results are presented in Fig. 2. The optimum argon flow rate was 125 ml/min as opposed to the optimum flow rate by the generation of organolead hydride products [30].

*Enrichment and atomization temperature*

The enrichment temperature, as well as the atomization temperature, is, in combination with the type of graphite furnace, a major parameter for the sensitivity of a method. Several investigations into the enrichment temperature and the theoretical foundations about the sorption and atomization are described [19,28].

The optimum high enrichment temperature of 600 °C we found in concordance with Aroza

Table 1
Standard operating conditions

| | |
|---|---|
| *Spectrometer* | |
| Lamp | EDL (440 mA) |
| Wavelength | 283.3 nm |
| Slit | 0.7 nm |
| Integration time | 5 s |
| Measurement type | peak height |
| BOC time | 2 s |
| *FIAS System* | |
| Pump speed | see Table 2 |
| Pump tubing | |
| Pump 1 | |
| Sample | 1.52 mm (i.d.) |
| Waste | 3.18 mm |
| Pump 2 | |
| Carrier | 1.52 mm |
| Reducing agents | 1.14 mm |
| Oxidants | 1.14 mm |
| Waste | 3.18 mm |
| Carrier gas flow | 100 ml/min |
| Sample loop | 500 µl |
| *Reagents* | |
| Carrier solution | 0.1% HCl + 0.15% Na cumol sulphonate |
| Reducing agents | 0.5% $NaBH_4$ in 0.05% NaOH |
| Oxidants | 5% $(NH_4)_2S_2O_8$ |
| *Furnace* | |
| Trapping temperature | 450 °C |
| Atomization temperature | 1800 °C |
| Temperature program | see Table 3 |

et al. [8] seems to favour a normal thermic decomposition to the element and rules out simple physisorption of the hydride or its decomposition product [19]. The determination of the enrichment temperature, i.e. the decomposition of the lead hydride, was carried out using an atomization temperature of 1600 °C. A steady increase of sensitivity was found (Fig. 3). Temperatures of more than 600 °C seem inappropriate in order to avoid unnecessary strain on the pipetting quartz tip. It will gradually be damaged. For routine analysis, an enrichment temperature of 450 °C was sufficient.

Other authors point out that a zirconium- or palladium-coated graphite tube show a more effective adsorption for hydrides in general and especially for lead hydride [11,20,25,28]. This allowed lower enrichment temperatures to be used. The reason for this seems to be a catalytic dissociation on zirconium carbide or palladium rather than a thermal decomposition [11,19].

Since we could not detect significant differences at the temperatures we used, we did not modify graphite tubes with zirconium or palladium solutions. The graphite tubes for the Perkin-Elmer 4100 ZL obviously have a surface that is well suited for the decomposition of lead hydrides. But the decisive reason for not modifying the graphite tube was the instability of plumbane. At higher temperatures it decomposes spontaneously, in contrast to the relatively stable hydrides, e.g. of arsenic or antimony. No catalytic process is needed for the decomposition of plumbane. By using a modifier for signals with decreased peaks heights, large peak areas were obtained.

The surface of the graphite tube is also a significant parameter for the atomization temperature [28]. Modifying the graphite tube after enriching the hydrides with palladium or zirconium also influences the atomization of lead [31]. The modification seems impractical in this case for routine applications because the enrichment technique has no programmable step and no device for automatic pipetting of a modifier. We settled for a tube treatment after hydride enrichment, and we experienced no loss of reproducibility or sensitivity. We determined an atomization temperature of 1800 °C and an enrichment temperature of 450 °C to be satisfactory (Table 3).

Table 2
FIAS-program for the enrichment step

| Step number | Time (s) | Pump speed no. 1 (U/min) | Pump speed no. 2 (U/min) | Valve position |
|---|---|---|---|---|
| Prefill | 10 | 100 | 0 | fill |
| 1 | 10 | 100 | 80 | fill |
| 2 | 8 | 0 | 0 | inject |
| 3 | 20 | 120 | 70 | inject |
| 4 | 8 | 0 | 0 | inject |
| 5 | 5 | 120 | 0 | fill |

*Tube life-time*

The total measurements here were carried out with two graphite tubes. Consequently, the life-time of one graphite tube was greater than 4000 firings. It showed no dependence on the sample matrix in contrast to the conventional graphite furnace technique, where the life-time of the tube directly depends on the matrix. The tube gets broken because of the normal wearing process.

The chemical parameters were optimized with the physical parameters listed in Table 1.

*Acid*

For the determination of lead it is very important, besides finding the optimum concentration, to choose the right type of acid. This has already been described in the literature for other hydride-forming elements [32,33]. Hydrochloric acid again proved to be the most appropriate acid. Nitric acid or weak acids such as acetic acid did not produce as good a sensitivity as hydrochloric acid (Fig. 4). Even tartaric acid, which has been used until now [13], did not reproduce the sensitivity of hydrochloric acid in combination with the oxidation agents used here.

We found a direct correlation between the maximum sensitivity and the pH of the acid. This can be explained by the fact, that the oxidation power of ammonium peroxodisulphate depends directly on the concentration of $H^+$. We found a pH of ca. 1.7 to be the optimum with the three acids we used. Even small variations of the optimum pH showed a drastic decrease in sensitivity. Therefore, it is important to adjust the pH to the optimum value by treating the samples with ammonia or sodium hydroxide when preparing the samples.

*Sodium borohydride reductant*

Sodium borohydride is still considered to be the best reductant for AAS. The signal intensity steadily increased with an increasing concentration of $NaBH_4$ (Fig. 5). The limiting factor though is the fact, that concentrations of more than 1% (w/v) $NaBH_4$ lead to so much foaming that parts of the liquid in the gas–liquid separator will be transferred into the Teflon tube and the graphite oven. On addition of an anti-foaming agent the plumbane generation efficiency is increased very little with higher concentrations of $NaBH_4$. However, this effect influences the signal intensity less than the effect caused by the use of surface active substances, which tend to foam in the reactor (see

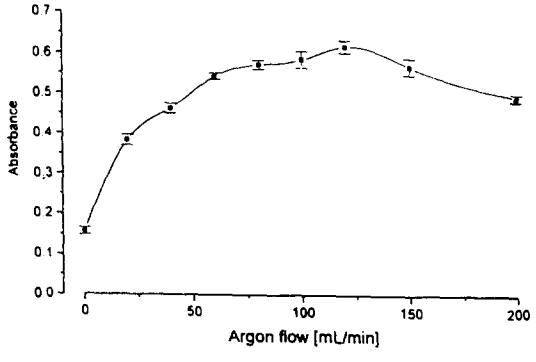


Fig. 2. Influence of the argon flow rate on the signal intensity.

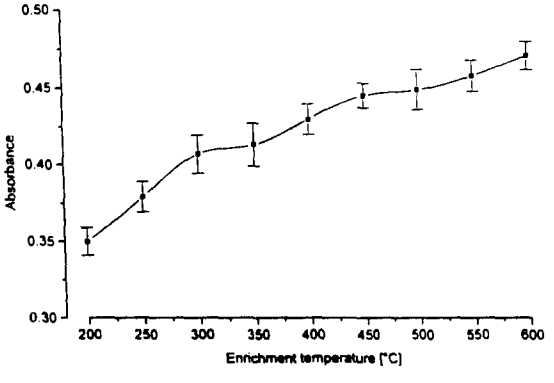


Fig. 3. Signal intensity by increasing enrichment temperature.

Table 3
Temperature program for the graphite furnace routine

| Step | Temperature (°C) | Ramp (s) | Hold (s) | Gasflow (ml/min) |
|---|---|---|---|---|
| Enrichment | 450 | | | |
| Pre-treatment | 450 | 1 | 20 | 250 |
| Atomization | 1800 | 0 | 5 | 0 read |
| Glow out | 2300 | 1 | 2 | 250 |

Effect of surface active substances). To achieve good results, a concentration of 0.5% (w/v) was quite sufficient for the hydride generation. The lead content in the $NaBH_4$ is no problem, as expected, the plot show a linear increase (Fig. 5).

*Ammonium peroxodisulphate oxidant*

A successful determination of lead requires that, prior to reduction, all lead must be oxidized to Pb(IV) by some oxidant, because only Pb(IV) forms sufficiently stable hydrides [15,34]. Several oxidants, such as potassium permanganate, potassium dichromate and hydrogen peroxide, have been more or less successfully tried out. As other authors found, ammonium peroxodisulphate proved to be the optimum oxidant for oxidizing lead(II) ions [4,8,12]. When using a FIA system, it is necessary to follow the proper sequence when adding the various substances (see Fig. 1). An increase of ammonium peroxodisulphate show a similar linear increase in sensitivity in Fig. 6, as well as $NaBH_4$.

In order to save material, all the following determinations have been carried out with a concentration of 5% (w/v) and not with the concentration for maximum sensitivity. This also leads to much less foaming owing to higher concentrations in some samples.

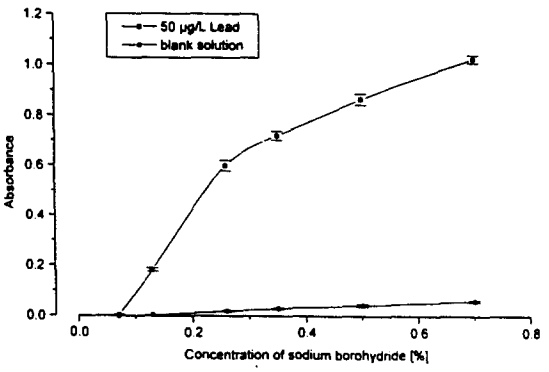


Fig. 5. Dependence between signal intensity and reducing reagent.

*Effect of surface active substances*

Surfactant organized substances or organized molecular assemblies have an enormous influence on the chemical equilibrium, reaction rates and other important chemical features owing to their capacity to create a special microenvironment for reactions at a molecular level [26]. It was shown, that surfactant organized substances greatly support the formation of hydrides [12,28]. In this work the addition of three types of this organized media were investigated to study the effect on plumbane generation. Sodium cumol sulphonate (SCS), Triton 100 and tetrabutylammonium hydrogensulphate (TBHS) were tested. The effect of those substances on plumbane formation is shown in Fig. 7. It can be seen that the absorption signal increased with increasing surfactant substances concentration until a plateau was reached. Those substances have been added to the carrier. Though higher signals can be achieved by adding the substances directly to the sample solution, the sample preparation will be much easier when the required substances are combined in the FIA system. Especially as the signal gain is only 20–30%.

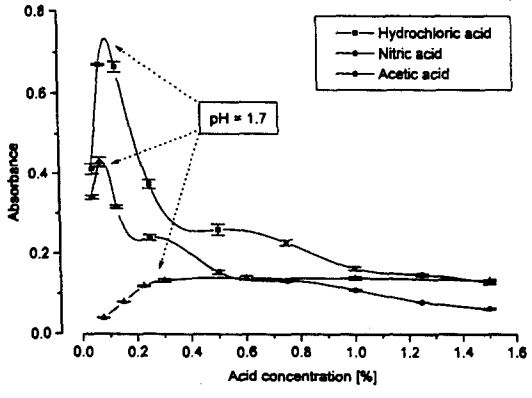


Fig. 4. Influence of different acids on the signal intensity.

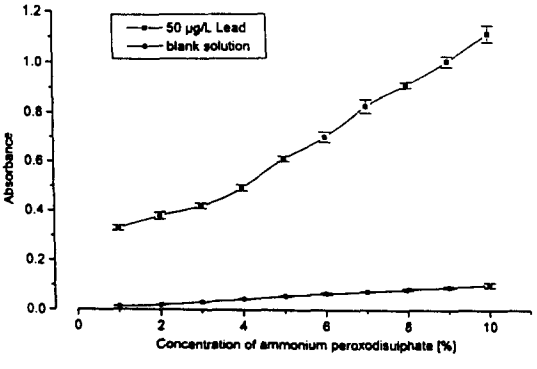


Fig. 6. Signal intensity by increasing the oxidant.

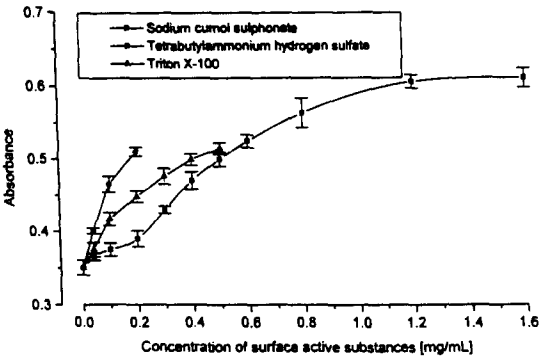


Fig. 7. Effect of surface active substances on the lead determination.

The maximum concentration was also limited by foaming in the gas–liquid separator, which drives some of the liquid into the Teflon tube or the graphite furnace. The additional membrane for this separator, manufactured by Perkin-Elmer somewhat reduces this effect, and can increase the signal by a factor of 1.3 to two as other authors also found [12]. The signal mainly depends on the degree of foaming in the sample solution. Sodium cumol sulphonate showed the best results, because it barely foamed even in large concentrations. Real samples could be determined best when using SCS, because SCS could buffer varying pH values in the sample solutions.

*Sample preparation*

The standard reference materials were first dried as described in the BCR information reports about the certification details. After drying the reference materials were digested with aqua regia according to DIN 38414-S7 [35]. For the sample aquatic moss CRM 061, an aqua regia disintegration with reverse acid ratio (invers aqua regia) was accomplished because of its better decomposition [36]. These solutions are not filtered but after filling into graduated flasks were decanted into polyethylene bottles. These solutions were diluted to demand with suprapure water and neutralized with ammonia to pH ca. 2, (pH paper accuracy is sufficient).

*Interferences from other heavy metals*

The interfering effect of some metals for the determination of lead were investigated (Table 4). The listed elements are normally the main metal components in real samples after aqua regia extraction.

Every determination using hydride techniques have so far shown interferences that influence the determination to various degrees [32,37,38]. Two mechanisms of interference are generally possible. First the formation of the hydride is inhibited in the presence of transition metals and second, other hydride-forming substances as well as other gaseous substances interfere with the determination itself [26]. The interference through transition metals are influenced by the parameters concentration and type of acid, type of reductant and the contact time between the sample solution and the reductant during the hydride formation. The interferences in flow injection analysis tend to be one or two orders of magnitude lower than in batch systems because the normally slow interfering reactions are often suppressed by using short reaction coil lengths. Another aspect is the high flow rate of the sample and reagent through the reaction coil and the gas–liquid separator. Because of the high flow rate the possibility of accumulating reduced metals or metal borides therein is very small. Such deposits are often considered to be important sources of interferences in hydride generation [25]. Also, the small sample volumes introduces smaller absolute amount of interferent into the hydride generation system. This is important because the absolute amount of interferent has often been shown to be more important than its relative concentration.

Table 4
Interferences of some heavy metals on the determination of lead

| Interferent | Relation | Recovery (%) |
|---|---|---|
| Mn(II) | 1:100 | no influence |
| Mn(VII) | 1:50 | positive interference (+20%) |
| Cu | 1:100 | no influence |
| Zn | 1:1000 | no influence |
| Cd | 1:500 | no influence |
| Co | 1:100 | no influence |
| V(V) | 1:100 | no influence |
| Hg | 1:250 | positive interference (+20%) |
| As(III) | 1:100 | no influence |
| As(V) | 1:100 | no influence |
| Sb(V) | 1:100 | no influence |
| Fe | 1:1000 | no influence |
| Sn | 1:100 | no influence |
| Bi | 1:100 | no influence |
| Ni | 1:100 | no influence |
| Ti | 1:250 | no influence |
| Se | 1:100 | negative interference (−70%) |
| Cr(III) | 1:100 | no influence |
| Cr(VI) | 1:50 | positive interference (+10%) |

Table 5
Fundamental calibration and characteristical data

| | Linear regression (0–50 µg/l) | Quadratic regression (0–200 µg/l) |
|---|---|---|
| Slope $a$ (abs. *l/µg) | 5.97E-3 | 2.32E-2 |
| Intercept $b$ (abs.) | 3.03E-2 | 6.85E-3 |
| Quadratic coefficient $c$ (abs. *$l^2$/µ$g^2$) | — | −1.48E-5 |
| Coefficient of regression | 0.9998 | 0.9994 |
| Residual standard deviation $s_y$ (abs.) | 1.97E-3 | 5.71E-3 |
| Operation standard deviation $s_{xo}$ (µg/l) | 0.33 | 1.10 |
| Relative operation standard deviation $V_{xo}$ (%) | 1.56 | 1.97 |
| Mean value $x$ (µg/l) | 21.14 | 56.05 |
| Mean value $y$ (abs.) | 0.157 | 0.307 |
| Sensitivity $E$ (abs. *l/µg) | — | 5.18E-3 |
| Number of measurement ($N$) | 14 | 20 |

Those hydrides produced as a by-product mainly interfere in the atomization phase (when using a quartz cell) but, since there is no direct atomization in the graphite tube, there should be no further interference [26]. Because Table 4 shows a strong signal depression for selenium it is possible that hydride forming substances may already interfere during the reduction in the reactor. Transition metals, as oxidants, and mercury induce/introduce a positive interference because, in the case of dichromate and permanganate, they increase the mobility of lead through their oxidation power in the reaction.

Therefore, interferences for the determination of lead with this method should be expected, but they can be minimized with the parameters mentioned above. Only selenium causes significant interference. But selenium seems to interfere with every hydride technique [3,26,32].

## 3. Results and discussion

The calibration shows a linear range in the concentration range up to ca. 50 µg/l lead and then changes into a typical second order function. The absolute sensitivity, the characteristic mass, defined as the amount of lead required to give 1% absorption (peak height A = 0.0044) is 368 pg. The characteristic mass of lead reported in the literature was 10 pg for GF-AAS [39]. The large difference between the characteristic masses can be explained with the inefficient generation of plumbane by the hydride generation technique. For comparing with the graphite furnace technique the characteristic concentration is decisive and not the characteristic mass, because the concentration criterion is dependent on the available volume. Because the large sample volumes in the enrichment technique the poor yield of hydride products can be compensated for. The resulting characteristic concentration was 0.74 µg/l for a 500 µl sample volume. The characteristic concentration reported for GF-AAS was 0.2 µg/l for a 50 µl sample volume [39]. By using a greater sample volume or the continuous mode, lower characteristic concentrations in the same range or less like GF-AAS are obtainable by the hydride generation technique. The detection limit, defined as the amount of lead required to give an absorbance equal to three-fold standard deviation of the blank absorbance [40], was 0.70 µg/l for a 500 µL sample volume. For GF-AAS the detection limit is 0.1 µg/l for a 50 µl sample volume. The characteristic data of the method computed by formulas taken from Funk et al. [41] are presented in Table 5.

In order to compare GF-AAS hydride generation with other AAS methods, we determined the lead contents of some standard reference material samples. The reliability of the method was tested by measuring the content of lead in several real samples. Organic and inorganic materials with different matrices were decomposed with aqua regia and measured with the described method. The parameter for weight-in-quantities, dry processes of the samples, the decomposition method (aqua regia or invers aqua regia) and the results found with the described technique are presented in Table 6. The results obtained by this method were compared with those obtained by graphite furnace absorption spectrometry and the new multi

Table 6
Results and recoveries by the determination of lead with the flow injection analysis system–hydride generation–graphite furnace atomic absorption spectrometry (FIAS–HG–GFAAS)

| Reference material | Weight (g) | Dry process | Decomposition method | Mean value (μg/g) | Certification (μg/g) | Recovery (%) |
|---|---|---|---|---|---|---|
| Pine needles SRM 1575 | 2.3 | 2 hr, 85 °C | aqua regia | 13.7 ± 1.2 | 10.8 ± 0.5 | 127 |
| Rye gras CRM 281 | 3.3 | 2 hr, 105 °C | aqua regia | 3.43 ± 0.33 | 2.38 ± 0.11 | 144 |
| Aquatic moss CRM 061 | 3.0 | 24 hr, $P_2O_5$ | aqua regia inv. | 61.1 ± 2.8 | 64.4 ± 3.5 | 95 |
| Estuarine sediment CRM 277 | 3.0 | 1 hr, 105 °C | aqua regia | 155.8 ± 5.6 | 135.8 ± 3.3 | 107 |

Table 7
Comparison of the recovery of lead by different measurement systems

| Reference material | Pine needles SRM 1575 (μg/g) | Rye gras CRM 281 (μg/g) | Aquatic moss CRM 061 (μg/g) | Estuarine sediment CRM 277 (μg/g) |
|---|---|---|---|---|
| FIAS–HG–GFAAS | 13.7 ± 1.2 | 3.43 ± 0.33 | 61.1 ± 2.8 | 155.8 ± 5.6 |
| ZL 4100 | 11.3 ± 1.2 | 3.4 ± 1.0 | 57.1 ± 2.2 | 150.4 ± 3.4 |
| FremsAAS | 12.0 ± 1.0 | 4.6 ± 0.8 | 61.0 ± 4.2 | — |
| Certification | 10.8 ± 0.5 | 2.38 ± 0.11 | 64.4 ± 3.5 | 145.8 ± 3.3 |

FIAS–HG–GFAAS: flow injection analysis system–hydride generation–graphite furnace AA spectrometer; ZL 4100: GFAAS with longitudinal Zeeman background correction; FremsAAS: frequency modulated simultaneous GFAAS with deuterium background correction.

element-GFAAS. Satisfactory results with very good agreement by all three methods were observed. The accuracy of the results are also in accordance with the certification (Table 7).

## 4. Conclusion

This vapor generation and enrichment method offers many advantages with respect to simplicity and speed and substantially improved sensitivity. Additionally, it was observed that this technique is mostly free from interferences. The detection limit in the flow injection system was 0.70 μl for a 500 μl-sample loop. By enrichment of greater sample volumes with a continuous flow step, the sensitivity increases by more than a factor of 10. Naturally, because of the different stabilities of the hydride products of organolead compounds and lead itself, the method is more sensitive for organolead compounds. The method works well for organolead compounds, and also works satisfactorily for the inorganic compound.

Because the detection limit reached by this method is higher than that provided by the conventional graphite furnace, application in a continuous mode is paramount. In biological materials, where the content of lead is very small, the enrichment step in continuous mode allowed the detection of lead in the pg/g range. In this study a continuous mode was unnecessary to obtain good results because of the great weight-in-quantities.

This method in flow injection mode is simple to carry out and can be conveniently used for the analysis of large numbers of samples on a routine basis. Accurate results can be obtained if the concentration levels of the interfering metals are less than the lead concentration. This is safely possible for materials like fly ashes or sediments. Significant interference effects have been encountered when analysing biological materials. By using the standard addition method, most problems can be eliminated, only the sensitivity of the lead signal decreased.

The measurements of standard reference materials have shown accurate results according to the certification of these materials. No problems were found using the standard addition method if the evaluation of the signals are carried out by measuring peak area instead of peak height.

Using surfactant substances the sensitivity of lead determination increases and positive influences by the suppression of some interferences have been observed.

## Acknowledgement

The authors kindly acknowledge the financial support of the Land "Nordrhein-Westfalen".

## References

[1] K.C. Thompson and D.R. Thomerson, Analyst, 99 (1974) 595.
[2] P.N. Vijan and G.R. Wood, Analyst, 101 (1976) 966.
[3] H.D. Fleming and R.G. Ide, Anal. Chim. Acta, 83 (1976) 67.
[4] K. Jin, M. Taga, H. Yoshida and S. Hikime, Jpn. Anal. (Bunseki Kagaku), 27 (1978) 759.
[5] P.N. Vijan and R.S. Sadana, Talanta, 27 (1980) 321.
[6] M. Ikeda, J. Nishibe, S. Hamada and R. Tujino, Anal. Chim. Acta, 125 (1981) 109.
[7] J.R. Castillo, J.N. Mir, J. Val, M.P. Colón and C. Martinez, Analyst, 110 (1985) 1219.
[8] I. Aroza, M. Bonilla, Y. Madrid and C. Cámara, J. Anal. At. Spectrom., 4 (1989) 163.
[9] J.-X. Li, Y.-M. Liu and T.-Z. Lin, Anal. Chim. Acta, 231 (1990) 151.
[10] Y. Madrid, M. Bonilla and C. Cámara, Analyst, 115 (1990) 563.
[11] X.-P. Yan and Z.-M. Ni, J. Anal. At. Spectrom., 6 (1991) 483.
[12] M.C. Valdé-Hevia y Temprano, B. Aizpún Fernández, M.R. Fernández de la Campa and A. Sanz-Medel, Anal. Chim. Acta, 283 (1993) 175.
[13] D. Erber, L. Quick, J. Roth and K. Cammann, in K. Dittrich and B. Welz' (Eds.) CANAS'93, Universität Leipzig and UFZ-Umweltforschungszentrum Leipzig-Halle, Leipzig, 1993, p. 557.
[14] Gmelin, Handbook of Inorganic Chemistry, 8th edn., B1, VCH, Weinheim, 1972, p. 354.
[15] Gmelin, Handbook of Inorganic Chemistry, 8th edn., C1, VCH, Weinheim, 1969, p. 47.
[16] R.E. Sturgeon, S.N. Willie and S.S. Berman, J. Anal. At. Spectrom., 1 (1986) 115.
[17] G.V. Drasch, L. Meyer and G. Kauert, Fresenius Z. Anal. Chem., 304 (1980) 141.
[18] R.E. Sturgeon, S.N. Willie and S.S. Berman, Anal. Chem., 57 (1985) 2311.
[19] R.E. Sturgeon, S.N. Willie, G.I. Sproule and S.S. Berman, J. Anal. At. Spectrom., 2 (1987) 719.
[20] L. Zhang, Z.-M. Ni and X.-Q. Shan, Spectrochim. Acta, 44B (1989) 339.
[21] I.L. Shuttler, M. Feuerstein and G. Schlemmer, J. Anal. At. Spectrom., 7 (1992) 1299.
[22] G. Schlemmer and M. Feuerstein, in K. Dittrich and B. Welz' (Eds.), CANAS'93, Universität Leipzig and UFZ-Umweltforschungszentrum Leipzig-Halle, Leipzig, 1993, p. 431.
[23] D.S. Lee, Anal. Chem., 54 (1982), 1682.
[24] The FIAS-Furnace Technique, Recommended Analytical Conditions and General Information, Bodenseewerk Perkin-Elmer, 1993.
[25] Z. Fang, Flow Injection Separation and Preconcentration, VCH, Weinheim, 1993.
[26] L.J.C. Love, J.G. Habarta and J.G. Dorsey, Anal. Chem., 56 (1984) 1132A.
[27] E. Pelizzetti and E. Pramauro, Anal. Chim. Acta, 169 (1985) 1.
[28] B. Aizpún-Fernández, C. Valdés-Hevia y Temprano, M.R. Fernández de la Campa and A. Sanz-Medel, Talanta, 39 (1992) 1517.
[29] F. Winter, L. Quick, M. Bradter and K. Cammann, in B. Welz'(Eds.)6.Colloquium Atomspektrometrische Spurenanalytik, Bodenseewerk Perkin-Elmer, Überlingen, 1991, p. 489.
[30] D. Erber, J. Bettmer and K. Cammann, Fresenius J. Anal. Chem., 349 (1994) 738.
[31] P.-Y. Yang, Z.-M. Ni, Z.-X. Zhuang, F.-C. Xu and A.B. Jiang, J. Anal. At. Spectrom., 7 (1992) 515.
[32] A. Meyer, C. Hofer, G. Tölg, S. Raptis and G. Knapp, Fresenius Z. Anal. Chem., 296 (1979) 337.
[33] B. Welz and M. Melcher, Spectrochim. Acta, 36B (1981) 439.
[34] A.F. Hollemann and E. Wiberg, Lehrbuch der Anorganischen Chemie, Walter de Gruyter, Berlin, 1985, p. 806.
[35] Deutsche Einheitsverfahren zur Wasser-. Abwasser- und Schlammuntersuchung, Bd. 3, S7, VCH, Weinheim, 1983.
[36] H. Edel, Diploma thesis, University of Münster, 1994.
[37] B. Welz and M. Melcher, Anal. Chim. Acta, 131 (1981) 17.
[38] J. Dedina, Anal. Chem., 54 (1982) 1097.
[39] B. Welz, in H. Naumer and W. Heller's (Eds.), Untersuchungsmethoden in der Chemie, pp. 226 and 235, Georg Thieme, Stuttgart, 1990.
[40] K. Doerffel, Statistik in der Analytischen Chemie, VCH, Weinheim, 1987, p. 91.
[41] W. Funk, V. Dammann and G. Donnevert, Qualitätssicherung in der Analytischen Chemie, VCH, Weinheim, 1992.

ELSEVIER

Talanta 42 (1995) 937–943

Talanta

# Simultaneous determination of sulphide and sulphite by gas-phase molecular absorption spectrometry. Comparative study of different calculation methods

S. Cabredo Pinillos [a], I. Sanz Vicente [a], J. Sanz Asensio [a,*], J. Galbán Bernal [b]

[a] *Chemistry Department, Analytical Chemistry Section, University of La Rioja, Logroño-26001, Spain*
[b] *Analytical Chemistry Department, Faculty of Sciences, University of Zaragoza, Zarogoza-50009, Spain*

Received 25 October 1994; revised 21 December 1994; accepted 13 January 1995

**Abstract**

A method for the simultaneous determination of sulphide and sulphite is described, which involves continuous $H_2S$ and $SO_2$ generation, preconcentration in a liquid nitrogen trap and measurement of the molecular absorption spectra of volatiles in the gas phase in 190–220 nm range. Under the recommended conditions (sample flow: 50 ml/min and concentrated sulphuric acid flow: 12 ml/min; generation time: 4 min) linear response ranges from 0.05 μg/ml for $S^{2-}$ and 0.20 μg/ml for $SO_3^{2-}$ are obtained with detection limits of 0.05 and 0.20 μg/ml respectively. Synthetic mixtures of the two components have been solved and a comparative study of different calculation methods has been made. In conclusion, multiwavelength methods offer better precision and accuracy.

## 1. Introduction

Classical approaches to the simultaneous determination of sulphur anions, i.e. titration [1], spectrophotometry [2,3] or polarography, typically involve differential assays, reaction of the sample with iodine, bromine compounds of many others [4,5] under different conditions. In many cases, the need for extensive manipulation of samples, subtraction of large numbers from each other, and substantial time investment per sample limit their applications. Automatized or semi-automatized methods offer opportunities to approach the problem. Burguera and Burguera [6] have attempted the simultaneous determination of several sulphur anions using a relatively uncommon technique, molecular emission cavity analysis (MECA); Hauge [7] and Sonne [8] have described a complicated simultaneous photometric flow injection determination of sulphide, polysulphide, thiosulphate, sulphite and sulphate based on different chemical reactivities, differing p$K_a$s and volatilities of the various sulphur-containing acids, and kinetic differences.

Many papers about several sulphur-containing anions determination are based on chromatographic separation and later determination. So Story [9] has indeed demonstrated the successful determination of a large number of sulphur anions with postcolumn reaction detection. Other authors that use chromatographic separation are Shpigun et al. [10] for determining sulphide, sulphite, sulphate and thiosulphate, or Steudel et al. [11] for sulphide, sulphite, thiosulphae and polysulphide.

Although previous methods offer good results, they all show different problems; for example, instrumental complexity (as MECA), sensitivity (as Sonne's method) or the excessive manipulation of samples (as methods with post-column deviation). Furthermore, the methods described are in fact sequential, not simultaneous, which leads to more complex

* Corresponding author.


*SSDI* 0039-9140(95)01529-9

procedures. The introduction of diode-array detection systems in UV-visible spectrophotometers allows new developments in GPMAS (Gas Phase Molecular Absorption Spectrometry) by Sanz et al. for single [12–15] and multicomponent simultaneous determinations [16–18]. The first papers on this technique were published by Cresser and Syty, independently. Both of them used a mono-channel detection system (an atomic absorption spectrometer with hollow cathode or deuterium lamps as radiation sources) so they were not able to perform simultaneous determination; Syty reported only single sulphide (by $H_2S$ generation) [19] or sulphite (by $SO_2$ generation) [20] determination.

From this period on, few works have been published on sulphite or sulphide [21] single determination of GPMAS. Simultaneous determination has only recently been proposed by Jin et al [22]. Using a similar approach to Syty, they perform simultaneous determination by measuring sequentially from two different radiation sources (magnesium and tellurium hollow cathode lamps) emitting at 202.6 and 214.3 nm; these wavelengths are far from the maximum molecular absorption of $SO_2$ and $H_2S$ (198 and 196 nm, respectively) and two problems could arise: low sensitivity (which can be avoided by using a more expensive long path cell) and low precision (reproducibility values are not indicated by the authors). In addition, owing to the high overlap of the molecular absorption spectra of both volatiles, the use of the two-wavelength method for simultaneous determination is prone to inaccuracy.

In this paper generation of sulphur volatiles in a continuous mode, coupled to a retention in liquid nitrogen, permits the use of GPMAS with diode-array detection for the simultaneous determination of sulphide and sulphite at low concentration levels. Different mathematical data treatments for binary determinations of these compounds have been compared; the multiwavelength method give more accuracy and precision than the two wavelength methods.

## 2. Experimental

### 2.1. Apparatus

All measurements were performed using a Hewlett-Packard model HP 8451A diode-array spectrophotometer furnished with a quartz flow cell of 1 cm path length (Hellma 174 QS) and equipped with a Keyboard HP98155A (Hewlett-Packard), a floppy disk drive for bulk data storage (Hewlett-Packard HP9121) and a graphics plotter (HP7475A). For mathematical treatment a Hewlett-Packard Vectra microprocessor with Eureka® software was used. Masterflex models 7518-10 and 7016-20 peristaltic pumps (Cole Parmer Instrument Co. Chicago, Illinois 60648), were employed throughout.

### 2.2. Reagents

All reagents used were of analytical-grade quality. Doubly distilled water was used.

Standard sulphide solution was prepared by dissolving $Na_2S \cdot 9H_2O$ (0.75 g) in 100 ml water, and then titration with ferricyanide. This and working standard solutions (perpared by serial dilution of the stock solution), were prepared daily.

Standard sulphite solution was prepared by dissolving $Na_2SO_3 \cdot 7H_2O$ in a 5% glycerin water solution as stabilizer. Working standards were prepared by serial dilution of the stock solution, immediately before use.

Concentrated perchloric (70%, 1.67 g/ml) and sulphuric (96%, 1.84 g/ml) acids were also used.

### 2.3. System description. Procedure

Volatiles generation and cold trap systems are shown in Fig. 1. Two peristaltic pumps were used for mixing analytes solution (50 ml/min) and concentrated sulphuric acid (12 ml/min). $H_2S$ and $SO_2$ generated into the mixing coil (in which an additional 600 ml/min nitrogen gas-auxiliary carrier flow, AF, was flowing) were separated in a first gas–liquid separator where there was a nitrogen flow (transport flow, TF, 100 ml/min) and the remaining liquid phase reached a second gas–liquid separator. The volatiles were swept through a water trap (a flask full of Raschig rings and immersed in an ice and salt bath at $-10\,^{\circ}C$) and were finally condensed in the U-tube immersed in liquid nitrogen which contained a small quantity of glass spheres (2 mm diameter). The Raschig rings and the small glass spheres were both silanized.

After generation and trapping of volatile compounds for 4 min, the U-tube was closed, removed from the liquid nitrogen and left at

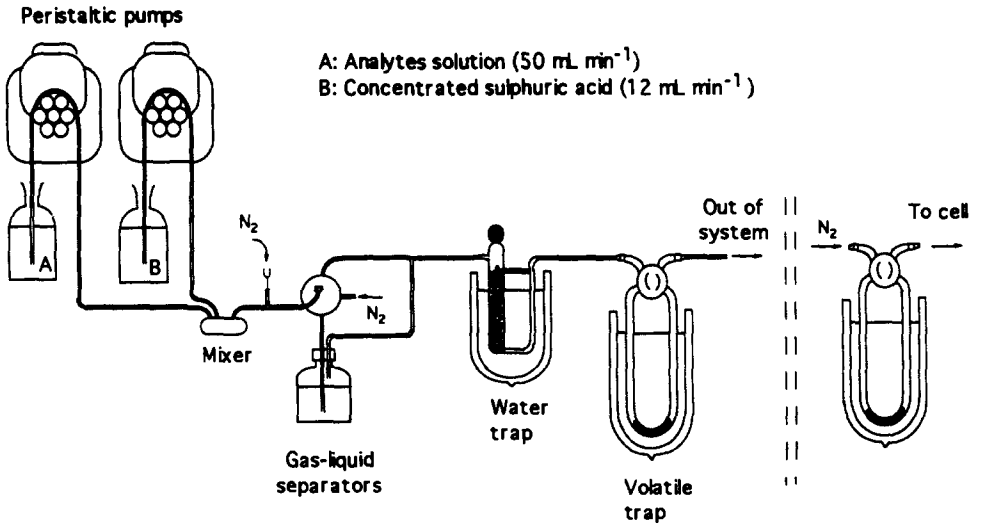


Fig. 1. Schematic diagram of the system (see explanation in the text).

room temperature. After 10 min the volatiles were transported to the continuous flow cell, placed in the spectrophotometer, with a nitrogen flow (measuring flow, MF) of 2000 ml/min.

To measure the transient signal, the spectrophotometer was programmed with a BASIC program that permitted us to obtain and store molecular absorption spectra in the 190–250 nm range, with a time interval of 0.2 s. All determinations of mixtures and standards were made at least in triplicate.

To determine $S^{2-}$ and $SO_3^{2-}$ contents in a mixture, the maximum absorbance values for every wavelength between 190 and 220 nm were obtained (the spectral bandwidth of the spectrophotometer was 2 nm, so 16 absorbance values were used).

## 3. Results and discussion

### 3.1. Optimization of parameters

Generation and preconcentration of volatiles were performed using a system which is based on another described in a previous paper [18]. This system had been used for hydride generation so many parameters had to be reoptimized because the nature of the compounds to be generated is quite different.

Although other mixers have been employed, the results obtained using that shown in Fig. 1 were the best. With respect to the glass reaction coil, different lengths were studied (3, 10 and 40 cm), and almost no influence on the absorbance or signal shape was observed, so a reaction coil length of 3 cm (the minimum possible) was chosen. Using 40 cm instead of 3 cm gives a slight decrease in absorbance (about 10%) observed.

In most manifolds used in continuous flow determinations involving a gas–liquid separation process, a single gas–liquid separation step is used. In this work we observed that two serial gas–liquid separators produce signal increases of 35% compared to the use of only one separator. This increase is explained if one considers that the temperature of the solution to be separated is higher than ambient (owing to the heat liberated during the mix of aqueous analyte solution and concentrated sulphuric acid) so the separation process continues in the second gas–liquid separator; in addition, the shape of this second gas–liquid separator favours the process further.

Nitrogen TF is one of the parameters which most affects the analytical signal. As has been described for hydride generation [18], the TF must be the lowest possible to obtain the maximum retention yield in the liquid nitrogen trap. This is logical considering that the larger the flow, the less the residence time of the volatiles in the trap. However, when we employed low flows (as hydride) for sulphur volatiles, a retention of the nitrogen in the cryogenic trap was observed; when the trap was later brought to room temperature, the nitrogen suddenly escaped from the valve and allowed the volatiles to escape. In order to avoid this problem, three alternatives were tested.

Table 1
Variation of $SO_2$ signal with AF/TF ratio (total flow = 1200 ml/min)

| AF (ml/min) | TF (ml/min) | AF/TF (ml/min) | Signal |
|---|---|---|---|
| 1100 | 100 | 11 | 0.036 |
| 1030 | 170 | 6 | 0.040 |
| 600 | 600 | 1 | 0.030 |
| 100 | 1100 | 0.1 | 0.025 |

AF = Auxiliary flow, TF = transport flow.

(a) Changing the cryogenic trap to another at a higher temperature, so that nitrogen gas could not be held. A liquid nitrogen–ethanol bath (ca. −117 °C) was used, but a large decrease in absorbance values was observed which indicated a low retention yield for sulphur volatiles.

(b) Addition to the analyte solution of a substance capable of forming a gas in an acidic environment; this gas could act as an internal carrier gas [21]. $NaBH_4$ can not be used because it is a reducing agent and would transform sulphite into sulphide. Low carbonate concentrations were employed, but $CO_2$ causes the same problem as nitrogen.

(c) Increasing the nitrogen flow. To do this an AF was bubbled through the reaction coil (between mixer and first gas–liquid separator). This alternative gives successful results.

Nitrogen TF and AF were studied in a wide range of possible flow-rate combinations. $H_2S$ and $SO_2$ were optimized separately. Table 1 shows $SO_2$ absorbance for different AF/TF ratios (maintaining a total flow of 1200 ml/min). The optimum value was for a ratio equal to 6. Table 2 shows the $SO_2$ absorbance variation with total flow (maintaining an AF/TF of 6). The best results were obtained using 700 ml/min total flow. A total flow of nitrogen of less than 400 ml/min produced the retention of $N_2$ in the cryogenic trap. Contrary to what happened with $SO_2$ absorbance, the $H_2S$ optimization showed the best results using a total flow of 2000 ml/min. Finally, 700 ml/min total flow (AF = 600 ml/min and TF = 100 ml/min) was used because sulphite sensitivity was poorer than sulphide. With respect to the nitrogen MS, 2000 ml/min was found to be the optimum for different reasons, as discussed previously [18].

Table 2
Variation of $SO_2$ signal with total flow (AF/TF ratio = 6)

| AF (ml/min) | TF (ml/min) | Total flow (ml/min) | Signal |
|---|---|---|---|
| 1800 | 300 | 2100 | 0.027 |
| 1030 | 170 | 1200 | 0.040 |
| 600 | 100 | 700 | 0.063 |
| 430 | 70 | 500 | 0.044 |

AF = Auxiliary flow, TF = transport flow.

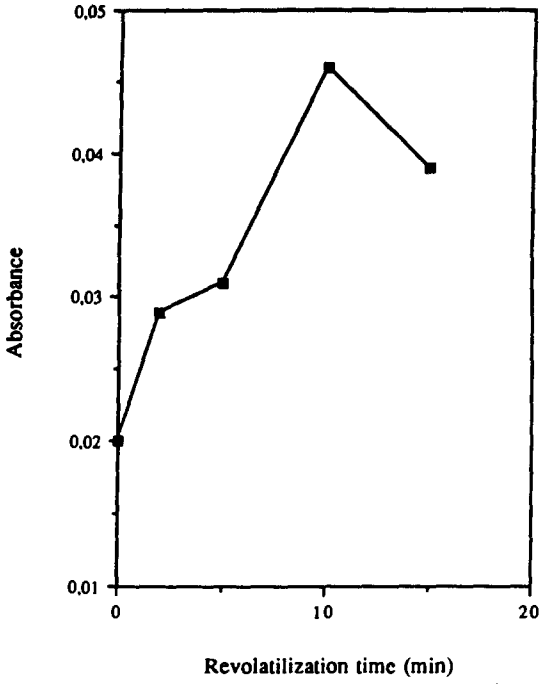


Fig. 2. Variation of absorbance with revolatilization time.

An exhaustive study was also performed of the time necessary for volatiles revolatilization at room temperature from the nitrogen trap; Fig. 2 shows peak height variation with this time (from 0 to 15 min). Other assays were performed by heating the U-tube after this time, but no improvements in the analytical signal were observed.

Sulphuric and perchloric acids at various concentrations were used both to achieve optimum acidity of the medium and to obtain quantitative generation of $H_2S$ and $SO_2$. These acids were selected because they are used for batch generation of $H_2S$ and $SO_2$, respectively. A first comparison for both acids in a 50% (v/v) solution, indicated better results by using 50% $H_2SO_4$; the reason was, perhaps, the high temperature of the acid solution that favours the volatilization of $H_2S$ and $SO_2$. In a second series of assays, the absorbance values obtained using different concentrations of sulphuric acid indicated that concentrated acid gives much higher results than any other acid concentra-

Table 3
Optimization of analyte flow/acid flow ratio

| Analyte flow (ml/min) | Acid flow (ml/min) | $H_2S$ signal | $SO_2$ signal | Analyte/acid |
|---|---|---|---|---|
| 50 | 2 | 0.022 | 0.027 | 24:1 |
| 50 | 6 | 0.021 | 0.035 | 8:1 |
| 50 | 12 | 0.023 | 0.048 | 4:1 |

tion, which confirms the positive heating effect obtained with this acid.

Another optimized chemical parameter was the acid flow/analytes flow ratio. Ratios ranging from 24:1 and 4:1 did not produce variations in absorbance for $H_2S$, whereas the best results for $SO_2$ appeared when a 4:1 ratio or lower is used (Table 3). On the other hand, maintaining the 4:1 ratio and decreasing flow (acid flow = 3 ml/min and analyte flow = 12 ml/min, for example) gave a slight enhancement in signal (about 15%) but the analysis time increased.

The best conditions for the simultaneous determination of sulphide and sulphite by GP-MAS are given in Table 4.

### 3.2. Analytical characteristics

Under the compromise conditions found for $S^{2-}$ and $SO_3^{2-}$, individual calibration studies were performed by measuring the absorbance at the corresponding wavelengths of maximum absorbance (196 and 198 nm for $S^{2-}$ and $SO_3^{2-}$, respectively). The equations of the calibration graphs obtained by the method of least squares were:

$$Y = 1.46 \times 10^{-3} + 5.03 \times 10^{-2}[S^{2-}] \qquad r = 0.998$$

$$Y = 1.65 \times 10^{-3} + 1.57 \times 10^{-2}[SO_3^{2-}] \qquad r = 0.998$$

A linear response from 0.05 μg/ml to at least 5 μg/ml for sulphide and from 0.2 μg/ml to at least 20 μg/ml for sulphite was obtained; reproducibility values (expressed as RSD) were 2.9% (for 0.2 μg/ml $S^{2-}$) and 3.1% (for 0.8 μg/ml $SO_3^{2-}$). Detection limits calculated from a signal three times the height of the background of the blank measurement were 0.05 μg/ml for sulphide and 0.2 μg/ml for sulphite.

In conclusion, the sensitivity of this method (expressed as specific absorptivity, in ml $\mu g^{-1}$ $cm^{-1}$) is 10 times higher than we obtained by batch model [21]. With regards to the results obtained by other authors, it is very difficult to make comparisons; as we have used a 1 cm optical path length cell while other authors have used larger cells (normally, 15 cm optical path length). Using specific absorptivity as the comparison parameter, the values obtained by this method are about 15 times higher than obtained by other authors [22].

Table 4
Optimum conditions for simultaneous determination of sulphide and sulphite

| | |
|---|---|
| Analytes solution | 50 ml/min |
| $H_2SO_4$ | 12 ml/min |
| $N_2$ Auxiliary flow | 600 ml/min |
| $N_2$ Transport flow | 100 ml/min |
| $N_2$ Measurement flow | 2000 ml/min |
| Generation time | 4 min |
| Revolatilization time | 10 min |

Table 5
Results obtained for simultaneous determination of sulphide and sulphite by MLRA and MLRA-TA

| Mixtures[a] | | MLRA | | MLRA-TA | |
|---|---|---|---|---|---|
| Mixture 1 | $[S^{2-}] = 0.50$ | 0.43 | 0.43 | 0.51 | 0.52 |
| | $[SO_3^{2-}] = 2.0$ | 1.7 | 1.8 | 1.7 | 1.5 |
| Mixture 2 | $[S^{2-}] = 0.50$ | 0.62 | 1.2 | 0.62 | 0.78 |
| | $[SO_3^{2-}] = 15.0$ | 15.7 | 15.5 | 16.0 | 15.1 |
| Mixture 3 | $[S^{2-}] = 1.5$ | 1.7 | 1.6 | 1.4 | 1.5 |
| | $[SO_3^{2-}] = 3.0$ | 2.6 | 2.7 | 2.3 | 2.5 |

[a]Concentrations in μg/ml.

### 3.3. Simultaneous determination

In this work several mathematical procedures for the resolution of three synthetic samples of sulphite and sulphide have been tested, involving different versions of the two-wavelength method and multiwavelength methods.

### 3.4. Two-wavelength methods

In these methods, absorbance is measured at two appropriate wavelengths; the concentrations of both components were determined by resolving the following equations system:

$$\mathrm{Abs}_{(\lambda 1)} = a_{(\lambda 1)^{\bullet}}^{\mathrm{Sulphide}}[S^{2-}] + a_{(\lambda 1)^{\bullet}}^{\mathrm{Sulphite}}[SO_3^{2-}] - \mathrm{Abs}_{(\lambda 1)}^{\mathrm{blak}}$$

$$\mathrm{Abs}_{(\lambda 2)} = a_{(\lambda 2)^{\bullet}}^{\mathrm{Sulphide}}[S^{2-}] + a_{(\lambda 2)^{\bullet}}^{\mathrm{Sulphite}}[SO_3^{2-}] - \mathrm{Abs}_{(\lambda 2)}^{\mathrm{blak}} \qquad (1)$$

where $\mathrm{Abs}_{(\lambda 1)}$ and $\mathrm{Abs}_{(\lambda 2)}$ are the absorbance

Table 6
Results obtained for simultaneous determination of sulphide and sulphite by CMM

| Range (nm) | Mixture 1 | | Mixture 2 | | Mixture 3 | |
|---|---|---|---|---|---|---|
| | $[S^{2-}]$ 0.50 μg/ml | $[SO_3^{2-}]$ 2.0 μg/ml | $[S^{2-}]$ 0.50 μg/ml | $[SO_3^{2-}]$ 15.0 μg/ml | $[S^{2-}]$ 1.5 μg/ml | $[SO_3^{2-}]$ 3.0 μg/ml |
| 190–220 | 0.42 | 1.8 | 0.43 | 17.8 | 1.4 | 3.5 |
| 190–210 | 0.51 | 1.5 | 0.42 | 18.0 | 1.3 | 3.7 |
| 190–214 | 0.50 | 1.6 | 0.40 | 18.2 | 1.4 | 3.5 |
| 190–216 | 0.44 | 1.8 | 0.39 | 17.7 | 1.4 | 3.5 |
| 198–208 | 0.26 | 2.1 | 0.21 | 18.3 | 1.3 | 3.6 |
| 198–210 | 0.05 | 2.3 | 0.25 | 18.0 | 1.3 | 3.6 |
| 198–212 | 0.05 | 2.5 | 0.17 | 17.6 | 1.2 | 3.7 |
| 198–214 | 0.05 | 2.5 | 0.05 | 19.3 | 1.2 | 3.6 |
| 198–216 | 0.05 | 2.6 | 0.05 | 19.0 | 1.2 | 3.7 |
| 204–220 | 0.07 | 2.5 | 0.13 | 18.8 | 1.3 | 3.5 |
| 198–220 | 0.05 | 2.6 | 0.10 | 18.6 | 1.6 | 2.7 |
| 210–220 | 0.51 | 1.6 | 0.93 | 17.3 | 2.1 | 1.7 |
| 212–220 | 0.53 | 1.6 | 0.80 | 16.8 | 1.9 | 2.5 |

of the mixture at each of the two wavelengths; $a_{(\lambda 1)}^{\text{Sulphite}}$, $a_{(\lambda 1)}^{\text{Sulphide}}$, $a_{(\lambda 2)}^{\text{Sulphite}}$, $a_{(\lambda 2)}^{\text{Sulphite}}$, $a_{(\lambda 2)}^{\text{Sulphide}}$ are the specific absorptivity (slope of calibration graph) of the individual compounds at the wavelength specified. The selection of $\lambda_1$ and $\lambda_2$ were performed on the basis of two analytical parameters as follows.

(i) Optimum sensitivity. This is the more used criteria for wavelength selection and corresponds to the maximum absorbance value of each of the two volatiles, i.e. 196 and 198 nm.

(ii) Optimum precision. The two wavelengths were calculated by applying a procedure described by DiTusa et al. [23], resulting in 196 and 212 nm for this case.

By using both methods, the results were very unsatisfactory (negative concentration values were obtained in some cases), so new alternatives were tested.

(i) Wavelength average. In this method each of the absorbance values is obtained as the average of the absorbance at three close wavelengths; firstly, the average at 192, 196 and 200 nm and secondly the average at 194, 198 and 202 nm. By this method the wavelength inaccuracy of the spectrophotometer is partially avoided.

(ii) Time average. As has been indicated above, we obtained a sequence of 50 spectra in each measurement and we used the maximum absorbance spectrum for obtaining the absorbance values at the selected wavelength. In many cases the maximum absorbance values spectrum appears close to other spectra of a similar area. This method, therefore, uses the average absorbance values at similar times (taking the two spectra before the maximum and the two after the maximum), in order to correct the time inaccuracy.

(iii) Wavelength and time averages. This method is a combination of the previous two.

The results obtained using these alternatives were unsatisfactory too, so multiwavelength methods were applied.

### 3.5. *Multiwavelength methods*

In this method absorbance values obtained in a wavelength range is employed. Blanco et al. [24] demonstrated that the best results in the resolution of mixtures of species with overlapped spectra are obtained when the widest possible wavelength range is used. Such a range was 190–220 nm throughout this work. Two different methods has been tested:

(i) Multiwavelength Linear Regression Analysis (MLRA), proposed by Blanco et al. [25]. Table 5 shows the results obtained. Concentrations found agreed reasonably with known values. This method was also applied after performing a time average of absorbance values, but no better results were observed.

(ii) Complete Multiwavelength Method (CMM). This method basically consists of solving a set of equations similar to Eq. (1); the number of the equations is selected empirically but normally corresponds [24] to the wavelength range in which a higher overlapping of the spectra is observed. In order to solve the equations, mathematical program (Eureka®)

using an iterative procedure was employed. Different wavelength intervals were assessed and the best results were obtained using all wavelengths between 190 and 220 nm (which means a set of 16 equations, because the spectral bandwidth of the spectrophotometer is 2 nm). The results obtained for several ranges are shown in Table 6. All results are the average of three determinations and the RSD values were, in all cases, lower than 4%. The time average of the absorbance values did not give better results either.

It can be concluded that two-wavelength methods produce imprecise and inaccurate results; using either MLRA or CMM the results are satisfactory.

## 4. Conclusions

This procedure shows some advantages against previous GPMAS determination, such as higher sensitivity and the possibility of using the whole molecular absorption spectrum, allowing better reproducibility and accuracy in the results. Also it is possible to forecast the spectral interferences present. As opposed to other methods, sensitivity values are similar, neither complex nor specific instrumental is required and it is easy to apply.

## Acknowledgements

This work was supported by CICYT (project No. 541 A. 783) and Caja Rioja-University of La Rioja agreement. S. Cabredo is grateful to the FPI grant to 'Instituto de Estudios Riojanos' of La Rioja (Spain).

## References

[1] C.M. Das, Talanta, 38 (1991) 347.
[2] T. Koh and Y. Okabe, Anal. Sci., 3 (1992) 285.
[3] T. Koh, Y. Okabe and Y. Miura, Analyst, 118 (1993) 669.
[4] J.F. Verchere and A.M. Don, Analusis, 20(1992) 437.
[5] M. García-Vargas, M. Milla and J.A. Pérez Bustamante, Analyst, 108 (1986) 1417.
[6] J.L. Burguera and M. Burguera, Anal. Chim. Acta, 157 (1984) 177.
[7] S. Hauge, K. Maroy and A. Thorlacius, Anal. Chim. Acta, 251 (1991) 197.
[8] K. Sonne and P.K. Dasgupta, Anal. Chem., 63 (1991) 427.
[9] J.N. Story, J. Chromatogr. Sci., 21 (1983) 277.
[10] D.A. Shpigun, D.N. Obrezkov, J. Funk and G. Werner, Vestn. Mosk. Univ. Ser. 2: Khim., 30 (1989) 273.
[11] R. Steudel, G. Holdt and T. Goebel, J. Chromatogr., 475 (1989) 442.
[12] J. Sanz, F. Gallarta, J. Galbán and J. R. Castillo, Fresenius'Z. Anal. Chem., 330 (1988) 510.
[13] J. Sanz, F. Gallarta, J. Galbán and J.R. Castillo, Analyst, 113 (1988) 1387.
[14] J. Sanz, L.A. Ortega, J. Galbán and J.R. Castillo, Microchem. J., 41 (1990) 29.
[15] J. Sanz, S. de Marcos, O. Muro and J. Galbán, Microchim. Acta, 110 (1993) 193.
[16] J. Sanz, F. Gallarta and J. Galbán, Anal. Chim. Acta, 225 (1991) 113.
[17] J. Sanz, S. de Marcos, J. Galbán and F. Gallarta, Analusis, 21 (1993) 27.
[18] S. Cabredo, J. Sanz and J. Galbán, Anal. Chim. Acta., in press.
[19] A. Syty, Anal. Chem., 51 (1979) 911.
[20] A. Syty, Anal. Chem., 45 (1973) 1744.
[21] J. Sanz, S. Cabredo and J. Galbán, Anal. Lett., 25 (1992) 2095.
[22] Q. Jin, H. Zhang, Y. Duan, A. Yu, X. Liu and L. Wang, Talanta 39 (1992) 967.
[23] M.R. DiTusa and A.A. Schilt, J. Chem. Educ., 62 (1985) 541.
[24] M. Blanco, J. Gené, H. Iturriaga and S. Maspoch, Analyst, 112 (1987) 619.
[25] M. Blanco, H. Iturriaga, S. Maspoch and P. Tarin, J. Chem. Educ., 66 (1989) 179.

ELSEVIER

Talanta 42 (1995) 945–948

Talanta

# Determination of carbonate, bicarbonate and phosphate in uranium leach liquors containing $KMnO_4$ as oxidant

D.S.R. Murty *, A. Thangaraj, R. Radhamani, R. Rangaswamy

*Atomic Minerals Division, Department of Atomic Energy, Nagarbhavi, Bangalore – 560 072, India*

Received 4 November 1994; revised 16 January 1995; accepted 19 January 1995

**Abstract**

A simple, rapid and economic method has been developed for the reduction of potassium permanganate in alkaline carbonate uranium leach liquors to a colourless solution. The pink colour of permanganate, if not reduced, seriously impedes the determination of carbonate, bicarbonate and phosphate by titrimetry and spectrophotometry. Out of 17 reductants investigated, commercial sugar has been found to be the most effective, rapid, simple and interference free for further estimations. To the best of the authors' knowledge, this is the first time that sugar as a reductant has been made use of in analytical investigations.

## 1. Introduction

Tetravalent uranium present in primary and secondary uranium ores does not dissolve in sulphuric acid or carbonate solution at discernible rates, and requires the addition of an oxidant for its oxidation to the hexavalent state. Potassium permanganate is an effective oxidant and hence accepted as an additive in alkaline carbonate leaching for uranium [1]. Because hydroxyl ions are formed during carbonate leaching, it is imperative also to add bicarbonate to prevent the precipitation of leached uranium by providing the required amount of hydrogen ions. The potassium permanganate added imparts a pink colour to the uranium leach liquors, thus vitiating the methods of estimation of carbonate and bicarbonate by titration and phosphate by spectrophotometry. The determination of these three anions in alkaline uranium leach liquors is of immense use for the economic exploitation of leaching procedures, and hence investigations were carried out to overcome the interference of the pink colour of the permanganate in the estimation procedures. These experiments were carried out on uranium leach liquors of phosphatic siliceous calcite-dolostone samples from Cuddapah Basin, Andhra Pradesh, India. The results are presented in this paper.

## 2. Experimental

### 2.1. Reagents

20% sugar solution is prepared by dissolving 20 g of commercial sugar in water and making up to 100 ml. The solution is filtered through Whatman No. 40 filter paper. Fresh solution is prepared every day as the sugar solution develops bacterial growth due to fermentation on standing, making it unsuitable for pipetting. All other chemicals used are of Analar quality.

### 2.2. Instrumentation

A Shimadzu UV-240 model double beam spectrophotometer was used for the absorption measurements.

* Corresponding author. Fax: (91)80-335-1511.


*SSDI* 0039-9140(95)01530-0

Table 1
Percentage recovery of carbonate, bicarbonate and phosphate

| No. | Carbonate | | | Bicarbonate | | | Phosphate | | |
|---|---|---|---|---|---|---|---|---|---|
| | Added (mg) | Found (mg) | Recovery (%) | Added | Found (mg) | Recovery (mg) | Added (%) | Found (mg) | Recovery (mg)(%) |
| 1 | 3.0 | 3.0 | 100 | 5.0 | 4.9 | 98 | 3.0 | 2.8 | 93 |
| 2 | 6.0 | 5.8 | 97 | 10.0 | 9.7 | 97 | 5.0 | 4.7 | 94 |
| 3 | 9.0 | 8.8 | 98 | 15.0 | 15.2 | 101 | 8.0 | 7.9 | 99 |
| 4 | 10.0 | 9.6 | 96 | 20.0 | 20.1 | 100 | 10.0 | 9.7 | 97 |
| 5 | 12.0 | 11.7 | 98 | 25.0 | 25.0 | 100 | 14.0 | 13.4 | 96 |

### 2.3. Procedure

A 50.0 ml aliquot of the carbonate leach liquor of uranium containing potassium permanganate as an oxidant is taken in a 100 ml beaker. Freshly prepared 20% sugar solution (10.0 ml) is added and stirred with a glass rod. The permanganate in the liquor is reduced to $MnO_2xH_2O$ and the precipitate settles to the bottom within 30 min, leaving a clear, colourless supernatant liquid. Three aliquots, 10.0 ml each of the supernatant solution, are taken into three separate breakers for analysis. From the first two beakers, carbonate and bicarbonate are determined by titration with standard HCl solution [2], using phenolphthalein and bromocresol green as indicators. In the third aliquot, phosphate is determined spectrophotometrically using a vanadomolybdo reagent [3]. A 10.0 ml aliquot of the 20% sugar solution is taken as a blank for each determination.

## 3. Results and discussion

Because of the presence of dolomitic limestone in Cuddapah basin samples only carbonate leaching for uranium extraction is to be adopted, as the acid consumption in acid leaching is very high. Under alkaline carbonate leaching parameters, uranium present in association with phosphates and Fe–Ti mineral complexes is not solubilised [4]. Potassium permanganate is one of the oxidants studied for oxidising tetravalent uranium to the hexavalent state. As little as 0.01 ml of 0.02 M permanganate imparts a pale pink colour to 100 ml of water [2], so it has to be decolourised to avoid interferences in the determination of carbonate, bicarbonate and phosphate. 17 reductants were tried to reduce the pink coloured permanganate ion either to the colourless manganous ion or to the precipitation of manganese dioxide. All reductants studied are able to decolourise the alkaline leach liquor, but each reductant except sugar has its own advantages and disadvantages for uniform applicability.

Sodium chloride or hydrochloric acid decolourises the leach liquors only on heating, whereas hydroxylamine hydrochloride and stannous chloride reduce even in cold conditions. The resulting solution can be used for phosphate estimation only, but carbonate and bicarbonate cannot be estimated quantitatively. Sodium thiosulphate and hydrogen sulphide decolourise, but the resulting solution is very turbid and hence not useful for further estimations. Sodium sulphate and sulphurous acid also reduce permanganate. Although there is no interference for the phosphate estimation, the same cannot be assumed for other estimations. In the presence of potassium iodide the liberated iodine imparts an unwanted brown colour to the solution rendering it useless for further estimations. When ferrous iron is used for reduction, the iron precipitates and interferes in all the estimations.

Ethyl alchohol or ascorbic acid also give colourless solutions; they not only give turbidity to the leach liquors, but also reduce the molybdovanadate reagent used for phosphate estimation. If hydrogen peroxide is used, the excess should be boiled off. Oxalic acid reduces only on heating, disturbing the carbonate/bicarbonate system. The reducing effect of activated charcoal on permanganate is very slow and also leads to inaccurate values for carbonate and bicarbonate.

The fact that permanganate is inherently unstable in the presence of manganese(II) ions, particularly in an alkaline medium [2], has been made use of for decolourisation. In the result-

Table 2
Analytical data of carbonate, bicarbonate and phosphate in uranium leach liquors

| No. | Sample | Carbonate ($g l^{-1}$) | | Bicarbonate ($g l^{-1}$) | | Phosphate ($g l^{-1}$) | |
|---|---|---|---|---|---|---|---|
| | | Present method | pH titration | Present method | pH titration | Present method | Emission method |
| 1 | AMD-1 | 6.3 | 6.5 | 2.4 | 2.3 | 0.2 | 0.1 |
| 2 | AMD-2 | 14.5 | 14.3 | 4.8 | 4.9 | 6.0 | 6.1 |
| 3 | AMD-3 | 41.4 | 41.4 | 23.2 | 23.1 | 5.3 | 5.4 |
| 4 | AMD-4 | 8.2 | 8.5 | 2.7 | 2.5 | 2.1 | 2.1 |
| 5 | AMD-5 | 18.3 | 18.3 | 5.1 | 5.3 | 30.4 | 30.8 |
| 6 | AMD-6 | 9.1 | 9.3 | 3.1 | 3.0 | 17.9 | 18.1 |
| 7 | AMD-7 | 11.2 | 11.4 | 1.0 | 1.0 | 1.6 | 1.5 |
| 8 | AMD-8 | 6.5 | 6.3 | 1.2 | 1.4 | 35.6 | 35.9 |
| 9 | AMD-9 | 16.1 | 16.0 | 5.1 | 5.3 | 4.9 | 4.9 |
| 10 | AMD-10 | 4.6 | 4.6 | 1.0 | 1.1 | 0.6 | 0.5 |

ing solution, phosphate can be determined; however, the carbonate and bicarbonate values are not accurate.

Although sucrose, the commercial sugar is a non-reducing sugar [5], as far as the reduction of Fehling solution is concerned, because of the linkage of the aldehyde group of the glucose part with the ketonic group of the fructose part, its addition to the pink coloured alkaline leach liquors causes the reduction of $Mn^{7+}$ to $MnO_2xH_2O$. This may be due either to the presence of monosaccharide (glucose/fructose) which is a reducing sugar or to the high redox potential of the permanganate [5]. In the supernatant solution of leach liquors after decolourisation by the addition of sugar solution, phosphate is determined by the molybdovenadate method [3], and carbonate and bicarbonate are determined by titration with standard HCl [2] using phenolphthalein and bromocresol green as indicators without any interference. Glucose also reduces the pink colour of permanganate. However, in the case of pure glucose, the only advantage is that the reduction takes place within 10–15 min as opposed to the 30 min necessary for commercial sugar. However, this time factor is outweighed by the cost of glucose with respect to commercial sugar, to provide an economic method.

Percentage recovery values calculated by adding known amounts of phosphate, carbonate and bicarbonate and determined by the present procedure are given in Table 1. The recovery values obtained vary from 93 to 101%. The values of phosphate, carbonate and bicarbonate in some alkaline permanganate leach liquors of uranium after decolourisation with sugar solution are presented in Table 2. The values of carbonate and bicarbonate obtained by pH titration with a pH meter [2] and phosphate values obtained by a plasma emission technique [6] are also presented in this table. The values are in fairly good agreement, reflecting the accuracy of the method.

## 4. Conclusion

The pros and cons of various reagents for the reduction of permanganate show that sucrose is the best reductant to obtain a clear and colourless solution for the estimation of carbonate and bicarbonate by titrimetric, and phosphate by absorptiometric methods without any interference. The advantages of this procedure are simplicity, rapidity, economy, and freedom from interference to give uniform applicability.

## Acknowledgements

The authors are thankful to Sri.KK. Dwivedy, Director, AMD and to Sri.M. Vasudeva Rao for permission to publish the paper, and for encouragement. The inspiration in the form of continuous guidance from Sri.K.P. Cheria is gratefully acknowledged. The authors are also thankful to R. Anupama for her technical assistance.

## References

[1] Rober C. Merritt, The Extractive Metallurgy of Uranium, prepared under contract with the United States

Atomic Energy Commission (USAEC), Washington, 1971, pp. 85, 104.
[2] A.I. Vogel, Text Book of Quantitative Chemical Analysis, 5th edn. (revised), ELBS Longman, London, 1991, pp. 299, 369, 279.
[3] L. Shapiro, Rapid analysis of silicate, carbonate and phosphate rocks, revised edn., Geological Survey Bulletin No. 1401, Washington, 1975, p. 37.
[4] Ravi Kaul, R.N. Shankaran, Y. Lakshminarayana and Minati Roy Exploration and Research for Atomic Minerals, Vol. 4, AMD, Hyderabad, India, 1991, p. 197.
[5] I.L. Finar, Organic Chemistry, Vol. 1, ELBS, Longman, London, 1964, pp. 461, 439.
[6] R.K. Winge, C.A. Fassel, V.J. Peterson and M.A. Floyd, Inductively Coupled Plasma-Atomic Emission Spectroscopy, Elsevier, Amsterdam, 1987.

ELSEVIER

Talanta 42 (1995) 949–955

Talanta

# Determination of total selenium content in sediments and natural water by graphite furnace-atomic absorption spectroscopy after collection as a selenium(IV) complex on activated carbon

Toshio Kubota *, Kazuhiro Suzuki, Tadao Okutani

*College of Science and Technology, Nihon University, 1-8-14, Kanda-Surugadai, Chiyoda-ku, Tokyo, 101 Japan*

Received 31 May 1994; revised 23 January 1995; accepted 24 January 1995

**Abstract**

A trace level of Se was collected on activated carbon (AC) as the Se(IV)-3-phenyl-5-mercapto-1,3,4-thiadiazole-2(3*H*)-thione (Bismuthiol II) complex. The AC was directly introduced as an AC-suspension into the graphite tube atomizer and the Se concentration was determined by atomic absorption spectroscopy (T. Okutani, T. Kubota, N. Sugiyama and Y. Turuta, Nippon Kagaku Kaishi, (1991) 375). The amount of Se in heavily contaminated samples including sediment, lake water and seawater was determined using this method. The sediments were digested with $HNO_3$–$HClO_4$–HF and the interference from $AlF_3$ was removed using $H_3BO_3$–$HClO_4$. Lake water and seawater were acidified with $H_2SO_4$ and digested with $KMnO_4$. The Se concentrations of these samples were determined by this method with satisfactory results.

The above method is simple, rapid and applicable to heavily contaminated samples.

## 1. Introduction

Se is an essential trace nutrient, and Se deficiency diseases are known in veterinary medicine, but the ingestion of greater than trace levels of Se is toxic to animals and humans.

Se and Se compounds are listed as the Basel convention on the control of transboundary movements of hazardous waste and their disposal [1].

Therefore, the determination of Se in the environment has become important. Se has been determined by atomic absorption spectroscopy (AAS), ICP atomic emission, fluorometry, etc. Hydride generation/electrothermal AAS [2] and fluorometry with 2,3-diamino naphthalene [3,4] are the most sensitive techniques, and currently applicable to environmental samples. However, the former is subject to interferences from coexisting ions, while the latter has a large blank absorption which makes it necessary to remove coexisting materials, so HPLC has to be used.

The authors reported a method [5] in which the activated carbon (AC) collected Se(IV)-3-phenyl-5-mercapto-1,3,4-thiadiazole-2(3*H*)-thione (Bismuthiol II) complex was directly introduced as an AC-suspension into the graphite furnace (GF) for AAS. This method is simple, rapid and relatively free from interferences caused by coexisting ions. Therefore, it was applied to heavily contaminated samples such as sediments, seawater and lake water.

Sediments contain large amounts of Al, Fe, Si and organic matter. The digestion of the sediment to determine the concentration of volatile elements such as Se is very difficult. Se

* Corresponding author. Fax: (81) 474-69-5324.


*SSDI* 0039-9140(95)01535-3

Table 1
Operating conditions of GF-AAS

| | |
|---|---|
| Atomic absorption spectrometer | |
| Light source | Se-HCl, 15 mA |
| Wave length | 196.0 nm |
| Spectral band width | 1.0 nm |
| Graphite furnace | |
| Drying conditions | 150 °C, 20 s (ramp mode) |
| Ashing conditions | 1050 °C, 60 s (ramp mode) |
| Atomization | 2500 °C, 3 s (temperature control mode) |
| Purge gas | Ar, 2.5 l $min^{-1}$ (continuous) |

values in the sediment (NIST, SRM-1645) reported so far are in the 0.85–24 μg $g^{-1}$ [6]. This is mainly caused by differences in the digestion methods. Therefore, the authors renewed their investigation into the digestion methods. From the results, the sediments were digested with $HNO_3$–$HClO_4$–HF, and the interferences from $AlF_3$ were removed using $H_3BO_3$–$HClO_4$. The sediments could be digested in a shorter time without Se volatilization using this method.

In natural water, Se exists as organic and inorganic forms. It has been pointed out that when Se is determined as the Se(IV) organic derivative and the organic compounds do not completely digest, the interference from the organic compounds will remain [7]. Therefore, preparation of natural water was investigated. From the results, natural water was acidified with $H_2SO_4$ and prepared by heat treatment after adding $KMnO_4$. Seawater and lake water could be completely prepared using this method.

These preparations were applied to the environmental samples, and Se content was then determined by the reported method with satisfactory results.

## 2. Experimental

### 2.1. Apparatus

A Seiko Model SAS 727 atomic absorption spectrometer equipped with a Model SAS 705V GF atomizer, a Se hollow-cathode lamp and a deuterium background corrector (BGC – $d_2$) was used. The optimum operating conditions are listed in Table 1. Ultrasonic cleaner Model B2200 (Bransonic) and aluminum dry block bath Model AL1000 (Scinics) were used.

### 2.2. Reagents

The standard Se(IV) solution was prepared by dilution of a 1000 μg $ml^{-1}$ atomic absorption standard (Wako Pure Chemicals Co., Ltd.) with 0.1 M HCl. The standard Se(VI) solution was prepared by dissolution of $Na_2SeO_4$ (Soekawa Rika Co., Ltd.), and diluted with water. Pd solution (2000 μg-Pd $ml^{-1}$) was prepared by dissolution of 1 g $PdCl_2$ in 300 ml 1 M HCl. 2-Amino-4-(methylseleno) butanoic acid (Se-methionine) (Sigma) and 3-phenyl-5-mercapto-1,3,4-thiadiazole-2(3*H*)-thione (Bismuthiol II) (Dojindo Laboratories) were used without further purification. AC (Merck No. 2186, <300 Tyler mesh) was soaked in 3 M HCl for 1 day, and washed with deionized water until it was neutral, then dried at 120 °C for 2 h. All other reagents were of analytical grade.

### 2.3. Preconcentration and determination [5]

A sample solution (100–1000 ml) containing less than 0.5 μg of Se(IV) was put in a beaker. The solution was adjusted to 1.5 M HCl by the addition of conc. HCl followed 5 ml of 0.1% Bismuthiol II solution, and the solution was then stirred for 5 min to form the complex. 50 mg of AC was added and stirred for 5 min for collection of the complex. The AC was separated from the aqueous phase through a membrane filter (8 μm pore size) (Filtration B), and the AC phase on the filter was then dispersed in 5 ml of water (containing 0.5 ml of 2000 μg-Pd $ml^{-1}$ solution) using an ultrasonic cleaner for 30 s (AC-suspension). 10 μl of magnetically stirred AC-suspension was pipetted into the graphite furnace. The peak height was measured under the conditions shown in Table 1.

### 2.4. Digestion of sediment [8]

A dried sample (0.1–0.2 g, containing less than 0.5 μg-Se) was put in a 50 ml Teflon beaker, followed by addition of 4 ml of $HNO_3$, 3 ml of $HClO_4$ and 5 ml of HF. The solution was allowed to stand for 30 min to avoid any loss of the volatile Se compound. The beaker was capped with a Teflon lid and then heated on a dry block bath at 165 °C until 2–3 ml of the volume remained in the draft chamber equipped with a hand-made air filter to avoid contamination. If the digestion was incomplete and the final solution was not clear yellow, the acid mixture was added and heated again. After the solution was cooled, 4 ml of 4% $H_3BO_3$ solution and 0.5 ml of $HClO_4$ were added, and the solution was heated at 165 °C until approximately 2 ml of volume remained. The residual solution was diluted to 100 ml with water, and then filtered using a membrane filter.

### 2.5. Preparation of natural water

A sample of water (100–1000 ml) containing less than 0.5 μg of Se was put into a digestion vial. 100 ml of 4.5 M $H_2SO_4$ and 20 ml of 5% $KMnO_4$ solution were added per 100 ml of sample volume. The mixture was heated at 110 °C for 1 h in an oil bath. After cooling, the vial was opened. A few drops of 10% $NH_2OH$–HCl solution was added until residual $MnO_2$ was dissolved. In order to reduce Se(VI) to Se(IV), the sample water was adjusted to 1.5 M HCl using conc. HCl, and 4.5 g of KBr was added per 100 ml of sample volume. The mixture was heated at 90 °C in a water bath for 30 min [5]. If the solution was colored, a small amount of $NaHSO_3$ was added until it was colorless. This solution was employed for the determination of Se concentration.

## 3. Results and discussion

### 3.1. Matrix modifier

In the reported method [5], 10 μl of Rh solution (500 μg-Rh $ml^{-1}$) was injected into the GF as a modifier. The GF was heated to dryness, and then 10 μl of the AC-suspension was injected and GF-AAS performed. Using the established procedure, Se sensitivity was varied in relation to heating times of exposed GF. The matrix modifiers, $Rh(NO_3)_3$, $Ni(NO_3)_2$ and $PdCl_2$ were investigated using the AAS standard solution (1000 μg $ml^{-1}$). The data are shown in Table 2. The use of these modifiers shows an almost equal increase in sensitivity. However, the Ni and Rh solutions contained much Se, but the Pd solution contained very little, so the Pd solution was used for the matrix modifier of the Se determination. The absorbance of Se became almost constant by adding more than 200 μg $ml^{-1}$ of the Pd solution. The two methods for the addition of Pd solution were compared, i.e. the Pd solution and AC-suspension were separately injected into the GF. In contrast, a mixture of the Pd solution and AC-suspension was injected into the GF. In addition to this method, both sample suspensions were previously exposed to ultrasonic cleaning for 30 s. The latter method resulted in either an increase in sensitivity or an improvement in reproducibility.

### 3.2. Effect of foreign ions

In a previous paper [5], the effects of foreign ions were investigated. The digest of sediment should have a higher concentration of foreign ions. Therefore, the solution containing 0.25 μg of Se and foreign ions of equal weight included in 0.2 g of pond sediment (NIES No. 2) was digested and diluted to 100 ml. The solution was concentrated to 5 ml of AC-suspension, and Se content was determined by the proposed method [5]. Because the recovery of Se was 100 ± 10%, the presence of foreign ions was regarded as having no effect. From the results, the following had no effect:

Table 2
Comparison of the effects of Pd, Rh and Ni on Se sensitivity

| Metal amount (μg) | Peak height (mm) | |
|---|---|---|
| | Reagent blank | Se [a] |
| – | 6 [b] | – |
| Pd 5 | 6 | 44 |
| Rh 5 | 8 | 40 |
| Ni 5 | 26 | 41 |

Metal solution is injected into GF as a modifier, GF is heated to dryness, and then 0.2 ng Se is injected and GF is operated.
Metal solution used Pd: $PdCl_2$, Rh: $Rh(NO_3)_3$, Ni: $Ni(NO_3)_2$.
[a] Reagent blank is substracted.
[b] Background signal.

500 μg ml$^{-1}$ of Al(III), K(I) and $SiO_3^{2-}$; 2 μg ml$^{-1}$ of Zn(II); 1 μg ml$^{-1}$ of Cr(III), Cr(VI) and V(V); 0.2 μg ml$^{-1}$ of Co(II), Ni(II), Cd(II), $AsO_3^{3-}$ and $AsO_4^{3-}$.

### 3.3. Reduction of Se(VI) to Se(IV)

Se(VI) in prepared natural water was reduced to Se(IV) using the previously reported method [5]. However, in the case of the sediment, the sample volume after digestion was less than 2 ml, so Se(VI) was reduced using only HCl. We then referred to the report of Yamada et al. [4]. 2 ml of 6 M HCl was added to the digest. Se(VI) was then reduced to Se(IV) by heating in boiling water for 15 min. The solution was diluted to 100 ml (about pH 1) with water and filtered with a membrane filter (5 μm pore size), and the precipitate was removed. The filtrate was employed for the determination of Se. Using this method, standard Se(VI) solution was reduced and determined, and the value was in agreement with the equal concentration of the standard Se(IV) solution.

### 3.4. Digestion of sediments

#### $HNO_3$–$HClO_4$–HF digestion

In a previous paper [8], the sediments were completely digested in a short time using the $HNO_3$–$HClO_4$–HF mixture. The method was applied to the determination of Se in the sediment. The sediments were digested in the same manner when reconstituted digest was evaporated to dryness. 2 ml of 6 M HCl was then added to the residue, and the Se(VI) was reduced by heating and then diluted to 100 ml with water. The precipitate was removed by filtration with a membrane filter (Filtration A). Se in the filtrate was preconcentrated using Bismuthiol II and AC, and its concentration determined. Se values of the pond sediment (NIES No. 2) varied widely from 0.5 to 1.0 μg g$^{-1}$. Further, when the residue after evaporation to dryness became white, Filtration A was easily used and the white precipitate was obtained. When the residue (after evaporation to dryness) became black–brown, the precipitate was not obtained after Filtration A. Filtration B in the preconcentration process was difficult, and atomic absorption could not be measured because of a large molecular absorption. The causes of these phenomena were then investigated.

### 3.5. Interference from coexisting ions with the digestion

The influences of various ions in the sediment on $HNO_3$–$HClO_4$–HF digestion and preconcentration were investigated. A 1% solution of each of $SiO_3^{2-}$, Al(III) and Fe(III) was prepared, and the same quantity of each ion contained in 0.2 g of the standard pond sediment (NIES No. 2) was put in separate Teflon beakers. Se(IV) solution (containing 0.1 μg of Se) and 3 ml of mixed acid ($HNO_3$:$HClO_4$:HF = 4:3:5) were added. The digestion, preconcentration and determination were then normally run. From the results, $SiO_3^{2-}$ and Fe(III) did not entirely interfere with these processes. However, Al(III) interfered with the filtration during the digestion process, and Filtration A became very difficult. Further, when the digestion was incomplete, the atomic absorption of Se could not be measured because of the large molecular absorption, even if BGC-$d_2$ was used. These phenomena were the same as during the digestion of sediment. A small amount of the white precipitate obtained from Filtration A was then injected into the GF, and GF-AAS was performed. A large degree of molecular absorption was observed, and atomic absorption due to Se could not be determined.

Therefore, the chemical binding energy and crystal structure of the white precipitates were investigated using X-ray photoelectron spectroscopy (XPS) and X-ray diffraction (XRD). The observed binding energy and the peak strength ratio of Al to F in the white precipitate nearly agreed with those of the reagent $AlF_3$. XRD spectra of the white precipitate agreed with $AlF_3$ spectra from the powder diffraction file No. 31-0011 [9], but unknown spectra still partly remained. The white precipitate was mainly made up of $AlF_3$.

$AlF_3$ formed by the reaction of Al(III) and HF does not dissolve in water, but forms a stable hydrate [10]. If $AlF_3$ is not formed, the interferences with preconcentration and determination processes should not occur. Therefore, the method to prevent formation of $AlF_3$ was investigated. Yamada et al. [4] reported that HF could be masked using $H_3BO_3$. If HF is masked, $AlF_3$ should not be formed.

In contrast, the Se values determined by this method varied widely. This is how Se was thought to volatilize through a process of evaporation to dryness.

Table 3
Analytical results of selenium in sediments

| Sample | Found value ($\mu g\ g^{-1}$) | | Reported value ($\mu g\ g^{-1}$) |
|---|---|---|---|
| | Standard addition method | Calibration curve method | |
| NIES No. 2 Pond sediment | 0.92 | $0.95 \pm 0.04$ [a] ($n = 11$) | $0.73 \pm 0.06$ [4] 0.50 [11]0.576 [11] |
| NIST SRM 1646 Estuarine sediment | 0.68 | $0.68 \pm 0.03$ [a] ($n = 7$) | 0.43 [6], 0.58 [6], 0.59 [6] $0.61 \pm 0.018$ [12] |

[a] Average and standard deviation.

Table 4
Preparation of artificial water samples

| Method | Reagents | Preparation procedure | Recovery (%) |
|---|---|---|---|
| A | $K_2S_2O_7$ (0.8 g) | 30 min at 120 °C in pressure cooker | 80 |
| B | $KMnO_4$ (0.08% 20 ml) $H_2SO_4$(6 M 20 ml) | In boiling water for 30 min | 83 |
| C | $H_2O_2$(30% 8 ml) NaOH (1 M 4 ml) | Boil until fine bubbles subside | 101 |
| D | $KMnO_4$ (5% 20 ml) $H_2SO_4$ (4.5 M 100 ml) | 60 min at 110 °C | 100 |

Sample water is spiked with Se-methionine (0.25 μg Se) in pure water (100 ml).

In order to improve these results, new procedures were investigated. During the digestion process, the digest did not evaporate to dryness, but evaporation stopped with 2–3 ml remaining. After the residue was cooled, 4 ml of 4% $H_3BO_3$ solution and 0.5 ml of $HClO_4$ were added, and the solution was heated (at 165 °C) until approximately 2 ml remained. 2 ml of 6 M HCl was then added to the residue, and heated for 15 min in boiling water, reducing Se(VI) to Se(IV). Using the Al(III) solution, Al(III), Fe(III) and $SiO_3^{2-}$ mixed solution containing 0.1 μg of Se, this procedure was investigated. From these experiments, Filtration A in the digestion process, and Filtration B in the preconcentration process were easily operated for a short time. Se in these solutions was quantitatively recovered.

### 3.6. Determination of total selenium in sediments

The proposed method was applied to the determination of total Se in the sediments. The results obtained are listed in Table 3. In both samples, the standard addition curves are parallel to the calibration curve. The values from both determinations agree well, and the relative standard deviation is 4–5%. However, Se values obtained from both samples are larger than the other values already reported [4,6,11,12]. It seems that the NIES and NIST sediments could be digested without Se volatilization by the proposed method.

### 3.7. Preparation of natural water

Preparation procedures were investigated using the sample water, which was prepared by the addition of Se-methionine to deionized water and natural water.

Deionized water spiked with Se-methionine was used to investigate various digestion methods. The results are shown in Table 4. Tested digestion methods are (A) persulfate digestion for total phosphorus determination [13], (B) permanganate digestion for chemical oxygen demand determination [13], (C) alkaline hydrogen peroxide digestion [14], (D) permanganate digestion [14]. Methods C and D completely decomposed Se-methionine into Se(IV).

The lake water spiked with Se-methionine was also examined using methods C and D. The results are shown in Table 5. Only method

Table 5
Preparation of natural water

| Method | Reagents | Preparation procedure | Recovery (%) |
|---|---|---|---|
| C | $H_2O_2$ (30% 8 ml)<br>NaOH (1 M 4 ml) | Boil until fine bubbles subside | 8 |
| D | $KMnO_4$ (5% 20 ml)<br>$H_2SO_4$ (4.5 M 100 ml) | 60 min at 110 °C | 100 |

Lake water is filtered through a 0.45 μm pore size membrane filter.
Sample water is spiked with Se-methionine (0.25 μg Se) in 100 ml of natural water.

Table 6
Analytical results of selenium in natural water

| Sample | Filterable ($\mu g\,l^{-1}$) | | Non-filterable ($\mu g\,l^{-1}$) [b] |
|---|---|---|---|
| | Standard addition method | Calibration curve method | Calibration curve method |
| Lake water (Lake-Inba in Chiba) [c] | 0.15 | $0.15 \pm 0.01$ [a] ($n = 6$) | 0.043 ($n = 2$) |
| Sea water (Ichikawa coast of Tokyo bay) [d] | 0.19 | $0.18 \pm 0.01$ [a] ($n = 6$) | 0.036 ($n = 2$) |

[a] Average and standard deviation.
[b] Se contents of non-filterable compound in 1 l of sample volume.
[c] Sample taken 26 August 1993.
[d] Sample taken 2 September 1993.

D completely decomposes Se-methionine. Therefore, in subsequent experiments, method D was adopted.

### *3.8. Determination of total selenium in natural water*

The method was applied to heavily contaminated natural water. The sample water was first filtered using a membrane filter (0.45 μm pore size), and then the filtrate was prepared by the proposed method and total Se was determined. The non-filterable compound was digested by the same method with the sediment.

The results are shown in Table 6. The standard addition curves of both samples are parallel to the calibration curve. Total Se values of the filtrate agree well with the standard addition method and the calibration curve method. Non-filterable Se values are indicated per sample volume, and are 20–30% of the filterable Se value.

## Acknowledgment

The authors thank Dr. Hiroshi Yamamoto and Dr. Hiroyuki Sango, College of Science and Technology, Nihon University, Tokyo, Japan, for the XRD and XPS measurements and analyses.

## References

[1] The Basel convention on the control of transboundary movements of hazardous waste and their disposal, Basel, 22 March 1989.
[2] K. Yamaya, T. Aoki and Y. Kim, Bunseki Kagaku, 41 (1992) 263.
[3] K. Itoh, M. Nakayama, M. Chikuma and H. Tanaka, Fresenius' Z. Anal. Chem., 325 (1986) 539.
[4] H. Yamada, T. Hattori, S. Matuda and Y. Kang, Bunseki Kagaku, 36 (1987) 542.
[5] T. Okutani, T. Kubota, N. Sugiyama and Y. Turuta, Nippon Kagaku Kaishi, (1991) 375.
[6] E.S. Gladney, B.T. O'Malley, I. Roelandts and T.E. Gills, NBS Special Publication, Vol. 260–111, Na-

tional Bureau of Standards, Washington, DC, 1987, p. 1646–5.
[7] Y. Koike, Y. Nakaguchi and K. Hiraki, Bunseki Kagaku, 42 (1993) 285.
[8] T. Kubota, K. Uchida, T. Ueda and T. Okutani, Bunseki Kagaku, 37 (1988) 381.
[9] Joint Committee on Powder Diffraction Standard, Powder Diffraction File, Inorganic, No. 31-0011, 1988.
[10] Kirk-Othmer, Encyclopedia of Chemical Technology, 3rd Edn., Vol. 10 Wiley New York, 1980, p. 661.
[11] K. Okamoto, Research Report from the National Institute for Environmental Studies Japan, Vol. 38, 1982, pp. 41, 95.
[12] A. Dong, V.V. Rendig, R.G. Burau and G.S. Besga, Anal. Chem., 59 (1987) 2728.
[13] Nihon Bunseki Kagakukai Hokkaidou-Shibu, Mizunobunseki 3rd edn., Kagaku-dojin, Kyoto, 1985, pp. 241, 361.
[14] L.S. Clesceri, A.E. Greenberg and R.R. Trussell, Standard Methods for the Examination of Water and Wastewater, 17th edn., American Public Health Association, Washington, DC, 1989, pp. 3-132, 3-133.

ELSEVIER

Talanta 42 (1995) 957–965

Talanta

# Transport of iron halides through polyurethane ether-type membranes

R.D. Oleschuk, A. Chow *

*Department of Chemistry, University of Manitoba, Winnipeg, Man. R3T 2N2, Canada*

Received 19 September 1994; revised 23 January 1995; accepted 25 January 1995

**Abstract**

The transport of iron(III) using polyether-based polyurethane membranes was studied. The rate at which iron passes through the membrane depends on the formation of the $HFeX_4$ species, which is related to the initial acid and salt concentration of the metal solution. Iron is quantitatively transported from a cell of high acid-halide concentration to one with low concentration.

## 1. Introduction

The isolation of selected metals from solution has been a problem in industry and for analysis. In sample preparation and in actual analysis, separation is an important aspect of analytical chemistry, and in most cases the separations are neither quick nor quantitative. When measurement techniques are used to determine a species or compound in a sample, interferences from extraneous substances in that sample can cause significant problems. Thus, the removal of interferences or the isolation of the analytical species is of considerable importance. In industry, separations are needed to produce purer materials and cleaner effluents. In many instances, quantitative separations are not needed or are not possible; in others, speed is not a major factor.

Membranes used for separations are barriers separating two phases that are permeable and often selective towards a particular species present in one of the phases. Several materials have been used as membranes, ranging from bi-layers that surround living cells to thin semi-permeable polymeric barriers. Ideally, analytical membranes would provide quantitative separation of a permeating species, but in most cases they provide partial enrichment of one of the phases. The term "membrane" in polyurethane chemistry has been applied to two separate solid physical forms: non-porous polymer film membranes, as used in this investigation, and those which are porous, made of polyurethane foam that allows solutions to percoalate through the membrane. The non-porous membranes, although providing a lower surface area, separate the two solutions and prevent them from mixing.

Polyurethane foams (PUFs) were first shown by Bowen [1] to act as selective absorbents for a number of substances from aqueous media. The mechanism by which the sorption occurs has been investigated by several authors. The first to emerge was the solvent extraction mechanism [1], which showed that compounds extracted by ether-based polyurethane foams were analogous to those extracted by diethyl ether. From this, it was proposed that polyurethane foams could be used as solid substitutes for diethyl ether [2,3]. An ion-exchange mechanism was later suggested, where sorption was explained by the interaction of ions and the weak or strong anion exchange sites of PUF.

* Corresponding author. Fax: (204)275-0905.


*SSDI* 0039-9140(95)01537-X

The third mechanism, the cation chelation [4] mechanism, explained that sorption was due to the helical structure of the polyether-type PUF that possesses a receptive site for extraction. Each site forms a cage with a metal complex possessing the appropriate cation to "fit" the cage. The order of extraction of complexes with differing cations was found to be ($Li^+ < Na^+ < Cs^+ < K^+$), which is similar to the cyclic polyether dicyclohexyl-18-crown-6. The mechanism and many uses of polyurethane sorption have been reviewed by several authors [5–8].

It has previously been shown that some iron and gallium chloride complexes [9] and cobalt thiocyanate [10] complexes can be extracted and transported through polyurethane membranes, demonstrating their possible use for metal separations. The extent of the metal halide complex formation depends on the stability constants of the individual complex and the concentration of the halide present. These properties control the proportion of metal halide complex present and therefore can probably be used to facilitate the selective transport and separation of metals. In this paper, iron is used as a probe into the nature and mechanism of the separation because of its well-known propensity to form $HMX_4$ complexes. The effects of varying concentrations of different acids and halides on the transport of the metal through the membrane were investigated. As well as the effects of different salts, temperatures and membrane thicknesses were studied. Previous publications [9,10] describing the use of polyurethane membranes have shown promising results for possible separation of metal mixtures. The present investigation of iron transport through the membrane was undertaken to obtain a better understanding of the transport process essential to establishing the potential of this process.

## 2. Experimental

### 2.1. Apparatus and reagents

All iron analyses were performed with a Varian SpectrAA-20 atomic absorption spectrometer equipped with a Cathodeon hollow cathode lamp and a Varian Mark VI burner head coupled with an air–acetylene flame. The wavelength observed was 248.3 mm with a slit width of 0.2 nm, and the lamp current was set at 6 mA. All chemicals used were of reagent grade. Stock iron solutions were prepared using ferric nitrate supplied by Fisher Scientific. Hydrochloric and hydriodic acids were supplied by Mallinckrodt, and hydrobromic acid by Fisher Scientific. All water used was purified by a Barnsted Nanopure™ II system using reverse osmosis-treated feeedstock. The membranes used were of the polyurethane ether type (XPR-625-FS) in two different thicknesses (0.025 mm and 0.050 mm) and were provided by Stevens Elastomerics/Urethane Products Northhampton, MA.

The apparatus used for membrane testing consisted of two separate cells (a starting and receiving cell). The starting cell was a Nalgene 125 ml PETG (polyethylene terephthalate copolyester) media bottle (cat # 2015–0125) with a 2 cm diameter hole drilled into the screw cap. A small notch was also cut at the side of the drilled hole to prevent air bubbles from being trapped along the membrane surface. The receiving cell consisted of a 100 ml beaker, cut to an appropriate height to allow a smaller volume of receiving solution to be used. Media bottles are very well suited for the starting cells because they enable a quick easy way of fastening the membrane to the bottle with an air and water tight seal. For units to be run at elevated temperatures, a small hole was drilled into the edge of this starting cell to prevent any pressure build-up. Membranes were cut into 5 cm × 5 cm squares and placed on top of the open media bottle holding a sample. The cap was placed on the bottle and carefully tightened, yielding a membrane with an active surface area of 5.3 $cm^2$. The media bottle was then inverted and immersed in the solution held by the receiving cell, and the air bubbles removed through the notch with the membrane separating the two solutions. Each unit was then wrapped in Parafilm™ to prevent evaporation of the solution. At elevated temperatures Parafilm softened and melted, and instead a plastic wrap, Resinite by Borden Chemical, was substituted. For each experiment a number of units were prepared and then stopped after various times during the experiment to obtain a separation profile and establish reproducibility. After the cells were stopped by removing the starting flask from the receiving cell, each cell was individually weighed to determine any solution losses due to either evaporation or leakage through the membrane. The volume of solution was calculated using the solution den-

Table 1
Percentage of Iron in the $FeCl_4^-$ complex at various HCl concentrations and time required for quantitative transport

| HCl concentration (M) | % Fe in the $FeCl_4^-$ complex | Time required for quantitative transport (h) |
|---|---|---|
| 9.0 | 53.4 | 4 |
| 7.0 | 25.8 | 7.5 |
| 5.0 | 7.7 | 48 |
| 3.0 | 1.0 | – |
| 1.0 | 0.02 | – |
| 0.1 | $1.15 \times 10^{-5}$ | – |

sity. The final volumes in the top and bottom cell were close to the initial values for trial where no iron movement was observed. Where iron was transported, the volume changed only slightly unless the membrane failed, and then significant leakage occurred.

All iron solutions were prepared from a 1000 mg $l^{-1}$ standard prepared by dissolving $Fe(NO_3)_3 \cdot 9H_2O$ in water in a 1000 ml volumetric flask.

## 3. Results and discussion

### 3.1. Effect of HCl concentration

The stability constants of iron(III) species with chloride ions in the aqueous phase can be represented as follows:

$$Fe^{3+} + nCl^- \rightleftharpoons FeCl_n^{3-n}$$

Using the iron chloride complex stability constants [11], the data in Table 1 were calculated. The chloride concentration was taken to be equal to the activity of the chloride ion. As the HCl concentration increases, the percentage of iron as the $HFeCl_4$ complex also increases. To study the effects of varying concentrations of HCl, and consequently varying proportions of the $HFeCl_4$ complex in solution on the separation, 15 mg $l^{-1}$ iron solutions were prepared with several HCl concentrations (0, 1.0, 3.0, 5.0, 7.0, 9.0 M).

A separation experiment was performed with each of the different acid solutions in the starting cell with all the receiving cells containing 0.1 M HCl. The 0.1 M HCl was needed to prevent hydrolysis of the iron once it had passed through the membrane. At concentrations of zero and 1.0 M HCl, no iron is transported from the starting to the receiving cell over the time that the experiment was run. With 3.0 M acid, only a small amount of iron was transported across the membrane. At HCl concentrations of 5.0 M and greater, it was found that the iron is quantitatively transported to the receiving cell, and a smooth separation profile is obtained where the transport rate increases with an increase in HCl concentration. This supports a previous suggestion [12] that the transport of iron through the polyurethane membrane is due to the $HFeCl_4$ complex. In Table 1 it is shown that for solutions containing less than 3.0 M HCl, less than 1% of the iron is in the $FeCl_4^-$ complex, and most of this is present as the extractable $HFeCl_4$ complex at these high acidities. At higher HCl concentrations, there are significant amounts of the $HFeCl_4$ present to facilitate transport across the membrane. With an increase in concentration of the species required for transport, we would expect to see an increase in the rate of transport as well. This should continue to occur if more of the $HFeCl_4$ complex is present, or until the membrane becomes saturated, at which point the rate of transport will have reached a maximum. This can be seen in the results; with each increase in HCl concentration there was a corresponding increase in the rate of transport as shown in Figs. (1a) and (1b), although no maximum was observed. The quantitative transport of iron to the receiving cell from 5.0 M HCl required 48 h, while only requiring 9 h when the HCl concentration was increased to 9.0 M. The acid concentrations of the starting and receiving cells were found to equalize when an equilibrium between them had eventually been established. This phenomenon was only apparent when concentrations of 5.0 M HCl or greater were used. The transparent membrane gradually became cloudy and translucent, and then white, opaque and "puckered". In the experiments run at room temperature over a period of 48 h, the physical changes did not appear to play a part in the separation.

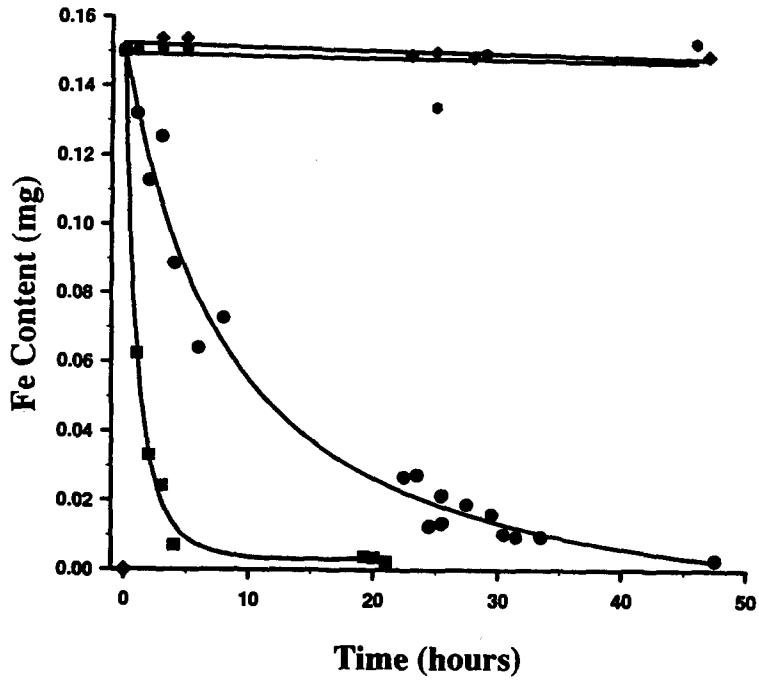


(a)

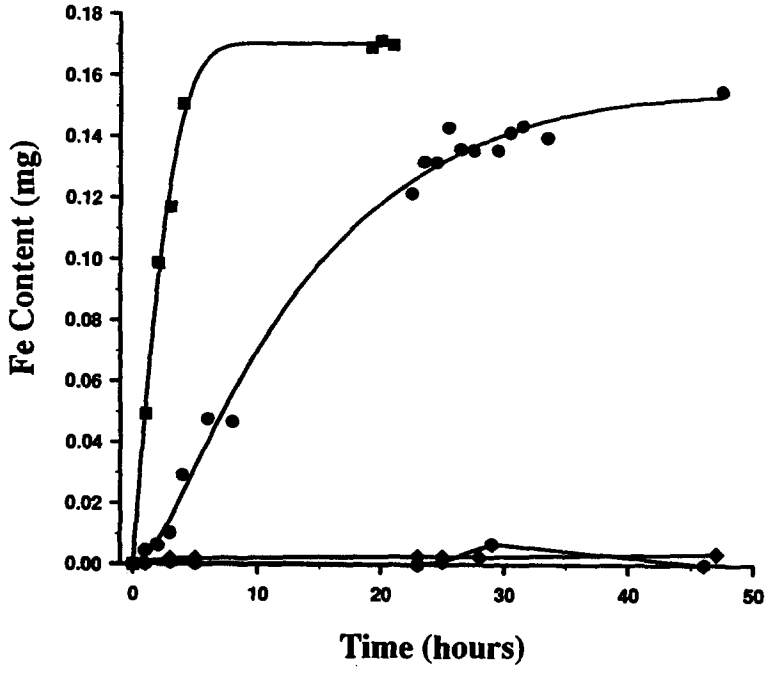


(b)

Fig. 1. (a) Iron separation profile for starting cells containing 10 ml of 15 mg $l^{-1}$ iron: ●, no HCl added; ◆, 1.0 M HCl; ●, 5.0 M HCl; ■, 9.0 M HCl. (b) Receiving cell iron contents corresponding to each of the starting cell HCl concentrations in (a). Each receiving cell initially contained 30 ml of 0.1 M HCl.

### *3.2. Effect of other halo-acids*

Experiments using HBr and HI in place of HCl in both the starting (5.0 M) and receiving flasks (0.1 M) were performed. The use of HBr produced a five-fold increase in transport rate as compared to HCl. This phenomenon can be attributed to two possible factors: the $HFeBr_4$ complex may form more readily because of higher stability constants, and the complex is a weaker acid so it would be in higher concentration than the chloride analogue. The relative

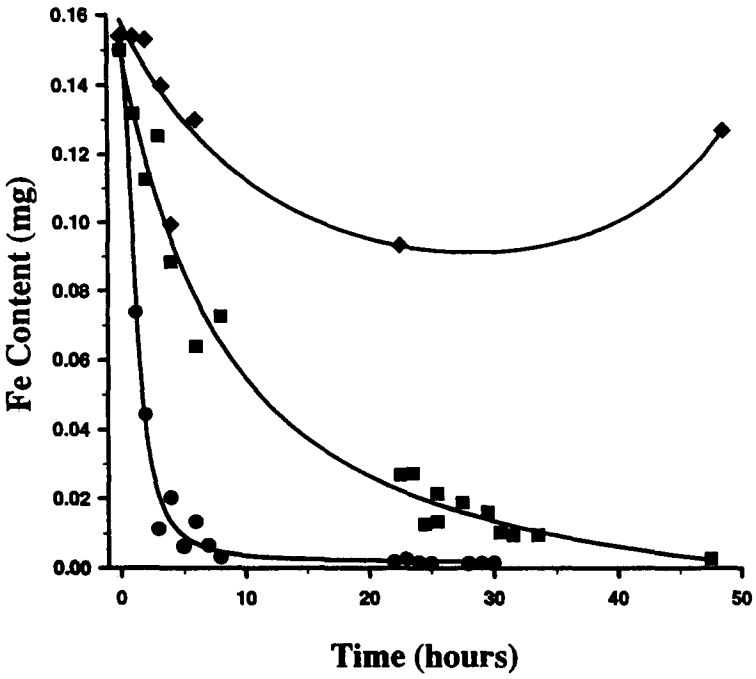


Fig. 2. Iron separation profile for starting cells containing 10 ml of 15 mg $l^{-1}$ iron with a concentration of 5.0 M HCl: ◆, hydriodic acid; ■, hydrochloric acid; ●, hydrobromic acid.

strength of the complexes is determined by respective ionic sizes and electronegativities. In the early stages of the separation using hydriodic acid, no iron is transported through the membrane. After 3 h the membrane becomes porous, so that iron and acid solution can pass through it. Because it does not form a tetrahedral complex in the presence of iodide ions, iron is not transported through the membrane. The results of the separations performed using the different halo-acids are presented in Fig. 2.

It is important to note that when HCl and HBr were used the iron was quantitatively (>98%) transported from the starting to the receiving cell, and then remained in the receiving cell. Also, the phenomena occurring in our case is not diffusion, as other authors [13] using polyurethane membranes have reported. Rather, an uphill transport process predominates. Our investigation has shown that a quantitative separation of iron is possible with our membrane, which would not occur if simple diffusion was the sole process acting on the system. Once the iron is transported from the starting to the receiving cell, it is then in an environment that contains less halide than the starting cell. The equilibrium is then shifted from the $HMX_4$ complex to other species that do not possess the ability to be extracted and transported through the membrane. The iron is therefore trapped in the receiving cell, and cannot proceed back through the membrane to the starting cell until sufficient halide is present to re-form the complex or the membrane becomes porous allowing diffusion back into the starting flask.

### 3.3. Membrane thickness

To determine the effects that the thickness of the membrane had on the rate of transport, a 0.025 mm membrane was used that was half as thick as that used previously. As expected, the iron was transported across the thinner membrane twice as fast as across the thicker membrane, as shown in Fig. 3. This indicates that the rate-determining step of the separation is the movement of the iron through the polymer rather than its sorption onto the polymer surface. Further, if the polymeric membrane could be made thinner then a faster separation might be possible, although this may cause some mechanical problems.

### 3.4. Effect of temperature

The effect of temperature on the rate of transport was studied using the following set of conditions. The starting flask contained 10 ml of 15 p.p.m. Fe in 5.0 M HCl and the receiving

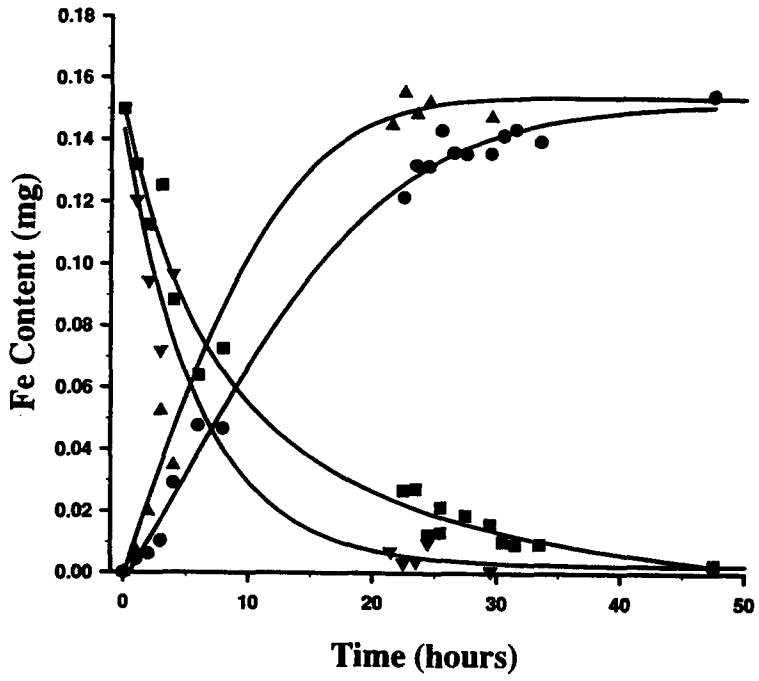


Fig. 3. Iron separation profile using two different membrane thicknesses. Starting cells contained 10 ml of 15 mg $l^{-1}$ iron in 5.0 M HCl, and receiving cells 0.1 M HCl: ■, starting cell using a 0.050 mm thick membrane; ●, receiving cell using a 0.050 mm thick membrane; ▲, receiving cell using a 0.025 mm thick membrane.

flask containing 30 ml of 0.1 M HCl. These conditions were chosen because the iron is quantitatively transported through the membrane in a reasonable amount of time (less than 2 days at room temperature). Under these conditions five experiments were run at different temperatures (5, 22, 37, 50, 65°C) to obtain thermodynamic data. As expected, the rate of transport increased markedly with an increase in temperature. The reason for the increase in transport rate may be due to two factors. The increase in temperature allows more molecules to overcome the activation barrier and may also cause a shift in the equilibrium of favour further $HFeCl_4$ formation. Separation data are presented in Table 2.

Table 2
Time required for quantitative transport of iron at vrious temperatures

| Temperature (°C) | Time required for quantitative transport (h) |
|---|---|
| 5 | 250 |
| 22 | 48 |
| 37 | 22 |
| 50 | 10 |
| 65 | 4 |

The energy of activation was calculated to be 50 kJ $mol^{-1}$ using an Arrhenius plot, as shown in Fig. 4. This value is consistent with values [14,15] found for the sorption and transport of aqueous salt and acetic acid solutions in polyurethane membrane material. It was assumed that during the experiment the same percentage of iron remained as the $FeCl_4^-$ complex. If the temperature affected the equilibrium of the iron chloride complex there would be a deviation from linearity. Considering the linearity of the plot in Fig. 4, the effects of the different temperatures on the equilibrium appear to be minimal.

As in the experiments at room temperature, the membrane became white, opaque and puckered, but at 65°C the membrane became porous as well. The porosity of the membrane led to the back flow of iron from the receiving cell into the starting cell. Extended experiments at lower temperatures also resulted in the same condition, but required more time to do so. This phenomenon was shown to be caused by the swelling and "puckering" of the membrane, subsequently causing the formation of microscopic holes which can be seen by optical or scanning electron microscope. These holes then allow the restricted, but non-selective, passage of acid from the starting to the receiving cell. The formation of holes was observed to be

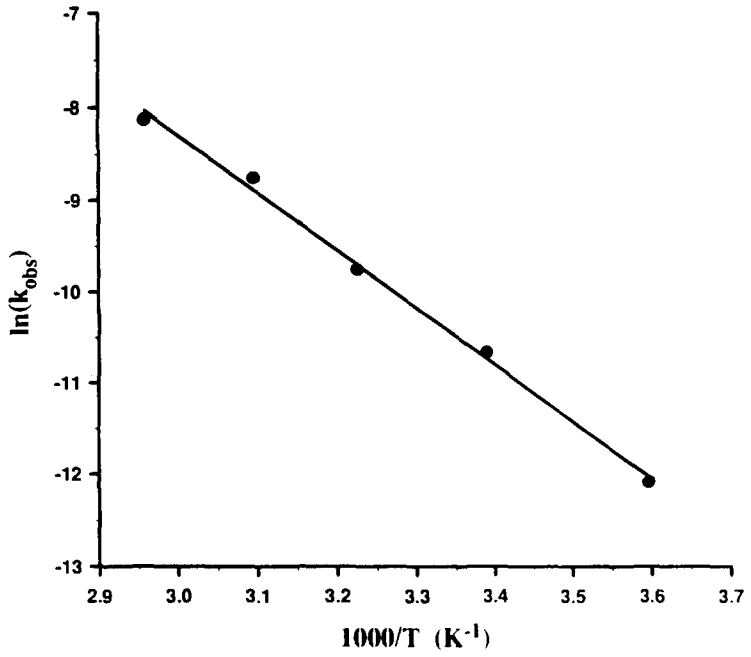


Fig. 4. Arrhenius plot of 0.050 mm membrane at 5, 22, 37, 50, and 65°C. Starting cells contained 15 mg $l^{-1}$ Fe in 5.0 M HCl, and receiving cells 0.1 M HCl.

separate from the transport of iron, and primarily due to the harsh conditions to which the membrane was subjected.

### 3.5. Salt effects

It is possible to form the $FeCl_4^-$ complex by the addition of chloride salts. Preliminary investigations performed using 5.0 M HCl with 0.5 M salts (NaCl, KCl, LiCl) yielded no difference in transport rate. A further experiment was undertaken where a high concentration of a salt was used in the place of a high concentration of HCl. LiCl was chosen for its high solubility in water. Some acid was needed to keep the iron in solution, so the experiment was performed with 60 p.p.m. iron in 4.8 M LiCl and 0.2 M HCl in the starting flask, and 0.1 M HCl in the receiving flask. The larger iron concentration was necessary because the salt solutions needed dilution by a factor of four before analysis by atomic absorption spectrophotometry. The results of the separation are presented in Fig. 5. The separation profile looks quite different when compared to that of the experiment performed with 5.0 M HCl in the starting flask, although the total chloride concentrations are identical. When LiCl was used, the separation proceeded much more slowly and was not quantitative within the time of the experiment. Using stability constants [6], the percentage of iron in the iron–tetrachloro complex in this LiCl solution was calculated to be 5.5%. Although this is less than the 7.7% with 5.0 M HCl is used, the lower concentration does not fully explain the dramatic change in transport behaviour. This indicates that the acid must play an integral part in the transport together with the chloride concentration. It is probable that ether groups present in the polymer, which we believe participate in the chelation of the iron complex, need to be protonated in order for the iron complex to be sorbed and transported through the membrane. In the LiCl experiment the transporting complex is $LiFeCl_4$, compared to $HFeCl_4$ in the previous HCl experiments, highlighting the role that the size of the cation plays in the transport of the metal across the membrane. Previous studies by Hamon et al. [4] indicate that the cation does indeed play a paramount role in the extraction of a metal complex by PUF. They found that the cation complexes were increasingly extracted in the following order ($Li^+ < Na^+ < Cs^+ < Rb^+ < K^+$), but this phenomenon was not observed in the current investigation. The difference may be due to the fact that this polyurethane is a different type produced by a different manufacturer. To a lesser degree, the differences may be due to the polymer being in a different physical form, the membrane being a film rather than an open cell

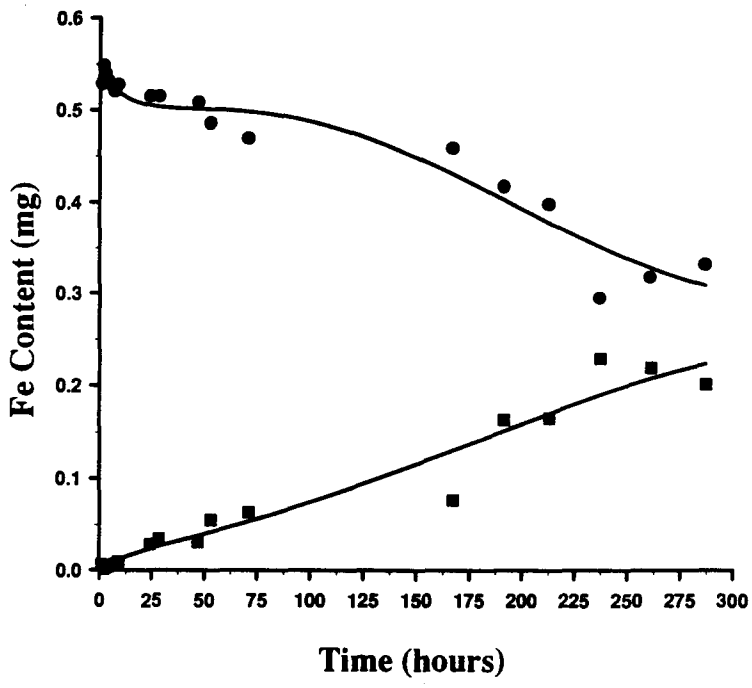


Fig. 5. Iron separation profile, with 10 ml of 60 ml $l^{-1}$ Fe in 4.8 M LiCl and 0.2 M HCl in the starting cell, and 30 mL of 0.1 M HCl in the receiving cell: ●, starting cell; ■, receiving cell.

PUF. Therefore, the "sites" available in the membrane may have a different size preference for accepting different-sized cations, and thus the complexes will be extracted and transported to differing degrees.

## 4. Conclusions

The transport of iron from hydrochloric acid solutions of concentrations less than 1.0 M does not occur through polyurethane membrane material. At 3.0 M HCl, transport of iron begins but is quite slow; at concentrations of 5.0 M and greater, the transport becomes quantitative (>99%). This effect is due to the increased formation of the $HFeCl_4$ complex, which is the species extracted into the polyurethane membrane. The higher the HCl concentration, the greater the percentage of iron in the ferric–tetrachloro complex, which results in faster transport rates. Substituting hydrobromic acid, the transport rates quintuple, primarily due to the $HFeBr_4$ being a weaker acid. Thus more of the iron–bromide complex is in the protonated form, which leads to a higher extraction rate and faster transport.

The transport of iron from hydrochloric acid is aided by an increase in temperature. At 5°C the quantitative transport of iron requires more than 10 days in comparison to 7 h at 65°C. Membrane thickness also plays an important role in the time needed for transport. Quantitative transport through a membrane 0.050 mm thick requires 48 h, as compared to 24 h with a thickness of 0.025 mm.

The use of salt rather than hydrochloric acid to form the ferric–tetrachloro complex leads to a slower process that does not allow quantitative separation. This is possibly due to two factors: the size of the complex and the need for the ether groups present in the polymer to be protonated in order for transport to occur.

The phenomenon of quantitative transport across an ether-type polyurethane membrane provides evidence that the polymer may be used to separate mixtures of metals based on their ability to form halide complexes. Although the active transport of iron presented in this paper is not presently practical for its separation, it demonstrates the ability of polyurethane membranes to quantitatively transport a metal from one phase to another. The method is inherently simple and inexpensive compared to other available techniques, and may prove an interesting alternative to other separation processes presently available for both analytical and industrial applications.

## Acknowledgements

This work is supported by the Natural Science and Engineering Research Council of Canada. We thank Stevens Elastomerics for supplying the polyurethane membrane material.

## References

[1] H.J.M. Bowen, J. Chem. Soc. A, (1970) 1082.
[2] H.G. Gesser, E. Bock, W.G. Baldwin, A. Chow, D.W. McBride and W. Lipinski, Sep. Sci., 11 (1976) 317.
[3] H.D. Gesser and G.A. Horsfall, J. Chim. Phys., 74 (1977) 1072.
[4] R.F. Hamon, A.S. Khan and A. Chow, Talanta, 29 (1982) 313.
[5] Zeev B. Alfassi and Chien M. Wai, Preconcentration Techniques for Trace Elements, CRC Press, Boca Raton, FL, 1992, p. 364.
[6] T. Braun, J.D. Navratil and A.B. Farag, Polyurethane Foam Sorbents in Separation Science, CRC Press, Boca Raton, FL, 1985.
[7] T. Braun, Fresenius' Z. Anal. Chem., 333 (1989) 785.
[8] G.J. Moody and J.D.R. Thomas, Chromatographic Separation and Extraction with Foamed Plastics and Rubbers, Marcel Dekker, New York, 1982.
[9] H.D. Gesser, G.A. Horsfall, K.M. Gough and B. Krawchuk, Nature, 268 (1977) 323.
[10] R.F. Hamon, Ph.D. Thesis, University of Manitoba 1981, p. 423.
[11] J. Bjerrum and I. Lukes, Acta Chem. Scand., 40 (1986) 31.
[12] J.J. Oren, K.M. Gough and H.D. Gesser, Can. J. Chem., 57 (1978) 2032.
[13] William A. Hunke and Lloyd E. Matheson, J. Pharm. Sci., 70 (1981) 1313.
[14] Shivaputrappa B. Harogoppad, Tejraj M. Aminabhavi and Ramachandra H. Balundgi, J. Appl. Polym. Sci., 42 (1991) 1297.
[15] S.B. Harogoppad and T.M. Aminabhavi, Polymer, 31 (1990) 2346.

ELSEVIER

Talanta 42 (1995) 967–970

Talanta

# Determination of polycyclic aromatic hydrocarbons in drinking and surface waters from Galicia (N.W. Spain) by constant-wavelength synchronous spectrofluorimetry

M.J. López de Alda Villaizán, J. Simal Lozano, M.A. Lage Yusty *

*Department of Analytical Chemistry, Nutrition and Bromatology, Area of Nutrition and Bromatology, Faculty of Pharmacy, University of Santiago de Compostela, E-15706 Santiago de Compostela, La Coruña, Spain*

Received 1 November 1994; revised 3 January 1995; revised 26 January 1995; accepted 27 January 1995

**Abstract**

We describe a fast, new method for determination of the joint concentration of the six polycyclic aromatic hydrocarbons (PAHs), designated by current legislation as indicators of the quality of drinking waters and surface waters intended for the abstraction of drinking waters. The limit of detection of the new method was 6 ng $l^{-1}$, its limit of quantification 20 ng $l^{-1}$, its precision (CV%) 2.48 and its recovery 94.05%. Its speed allowed rapid PAH screening of 404 samples of surface and drinking water from Galicia (N.W. Spain).

## 1. Introduction

Since 1930, when Kennaway and Hieger according to Fabre and Truhaut [1] found dibenz[*a*,*h*]anthracene to be carcinogenic, interest in the determination of polycyclic aromatic hydrocarbons (PAHs) in foodstuffs and the environment has been spurred by progressively increasing knowledge and awareness of their toxic and carcinogenic properties, and by the increase in PAH emissions by industry. As a result, their study has been given priority by various environmental and public health authorities [2–4]. In European Community legislation [5–7], PAH concentration in drinking water and waters destined for use as such is limited in terms of the joint concentration of six fluorescent indicator PAHs (fluoranthene, benzo[*b*]fluoranthene, benzo[*k*]fluoranthene, benzo[*a*]pyrene, indeno[123-*cd*]pyrene and benzo[*ghi*]perylene), even though other fluorescent contaminants and also quenchers may be present. The maximum admissible joint concentration for drinking water and class $A_1$ and $A_2$ surface waters is 0.2 μg $l^{-1}$, while the maximum for class $A_3$ surface waters is 1 μg $l^{-1}$. The established minimum annual sampling frequency is 1 for surface waters, and ranges from 1 to 20 for drinking water (depending on the volume of water produced or distributed and the size of the population affected); special provisions are also made for occasional sampling in accidental or particular situations.

Methods proposed for the determination of PAHs in aqueous systems have been based on a wide variety of analytical techniques, the most frequently used being chromatography. Nevertheless, chromatographic methods often prove to be heavy consumers of both time and materials, and most of them do not conform to the reference methods which, according to European legislation, should be employed wherever possible for the determination of toxic substances in water. These reference methods require "measurements of UV fluorescence after extraction with hexane; gas chromatography or measurement of the UV fluorescence after thin layer chromatography; measurements in comparison with those of standard mixtures containing equal concentrations of the six indicator substances" [6,7].

* Corresponding author.


*SSDI* 0039-9140(95)01545-0

In view of the above observations, we previously developed a method [8] for determination of PAHs in water based on extraction with hexane and measurement of UV fluorescence, as recommended in the European legislation. The method precision (CV% = 3.8) and accuracy (recovery = 77%) and its detection limit (5 ng $l^{-1}$) meet those exacted in the legislation [6] in addition, this method is simple and does not consume large amounts of reagent.

In this work, we report the optimization of this method, which led to improved precision and very much improved accuracy without significant increases in limits of quantification or detection, and increased sample throughput. We also describe the application of the new, optimized method to screening of drinking and surface waters sampled in Galicia (N.W. Spain).

## 2. Experimental

### 2.1. Reagents

Fluoranthene and benzo[*a*]pyrene standards were purchased from Aldrich, and benzo[*b*]fluoranthene, benzo[*k*]fluoranthene, indeno-[123-*cd*]pyrene and benzo[*ghi*]perylene standards from Sugelabor.

Residue analysis grade granulated anhydrous sodium sulphate and *n*-hexane, and analytical grade sulphuric acid, were all purchased from Merck. The sulphuric acid was extracted with *n*-hexane prior to use (we recommend that the purity of all reagents be verified under analysis conditions prior to measurement).

### 2.2. Water samples

Water sampling was carried out in 1991 by personnel of the Servicio Galego de Saude of the Xunta de Galicia. A total of 404 water samples were taken over two sampling periods (January 29–June 3, and June 24–December 16) from the network supplying the 60 most highly populated municipalities of Galicia, N.W. Spain. Sampling points were grouped into zones C, D and T, corresponding respectively to water catchment areas (the inlets of water treatment plants), the distribution network (points between the outlets of those plants and the distribution network), and consumers' taps, thus enabling water quality to be monitored along the length of the supply system.

### 2.3. Apparatus

All spectrofluorimetric measurements were performed with a Perkin-Elmer LS-50 luminescence spectrometer equipped with a xenon discharge lamp, Monk-Gillieson monochromators and 1 cm quartz cuvettes. For acquisition and processing of spectral data by Fluorescence Data Manager software, the LS-50 was serially interfaced (RS232C) to a Handok HNS-286 PC linked to a Nec Pinwriter P6+ colour printer for hard copy.

The spectra were obtained with the following instrumental parameters: both excitation and emission slits 5 mm, scan speed 1500 nm $min^{-1}$, constant wavelength interval between excitation and emission monochromators 120 nm. Synchronous spectra were recorded between 245 and 450 nm at 20 °C.

### 2.4. Procedure

100 μg $l^{-1}$ and 100 mg $l^{-1}$ stock standards of each PAH in *n*-hexane (which were prepared in the laboratory and were stable under refrigeration) were diluted with *n*-hexane as appropriate. Seven working standards containing equal concentrations (0.1, 0.2, 0.4, 0.6, 0.8, 1.0 and 2.0 μg $l^{-1}$) of each of the six PAHs were prepared by mixing suitable volumes of these individual stock solutions and diluting with *n*-hexane. The spectra of these standards were run and the spectral area between 275 and 395 nm was regressed on the known total concentration in order to obtain a calibration curve. The PAH content of water samples was determined by extracting 1 l of sample as described previously (Fig. 1) [8], running the extract with the spectrofluorimeter settings specified above, and using the calibration line to obtain PAH concentration from the spectral area between 275 and 395 nm.

## 3. Results and discussion

The new, optimized method employs wider excitation and narrower emission slit widths (now both 5 nm), a faster scan speed (1500 nm $min^{-1}$), and quantification of the PAHs by integration of peak area over a narrower wavelength interval (275–395 nm) than described previously [8]. Under these conditions, method precision and accuracy are much improved without significant increases in limits

of detection and quantification. Determination of the joint concentration of the six PAHs is also much faster, speed being a particularly important consideration in the analysis of drinking water, as screening for PAHs is generally carried out on a large number of samples and on a frequent basis [6,7].

Under the new conditions, instrumental response was highly linear (the correlation coefficient of the calibration line was 0.9955) and the limit of detection (calculated, following ACS guidelines [9] for reducing the risk of false positives, as the concentration corresponding to a spectral area equal to the average measured area for blanks plus six standard deviations) was 6 ng $l^{-1}$, well below the officially stipulated limit of 40 ng $l^{-1}$ [6]. It was verified experimentally that this quantity of PAH was indeed detected in water samples. The limit of quantification, calculated as the concentration corresponding to a spectral area equal to the average measured area for blanks plus 10 standard deviations, was 20 ng $l^{-1}$. Method precision, calculated as the coefficient of variation of the results obtained when the whole extraction/spectrometry procedure was applied to six replicate 1 l water samples spiked with 0.03 μg of each indicator PAH, was 2.48%, much better than the officially stipulated 50% [6]. Mean recovery from six water samples spiked at levels close to the official maximum allowable PAH concentration was 94.05%.

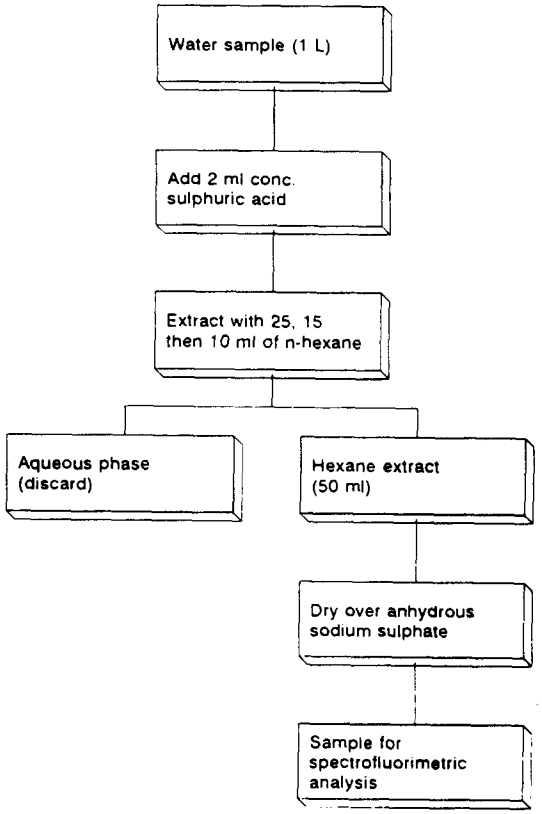


Fig. 1. Treatment of water samples prior to determination of polycyclic aromatic hydrocarbons by constant-wavelength synchronous spectrofluorimetry.

PAH screening of the 404 water samples by this optimized method indicated that: levels were below the maximum allowed concentration [5,7] of 200 ng $l^{-1}$ in all cases; quantifiable levels were present in only one in three samples; where quantifiable, PAH levels were generally well below the maximum. These results confirm the high quality of both the raw and the treated water.

In order to determine whether there were significant differences between the PAH levels in (a) samples taken during the first sampling period and those taken during the second, and (b) samples taken from the three sampling zones, we used one-way analysis of variance (ANOVA) to compare mean results. The means for the two sampling periods (15 ng $l^{-1}$ for Jan.–June; 9 ng $l^{-1}$ for June–Dec.) were found to be different at the 95% confidence level (signification level = 0.0085 for 402 degrees of freedom within sampling periods). These differences are attributable to variations in rainfall during the sampling periods: according to data from the Galician Meteorological Centre [10], for the first sampling period, most of the samples were taken during the driest months of 1991, while for the second period sampling coincided with the wettest months of 1991.

Significant differences (signification level = 0.0369) were observed between the mean PAH levels found in zones C (catchment), D (distribution) and T (consumers' taps). The least significant difference (LSD) intervals at the 95% confidence level indicated that PAH levels in samples from zone C (mean $\approx$16 ng $l^{-1}$) were significantly higher than in those from zones D and T (both means $\approx$10 ng $l^{-1}$). These results confirm that the water treatment system is effective, and that PAH levels are not significantly altered during water distribution.

In conclusion, we propose that the above-described method be adopted for determination of the joint concentration of the six PAHs designated by current European legislation as indicators of the quality of drinking waters and surface waters destined for use as such. Its

precision (coefficient of variation) is 2.48% in contrast with the officially stipulated 50%, its detection limit 10 ng $l^{-1}$ as opposed to the officially stipulated 40 ng $l^{-1}$, and its limit of quantification 28 ng $l^{-1}$. Recovery (94.05%) is likewise better than official requirements (50%). Additional advantages over the reference methods laid down in European legislation are greater speed, greater operational simplicity and lower maintenance costs. Application of this method to the PAH screening of water used to produce drinking water in Galicia (N.W. Spain) confirmed them to be of high quality.

## Acknowledgements

The authors thank the Conselleria de Sanidad of the Xunta de Galicia for financial support of this work, and the Xunta de Galicia for concession of a bursary to M.-J. López de Alda-Villaizán.

## References

[1] R. Fabre and R. Truhaut, Toxicologia, Vol. 1, Paraninfo, Madrid, 1976.
[2] World Health Organization (WHO), Guidelines for Drinking-Water Quality, Vol. 2, World Health Organization, Geneva, 1984.
[3] Commission of the European Communities, Measurements & Testing Newsletter, 1 (1993) 1.
[4] US Environmental Protection Agency (USEPA), Drinking Water Regulations and Health Advisories, Office of Water, US Environmental Protection Agency, Washington, DC, 1994.
[5] Council of the European Communities, Directive 75/440/EEC, Off. J. Eur. Communities, L194 (1975) 26.
[6] Council of the European Communities, Directive 79/869/EEC, Off. J. Eur. Communities, L271 (1979) 44.
[7] Council of the European Communities, Directive 80/778/EEC, Off J. Eur. Communities, L229 (1980) 11.
[8] M.J, López de Alda, S. García, M.A. Lage and J. Simal J. AOAC Int., 78(2) (1995) 402.
[9] American Chemical Society (ACS) Subcommittee on Environmental Analytical Chemistry, Anal. Chem., 52(14) (1980) 2242.
[10] P. Carmona, personal communication, 1994, Centro Meteorológico Territorial de Galicia, La Coruña, Spain.

ELSEVIER

Talanta 42 (1995) 971–977

Talanta

# A new sample cell design for studying solid-matrix room-temperature phosphorescence moisture quenching

S.W. Tjioe, R.J. Hurtubise *

*Department of Chemistry, University of Wyoming, Laramie, WY 82071-3838, USA*

Received 15 December 1994; revised 26 January 1995; accepted 31 January 1995

**Abstract**

A new sample chamber was developed that can be used in the measurement of the effects of moisture on the room-temperature solid-matrix phosphorescence of phosphors adsorbed onto filter paper. The sample chamber consists of a sealed quartz cell that contains a special teflon sample holder. Sulfuric acid solutions in the quartz cell determine the percentage relative humidity in the cell and also determine the amount of moisture adsorbed onto the filter paper. The new sample chamber is much easier to use than a flowing nitrogen gas system. Results from both systems are compared with respect to ease of use and the amount of moisture adsorbed onto the filter paper.

## 1. Introduction

Solid-matrix room-temperature luminescence is a very useful analytical method for the trace analysis of organic compounds. The adsorption of organic molecules onto dry filter paper can reduce the non-radiative decay of a phosphor from the triplet state [1,2]. Solid-matrix room-temperature phosphorescence (SMRTP) and fluorescence (SMRTF) give greater quantum yields, in many cases, than the corresponding solution at low temperature [3]. In general, hydrogen-bonding interactions between the filter paper and the lumiphor is one of the main mechanisms responsible for the strong luminescence observed at room temperature [4]. The rigid environment provided by the filter paper reduces non-radiative transitions of the excited molecules and enhances luminescence.

Nissan [5] pointed out that the strength and number of hydrogen bonds in hydrogen-bond dominated solids, as measured by Young's modulus, decreases drastically upon the adsorption of moisture. The decrease in modulus is directly related to two regions of hydrogen-bond dissociation in paper [6]. The first region extends from zero moisture content to a point where a BET monomolecular layer of moisture has been established in the filter paper. The weight fraction of moisture at such monolayer coverage is designated as $W_M$. Within this region, only a single hydrogen bond is broken upon the adsorption of a water molecule. After the moisture content of the solid matrix exceeds $W_M$, cooperative hydrogen-bond dissociation dominates. In this region, groups of hydrogen bonds dissociate upon the adsorption of a single water molecule. Consequently, a more drastic decrease in the rigidity of the solid matrix is observed.

Schulman and Parker [7] presented evidence to indicate that the adsorption of moisture by filter paper permitted oxygen to penetrate the paper more efficiently. Citta and Hurtubise [8] reported that the SMRTP intensity of model aromatic compounds adsorbed onto filter paper decreased dramatically in the presence of humid nitrogen gas. In the presence of humid oxygen gas of 75% relative humidity (% RH), the SMRTP of the model compound they in-

* Corresponding author. Fax: (307)766-2807.


*SSDI* 0039-9140(95)01548-5

vestigated was completely quenched. Purdy and Hurtubise [9] observed that SMRTP lifetimes of model compounds were comparatively insensitive to moisture in nitrogen gas. The quenching of SMRTP was primarily a result of diminished filter paper matrix rigidity [9]. The moisture quenching of SMRTP for phosphors on filter paper was thus referred to as "matrix quenching" in contrast to the conventional static quenching in solution [9]. Chen et al. [10] introduced an equation that describes the changes in the SMRTP intensity as a function of SMRTP lifetime ratios and an exponential expression that included the weight percent of adsorbed moisture. Further, Chen and Hurtubise [11] introduced a model for the moisture quenching of SMRTP via the decrease in the Young's modulus of filter paper.

In previous studies of solid-matrix moisture quenching, moisture was introduced into the sample compartment of the luminescence spectrometer containing the filter paper sample via a flow of humid gas [8–11]. The amount of moisture in the flowing gas was determined by the flow rate of the gas through a series of sulfuric acid solutions [12]. In this work, a much simpler system was developed to obtain constant humidity in a sample chamber that contained the filter paper sample. This new sample chamber consists of a quartz cell and a teflon filter paper sample holder. Sulfuric acid solutions were added to the cell to create a humid environment surrounding the sample holder. It can be placed inside the sample compartment of a luminescence spectrometer, which eliminates the need to flow humidified nitrogen gas into the cell compartment.

## 2. Experimental

### 2.1. Apparatus

Intensity and lifetime measurements were obtained with a Fluorolog 2+2 spectrofluorometer (Spex Industries, Edison, NJ) interfaced with a Spex Datamate computer and the Spex 1934C phosphorimeter accessory. The excitation source was a 50 W programmable pulsed lamp. A cooled Hamamatsu R928 photomultiplier tube was employed. The % RH in the sample compartment of the spectrofluorometer and in the procedure used to obtain adsorption isotherms was measured with a Vaisala HMI 31 hygrometer (Vaisala, Helsinki, Finland).

### 2.2. Reagent and chemicals

Absolute methanol (Baker, HPLC grade) was mixed with water (Baker, HPLC grade) in a 1:1 ratio. Thallium acetate (Aldrich, 99.99%) and glacial acetic acid (ACS Reagent grade, Fisher Scientific) were added to the above solvent to give 0.5 M thallium acetate and 0.3 M acetic acid. Benzo[*a*]pyrene-*r*-7,*t*-8,9,*c*-10-tetrahydrotet-rol (tetrol I-1) was used as the model phosphor (Midwest Research Institute, Kansas City, MO), The tetrol solution was prepared by directly dissolving a weighed amount of tetrol in the thallium acetate solution as described previously [13]. The concentration of the tetrol solution was 40 ng $\mu l^{-1}$. Sulfuric acid (ACS reagent) was diluted in distilled water to various concentrations and stored in stopped bottles [12].

### 2.3. Materials

Whatman No. 1 filter paper (Whatman Co., Clifton, NJ) was developed three times in absolute methanol, dried at 110 °C for 30 min and stored in a desiccator. Small circular disks of filter paper that were 0.4 cm in diameter were obtained from the developed filter paper sheet using a commercial paper punch. A teflon sampler holder and a delrin sample holder were custom made to hold the filter paper samples (Fig. 1). A quartz cell (Wilmad Co., Buena, NJ) was used as the sample chamber to contain the teflon sample holder. Compressed nitrogen gas (US Welding, Golden, CO) was filtered through an oxygen trap (Oxyclear, Oakland, CA) and Drierite (W.A. Hammond Drierite Company, Xenia, OH). Chemical resistant Duraseal film (Diversified Biotech, Boston, MA) was used to seal the top of the 1 cm quartz cell. This film allows only 0.00807 $cm^3\ cm^{-2}\ h^{-1}$ of $O_2$ and 0.646 $\mu g\ cm^{-2}\ h^{-1}$ of $H_2O$ to penetrate when used as described. An analytical balance was placed inside an Atomsbag (Aldrich) for the measurement of the weight increase of filter paper samples upon moisture adsorption in obtaining adsorption isotherms [10].

## 3. Experimental designs and procedures

### 3.1. Adsorption isotherm

An adsorption isotherm for water was obtained for thallium acetate treated paper as

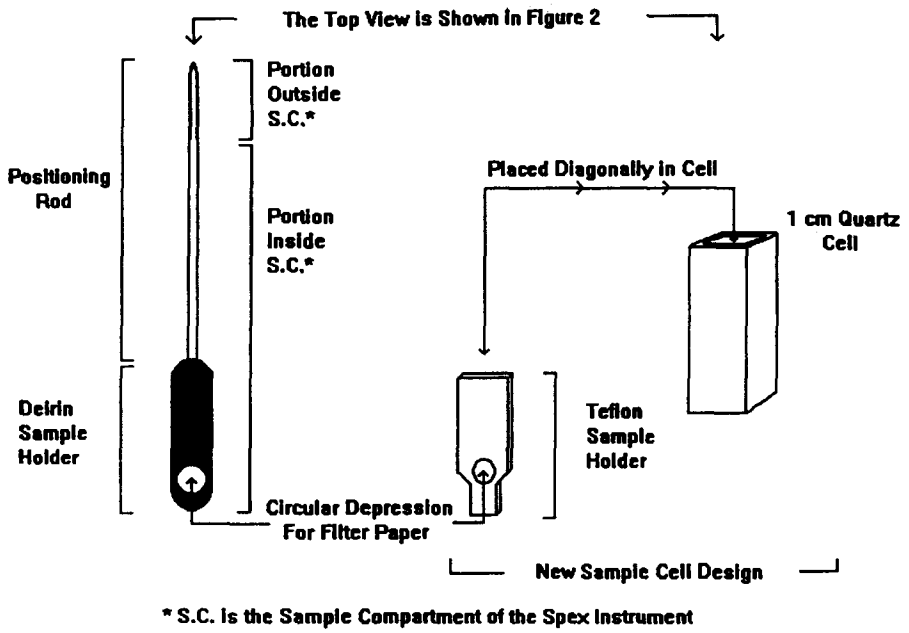


Fig. 1. Delrin and teflon sample holders.

described by Chen et al. [10]. Thallium acetate treated filter paper samples were suspended above sulfuric acid solutions of various concentrations for 45 min in stopped plastic bottles. The filter papers were weighed before and after this period of time. The adsorption isotherm was constructed by plotting the weight gained due to moisture adsorption against the % RH in the bottles. The % RH in the bottle was determined by the concentration of sulfuric acid, and the wt% of moisture at monolayer coverage ($W_M$) of thallium acetate treated filter paper was calculated using the BET method [14]. The data are given in Table 1.

The SMRTP quenching of I-1 was then determined in relation to the moisture content of the filter paper at various % RH. In general, the SMRTP intensities and phosphorescence decay curves were measured before and after the filter paper had acquired moisture. Moisture was introduced onto the filter paper via either a flow of humid nitrogen gas, or by suspending the filter paper sample above a solution of sulfuric acid in a sealed 1 cm quartz cell sample chamber. In both designs, filter paper samples were fitted into the sample holder. The sample holder was then placed in a sample chamber in which constant % RH was established. This is described in more detail below.

### 3.2. SMRTP quenching with flowing humid nitrogen gas

A delrin sample holder (see Fig. 1) was used to hold the filter paper samples. As indicated in the Figure, a positioning rod was attached to the upper part of the sample holder. The sample holder was placed on a stage inside the sample compartment of the spectrofluorometer.

Table 1
Adsorption isotherm data for thallium acetate treated whatman No. 1 filter paper

| % RH | Moisture (wt%) |
|---|---|
| 0 | 0.00 |
| 10 | 1.07 |
| 20 | 2.12 |
| 30 | 2.97 |
| 40 | 3.63 |
| 50 | 4.52 |
| 60 | 5.13 |
| 70 | 7.09 |
| 80 | 8.14 |
| 90 | 10.23 |
| 100 | 16.00 |

Each data point is the average of at least five trials. The standard deviation associated with each data point is less than 5%.
The linear region between 10 and 50% RH was used to calculate monolayer coverage, $W_M$. The calculated value of $W_M$ was 2.47 wt% moisture. The linear correlation coefficient was 0.999 for the region from 10 to 50% RH.

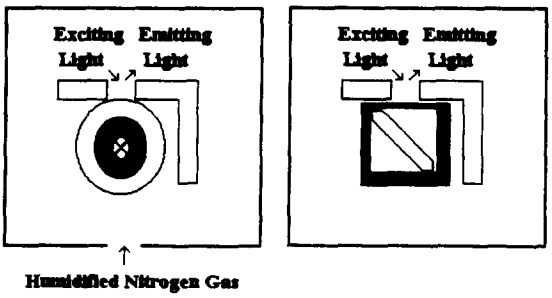


Fig. 2. Top view of sample holders in the cell compartment.

Fig. 2 illustrates the sample compartment of the instrument viewed from the top. The stage is indicated as a clear circle (left) and dark square (right) around the sample holders in Fig. 2. The upper 3 cm of the positioning rod was outside the sample compartment, so that the rotational orientation of the sample holder could be manipulated to obtain the maximum SMRTP intensity. The design on the left in Fig. 2 was used for flowing humid nitrogen gas. Compressed nitrogen gas was passed into the sample compartment via two paths. The nitrogen gas which came in via path (1) contained no moisture and provided 0% RH inside the sample chamber. The nitrogen gas which came in via path (2) was filtered through an oxygen trap and a set of three water bottles. Each water bottle contained approximately 500 ml of distilled water. The amount of moisture brought into the sample compartment via path (2) was determined by the flow rate of nitrogen gas. The %RH inside the sample chamber was constantly monitored by a digital hygrometer. It could be altered by adjusting the flow of gas through either path (1) or path (2).

One microliter of blank solvent was spotted on the surface of a filter paper sample which was on top of four other pieces of filter paper in the circular depression of the delrin sample holder (Fig. 1). The entire sample holder was dried in a oven at 110 °C for 30 min. It was then cooled at room temperature for 5 min under dry nitrogen gas inside the sample compartment. Both the blank and the sample were protected from the excitation light prior to the measurement step. The steady-state intensity of the blank filter paper was measured before the SMRTP decay curve of the blank filter paper was recorded. Dry nitrogen gas was continuously passed into the sample compartment throughout the measuring period. After obtaining SMRTP data under dry conditions, humid nitrogen gas from path (2) was directed into the sample compartment. Dry nitrogen gas inside the sample chamber was quickly displaced by the humid nitrogen gas. A fixed % RH was established inside the sample chamber within 20 min. The SMRTP intensity or phosphorescence decay curve of the humid blank filter paper sample was measured 45 min after a constant % RH inside the sample chamber was established. After blank measurement, the delrin sample holder was removed from the sample compartment and dried again at 110°C for 30 min. One-microliter aliquots of tetrol I-1 solution were transferred onto the top surface layer of the filter paper samples. After drying (30 min at 110 °C and then 5 min under dry nitrogen gas at room temperature), the steady-state SMRTP intensity and phosphorescence decay curve of I-1 on filter paper were measured. Mositure was then introduced again, and the SMRTP intensity and phosphorescence decay curve were obtained under humid conditions. The SMRTP intensity and phosphorescence decay curve from the blank filter paper samples were subtracted from the corresponding SMRTP intensity and phosphorescence decay curve of tetrol I-1 on dry and humid filter paper samples. The phosphorescence lifetimes of I-1 were calculated for dry and humid filter paper samples and are presented in Table 2 with respect to the moisture content of the filter paper.

### *3.3. SMRTP quenching within a Quartz cell sample chamber*

A teflon sample holder was custom made to hold the filter paper samples (Fig. 1). A 1 cm quartz cell was used to hold the teflon sample holder. It was sealed with a piece of Duraseal film and fitted snugly on a metal stage inside the sample compartment of the spectrofluorometer (Fig. 2). The teflon sample holder containing the blank filter paper samples was dried under identical conditions to the delrin sample holder. It was transferred to the sample compartment of the spectrofluorometer and placed diagonally into a quartz sample cell (Fig. 1). Dry nitrogen gas was directed into the quartz sample cell via a glass pipette for 5 min before it was sealed with a square piece of airtight Duraseal film. The SMRTP intensity and phosphorescence decay curves of the blank filter paper samples were recorded under the identical instrumental conditions as the flowing nitrogen gas system. After the RTP data on dry filter paper sample was recorded, the

Table 2
$\tau_0/\tau$ and $P_0/P$ values for tetrol I-1 with flowing nitrogen gas and a quartz cell system

| Moisture (wt%) | Flowing nitrogen gas [a] | | Within quartz cell | |
|---|---|---|---|---|
| | $\tau_0/\tau$ | $P_0/P$ | $\tau_0/\tau$ | $P_0/P$ |
| 0.00 | 1.00 | 1.00 | 1.00 | 1.00 |
| 1.42 | 1.12 | 1.05 | 1.05 | 1.08 |
| 1.87 | – | – | 1.07 | – |
| 2.12 | 1.20 | 1.38 | 1.10 | 1.17 |
| 2.97 | 1.22 | 1.78 | 1.26 | 1.27 |
| 3.63 | 1.24 | 1.98 | 1.27 | 2.54 |
| 4.52 | 1.17 | 2.63 | 1.38 | 4.37 |
| 5.38 | – | – | 1.52 | – |
| 5.57 | – | – | 1.60 | – |
| 7.09 | 1.17 | 3.80 | 1.77 | 9.66 |
| 7.50 | – | – | 1.90 | – |

[a] The $\tau_0/\tau$ and $P_0/P$ data were taken from Ref. [10].

Duraseal film was removed and 0.6 ml of a sulfuric acid solution was added to the quartz sample cell. A gentle stream of dry nitrogen gas was continuously passed into the quartz sample cell at 0.5 psi during the addition of sulfuric acid solution. The quartz sample cell was sealed again with a fresh piece of Duraseal film. The SMRTP intensity and decay curve of blank filter paper sample were recorded again after 45 min. After the measurements, the teflon sample holder was removed from the quartz cell and dried at 110 °C for 30 min. Sulfuric acid solution inside the quartz sample cell was discarded and the cell was rinsed with soap, nitric acid, tap water, distilled water and distilled ethanol, before being placed back onto the metal stage in the sample compartment. After drying, the teflon sample holder was cooled under dry nitrogen gas for 5 min at room temperature. One microliter of tetrol I-1 solution was spotted onto the top filter paper sample. The entire sample holder was dried again at 110 °C for 30 min. It was placed back into the quartz sample cell and cooled under dry nitrogen gas. The SMRTP intensity and phosphorescence decay curve of the tetrol on dry and humidified filter paper samples were recorded in the same fashion as the blank filter paper samples. The blank SMRTP intensity and phosphorescence decay curve data were subtracted from the corresponding sample data for I-1. The results are presented in Table 2.

### *3.4. Measuring the steady state SMRTP intensity and lifetime*

The steady state SMRTP intensity of the tetrol was measured by setting both the excitation and emission monochromators at appropriate wavelengths ($\lambda_{ex} = 345$ nm and $\lambda_{em} = 608$ nm). The initial delay was set at 0.1 ms, the gatetime (specified as "window" in Spex) was set at 5 ms, and the average intensity was obtained from 20 intensity values. The SMRTP decay curves of the filter paper and tetrol I-1 were also recorded at the excitation and emission wavelengths mentioned above. A phosphorescence lifetime program was loaded into the Datamate computer to obtain the phosphorescence decay curve. The phosphorescence decay curves obtained from filter paper samples with various moisture contents were all measured with 0.03 ms delay, 5 ms gatetime, and five flashes per data point. A time period of 0.07 ms was allowed between each flash, with 0.1 ms between consecutive data points. A total of 200 points was collected in constructing the phosphorescence decay curve. After subtracting the blank decay curve, the data for the phosphorescence decay curve from 0.03 to 12.75 ms were used in a linear regression program. The SMRTP lifetimes of the tetrol samples were calculated from the slope of the regression line.

## 4. Results and discussion

The weight percent (wt%) moisture values obtained on thallium acetate treated filter paper samples at a given %RH are presented in Table 1. The moisture content of filter paper increased linearly between 5 and 50% RH, and then more drastically above 70% RH. The linear correlation coefficient between 5 and 50%

RH was over 0.999. Using the linear portion between 5 and 50% RH, the monolayer coverage of water ($W_M$) was calcualted to be 2.47% using the BET method. This corresponds to approximately 24% RH. The point at which $W_M$ occurs is important because, as discussed in the Introduction, it separates two regions of hydrogen bond dissociation.

Table 2 lists the ratios of SMRTP intensities ($P_0/P$) and lifetimes ($\tau_0/\tau$) in relation to various percentages of moisture content in the filter paper. $P_0$ represents the SMRTP intensity on dry filter paper and $P$ represents the corresponding intensity with moisture. Similarly, the term $\tau_0$ is the SMRTP lifetime without moisture, and $\tau$ is the corresponding lifetime with moisture present. Each data point in Tables 1 and 2 represents the average of at least two trails.

As indicated in Table 2, the SMRTP intensity of I-1 was not affected much by moisture before $W_M$. The $\tau_0/\tau$ values also changed little for the flowing nitrogen gas system. After the wt% of water had reached about 2.0%, the $P_0/P$ values changed more rapidly with the flowing nitrogen gas system compared to the $\tau_0/\tau$ values with this system. The $\tau_0/\tau$ results from the quartz cell showed a similar trend compared to the flowing nitrogen gas system up to approximately 3.6 wt% water. After about 4.5 wt% water was adsorbed, the $\tau_0/\tau$ values became larger compared to the $\tau_0/\tau$ values obtained from the flowing nitrogen gas system. The $P_0/P$ ratios with the quartz cell system were considerably larger after about 4.5 wt% water, compared to the $P_0/P$ ratios from the flowing nitrogen gas system. Fig. 3 illustrates the data in Table 2 for both systems.

In general, the results from the two systems gave similar trends. The adsorption of moisture can be separated into two regions, as discussed by Chen et al. [10]. In the first region, which extends from 1 to about 2.5 wt% water, dynamic quenching dominates the entire quenching process. The intensity and lifetime ratios were about the same. In the second region, the $P_0/P$ ratio increased much faster than the $\tau_0/\tau$ ratios (Fig. 3). Fig. 3 clearly showed that identical quenching was not obtained for both systems over the entire wt% water range for the corresponding $\tau_0/\tau$ and $P_0/P$ ratios. This is most likely related to the fundamental differences between the two systems. With the flowing nitrogen gas system, the humidified nitrogen gas flows into and also exits the sample chamber. The nitrogen gas is constantly in motion, and thus moisture would not absorb as readily onto the filter paper as with a static system. The quartz cell sample chamber can be considered as a static system. As Fig. 3 shows, at greater than 3.5 wt% moisture, more water was adsorbed by the filter paper as indicated by the greater change in the $P_0/P$ ratios with the quartz cell compared to the flowing system. This is a result of the moisture being in more intimate contact with the filter paper in the quartz cell. In the flowing system, the cell compartment is very large and the humidified nitrogen is readily dispersed compared to the closed 1 cm quartz cell. The results in Fig. 3 showed that the type of system used to study moisture adsorption on filter paper is important, and the results are influenced by the design of the system. Thus, it would be important to use the same system for a given set of experiments to acquire consistent results.

Another important consideration related to the results in Fig. 3 is that the wt% water adsorbed onto the filter paper was obtained by

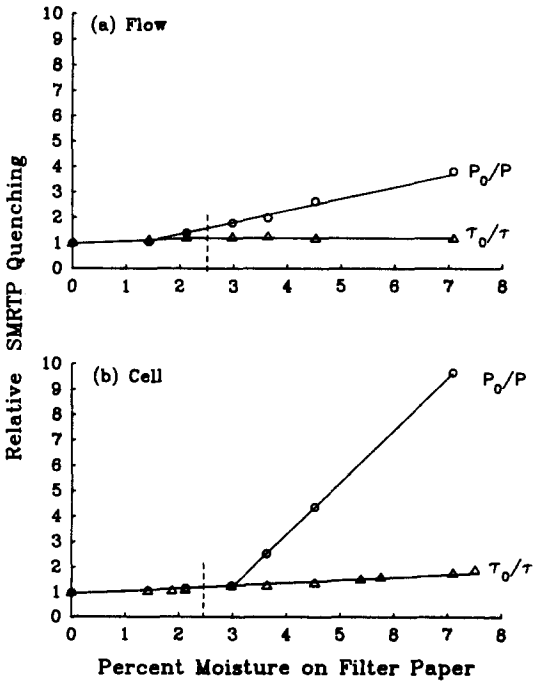


Fig. 3. SMRTP quenching of tetrol I-1(a) on Whatman No. 1 filter paper treated with thallium acetate-acetic acid solution under a flow of humid nitrogen gas (data from Ref. [10]), and (b) inside a sealed quartz sample cell. The ratio $P_0/P$ refers to the phosphorescence intensity ratio, and the ratio $\tau_0/\tau$ refers to the phosphorescence lifetime ratio. See text for additional details.

first suspending filter paper samples in bottles containing sulfuric acid solutions, and then weighing the samples in a humidity controlled environment. Most likely, the wt% moisture obtained under these conditions would be very similar to that in the quartz sample chamber. However, because all three systems (quartz cell, flowing system, and bottles with sulfuric acid) are not identical, the wt% moisture values in Table 1 would be proportional to the true wt% moisture adsorbed for the two systems investigated. This is indicated by the results in Fig. 3. The wt% moisture used in Figs. 3(a) and 3(b) is identical for both wt% moisture axes, but beyond 3.5 wt% moisture the $P_0/P$ values for the two systems become considerably different.

The trends in $\tau_0/\tau$ ratios obtained from the two systems are different. With the quartz cell, the $\tau_0/\tau$ ratio gave an approximate linear relationship with wt% moisture. The $\tau_0/\tau$ ratios for the flowing nitrogen gas system essentially reached a constant value above about 2.12 wt% water. Matrix quenching was more effective in the new sample chamber as indicated in Fig. 3 with the much greater slope of the $P_0/P$ plot in the region beyond 3.0 wt% water for the quartz cell. Matrix quenching involves the participation of moist filter paper in the quenching process. This type of quenching has been discussed by Chen et al. [10]. The separation between the two regions of SMRTP quenching discussed was also better clarified using the new design. It occurred slightly beyond $W_M$ at 3% moisture content (compare Figs. 3(a) and 3(b)). Using the new quartz cell design, the effects of a humid environment can be studied in the sample compartment of commercial luminescence instruments. In addition, the quartz sample cell can be transferred easily so that data can be obtained from instrument to instrument.

## Acknowledgment

Financial support for this project was provided by the United States Environmental Protection Agency, Grant No. R817678.

## References

[1] R.J. Hurtubise, Solid Surface Luminescence Analysis: Theory, Instrumentation, Applications, Marcel Dekker, New York, 1981.
[2] R.J. Hurtubise, Phosphorimetry: Theory, Instrumentations, and Applications, VCH, New York, 1990.
[3] R.J. Hurtubise and S.M. Ramasamy, Appl. Spectrosc., 47 (1993) 116.
[4] R.A. Dalterio and R.J. Hurtubise, Anal. Chem., 56 (1984) 336.
[5] A.H. Nissan, Macromolecules, 9 (1976) 840.
[6] G.L. Batten and A.H. Nissan, Tappi, 70 (1987) 119.
[7] E.M. Schulman and R.J. Parker, J. Phys. Chem., 81 (1977) 1932.
[8] L.A. Citta and R.J. Hurtubise, Appl. Spectrosc., 45 (1991) 1547.
[9] B.B. Purdy and R.J. Hurtubise, Anal. Chem., 64 (1992) 1400.
[10] J. Chen, S.W. Tjioe and R.J. Hurtubise, Appl. Spectrosc., 48 (1994) 1242.
[11] J. Chen and R.J. Hurtubise, Appl. Spectrosc., 49 (1995) 98.
[12] J.A. Dean (Ed.), Lange's Handbook of Chemistry, McGraw-Hill, New York, 1992, Chapter 11.7.
[13] S.W. Tjioe and R.J. Hurtubise, Anal. Lett., 26 (1993) 557.
[14] D.M. Ruthen, Principles of Adsorption and Adsorption Processes, Wiley, New York, 1984.

ELSEVIER

Talanta 42 (1995) 979–982

Talanta

Short communication

# Correlation between retention behaviour and GC–FTIR data in the study of flavonoids

E. Horváth [a,*], J. Mink [b], E. Bottari [c], M.R. Fest [c]

[a] *Research Group for Analytical Chemistry of Hungarian Academy of Sciences, 8201 Veszprém, P.O.B. 158, Hungary*
[b] *Veszprém University, Department of Analytical Chemistry, 8201 Veszprém, P.O.B. 158, Hungary*
[c] *"La Sapienza" University, Department of Chemistry, Ple Aldo Moro 5, 00185 Roma, Italy*

Received 18 August 1994; revised 16 January 1995; accepted 16 January 1995

**Abstract**

Trimethylsilyl derivatives of 10 different hydroxy- and methoxyhydroxyflavonoid compounds were studied by the GC–FTIR technique. Optimal deviation parameters were determined for the flavonoids studied. The correlation found between retention and gas-phase IR data can successfully be used in structural identification of compounds having very similar chromatographic behaviour. The shift of the carbonyl frequency gives information on the presence of substituting agents

## 1. Introduction

Flavonoids are the most diverse and ubiquitous compounds of plants. Currently, the most common techniques used for the analysis of flavonoids are thin layer chromatography and reversed phase HPLC [1–4], in spite of the fact that it is difficult to handle problems originating from the similarity of retention behaviour and the use of classical detection methods. This is the reason why efforts are made to correlate retention and spectroscopic data or to use coupled techniques [5–7]. Coupling of thin layer and liquid chromatography with infrared spectroscopy as a detection technique encounters several practical difficulties and cannot be considered a routine method [8]. Therefore, the GC–FTIR technique has its advantage in the structural identification of compounds suitable for GC analysis either directly or indirectly (via derivatization). In the present work correlations between retention behaviour and the gas phase IR spectroscopic data are discussed.

## 2. Experimental

### 2.1. Materials

The flavonoid samples (min. 98% purity) used throughout the experiments are as follows: 3-hydroxyflavone (flavonol), 5,7-dihydroxyflavone, 4′,5,7-trihydroxyflavone (naringenin), 2′,3,4′,5,7-pentahydroxyflavone (morin), 3,3′,4′,5,7-pentahydroxyflavone (quercetin), 7-methoxyflavanone, 3-hydroxy-4′-methoxyflavone, 5,7-dihydroxy - 2′,3 - dimethoxyflavone,3′,5,7 - trihydroxy-4-methoxyflavone (hesperetin) and 3′,3,4′,5-tetrahydroxy-7-methoxyflavone (rhamnetin).

Compounds used as derivatization agents were 2,2,2-trifluoro-*N*,*O*-bis(trimethylsilyl)acetamide (BSTFA; Fluka and Merck), *N*-

* Corresponding author.


*SSDI* 0039-9140(95)01587-6

(trimethylsilyl)imidazole (Tri-Sil Z; Pierce), 1,1,1,3,3,3-hexamethyldisilazane (HMDS; Fluka) and trimethylchlorsilane (TMCS; Fluka). Hexane (Carlo Erba) and methanol (Reanal, Budapest) used as solvents were of chromatographic purity.

### 2.2. Derivatization

Two methanolic stock solutions (mixtures A and B) were prepared from both hydroxyflavonoids and methoxyhydroxyflavonoids. Mixture A contains flavonol, 5,7-dihydroxyflavone, naringenin, morin and quercetin in equal concentrations of 1 mg/ml. Mixture B contains 7-methoxyflavanone, 3-hydroxy-4'-methoxyflavone, 5,7-dihydroxy-2'3-dimethoxyflavone, hesperetin and rhamnetin of the same concentration (1 mg/ml). In order to evaporate the solvent, a given quantity (100–200 µl) was exposed to the air for some 12 h. In the case of mixture A 300 µl Tri-Sil Z and 200 µl hexane were added to the dry residue and silanization was maintained at 85 °C for 30 min. For mixture B, 300 µl BSTFA and 200 µl hexane were added, and the reaction was allowed to proceed at 70 °C for 60 min. Then the mixtures were made up to 1 ml with hexane.

### 2.3. Gas chromatographic separation

Separation of the components of mixtures A and B was made by means of a HP-588OA (Hewlett-Packard) type gas chromatograph. A HP-1 type fused silica capillary column (Hewlett-Packard; $l = 12$ m, 0.2 mm i.d., 0.33 µm film thickness) was used. Separations were made with programmed heating ($T = 180$ °C for 1 min, then 5 °C/min to 280 °C, and finally $T = 280$ °C for 5 min) using splitless injection (350 °C injector temperature) and a flame ionization detector (FID).

### 2.4. GC–FTIR analysis

GC–FTIR runs were performed by means of a HP-5880A gas chromatograph connected to a Bio-Rad FTS-45 type FTIR spectrometer via a Bio-Rad GC-32 interface equipped with a high sensitivity mercury cadmium tellurid (MCT) detector. Therefore, it was possible to carry out simultaneous FID and IR detection. The temperature of the transfer line and the light pipe (15 cm long, 1 mm i.d., gold-plated inside) was thermostated to 300 °C. The software-generated chromatogram was obtained by the Gram-Schmidt vector orthogonalization method. Spectra were recorded at a resolution of 8 $cm^{-1}$.

## 3. Results and discussion

### 3.1. Derivatization

The preparation of the trimethylsilylated derivatives of flavonoid compounds is widely discussed in the literature [9–11]. Although no difficulties associated with derivatization are reported, we found that complete derivatization (100% conversion) can only be achieved with flavonoids of low substitution owing to the strong intramolecular hydrogen bonds of polysubstituted flavonoids. The breaking of these bonds requires stronger derivatization agents, or an increase in the temperature of the silanization reaction which, on the other hand, may result in the decomposition of the molecule or the occurrence of side-reactions. Our observations are in good agreement with those of Brownbridge [12]. It was also recognized that the FID is rather insensitive to trimethylsilyl derivatives of flavonoids (e.g. the detection limit for derivatized quercetin was 0.04 mg/ml) which is probably a result of the high thermal stability of these compounds [9,10]. This is one of the reasons why relatively high concentrations were used.

Both mixtures (A and B) were reacted with BSTFA, Tri-Sil Z and HMDS:TMCS (2:1 v/v) reagetns for different times at various temperatures. It was found that mixture B was very sensitive to the strength of the derivatization agent and to the temperature of the reaction. This is supported by the linear FID response (in the 0.05–1.0 mg/ml concentration range) to reaction products obtained during the derivatization of quercetin with BSTFA in a microwave oven (Philips M610; stage 6; 2 × 5 minutes). Similar results were obtained with the Tri-Sil Z derivatization agents. The regression coefficients obtained in the above concentration range with derivatization agents BSTFA and Tri-Sil Z were $R = 0.9998$ and 0.9996, respectively, in spite of the fact that—unlike the literature results [9–11]—complete decolourization was not observed.

The optimal parameters for the reaction of hydroxyflavonoids were 30 min reaction time and 80 °C reaction temperature with Tri-Sil Z derivatization agent. For the reaction of

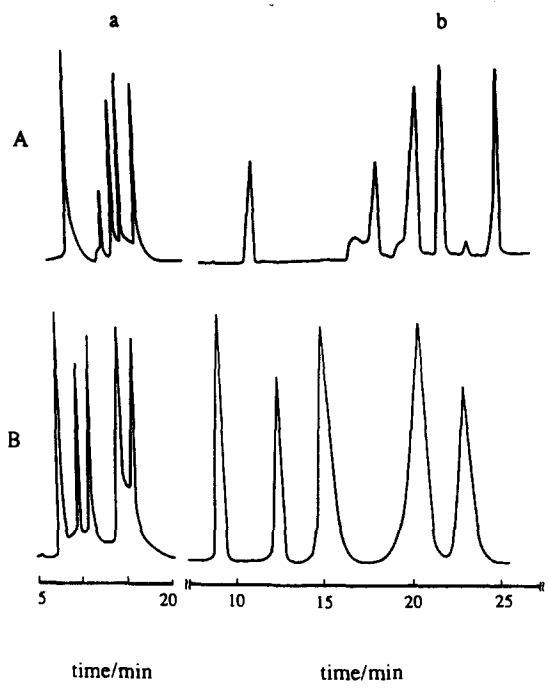


Fig. 1. Chromatograms of silanized flavonoid compounds. (A) mixture A; (B) mixture B; (a) FID response; (b) reconstructed Gram–Schmidt chromatogram; Elution sequence: mixture A: flavonol, 5,7-dihydroxyflavone, naringenin, morin, quercetin. Mixture B: 7-methoxyflavanone, 4′-methoxy-3-hydroxyflavone, 2′,3-dimethoxy-5,7-dihydroxyflavone, hesperetin, rhamnetin.

methoxyhydroxyflavonoids, the use of BSTFA reagent at 70 °C for 60 min was found to be optimal. The FID and reconstructed Gram–Schmidt chromatograms recorded under the above conditions are shown in Fig. 1.

### 3.2. GC–FTIR analysis

Gas spectra with a good signal-to-noise ratio were obtained only when the amount of the compound to be detected in the light pipe was a minimum of 80–100 ng. This is an additional reason to use relatively high sample concentrations.

The symmetrical deformation vibration of the siloxane methyl groups connecting to silicon appears at 1260 $cm^{-1}$ in the form of a characteristic band. The methyl rocking band occurs at $850 \pm 30$ $cm^{-1}$ including the Si–C stretching mode. The Si–O–C band appears at $1100 \pm 100$ $cm^{-1}$. This frequency, however, strongly depends on the chemical environment. In the spectra of flavonoid derivatives the Si–O–C stretching and the methyl rocking bands occur in the 1305–1166 $cm^{-1}$ and the 920–840 $cm^{-1}$ ranges, respectively.

In order to compensate for errors originating from the changing concentration of components in the light-pipe, the peak intensity ratios of the Si–O–C stretching ($\nu_{Si-O-C}$) and the methyl rocking ($\rho_{CH_3(Si-CH_3)}$) bands ($A\nu_{Si-O-C}/A\rho_{CH_3(Si-CH_3)}$) were related to the relative retention. Since the increase of the number of $-O-Si(CH_3)_3$ substituents on the flavone molecule results in the increase in intensity of both the Si–O–C stretching and the methyl rocking bands, and the retention time increases with the molecular weight on an apolar column, it seemed to be logical to correlate the relative intensity with the relative retention. For calculation of the relative retention $t_R/t_{R'}$, the flavonoid (flavonol) having the lowest retention time was selected as a reference. Data obtained from the spectra are summarized in Table 1. There was a close correlation between the relative retention and the peak intensity ratio of the $\nu_{Si-O-C}$ and $\rho_{CH_3(Si-CH_3)}$ bands (Fig. 2). In the $t_R/t_{R'} < 2$ range a significant difference can be observed in the curves ob-

Table 1
Correlation between relative retention $t_R/t_{R'}$ and some data of gas phase IR spectra

| Compound | $t_R/t_{R'}$ | $\nu_{C=O}$ ($cm^{-1}$) | $\nu_{Si-O-C}/\rho_{CH_3(Si-CH_3)}$ | $\Delta\nu_{C=O}$ ($cm^{-1}$) |
|---|---|---|---|---|
| Flavonol | 1 | 1661 | 1.78 | −45 |
| 5,7-Dihydroxyflavone | 1.8 | 1666 | 0.85 | −40 |
| Naringenin | 2.08 | 1696 | 0.61 | −10 |
| Morin | 2.27 | 1652 | 0.65 | −54 |
| Quercetin | 2.70 | 1650 | 0.67 | −56 |
| 4′-Methoxy-3-hydroxyflavone | 1.33 | 1659 | 2.07 | −47 |
| 2′,3-Dimethoxy-5,7-dihydroxyflavone | 1.52 | 1650 | 1.28 | −56 |
| Hesperetin | 2.02 | 1692 | 0.71 | −9 |
| Rhamnetin | 2.28 | 1650 | 0.69 | −56 |

Carbonyl reference frequency: 1706 $cm^{-1}$.

tained for methoxyhydroxy and hydroxyflavonoids. In the $t_R/t_{R'} > 2$ range, however, a constant intensity ratio of 0.6–0.7 is expected. In the "substituent sensitive" region of the relative peak intensities (between 2.1 and 0.7) the number of the $-O-Si(CH_3)_3$ substituents or the expected retention times of the derivatives can be estimated. A further study is necessary to investigate which spectral properties can be used to estimate the retention time of highly substituted derivatives.

The carbonyl stretching frequency of the substituted flavone molecule differs strongly from that of the nonperturbated one, depending on the position of the substituent. IR spectra available in the literature [1,2,13] were recorded in KBr, nujol, $CCl_4$ and dioxane matrices, only. Therefore, it seemed reasonable to select the vapour phase C=O stretching band of 7-methoxyflavanone as a 'nonperturbated' reference frequency (1706 $cm^{-1}$). The frequency shifts of the carbonyl bands relative to this frequency ($\Delta\nu_{C=O}$) are given in the last column of Table 1. It can be seen from the band shifts that the carbonyl frequencies of the derivatives of naringenin, hesperetin and 7-methoxyflavanone used as reference material are observed around 1700 $cm^{-1}$, while those of the flavonol, morin, quercetin, 3-hydroxy-4'-methoxyflavanone and rhamnetin derivatives show band shifts of 45–56 $cm^{-1}$. The shift of the $\nu_{C=O}$ stretching frequency relative to the reference position (1706 $cm^{-1}$) may be due to steric hindrances. It is interesting to note that with molecules substituted at the C-3 position (flavonol, 3-hydroxy-4'-methoxyflavone) a frequency shift of 45–47 $cm^{-1}$ was observed. On the other hand, the carbonyl vibration is less hindered in molecules substituted at the C-5 position (e.g. for naringenin $\Delta\nu = 10\ cm^{-1}$). For molecules substituted at both the C-3 and C-5 positions frequency shifts of 54–56 $cm^{-1}$ were observed. The influence is not additive and it seems that the effect of substituents at the C-5 position is stronger than at the C-5 one.

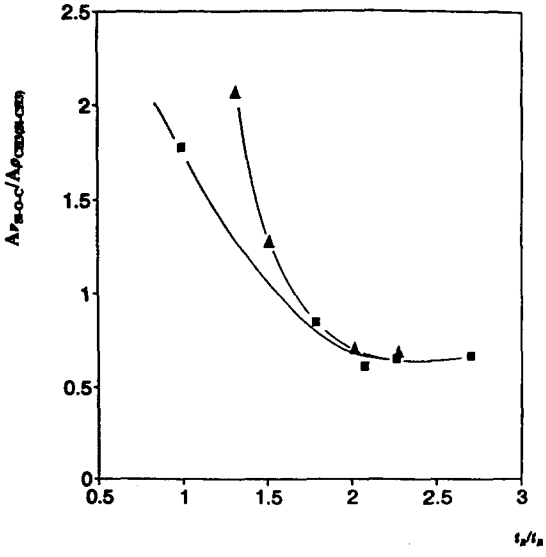


Fig. 2. Correlation between relative retention ($t_R/t_{R'}$) and the peak intensity ratio of the $\nu_{Si-O-C}$ and $\rho_{CH_3(Si-CH_3)}$ bands. ▲, Methoxyhydroxyflavonoids; ■, hydroxyflavonoids.

## 4. Conclusion

Based on the results obtained it can be stated that the GC–FTIR method has advantages over HPLC or TLC techniques when the identification of structure is difficult owing to similarities in retention behaviour and/or to limitations of classical detection methods. The shift of the carbonyl band frequency is particularly sensitive to C-3 and C-5 substitution. With the correlation between relative retention and the $\nu_{Si-O-C}/\rho_{CH_3(Si-CH_3)}$ band ratio, the number of substituents can be estimated.

## References

[1] J.B. Harborne and T.J. Mabry, The Flavonoids: Advances in Research, Chapman & Hall, London, 1975.
[2] K.R. Markham, Techniques of Flavonoid Identification, Academic Press, New York, 1982.
[3] P. Gamache, E. Ryan and I.N. Acworth, J. Chromatogr., 635 (1993) 143.
[4] D. Heimler, L. Mittempergher, P. Buzzini and V. Boddi, Chromatographia, 29 (1990) 16.
[5] M.C. Pietrogrande, P. Reschiglian and F. Dondi, J. Chromatogr., 592 (1992) 65.
[6] E. Bombardelli, A. Bonati, B. Gabetta, E.M. Martinelli and G. Mustich, J. Chromatogr., 120 (1976) 115.
[7] E. Bombardelli, A. Bonati, B. Gabetta, E.M. Martinelli and G. Mustich, J. Chromatogr., 139 (1977) 111.
[8] E.G. Brame (ed.), Practical Spectroscopy, Series A, Vol. 10, Chap. 3,4 Marcel Dekker, New York, 1990.
[9] T. Furuya, J. Chromatogr., 19 (1965) 607.
[10] A.E. Pierce, Silylation of Organic Compounds, Pierce Chemical Company, Rockford, Illinois, 1977.
[11] K. Blau and G.S. King (Eds.), Handbook of Derivatives for Chromatography, Heyden, London, 1978.
[12] P. Brownbridge, Synthesis, 1 (1983) 1.
[13] Ph. Lebreton and J. Chopin, Spectrochim. Acta, 19 (1963) 2099.

ELSEVIER

Talanta 42 (1995) 983–984

Talanta

# Letter to the Editors

Dear Sir,

An analytical method for speciation of mercury by GC/CVAFS after aqueous phase ethylation and room temperature precollection has been originally published by Bloom [1], and improved by Liang et al. [2]. The method has been extensively used in more and more laboratories for the determination of mercury species in a variety of environmental and biological materials.

Using the original method [1], the ethylation derivatives are precollected on Carbotrap® columns. As described in our paper [2], because of its catalytic activity as well as other unknown factors, the Carbontrap® may sometimes cause a decomposition of organo-Hg species during thermal desorption of these compounds from the Carbontrap® column to a GC column. To eliminate this problem, we have suggested the use of Tenax® traps in the improved method. We found that the Tenax® has an excellent trapping efficiency, which does not cause the decomposition of organo-Hg species, indicating that it is a good trapping material. We have also found, however, that when these traps were used, the sensitivity decreased with increasing measurement number, especially when new traps were used. The magnitude of decrease was found to depend on the measurement frequency. For instance, in a frequency of 10 measurements per day, no significant decrease was observed, but if 10 measurements were completed per hour, a gradual decrease in sensitivity appeared after about 10 measurements, and, sometimes even, no signals were observed after about 40 measurements. We found that letting the GC column stay at the measurement temperature or higher overnight, the sensitivity returned to normal. On the next day, however, the same pattern in the sensitivity was observed again. The reason for this is probably because the Tenax® is a polymer containing numerous volatile compounds such as aromatic hydrocarbons. The volatile compounds from the Tenax® may release to and deposit on the GC column while heating the Tenax® trap at a higher temperature for desorbing organo-Hg species resulting in interference in the GC process.

Based on the above explanation, in order to protect the GC column from the deposition of the volatile compounds released from the Tenax® trap, a precolumn was inserted between the Tenax® trap and GC column, and was kept at room temperature. The precolumn was constructed by packing a small amount of OV-3, the same material as used for packing the GC column, into the same quartz tubing as used for packing the Tenax® trap [1]. After inserting this precolumn, the gradual decrease in the sensitivity with increasing measurement number was no longer observed, thus, the interference was eliminated. It was indicated that here the precolumn played the role of a filter, and the compounds released from the Tenax® could not go through the precolumn at room temperature, while the organo-Hg compounds can go through with no retention. The only problem is that after inserting the precolumn, the peaks broadened and the retention time extended, thus the peak height sensitivity decreased and the throughput reduced. To avoid this problem, the amount of OV-3 used for packing the precolumn was minimized. The optimal amount was found to be about 20 mg. Further, to shorten the retention time the temperature of the GC column was slightly increased. Both the peak height sensitivity and the throughput were finally compensated. We cleaned the precolumn every day before starting the analysis by heating it with the wire used for heating the trapping column to desorb the organo-Hg species [1] at about 200°C for 5 min, while disconnected from the GC column. A precolumn can be used for at least 6 months with excellent protection efficiency.

17 April 1995

## References

[1] N.S. Bloom, Determination of picogram levels of methylmercury by aqueous phase ethylation, followed by cryogenic gas chromatography with cold vapor atomic fluorescence detection, Can. J. Fish Aq. Sci., 46 (1989) 1131–1140.
[2] L. Liang, M. Horvat and N.S. Bloom, An improved speciation method of mercury by GC/CVAFS after aqueous phase ethylation and room temperature precollection, Talanta, 41 (1994) 371–379.

Lian Liang
Department of Environmental Medicine
University of Rochester
575 Elmwood Avenue
Box EHSC
Rochester, NY 14642, USA

Milena Horvat
IAEA-MEL
19 Avenue des Castellans
MC 98012, Principality of Monaco

Paul Danilchik
Brooks Rand, Ltd.
3950 6th NW
Seattle, WA 98107, USA

ELSEVIER

Talanta 42 (1995) 987–997

Talanta

# Investigation of the contact charge transfer absorption of organic solvents with oxygen for use in oxygen determination

Ming Fat Choi *, Peter Hawkins

*Faculty of Applied Sciences, University of the West of England, Coldharbour Lane, Frenchay, Bristol, BS16 1QY, UK*

Received 4 March 1994; accepted 13 April 1994

**Abstract**

The contact charge transfer (CCT) absorption spectra of dimethylsulphoxide (DMSO), *N,N*-dimethylformamide (DMF), *N,N*-dimethylacetamide (DMA), ethanol, methanol, water, benzene (Bz), *N,N'*-diethylaniline (DEA), *N,N'*-dimethyl-*p*-toluidine (DMT) and *N,N'*-diethyl-*p*-toluidine with molecular oxygen have been investigated. These solvents form strong ultraviolet/visible CCT absorption spectra with intensities that are related to the partial pressure of the applied oxygen. DMSO, DMF, DMA, Bz, DEA and DMT are shown to form 1:1 molecular contact complexes with molecular oxygen. A simple oxygen sensing system is described using CCT absorption spectroscopy of DMT at a wavelength of 400 nm, with a gas flow rate of 60 $cm^3$ $min^{-1}$ through the solvent in a cuvette with a pathlength of 1 cm. Inexpensive plastic fibres are used to relay the light from a xenon lamp source to the cuvette and back to a photo-detector. The response of the sensing system to changes in oxygen concentration is reversible, non-linear and in good agreement with the Beer–Lambert law. The most sensitive response region is from 0 to 20% $O_2$ with a change in signal level of about 35%. The solvent used shows no deterioration in performance over a long period and can be used to determine gaseous oxygen concentrations from 0 to 100%. It does not respond to carbon dioxide.

## 1. Introduction

The determination of oxygen concentrations in various gaseous and liquid samples, and biological fluids has important applications in environmental, clinical and analytical chemistry, and oxygen concentrations are often closely related to the progress of many chemical and biochemical reactions. Considerable effort has been devoted over many years to the development of new techniques for the measurement of the oxygen concentrations. A very common oxygen sensor is the Clark-type electrode, which is one form of a direct amperometric gas sensor, or its modifications [1,2]. It is easily calibrated and has a relatively rapid response. However, this electrode usually requires a steady supply of oxygen to the sensor surface for a reliable response as it consumes oxygen (irreversible), and so is not recommended for use in a very small static sample. It also has a limited working life and is easily poisoned by $H_2S$, proteins and various organic compounds. Other electrochemical oxygen sensors have been developed, including conductometric sensors [3] and potentiometric sensors [4–6]. One alternative to the electrochemical oxygen sensors uses the paramagnetic nature of molecular oxygen to alter the force of attraction between a diamagnetic material and a steady magnetic field [7]. This system has limited applications and cannot be used with liquid samples. Other alternative methods are the luminescence-based optical fibre sensors which have increased in importance in recent years. The sensor is usually made from a fluorescent

* Corresponding author.

compound attached to the tip of a fibre-optic cable. Excitation light, after passing along a light fibre, interacts with the fluorescent compound and the fluorescence, picked up by the same or another fibre, is transmitted to a detector. The principle of the measurement is based upon the fluorescence quenching or lifetime changes of the fluorescent compound exposed to different oxygen concentrations [8–12]. Unfortunately, the optical fibre fluorosensors are subject to several limitations such as: the time-consuming preparation of the sensing material; poor long-term stability of the sensing material; and a generally limited dynamic range. Another type of fibre-optic sensor is based on the absorption change of a metallic-organic compound; however, its response is also pH-dependent [13].

It has been found that some organic solvents exhibit new absorption bands when in contact with oxygen [14]. Tsubomura and Mulliken [15] concluded that this is caused by the formation of contact charge transfer (CCT) pairs between the organic solvents and molecular oxygen. A theoretical investigation of the absorption spectra caused by oxygen has also been given by them. Molecular oxygen acting as an electron acceptor via its triplet electronic state ($^3O_2$) can form a donor–acceptor (D–$^3O_2$) contact pair with some solvents acting as electron donors (D). Radiation absorbed by the ground state D–$^3O_2$ contact pair gives an excited state (D–$^3O_2$)* which subsequently dissipates the excess energy via several different possible mechanisms. If the difference in energy between the excited and ground states is relatively small, especially for those donors with low ionization potentials, then de-excitation to the ground state usually occurs without any photodecompostion of the donor and the acceptor [16]. The CCT absorption bands lie in longer wavelength regions if the solvents have lower ionization potentials, and usually appear as extensions to the long wavelength edge of the absorption spectra of the de-oxygenated solvents. The peaks of the CCT absorption bands are generally masked by the much stronger absorption bands of the solvent itself. The CCT absorption intensity of the organic solvents is also related to the partial pressure of oxygen in the gas mixtures above the solvents, and the reaction between the solvents and oxygen is reversible [17].

The purpose of the investigation was to study the CCT absorption spectra of a number of different solvents with oxygen and then to explore the possibility of building a simple detecting system for oxygen using one of the solvents. The solvents studied in the investigation were dimethylsulphoxide (DMSO), *N,N*-dimethylformamide (DMF), *N,N*-dimethylacetamide (DMA), ethanol (EtOH), methanol (MeOH), water ($H_2O$), benzene (Bz), *N,N'*-diethylaniline (DEA), *N,N'*-dimethyl-*p*-toluidine (DMT) and *N,N'*-diethyl-*p*-toluidine (DET). The results of this investigation show that DMT has strong CCT absorption bands extending into the visible region and it was chosen for use in the detecting system for oxygen. This detecting system has several advantages: inexpensive plastic optical fibre can be used; DMT is inexpensive and readily available (without the time-consuming preparation of oxygen-sensitive material); it can detect a wide range of concentrations of gaseous oxygen; it can possibly be further developed into a multi-analyte sensing system; the solvent used is stable for a long period without loss of sensitivity.

## 2. Experimental

### 2.1. Chemicals and reagents

DMSO (99.9%, HPLC grade), acetonitrile (MeCN, >99.9%, HPLC grade), DMA (>99.9%, HPLC grade), DMF (>99.9%, HPLC grade), DEA (>99%), DMT (>99%), MeOH (>99.9%, HPLC grade), EtOH (denatured with 5% isopropyl alcohol, HPLC grade), Bz (>99.9%, HPLC grade) and *n*-heptane (99%, spectrophotometric grade) were purchased from Aldrich. DET (99%) was obtained from Kodak Laboratory Research Products, UK. Water was deionized by the Purite R0200-Stillplus HP system. 'White spot' nitrogen gas (oxygen free), oxygen gas, carbon dioxide and hydrogen gas were obtained from BOC Limited, UK.

### 2.2. The gas mixing system

The gas mixing system is shown in Fig. 1. Different oxygen concentrations (in the range 0–100%) in the gas stream were produced by controlling the flow rates of the oxygen and the diluent nitrogen gas entering the mixing chamber. The gas mixture was passed through a portable oxygen meter (Oxywarn 100I from

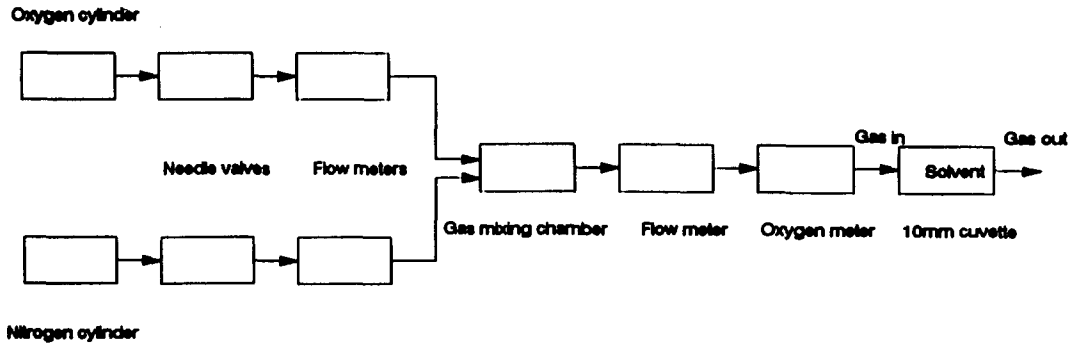


Fig. 1. Schematic diagram of the gas mixing system for generating oxygen standards.

Draeger Manufacturing, UK), where the oxygen concentration in the gas mixture was determined before passing through the solvent contained in a 1 cm pathlength spectrophotometer cuvette.

### 2.3. Instrumentation

CCT absorption spectra were measured on a Perkin-Elmer Lambda 15 Spectrophotometer. In the sensing system for oxygen, a laboratory-made optical system was set up (Fig. 2). An intense beam of ultraviolet/visible (UV/vis) radiation of a known wavelength was produced using the internal 150 W xenon lamp and monochromator (bandpass width 34 nm) of a Perkin-Elmer MPF-3 Fluorescence Spectrophotometer, and then modulated by passing it through a frequency-stabilized light chopper operating at a frequency of 211 Hz (Model 9000 from Monolight Instruments, UK) before being launched into a bundle of plastic optical fibres (1 m length and 2 mm diameter from RS Components, UK). The transmitted radiation from the fibres irradiated the front surface of a 1 cm quartz cuvette containing 3 ml of the solvent, with gaseous oxygen standards continuously passing through it at a flow rate of 60 $cm^3$ $min^{-1}$. A second bundle of plastic fibres (each of 0.5 m length, 2 mm diameter) was placed on the back surface of the cuvette to collect the transmitted light. The other end of this bundle led directly onto the front surface of a 100 $mm^2$ silicon photo-voltaic detector (RS Components, UK), and the output signal connected to a Bentham 277 current pre-amplifer and a Bentham 223 lock-in amplifer (Bentham Instruments Ltd, UK) which was synchronised to the modulated light beam by a reference signal provided by the light chopper. The signal from the amplifier was recorded on a Gould BS-271 recorder (Gould Bryans Instrument Ltd., UK) or displayed on a Bentham 217 digital unit.

## 3. Results and discussion

### 3.1. The CCT absorption spectra of the solvents using the spectrophotometer

Corrections for the UV/vis absorptions were done automatically by filling the reference beam cuvette in the spectrophotometer with the solvents saturated with air. Different oxygen concentrations of the gaseous standards at flow rates of about 30 $cm^3$ $min^{-1}$ were passed through the solvents to be investigated until they were totally gas saturated (about 3 min) and the UV/vis absorption spectra were recorded immediately.

In addition to all the solvents listed above, the CCT absorption spectra for different mole fraction mixtures of DMSO/MeCN, DMF/MeCN, DMA/MeCN, Bz/MeCN, DEA/*n*-heptane and DMT/*n*-heptane were also recorded.

The CCT absorption spectra of $H_2O$, MeCN, MeOH, EtOH, *n*-heptane, Bz, DMSO, DMF, DMA, DMT, DEA and DET with oxygen are shown in Fig. 3. The CCT absorption bands are broad and extend from the UV to the vis regions, depending on the solvent, and are related to the ionization potentials of the individual solvents as described by Jortner and Sokolov [18]. The lower the ionization potential of the solvent, the larger the red-shift of the CCT absorption spectrum. The ionization potentials of these solvents are given in Table 1. The results agree with the conclusions of Jortner and Sokolov; DMT, DEA and DET, with the lowest ionization potentials, have the most red-shifted CCT absorption bands lying in the

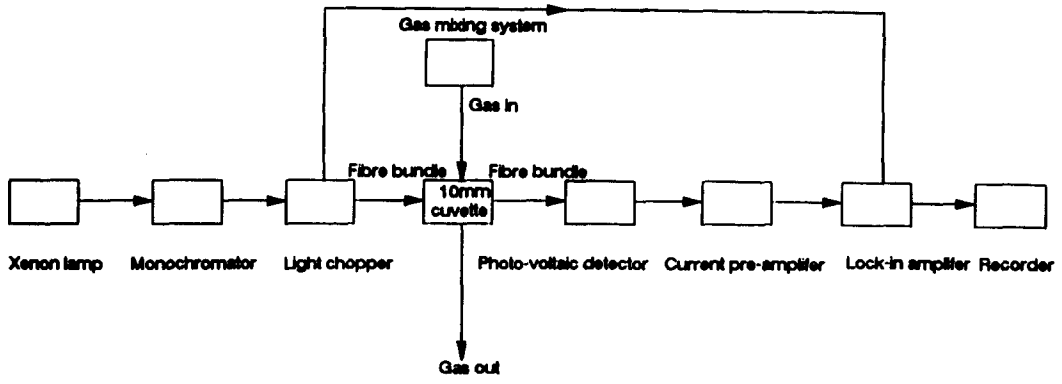


Fig. 2. Schematic diagram of the sensing system for the determination of oxygen.

visible region, whereas MeOH, EtOH, *n*-heptane, Bz, DMSO, DMF and DMA, with higher ionization potentials, have CCT absorption spectra in the UV region. $H_2O$ and MeCN, with the highest ionization potentials of the solvents investigated, have a CCT absorption band extending possibly into the vacuum UV region. The CCT absorption bands disappear when the dissolved oxygen is removed by purging the solvents with nitrogen, carbon dioxide or hydrogen. The CCT absorption band maxima could not be determined accurately in the region under investigation because of the overlap of the continuous bands with the much stronger absorption band of the solvent itself. The apparent CCT absorption band maxima of MeOH, EtOH, *n*-heptane, Bz, DMSO, DMF, DMA, DMT, DEA and DET with oxygen shown in Fig. 3 are almost certainly distorted, particularly at shorter wavelengths (stray effect occurs), by instrumental errors arising when the strong absorption of the solvent itself causes the intensity of the transmitted radiation through the sample and reference cuvettes to fall below the detection limit of the detector in the spectrophotometer. For $H_2O$ and MeCN, the CCT absorption bands appear to have maxima which occur at less than 190 nm and beyond the range of the spectrophotometer.

### *3.2. The effect of oxygen concentration on the CCT absorption spectra*

Suppose $x$ donor molecules, D, react with an oxygen molecule to form a CCT complex D$x$–$O_2$ which is responsible for the CCT absorption:

$$x\mathrm{D} + \mathrm{O_2} \rightleftharpoons \mathrm{D}x\text{–}\mathrm{O_2}$$

The concentration of the D$x$–$O_2$ CCT complex can be represented by

$$[\mathrm{D}x\text{–}\mathrm{O_2}] = K[\mathrm{D}]^x[\mathrm{O_2}] \quad (1)$$

where [D] and [$O_2$] are the mole fractions of donor (in this case, the solvent) and dissolved oxygen respectively, and $K$ is the equilibrium constant. According to the Beer–Lambert law, the absorbance of the D$x$–$O_2$ CCT complex, $A_{O_2}$, will follow the equation

$$A_{\mathrm{O_2}} = [\mathrm{D}x\text{–}\mathrm{O_2}]ba \quad (2)$$

where $b$ is the optical pathlength of the cuvette and $a$ is the molar absorptivity of the CCT complex. Substituting [D$x$–$O_2$] from Eq. (1) into Eq. (2):

$$A_{\mathrm{O_2}} = K[\mathrm{D}]^x[\mathrm{O_2}]ba \quad (3)$$

The mole fraction of the dissolved $O_2$ in a solvent is proportional to the partial pressure of $O_2$, $P_{O_2}$, applied to it. Eq. (3) can be modified to give

$$A_{\mathrm{O_2}} = K[\mathrm{D}]^x(P_{\mathrm{O_2}}/k')ba \quad (4)$$

where $k'$ is Henry's constant for the solvent and oxygen. $K$, $k'$, $b$ and $a$ can be replaced by another constant, $k_1$, and so Eq. (4) can be further reduced to

$$A_{\mathrm{O_2}} = k_1[\mathrm{D}]^x P_{\mathrm{O_2}} \quad (5)$$

As [D] is the concentration of the solvent which can be assumed to remain constant over the range of oxygen concentrations used, the absorbance of the CCT complex will be directly proportional to $P_{O_2}$. This theoretical result is supported by the CCT absorption spectra shown in Fig. 4(a) for DMT. The other solvents were tested and all produced similar results to DMT, but these are not shown in this paper. The graphs in Fig. 4(b), however, show

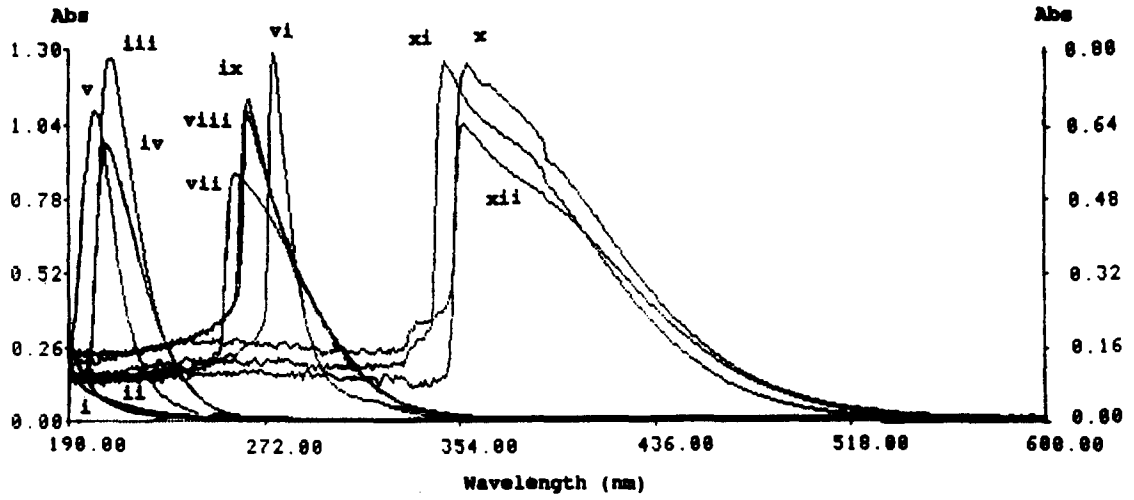


Fig. 3. Effect of oxygen on the CCT absorption spectra of the solvents. Absorbance ranges: (i) $H_2O$, 0.00–0.80; (ii) MeCN, 0.00–0.80; (iii) MeOH, 0.00–1.30; (iv) EtOH, 0.00–1.30; (v) *n*-heptane, 0.00–1.30; (vi) Bz, 0.00–0.80; (vii) DMSO, 0.00–0.80; (viii) DMF, 0.00–0.80; (ix) DMA, 0.00–1.30; (x) DMT, 0.00–1.30; (xi) DEA, 0.00–1.30; (xii) DET, 0.00–1.30. All solvents were saturated with 100% oxygen. The optical pathlength of cuvettes is 1 cm and the reference is the corresponding air-saturated solvent.

the results for all the solvents of $A_{O_2}$ plotted against $P_{O_2}$, where $A_{O_2}$ = absorbance of the solvent containing oxygen with a partial pressure of $P_{O2}$ – absorbance of the solvent saturated with nitrogen, i.e. $P_{O_2} = 0$. The slopes, *y*-intercepts and correlation coefficients of the graphs are tabulated in Table 1, and show that $A_{O_2}$ varies linearly with $P_{O_2}$. Similar straight line graphs are obtained for the solvent when other wavelengths in the CCT absorption bands are used and clearly plots of $A_{O_2}$ against $P_{O_2}$ will have the greatest slope for wavelengths at the maximum of the absorbance peak for the CCT spectrum. However, reliable results can only be obtained using wavelengths near the red end of the CCT absorption spectrum, because of problems caused by the strong absorption of the solvent at the peak of the CCT absorption as described earlier.

### 3.3. The effect of the concentration of the solvent on the CCT absorption

If $P_{O_2}$ is kept constant, Eq. (5) can be expressed as

$$A_{O_2} = k_2[\mathrm{D}]^x \quad (6)$$

where $k_2 = k_1 P_{O_2}$. Taking the logarithm on both sides of Eq. (6), the expression becomes

$$\log(A_{O_2}) = x \log[\mathrm{D}] + \log k_2 = x \log[\mathrm{D}] + k_3 \quad (7)$$

where $k_3$ is a constant. Plotting $\log(A_{O_2})$ against log[D] will produce a straight line graph with a slope equal to $x$. The values of

Table 1
The ionization potential (I.P.) of the solvents [19], and the slopes, *y*-intercepts and correlation coefficients of Fig. 4(b)

| Solvent | I.P. (eV) | Slope ($10^{-3}\%^{-1}$) | *y*-intercept ($10^{-3}$) | Correlation coefficient |
|---|---|---|---|---|
| DMSO | 9.35 [a] | 4.81 | 7.39 | 0.9996 |
| DMF | 9.12 ± 0.02 | 5.06 | 3.63 | 0.9997 |
| DMA | 8.81 ± 0.03 | 4.92 | −1.16 | 0.9970 |
| Bz | 9.24 | 11.69 | −4.43 | 0.9998 |
| MeOH | 10.84 | 16.50 | 8.20 | 0.9995 |
| EtOH | 10.49 | 16.01 | 40.03 | 0.9945 |
| $H_2O$ | 12.6 | 2.01 | −0.28 | 0.9983 |
| DEA | 6.99 | 8.04 | 5.88 | 0.9998 |
| DMT | 7.33 | 10.20 | 4.95 | 0.9995 |
| DET | 6.93 | 8.18 | 7.80 | 0.9988 |

[a] Calculated using Ref. [20]

[D] were varied experimentally by diluting some of the solvents with MeCN or *n*-heptane which have no CCT absorption bands at the wavelengths used and the values of $x$ determined by plotting $\log(A_{O_2})$ against log[D] for a series of DEA/*n*-heptane, DMT/*n*-heptane, Bz/MeCN, DMSO/MeCN, DMF/MeCN and DMA/MeCN mixtures at a particular partial pressure of oxygen. The results for the CCT absorption spectra of DMT/*n*-heptane mixtures are shown in Fig. 5(a). The other solvent mixtures behave in a similar way to the DMT/*n*-heptane mixture, although these results are not reported in the paper. The plots of $\log(A_{O_2})$ against log[D] for all the solvent mixtures are shown in Fig. 5(b). The results in Table 2 show that the slope of each line is close to unity, which means that in each case the CCT complex is formed from one donor and one oxygen molecule. In the analysis of the results, it has been assumed that for a particular series of solvent mixtures, the concentration of dissolved oxygen (or Henry's constant) is the same in each case: this assumption is reasonable since, even for the most dilute mixture used, the solvent concentration is much greater than the concentration of dissolved oxygen.

### 3.4. The design of a sensing system for oxygen

The experimental results of the CCT absorption spectra of the solvents show that DMT is

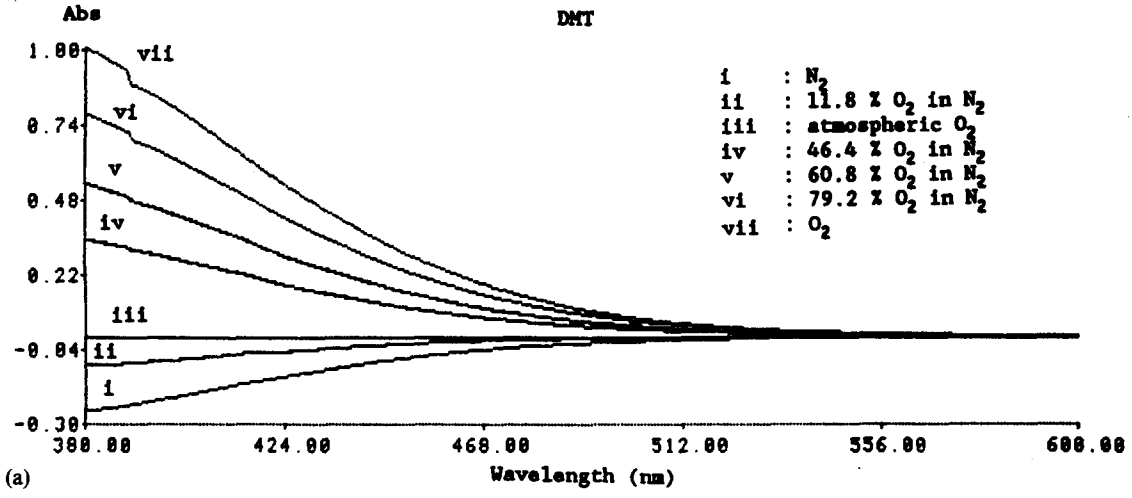


(a)

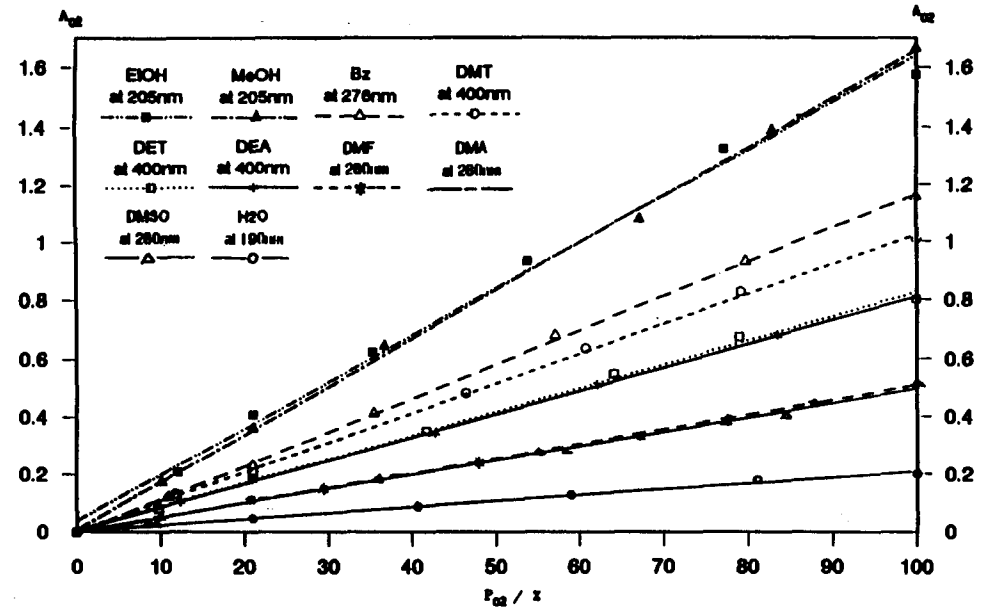


(b)

Fig. 4. (a) Effect of different oxygen concentrations on the CCT absorption spectra of DMT. The optical pathlength of the cuvettes is 1 cm and the reference is air-saturated DMT. (b) Effect of different oxygen concentrations on the CCT absorption of the solvents. The plots are the absorbance of the solvent, $A_{O_2}$, at the wavelengths shown for the different solvents against the partial pressure of applied oxygen, $P_{O_2}$ in the solvent.

a promising solvent to be used in the development of a sensing system for oxygen. It has a CCT absorption spectrum extending well into the visible region so it can be used with inexpensive plastic fibres; it is also more sensitive to oxygen than DEA or DET. In addition, many amino compounds like DMT, exhibiting CCT absorption, do not result in any products on irradiation and are recovered unchanged [16]; it is also an inexpensive and readily available solvent. Using the apparatus described earlier (Fig. 2), the response, reproducibility and total signal change of the sensing system were investigated with light at a wavelength of 400 nm and gas at a flow rate of 60 $cm^3$ $min^{-1}$ through the solvent in a 1 cm pathlength cuvette. Fig. 6 shows the response of the sensing system to step changes in gas concentrations from 100% $O_2$ to 100% $N_2$ (0%$O_2$) and back to 100% $O_2$, and then from 100% $O_2$ to 100% $CO_2$ (0% $O_2$) and back again to 100% $O_2$. The reversibility of the sensing system is good and there is no cross interference from $CO_2$. The response time is 1.3 min and 2.2 min for a 90% signal change from $N_2$ to $O_2$ and from $O_2$ to $N_2$, respectively.

The response of the sensing system when subjected to different levels of oxygen was investigated (Fig. 7). As expected, the decrease in signal level with increasing oxygen concentration is non-linear (Fig. 8(a)). The sensitivity (indicated by the slope of the graph) decreases as the concentration of oxygen increases and

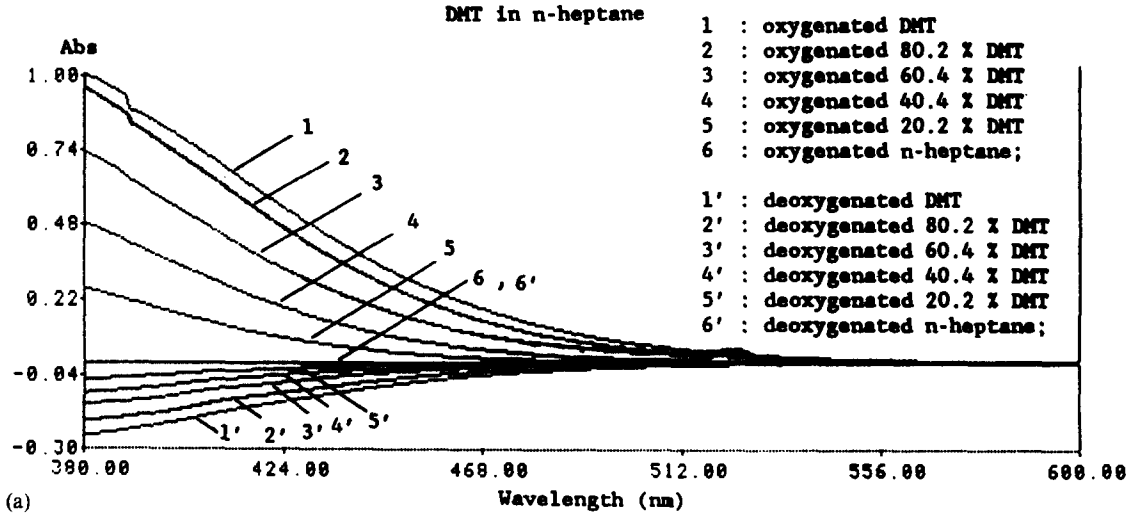


(a)

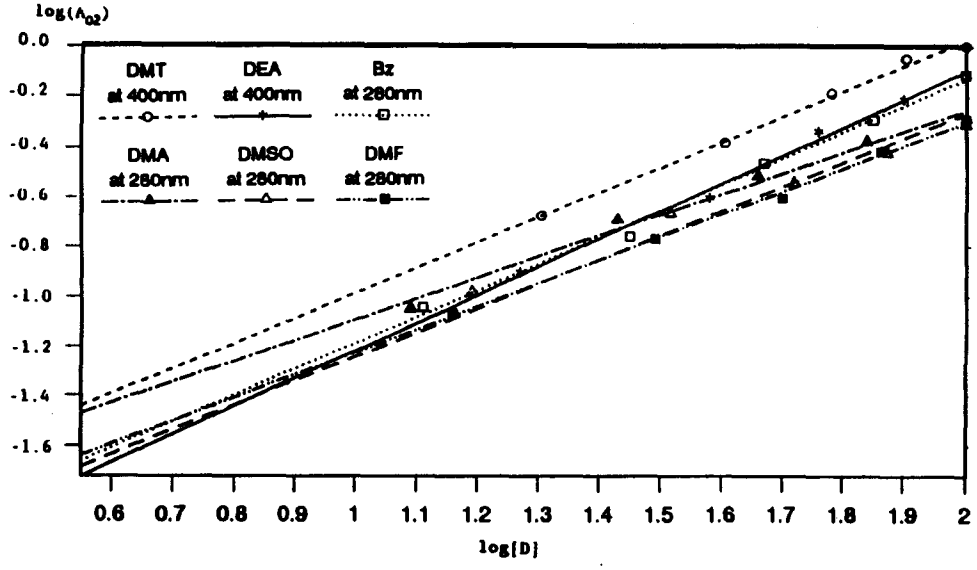


(b)

Fig. 5. (a) CCT absorption spectra of DMT/*n*-heptane solvent mixtures. Solvent mixtures are in mole percentages. The measurement conditions are the same as Fig. 4(a). (b) Effect of the concentration of the different solvents [D] on CCT absorption. Plots of $\log(A_{O_2})$ against log [D].

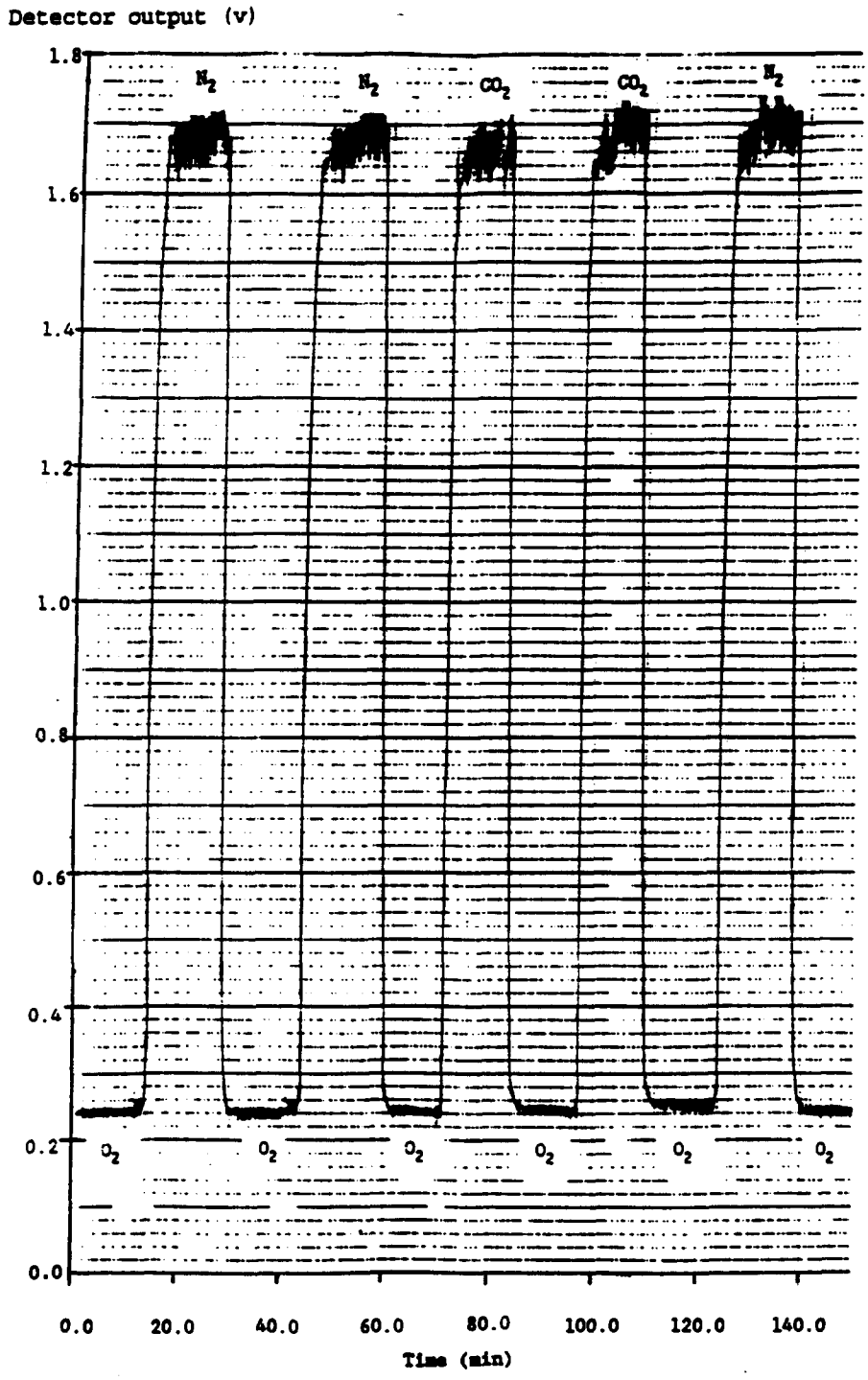


Fig. 6. Response time, reproducibility and total signal change of the sensing system for oxygen when subjected to rapid changes between oxygen → nitrogen → oxygen and oxygen → carbon dioxide → oxygen. 3.0 ml of DMT in a 1 cm cuvette was used with light of wavelength 400 nm and a gas flow rate through the DMT of 60 $cm^3$ $min^{-1}$.

the most sensitive region is between 0 and 20% $O_2$ with about a 35% change in signal level. The sensing system responds over the range 0–100% $O_2$ with a response which is in agreement with the Beer–Lambert law, so that a linear graph (slope = 0.008 21% and correlation coefficient = 0.9968) is obtained when $\log(I_{N_2}/I_{O_2})$ is plotted against $[O_2]$; $I_{N_2}$ is the signal level recorded in nitrogen only (i.e. $[O_2] = 0$) and $I_{O_2}$ is the level recorded in a gas mixture having an oxygen concentration of $[O_2]$ (Fig. 8(b)).

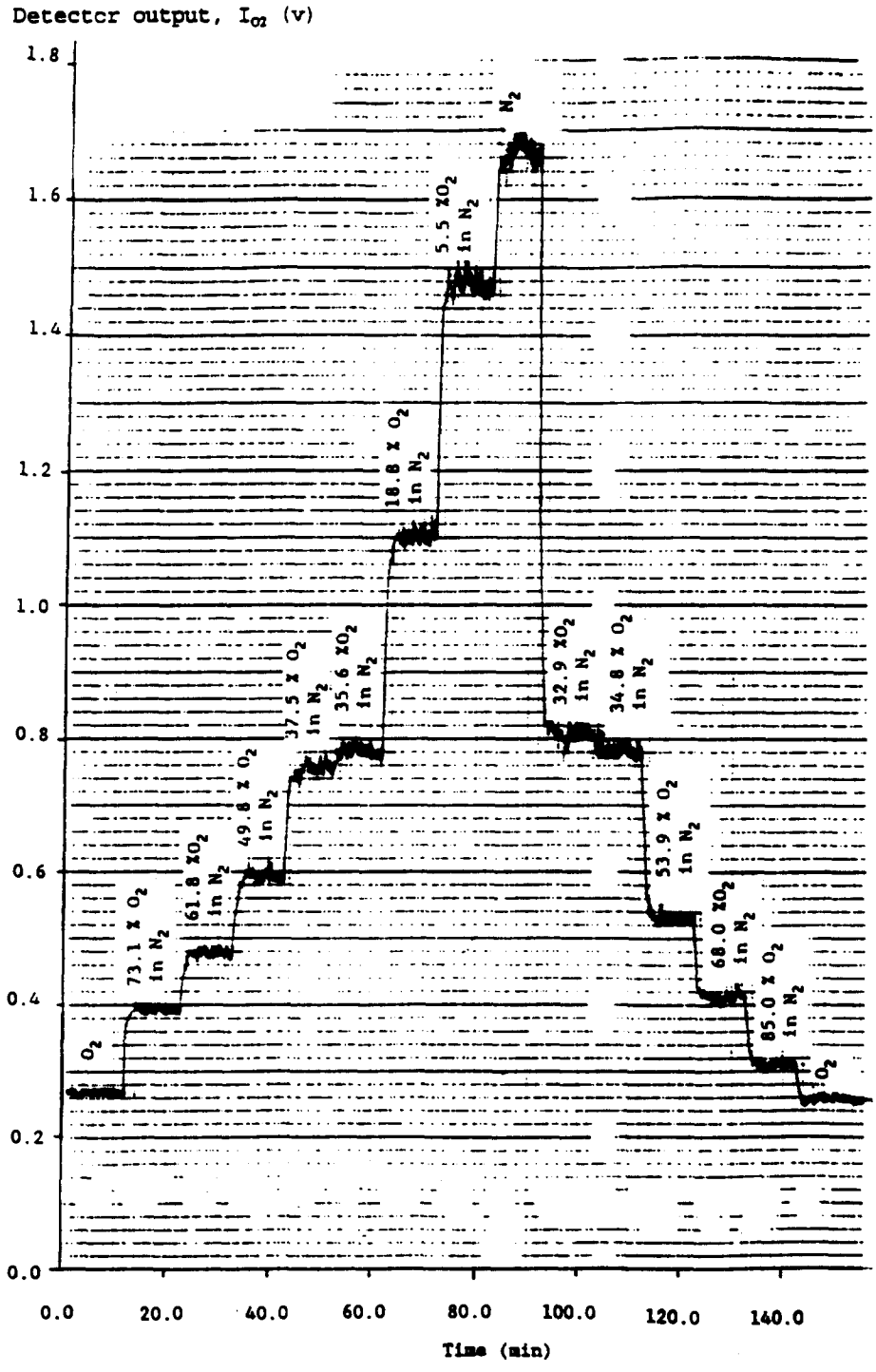


Fig. 7. Variation in output signal level $I_{O_2}$ of the sensing system for oxygen when subjected to different oxygen concentrations. Measurement conditions were the same as in Fig. 6.

The solvent used has very good stability with no noticeable change in the response to oxygen over a long period under the experimental conditions.

## 4. Conclusions

This study demonstrated the possibility of using some aniline derivatives or other solvents

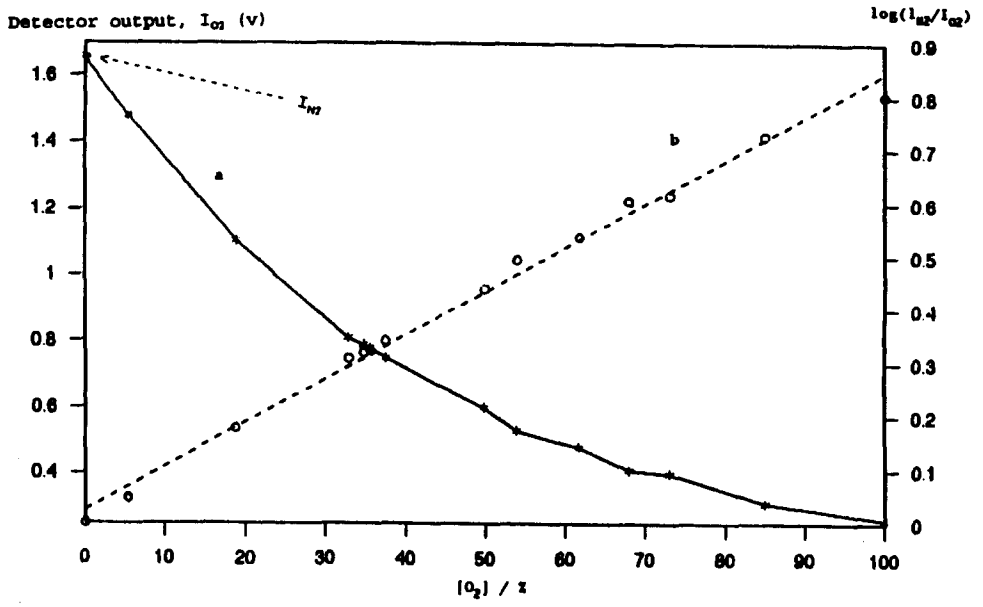


Fig. 8. Graphs plotted using data from Fig. 7. (a) Plot of the detector output ($I_{O_2}$) against $[O_2]$. (b) Plot of $\log(I_{N_2}/I_{O_2})$ against $[O_2]$, where $I_{N_2}$ is the signal level with nitrogen passing through DMT.

having low ionization potentials (e.g. DMT) as an oxygen-sensitive material for the determination of gaseous oxygen. The response time of the above sensing system is slow, but it can be reduced substantially by using a miniaturized, thin-wall cuvette which fits on the end of the fibre bundles. Although the present sensing system is a single wavelength monitoring system, the stability of the signal can be further improved by placing a light beam splitter in front of the cuvette and ratioing the output of the sample beam to the output of the reference beam. A further advantage of using DMT is that other analyte-sensitive materials can be incorporated to give a multi-analyte-sensitive material. An example is the dissolution of the pH-sensitive dye in the solvent for simultaneously sensing oxygen (based on the CCT absorption of solvent) and carbon dioxide (based on the change of absorbance of dye). Some of our preliminary experiments show that the principle is working, and further investigation is still being undertaken. One possible disadvantage of the sensing system is the cross interference from strong acidic gases such as hydrogen chloride [15] and other electron acceptors such as nitric oxide [18].

Table 2
The slopes, $y$-intercepts and correlation coefficients of Fig. 5(b)

| Solvent | Slope | $y$-Intercept | Correlation coefficient |
|---|---|---|---|
| DEA | 1.12 | −2.34 | 0.9973 |
| DMT | 1.01 | −2.00 | 0.9979 |
| Bz | 1.06 | −2.24 | 0.9965 |
| DMSO | 0.98 | −2.22 | 0.9938 |
| DMF | 0.92 | −2.15 | 0.9985 |
| DMA | 0.84 | −1.93 | 0.9943 |

## Acknowledgements

The authors would like to express their thanks to Dr. A. Tubb for the use of his oxygen meter and to the University of the West of England, Bristol, for providing the financial support.

## References

[1] M.L. Hitchman, Measurement of Dissolved Oxygen, Wiley, New York, 1978, pp. 132–138.
[2] T.W. Rejda, J.D.N. Bunschoten and G.A.J. Kalis, Anal. Chim. Acta, 190 (1986) 275.
[3] E.Y. Gutman and I.A. Myasnikov, Sensors Actuators, B1 (1990) 210.
[4] S.V. Chernov, A.L. Moskvin, A.N. Katruzov and I.V. Murin, Zh. Anal. Khim., 45 (1990) 1668; Anal. Abstr., 53 (1991) 11A61.
[5] J.P. Lukaszewicz, N. Miura and N. Yamazoe, Sensors Actuators, B1 (1990) 195.
[6] H.-S. Yim and M.E. Meyerhoff, Anal. Chem., 64 (1992) 1777.

[7] M.L. Hitchman, Measurement of Dissolved Oxygen, Wiley, New York, 1978 pp. 178–182.
[8] O.S. Wolfbeis and F.M. Carlini, Anal. Chim. Acta, 160 (1984) 301.
[9] O.S. Wolfbeis, H.E. Posch and H.W. Kroneis, Anal. Chem., 57 (1985) 2556.
[10] J.R. Bacon and J.N. Demas, Anal. Chem., 59 (1987) 2780.
[11] M.E. Lippitsch, J. Pusterhofer, M.J.P. Leiner and O.S. Wolfbeis, Anal. Chim. Acta, 205 (1988) 1.
[12] P.Y.F. Li and R. Narayanaswamy, Analyst, 114 (1989) 1191.
[13] A.D. Bianco, F. Baldini, M. Bacci, I. Klimant and O.S. Wolfbeis, Sensors Actuators, B11 (1993) 347.
[14] D.F. Evans, J. Chem. Soc., (1953) 345.
[15] H. Tsubomura and R.S. Mulliken, J. Am. Chem. Soc., 82 (1960) 5966.
[16] K. Onodera, G. Furusawa, M. Kojima, M. Tsuchiya, S. Aihara, R. Akaba, H. Sakuragi and K. Tokumaru, Tetrahedron, 41 (1985) 2215.
[17] A.U. Munck and J.F. Scott, Nature, 177 (1956) 587.
[18] J. Jortner and U. Sokolov, J. Phys. Chem., 65 (1961) 1633.
[19] R.C. Weast (Ed.), CRC Handbook of Chemistry and Physics, CRC Press, Boca Raton, FL, 65th edn., 1984, pp. E70–76.
[20] MOPAC 93, General Molecular Orbital Package, Quantum Chemistry Programme Exchange, 1993.

ELSEVIER

Talanta 42 (1995) 999–1004

Talanta

# A polymer membrane potentiometric sensor for silver

Marie-Rose M. Bates, Terence J. Cardwell, Robert W. Cattrall *, Leslie W. Deady, C. Grace Gregorio

*Centre for Scientific Instrumentation, School of Chemistry, La Trobe University, Bundoora, Vic. 3083, Australia*

Received 22 December 1994; revised 4 January 1995; accepted 13 January 1995

**Abstract**

Four new sulfur-containing compounds based on pyridine, benzene, 1,8-naphthyridine and 1,10-phenanthroline have been synthesized. These molecules have been incorporated into a polymeric matrix as neutral carriers and evaluated as silver sensors. Two of the compounds (pyridine and benzene) show high selectivity for $Ag^+$. The sensor with the pyridine-based compound, in particular, shows near-Nernstian response and good sensitivity towards $Ag^+$ with a short response time (<10 s), making it ideal for use in flow analysis.

## 1. Introduction

A significant number of macrocycles ranging from crown ethers to acyclic dithia benzene derivatives have been reported to possess good to excellent selectivity for silver when used in polymeric membrane electrodes [1–7]. The affinity exhibited by these molecuels for this $d^{10}$ metal is primarily due to the presence of sulfur atoms that serve as donor atoms for complexation.

We previously reported a work [8] describing a series of pyridine-based macrocycles containing sulfur and/or oxygen atoms in a two- to six-atom bridge unit. The reagents containing sulfur atoms showed high bonding affinities for class b acceptors, particularly silver and mercury. The ionophores in this series all contained an octyloxy group in the pyridine ring to convey lipophilicity to the molecule, making it more compatible with poly(vinyl chloride) which was used as the matrix in the sensor membrane.

We have carried out further work on sulfur-containing molecules for use in sensors for the silver ion, which are described in this paper. The four molecules studied are all open chain thiol esters based on pyridine, benzene, 1,8-naphthyridine and 1,10-phenanthroline. The molecules which have been synthesized and investigated are shown in Fig. 1. It is interest-

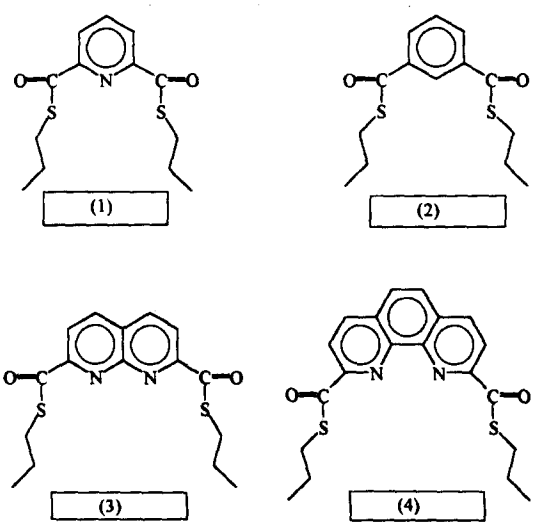


Fig. 1. Structures of pyridine thiol ester (1), benzene compound (2), naphthyridine compound (3) and phenanthroline compound (4).

* Corresponding author.


*SSDI* 0039-9140(95)01533-7

ing to note that these compounds, dissolved in a suitable plasticizer, showed good compatibility with PVC without the necessity of having a long alkyl chain in their structure.

## 2. Experimental

### 2.1. Preparation of compounds

The synthesis of the four compounds was similar in that the appropriate dicarbonyl chloride was reacted with propanethiol. The reaction to form the benzene derivative took longer and produced a yellow oil, while the other three eventually produced solids.

*(a) S,S-Dipropyl-2,6-pyridinedicarbothiolate (1)*

A mixture of 2,6-pyridinedicarboxylic acid (5.0 g), thionyl chloride (20 ml) and a drop of dimethylformamide was refluxed for 3 h. The thionyl chloride was removed in vacuo and the dicarbonyl chloride was recrystallized from light petroleum (b.p. 60–90 °C) before being used immediately in the next step.

Propanethiol (6 ml) was added to the dicarbonyl chloride and dichloromethane (50 ml) in a flask protected by a calcium chloride drying tube. The mixture was refluxed for 1 h. The cooled solution was then washed with NaOH (10%) (3 × 50 ml) and water (3 × 50 ml). The organic layer was separated, dried ($MgSO_4$) and the solvent evaporated to leave white crystals, which were recrystallized from methanol/water (15:1) to give the thiol ester (1) (5.28 g, 71%), m.p. 40–42 °C. $^1$H NMR ($CDCl_3$, 90 MHz) $\delta$: 1.18, t, $J$ 9 Hz, $CH_3$; 1.85, h, $J$ 9 Hz, $CH_2\underline{CH_2}CH_3$; 3.18, t, $J$ 9 Hz, S-$CH_2$; 8.05–8.38, m, ArH. Analysis: Calcd. for $C_{13}H_{17}NO_2S_2$: C, 55.1; H, 6.0; N, 4.9. Found: C, 55.4; H, 6.3; N, 5.2.

*(b) S,S-Dipropyl-1,3-benzenedicarbothiolate (2)*

The thiol ester (2) was prepared as for 1 from isophthaloyl dichloride (2 g) and propanethiol (2 ml), and refluxed for 8 h, to give a yellow oil. $^1$H NMR $\delta$: 1.13, t, $J$ 9 Hz, $CH_3$; 1.80, h, $J$ 9 Hz, $CH_2\underline{CH_2}CH_3$; 3.20, t, $J$ 9 Hz, S-$CH_2$; 7.62, t, $J$ 8 Hz, H-5; 8.25, d, $J$ 8 Hz, H-4,6; 8.65, s, H-2.

*(c) S,S-Dipropyl-1,8-naphthyridine-2,7-dicarbothiolate (3)*

The thiol ester (3) was prepared as for 1 from 1,8-naphthyridine-2,7-dicarbonyl chloride [9] (0.7 g) and propanethiol (1 ml) to yield a red viscous oil, which was solidified in dry ice/acetone and then recrystallized repeatedly from hexane to yield a yellow solid (50 mg), m.p. 77–79 °C. $^1$H NMR $\delta$: 1.10, t, $J$ 9 Hz, $CH_3$; 1.80, h, $J$ 9 Hz, $CH_2\underline{CH_2}CH_3$; 3.12, t, $J$ 9 Hz, S-$CH_2$; 8.24 + 8.50, d + d, $J$ 9 Hz, ArH. Analysis: Calcd. for $C_{16}H_{18}N_2O_2S_2$: C, 57.5; H, 5.4; N, 8.4. Found: C, 57.4; H, 5.6; N, 8.3.

*(d) S,S-Dipropyl-1,10-phenanthroline-2,9-dicarbothiolate (4)*

The thiol ester (4) was prepared as for 1 from 1,10-phenanthroline-2,9-dicarbonyl chloride [9] (0.8 g) and propanethiol (1 ml) to yield a solid which was recrystallized from methanol (0.5 g; 50%), m.p. 133–135 °C. $^1$H NMR $\delta$: 1.17, t, $J$ 9 Hz, $CH_3$; 1.89, h, $J$ 9 Hz, $CH_2\underline{CH_2}CH_3$; 3.22, t, $J$ 9 Hz, S-$CH_2$; 8.08, s, H-5,6, 8.45 + 8.55, d + d, $J$ 9 Hz, H-3, 4, 7, 8. Analysis: Calcd. for $C_{20}H_{20}N_2O_2S_2$: C, 62.5; H, 5.2; N, 7.3. Found: C, 62.5; H, 5.3; N, 7.3.

### 2.2. Construction of electrodes

Mixtures of poly(vinyl chloride) (34 mg), *o*-nitrophenyl-*n*-octylether (NPOE) (63.5 mg), reagent (2 mg) and potassium tetrakis(*p*-chlorophenyl)borate (0.5 mg) were dissolved in 1 ml of freshly purified tetrahydrofuran (THF) [8]. Approximately eight drops of each membrane solution were added dropwise into a glass electrode barrel (length 100 mm; i.d. 3 mm; o.d. 10 mm) clamped vertically onto a glass microscope slide. The solvent was allowed to evaporate and a clear homogeneous membrane was obtained which adhered firmly to the end of the barrel.

An internal reference element (Ag/AgCl) was then fitted inside the electrode barrel which was filled with an appropriate internal solution ($10^{-1}$ M KCl or $KNO_3$ with 2 drops of 0.1 M $AgNO_3$). Electrodes were conditioned overnight in a 0.1 M solution of the primary ion.

An Orion Ag–AgCl double-junction reference electrode with an outer chamber filling solution of 10% $KNO_3$ solution was used in conjunction with the working electrodes. The electrochemical cell for this study was as follows:

Ag–AgCl/internal solution/sensor membrane/test solution//reference electrode.

Potential measurements were made, as previously described [8], with an Orion 901 Iona-

lyzer digital pH/mV meter interfaced to an Apple IIe microcomputer through a switching box to allow evaluation of several electrodes at one time.

### 2.3. Response characteristics

Initial response tests were done in KCl or $KNO_3$ solutions in the concentration range of $10^{-5}$ to $10^{-1}$ M to ensure the electrodes were functioning. Subsequent electrode response studies were done in $Ag^+$ solutions, since $Ag^+$ was found to be the preferred ion based on preliminary selectivity studies performed against $K^+$ as the primary ion. A criterion of stability [8] was employed in all e.m.f. measurements such that the steady-state potential was defined as the value which did not change by more than $\pm 0.1$ mV over a period of 2 min.

### 2.4. Selectivity study

As mentioned above, all the ligands reported here showed a high selectivity for the $Ag^+$ ion, and so further selectivity studies were carried out using $Ag^+$ as the primary ion. The two-point mixed-solution method [10] was used for this purpose. This was carried out by measuring the potential in a $10^{-3}$ M solution $Ag^+$ and then in a mixed solution containing $10^{-3}$ M of $Ag^+$ and $10^{-1}$ M of the interfering ion. Owing to the narrow linear range of compound **2**, a $10^{-4}$ M solution of $Ag^+$ and a mixed solution of $10^{-4}$ M $Ag^+$ and $10^{-2}$ M of the interfering ion were used for the pertinent selectivity study. Selectivity coefficients were then calculated using the Nicolsky equation. Ion activities were estimated using the Debye–Hückel equation.

All inorganic salts were of analytical reagent grade and all solutions were made up in NANO pure water (17 MΩ cm, Barnstead, Dubuque, IA, USA).

### 2.5. Flow system

The flow injection (FI) system used consisted of a Gilson Minipuls 2 peristaltic pump, an automatic injector system [11], a multi-channel potentiometric flowcell [11,12] and a PC-based data acquisition unit. Teflon tubing of 0.5 mm i.d. was used in the manifold.

Data collection and analysis were achieved using the flow control system (FCS) software [13] designed for flow injection work. The software utilizes an A/D card which collects and converts analytical signals from a maximum of eight detectors at a specified sampling rate. Data processing routines such as peak measurement (i.e. height, width, area), data smoothing, noise filtering, baseline correction and statistical analysis are done by the software.

The automatic injector system [11] was composed of two miniature two-way solenoid valves (Lee Co., CT, USA) which deliver the desired sample volume (50 μl for this work) and the carrier solution to the flow injected manifold. The software controls the sample volume injected using an electronically-controlled pulse to switch the solenoid valve on for sample delivery.

The multi-channel potentiometric flowcell [11,12] used in this study is an improved version of a miniature flowcell [14] previously reported in the literature. The flowcell consisted of four silver wires which served as contacts for the $Ag^+$ sensing membrane. The reference electrode was Ag/AgCl with its own reference stream consisting of 0.1 M $NH_4NO_3$ with $10^{-6}$ M $AgNO_3$. The same solution was used as carrier and all standard $AgNO_3$ solutions were made up in 0.1 M $NH_4NO_3$.

### 2.6. Steady-state measurements

Steady-state measurements were done by continuously pumping each silver standard solution into the flowcell until equilibrium was attained.

## 3. Results and discussion

### 3.1. Silver ion response

The potential responses in $AgNO_3$ solutions of the PVC electrodes based on the four neutral carriers synthesized are summarized in Table 1. The pyridine-based neutral carrier (**1**) exhibits Nernstian behavior in the activity range of $10^{-5}$–$10^{-1}$ M, with a slope of 58 mV/decade change in $Ag^+$ activity. The dithiabenzene compound (**2**) shows a near-Nernstian slope of 55 mV/p$Ag^+$ activity in the range of $10^{-4}$–$10^{-2}$ M. However, for the naphthyridine (**3**) and phenanthroline (**4**) based carriers, a non-Nernstian response is observed with slopes of 49 mV/p$Ag^+$ between $10^{-4}$ and $10^{-1}$ M, and 36 mV/p$Ag^+$ between $10^{-4}$ and $10^{-2}$ M,

Table 1
Potential responses of silver-selective membrane electrodes based on ionophores **1–4**

| Compound | % ionophore (m/m) | Slope (mV/pAg$^+$) | Concentration range (M) |
|---|---|---|---|
| **1** | 2% | 58.0 | $10^{-5}$–$10^{-1}$ |
| **2** | 2% | 55.0 | $10^{-4}$–$10^{-2}$ |
| **3** | 1% | 55.0 | $10^{-5}$–$10^{-1}$ |
| **3** | 2% | 49.0 | $10^{-4}$–$10^{-1}$ |
| **3** | 5% | 41.0 | $10^{-4}$–$10^{-1}$ |
| **4** | 2% | 36.0 | $10^{-4}$–$10^{-2}$ |
| **4** | 2% | −53.0 | $10^{-2}$–$10^{-1}$ |

respectively. Attempts were made to improve the response of the former by varying the amount of the reagent. Increasing the ionophore content to 5% (m/m) gave a slope of 41 mV/pAg$^+$ over $10^{-4}$–$10^{-1}$ M, while reducing it to 1% (m/m) improved the slope to 55 mV/pAg$^+$ in the activity range of $10^{-5}$–$10^{-1}$ M.

Very good response times were obtained for compounds **1** and **2**, the $t_{95\%}$ being no more than 10 s with good reproducibility. Significantly slower response times were found for compounds **3** and **4**.

Between $10^{-2}$ and $10^{-1}$ M, the phenanthroline compound (**4**) showed a negative slope of −53 mV/pAg$^+$, a response close to that expected for a monovalent anion. Such behavior has been observed in previous work [8] and is explained as being due to strong complexation of the silver ion by the ligand which inhibits metal ion exchange with the resulting positively charged complex. Such a complex can, however, extract a charge-satisfying anion such as nitrate, thus giving rise to an anion response.

### 3.2. Selectivities

Selectivity coefficients for Ag$^+$ with respect to other cations for the electrodes based on the three ionophores **1**, **2** and **3** are summarized in Fig. 2. It can be seen that the electrodes for the three ionophores are highly selective for the silver ion, particularly in the presence of other heavy metal ions. The one exception to this is Hg$^{2+}$, which irreversibly poisons the membrane in each case. In fact, there is evidence [15] for the pyridine-based ligand that reaction with mercury leads to disintegration of the ionophore structure. Work is continuing on an investigation of this phenomenon [15].

Attempts to carry out selectivity studies for the phenanthroline derivative (**4**) failed because most metal ions interfered strongly and irreversibly. This is not surprising as phenanthroline is known to be a very effective chelating agent for transition metals.

The high selectivity towards Ag$^+$ exhibited by compounds **1** and **2** is an indication that, although the binding between the metal and the ionophores is relatively strong, the complex formed is quite labile. The presence of the sulfur atoms in the propyl side chains, which serve as excellent receptors for the Ag$^+$, is the key factor in the high selectivity demonstrated by ionophores **1** and **2**. This is consistent with previous work describing a number of macrocycles [8], in which oxygen atoms in the rings were substituted by sulfur atoms resulting in much higher bonding affinities towards class b acceptors such as Ag$^+$ and Hg$^{2+}$. This work also demonstrates that it is not necessary to form a macrocyclic ring in order to obtain high selectivity for a particular ion.

The only structural difference between compounds **1** and **2** is the presence of the nitrogen atom in the former. The lower selectivity for Ag$^+$ is attributable to this nitrogen atom which can be involved in complexation, particularly with transition metals.

Compounds **1** and **2** share some similarities with a group of ionophores reported in the literature [7]. The benzene-based compound (**2**) is similar to a family of acyclic dithia benzene derivatives [7] which display a Nernstian response towards Ag$^+$. The main structural difference lies in the presence of the thiocarboxylate groups and two propyl pendant chains in **2**, whereas the reported dithia benzene derivatives either had shorter or longer side chains and no CO functional groups. The same work also reported a group of acyclic $NS_2$ ligands which resembled the parent molecule of compound **1** in a similar way. Although the structural differences between one of the reported molecules and compound **1** are only minor, it is interesting to note that no special selectivity has apparently been found for that particular ligand and the rest of the group.

We have, evidently, developed a highly sensitive and selective silver sensor based on a pyridine thiol ester (**1**), which displays a Nernstian response over a wide concentration range. It also has a very fast response of less than 10 s and exhibits excellent electrode reproducibility.

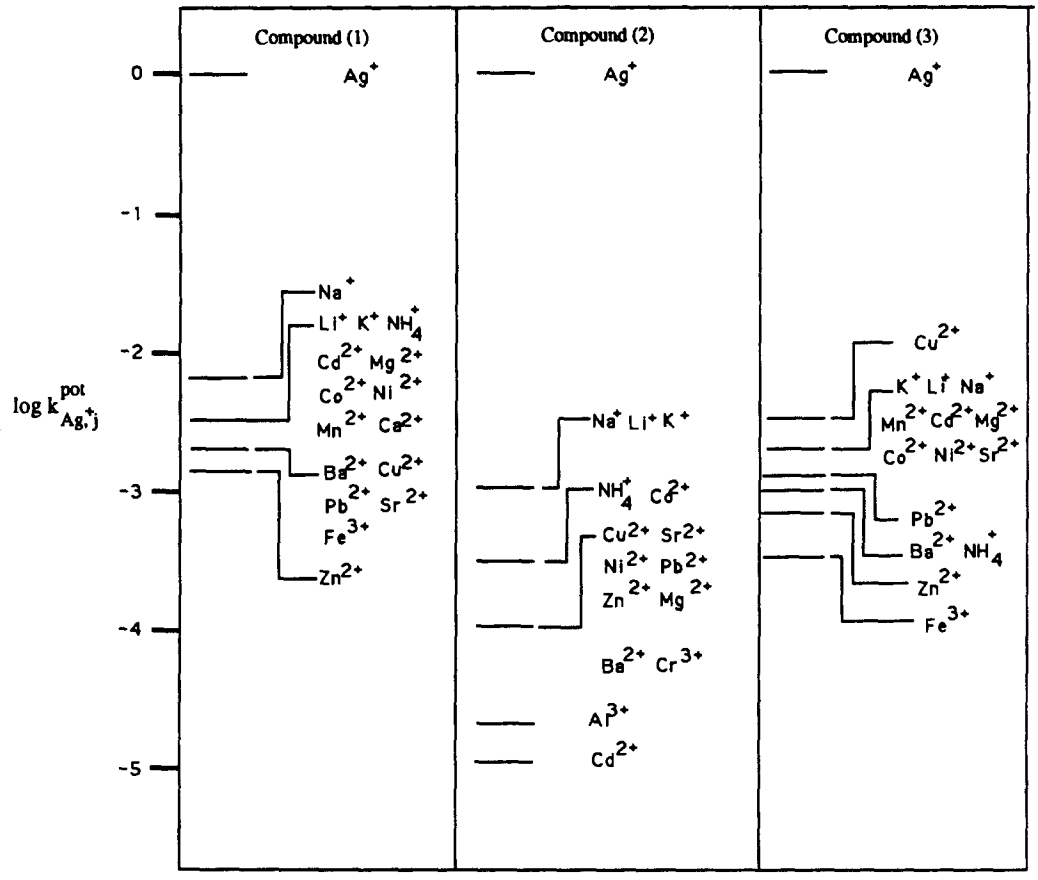


Fig. 2. Selectivities of ionophores 1, 2 and 3 for various metals against $Ag^+$ as the primary ion.

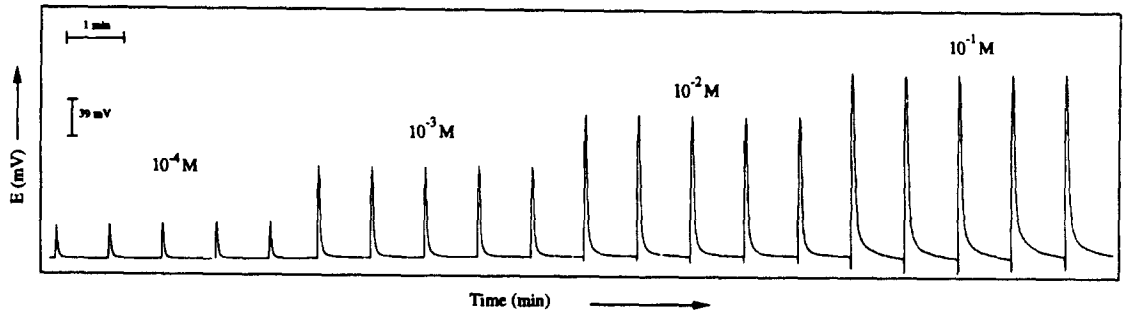


Fig. 3. Typical flow injection calibration plot for the silver-selective sensor based on ionophore 1.

Although the dithiabenzene compound (2) appears to possess good selectivity, its response characteristics are inferior compared to the pyridine thiol ester (1).

Because of its excellent reproducibility and fast response, the sensor has particular advantages in flow analysis. It has been applied to flow injection for the direct measurement of silver, and a typical output generated by the FCS software [13] is shown in Fig. 3. It can be seen that the peaks are very sharp with good precision (RSDs for the peak height measurements of 1% for $10^{-3}$–$10^{-1}$ M and <2% for $10^{-4}$ M).

A typical calibration graph for a range of silver standards with $10^{-4}$–$10^{-1}$ M $Ag^+$ is shown in Fig. 4, and is compared with that obtained from steady-state measurements. It can be seen that the FI calibration is almost identical to the steady-state case which demonstrates the very fast response of the sensor, making it ideal for use in flow injection.

Further work [12] is presently being done on the application of this pyridine-based silver sensor in the indirect determination of chloride in water samples.

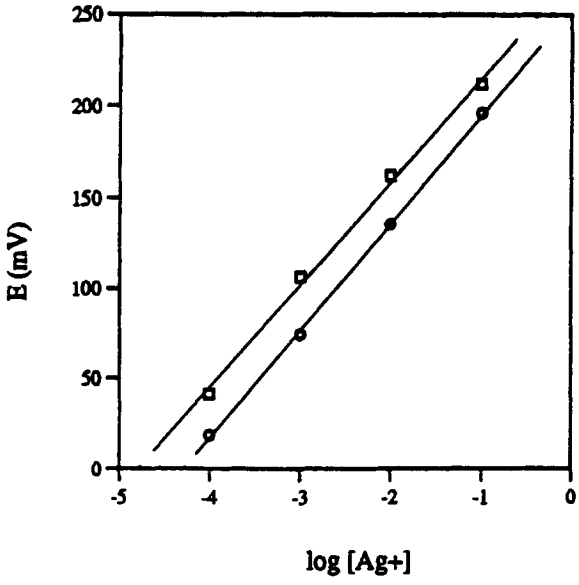


Fig. 4. A comparison of the silver sensor response in steady-state and flow injection modes: □, FI mode; ○, steady-state mode.

## Acknowledgments

We wish to thank the Australian Research Council (ARC) for financial support. One of the authors, C.G. Gregorio, is grateful for an Australian International Development Assistance Bureau award.

## References

[1] M.T. Lai and J.S. Shih, Analyst, 111 (1986) 891.
[2] M. Oue, K. Kimura, K. Akama, M. Tanaka and T. Shono, Chem. Lett., (1988) 409.
[3] M. Oue, K. Akama, K. Kimura, M. Tanaka and T. Shono, J. Chem. Soc., Perkin Trans., 1 (1989) 1675.
[4] K.M. O'Connor, G. Svehla, S.J. Harris and M.A. Mc-Kervey, Anal. Proc., 30 (1992) 137.
[5] K.M. O'Connor, G. Svehla, S.J. Harris and M.A. Mc-Kervey, Talanta, 39 (1993) 1549.
[6] Z. Brzozka, P.L.H. Cobben, D. Reinhouldt, J.J.H. Edema, J. Butler and R.M. Kellogg, Anal. Chim. Acta, 273 (1993) 139.
[7] J. Casabo, T. Flor, M.I. Romero, F. Teixidor and C. Perez-Jimenez, Anal. Chim. Acta, 294 (1994) 207.
[8] M.R.M. Bates, T.J. Cardwell, R.W. Cattrall, L.W. Deady and K. Murphy, Aust. J. Chem., 44 (1991) 1603.
[9] C.J. Chandler, L.W. Deady, J.A. Reiss and V. Tzimos, J. Heterocyc. Chem., 19 (1982) 1017.
[10] K. Srinivasan and G.A. Rechnitz, Anal. Chem., 41 (1969) 1203.
[11] T.J. Cardwell, R.W. Cattrall, G.J. Cross and I.C. Hamilton, unpublished work, 1993.
[12] T.J. Cardwell, R.W. Cattrall and C.G. Gregorio, unpublished work, 1993.
[13] Flow Control System (FCS) software, A-Chem. Technologies, Melbourne, Victoria, Australia.
[14] T.J. Cardwell, R.W. Cattrall, P.C. Hauser and I.C. Hamilton, Anal. Chim. Acta, 358 (1988) 214.
[15] A.M. Bond, R.W. Cattrall and R. Webster, unpublished work, 1994.

ELSEVIER

Talanta 42 (1995) 1005–1006

Talanta

# Book reviews

***Physical Chemistry***, 5th edn., by P.W. Atkins, Oxford University Press, Oxford, 1994, xix + 1031 pp. + about 100 pp. of additional information, softback, £24.00. ISBN 0-19-855730-2.

The first edition of this book appeared in 1978 and there has been a new edition every 4 years. Its low price is a reflection of its popularity and it is claimed by Oxford University Press to be the world's best-selling textbook on physical chemistry. It is certainly purchased in great numbers by students studying chemistry at university.

So what is new for this edition? Well, the most obvious addition is the use of a colour — blue — to enhance many of the diagrams and headings. *Justifications* are also introduced where, for example, derivations of mathematical formulae are presented. This separates some of the in-depth treatment, which may seem daunting at first, from the text. Other details also considered to be somewhat intrusive are given as *Further information* at the end of the book.

The main layout of the text is still in three parts: Part 1—*Equilibrium*; Part 2—*Structure*; and Part 3—*Change*. The 29 chapters are prefixed with chapter 0 which gives an overview of the book's content. New to Part 1 is the introduction of *Molecular interpretations* which show the interpretation of a bulk result in terms of atomic and molecular properties. These interpretations supplement the rigour of thermodynamics and are an addition which will be welcomed by many students. At the end of each chapter a checklist of key ideas is now present, a feature which formerly appeared at the beginning of each chapter. However, each chapter now starts with an abstract of the contents so, overall, the important concepts are more than adequately emphasised.

Numerous problems (with answers) are also presented at the ends of chapters and a separate Solutions Manual may be purchased. In addition there are many worked examples in the text and each of these are clearly explained under the headings: *Method*, *Answer* and *Comment*.

This is a book which attempts to cover a very wide number of topics and hence some will only be dealt with at a cursory level.

A *Further reading* section addresses this criticism where references to articles of general interest and texts and sources of data and information for each chapter are grouped together. I found the treatment of tables in the text somewhat disjointed as some are contained in the relevant chapter, some are presented in a shortened form in the chapter and in a longer form in a *Data section* and others — some short, some long — are only given in the *Data section*.

Many academic staff from the UK and USA have made contributions to the preparation of this book and I am sure this edition will be welcomed by them as many up-to-date changes have been made since the fourth edition. The book must first find favour with academic staff who recommend books for students to purchase. It is to be hoped that the many innovations in the text will find favour amongst both staff and students.

P.J. Cox

***Photochemical Vapor Deposition*** by J.G. Eden, Wiley, Chichester, 1992, xi + 193 pp., £43.95. ISBN 0-471-55083-3.

Photochemical vapour deposition (photo-CVD) is a recent development of CVD, where the introduction of visible or UV light into the CVD reactor opens up new possibilities of reducing film-growth temperatures and for producing novel materials. These materials include abrasion-resistant coatings, epitaxial layers for semiconductor lasers and low scatter films for optical components such as mirrors and beam splitters. This is clearly a topic of enormous technological importance, where experimental techniques may change as a result of ongoing

ELSEVIER

Talanta 42 (1995) 1005–1006

Talanta

# Book reviews

***Physical Chemistry***, 5th edn., by P.W. Atkins, Oxford University Press, Oxford, 1994, xix + 1031 pp. + about 100 pp. of additional information, softback, £24.00. ISBN 0-19-855730-2.

The first edition of this book appeared in 1978 and there has been a new edition every 4 years. Its low price is a reflection of its popularity and it is claimed by Oxford University Press to be the world's best-selling textbook on physical chemistry. It is certainly purchased in great numbers by students studying chemistry at university.

So what is new for this edition? Well, the most obvious addition is the use of a colour — blue — to enhance many of the diagrams and headings. *Justifications* are also introduced where, for example, derivations of mathematical formulae are presented. This separates some of the in-depth treatment, which may seem daunting at first, from the text. Other details also considered to be somewhat intrusive are given as *Further information* at the end of the book.

The main layout of the text is still in three parts: Part 1—*Equilibrium*; Part 2—*Structure*; and Part 3—*Change*. The 29 chapters are prefixed with chapter 0 which gives an overview of the book's content. New to Part 1 is the introduction of *Molecular interpretations* which show the interpretation of a bulk result in terms of atomic and molecular properties. These interpretations supplement the rigour of thermodynamics and are an addition which will be welcomed by many students. At the end of each chapter a checklist of key ideas is now present, a feature which formerly appeared at the beginning of each chapter. However, each chapter now starts with an abstract of the contents so, overall, the important concepts are more than adequately emphasised.

Numerous problems (with answers) are also presented at the ends of chapters and a separate Solutions Manual may be purchased. In addition there are many worked examples in the text and each of these are clearly explained under the headings: *Method*, *Answer* and *Comment*.

This is a book which attempts to cover a very wide number of topics and hence some will only be dealt with at a cursory level.

A *Further reading* section addresses this criticism where references to articles of general interest and texts and sources of data and information for each chapter are grouped together. I found the treatment of tables in the text somewhat disjointed as some are contained in the relevant chapter, some are presented in a shortened form in the chapter and in a longer form in a *Data section* and others — some short, some long — are only given in the *Data section*.

Many academic staff from the UK and USA have made contributions to the preparation of this book and I am sure this edition will be welcomed by them as many up-to-date changes have been made since the fourth edition. The book must first find favour with academic staff who recommend books for students to purchase. It is to be hoped that the many innovations in the text will find favour amongst both staff and students.

P.J. Cox

***Photochemical Vapor Deposition*** by J.G. Eden, Wiley, Chichester, 1992, xi + 193 pp., £43.95. ISBN 0-471-55083-3.

Photochemical vapour deposition (photo-CVD) is a recent development of CVD, where the introduction of visible or UV light into the CVD reactor opens up new possibilities of reducing film-growth temperatures and for producing novel materials. These materials include abrasion-resistant coatings, epitaxial layers for semiconductor lasers and low scatter films for optical components such as mirrors and beam splitters. This is clearly a topic of enormous technological importance, where experimental techniques may change as a result of ongoing

developments. The appearance of this authoritative monograph by Professor Eden is therefore very welcome.

After a brief Introduction in Chapter 1, Chapter 2 covers the fundamental aspects of photo-CVD including a general classification of photo-assisted deposition processes, the optical characteristics of molecular ad-layers and surface kinetics. Chapter 3 deals with reactors, optical sources and all the associated equipment. Subsequent chapters present a systematic overview of the applications of these methods in the deposition of metal films, semiconductors (such as elemental C and Si and various compounds and Ga, for example), dielectrics (such as $SiO_2$ and $Al_2O_3$) and indeed of polymer films.

The presentation throughout is clear and straightforward with easy-to-follow diagrams and useful tables. This book can be commended to industrialists interested in these applications, to experienced researchers, and to new students approaching this topic for the first time.

M.D. Ingram

***Kirk-Othmer Encyclopedia of Chemical Technology***, Vol. 12, 4th edn. (Fuel Resources to Heat Stabilizers, edited by J.I. Kroschwitz and M. Howe-Grant), Wiley, New York, 1994, xxviii + 1091 pp., £185.00. ISBN 0-471-52681-9 (v. 12).

Well over 12 000 pages of this encyclopedia, which contains a wide variety of topics related to chemical technology, have now been published. The entries are arranged in alphabetical order and volume 12 extends to the letter 'H'.

Four different elements and their compounds are covered in this current volume: gallium, germanium, gold and hafnium. In each case physical and chemical properties are given along with details of occurrence, manufacture, economic aspects, analytical procedures, health and safety, and uses.

Several entries deal with fuel. These include fuel resources, fuels from biomass, fuels from waste, fuels — synthetic, furnaces — fuel fired, gas — natural and gasoline, and other motor fuels. Many tables, flow-charts and graphs are included here and as with all entries a substantial number of references are given.

Other entries which clearly relate to chemical engineering include the topics: fusion energy, geothermal energy, geotextiles, groundwater monitoring, hardness, hazard risk analysis and heat-exchange technology.

The related entries — glass, glass-ceramics, glasses (organic–inorganic hybrids) and glassy metals cover over 120 pages with photographs supplementing the tables and figures.

Classes of chemical compounds in this volume include glycols and Grignards and there are separate entries for gelatin and glycerol. Several chemical structures and reactions are presented. Other diverse entries which I found to be of interest — and will no doubt refer to again — deal with fungicides-agricultural, gastrointestinal agents, gemstones, genetic engineering, growth regulators, gums, and hair preparations.

As with previous volumes a wealth of information is presented on a wide variety of diverse topics that should satisfy the intellectual curiosity of most, if not all, chemists.

P.J. Cox

developments. The appearance of this authoritative monograph by Professor Eden is therefore very welcome.

After a brief Introduction in Chapter 1, Chapter 2 covers the fundamental aspects of photo-CVD including a general classification of photo-assisted deposition processes, the optical characteristics of molecular ad-layers and surface kinetics. Chapter 3 deals with reactors, optical sources and all the associated equipment. Subsequent chapters present a systematic overview of the applications of these methods in the deposition of metal films, semiconductors (such as elemental C and Si and various compounds and Ga, for example), dielectrics (such as $SiO_2$ and $Al_2O_3$) and indeed of polymer films.

The presentation throughout is clear and straightforward with easy-to-follow diagrams and useful tables. This book can be commended to industrialists interested in these applications, to experienced researchers, and to new students approaching this topic for the first time.

M.D. Ingram

***Kirk-Othmer Encyclopedia of Chemical Technology***, Vol. 12, 4th edn. (Fuel Resources to Heat Stabilizers, edited by J.I. Kroschwitz and M. Howe-Grant), Wiley, New York, 1994, xxviii + 1091 pp., £185.00. ISBN 0-471-52681-9 (v. 12).

Well over 12 000 pages of this encyclopedia, which contains a wide variety of topics related to chemical technology, have now been published. The entries are arranged in alphabetical order and volume 12 extends to the letter 'H'.

Four different elements and their compounds are covered in this current volume: gallium, germanium, gold and hafnium. In each case physical and chemical properties are given along with details of occurrence, manufacture, economic aspects, analytical procedures, health and safety, and uses.

Several entries deal with fuel. These include fuel resources, fuels from biomass, fuels from waste, fuels — synthetic, furnaces — fuel fired, gas — natural and gasoline, and other motor fuels. Many tables, flow-charts and graphs are included here and as with all entries a substantial number of references are given.

Other entries which clearly relate to chemical engineering include the topics: fusion energy, geothermal energy, geotextiles, groundwater monitoring, hardness, hazard risk analysis and heat-exchange technology.

The related entries — glass, glass-ceramics, glasses (organic–inorganic hybrids) and glassy metals cover over 120 pages with photographs supplementing the tables and figures.

Classes of chemical compounds in this volume include glycols and Grignards and there are separate entries for gelatin and glycerol. Several chemical structures and reactions are presented. Other diverse entries which I found to be of interest — and will no doubt refer to again — deal with fungicides-agricultural, gastrointestinal agents, gemstones, genetic engineering, growth regulators, gums, and hair preparations.

As with previous volumes a wealth of information is presented on a wide variety of diverse topics that should satisfy the intellectual curiosity of most, if not all, chemists.

P.J. Cox

ELSEVIER

Talanta 42 (1995) 1007–1030

Talanta

Review

# Metal speciation in solid matrices

Arabinda K. Das [1], Ruma Chakraborty [1], M. Luisa Cervera, Miguel de la Guardia *

*Department of Analytical Chemistry, University of Valencia, 50 Dr. Moliner St., 46100 Burjassot, Valencia, Spain*

Received 17 November 1994; revised 16 January 1995; accepted 7 February 1995

**Abstract**

The literature on metal ion speciation in solid matrices is reviewed, taking into account its applications in the analysis of soil, sediment, biological materials, foodstuff and other solid samples. The pretreatment methods of various solid materials required for carrying out speciation studies have been highlighted. The basis of the methods of separation of different species from matrices, such as sequential extraction, selective extraction, etc. is discussed. The instrumental techniques used for the characterization of different chemical species in solid matrices have been mentioned. The literature survey reveals the analytical details of the developed methodologies, and these have been examined in terms of the limit of detection, precision and accuracy.

## 1. Introduction

An increasing number of recent publications have dealt with the study of chemical speciation of trace elements. At present, the necessity to advance our knowledge of the mobility of chemicals in soils and the physiological activity of the inorganic elements makes necessary not only the determination of the total amount of these elements, but also the exact determination of the concentration of their different chemical forms [1].

Speciation analysis normally refers to the determination of species of metals and metalloids including organometallic compounds. As a matter of fact, speciation is very significant when applied to trace elements, because the analytical difficulties are related to the choice of relevant techniques for measurement of the individual species.

Speciation studies of trace elements in various phases in the environment are widely used in investigating the effects of a particular element in the ecosystem. Speciation analysis is also concerned with the characterization of poorly defined forms of metal ions.

Different aspects of speciation have been discussed in some recent review articles and books [2–6]. For example, the different general aspects of speciation analysis were reviewed by Lund [2]. Also, Van Loon and Barefoot [3] reviewed a selection of major developments in the field of analytical methodology for elemental speciation for the period from January 1986 to December 1990. Nevertheless, much of the published work on metal speciation has dealt with the determination of trace metal species in natural waters. It also transpires that papers on speciation in solid matrices are scattered in the literature.

Although it is now possible to determine various elements at the nanogram per gram level in different samples with the aid of currently available analytical instrumentation, the same measure of success has not yet been

* Corresponding author.

[1] Permanent address: Department of Chemistry, University of Burdwan, Burdwan-713 104, India.



*SSDI* 0039-9140(95)01557-4

achieved for the determination of the same elements in solid matrices. This is currently due to changes in the species during the pretreatment of samples. Also, inaccurate results are sometimes obtained because of the differences in the analytical response of the various physical and chemical forms of the same element. A further problem that is encountered in chemical speciation of solids is that the analytical sensitivity for certain elements is inadequate, as we are dealing with only fractions of the total content. Thus it will be highly interesting to study different aspects of speciation studies in various types of solid samples, in order to evidence the present state of the art.

The references for which the present work has been carried out were collected from the Analytical Abstracts database (period 1980–March 1994) and from the Chemistry Citation Index (1991–March 1994).

The papers that have been found in the present literature review could be classified into three groups depending on a matrix criterion (for the convenience of the readers, the reference numbers of the respective groups are given in square brackets): (i) speciation of soil and sediment samples [2,7,9,10,13,17,20–27,31–41,45–72]; (ii) speciation of solid biological and food materials [5,16,23,65,75–77, 80–133]; and (iii) speciation of miscellaneous solid samples [16,32,42–44,134–143].

## 2. Speciation of soil and sediment samples

Soils and sediments constitute concentrated reservoirs of trace metals in which amounts are more magnified than those present in other adjacent phases of the environment, e.g. water, air. In the literature, speciation studies of soils and sediments are usually reported independently. This is because most natural soils are characterized by oxidized conditions, whereas non-polluted sediments are usually deposited under oxygen-deficient conditions [7]. In the environment, different situations as a consequence of the anthropogenic activity may also occur. Thus waste deposits with a high coal ash content may show a high diversity in surface layers, resulting in reducing conditions underneath; or dredged anoxic sediments may be deposited under aerobic conditions. Hence the composition of soils and sediments reflects the nature of the original base rock, the degree of degradation and leaching introduced by weathering cycles, and the influence of external inputs [8]. Metal cations in soils may be present in several different physicochemical forms, i.e. as simple or complex ions, as easily exchangeable ions, as organically bound, as occluded by or coprecipitated with metal oxides or carbonates or phosphates and secondary minerals, or as ions in crystal lattices of primary minerals [9]. From the chemical point of view, the chemical compounds of a sediment may be carbonates, hydroxides, silicates, sulfides, phosphates and organics in various stages of crystallization, stoichiometry, water content, and so on [10]. Again, the principal metal forms in sludge are soluble, being present as precipitated or coprecipitated in metal oxides, adsorbates and associated with biological residues [11].

### 2.1. Pretreatment

Storage and preparation of soil or sediment samples prior to leaching with selective reagents may affect the extractability of elements. For example, exchangeable potassium can be converted into a non-exchangeable form when samples are dried [12]. Manganese and iron solubilities decreased dramatically on air-drying, but after oven-drying, the solubility of manganese exceeded by several times that found in moist samples [13]. Nevertheless, soils and sediments all vary in their moisture content depending on the location and the time of sampling. Provided that the metal species are stable the matrix should be dried either by freeze-drying or by air-drying at 40 °C. Most trace organics associated with them are bound to the organic surfaces of the matrix. The metal species may be leached from such samples by soaking and stirring or sonicating the sediment with HCl, and extracted into the organic solvent i.e. ethyl acetate [14]. Other workers reported [15] a similar use of acid to leach the compounds from the sediment along with methanol as an additive. Alternately, the metal species may be exhaustively extracted in a Soxhlet apparatus, after acidification with HCl. A weakly bonded/adsorbed fraction may be removed by sonication with an electrolyte such as $NH_4Cl$, followed by extraction with solvents of increasing polarity. The strength of the extraction medium can be further increased with dilute and then with more concentrated HCl, followed by organic solvent and acetic acid mixtures. Additional solvent extraction, by boiling with 2-mercaptoethanol in Tris–buffer

will disrupt the S–S linkage and release the more strongly bound organometallic compounds. Nevertheless, the concentration of many metal species in soil and sediment is completely dependent on the method used for extraction [16].

The effects of pretreatments on the leaching of elements vary from element to element and seem to depend on the form of occurrence of the element in the sediment sample. The drying of organic stream sediment tends to decrease the concentration of readily extractable elements [17].

Various approaches to sampling and sample pretreatments for metal speciation in soils and sediments have recently been reviewed by Rubio and Ure [18]. They have discussed the avoidance of contamination and loss, field sampling and subsampling of air-dried soils and sediments. Location of sampling points, kinds of sample and sampling apparatus for suspended sediments, bottom sediments and interstitial water, measurement in situ, and pretreatment and storage of the sample have also been presented.

### 2.2. Extraction techniques

In order to assess the reactivity of the species or binding forms of heavy metals in solid soil, sediment and sludge samples, extraction procedures have been applied both as single leaching steps and combined in sequential extraction schemes [19] with a representative sample size and without the need of any sample preparation. Extraction media could be neutral electrolytes, like $CaCl_2$ or $MgCl_2$, buffers of weak acids, like acetic acid or oxalic acid, chelating agents, like EDTA or DTPA, redox agents, like $NH_2OH$, strong acids, like HCl, $HNO_3$, $HClO_4$ or HF, or bases, like NaOH or $Na_2CO_3$.

The ability of various extracting agents to release metal ions depends on their association with particular soil fractions. Extractants like electrolytes, weak acids and chelating agents release metals from coordination sites, while strong acids and other redox agents are capable of releasing additional quantities of metal as a result of the decomposition of the soild matrix.

Sequential extraction schemes have been described by several workers [20] for sediments and dredged material also. Consecutive leaching techniques allow us to obtain information about the mobilities of major and trace constituents under different environmental conditions such as acidic or alkaline, oxidizing or reducing behaviour, the action of chelating agents, and so on. From this study, the actual chemical form of the investigated species occurring in soil or sediment can be concluded, leading to predictions about both origin and bioavailability [21].

Subjecting soil and sediment samples to multiple extraction has not been proved as an attractive alternative to sequential extraction, possibly because the latter approach tends to more readily identify the sediment component(s) responsible for retaining the majority of the elements of interest. The most appropriate sequence can be determined by the type of soil or sediment being examined, the horizon involved, the elements of interest, and so on [22].

As a matter of fact, sequential extraction provides more information than single extraction and has several advantages [7].

(i) Extractive procedures applied are comparable to those occurring in nature. In natural environments, soil and sediments are subject to similar leaching procedures by natural and anthropogenic electrolyte solutions.

(ii) The total sum of all fractions should be more-or-less 100%, so the results are self-checking.

(iii) It is an essential tool in establishing element partitioning with natural samples.

(iv) Chemical extraction sequences can be used for the estimation of the potential remobilization of metals under changing environmental conditions.

Microwave-assisted extraction techniques have been very useful in the study of the speciation of metals not only in geological and environmental samples but also in biological samples [23–25]. This is because the use of microwave ovens in chemistry provides a very effective means for supplying high temperatures in a short time [26]. Extraction rate experiments using conventional and microwave-assisted heating showed that microwave-assisted heating produces results comparable to those of the conventional procedure. Sequential microwave extraction procedures were established from the results of extraction rate experiments [27].

Other operationally defined speciation schemes include the use of the combination of a chromatographic fractionation of the soil solution followed by the analysis of the fraction by a sensitive analytical procedure. Thus Gardiner et al. [28], used size-exclusion HPLC

with electrothermal-atomic absorption spectrometric analysis (ET-AAS) to identify aluminium species in soil solutions. Speciation schemes also make use of combinations of anion- and cation-exchange columns to fractionate various species of metals like cadmium and lead in soil solution [29]. Supercritical fluid extraction is fast becoming an alternative technique to the more conventional methods for soils and sediments [30].

### 2.3. General procedures

It has already been mentioned that for speciation studies in soils, sediments and similar materials, sequential extraction schemes are widely used. In an elaborate review article, Pickering [22] summarized the different extraction schemes as described in the pertinent literature. In Table 1 various frequently used sequential extraction procedures [31–39] are presented.

The groupings used in descriptions of distribution patterns are somewhat arbitrary, but the fractions more commonly considered appear to be the ion-exchangeable, the weakly absorbed, organic-bound, hydrous oxide component and lattice component material. The latter component has been termed as "residual", with the sum of the other fractions being "non-residual".

The behaviour of each fraction differs according to the type of reagent required for the release of a specific fraction [8] of the target elements in the target sample, thus providing the specific characteristics of each sample. Nevertheless, the extraction sequence proposed by Tessier et al. [32] had been most widely used [7,10,40,41] and applied not only to soils and sediments, but also to atmospheric particulate matter [42–44].

Although some workers water-wash the samples prior to sequential extraction without their analysis, Gatehouse et al. [31] considered water treatment as one of the extraction steps. The use of hydrazine for the extraction of non-silicate Fe phases is unique in comparison to other extraction schemes.

The extraction scheme presented by Sposito et al. [33] was effective for arid-zone field soils enabling an experimental precision at any extraction step of better than 5%. Miller and McFee [34] applied their technique for the speciation of Cd, Cu, Pb and Zn in soils, making use of a sequential extraction procedure for sewage sludges and a selective extraction procedure for manganese oxides.

The method of Psenner et al. [35] has been used for the evaluation of the speciation of inorganic constituents in sediments of the Danube [10] river. The grain size of the sediment is the most decisive parameter in such an analysis. However, dithionite must be avoided because it contains a lot of impurities of heavy metals and can cause problems in flame atomic absorption spectrometric determinations. On the other hand, the presence of $S^{-2}$ in dithionite must be avoided [45].

The special feature of the Shuman and Hargrove [36] method is the use of NaOCl as an oxidizing agent. The effect of $OH^-$ ions present makes the organic fraction more accessible and easily removable. This reagent is also considered to cause less damage to amorphous constituents and clay minerals, but it can oxidize some Mn to $MnO_4^-$. Another disadvantage is the associated precipitation of released metal ions in the alkaline solution. For extraction of exchangeables, e.g. by using $NH_4NO_3$, it may, however, lower the pH sufficiently for $H^+$ ion competition for sites to be discernible, and hydrolysis of clays will be promoted. Extraction with $NH_4Ac$, as proposed by Kersten and Förstner [37], avoids the aforementioned effect by acting as a buffer.

In the course of the elution sequence of the procedure of Zeien and Brümmer [38], the acidity of the extractants increases. The heavy metals are fractionated according to their mobility during the first two steps of the extraction sequence, whereas steps three to seven fractionate according to their binding characteristics. However, this method is only applicable to oxidized soils with below 5% $CaCO_3$.

Hirner et al. [39] proposed an extraction sequence based on the specific isolation of soluble (by solvent extraction) and insoluble (by demineralization) organic constituents. The last step of any sequential procedure is the quantitative dissolution of the final extraction residue.

The different extraction procedures cited above are not always selective. It seems that all the reagents used in the various schemes have advantages and disadvantages and there is not an ideal reagent. This is because chemical reagents may themselves alter the indigenous speciation of a trace element, and in the choice of extractants, less powerful leaching solutions will probably be more selective for specific

Table 1
Commonly used sequential extraction procedures for extracting various components of soils and sediments

| Authors | Extractant [a] | Fraction |
|---|---|---|
| Gatehouse et al. [31] | $H_2O$ | Water-solubles |
| | $NH_4Ac/HAc$ | Exchangeables |
| | $NH_2OH \cdot HCl/HAc$ | Oxides |
| | $H_2O_2/HNO_3$ | Sulfides and organics |
| | $N_2N_4 \cdot HCl$ | Non-silicate Fe phases |
| | $HClO_4$ | Residuals |
| Tessier et al. [32] | $MgCl_2$ | Exchangeables |
| | NaAc/HAc | Carbonates |
| | $NH_2OH \cdot HCl/HAc$ | Oxides |
| | $H_2O_2/HNO_3/NH_4Ac$ | Organics |
| | $HF/HClO_4$ | Residuals |
| Sposito et al. [33] | $KNO_3$ | Exchangeables |
| | NaOH | Sorbed components |
| | EDTA | Organics |
| | $HNO_3$ | Carbonates and sufildes |
| Miller and McFee [34] | $H_2O$ | Water–solubles |
| | $KNO_3$ | Exchangeables |
| | $Na_4P_2O_7$ | Organics |
| | EDTA | Carbonates, Fe occluded (amorphous) |
| | $NH_2OH \cdot HCl/HNO_3$ | Mn-oxide occluded |
| | Na-citrate/$NaHCO_3/Na_2S_2O_4$ | Crystalline Fe-oxide occluded |
| | $HNO_3$ | Sulfides |
| | $HNO_3/H_2O_2$ | Residuals |
| Psenner et al. [35] | $HCO_3^-/S_2O_4^{2-}$ | Organics and humics (partially) |
| | NaOH | Humics |
| | HCl | Carbonates, Fe hydroxides, sulfides (partially) |
| | Hot NaOH | Kaolinite (partially), sulfides |
| Shuman and Hargrove [36] | $Mg(NO_3)_2$ | Exchangeables |
| | NaOCl | Organics |
| | $NH_2OH \cdot HCl/NH_4Ac$ | Mn oxides |
| | $(NH_4)_2Ox$ | Fe oxides (amorphous) |
| | Ascorbic acid/oxalate buffer | Fe oxides (crystalline) |
| | $HCl/HF/HNO_3$ | Residuals |
| Kersten and Förstner [37] | $NH_4Ac$ | Exchangeables |
| | NaAc/HAc | Carbonates |
| | $NH_2OH \cdot HCl/HNO_3$ | Mn oxides |
| | Oxalate buffer | Fe oxides (amorphous) |
| | $H_2O_2/HNO_3/NH_4Ac$ | Sulfides and organics |
| | $HNO_3$ | Residuals |
| Zeien and Brümmer [38] | $NH_4NO_3$ | Exchangeables (non-specifically adsorbed) |
| | $NH_4Ac$ | Exchangeables (specifically adsorbed) |
| | $NH_2OH \cdot HCl/NH_4Ac$ | Mn oxides |
| | $(NH_4)_2EDTA$ | Organics |
| | $(NH_4)_2Ox$ | Fe oxides (amorphous) |
| | Ascorbic acid/oxalate buffer | Fe oxides (crystalline) |
| | $HF/HClO_4/HNO_3$ | Residual |
| Hirner et al. [39] | $H_2O$ | Water solubles |
| | $NH_4Ac$ | Exchangeables |
| | $C_6H_6/CH_3OH$ | Soluble organics (solvent extractables) |
| | $C_6H_6/CH_3OH/KOH$ | Soluble organics (humic and fulvic acids) |
| | HCl | Mineral matrix (easily soluble) |
| | HF | Mineral matrix (hardly soluble) |
| | $HCl/HClO_4/HNO_3$ | Insoluble organics |

[a] The different extractants are employed sequentially and each one provides leaching of the noted metal fractions, as indicated by the authors.

fractions than more severe reagents, which may attack in other forms, although the overall efficiency of extraction may be lower [9]. Also to be taken into consideration are factors such as readsorption processes, the time required to carry out the experiments, the effect of temperature and the ratio between the solid mass and the volume of the extractant solution.

One serious concern about the extraction schemes stated in Table 1 and other similar schemes is that the rate of extraction is slow and takes several days to complete the analysis. For example, the procedure of Tessier et al. [32] needs 5 overnights [10] for the extraction steps to be completed during the analysis of a sediment sample whereas the procedure after Miller and McFee [34] needs more than 77 h [46] for sequential extraction for soil speciation. Use of PTFE reactors and microwave-assisted digestion procedures at high pressures and temperatures has usually been effective to overcome this problem [22–26]. Another way by which the speciation studies have been made rapid is by using on-line treatment. In an experiment for studying speciation of heavy metals like Cd, Zn, Cu and Pb performed by Scokart et al. [47], a small column (0.5 cm in diameter) was packed with soil (1 g) and eluted successively with water, $BaCl_2$, acetate buffer/EDTA and $HNO_3$ furnished by a peristaltic pump. The leachates were directly injected into an inductively coupled plasma-optical emission spectrometer in order to analyze immediately the extracted solution. Actually, it gives a kind of chromatogram of the chemical species of the elements studied which may be considered as a picture of their availability.

### 2.4. *Modifications of the usual extraction sequence*

When the requirement is not the complete analysis of the soil or sediment but to study the speciation of specific component(s), modification of the usual extraction sequence has been proposed. An improvement in analytical measurements for single and sequential procedures applied to soil and sediment analysis has been reported by Quevauviller et al. [48]. The study indicated that broadly acceptable extraction schemes can be established, e.g. a single-extraction (EDTA/acetic acid/ammonium acetate) method for soil and a sequential extraction (with acetic acid, hydroxylammonium chloride, ammonium acetate and $H_2O_2$) method for sediment. Few specific examples may be cited here.

For Cd speciation, sequential extractions were performed with $H_2O$, $CaAc_2$, NaAc, NaOH and Na citrate [49]. Columns packed with Amberlite IR-120 cation-exchange resin were used together with Amberlite XAD-2 absorbent resin to investigate Cd speciation in solutions of sewage-sludge-amended soils [50].

Similarly, Cu species may be sequentially extracted by using $CaCl_2$, HAc, $K_4P_2O_7$, oxalate buffer and HF [51]. For marine sediments, extraction of the organic-bound fraction by hot (100 °C) sodium dodecylsulfate–sodium bicarbonate at pH 9.2 has been recommended [52].

The speciation studies of aluminium were performed by extracting soil samples with $CaCl_2$, then with KCl, and the separation of the aluminium species was carried out by the ion-chromatographic method [53].

For the evaluation of the speciation of tin in finely grained sediments of the Danube river, a leaching sequence was presented [20] which consisted of treatment with ethanol, $NH_2OH \cdot HCl$/HAc, oxalate buffer, $KMnO_4$/$HNO_3$, $NH_4I$ and tartaric acid. Owing to the very high toxicity for marine organisms of tributyltin, there is great interest in its speciation in environmental samples. The sediment samples collected from Porto Vecchio Bay (Corsica, France) were analyzed by three different speciation methods of which extraction of tin species in HAc followed by hydride generation, cold trapping, separation on a GC column and determination by graphite furnace-AAS furnished the best results [54]. The extraction of tributyltin from spiked sediment by a supercritical fluid ($CO_2$ containing 5.1 M methanol) has been reported by Dachs et al. [55]. Extracts were derivatized with 20% $C_2H_5MgCl$ in tetrahydrofuran and analyzed by GC with flame photometric detection. Recently, the speciation of some tributyltin compounds has been studied by using Mössbauer spectroscopy, in anoxic and oxic estuarine sediments [56]. The study indicated that tributyltin fluoride remains in its polymeric form after interaction with both types of sediments.

The extraction and speciation of inorganic arsenic ($As^{3+}$ and $As^{5+}$) in soil and sediment samples have been reported by various workers [57,58]. The method involves extraction with 60% $HNO_3$ followed by hydride generation-AAS. To determine the amount of arsenic com-

pounds such as arsenate, arsenite, monomethyl arsonate and dimethyl arsinate in Japanese soils, Takamatsu et al. [59] developed an analytical technique that consisted of sequential extraction with HCl, HCl/KI, benzene, and $H_2O/H_2O_2$ followed by anion-exchange chromatography and final determination of arsenic by flameless atomic absorption spectrometry.

A sequential extraction procedure [60] using the following reagents in the order $H_2O$, $NH_4Ac$, NaAc/HAc, $NH_2OH \cdot HCl$/HAc, $H_2O_2/NH_4Ac$, $HNO_3$ was applied to study the speciation of Chernobyl-derived radionuclides, i.e. $^{137}Cs$ and $^{90}Sr$ in soils. In general, both $^{137}Cs$ and $^{90}Sr$ had lower mobility factors in the Russian soils compared to the Norwegian soils. Speciation of $^{137}Cs$ and $^{90}Sr$ in soils and bottom sediments in the Chernobyl accident zone was also studied by Konoplev et al. [61] who found that the adsorption of $^{137}Cs$ and $^{90}Sr$ in the environment is controlled by the cation-exchange capacity and the selectivity of the solid phase and the cationic composition of the liquid phase.

Speciation of $Ca^{2+}$ ions and particulate calcium as $Ca_3(PO_4)_2$ needs neither sample preparation nor extraction step and the species were studied by flame AAS using slurries [62].

On the other hand, speciation between $Sb^{3+}$ and $Sb^{5+}$ is difficult in the solid samples because a quantitative recovery is only obtained in $HF + HNO_3 + H_2SO_4 + HClO_4$, which alters the oxidation state. To determine Sb in solid samples, the batch hydride generation method is recommended in preference to automated (flow injection analysis (FIA) or continuous) methods, because a clear solution is not obtained after any of the sample treatments used. In the FIA and continuous methods, previous filtration of the suspension is required before analysis to avoid clogging of Teflon tubing [63].

Organometallic compounds are often difficult to determine in soil and sediment samples [2]. There are few reports on the study of organomercury compounds in soils and sediments [64]. A search for new methods of mercury speciation based on liquid chromatography, as well as quality control and application to sediments, has been described by Cela et al. [65]. The speciation of mercury in soils and sediments has also been studied by a thermal evaporation technique [66]. The determinations of organomercury and total mercury were carried out by HPLC–AFS and cold vapour AAS respectively.

Selenium exists in soil in several oxidation states and as a variety of inorganic and organic compounds. Speciation studies on this element, particularly in soil samples, are scanty [67,68].

Recently, for studying the speciation of Fe(II) and Fe(III) in contaminated aquifer sediments, single-step extraction including 1 M $CaCl_2$, NaAc, oxalate, dithionite, Ti(III)-EDTA, 0.5 M HCl, 5 M HCl, hot 6 M HCl and a sequential extraction by HI and $Cr^{2+}$HCl were tested on saturated iron minerals and nine aquifer sediments [69].

### 2.5. Analytical details

Table 2 summarizes details of the analytical performance of some speciation methods for soil and sediment samples. It transpires that sequential extraction is the most common technique for the preferential separation of various components. The resultant extract solutions are usually then analyzed by instrumental techniques suitable for the chemical multielement analysis of liquids, i.e. atomic absorption spectrometry (flame and graphite furnace), and inductively coupled plasma spectrometry (ICP-OES and ICP-MS). However, the complementary approach, i.e. analysis of the solid extraction residues by X-ray fluorescence spectrometry is also possible [7]. Of these techniques, AAS has been used widely because of its simplicity and low cost. By introducing flow injection analysis (FIA), sensitivity is further increased. Thus a 5.5-fold to 60-fold increase in the sensitivity is obtained for flame AAS and a 15 fold to 50 fold increase for ET-AAS [73].

From Table 2 it is also evident that the information about the analytical performance of the developed methodologies is scarcely reported. The limits of detection obtained are in the parts-per-million to parts-per-billion range. The precision is usually adequate for these determinations (relative standard deviations between 0.4 and 8%).

The usual speed of analysis in conventional extraction methods is enhanced with a microwave-assisted treatment, as previously indicated, and is also further improved by use of an ICP-S method of determination. A typical sixfold to fifteenfold increase in speed has been reported [27,74].

Accuracy data have been reported in a few papers, and in general these data concern the determination of the total content of metals and not the accuracy of determination of each

Table 2
Analytical details of metal ion speciation studies of soil and sediment samples

| Element | Species | Matrix | Separation and measuring technique | LOD [a] | R.S.D. [b] (%) | Recovery (%) | Ref. |
|---|---|---|---|---|---|---|---|
| Al, As, Ca, Co, Cr, Cu, Fe, K, Mg, Mn, Ni, P, Pb, Zn | Animal and plant tissues partially humics; humics, rest of animal and plant tissues; carbonates, iron hydroxides, some sulfides; part of kaolinite, rest of sulfides | Lacustrine sediment (Danube river Austria) | Sequential, AAS, ICP and photometry | – | – | – | [10] |
| Al, Ca, Co, Cu, Fe, K, Mg, Mn, Na, Ni, Pb, Zn | Exchangeable cations, fulvic fraction, humic fraction, secondary manganese oxide fraction, secondary iron oxide fraction, residue | Sediment (Plynlimon, U.K.) | Sequential, flame AAS | Na, K, Mg:1 ppm; Ca, Fe:5 ppm; Al, Mn: 2 ppm; Pb:0.5 ppm; Co, Ni, Cu:0.2 ppm; Zn:0.1 ppm | – | – | [13] |
| Al, As, Cd, Co, Cu, Cr, Fe, Pb, Mn, Ni, Zn | Mobile (weak extraction) fraction, acid digestion fraction | Organic stream sediment (Finland) | Selective, AAS (Flame, GF-) | – | – | – | [17] |
| Sn | Organics, carbonates, Fe and Mn hydroxides, sulfides, cassiterite | Sediments and soils (Danube river, Austria) | Sequential, ET-AAS | – | – | – | [21] |
| Ca, Cr, Fe, Mn, Pb, Zn | Exchangeables, carbonate bound, bound to Fe and Mn oxides, organic material | Sediment (California Gulch Colorado) | Sequential, ICP-S | – | 11 | 76–120 (conventional) 62–120 (microwave) | [27] |
| Cd, Cr, Cu, Ni, Pb, Zn | Carbonate, Fe and Mn oxides, organic matter and silica | Sediment (Besos river, Spain) | Sequential, AAS (Flame, GF-), XRF | – | – | – | [40] |
| Ba, Ca, Cr, Cu, Fe, K, Mn, Rb, Sr, Ti, Zn | Exchangeables, bound to carbonates, Fe and Mn (hydr)oxides, organics, silicates | Soil (Sardinia, Italy) | Sequential, total reflection XRF | $<1$ mg $kg^{-1}$ for trace Elements; 20–100 mg $Kg^{-1}$ for major elements | – | – | [41] |

Table 2 (contd.)

| Element | Species | Matrix | Separation and measuring technique | LOD [a] | R.S.D. [b] (%) | Recovery (%) | Ref. |
|---|---|---|---|---|---|---|---|
| Cd, Cu, Pb, Zn | Water soluble ions; easily exchangeable ions; strongly adsorbed, chelated or complexed ions; secondary clay minerals and metal oxides; primary minerals or highly fixed ions | Soil | Selective, ICP-S | – | – | – | [47] |
| Al | $Al(H_2O)_6^{3+}$, $[Al(OH)_n(H_2O)_{6-n}]^{(3-n)+}$, $[AlF(H_2O)_5]^{2+}$, $[AlF_2(H_2O)_4]^{+}$, $[Al(oxal)(H_2O)_4]^{+}$, $[Al(Hcitrate)(H_2O)_4]^{+}$ | Soil | Selective ion chromatography | 0.455 ppb | – | – | [53] |
| Sn | Tributyltin | Marine sediments (Porto Vecchio Bay, France) | Selective GF-AAS | 25 ng $g^{-1}$ | 9 | – | [54] |
| Sn | Tributyltin | Sediment | Supercritical fluid extraction, GC | – | 9.2 | 82 | [55] |
| As | $AsO_4^{3-}$, $AsO_3^{3-}$, monomethyl arsonate, dimethyl arsinate | Soil (Japan) | Solvent extraction, anion exchange chromatography, flameless AAS | – | – | 91–103 | [59] |
| Cs, Sr | $^{137}Cs$, $^{90}Sr$ | Soils (Norway, USSR) | Sequential, $\gamma$-spectrometry, Čerenkov counting, NAA | – | – | – | [60] |
| Sb | Sb(III), Sb(V) | Soils, lake sediments (Madrid, Spain) | Batch, GF-AAS, FIA, HG-AAS | 0.007 ng FIA; 0.01 ng GF-AAS; 2.97 ng batch | 0.4 (0.5 ng)FIA 3.8 (0.8 ng) GF-AAS 6.6(10 ng) batch | 107 ± 6.1 18.8 ± 8.4 | [63] |

Table 2 (contd.)

| Element | Species | Matrix | Separation and measuring technique | LOD [a] | R.S.D. [b] (%) | Recovery (%) | Ref. |
|---|---|---|---|---|---|---|---|
| Hg | Inorganic mercury, methylmercury | Sediment (Ria de Pontevedra, Galicia, Spain) | Selective, chromatography | – | | – | [65] |
| Se | Se(IV) | Soil | Selective, ion chromatography | 20 ppb | – | – | [67] |
| Se | Se(IV), Se(VI) | Soil | Selective, ion chromatography | 30 ppb | – | | [68] |
| Al, Cd, Cu, Pb and Zn | Bound to carbonates, bound to Fe and Mn oxides, organic matter bound, bound to silicates | Sediment (semi-rural area of Belgium | Sequential, AAS (Flame, GF-), ICP | | 5–8 | – | [70] |
| Al, As, Co, Cr, Cu, Fe, K, Mg, Ni, P, Pb, Zn | Animals and plant tissues, humics, carbonates, hydroxides, sulfides, kaolinite | River sediments and soils | Sequential, AAS, ICP and photometry | – | – | | [71] |
| Sn | Cassiterite | Rock | Selective, HG-AAS | – | – | – | [72] |

[a] LOD, limit of detection

[b] R.S.D., relative standard deviation.

one of the species or fractions analyzed. Thus recoveries of total metals in certified sediment samples ranged from 76 to 120% for the conventional procedure and 62 to 120% for the microwave procedure. Recoveries of total metals using microwave and conventional techniques were reasonably comparable except for iron (62% by microwave as against 75% by conventional). Substitution of an aqua regia/HF extraction for total/residual metals results in essentially complete recovery of metals [27].

The precision obtained from 31 replicate samples of the California Gulch (Colorado) sediment which yielded about an average of 11% R.S.D. excludes the exchangeable fraction which was more variable [27].

In the case of the speciation studies of Sb(III) and Sb(V), very low recoveries ($18.8 \pm 8.4$–$48.2 \pm 2.2\%$) have been reported. Again, when a quantitative recovery ($107.1 \pm 6.1\%$) is obtained, the oxidation state of antimony is altered yielding errors in speciation [63].

## 3. Speciation of solid biological and food materials

In contrast to inorganic materials where the number of element species is relatively small, trace elements can be present in living matter in a large variety of chemical forms. The purpose of most investigations into the chemical speciation of trace elements in biological systems has been to identify the physiologically active forms, the storage and transport of species, the metabolites of trace-element-containing drugs and to find sensitive indices of the status of trace elements [75]. With increasing knowledge of the metabolism and biological effects of trace elements, it has become increasingly apparent that there is a need not only to determine the total levels of an element in tissues and body fluids but also to measure its different chemical forms quantitatively.

The toxicity of chemical species of different elements is a function of both the target element and the chemical structure of the compounds considered, and it depends on the absorption pathways of the elements. Most of the species of interest in the toxicology of trace elements are small molecules. Many metals are capable of forming organometallic compounds and their toxic effects in some cases exceed by far those of the inorganic forms of the elements or the compounds formed with large molecules. In general, in the investigation of the toxic effects, the speciation of small molecules is of concern, whereas in the investigation of the biological functions the determination of large molecules has priority. Again most of the essential species of the trace elements, i.e. metalloenzymes, are produced in the organism after transformation of the different chemical forms of the elements present in the diet. The content of an essential compound decreases with insufficient dietary element supply and is thus related to the total element content [26].

Although the speciation of metals is widely recognized as a desirable goal in the analysis of biological materials (this has been particularly the case for clinical and environmental samples) interest is now being widened to include foods [77], because the bioavailability of metal species in food has been correlated with the extractability obtained by enzymolysis with gastric and intestinal fluids [78]. Quality control measures for toxic metals, neglected in many cases in food analysis, should be rigorously followed. No effort should be spared in determining the accuracy and precision for each separate food matrix, since each foodstuff is a different chemical matrix and requires special control of interferences [79].

### *3.1. Pretreatment of biological materials for carrying out speciation studies*

For speciation studies of biological materials, more stringent conditions have to be fulfilled during sample collection, pretreatment and storage [75]. It is necessary not only to collect a representative sample and to avoid chemical contamination, but also the integrity of the chemical species has to be maintained. During and after sampling, changes in parameters such as temperature, ionic strength, pH, redox potential, oxygen level, irradiation with UV light, etc. to which the sample is exposed, can influence the distribution of chemical species. As a matter of fact, the act of sampling itself may create conditions that could induce changes which may affect the types and prevalence of species found for a given element. In order to minimize the effect of the above changes, it is essential to choose those analytical conditions, in particular the pH and ionic strength of the working media, which do not differ markedly from those found in the original system.

The choice of sample storage containers is also a critical factor. In general, the most ap-

propriate action is to deep freeze samples immediately on collection to minimize any bacterial or enzyme degradation, loss through volatility or contamination of the sample. According to Uthe and Chou [80], biological tissue should be dissected at the sampling site and frozen in liquid nitrogen and then stored in a deep freeze to reduce enzyme release of heavy metals. Most studies on biological matrices are undertaken on wet tissue, rather than lyophilized materials, which is either extracted as fresh material or has previously been dissected and rapidly frozen.

Pretreatment techniques can only be chosen when the nature of the problem and the information required from the analysis of the sample have been understood clearly. Again the effect of storage on the distribution and the genuineness of the chemical species are both associated with such problems. For example, as stated above, biological tissue samples after collection are usually frozen until required, but such freezing of samples slows down on-going biochemical reactions which would otherwise disrupt the complexes or completely changes the distribution profile of a given element. The extent of damage to any constituent of interest would depend upon the conditions and time period of storage. Mechanical and physical effects of the ice crystals formed could denature proteins and may deactivate enzymes. Also, oxidation or reduction of side chains and light-catalyzed degradation of various proteins could continue to occur in the material during storage, particularly when transition metals are present [81].

Usually, sample preparation procedures for biological materials fall into two categories [77]. Firstly, those methods where the sample is analyzed after a minimal pretreatment by using slurry or solid sample introduction systems or alternately after dilution with an appropriate reagent for deproteinization, metal release or cell disruption. Secondly, there are methods where considerable sample pretreatment such as separation, extraction or destruction of the organic component by heat, solubilizing agents or oxidizing agents is necessary before determinations can be carried out.

### 3.2. Extraction techniques

The information required for speciation studies in the case of biological materials may be the oxidation state of the metal, the concentration of molecular species or the identity of the organometallic complex. The most common technique for obtaining such information involves separation procedures which isolate selectively the species of interest [82] or a separating column which generates a series of fractions containing organometallic complexes [83].

In principle, most of the separation modes available for liquid chromatography such as size-exclusion, normal-phase, reversed-phase, paired-ion reversed-phase and ion-exchange should be applicable to biological systems. Of these, fractionation according to size has been most frequently used. When chromatographic techniques are used to separate organometallic complexes, information on the concentration of organic molecules may also be obtained concomitantly from the elution pattern [84]. For efficient separation of sensitive non-stable species, gel permeation chromatography with aqueous eluents is used. Other techniques like ion-exchange chromatography may have the problem of loading the species, with separation of specific charges and/or substrates from either the column matrix or the buffer systems. This may result in changes in the original species. Thus leaching procedures are not much use in speciation analysis of biological samples [2]. For stable species only, electrophoretic separation can be applied in the form of a continuous flow-through or a capillary system [85].

Biological samples can also be extracted by blending as a paste or slurry with the selected solvent or solvent mixtures [86,87]. Sample tissue or plant material can be pulverized in liquid nitrogen to break up the matrix. Ionic lead species in grass and tree leaves may be solubilized with tetramethylammonium hydroxide from the crushed leaves in sodium diethyldithiocarbamate prior to extraction with pentane [88].

In general, organometals are more strongly bound to the protein, and for studying these systems, rupture of the protein–metal linkage is required. In such cases, enzymes can be used to destroy the substrate and release the organometal intact. For example, pepsin can be used to rupture the S–S bonds and bacterial protease K can be used to release organometals bound to proteins [16].

Recently, successful use has been made of pressure digestion in a microwave oven as an alternative procedure for solubilizing samples, because of the advantages it offers of reducing digestion time and reagents, thus decreasing

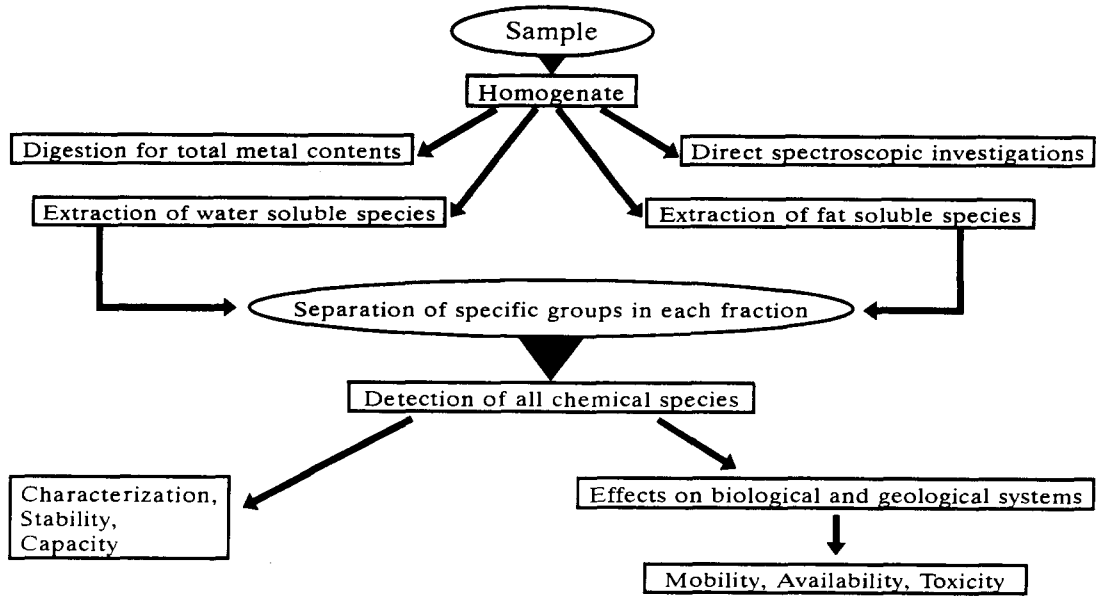


Fig. 1. General scheme that may be applied for metal ion speciation studies in biological materials.

contamination problems. Unfortunately, only a few studies on foods and biological matters have been published [23,89]. Supercritical fluid extraction is more suitable for isolating labile compounds and is an ideal technique for on-line automation. The method has been applied to speciation studies in biological tissues [90].

### 3.3. General procedure

For most speciation analyses, it is important to relieve the preferred species of other undesirable components of the sample matrix by selective extraction of either water- or fat-soluble forms. After selective separation, sensitive detection procedures followed by effects on biological systems, uptake and toxicological experiments which mimic real processes are carried out for complete speciation studies [91]. Various schemes like that shown in Fig. 1 are used to fulfil the requirements of speciation analysis.

For the elucidation of the structure, stability and capacity or the evaluation of the mobility, availability and toxicity of the metal species, different methods have to be used. Some of the instrumental techniques [75] that can be used to characterize chemical species in biological matters and the information that they may provide are summarized in Table 3.

Evidently, there is no unique procedure for speciation studies of all different types of biological materials. But depending on the nature of the material, some direct or combined method may be suggested. In some cases chemical species can be measured directly in the sample without interference from other components. For example, with several metal-containing enzymes, the enzymic activity can be taken as a measure of the concentration of the compound. Again enzyme systems specifically affected by the toxic form of the element may be monitored so that the inhibition of the enzymic activity can be taken as a measure of the toxic species. Immunoassay may be another direct way for the speciation of trace element compounds with antigenic properties [76].

On the other hand, various combined methods can be used in speciation studies. With some elemental species, relatively simple procedures may be used, i.e. volatilization of compounds or a single absorption or extraction step. For the speciation of small molecules like organometallic compounds, gas chromatography or high-performance liquid chromatography have been combined with analytical methods such as AAS and applied for routine analysis [5].

### 3.4. Various speciation methods

The procedures used for solubilization of the biological samples and subsequent determination of the analyte(s) by techniques like AAS, ICP-S, etc. are very wide. A critical examination of this subject reveals that major work has

Table 3
Major techniques for the characterization of chemical species in various matrices

| Instrumental techniques(s) | Information |
|---|---|
| AAS, ICP-AES, XRF, neutron activation, anodic stripping voltametry | Total metal content, detection of species, characterization of species is possible if the technique is coupled with a separation method |
| XRD | Determination of specific structures, principally crystalline compounds in tissues |
| IR and Raman spectroscopy | Structure and conformational changes |
| NMR | Structure, equilibrium and kinetic properties |
| Mass spectroscopy | Characterization of species |
| Mössbauer spectroscopy | Electronic structure, spatial arrangement, spin and oxidation states of the metal in the prosthetic group |
| Circular dichroism | Interaction between ligands and proteins, secondary structure of proteins and binding of metals at the active sites in enzymes |
| Molecular UV absorption and luminescence | Determination of specific species containing chromogenic or fluorogenic structures |

been done on the speciation of arsenic followed by that of mercury. The work on the speciation of other elements in biological materials are not many in number. This may be evident from the following discussions.

For the speciation of arsenic chemicals by atomic spectrometry, a series of procedures based on the use of a selective liquid–liquid extraction has been developed. The selective determination of inorganic arsenic and organic compounds in foods has been carried out by Münz and Lorenzen [92] by liquid–liquid extraction and hydride generation. Previously mineralized samples with $HNO_3$ were treated with ascorbic acid, to reduce As(V) to As(III), extracted from 7–9 M HCl into $CH_2Cl_2$. Inorganic arsenic was determined after a back extraction of the $CH_2Cl_2$ phase with water; the determination of organic arsenicals was achieved by evaporation of the remaining HCl phase, decomposition with $HNO_3$ and subsequent measurement by HG-AAS.

Inorganic arsenic species found in foods may also be selectively extracted with dilute $H_2SO_4$ from the lyophilized solid samples. Under these conditions organically bound arsenic remains stable [93].

For the determination of total inorganic arsenic in fish [94], solid samples were treated with NaOH and $Na_2SO_4$ on a boiling water bath for 20 min, after which HCl was added and arsenic was extracted with ammonium pyrrolidine dithiocarbamate (APDC) in MIBK. The arsenic was back-extracted with $HNO_3$ and then treated with a$H_2SO_4$ before measurements were carried out by the hydride generation technique.

Inorganic As(III) and As(V) were determined in biological materials [95] after solubilization with HCl, extraction into toluene and back-extraction with water. Organic arsenic was retained in the acidic solution. The total arsenic was determined after digestion with $HNO_3$, $H_2SO_4$ and $HClO_4$.

For selective determination of As(III) in foods, in the presence of As(V), the liquid–liquid extraction of $AsCl_3$ in $CHCl_3$ was proposed. The determination was carried out by hydride generation after back-extraction in water [96]. At pH 4–5 the hydride generation of arsenic with $NaBH_4$ permits the selective determination of As(III) in a mixture of As(III) and As(V). On the other hand, total arsenic can be determined by hydride generation from 5 M HCl. For the speciation of arsenic in solid biological samples and to avoid the oxidation of As(III), the use of concentrated $HNO_3$ and $H_2SO_4$ was substituted by the use of those acids diluted 1 + 2 with water [97].

A method for the separation of arsenic species from solid samples of orchard, tomato and oak leaves has been described by Sarx and Bächmann [98]. The volatilized arsenic species were separated into various fractions and determined by graphite furnace-atomic absorption spectrometry and microwave-induced plasma-optical emission spectrometry.

The major form of arsenic in fish and crustaceans is arsenobetaine. Although this compound has been shown to be non-toxic, for reasons of toxicological reassurance, its concentration and that of other arsenicals in foodstuffs of marine origin must be determined by some routine method [99]. Extraction of arsenobetaine from fish tissue homogenates may be performed by using $CHCl_3$–$CH_3OH$ mixtures. A recovery of 101 ± 4% was reported for the 1:2 solvent mixture extraction of freeze-dried fish muscle spiked with arsenobetaine [100]. For the routine analysis of arsenobetaine in marine samples, HPLC–ICP-AES would be a good choice in terms of sensitivity, selectivity and ease of operation [101], but even better sensitivity could be achieved with HPLC–ICP-MS [99].

In the determination of organoarsenic species by HPLC–ICP-MS, dried fish (1 g) was extracted with $CHCl_3$ or aqueous trypsin and the extracts were analyzed on an HPLC column containing anion-exchange resin with a mobile phase of alkaline potassium sulphate and with ICP-MS detection [102]. Recoveries ranged between 80 and 115% for arsenobetaine and arsenate. No monomethylarsonic acid was observed in any of the fish, though dimethylarsinic acid was detected.

The method proposed by Lunde [103] for the separation and analysis of organic-bound and inorganic arsenicals in marine organisms by neutron activation and X-ray fluorescence, based on the extraction of arsenic as $AsCl_3$ and subsequent removal by distillation at 100 °C, can be adapted for the analysis of inorganic arsenic in seafood products by HG-AAS after in-line microwave-assisted distillation of $AsCl_3$ [104].

Although the most popular way for the speciation of mercury is based on the selective reduction to $Hg^0$ following the procedure proposed by Magos [105], organic mercury can be determined by solvent extraction into toluene and electrothermal atomic absorption [106]. For this purpose, the solid residue of an extract in acetone from homogenized biological materials is treated with acid bromide and $CuSO_4$, and then the mercury is extracted into toluene. For the stabilization of methylmercury in the furnace, dithiozone was added to samples and standards and the mercury was atomized at 950°C. This method provides an average recovery of 97 ± 5% and supplies an alternative to the gas–liquid chromatographic method [107].

From the published papers on mercury speciation, it can be concluded that the reduction of mercurials can be selectively carried out by using different reduction steps with $SnCl_2$ and with $SnCl_2 + CdCl_2$. On the other hand, the pH strongly affects the reduction of mercurials by $NaBH_4$, specially in the presence of Fe(III), and finally it seems that a combination of $SnCl_2$ and $NaBH_4$ could be very convenient in order to carry out the speciation of mercury in biological samples [108]. Magos' method [105] was used for the speciation of mercury in brain tissue from monkeys [109] where the direct determination of mercury in 1 g of solubilizate was performed for total mercury by $CdCl_2 + SnCl_2$ reduction and for inorganic mercury by $SnCl_2$ reduction.

The extraction of $CH_3Hg^+$ as the bromide from fish samples by $CHCl_3$ and its direct determination in organic medium by cold vapour atomic absorption spectrometry was described by Rezende et al. [110]. Fresh fish muscle was cut into small pieces, prepared as a homogenate and mixed in a centrifuge tube with water, $H_2SO_4$ and KBr. Extraction with $CHCl_3$ was performed and methylmercury was determined by mixing the organic extract with 50% $HNO_3$ in DMF and 2% $NaBH_4$ in DMF (1:2:1).

A procedure for the determination of organic and inorganic mercury in biological materials like fish, oyster, meat, milk (dried), banana (dried), and wheat flour by GF-AAS has been reported [111]. To 0.5 g of the homogenate, 1% NaCl in 1 M HCl and benzene were added. Organic mercury extracted as chloride was re-extracted by 0.01 M thiosulphate solution. The organic mercury thiosulphate extract was next treated with 0.5 M $CuCl_2$, re-extracted in the benzene layer, and analyzed by GLC for speciation. Inorganic mercury was converted into a methyl chloride derivative by methanolic tetramethyltin (0.4 M) prior to extraction.

For rapid speciation studies on organomercury compounds in molluscs, a separation based on chromatography has been reported [65]. Frozen fish (0.5 g) was homogenized with water and 1 M $CuSO_4$. Acid potassium bromide and benzene were then added and the mixture was centrifuged. The organic layer (5 μl) was analyzed by capillary gas chromatography interfaced with AAS [86].

Trialkyltins are the class of organotins which have the greatest biocidal activity in mammals.

Arakawa et al. [112] reported the determination of tetraalkyltin and trialkyltin homologues in mammalian tissues. This technique involves the isolation of alkyltins from tissue homogenates as chlorides by simultaneous extraction with HCl and ethyl acetate, followed by extraction with *n*-hexane and stepwise elution with *n*-hexane + ethyl acetate on a silica gel column. The column eluate is injected directly into a gas chromatographic column. The method involves at least nine steps requiring six transfers of sample. This time-consuming process has been improved by Means and Hulebak [113]. In their method, methyltin compounds (monomethyl-, dimethyl-, trimethyl- and tetramethyl-) are purged from freshly homogenized mouse kidney and brain tissues using $NaBH_4$. The volatile organotin hydrides produced are cryogenically trapped on the head of a gas chromatographic column (at −40 °C) and eluted. The compounds are detected using selected ion monitoring in a mass spectrometer.

Determination of organometallic compounds in biological matrices is not very easy. Derivatization reactions including hydride generation and other sample treatments that lead to volatilization are employed, finally followed by GC separation [2]. Such procedures have been applied for the determination of Hg, As, Se, Sn and Pb species in biological samples [114,115]. AAS is used to quantify the elements in these cases. In a few cases, organometallic compounds of mercury, tin and arsenic have been determined in biological samples by HPLC with spectroscopic detectors [116]. Caroli et al. [117] used HPLC followed by ICP-AES to determine the iron proteins ferritin, transferrin, cytochrome C and iron protein succinate in a number of iron-based pharmaceuticals.

In order to investigate chemical speciation analysis in foodstuffs, protein-, pectin- and lipid-splitting enzymes like pepsin, pectinase, papain, bromelain and lipase have been used in stepwise extraction procedures [118]. The use of enzymes in the extraction procedures indicated clear differences in the solubility of the metal species, i.e. iron and manganese species, by pectinase from oat flakes and iron compounds by papain/lipase from wheat germ. The application of gradient gel electrophoresis provides a useful method for the separation of zinc, nickel and copper species in soybean fluor extracts [119]. The separated substances were electrophoretically eluted, followed by flame AAS determination of the metals. Thus is a sensitive separation method with a high resolving power that can provide various information concerning the metal species, e.g. molecular size, charge and stability.

Speciation of zinc and cadmium in different vegetable foodstuffs has been reported [120] where the cell breakdown was carried out by liquid shearing (ultraturrax treatment) of the crushed plants in a Tris–HCl buffer (pH 8). The homogenates were separated into cytosols (liquid fractions) and pellets (solid fractions) by centrifugation. The cytosols were again separated by gel permeation chromatography. The metal in each fraction was determined by GF-AAS after wet digestion in $HNO_3$.

Chau et al. [121] used tetramethylammonium hydroxide as tissue solubilizer to dissolve biological samples like fish without altering the chemical species of the alkyllead species. The various alkyllead species were isolated quantitatively by chelation extraction with sodium diethyldithiocarbamate, followed by *n*-butylation to their corresponding tetraalkyl forms, $R_nPbBu_{(4-n)}$ and $Bu_4Pb$ respectively (where R is Me, Et), all of which were determined by a GC–AAS method. The method could determine simultaneously the following species in one sample: tetraalkyllead ($Me_4Pb$, $Me_3EtPb$, $Me_2Et_2Pb$, $MeEt_3Pb$, $Et_4Pb$); ionic alkyllead ($Me_2Pb^{2+}$, $Et_2Pb^{2+}$, $Me_3Pb^{+}$, $Et_3Pb^{+}$); $Pb^{2+}$ ion.

Methyltin and butyltin and inorganic tin in oysters were extracted from frozen tissue with methanol and hydrochloric acid. The extracts were then treated by a hydride generation-AAS method [122].

### 3.5. Analytical details

As indicated in Table 4, it is clearly evident that there has been continuous interest in speciation studies of arsenic and mercury in biological materials. The decreasing order of toxicity of arsenic compounds has been found to be the following: metallic As, As(III), As(V), monomethylarsinic acid (MMA), dimethylarsinic acid (DMA). Again, compounds such as arsenobetaine, arsenocholine and arsenosugars are believed to be non-toxic. Consequently, a variety of procedures have been developed for determination of organic and organic species of arsenic, together with total arsenic in biological samples [92,93,96,98,100,102,104,

Table 4
Analytical details of metal ion speciation studies of biological and food materials in solid state

| Element | Species | Matrix | Separation and measuring technique | LOD | RSD (%) | Recovery (%) | Ref. |
|---|---|---|---|---|---|---|---|
| Hg | Organomercury | Molluscs, mussel tissue, tuna muscle | Extraction, GC | – | 10 | – | [65] |
| Hg | Organomercurials | Fish | Extraction, GC–AAS | 0.1 ng Hg | – | 95 | [86] |
| As | Inorganic As, DMA Phenylarsonic acid derivative | Food | Extraction, HG–AAS | – | – | – | [92] |
| As | Inorganic and organic arsenic | Dutch total diet | Extraction, spectrometry | – | – | 94–122 (inorganic As) 87–104 (organic bound As) | [93] |
| As | As(III), As(V) | Lobster, tuna, scallops, squid | Extraction, HG-AAS | – | – | 81–97 | [96] |
| As | DMA | Leaves of orchard, tomato, oak | Volatilization, AAS, MIP-OES | 10ppb(AAS) 0.1 ppb (MIP-OES) | – | – | [98] |
| As | Arsenobetaine, As(III), As(V), MMA, DMA, arsenocholine | Dogfish muscle | Extraction, HPLC–ICP-MS GF-AAS | 0.3 ng As (HPLC–ICP-MS), 0.02 ng As(GF-AAS) | – | $101 \pm 4$ | [100] |
| As | Organoarsenic species | Fish | HPLC, ICP-MS | – | – | 80–115 | [102] |
| As | Inorganic arsenic | Seafood | Microwave distillation, HG-AAS | 0.068 mg $kg^{-1}$ (dry mass) 0.023 mg $kg^{-1}$ (wet mass) | 9 | $97 \pm 3$ ($As^{III}$) $100 \pm 3$ ($As^{V}$) | [104] |
| Hg | Methylmercury | Homogenized tissue | Extraction, GF-AAS | 0.08 mg $kg^{-1}$ | – | $97.7 \pm 5.5$ | [106] |
| Hg | Organic and inorganic mercury | Hair, fish | Cold vapour AAS | 0.003–0.005 ppb | – | – | [108] |
| Hg | Total, inorganic and organic mercury | Brain tissue from monkeys | Cold vapour AAS | – | 31–41 (inorg Hg) 2–8 (methylHg) | – | [109] |

Table 4 (contd.)

| Element | Species | Matrix | Separation and measuring technique | LOD | RSD (%) | Recovery (%) | Ref. |
|---|---|---|---|---|---|---|---|
| Hg | $CH_3Hg^+$ | Fish | Extraction, cold vapour AAS | 25 ng Hg | – | 102 ± 2 | [110] |
| Hg | Methyl-, ethyl-, phenyl- and inorganic mercury | Meat, fish, oyster, dried banana, wheat flour | Extraction, GLC, GF-AAS | 0.003 ng $\mu l^{-1}$ methyl- and ethylHg 0.125 ng $\mu l^{-1}$ phenylHg | 2.1–8.1 | 96–105 | [111] |
| Sn | Tetra- and trialkyltin homologues | Mammalian tissues | GLC | 1 pg trialkylSn | – | 97–106 | [112] |
| Sn | Methyltins | Mouse tissue | GC–MS | 1 ng trialkylSn per g tissue | – | 89.1–969 | [113] |
| Fe | Ferritin, Transferrin, Fe protein-succinate, cytochrome C | Drugs | Extraction, HPLC, ICP-AES | – | – | – | [117] |
| Fe, Mn | Protein, pectin and lipid bound metals | Milk powder, wheat germ, oak flakes, lentils, rice and rye flour) | Extraction, flame AAS | – | – | – | [118] |
| Cu, Ni, Zn | Protein bound metals | Soybean flour | Gradient gel electrophoresis, flame AAS | – | – | – | [119] |
| Cd, Zn | Protein bound metals | Vegetable foodstuffs | Sephadex column separation, GF-AAS | – | – | – | [120] |
| Pb | Tetraalkyl- and ionic alkyllead, $Pb^{2+}$ | Fish tissue | GC, AAS | 7.5 ng $g^{-1}$ | 6.5 (triethylPb) 20 (diethylPb) | 71–101 for diethylPb | [121] |
| Sn | Methyl-, butyl- and, inorganic tin | Oyster | Extraction, HG-AAS | 1–2.5 ng | – | – | [122] |
| Hg | Methyl-, and ethyl-mercury, thimerosal | Tuna, biological products | HPLC(RP), cold vapour, ICP-MS | 7–20 ppb | – | – | [123] |
| Sn | Monobutyl-, dibutyl-, tributyl-, tetrabutyltin | Fish, shellfish | Extraction, GC | – | – | – | [124] |
| Sn | Cyclohexyl- and butyltin | Oyster | Extraction, HPLC–AAS, GC-MS, HPLC–MS | – | – | – | [125] |

Table 4 (contd.)

| Element | Species | Matrix | Separation and measuring technique | LOD | RSD (%) | Recovery (%) | Ref. |
|---|---|---|---|---|---|---|---|
| Pb | Tetraalkyl- and ionic alkyllead | Fish | Extraction, GC–AAS, GC-MS | – | – | – | [126] |
| As | Arsonobetaine | Lobster | Extraction, single crystal X-ray | – | – | – | [127] |
| As | Arsenobetaine, cacodylate, tetrametylarsonium ions | Dogfish musxle | Extraction, HPLC, ICP-AES | – | – | – | [128] |
| As | MMA, DMA, arsenobetaine, arsenocholine, tetramethyl arsonium iodide, inorganic arsenic | Shark tissue | Extraction, IR, NMR, GC-MS, ET-AAS | – | – | – | [129] |
| Cd | Metallothionein-like protein bound | Pig kidney | HPLC (size exclusion chromatography), ICP-MS | – | – | – | [130] |
| Cd | Protein complexed form | Crab meat | HPLC(RP), ET-AAS | – | – | – | [131] |
| Se | Selenomethionine | Soybean | GC–MS | – | – | – | [132] |
| Se | Selenomethionine, methyl selenocysteine | Healthfoord supplements | HPLC, AAS | – | – | – | [133] |

127–129]. Many of these have evolved by coupling a gas- or liquid-chromatographic technique with an element-specific detector. Of the instrumental methods, atomic spectrometry is most widely used and most effectively developed, both in respect of methods using hydride generation coupled to atomic absorption or emission [92,96,104] and inductively coupled plasma-spectrometry [128] and electrothermal methods with graphite furnace [129]. Recently, ICP-MS has been used for the detection of arsenic [100,102]. In such cases, GC or HPLC was used as the method of separation. It can be shown from Table 4 that below-nanogram-level detection limits can be achieved in some methods [98,100,104]. Also the accuracy of some of the methods is very good [96,102,104]. However, only a few data are available concerning these aspects.

One question that arises when speciation of mercury is to be performed is the sample pretreatment used to bring the mercury species into solution. The treatment must be capable of solubilizing the species from the sample under investigation without breaking the C–Hg bond. In general, the chromatographic methods make use of solvent extraction for this purpose, using non-polar solvents, the organic mercury being extracted as chloride or bromide. Thus most of the speciation methods for mercury in solid biological materials depend on chromatographic separations with detection by means of cold vapour atomic absorption spectrometry [108–110]. Mercury has been detected by GF-AAS [106–111] and ICP-MS [123] by some workers in biological samples. It can be seen from data in Table 4 that the detection limits for various organomercury species are mostly in the parts per billion range or below [86,106,108,110,111,123]. Typical R.S.D. values lie within 10% [65,109,111] for organomercurials but for inorganic mercury they may be poor [109]. The recovery of the reported methods in cases in which this parameter has been reported is excellent [86,106,110,111].

Hydride generation has been satisfactory for the determination of alkyltin compounds containing carbon chains of four atoms or less; derivatization is required for more than four carbon atoms in the chain. Various workers have analyzed biological samples for organotins by extraction followed by GLC or GC–MS [112,113,124,125]. In such cases a better LOD value, i.e. 1 pg for trialkyltin [112], may be attained compared with HG-AAS (1–2.5 ng) [122].

Not many papers have been published on the speciation of Pb, Mn, Zn, Ni, Cu, Cd or Se in biological materials in the solid phase. Speciation studies of metalloproteins of these elements have been accomplished by extraction [117,118], separation by gel electrophoresis [119], on a Sephadex column [120] or by gas chromatography [126] followed by AAS determination of the analyte. Investigations of the different biochemical forms of selenium have been made by using GC–MS [132] or HPLC–AAS [133]. In most of these cases, the analytical parameters have not been stated. Nevertheless, in a typical study of inorganic and organic lead compounds in fish tissues by GC–AAS, an LOD of 7.5 ng $g^{-1}$, an R.S.D. of 6.5% for triethyllead and a recovery of 71–101% for diethyllead have been reported [121].

## 4. Speciation of miscellaneous solid samples

In this section we would like to discuss some papers concerning different solid matrices, in which speciation studies have been carried out on samples other than soil, sediment, biological or food samples. For example, details of metal speciation in atmospheric particulates and also speciation in wood, and coal, which have been developed in recent years, are presented below.

Several experimental procedures, varying in manipulative complexity, have been proposed for determining several chemical speices of particulate trace metals. Thus atmospheric particulates collected on a glass fibre filter can be acidified by soaking in HCl and extracted by shaking with toluene, ethyl acetate or methanol or by refluxing in a Soxhlet apparatus. Continuous Soxhlet extraction is sometimes preferred since the cycling time can be controlled and the exhaustive technique exposes fresh solvent, which can percolate into the pores of particles like fly ash which may have a hollow structure [16].

A sequential extraction procedure, originally applied in the study of soil sample [32], has been used for the analysis of urban dust particles [134]. In such a case, exchangeable metals were determined by extraction with $MgCl_2$, metals bounded to carbonate by leaching with an acetic acid buffer, metals bounded to Fe–Mn oxides by extraction with hydroxylamine at 96 °C, those bounded to organic matter by extraction with $H_2O_2$ at 85 °C, and residual metals by digestion with an $HF–HClO_4$ mixture.

Complex analytical methods were proposed for determining chemical species of selected trace metals in fly ash [135]. Morphological investigations and single particle analysis were performed by SEM/EDAX method. A survey of mineral-logical phases was made by X-ray powder diffraction and IR spectrometry. Sequential solvent-leaching experiments were carried out to obtain information on the mobility of metal species. Cu, Ni, Co, Cr, Pb and Cd were studied for determining exchangeable metals, carbonate, Mn oxides, organic matter, non-crystalline iron oxides, crystalline iron oxides and residual fractions.

Chemical species of iron, i.e. metal iron, soluble iron ($H_2O$, $H^+$), $Fe^{2+}$, $Fe^{2+}$ (ionic), $Fe^{3+}$ (ionic), $Fe_3O_4$ (magnetite), $Fe_2O_3$ (hematite) and FeO(OH) (goethite), have been determined in atmospheric particulate samples. Filtration, ultrafiltration, ion chromatography, extraction ($H_2O$, 0.02 M citric acid, 0.1 M HCl) and Mössbauer spectroscopy have been used for their characterization [136,137].

Speciation of Cu, Pb, Zn and Cr in dust of different origins and particle diameters has been reported by Gao et al. [138]. Major parts of these metals were bound to organic matter, Fe–Mn oxides and the rest as residuals. The exchangeable metals bound to carbonates and Fe–Mn oxides of these four heavy metals in small particles were superior to those in large particles. This illustrated that heavy metals in small particles are more active and toxic; the activity order being Zn > Pb > Cu > Cr.

Determination and speciation of ionic alkyllead compounds have presented a serious challenge for analytical chemist. In the environment these compounds have an anthropogenic origin but they may also be produced from biological transformations of $Pb^{2+}$ ions. Triethyllead, tetraethyllead and other alkyllead species in environmental samples have been studied by GC–AAS after extraction [139].

Possanzini et al. [140] developed a method for the speciation and separate determination of inorganic $NH_4^+$ salts in atmospheric aerosols. The speciation and quantification of organosilicon compounds at below parts-per-million levels in environmental and industrial samples require the separation of the compounds of interest coupled with sensitive, selective detection [141]. The combination of HPLC for separation and ICP-AES for detection is ideal for the determination of various organosilicon compounds. Separation of non-polar, high molecular mass poly(dimethylsiloxane) polymers was performed by size-exclusion chromatography with tetrahydrofuran or xylene as the mobile phase. Again, separation of polar, low molecular mass silanols was accomplished by reversed-phase HPLC with water–acetonitrile as mobile phase.

Methods for the determination of Cu, Cr and As and for the speciation of Cr(VI), As(III) and As(V) in wood and dust from impregnated timber (with those metal ions as preservatives) are given by Nygren and Nilsson [142]. Weak-acid-soluble Cr(VI) was determined by soaking a dust sample twice in NaAc buffer on a shaker for 5 min. the two extracts were filtered off using a membrane filter, combined and Cr(VI) was determined. For speciation studies of arsenic, a dust sample was leached twice in 45 ml of 6 M HCl for 1 h. The extracts were filtered through Millipore filter, combined and the volume adjusted to 100 ml. To 10 ml of the extract, 10 ml of 12 M HCl and 10 ml toluene were added. As(III) was re-extracted from the organic phase and determined by GF-AAS. After separation of As(III), As(V) was determined in the remaining solution after reduction with KI and following the same procedure.

Brown coal samples from different deposits have been analyzed [143] for the binding forms of their inorganic components. Besides the analysis of dried coals, ashing techniques and extraction procedures with different solvents (acids, bases, complexing agents, organic solvents with different polarity) have been investigated. ESCA, PIXE, INAA, ICP-AES, NMR and ion chromatography have been applied to the analysis of coals, ashes, wet ashes and extraction products. The bonding behaviour of more than 40 elements was characterized. Species identified in such cases were kaolinite, muscovite, calcite, apatite, iron pyrites, siderite, mica, rutile, quartz, bassanite, gypsum, anhydrite and hematite. On the other hand, major species in the coal ash were $SiO_2$, CaO, $Fe_2O_3$, $Al_2O_3$ and MgO.

Although the methodologies of the speciation studies included in this section are described in details, except in a few cases, the analytical characteristics are not stated, e.g. LOD [141]; 1–4 ng Si for methylsilanediols, 4–5 ng Si for polydi-methylsiloxane. Recoveries and coefficient of variation values are indicated only in some cases [142], and for Cr(VI), As(III) and As(V) they are, respectively, 94%, 1–8%; 82%, 4–5%; 89%, 4–12%.

## 5. Conclusion

In the investigation of the toxic and essential effects of trace constituents, a speciation study is often indispensable. It is clear that this is one of the important areas in speciation that has developed more rapidly. In the near future, an appreciable increase in applications can be expected because in recent years, the coupling of different separation and preconcentration techniques with various instrumentation has been established as an appropriate methodology for speciation.

It is evident that speciation studies have been carried out by two different approaches, one to identify unknown species by rigorous methods and other to identify compounds in experimental samples by comparison with standard compounds. The continued application and development of both approaches is necessary for complete speciation of various solid samples, and in this respect the availability of stable certified materials for different chemical species is an important challenge which will be a great help for the validation of new strategies.

On the other hand, in order to obtain accurate information on the chemical species in a sample, due consideration should be given to the sample collection, pretreatment and storage steps. More studies and applications of fast speciation analysis for solid samples in order to measure the very small concentrations of species are eagerly awaited.

## Acknowledgement

Funds to carry out this work were provided by the Universidad de Valencia (Spain) for which two of the authors (A.K.D., R.C.) are deeply indebted.

## References

[1] M. de la Guardia, Non-Chromatographic Methods for the Element Speciation by Atomic Spectrometry, in S. Caroli (Ed.), Element Speciation in Bioionorganic Chemistry, in press.
[2] W. Lund, Fresenius Z. Anal. Chem., 337 (1990) 557.
[3] J.C. Van Loon and R.R. Barefoot, Analyst, 117 (1992) 563.
[4] J.R. Kramer and H.E. Allen (Eds.), Metal Speciation, Theory, Analysis and Applications, Lewis Publishers, Chelsea, 1988, pp. 155–194.
[5] G.E. Batley (Ed.), Trace Element Speciation: Analytical Methods and Problems, CRC Press, Boca Raton, FL, 1989, pp. 77–342.
[6] J.W. Patterson and R. Passino (Eds.), Metal Speciation, Separation and Recovery, Vol. 2, Lewis Publishers, Chelsea, 1990, pp. 237–319.
[7] A.V. Hirner, Int. J. Environ. Anal. Chem., 46 (1992) 77.
[8] W.F. Pickering, Crit. Rev. Anal. Chem., Nov. (1981) 233.
[9] D.L. Lake, P.W.W. Kirk and J.N. Lester, J. Environ. Qual., 13 (1984) 175.
[10] M. Sager, R. Pucsko and R. Belocky, Arch. Hydrobiol. Suppl., 84 (1990) 37.
[11] J.N. Lester, Sci. Total Environ., 30 (1983) 1.
[12] P.R. Hesse, A Textbook of Soil Chemical Analysis, Murray, London, 1971, p. 116, 128.
[13] N. Breward and D. Peachey, Sci. total Environ., 29 (1983) 155.
[14] T. Tusuda, H. Nakanisi, S. Aoki and J. Takebayashi, J. Chromatogr., 387 (1987) 361.
[15] R.M. Harrison and S. Rapsomanikis, Environmental Analysis using Chromatography Interfaced with Atomic Spectroscopy, Ellis Horwood, 1989.
[16] D.E. Wells, Microchim. Acta, 109 (1992) 13.
[17] M.L. Räisänen, L. Hämäläinen and L.M. Westerberg, Analyst, 117 (1992) 623.
[18] R. Rubio and A.M. Ure, Int. J. Environ. Anal. Chem., 51 (1993) 205.
[19] W. Salomons and U. Förstner, Environ. Technol. Lett., 1 (1980) 506.
[20] U. Förstner, W. Calmano, K. Conradt, H. Jaksch, C. Schimkus and J. Schoer, Proc. Int. Conf. Heavy Metals in the Environment, Amsterdam, 1981, p. 698.
[21] M. Sager, Mikrochim. Acta, 3 (1986) 129.
[22] W.F. Pickering, Ore Geol. Rev., 1 (1986) 83.
[23] R.A. Nadkarni, Anal. Chem., 56 (1984) 2233.
[24] S. Nakashima, R.E. Sturgeon, S.N. Willie and S.S. Berman, Analyst, 113 (1988) 159.
[25] M. Bettinelli, U. Baroni and N. Pastorelli, Anal. Chim. Acta, 225 (1989) 159.
[26] M. de la Guardia (Ed.), Empleo de los Hornos de Microondas en Química, University of Valencia, 1990.
[27] K.I. Mahan, T.A. Foderaro, T.L. Garza, R.M. Martinez, G.A. Maroney, M.R. Trivisonno and E.M. Willging, Anal. Chem., 59 (1987) 938.
[28] P.E. Gardiner, R. Schierl and K. Kreutzer, Plant Soil, 103 (1987) 151.
[29] A.R. Tills and B.J. Alloway, Int. Conf. Heavy Metals in the Environment, Heildelberg, Vol. 2, C.E.P. Consultants, Edinburgh, 1983, p. 1212.
[30] C. Berger and M. Perrut, J. Chromatogr., 505 (1990) 37.
[31] S. Gatehouse, D.W. Russel, J.C. van Moort, J. Geochem. Explor., 8 (1977) 483.
[32] A. Tessier, P.G.C. Campbell and M. Bisson, Anal. Chem., 51 (1979) 844.
[33] G. Sposito, L.J. Lund and A.C. Chang, Soil. Sci. Soc. Am. J., 46 (1982) 260.
[34] W.P. Miller and W.W. McFee, J. Environ. Qual., 12 (1983) 29.
[35] R. Psenner, R. Pucsko and M. Sager, Arch. Hydrobiol. Suppl., 70 (1984) 111.

[36] L.M. Shuman and W.L. Hargrove, Soil. Sci. Soc. Am. J., 49 (1985) 1117.
[37] M. Kersten and U. Förstner, Water Sci. Technol., 18 (1986) 121.
[38] H. Zeien and G.W. Brümmer, Mitt. Dt. Bodenkundl. Ges., 59 (1989) 505.
[39] A.V. Hirner, K. Kritsotakis and H.J. Tobschall, Appl. Geochem., 5 (1990) 491.
[40] R. Rubio, J.F. Lopez-Sanchez and G. Rauret, An. Quim., 87 (1991) 599.
[41] G.A. Battiston, R. Gerbasi, S. Degetto and G. Sbrignadello, Spectrochim. Acta, Part B, 48 (1993) 217.
[42] R.M. Harrison, D.P.H. Laxen and S.J. Wilson, Environ. Sci. Technol., 15 (1981) 1378.
[43] J.L. Fraser and K.R. Lum, Environ. Sci. Technol., 17 (1983) 52.
[44] A. Wadge and M. Hutton, Environ. Pollut., 48 (1987) 85.
[45] B. Welté, N. Bles and A. Montiel, Environ. Technol. Lett., 4 (1983) 79.
[46] A.M. Ure, Mikrochim. Acta, 2 (1991) 49.
[47] P.O. Scokart, K. Meeus-Verdinne and R. De Borger, Int. J. Environ. Anal. Chem., 29 (1987) 305.
[48] P. Quevauviller, A. Ure, H. Muntau and B. Griepink, Int. J. Environ. Anal. Chem., 51 (1993) 129.
[49] L. Viereck, K. Tenhaken, P. Obermann and E. Schrammeck, Assessment of heavy Metal Contamination in Soils, Dechema, Frankfurt, 1989, pp. 169–188.
[50] F.E. Butterworth and B.J. Alloway, Int. Conf. Heavy Metals in the Environment, Amsterdam, C.E.P. Consultants, Edinburgh, 1981, p. 713.
[51] R.G. McLaren and D.V. Crawford, J. Soil Sci., 24 (1973) 172.
[52] J.M. Robbins, M. Lyle and G.R. Heath, Report 84-3, College of Oceanography, Oregon State University, Corvallis, U.S.A., 1984.
[53] J.A.E. Gibson and I.R. Willett, Commun. Soil Sci. Plant. Anal., 22 (1991) 1303.
[54] A. Astruc, R. Lavigne, V. Desauziers, R. Pinel and M. Astruc, Appl. Organomet. Chem., 3 (1989) 267.
[55] J. Dachs, R. Alzaga, J. M. Bayona and P. Quevauviller, Anal. Chim. Acta., 286 (1994) 319.
[56] L. May, L. Berhane, M. Berhane, C. Counsil, M. Keane and B.B. Reed, Water, Air, Soil Pollut., 75 (1994) 293.
[57] G. Bombach, A. Pierra, W. Klemm, Fresenius' Z. Anal. Chem., 350 (1994) 49.
[58] E.G. Soto, E.A. Rodriguez, D.P. Rodriguez. P.L. Mahia and S.M. Lorenzo, Sci. Total Environ., 141 (1994) 87.
[59] T. Takamatsu, H. Aoki and T. Yoshida, Soil Sci., 133 (1982) 239.
[60] D.H. Oughton, B. Salbu, G. Riise, H. Lien, G. Ostby and A. Noren, Analyst 117 (1992) 481.
[61] A.V. Konoplev, A.A. Bulgakov, V.E. Popov and Ts.I. Bobovnikova, Analyst, 117 (1992) 1041.
[62] R. Martinez Avila, A. Salvador and M. de la Guardia, Analusis, 19 (1991) 213.
[63] M.B. de la Calle Guntiñas, Y. Madrid and C. Cámara, Mikrochim. Acta., 109 (1992) 149.
[64] P. Quevauviller, O.F.X. Donard, J.C. Wasserman, F.M. Martin and J. Schneider, Appl. Organomet. Chem., 6 (1992) 221.
[65] R. Cela, R.A. Lorenzo, M.C. Mejuto, M.H. Bollaín, M.C. Casais, A. Botana, E. Rubí and M.I. Medina, Mikrochim. Acta, 109 (1992) 111.
[66] G. Bombach, K. Bombach and W. Klemm, Fresenius' Z. Anal. Chem., 350 (1994) 18.
[67] U. Karslon and W.T. Frankenberger, Jr., Soil Sci. Soc. Am. J., 49 (1985) 592.
[68] S.L. McGeehan and D.V. Naylor, J. Environ. Qual., 21 (1992) 68.
[69] G. Heron, C. Crouzet, A.C.M. Bourg and T.H. Christensen, Environ. Sci. Technol., 28 (1994) 1986.
[70] M. Thomas, D. Petit, B. Kenis and L. Lamberts, Analusis, 13 (1985) 76.
[71] M. Sager, R. Belocky and R. Pucsko, Acta Hydrochim. Hydrobiol., 18 (1990) 157.
[72] M. Sager, Fresenius' Z. Anal. Chem., 320 (1985) 274.
[73] V. Carbonell, A. Salvador and M. de la Guardia, Fresenius' Z. Anal. Chem., 342 (1992) 529.
[74] A.M. Ure, Fresenius' Z. Anal. Chem., 337 (1990) 577.
[75] P.E. Gardiner, J. Anal. At. Spectrom., 3 (1988) 163.
[76] D. Behne, Analyst, 117 (1992) 555.
[77] J.B. Dawson, Fresenius' Z. Anal. Chem., 324 (1986) 463.
[78] H.M. Crews, J.A. Burrell and D.G. McWeeny, J. Sci. Food Agric., 34 (1983) 997.
[79] M.L. Cervera and R. Montoro, Fresenius' Z. Anal. Chem., 348 (1994) 331.
[80] J.F. Uthe and C.L. Chou, Sci. Total Environ., 71 (1988) 67.
[81] P.E. Gardiner, Fresenius' Z. Anal. Chem., 345 (1993) 287.
[82] M. Yu, G. Liu and Q. Jin, Talanta, 30 (1983) 265.
[83] D.C. Chilvers, J.B. Dawson, M.H. Bahreyni-Toosi and A. Hodgkinson, Analyst, 109 (1984) 871.
[84] J.B. Dawson and D.C. Chilvers, Analyst, 109 (1984) 473.
[85] L. Dunemann, Fresenius' Z. Anal. Chem., 342 (1992) 802.
[86] J. Gui-Bin, N. Zhe-Ming, W. Shun-Rong and H. Heng-Bin, Fresenius' Z. Anal. Chem., 334 (1989) 27.
[87] D.E. Wells, Pure Appl. Chem., 60 (1988) 1437.
[88] R. Van Cleuvenbergen, D. Chakraborti and F. Adams, Anal. Chim. Acta, 228 (1990) 77.
[89] N. Ybañez, M.L. Cervera, R. Montoro and M. de la Guardia, J. Anal. At. Spectrom., 6 (1991) 379.
[90] V. Lopez-Avila, N.S. Dodhiwala and W.F. Berkert, J. Chromatogr. Sci., 28 (1990) 468.
[91] P.H. Brown, L. Dunemann, R. Schulz and H. Marschner, Z. Pflanzenernaehr Bodenk, 152 (1989) 85.
[92] H. Münz and W. Lorenzen, Fresenius' Z. Anal. Chem., 319 (1984) 395.
[93] H.A.M.G. Vaessen and A. Van Ooik, Z. Lebensm. Unters. Forsch., 189 (1989) 232.
[94] P.J. Brooke and W.H. Evans, Analyst, 106, (1981), 514.
[95] A. Yasui, C. Tsutsumi and S. Toda, Agric. Biol. Chem., 42 (1978) 2139.
[96] W. Holak and J.J. Specchio, At. Spectrosc., 12 (1991) 105.
[97] J. Aggett and A.C. Aspell, Analyst, 101 (1976) 341.
[98] B. Sarx and K. Bächmann, Fresenius' Z. Anal. Chem., 316 (1983) 621.
[99] M. Morita and J.S. Edmonds, Pure Appl. Chem., 64 (1992) 575.

[100] D. Beauchemin, M.E. Bednas, S.S. Berman, J.W. McLaren, K.W.M. Siu and R.E. Sturgeon, Anal. Chem., 60 (1988) 2209.
[101] M. Morita, T. Uehiro and K. Fuwa, Anal. Chem., 53 (1981) 1806.
[102] S. Branch, L. Ebdon and P. O'Neill, J. Anal. At. Spectrom., 9 (1994) 33.
[103] G. Lunde, J. Sci. Food Agric., 24 (1973) 1021.
[104] J.C. López, C. Reija, R. Montoro, M.L. Cervera and M. de la Guardia, J. Anal. At. Spectrom., 9 (1994) 651.
[105] L. Magos, Analyst, 96 (1971) 847.
[106] G.T.C. Shum, H.C. Freeman and J.F. Uthe, Anal. Chem., 51 (1979) 414.
[107] J.F. Uthe, J. Solomon and B. Grift, J. Assoc. Off. Anal. Chem., 55 (1972) 583.
[108] C.E. Oda and J.D. Ingle, Jr., Anal. Chem., 53 (1981) 2305.
[109] B. Lind, R. Body and L. Friberg, Fresenius' Z. Anal. Chem., 345 (1993) 314.
[110] M.C.R. Rezende, R.C. Campos and A.J. Curtius, J. Anal. At. Spectrom., 8 (1993) 247.
[111] M. Filippelli, Anal. Chem., 59 (1987) 116.
[112] Y. Arakawa, O. Wada, T.H. Yu and I. Hideaki, J. Chromatogr., 216 (1981) 209.
[113] J.C. Means and K.L. Hulebak, Neurotoxicology, 4 (1983) 37.
[114] J.C. Van Loon, Selected Methods of Trace Metal Analysis: Biological and Environmental Sample, Wiley, New York, 1985.
[115] P.J. Craig (Ed.)., Organometallic Compounds in the Environment. Principles and Reactions, Longman, Harlow, 1986.
[116] W. Langseth, Anal. Chim. Acta, 185 (1986) 249.
[117] S. Caroli, F. La Torre, F. Petrucci, O. Senofonte and N. Violante, Trace Elements Anal. Chem. Med. Biol. 6 (1992) 311.
[118] G. Schwedt and K.-D. Neumann, Z. Lebensm. Unters. Forsch., 194 (1992) 152.
[119] L. Dunemann and H. Reinecke, Fresenius' Z. Anal. Chem., 334 (1989) 743.
[120] K. Günther and H. Waldner, Anal. Chim. Acta, 259 (1992) 165.
[121] Y.K. Chau, P.T.S. Wong, G.A. Bengert and J.L. Dunn, Anal. Chem., 56 (1984) 271.
[122] J.S. Han and J.H. Weber, Anal. Chem., 60 (1988) 316.
[123] D.S. Bushee, J.R. Moody and J.C. May, J. Anal. At. Spectrom., 4 (1989) 773.
[124] I.S. Krull, K.W. Panaro, J. Noonan and D. Erickson, Appl. Organomet. Chem., 3 (1989) 295.
[125] W.R. Cullen, G.K. Eigendorf, B.U. Nwata and A. Takatsu, Appl. Organomet. Chem., 4 (1990) 581.
[126] D.S. Forsyth, R.W. Dabeka and C. Cleroux, Appl. Organomet. Chem., 4 (1990) 591.
[127] J.S. Edmonds, K.A. Francesconi, J.R. Cannon, C.L. Raston, B.W. Skelton and A.H. White, Tetrahedron Lett., 18 (1977) 1543.
[128] Y. Shibata and M. Morita, Anal. Chem., 61 (1989) 2116.
[129] T. Kaise and S. Fukui, Appl. Organomet. Chem., 6 (1992) 155.
[130] H.M. Crews, J.R. Dean, L. Ebdon and R.C. Massey, Analyst, 114 (1989) 895.
[131] K.O. Olayinka, S.J. Haswell and R. Grzeskowiak, J. Anal. At. Spectrom., 4 (1989) 171.
[132] K. Yasumoto, T. Suzuki and M. Yoshida, J. Agric. Food Chem., 36 (1988) 463.
[133] T. Lei and W.D. Marshall, 38th Canadian Spectroscopy Conf., Trent University, Peterborough, Ontario, 1992.
[134] U. Förster, in M. Bernhard, F.E. Brinckman and P. J. Sadler (Eds.), The Importance of Chemical Speciation in Environmental Processes, Springer, Berlin, 1986.
[135] K. Polyák, I. Bódog and J. Hlavay, Talanta, 41 (1994) 1151.
[136] A.N. Dedik, P. Hoffmann and J. Ensling, Atmos. Environ., 26A (1992) 2545.
[137] P. Hoffmann, T. Sinner, A.N. Dedik, V.K. Karandashev, A.A. Malyshev, S. Weber and H.M. Ortner, Fresenius' Z. Anal. Chem., 350 (1994) 34.
[138] L.C. Gao, G.H. He, S.R. Wang and S.P. Feng, Chin. Chem. Let., 4 (1993) 1109.
[139] P.T.S. Wong, Y.K. Chau, J. Yaromich, P. Hodson and M. Whittle, Appl. Organomet. Chem., 3 (1989) 59.
[140] M. Possanzini, P. Masia and V. Dipalo, Atmos. Environ., 26A (1992) 1995.
[141] S.B. Dorn and E.M. Skelly Frame, Analyst, 119 (1994) 1687.
[142] O. Nygren and C.A. Nilsson, Analusis, 21 (1993) 83.
[143] C. Vogt, Fresenius' Z. Anal. Chem., 350 (1994) 89.

ELSEVIER

Talanta 42 (1995) 1031–1036

Talanta

# Sorption and preconcentration of some heavy metals by 2-mercaptobenzothiazole–clay

Newton L. Dias Filho [a,*], Wagner L. Polito [b], Yoshitaka Gushikem [c]

[a] *Departamento de Ciências, UNESP, C.P. 31, 15378-000, Ilha Solteira, SP, Brazil*
[b] *Instituto de Química, USP, 13560-250, São Carlos, SP, Brazil*
[c] *Instituto de Química, UNICAMP, CP 6154, 13083-970, Campinas, SP, Brazil*

Received 12 August 1994; revised 2 December 1994; accepted 7 December 1994

**Abstract**

2-Mercaptobenzothiazole loaded on previously treated clay was prepared, characterized and used for sorption and preconcentration of Hg(II), Pb(II), Zn(II), Cd(II), Cu(II) and Mn(II) from an aqueous solution. The support used was a natural clay previously treated with sulphuric acid solution. Adsorption isotherms of metal ions from aqueous solutions as function of pH were studied at 298 K. Conditions for quantitative retention and elution were established for each metal by batch and column methods. The chemically treated clay was very selective to Hg(II) in solution in which Zn(II), Cd(II), Pb(II), Cu(II) and Mn(II) were also present.

## 1. Introduction

The use of clays for adsorption and ion exchange studies [1–5], hydrolysis reactions [6], esterification of carboxylic acids [7] and whitening of oils [8] have been of interest to many researchers using natural aluminium silicates as rigid support.

Previously, Terada et al. [9,10] reported that 2-mercaptobenzothiazole (MBT) impregnated on silica gel surface can be used in preconcentration of metal ions present in water samples. MBT is insoluble in water but soluble in many organic solvents and can, therefore, be used in the preconcentration process of trace metals present in natural water [10].

Impregnation of organic molecules on a solid surface is a different process of organofunctionalization, e.g. grafting of organic molecules on silica gel surface. In the latter case, organic molecules are attached on the support by means of chemical bonding [11–15], while in the former case it is by means of physical interactions. Using the first process, sorbents are much easier prepared and under steric ground, the physically adsorbed reagents do not present any restrictions in coordinating with the metal ions on the surface. Quantitative retention of the metal ions complex species on the surface is achieved provided that they are insoluble in the solvent.

This work focuses on the preparation and utilization of treated natural clay as support for MBT looking at the following properties: (a) selective adsorption of heavy metal ions, (b) utilization as chromatographic columns packing material and (c) utilization in the preconcentration processes of heavy metal ions.

## 2. Experimental

All reagents were of analytical grade and used without further purification.

* Corresponding author. Fax: (55) 187-62-2735.


*SSDI* 0039-9140(95)01505-1

Table 1
Composition (%) and specific surface area ($S_{BET}$ ($m^2/g$)) of the clay samples

| Sample | $S_{BET}$ | $SiO_2$ | $Al_2O_3$ | $Fe_2O_3$ | CaO | MgO | $Na_2O$ | $K_2O$ | $SO_3$ | $MnO_2$ |
|---|---|---|---|---|---|---|---|---|---|---|
| a | 5.3 | 66.8 | 23.6 | 5.3 | 0.60 | 0.85 | 0.20 | 0.71 | — | — |
| b | 37.3 | 83.4 | 9.7 | 2.4 | 0.04 | 0.15 | 0.08 | 0.38 | 0.07 | — |
| c | 39.8 | 86.8 | 6.5 | 1.6 | 0.40 | 0.12 | 0.05 | 0.38 | 0.05 | 0.13 |
| d | 54.8 | 86.6 | 5.2 | 3.5 | 0.38 | 0.17 | 0.06 | 0.38 | — | 0.12 |
| e | 72.6 | 89.4 | 5.0 | 1.4 | 0.34 | 0.09 | 0.09 | 0.20 | — | 0.12 |
| f | 100.5 | 92.0 | 1.7 | 1.8 | 0.02 | 0.12 | 0.05 | 0.10 | 0.07 | 0.04 |
| g | 89.4 | 94.7 | 3.4 | 0.6 | 0.02 | 0.05 | 0.08 | 0.18 | 0.06 | 0.15 |

Sample (a) Natural clay; samples (b–g) chemically treated clay according to the procedures described.

### 2.1. Sample preparations

Natural clay from Jupia, city of São Paulo State, was used in this work. The clay was obtained by the dispersion and sedimentation method [16]. Various chemical treatments were applied to the material before use. A general procedure is as follows: the clay was treated with 0.5 M solution of potassium permanganate acidified with sulphuric acid solution (6.0 M). The mixture was gently shaken at different times (between 2 and 12 h) at 353 K and then filtered, washed with water and dried at temperatures between 353 and 873 K. The material was ground and sieved.

### 2.2. Chemical analysis and characterization

The samples were chemically analyzed and the results are summarized for various treatments in Table 1. The specific surface areas were determined by the BET technique using CG Scientific Instruments equipment.

### 2.3. Impregnation procedure

About 50 g of treated clay sieved between 70 and 200 mesh was immersed in 50 $cm^3$ of MBT acetone solution (8 w/v%) and shaken for few min and then the solvent was evaporated at room temperature under vacuum. The material was washed with deionized water and dried at 353 K under vacuum.

### 2.4. Isotherm of adsorption

The isotherms of adsorption of metal ions by MBT–clay were determined for Zn(II), Cd(II), Hg(II), Pb(II), Cu(II) and Mn(II) metal ions in aqueous solutions. About 0.5 g of the solids were shaken in 25 $cm^3$ of metal ion solutions (concentrations between $1.0 \times 10^{-3}$ and $1.0 \times 10^{-4}$ M) at $298.0 \pm 0.2$ K for 30 min. The quantity of metal ions in the supernatant solutions were determined by atomic absorption spectroscopy (AAS).

Adsorption isotherms of metal ions from solutions at different pH were also studied. In this case 0.5 g of the sorbent was immersed in 25 $cm^3$ solutions of metal ions of $9.0 \times 10^{-4}$ M and shaken for 30 min at $298 \pm 0.2$ K. The quantity of the metal ion in the supernatant in each flask was determined by AAS.

The quantity of adsorbed metal, $N_f$, was calculated by applying the equation

$$N_f = (N_a - N_s)/m$$

where $N_a$ is the initial mole number of the metal ion, $N_s$ is the metal mole number under equilibrium conditions and $m$ is the mass of the sorbent.

### 2.5. Preconcentration experiments

In the preconcentration experiments using the batch method, solutions of metal ions (25 $cm^3$) with a concentration of $2.0 \times 10^{-4}$ M at various pH were shaken with 1.0 g of MBT-clay at $298 \pm 0.2$ K for 30 min. The amount of metal ions in the supernatant solutions were measured by AAS.

For preconcentration experiments using the column method, a glass column of 20 cm height and 0.8 cm internal diameter was packed with about 8 g of the sorbent. About 10 $cm^3$ of metal ion solution at a suitable pH was passed through the column with a flow rate between 0.5 and 1.0 $cm^3\ min^{-1}$. The column was washed with 20 $cm^3$ of deionized water. The adsorbed metal ions were eluted passing 20 $cm^3$ of eluent (HCl solution) with a suitable composition and the effluent collected for analysis of the metal ions by AAS.

## 3. Results and discussion

X-ray diffraction patterns of the natural clay showed the presence of mixture including kaolinite, montmorillonite, illite and quartz. This is a common composition of the clay mineral found in the region [16]. The chemical treatments applied to the clay samples changed the composition and the specific surface areas as shown in Table 1. It is very clear that decreasing the $Al_2O_3$ content by acid treatment of the natural clay increases the specific surface area and the material becomes more porous [8]. The clay sample resulting from treatment f was used throughout this work.

### *3.1. Amount of reagent loaded on the supporting material*

The amount of MBT supported on the chemically treated surface was determined as follows: 0.5 g of the dried material was packed in a glass column tube and then 20 $cm^3$ of ethanol was passed to quantitatively elute MBT. The quantity of MBT was determined spectrophotometrically.

The amount of reagent loaded on the supporting material was 5.1 mg MBT clay. Under this treatment a reasonable surface coverage with MBT was possible achieving a loading values similar to those obtained using more porous materials such as silica gel [17–21].

### *3.2. Isotherms of adsorption*

Adsorption of metal ions from solution by a solid phase can occur with formation of surface complex between the adsorbed ligand and the metal. However, the sites responsible for the adsorption process are not exclusively due to the adsorbed organic molecule. Other sites on activated clay surface can also contribute to the adsorption process [1–8].

Initially the isotherms were carried out in aqueous solutions without prior adjusting of the pH. The curves resulting by plotting $N_f$ vs. $C$, where $C$ is the equilibrium concentration of the metal ion in solution in contact with the solid phase, are shown in Fig. 1. The adsorption capacities determined for each metal at saturation condition were (in $\mu mol\ g^{-1}$): Hg(II) = 13.5, Cd(II) = 10.0, Zn(II) = 6.9, Pb(II) = 3.5, Cu(II) = 11.0 and Mn(II) = 2.8. Fixing the initial concentration of metal ion and changing the pH solutions and plotting $N_f$ vs. pH, the set of curves shown in Fig. 2 were obtained. Fig. 2A shows that adsorption of Hg(II) by MBT–clay is independent of pH solution. Adsorption of the ion by untreated clay is negligible below pH 3 and at 6, the adsorption is about half of that of observed for treated clay (isotherm not shown). The high affinity of MBT–clay in all the pH solutions range by Hg(II) is explained well by the Pearson rule [22] because MBT and Hg(II) are soft base and acid, respectively. It can be observed that adsorption for the remaining metals is dependent of changes in pH solutions and increased when they vary from 1 to 6.

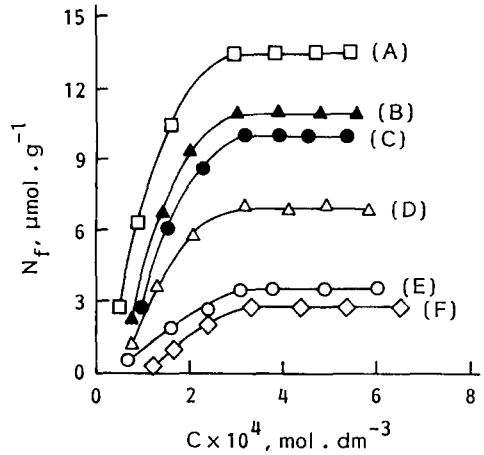


Fig. 1. Isotherms of adsorption of metal ions from solutions by MBT–clay. (A) Hg(II), (B) Cu(II), (C) Cd(II), (D) Zn(II), (E) Pb(II) and (F) Mn(II).

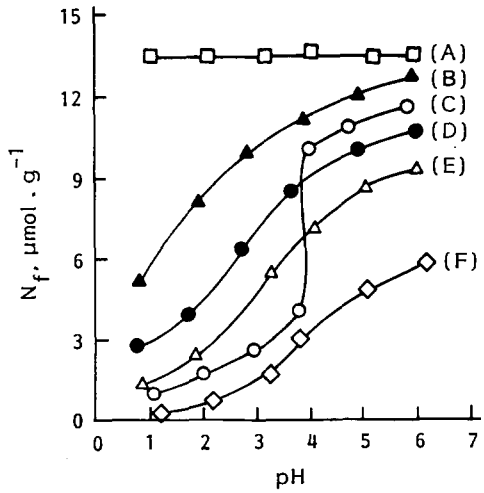


Fig. 2. Isotherms of adsorption of metal ions from solutions by MBT–clay as function of pH. (A) Hg(II), (B) Cu(II), (C) Pb(II), (D) Cd(II), (E) Zn(II) and (F) Mn(II).

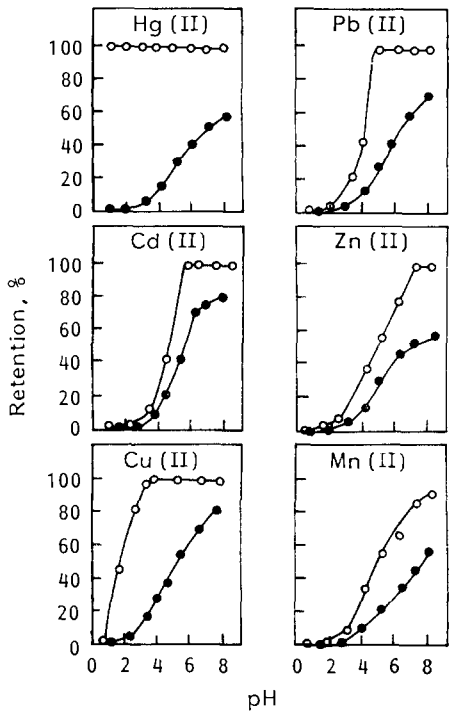


Fig. 3. Preconcentration of metal ions from aqueous solutions by MBT–clay as function of solution pH. Blank points of plots are MBT–clay and full points of plots are untreated clay.

### 3.3. Preconcentration of individual metal ions

*Batch method*

Preconcentration of each metal ion by MBT–clay from an aqueous solution at various pH solutions was examined by batch technique. In the experiments, the equilibrium pH solutions were measured for each experimental point. The results, expressed in per cent extraction, are presented in Fig. 3.

Hg(II) was quantitatively retained from pH 1 up to pH 8. Cu(II) was quantitatively retained on the chelating material from pH 3.5 up to pH 8, whereas untreated clay began to adsorb Cu(II) at pH 3. Pb(II) and Cd(II) showed nearly similar behaviors and were quantitatively retained at pH values of 5 and 5.5, respectively. Zn(II) was completely retained at pH 7.5 and Mn(II) was not quantitatively retained in the pH range of 1–8. In case of Zn(II), despite the high pH value, precipitation of metal hydroxide was not visually detected because the initial concentration of metal ions was very low ($10^{-4}$ M). In all these cases, a pronounced difference in adsorbability between MBT–clay and untreated material was observed.

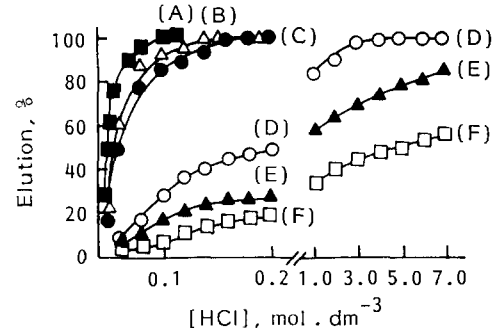


Fig. 4. Elution of metal ions adsorbed on MBT–clay by acid solutions. (A) Mn(II), (B) Zn(II), (C) Cd(II), (D) Pb(II), (E) Cu(II) and (F) Hg(II).

*Column method*

In the column experiment, each metal was quantitatively adsorbed adjusting the solutions pH according to the values found in the previous batch method. In every run, the effluent was collected and a quantity of metal ion analysed. Elution of the metals from the column were made passing 20 cm$^3$ of hydrochloric acid of different concentrations. The results are shown in Fig. 4.

It can be observed that, in the experimental conditions used, only Zn(II), Cd(II) and Mn(II) could be quantitatively eluted with 0.2 M HCl while 49% of Pb(II), 27% of Cu(II) and 19% of Hg(II) were eluted. Quantitative elution of Pb(II) was achieved passing 20 cm$^3$ of 4 M HCl solution while using this condition, 47% of Hg(II) and 73% of Cu(II) were eluted. Quantitative elution of Hg(II) and Cu(II) was possible by passing 20 cm$^3$ of 0.2 M thiourea solution acidified with 1 M HCl solution (Fig. 5).

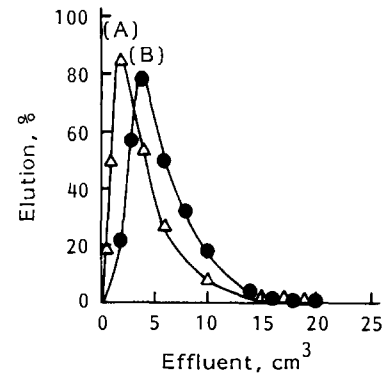


Fig. 5. Elution of (A) Cu(II) and (B) Hg(II) adsorbed on MBT–clay by 0.2 M thiourea solution in HCl (1.0 M).

Table 2
Recovery of metal ions from a mixture

| Ion | Concentration/$10^{-3}$ M | Recovery (%) [a] | | | | | |
|---|---|---|---|---|---|---|---|
| | | Zn(II) | Cd(II) | Hg(II) | Pb(II) | Cu(II) | Mn(II) |
| Zn(II) | 0.2 | — | 97 | 100 | 96 | 91 | 94 |
| | 2.0 | — | 67 | 100 | 54 | 66 | 47 |
| Cd(II) | 0.2 | 95 | — | 100 | 96 | 100 | 92 |
| | 2.0 | 24 | — | 100 | 59 | 96 | 43 |
| Hg(II) | 0.2 | 97 | 93 | — | 91 | 90 | 98 |
| | 2.0 | 92 | 61 | — | 62 | 43 | 43 |
| Pb(II) | 0.2 | 94 | 95 | 100 | — | 100 | 96 |
| | 2.0 | 44 | 66 | 97 | — | 78 | 68 |
| Cu(II) | 0.2 | 98 | 97 | 98 | 94 | — | 100 |
| | 2.0 | 94 | 65 | 92 | 63 | — | 100 |
| Mn(II) | 0.2 | 98 | 98 | 100 | 97 | 95 | — |
| | 2.0 | 70 | 82 | 100 | 78 | 82 | — |
| Co(II) | 0.2 | 100 | 100 | 100 | 95 | 100 | 100 |
| | 2.0 | 97 | 97 | 100 | 71 | 67 | 97 |
| Ni(II) | 0.2 | 98 | 100 | 100 | 93 | 89 | 100 |
| | 2.0 | 95 | 98 | 98 | 19 | 58 | 98 |

[a] Concentration of each ion was $0.1 \times 10^{-3}$ M.

### 3.4. Adsorption and recovery of a mixture of ions

Adsorption and elution studies of a mixture of metal ions as well as interference of Co(II) and Ni(II) were also carried out. In these studies, a series of solutions were prepared in which the metal ions concentrations were fixed at $0.1 \times 10^{-3}$ M except for one of them fixed at $2.0 \times 10^{-3}$ or $0.2 \times 10^{-3}$ M. The results are presented in Table 2.

Recovery of Hg(II) in the presence of other metal ions in concentrations twice or 20 times, was not significantly affected. However, Hg(II) at $2.0 \times 10^{-3}$ M significantly affected the recovery of Zn(II), Cd(II), Pb(II), Cu(II) and Mn(II) in a mixture containing these six ions. In the presence of transition metal ions at a concentration of $2.0 \times 10^{-3}$ M, only the recovery of Hg(II) was not affected.

## 4. Conclusions

MBT–clay has been shown to be an effective solid-phase selective sorbent for Hg(II). Formation of a stronger metal to sulphur donor atom bond accounts for the high affinity shown by MBT for Hg(II) on the basis of the Pearson hard–soft acid–base rule. The material can selectively adsorb Hg(II) from a solution and the presence of other heavy metals or some transition metals do not significantly interfere. An advantage in using this material as sorbent is the abundance of natural clay and the facility of preparation of the modified clay.

## Acknowledgements

N.L.D.F. is indebted to Fundação de Amparo a Pesquisa do Estado de São Paulo (FAPESP) and the Fundação para o Desenvolvimento da UNESP (FUNDUNESP) for financial support.

## References

[1] S. Yariv, Thermochim. Acta, 88 (1985) 49.
[2] M.S. Stul, L. Van Leemput and J.B. Uytterhoeven, Clays Clay Min., 31 (1983) 158.
[3] L. Van Leemput, M.S. Stul, A. Maes, J.B. Uytterhoeven and A. Cremers, Clays Clay Min., 31 (1983) 261.
[4] R.M. Barrer and D.M. MacLeod, Trans. Faraday Soc., 51 (1955) 1290.
[5] M.B. MacBride and M.M. Mortland, Clay Min., 10 (1975) 357.
[6] M.M. Mortland and V. Berheiser, Clays Clay Min., 24 (1976) 60.
[7] J. Shabtai, N. Frydman and R. Lazar, Proc. 6th Int. Congr. Catal., Vol. 2, London, 1976, p. 660.
[8] A.O. Orazmuradov, O.O. Khodzhamuradova and A.K. Mukhamedkuliev, Ser. Fiz. Tekh. Khim. Geol. Nauk., 5 (1986), 73.
[9] K. Terada, K. Morimoto and T. Kiba, Bull. Chem. Soc. Jpn, 53 (1980) 1605.
[10] K. Terada, K. Matsumoto and H. Kimura, Anal. Chim. Acta, 153 (1983) 237.

[11] N.L. Dias Filho, Y. Gushikem, E. Rodrigues, J.C. Moreira and W.L. Polito, J. Chem. Soc. Dalton Trans., (1994) 1493.
[12] N.L. Dias Filho and Y. Gushikem, J. Mol. Struct., in press.
[13] N.L. Dias Filho, Y. Gushikem, J.C. Moreira, W.L. Polito and E. Rodrigues, J. Brazilian Chem. Soc., 5 (1994) 1.
[14] E.I.S. Andreotti and Y. Gushikem, J. Colloid Interface Sci., 142 (1991) 97.
[15] J.C. Moreira and Y. Gushikem, Anal. Chim. Acta, 176 (1985) 263.
[16] P.S. Santos, Clay Technologies Applied to Brazilian Clays, Vol. 1, Edgard Blücher, 1982, p. 282.
[17] K. Terada, A. Inoue, J. Inamura and T. Kiba, Bull. Chem. Soc. Jpn, 50 (1977) 1060.
[18] C. Samara and T.A. Kouimtzis, Anal. Chim. Acta, 174 (1985) 305.
[19] K. Terada, K. Matsumoto and Y. Taniguchi, Anal. Chim. Acta, 147 (1983) 411.
[20] K. Terada, K. Matsumoto and T. Inaba, Anal. Chim. Acta, 158 (1984) 207.
[21] A. Tong, Y. Akama and S. Tanaka, Anal. Chim. Acta, 230 (1990) 175.
[22] R.G. Pearson, J. Am. Chem. Soc., 85 (1963) 3533.

ELSEVIER

Talanta 42 (1995) 1037–1044

Talanta

# Micellar medium for the analysis of complex mixtures of molybdenum and tungsten by derivative synchronous spectrofluorimetry in steels

C. Cruces Blanco *, A.M. García Campaña, F. Alés Barrero, M. Román Ceba

*Department of Analytical Chemistry, Faculty of Sciences, University of Granada, 18071 Granada, Spain*

Received 17 January 1994; revised 9 December 1994; accepted 12 December 1994

**Abstract**

The cationic surfactant hexadecyltrimethylammonium bromide enhances the fluorescence intensity of both molybdenum and tungsten complexes obtained with Alizarin Red S. This characteristic has been used for a sensitive simultaneous spectrofluorimetric determination of both ions over the range 32–4000 ng/ml and 49–2500 ng/ml for Mo and W, respectively. Good selectivity is achieved applying the well known synchronous derivative technique with a minucious pH selection. The proposed method has been applied to a certified steel sample with recoveries between 96 and 102%.

## 1. Introduction

Micellar media, primarly those formed by synthetic detergent molecules, have been used in luminescence analysis to enhance or otherwise modify the luminescence properties of molecules [1–3], especially improving the sensitivity of many spectrofluorimetric methods which already exist [4,5]. In the literature, several organic ligands for the individual spectrofluorimetric determination of molybdenum [6–8] and tungsten [6,9–13] have been proposed.

Alizarin Red S (ARS, the sodium salt of 1,2-dihydroxyanthraquinone-3-sulphonic acid) is a widely used reagent for the spectrophotometric and spectrofluorimetric determination of several inorganic species [14,15], including W and Mo [16,17]. Because of the similar spectral features of the inorganic complexes obtained with the same spectrofluorimetric reagent (Alizarin Red S), the determination of these ions in binary mixtures is not feasible. However, there are some simple and rapid instrumental approaches which allow the simultaneous determination of both complexes with overlapping spectral profiles without prior separation. Synchronous spectrofluorimetry offers improved selectivity over conventional spectrofluorimetry thanks to the narrower spectral bandwidth, which depends greatly on the wavelength increment chosen. Also, the application of derivatives to synchronous fluorescence spectrometry has proved a highly useful analytical technique for the direct resolution of mixtures, especially of two components of different compounds [18–22].

In this paper, the influence of several surfactants (anionic, cationic and non-ionic) on the fluorescence of the complexes of Mo(VI) and W(VI) with Alizarin Red S have been studied. The combination of these effects and the application of the synchronous derivative methodology have allowed the simple resolution of molybdenum and tungsten mixtures in real samples.

* Corresponding author.


*SSDI* 0039-9140(95)01506-X

## 2. Experimental

### 2.1. Apparatus

Fluorescence was monitored with a Perkin-Elmer Model MPF-66 spectrofluorimeter, equipped with a 150 W xenon arc lamp and a R-928 photomultiplier. All measurements were performed in standard 10-mm path length quartz cells, thermostatically controlled at $25 \pm 0.5$ °C with a water-bath circulator (Frigiterm S-382). Excitation and emission monochromators were locked together and scanned simultaneously with a wavelength constant difference $\Delta\lambda = \lambda_{em} - \lambda_{ex}$. The scanning speed and response time of the spectrophotometer were set at 480 nm/min and 0.5 s respectively.

The spectrophotometer was connected to a Perkin-Elmer Model 7300 Professional computer provided with a PETLS application software (C 646-0280). A 101 Rhodamine quantum counter sample (Perkin-Elmer) was used for source intensity adjustment. Fluorescence data are given without spectral correction.

A Crison Digit-501 pHmeter was used for all pH measurements.

### 2.2. Reagents

All experiments were carried out with analytical reagent grade chemicals using doubly distilled and demineralized water.

Alizarin Red S solution ($1.0 \times 10^{-3}$ M) was prepared by weighing exactly 0.171 g of the reagent (Carlo Erba) and diluting to 500 ml with doubly distilled water.

Stock solutions of the following surfactant agents were prepared: sodium dodecylsulphate (SDS) (Merck, 0.18 M), polyoxyethylenedodecylether (Brij-35) (Merck, $4.2 \times 10^{-2}$ M), and hexadecyltrimethylammonium bromide (HTAB) (Merck, 0.14 M).

Molybdenum stock solution (0.1 mg/ml) was prepared from $(NH_4)_6Mo_7O_{24} \cdot 4H_2O$ (Merck) in doubly distilled water and standardized gravimetrically [23].

Tungsten stock solution (0.1 mg/ml) was prepared from $Na_2WO_4 \cdot 2H_2O$ (Merck) in doubly distilled water and standardized gravimetrically [24]. More dilute solutions were prepared by appropriate dilutions with doubly distilled water.

Buffer solutions of the required pH (4.3) were prepared from 1 M acetic acid and 1 M sodium acetate.

### 2.3. Procedure

*General*

An aliquot of sample containing 0.5–2.5 μg of molybdenum and 0.3–3.0 μg of tungsten with 0.3 ml of Alizarin Red S standard solution ($1 \times 10^{-3}$ M) or 4.7–40.0 μg Mo and 2.6–25.0 μg W with 0.5 ml Alizarin Red S standard solution ($1 \times 10^{-3}$ M) was added to 2 ml of 1 M acetic acid/acetate buffer solution (pH 4.3), 2 ml of 0.14 M HTAB solution and the mixture diluted to a final volume of 10 ml with demineralized water. A blank solution containing all the reagents, except both molybdenum and tungsten, was prepared and treated in the same way as described above. The synchronous fluorescence spectrum was recorded against the reagent blank, thermostatting the samples at $25 \pm 0.5$ °C with the following fixed instrumental parameters: $\Delta\lambda = \lambda_{em} - \lambda_{ex} =$ 110 nm; scan speed, 480 nm/min and a spectrometer response time of 0.5 s. The spectra were then archived on a disk file and the first-derivative was calculated by the Savitzky–Golay [25] method with 25 derivative points.

First-derivative measurements were taken as the vertical distance from the first-derivative synchronous spectrum at 486 nm to the base line for molybdenum and at 502 nm to the base line for tungsten.

The fluorescence intensities of these derivative signals are directly related to the concentration of each ion in their individual calibration graphs.

*Analysis of steel samples*

A BCS/SS Carbon Steel No. 451/1 with a certified content of C (0.054%), Si (0.116%), Mn (0.62%), P (0.009%), S (0.014%), Cr (0.104%), Mo (0.039%), Ni (0.016%), As (0.041%), Cu (0.47%), Sn (0.002%), Ti (0.105%) and W (0.099%), was analyzed. The sample (0.5 g) was dissolved in 25 ml of concentrated hydrochloric acid, 10 ml of nitric acid was added, the oxides of nitrogen boiled off and diluted to 50 ml. It was cooled, filtered and the filter washed with hot dilute hydrochloric acid and finally with hot water and diluted to 100 ml. The interference from Fe(III) was avoided by its precipitation as hydrated iron(III) oxide [26–28] by adding a 2 M NaOH solution to 10 ml sample solution. The resulting solution was filtered, neutralized and diluted to 100 ml. Aliquots (4 ml) of this solution

were used for the spectrofluorimetric determination of both ions.

## 3. Results and discussion

### 3.1. Effect of experimental variables

Alizarin Red S forms fluorescent complexes with Mo(VI) and W(VI) in aqueous media. The molybdenum complex has an excitation maximum of 488 nm and the tungsten complex at 478 nm. The emission spectra show maxima of 618 and 605 nm, respectively.

In order to choose an appropriate micellar medium to enhance the analytical signal of both complexes and to achieve the best separation between fluorescence maxima, cationic, anionic and non-ionic surfactants were tested.

Of the various surfactants tested, the greatest increase in the emission intensities of both complexes are obtained in the presence of the cationic surfactant (HTAB) and, for that reason, all further research has been carried out in this medium.

The fluorescence spectra of both complexes in the micellar medium selected are shown in Fig. 1. When these spectra were compared with those obtained without the micellar medium, a considerable increase in the fluorescence intensity of both complexes was obtained, but no appreciable changes in wavelength maxima were observed. For this reason, in this particular case an increase in sensitivity of the analytical determination of both ions using micellar medium is achieved, but they closely overlap and, consequently, the selectivity of the determination is not improved.

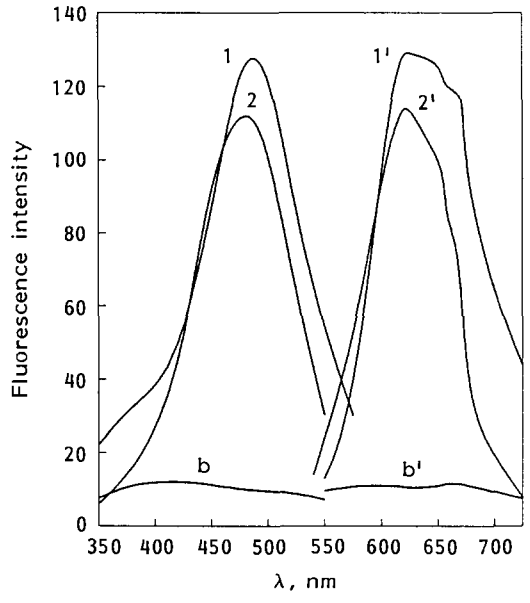


Fig. 1. Fluorescence spectra of molybdenum (1, 1') and tungsten (2, 2') complexes with Alizarin Red S in the presence of HTAB, with respect to the reagent blank. [Mo] = 250 ng/ml, [W] = 250 ng/ml, [ARS] = $3 \times 10^{-5}$ M, [HTAB] = $2.8 \times 10^{-2}$M, pH 4.3.

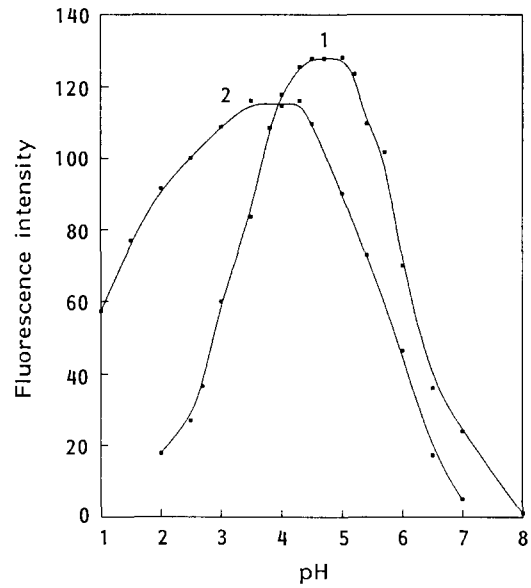


Fig. 2. Influence of pH on the fluorescence intensity of the Mo complex (1) and W complex (2). [Mo] = [W] = 250 ng/ml, [ARS] = $1 \times 10^{-5}$ M, [HTAB] = $1.4 \times 10^{-2}$ M.

Once the surfactant medium was selected, a minucious study of the appropriate pH to obtain the highest fluorescence intensity of each complex was carried out.

The reaction between molybdenum and tungsten with Alizarin Red S in the presence of the micellar medium selected (HTAB) in a concentration over its c.m.c. requires, in both cases, an acidic medium between 3.5 and 5.5 (Fig. 2). The greatest fluorescence intensity for both complexes simultaneously is obtained at a working pH of 4.3, which was selected for the rest of the experimental work. An acetic acid/acetate buffer solution of pH 4.3 gave the desired acid medium. The concentration of this buffer solution was studied and no effect on the fluorescence intensity of both complexes was observed, for which a final concentration of 0.2 M was therefore used.

Once the optimum pH for the formation of two complexes in the presence of the cationic surfactant HTAB was selected, the influence of its concentration on their fluorescence intensity

was studied. Different concentrations of HTAB around its c.m.c. were tested, showing that a concentration of $2.8 \times 10^{-2}$ M gave the best results.

The effect of the Alizarin Red S concentration was examined, over the concentration range $2 \times 10^{-6}$–$6 \times 10^{-5}$ M. A 2:1 (ARS:Mo) and 3:1 (ARS:W) molar ratio was needed to ensure maximum fluorescence intensity of both complexes and to avoid the decreased reproducibility of the measurements observed at higher concentrations.

The formation of both complexes is instantaneous and the fluorescence intensities remained constant almost 3 h after sample preparation, for which no precautions in fluorescence measurement have to be considered.

The dependence of the fluorescence intensity of both complexes on the temperature is critical. A temperature of $25 \pm 0.5$ °C gave the best results and it was chosen to carry out fluorescence measurements. The temperature control was carried out by thermostatting the sample compartment for the rest of the experimental work.

As was observed after different order of mixing of the different reagents for the complex formation, the addition of the surfactants before or after the complexes are formed did not play any significant role in the fluorescence intensity. Despite this absence of fluorescence modifications, an order of mixing of ions, Alizarin Red S, buffer solution and surfactant solution was chosen as the most convenient for the rest of the experimental work.

### *3.2. Synchronous derivative spectrofluorimetric conditions and instrumental variables*

As can be deduced from the excitation and emission maxima of these complexes in micellar medium, a preseparation should be carried out before their determination in a mixture.

Analytical advantages offered by synchronous derivative spectrofluorimetry have been made use of to analyze a mixture containing these two ions without any prior separation. For this purpose, a detailed study of the synchronous spectra for each complex alone in a range of wavelength intervals near the Stokes shift of each ion (130 and 127 nm for Mo and W, respectively), was performed. After careful observation of the spectral shapes of the different synchronous spectra, we selected a 110 nm wavelength scanning interval as the most appropriate to obtain the narrowest spectral shape and the best separation between fluorescence maxima (Fig. 3).

Despite a quite good separation of both synchronous spectra maxima being achieved, a considerable spectral overlap already existed. For this reason, the use of the additional resolution capability offered by derivative spectroscopy, is also needed. The synchronous first derivative spectra of two series of solutions containing increasing amounts of Mo and W complexes are shown in Fig. 4a. At the base line two isodifferential points at 486 and 502 nm can be observed for W and Mo complexes, respectively. Preliminary experiments showed that the fluorescence signals of the synchronous first derivative at 486 nm (working zero-crossing wavelength of W) are proportional to the Mo concentration and the fluorescence signals of the synchronous first derivative at 502 nm (working zero-crossing wavelength of Mo) are proportional to the W concentration.

Owing to the fact that at these wavelengths the changes in the fluorescence signal values with changing concentrations arise from each chelate while the other is zero, one compound can be determined without the interference of the other.

The zero-crossing method used in this paper to discriminate the overlapping bands needs

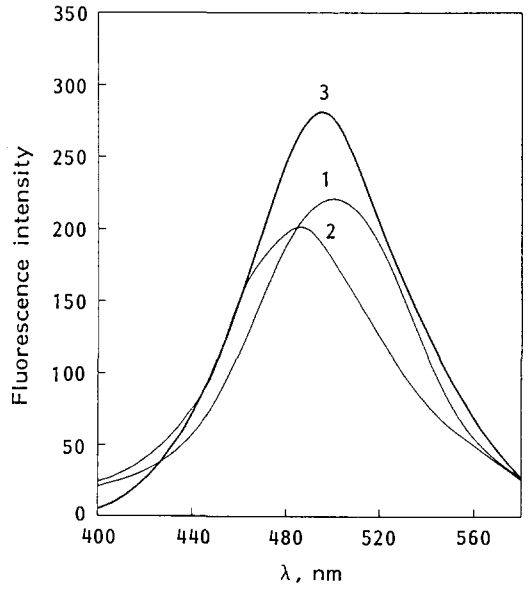


Fig. 3. Synchronous fluorescence spectra for the Mo complex (curve 1), W complex (curve 2) and a mixture of both complexes (curve 3) at $\Delta\lambda = 110$ nm. [Mo] = [W] = 1000 ng/ml. Wavelength scanning speed = 480 nm/min, response time = 0.5 s.

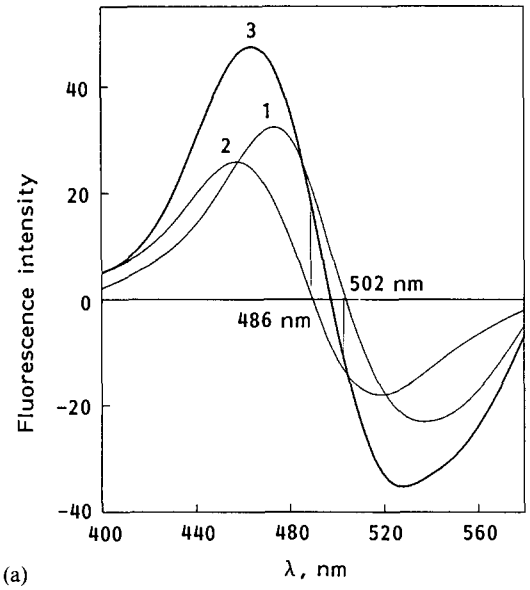


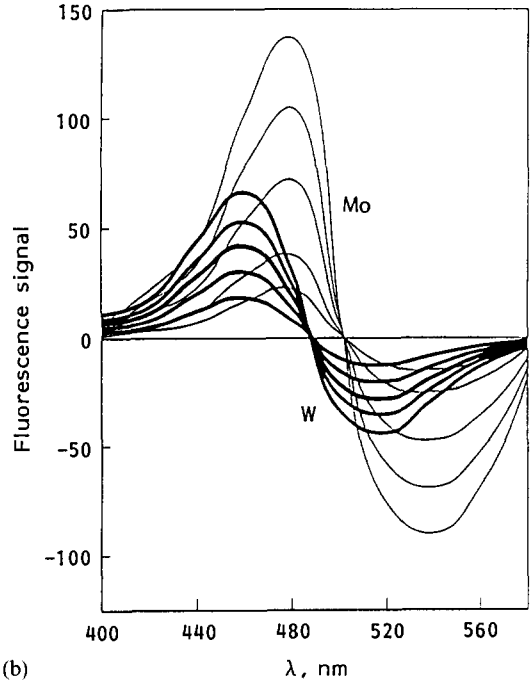


Fig. 4. (a) First-derivative synchronous spectra of the Mo complex (curve 1), W complex (curve 2) and a mixture of both complexes (curve 3) and (b) superimposed first-derivative synchronous spectra of two series of molybdenum and tungsten complexes covering the ranges for Mo (0.5, 1.0, 2.0, 3.0, 4.0 μg/ml) and W (0.5, 1.0, 1.5, 2.0, 2.5 μg/ml). Arrows indicate graphical measurements based on isodifferential points. Analytical parameters as in Fig. 3.

Beer's law to be obeyed in the full concentration range studied. This fact was proved with two solutions containing each analyte and a mixture of both. The resolution of the two equations satisfactorily resolves the mixture, indicating that the law is satisfied in the concentration range studied. The measurement wavelengths for both compounds using $\Delta\lambda = 110$ nm are indicated in Fig. 4b.

The use of the zero-crossing method in synchronous derivative spectrofluorimetry for resolving a mixture of chromophores with overlapped spectra produces a considerable loss of accuracy and sensitivity. This problem arises because the measurements are taken at a very critical wavelength, the localization of which is sometimes very difficult (see Fig. 4b).

The instrumental variables to be optimized when applying the derivative technique to the synchronous spectra are wavelength scanning speed, differentiation constant, spectrofluorimeter time constant and slit widths. All of them have a critical effect on the sensitivity and selectivity of the determination as they affect both the resolution and the fluorescence signal intensity because they modify the wavelength ranges and the relative intensity of derivative peaks.

Different values for these variables were tested, observing that the best resolution with the better signal-to-noise ratio was obtained when using a scan speed of 480 nm/min, a differentiation constant of 25 points (convoluting according to the Savitsky and Golay algorithm), a spectrofluorimeter time constant of 0.5 s and slit widths of 10 and 5 nm, depending on the calibration graph.

### 3.3. Analytical parameters

Having established the experimental and instrumental conditions, calibration graphs for the determination of Mo were prepared by measuring changes in the fluorescence signal at 486 nm, i.e. the isodifferential point of tungsten complex. Similarly for W, changes in the fluorescence signal at 502 nm, the isodifferential point of molybdenum, were measured.

These calibration graphs obtained by plotting fluorescence signal vs. molybdenum and tungsten concentrations are linear for 32–4000 ng/ml for Mo and for 49–2500 ng/ml for W. For concentrations of both ions higher than 500 ng/ml, a $5 \times 10^{-5}$ M reagent concentration should be used in order to retain the required ARS/ion molar ratio. Also, owing to the high fluorescence intensity of both complexes, a reduction of slit band width from 10 to 5 nm when applying higher concentrations is also needed.

Table 1
Analytical parameters of the proposed methods

| Element | Dynamic range (ng/ml) | Sensitivity, $S_A$ (ng/ml) | LOD (ng/ml) | LOQ (ng/ml) | RSD [a] (%) |
|---|---|---|---|---|---|
| Mo | 50–250 | 3.2 | 9.5 | 31.6 | 1.4 |
| | 500–4000 | 49.0 | 141.0 | 471.0 | 3.3 |
| W | 50–300 | 8.1 | 14.7 | 49.0 | 3.1 |
| | 500–2500 | 36.0 | 77.4 | 258.0 | 2.3 |

[a] Relative standard deviations for Mo and W at 150 ng/ml (lower ranges) and 1000 ng/ml (higher ranges), calculated from the calibration data set, $n = 3$.

Three replicates for each concentration value, with the blank signal included, were used in all cases to calculate the following equations of the corresponding equation lines [29,30].

Lower dynamic range

$$RFI = -2.43[Mo] + 8.67 \times 10^{-2} \qquad r^2 = 99.8\%$$

$$RFI = 4.95[W] + 4.63 \times 10^{-2} \qquad r^2 = 99.4\%$$

Higher dynamic range

$$RFI = 3.05[Mo] + 1.65 \qquad r^2 = 99.9\%$$

$$RFI = 2.13[W] + 7.78 \qquad r^2 = 99.8\%$$

As is evidenced by their determination coefficients ($r^2$), the linear regression analysis of the change in fluorescence signals at the isodifferential points selected shows good linear fit.

The main analytical parameters of the individual methods developed for Mo and W by using the derivative synchronous fluorescence spectrometry are summarized in Table 1. The analytical sensitivity, $S_A$, characteristic of the instrumental calibration method (calculated through the expression $S_{R,c}/b$, where $S_{R,c}$ indicates the regression standard deviation of instrumental response to concentration and $b$, the slope of the regression line) [30] and the precision expressed by the relative standard deviation calculated from the data set of calibration experiment for any concentration value [30], and detection (LOD) and quantitation limits (LOQ) [31], are indicated.

As can be observed from Table 1, very similar values of detection limits and other analytical parameters were obtained for both ions using first-derivative synchronous spectrofluorimetry. The relative standard deviation (RSD), also given in Table 1, shows good precision of both Mo and W determination.

Studies with mixtures of Mo and W at different concentration ratios (Table 2) revealed that the amplitude selected for the individual quanti-

Table 2
Determination of molybdenum and tungsten in binary mixtures

| Mo/W ratio | Taken (μg/ml) | | Found (μg/ml) | | Recovery (%) | |
|---|---|---|---|---|---|---|
| | Mo | W | Mo | W | Mo | W |
| 20:1 | 4.0 | 0.2 | 4.26 | 0.16 | 106.5 | 80.0 |
| 10:1 | 2.0 | 0.2 | 2.20 | 0.22 | 110.0 | 110.0 |
| 7:1 | 1.4 | 0.2 | 1.27 | 0.19 | 90.7 | 95.0 |
| 5:1 | 1.0 | 0.2 | 0.91 | 0.19 | 91.0 | 95.0 |
| 3:1 | 0.6 | 0.2 | 0.57 | 0.20 | 95.0 | 100.0 |
| 2:1 | 0.4 | 0.2 | 0.35 | 0.20 | 87.5 | 100.0 |
| 1:1 | 0.2 | 0.2 | 0.18 | 0.20 | 90.0 | 100.0 |
| 1:2 | 0.2 | 0.4 | 0.18 | 0.35 | 90.0 | 87.5 |
| 1:3 | 0.2 | 0.6 | 0.19 | 0.52 | 95.0 | 86.7 |
| 1:5 | 0.2 | 1.0 | 0.21 | 0.88 | 105.0 | 88.0 |
| 1:10 | 0.2 | 2.0 | 0.14 | 1.67 | 85.0 | 83.5 |

Table 3
Effect of foreign species on the simultaneous determination of molybdenum and tungsten (200 ng/ml)

| Tolerance ratio (w:) | Molybdenum DSI | Tungsten DSI |
|---|---|---|
| 1000 | $SCN^-$, $Mn^{2+}$, $IO_3^-$, $NO_3^-$, $Br^-$, $SO_4^{2-}$ | $SCN^-$, $Mn^{2+}$, $NO_3^-$, $IO_3^-$, $SO_4^{2-}$ |
| 500 | $Ca^{2+}$, $Ni^{2+}$, $SiO_3^{2-}$, $PO_4^{3-}$ | $Ca^{2+}$, $Ni^{2+}$, $Br^-$, $SiO_3^-$, $PO_4^{3-}$ |
| 100 | $Zn^{2+}$, $Mg^{2+}$, $CrO_4^{2-}$, $Co^{2+}$, $Ba^{2+}$ | $Zn^{2+}$, $Mg^{2+}$, $CrO_4^{2-}$, $Co^{2+}$, $C_2O_4^{2-}$, $Ba^{2+}$ |
| 50 | $Sr^{2+}$ | $Sr^{2+}$ |
| 25 | $Cu^{2+}$, $C_2O_4^{2-}$ | $Cu^{2+}$ |
| 10 | $F^-$, $BO_3^{3-}$ | $F^-$, $Sb^{3+}$, $BO_3^{3-}$ |
| 5 | | $Pb^{2+}$ |
| 3 | $Zr^{4+}$, $As^{3+}$ | $Zr^{4+}$, $As^{3+}$, $Al^{3+}$ |
| 1 | $Fe^{3+}$, $Pb^{2+}$, $V^{5+}$, $Sn^{4+}$, $Sb^{3+}$, $Al^{3+}$ | $Fe^{3+}$, $Sn^{4+}$ |
| 0.5 | citrate | citrate, $V^{5+}$ |

Table 4
Simultaneous determination of molybdenum and tungsten in a BCS carbon steel

| Element | Content [a] (RDS%) (μg/g) | Found [b] (RSD%) (μg/g) | Recovery (%) |
|---|---|---|---|
| Mo | 390 (4.2) | 399.4 (1.8) | 102.4 |
| W | 990 (6.0) | 950.9 (3.4) | 96.1 |

[a] Certified values (mean of five determinations).
[b] Mean of three determinations.

tation of the ions is appropriate. It can be concluded that with the application of the synchronous derivative technique, good recoveries of Mo are obtained when W is in a 10-fold excess, and W with a 20-fold excess of Mo if present in the same solution. Although mixtures of these compounds in higher proportions could cause some interference, the application of synchronous derivative using the zero-crossing graphical model would permit the simultaneous determination of these ions in the usual proportions found in real samples.

### 3.4. Interference study

Quantitative recovery is only one aspect to be considered in evaluating the applicability of the method to these ions. The other aspect is selectivity. Selectivity is a function of the ability to eliminate components which would be detected with the determination procedure.

To test the efficiency and selectivity of the proposed analytical procedure to real samples, a systematic study was made of the effect of various species, in a wide range of concentrations, on the determination of $Mo^{VI}$ and $W^{VI}$ at the 200 ng/ml level by synchronous first derivative spectrofluorimetry.

If interference occurred, the ratio was progressively reduced until interference ceased. The tolerance criterion used was a deviation of twice the standard deviation, $S_s$, of the mean value of three measurements of 200 ng/ml of molybdenum and tungsten by the different methods proposed.

The results obtained are shown in Table 3. The analytical signal corresponding to each ion was converted into concentration using their corresponding equation lines. These results show that the great tolerance ratios of many ions frequently accompanying Mo and W in real samples are well tolerated without any prior separation technique.

## 4. Applications

### 4.1. Determination of molybdenum and tungsten in a certified steel

A British Chemical Standard (B.C.S) carbon steel $N_o$ 451/1 containing certified amounts of molybdenum and tungsten of 390 and 990 μg/g, respectively, was analyzed directly by measuring the fluorescence signal of the first derivative synchronous spectra. The average molybdenum and tungsten contents in the sample studied, based on three determinations, are shown in Table 4. In all cases there is very good agreement between officially certified values and those obtained by the method proposed.

In conclusion, the present paper shows a practical application of the synchronous derivative spectrofluorimetric technique in combination with the use of micellar media, which permitted an accurate and precise determination of two complexes with very similar fluorescence spectra, in only one simple scan, without any prior separation technique. The method could be easily applied to the analysis of both ions in different real samples.

## References

[1] W.L. Hinze, in K.L. Mittal (Ed.), Solution Chemistry of Surfactants, Vol. 1, Plenum Press, New York, 1979, p. 79.
[2] T. Taketatsu and A. Sato, Anal. Chim. Acta, 108 (1979) 429.
[3] E. Pelizzetti and E. Pramauro, Anal. Chim. Acta, 169 (1985) 1.
[4] P.M. Ritenour Hertz and L.B. McGown, Anal. Chem., 64 (1979) 2920.
[5] M. Falcon, J. Guiteras, A. Izquierdo and M.D. Prat, Talanta, 40 (1993) 17.
[6] G.F. Kirkbright, T.S. West and C. Wooward, Talanta, 13 (1966) 1637.

[7] Y. Titkov, Ukr. Khim. Zh., 36 (1970) 613.
[8] P.R. Haddad, P.W. Alexander and L.E. Smythe, Talanta, 22 (1975) 61.
[9] R.S. Bottei and B.A. Trusk, Anal. Chem., 35 (1963) 1910.
[10] R.S. Bottei and B.A. Trusk, Anal. Chim. Acta, 37 (1967) 409.
[11] A.T. Pilipenko, A.I. Zhebentyev and A.I. Volkova, Ukr. Khim. Zh., 41 (1975) 1087.
[12] A.T. Pilipenko, A.I. Zhebentyaev and A.I. Volkova, Zh. Anal. Khim. 29 (1974) 1854.
[13] F. Capitán, J.P. De Gracia, A. Navalón, L.F. Capitán-Vallvey and J.L. Vilchez, Analyst, 115 (1990) 849.
[14] A. Navas Díaz, Talanta, 38 (1991) 6, 571.
[15] A. García Campaña, F. Alés Barrero and M. Román Ceba, Analyst, 117 (1992) 1189.
[16] C. Cruces Blanco, A. García Campaña, F. Alés Barrero and M. Román Ceba, Anal. Chim. Acta, 283 (1993) 213.
[17] A. García Campaña, F. Alés Barrero, M. Román Ceba and A. Fernández Gutierrez, Analyst, 119 (1994) 1903.
[18] S. Rubio, A. Gómez-Hens and M. Valcárcel, Anal. Chem., 57 (1985) 1101.
[19] A. Muñoz de la Peña, F. Salinas, M.E. Sánchez and J.A. Murillo, Analyst, 113 (1988) 1435.
[20] F. García Sánchez, J.C. Márquez Gómez and M. Hernández López, Analyst, 112 (1987) 649.
[21] F. Capitán, G. Sánchez-Palencia, A. Navalón and L.F. Capitán-Vallvey, Anal. Chim. Acta, 259 (1992) 345.
[22] D.G. Kostantianos and P.C. Ioannou, Analyst, 117 (1992) 877.
[23] F.D. Snell and L.S. Ettre (Eds.), Encyclopedia of Industrial Chemical Analysis, Vol. 16, Interscience, New York, 1971, p. 156.
[24] F.D. Snell and L.S. Ettre (Eds.), Encyclopedia of Industrial Chemical Analysis, Vol. 16, Interscience, New York, 1971, p. 204.
[25] A. Savitsky and M.J.E. Golay, Anal. Chem., 36 (1964) 1627.
[26] H. Hildebrand and M. Dundell, Applied Inorganic Analysis, Wiley, New York, 1929.
[27] F. Salinas, M. Jiménez Arrabal and I. Durán Merás, Ann. Chim., 77 (1987) 705.
[28] J.L. Martinez Vidal, A.R. Fernández Alba and F. Salinas, Analyst, 115 (1990) 329.
[29] J.C. Miller and J.N. Miller, Statistic for Analytical Chemistry, Ellis Horwood, Chichester, U.K., 1988.
[30] L. Cuadros Rodriguez, A. García Campaña, C. Jiménez Linares and M. Román Ceba, Ann. Lett., 26 (1993) 1243.
[31] Nomenclature, symbols, units and their usage in spectrochemical analysis II, Spectrochim. Acta, 33B (1978) 242.

ELSEVIER

Talanta 42 (1995) 1045–1050

Talanta

# Flow injection analysis chemiluminescence detection of residual ozone

K.A. McGowan, G.E. Pacey *

*Department of Chemistry, Miami University, Oxford, OH 45056, USA*

Received 8 August 1994; revised 21 November 1994; accepted 28 November 1994

**Abstract**

Chemiluminescent reagents for the determination of residual ozone were compared. Each method was automated using gas diffusion flow injection analysis. The luminol method gave a four order of magnitude working range with an LOD of 0.008 mg $O_3$/l. The luminol method has better analytical characteristics than the standard colorimetric Indigo Blue methods

## 1. Introduction

In 1986 the United States Environmental Protection Agency (USEPA) enacted the safe drinking water act amendment. Some of the changes affecting water disinfection are: 99.9% inactivation of *Giardia lamblia* cysts; 99.99% inactivation of enteric viruses, legionella bacteria and heterotrophic plate count organisms; and trihalomethanes (THMs) must be kept below a yet to be determined range (possibly 0.10–0.01 mg/l). These specific changes apply to all surface water and surface water affected drinking water supplies [1]. These regulations mean that of the over 200 000 drinking water treatment plants in the United States, at least 30% will be affected. Many speculate that the drinking water treatment plants will change from chlorination, to one of the following disinfecting agents: ultraviolet radiation, ozone, chlorine dioxide, or chloramines [2].

For the past 90 years chlorine has been the predominant drinking and wastewater disinfectant and biocide used in the United States [3]. The use of chlorine as a disinfectant is primarily based on its strong germicidal properties, high oxidizing power, ease of application, measurement and control properties, and its relatively low cost. However, chlorination exhibits some significant shortcomings in satisfying the 1986 safe drinking water amendment, such as ineffective *Giardia lamblia* cyst inactivation and THMs production.

In many situations, ozone is the best choice as a replacement for chlorination since it has the potential to satisfy all criteria for potential alternative oxidants. These criteria were proposed by Symons for the USEPA [2].

1. The oxidant must be easily generated and in widespread use.
2. The oxidant must be an effective biocide.
3. The oxidant must provide an easily measured residual.
4. The oxidant must produce fewer undesirable by-products than choline.
5. The oxidant must be cost effective.

Current analytical methods for the determination of residual ozone are: standard iodometry [4], amperometry [4], arsenic(III) back titration [5], diethyl-*p*-phenylenediamine (DPD) [6] and Syringaldazine (FACTS) [7] all based on the oxidation of iodide ion to iodine, making them highly susceptible to interference from other oxidizing agents, such as atmospheric oxygen and hydrogen peroxide. These methods are not recommended [8]. The Acid

* Corresponding author. Fax: (513) 529-7284.


*SSDI* 0039-9140(95)01508-6

Chrome Violet K (ACVK) [9], the Leuco Crystal Violet [10] the arsenic(III) direct oxidation [11] the bis(terpyridine) iron(II) [12] and the Indigo Blue method [13,14] are colorimetric methods. In these methods, interferences from strong oxidizing agents other than ozone, such as chlorine and oxidized forms of manganese, are of some concern. For many of these methods, masking reagents like malonic acid and glycine, are used to minimize the interferences. The Indigo Blue method is currently the accepted method [15]. Two other methods are direct UV absorption at 260 nm [16,17], and an amperometric electrode method [18]. Under ultra-pure laboratory water conditions the direct UV measurement of ozone is recommended. However, dissolved organic and inorganic matter present in the ozone samples may interfere by absorbing in the 200–300 nm wavelength region [19]. Also, the detection limit for direct UV absorption in high [16,17].

The objective of this paper was to investigate chemiluminescent methods for the determination of residual ozone. Although there have been numerous publications about gas phase ozone chemiluminescent methods, the number of investigations for aqueous phase chemiluminescent measurements is limited. In particular the work of Takeuchi and Taskashi [20], which suggested that indigo disulphonate was an excellent choice for a chemiluminescent ozone method, did not investigate the obvious reagents. All methods are designed as gas diffusion flow injection analysis (GD-FIA) methods since FIA is inherently more precise especially for fast reactions like the chemiluminescence and volatile analytes like ozone. The reagent chemistries tested were indigo disulphonate (IDS), indigo trisulphonate (ITS) and luminol. Each system was optimized with respect to sensitivity, working range and LOD evaluated. Comparison to the previously reported colorimetric GD-FIA indigo method is made.

## 2. Experimental

All ozone methods examined were automated using GD-FIA. A diagram of the typical GD-FIA manifold used in these experiments is shown in Fig. 1. The gas diffusion manifold consisted of two PVC blocks with small channels bored as mirror images. A microporous teflon 0.45 micron gas diffusion membrane (W.L. Gore) is placed between the blocks. Teflon was chosen because of its excellent diffusion characteristics, resistance to the oxidizing capabilities of ozone and nonwetting characteristics which only allow a gas to be transferred through the membrane. Gas diffusion was incorporated into the FIA system to increase selectivity and matrix optimization for ozone measurements. Some of the decomposition products of ozone $O_3^-$, $HO_2^-$, $O_2^-$, OH, $HO_2$, and $H_2O_2$ will interfere by initiating chemiluminescence. However, the gas diffusion membrane allows only gaseous species to pass. Matrix modification allows a sample to be transferred from a matrix that may not be favorable for the chemistry being performed into a matrix that is more favorable toward that particular chemistry. In other words the solution in the donor stream side of the manifold inhibits the desired reaction, while the solution in the acceptor stream is optimized for the desired reaction.

A spiral-T-cell was positioned in a front of the PMT. One conduit carries the chemiluminescent reagent, while the other conduit (the accepter stream side of the gas diffusion manifold), carries the sample. The sample, ozone, and the reagent merge and the chemiluminescent reaction takes place in the spiral. The spiral-T-cell was designed using quartz tubing, which greatly enhanced the transmission of produced photons. Also, the back of the spiral was mirrored in order to increase, even further, the number of photons striking the PMT. The PMT signal was amplified through a Keithly electrometer.

The procedures for the experiments are as follows. Ozone was generated by an Ozone Research and Equipment model 03V9-9 ozonator. The generated ozone was then allowed to contact a 0.1 M phosphate buffer solution of

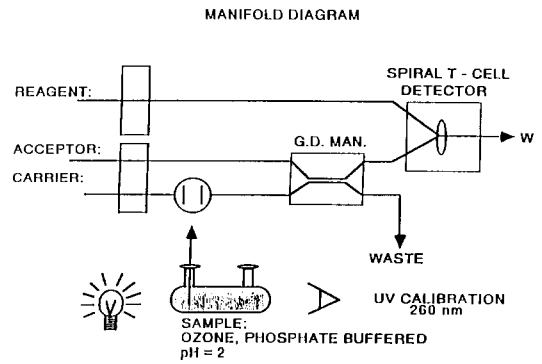


Fig. 1. Typical GD-FIA manifold for the residual ozone determinations.

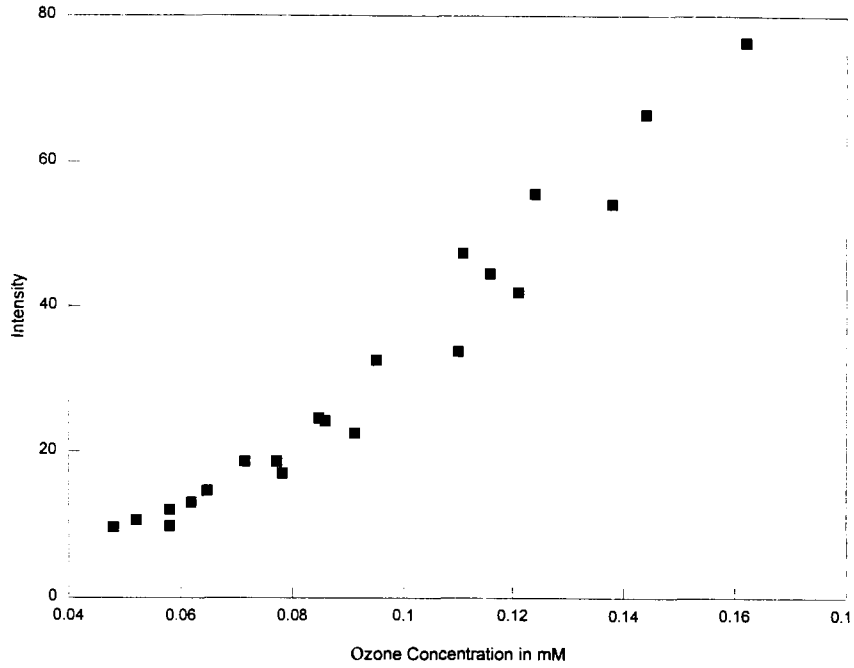


Fig. 2. Ozone chemiluminescent response to indigo disulphonate IDS. Electrometer setting at $10^{-8}$ A. ■, Ozone signal.

pH 2.12 by bubbling the ozone into a 3000 ml contractor vessel containing the solution. The solution in the vessel was used to make the standard ozone solutions. A 0.1 M phosphate buffer solution of pH 2 was chosen to minimize the instability of ozone. Ozone stability is greatest at this concentration and pH of buffer. Standard ozone solutions of varying concentrations were prepared by bubbling air, from a compressed air tank, into the contractor [21]. The bubbling of the air was then stopped and the solution was then standardized by direct UV absorption at 260 nm. The bubbling of air was then resumed in order to obtain a standard containing a lower concentration of ozone than the previous sample. This was continued until the method under investigation produced no signal above background. Depending on ozone concentrations, solutions were standardized in 2.5, 5.0, or 10.0 cm cuvettes. Ozone standards were then pumped directly out of the cuvettes into the FIA system. In this way, ozone standards were not allowed to come in contact with the laboratory environment. Lower concentrations of ozone standards ($< 10^{-6}$ M) were made by using a shrinking bottle device. The shrinking bottle is simply a large syringe into which previously standardized ozone of a higher concentration is placed. Known volumes of the standardized ozone from the shrinking bottle are then injected into sealed vessels of known volume. The injected standard is then diluted to a known volume with ozone demand free solution of the same buffer concentration and pH.

All carrier streams in these experiments were 0.1 M phosphate buffer of pH 2. The first reagent investigated, IDS, previously been optimized and these parameters were incorporated into the FIA system. The optimum IDS concentration is $2.14 \times 10^{-5}$ M (10 mg/l). This solution was prepared by dissolving 10 mg IDS in 1 l of 2 mM phosphate buffer, pH 7.2. The phosphate buffer was prepared by dissolving 0.174 g $K_2HPO_4$ and 0.136 g $KH_2PO_4$ in 1 l water. This buffer also comprised the acceptor stream.

The second reagent investigated, ITS, needed reaction conditions to be optimized. The ITS concentration was varied from 2 to 20 mg/l. A 1009 mg/l ITS stock solution was made by dissolving 100 mg ITS in 1 l 2 mM pH 7.2 phosphate buffer. Concentrations of 2–20 mg/l were made by diluting the appropriate amount of stock solution with the 2 mM, pH 7.2 buffer. The buffer solution pH was then varied in order to determine the optimum pH. The pH was varied from 5.2 to 10.28 in order to determine its optimum concentration. This was accomplished by dilution of a 50 mM stock solution. The acceptor stream was the buffer whose concentration and pH were determined to be optimum.

Luminol concentration, buffer pH, and buffer concentration for the reagent were previously optimized [21]. The optimum luminol concentration is $1 \times 10^{-4}$ M (17.70 mg/l). This solution was prepared by dissolving 17.70 mg in 1 l 0.1 M, pH 12.3 phosphate buffer. The buffer was prepared by dissolving 6.0 g $NaH_2PO_4$ and 3.4 ml $H_3PO_4$ in 1 l water. The acceptor stream in this experiment was deionized water.

Interference studies used diluted 30% hydrogen peroxide in the same sample matrix as the ozone and permanganate ion (from potassium permanganate) which is the reaction product between ozone and lower valence state manganese compounds.

All water in this experiment was distilled and deionized by a model D3600 Barnstead Nanopure double still system with a UV attachment. All chemicals were reagent grade.

## 3. Results and discussion

The data for the IDS experiment are shown graphically in Fig. 2. The results of three separate runs, five injection per data point, are fit. A nonlinear fit was observed but was not unexpected since a chemiluminescent event is not governed by Beer's Law. Unfortunately, a working range of only $5.20 \times 10^{-5}$ to $1.24 \times 10^{-4}$ M is observed. A working range at least three orders of magnitude wide is needed. The LOD of the method, as defined by three times signal-to-noise, was $5.20 \times 10^{-5}$ M.

For the ITS experiment, an optimization of the chemistry was required. The first optimization was that of the ITS concentration. Concentration of ITS were varied from 2 to 30 mg/l while the buffer solution pH and concentration were held constant at 7.2 and 2 mM respectively. The optimum concentration seems to be 14 mg/l. This ITS concentration was used throughout the investigation. The next variable to be optimized was the pH of the buffer solution. Solutions of varying pHs, 6.87–11.58, where made by the addition of dilute HCl. The ITS concentration was kept constant at 14 mg/l and the buffer concentration was also kept constant at 2 mM. The optimum pH seems to be between 7 and 9.5, therefore, it was decided to use a pH 7.2 buffer. For the optimized of the buffer concentration solutions were made with varying buffer concentrations, 0.28–10.28 mM. The concentration of ITS in the solutions was kept constant at 14 mg/l and the pH was kept constant at 7.2. The optimum buffer concentration seems to be in the range 1–5.28 mM. It was, therefore, decided to maintain the buffer concentration at 2 mM.

The data for the optimized ITS experiment are shown graphically in Fig. 3. The data represents three separate experiments with each data point representing five injections. This data did produce a linear fit, $R_2 = 0.993$; however, again the working range is limited. In this case the working range is $1.72 \times 10^{-5}$ to $1.03 \times 10^{-4}$ M with the lower concentration being the actual LOD.

The luminol method was investigated using the conditions previously used [21]. An acceptor stream of pH 3.0 phosphate buffer was reported as optimum. However, an acceptor stream of water was not examined. Upon examining the use of water it was discovered that the signal was increased 5.5 times that of the previously used acceptor stream. This is most likely due to the fact that luminol reacts best in highly alkaline conditions. However, when an acceptor stream having any buffer capacity of low pH is merged with the reagent stream the conditions for the luminol reaction become less than optimized, thereby resulting in a smaller signal.

The data for the luminol experiment are shown graphically in Fig. 4. It should be noted that both the IDS and ITS graphs have $y$-axis in the 10–100 intensity range while the luminol $y$-axis intensity is 100–500,000. The emission intensity of the luminol system is superior to IDS and ITS. The data represents three separate experiments and each data point is an average of five injections. The luminol method offers a much larger working range than either the ITS of IDS method. The working range is $4.84 \times 10^{-5}$ to $1.55 \times 10^{-4}$ M ozone. The lower concentration is the actual LOD. The working range encompasses approximately four orders of magnitude. The luminol system is measured at an electrometer setting of $10^{-5}$ A while the other two are at $10^{-8}$ A. Lower detection of ozone does appear to be possible.

A comparison of the manual standard method, the FIA automated standard method, the GD-FIA automation of the standard method and the GD-FIA luminol method is gives in Table 1. As can be seen the luminol method has lower detection, long working

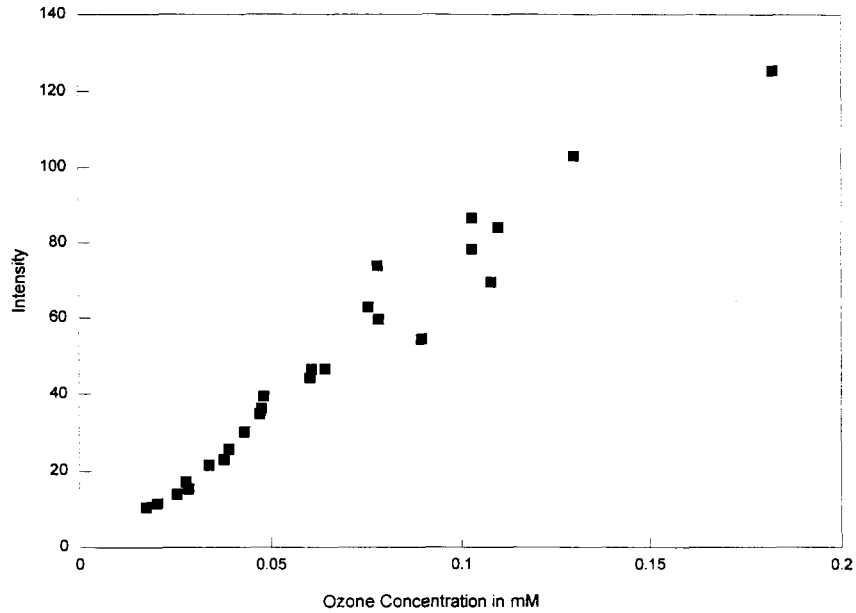


Fig. 3. Ozone chemiluminescent response to indigo trisulphonate ITS. Electrometer setting at $10^{-8}$ A. ■, Ozone signal.

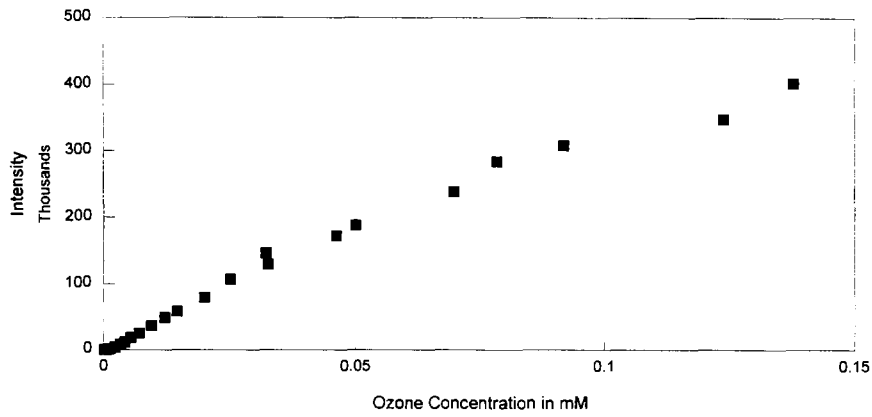


Fig. 4. Ozone chemiluminescent response to luminol. electrometer setting at $10^{-5}$ A. ■, Ozone signal.

range and less interferences than the other methods. Its sample throughput is the second largest. Given the simplicity of the hardware and the selectivity of the procedure, the luminol method should be given some consideration as a standard method for residual ozone.

Table 1
Comparison of FIA based ozone methods

| Method | Manual indigo | FIA indigo | GD-FIA indigo | GD-FIA luminol |
|---|---|---|---|---|
| Linear range (mg $O_3$/l) | 0.05–0.5 | 0.2–4 | 0.03–4 | 0.002–8 |
| Sample/hr | 20 | 120 | 65 | 100 |
| Interferences [a] | | | | |
| $H_2O_2$ | none | none | none | none |
| Mn 1 mg/l | 0.8 mg/l | 0.44 mg/l | none | none |

[a] The specified interference level produced a signal equal to the stated amount of ozone.

## 4. Conclusion

If one was to compare the three chemiluminescence methods the results would show that luminol is better than ITS and ITS is better than IDS. However, realistically neither ITS nor IDS compare in any manner to luminol. Two advantages of the luminol method over other reported methods are a direct result of automation with FIA. First, the response time is very fast when compared to the batch methods and second the sample volume required for the analysis is very small, allowing for conservation of a limited amount. Finally, there is the potential for gas phase detection incorporating reverse dual phase gas diffusion FIA.

## References


[1] Federal Register, Part II, EPA National Primary Drinking Water Regulations (Proposed Rules); Filtration and Disinfection; Giardia lamblia, Viruses, Legionella and Heterotrophic Bacteria, 421178-422 1987.

[2] J.M. Symons et al., in R.L. Jolley (Ed.), Water Chlorination: Environmental Impact and Health Effects, Vol. 2, Ann Arbor Science Publishers Ann Arbor, MI, 1979, pp. 555–560.

[3] G.C. White, Handbook of Chlorination. Van Nostrand Reinhold, New York, 1977.

[4] Standard Methods for the Examination of Water and Waste Water, 14th edn., American Public Health Association, Washington, DC, 1975.

[5] D.E. Sullivan, L.C. Hall, M. D'Ambrosi and J.A. Roth, Ozone Sci. Eng., 2 (1980) 183.

[6] A.T. Palin, J. Inst. Water Eng., 28 (1974) 129.

[7] J. Lieberman Jr., N.M. Roscher, E.P. Meier and W.J. Copper, Environ. Sci. Technol., 14 (1980) 13[illegible]

[8] G. Gordon and J. Grunwell, Proc. 6th Worl[illegible] Ozone Conference: A Comparison of Analytical Methods for Residual Ozone, Washington, DC, 1983.

[9] W.J. Masschelein and G. Fransolet, J. Am. Water Works, 69 (1977) 461.

[10] R.F. Layton and R.N. Kinman, Proc. National Specialty Conference on Disinfection, American Society of Civil Engineers, New York, 1970.

[11] J.H. Stanley and J.D. Johnson, Anal. Chem., 51 (1979) 2144.

[12] H. Tomiyasu and G. Gordon, Anal. Chem., 56 (1984) 752.

[13] H. Bader and J. Hoigne, J. Water Res., 15 (1981) 449.

[14] H. Bader and J. Hoigne, Ozone Sci. Eng., 4 (1982) 169.

[15] Standard Methods for the Examination of Water and Waste Water, 17th edn. American Public Health Association, Washington DC, 1990.

[16] D. Bahnerman and E.J. Hart, J. Phys. Chem., 86 (1982) 252.

[17] L. Forni, D. Bahnemann and E.J. Hart, J. Phys. Chem., 86 (1982) 255.

[18] J.H. Stanley and J.D. Johnson, Anal. Chem., 51 (1979) 2144.

[19] G. Gordon, W.J. Copper, R.G. Rice and G.E. Pacey, Disinfectant Residual Measurement Methods, American Water Works Association, Denver, CO, 1987.

[20] K. Takeuchi and I. Takashi, Anal. Chem., 61 (1989) 619.

[21] M. Straka, Ph.D. Dissertation, Miami University, 1983.

ELSEVIER

Talanta 42 (1995) 1051–1056

Talanta

# Flow-injection photometric determination of nanogram levels of iron based on the catalysis of oxidative coupling of *N*-phenyl-*p*-phenylenediamine with *m*-phenylenediamine in a micellar medium

Shigenori Nakano [a,*], Keisuke Tsujii [a], Takuji Kawashima [b]

[a] *Chemical Institute, Faculty of Education, Tottori University, Koyama-cho, Tottori 680, Japan*
[b] *Laboratory of Analytical Chemistry, Department of Chemistry, University of Tsukuba, Tsukuba 305, Japan*

Received 14 August 1994; revised 14 November 1994; accepted 28 November 1994

**Abstract**

A highly sensitive photometric flow-injection method is described for the determination of iron(II, III) based on the catalytic action on the oxidative coupling of *N*-phenyl-*p*-phenylenediamine with *m*-phenylenediamine in the presence of hydrogen peroxide. The sensitivity of the method was enhanced by the addition of Tween 80 as a surfactant. The dynamic range was 0.5–30 ng/ml of iron(II, III) with the relative standard deviations below 3% at a sampling rate of 30 $h^{-1}$. The proposed method was subject to few interferences from coexisting metal ions and was successfully applied to the determination of iron in natural water samples.

## 1. Introduction

The kinetic-catalytic method has proved to be an attractive means for trace analysis. Ultra-trace levels of chemical species which act as catalysts on an appropriate indicator reaction can be determined under the optimal conditions with simple instrumentation [1,2]. The addition of a ligand as an activator to the metal-catalyzed reaction improves the sensitivity and/or selectivity of these methods [1–3]. Another way for improving the sensitivity is the use of a surfactant which has the ability to form organized assemblies (micelles, microemulsions, monolayers, bilayers and vesicles) and can accelerate the rate of the catalyzed reaction [4,5].

Many batch procedures for the catalytic determination of iron have recently been reported, based on its catalytic action on the oxidation of organic substrates with hydrogen peroxide [6–9], perdisulfate [10] or periodate [11,12]. Though these methods allowed the determination of iron at sub-ppb and/or ppb levels, they include time as a variable to be strictly controlled and measured.

Flow-injection analysis (FIA) is well suited for kinetic-based methods, because it can easily control the reagent addition and the reaction time [1–3,13]. The catalytic flow-injection methods offer better accuracy, precision and speed, as well as higher sensitivity. Some iron(II, III)-catalyzed redox reactions have been applied to the flow-injection systems [3,14–18]. The oxidation of leuco Malachite Green with hydrogen peroxide was employed for the determination of 0.1–1.0 μg/ml of iron [14,15]. Cerda et al. [16] reported a flow-injection determination method for iron(III) based on the catalytic effect of iron(III)–EDTA complex on the oxidation of hydroxylamine by dissolved oxygen, by detecting nitrite produced

* Corresponding author.


*SSDI* 0039-9140(95)01509-4

by the Griess reaction. Iron(III) at 3.5–150 ng/ml was determined. An iron(II)-catalyzed chemiluminescent reaction of brilliant sulfoflavin with hydrogen peroxide was adopted to the flow-injection determination of iron(II) [17]; iron(II) and total iron in sea-water were determined using this reaction system after preconcentrating iron with a cation-exchange column in the sample loop [18]. The oxidative coupling of *p*-anisidine with *N*,*N*-dimethylaniline was adopted to a FIA system [3]; levels as low as 0.5 ng/ml of iron(III) can be determined. However, the calibration curve was not linear.

In an earlier paper [19], we reported a catalytic method with a batch mode for the determination of 0.6–6 ng/ml of iron(II, III) using an oxidative coupling of *N*-phenyl-*p*-phenylenediamine (PPDA) with *N*,*N*-dimethylaniline (DMA) in the presence of hydrogen peroxide. This method had a high sensitivity, but needed care in the mixing of sample and reagents at regular time intervals to obtain reproducible results. On the basis of this iron-catalyzed reaction, the highly sensitive and selective flow-injection photometric determination of iron has been developed. In the present system, *m*-phenylenediamine (PDA) was replaced with DMA owing to the higher solubility of PDA. Furthermore, the reaction was carried out in a micellar medium in order to accelerate the rate of the catalyzed reaction and to prevent the adsorption of the reaction product in the reaction coil. In the presence of Tween 80 as a surfactant, the sensitivity and sampling frequency of the method was increased. The concentration of hydrogen peroxide used was several orders of magnitude larger than the total iron concentration in the sample so that the iron was predominantly in the iron(III) form regardless of the initial amounts of iron(II) and iron(III). The proposed method could determine the total iron concentration in the range 0.5–30 ng/ml at a sampling rate of 30 $h^{-1}$.

## 2. Experimental

### 2.1. Reagents

All reagents used were of analytical-reagent grade. All solutions were prepared with deionized water purified with a Millipore Milli-Q system.

Standard iron(II) and iron(III) solutions (1.0 mg/ml) were prepared by dissolving weighted amounts of ammonium iron(II) sulfate and ammonium iron(III) sulfate in sulfuric (0.05 M) and hydrochloric (0.1 M) acids, respectively. These solutions were standardized by EDTA. The working standard solutions were prepared daily by diluting the stock solutions with the same acids.

*N*-Phenyl-*p*-phenylenediamine hydrochloride (PPDA) was obtained from Aldrich and used without further purification. A $2.0 \times 10^{-3}$ M PPDA solution containing polyoxyethylene(20) sorbitan monooleate (Tween 80, 0.2 wt%) was prepared. *m*-Phenylenediamine dihydrochloride (PDA) was purified by recrystallization from hydrochloric acid and a $1.0 \times 10^{-2}$ M PDA stock solution was prepared. A hydrogen peroxide solution (0.4 M) was prepared by dilution of a 30% solution (Mitsubishi Gasu Kagaku) with water. Ammonium acetate (2 M) and triethylenetetramine (trien, $1.0 \times 10^{-2}$ M) stock solutions were also prepared. Surfactants such as decyltrimethylammonium bromide (DETAB), dodecyltrimethylammonium bromide (DOTAB), tetradecyltrimethylammonium bromide (TTAB), tetradecyldimethylbenzylammonium chloride (zephiramine, TDBAC), hexadecyltrimethylammonium bromide (HTAB), hexadecylpyridinium chloride (HPC), sodium dodecylsulphate (SDS), polyoxyethylene(23) dodecanol (Brij-35), polyoxyethylene(9.5)p-1,1,3,3,-tetramethylbutylphenol (Triton X-100), polyoxyethylene(20) sorbitane monolaurate (Tween 20) and Tween 80 were used as received.

A working mixed solution of PDA ($4.0 \times 10^{-4}$ M), ammonium acetate (0.5 M) and trien ($1.2 \times 10^{-4}$ M) was prepared by mixing the stock solutions; the pH of the solution was adjusted to about 5.1 with 1.0 and 0.1 M hydrochloric acid.

### 2.2. Apparatus

A diagram of the flow-injection system for iron(II, III) determination is shown in Fig. 1, together with appropriate experimental parameters. The system was assembled from Teflon tubing (0.5 mm i.d.) and constructed using two double-plunger micropumps (Sanuki Kogyo, DMX-2400T), a sixway injection valve (Sanuki Kogyo SVM-6M2) with a loop, a circulating thermostatted bath (Toyo LH-1000C), a spectrophotometer (Soma Kougaku S-3250)

with a 10-mm micro flow-cell (8 μl) and a recorder (Nippon Denshi Kagaku V1250). A Hitachi 200-10 double-beam spectrophotometer with 10-mm cells and a Toa Model HM-5S pHmeter were also used.

### 2.3. Flow injection analysis

A carrier solution (R1, 0.1 M hydrochloric acid) was pumped into the analytical line at a flow rate of 0.8 ml/min (Fig. 1). At the same flow rate, the reagent solutions in the reservoirs R2 (hydrogen peroxide), R3 (PPDA and Tween 80) and R4 (PDA, trien and acetate) were pumped to the carrier stream at confluence points downstream. An aliquot of the sample solution (180 μl) was introduced into the carrier flow line by a loop-valve injector, and then merged in the reagent solutions. The color-forming reaction of PPDA with PDA proceeded in the reaction coil (RC, length 5 m) kept at 55.0 ± 0.1 °C. The absorbance of the colored product was monitored at 620 nm.

## 3. Results and discussion

In the presence of hydrogen peroxide, PPDA reacts with PDA to form a blue dye, which is thought to be *N*-phenyl-*N'*(2',4'-diaminobenzene-1,4-benzoquinone diiminonium ion. Iron(III) catalyzes this color-forming reaction in the slightly acidic medium. Iron(II) also catalyzes the reaction, being oxidized to iron(III) by hydrogen peroxide. Thus, the above two species of iron can act as the catalyst in the coloration and the total amounts of iron can be determined by measuring the absorbance of the dye produced at a constant time.

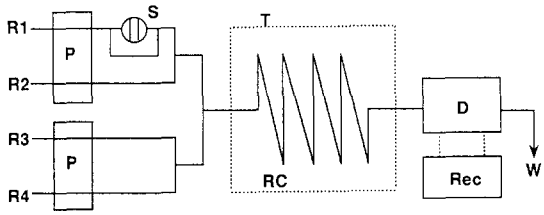


Fig. 1. Flow diagram for the determination of iron(II, III). R1, carrier (0.1 M HCl); R2, 0.4 M $H_2O_2$; R3, mixture of $2.0 \times 10^{-3}$ M PPDA and 0.2 wt% Tween 80; R4, mixture of $4.0 \times 10^{-4}$ M PDA, 0.5 M ammonium acetate and $1.2 \times 10^{-4}$ M trien; P, micropump (0.8 ml/min); S, sample injector (180 μl); RC, reaction coil (5 m); T, thermostatted bath (55 °C); D, spectrophotometer (620 nm); Rec, recorder; W, waste (pH 4.6).

Table 1
Effect of surfactants on the peak height for 10 ng/ml of iron(III) solution injected [a]

| Surfactant [b] | CMC [c] ($10^{-3}$ M) | Relative peak height |
|---|---|---|
| None | — | 1.0 |
| Cationic ($5.0 \times 10^{-3}$ M) | | |
| DETAB | 65 | 1.1 |
| DOTAB | 15 | 0.9 |
| TTAB | 3.5 | 1.6 |
| TDBAC | 1.9 | 1.9 |
| HTAB | 0.92 | 1.7 |
| HPC | 0.9 | 1.5 |
| Non-ionic (0.2 wt%) | | |
| Brij-35 | 0.091 | 2.3 |
| Triton X-100 | 0.3 | 2.2 |
| Tween 20 | 0.059 | 1.9 |
| Tween 80 | 0.012 | 2.4 |

[a] Conditions as in Fig. 1 except for iron(III) and surfactant concentrations.
[b] See text for names and abbreviations.
[c] From Refs. [20–22].

The absorption maximum of the dye was at 620 nm in the presence of Tween 80. The absorbance at this wavelength was, therefore, measured in the FIA system.

### 3.1. Choice of surfactant

As iron(III) standard solutions were injected to the FIA system in the absence of a surfactant, it appeared that the peaks were broader and the tailing of the peaks became appreciable. It seemed to be a result of the adsorption of the dye produced on the inner surface of the reaction coil and led to lower sampling frequency. To overcome the drawbacks, an attempt was made to add a surfactant to the reaction system. Furthermore, it was expected that micelles modified the rate of the iron-catalyzed reaction through the large electrostatic potential at the micellar surface or through hydrophobic forces [4,5]. Since the addition of SDS to the reaction system was observed the precipitate formed, cationic and non-ionic surfactants were tested. The relative peak heights in the absence and presence of surfactants are shown in Table 1. As can be seen in this table, the surfactants at the concentrations above critical micelle concentration (CMC) have an enhancing effect. In addition, the tailing of the peaks became smaller. The peak height for iron(III) increased as the concentration of Tween 80 increased and eventually became less dependent on the surfactant concentrations; on

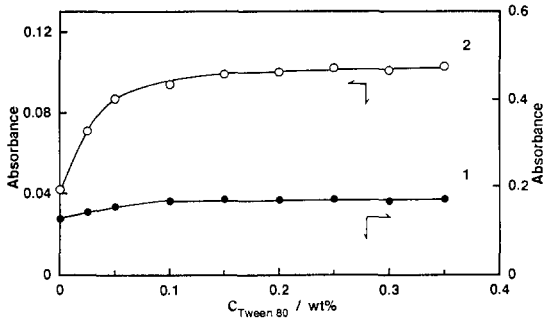


Fig. 2. Effect of Tween 80 concentration on the uncatalyzed (1) and catalyzed (2) reactions. Conditions as in Fig. 1, except for Tween 80 concentration. $C_{Fe(III)}$, 10 ng/ml.

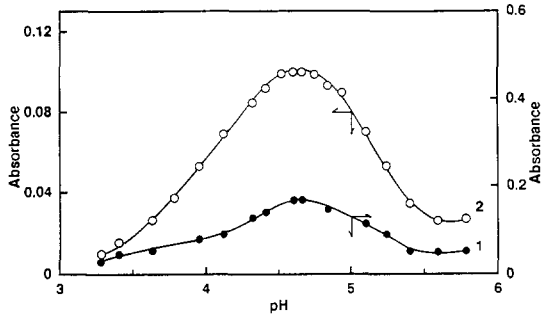


Fig. 4. Effect of pH on the uncatalyzed (1) and catalyzed (2) reactions. Conditions as in Fig. 1, except for pH. $C_{Fe(III)}$, 10 ng/ml.

the other hand, the height of baseline was almost constant (Fig. 2). The effects of concentration of other surfactants were similar to that of Tween 80. In this system, Tween 80 (0.2 wt%) was used as a surfactant. To check whether the micelle accelerated the catalyzed reaction or not, the absorbance–time curves were prepared in the absence and presence of Tween 80 (Fig. 3). The initial rate of the catalyzed reaction in the presence of the surfactant was slightly raised compared to that in the absence of surfactant, and the higher stability of the dye produced was obtained by adding surfactant. The above results suggest that the surfactant accelerates the iron-catalyzed reaction and stabilizes the dye produced. Furthermore, it suppressed the adsorption of the dye on the reaction coil.

### 3.2. *Effect of reaction variables*

To obtain the optimum conditions for the determination of iron(II, III), FIA variables were examined in the presence of Tween 80. Some preliminary experiments showed that

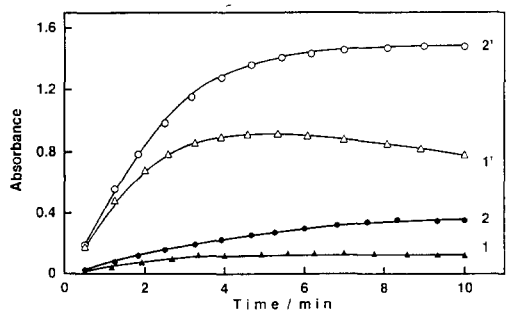


Fig. 3. Absorbance–time curves for the uncatalyzed (1, 2) and catalyzed (1′, 2′) reactions in an aqueous (1, 1′) and Tween 80 (2, 2′) medium. $C_{Fe(III)}$, 10 ng/ml; $C_{PPDA}$, $2.0 \times 10^{-4}$ M; $C_{PDA}$ $1.0 \times 10^{-4}$ M; $C_{H_2O_2}$ $2.0 \times 10^{-2}$ M; $C_{acetate}$, 0.13 M, $C_{Tween\ 80}$, 0.5 wt%. All at pH 4.6 at 55 °C.

heights of peak and baseline increased at the lower flow rate, owing to increase in the reaction time. By considering the stability of baseline and the sampling frequency, a 0.8 ml/min flow rate of carrier and reagent streams was selected for the procedure. By lengthening the reaction coil, the heights of peak and baseline were increased because of the longer reaction time. Since the lower height of baseline owing to the uncatalyzed reaction was favorable, a 5 m reaction coil was used. The peak height and peak width increased with increasing sample size; a 180-μl sample volume was adopted for the method. As the reaction temperature was elevated, there was an increase in the rates of the uncatalyzed and catalyzed reactions. For the sake of sensitivity, the temperature of the reaction coil was kept at 55 °C.

The effect of pH on the uncatalyzed and catalyzed reactions in the range 3.3–5.8 is shown in Fig. 4; a maximum peak height owing to the catalyzed reaction exists at about pH 4.6–4.7. The reaction was carried out in this pH range. Acetate was chosen as a buffer because it acted as an activator [19]. The peak height increased with increasing acetate concentration up to 0.4 M, above which it gradually increased; a 0.5 M acetate concentration was selected for the procedure.

An increase in the concentration of PPDA caused an increase in the rates of uncatalyzed and catalyzed reactions (Fig. 5). A concentration of $2.0 \times 10^{-3}$ M PPDA was chosen because of the desire to minimize the baseline readings owing to uncatalyzed reaction. With an increase in PDA concentration, the rate of the catalyzed reaction increased, reaching a maximum at a concentration above $2.0 \times 10^{-4}$ M; on the other hand, the rate of the uncatalyzed reaction gradually increased. A $4.0 \times 10^{-4}$ M PDA solution was used for the

procedure. As the hydrogen peroxide concentration increased, the rates of uncatalyzed and catalyzed reactions also increased. At concentrations above 0.3 M, the peak height for the catalyzed reaction was kept constant. A 0.4 M hydrogen peroxide concentration was selected as optimal.

### 3.3. Calibration graph

The calibration graphs for iron(II) and iron(III) were prepared by the recommended procedure using the flow system as shown in Fig. 1. The graphs were linear up to 30 ng/ml of both species of iron. The slopes of both graphs agree with each other within experimental error; the present method allows the determination of total iron. The detection limit for a signal-to-noise ratio of two was 0.2 ng/ml. The coefficients of variation for the determination of 5 and 10 ng/ml of iron(III) were 2.6 and 1.4%, respectively. The sample rate throughout was about 30 $h^{-1}$. In general, catalytic flow-injection methods have a lower sensitivity than batch methods as a result of shorter reaction time. The proposed flow-injection method, in which the reaction is carried out in a micellar medium, has a higher sensitivity, wider dynamic range and better reproducibility than the batch method reported previously [19].

### 3.4. Interference study

From preliminary experiments, copper(II) also catalyzed this indicator reaction. Some complexing agents for copper(II) were examined such as trien, *N*-(dithiocarboxy)sarcosine and triethanolamine. Among them, trien effectively suppressed the catalytic effect of copper(II) at concentrations below 100 ng/ml and did not affect the iron(III)-catalyzed reaction up to $2.4 \times 10^{-2}$ M; $1.2 \times 10^{-4}$ M trien was used.

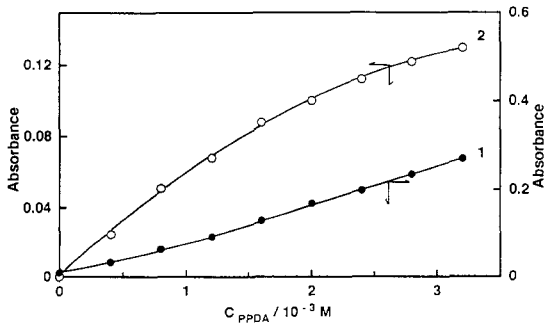


Fig. 5. Effect of PPDA concentration on the uncatalyzed (1) and catalyzed (2) reactions. Conditions as in Fig. 1 except for pH. $C_{Fe(III)}$, 10 ng/ml.

TAL 42-8-E

Table 2
Tolerance limits for foreign ions on the determination of 5 ng/ml of iron(III)

| Tolerance limit (ng/ml) | Ion added |
|---|---|
| 100 000 | As(V), Ba(II), Ca(II), K(I), Mg(II), Na(I), Sr(II), $BO_3^{3-}$, $Br^-$, $ClO_4^-$, $NO^{-3}$, $SO_4^{2-}$ |
| 10 000 | Ce(III), Hg(II), Se(IV), Te(IV), W(VI), $PO_4^{3-}$ |
| 1000 | Ag(I), As(III), Bi(III), Mo(VI), Zn(II), $F^-$, $I^-$, $NO_2^-$ |
| 500 | Al(III), Ce(IV), Cd(II), Mn(II), Ni(II), Pb(II), V(V), tartrate |
| 100 | Co(II), Cu(II), Cr(III), Cr(VI), Ti(IV) |
| 50 | Sn(II), Sn(IV), oxalate |
| 5 | $P_2O_7^{2-}$, citrate, EDTA |

The effect of other coexisting ions on the determination of 5.0 ng/ml iron(III) was examined in the presence of trien. The tolerance limits with an error of 5% are summarized in Table 2. Most of the ions listed in the table did not interfere in concentrations up to at least 100-fold excesses (by weight). Positive interferences were observed for Co(II), Cr(VI) and Ti(IV) at concentrations indicated in Table 2. Chromium(III) and tin(II, IV) caused negative error; however, these ions were allowed to coexist in up to 10-fold excesses. The selectivity of the proposed method is higher than that of the previous one [19]. The tolerance limits for these metal ions are greater than the levels normally present in natural water samples. Diphosphate, citrate, EDTA and oxalate interfered with the catalytic action of iron by the formation of complexes with iron(III).

### 3.5. Application

The proposed method was applied to the determination of iron in natural water to evaluate its usefulness. River, lake and sea-water samples were filtered through a Millipore filter (pore size 0.45 μm) and the filtrates were acidified with hydrochloric acid to about pH 1. Then iron was determined according to the recommended procedure by applying the calibration curve and standard addition methods. The results which were obtained from the calibration curve and the standard addition methods were in good agreement (Table 3).

Table 3
Determination of iron in river, lake and sea-water samples

| Sample [a] | Dilution | Iron in sample [b] (ng/ml) | |
|---|---|---|---|
| | | (I) [c] | (II) [d] |
| River water | | | |
| Gamou-gawa | 1:10 | 49.4 ± 0.8 | 49.9 ± 0.8 |
| Sendai-gawa | 1:2 | 11.5 ± 0.4 | 11.3 ± 0.2 |
| Tenjin-gawa | 1:5 | 32.6 ± 0.7 | 32.4 ± 0.8 |
| Hino-gawa | 1:5 | 28.2 ± 0.1 | 28.1 ± 0.4 |
| Lake water | | | |
| Tanega-ike | 1:10 | 38.1 ± 0.6 | 38.0 ± 0.8 |
| Hatiman-ike | 1:2.5 | 17.2 ± 0.4 | 17.6 ± 0.4 |
| Koyama-ike | 1:2 | 8.9 ± 0.2 | 8.6 ± 0.2 |
| Togo-ike | 1:2.5 | 13.6 ± 0.3 | 13.2 ± 0.5 |
| Seawater | | | |
| Uradome | 1:1.25 | 2.4 ± 0.1 | 2.3 ± 0.1 |
| Karo | 1:1.25 | 3.4 ± 0.1 | 3.5 ± 0.2 |
| Kaike | 1:2 | 6.9 ± 0.2 | 6.8 ± 0.1 |
| Yonago | 1:2.5 | 12.5 ± 0.2 | 12.1 ± 0.3 |

[a] Collected in Tottori Prefecture, Japan.
[b] Corrected for addition ($n = 3$).
[c] Calibration graph method.
[d] Standard addition method.

## 4. Conclusions

A simple and rapid flow-injection method is proposed for the determination of iron in the range 0.5–30 ng/ml by using the iron-catalyzed reaction of PPDA with PDA in the presence of hydrogen peroxide and Tween 80. The addition of the surfactant to the reaction system has some advantages, viz. the catalyzed reaction can be accelerated, and the dye produced can be stabilized and its adsorption suppressed to the inner coil surface, leading to a higher sensitivity and sampling frequency. The proposed method can be applied to the analysis of natural water without preconcentration and separation. Compared with other catalytic flow-injection methods [3,14–18], the present method offers a higher sensitivity and a more extended dynamic range.

## References

[1] H.A. Mottola, Kinetic Aspects of Analytical Chemistry, Wiley, New York, 1988.
[2] D. Perez-Bendito and M. Silva, Kinetic Methods in Analytical Chemistry, Horwood, Chichester, 1988.
[3] T. Kawashima and S. Nakano, Anal. Chim. Acta, 261 (1992) 167.
[4] M.L. Lunar, S. Rubio and D. Perez-Bendito, Anal. Chim. Acta, 237 (1990) 207.
[5] M.L. Lunar, S. Rubio and D. Perez-Bendito, Talanta, 39 (1992) 1163.
[6] D.G. Themelis and G.S. Vasilikiotis, Analyst, 112 (1987) 791.
[7] A.Ch. Zotou and C.G. Papadopoulos, Analyst, 112 (1987) 787.
[8] K. Hirayama and N. Unohara, Anal. Chem., 60 (1988) 2573.
[9] D. Guo-Zhong and J. Zhi-Liang, Talanta, 36 (1989) 1107.
[10] I. Mori, Y. Fujita, K. Ikuta, Y. Nakashima, K. Kato, K. Tamura and M. Ohji, Fresenius' Z. Anal. Chem., 334 (1989) 49.
[11] A.A. Alexiev and A.M. Stoyanova, Anal. Lett., 21 (1988) 1515.
[12] R. Forteza, J.M. Estela and V. Cerda, Analyst, 115 (1990) 749.
[13] J. Ruzicka and E.H. Hansen, Flow Injection Analysis, 2nd edn., Wiley, New York, 1988.
[14] H. Muller and V. Muller, Z. Chem., 26 (1986) 142.
[15] H. Muller, V. Muller and E.H. Hansen, Anal. Chim. Acta, 230 (1990) 113.
[16] A. Cladera, E. Gomez, J.M. Estela and V. Cerda, Analyst, 116 (1991) 913.
[17] M. Yamada, A. Sudo and S. Suzuki, Chem. Lett., (1985) 801.
[18] V.A. Elrod, K.S. Johnson and K.H. Coale, Anal. Chem., 63 (1991) 893.
[19] S. Nakano, M. Odzu, M. Tanaka and T. Kawashima, Mikrochim. Acta, 1 (1983) 403.
[20] J.H. Fendler and E.J. Fendler, Catalysis in Micellar and Macromolecular systems, Academic Press, New York, 1975.
[21] A. Helenlus, D.R. McCaslin, E. Fries and C. Tanford, in S. Fleischer and L. Packer (Eds.), Methods in Enzymology, Vol. LVI, Academic Press, New York, 1979, pp. 734–749.
[22] H. Suzuki, J. Am. Oil Chem. Soc., 47 (1970) 273.

ELSEVIER

Talanta 42 (1995) 1057–1065

Talanta

# Solid-phase spectrophotometric determination of trace amounts of vanadium at sub-ng/ml level with 4-(2-pyridylazo)resorcinol

M.L. Fernández-de Córdova [a], A. Molina-Díaz [a,*], M.I. Pascual-Reguera [a], L.F. Capitán-Vallvey [b]

[a] *Department of Physical and Analytical Chemistry, Faculty of Experimental Sciences, University of Jaén, E-23071 Jaén, Spain*

[b] *Department of Analytical Chemistry, Faculty of Sciences, University of Granada, E-18071 Granada, Spain*

Received 5 December 1994; accepted 3 January 1995

**Abstract**

Solid-phase spectrophotometry has been applied to analysis for trace amounts of vanadium. Vanadium was sorbed in a styrene–divinylbenzene-type anion-exchanger Dowex 1-X8 as a vanadium-4-(2-pyridylazo)resorcinol complex. Resin phase absorbances at 562 and 800 nm were measured directly which allowed the determination of vanadium in the range of 0.1–2.4 ng/ml with a RSD of 1.5%. The method has been applied to the determination of vanadium in different samples, namely toadstool tissue, mussel tissue, petroleum crudes and swamp water.

## 1. Introduction

There are several biological systems which contain significant levels of vanadium-containing compounds. Plants have a baseline mean vanadium content of about 1–2 μg/g, and animals of less than 1 μg/g [1]. Comparisons between these levels and those in certain plants and animals indicate large accumulations of vanadium. So, the toadstool *Amanita muscaria* was found to contain unusually large concentrations of vanadium [2] and certain species of marine animals, *Ascidians*, concentrate vanadium in their blood to a level comparable to that of iron in the human blood [3]. The accumulation by tunicates and *Amanita* toadstools may have started at an earlier stage, with atmospheric oxygen still at a rather low level.

Vanadium's role in physiological systems includes participation in various enzyme systems as an inhibitor and a cofactor [4], catalysis of the oxidation of various amines [5] and normalization of sugar levels. Vanadium in trace amounts is an essential element for all cell growth, but is toxic in high concentrations [6]. The toxicity of vanadium to humans through industrial exposure increases with the oxidation state of the vanadium compound, with the +5 oxidation state being the most toxic [7]. The dumping of petroleum crudes is one of the most important marine pollution sources. Vanadium, together with nickel, is always present in petroleum crudes, especially those from Canada and Venezuela, in the form of vanadium porphyrins [7]. Since some marine animals, such as molluscs, grow in places where this effect is especially strong, the determination of vanadium in the tissue of these species can be used as a control parameter of the pollution levels.

Thus it is of importance to develop sensitive methods for determining vanadium. Spec-

* Corresponding author.


*SSDI* 0039-9140(95)01516-7

trophotometry is the most common technique used for vanadium determination, owing to its high sensitivity and selectivity. The most useful method involving complex formation in aqueous solution appears to be that using the chromogenic agent 4-(2-pyridylazo)resorcinol (PAR) [8] in the presence of the masking agent CDTA. However, for the spectrophotometric determination of V(V) at sub-ng/ml levels in solution a previous preconcentration step is required. In this paper we have developed a very sensitive and selective method for the determination of vanadium with PAR by using solid-phase spectrophotometry (SPS). This technique introduced in 1976 [9] presents various important advantages: the sensitivity (expressed as molar absorptivity) is much higher (from $10^3$ to $10^4$ times) than the corresponding spectrophotometry in solution, it does not require an expensive instrumentation and the species interfering in spectrophotometry in solution can be excluded from the ion-exchanger in adequate conditions. Solid-phase spectrophotometry (SPS) combines the use of a solid support, usually an ion-exchanger, to preconcentrate the analyte with the aid of a chromogenic reagent and subsequent direct measurement of the absorbance of solid phase [10].

The proposed method has been satisfactorily applied to the determination of vanadium in diverse natural samples.

## 2. Experimental

### 2.1. Reagents

Analytical-reagent grade chemicals and doubly distilled water were used throughout. All experiments were carried out at room temperature.

Vanadium(V) stock solution was 1000 mg/l, as chloride (Aldrich). Solutions of lower concentration were prepared by dilution with doubly distilled water.

Ion exchanger: Dowex 1-X8 (200–400 mesh) anion-exchange resin (Aldrich) was used in the chloride form. The resin was washed several times with doubly distilled water, then treated with 2 M HCl for 4 h and finally with doubly distilled water until the washing was free from chloride. It was air-dried and stored in a polyethylene container.

Buffer solution HOAc/NaOAc of pH 3.8, was prepared by dissolving 2.7216 g of sodium acetate trihydrate, $NaOAc \cdot 3\,H_2O$ (Merck), and 8 ml of acetic acid in 1000 ml of water.

4-(2-pyridylazo)resorcinol solutions (PAR): solutions of various concentrations were prepared by dissolving 4-(2-pyridylazo)resorcinol monosodium salt (monohydrate) (Merck), in water. These solutions were stored under refrigeration and in absence of light. In these conditions they are stable for at least 4 days.

### 2.2. Apparatus

A single beam GBC 911A microprocessor-controlled UV-Vis spectrophotometer, from GBC Scientific Equipment Ply Ltd, with 1 mm glass cells was used for all spectral measurements. The spectra were obtained with a scan rate of 250 nm/min. The GBC 911A UV-Vis spectrophotometer was connected to a BRAVO AST/286 microcomputer by means of a serial port. The program GBC SCAN MASTER V 1.62 was used for data acquisition and treatment. A COMX PL80 plotter was used for graphical representations. Other apparatus consisted of an Agitaser 2000 rotating bottle agitator, a Selecta Model S-240 desk centrifuge and a Crison Model 2002 pH-meter fitted with a glass-saturated calomel electrode assembly and a temperature probe for pH measurements.

### 2.3. Absorbance measurements

The absorbance (really attenuation) of the PAR–V complex sorbed on the resin was measured in a 1 mm cell at 562 nm (corresponding to the absorption maximum of the coloured species) and 800 nm (the latter is in the range where only the resin absorbs light), compared with a 1 mm cell packed with resin equilibrated with blank solution. The net absorbance was calculated as in a previous report [11].

### 2.4. Procedures

(A) For 100 ml samples, an appropriate volume of sample containing 0.15–2.1 μg (1.5–21 ng/ml) of vanadium(V) was transferred into a 1 l-polyethylene bottle and then 10 ml of $1.47 \times 10^{-5}$ M PAR solution, 10 ml of pH 3.8 HOAc/NaOAc buffer solution and 70 mg of Dowex 1-X8 (200–400 mesh) resin were added, after levelling off to 100 ml.

The mixture was stirred mechanically for 15 min and the coloured resin beads were collected by filtration under suction and, with the aid of a small pipette, packed into a 1 mm-cell together with a small volume of the filtrate. The cell was centrifuged at 5000 rpm for 2 min. A blank solution containing all reagents except vanadium was prepared and treated in the same way as the sample. The absorbance difference between sample and blank, measured as described under Absorbance measurements, provides an estimation of the net absorbance.

(B) For 500 ml samples, an appropriate volume of sample containing 0.125–2.25 μg (0.25–4.5 ng/ml) of vanadium(V) was transferred into a 1 l-polyethylene bottle and then 10 ml of $2.64 \times 10^{-5}$ M PAR solution, 50 ml of pH 3.8 HOAc/NaOAc buffer solution and 70 mg of Dowex 1-X8 (200–400 mesh) resin were added, after levelling off to 500 ml. The mixture was shaken mechanically for 50 min, operating as indicated in the above procedure.

(C) For 1000 ml samples, an appropriate volume of sample containing 0.125–2.4 μg (0.125–2.4 ng/ml) of vanadium(V) was transferred into a 2l-polyethylene bottle and then 10 ml of $3.53 \times 10^{-5}$ M PAR solution, 100 ml of pH 3.8 HOAc/NaOAc buffer solution and 70 mg of Dowex 1-X8 (200–400 mesh) resin were added, after making up to volume. The stirring time was increased to 60 min. Other details were as above.

The calibration graphs were constructed in the same way, using vanadium solutions of known concentration.

### 2.5. Treatment of samples

*Water*

Natural water was filtered through a 0.45 μm membrane filter (Millipore) and collected in a polyethylene container carefully cleaned with nitric acid. The samples were stored at 4 °C until analysis. Analyses were performed with the least possible delay. The usual general precautions were taken to avoid contamination.

*Toadstool tissue (Amanita muscaria)*

Firstly all foreign matter, especially adhering soil, was removed from the sample by means of successive washings with distilled water, 0.1 M HCl and doubly distilled water (we avoided an excessive washing to prevent leaching). The sample was immediately dried into a forced-draft oven for 24 h at 70 °C to prevent decomposition or weight loss by respiration and ground in a hand-mill. A suitable aliquot was weighed (1.0659 g dry material) into a quartz crucible and placed in a cool furnace; the mineralization was carried out by heating slowly to 450 °C for 2 h and holding at this temperature for a further 2 h. The sample was removed and cooled and the ashes were wet carefully with a fine stream doubly distilled water, then adding 1 ml of 4 M NaOH; the crucible was covered with a watch glass, heated cautiously on a hot plate to boiling and finally let stand for a few min. Then, the solution was filtered through Whatman no. 42 paper over a 100 ml standard flask, diluting to volume after addition of 0.75 ml HCl. The vanadium content was determined on an aliquot, as described in the 100 ml procedure.

*Mussel tissue (Mytilus galloprovincialis)*

The sample was dried in a forced-draft oven at 70 °C to constant mass and then ground into a fine powder. A suitable aliquot was weighed (19.6253 g dry material) into a quartz crucible and placed in a cool furnace; the mineralization was carried out by heating slowly to 550 °C for 2 h and holding at this temperature for a further 2 h. The sample was removed and cooled and the ashes were wet carefully with a fine stream doubly distilled water, then adding 2 ml of 4 M NaOH; the crucible was covered with a watch glass, heated cautiously on hot plate to boiling and finaly let stand for a few minutes. Then, the solution was filtered through Whatman no. 42 paper over a 100 ml standard flask, diluting to volume after addition of 0.8 ml HCl. The vanadium content was determined on an aliquot, as described in the 100 ml procedure.

*Petroleum crudes*

A suitable weight of petroleum sample (from 0.501 to 7.529 g, depending on the vanadium content) was treated in a Vycor vessel with sulphuric acid (1 ml for each gram of sample) in a sand-bath with continuous agitation to avoid foam formation, followed by combustion of carbonaceous ash at 525 ± 25 °C. The inorganic residue was treated with 1:1 hydrochloric acid and heated to effect complete dissolution. After concentration, a few drops of nitric and sulphuric acids were added and the solution was heated gently until white fumes were formed and the small carbonaceous residue not ignited was destroyed. After, the Vycor vessel

was washed carefully, the solution was heated to boiling and neutralized and pH was fixed between 3 and 5 with sulphuric acid. Finally, the solution was diluted to 50 ml with doubly distilled water.

### 2.6. Distribution measurements

PAR solution, buffer solution and 70 mg of Dowex 1-X8 (200–400 mesh) were added to a 100 ml water solution containing 3.93 μmol of V(V). After 30 min equilibration, the resin beads were separated by filtration under suction. Then, the equilibrium concentration of V(V) in the solution was determined as described in the 100 ml procedure. The distribution ratio $D$ was calculated from the initial and equilibrium concentrations in the solution. An average value of $(218.2 \pm 3.2) \times 10^3$ ml/g was obtained from five replicate determinations.

## 3. Results and discussion

### 3.1. Absorption spectra in solid phase

PAR reacts with V(V) in solution to give a 1:1 violet complex [12], with an absorption maximum at 533 nm, suitable for colorimetric determination of the latter. Between pH 2 and 8 this complex is sorbed on Dowex 1-X8 anion-exchange resin shifting the absorption maximum at 562 nm. PAR is fixed on this resin showing a yellow-orange colour with an absorption maximum at 409 nm (415 nm in solution). The spectra of the complex in solution and resin phases, from which the increase of the sensitivity in the resin phase is evident are shown in Fig. 1.

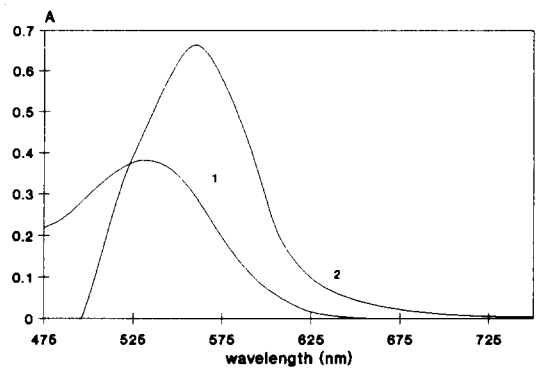


Fig. 1. Net absorption spectra of V(V)–PAR species. (1) in solution $[V(V)] = 1.96 \times 10^{-5}$ M, $[PAR] = 3.93 \times 10^{-4}$ M, pH = 3.9, 10 mm optical path length; (2) on resin. $[V(V)] = 2.94 \times 10^{-7}$ M, $[PAR] = 5.88 \times 10^{-6}$ M, pH 3.9, 70 mg of resin, 1 mm optical path length, stirring time = 15 min, $V = 100$ ml.

### 3.2. Optimization of variables

*pH dependence*

This variable was studied by applying the 100 ml procedure. Optimum pH for the formation and fixation of the species fell in the range 3–4.5 (Fig. 2). At pH values below 3 and above 6 the absorbance decreased significantly. Different buffer solutions ($HCOOH/HCOO^-$, potassium phthalate/HCl, HOAc/NaOAc) were tested. The HOAc/NaOAc buffer (pH 3.8) was found to yield the best results.

Absorbance was independent on ionic strength, adjusted with the buffer solution, up to a concentration of $3.2 \times 10^{-2}$ M. For higher values the absorbance decreased quickly as usual in SPS studies, probably owing to competition between the anions of the buffer for the anionic sites of the resin.

*PAR concentration*

Absorbance increases together with PAR concentration, up to a molar [PAR]/[V(V)] ratio 4 (for 100 ml sample). Consequently, a [PAR]/[V(V)] ratio of 5 was chosen for 100 ml. Similarly, for 500 and 1000 ml molar [PAR]/[V(V)] ratios of 9 and 12 were chosen, respectively.

*Other experimental conditions*

The optimum stirring times were 15, 50 and 60 min for 100, 500 and 1000 ml sample volumes, respectively. The fixed complex was stable for at least 120 min after equilibration. The order of addition of reagents did not affect the results obtained and the one used here was:

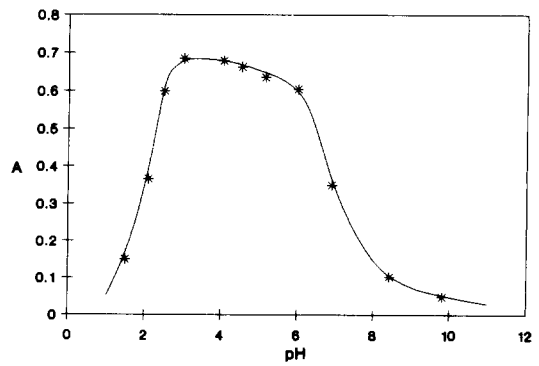


Fig. 2. Influence of pH. $[V(V)] = 2.94 \times 10^{-7}$ M, 70 mg of resin, stirring time = 15 min, $V = 100$ ml, 1 mm optical path length.

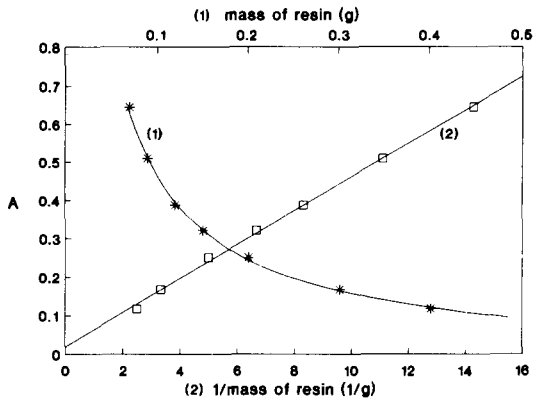


Fig. 3. Influence of the amount of resin. (1) $A$ vs. mass of resin; (2) $A$ vs. 1/mass of resin. $[V(V)] = 2.94 \times 10^{-7}$ M, $[PAR] = 2.94 \times 10^{-6}$ M, pH 3.8, stirring time = 15 min, $V = 100$ ml, 1 mm optical path length.

sample–PAR–buffer–resin. The use of a large amount of resin ($m_r$, in g) lowered absorbance values, as usual [10]. The minimum amount of dry resin required to fill the cell and facilitate handling, i.e. 70 mg, was used for all the measurements. The reduction of absorbance was according to the empirical equation $A_c m_r^{0.958} = 0.051$ (Fig. 3, curve 1). When absorbance $A_c$ is represented vs. $1/m_r$ (Fig. 3, curve 2) we found that absorbance decreased according to the equation $A_c = 0.020 + 0.044/m_r$ ($r = 0.999$).

We can calculate the agreement of the slope with molar absorbance as follows [13]:

$$A_c = \epsilon_c l_R C_o V 1000/(m_r + V/D) \quad (1)$$

where $\epsilon_c$ is the molar absorptivity of the sample species in the ion-exchanger phase (15.700 kg $mol^{-1}$ $cm^{-1}$), $l_R$ the mean light-path length through the solid phase (cm), $C_o$ the initial concentration of V(V) (M), $V$ the volume of sample solution (1), $D$ the distribution ratio (l/g) and $m_r$ the mass of ion-exchanger (g). In our case, owing to the large value of $D$, the fraction $V/D$ can be neglected as compared with $m_r$ for all the values of this latter and then we obtain the equation which relates the absorbance with the mass of ion-exchanger:

$$A_c = \epsilon_c l_R C_o V 1000/m_r = K/m_r \quad (2)$$

where $K = \epsilon_c l_R C_o V 1000$ is the slope of the graphic representation of $A_c$ vs. $1/m_r$. Supposing $l_R = 0.1$ cm, the expected value for $K = 15.700 \times 0.1 \times 2.94 \times 10^{-7} \times 0.100 \times 1000 = 0.046$ which is in excellent agreement with the experimental value 0.044.

*Nature of the fixed complex*

The composition of the fixed V(V)–PAR complex on Dowex 1-X8 resin was studied at the working pH 3.8 using the *molar ratio* [14,15] and the *Job* [16] methods.

The plot $A$ vs. [PAR]/[V(V)] molar ratio, obtained by varying the PAR concentration, showed an inflexion at 1 molar ratio indicating the presence of one molecule of PAR in the fixed complex. Moreover, the *Job* method shows a ratio [PAR]/[V(V)] = 1. Consequently, these results indicated that the stoichiometry is [V(V)]:[PAR] = 1:1 and agreed with those found in aqueous solution [12].

PAR may be considered to act as terdentate ligand having three donor atoms in a plane. The metal is coordinated through the pyridinic nitrogen, the azo nitrogen further from the heterocyclic ring, and the *ortho* hydroxyl group of the reagent [17,18].

Corsini [19] studying the formation of complexes between PAR and various metalic ions in aqueous solution found that the $pK_{a2}$ value of the *p*-OH group of PAR increases notably by the chelation. On the other hand, other authors who have utilized a PAR-like chromogenic reagent in SPS admit that the fixation of the metal–PAR complex on an anion-exchange resin promotes the dissociation of the *para*-hydroxyl group [20].

According to this, the global complexation–fixation process could be presented in this case by the following scheme:

$$VO_2^+ + H_2L + X^- \rightleftarrows VO_2LHX^- + H^+$$

(complexation process)

$$VO_2LHX^- + Cl_m^- R^{m+} \rightleftarrows VO_2LX^{2-}Cl_{m-2}^- R^{m+} + 2Cl^- + H^+$$ (fixation process)

$$VO_2^+ + H_2L + X^- + Cl_m^- R^{m+} \rightleftarrows VO_2LX^{2-}Cl_{m-2}^- R^{m+} + 2Cl^- + 2H^+$$

(global process)

where X represents an unidentate anion, (e.g. $Cl^-$, $AcO^-$), which would be fulfilling the sixth coordination position of the vanadium(V) atom, and $Cl_m^- R^{m+}$ the anionic resin.

In fact, the V(V)–PAR complex is apparently anionic in nature, whereby it is extracted into methyltrioctylammonium chloride solution (Adogen 464) in toluene, whereas it is not extracted into toluene of tetrachloromethane. The above proposed structure for the V(V)–PAR complex in the resin phase is in agree-

Table 1
Analytical parameters for SPS vanadium(V) determination

| | Volume of sample system | | |
|---|---|---|---|
| | 100 ml | 500 ml | 1000 ml |
| Intercept | 0.014 | 0.016 | 0.002 |
| Slope | 0.043 | 0.212 | 0.406 |
| Linear dynamic range (ng/ml) | 1.5–21.0 | 0.2–4.5 | 0.1–2.4 |
| Correlation coefficient | 0.9997 | 0.9993 | 0.9989 |
| Detection limit ($K = 3$) [a] (ng/ml) | 0.29 | 0.023 | 0.018 |
| Determination limit ($K = 10$) [b] (ng/ml) | 0.96 | 0.077 | 0.060 |
| RSD (%) ($n = 10$) | 1.4 (15) [c] | 1.7 (3) [c] | 1.5 (1.5) [c] |

[a] From Ref. [34].
[b] From Ref. [35].
[c] Vanadium (V) concentration (ng/ml) used for the determination of reproducibility.

ment with that proposed in solution for complexes 1:1 between PAR and metallic ions with coordination index [21].

### 3.3. Analytical data

The analytical parameters are summarized in Table 1. It was verified that one of the main contributions to the RSD comes from the variability of the packing of the ion-exchanger. The relative standard deviation (RSD) was 7.0% without centrifugation for the 100 ml sample and 10 determinations. With centrifugation for 2 min at 5000 rpm before the absorbance measurements were carried out, the RSD decreased at 1.4% and the absorbance values increased at about 9%.

The sensitivity, expressed as apparent molar absorptivity, of the proposed methods, is compared with that of spectrophotometric procedures in the literature (Table 2). It is shown that the increase in sensitivity obtained with the proposed methods is substantial, especially in relation to the solution methods using the same reagent.

According to the equation $A_c = \epsilon_c l_R C_o V 1000/(m_r + V/D)$, the sensitivity in SPS methodology can be enhanced by increasing the sample volume. In our case, the fraction $V/D$ can be neglected as compared with $m_r$ for all the values of $V$ lower than 11 and then we obtain the equation which relates absorbance with sample volume:

$$A_c = \epsilon_c l_R C_o V 1000/m_r = K'V \quad (3)$$

where $K' = \epsilon_c l_R C_o 1000/m_r$ is the slope of $A_c$ vs. $V$ (for $V$ values lower than 11). The expected value for $K' = 15.700 \times 0.1 \times 2.94 \times 10^{-8} \times 1000/0.07 = 0.659\ l^{-1}$.

The increase of absorbance with sample volume can be evaluated by measuring the absorbance of resin equilibrated with different volumes of solutions containing the same concentration of vanadium ($V$) and proportional amounts of the other reagents. Fig. 4 shows the increase in the absorbance with sample volume $V$. Absorbance increases according to the empirical equation $A_c = 0.634V$ ($r = 0.997$), for $V$ values lower than 11. The experimental value of the slope, $0.634\ l^{-1}$, is in excellent agreement with the theoretical value $0.659\ l^{-1}$.

The factor $m_r$ can be neglected compared with $V/D$ at higher sample volume values and then the absorbance becomes independent of sample volume: $A_c = \epsilon_c l_R C_o 1000D = K''$. In practice, absorbance becomes independent of sample volume for $V$ values lower than values predicted theoretically (Fig. 4); probably owing to the stirring time required for high volumes being greater than the experimental one used.

In practice, the increase in the absorbance with sample volume can be also predicted from the slope of the calibration graphs. The sensitivity ratios ($S$) for the samples analysed here are: $S_{1000/500} = 1.92$; $S_{1000/100} = 9.44$ and $S_{500/100} = 4.93$. The theoretical expected values obtained using the distribution ratio value [33] $D$ are 1.94, 9.45 and 4.87, respectively.

The standard deviations of the background absorbance for the blanks, necessary for calculating the IUPAC detection limit (K = 3) [34], measured as the average of 10 determinations and expressed as SD units, were 0.004, 0.002 and 0.002, for 100, 500 and 1000 ml sample volumes, respectively. The detection limits of the proposed methods are similar to those obtained by other sensitive techniques such as

Table 2
Comparison of sensitivities for determination of vanadium(V)

| Reagent | Molar absorptivity | Ref. |
|---|---|---|
| Tungstophosphovanadic acid [a] | $1.4 \times 10^3$ | 22 |
| 8-Hydroxyquinoline [b] | $3.0 \times 10^3$ | 23 |
| *N*-Benzoyl-*N*-phenylhydroxylamine [a] | $4.8 \times 10^3$ | 24,25 |
| 4-(2-Pyridylazo)resorcinol–$H_2O_2$ [a] | $1.64 \times 10^4$ | 26 |
| 1-(2-Pyridylazo)-2-naphthol [a] | $1.7 \times 10^4$ | 27 |
| 4-(2-Pyridylazo)resorcinol [a] | $3.6 \times 10^4$ | 28 |
| 2-(3,5-Dibromo-4-methyl-2-pyridylazo)-5-diethylaminophenol–$H_2O_2$ [a] | $5.43 \times 10^4$ | 29 |
| Malachite Green–molybdovanadophosphate [c] | $1.8 \times 10^5$ | 30 |
| Benzohydroxamic acid [d] (500 ml) | $3.9 \times 10^5$ [e] | 31 |
| 5-Br-Salicylhydroxamic acid [d] (1000 ml) | $1.1 \times 10^7$ [e] | 32 |
| 4-(2-Pyridylazo)resorcinol [d] (100 ml) | $2.2 \times 10^7$ [e] | proposed method |
| 4-(2-Pyridylazo)resorcinol [d] (500 ml) | $1.1 \times 10^8$ [e] | proposed method |
| 4-(2-Pyridylazo)resorcinol [d] (1000 ml) | $2.1 \times 10^8$ [e] | proposed method |

[a] Solution method.
[b] Extractive method.
[c] Method based on extractable ion-pair with basic dye.
[d] Solid phase spectrophotometry.
[e] Apparent molar absorptivity (absorbance value of the complex sorbed on the resin from a 1 M aqueous solution of V(V) and supposing that it was measured in a 10 mm optical path length cell).

EAAS, AFS and ICPS (Table 1). The accuracy and precision of the proposed SPS methods are similar to the ones obtained by the techniques indicated above.

### 3.4. *Effect of foreign ions*

A detailed study of interference effects was carried out for cations and anions, in amounts ranging up to 1000 μg, with 1.5 μg of vanadium. Ions were considered as not interfering if they produced an error of less than ± 5% in the determination of analyte. The tolerance limits for the ions studied are shown in Table 3.

Of the ions tested, the only major interferences were from Co(II) and Cu(II) owing to the formation of complexes with PAR which fix on the solid phase and absorb at the working wavelength [10,36]. Therefore, we can confirm that the proposed methods are sufficiently selective.

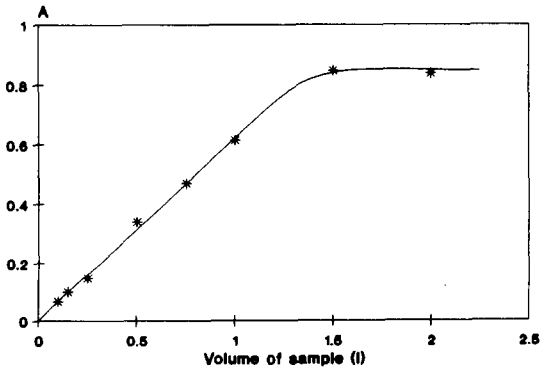


Fig. 4. Influence of the sample volume on colour development. $[V(V)] = 2.94 \times 10^{-8}$ M, $[PAR] = 2.94 \times 10^{-7}$ M, 70 mg of resin, pH 3.8, stirring time = 15–160 min.

Table 3
Effect of foreign ions on the determination of 15 ng/ml of vanadium(*V*) (*V* = 100 ml)

| Foreign ion or species | Tolerance level (ng/ml) |
|---|---|
| $NO_3^-$, $NO_2^-$, $Cl^-$, Mn(II), $I^-$, $C_2O_4^{2-}$, $H_2PO_4^-$, $SO_4^{2-}$ | >10000 |
| $CO_3^{2-}$, Ca(II), Mg(II) | 5000 |
| $F^-$, Zn(II) | 2000 |
| Al(III) | 1000 |
| Cr(III) | 500 |
| Fe(III), EDTA | 50 |
| Cu(II) | 5 |
| Co(II) | 2 |

Table 4
Analytical applications

| Sample | | Vanadium content found (μg/g) | Vanadium content found by standard method (μg/g) |
|---|---|---|---|
| Toadstool [f] (*Amanita muscaria*) | | 8.32 ± 0.20 [a] | 8.01 ± 0.48 [c] |
| Mussel [e] (*Mytilus galloprovincialis*) | | 0.802 ± 0.026 [a] | 0.827 ± 0.030 [c] |
| Petroleum crudes [f] | Arabia ligero | 15.9 ± 0.2 [b] | 15.9 ± 0.1 [d] |
| | Qatar Terrestre | 5.3 ± 0.1 [b] | 5.2 ± 0.1 [d] |
| | Zueitina | 1.06 ± 0.01 [b] | 1.06 ± 0.02 [d] |
| | Irán Ligero | 19.0 ± 0.3 [b] | 18.6 ± 0.4 [d] |

[a] Average values of three determinations.
[b] Average values of four determinations.
[c] Electrothermic atomic absorption spectroscopy.
[d] ASTM.
[e] Standard addition calibration graph method; 100 ml sample.
[f] Standard calibration graph method; 100 ml sample.

### 3.5. Analytical applications

The proposed method has been applied to the determination of vanadium in toadstool tissue, mussel tissue, petroleum crudes and swamp water. The determination of vanadium in toadstool tissue (*Amanita muscaria*) was performed using the standard calibration graph method, since no matrix effect was observed (Table 4). Sample was collected from near the city of Viso del Marqués (Ciudad Real, Spain). Mussel tissue (*Mytilus galloprovincialis*) came from Galicia (Spain) and was analysed by the standard addition calibration graph method (Table 4). The loss of sensitivity caused by matrix effects (evaluated by the slope's quotient between the standard addition calibration graph and the standard calibration graph) was 0.77. The results obtained in both cases are in excellent agreement with those found by EAAS.

The vanadium content in four petroleum samples of different origin, composition and density was analysed by the standard calibration graph method (Table 4). As a reference method, the ASTM procedure, based on tungstophosphovanadic acid formation and absorbance measurement at 436 nm [37], was employed but, in this case, a larger amount of sample than in the SPS method (from 20.050 to 301.180 g) was used. The statistical study of precision and accuracy of the proposed method and the reference ASTM method was made from $F$-criterion and the $t$-test, respectively. The results showed that both methods have the same precision and accuracy.

The method was also applied to the determination of vanadium in Quiebrajano swamp water (Jaén, Spain) by the standard addition calibration graph method obtaining an average content ($n = 3$) of 0.49 ± 0.02 ng/ml of vanadium. The loss of sensitivity caused by the matrix effect (evaluated as indicated above) was 0.68. In this case, in order to check the accuracy of the proposed method a study of recovery was performed. For this, 0.75 and 1.05 ng/ml of vanadium were added to 1000-ml water samples, obtaining recovery precentages of 98.7 and 96.2%, respectively.

## Acknowledgements

This work was supported by the Dirección General de Universidades e Investigación de la Junta de Andalucía (Spain), Annual Grant No 1066. The authors thank A. Navalón Montón (Department of Analytical Chemistry, Faculty

of Sciences, University of Granada) for his help in realizing this work.

## References

[1] J.D. Saxby, Rev. Pure Appl. Chem., 19 (1969) 131.
[2] H. Ter Meulen, Rec. Trav. Chim. Pays-Bas, 50 (1931) 491.
[3] D.B. Carlisle, Proc. Roy. Soc. (Lond.), Ser. B, 171 (1968) 31.
[4] D.C. Crans, M. Shaia Gottlieb, J. Tawara, R.L. Bunch and L.A. Thiesen, Anal. Biochem., 188 (1990) 53.
[5] H.E. Stokinger, in G.D. Clayton and F.E. Clayton (Eds.), Patty's Industrial Hygiene and Toxicology, 3rd edn., Wiley-Interscience, Vol. 2A, New York, 1981.
[6] E. Berman, in L. Thomas (Ed.), Toxic Metals and Their Analysis, Heyden, London, 1980.
[7] M.J. Kendrick, M.T. May, M.J. Plishka and K.D. Robinson, Metals in Biological Systems, Ellis Horwood, Chichester, 1992.
[8] T. Yotsuyanagi, J. Ito and K. Aomura, Talanta, 16 (1969) 1611.
[9] K. Yoshimura, H. Waki and S. Ohashi, Talanta, 23 (1976) 449.
[10] M.L. Fernández-de Córdova, A. Molina-Díaz, M.I. Pascual-Reguera and L.F. Capitán-Vallvey, Fresenius J. Anal. Chem., 348 (1994) 1668.
[11] A. Molina-Díaz, J.M. Herrador-Mariscal, M.I. Pascual-Reguera and L.F. Capitán-Vallvey, Talanta, 40 (1993) 1059.
[12] O. Budevski and L. Johnova, Talanta, 12 (1965) 291.
[13] K. Yoshimura and H. Waki, Talanta, 32 (1985) 345.
[14] J.H. Yoe and A.L. Jones, Ind. Engng. Chem. Anal. Ed., 16 (1944) 111.
[15] J.H. Yoe and A.E. Harvey, J. Am. Chem. Soc., 70 (1948) 648.
[16] P. Job, Ann Chim., 9 (1927) 114.
[17] Y. Muto, Bull. Chem. Soc. Jpn., 31 (1958) 1017.
[18] H.A. Flaschka and A.J. Barnard Jr., Chelates in Analytical Chemistry Marcel Decker, New York, 1972.
[19] A. Corsini, Talanta, 15 (1968) 993.
[20] J.M. Bosque Sendra, M.C. Valencia and L.F. Capitán-Vallvey, Int. J. Environ. Anal. Chem., 38 (1990) 551.
[21] T. Yotsuyanagi and H. Hoshino, Bunseki, (1976) 743.
[22] R. Bock and B. Jost, Z. Anal. Chem., 250 (1970) 358.
[23] P. Bermejo-Barrera, A. Bermejo-Barrera and F. Bermejo-Martínez, Microchem. J., 25 (1980) 458.
[24] D.E. Ryan, Analyst, 85 (1960) 569.
[25] E.S. Pilkington and W. Wilson, Anal. Chim. Acta, 43 (1969) 461.
[26] K.N. Bagdasarov, H.A. Akhmedova and O.A. Tataev, Zav. Lab., 35 (1969) 12,
[27] F.W. Staten and E.W. Huffman, Anal. Chem., 31 (1959) 2003.
[28] O.I. Karpova, V.V. Lukachina and A.T. Pilipenko, Ukr. Khim. Zh., 39 (1973) 195.
[29] E. Kiss, Anal. Chim. Acta, 77 (1975) 205.
[30] A.T. Pilipenko, E.A. Shpak and G.T. Kurbatova, Zh. Anal. Khim., 22 (1967) 1014.
[31] F. Capitán, M.C. Valencia, L. Cuadros and L.F. Capitán-Vallvey, Microchem. J., 31 (1985) 396.
[32] M.I. Pascual-Reguera, A. Molina-Díaz, N. Ramos-Martos and L.F. Capitán-Vallvey, Anal. Lett., 24 (1991) 2245.
[33] K. Yoshimura and S. Ohashi, Talanta, 25 (1978) 103.
[34] IUPAC, nomenclature, symbols, units and their usage in spectrometrical analysis, Pure Appl. Chem., 105 (1976) 45.
[35] Guidelines for data acquisition and data quality evaluation in environmental chemistry, Anal. Chem., 52 (1980) 2242.
[36] M.L. Fernández-de Córdova, A. Molina-Díaz, M.I. Pascual-Reguera and L.F. Capitán-Vallvey, Anal. Lett., 25 (1992) 1961.
[37] 1975 Book of ASTM Standards, Part 23, Method D 1548-63, American Society for Testing and Materials, Philadelphia, 1975.

ELSEVIER

Talanta 42 (1995) 1067–1079

Talanta

# Extrapolation of molar equilibrium constants to zero ionic strength and parameters dependent on it. Copper(II), nickel(II), hydrogen(I) complexes with glycinate ion and calcium(II), hydrogen(I) complexes with nitrilotriacetate ion

Giorgio Anderegg *, Sherif Kholeif [1]

*Laboratory of Inorganic Chemistry, Swiss Federal Institute of Technology (ETHZ), Universitätstrasse 6, CH-8092 Zurich, Switzerland*

Received 3 October 1994; revised 3 January 1995; accepted 3 January 1995

**Abstract**

The stability constants of the complexes of glycinate ion with copper(II), nickel(II) and hydrogen(I) and of nitrilotriacetate ion with calcium(II) and hydrogen(I) and the ionic product of water ($K_w$) were determined potentiometrically. The measurements were carried out at 25.0 °C in four different ionic strengths up to $I\ (=I_c) = 2.50$ and two different ionic media ($KNO_3$ and $(CH_3)_4NNO_3$). Extrapolation of equilibrium constants to zero ionic strength and ionic strength corrections to equilibrium constants were carried out with the data obtained from both media using the TEC (thermodynamic equilibrium constant) equation and computer program. The constants of the potassium complexes with nitrilotriacetic acid at low ionic strength are also given. Successful attempts to predict equilibrium constants for other ionic media using TEC parameters and the procedure of the specific ion-interaction theory (SIT) are given. The variations of equilibrium constants with the ionic strengths and ionic media are demonstrated.

## 1. Introduction

One of the most important tasks in aqueous solution chemistry is speciation, i.e. the exact description of a system with different metal ions and ligands in terms of the concentrations of the species present at given conditions (temperature, ionic strength $I$, and inert salt) and known total concentrations of the components. This is only possible if the equilibrium constants for all the species present in the system at the chosen conditions are known. As this is not always possible, the unknown constants can still be estimated starting from known values evaluated under other experimental conditions. Two of the important parameters affecting the values of the equilibrium constants are the ionic strength and the inert salt. Their dependence may be described using expressions containing terms for the activity coefficients of the species involved in equilibrium [1]. We have recently published a paper [1] introducing the TEC (thermodynamic equilibrium constant) equation for use with such calculations. The results obtained by TEC using the literature data were discussed and compared with those obtained by the SIT (specific ion-interaction theory) equation or its synonym the BGS (Brønsted–Gugenheim–Scatchard) equation.

* Corresponding author.

[1] Permanent address: Alexandria University, Faculty of Science, Chemistry Department, Horreya Avenue, Elchatby, Alexandria, Egypt.


*SSDI* 0039-9140(95)01518-3

In this paper, our own experimental results of some simple systems are analysed with the above equation using statistical quantities defined in our earlier paper [1] and given in the footnotes of Table 4. The values of some equilibrium constants with glycinate and nitrilotriacetate ions in presence of two inert salts and a wide ionic strength range have been obtained ($I = 0.050–2.50\ M$). This allows the interpolation of the same stability constants for arbitrary conditions at $I < 3$ and the extrapolation of the same values to $I = 0$. The resulting values are discussed in terms of their precision and reliability as well as the possibility equilibrium constants values in presence of other inert salts.

The practical standard state for a solute B in a solution is a hypothetical solution at the standard state pressure with concentration $c_B = 1\ M$ and activity coefficient $y_B = 1$. To avoid using activity coefficients, the measurements are always done in presence of an inert electrolyte that should not react with the studied species but maintain the activity coefficients of all investigated species as constant. From measurements at different $I$ values, it is often possible to calculate the equilibrium constant at $I = 0$ in the standard state studied by extrapolation using extended Debye–Hückel equations referred to the molar ionic activity coefficients $\gamma_i$.

Recently, a critical survey on equilibrium constant data of glycine and its metal complexes has been published [2]. Some mentioned papers give exact values for the protonation of glycinate ion in solution [3–5] at different ionic strength ($I \simeq 0.01–0.1$) with a few recommended values also for the metal complex formation with the same anion. Another critical survey on equilibrium constants data of nitrilotriacetate and its metal complexes is found in the literature [6] and includes recommended values for the protonation constants of nitrilotriacetate (NTA) at $I = 0.1$(KCl or $KNO_3$) and for the stability constant of the complex with calcium at $I = 0.1(KNO_3)$. In both cases, the number of values is too limited to allow an exact evaluation of the involved constants required for the inert salt concentrations with $I \leqslant 3\ M$.

While a single article appeared on the subject of the $K^+$ complex with glycine [7], a few articles [8–10] have reported a complex of $K^+$ with NTA ($KL^{2-}$ where L = NTA) at $I = 0.1$. Only one article [8] reported the constant of the protonated species $KHL^-$ at the same ionic strength with a large standard deviation. As the stability constants of the potassium complexes are small in magnitude and difficult to be evaluated, it is important to know their values at all ionic strengths because of the applications of potassium salts as supporting electrolytes in potentiometric titrations. Similar remarks can be generalized for $Na^+$ normally forming more stable complexes with polyaminopolycarboxylate ligands than $K^+$ and present in biological systems ($I = 0.15$(NaCl)) and seawater ($I = 0.7$).

## 2. Experimental

### 2.1. Reagents

Glycine (HL) and nitrilotriacetic acid ($H_3L$), Fluka puriss 99%, were checked for purity using elemental analysis. Potassium nitrate, Merck pro analysi 99% was dried in an oven at 80 °C. Potassium hydroxide solution was prepared from a Titrisol Merck ampoule and standardized against three different standard solutions of potassium hydrogen phthalate. The solid potassium hydrogen phthalate was Merck pro analysi titration grade 99.95–100.05%. Nitric acid solutions were prepared from a Titrisol Merck ampoule. The disodium salt of ethylenediaminetetraacetic acid (EDTA) was standardized against standard zinc chloride solution prepared from zinc metal, Fluka 99.999%. Copper nitrate and nickel nitrate, both AnalaR grade, were standardized by titration against standard EDTA solution. Tetramethylammonium nitrate (Fluka), was checked for purity using elemental analysis. Tetramethylammonium hydroxide (Fluka) was standardized against standard potassium hydrogen phthalate. Both tetramethylammonium compounds were checked for the presence of metal impurities. Mercury (Merck) analysis and polarography grade was used.

### 2.2. Potentiometric system

The measuring system consists of a 10 ml thermostated jacket cell (temperature adjusted using a Lauda MS M3 thermostat) containing a micro glass electrode and an external 'homemade' calomel electrode (Pt | Hg, $Hg_2Cl_2$, $xM(N\text{Cl})$, $x'M(N\text{NO}_3)$, where $x = 10\%$ of the total solution concentration $(x + x')M$ and

$N = K^+$ or $(CH_3)_4N^+$) connected to the measuring solution through a salt bridge filled with the aqueous solution of the inert salt alone at the given $I$ ($=x+x'$) value. Its cell potential, $E$, was measured at 25.0 °C using an Orion SA 720 potentiometer. The strong base was added stepwise from a 1.000 ml motor burette (Metrohm 665 Dosimat) to 5.00 ml of the measured acidic solutions. The whole titration system was monitored using an IBM AT computer and the TIT212 data acquisition–titration control software [11].

### 2.3. Procedure

The cell was calibrated by titrating 5.00 ml standard nitric acid solutions at $I = 0.050$, 0.300, 1.00 and 2.50 against either standard potassium hydroxide or tetramethylammonium hydroxide. The calibration parameters (the apparent standard electrode potential $E°'$ and the negative logarithm of the ionic product of water $pK_w$) were computed [12] using the experimental data obtained, i.e. $E$ value for each base addition. An extra term was added to the Nernst equation accounting for the Henderson's liquid junction potential correction [13] owing to $H^+$ and $OH^-$ concentrations. All measured solutions and titrants were maintained at a given ionic strength with the same ionic medium used. During the alkalimetric titration, a reduction in the concentration of the inert salt and $I$ occurs becuase of the neutralization of $H^+$ and dilution. The maximum reductions of the ionic strnegth computed from a strong acid–strong base titration is 0.002 and 0.004 at the ionic strengths of 0.050 and 2.50, respectively. It is in general possible to reach the exact ionic strength in the pH range from which the constants are determined. The calibration parameters were later used to convert the $E$(mV) reading (by the glass electrode) of the measured solutions under investigation to pH. The Nernst slope is set constant to 59.16 mV and the errors obtained for $E°'$ were between $\pm 0.04$ and 0.2 mV corresponding to 0.0007 and 0.003 pH unit, respectively. The deionized water used was previously degassed for 2 h and then saturated with pure argon or nitrogen gas. The gas was first passed through a solution with the same ionic medium and ionic strength of the whole system and then allowed to evolve above the measured solution in the covered measuring cell. The glycinate ion in its fully protonated form ($H_2L^+$) was titrated alone and in presence of copper or nickel metal nitrates, the nitrilotriacetate ion as $H_3L$ was titrated alone and in the presence of calcium nitrate in $KNO_3$ and $(CH_3)_4NNO_3$ media at $I$ values of 0.050, 0.300, 1.00 and 2.50 $M$. The weighted equilibrium constants were then computed using both KONST [14] and SUPERQUAD [15] computer programs. The differences between the constants computed using both programs are negligible (mainly owing to differences in the weighting procedures) and within the uncertainties of the constants. Each equilibrium constant is computed from three or more different solutions and hence three or more different titration curves in ml–mV.

## 3. Extrapolation model

The extrapolation of equilibrium constants to zero ionic strength and the ionic strength correction of equilibrium constants in $KNO_3$ and $(CH_3)_4NNO_3$ were carried out using the TEC approach [1] (Eq. (3)) for equilibrium (1), where ${}^*\beta_{n,p,m}$ and ${}^*\beta°_{n,p,m}$ are the

$$mM + nL + pH_2O \rightleftharpoons M_mL_n(OH)_p + pH^+ \quad (1)$$

$${}^*\beta_{n,p,m} = \frac{[M_mL_n(OH)_p][H^+]^p}{[M]^m[L]^n} \quad (2)$$

$$\log {}^*\beta_{n,p,m} - p \log a_{H_2O} = \log {}^*\beta°_{n,p,m} - \frac{\Delta z^2 A\sqrt{I}}{1 + B\alpha\sqrt{I}} + \Delta CI + \Delta DI^2 + \cdots \quad (3)$$

equilibrium constant and the thermodynamic equilibrium constant, respectively, $a_{H_2O}$ is the activity of water, $\Delta z^2$ ($\Delta z^2 = mz_M^2 + nz_L^2 - z^2_{M_mL_n(OH)_p} - p$) is the net charge, $A$ and $B$ are the Debye–Hückel (D.H.) constants and the quantities $\log {}^*\beta°_{n,p,m}$, $\alpha$, $\Delta C$ and/or optionally $\Delta D$ are adjustable parameters and defined elsewhere [1].

## 4. Results and discussion

### 4.1. Equilibrium constants data at different ionic strengths

The weighted mean equilibrium constants of glycinate ion with hydrogen, copper and nickel and nitrilotriacetate ion with hydrogen and calcium at different ionic strengths in $KNO_3$

and $(CH_3)_4NNO_3$ media at 25.0 °C are collected in Tables 1 and 2, the $pK_w$ are collected in Table 3 and the literature values for the same conditions are given in the footnotes. The individual constants are those computed using SUPERQUAD program. The stability constants of copper and nickel glycine complexes or calcium NTA complexes determined in $KNO_3$ medium and given in Tables 1 and 2 are computed as usual without allowing for the potassium complex with the mentioned ligands.

For glycine (Table 1) it is, however, very difficult to discuss the reliability of the literature data obtained in Ref. [16] with $H^+$. Indeed, the extrapolated data at $I=0$ given in that paper with $\log {}^*\beta^\circ_{1,0,1} = 9.85$ and $\log {}^*\beta^\circ_{1,0,2} = 12.39$ differ strongly from those obtained by different authors [3–5] (all lying within 0.01 log unit) that systematic errors cannot be excluded. The above values are fully beyond the limits of those recommended by the IUPAC [2]: $\log {}^*\beta_{1,0,1} = 9.78 \pm 0.01$ and $\log {}^*\beta_{1,0,2} = 12.14 \pm 0.02$. The other values in the footnotes of Table 1 were given with the classification of the IUPAC critical survey [2]. The three values of $Ni^{2+}$, $\log {}^*\beta_{i,0,1}$ ($i = 1, 2, 3$), at $I = 1(KNO_3)$ lie within the limits given in a publiction [19] based on the measurements of several laboratories for the same system ($\log {}^*\beta_{1,0,1}$: 5.64–5.68; $\log {}^*\beta_{2,0,1}$: 10.24–10.4 and $\log {}^*\beta_{3,0,1} = 13.9$ at $I = 1$(NaCl)). By comparing our own values obtained in both inert salts at the same ionic strength, it was found that, for $I = 0.05$ and 0.3, the same values for all constants with $Cu^{2+}$ and $Ni^{2+}$ are obtained within $\pm 0.04$ log unit. For the equilibrium constant values of nitrilotriacetate ion with hydrogen or calcium, no literature data at the experimentally measured ionic strength in $KNO_3$ or $(CH_3)_4NNO_3$ media were found for comparison. However, interpolated values at $I = 0.1$ and 0.5 using TEC are compared with

Table 1
Experimental stability constants of glycinate ion with $H^+$, $Cu^{2+}$ and $Ni^{2+}$ at different ionic strengths in $KNO_3$ and $(CH_3)_4NNO_3$ media and 25.0 °C

| Medium | M | $I$ | $n, p, m$ [a] | $\log {}^*\beta_{n,p,m}$ | M | $I$ | $n, p, m$ [a] | $\log {}^*\beta_{n,p,m}$ |
|---|---|---|---|---|---|---|---|---|
| $KNO_3$ | $H^+$ | 0.050 | 1, 0, 1 | 9.589(3) [b] (0.007) | $Ni^{2+}$ | 0.050 | 1, 0, 1 | 5.827(8) (0.02) |
| | | | 1, 0, 2 | 11.92(1) [b] (0.04) | | | 2, 0, 1 | 10.647(7) (0.02) |
| | | 0.300 | 1, 0, 1 | 9.5546(4) (0.001) | | | 3, 0, 1 | 13.973(4) (0.01) |
| | | | 1, 0, 2 | 11.956(7) (0.02) | | 0.300 | 1, 0, 1 | 5.678(1) (0.004) |
| | | 1.00 | 1, 0, 1 | 9.640(4) (0.007) | | | 2, 0, 1 | 10.448(5) (0.01) |
| | | | 1, 0, 2 | 12.090(8) (0.01) | | | 3, 0, 1 | 13.84(1) (0.04) |
| | | 2.50 | 1, 0, 1 | 9.880(5) (0.01) | | 1.00 | 1, 0, 1 | 5.682(8) (0.02) |
| | | | 1, 0, 2 | 12.50(1) (0.04) | | | 2, 0, 1 | 10.48(2) [d] (0.05) |
| | $Cu^{2+}$ | 0.050 | 1, 0, 1 | 8.230(7) (0.01) | | | 3, 0, 1 | 13.94(3) [d] (0.08) |
| | | | 2, 0, 1 | 15.10(1) (0.02) | | 2.50 | 1, 0, 1 | 5.82(1) [e] (0.02) |
| | | 0.300 | 1, 0, 1 | 8.074(2) (0.006) | | | 2, 0, 1 | 10.74(2) (0.07) |
| | | | 2, 0, 1 | 14.884(4) (0.01) | | | 3, 0, 1 | 14.31(4) (0.1) |
| | | 1.00 | 1, 0, 1 | 8.074(1) (0.004) | | | | |
| | | | 2, 0, 1 | 14.939(3) (0.008) | | | | |
| | | 2.50 | 1, 0, 1 | 8.304(2) [c] (0.005) | | | | |
| | | | 2, 0, 1 | 15.380(4) (0.01) | | | | |

Table 1 (continued)

| Medium | M | $I$ | $n, p, m$ [a] | $\log {}^*\beta_{n,p,m}$ | M | $I$ | $n, p, m$ [a] | $\log {}^*\beta_{n,p,m}$ |
|---|---|---|---|---|---|---|---|---|
| $(CH_3)_4NNO_3$ | $H^+$ | 0.050 | 1, 0, 1 | 9.5943(6) (0.001) | $Ni^{2+}$ | 0.050 | 1, 0, 1 | 5.850(2) (0.006) |
| | | | 1, 0, 2 | 11.958(5) (0.01) | | | 2, 0, 1 | 10.691(2) (0.006) |
| | | 0.300 | 1, 0, 1 | 9.509(1) (0.004) | | | 3, 0, 1 | 14.118(7) (0.02) |
| | | | 1, 0, 2 | 11.86(2) (0.05) | | 0.300 | 1, 0, 1 | 5.683(4) (0.01) |
| | | 1.00 | 1, 0, 1 | 9.527(3) (0.009) | | | 2, 0, 1 | 10.441(5) (0.01) |
| | | | 1, 0, 2 | 12.051(2) (0.007) | | | 3, 0, 1 | 13.78(1) (0.04) |
| | | 2.50 | 1, 0, 1 | 9.6594(4) (0.001) | | 1.00 | 1, 0, 1 | 5.7489(4) (0.001) |
| | | | 1, 0, 2 | 12.5052(4) (0.001) | | | 2, 0, 1 | 10.605(1) (0.004) |
| | $Cu^{2+}$ | 0.050 | 1, 0, 1 | 8.220(2) (0.006) | | | 3, 0, 1 | 14.16(2) (0.06) |
| | | | 2, 0, 1 | 15.094(1) (0.002) | | 2.50 | 1, 0, 1 | 6.064(6) (0.02) |
| | | 0.300 | 1, 0, 1 | 8.064(8) (0.02) | | | 2, 0, 1 | 11.275(5) (0.01) |
| | | | 2, 0, 1 | 14.864(9) (0.02) | | | 3, 0, 1 | 15.17(1) (0.02) |
| | | 1.00 | 1, 0, 1 | 8.16(1) (0.04) | | | | |
| | | | 2, 0, 1 | 15.06(2) (0.06) | | | | |
| | | 2.50 | 1, 0, 1 | 8.56(1) (0.02) | | | | |
| | | | 2, 0, 1 | 15.82(2) (0.07) | | | | |

The values in parentheses are the standard deviations and those beneath them are the confidence intervals at 95% confidence level.

[a] $mM + nL + pH_2O \rightleftharpoons M_mL_n(OH)_p + pH$; L = glycinate.

[b] $\log {}^*\beta_{1,0,1} = 9.721(6)$; $\log {}^*\beta_{1,0,2} = 12.023(8)$ [16].

[c] $\log {}^*\beta_{1,0,1} = 8.38$[D] [17].

[d] $\log {}^*\beta_{2,0,1} = 10.55$[T]; $\log {}^*\beta_{3,0,1} = 14.06$[T] [18].

[e] $\log {}^*\beta_{1,0,1} = 5.33$[D] [17].

The reviewer classification [2] are: [D] = doubtful and [T] = tentative.

the literature data in the next section. For the ionic product of water (Table 3), it is important to find literature values in $(CH_3)_4NNO_3$ or $KNO_3$ ($I \geqslant 0.2$) to be compared with ours. This is also needed to detect any eventual systematic errors due to our glass electrode or the Nernst slope. In dilute solutions ($I \leqslant 0.1$), the activity coefficients of the uni-univalent electrolytes may be considered practically independent of the electrolyte type dissolved. Therefore, the corresponding values for the equilibrium constants should be the same and independent of the inert salt used as far as the ionic strength is the same. Thus the $pK_w$ value obtained with each alkali halide salt at $I = 0.05$ [20] should be identical to those in our two inert salt solutions. The value in $(CH_3)_4NNO_3$ is within the limits of error and that in $KNO_3$ is a little bit low.

Some information about the stability of the potassium complexes with the two ligands can be obtained by comparing the values of $\log {}^*\beta_{1,0,m}$ ($M = H^+$) in presence of the two inert salts (glycine: $m = 1$, 9.589(7); $m = 2$, 11.92(4) in $KNO_3$ and 9.594(1) and 11.958(10) in $(CH_3)_4NNO_3$, respectively; nitrilotriacetic acid: $m = 1$, 9.726(20); $m = 2$, 12.32(6) in $KNO_3$ and 9.867(20) and 12.527(10) in $(CH_3)_4NNO_3$, respectively). Already at $I = 0.050$, for which the medium effect is negligible, low values are found in presence of $K^+$. This may be explained by the formation of $K^+$

Table 2
Experimental stability constants of nitrilotriacetate ion with $H^+$ and $Ca^{2+}$ at different ionic strengths in $KNO_3$ and $(CH_3)_4NNO_3$ media and 25.0 °C

| $KNO_3$ | | | | $(CH_3)_4NNO_3$ | | | |
|---|---|---|---|---|---|---|---|
| M | $I$ | $n, p, m$ [a] | $\log {}^*\beta_{n,p,m}$ | M | $I$ | $n, p, m$ [a] | $\log {}^*\beta_{n,p,m}$ |
| $H^+$ | 0.050 | 1, 0, 1 | 9.729(7) | $H^+$ | 0.050 | 1, 0, 1 | 9.867(7) |
| | | | (0.02) | | | | (0.02) |
| | | 1, 0, 2 | 12.32(2) | | | 1, 0, 2 | 12.527(3) |
| | | | (0.06) | | | | (0.01) |
| | | 1, 0, 3 | 14.24(5) | | | 1, 0, 3 | 14.490(9) |
| | | | (0.1) | | | | (0.02) |
| | 0.300 | 1, 0, 1 | 9.441(4) | | 0.302 | 1, 0, 1 | 9.648(2) |
| | | | (0.01) | | | | (0.005) |
| | | 1, 0, 2 | 11.82(1) | | | 1, 0, 2 | 12.064(5) |
| | | | (0.03) | | | | (0.01) |
| | | 1, 0, 3 | 13.72(5) | | | 1, 0, 3 | 13.89(3) |
| | | | (0.1) | | | | (0.08) |
| | 1.00 | 1, 0, 1 | 9.284(3) | | 1.00 | 1, 0, 1 | 9.592(6) |
| | | | (0.008) | | | | (0.01) |
| | | 1, 0, 2 | 11.616(7) | | | 1, 0, 2 | 12.006(7) |
| | | | (0.02) | | | | (0.02) |
| | | 1, 0, 3 | 13.34(2) | | | 1, 0, 3 | 13.79(2) |
| | | | (0.05) | | | | (0.05) |
| | 2.50 | 1, 0, 1 | 9.410(2) | | 2.50 | 1, 0, 1 | 9.785(6) |
| | | | (0.005) | | | | (0.01) |
| | | 1, 0, 2 | 11.82(1) | | | 1, 0, 2 | 12.41(1) |
| | | | (0.02) | | | | (0.02) |
| | | 1, 0, 3 | 13.72(2) | | | 1, 0, 3 | 14.47(2) |
| | | | (0.07) | | | | (0.05) |
| $Ca^{2+}$ | 0.050 | 1, 0, 1 | 6.72(1) | $Ca^{2+}$ | 0.050 | 1, 0, 1 | 6.743(5) |
| | | | (0.04) | | | | (0.01) |
| | | 2, 0, 1 | 9.31(4) | | | 2, 0, 1 | 9.35(2) |
| | | | (0.1) | | | | (0.05) |
| | 0.304 | 1, 0, 1 | 6.007(1) | | 0.301 | 1, 0, 1 | 6.245(6) |
| | | | (0.004) | | | | (0.01) |
| | | 2, 0, 1 | 8.873(4) | | | 2, 0, 1 | 8.97(2) |
| | | | (0.01) | | | | (0.07) |
| | 1.00 | 1, 0, 1 | 5.554(4) | | 1.00 | 1, 0, 1 | 5.92(3) |
| | | | (0.01) | | | | (0.07) |
| | | 2, 0, 1 | 8.669(4) | | | | 8.80(6) |
| | | | (0.01) | | | | (0.2) |
| | 2.50 | 1, 0, 1 | 5.32(1) | | 2.50 | 1, 0, 1 | 6.01(1) |
| | | | (0.04) | | | | (0.04) |
| | | 2, 0, 1 | 8.47(4) | | | 2, 0, 1 | 9.35(3) |
| | | | (0.1) | | | | (0.08) |

The values in parenthesis are the standard deviations and those beneath them are the confidence intervals at 95% confidence level.
[a] $mM + nL + pH_2O \rightleftharpoons M_mL_n(OH)_p + pH$; L = nitrilotriacetate.

complexes with the ligand species according to Eq. (1). This effect is particularly evident for nitrilotriacetic acid forming, in its deprotonated form, complexes with stability constants that are at least five order of magnitude larger with respect to those of glycine ($\log {}^*\beta_{1,0,1}$ for glycinate [2]: $Ca^{2+} \sim 1.4$ and $Cu^{2+} \sim 8.1$ and nitrilotriacetate [6]: $Ca^{2+} \sim 6.5$ and $Cu^{2+} \sim 13$). On the contrary, in the case of glycine in the two ionic media studied the change of $\log {}^*\beta_{1,0,1}$ is within the estimated errors of the values. For $\log {}^*\beta_{1,0,2}$ the change is larger but always within the estimated errors of the constants. The possible existence of $KHL^-$ may be excluded after examining the data of $Ni^{2+}$ and $Cu^{2+}$ obtained in the two inert salt solutions at $I = 0.050$ that are practically identical. If $KHL^-$ was present in the solution, lower values of ${}^*\beta_{1,0,1}$ for the complexes in $0.050(KNO_3)$ would be expected.

Table 3
The negative logarithm of the ion-product of water, $pK_w$, at 25.0 °C in $KNO_3$ and $(CH_3)_4NNO_3$

| $KNO_3$ | | $(CH_3)_4NNO_3$ | |
|---|---|---|---|
| $I$ | $pK_w$ | $I$ | $pK_w$ |
| 0.050 | 13.808(8) [a] (0.006) | 0.050 | 13.823(5) [a] (0.005) |
| 0.300 | 13.733(2) (0.002) | 0.300 | 13.76(1) (0.008) |
| 1.00 | 13.762(2) (0.003) | 1.00 | 13.93(1) (0.01) |
| 2.50 | 13.953(2) (0.004) | 2.50 | 14.451(8) (0.009) |

[a] At $I \leq 0.1$, the activity coefficients are independent from the inert salt used. Using the data of Harned and Mannweiler [20], for $I = 0.05$: $\log(m_H \cdot m_{OH}) = -13.8285$ which corresponds to $-13.8288$ in the molarity scale.

The use of this large concentration of $K^+$ in detecting its complexes is due to the fact that monovalent alkali ions form weaker complexes with respect to other metal ions of larger charge, i.e. the divalent alkaline earth or 3d metal ions. This is also the reason for using salts of the alkali metal ions as inert salts in ionic equilibrium studies in order to minimize the effect of the components of the inert salts on the equilibria investigated. In case of nitrilotriacetate ion, the stability constants of the potassium complexes at $I = 0.050\ M$ are obtained from the corresponding $^*\beta_{1,0,m}$ with the assumption [21] that the decrease of their values are only due to $K^+$ complex formation giving for $\log([KL^{2-}]/([K^+][L^{3-}])) = 0.83(8)$ and $\log([KHL^-]/([K^+][HL^{2-}])) = 0.47(20)$, with the errors in parentheses calculated at 90% confidence. The percentage of $KHL^-$, calculated using the latter constant, is 12% in 0.050 $M$ $KNO_3$ solution but already 45% in 0.30 $M$ ($KNO_3$) solution. For this reason the constant $^*\beta_{1.0,1}$ with $Ca^{2+}$ (Table 2) at $I = 0.304(KNO_3)$ is only $10^{6.007}$ with respect to $10^{6.245}$ at $I = 0.301((CH_3)_4NNO_3)$.

At $I > 0.1$, the use of different inert salts results in different activity coefficient values specific for each salt. Thus a quantitative determination of a stability constant of $K^+$ complex cnanot be obtained from the results in Tables 1 and 2. The use of a $K^+$ electrode or the solubility measurements with a $K^+$ salt at high ionic strength can give more exact information on this important problem.

A discussion about the reasons of variation of $^*\beta_{n,p,m}$ values with the ionic strength and the inert salt is not a quite simple problem because of the different types of possible interactions among all species present in the given solution. The first problem that needs to be resolved is an explanation of the values of the activity coefficients $\gamma_i$ of single inert salts at different $I$ values. This should also explain the reasons for the different $\gamma_i$ values obtained by changing the inert salt. Indeed the fit of $\gamma_i$ values at different $I$ with the calculated values using the preferred D.H. expression is attained by adjusting some constant parameters in the selected expression. An interpretation of the parameters obtained stand out. The D.H. expressions take into consideration only the electrostatic cation anion interaction without inclusion of other resulting species. Without this preliminary step, each intuitive interpretation of the variation of $^*\beta_{n,p,m}$ with $I$ can only be considered as speculation. On the basis of the known studies in this direction it is not certain that the interpretation of the activity coefficients of pure inert salts at different $I$ values can be considered a fully resolved puzzle.

### 4.2. Extrapolation to zero ionic strength and interpolation to a given I value

The extrapolation of equilibrium constants to zero ionic strength and the ionic strength correction of equilibrium constants in $KNO_3$ and $(CH_3)_4NNO_3$ were carried out using a TEC approach (Eq. (3)) for $\Delta z^2 \neq 0$ and $\Delta z^2 = 0$ [1] as well. The thermodynamic equilibrium constants ($\log {}^*\beta^\circ_{n,p,m}$) computed together with the parameters of Eq. (3) are collected in Table 4.

A comparison of our data with those recommended elsewhere–IUPAC critical survey [2,6] or 'critical' stability constants of Martell and

Table 4
Thermodynamic equilibrium constants $\beta^{\circ}_{n,p,m}$, TEC parameters [1] of different equilibrium systems at 25.0 °C in $KNO_3$ and $(CH_3)_4NNO_3$ media

| Medium | M | L | $n, p, m$ | $\log {}^{*}\beta^{\circ}_{n,p,m}$ | $\alpha \times 10^8$ | $\Delta C$ | $\Delta D$ | SSR | $\sigma_{est}$ | $P$ |
|---|---|---|---|---|---|---|---|---|---|---|
| $KNO_3$ | $H^+$ | $OH^-$ | 1, 0, 1 | 13.993 [a] | 5.4(2) | 0.165(3) | 0 | 0.442 | 0.0015 | 0.51 |
| | | | | (0.008) | (0.4) | (0.005) | | | | |
| | $H^+$ | gly | 1, 0, 1 | 9.743 [a] | 8.7(5) | 0.183(4) | 0 | 1.41 | 0.00093 | 0.23 |
| | | | | (0.01) | (0.91) | (0.008) | | | | |
| | | | 1, 0, 2 | 12.03(5) | 13(6) | 0.27(2) | 0 | 7.71 | 0.023 | 0.0055 |
| | | | | (0.1) | (12) | (0.04) | | | | |
| | $Cu^{2+}$ | gly | 1, 0, 1 | 8.55(1) | 6.0(2) | 0.218(5) | 0 | 2.90 | 0.0027 | 0.088 |
| | | | | (0.02) | (0.3) | (0.009) | | | | |
| | | | 2, 0, 1 | 15.554(7) | 6.3(1) | 0.383(4) | 0 | 0.421 | 0.0026 | 0.52 |
| | | | | (0.01) | (0.2) | (0.007) | | | | |
| | $Ni^{2+}$ | gly | 1, 0, 1 | 6.11(2) | 7.5(7) | 0.15(1) | 0 | 2.93 | 0.0033 | 0.087 |
| | | | | (0.04) | (1.3) | (0.02) | | | | |
| | | | 2, 0, 1 | 11.07(1) | 7.9(3) | 0.25(1) | 0 | 0.646 | 0.0062 | 0.42 |
| | | | | (0.02) | (0.5) | (0.02) | | | | |
| | | | 3, 0, 1 | 14.363(7) | 9.4(4) | 0.31(1) | 0 | 0.361 | 0.0044 | 0.55 |
| | | | | (0.01) | (0.7) | (0.02) | | | | |
| | $H^+$ | NTA | 1, 0, 1 | 10.19(1) | 6.7(1) | 0 | 0.047(1) | 1.48 | 0.0036 | 0.22 |
| | | | | (0.02) | (0.2) | | (0.002) | | | |
| | | | 1, 0, 2 | 13.13(2) | 5.4(2) | 0.32(1) | 0 | 0.870 | 0.0090 | 0.35 |
| | | | | (0.04) | (0.3) | (0.02) | | | | |
| | | | 1, 0, 3 | 15.2(1) | 6.4(5) | 0 | 0.12(1) | 2.33 | 0.040 | 0.13 |
| | | | | (0.2) | (1.0) | | (0.02) | | | |
| | $Ca^{2+}$ | NTA | 1, 0, 1 | 7.699(2) | 5.38(1) | 0.070(1) | 0 | 0.0141 | 0.00078 | 0.90 |
| | | | | (0.003) | (0.02) | (0.002) | | | | |
| | | | 2, 0, 1 | 9.66(3) | 6.3(3) | 0 | 0 | 11.1 | 0.013 | 0.0037 |
| | | | | (0.04) | (0.4) | | | | | |
| $CH_3)_4NNO_3$ | $H^+$ | $OH^-$ | 1, 0, 1 | 13.982(5) | 3.6(3) | 0.41(1) | 0 | 0.518 | 0.0052 | 0.47 |
| | | | | (0.009) | (0.5) | (0.02) | | | | |
| | $H^+$ | gly | 1, 0, 1 | 9.749(3) | 5.6(2) | 0.128(4) | 0 | 7.20 | 0.0016 | 0.0072 |
| | | | | (0.005) | (0.4) | (0.008) | | | | |
| | | | 1, 0, 2 | 12.11(2) | 4.5(4) | 0.350(8) | 0 | 5.74 | 0.0018 | 0.016 |
| | | | | (0.03) | (0.8) | (0.02) | | | | |
| | $Cu_{2+}$ | gly | 1, 0, 1 | 8.527(6) | 5.6(3) | 0.35(2) | 0 | 1.80 | 0.0050 | 0.18 |
| | | | | (0.01) | (0.6) | (0.03) | | | | |
| | | | 2, 0, 1 | 15.566(5) | 4.9(2) | 0.65(2) | 0 | 1.14 | 0.0021 | 0.28 |
| | | | | (0.01) | (0.4) | (0.04) | | | | |
| | $Ni^{2+}$ | gly | 1, 0, 1 | 6.15(1) | 6.1(4) | 0.28(2) | 0 | 20.9 | 0.0035 | $<0.001$ |
| | | | | (0.02) | (0.8) | (0.04) | | | | |
| | | | 2, 0, 1 | 11.15(1) | 5.3(3) | 0.56(2) | 0 | 27.2 | 0.0090 | $<0.001$ |
| | | | | (0.02) | (0.5) | (0.04) | | | | |
| | | | 3, 0, 1 | 14.62(7) | 3(1) | 1.0(2) | 0 | 48.3 | 0.067 | $\ll 0.001$ |
| | | | | (0.1) | (2) | (0.3) | | | | |
| | $H^+$ | NTA | 1, 0, 1 | 10.31(3) | 7.4(6) | 0.19(2) | 0 | 7.90 | 0.0098 | 0.0049 |
| | | | | (0.05) | (1.1) | (0.03) | | | | |
| | | | 1, 0, 2 | 13.305(9) | 5.8(2) | 0.45(2) | 0 | 3.39 | 0.0086 | 0.065 |
| | | | | (0.02) | (0.3) | (0.03) | | | | |
| | | | 1, 0, 3 | 15.471(8) | 4.8(1) | 0.72(2) | 0 | 0.336 | 0.0085 | 0.56 |
| | | | | (0.02) | (0.2) | (0.03) | | | | |
| | $Ca^{2+}$ | NTA | 1, 0, 1 | 7.62(3) | 7.6(4) | 0.14(3) | 0 | 8.82 | 0.021 | 0.0029 |
| | | | | (0.05) | (0.8) | (0.06) | | | | |
| | | | 2, 0, 1 | 9.857(5) | 4.81(8) | 0 | 0.140(2) | 0.0356 | 0.0047 | 0.85 |
| | | | | (0.009) | (0.1) | | (0.004) | | | |

Values in parentheses are the least-squares unbiased estimates (estimated standard error of the parameters) and the values in parentheses beneath them are the 68.3% confidence or the estimate of $1\sigma$.
SSR = Weighted sum of squared residuals.
$\sigma_{est}$ = Estimated standard deviation of equilibrium constant using the TEC equation.
P = Computed probability based on SSR and the degrees of freedom.
[a] For correction see text.

Smith [22] for given $I$ vlaues–is only possible if the inert salt used is also given. The known experimental data show different ionic strength dependence of the involved constant with the inert salts. Thus the use of the same $^*\beta_{1,0,1}$ value for a constant at the same ionic strength [8] for salts of the same cation (or alkali metal cation) as claimed by Martell and Smith [22] as well as for all salts as assumed by Kiss et al. [2] cannot be accepted. For this reason, their recommended values have scarce importance and are not further considered. On the basis of the literature data given in the IUPAC critical survey, after using statistical estimations of their precision (Table 5a), it was possible to obtain the required quantities for the extraolation and interpolation in other inert salts (Table 5b). The corresponding results for the formation of HL in case of glycine are reproduced in Fig. 1. The values of $\log {}^*\beta^\circ_{1,0,1}$ for the same $I$ value in different inert salts given in the figure show a large variation and are not equal. This is partly due to systematic errors in the different values. In general, the quantity of information given by the authors in the experimental part of the published papers is not complete enough to allow a clear identification of the type of calibration used and the precautions taken to avoid liquid junction potentials errors of some 0.01 pH units. In this context, one has to realize that the more accurate known value for $\log {}^*\beta_{1,01}$ of the system under consideration is 9.778 and values in the limit of $\pm 0.03$ can be considered acceptable in consideration of the large errors of extrapolation and large change of $\log {}^*\beta_{1,0,1}$ caused by small variation of $I$ at $I < 0.1$. By comparing all our values obtained with the accepted ones, it appears that at the lowest $I$ in $KNO_3$ they are lower by 0.02 to 0.03 log unit for the case of glycine ($\log {}^*\beta^\circ_{1,0,1} = 9.718$) and the ionic product of water ($\log {}^*\beta^\circ_{1,0,1} = 13.968$). Increasing our values by 0.025 log unit results (Tables 4 and 6) in an excellent agreement among all data. This can be explained by a small systematic error owing to the strict use of the Nernst value $(RT/F)\ln 10$ that is 59.159 mV for every one pH unit. As shown in Table 6, the agreement of the literature experimental mean values treated statistically and our results is then satisfactory for both glycine and NTA equilibrium systems. Other thermodynamic stability constant values are found in the literature. For glycine [7]: $\log {}^*\beta^\circ_{1,0,1} = 9.75$ and $\log {}^*\beta^\circ_{1,0,2} = 12.08$ extrapolated from a medium in $(C_2H_5)_4NI$. They are in good agreement with our values in Table 6. For NTA [8], the calculated thermodynamic constants are: $\log {}^*\beta_{1,0,1} = 10.39$, $\log {}^*\beta_{1,0,2} = 13.33$ and $\log {}^*\beta_{1,0,3} = 15.31$ extrapolated from media in $(C_2H_5)_4N^+$ or $(C_3H_7)_4N^+$ with the anions of bromide and iodide. They show slight deviation from our values extrapolated in $(CH_3)_4NNO_3$ medium and given in Table 6.

### 4.3. Estimation of $\Delta C$ parameters

The parameter $\Delta C$ of Eq. (3) may be estimated from other individual $C$ parameters. This treatment help estimating equilibrium constants in ionic media other than those measured presuming that the thermodynamic equilibrium constant is known. The combined $\Delta C$ parameters for the equilibrium systems in this work are given in Table 4.

The combined $\Delta C$ parameter of the $pK_w$ in $KNO_3$ and $(CH_3)_4NNO_3$ media may be represented by the following relations,

$$\Delta C = C_{KOH} + C_{HNO_3} \tag{4}$$

$$\Delta C = C_{(CH_3)_4NOH} + C_{HNO_3} \tag{5}$$

From Eq. (5), the individual parameter $C_{(CH_3)_4NOH}$ amounts to 0.35(2) where $C_{HNO_3}$ is computed separately from mean activity coefficient data [23,24] at different ionic strengths and 25.0 °C using the PDHE computer program and the polynomial Debye–Hückel equation (6) for the molar mean activity coefficient $\gamma_\pm$.

$$\log \gamma_\pm = \frac{-Az_+z_-\sqrt{I}}{1 + B\alpha\sqrt{I}} + CI + DI^2 + \cdots \tag{6}$$

The computed parameters of Eq. (6) for 12 common electrolytes are given in Table 7 and are valid in the range $2.50 \geqslant I \geqslant 0$ in molar scale. The activity coefficients required are obtained from those in the molal scale, which are identical with the values in molar scale but setting the concentration $c = (1000 \cdot d \cdot m)/(1000 + M_w \cdot m)$, where $d$ is the density of the involved solution. To avoid confusion in Eq. (6), the molar ionic strength $I_c$ is used. It is noticed that two different parameters $C$ and $D$ are obtained. By examining their values, only the first one is important; the second being 10 times smaller except for the cases of NaCl, KCl and $HClO_4$. For the equilibria investigated, the values of $\Delta D$ in Table 4 are negligible. The standard deviations obtained for $C$ and $D$ de-

Table 5
(a) Mean values of the stability constants of glycine in different ionic media at 25 °C using literature data with statistical estimation of their precision

| I | $NaClO_4$ | | KCl | NaCl | |
|---|---|---|---|---|---|
| | log $*\beta_{1,0,1}$ | log $*\beta_{1,0,2}$ | log $*\beta_{1,0,1}$ | log $*\beta_{1,0,1}$ | log $*\beta_{1,0,2}$ |
| 0.050 | | | 9.61(5) [a] | | |
| 0.0995 | | | | 9.60(2) [b] | 11.96(4) [b] |
| 0.1 | 9.61(6) | 11.95(6) | 9.66(3) [a] | 9.62(2) [b] | |
| 0.15 | 9.58(6) | 11.97(9) | | 9.60(2) [b] | 11.97(4) [b] |
| 0.2 | | | 9.62(9) [a] | | |
| 0.297 | | | | 9.58(2) [b] | 11.94(4) [b] |
| 1.0 | 9.68(5) | 12.13(6) | 9.67(1) [a] | 9.65(1) | 12.08(3) |
| 3.0 | 10.14(10) | 12.88(12) | | | |

[a] Interpolation between $I = 0.2$ and 1.0.
[b] Errors assumed.
Values in parentheses are the standard deviation of the mean unless otherwise stated.

(b) TEC parameters for the extrapolation of the literature data in Table 5a to zero ionic strength at 25 °C

| Electrolyte | log $*\beta^{\circ}_{1,0,1}$ | $\alpha \times 10^8$ | $\Delta C$ | log $*\beta^{\circ}_{1,0,2}$ | $\alpha \times 10^8$ | $\Delta C$ |
|---|---|---|---|---|---|---|
| $NaClO_4$ | 9.79(2) | 4.7(9) | 0.28(2) | 12.14(2) | 4(1) | 0.42(3) |
| | (0.04) | (2.0) | (0.04) | (0.04) | (2.0) | (0.05) |
| KCl | 9.77(9) | 10(8) | 0.13(7) | | | |
| | (12) | (10) | (0.09) | | | |
| NaCl | 9.80(2) | 5(2) | 0.23(6) | 12.16(6) | 4(4) | 0.35(18) |
| | (0.03) | (2) | (0.08) | (0.08) | (5) | (23) |

Values in parentheses are the least squares errors and beneath them those adjusted to $1\sigma$.

pend on their magnitude but in general are much lower with respect to those obtained using $C$ and Eqs. (4), (5) and (7)–(13).

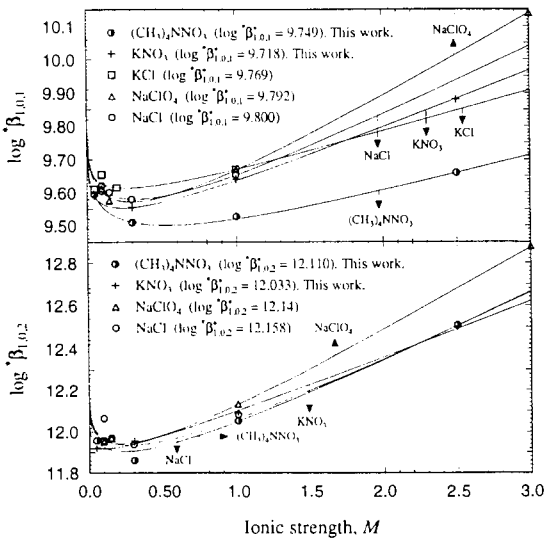


Fig. 1. Variation of stability constants of glycine with ionic strength $I$ and ionic media at 25 °C. Extrapolated data obtained from this work are prompted in the legend of the figures otherwise the data are obtained from the literature and statistically treated to obtain mean values.

The stability constants of copper glycine complexes are relatively high. Their ionic strength dependent parameters $\Delta C$ may be used to retrieve some individual $C$ parameters as an example. For the first and second stability constant of copper glycine complexes, the ionic strength dependent parameters $\Delta C_1$ and $\Delta C_2$ may be represented by the following relations,

$$\Delta C_1 = C_{Cu(NO_3)_2} + C_{NL} - C_{CuLNO_3} \quad (7)$$

$$\Delta C_2 = C_{Cu(NO_3)_2} + 2C_{NL} - C_{CuL_2} \quad (8)$$

where $N = K^+$ or $(CH_3)_4N^+$ and L is the fully deprotonated form of glycine. The difference between $\Delta C_1[(CH_3)_4NNO_3]$ and $\Delta C_1(KNO_3)$, in which $\Delta C_1$ is expressed by Eq. (7), is found to be 0.13(3) l mol$^{-1}$ and is expected to be totally due to the difference between $C_{(CH_3)_4NL}$ and $C_{KL}$. This is ascertained by the difference between $\Delta C_2[(CH_3)_4NNO_3]$ and $\Delta C_2(KNO_3)$ for the same equilibrium system in which $\Delta C_2$ is expressed by Eq. (8). This difference is again believed to be totally attributed to $2C_{(CH_3)_4NL} - 2C_{KL}$ and found to be 0.267 l mol$^{-1}$. Thus $C_{(CH_3)_4NL} - C_{KL}$ is again 0.13(4) l mol$^{-1}$.

Table 6
Interpolated logarithmic equilibrium constants of glycinate ion with $H^+$, $Cu^{2+}$ and $Ni^{2+}$ and nitrilotriacetate ion with $H^+$ and $Ca^{2+}$ using TEC in $KNO_3$ and $(CH_3)_4NNO_3$ medium and the numerically treated literature data in $KNO_3$ medium at 25 °C

| | | | IUPAC publ. [2,6] $KNO_3$ | | | TEC $KNO_3$ | | | TEC $(CH_3)_4NNO_3$ | | |
|---|---|---|---|---|---|---|---|---|---|---|---|
| M | L | I | $^*\beta_{1,0,1}$ | $^*\beta_{1,0,2}$ | | $^*\beta_{1,0,1}$ | $^*\beta_{1,0,2}$ | | $^*\beta_{1,0,1}$ | $^*\beta_{1,0,2}$ | |
| $H^+$ | gly | →0 | 9.778(2)[i] | 12.133(8)[ii] | | 9.74 [a] | 12.03(10) | | 9.749(5) | 12.11(3) | |
| | | 0.10 | 9.574(7)[iii] | 11.94(2)[iii] | | 9.566(4) | 11.92(3) | | 9.558(3) | 11.93(2) | |
| | | 0.11 | 9.54(1)[iv] | 11.89(2)[iv] | | 9.564(4) | 11.92(3) | | 9.553(3) | 11.92(2) | |
| | | 0.20 | 9.58(4)[vi] | 11.92(2)[vi] | | 9.554(2) | 11.93(3) | | 9.525(4) | 11.91(1) | |
| | | 0.50 | | | | 9.570(2) | 11.98(3) | | 9.501(2) | 11.93(1) | |
| | | 1.0 | | | | 9.636(4) | 12.10(3) | | 9.520(6) | 12.051(9) | |
| | | 3.0 | | | | 9.97(1) | 12.62(7) | | 9.714(4) | 12.667(5) | |
| | | | $^*\beta_{1,0,1}$ | $^*\beta_{2,0,1}$ | $^*\beta_{3,0,1}$ | $^*\beta_{1,0,1}$ | $^*\beta_{2,0,1}$ | $^*\beta_{3,0,1}$ | $^*\beta_{1,0,1}$ | $^*\beta_{2,0,1}$ | $^*\beta_{3,0,1}$ |
| $Cu^{2+}$ | gly | →0 | 8.59(2)[v] | 15.78(7)[v] | | 8.55(2) | 15.55(1) | | 8.53(1) | 15.57(1) | |
| | | 0.10 | 8.17(2)[i] | 15.08(2)[i] | | 8.17(1) | 15.006(7) | | 8.152(6) | 14.988(5) | |
| | | 0.20 | 8.16[iv] | 14.98[iv] | | 8.103(7) | 14.919(5) | | 8.09(1) | 14.90(1) | |
| | | 0.50 | | | | 8.050(3) | 14.866(3) | | 8.07(2) | 14.88(2) | |
| | | 1.0 | | | | 8.074(3) | 14.940(3) | | 8.15(2) | 15.04(2) | |
| $Ni^{2+}$ | gly | →0 | 6.175(8)[ii] | 11.12(1)[ii] | 14.3(2)[vi] | 6.11(4) | 11.07(2) | 14.36(1) | 6.15(2) | 11.15(2) | 14.6(1) |
| | | 0.10 | 5.75(1)[i] | 10.62(2)[i] | 14.1(2)[ii] | 5.76(2) | 10.560(7) | 13.907(2) | 5.78(1) | 10.59(2) | 13.98(7) |
| | | 0.50 | | | | 5.658(7) | 10.428(9) | 13.847(6) | 5.69(1) | 10.47(1) | 13.8(1) |
| | | 1.0 | | 10.55[iv] | 14.06[iv] | 5.67(1) | 10.46(1) | 13.933(7) | 5.749(3) | 10.60(1) | 14.0(2) |
| | | | $^*\beta_{1,0,1}$ | $^*\beta_{1,0,2}$ | $^*\beta_{1,0,3}$ | $^*\beta_{1,0,1}$ | $^*\beta_{1,0,2}$ | $^*\beta_{1,0,3}$ | $^*\beta_{1,0,1}$ | $^*\beta_{1,0,2}$ | $^*\beta_{1,0,3}$ |
| $H^+$ | NTA | →0 | | | | 10.19(2) | 13.13(4) | 15.2(2) | 10.31(5) | 13.30(2) | 15.47(2) |
| | | 0.10 | 9.62(9)[ii] | 12.3(1)[ii] | 13.97[iv] | 9.62(1) | 12.13(2) | 14.0(1) | 9.78(2) | 12.342(9) | 14.245(9) |
| | | 0.50 | 9.57(1)[iv] | 12.21(4)[iv] | 13.78(7)[iv] | 9.359(5) | 11.70(1) | 13.49(5) | 9.61(1) | 11.99(2) | 13.77(2) |
| | | 1.0 | | | | 9.285(6) | 11.62(1) | 13.35(6) | 9.60(2) | 12.00(2) | 13.80(2) |
| | | | $^*\beta_{1,0,1}$ | $^*\beta_{2,0,1}$ | | $^*\beta_{1,0,1}$ | $^*\beta_{2,0,1}$ | | $^*\beta_{1,0,1}$ | $^*\beta_{2,0,1}$ | |
| $Ca^{2+}$ | NTA | →0 | | | | 7.699(3) | 9.66(4) | | 7.62(5) | 9.857(9) | |
| | | 0.10 | 6.4(1)[vi] | | | 6.462(2) | 9.08(1) | | 6.55(2) | 9.212(5) | |
| | | 0.50 | | | | 5.807(1) | 8.785(6) | | 6.12(4) | 8.868(8) | |
| | | 1.0 | | | | 5.5539(8) | 8.667(8) | | 6.00(4) | 8.81(1) | |

[i] $N = 6$, [ii] $N = 5$, [iii] $N = 8$, [iv] $N = 1$, [v] $N = 3$, [vi] $N = 2$.
The values in parentheses are the estimates of $1\sigma$. All values of TEC are derived from four points ($N = 4$) and have one degree of freedom.
The extrapolated values to $I = 0$ under 'IUPAC publication–$KNO_3$' are calculated from different ionic media.
[a] For correction see text.

The $\Delta C$ constants of nickel glycine may be represented by the following relations,

$$\Delta C_1 = C_{Ni(NO_3)_2} + C_{\mathcal{N}L} - C_{NiLNO_3} \quad (9)$$

$$\Delta C_2 = C_{Ni(NO_3)_2} + 2C_{\mathcal{N}L} - C_{NiL_2} \quad (10)$$

$$\Delta C_3 = C_{Ni(NO_3)_2} + 3C_{\mathcal{N}L} - C_{NiL_3N} \quad (11)$$

The same result was observed for the first stability constant of the relatively strong nickel glycine complex. A difference between $\Delta C_1((CH_3)_4NNO_3)$ and $\Delta C_1(KNO_3)$, in which $\Delta C_1$ is expressed by Eq. (9), is found to be $0.13(4)\,l\,mol^{-1}$. The difference between $\Delta C_2((CH_3)_4NNO_3)$ and $\Delta C_2(KNO_3)$, in which $\Delta C_2$ is represented by Eq. (10), shows slight deviation from the value of 0.13. The actual value is found to be $0.16(4)\,l\,mol^{-1}$. However, this difference is within the estimated errors.

The $\Delta C$ parameters for the system of glycine may be represented by the following relations,

$$\Delta C_1 = C_{HNO_3} + C_{\mathcal{N}L} - C_{\mathcal{N}NO_3} \quad (12)$$

$$\Delta C_2 = 2C_{HNO_3} + C_{\mathcal{N}L} - C_{H_2LNO_3} \quad (13)$$

The difference between $\Delta C_2((CH_3)_4NNO_3)$ and $\Delta C_2(KNO_3)$ in which $\Delta C_2$ is represented by

Table 7
PDHE parameters for some electrolytes at 25.0 °C applicable until $I = 2.50$

| Electrolyte | $a \times 10^8$ | $C$ | $D$ |
|---|---|---|---|
| HCl | 4.596(7) | 0.1063(3) | 0.00772(8) |
| NaCl | 4.42(2) | 0.0197(6) | 0.0060(2) |
| KCl | 3.951(2) | −0.0018(1) | 0.00376(3) |
| $HNO_3$ | 4.767(5) | 0.0633(1) | |
| $NaNO_3$ | 3.84(2) | −0.0405(8) | |
| $KNO_3$ | 3.04(1) | −0.1092(8) | 0.0052(2) |
| $HClO_4$ | 5.31(2) | 0.0862(5) | 0.0212(2) |
| $NaClO_4$ | 4.48(2) | 0.0028(7) | 0.0032(2) |
| NaOH | 3.80(2) | 0.0541(7) | 0.0018(2) |
| KOH | 3.50(1) | 0.0998(6) | 0.0034(2) |
| $Cu(NO_3)_2$ | 4.886(1) | 0.0317(2) | 0.00392(6) |
| $Ni(NO_3)_2$ | 4.855(1) | 0.0587(2) | 0.00265(7) |

Values in parentheses are the least-squares unbiased estimates or estimated standard error of the parameters.
$C_{Cu(NO_3)_2}$ and $C_{Ni(NO_3)_2}$ should be multiplied by three to be compatible with the $\epsilon$ vlaues calculated using the SIT equation.

Eq. (13), should also produce the value of 0.13 l mol$^{-1}$, however, it is found to be only 0.08(4) that is still within the large error limits. The difference between $\Delta C_1((CH_3)_4NNO_3)$ and $\Delta C_1(KNO_3)$, in which $\Delta C_1$ is represented by Eq. (12), is given as follows,

$$C_{(CH_3)_4NL} - C_{KL} - C_{(CH_3)_4NNO_3} + C_{KNO_3} = -0.055(11) \quad (14)$$

Substituting the value of 0.13 in relation (14), the value of $C_{(CH_3)_4NNO_3}$ is obtained. This value is found to be 0.076(31). It is then substituted in Eq. (12), in which $N = (CH_3)_4N^+$, to obtain the value of $C_{(CH_3)_4NL}$. This value is found to be 0.14(3). Consequently, the value of $C_{KL}$ is found to be 0.01(4). Similarly, the value of $C_{CuLNO_3}$ can be readily obtained from Eq. (7) for which $N = (CH_3)_4N^+$ or $K^+$. A value of −0.11(4) is then found. The other individual $C$ parameters for the $Ni^{2+}$ system may be obtained in a similar way. The estimation of $\Delta C$ parameters are necessary to estimate or predict equilibrium constants in other ionic media.

### 4.4. Prediction and estimation of equilibrium constants

The equilibrium constants for a system in a given inert salt at ionic strength $I$ ($\leqslant 3$) can be calculated using Eq. (3) if the thermodynamic constant $^*\beta^\circ_{n,p,m}$ and the parameters $\alpha$ and $\Delta C$ are known. Sometimes $\Delta C$ can be estimated from known values of $C$ for the same or similar electrolytes. In the last case, the knowledge of one suitable $^*\beta_{n,p,m}$ in the range $0.2 < I < 2.5$ is enough to obtain $\alpha$. Otherwise, two values for $^*\beta_{n,p,m}$ are required to obtain the two unknown parameters.

As an example, the $pK_w$ in $NaClO_4$ medium at different $I$ are estimated using the two procedures mentioned above. The $pK^\circ_w = 13.982(9)$ computed from the data in this work measured in $(CH_3)_4NNO_3$ medium and the two literature data of $pK_w$ [25] (13.78(1) at $I = 0.1$ and 13.97(1) at $I = 2$ in $NaClO_4$) are used. In the first procedure, the two TEC equations are solved for $\alpha$ and $\Delta C$. The values found are: $\alpha = 4.14 \times 10^{-8}$ and $\Delta C = 0.241$. The least-squares analysis for the set of literature data given in the ionic strength range of 0.1–3.8 M resulted in the following parameters: $pK^\circ_w = 13.99(2)$, $\alpha = 3.6(6) \times 10^{-8}$, $\Delta C = 0.26(2)$. Thus the calculated parameters from the two data points are within the errors computed by the least-squares analysis. The calculated constants using two data points at $I = 0.10$, 0.50, 1.00, 2.00, 2.99 and 3.80 are: 13.78, 13.73, 13.79, 13.97, 14.18 and 14.35, respectively. They are comparable to the experimental constants at the same ionic strength: 13.78(1), 13.74(1), 13.80(1), 13.97(1), 14.20(1), 14.42(2). The selection of a correct thermodynamic constant $\log {}^*\beta^\circ_{n,p,m}$ is of particular importance. This method can also be used with most of the equations discussed previously [1] although they have not been tested for these procedures; a case that is beyond the scope of this article. The reader is expected to consult Ref. [1] before making the final choice.

In the second procedure, we assume that $\Delta C$ is known along with one equilibrium constant at $I \geqslant 0.5$ and $\log {}^*\beta^\circ_{n,p,m}$. The $\Delta C$ may be calculated from the individual $C$ parameters obtained from Eq. (6) and given in Table 7. For this case, Eqs. (4) or (5) may be used as a guide. For the $pK_w$ system in $NaClO_4$, the estimated $\Delta C = 0.140$ and $\Delta D = 0.023$. The $\alpha$ value may then be calculated using Eq. (15) obtained from Eq. (3) for $p = 0$.

$$\alpha = -\left[\frac{\log {}^*\beta^\circ_{n,p,m} - \log {}^*\beta_{n,p,m} - \Delta z^2 A\sqrt{I} + \Delta CI + \Delta DI^2}{B\sqrt{I}(\log {}^*\beta^\circ_{n,p,m} - \log {}^*\beta_{n,p,m} + \Delta CI + \Delta DI^2)}\right] \quad (15)$$

Thus $\alpha$ is found to be $5.93 \times 10^{-8}$ using the $pK_w$ at $I = 2.0$. The estimated $pK_w$ at $I = 0.10$, 0.50, 1.00, 2.00, 2.99 and 3.80 are: 13.80, 13.75, 13.80, 13.97, 14.20 and 14.43, respectively, to be compared to the experimental values given above. If the $pK_w$ at $I = 0.5$ is used, the calculated $\alpha$ is $5.48 \times 10^{-8}$ and the estimated $pK_w$ at the same ionic strenths are: 13.79, 13.74, 13.78, 13.95, 14.18 and 14.40 to be compared again to the experimental values above. Another possibility for calculating $\alpha$ in this procedure by using the $pK_w$ at $I = 0.10$ and setting both $\Delta C$ and $\Delta D$ to zero in Eq. (15). In this case, $\alpha$ is found to be $5.78 \times 10^{-8}$. It is used beside the other estimated parameters $\Delta C$, $\Delta D$ and $\log {}^*\beta^\circ_{n,p,m}$ in Eq. (3) to estimate the $pK_w$ at the other ionic strengths given earlier.

The choice of the ionic strength value, in which $\alpha$ is calculated, is not arbitrary. This ionic strength is selected in such a way to equal or exceed $I_{crit}$ to a certain limit. In most of the time this is realized in the ionic strength range $1.5 > I \geqslant 0.2$. The range of $I < 0.1$ is avoided because of the large variation of $\alpha$ with the ionic strength and the strong dependence of $C$ on $\alpha$.

When data in the literature are not enough to extract all individual $C$ parameters required for a given system, the first procedure may then be used.

## References


[1] G. Anderegg and S. Kholeif, Talanta, 41 (1994) 1507.
[2] T. Kiss, I. Sóvágó and A. Gergely, Pure Appl. Chem., 63 (1991) 597.
[3] B.B. Owen, J. Am. Chem. Soc., 56 (1934) 24.
[4] E.J. King, J. Am. Chem. Soc., 73 (1951) 155.
[5] S.P. Datta and A.K. Grzybowski, Trans. Faraday Soc., 54 (1958) 1179.
[6] G. Anderegg, Pure Appl. Chem., 54 (1982) 2693.
[7] P.G. Daniele, A. De Robertis, C. De Stefano, S. Sammartano and C. Rigano, J. Chem. Soc., Dalton Trans., (1985) 2353.
[8] P.G. Daniele, C. Rigano and S. Sammartano, Anal. Chem., 57 (1985) 2956.
[9] L. Harju, Finn. Chem. Lett., (1985) 235.
[10] G. Anderegg, Helv. Chim. Acta, 50 (1967) 2333.
[11] R. Kissner, "AUTOTIT" version 2.00, 1989–1990; S. Kholeif, "TIT212" version 2.10–2.12, 1990, unpublished work.
[12] G. Anderegg, "EICHUNG" program, unpublished work.
[13] P. Henderson, Z. Physik. Chem., 59 (1907) 118; 63 (1908) 325.
[14] H. Stünzi and G. Anderegg, J. Coord. Chem., 7 (1978) 239.
[15] P. Gans, A. Sabatini and A. Vacca, J. Chem. Soc., Dalton Trans. (1985) 1195.
[16] F. Rey, A. Varela, J. Antelo and F. Arce, J. Chem. Engng. Data, 34 (1989) 35.
[17] A.J. Fridman, G.M. Sycheva and J.A. Afanasev, Soviet J. Coord. Chem., 5 (1979) 1132.
[18] R.A. Fridman and R.A. Veresova, Russ. J. Inorg. Chem., 13 (1968) 399.
[19] E. Bottari, A. Braibanti, L. Ciavatta, A.M. Currie, P.G. Daniele, F. Dallavalle, M. Grimaldi, A. Mastroianni, G. Mori, G. Ostacoli, P. Paoletti, E. Rizzarelli, G. Sammartano, C. Severini, A. Vacca and D.R. Williams, Ann. Chim., 68 (1978) 813.
[20] H.S. Harned and G.E. Mannweiler, J. Am. Chem. Soc., 67 (1935) 1873.
[21] G. Anderegg, Inorg. Chim. Acta, 194 (1992) 31.
[22] A.E. Martell and R.M. Smith, Critical Stability Constants, Vols 1–6, Plenum Press, New York, 1974–1989.
[23] W.J. Hamer and Y. Wu, J. Phys. Chem. Ref. Data, 1 (1972) 1047.
[24] B.R. Staples and R.L. Nuttall, J. Phys. Chem. Ref. Data, 6 (1977) 385.
[25] R. Fischer and J. Byé, Bull. Soc. Chim. (Fr.), (1964) 2920.

ELSEVIER

Talanta 000 (1995) 1081–1088

Talanta

# An optimized on-line preconcentration system for analysis of trace gold in ore samples

P. Di, D.E. Davey *

*School of Chemical Technology, University of South Australia, The Levels, SA 5095, Australia*

Received 12 August 1994; revised 5 December 1994; accepted 27 December 1994

**Abstract**

A flow injection on-line preconcentration technique, combined with graphite furnace atomic absorption spectrometry for the determination of gold in ore samples has been presented. An α-amino pyridine resin (AP) was loaded onto a microcolumn as the preconcentration reagent and a solution of 90% acetone–5% HCl–5% $H_2O$ was used for the gold elution. The Scaled Simplex Method was employed to optimize the flow injection manifold. The selected factors were optimized by the simultaneous consideration of two responses, absorbance and column retention efficiency, with only 12 tests. A detection limit of 0.065 μg Au/l ($3\sigma$) with a relative standard deviation of 4.3%, was achieved. Ore samples containing gold have been analysed successfully using the proposed method.

## 1. Introduction

On-line preconcentration techniques with flow injection analysis (FIA) have significantly increased the sensitivity of flame atomic absorption spectrometry (FAAS) for trace elements [1–4]. The applications of this technique to graphite furnace AAS are few, owing to the necessity of non-continuous flow in the sample introduction stage, which causes difficulties in both the manifold design and the experimental optimization of the FI system. The use of either a fraction collector or an autosampler as the interface between FIA system and GFAAS has been reported [5–9]. Such combinations have disadvantages in being time-consuming, and introduce a high risk of contamination from the equipment and the laboratory environment. In addition, by collecting the total eluate volume and injecting only small part of it into the graphite tube, the effect of the preconcentration is in part lost by the inherent dilution.

Fang and coworkers described a unique FIA manifold for sorbent extraction preconcentration systems using an autosampler arm and capillary as the sample collector and the interface between FIA and GFAAS. A microcolumn with a packing volume of only 15 μl and a very slow elution rate of 0.15 ml/min were used to limit the eluate volume so that the sensitivity was not reduced too much. All the procedures prior to the sample introduction were carried out in an enclosed stream to reduce any contamination risk. The fraction of eluate containing a high concentration of the analyte was introduced into the furnace. Thus, a semi-on-line approach was developed which exhibited all the basic advantages of an on-line procedure [10–13].

Although the combination of the on-line preconcentration technique with the GFAAS is more difficult than that with FAAS or ICP-AES, it is attractive for those systems where matrix influences are significant and where a sensitive determination is required, such as in the analyses of rare or noble metals in mineral samples. As an extension of our previous work for noble metal analysis by on-line preconcen-

* Corresponding author. Fax: (61) 8-302-3390.


*SSDI* 0039-9140(95)01524-8

tration with FAAS [14,15], we have attempted to apply the on-line preconcentration technique to GFAAS detection of trace gold in ore samples. Since the gold content of mineral samples is normally at the parts per million level and gold-containing samples are also expensive, more attention has had to be paid to the column efficiency than previously, to insure that most of the sample treated in the column can be detected. Therefore, a larger column was selected, which has required us to carefully optimize the controlling parameters.

A simplex method was adopted to optimize the FIA section of the manifold. The technique was initially proposed by Spendley [16] and used in analytical chemistry by Long [17]. Since then, some modifications of this method have been presented [18,19] and applications in FIA have also been reported [20–22]. In our experiments, the simplex method has been used to optimise the preconcentration and elution parameters in the FIA manifold, allowing flame AAS to be employed to monitor the changing response. This approach simplifies the operational procedure. The optimized configuration was, then, employed in the GFAAS determination for gold in reference ore samples with acceptable recoveries and precision observed.

## 2. Experimental

### 2.1. AAS determination

A GBC 901 atomic absorption spectrometer fitted with a GBC 900 graphite furnace was used for trace gold analysis, whilst a GBC 905 model flame atomic absorption spectrometer (GBC Scientific Equipment Pty Ltd, Australia) was used in the parameter optimization for the FIA preconcentration stage. Simultaneous background corrections were made using deuterium lamps in both flame AAS and GFAAS. The graphs and data were printed with an Epson RX 80 printer (Epson Corporation, Japan) and the signals from the GFAAS were recorded by a OmniScribe recorder (Houston Instruments, Austin, TX, USA). The GFAAS parameters are listed in Table 1. GBC graphite cups were selected for the GFAAS determination because larger volumes than usual samples were needed (about 50 μl).

Table 1
Parameters of GFAAS determination for gold

| | |
|---|---|
| Wavelength (nm) | 242.8 |
| Slit (nm) | 0.5 |
| Lamp current (mA) | 10.0 |
| Dry temperature (°C) | 140–240, 1.5 °C/s |
| Ash temperature (°C) | (1) 250–450, 15 °C/s |
| | (2) 500–1100, 50 °C/s |
| Atomization temperature (°C) | 3000, 450 °C/s |

### 2.2. On-line preconcentration methodology

The preconcentration FIA-GFAAS technique used in this work employed a single column (Fig. 1) controlled by a Flow Injection Control System (FICS, homemade). Software which allows the time parameters to be set in the computer prior to the analysis was developed to control the operations of both the preconcentration stage and the sample injection into the graphite furnace.

In the sampling stage, pump 2 (P2, Mini-S 860, ISMATEC, Switzerland) started and carried samples through the column (C, homemade). After a selected period of time for sample introduction (60 s in this work), P2 was stopped and pump 1 (P1, multi-speed pump, Gilson, France) ran for 10 s. A 2 M HCl solution was then passed through the column to remove matrix elements (if required). Then, both P1 and P2 were stopped and a 5 s rest period was set to allow manual switching of the four-way rotary valve (V, Rheodyne Incorporated, U.S.A.) from the sampling to the eluting position. P1 was then started again. The analyte was washed out of the column and collected in a PTFE loop (L, 2.0 m in length, 0.5 mm i.d.). The initial fraction of the eluate went to waste, and P1 was stopped when the concentrated fraction of the eluate flowed to the end of the PTFE loop. This time interval obviously needed to be carefully optimised. A manual step was used here to insert the PTFE

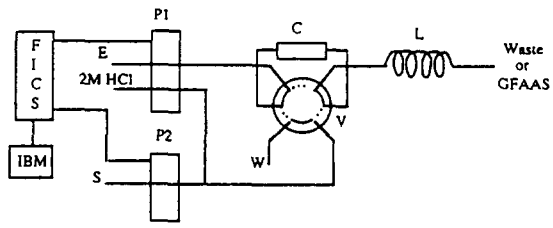


Fig. 1. The manifold of the preconcentration system combined with GFAAS. S, Sample; E, eluent and W, waste. The value is shown in the elution position.

Table 2
Programmed sequence of the FI preconcentration of GFAAS determination

| Step | Time (s) | State of pump 1 | State of pump 2 | Position of the valve | Operation stage |
|---|---|---|---|---|---|
| 1 | 60 | Stop | Go | Sampling | Preconcentration |
| 2 | 10 | Go | Stop | Sampling | Matrix removal |
| 3 | 5 | Stop | Stop | Switching | Valve position change |
| 4 | 8 | Go | Stop | Elution | Elution and removal of the initial eluate fraction |
| 5 | 5 | Stop | Stop | Elution | Capillary insertion into the GC[a] |
| 6 | 1 | Go | Stop | Elution | Sample injection |
| 7 | 20 | Go | Stop | Elution | Remaining eluate to waste |

[a] GC: Graphite cup.

loop into the graphite cup, and then P1 was restarted for 1 s to inject the sample (about 50 μl) into the cup. After the loop was withdrawn for the graphite cup, the heating program could be started. The programmed operation steps are shown in Table 2.

An organic solvent resistant tube (2.06 mm i.d., A.I. Scientific Pty Ltd, Australia) was used for the acetone-based eluent, and Tygon pump tubes (2.06 mm i.d.) for the sample solutions and matrix removal. The sample loading flow rate was 12.6 ml/min, and the elution flow rate, 6.0 ml/min. A microcolumn with the dimensions 3.0 (l) × 50 (i.d.) mm was used in the preconcentration stage. The manifold without the effluent collection loop (L) was used to optimize the preconcentration configuration and the elution step. The Scaled Simplex Method and flame AAS detection were selected for manifold optimization.

### 2.3. Reagents

A 1.00 mg/ml gold solution (BDH Chemicals Ltd, Poole, UK) was used as the stock solution for gold standards. An α-amino pyridine (AP) resin (60–80 mesh, Institute of Polymer Chemistry, Nankai University, China) was employed as the preconcentration reagent. The eluent was a solution of 90% acetone–5% HCl–5% $H_2O$ [23]. The other chemicals used in this work were all analytical-grade.

### 2.4. Ore sample digestion

A 2 g ore sample was first heated in a porcelain crucible at 600 °C in a Muffle Furnace for 3 h. After cooling for 0.5 h, it was transferred into a porcelain evaporating dish, and then 20 ml aqua regia (1:1) was added to the sample. The sample was dissolved on a hot plate in a fume hood and boiled for 1 h with regularly stirring. The dissolved sample was then filtered, and the residues were washed about five times with 0.1 M HCl solution. The sample was finally diluted to the mark in a 100 ml volumetric flask.

### 2.5. Application of scaled simplex method

Although the Modified Simplex Method (MSM) [18] had been successfully applied to our previous work [14], in this present study, the Scaled Simplex Method (SSM) proposed by Morgan and Deming [19] was also used. It is particularly suited where the factors or responses have different units or different regions of interest. The critical idea is one of scaling all factors and responses in such a way that their domains extend from 0 to 1 (or from 0% to 100%). This is accomplished by the equations:

$$X_s = \frac{X_s - X_{al}}{X_{ah} - X_{al}} \quad (1)$$

or

$$R_s = \frac{R_a - R_{al}}{R_{ah} - R_{al}} \quad (2)$$

where $X_s$ or $R_s$, is the scaled value of factor or response; $X_a$ or $R_a$, is the real value used, or obtained, in the experiment; $X_{al}$ or $R_{al}$, is the lowest value; and $X_{ah}$ or $R_{ah}$, is the highest value in the region of interest.

There were two responses used in this study: absorbance ($R1$) and the retention efficiency of the analyte on the column ($R2$). The weights of

these two responses were taken into account in the optimization. The response function used was

$$R_{\text{total}} = R1_s \times 0.7 + R2_s \times 0.3 \quad (3)$$

where $R_{\text{total}}$ is the toal desired response, and $R1_s$ and $R2_s$ are the scaled absorbance and the scaled retention efficiency, respectively. Since the absorbance, which reflects sensitivity, was considered more important in this work, the weighting of 70% was given to it, and 30% to the column efficiency.

A computer program which had been developed for the MSM approach described in our recent work [14] was again used here to calculate new factor values by SSM.

## 3. Results and discussion

### 3.1. Preconcentration and elution

The α-amino pyridine (AP) resin is formed by bonding α-amino pyridine to a cross-linked poly-phenylethene support. Li investigated AP resin gold adsorption by infrared spectroscopy and proposed that the mechanism could involve a combination of coordination through the pyridine N lone pair, and ion pair formation via the protonated amine group, $-NH_3^+$, to the complex anion $AuCl_4^-$. The structure could be thus represented as shown.

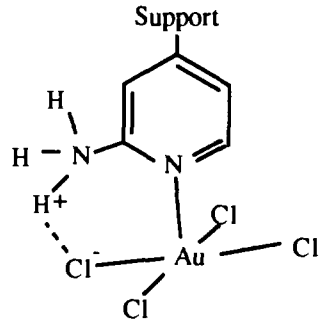


The planar structure of $AuCl_4^-$ provides sufficient space for the coordinating N, whilst the association of $H^+$ and $Cl^-$ is favoured by the ring arrangement shown, reflecting the strong Au affinity observed for the resin. The adsorptive capacity for gold was found to be 500–600 mg Au/g resin [23].

A fast initial reaction between AP resin and gold was observed by us during on-line preconcentration, and the retention efficiency of the microcolumn was still about 90% even with a fast sampling flow rate of 12 ml/min. The effect of sample acidity on the on-line preconcentration stage was found negligible, there being no change in response with 0.1–4.0 M HCl as sample media. A 0.1 M HCl solution was selected in further experiments.

AP resin had previously been used by us to preconcentrate Pd, Pt and Ir using on-line techniques [15]. A 0.5 M HCl–0.5 M $HClO_4$–0.5 M $Mg(ClO_4)_2$ solution was found suitable on that occasion as a group eluent for Pd, Pt and Ir. This solution could, however, not be used for elution here due to the strong combination of gold with the resin. Even thiourea solution, which had also been successfully used previously as a gold eluent [14], did not perform satisfactorily here. An organic-mixed solution, 90% acetone–5% HCl–5% $H_2O$, studied by some authors [24,25], was then selected as the gold eluent and brought success. Gold, with the concentration range 0.1 ppb–1 ppm, could be fully eluted and the column could be regenerated using this solution. The column also possessed an excellent lifetime (over a hundred reuses). The acetone–HCl eluent was thus selected for all further experiments in this study.

### 3.2. Optimization of the preconcentration manifold

In the optimization study, three factors, column length, sample flow rate and elution flow rate, were chosen, while two responses, absorbance and column retention efficiency, were taken into account. The selection was based on our previous experience, and on precedents in the literature [14].

To determine the column retention efficiency, the loss of gold in the sampling stage was measured. The retention efficiency ($R2$) was than calculated by Eq. (4).

$$R2 = \frac{C_t - C_d}{C_t} \times 100\% \quad (4)$$

where $C_t$ is the total amount of gold carried through the column, and $C_d$ is the gold lost in the sampling stage. The factors, the column length (F1), the sample flow rate (F2), and the elution flow rate (F3), were selected, as stated above. The actual boundary values of the factors ($X_{al}$, $X_{ah}$) and the response values ($R_{al}$, $R_{ah}$) are shown in Table 3. The basic parameters of the simplex optimization are shown in Table 4.

Table 3
Actual boundary values for each factor and response

| Factor | Low value ($X_{al}$) | High value ($X_{ah}$) | Response | Low value ($R_{al}$) | High value ($R_{ah}$) |
|---|---|---|---|---|---|
| F1 (mm) | 5 | 80 | R1 | 0.020 | 0.200 |
| F2 (ml/min) | 2.5 | 13.5 | R2 (%) | 50 | 100 |
| F3 (ml/min) | 1.4 | 6.0 | | | |

Table 4
Parameters of the scaled simplex method

| Factor | Lower limit | | Upper limit | | Step size[b] | | Initial value | | Convergence coefficient |
|---|---|---|---|---|---|---|---|---|---|
| | Actual | %[a] | Actual | %[a] | Actual | %[a] | Actual | %[a] | |
| F1 (mm) | 5.0 | 0 | 80.0 | 100 | 35 (20) | 40 (20) | 27.5 | 30.0 | |
| F2 (ml/min) | 2.5 | 0 | 13.5 | 100 | 6.9 (3.6) | 40 (10) | 5.5 | 27.3 | 0.1 |
| F3 (ml/min) | 1.4 | 0 | 6.0 | 100 | 3.2 (2.1) | 40 (15) | 4.2 | 60.8 | |

[a] % values are scaled by Eqs. (1) and (2).
[b] The values in the parentheses are the small step sizes used in the initial test.

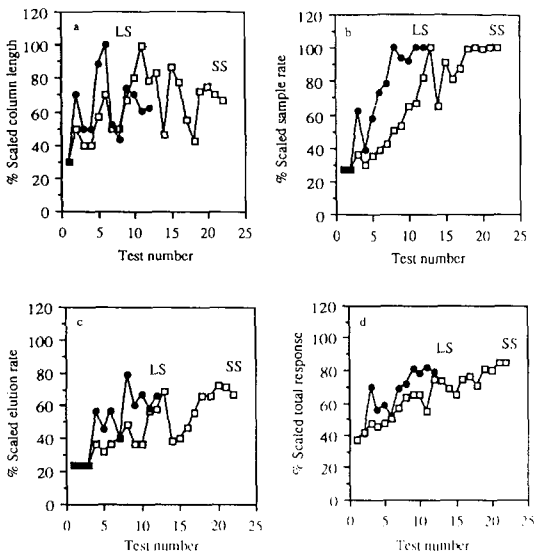


Fig. 2. SSM progression. (a–c) Progress of the factors, (d) total scaled response. LS, large step size; SS, small step size.

As discussed by Yarbro [26] and observed in our earlier work [14] the step size chosen in the simplex method is crucial to success in gaining optimization. In this present study, it was found that rather than starting with an initial simplex using small step sizes, which may prolong the time to reach an optimum, a large initial simplex covering more factor space led quickly to the optimum area. In Fig. 2, the graphs (a–c) show the differences in the optimization of the factor levels by using different step sizes. Although the initial tests were started at the same factor levels, the progress of optimization was slow with small step sizes, and a large step size was found preferable and quickly led to optimization (Fig. 2d). Only 12 tests were needed using this approach. The optimal areas are listed in Table 5. An observed range of 85–94% for the retention efficiency was achieved, while the absorbance was maintained satisfactorily.

### 3.3. Sample injection

The interface between a FIA system and graphite furnace AAS is the critical area in linking these two techniques together, owing to the non-flow-through nature of GFAAS. Initial efforts were made using a vessel to collect sample from the FI stream, followed by normal GFAAS procedures [1,9]. However, an effective loss of sample, and decrease in sensitivity, was observed with a large sample collection and, in fact, only a small portion reached the furnace. A better approach was developed using an autosampler arm as an interface. Only the concentrated portion in the stream was injected into the furnace, and subsequently sensitivity was increased and contamination risk reduced [10–13].

In this study, a PTFE tube was employed to collect and directly introduce eluates into the furnace. The PTFE tube was manually inserted, and all the solutions were kept in an enclosed stream prior to the injection, which both avoided any sample loss or contamina-

Table 5
Optimal factor areas obtained by the scaled simplex method

| | Column length | Sample flow rate | Elution flow rate |
|---|---|---|---|
| Scaled value | 49-73% | 78-100% | 59-78% |
| Actual value | 42-60 (mm) | 11.1-13.5 (ml/min) | 4.1-5.0 (ml/min) |

tion, and kept the manifold and the program simple. We intend to fully automate this step in future work.

It was most important to control the sample injection time into the furnace to insure that sensitivity and precision were not lost. A computer was used to operate the eluent pump (P1) to start and stop the sample injection. The elution curves obtained by determining the eluate during 1 s intervals are given in Fig. 3. It can be seen that each curve has a plateau in the range from 5 s (0.5 ppb) to 10 s (5.0 ppb), which was brought about by the use of a longer column. Although the gold in the plateau region does not in fact contribute to an improved sensitivity, it improves the reproducibility of the determination, and compensates for any variation in the position of the most concentrated fraction of the gold in the sample stream, in turn caused by any variation of flow rate (e.g. as pump tubing wears out). As shown in Fig. 3, the signal became stable after 8 sec elution, i.e. a period of 8 s were needed to elute the gold from the column, and remove the initial fraction of the effluent. Pump 1 was then stopped for 5 s, the PTFE loop inserted into the furnace, and the pump started again for 1 s to inject the sample (see steps 4-6, Table 2).

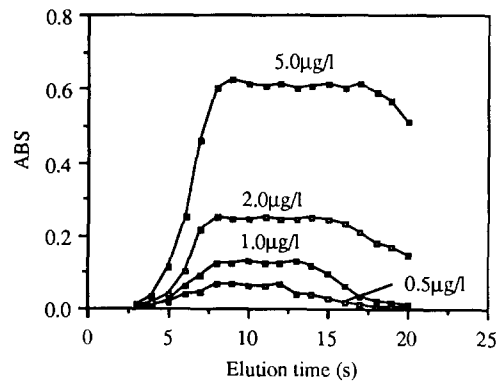


Fig. 3. The elution curves detected by the graphite furnace AAS method. The first sample was injected after 3 sec elution. All the samples were injected for 1 sec.

### 3.4. Interference study

As mentioned earlier, the noble metals, Pd, Pt and Ir, could be eliminated as potential interferents using a 0.5 M HCl-0.5 M $HClO_4$-0.5 M $Mg(ClO_4)_2$ solution [15]. Furthermore, salt matrices such as, $KNO_3$ (4000), NaCl (29 000), $CaCl_2$ (5000), $MgSO_4$ (6000), $AlCl_3$ (800), $Fe(NO_3)_3$ (100), $CrCl_3$ (480), $NiSO_4$ (280), $Pb(NO_3)_2$ (200), and $Cu(NO_3)_2$ (400 mg/l), were studied and found not to markedly affect gold preconcentration or determination by the proposed method. The recoveries of gold in the presence of these elements were above 95%, which was considered satisfactory. All the above matrix elements could be eliminated using 2 M HCl solution prior to the gold elution.

### 3.5. Calibration standard, detection limit and precision

A standard solution series, 0, 0.5, 1.0, 2.0, and 5.0 μg/l, in gold was determined. Each was passed through the column for 60 s and eluted for 8 s, using the graphite furnace AAS method outlined previously. A linear calibration with a good correlation coefficient was obtained, where: absorbance = 0.00206 ($\pm$0.00308) + 0.119 ($\pm$0.00125) Au concentration (μg/l); $R^2 = 0.998$.

A solution containing 0.5 μg/l of gold was determined for 10 replicates. The detection limit found was 0.065 μg/l ($3\sigma$) and the relative standard deviation (%RSD) was 4.3%. In our view, the key source of imprecision in this system was flow rate variation. Although a solvent-resistant pump tube was used in the elution stream, it was observed to soften with acetone contact, causing some stretching and flow rate change over time.

### 3.6. Sample analysis

A mixed composition standard solution and two certified reference ore samples of gold were

Table 6
Analysis results for a prepared mixed standard and ore samples

| Sample | Reference value | | Observed value | |
|---|---|---|---|---|
| | Concentration of Au (g/t) | Standard deviation | Concentration of Au (g/t) | Standard deviation ($n = 6$) |
| Mixed composition standard[a] | 0.50 | — | 0.49 | ±0.02 |
| OREAS 1C[b] | 0.200 | ±0.022 | 0.189 | ±0.032 |
| 7814490[c] | 0.20 | ±0.01 | 0.203 | ±0.015 |

All concentrations are given in g/t for comparison purposes, although the mixed composition standard was prepared in μg/l.
[a] Prepared using a gold standard solution with 10 matrix elements, as listed in the Interference Study section.
[b] Provided by the Chemistry Centre, Western Australia.
[c] Provided by Shandong Geological Exploration Company, China.

determined under the conditions proposed. The results are shown in Table 6. The values obtained corresponded well with the certified values.

## 4. Conclusion

The non-continuous aspect of graphite furnace AAS causes some difficulties in combination with an on-line preconcentration FIA system. This combination is, however, still very attractive for trace element analysis. First of all, pre-matrix removal is a significant advantage of the on-line preconcentration technique. Matrix problems are often encountered in GFAAS determinations, and are removed in the procedure described. Secondly, effective preconcentration reagents and eluents also lead to increased sensitivity. The AP resin described, when combined with an eluent composed of 90% acetone–5% HCl–5% $H_2O$, has epitomized this ideal. Fast sampling and elution speed are added bonuses. Certified Au ore samples have been analysed using the proposed method, and good agreement between the reference values and determined values has been achieved.

Thirdly, the scaled simplex method (SSM) has provided an excellent tool to optimize the control parameters. Although a complicated on-line preconcentration FIA system was involved, SSM allowed more than one response to be considered simultaneously, and significantly simplified the experimental procedure. Larger step sizes were found preferable to quickly reach the optimum area. Only 12 tests were needed to reach the performance plateau. A longer column (50.0 mm) was found beneficial in providing reproducible sample injection and determination.

Finally, an enclosed environment was provided for the sample by simply using the PTFE capillary of the FIA system as the interface between the FIA and GFAAS. FIA methods provided an obvious way to avoid contamination from the laboratory surrounds, and thus furnish the experimenter with a 'poorman's clean room'.

## References

[1] F. Malamas, M. Bengtsson and G. Johansson, Anal. Chim. Acta, 160 (1984) 1.
[2] Z. Fang, S. Xu, and S. Zhang, Anal. Chim. Acta, 169 (1985) 321.
[3] Z. Fang, J. Ruzicka and E.H. Hansen, Anal. Chim. Acta, 164 (1984) 23.
[4] M.J.C. Taylor, D.E. Barnes and G.D. Marshall, Anal. Chim. Acta, 265 (1992) 71.
[5] H. Koizumi, T. Hadeishi, and R. McLaughlin, Anal. Chem., 50 (1978) 387.
[6] F.E. Brinckman, W.R. Blair, K.L. Jewett, and W.P. Iverson, J. Chromatogr. Sci., 15 (1977) 493.
[7] K. Backstrom and L.G. Danielsson, Anal. Chem., 60 (1988) 1354.
[8] F. Malamas, M. Bengtsson, and G. Johansson, Anal. Chim. Acta, 160 (1984) 1.
[9] S. Nakashima, R.E. Sturgeon, S.N. Willie, and S.S. Berman, Fresenius Z. Anal. Chem., 330 (1988) 592.
[10] Z. Fang, M. Sperling, and B. Welz, J. Anal. At. Spectrom., 5 (1990) 639.
[11] M. Sperling, X. Yin, and B. Welz, J. Anal. At. Spectrom., 6 (1991) 295.
[12] B. Welz, X. Yin, and M. Sperling, Anal. Chim. Acta, 261 (1992) 477.
[13] M. Sperling, X. Yin, and B. Welz, Spectrochim. Acta, 46B (1991) 1789.
[14] P. Di and D.E. Davey, Talanta, 41 (1994) 565.
[15] P. Di and D.E. Davey, Talanta, 42 (1995) 685.

[16] W. Spendley, G.R. Hext and F.R. Himswort, Technometrics, 4 (1962) 411.
[17] D.E. Long, Anal. Chim. Acta, 46 (1969) 308.
[18] J.A. Nelder and R. Mead, Comput. J., 7 (1965) 308.
[19] S.L. Morgan, S.N. Deming, Anal. Chem., 46 (1974) 117.
[20] J. Alonso, J. Bartroli, J. Coello and M. del Valle, Anal. Lett., 20 (1987) 1247.
[21] T.A.H.M. Janse, P.F.A. Van der Wiel, Van and G. Kateman, Anal. Chim. Acta, 155 (1983) 89.
[22] D. Betteridge, T.J. Sly and A.P. Wade, Anal. Chem., 55 (1983) 1292.
[23] L. Li, Y. Zhou, Z. Yin, and S. Wang, Fenxi Huaxue, 15 (1987) 297.
[24] J.S. Fritz, Talanta, 18 (1971) 323.
[25] C. Pohlandt, J.S. Fritz, J. Chromatog., 176 (1979) 189.
[26] L.A. Yarbro and S.N. Deming, Anal. Chim. Acta, 73 (1974) 391.

ELSEVIER

Talanta 42 (1995) 1089–1093

Talanta

# Technique for the isolation of secondary phases in processed magnesite

P. Arjunan, A. Kumar *, M. Chaudhuri, G. Banerjee

*Central Glass and Ceramic Research Institute, Jadavpur, Calcutta 700 032, India*

Received 3 June 1994; revised 22 December 1994; accepted 27 December 1994

**Abstract**

The study describes a new wet chemical technique, termed ANM, for the isolation of secondary phases in magnesite processed at a temperature of 1650 °C. The major MgO (periclase) phase in processed magnesite was preferentially extracted as ammonium nitrate magnesium double salt by ammonium nitrate in ethanol medium. The residues containing enriched secondary phases were identified by XRD.

## 1. Introduction

Secondary phases and impurities present in small amounts control the behavior of many ceramic materials. Identification of these secondary phases by X-ray powder diffraction is rather difficult owing to their low concentrations in the as-processed samples. Leipold [1] reported a technique for the detection of grain boundary impurities in polycrystalline ceramics through the use of electron beam microprobe (EBM) techniques to determine the distribution of grain boundary impurities like Si, Al, Ca, etc., which are present in ppm levels. The nature of electron techniques do not permit evaluation of the entire matrix owing to the localized nature of the method.

In refractories, secondary phases give rise to critical liquid-forming phase at lower temperatures that control processing behavior. The magnesia system is significantly affected by the presence of such secondary phases, the determination of which are quite difficult [2]. Alper [3] has suggested the use of dilute hydrochloric acid to dissolve the major MgO phase in magnesite refractories in an attempt to concentrate impurities for further analysis and identification through X-ray studies. Methods to isolate metallic and oxide fractions of magnesium in slags have been reported [4]. This paper describes a new wet chemical method to concentrate secondary phases in magnesite which enables easy identification through subsequent XRD.

The method is dependent on ammonium nitrate which has been used for the estimation of uncombined or free MgO (periclase) in cement and cement clinkers by Bogue and Taylor [5]. In the original method, free MgO was extracted from cement clinker as a double salt of ammonium nitrate in the presence of ethanol–glycerol solvent medium. Later, the Bogue–Taylor technique was modified [6] in which only ethanol was used as a solvent. It was observed that use of ethanol as the solvent enhanced the rate of reaction and the extraction period reduced considerably.

The present paper discusses a technique, which has been developed on the basis of previous work [6] in Portland cement, to remove the major MgO phase in processed magnesite through preferential dissolution. The technique is termed the Ammonium Nitrate Method (ANM). The extracted residue can be analyzed

* Corresponding author.


*SSDI* 0039-9140(95)01525-6

by X-ray powder diffraction to identify secondary phases.

## 2. Experimental

### 2.1. Raw materials

Two natural magnesite samples from two different regions of India were selected for the experiments. The first was Salem magnesite, termed S, from the Salem region of Tamil Nadu, India. This magnesite is rich in silica, present as quartz veins or lenses within the raw magnesite [7]. The other was magnesite from the Almora region of Uttar Pradesh, India, termed A, with iron present as solid solution with magnesite [7].

The magnesities were crushed, ground and pelletized before processing. The pelletized magnesite samples were processed at 1650 °C with 1 h soaking at maximum temperature. This processing reduced the magnesium carbonate to the oxide and produced a compact mass. The compact processed mass was crushed and ground for phase analyses. Phase analyses of these processed samples was done with the help of X-ray powder diffraction technique using Cu K$\alpha$ radiation with Ni filter at a scan speed of 2° 2$\theta$ per minute using a Philips PW-1730 XRD unit. Because these samples contained magnesia (periclase) as the major phase, the secondary phases did not appear in a reasonably identifiable form as will be detailed later. To identify the secondary phases, the processed samples were ground to $-300$ mesh BS ($-52$ μm) and taken for extraction by ANM. After extraction the residue was dried, and the secondary phase were identified using powder XRD.

### 2.2. Apparatus for extraction

Standard chemical laboratory equipment was used for the extraction step in ANM. Refluxing assembly, consisting of a flat-bottom short neck Erlenmeyer flask 500 ml capacity. The water cooler refluxing condenser had a minimum length of 300 mm. The flask and reflux condenser were connected with standard tapered ground glass joints. A heating assembly consisting of a heating mantle with a capacity of 1 l attached with an energy regulator was used. A filtration unit consisting of a standard glass funnel set-up with Whatman No. 41 filter paper was used.

### 2.3. Reagents and materials

The following were used: ammonium nitrate, (AR/GR Grade); ethanol, (purity 99.5%); glass boiling beads; high temperature processed magnesite powder.

### 2.4. Extraction technique

In the ANM, for identification of secondary phases in processed magnesia, the following steps were conducted. About 5 g of powdered ($-52$ μm) sintered magnesia sample was taken in a 500 ml Erlenmeyer flask fitted with a refluxing condenser. About 300 ml absolute ethanol and 20 g of ammonium nitrate and a few small glass beads to aid smooth boiling were added to the sample. The contents were refluxed at a controlled temperature of 70 °C on a heating mantle for about 10–15 h. At regular intervals the flask was shaken well to disturb the settling of fine magnesite powders at the bottom of the flask. Intermittently, the condenser was removed from the flask to release the ammonia formed from the reaction between MgO and ammonium nitrate.

After completion of refluxing the contents were cooled to room temperature and filtered. The glass beads were carefully removed and the residue was washed three to four times in absolute alcohol. The residue was dried at $100 \pm 5$ °C for 1 h and taken for X-ray analysis. If necessary, the filtrate was collected and analyzed complexometrically to determine the total MgO extracted.

## 3. Results and discussion

### 3.1. Phases in as-sintered magnesite

Initial phase analyses of raw materials using XRD and microscopy showed that natural Salem magnesites contain quartz and serpentine as the commonly associated minerals while Almora contains calcite and dolomite and both magnesites contain a minor amount of talc. These associated minerals in the raw material are bound to give rise to secondary phases in magnesite processed at high temperature. The composition of the secondary matrix varies depending on the composition of raw materials. Identification of these secondary phases requires much attention, but at the same time this is difficult owing to the low phase concen-

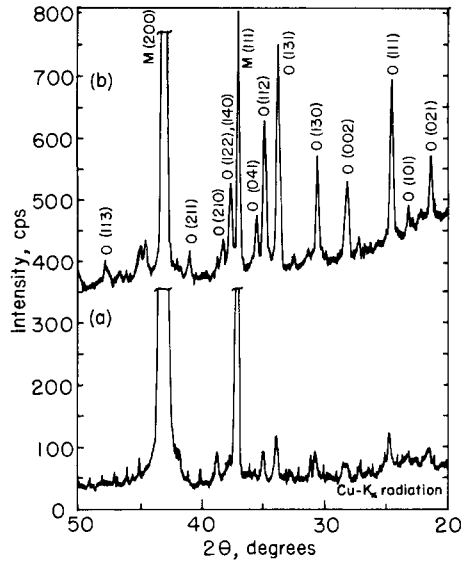


Fig. 1. Powder X-ray diffraction patterns for Salem magnesite processed at 1650 °C. (a) Before and (b) after extraction of the major portion of the periclase phase (M) using ANM showing monticellite (O) to be the crystalline secondary phase.

tration compared to the large amount of periclase grains.

The results of powder XRD analysis of as-fired samples are given in Figs. 1(a) and 2(a). The two patterns show the characteristic (200) and (111) reflections at $d$-spacings of 0.243 and 0.210 nm respectively (at about 43° and 37° $2\theta$ for Cu K$\alpha$ radiation) for periclase (JCPDS 4-0829). The (220) reflection for $d$-spacing of 0.149 nm was identified but this has not been reproduced in the figures for the sake of brevity. Other reflections for secondary phases were present at a low intensity level. It is evident from both figures that the dominant MgO phase does not permit the ready identification of secondary phases. However, even these powder patterns of the as-fired MgO do confirm the presence of secondary phases.

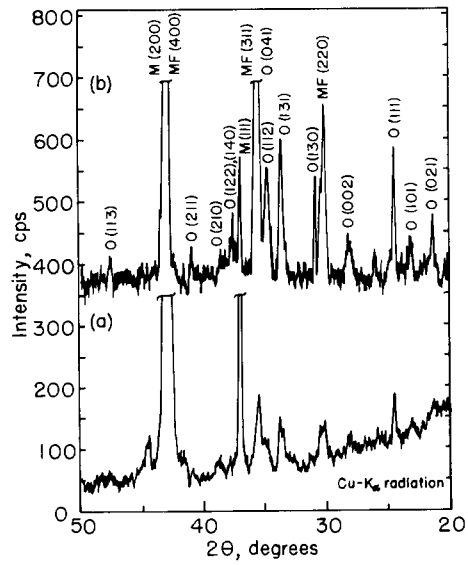


Fig. 2. Powder X-ray diffraction patterns for Almora magnesite processed at 1650 °C. (a) Before and (b) after extraction of the major portion of the periclase phase (M) using ANM showing enhanced magnesioferrite (MF) and monticellite (O) to be the crystalline secondary phases.

Table 1
Periclase, MgO, extracted from processed magnesite

| Sample code | Material | Refluxing time (h) | MgO Extracted (%) |
|---|---|---|---|
| S | Processed Salem magnesite | 9 | 86 |
| A | Processed Almora magnesite | 13 | 89 |

Solvent volume: 300 ml; sample weight: 5 g. Ammonium nitrate: 20 g.

### 3.2. Phases in periclase extracted samples

The results of the chemical extraction using ANM on two samples are given in the Table 1. Alcoholic ammonium nitrate during refluxing with processed magnesite forms a double salt of magnesium with the extracted periclase according to the following equation:

$$MgO + 4NH_4NO_3 \rightarrow Mg(NO_3)_4(NH_4)_2 + 2NH_3 + H_2O \quad (1)$$

An alcoholic solvent was used to prevent possible hydrolysis of magnesium and calcium bearing phases. The ethanol used for the experiments had a water content of less than 0.5%. The processed sample of Almora magnesite with high iron impurity required a longer refluxing period of 13 h compared to samples of processed Salem magnesite which required about 9 h to extract about 85–90% of the sample of MgO (Table 1). This slow reaction time may be attributed to the presence of iron as solid solution in all phases in Almora magnesite preventing easy dissolution of MgO phase.

The solvent volume also affected the extraction time in ANM. The solvent volume below an optimum level increases the extraction period considerably. The optimum solvent level here may be considered as the volume at which

Table 2
Intensity of powder XRD reflections before and after extraction in processed magnesites

| Phases (JCPDS) | *hkl* index | $I/I_0$ | Intensity (*cps*) | | | |
|---|---|---|---|---|---|---|
| | | | Salem | | Almora | |
| | | | Before | After | Before | After |
| Periclase | 200 | 100 | >9000 | >5000 | >5000 | >2000 |
| (4-0829) | 111 | 10 | 850 | 420 | 460 | 200 |
| Monticellite | 131 | 100 | 75 | 360 | 90 | 250 |
| (11-0353) | 130 | 35 | 50 | 170 | 70 | 180 |
| | 111 | 40 | 50 | 280 | 110 | 250 |
| Magnesioferrite | 311 [a] | 100 | — | — | 130 | >700 |
| (17-0464) | 220 | 40 | — | — | 70 | 300 |

[a] Overlaps with monticellite (041) reflection.

the ammonium nitrate dissolves completely at room temperature. According to Eq. (1), 1 g MgO requires 4 g of ammonium nitrate for the reaction. About 20 g of ammonium nitrate were taken for 5 g sample. The optimum solvent volume for 20 g ammonium nitrate was found to be 300 ml ethanol. However, no experiment was conducted to ascertain the effect of solvent volume above the optimum. The non-solubility of phases other than periclase was confirmed by analyzing the resultant filtrate after ANM extraction for elements like Ca, Fe, and Si and none were found. Through repeated trial experiments, it was determined that a minimum refluxing time of about 8 h is required to extract about 80 wt% of the periclase (MgO) phase. Extraction of MgO up to this level of about 80 wt% is considered satisfactory for subsequent identification of secondary phases by XRD.

Phase identification through powder XRD was done after the ANM magnesia extraction to identify the secondary phases present in the sintered magnesites. It was observed that the secondary phases were easily identifiable. The major secondary phase in processed cryptocrystalline Salem magnesite was monticellite with extremely minor amounts of forsterite. The level of forsterite is so low in the material that it is just detectable even after extraction of about 86% of the parent sample as MgO. The major reflections of monticellite (JCPDS 11-0353) are marked O in Fig. 1(b). Dicalcium silicate present as an amorphous mass gave rise to the hump in the XRD pattern at around 20° $2\theta$ Cu K$\alpha$, typical of silicate bearing amorphous phases.

In coarse crystalline Almora magnesite processed material, monticellite and magnesioferrite (JCPDS 17-0464) were the two major crystalline phases revealed after ANM extraction as shown in Fig. 2(b). The iron impurity in this magnesite manifested itself as magnesioferrite after the high temperature processing. XRD of the processed magnesite itself before extraction (Fig. 2(a)) revealed the presence of magnesioferrite and monticellite through the presence of the (311) and (131) reflections of the two phases, respectively. After extraction, the intensity of the various reflections for the two crystalline secondary phases was enhanced considerably as shown in Fig. 2(b). This enhanced XRD pattern through extraction confirmed the absence of significant quantities of any other crystalline secondary phase.

The enhanced intensity of the major secondary crystalline phase reflections and the reduction in intensity of the periclase reflections after the ANM magnesia extraction are given in Table 2. The background noise in the case of Almora magnesite after extraction was high owing to the fluorescence from the relatively large amount of iron in the magnesioferrite. The (200) and (111) reflections for MgO were reduced by over one-half, from over 5000 cps to over 2000 cps and from 460 to 200 cps for the two peaks, respectively (Table 2). The 100% reflection of the monticellite, $CaMgSiO_4$, increased three to five times owing to extraction while magnesioferrite reflections were suitably improved by a factor of four. On the basis of these observations, it can be said that the ANM solution extraction technique was helpful in identification of small amounts of secondary phases in magnesia refractory material.

## 4. Conclusions

A wet chemical technique has been established for the isolation of secondary phases in processed magnesite samples. In this technique, the major MgO phase (periclase) in high temperature processed magnesite was preferentially dissolved by ammonium nitrate in ethanol medium. The filtered residue containing isolated secondary phase concentrate enabled identification of mineral phases when subjected to powder XRD. The technique is easy to perform and requires minimum operational attention during the extraction step.

## Acknowledgments

The authors are grateful to Dr B.K. Sarkar, Director, CGCRI, for his kind permission to carry out this study and publish these results. The authors are greatly indebted to Dr H.S. Maiti, Head, Analytical Chemistry Division, for his kind permission and advice during the entire study.

## References

[1] M.H. Leipold, in R.M. Fulrath and J.A. Pask (Eds.), Proc. Third Intl. Materials Symp., University of California, Berkeley, John Wiley, New York, 1968, p. 289.
[2] M. Nath Chaudhuri, A. Kumar, A.K. Bhadra, G. Banerjee and S.L. Sarkar, Bull. Am. Ceram. Soc., 71 (1992) 345.
[3] A. Alper, in R.M. Fulrath and J.A. Pask (Eds.), Proc. Third Intl. Materials Symp., University of California, Berkeley, John Wiley, New York, 1968, p. 295.
[4] R.S. Young, Chemical Phase Analysis, 1st edn., Charles Griffin, London 1974, p. 74.
[5] R.H. Bogue and H.F.W. Taylor, in F.M. Lea (Ed.), The Chemistry of Cement and Concrete, 2nd edn., Edward Arnold, London, 1956, p. 108.
[6] P. Arjunan and A. Kumar, Cement Concrete Res., 24(2) (1994) 343.
[7] M. Chaudhuri, A. Kumar, A.K. Bhadra and G. Banerjee, Interceram, 39(4/5) (1990) 26.

ELSEVIER

Talanta 42 (1995) 1095–1098

Talanta

# Determination of antimony, arsenic, bismuth, selenium, tellurium and tin by low pressure atomic absorption spectrometry with a quartz tube furnace atomizer and hydride generation with air addition

Baogui Zhang *, Yan Wang, Xinsheng Wang, Xulong Chen, Jianxing Feng

*Department of Environmental Science, Nankai University, Tianjin, People's Republic of China*

Received 19 October 1994; revised 11 January 1995; accepted 13 January 1995

**Abstract**

A new method has been developed for the determination of antimony, arsenic, bismuth, selenium, tellurium and tin by hydride generation–atomic absorption spectrometry in an electrically heated quartz tube furnace under sub-atmospheric pressure. The hydride generator, operating at a pressure lower than atmospheric, is used to generate and collect the hydrides of these elements. A certain volume (at atmospheric pressure) of air is then added to the generator after the formation of the volatile hydride. The gaseous mixture of the hydride and air is drawn into an evacuated, heated quartz tube by a vacuum pump. The proposed method gives improved sensitivities and detection limits.

## 1. Introduction

Elements forming covalent hydrides such as antimony, arsenic, bismuth, selenium, tellurium, tin, etc., are often determined after hydride generation by atomization of the hydride and measurement by atomic absorption spectrometry. Quartz tubes are the most widely used atomizers for hydrides. Investigations of many authors showed that addition of oxygen to air to the purge gas increased the sensitivities [1–4] and the highest sensitivities were found for extremely fuel-rich hydrogen–oxygen (or hydrogen–air) flames burning inside unheated quartz tube atomizers [5–7]. Dedina and Rubeska [7] and Welz and Melcher [8] studied the atomization of gaseous hydrides and the effect of oxygen on the sensitivity of hydride-forming elements. They concluded that the atomization of volatile hydride-forming elements was caused by collision with free hydrogen radicals and the role of oxygen was that it was able to increase the concentration of hydrogen radicals, the possibility of collision with hydride molecules and the atomization efficiency.

A method for the determination of antimony, arsenic, selenium and tin by low pressure furnace atomic spectrometry has been established [9–11]. On the basis of these works, a new method for the detemination of antimony, arsenic, bismuth, selenium, tellurium and tin has been developed. The hydrides are generated by adding dilute (1% m/v) sodium borohydride solution to acidified samples in a low pressure (state pressure approx. 9.8 kPa) generator. A certain amount of air is then added to the generator. The gaseous mixture is drawn into an evacuated, heated quartz tube where the atomic absorption occurs. It is most important to optimize the amount of air added so that the sensitivities are not reduced by the liberated hydrogen. The oxygen added reacts with the hydrogen and forms water. This pro-

* Corresponding author.


*SSDI* 0039-9140(95)01526-4

cedure removes the unnecessary hydrogen and reduces the dilution by hydrogen of the atomic concentration of the analyzed elements inside the quartz tube. The effects of various experimental conditions have been thoroughly studied.

## 2. Experimental

### 2.1. Apparatus

A Varian-Techtron AA6 atomic absorption spectrometer was equipped with a Model XWT-200 amplifier-strip chart recorder (Shanghai, China). The recorder has a full-scale pen response of 0.5–0.8 s. This recorder and the Varian AA6 were sufficiently fast to accurately record the transient signals of atomic absorption in our experiments. Varian Techtron hollow cathode lamps were used for all elements. A low pressure hydride generator was employed for the hydride generation and collection. The atomizer was an electrically heated, evacuated quartz tube, which had quartz windows at two sides. The length and the diameter of the tube were 16 and 0.8 cm, respectively. A certain length of capillary pipe used as a damper was connected to the gaseous outlet of the quartz tube. The purpose was to increase the retention period of the analyte atoms inside the quartz tube. If the diameter of the capillary damper was 0.2 cm, the length used was 10–70 cm [9]. A model 2XZ-4 vacuum pump (Shanghai, China) was used to draw out the mixture from the generator into the quartz tube. The limit vacuum of the pump is $6 \times 10^{-5}$ kPa. The apparatus for the low pressure generation of the hydrides and low pressure measurements is shown schematically in Fig. 1.

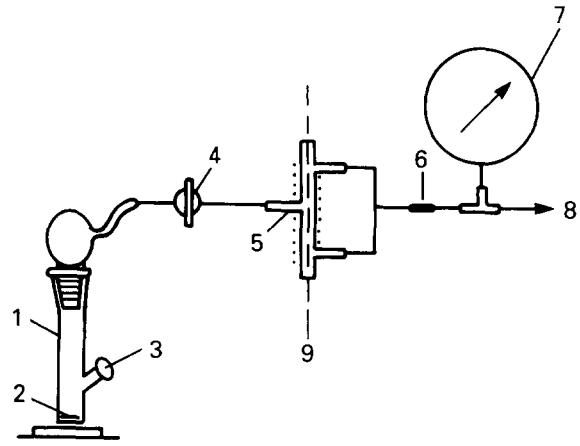


Fig. 1. Schematic diagram of the apparatus for sub-atmospheric pressure hydride generation and measurement in an evacuated, heated quartz tube: 1, hydride generator, 2, magnetic follower; 3, silicone rubber septum; 4, two-way stopcock; 5, electrically heated vacuum quartz tube; 6, capillary damper; 7, monometer, 8, to vacuum pump; 9, optical path.

### 2.2. Reagents

Analytical reagent grade chemicals and doubly distilled water were used throughout. The standard solution contained 1000 μg/ml of ether As, Bi, Sb, Se, Sn or Te. A solution of 1% (m/v) $NaBH_4$ was prepared by dissolving $NaBH_4$ powder in 0.1% (m/v) NaOH, and the solution was filtered through a 0.45 μm membrane filter. The operating conditions for the elements tested are summarized in Table 1.

### 2.3. Analytical procedure

A certain amount of sample solution (about 1–2 ml) and a certain volume of 6 M HCl solution were added to the generator (Table 1). The generator was connected to the apparatus. The two-way stopcock was opened and the air in it drawn out by a vacuum pump for about 20 s. Then the stopcock was closed. A certain volume of 1% $NaBH_4$ solution (Table 1) was injected into the generator through a silicon–

Table 1
Operating conditions and solution specifications

| Element | Wavelength (nm) | Lamp current (Ma) | Spectral bandwidth (nm) | 6 M HCl addition volume (ml) | 1% $NaBH_4$ addition volume (ml) | Air addition volume (ml) |
|---|---|---|---|---|---|---|
| As | 193.7 | 7 | 1.0 | 1.0 | 0.8 | 4 |
| Sb | 217.6 | 5 | 0.2 | 1.0 | 0.5 | 5 |
| Bi | 223.1 | 5 | 0.2 | 0.5 | 0.3 | 4 |
| Sn | 224.6 | 5 | 0.5 | 0.2 | 1.0 | 0.8 |
| Se | 196.0 | 8 | 1.0 | 1.0 | 0.3 | 4 |
| Te | 214.3 | 6 | 0.2 | 1.0 | 0.5 | 3 |

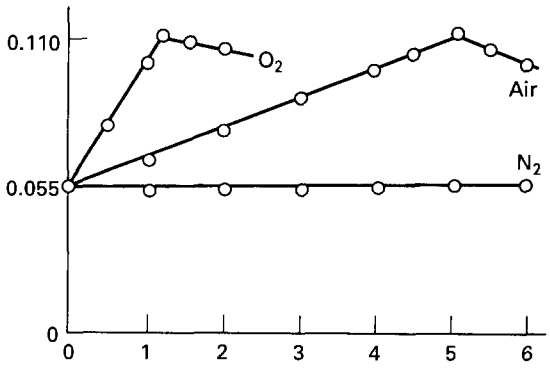


Fig. 2. Effect of the volumes of oxygen, air and nitrogen added on the absorbances of 2 ng atimony.

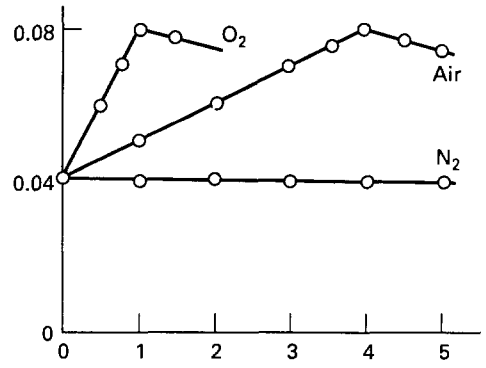


Fig. 3. Effect of the volumes of oxygen, air and nitrogen added on the absorbances of 5 ng arsenic.

rubber septum. The reduction proceded very fast under stirring. After 10 s a certain amount of air was injected into the generator. The stopcock was then opened for drawing out the mixture of the hydride and air into the evacuated, heated quartz tube. The peak absorbance of the sample was recorded instantly.

## 3. Results and discussion

### *3.1. Selection of the temperature inside the electrically heated, evacuated quartz tube*

The temperature inside the central section of the quartz tube was measured using a thermocouple to observe the effect of atomizer tube temperature on the sensitivities of elements. No effect on the results was observed when the temperature was within 800–850 °C. Thus 850 °C is recommended.

### *3.2. Effect of air, oxygen and nitrogen on the sensitivities of elements*

It has been found that the sensitivities of these elements can be increased if a certain amount of air or oxygen is added to the generator, but nitrogen can not be utilized to increase the sensitivities. The experimental results are compared in Figs. 2–7: the sensitivities of antimony, arsenic, bismuth, selenium and telleurium are increased by a factor of approximately two, and the optimum air amounts of these elements are 5, 4, 4, 4, and 3 ml, respectively, whereas the optimum oxygen amounts are 1.2, 1.0, 1.0, 1.0, and 0.6 ml, respectively; this technique is crucial for the determination of tin because the absorbance of 5.0 ng Sn is nearly zero when using the no addition procedure.

### *3.3. Increasing sensitivities by adding oxygen*

When a small amount of air or oxygen is added, a weak flash is seen inside the evacuated, heated quartz tube at the gas inlet. The more air or oxygen is added, the more obvious the flash. This phenomenon is generated by reaction of the hydrogen produced by the decomposition of sodium borohydride with the oxygen added. If air or oxygen is not added, a large amount of hydrogen liberated from the decomposition of sodium tetrahydroborate dilutes the atomic concentration of hydrides.

When air or oxygen is added, the oxygen reacts with the hydrogen and forms water.

$$2H_2 + O_2 = 2H_2O$$

This procedure removes unnecessary hydrogen and reduces the dilution by hydrogen of the atomic concentration of the analyzed elements inside the quartz tube so that the sensitivities are increased.

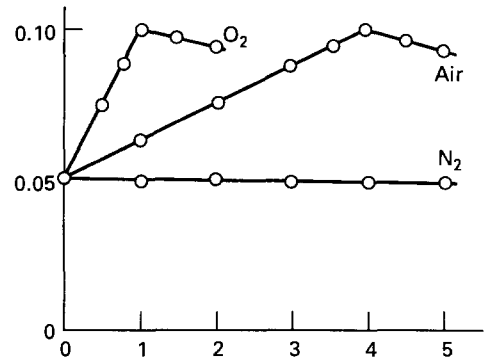


Fig. 4. Effect of the volumes of oxygen, air and nitrogen added on the absorbances of 2 ng bismuth.

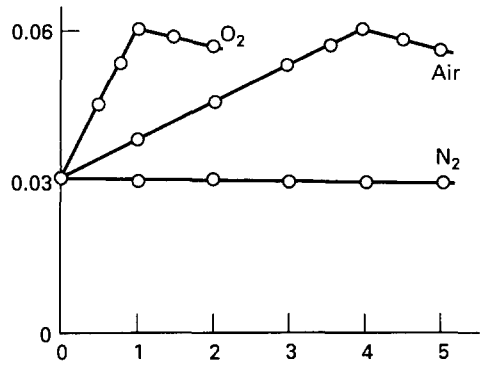


Fig. 5. Effect of the volumes of oxygen, air and nitrogen added on the absorbances of 1 ng of selenium.

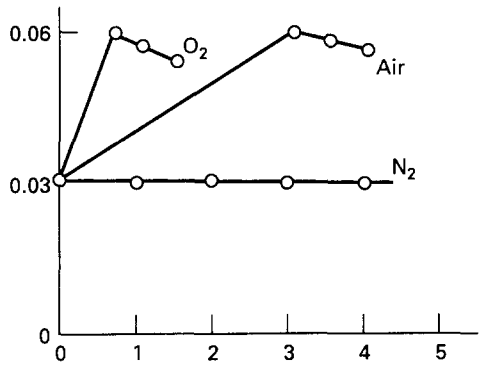


Fig. 6. Effect of the volumes of oxygen, air and nitrogen added on the absorbances of 2 ng of tellurium.

### 3.4. Sensitivity and detection limit

The typical sensitivities of the low pressure technique for arsenic, antimony, bismuth, selenium, tellurium and tin are 290, 80, 90, 73, 140 and 110 pg, respectively; whereas the detection limits ($3\sigma$) of this method for these elements are 610, 100, 50, 60, 26 and 200 pg, respectively.

In order to document the improvement in sensitivity achieved by using a vacuum system, a experiment with carrier gas ($N_2$) has been done. The optimum nitrogen flow-rate was 1.0 l/min for the elements except selenium and tellurium when a flow-rate of 2.6 l/min was used. The other experimental conditions are identical with the vacuam method except for the procedure of adding oxygen or air. The sensitivities of the carrier gas technique for the above elements were 600, 550, 450, 2000, 1600 and 500 pg, respectively. A comparison of the sensitivities between the two methods illustrates that it is beneficial to generate, collect and atomize the hydrides under sub-atmospheric pressure.

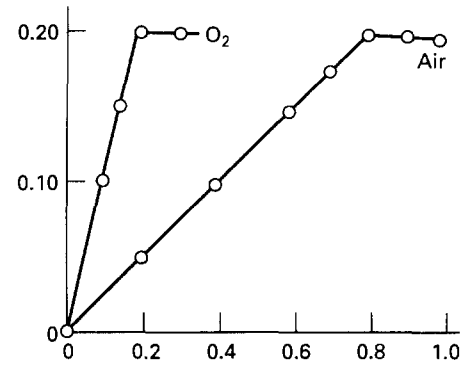


Fig. 7. Effect of the volumes of oxygen, air and nitrogen added on the absorbances of 5 ng of tin.

## 4. Conclusion

As compared with the conventional carrier gas method [12–14], the key features of our method are the hydride generation at less than atmospheric pressure, the vacuum atomization and the elimination of the influence of the hydrogen liberated from the decomposition of sodium borohydride.

## References

[1] P.D. Goulden and P. Brooksbank, Anal. Chem., 46 (1974) 1431.
[2] P.N. Vijan and G.R. Wood, Talanta, 23 (1976) 89.
[3] F.D. Pierce, T.C. Lamoreaux, H.R. Brown and R.S. Fraser, Appl. Spectrosc., 30 (1976) 38.
[4] M.P. Andreae, Anal. Chem., 49 (1977) 820.
[5] D.D. Siemer, and L. Hageman, Anal. Lett., 8 (1975) 323.
[6] D.D. Simer, P. Koteel and V. Jariwala, Anal. Chem., 48 (1976) 836.
[7] J. Dedina and I. Rubeska Spectrochim. Acta, 35B (1980) 119.
[8] B. Welz and M. Melcher, Analyst, 108 (1983) 213.
[9] B.G. Zhang, K.Y. Tao and J.X. Feng, Spectrochim. Acta, 44B (1989) 247.
[10] B.G. Zhang, K.Y. Tao and J.X. Feng, Acta Scientiarum Naturalium Universitatis Nankainensis, 2 (1987) 83.
[11] B.G. Zhang, K.Y. Tao and J.X. Feng, Proceedings of 2nd Beijin Conference and Exhibition on Instrumental Analysis 1987, p. 615.
[12] K.C. Thompson and D.R. Thomerson, Analyst, 99 (1974) 595.
[13] V. Cheam and H. Agemian, Anal. Chim. Acta, 113 (1980) 237.
[14] R.G. Godden and D.R. Thomerson, Analyst, 105 (1980) 1137.

ELSEVIER

Talanta 42 (1995) 1099–1102

Talanta

# A gas chromatographic method for the determination of nitrite ions in natural waters ☆

I. Sarudi *, I. Nagy

*Department of Chemistry, Faculty of Animal Science, Pannon Agricultural University, Kaposvár, Hungary*

Received 4 November 1994; revised 28 February 1995; accepted 28 February 1995

**Abstract**

Following the treatment of the sample with zinc hydroxide, nitrite reacts with potassium iodide in the presence of acetone and sulphuric acid. The released iodine and the propanone derivative resulting from the acetone are extracted in *n*-hexane. The extract is subjected to gas chromatographic separation and detection using an electron capture detector. The calibration curve was found to be linear up to a concentration of 2.5 mg $l^{-1}$ $NO_2^-$. The detection limit calculated from the threefold noise level and the slope of the calibration curve is 0.008 mg $l^{-1}$. The relative standard deviation (including that of the blank) was less than 8%. The reliability of the method is adequate for practical uses. Amongst the advantages is that the method does not require the use of exceedingly toxic reagents. On the other hand, the method is applicable for samples that even after being subjected to clarification procedures still do not become fully transparent.

*Keywords:* Natural waters; Nitrite ions; Gas chromatography

## 1. Introduction

In the decades that have elapsed since the emergence of flow injection analysis (FIA), several automated methods have been developed for the microquantitative determination of nitrite (FIA spectrometry [1–4], FIA–AAS [5], FIA–voltammetry [6–8], etc.). However, the most widely used practical procedures are still based on spectrophotometric methods [9–12]. Generally the sensitivity of spectrophotometric nitrite determinations satisfies the requirements. However, many of these methods have the drawback that they imply the use of highly toxic and/or carcinogenic chemical reagents [13,14]. Increased precautions are necessary in the case of methods based on the use of azo dyes. Yet another drawback of these methods is that in the case of turbid or opalescent samples, the measurement itself may be hindered, as the clarifying agents used in practice are far from ideal (i.e. the Hungarian Standard [15] recommends the use of zinc hydroxide).

The aim of the present paper is to describe a method that may be used for the determination of the nitrite content in natural waters. The method advocated by us does not require the use of special precautionary measures. On the other hand, our method is applicable even in the cases of samples that, after clarification with zinc hydroxide, still do not provide a transparent, clear solution. The zinc hydroxide treatment of the sample is still recommended, as this happens to be an efficient means of eliminating from the liquid phase interfering heavy metal ions (i.e. $Fe^{3+}$ and $Cu^{2+}$).

* Corresponding author.

☆ In honour of Professor Inczedy.



*SSDI* 0039-9140(95)01576-0

## 2. Experimental

### 2.1. Chemicals and reagents

Analytical reagent grade chemicals were used throughout. Distilled water was prepared starting from 2 l of chlorinated tap water, and the chlorine was removed by boiling vigorously for 10 min. After the addition of 2 g of sodium hydroxide, the remaining water was redistilled. All the solutions were prepared using the distilled water obtained according to the above procedure.

Clarifying agents used were 0.6 M $ZnSO_4$ and 2 M NaOH. Other solutions and chemicals were 3.5 M $H_2SO_4$, a mixture of acetone and redistilled water (2:3), $5 \times 10^{-4}$ M KI solution prepared from iodine-free potassium iodide, and finally *n*-hexane. Before use, acetone and *n*-hexane were redistilled and nitrogen gas was bubbled through the KI solution in the test tube for 2 min.

Aqueous standard solutions containing 0.05, 0.10, 0.25, 0.50, 1.00, 1.50, 2.00 and 2.50 mg $l^{-1}$ $NO_2^-$ respectively were prepared by dilution from a 100 mg $l^{-1}$ $NO_2^-$ stock solution which was made up from $KNO_2$.

### 2.2. Apparatus and chromatographic conditions

A Packard-Becker model 419 gas chromatograph was used, equipped with a $^{63}Ni$ electron capture detector and a glass capillary column (30 m × 0.75 mm) coated with SPB-35 (Supelco Inc., USA). The chromatograph was interfaced to a Shimadzu Chromatopac C-R3A integrator. Nitrogen was used as carrier gas at a flow rate of 40 ml $min^{-1}$. The tests were carried out under isothermal conditions. The temperature of the column, inlet and the detector were 110 °C, 170 °C and 300 °C respectively.

### 2.3. Procedure

A portion (2 ml) of $ZnSO_4$ solution and 1 ml of NaOH solution were added to 100 ml of the sample. After sedimentation of the zinc hydroxide precipitate, the clear supernatant was used for the analysis.

A portion (4.5 ml) of the acetone/water mixture, 1.0 ml of the $H_2SO_4$ solution and 2.50 ml of the clarified sample were introduced into a 14 ml vial. Subsequently, nitrogen gas was bubbled through the vial for 2 min, after which 0.5 ml of KI solution and 2.50 ml of *n*-hexane were added to the liquid. The vial was then closed and allowed to stand for 1 h, with vigorous shaking every 15 min. Finally, 5 µl aliquots of the organic phase were manually injected with a micropipette into the gas chromatograph. Three injections were made for each sample. The peak area was used for quantitation and for the calculations. The blank (redistilled water) and the standard solutions were treated in the same manner as the sample. Standard curves were constructed daily.

## 3. Results and discussion

In the above described method, the nitrite ions reacted with iodide ions in the presence of sulphuric acid and acetone, and the released iodine was measured with the GC method of Hasty [16]. Since oxygen oxidizes the iodide ions and this reaction is catalyzed by the NO formed during the reaction between iodide and nitrite, the dissolved oxygen was removed from the sample.

In agreement with the findings of Hasty [16], under the described experimental conditions we also found the existence of a single reaction product, namely monoiodoacetone. The compound 1,1-di-iodoacetone does not appear if the $H_2SO_4$ concentration of the reaction medium is in the range 0.1–1.0 mol $l^{-1}$ (see Refs. [16,17]). The retention time of *n*-hexane and monoiodoacetone were 1.1 and 2.7 min respectively. In reasonable agreement with the findings of other workers [16,18], the partition coefficient of monoidoacetone was found to be 1.85 between *n*-hexane and water at room temperature ($C_{org}/C_{aq}$).

The detector response to monoiodoacetone extracted into *n*-hexane was directly proportional to the $NO_2^-$ concentration of the sample up to a concentration of 2.5 mg $l^{-1}$ of $NO_2^-$. The regression equation of a typical standard curve was $y = 1.93 + 82.54x$, where $x$ is the $NO_2^-$ concentration in milligrams per litre and $y$ is the peak area in arbitrary units. The standard deviation of the regression constant (intercept) and the regression coefficient (slope) were 0.28 and 0.77 respectively. It was shown by the test that the regression constant is significantly different from zero ($p < 0.05$). It appears that the intercept is due to the impurities existing in the reagents.

Table 1
Results of comparative $NO_2^-$ determinations in water samples (mg $l^{-1}$)

| Sample | Gas chromatographic method | | | Spectrophotometric method [a] | | |
|---|---|---|---|---|---|---|
| | $n$ | $\bar{x}$ | SD | $n$ | $\bar{x}$ | SD |
| Rainwater | 7 | 0.069 | 0.005 | 5 | 0.063 | 0.008 |
| Drinking water (unchlorinated) | 5 | 0.078 | 0.007 | 5 | 0.087 | 0.008 |
| Lake water (I) | 6 | 0.103 | 0.008 | 6 | 0.094 | 0.007 |
| Lake water (II) | 7 | 0.329 | 0.024 | 5 | 0.368 | 0.039 |
| Marsh water | 8 | 1.481 | 0.108 | 5 | 1.352 | 0.102 |

[a] Reagents: *N*-(1-naphthyl)ethylendiamine dihydrochloride and sulphanilic acid (see Ref. [21]).

To establish the limit of detection, the blank (redistilled water) was subjected ten times to the complete procedure, including the pretreatment, as previously described, with clarifying agents. The mean and the standard deviation of the obtained signals were 2.51 and 0.22 respectively in arbitrary units. The limit of detection (LOD) was calculated from the standard deviation of the blank signals (noise, $N$) and the slope of the calibration curve ($S$) as follows [19]: $LOD = 3N/S = 0.008$ mg $l^{-1}$ $NO_2^-$ in the water sample. This concentration value calculated corresponds to about 40 pg of $NO_2^-$ ions in the sample if a 5 µl aliquot of the organic phase is injected into the gas chromatograph.

In order to check the reproducibility, the complete procedure described above was repeated seven times with one sample of unchlorinated, poor-quality drinking water. The sample contained 81.6 mg of $Na^+$, 12.1 mg of $K^+$, 248.8 mg of $Ca^{2+}$, 47.3 mg of $Mg^{2+}$, 0.26 mg of $Fe^{2+}$, 0.10 mg of $Mn^{2+}$ and 0.22 mg of $NH_4^+$ cations, as well as 824.3 mg of $HCO_3^-$, 101.2 mg of $Cl^-$, 79.4 mg of $NO_3^-$, 111.9 mg of $SO_4^{2-}$, 16.0 mg of $SiO_3^{2-}$ and 0.003 mg of $SeO_3^{2-}$ anions per litre, while the permanganate index [20] was 6.4 mg $l^{-1}$ of oxygen. The mean and the relative standard deviation (RSD) of the obtained results were 0.347 mg $l^{-1}$ $NO_2^-$ and 5.8% respectively.

To check the day-to-day reproducibility, the $NO_2^-$ concentration of the same water sample as mentioned above was determined once a day for five consecutive days. The mean of the obtained results was 0.328 mg $l^{-1}$ $NO_2^-$ and the RSD was 7.4%. (We have used the same detector and column every time. The sensitivity of the measuring system has a fluctuation of ±5.5% from day to day.)

We investigated the interfering effect of various ions on the determination of 0.75 mg $l^{-1}$ $NO_2^-$. It was found that up to 500 mg $l^{-1}$ level, $F^-$, $Cl^-$, $Br^-$, $H_2PO_4^{2-}$, $SiO_3^{2-}$, and $B_4O_7^{2-}$ ions do not interfere. The upper tolerance limits regarding several potentially interfering ions are as follows: 350 mg $l^{-1}$ for $NH_4^+$, 250 mg $l^{-1}$ for $NO_3^-$, 40 mg $l^{-1}$ for $Mn^{2+}$, 25 mg $l^{-1}$ for $Fe^{2+}$, $Fe^{3+}$ and $Cr^{3+}$, 15 mg $l^{-1}$ for $Cu^{2+}$, 2 mg $l^{-1}$ for $SeO_3^{2-}$, 0.5 mg $l^{-1}$ $AsO_2^-$ and $AsO_4^{3-}$, 0.2 mg $l^{-1}$ for $S^{2-}$ and finally less than 0.1 mg $l^{-1}$ for $ClO^-$ and $IO_3^-$. It is obvious the fairly high tolerance limits for the heavy metal ions is due to the clarification of the sample.

Several water samples were analysed by the method described in the present paper as well as by a widely accepted [21] spectrometric method. As shown in Table 1, the results obtained by the two methods are in close agreement. The difference between the corresponding mean values was not significant at the 5% probability level in either case. The RSD of the gas chromatographic results was lower than 8%.

We intend to apply the described gas chromatographic method for the analysis of various food products, with special emphasis on the analysis of samples difficult to discolour such as fruit juices. In the case of celery juice we have already applied the method developed by us. The nitrite content of the celery juice was determined in the described manner, performing five parallel analyses. The mean value was 1.428 mg $l^{-1}$ and the RSD was 7.3%.

The original nitrite content of celery juice was decomposed quantitatively [5] with the aid of sulphaminic acid, then $KNO_2$ was added to the sample so as to achieve a 1.00 mg $l^{-1}$ concentration of nitrite. Following this procedure we performed three parallel determinations ac-

cording to the above described procedure. The obtained results were 0.92, 0.99 and 1.05 mg $l^{-1}$.

## 4. Conclusions

On the basis of our results we may safely conclude that the gas chromatographic method developed by us proved adequate for the determination of nitrite ions in natural waters and unchlorinated potable waters. The sensitivity and reliability of the method meets the practical requirements. It is worth mentioning that the method does not necessitate the use of highly toxic reagents and the samples do not need to be transparent. We believe that the present method is applicable in food analysis, primarily in the case of samples that are difficult to discolour.

## Acknowledgement

Financial support from the National Fund of Scientific Research (OTKA) is gratefully acknowledged.

## References

[1] H. Bergamin, B.F. Reis and E.A.G. Zagatto, Anal. Chim. Acta, 97 (1978) 427.
[2] E.A.G. Zagatto, A.O. Jacintho, J. Mortatti and H. Bergamin, Anal. Chim. Acta, 120 (1980) 339.
[3] R.C. Schothorst, J.M. Reijn, H. Poppe and G. von den Boef, Anal. Chim. Acta, 145 (1983) 197.
[4] S. Nakashima and M. Yagi, Anal. Chim. Acta, 155 (1983) 263.
[5] M. Gallego, M. silva and M. Valcarcel, Fresenius' Z. Anal. Chem., 323 (1986) 50.
[6] A.G. Fogg, N.K. Bsebsu and M.A. Abdalla, Analyst, 107 (1982) 1040.
[7] A.G. Fogg, A.Y. Chamsi and M.A. Abdalla, Analyst, 108 (1982) 464.
[8] A.G. Fogg and N.K. Bsebu, Analyst, 109 (1984) 19.
[9] D.F. Boltz and J.A. Howell, Colorimetric Determination of Nonmetals, 2nd edn., Interscience, New York, 1956, Chapter 7, p. 201.
[10] W.J. Williams, Handbook of Anion Determination, Part 1, 1st edn., Butterworth, London, 1979, p. 144.
[11] E. Sawicki, T.W. Stanley, J. Pfaff and A. D'Aminco, Talanta, 10 (1963) 641.
[12] M. Nakamura, T. Mazuka and M. Yamashita, Anal. Chem., 56 (1984) 2242.
[13] S.E. Allen, Chemical Analysis of Ecological Materials, Blackwells, Oxford, 1974, p. 203.
[14] A. Foris and T.R. Sweet, Anal. Chem., 37 (1965) 701.
[15] Drinking water analysis: determination of nitrate and nitrite ions, Hungarian Standard MSZ 448/12-82. 3.3.2.
[16] R.A. Hasty, Mikrochim Acta, 1971, 348.
[17] S.T. Grys, J. Chromatogr., 100 (1974) 43.
[18] L. Maros, M. Káldy and S. Igaz, Anal. Chem., 1989. 61, 733.
[19] E. Pungor, Analítikusok kézikönyve (Handbook of Analysts), Vol. 17, Mûszaki Könyvkiadó, Budapest, 1987, p. 380 (in Hungarian).
[20] Drinking water analysis: determination of the chemical oxygen demand with potassium permanganate (permanganate index), Hungarian Standard MSZ 448/20.4.
[21] H.A.C. Montgomery and J.F. Dymock, Analyst, 86 (1961) 414.

ELSEVIER

Talanta 42 (1995) 1103–1110

Talanta

# Determination of Michaelis–Menten and inhibitor constants by an open–closed flow injection approach (Application to the alkaline phosphatase/theophylline system)

M. Sánchez-Cabezudo [1], J.M. Fernández-Romero, M.D. Luque de Castro *

*Department of Analytical Chemistry, Faculty of Sciences, University of Córdoba, Córdoba, E-14004, Spain*

Received 11 October 1994; revised 27 December 1994; accepted 20 January 1995

**Abstract**

An automatic method for the estimation of Michaelis–Menten and inhibitor constants in biochemical systems was developed using an unsegmented open–closed flow manifold, and the Lineweaver–Burk and Dixon plot methods. The methods were applied to both the determination of $K_m$ of the enzymatic reaction catalyzed by bovine alkaline phosphatase using 4-methylumbelliferone phosphate as substrate, and the determination of the $K_i$ constant from theophylline as an inhibitor of this biochemical system. The data treatment and comparative results are presented. The values obtained agree with those provided by a conventional method with the biocatalyst in solution.

## 1. Introduction

The development of continuous flow methods coupled with enzymatic reactions has increased the degree of automation in analytical chemistry over the last two decades [1, 2]. However, little attention has been paid to the development of a method for the determination of kinetic constants, stoichiometries, etc. Some papers concerning enzymatic systems (e.g. alcohol dehydrogenase/NADPH dehydrogenase/monooxygenase [3] dihyldrofolate reductase [4], lactic dehydrogenase [5], and glucose oxidase [6]) provide information on enzyme kinetic constants. One of these works deals with the determination of the Michaelis constant of the substrate and antifolate inhibition constant in the NADPH/dihydrofolate reductase system using potentiometric titrations [4].

The applicability of cyclic flow injection systems to non-determination studies has been demonstrated in a variety of methods (e.g. estimation of kinetic [7] and stoichiometry constants [8], amplification methods [9], speciation [10], reaction rate measurements [11–13] and interference removal [14]).

The phenomenon of catalysis inhibition shown by some chemical substances is frequently used to develop methods for the determination of inhibitors [15–27]. Knowledge of the kinetic parameters involved in the biochemical reaction and the inhibitors has contributed to the clarification of inhibition mechanisms.

Inhibitors can influence the enzymatic reaction in such a way that the Michaelis constant ($K_m$) is apparently increased, the maximum reaction rate ($v_{max}$) is apparently decreased or both parameters are apparently changed. The first case is known as competitive inhibition, and the second as non-competitive inhibition. The third type, the special case in which $K_m$ and $v_{max}$ are apparently equally changed, is known as uncompetitive inhibition [28].

* Corresponding author.

[1] Permanent address: Laboratory of Instrumental Techniques, Department of Analytical Chemistry, Faculty of Pharmacy, UCM. 2840-Madrid, Spain.


*SSDI* 0039-9140(95)01532-9

The aim of this work was to show the availability of open–closed flow-injection systems for monitoring inhibitory effects using theophylline as an inhibitor of immobilized alkaline phosphatase. The application of different mathematical algorithms (such as the Lineweaver–Burk method [29] and the Dixon plot method [30] to the multipeak recording achieved in the absence or presence of theophylline as inhibitor, permits the estimation of the apparent Michaelis–Menten constants of immobilized alkaline phosphatase and also the determination of the apparent inhibition constants of this system.

The biochemical reaction involved hydrolysis of a 7-hydroxy-4-methylcoumarin derivative [31] (4-methylumbelliferyl phosphate), catalyzed by phosphatase in a basic medium to yield 4-methylumbelliferone and phosphate, according to the following reaction:

4-methylumbelliferyl phosphate + $H_2O$

$$\xrightarrow{\text{Alkaline phosphatase}} \text{4-methylumbelliferone} + HPO_4^{2-}$$

The fluorescence of 4-methylumbelliferone in a basic medium was monitored at $\lambda_{ex} = 365$ nm, $\lambda_{em} = 445$ nm.

Alkaline phosphatase was immobilized on controlled pore glass in preparation to catalyze the conversion of 4-methylumbeliferone phosphate into 4-methylumbelliferone. As the sample passed through the reactor packed with the immobilized biocatalyst, the theophylline present was bound to some groups of the enzyme–substrate complex modifying its catalytic activity; thus the reaction took place to a lesser extent, the amount of 4-methylumbelliferone formed being inversely proportional to the concentration of the inhibitor.

## 2. Experimental

### 2.1. Apparatus and materials

A Kontron Instruments SFM 25 spectrofluorimeter furnished with a Hellma 138.QS flow cell and equipped with a Perkin-Elmer R-100 recorder and a Selecta 382-S recirculating thermostat was used. A Gilson Minipuls-2, four-channel peristaltic pump with a rate selector, a laboratory-made dual injection valve built from two Rheodyne 5041 injection valves, a Rheodyne 5041 injection valve (modified to act as a switching valve) and Teflon tubing of 0.5 mm i.d. were also used. A Zenit ZDS 625 nl PC-Bull System connected via a RS-232 interface was used for absorbance–time data acquisition, processing and delivery.

### 2.2. Reagents

The buffer used was a 500 mmol $l^{-1}$ aqueous solution of tris(hydroxymethyl)aminomethane (Merck N. 8382) adjusted to pH 10 with 1 mol $l^{-1}$ hydrochloric acid (Merck N. 319). A solution of 2.0 mmol $l^{-1}$ 4-methylumbelliferyl phosphate (Sigma M. 8883) was prepared in the above-mentioned buffer. A standard stock solution of alkaline phosphatase (orthophosphoric monoester phosphohydrolase, alkaline optimum, E.C. 3.1.3.1, Sigma P-2897, type I-S from *Bovine intestinal mucose*, 5.8 U $mg^{-1}$) was prepared by dissolving the content of a vial in the 1 mmol $l^{-1}$ theophylline buffer solution (Sigma T. 1633).

The reagents 3-aminopropyltriethoxysilane (Aldrich N. 11, 339-5), glutaraldehyde (Merck N. 820603) and controlled-pore glass (Sigma, CPG-240-200, 120/200 mesh) were used for the biocatalyst immobilization. All solutions were prepared using bi-distilled water of high purity obtained from a Millipore Milli-Q plus system.

### 2.3. Enzyme immobilization

Alkaline phosphatase was immobilized using Masoom and Townshend's method [32,33] and stored at 4 °C in 100 mmol $l^{-1}$ potassium dihydrogen phosphate buffer at pH 7.0. Glass tubes of different lengths and 1 mm i.d. were packed with the support–enzyme conjugate. The alkaline phosphatase reactors preserved their activity for at least 2 months (loss of activity smaller than 2%).

### 2.4. Manifold and procedure

Fig. 1 depicts the open–closed approach used. The theophylline solution (S), diluted to an appropriate extent with tris-HCl buffer, and the substrate solution (R) are simultaneously injected via the dual valve ($IV_1$ and $IV_2$) into two streams of the same buffer (B), and merge at point "a". The inhibitor–substrate plug passes through the valve (SV) and is then trapped in the closed circuit by switching the valve at suitable time interval after injection. The plug passes through the alkaline phos-

phatase reactor where the enzymatic reaction takes place to an appropriate extent. The cycling of the plug into the circuit provides a multipeak recording in which the peak height increases gradually after each new substrate/catalyst contact, thus providing an additional amount of the monitored product. As the buffer solution is injected instead of the theophylline solution the enzymatic reaction occurs to a greater extent and the multipeak recording achieved is used as the blank signal. In the presence of the inhibitor, the catalyzed reaction occurs to a lesser extent. The difference between the signal obtained in the absence and presence of the inhibitor is proportional to the concentration of the inhibitor in the sample.

### 2.5. Analytical signal and data treatment

The iterative passage of the bolus through the immobilized enzyme reactor (IMER) and detector provides the typical recording shown in Fig. 2, in which the successive evolution of the fluorescence signal corresponds to the development of the enzymatic reaction in the absence and presence of the inhibitor (See Fig. 2(A).

The manual method for the determination of $K_m$ involves measurement of the initial reaction rate at different substrate concentrations. The reaction rate vs. substrate concentration plot is a typical exponential curve with a maximum, constant reaction rate ($v_{max}$) at high substrate concentration. $K_m$ is defined as the substrate concentration corresponding to a reaction rate equal to $v_{max}/2$.

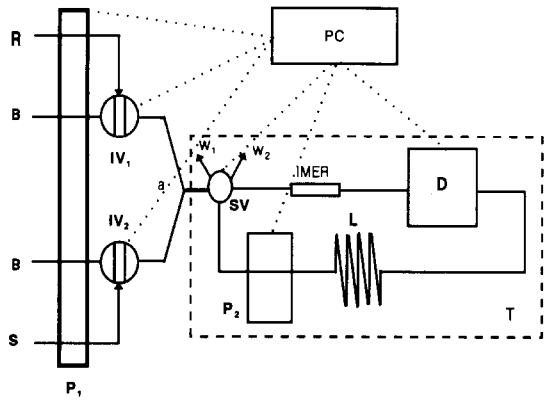


Fig. 1. Open–closed system: R, substrate; B, buffer; S, sample; $P_1$ and $P_2$, peristaltic pumps; $IV_1$ and $IV_2$, double injection valve; a, merging point; SV, switching valve; $W_1$ and $W_2$, waste; IMER, immobilized enzyme reactor; D, detector; L, open reactor; PC, personal computer.

The wealth of information supplied by each recording enables the use of different procedures for obtaining initial reaction rates values.

The multipeak recording in Fig. 2(B) allows different measurements based on fluorescence differences between peaks, whether consecutive or not. Thus, three reaction rate values were obtained from the recording, namely $V_1$, $V_2$ and $V_3$ from the equation $V_i = (A_{i+1} - A_i)/(t_{i+1} - t_i)$, where $A_{i+1}$ and $A_i$ are consecutive maxima or minima obtained at times $t_{i+1}$ and $t_i$, respectively. It is also possible to obtain measurements between non-consecutive peaks, from the equation $V_{31} = (A_3 - A_1)/(t_3 - t_1)$ where $V_{31}$ is the reaction rate calculated from maxima 3 and 1 at times $t_3$ and $t_1$, respectively.

A number of methods [28] have been used to foretell the type of inhibition. However, only two of these methods are widely used; these are discussed below.

(a) A straight line for each concentration of inhibitor is obtained when $1/V_i$ is plotted against $1/[S]$, according to Lineweaver and Burk [29]. These straight lines generally have different slopes for different inhibitor concentrations. Depending on the intercept and the slopes it is possible to predict the type of inhibition. When $1/V$ is plotted against $1/[S]$ in the absence of inhibitor, the constant achieved is the apparent $K_m$ of the enzyme.

(b) A more convenient method is that described by Dixon [30] which enables estimation of $K_i$ by two different procedures: (i) at constant substrate concentration $V_i$ is calculated at several concentrations of the inhibitor, and $1/V_i$ is plotted vs. inhibitor concentration. (ii) $1/K'_m$ is plotted vs. inhibitor concentration ($K'_m$ is the apparent Michaelis constant calculated by the Linewaver–Burk method for each inhibitor concentration). Every type of inhibition provides a straight line for each substrate concentration. In both cases (i and ii) the $x$-axis intercept provides the values of $-K_i$.

## 3. Results and discussion

### 3.1. Optimization of variables

The open–closed approach was optimized using the univariate method. This study was aimed at obtaining the best analytical response of the system in the absence of the inhibitor. The variables were classified into physical, chemical and those characteristic of the hydro-

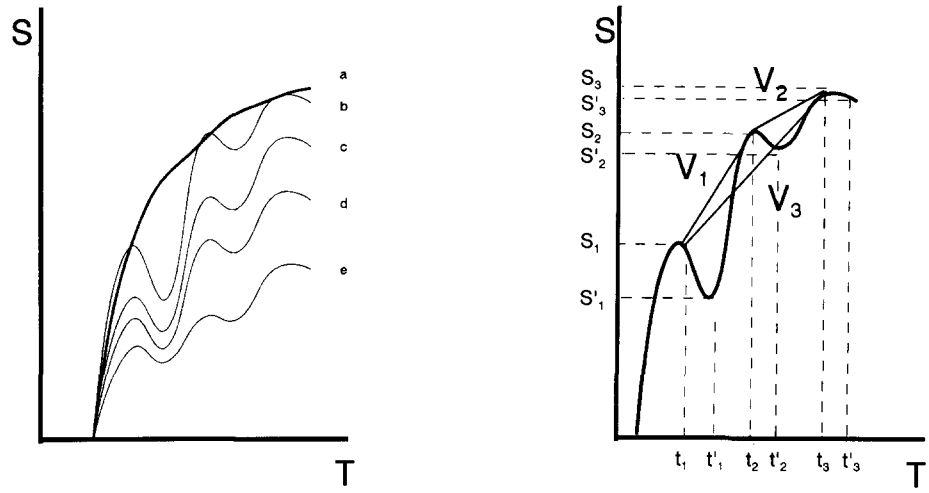


(A) (B)

Fig. 2. (A) Kinetic curves from (a) conventional method, (b–e) open–closed FI method (b, blank; c–e, different theophylline concentrations). (B) Types of measurement; $S$, analytical signal; $T$, time; $S_1$, $S_2$ and $S_3$, maxima obtained at times $t_1$, $t_2$ and $t_3$, respectively; $S'_1$, $S'_2$ and $S'_3$, minima obtained at times $t'_1$, $t'_2$ and $t'_3$, respectively; $V_1$, $V_2$ and $V_3$, reaction rate measurements (see text for details).

Table 1
Study of the variables

| Type | Variable | Range studied | Optimum value |
|---|---|---|---|
| Physical | Temperature (°C) | 20–45 | 40 |
| FIA | Flow-rate (ml $min^{-1}$) | 0.6–3.2 | 1.3 |
| | $IV_1$ injection volume (μl) | 50–500 | 225 |
| | | 50–1000 | 500 |
| | $IV_2$ injection volume (μl) | 50–500 | 100 |
| | | 0.1–1.0 | 0.2 |
| | Length of coil $L_1$ (cm) | 40–100 | 70 |
| | Length of IMER (cm) | 0.1–1.0 | 0.2 |
| | Switching time (s) | 6.0–10.0 | 8.4 |
| Chemical | [Tris-HCl] (mmol $l^{-1}$) | | |
| | pH | | |

dynamic system. Table 1 shows the range studied and the optimum values found.

An increase in temperature had a favourable effect on the analytical signal. Over 40 °C the signal did not increase, probably owing to biocatalyst denaturation.

The flow-rate had a marked influence on the evolution of the signal in the closed system, as it conditioned both the dispersion of the plug and the substrate–enzyme–inhibitor contact. Low flow-rates provided high development of the enzymatic reaction, but also a lower number of iterative passages through the enzyme reactor. A flow-rate of 1.3 ml $min^{-1}$ was chosen to obtain sufficient peaks in the multipeak recording. Both substrate and inhibitor injection volumes influenced the development of the multisignal. Substrate injection volumes ($IV_1$) above 225 μl increased the dispersion in the closed system. A 500 μl injection volume of inhibitor ($IV_2$) produced the highest inhibitory response. The IMER length had a strong influence on the analytical response. A long length provided higher development of the enzymatic reaction and a lesser inhibitory effect, probably as a consequence of more active sites in the enzyme reactor. A 0.2 cm long alkaline phosphatase reactor provided the highest difference between blank and sample recording.

At the flow-rate selected (1.3 ml $min^{-1}$), a 100 cm length of coil L and a switching time of 70 s after injection provided the best hydrodynamic conditions for optimal development of the biochemical reactions taking place in the open–closed approach.

Table 2
Calculation of the Michaelis constants

| Method | Type of measurement | Lineweaver–Burk lines | | | Kinetic parameter | |
|---|---|---|---|---|---|---|
| | | Slope | Intercept | $r^2$ | $K_m$ (mmol $l^{-1}$) | $V_{max}$ (mmol $l^{-1}$ $s^{-1}$) |
| Open–closed | Maxima | | | | | |
| | $V_1$ | 2.099 | 5.881 | 0.9972 | 0.357 | 0.170 |
| | $V_3$ | 2.260 | 4.804 | 0.9990 | 0.470 | 0.208 |
| | Minima | | | | | |
| | $V'_1$ | 0.736 | 3.445 | 0.9985 | 0.211 | 0.287 |
| | $V'_2$ | 1.213 | 4.957 | 0.9930 | 0.244 | 0.207 |
| Conventional | | 2.664 | 6.478 | 0.9982 | 0.411 | 0.154 |

A 0.5 mol $l^{-1}$ tris solution, adjusted to pH 8.5 with 1 M hydrochloric acid, was selected as buffer. All the ingredients of the enzymatic reaction (substrate and inhibitor solutions) were prepared in this buffer.

### *3.2. Determination of the Michaelis–Menten constants*

*(a) By the proposed method*

The Michaelis–Menten constant and the maxima reaction rate were calculated by applying the Lineweaver–Burk method in the open–closed system in the absence of inhibitor. Five 4-methylumbelliferyl phosphate solutions with concentrations between 0.04 and 4.0 mmol $l^{-1}$ were injected in triplicate into the system and the multipeak recording from each solution was obtained. A simple computer processing of the data provided the reaction rate values and also allowed estimation of $K_m$ and $V_{max}$. Table 2 shows the results found using different types of measurement.

*(b) By the conventional method*

The Lineweaver–Burk method [29] was applied to the manual kinetic data for calculation of reaction rates with the enzyme in solution. Five millilitres of the reagent solution containing different concentrations of substrate were added to a test tube containing 100 µl of alkaline phosphatase (10 U $l^{-1}$). The mixture was poured into a conventional cell, placed in the fluorimeter and the fluorescence intensity vs. time was plotted. A data treatment similar to that used in the open–closed flowing method was performed.

*(c) Comparison of the results*

The envelopes of the multipeak signal provided by the open–closed system were quite similar to the kinetic curves obtained using the conventional method. This enables conventional treatment of the information obtained using the automatic method, and comparison of the results obtained with thoses provided by the conventional method.

The linear reaction rate interval achieved in the closed circuit is lower than the linear reaction rate interval obtained by the conventional method. Both the highest linear reaction rate range and the values of $K_m$ and $v_{max}$ closer to the conventional method were obtained when they were based on the average of different reaction rate ranges.

### *3.3. Determination of the inhibitor constants*

*(a) By the proposed method*

The inhibition constants for thephylline were calculated by applying both the Lineweaver–Burk and the Dixon plot methods. Inhibitor solutions containing 0, 0.5, 1.0 and 5.0 mmol $l^{-1}$ were injected in triplicate into the system. The treatment of the data provided information about the type of inhibition and also permitted estimation of $K_i$ from different measurements in the multipeak recording. Figs. 3 and 4, illustrate models of the different types of measurement. Table 3 shows some of the results obtained.

*(b) By the conventional method*

Lineweaver–Burk and Dixon plot methods were applied to the manual kinetic data for calculation of reaction rates with the enzyme in solution. 5 ml of the reagent solution containing different concentrations of substrate were

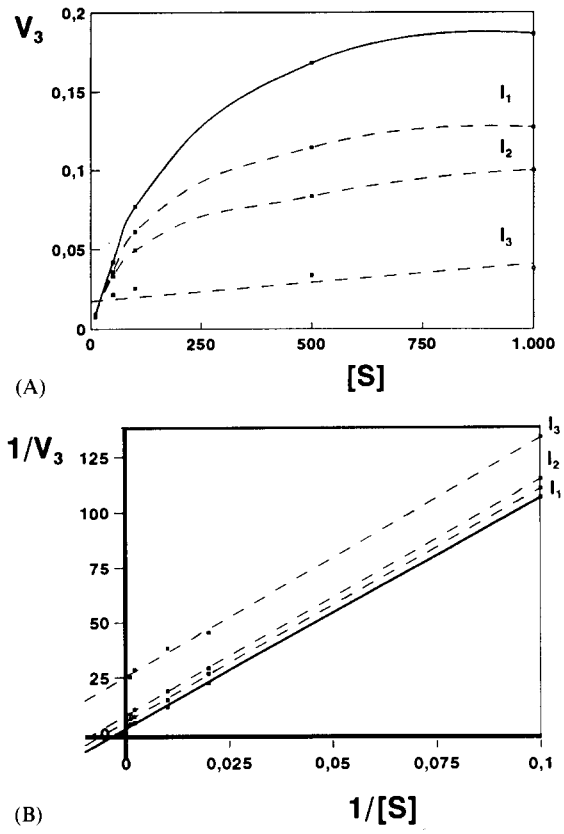


Fig. 3. (A) Reaction rate vs. substrate from $V_3$ measurement: in the absence of theophylline (——) and with different theophylline concentrations $I_1$, $I_2$ and $I_3$ (– – –). (B) Lineweaver–Burk lines from $V_3$ measurements: without theophylline (——) and with different theophylline concentrations $I_1$, $I_2$ and $I_3$ (– – –).

added to a test tube containing 100 µl of standard solution of theophylline were added to a test tube containing 100 µl of standard solution of theophylline (containing 0, 0.5, 1.0 and 5.0 mmol $l^{-1}$) and 100 µl of alkaline phosphatase (10 U $l^{-1}$). The procedure was similar to that used in the manual method previously described.

*(c) Comparison of the results*

Figs. 3 and 4 are typical inhibition plots. The straight lines obtained in all instances denote that theophylline is an uncompetitive inhibitor of bovine alkaline phosphatase. Table 3 summarizes the features of the lines obtained by both the conventional and the proposed open–closed method.

Comparison of the two sets of results shows the correlation found when the Lineweaver–Burk method is applied:

$$Y = 0.65X + 3.37 \qquad (r = 0.9836)$$

where $X$ refers to the conventional kinetic method and $Y$ refers to the open–closed method. The parameters of this equation are as follows:

$$\Sigma_{\text{intercept}} = 0.64$$

$$\Sigma_{\text{slope}} = 0.08$$

$$\Sigma_{y/x} = 0.49$$

which shows an acceptable correlation between both methodologies.

## 4. Final remarks

The study reported here shows the capability of open–closed systems for the implementation of methodologies for predicting the type of inhibition in enzyme-based processes.

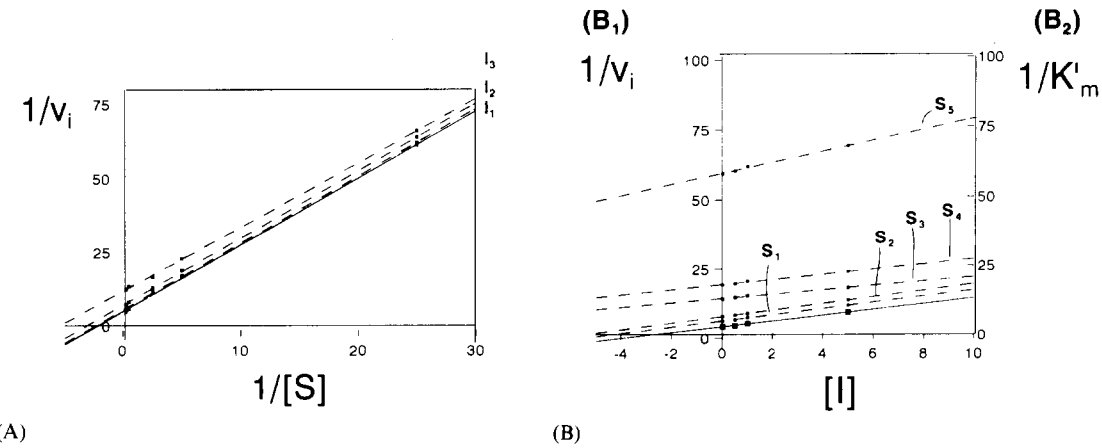


Fig. 4. (A) Lineweaver–Burk lines from $V_1$ measurement: without theophylline (——) and with different theophylline concentrations $I_1$, $I_2$ and $I_3$ (– – –) lines). (B) Dixon plot method: ($B_1$) from [I] vs. $1/v_i$ (at different substrate concentrations $S_1$, $S_2$, $S_3$, $S_4$ and $S_5$); ($B_2$) from [I] vs. $1/K'_m$.

Table 3
Estimation of the inhibitor constant (based on $V_i$ measurement)

| Method mate | [Inhibitor] Inhibition (mmol/$l^{-1}$) − 1) | Slope (mmol $l^{-1}$) | Intercept degree [a] | $r^2$ | $K_m$ (mmol $l^{-1}$) | $V_{max}K_i$ esti- (mmol/$l^{-1}$ s |
|---|---|---|---|---|---|---|
| (a) Lineweaver–Burk | | | | | | |
| Open–closed | 0 | 5.881 | 2.099 | 0.9972 | 0.3569 | 0.1700– – |
| | 0.5 | 6.586 | 2.108 | 0.9974 | 0.3201 | 0.15180.23900 |
| .11 | | | | | | |
| | 1.0 | 8.495 | 2.150 | 0.9983 | 0.2531 | 0.11770.44400 |
| .31 | | | | | | |
| | 5.0 | 10.81 | 2.170 | 0.9987 | 0.2010 | 0.09250.16760 |
| .46 | | | | | | |
| Conventional | 0 | 4.080 | 2.260 | 0.9997 | 0.5530 | 0.2450– – |
| | 0.5 | 5.379 | 2.269 | 0.9996 | 0.4097 | 0.18590.63580 |
| .26 | | | | | | |
| | 1.0 | 6.988 | 2.276 | 0.9997 | 0.3257 | 0.14310.59340 |
| .41 | | | | | | |
| | 5.0 | 11.740 | 2.169 | 0.9996 | 0.1847 | 0.08520.37510 |
| .85 | | | | | | |
| (b) Dixon plot [b] | | | | | | |
| Open–closed | – | 2.766 | 1.045 | 0.9972 | – | –0.3770– |
| Conventional | – | 1.808 | 1.262 | 0.9999 | – | –0.6930– |

[a] Calculated as $[I] = (1 - V'/V)$ [34].
[b] From the second procedure ($1/K'_m$ vs. [I]).

A pattern of inhibition of different enzymatic systems can be established using open–closed manifolds and other potential inhibitors.

## Acknowledgement

The Comisión Interministerial de Ciencia y Tecnología (CICyT) is thanked for financial support (Project No. PB93-0827).

## References

[1] J. Ruzicka and E.H. Hansen, Flow Injection Analysis, Wiley, New York, 1988.
[2] M. Valcárcel and M.D. Luque de Castro, Flow Injection Analysis: Principles and Applications, Ellis Horwood, Chichester, 1987.
[3] S. Girotti, A. Roda, S. Chini, A.L. Piacentini, G. Carrera and R.A. Bovara, Anal. Chim. Acta., 183 (1986) 187.
[4] R. Gillis, J.C. Sari, L. Sica, B. Bourdeaux and C. Briand, Anal. Biochem., 152 (1986) 1.
[5] J.M. Fernández-Romero, M.D. Luque de Castro and M. Valcárcel, Anal. Chim. Acta., 219 (1989) 191.
[6] J. Marcos, A. Ríos and M. Valcárcel, Anal. Chim. Acta., 283 (1993) 429.
[7] A. Ríos, M.D. Luque de Castro and M. Valcárcel, Anal. Chem., 57 (1985) 1803.
[8] A. Ríos, M.D. Luque de Castro and M. Valcárcel, J. Chem. Educ., 63 (1986) 552.
[9] A. Ríos, F. Lázaro, M.D. Luque de Castro and M. Valcárcel, Anal. Chim. Acta., 199 (1987) 15.
[10] A. Fernández, M.D. Luque de Castro and M. Valcárcel, Quím. Anal., 6 (1987) 314.
[11] J.M. Fernández-Romero, M.D. Luque de Castro and M. Valcárcel, J. Biotech., 14 (1990) 43.
[12] J.M. Fernández-Romero, M.D. Luque de Castro and M. Valcárcel, Anal. Chim. Acta, 274 (1993) 99.
[13] J.M. Fernández-Romero, M.D. Luque de Castro and M. Valcárcel, Sensor Actuators, B.10 (1993) 203.
[14] R. Quilles-Zafra, J.M. Fernández-Romero, M.D. Luque de Castro and M. Valcárcel, Anal. Proc., 31 (1994) 233.
[15] G.G. Guibault, Anal. Chem., 38 (1966) 527R.
[16] G.G. Guilbault, Anal. Chem., 40 (1968) 459R.
[17] G.G. Guilbault, Anal. Chem., 42 (1970) 334R.
[18] J. Delga and P. Foulhous, Prod. Probl. Pharm., 24 (1969) 57.
[19] J. Cohen, R. Oostembaan and F. Berends, Methods Enzymol., 11 (1968) 686.
[20] C. Mendoza, P. Wales, H. McLeod and W. Mckinley, Analyst, 34 (1986) 93.
[21] G.G. Guilbault, M. Sacar and M. Zimmer, Anal. Chim. Acta, 44 (1969) 361.
[22] A. Townshend and A. Vaughan, Talanta, 17 (1969) 289.
[23] W.H.R. Shaw and D.N. Raval, J. Am. Chem. Soc., 83 (1961) 3184.
[24] Y. Shirokane, M. Nakajima and K. Misusawa, Clin. Chem., 37(3) (1991) 478.

[25] M.A. Saka-Aumini, J.J. Vallon and S. Lartillot, Anal. Chim. Acta, 245 (1991) 129.
[26] K.J. Sweadner, Anal. Biochem., 194 (1991) 130.
[27] N.C. Fould, J.M. Wilshere and M.J. Green, Anal. Chim. Acta, 229 (1990) 57.
[28] H.U. Bergmeyer and K. Gawehn, Principles of Enzymatic Analysis, Verlag Chemie, Weinheim, 1978.
[29] H. Lineweaver and D. Burk, J. Chem. Soc., 56 (1934) 658.
[30] M. Dixon and E.C. Webb, Nature, 184 (1959) 1298.
[31] E. Koller and O. Wolfbeis, Anal. Biochem., 143 (1984) 146.
[32] M. Masoom and A. Townshend, Anal. Chim. Acta, 166 (1984) 111.
[33] M. Masoom and A. Townshend, Anal. Chim. Acta, 174 (1984) 293.
[34] J. Cárdenas, E. Fernández, F. Galván, A.J. Márquez and J.M. Vega, Problemas de Bioquímica, Alhambra, Madrid, 1988.

ELSEVIER

Talanta 42 (1995) 1111–1119

Talanta

# Prediction of chemical structure of aromatic hydrocarbons by pattern recognition of spectral lines obtained by fluorescence spectrometry in a supersonic jet

Cheng-Huang Lin, Totaro Imasaka *

*Department of Chemical Science and Technology, Kyushu University, Hakozaki, Fukuoka 812, Japan*

Received 14 September 1994; revised 23 January 1995; accepted 24 January 1995

**Abstract**

A technique based on pattern recognition of data obtained by supersonic jet spectrometry is employed for the prediction of chemical structure. The degree of similarity is evaluated quantitatively by calculating a cross correlation factor between sample and reference molecules. A probability density function is determined by fitting the data to a specified equation. The functional group and its position are also predicted by a similar technique. The pattern recognition provides a method for prediction of the chemical structure and is applicable to samples that have not been examined by supersonic jet spectrometry.

## 1. Introduction

Supersonic jet spectrometry provides sharp line structure in ultraviolet and visible spectra [1–4]. This analytical method, therefore, shows selectivity and allows spectrometric differentiation between molecules with similar chemical structures. The application of mass spectrometry after multiphoton ionization gives information relating to the molecular weight of the sample. This information alone, however, is not always sufficient for differentiating between isomers. Although the advantage of supersonic jet spectrometry lies in its well-resolved spectral features, the mass resolution of this technique could be improved by expanding the gas and decreasing its velocity distribution, since a better mass resolution can be obtained by other techniques such as ion cyclotron resonance. It is the sharp spectral features given by supersonic jet spectrometry that are important and useful in the assignment of chemical species and structure.

When a complete database is available, a sample molecule can be accurately identified using the spectral data accumulated for a series of authentic compounds. Recently, a database constructed by accumulating the wavelengths of pure electronic (0–0) transitions was used for the assignment of aromatic hydrocarbons [5–7]. This approach is reliable, because of the sharp line structure of the spectrum. However, there is no straightforward relationship between spectrum and chemical structure. It is, therefore, difficult to assign the chemical species when no standard spectrum is available in the database for that species. It would be useful, therefore, to develop a new method for data analysis, which can be applied to samples whose spectra are not available, i.e. which have not been reported.

One possible approach to this problem involves theoretical calculations of spectral parameters. The energy for the 0–0 transition is estimated by calculation of the molecular orbital by the Pariser–Parr–Pople (PPP) method and by the complete neglect of differential overlap method for spectroscopy (CNDO/S) [8]. These methods are useful for

* Corresponding author. Fax: (81) 92-651-5606.


*SSDI* 0039-9140(95)01536-1

reducing the number of candidates in the assignment. However, the error in the estimation of the wavelength for the 0–0 transition is 1–3%, which is much larger than the error of the peak position obtained experimentally (<0.01%). For more accurate discussion, it is necessary to use a spectral pattern for assignment. In physical chemistry, the spectral profile, i.e. transition energy and intensity, is calculated from the wave function and the Franck–Condon factor by solving a Schrödinger equation. This may give additional information for assignment of the chemical species. However, this approach is not altogether accurate, and the error in the calculation of the vibrational energy sometimes exceeds 10%. In addition, such an approach is complicated and time-consuming even for a single molecule, and as a result is not suitable for applications to analytical spectroscopy. What is ideally needed is a method which will provide sufficient information for the prediction of chemical structure without a standard spectrum of the sample or a complicated theoretical calculation of spectral parameters.

This study describes an approach involving the recognition of patterns of spectral lines which are produced as a result of supersonic jet spectrometry. In order to correlate spectral feature with chemical structure, we calculate a cross correlation factor (CCF) between the spectra obtained for the sample and reference molecules. The line shape in the supersonic jet spectrum is so narrow that almost all the CCF values become zero when they are calculated for different compounds. The data, therefore, were optimized by expanding the spectral line to a specified function, e.g. a gaussian function, thus giving useful information. In order to evaluate the degree of spectral similarity quantitatively, the probability density is plotted against the CCF value for a series of aromatic hydrocarbons. In addition, the spectral data of the 0–0 transition are used for prediction of the chemical structure. The wavelength of the 0–0 transition hardly coincides with that of a different compound, but is correlated quantitatively with a probability density function, providing useful information for structure prediction. The probability densities obtained independently by the above two methods are then multiplied to improve the accuracy of prediction. The advantage of this pattern recognition is demonstrated by differentiation of the anthracene derivatives against non-anthracene compounds. The functional group and its position can also be predicted relatively. The present approach requires neither a standard spectrum of the sample nor a knowledge of complicated quantum chemistry, and it works quite well for assignment of the chemical species in supersonic jet spectrometry.

## 2. Experimental

### 2.1. Calculation

Fig. 1 shows a bar graph of the fluorescence excitation spectra for anthracene and its derivatives obtained by supersonic jet spectrometry. Similar vibrational structure is observed in the spectra of the compounds with similar chemical structure. This is consistent with the fact that vibrational structure is strongly associated with skeletal vibration of the anthracene ring. These similarities can be visually observed, but for quantitative purposes the degree of similarity should be calculated mathematically. It is possible to use a CCF value for evaluation of the similarity between the standard and reference molecules [9]. However, the spectral line is so narrow (<0.01 nm) that almost all the CCF values between different compounds become zero. Therefore, optimization is necessary to evaluate the degree of similarity.

In this study, the signal peak in the supersonic jet spectrum is assumed to have a gaussian distribution:

$$I_k(\nu) = \exp[-(\nu - \nu_k)^2/r^2] \quad (1)$$

where $I_k(\nu)$ is the fluorescence intensity at the excitation frequency of $\nu$ for peak $k$, and $r$ is the linewidth assumed. The spectra of the chemical species $X(\nu)$ and $Y(\nu)$ are represented by

$$X(\nu) = \sum_1^n X_k(\nu) \quad (2)$$

$$Y(\nu) = \sum_1^n Y_k(\nu) \quad (3)$$

where $n$ is the total number of spectral lines. In order to compare the vibrational structure in the excitation spectrum, it is necessary to subtract the frequency of the 0–0 transition from each peak position. The CCF value, $C$, is calculated between the standard and reference spectra by

$$C = \frac{\left[\int X(\nu - \nu_{0X}) \cdot Y(\nu - \nu_{0Y})\, d\nu\right]}{\left[\int X^2(\nu - \nu_{0X})\, d\nu \cdot \int Y^2(\nu - \nu_{0Y})\, d\nu\right]^{1/2}} \quad (4)$$

where $\nu_{0X}$ and $\nu_{0Y}$ are the frequencies of the 0–0 transition for compounds X and Y, respectively. The denominator is a normalization factor. The CCF value is close to unity when the spectral feature of the standard is similar to that of the reference; CCF = 1 when CCF is calculated between the same compounds. In contrast, the CCF value is close to zero when the spectral features are completely different from each other. The CCF value also depends on the parameter $r$. In order to differentiate between the compounds giving similar spectra, this value should be small. However, if it is too small, all the CCF values become zero. Thus, appropriate fuzziness must be introduced by optimizing this parameter.

The CCF value was calculated using a notebook-type personal computer (NEC, PC-9801n). The program was written in BASIC. All the spectral data were cited from the references reported by other authors and from the data measured by ourselves. After digitizing the spectral data (frequency and intensity), the excitation spectrum was calculated using the assumed value for $r$. The CCF value was calculated between the spectra for the standard and reference molecules. The time period of calculation was typically 10 min.

## 3. Results and discussion

### 3.1. Preliminary study

The CCF values are calculated for various anthracene derivatives using 2-ethylanthracene as a standard sample. These results are shown in Table 1. The linewidth, $r$, is changed from 0.1 to 10 $cm^{-1}$. When $r$ is assumed to be 0.1 $cm^{-1}$, it is difficult to evaluate the degree of similarity properly. In the present study, the optimum value of $r$ appears to be between 1 and 10 $cm^{-1}$. The CCF values calculated for alkylanthracenes are significantly larger than those for chloroanthracenes, suggesting that the standard sample contains an alkyl group rather than a chlorine atom. The CCF values for anthracene derivatives substituted at position 2 are larger than those substituted at position 9, indicating a substituent group at position 2. The CCF value is not unity for 2-methylanthracene, indicating that the sample is not 2-methylanthracene. However, the large CCF value for 2-methylanthracene implies that the chemical structure is closely related, structurally, to 2-methylanthracene, and is possibly 2-ethylanthracene. This success in the preliminary study strongly encouraged us to perform further systematic investigations.

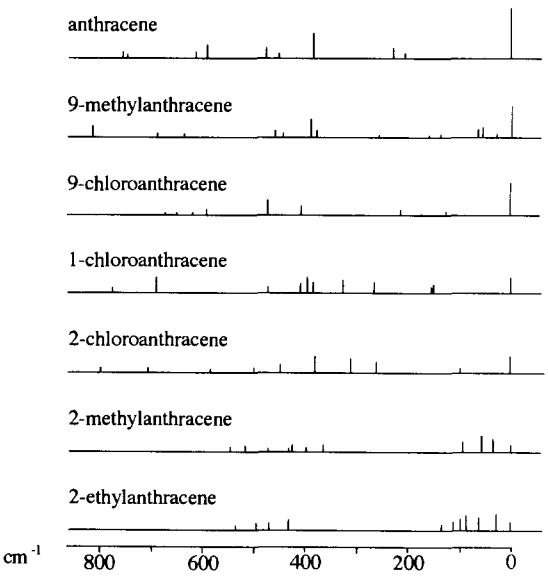


Fig. 1. Fluorescence excitation spectra for anthracene derivatives.

### 3.2. Skeletal structure

The CCF values were calculated for various aromatic hydrocarbons with different skeletons using 9-methylanthracene as a standard sample. A similar study was carried out using 1-methylnaphthalene. The results are shown in Table 2. The CCF values are the largest for the compounds with the same skeletons. Thus the skeletal structure can readily be predicted by this method.

Table 1
CCF values calculated for various aromatic hydrocarbons using 2-ethylanthracene as a standard sample

| Compound | $r = 0.1$ | $r = 1$ | $r = 10$ | Ref. |
|---|---|---|---|---|
| 2-Ethylanthracene | 1 | 1 | 1 | [6] |
| 2-Methylanthracene | 0.243 | 0.301 | 0.495 | [6] |
| 9-Methylanthracene | 0.001 | 0.060 | 0.236 | [6] |
| 2-Chloroanthracene | $10^{-4}$ | 0.008 | 0.048 | [6] |
| 9-Chloroanthracene | $10^{-12}$ | 0.004 | 0.040 | [6] |
| Anthracene | $10^{-19}$ | $10^{-4}$ | 0.002 | [6] |
| 1-Chloroanthracene | $<10^{-20}$ | $<10^{-20}$ | 0.001 | [6] |

$r$: $cm^{-1}$.

Table 2
CCF values calculated for various aromatic hydrocarbons with different skeletons using 9-methylanthracene and 1-methylnaphthalene as standard samples

| Compound | 9-Methylanthracene | | 1-Methylnaphthalene | | Ref. |
|---|---|---|---|---|---|
| | $r = 1$ | $r = 10$ | $r = 1$ | $r = 10$ | |
| Benzene | 0.002 | 0.017 | $10^{-15}$ | 0.004 | [12] |
| Indole | $10^{-15}$ | 0.001 | $<10^{-20}$ | $10^{-5}$ | [13] |
| Naphthalene | $10^{-6}$ | 0.012 | 0.044 | 0.058 | [14] |
| Fluorene | $<10^{-20}$ | $10^{-5}$ | $10^{-6}$ | 0.036 | [15] |
| Anthracene | 0.080 | 0.605 | $10^{-10}$ | 0.001 | [6] |
| Pyrene | 0.002 | 0.026 | $10^{-5}$ | 0.003 | [16] |

$r$: $cm^{-1}$.

A similar comparison was also carried out using toluene (methylbenzene) as a standard sample. The CCF values calculated for the same aromatic hydrocarbons are shown in lines 1–6 (benzene–pyrene) of Table 3. Surprisingly, the value for benzene is small; the values for pyrene and naphthalene are much larger at $r = 1\ cm^{-1}$ and those of indole and naphthalene at $r = 10\ cm^{-1}$. As a result, the CCF values were also calculated for naphthalene derivatives (7–11, Table 3). However, the CCF values are not so large for naphthalene derivatives. The values for benzene derivatives were also calculated as trials. The results are shown in lines 12–26 of Table 3. Clearly, large CCF values are obtained for benzene derivatives, especially for alkylbenzenes. It should be noted that benzene has a high molecular symmetry ($D_{6h}$) and, as a result, the electronic transition ($^1A_{1g}$–$^1B_{2u}$) is essentially forbidden. Consequently, the spectrum is observed only when the electronic transition is coupled with vibrations breaking $D_{6h}$ symmetry. This situation is completely different from other benzene derivatives. Thus benzene is a special case and is not a representative molecule for benzene derivatives. The compound with an OH or $NH_2$ substituent, e.g. *p*-cresol or *p*-toluidine, gives a small CCF value. Such compounds could be easily differentiated from benzene derivatives which contain only alkyl groups. The effect of substituent groups is further discussed in later sections.

### 3.3. Probability density function

In order to differentiate anthracene derivatives from non-anthracene compounds, the degree of similarity was evaluated by calculating the CCF values for various aromatic hydrocarbons using anthracene as a standard sample. The result is shown in column 2 of Table 4. It is apparent that compounds with an anthracene ring have larger CCF values. Fig. 2 shows the probability density of anthracene derivatives plotted against the CCF value. The solid curve was obtained by fitting the data to the following equation:

Table 3
CCF values calculated for various aromatic hydrocarbons using toluene as a standard sample

| Compound | $r = 1$ | $r = 10$ | Ref. |
|---|---|---|---|
| *Skeletal molecules* | | | |
| Benzene | 0.002 | 0.043 | [12] |
| Indole | $10^{-4}$ | 0.158 | [13] |
| Naphthalene | 0.010 | 0.133 | [14] |
| Fluorene | $10^{-6}$ | 0.026 | [15] |
| Anthracene | 0.002 | 0.024 | [6] |
| Pyrene | 0.015 | 0.040 | [16] |
| *Naphthalene derivatives* | | | |
| 2-Methylnaphthalene | 0.021 | 0.034 | [14] |
| Naphthalene | 0.010 | 0.133 | [14] |
| 1-Methylnaphthalene | $10^{-4}$ | 0.008 | [14] |
| 2-Ethylnaphthalene | $10^{-4}$ | 0.062 | [14] |
| 1-Naphthol | $10^{-6}$ | 0.023 | [17] |
| *Benzene derivatives* | | | |
| Benzene | 0.002 | 0.043 | [12] |
| Ethylbenzene | 0.721 | 0.806 | [18] |
| *n*-Butylbenzene | 0.561 | 0.711 | [18] |
| *n*-Propylbenzene | 0.544 | 0.640 | [18] |
| *n*-Hexylbenzene | 0.516 | 0.737 | [18] |
| *tert*-Butylbenzene | 0.474 | 0.601 | [18] |
| *n*-Pentylbenzene | 0.423 | 0.482 | [18] |
| Isopropylbenzene | 0.246 | 0.447 | [18] |
| 1-Phenyl-1-butyne | 0.124 | 0.265 | [20] |
| *p*-Aminophenol | 0.040 | 0.100 | [19] |
| *p*-Difluorobenzene | 0.041 | 0.012 | [20] |
| 1-Phenylpropyne | 0.013 | 0.324 | [20] |
| *p*-Cresol | $10^{-6}$ | 0.000 | [19] |
| *p*-Toluidine | $10^{-7}$ | 0.067 | [19] |
| *p*-Fluorophenol | $10^{-15}$ | 0.001 | [19] |

$r$: $cm^{-1}$.

Table 4
CCF values and similarities calculated for various aromatic hydrocarbons using anthracene as a standard sample.

| Compound | CCF | Similarity (%) | Ref. |
|---|---|---|---|
| 9-Hexylanthracene | 0.606 | 100.0 | [21] |
| 9-Methylanthracene | 0.600 | 100.0 | [21] |
| 2-Chloroanthracene | 0.406 | 99.9 | [6] |
| 2-Phenylanthracene | 0.270 | 96.0 | [22] |
| 9-Cyanoanthracene | 0.267 | 95.7 | [23] |
| 9-Bromoanthracene | 0.220 | 88.3 | [23] |
| 1-Chloroanthracene | 0.181 | 76.7 | [6] |
| 2-Methylnaphthalene | 0.174 | 73.9 | [14] |
| 9,10-Dibromoanthracene | 0.122 | 48.3 | [23] |
| 9-Phenylanthracene | 0.095 | 33.0 | [22] |
| *trans*-2-Naphthol | 0.089 | 17.9 | [17] |
| 2-Methylanthracene | 0.062 | 15.7 | [6] |
| 9-Methoxyanthracene | 0.051 | 10.9 | [24] |
| *n*-Propylbenzene | 0.050 | 10.5 | [18] |
| 9-Chloroanthracene | 0.042 | 7.1 | [6] |
| Tryptamine | 0.038 | 6.2 | [24] |
| Tryptophan | 0.035 | 5.2 | [25] |
| 7-Azaindole | 0.032 | 4.4 | [26] |
| 3-Methylindole | 0.032 | 4.4 | [13] |
| *n*-Hexylbenzene | 0.029 | 3.6 | [18] |
| 9,10-Dichloroanthracene | 0.025 | 2.7 | [23] |
| Toluene | 0.024 | 2.5 | [18] |
| 1-Naphthol | 0.023 | 2.3 | [17] |
| *cis*-2-Naphthol | 0.023 | 2.3 | [17] |
| 3-Indole acetic acid | 0.010 | 0.4 | [27] |
| 2-Ethylanthracene | 0.009 | 0.3 | [6] |
| 1-Phenylpropyne | 0.005 | 0.1 | [20] |
| 1-Phenyl-1-butyne | 0.002 | 0.0 | [20] |
| 1-Methylnaphthalene | 0.002 | 0.00 | [14] |
| Phenylethyne | 0.001 | 0.0 | [20] |
| 2-Indole propionic acid | 0.000 | 0.0 | [27] |
| 1-phenyl-1-hexyne | 0.000 | 0.0 | [20] |

The linewidth, $r$, is assumed to be $10\,cm^{-1}$.

$$P = 1 - \exp(-C^2/k^2) \quad (5)$$

where $P$ is the probability of an anthracene derivative, $C$ is the CCF value, and $k$ is the constant obtained by fitting the data to the above equation. This curve is useful for quantifying the "similarity" of the spectrum by calculating the probability from the CCF value using Eq. (5). This "similarity" is listed in the third column of Table 4. The value for 9-hexylanthracene or 9-methylanthracene is 100%, indicating a high spectral similarity, and implying a high probability to be assigned to an anthracene derivative. It should be noted that the curve in Fig. 2 is saturated at high CCF values. In order to differentiate between compounds with closely related structures, the linewidth can be reduced, e.g. to $\approx 1\,cm^{-1}$. It is interesting to note that the first seven compounds are anthracene derivatives in Table 4, but the similarity of other anthracene derivatives such as 9,10-dichloroanthracene and 2-ethylanthracene are much lower than those for non-anthracene derivatives. Thus the reliability given by the present approach is not necessarily perfect.

In order to improve the accuracy of prediction, it is necessary to use an additional, simultaneous parameter, different from the CCF value, in order to discriminate against compounds having different spectral properties.

### 3.4. Wavelength of the 0–0 transition

In the previous section, only the vibrational structure of the spectrum is used for prediction of the chemical structure after subtraction of the frequency of the 0–0 transition. However, this frequency contains important information about the extension of $\pi$ electrons in a molecule, which is related to the ring size. The second column of Table 5 shows the wavelengths of the 0–0 transition for compounds whose excitation spectra have been previously reported. The 14 anthracene derivatives are located between 364 and 387 nm, although two other compounds (pyrene and pyrazine) are also located in this spectral region. This implies that the wavelength of the 0–0 transition can be used to advantage for differentiation of anthracene derivatives. The probability density of the anthracene derivative is plotted against the wavelength of the 0–0 transition in Fig. 3. The probability density increases rapidly at shorter wavelengths and then decays gradually

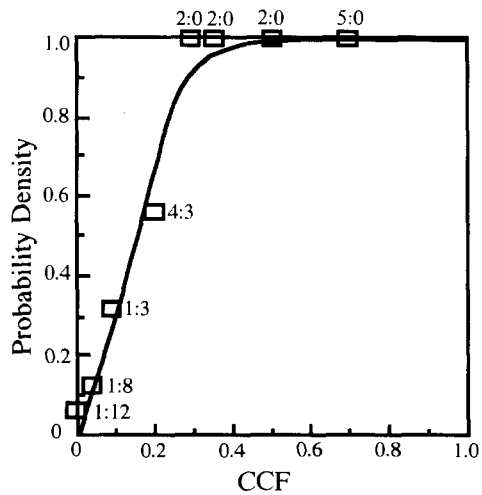


Fig. 2. Probability density of anthracene derivatives versus CCF value. The number in the Figure indicates the number of anthracene (left) and non-anthracene (right) compounds. The solid curve is calculated from Eq. (5) by fitting the experimental data to $k = 0.2$.

Table 5
Wavelengths of the 0–0 transitions for various aromatic hydrocarbons and probabilities of anthracene derivatives

| Compound | 0–0 transition (nm) | Probability (%) | Ref. |
|---|---|---|---|
| *n*-Propylbenzene | 266.08 | 0.0 | [18] |
| *n*-Hexylbenzene | 266.15 | 0.0 | [18] |
| Toluene | 266.83 | 0.0 | [18] |
| Phenylethyne | 274.94 | 0.0 | [20] |
| 1-Phenylpropyne | 275.96 | 0.0 | [20] |
| 1-Phenyl-1-butyne | 276.49 | 0.0 | [20] |
| 1-Phenyl-1-hexyne | 276.54 | 0.0 | [20] |
| 3-Indole acetic acid | 285.40 | 0.0 | [27] |
| 3-Indole propionic acid | 285.88 | 0.0 | [27] |
| Tryptamine | 286.39 | 0.0 | [24] |
| 3-Methylindole | 286.68 | 0.0 | [13] |
| Tryptophan | 286.75 | 0.0 | [25] |
| 7-Azaindole | 288.73 | 0.0 | [26] |
| Naphthalene | 312.30 | 0.0 | [14] |
| 1-Methylnaphthalene | 314.73 | 0.0 | [14] |
| 2-Methylnaphthalene | 315.40 | 0.0 | [14] |
| 1-Naphthol | 317.90 | 0.0 | [17] |
| *trans*-2-Naphthol | 323.57 | 0.0 | [17] |
| *cis*-2-Naphthol | 326.94 | 0.0 | [17] |
| 2-Ethylanthracene | 364.54 | 61.0 | [6] |
| 2-Methylanthracene | 365.07 | 60.5 | [6] |
| 2-Chloroanthracene | 367.09 | 59.5 | [6] |
| 1-Chloroanthracene | 367.31 | 59.0 | [6] |
| Pyrene | 367.44 | 58.8 | [16] |
| 2-Phenylanthracene | 370.80 | 52.0 | [22] |
| 9-Phenylanthracene | 371.14 | 51.2 | [22] |
| 9-Methylanthracene | 371.15 | 51.0 | [21] |
| Pyrazine | 372.80 | 49.5 | [28] |
| 9-Hexylanthracene | 373.03 | 48.2 | [21] |
| 9-Chloroanthracene | 373.25 | 47.2 | [6] |
| 9-Methoxyanthracene | 373.40 | 47.0 | [24] |
| 9-Bromoanthracene | 374.20 | 46.5 | [23] |
| 9-Cyanoanthracene | 382.10 | 32.4 | [23] |
| 9,10-Dichloroanthracene | 385.35 | 30.5 | [23] |
| 9,10-Dibromoanthracene | 386.45 | 30.0 | [23] |
| Benzo[a]pyrene | 395.90 | 18.5 | [29] |
| Fluoranthene | 396.56 | 18.0 | [30] |
| Perylene | 415.45 | 7.5 | [31] |
| Tetracene | 446.37 | 1.0 | [32] |
| Ovalene | 466.22 | 0.0 | [33] |
| Pentacene | 536.90 | 0.0 | [34] |

at longer wavelengths. These data were fitted to the chi-square distribution function:

$$F_m(x) = [(1/2)\Gamma(m/2)](x/2)^{m/2-1} \exp(-x/2) \quad (6)$$

where $\Gamma(m/2)$ is the gamma function, $m$ is the degree of freedom, and $x$ is the wavelength. The probability to be assigned to an anthracene derivative is listed in column 3 of Table 5. The probabilities for pyrene and pyrazine are rather high, indicating the limitation of this method alone.

### 3.5. Product of probabilities

In order to improve the accuracy of prediction, the probabilities obtained independently (third columns of Tables 4 and 5) may be multiplied. The result is shown in Table 6. It is noteworthy that the first 14 compounds are anthracene derivatives and the probabilities for non-anthracene derivatives are completely zero. Thus, the discrimination of anthracene derivatives from other compounds is perfect for all

the compounds whose spectra are so far available in the reference literature. In this study, anthracene was used simply as a representative molecule of anthracene derivtives in calculation of the CCF values. More accurately, the calculation must be performed using the "averaged spectrum" of anthracene derivatives, which is obtained by accumulating all the spectra for anthracene derivatives. This procedure may further improve the accuracy of prediction.

### 3.6. Functional group

For complete knowledge of the chemical structure, the functional group and its position must also be predicted properly. Table 7 shows the CCF values calculated for various benzene derivatives using toluene as a standard sample. As expected, alkylbenzenes, especially *n*-alkylbenzenes, give large CCF values. Fig. 4 shows the probability of alkylbenzene derivatives plotted against the CCF value. Fig. 5 shows the probability density for alkylbenzenes calculated from the frequency shifts of the 0–0 transitions. The typical shifts by substitution with an alkyl group are 500–1000 $cm^{-1}$. The product of the probabilities is shown for benzene derivatives in column 6 of Table 7. Apparently, ethylbenzene gives the largest value among these compounds, indicating the distinct merit of the present pattern recognition.

A similar comparison was also performed using 9-methylanthracene as a standard sample. As expected, 9-alkylanthracene, i.e. 9-hexylanthracene, gives the largest CCF value, implying the presence of an alkyl group at the 9-position. It is interesting to note that the CCF values for anthracene derivatives substituted at the 2-position with an alkyl group are rather small. This is ascribed to vibrational and rotational motions of the methyl group, providing many split lines due to a shallow potential curve.

Owing to a lack of spectral data, a more accurate discussion is difficult. However, it is generally true that the functional group and its position can be predicted fairly well as the probability is always high when the CCF value is calculated using the standard sample with a closely related chemical structure.

Table 6
Products of probabilities of anthracene derivatives obtained from CCF values and wavelengths of the 0–0 transition

| Compound | Product of probabilities (%) |
|---|---|
| 2-Chloroanthracene | 59.4 |
| 9-Mthylanthracene | 51.0 |
| 2-Phenylanthracene | 49.9 |
| 9-Hexylanthracene | 48.2 |
| 1-Chloroanthracene | 45.3 |
| 9-Bromoanthracene | 41.0 |
| 9-Cyanoanthracene | 31.0 |
| 9-Phenylanthracene | 16.8 |
| 2-Methylanthracene | 9.5 |
| 9-Methoxyanthracene | 5.1 |
| 9-Chloroanthracene | 1.4 |
| 9,10-Dichloroanthracene | 0.9 |
| 9,10-Dibromoanthracene | 0.8 |
| 2-Ethylanthracene | 0.2 |
| 2-Methylnaphthalene | 0.0 |
| *n*-Propylbenzene | 0.0 |
| *trans*-2-Naphthol | 0.0 |
| Tryptamine | 0.0 |
| Tryptophan | 0.0 |
| 7-Azaindole | 0.0 |
| 3-Methylindole | 0.0 |
| *n*-Hexylbenzene | 0.0 |
| Toluene | 0.0 |
| 1-Naphthol | 0.0 |
| *cis*-2-Naphthol | 0.0 |
| 3-Indole acetic acid | 0.0 |
| 1-Phenylpropyne | 0.0 |
| 1-Phenyl-1-butyne | 0.0 |
| 1-Methylnaphthalene | 0.0 |
| Phenylethyne | 0.0 |
| 3-Indole propionic acid | 0.0 |
| 1-Phenyl-1-hexyne | 0.0 |

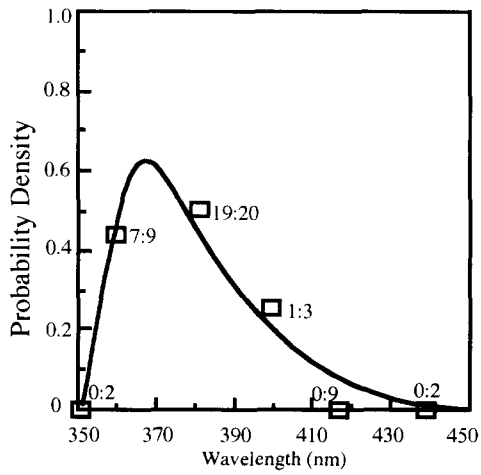


Fig. 3. Probability density of anthracene derivative against the wavelength of the 0–0 transition. The number in the figure indicates the number of anthracene (left) and non-anthracene (right) compounds. The solid curve is calculated from Eq. (6) by fitting the experimental data to $m = 4$.

Table 7
Probabilities calculated from CCF values using toluene as a standard sample and from frequency shifts of the 0–0 transition from benzene

| Benzene derivative | CCF | PC (%) | FS ($cm^{-1}$) | PFS (%) | P (%) |
|---|---|---|---|---|---|
| Ethylbenzene | 0.806 | 98.3 | 501.1 | 73.3 | 72.0 |
| *n*-Hexylbenzene | 0.737 | 96.6 | 516.6 | 73.5 | 71.0 |
| *n*-butylbenzene | 0.711 | 95.8 | 512.4 | 73.4 | 70.3 |
| *n*-Propylbenzene | 0.640 | 92.3 | 506.8 | 73.3 | 67.6 |
| *tert*-Butylbenzene | 0.601 | 89.5 | 393.4 | 72.2 | 64.6 |
| *n*-Pentylbenzene | 0.482 | 76.6 | 515.2 | 73.5 | 56.3 |
| Isopropylbenzene | 0.447 | 71.3 | 430.3 | 72.8 | 51.9 |
| *p*-Aminophenol | 0.100 | 6.1 | 6690.3 | 0.0 | 0.0 |
| *p*-Toluidine | 0.67 | 2.8 | 4993.3 | 0.0 | 0.0 |
| 1-Naphthol | 0.023 | 0.3 | 6633.0 | 0.0 | 0.0 |
| *trans*-2-Naphthol | 0.018 | 0.2 | 7184.2 | 0.0 | 0.0 |
| *cis*-2-Naphthol | 0.010 | 0.1 | 1722.9 | 21.7 | 0.0 |
| *p*-Fluorophenol | 0.001 | 0.0 | 2963.5 | 3.1 | 0.0 |

The linewidth, $r$, is assumed to be $10\,cm^{-1}$.
CCF, cross correlation factor; PC, probability from CCF (%); FS, frequency shift ($cm^{-1}$); PFS, probability from frequency shift (%); $P$, product of probabilities (%).

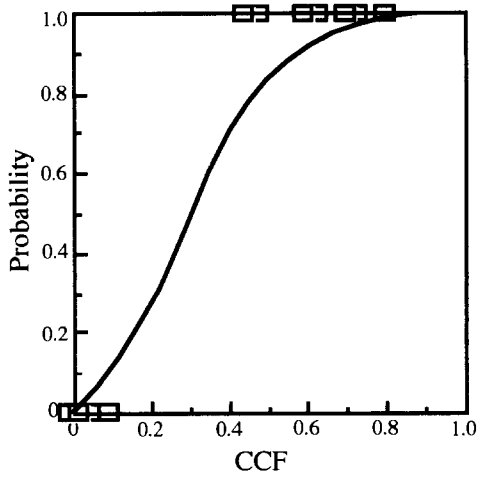


Fig. 4. Probability of alkylbenzenes against CCF value. Owing to the small number of compounds available, the data (0 or 1) are directly plotted in the Figure. The solid curve is calculated from Eq. (5) by fitting the experimental data to $k = 0.4$.

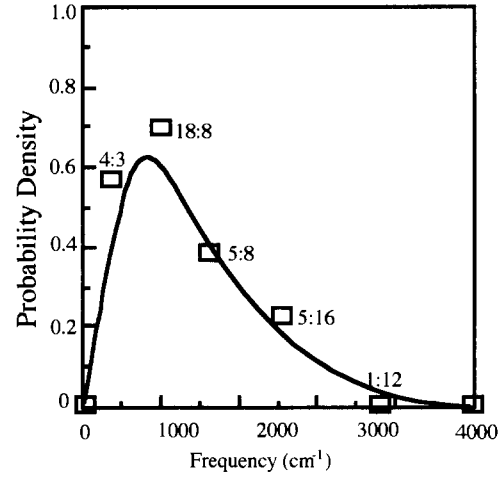


Fig. 5. Probability density of alkylbenzene against the frequency shift of the 0–0 transition from that of benzene. The solid curve is calculated from Eq. (6) by fitting the experimental data to $m = 4$.

## 4. Conclusion

A supersonic jet spectrum contains information concerned with skeletal vibrations, so that the skeletal structure can be well-predicted by pattern recognition. The wavelength of the 0–0 transition also contains information on the chemical structure. Thus the accuracy in prediction is improved by multiplying the above two probabilities obtained independently. Additional data concerned with fluorescence and multiphoton ionization spectra might also be useful for this purpose. Pattern recognition may be applied to analysis of the mass fragment spectrum for more accurate prediction of the chemical structure.

In this study, the determination of functional group position must be regarded as preliminary, since the number of supersonic jet spectra reported is small at the present time. By increasing the number of accumulated data, it will become possible to discuss the effect of other substitutional groups, such as OH or $NH_2$. Their CCF values are quite small when an alkylbenzene is used as a standard sample, suggesting that it may be possible to discrimi-

nate such compounds from other aromatic hydrocarbons, especially alkylbenzene.

For more accurate prediction of chemical structure, it is necessary to accumulate a large number of spectra in the database, as described. For this purpose, it is necessary to develop an instrument which allows measurements of the supersonic jet spectrum in a short time period. For example, the sample should be replaced immediately without changing the conditions of the nozzle and the vacuum system [10]. Further, a widely-tunable laser source may be essential, because the tunable range of the dye laser currently used is very limited and is not suitable for application to unknown samples. A titanium-doped sapphire laser or an optical parameteric oscillator coupled with a frequency conversion system is quite attractive. A multi-frequency laser may be also used to reduce the time for recording a spectrum [11]. Such hardware developments are essential not only for construction of the database, but also for practical use of supersonic jet spectrometry in routine work.

## References


[1] J.M. Hayes and G.J. Small, Anal. Chem., 55 (1983) 565 A.
[2] M.V. Johnston, Trends Anal. Chem., 3 (1984) 58.
[3] D.M. Lubman, Anal. Chem., 59 (1987) 31A.
[4] T. Imasaka and N. Ishibashi, Prog. Quantum Electron., 14 (1990) 131.
[5] T. Imasaka and N. Ishibashi, Spectrochim. Acta., Part B, 43 (1988) 661.
[6] C.H. Lin, H. Fukii, T. Imasaka and N. Ishibashi, Anal. Chem., 63 (1991) 1433.
[7] T. Imasaka and N. Ishibashi, Report For Grant-in-Aid for Scientific Research from the Ministry of Education of Japan, Project No. 01470065, 1991.
[8] T. Imasaka, K. Sakaki and N. Ishibashi, Chemom. Intell. Lab. Syst., 6 (1989) 281.
[9] T. Imasaka, K. Sakaki and N. Ishibashi, Spectrochim. Acta, Part B, 43 (1988) 703.
[10] T. Imasaka, T. Okamura and N. Ishibashi, Anal. Chem., 58 (1986) 2152.
[11] M. Nishida, C.H. Lin and T. Imasaka, Anal. Chem., 65 (1993) 3326.
[12] T.A. Stephenson, P.L. Radloff and S.A. Rice, J. Chem. Phys., 81 (1984) 1060.
[13] R. Bersohn, U. Even and J. Jorther, J. Chem. Phys., 80 (1984) 1050.
[14] S.M. Beck, D.E. Powers, J.B. Hopkins and R.E. Smalley, J. Chem. Phys., 73 (1980) 2019.
[15] A. Amirav, U. Even and J. Jortner, J. Chem. Phys., 67 (1982) 1.
[16] N. Ohta and H. Baba, Chem. Phys. Lett., 133 (1987) 222.
[17] A. Oikawa, H. Abe, N. Mikami and M. Ito, J. Phys. Chem., 88 (1984) 5180.
[18] J.B. Hopkins, D.K. Powers and R.E. Smalley, J. Chem. Phys., 72 (1980) 5039.
[19] R. Tembruell, T.M. Dunn and D.M, Lubman, Spectrochim. Acta, Part A, 42 (1986) 899.
[20] A.E.W. Knight and S.H. Kable, J. Chem. Phys., 89 (1988) 7139.
[21] J.A. Syage, P.M. Felker, D.H. Semmes, F.A. Adel and A.H. Zewail, J. Chem. Phys., 82 (1985) 2896.
[22] D.W. Werst, A.M. Brearley, W.R. Gentry and P.F. Parbara, J. Am. Chem. Soc., 109 (1987) 32.
[23] A. Amirav, C. Horwitz and J. Jortner, J. Chem. Phys., 88 (1988) 3092.
[24] S. Hirayama and F. Tanaka, Chem. Phys. Lett., 153 (1988) 112.
[25] T.R. Rizzo, Y.D. Park, L.A. Peteanu and D.H. Levy, J. Chem. Phys., 84 (1986) 2534.
[26] K. Fuke, H. Yoshiuchi and K. Kaya, J. Phys. Chem., 88 (1984) 5840.
[27] Y.D. Park, T.R. Rizzo, L.A. Peteanu and D.H. Levy, J. Chem. Phys., 84 (1986) 6539.
[28] J.L. Tomer, K.W. Holtzclaw and D.W. Pratt, J. Chem. Phys., 88 (1988) 1528.
[29] G.D. Greenblatt, E. Nissani, E. Zaroua and H. Yehuda, J. Phys. Chem., 91 (1987) 570.
[30] I.Y. Chan and M. Dantus, J. Chem. Phys., 82 (1985) 4771.
[31] M. Sonnenschein, A. Amirav and J. Jortner, J. Phys. Chem., 88 (1984) 4214.
[32] A. Amirav, U. Even and J. Jortner, J. Chem. Phys., 75 (1981) 3770.
[33] A. Amirav, U. Even and J. Jortner, Chem. Phys. Lett., 69 (1980) 14.
[34] A. Amirav, C. Horwitz and J. Jortner, Chem. Phys. Lett., 72 (1980) 21.

ELSEVIER

Talanta 42 (1995) 1121–1126

Talanta

# Photometric assay of 1-naphthylamine by azo dye formation with diazotized sulfisomidine — application to waters

Thaira I. Younis, W.A. Bashir *

*Department of Chemistry, College of Science, Mosul University, Mosul, Iraq*

Received 3 June 1994; revised 5 October 1994; accepted 1 February 1995

**Abstract**

A simple and sensitive photometric method for the trace determination of 1-naphthylamine has been worked out. The method is based on the coupling reaction of the determinand in acidic medium with diazotized sulfisomidine, to form a purplish violet water-soluble mono azo dye that shows maximum absorption at 540 nm with a molar absorptivity of $4.47 \times 10^4$ l mol$^{-1}$ cm$^{-1}$. Beer's law is obeyed over the concentration range 5–70 μg of 1-naphthylamine in a final volume of 25 ml, i.e. 0.2–2.8 p.p.m. with a relative error of −0.7 to +1.7% and a relative standard deviation of 0.35–4.2%, depending on the concentration level. Moreover, the method does not require either temperature control or solvent extraction. Interferences due to foreign species have been examined. The developed method has been applied to the determination of 1-naphthylamine in river water and sea water.

## 1. Introduction

1-Naphthylamine, being a first-class carcinogen, is important from the view point of toxicology [1,2], and therefore its assay is very desirable. The methods available for the determination of 1-naphthylamine are mainly spectrophotometric because of their outstanding features [3]. The commonly used methods for the determination of the intended compound can be grouped into three types. Type I methods involve treatment of 1-naphthylamine with nitrite in acidic medium to form a diazonium cation; this is subsequently coupled with an activated aromatic nucleus in either acidic [4] or basic [5] medium, depending on the nature of the coupling component, to form a colored azo dye for measurement of 1-naphthylamine. These methods are rather time-consuming, not sensitive and involve a several-step procedure. Further, sometimes toxic reagents are used such as 2-naphthol [6].

Type II methods comprise the coupling of 1-naphthylamine with diazotized reagent to form an intensely-colored azo dye. In this respect, diazotized sulfanilic acid [7], diazotized 3,5-dichloraniline [8], diazotized *p*-aminoacetophenone [9], diazotized *p*-nitroaniline [10], and diazotized *p*-aminobenzophenone [11] have been reported for the determination of 1-naphthylamine. Type III methods involve condensation of the determinand with a nitroso aromatic compound to form the corresponding colored azo dye [12]. This technique is time-consuming, insensitive and the reaction medium should be 30% in acetic acid for the performance of the method.

Type II methods are characterized by simplicity, rapidity, and sensitivity, but a review of these methods reveals that the investigations performed using these procedures [9–11] require further study. This paper is devoted to a detailed investigation of the coupling reaction conditions of 1-naphthylamine with diazotized

* Corresponding author.


*SSDI* 0039-9140(95)01546-9

sulfisomidine. The developed method has proved successful, and has been applied to the assay of 1-naphthylamine in river and sea waters.

## 2. Experimental

### 2.1. Reagents

Caution-gloves are worn in weighing, and all transfers of 1-naphthylamine solutions should be made with a pipette filler.

*Stock 1-naphthylamine solution, 10 mg ml$^{-1}$*

1-Naphthylamine (0.10000 g) (Hopkins and William) is dissolved in ethanol (Fluka), and the volume is then made up to 10 ml in a volumetric flask.

This solution, when stoppered tightly and kept in the refrigerator ($\approx$5 °C), is stable for at least 3 months.

*Working 1-naphthylamine solution, 50 μg ml$^{-1}$*

A 0.5 ml volume of the stock 1-naphthylamine solution is transferred into a 100 ml volumetric flask, and diluted to the mark with distilled water. This solution is stable for at least 1 week.

*Diazotized sulfisomidine solution, 3 mM*

A 22.4 ml volume of 6.7 mM sulfisomidine (Sigma) solution is transferred to a 50 ml volumetric flask. 3 ml of sodium nitrite (BDH) solution (0.0035 g ml$^{-1}$) is then added and, after adding water to 40 ml, the mixture is cooled to 5 °C. A 3 ml volume of 1 M $H_3PO_4$ (Fluka) solution is added, the mixture is stirred occasionally for 10 min and the volume is made up to 50 ml with additional ($\approx$5 °C) cooled distilled water. This solution is stored in darkness over ice and used after 20 min. The reagent when kept in the refrigerator ($\approx$5 °C) is stable for at least 9 days.

*Foreign compound solutions, 1 mg ml$^{-1}$*

These are prepared in either distilled water or ethanol.

### 2.2. Instruments

Absorbance and spectral measurements are performed on a Pye Unican SP 30 UV double-beam digital spectrophotometer using 1 cm optical silica matched cells.

pH measurements (at 20–25 °C) are carried out using a Philips PW 9421 pH meter, reading to three decimal places.

### 2.3. Procedure

To a series of 25 ml volumetric flasks are added 5–70 μg samples of 1-naphthylamine. Distilled water (10 ml) and 3 ml of 1 M $H_3PO_4$ solution are then added, and the mixture is shaken. A 2 ml volume of 3 mM diazotized sulfisomidine solution is then added and the volume is diluted to the mark with distilled water. After standing for 20–30 min, the absorbances are measured against the corresponding blank at 540 nm using 1 cm cells. The apparent molar absorptivity of the wavelength of measurement is $4.47 \times 10^4$ l mol$^{-1}$ cm$^{-1}$. The stability period of at least 30 min is sufficient for many measurements to be made at the same time.

For the subsequent experiments, 50 μg of 1-naphthylamine is taken and the final volumes are 25 ml.

## 3. Results and discussion

### 3.1. Study of the optimum reaction conditions

The effects of various parameters on the absorption intensity of the azo dye are studied and the reaction conditions are optimized.

### 3.2. Choice of diazotized reagent

Several previously unreported diazotized reagents have been examined for the photometric assay of 1-naphthylamine. These reagents are: diazotized sulfisomidine, sulfameter (5-methoxysulfadiazine), sulfamethazine, sulfamethizole, sulfanilamide, sulfanilic acid, sulfapyridine, sulfathiazole, and sulfaisoxazole. Diazotized sulfisomidine has been selected because it satisfies certain requirements [9] (intensity of the azo dye formed and the relatively rapid coupling rate). This reagent is also easily diazotized and remains stable for several days when stored at about 5 °C in darkness. Further, diazotized sulfisomidine gives a water-soluble azo dye with 1-naphthylamine under the experimental conditions, thus avoiding a time-consuming extraction process. The foregoing characteristics recommend diazotized sulfisomidine as a reagent for the assay of 1-naphthylamine.

### 3.3. Effect of acid

It is well-known that aromatic amines couple with diazonium salts in acidic to nearly neutral medium [3]. Different amounts (1–10 ml of 1 M) of different acids (HCl, $HClO_4$, $HNO_3$, $H_2SO_4$, $H_3PO_4$ and $CH_3COOH$) have been examined for their effect on the color intensity of the azo dye. The experimantal data reveal that in the case of strong acids, both the amount and order of the acid (sample + acid + diazotized reagent or sample + diazotized reagent + acid) added affect the intensity of the colored azo dye, and are immaterial when the acids are weak.

### 3.4. Effect of base

Different amounts (1–10 ml of 1 M) and orders (sample + base + diazotized reagent or sample + diazotized reagent + base) of various bases ($CH_3COONa$, $NaHCO_3$, $Na_2CO_3$, $NH_3$, NaOH and KOH) have been investigated for their effect on the color intensity of the azo dye. The color of the azo dye changes from violet in acidic media to orange then to yellowish-brown as the amount of base increases in the reaction medium. In addition, the blank changes from colorless in acidic media to yellow in basic media.

Acidic medium is preferred over basic medium because of: (a) strong color contrast, (b) higher sensitivity, and (c) better expected selectivity of determination because most compounds are activated towards coupling in basic medium.

A 3 ml volume of 1 M $H_3PO_4$ acid (final pH of the reaction mixture $\approx 1.5$) is selected for the subsequent experiments. This is because $H_3PO_4$ can act as a masking agent for cations such as iron(III), aluminium, and calcium, which may be present with the determinand in the same sample and are expected to interfere.

### 3.5. Formation of diazotized sulfisomidine

The diazotization reaction proceeds according to the following equation:

$$ArNH_2 + NaNO_2 + 2HX \xrightarrow{0-5\ ^\circ C} ArN_2X + NaX + 2H_2O$$

From the above equation, it is observed that the formation of diazonium salt is related to three components: the amine, the acid and the nitrite. Therefore, in the subsequent experiments the effect of each has been investigated.

### 3.6. Effect of acid-to-amine ratio

From the above equation, it can be observed that the acid reacts with the amine in a 2:1 ratio to form the diazonium salt. Different ratios of different acids (strong and weak) have been examined for their effect on the yield of the colored azo dye.

The experimental data have drawn the following observations.

(i) The diazotization of sulfisomidine can be carried out equally well in strong acid medium and weak acid medium.

(ii) In general, the absorbance of the colored azo dye becomes independent of the acid-to-amine ratio when the latter is greater than or equal to 2.

(iii) Generally, the absorbance of the colored azo dye becomes independent of the amount of diazotized reagent when the latter is greater than $2 \times 10^{-3}$ mmol per 25 ml final volume.

(iv) The same absorbance is essentially obtained when nitrite and sulfisomidine are mixed (in the absence of acid) and added to the sample solution containing 3 ml of 1 M $H_3PO_4$ per 25 ml final volume. This indicates that the diazotization of sulfisomidine is very fast. However, the 3 ml of 1 M $H_3PO_4$ is omitted and the procedure repeated, only a faint orange–red color is obtained (0.005 A unit).

(v) At a higher acidity ratio in HCl medium, the yield of the colored azo due decreases, probably because nitrous acid will exert an oxidizing rather than a nitrosating effect [14]:

$$2NO_2^- + 2Cl^- + 4H^+ \rightarrow 2NO + Cl_2 + 2H_2O$$

(vi) Phosphoric acid is recommended for diazotization because, in this acid, diazotization is fast, the color of the diazonium salt formed in more faint than in other acids, and the excess which remains can act as a masking agent [15].

### 3.7. Effect of amine-to-acid ratio

Amine solutions of concentrations 1, 3 and 5 mM have been prepared in phosphoric acid at acid-to-amine ratios between 2:1 and 100:1 for the concentrations of the amine. From the results obtained, a 3 mM solution has been selected for the subsequent experiments. This concentration of the diazotized reagent has

been selected as a compromise between sensitivity and stability of the diazonium salt. The stability of diazonium salts decreases as their amounts increase [16].

### 3.8. Effect of nitrite-to-amine ratio

At a constant amine-to-acid ratio of 1:20, the effect of nitrite-to-amine ratio has been evaluated for optimal color intensity using 1, 3 and 5 ml of the prepared diazotized reagent solution. As the ratio of nitrite to amine becomes more than 1:1 and a higher volume of diazotized reagent is used, the color changes from violet to pinkish-orange. Therefore, a 1:1 nitrite-to-amine ratio is recommended for subsequent experiments.

### 3.9. Mode of preparation of diazotized reagent

There are three possible modes for the preparation of diazotized sulfisomidine. Mode II of preparation (amine + $NaNO_2$ then acid) is chosen for subsequent experiments, because the diazonium salt prepared by this mode has the least faint color.

### 3.10. Amount of diazotized reagent

0.5–10 ml of 3 mM diazotized sulfisomidine reagent was examined over the range 5–100 μg of 1-naphthylamine per 25 ml final volume for optimal readings of absorbance. The experimental data reveal that the absorbance increases significantly with increasing amount of diazotized sulfisomidine, and remains approximately constant in the range 2–7 ml of 3 mM diazotized reagent solution. Larger amounts decrease the absorbance and cause hypsochromic shift. The shift may be due to multiple coupling [17]. A 2 ml volume of 3 mM diazotized reagent has been selected for the procedure, because a good correlation between abosrobance and determinand concentration exists. Also, the stability period of the colored azo dye is suitable, the sensitivity of the colored azo due is adequate, and at lower reagent amounts the selectivity of determination will increase.

### 3.11. Effect of temperature

The experimental data show that the absorbance of the azo dye increases as the temperature increases in the range 0–20 °C, reaches a maximum at 20 °C, and remains constant up to 45 °C. Therefore, it has been recommended to carry out reactions at room temperature (20 °C).

### 3.12. Absorption spectra

When a dilute solution of 1-naphthylamine in the presence of phosphoric acid, under the above-established conditions, is mixed with diazotized sulfisomidine reagent, a purplish-violet colored azo dye forms. This shows maximum absorption at 540 nm, in contrast to the colorless reagent blank which shows no absorption at the wavelength of maximum absorption. Fig. 1 shows the absorption spectra of the azo dye and the corresponding reagent blank. The wavelength of maximum absorption at 540 nm has been adapted for the subsequent work.

### 3.13. Kinetics of diazotized sulfisomidine reagent formation

The formation of the diazotized reagent (from its components) has been followed by taking 2 ml of 3 mM solution of the diazotized reagent at various time intervals and measuring the absorbance of the treated standard (according to the recommended procedure). The obtained results indicate that the diazotized reagent solution can be used after 20–30 min from preparation and up to at least 10 days, provided it is kept in the dark at about 5 °C.

### 3.14. Accuracy and precision of the method

To check the accuracy and precision of the method, 1-naphthylamine has been determined at three concentrations. The results are shown in Table 1 and indicate that the method is satisfactory.

Table 1
Accuracy and precision of the method

| Amount of l-naphthylamine taken (μg) | Relative error [a] (%) | Relative standard deviation [a] (%) |
|---|---|---|
| 5 | +1.7 | ±4.2 |
| 30 | −0.7 | ±1.0 |
| 70 | 0 | ±0.4 |

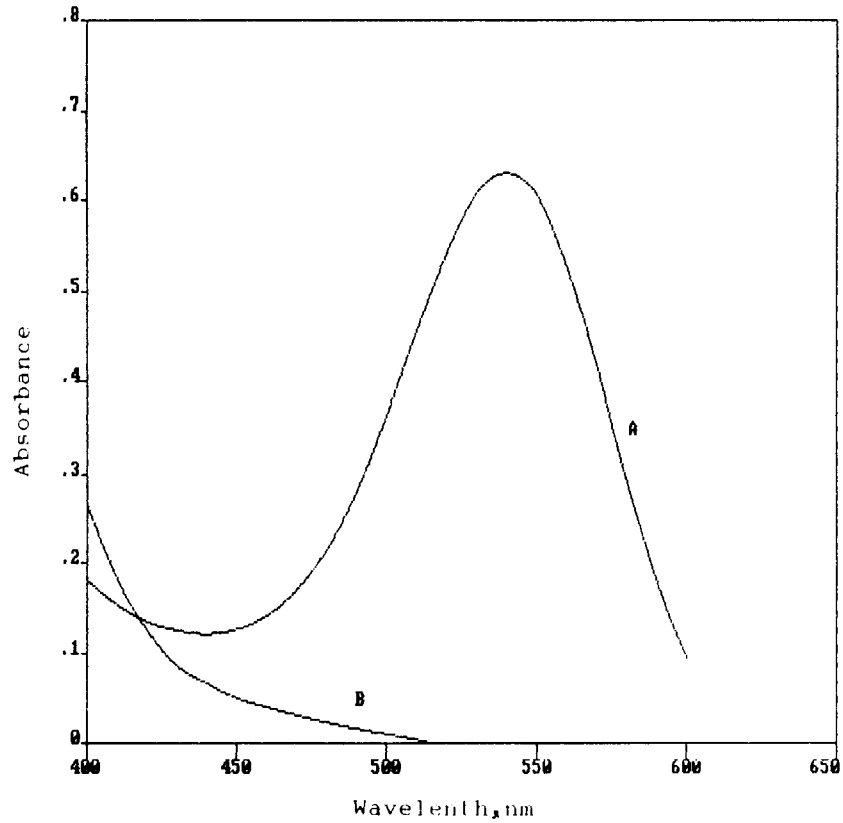


Fig. 1. Absorption spectra of 50 μg of 1-naphthylamine/25 ml measured against: (A) blank; (B) blank against distilled water.

### 3.15. Nature of the dye

The composition of the colored azo dye has been established using Job's method of continuous variation. The results indicate that the dye has been obtained by a 1:1 combining ratio of diazotized sulfisomidine to 1-naphthylamine, revealing a mono azo dye. 1-Naphthylamine couples with diazonium salts at the 4-position, and the structure of the azo dye may be written as follows:

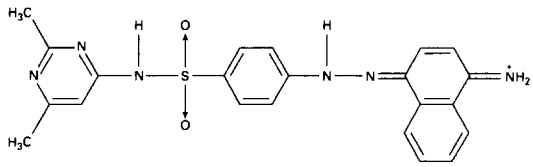

The apparent stability constant has been calculated [18] and is found to be $3.3 \times 10^4$.

### 3.16. Effect of organic solvents

Basic solvents cause hypsochromic shift and sensitivity decrease. Water is shown to be a good medium from the points view of sensitivity and economy. Common immiscible organic solvents only partially (if at all) extract the colored azo dye.

### 3.17. Interferences

In order to assess the possible analytical applications of the present proposed method, the interfering effects of foreign substances (organic and inorganic) at various levels on the determination of 50 μg of 1-naphthylamine by the recommended method have been examined, and the results are given in Table 2.

From the data given in Table 2, it can be observed that some compounds exist that can interfere with the analyte. However, extraction or chromatography can successfully remove these interferences.

### 3.18. Application of the method

*Determination in river water*

1-Naphthylamine may find its way into river water through the discharge of some dye factories. The results for the determination of the compound are shown in Table 3.

Table 2
Effect of foreign compounds on the determination of 50 μg of 1-naphthylamine

| Interferent | Form added | Minimum tolerable amount [a] (μg) |
|---|---|---|
| Aluminium | $AlCl_3 \cdot 6H_2O$ | 500 |
| Ammonium | $NH_4Cl$ | 1000 |
| Aniline | – | 500 |
| Ascorbic acid | – | <50 |
| Benzidine | – | 1000 |
| Benzoic acid | – | 1000 |
| Bicarbonate | $NaHCO_3$ | 1000 |
| Boric acid | – | 1000 |
| Carbonate | $Na_2CO_3$ | 1000 |
| Chloride | NaCl | <100 |
| Copper(II) | $CuCl_2$ | 1000 |
| Diphenylamine | – | <50 |
| EDTA | Disodium salt dihydrate | 1000 |
| Hydroxylamine | Hydrochloride | 50 |
| Indole | – | <50 |
| Iodide | NaI | <50 |
| Iron(III) | $FeCl_3 \cdot 6H_2O$ | 500 |
| Magnesium | $MgCl_2 \cdot 6H_2O$ | 200 |
| Malonic acid | – | 200 |
| α-Naphthol | – | 200 |
| β-Naphthol | – | <50 |
| Nitrate | $NaNO_3$ | 1000 |
| Oxine | – | 1000 |
| Phloroglucinol | – | 200 |
| 1,10-Phenanthroline | Hydrochloride monohydrate | 1000 |
| Phenol | – | 1000 |
| Phosphate | $NaH_2PO_4$ | 1000 |
| Picolinic acid | – | 1000 |
| Potassium | KCl | <50 |
| Pyrrole | – | <50 |
| Resorcinol | – | <50 |
| Salicylate | Sodium salicylate | 1000 |
| Silicate | $Na_2SiO_3 \cdot 5H_2O$ | 1000 |
| Sulphate | $Na_2SO_4$ | 500 |
| Urea | – | 500 |

[a] Amount of interferent causing a relative error equal to or better than ±2.5% in the absorbance reading of 50 μg 1-naphthylamine.

*Determination in sea water*

The compound may find its way into sea water by ship accident. To simulate this, synthetic sea water has been prepared [19] and 1-naphthylamine has been assayed in sea water by the present method, and the results are shown in Table 4.

Table 3
Determination of 1-naphthylamine in river water

| 1-Naphthylamine added (μg) | Recovery (%) of 1-naphthylamine per ml of river water used | | | | | |
|---|---|---|---|---|---|---|
| | 1 | 3 | 5 | 7 | 10 | 15 |
| 5 | 97.0 | 98.3 | 101.4 | 97.1 | 96.4 | 105.4 |
| 30 | 104.4 | 99.1 | 101.6 | 100.8 | 102.0 | 101.8 |
| 70 | 99.8 | 100.2 | 100.7 | 100.3 | 100.7 | 100.5 |

Table 4
Determination of 1-naphthylamine in sea water

| 1-Naphthylamine added (μg) | Recovery (%) of 1-naphthylamine per ml of sea water used | | | | | |
|---|---|---|---|---|---|---|
| | 1 | 3 | 5 | 7 | 10 | 15 |
| 5 | 105.1 | 95.2 | 101.4 | 97.0 | 101.5 | 105.1 |
| 30 | 99.1 | 99.2 | 100.3 | 97.8 | 98.3 | 98.0 |
| 70 | 97.9 | 97.9 | 97.1 | 95.2 | 93.8 | 90 |

## References

[1] R.F. Straub, R.D. Voyksner and J.T. Keever, Anal. Chem., 65 (1993) 2131.
[2] J.S. Wishnok, Anal. Chem., 64 (1992) 1126A.
[3] J.A. Howell and L.G. Hargis, Anal. Chem., 54 (1982) 171R.
[4] G. Norwitz and P.N. Keliher, Talanta, 33 (1986) 311.
[5] M.A. El-Deb, J. ADAC, 54 (1971) 1383.
[6] F.L. English, Anal. Chem., 19 (1947) 457.
[7] V. Lenkhold, Anilinokrasochnaya, prom., 3 (1933) 87; Chem. Abst., 27 (1933) 5277.
[8] B.A. Lugg, Anal. Chem., 35 (1963) 899.
[9] B. Sulaiman and W.A. Bashir, Analyst, 109 (1984) 1409.
[10] N.D. Ismail, M.Sc. Thesis, Mosul University, 1986, P. 43.
[11] A.A. Al-Hatim and B.B. Ibraheem, Anal. Lett., 22 (1989) 2091.
[12] I.Ya. Korenman, Trans. Khim. Khim. Tekhnol, (Gor'kii) 1 (1967) 113; Anal. Abst., 15 (1968) 5403.
[13] K.H. Saunders and R.L.M. Allen, Aromatic Diazo Compounds, 3rd edn., Edward Arnold, London, 1985, P. 295.
[14] H. Zollinger, Azo and Diazo Chemistry, Interscience, New York, 1961, p. 16.
[15] G. Wilkinson (Ed.), Comprehensive Coordination Chemistry, Pergamon, Oxford, 1987, Vol. 1, p. 337.
[16] G. Norwitz and P.N. Keliher, Anal. Chem., 53 (1981), 56.
[17] L.R. Whitlock, S. Siggia and J.E. Smola, Anal. Chem., 44 (1972) 532.
[18] T.S. Al-Chabsha, M.Sc. Thesis. University of Mosul, 1975, p. 107.
[19] A. Henriksen, Analyst, 90 (1965) 83.

ELSEVIER

Talanta 42 (1995) 1127–1133

Talanta

# Application of a macroporous resin containing imidazoline groups to preconcentration and separation of gold, platinum and palladium prior to ICP-AES determination

Zhi-Xing Su, Qiao-Sheng Pu *, Xing-Yin Luo, Xi-Jun Chang, Guang-Yao Zhan, Feng-Zhi Ren

*Department of Chemistry, Lanzhou University, Lanzhou, 730000, People's Republic of China*

Received 7 October 1994; revised 31 January 1995; accepted 3 February 1995

**Abstract**

A new functional resin with a long functional side chain was synthesized by modification of aminated macroporous poly(vinyl chloride) resin with cyanoethylene and ethylenediamine. Traces of Au(III), Pt(IV) and Pd(II) in aqueous solution were quantitatively adsorbed in the acidity range of pH $\leqslant 4$ and $C_{H^+} \leqslant 3$ M. The rate of equilibration is high; $Cu^{2+}$, $Fe^{3+}$, $Ni^{2+}$, etc. exhibit little interference on the adsorption of the sought noble metals. The saturated adsorption capacities for Au(III), Pt(IV), Pd(II) and Ir(IV) in 2 M HCl were $\geqslant 4.0$, 1.57, 2.26, 1.85 mmol $g^{-1}$. Adsorbed ions can be quantitatively desorbed by 4% thiourea + 0.25 M $H_2SO_4$. The resin has good reusability, and can be used for preconcentration and separation of Au(III), Pt(IV) and Pd(II) prior to their determination by ICP-AES with satisfactory results.

## 1. Introduction

Adsorption methods are widely used and are the most effective methods for preconcentration and separation of noble metal ions from aqueous solution. Many different adsorbents have been used in this respect [1–8]. However, the mechanisms of adsorption of noble metals are not well defined because of the complication of the form of these elements in aqueous solution. Optimization of the adsorption conditions is also difficult [9]. To date, although a wide variety of different adsorbents used for preconcentration and separation of noble metal ions prior to their determination have been described, the methods do not meet all analytical requirements [3]. In general, adsorption of noble metal ions onto chelating adsorbents takes place on prolonged shaking or heating, owing to their low rate of ligand exchange [10]. Meanwhile, the desorption of these ions is difficult for many adsorbents. In analytical procedures these adsorbents have to be destroyed by ashing at high temperature or heating with a perchloric–sulfuric acid mixture to recover the adsorbed elements [11]. It is valuable to synthesize novel adsorbents with high selectivity, high adsorption rate, and from which adsorbed metal ions can be readily desorbed. We attempt to improve the kinetic characteristic of the adsorbent by increasing the chain length between the macromolecular network and functional groups. This can increase the flexibility of the sidechain which contains the functional group and improve the access of metal ions to the functional groups.

According to Myasoedova et al. [11], functional resins containing nitrogen-heterocyclic groups are highly selective for noble metals. In this work, a macroporous adsorbent which has a long functional sidechain is synthesized. The selectivity of this adsorbent for Au(III), Pt(IV)

* Corresponding author. (ZR-94-004).


*SSDI* 0039-9140(95)01553-1

and Pd(II) is high. Desorption of these ions from the adsorbent is easy. The adsorbent can be successfully applied to the determination of Au, Pt and Pd in a sample.

## 2. Experimental

### 2.1. Instrumentation and reagents

An ICP 6500 inductively coupled plasma optical emission spectrometer (Perkin-Elmer), a Nicolet 170-SX Fourier transform-infrared (FT-IR) spectrometer, a Model pHs-2 precision pH-meter (the second Analysis instrument factory at Shanghai, China) were used. The sorption column was a glass tube (4.5 mm i.d., 10 cm length) in which a small pad of cotton-wool had been placed beforehand. A stock solution of Au, Pt, Pd, Ir and Ru was prepared by dissolving spectroscopically pure $HAuCl_4 \cdot 2H_2O$, $(NH_4)_2PtCl_6$, $PdCl_2$, $(NH_4)_2IrCl_6$, and $(NH_4)_2RuCl_6$ in dilute HCl. All other reagents were analytical grade. Demineralized distilled water was used for preparing aqueous solutions.

### 2.2. Synthesis of adsorbent

The macroporous cyanoethylamino resin (CEA) was synthesized as described previously [12].

Imidazolinyl ethyl amino resin (IEA) was prepared by the following procedure. Twenty grams of CEA, 50 ml ethylene diamine, 40 ml toluene and a little amount of sulfur powder were added to a 250 ml three-necked flask with a reflux condenser, a thermometer, and an agitator. The mixture was refluxed for 7 h. The resulting product was filtered. After washing with ethanol several times the resin was extracted with 75% ethanol until the extract was colorless. The product was dried at 80 °C under vacuum for later use. The nitrogen content of IEA was 11.96%.

The synthetic route of the IEA can be described schematically as

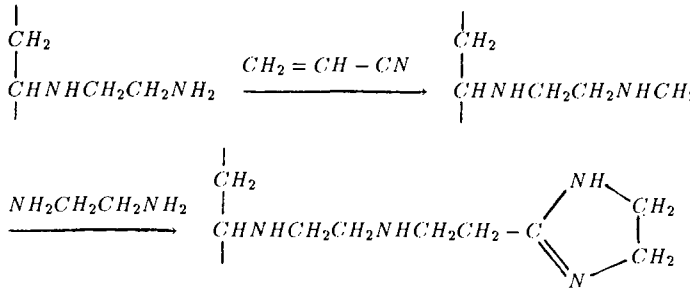

### 2.3. Determination of equilibration rate

Sixty milliliters of 2 M HCl containing Au(III), Pt(IV), and Pd(II) (50.0 μg of each) was added to a vessel fitted with a glass stopper. 0.1 g of IEA resin was added, and the vessel was shaken for the necessary time on a mechanical vibrator. The supernatant was decanted immediately. The metal ions in supernatant were determined by ICP-AES (forward power 1100 W; viewing height 17 mm; argon plasma gas flow rate 14 l $min^{-1}$, argon auxiliary gas flow rate 0.4 l $min^{-1}$, argon nebulizer gas flow rate 1.0 l $min^{-2}$, wave length Au 242.795, Pt 214.423, Pd 229.651, Ir 224.268, Ru 240.272 nm). The rate of adsorption at different shaking times was calculated.

### 2.4. Adsorption procedure

IEA resin (0.1 g) which had been soaked in distilled water for 24 h was loaded into the sorption column and washed with HCl of the same concentration as that in the test solution. The test solution (60–100 ml) was then passed through the column at 0.5–1.0 ml $min^{-1}$, and the resin bed was washed with about 5 ml HCl of the same concentration. The solution which passed the column was evaporated to about 5 ml, transferred into a 10 ml volumetric flask, and diluted to the mark with distilled water. The metal ions in the solution were determined by ICP-AES. The efficiency of adsorption was calculated using $S\% = [(a - CV)/a] \times 100\%$, where $a$ is the initial amount of the metal ion in the test solution (μg) $C$ is the concentration of metal ion in volumetric flask (μg $ml^{-1}$), and $V$ is the volume of volumetric flask (ml).

Adsorbed Au(III), Pt(IV) and Pd(II) were desorbed with preselected eluant and transferred into a 10 ml volumetric flask, diluted to the mark. Metal ions were determined by ICP-AES. Recovery was calculated.

### 2.5. Metal adsorption capacities

A batch equilibrium technique was used to determine metal adsorption capacities. Ten milligrams of IEA resin was added to each of four vessels with glass stoppers. Ten milliliters of 2 M HCl containing different amounts of Au(III) was added to each vessel. These vessels were then shaken on a mechanical vibrator for 10 h. A portion of supernatant was removed and the metal ion was determined by ICP-AES. The adsorption capacity of Au(III) was calculated. The adsorption capacities of Pt(IV), Pd(II) and Ir(IV) were determined by same procedure.

### 2.6. Analysis of sample

A 0.2 g smelter sample was added to a nickel crucible containing a 0.5 g $Na_2CO_3$ and 1.5 g $Na_2O_2$ mixture, and was covered with a little amount of $Na_2CO_3$–$Na_2O_2$ mixture. The sample was then fused in an electric muffle at 700 °C for 10 min. After cooling, it was dissolved in hot water and transferred into a beaker. Conc. HCl was added to adjust the acidity. The solution was boiled for 30 min, and then filtered. The residue and filter paper were washed with 2 M HCl several times. Au, Pt and Pd were adsorbed, and determined following the above procedure.

The standard nickel alloy reference sample (102-A-7) was analyzed following the same procedure after being dissolved in aqua regia.

## 3. Results and discussion

### 3.1. Solution acidity

Fig. 1 shows the effects of pH and acidity on the adsorption of Au(III) (0.82 μg $ml^{-1}$), Pt(IV) (0.86 μg $ml^{-1}$), Pd(II) (0.92 μg $ml^{-1}$), Ir(IV) (1.17 μg $ml^{-1}$) and Ru(IV) (1.00 μg $ml^{-1}$). Pd(II) could be quantitatively adsorbed by the IEA resin at pH ≤ 6.0 and $C_{H^+} \leq 6$ M, Au(III) at pH ≤ 4.0 and $C_{H^+} \leq 6$ M, Pt(IV) at pH ≤ 6.0 and $C_{H^+} \leq 3$ M, and Ir(IV) at pH ≥ 2.

### 3.2. Extraction time

Under batch conditions, the degree of adsorption in 2 M HCl was determined after shaking for between 2 min and 4 h. A quantitative adsorption of microquantities of Au(III), Pt(IV) and Pd(II) was reached in 2 min. The high rate of equilibration may be due to the high flexibility of the functional group and the hydrophilicity of the sidechain. These properties of the adsorbent enabled the ions in aqueous solution to readily approach the functional group.

### 3.3. Desorption conditions

Thiourea and mineral acid mixtures of different concentrations were used as eluants after Au(III), Pt(IV) and Pd(II) had been adsorbed by the IEA resin. The results showed that 4% thiourea + 0.5 M mineral acid could quantitatively desorb the above metal ions. Figs. 2 and 3 show the desorption curves of 4% thiourea + 0.5 M HCl and 4% thiourea + 2% $H_2SO_4$ + 1% KSCN as eluants. Multiple experiments showed that 4% thiourea + 0.25 M $H_2SO_4$ was the best eluant. The recovery of Au(III), Pt(IV) and Pd(II) using this eluant was 96.0%, 99.3% and 99.0%, respectively. Because of the high dissolved solid content of the eluant, the recovery values of the single determination were mostly in the 90–110% region. However, the precision is acceptable in the determination of trace amounts of elements. We also found that after the adsorption of the above metal ions, the desorption must be performed immediately. If the time between adsorption and desorption was more than 6 h, the

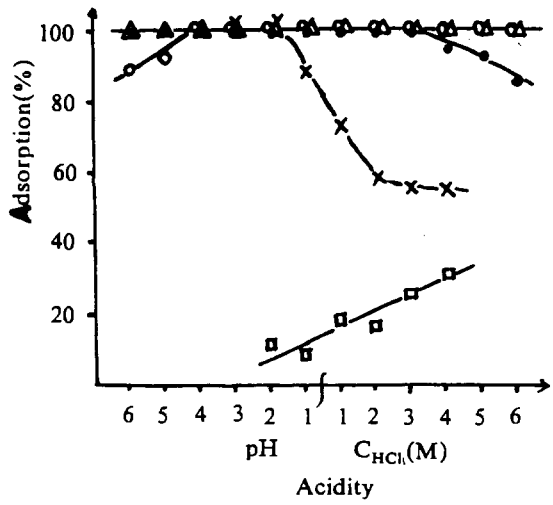


Fig. 1. Effect of acidity on adsorption of 49.4 μg Au(III) (○), 51.6 μg Pt(IV) (●), 55.5 μg Pd(II) (Δ), 70.0 μg Ir(IV) (X), and 60.0 μg Ru(IV) (□) on IEA resin. Solution volume 60 ml, sorbent 0.1 g, flow rate 1.0 ml $min^{-1}$.

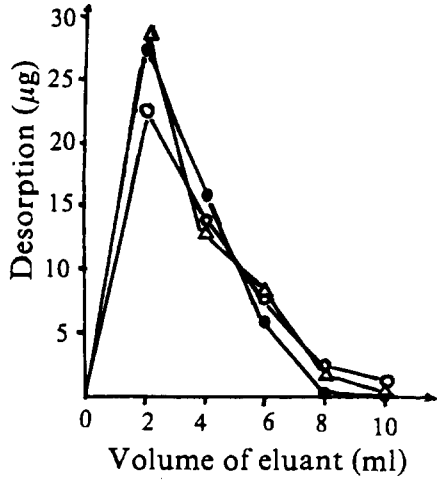


Fig. 2. Desorption curve of 49.4 μg Au(III) (○), 51.6 μg Pt(IV) (●) and 55.5 μg Pd(II) (△) with 4% thiourea + 0.5 M HCl. Sorbent 0.1 g, flow rate 2.0 ml $min^{-1}$.

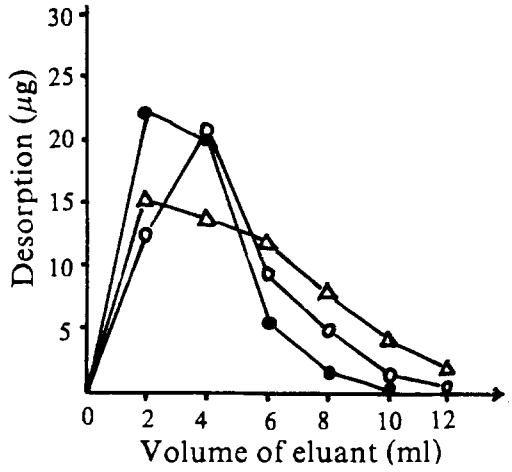


Fig. 3. Desorption curve of 49.4 μg Au(III) (○), 51.6 μg Pt(IV) (●) and 55.5 μg Pd(II) (△) with 4% thiourea + 2% $H_2SO_4$ + 1% KSCN. Sorbent 0.1 g, flow rate 2.0 ml $min^{-1}$.

recovery of Pt(IV) and Pd(II) was less than 90%. If the time was more than a day, only half of Pt(IV) and Pd(II) was desorbed. In addition, determination of Au(III), Pt(IV) and Pd(II) in the eluant by ICP-AES had to be carried out in 2 h. Otherwise, the results would be incorrect, owing to the reduction of these ions by thiourea.

### 3.4. *Effects of accompanying ions*

Table I shows the effects of accompanying ions on the adsorption of Au(III), Pt(IV) and Pd(II) (50.0 μg in 60 ml) by IEA resin. None of these ions caused interference to the adsorption or the determination of Au(III), Pt(IV) and Pd(II). The selectivity of this resin for these noble metal ions is high.

### 3.5. *Adsorption of Au(III), Pt(IV) and Pd(II) from the p.p.b. range*

500 ml of 2 M HCl containing Au(III) 39.6 p.p.b., Pt(IV) 41.2 p.p.b., and Pd(II) 41.4 p.p.b. was passed through 0.1 g of the IEA resin following the above procedure, and was then desorbed with 10 ml 4% thiourea + 0.25 M $H_2SO_4$. The recovery is shown in Table 2.

Au(III) 39.6, Pt(IV) 41.2, Pd(II) 44.4 p.p.b. in 500 ml solution (pH 1.0) containing $Cu^{2+}$, $Fe^{3+}$, $Zn^{2+}$ (100 p.p.m. each), $Ni^{2+}$, $Mn^{2+}$, $Cr^{3+}$, $Ca^{2+}$, $Mg^{2+}$ (10 p.p.m. each) were adsorbed and desorbed following the same procedure. The recovery is also shown in Table 2.

The results showed that at 2 M HCl the recovery of adsorption of Au(III), Pt(IV) and Pd(II) from the p.p.b. range solution was not satisfactory. However, at pH 1.0, in spite of the existence of a large amount of accompanying ions, the p.p.b. range of Au(III), Pt(IV) and Pd(II) could be adsorbed at a high flow rate with acceptable results.

### 3.6. *Stability and reusability of the resin*

In one experiment, Au(III), Pt(IV) and Pd(II) were adsorbed and desorbed following the above procedure, the column was then washed with distilled water until neutral, and another adsorption–desorption cycle was carried out. After 10 cycles of adsorption–desorption, the efficiency of adsorption and recovery of desorption showed virtually no change (Table 3). Thus the stability and reusability of IEA resin is satisfactory.

### 3.7. *Saturated capacity of adsorption*

Fig. 4 shows the results of the determination of the saturated capacity of IEA resin. The amounts of Pt(IV), Pd(II) and Ir(IV) were 1.57, 2.26 and 1.85 mmol per gram of dry resin, respectively. However, Au(III) did not reach saturated adsorption until 8.19 mg Au(III) in solution. This was due to the reduction of Au(III) to Au(0). In these experiments, after the vessels containing Au(III) solution and IEA resin were shaken for several hours, a powder with a golden glitter was observed on the bottom of the vessel and on the surface of the resin.

Table 1
Effects of accompanying ions on recovery (%) of 50 μg Au(III), Pt(IV) and Pd(II)

| | Accompanying ion (mg) | | | | | | | |
|---|---|---|---|---|---|---|---|---|
| | $Cu^{2+}$ (50) | $Fe^{3+}$ (50) | $Zn^{2+}$ (50) | $Ni^{2+}$ (5) | $Mn^{2+}$ (5) | $Cr^{3+}$ (5) | $Ca^{2+}$ (5) | $Mg^{2+}$ (5) |
| Au(III) | 92.2 | 105.1 | 88.4 | 93.9 | 102.4 | 96.8 | 96.4 | 103.0 |
| Pt(IV) | 94.9 | 91.1 | 98.2 | 91.5 | 92.5 | 99.4 | 91.8 | 96.3 |
| Pd(II) | 98.8 | 98.6 | 92.3 | 94.3 | 95.9 | 105.4 | 93.5 | 91.4 |

Solution volume 60 ml, sorbent 0.1 g, flow rate 1.0 ml $min^{-1}$.

Table 2
Recovery (%) of Au(III), Pt(IV) and Pd(II) adsorption from the p.p.b. range

| | Au(III) | Pt(IV) | Pd(II) |
|---|---|---|---|
| 2 M HCl [a] | 83.8 | 82.6 | 66.2 |
| pH 1.0 [b] | 94.5 | 86.6 | 80.6 |

[a] Flow rate 1.0 ml $min^{-1}$.
[b] Flow rate 16.0 ml $min^{-1}$.
Solution volume 500 ml, sorbent 0.1 g.

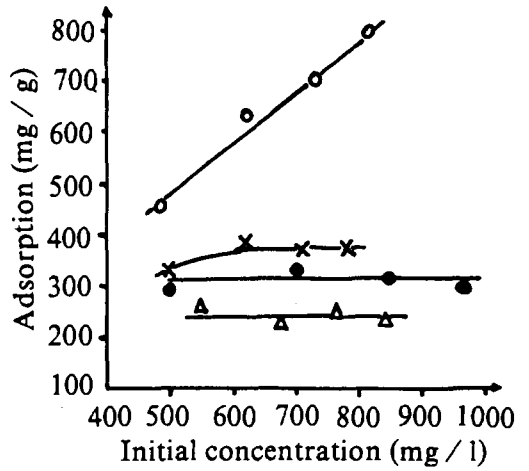


Fig. 4. Effect of concentration on capacity of adsorption of IEA resin for Au(III) (○), Pt(IV) (●), Pd(II) (△) and Ir(IV) (X). Solution volume 10 ml, sorbent 10 mg, shaking time 10 h.

### 3.8. Analytical application

Au, Pt and Pd in a sample from a smelter and a standard nickel alloy reference sample were adsorbed and determined by the above procedure. The reliability of the procedure for the smelter sample was confirmed by the standard addition method (Tables 4 and 5).

### 3.9. IR spectra of the IEA resin and IEA-Pd

The IR absorption bands of IEA resin alone and saturated with Pd(II) ions (IEA-Pd) were assigned according to Refs. [13–15] (Table 6). Absorption at 2244 $cm^{-1}$ of IEA was due to the unreacted cyanogroup. It disappeared after saturation with Pd owing to hydrolysis. After

Table 3
Effects of adsorption–desorption cycles on adsorption of 49.4 μg Au(III), 51.6 μg Pt(IV) and 55.5 μg Pd(II)

| Cycle | Adsorption (%) | | | Desorption recovery (%) | | |
|---|---|---|---|---|---|---|
| | Au(III) | Pt(IV) | Pd(II) | Au(III) | Pt(IV) | Pd(II) |
| 1 | 99.5 | 100.0 | 98.7 | – | – | – |
| 2 | 98.8 | 100.0 | 100.0 | 103.6 | 103.0 | 101.2 |
| 3 | 99.3 | 97.3 | 100.0 | 91.5 | 97.8 | 97.6 |
| 4 | 99.2 | 100.0 | 100.0 | 101.4 | 105.6 | 103.8 |
| 5 | 97.7 | 100.0 | 100.0 | 95.6 | 93.7 | 106.0 |
| 6 | 98.6 | 100.0 | 99.5 | 88.7 | 103.0 | 102.0 |
| 7 | 100.0 | 100.0 | 100.0 | 98.1 | 103.0 | 95.3 |
| 8 | 98.4 | 100.0 | 100.0 | 102.1 | 95.5 | 92.5 |
| 9 | 99.4 | 95.7 | 100.0 | 91.5 | 95.4 | 102.0 |
| 10 | 100.0 | 96.3 | 100.0 | 92.5 | 94.9 | 96.4 |

Solution volume 60 ml, sorbent 0.1 g, eluent volume 10 ml, adsorption flow rate 1.0 ml $min^{-1}$, desorption flow rate 2.0 ml $min^{-1}$.

Table 4
Results for the determination of a smelter sample ($n = 3$) [a] ($\mu g\ g^{-1}$)

| Element | Found ±S.D. | Added | Total found ±S.D. | Recovery (%) | Added | Total found ±S.D. | Recovery (%) |
|---|---|---|---|---|---|---|---|
| Au | 221 ± 11 | 127 | 339 ± 5 | 92.9 | 253 | 461 ± 14 | 94.9 |
| Pt | 637 ± 16 | 132 | 761 ± 26 | 94.0 | 263 | 896 ± 30 | 98.5 |
| Pd | 403 ± 4 | 142 | 538 ± 15 | 95.1 | 284 | 687 ± 45 | 100.0 |

[a] Compositions stated by the smelter for the sample were 0.023, 0.066 and 0.040% Au, Pt and Pd, respectively.

Table 5
Results for determination of the standard reference sample (102-A-7) ($n = 3$) ($\mu g\ g^{-1}$)

| Element | Found | Certified |
|---|---|---|
| Au | 136 ± 8 | 144 |
| Pt | 310 ± 9 | 306 |
| Pd | 183 ± 12 | 189 |

Pd(II) was adsorbed by the IEA, the peak at 3251 $cm^{-1}$ of $\nu$(N–H) became broad. The 1660 and 1592 $cm^{-1}$ peaks of $\nu$(C=C) + $\nu$(C=N) shifted to 1625 $cm^{-1}$, and the 1440 $cm^{-1}$ and 755 $cm^{-1}$ peaks of $\delta$(N–H) shifted to 1442 and 760 $cm^{-1}$, respectively. The 1129 $cm^{-1}$ peak of $\nu$(C–N) shifted to 1169 $cm^{-1}$, and the 995 $cm^{-1}$ peak of the skeletal vibration of the heterocycle shifted to 1045 $cm^{-1}$. All of these indicated that the nitrogen atom participated in the coordination. The new peaks at 533 $cm^{-1}$, 271 $cm^{-1}$ and 319 $cm^{-1}$ were due to $\nu$(Pd–N), $\delta$(N–Pd–N) and $\nu$(Pd–Cl) respectively. Accordingly, the structure formed from IEA resin with Pd(II) might be:

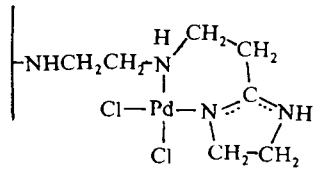

or

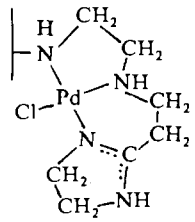

Table 6
Assignment of major IR bands of IEA resin and IEA saturated with Pd(II) ($cm^{-1}$)

| Resin | Resin saturated with Pd(II) | Assignments |
|---|---|---|
| 3251 | 3249 | $\nu_{N-H}$ |
| 2926, 2856 | 2919 | $\nu_{CH_2}$ |
| 2244 | – | $\nu_{C\ N}$ |
| 1660, 1592 | 1625 | $\nu_{C\ C} + \nu_{C\ N}$ |
| 1440 | 1442 | $\delta_{NH}$ |
| 1347 | 1348 | $\delta_{CH_2}$ |
| 1129 | 1169 | $\nu_{C\ N}$ |
| 995, 988 | 1045, 988 | Skeletal vibration of heterocycle |
| 755 | 760 | $\delta_{N\ H}$ |
| – | 533 | $\nu_{Pd-N}$ |
| – | 319 | $\nu_{Pd-Cl}$ |
| – | 271 | $\delta_{N-Pd-N}$ |

## 4. Conclusion

IEA resin has high adsorption selectivity for Au(III), Pt(IV) and Pd(II). It can quantitatively adsorb these ions over a wide range of acidities. The adsorbed ions can be readily desorbed by a thiourea and mineral acid mixture. The resin also has the advantage of a high rate of equilibration, low interference, large adsorption capacity, high stability and good reusability. Preconcentration by this resin combined with ICP-AES can be reliably applied to the determination of Au, Pt and Pd in mineral samples.

## References

[1] R.M. Barnes and A. Diallo, in L.R.P. Butler (Ed.), Analytical Chemistry in the Exploration, Mining and Processing of Materials, Blackwell, Oxford, 1986, pp. 3–13.
[2] Y.S. Chung and R.M. Barnes, J. Anal. At. Spectrom., 3 (1988) 1079.
[3] Zs. Horvath, A. Lasztity and R.M. Barnes, Spectrochim. Acta Rev., 14 (1991) 45.

[4] G. Koster and G. Schmuekler, Anal. Chim. Acta, 38 (1967) 179.
[5] A. Warshawsky, M.M.B. Fieberg, P. Mihalik, T.G. Murphy and Y.B. Ras, Sep. Purif. Methods, 9 (1980) 209.
[6] Sandeep Srivastava and Gadepalli N. Rao, Analyst, 115(12) (1990) 1607.
[7] Frederick Vernon, Pure Appl. Chem., 54 (1982) 2151.
[8] S. Siddhanta and H.R. Das, Talanta, 32 (1985) 457.
[9] T.I. Tikhmirova, V.I. Fadeeva, G.V. Kudryavtsev, P.N. Nesterenko, V.M. Ivanov, A.T. Savitchev and N.S. Smirnova, Talanta, 38 (1991) 267.
[10] L.Y. Li, X.W. Xu, Y. An and J.Q. Ma, Chem. J. Chin. Univ., 10 (1989) 1147.
[11] G.V. Myasoedova, I.I. Antokol'skaya and S.B. Savvin, Talanta, 32 (1985) 1105.
[12] Z.X. Su, D.R. Cao and Z.C. Zhang, Ion Exchange and Adsorption, 4 (1988) 574.
[13] Z.M. Wang, X.X. He and D.Q. Sun, Practical Infrared Spectroscopy, Publishing House of Oil Industry, Beijing, 1982, pp. 224, 249.
[14] J. Dehand and J. Jordanov, Inorg. Chim. Acta, 17 (1976) 37.
[15] G.W. Watt and D.D. Klett, Spectrochim. Acta, 20 (1964) 1053.

ELSEVIER

Talanta 42 (1995) 1135–1142

Talanta

# Spectrophotometric determination of aluminium by morin

M. Jamaluddin Ahmed *, Jamal Hossan

*Laboratory of Analytical Chemistry, Department of Chemistry, University of Chittagong, Chittagong, Bangladesh*

Received 10 November 1994; revised 31 January 1995; accepted 3 February 1995

**Abstract**

A direct spectrophotometric method for the determination of aluminium with morin has been developed. Morin reacts in slightly acidic 50% ethanolic media (0.0001–0.0015 M $H_2SO_4$) with Al to give a deep-yellow chelate which has an absorption maximum at 421 nm. The average molar absorptivity and Sandell's sensitivity were found to be $5.3 \times 10^3$ l mol$^{-1}$ cm$^{-1}$ and 5 ng of Al cm$^{-2}$, respectively. The reaction is instantaneous and absorbance remains stable for 48 h. The colour system obeys Beer's law from 10 ng ml$^{-1}$ to 5.0 μg ml$^{-1}$ of Al; the stoichiometric composition of the chelate is 2:3 (Al:morin). The interference from over 50 cations, anions and complexing agents has been studied at 0.1 μg ml$^{-1}$ of Al. The method was applied successfully to some certified reference material samples (alloys and steels), environmental waters (inland and surface), biological samples (human blood, urine and gallstone), soils and complex synthetic mixtures.

## 1. Introduction

Aluminium has long been considered as virtually non-toxic and non-absorbable from the gastrointestinal tract. More recent studies on humans, however, expose its acute toxicity [1], including impaired memory, convulsions, characteristic EEG changes, uremia, Shaver's disease (lung) [2], Alzheimer's disease (brain) [3] and also increased risks of cancer [4] of the lung and pancreas, and leukaemia. Al at trace and sub-trace levels in the water used for dialysis can cause brain damage, bone disease and anaemia [5]. All these findings cause alarming concern in public health, demanding accurate determination of this metal ion at trace and sub-trace levels.

Miller and Andelman [6] reviewed methods for the determination of Al species in water. Several recently published spectrophotometric methods [7–18] based on use of various reagents are reported for the determination and detection of the metal ion. Some of these methods are not sensitive [10–14] or suffer from interferences [15–18]. The present paper describes a sensitive spectrophotometric method for the determination of Al using morin. The method is based on the selective complexation of the non-absorbent reagent, morin, in slightly acidic medium (0.0001–0.0015 M $H_2SO_4$) with Al to produce a deep-yellow chelate, followed by direct measurement of the absorbance in 50% ethanolic solution.

## 2. Experimental section

### 2.1. Apparatus

A Shimadzu (Model-160) double beam UV/visible recording spectrophotometer and Philips PW 9418 pH-meter with combination electrodes were used for measurements of absorbance and pH, respectively. Biological samples were analyzed for trace amounts of Al by a Perkin-Elmer Model 560 atomic absorption spectrophotometer at 309.3 nm, using a nitrous oxide–acetylene flame.

* Corresponding author.


*SSDI* 0039-9140(95)01554-X

### 2.2. Reagents and solutions

All the chemical used were of analytical grade of the highest purity available. Triply-distilled ethanol (from lime) and high-purity deionized water, non-absorbent under UV radiation, were used throughout. High-purity water was obtained by passing tap water through a cellulose absorbent and two mixed-bed ion exchange columns, followed by distillation in a Corning AG-11 unit. The Al level in the high-purity water was found to be below the spectrophotometric detection limit (three times the standard deviation of the blank) of 6 ng $ml^{-1}$. Glass vessels were cleaned by soaking in acidified solutions of $KMnO_4$ or $K_2Cr_2O_7$ followed by washing with concentrated $HNO_3$, and rinsed several times with high-purity deionized water. Stock solutions and environmental water samples (1000 ml each) were kept in polypropylene bottles containing 1 ml conc. $HNO_3$.

*Morin solution, $1.35 \times 10^{-3}$ M*

40.27 mg of morin (BDH Chemicals) was dissolved in 100 ml of triply-distilled ethanol. This solution was diluted further as required.

*Al standard solutions*

100 ml stock solution of Al ($3.71 \times 10^{-2}$ M) was prepared by dissolving 1.7582 g of $AlK(SO_4)_2 \cdot 12H_2O$ (Merck analytical grade) in deionized water. Working standard solutions were prepared after suitable dilutions of the stock solution.

*EDTA solution*

100 ml stock solution of EDTA (0.01%) was prepared by dissolving 10 mg of A.C.S. grade

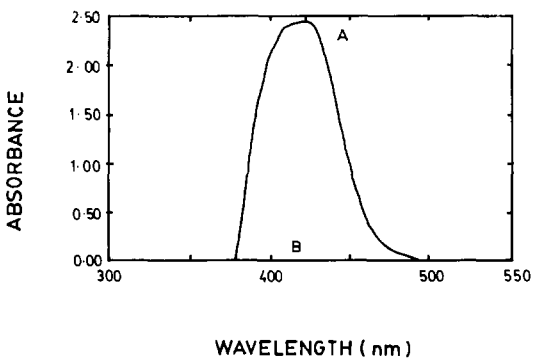


Fig. 1. A and B absorption spectra of the Al–morin system and the reagent blank ($\lambda_{max} = 421$ nm) in 50% ethanolic solutions.

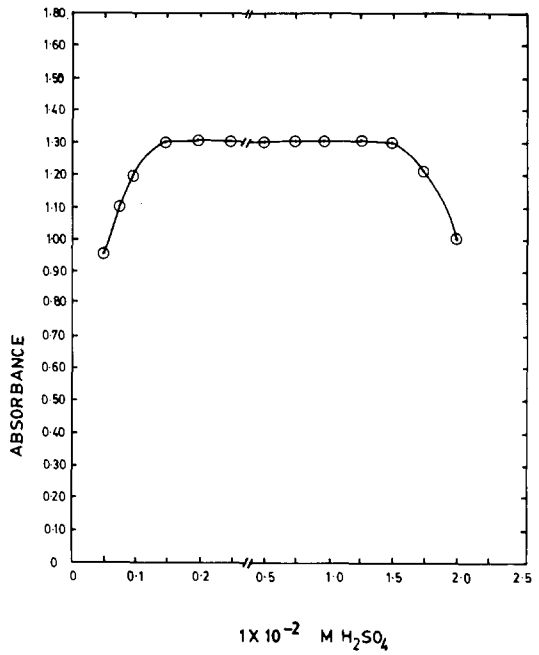


Fig. 2. Effect of acidity on the absorbance of the Al (0.1 μg $ml^{-1}$)–reagent system.

(≥99%) ethylenediaminetetraacetic acid, disodium salt dihydrate in (100 ml) deionized water.

*Tartrate solution*

100 ml stock solution of tartrate (0.01%) was prepared by dissolving 10 mg of A.C.S. grade (99%) potassium sodium tartrate tetrahydrate in (100 ml) deionized water.

*Dilute ammonium hydroxide solution*

A 100 ml solution of dilute ammonium hydroxide was prepared by diluting 10 ml conc. $NH_4OH$ (28–30%, A.C.S. grade) to 100 ml with deionized water. The solution was stored in a polypropylene bottle.

*Other solutions*

Solutions of a large number of inorganic ions and complexing agents were prepared from their water-soluble salts (or the oxides and carbonates in hydrochloric acid); solutions of titanium, zirconium and hafnium were specially prepared from their corresponding oxides (Specpure, Johnson Matthey) according to the recommended procedures of Mukharji [19].

### 2.3. Procedure

To 0.1–1.0 ml of a neutral aqueous (pH 6) solution containing 0.1–50 μg of aluminium in

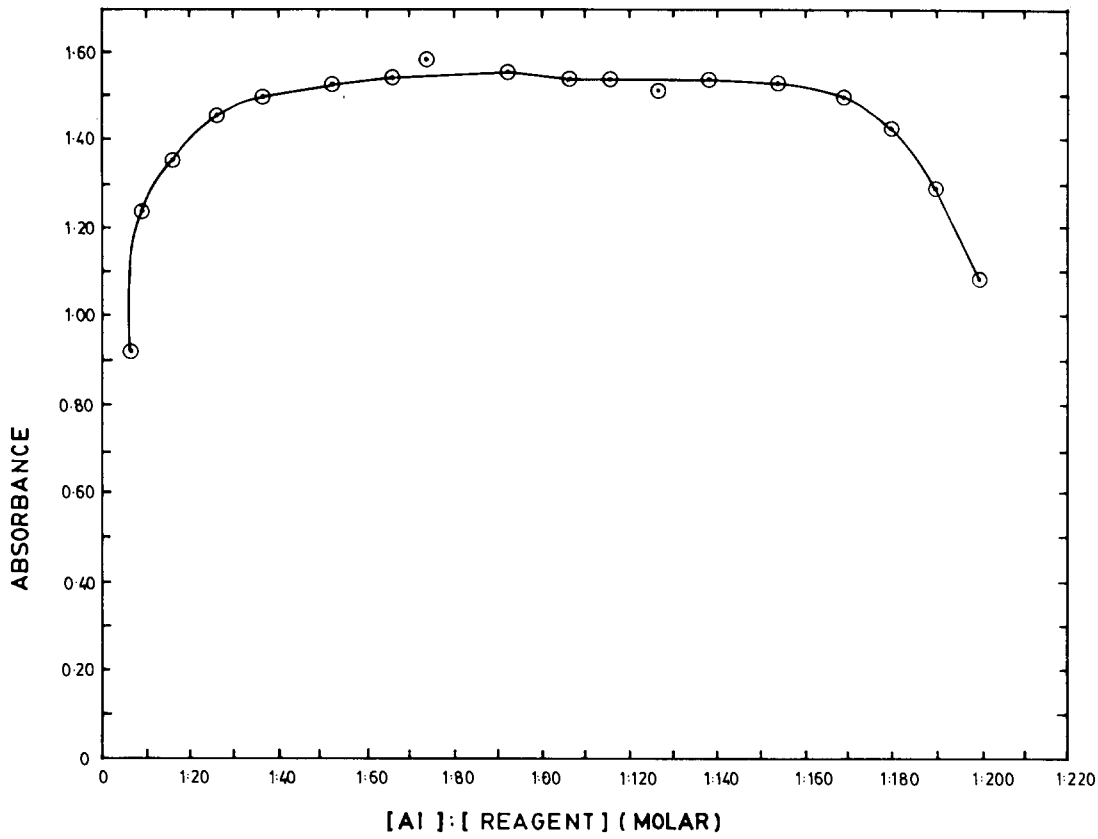


Fig. 3. Effect of the reagent (morin: Al molar concentration ratio) on the absorbance of the Al (0.5 μg $ml^{-1}$)–reagent system.

a 10 ml volumetric flask was added 2.0 ml of $1.35 \times 10^{-3}$ M of the morin reagent solution, followed by the addition 0.2 ml of 0.025 M (0.005 M) sulphuric acid. The solution was mixed well and allowed to stand for 1 min, after which 5 ml of ethanol was added. The mixture was diluted up to the required volume with deionized water. The absorbance was measured at 421 nm against a corresponding reagent blank. A calibration graph was used for unknown samples.

### 2.4. Analytical applications

#### A. Determination of Al in alloys and steels

A 0.1 g amount of an alloy or steel sample containing 3.34–90.5% Al was weighed accurately and placed in a 50 ml Erlenmayer flask. To this was added 5 ml each of concentrated sulphuric and nitric acids, and the mixture was heated gently. 1 ml of perchloric acid (sp. gr. 1.70) was added to the solutions and evaporated until strong fuming occurred. The solution was cooled to room temperature after complete dissolution of the sample. The soluble salts were dissolved in deionized water. The solution was filtered through a Whatman No. 40 filter paper into a 100 ml calibrated flask; the residue (silica and tungstic acid) was washed with a small volume (5 ml) of hot (1:99) sulphuric acid followed by water. The filtrate and washings were collected in the same calibrated flask. The content of the flask was neutralized (pH 6) with dilute $NH_4OH$ in the presence of 1–2 ml of 0.01% (w/v) tartrate and/or EDTA solution, and the volume was made up to the mark with deionized water. An aliquot (1–2 ml) of this solution was pipetted into a 10 ml calibrated flask, and the Al content was determined as described in section 2.3.

#### B. Determination of Al in environmental water samples

Each filtered (through a Whatman No. 40 filter paper) environmental water sample (50 ml) was heated with a mixture of 1 ml conc. $H_2SO_4$ and 2.5 ml conc. $HNO_3$ until sulphur trioxide fumes appeared. After cooling, addition of 2.5 ml conc. $HNO_3$ and heating was repeated until dense white fumes were ob-

Table 1
Determination of Al in synthetic mixtures

| Sample | Composition of mixture ($\mu g\ ml^{-1}$) | Al found [a] ($\mu g\ ml^{-1}$) | Error [a] (%) |
|---|---|---|---|
| A | Al (0.5) + $Ce^{3+}$(25) + $Cr^{3+}$(25) Tartrate + EDTA | 0.499 | 0.20 |
| B | A + Mg(25) + $Bi^{3+}$(25) | 0.497 | 0.60 |
| C | B + $Sn^{2+}$(25) + Zn(25) | 0.495 | 1.00 |
| D | C + $Ag^{+}$(25) + Ba(25) | 0.507 | 1.40 |

[a] Average of five determinations.

Table 2
Analysis of high-speed steels and alloys

| Sample | Certified reference material composition (%) | Al (%) | | Standard deviation | Error [a] (%) |
|---|---|---|---|---|---|
| | | Certified value | Amound found [a] | | |
| 1 | Bureau of Analysed Samples Ltd. No. BAS-10g (high tensile) (Cu, 60.8; Sn, 0.21; Zn, 30.0; Al, 3.34; Pb, 0.023; Ni, 0.16; Fe, 1.56; Mn, 1.36) | 3.34 | 3.335 | ±0.004 | 0.0025 |
| 2 | Bureau of Analysed Samples Ltd. No. BAS-20b (Al-alloy) (Al, 90.5; Mg, 1.6; Cu, 4.1; Ni, 1.9; Fe, 0.43; Mn, 0.19; Si, 0.24) | 90.50 | 90.495 | ±0.006 | 0.004 |

[a] Average of 10 determinations.

served, or until the solution became colourless. The solution was then cooled and neutralized (pH 6) with dilute $NH_4OH$ in the presence of 1–2 ml of 0.01% (w/v) EDTA and/or tartrate solution. It was transferred into a 50 ml volumetric flask and diluted up to the mark with deionized water. 1 ml of the final solution was pipetted into a 10 ml calibrated flask and the Al content was determined as described in section 2.3.

*C. Determination of Al in biological samples*

Human blood (10–20 ml), urine (10–50 ml) or human gallstone (0.1–0.5 g) was added to a 100 ml micro-Kjeldahl digestion flask. A glass bead and 10 ml of conc. $HNO_3$ were added and heated gently on the digester. When the initial brisk reaction was over, the solution was removed and cooled. Conc. $H_2SO_3$ (2.5 ml) was added carefully, followed by the addition of 70% perchloric acid (1 ml); heating was continued until dense white fumes were observed, repeating $HNO_3$ addition if necessary. Heating was continued for at least 30 min, followed by cooling. The content of the flask was neutralized (pH 6) with dilute $NH_4OH$ in the presence of 1–2 ml of 0.01% (w/v) tartrate and/or EDTA solution, transferred quantitatively into a 50 ml volumetric flask and made up to the mark with deionized water. An aliquot (1–2 ml) of the final solution was pipetted into a 10 ml calibrated flask and the Al content was determined as described in section 2.3.

*D. Determination of Al in soil samples*

A 10–20 g amount of air-dried soil sample was weighed accurately and placed in a 100 ml micro-Kjeldahl flask. The sample was digested according to the method recommended by Jackson [20]. The contents of the flask were filtered through Whatman No. 40 filter paper into a 25 ml calibrated flask, neutralized (pH 6) with dilute ammonia and diluted to the volume with deionized water. Suitable aliquots (1–2 ml) were transferred to a 10 ml volumetric flask and the calculated amount of

Table 3
Determination of Al in some environmental water samples

| Environmental water sample | Al "spiked" | | | Aluminium "unspiked" found ($\mu g\ ml^{-1}$) |
|---|---|---|---|---|
| | Added ($\mu g\ ml^{-1}$) | Found ($\mu g\ ml^{-1}$) | Recovery (%) | |
| Tap water | 1.00 | 1.51 [a] | 99.3 ± 0.5 [b] | 0.52 |
| | 0.10 | 0.605 | 99 ± 0.1 | 0.51 |
| Pond water | 1.00 | 0.99 | 99 ± 0.6 | 0.00 |
| | 0.10 | 0.098 | 98 ± 0.5 | 0.00 |
| Well water | 1.00 | 1.25 | 100.8 ± 1.0 | 0.24 |
| | 0.10 | 0.36 | 99.3 ± 0.8 | 0.27 |
| River water | | | | |
| (i) Halda (upper stream) | 1.00 | 1.131 | 100 ± 1.0 | 0.131 |
| | 0.10 | 0.231 | 99.6 ± 1.5 | 0.132 |
| (ii) Halda (lower stream) | 1.00 | 1.125 | 99.9 ± 0.5 | 0.126 |
| | 0.10 | 0.225 | 100.4 ± 2.0 | 0.124 |
| (i) Karnaphuly (upper) | 1.00 | 1.164 | 100 ± 1.0 | 0.163 |
| | 0.10 | 0.266 | 100.3 ± 0.8 | 0.165 |
| (ii) Karnaphuly (lower) | 1.00 | 1.165 | 100 ± 0.6 | 0.164 |
| | 0.10 | 0.265 | 99.6 ± 1.2 | 0.166 |
| Sea water | | | | |
| (i) Bay of Bengal (upper) | 1.00 | 1.176 | 99.8 ± 1.0 | 0.178 |
| | 0.10 | 0.277 | 100.7 ± 0.5 | 0.175 |
| (ii) Bay of Bengal (lower) | 1.00 | 1.174 | 100.1 ± 0.8 | 0.173 |
| | 0.10 | 0.272 | 99.3 ± 1.5 | 0.174 |
| Drain water | | | | |
| (i) Madina Tannery [c] | 1.00 | 1.398 | 99.8 ± 0.6 | 0.399 |
| | 0.10 | 0.498 | 100.2 ± 1.0 | 0.397 |
| (ii) Delhi Aluminum Factory [d] | 1.00 | 1.335 | 100.2 ± 1.2 | 0.333 |
| | 0.10 | 0.432 | 99.6 ± 1.3 | 0.334 |
| (iii) Karnaphuly Paper Mill [e] | 1.00 | 1.444 | 100 ± 0.8 | 0.443 |
| | 0.10 | 0.542 | 99.9 ± 1.5 | 0.443 |

[a] Values given represent the average of five analyses of each sample.
[b] Standard deviation is a measure of precision.
[c] Madina Tannery, Jalalabad, Chittagong.
[d] Delhi Aluminum Factory, Biojid-Bostami, Chittagong.
[e] Karnaphuly Paper Mill, Chandraghona, Chittagong.

0.025 M $H_2SO_4$ needed to give a final acidity of 0.0001–0.0015 M was added, followed by 1–2 ml of 0.01% (w/v) tartrate and/or EDTA solution. Al content was then determined as in section 2.3.

## 3. Results and discussion

### 3.1. Development of the method

*Spectral characteristics*

The absorption sepctra of the Al–morin system in 0.025 M $H_2SO_4$ medium was recorded using the spectrophotometer. The absorption spectra of Al–morin as a symmetric curve with maximum absorbance at 421 nm and an average molar absorptivity of $5.3 \times 10^3\ l\ mol^{-1}\ cm^{-1}$ is shown in Fig. 1. The reagent blank exhibited negligible absorbance despite having a wavelength at 421 nm. The reaction mechanism of the present method is as reported earlier [21].

### 3.2. Effect of solvent

Chloroform, benzene, carbon tetrachloride, isobutanol and ethanol were tested as solvents for the system. No absorbance was observed in the organic phase. In 50 ± 2% (v/v) ethanolic medium, however maximum absorbance was observed; hence, a 50% ethanolic solution was used in the recommended procedure.

### 3.3. Effect of acidity

The absorbance was at a maximum and constant when the 10 ml of solution (0.1 $\mu g\ ml^{-1}$)

Table 4
Concentration levels ($\mu g\ ml^{-1}$ or $\mu g\ g^{-1}$) of Al in biological samples under pathological conditions

| Serial No. | Name of sample | Concentration of aluminium (mean value [a] ± SD(%)) | | Sample source |
|---|---|---|---|---|
| | | AAS method | Proposed method | |
| 1 | a. Blood | 0.27 ± 0.8 | 0.28 ± 0.5 | Cancer (leukaemia) patient |
| | b. Urine | 0.10 ± 1.3 | 0.12 ± 1.0 | Chittagong M.C. Hospital |
| 2 | a. Blood | 0.29 ± 1.5 | 0.29 ± 1.0 | Cancer (lung) patient |
| | b. Urine | 0.13 ± 1.0 | 0.14 ± 1.2 | Chittagong M.C. Hospital |
| 3 | a. Blood | 0.19 ± 1.4 | 0.18 ± 0.6 | Neurotic patient (female) |
| | b. Urine | 0.08 ± 2.0 | 0.07 ± 1.4 | Chittagong M.C. Hospital |
| 4 | a. Blood | 0.12 ± 1.6 | 0.13 ± 0.8 | Normal adult (male) |
| | b. Urine | 0.04 ± 0.8 | 0.04 ± 0.2 | Chittagong M.C. Hospital |
| 5 | Human gall-stone | 37.00 ± 1.2 | 36.75 ± 1.0 | Gall-stones patient (male) Chittagong M.C. Hospital |

[a] Average of five determinations.

contained 0.001–0.015 M $H_2SO_4$ at room temperature (25 ± 5°C). Outside this range of acidity, the absorbance decreased (Fig. 2). For all subsequent measurements, 0.2 ml of 0.025 M (0.005 M) $H_2SO_4$ was added.

### 3.4. Effect of time

The reaction is instantaneous. The Al–morin system attained maximum and constant absorbance immediately (within 1 min) after diluting the solution to the final volume, which then remained stable for at least 48 h. A longer period of time was not studied.

### 3.5. Effect of reagent

The excess of reagent is not critical. In tests with 0.5 $\mu g\ ml^{-1}$ Al, the Al/reagent mole ratio was varied from 1:10 to 1:200. Constant maximum absorbance was obtained for mole ratios between 1:40 and 1:170 (Fig. 3). For the different Al concentrations (1 and 0.1 $\mu g\ ml^{-1}$), an identical effect of varying the reagent concentration was noticed.

### 3.6. Calibration graph and Beer's law

Plots of absorbance against Al concentration were linear and passed through the origin for a wide range (10 $ng\ ml^{-1}$ to 5 $\mu g\ ml^{-1}$) of Al concentrations, when different scale expansions were used. The average molar absorptivity and the Sandell's sensitivity [22] were found to be $5.3 \times 10^3\ l\ mol^{-1}\ cm^{-1}$ and 5 ng of Al $cm^{-2}$, respectively.

### 3.7. Precision and accuracy

The precision of the present method was evaluated by determining different concentrations of Al (each analyzed at least five times). Standard deviations in the range 0.001–2.0 for 0.1–50 μg of Al in 10.0 ml were achieved, indicating that this method is highly precise and reproducible. The detection limit (three times the standard deviation of the blank) for Al were found to be 6 $ng\ ml^{-1}$. The reliability of the proposed procedure was assessed by analyzing the Bureau of Analyzed Samples (Table 2) and a series of synthetic mixtures of various compositions (Table 1). Note from Table 2 the good agreement for Al found with the certified values. A few synthetic mixtures of various compositions containing Al and diverse ions of known concentrations were determined by the present method using tartrate and/or EDTA as masking agents, and the results (Table 1) were found to be highly reproducible. The reliability of our procedure was also tested by doing recovery studies. The average recovery obtained for the addition of Al spikes to some environmental water samples was quantitative, as shown in Table 3. The results of the analysis of biological samples by our procedure were found to be in excellent agreement with those obtained by an atomic absorption spectrophotometric method, as shown in Table 4. Hence, the precision and accuracy of the method were found to be excellent.

### 3.8. Effect of foreign ions

More than 50 anions and cations were studied individually to investigate their effect on the determination of 0.1 $\mu g\,ml^{-1}$ of Al. The criterion for an interference was an absorbance value varying by more than 5% from the expected value for Al alone [23]. There was no interference from the following: 1000-fold amounts of tartrate, nitrate, sulphate, citrate, fluoride, bromide, oxalate, alkali metals or acetate; 500-fold amounts of azide, chromium(III), cerium(IV), magnesium, barium or sulphide; 100-fold amounts of tin (II and IV), silver(I) cadmium, manganese(II), bismuth, chromium(VI), copper(II), strontium, vanadium(V), molybdenum(VI), selenium(IV and VI), arsenic(III), uranium(VI) or EDTA. Sodium tartrate prevented the interference of a 100-fold amount of lead(II), iron(II and III), zinc, nickel(II), calcium, mercury(II), tungsten(VI), chloride or cyanide, A 50-fold excess of thiocyanide and thiourea have been tolerated. Interference from persulphate, permanganate or hydrogen peroxide was removed simply by using sodium azide and boiling the solution.

### 3.9. Nature of the complex

Job's method [24] of continuous variation and the molar-ratio [25] method were applied to ascertain the stoichiometric composition of the complex. A 2:3 (Al:morin) complex was indicated by both the methods.

### 3.10. Comparative study

The method is rapid, simple, sensitive and reproducible. It is well suited for routine analysis of trace amounts of Al.

### 3.11. Applications of the method

The proposed method was used to determine the Al content of a series of synthetic environmental samples to test its general/specific applications. The method was also applied to the determination of the Al content in a number of standard samples (alloys and steels), environmental waters (inland and surface), biological samples (human gallstone, blood and urine), and soil samples. In view of the unknown composition of the environmental water samples, the same aliquots were analyzed for their aluminium content, both "spiked" and "unspiked". The mean error and standard deviations for each series of determination were calculated.

A few synthetic mixtures of varying composition containing Al and diverse ions of known concentrations were determined by the present method using tartrate and/or EDTA as masking agents, and the corresponding results are given in Table 1. The reliability of the proposed method was assessed by analyzing the Bureau of Analyzed samples and the corresponding results are shown in Table 2. The analysis of water from various sources for Al is shown in Table 3. The high values for treated waters are probably due to leakage and/or excess addition of alum used as a flocculant in the water-treatment plants. The occurrence of such high values of Al content are also reported in the treated waters of some developed countries [26]. The results of the analysis of biological samples by our procedure were found to be in excellent agreement with those obtained by atomic absorption spectrophotometric methods and are shown in Table 4. The average value of Al in ten different surface soil samples of Bangladesh was found to be 8.5 $\mu g\,ml^{-1}$. The method is very reliable, and the concentration in the $ng\,g^{-1}$ range in 50% ethanolic medium at room temperature ($25 \pm 5$ °C) can be measured in a very simple and rapid way for routine analysis of Al.

## Acknowledgements

The authors acknowledge the gift of some standard samples by Professor B.K. Pal of Jadavpur University, Calcutta, India. We are specially indebted to the authorities of Chittagong Medical College Hospital for their generous help in supplying biological samples. The authors thank Mr. S.M, Amjad Hossain, Deputy Chief Chemist, CUFL, Chittagong for analyzing the biological samples by AAS.

## References

[1] C.G. Elinder and B. Sjogren, Aluminium, in L. Friberg, G.F. Nordberg and V.B. Vouk (Eds.), Handbook on the Toxicology of Metals, 2nd edn., Vol. 2, 1986, Chapter 1, Elsevier, Amsterdam, pp. 1–20.

[2] B. Venugopal and T.D. Luckey, Aluminium, in Metal Toxicity in Mammals 2, Plenum, New York, 1979, pp. 104–112.

[3] D.R. Craper, S.S. Krishnan and A.J. Dalton, Brain aluminium distribution in Alzheimer's disease and experimental neurofibrillary degeneration, Science, 108 (1973) 511.
[4] R.K. Iyer and S.G. Jadhav, Science Today, 24 (1990) 9.
[5] A.K. De, Chemical Toxicology, in Environmental Chemistry, Wiley Eastern Limited, New Delhi, 1989, p. 66.
[6] J.R. Miller and J.B. Andelman, Chem. Environ., Proc. Int. Conf., J.N. Lester, R. Perry and R.M. Sterritt (Eds.), Selper, London, 1986, pp. 26–35.
[7] J. Dewis and F. Freitas (Eds.), Physical and Chemical Methods of Soil and Water Analysis, Food and Agriculture Organizaton of the United Nations, Rome, 1976, pp. 138–140.
[8] O. Røyset, Anal. Chim. Acta, 185 (1986) 75.
[9] O. Røyset, Anal. Chem., 59(6) (1987) 899.
[10] R.L. Benson, P.J. Worsfold and F.W. Sweeting, Anal. Chim. Acta, 238(1) (1990) 177.
[11] N. Clarke, L. Danielsson and A. Sparen, Int. J. Environ. Anal. Chem., 48(2) (1992) 77.
[12] Yun Zhang, Yejin Fenxi, 10(4) (1990) 57.
[13] Zhonfang Liu, Liu Shaopu and Wang Xuechao, Yejin Fenxi, 10(4) (1990) 9.
[14] C. Woodward and H. Freiser, Talanta, 15(1–6) (1968) 321.
[15] Teiko Ohmori, Kogyo Youi, 409 (1992) 58.
[16] Nishida Hiroshi, Bunseki Kagaku, 42(5) (1993) 293.
[17] L.M. Shafic and H. Ibrahim, Delta J. Sci., 15(1) (1991) 67.
[18] J. Bassett, R.C. Denny, G.H. Jeffery and J. Mendham (Eds.), Vogel's Textbook of Quantitative Inorganic Analysis, 4th edn., English Language Book Society/Longman, London, 1978, p. 729.
[19] A.K. Mukharji, Analytical Chemistry of Zirconium and Hafnium, 1st edn., Pergamon Press, New York, 1970, p. 12.
[20] M.L. Jackson, Soil Chemical Analysis, Prentice-Hall, New Jersey, 1965, p. 297.
[21] N. Bobrov, Handbook of Analytical Chemistry, Ju. Lurie (Ed.), Mir Publishers, Moscow, 1975, p. 382.
[22] E.B. Sandell, Colorimetric Determination of Traces of Metals, 3rd edn., Interscience, New York, 1965, p. 269.
[23] C. Bosch Ojeda, A. Garcia De Torres, F. Sanchez Rojas and J.M. Cano Pavon, The Analyst, 112 (1987) 1499.
[24] P. Job, Ann. Chim. (Paris), 9 (1928) 113.
[25] J.A. Yoe and A.L. Jones, Ind. Eng. Chem. Anal. Ed., 16 (1944) 11.
[26] Nobuo Uehara, Makoto Kanbayashi, Hitoshi Hosino and Takao Yotsuyanagi, Talanta, 36 (1989) 1031.

ELSEVIER

Talanta 42 (1995) 1143–1149

Talanta

# Determination of strontium at low concentration levels by flame atomic absorption spectrometry associated on-line with continuous coprecipitation preconcentration

Soulin Lin *, Chunsung Zheng, Houjin Zu

*Department of Applied Chemistry, China University of Geosciences, Wuhan 430074, People's Republic of China*

Received 2 August 1994; revised 26 January 1995; accepted 3 February 1995

**Abstract**

A sensitive method for the determination of strontium has been developed. In this work strontium was determined by flame atomic absorption spectrometry using a continuous copreconcentration dissolution procedure based on the formation of lead sulfate followed by elution with hot EDTA solution. Manifold parameters and chemical conditions are described in detail. A concentration factor of up to 61 can be achieved at a sampling rate of 20–30 $h^{-1}$. The detection limit for strontium was 0.9 ng $ml^{-1}$ ($3\sigma$) and the relative standard deviation was 3.5% ($n = 8$) at a concentration level of 100 ng $ml^{-1}$.

## 1. Introduction

It is a matter of fact that the absorption signal for strontium in the air–acetylene flame is depressed in the presence of Al, Si, Ti or phosphates and these effects can be minimized by the addition of releasing agents. In early work reported on the determination of this element with flame atomic absorption spectrometry (FAAS), lanthanum [1] or calcium [2], 8-hydroxyquinoline and lanthanum [3], and EDTA and lanthanum [4] were used to suppress interferences in the air–acetylene flame. Ion exchange procedures were employed by Hofer [5] and David [6] to separate strontium from matrix components for the analysis of phosphate rocks and biological materials respectively. Curnow et al. [7] have reported a method for the determination of strontium. In the method described by these authors, strontium was coprecipitated with calcium oxalate, the precipitate was dissolved in hydrochloric acid and lanthanum chloride was added prior to nebulization. Other than FAAS, methods using spectrophotometric detection have been reported [8,9]. In these methods simultaneous determinations of magnesium and strontium [8], and calcium and strontium [9] were carried out with flow injection (FI) differential kinetic analysis. The determinations were carried out at 40 $h^{-1}$ and the injected sample volumes were 25–250 µl. No detection limits and precision values were reported.

Recently, Gong [10] reported a method for the determination of strontium in rocks. Strontium was coprecipitated with lead sulfate, the precipitate was centrifuged, then dissolved in hot EDTA solution and finally nebulized into the air–acetylene flame. The author claimed that satisfactory results can be obtained with the proposed separation procedure. However, this procedure is laborious and time consuming.

Since 1987, there have been several reports involving the use of on-line precipitation techniques in the FI literature. In 1987, Valcarcel and co-workers published their first paper on the use of on-line precipitation which dealt

* Corresponding author. Fax: (86) 27-701-763.


*SSDI* 0039-9140(95)01555-8

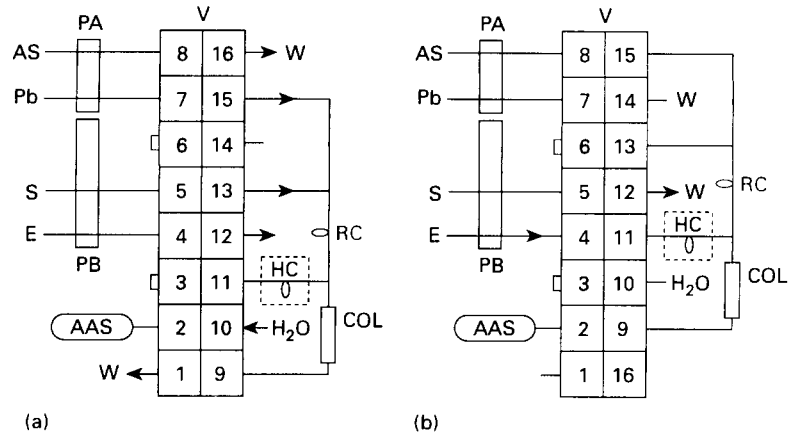


Fig. 1. Manifold for the co-precipitation preconcentration and AA determination of Sr. V-8 channel rotary injection valve, with channel 3 and 6 blocked. The left part is the stator and the right part the rotator; PA, PB-3 channel peristaltic pumps; RC—reaction coil, 30 cm; HC—heating coil, 40 cm (for tube diameters see text): COL—filter; AAS—atomic absorption spectrometer; S—sample plus 1% $H_2SO_4$ plus 20% ethanol; Pb—0.2% $Pb(AC)_2$; AS—2% $(NH_4)_2SO_4$; E—5% EDTA plus 1% KH phthalate; W—waste. (a) Preconcentration position; (b) elution position.

with the separation and preconcentration of lead [11]. In their work, lead in tap water was determined by precipitation with ammonia. A sintered stainless steel filter for solvent filtering in HPLC was used to trap the precipitate, which was then dissolved in a stream of nitric acid to give a transient signal. The technique has also been applied to the determination of copper [12] and cobalt [13] in silicate rocks with dithiooxamide and 1-nitroso-2-naphthol, respectively. In a recent report, the use of disposable membrane filters has been suggested by Tyson and co-workers [14] for the retention of the precipitates of calcium (as oxalate) and copper (as hydroxide). Recently, Fang et al. [15] demonstrated the merit of coprecipitation, which expands the scope of precipitation for separation and preconcentration. This brings the possibility that other sample components and those added externally could aid the collection of analyte species by various processes of coprecipitation. In the paper reported by these authors, the precipitate was collected in an open knotted tube reactor for the determination of lead by coprecipitation with iron(III) by hexamethylene ammonia hexamethylene dithiocarbamate.

In an attempt to improve the performance and to automize the procedure for strontium described above, we have designed a flow system for con-tinuous coprecipitation preconcentration in combination on-line with atomic absorption measurement. In this work, a demountable Perspex glass column with a disposable piece of silk fabric as the filter screen was constructed. The performance of the silk fabric filter is demonstrated by the alleviated pressure in the manifold as well as the rather good precision.

## 2. Experimental

### 2.1. Apparatus and reagents

The flow injection system used was an IFIS-A intelligent flow injection sampler (XIAN Spring Institute, China) comprising an eight-channel rotary injection valve and two three-channel peristaltic pumps. A WFX-1A atomic absorption spectrometer (Beijing Second Optical Instrument Factory, China), a strip chart recorder (PM 8251, Philips, U.K.) and a Sr hollow cathode lamp with an operating current of 6 mA were employed. A fuel-rich air–acetylene flame and a spectral bandpass of 0.2 nm were adopted in all the experiments.

The manifold described in this paper (Fig. 1) has been designed to minimize the dead volumes of the filter and the coils. All transport tubes are of 1.06 mm i.d. Teflon tubing. The heating coil (HC) was made by winding 40 cm of Teflon tubing into coils 30 cm in diameter and placing them in a Thermostat (95 °C).

The construction of the filter is shown in Fig. 2. The demountable column jacket is made of Perspex glass. The total volume of the column is 100 μl (φ2 mm × 32 nm) and is divided by the disposable silk fabric screen. In order to decrease the dispersion of analyte species, the

position of the screen is arranged such that the downstream part of the column for elution is as short as possible. Any super quality silk fabrics with a pore size of approximately 150 μm available in the market may serve as the filter screen.

All reagents are of analytical grade. Water from subboiling distillation was used throughout.

To prepare 10% lead acetate solution, 2.5 g of lead acetate are dissolved in water, 1.5 ml of glacial acetic acid are added and the solution is diluted to 250 ml with water. This solution is diluted further to give a working solution of 2000 μg $ml^{-1}$ of lead. For preparing Sr standard solution, 1.685 g of strontium carbonate are dissolved in a suitable amount of hydrochloric acid, the solution is made up to 80 ml with the same acid, and the resulting solution is transferred to a 1000 ml volumetric flask and is diluted to the mark with water; 1 ml equals 1 mg of strontium. This solution is diluted successively to give a standard series for calibration. Eluting solution, 5% EDTA plus 1% KH phthalate plus 1% NaOH; analytical solution, sample or standard solution plus 0.2% sulfuric acid plus 20% ethanol; wash solution, 2% ammonium sulfate.

### 2.2. Manifold program and time cycle

The manifold program and the time cycle of determinations are shown in Tables 1 and 2, respectively. Values of flow rate corresponding to pump speeds higher than 40 rev $min^{-1}$ can be obtained by extrapolation.

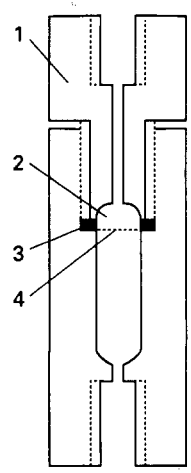


Fig. 2. Construction of the filter. (1) Perspex glass column; (2) cavity; (3) seal ring, (4) silk fabric screen.

Table 1
Manifold program

| Variable | Step | | | | | |
|---|---|---|---|---|---|---|
| | 0 | 1 | 2 | 3 | 4 | 5 |
| Pump A | | | | | | |
| Time (s) | 15 | 2 | 5 | 120 | 15 | 20 |
| Pump speed (rev $min^{-1}$) | 0 | 0 | 65 | 10 | 85 | 0 |
| Pump B | | | | | | |
| Time (s) | 15 | 2 | 5 | 120 | 15 | 20 |
| Pump speed (rev $min^{-1}$) | 85 | 0 | 85 | 50 | 0 | 80 |
| Valve position | a | a | a | a | b | b |

(b) Flow rate corresponding to the pump speed is as follows

| | Pump speed (rev $min^{-1}$) | | | | |
|---|---|---|---|---|---|
| | 5 | 10 | 20 | 30 | 40 |
| Flow rate (ml $min^{-1}$) | 0.35 | 0.72 | 1.4 | 2.1 | 2.8 |

### 2.3. Procedures

*Effect of sulfuric acid concentration*

A series of standard solutions containing the same amount of Sr (200 ng $ml^{-1}$), the same amount of ethanol (20%) and different amounts of sulfuric acid (0.5, 1.0, 2.0, 3.0%) at a pump speed of 50 rev $min^{-1}$ were merged with a solution of 2000 μg $ml^{-1}$ of Pb at a pump speed of 10 rev $min^{-1}$. The dissolving solution stream was 5% EDTA at a pump speed of 82 rev $min^{-1}$.

*Effect of EDTA concentration*

By using the same Sr standard solution of 1% sulfuric acid and flow conditions as were used for investigating the sulfuric acid concentration, the dissolving EDTA solution was varied over a number of concentrations in the range 1–9% at 1% intervals. The dissolving solution was 5% EDTA.

*Effect of pump speed of the sample solution*

With the same dissolving solution at a pump speed of 82 rev $min^{-1}$ and a Sr standard solution of 1% sulfuric acid, the pump speed of the sample solution was varied in the range 40–60 rev $min^{-1}$ at 5 rev $min^{-1}$ intervals.

*Effect of pump speed of EDTA solution*

By using the same solutions as were used for the investigation of the pump speed of the sample solution, the pump speed of the EDTA solution was varied in the range 70–100 rev $min^{-1}$ at 10 rev $min^{-1}$ intervals.

Table 2
Time cycle for determination

| Time (s) | Function |
|---|---|
| 0–15 | PA stops, PB goes, V turns to position a. Wash RC and COL with water. |
| 16–17 | PA and PB stop. Replace water with sample solution. |
| 18–22 | PA and PB go. Rapidly propel water out of RC and COL with the sample and lead acetate solutions. |
| 23–142 | PA and PB go. Start of preconcentration. The precipitate is formed at the confluence point and is subsequently trapped by the filter screen. |
| 143–157 | PA goes, PB stops. V turns to position b. Wash the precipitate with ammonium sulfate. |
| 158–177 | PA stops, PB goes, V remains in position b. Start of elution by flushing a stream of eluting solution. The eluent is propelled into the nebulizer for atomic absorption measurement. |

Key: PA, pump A; PB, pump B; V, valve; RC, reaction coil; COL, column.

*Sample preparation*

*Tea.* Weigh out 0.4 g of the dried sample into a porcelain crucible, ash at 600 °C for 15 min. Dissolve the residue with nitric acid and extract with water. Transfer to a 50 ml volumetric flask, add 10 ml of 5% sulfuric acid and 10 ml of ethanol. Dilute to the mark with distilled water.

*Mineral water.* Pipette 10 ml of the water sample into a 25 ml volumetric flask, and add 5 ml of 5% sulfuric acid and 5 ml of ethanol. Dilute to the mark with distilled water.

*Rock.* Weigh out 0.1 g of the rock sample into a PTFE crucible, and wet with water. Add 0.5 ml of perchloric acid, 5 ml of hydrofluoric acid and 1 ml of hydrochloric acid. Heat on a hotplate to produce copious fumes of perchloric acid. Continue heating until no more fumes appear. Add 1 ml of hydrochloric acid to dissolve the residue and transfer to a 50 ml volumetric flask. Add 10 ml of 5% sulfuric acid and 10 ml of ethanol, and dilute to the mark with distilled water.

## 3. Results and discussion

### 3.1. Optimization of chemical conditions

The selection of the sulfuric acid concentration and the corresponding pump speed are shown in Fig. 3. We can see from the upper curve that a lower concentration (1%) of sulfuric acid gives a higher sensitivity. This can probably be attributed to the formation of finer particles of lead sulfate that are readily dissolved in hot EDTA at this concentration. We used a higher pump speed (50 rev $min^{-1}$) for sample solutions and a lower pump speed (fixed at 10 rev $min^{-1}$) for the lead ions so that a high ratio of strontium to lead, and thus higher sensitivity, can be obtained.

The influence of lead ion concentration on the absorption sensitivity has been studied. As is evident from Fig. 4, it was found that the lead concentration was not critical provided that it was held in the range 1800–2200 μg $ml^{-1}$; 2000 μg $ml^{-1}$ would be the best choice.

Experimental results showed that the absorption sensitivity reached a maximum value and

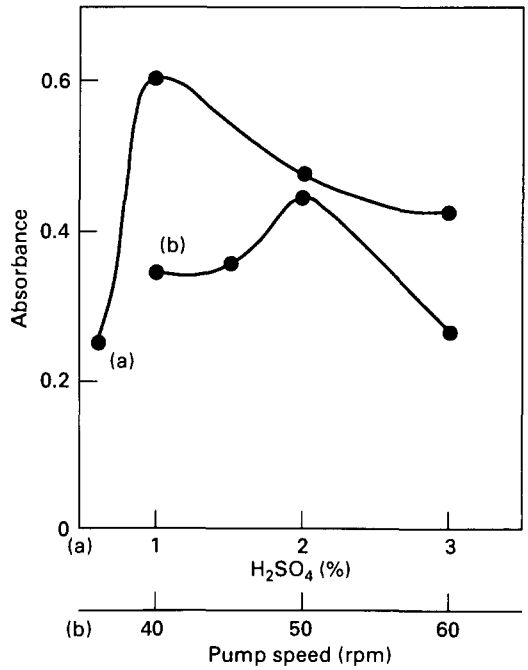


Fig. 3. Effect of $H_2SO_4$ concentration and the corresponding pump speed on the absorption sensitivity. (a) Sr 200 ng/ml, Pb 0.2% (at a fixed pump speed of 50 rpm) and ethanol 20%. (b) Sr 200 ng/ml, Pb 0.2%, $H_2SO_4$ 1% and ethanol 20%.

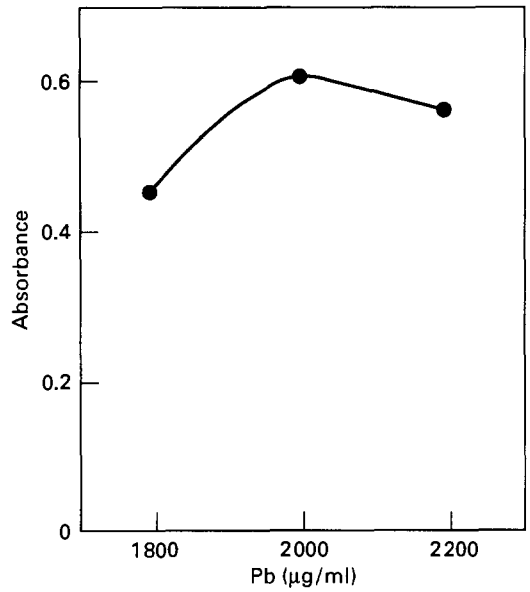


Fig. 4. Effect of Pb concentration on the absorption sensitivity. Sr 200 ng/ml, $H_2SO_4$ 1% and ethanol 20%.

remained constant over a wide range of EDTA concentrations at levels of greater than 5%. In order to avoid the introduction of an excess amount of dissolved solids and to prevent the nebulizer from possible clogging, a concentration of 5% was selected throughout.

The temperature of the EDTA solution is a very critical factor. Lead sulfate can dissolve rapidly in EDTA solution at temperatures higher than 90 °C, while at lower temperatures lead sulfate dissolves much more slowly, yielding a broad signal and much lower peak height.

### 3.2. Interference study

In order to examine the effectiveness of the separation procedure, studies of the effects of coexisting ions have been carried out. With the optimized chemical and flow conditions, no suppression of the absorption signal for 200 ng $ml^{-1}$ of Sr by the following ions (μg/ml) was observed: Al, 100; Ca, 100; Fe, 100; Mg, 100; Si, 20; Ti, 20.

Two reagents were used to improve the analytical performance. Firstly, the sample solutions were made alcoholic by the addition of 20% ethanol to reduce the solubility product of lead sulfate and to accelerate the formation of the precipitate; and secondly, 1% of KH phthalate was added to the eluting solution to eliminate residue interferences, if any [10]. It was shown that KH phthalate was very effective for this purpose. However, the reaction mechanism is not quite understood at present.

### 3.3. Manifold parameters

As lead sulfate was quickly dissolved in EDTA solution at elevated temperature (95 °C), a higher pump speed for the EDTA solution was therefore preferred. This was consistent with the plot in Fig. 5. Nevertheless, the selection of the pump speed was very critical in that it caused a rapid decrease of the absorption signal at values greater than 82 rev $min^{-1}$. The reason was very likely due to the fact that the response of the recorder lagged behind the instantaneous signals.

The absorption sensitivity depends on the preconcentration time, as shown in Fig. 6. A compromise should be made between the two parameters for the concentration levels of interest.

### 3.4. Calibration graph

Calibration graphs were constructed by using Sr standards of 0, 50, 75, 100, 200 ng $ml^{-1}$and 0, 500, 1000, 2000, 3000, 4000 ng $ml^{-1}$ with and without preconcentration, respectively. The data were fitted by the linear equation $y = ax + b$, where $y$ is the peak height in absorbance units and $x$ is the concentration of strontium in nanograms per milliliter. The resulting equations were $y = 2.54 \times 10^{-3}x + 0.003$ (with preconcentration) and $y = 4.70 \times 10^{-5}x + 0.001$ (without preconcentration). The correlation coefficients were 0.998 and 0.997, respectively.

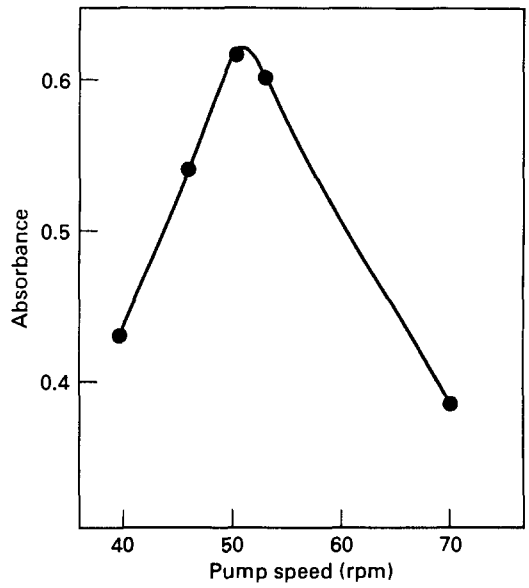


Fig. 5. Effect of pump speed of EDTA on the absorption sensitivity. Sr 200 ng/ml and EDTA 5%.

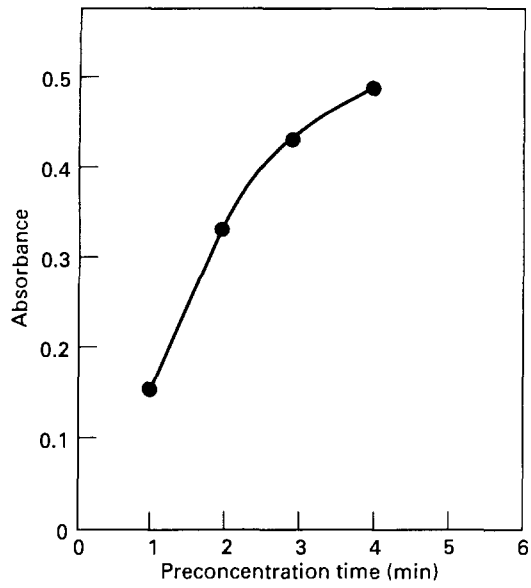


Fig. 6. The absorbance as a function of the preconcentration time. Sr 100 ng/ml, pump speed: 10 rev $min^{-1}$ for sample solutions and 50 rev $min^{-1}$ for Pb.

### 3.5. Sensitivities, detection limits and precision

The analytical performance achieved by the proposed procedure, including sensitivity, detection limit and precision, along with those obtained by direct nebulization, are listed in Table 3. Slopes of the calibration graph were used for comparisons of sensitivities and for calculations of concentration factors. Detection limits were calculated based on $3\sigma$.

### 3.6. Real sample analysis

A variety of samples were analyzed using the proposed procedure to evaluate the reliability and accuracy of the method. Analytical results are listed in Table 4. For rock samples, the analytical data were compared with certified values of standard geological reference materials. For the tea sample, the accuracy was evaluated with a spiked standard and the recovery was satisfactory.

## 4. Conclusion

It has been shown that a simple, inexpensive, disposable and non-metallic filter can be used in a continuous-flow precipitation manifold to collect suspended substances. The FI method described above for the determination of strontium provides a precise and rapid technique that satisfied most of the requirements in routine analysis. An intelligent flow injection sampler equipped with an eight-channel switching/injection valve can serve to control both the precipitation and elution processes automatically.

Table 3
Comparison of analytical performance

| Performance parameter | With preconcentration | Without preconcentration | $S_a/S_b$ | $DL_b/DL_a$ |
|---|---|---|---|---|
| Sensitivity, $A$ (ng $ml^{-1}$) | $2.54 \times 10^{-3}$ | $4.70 \times 10^{-5}$ | 61 | – |
| Detection limit (ng $ml^{-1}$) | 0.9 | 50 | – | 55 |
| Precision, R.S.D. (%) | 3.5 ($n = 8$) [a] | 3.2 ($n = 11$) [b] | – | – |

Key: $S_a$, $S_b$, sensitivities with and without preconcentration; $DL_a$, $DL_b$, detection limits with and without preconcentration.
[a] Sr concentration, 100 ng $ml^{-1}$.
[b] Sr concentration, 200 ng $ml^{-1}$.

Table 4
Analytical results for Sr

| Sample | Found | Certified | Recovery (%) |
|---|---|---|---|
| GSD4 | 137 μg $g^{-1}$ | 142 μg $g^{-1}$ | – |
| GSD6 | 269 μg $g^{-1}$ | 263 μg $g^{-1}$ | – |
| Mineral water | 0.42 μg $ml^{-1}$ | 0.4 μg $ml^{-1}$ [a] | – |
| Tea | 1.75 μg $g^{-1}$ | – | 106 |

[a] Nominal value.

## Acknowledgment

The authors are grateful to the Project for Developing the Geological Science and Technology of China for financial support.

## References

[1] C.B. Belcher and K.A. Brookes, Anal. Chim. Acta, 29 (1963) 202.
[2] G. Tanaka, A. Tamikawa, H. Kanamura and Y. Oyagi, J. Chem. Soc. Jpn., Pure Chem. Section, 89 (1968) 175.
[3] B. Moldan and M. Miksovsky, Collect. Czech. Chem. Commun., 36 (1971) 1673.
[4] P.B. Adams and W.O. Possmore, Anal. Chem., 38 (1966) 630.
[5] A. Hofer, Z. Anal. Chem., 249 (1970) 115.
[6] D.J. David, Analyst, 87 (1962) 576.
[7] D.C. Curnow, D.H. Gutteride and E.D. Horgan, At. Absorpt. Newsl., 7 (1968) 45.
[8] J.H. Dahl, D. Esperson and A. Jensen, Anal. Chim. Acta, 105 (1979) 327.
[9] Henrik Kagenow and Arne Jensen, Anal. Chim. Acta, 114 (1980) 227.
[10] Z. Gong, Yankuang Ceshi, 5 (1986) 9.
[11] P. Matinez-Jimenez, M. Gallego and M. Valcarcel, Analyst, 112 (1987) 1233.
[12] R.E. Santelli, M. Gallego and M. Valcarcel, Anal. Chem., 61 (1989) 1427.
[13] R.E. Santelli, M. Gallego and M. Valcarcel, J. Anal. At. Spectrom., 4 (1989) 547.
[14] E. Debrah, C.E. Andeeyinwo, S.R. Bysouth and J.F. Tyson, Analyst, 115 (1990) 1543.
[15] Z. Fang, M. Sperling and B. Welz, J. Anal. At. Spectrom., 6 (1991) 301.

ELSEVIER

Talanta 42 (1995) 1151–1155

Talanta

# Chromium speciation by a surfactant-coated alumina microcolumn using electrothermal atomic absorption spectrometry

Jamshid L. Manzoori *, Mohammad H. Sorouraddin, Farzaneh Shemirani

*Department of Analytical Chemistry, Faculty of Chemistry, University of Tabriz, Tabriz, Iran*

Received 4 November 1994; revised 7 February 1995; accepted 7 February 1995

**Abstract**

A simple and convenient method has been developed for the speciation of chromium(III) and chromium(VI) in aqueous solutions using a sodium dodecyl sulphate coated alumina micro-column (1.5 cm × 5 mm i.d.) and graphite furnace-atomic absorption spectrometry (GF-AAS). Under the optimized conditions (pH 0.6, adjusted with hydrochloric acid; flow rate, 1 ml $min^{-1}$) chromium(VI) is retained on the column and chromium(III) is collected and determined by GF-AAS. Total chromium is directly determined by GF-AAS and chromium(VI) is calculated by difference. The relative standard deviations (10 replicate analyses) at the 20 μg $l^{-1}$ level for chromium(III) and chromium(VI) and at the 40 μg $l^{-1}$ level for total chromium were 1.4%, 3.6% and 1.8%, and the corresponding limits of detection (based on $3\sigma$) were 0.57 μg $ml^{-1}$, 0.61 μg $ml^{-1}$ and 0.35 μg $l^{-1}$ respectively. No large interference effects have been observed from other investigated species and the method has been successfully applied to a range of water samples.

## 1. Introduction

Chromium may exist in many chemical forms and in nature it is usually encountered in the oxidation states III and VI. Chromium(III) probably exists in natural waters in the form of many different species, hydrolyzed, complexed and some even adsorbed on colloidal matter. Such species decompose on the addition of acid, so that in the analysis of water one will have a mixture of anionic chromate and cationic chromium(III) species [1]. Hexavalent chromium finds its way into natural waters, chiefly in the effluents from the electroplating and tanning industries, from dyeing, from sanitary landfill leaching and from water cooling towers [2]. It is well known that each of these oxidation states has very different biological and toxicological properties. Chromium(III) is an essential element for mammals, whereas chromium(VI) is reported to have particularly adverse effects on the lungs, liver and kidneys [3].

A number of papers have described specific analytical procedures for the speciation of chromium ions. However, in spite of the existence of powerful instrumental determination methods, most trace metal analyses performed to date have required some pretreatment of the sample, not only to concentrate the desired trace metals but also to avoid interferences from coexisting elements [4]. Novel combined procedures based on preliminary chelation [5], ion exchange [6,7], solvent extraction [8,9] and electrochemical separation [10] have been developed for the speciation of chromium. All these preconcentration methods introduce additional laborious and time-consuming sample manipulation steps with their associated well-known sources of error. To overcome these problems, an on-line solid sorbent extractions method using a C18 bonded silica reversed-

* Corresponding author.


*SSDI* 0039-9140(95)01556-6

phase sorbent as the column material has been employed for the differential determination of chromium(III) and chromium(VI) in natural waters [11]. A microcolumn of activated alumina in combination with direct current plasma (DCP) [12] or inductively coupled plasma (ICP) [13] atomic emission spectrometry and flame atomic absorption spectrometry [14] has also been used for the sequential determination of chromium(III) and chromium(VI). As a part of our project on trace element determination in environmental samples, we recently described a method for the determination of chromium in serum and lake water samples by electrothermal atomic absorption spectrometry [15]. In this report, a method for the separation and determination of chromium(VI) and chromium(III) using a microcolumn of sodium dodecyl sulphate coated alumina and GF-AAS is described. This method combines the selectivity and separation power of the surfactant-coated alumina with the excellent sensitivity of GF-AAS.

## 2. Experimental

### 2.1. Apparatus

The experiments were performed using a Shimadzu atomic absorption spectrometer model AA 670G with a graphite furnace atomizer GFA-4A, an autosample changer 60G and a graphic printer PR4. A chromium hollow cathode lamp (Hamamatsu Photonics K.K., Japan) and pyrolytic graphite coated graphite tubes were used with sample injection directly onto the tube wall. The sample injection volume was 10 μl in all experiments. The instrumental parameters and temperature programme for the graphite atomizer are listed in Table 1.

### 2.2. Reagents

Analytical reagent-grade chemicals and triply distilled deionized water were used. All glassware was soaked in 5% (v/v) nitric acid for at least 24 h and washed with water.

Alumina powder: alumina (particle size, 10–50 μm; chromatographic grade; Katayama Chemicals, Japan) was purified prior to use by shaking with 5 mol $l^{-1}$ nitric acid, and washing three times with water.

Sodium dodecyl sulphate (SDS): the analytical-grade reagent (Katayama Chemicals) was used without further purification.

SDS-coated alumina: to a 50 ml Erlenmeyer flask were added 1.5 g of alumina, 100 mg of SDS and 50 ml of hydrochloric acid (0.24 mol $l^{-1}$) and the flask was shaken mechanically for 15 min. After this step, the SDS-coated alumina was packed into a microcolumn (1.5 cm × 5 mm i.d.).

Stock solutions of 1000 μg $ml^{-1}$ of chromium(III) and chromium(VI) were prepared from chromium(III) chloride hexahydrate and potassium dichromate, respectively. Working solutions were prepared daily from the stock solutions by serial dilutions with water.

Lake water samples collected from Uromieh Lake, north-west of Iran, were filtered through a 0.45 μm Nucleopore filter prior to storage.

### 2.3. Recommended procedure

A 4 ml portion of sample solution containing chromium(VI) and chromium(III) is transferred to a 10 ml beaker and the pH of the solution is adjusted to 0.6 with 1 mol $l^{-1}$ hydrochloric acid solution. The glass electrode is rinsed with 0.24 mol $l^{-1}$ hydrochloric acid solution and the final volume of the solution is adjusted to 10 ml using 0.24 mol $l^{-1}$ hydrochloric acid solution. The solution is passed through the surfactant-coated alumina with a flow rate of 1 ml $min^{-1}$. The effluent is then collected by suction and chromium(III) is determined by GF-AAS under

Table 1
Instrumental parameters for chromium determination

Spectrometer

| Parameter | Value |
|---|---|
| Wavelength (nm) | 357.9 |
| Slit width (nm) | 0.5 |
| Lamp current (mA) | 7 |
| Integration time (s) | 4 |

Absorbance measurement was by peak height

Graphite atomizer

| Stage | Temperature (°C) | Time (s) | | Argon gas flow (ml $min^{-1}$) |
|---|---|---|---|---|
| | | Ramp | Hold | |
| Drying | 120 | 10 | 20 | 500 |
| Pyrolysis I | variable | 15 | – | 500 |
| Pyrolysis II | variable | – | 20 | 500 |
| Atomization | 2300 | – | 4 | 0 |
| Cleaning | 2600 | – | 2 | 500 |
| Cooling | 50 | – | 3 | 500 |

Table 2
Analytical recovery of chromium added to some water samples [a]

| Sample [b] | Recovery at 20 μg l$^{-1}$ "spike" (%) | |
|---|---|---|
| | Cr(III) | Cr(VI) |
| Lake water | 100.4 ± 2.0 | 98.6 ± 3.2 |
| Waste water | 99.8 ± 1.3 | 100.2 ± 1.5 |
| Tap water | 99.0 ± 1.8 | 101.0 ± 3.0 |

[a] The values given represent the average and standard deviation of the three determinations of each sample.
[b] The endogenous levels of chromium(III) and chromium(VI) in the lake and tap water were below the GF-AAS and in waste water were 19.0 μ l$^{-1}$ respectively.

the optimized conditions shown in Table 1, using a calibration graph prepared by injecting pure chromium solutions. The total chromium in the sample is directly determined by GF-AAS and chromium(VI) is calculated by difference. In the case of the recovery experiments with spiked water samples (Table 2) total chromium and chromium(III) are determined by GF-AAS using a vanadium(V)–molybdenum(VI) chemical modifier [15].

## 3. Results and discussion

### 3.1. Adsorption of chromium(VI) by SDS-coated alumina

The separation of chromium(III) and chromium(VI) on SDS-coated alumina is attributed to the property of the modified alumina surfaces to adsorb non-ionic compounds in preference to ionic species. Negatively charged SDS is adsorbed on the positively charged alumina surface and forms aggregates know as hemi-micelles or admicelles, which can trap molecules homogeneously. On the addition of a mixture of chromium(III) and chromium(VI) in strongly acidic solutions (HCl; 0.24 mol l$^{-1}$) the latter species, which is in the non-ionic state, is retained quantitatively, while the former species, which is cationic, remains unadsorbed. In the present work an attempt was made to adsorb chromium(VI) on unmodified activated alumina. In spite of the reports of quantitative adsorption of chromium(VI) on alumina at pH 2, no adsorption of chromium(VI) on alumina was observed in aqueous hydrochloric acid medium (0.24 mol l$^{-1}$). This observation indicates the non-ionic nature of chromium(VI), presumably in the form of $H_2CrO_4$ or $HCrO_3Cl$.

In order to avoid chromium(VI) entrapment into the micelles in the aqueous phase, the SDS concentration was fixed at 2 mg ml$^{-1}$, which is below the CMC [16].

### 3.2. Effect of pH

In coating alumina surfaces, the adsorption of SDS on alumina is highly dependent on the solution pH [16]. Negatively charged SDS was more effectively adsorbed on the positively charged alumina surfaces at lower pH values. Almost complete adsorption was achieved at pH 1–4 by shaking SDS solution with alumina for 15 min. The effect of the solution pH on SDS adsorption on alumina is shown in Fig. 1.

In order to study the effect of pH on the adsorption of chromium(VI) on SDS-coated alumina, solutions of different pH in the range 0.0–6.0 containing 50 μg l$^{-1}$ of chromium(VI) were passed through the microcolumn and the percentage of chromium adsorption on the surfactant-coated alumina microcolumn was evaluated. This experiment was repeated for the solutions containing 50 μg l$^{-1}$ of chromium(III). The results are shown in Fig. 2. This figure indicates that at pH 0.6 nearly all the chromium(III) passes through the column while nearly all the chromium(VI) is retained on the column. The decrease in the adsorption of chromium(VI) at pH values greater than 0.8 can be attributed to the transition of chromium(VI) from the non-ionic form to the ionic form, which is not adsorbed on SDS-coated

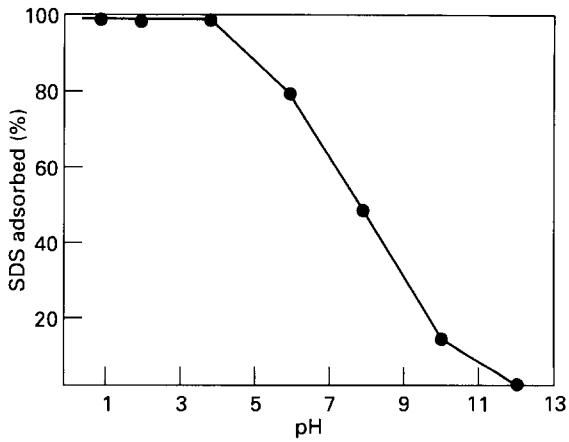


Fig. 1. Effect of the pH on the adsorption of SDS on alumina. (Conditions: 100 mg of SDS and 1.5 g of alumina in 50 ml of hydrochloric acid solution with known pH, mixed for 15 min.)

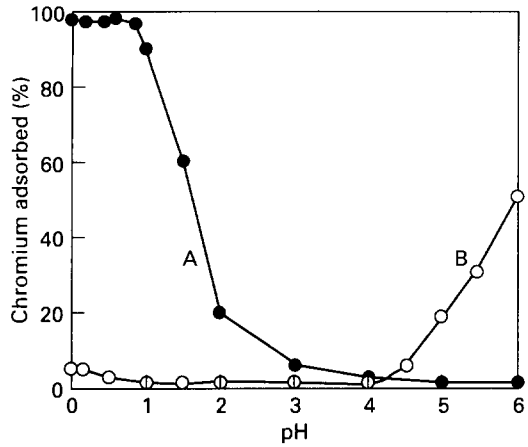


Fig. 2. Effect of the pH on the adsorption of (curve A) chromium(VI) and (curve B) chromium(III) each 50 μg $l^{-1}$ on SDS-coated alumina.

alumina. The increase in the adsorption of chromium(III) at pH values greater than 4.5 is most probably due to the formation of the uncharged $Cr(OH)_3$ species which is easily adsorbed on SDS-coated alumina.

### 3.3. Interference effects

Some experiments were carried out in order to examine the effects of common coexisting ions on the adsorption of chromium(VI) on SDS-coated alumina. In these experiments, solutions of 100 μg $l^{-1}$ of chromium(VI) containing the added interfering ion were treated according to the recommended procedure. The chromium content of the effluents was determined in order to calculate the deposition efficiency of chromium(VI). The tolerances of the coexisting ions, defined as the largest amount yielding a change of less than 5% in the adsorption efficiency of 100 μg $l^{-1}$ of chromium(VI), are given in Table 3. From the results obtained, it can be deduced that the presence of major cations and oxyanions (the most serious interferents on an activated alumina column [14]) have no large influence on chromium(VI) adsorption under the conditions used here.

Table 3
Tolerance limits for coexisting ions in the adsorption of 100 μg $l^{-1}$ of chromium(VI)

| Tolerance limit of ions to Cr(VI) (mg $l^{-1}$) | Coexisting ion |
|---|---|
| 5000 | $K^+$, $Ca^{2+}$, $Mg^{2+}$ |
| 1000 | $Zn^{2+}$, $Cu^{2+}$, $NO_3^-$, $PO_4^{3-}$ |
| 600 | $Mn^{2+}$ |
| 550 | $Al^{3+}$ |
| 500 | $Co^{2+}$, $Fe^{3+}$ |
| 400 | Mo(VI), $SO_4^{2-}$ |

Table 4
Results of chromium(III) and chromium(VI) determinations in synthetic mixtures

| Added (μg $l^{-1}$) | | Found [a] (μg $l^{-1}$) | | |
|---|---|---|---|---|
| Cr(III) | Cr(VI) | Cr(III) | Cr(VI) | Cr (total) |
| 20 | 20 | 20.3 ± 0.3 | 19.9 ± 0.7 | 40.2 ± 0.7 |
| 31 | 21 | 30.6 ± 0.6 | 20.7 ± 0.6 | 51.3 ± 0.8 |
| 22 | 47 | 21.7 ± 0.6 | 48.4 ± 0.7 | 70.1 ± 0.7 |

[a] Average and standard deviation of three determinations

The interferences from high concentrations of matrix ions on chromium(III) and total chromium determinations were overcome by adding vanadium(V) plus molybdenum(VI), 20 μg of each, as chemical modifier.

### 3.4. Calibration, precision and detection limit

The calibration graphs for the determination of total chromium and chromium(III) were both linear up to 100 μg $l^{-1}$ of chromium. The repeatability of the measurements were tested for different amounts of chromium(III) and chromium(VI). At the 40 μg $l^{-1}$ level of total chromium (20 μg $l^{-1}$ with respect to each species), the relative standard deviations (10 replicate analyses) were 1.4%, 3.6% and 1.8% for chromium(III), chromium(VI) and total chromium respectively. This indicates that the precision of chromium(VI) determination is not significantly impaired by the presence of chromium(III). Detection limits defined as three times the standard deviation of a blank determination were 0.57 μg $l^{-1}$, 0.61 μg $l^{-1}$ and 0.35 μg $l^{-1}$ for chromium(III), chromium(VI) and total chromium, respectively, based on ten replicate determinations of the blank.

### 3.5. Application to samples

In order to establish the validity of the proposed procedure, the method has been applied to the determination of some simple mixtures of chromium(III) and chromium(VI). The results are given in Table 4. The reliability of the proposed procedure was also tested by carrying out recovery studies. The average per cent recoveries obtained for the addition of chromium(III) and chromium(VI) spikes to lake, waste and tap water samples are given in

Table 2. The results of Table 2 show that the recoveries of chromium(III) and chromium(VI) were correct to within ±1%.

## 4. Conclusion

A method using a microcolumn of SDS-coated alumina combined with GF-AAS has been developed for the determination of chromium(III) and chromium(VI). Attractive features of this novel method are its good sensitivity, good selectivity and improved simplicity provided by the SDS aggregates. In this method, unlike that using unmodified alumina, there is no need for an additional elution step. Chromium(III) is determined in the effluent while the total chromium concentration is directly determined by GF-AAS, and chromium(VI) is then calculated by difference.

## References

[1] J.F. Pankow and G.E. Janauer, Anal. Chim. Acta, 69 (1974) 97.
[2] V.M. Rao and M.N. Sastri, J. Sci. Ind. Res., 41 (1982) 607.
[3] E. Berman, Toxic Metals and their Analysis, Heyden, London, 1980.
[4] Yu.A. Zolotov and N.M. Kuzmin, Preconcentration of Trace Elements, Elsevier, Amsterdam, 1990.
[5] M.J. Fishman, D.E. Erdmann and J.R. Garbarino, Anal. Chem., 55 (1983) 104R.
[6] J.F. Ponkow, D.P. Leta, J.W. Lin, S.E. Out, W.P. Shum and G.E. Janauer, Sci. Total Environ., 7 (1977) 17.
[7] G.-L. Ou-Yang and J.-F. Jen, Anal. Chim. Acta, 279 (1993) 329.
[8] K.S. Subramanian, Anal. Chem., 60 (1988) 11.
[9] R.K. Mugo and K.J. Orians, Anal. Chim. Acta, 271 (1993) 1.
[10] G.E. Batley and J.P. Matousek, Anal. Chem., 52 (1980) 1570.
[11] M. Sperling, X. Yin and B. Welz, Analyst, 117 (1992) 629.
[12] S. Ahmad, R.C. Murthy and S.V. Chandra, Analyst, 115 (1990) 287.
[13] A.G. Cox, I.G. Cook and C.W. McLeod, Analyst, 110 (1985) 331.
[14] M. Sperling, S. Xu and B. Welz, Anal. Chem., 64 (1992) 3101.
[15] J.L. Manzoori and A. Saleemi, J. Anal. At. Spectrom., 9 (1994) 337.
[16] M. Hiraide, M.H. Sorouradin and H. Kawaguchi, Anal. Sci., 10 (1994) 125.

ELSEVIER

Talanta 42 (1995) 1157–1163

Talanta

# Characterization of the ionization and spectral properties of sulfonephthalein indicators. Correlation with substituent effects and structural features. Part II

M. Carla Aragoni, Massimiliano Arca, Guido Crisponi *, Valeria M. Nurchi, Roberta Silvagni

*Dipartimento di Chimica e Tecnologie Inorganiche e Metallorganiche, Via Ospedale 72, 09124 Cagliari, Italy*

Received 22 November 1994; revised 13 February 1995; accepted 13 February 1995

**Abstract**

A spectrophotometric study is presented on the first ionization equilibrium of a class of substituted sulfonephthaleins, whose second ionization was the subject of the first part of this work. The present study was more difficult than the previous in that highly acid media and acidity functions had to be used. Nevertheless the results were of sufficient accuracy to allow the dual substituent analysis of Swain and Lupton (C.G. Swain and A.C. Lupton, Jr., J. Am. Chem. Soc., 90 (1968) 4328). Generally speaking, the dependences of equilibrium and spectral parameters on field and resonance parameters found in this and the previous paper were very similar.

## 1. Introduction

Sulfonephthaleins are a class of arylsulfonic acids whose general formula is shown in Fig. 1.

All the indicators are summarized in Table 1. These molecules are characterized by the three following acidic groups: sulfonic, hydroquin-onic and phenolic. The ionizations of these substances can be represented by the equilibria shown below (form 1). The object of the present work is the spectrophotometric measurement of p$K$ values for the first ionization equilibrium and the study of the related spectral features in order to confirm, on these bases, the attribution of this ionization to the hydroquinonic group, the sulfonic groups behaving as stronger acids. A correlation study between the equilibrium and spectral properties and the various substituents characterizing each molecule is proposed. With this information it is possible to complete the data acquisition in this class of indicators reported in a previous work [1] for second dissociation p$K_2$ values. An analogous $^{13}C$ NMR analysis is unworkable because the solubility of

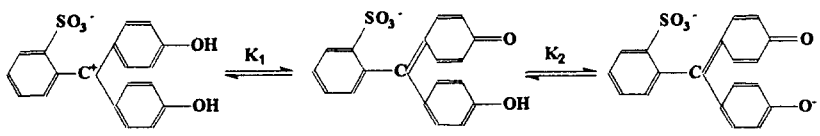


I II III

Form 1

* Corresponding author.


*SSDI* 0039-9140(95)01559-0

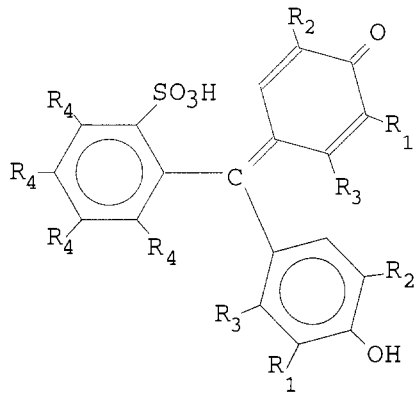


Fig. 1. General formula of sulfonephthaleins.

sulfonephthalein is insufficient in acidic solutions.

The estimation of the $pK_1$ values also requires high acid concentrations. Because of the high concentration of our acidic solutions we had to use a suitable acidity function. The results of this study clarify the behaviour of a class of very versatile indicators with a wide range of colours and p$K$s.

## 2. Experimental

### 2.1. Materials

The studied sulfonephthaleins were Aldrich products, used without further purification. Their purity was checked in the previous work [1] by the appearance of their NMR spectra.

### 2.2. Spectrophotometric measurements

Absorption spectra were recorded at 25 °C, on a Hewlett–Packard 8452 diode array spectrophotometer using a 1 cm quartz cell.

The acid chosen as solvent had to be non-absorbing and strong enough to allow the observation of reliable colour changes (p$K$ values −4.4 to 1.1). Although insufficient to obtain completely the diprotonated form of some indicators, hydrochloric acid proved the most suitable among the acids tried, also in view of its non-oxidizing nature.

A set of 14 HCl solutions from $10^{-2}$ to 11 M were therefore prepared from 37% fuming hydrochloric acid (Merck) and from volumetric standards 1.012 N and 0.1041 N (Aldrich). The titres of the 14 solutions were confirmed potentiometrically.

For each substance 14 samples were then prepared by mixing 0.500 ml of an aqueous solution of approximately $1 \times 10^{-4}$ M indicator and 2.50 ml of the acid solution.

Each sample was then spectrophotometrically analyzed in the range from 190 to 820 nm, obtaining 14 spectra, as for Chlorophenol Red shown in Fig. 2 as an example.

### 2.3. Calculation of ionization constants

Spectral data were analyzed with the program SPECFIT [2] as in the first part of this work [1].

Table 1
Substituents $R_1$, $R_2$, $R_3$ and $R_4$ of the 15 studied sulfonephthaleins

| Indicator name | Compound | $R_1$ | $R_2$ | $R_3$ | $R_4$ |
|---|---|---|---|---|---|
| Cresol Red | 1 | H | $CH_3$ | H | H |
| Phenol Red | 2 | H | H | H | H |
| 3,4,5,6-Tetrabromophenol sulfonephthalein | 2Br | H | H | H | Br |
| Bromocresol Purple | 3 | Br | $CH_3$ | H | H |
| Chlorophenol Red | 4 | H | Cl | H | H |
| Bromochlorophenol Blue | 5 | Br | Cl | H | H |
| Bromophenol Blue | 6 | Br | Br | H | H |
| Tetrabromophenol Blue | 6Br | Br | Br | H | Br |
| 3′,3″,5′,5″-Tetraiodophenol sulfonephthalein | 7 | I | I | $CH_3$ | H |
| Xylenol Blue | $1CH_3$ | H | $CH_3$ | $CH_3$ | H |
| Thymol Blue | $'1CH_3$ | H | $CH(CH_3)_2$ | $CH_3$ | H |
| Cresol Purple | $2CH_3$ | H | H | $CH_3$ | H |
| Bromoxylenol Blue | $3CH_3$ | Br | $CH_3$ | $CH_3$ | H |
| Bromothymol Blue | $3'CH_3$ | Br | $CH(CH_3)_2$ | $CH_3$ | H |
| Bromocresol Green | $6CH_3$ | Br | $CH_3$ | H | |

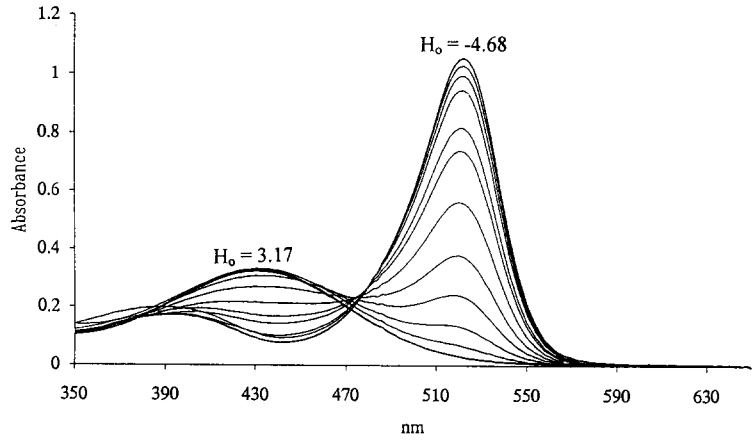


Fig. 2. Experimental spectra of Chlorophenol Red.

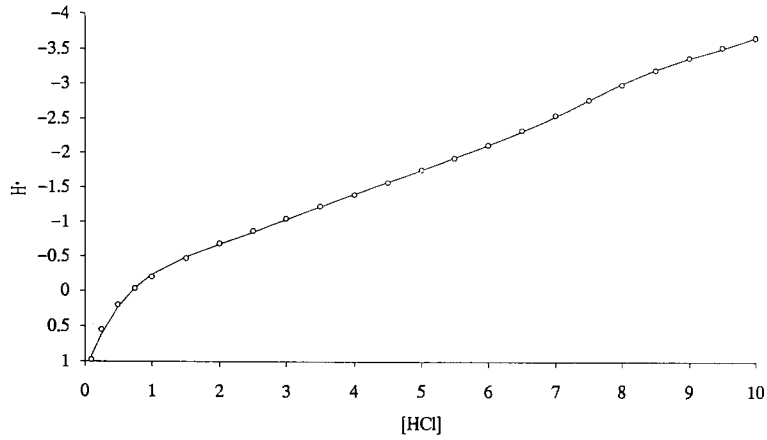


Fig. 3. Literature $H_0$ values fitted with a seven degree polynomial model.

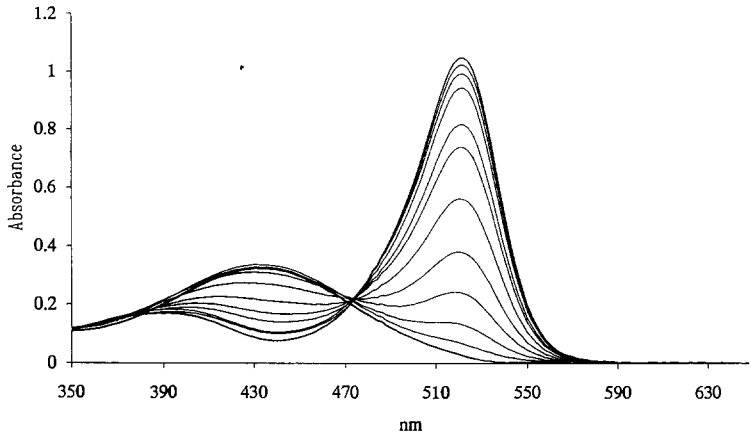


Fig. 4. Reconstructed spectra of Chlorophenol Red.

## 3. Results and discussion

### 3.1. Equilibrium data

In the previous study all measurements were made at an ionic strength of 0.1 M $KNO_3$, and $[H^+]$ was adjusted by titrating a mixture of approximately $10^{-2}$ M in different acids. In the present case we had to use much higher acid concentrations. It was therefore no longer possible to control the ionic strength or to use directly the acid concentration; it became neces-

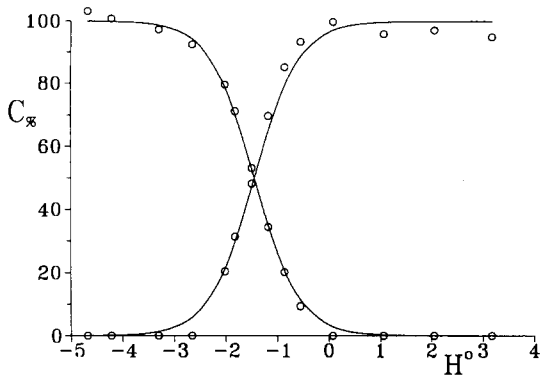


Fig. 5. Distribution curves for the first ionization of Chlorophenol Red.

sary therefore to resort to an acidic function. The $H_0$ function proposed by Hammet and Deyrup [3] was used. The literature [4] values were fitted with a seventh degree polynomial model to extrapolate the values for the hydrogen ion concentrations used, as shown in Fig. 3.

For dilute solutions, $-\log[H^+]$ was used. The experimental absorbance data were analyzed by evolving factor analysis (EFA), using the above $H_0$ function as a continuous variable. As an example we report the experimental spectra of Chlorophenol Red in the $H_0$ range 3.2 to −4.7 (Fig. 2). These data do not present a well-defined isosbestic point. This is presumably to be ascribed to spectral changes connected with the remarkable variation in ionic strength. The same spectra reconstructed taking into account the first two eigenvalues in the factor analysis are presented in Fig. 4. In these spectra all the contributions not determined by ionization were removed.

The evolving factor analysis (EFA) on these data indicates the presence of two absorbing species in the examined range.

Table 2
The $pK_I$ values of the 15 studied sulfonephthaleins

| Compound | $pK_I$ [a] |
|---|---|
| 1 | 1.11 ± 0.01 |
| 1$CH_3$ | 1.42 ± 0.01 |
| 1'$CH_3$ | 1.49 ± 0.01 |
| 2 | 1.16 ± 0.01 |
| 2BR | 0.64 ± 0.01 |
| 2$CH_3$ | 1.57 ± 0.02 |
| 3 | −2.00 ± 0.01 |
| 3$CH_3$ | −1.54 ± 0.01 |
| 3'$CH_3$ | −1.55 ± 0.06 |
| 4 | −1.45 ± 0.01 |
| 5 | −3.6 ± 0.1 |
| 6 | −4.3 ± 0.1 |
| 6Br | −1.4 ± 0.1 |
| 6$CH_3$ | −4.4 ± 0.1 |
| 7 | −4.2 ± 0.1 |

[a] Errors were evaluated as $3\sigma$, where $\sigma$ is the standard deviation furnished by SPECFIT

The distribution curves in Fig. 5 and the spectra in Fig. 6 obtained with EFA without any model assumption are reported as symbols. SPECFIT, moreover, allows a least-squares optimization based on an equilibrium model. We therefore assigned to structures I and II the two absorbing species indicated by EFA, which are connected by a single ionization equilibrium. The relative $pK_I$ estimate was therefore optimized. The resulting distribution curves and spectra are reported as continuous lines in Figs. 5 and 6. With the two procedures, the results are in good agreement. This proves that the experimental measurements were correct. The $pK_I$ values for all the 15 indicators were evaluated with the same procedure outlined above for Chlorophenol Red. These ionization parameters are reported with their respective errors in Table 2. The same $pK_I$

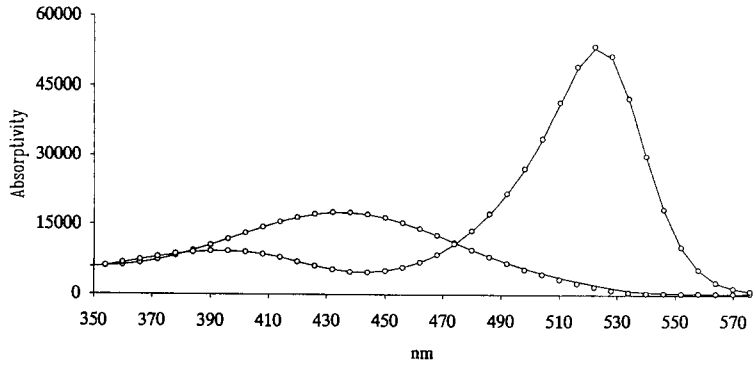


Fig. 6. Absorptivity spectra of the basic and acid forms of Chlorophenol Red.

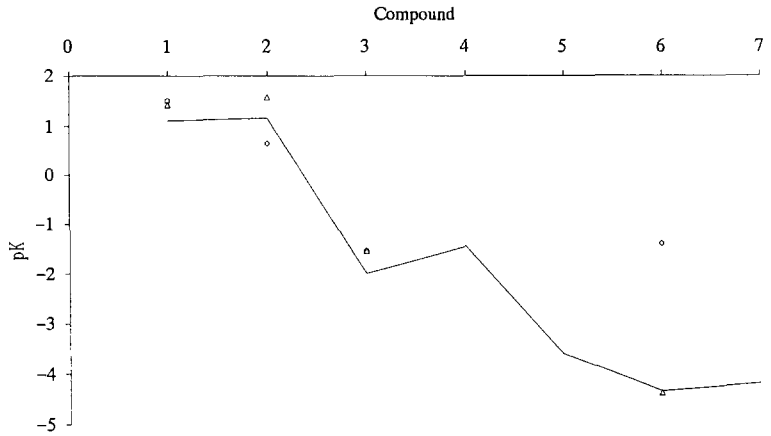


Fig. 7. The p$K_1$ values reported as a substituent function. Continuous line, compounds 1 to 7; △, $1CH_3$, $2CH_3$, $3CH_3$, and $6CH_3$; ○, $1'CH_3$ and $3'CH_3$; ◇, 2Br and 6Br.

values are graphically reported as a function of ortho substituents in Fig. 7. They show a very similar behaviour to that found for the second ionization. The anomalous outlying result for the 6Br compound will be discussed later.

### 3.2. UV-visible spectra

The UV-visible spectra of the 15 indicators, collected as reported above, were decomposed with SPECPEAK [5] and the maximum wavelengths of the component Gaussian peaks in the 300–600 nm range were obtained. These data are reported in Table 3. Peak III was not reported because it is unaffected when the substituents are changed.

Some qualitative observations may be made on the trend of maximum wavelengths reported in Fig. 8 as a function of the substituents.

(i) Indicators 1–7 present a regular trend although maximum wavelengths and p$K_1$ values of indicators 5, 6 and 7 are affected by considerable errors due to their acid strength.

(ii) The $CH_3$ and $CH(CH_3)$ substituents in compounds $1CH_3$, $2CH_3$, $3CH_3$, $6CH_3$, and $1'CH_3$, $3'CH_3$ respectively cause shifts that vary with respect to the trend of related substances with only $R_1$ and $R_2$ substituents.

The presence of Br in position $R_4$ produces a very irregular trend. The basic band at approximately 450 nm, corresponding to the p$K_2$ acid band, confirms a negligible variation with the substituents.

Table 3
Parameters of the most intense Gaussian bands

| Indicator | Peak I | | | Peak II | | | Peak IV | | | Peak V | | |
|---|---|---|---|---|---|---|---|---|---|---|---|---|
| | $\lambda_{max}$ | $W$ | $H$ | $\lambda_{max}$ | $W$ | $H$ | $\lambda_{max}$ | $W$ | $H$ | $\lambda_{max}$ | $W$ | $H$ |
| 1 | 318 | 57 | 122 | 370.1 | 61.3 | 165 | 505.9 | 56.5 | 581 | 520 | 29 | 600 |
| 2 | 325.0 | 46.1 | 134 | 372.6 | 48.6 | 215 | 493 | 51.5 | 666 | 507.9 | 28.9 | 1024 |
| 3 | 325 | 80 | 194 | 391.1 | 56 | 270 | 513.1 | 59.1 | 670 | 534.3 | 34.5 | 1420 |
| 4 | 324 | 74 | 134 | 390.1 | 70 | 173 | 508.2 | 58 | 446 | 525.8 | 32.2 | 703 |
| 5 | 327.2 | 98 | 353 | 431.5 | 83.6 | 980 | – | – | – | 532.3 | 47.9 | 230 |
| 6 | 328 | 93 | 189 | – | – | – | 483 | 63 | 61 | 532.3 | 46 | 141 |
| 7 | 301 | 300 | 157 | – | – | – | 489 | 121 | 40 | 549.2 | 47 | 70 |
| $1CH_3$ | 290 | 200 | 200 | 368.4 | 56 | 137 | 496.8 | 33 | 61 | 544.9 | 60.8 | 717 |
| $2CH_3$ | 314 | 110 | 145 | 394 | 64 | 210 | 491 | 59 | 150 | 529.7 | 49.7 | 680 |
| $3CH_3$ | 322 | 130 | 188 | 411 | 54.5 | 174 | 530 | 69 | 200 | 563.4 | 53.2 | 700 |
| $6CH_3$ | 341.7 | 88 | 224 | – | – | – | 536 | 96 | 131 | 566.5 | 55 | 232 |
| $1'CH_3$ | 321 | 78 | 180 | 387.1 | 56 | 179 | 498.5 | 35 | 91 | 545.3 | 58.1 | 879 |
| $3'CH_3$ | 300 | 230 | 250 | 412.6 | 54.4 | 247 | 547.6 | 79.9 | 480 | 563.8 | 47.1 | 710 |
| 2Br | 290 | 100 | 190 | 357.5 | 44 | 118 | 511.9 | 54.1 | 420 | 526.3 | 26.6 | 498 |
| 6Br | – | – | – | 366 | 96 | 70 | 510 | 190 | 51 | – | – | – |

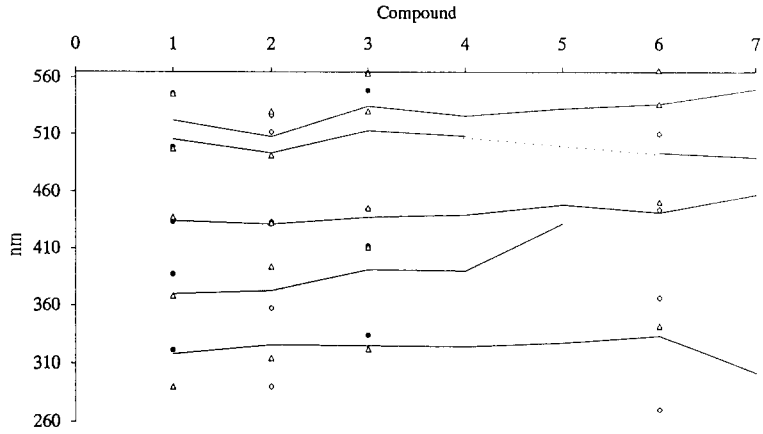


Fig. 8. The wavelength of all indicator peaks. Continuous line, compounds 1 to 7; △, $1CH_3$, $2CH_3$, $3CH_3$, and $6CH_3$; ○, $1'CH_3$ and $3'CH_3$; ◇, 2Br and 6Br.

Table 4
Results of Swain–Lupton analysis

| | Set | $y^\circ$ | $r_1$ | $r_2$ | Std. error | $\Sigma r^2$ | Correl. Coeff. |
|---|---|---|---|---|---|---|---|
| $pK_1$ | 1 | 1.243 | −5.213 | 1.778 | 0.290 | 0.336 | 0.995 |
| | 2 | 1.574 | −6.744 | −0.222 | 0.135 | 0.055 | 0.999 |
| $\lambda_{max}$ | 1 | 508.6 | −2.380 | −71.55 | 5.912 | 139.8 | 0.927 |
| | 2 | 529.7 | 0.064 | −83.62 | 0.257 | 0.198 | 1.000 |
| $pK_1$ vs. $\mathcal{F}$ | 1 | 1.072 | −5.939 | – | 0.303 | 0.459 | −0.993 |
| | 2 | 1.604 | −6.651 | – | 0.119 | 0.057 | −0.999 |
| $\lambda_{max}$ vs. $\mathcal{R}$ | 1 | 508.8 | – | −66.91 | 5.308 | 140.8 | −0.972 |
| | 2 | 529.7 | – | −83.74 | 0.223 | 0.199 | −1.000 |

## 4. Concluding remarks

A Swain and Lupton [6] dual substituent analysis was carried out as in the first part of this work [1], but the more recent $\mathcal{F}$ and $\mathcal{R}$ values reported by Hansch et al. [7] were used; the results are reported in Table 4. The $pK_1$ values and maximum wavelengths $\lambda_{max}$ can in fact be well fitted with the equation $y = y^0 + r_1\mathcal{F} r_2\mathcal{R}$, where $\mathcal{F}$ and $\mathcal{R}$ are the sum of the tabulated values for the ortho substituent, since the effects of the $R_1$ and $R_2$ substituents can be considered additive.

Sets 1 and 2 in Table 4 represent the seven (1–7) and six ($1CH_3$–$6CH_3$) compounds respectively. As can be seen the goodness parameters (standard error, $\Sigma r^2$, correlation coefficient) referring to set 1 are very bad con-

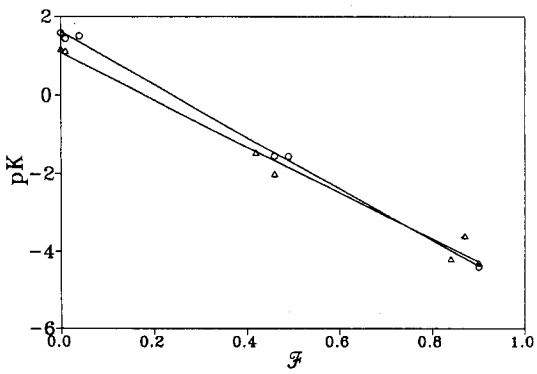


Fig. 9. The p$K$ values of set 1 and set 2 reported as a function of the $\mathcal{F}$ variable.

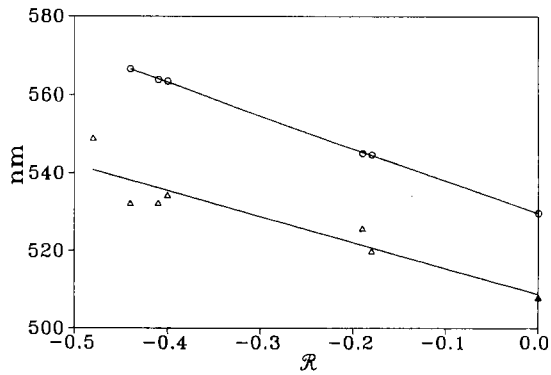


Fig. 10. The $\lambda_{max}$ values for set 1 and set 2 reported as a function of $\mathcal{R}$.

sidering the acidic strength of indicators 5, 6 and 7.

The p$K$ values and the maximum wavelengths of first dissociation depend on the $R_1$ and $R_2$ substituents with a trend analogous to that found for the second equilibrium. Also in this case the $\mathcal{F}$ field variable alone accounts for 86% and 77% of the p$K_1$ variability around the reference value of the unsubstituted compound 2, respectively, for sets 2 and 1. The linear regression with only $\mathcal{F}$ as an independent variable nevertheless shows a standard error and $\Sigma r^2$ very similar to those of the two-variable regression. In Fig. 9 p$K_1$ values versus $\mathcal{F}$ are reported for the two sets: set 1 again is poorer than set 2. The two lines are indistinguishable on the basis of the large errors by which they are affected. Nevertheless, by comparing the most accurate p$K_1$ values of 1 with $1CH_3$ and $1'CH_3$, 2 with $2CH_3$ and 3 with $3CH_3$ and $3'CH_3$, a difference of about 0.5 p$K$ units, corresponding to the meta $CH_3$ effect, can be remarked. These findings are in line with those for the first ionization.

The meta $CH_3$ effect is more significant than that of the ortho substituent because of the steric factor which causes a torsion of the phenolic rings. As can be seen from 1 and 2 or from $1CH_3$, $1'CH_3$ and $2CH_3$ indicators, the ortho substituents do no affect p$K_1$ values. When $R_1$ and $R_2$ are halogens an inductive $-I$ effect causes an increase in acidity as shown in the series 2, 3, and 6 or in the corresponding sequence $2CH_3$, $3CH_3$, $6CH_3$. The trend of maximum wavelengths of the most intense band VI may be seen in Fig. 10. This band was analyzed with the Swain–Lupton method and the parameters shown in Table 4 were obtained. While p$K_1$ values can be evaluated with the $\mathcal{F}$ parameter alone, the band position for both sets shows an 80.5% and an 91% dependence on the resonance $\mathcal{R}$ parameter for sets 1 and 2, respectively. Fig. 10 reports $\lambda_{max}$ values vs. $\mathcal{R}$. A shift of 21 nm between the intercepts of set 2 with respect to set 1 is observed. Analogously to the previous study, the half-bandwidths of set 2 spectra are larger than those of set 1.

In conclusion, it should be pointed out that ionization of the first exchangeable proton takes place at a p$K_1$ value which is normally approximately 7 units lower than the second ionization and the spectral properties of the biprotonated form and of the completely deprotonated form have very similar spectra. This observation substantiates the sequence of ionization equilibria proposed above. In fact the similarity of the spectra is well explained by their assignment to the two symmetric forms I and III, as discussed by Schwarzenbach [8]. The first ionization of the sulfonic group, on the contrary, should give two non-symmetric forms with different spectral properties. This attribution is furthermore supported by the high similarity in the values of the dual substituent analysis on p$K_1$ and p$K_2$.

The difference between the trends of p$K_1$ and p$K_2$ observed when bromine is $R_4$ has to be explained. While p$K_2$ values are not affected, p$K_1$ in fact shows an ambiguous behaviour. The acidity of the 2Br sulfonephthalein increases and that of 6Br decreases. We can tentatively explain this behaviour by a decrease of sulfonic group acidity to $pK \cong -1.4$ due to resonance effects of the four bromine atoms. The ionization order of sulfonic and hydroquinonic groups, which is unaffected in the 2Br compound, is in contrast, reversed in 6Br. The ionization of the hydroquinonic group in the last compound is expected, in fact, at $pK \cong -4$. Further support of sulfonic ionization is given by the spectral features of 6Br which is the only indicator whose acidic species is not coloured.

## References

[1] R. Casula, G. Crisponi, F. Cristiani, V.M. Nurchi, M. Casu, and A. Lai, Talanta, 40 (1993) 1781.
[2] H. Gampp, M. Maeder, Ch.J. Meyer and A.D. Zuberbhuler, Talanta, 32 (1985) 1133; 33 (1986) 943; Anal. Chim. Acta, 193 (1987) 287.
[3] L.P. Hammet and A.J. Deyrup, J. Am. Chem. Soc., 54 (1932) 2721.
[4] M.A. Paul and P.A. Long, Chem. Rev., 57 (1957) 1.
[5] M.C. Aragoni, M. Arca, G. Crisponi, V.M. Nurchi, 11th Congr. Nazionale Chimica Analitica, Cagliari, 12–16 September 1994.
[6] C.G. Swain and A.C. Lupton, Jr., J. Am. Chem. Soc., 90 (1968) 4328.
[7] C. Hansch, A. Leo and R.W. Taft, Chem. Rev., 91 (1991) 165.
[8] G. Schwarzenbach, Helv. Chim. Acta, 20 (1937) 490, 498, 627, 654.

ELSEVIER

Talanta 42 (1995) 1165–1170

Talanta

# Labelling of organotin compounds for fluorimetric detection

C. Leal, M. Granados, M.D. Prat *, R. Compañó

*Departament de Química Analítica, Universitat de Barcelona, Diagonal 647, E-08028 Barcelona, Spain*

Received 25 October 1994; revised 15 February 1995; accepted 15 February 1995

**Abstract**

A systematic study of the fluorescence of complexes of some flavone derivatives with organotin compounds in hexane and in an aqueous micellar medium on Triton X-100 is reported. Some relationships between fluorescence intensity and the structure of the fluorogenic reagent or that of the organotin compound can be deduced, and the most suitable reagent for each organotin species can be chosen on the basis of sensitivity and selectivity. Results point out that flavone derivatives are appropriate post-column derivatization reagents for organotin compounds in liquid chromatography.

## 1. Introduction

Aryl and alkyl derivatives of tin are extensively used as PVC stabilizers, biocides, and catalysts and in antifouling paints. The variety of pathways for their entry into the environment, together with their toxicity, has brought about investigations of methods for their separation and detection in environmental samples. Separation is usually carried out by gas chromatography [1,2] or liquid chromatography [3]. For the latter, most detection systems are based on atomic spectroscopic techniques or molecular fluorscence.

As organotin compounds are not intrinsically fluorescent, a fluorogenic derivatization process is needed when detection is performed with fluorimetry. Derivatization can be carried out either pre-column, on-column or post-column, which is the most frequent. Flavone derivatives, which are well-known fluorogenic reagents for inorganic tin [4], have also been proposed for the fluorimetric determination of organotin species [5–7] and they have been used for derivatization in liquid chromatography (LC) [8–14]. However there is a need for systematic study of the relative fluorescence intensities of organotin complexes with flavones in media commonly used in LC, which would allow the selection of the most suitable reagent for each specific problem.

This paper describes a systematic study of the fluorescence properties of several flavone derivatives as labelling reagents for methyltin, butyltin, cyclohexyltin and phenyltin species. In Fig. 1 the structural formulae, the systematic

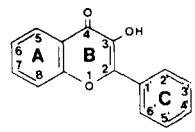


| SYSTEMATIC NAME | ORDINARY NAME |
|---|---|
| 3-hydroxyflavone | Flavonol |
| 5,7-dihydroxyflavone | Chrysin |
| 3,5,7-trihydroxyflavone | Galangin |
| 3,4',5,7-tetrahydroxyflavone | Kaempferol |
| 3,3',4',7-tetrahydroxyflavone | Fisetin |
| 3,3',4',5,7-pentahydroxyflavone | Quercetin |
| 3,5,7,2',4'-pentahydroxyfflavone | Morin |

Fig. 1. Structural formulae, systematic names and ordinary names of the flavone derivatives.

* Corresponding author.


*SSDI* 0039-9140(95)01560-4

names and the ordinary names of the flavone derivatives studied are shown.

Hexane, which is a suitable mobile phase for normal-phase LC of organotin compounds, is one of the reaction media selected. Furthermore, it has been reported that, in comparison with hydro-organic media, non-ionic and cationic surfactants enhance the fluorescence of organotin complexes with flavone derivatives [6,9,15]. Among the micellar media tested, the best results in terms of sensitivity are obtained with non-ionic Triton X-100. Therefore Triton X-100 micellar solutions may be a good alternative for fluorimetric detection of organotin species after chromatographic separation by reverse phase or ion exchange. Thus, the fluorescence of these complexes in 1% (m/v) Triton X-100 was also studied.

## 2. Experimental

### 2.1. Reagents

Solutions were prepared in doubly deionized water (Culligan Ultrapure GS) of 18.3 MΩ cm resistivity.

Triphenyltin chloride (TPhTCl), diphenlytin chloride (DPhTCl), monophenyltin chloride (MPhTCl), tributyltin chloride (TBTCl), dibutyltin chloride (DBTCl), monobutyltin chloride (MBTCl), trimethyltin chloride (TMTCl), and tricyclohexyltin chloride (TCHTCl) were purchased from Fluka or Aldrich (purity above 95%) and were used without further purification. Stock solutions (0.5 g $l^{-1}$ as tin) were prepared with methanol (Merck), except for TCHTCl, which was prepared with cyclohexane. These solutions were stored at 4 °C in dark glass bottles, and working solutions (1–25 mg $l^{-1}$) were prepared freshly prior to use, by dilution with methanol and water, or hexane (Merck).

Ethanol solutions ($3 \times 10^{-4}$–$5 \times 10^{-3}$ M) of flavonol (Aldrich), galangin (Aldrich), kaempferol (Fluka), quercetin (Merck), morin (Merck), fisetin (Aldrich), chrysin (Aldrich) and 7,8-dihydroxy-flavone (Toyko Kasey) were prepared daily.

Buffer solutions of 0.05 M formic acid–solution hydroxide (pH 3–4), 0.05 M succinic acid–sodium hydroxide (pH 5–6) and 0.05 M Tris–hydrochloric acid (pH 7–8) were used; pH values below 3 were adjusted with hydrochloric acid.

A stock aqueous solution of 8.3% (m/v) Triton X-100 (Merck) was used.

### 2.2. Apparatus

Fluorescence measurements were performed on a Perkin-Elmer LS-50 spectrofluorimeter equipped with a xenon discharge lamp and 10-mm pathlength quartz cells. The slit widths were adjusted to 3 or 10 nm in both monochromators depending on the fluorescence of the complexes. Measurements were performed at 20 °C in a thermostatted room. The spectrofluorimeter was calibrated daily using a Perkin-Elmer fluorescence intensity standard of ovalene. All fluorescence data are given without spectral correction.

Spectrophotometric measurements were carried out on a Perkin-Elmer Lambda 19 double-beam spectrophotometer, using 10-mm quartz cells.

A Crison Digilab-517 pH meter equipped with an Orion combined electrode was used for pH measurements. The potentiometric system was calibrated prior to use with buffer solutions, at pH 4.008 and 6.863, prepared from Merck salts according to DIN 19 266.

All glassware used for experiments was previously soaked in 10% nitric acid (Merck) for 24 h and rinsed with doubly deionized water.

### 2.3. Procedures

*Fluorescence measurements*

Hexane medium: transfer 2 ml of the hexane organotin compound solution (1 mg $l^{-1}$) into a 10 ml volumetric flask containing 0.5 ml of the flavone solution ($3.4 \times 10^{-4}$ M) and dilute to volume with hexane. When estimating detection limits, more diluted solutions of organotin compounds were used.

Micellar medium: transfer 1 ml of aqueous organotin compound solution (5 mg $l^{-1}$) into a 25 ml volumetric flask containing 0.5 ml of the flavone solution ($2.1 \times 10^{-3}$ M), 2.5 ml of buffer solution and 3 ml of Triton X-100 solution, and dilute to volume with water.

Immediately after the preparation, excitation and emission spectra were recorded and the fluorescence intensity at optimal wavelengths was read. The fluorescence intensity was read again 1 h later. Blank solutions were prepared and measured at the optimal wavelengths of the complex.

Table 1
Wavelength of the excitation and emission maxima ($\lambda_{ex}$, $\lambda_{em}$) and relative fluorescence intensities ($I_F$) of the complexes of organotin compounds (200 $\mu g\,l^{-1}$) with flavone derivatives in hexane

| Flavone derivative | DBT | | | MBT | | | DPhT | | | MPhT | | |
|---|---|---|---|---|---|---|---|---|---|---|---|---|
| | $\lambda_{ex}$ | $\lambda_{em}$ | $I_F$ | $\lambda_{ex}$ | $\lambda_{em}$ | $I_F$ | $\lambda_{ex}$ | $\lambda_{em}$ | $I_F$ | $\lambda_{ex}$ | $\lambda_{em}$ | $I_F$ |
| Flavonol | 396 | 445 | 13 | 400 | 454 | 48 | 396 | 445 | 44 | 400 | 452 | 27 |
| Galangin | 434 | 488 | 0.4 | 416 | 474 | 8 | 429 | 483 | 2 | 418 | 475 | 7 |
| Kaempferol | 420 | 468 | 5 | 428 | 476 | 78 | 426 | 469 | 47 | 429 | 475 | 37 |
| Quercetin | 426 | 482 | 28 | 432 | 487 | 81 | 432 | 486 | 85 | 436 | 485 | 40 |
| Morin | 418 | 488 | 51 | 425 | 498 | 39 | 425 | 491 | 86 | 425 | 495 | 42 |
| Fisetin | 418 | 481 | 97 | 421 | 488 | 43 | 421 | 482 | 100 | 421 | 483 | 45 |

*UV absorption spectra*

Solutions used to obtain the UV absorption spectra were prepared by one of the procedures described above, but using more concentrated solutions of organotin compounds and flavones. The final concentration of the organotin compound was 1 $mg\,l^{-1}$ with a ten-fold excess of reagent. Absorption spectra of the complexes were recorded against a blank.

## 3. Results and discussion

### 3.1. Fluorescence in hexane

The fluorescence intensities (relative to that of the DPhTCl–Fisetin complex, taken as 100), as well as the wavelengths of the excitation and emission maxima, of the complexes of some organotin compounds with six flavone derivatives are given in Table 1. Values corresponding to other species, such as TBT, TPhT, TMT and TCHT, are not given because they exhibited very weak fluorescence with all the flavone derivatives.

In all the cases, both the excitation and emission spectra consisted of a single structureless broad band with the excitation maximum in the range 410–435 nm and the emission maximum in the range 470–500 nm, except for complexes with flavonol ($\lambda_{exc}$ = 390–400 nm; $\lambda_{em}$ = 445–460 nm). The emission intensities did not change significantly for 1 h after the preparation of the solutions.

Values in Table 1 show that, in this medium, the complexes of diorganotin and monoorganotin compounds with the reagents studied are highly fluorescent. Most fluorescent systems, like fisetin or morin complexes of MBT, DBT, MPhT and DPhT, allow limits of detection to be reached at about 0.1 $\mu g\,l^{-1}$, which makes them suitable as labelling reagents in environmental analysis.

The fact that the fluorescence of trialkyl and triaryl complexes in hexane is much less intense than that of monoorganotin and diorganotin compounds, has already been reported by Arakawa et al. [5] and Langseth [16] in the case of morin, and has been attributed to the shielding of the tin atom by the carbon chains of the triorganotin compounds, which hinders the formation of the complex. To confirm this assumption, the UV absorption spectra of solutions containing, respectively, TBT, TPhT, DBT or DPhT and a ten-fold excess of morin or flavonol were compared with the corresponding reagent blanks. No change in the spectrum of the reagent was observed when TBT or TPhT was added to the solution, whereas a new band appeared in the region of 380–430 nm in the case of DBT and DPhT, which suggests that complex formation for triorganotin compounds takes place to a much lesser extent than for diorganotin derivatives. This behaviour agrees with data reported on the complexation of flavonol with butyltin species in methanol, chloroform and toluene [17]. In all the solvents stability constants for TBT were lower than those corresponding to DBT and MBT.

Comparing the emission intensities given by the complexes of the different flavone derivatives (Table 1), some relationships between the structure and the fluorescence of the complex can be deduced. First, the presence of a hydroxyl group at position 3 is essential to fluorescence, as shown by the fact that 7,8-dihydroxyflavone and chrysin do not form fluorescent complexes. On the other hand, the presence of hydroxyl groups in ring A seems to decrease the fluorescence of the complexes, whereas their presence in ring C increases the

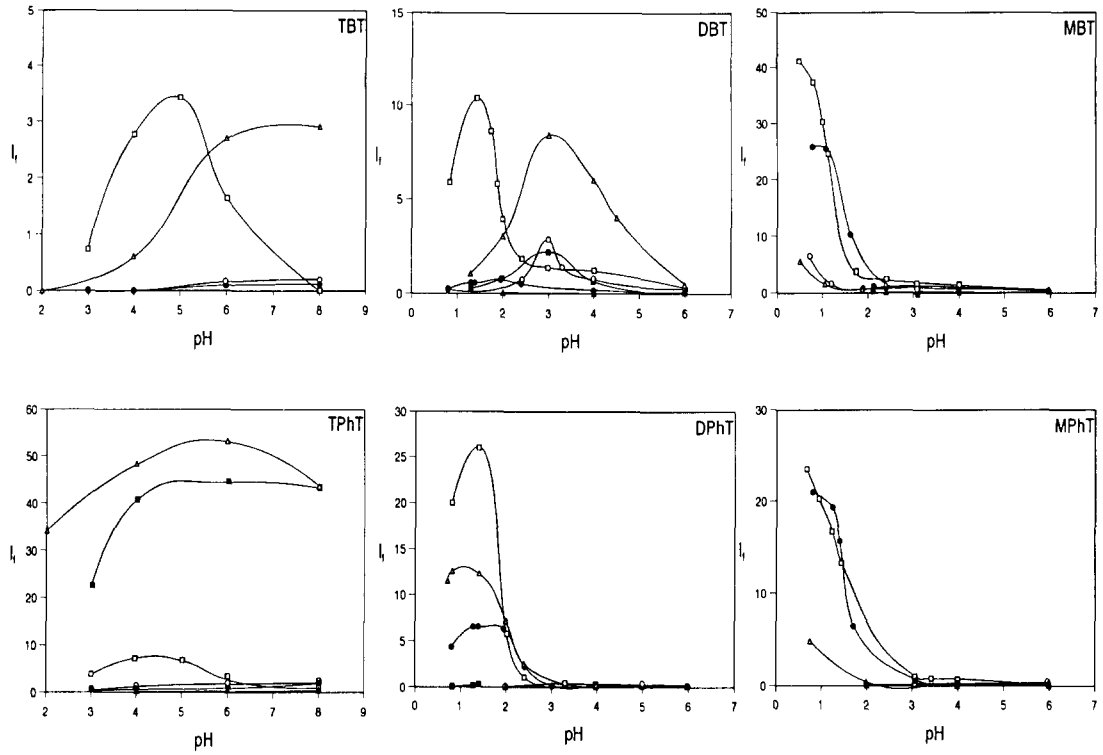


Fig. 2. The pH dependence of the fluorescence intensity of the complexes of organotin compounds in 1% (m/v) Triton X-100. ([Organotin = 200 μg $l^{-1}$].) □, morin; ○, quercetin; ●, kaempferol; ▲, galangin; △, fisetin; ■, flavonol.

emission intensity. In comparison with flavonol, which has no hydroxyl groups in these rings, in galangin, the addition of two OH groups in ring A causes a clear decrease in the fluorescence. In the case of kaempferol, one OH group has been introduced in ring C, increasing the fluorescence of the complexes in relation to galangin. When considering morin or quercetin, which contain two OH groups in ring C, a significant rise in the emission is observed. Finally, fisetin, which has lost a hydroxyl group in ring A, shows the highest fluorescence intensity.

### 3.2. *Fluorescene in Triton X-100 medium*

Fig. 2 shows the influence of pH on the fluorescence of organotin complexes, and in Table 2 excitation and emission maxima wavelengths are given for each complex in 1% (m/v) Triton X-100. Data corresponding to TMT and TCHT are not given, because their complexes exhibit very low fluorescence. As observed in hexane medium, all the spectra show a single broad band.

The fluorescence of organotin complexes in this micellar medium is strongly dependent on pH. As the number of substituents in the tin atom increases, there is a shift of the optimum pH range towards higher values. This behaviour is observed with both butyltin and phenyltin species, and agrees with the data reported [9,15]. On the other hand, in most cases the fluorescence of butyltin species takes place at a slightly higher pH than for the corresponding phenyltin species and this effect is more pronounced for diorganotin species.

No fluorescence was detected from solutions containing chrysin or 7,8-dihydroxyflavone and any of the organotin species tested, in the pH range covered in this study. In order to ascertain whether complexes are formed in these systems, a UV-visible spectrophotometric study was carried out and TPhT was selected as the organotin compound model. From pH 4, significant differences are observed between the absorption spectra of solutions containing TPhT and 7,8-dihydroxy-flavone and those corresponding to the reagent blank. This confirms that complexation takes place, but the new species is not fluorescent. Nevertheless in the system TPhT–chrysin, spectra of the solutions containing both the organotin and the flavone reagent do not show any change in relation to the spectra of the reagent blank, which leads us to conclude that complexes are not formed.

Table 2
Wavelength of the excitation and emission maxima (and relative fluorescence intensities of the complexes of organotin compounds (200 μg $l^{-1}$) with flavone derivatives in 1% (m/v) Triton X-100

| Flavone derivative | TBT | | | DBT | | | MBT | | | TPhT | | | DPhT | | | MPhT | | |
|---|---|---|---|---|---|---|---|---|---|---|---|---|---|---|---|---|---|---|
| | $\lambda_{ex}$ | $\lambda_{em}$ | $I_F$[a] | $\lambda_{ex}$ | $\lambda_{em}$ | $I_F$[a] | $\lambda_{ex}$ | $\lambda_{em}$ | $I_F$[a] | $\lambda_{ex}$ | $\lambda_{em}$ | $I_F$[a] | $\lambda_{ex}$ | $\lambda_{em}$ | $I_F$[a] | $\lambda_{ex}$ | $\lambda_{em}$ | $I_F$[a] |
| Flavonol | – | - | – | 397 | 452 | 3 | 400 | 456 | 0.3 | 392 | 490 | 44 | 392 | 490 | 0.2 | 400 | 462 | 0.4 |
| Galangin | – | – | – | 426 | 492 | 0.1 | 422 | 486 | 0.2 | – | – | – | 420 | 477 | 0.1 | 424 | 478 | 0.1 |
| Kaempferol | 414 | 500 | 0.1 | 430 | 484 | 0.7 | 430 | 481 | 26 | 418 | 493 | 2 | 430 | 83 | 7 | 430 | 482 | 21 |
| Quercetin | 420 | 510 | 0.2 | 434 | 485 | 2 | 433 | 485 | 6 | 424 | 497 | 2 | 428 | 492 | 0.3 | 434 | 489 | 0.2 |
| Morin | 407 | 543 | 3 | 418 | 493 | 10 | 422 | 500 | 41 | 411 | 525 | 7 | 411 | 525 | 26 | 422 | 500 | 23 |
| Fisetin | 410 | 504 | 3 | 418 | 478 | 8 | 423 | 485 | 6 | 410 | 494 | 53 | 412 | 493 | 12 | 431 | 486 | 5 |

[a] Value corresponding to optimum pH for each complex.

The behaviour of 3-hydroxyflavone differs from that shown by the other flavone derivatives. It is an extremely sensitive reagent for TPhT, gives some fluorescence with DBT, and very low or no response with any of the other organotin species tested. A spectrophotometric study pointed out that absorption spectra of solutions containing TPhT and 3-hydroxyflavone show the same trends as those of solutions containing TBT and 3-hydroxyflavone, which reveals that the lack of fluorescence of the TBT solution is not due to poor or no complexation, but to very low quantum yields.

In comparison with the hexane medium, in Triton X-100 solutions the pH is an additional parameter that affects the fluorescence. In consequence, the search for relationships between the fluorescence of the complexes and the structure of the fluorogenic reagent is more difficult. Nevertheless, some of the relationships that have been found in hexane are also valid for Triton X-100 medium. Thus fluorescence is obtained only if the flavone derivative has a hydroxyl group in position 3. On the other hand, as observed in hexane, galangin is the 3-hydroxy derivative that provides the lowest fluorescence intensities, and this behaviour may be related with the presence of hydroxyl groups in ring A, but not in ring B. Finally our data suggest that, in general, reagents that have hydroxyl groups in ring B, such as quercetin, kaempferol, morin and fisetin, provide more intense fluorescence.

The intense fluorescence shown by some of these complexes allows very low limits of detection to be attained. Thus the obtained value for the batch determination of TPhT with flavonol [6] is 0.07 μg $l^{-1}$ and, when this reagent is used as the TPhT labelling reagent after the LC separation [12], the detection limit is 0.1 μg $l^{-1}$ (injected volume, 200 μl). Current studies that we are carrying out show that, when fisetin is used coupled with LC, limits of detection for TBT and TPhT are 4.5 μg $l^{-1}$ and 0.15 μg $l^{-1}$, respectively (injected volume 200 μl). Similar values can also be reached for monoorganotin and diorganotin species with the appropriate reagent.

## 4. Conclusions

The fluorescence intensity values corresponding to a hexane medium show that morin and fisetin are the reagents that provide the highest fluorescence intensities in this solvent with DBT, MPhT and DPhT, and fisetin is slightly superior. The most fluorescent MBT complexes are formed with kaempferol and quercetin, but morin and fisetin complexes of MBT also show strong fluorescence, with values comparable to those of MPhT. From these considerations, and taking into account that all morin and all fisetin complexes have very similar excitation and emission wavelengths, both reagents are suitable for the fluorimetric detection of these organotin species after normal-phase chromatographic separation and they are comparable in terms of sensitivity. Nevertheless, if only MBT, or MBT and MPhT, are to be determined, kaempferol or quercetin is a better choice.

In Triton X-100 solution, morin and fisetin are the most general reagents, and morin is clearly superior for the monoorganotin species, whereas fisetin is the most sensitive reagent for triphenyltin. Kaempferol also provides excellent sensitivity for the monoorganotin species. If a general screening of butyl and/or phenyl

organotin compounds is to be performed by ion-exchange or reverse-phase LC, either morin or fisetin can be used for post-column derivatization before fluorimetric detection. The choice between morin and fisetin depends on the need of sensitivity for monoorganotin vs. triorganotin. In any case, a change of pH of the solution to be detected will be required during the analysis, as optimum conditions for diorganotin and monoorganotin are more acidic (pH below 2) than those required for the detection of triorganotin (pH above 4).

Finally it can be concluded that the fluorescence of the complexes of monoorganotin and diorganotin compounds in hexane is higher than in Triton X-100. In contrast the emission of triorganotin complexes is more intense in the micellar medium, although it is weaker than that of monoorganotin and diorganotin derivatives.

## Acknowledgements

An FPI grant to C. Leal by the Spanish Ministry of Education and Science is gratefully acknowledged. The authors thank the CICYT (project NAT91-1339) for supporting this study.

## References

[1] I. Tolosa, J.M. Bayona, J. Albaigés, L.F. Alencastro and J. Tarradellas, Fresenius' Z. Anal. Chem., 339 (1991) 646.
[2] Y. Cai, S. Rapsomanikis and M.O. Andreae, Anal. Chim. Acta, 274 (1993) 243.
[3] X. Dauchy, A. Astruc, M. Borsier and M. Astruc, Analusis, 20 (1992) 41.
[4] A. Fernández-Gutiérrez and A. Muñoz de la Peña, in S.G. Schulman (Ed.), Molecular Luminescence Spectroscopy, Part 1, John Wiley, New York, 1985, Chapter 4.
[5] Y. Arakawa, W. Osamu, and M. Manabe, Anal. Chem., 55 (1983) 1901.
[6] R. Compañó, M. Granados, C. Leal and M.D. Prat, Anal. Chim. Acta, 283 (1993) 272.
[7] W.N. Aldrige and B.W. Street, Analyst, 106 (1981) 60.
[8] T-H. Yu and Y. Arakawa, J. Chromatogr., 258 (1983) 189.
[9] L. Ebdon and J.I. Garcia Alonso, Analyst, 112 (1987) 1551.
[10] J.A. Stäb, J.M.M. Rozing, B. Van Hattum, P. Cofino and U.A. Brinkman, J. Chromatogr., 609 (1992) 195.
[11] J.I. Garcia Alonso, A. Sanz Medel and L. Ebdon, Anal. Chim. Acta, 283 (1993) 261.
[12] R. Compañó, M. Granados, C. Leal and M.D. Prat, Anal. Chim. Acta, 302 (1995) 185.
[13] W. Kleiböhmer and K. Cammann, Fresenius' Z. Anal. Chem., 335 (1989) 780.
[14] M. Pfeffer, B. Gelbe, P. Hampe and B. Steinberg, Fresenius' Z. Anal. Chem., 342 (1992) 839.
[15] W. Kleiböhmer and K. Cammann, Fresenius' Z. Anal. Chem. 335 (1989) 775.
[16] W. Langseth, J. Chromatogr., 315 (1984) 351.
[17] W. Langseth, Inorg. Chim. Acta, 90 (1984) 53.

ELSEVIER

Talanta 42 (1995) 1171–1177

Talanta

# The equilibrium constants of cadmium(II)–, lead(II)–, magnesium(II)–, and zinc(II)–α,β,γ,δ-tetrakis(1-methylpyridinium-4-yl)porphine complexes

Shukuro Igarashi *, Hitoshi Suzuki, Takao Yotsuyanagi

*Department of Molecular Chemistry and Engineering, Faculty of Engineering, Tohoku University, Aoba, Aramaki, Sendai 980, Japan*

Received 14 March 1994; revised 19 January 1995; accepted 23 February 1995

**Abstract**

The equilibrium constants of α,β,γ,δ-tetrakis(1-methylpyridinium-4-yl)porphine (TMPyP) complexes of cadmium(II), lead(II), magnesium(II), and zinc(II) were spectrophotometrically determined using the absorption spectra at the Soret band and the fluorescence spectra. The values of the following constants at 25 °C and ionic strength 0.1 M were evaluated: $K_{Pb-P} = 10^{-8.07 \pm 0.09}$, $K_{Cd-P} = 10^{-7.68 \pm 0.03}$, $K_{Zn-P} = 10^{1.72 \pm 0.08}$, and $K_{Mg-P} = 10^{-7.40 \pm 0.08}$ by the acid hydrolysis reaction of the TMPyP–metal complex at various pHs; $K_{Pb-P} = 10^{-7.80 \pm 0.04}$ and $K_{Cd-P} = 10^{-7.38 \pm 0.04}$ were determined by the ligand exchange reaction between TMPyP and nitrilotriacetic acid.

## 1. Introduction

It is well known that porphyrin compounds form very stable complexes with metal ions such as vanadium(V), cobalt(II), copper(II), etc. With respect to the stability of these complexes, Falk reported the following qualitative order by using the elimination reaction of the metal ion with strong acid [1]: Pt(II) > Pd(II) > V(V) > Ni(II) > Co(II) > Ag(II) > Cu(II) > Fe(II) > Mn(II) > Zn(II) > Mg(II) > Cd(II) > Ca(II) > Sn(II) > Pb(II) > $Li(I)_2$ > Ba(II) > $Ag(I)_2$. Recently, highly sensitive spectrophotometric determinations of various metal ions with water-soluble porphyrins have been developed using the absorption spectra at the Soret band (around $\varepsilon = (20-70) \times 10^4$ $M^{-1}$ $cm^{-1}$ at around 400–500 nm) or the fluorescence spectra at 600–700 nm [2–5].

The investigation of the porphyrin–metal complex in solution chemistry has mainly centered on the kinetics of complexation or adduct formation equilibrium of the porphyrin complex with axial ligands, such as $SCN^-$ for the α,β,γ,δ-tetrakis(1-methylpyridinium-4-yl)-prophine (TMPyP)–cobalt(III) complex [6]. However, systematic studies on the formation equilibria of water-soluble porphyrin complexes are relatively few. Tabata et al. determined the formation constants of the α,β,γ,-δ-tetrakis(4-sulfophenyl)porphine (TPPS) complexes of mercury(II), zinc(II), and cadmium-(II) by using a kinetic model for the metal exchange reaction [7]. Hambright et al. estimated the constant for the TMPyP–cadmium-(II) complex to be $2.0 \times 10^{-8}$ using a spectrophotometric method for the Q band at around 500–700 nm [8].

* Corresponding author. Present address: Department of Materials Science, Faculty of Engineering, Ibaraki University, Nakanarusawa 4-12-1, Hitachi-shi, Ibaraki, 316 Japan.


*SSDI* 0039-9140(95)01564-7

In this paper, the equilibrium constants ($K$) of TMPyP–lead(II), –cadmium(II), –magnesium(II), and –zinc(II) complexes were determined by a spectrophotometric method using absorption spectra at the Soret band and the fluorescence spectra.

$$M^{2+} + H_2P \rightleftharpoons MP + 2H^+, \qquad K = \frac{[MP][H^+]^2}{[M^{2+}][H_2P]}$$

Moreover, the equilibrium constants for the TMPyP–lead(II) and TMPyP–cadmium(II) complexes were also determined by the ligand exchange reaction with nitrilotriacetic acid.

## 2. Experimental

### 2.1. Apparatus

A Shimazu model UV-365 recording double-beam spectrophotometer with 1 cm glass cells was used for the absorbance measurements. A Hitachi model 850 recording fluorimeter with 1 cm glass cells was used for the relative fluorescence intensity measurements. A Hitachi–Horiba model F-7ss pH meter with Horiba model 6026 glass–Ag/AgCl combined electrode was used. A Komatsu-Yamato model CRT-220 coolnics was used as the water thermostat (25.0 ± 0.1 °C) for the sample solution and the cell holder in the spectrophotometer. An NEC personal computer model PC-9801 was used for the calculation of the equilibrium constant.

### 2.2. Reagents

All reagents used were of analytical-reagent grade unless otherwise described. The synthesis of TMPyP and the preparation of $10^{-4}$ M TMPyP solution was as follows. TMPyP tetratosylate was synthesized and purified as described elsewhere [9]. TMPyP solution was prepared by dissolving 34.9 mg of TMPyP tetratosylate in 250 ml of distilled water. The standardization of TMPyP solution was done by photometric titration (molar ratio method) with a standard copper(II) solution [10]. All standard metal ion solutions ($10^{-2}$M) were prepared from metal nitrates (Wako Junyaku Co.) and the concentrations were determined by EDTA titration. Nitrilotriacetic acid (NTA) (Wako Junyaku Co.) was purifed by the reported method [11]. The $1 \times 10^{-4}$ M solutions of each metal ion and NTA were prepared by dilution with distilled water. The pH buffer reagents, 3-($N$-morpholine)propanesulfonic acid (Mops; Dotaito), tris(hydroxymethyl)-aminomethane (Tris; Wako Junyaku Co.), hexamethylenetetramine (hexamine; Wako Junyaku Co.), sodium tetraborate (borax; Kanto Kagaku Co.), sodium hydroxide, and hydrochloric acid (Wako Junyaku Co.) were used.

### 2.3. Procedure

#### 2.3.1. Determination of equilibrium constants by analysis of pH–absorbacne and pH–fluorecence intensity curves

The dissociation reaction of the porphyrin metal complex was observed for the determination of the equilibrium constant. Each metal complex was prepared by a previous described method [3,12]. Namely, the reaction conditions were as follows. Zinc(II) complex: $[Zn^{2+}]_{Total} = 0.98 \times 10^{-5}$ M, $[H_2P]_{Total} = 4.30 \times 10^{-6}$ M, pH 9.3 (0.1 M borax), reaction time; 30 min (20 °C); magnesium(II) complex: $[Mg^{2+}]_{Total} = 3.99 \times 10^{-5}$ M, $[H_2P]_{Total} = 3.37 \times 10^{-6}$ M, $[oxine]_{Total} = 8.00 \times 10^{-5}$ M, pH 9.3 (0.1 M borax), reaction time, 90 min (95 °C); cadmium(II) complex: $[Cd^{2+}]_{Total} = 0.96 \times 10^{-5}$ M, $[H_2P]_{Total} = 4.30 \times 10^{-6}$ M, pH 9.8 (0.1 M hexamine–0.1 M Tris buffer solution), reaction time, 10 min (20 °C); lead(II) complex: $[Pb^{2+}]_{Total} = 1.82 \times 10^{-5}$ M, $[H_2P]_{Total} = 4.30 \times 10^{-6}$ M, pH 7.66 (0.1 M Mops–0.1 M NaOH buffer solution), reaction time, 30 min (20 °C).

Owing to the dissociation reaction of each complex, 2.5 ml of 2 M $NaNO_3$ solution are added to the system in order to maintain the ionic strength at $I = 0.1$ M, 20 °C. Next, after achieving the prescribed pH with a small amount of 2 M HCl solution, the mixture was diluted with distilled water to the mark in the 25 ml amber volumetric flask. The sample solution was then placed in a 50 ml amber sample bottle, and allowed to stand for the prescribed time at 20 °C in the thermostat. The absorbance of the cadmium(II) complex was measured at 448 nm after 2 days, that of the lead(II) complex at 476 nm after 10 min, the relative fluorescence intensity of the zinc(II) complex at 631 nm (excitation wavelength, 438 nm) after 30 days, and that of the magnesium(II) complex at

648 nm (excitation wavelength, 453 nm) after 27 days.

*2.3.2. Determination of equilibrium constants based on ligand exchange reaction*

The preparation of the lead(II) or cadmium(II) complex solution was as follows. A 2.5 ml sample of $10^{-4}$ M lead(II) or cadmium(II) standard solution was allowed to stand for 30 min at room temperature after achieving a pH of 10.7 with 2 ml of 0.1 M borax–0.1 M Tris–0.1 M NaOH mixed buffer solution. Next, 2.5 ml of 2 M $NaNO_3$ solution are added in order to set the ionic strength at $I = 0.1$ M, and 5 ml of $10^{-4}$ M NTA standard solution, and small amounts of 2 M HCl solution to achieve the prescribed pH were added, respectively. The sample solution was then placed in a 50 ml amber bottle, and allowed to stand for the prescribed time at 20 °C in the thermostat. The absorbance at 476 nm of the lead(II) complex and that at 448 nm of the cadmium(II) complex were measured after 2 days.

The concentration of $H_2P$ was determined by measuring the absorbance at 423 nm or the relative fluorescence intensity at 641 nm (excitation wavelength, 423 nm) in both the above procedures.

## 3. Results and Discussion

Many methods have been reported for the determination of the equilibrium constant of complexation. In this paper, a highly sensitive and reproducible spectrophotometric and fluorescence method was used. The absorption spectra in the Soret band and the fluorescence spectra of each metal complex are shown in Figs. 1 and 2, respectively. Since the Soret bands of the zinc(II) complex and the magnesium(II) complex significantly overlap with that of free reagent, the fluorescence spectra were used for their concentration measurements. The complexation of the metal ion (M) and free-base type porphyrin ($H_2P$) is given as follows

$$M + H_2P \overset{K}{\rightleftharpoons} M\text{–}P + 2H$$

$$K = \frac{[M\text{–}P][H]^2}{[M][H_2P]} \quad (1)$$

where $K$ is the equilibrium constant. The species charge was omitted.

*3.1. Equilibrium constants for TMPyP–cadmium(II), –magnesium(II), –lead(II), and –zinc(II) complexes*

*3.1.1. Cadmium(II), magnesium(II), and lead(II) complexes (pH 5.5–7.5)*

The hydrolysis species of the metal ion (MOH, $M(OH)_2$) was considered and the concentration [M] of the unreacted metal ion and side reaction coefficient (herein after, the $\alpha$ coefficient [13]) were defined

$$[M]_{Free} = [M] + [MOH] + [M(OH)_2]$$

$$\alpha_M = \frac{[M]_{Free}}{[M]} = 1 + \frac{[MOH]}{[M]} + \frac{[M(OH)_2]}{[M]}$$

The $\alpha_M$ coefficient was calculated by using a constant with respect to the hydrolysis reaction

Cd [14]:
$$\beta_1^{Cd} = \frac{[CdOH][H]}{[Cd]} = 10^{-7.92}$$

$$\beta_2^{Cd} = \frac{[Cd(OH)_2][H]}{[CdOH]} = 10^{-11.38}$$

Mg [15]:
$$\beta_1^{Mg} = \frac{[MgOH][H]}{[Mg]} = 10^{-11.40}$$

Pb [16]:
$$\beta_1^{Pb} = \frac{[Ph(OH)][H]}{[Pb]} = 10^{-8.84}$$

$$\beta_2^{Pb} = \frac{[Pb(OH)_2][H]}{[PbOH]} = 10^{-7.11}$$

From these $\alpha_M$ coefficents, the equilibrium constant $K$ of Eq. (1) was as follows

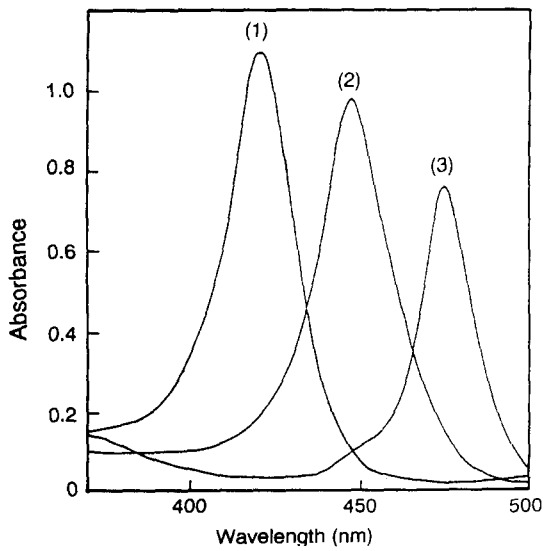


Fig. 1. Absorption spectra of TMPyP, TMPyP–cadmium(II) and TMPyP–lead(II) complexes. Curve (1), TMPyP; curve (2), TMPyP–Cd(II); curve (3), TMPyP–Pb(II). (Measurement conditions: pH 9.30; 20 °C; $[TMPyP]_{Total} = 4.30 \times 10^{-6}$ M; $[Cd^{2+}]_{Total} = 0.96 \times 10^{-5}$ M; $[Pb^{2+}]_{Total} = 1.82 \times 10^{-5}$ M.)

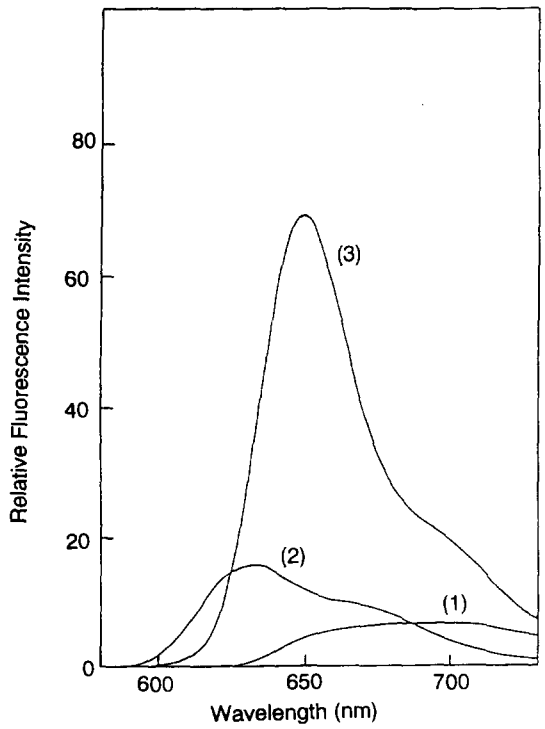


Fig. 2. Fluorescence spectra of TMPyP, TMPyP–magnesium(II) and TMPyP–zinc(II) complexes. Curve (1), TMPyP (excitation wavelength $\lambda_{ex} = 423$ nm); curve (2), TMPyP–Zn(II) ($\lambda_{ex} = 438$ nm); curve (3), TMPyP–Mg(II) ($\lambda_{ex} = 453$ nm). (Measurement conditions: pH 9.30; 20 °C; $[TMPyP]_{Total} = 4.30 \times 10^{-6}$ M; $[Zn^{2+}]_{total} = 0.98 \times 10^{-5}$ M; $[Mg^{2+}]_{Total} = 3.99 \times 10^{-5}$ M.)

$$K = \frac{[M-P][H]^2}{[M]_{Free}[H_2P]}\alpha_M \qquad (2)$$

where $[M]_{Free} = [M]_{Total} - [M-P]$, and $[P]_{Total} = [H_2P] + [M-P]$. The concentration of M–P and $H_2P$ were determined by measuring the absorbance and relative fluorescence intensity at their respective maximum wavelenghts. Based on these data, the equilibrium constant $K$ of Eq. (2) was calculated.

### 3.1.2. Zinc(II) complex (pH 1.0 ~ 3.0)

Species of $H_3P$ and $H_4P$ and $H_4P$ for TMPyP are considered and the side-reaction coefficient ($\alpha_P$) was defined. Also, the side-reaction coefficient ($\alpha_M$) due to hydrolysis of the metal ion was neglected in this pH range.

$$[P]_{Free} = [H_2P] + [H_3P] + [H_4P]$$

$$\alpha_p = \frac{[P]_{Free}}{[H_2P]} = 1 + \frac{[H_3P]}{[H_2P]} + \frac{[H_2P]}{[H_2P]}$$

The $\alpha_p$ coefficient was calculated by using the acid dissociation constant [17]

$$Ka_3 = \frac{[H_3P]}{[H_2P][H]} = 10^{2.06} \quad Ka_4 = \frac{[H_4P]}{[H_3P][H]} = 10^{0.80}$$

From this $\alpha_p$ coefficient, the equilibrium constant $K$ in Eq. (1) because

$$K = \frac{[M-P][H]^2}{[M][P]_{Free}}\alpha_p \qquad (3)$$

where $[M] = [M]_{Total} - [M-P]$, $[P]_{Free} = [P]_{Total} - [M-P]$

The concentration of M–P was determined by measuring the relative fluorescence intensity. The equilibrium constant $K$ of Eq. (3) was then determined. Results of sections 3.1.1. and 3.2.2. are shown in Table 1 and Fig. 3.

### 3.2. Determination of equilibrium constant of lead(II) and cadmuim(II) complexes by ligand exchange reaction

Nitrilotriacetic acid ($H_3Y$) was selected as the reagent for the ligand exchange reaction. The material balance equation for the metal ions is given by

$$[M]_{Free} = [M] + [MOH] + [M(OH)_2] + [M-Y]$$
$$= [M]_{Total} - [M-P] \qquad (4)$$

where $[M-Y] = K_Y[M][Y]_{Total}/K_Y[M] + \alpha_Y$. The side-reaction coefficent of NTA ($\alpha_Y$) is given by

$$\alpha_Y = 1 + \frac{[HY]}{[Y]} + \frac{[H_2Y]}{[Y]} + \frac{[H_3Y]}{[Y]}$$

Therefore, Eq. (4) can be rearranged to

$$[M]_{Free} = [M] + \frac{\beta_1^M}{[H]}[M] + \frac{\beta_1^M\beta_2^M}{[H]^2}[M] + \frac{K_Y[M][Y]_{Total}}{K_Y[M] + \alpha_y} \qquad (5)$$

and the value of $\alpha_Y$ was then calculated from the acid dissociation constants of $H_3Y$ [18]

$$Ka_1^Y = \frac{[HY]}{[Y][H]} = 10^{9.73} \quad Ka_2^Y = \frac{[H_2Y]}{[HY][H]} = 10^{2.49}$$

$$Ka_3^Y = \frac{[H_3Y]}{[H_2Y][H]} = 10^{1.89}$$

The hydrolysis constants of $\beta_1^{Pb}$, $\beta_2^{Pb}$, $\beta_1^{Cd}$, and $\beta_2^{Cd}$ are the same as that previously mentioned. The $K_Y$ value was calculated from the formation constants of the NTA metal complex

$$K_Y^{Cd} = \frac{[CdY]}{[Cd][Y]} = 10^{10.0}\ [19]$$

$$K_Y^{Pb} = \frac{[PbY]}{[Pb][Y]} = 10^{11.47}\ [20].$$

Table 1
The pH dependence in the TMPyP–metal ion reaction system and the calculation of equilibrium constants $K$ at 20 °C and $I = 0.1$ M ($NaNO_3$)

| Cd | | | Pb | | | Mg | | | Zn | | |
|---|---|---|---|---|---|---|---|---|---|---|---|
| pH | log $A$ [a] | log $K$ | pH | log $A$ [a] | log $K$ | pH | log $A$ [a] | log $K$ | pH | log $A$ [a] | log $K$ |
| 7.07 | 6.49 | −7.65 | 6.49 | 4.85 | −8.13 | 7.34 | 7.21 | −7.46 | 2.01 | 5.71 | 1.69 |
| 6.94 | 6.19 | −7.69 | 6.33 | 4.60 | −8.06 | 7.19 | 6.90 | −7.48 | 1.96 | 5.63 | 1.72 |
| 6.82 | 5.96 | −7.69 | 6.09 | 4.20 | −7.98 | 7.06 | 6.82 | −7.30 | 1.90 | 5.57 | 1.77 |
| 6.77 | 5.82 | −7.71 | 5.89 | 3.75 | −8.03 | 6.96 | 6.53 | −7.38 | 1.82 | 5.42 | 1.78 |
| 6.67 | 5.65 | −7.70 | 5.72 | 3.41 | −8.02 | 6.84 | 6.31 | −7.37 | 1.70 | 5.14 | 1.74 |
| 6.55 | 5.42 | −7.69 | 5.69 | 3.32 | −8.03 | 6.74 | 6.07 | −7.41 | 1.62 | 4.87 | 1.64 |
| 6.47 | 5.26 | −7.68 | – | – | – | 6.60 | 5.82 | −7.37 | – | – | – |
| 6.36 | 5.05 | −7.66 | – | – | – | 6.46 | 5.55 | −7.36 | – | – | – |
| – | – | – | – | – | – | 6.33 | 5.28 | −7.38 | – | – | – |
| – | – | – | – | – | – | 6.15 | 4.84 | −7.47 | – | – | – |
| | | Average, −7.68 ± 0.03 | | | Average, −8.04 ± 0.09 | | | Average, −7.40 ± 0.08 | | | Average, 1.72 ± 0.08 |

[a] $A = [M-P]/[H_2P][M]$ was calculated from Eqs. (2) or (3) with the observed parameters

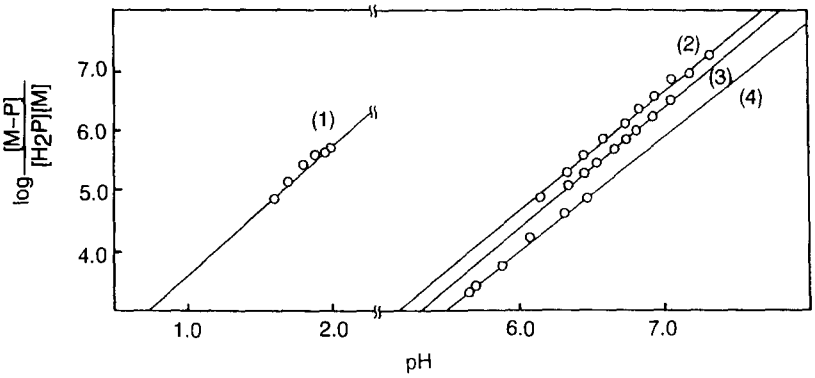


Fig. 3. Plots of log [M–P]/[$H_2$P][M] vs. pH for the dissociation reaction of TMPyP–metal(II) complexes at 20 °C and $I = 0.1$ M ($NaNO_3$). Line (1), TMPyP–Zn(II) (slope, 2.11); line (2), TMPyP–Mg(II) (slope, 1.99); line (3), TMPyP–Cd(II) (slope, 2.00); line (4), TMPyP–Pb(II) (slope, 1.90).

The solution of the quadratic Eq. (5) for [M] was calculated; $K$ can be determined by substituting this solution in Eq. (1)

The results are shown in Table 2 and Fig. 4. The equilibrium constants obtained in this study are summarized in Table 3. The values of log $K$ in Figs. 3 and 4 were also obtained from the $y$-intercept in the relationship log $A$ vs. pH. In Fig. 3, this analysis method gave the following values: $\log K_{TMPyP-Pb} = -7.44$ (slope, 1.90); $\log K_{TMPyP-Cd} = -7.71$ (slope, 2.00); $\log K_{TMPyP-Mg} = -7.32$ (slope, 1.99); and $\log K_{TMPyP-Zn} = 1.53$ (slope, 2.11). Moreover, similarly in Fig. 4, the values were $\log K_{TMPyP-Pb} = -7.93$ (slope, 2.01) and $\log K_{TMPyP-Cd} = -7.05$ (slope, 1.96). However, this method was not adopted, because the pH region of the experimental points was narrow and the slope of the straight line obtained by the least-square method slightly deviated from the 2.00 theoretical value. The average value of $K$ obtained from each experimental point was adopted as an equilibrium constant of the porphyrin complex in this study. The order of stability for each metal complex agreed well with that (Zn(II) > Mg(II) > Cd(II) > Pb(II)) reported by Falk [1]. With respect to the lead(II) complex, the measurement of the equilibruim constant based on the ligand exchange reaction is useful because of being able to reduce the influence of hydrolysis. As a result, the straight line (slope, 2.01) in Fig. 4 was better than that in Fig. 3 (slope, 1.90), since that in Fig. 4 is close to the theoretical value (slope, 2.00) of the two-proton reaction. Compared with the equilibrium constant in this study and those of Tabata et al. [7], reported for the TPPS–cadmium(II), –zinc(II) and

Table 2
The pH dependence in the TMPyP–metal ion–NTA ligand exchange reaction system and the calculation of equilibrium constants $K$

| Cd | | | Pb | | |
|---|---|---|---|---|---|
| pH | log $A$ [a] | log $K$ | pH | log $A$ [a] | log $K$ |
| 8.42 | 9.47 | −7.37 | 10.06 | 12.36 | −7.76 |
| 8.34 | 9.28 | −7.40 | 9.95 | 12.12 | −7.79 |
| 8.24 | 9.07 | −7.40 | 9.85 | 11.90 | −7.80 |
| 8.13 | 8.87 | −7.39 | 9.78 | 11.77 | −7.78 |
| 8.05 | 8.70 | −7.40 | 9.67 | 11.53 | −7.81 |
| 7.97 | 8.53 | −7.41 | 9.57 | 11.30 | −7.84 |
| 7.83 | 8.23 | −7.39 | 9.43 | 11.07 | −7.79 |
| 7.78 | 8.18 | −7.37 | 9.37 | 10.89 | −7.84 |
| 7.61 | 7.85 | −7.37 | 9.23 | 10.68 | −7.78 |
| 7.56 | 7.77 | −7.36 | 9.15 | 10.48 | −7.81 |
| 7.48 | 7.59 | −7.36 | 9.01 | 10.23 | −7.79 |
| 7.34 | 7.34 | −7.35 | 8.92 | 10.05 | −7.79 |
| 7.25 | 7.15 | −7.34 | 8.82 | 9.83 | −7.81 |
| | | Average, −7.38 ± 0.04 | | | Average, −7.80 ± 0.04 |

[a] $A = [M-P]/[H_2P][M]$ was calculated from Eqs. (5) and (1) with the observed parameters

Table 3
Summary of the equilibrium constants for TMPyP–lead(II), –magnesium(II), –zinc(II), and –cadmium(II) complexes[a]

| Equilibrium Constant | Pb | Cd | Zn | Mg |
|---|---|---|---|---|
| log $K$ [b] | −8.04 ± 0.09 | −7.68 ± 0.03 | −1.72 ± 0.08 | −7.40 ± 0.08 |
| log $K$ [c] | −7.80 ± 0.04 | −7.38 ± 0.04 | – | – |

[a] All measurement conditions were described in the experimental section.
[b] Equilibrium constants based on the dissociation reaction of TMPyP complexes (pH dependent, see Table 1).
[c] Equiliblium constants based on the NTA ligand exchange (Table 2).

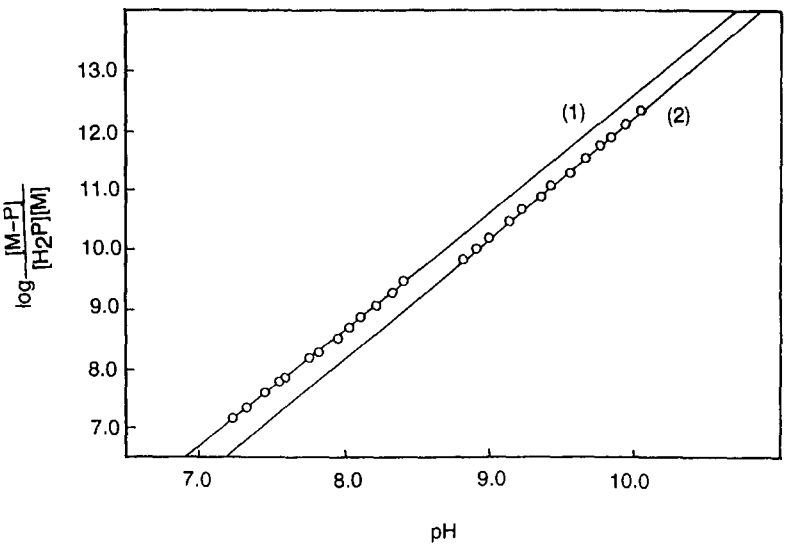


Fig. 4. Plots of log [M–P]/[$H_2$P][M] vs. pH for the dissociation reactions of TMPyP–cadmium(II) and –lead(II) complexes by NTA ligand change at 20 °C and $I = 0.1$ M ($NaNO_3$). Line (1), TMPyP–Cd(II)(slope, 1.96); line (2), TMPyP–Pb(II)(slope, 2.01).

– lead(II) complexes, the different values of the formation constants (i.e. log $K_{TPPS} - \log K_{TMPyP}$ were $-2.17 \pm 0.09$ for any of them. Also, the equilibrium constant $K$ value with respect to the TMPyp–cadmium(II) complex approximately agrees with the value previously reported by Hambright et al. [17].

## References


[1] J.E. Falk, Porphyrins and Metalloporphyrins, Elsevier, Amsterdam, 1964, pp. 30–40.
[2] K.L. Cheng, K. Ueno and T. Imamura, Handbook of Organic Analytical Reagents, CRC Press, Inc., Florida, 1982, p. 355, and refs. therein.
[3] M. Tabata and Kaneko, Analyst, 116 (1991) 1185.
[4] J.A. Schneider and J.F. Hornig, Analyst, 118 (1993) 933.
[5] S. Igarashi and T. Yotsuyanagi, Anal. Chim. Acta, 281 (1993) 347.
[6] R.F. Pasternack and M.A. Cobb, J.Inorg. Nucl. Chem., 35 (1973) 4327.
[7] M. Tabata and M. Tanaka, J. Chem. Soc., Chem. Commun., (1985) 42.
[8] A. Shamin and P. Hambright, Inorg. Chem., 19 (1980) 564.
[9] R.F. Pasternack, P.R. Huber, P. Boyd, G. Engasser, L. Francesconi, E. Gibbs, P. Fasella, G.C. Venturo and L.deC. Hinds, J. Am. Chem. Soc., 94 (1972) 4511.
[10] T. Makino and J. Itoh, J. Clin. Chem., 8 (1979) 296.
[11] T.Moeller and R. Ferrus, Inorg. Chem., 1 (1962) 49.
[12] S. Igarashi, J. Kobayashi, T. Yotsuyanagi and K. Aomura, Nippon Kagaku Kaishi, (1979) 602 (in Japanese).
[13] A. Ringbom, Complexation in Analytical Chemistry, John Wiley and Sons Inc., New York, 1963.
[14] V.B. Spivakovskii and L.P. Moisa, Zh.Neorg. Khim., 9 (1964) 2287.
[15] P.B. Hostetler, Am.J. Sci., 261 (1963) 238.
[16] R. Hugel, Bull. Soc. Chim. Fr., (1965) 968.
[17] P. Hambright, P.B. Chok, J. Am. Chem. Soc., 96 (1974) 3123.
[18] W. Noddak and G. Oertel, Z. Electrochem., 61 (1957) 121.
[19] V. Jokl, J.Chromatogr., 14 (1964) 71.
[20] J. Stary, Anal. Chim. Acta, 28 (1963) 132.

ELSEVIER

Talanta 42 (1995) 1181–1188

Talanta

# Dopamine sensing and selectivity of Nafion-coated plant tissue powder sensors

Y. Chen, T.C. Tan *

*Department of Chemical Engineering, National University of Singapore, 10, Kent Ridge Crescent, 0511 Singapore*

Received 22 July 1994; accepted 1 November 1994

**Abstract**

Dopamine tissue sensors were prepared using biofilms containing pretreated tissue powder of potato, banana, mushroom and apple. These sensors showed good stability, reproducibility and service life span of more than 200 days involving 300 to 500 measurements. Overlaying the sensors with a Nafion coating considerably improved the sensor selectivity for dopamine by effectively precluding neutral and anionic solutes from entering the biofilm thus removing the interference of most of the 23 solutes examined in this study. The response of the Nafion-coated apple powder sensor in a mixture containing dopamine and the three strong interferents (arterenol, histidine and tyrosine), at concentrations within their respective linear calibration range, was linear with respect to the concentration of each of the solutes. The sensitivity of each of the components in the mixture was higher than the corresponding single component linear range sensitivity.

## 1. Introduction

Polyphenolase, an enzyme present in many fruits, fungi and vegetables, catalyses the oxidation of phenolic and allied compounds including dopamine [1,2], an important neurotransmitter associated with Parkinson's disease, muscular immobility and tumour when its concentration deviates from its normal level [3]. Polyphenolase sensors have been prepared with biofilm fabricated from tissues of apple [4–6] banana [5,7,8] potato, mushroom [5,9] and avocado [9]. In most cases, fresh tissues were used either by themselves [4,7,9,10] or mixed with a conductive material such as carbon paste [8]. They were characterized by very short service life owing to microbial degradation. They were normally stored at 4 °C to −10 °C when they were not being used. Tan and Chen [4,5] overcame the deterioration problem by removing water-soluble biodegradable materials from the tissue prior to its use for the biofilm preparation. They reported a service life of more than 3 months and were stored in phosphate buffer at room temperature when they were not in use. The sensors also showed better reproducibility, stability and sensitivity than the untreated tissue sensors. Polyphenolase also catalyses the oxidation of many other biogenic amines, amino acids and phenolic compounds. As a result, polyphenolase based biosensors generally showed poor selectivity. The selectivity problem is more serious with tissue sensors since the tissue also contained many other types of enzymes besides polyphenolase. Dopamine selectivity has been enhanced by overlaying the sensor with functional membranes such as base-hydrolysed cellulosic film to preclude larger molecule interferents [11], protonated poly(4-vinylpyridine) film to remove cationic interferents [12] and Nafion to remove anionic interferents [6,13]. Enzyme inhibitors and activators have also been used to improve the selectivity of tissue-based adenosine sensor [14].

* Corresponding author.


*SSDI* 0039-9140(95)01507-8

This paper reports the effects of overlaying four different tissue powder sensors with a Nafion film on their efficacy and selectivity for dopamine sensing.

## 2. Experimental

### 2.1. Materials and preparation

All the chemicals used in this study were analytical reagent grade. Stock solutions of 0.05 M disodium hydrogen phosphate ($Na_2HPO_4 \cdot 2H_2O$, Merck) and 0.05 M sodium dihydrogen phosphate ($NaH_2PO_4 \cdot 2H_2O$, Merck) were prepared. Appropriate amounts of the two stock solutions were mixed when required to give 0.05 M phosphate buffers of pH ranging from 4.89 to 8.49. The pH was measured using a Hanna pH meter (Model 8417). Altogether 22 compounds of various biogenic amines, catecholamines, amines, amino acids and phenolic compounds were used to examine the sensitivity of the tissue sensors relative to dopamine. All compounds except phenol (BDH) were obtained from Sigma. Solutions of unstable and easily oxidizable compounds such as biogenic amines were prepared as required using nitrogen-deaerated deionized water.

### 2.2. Sensor fabrication and experimental procedure

Four Nafion-coated tissue power sensors were prepared using biofilms containing approximately the same mass of immobilized potato, banana, mushroom and apple pretreated powder according to the procedure described in an earlier paper [6]. The fabrication involved pretreating the tissue to remove water-soluble biodegradable solutes, immobilizing the tissue powder on polycarbonate membrane, coating Nafion on a polycarbonate membrane and finally securing these membranes over a dissolved oxygen probe (YSI Model 50, Yellowstone Instrument).

The sensor was placed in a jacketed beaker containing 50 ml of 0.05 M phosphate buffer of known pH and constant temperature. The solution was saturated with dissolved oxygen by bubbling air continuously through it. A Pine AFRDE4 potentiostat maintained the dissolved oxygen probe at $-0.8$ V and the current output was monitored continuously on a HP 3466A digital multimeter and simultaneously recorded on a Rikadenki chart recorder. At steady-state, the baseline current, $I_0$ was noted. A known amount of the test solute was added to the buffer. The new steady-state current, $I_s$ was recorded. The difference, $\Delta I$ $(=I_0 - I_s)$, was noted as the sensor response corresponding to the concentration of the test solute in the buffer solution. The response time for the system to equilibrate after the addition of the test solute was also recorded. The sensor was removed, washed with deionized water and returned to the jacketed beaker which was refilled with 50 ml of fresh buffer solution. The recovery time for the sensor current to return to its baseline value was noted before starting the next measurement. Measurements were carried for each of the four sensors at different pHs, temperatures and concentrations of dopamine and other solutes. To obtain good reproducibility and stability, the sensor has to be preconditioned when new or has been left unused for several weeks, and also each time the pH or temperature of the solution was changed. This was done by repeating the measurement procedure several times in the new environment with the same solute concentration until the results were reproducible.

The selectivity and interference effects of the 22 compounds were examined at 298 K and at the respective optimum pH of the sensor by comparing the sensor response of the solute with dopamine at the same concentration of 40.1 μM. Solutes showing a relative sensitivity (response) with respect to dopamine equal or greater than 10% were considered as strong interferents. For the sensor which showed the least number of such strong interferents, linear range calibration was carried out for each of the strong interferents. Measurements were also made in solutions containing different concentrations of dopamine and these strong interferents.

## 3. Results and discussion

### 3.1. Effect of pH

The response of the four Nafion-coated sensors generally increases with decreasing pH of the solution with a slight maximum shown by the apple sensor at pH about 5.56 (Fig. 1a). Without the Nafion coating, the sensors showed optimum response at pH 6.50 for

potato, 5.56 for apple and banana and 7.40 for mushroom [5]. A similar pH effect is shown in Fig. 1(b) on the ratio of the response of Nafion-coated sensor ($\Delta I_c$) to that without the Nafion coating ($\Delta I_u$). All the data for the uncoated sensors were obtained in a previous study [5]. These observations may be attributed to the increased swelling of the Nafion film at lower pH [15] resulting in higher solubility and diffusivity of the solute and hence better mass transfer [16]. Although Alhaique et al. [15] reported no pH effect on the permeability of cationic exchange Nafion film towards positively charged species such as dopamine, the diffusion rate of dopamine through the Nafion film would nevertheless vary with pH by virtue of its effect on the hydrolysis of dopamine in the solution. Since lower pH favours the hydrolysis of dopamine, the concentration of its positively charged species would, therefore, increase with decreasing pH. Its diffusion rate through the Nafion film would increase, resulting thereby in a higher sensor response. In the absence of the Nafion coating, the hydrolyis of dopamine has no effect on its diffusion through the polycarbonate membrane. The reduced sensor response of the Nafion-coated sensors is, however, a measure of the mass transfer resistance and the cationic exchange activity of the Nafion film.

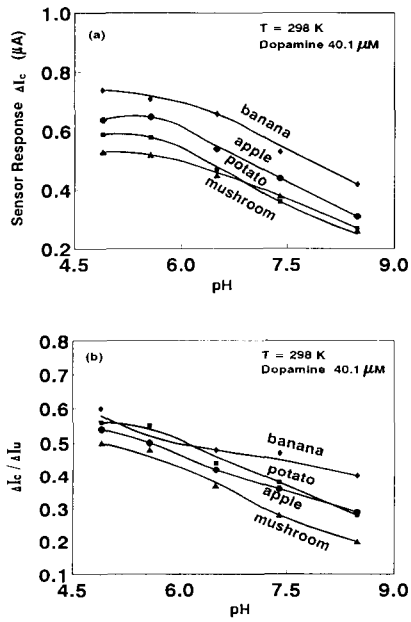


Fig. 1. pH effect on sensor response to dopamine.

TAL 42-8-H

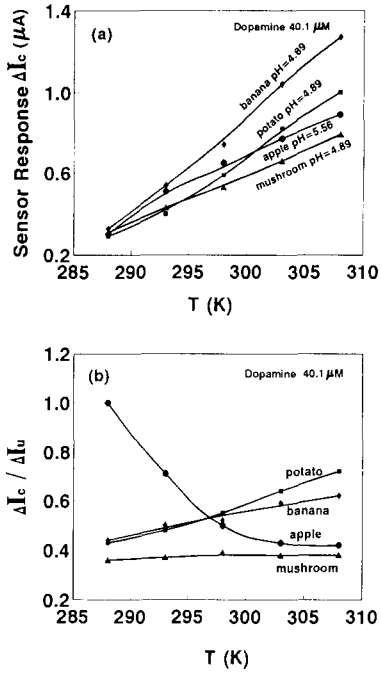


Fig. 2. Temperature effect on sensor responses of Nafion-coated sensors and the ratio $\Delta I_c/\Delta I_u$.

### 3.2. Effect of temperature

The response of all the four sensors increased monotonically with temperature increasing from 288 to 308 K (Fig. 2a). The data for the uncoated sensors were obtained in a previous study [5] at their respective optimum pH. The response of the Nafion-coated sensors relative to the uncoated sensors is shown in Fig. 2(b). Only the apple sensor showed a decreasing trend. Since measurements using the apple sensor with and without the Nafion coating were made at the same pH, the temperature effect on the reaction constant and diffusion through the polycarbonate membrane and biofilm should be the same for both cases. The decrease in the relative response is, therefore, a measure of the temperature effect on the hydrolysis of dopamine, the extent of swelling and the cation transport property of the Nafion film. In the other three cases, the increase in the relative response with temperature would also include the effects due to operating the Nafion-coated sensors at lower pH.

### 3.3. Response and baseline recovery

The response time of the Nafion-coated sensors generally increased with increasing dopamine concentration. The response time at 298 K was about 3–14 min in the linear concentration range of pH 5.56 for apple and 4.89

Table 1
Sensing characteristics for dopamine in 0.05 M phosphate buffer

| Parameters | Potato | Banana | Mushroom | Apple |
|---|---|---|---|---|
| Temperature (K) | 298 | 298 | 298 | 298 |
| pH | 4.89 | 4.89 | 4.89 | 5.56 |
| | (6.5) | (5.56) | (7.4) | (5.56) |
| Mass immobilized (mg) | 30.1 | 30.0 | 30.0 | 30.2 |
| Linear range (μM) | 4–40.1 | 4–40.1 | 4–79.9 | 4–79.9 |
| | (4–99.7) | (4–60.1) | (4–129) | (4–60.1) |
| Sensitivity (μA/μM) | 0.0147 | 0.0184 | 0.0137 | 0.0167 |
| | (0.0271) | (0.0344) | (0.0329) | (0.0325) |
| Response time (min) | 3.1–11 | 3–9 | 3.3–14.2 | 4.2–9 |
| | (5–11) | (4.4–7.4) | (3.8–8.8) | (3.6–9) |
| Recovery time (min) | 3–16 | 2–13.5 | 4.3–25 | 3–27 |
| | (7–30) | (7–13) | (5–12) | (10–30) |
| Service life (day) | >240 | >235 | >206 | >214 |

Figures in parenthese are for the uncoated sensors obtained from Ref. [5].

for the other three sensors (Table 1). These were comparable with the response time (values in parentheses in Table 1) of those without the Nafion coating and operating at their respective optimum pH and higher linear concentration range [5]. The negligible change in the response time with the addition of the Nafion film could be due to the lower concentration involved and operating at lower pH (except for apple). Carr [17] and Chen and Tan [5] found that the response time is longer with lower operating temperature, higher concentration and lower diffusivity of the substrate.

Good reproducibility, stability and service life span were obtained by leaving the sensor after each measurement in a fresh phosphate solution to allow it to return to its baseline value. The baseline recovery time for the Nafion-coated sensors varied from 2–27 min compared with 5–30 min for the uncoated sensors [5] for the same reasons of lower substrate concentration in the biofilm and pH.

### 3.4. *Reproducibility, stability and service life*

The stability and reproducibility of the four sensors with and without the Nafion coating was examined over a period of more than 200 days by repeating the steady-state measurement in a 0.05 M phosphate buffer containing 40.1 μM dopamine at 298 K and at their respective operating pH. The sensors were used in between these measurements for other parametric studies involving more than 300 measurements for the mushroom sensor and more than 500 measurements for the other three sensors. They were stored in substrate-free phosphate buffer at room temperature when they were not in use. The time plot of the relative response expressed as per cent of the initial value corresponding to the first steady-state measurement immediately after its preconditioning is shown in Fig. 3. All the four sensors showed a mean relative response of 100.1–104.1% with a standard deviation of 1.46–4.25 and a coefficient of variation (CV) of 1.5–4.1%. These results showed conclusively that the pretreated tissue powder sensors have

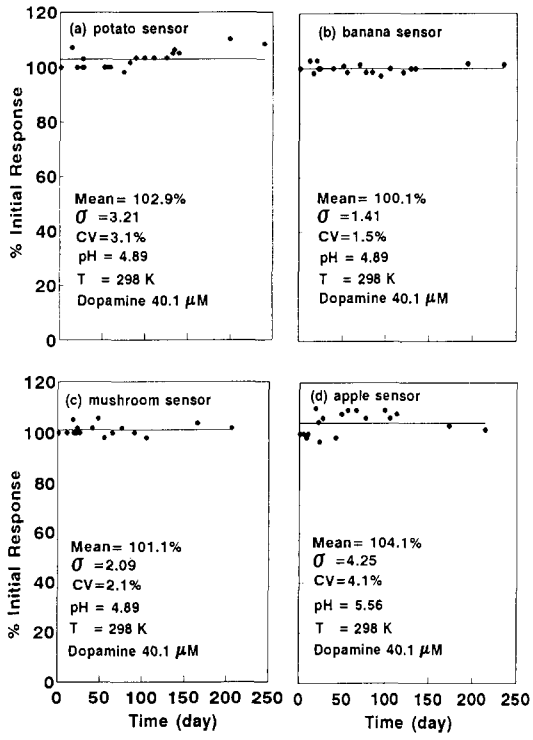


Fig. 3. Stability and reproducibility of the sensor response.

considerably better stability, reproducibility and longer service life compared with sensors using untreated tissues [4,7,9,10] or purified tyrosinase [18]. Moreover, the storage of the present sensors when they were not in use was considerably more convenient in phosphate buffer at room temperature compared with −10° to 4 °C storage conditions for the untreated tissue sensors. The Nafion coating further reduced the contamination and deactivation of the enzyme in the tissue powder by precluding most of the interferents from entering the biofilm.

### 3.5. Calibration against dopamine

The results of the calibration of the four Nafion-coated sensors against dopamine at 298 K and pH 5.56 for the apple sensor and 4.89 for the other three sensors are given in Table 1. Corresponding values for the uncoated sensors obtained in a previous study [5] are given in parentheses for comparison. Linear response was observed over the concentration range of 4–40.1 μM for potato and banana sensors and 4–79.9 μM for mushroom and apple sensors with sensitivity of about 0.0137–0.0183 μA/μM compared with 0.0271–0.0344 μA/μM reported earlier for the uncoated sensors [5]. The presence of the Nafion film, therefore, reduced the sensitivity to about half that of the uncoated sensors. A similar drop in sensitivity was observed by Gerhard et al. [19] and Harrison et al. [20] for their Nafion-coated sensors.

### 3.6. Selectivity and interference

The response of the four sensors to 22 solutes relative to their response to dopamine at the same concentration of 40.1 μM at different pHs are shown in Fig. 4(a–d). The data for the uncoated sensors [5] given as PU 6.5 in Fig. 4(a), BU 5.56 in Fig. 4(b), MU 7.4 in Fig. 4(c) and AU 5.56 in Fig. 4(d) were included for comparison. The anionic repulsion property of the Nafion film significantly reduced or totally eliminated the interference of anionic interferents including amino acid with p$I$ values less than the pH of the solution such as DOPAC (Dc), homovanillic acid (H), vanillymandelic acid (V), L-histidine (Hd), L-tryptophan (Tp), L-DOPA (Da), L-tyrosine (Ty), L-cysteine (Ce), L-cystine (C) and 3-indolylacetic acid (I). On the other hand, its cationic exchange property enhanced the sensor sensitivity towards cationic solutes while the reduced sensitivity towards the neutral solutes such as catechol (Ct) could be due to its mass transfer resistance. The exclusion of anions and neutral molecules reduced the contamination and deactivation of the enzymes in the tissue and further improved the stability, reproducibility and service life span of the sensor. Among the four sensors, dopamine sensing by the apple powder sensor was affected by the least number of interfering solutes and the number was further reduced by the Nafion coating. The present sensors showed significantly lower sensitivity to the interferents reported for a purified mushroom tyrosinase sensor [18].

The effect of concentration on the extent and nature of interference was studied using the Nafion-coated apple sensor at a pH of 5.56. The results showed that increase in the solute concentration did not affect the interference of epinephrine (E), H, V, tryptamine (T), C, I, phenol (P), ascorbic acid (Aa), 3-methoxytyramine hydrochloride (M), serotonin (S), Tp, Da, adenine (Ad), riboflavin (R), DOPEG (Dg) and Ct up to a concentration as high as 100 μM. The results confirmed that these solutes have little or no interference on dopamine sensing within the linear calibration range of dopamine. However, the relative selectivity of uric acid (Ua) with respect to dopamine at the same concentration decreased from 17% at 40.1 μM to 3% at 98.3 μM. This showed that the sensitivity of dopamine is more concentration dependent than that of uric acid outside the linear range. Linear calibration was carried out for arterenol (Ar), Dc, Ty, Hd and Ce. The results are given in Table 2. The linear range sensitivity of arterenol, histidine and tyrosine to dopamine was about 11–12% that of dopamine. Their interference in a mixture with dopamine was examined by determining the sensor response at different concentrations of the four components in the mixture. The concentration of each of the components was limited to within its linear calibration range. The experimental sensor response–composition data were correlated assuming linear interaction and the results obtained given by:

$$\Delta I_{\text{mixture}} = 0.0178C_{\text{dopamine}} + 0.0033C_{\text{arterenol}} + 0.0037C_{\text{histidine}} + 0.0023C_{\text{tyrosine}}$$

The correlation showed a mean fractional error of 0.088 with a standard deviation of 0.12 and

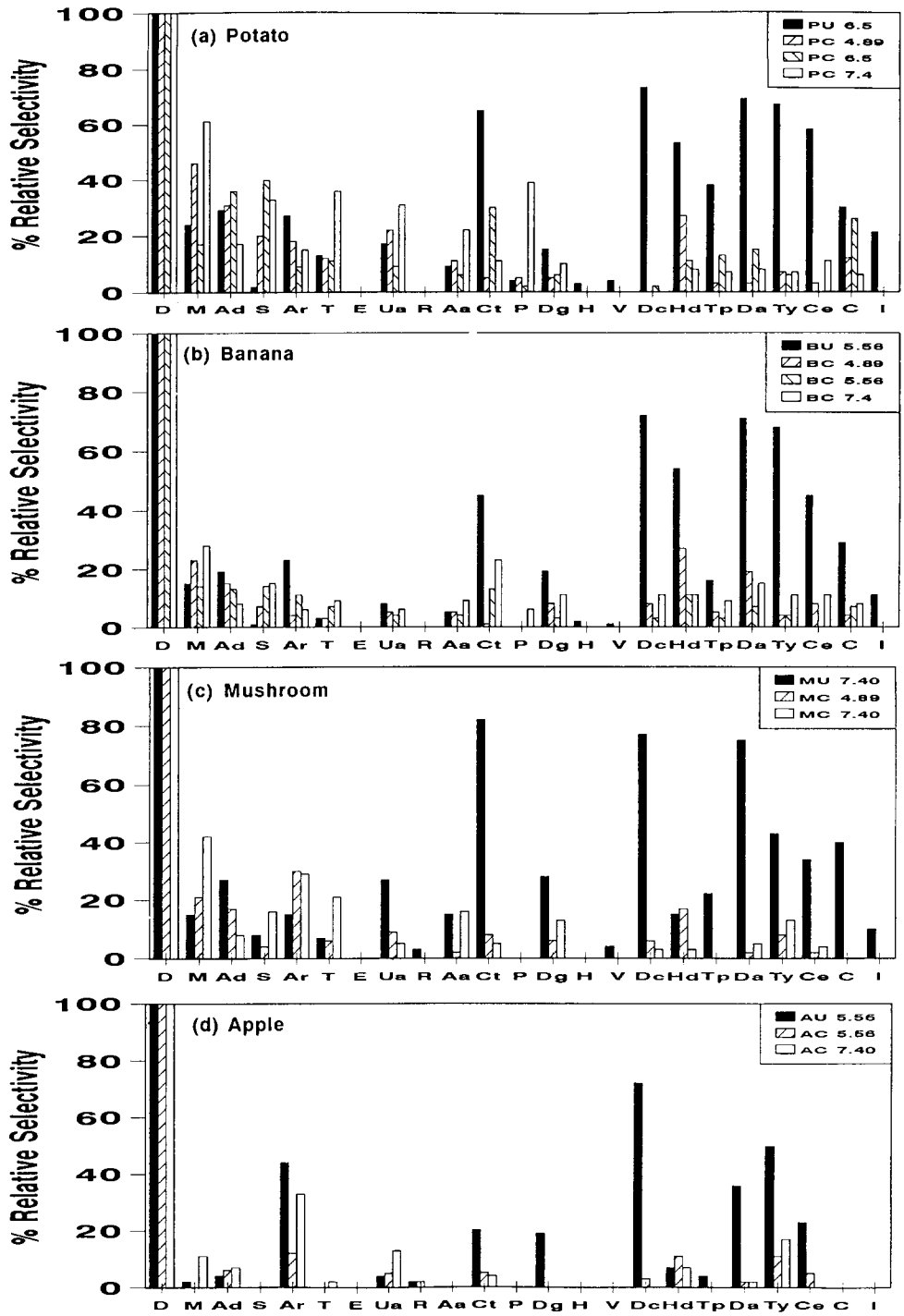


Fig. 4. Relative selectivity of sensors with and without the Nafion coating for 22 solutes with respect to dopamine—D(dopamine), M(3-methoxytramine hydrochloride), Ad(adenine) S(serotonin), Ar(arterenol), T(tryptamine), E(epinephrine), Ua(uric acid), R(riboflavin), Aa(ascorbic acid), Ct(catechol), P(phenol), Dg(DOPEG), H(homovanillic acid), V(vanillylmandelic acid), Dc(DOPAC), Hd(histidine), Tp(tryptophan), Da(DOPA), Ty(tyrosine), Ce(cysteine), C(cystine) and I(3-indolylacetic acid). (The data for the uncoated sensors were obtained from Ref. [5].)

a mean ratio of calculated to experimental response of 1.064 with a standard deviation of 0.135. The component sensitivity in a mixture was higher than the corresponding pure component sensitivity for all the components. The increase is in the order of decreasing molecular weight of the components: dopamine (MW 189.6) increased by 5.4%, tyrosine (MW 181.2)

Table 2
Calibration and relative selectivity of apple tissue powder sensor

| Solute | Linear range (μM) | Sensitivity (μA/μM) | % relative selectivity coated (uncoated) |
|---|---|---|---|
| Dopamine | 4–79.9 | 0.0169 | 100.0(100.0) |
| Arterenol | 4–95.0 | 0.0019 | 11.6(51.7) |
| Histidine | 4–60.0 | 0.0018 | 10.8(12.0) |
| Tyrosine | 4–40.3 | 0.0018 | 10.5(49.8) |
| Cysteine | 4–23.7 | 0.0012 | 7.4(22.8) |
| DOPAC | 4–40.2 | 0.0005 | 3.0(72.0) |

by 32.3%, arterenol (MW 169.2) by 71.7% and histidine (MW 155.2) by 107.8%. Solute diffusing in the same direction mutually increased their mass transfer rates and the increase was higher with smaller molecules. This would, therefore, explain the mutual increase in the response and sensitivity of the components in the mixture. The increase may also be attributed to the difference in the affinity of the Nafion film for the various components depending on their positivity at the operating pH.

## 4. Conclusions

Four Nafion-coated tissue powder sensors were fabricated using tissues of potato, banana, mushroom and apple which have been pretreated to remove the water-soluble biodegradable solutes contained in the tissue. They showed good stability, reproducibility and service life span of over 200 days involving 300–500 measurements compared to the few days life span of untreated tissue and purified polyphenolase sensors. The sensors were stored in phosphate buffer at room temperature unlike the raw tissue sensors which have to be stored at 4 to −10 °C. Overlaying the sensors with a Nafion coating considerably increased sensor selectivity for dopamine and decreased the number of interferents among the 22 solutes examined in this study by effectively precluding the neutral and anionic solutes from entering the biofilm. This further reduced the contamination and deactivation of the enzymes in the tissue. Apple tissue powder sensor showed the least number of interferents. Its response to a mixture of dopamine and three other strong interferents (arterenol, histidine and tyrosine) was linear with respect to the concentration of the components. The component sensitivity of all the components in the mixture was higher than the respective single component sensitivity. The long service life span of these sensors and the effectiveness of Nafion coating in reducing interference of most of the solutes have enhanced their potential applications in clinical analysis of dopamine in physiological fluids and as a detector for liquid chromatograph.

## Acknowledgements

The authors gratefully acknowledge the funding of the sensor project by the National University of Singapore and the award of a research scholarship to Y. Chen for her graduate study.

## References

[1] J.K. Palmer, Plant Physiol., 38 (1963) 508.
[2] T.C. Tan and Y. Chen, Int. J. Chem. Kinetics, 24 (1992) 1023.
[3] R. Chirakal, E.S. Garnett, G.J. Schrobilgen, C. Nahmias and G. Firnau, Chem. Br., 27 (1991) 47.
[4] T.C. Tan and Y. Chen, Sensors Actuators B, 17 (1994) 101.
[5] Y. Chen and T.C. Tan, Sensors Actuators B, in press.
[6] Y. Chen and T.C. Tan, Biosensors Bioelectron., 9 (1994) 401.
[7] J.S. Sidwell and G.A. Rechnitz, Biotechnol. Lett., 7 (1985) 419.
[8] J. Wang and M.S. Lin, Anal. Chem., 60 (1988) 1545.
[9] F. Mazzei, F. Botrè, M. Lanzi, G. Lorenti, F. Porcelli and C. Botrè, Sensors Actuators B, 7 (1992) 427.
[10] M.V. Deshpande and E.A.H. Hall, Biosensors Bioelectron., 5 (1990) 431.
[11] J. Wang and L.D. Hutchins, Anal. Chem., 57 (1985) 1536.
[12] J. Wang, T. Golden and P. Tuzhi, Anal. Chem., 59 (1987) 740.
[13] J. Wang and P. Tuzhi, Anal. Chem., 58 (1986) 3257.
[14] M.A. Arnold and G.A. Rechnitz, Anal. Chem., 53 (1981) 515.
[15] F. Alhaique, A. Memoli, E. Santucci and F. Olana, J. Membr Sci., 45 (1989) 55.

[16] H.L. Yeager, in A. Eisenberg and H.L. Yeager (Eds.), Perfluorinated Ionomer Membrane, American Chemical Society, Washington, DC., 1982, p. 42.
[17] P.W. Carr, Anal. Chem., 47 (1977) 799.
[18] C.R. Tillyer and P.T. Gobin, Biosensors Bioelectron., 6 (1991) 569.
[19] G.A. Gerhardt, A.F. Oke, G. Nagy, B. Moghaddam and R.N. Adams, Brain Res., 29 (1984) 390.
[20] D.J. Harrison, R.F.B. Turner and H.P. Baltes, Anal. Chem., 60 (1988) 2002.

ELSEVIER

Talanta 42 (1995) 1189–1193

Talanta

# Book reviews

***Information Theory in Analytical Chemistry***, by K. Eckschlager and K. Danzer, Wiley, Chichester, 1994, xv + 275 pp., £54.00. ISBN 0-471-59507-1.

Imagine, if you will, a book on relativity that does not mention Einstein. It would be hard to take very seriously as a work of authority. Eckschlager and Danzer's book is concerned with information theory, a subject which was pioneered by Claude Shannon and developed in numerous areas of physics by Ed Jaynes. These men are the giants of the field, and indeed, major contributors to 20th century science, but Shannon receives only a passing reference, and Jaynes is ignored altogether! This sets the tone for what I regard as a very unsatisfactory book.

It is unsatisfactory first of all because of a tendency to gloss over key issues. For example, the use of entropy in an information theory context is still a subject of controversy, yet this problem is completely ignored: "*Entropy is a universally valid measure of uncertainty, disorder, irrespective of the system whose order is characterised by it*" state the authors. This is their belief, but at the very least there should be some references to the literature here from which the reader can explore this rich seam of controversy.

Bayes' theorem (called rather quaintly "*Bayes' relation*" in the book) is a key ingredient in the use of information theory. It enables you to code into the calculations suitable prior knowledge of the parameters being sought. It too gets scant attention. This is another unsatisfactory tendency; information theory is presented as an isolated edifice. There are numerous discussions of increases in information content when certain mathematical techniques are used, but often it is just traditional statistics in another guise, when what is needed is a Bayesian method in which the entropy functional is used in conjunction with Bayes' theorem.

The reader will have noticed that the English of the quotation in paragraph two above is rather stilted; this is characteristic of the whole book. Sentences are not grammatically incorrect in general, but they are rather unusual in their grammar and use of words; the text does not flow easily. So if you are an analytical chemist looking for a useful book on information theory, this is not the one, but if you do purchase it be aware that the method is much more wide ranging and intellectually stimulating than this.

C.J. Gilmore

***Quality Assurance for Biopharmaceuticals***, by J.F. Huxsoll, Wiley, New York, 1994, 206 pp., £49.50. ISBN 0-471-03656-0.

This book is an excellent, instructive, concise, easily readable, reference source on quality assurance (QA). It deals with general basic principles and the particular problems associated with manufacture and control to assure the quality of biopharmaceuticals. Testing, documentation, labeling, validation, audit, training, safety and waste management — all have their place in the book. The frequent use of lists summarising the requirements for, e.g. QC, documentation, validation, etc., and lists explaining the multitude of abbreviations used in QA literature is to be commended. All who work in QA know that statistical analysis is required. The relevant chapter represents a basic, concise guide to all the statistical methods required in the control of QA processes. For those with an interest in marketing biopharmaceutical products in the USA, Europe and Japan, the last three chapters in the book deal with the regulatory issues and variations in requirements between these three major markets.

All eleven chapters in the book are written in the same concise style. All contain appropriate references at the end of each chapter for further reading. A minor criticism, from the point of the reader outside the USA, is that the book

ELSEVIER

Talanta 42 (1995) 1189–1193

Talanta

# Book reviews

***Information Theory in Analytical Chemistry***, by K. Eckschlager and K. Danzer, Wiley, Chichester, 1994, xv + 275 pp., £54.00. ISBN 0-471-59507-1.

Imagine, if you will, a book on relativity that does not mention Einstein. It would be hard to take very seriously as a work of authority. Eckschlager and Danzer's book is concerned with information theory, a subject which was pioneered by Claude Shannon and developed in numerous areas of physics by Ed Jaynes. These men are the giants of the field, and indeed, major contributors to 20th century science, but Shannon receives only a passing reference, and Jaynes is ignored altogether! This sets the tone for what I regard as a very unsatisfactory book.

It is unsatisfactory first of all because of a tendency to gloss over key issues. For example, the use of entropy in an information theory context is still a subject of controversy, yet this problem is completely ignored: "*Entropy is a universally valid measure of uncertainty, disorder, irrespective of the system whose order is characterised by it*" state the authors. This is their belief, but at the very least there should be some references to the literature here from which the reader can explore this rich seam of controversy.

Bayes' theorem (called rather quaintly "*Bayes' relation*" in the book) is a key ingredient in the use of information theory. It enables you to code into the calculations suitable prior knowledge of the parameters being sought. It too gets scant attention. This is another unsatisfactory tendency; information theory is presented as an isolated edifice. There are numerous discussions of increases in information content when certain mathematical techniques are used, but often it is just traditional statistics in another guise, when what is needed is a Bayesian method in which the entropy functional is used in conjunction with Bayes' theorem.

The reader will have noticed that the English of the quotation in paragraph two above is rather stilted; this is characteristic of the whole book. Sentences are not grammatically incorrect in general, but they are rather unusual in their grammar and use of words; the text does not flow easily. So if you are an analytical chemist looking for a useful book on information theory, this is not the one, but if you do purchase it be aware that the method is much more wide ranging and intellectually stimulating than this.

C.J. Gilmore

***Quality Assurance for Biopharmaceuticals***, by J.F. Huxsoll, Wiley, New York, 1994, 206 pp., £49.50. ISBN 0-471-03656-0.

This book is an excellent, instructive, concise, easily readable, reference source on quality assurance (QA). It deals with general basic principles and the particular problems associated with manufacture and control to assure the quality of biopharmaceuticals. Testing, documentation, labeling, validation, audit, training, safety and waste management — all have their place in the book. The frequent use of lists summarising the requirements for, e.g. QC, documentation, validation, etc., and lists explaining the multitude of abbreviations used in QA literature is to be commended. All who work in QA know that statistical analysis is required. The relevant chapter represents a basic, concise guide to all the statistical methods required in the control of QA processes. For those with an interest in marketing biopharmaceutical products in the USA, Europe and Japan, the last three chapters in the book deal with the regulatory issues and variations in requirements between these three major markets.

All eleven chapters in the book are written in the same concise style. All contain appropriate references at the end of each chapter for further reading. A minor criticism, from the point of the reader outside the USA, is that the book

is aimed at a USA public and thus the text uses USA legislative requirements for illustrative examples.

R.R. Moody

***Pharmaceutical and Biomedical Applications of Liquid Chromatography***, edited by C.M. Riley, W.J. Lough and I.W. Wainer, Elsevier, Oxford, 1994, x + 379 pp., £85.00. IBSN 0-08-041009-X.

As is outlined in the Introduction, this text is a sequel to a previous volume edited by I.W. Wainer on Liquid Chromatography in Pharmaceutical Development. As such it is a valuable addition to the literature in this area since it deals with developments in LC which have been developed or which have assumed greater importance since the publication of the earlier book.

The book is divided into four parts, each dealing with different aspects of a general area. Part 1 deals with two aspects of on-column separations namely the very general amine-containing compounds such as primary amines, amino acids and peptides and also methods of obtaining fast separations of enantiomers. The chapter on capillary electrophoresis with which this part begins could usefully have been omitted. Half of it is devoted to standard electrophoretic theory and the remainder is a very general overview which requires to be dealt with in much greater detail to be useful.

Part 2 consists of four chapters each dealing with a topic representing a variant on sample pretreatment. The chapter on solid phase extraction, while short, is a good general account of the process. The chapter on on-line microdialysis pretreatment combines good treatment of theoretical considerations with numerous specific applications of the technique. This part of the text concludes with a short but readable account of column switching as applied to chiral separations.

The third part of the book focuses on the use of liquid chromatography as a preparative method. One chapter deals generally with the problems of obtaining pure samples of drugs for evaluation studies using liquid chromatography. The other is concerned specifically with the purification of naturally occurring biomolecules. This chapter reviews different chromatographic modes of operation as well as discussing the different retention mechanisms which have been employed for proteins and peptides.

The concluding part contains two chapters each concerned with the validation of assays based on liquid chromatography. The first of these, Chapter 10, deals with the strategic aspects of developing a separation and this is followed with a short account of validation parameters. Here the separate validation requirements for main component and impurity assay are nicely distinguished. The last chapter is a much more in-depth account of assay validation including useful flow charts and necessary statistical relationships.

Overall this is an excellent companion volume to the previous Liquid Chromatography in Pharmaceutical Development. Most practising chromatographers will find chapters directly relevent to their own current interests. In addition, the coverage of the developments which have taken place over the last few years is so well balanced that all of us will find this book useful in obtaining at least a nodding acquaintanceship with areas outside our direct interest as well as providing a useful range of references for further reading.

R.B. Taylor

***Reviews on Analytical Chemistry — Euroanalysis VIII***, edited by D. Littlejohn and D. Thorburn Burns, The Royal Society of Chemistry, Cambridge, 1994, x + 365pp., £75.00. ISBN 0-85186-982-3.

The compilation of papers which go together to make this book represents 25 of the invited lectures presented at the Euroanalysis VIII conference held in Edinburgh in 1993. They consist of a very diverse range of subjects and vary in their style from reviews to more research-based papers. The editors have attempted to give some structure to the chapters, but the text covers a wide range of subject areas and by its nature lacks cohesion. Readers are advised to look closely at the contents of the book as many major areas of analytical science were obviously not presented as papers at the conference. Nevertheless, given that the text was prepared as a summary of the papers at Euroanalysis VII, it clearly achieves its aim, with a set of well written and easy-to-read papers. I would question, however, the review aspects of some of the chapters and this may be a misleading feature of the title.

is aimed at a USA public and thus the text uses USA legislative requirements for illustrative examples.

R.R. Moody

***Pharmaceutical and Biomedical Applications of Liquid Chromatography***, edited by C.M. Riley, W.J. Lough and I.W. Wainer, Elsevier, Oxford, 1994, x + 379 pp., £85.00. IBSN 0-08-041009-X.

As is outlined in the Introduction, this text is a sequel to a previous volume edited by I.W. Wainer on Liquid Chromatography in Pharmaceutical Development. As such it is a valuable addition to the literature in this area since it deals with developments in LC which have been developed or which have assumed greater importance since the publication of the earlier book.

The book is divided into four parts, each dealing with different aspects of a general area. Part 1 deals with two aspects of on-column separations namely the very general amine-containing compounds such as primary amines, amino acids and peptides and also methods of obtaining fast separations of enantiomers. The chapter on capillary electrophoresis with which this part begins could usefully have been omitted. Half of it is devoted to standard electrophoretic theory and the remainder is a very general overview which requires to be dealt with in much greater detail to be useful.

Part 2 consists of four chapters each dealing with a topic representing a variant on sample pretreatment. The chapter on solid phase extraction, while short, is a good general account of the process. The chapter on on-line microdialysis pretreatment combines good treatment of theoretical considerations with numerous specific applications of the technique. This part of the text concludes with a short but readable account of column switching as applied to chiral separations.

The third part of the book focuses on the use of liquid chromatography as a preparative method. One chapter deals generally with the problems of obtaining pure samples of drugs for evaluation studies using liquid chromatography. The other is concerned specifically with the purification of naturally occurring biomolecules. This chapter reviews different chromatographic modes of operation as well as discussing the different retention mechanisms which have been employed for proteins and peptides.

The concluding part contains two chapters each concerned with the validation of assays based on liquid chromatography. The first of these, Chapter 10, deals with the strategic aspects of developing a separation and this is followed with a short account of validation parameters. Here the separate validation requirements for main component and impurity assay are nicely distinguished. The last chapter is a much more in-depth account of assay validation including useful flow charts and necessary statistical relationships.

Overall this is an excellent companion volume to the previous Liquid Chromatography in Pharmaceutical Development. Most practising chromatographers will find chapters directly relevent to their own current interests. In addition, the coverage of the developments which have taken place over the last few years is so well balanced that all of us will find this book useful in obtaining at least a nodding acquaintanceship with areas outside our direct interest as well as providing a useful range of references for further reading.

R.B. Taylor

***Reviews on Analytical Chemistry — Euroanalysis VIII***, edited by D. Littlejohn and D. Thorburn Burns, The Royal Society of Chemistry, Cambridge, 1994, x + 365pp., £75.00. ISBN 0-85186-982-3.

The compilation of papers which go together to make this book represents 25 of the invited lectures presented at the Euroanalysis VIII conference held in Edinburgh in 1993. They consist of a very diverse range of subjects and vary in their style from reviews to more research-based papers. The editors have attempted to give some structure to the chapters, but the text covers a wide range of subject areas and by its nature lacks cohesion. Readers are advised to look closely at the contents of the book as many major areas of analytical science were obviously not presented as papers at the conference. Nevertheless, given that the text was prepared as a summary of the papers at Euroanalysis VII, it clearly achieves its aim, with a set of well written and easy-to-read papers. I would question, however, the review aspects of some of the chapters and this may be a misleading feature of the title.

is aimed at a USA public and thus the text uses USA legislative requirements for illustrative examples.

R.R. Moody

***Pharmaceutical and Biomedical Applications of Liquid Chromatography***, edited by C.M. Riley, W.J. Lough and I.W. Wainer, Elsevier, Oxford, 1994, x + 379 pp., £85.00. IBSN 0-08-041009-X.

As is outlined in the Introduction, this text is a sequel to a previous volume edited by I.W. Wainer on Liquid Chromatography in Pharmaceutical Development. As such it is a valuable addition to the literature in this area since it deals with developments in LC which have been developed or which have assumed greater importance since the publication of the earlier book.

The book is divided into four parts, each dealing with different aspects of a general area. Part 1 deals with two aspects of on-column separations namely the very general amine-containing compounds such as primary amines, amino acids and peptides and also methods of obtaining fast separations of enantiomers. The chapter on capillary electrophoresis with which this part begins could usefully have been omitted. Half of it is devoted to standard electrophoretic theory and the remainder is a very general overview which requires to be dealt with in much greater detail to be useful.

Part 2 consists of four chapters each dealing with a topic representing a variant on sample pretreatment. The chapter on solid phase extraction, while short, is a good general account of the process. The chapter on on-line microdialysis pretreatment combines good treatment of theoretical considerations with numerous specific applications of the technique. This part of the text concludes with a short but readable account of column switching as applied to chiral separations.

The third part of the book focuses on the use of liquid chromatography as a preparative method. One chapter deals generally with the problems of obtaining pure samples of drugs for evaluation studies using liquid chromatography. The other is concerned specifically with the purification of naturally occurring biomolecules. This chapter reviews different chromatographic modes of operation as well as discussing the different retention mechanisms which have been employed for proteins and peptides.

The concluding part contains two chapters each concerned with the validation of assays based on liquid chromatography. The first of these, Chapter 10, deals with the strategic aspects of developing a separation and this is followed with a short account of validation parameters. Here the separate validation requirements for main component and impurity assay are nicely distinguished. The last chapter is a much more in-depth account of assay validation including useful flow charts and necessary statistical relationships.

Overall this is an excellent companion volume to the previous Liquid Chromatography in Pharmaceutical Development. Most practising chromatographers will find chapters directly relevent to their own current interests. In addition, the coverage of the developments which have taken place over the last few years is so well balanced that all of us will find this book useful in obtaining at least a nodding acquaintanceship with areas outside our direct interest as well as providing a useful range of references for further reading.

R.B. Taylor

***Reviews on Analytical Chemistry — Euroanalysis VIII***, edited by D. Littlejohn and D. Thorburn Burns, The Royal Society of Chemistry, Cambridge, 1994, x + 365pp., £75.00. ISBN 0-85186-982-3.

The compilation of papers which go together to make this book represents 25 of the invited lectures presented at the Euroanalysis VIII conference held in Edinburgh in 1993. They consist of a very diverse range of subjects and vary in their style from reviews to more research-based papers. The editors have attempted to give some structure to the chapters, but the text covers a wide range of subject areas and by its nature lacks cohesion. Readers are advised to look closely at the contents of the book as many major areas of analytical science were obviously not presented as papers at the conference. Nevertheless, given that the text was prepared as a summary of the papers at Euroanalysis VII, it clearly achieves its aim, with a set of well written and easy-to-read papers. I would question, however, the review aspects of some of the chapters and this may be a misleading feature of the title.

Chapter 1 gives a historical perspective of Scottish analytical chemistry and contains many facts, elucidating many of the relationships between alchemy, scientific chemistry and analytical science. Individual sections describe the life and work of some notable chemists and contain many interesting anecdotes. With the growing importance of validation and data quality it is not surprising that papers 2 and 3 focus on this subject. *Traceability to the Mole: A New Initiative by CIPM* might not seem a wildly attractive title to the analyst but the text is an excellent review on calibration techniques mainly using isotope dilution mass spectrometry. The third paper is a very provocative view of the quality of analytical methods and demonstrates an interesting analogy to the presence of towers on the Dutch landscape. The next two papers focus on initiatives to improve the quality of food analysis and in particular the regulatory requirements. Paper 6 looks at water quality standards, identifying the good and the bad guys and states what effluents should or should not contain. Factors that influence elemental species in sediments form the basis of a detailed review whilst the speciation of organic sulphur in hydrocarbons is given a very thorough discussion in a complimentary paper. The final four papers in the book deal with clinical applications of analytical science, mainly the use of capillary electrophoresis as a diagnostic tool, magnesium determinations, the use of stable isotopes in clinical studies and assays based on antibody screening. The remaining 12 papers tend to be orientated mainly towards techniques rather than applications and include a review on plasma mass spectrometry and the use of mass spectrometry in process analysis. These topics based papers continue with laser induced molecular luminescence, a most interesting review of high resolution imaging techniques, neural networks including the use of fuzzy logic, electrochemical applications including microelectrodes, modified electrodes for sensor and in-vivo monitoring, and two reviews on flow analysis. The papers vary in length but are very readable taking anything from 20 to 40 minutes to complete any one article. Each paper is packed with information and high quality tables and diagrams can be found throughout the text. There is a limited index for reference purposes, but the real value of the book does not lie in its reference capability, but in the fact that it offers a snapshot 'state of the art' view on particular topics and how they are developing. As indicated earlier many of the more traditional aspects of analytical chemistry are not covered in the book, but those included are recommended to the reader who wishes to consolidate their current knowledge or just browse into other areas of analytical methodology.

S.J. Haswell

***Handbook of Surfactants***, 2nd ed., by M.R. Porter, Blackie, London, 1994, xii + 324 pp., £75.00. ISBN 0-7514-0170-6.

As implied in the title, this is a practical book aimed at those who work with surface-active agents. Compared to the first edition the book has been updated and extended and the chapters on surfactant theory and polymeric surfactants have been completely rewritten.

Following a short introduction, a general approach to using surfactants in formulations is given. The author's experience is very much in evidence both here and in the following chapter on information sources where his opinions on certain published works and databases are confidently stated, e.g. "By far the best book on. . . ", "Good but more theoretical than practical", and "Does not quite live up to title".

There then follows a comprehensive chapter (63 pp.) on surfactant theory which is superbly illustrated with 59 diagrams and contains many up-to-date references from the 1990s. This chapter presents a very good, non-mathematical description of surfactant theory, with details such as the definition of HLB number and the experimental observation (by light scattering) that there are about 71 sodium lauryl sulphate molecules in a micelle at 23 °C.

The following four chapters, which make up more than half of the book, are devoted to the four main classes of surfactant: anionic, nonionic, cationic and amphoteric. These chapters start with an introduction and then the main types are discussed under sub-headings such as Nomenclature, Description, General properties, Applications, and Specification. As expected, the chapter on anionics (70 pp.) is dominated by the sulphates and sulphonates but the carboxylates, isethionates, phosphates, sulphosuccinates, sulphosuccinamates and taurates are also mentioned. A total of 15 sub-divisions are made to cover the nonionic surfactants (79 pp.) with the Tweens and Spans (Atlas trade names) discussed under Sorbitan derivatives. The chemistry of ethoxylation is also given in this chapter.

Chapter 1 gives a historical perspective of Scottish analytical chemistry and contains many facts, elucidating many of the relationships between alchemy, scientific chemistry and analytical science. Individual sections describe the life and work of some notable chemists and contain many interesting anecdotes. With the growing importance of validation and data quality it is not surprising that papers 2 and 3 focus on this subject. *Traceability to the Mole: A New Initiative by CIPM* might not seem a wildly attractive title to the analyst but the text is an excellent review on calibration techniques mainly using isotope dilution mass spectrometry. The third paper is a very provocative view of the quality of analytical methods and demonstrates an interesting analogy to the presence of towers on the Dutch landscape. The next two papers focus on initiatives to improve the quality of food analysis and in particular the regulatory requirements. Paper 6 looks at water quality standards, identifying the good and the bad guys and states what effluents should or should not contain. Factors that influence elemental species in sediments form the basis of a detailed review whilst the speciation of organic sulphur in hydrocarbons is given a very thorough discussion in a complimentary paper. The final four papers in the book deal with clinical applications of analytical science, mainly the use of capillary electrophoresis as a diagnostic tool, magnesium determinations, the use of stable isotopes in clinical studies and assays based on antibody screening. The remaining 12 papers tend to be orientated mainly towards techniques rather than applications and include a review on plasma mass spectrometry and the use of mass spectrometry in process analysis. These topics based papers continue with laser induced molecular luminescence, a most interesting review of high resolution imaging techniques, neural networks including the use of fuzzy logic, electrochemical applications including microelectrodes, modified electrodes for sensor and in-vivo monitoring, and two reviews on flow analysis. The papers vary in length but are very readable taking anything from 20 to 40 minutes to complete any one article. Each paper is packed with information and high quality tables and diagrams can be found throughout the text. There is a limited index for reference purposes, but the real value of the book does not lie in its reference capability, but in the fact that it offers a snapshot 'state of the art' view on particular topics and how they are developing. As indicated earlier many of the more traditional aspects of analytical chemistry are not covered in the book, but those included are recommended to the reader who wishes to consolidate their current knowledge or just browse into other areas of analytical methodology.

S.J. Haswell

***Handbook of Surfactants***, 2nd ed., by M.R. Porter, Blackie, London, 1994, xii + 324 pp., £75.00. ISBN 0-7514-0170-6.

As implied in the title, this is a practical book aimed at those who work with surface-active agents. Compared to the first edition the book has been updated and extended and the chapters on surfactant theory and polymeric surfactants have been completely rewritten.

Following a short introduction, a general approach to using surfactants in formulations is given. The author's experience is very much in evidence both here and in the following chapter on information sources where his opinions on certain published works and databases are confidently stated, e.g. "By far the best book on. . . ", "Good but more theoretical than practical", and "Does not quite live up to title".

There then follows a comprehensive chapter (63 pp.) on surfactant theory which is superbly illustrated with 59 diagrams and contains many up-to-date references from the 1990s. This chapter presents a very good, non-mathematical description of surfactant theory, with details such as the definition of HLB number and the experimental observation (by light scattering) that there are about 71 sodium lauryl sulphate molecules in a micelle at 23 °C.

The following four chapters, which make up more than half of the book, are devoted to the four main classes of surfactant: anionic, nonionic, cationic and amphoteric. These chapters start with an introduction and then the main types are discussed under sub-headings such as Nomenclature, Description, General properties, Applications, and Specification. As expected, the chapter on anionics (70 pp.) is dominated by the sulphates and sulphonates but the carboxylates, isethionates, phosphates, sulphosuccinates, sulphosuccinamates and taurates are also mentioned. A total of 15 sub-divisions are made to cover the nonionic surfactants (79 pp.) with the Tweens and Spans (Atlas trade names) discussed under Sorbitan derivatives. The chemistry of ethoxylation is also given in this chapter.

The short chapter on cationic surfactants (10 pp.) briefly discusses quaternary ammonium, amine and imidazoline salts and I recognised Cetrimide BP (an antiseptic detergent) as being in this category. Amphoterics (18 pp.) covers betaines, glycinates and amino propionates and mentions their mildness on skin and mucous membrane compared with other types of surfactants. A further short chapter is concerned with speciality surfactants and includes Bolaform surfactants (polar groups at both ends of the hydrophobic group) and Gemini surfactants (two surfactant molecules linked with an organic spacer via the two hydrophilic groups). The final chapter covers polymeric surfactants and is followed by two appendices — the first on names of hydrophobes and average composition of fats and oils and the second on the all important ecological and toxicity requirements.

Overall, I found this book very detailed. Having read it from cover-to-cover I find it difficult to retain all the information offered and I will have to revert to using it as intended, i.e. as a handbook. It includes much practical information such as details of surfactant mixtures and compatibilities and the theory and practical chapters compliment each other extremely well. It will be a very worthwhile purchase for all those involved with surfactants.

P.J. Cox

***Principles and Applications of Electrochemistry***, by D.R. Crow, Chapman and Hall, London, 1994, xi + 282pp., Softback, £16.99. ISBN 0-7514-0168-4.

This well known text is now into its 4th edition. It has undergone extensive revision but has maintained a traditional approach in bringing the text up-to-date with the content requirements of modern undergraduate courses in chemistry. The book is divided into two parts. Part I (153 pp.) covers the principles of ionic interactions, ionic equilibria, conductivity, interfacial phenomena, electrochemical cells and electrode processes. The author's teaching experience shows in the clear and lucid way in which the fundamental principles are presented and appropriately illustrated with suitable diagrams, tables or problems. Part II (98 pp.) gives the applications which have as their basis the theoretical considerations given in Part I. These include equilibrium constant determinations by both conductivity and pH measurement, polarography, amperometric titration and coulometric methods. The last but one chapter gives a brief overview of electrochemical sensors and in the final chapter, the exploitation of electrode processes, e.g. as sources of energy in industry, is explained and exemplified.

As an aid to understanding the text, problems are given at the end of each chapter and answers in an Appendix. Each chapter also has suggestions for further reading. In this day and age where self study is becoming more important a text such as this is recommended.

R.R. Moody

***Analysis of Addictive and Misused Drugs***, edited by J.A. Adamovics, Dekker, New York, 1994, viii + 671pp., US$195.00. ISBN 0-8247-9238-6.

Approximately half of this text consists of separate chapters devoted to individual analytical techniques used for the quantification of drugs. The remainder of the book, some 300 pages, consists of an appendix in the form of a reference table of analytical methods for approximately 400 compounds listed as controlled substances by the U.S. Drug Enforcement Agency or as banned drugs by the International Olympic Committee. The data provided in this appendix include, for each compound, the matrix, analytical technique, any sample pretreatment required, stationary and mobile phases for chromatographic analyses (which constitute the vast majority of the methods cited), detection method, comments including additional references and original literature reference.

This section will be useful as a source of analytical information for those requiring to undertake analysis of such durgs in that it assembles information into a concise and useable format. While this appendix is not exhaustive, it does serve the more general purpose of indicating the relative degree of use of different analytical techniques in this field. In this sense it shows current usage of the different techniques discussed in the individual chapters. It is stated in the text that the purpose of the appendix is to complement the material in individual chapters. It seems approproate, there-

The short chapter on cationic surfactants (10 pp.) briefly discusses quaternary ammonium, amine and imidazoline salts and I recognised Cetrimide BP (an antiseptic detergent) as being in this category. Amphoterics (18 pp.) covers betaines, glycinates and amino propionates and mentions their mildness on skin and mucous membrane compared with other types of surfactants. A further short chapter is concerned with speciality surfactants and includes Bolaform surfactants (polar groups at both ends of the hydrophobic group) and Gemini surfactants (two surfactant molecules linked with an organic spacer via the two hydrophilic groups). The final chapter covers polymeric surfactants and is followed by two appendices — the first on names of hydrophobes and average composition of fats and oils and the second on the all important ecological and toxicity requirements.

Overall, I found this book very detailed. Having read it from cover-to-cover I find it difficult to retain all the information offered and I will have to revert to using it as intended, i.e. as a handbook. It includes much practical information such as details of surfactant mixtures and compatibilities and the theory and practical chapters compliment each other extremely well. It will be a very worthwhile purchase for all those involved with surfactants.

P.J. Cox

***Principles and Applications of Electrochemistry***, by D.R. Crow, Chapman and Hall, London, 1994, xi + 282pp., Softback, £16.99. ISBN 0-7514-0168-4.

This well known text is now into its 4th edition. It has undergone extensive revision but has maintained a traditional approach in bringing the text up-to-date with the content requirements of modern undergraduate courses in chemistry. The book is divided into two parts. Part I (153 pp.) covers the principles of ionic interactions, ionic equilibria, conductivity, interfacial phenomena, electrochemical cells and electrode processes. The author's teaching experience shows in the clear and lucid way in which the fundamental principles are presented and appropriately illustrated with suitable diagrams, tables or problems. Part II (98 pp.) gives the applications which have as their basis the theoretical considerations given in Part I. These include equilibrium constant determinations by both conductivity and pH measurement, polarography, amperometric titration and coulometric methods. The last but one chapter gives a brief overview of electrochemical sensors and in the final chapter, the exploitation of electrode processes, e.g. as sources of energy in industry, is explained and exemplified.

As an aid to understanding the text, problems are given at the end of each chapter and answers in an Appendix. Each chapter also has suggestions for further reading. In this day and age where self study is becoming more important a text such as this is recommended.

R.R. Moody

***Analysis of Addictive and Misused Drugs***, edited by J.A. Adamovics, Dekker, New York, 1994, viii + 671pp., US$195.00. ISBN 0-8247-9238-6.

Approximately half of this text consists of separate chapters devoted to individual analytical techniques used for the quantification of drugs. The remainder of the book, some 300 pages, consists of an appendix in the form of a reference table of analytical methods for approximately 400 compounds listed as controlled substances by the U.S. Drug Enforcement Agency or as banned drugs by the International Olympic Committee. The data provided in this appendix include, for each compound, the matrix, analytical technique, any sample pretreatment required, stationary and mobile phases for chromatographic analyses (which constitute the vast majority of the methods cited), detection method, comments including additional references and original literature reference.

This section will be useful as a source of analytical information for those requiring to undertake analysis of such durgs in that it assembles information into a concise and useable format. While this appendix is not exhaustive, it does serve the more general purpose of indicating the relative degree of use of different analytical techniques in this field. In this sense it shows current usage of the different techniques discussed in the individual chapters. It is stated in the text that the purpose of the appendix is to complement the material in individual chapters. It seems approproate, there-

The short chapter on cationic surfactants (10 pp.) briefly discusses quaternary ammonium, amine and imidazoline salts and I recognised Cetrimide BP (an antiseptic detergent) as being in this category. Amphoterics (18 pp.) covers betaines, glycinates and amino propionates and mentions their mildness on skin and mucous membrane compared with other types of surfactants. A further short chapter is concerned with speciality surfactants and includes Bolaform surfactants (polar groups at both ends of the hydrophobic group) and Gemini surfactants (two surfactant molecules linked with an organic spacer via the two hydrophilic groups). The final chapter covers polymeric surfactants and is followed by two appendices — the first on names of hydrophobes and average composition of fats and oils and the second on the all important ecological and toxicity requirements.

Overall, I found this book very detailed. Having read it from cover-to-cover I find it difficult to retain all the information offered and I will have to revert to using it as intended, i.e. as a handbook. It includes much practical information such as details of surfactant mixtures and compatibilities and the theory and practical chapters compliment each other extremely well. It will be a very worthwhile purchase for all those involved with surfactants.

P.J. Cox

***Principles and Applications of Electrochemistry***, by D.R. Crow, Chapman and Hall, London, 1994, xi + 282pp., Softback, £16.99. ISBN 0-7514-0168-4.

This well known text is now into its 4th edition. It has undergone extensive revision but has maintained a traditional approach in bringing the text up-to-date with the content requirements of modern undergraduate courses in chemistry. The book is divided into two parts. Part I (153 pp.) covers the principles of ionic interactions, ionic equilibria, conductivity, interfacial phenomena, electrochemical cells and electrode processes. The author's teaching experience shows in the clear and lucid way in which the fundamental principles are presented and appropriately illustrated with suitable diagrams, tables or problems. Part II (98 pp.) gives the applications which have as their basis the theoretical considerations given in Part I. These include equilibrium constant determinations by both conductivity and pH measurement, polarography, amperometric titration and coulometric methods. The last but one chapter gives a brief overview of electrochemical sensors and in the final chapter, the exploitation of electrode processes, e.g. as sources of energy in industry, is explained and exemplified.

As an aid to understanding the text, problems are given at the end of each chapter and answers in an Appendix. Each chapter also has suggestions for further reading. In this day and age where self study is becoming more important a text such as this is recommended.

R.R. Moody

***Analysis of Addictive and Misused Drugs***, edited by J.A. Adamovics, Dekker, New York, 1994, viii + 671pp., US$195.00. ISBN 0-8247-9238-6.

Approximately half of this text consists of separate chapters devoted to individual analytical techniques used for the quantification of drugs. The remainder of the book, some 300 pages, consists of an appendix in the form of a reference table of analytical methods for approximately 400 compounds listed as controlled substances by the U.S. Drug Enforcement Agency or as banned drugs by the International Olympic Committee. The data provided in this appendix include, for each compound, the matrix, analytical technique, any sample pretreatment required, stationary and mobile phases for chromatographic analyses (which constitute the vast majority of the methods cited), detection method, comments including additional references and original literature reference.

This section will be useful as a source of analytical information for those requiring to undertake analysis of such durgs in that it assembles information into a concise and useable format. While this appendix is not exhaustive, it does serve the more general purpose of indicating the relative degree of use of different analytical techniques in this field. In this sense it shows current usage of the different techniques discussed in the individual chapters. It is stated in the text that the purpose of the appendix is to complement the material in individual chapters. It seems approproate, there-

fore, that each of the analytical methods in these chapters is treated from a different standpoint.

In Chapter 1 the principles of enzyme immunoassays are covered together with some of the commercially available technology while in Chapter 2 biosensors based on enzyme reactions and bioaffinity are described in general terms. Chapter 3 is an account of a single commerical TLC system. Chapter 4 provides considerable information on the general principles of obtaining LC separations including choice of stationary and mobile phase composition. Numerous applications of these to forensic situations are described. The relative state of use of capillary electrophoresis is shown in Chapter 5 in that the majority of information is concerned with explaining the principles of separation in the various modes of CE and limiting examples to essentially bulk material. Chapter 6 is an amalagam of TLC and coupled GC–MS. These appear to have been included in a single chapter in order to describe the principle of initial screening for abused drugs in biological fluids and subsequent confirmation. This chapter also contains a large tabulation of TLC and GC–MS data for different drugs.

The last two chapters are somewhat extraneous to the main thrust of this text. The chapter on drug testing of athletes is basically a detailed account of particular screening and confirmation procedures. Likewise, that on drug analysis in South America, describes operating procedures rather than extending the analytical content of the book. These chapters will have a much less general appeal than the rest of this text which will be a useful addition to the analytical literature concerned with testing for drug abuse and misuse.

R.B. Taylor

ELSEVIER

Talanta 42 (1995) 1195–1214

Talanta

Review

# Recent developments in derivative ultraviolet/visible absorption spectrophotometery

C. Bosch Ojeda, F. Sanchez Rojas, J.M. Cano Pavon *

*Department of Analytical Chemistry, Faculty of Sciences, University of Málaga, 29071 Málaga, Spain*

Received 11 October 1994; accepted 10 March 1995

**Abstract**

The instrumental development and analytical applications of derivative ultraviolet/visible region absorption spectrophotometry produced in the last seven years (since 1987) are reviewed.

## 1. Introduction

In a review published some years ago [1] we exposed the theoretical aspects, instrumental devices and analytical applications of derivative ultraviolet/visible spectrophotometry (DS) until 1986. Although this technique does not really constitute a very important innovation, its ability to solve problems, especially for binary and ternary mixtures of compounds whose spectra show considerable overlapping, have made its use grow spectacularly over the last few years, especially in pharmaceutical, clinical and biochemical, as well as in inorganic and organic analysis.

The purpose of this paper is to review the publications on instrumental and theoretical aspects of derivative spectrometry and its use in the diverse fields of applications published since 1987, in order to fill the gap existing since the publication of our first review.

## 2. Theoretical and instrumental aspects

Over the last few years, the use of digital differentiation by means of computers to obtain derivative spectra has been the usual procedure. Higher order derivatives can easily be obtained. General principles of these methods have been reviewed [2], and diverse interferences for coupling conventional spectrophotometers to microcalculations have been developed [3]; diverse algorithms (such as those of Fourier and Savitzky–Golay) are often used for obtaining the derivative spectra [4].

Diode-array spectrophotometers are actually widely used owing to their speed. Different computer-based data-acquisition systems for use with diode-array spectrophotometers have been described [5]. Diverse programs were developed to control the system and to process the results. Program functions usually included: (i) acquisition of data and correction for diode sensitivity, (ii) correction for positional shifts in array, (iii) creation of the data-base, (iv) fitting of the baseline, location of peaks, conversion to wavelength and identification of elements present, (v) display of raw and enhanced data from individual arrays, and (vi) use of an artificial intelligence approach to identify components of a sample [6].

The attained derivative spectra have been assayed by other procedures, e.g. by subtrac-

* Corresponding author.

tion of delayed spectra. In this procedure, production of a derivative spectrum is achieved with the use of a single data system without the creation of noise and without the need for computer software; the spectrum is stored in one half of the memory. A small horizontal shift is made, the size of which is not critical, and the resultant is transferred to the second half of the memory; the derivative spectrum is then created by subtraction of one half from the other [7].

An inconvenience of the derivative technique is that the signal-to-noise ratio (S/N) becomes progressively worse for higher orders. For this reason, practical derivative techniques include some degree of low-pass filtering or smoothing to control the increase in noise. Over the last few years, this problem has usually been solved by three types of digital filtering: ensemble averaging, least-squares polynomial smoothing and Fourier smoothing. Several computer programs were written for the actual applications of the concepts of these digital filters on UV/visible spectrophotometer systems; as a result, ensemble averaging could not be applied as a routine operation for the spectrophotometer used; the maxima S/N enhancement factors achieved by least-squares polynomial smoothing were 6.17 and 7.47 for the spectra of Gaussian and Lorentzian distribution models, and 16.42 and 11.78 by Fourier smoothing for the spectra of the two models, respectively [8]. Talsky concludes that, in general, the more favourable S/N was obtained from four to six orders of derivative when electronic differentiation combined with diverse filtering systems was used [9].

The precision and accuracy in derivative spectrophotometry have been evaluated in a wide variety of situations. Using a computerized numerical method, it has been concluded [10] that if the spectrophotometric measurements are accurate to four significant figures, the relative error of the first numerical derivative is 0.6%; if measurements are accurate to three significant figures, the relative error of the first numerical derivative is 6%. Compared with conventional spectrophotometry, the first derivative from a recording spectrophotometer caused an average error of $\approx 4\%$, but at the peak of the first derivative the error was $\approx 2\%$. Kimbrell et al. [11] recently developed a theoretical study on the multiple interacting factors which determine precision in derivative spectrometry. According to this work, the precision varies by close to an order of magnitude when reasonable combinations of factors levels are used; the derivative order typically interacts strongly with the polynomial degree of the smoothing and derivatizing functions, and with the window width of these functions.

Enhancement of the precision and accuracy in derivative spectrophotometry of highly absorbing samples has been investigated using transmittance-ratio methods [12]. The precision and accuracy obtained in multi-component determinations have also been considered, especially in mixtures of pharmaceuticals [13,14]. Detection limits have been evaluated for different substances using diverse derivative orders [15]; in general, no appreciable differences from conventional photometry are observed.

### 2.1. *Multicomponent analysis*

Derivative UV/visible spectrophometry has been widely used over the last few years in the analysis of multicomponent mixtures. For this reason, diverse procedures for the resolution of overlapped derivative peaks have been applied. Thus, the zero-crossing method has been used for the first- and second-derivative spectra in diverse mixtures [16]. Another procedure used is the named "$K$-ratio" method, in which the $K$-coefficient dual wavelength spectrophotometric method is taken as the mathematical model in order to resolve the difference $n$th-derivative spectral data at one wavelength for determining diverse two-component systems with zeroth-derivative and $n$th-derivative spectra that were seriously interfered with [17,18].

Diverse computer programs have been applied to the analysis of multicomponents using derivative spectra. Delaye et al. [19] developed a program (DESPI) for the computerized recognition of the spectral components in known binary mixtures, whereas Park et al. [20] describe another program (SPECMAN PLUS), written in Pascal, which provides automated spectral comparison techniques, utilizing the value of the root-mean square (RMS) of each difference; this comparison routine of the program can deal with spectra of compounds of different concentrations and different spectral recording resolutions. Recently, a multivariate statistical tool, the partial least-squares (PLS) method, has been applied to derivative data with good results [21]; the PLS technique has a calibration step where the relationship is estimated from a set of reference samples, and this

step is followed by prediction in which the results of the calibration are used to predict or estimate the component concentration from the unknown sample spectrum.

Other procedures for multicomponent analysis using computer calculations have also been reported. The FDAS-SL method [22], which is a means of measuring the shift-length (SL, nm) of the maximum absorption wavelength of a compound by utilizing the first-derivative absorption spectrum (FDAS), was used in the simultaneous determination of binary mixtures; this method utilizes the shift of the absorption spectrum of a compound at surfactant concentrations above the critical micelle concentration and the mixed molar ratio is obtained from the shift-length; each concentration of the compound is calculated by Beer's law. Karstang and Kvaleim [23] describe a technique based upon regression modelling of spectra for accurate estimation of the concentration of analytes in the presence of background constituents; this novel technique gives reliable predictions, while all the contaminated samples are detected as outliers in the conventional approach.

### *2.2. Combination of DS with flow injection, liquid chromatography and kinetic analysis*

The advent of a multi-dimensional detection system and the affordability of personal computers provided with software that allows storage and subsequent processing of data has fostered developments of new experimental procedures in which DS is used in combination with dynamic techniques, such as flow-injection and liquid chromatography.

The simultaneous determination of compounds in two-, three- and four-component mixtures with completely overlapping spectra was achieved by flow-injection with a diode-array detection system, using the third-derivative spectra in the range 214–290 nm. The absorbance spectrum of each solution was recorded 10.7 s after sample injection with an integration time of 0.4 s [24].

In liquid chromatography, the information supplied by derivative spectroscopy used as a detection system has been exploited in three different ways, namely: (i) using the first derivative of the elution profile obtained at the wavelength of the absorption maximum; in theory, the derivative should be zero at this point and therefore the disappearance of the main peak reveals the presence of other constituents with different absorption features; this procedure is called the "null spectral derivative technique"; (ii) using the complete derivative obtained by recording the elution profile; this procedure is known as the "spectral derivative mapping technique" [25,26]; (iii) using the derivative spectra of the components obtained around the maxima signal of the overlapped chromatographic peaks; the detector was set to collect a spectrum every 1 s, over an adequate wavelength range; this procedure makes possible the easy transformation of a chromatographic problem in a spectrophotometric problem [27].

Derivative techniques have also been used in kinetic analysis. A selective empirical data processing method based on a modification of the conventional kinetic derivative method has been reported [28]. The method is based on parameters not directly correlated with the initial rate, but which are similar to those used in derivative spectrometry as the distance between two peaks or the value of the derivative at a single time. Two types of kinetic curves were tested, namely curves with and without induction periods. Different-order derivatives were obtained by numerical differentiation using the Savitzky–Golay method. The proposed method is shown to provide improved selectivity.

## 3. Applications

### *3.1. Inorganic analysis*

The use of DS in inorganic analysis, especially in the determination of mixtures of metal ions, has undergone an appreciable increase in the last few years. Diverse chromogenic reagents (EDTA, dithizone, 8-hydroxyquinoline, some hydrazones, etc.) have been proposed. The different determinations achieved are described in Table 1. However, the analysis of anions has hardly been investigated; only the simultaneous determination of nitrite and nitrate in water using linear regression DS has been described [76].

### *3.2. Organic compounds*

Binary and ternary mixtures of organic compounds have been widely analyzed using DS. Although pharmaceutical formulations are the mixtures most frequently assayed, and are es-

Table 1
Determination of metal ions

| Elements | Reagents | Remarks | Ref. |
|---|---|---|---|
| Al, Fe(III), Cu, Ti, Ni | 8-Hydroxyquinoline | 1st deriv., extraction into chloroform; binary, ternary and quaternary mixtures were analyzed | 28 |
| Be | Beryllon III | 3rd deriv. | 29 |
| Be, Al | 5,8-Dihydroxy-1, 4-naphthoquinone | Simultaneous determination; 7.2–396 and 10.8–1080 ng $ml^{-1}$, respectively | 30 |
| Co | 8-Hydroxyquinoline | 1st deriv., cobalt is oxidized by air only in the presence of Fe(III) or V(V), extraction into chloroform is used | 31 |
| Co, Fe(II) | 3-(4-Phenyl-2-pyridinyl)-1,2,4-triazine | 1st deriv., simult. determ., extraction into dichloroethane, 57–2000 and 2–200 ng $ml^{-1}$, respectively | 32 |
| Co, Cu | Methylenediamine tetraacetic acid | 1st deriv., simult. determ. | 33 |
| Cu, Fe(III) | 2-(5-Bromo-2-pyridylazo)-5-diethylaminophenol | Simult. determ., 2–10 μg $ml^{-1}$ of each ion | 34 |
| Cu, Ni | Sodium cyanide | 3rd deriv., simult. determ., 0.55–5.8 and 0.55–6.8 μg $ml^{-1}$, respectively | 35 |
| Cu, Ni | – | 1st deriv., aqueous solutions of both metal ions were analyzed | 36 |
| Cu, Zn | 5,10,15,20-Tetrakis-(4-trimethylammonio-ohenyl)porphine | 4th deriv., determinations were performed in the presence of sodium dodecylsulphate | 37 |
| Cu, Zn, Mn(II) | 2-(5-Bromo-2-pyridylazo)-5-diethylaminophenol | 1st and 2nd deriv., simult. determ., using the equation set of solutions and the least-squares method | 38 |
| Fe(III) | EDTA | 1st and 2nd deriv. | 39 |
| Fe(II) | 1,10-Phenanthroline | 2nd deriv., 1–12 μg $ml^{-1}$, iron is determined in bronze | 40 |
| Fe(III), Bi | EDTA | 1st deriv., 0.5–8.0 and 0.1–35.7 μg $ml^{-1}$, respectively | 41 |
| Hg | Iodide + Pyronine G | 3rd deriv., 0.04–0.8 μg $ml^{-1}$ | 42 |
| Hg, Co | Benzyl-2-pyridylketone-2-quinolylhydrozone | 1st deriv., simult. determ. | 43 |
| Ir, Rh, Pt, Ag | Sulfochlorophenoazo-rhodanine | | 44 |
| La, Pr, Nd, Sm, Eu, Ho, Er | Triethylenetetramine-hexaacetic acid (TTHA) | 3rd deriv. | 45 |
| Mn | $(NH_4)_2S_2O_8$ + Ag(I) | 1st deriv., manganese is oxidized to permanganate | 46 |
| Mo | Bromopyrogallol red | 3rd deriv., simultaneous determ. | 47 |
| Mo, Ti | Salicylfluorone + hexadecylmethylammonium bromide | 3rd deriv., simult. determ. | 48 |

Table 1 (continued)

| Elements | Reagents | Remarks | Ref. |
|---|---|---|---|
| Nd | Tiron | 3rd deriv. | 49 |
| Nd | Ascorbic acid | 5th deriv., Nd is determined in magnesium alloys | 50 |
| Nd, Er | 5,7-Dibromoquinolin-8-ol | 3rd deriv., simult. determ., Trition X-100 is used as surfactant, up to 18 $\mu g\ ml^{-1}$ of Nd and up to 21 $\mu g\ ml^{-1}$ of Er | 51 |
| Nd, Er | 5-Sulfo-7-iodoquinolin-8-ol (ferron) + diethylamine | 3rd deriv., up to 14 $\mu g\ ml^{-1}$ for Nd and up to 13 $\mu g\ ml^{-1}$ for Er | 52 |
| Nd, Er | 4-Benzoyl-3-methyl-1-phenylpyrazolin-5-one | 3rd deriv., simult. determ., 5.8–29 and 6.7–40 $\mu g\ ml^{-1}$, respectively | 53 |
| Nd, Er | 8-Hydroxyquinoline + diethylamine | 3rd deriv., 3–18 and 4.5–21 $\mu g\ ml^{-1}$, respectively | 54 |
| Nd, Sm, Eu, Gd, Tb, Dy | HCl | 1st deriv. | 55 |
| Ni, Co | 2-(4,5-Dimethyl-2-thiozolylazo)-5-dimethylaminobenzoic acid | 1st deriv., simult. determ., the method makes possible the determination of both elements in nickel minerals | 56 |
| Ni, Co | Benzyl-2-pyridylketone-2-quinolylhydrazone | 1st deriv., 480 and 512 nm, simult. determ. | 57 |
| Ni, Cu, V | 2-(5-Bromo-2-pyridylazo-5-diethylamino)phenol | 1st deriv., simult. determ., these elements have been determined in petroleum samples | 58 |
| Ni, Cu, Zn | 4-(2-Pyridylazo)resorcinol | 1st deriv., simult. determ., Kalman filter is used | 59 |
| Ni, Cu, Zu | 1-(2-Pyridylazo)-2-naphthol | 2nd deriv., simult. determ., 0.3–2.0, 0.5–3.0 and 0.5–3.0 $\mu g\ ml^{-1}$, respectively | 60 |
| Pb | 1,10-Phenanthroline + Rose Bengal | 4th deriv., extraction of the complex into chloroform | 61 |
| Pd, Pt | Dithizone | 5th deriv., simult. determ., extraction into carbon tetrachloride | 62 |
| Pd, Pt | *N*,*N*-Diethyl-4-nitrosoaniline | 1st deriv., simult. determ., 567.5 and 549.2 nm, respectively | 63 |
| Pd, Nd, Sm, Eu, Ho, Er | EDTA and oxalic acid | 2nd and 4th deriv., Sm and Eu can be determined in the presence of other metals | 64 |
| Pr, Nd, Eu, Ho, Er, Tm | 2-Thenoyltrifluoroacetone and 2,6-dimethylpyridine | 2nd deriv. | 65 |
| Pr, Nd, Dy | – | 2nd deriv., spectra in acid solutions were measured | 66 |
| Sm, Gd, Dy, Nd | | 2nd deriv., 4th deriv., spectra in acid solutions ($HClO_4$) were measured | 67 |
| Ta | 5-Bromo-2-(2-pyridylazo)-5-diethylaminophenol | 1st deriv., Ta is determined in nickel-based alloys containing niobium | 68 |

Table 1 (continued)

| Elements | Reagents | Remarks | Ref. |
|---|---|---|---|
| Ti | Hydrogen peroxide | 2nd deriv., up to 10 μg ml$^{-1}$, Ti is determined in steels | 69 |
| U, Th | Carminic acid | 1st deriv., simult. determ., 2–50 and 1–40 μg ml$^{-1}$, respectively | 70 |
| U, Th | 4-(2′-Thiazolylazo) resacetophenone oxime | 1st deriv., simult. determ. | 71 |
| V, Co | 4-(1′*H*-1′, 2′,4′-Triazol-3′-ylazo)-2-methylresorcinol | 2nd deriv., simult. determ., 0.10–1.02 and 0.12–1.18 μg ml$^{-1}$, respectively | 72 |
| W, Mo | Sacilylfluorone and cetyltrimethylammonium bromide | | 73 |
| Zn | *meso*-Tetrakis (3,5, dibromo-4-hydroxyphenyl)porphyrin (T(DBHP)P) | 2nd deriv., up to 0.24 μg ml$^{-1}$, zinc can be determined in biological samples | 74, 75 |

pecially considered in the next paragraph, other diverse mixtures (antioxidants, pesticides, herbicides, etc.) have been determined with good results. Table 2 shows the diverse procedures described since 1987. Li and Shi [100] reviewed years ago the articles published on organic compounds (including pharmaceuticals and clinical samples) until 1988.

### 3.3. Pharmaceutical analysis

The application of DS in pharmaceutical analysis has undergone explosive growth over the last 5 years. This fact is due to the easy application of this technique to pharmaceutical formulations, which are usually mixtures of two or three components of different chemical structures, and therefore show UV/visible spectra with different peaks and/or different amplitudes. DS has also proved particularly useful in eliminating matrix interferences, including those of aromatics, which have weak absorption in the near ultraviolet.

More than a hundred methods for pharmaceutical mixtures have been described over the last few years [101–215], and are shown in Table 3. Particularly numerous are the determinations referring to mixtures of antidepressives and transquilizers, as well as to formulations containing caffeine with other stimulants and antihystaminics, or mixtures of diverse sulphamides or antibiotics.

### 3.4. Analysis of amino acids, proteins and other biological compounds

DS has been widely used in the analysis of binary and ternary mixtures of amino acids. Mixtures of phenylalanine, tyrosine and triptophane have been especially studied. Procedures described since 1987 [216–235] are shown in Table 4.

### 3.5. Clinical and forensic analysis

DS has been proposed for the identification of compounds in mixtures of special interest in clinical and forensic analysis, and diverse general reports have been published in recent years [236,237]. Specific procedures are summarized [238–257] in Table 5. Diverse procedures using second derivative spectra have been described for the determination of haemoglobin and carboxyhaemoglobin in blood, as well as for the analysis of diverse pharmaceutical compounds in biological fluids.

### 3.6. Food analysis

Procedures involving the application of UV/visible DS to food analysis are summarized [258–271] in Table 6. In general, derivative technique has been especially used in the determination of additives (colouring, flavour enhancers) in foods.

Table 2
Determination of organic compounds

| Compounds | Remarks | Ref. |
|---|---|---|
| Alkaloids | Total alkaloids of Coptis chinensis were extracted in HCl–MeOH and determined | 77 |
| Antioxidants (butylated hydroxyanisole, butylated hydroxytoluene and Pr gallate) | 3rd and 4th deriv. was used | 78 |
| Carbaryl and chlorpyrifos | PLS was also applied to simultaneous determination | 79 |
| Carbendazim | 2nd deriv., the compound is determined in Kolfugo extra formulations | 80 |
| Chlorophenols | 1st deriv., two-, three- and four-component mixtures were possible using multivariate calibration | 81, 82 |
| Chlorpromazine and $\beta$-cyclodextrin | 2nd deriv., the binding constant between both compounds in aqueous solution was determined by means of an iterative calculation method | 83 |
| Cocaine | 1st and 2nd deriv., the compound (up to 10 $\mu g\ ml^{-1}$) is determined in methanol | 84 |
| 2-Furfuraldehyde, 5-hydroxymethyl furfuraldehyde and malonaldehyde | Simult. determ., the three chemicals were reacted previously with 2-thiobarbituric acid, PLS analysis is used | 85 |
| 5-Hydroxyflavonoids | 1st deriv. | 86 |
| Indulin C | 2nd deriv., spectra are used for studies of degradation of lignin | 87 |
| Indazole-3-carboxylic acid | 2nd, 3rd and 4th deriv., several isomers $N_1$ and $N_2$ substituted were identified using this technique | 88 |
| Nicotine | 1st and 2nd deriv., nicotine is determined in tobacco products | 89 |
| Paeonol | 1st deriv., the derivative values at 279 and 242 nm were used for quantification of paeonol, and their difference was proportional to up to 10 $\mu g\ ml^{-1}$ of this substance | 90 |
| Phenol compounds | 1st and 2nd deriv., mixture of to up to nine phenols (phenol and halogen, nitro-, methoxy- and methyl-derivatives, 1–100 $\mu M$) were determined with use of the mathematical algorithm MULTI3 | 91 |
| Phloroglucinols | 2nd deriv., flow-injection analysis coupled with liquid chromatography and a diode array detector was used | 92 |
| Piperonyl butoxide, neopynamine, permethrin and fenitrothion | 2nd deriv., binary mixtures can be resolved | 93 |
| Polymers | 1st and 4th deriv., polystyrene and mixtures of several prepolymers were studied | 94 |
| Polymers | 2nd deriv. | 95 |
| Salicylaldehyde and *para*-hydroxybenzaldehyde | 2nd deriv., simult. determ. | 96 |

Table 2 (continued)

| Compounds | Remarks | Ref. |
|---|---|---|
| Salicylaldehyde, 3-hydroxybenzaldehyde and 4-hydroxybenzaldehyde | 1st deriv., simult. determ. | 97 |
| Tocopherols | 2nd deriv., individual $\alpha$-, $\beta$-, $\gamma$- and $\delta$-tocopherols were determined | 98 |
| Trifluralin, benfluralin, isopropalin and oryzalin (herbicides) | 1st deriv., detection range found was 1–7 $\mu g\ ml^{-1}$ | 99 |

Table 3
Methods described for the analysis of compounds in pharmaceutical formulations

| Compounds | Remarks | Ref. |
|---|---|---|
| Acetylsalicylic acid and chlormezanone | 4th deriv., 0.02–0.2 $mg\ ml^{-1}$ for each compound | 101 |
| Acetylsalicylic acid and paracetamol | 276, 286, 304 and 314 nm for acetylsalicylic acid; 256 and 320 nm for paracetamol. Regression equations must be used | 102 |
| Aliphatic thiol drugs | 2nd and 3rd deriv., 4-(6-methylnaphthalen-2-yl)4-oxobut-2-enoic acid is used as reagent | 103 |
| Acetaminophen and orphenedrine, ibuprofen or chlorzoxazone | Binary mixtures only | 104 |
| Aminazine and diprazine | 250–255 nm | 105 |
| 4-Aminophenol | 2nd deriv., 224 nm, 0.5–38% of 4-aminophenol can be determined in the presence of paracetamol | 106 |
| Aminodarone hydrochloride | 1st and 2nd deriv. | 107 |
| Amitriptyline and chlordiazepoxide or perphenazine | 1st deriv. | 108 |
| Amoxycillin | 2nd deriv., 280 nm, 3.3–55.4 $\mu g\ ml^{-1}$ | 109 |
| Amoxycillin and cephalexin | 2nd deriv., up to 90 $\mu g\ ml^{-1}$ for amoxycillin (276 nm) and up to 60 $\mu g\ ml^{-1}$ for cephalexin (267.5 nm) | 110 |
| Ascorbic acid and analgin | 1st deriv. | 111 |
| Asparaginase | 259 nm, 0.05–0.125 $mg\ ml^{-1}$ | 112 |
| Benzalkonium HCl | 2nd deriv., 255–275 nm, determination can be achieved in the presence of pilocarpine, hypromellose and polivinyl alcohol | 113 |
| Benzodiazepines | 1st and 2nd deriv., single compounds only | 114 |
| Benzodiazepines and/or their metabolites | 2nd deriv., 19 compounds can be clearly identified, whereas four can only be differentiated two by two (diazepam–prazepam and alprazolam–estazolam) | 115 |
| Benzodiazepines and benzophenones | Determination in biological fluids | 116 |

Table 3 (continued)

| Compounds | Remarks | Ref. |
|---|---|---|
| Bretylium tosylate, hyoscine Bu bromide, oxyphenonium bromide, cetrimide and benzalkonium chloride | 1st deriv., picric acid is used as reagent, 5–20 $\mu g\ ml^{-1}$ for each compound | 117 |
| Bromazepam | 2nd deriv., 237–247 nm, up to 30 $\mu g\ ml^{-1}$ | 118 |
| Bufotoxin lactone | 2nd deriv., 359 and 376 nm, determination is made in Houzhenwan (traditional chinese antipyretic) | 119 |
| Caffeine and amidopyrine | 1st deriv., 275–296 nm, linear regression method of multiwavelength is used | 120 |
| Caffeine and antihistaminics | 1st deriv. | 121 |
| Caffeine and sodium benzoate | 9–33 $\mu g\ ml^{-1}$(269 nm) for caffeine and 6.5–19.5 (241 nm) for sodium benzoate | 122 |
| Canrenone | 2nd deriv., 300 nm, 2–10 $\mu g\ ml^{-1}$, determination in the presence of spironolactone | 123 |
| Carbimazole and methimazole | 3rd deriv., 265 and 295 nm, respectively | 124 |
| Cephalosporins and their degradation products | 2nd deriv., 4–24 $\mu g\ ml^{-1}$ | 125 |
| Clomiphene citrate and tamoxifen citrate | 1st deriv. | 126 |
| Chlorpheniramine maleate | 2nd deriv., 228–260 nm, 4–36 $\mu g\ ml^{-1}$ | 127 |
| Chlorpheniramine maleate and phenylephrine–HCl | | 128 |
| Chlorphenoxamine and caffeine | 225, 232 nm for chlorphenoxamine and 256, 283 nm for caffeine | 129 |
| Chlorpromazine and its sulphoxide | 3rd deriv. | 130 |
| Clotrimazole | 1st deriv., 266 nm | 131 |
| Captotril and hydrochlorothiazide | 1st deriv., 228–248 nm | 132 |
| Cytarabine and acyclovir | 1st and 2nd deriv., 268 and 272, respectively | 133 |
| Danthron and phanquone | 1st deriv., previous formation of complexes with metal ions | 134 |
| Diazepam and oxazepam | 4th deriv. | 135 |
| Diazepam and otilonium bromide | 1st deriv., 264 and 406–408 nm, respectively | 136 |
| Dicloxacillin and ampicillin | 2nd deriv., up to 60 $\mu g\ ml^{-1}$ for each compound | 137 |
| 2,6-Diisopropylphenol | 2nd deriv., 0.10–0.25 $\mu g\ ml^{-1}$ | 138 |
| Diphenhydramine or naphazoline, and methylene blue | 2nd deriv., extraction into chloroform | 139 |
| Diphenhydramine | 2nd deriv., 215 or 251 nm | 140 |
| Diphenhydramine, ephedrine and pentoxyverine | 1st and 4th deriv. | 141 |

Table 3 (continued)

| Compounds | Remarks | Ref. |
|---|---|---|
| Diloxanide furoate and metronidazole | 1st and 2nd deriv., 0.02–0.1 mg $ml^{-1}$ (262 nm) and 0.04–0.2 mg $ml^{-1}$ (248 nm), respectively | 142 |
| Domperidone | 1st deriv. | 143 |
| Enalapril maleate | 4th deriv. | 144 |
| Estradiol and progesterone or testosterone | | 145 |
| Estrone, equilin, 17-α-estradiol and 17-α-dihydroequilin | 1st, 2nd, 3rd and 4th deriv., 280 and 338 nm | 146 |
| Ethinyl oestradiol and norethisterone | 1st and 2nd deriv. | 147 |
| Famotidine | 2nd deriv., 304 nm | 148 |
| Febuprol | 276 and 280 nm | 149 |
| Fendiline HCl and other related compounds | 2nd deriv., 0.25–1 g $l^{-1}$ | 150 |
| Glibenclamide, mebeverine and clopamide | 2nd deriv., determination can be achieved in the presence of their degradation products | 151 |
| Hydrochlorothiazide and amiloride HCl | 1st deriv., 284.7 nm | 152 |
| Hydrocortisone, dexamethasone, prednisolone and prednisone | 1st deriv. | 153 |
| 4-Hydroxyphenoxymethyl penicillin | 4th deriv., 304–314 nm, 0.06–0.30 mg $ml^{-1}$ | 154 |
| Imipramine and amitriptyline | 1st and 2nd deriv., 0.62–10.14 μg $ml^{-1}$ and 0.63–10.40 μg $ml^{-1}$, respectively | 155 |
| Imipramine, trimipramine, amitriptyline, dothiepin and cyproheptadine | 1st and 2nd deriv. | 156 |
| Insulin | 7th deriv., bovine and porcine insulin can be discriminated | 157 |
| Isoniazid and pyridoxine or thiacetazone | 1st deriv., 8.2–41.1 μg $ml^{-1}$ and 7.1–23.6 μg $ml^{-1}$ | 158 |
| β-Lactam antibiotics | Determination in turbid solutions containing liposomes | 159 |
| Levamisole hydrochloride | 1st deriv., 239 nm | 160 |
| Levodopa | 2nd deriv., 267 nm | 161 |
| Levodopa | 2nd deriv., 280–290 nm, 2.4–120 μg $ml^{-1}$ | 162 |
| Lidocaine | 3rd deriv. | 163 |
| Methylene blue, hexamethylene tetramine and resorcinol | 1st deriv., 273, 221 and 300 nm, respectively | 164 |
| Minoxidil and retinoic acid | 1st deriv., 290 and 351 nm, respectively | 165 |
| Nifedipine | 1st deriv., 402 nm | 166 |
| Nitofurantoin and phenazopyridine | 1st deriv., 335 and 317 nm, respectively | 167 |
| Notriptyline and perphenazine | 4th deriv., 239.6 and 268.8 nm, respectively | 168 |

Table 3 (continued)

| Compounds | Remarks | Ref. |
|---|---|---|
| Oestradiol | 3–12 μg ml$^{-1}$ | 169 |
| Oxytetracycline | | 170 |
| Parabens | | 171 |
| Paracetamol | 2nd deriv. | 172 |
| Paracetamol and chlorzoxazone | 2nd deriv., 270.8 and 278.9 nm, respectively | 173 |
| Paracetamol and methocarbamol | 2nd deriv., 250.2 and 227.6 nm, respectively | 174 |
| Paracetamol and phenylpropanolamine HCl | 1st deriv., 256.7 and 242.8 nm, respectively | 175 |
| Penicillins and cephalosporins | 1st, 2nd and 3rd deriv., 13 penicillins and five cephalosphorins in different combinations were assayed | 176 |
| Perphenazine and amitriptyline | 1st and 2nd deriv., 1–8 μg ml$^{-1}$ and 1–30 μg ml$^{-1}$, respectively | 177 |
| Perphenazine and amitriptyline | 1st and 2nd deriv., other tranquilizers and antidepressants were also assayed | 178 |
| Phenothiazines | 1st and 2nd deriv. | 179 |
| Phenothiazines | 2nd and 4th deriv. | 180 |
| Phenothiazines | 2nd deriv., binary mixtures | 181 |
| Phenylephrine | 1st deriv., determination is in the presence of chlorapheramine, sulphacetamide or prednisolone | 182 |
| 1-Phenylethylamine | Determination is in the presence of fosfomycin | 183 |
| Phenylephrine HCl and carbinoxamine maleate | 1st deriv., 275 and 237 nm, respectively; related compounds were also assayed | 184 |
| Phenytoin and phenobarbital | 2nd deriv. | 185 |
| Phenytoin | 2nd deriv., 4.5–160 μmol l$^{-1}$ | 186 |
| Prazosin and polythiazide | 2nd deriv., 346 and 236 nm, respectively | 187 |
| Prenylamine lactate and other related compounds | 2nd deriv. | 188 |
| Propofol | 2nd deriv., 286 nm, 0.1–0.25 mg ml$^{-1}$ | 189 |
| Pseudoephedrine and chlorpheniramine | 1st deriv. | 190 |
| Pseudoephedrine, chlorpheniramine and dextromethorphan | 2nd deriv., 240–300 nm | 191 |
| Puerarin | 1st deriv., 3.2–16 μg ml$^{-1}$ | 192 |
| Rifamixin | 2nd deriv. 2–40 μg ml$^{-1}$ | 193 |
| Salbutamol | 1st deriv., 286 nm | 194 |
| Salbutamol | 2nd and 4th order, 1–80 μg ml$^{-1}$, determination is in the presence of gelatine | 195 |
| Salicylic and salicyluric acids | 1st deriv., 2.6–52 μg ml$^{-1}$ and 2.1–42 μg ml$^{-1}$ | 196 |
| Simvastatin | | 197 |

Table 3 (continued)

| Compounds | Remarks | Ref. |
|---|---|---|
| Spironolactone and hydrochlorothiazide | | 198 |
| Sulfamethoxazole and trimethroprim | 280 and 290 nm, respectively | 199 |
| Sulfacetamide, sulfadimidine and sulfathiourea | 1st deriv. | 200 |
| Sulfonamides | 1st and 4th deriv., Bratton–Marshall reaction combined with derivative photometry is used | 201 |
| Sulphamethizole | 1st deriv., up to 43 μg $ml^{-1}$, determination is in the presence of nitrofurantoine | 202 |
| Sulphaquinoxaline and pyrimethamine | 1st deriv., 1–25 mg $ml^{-1}$ and 1–50 mg $ml^{-1}$, respectively | 203 |
| Synephrine | 1st deriv. | 204 |
| Tetracyclines | 2nd deriv. | 205 |
| Theophylline | 1st deriv., 284, nm | 206 |
| Thiamine, riboflavine, nicotinamide, pyridoxine and ascorbic acid | Multiple linear regression analysis is used | 207 |
| Thiamine, riboflavine, nicotinamide, pyridoxine and calcium pantothenate | 1st deriv., multicomponent program is used | 208 |
| Thiobarbituric acid | 2nd deriv., determination is in the pressure of reactive products of lipid peroxidation in plants | 209 |
| Thioxanthenes | 1st deriv., 4–40 μg $ml^{-1}$ | 210 |
| Tocopherols | $\alpha$-, $\beta$-, $\gamma$- and $\delta$-tocopherols were determined at 298, 302, 304 and 306 nm, respectively | 211 |
| Tolazoline, atropine homatropine, tetrahydrozoline and xylometazoline | 1st deriv., picric acid is used as reagent, extraction is made into chloroform | 212 |
| Triamterene and hydrochlorothiazide or xipamide | 1st deriv. | 213 |
| Triamphenicol glycinate and *N*-acetylcisteine or 4-hydroxyisophthalic acid | 2nd deriv., 274–278 nm, 6–55 μg $ml^{-1}$ for triamphenicol | 214 |
| Trimethroprim and sulfamethoxazole | | 215 |

### 3.7. *Environmental analysis*

A few applications of derivative UV spectrophotometry to environmental analysis have been described over the last few years. High-order derivative absorption spectrophotometry has been used in the determination of oil in waste water to avoid complex sample extraction and to eliminate interference by other chemical species; the calibration curve varied rectilinearly up to 100 mg $l^{-1}$ of oil, with 0.05 N $H_2SO_4$ as reference standard and light petroleum as blank [272].

Derivative spectrophotometry has also been used in combination with thermal soil desorption in the field screening of benzene–toluene–

Table 4
Methods for the analysis of amino acids and proteins

| Compounds | Remarks | Ref. |
|---|---|---|
| Adenine and thymine | 2nd deriv., adenine and thymine were determined in DNA (not more than 10 μg DNA is required) | 216 |
| Amino acids | 2nd deriv., aromatic amino-acids were tested | 217 |
| Amino acids | 2nd deriv, and size-exclusion HPLC were combined and applied to the determination of aromatic amino acids of polypeptides | 218 |
| Chlorophylls a and b | 1st deriv., 671 nm for a and 467 nm for b | 219 |
| Metaloporphyrins | 3rd deriv., the method is based on variation of the Soret band wavelength with the type of functional group structure of the 20-carbon porphyrin chromophore | 220 |
| Phenylalanine, tyrosine and triptophane | Factorial analysis procedure for interpreting derivative spectra is proposed; application is made to the determination of these compounds in the presence of aromatic chromophores content in mitochondrial proteins | 221 |
| Ibidem | 2nd deriv. | 222 |
| Ibidem | Phenylalanine is determined in the presence of the other compounds by means of the negative derivative peak near 258 nm | 224 |
| Phospholipids | HPLC 2nd deriv. is used; phosphatidylcholine, phosphatidylethanolamine, phosphatidylserine and phosphatidic acid were characterized | 225 |
| Phosphotyrosine | HPLC 2nd deriv. is used, phosphatyrosine residues in peptides were identified | 226 |
| Polynucleotides | Conformational isomerizations of polynucleotides are studied by means of 4th deriv. spectrophotometry | 227, 228 |
| Proteins | HPLC deriv. spectrophotometry is used for the separation and detection of proteins and peptides | 229 |
| Proteins | 4th deriv. is used for protein quantification during purification | 230 |
| Proteins | Size-exclusion HPLC derivative spectrophotometry is used | 231 |
| Proteins and phenol | Detection of diverse proteins and phenol were achieved in DNA samples | 232 |
| Somatotropin | 2nd deriv., proteolysis of native bovine somatotropin is studied | 233 |
| Tryptophan | 2nd deriv., presence of tryptophan in peptides is studied | 234 |
| Tryptophan and tyrosine | 2nd deriv., both amino acids were determined in synthetic peptides | 235 |

Table 5
Clinical and forensic analysis

| Substances | Type of sample | Remarks | Ref. |
|---|---|---|---|
| Allopurinol and uric acid | Urine | 1st and 2nd deriv. (284 and 243 nm, respectively), 2–12 μg $ml^{-1}$ | 238 |
| Bile salts | | 2nd deriv., critical micellar concentrations of bile salts were determined | 239 |
| Bilirrubin, methaemoglobin and oxyhaemoglobin | Cerebroespinald fluid | 1st and 2nd deriv., simultaneous determination, effects of turbidity are minimized | 240 |
| Carboxyhaemoglobin | Blood | 2nd deriv., 418 nm | 241 |
| Carboxyhaemoglobin | Blood | Soret region of the UV spectrum is used, method has been applied in postmortem blood samples | 242 |
| Ceftizoxime | Plasma | 2nd deriv., 281 nm, 1–100 μg $ml^{-1}$ | 243 |
| Clonazepam | Urine | 3rd deriv., limit of detection is 150 ng $ml^{-1}$ | 244 |
| Haemoglobin | Plasma or serum | 1st deriv. | 245 |
| Haemoglobin (total) and carboxyhaemoglobin | Blood | 3rd deriv., carboxyhaemoglobin shows a maximum at 565 nm, and oxyhaemoglobin crosses the zero line at 565 nm | 246 |
| Haemoglobin and urinary porphirins | Plasma | 2nd deriv., limits of detection are 0.060 μmol for haemoglobin and 10 mmol $l^{-1}$ for coproporphyrin and uroporphyrin | 247 |
| Imipenem | Plasma | 3rd deriv., 306–312 nm, detection limit is 3 μg $ml^{-1}$ | 248 |
| Lipids | Plasma | 2nd deriv., lipid dienes as markers of lipid peroxidation in heptane extracted from plasma from patients with arthritis are analyzed | 249 |
| Lipids | Plasma | Lipid peroxidation is used, and hydroperoxidienes formed were studied by derivative spectrophotometry | 250 |
| Myoglobin | | 2nd deriv., myoglobin is determined in the presence of haemoglobin; diverse algorithms were used | 251 |
| Nitrazepam and clorazepam | Biological fluids | 5th deriv., limits of detection are 1 μg $ml^{-1}$ and 1.5 μg $ml^{-1}$, respectively | 252 |
| Paracetamol and salicylate | Plasma | 2nd deriv., recovery is slow | 253 |
| Pesticides | Serum and gastric juice | 2nd deriv., 245 nm, carbamate pesticides were analyzed, detection limit for carbaryl is 250 μg $ml^{-1}$ | 254 |
| Phenylbutazone and oxyphenbutazone | Plasma | 4th deriv., 1–5 μg $ml^{-1}$ for phenylbutazone and 3–8 μg $ml^{-1}$ for oxyphenbutazone | 255 |
| Porphyrins | Urine | 2nd deriv. | 256 |
| Rifampicin | Plasma | Binding of rifampicin by plasma proteins is studied | 257 |

Table 6
Food analysis

| Substances | Type of sample | Remarks | Ref. |
|---|---|---|---|
| $\alpha$- and $\beta$-acids | Hops | 2nd deriv., simult. determ. | 258 |
| Chlorogenic acids | Instant coffee | 2nd deriv., 325 nm, chicory does not interfere | 259 |
| Enzymes | Red fruited pears | 4th deriv., of peroxidase, esterase and acid phosphatase were determined | 260 |
| Flavour enhancers | Food preparations | 1st and 2nd deriv., partial least-squares and principal component regression modelling of spectrophotometric data have been used | 261 |
| Food colours (synthetic) | Foods | 2nd deriv., Amaranth, Tartrazide, New Coccine, Sunset Yellow and Brillant Blue were determined in binary mixtures | 262 |
| Food colours (synthetic) | Foods | 1st deriv., Acid Blue, Food Red, Acid Red and Food Yellow were determined simultaneously | 263 |
| 2-Furfuraldehyde and 5-(hydroxymethyl)-2-furfuraldehyde | Orange juice | 1st deriv., thiobarbituric acid is used as reagent, 436 and 414 nm were used | 264 |
| Lipid oxidation products | Vegetable oils | 2nd deriv., degree of rancidity of diverse vegetable oils (peanut, sunflower, corn, soybean, grape seed) was determined | 265 |
| Pigments | Orange-drink powder | 1st deriv., carminic acid and citron yellow were determined at 468 and 548 nm, respetively | 266 |
| Quinine | Soft drinks | 4th deriv., limit of detection is 5 ng $ml^{-1}$ | 267 |
| Refined oil | Virgin olive oils | 2nd deriv., interfering oxidizing products were removed with alumina | 268 |
| Saccharin, benzoic acid and ethyl-4-hydroxybenzoate | Beverages | | 269 |
| Seed oils | Olive oils | 2nd deriv., peanut, sunflower, corn, soybean, grapeseed oils were determined | 270 |
| Sorbic and benzoic acids | Soft drinks | 2nd deriv., 1–7 $\mu g\ ml^{-1}$ | 271 |

ethylbenzene–xylene in solids [273]. Another method has been developed for the analysis of environmental polycyclic aromatic hydrocarbons (PAHs) utilizing an algorithm in which the samples spectrum was used to build a vector containing the second to fifth derivatives; this was multiply regressed against similar vectors containing the corresponding derivative of the unit molar UV spectra of the target PAH; the PAHs selected in this step were used for a second multiple regression filter, fitting all possible compounds into a

single Beer's law model; a third filter, based on sensitivity analysis, selected the significant components of the sample system [274].

Finally, a second-derivative UV spectrophotometry method is described for the determination of nitrate in soils; ammonium nitrite and urea may be determined in the same experiments [275].

## References


[1] F. Sánchez Rojas, C. Bosch Ojeda and J.M. Cano Pavón, Talanta, 35 (1988) 753.
[2] I.M. Dubrovkin, Probl. Anal. Khim., 9 (1989) 50.
[3] I.M. Dubrovkin, A.S. Lozovitskii and V.G. Velikov, Zavod. Lab., 54 (1988) 19.
[4] K. Kitamura and K. Hozumi, Anal. Chim. Acta, 201 (1987) 301.
[5] M. Ryan-Hotchkiss and J.D. Ingle, Talanta, 34 (1987) 619.
[6] L. Brett, A. Kalsi, S. Cummins and D. Thombs, Anal. Proc., 28 (1991) 224.
[7] P.G. Craven, S.A. Fainhurst and L.H. Sutcliffe, Spectrochim. Acta, Part A, 44 (1988) 539.
[8] M.K. Park and J.H. Cho, Arch. Pharmacol. Res., 10 (1987) 1.
[9] G. Talsky, Fresenius' Z. Anal. Chem., 333 (1989) 702.
[10] Q. Du, G. Zhang and X. Zhang, Fenxi Shiyanshi, 9 (1990) 16.
[11] S.M. Kimbrell, K. Booksh and R.J. Stolzberg, Appl. Spectrosc., 46 (1992) 704.
[12] I. Dol, M. Knochen and C. Altesor, Analyst, 116 (1991) 69.
[13] A.I. Grizodub, N.N. Asmolova, M.G. Levin and V.P. Georgievskii, Zh. Anal. Khim., 43 (1988) 2170.
[14] L.L. Juhl and J.H. Kalivas, Anal. Chim. Acta, 207 (1988) 125.
[15] X. Hu, R. Qu, Z. Zhaoi and Y. He, Huaxue Fence, 26 (1990) 249.
[16] J. Li, Q. Luo and Y. Zeng, Huaxue Xuebao, 46 (1988) 590.
[17] G.M. Liu, G.X. Song and X.D. Zhou, Spectrosc. Lett., 25 (1992) 565.
[18] J. Li, C. Xi and H. Shi, Fenxi Huaxue, 17 (1989) 217.
[19] F. Delaye, M.D. Gaye and J.J. Aaron, Anal. Chim. Acta, 223 (1989) 395.
[20] M.K. Park, J.H. Park and J.H. Cho, Arch. Pharmacol. Res., 12 (1989) 289.
[21] A. Espinosa Mansilla, A. Muñoz de la Peña, F. Salinas and A. Zamora, Anal. Chim. Acta, 252 (1992) 47.
[22] K. Shimizu, Y. Motoyama and M. Iwatsuru, Chem. Pharm. Bull, 40 (1992) 2817.
[23] T.V. Karstang and O. Kvaleim, Anal. Chem., 63 (1991) 767.
[24] M. Blanco, J. Gene, H. Iturriaga and S. Maspoch, Analyst, 112 (1987) 619.
[25] A. Grant and P.K. Bhattacharyya, J. Chromatogr., 347 (1985) 219.
[26] A.A. Fasanmade and A.F. Fell, Anal. Chem., 61 (1989) 720.
[27] J.A. Jimena García, J. Giménez Plaza and J.M. Cano Pavón, J. Liq. Chromatogr., 17 (1994) 277.
[28] M. Blanco, J. Coello, F. González, H. Iturriaga and S. Maspoch, Anal. Chim. Acta, 226 (1989) 271.
[29] Y. Zhu and J. Shao, Analyst, 114 (1989) 97.
[30] N.K. Agnihotri, H.B. Singh, R.L. Sharma and V.K. Singh, Talanta, 40 (1993) 415.
[31] M. Blanco, J. Coello, F. González, H. Iturriaga and S. Maspoch, Anal. Chim. Acta, 230 (1990) 221.
[32] M.I. Toral, P. Richter, L. Silva and A. Salinas, Microchem. J., 48 (1993) 221.
[33] J.M. Castro Romero, J. Fernández Solís, M.H. Bollaín Rodríguez and F. Bermejo Martínez, Microchem. J., 43 (1991) 104.
[34] W. Sun, R. Xiang and H. Mao, Fenxi Shiyanshi, 11 (1992) 26.
[35] N.X. Wang, W.A. Liang and P. Qi, Talanta, 40 (1993) 897.
[36] P.S. Ramanathan, V.S. Sarang and A.P. Walkevar, Indian J. Chem. A, 26 (1987) 320.
[37] H. Li and J. Yan, Fenxi Huaxue, 15 (1987) 52.
[38] J.Y. Zhang, Y. Ren and X.L. Yin, Guangpuxue Yu Guangpu Fenxi, 12 (1992) 113.
[39] H. Salem, M. El-Maamli, M. El-Sadek and A.A. Kheir, Zh. Prikl. Spektrosk., 57 (1992) 264.
[40] Z. Wang, Z. Zheng and Z. Wu, Fenxi Huaxue, 15 (1987) 251.
[41] A. Bermejo Barrera, M.P. Bermejo Berrera, M.M. Guisasola Escudero and F. Bermejo Martínez, Analyst, 112 (1987) 481.
[42] S. Mathew, R. Sukumar, T. Prasada Rao and A.D. Damodarán, Anal. Lett., 25 (1992) 1941.
[43] F. García Sánchez, M. Hernández and J.C. Márquez Gómez, An. Quim., 86 (1990) 652.
[44] R.F. Gureva and S.B. Savvin, Zh. Anal. Khim., 43 (1988) 476.
[45] J. Li, Q. Luo and Y. Zeng, Fenxi Shiyanshi, 7 (1989) 16.
[46] C. Jhiang and Z. Li, Fenxi Shiyanshi, 7 (1988) 59.
[47] J. Hernández Méndez, B. Moreno Cordero and L. Gutierrez Dávila, Analyst, 112 (1987) 1507.
[48] H. Shi, L. Kong, J. Li and L. Wang, Huaxue Shiji, 12 (1990) 321.
[49] S. Zou and Z. Li, Gaodeng Xuexiao Huaxue Xuebao, 9 (1988) 850.
[50] N.A. Kanaev, A.P. Ivchenko, T.A. Belova and N.V. Gundobin, Zavod. Lab., 59 (1993) 1.
[51] N.X. Wang, Q.C. Wu, J.B. Shi and P. Qi, Mikrochim. Acta, 110 (1993) 119.
[52] N. Wang, W. Liang, S. Zhou and P. Qi, Anal. Chim. Acta, 262 (1992) 253.
[53] J. Zhou, W.A. Liang and S.F. Zhou, Yankuang Ceshi, 11 (1992) 333.
[54] N.X. Wang, W.A. Liang and P. Qi, Fenxi Huaxue, 21 (1993) 90.
[55] Y. Hayashibe, M. Takeya and Y. Sayama, Bunseki Kagaku, 42 (1993) 99.
[56] Q. Hu, C.X. Xie and S.Z. Yang, Fenxi Huaxue, 20 (1992) 1439.
[57] M. Hernández López, J.C. Márquez Gómez, J. Medinilla and F. García Sánchez, Quim. Anal., 7 (1988) 341.
[58] S.L. Zhao, P. Li, L.J. Zhang and Y.J. Wang, Fenxi Huaxue, 21 (1993) 336.
[59] S.L. Zhao, P. Li and X.B. Wu, Fenxi Huaxue, 20 (1992) 1195.

[60] A. Gallardo Melgarejo, A. Gallardo Céspedes and J.M. Cano Pavón, Analyst, 114 (1989) 109.
[61] D. Sreevalsan Nair, T. Prasada Rao, C.S.P. Iyer and A.D. Damodarán, Anal. Lett., 26 (1993) 523.
[62] S. Kus and Z. Marczenko, Analyst, 112 (1987) 1503.
[63] G. Mai, J. Gao, H. Sui and S. Wang, Huaxue Shijie, 28 (1987) 22.
[64] G. Bai, J. Kang and R. Chen, Fenxi Huaxue, 15 (1987) 902.
[65] P. Chen, Q. Luo and Y. Zeng, Guangpuxue Yu Guangpu Fenxi, 7 (1987) 5.
[66] N.N. Aleksandrova, V.T. Mishchenko, N.S. Poluektov and L.P. Shilova, Ukr. Khim. Zh., 53 (1987) 297.
[67] G.Q. Lao and L.R. Chen, Huaxue Fence, 28 (1992) 353.
[68] R. Sun, Fenxi Shiyanshi, 10 (1991) 68.
[69] S. Kus, Z. Marczenko and N. Obarski, Chem. Anal., 37 (1992) 569.
[70] P.L. López de Alba and L. Martínez, J. Radioanal. Nucl. Chem., 164 (1992) 309.
[71] A. Ramesh, J. Krishamacharyulu, L.K. Ravindranath and S.B. Rao, J. Radional. Nucl. Chem., 170 (1993) 181.
[72] A.I. Jiménez, F. Jiménez and J.J. Arias, Analyst, 114 (1989) 93.
[73] J. Zhang, Y. Ren and P. Miao, Yingyong Huaxue, 7 (1990) 34.
[74] Z.J. Li, J.M. Pan and Z.J. Xu, Huaxue Fence, 28 (1992) 259.
[75] J.M. Pan, Z.J. Li and Z.J. Xu, Huaxue Fence, 29 (1993) 76.
[76] L. Liu, P. Li, W. Xu and H. H. Lu, Fenxi Huaxue, 19 (1991) 1228.
[77] L. Lin, Zhongguo Zhongyao Zazhi, 15 (1990) 32.
[78] D. Ivanovic, E. Guernet-Nivaud and M. Guernet, Anal. Lett., 23 (1990) 1123.
[79] A. Espinosa Mansilla, A. Muñoz de la Peña, F. Salinas and A. Zamora, Anal. Chim. Acta, 258 (1992) 47.
[80] G. Milch and E. Szabo, Acta Phys. Hung., 63 (1988) 165.
[81] F. Navarro Villoslada, M.E. León González, L.V. Pérez Arribas, M.J. Santos Delgado and L.M. Polo Diez, Microchem. J., 44 (1991) 339.
[82] F. Navarro Villoslada, L.V. Pérez Arribas, M.E. León González, M.J. Santos Delgado and L.M. Polo Diez, Talanta, 38 (1991) 1341.
[83] K. Kitamura and N. Imayoshi, Anal. Sci., 8 (1992) 497.
[84] V. Singh, J.S. Mahanwal and S.K. Shukla, Indian J. Forensic Sci., 4 (1990) 161.
[85] A. Espinosa Mansilla, A. Muñoz de al Peña, F. Salinas and M. Martínez Galera, Anal. Chim. Acta, 276 (1993) 141.
[86] A.A.S. El-Din, Alexandria J. Pharm. Sci., 1 (1987) 57.
[87] J. Gabriel, L. Homolka and R. Krejci, Collect. Czech. Chem. Commun., 55 (1990) 1866.
[88] C. Vetuschi, G. Ragno, L. Baiocchi and P. Ridolfi, Spectrosc. Lett., 22 (1989) 375.
[89] J.S. Mahanwal, V. Singh and S.K. Shukla, Indian J. Forensic Sci., 5 (1991) 176.
[90] T.F. Li, Fenxi Huaxue, 20 (1992) 1481.
[91] A. Cladera, E. Gómez, J.M. Estela and V. Cerdá, Anal. Chim. Acta, 267 (1992) 95.
[92] A.F. Fell, T.Z. Woldermarian, P.A. Linley, J. Ge, M.D. Luque de Castro and M. Valcarcel, Anal. Chim. Acta, 234 (1990) 89.
[93] J.A. Jimena García, J. Giménez Plaza and J.M. Cano Pavón, Anal. Chim. Acta, 268 (1992) 153.
[94] S. Mori, J. Appl. Polym. Sci., 33 (1987) 1923.
[95] L. Meal, J. Appl. Polym. Sci., 41 (1990) 2521.
[96] C.Z. Zhao, Z. Tan and X.L. Song, Fenxi Shiyanshi, 12 (1993) 47.
[97] J.J. Berzas Nevado, C. Guiberteau Cabanillas and F. Salinas, Talanta, 39 (1992) 547.
[98] G.J. Bukovits and A. Lezerovich, J. Am. Oil Chem. Soc., 64 (1987) 517.
[99] S. Traore and J.J. Aaron, Analyst, 114 (1989) 609.
[100] J. Li, P. Peng and H. Shi, Huaxue Shiji, 11 (1989) 220.
[101] D. Ivanovic, C. Herrenknecht, E. Guernet-Nivaud and M. Guernet, Anal. Lett., 25 (1992) 1693.
[102] R. Lu, Yaoxue Xuebao, 26 (1991) 219.
[103] V. Cavrini, R. Gatti, P. Roveri and M.R. Cesaroni, Analyst, 113 (1988) 1447.
[104] M.K.S. El-Din, M.A. Abuirjeie and M.H. Abdel-Hay, Anal. Lett., 24 (1991) 2187.
[105] S.G. Tiraspolskaya, G.I. Lukyanchikova, G.V. Alfimova, T.I. Maksimenko and O.G. Strusovskaya, Farmatsiya, 40 (1991) 74.
[106] A. Yesilada, H. Erdogan and M. Ertan, Anal. Lett., 24 (1991) 129.
[107] A.M. Di Pietra, V. Cavrini, R. Gatti and M.A. Raggi, Pharm. Res., 5 (1988) 709.
[108] F. Belal, F. Ibrahim, S.M. Hassan and F.A. Aly, Microchem. J., 41 (1990) 305.
[109] A. Yesilada and M. Ertan, Anal. Lett., 24 (1991) 2033.
[110] J.A. Murillo, J. Rodríguez, J.M. Lemus and A. Alanon, Analyst, 115 (1990) 1117.
[111] M. El Sadek, H. Salem and A. Aboul Khier, Spectrosc. Lett., 23 (1990) 77.
[112] B. Zhang, Zhongguo Yaoxeu Zazhi, 27 (1992) 485.
[113] J.E. Parkin, J. Pharm. Biomed. Anal., 11 (1993) 609.
[114] V. Singh, S.K. Shukla and J.S. Mahanwal, Indian J. Forensic Sci., 4 (1990) 89.
[115] L. Duhau, P. Lafargue, P. Levillain, M. Galliot and R. Bourdon, Analusis, 17 (1989) 553.
[116] P. Corti, C. Aprea, G. Corbini, E. Dressi and L. Celesti, Pharm. Acta. Helv., 66 (1991) 50.
[117] M.S. Mahrous, H.G. Daabees and Y.A. Beltagy, Spectrosc. Lett., 25 (1992) 389.
[118] P. Richter, Int. J. Pharm., 72 (1991) 207.
[119] B. Xu and Q. Liu, Zhongguo Zhongyao Zazhi, 18 (1993) 35.
[120] T. Bai and J.H. Jia, Yaoxue Xuebao, 23 (1988) 616.
[121] M.E. Abdel-Moety, M.F. El-tarras, B.E.A. El-Zeany and K.O. Kelani, Arch. Pharmacol. Res., 13 (1990) 215.
[122] X. Weng, Yaowu Fenxi Zazhi, 8 (1988) 187.
[123] A.A.M. Wahbi, M.S. Mahrous, Y.A. Beltagy, A.S. Issa and H. Lymona, Spectrosc. Lett., 25 (1992) 721.
[124] M.G. El-Bardicy, Y.S. El-Saharty and M.S. Tawakkol, Spectrosc. Lett., 24 (1991) 1079.
[125] M.A. Korany, M. Abdel-Hady, Elsayed and S.M. Galal, Anal. Lett., 22 (1989) 159.
[126] I.I. Hewala, Anal. Lett., 26 (1993) 625.
[127] W.M. He and Q. Wang, Zhongguo Yiyao Gongye Zazhi, 22 (1991) 508.
[128] H. Mahgoub, Drug Dev. Ind. Pharm., 16 (1990) 2135.

[129] N. Magda, H. El-Henawee, M. Saleh, N. El-Bolkiny and M.N. Ayad, Spectrosc. Lett., 23 (1990) 273.
[130] A.A. Fasanmade and A.F. Fell, Analyst, 110 (1985) 1117.
[131] Y. Zhou, Yaowu Fenxi Zazhi, 6 (1986) 359.
[132] H. Mahgoub, F.A. El-Yazbi and M.H. Barary, Sci. Pharm., 60 (1992) 239.
[133] M.S. Mahrous, M.M. Abdel-Khalek, H.G. Daabees and Y.A. Beltagy, Anal. Lett., 25 (1992) 1491.
[134] M.M. Amer, M. Fayez El-Tarras, S. Abd El Fattah and F.H. Metwally, Anal. Lett., 21 (1988) 773.
[135] M.E. Abdel-Hamid and M.A. Abuirjeie, Analyst, 113 (1988) 1443.
[136] C. Mannuci, J. Bertini, A. Cocchini, A. Perico, F. Salvagnini and A. Triolo, J. Pharm. Sci., 81 (1992) 1175.
[137] B. Morelli, J. Pharm. Sci., 77 (1988) 1042.
[138] L.C. Bailey, K.T. Tang and B.A. Rogozinski, J. Pharm. Biomed. Anal., 9 (1991) 501.
[139] M.A. Korany, M.M. Bedair and A. El-Gindy, Drug. Dev. Ind. Pharm., 16 (1990) 1555.
[140] J. Guan, M. Xu and S. Cao, Zhongguo Yiyuan Yaoxue Zazhi, 13 (1993) 120.
[141] L. Lin, S. Yu and B. Xu, Fenxi Huaxue, 20 (1992) 680.
[142] S.M. Galal, M.M. Bedair and M.A. El-Sayed, J. Pharm. Belg., 45 (1991) 315.
[143] M.E. Mohamed, H.A. Al-Khamees, M. Al-Awadi and K.I. Al-Khamis, Farmaco., 44 (1989) 1045.
[144] L. Nobile and M.A. Raggi, Farmaco., 47 (1992) 811.
[145] F.A. El-Yazbi, M.A. Korany, O. Abedel-Razak and M.A. El-Sayed, Alexandria J. Pharm. Sci., 2 (1988) 160.
[146] J. Novakovic and I. Nemcova, Pharmazie, 45 (1990) 439.
[147] M.A. Korany, F.A. El-Yazbi, O. Abdel-Razak and M.A. Elsayed, Pharm. Weekbl., Sci. Ed., 7 (1985) 163.
[148] F.A. El-Yazbi, Spectrosc. Lett., 25 (1992) 1011.
[149] X. Yuan and H. Ding, Zhongguo Yaouxue Zazhi, 27 (1992) 554.
[150] G. Milch and E. Szabo, Analusis, 16 (1988) 59.
[151] M.M. Bedair, M.A. Korany, M.A. Ebdel-Hay and A.A. Azza, Analyst, 115 (1990) 449.
[152] C. Yucesoy, Turk Eczacilari Birligi Dergisi Pharmacia, 30 (1990) 53.
[153] F.A. El-Yazbi, M.A. Korany, O. Abdel-Razek and M.A. El-Sayed, Alexandria J. Pharm. Sci., 1 (1987) 1.
[154] K. Kovacs-Hardady, I.T. Kiss, M. Kiss and K. Barna-Katona, Analyst, 113 (1988) 569.
[155] J.M. García Fraga, A.I. Martínez Abizanda, F. Jiménez Moreno and J.J. Arias León, J. Pharm. Biomed. Anal., 9 (1991) 109.
[156] R. Kashyap, L.R. Iyer and M.M. Singh, Indian J. Forensic Sci., 4 (1990) 203.
[157] A. Yesilada, A.E. Theobald and R.C. Hidder, J. Pharm. Biomed. Anal., 10 (1992) 699.
[158] F. Onur and S. Dermis, S.T.P. Pharma, 6 (1990) 464.
[159] A. Di Giulio, G. Maurizi, M.A. Antonietta, G. Amicosante, P. Mazzeo and A. Oratore, J. Pharm. Biomed Anal., 7 (1989) 1159.
[160] L. Liang and Z. Tao, Yaowu Fenxi Zazhi, 12 (1991) 238.
[161] S.T. Hassib, Anal. Lett., 23 (1990) 2195.
[162] X. Mei and G. Yang, Yaowu Fenxi Zazhi, 12 (1992) 172.
[163] H. Li, Yaoxue Tongbao, 22 (1987) 221.
[164] F. Onur and N. Acar, Int. J. Pharm., 78 (1992) 89.
[165] M.S. Mahrous, M.M. Abdel-Khalek and Y.A. Beltagy, Anal. Lett., 25 (1992) 1673.
[166] A.M. El Walily, M.A. Korany, F.M. El-Anwar and S.M. Zamel, Anal. Lett., 25 (1992) 81.
[167] J.J. Berzas Nevado, J. Rodríguez Flores and M.L. De la Morena Pardo, Analusis, 21 (1993) 33.
[168] S. Atmaca, Z. Bilgic and M. Acikkol, Pharmazie, 46 (1991) 532.
[168] D.N. Xie, J.H. Ge, Q.T. Lan, R.G. Yu and J.Y. Cui, Zhongguo Yaoke Daxue Xuebao, 23 (1992) 183.
[170] L.M. Lin, Y.H. Liu and J.M. Wang, Zhongguo Yiyao Gongye Zazhi, 23 (1992) 220.
[171] K. Shimizu, Y. Motoyama and M. Iwatsuru, Chem. Pharm. Bull., 40 (1992) 2817.
[172] G. Milch and E. Szabo, J. Pharm. Biomed. Anal., 9 (1991) 1107.
[173] C. Yucesoy, FABAD Farm. Bilimler Derg., 15 (1990) 175.
[174] S. Kir, C. Safak, A. Tureli and A. Temizer, Fresenius' J. Anal. Chem., 339 (1991) 264.
[175] F. Onur and N. Acar, Analusis, 18 (1990) 560.
[176] M.K. Par, J.H. Cho and Y.H. Park, Soul Taehakkyo Yakhak Nonmunjip, 12 (1987) 67.
[177] J.M. García, A.I. Jiménez, F. Jiménez and J.J. Arias, Anal. Lett., 25 (1992) 1511.
[178] F.A. El-Yazbi, M.A. Korany, H.H. Abdine and M.A. Elsayed, Spectrosc. Lett., 24 (1991) 437.
[179] M.H. Abdel-Hay, M.H. Barary, E.M. Hassan and M.A.H. Elsayed, Spectrosc. Lett., 22 (1989) 1025.
[180] P. Ryclovsky and I. Nemcova, Cesk. Farm., 38 (1989) 241.
[181] R. Kashyap, L.R. Iyer and M.M. Singh, Indian J. Forensic Sci., 5 (1991) 73.
[182] H. Salem, H.E. Abdel Latef, M.A. Elsadek and A. Aboul-Kheir, Spectrosc. Lett., 23 (1990) 1065.
[183] G. Gazzani, G. Stoppini, C. Gandini and A. Bettero, J. Chromatogr., 609 (1992) 391.
[184] I. Shoukrallah, Anal. Lett., 24 (1991) 2043.
[185] L.S. Rosenberg and J.L. Jackson, Drug Dev. Ind. Pharm., 15 (1989) 373.
[186] P. Mura, G. Santoni and S. Pinzauti, Pharm. Acta Helv., 62 (1987) 226.
[187] B. Panzova, M. Ilievska, G. Trendovska and B. Bogdanov, Int. J. Pharm., 70 (1991) 187.
[188] G. Milch and E. Szabo, Acta Chim. Hung., 124 (1987) 883.
[189] L.C. Bailey, K.T. Tang and B.A. Rogozinksi, J. Pharm. Biomed. Anal., 9 (1991) 501.
[190] J.M. Hoover, R.A. Soltero and P.C. Bansal, J. Pharm. Sci., 76 (1987) 242.
[191] J.L. Murtha, T.N. Julian and G.W. Radebaugh, J. Pharm. Sci., 77 (1988) 715.
[192] R. Zhang, Y. Hu and C. Xu, Zhongcaoyao, 19 (1988) 159.
[193] P. Corti, L. Savini, L. Celesti, G. Ceramelli and L. Montecchi, Pharm. Acta Helv., 67 (1992) 76.
[194] E.R.M. Hackmann, S.A. Benetton and M.I.R.M. Santoro, J. Pharm. Pharmacol., 43 (1991) 285.
[195] G. Mukherji and N. Aggarwal, Int. J. Pharm., 71 (1991) 187.
[196] F. Salinas, J.J. Berzas Nevado and A. Espinosa Mansilla, Talanta, 37 (1990) 347.
[197] G. Carlucci and P. Mazzeo, Farmaco, 47 (1992) 817.

[198] H. Salem, M. El-Maamli, M. El-Sadek and A.A. Kheir, Spectrosc. Lett., 24 (1991) 451.
[199] S. Othman, Int. J. Pharm., 63 (1990) 173.
[200] H.E. Abdellatef, M.N. Elbalkiny and A. Aboulkheir, J. Pharm. Biomed. Anal., 7 (1989) 571.
[201] F. Salinas, A. Espinosa Mansilla and J.J. Berzas Nevado, Anal. Chim. Acta, 233 (1990) 289.
[202] J.J. Berzas Nevado, J. Rodríguez Flores and M.L. de la Morena Pardo, Talanta, 38 (1991) 1261.
[203] J.J. Berzas Nevado, J.M. Lemus Gallego and G. Castañeda Penalvo, J. Pharm. Biomed. Anal., 11 (1993) 601.
[204] Z. Zu, Yaowu Fenxi Zazhi, 7 (1987) 100.
[205] P.K. Hon and W.K. Fun, Analyst, 116 (1991) 751.
[206] X. Zhang, T. Li and X. Ping, Yaowu Fenxi Zazhi, 12 (1992) 348.
[207] M. Park and J. Cho, Arch. Pharmacol. Res., 11 (1988) 45.
[208] J. Petiot, P. Prognon, E. Postaire, M. Larue, F. Laurencon-Courteille and D. Pradeau, J. Pharm. Biomed. Anal., 8 (1990) 93.
[209] M.N. Merzlyak, T.V. Zhigalova and V.V. Shevyreva, Phytochem. Anal., 3 (1992) 105.
[210] F.A. Aly, Mikrochim. Acta, 110 (1993) 187.
[211] G.J. Bukovits and A. Lezerovich, J. Am. Oil Chem. Soc., 64 (1987) 517.
[212] M.S. Mahrous, M.E. Abdel-Hamid, H.G. Dabees and Y.A. Beltagy, J. Pharm. Belg., 47 (1992) 135.
[213] M.M. Bedair and M.H. Barary, Bull Fac. Pharm., 29 (1991) 1.
[214] L. Nobile, V. Cavrini, M.A. Raggi and A.M. Di Pietra, Int. J. Pharm., 40 (1987) 85.
[215] L.M. Lin, Yaoxue Xuebao, 26 (1991) 858.
[216] R. Marquet and C. Houssier, Anal. Biochem., 176 (1989) 265.
[217] V.S. Saakov, A. Semenova, V.G. Leontev and B.V. Shiryaev, Fiziol. Rast., 37 (1990) 180.
[218] D.E.H. Palladino and K.A. Cohen, J. Chromatogr. Sci., 29 (1991) 91.
[219] Z.B. Wang, Z.Z. Zheng and L.L. Ouyang, Fenxi Huaxue, 20 (1992) 987.
[220] D.H. Freeman, D.C. San Martín and C.J. Boreham, Energy Fuels, 7 (1993) 194.
[221] A.V. Semenova and V.S. Saakov, Fiziol. Rast., 36 (1989) 1207.
[222] Y. Nozaki, Arch. Biochem. Biophys., 277 (1990) 324.
[223] Reference deleted.
[224] H. Mach., J.A. Thomson, C.R. Middaugh and R.V. Lewis, Arch. Biochem. Biophys., 287 (1991) 33.
[225] L.L. Holte, F.J. Van Kuijk and E.A. Dratz, Anal. Biochem., 188 (1990) 136.
[226] C.W. Turck, Pept. Res., 5 (1992) 156.
[227] P. Garriga, J. Sagi, D. García Quintana, M. Sabes and J. Manyosa, J. Biomol. Struct. Dyn., 7 (1990) 1061.
[228] P. Garriga, D. García Quintana and J. Manyosa, Eur. J. Biochem., 210 (1992) 205.
[229] H. Goetz, Biochromatography, 4 (1989) 159.
[230] C. Wilson, R.L. Greasham, M. Will and R.A. Copeland, Anal. Biochem., 182 (1989) 141.
[231] M.T.W. Hearn, M.I. Aguilar, T. Nguyen and M. Fridman, J. Chromatogr., 435 (1988) 271.
[232] H. Mach, C.R. Middaugh and R.V. Lewis, Anal. Biochem., 200 (1992) 20.
[233] M.A. Ramzan, E.J. Cookson and R.J. Beynon, Biochem. Soc. Trans., 19 (1991) 296.
[234] M. Meys and S.A. Cohen, LC-GC, 9 (1991) 422.
[235] J. Bertini, C. Mannucci, R. Noferini, A. Perico and P. Rovero, J. Pharm. Sci., 82 (1993) 179.
[236] A.T. Dadd, Int. Lab., 21 (1991) 26.
[237] F.N. Kakhanovskii and S.V. Melenevskii, Sud.-Med. Ekspert., 35 (1992) 19.
[238] M.H. Abdel-Hay, M.H. Barary, M.A. Elsayed and E.M. Hassan, Anal. Lett., 24 (1991) 1517.
[239] W. Spivak, C. Morrison, D. Devinuto and W. Yuey, Biochem. J., 252 (1988) 275.
[240] J.W. Stroes and H.J.M. Van Rijn, Ann. Clin. Biochem., 24 (1987) 189.
[241] H. Verweij and H.A. Bonte, Ann. Clin. Biochem., 28 (1991) 179.
[242] B.J. Perrigo and B.P. Joint, J. Anal Toxicol., 13 (1989) 37.
[243] S. Wu and M. Liu, Huaxi Yaoxue Zazhi, 8 (1993) 9.
[244] F. Randez-Gil, A. Salvador and M. de la Guardia, Microchem. J., 44 (1991) 249.
[245] B.E. Copeland, P.J. Dyer and A.J. Pesce, Ann. Clin. Lab. Sci., 19 (1989) 383.
[246] A. Cruz, M. López Rivadulla, I. Sánchez, A.M. Bermejo and P. Fernández, Anal. Lett., 26 (1993) 1087.
[247] A. Iordache, A. Beamonte, A.M. Soummer and P. Chambon, Pathol. Biol., 38 (1990) 80.
[248] G. Carlucci, P. Mazzeo and M. Bologna, J. Pharm. Biomed. Anal., 9 (1991) 1169.
[249] R.D. Situnayake, B.J. Crump, A.V. Zezulka, M. Davis, B. McConkey and D.I. Thurham, Ann. Clin. Biochem., 27 (1990) 258.
[250] F.P. Corongiu, S. Banni and M.A. Dessi, Free Radical Biol. Med., 7 (1989) 183.
[251] L.S.L. Arakaki and D.H. Burns, Appl. Spectrosc., 46 (1992) 1919.
[252] F. Randez Gil, J.A. Daros, A. Salvador and M. de la Guardia, J. Pharm. Biomed. Anal., 9 (1991) 539.
[253] A.M. Bermejo, M. López Rivadulla, P. Fernández and A. Cruz, Anal. Lett., 24 (1991) 1147.
[254] H.D. Li, X.H. Yan and H. Zheng, Yaowu Fenxi Zazhi, 12 (1992) 323.
[255] M.M. Abdel-Khalek, M.S. Mahrous, H.G. Daabees and Y.A. Beltagy, Anal. Lett., 25 (1992) 1851.
[256] A.W. Van de Giessen and E.M. Van Wijk, J. Clin. Chem. Clin. Biochem., 28 (1990) 605.
[257] N. Martín, P. Lafargue, P. Levillain and G. Houin, Report 1989, CERMA-89/25, Order No. PB90-168923.
[258] M.C. Gutierrez, J. Inst. Brew., 98 (1992) 277.
[259] C.J. Humphrey and R. Macrae, Colloq. Sci. Int. Cafe, 12 (1987) 179.
[260] L.S. Daley, R.A. Menéndez and R.L. Stebbins, J. Environ. Hortic., 5 (1987) 25.
[261] I. Durán Meras, A. Muñoz de la Peña, A. Espinosa Mansilla and F. Salinas, Analyst, 118 (1993) 807.
[262] Y. Chen and Z. Zhuo, Fenxi Huaxue, 16 (1988) 9.
[263] S.P. Feng, S.R. Wang, R.L. Chen, G.L. Li and L.Z. Wang, Fenxi Huaxue, 21 (1993) 294.
[264] D. Tu, S. Xue, C. Meng, A. Espinosa Mansilla, A. Muñoz de la Peña and F. Salinas López, J. Agric. Food Chem., 40 (1992) 1022.
[265] R. Calapaj, S. Chiricosta, G. Saija and E. Bruno, Riv. Ital. Sostanze Grasse, 67 (1990) 35.
[266] Z. Wang, Z. Zheng and S. Jiang, Fenxi Huaxue, 15 (1987) 383.

[267] J.C. García Castro, M.J. Sánchez, M.A. Rodríguez Delgado and C. Diaz Romero, Mikrochim. Acta., 110 (1993) 263.
[268] S. Chiricosta, R. Calapaj, G. Saija and E. Bruno, Riv. Ital. Sostanze Grasse, 66 (1989) 91.
[269] P. Deng, Shipin Kexue, 136 (1991) 49.
[270] S. Chiricosta, R. Calapaj, G. Saija and E. Bruno, Riv. Ital. Sostanze Grasse, 69 (1992) 457.
[271] J.C. García Castro, M.A. Rodríguez Delgado, M.J. Sánchez and F. García Montelongo, Anal. Lett., 25 (1992) 2367.
[272] M. Zou, Huaxue Fence, 24 (1988) 52.
[273] R.N. Hager and V.T. Jones, Hydrocarbon Contam. Soils, 1 (1991) 193.
[274] J. Ares, Anal. Chim. Acta, 268 (1992) 135.
[275] K. Putamma and E.V.S. Rao, Commun. Soil Sci. Plant. Anal., 24 (1993) 737.

ELSEVIER

Talanta 42 (1995) 1215–1227

Talanta

Review

# Speciation with unsegmented continuous systems

M.D. Luque de Castro *, D.W. Bryce, A. Izquierdo

*Department of Analytical Chemistry, Faculty of Sciences, University of Córdoba, E-14004 Córdoba, Spain*

Received 6 December 1994; revised 10 March 1995; accepted 11 March 1995

**Abstract**

Speciation applications of the flow-injection technique are discussed in relation to the hydrodynamic manifold components that are adapted for this purpose. Alterations include double halting of the propulsion system, coupling of injection valves, modifications of the transport-reaction zone, use of switching valves, and merging and splitting points. Detector remodelling, the use of sensors and special detectors, and data processing methodologies are also reviewed in connection with the flow-injection/chromatography coupling. Finally, foreseeable trends and desirable advances are outlined.

## 1. Introduction

One of the toughest problems facing analytical chemists on the verge of the 21st century is that of specification, towards which substantial portions of R&D budgets are being alloted in developed countries.

The environment is one of the areas most seriously affected by problems arising from certain toxic physicochemical forms of elements and compounds. The vast amounts of pollutants that are being discharged into the environment, and their usually rapid interconversion, demand continuous or the least frequent monitoring of many such species. This entails developing expeditious, precise methods capable for monitoring environmentally hazardous substances in real or near-real time.

Flow-injection analysis (FIA) is one of the most attractive approaches to speciation on account of its high flexibility, throughput and automatability, as can be inferred from the abundance of literature on this topic [1–7]. As in other areas of social interest, the potential of FIA for speciation has not been fully explored; a call of the analytical community's attention to the great capabilities of FIA in this respect is, therefore, in order.

There is a current trend to refer to this technique as flow-injection (FI), on the reasoning that only in certain instances does sample treatment by this unsegmented flow approach involve true analysis.

Developments in FI/speciation coupling have so far relied on alterations of one or more of the basic elements of a hydrodynamic manifold, namely the propulsion unit, injection system, transport and/or reaction zone and detector. Speciation can also be accomplished prior to introducing the sample into an FI system [8]. In such a case, the manifold is intended to facilitate interference removal and/or derivatization, as well as (obviously) transfer the analyte to the detector. Coupling an FI manifold to a high-discrimination instrument or data processing detector can also be of assistance for speciation. Fig. 1 shows a global view of these approaches, typical examples of which are discussed below.

* Corresponding author. Tel: 957-218616. Fax: 957-218606.


*SSDI* 0039-9140(95)01590-6

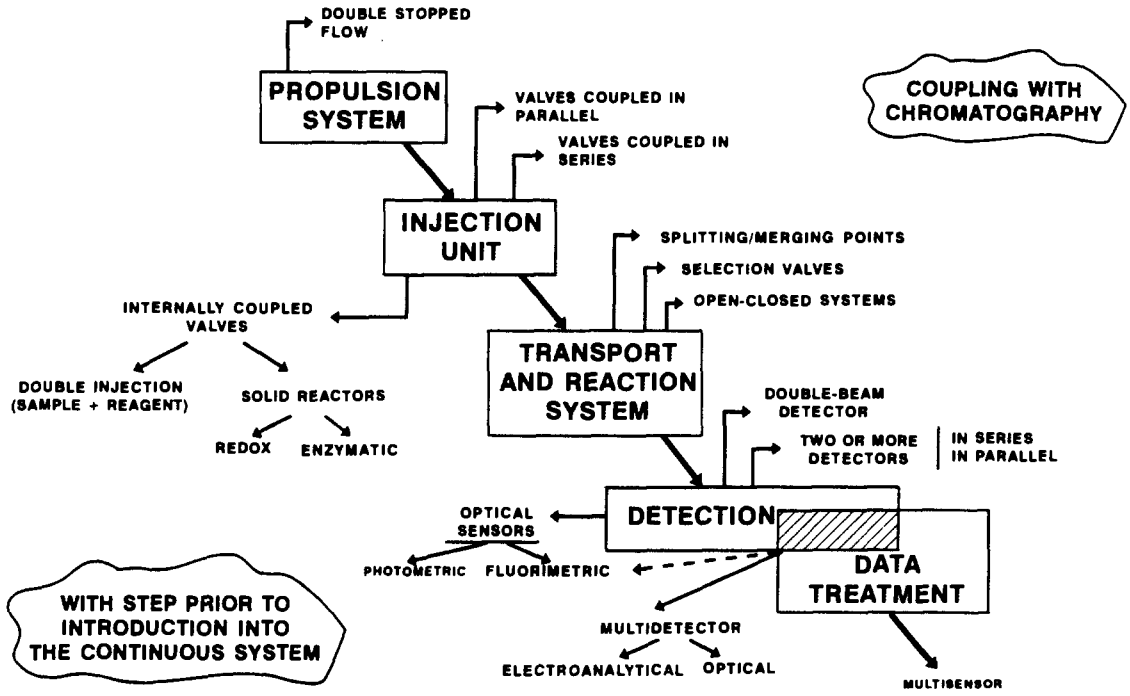


Fig. 1. Approaches to speciation in flow-injection analysis.

We should note that the conventional chemical criteria for speciation in environmental analyses (e.g. oxidation state, coordination form, electron configuration) [9] do not apply in pharmaceutical analyses, where the target problem is discrimination of chiral compounds [10–17], nor in clinical analyses, which include such well-known systems as free and esterified cholesterol [18–20] or free and combined calcium [21–25], in addition to isoenzyme discrimination, a key to diagnosing diseases of great social concern such as infarction [26–33]. This article reviews examples of speciation methods based not only on these, but also on other criteria.

## 2. Speciation prior to flow injection

Sample treatment, usually with an acid, facilitates conversion of species into forms that can be measured by the detector. Thus, alternate introduction of treated and untreated samples into the FI manifold the sequential speciation of two forms of a given compound. Such is the case of selenium speciation as Se(IV)/Se(VI) by the catalytic action of Se(IV) on the reaction

$$ClO_3^- + 5Cl^- + 6H^+ \rightleftharpoons 3Cl_2 + 3H_2O$$

The oxidation product of *o*-tolidine with $Cl_2$ is used for the quantitation at 440 nm. Selenium(VI) is reduced off-line to Se(IV) by boiling HCl [34]. The speciation of this element in sediments and planktonic material entails multistep digestion with $HNO_3$/$HClO_4$ to dissolve all the selenium, as well as dilute sodium hydroxide to relate selenite and selenate. The dissolved species are subsequently determined using a selective hydride generation/atomic absorption method [35].

Voltammetric stripping methods afford very low detection limits for selenium by virtue of preconcentration at the electrode, which is typical in stripping methods. Both the cathodic and anodic modes have been used for selenium(IV) determination with a gold working electrode (anodic stripping [36]) or a glassy carbon working electrode (cathodic stripping [37]). Alternate pretreatment of samples with hot concentrated HCl enables speciation by reduction of Se(VI). A continuous flow manifold facilities not only the removal of interferents for cationic species by use of an ion-exchange microcolumn in the sample stream prior to the injection valve, but also automatic regeneration of the Hg film of the working electrode and automatic switching of electrolyte solutions between the preconcentration and stripping step, thus dramatically increasing automatability, throughput and precision.

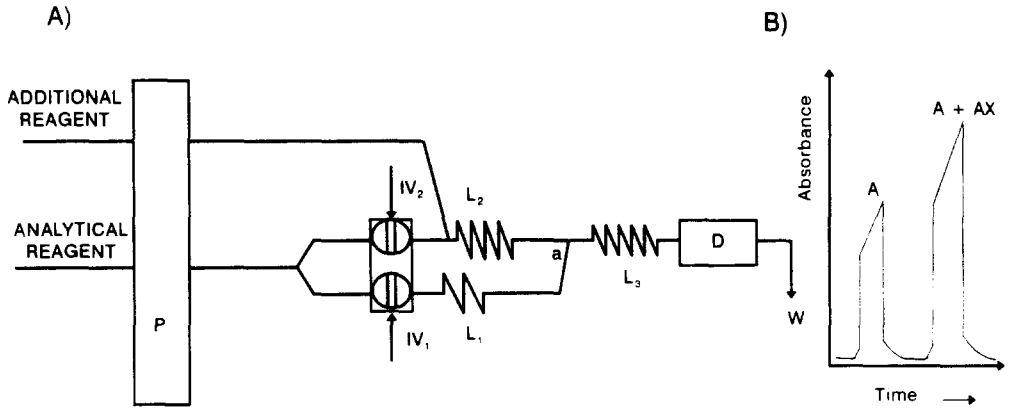


Fig. 2. Merging zones/doubly stopped-flow manifold for speciation of free and bound $SO_2$. P, IV, L, a, D, W, A and AX denote peristaltic pump, injection valve, reaction coil, confluence point, detector, waste, absorbance of free $SO_2$ and absorbance of total $SO_2$, respectively.

## 3. Speciation with a modified propulsion system

Alterations of an ordinary propulsion unit such as a peristaltic pump have opened up a wide range of FI uses such as gradient technique [38–41] (by use of programmed drum rotation speeds), reversed FI, which is particularly effective for accomplishing liquid–liquid extraction without phase separation [42–45], and reaction-rate measurements [46,47] with alternate changes in the drum rotation direction. In any case, the simplest way of manipulating a peristaltic pump is by alternately starting an stopping the flow. This approach, in combination with the merging-zones mode, enables the simultaneous determination of free and bound $SO_2$ in wine. The procedure involves simultaneous dual injection via two parallel valves and stopping the flow twice sequentially as shown in Fig. 2(A). The flow is first stopped when $plug_1$ reaches the detector, where the indicator reaction is monitored to quantify free $SO_2$. Simultaneously, $plug_2$ is stopped at $L_2$, where the bound analyte is subjected to alkaline hydrolysis. Restarting the pump flushes $plug_1$ out of the system and drives $plug_2$ to the detector, after merging at point **a** with the reacting mixture. The flow is stopped again when $plug_2$ reaches the detector. The measured absorbance changes comprise the contributions of both free and bound $SO_2$ [48].

## 4. Speciation with a customized injection unit

The injection system is one of the FI units that can be most readily altered by means available to ordinary research laboratories and not surprisingly has received by far the most attention by workers on FI/speciation [49–53]. Two or more injection valves can be arranged serially or in parallel, or be coupled internally. They can also accommodate solid reactors of different nature in their loops in order to facilitate conversion of the target analytes into their most suitable forms for subsequent derivatization-detection. By way of example, Fig. 3 shows some typical valve arrangements used for nitrogen speciation.

*Two valves connected in series or parallel* (Fig. 3(A)) have been used for nitrogen speciation as ammonia/urea [54], with fluorimetric monitoring of the $NH_3$/OPA (*o*-phthalaldehyde + mercapto-ethanol) reaction product. Simultaneous injection of two sample aliquots into the FI manifold is used to determine endogenous $NH_3$ in the plug with the shorter residence time; the other plug, delayed by passage through an enzyme reactor containing urease immobilized on controlled-pore glass (CPG), is employed to determine both nitrogen forms initially present in the sample after urea is converted into ammonia. These nitrogen species can also be determined by photometric monitoring using an asymmetric merging-zones manifold (Fig. 3(B)), where one valve is loaded with buffer and the other with Nessler's reagent. As the injection valves are simultaneously switched to their inject position, the head of the Nessler's plug reacts with the sample (carrier) to produce a signal proportional to the ammonia concentration. The buffer injected via the first valve restores the baseline before the carrier is passed through the immobilized enzyme reactor (IMER), where the urea is con-

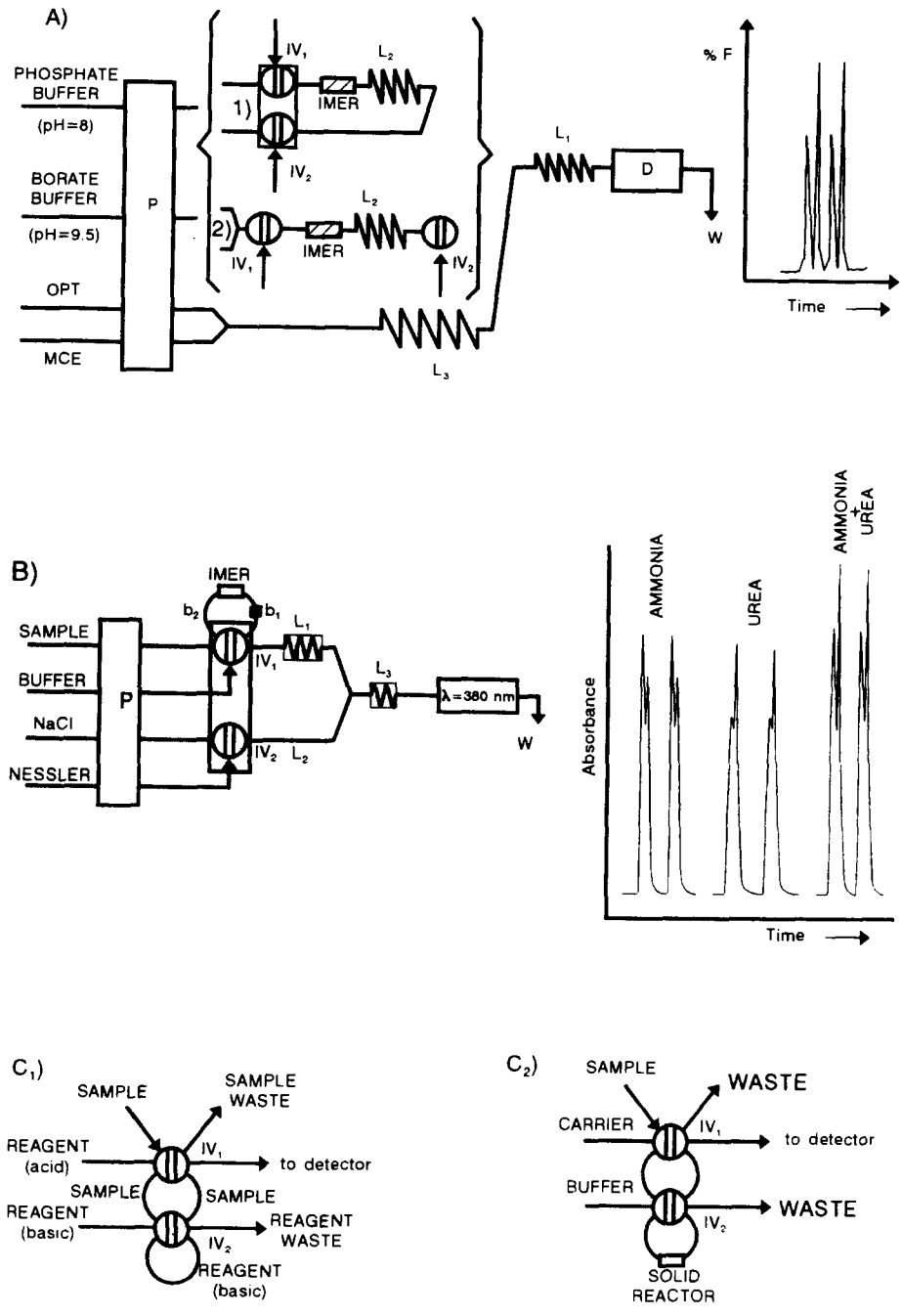


Fig. 3. Manifolds for speciating N based on an altered injection system: (A) with valves in a serial or parallel arrangement for the fluorimetric determination of $NH_3$–urea; (B) by reversed FIA using the asymmetric merging-zones mode (Nessler's reagent is used as derivatizer and the reaction product is monitored photometrically); IMER and b denotes immobilized enzyme reactor and sample sub-loops, respectively; (C) with internally coupled valves ($C_1$) and an optional solid reactor ($C_2$). OPT and MCE are *o*-phthalaldehyde and mercaptoethanol, respectively.

verted into ammonia, which subsequently merges with the tail of Nessler's plug to give a signal proportional to the concentration of ammonia plus urea. The urea concentration is then obtained by difference [55].

The *internally coupled injection valves* used to establish pH gradients [56] provide an excellent means for accomplishing speciation. One such arrangement was used in conjunction with the $NH_3/NH_2$–$NH_2$ + OPA chemical system for speciation of these nitrogen forms, based on the fact that OPA reacts with $NH_3$ in basic medium whereas hydrazine yields a fluorescent product in acid medium. OPA solutions at two different pH values are used; one acts as carrier, the other filling the loop of the secondary

injection valve (that of the main valve is filled with sample), as shown in Fig. 3($C_1$). Simultaneous injection from the two valves produces a profile including four sample/reagent interfaces, and gives rise to a pH difference between the terminal and central interfaces that is as large as required by the chemical system and which can be manipulated through the loop of both valves. The two central interfaces can give rise to a single peak providing the loop of the secondary valve is small enough. Only three peaks appear on the recording; the two outer peaks correspond to hydrazine and the central peak to ammonia [57].

One other way of using internally coupled valves is by placing a solid reactor (whether redox or enzymatic) [58] *in the loop of the secondary valve*, as shown in Fig. 3($C_2$). The assembly, including a copperized cadmium microcolumn, was used for speciation of nitrogen as nitrite/nitrate. Both sub-loops of the main valve were filled with sample, and the secondary loop with carrier. By switching both valves to their inject positions, the carrier was passed through the redox column in the opposite direction to which it was filled in order to prevent overpacking the column, which would have been a problem otherwise. The first sample sub-plug, which was not reduced, was allowed to reach the detector, where it gave a signal proportional to the nitrite concentration. The second portion passed through the redox column to reduce nitrate to nitrite, thereby effectively giving a signal proportional to nitrate plus nitrite. The nitrate concentration was then obtained by difference [58]. A similar arrangement was used for iron speciation as [Fe(II)/Fe(III)] with 1,10-phenanthroline as the derivatizing reagent. The manifold was a part of an analyzer that also enables the determination of sulphate and ammonia, and the preconcentration of the analytes on an ion-exchange microcolumn located in the loop of an auxiliary valve. A series of switching valves circulate the appropriate reagents for each determination, the reaction products being monitored with a single, conventional photometric detector [59,60].

The above system enables the simultaneous determination of the analytes according to the FI criterion, by which simultaneous determinations are those based on a single injection operation [61]. However, sequential determination of two forms of a compound can be performed with a simpler assembly, such as that reported by Sperling et al. for chromium speciation [as Cr(III)/Cr(VI)] by *on-line preconcentration with selective adsorption* on activated alumina and flame atomic absorption detection. They use a conical microcolumn designed by themselves [62] that is placed in the loop of a commutator; preconcentration and elution are done in opposite directions in order to avoid both the gradually increasing compactness of the column and passage of the sample matrix through the detector. It is worth emphasizing the low detection limits thus achieved (1.0 and 0.8 ng $ml^{-1}$ for Cr(III) and Cr(VI), respectively) [63].

## 5. Speciation with an altered reaction/transport unit

Modifications of the reaction/transport unit mainly involve using diverting/switching valves [64] and/or splitting/merging points [65]. A manifold including one such unit allows speciation in a single injection operation with fixed-time or reaction-rate measurements. Cerium speciation as [Ce(III)/Ce(IV)] was accomplished using a manifold such as that shown in Fig. 4(A), with a redox reactor in one of the *split channels*, and monitoring the native fluorescence of Ce(III). The injected plug is split into two portions, one of which is rapidly driven to the detector, where endogenous Ce(III) is monitored. The other portion is delayed by passage through the redox reactor; it does not overlap with the first portion on passage through the detector, but produces a signal that consists of the contributions from both cerium forms initially present in the sample [66].

The speciation of free- and esterified-cholesterol in serum was also accomplished using a manifold with *splitting/merging points* [67,68]. A cholesterol esterase solid reactor inserted in one of the split channels produced the enzymatic hydrolysis of esterfied cholesterol in the sub-plug circulated through the channel, while the plug in the other channel underwent no hydrolysis. A cholesterol oxidase reactor placed beyond the merging point catalyzed the oxidation of cholesterol from the two plugs, which reached the reactor and detector sequentially. An enzyme electrode (peroxidase immobilized on a gold electrode) produced a signal due to the reduction of the hydrogen peroxide formed in the previous enzymatic step.

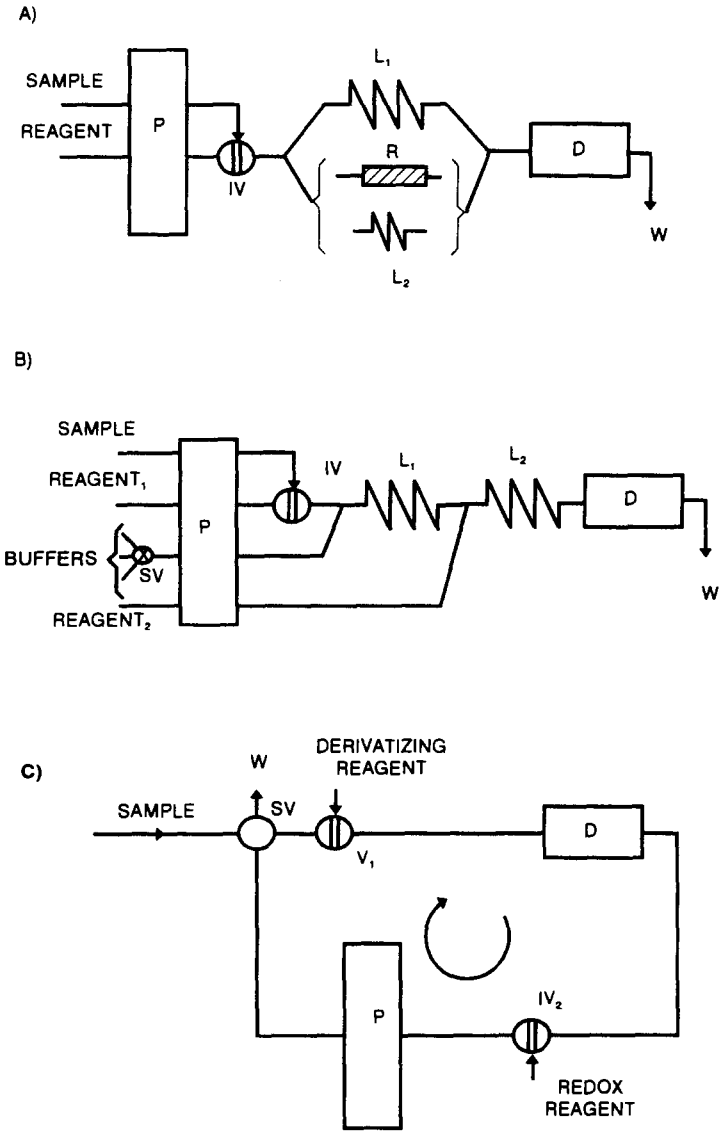


Fig. 4. Modifications of the transport/reaction zone for specification: (A) splitting and merging points, with or without a redox reactor, with fixed-time or reaction-rate monitoring, respectively; (B) selection of the reaction medium; (C) open–closed manifold for fixed-time and reaction-rate measurements for multipeak recordings. R and SV denote redox reactor and switching valve, respectively.

The different reaction-rate of cyanide with $B_6$ vitamins to yield fluorescent products also affords speciation of these compounds (as pyrodoxal-Py- and pyridoxal-5-phosphate-Py5P) in serum by means of an FI manifold with *splitting/merging points* (Fig. 4(A)). A two-peak recording is obtained per injected sample; the first peak is due to the reaction product of Py5P/cyanide, with faster kinetics; the second is due to the products of both vitamins [69]. The main drawback of this approach is the need for a compromise in the pH to be made for development of the derivatizing reactions of both analytes which detracts from the sensitivity. The sequential determination of these analytes by means of a manifold including a switching valve circumvents this shortcoming, as it allows a solution at the optimum pH for each reaction to be selected. The ensuing method is somewhat slower as it requires one sample injection per analyte; this augments sample consumption, which can be a serious drawback for clinical analyses [69].

The use of *valves for selecting* the most suitable reaction medium for each analyte has also been reported in connection with arsenic speciation (as arsenite/arsenate), and phosphate determination by measurement of the formation

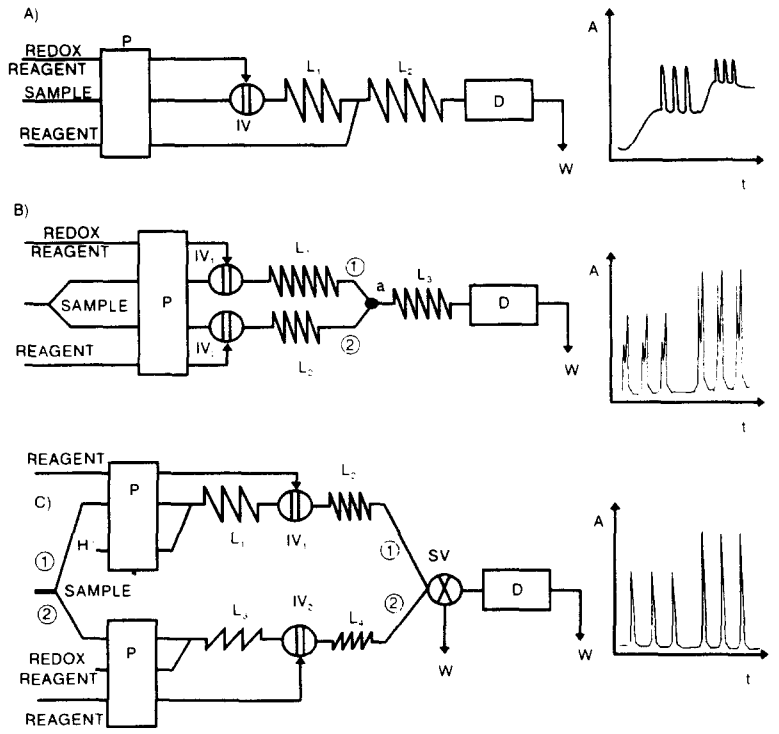


Fig. 5. Reversed FI manifolds for chromium speciation and typical recordings obtained: (A) with continous monitoring of Cr(VI) and periodic measurement of Cr(III); (B) by the asymmetric merging-zones mode (simultaneous determination); (C) by sequential determination of Cr(VI) (manifold 1) and Cr(VI) + Cr(III) (manifold 2). a is a merging point.

of a heteropolyacid with Mo(VI) and reduction to Molydenum Blue in the presence of ascorbic acid. The switching valve in Fig. 4(B) facilitates merging of the main channel with a stream of water (determination of arsenate), $KIO_3$ (determination of the arsenite/arsenate mixture) or $H_2SO_4$ (determination of $PO_4^{3-}$) [70]. Speciation of the two arsenic forms has also been accomplished using Fleitman's reaction for the selective formation of arsine, followed by efficient trapping of this volatile hydride and measurement by electrothermal atomic absorption spectrometry [71]. Rüde and Puchelt [72] recently reported a method based on flow-injection/hydride generation/atomic absorption spectrometry (FI/HG/AAS). The FI manifold provides a suitable acid medium for hydride formation for arsenic, arsenous, monomethylarsonic and dimetylarsinic acids. Switching to the specific medium by means of the valve is followed by injection of a sample aliquot for the determination of a single analyte, so only sequential determinations are feasible.

*Reversed FI* has been used to develop a wide range of speciation methods, particularly for chromium as [Cr(III)/Cr(VI)]. The derivatizing reaction involves chromic ion and diphenylcarbazide (DPC). Chromium(III) does not react with DPC, so it must have been oxidized previously, usually with Ce(IV). The most serious shortcoming of reversed FI is a high sample consumption relative to normal FI. However, this poses no problem with water samples (tap, sea, waste, etc.), which are usually abundant. The three configurations outlined in Fig. 5 were tested for speciation of chromium in water with the Cr(VI)/DPC system as indicator. Configurations A and B allow the simultaneous determination of the two oxidation states of the metal, while configuration C permits their sequential determination. Fig. 5(A) demonstrates continuous monitoring for Cr(VI) and periodical determination of Cr(III). In Fig. 5(B), asymmetric merging of a large DPC plug and a small oxidant plug gives two peaks related to the concentration of Cr(VI) and the sum of the two oxidation states, respectively. Valve SV in Fig. 5(C) is used to switch between the determination of Cr(VI) (upper manifold) and [Cr(VI)/Cr(III)] (lower manifold) [73].

A switching valve can also be employed to construct an *open–closed system* [74] for use in the reverse FI mode in order to accomplish efficient speciation with fixed-time or reaction-rate measurements. The manifold in Fig. 4(C) was used for the speciation of chromium [75]

and iron [76] by simultaneous injection of the derivatizing reagent (diphenylcarbazide and 1,10-phenanthroline, respectively) and a redox agent (Ce(IV) and hydroxylamine, respectively). The reagent injection provided several peaks for one of the analytes (Cr(VI) or Fe(II)); after the contents of the closed circuit were dispersed, the derivatizing reagent/sample mixture met the redox agent plug. Subsequent measurements consisted of the contributions from the two oxidation states.

## 6. Speciation with a modified detection unit

Discrimination between chemical forms can be accomplished using one or more detectors which can be interfaced to a computer to expedite data processing. *Two flow-cells arranged in series or parallel* in a double-beam spectrophotometer, or aligned within the optical path of a single-beam spectrophotometer, allow two peaks to be obtained per sample injection. The first peak corresponds to the species that reacts with the derivatizing reagent, and the second to both forms initially present in the sample. With serially connected cells, the point of merging of the redox agent lies between the cells, so the double peak is due to the above-described contributions. With parallel cells or cells aligned within optical path of a single-channel detector, a splitting point for the sample is used after the injection system. Each of the channels is merged with suitable reagents and leads to one of the cells. For a double peak to be obtained, the arrival of either reacting plugs at the flow-cells must be delayed in order to avoid overlap in the optical path [77].

Manifolds including *several detectors* are simpler, but also costlier, to construct. Coupled spectrophotometers have been used in combination with selective reactions for Fe(III) and Fe(II) complex formation with thiocyanate and 1,10-phenanthroline, respectively, for the determination of both oxidation states in mixed process liquors [78]. A molecular spectrometer and an atomic detector in a serial arrangement were also used for speciating Fe(II)/Fe(III) and Cr(III)/Cr(VI) (determination of one oxidation state and the total concentration) [79].

A more complex assembly consisting of *three detectors arranged in series* was used for the speciation of nitrogen (as $NH_3/NO_2^-$) and determination of pH, conductivity and residual chloride in waters [80]. The configuration is an excellent example of the versatility of FIA, in that a single-channel configuration affords five determinations under optimum conditions (pH, reagents and residence time), and switching between normal and reversed FIA as required.

*Flow-through (bio)chemical sensors* are among the most promising types of sensors on account of their ability to solve a host of real analytical problems [81]. They can play a variety of roles in speciation. Some entail no special data processing as speciation does not take place in the sensor itself, but in the hydrodynamic manifold prior to the sensor. Such is the case with the speciation of aluminium based on manipulation of the sample prior to insertion in order to discriminate reactive and total Al, and passage through an ion-exchange column to determine non-labile mono-meric Al [82–84]. Acid soluble Al and labile monomeric Al can be determined by difference. The principal use of this flow-through sensor (flow-cell packed with silica beads and $C_{18}$ as the bonded phase) is for in situ concentration in order to enhance the sensitivity [85].

## 7. Speciation based on data treatment

Most of the approaches dealt with in this section could also be included in section 6 in that they entail use of an unconventional detector, which in turn generally requires a computer for data acquistion and processing.

The simplest such devices are *fast scan voltammetric detectors*, which can be connected to $x-y$ and $x-t$ recorders (the latter are assisted by an electronic device) to obtain normal and derivative cyclic voltammograms, as in the resolution of a mixture of phenol, guaiacol and 2–4 dichlorophenol [86]. Despite the fact that the method has been applied with no computer, data treatment using one of these devices instead of direct measurement of the plateau or peaks of the recordings (normal and derivative measurements, respectively) would have ensured more accurate and reproducible results.

*Detectors with multidetection capabilities* (e.g. diode array spectrophotometers, DAS) must inevitably be interfaced to a computer in order that data may be acquired as they are produced by the detector. The reaction products of organic isomers such as 1- and 2-naphthol, or *o*-, *m*-, and *p*-cresol with 2-aminobenzothiazole/nitrite ion provide very similar absorption spectra. Binary and ternary mixtures of these

isomers have been resolved using FI-DAS for simultaneous monitoring at the 10–20 wavelengths where spectral differences between products are maximal [87]. A DAS-based multisensor was used for the speciation of aromatic amines by differences in the absorption spectra of the analytes of 10 wavelengths, using a flow-cell packed with $C_{18}$ bonded silica in a single-channel manifold with 40:60 v/v methanol/phosphate buffer as carrier-eluent. Analyte concentrations of $5 \times 10^{-7}$ M were thus resolved [88]. A similar flow-through multisensor, in a somewhat more complex FI modified effecting both hydrolysis and derivatization (Griess reaction), was applied to the speciation of carbamate pesticides. Retention of azo dyes on the solid packing of the flow-cell afforded determination limits 50 times lower than that of the conventional FI method [89].

The joint use of *FI-flow-through sensors-synchronous derivative spectrofluorimetry* [90–92] is one other approach to speciation where FI affords automated sample conditioning and derivatization. The sensor provides enhanced sensitivity, while the detector enables selectivity improvements by synchronizing the excitation/emission scan and processing data for delivering results based on a derivative signal. One such triple combination was used for speciation of $B_6$ vitamins (as pyridoxal, pyridoxal-5-phosphate and pyridoxic acid) by derivatization with cyanide to produce fluorescent compounds that were retained on $C_{18}$ bonded silica beads packed in a flow-cell. Elution/regeneration was realized with a switching valve that enabled passage of a 2 M HCl stream through the sensor. Analytes were thus determined in serum [93]. A similar assembly was used for the speciation of PAHs [94]. Halting the flow after retention was found to provide more reproducible results as regards data acquistion. A comparison of numerical vs. electronic derivation showed the best results in terms of sensitivity and reproducibility to be obtained with the former.

Multispeciation of up to seven forms of chromium (molecular, anionic and dimeric Cr(VI), and hydroxylated Cr(III)) was accomplished using a *reserved asymmetric merging-zones manifold* as described above [73], where a *glass-calomel* microelectrode was placed in the sample stream. Use of suitable *computer software* to process pH and total Cr(VI) and Cr(III) concentration data, in addition to the *acid–base equilibrium constants*, enabled calculation of the concentration of the seven forms [95].

## 8. Use of FI-chromatography for speciation

Although chromatography, particularly HPLC [96–105], provides a means for enhancing resolution in speciation analyses, its potential in this context can be further expanded by coupling with FI.

Stockwell and Corns [106] recently elaborated on commercially available continuous systems devised by them for coupling to *atomic fluorescence detectors* (AFS) for speciation of Hg, As and Se, which afford detection limits below the parts-per-trillion level. These hyphenated HPLC-FI-AFS and GC-FI-AFS systems enable optimum pretreatment/speciation of the sample components prior to atomic detection [107].

One *FI-HPLC approach* with a wide range of applications in routine analysis involved the two-fold use of the FI manifold as a screeming system and a post-column derivatizing system for analytes with similar chemical properties. The most receptive field for this type of hyphenated system is the analysis of large sample batches including only a few of interest on account of their toxicity or potential use as disease indicators. One typical example is the food analysis for aflatoxins. Screening of about 300 food samples for this type of carcinogen revealed their presence in only 6% [108]. A straightforward single-channel FI system permits measurement of up to 150 samples $h^{-1}$. A bromine solution is used as the carrier/reagent in order to enhance the fluorescence of the oxidized forms of the analytes. Only those few samples that produce signals corresponding to toxicity of suspected concentrations of the analytes are injected/separated in the chromatograph and the eluent derivatized/monitored in the FI manifold [109]. A similar assembly including an immobilized enzyme reactor for derivatization can be used for the screening/separation determination of bile acids in order to avoid overloading clinical laboratories with samples for patients with liver disorders [110].

*FI-HPLC* assemblies, such as those described above, have been used for the total and individual determination of polluting pesticides with photometric detection of the Griess product [111]. The sensitivity can be signifi-

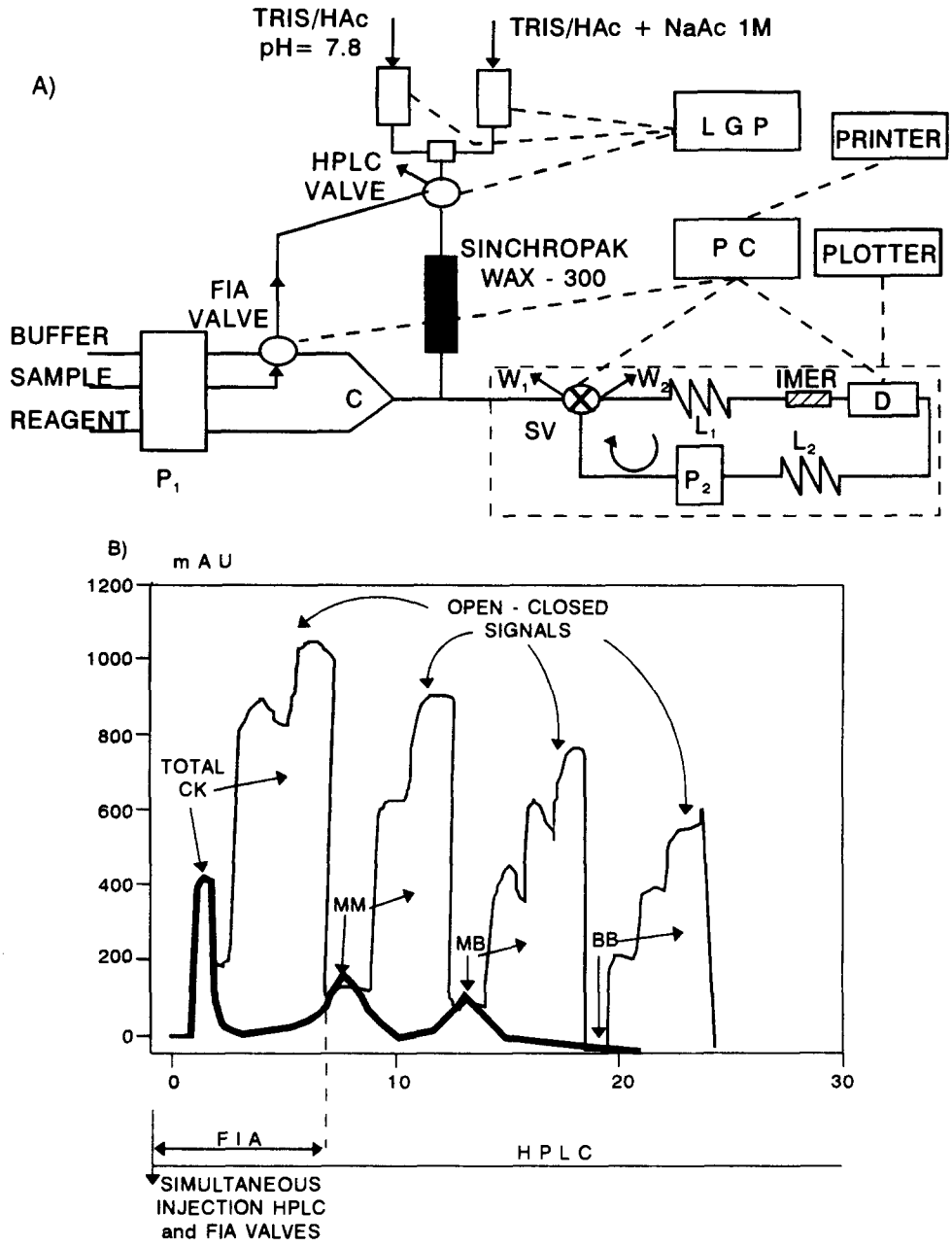


Fig. 6. (A) HPLC/FIA open–closed assembly for the total and individual determination of creatine kinase isoenzyme activities. LGP and PC denote liquid gradient programmer and personal computer, respectively. The sample stream can load both the FI and chromatographic valves or only one, depending on their positions. The lower part (FI manifold) is used for screening purposes; the upper system has a separative function, the FI manifold acting in this case as a post-column derivatization/detection system of the separated isoenzymes. (b) Recording obtained by simultaneously inserting the sample into the flow-injection system and the chromatographic column through the pertinent injection valves shown in (A). The bold line corresponds to a normal FI system (with the switching valve in the open position). The multiple-peak recording (thin line) was obtained by actuating the switching valve and trapping each zone in the closed circuit during the intervals between elution of successive isoenzymes. CK is creatine kinase, and MM, MB and BB are its isoenzymes.

cantly enhanced (50–100 times) by coupling with a flow-through sensor for preconcentration of the monitored product at the point of detection. One such set-up was used for the determination of mixtures of pesticides [112], and carbaryl and its hydrolysis product [113].

One effective way of increasing the sensitivity of an *FI-HPLC* method is by replacing the conventional manifold with an *open–closed system* [74–76] (see Fig. 6). This approach was

used for the individual and total determination of creatine kinase activities using two coupled enzymatic reactions [114]:

creatine phosphate
$$+ \text{ADP} \underset{Mg^{2+}}{\overset{CK}{\rightleftharpoons}} \text{creatine} + \text{ATP}$$
$$\text{ATP} + \text{D-glucose} \overset{HK}{\rightleftharpoons}$$
$$\text{D-glucose-6-phosphate} + \text{ADP}$$
$$\text{D-glucose-6-phosphate} + \text{NADP}^+ \overset{G6PDH}{\rightleftharpoons}$$
$$\text{D-glucose-}\delta\text{-lactone-6-phosphate} + \text{NADPH} + \text{H}^+$$

where CK, HK and G6PDH denote creatin-kinase, hexokinase and glucose-6-phosphate dehydrogenase, respectively. The two enzymes are immobilized together and the packed reactor is inserted into the open–closed circuit. Injections through an FI valve produce multipeak recordings that provide the total isoenzyme concentration. Injection through the HPLC valve, followed by sequential trapping in the circuit of each individual isoenzyme, gives rise to a multipeak recording for each isoenzyme, which enhances the sensitivity (see Fig. 6(B), which shows signals corresponding to the total determination, the conventional individual determination (with a single passage of the eluent through the detector) and the typical multipeak recording). The ensuing method was successfully applied to serum samples [114].

An *FI* system and a *gas chromatograph* are always naturally coupled in the precolumn portion. Derivatization of the analytes [115] or a two-fold derivatization/separation step by liquid–liquid [116] or ion-exchange [117] is quite common place in this context. An automatic method for the on-line preparation of fatty acid methyl esters from olive oil and other types of oil prior to their gas chromatographic determination provides excellent results [115]. Free fatty acids in dairy products can also be determined by directly coupling a continuous preconcentration ion-exchange/derivatization module to a gas chrom-atograph [117]. Pesticides of the *N*-methylcarbamate family have been quantified by use of an electron capture detector (ECD) with on-line derivatization/liquid–liquid extraction/gas chromatography. The hydrolysis products of *N*-methylcarbamates (phenols) are derivatized and extracted in a continuous fashion using pentafluoropropionic anhydride (the derivatizer) in *n*-hexane as extractant. In this way, the thermal instability of *N*-methylcarbamates is overcome by formation of fluorinated derivatives that can be identified and quantified at the ng $ml^{-1}$ level with an ECD [116].

## 9. Future of speciation analysis

As in many other areas of social interest, if the analytical process is resolved into several stages, including sampling, storage, preliminary operations, measurement-transducing, and data acquistition and processing, one can conclude that different extents of speciation development have been reached at each stage. Thus, the later stages have been the subject of more extensive research than the earlier steps. It can therefore be expected that reasearch will be focussed on such comparatively less developed stages in the future.

The main aim of sampling-storage is to preserve the integrity of the species to be determined by avoiding interconversion and losses. The principle technical choices for this purpose are as follows

(1) *Probe and flow-through sensors.* Probe and flow-through sensors enable in situ and on-line measurements, respectively, thus avoiding the need for minimizing manipulations prior to measurements. The type of sensor to be used depends on the nature of the sample matrix.

(2) *Sampling minicolumns.* These enable specific retention of each analyte form to be determined, but demand careful choice of the column.

(3) *Chemical treatment.* Chemical treatment of samples is aimed at preventing interconversion or loss of analytes. It entails thorough investigation and the use of automatic designs in order to minimize manipulation.

(4) *In situ separation techniques.* These are also intended to avoid analyte interconversions and losses; however, the target analytes are separated physically whether in different phases or as a whole.

Use of one or more of the above approaches prior to speciation-discrimination steps using a continuous separation technique, be it chromatographic or otherwise, and the most convenient hydrodynamic manifold in each case, should provide the optimal solution for each specific problem. The use of detectors with a high discrimination power (e.g. MS, FT-IR, etc.) in combination with continuous unseg-

mented techniques is also bound to play a central role in speciation analysis in the near future. All these approaches demand substantial investments in research and development if speciation is to take the place it deserves in chemical analysis.

## Acknowledgements

Dirección General de Investigación Científica y Técnica is thanked for financial support (project No. PB93/0827). One of the authors (D.W.B.) wishes to express his gratitude to the Community Bureau of Reference for award of a doctoral grant covering the expenses incurred during his stay in Spain.

## References

[1] M. Valcárcel and M.D. Luque de Castro, Flow Injection Analysis: Principles and Applications, Ellis Horwood, Chichester, 1987.
[2] J. Ruzicka and E.H. Hansen, Flow Injection Analysis, 2nd edn., Wiley, New York, 1988.
[3] M.D. Luque de Castro, Talanta, 33 (1986) 45.
[4] M.D. Luque de Castro, Trends Anal. Chem., 11 (1992) 149.
[5] J.S. Cosano, J.L. Calle, J.L. Pinillos, P. Linares and M.D. Luque de Castro, Tech. Lab., 147 (1988) 32.
[6] M.D. Luque de Castro, Mikrochim. Acta, 109 (1992) 165.
[7] Proceedings of the A.M.S.E. Meeting, Advances in Elemental Species Analysis — Concepts, Findings and Evaluation, Fresenius' J. Anal. Chem., 350 (1994) 1.
[8] M.D. Luque de Castro and M. Valcárcel, Analyst, 109 (1984) 413.
[9] F.H. Frimmel and T. Gremm, Fresenius' J. Anal. Chem., 350 (1994) 7.
[10] S.G. Allenmark, Chromatographic Enantioseparation, Methods and Applications, Ellis Horwood, Chichester, 1988.
[11] T. Kaneda, J. Chromatogr., 366 (1986) 217.
[12] G. Blaschke, J. Liq. Chromatogr., 9 (1986) 341.
[13] D.W. Amstrong and S.M. Han, CRC Crit. Rev., 19 (1988) 175.
[14] K.S. Litwiler, G.C. Catena and F.V. Bright, Anal. Chim. Acta, 237 (1990) 485.
[15] D.W. Amstrong, Y. Tang, T. Ward and M. Nichols, Anal. Chem., 65 (1993) 1114.
[16] N.W. Smith, J. Chromatogr., 653 (1993) 63.
[17] M. Schleimer, M. Fluk and V. Shurig, Anal. Chem., 66 (1994) 2893.
[18] C.L.E. Jacklyn, M.H. Tan, V.A. Storm, C.L. Cousins and M.A. MacAulag, Clin. Biochem., 18 (1985) 134.
[19] K.R. Kulkarus, D.W. Garber, C.F. Schmidt, S.M. Marcovina, M.H. Ho, B.J. Wilwhite, K.R. Bleanchie and J.P. Segrest, Clin. Chem., 38 (1992) 1898.
[20] M.H. Herrner, W.E. Kluitenberg and F.M.J. Zuijderhondt, Eur. J. Chin. Chem. Clin. Biochem., 30 (1992) 153.
[21] F. Lagerlof and S. Matsuo, Clin. Chim. Acta, 190 (1991) 175.
[22] P. Agelova-Gateva and D.J. Koev, Clin. Chem., 35 (1989) 491.
[23] D.A. Dileva, R.N. Walueley and C.G. Fraser, Clin. Chem., 29 (1983) 1856.
[24] D. Pilz, H. Koehler and W. Rotzsch, Z. Chem. Lavorat., 20 (1979) 348.
[25] W.G. Roberseh and R.W. Marshall, CRC. Crit. Rev. Clin. Lab. Sci, 11 (1979) 271.
[26] C.P. Fitzpatrick and H.L. Pardue, Clin. Chem., 38 (1992) 238.
[27] J. Vuori, S. Rasi, T. Takala and K. Vaananen, Clin. Chem., 37 (1991) 2087.
[28] S. Kudoh and H. Nakamura, Anal. Sci., 7 (1991) 267.
[29] V.A. Amelyshkine, N.A. Bochkova, I.F. Chernyadeva and V.N. Titov, Lab. Delo, 3 (1990) 46.
[30] S.E. Szedlacsek, V. Ostafe, S. Mogos and S.A. Hulea, Biochem. Int., 12 (1986) 279.
[31] T. Karpetskym, G.E. Brown, F. McFarland, S.T. Brady, W. Roth, A. Rahman and P. Jewett, Biochem. J., 219 (1984) 553.
[32] W. Martin, Aerztl. Lab., 29 (1983) 165.
[33] S.A. Saeed and T.R.C. Boyde, Biochem. Soc. Trans., 19 (1991) 219S.
[34] P. Linares, M.D. Luque de Castro and M. Valcárcel, Analyst, 111 (1986) 1405.
[35] G.A. Cutter, Anal. Chem., 57 (1985) 2951.
[36] D.W. Bryce, A. Izquierdo and M.D. Luque de Castro, Anal. Chim. Acta, 308 (1995) 96.
[37] Idem, Fresenius' J. Anal. Chem., 351 (1995) 433.
[38] M. Agudo, J. Marcos, A. Ríos and M. Valcárcel, Anal. Chim. Acta., 239 (1990) 211.
[39] J. Marcos, A. Ríos and M. Valcárcel, Trends Anal. Chem., 11 (1992) 373.
[40] J. Marcos, A. Ríos and M. Valcárcel, Anal. Chem., 62 (1992) 2237.
[41] J. Marcos, A. Ríos and M. Valcárcel, Anal. Chim., Acta, 261 (1992) 489.
[42] A. Ríos, M.D. Luque de Castro and M. Valcárcel, Anal. Chem., 60 (1988) 1540.
[43] F. Cañete, A. Ríos, M.D. Luque de Castro and M. Valcárcel, Anal. Chim. Acta, 224 (1989) 169.
[44] F. Cañete, A. Ríos, M.D. Luque de Castro and M. Valcárcel, Anal. Chem., 60 (1988) 2354.
[45] J.A. García-Mesa, M.D. Luque de Castro and M. Valcárcel, Lab. Rob. Autom., 5 (1993) 29.
[46] J.M. Fernández-Romero, M.D. Luque de Castro and M. Valcárcel, J. Biotechnol., 14 (1990) 43.
[47] J.M. Fernández-Romero, M.D. Luque de Castro, J. Pharm. Biomed. Anal., 9 (1991) 679.
[48] F. Lázaro, M.D. Luque de Castro and M. Valcárcel, Anal. Chem., 59 (1987) 950.
[49] J.F. van Staden, Anal. Chim. Acta, 138 (1982) 403.
[50] K.S. Johson and R.L. Petty, Limnol, Oceanogr., 28 (1983) 1260.
[51] A. Hulanicki, W. Matuszewski and M. Trojanovicz, Anal. Chim. Acta, 194 (1987) 119.
[52] L. Anderson, Anal. Chim. Acta, 110 (1979) 123.
[53] X. Shukun and F. Zhaolun, Inst. For. Soil Sci., 11 (1981) 93.

[54] A. Izquierdo, P. Linares, M.D. Luque de Castro and M. Valcárcel, Fresenius' J. Anal. Chem., 336 (1990) 490.
[55] J.S. Cosano, J.L. Calle, J.L. Pinillos, P. Linares and M.D. Luque de Castro, Anal. Chim. Acta, 221 (1989) 173.
[56] A. Ríos, M.D. Luque de Castro and M. Valcárcel, Anal. Chem., 58 (1986) 663.
[57] A. Ríos, M.D. Luque de Castro and M. Valcárcel, Anal. Chim. Acta, 187 (1986) 139.
[58] B. Bermúdez, A. Ríos, M.D. Luque de Castro and M. Valcárcel, Talanta, 35 (1988) 810.
[59] J.S. Cosano, M.D. Luque de Castro and M. Valcárcel, J. Autom. Chem., 15 (1993) 141.
[60] J.S. Cosano, M.D. Luque de Castro and M. Valcárcel, J. Autom. Chem., 15 (1993) 147.
[61] M.D. Luque de Castro and M. Valcárcel, Trends Anal. Chem., 5 (1986) 71.
[62] Z. Fang and B. Welz, J. Anal. At. Spectrom., 4 (1989) 543.
[63] M. Sperling, S. Xu and B. Welz, Anal. Chem., 64 (1992) 3101.
[64] A. Ríos, M.D. Luque de Castro and M. Valcárcel, J. Autom. Chem., 9 (1987) 30.
[65] A. Fernández, M.D. Luque de Castro and M. Valcárcel, Anal. Chim. Acta, 193 (1987) 107.
[66] K.H. Al-Sowdani and A. Townshend, Anal. Chim. Acta, 179 (1986) 469.
[67] T. Yao, M. Sato, Y. Kobayashi and T. Wasa, Anal. Biochem., 149 (1985) 387.
[68] T. Yao and T. Wasa, Anal. Chim. Acta, 207 (1988) 319.
[69] P. Linares, M.D. Luque de Castro and M. Valcárcel, Anal. Chem., 57 (1985) 2101.
[70] P. Linares, M.D. Luque de Castro and M. Valcárcel, Anal. Chem., 58 (1986) 120.
[71] M. Burguera and J.L. Burguera, J. Anal. Atom. Spectrom., 8 (1993) 229.
[72] T.R. Rüde and H. Puchelt, Fresenius' J. Anal. Chem., 350 (1994) 44.
[73] J. Ruz, A. Ríos, M.D. Luque de Castro and M. Valcárcel, Fresenius' Z. Anal. Chem., 322 (1985) 499.
[74] A. Ríos, M.D. Luque de Castro and M. Valcárcel, Anal. Chem., 57 (1985) 1803.
[75] J. Ruz, A. Ríos, M.D. Luque de Castro and M. Valcárcel, Talanta, 33 (1986) 199.
[76] A. Ríos, M.D. Luque de Castro and M. Valcárcel, Quim. Anal., 6 (1987) 314.
[77] J. Ruz, A. Ríos, M.D. Luque de Castro and M. Valcárcel, Anal. Chim. Acta, 186 (1986) 139.
[78] T.P. Lynch, N.J. Kernoghan and J.N. Wilson, Analyst, 109 (1984) 843.
[79] T.P. Lynch, N.J. Kernoghan and J.N. Wilson, Analyst, 109 (1984) 839.
[80] F. Cañete, A. Ríos, M.D. Luque de Castro and M. Valcárcel, Analyst, 113 (1988) 739.
[81] M. Valcárcel and M.D. Luque de Castro, Flow-Through (Bio)chemical Sensors, Elsevier, Amsterdam, 1994.
[82] J.I. García Alonso, A. López García, A. Sanz-Medel, E. Blanco González, L. Ebdon and P. Jone, Anal. Chim. Acta, 225 (1989) 339.
[83] B. Fairman and A. Sanz-Medel, Int. J. Environ. Anal. Chem., 50 (1993) 161.
[84] M.J. Quintela, M. Gallego and M. Valcárcel, Analyst, 118 (1993) 1199.
[85] P. Cañizares and M.D. Luque de Castro, Anal. Chem. Acta, 295 (1994) 59.
[86] F. Cañete, A. Ríos, M.D. Luque de Castro and M. Valcárcel, Anal. Chim. Acta, 214 (1988) 375.
[87] B. Bermúdez, F. Lázaro, M.D. Luque de Castro and M. Valcárcel, Analyst, 112 (1987) 535.
[88] B. Fernández-Band, F. Lázaro, M.D. Luque de Castro and M. Valcárcel, Anal. Chim. Acta, 229 (1990) 177.
[89] B. Fernández-Band, P. Linares, M.D. Luque de Castro and M. Valcárcel, Anal. Chem., 63 (1991) 1672.
[90] G.L. Green and T.C. O'Haver, Anal. Chem., 46 (1974) 2191.
[91] J.B.F. Lloyd, Nature, 231 (1971) 64.
[92] T. Vo-Dinh, Anal. Chem., 50 (1978) 396.
[93] D. Chen, M.D. Luque de Castro and M. Valcárcel, Anal. Chim. Acta, 261 (1992) 269.
[94] P. Cañizares and M.D. Luque de Castro, Anal. Chim. Acta, 295 (1994) 59.
[95] J. Ruz, A. Torres, A. Ríos, M.D. Luque de Castro and M. Valcárcel, J. Autom. Chem., 8 (1986) 70.
[96] R. Lobinski, W.M.R. Dirkx, M. Ceulemans and F.C. Adams, Anal. Chem., 64 (1992) 159.
[97] T. Kato, T. Uehiro, A. Yasuhara and M. Morita, J. Anal. At. Spectrom., 7 (1992) 15.
[98] E. Bulska, D.C. Baxter and W. Frech, Anal. Chim. Acta, 249 (1991) 545.
[99] S. Rapsomanikis and P.J. Craig, Anal. Chim. Acta, 248 (1991) 563.
[100] F. Laborda, M.T.C. De Loos Vollebregt and L. De Galan, Spectrochim. Acta, Part B, 46 (1991) 1089.
[101] P. Morin, M.B. Amran, S. Favier, R. Heimburger and M. Leroy, Fresenius' J. Anal. Chem., 339 (1991) 504.
[102] J.W. Robinson, J. Chin. Chem. Soc., 37 (1990) 313.
[103] A.K. Datta, P.J. Wedlund and R.A. Yokel, J. Trace Elem. Electrolytes Health Dis., 4 (1990) 107.
[104] S.B. Roychowdhury and J.A. Koropchak, Anal. Chem., 62 (1990) 484.
[105] W.A.J. De Waal, S. Heemstra, J.C. Krak and R.J. Jonker, Chromatographia, 30 (1990) 38.
[106] P.B. Stockwell and W.T. Corns, Intern. Lab., 34 (1994) 33.
[107] P.B. Stockwell and J.N. Lester, Anal. Chim. Acta, in press.
[108] P.A. Burdaspal and A. Gorostidi, Alimentaria, 186 (1985) 457.
[109] F.Lázaro, M.D. Luque de Castro and M. Valcárcel, J. Chromatogr., 448 (1988) 173.
[110] A. Membiela, F. Lázaro, M.D. Luque de Castro and M. Valcárcel, Anal. Chim. Acta, 249 (1991) 461.
[111] M.T. Tena, M.D. Luque de Castro and M. Valcárcel, Chromatographia, 33 (1992) 449.
[112] M.T. Tena, M.D. Luque de Castro and M. Valcárcel, J. Liq. Chromatogr., 15 (1992) 2373.
[113] M.T. Tena, M.D. Luque de Castro and M. Valcárcel, J. Chromatogr. Sci., 30 (1992) 276.
[114] M.D. Luque de Castro and J.M. Fernández-Romero, Anal. Chim. Acta, 263 (1992) 43.
[115] E. Ballesteros, M. Gallego and M. Valcárcel, Anal. Chim. Acta, 282 (1993) 581.
[116] E. Ballesteros, M. Gallego and M. Valcárcel, Anal. Chem., 65 (1993) 1773.
[117] E. Ballesteros, M. Gallego and M. Valcárcel, Anal. Chem., 66 (1994) 628.

ELSEVIER

Talanta 42 (1995) 1229–1237

Talanta

# Kinetic studies of complexation reactions of water-soluble hydrazones with nickel(II) and palladium(II) ions

Tsugikatsu Odashima *, Mitsuru Yamaguchi [1], Hajime Ishii

*Institute for Chemical Reaction Science, Tohoku University, Katahira, Aoba-ku, Sendai, Miyagi 980, Japan*

Received 1 August 1994; revised 21 February 1995; accepted 23 February 1995

**Abstract**

The kinetics of complexation reactions of five water-soluble heterocyclic hydrazones with nickel(II) and palladium(II) ions have been investigated by stopped-flow spectrophotometry. Rates of complexations with nickel(II) and palladium(II) in the absence of chloride ion were found to be proportional to the first order of the ligand and metal ion concentrations and to the inverse first order of the hydrogen ion concentration except for the complexation of α-(2-benzimidazolyl)-α-(5-nitro-2-pyridyl)hydrazono-3-toluenesulfonic acid with palladium(II). Rates of complexation with palladium(II) in the presence of chloride ion were best described by a two-term expression, both terms being first order in the palladium ion and ligand concentrations and inverse first order in the hydrogen ion concentration. The first term has zero dependence of the chloride ion concentration, whereas the second is first order with respect to the chloride ion concentration. The rate constant for each complexation reaction was determined. The complexation of the hydrazones with nickel(II) was estimated to go according to an Eigen mechanism and that with palladium (II) according to the associative mechanism.

## 1. Introduction

Among the water-soluble hydrazones which consist of 5-nitro-2-pyridylhydrazine and heterocyclic ketones having one or two sulfo groups in their molecules, α-(5-nitro-2-pyridyl)hydrazono-α-(2-pyridyl)-3-toluenesulfonic acid (NPHPTS) [1], α-(5-nitro-2-pyridyl)hydrazono-α- (2-quinolyl)-3-toluenesulfonic acid (NPHQTS) [2], α-(2-benzothiazolyl) -α-(5-nitro-2-pyridyl)hydrazono-3-toluenesulfonic acid (BTNPHTS) [2], α-(2-benzimidazolyl)-α-(5-nitro-2-pyridyl)hydrazono-3-toluenesulfonic acid (BINPHTS) [2] and disulfonated (2-benzimidazolyl)(phenyl)methanone 5-nitro-2-pyridylhydrazone (DSBINPH) [3] were recently found to be very useful as highly sensitive spectrophotometric reagents for metals. Some of them were applied to the determination of trace amounts of cobalt [1,4] and nickel [3,5]. In addition, complexation equilibria between the above-mentioned five hydrazones and metal ions including cadmium(II), cobalt(II), copper(II), iron(II), palladium(II) and zinc(II) were investigated previously [6]. In this work kinetics of complexation reactions of these five hydrazones with nickel(II) and palladium(II) have been studied in detail by stopped-flow spectrophotometry in order to more fully understand these complexation reactions.

## 2. Experimental

### 2.1. Reagents

All reagents were of analytical-reagent grade

* Corresponding author.

[1] Present address: Analytical Research Center, Central Research Laboratory, Research & Development Division, Japan Energy Corporation, 3-17-35, Niizo-minami, Toda-shi, Saitama 335, Japan.


*SSDI* 0039-9140(95)01565-5

and all solutions were prepared with distilled, demineralized water, unless stated otherwise.

Hydrazone solutions, $5.0 \times 10^{-4}$ or $1.0 \times 10^{-3}$ M, were prepared by dissolving each hydrazone, synthesized as in earlier work [1–3], in water or 0.01 M sodium hydroxide solution. These solutions were further diluted with water if necessary.

Standard solutions of nickel(II) and palladium (II), about 0.5 mg $cm^{-3}$, were prepared by first dissolving their nitrates in 0.01 M perchloric acid and then standardizing by EDTA titration. Working solutions were prepared by dilution of these solutions with water.

Buffer solutions were prepared by mixing 0.2 M tris(hydroxymethyl)aminomethane (Tris) solution and 0.2 M nitric acid.

### 2.2. Apparatus

A JASCO KS-100M stopped-flow system was used, which consists of a stopped-flow module with a flow cell of optical path 10 mm, a diode-array spectrophotometer, an oscilloscope, an X–Y plotter, a microcomputer and a thermostatic bath. This system has a minimum dead-time of 2 ms and affords, on both the oscilloscope screen and the plotter, a three-dimensional (time-resolved) adsorption spectrum (corrected by subtracting the blank signal of the reaction product over the region of $\pm 170$ nm from a fixed wavelength, and its absorbance changes with time (kinetic curves) at repeated arbitrary wavelengths.

### 2.3. Procedure

Kinetic runs were performed under pseudo-first-order conditions with respect to hydrazone. Each run was repeated five times, the average signal being adopted.

Equal volumes of nickel(II) (or palladium(II)) and hydrazone solutions, both of which were buffered at a fixed pH between 7.0 and 8.5 (or adjusted to a fixed acidic pH value between 1.0 and 2.0 for the palladium(II) complex) with a constant ionic strength of 0.2 M (or 2.0 M for the palladium(II) complex), were mixed in the mixing chamber of the stopped-flow apparatus. The temperature was controlled at $25 \pm 0.1$ °C. A kinetic curve at the absorption-maximum wavelength of the complex was recorded on the oscilloscope screen and by the recorder. The absorbance values were collected regularly and processed by linear regression using programs provided with the microcomputer for the application of first-order reaction plots (Eq. (4)) and Kezdy–Swinbourne's plots (Eq. (6)) [7,8].

Kinetics measurements for the complexation of NPHQTS and BTNPHTS with nickel(II) were performed in 10% (v/v) 1,4-dioxane/$H_2O$ because of their low solubilities in water.

## 3. Results and discussion

In general, since the rate of complex formation depends on the concentrations of metal ion, ligand, and hydrogen ion, the rate of formation of the metal–hydrazone complex is assumed to be

$$-\frac{d[M]}{dt} = k^*[M]^a[R]^b[H^+]^c \quad (1)$$

where $t$ is the reaction time, $k^*$ is the rate constant, M is the metal ion, R is the hydrazone and $a$, $b$ and $c$ are the reaction orders with respect to the concentrations of metal ion, hydrazone and hydrogen ion, respectively.

Under a pseudo-first-order excess of the hydrazone and at a constant pH, the reaction rate can be expressed as

$$-\frac{d[M]}{dt} = k_{obsd}[M]^a \quad (2)$$

where $k_{obsd}$ is the observed pseudo-first-order rate constant, assuming $a = 1$. By integrating Eq. (2), taking the mass balance into consideration and then applying Beer's law, Eq. (3) can be derived, which is rewritten as Eq. (4).

$$A_\infty - A_t = (A_\infty - A_0)\exp(-K_{obsd}t) \quad (3)$$

$$-\ln(A_\infty - A_t) = -\ln(A_\infty - A_0) + k_{obsd}t \quad (4)$$

where $A_0$, $A_t$ and $A_\infty$ are the absorbance of the reaction system at $t = 0$, $t$ and $\infty$, respectively.

### 3.1. Kinetics of formation of nickel complexes

#### 3.1.1. Reaction order with respect to nickel-ion concentrations

Fig. 1 shows a kinetic curve measured in the presence of a large excess of DSBINPH and at pH 7.43 for the complex formation of DSBINPH with nickel(II), along with a $-\ln(A_\infty - A_t)$ vs. $t$ plot prepared from this

kinetic curve. The plot gives a straight line with a slope of 0.0436, which indicates that the rate of complexation is first order with respect to the nickel(II) concentration, i.e. $a = 1$ in Eq. (1), and the $k_{obsd}$ is $4.36 \times 10^{-2}\ s^{-1}$ under the experimental conditions given in Fig. 1.

In the complex formation of the other hydrazones with nickel(II), however, more than 20 h were required for attaining equilibrium. Accordingly the absorbances at infinite time ($A_\infty$) were not obtained within the experimental period (about 1 h). Therefore the kinetics analysis for these complexation reactions was performed according to Kezdy–Swinbourne's method [7,8] as follows. As is clear from Eq. (3), after the elapse of a fixed time, $\Delta t$, from $t$, Eq. (5) holds

$$A_\infty - A_{t+\Delta t} = (A_\infty - A_0)\exp[-k_{obsd}(t+\Delta t)] \quad (5)$$

From Eqs. (3) and (5), Eq. (6) is obtained

$$A_t = A_\infty[1 - \exp(k_{obsd}\Delta t)] + A_{t+\Delta t}\exp(k_{obsd}\Delta t) \quad (6)$$

Eq. (6) implies that a plot of $A_t$ versus $A_{t+\Delta t}$ gives a straight line with a slope of $\exp(k_{obsd}\Delta t)$. As the value of $\Delta t$ is known, the $k_{obsd}$ value can be calculated from this slope. Furthermore, $A_t$ is equal to $A_{t+\Delta t}$ and also equal to $A_\infty$ at $t = \infty$, so an intersecting point of this line with a straight line $A_t = A_{t+\Delta t}$ (i.e. a line with a slope of unity passing through the origin) should give the value of $A_\infty$. Fig. 2 shows a plot of $A_t$ versus $A_{t+\Delta t}$ for the BINPHTS–nickel(II) system as an example, in which the plot gives a straight line with a slope of 1.92. Similar results to that shown in Fig. 2

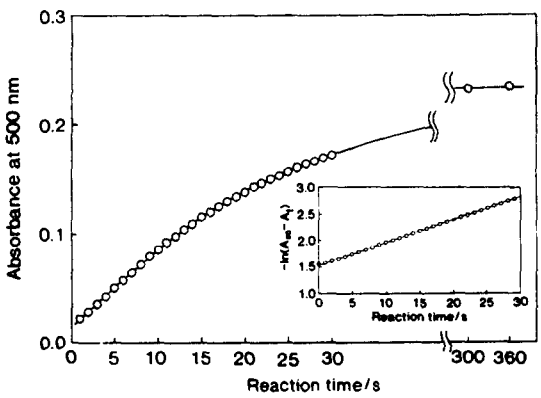


Fig. 1. Reaction curve and plot of $-\ln(A_\infty - A_t)$ vs. $t$ for the formation of DSBINPH–nickel(II) complex. (DSBINPH, $8.3 \times 10^{-5}$ M; Ni(II), $2.5 \times 10^{-6}$ M; pH 7.43; ionic strength, 0.2 M ($NaClO_4$); temperature, $25 \pm 0.1$ °C.)

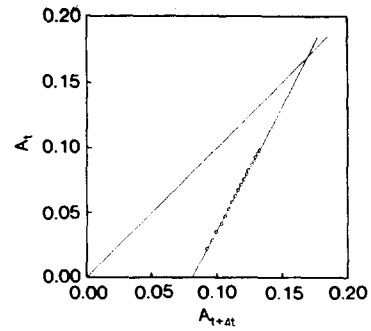


Fig. 2. Kezdy–Swinbourne plot for the BINPHTS–nickel(II) system. (BINPHTS, $7.5 \times 10^{-5}$ M; pH 7.52; Wavelength, 500 nm. Other conditions are the same as those in Fig. 1.)

were obtained for NPHPTS–, NPHQTS– and BTNPHTS–nickel(II) systems, which indicates that the rate of complexation in these systems is first order with respect to the nickel(II) concentration, i.e. $a = 1$.

### 3.1.2. Reaction order with respect to hydrazone concentration

From the above results the rate equation for the formation of the nickel complexes can be written as follows

$$-\frac{d[Ni(II)]}{dt} = k_{obsd}[Ni(II)] = k_{0(H)}[Ni(II)][R]^b \quad (7)$$

$$k_{obsd} = k_{0(H)}[R]^b \fallingdotseq k_{0(H)}C_R^b \quad (8)$$

where $k_{0(H)}$ is the conditional second-order rate constant and $C_R$ is the total concentration of the hydrazone. The effect of the hydrazone concentration on the observed rate constant was examined in order to determine the reaction order with respect to the hydrazone concentration. Fig. 3 shows the result for the DSBINPH–nickel(II) system, in which plots of $k_{obsd}$ versus $C_R$ give straight lines passing

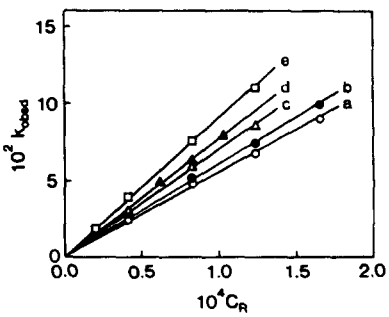


Fig. 3. Plots of $k_{obsd}$ vs. $C_R$ for DSBINPH–nickel(II) system at pH: curve a, 7.43; curve b, 8.01; curve c, 8.28; curve d, 8.37; curve e, 8.52. Other conditions are the same as those in Fig. 1.

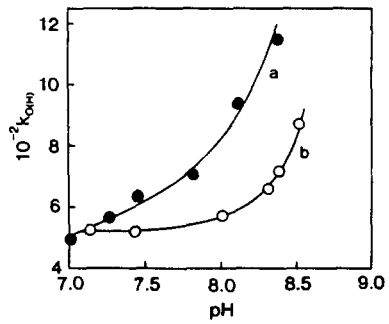


Fig. 4. Plots of $k_{0(H)}$ vs. pH for (curve a) BINPHTS–nickel(II) and (curve b) DSBINPH–nickel(II) systems. $C_R$: curve a, $9.4 \times 10^{-5}$ M; curve b, $1.0 \times 10^{-4}$ M. Other conditions are the same as those in Fig. 1.

through the origin. Similar results to that in Fig. 3 were obtained for the other hydrazone–nickel(II) systems, which indicates that the rate of complexation in these systems in first order, dependent on the hydrazone concentration, i.e. $b = 1$.

### 3.1.3. *Effect of hydrogen-ion concentration*

The effect of pH on the observed rate constant was studied, values of $k_{0(H)}$ ($\fallingdotseq k_{obsd}/C_R$) being plotted against pH for each hydrazone–nickel(II) system. According to the results, the $k_{0(H)}$ value decreased with increasing pH in the NPHQTS–nickel(II) system, but it increased with increasing pH in the other systems. This indicates that there are two controlling reactions; one is independent of, and the other is inverse first order, dependent on the hydrogen-ion concentration. Two examples of these plots are shown in Fig. 4.

### 3.1.4. *Rate-determining steps and rate constants*

Since the species of nickel in the pH range 7.0–8.5 studied in this work are $Ni(H_2O)_6^{2+}$ and $NiOH(H_2O)_5^{+}$ and those of the hydrazones are $HL^-$ for NPHPTS, NPHQTS and BTNPHTS, $H_2L^-$ for BINPHTS and $H_2L^{2-}$ for DSBINPH (where L denotes the undissociable part of the hydrazone), as is evident from the values of their acid dissociation constants [6], the equilibria and the reactions for the formation of monoligated complexes are expresseed by Eqs. (9)–(15).

For the hydrolysis of nickel(II)

$$Ni^{2+} + H_2O \overset{K_{Ni}}{\rightleftharpoons} NiOH^+ + H^+ \quad (9)$$

$$K_{Ni} = \frac{[NiOH^+][H^+]}{[Ni^{2+}]}$$

where $K_{Ni}$ is the hydrolysis constant of nickel(II).

For the formation of the NPHPTS, NPHQTS and BTNPHTS complexes, Eqs. (10) and (11) hold

$$Ni(H_2O)_6^{2+} + HL^- \xrightarrow{k_1} NiL + H^+ + 6H_2O \quad (10)$$

$$NiOH(H_2O)_5^{+} + HL^- \xrightarrow{k_2} NiL + 6H_2O \quad (11)$$

for the formation of the BINPHTS complex, Eqs. (12) and (13) hold

$$Ni(H_2O)_6^{2+} + H_2L^- \xrightarrow{k_1} Ni(HL) + H^+ + 6H_2O \quad (12)$$

$$NiOH(H_2O)_5^{+} + H_2L^- \xrightarrow{k_2} Ni(HL) + 6H_2O \quad (13)$$

and for the formation of the DSBINPH complex, Eqs. (14) and (15) hold

$$Ni(H_2O)_6^{2+} + H_2L^{2-} \xrightarrow{k_1} [Ni(HL)]^- + H^+ + 6H_2O \quad (14)$$

$$NiOH(H_2O)_5^{+} + H_2L^{2-} \xrightarrow{k_2} [Ni(HL)]^- + 6H_2O \quad (15)$$

where $k_1$ and $k_2$ represent the rate constants of respective reaction steps.

Here we consider the DSBINPH–nickel(II) system as an example. On the basis of the results described above and the assumption that the rate-determining steps are competitive reactions shown by Eqs. (14) and (15), the rate equation can be expressed as

$$-\frac{d[Ni(II)]}{dt} = k_1[Ni^{2+}][H_2L^{2-}] + k_2[NiOH^+][H_2L^{2-}] \quad (16)$$

From Eqs. (7), (8), (9) and (16), Eq. (17) can be derived.

$$k_{0(H)} = \frac{k_1 + (k_2K_{Ni}/[H^+])}{1 + (K_{Ni}/[H^+])} \quad (17)$$

Also for the complexation reactions of the other hydrazones, Eq. (17) can be derived by similar treatment. Values of $k_1$, $k_2$ and $K_{Ni}$ were calculated by the Simplex method using the data of the $k_{0(H)}$ vs. pH plot obtained already. The results are given in Table 1 and theoretical curves for the $k_{0(H)}$ vs. pH plots are shown by solid lines in Fig. 4. The $K_{Ni}$ values obtained in this work are nearly equal to that ((0.1–about 6.3) $\times 10^{-10}$ M) reported in the literature [9]. The values of $k_1$ and $k_2$ of each complexation reaction are also almost the same in the order, respectively, and the $k_2$ values are

Table 1
Rate constants of complexation reactions of hydrazones with nickel(II) and hydrolysis constant of nickel(II) at 25 ± 0.1 °C and an ionic strength of 0.2 M ($NaClO_4$)

| Hydrazone | $k_1$ ($M^{-1}s^{-1}$) | $k_2$ ($M^{-1}s^{-1}$) | $K_{Ni}$ (M) |
|---|---|---|---|
| NPHPTS | $3.6 \times 10^2$ | $3.6 \times 10^3$ | $1.1 \times 10^{-10}$ |
| NPHQTS | –[a] | –[a] | –[a] |
| BTNPHTS[b] | $5.5 \times 10$ | $1.8 \times 10^3$ | $1.0 \times 10^{-10}$ |
| BINPHTS | $2.5 \times 10^2$ | $1.8 \times 10^4$ | $1.0 \times 10^{-10}$ |
| DSBINPH | $2.4 \times 10^2$ | $5.3 \times 10^3$ | $0.99 \times 10^{-10}$ |

[a] Not determined.
[b] Determined in aqueous 10% (v/v) 1,4-dioxane.

close to the releasing rate constant ($1.5 \times 10^4\ s^{-1}$) [10] of a water molecule from the nickel aquo-ion, although the $k$ value of the BTNPHTS–nickel(II) system is somewhat small. This suggests that the complexation reactions between the hydrazones and nickel(II) proceed according to an Eigen mechanism.

### 3.2. Kinetics of formation of palladium complexes in the absence of chloride ion

#### 3.2.1. Reaction order with respect to palladium-ion concentration

All kinetics experiments were performed in strongly acidic media because the complexation reaction between the hydrazones and palladium (II) was too fast to measure in weakly acidic media. Fig. 5 shows a $-\ln(A_\infty - A_t)$ vs. $t$ plot for the formation of a BTNPHTS–palladium(II) complex measured in the presence of a large excess of DSBINPH and at an acidity of 1.16 M. The plot gives a sraight line. Similar results to those in Fig. 5 were obtained for the

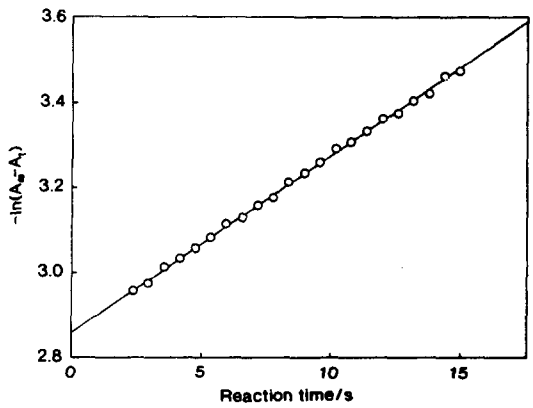


Fig. 5. Plot of $-\ln(A_\infty - A_t)$ vs. $t$ for formation of BTNPHTS–palladium(II) complex. (BTNPHTS, $7.8 \times 10^{-5}$ M; Pd(II), $2.1 \times 10^{-6}$ M; $[H^+]$, 1.16 M; ionic strength, 2.0 M ($NaNO_3$); temperature, 25 ± 0.1 °C.)

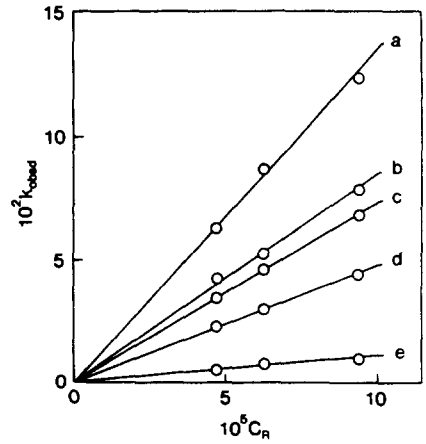


Fig. 6. Plots of $k_{obsd}$ vs. $C_R$ for BTNPHTS–palladium(II) system at pH: curve a, 0.77; curve b, 0.97; curve c, 1.16; curve d, 1.45; curve e, 1.93; wavelength, 590 nm. Other conditions are the same as those in Fig. 5.

formation of the other hydrazone–palladium (II) complexes. These results indicate that the complexation reactions between the hydrazones and palladium(II) are all first order with respect to the palladium (II) concentration, i.e. $a = 1$.

#### 3.2.2. Reaction order with respect to hydrazone concentration

Fig. 6 shows the effect of the concentration of BTNPHTS on the observed rate constant at various acidities. The plots of $k_{obsd}$ versus $C_R$ give straight lines passing through the origin. Similar results to those in Fig. 6 were obtained for the other hydrazone–palladium(II) systems, which indicates that the complexation reactions of these systems are all first order with respect to the hydrazone concentration, i.e. $b = 1$.

#### 3.2.3. Reaction order with respect to hydrogen-ion concentration

Curve a in Fig. 7 shows a $k_{0(H)}$ vs. $1/[H^+]$ plot for the formation of the DSBINPH–palladium (II) complex. The plot gives a straight line passing through the origin. Similar results to those shown by curve a in Fig. 7 were obtained for the formation of the other hydrazone complexes except for the BTNPHTS complex, for which a $k_{0(H)}$ vs. $1/[H^+]$ plot shown by curve b in Fig. 7 was obtained. These results indicate that the reaction order with respect to the hydrogen-ion concentration is inverse first order (i.e. $c = -1$) for the formation of the hydrazone complexes except for the BTNPHTS complex, and is measured as a complicated function of the hydrogen-ion concentration in

the BTNPHTS system. This discrepancy seems to be influenced by an intramolecular hydrogen bond in BTNPHTS. At the present stage, however, we cannot give a clear chemical interpretation for the intramolecular hydrogen bond.

*3.2.4. Rate-determining steps and rate constants*

The species of palladium under the conditions studied is $Pd(H_2O)_4^{2+}$ and those of the hydrazones are considered to be $H_3L^+$ and $H_2L$ for NPHPTS, NPHQTS and BTNPHTS, $H_4L^+$ and $H_3L$ for BINPHTS and $H_4L$ and $H_3L^-$ for DSBINPH. Taking into consideration the results described above, however, only Eqs. (18)–(20) are feasible as formation reactions of monoligated complexes between the hydrazones and palladium (II). For NPHPTS and NPHQTS

$$Pd(H_2O)_4^{2+} + H_3L^+ \xrightarrow{k_1} [Pd(H_2L)]^{2+} + H^+ + 4H_2O \quad (18)$$

for BINPHTS

$$Pd(H_2O)_4^{2+} + H_4L^+ \xrightarrow{k_1} [Pd(H_3L)]^{2+} + H^+ + 4H_2O \quad (19)$$

and for DSBINPH

$$Pd(H_2O)_4^{2+} + H_4L \xrightarrow{k_1} [Pd(H_3L)]^{+} + H^+ + 4H_2O \quad (20)$$

The rate equation can be expressed by Eq. (21) for every reaction system, except the BTNPHTS–palladium(II) system.

$$-\frac{d[Pd(II)]}{dt} = k_1[Pd^{2+}]\frac{C_R/[H^+]}{1+(K_{al}/[H^+])} \quad (21)$$

where $K_{al}$ is the acid dissociation constant of each hydrazone. From Eqs. (2), (8) and (21)

$$k_{0(H)}[1+(K_{al}/[H^+])] = k_1/[H^+] \quad (22)$$

is obtained. Eq. (22) means that the plot of $k_{0(H)}[1+(K_{al}/[H^+])]$ versus $1/[H^+]$ gives a straight line with a slope of $k_1$ passing through the origin. Actually this plot for each hydrazone–palladium (II) system gave a straight line. The value of $k_1$ obtained for each reaction system is given in Table 2.

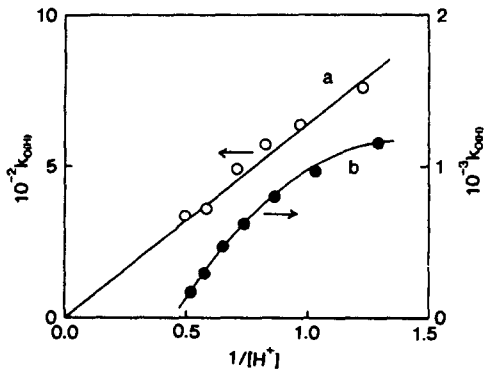


Fig. 7. Plots of $k_{0(H)}$ vs. $1/[H^+]$ for (curve a) DSBINPH–palladium(II) and (curve b) BTNPHTS–palladium(II) systems at $C_R$: curve a, $8.2 \times 10^{-5}$ M; curve b, $7.8 \times 10^{-5}$ M. Other conditions are the same as those in Fig. 5.

Table 2
Rate constants of complexation reactions of hydrazones with palladium(II) in the absence of chloride ion at $25 \pm 0.1$ °C and an ionic strength of 2.0 M ($NaClO_4$)

| Hydrazone | $k_1$ ($M^{-1}s^{-1}$) | $k_{-1}/K'_a$ ($M^{-1}s^{-1}$) |
|---|---|---|
| NPHPTS | $3.0 \times 10^3$ | – |
| NPHQTS | $2.7 \times 10^2$ | – |
| BTNPHTS | $1.5 \times 10^3$ | $7.7 \times 10^{-4}$ |
| BINPHTS | $4.3 \times 10^2$ | – |
| DSBINPH | $7.6 \times 10^2$ | – |

As for the BTNPHTS–palladium(II) system, on the other hand, the reverse reaction was taken into consideration in addition to the forward one as shown in Eq. (23) because the reaction order with respect to the hydrogen-ion concentration was not inverse first order but complex, as was already shown by curve b in Fig. 7.

$$Pd^{2+} + H_3L^+ \underset{k_{-1}}{\overset{k_1}{\rightleftharpoons}} [Pd(H_2L)]^{2+} + H^+ \quad (23)$$

where $k_{-1}$ is the rate constant of the reverse reaction.

The rate equation is expressed by Eq. (24)

$$-\frac{d[Pd(II)]}{dt} = k_1[Pd^{2+}][H_3L^+][H^+]^{-1} - k_{-1}[Pd(H_2L)^{2+}][H^+] \quad (24)$$

The complexation reaction of BTNPHTS with palladium(II) is represented by Eq. (25), its equilibrium constant, $K_{eq}$, being given by Eq. (26) [6]

$$Pd^{2+} + H_3L^+ \underset{}{\overset{K_{eq}}{\rightleftharpoons}} Pd(HL)^+ + 2H^+ \quad (25)$$

$$K_{eq} = \frac{[Pd(HL)^+][H^+]^2}{[Pd^{2+}][H_3L^+]} = 10^{4.9} \quad (26)$$

The proton dissociation of the complex $Pd(H_2L)^{2+}$ is represented by Eq. (27), its proton dissociation constant, $K'_a$, being given by Eq. (28).

$$Pd(H_2L)^{2+} \underset{}{\overset{K'_a}{\rightleftharpoons}} Pd(HL)^+ + H^+ \quad (27)$$

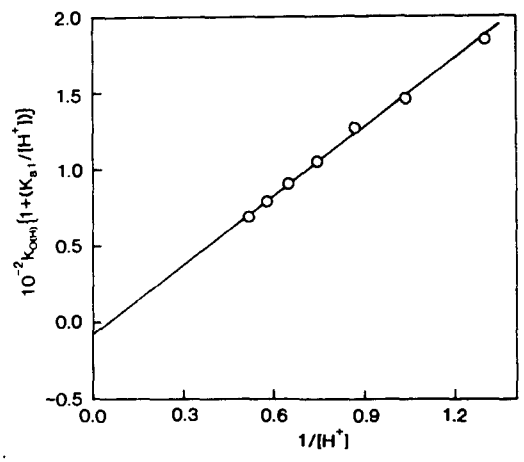


Fig. 8. Plot of $k_{0(H)}(1 + K_{a1}/[H^+])$ vs. $1/[H^+]$ for BT-NPHTS–palladium(II) system at $C_R$, $7.8 \times 10^{-5}$ M. Other conditions are the same as those in Fig. 5.

$$K'_a = \frac{[Pd(HL)^+][H^+]}{[Pd(H_2L)^{2+}]} \quad (28)$$

From Eqs. (7), (8), (24), (26) and (28), Eq. (29) can be derived, which is rewritten as Eq. (30)

$$-\frac{d[Pd(II)]}{dt} = \frac{[Pd^{2+}]C_R}{1 + (K_{a1}/[H^+])} \times (k_1/[H^+] - K_{eq}k_{-1}K'_a) = k_{0(H)}[Pd^{2+}]C_R \quad (29)$$

$$k_{0(H)}[1 + (K_{a1}/[H^+])] = k_1/[H^+] - K_{eq}k_{-1}/K'_a \quad (30)$$

Eq. (30) means that the plot of $k_{0(H)}[1 + (K_{a1}/[H^+])]$ versus $1/[H^+]$ gives a straight line, the values of $k_1$ and $k_{-1}/K'_a$ being calculated from the slope and the intercept of the line, respectively. Fig. 8 shows this plot for the BT-NPHTS–palladium(II) system, which gives a straight line. The values of $k_1$ and $k_{-1}/K'_a$ calculated are given in Table 2.

### 3.3. Kinetics of formation of palladium complexes in the presence of chloride ion

#### 3.3.1. Reaction orders with respect to concentrations of palladium ion, hydrazone and hydrogen ion

Fig. 9(A) shows an $\ln(A_\infty - A_t)$ vs. $t$ plot for the complexation of DSBINPH with palladium (II) in the presence of large excesses of DS-BINPH and chloride ion and at a constant acidity of 1.06 M. The plot gives a straight line. Figs. 9(B) and 9(C) show $k_{obsd}$ vs. $C_R$ plots at various acidities and a $k_{0(H)}$ vs. $1/[H^+]$ plot, respectively, for the DSBINPH–palladium(II) system. Every plot gives a straight line passing through the origin. Similar results to those shown in Figs. 9(A)–9(C) were obtained for the other hydrazone–palladium(II) systems. These results reveal that the reaction orders with respect to the concentrations of both palladium(II) and the hydrazone are first order.

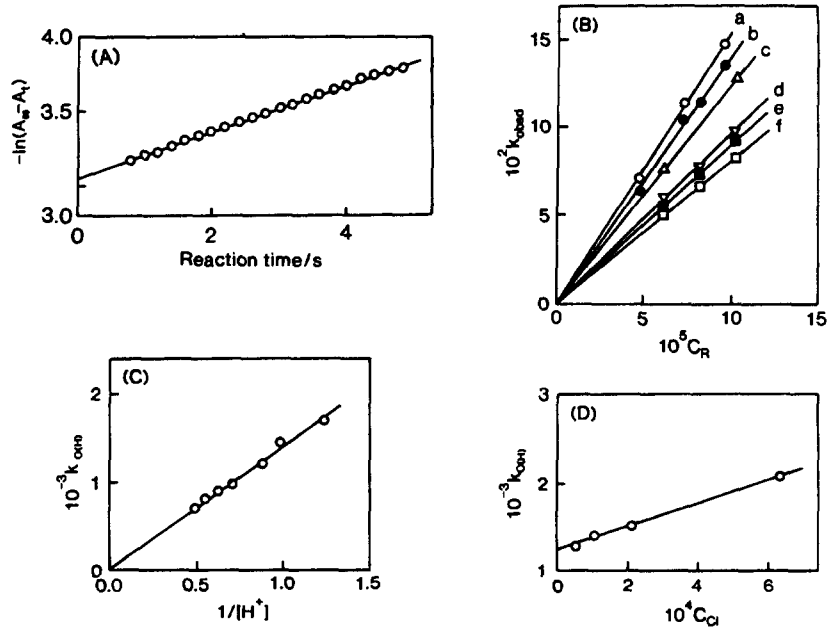


Fig. 9. Plots of (A) $-\ln(A_\infty - A_t)$ vs. $t$, (B) $k_{obsd}$ vs. $C_R$, (C) $k_{0(H)}$ vs. $1/[H^+]$ and (D) $k_{0(H)}$ vs. $C_{Cl}$ for DSBINPH–palladium(II)–chloride system. DSBINPH, $8.2 \times 10^{-5}$ M; (A), (C), (D) Pd(II), $2.1 \times 10^{-6}$ M; (B) $[H^+]$: (curve a) 0.81, (curve b) 1.01, (curve c) 1.22, (curve d) 1.42, (curve e) 1.72, (curve f) 2.03; (A), (D) $[H^+]$, 1.06; (A), (B), (C) $[Cl^-]$, $2.12 \times 10^{-4}$ M; ionic strength, 2.0 M ($NaNO_3$); wavelength, 564 nm; temperature, $25 \pm 0.1$ °C.

that with respect to the hydrogen-ion concentration being inverse first order.

### 3.3.2. Reaction order with respect to chloride-ion concentration

Fig. 9(D) shows a $k_{0(H)}$ vs. $C_{Cl}$ plot for the DSBINPH–palladium(II) system, which gives a straight line with an intercept. Similar results to those shown in Fig. 9(D) were obtained for NPHPTS– , NPHQTS– and BINPHTS–palladium (II) systems, but no such result was obtained for the BTNPHTS–palladium(II) system. These results indicate that the reaction order with respect to the chloride-ion concentration for the complex formation between palladium(II) and the hydrazones, except BTNPHTS, under the conditions studied is zero order and first order.

### 3.3.3. Rate-determining steps and rate constants

The species of palladium(II) under the conditions studied are regarded as $Pd(H_2O)_4^{2+}$, $PdCl(H_2O)_3^{+}$ and $PdCl_2(H_2O)_2$. On the basis of the above results, however, potential complexation reactions between the hydrazones and palladium(II) are restricted to Eqs. (31)–(36) and each pair of reactions is considered to proceed competitively and govern the complexation reaction in each hydrazone–palladium(II) system. For NPHPTS and NPHQTS

$$Pd(H_2O)_4^{2+} + H_3L^{+} \xrightarrow{k_1} Pd(H_2L)^{2+} + H^{+} + 4H_2O \quad (31)$$

$$PdCl(H_2O)_3^{+} + H_3L^{+} \xrightarrow{k_2} Pd(H_2L)Cl^{+} + H^{+} + 3H_2O \quad (32)$$

for BINPHTS

$$Pd(H_2O)_4^{2+} + H_4L^{+} \xrightarrow{k_1} Pd(H_3L)^{2+} + H^{+} + 4H_2O \quad (33)$$

$$PdCl(H_2O)_3^{+} + H_4L^{+} \xrightarrow{k_2} Pd(H_3L)Cl^{+} + H^{+} + 3H_2O \quad (34)$$

and for DSBINPH

$$Pd(H_2O)_4^{2+} + H_4L \xrightarrow{k_1} Pd(H_3L)^{+} + H^{+} + 4H_2O \quad (35)$$

$$PdCl(H_2O)_3^{+} + H_4L \xrightarrow{k_2} Pd(H_3L)Cl + H^{+} + 3H_2O \quad (36)$$

where $k_1$ and $k_2$ represent the rate constants. The rate equation for these complexation reactions can be expressed as

Table 3
Rate constants of complexation reactions of hydrazones with palladium(II) in the presence of chloride ion at 25 ± 0.1 °C and ionic strength of 2.0 M ($NaClO_4$)

| Hydrazone | $k_1$ ($M^{-1}s^{-1}$) | $k_2$ ($M^{-1}s^{-1}$) |
|---|---|---|
| NPHPTS | $8.0 \times 10^3$ | $1.9 \times 10^4$ |
| NPHQTS | $5.6 \times 10^2$ | $7.4 \times 10^3$ |
| BTNPHTS | –[a] | –[a] |
| BINPHTS | $3.9 \times 10^2$ | $8.1 \times 10^3$ |
| DSBINPH | $1.5 \times 10^3$ | $1.7 \times 10^4$ |

[a] Not determined.

$$-\frac{d[Pd(II)]}{dt} = k_1\frac{[Pd(II)][L]}{[H^+]} + k_2\frac{[Pd(II)][L][Cl^-]}{[H^+]} \quad (37)$$

By taking into consideration the acid dissociation of the hydrazones and the mass balance of the hydrazones and palladium(II) and using the side-reaction coefficient, $\alpha_{(Cl)}$, of palladium(II) for chloride ion and the formation constant, $\beta_1$, of the monochloro complex of palladium(II), Eq. (38) can finally be derived from Eq. (37)

$$k_{0(H)} = \frac{1}{\left(1 + \frac{k_{al}}{[H^+]}\right)[H^+]}\left[k_1 + k_2\frac{C_{Cl}\beta_1}{\alpha_{(Cl)}}\right] \quad (38)$$

where $C_{Cl}$ is the total concentration of chloride ion.

Eq. (38) means that the $k_{0(H)}$ vs. $C_{Cl}$ plot, which is equivalent to Fig. 9(D) gives a straight line; the values of $k_1$ and $k_2$ can be calculated from the intercept and the slope of this line, respectively. The results obtained are summarized in Table 3.

### 3.3.4. Mechanism of formation of palladium complexes

Palladium(II) usually forms the square planar complex [11]. As is clear from Table 3, the rate constants for the complexation of palladium(II) obtained in this work depend on the kind of hydrazone, which suggests that the complexation reaction of the hydrazones with palladium(II) goes according to the associative mechanism. The value of $k_2$ is larger than that of $k_1$ for every hydrazone–palladium(II) system, indicating that the palladium aquo-ion is activated by the formation of monochloro ion. Also, the $k_1$ values obtained here are in accordance with those obtained in the absence of chloride ions, demonstrating the reliability of this work.

## References


[1] T. Odashima, T. Kikuch, W. Ohtani and H. Ishii, Analyst, 111 (1986) 1383.

[2] K. Kohata, Y. Kawamonzen, T. Odashima and H. Ishii, Bull. Chem. Soc. Jpn., 63 (1990) 3398.

[3] T. Odashima, M. Yamaguchi and H. Ishii, Mikrochim. Acta. I (1991) 267.

[4] H. Ishii, T. Odashima and Y. Kawamonzen, Anal. Chim. Acta, 244 (1991) 223.

[5] H. Ishii, T. Odashima and Y. Kawamonzen, Bull. Chem. Soc. Jpn., 63 (1990) 3405.

[6] H. Ishii, M. Yamaguchi and T. Odashima, Talanta, 39 (1992) 1181.

[7] F.J. Kezdy, J. Kaz and A. Bruylants, Bull. Soc. Chim. Belges, 67 (1958) 687.

[8] E.S. Swinbourne, J. Chem. Soc., (1960) 2371.

[9] L.G. Sillen and A.E. Martell, Stability Constants of Metal-Ion Complexes, Special Publication No. 17, The Chemical Society, London, 1964, p. 56.

[10] M. Eigen and K. Tamm, Z. Elektrochem., 66 (1962) 107.

[11] F. Basolo and R.G. Pearson, Mechanisms of Inorganic Reactions. A Study of Metal Complexes in Solution, 2nd edn., John Wiley, New York, 1967 p. 414.

ELSEVIER

Talanta 42 (1995) 1239–1244

Talanta

# Robust regression methods to calibrate a continuous flow analyzer in the colorimetric analysis of inorganic phosphorus in seawater

M. Mecozzi

*ICRAM, Istituto Centrale per la Ricerca Scientifica e Tecnologica Applicata al Mare, via L. Respighi n.5, 00197 Roma, Italy*

Received 27 September 1994; revised 22 November 1994; accepted 17 February 1995

**Abstract**

The presence of a salinity effect in the automated analysis of phosphorus in seawater performed by a phosphomolybdate complex can cause the inaccurate estimation of the true amount, because the calibration procedure performed by least-squares regression does not take into account the different analytical response of samples and standard solutions. The error arising from this salt effect is corrected by calibrating the autoanalyzer with robust regression methods (RRMs), which allow definition of the range of salinity in which the analytical response of the autoanalyzer is only dependent on the concentration of marine nutrients. The RRMs are especially helpful in the analysis of oligotrophic samples where the salinity effect is particularly relevant.

## 1. Introduction

The study of phenomena such as eutrophication or algal blooms requires the analysis of many samples to detect the amount of principal marine nutrients such as phosphate, silicate and nitrogen compounds.

The colorimetric methods generally employed are often performed by a continuous flow autoanalyzer, which allows completion of the analysis in a short time and with good detection limits [1]. However, some interferences can be observed, either when calibration solutions and samples have different salinity (baseline drifts) or when the linearity range concentration vs. analytical response of the autoanalyzer is not well identified. In fact the analytical response of the instrument generally tends to increase with increasing salinity (Fig. 1), either a result of refractive index differences or as a stray-light effect depending on the general characteristics of the autoanalyzer. These interferences cause incorrect determinations of nutrients when the calibration is performed by a global least-squares (LS) regression.

This effect of automated techniques is called "density fluctuation", and in the analysis of phosphorus based on ion pair formation between molybdophosphate and malachite green it can be corrected by a reducing agent ($S_2O_3^{2-}$) with a modified instrument [2] and by a standard addition method (MOSA).

In this paper, new univariate calibration procedures based on different methods of robust linear regression analysis are employed in order to correct the density fluctuation in the analysis of phosphorus. The two procedures examined are the non-parametric regression according to Theil's complete method (TCM) [3] and the least median or squares (LMS) [4]. The main advantages of robust regression methods (RRMs) are no modification of the autoanalyzer is required and the operator has the potential to determine the linearity range of nutrient vs. analytical response according to the salinity characteristics of each sample.


*SSDI* 0039-9140(95)01566-3

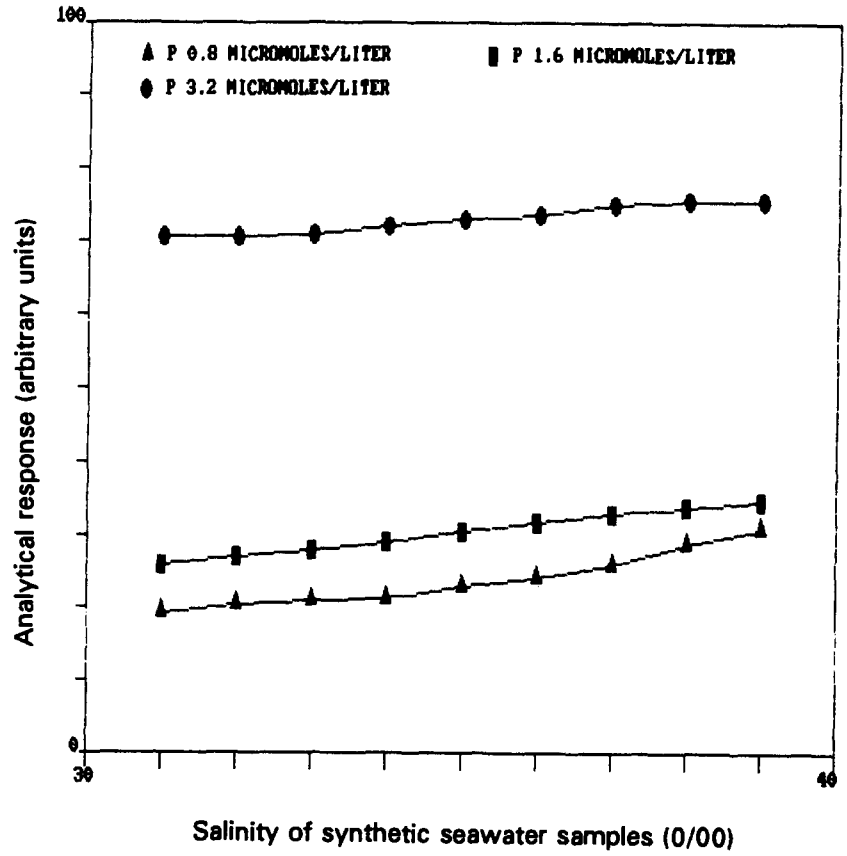


Fig. 1. Evidence of salt effect: increase in the instrumental response of identical concentrations of P with the salinity of synthetic seawater samples.

TCM and LMS regressions were applied to the analysis of phosphorus in synthetic seawater samples to verify the precision of the proposed method, and were compared with other methods of calibration such as MOSA and multilinear regression (MLR) analysis. The results were more precise than those obtained by unmodified LS regression and comparable with MOSA.

## 2. Experimental

All the measurements were performed using an Integral Alliance continuous flow autoanalyzer supported by an AST Premium 286 PC, according to the modified phosphomolybdate complex method for the analysis of inorganic P in seawater [5].

All the chemicals were of analytical reagent grade and only MilliQ deionized water was used to prepare the solutions.

Synthetic seawater samples, having a salinity of 31–39‰ and a P content of 0–3.5 μmol $cm^{-3}$, were considered in this study, and the salinity values were prepared according to the table of the major ions in seawater in relation to salinity [6].

In every test, synthetic seawater, having the lowest salinity value of the considered range, was always used as the spectroscopic blank. Such care was necessary, because the instrumental response increases with salinity (Fig. 1). Within a salinity range, baseline drifts or ghost peaks can sometimes be observed owing to the salt effect when an intermediate value of salinity is considered as the spectrophotometric blank, instead of the lowest value.

Triplicate measurements of each synthetic sample were performed to avoid outliers resulting from uncorrected concentrations of P.

LS regression, MLR, TCM and the residual regression analysis of TCM according to the studentized residual method [3] were carried out using home-made software written in GW-BASIC (ver. 3.22). LMS were performed by the PROGRESS software [7], which also includes residual regression analysis by the standardized residual method [3].

## 3. Results and discussion

The importance of applying RRMs can be illustrated by some practical examples. Let us consider the determination of phosphorus in a marine sample set having salinity between 31 and 36‰ (Table 1). This range is very common in the Adriatic Sea, where the salinity may vary from 30 to higher than 39‰ [8]. If we assume an a priori linear relationship concentration of $P$ vs. analytical response, we could inadvertently include some outliers in the automated calibration performed by LS regression. LS regression is based on the assumption of an independent and normal error distribution having a constant variance; this means that the regression residuals are presumed to have a gaussian distribution [9]. In the analysis of marine nutrients performed by an autoanalyzer, the conditions of normality could not be verified because the salinity can cause a non-gaussian distribution of residual regression.

A good procedure to correct the interference of this salt effect is the identification of sub-ranges of salinity within the sample set, where the analytical response of the autoanalyzer depends only on the concentration of P. RRMs such as TCM and LMS were considered for this purpose.

RRMs are designed to be as independent as possible of the presence of outliers [10–13]. This behaviour, defined as the breakdown point (BDP), is the percentage of outlier points on the calibration graph that can be tolerated before the regression line is significantly altered. BDP, which is equal to 0% for LS regression, ranges between 20 and 50% for RRM [3,4].

Table 1
Example of application of TCM and LMS to a data set of standard solutions of salinity between 31 and 36‰

| Salinity (‰) | P (μmol dm$^{-3}$) | Analytical response mean values of three replicates (arbitrary units) |
|---|---|---|
| 31 | 0.8 | 18.1 ± 0.18 [a] |
| 32 | 3.3 | 76.2 ± 0.20 |
| 33 | 1.3 | 36.5 ± 0.22 |
| 34 | 2.4 | 59.1 ± 0.31 |
| 35 | 0.9 | 25.9 ± 0.23 |
| 36 | 1.6 | 42.4 ± 0.32 |

| | LS 31–36‰ | LS-out$_{TCM}$ 32–36‰ | LS-out$_{LMS}$ 32–36‰ |
|---|---|---|---|
| Corr. coeff. | 0.991 | 0.998 | 0.998 |
| Res. std. Dev. [b] | 3.04 | 1.17 | 1.17 |

[a] Outlier by TCM and LMS residual analysis.
[b] Residual standard deviation, calculated according to Refs. [12] and [26].

A general property of robust methods when outliers are present is that the non-parametric regression estimators have smaller standard deviations than LS regression for all sample sizes [14], and this could suggest direct substitution of LS regression with TCM. Cruz et al. [15] instead suggested a difference procedure which allows exploitation of the power of RRMs to detect groups of aligned or unaligned experimental data by analysis of the regression residual [3,7]. This procedure is reported below.

Step 1. Application of TCM and LMS to the experimental data of calibration (having the same salinity range as the marine sample set) to obtain the robust equation $Y = A + BX$.

Step 2. Evaluation of the standardized residuals in order to detect outliers and determination of the linearity range with respect to the salinity.

Step 3. Application of LS regression —outliers excluded in order to obtain the robustly corrected equation $Y = A + BX$ according to the salinity range.

A practical application of this procedure in the analysis of P is reported in Table 1.

The results obtained showed that the linearity range lies between 32 and 36‰. The exclusion of the 31‰ solution, designated as an outlier by both TCM and LMS, improved the correlation coefficient and reduced the residual standard deviation. Hence, original salinity range was divided into two different calibration sets, the first including samples having 32–36‰ and the second one with only 31‰ samples. The linear relationships between concentration of P and analytical response were subsequently established again for each sub-set of aligned data by LS regression, as it is the most precise of all the exact estim-ations [15].

Therefore, it is possible to say that RRM can designate salinity ranges where the bias error of the determination is included in the random error of the applied analytical method.

### 3.1. Comparison between TCM and LMS

The results of Table 1 showed that TCM and LMS have similar power to detect outliers in a calibration set. However, this similarity of results is not always the case, because the BDP is

Table 2
Comparison of the power of TCM and LMS to detect outliers in a data set of synthetic seawater solutions of salinity between 35 and 39‰

| Salinity (‰) | P (μmol dm$^{-3}$) | Analytical response mean values of three replicates (arbitrary units) |
|---|---|---|
| 39 | 1.0 | 31.3 ± 0.37 [a] |
| 38 | 1.1 | 36.9 ± 0.41 |
| 35 | 1.62 | 39.9 ± 0.44 [a] |
| 36 | 2.42 | 60.3 ± 0.45 |
| 37 | 3.23 | 75.7 ± 0.39 |

$Y = 12.27_{LS} + 19.50_{LS}X$
$Y = 12.84_{TCM} + 19.46_{TCM}X$
$Y = 16.75_{LMS} + 18.17_{LMS}X$

| | LS 35–39‰ | LS–out$_{LMS}$ 36–38‰ |
|---|---|---|
| Corr. coeff. | 0.990 | 0.999 |
| Res. std. dev. | 3.00 | 0.52 |

$Y$ analytical response; $X$ = concentration of P.
[a] Outliers after LMS residual analysis by PROGRESS software

the limiting factor in the application of RRMs. In fact, the BDP value of TCM in 30% and LMS has a BDP value of up to 50% for both univariate and multivariate regressions [16,17]. This high BDP is seldom necessary in analytical chemistry, but can be usefully employed in the calibration of an autoanalyzer. The power to detect outliers tends to diminish when a small number of solutions (three or four) is included in the calibration set. The example of Table 2, referring to another range of salinity, showed the high power of LMS to detect outliers. Here the salinity range between 35 and 39‰, but only five synthetic seawater samples were included in the calibration set.

In Table 2, the equations for LS regression, TCM and LMS are reported. The LS and TCM equations are quite similar, while the LMS is different. TCM was not able to detect outliers; on the contrary, LMS detected two outliers, the samples with 35‰ and 39‰. This means that the original range of salinity must be divided into three calibration sets (the first 35‰, the second 36–38‰ and the third 39‰) to always obtain linear relationships between concentration of P and analytical response. This result also underlines a general rule of calibrating an autoanalyzer by robust methods having different BDP values: the greater the number of points in the calibration set, the greater the possibility of detecting outliers with the same power. When the number of points is small (such as the example of Table 2), the LMS with its high BDP has greater power than TCM.

### 3.2. Comparison between RRMs and MLR

A fast and simple method to correct the effect of salinity is to include the variable salinity in the calibration model using MLR analysis. In the re-examination of the data reported in Tables 1 and 2, it was always possible to obtain a good correlation according to the global equation

$$Y = a_1 S + a_2 C + \cos t$$

where $S$ is salinity, $C$ is the concentration of marine nutrient and $Y$ is the analytical response.

In fact, for the data of Table 1, the coefficient of MLR and the residual standard deviation are 0.996 and 2.25 respectively; for the data of Table 2, the coefficient of MLR and the residual standard deviation are 0.994 and 2.85 respectively. However, the multivariate calibration model has a problem in calculating the limit of detection (LOD), because it is not as unique as the univariate regression.

Lorber [18] proposed the net analytical response theory to define the LOD of multivariate regressions; Bauer et al. [19] proposed the propagation error theory to estimate the LOD of MLR; Delaney [20] and Singh and Garner [21] used the chemometrical approach based on principal component analysis to estimate the LOD in multivariate calibration. All these methods have both advantages and disadvantages [22], so the univariate RRMs are easier applications because they allow a direct and unique identification of the LOD.

### 3.3. Comparison between RRMs and MOSA

Another good procedure which avoids the salt effect is to perform the "in situ calibration" of MOSA, which works well independently of salinity and does not require knowledge of this value. This peculiarity is an advantage of MOSA in comparison with RRMs, but MOSA can also have some drawbacks compared to RRMs. In fact, in an extensive study about the properties of MOSA, Garner and Gunn [23] recommended the use of double additions up to the top of the linear range, combined with

calculation of results by a weighted linear regression in order to improve the analytical precision. This characteristic makes MOSA generally more time consuming than RRMs, because each sample needs a convenient calibration, and a short time of analysis is another critical step in the determination of marine nutrients. In fact, Koroleff [5] recommends that the analysis of P in seawater should be commenced as soon as possible, certainly within 2 h from the sampling or from the defrosting of samples.

RRMs are, in contrast, fast procedures, because their application can be performed in a single and automated step using the proper software and before starting the sample analysis. Therefore, the identification of the linear range between concentration and analytical response allows the application of MOSA to be avoided for all the samples and the time of analysis to be reduced.

Hence, the necessity of knowing the value of the salinity for each sample in the application of RRMs is only apparently a drawback because marine nutrients are often included in monitoring studies of seawater, where salinity is jointly measured with other parameters such as dissolved oxygen content, temperature, conductivity, density, and Redox potential by a multiparametric probe [24].

Finally, RRMs have a precision which can be compared with that of MOSA (Table 3).

Table 3
Oligotrophic ([P] < 2 μmol $dm^{-3}$) and eutrophic synthetic seawater samples ([P] > 2 μmol $dm^{-3}$). Comparison among results obtained by LS and LS-out and MOSA determinations. For this comparison both TCM and LMS were used for LS-out results, and MOSA results were obtained according to Ref. [23]

| True value μmol $dm^{-3}$ | LS μmol $dm^{-3}$ | LS-out μmol $dm^{-3}$ | MOSA μmol $dm^{-3}$ |
|---|---|---|---|
| 0.62° | 0.76 ± 0.19 | 0.57 ± 0.04 | 0.57 ± 0.04 |
| 0.81° | 0.98 ± 0.18 | 0.80 ± 0.04 | 0.82 ± 0.03 |
| 0.71° | 0.86 ± 0.18 | 0.74 ± 0.04 | 0.75 ± 0.05 |
| 0.90° | 1.20 ± 0.18 | 1.04 ± 0.04 | 0.98 ± 0.05 |
| 1.62° | 1.65 ± 0.18 | 1.53 ± 0.04 | 1.71 ± 0.05 |
| 1.16° | 1.45 ± 0.19 | 1.21 ± 0.04 | 1.18 ± 0.05 |
| 0.81° | 1.15 ± 0.17 | 0.88 ± 0.04 | 0.86 ± 0.04 |
| 0.81° | 0.91 ± 0.17 | 0.73 ± 0.04 | 0.84 ± 0.04 |
| 3.23ᵉ | 3.07 ± 0.18 | 3.05 ± 0.04 | 3.16 ± 0.06 |
| 2.42ᵉ | 2.42 ± 0.17 | 2.35 ± 0.04 | 2.38 ± 0.07 |
| 2.65ᵉ | 2.75 ± 0.17 | 2.70 ± 0.04 | 2.78 ± 0.07 |

o: oligotrophic sample; e: eutrophic sample.

TAL 42:9-D

### 3.4. *Final consequences of applying robust regressions in the analysis of marine nutrients*

The entity of density fluctuation and the relative linearity range depend on the general characteristics of the autoanalyzer, and different measurements are necessary to establish the best conditions of analysis. The direct consequence of including one or more outliers in the calibration is the underestimation or overestimation of the pertinent analytes in a real sample. A re-examination of Fig. 1 shows that the lowest concentration of P corresponding to the highest percentage analytical error. Therefore, it is possible to say that the density fluctuation has the greatest effect at the lowest concentrations, i.e. for oligotrophic samples ([P] < 2 μmol $dm^{-3}$), while it is negligible for eutrophic samples.

The example of Table 3, in which only synthetic seawater samples have been considered, confirmed this general trend. The main reason for using synthetic seawater samples instead of real marine samples was because of the necessity of comparing the calculated values of [P] with the real ones. In fact, it is well known that in many chemical and biological investigations, seawater of a known composition of the major ions is needed [6].

For eutrophic samples, there is no evidence of density fluctuation because of the overlapping results calculated by LS and LS-out, regression. For oligotrophic samples, the LS-out values are closer to the true values than the LS ones. This result is really important in monitoring the activity of oligotrophic seawater, such as that from the Mediterranean [25].

## 4. Conclusion

RRMs such as TCM and LMS were shown to be good tools to detect outliers in the colorimetric analysis of P in seawater performed by a continuous flow autoanalyzer. The presence of outliers in the calibration step can be due to a salinity effect because analytical response vs. concentration is not linear, causing corrupted estimations of nutrients especially in oligotrophic marine samples. The advantage of applying an RRM is that no modification of the autoanalyzer is required to correct the salinity effect, while modifications of the autoanalyzer are required by other methods. A second advantage of robust methods is that they generally require a shorter time of analysis

than MOSA, although they have similar analytical precision.

This study on the determination of inorganic P was performed because a density fluctuation has only been observed for this nutrient. However, the application of RRMs can be extended to the determination of different nutrients (total P, Si and nitrogen nutrients such as $NH_3$, $NO_2^-$ when the salt effects are observed.

## Acknowledgements

The author is grateful to Dr. M. Cruz Ortiz and Dr. L.A. Sarabia of Colegio Universitario of Burgos, Spain, for the helpful discussion about the applications of RRMs. The author is also grateful to Miss C. Gesumundo and Miss M. Amici for their technical assistance.

## References

[1] W.A. Coakley, Handbook of Automated Analysis: Continuous Flow Techniques, Marcel Dekker, New York, 1981.
[2] M. Aoyagi, Y. Yasumasa and A. Nishida, Anal. Chim. Acta, 214 (1988) 229.
[3] J.N. Miller, Analyst, 118 (1993) 455.
[4] D.L. Massart, L. Kaufman, P.J. Roussew and A. Leroy, Anal. Chim. Acta, 187 (1986) 171.
[5] F. Koroleff, in K. Grassoff, K. Ehrardt and K. Kremling (Eds.), Methods of Seawater Analysis, 2nd edn., Verlag Chemie, Weinheim, 1983, Chapter 3.
[6] K. Kremling, in K. Grassoff, K. Ehrardt and K. Kremling (Eds.), Methods of Seawater Analysis, 2nd 2dn., Verlag Chemie, Weinheim, 1983, Chapter 11.
[7] P.J. Rousseeuw and A.M. Leroy, Robust Regression & Outliers Detection, Wiley, New York, 1987.
[8] M. Giani, M. Mecozzi, R. Morlino, M.G. Natale, L. Salvatori and F. Savelli, in Studies and characteristics of Marine Snow in Northen Adriatic Sea, ICRAM, Roma, 1991, Chapter 3.
[9] G.R. Phillips and E.M. Eyring, Anal. Chem., 55 (1983) 1134.
[10] J.N. Miller, Analyst, 116 (1991) 3.
[11] R. Wolters and G. Kateman, J. Chemometrics, 3 (1989) 329.
[12] J.C. Miller and J.N. Miller, Statistics for Analytical Chemistry, Ellis Horwood Series, Chichester, 1989.
[13] M. Forina, Introduzione alla Chimica Analitica con Elementi di Chemiometria, ECIG, Genova Italia, 1993.
[14] P.P. Talwar, Comput. Stat. Data Anal. 15 (1993) 309.
[15] M. Cruz Ortiz, J. Arcos, J.V. Juarros, J. Lopez Palacios and L.A. Sarabia, Anal. Chem., 65 (1993) 678.
[16] P.J. Rousseuw, J. Am. Stat. Assoc., 79 (1984) 871.
[17] P.J. Rousseuw, J. Chemometrics, 5 (1991) 1.
[18] A. Lorber, Anal. Chem., 58 (1986) 1167.
[19] G. Bauer, W. Wegscheider and H.M.F. Ortner, J. Anal. Chem., 340 (1991) 135.
[20] M.F. Delaney, Chemom. Intell. Lab. Syst., 3 (1988) 45.
[21] A. Singh and F.C. Garner, Anal. Chim. Acta, 277 (1993) 205.
[22] R. Boque and F.X. Rius, Congress 3rd Colloquium Chimiometricum Mediterraneum, International Chemometrics Society, 7–9 June 1994, Abstract p. 21.
[23] M.J. Gardner and A.M. Gunn, Fresenius' Z. Anal. Chem., 325 (1986) 263.
[24] M. Innammorati, I. Ferrari, D. Marino and Ribera D'Alcalà, in Ecological Methods in the Study of Marine Plancton, Nova Thalassia, Trieste, Italy, Vol. 11, 1990, p. 111.
[25] Società Chimica Italiana, Workshop on Depollution planning of Mediterranean Sea, Italian Society of Chemistry Edition, Rome, 1992.
[26] M.H. Feinberg, J. Chemometrics, 3 (1988) 103.

ELSEVIER

Talanta 42 (1995) 1245–1250

Talanta

# Simultaneous spectrophotometric determination of Thymol Blue, Semimethylthymol Blue and Methylthymol Blue II. Monitoring of the syntheses of Semimethylthymol Blue and Methylthymol Blue

S. Kiciak *, H. Gontarz, E. Krzyżanowska

*Institute of Chemistry and Technical Electrochemistry, Politechnika Poznańska, PL-60-965 Poznań, Poland*

Received 25 October 1994; revised 21 February 1995; acepted 22 February 1995

**Abstract**

A new version of the direct spectrophotometric method for the simultaneous determination of Thymol Blue, Semimethylthymol Blue (SMTB) and Methylthymol Blue (MTB) was developed and used for monitoring syntheses of SMTB and MTB.

## 1. Introduction

The method for the simultaneous determination of Thymol Blue (TB), Semimethylthymol Blue (SMTB) and Methylthymol Blue (MTB) given in a previous paper [1] was based on measurements of the absorbances of three solutions of these compounds in 1, 4 and 7 M sulphuric acid. Some possibilities were shown using this method for the determination of TB, SMTB and MTB in spectrophotometric reagents and in mixtures obtained during syntheses of SMTB.

In spite of the obtained results being relatively good, two aspects of the method were not satisfactory enough for the authors. The first was the necessity of preparating three solutions for each tested sample, two of them with relatively high sulphuric acid concentrations (4 and 7 M). Secondly, the drawing of figures for the given graphical version of the method was time consuming and the exact read-out of the results given in such figures was relatively difficult. The first problem was resolved when we found that good results of absorbance measurements could be obtained using solutions with a 0.5 M sulphuric acid concentration not only near 548 nm but also at 485 and 455 nm. The second problem was overcome by rearranging the newly obtained dependences of the relative absorbances on the mole fractions of SMTB and MTB ($A_{R1}=f(X_{SMTB},X_{MTB})$ and $A_{R_2}=f(X_{SMTB},X_{MTB})$ to $X_{SMTB}=f(A_{R1},A_R)$ and $X_{MTB}=f(A_{R1},A_{R2})$. This allows the calculation of mole fractions of the dyes determined without using additional figures and shows the route of the syntheses more exactly than before [1]. However, the limitation of spectrophotometrically active reagents to three main components present during the described syntheses, without taking into account the byproducts occurring in trace or low amounts [2–4] is a necessary simplification. This can be the reason for the low relative errors (mainly much below 5%).

* Corresponding author.


*SSDI* 0039-9140(95)01567-1

## 2. Experimental

### 2.1. Apparatus

The absorption measurements were made with a Zeiss-Jena spectrophotometer (Specord M40) with 1-cm cells. A conventional thermostated glass apparatus with a reflux condenser was used for the syntheses.

### 2.2. Reagents

MTB (Merck) containing approximately 90% of the dye was purified by extraction in a dilute sulphuric acid–1-butanol system.

SMTB (from our own synthetic mixture containing approximately 40% of the dye) was purified by the previously reported method [5].

A commercial sample of TB was recrystallized from ethanol. All other reagents were of analytical grade. Standard solutions of the three dyes (0.001 M) were prepared in 0.01 M sulphuric acid for MTB and SMTB and in 1:1 (v/v) ethanol–aqueous 0.02 M sulphuric acid mixture for TB.

### 2.3. Syntheses and Sampling

Dissolve 235 mg of TB in approximately 50 ml of glacial acetic acid. Add the required amount of iminodiacetic acid (IDAA) and anhydrous sodium acetate, stir and heat the mixture to the required temperature — not lower than 55 °C and not higher than 65 °C. At the lower temperature the reaction rate is too slow; at the higher temperature the formation of byproducts must be taken into account. Transfer $0.25 \pm 0.05$ ml of a solution of the obtained mixture to a 50-ml standard flask (sample "zero"), Then start the synthesis by adding the required amount of formaldehyde to the stirred thermostatted mixture. The ranges of the ratios of mole concentrations used in the experiments were: $C_{IDAA}/C_{TB}$, 1.00–4.0; $C_{CH_3COONa}/C_{IDAA}$, 2.0–8.0; and $C_{HCHO}/C_{IDAA}$, 2.2–4.2. Next, remove samples after defined time intervals from the beginning of the synthesis — at first after every 1 h period, then after periods of 2 or more h. The total time of the syntheses was, 24 or 36 h.

To each of the $0.25 \pm 0.05$ ml samples (the "zero" sample and those transferred during the synthesis to 50-ml standard flasks), add 5 ml of 0.05 M sulphuric acid and dilute to the mark with water (solutions $S_0$). There is no need to remove exactly the same known amounts of reaction mixture because the relative absorbances used (in the given ranges) are practically not dependent on the concentration of solution $S_0$. Transfer 10.0-ml aliquots of solution $S_0$ to two 25-ml standard flasks for each sample. Add 10.0 ml of 1.25 M $H_2SO_4$ to each 25-ml flask containing the examined sample, and make up to the mark with water (solutions $S_{0.5}$). Solutions $S_0$ are much more stable than solutions $S_{0.5}$. The former can be used 0.1–8 h after preparation without remarkable changes occurring, but absorbance measurements on solutions $S_{0.5}$ should be performed no longer than 0.5 h after their preparation.

### 2.4. Measurements and Calculations

Measure the absorbances of the solutions $S_{0.5}$ at 455, 485 and 545 nm (1-cm path-length cells). Calculate the relative absorbances $A_{R1}$ and $A_{R2}$ and the mole fractions of the components as given below (Eqs. (6)–(10)). Use the obtained results to show the route of the synthesis on a Gibbs triangle. The molar absorptivities of pure samples of the three dyes should be determined with the equipment used, and substituted for those quoted, if there is a difference.

## 3. Results and discussion

### 3.1. Conditions for absorbance measurements

More detailed investigations than were previously carried out [1] of the dependences of the molar absorptivities of TB, SMTB and MTB on the sulphuric acid concentration show that at a much lower concentration of the acid, the absorbance measurements can be performed at 545, 485 and 455 nm in solutions with 0.5 M sulphuric acid. The molar absorptivities of the dyes, under the chosen conditions, are given in Table 1.

Table 1
Molar absorptivites of TB, SMTB and MTB (in 0.5 M sulphuric acid)

| Dye | $\varepsilon$ ($dm^3\ cm^{-1}\ mol^{-1}$) | | |
|---|---|---|---|
| | 455 nm | 485 nm | 545 nm |
| TB | 4800 | 7350 | 36400 |
| SMTB | 11100 | 11200 | 13900 |
| MTB | 18900 | 11800 | 4450 |

It is advantageous here that in 0.5 M sulphuric acid at 455 nm, the molar absorptivites of SMTB and MTB are much greater than that of TB, and at 545 nm the molar absorptivities of TB and SMTB are much greater than that of MTB.

### 3.2. Equations used for the calculations

It was stated that under the given conditions Beer's law is obeyed and the absorbances are additive over the concentration range (0.5–25) $\times 10^{-6}$ M, so according to the given molar absorptivities of the three dyes, for a path length of 1 cm, the absorbances ${}_{455}A$, ${}_{485}A$ and ${}_{545}A$ (in 0.5 M sulphuric acid) are

$${}_{455}A = (4.8C_{TB} + 11.1C_{SMTB} + 18.9C_{MTB}) \times 10^3 \quad (1)$$

$${}_{485}A = (7.35C_{TB} + 11.2C_{SMTB} + 11.8C_{MTB}) \times 10^3 \quad (2)$$

$${}_{545}A = (36.4C_{TB} + 13.9C_{SMTB} + 4.45C_{MTB}) \times 10^3 \quad (3)$$

It follows from Eqs. (1)–(3), that

$$A_{R1} = \frac{{}_{455}A}{{}_{485}A} = \frac{(4.8C_{TB} + 11.1C_{SMTB} + 18.9C_{MTB}) \times 10^3}{(7.35C_{TB} + 11.2C_{SMTB} + 11.8C_{MTB}) \times 10^3} \quad (4)$$

$$A_{R2} = \frac{{}_{545}A}{{}_{485}A} = \frac{(36.4C_{TB} + 13.9C_{SMTB} + 4.45C_{MTB})q \times 10^3}{(7.35C_{TB} + 11.2C_{SMTB} + 11.8C_{MTB}) \times 10^3} \quad (5)$$

where $A_{R1}$ and $A_{R2}$ are the chosen relative absorbances.

The mole fractions of TB, SMTB and MTB are

$$X_{TB} = \frac{C_{TB}}{\sum C_i} X_{SMTB} = \frac{C_{SMTB}}{\sum C_i} X_{MTB} = \frac{C_{MTB}}{\sum C_i}$$

where $\Sigma C_i = C_{TB} + C_{SMTB} + C_{MTB}$ and $X_{TB} + X_{SMTB} + X_{MTB} = 1$. Division of the numerators and denominators of Eqs. (4) and (5) by $\Sigma C_i$ and introduction of $X_{TB} = 1 - X_{SMTB} - X_{MTB}$ gives

$$A_{R1} = \frac{4.8 + 6.3X_{SMTB} + 14.1X_{MTB}}{7.35 - 3.85X_{SMTB} - 4.45X_{MTB}} \quad (6)$$

$$A_{R2} = \frac{36.4 - 22.5X_{SMTB} - 31.95X_{MTB}}{7.35 - 3.85X_{SMTB} - 4.45X_{MTB}} \quad (7)$$

By rearranging Eqs. (6) and (7) we obtain

$$X_{SMTB} = \frac{666.6 - 396.9A_{R2} - 82.3A_{R1}}{22.9A_{R1} + 26.25A_{R2} + 116.0} \quad (8)$$

$$X_{MTB} = \frac{305.5A_{R1} + 27.8A_{R2} - 337.3}{22.9A_{R1} + 26.25A_{R2} + 116} \quad (9)$$

and because $X_{TB} = 1\text{-}X_{SMTB}\text{-}X_{MTB}$

$$X_{TB} = \frac{114.3A_{R1} + 80.75A_{R2} - 213.3}{22.9A_{R1} + 26.25A_{R2} + 116} \quad (10)$$

### 3.3. Results of monitoring the syntheses of SMTB and MTB

The experiments carried out at the beginning of this work showed that if the molar concentration of formaldehyde was over twice to four times greater than the concentration of iminodiacetic acid, then the results of the syntheses were mainly dependent on the ratios between the molar concentrations of sodium acetate, iminodiacetic acid and Thymol Blue and on the applied temperature.

Therefore these dependences were examined in this work.

The dependence of the course of the syntheses on time, for different ratios of the initial molar concentrations of $C_{0CH_3COONa}$:$C_{0TB}$ and for a constant concentration ratio $C_{0HCHO}$:$C_{0IDAA}$:$C_{0TB}$ = 8:2:1, was investigated at constant temperatures (55, 65 or 75 °C).

The results obtained showed that at 75 °C the reaction rate and the compositions of the mixtures forming are considerably dependent on concentration changes at low concentrations of sodium acetate, but are almost independent of concentration at higher concentrations (over three times higher than the concentration of iminodiacetic acid and six times higher than the concentration of Thymol Blue).

At lower temperatures (65 and 55 °C) the influences on the reaction path of concentration changes at low concentrations of sodium acetate are much smaller than those at 75 °C.

The dependences of the course of the syntheses on time at constant temperature (65 °C) for different concentrations of iminodiacetic acid at constant concentrations of formaldehyde, sodium acetate and Thymol Blue are given in Fig. 1.

It follows from the data given in Fig. 1 that the rate of reaction considerably accelerates

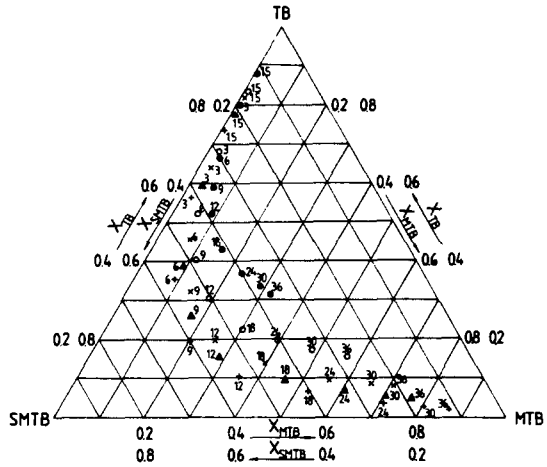


Fig. 1. The dependence of the compositions (given in mole fractions $X_i$) of TB, SMTB and MTB mixtures on the time of synthesis (h) carried out at 65 °C, for a constant ratio of the initial molar concentrations $C_{0HCHO}:C_{0CH_3COONa}:C_{0TB} = 8:8:1$ and for different ratios of $C_{0IDAA}:C_{0TB}$:(●) 1.0; (○) 1.5; (×) 2.0; (△) 3.0; (+) 4.0.

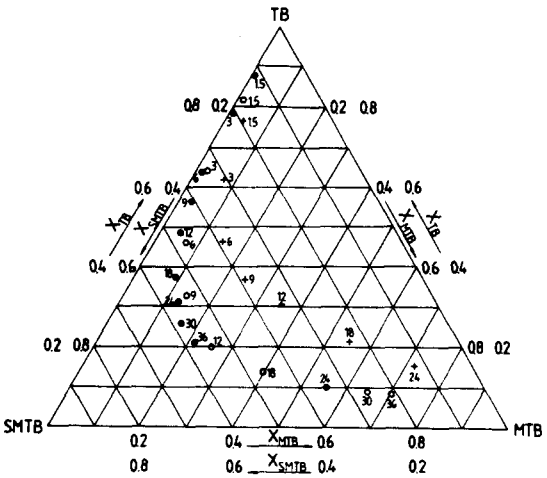


Fig. 2. The dependence of the compositions (given in mole fractions $X_i$) of TB, SMTB and MTB mixtures on the time of synthesis (h), for a constant ratio of the initial molar concentrations $C_{0IDAA}:C_{0HCHO}:C_{0CH_3COONa}:C_{0TB} = 2:8:8:1$, carried out at different temperatures: (●) 55 °C; (○) 65 °C; (+) 75 °C.

with the increase in the amount of iminodiacetic acid used. During the first period of the reaction (about 9 h) the dominant product is Semimethylthymol Blue, but in the next period the formation of Methylthymol Blue dominates.

The dependences of the course of the syntheses on time at different temperatures, at constant concentrations of sodium acetate and formaldehyde and at constant ratios of the initial molar concentrations of iminodiacetic acid and Thymol Blue, are given in Figs. 2 (for $C_{0IDAA}:C_{0TB} = 2:1$) and 3 (for $C_{0IDAA}$: $C_{0TB}$ = 4:1). The results obtained for $C_{0IDAA}$: $C_{0TB}$ = 1:1 as well as those given in Figs. 2 and 3 show that a temperature increase of the reaction mixtures accelerates the reaction rates and changes the paths of the proceeding reactions. This is clearly seen by a comparison of the values of the reaction periods necessary to obtain the maximum mole fraction for Semimethylthymol Blue ($t_{maxSMTB}$) and by a comparison of the values of these fractions ($X_{maxSMTB}$) at different temperatures and at constant ratios of initial molar concentrations of iminodiacetic acid and Thymol Blue (Table 2).

To obtain more conclusions concerning the kinetics of the investigated processes it is necessary to present dependences of mole fractions ($X_i$) on time ($t$) for each of the three dyes, as is shown in Fig. 4.

The shapes of the dependences suggest that both reactions TB → SMTB and SMTB → MTB are first order. This was confirmed by calculation of the rate constants $k_1$ and $k_2$ by using the equations

$$k_1 = -\frac{1}{t} \ln X_{TB} \tag{11}$$

$$k_2 = \frac{\Delta X_{MTB}}{X_{SMTB} \Delta t} \tag{12}$$

where $X_{TB}$ is the mole fraction of TB $t$ h from the beginning of the synthesis, $X_{SMTB} = (\Sigma X_i)_{SMTB}/n$ is the mean value of $X_{SMTB}$ for the reaction period $\Delta t = t_2 - t_1$ for $n \geq 5$ values of $X_{SMTB}$ taken every 1.5 or 3 h during the reac-

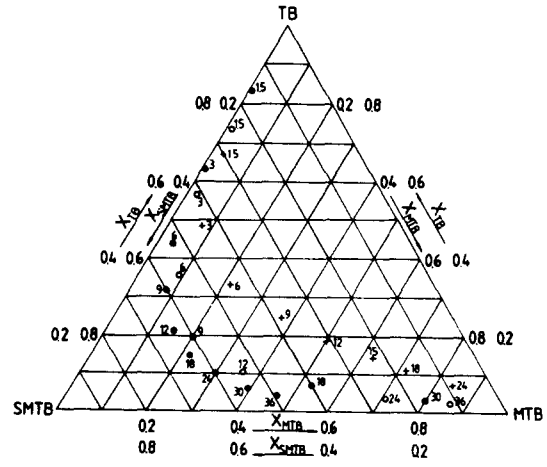


Fig. 3. The dependence of the compositions (given in mole fractions $X_i$) of TB, SMTB and MTB mixtures on the time of synthesis (h) for a constant ratio of the initial mole concentrations $C_{0IDAA}:C_{0HCHO}:C_{0CH_3COONa}:C_{0TB} = 4:8:8:1$, carried out at different temperatures: (●) 55 °C; (○) 65 °C; (+) 75 °C.

Table 2
Dependence of the maximum molar fractions of Semimethylthymol Blue ($X_{maxSMTB}$) on temperature and reaction periods ($t_{maxSMTB}$) necessary for obtaining $X_{SMTB}$ at constant ratios of the initial molar concentrations of iminodiacetic acid and Thymol Blue ($C_{0IDA}/C_{0TB}$)

| $C_{0IDAA}/C_{0TB}$ | 55 °C | | 65 °C | | 75 °C | |
|---|---|---|---|---|---|---|
| | $X_{maxSMTB}$ | $t_{maxSMTB}$ (h) | $X_{maxSMTB}$ | $t_{maxSMTB}$ (h) | $X_{maxSMTB}$ | $t_{maxSMTB}$ (h) |
| 1:1 | 0.45 | 40 | 0.41 | 18 | 0.38 | 7.0 |
| 2:1 | 0.58 | 34 | 0.54 | 10 | 0.40 | 6.0 |
| 4:1 | 0.63 | 12 | 0.60 | 8.5 | 0.46 | 4.5 |

tion period $\Delta t$, and $\Delta X_{MTB} = (X_2 - X_1)$ is the difference in $X_{MTB}$ for the reaction period $\Delta t$.

Examples of calculations of $k_1$ and $k_2$ are given in Tables 3 and 4.

The $k_1$ and $k_2$ values calculated according to Eqs. (11) and (12) for the synthesis performed at 65 °C under the given conditions (Tables 3 and 4), as well as that performed at 55 °C, are reaction rate constants of the first order.

The constants $k_1$ and $k_2$ and their standard deviations are:

for 55 °C, $_{55}k_1 = 0.132 \pm 0.008\ h^{-1}$ and $_{55}k_2 = 0.0258 \pm 0.0008\ h^{-1}$;

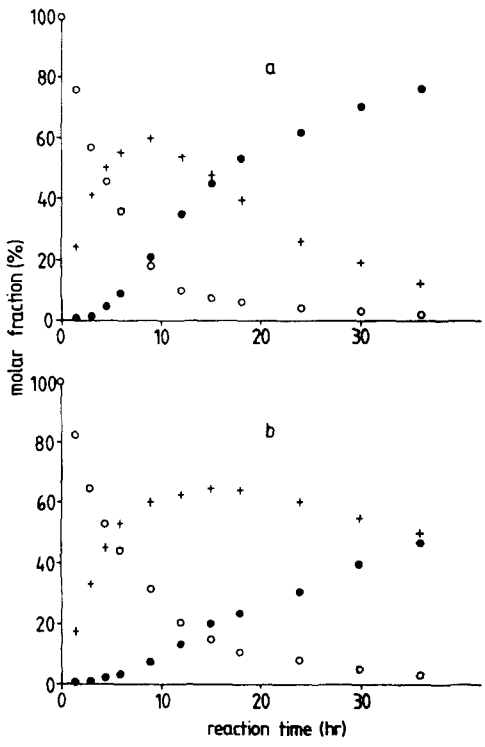


Fig. 4. Dependence of mole fractions of TB, SMTB and MTB found in the mixtures on the time of synthesis, for a constant ratio of the initial mole concentrations $C_{0IDAA}$: $C_{0HCHO}$:$C_{0CH_3COONa}$:$C_{0TB}$ = 4:8:8:1, carried out at (a) 65 °C and (b) 55 °C. (○) $X_{TB}$; (+) $X_{SMTB}$; (●) $X_{MTB}$.

for 65 °C, $_{65}k_1 = 0.179 \pm 0.009\ h^{-1}$ and $_{65}k_2 = 0.0696 \pm 0.0019\ h^{-1}$.

Comparison of these constants allows us to confirm that at 55 °C the reaction rate constant for the SMTB synthesis ($k_1$) is about five times greater than the rate constant obtained for MTB synthesis ($k_2$). However, the increase of temperature to 65 °C causes only about a 35% increase in $k_1$ ($_{65}k_1/_{55}k_1 = 1.356$) whereas the $k_2$ value then increases more than 2.5 times ($_{65}k_2/_{55}k_2 = 2.70$).

Similar calculations carried out when using the results obtained for syntheses performed at 75 °C and at lower ratios of the initial concentrations of the used reagents to the initial concentration of TB did not give stable values of $k_1$ and $k_2$.

## 4. Conclusions

The new version of the spectrophotometric method for the simultaneous determination of TB, SMTB and MTB is simpler and gives more information concerning the SMTB and MTB syntheses than the method used before [1].

The method allows us to perform relatively exact observations of the progress of the reaction during 24–36 h of the syntheses carried out below 70 °C.

The results of monitoring the syntheses of SMTB and MTB obtained by using this method can be helpful for the optimization of these syntheses. In our experiments, the highest yield for SMTB (60% or above) was reached after 12 h of reaction carried out at 55 °C and at an initial molar concentration ratio $C_{0IDAA}/C_{0TB} = 4:1$, or at 65 °C after 8.5 h, at the same ratio of $C_{0IDAA}/C_{0TB}$. However, for the MTB synthesis, the highest yield (80% or above) was obtained after 30–36 h of reaction carried out at 65 °C and at the same ratio of $C_{0IDAA}/C_{0TB} = 4:1$.

Table 3
Results of the calculation of the rate constant $k_1$ for the reaction TB → SMTB at 65 °C for a constant ratio of the initial molar concentrations of the reagents used ($C_{0TB}$:$C_{0IDAA}$:$C_{0ICHCOONa}$:$C_{0HCHO}$ = 1:4:8:8)

| | | | | | | | | |
|---|---|---|---|---|---|---|---|---|
| $t$(h) | 1.5 | 3.0 | 4.5 | 6.0 | 9.0 | 12.0 | 15.0 | 18.0 |
| $X_{TB}$ | 0.760 | 0.565 | 0.445 | 0.360 | 0.185 | 0.110 | 0.075 | 0.050 |
| $-\ln X_{TB}$ | 0.274 | 0.571 | 0.810 | 0.510 | 1.687 | 2.207 | 2.190 | 2.996 |
| $k_1(h^{-1})$ | 0.183 | 0.190 | 0.180 | 0.170 | 0.187 | 0.184 | 0.173 | 0.166 |

Table 4
Results of the calculation of the rate constant $k_2$ for the reaction SMTB → MTB at 65 °C for $C_{0TB}$:$C_{0IDAA}$:$C_{0CH_2COONa}$:$C_{0HCHO}$ = 1:4:8:8

| | | | | | | | | |
|---|---|---|---|---|---|---|---|---|
| $t_2$ (h) | 12.0 | 12.0 | 15.0 | 15.0 | 15.0 | 18.0 | 18.0 | 18.0 |
| $t_1$ (h) | 6.0 | 4.5 | 6.0 | 4.5 | 3.0 | 4.5 | 3.0 | 1.5 |
| $\Delta t$ (h) | 6.0 | 7.5 | 9.0 | 10.5 | 12.0 | 13.5 | 15.0 | 16.5 |
| $X_{SMTB}$ (for $n$) | 0.570 (5) | 0.558 (6) | 0.549 (7) | 0.542 (8) | 0.528 (9) | 0.518 (10) | 0.508 (11) | 0.485 (12) |
| $\Delta X_{MTB}$ | 0.245 | 0.295 | 0.355 | 0.405 | 0.435 | 0.490 | 0.520 | 0.530 |
| $k_2$ ($h^{-1}$) | 0.071 | 0.070 | 0.072 | 0.071 | 0.069 | 0.070 | 0.068 | 0.066 |

The constant values of the rate constants obtained for the SMTB and MTB syntheses, carried out at 55 and 65 °C, confirm the assumption that the sum of the mole fractions given by the equation $X_{TB} + X_{SMTB} + X_{MTB} = 1$ is correct. However, the results obtained for the syntheses carried out at 75 °C showed that at this temperature deviations from the equation may be significant.

## Acknowledgement

This work was financed by the Committee for Scientific Investigations (K.B.N.).

## References

[1] S. Kiciak and M.A. Mehdi, Talanta, 39 (1992) 265.
[2] T. Yoshino, S. Murakami and M. Kagawa, Talanta, 21 (1974) 199.
[3] N.F. Kosenko, T.W. Malkowa and K.B. Yatsimirskij, Zh. Anal. Khim., 30 (1975) 2245.
[4] N. Nakayama, S. Tachiyashiki and E. Shimizu, Anal. Sci., 4 (1988) 595.
[5] S. Kiciak, H. Gontarz, P. Koschel and M.A. Mehdi, Microchim. Acta, 108 (1992) 73.

ELSEVIER

Talanta 42 (1995) 1251-1258

Talanta

# Tensammetric determination of non-ionic surfactants combined with BiAS separation procedure (Wickbold) 2. Optimisation of the precipitation and investigation of interferences

Bogdan Wyrwas, Andrzej Szymanski, Zenon Lukaszewski *

*Technical University of Poznan, Institute of Chemistry, PL-60-965 Poznan, Poland*

Received 1 November 1994; revised 22 February 1995; accepted 24 February 1995

**Abstract**

The precipitation step in the developed procedure (BiAS–ITM) was optimised with the aim of achieving a lower detection limit. Losses during filtration using Triton X-100 as representative non-ionic surfactant (NS), the indirect tensammetric method (ITM) and adsorptive stripping tensammetry (AdST) for the determination of the concentration of the surfactant in the precipitate and in the filtrate were investigated. The G4 glass filter recommended up to now was found to be insufficiently effective and a source of loss. The new version of the procedure developed works within the range 2–1000 μg of NS in the sample, and thus two orders of magnitude lower than the former version of the procedure, showing satisfactory recovery and precision. The detection limit (3 × S.D.) was found to be below 1.5 μg in the sample.

Interferences of anionic surfactants (ASs) e.g. sodium dodecylbenzenesulphonate and sodium lauryl sulphate, lipids, e.g. glycerol trioleate (GTO), and chlorophyll were investigated. GTO and AS show no effect on the BiAS–ITM results although strong adsorption of ASs on the glass filter as well as a slight adsorption on the precipitate was found. Chlorophyll does not interfere with the determination up to 30 μg in the sample, whereas higher concentrations produce results that are too high.

## 1. Introduction

Control of non-ionic surfactants (NSs) in surface water requires more effective methods than those currently used. The classical BiAS procedure [1,2] though widely used in Europe, gives poor results for an NS amount lower than 100–200 μg in the sample due to an unavoidable loss of precipitate during its washing with glacial acetic acid [3]. A recently developed modification of this procedure combining the precipitation of NSs with modified Dragendorff reagent and quantification by the indirect tensammetric method (BiAS–ITM) shows several advantages in comparison with the classical BiAS procedure [4]. First of all, the BiAS–ITM does not need the washing of the precipitate with glacial acetic acid. In this way the main source of error in the classical BiAS procedure is eliminated. Additionally, the BiAS–ITM exhibits considerably fewer differences in the slopes of the calibration graphs of different NSs than the classical BiAS method and therefore shows a substantially lower "error of choice of standard" (the error when one surfactant is determined using a calibration curve for another surfactant (standard)). The BiAS–ITM can be used for the determination of NSs having 3–30 oxyethylene subunits while the classical BiAS method only applies to NSs having 5–30 subunits.

Precipitation according to the classical BiAS procedure is applied within the range 100–

* Corresponding author.


SSDI 0039-9140(95)01568-X

1000 μg of NS whereas the ITM final assay requires only 2–25 μg in the sample [5]. Therefore the sample obtained after precipitation and dissolution of the precipitate should be diluted prior to the final measurement (an aliquot is used). A much better agreement of the precipitation step with the final measurement would be achieved if a lower amount of NS was precipitated. Thus the optimisation of the precipitation step was the main aim of this work. In preliminary experiments it was found that the solubility of Triton X-100 precipitate with 75 ml of Dragendorff reagent corresponds to only 0.12 μg of Triton X-100. Hence, it should be possible to precipitate several micrograms of NS. It was also observed that the temperature of precipitation within the range −5–60 °C has no marked influence on the recovery of the surfactant. A further aim of this work was the study of possible interferences from the water matrix. Anionic surfactants, lipids and chlorophyll were investigated as potential interferents. Anionic surfactants are usually present in excess compared with NSs in surface water. Lipids (one of the components of surface water) are preconcentrated during extracion or gas stripping in the boundary layer between the water and the organic phases. Numerous water samples show a fat layer on the phase boundary. Chlorophyll extracted from plants is the most serious interferent in the ITM measurements [5]. Triton X-100 was used as a representative non-ionic surfactant in all the experiments.

The ITM, which was used for the final measurement in the BiAS–ITM procedure, is a method recently developed for the determination of the total concentration of surfactants [6–8]. The lowering of the ethyl acetate tensammetric peak (the monitoring substance) is the analytical signal in the ITM. The signals of different NSs are roughly additive [8] and are sufficiently tolerant to anionic surfactants [7]. ITM can be applied both as final measurement in a separate procedure as well as in combination with the BiAS procedure [5]. Apart from the ITM, adsorptive stripping tensammetry (AdST) was used as an auxiliary technique. The analytical signals in AdST are specific and highly sensitive to the effects of mixtures. Therefore AdST can hardly be used for the final measurement. On the other hand, its high sensitivity and specificity make AdST an excellent technique for different model investigations with a single surfactant [3,9].

The experiments in this study were performed over a comparatively long period of time and the precipitation procedure was gradually improved. Thus some of the experiments were performed using much higher Triton X-100 spike concentrations and 0.5 M sodium sulphate as supporting electrolyte. Later experiments were performed under the modified conditions with lower NS spike concentrations and a supporting electrolyte containing mainly sodium chloride.

## 2. Experimental

### 2.1. Apparatus and reagents

The apparatus, cell and measuring procedure used were described in part 1 [4]. Briefly, a scan voltage of 400 mV $min^{-1}$ and an alternating voltage amplitude of 2 mV were applied. A quartz beaker instead of a glass one was used and protection of a ceramic frit on the end of a salt bridge was applied, to prevent adsorptive loss of surfactant [10].

Glass filters G1, G2, G3, G4 and G5 (Schott-Geräte) were used.

Triton X-100 (Rohm and Haas) was used without additional purification.

Chlorophyll was extracted from *Scindapsus* with acetone. Its concentration was determined by the ITM [5].

Purified sodium sulphate and sodium chloride were used for the preparation of the aqueous base electrolytes. All solutions were prepared in water triply distilled from quartz. Only freshly distilled water was used.

The modified Dragendorff reagent [1] was prepared by mixing solutions A and B before use. Solution A comprised 1.7 g of basic bismuth (III) nitrate, 65 g of potassium iodide and 220 ml of glacial acetic acid per 1000 ml. Solution B was an aqueous solution containing 290 g of barium chloride dihydrate in 1000 ml.

The solution for dissolving the precipitate (solution C) was prepared from 12.4 g of tartaric acid and 18 ml of ammonia solution (25%) made up with water to 1000 ml. For the purification of this solution of silica gel cartridge (Bakerbond spe silica gel 7086–03) was used.

### 2.2. Procedures

#### 2.2.1. Precipitation of NSs with modified Dragendorff reagent according to the BiAS procedure

*Procedure A* The surfactant sample was dissolved in a mixture of 2 ml of methanol and 16 ml of water. Solution A (8 ml) and solution B (4 ml) of the modified Dragendorff reagent were mixed and added to the sample. The reaction mixture was stirred for 20 min and left for 10 min, with the exception of the experiments related to the study of the effect of ageing of the precipitate. The orange-coloured precipitate was filtered through a glass filter (usually G5). No washing of the precipitate was used.

The precipitate was dissolved in 20 ml of hot solution C. The filter and the beaker were then washed with 3–4 ml of water; this portion of water was added to the solution containing the dissolved precipitate. After cooling, the solution volume was made up to 25 ml with water.

#### 2.2.2. ITM measurement of concentration of NSs in the precipitate

*Procedure B* An aliquot of solution obtained by dissolving the precipitate was transferred to a 25 ml volumetric flask, 12.5 ml of 1 M aqueous sodium sulphate and 1.5 ml of ethyl acetate were added, and the flask was filled to the mark with water. The mixture, containing an excess of ethyl acetate, was vigorously shaken and the emulsion transferred into the voltammetric cell. The emulsion was stirred for 10 min to achieve clarity of the solution due to evaporation of the excess ethyl acetate. This excess ethyl acetate extracts surfactants and therefore it must be removed; this is demonstrated by the disappearance of turbidity. After a quiescent period (30 s) the tensammetric curve of ethyl acetate was recorded in the cathodic direction starting from −1.20 V (vs. SCE) using a new mercury drop. The difference between the height of the ethyl acetate peak (recorded in a separate measurement) and the peak height of ethyl acetate in the presence of NS is the analytical signal. The results were quantified using a calibration curve of Triton X-100.

#### 2.2.3. ITM measurement of concentration of NSs in the precipitate

*Procedure C* An aliquot of solution obtained by dissolving the precipitate (0.5/25, 4/25 or 20/25) was transferred to a 25 ml volumetric flask, 2.5 ml of 5 M aqueous sodium chloride and 1.8 ml of ethyl acetate were added, and the flask was filled to the mark with water. The method was further continued according to procedure B.

#### 2.2.4. AdST measurement of concentration of NSs in the precipitate

*Procedure D* An aliquot of solution obtained by dissolving the precipitate was transferred to a 25 ml volumetric flask, 12.5 ml of 1 M aqueous sodium sulphate was added, and the flask was filled to the mark with water. The AdST measurement was run. The preconcentration was performed at a new mercury drop in a stirred solution at −1.20 V (vs SCE). The preconcentration time (5 min) was measured from the moment of drop formation. The tensammetric curve was recorded in the cathodic direction after a 30 s quiescent period. The analytical signal was the height of the "wide" tensammetric peak of Triton X-100 [11]. The results were quantified using a calibration graph of Triton X-100.

#### 2.2.5. AdST measurement of concentration of NSs in the filtrate

*Procedure E* Sodium chloride (10 g) was added to the filtrate in a 100 ml volumetric flask, and the flask was filled to the mark with water. NSs were extracted from the sample with 10 ml of ethyl acetate. An aliquot of the extract (50 µl) was dissolved in the 0.5 M sodium sulphate base electrolyte. The AdST measurement was performed. The preconcentration was performed at a new mercury drop in a stirred solution at −1.20 V (vs SCE). The preconcentration time (5 min) was measured from the moment of drop formation. The tensammetric curve was recorded in the cathodic direction after a 30 s quiescent period. The analytical signal was the height of the "wide" tensammetric peak of Triton X-100 [11]. The results were quantified using a calibration graph of Triton X-100 obtained in the presence of 50 µl of ethyl acetate.

*2.2.6. Determination of the concentration of anionic surfactants (ASs) in the precipitate and in the filtrate*

ASs in the precipitate were determined according to the MBAS procedure [12] after their dissolution in solution C, the AS in the filtrate being determined by AdST. The determination of AS in the filtrate by AdST was carried out in the samples after extraction of non-ionic surfactants and the bismuth (III) complex with iodide. Sodium chloride (20 g) was added to this solution which was free of NSs. ASs were extracted with 10 ml of ethyl acetate. An aliquot of the extract was evaporated and dissolved in 0.5 M sodium sulphate base electrolyte. The AdST measurement was performed using 5 min preconcentration at −1.0 V (vs SCE). The analytical signal was the height of the tensammetric peak of the corresponding surfactant. The results were quantified using calibration graphs of corresponding ASs.

## 3. Results and discussion

### *3.1. Optimisation of the procedure*

*3.1.1. Study of the influence of the porosity of the glass filter used on the loss of Triton X-100 spike*

Additional sources of the loss of surfactant become important after the elimination of the most important source of error (loss of the precipitate due to dissolution in glacial acetic acid). The loss of precipitate during filtration due to an insufficiently effective glass filter can be one of the potential reasons for the poor recovery. The use of a G4 glass filter is recommended in the classical BiAS procedure [1]. In the present study the effectiveness of filtration of the precipitate through glass filters of different porosities was examined. For this purpose, G1 (100–160 μm), G2 (40–100 μm), G3 (16–40 μm), G4 (5–16 μm) and G5 (1.6–5 μm) glass filters were used. Samples with spikes of 200 μg of Triton X-100 precipitated with modified Dragendorff reagent were filtered through these filters. The precipitates were then dissolved in hot ammonium tartrate solution (see procedure A, section 2.2.1. for details). The amount of Triton X-100 was determined by ITM (procedure B, section 2.2.2.) as well as by AdST techniques (procedure D, section 2.2.4.). The filtrate was extracted with ethyl acetate. It is necessary to stress that particles of the precipitate dispersed in the filtrate are decomposed by ethyl acetate during extraction and NSs are thus transferred into ethyl acetate. The amount of Triton X-100 in the filtrate was determined by AdST (see procedure E, section 2.2.5.). The results are shown in Fig. 1. Except for the amounts of Triton X-100 in the precipitate (as determined both by ITM and AdST) and in the filtrate, the total amount of Triton X-100 is given. The G4 filter proves to be insufficient for effective filtration as roughly 25 μg of Triton X-100 (from the initial 200 μg of the surfactant) are lost. The G5 filter is much better although loss of trace amounts is still found. The G5 filter was used in further investigations, taking into account these results.

*3.1.2. The effect of "time of precipitation"*

The precipitation of NSs with modified Dragendorff reagent depends on the period of time between the mixing of the reagents and the filtration of the precipitate, called here the "time of precipitation". The time of precipitation consists of the time of formation of the complex precipitate and the time of ageing of the precipitate in the reaction mixture prior to filtration. For the precise determination of the time of precipitation, a series of experiments involving the precipitation of 100 μg of Triton X-100 were performed. The amount of Triton X-100 was determined both in the precipitate

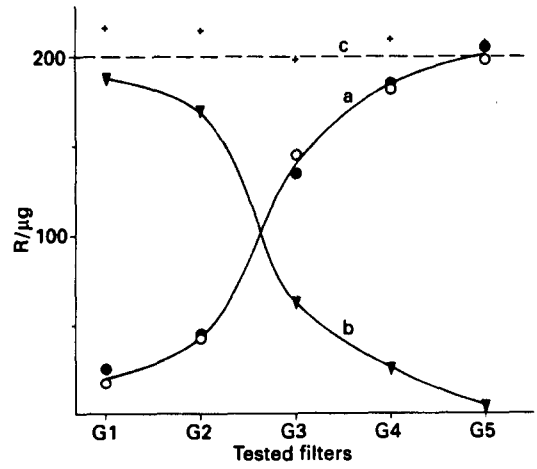


Fig. 1. Dependence of the recovery (R) of a 200 μg spike of Triton X-100 on the porosity of the glass filters used in the procedure, as determined by ITM (curve a; empty circles) and AdST (curve a; filled circles). Curve (b) shows the amount of Triton X-100 lost in the filtrate. Crosses show the sum of Triton X-100 in both fractions. The broken line (c) shows the spike of Triton X-100.

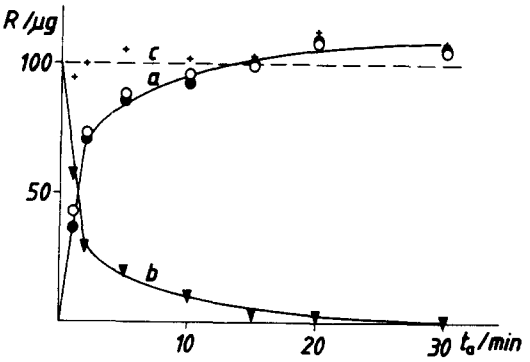


Fig. 2. Dependence of the recovery (R) of a 100 µg spike of Triton X-100 on the "time of precipitation" ($t_a$) of the precipitate, as determined by ITM (curve a; empty circles) and AdST (curve a; filled circles). Curve (b) shows the amount of Triton X-100 lost in the filtrate. Crosses show the sum of Triton X-100 in both fractions. The broken line (c) shows the spike of Triton X-100.

(by ITM, procedure B, and AdST, procedure D) and in the filtrate (by AdST, procedure E). The results are given in Fig. 2. The minimum period of time necessary to avoid serious losses of surfactant in this step of the procedure is 15 min. A further ageing time of up to 30 min seems to have some positive effect.

### *3.1.3. Preliminary attempts to precipitate sub-100 µg amounts of Triton X-100*

The elimination of several sources of error in the precipitation step of the BiAS procedure (such as removal of the washing with glacial acetic acid, a properly selected porosity of the glass filter and an optimum time of precipitation) makes the precipitation of amounts of NS below 100 µg feasible. The aim of the present study was to check whether 10–100 µg amounts of Triton X-100 are quantitatively precipitated with modified Dragendorff reagent. Spikes of Triton X-100 were precipitated with modified Dragendorff reagent [1] filtered and dissolved in hot ammonium tartrate (solution C). Triton X-100 was extracted with 10 ml of ethyl acetate. Portions (0.1–1.0 ml) of ethyl acetate solution were transferred to a 25 ml volumetric flask, 12.5 ml of 1 M aqueous sodium sulphate were added and the volumetric flask was filled to the mark with water. Triton X-100 was determined by AdST after 5 min preconcentration at −1.20 V (vs. SCE). The specific signal of Triton X-100 was used for the determination of the concentration, using a calibration curve prepared in the presence of a fixed amount of ethyl acetate. AdST was applied in this series to certify the precipitation of Triton X-100. The results are shown in Table 1. They show that spikes of Triton X-100 are correctly recovered within the investigated range, as the Triton X-100 is almost quantitatively precipitated.

### *3.1.4. Modification of the ITM measurement for the determination of small amounts of NSs*

The procedure described in the previous paper [4] is limited to the determination of NSs in amounts higher than 100 µg in the sample. Only aliquots of solution obtained after dissolution of the precipitate were used according to this procedure. However, if larger portions of the dissolved precipitate are introduced into the measuring system, the barium ions from the dissolved precipitate react with sulphate ions from the base electrolyte, forming a precipitate of barium sulphate. This concerns not only barium ions from the dissolved precipitate but also barium ions from the excess of Dragendorff reagent not removed by washing. The other factor which must be taken into account is the presence of high concentrations of tartrates, which slightly modifies the measuring conditions in the ITM procedure. Therefore the conditions for the ITM measurement were modified. Sodium chloride (0.5 M) was used instead of 0.5 M sodium sulphate as the base electrolyte (compare procedures B and C). The influence of tartrates was taken into account for the construction of the calibration graphs. A range of 2–1000 µg NS in the sample was aimed at in the modified procedure. Such a wide range could not be covered using only one calibration curve. Thus three ranges for the amount of NSs in the samples were selected: 2–20 µg, 10–100 µg and 50–1000 µg respectively. The NSs precipitated with modified Dragendorff reagent were dissolved in 20 ml of

Table 1
Recovery of Triton X-100 spikes below 100 µg precipitated with modified Dragendorff reagent (as determined by AdST)

| Added (µg) | Found (µg) | Recovery (%) |
|---|---|---|
| 0 | 1.3 | – |
| 10 | 8.1 | 81 |
| 20 | 17.7 | 89 |
| 40 | 39.0 | 97 |
| 60 | 58.6 | 98 |
| 80 | 77.1 | 96 |
| 100 | 97.6 | 98 |

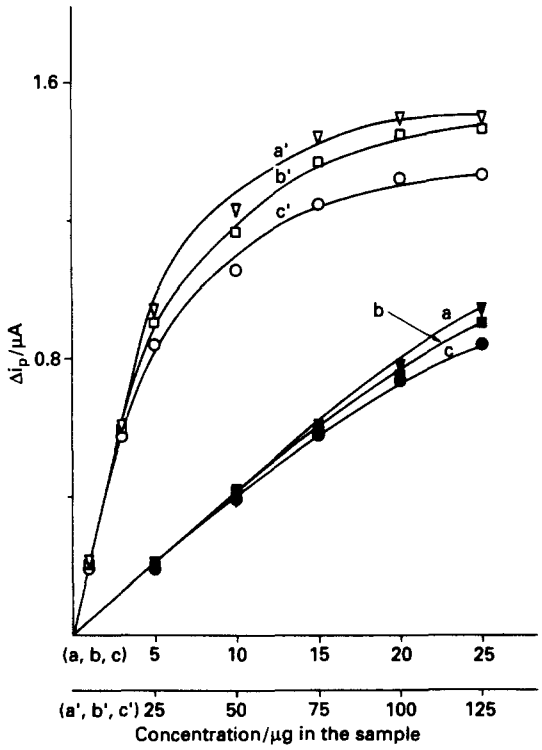


Fig. 3. Calibration graphs of Triton X-100 corresponding to the use of three different aliquots of the dissolved precipitate: curve a, 0.5/25; curve b, 4/25; curve c, 20/25.

hot ammonium tartrate solution (according to the classical BiAS procedure with additional filtration of the solution through an spe silica gel cartridge); the solution was then placed in a 25 ml volumetric flask and filled to the mark with water. For the range 50–1000 μg, a 0.5 ml aliquot is used. Further processing of the aliquot was performed according to procedures C and B. If the result obtained was below this range, the measurement was repeated with a 4 ml aliquot of sample in the range 10–100 μg. Finally, if the result was still below this range, a 20 ml aliquot of a solution (range 2–20 μg) was used. As each of these aliquots contains different amounts of tartrates, slight changes in the calibration graph result. Therefore three calibration graphs should be used, with tartrates in concentrations corresponding to the 0.5, 4 and 20 ml aliquots, respectively. The calibration graphs performed under these conditions with standard Triton X-100 are shown in Fig. 3. Curves a', b' and c' cover a wide range of concentration showing typical Γ-shape curves, while curves a, b and c cover the almost linear, most frequently used sections of the calibration graphs. Differences between the curves are best explained by the influence of tartrates or impurities introduced with the tartrates. The more tartrates, the stronger their influence on the analytical signal.

### *3.1.5. Recovery and precision according to the improved analytical procedure*

Recovery and precision were checked in model studies involving precipitation of Triton X-100 spikes, dissolution of the precipitate and the ITM measurement (following procedures A and C). The recovery was tested within the range 2–1000 μg of Triton X-100. The results are shown in Table 2. In several cases the measurements were performed using two different aliquots of the same precipitated Triton X-100 spike. The results support the possibility of precipitation and determination of NSs at concentrations below 100 μg up to 2 μg in the sample, using the BiAS–ITM procedure. The recoveries are satisfactory, although they are

Table 2
Recovery of different spikes of Triton X-100 (model studies)

| Added (μg) | Calibration graph | Found (μg) | Recovery (%) |
|---|---|---|---|
| 1000 | I | 1012 | 101 |
| 700 | I | 708 | 101 |
| 400 | I | 392 | 98 |
| 200 | I | 192 | 96 |
| 100 | II | 95.6 | 96 |
| 50 | II | 47.9 | 96 |
| 30 | II | 28.1 | 94 |
| 30 | III | 26.0 | 87 |
| 25 | II | 25.0 | 100 |
| 25 | III | 22.0 | 88 |
| 20 | II | 17.7 | 89 |
| 20 | III | 18.9 | 95 |
| 15 | II | 11.5 | 77 |
| 15 | III | 14.1 | 94 |
| 10 | II | 8.4 | 84 |
| 10 | III | 9.6 | 91 |
| 5 | III | 4.5 | 90 |
| 2 | III | 2.0 | 100 |

Table 3
Precision of the determination of different Triton X-100 spikes for the complete measuring cycle of model solutions [a]

| Added (μg) | Found (μg) | SD (μg) | R.S.D. |
|---|---|---|---|
| 1000 | 1012 | 15 | 0.015 |
| 100 | 95.6 | 3.0 | 0.03 |
| 5 | 4.5 | 0.42 | 0.09 |

[a] Number of measurements, 5.

Table 4
The influence of anionic surfactants on the determination of Triton X-100 spikes by the BiAS–ITM procedure

| Added (μg) | | | Found (μg) | | | |
|---|---|---|---|---|---|---|
| Triton X-100 | DBS | LS | Triton X-100 | | DBS or LS | |
| | | | ITM | AdST | P [a] | F [b] |
| 0 | 1000 | 0 | 0 | 0 | 220 | 784 |
| 100 | 1000 | 0 | 90 | 100 | 226 | 784 |
| 200 | 1000 | 0 | 194 | 224 | 274 | 734 |
| 1000 | 1000 | 0 | 970 | 990 | 306 | 666 |
| 0 | 0 | 1000 | 5 | 2 | 422 | 631 |
| 100 | 0 | 1000 | 97 | 94 | 412 | 660 |
| 200 | 0 | 1000 | 206 | 212 | 433 | 631 |
| 1000 | 0 | 1000 | 994 | 988 | 456 | 579 |

[a] P represents DBS or LS in the precipitate or on the filter as determined by the MBAS procedure.
[b] F represents DBS or LS in the filtrate as determined by AdST.

usually slightly below 100%, especially for the lower concentration range. It is usual for trace analysis that at the lower concentrations the loss is more pronounced.

The precision was tested for 1000, 100 and 5 μg Triton X-100 spikes. The results are shown in Table 3. The precision is very good for the larger spikes and acceptable for the 5 μg spikes, typical for trace analysis. The detection limit of the BiAS–ITM procedure calculated on the basis of 3 × S.D. lies slightly below 1.5 μg NS in the sample.

### 3.2. *Interferences*

#### 3.2.1. *Anionic surfactants*

The ITM is tolerant to anionic surfactants [7]. However, it was necessary to check the influence of ASs on the precipitation step. To do this, 100, 200 and 1000 μg spikes of Triton X-100 were precipitated in the presence of 1000 μg of sodium dodecylbenzenesulphonate (DBS) or sodium lauryl sulphate (LS). Triton X-100 was determined according to the procedure B. Additionally, the precipitated surfactant was determined by AdST (procedure D). DBS and LS were also controlled in the precipitate using the MBAS method [12] and in the filtrate by AdST (see section 2.2.6.). The amount of surfactant in the precipitate fraction also included the surfactants adsorbed on the glass filter and surfactants washed out simultaneously with the precipitate. The results are shown in Table 4. The results obtained by the BiAS–ITM and AdST techniques are basically the same. No substantial influence of the anionic surfactants on the results for Triton X-100 is observed. Very interesting results concern the anionic surfactants. Both DBS and LS are strongly adsorbed on the glass filter, as is seen from the results of measurements in the absence of Triton X-100. No Triton X-100 spike means no precipitate formed. Therefore only the glass filter used is responsible for a roughly 20% presence of DBS and a roughly 40% presence of LS in the "precipitate" frac-

Table 5
The influence of glycerol trioleate (GTO) on the determination of Triton X-100 spikes by the BiAS–ITM procedure

| Added (μg) | | Found (μg) | |
|---|---|---|---|
| Triton X-100 | GTO | Triton X-100 | |
| | | ITM | AdST |
| 100 | 1000 | 102 | 108 |
| 1000 | 1000 | 992 | 974 |

Table 6
Recovery of Triton X-100 spike in the presence of chlorophyll (calibration curve III)

| Added (μg) | | Found (μg) | Recovery (%) |
|---|---|---|---|
| Triton X-100 | Chlorophyll | | |
| 10 | 0 | 9.6 | 96 |
| 10 | 10 | 9.4 | 94 |
| 10 | 30 | 9.8 | 98 |
| 10 | 50 | 12.1 | 121 |
| 10 | 100 | 16.5 | 165 |

tion. A corresponding loss in the filtrate fraction supports this conclusion. Some DBS and LS is also adsorbed on the Triton X-100-containing precipitate, as must be derived from the fact that the amount of the anionic surfactants in the precipitate fraction increases with the increase of the spike of Triton X-100, whereas the amount of AS in the filtrate respectively decreases.

*3.2.2. Lipids*

Lipids were represented by glycerol trioleate (GTO). Spikes (100 and 1000 μg) of Triton X-100 were processed in the presence of 1000 μg of GTO. Triton X-100 in the dissolved precipitate was determined using procedure B. The results are summarised in Table 5. No substantial effect of GTO was observed.

*3.2.3. Chlorophyll*

Chlorophyll is the most serious interferent in the ITM measurements, showing much stronger signals than NSs. Therefore, water samples for the ITM measurement of NS concentration must be filtered, thereby any information concerning the amount of NSs adsorbed on particles in the surface water is lost. Loss of chlorophyll during the precipitation step is foreseeable. Experiments involving the precipitation of a 10 μg spike of Triton X-100 in the presence of increasing amounts of chlorphyll (from 10–100 μg in the sample) were carried out. The chlorophyll concentration was measured by the ITM. The Triton X-100 in the precipitate was determined according to procedure C. The results are shown in Table 6. It is apparent that 30 μg of chlorophyll are tolerated while 50 μg of chlorophyll are not. Thus, a 3:1 excess of chlorophyll is tolerated. The result is satisfactory as an excess of chlorophyll vs. NSs is not to be expected.

## Acknowledgement

This work was supported by the Committee of Scientific Research (institutional grant for Institute of Chemistry of Technical University of Poznan, No 31-447/94/DS).

## References

[1] R. Wickbold, Tenside Deterg., 9 (1972) 173.
[2] J. Waters, J.T. Garrigan and A.M. Paulson, Water Res., 20 (1986) 247.
[3] B. Wyrwas, A. Szymanski and Z. Lukaszewski, Anal. Chim. Acta, 278 (1993) 197.
[4] B. Wyrwas, A. Szymanski and Z. Lukaszewski, Talanta, 41 (1994) 1529.
[5] A. Szymanski, B. Wyrwas and Z. Lukaszewski, Anal. Chim. Acta, 305 (1995) 256.
[6] A. Szymanski and Z. Lukaszewski, Anal. Chim. Acta, 260 (1992) 25.
[7] A. Szymanski and Z. Lukaszewski, Anal. Chim. Acta, 273 (1993) 313.
[8] A. Szymanski and Z. Lukaszewski, Anal. Chim. Acta, 293 (1994) 77.
[9] A. Szymanski and Z. Lukaszewski, Anal. Chim. Acta, 281 (1993) 443.
[10] A. Szymanski and Z. Lukaszewski, Anal. Chim. Acta, 231 (1990) 77.
[11] Z. Lukaszewski, H. Batychka and W. Zembrzuski, Anal. Chim. Acta, 175 (1985) 55.
[12] Polish Standard PN-85-C-04550/02, Determination of anionic synthetic surface active agents by colorimetric method with Methylene Blue, Polish Committee for Standardisation, Measures and Quality Control, 1985.

ELSEVIER

Talanta 42 (1995) 1259–1263

Talanta

# Flame AAS determination of dopants and trace metal impurities in single crystals of potassium titanylphosphate

E. Ivanova *, I. Havezov

*Institute of General and Inorganic Chemistry, Bulgarian Academy of Sciences, BG113 Sofia, Bulgaria*

Received 14 December 1994; revised 22 February 1995; accepted 22 February 1995

**Abstract**

A flame AAS method is used for the determination of dopants and impurities in potassium titanylphosphate (KTP) single crystals. Sample digestion using sulphuric acid and hydrofluoric acid is proposed as being the most appropriate procedure. The effect of major and minor components in the sample solution on the analytical signal is studied. The content of the dopants Cr, Mn and Ni (at a level of about 1 mg $g^{-1}$) as well as the content of the impurities Fe, Na, Mg, W and Al (from 4 μg $g^{-1}$ to 4 mg $g^{-1}$, depending on the trace metal) in the KTP single crystals is determined. The precision of the method is characterized by a relative standard deviation of 3–10%. The accuracy is checked by comparison with ICP-AES data for the trace element content in the KTP single crystals.

*Keywords:* Dopants; Flame AAS; Potassium titanylphosphate; Single crystals; Trace metal impurities

## 1. Introduction

Potassium titanylphosphate (KTP) possesses a unique combination of properties making it a superior optical crystal for second harmonic generation and electro-optic applications [1,2]. Ionic conductivity is important in the processing of waveguides in the material and in waveguide device stability [3]. The damage susceptibility of KTP has been shown to increase with increasing ionic conductivity of the crystal [3]. Doping is a way of reducing the ionic conductivity. For example, doping with chromium reduces the ionic conductivity of KTP from $10^{-6}$ to $10^{-8}\ \Omega^{-1}\ cm^{-1}$.

Along with dopants intentionally added in order to achieve specific properties, impurities can be unintentionally introduced into the crystal from the starting materials or during the crystal growth. The structural properties of typical non-linear optical oxides lead to high distribution coefficients of trace elements, and little if any purification occurs during the growth process [3]. Therefore the use of high-purity starting materials is very important for lowering the impurity level in the crystals themselves.

The correct interpretation of the specific properties of the crystals and the control of their quality requires a precise knowledge of the content of dopants and impurities incorporated.

The aim of the present work was to develop a reliable sample decomposition and flame atomic absorption procedure in order to determine the concentration of trace elements (dopants and impurities) in KTP single crystals.

## 2. Experimental

### 2.1. Reagents

Reagents of the highest available purity grade were used — 96% $H_2SO_4$ and 40% HF

* Corresponding author.


*SSDI* 0039-9140(95)01570-1

(Suprapur, Merck), 30% $H_2O_2$ (z.S., Merck), and redistilled water. Plastic or PTFE ware was used throughout.

### 2.2. Apparatus

The measurements were performed using the flame AAS spectrometer Pye Unicam SP 192, at the most sensitive analytical lines of the elements recommended in the manual. Deuterium background correction and an adjustable Pt–Ir nebulizer with an impact bead were used. A lean air–acetylene flame was used for Ni, Mn, Na, Fe, Mg, Pt and Cr; a rich $N_2O$–acetylene flame was used for Al and W. The heights of the "red feather" were 1 cm and 2.5 cm, respectively. Calibration was performed by the standard additions method.

### 2.3. Dissolution procedure

The KTP crystal was crushed into pieces and finely ground in an agate mortar. A portion (200 mg) of the sample was transferred to a PTFE beaker of 100 ml volume, and 2 ml of concentrated $H_2SO_4$ and 6 ml of 40% HF were added. The beaker was heated on a hot plate until sample dissolution occurred with subsequent removal of the excess HF. The beaker was cooled, the walls were washed with several milliliters of redistilled water and heating was repeated until $SO_3$ vapours appeared. The solution obtained was diluted with 3–4 ml of redistilled water and 0.4 ml of 30% $H_2O_2$ were added dropwise under stirring. The obtained orange-coloured solution was transferred to a 25 ml polypropylene graduated flask and was brought up to volume with redistilled water. The concentration of KTP in the solution was 0.8%, and the concentration of $H_2SO_4$ was 1.5 mol $dm^{-3}$. Where necessary, an aliquot of the sample solution was diluted with water in a polypropylene tube.

A blank sample was subjected to the whole procedure.

## 3. Results and discussion

The chemical resistance and the low solubility of KTP are among its advantages as an optical crystal. These are disadvantages, however, when considering its analysis by means of AAS, since preliminary dissolution of the sample is required.

For the dissolution of phosphates and titanates, sample digestion with sulphuric acid is proposed. The process is accelerated by the addition of ammonium sulphate [4]. The residue is dissolved in sulphuric acid with a concentration above 5% in order to avoid hydrolysis and the precipitation of titanium. A better dissolution of the residue is achieved by the addition of $H_2O_2$, tartaric or oxalic acid. Titanium oxide is readily soluble in HF [4]. In many cases, good results are obtained by fusion with potassium pyrosulphate or sodium hydroxide/sodium peroxide [4]. Titanium-containing silicate samples are digested with a mixture of $H_2SO_4$ and HF. Sulphuric acid is added in order to avoid partial losses of volatile fluorides [4].

The method of sample digestion should be in accordance with the subsequent method of analysis. From this point of view, sample digestion by fusion is not appropriate for the AAS determination of the trace element content in KTP crystals due to the high salt content of the final solution, leading to severe matrix interferences and high blank values as well as to a drift in the flame characteristics (or even burner blockage).

The method of sample digestion should also take into consideration the analyte elements in order to provide their complete dissolution without losses or contamination.

Two modes of acid digestion of the KTP crystals were tested.

(i) Digestion with a mixture of $H_2SO_4$ and $(NH_4)_2SO_4$. A 100 mg portion of the sample was heated on a hot plate with 1.2 ml of concentrated $H_2SO_4$ and 0.5 g of $(NH_4)_2SO_4$ for 1 h. After cooling, 3–4 ml of water and 0.5 ml of 30% $H_2O_2$, dropwise were added. The latter was introduced in order to maintain the titanium in solution as the complex acid $H_2[TiO_2(SO_4)_2]$ [4]. The solution became orange-coloured (the colour of the complex), a small amount of a white precipitate also being observed. Qualitative analysis of the precipitate by atomic emission spectrometry pointed to the presence of silicon, aluminium and magnesium. It may hence be assumed that the KTP crystals had been contaminated with silicon (from the furnace materials) during the synthesis and the silicic acid precipitate formed during digestion sorbed aluminium, magnesium and probably other trace elements, thus interfering with their quantitative determination in the analyte solution.

It follows then that silicic acid should be removed from the solution during digestion, as accomplished in procedure (ii).

(ii) Digestion with a mixture of $H_2SO_4$ and HF. A portion (100 mg) of the sample was heated on a hot plate (PTFE beaker) with 1.5 ml of concentrated $H_2SO_4$ and 5 ml of 40% HF. After heating for 5–10 min, a clear solution was obtained. Heating was continued in order to remove the excess HF since fluoride ions would interfere with the subsequent formation of the complex $H_2[TiO_2(SO_4)_2]$ [4]. During HF removal, a fine white precipitate appeared in the solution. After cooling, diluting with water and adding 0.5 ml of $H_2O_2$, this precipitate dissolved completely. The appearance of the precipitate upon the removal of HF and its redissolution by the addition of $H_2O_2$ gives grounds to assume that the precipitate was titanium.

The trace elements to be determined in the present study were Cr, Mn, Ni, Fe, W, Pt, Mg, Al and Na. Preliminary experiments with spiked samples showed that these elements were brought into solution quantitatively by the above digestion method. The optimized conditions of the digestion method used are given in the dissolution procedure. All the cited trace elements were determined in the solution of KTP thus obtained, some after additional 2–5-fold dilution with water.

The following KTP single crystals were analysed:

undoped KTP (four samples);
KTP doped with Mn (one sample);
KTP doped with Cr (one sample);
KTP doped with Ni (one sample).

### 3.1. Determination of dopants

The concentration of dopants in optical crystals is usually in the range of hundreds of micrograms per gram which considerably exceeds the dynamic range of flame AAS (the corresponding flame AAS limits of detection in a 0.8% solution of KTP are shown in Table 1). This allowed us to apply a 2–5-fold dilution of the sample solutions. It was important to find out whether the matrix KTP or the dissolution reagent $H_2SO_4$ affected the analytical signal. This effect was estimated by comparing the slopes of the calibration curves for various concentrations of KTP or $H_2SO_4$ with that of an aqueous calibration curve. The results of this study are shown in Tables 2 and 3. As can be seen, the matrix KTP still strongly suppresses the analytical signal of Cr, Mn and Ni at the lowest concentration examined — 0.16%, which corresponds to a five-fold dilution of the sample solution. The effect is most strongly expressed for Cr, most weakly for Ni. It may hence be assumed that at the temperature of the air–acetylene flame, the droplets produced by the nebulizer had given rise to solid particles (e.g. a Cr–Ti compound) which, because of their high vaporization temperature, are not completely converted to atomic vapour. The effect of $H_2SO_4$ is less pronounced for all three elements, i.e. viscosity and surface tension effects are negligible in the examined $H_2SO_4$ concentration range.

Reviewing the data presented in Tables 2 and 3 it may be concluded that accurate results for the content of Cr, Mn and Ni in KTP solutions can be obtained by means of flame AAS when calibration is performed by the standard additions method or if the calibration standards contain the same concentration of an undoped crystal matrix. Where possible, sample dilution is recommended.

Table 1
Flame AAS limits of detection ($3\sigma$ criterion) of the elements in a 0.8% KTP solution

| Element | Limit of detection ($\mu g\ g^{-1}$) |
|---|---|
| Cr | 17 |
| Mn | 2.8 |
| Ni | 8 |
| W | 500 |
| Al | 150 |
| Pt | 11 |
| Fe | 7 |
| Na | 1.7 |
| Mg | 0.35 |

Table 2
Ratio slopes of the calibration curves for various KTP contents and the slope of an aqueous calibration curve

| Element | KTP in solution | | | |
|---|---|---|---|---|
| | 0.16% | 0.4% | 0.8% | 1.0% |
| Cr | 0.6 | 0.5 | 0.4 | 0.3 |
| Mn | 0.7 | 0.6 | 0.5 | 0.5 |
| Ni | 0.9 | 0.8 | 0.7 | – |
| Na | 0.9 | 0.9 | 0.8 | 0.7 |
| Fe | 0.7 | – | 0.5 | – |
| Mg | 0.5 | 0.3 | 0.15 | – |

Table 3
Ratio slopes of the calibration curves for various $H_2SO_4$ concentrations and the slope of an aqueous calibration curve

| Element | Sulphuric acid | |
|---|---|---|
| | 0.3 mol $dm^{-3}$ | 1.5 mol $dm^{-3}$ |
| Cr | 1.0 | 0.9 |
| Mn | 1.0 | 0.9 |
| Ni | 1.0 | 0.9 |
| Na | 1.0 | 0.9 |
| Fe | 1.0 | 0.9 |
| Mg | 0.9 | 0.8 |

### 3.2. Determination of impurity elements

The growth of KTP crystals takes place from a molten mixture of the composition $K_2O$–$P_2O_5$–$TiO_2$–$WO_3$, where $WO_3$ serves as a high-temperature solvent. The presence of a large amount of $WO_3$ in the growth solution leads to its incorporation in the crystal. That is why the tungsten content in the latter is of interest.

The KTP crystals may be also contaminated with platinum from the crucible used for the synthesis.

Traces of Mg, Al, Fe and Na can be incorporated in the crystal from the starting substances, from the furnace materials and from the ambient air.

The limits of detection of W, Al, Pt, Fe, Na and Mg in a 0.8% solution of KTP determined by flame AAS are presented in Table 1.

Preliminary experiments performed by means of ICP-AES revealed that the concentration of W in the KTP crystals was about 1000–4000 mg $g^{-1}$. A comparison of this concentration range with the data of Table 1 reveals that the reliable flame AAS determination of W in 0.8% solutions of KTP is hardly possible. The W content was determined only in sample 1 of the undoped KTP crystal which had the highest W content.

The content of Pt in the analysed KTP crystals was below the limits of detection shown in Table 1.

Preliminary studies of the Al content of the KTP crystals (ICP-AES) pointed to a content of about 200–700 μg $g^{-1}$. The data for Al shown in Table 1 revealed that the determination of Al in the KTP solutions is as discussed for W. Only sample 3 of the undoped KTP crystal (that with the highest Al content) was analysed for Al.

The content of Fe, Na and Mg in the KTP crystals was higher than the limits of detection shown in Table 1. Care was taken to avoid contamination from reagents and laboratory ware.

The effects of the KTP and $H_2SO_4$ contents in the solution on the analytical signals of Fe, Na and Mg are shown in Tables 2 and 3. As can be seen, the dependences are the same as for Cr, Mn and Ni: the effect of KTP is much higher than that of $H_2SO_4$. The effect of KTP is most pronounced for Mg. Fortunately the content of this element in the analysed crystals permitted its determination after five-fold dilution of the solution.

### 3.3. Analysis of KTP single crystals

The content of dopants and impurity elements in the KTP crystals was determined as described in the Section 2.2. The results are shown in Table 4. The mean value was determined from the analysis of three separate portions of each single crystal.

Table 4
Content of dopants and impurities in KTP single crystals

| Element (μg $g^{-1}$) | Undoped KTP | | | | Cr-doped | Mn-doped | Ni-doped |
|---|---|---|---|---|---|---|---|
| | 1 | 2 | 3 | 4 | | | |
| Cr | – | – | – | – | 837 | – | – |
| Mn | – | – | – | – | – | 862 | – |
| Ni | – | – | – | – | – | – | 1146 |
| Fe | 108 | 94 | 76 | 59 | 48 | 51 | 47 |
| Na | 435 | 457 | 542 | 343 | 540 | 825 | 772 |
| Mg | 4.8 | 12.0 | 12.3 | 4.3 | 6.3 | 7.3 | 5.7 |
| W | 4420 [a] | – | – | – | – | – | – |
| Al | – | – | 750 | – | – | – | – |

[a] Single determination.

Table 5
Trace element determination in the Mn-doped sample by flame AAS and ICP-AES

| | ($\mu g\ g^{-1}$) | ($\mu g\ g^{-1}$) |
|---|---|---|
| Mn | $862 \pm 25$ | $835 \pm 30$ |
| Fe | $51 \pm 5.5$ | $55.6 \pm 6.0$ |
| Na | $825 \pm 39$ | $822 \pm 16$ |
| Mg | $7.3 \pm 0.50$ | $8.0 \pm 0.50$ |

The precision of the method is characterized by a relative standard deviation of 3–10%. The accuracy of the flame AAS determination of the trace element content (dopants and impurities) in KTP single crystals was checked by comparison with the results obtained by the ICP-AES analysis [5] of a sample solution obtained as described in the dissolution procedure. Results for the analysis of the Mn-doped sample are shown in Table 5. Using Student's criterion, no statistical difference between the results obtained by the two methods was found.

## Acknowledgements

Thanks are due to the National Fund "Scientific Research" of the Ministry of Science and Education of Bulgaria for financial support of this work.

## References

[1] F.C. Zumsted, J.D. Bierlein and T.E. Gier, J. Appl. Phys., 47 (1976) 4980.
[2] J.D. Bierlein and C.B. Arweiler, Appl. Phys. Lett., 49 (1986) 917.
[3] P.A. Morris, A. Ferretti and J.D. Bierlein, J. Cryst. Growth, 109 (1991) 367.
[4] A.I. Ponomarev, Metody Khimicheskogo Analiza Silikatnykh i Karbonatnykh Porod, Izd. AN SSSR, Moscow, 1961 (in Russian).
[5] N. Daskalova, P. Slavova and S. Velichkov, Spectrochim. Acta B, submitted for publication.

ELSEVIER

Talanta 42 (1995) 1265-1271

Talanta

# Analysis of cement and cement raw meal by atomic absorption spectrophotometry using a new fusion agent

Oi-Wah Law [a,*], Lik Lam [a], Shiu-Fai Luk [b]

[a] *Department of Chemistry, The Chinese University of Hong Kong, Shatin, N.T., Hong Kong*
[b] *Applied Science Department, Sha Tin Technical Institute, Shatin, Hong Kong*

Received 18 November 1994; revised 22 February 1995; accepted 2 March 1995

**Abstract**

A new fusion agent is proposed for the analysis of cement and cement raw meal using AAS. In the described method, 0.8 g of the fusion agent, consisting of equal portions of oxalic acid, lithium carbonate and lithium tetraborate, was mixed with 0.2 g of the sample, and the mixture was fused for 10 min at 925 °C in a platinum crucilbe. The fusion cake was dissolved with dilute hydrochloric acid (1 + 10) and diluted to 500 ml for the determination of Si, Al, Fe, Ti, Na and K expressed as $SiO_2$, $Al_2O_3$, $Fe_2O_3$, $TiO_2$, $Na_2O$, and $K_2O$ respectively. For the determination of Ca and Mg (expressed as CaO and MgO respectively), 10 ml of the previous sample solution were mixed with 4 ml of 6% (m/v) lanthanum nitrate solution and the solution was diluted to 100 ml. The method was found to have good accuracy and precision. The time required to determine the eight elements was around 80 min for each sample.

*Keywords:* Atomic absorption spectrophotometry; Cement; Fusion method; Limestone; Raw meal

## 1. Introduction

In the cement industry, limestone, clay and iron ore are used as raw materials and are mixed in controlled proportions and ground to form the raw meal, which is ignited at high temperature to form clinker. The clinker is ground with gypsum to give cement. Inside the cement plant, on-line control of the composition of raw meal is needed to maintain the composition of cement to within strict requirements. This is usually achieved in the cement industry by determining the content of each element of interest, expressed in terms of the respective oxide. The final composition of a typical cement is as follows: 65% CaO, 22% $SiO_2$, 3.8% $Al_2O_3$, 4.2% $Fe_2O_3$, 1.0% MgO, 0.6% $Na_2O$, 0.2% $K_2O$, 0.2% $TiO_2$.

The instrumental method commonly used for the analysis of cement and cement raw meal is X-ray fluorescence (XRF) spectrometry [1,2]; however, the instrument is expensive. Further, for the determination of trace elements in cement using XRF, tedious steps are needed to separate the analyte from the matrix [3]. Other instrumental methods applicable are UV-vis spectrophotometry [4], atomic absorption spectrophotometry (AAS) [5] and inductively coupled plasma-atomic emission spectrometry (ICP-AES) [6]. The standard methods [7,8] for cement analysis are complicated and require a long time to complete a full analysis for a single sample. Among these methods, AAS is most suitable for the analysis of cement and raw meal because it is selective, rapid and the instrument employed is cheaper and the running cost lower than those for XRF and ICP-AES, however, it requires the sample to be completely soluble.

Raw meals containing appreciable amounts of silica are difficult to dissolve and they are

* Corresponding author.


*SSDI* 0039-9140(95)01571-X

Table 1
Instrumental operating conditions for the AAS determinations

| Element | Spectrophotometer | | | Fuel type | Flow rate | |
|---|---|---|---|---|---|---|
| | Lamp curent (mA) | Wavelength (nm) | Slit (nm) | | Fuel ($l\ min^{-1}$) | Oxidant ($l\ min^{-1}$) |
| Fe | 10 | 248.3 | 0.2 | A | 1.7 | 13.6 |
| Al | 10 | 309.3 | 1.3 | N | 5.5 | 6.6 |
| Si | 10 | 251.6 | 0.2 | N | 5.8 | 6.3 |
| Mg | 7.5 | 285.2 | 0.4 | A | 1.7 | 13.6 |
| Ca | 10 | 422.7 | 0.2 | A | 1.7 | 15.0 |
| Na | 7.5 | 589.0 | 0.4 | A | 1.5 | 15.0 |
| K | 7.5 | 766.5 | 1.3 | A | 1.5 | 13.6 |
| Ti | 7.5 | 364.3 | 0.4 | N | 5.8 | 6.0 |

Key: A, air–acetylene flame; N, nitrous oxide–acetylene flame.

either decomposed by hydrofluoric acid or by fusion. Hydrofluoric acid decomposition takes more than 1 h to complete and is not suitable for rapid analysis. In the fusion method, the agents used include sodium carbonate [9], lithium metaborate [10–13], and lithium tetraborate [14,15]. Sodium carbonate is not efficient to convert silica into a soluble form. Lithium metaborate and tetraborate are effective but are expensive and require a long time for dissolving the fusion cake. We observed that when lithium tetraborate was used, silica was precipitated during the course of dissolving the fusion cake. The lithium tetraborate–sodium carbonate system [15] does not have these drawbacks, and has been successfully applied to the analysis of cement and flyash containing up to 50% of silica; however, sodium in the samples cannot be determined.

It is the purpose of the present work to develop a new fusion agent for the rapid analysis of cement and cement raw meal using AAs, which is superior to other published fusion systems in terms of the time required for fusion and dissolution and the number of elements that can be determined.

## 2. Experimental

Analytical reagent grade chemicals and distilled water were used throughout the procedure.

### 2.1. Instrument

A Hitachi Z6100 Zeeman atomic absorption spectrophotometer was used for the absorbance measurements. The measurement conditions are shown in Table 1.

### 2.2. Reagents

To prepare the fusing agent, oxalic acid, lithium tetraborate and lithium carbonate were thoroughly mixed in equal proportions in mass and ground in a mortar with a pestle to give a homogeneous mixture.

Lanthanum nitrate solution (6%; m/V) was prepared by dissolving 30 g of the compound in 20 ml of concentrated HCl and diluting the solution to 500 ml with distilled water.

### 2.3. Procedure

A portion of the sample (0.200 g) was weighed accurately and mixed thoroughly with 0.8 g of the fusing agent in a platinum crucible, which was then covered with its lid and placed in a muffle furnace at 295 °C for 10 min. The crucible lid was then transferred to a 400 ml beaker containing 100 ml of boiling distilled water and 10 ml of concentrated hydrochloric acid. The crucible was cooled by washing its exterior wall with a stream of water, and was then placed in the same beaker, which was subsequently covered with a watch glass. The solution was heated on a water bath until the fusion cake was dissolved. The solution was then cooled and diluted to 500 ml with distilled water in a calibrated flask. This sample solution was reserved for the Si, Fe, Al, K, Na and Ti determinations. For the Ca and Mg determinations, 10 ml of the above sample solution were pipetted into a 100 ml calibrated flask and 4 ml of the 6% (m/v) lanthanum nitrate solution were added, as ionization buffer, and the resulting solution

was diluted to the mark with distilled water.

For standards preparation, 0.5000 g of a cement standard, e.g. BCS 372/1, was mixed with 2.0 g of the fusing agent and the mixture was treated similarly as for the sample, except that 20 ml of concentrated HCl instead of 10 ml were used for dissolving the fusion cake. The sample solution was diluted with distilled water to 250 ml in a calibrated flask and labelled as stock solution A. Standard solutions were prepared by pipetting 25, 35, 50, and 75 ml of the stock solution A separately into a series of 250 ml calibrated flasks and diluting to the mark with distilled water. These standard solutions were used for $SiO_2$, $Fe_2O_3$, $Na_2O$, $K_2O$, $TiO_2$ and $Al_2O_3$ determinations.

Standards for the CaO and MgO determinations were prepared by first fusing 0.2000 g of a cement standard with 0.8 g of the fusing agent for 10 min. After dissolving in hydrochloric acid (1 + 10), the solution was diluted to 500 ml in a calibrated flask and labelled as stock solution B. Standard solutions were prepared by pipetting 10, 20, 25 and 40 ml of stock solution B separately into a series of 250-ml calibrated flasks, adding 10 ml of the lanthanum nitrate solution to each flask and diluting to the mark with distilled water.

The respective reagent blanks were prepared similarly as for the sample solutions, except that no sample was used in the fusion procedure.

## 3. Results and discussion

The recently developed system sodium carbonate–lithium tetraborate [15] is efficient at converting silica into the soluble form and can save a lot of time taken up in fusion and dissolution. However, as sodium carbonate is used, it is not possible to determine sodium in the sample. To remedy the situation, sodium carbonate needs to be replaced by an appropriate compound. Lithium carbonate was chosen for the present study because it has a lower melting point so that fusion can be carried out at a lower temperature. Although lithium tetraborate is expensive, it can convert silica into the solution form, and hence should not be excluded from the system. Lithium tetraborate is preferable to lithium metaborate because it is difficult to obtain the latter in high purity. Oxalic acid is included as it was found to shorten the dissolution time when present. As the loss of alkali was reported at temperatures above 950 °C [16] the temperature used was 925 °C.

Four fusion systems were prepared to contain different proportions of lithium tetraborate, lithium carbonate and oxalic acid. The recoveries of silica in cement and flyash obtained after fusion with these systems are summarized in Table 2, where it can be seen that the proposed system gave the best recoveries for both samples. Further, the dissolution time was shortened from 30 min to less than 10 min. Also, no precipitation of silicon was observed and hence a better recovery can be obtained.

It was found that a graphite crucible was not suitable for the proposed system as the melt after fusion solidified rapidly and was difficult to transfer completely to the beaker. Further, fine particles of charcoal were also found to have been transferred, and these needed to be removed by filtration. A platinum crucible was found to be satisfactory for the proposed method.

### 3.1. Accuracy

The concentration of oxides in a number of cement, raw meal, and limestone samples were determined using the proposed and the XRF methods, and the results are shown in Tables 3 and 4, respectively. The average absolute differences between experimental and known concentrations were calculated for the cement and raw meal samples, and the ASTM-allowed differences [8] are also included for comparison. It can be seen that the average absolute differences obtained by the proposed method were all equal to or less than the respective

Table 2
Determination of $SiO_2$ by AAS using different fusion systems

| Fusion system [b] | $SiO_2$ concentration (%) | | | | |
|---|---|---|---|---|---|
| | Found [a] | | | | Known |
| | A | B | C | D | |
| Cement | 20.57 (98.5) | 20.83 (98.5) | 20.80 (99.6) | 20.93 (100.2) | 20.88 |
| Flyash | 43.27 (91.5) | 45.79 (96.8) | 45.20 (95.6) | 47.30 (100) | 47.3 |

[a] Per cent recovery given in parentheses.
[b] A, lithium tetraborate; B, lithium tetraborate–lithium carbonate (1:1); C, lithium tetraborate–oxalic acid (1:1); D, lithium tetraborate–lithium carbonate–oxalic acid (1:1:1).

Table 3
Analysis of standard reference materials using AAS with the proposed fusing agent

| Sample type | Concentration (%) | | | | | | | | |
|---|---|---|---|---|---|---|---|---|---|
| | Known/Found | $Fe_2O_3$ | $TiO_2$ | CaO | $SiO_2$ | $Al_2O_3$ | $Na_2O$ | MgO | $K_2O$ |
| Cement | | | | | | | | | |
| SRM 633 | Known | 4.20 | 0.24 | 64.50 | 21.88 | 3.79 | 0.64 | 1.04 | 0.17 |
| | Found | 4.14 | 0.27 | 64.69 | 21.86 | 3.65 | 0.66 | 1.00 | 0.18 |
| SRM 637 | Known | 1.80 | 0.21 | 66.04 | 23.07 | 3.30 | 0.13 | 0.68 | 0.25 |
| | Found | 2.05 | 0.23 | 66.08 | 23.00 | 3.16 | 0.14 | 0.65 | 0.27 |
| SRM 1881 | Known | 4.68 | 0.25 | 58.67 | 22.25 | 4.16 | 0.04 | 2.63 | 1.17 |
| | Found | 4.67 | 0.21 | 58.53 | 22.40 | 4.21 | 0.05 | 2.53 | 1.17 |
| SRM 1885 | Known | 4.40 | 0.20 | 62.14 | 21.24 | 3.68 | 0.38 | 4.02 | 0.83 |
| | Found | 4.46 | 0.21 | 62.03 | 21.16 | 3.55 | 0.40 | 3.79 | 0.83 |
| SRM 1887 | Known | 2.16 | 0.27 | 62.88 | 19.98 | 5.59 | 0.10 | 1.26 | 1.27 |
| | Found | 2.11 | 0.30 | 62.74 | 20.02 | 5.54 | 0.10 | 1.22 | 1.26 |
| BCS-CRM 353 | Known | 4.82 | 0.16 | 64.80 | 20.50 | 3.77 | 0.10 | 2.42 | 0.49 |
| | Found | 4.78 | 0.13 | 64.71 | 20.46 | 3.71 | 0.11 | 2.35 | 0.51 |
| Raw meal [a] | | | | | | | | | |
| | Known | 2.98 | 0.24 | 43.41 | 11.00 | 6.84 | 0.30 | 0.34 | 1.16 |
| | Found | 3.08 | 0.21 | 43.43 | 11.12 | 6.95 | 0.28 | 0.28 | 1.13 |
| | Known | 4.63 | 0.24 | 43.41 | 13.28 | 4.30 | 0.05 | 0.48 | 0.16 |
| | Found | 4.83 | 0.24 | 43.23 | 13.36 | 4.30 | 0.14 | 0.49 | 0.12 |
| | Known | 1.80 | 0.16 | 47.21 | 12.32 | 2.06 | 0.13 | 0.59 | 0.06 |
| | Found | 1.90 | 0.11 | 47.24 | 12.37 | 2.04 | 0.12 | 0.62 | 0.03 |
| Average absolute difference | | 0.10 | 0.03 | 0.10 | 0.07 | 0.08 | 0.02 | 0.07 | 0.02 |
| Standard deviation | | 0.08 | 0.02 | 0.06 | 0.04 | 0.05 | 0.03 | 0.07 | 0.01 |
| ASTM allowed difference [b] | | ±0.10 | ±0.03 | ±0.3 | ±0.2 | ±0.2 | ±0.05 | ±0.2 | ±0.05 |
| Limestone | | | | | | | | | |
| BCS-CRM 393 | Known | 0.05 | | 55.40 | 0.70 | 0.12 | | 0.15 | 0.02 |
| | Found | 0.05 | | 55.34 | 0.63 | 0.08 | | 0.10 | 0.05 |
| SRM 1c | Known | 0.55 | | 50.30 | 6.84 | 1.30 | | | 0.28 |
| | Found | 0.51 | | 50.95 | 6.62 | 1.21 | | | 0.28 |
| SRM 88b | Known | 0.28 | | 29.95 | 1.13 | 0.34 | | 21.03 | 0.10 |
| | Found | 0.33 | | 30.21 | 1.08 | 0.29 | | 20.60 | 0.11 |

Minor oxide analysis of BCS-CRM 372/1:

| | BaO | $Cr_2O_3$ | $Mn_2O_3$ |
|---|---|---|---|
| Known (%) | 0.01 | 0.012 | 0.074 |
| Found (%) | 0.011 | 0.012 | 0.081 |

[a] Prepared by mixing known amounts of appropriate standard reference materials.
[b] From Ref. [8].

ASTM-allowed difference, whereas the same is not true for the XRF method. The proposed method can yield better results than the XRF method, especially for the light elements such as $Na_2O$ and MgO and for those oxides with contents of below 1%. The XRF flux yields of the light elements are very low and are easily absorbed by the environment, resulting in poor accuracy in the determination. Further, for high accuracy in XRF, the nature of the standards used must be close to the sample to be analysed. If the concentrations did not fall within the calibration range, e.g. CaO in BCS-CRM354 (Table 4), great deviations were observed.

The oxides of some of the trace elements, namely BaO, $Cr_2O_3$ and $Mn_2O_3$, have also been determined by the AAS method using the standard additions technique, yielding satisfactory results (see Table 3).

Three limestone reference standard materials were analysed using the AAS method. The accuracy is good except for those oxides with concentrations less than 0.1%.

Table 4
Analysis of standard reference material using XRF

| Sample type | Concentration (%) | | | | | | | | |
|---|---|---|---|---|---|---|---|---|---|
| | Known/Found | $Fe_2O_3$ | $TiO_2$ | CaO | $SiO_2$ | $Al_2O_3$ | $Na_2O$ | MgO | $K_2O$ |
| Cement | | | | | | | | | |
| SRM 634 | Known | 2.84 | 0.29 | 62.58 | 20.73 | 5.21 | 0.15 | 3.30 | 0.40 |
| | Found | 2.80 | 0.29 | 62.00 | 20.84 | 5.06 | 0.16 | 2.22 | 0.43 |
| BCS-CRM 353 | Known | 4.82 | 0.16 | 64.80 | 20.50 | 3.77 | 0.10 | 2.42 | 0.49 |
| | Found | 4.75 | 0.19 | 64.90 | 20.20 | 4.28 | 0.16 | 2.65 | 0.46 |
| BCS-CRM 354 | Known | 0.30 | – | 70.00 | 21.80 | 4.85 | 0.10 | 0.42 | 0.11 |
| | Found | 0.30 | – | 68.00 | 22.05 | 5.06 | 0.25 | 0.81 | 0.00 |
| BCS-CRM 372/1 | Known | 3.42 | 0.28 | 65.30 | 20.30 | 5.37 | 0.10 | 1.31 | 0.76 |
| | Found | 3.52 | 0.29 | 64.20 | 20.80 | 5.60 | 0.18 | 1.27 | 1.05 |
| SRM 1881 | Known | 4.68 | 0.25 | 58.67 | 22.25 | 4.16 | 0.04 | 2.63 | 1.17 |
| | Found | 4.58 | 0.20 | 57.80 | 22.40 | 4.19 | 0.04 | 2.81 | 1.34 |
| SRM 1884 | Known | 3.30 | 0.16 | 64.01 | 23.19 | 3.31 | 0.13 | 2.32 | 0.51 |
| | Found | 3.26 | 0.17 | 65.07 | 23.52 | 3.20 | 0.08 | 2.02 | 0.49 |
| Raw meal | Known | 2.56 | 0.16 | 41.37 | 18.65 | 3.70 | 0.05 | 0.66 | 0.37 |
| | Found | 2.77 | 0.24 | 41.00 | 18.32 | 3.91 | 0.25 | 1.00 | 0.38 |
| | Known | 1.35 | 0.06 | 40.52 | 20.25 | 3.00 | 0.26 | 0.37 | 1.41 |
| | Found | 1.70 | 0.16 | 39.60 | 20.83 | 3.06 | 0.50 | 0.12 | 1.20 |
| Average absolute difference | | 0.11 | 0.04 | 0.88 | 0.31 | 0.19 | 0.10 | 0.35 | 0.11 |
| Std. deviation | | 0.11 | 0.04 | 0.57 | 0.14 | 0.15 | 0.09 | 0.31 | 0.10 |
| ASTM-allowed difference [a] | | ±0.10 | ±0.03 | ±0.02 | ±0.2 | ±0.2 | ±0.05 | ±0.2 | ±0.05 |

[a] From Ref. [8].

### 3.2. Interference studies

It has been reported that $Al^{3+}$ ions interfered with the determination of silicon [17], and silicon and aluminium interfered with the determination of calcium [16] by AAS. The effects of some common interfering ions were assessed by measuring the AAS absorbances of solutions with matrices simulating the fusion conditions and containing a fixed amount of the analyte and various amounts of the interferents. The relative deviation in the signal caused by the interferent was calculated and is tablulated in Table 5. With the matrix containing lithium tetraborate, no interference was observed for most of the interferents except CaO for the determination of $Na_2O$, where CaO caused a positive error at high concentration of Ca(II), and the interference was less in the matrix with a high concentration of lithium. Further, sulphate was found to cause a negative error in the determination of calcium, possibly due to the formation of calcium sulphate which can only be broken down at high temperatures. Nevertheless, the concentration of sulphate in cement samples is much less than that of Ca(II), and so its effect need not be considered except that sulphuric acid should not be used for dissolution purposes.

### 3.3. Calibration graph, detection limit and precision

The upper limits (3% deviation from the calibration graph), detection limits (defined for three times the standard deviation of the blank) and correlation coefficients for the calibration graphs for the determination of the eight oxides are shown in Table 6. The working ranges of the method are wide for these oxides, which enable samples with great variations in compositions to be determined.

The precision for the determination of the eight oxides using the proposed and XRF methods are shown by comparing the standard deviations for replicate determinations ($n = 4$) of the oxides in a cement sample. The results are presented in Table 7, where it can be seen that the precision using the AAS method is comparable or slightly better than that using the XRF method, except for $TiO_2$ for which the precision using the XRF method is better.

### 3.4. Real sample analysis

In real sample analysis, the XRF method was taken as the countercheck method. The $t$-values calculated for cement and raw meal are less than the theoretical values, indicating

Table 5
Effect of interferents on the proposed method

| Analyte | Interferent | Interferent/analyte ratio [a] | | | |
|---|---|---|---|---|---|
| $Na_2O$ | CaO | 56 | 108 | 140 | – |
| | | (2.3) | (4.9) | (6.4) | – |
| | CaO [b] | 32 | 80 | 128 | – |
| | | (4.1) | (5.1) | (7.9) | – |
| $K_2O$ | CaO | 28 | 56 | 65 | – |
| | | (−1.5) | (−3.0) | (−1.8) | – |
| | CaO [b] | 41 | 66 | – | – |
| | | (2.4) | (3.5) | – | – |
| CaO | $SiO_2$ | 50 | 70 | – | – |
| | | (−3.9) | (−5.8) | – | – |
| | $Al_2O_3$ | 5 | 7 | 14 | 23 |
| | | (−0.8) | (−3.5) | (−9.8) | (−11.2) |
| | $SO_4^{2-}$ | 7 | 16 | 34 | – |
| | | (−1.1) | (−5.4) | (−36.8) | – |
| MgO | $SiO_2$ | 7 | 17 | 23 | – |
| | | (2.5) | (2.2) | (2.8) | – |
| | $Al_2O_3$ | 0.3 | 3.3 | 23 | – |
| | | (0.4) | (0.4) | (1.8) | – |
| $SiO_2$ | $Al_2O_3$ | 2.5 | 4.8 | 7.1 | – |
| | | (−1.1) | (−2.3) | (2.2) | – |

[a] The value in parentheses is the per cent deviation from the value without interferent.
[b] Matrix free of lithium tetraborate.

that there is no significant difference between the proposed and countercheck methods (see Table 8).

In carbonate rock analysis, although the microwave oven technique [18] is time-saving, the oven used is a laboratory model (not a home appliance), which is less popular and expensive. Hence a muffle furance was used for the present investigation.

The proposed method can also be successfully applied to limestone determinations. This indicates the flexibility of the method.

For the classical gravimetric method [8], the cement and clinker samples are treated with hydrochloric acid and the amount of insoluble silica is negligible. This procedure cannot be applied to the raw meal and flyash blended cement samples without modification because they contain some acid-insoluble substances such as flyash and sand. For such samples, either fusion with sodium carbonate or clinkerization at 1400 °C must be carried out, and hence either sodium cannot be determined or a special muffle furnace (heating up to 1500 °C) is required for clinkerization. The fusion technique now proposed is shown to be effective for dissolving raw meal and flyash as well.

Table 6
Detection limits, upper limits and correlation coefficients for the calibration graphs [a]

| Oxide | Detection limit (%) | Upper limit (%) | Correlation coefficient |
|---|---|---|---|
| CaO | 0.12 | 70.0 | 0.9974 |
| MgO | 0.01 | 3.0 | 0.9996 |
| $Fe_2O_3$ | 0.01 | 5.0 | 0.9992 |
| $Al_2O_3$ | 0.03 | 6.8 | 0.9992 |
| $SiO_2$ | 0.24 | 42.5 | 0.9998 |
| $TiO_2$ | 0.06 | 0.75 | 0.9996 |
| $Na_2O$ | 0.03 | 0.33 | 0.9979 |
| $K_2O$ | 0.01 | 1.5 | 0.9988 |

[a] For definitions, see text.

Table 7
Precision analysis [a]

| Analyte | Concentration of the analyte in cement sample (%) | |
|---|---|---|
| | Proposed AAS method [b] | XRF method [b] |
| $SiO_2$ | 20.88 ± 0.11 (0.5) | 20.88 ± 0.13 (0.06) |
| $Al_2O_3$ | 5.58 ± 0.07 (1.2) | 5.58 ± 0.10 (1.8) |
| CaO | 65.01 ± 0.24 (0.4) | 65.01 ± 0.36 (0.6) |
| $Fe_2O_3$ | 2.85 ± 0.03 (1.0) | 2.85 ± 0.06 (2.10) |
| $Na_2O$ | 0.15 ± 0.01 (6.7) | 0.15 ± 0.02 (13.3) |
| $K_2O$ | 0.35 ± 0.01 (2.8) | 0.35 ± 0.01 (2.8) |
| MgO | 0.96 ± 0.03 (3.1) | 0.96 ± 0.06 (6.25) |
| $TiO_2$ | 0.27 ± 0.02 (7.4) | 0.27 ± 0.01 (3.7) |

[a] The sample solution was prepared as described in the Section 2.
[b] Relative standard deviation in per cent shown in parentheses.

Table 8
Analysis of real samples using the proposed (AAS) method

| Sample | Concentration (%) | | | | | | | | | | | | | | | |
|---|---|---|---|---|---|---|---|---|---|---|---|---|---|---|---|---|
| | $SiO_2$ | | $TiO_2$ | | $Al_2O_3$ | | $Fe_2O_3$ | | CaO | | $Na_2O$ | | $K_2O$ | | MgO | |
| | AAS | XRF | AAS | XRF | AAS | XRF | AAS | XRF | AAS | XRF | AAS | XRF | AAS | XRF | AAS | XRF |
| Limestone | 1.55 | 1.65 | – | – | 0.50 | 0.60 | 0.20 | 0.25 | 54.95 | 53.65 | 0.05 | 0.02 | 0.01 | 0.03 | 0.60 | 0.57 |
| Raw meal | 13.81 | 14.24 | 0.19 | 0.17 | 3.14 | 3.17 | 2.08 | 2.02 | 44.80 | 44.64 | 0.04 | 0.02 | 0.13 | 0.18 | 0.55 | 0.64 |
| | 14.55 | 14.53 | 0.16 | 0.15 | 2.91 | 3.01 | 2.35 | 2.20 | 44.76 | 44.44 | 0.05 | 0.02 | 0.13 | 0.16 | 0.53 | 0.51 |
| | 16.48 | 15.90 | 0.22 | 0.24 | 4.63 | 4.50 | 2.22 | 2.20 | 41.88 | 42.71 | 0.06 | 0.04 | 0.26 | 0.29 | 0.85 | 0.67 |
| Cement | 21.20 | 20.94 | 0.26 | 0.26 | 5.24 | 5.17 | 2.95 | 2.90 | 64.84 | 65.11 | 0.22 | 0.22 | 0.58 | 0.60 | 1.23 | 1.50 |
| | 20.57 | 20.85 | 0.23 | 0.25 | 4.58 | 4.59 | 3.10 | 3.00 | 64.46 | 64.30 | 0.26 | 0.24 | 0.52 | 0.56 | 1.07 | 1.06 |
| | 21.83 | 21.80 | 0.18 | 0.19 | 3.53 | 3.51 | 5.42 | 5.06 | 65.31 | 65.15 | 0.05 | 0.14 | 0.43 | 0.42 | 0.60 | 0.56 |
| | 20.88 | 20.81 | 0.29 | 0.27 | 5.58 | 5.51 | 2.86 | 2.89 | 65.06 | 65.12 | 0.15 | 0.20 | 0.37 | 0.31 | 0.95 | 1.05 |
| Flyash-blended | 29.14 | 29.84 | 0.47 | 0.49 | 8.84 | 8.98 | 3.60 | 3.65 | 50.08 | 50.20 | 0.17 | 0.20 | 0.78 | 0.72 | 2.46 | 2.06 |
| cement | 27.94 | 26.75 | 0.59 | 0.62 | 12.11 | 12.17 | 3.51 | 3.56 | 48.83 | 49.51 | 0.10 | 0.17 | 0.58 | 0.51 | 1.65 | 1.35 |
| | 27.28 | 27.10 | 0.42 | 0.40 | 7.27 | 7.31 | 3.35 | 3.31 | 54.77 | 54.79 | 0.15 | 0.17 | 0.77 | 0.73 | 2.49 | 2.62 |
| | 23.78 | 24.17 | 0.52 | 0.48 | 9.17 | 9.43 | 3.11 | 3.13 | 57.33 | 57.26 | 0.10 | 0.15 | 0.37 | 0.27 | 0.86 | 0.67 |
| $t$-Value | | | | | | | | | | | | | | | | |
| Calculated | 1.21 | | 1.52 | | 1.27 | | 1.75 | | 1.45 | | 1.41 | | 1.61 | | 1.77 | |
| Theoretical | 2.23 | | 2.23 | | 2.23 | | 2.23 | | 2.23 | | 2.23 | | 2.23 | | 2.23 | |

The standards for calibration are easily prepared from only one reference standard and can be used for calibrating all eight elements. For other published methods, different elements may require different sets of standards and chemicals [4]. Therefore, the proposed method is superior to the other method for standards preparation.

## 4. Conclusion

The proposed method is simple, rapid, accurate and has good precision. It can be applied to cement and raw meal with high silica contents of above 30%, and can also be applied to limestone samples. The standard preparation procedure is simplified, is better than other methods such as XRF, and is also applicable to determine trace elements in cement without tedious separation steps. The fusion agent is cheaper because part of the expensive lithium tetraborate is substituted with oxalic acid and lithium carbonate. The determination of eight elements for each sample can be completed within 80 min and therefore a large number of samples can be analysed within a working day.

## References

[1] G. Frechette, J.C. Hebert, T.P. Thinh, R. Rousseau and F. Claisse, Anal. Chem., 51 (1979) 957.
[2] H.Z. Yuen, Z.D. Wu, S.Y. Ding, Q.Y. Shi and G.H. Yin, Fenxi Huaxue, 14 (1986) 40.
[3] Y. Yamamoto, Y. Nishino and K. Ueda, Talanta, 32 (1985) 662.
[4] A. Nestoridis, Analyst, 95 (1970) 51.
[5] R.F. Gebhardt (Ed.), Rapid Methods for Chemical Analysis of Hydraulic Cement, ASTM, STP 985, 1988, p. 5–30.
[6] M.L.F. Sánchez, J.P. Suarez, E.F. Molina and A.S. Medel, J. Anal. At. Spectrom., 2 (1987) 491.
[7] BS 4550, Part 2, British Standard Institution, 1970.
[8] Annual Book of ASTM Standards, Part 4, ASTM, 1990, C114-88.
[9] Annual Book of ASTM Standards, Part 13, ASTM, 1980, C595-79.
[10] N.H. Suhr and C.O. Ingamells, Anal. Chem., 38 (1966) 730.
[11] J.W. Yule and G.A. Swanson, At. Absorpt. Newslett., 8 (1969) 30.
[12] J.H. Medlin, N.H. Suhr and J.B. Bodkin, At. Absorpt. Newslett., 8 (1969) 25.
[13] C.O. Ingamells, Anal. Chim. Acta, 52 (1970) 323.
[14] R.F. Gebhardt (Ed.), Rapid Methods for Chemical Analysis of Hydraulic Cement, ASTM, STP 985, 1988, p. 31–37.
[15] K.K. Choi, L. Lam and S.F. Luk, Talanta, 41 (1994) 1.
[16] J.C. Van Loon and C.M. Parissis, Analyst, 94 (1969) 1057.
[17] S.H. Omang, Anal. Chim. Acta, 46 (1969) 225.
[18] A.J. Kemp and C.J. Brown, Analyst, 115 (1990) 1197.

ELSEVIER

Talanta 42 (1995) 1273–1278

Talanta

# Catalytic determination of nanogram amounts from iron(III) using its catalytic effect on the oxidation of sodium pyrogallol-5-sulphonate by hydrogen peroxide ☆

Snežana S. Mitić *, Gordana Ž. Miletić, Mirjana V. Obradović

*Department of Chemistry, Faculty of Philosophy, University of Niš, 18000 Niš, Yugoslavia*

Received 3 November 1995; revised 21 February 1995; accepted 28 February 1995

**Abstract**

A kinetic method is described for the determination of iron(III) based on its catalytic effect on the oxidation of sodium pyrogallol-5-sulphonate by hydrogen peroxide. The reaction was followed spectrophotometrically by measuring the rate of change in the absorbance of the coloured product at 436.8 nm. Nanogram amounts of iron(III) (2.0–75.0 ng $cm^{-3}$) can be determined with good accuracy and reproducibility. The influence of foreign ions on the results was investigated and the method was found to be adequately selective. It has been applied satisfactorily to the determination of iron(III) in tap water samples. The kinetic parameters of both the catalysed and uncatalysed reactions are reported.

## 1. Introduction

The catalytic kinetic method [1] is one of the most attractive procedures for achieving the ultratrace determination of iron. The advantage of the catalytic kinetic method lies in the fact that the only instrumentation required is a spectrophotometer. Many indicator reactions for the catalytic kinetic method have been reported to determine microgram per cubic centimetre or submicrogram per cubic centimetre amounts of iron(III): the oxidation of Variamine Blue B base (*N*-(*p*-methoxyphenyl)-*p*-phenylenediamine) [2], its analogue (*N* - (*p* - methoxyphenyl) - *N'*, *N'* - dimethyl - *p*-phenylene-diamine) [3], 2-hydroxybenzaldehyde thiosemicarbazone [4], and chromotropic acid [5] by hydrogen peroxide and of *p*-phenetidine [6] by periodate in the presence of 2,2'-bipyridine. However, there are few methods that have sufficient sensitivity to determine iron(III) at the nanogram per cubic centimetre level or below: the oxidation of sodium 4,8-diamino-1,5-dihydroxyanthraquinone-2,6-disulphonate by dissolved oxygen (limit of detection, 18 ng $cm^{-3}$) [7] and *N*-methyl-*p*-aminophenolate by hydrogen peroxide (limit of detection, 0.8 ng $cm^{-3}$) [8]. Recently, Nakano et al. have developed a sensitive procedure for determining 0–6 ng $cm^{-3}$ iron(III) based on the oxidative coupling of *N*-phenyl-*p*-phenylene diamine with *N*,*N*-dimethylaniline by hydrogen peroxide [9]; however, the reaction must be performed at a higher temperature (40 °C). The catalytic oxidation of 3,5-diaminobenzoic acid dihydrochloride by hydrogen peroxide was also applied for the trace determination of iron [10]. The sensitivity of these reactions is 1 ng $cm^{-3}$, but the reaction must be performed at 35 °C. Dolmanova et al. [11] determined iron(III) by its catalytic effect on the oxidation of *o*-tolidine by periodate and 2,2'-bipyridine as an activator. The method has a high sensitivity 20 pg $cm^{-3}$, but manganese(II) interferes seriously with the determination even when present, in a amount equal to

☆ Presented at the 2nd Symposium the Physical Chemistry, Belgrade, Yugoslavia, 26–28 September, 1994.

* Corresponding author.



SSDI 0039-9140(95)01572-8

that of iron(III). Therefore, a still more sensitive and selective method for iron determination, the catalytic kinetic method is expected to achieve widespread application. For the development of a new indicator reaction for practical applications, attention should be paid to the following considerations: the reaction time to be analysed should be as short as possible within 20–30 min; the catalysed reaction should proceed at room temperature for convenient operation; the reaction rate can be followed spectrophotometrically by the differential tangent method; the indicator reaction preferably should be a simple mechanism, not involving a side reaction and an activator.

On the basis of the above concept, we present a new sensitive catalytic method of analysis for iron(III) based on the oxidation of sodium pyrogallol-5-sulphonate (PS) with hydrogen peroxide. The detection limit for this method was calculated to be 0.16 ng $cm^{-3}$. The method was successfully applied to the determination of trace iron in tap water without preconcentration and separation.

## 2. Experimental

### 2.1. Reagents

All chemicals were of analytical reagent grade, and were provired by Merck unless indicated otherwise. Solutions were made up in deionised water.

Hydrogen peroxide solution was prepared by appropriate dilution of the Merck pro analysi reagent and was standardised against potassium permanganate solution. PS was synthesised by dissolving 3.7833 g of pyrogallol in 100 $cm^3$ of the sulphuric acid (96%) [12]; a $8.8 \times 10^{-3}$ mol $dm^{-3}$ solution of the reagent was used. The stock iron solution, concentration 1 mg $dm^{-3}$, was prepared from iron(III) chloride and was determined by titration with EDTA using sulphosalicylic acid as indicator. Hydrolysis was prevented by adjusting the pH to about 1 with HCl [13]. A standard iron solution (100 ng $cm^{-3}$) was prepared by diluting the stock iron solution with deionised water. The perchloric acid solution (0.12 mol $dm^{-3}$) was prepared from the 70% reagent.

All the stock solutions were stored in polyethylene containers. Working solutions of iron, hydrogen peroxide and PS were prepared immediately before use.

All the polyethylene containers and glassware used were cleaned in aqueous HCl (1:1) and then thoroughly rinsed with deionised water.

### 2.2. Apparatus

A Perkin–Elmer Lamda 15 spectrophotometer, connected to a thermocirculating bath, was used for the absorbance measurements. The pH was measured by means of a Radiometer PHM 29b pH meter and a combined glass–calomel electrode, GK 2311C. The solutions were thermostatted at $25 \pm 0.1$ °C before the beginning of the reaction.

### 2.3. Procedure

Selected amounts of the reactants were transferred to a 10 $cm^3$ standard flask in the order PS, perchloric acid and catalyst. Water was added to give the predetermined volume. The flask was thermostatted for 10 min, and the solution was then made up to the mark with hydrogen peroxide and vigorously shaken. The spectrophotometer cell was rinsed well and filled with the solution. The absorbance at 436.8 nm, was measured every 30 s over a period of 5–8 min after the addition of hydrogen peroxide. The method of tangents was used and the slope of the linear section of the absorbance–time curve, $dA/dt = \tan \alpha$, was used as a measure of the reaction rate.

The measurements were made at $25 \pm 0.1$ °C.

## 3. Results and discussion

### 3.1. Catalytic oxidation of PS by $H_2O_2$

The absorption spectra were recorded of iron(III), and PS in perchloric acid solution (Fig. 1, curves 1 and 2, respectively), PS–perchloric acid–Fe(III) (curves 3 and 4) immediately after mixing (the absorption maxima is constant 1 h after mixing), PS–perchloric acid–hydrogen peroxide (curve 5) and PS–perchloric acid–hydrogen peroxide–Fe(III) (curve 6) 1 h after mixing.

The oxidation of PS with hydrogen peroxide at the higher concentrations of Fe(III) ($c_{Fe(III)} \geq 10^{-4}$ mol $dm^{-3}$) led to the formation of a yellow oxidation product at 436.8 nm, and also to the formation of a green complex at about 700 nm (curve 4). They are parallel reac-

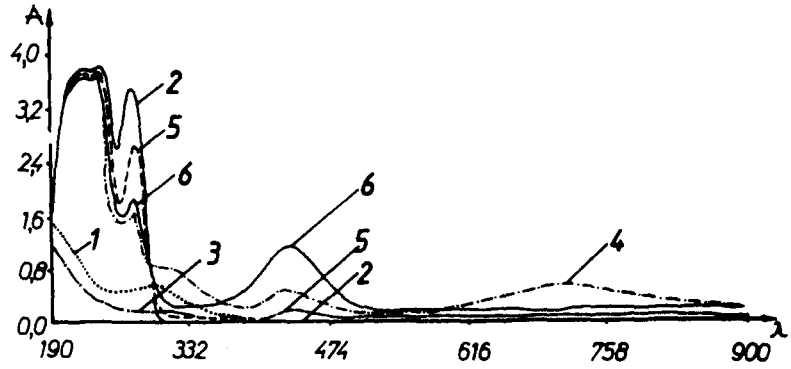


Fig. 1. Absorption spectra: spectrum 1, iron(III) aqueous solution; spectrum 2, PS in $HClO_4$; spectra 3 and 4, PS–$HClO_4$–Fe(III), immediately after the reagents were mixed; spectrum 5, PS–$HClO_4$–$H_2O_2$; spectrum 6, PS–$HClO_4$–$H_2O_2$–Fe(III) mixture 1 h after mixing.

tions, but both are under investigation. The aim of this paper is to study the catalytic effect of iron(III) on the oxidation of PS by the hydrogen peroxide reaction. For further work an iron(III) concentration of about $10^{-7}$ mol dm$^{-3}$ was selected. No characteristic absorption maxima are seen in the visible part of the spectrum of a PS–perchloric acid–Fe(III) solution mixture (curve 3) under the given optimum conditions for the iron(III).

However, the oxidation of PS by a higher concentration of hydrogen peroxide ($c_{H_2O_2}/c_{Fe(III)} \approx 10^5$) in the presence of perchloric acid is characterised by a slight maximum at 436.8 nm which significantly increases in the presence of iron(III). Therefore it can be concluded that iron(III) acts as a catalyst in the PS hydrogen peroxide oxidation reaction.

The dependence of the reaction rate on the $H_2O_2$ or PS concentration (see Figs. 3 and 4 below) indicates that the reaction proceeds through an intermediate complex of the catalyst–reductant–oxidant type [14], and, finally, the activated complex decomposes into the products and the catalyst

$$[PS\text{–}Fe(III)\text{–}H_2O_2] \rightarrow \text{Products} + Fe(II) \quad (1)$$

$$2Fe(II) + H_2O_2 \rightarrow 2Fe(III) + 2OH^- \quad (2)$$

It can be assumed that the second reaction proceeds much more quickly than the first.

The reduced iron(II) is oxidised to iron(III) by hydrogen peroxide, and then the formed iron(III) is allowed to react with PS again. Probably for this reason, a large excess of hydrogenperoxide with respect to the reagent is needed.

The oxidation product was not identified. However, PS could be oxidised by a one-electron mechanism to produce a resonance-stabilised product [15,16], a quinonoid species seems probable.

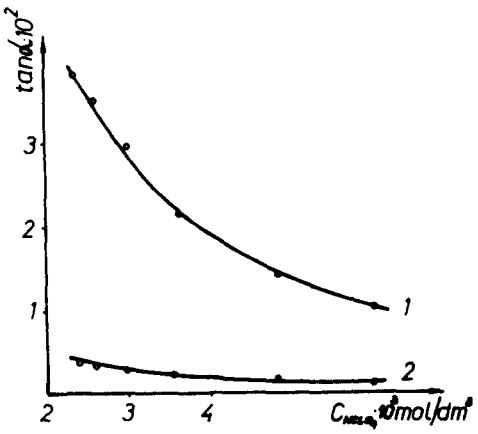


Fig. 2. Dependence of the reaction rate on $HClO_4$ concentration. Initial concentrations: PS, $8.8 \times 10^{-4}$ mol dm$^{-3}$; $H_2O_2$, 0.16 mol dm$^{-3}$; Fe(III), 0.3 μg cm$^{-3}$. Curve 1, catalytic reaction; curve 2, non-catalytic reaction.

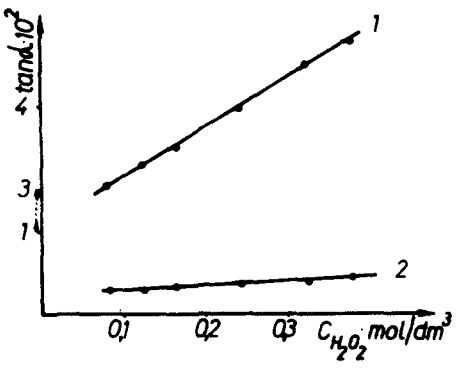


Fig. 3. Dependence of the reaction rate on $H_2O_2$ concentration. Initial concentrations: $HClO_4$, $2.6 \times 10^{-3}$ mol dm$^{-3}$; other concentrations as for Fig. 2 (except $H_2O_2$). Curve 1, catalytic reaction; curve 2, non-catalytic reaction.

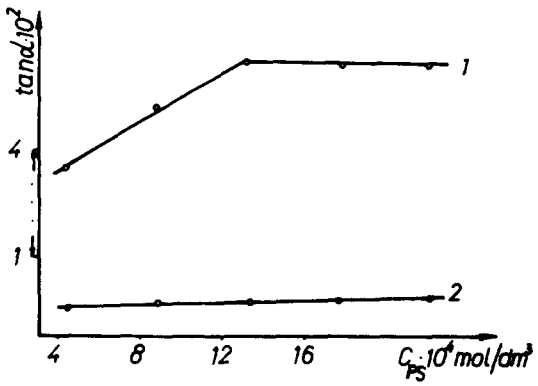


Fig. 4. Dependence of the reaction rate on PS concentration. Initial concentrations: $H_2O_2$, 0.32 mol dm$^{-3}$; $HClO_4$, $2.6 \times 10^{-3}$ mol dm$^{-3}$; Fe(III), 0.3 μg cm$^{-3}$. Curve 1, catalytic reaction; curve 2, non-catalytic reaction.

### 3.2. Effects of reaction variables

The influence of perchloric acid, temperature, and PS and hydrogen peroxide concentrations was studied for both the catalytic and non-catalytic reactions, in order to establish optimum conditions for the determination of iron(III).

Keeping all other experimental parameters constant, the perchloric acid dependence of the system was studied in the range $2.2 \times 10^{-3}$–$6 \times 10^{-3}$ mol dm$^{-3}$ (Fig. 2). It can be seen that the greatest difference between the reaction rates which occurs at $2.6 \times 10^{-3}$ mol dm$^{-3}$ maximally decreases the catalytic reaction rate. For further work a perchloric acid concentration of $2.6 \times 10^{-3}$ mol dm$^{-3}$ was selected.

The dependence of the reaction rate on $H_2O_2$ concentration is shown in Fig. 3, which shows that with increasing hydrogen peroxide concentration the difference between the rates of the catalytic and non-catalytic reactions increases. Both reactions are first order with respect to the $H_2O_2$ concentration. For further work an $H_2O_2$ concentration of 0.32 mol cm$^{-3}$ was selected.

The dependence of the reaction rates on the concentration of PS is shown in Fig. 4, which shows that the non-catalytic reaction is first order with respect to the PS concentration, whereas the catalytic reaction is first order with respect to PS concentration up to $1.32 \times 10^{-3}$ mol dm$^{-3}$ and zero order for higher concentrations. For further work, a PS concentration of $1.76 \times 10^{-3}$ mol dm$^{-3}$ was selected.

The influence of temperature on the reaction rate was studied in the range 22–34 °C (Fig. 5). The reaction rate increased as the temperature increased between 22 and 34 °C. The rate of the reaction increased by about 2 as the temperature was increased from 22 to 34 °C. However, although higher sensitivity could be obtained at the higher reaction temperature, it was troublesome to control the temperature precisely at the elevated temperature, hence a reaction temperature of 25 °C was chosen.

### 3.3. Calibration graph

A calibration graph was prepared for the optimum concentrations described above. There was a linear relationship between the reciprocal of tan α and the iron(III) concentration from $3.6 \times 10^{-8}$ to $1.3 \times 10^{-6}$ mol dm$^{-3}$ or from 2.0 to 75.0 ng cm$^{-3}$ of iron(III) in the final solution. Fig. 6 shows three calibration lines which can be used or the determination of the iron(III) concentration in the interval mentioned. The line 3 measured at 31 °C is steeper and more suitable for use than line 1, measured at 25 °C (or line 2, measured at 28 °C).

On the basis of our kinetic investigation, we formulated a kinetic equation for the oxidation of PS by hydrogen peroxide with iron as catalyst:

$$\frac{dx}{dt} = k_1 c_{HClO_4}^{-0.9} c_{H_2O_2} c_{PS} c_{Fe} \quad \text{for} \quad c_{PS} \leqslant 1.32 \times 10^{-3} \text{ mol dm}^{-3} \tag{3}$$

$$\frac{dx}{dt} = k_1 c_{HClO_4}^{-0.9} c_{H_2O_2} c_{Fe} \quad \text{for} \quad c_{PS} \geqslant 1.32 \times 10^{-3} \text{ mol dm}^{-3} \tag{4}$$

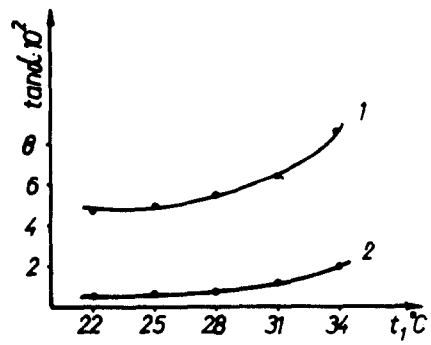


Fig. 5. Dependence of the reaction rate on temperature. Initial concentration: PS, $1.76 \times 10^{-3}$ mol dm$^{-3}$; other concentrations as for Fig. 4. Curve 1, catalytic reaction; curve 2, non-catalytic reaction.

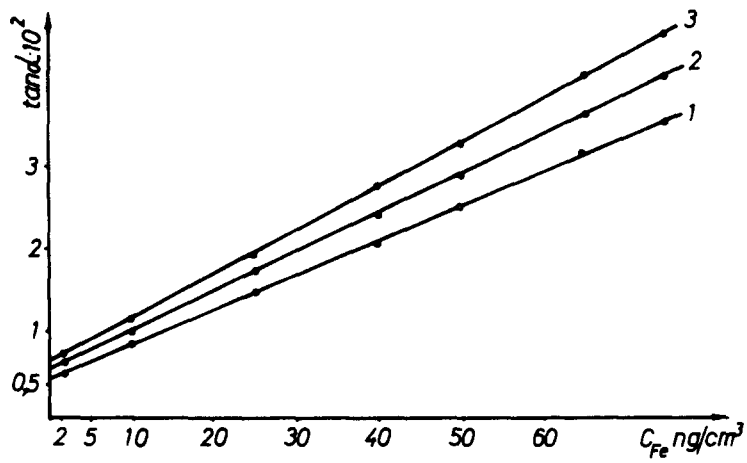


Fig. 6. Dependence of the reaction rate on Fe(III) concentration. Initial concentrations as for Fig. 5. Curve 1, 25 °C; curve 2, 28 °C; curve 3, 31 °C.

The kinetic equation for the non-catalytic reaction under the same conditions may be written as follows:

$$\frac{dx}{dt} = k_0 c_{HClO_4}^{-0.8} c_{H_2O_2} c_{PS} \quad (5)$$

where $k_1$ and $k_0$ are the relative rate constants for the catalytic and non-catalytic reactions. On the basis of these equations the rate constants for the catalytic and non-catalytic reactions were calculated.

The linear relationship between the logarithm of the relative rate constant and the reciprocal of the absolute temperature was found for the catalytic as well as the non-catalytic reaction. The activation energies were found to be 28.11 kJ mol$^{-1}$ for the catalytic reaction and 45.88 kJ mol$^{-1}$ for the non-catalytic reaction.

The minimum concentration of iron which could be determined by this method may be calculated by the method given by Yatsimirskii [17]

$$c_{min} \geqslant 0.1 \frac{k_0 c_{HClO_4}^{-0.8}}{k_1 c_{HClO_4}^{-0.9}} \quad (6)$$

By entering these values in the previous equation we find that $c_{min} \geqslant 2.9 \times 10^{-9}$ mol dm$^{-3}$ or 0.16 ng cm$^{-3}$.

The precision and accuracy of the method are also investigated. The relative error ranges from 0.5 to 7.2% in the iron(III) concentration range 75.0–2.0 ng cm$^{-3}$.

### 3.4. Interference studies

The interference effects of many cations and anions on the kinetic determination of Fe(III) ($c_{Fe(III)} = 50$ ng cm$^{-3}$) were examined and the tolerance limits for interfering ions are summarised in Table 1. It may be seen that Cu(II), Cr(VI) and I$^-$ in a 1:1 ratio with iron(III) interfere with the reaction. The other ions investigated have practically no influence on the determination of iron(III) by this method.

### 3.5. Application to tap water

The method was directly applied to the analysis of tap waters, because interfering ions (Table 2) in natural waters are tolerable. Tap water was acidified to pH 1 with hydrochloric acid (6 mol dm$^{-3}$) and then heated to remove chlorine. After this treatment, a 2 cm$^3$ portion

Table 1
Tolerance levels of interferents in the kinetic determination of 50 ng cm$^{-3}$ iron(III) using the optimum conditions as reported under the analytical procedure (Section 2.3)

| Tolerance level, $c_{ion}/c_{Fe(III)}$ | Ion added |
|---|---|
| $10^3$ | Ca(II), Sr(II), Mg(II), Ba(II) |
| $10^2$ | Zn(II), Cd(II), $AsO_4^{3-}$, $WO_4^{2-}$, $F^-$, $Br^-$, $SO_4^{2-}$, $PO_4^{3-}$ citrate, tartrate, $C_2O_4^{2-}$ |
| 10 | Pb(II), Hg(II), Ni(II), Co(II), Al(III), $SCN^-$ |
| 0.8 | Cu(II), $I^-$ |
| 0.5 | $Cr_2O_7^{2-}$ |

Table 2
Results for the determination of iron(III) in tap water using the optimum conditions reported under the application to tap water (Section 3.5)

| Sample | Sample taken ($cm^3$) | Fe(III) added ($ng\ cm^{-3}$) | Fe(III) [a] found ($ng\ cm^{-3}$) | Fe(III) in sample ($ng\ cm^{-3}$) | $G$ [b] (%) | Other method ($ng\ cm^{-3}$) |
|---|---|---|---|---|---|---|
| Tap | 2 | 0 | 9.44 | 47.20 | 3.1 | 50 [d] |
| Water [c] | 2 | 20.00 | 29.39 | 46.96 | 2.9 | |

[a] From the calibration graph for aqueous solutions.
[b] Relative error.
[c] Selected at University of Niš (25th August 1992).
[d] Value obtained by the AAS method.

of the sample was used for the recommended procedure. To examine the recovery of iron(III), known amounts of iron(III) were added to the samples.

The results are shown in Table 2. The recovery of added iron(III) is found to be quantitative and the reproducibility is satisfactory. Furthermore, the results obtained by the present method were compared with those obtained by the atomic absorption spectrophotometric method. The values for tap water samples are in good agreement with those obtained by the AAS method. From these results, the method seems to be applicable to the determination of soluble iron.

## References

[1] K.B. Yatsimirskii, Kinetic Methods of Analysis, Pergamon, Oxford, 1966.
[2] S. Kreingold and L.I. Sosenkova, Zh. Anal. Khim., 26 (1971) 332–337.
[3] T. Kawashima, Y. Kozuma and S. Nakano, Anal. Chim. Acta, 106 (1979) 355–360.
[4] A. Moreno, M. Silva, D. Perez-Bendito and M. Velcarcel, Anal. Chim. Acta, 157 (1984) 333–342.
[5] D.G. Themelis and G.S. Vasilikiotis, Analyst, 112 (1987) 787–789.
[6] I.F. Dolmanova, V.I. Rychkova and V.M. Peshkova, Zh. Anal. Khim., 28 (1973) 1763–1767.
[7] A. Navas Diaz and F. Sanchez Rojas, Analyst, 109 (1984) 1435–1438.
[8] A.P. Gumenyuk and S.P. Mushtakova, Zh. Anal. Khim., 39 (1984) 1278–1280; J. Anal. Chem. USSR (Engl. Transl.), 39 (1984) 1022–1024.
[9] S. Nakano, M. Odzu, M. Tanako and T. Kawashima, Mikrochim. Acta., 1, (1983) 403–411.
[10] A.Ch. Zotou and C.G. Papadopoulos, Analyst, 112 (1987) 787–789.
[11] I.F. Dolmanova, V.I. Rychkova and V.M. Peshkova, Zh. Anal. Khim., 32 (1977) 1387–1393.
[12] V.M. Obradović, S.D. Veselinović and S. Djordjević, 34rd Conf. Serbian Chem. Soc., Belgrade, 1992, p. 128.
[13] A.E. Smith, Analyst, 98 (1973) 65.
[14] P.R. Bontchev and S. Gantcheva, Talanta, 27 (1980) 899.
[15] W.V. Kaeding, J. Org. Chem., 28 (1963) 1063.
[16] J.L. Ferrer-Herranz and D. Pérez-Bendito, Anal. Chem. Acta, 132 (1981) 157–164.
[17] K.B. Yatsimirskii, Zh. Anal. Khim., 10 (1955) 299.

ELSEVIER

Talanta 42 (1995) 1279–1283

Talanta

# Selective extraction and photometric determination of trace vanadium with cinnamohydroxamic acid in MIBK and its application to steel and rock ore analysis

A.K. Chakrabarti

*Department of Inorganic and Analytical Chemistry, Jadavpur University, Calcutta 700 032, India*

Received 18 October 1990; revised 15 February 1995; accepted 28 February 1995

**Abstract**

A sensitive and selective photometric method for the trace determination of vanadium with cinnamohydroxamic acid extracted from 1.8 M HCl in methyl isobutyl ketone is described. The wine-red chelate formed under an optimum acidity of 1.3–2.6 M HCl absorbs with a maximum at 525 nm. Beer's law is obeyed in the range 0–8 ppm of vanadium(V) and the optimum range of determination of vanadium is found to be 1–8 ppm. The molar absorptivity and Sandell's sensitivity are $6.0 \times 10^3$ l mol$^{-1}$ cm$^{-1}$ and 0.0086 μg cm$^{-2}$ of vanadium(V) at 525 nm. The photometric determination of trace amounts of vanadium in materials such as alloys, minerals and rock ores is also reported. The solvent extraction methods are simple, rapid and highly selective with fluoride used as a masking agent for Fe and Ti. The standard deviations are minimal and the mean error is only 0.015%.

## 1. Introduction

The recovery with determination and rapid assay of vanadium metal present as the vanadate in rock ores [1] are performed by wet analysis and by spectrometric methods for the prospecting of metals in geological samples and others.

Vanadium occurs at the part-per-billion level in many natural systems, alloys and geochemical minerals [2,3]. Preconcentration with selective solvent extraction has been followed by the trace analysis of vanadium in the presence of iron(III) and titanium(IV). For an assay of the metal, molecular spectrophotometry has always been rapid, simple and the preferred choice over atomic absorption spectrometry and fluorimetry. The reported use of hydroxamic acids led to the development of a unique microchemical technique and the present method for analysing specialised alloys and ores.

Cinnamo hydroxamic acid (N-CHA) reacts with vanadium(V) in both the pH and the acidity range of the media for extractions in methyl isobutyl ketone. The reagent has been studied on limited occasions [4,5]. Moreover, vanadium(V) chemistry [6] is important in extraction equilibria and has been thoroughly studied with organic acids as model compounds. Vanadyl species with a square-planar arrangement in the hydroxamate have been investigated thoroughly [7]. The mechanisms of the extractions are governed in most cases by ion pair formation, the chelate effect, synergism and mixed-ligand complex formation. The specification studies and the adverse effect of alcohol have little importance as regards the oxidation state, the nature of the solvent and extraction behaviour. The extraction method is found to be simple, rapid and sensitive, with high precision and reproducibility. Its usefulness is shown by its rapid extraction behaviour over a wide acidity range. The higher tolerance limits have indicated a major utility factor. These are some of the highlights of the method.


*SSDI* 0039-9140(95)01574-4

In this paper the synthesis of very pure cinnamohydroxamic reagent is reported following a modified procedure. The reagent (N-CHA) was synthesised and utilised in the development of a selective and sensitive photometric method for the trace analysis of vanadium. Its application to the analysis of samples demonstrated advantages over other methods reported earlier [8–10]. The analytical uses of the selective reagent, N-CHA, in binary extraction procedures for the assay of vanadium in steels, minerals and ores in the presence of rarer and other base metals are reported and are described here.

## 2. Experimental

### 2.1. Reagents

*Ammonium vanadate solution*

The metal solution was prepared by dissolving ammonium metavanadate ($NH_4VO_3$; Merck) in 3 ml of concentrated ammonia and double-distilled water and then making the volume up to 250 ml. The solution was standardised both by complexometric titration [11] and photometrically with *N*-benzoyl-*N*-phenylhydroxylamine [12]. Aliquots from a standard stock solution containing 100 μg $ml^{-1}$ were always used.

*Cinnamohydroxamic acid solutions (0.031 M)*

The pure reagent N-CHA, was prepared by a modified procedure reported in the literature [13]. The reagent was found to be pure, stable in air, and was stored in a brown bottle. The reagent readily dissolves in methyl isobutyl ketone (MIBK). A freshly prepared solution of 0.5% reagent in MIBK was used for the binary extractions.

A standard stock solution of 6 M hydrochloric acid was prepared and a 0.1 M acid solution was obtained by dilution. A standard buffer of pH 4.0 was prepared from 0.2 M acetic acid and 0.2 M sodium acetate. All other chemicals used were A.R. or G.R. grade and the solvents were purified before use.

### 2.2. Procedure

Mix an aliquot of standard vanadium solution (0–100 μg $ml^{-1}$) with 5 ml of 0.5% cinnamohydroxamic acid in a 100 ml separating funnel. To this mixture add 10 ml of pure MIBK as solvent, followed by 3 ml of 6 M hydrochloric acid, and dilute to give 10 ml of the aqueous phase. Shake the mixture for 5 min, separate the organic layer containing the wine-red complex and dry it over anhydrous sodium sulphate in a 25 ml beaker. Extract again with 5 ml of MIBK. Combine the extracts and transfer them to a 25 ml flask. Make up the volume to the mark with MIBK. Prepare a reagent blank similarly. However, a solvent blank alone was found to be satisfactory. Measure the absorbance at 525 nm against the solvent blank.

### 2.3. Procedure for steel analysis

Dissolve 0.5 g of steel in 20 ml of sulphuric acid (1:1) in a beaker on a hotplate. Add 5 ml of concentrated nitric acid and evaporate to strong fumes of sulphur trioxide. Cool, add 50 ml of water, boil, filter with a Whatman no. 42 paper and wash the residue several times with hot dilute sulphuric acid and finally with hot water. Cool the filtrate and washings, transfer to a 250 ml standard flask, make up to the mark and mix well.

To 5 ml of this solution add 0.1% potassium permanganate solution until a pink colour persists. Add this mixture to hot 15% sodium hydroxide solution in excess and boil. Filter off the precipitate and redissolve it in dilute hydrochloric acid. Reprecipitate the hydroxides as above and filter. Combine the filtrates and evaporate to a low bulk. Cool, add 15 mg of sodium fluoride, and determine the vanadium content by the described procedure (acidity, 1.8 M). Measure the absorbance at 525 nm as appropriate.

### 2.4. Procedure for rock (mineral) analysis

Fuse 0.5 g of the sample for 2 h with 3 g of sodium carbonate and 1 g of sodium hydroxide in a nickel crucible. Cool the melt, leach with hot water and allow to stand overnight. Filter the solution through Whatman no. 42 filter paper, transfer to a 100 ml volumetric flask and make up the volume with double-distilled water. Take an appropriate amount of the solution and determine the vanadium content by the above procedure using 15 mg of fluoride as masking agent.

### 2.5. Procedure for ore analysis

Fuse 0.5 g of the sample for 2 h with 3 g of sodium carbonate and 1 g of sodium hydroxide in a nickel crucible. Cool the melt, leach with hot water and allow to stand overnight. The aqueous extract contains vanadium along with iron and titanium. Filter the solution through a Whatman no. 42 filter paper, transfer to a 100 ml volummetric flask and make up the volume with double-distilled water. Take an appropriate amount of the solution and determine the vanadium content by the above procedure using 15 mg of fluoride as masking agent.

## 3. Results and discussion

### 3.1. Absorbance spectra

The reagent mainly extracts V(V) quantitatively from 1.8 M HCl. The wine-red complex absorption maximum is at 525 nm with the solvent as reference.

### 3.2. Effects of acidity, reagent, time and stability

The optimum acidity range for the binary extraction is 1.3–2.6 M HCl (i.e. 2.2–4.4 ml of 6 M HCl). The acidity of 1.8 M was always adjusted by adding 3 ml of 6 ml HCl. The absorbances of the wine-red complexes remained constant with the optimum reagent required being 2–8 ml of a 0.5% solution in MIBK. A 5 ml amount of 0.5% CHA was always added. The per cent extraction was maximum with a water:MIBK ratio of 10:10 (v/v). The extraction time for complete reaction was 4–7 min. The complex was found to be stable for 24 h at room temperature.

### 3.3. Beer's law, optimum range, absorptivity, and sensitivity

The complex obeyed Beer's law in the range 0–8 ppm and the optimum range [15] of determination is 1–8 ppm of V(V) at 525 nm. The molar absorptivity (TMA) determined by the method of Chakrabarti and Bag based on the free ligand [16] concentration is $7.6 \times 10^3$ l mol$^{-1}$ cm$^{-1}$. The molar absorptivity and Sandell's sensitivity values are $6.0 \times 10^3$ l mol$^{-1}$ cm$^{-1}$ and 0.0086 μg cm$^{-2}$ of V(V) respectively.

### 3.4. Tolerance limits for diverse ions

Interference studies were carried out with 4 ppm of vanadium in a 1.8 M acid system, the tolerance limit being the amount causing a deviation of more than 0.005 absorbance units.

A large number of diverse ions have been studied, A 60-fold excess of acetate, oxalate, Cu(II), Cr(III), Zr(IV); a 12-fold excess of Ti(IV) and W(VI); a 30-fold excess of Mo(VI) and Pd(II), and a 150-fold excess of Ca(II), Mn(II), Co(II), Al(III) and fluoride were tolerated. A very large excess of citrate, tartrate, EDTA, nitrate, sulphate, phosphate, Ni(II), Zn(II), Cd(II), Hg(II), Th(IV) and Pb(II) was tolerated, the tolerance ratio being 500-fold excess for metal ions and 1000-fold amounts for anions. Only Fe(III) interferes, but with fluoride as masking agent the tolerance limit increased to a 25-fold excess. The method is thus rendered highly selective. The tolerance limits are given in Table 1.

### 3.5. Binary extraction with N-CHA in MIBK over the acid pH range

A yellow-brown or yellow-orange complex formed at pH 3.8–4.4, adjusted with 0.1 M HCl and a pH 4.0 acetate buffer. Its absorption

Table 1
Tolerance limits for the determination of vanadium (4 ppm) with N-CHA in the presence of interfering ions

| Ions | Tolerance limit (ppm) | Ion | Tolerance limit (ppm) |
|---|---|---|---|
| Acetate | 250 | Pd(II) | 125 |
| Oxalate | 250 | Cr(III) | 240 |
| Tartrate | 1000 | Mn(II) | 600 |
| Citrate | 1500 | Th(IV) | 1000 |
| EDTA | 1500 | Co(II) | 600 |
| Phosphate | 8000 | Ni(II) | 1000 |
| Fluoride | 600 | Al(III) | 600 |
| Phosphate | 8000 | Ni(II) | 1000 |
| Fluoride | 600 | Al(III) | 600 |
| Sulphate | 8000 | Hg(II) | 2000 |
| Nitrate | 8000 | Cd(II) | 2000 |
| Fe(III) | N.I.[a] (100[b]) | Zn(II) | 1000 |
| Ti(IV) | N.I.[a] (50[b]) | Pb(II) | 1000 |
| Mo(VI) | 120 | Cu(II) | 240 |
| W(VI) | 50 | Nb(V) | 40[b] |
| $UO_2$(II) | 400 | Ta(V) | 40[b] |
| Zr(IV) | 250 | Ba(II) | 600 |
| Ca(II) | 600 | Sr(II) | 600 |

[a] No interference; interferences were removed by double precipitation as the hydroxides using 15% NaOH.
[b] Fluoride used as masking agent.

maximum was at 430–460 nm. The chloro or acetate complexes were found to be unstable in the MIBK phase. Binary extractions of the wine-red chelate formed with 1.8 M HCl have been thoroughly investigated.

### 3.6. Stability of the reagent

With regard to the purity and stability of the reagent (N-CHA) in air it has been observed that its method of isolation as reported in the literature was found to result in an impure reagent with low yield. Moreover, it is unstable in the presence of light. Both these shortcomings were solved by making sure that the reagent was free from traces of ester. This additional step was considered and carefully controlled. thus, the yellow sodium salt of N-CHA was thoroughly washed with a petroleum ether three or four times to free it completely from ethyl cinnamate ester and other impurities. The reagent is generated in the pure form by acidification. The isolated solid (m.p. 100–111 °C) was stored in a brown bottle and was found to be stable for an indefinite period. Thus it is not available commercially and the reason is obvious.

### 3.7. Selectivity

The review in the monograph showed limited selectivity in the methods due to interferences normally by iron and titanium. A close association of V with Fe and Ti is very common for its matrices and analyte solutions. The tolerance ratio of V:Fe lies in between 1:10 and 1:50, and mostly this ratio is found to be 1:10 with or without the masking agents studied with such acid reagents. The adopted methods vary among those available to chemists, and the error is viewed differently [18,20]. The selectivity and tolerance limits with Fe and Ti are low and masking with fluoride greatly improved these effectively for a moderate excess of Fe and Ti. The major interferences of iron and titanium ores in a 25-fold excess have been removed by a double precipitation technique using 15% sodium hydroxide. The results were found to be accurate and reproducible, as reported for two of the ilmenite minerals and a bauxite ore.

### 3.8. Analysis of steel and rock ores

The ilmenite ores were processed before being used as the sample analytes and were passed through sieves for the bulk analyses. Their specifications were obtained. The method is highly reliable for all commercial low grade ores. Interfering ions were removed during the digestion with the reagents and the acids, and the filtration. The chief advantage is that the separations by extraction with recovery of vanadium from its ores are comparable for accurate and reproducible routine analyses. The method is simple and rapid. The results obtained after several runs were verified and compared with standard spectroscopic results or certified values. The results of the comparison give and reflect the method that is most rapid and has the highest accuracy. In conclusion, the aim of the work was to develop and devise an analytical technique that was obviously simple and rapid, for application as a routine assay in geochemical mining and prospecting of rocks [19].

Application of the technique to samples was tested using BAS 64b steel and two ilmenite samples collected from Putka Pahar, Madhya Pradesh (M.P.), India, and Tamil Nadu (Hornbendite rock), India, through the Geological Survey of India and IOL, Calcutta. The samples were finely ground (200 mesh) before direct analysis after separation. The methods were found to be excellent because of their high selectivity. The photometric procedures were found to be accurate, simple and highly reproducible when fluoride was used for masking more than a 25-fold ratio of Fe and Ti present in excess. The samples were analysed by a spectroscopic method [20] and the results agreed well. The results are shown in Table 2.

### 3.9. Nature of the complex

The primary aim was to investigate the choice of a solvent that would readily dissolve the N-CHA reagent and quantitatively distribute the metal as a red chelate in the organic phase in a single extraction. The solvent MIBK was found to be satisfactory for application over a wide acidity range of 1.3–2.6 M HCl for the extraction. A 1:2 complex, i.e. $VO(OH)(CHA)_2$ chelate, is formed in MIBK when extracted with 0.5% reagent. The composition of the complex was determined by Job's method and verified by the mole ratio method.

Table 2
Spectrometric determination of trace vanadium in steel, minerals and ores with cinnamohydroxamic acid reagent

| Sample | Vanadium in sample (%) | | Error (%) | Standard deviation |
|---|---|---|---|---|
| | Found | Certified | | |
| BAS Steel 64b | 1.977<br>1.975<br>1.976 | 1.99 | 0.014 | ±0.001 |
| Ilmenite I<br>Hornbendite rock | 0.089<br>0.085<br>0.091 | 0.1 | 0.012 | ±0.003 |
| Ilmenite II | 0.142<br>0.144<br>0.141 | 0.15 | 0.008 | ±0.002 |
| Bauxite (ore) | 0.223<br>0.225<br>0.221 | 0.2 | 0.023 | ±0.004 |

Stable V=O, V–O(H) and V–O(LH) bonds are formed with the highly stable closed five-membered ring ether structure. This has been established by elemental analysis and spectroscopic studies of such complexes. The configuration is similar to that of the vanadium complexes with other hydroxamic acid compounds reported previously [4,17]. The ligands do not simply coordinate but a molecule with tautomeric forms –C(O)–NH(OH) ⇌ –C(OH)=N(OH) enhances the phase transfer processes with enhancement of polarisation and rapid recovery via membrane transport. This has led to a selective extraction even in the presence of large amounts of other metal ions. Al:1(aqueous:organic) volume ratio leads to maximum sensitivity and high selectivity. Traces of alcohol are to be avoided because they cause a detrimental effect.

Complex formula: $VO(OH)(CHA)_2$
Tautomeric forms:
–C(O)–NH(OH) ⇌ –C(OH)=N(OH)

## Acknowledgements

The author gratefully acknowledges with thanks the technical assistance extended to him by Shri P.K. Chakraborty of IOL, India, to Professor S.P. Bag for his suggestions and the referee towards improvement of the paper.

Financial assistance received from C.S.I.R. is also hereby acknowledged with thanks.

## References

[1] W.H. Schoeller and A.R. Powell, The Analysis of Minerals and Ores of the Rarer Metals, 3rd edn., Longmans, London, 1955.
[2] P. Battistoni, P. Bruni, L. Cardelline, G. Fava and G. Gobbi, Talanta, 27 (1980) 623.
[3] G. Svehla and G. Tolg, Talanta, 23 (1976) 209.
[4] A.K. Chakrabarti, J. Inst. Chem., (India), 63 (1991) 174.
[5] S. Das, K.K. Sen and S.P. Bag, J. Indian Chem. Soc., 67 (1990) 441.
[6] A.S. Bhaduri, Z. Anal. Chem., 151 (1956) 109.
[7] D.E. Ryan, Analyst, 85 (1960) 569.
[8] E.S. Pilkington and W. Wilson, Anal. Chim. Acta, 41 (1968) 75.
[9] M. Tanaka and I. Kojima, Anal. Chim. Acta, 41 (1968) 461.
[10] A.I. Vogel, A Text Book of Quantitative Inorganic Analysis, 3rd. edn., Longmans, London, 1964.
[11] A.K. Majumdar, *N*-Benzoylphenylhydroxylamine and its Analogues, Pergamon, Oxford, 1972.
[12] A.H. Blatt, Organic Synthesis, Vol. 1, 2nd edn., Wiley, New York, 1945.
[13] J. Thiele and R.H. Pickard, Ann., 309 (1889) 194.
[14] A.I. Vogel, Practical Organic Chemistry, 3rd edn., Longmans, London, 1956.
[15] A. Ringbom, Z. Anal. Chem., 115 (1938) 332.
[16] A.K. Chakrabarti and S.P. Bag, Talanta, 23 (1976) 736.
[17] L.J. Bellamy, The Infrared Spectra of Complex Molecules, 2nd edn., Wiley, New York, 1958.
[18] S.P. Bag, A.B. Chatterjee, A.K. Chakrabarti, and P.R. Chakraborty, Talanta, 29 (1982) 526.
[19] L.H. Ahrens and S.R. Raylor, Spectrochemical Analysis — A Treatise on the D.C. Arc Analysis of Geological and Related Materials, 2nd edn., Addison-Wesley, Reading, MA, 1961.
[20] P.W.J.M. Boumans, Theory of Spectrochemical Excitation, Plenum, New York, 1966.

ELSEVIER

Talanta 42 (1995) 1285–1289

Talanta

# FIA-AAS determination of salicylic acid by a solid-phase reactor of copper carbonate incorporated in polyester resin beads

G.A. Rivas [1], J. Martínez Calatayud *

*Department de Química Analitica, Universitat de València., Moliner 50, Burjasot València, Spain*

Received 19 September 1994; revised 4 January 1995; accepted 28 February 1995

**Abstract**

The determination of salicylic acid was carried out by reaction of the drug with copper carbonate entrapped in a polymeric material in a solid-phase reactor; the released cupric ions were monitored by flame atomic absorption at 324.8 nm. The calibration graph is linear over the range 4.0–75 μg $ml^{-1}$ of salicylic acid, with a relative standard deviation of less than 1.5% and a sample throughput of 257 $h^{-1}$. The influence of foreign compounds was studied and the method was applied to the determination of salicylic acid content in two different pharmaceutical formulations.

*Keywords:* Flow injection analysis; Pharmaceutical analysis; Solid-phase reactor

## 1. Introduction

Salicylic acid is 2-hydroxybenzoic acid, and occurs as white or colourless aciculate crystals or a white crystalline powder. It is slightly soluble in water, freely soluble in ethanol and in ether, and sparingly soluble in chloroform. Salicylic acid has keratolytic properties and is applied topically in the treatment of hyperkeratotic and scaling skin conditions; it is often used in conjunction with many other agents. Salicylic acid also possesses fungicidal properties and is used in the treatment of skin fungal infections [1].

The analysis of the drug (official procedures) is established by titration in an ethanol–aqueous medium with sodium hydroxide, using phenol red as an indicator [2]. Different spectrophotometric procedures have been published for the determination of salicylic acid on the basis of the complex formed with Fe(III) [3] or Cu(II) [4]. The yellowish-green species with copper is stable in the pH range 5.5–6, and presents its maximum absorbance at 730 nm with a molar absorptivity of 20 l $mol^{-1}$ $cm^{-1}$. An FIA-electrochemical procedure [5] came to the notice of the authors when the work reported here had already been concluded; the method makes use of the enzyme salicylate hydroxylase immobilized on a solid-phase reactor, which should be sorted in buffer at 4 °C. The enzyme catalyses the conversion of salicylic acid to catechol, which can then be detected amperometrically.

The use of solid-phase reactors in continuous-flow manifolds is an advantageous alternative to reagents in solution. The interest is ascribed to different advantages offered over homogeneous systems, which have been discussed earlier [6]. The present paper deals with a solid-phase reactor placed in a flow manifold;

* Corresponding author.

[1] Present address: Dpto. Fisico Química, Fac. Ciencias Químicas, Universidad Nacional de Córdoba, Suc. 16 CC61. 5016, Córdoba, Argentina.


*SSDI* 0039-9140(95)01575-8

the immobilization is based on the physical entrapment of the reagent, copper carbonate [7], by means of the polymerization reaction of linear unsaturated polyester chains. The analytical procedure is based on the reaction of the injected sample with the immobilized copper carbonate and monitoring of the release of copper (complexed by salicylic acid) by an atomic absorption spectrometer.

## 2. Experimental

### 2.1. Reagents

Aqueous solutions of salicylic acid (Guinama, a.r.) were in distilled water. Urea, thymol, boric acid, benzocaine, resorcinol, procaine hydrochloride, lactic acid, glucose, sucrose and fructose (Guinama, a.r.) were used. All other reagents were of analytical grade unless stated otherwise.

### 2.2. FIA manifold

Fig. 1 shows the continuous-flow manifolds used. The sample injector was from Rheodyne, model 5041, and a Gilson Minipuls 2 pump was used. The determination of copper was carried out by means of an AA spectrometer from Varian, Model SpectrAA-10, at a wavelength of 324.8 nm. The PTFE tubing was of 1.2 mm internal diameter for the solid-phase bed reactor and 0.8 mm for the rest of the manifold.

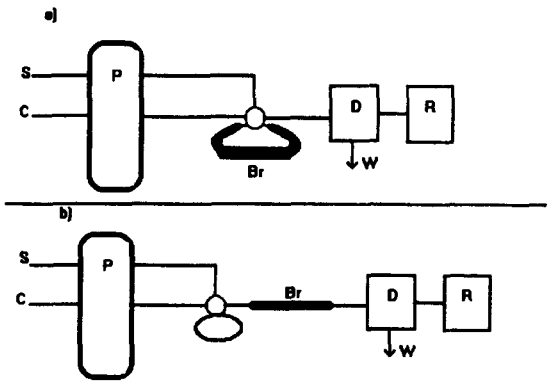


Fig. 1. Flow manifolds tested in preliminary experiments for the determination of salicylic acid. (Manifold (b) was selected for the optimization studies): P, pump; D, atomic absorption detector; R, recorder; Br, bed-reactor; S, sample solution; C, carrier stream; W, waste.

### 2.3. Procedures

*Preparation of the solid-phase reactor*

The bed-reactor was prepared as described previously [8]. A 45 g mass of $Cu(CO_3)$ $Cu(OH)_2 \cdot 10H_2O$ (Panreac) was added to 15 g of the resin solution AL-100 A (from Reposa); after homogenization by manual stirring, 1 ml of the catalyst (ethyl methyl ketone, from Azko) was added and stirred before it became solid. The obtained solid was reduced to small particles, washed with distilled water and dried at 80 °C. The particles selected by size, 90–200 μm, were washed and introduced into the PTFE tubing (1.2 mm internal diameter and 5.0 cm length) by suction. Specific conditions for storage were not required.

*Pharmaceutical formulations*

The proposed procedure was applied to two formulations: Callicida Gras and Pyralvex. The solution of Pyralvex (0.80 ml) was directly diluted in pure distilled water, filtered and levelled to 500 ml with distilled water; aliquots of the resulting solution were then injected into the carrier stream. The solution of Callicida Grass was weighed (about 2 g), dissolved in ethanol by ultrasonic stirring and levelled to 100 ml with ethanol. 1 ml of the resulting solution was diluted to 500 ml with pure distilled water and then injected as usual into the FIA manifold.

## 3. Results and discussion

### 3.1. Preliminary studies

Preliminary studies were designed to examine the reaction between the immobilized copper carbonate and the salicylic acid in a continuous-flow manifold. These experiments were carried out by means of a flow assembly in which the solution of salicylic acid in distilled water merged with different acidic or basic aqueous solutions; the resulting mixture was then passed through the solid-phase reactor and, after reaction, the released copper was measured by atomic absorption. The obtained transient signals (absorbance units) were contained as the mean value of 10 replicates at wavelength 324.8 nm and 0.5 nm slit window; the results obtained for different media and pH values (potentiometrically measured) are depicted in Table 1.

An increase in base-line noise was clearly observed when the sample solution merged

Table 1

| Medium | pH | Absorbance |
|---|---|---|
| $Na_2CO_3/NaHCO_3$ | 9.80 | 0.967 |
| $Na_2CO_3/NaHCO_3$ | 9.12 | 0.983 |
| $NaHCO_3$ | 8.33 | 0.853 |
| NaOH/HCl | 7.04 | 0.984 |
| Deionized water | | 1.081 |
| $CH_3$-COOH/NaOOC-$CH_3$ | 6.30 | 1.041 |
| $CH_3$-COOH/NaOOC-$CH_3$ | 6.10 | 0.856 |
| $CH_3$-COOH/NaOOC-$CH_3$ | 6.00 | 0.128 |
| HCl | 5.40 | 0.883 |
| HCl | 4.40 | 0.816 |

with acidic solutions (mainly with hydrochloric or acetic acid concentrated solutions), owing to the copper released by the acidic solvent. The presence of organic solvents like ethanol did not result in increased outputs. The highest peak-height was observed for acetic/acetate buffered solutions, which was slightly higher than that obtained with distilled water, i.e. 1.041 vs. 1.081 (absorbance units). As the difference is small, distilled water was the selected carrier for further work.

Further tests were devoted to the study of the suitable flow-injection assembly; the two assemblies depicted in Figs. 1(a) and 1(b) were pre-selected after some experiments. Different sets of injections (varying the flow-rates of carrier and sample solutions) were carried out to compare the behaviour of both manifolds. Transient outputs from the assembly in which the solid-phase reactor was nesting in the sample loop (Fig. 1(a)) were about 5% higher (peak-height) than those corresponding to the assembly with the reactor between the injector and detector (Fig. 1(b)). However, bearing in mind the life-span of the reactor (the former is continuously exposed to an acidic stream, pH of the sample solution 3.0) the assembly depicted in Fig. 1(b) was selected for further work.

Having selected the FIA manifold, the experimental parameters, temperature, "concentration" of the reagent (copper carbonate) in the polymeric matrix, reactor length, particle size, internal diameter of the reactor, sample volume and carrier flow-rate, were successively optimized by means of the univariate method. The injected sample solutions (salicylic acid in distilled water) contained 10, 40 or 100 μg $ml^{-1}$ of salicylic acid, respectively.

The tested range for each studied parameter and the optimum selected values are depicted in Table 2. A study on the influence of the temperature was carried out by introducing into a water bath: (a) the solution containers; (b) the solid-phase reactor; and (c) the whole assembly. The tested range was room temperature to 80 °C. The obtained results in series (b) revealed an increase of peak-height with temperature; the maximum increase, about 20% in the peak-height (compared with the peak-height at room temperature), was obtained at 60 °C. Higher values of the temperature then resulted in lower outputs. In contrast, the highest temperatures tested induced the release of cupric ions from the solid-phase reactor by passing the carrier, which meant a shorter life-span of the reactor. From these observations, it was decided that the slight gain in peak-height was not valuable, and room temperature was selected for further work.

The "concentration" of the reagent (mass of copper carbonate vs. mass of resin) in the solid-phase reactor showed a critical influence; the ratio (g/g) copper carbonate/resin solution was studied over the range 1/1–3/1; higher ratios were not tested as they resulted in solid particles without mechanical resistance. The ratio 3/1 was selected as giving the best output.

The influence of the reactor parameters, such as length, internal diameter and particle size, on the transient outputs was very important. The length was tested by injecting series of salicylic acid solutions of different concentrations, from 10 to 500 μg $ml^{-1}$. Fig. 2 depicts the calculated sensitivity (linear slope) of each tested reactor-length. A length of 5 cm was selected as resulting in the best output. This strategy of testing a series of salicylic acid concentrations was also used for studying the influence of the particle size and internal diameter of the reactor. The influence of the particle size was tested by preparing calibration

Table 2
Optimization of experimental parameters (for details set text)

| Parameter | Tested range | Selected value |
|---|---|---|
| Temperature (°C) | room–80 | room |
| Ratio copper carb./resin (g/g) | 1/1–3/1 | 3/1 |
| Reactor length (cm) | 5.0–30.0 | 5.0 |
| Particle size (μm) | 90–300 | 90–200 |
| Internal diameter reactor (mm) | 0.8–1.5 | 1.2 |
| Sample volume (μl) | 100.0–500.0 | 195.2 |
| Carrier flow-rate (ml $min^{-1}$) | 2.0–6.0 | 5.2 |

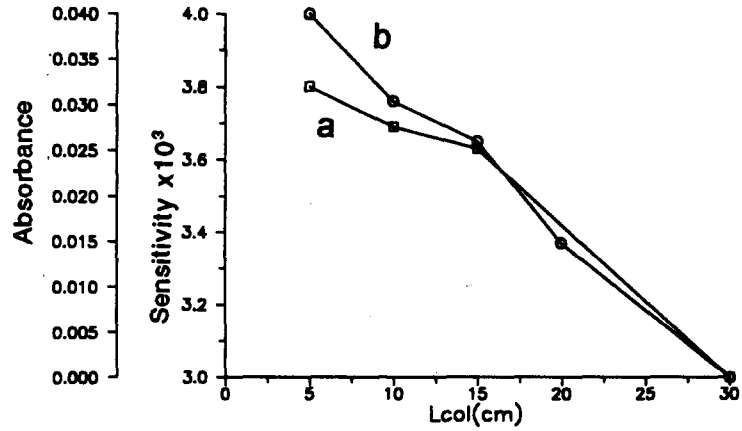


Fig. 2. Influence of the reactor-length on the peak-height. Right axis depicts the absorbance of injected solutions containing 10 μg ml$^{-1}$ of salicylic acid. Left axis depicts the sensitivity (slope of the linear graph) of the series of salicylic concentrations for each tested column length. Curve a, FIA outputs in absorbance units, obtained with salicylic concentration of 10.0 μg ml$^{-1}$. Curve b, slope of linear graphs.

graphs with each tested size; the obtained results showed that the best outputs for two different sizes, 200–300 μm and 90–200 μm, calculated from linear slopes (absorbance vs. concentration of salicylic acid in μg ml$^{-1}$) were 2.99 and 2.90 ($\times 10^{-3}$), respectively. The study of the internal diameter (tested in the range 0.8–1.5 mm internal diameter) revealed slightly better results with the thinner tube, but owing to the ease of the column preparation the 1.2 mm tube was selected.

The sample volume is also a critical parameter influencing peak-height and base-width. Fig. 3 depicts the absorbance of the peak vs. the sample volume; bearing in mind the best compromise of sensitivity/sample throughput, the selected value was 195 μl. The influence of the carrier flow-rate, tested for three different concentrations of acid salicylic, is depicted in Fig. 4, 5.2 ml min$^{-1}$ being the value selected as the optimum that could be obtained. The results of the optimization are depicted in Table 3.

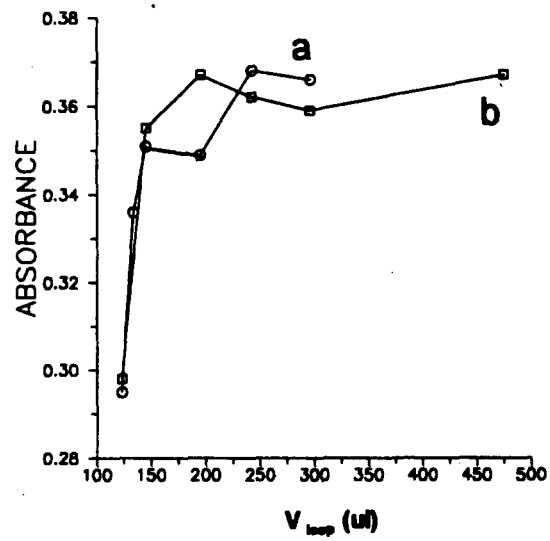


Fig. 3. Influence on the peak-height of the sample volume for two different solid-phase reactors. Reactor length: a, 10 cm; b, 5 cm.

## 4. Analytical application

The calibration graph shows linear behaviour over the range 4.0–75 μg ml$^{-1}$ of salicylic acid, with the equation Abs. $= 2.1 \times 10^{-3} + 3.8 \times 10^{-3}C$ ($C$ is the concentration of salicylic acid in μg ml$^{-1}$) and correlation coefficient 0.9991. The repeatabilities calculated as RSD (%) (salicylic acid concentration in μ ml$^{-1}$, number of replicates, mean absorbance, and RSD) were: 50.0, 16, 0.191, 1.5; 40, 6, 0.155; 0.0; 10, 13, 0.042, 0.0. The sample throughput, according to different studied concentrations of the sample, varied from 220 (40 μg ml$^{-1}$ of salicylic acid) to 257 (5 μg ml$^{-1}$) h$^{-1}$.

The day-to-day reproducibility was studied by preparing calibration graphs with independent solutions and using three different columns on different days (up to 21). The obtained results (column, day, linear slope of the calibration graph $\times 10^{-3}$ and correlation coefficient) are depicted in Table 3.

The influence of foreign compounds that are commonly found in pharmaceutical formulations containing salicylic acid was also investigated. The results in terms of concentration

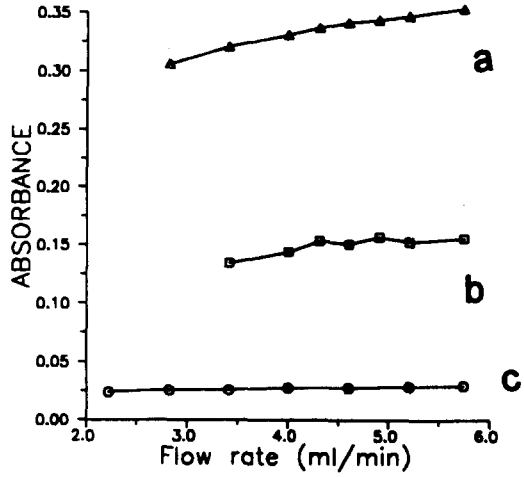


Fig. 4. Influence on the peak height of the carrier flow-rate for three different concentrations of salicylic acid ($\mu g\ ml^{-1}$): a, 100.0; b, 40.0; c, 10.0.

Table 3
Day-to-day reproducibility of the analysis using the solid-phase reactor

| Column | Day | Slope | Corr. coeff. |
|---|---|---|---|
| 1 | 1 | 3.80 | 0.9991 |
| 1 | 2 | 3.73 | 0.9990 |
| 1 | 8 | 3.82 | 0.9981 |
| 1 | 9 | 3.68 | 0.9941 |
| 2 | 1 | 3.89 | 0.9981 |
| 2 | 2 | 3.56 | 0.9978 |
| 2 | 21 | 3.52 | 0.9999 |
| 3 | 5 | 3.14 | 0.9991 |
| 3 | 13 | 3.17 | 0.9972 |

($\mu g\ l^{-1}$) and relative error (%) are depicted in Table 4. Procaine chlorhydrate, pilocarpine, methyl nicotinate, and the acetic, benzoic and lactic acids resulted in very serious interferences.

Salicylic acid was determined in two different pharmaceutical formulations: (a) Pyralvex (from Instituto Berna de España S.A.); declarated contents of anthraquinonic glucosides, 0.05 g $ml^{-1}$, and salicylic acid, 0.01 g $ml^{-1}$; (b) Callicida Grass (from Quimifar S.A.); declarated contents of salicylic acid, 250 mg $g^{-1}$, and ethanol, 365 mg $g^{-1}$. The relative errors (%) in the obtained results, according to the label claim, were: Pyralvex, 0.8%; Callicida Gras, 3.6%.

Table 4
Influence of foreign compounds on salicylic determination

| Compound | Conc. ($\mu g\ ml^{-1}$) | Rel. error (%) |
|---|---|---|
| Sorbitol | 1742 | 0.6 |
| Fructose | 2500 | 1.7 |
| Sucrose | 2500 | 0.9 |
| Glucose | 2500 | 5.0 |
| Nicotinamide | 412 | 4.4 |
| Menthol* | 125 | 0.0 |
| Alcanfor* | 50 | 4.2 |
| Lidocaine | 350 | 1.2 |
| Resorcinol | 1038 | 1.3 |
| Benzocaine | 256 | 0.6 |
| Boric acid | 606 | 1.2 |
| Thymol | 526 | 0.0 |
| Urea | 584 | 1.7 |

Salicylic acid concentration, 50 $\mu g\ ml^{-1}$; except for compounds marked with *, when it was 25 $\mu g\ ml^{-1}$.

## 5. Conclusions

An FIA-AAS procedure is proposed for the determination of salicylic acid by means of a solid-phase reactor of copper carbonate incorporated in polyester resin beads. The reactor is prepared from an easily available reagent by a quick and easy procedure, and the analytical properties of the resulting solid remain unchanged for more than two years. No special conditions are required.

The resulting manifold is suitable for the determination of salicylic acid in pharmaceutical formulations with competitive precision and high sample throughput.

## References

[1] Martindale, The Extra Pharmacopoeia, 30th edn., Pharmaceutical Press, London, 1992.
[2] BP, HMSO, London, 1993.
[3] U. Saha, IRCS Med. Sci., 11 (1983) 91.
[4] U. Saha and K. Baksi, Analyst, 110 (1985) 739.
[5] N. Neumayr, O. Friedrich, G. Sontag and F. Pitner, Anal. Chim. Acta., 273 (1993) 469.
[6] J.V. Garcia Mateo and J. Martínez Calatayud, Chem. Anal. (Warsaw), 38 (1993) 1.
[7] J.V. Garcia Mateo and J. Martínez Calatayud, Anal. Chim. Acta, 274 (1993) 275.
[8] L. Lahuerta Zamora, J.V. Garcia Mateo and J. Martínez Calatayud, Anal. Chim. Acta, 263 (1992) 81.

ELSEVIER

Talanta 42 (1995) 1291–1296

Talanta

# Extraction and spectrophotometric determination of lead(II) with pyridine-2-acetaldehyde salicyloylhydrazone

Muralidhar N. Bale, D.P. Dave, A.D. Sawant *

*Inorganic Chemistry Division, Institute of Science, 15, Madam Cama Road, Bombay 400032, India*

Received 15 July 1994; revised 24 February 1995; accepted 3 March 1995

**Abstract**

Lead(II) reacts with pyridine-2-acetaldehyde salicyloylhydrazone (PASH) in the pH range 8.6–9.3 to form a yellow-green, 1:2 chelate which can be extracted into chloroform. Beer's law is obeyed in the concentration range 1.5–6.2 $\mu g\,ml^{-1}$ of lead(II). The molar absorptivity of the extracted species is $1.93 \times 10^4$ $l\,mol^{-1}\,cm^{-1}$ at 380 nm. The proposed method is sensitive, simple, rapid, accurate and has been satisfactorily applied for the determination of lead in synthetic mixtures, alloys, water and soil samples.

## 1. Introduction

Lead is a transition metal and has significance in many industrial applications [1]. In spite of its various applications, lead is a very toxic and harmful element [2]. Hence it is very important to estimate lead at the trace level in different samples. Various reagents for the extractive spectrophotometric determination of lead, such as 8-hydroxy-7-[α-(2-methoxycarbonylanilino)-benzyl]quinoline [3], thio-2-thenoyltrifluoroacetone [4], *N*-(4-chlorophenyl)benzohydroxamic acid [5], 2-(salicylideneamino)benzenethiol [6], morphine-4-carbodithioate [7], *N,N'*-bis(2-hydroxy-5-nitrobenzyl)cryptand-22 [8], cyclohexane-1,3-dione-bis-(4-methylthiosemicarbazone) [9], monothiothenoyltrifluoroacetone [10], sodium *N,N*-diethyl-dithiocarbamate [11] and dithizone [12] have been reported. However these methods suffer from some limitations such as strict temperature control [6], long extraction times [4,6,8–10] and interference from some ions [3,4,6–10,12], etc. A method, superior in sensitivity to those reported in the literature [3,5,7,11], is developed for the extraction and spectrophotometric determination of lead(II) with pyridine-2-acetaldehyde salicyloylhydrazone (PASH). The method is rapid, simple and accurate. Earlier PASH was employed for the extractive spectrophotometric determination of vanadium(V) [13], iron(III) [14], nickel(II) [15], palladium(III) [16], copper(II) and ruthenium (III) [17]. PASH reacts with lead(II) to give a yellow-green coloured complex extractable in chloroform. The method is free from many limitations.

## 2. Experimental

### 2.1. Apparatus

A Bausch and Lomb Spectronic-20 spectrophotometer with glass cells, a ditigal ELICO pH meter (model LI-120) with a combined glass electrode and a Carl Zeiss Jena (DDR) atomic absorption spectrometer were used.

* Corresponding author.


*SSDI* 0039-9140(95)01578-7

### 2.2. Reagents

All chemicals used were of analytical grade unless otherwise stated. Double-distilled water was used.

*PASH*

The ligand was synthesised by the reaction of pyridine-2-acetaldehyde (Fluka) and salicyloylhydrazide (Aldrich) as reported in the literature [13]. A stock solution (10 mg $ml^{-1}$) of PASH was prepared by dissolving it in DMF. The appropriate volume was diluted to 100 ml with chloroform to give a 0.05% reagent solution of PASH.

*Lead(II) solution*

Lead nitrate (3.99 g) was dissolved in 3 ml of concentrated nitric acid, and the solution was diluted to 250 ml with double-distilled water and standardised by a known method [18].

*Lithium chloride (4M)*

Lithium chloride (17 g) was dissolved in 100 ml of distilled water.

*Buffer solution (pH 9.0)*

The pH of the aqueous (1:1) $NH_3$ solution was adjusted to the required pH with 4 N HCl using a pH meter.

### 2.3. Recommended procedure

To an aliquot of solution containing 15–62 μg of lead (II) in a separating funnel add 2 ml of 4 M lithium chloride solution and 2 ml of pH 9.0 buffer. Dilute the mixture to 10 ml with distilled water and equilibrate with 10 ml of a 0.05% reagent solution of PASH in chloroform for 1 min. Separate the two layers and measure the absorbance of the organic phase containing the complex at 380 nm against a reagent blank.

## 3. Results and discussion

### 3.1. Absorption spectra

The absorption spectra of PASH and the lead(II)–PASH complex are shown in Fig. 1. The absorption maximum of the ligand is at 345 nm and that of the complex is at 380 nm.

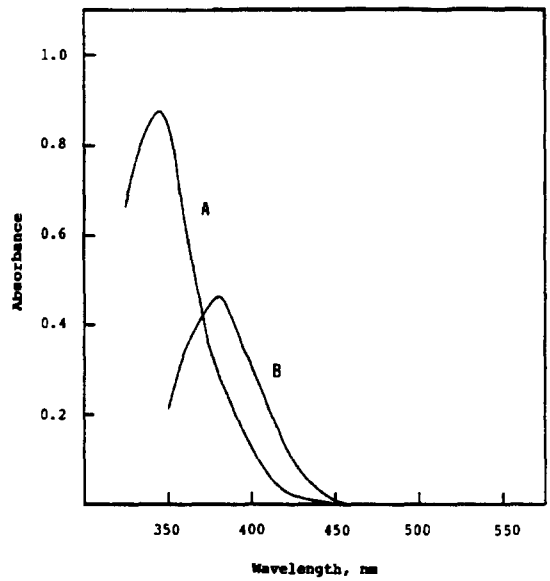


Fig. 1. Absorption spectra of PASH and its lead(II) complex extracted into chloroform. ([PB(II)] = 5 μg $ml^{-1}$; pH 9.0; [LiCl] = 0.8 M; [PASH] = 0.05%.) Spectrum A, PASH vs. chloroform; spectrum B, Pb(II)PASH complex vs. reagent blank.

### 3.2. Extraction conditions

Lead(II) was extracted over the pH range 2–11 from lithium chloride solution in the range 0.1–1.4 M with varying (0.005–0.060%) concentrations of PASH. The extraction coefficients were determined by atomic absorption spectrometry. At pH 8.6–9.3 the extraction reached a maximum, and lead(II)

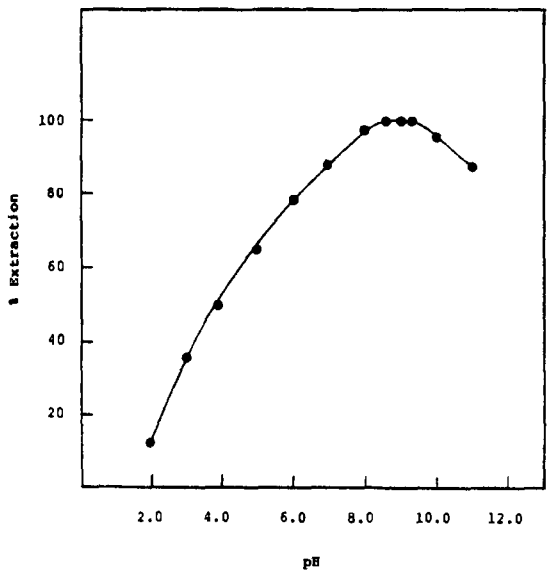


Fig. 2. The effect of pH on the extraction of lead(II) with PASH.

was quantitatively extracted as shown in Fig. 2. Therefore all extractions were performed at pH 9.0. The optimal concentrations of lithium chloride and PASH were found to be 0.8 M and 0.05%, respectively, for the extraction of lead(II). The equilibration time for the extraction of lead(II) was varied from 10–180 s, the minimum time required for the extraction of lead(II) was 60 s. A longer extraction time has no adverse effect. The lead(II) complex was stable for 40 h.

### 3.3. Effect of solvents

The effect of various solvents such as chloroform, benzene, xylene, toluene, carbon tetrachloride, methyl isobutyl ketone, amyl acetate and ethyl acetate on the extraction of lead(II) with PASH was studied and it was found that the extraction of lead(II) was quantitative with chloroform. The reagent solution of PASH (0.05%) in other solvents gave only 35–93% extraction of lead(II).

### 3.4. Beer's law and sensitivity

The absorbance is a linear function of lead(II) concentration in the range 1.5–6.2 μg $ml^{-1}$ of solution. The molar absorptivity is $1.93 \times 10^4$ 1 $mol^{-1}$ $cm^{-1}$ and the Sandell sensitivity is 0.0107 μg $cm^{-2}$.

### 3.5. Composition of the extracted species

The composition of the complex was determined by plotting of log $D$ against log $[PASH]_{org}$ at fixed pH, where $D$ denotes the distribution ratio of lead(II) between the two phases and $[PASH]_{org}$ is the equilibration concentration of PASH in the organic phase. As shown in Fig. 3, a straight line with a slope equal to about 2 shows that the metal-to-ligand ratio is 1:2.

### 3.6. Effect of foreign ions

The effect of various foreign ions on the extraction and determination of lead(II) was studied, and tolerance limits are shown in Table 1. The tolerance limit of the foreign ion was taken as the amount required to cause an error of not more than ±2% in the lead(II) recovery.

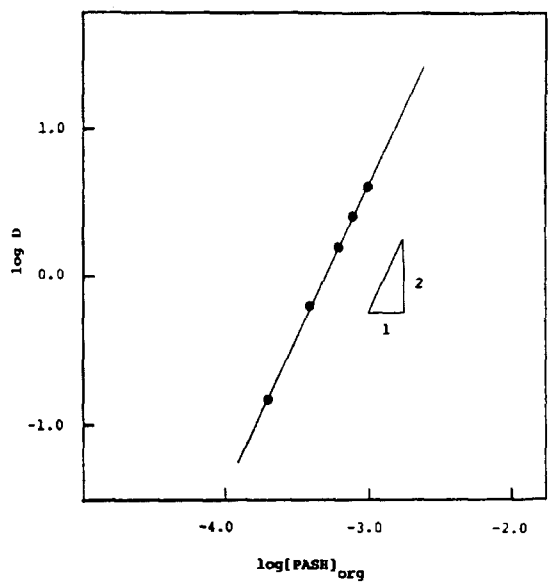


Fig. 3. Logarithmic plot of the distribution of lead(II) vs. concentration of PASH. ([Pb(II)] = 5 μg $ml^{-1}$; pH. 9.0; [LiCl] = 0.8 M; absorbance measurement at 380 nm.)

### 3.7. Application to the determination of lead in synthetic mixtures

The present method was applied to the determination of lead (30 μg) in various synthetic mixtures containing copper, nickel, zinc, iron, bismuth, tin, arsenic, antimony and manganese. The results are shown in Table 2.

Table 1
Effect of foreign ions on the extraction of 30 μg of lead(II) from 0.8 M LiCl solution with 0.05% PASH in chloroform

| Tolerance limit (μg) | Ions |
|---|---|
| 20000 | $Cl^-$, $Br^-$, $F^-$, $SO_3^{2-}$, $S_2O_3^{2-}$, $S_2O_8^{2-}$, $ClO_3^-$, $BrO_3^-$, $IO_3^-$, $NO_2^-$, $NO_3^-$, $CN^-$, $SCN^-$, urea, thiourea, oxalate, acetate, citrate, tartrate |
| 10000 | Ca(II), Sr(II) |
| 6000 | Co(II), Cd(II) |
| 5000 | Zn(II), Cr(III), W(VI) |
| 3500 | $I^-$ |
| 3000 | $SO_4^{2-}$ |
| 2500 | $MnO_4^-$ |
| 2000 | Mg(II), Fe(III) |
| 1000 | Mn(II), Hg(II) |
| 500 | Sn(II), Pd(II), Ru(III), V(V) |
| 200 | Sb(II), As(III), Ce(IV), Th(IV), U(VI) |
| 100 | Cu(II), Ni(II), Ti(IV) |
| 50 | Mo(III), Tl(IV) |
| 40 | Be(II), Bi(III) |
| 20 | Te(IV) |

Table 2
Analysis of synthetic mixtures

| Sample | Synthetic mixture composition [a] | Amount found [b] | Recovery (%) | Standard deviation | Coefficient of variation (%) |
|---|---|---|---|---|---|
| 1 | Pb(30), Cu(100), Ni(100), Zn(1000), Fe(1000) | 29.98 | 99.93 | 0.10 | 0.33 |
| 2 | Pb(30), Bi(40), Sn(100), As(200), Sb(200) | 30.00 | 100.00 | 0.10 | 0.33 |
| 3 | Pb(30), Bi(40), Sn(100), Cu(100), Mn(1000) | 29.92 | 99.73 | 0.47 | 1.57 |
| 4 | Pb(30), Cu(100), Sn(100), Fe(1000), Zn(1000) | 29.94 | 99.80 | 0.25 | 0.83 |
| 5 | Pb(30), Bi(40), Ni(100), Zn(1000), Fe(1000) | 29.94 | 99.80 | 0.08 | 0.26 |
| 6 | Pb(30), Sn(100), Sb(200), Zn(1000), Mn(1000) | 29.90 | 99.60 | 0.23 | 0.76 |
| 7 | Pb(30), Ni(100), Sn(100), Mn(1000), Fe(1000) | 29.96 | 99.86 | 0.42 | 1.40 |
| 8 | Pb(30), As(200), Fe(1000), Zn(1000), Mn(1000) | 30.00 | 100.00 | 0.14 | 0.46 |

[a] Numbers in parentheses are microgram amounts of the metals.
[b] Average of five determinations.

Table 3
Analysis of water and soil samples

| Sample | Present method [a] ($\mu g\ ml^{-1}$) | Standard deviation | Variation from mean | Atomic absorption ($\mu g\ ml^{-1}$) |
|---|---|---|---|---|
| A | 14.7 | 0.16 | $14.7 \pm 0.25$ | 14.7 |
| B | 24.9 | 0.11 | $24.9 \pm 0.18$ | 25.0 |
| C | 49.9 | 0.08 | $49.9 \pm 0.12$ | 50.0 |
| D | 50.2 | 0.14 | $50.2 \pm 0.22$ | 50.2 |
| E | 48.6 | 0.16 | $48.6 \pm 0.25$ | 48.8 |
| F | 45.4 | 0.08 | $45.4 \pm 0.12$ | 45.5 |

[a] Average of four determinations.
Key: A, Kotwali water tank; B, industrial waste water of Nocil; C, lead smelter, east side soil; D, lead smelter, west side soil; E, lead smelter, back ground soil; F, lead smleter, 15 cm depth soil.

### *3.7. Application to determination of lead in water samples*

Water samples were collected from a water tank at Kotwali and samples of industrial waste water from Nocil were also used. The samples were filtered and acidified with nitric acid. To 1–2 ml of the samples in a separating funnel were added 2 ml each of 4 M lithium chloride and pH 9.0 buffer. This mixture was diluted to 10 ml and extracted with 10 ml of a 0.05% reagent solution of PASH. After the separation of the two layers, the absorbance of the organic phase was measured at 380 nm against a reagent blank. The concentration of lead was determined from the standard curve. The results shown in Table 3 are in good agreement with each other and with those obtained by atomic absorption spectrometry.

### *3.8. Application to the analysis of soils*

The soil samples were collected from the area of a lead smelter.

*Sample dissolution*

To a 1 g soil sample in a beaker, 15 ml of aqua regia and 2 ml of perchloric acid were added and heated nearly to dryness. The process was repeated until a white residue was formed. The residue was dissolved in 30 ml of 5 N HCl and filtered through a Whatman no. 42 filter paper. The undissolved material was washed with 30 ml of distilled water and the volume of the filtrate was made up to 100 ml with distilled water. An aliquot of this solution was used for the determination of lead.

Table 4
Analysis of alloys

| Sample | Sample and its composition | Certified value | Amount found | Standard deviation (%) [a] | Coefficient of variation (%) |
|---|---|---|---|---|---|
| 1 | Leaded gunmetal (BCS 183/4) Cu, 84.06; Sn, 7.27; Zn, 3.47; Pb, 3.15; Ni, 1.30; Sb, 0.23; As, 0.13; Fe, 0.056; Bi, 0.005; P, 0.09 | 3.15% Pb | 3.13 | 0.212 | 0.67 |
| 2 | Tin base whitemetal (BCS, 178/2) Sn, 82.20; Sb, 9.45; Cu, 4.58; Pb, 3.18; Ni, 0.17; As, 0.15; Cd, 0.14; Bi, 0.11; Zn, 0.04; Fe, 0.02 | 3.18% Pb | 3.16 | 0.141 | 0.44 |
| 3 | Leaded brass (ITA Lab, 4016) Cu, 60.04; Zn, 33.02; Pb, 5.75; Al, 0.37; Sn, 0.30; Ni, 0.03; Fe, 0.18; Sb, 0.02; P, 0.02 | 5.75% Pb | 5.72 | 0.273 | 0.47 |
| 4 | Solder | 60.00 μg Pb [b] | 59.90 | 0.418 | 0.69 |

[a] Average of five determinations.
[b] 60 μg amount of Pb was taken.

*Determination of lead*

To 1 ml of the above solution in a separating funnel, 2 ml each of 4 M lithium chloride and pH 9.0 buffer were added. Iron(III) was masked with 3 ml of 2 M sodium citrate. The volume of the mixture was made up to 10 ml and extracted with 10 ml of a 0.05% reagent solution of PASH for 1 min. After the separation of two layers, the absorbance of the organic phase was measured at 380 nm against a reagent blank. The concentration of lead was determined from the standard curve. The results shown in Table 3 are in good agreement with each other and with those obtained by atomic absorption spectrometer.

### 3.9. Application to analysis of alloys

The proposed method was applied to the determination of lead in solder, brass, leaded gun metal and tin base white metal.

*Dissolution of solder, brass and leaded gun metal*

Alloy (0.01–0.1 g) was dissolved [19] in 5 ml of concentrated nitric acid. The solution was evaporated to dryness to remove excess of acid. The residue was dissolved in 5 M nitric acid, any metastannic acid was filtered off, and the filtrate was washed with hot dilute nitric acid and finally with 10 ml of hot water. The filtrate was diluted to 100 ml with distilled water.

*Dissolution of tin base white metal*

Alloy (0.1 g) was dissolved in 5 ml of 47% hydrobromic acid [19]. The solution was evaporated to dryness, cooled and 3 ml of 25% (v/v) sulphuric acid was added. Again, the mixture was evaporated nearly to dryness. Finally the white mass was dissolved in 4 ml of concentrated hydrochloric acid and diluted to 100 ml with distilled water.

*Determination of lead*

A 1 ml portion of the above prepared solution was taken in a separating funnel, and 2 ml each of 4 M lithium chloride and pH 9.0 buffer were added. To this mixture, 2 ml of a saturated solution of ammonium thiocyanate and sodium tartrate were added to mask the interfering ions. This mixture was diluted to 10 ml and extracted with 10 ml of a 0.05% reagent solution of PASH for 1 min. The two layers were separated and the absorbance of the organic phase was measured at 380 nm against a reagent blank. The concentration of lead was determined from the standard curve. The results are shown in Table 4.

## References

[1] T.W. Gilbert, Jr., in I.M. Kolthoff and P.J. Elving (Eds.), Treatise on Analytical Chemistry, Part II, Vol. 6, Interscience, New York, 1964.

[2] M. Sittig, Toxic Metals — Pollution Control and Worker Protection, Noyes Data Corporation, New Jersey, 1976.
[3] G. Roebisch, Anal. Chim. Acta, 47 (1969) 539.
[4] S.B. Akki and S.M. Khopkar, Bull. Chem. Soc. Jpn., 45 (1972) 167.
[5] Y.K. Agrawal and S.A. Patel, Bull. Soc. Chim. Belg., 88 (1979) 1027.
[6] G.N. Rao and A. Varadarajulu, J. Indian Chem. Soc., 59 (1982) 1009.
[7] C.L. Sethi, B.K. Puri and M. Satake, Microchem. J., 32 (1985) 272.
[8] Y. Sakai and N. Kawano, Talanta, 33 (1986) 407.
[9] F. Salinas, S.J.C. Jimenez and D.T. Galeano, Quim. Anal., 5 (1986) 197.
[10] T. Honjo, A. Okazaki, K. Terada and T. Kiba, Fresenius'. Z. Anal. Chem., 331 (1988) 647.
[11] Z. Zhou and Y. Liang, Yejin Fenxi, 11 (1991) 13.
[12] E.B. Sandell, Colorimetric Determination of Trace Metals, 3rd edn., Interscience, New York, 1959.
[13] M. Garcia-Vargas, M. Gallego and de la Guardia, Analyst, 105 (1980) 965.
[14] M. Garcia-Vargas, Michrochem. J., 27 (1982) 519.
[15] S.H. Sinha and A.D. Sawant, Indian J. Chem., 30A (1991) 641.
[16] S.H. Sinha and A.D. Sawant, Bull. Chem. Soc. Jpn., 65 (1992) 1622.
[17] S.H. Sinha, Doctoral Thesis, Bombay University, India, 1992.
[18] A.I. Vogel, Textbook of Quantitative Inorganic Analysis, 4th edn., English Language Book Society, London, 1978.
[19] N.M, Sundaramurthi and V.M. Shinde, Talanta, 38 (1991) 223.

ELSEVIER

Talanta 42 (1995) 1297–1303

Talanta

# Highly selective and sensitive detection of NADP coenzymes using co-immobilized glucose-6-phosphate dehydrogenase/diaphorase reactors as on-line amplifiers based on substrate recycling in a chemiluminometric flow-injection system

Toshio Yao *, Hirokuni Ogawa, Taketoshi Nakahara

*Department of Applied Chemistry, College of Engineering, University of Osaka Prefecture, 1-1 Gakuen-cho, Sakai, Osaka 593, Japan*

Received 15 December 1994; revised 2 March 1995; accepted 3 March 1995

**Abstract**

Two enzyme reactors prepared by the co-immobilization of two different glucose-6-phosphate dehydrogenases (G6PDH; from *Leuconostoc mescenteroides* (LM) and yeast (Y) and diaphorase are employed to enhance the sensitivity of NAD(P) coenzymes as on-line amplifiers based on substrate recycling in a chemiluminometric flow-injection system. The NAD(P) coenzymes are recycled enzymatically during passage through the reactor in the presence of sufficient glucose-6-phosphate and oxygen in the carrier solution to produce a large amount of hydrogen peroxide, which is detected chemiluminometrically in the subsequent flow line. The G6PDH(LM)/diaphorase co-immobilized reactor is not specific between the NAD and NADP coenzymes, but shows a six fold selectivity towards NADP coenzymes compared to NAD coenzymes; the amplification factors for NAD and NADP coenzymes are 60 and 380, respectively, at a flow rate of 0.3 ml $min^{-1}$. In contrast, the G6PDH(Y)/diaphorase co-immobilized reactor is specific for NADP coenzymes with an amplification factor of about 600 (at a flow rate of 0.3 ml $min^{-1}$). The detection limit is 6 fmol for both $NADP^+$ and NADPH.

*Keywords:* Chemiluminometric flow-injection; Co-immobilization; NADP coenzymes; Substrate recycling

## 1. Introduction

Enzymatic amplification based on substrate recycling is an interesting approach for enhancing sensitivity. The analyte is recycled by choosing a combination of coupled enzymes such that the product of the first enzyme is the substrate of the second. Such an amplification has been accomplished by incorporating a small reactor packed with co-immobilized coupled enzymes into an appropriate flow-injection analysis (FIA) system [1,2]. Considerable amplification has been achieved even with a short residence time of the sample zone in the enzyme reactor. The sensitivities of an on-line detection of L-lactate/pyruvate [3–6], L-glutamate [7], phosphate [8], purine nucleotides [9], adenosine-5′-triphosphate [10] and NAD coenzymes [11–13] have been increased by using the enzyme reactor and substrate recycling.

We are particularly interested in the on-line amplification of nicotinamide coenzymes which are physiologically important coenzymes. Previously [11], we proposed the usefulness of an amperometric FIA system with a glucose-6-phosphate dehydrogenase/lactate dehydro-

* Corresponding author.


*SSDI* 0039-9140(95)01579-5

genase/lactate oxidase co-immobilized reactor for the selective amplification of NAD coenzymes ($NAD^+$: oxi-dized form; NADH: reduced form) compared to NADP coenzymes ($NADP^+$: oxidized form; NADPH: reduced form). Kronkvist et al. [13] described the use of a glycerol dehydrogenase/diaphorase co-immobilized reactor for a similar purpose. However, an enzyme-amplified reactor that functions specifically for NADP coenzymes has not been developed as yet.

This paper describes a chemiluminometric FIA system with a glucose-6-phosphate dehydrogenase (G6PDH)/diaphorase co-immobilized reactor which permitted the selective detection with signal amplification of NADP coenzymes, due to differences in the substrate specifically between two varieties of the enzyme reactor prepared from different commercially available G6PDHs and diaphorase from *Clostridium kluyveri*. Diaphorase from *Clostridium kluyveri* catalyses the oxidation of NADPH to $NADP^+$ to produce hydrogen peroxide, consuming oxygen without a mediator such as hexacyanoferrate(III) [13].

## 2. Experimental

### 2.1. Materials

Distilled water purified with use of a Millipore Milli-Q system (Nippon Millipore Ltd., Tokyo) was used throughout. G6PDH (EC.1.1.1.49; 689 U $mg^{-1}$ from *Leuconostoc mescenteroides* and 468 U $mg^{-1}$ from yeast), diaphorase (EC.1.6.99; 399 U $mg^{-1}$, from *Clostridium kluyveri*), glucose-6-phosphate (G6P), $NAD^+$, NADH, $NADP^+$ and NADPH were purchased from Oriental Yeast (Tokyo) and flavin adenine dinucleotide, disodium salt (FAD), luminol (biochemical grade), potassium hexacyanoferrate(III) and glutaraldehyde were from Wako (Osaka). All other chemicals were of analytical reagent grade and were used as received. Controlled-pore glass (aminopropyl CPG; mean pore size, 527 Å; particle size, 120–200 mesh) was obtained from CPG Inc. (Fairfield, NJ) and was used as a support material for enzyme immobilization. For the determination of chemiluminescence (CL), 7 mM luminol and 200 mM potassium hexacyanoferrate(III) stock solutions were prepared according to a procedure described in the literature [14]. The carbonate buffers were prepared from sodium hydrogen carbonate.

### 2.2. Preparation of immobilized enzyme reactors

Aminopropyl CPG was packed into three glass columns (18 mm × 3 mm i.d.) furnished with small nylon nets (300 mesh) at each end. They were activated by circulating glutaraldehyde solution into the glass beads as previously described [15]. After washing with 0.1 M sodium carbonate buffer (pH 8.0), diaphorase (260 U) was loaded onto the column by circulating enzyme/sodium carbonate buffer solution (0.1 M; pH 8.0) through the column at 1.0 ml $min^{-1}$ for 2 h at room temperature. G6PDH from *Leuconostoc mescenteroides* (G6PDH(LM); 620 U) and diaphorase (260 U) were also co-loaded onto another column, and G6PDH from yeast (G6PDH(Y); 420 U) and diaphorase (260 U) were loaded onto the other column according to the same procedure. The weight ratio of coupled enzymes in the enzyme solution used for the preparation of the latter two reactors was 3:2 (G6PDH:diaphorase). This ratio was suitable for the substrate recycling experiments. When not in use, all the enzyme reactors were stored in 0.1 M sodium carbonate buffer (pH 7.5) in a refrigerator at 4 °C to minimize microbiological degeneration.

### 2.3. Apparatus and procedures

The FIA manifold used is outlined in Fig. 1. The reciprocating pump used was a multichannel Sanuki Kogyo (Tokyo) 4P3U model. A microsyringe was used to introduce the sample solution (20 µl) into an injector (Rheodyne model 7125) with a 100 µl loop, in the carrier stream (0.1 M sodium carbonate buffer, pH 8.0, containing 20 µM FAD and 1 mM G6P) pumped at a flow rate of 0.3 ml $min^{-1}$. The

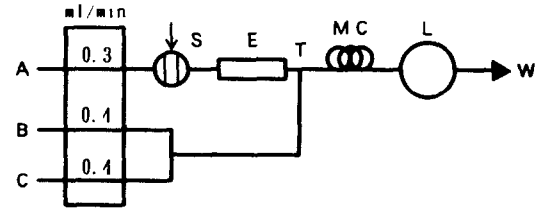


Fig. 1. Otimized chemiluminometric FIA manifold for the determination of NAD(P) coenzymes: A, carrier solution (0.1 M sodium carbonate buffer, pH 8.0); B, luminol solution (0.05 mM); C, potassium hexacyanoferrate(III) solution (50 mM); S, injector (20 µl); E, enzyme reactor; T, T-connector; MC, mixing coil (PTFE, 20 cm × 0.5 mm i.d.); L, luminometer; W, waste.

injected sample passed through the enzyme reactor inserted in the line as shown, where the substrate was oxidized by dissolved oxygen to form the product and hydrogen peroxide. After mixing at a confluence T with a mixed confluent of 0.05 mM luminol and 50 mM hexacyanoferrate(III) solutions pumped at 0.4 ml $min^{-1}$, respectively, the enzymatically generated hydrogen peroxide was detected as the intensity of light emitted in a luminol chemiluminescent reaction. The light intensity was measured with a luminometer (Yanagimoto, Kyoto) equipped with a 100 µl flow-through cell, which was directly attached to the photomultiplier tube operated at −700 V.

## 3. Results and discussion

### 3.1. System without amplification

Diaphorase is an enzyme that is most frequently employed for NADH (or NADPH) oxidation, but the presence of an acceptor, such as hexacyanoferrate(III), is required, as is shown in Eq. (1):

$$\text{NAD(P)H} + \text{acceptor} \xrightarrow{\text{diaphorase}} \text{NAD(P)}^+ + \text{reduced acceptor} \quad (1)$$

In the preliminary experiments, however, the enzyme reactor prepared by immobilizing diaphorase from *Clostridium kluyveri* was found to catalyse the subsequent reaction (Eq. (2)) incorporating an oxygen molecule as the acceptor:

$$\text{NAD(P)H} + \text{O}_2 \xrightarrow{\text{diaphorase}} \text{NAD(P)}^+ + \text{H}_2\text{O}_2 \quad (2)$$

However, repeated injections of NADH solution ($10^{-4}$ M; 20 µl) led to a gradual decrease in the response. This decrease was restored by passing 20 µM FAD solution through the enzyme reactor. This probably indicates that the activity of immobilized diaphorase decreases by releasing FAD from an active centre of the enzyme during the course of the reaction (Eq. (2)). Phosphate buffers (0.1 M) containing 20 µM FAD at various pH values were tested as the carrier solution. The resulting enzyme activity–pH plots showed a maximum plateau in the pH range 6.0–8.4. At pH values below 5.8 and above 8.6, the response decreased sharply. The conversion efficiency of NADH (or NADPH) to $NAD^+$ (or $NADP^+$) (and hydrogen proxide) was calculated from a comparison of the (CL) signals for NADH (or NADPH) and $H_2O_2$, and was found to be independent of the carrier flow rate and about 100% at every flow rate (0.3–1.5 ml $min^{-1}$) at room temperature.

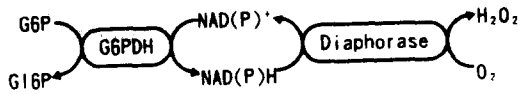


Fig. 2. Enzymatic recycling model of $NAD(P)^+$ and NAD(P)H in the co-immobilized glucose-6-phosphate dehydrogenase (G6PDH)/diaphorase reactor: G6P, glucose-6-phosphate; Gl6P, gluconolactone-6-phosphate.

In this system, NADH and NADPH gave nearly equal CL signals, because the diaphorase-immobilized reactor was not selective between the two coenzymes (NADH or NADPH). When 0.1 M phosphate buffer (pH 7.0) containing 20 µM FAD was pumped at a flow rate of 0.3 ml $min^{-1}$ as a carrier solution, the calibration graph for the CL signal was linear over the range $(1 \times 10^{-6})$–$(5 \times 10^{-4})$ M NADH. The calibration graph obtained for NADPH was essentially the same over the entire concentration range. The linear correlation coefficient was 0.998 ($n = 7$) for both graphs. The detection limit was $5 \times 10^{-7}$ M for both coenzymes (corresponding to 10 pmol).

### 3.2. System with amplification

Diaphorase is not specific between NADH and NADPH, while G6PDHs from two sources, *Leuconostoc mescenteroides* (LM) and yeast (Y), exhibited a difference in the reaction specificity for the coenzymes; the G6PDH(LM) is not specific between the coenzymes ($NAD^+$ and $NADP^+$) and G6PDH(Y) is specific for $NADP^+$. Two enzyme reactors prepared by co-immobilizing G6PDHs from different sources and diaphorase were tested for the amplification of NAD(P) coenzyme detection. The operating principle of the enzyme reactors used for the substrate recycling is shown schematically in Fig. 2. On passage through the enzyme reactor, the coupled enzymes (G6PDH and diaphorase) permit the recycling of NAD(P) coenzymes in the presence of G6P and oxygen in the carrier solution. Thus, the coenzymes are shuttled between the reduced and oxidized forms producing one molecule of hydrogen peroxide and gluconolactone-6-phosphate in each cycle. As a result, for every coenzyme molecule, a number of oxygen molecules are converted to form a large

Table 1
Optimization of variables for use in enzyme reactors

| Variable | Range studied | Enzyme reactor | |
|---|---|---|---|
| | | G6PDH(LM)/diaphorase[a] | G6PDH(Y)/diaphorase[b] |
| Chemical | | | |
| Buffer | Four kinds[c] | Carbonate (0.1 M) | Carbonate (0.1 M) |
| pH | 7.5–9.5 | 8.0 | 8.0 |
| G6P (mM) | 0.1–2.5 | 2.0 | 2.0 |
| NaCl (M) | 0.1–0.7 | 0.5 | 0.5 |
| FAD (μM) | 5–50 | 20 | 20 |
| Physical | | | |
| Reactor temperature (°C) | 16–42 | 32–37 | Above 42[d] |
| Flow rate (ml $min^{-1}$) | 0.2–1.0 | 0.3 | 0.3 |

[a] Glucose-6-phosphate dehydrogenase (from *Leuconostoc mescenteroides*)/diaphorase co-immobilized reactor.
[b] Glucose-6-phosphate dehydrogenase (from yeast)/diaphorase co-immobilized reactor.
[c] 0.1 M phosphate, carbonate, Tris–HCl and borate buffers.
[d] Sensitivity increases with the increase of temperature.

amount of hydrogen peroxide, which can be detected chemiluminometrically (Fig. 1).

Experiments were conducted to establish the optimum experimental conditions for the amplification and to evaluate the differences in the reaction specificity between the two enzyme reactors. Table 1 shows the range over which each variable was studied and the determined optimal values.

Four types of buffer (0.1 M; pH 8.0; phosphate, carbonate, Tris–HCl, and borate) containing 2 mM G6P and 20 μM FAD, were tested as the carrier solution, and were pumped at a constant flow rate of 0.5 ml $min^{-1}$ through the co-immobilized G6PDH(LM)/diaphorase reactor. A sodium carbonate buffer was used as the carrier solution as it provides the greatest signal for the amplification of NADH. The borate buffer greatly inhibited the G6PDH-catalysed reaction, while Tris–HCl buffer inhibited the chemiluminometric reaction of hydrogen peroxide (the sensitivity to hydrogen peroxide was approximately half of that in the carbonate buffer).

When 0.1 M carbonate buffer containing 2 mM G6P and 20 μM FAD was used as the carrier solution, the G6PDH(LM)/diaphorase reactor gave an amplified peak-shaped signal for NADH and $NAD^+$, but the G6PDH(Y)/diaphorase reactor produced no response for the same NAD coenzymes. Furthermore, both enzyme reactors gave a small broad signal for the NADP coenzymes (Fig. 3). However, the shape of the signal varied from a rounded to a sharp peak after the addition of NaCl to the carrier solution (Fig. 3). This is probably due to the ionic interactions between the NADP coenzyme and the CPG particles. As the NaCl concentration in the carrier was increased from 0 to 0.5 M, the sensitivity to NADP coenzymes was increased, but the increase was only slight at the higher concentration.

Without G6P in the carrier solution, only a negligibly small signal for NADPH was observed, with no signal for $NADP^+$ upon the

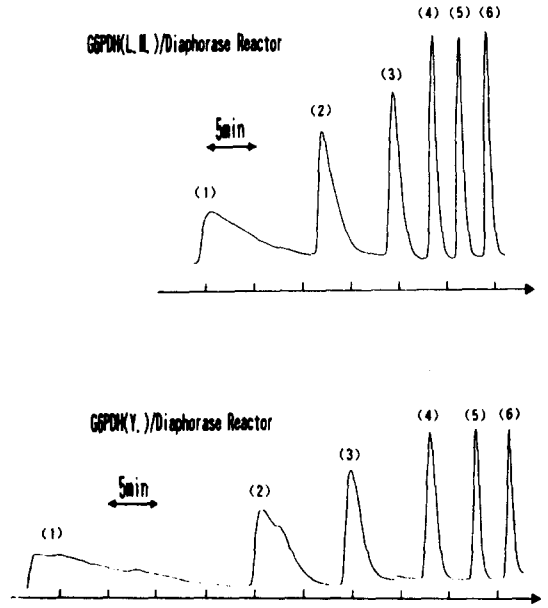


Fig. 3. Effect of NaCl addition to the carrier solution on the chemiluminescent signal for $NADP^+$. NaCl concentration: peak(1), 0; peak (2), 0.1 M; peak (3), 0.2 M; peak (4), 0.3 M; peak (5), 0.4 M; peak (6), 0.5 M. A 20 μl aliquot of $10^{-6}$ M $NADP^+$ solution was injected into the carrier stream (0.1 M carbonate buffer, pH 8.0, containing 2 mM G6P, 20 μM FAD and a variety of NaCl concentrations) pumped at 0.3 ml $min^{-1}$.

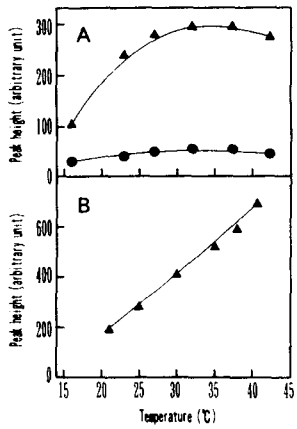


Fig. 4. Effect of reactor temperature on substrate amplification in the FIA system with (A) the G6PDH(LM)/diaphorase reactor and (B) the G6PDH(Y)/diaphorase reactor: amplified response for a 20 µl injection of $5 \times 10^{-7}$ M $NAD^+$ (●) and $5 \times 10^{-7}$ M $NADP^+$ (▲).

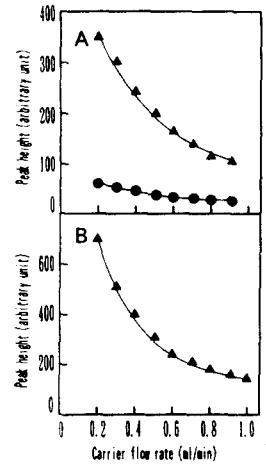


Fig. 5. Effect of carrier flow rate on substrate amplification in the FIA system with the G6PDH(LM)/diaphorase reactor (A) and the G6PDH(Y)/diaphorase reactor (B): amplified response for a 20 µl injection of $5 \times 10^{-7}$ M $NAD^+$ (●) and $5 \times 10^{-7}$ M $NADP^+$ (▲).

use of both enzyme reactors. When the G6P concentration in the carrier was increased from 0 to 2 mM, the sensitivity to NADPH was increased 380 times and 600 times, respectively, for the G6PDH(LM)/diaphorase and G6PDH(Y)/diaphorase reactors. This indicates that the recycling of $NADP^+$ and NADPH occurs effectively between the coupled enzymes in the presence of G6P because oxygen is dissolved in the carrier solution. However, the increase was only slight at higher concentrations of G6P, probably because of limited oxygen in the solution.

A 20 µM concentration of FAD in the carrier solution was selected as it provided reproducible signals for $NADP^+$ and NADPH after repeated injections.

The effect of the pH of the carrier solution (0.1 M sodium carbonate buffer containing 2 mM G6P, 20 µM FAD and 0.5 M NaCl) was investigated next. Maximum response for $NADP^+$ and NADPH was obtained at pH 8.0–8.5 for both enzyme reactors. At pH values below 7.5 and above 9.0, the response decreased sharply, probably because of the decrease in activity of immobilized G6PDHs. Therefore, 0.1 M sodium carbonate buffer (pH 8.0) containing 2 mM G6P, 20 µM FAD and 0.5 M NaCl was selected as the optimum carrier solution for both enzyme reactors.

The temperature of the enzyme reactors was increased by immersing them in a thermostatted water bath. Fig. 4A shows the effect of reactor temperature on the amplified response to $NAD^+$ and $NADP^+$ in the system with a G6PDH(LM)/diaphorase reactor; the maximum response was obtained at 32–37 °C and at higher temperature the response decreased gradually, probably because of a decrease in the activity of the G6PDH(LM). However, in the system with the G6PDH(Y)/diaphorase reactor (Fig. 4B), the amplified response to $NADP^+$ increased with an increase of the temperature up to 42 °C. This difference may be attributed to the thermostability of immobilized G6PDH(Y) compared with immobilized G6PDH(LM).

The carrier flow rate is related to the residence time of the sample zone in the reactor (i.e. the turnover numbers of recycling) and, therefore, the signal intensity increased with

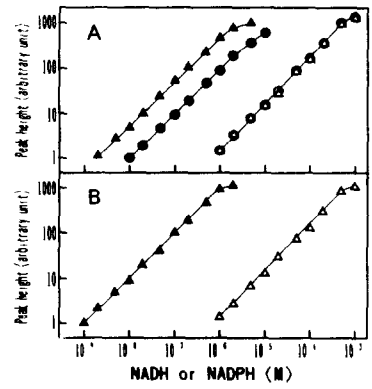


Fig. 6. Calibration graphs for NAD(P)H coenzymes obtained by FIA with the G6PDH(LM)/diaphorase reactor (A) and the G6PDH(Y)/diaphorase reactor (B): ○ and △, no amplified response for NADH and NADPH, respectively; ● and ▲, amplified response for NADH and NADPH, respectively. (Injection volume, 20 µl.)

decreasing flow rate (Fig. 5). Fig. 6 shows the calibration graphs for coenzymes with and without G6P in the carrier solution at a flow rate of 0.3 ml $min^{-1}$. When the G6PDH(LM)/diaphorase reactor was used (Fig. 6A) without G6P in the carrier solution, the response depended linearly on the NADH concentration up to $5 \times 10^{-4}$ M, and the detection limit was $5 \times 10^{-7}$ M; the linear correlation coefficient was 0.999 ($n = 7$). In contrast, the presence of 2 mM G6P in the same carrier solution resulted in a greatly increased signal. The calibration graphs for the amplified response were linear over the range $10^{-8}$–$5 \times 10^{-6}$ M NADH and $2 \times 10^{-9}$–$10^{-6}$ M NADPH; the correlation coefficients were 0.998 for NADH and 0.999 for NADPH, respectively. The detection limit was $8 \times 10^{-9}$ M for NADPH (corresponding to 160 fmol and 12 fmol, respectively). The cycle could also be initiated with $NAD^+$ and $NADP^+$, and so the calibration graphs obtained for them were essentially the same over the entire concentration range as those for NADH and NADPH, respectively. Similarly, in the system with the G6PDH(Y)/diaphorase reactor, the calibraiton graphs were amplified greatly for $NADP^+$ and NADPH over the range $10^{-9}$–$10^{-6}$ M; the calibration graphs for two NADP coenzymes were essentially the same, and were linear with a correlation coefficient of 0.999 ($n = 9$). The detection limit was $3 \times 10^{-10}$ M for both coenzymes (corresponding to 6 fmol). In this system NADH and $NAD^+$ gave no signal, because the G6PDH(Y) used was specific for $NADP^+$. Therefore, this system is useful for the highly sensitive detection of the $NADP^+$ and NADPH pair.

The reproducibility of the measurements was tested by repeated injections ($n = 10$) of $10^{-7}$ M $NADP^+$ and NADPH. The relative standard deviations were 1.5–2.3% for the systems with the two different reactors.

The immobilized enzyme reactors were used repeatedly to confirm the instability with time; even after repetitive use (about 10 samples per day) for 2 months, the enzyme reactors retained over 95% of their original activities.

## 4. Conclusions

A FIA approach with an immobilized enzyme reactor involving amplification by substrate recycling is very attractive with respect to the enhancement of the sensitivity for the selective detection of substrate in the nanomolar to micromolar range. The amplification of nico-tinamide coenzymes is particularly important, because they furnish the redox driving force for many dehydrogenase-catalysed reactions and are frequently used as substrates in enzyme immunoassays. This work demonstrated the usefulness of two enzyme reactors prepared by co-immobilizing two different commercially available G6PDHs and diaphorase for *Clostridium kluyveri* in order to increase greatly the sensitivity of NAD(P) coenzymes by substrate recycling. In particular, the G6PDH(Y)/diaphorase coimmobilized reactor was specific for NADP coenzymes with an amplification factor of about 600 (at a flow rate of 0.3 ml $min^{-1}$) in the determination of $NADP^+$ and NADPH. The difference in the specificity obtained by the combination of the coupled enzymes is very attractive for the specific detection of NAD(P) coenzymes. However, the proposed FIA system was not specific between the oxidized and reduced forms of NAD(P) coenzymes, because the cycle was initiated with each of them. This disadvantage can be overcome by using this amplified FIA system as a postcolumn detector for liquid chromatography. Also, the FIA system with the G6PDH(Y)/diaphorase coimmobilized reactor should prove useful as a highly sensitive detection system for enzyme immunoassays when using alkaline phosphatase as a label and $NADP^+$ (or NADPH) as the substrate.

## References

[1] F. Scheller and F. Schubert, Biosensors, Elsevier, Amsterdam, 1992.
[2] T. Yao, J. Flow Injection Anal., 9 (1992) 2.
[3] F. Scheller, N. Siegbahn, B. Danielsson and K. Mosback, Anal. Chem., 57 (1985) 1740.
[4] M.U. Asouzu, W.K. Nonidez and M.H. Ho, Anal. Chem., 62 (1990) 708.
[5] T. Yao, N. Kobayashi and T. Wasa, Electroanalysis, 3 (1991) 493.
[6] E.H. Hansen, L. Norgaard and M. Pedersen, Talanta, 38 (1991) 275.
[7] T. Yao, N. Kobayashi and T. Wasa, Electroanalysis, 2 (1990) 563.
[8] T. Yao, N. Kobayashi and T. Wasa, Anal. Chim. Acta, 238 (1990) 339.
[9] T. Yao and K. Tsureyama, Electroanalysis, 6 (1994) 165.

[10] D. Kirstein, B. Danielsson, F. Scheller and K. Mosback, Proc. 4th Eur. Congr. Biotechnol., Elsevier, Amsterdam, 1987, p. 215.
[11] Y. Yao, N. Kobayashi and T. Wasa, Anal. Chim. Acta, 248 (1991) 345.
[12] A.M. Almuiabed and A. Townshend, Anal. Proc., 26 (1989) 56.
[13] K. Kronkvist, K. Wallentin and G. Johansson, Anal. Chim. Acta, 290 (1994) 335.
[14] M. Tabata, C. Fukunaga, M. Ohyabu and T. Murachi, J. Appl. Biochem., 6 (1984) 251.
[15] T. Yao, M. Satomura and T. Nakahara, Anal. Chim. Acta, 296 (1994) 271.

ELSEVIER

Talanta 42 (1995) 1305–1324

Talanta

# A multivariate chemometric approach to fluorescence spectroscopy

Lars Nørgaard

*Royal Veterinary and Agricultural University, Department of Dairy and Food Science, Food Technology, Thorvaldsensvej 40, DK-1871 Frederiksberg, Denmark*

Received 29 December 1994; revised 7 March 1995; accepted 10 March 1995

**Abstract**

A multivariate approach to the solution of problems often encountered in the spectrofluorometry of natural samples, utilising information from whole spectra is presented. (a) Piecewise direct standardisation is implemented and employed to transfer emission spectra measured with two different xenon lamps of different ages as if the spectra were measured with the same lamp. (b) It has been shown using a multivariate analysis approach that it is possible to use the raw data points instead of the smoothed data based on an algorithm included in the instrument software by the manufacturer. (c) It is documented that Raman scattering does not hamper the performance of multivariate calibration; on the contrary, in an experiment with sugar samples the concentration prediction errors become about five times lower by including the whole emission spectrum in the analysis instead of using a univariate calibration based on an emission wavelength that only reflects the analyte of interest. (d) An algorithm for variable selection is implemented and employed in the selection of optimal excitation wavelengths. Among 13 emission spectra recorded for a sugar sample at different excitation wavelengths, four of these are chosen that describe 98.51% of the total variance in the original data. (e) Finally the combination of fluorescence spectroscopy and multivariate calibration with conventional chemical data according to the near-infrared black box model is presented. The refined sugar quality parameter, the ash content and the fluorescence emission spectra are correlated by a partial least-squares regression model. Five experiments employing different monochromator slit widths and sugar concentrations are performed, and the best correlation obtained by full cross-validation of the 15 sugar samples is $R = 0.98$.

## 1. Introduction

Fluorescence spectroscopy has been used for decades as a powerful analytical tool in all sorts of chemical, biochemical, food and environmental laboratories due to its two principal properties: excellent sensitivity and specificity. The use of fluorescence excitation and emission spectra has so far mostly been qualitative, with the purpose of finding a pair of excitation–emission wavelengths where the analyte of interest is the only chemical component giving rise to the recorded signals [1,2].

On searching the literature, very few papers are encountered dealing with the application of multivariate chemometric methods in fluorescence spectroscopy. This seems especially striking bearing in mind the enormous number of publications using chemometrics in combination with traditional spectroscopic techniques like near-infrared (NIR) spectroscopy [3–6]. In the majority of the papers dealing with fluorescence spectroscopy and chemometrics, only synthetic samples or natural samples containing very few chemical species are analysed with the aim of resolving a measured excitation–emission matrix (EEM) into pure excitation and emission spectra of the chemical components in the samples, and with the aim of


*SSDI* 0039-9140(95)01586-8

predicting analyte concentrations by rank annihilation methods [7–12]. When the number of signal-producing chemical components in a sample becomes larger than 5–6 it is very difficult to perform this resolution within acceptable limits of accuracy and precision [9].

In studies by Lindberg et al. [13] and Sjöström et al. [14] concentrations of two- and three-component synthetic mixtures are successfully predicted from fluorescence emission spectra by the method of partial least-squares regression. In Refs. [15–18] fluorescence spectroscopy in combination with partial least-squares regression is used for predicting botanical tissue components of complex wheat flour samples. The latter example is analogous to the widespread use of multivariate calibration in NIR spectroscopy [3–6], and illustrates how the chemical information for "dirty" natural samples can be enhanced by fluorescence spectroscopy in combination with multivariate statistical methods.

In this paper, the focus is on the analysis of spectra from refined sugar samples in order to investigate different intrinsic instrumental parameters as well as the combination of fluorescence spectroscopy of given samples and multivariate calibration. The study both serves as a general investigation of how to enhance the potential of fluorescence spectroscopy by chemometrics as well as a special investigation of how fluorescence spectroscopy of sugar samples can be approached in a multivariate sense. Sugar samples are real samples and all topics treated reflect the problems of measuring fluorescence spectra on real samples.

Refined sugar is a very pure foodstuff containing only small concentrations of impurities (below 1%). These impurities, such as phenolic compounds, amino acids, melanoidins, and melanins [19], stem from the sugar beet delivered to the sugar factory superimposed the chemical compounds produced at the individual unit operations of the factory. It is the long-term purpose of the project, of which this publication is a part, to use fluorescence spectroscopy for the on-line prediction of (a) refined sugar quality [20] and (b) optimal adjustment of process parameters. The fluorescence measured is autofluorescence (or primary fluorescence), i.e. the native fluorescence of the impurities in the dissolved sugar sample. The beauty of this approach rests in the fact that nature and processing combined respond with a multivariate fluorescent fingerprint [21].

Using several examples, the potential of multivariate analysis in fluorescence spectroscopy will be demonstrated. The topics addressed are as follows.

(i) Transferring spectra between different instrumental set-ups. Spectrofluorimeters are all different due to differences in lamps, monochromators and photomultipliers [2]. When analysing large sample sets, which is the case in on-line/at-line process applications, it is essential in the case of instrument break-down to be able to compare samples measured with different set-ups or even on different instruments. It is outlined how this problem can be solved by the piecewise direct standardisation algorithm originally developed for the standardisation of NIR instruments [22–24].

(ii) Smoothing of spectral data. The spectrofluorimeter employed for analysis automatically smooths the measured emission spectra. Raw data will be compared to data smoothed with binomial and Savitzky-Golay smoothing algorithms.

(iii) Raman scattering. This often overlaps the analyte emission spectra. The classical way of circumventing the problem of Raman scattering is to employ suitable filters [25] (if available), to subtract a blank emission spectrum from all the samples [25], or to change the excitation wavelength [25]. An example will be given of how multivariate methods are capable of overcoming the problem of the Raman scattering peaks by including whole emission spectra in the mathematical analysis.

(iv) Selection of wavelengths. The measurement of fluorescence emission spectra at a large number of excitation wavelengths is a time-consuming operation. It will be demonstrated how the principal variable algorithm [26] chooses a small but optimal number of excitation wavelengths describing the main variations in the excitation–emission data matrix. The wavelength selection is especially important in the multivariate calibration of large sample sets as well as for fast on-line prediction of analyte concentrations in future samples.

(v) Multivariate calibration. Multivariate calibration [27] of the sugar quality parameter ash content in refined sugar samples is performed. Experiments with different excitation monochromator and emission monchromator slit widths and sugar concentrations are performed in order to investigate their influence on the multivariate calibration models. The influence of pH and the use of corrected/not

corrected emission spectra in connection with multivariate modelling will be touched on.

## 2. Materials and methods

### 2.1. Instrumentation

All experiments are performed on a Perkin–Elmer LS 50B spectrometer. The computer controlling the instrument through an RS232C interface is an IBM-compatible 486/50 MHz PC. Uncorrected fluorescence spectra samples with 0.5 nm intervals are recorded in all experiments.

### 2.2. Programs

Calculations are performed with Matlab for Windows version 4.2c.1 (MathWorks, Inc.) and Unscrambler version 5.5 (CAMO A/S). A chemometric toolbox made by B.M. Wise [28] is used for piecewise direct standardisation. The Perkin-Elmer LS50 FLDM Instrument program (version 4.00) is used for controlling the instrument. Spectral data are converted to ascii files by a program made in the OBEY language furnished by Perkin-Elmer (OBEY, version 3.50). An OBEY program made by S. Huckins, Perkin-Elmer, is applied to obtain the raw fluorescence emission spectra from the instrument.

### 2.3. Measurement conditions

In experiments including several excitation wavelengths, the measurement always starts with the largest excitation wavelength and ends with the lowest excitation wavelength in order to minimise photodecomposition of the sample. This problem needs no further concern as long as each sample in a given experiment is subject to exactly the same measurement cycle. In all experiments the sample holder is thermostatted to 24 °C ± 0.1, which is the average room temperature during a normal working day.

### 2.4. Samples

Double ion exchanged water was used for all sugar solutions and dilutions. There was a high degree of repeatability of the sample measurements (see Figs. 12 and 15). The buffer capacity of refined sugar is extremely low and it is impossible to obtain reliable pH measurements of such samples. In the pH experiment, phosphate buffers with $C = 0.1$ M were prepared from sodium dihydrogen phosphate. The glassware and cuvettes were kept extremely free from contamination by washing with methanol and a 2% Extran solution (Merck). The sample sets analysed are arranged as follows (including relevant instrumental parameters).

(i) Sample set A (Piecewise Direct Standardisation) comprises solid standard blocks nos. 1 (anthracene and naphthalene mixture), 2(ovalene), 3(*p*-terphenyl), 4(tetraphenylbutadiene), and 5(compound 610) from the Perkin-Elmer C 520-7440 standard set, and a refined sugar sample (15.00 g of refined sugar added to 15.00 ml of water); six samples in total. Instrumental parameters were excitation wavelength, 300 nm; emission range recorded, 320–540 nm; excitation monochromator slit width, 5.0 nm; emission monochromator slit width, 5.0 nm; and emission scan velocity, 500 nm $min^{-1}$. The spectra are binomial smoothed (filter factor 9) by the FLDM software.

(ii) Sample set B (smoothing of spectra) comprises standard block 2 (ovalene) from the Perkin-Elmer set. Instrumental parameters were excitation wavelength, 342 nm; emission range recorded, 440–600 nm; excitation monochromator slit width, 3.0 nm; emission monochromator slit width, 5.0 nm; and emission scan velocity, 500 nm $min^{-1}$.

(iii) For sample set C (Raman scattering), a stock solution consisting of 25.00 g of refined sugar added to 50.0 ml of water was prepared. From this stock solution, 10 samples were prepared containing from 0.5 ml to 5.0 ml (with 0.5 ml intervals). All solutions were diluted to 10.0 ml with water, i.e. the concentrations are given as 5.0, 10.0, . . . , 50.0% v/v of the stock solution. A blank solution (water) was prepared. Instrumental parameters were excitation wavelength, 300 nm; emission range recorded, 315–540 nm; excitation monochromator slit width, 8.0 nm; emission monochromator slit width, 5.0 nm; and emission scan velocity, 1000 nm $min^{-1}$. The emission spectra are not smoothed.

(iv) Sample set D (multivariate calibration of fluorescence spectra) was as follows. (I) Fifteen different refined sugar samples consisting of 15.00 g of sugar added to 15.00 ml of $H_2O$ (approximately 50% (w/w)). (II) Each sample in sample set 1 was diluted 1:1 (10.00 ml of sugar solution added to 10.00 ml of $H_2O$). (III) The same original 15 sugar samples but with

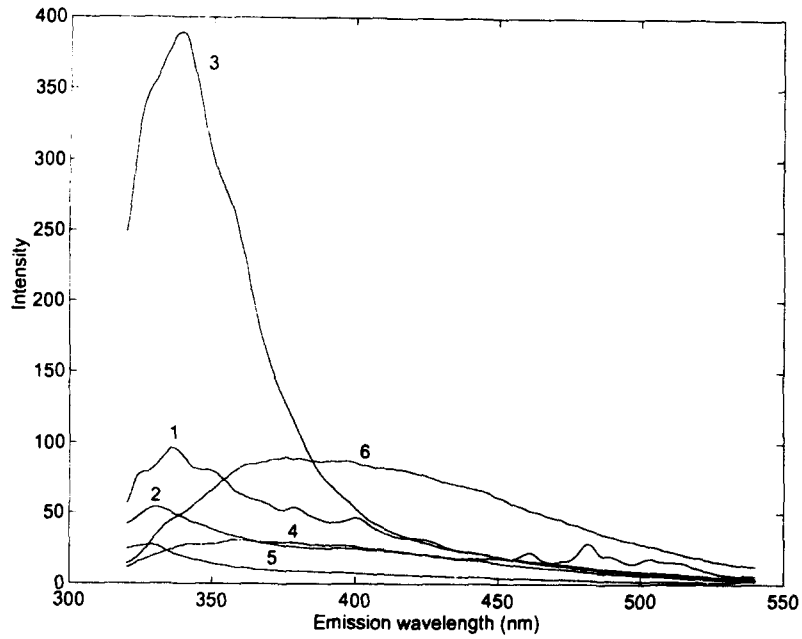


Fig. 1. Emission spectra of the 6 samples used in piecewise direct standardisation measured with lamp 1 mounted. The numbers correspond to sample set A.

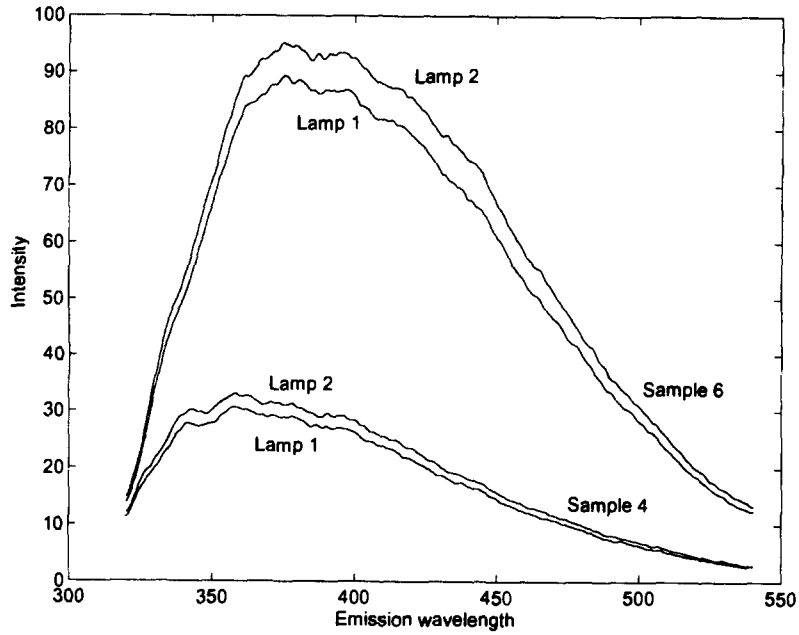


Fig. 2. Emission spectra of samples 4 and 6 measured with two different lamps mounted. Lamp 1 is older than lamp 2.

1.50 g of sugar added to 15.00 ml of $H_2O$ (approximately 10% (w/w)). Instrumental parameters were excitation wavelengths, 230 nm (emission, 245–435 nm), 240 nm (emission, 255–455 nm), 290 nm (emission, 305–555 nm), and 330 nm (emission, 345–635 nm), (1864 data points in total); and emission scan velocity, 1000 nm $min^{-1}$. The emission spectra are not smoothed.

### 2.5. Chemometric methods

The chemometric methods employed are described in detail in the literature, so only a brief description including the relevant literature references will be given here. Nomenclature: capital, italic bold face letters symbolise matrices, small, italic bold letters symbolise vectors and small italic characters are scalars. The number

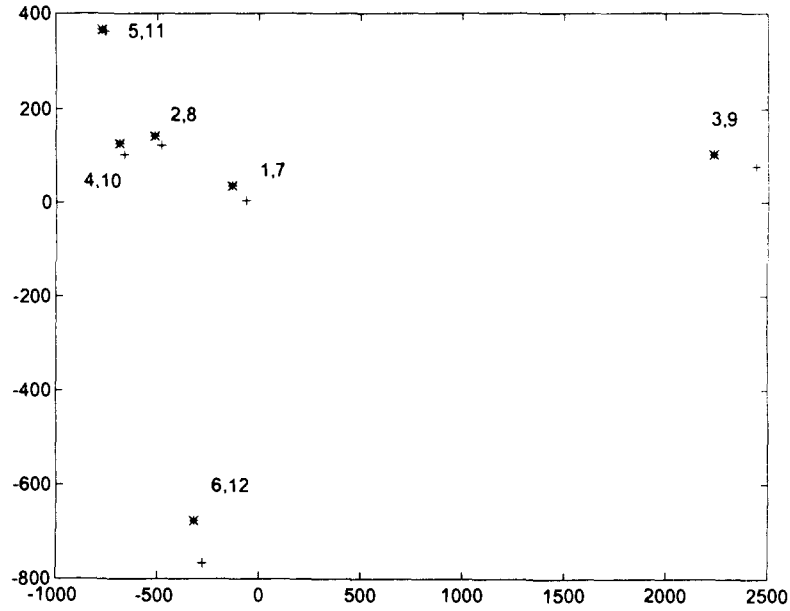


Fig. 3. Score plot (first two PCs) of 12 emission spectra before standardisation. Samples marked * (1–6) are measured with lamp 1 and samples marked + (7–12) are measured with lamp 2. Corresponding pairs of samples are 1, 7; 2, 8; . . . ; 6, 12.

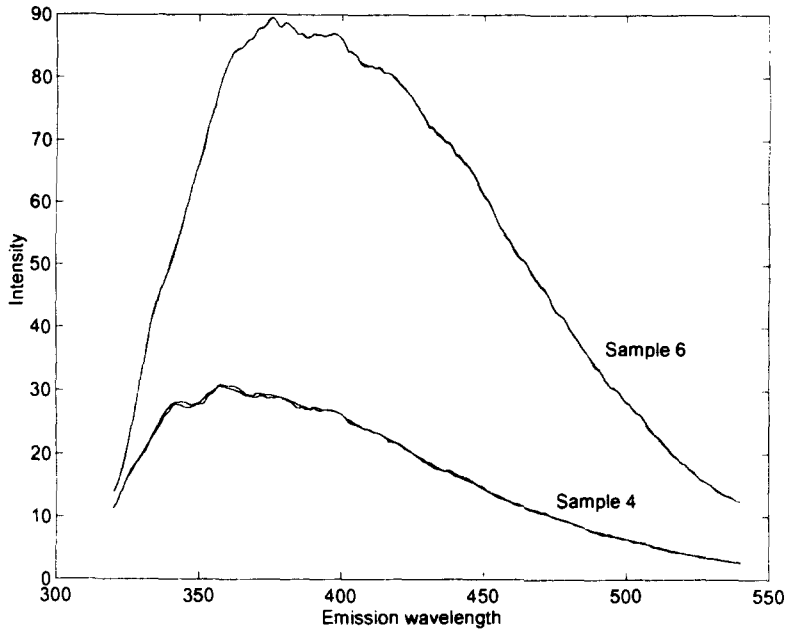


Fig. 4. Emission spectra of samples 4 and 6 measured with lamp 1 and the transformed spectra of the same samples originally measured with lamp 2. The spectral differences after transformation are very small.

of samples, the wavelength, and factors are denoted by $s$, $w$ and $f$, respectively.

*Principal component analysis (PCA)*

Principal component analysis finds the main variation in a multidimensional data set by creating new linear combinations of the raw data [27,29]. In matrix form we have

$$\boldsymbol{X} = \boldsymbol{TP}'$$

where $\boldsymbol{X}$ is the analysed data matrix with dimensions $s \times w$, $\boldsymbol{T}$ is the score matrix with dimensions $s \times min(s, w)$, and $\boldsymbol{P}'$ is the loading matrix with dimensions $w \times min(s, w)$. Only the significant number of principal components (PCs), $f$, equal to the chemical rank of the $\boldsymbol{X}$

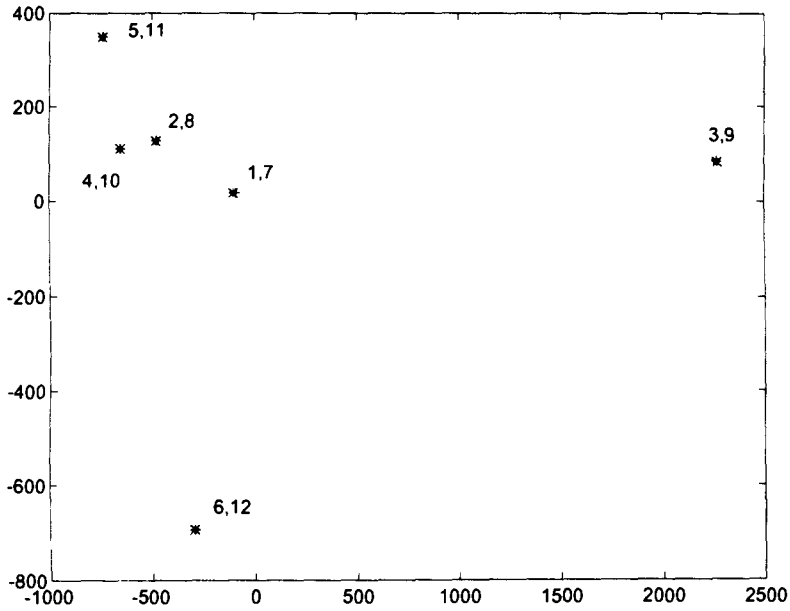


Fig. 5. Score plot (first two PCs) of 12 emission spectra after standardisation. Samples marked * (1–6) are measured with lamp 1 and samples marked + (7–12) originally measured with lamp 2 are transformed as if they were measured with lamp 1. Corresponding pairs of samples are 1, 7; 2, 8; . . . ; 6, 12. Samples 2, 3, and 6 are used as transformation standards.

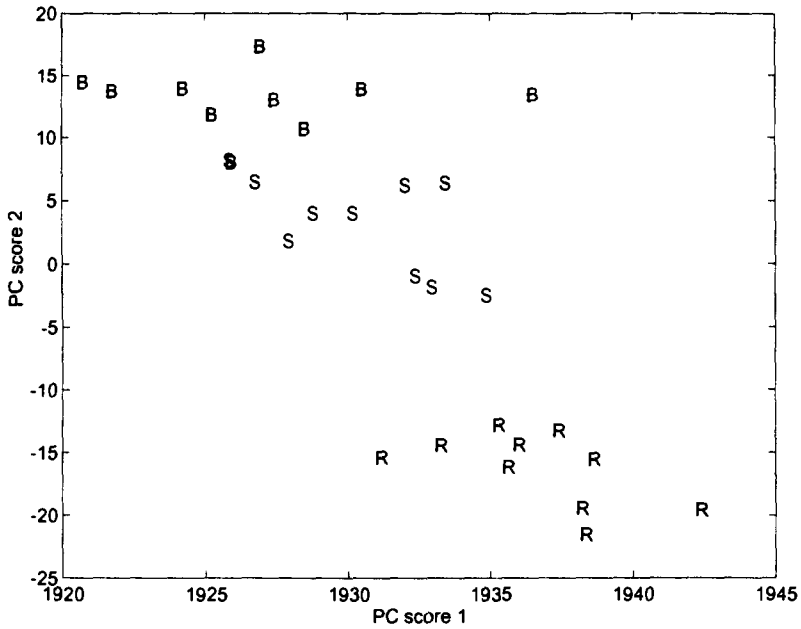


Fig. 6. Score plot (PC1 versus PC2) of 30 emission spectra of standard block 2. Three clusters are observed: binomial (B) smoothed, Savitzky-Golay (S) smoothed and raw (R) data. Two S and B samples are overlapping.

matrix is relevant in describing the information in $X$. This leads to the following decomposition of $X$

$$X = T_f P_f' + E$$

where $T_f$ is the score matrix with dimensions $s \times f$, $P_f$ is the loading matrix with dimensions $w \times f$, and $E$ is a residual matrix with the same dimensions as $X$.

*Partial least-squares regression (PLS)*

The purpose of regression is to build a model between $X$ and $y$, where $X$ (see above) contains the fluorescence spectra and $y$ ($s \times 1$) is a vector containing the property of interest (if several properties have to be modelled, we have a matrix $Y$ with dimensions $s$ multiplied by the number of properties). In principal component regression [27,30] (PCR) a multiple linear re-

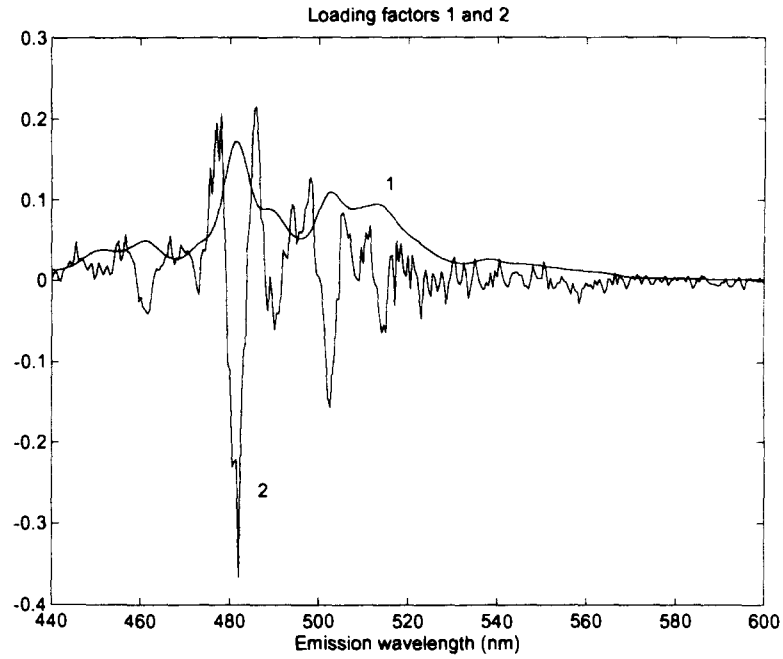


Fig. 7. Loadings from the PCA on 30 emission spectra (smoothed and raw). Loading vector 1 is smooth, while loading vector 2 indicates the spectral differences between the three data types.

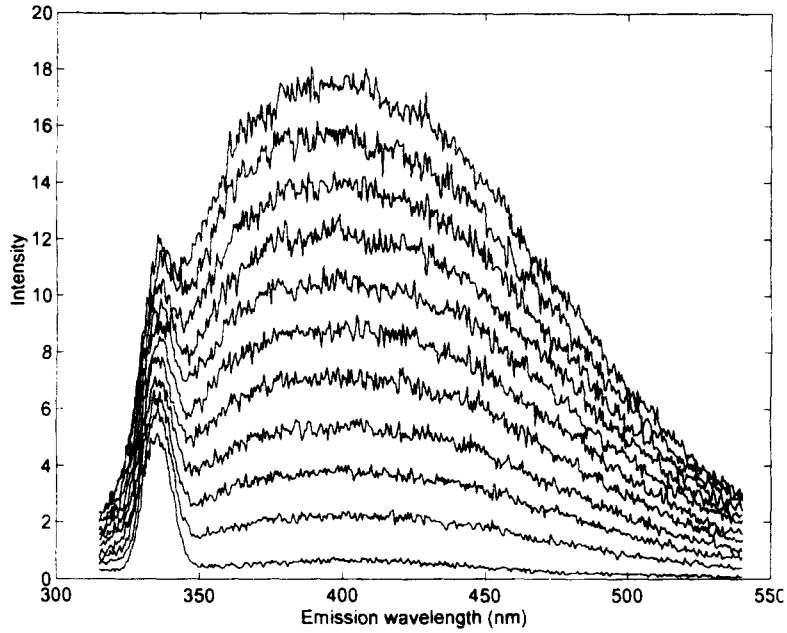


Fig. 8. Emission spectra of 11 samples with different concentrations of the same refined sugar sample (including a blank sample). The Raman scattering overlaps the analyte spectrum in the region around 334 nm.

gression model is built between the significant PCA scores ($T_f$) and $y$. PCR maximises the variance in $X$ followed by a regression to $y$. In partial least squares the significant score values $T_f$ are found in a slightly different way, taking into account the variation in $y$ during the decomposition of $X$, i.e. in PLS the covariance between $X$ and $y$ is maximised [27, 30–33].

The number of factors (principal components or partial least-squares components) to include when applying the above mentioned methods is found by test set validation [27]. In the case of small data sets, cross-validation [27,34] is an alternative way of validating the model performance.

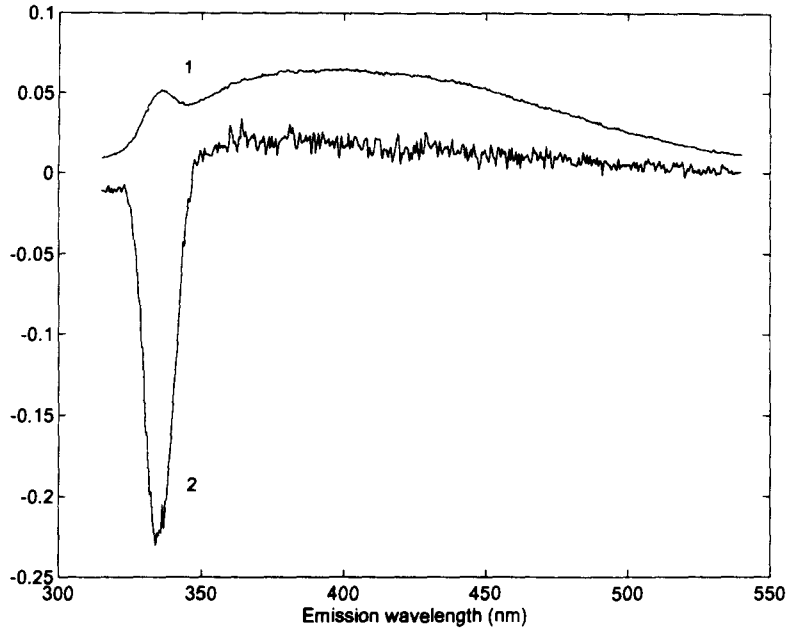


Fig. 9. Loading weights 1 and 2 for the PLS prediction of sugar concentration. The Raman scattering contributes to both loading vectors.

Table 1
Prediction of sugar concentrations
(A) Results of PLS calibration (with and without mean centring) and univariate calibration based on raw data

| | With mean centring RMSEP [a] | $R$ [b] | Without mean centring RMSEP [a] | $R$ [b] |
|---|---|---|---|---|
| One PLS component | 0.017 | 0.9999 | 0.134 | 1.000 |
| Two PLS components | – | – | 0.020 | 0.9999 |
| Univariate calibration | – | – | 0.105 | 0.9988 |

(B) Results of PLS calibration (with and without mean centring) based on Savitzky-Golay smoothing

| | With mean centring RMSEP [a] | $R$ [b] | Without mean centring RMSEP [a] | $R$ [b] |
|---|---|---|---|---|
| One PLS component | 0.025 | 0.9999 | 0.144 | 0.9999 |
| Two PLS components | – | – | 0.029 | 0.9998 |

[a] RMSEP $= \sqrt{\Sigma_{i=1}^{N} (C_i^{\text{predicted}} - C_i^{\text{reference}})^2/N}$, where $C_i^{\text{predicted}}$ is the model estimated concentration, $C_i^{\text{reference}}$ is the reference value and $N$ is the number of samples.
[b] Correlation coefficient.

*Piecewise direct standardisation (PDS)*

Piecewise direct standardisation [22–24] works on two data matrices $\boldsymbol{A}$ and $\boldsymbol{B}$. These matrices contain spectra of the same standards measured under two different instrumental conditions $\boldsymbol{A}$ and $\boldsymbol{B}$ (dimensions are number of standards multiplied by $w$). No data preprocessing is performed prior to the standardisation. A multiple of local multivariate regression models between each spectral point (wavelength) in $\boldsymbol{A}$ and a window of spectral points (including the wavelength chosen in $\boldsymbol{A}$) in $\boldsymbol{B}$ are then built. This yields a banded transfer matrix $\boldsymbol{M}$ ($w \times w$) with a window of non-zero regression elements along the matrix diagonal and zeros elsewhere [22]. In matrix notation, we have

$$\boldsymbol{A} = \boldsymbol{BM}$$

Future measurement of a sample under instrumental condition $B$ can now be transformed as if it were measured under instrumental condition $A$ by

$$\boldsymbol{a}'_{\text{rec}} = \boldsymbol{b}'_{\text{new}}\boldsymbol{M}$$

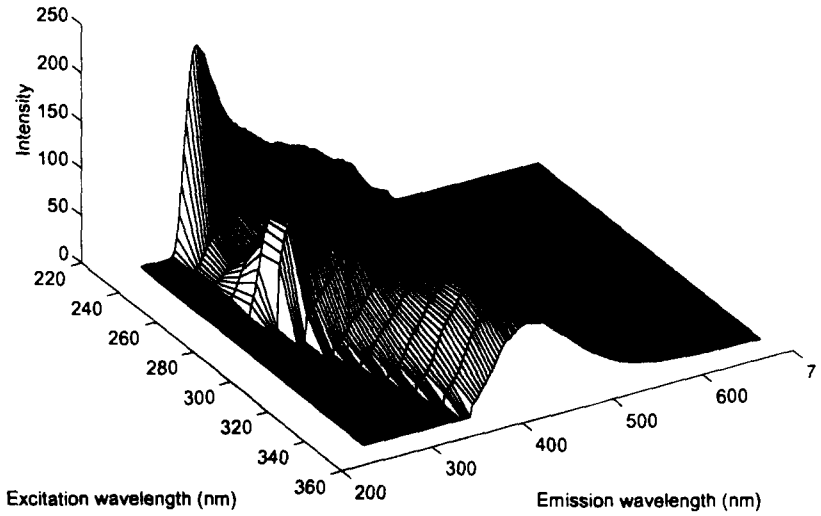


Fig. 10. A three-dimensional plot of an excitation–emission matrix (EEM) measured on a refined sugar sample. (Every 2.5 nm of the emission spectra are used in the plot).

where $b_{new}$ is a column vector containing the measured spectrum and $a_{rec}$ is the reconstructed spectrum. The selection of appropriate standards is important [22].

*Principal variables (PV)*

Assume that we have a matrix $X$ ($s \times w$). The method of principal variables [26] aims at finding few variables (in this case columns corresponding to wavelengths) that describe as much of the total variance in the data matrix as possible. The method is based on finding the largest diagonal value of

$$X'XX'X \quad (1)$$

with the dimension $w \times w$. The wavelength variable indexed by this value is the first principal variable, designated $w$ ($s \times 1$). In the next step $X$ is orthogonalised with respect to the chosen variable

$$k = (X'w)/(w'w) \quad (2)$$

$$X_{new} = X - wk' \quad (3)$$

where $w$ ($s \times 1$) and $k$ ($w \times 1$) are column vectors. The next PVs are found by repeating the procedure from step 1 to 3 with $X_{new}$ found in step 3. The number of PVs to choose depends on the actual problem to be solved. By analysing the matrix $X'yy'X$ instead of $X'XX'X$, the method of principal variables is extendible to deal with the selection of wavelength variables to obtain optimal correlations with properties of interest ($y$ values).

Table 2
Experiments performed to investigate the multivariate calibration of sugar samples with respect to ash content

| | | Sample set [a] | | |
|---|---|---|---|---|
| | | DI | DII | DIII |
| Ex 3.5 | Em 3.5 | Expt. 1 | – | – |
| Ex 8.0 | Em 5.0 | Expt. 2 | Expt. 3 | Expt. 4 |
| Ex 15.0 | Em 20.0 | – | – | Expt. 5 [b] |

[a] Description of the sample sets is given in the text.
[b] Emission ranges are 260–420 nm (ex. 230 nm), 270–440 nm (ex. 240 nm), 320–540 nm (ex. 290 nm), 360–620 nm (ex. 330 nm) (1624 data points in total).

## 3. Results and discussion

### 3.1. Piecewise direct standardisation

When using multivariate methods including many calibration samples, it is very important to be able to transfer spectra between different instrumental set-ups (lamps, slit widths, scan velocities) of the same spectrofluorimeter and, if necessary, between different instruments. Furthermore, the xenon lamp in the spectrofluorimeter also needs continuous standardisation due to a change of spectral characteristics during ageing. If, by accident, for example, the lamp breaks down after the measurement of 100 calibration samples, it is of the utmost importance to be able to use the calibration models based on these samples for the concentration prediction of samples measured with a new lamp with other spectral characteristics.

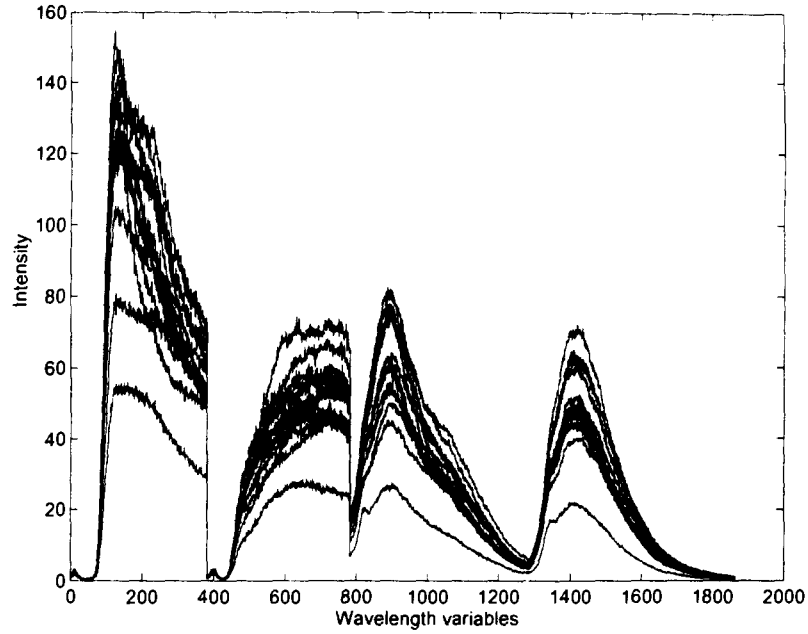


Fig. 11. Concatenated emission spectra of 15 different sugar samples (experiment 3, sample set DII) measured at four excitation wavelengths (230, 240, 290 and 330 nm). Emission variables 1–381 correspond to 245–435 nm; variables 382–782 correspond to 255–455 nm, variables 783–1283 correspond to 305–555 nm, variables 1284–1864 correspond to 345–635 nm.

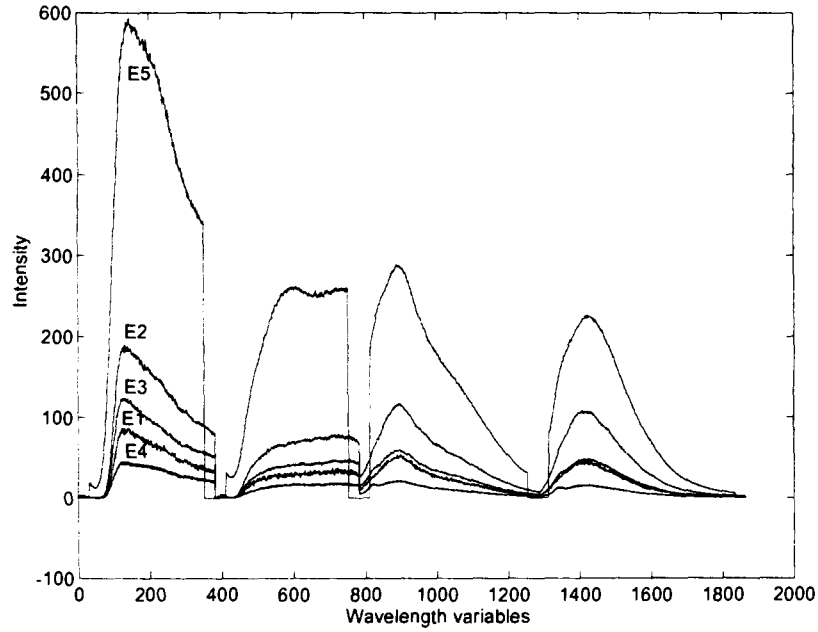


Fig. 12. Concatenated emission spectra of sugar sample 4 from experiments 1–5 (E1–E5). A replicate made in experiment 4 is included to illustrate the small replicate and measurement variation.

In order to make a preliminary investigation of the potential of using piecewise direct standardisation (PDS) on the fluorescence spectra, two experiments were performed with the same fluorescence spectrometer. In the first experiment, six samples (sample set A) are measured with xenon lamp 1 (old) mounted on the apparatus, while in the second experiment the samples are measured with xenon lamp 2 (new) fitted. The raw fluorescence emission spectra of all six samples measured with excitation at 300 nm and with xenon lamp 1 are shown in Fig. 1. In Fig. 2 the emission spectra of samples 4 and 6 measured with both lamps are shown. A distinct difference between the spectra is observed and principal component analy-

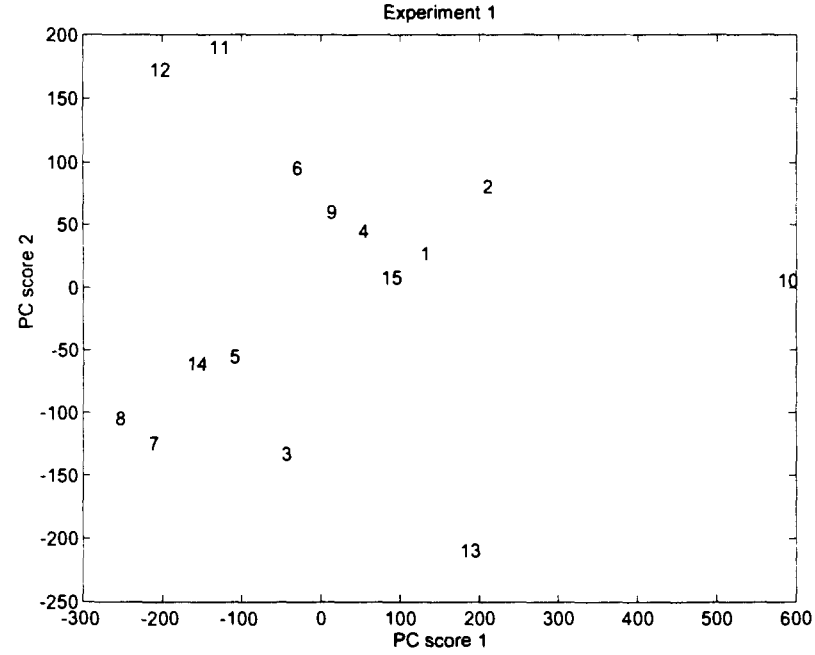


(a)

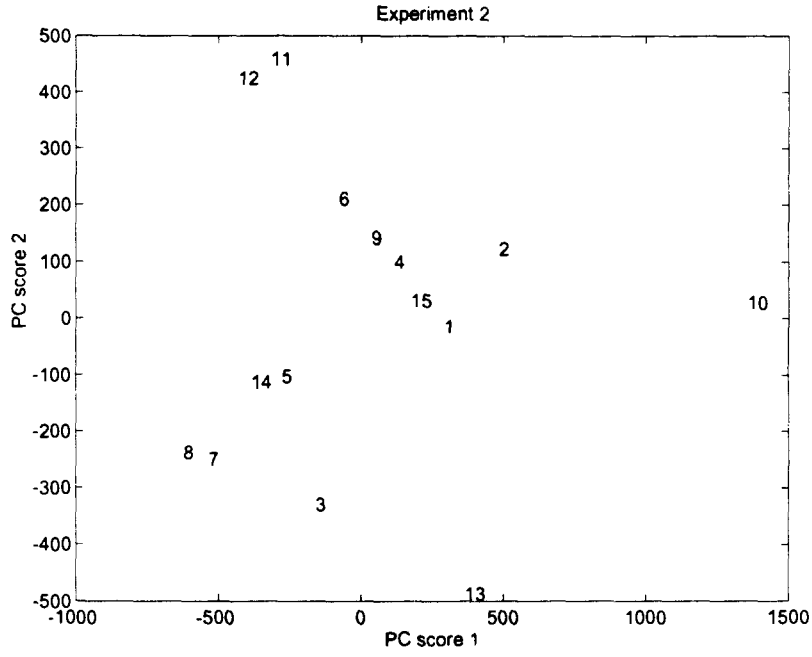


(b)

Fig. 13 (a) and (b).

sis of all 12 emission spectra shows the displacement of identical samples as seen in the score plot in Fig. 3. Samples 2, 3 and 6 are chosen as transfer standards in the PDS algorithm (how to select appropriate standards is described in Ref. [22]). The PDS algorithm calculates a matrix capable of transforming the spectra measured with lamp 2 as if they were measured with lamp 1.

$$\boldsymbol{A}_{\text{rec}} = \boldsymbol{B}\boldsymbol{M}_{\text{transfer}}$$

where $\boldsymbol{A}_{\text{rec}}$ is a matrix with 6 objects and 441 variables containing the reconstructed spectra, $\boldsymbol{B}$ is a $6 \times 441$ matrix containing the spectra measured with lamp B and $\boldsymbol{M}_{\text{transfer}}$ is a $441 \times 441$ transfer matrix. In this case the optimal window size was found to be 7, i.e. 7 spectral points in $\boldsymbol{B}$ (this corresponds to an emission range of 3 nm) are used to model the chosen wavelength in $\boldsymbol{A}$.

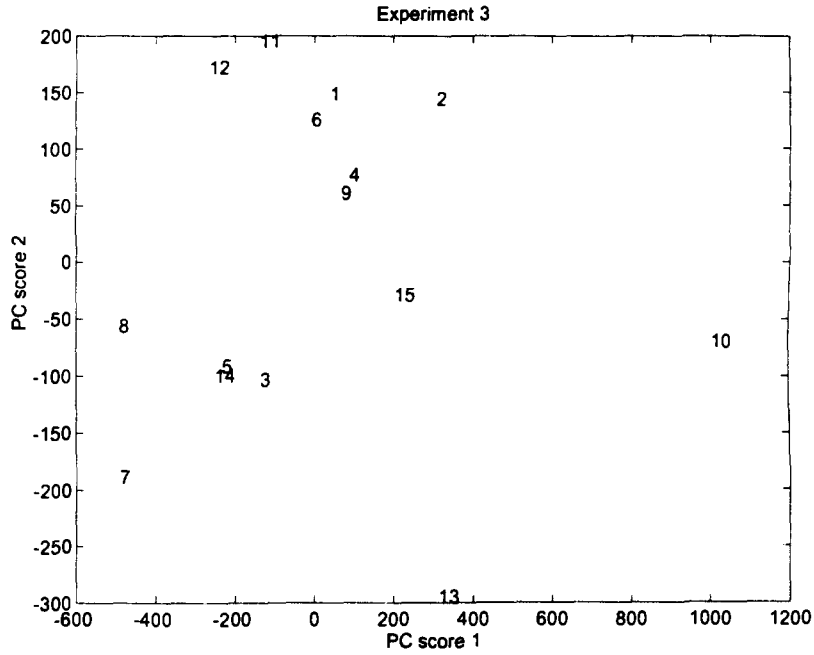


(c)

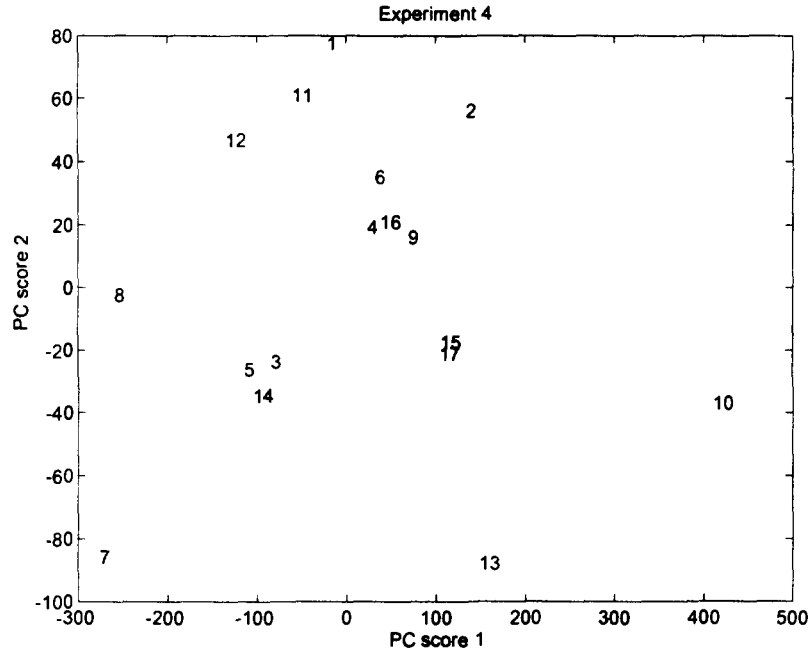


(d)

Fig. 13 (c) and (d).

In order to estimate the efficiency of PDS transformation, the true spectra measured with lamp 1 are compared with the transformed (reconstructed) spectra (Fig. 4). A PCA score plot of the 6 original lamp 1 spectra and the 6 transformed spectra is given in Fig. 5. As expected, the spectra of the three standards used in calculating the transfer matrix compare very well, but the three samples not included in the transfer calculation also compare satisfactorily.

This example indicates that the PDS is a valuable tool in transferring fluorescence spectra between different instrumental set-ups for the same fluorescence instrument and between different instruments. An extensive investigation of the performance of the PDS algorithm in combination with multivariate calibration methods of fluorescence spectra (including a larger sample set) is presented in Ref. [35].

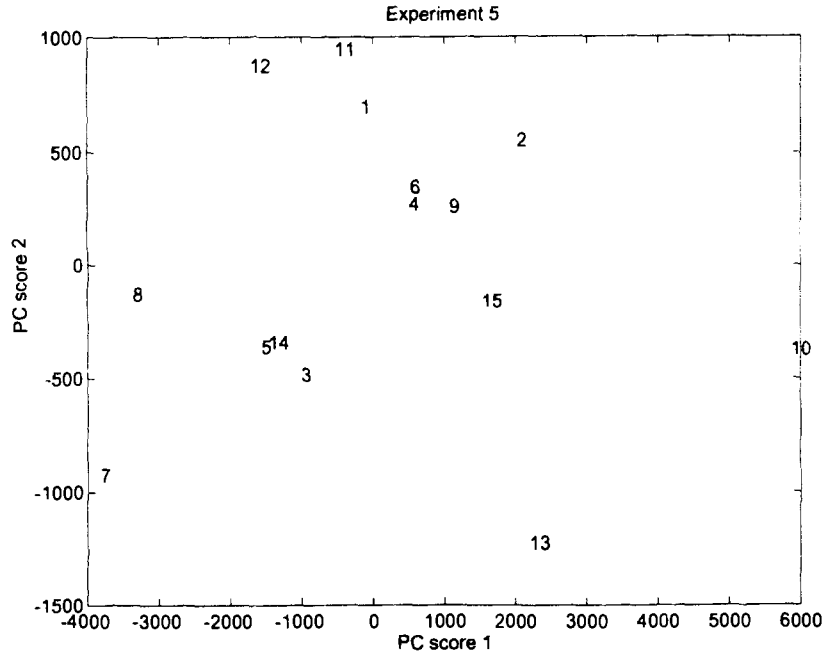


(e)

Fig. 13. Score plots (PC1 against PC2) for (a) experiment 1; (b) experiment 2; (c) experiment 3; (d) experiment 4; and (e) experiment 5. In experiment 4 replicates of samples 4 and 15 are included (nos. 16 and 17, respectively).

### 3.2. Smoothing of spectra

The Perkin-Elmer LS 50B instrument is sold with two types of software smoothing filters, i.e. the chemist must choose either binomial or Savitzky-Golay smoothing of the raw data. To investigate the smoothing effect on spectral shape an OBEY program was written to obtain the raw unsmoothed data as output from the instrument (see Section 2). Ten emission spectra were recorded on standard block 2 (sample set B) for each smoothing type. A PCA of the 30 spectra shows three clusters each for one of the data types (Fig. 6). The data were not preprocessed in any way in order to illustrate the sizes of the two significant principal components (the first PC explains 99.988% of the total variance and the second PC explains 0.004% of the total variance). In Fig. 7 the corresponding loadings are plotted. The first loading vector primarily describes the intensity level, while the second loading substantiates that the differences indeed are very small but still significant. Furthermore, the second derivative shape of the second loading vector at peak locations might indicate peak broadening. This agrees with the broadening effect of the smoothing algorithms.

In the section below (3.3) it is shown that instrumental Savitzky-Golay smoothing of data during recording of the spectra produces slightly larger prediction errors than when raw data are used as spectral input into a multivariate calibration model of the sugar concentration. It is concluded that no special smoothing algorithms are needed when the multivariate data approach is used.

### 3.3. Raman scattering

Raman scattering appears as a solvent-dependent emission occurring at longer wavelengths than the excitation wavelength [25]. Furthermore, the Raman frequency shifts are independent of the excitation frequency [25]. This can be a problem in classical univariate calibration if the spectral region of the analyte of interest is overlapped by the Raman scattering caused by the actual solvent (in this case water). A way of circumventing the influence of the Raman scattering is [25] (a) to subtract the blank spectrum from each of the sample spectra, assuming that the Raman scattering is independent of the analyte concentration and that the blank measurement is possible; (b) to employ appropriate filters (if it is possible in the actual case); or (c) to use another excitation wavelength with the risk of loosing relevant analyte information.

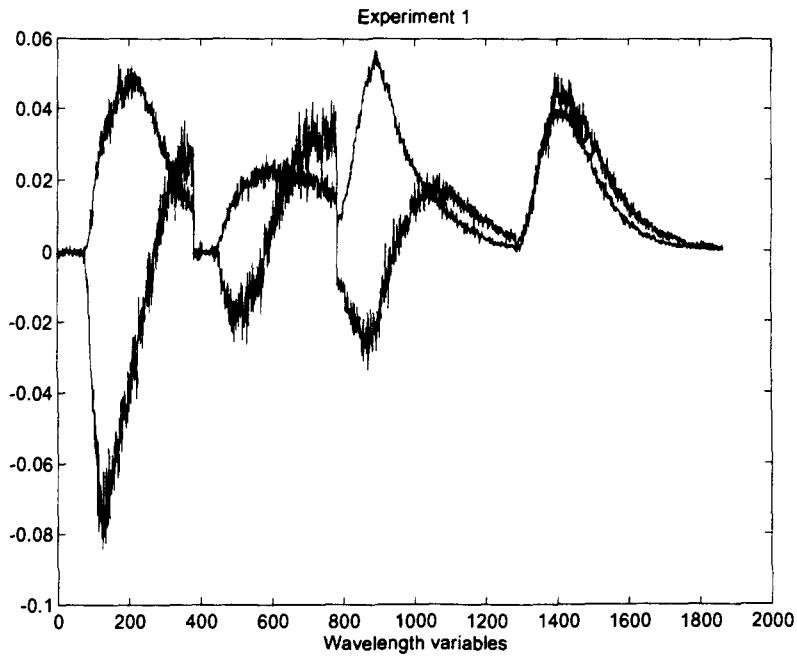


(a)

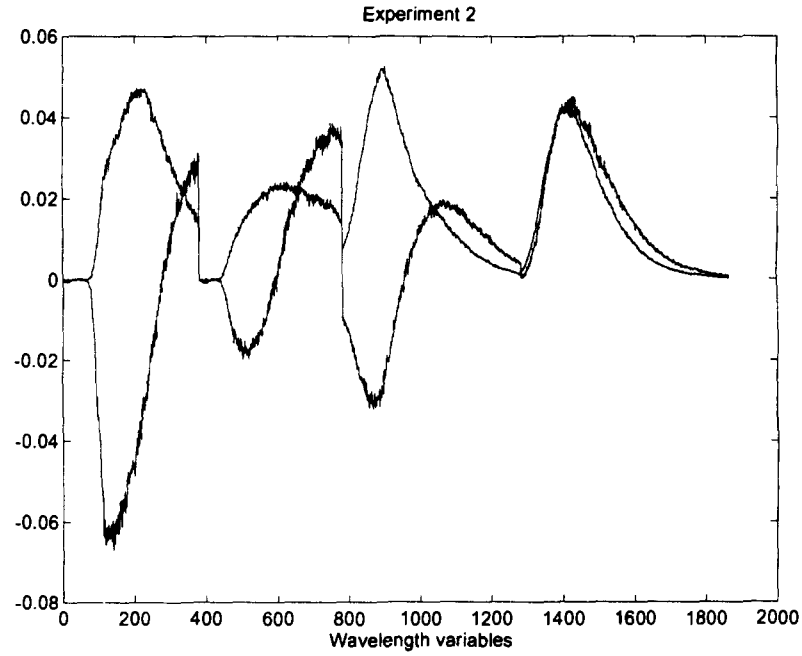


(b)

Fig. 14 (a) and (b).

A multivariate approach to the problems of Raman scattering is to analyse the whole emission spectrum including the Raman scatter. In multivariate calibration the Raman signals are treated as interferent(s) and cause no problems for the multivariate modelling of the analyte emisison spectra. This is illustrated by the following examples.

The emission spectra of 11 solutions of a given refined sugar sample having different concentrations are measured at an excitation wavelength of 300 nm (sample set C). At this excitation wavelength, Raman scattering will occur at around 334 nm, overlapping the emission spectrum of the sample. The fluorescence emission spectra are depicted in Fig. 8. A full cross-validated PLS model with the fluores-

(c)

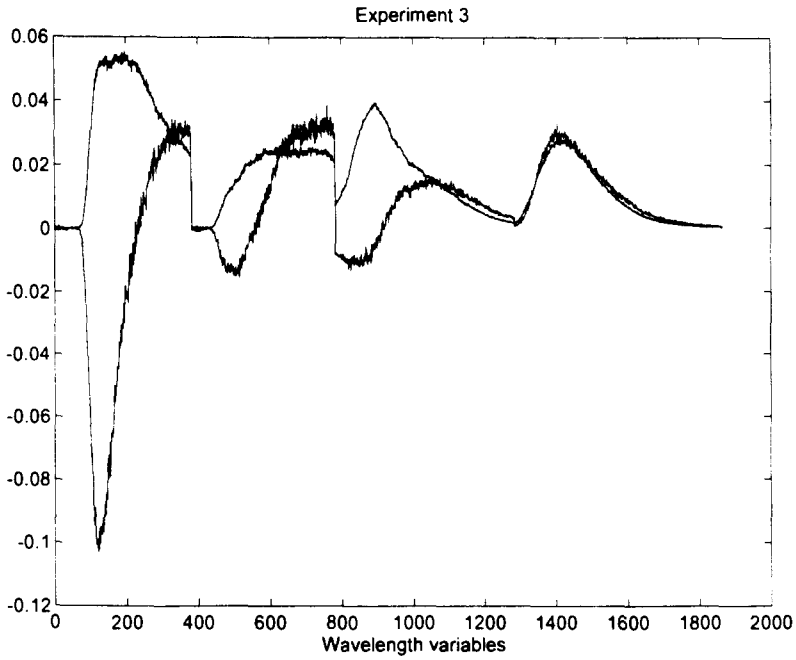


(d)

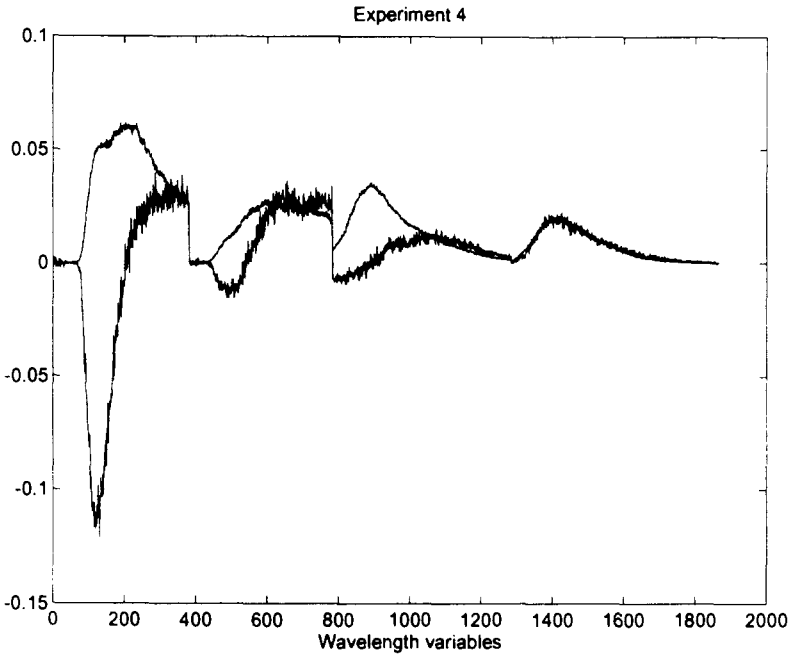


Fig. 14 (c) and (d).

cence emission spectra in $X$ (11 × 451) and the concentrations in $y$ (11 × 1) shows two significant components; the loading weights of the PLS analysis are given in Fig. 9. The Raman effect is seen in both loading vectors, i.e. both components are necessary in a full description of the data set (see Table 1). The PLS model was built without any preprocessing of the data to illustrate how PLS takes into account the Raman scattering. If the data are mean centred, a one-factor solution is achieved due to the fact that the Raman scattering has the same intensity in all the samples. The results are compared with full cross-validated univariate calibration (at emission wavelength, 395 nm) in Table 1(A). The prediction errors obtained when using multivariate models are approximately five times smaller than the error

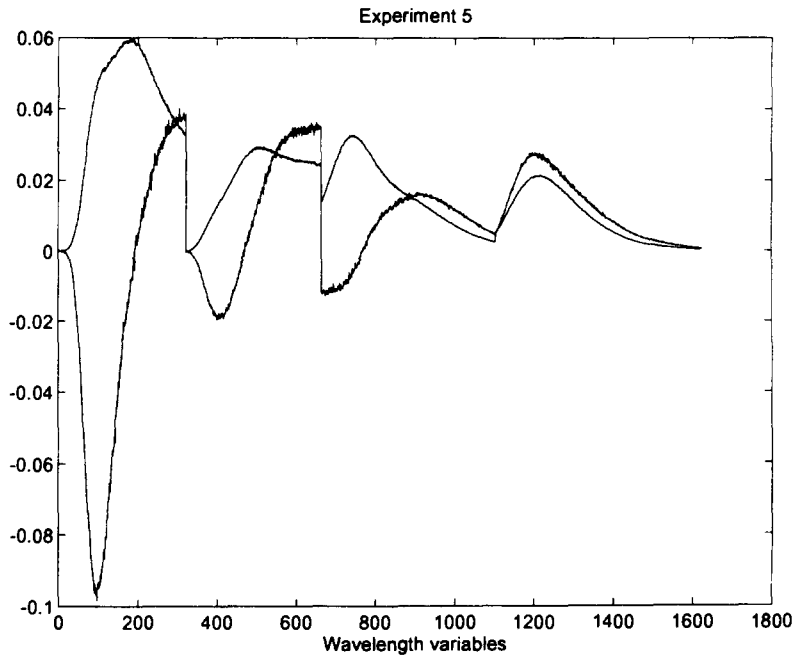


(e)

Fig. 14. The first two loading vectors for (a) experiment 1; (b) experiment 2; (c) experiment 3; (d) experiment 4; and (e) experiment 5. See comments in the text.

obtained in univariate calibration, i.e. even in the case of single analyte calibration multivariate modelling should be used. The prediction errors obtained with and without mean centring are of comparable size. In the case of no centring two factors are included in the model to handle the interfering Raman scattering.

The effect of the instrumental Savitzky-Golay smoothing of the raw data during recording of the spectra as input to the PLS model is shown in Table 1(B). The prediction errors obtained by this data preprocessing are slightly larger than when using raw data in the PLS model (see smoothing of spectra, section 3.2.).

In this one-analyte example (the same sugar solution diluted several times) PLS is capable of predicting the sugar concentrations of the samples without removal of the Raman signal in advance; in the case of several analytes being present and possible interaction between the Raman signals and the analyte signals, it is a necessity to use multivariate methods.

### 3.4. Selection of excitation wavelengths

The selection of a subset of excitation wavelengths is essential in order to minimise the time necessary to analyse a chemical sample. It takes approximately 40 s automatically to record one emission spectrum by the OBEY software at a given excitation wavelength (including the adjustment of the excitation monochomator), i.e. to be able to measure at least 20 samples per hour for on-line/at-line purposes, four to five excitation wavelengths have to be chosen. One way of selecting the excitation wavelengths from a large excitation–emission matrix (EEM) is the principal variable [26] (PV) algorithm, which is illustrated by the analysis of a refined sugar sample (sample 1 from sample set DI). An EEM is recorded at the excitation wavelengths 230–350 nm with 10 nm intervals, i.e. 13 emission spectra are obtained in the emission range 245–685 nm (excitation and emission monochromator slit widths were 8.0 nm and 5.0 nm, respectively). Rayleigh scattering peaks are removed from the emission spectra by filling with zeroes. In Fig. 10 a three-dimensional plot of the EEM is depicted. The PV algorithm applied to this EEM determines the optimal subset of excitation wavelengths to be 230 nm, 330 nm, 290 nm and 240 nm. The variances computed explain 60.28%, 33.91%, 3.57% and 0.75%, respectively, of the total variance. In total 98.51% of the original variance is explained. "Optimal" signifies a compromise between variance explained and the precision (see Ref. [26]).

### 3.5. Multivariate calibration of fluorescence spectra

The multivariate calibration of the ash content in sugar samples is important in developing fast on-line/at-line methods for detecting the end-product quality, which among others, is described by the ash content. Clear solutions of 15 refined sugar samples with measured levels of ash content determined at the laboratory of The Danish Sugar Factories (International Commision for Unified Methods of Sugar Analysis, ICUMSA) are analysed by spectrofluorimetry without pH correction.

Table 3
Prediction of ash content. Performance of PLS modelling in the five experiments performed

| | | $10^3$ RMSEP [a] | $10^3$ Bias [b] | $R$ [c] |
|---|---|---|---|---|
| Expt. 1 | (a) | 1.06 | −0.067 | 0.903 |
| | (b) | 1.11 | −0.071 | 0.763 |
| Expt. 2 | (a) | 1.06 | −0.200 | 0.916 |
| | (b) | 1.07 | 0.000 | 0.788 |
| Expt. 3 | (a) | 0.775 | 0.067 | 0.951 |
| | (b) | 1.04 | 0.071 | 0.826 |
| Expt. 4 | (a) | 0.516 | 0.000 | 0.979 |
| | (b) | 0.463 | −0.071 | 0.966 |
| Expt. 5 | (a) | 0.683 | −0.20 | 0.967 |
| | (b) | 0.707 | −0.21 | 0.933 |

Key: (a), All 15 samples; (b), sample 10 left out.
[a] RMSEP = $\sqrt{\Sigma_{i=1}^{N}(C_i^{\text{predicted}} - C_i^{\text{reference}})^2/N}$, where $C_i^{\text{predicted}}$ is the PLS estimated concentration, $C_i^{\text{reference}}$ is the reference value and $N$ is the number of samples.
[b] Bias = $\Sigma_{i=1}^{N}(C_i^{\text{predicted}} - C_i^{\text{reference}})/N$.
[c] Correlation.

Table 4
Ash content reference value and predicted ash content, from PLS modelling of fluorescence spectra measured on sugar samples in experiment 3

| Sample | Reference | Predicted |
|---|---|---|
| 1 | 0.012 | 0.011 |
| 2 | 0.009 | 0.010 |
| 3 | 0.012 | 0.012 |
| 4 | 0.010 | 0.010 |
| 5 | 0.011 | 0.011 |
| 6 | 0.010 | 0.011 |
| 7 | 0.010 | 0.011 |
| 8 | 0.014 | 0.014 |
| 9 | 0.009 | 0.010 |
| 10 | 0.003 | 0.003 |
| 11 | 0.012 | 0.011 |
| 12 | 0.012 | 0.011 |
| 13 | 0.008 | 0.007 |
| 14 | 0.010 | 0.011 |
| 15 | 0.008 | 0.008 |

Based on the results in the previous paragraph, the chosen excitation wavelengths are 230 nm, 240 nm, 290 nm and 330 nm, with the respective emission wavelength ranges 245–435 nm, 255–455 nm, 305–555 nm and 345–635 nm. The four emission spectra are concatenated, i.e. one sample is associated with 1864 spectral data points.

Five experiments were performed to investigate the influence of excitation monochromator and emission monochromator slit widths as well as the sugar concentration on the modelling of the ash content (Table 2). Rayleigh scattering becomes very broad when the slit widths are fully open, so the region of each recorded emission spectrum in experiment 5 is reduced by 30 nm (see Table 2).

Raw emission spectra from the 15 measurements in experiment 3 are illustrated in Fig. 11, and raw emission spectra of sample 4 from all five experiments, including a replicate from experiment 4, are given in Fig. 12. For qualitative comparison of the spectral shapes produced under different experimental conditions, a PCA was performed on each of the data sets. In Figs. 13a–13e, score plots (score 1 against score 2) including two replicates in experiment 4, are shown. The orders of samples are much alike in experiments 1 and 2 and in experiments 4 and 5, and it is seen that experiment 3 fits into the shift of the samples between experiments 2 and 4. The amount of variance explained by the first two significant factors are 81.6%, 86.4%, 89.9%, 91.3% and 93.7%, respectively. Figs. 14a–14e shows the first two loading vectors of each experiment. The shapes of the loading vectors are much alike, indicating that the experimental conditions give rise to the same kind of measured emission spectra. Moreover, it is observed that the noise level increases with decreasing slit widths and that it increases with decreasing sugar concentration.

A quantitative measure is obtained by looking at PLS models of the ash content. For each experiment, a full cross-validated [27,34] PLS model of the ash content is performed. RMSEP, Bias and the correlation coefficient $R$ for all experiments with and without sample number 10 are given in Table 3. Reference values and predictions obtained in experiment 3 are given in Table 4. Sample 10 has a low level of ash content but it is still very well predicted by the PLS models. It should be stressed that the prediction of sample 10 is based on models excluding this sample, i.e. sample 10 is a

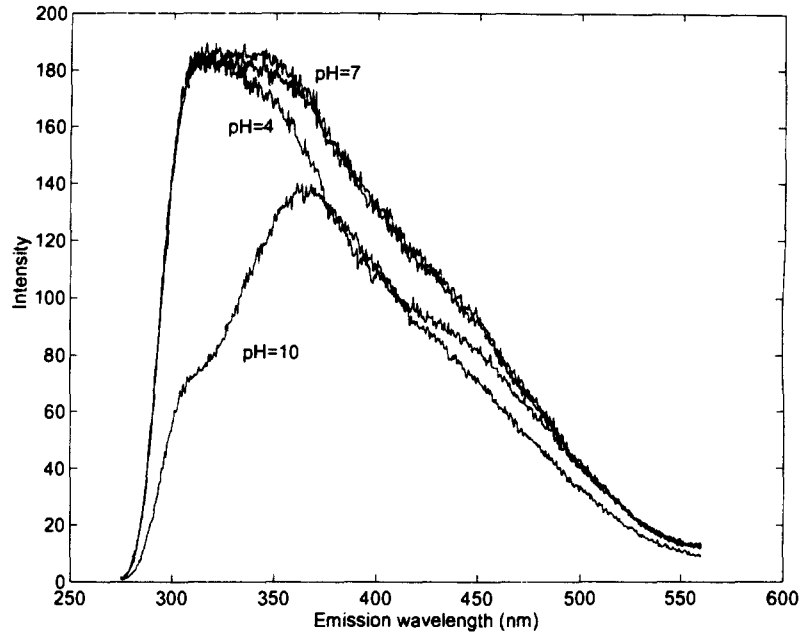


Fig. 15. Emission spectra of a refined sugar sample dissolved in buffer solutions at pH 4, 7, 10. The excitation wavelength is 230 nm. A replicate is made of the sample buffered to pH 7.

"good" outlying sample stabilising the models, as seen when comparing RMSEP and $R$.

From the prediction results it is seen that the selective wavelength information lost by using fully open slit widths is recovered in the signal-to-noise ratio by the employment of multivariate modelling. Furthermore, low concentrations of sugar yield lower prediction errors, indicating some kind of quenching or perhaps a viscosity effect. The conclusion is that the sugar concentration should be within the range 10–20% and the slit widths should be in the middle region of their respective extremes (excitation slit, 2.5–15 nm; emission slit, 2.5-20 nm). However, it is a very small difference in correlation ($R$) from the middle region slits to the fully open slits.

It is demonstrated how the multivariate method PLS is capable of utilising the information in fluorescence spectra despite very different conditions of measurement with respect to slit widths and sugar concentrations. These promising results are confirmed on a larger scale when about 90 refined sugar samples with and without pH correction are analysed [20]. Similar correlations to the ash content ($R = 0.93$) are documented as well as high correlations to quality parameters like amino-nitrogen and colour.

### 3.6. The pH and corrected spectra

*pH*

It is well known that the spectral shapes of fluorescing components are pH-dependent. This is confirmed in Fig. 15 where the difference in spectral shape obtained at pH 4.0, 7.0 and 10.0 for a given refined sugar sample is illustrated. The measurement at pH 7.0 has been repeated to show the uncertainty of a sample replicate. In ref. [20] comparisons of prediction errors from a large sample set of refined sugar sampes (about 90) dissolved in pure water and in buffer solution at pH 7.0 are presented. The value of $R$ with respect to the ash content is shown to be 0.92 with pH correction and 0.93 without correction. Even though the difference in prediction error is insignificant, the spectral shapes are systematically different in the two experiments, indicating that the information content is changed when going from water solutions to buffered solutions. It may be that some sample and process information is lost on pH correction of the solutions.

*Corrected emission spectra*

Throughout this presentation, uncorrected spectra are recorded in all experiments. When the fluorescence spectra are corrected [36] all spectra are wavelength multiplied by the same correction spectrum which stems from a stan-

dard measurement of, for example, a quinine sulphate solution, which introduces a reproducible small bias because of the inherent limitations in the choice of the standard. In multivariate calibration methods like PCR and PLS, however, a more general optimal weighting of wavelengths is found by the algorithms, so the present choice is not to correct the fluorescence spectra before they are introduced to the multivariate calibration model. In the area of transferring spectra between instruments, the method of piecewise direct standardisation using several transfer standards is much more preferable than using corrected spectra based on only one standard sample.

It should be noted that if resolution methods like rank annihilation factor analysis [9] (RAFA) and the generalised rank annihilation method [37] (GRAM) are employed and a library search of the resolved fluorescence spectra is performed, the measured spectra have to be corrected to compare with library spectra.

## 4. Conclusions

The outlined multivariate problems with regard to the evaluation of different data, all due to complex natural samples, individual spectrofluorimeters, Raman scattering, smoothing algorithms, and selection of excitation/emission wavelengths, may in part explain why fluorescence spectroscopy is a tool infrequently chosen by the analytical chemist as opposed to other spectroscopic methods. It has been demonstrated that by the use of multivariate chemometric methods, these problems are circumvented and fluorescence spectroscopy can be an important tool for the analytical chemist.

The NIR analogy of predicting reference values from spectra has been transferred to spectrofluorimetry, by determining the ash content in refined sugar samples from concatenated emission spectra. The potential of autofluorescence in this context is enormous for the analysis of all kinds of chemical, biological and environmental samples including on-line/at-line process analyses [21]. A further enhancement of spectrofluorimetry can be obtained by utilising the instrumental methods of polarisation and synchronous fluorimetry in combination with multivariate statistics and by the development and implementation of N-way algorithms [37–40] capable of dealing with the higher-order data structures produced by a full excitation–emission scan.

TAL 42:9-I

## Acknowledgements

The author thanks Ole Hansen, Lars Bo Jørgensen and John Jensen, The Danish Sugar Factories (DDS Development Centre, Maribovej 2, Post Box 119, DK-4900 Nakskov, Denmark) for a stimulating cooperation and for providing the sugar samples. Professor Lars Munck is acknowledged for valuable and inspiring discussions during the experimental work and during the preparation of the manuscript. The investigation is sponsored by funds to Professor Lars Munck from the Danish Research Councils 13-4804-1 (agriculture) and 16-5180-1 (technology) and from the Nordic Industry Foundation project P93149.

## References

[1] G.G. Guilbault, Practical Fluorescence, 2nd edn., Marcel Dekker, New York, 1990.
[2] C.A. Parker, Photoluminescense of Solutions, Elsevier, 1968.
[3] S.D. Brown, T.B. Blank, S.T. Sum and L.G. Weyer, Anal. Chem., 66 (1994) 315R.
[4] W.F. McClure, Anal. Chem., 66 (1994) 43A.
[5] T. Isaksson, Doctoral Thesis, Chalmers Tekniska Högskola, 1990.
[6] D. Bertrand and C.N.G. Scotter, Appl. Spectrosc., 46 (1992) 1420.
[7] C.-N. Ho, G.D. Christian and E.R. Davidson, Anal. Chem., 50 (1978) 1108.
[8] C.-N. Ho, G.D. Christian and E.R. Davidson, Anal. Chem., 52 (1980) 1071.
[9] C.-N. Ho, G.D. Christian and E.R. Davidson, Anal. Chem., 53 (1981) 92.
[10] C.J. Appellof and E.R. Davidson, Anal. Chim. Acta, 146 (1983) 9.
[11] S.L. Neal, E.R. Davidson and I.M. Warner, Anal. Chem., 62 (1990) 658.
[12] D.S. Burdick, X.M. Tu, L.B. McGown and D.W. Millican, J. Chemometrics, 4 (1990) 15.
[13] W. Lindberg, J.-Å. Persson and S. Wold, Anal. Chem., 55 (1983) 643.
[14] M. Sjöström, S. Wold, W. Lindberg, J. Persson and H. Martens, Anal. Chim. Acta, 150 (1983) 61.
[15] B. Pedersen and H. Martens, in L. Munck (Ed.), Fluorescence Analysis in Foods, Longman, Singapore, 1989, Chapter 13.
[16] S.A. Jensen, L. Munck and H. Martens, Cereal Chem., 1982, 59, 477.
[17] S.A. Jensen and H. Martens, Cereal Chem., 60 (1983) 171.
[18] S.A. Jensen and H. Martens, in H. Martens and H. Russwurm (Eds.), Food Research and Data Analysis, Applied Science, London, 1982, pp. 253–69.
[19] R.F. Madsen, W. Kofod Nielsen, B. Winstrøm-Olsen and T.E. Nielsen, Sugar Technol. Rev., 6 (1978/79) 49.
[20] L. Nørgaard, Classification and prediction of quality and process parameters of beet sugar and thick juice by fluorescence spectroscopy and chemometrics, Zuckerindustrie, in press.

[21] L. Munck, Chapter 1 in Fluorescence Analysis in Foods, Edited by L. Munck, Longman, 1989.
[22] Y. Wang, D.J. Veltkamp and B.R. Kowalski, Anal. Chem., 63 (1991) 2750.
[23] Y. Wang and B.R. Kowalski, Anal. Chem., 65 (1993) 1174.
[24] Y. Wang, M.J. Lysaght and B.R. Kowalski, Anal. Chem., 64 (1992) 562.
[25] C.A. Parker, Analyst, 84 (1959) 446.
[26] A. Höskuldsson, Chemometr. Intell. Lab. Syst., 23 (1994) 1.
[27] H. Martens and T. Næs, Multivariate Calibration, 2nd edn., Wiley, New York, 1993.
[28] B.M. Wise, Chemometrics Toolbox, Version 1.3 (ftp://ra.nrl.navy.mil/MacSciTech/chem/chemometrics/PLSToolbox13/).
[29] S. Wold, K. Esbensen and P. Geladi, Chemometr. Intell. Lab. Syst., 1987, 2, 37.
[30] P. Geladi and B.R. Kowalski, Anal. Chim. Acta, 185 (1986) 1.
[31] A. Höskuldsson, J. Chemometrics, 2 (1988) 185.
[32] P.J. Brown, Anal. Proc., 27 (1990) 303.
[33] P. Geladi and B.R. Kowalski, Anal. Chim. Acta, 185 (1986) 19.
[34] S. Wold, Technometrics, 20(4) (1978) 397.
[35] L. Nørgaard, Direct standardisation in multi wavelength fluorescence spectroscopy, Chemometrics and Intelligent Laboratory Systems, in press.
[36] J.W. Hofstraat, and M.J. Latuhihin, Appl. Spectrosc., 48 (1994) 436.
[37] E. Sanchez and B.R. Kowalski, Anal. Chem., 58 (1986) 496.
[38] S. Wold, P. Geladi, K. Esbensen and J. Öhman, J. Chemometrics, 1 (1987) 41.
[39] H. Henrion, Chemometr. Intell. Lab. Syst., 25 (1994) 1.
[40] A.K. Smilde and D.A. Doornbos, J. Chemometrics, 5 (1991) 345.

ELSEVIER

Talanta 42 (1995) 1325–1334

Talanta

# On-line flow injection analysis of volatile organic compounds in seawater by membrane introduction mass spectrometry

N. Kasthurikrishnan, R.G. Cooks *

*Department of Chemistry, Purdue University, West Lafayette, IN 47907-1393, USA*

Received 27 December 1994; revised 14 March 1995; accepted 14 March 1995

**Abstract**

The combination of flow injection analysis with membrane introduction mass spectrometry for analysis of volatile organic compounds (VOCs) in seawater is examined and is compared to measurements made in water. Membrane introduction mass spectrometry is performed using a benchtop ion trap mass spectrometer, and characterization of various aspects of the flow injection and ion trap combination for the analysis of volatile organic compounds (including anthropogenic halocarbons) in seawater is carried out. The analyte responses are shown to be linear over several orders of magnitude (e.g. for methylene chloride), independent of seawater pH (e.g. for chlorobenzene) and independent of matrix effects for the VOCs studied. A comparison of the performance of a microporous (Teflon) membrane with that of an amorphous silicone membrane is made, and the former is shown to provide lower detection limits which are in the parts-per-trillion range (300 ppt for chlorobenzene, 190 ppt for *trans*-1,2-dichloroethene). The microporous membrane provides faster response times by a factor of four to five for relatively more polar compounds, such as chlorobenzene. An analysis of a seven-component mixture demonstrates the ability of this on-line combination to allow multicomponent analysis of mixtures of some complexity.

## 1. Introduction

Seawater is a complex mixture consisting of many salts, suspended silts, various dissolved gases, living matter and decaying organic material. The analysis of various organic species in marine water is of great importance for monitoring water quality [1]. Among the volatile organic compounds (VOCs), anthropogenic and biogenic halocarbons are significant indicators of pollution in environmental samples. These halocarbons are usually present at low (ppb) levels in seawater samples, and may thus require a preconcentration step before identification and quantification by conventional techniques, such as gas chromatography/mass spectrometry. Common methods of preconcentration include the dynamic headspace technique which uses cold trapping [2] and liquid–liquid extraction with organic solvents [3]. Although preconcentration can extend absolute and relative detection limits, and may be essential for determinations of some compounds, it requires increased analysis times and carries the risk of contamination, and the possibility of loss of trace analytes. In addition, volatile halocarbons produced by marine organisms may interfere with the analysis [4]. Membrane introduction mass spectrometry (MIMS) is a specific yet sensitive method of analysis of volatile compounds in water, which often does not require a preconcentration step and which nevertheless displays good molecular specificity. As such, it may prove useful for the analysis of a whole range of VOCs in seawater.

* Corresponding author. Fax: (317) 494-0239.

0039-9140/95/$09.50 
*SSDI* 0039-9140(95)01588-4

MIMS has been applied to environmental [5–7] and bioreactor monitoring [5,7,8], and the technique has been reviewed [5,9,10]. MIMS is a relatively simple method which is flexible in terms of choice of membranes (amorphous silicone or microporous Teflon among many others, sheet or capillary configuration), is easily automated, has fast response times, and exhibits a response that is linear over a few orders of magnitude. It can be adapted to various sample introduction systems, especially flow injection analysis (FIA), and to different mass analyzers (triple quadrupole, ion trap and sector instruments inter alia). If a number of VOCs are present in the sample, the response is the sum of those for the separate analytes. When MIMS is used with a triple quadrupole mass spectrometer capable of tandem mass spectrometry, the spectra of individual compounds can be recorded [23]. A major drawback of the MIMS technique is the difficulty of analyzing compounds with molecular weight >300 dalton and polar compounds.

A number of improvements in the analysis of organic compounds by MIMS have been reported. For example, MIMS experiments have been shown to provide detection limits in the ppt (ng $l^{-1}$) range, i.e. at levels below the limits of quantification set by the US EPA [10] for a number of VOCs in aqueous solutions examined without preconcentration. On-line monitoring of chloroethylenes generated in bioreactors at low ppt levels has also been reported [11]. Detection of some organic compounds in air at ppt levels has been achieved using a membrane/jet separator interface and ion trap mass spectrometer [12]. On-site analysis of environmental pollutants in complex matrices has been demonstrated using a membrane inlet mass spectrometric method in a mobile analytical laboratory [13]. For example, a toluene concentration of 58 ppm and a trichloroethylene concentration of 30 ppb were measured in a contaminated ground water sample. Recently, stored waveform inverse Fourier transform (SWIFT) methods of selective ionization in the ion trap have been combined with MIMS to further improve detection limits. Measurements have been made in the ppq range in the ideal cases of toluene and dichloroethylene in pure aqueous solutions [14]. All of the above establish that MIMS can be used to analyze at least some VOCs at very low levels. Thus, MIMS is an attractive choice for analyzing VOCs in seawater, and indeed Bauer and Solyom have already presented data on these samples [15]. A direct insertion capillary probe fitted with a silicone capillary membrane, a 1 ml flow injection sample volume and an ion trap mass spectrometer were used to study 59 VOCs at the ppt level. Analysis of VOCs in seawater samples (Atlantic Ocean at Dayton Beach, FL) produced good quality mass spectra and showed no matrix effects.

There are a number of MIMS configurations in existence [16–18], among which the more recently introduced versions have yielded the lowest detection limits. In one of the earlier interfaces, the membrane was located at some distance from the mass spectrometer and the analyte solution was in contact with the membrane [16]. Although this configuration was employed for various successful applications, the vapor phase transport of the permeate led to the drawbacks of poor response times, memory effects, and analyte dilution problems. This led to modified versions of MIMS interfaces in which the membrane was located within a probe which could be inserted into the ion source of the mass spectrometer [17]. The probe could be fitted with either a sheet membrane or a capillary membrane. Slivon et al. were the first to pneumatically assist the transport of the analyte from a remote membrane into the mass spectrometer [19]. This concept was incorporated in a later membrane/jet separator combination which used a jet separator to provide enrichment of the analyte [18]. One of the advantages of this configuration is that the membrane is easily accessible. Studies on membrane inlet geometries by LaPack et al. have shown improved rates of permeation for a configuration where the sample flows on the inside and the permeate gas flows on the outside of a capillary membrane, as opposed to the reversed configuration [20]. A recent membrane/jet separator combiantion which uses this configuration requires lower sample flow rates for optimum analyte response [21]. Thus, the newer versions of membrane interfaces promise equal or lower detection limits with reduced analysis time, and these systems may be well suited for the analysis of VOCs in seawater samples. The highly sensitive ion trap mass spectrometer is an appropriate choice of analyzer for this type of experiment.

One concern in analyzing VOCs in seawater samples using a membrane and an ion trap mass analyzer is the corrosive nature of seawater and the possibility of membrane clogging.

Hence, special care was taken to minimize sample volumes using FIA to provide sample to the membrane for short periods of time as a narrow plug. As many as 12–15 samples per hour can be determined with FIA using an alternating standard/sample cycle (with a custom-built FIA unit [22]), as opposed to a rate of a few samples per hour in continuous aspiration experiments in which equilibrium response is measured. Although some loss is suffered in terms of signal magnitude, it is more than compensated for by the increased speed of analysis, high reproducibility, absence of clogging, and automation capability offered by FIA. The choice of FIA in combination with MIMS for analyzing VOCs in seawater was therefore made.

In this work we characterize various aspects of the analysis of VOCs (including anthropogenic halocarbons) on-line in a seawater matrix. Of particular interest is the effect of the seawater matrix on signal response, response times, and detection limits of VOCs. The effects of pH, flow rate, and sample volume on signal response are also studied. A few volatile organic compounds in seawater are quantified with two types of capillary membranes (microporous and silicone) and a comparison between the membranes is made. To facilitate this comparison, a seven-component mixture in seawater is analyzed.

## 2. Experimental

### 2.1. Instrumentation

A Finnigan (San Jose, CA, USA) ITS 40 quadrupole ion trap mass spectrometer was used for all experiments. This instrument has been modified to accommodate a two-stage analyte enrichment system (membrane/jet separator) described elsewhere [21]. The operating conditions of the ion trap were 50 °C manifold temperature, 80 μA filament current, electron impact ionization, and 25 ms ionization time. Data were acquired by scanning at 2 s per scan over the $m/z$ range of 40–160 using the ITS 40 data acquisition system.

### 2.2. Membrane interface

The membrane (4 cm in length) is encased in a 3/16″ stainless steel tube in a coaxial arrangement. All experiments were performed by flowing the analyte solution through the membrane while passing helium gas over its surface in the opposite direction [21]. The capillary membranes used were of two types: silastic and microporous. The dimensions of the membranes were 0.635 mm i.d. ± 1.19 mm o.d. for silicone (Dow Corning, Midland, MI) and 1 mm i.d. × 1.8 mm o.d. for the microporous PTFE (2 μm pore size, Anspec, Ann Arbor, MI). The ends of the silicone membranes were soaked in *n*-hexane prior to assembly for a tight fit onto the fluid transport lines.

### 2.3. Jet separator assembly

The coaxial membrane assembly is connected to a glass jet separator (Finnigan, San Jose, CA, USA, Part No. 10008-40010) which is connected to a mechanical vacuum pump (Alcatel, Kurt Lesker, Clairton, PA, USA, Model M2008A). This helps to enrich the permeate stream in the analyte by removing helium and water. The flow of helium is controlled by a variable gas flow controller of the Finnigan ITS 40 system. Higher pressures of helium gas led to the formation of bubbles due to helium gas permeation to the solution side of the membrane, and lower pressures led to reduced signal intensity. Thus, an optimum helium pressure (nominal 5 psi) was maintained throughout the experiments. A 51 cm stainless tube (1.588 mm o.d. × 0.762 mm i.d.) connected the jet separator interface to the ion trap via the GC transfer line and a Teflon front ferrule was used for sealing. The introduction of samples was carried out with the help of a custom-built FIA unit [22].

### 2.4. Heating assembly

The jet separator and the membrane assembly were heated individually by programmable heater controllers (Omega Engineering Inc., Stamford, CT, Model CN(*) 20). The jet separator and the membrane assembly were heated using 1/4″ adhesive heating tape (Clayborn, Roseville, CA, Model K16) and an 8″ × 8″ Kapton insulated heater (Omega Engineering Inc., Stamford, CT), respectively. Optimum temperatures for the jet separator and the membrane assembly were 150 °C and 80 °C, respectively [21].

### 2.5. FIA system

A schematic diagram of the FIA system is given elsewhere [22]. Plugs of solutions of desired volume were injected into a stream of carrier solution (water) by a Waters (Milford, MA) Filter Acquisition Module (FAM, Model 000024). The volume of the sample loop was 250 μl for some studies and 1 ml in the case of others. The FAM contains a TTL controllable sample/standard switching valve and a Rheodyne six port HPLC sampling valve (Biochem Valve Corporation, East Hanover, NJ). All the valves are controlled manually by a custom-built FIA control unit. In this unit, sample or standard could be loaded and injected by depressing a switch; no syringes were needed for loading purposes. The water, sample, and standard streams were maintained at a flow rate of 1–1.2 ml $min^{-1}$ for most of the experiments, except when the effect of flow rate was of interest. An Ismatec multichannel peristaltic pump (Cole-Parmer, Niles, IL) was used for maintaining flow rates between 1 and 1.2 ml $min^{-1}$, and a Masterflex pump (Cole-Parmer, Niles, IL) was used for the flow rate effect study.

### 2.6. Sample preparation

Commecially available reagents were purchased from Mallinckrodt (St. Louis, MO) or Fisher (Pittsburgh, PA) and were of analytical reagent grade. In all cases, aqueous solutions of VOCs were prepared by dissolving 1 ml of the commercially available reagent in 100 ml of methanol (stock solution), followed by serial dilution in water and seawater. VOCs dissolved in water (deionized water) were used as standards, and solutions in seawater constituted the sample. The seawater used a synthetic material prepared according to ASTM standard specifications for ocean water substituents (D1141-52).

## 3. Results and discussion

Optimization of the FIA-MIMS experiment was sought for the effects of flow rate, sample volume, membrane length and temperature. Previous studies using FIA with direct insertion probes have shown the flow rate to be at an optimum around 1 ml $min^{-1}$ [23]. In contrast, continuous monitoring experiments are often performed at higher flow rates to minimize boundary layer effects at the membrane surface. The present membrane/jet separator assembly showed no significant flow rate effect from 1 to 6 ml $min^{-1}$. The flow rate independence of FIA-MIMS offers flexibility of sample, carrier, standard and reagent volume. In order to simplify sample handling, the flow rate was maintained at 1.0–1.2 ml $min^{-1}$ for all experiments.

The volume of the sample loop plays an important role in experiments with short sample plugs introduced by FIA. In an FIA-MIMS system, the analyte signal increases with the sample volume, until equilibrium is achieved. Based on such studies, a range of sample volumes of 250 μl–1 ml was determined to be the optimum for analyzing VOCs in seawater. The optimum membrane temperature, jet separator temperature and membrane length were determined to be 80 °C, 150 °C and 4 cm, respectively [21].

Since the pH of seawater may vary, an attempt was made to study the effect of pH. The seawater pH was adjusted by adding sodium hydroxide and the range of pH 7–12 was examined. Fig. 1 shows results obtained using a silicone membrane and 100 ppb chlorobenzene solution. The analyte signal intensity is found to be almost independent of seawater pH. Studies on seawater by Bauer and Solyom also indicated no pH effect, except when organic acids and bases are present in the sample [15]. Microporous membranes show a similar lack of pH effect, and based on these results no pH adjustment is deemed necessary in the case of real samples.

Seawater matrix contains dissolved electrolytes of very high ionic strengths, and an important step in developing methodology for analyzing VOCs in seawater samples by FIA-MIMS is to determine matrix effects. In the membrane/jet separator combination, matrix effects may occur owing to the difference in concentration gradient or pressure gradient (seawater vs. helium, water vs. helium). In an FIA-MIMS system, the salts and ionic compounds do not pass through the membrane; nevertheless, in spite of small volumes of sample input, fouling of the membrane might be expected after prolonged operation. This is especially true with microporous membranes, as they are more prone to membrane fouling compared to amorphous membranes such as silicone. In these studies we used microporous

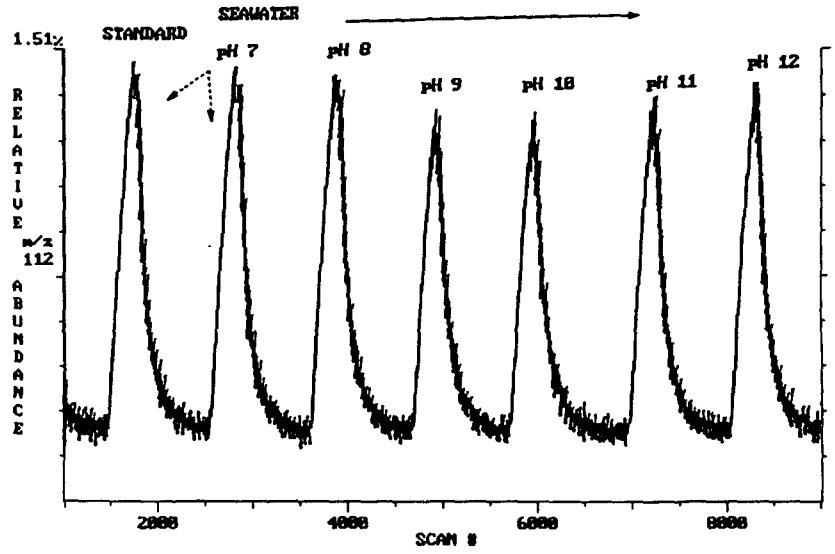


Fig. 1. Response of chlorobenzene ($m/z$ 122) in seawater at different pH (7–12) compared to water solutions. The standard (first peak) constitutes the response for chlorobenzene in water and all other peaks represent the response in seawater. The study was performed using the FIA-MIMS system, 250 µl sample volume, the silicone membrane, 100 ppb chlorobenzene ($m/z$ 112), and sodium hydroxide 0.1 M to adjust the pH.

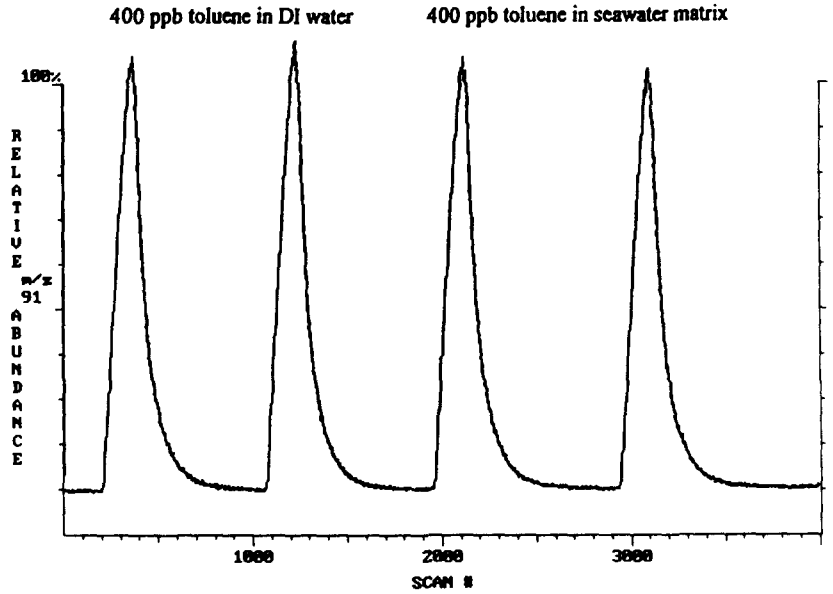


Fig. 2. Response due to toluene in water and seawater. This study was performed using the silicone membrane, 250 µl sample volume and 400 ppb of toluene monitored as $m/z$ 91.

membranes for 2–3 h of continuous operation without encountering clogging problems.

Fig. 2 shows the effect of the seawater matrix on the response of toluene using a silicone membrane. Two 250 µl injections, both of 400 ppb toluene, in water and seawater were made. This preliminary experiment failed to show any matrix effect. The experiment was repeated with randomly chosen concentrations of toluene (within the linear dynamic range of the ion trap) and no matrix effect was observed. This absence of a matrix effect is noteworthy. Since water and seawater have different solubilities for organic compounds, it would not be surprising for the nature of the mobile phase to have an effect.

In order to explore matrix effects further, an experiment was performed with three analytes (toluene, chlorobenzene, nitrobenzene) of different polarities (nitrobenzene > chlorobenzene > toluene). Each analyte, dissolved in water and then in seawater, was passed across the

membrane until equilibrium was reached. A typical result is shown in Fig. 3. Note that the widths of the peaks in this experiment have no particular significance; equilibrium was established making the peak heights the significant parameter. In each of these cases the analyte showed modest effects due to differences which may be associated with analyte polarity. These could be analogous to some of the salt effects observed in a reverse-phase LC system [24]. The change in the polarity of the mobile phase upon addition of salts may cause the analyte signal to increase or decrease depending on the ionic strength of the solution. In these experiments, salt concentrations were such as to decrease the analyte signal for the less polar compounds. Nitrobenzene, the most polar analyte, was least affected by seawater, whereas

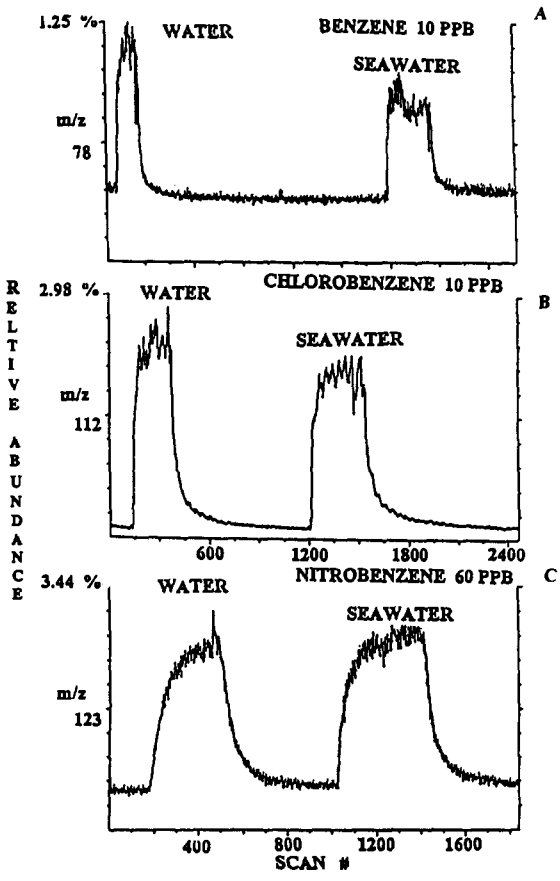


Fig. 3. (A) Response obtained for benzene (10 ppb, $m/z$ 78) in water and seawater with continuous aspiration and a microporous membrane. (B) Response obtained for chlorobenzene (10 ppb, $m/z$ 112) in water and seawater with continuous aspiration and a microporous membrane. (C) Response obtained for nitrobenzene (60 ppb, $m/z$ 123) in water and seawater with continuous aspiration and a microporous membrane. The widths of the peaks carry no significance.

benzene, the least polar, showed the largest reduction in signal. The study was repeated using FIA methods to provide small injection volumes for both silicone and microporous membranes, as shown in Fig. 4. This experiment failed to show any significant change in analyte signal with changes in the analyte and in mobile phase polarity. The lack of matrix effects in the FIA experiment cannot be fully explained because of operating away from equilibrium in the MIMS system, and we are still investigating this effect. Thus, it appears from preliminary studies that no compromise in detection limits or in the speed of the analysis need to be made when analyzing VOCs in seawater with FIA.

Figs. 5 and 6 depict the background subtracted mass spectrum of 100 ppb toluene in water and seawater obtained using an amorphous silicone membrane. The mass spectrum recorded in seawater is similar to and shows slightly better signal to noise characteristics than the spectrum of the same compound in water. One possible reason that the relative abundances of the $(M + H)^+$ ions are not the same is the difference in partial pressure of the analyte in water and seawater.

A typical log–log plot of signal intensity vs. concentration in water and seawater for methylene chloride solutions examined with a microporous membrane by FIA-MIMS is shown in Fig. 7. The data show a highly linear response over several orders of magnitude of analyte concentrations. The lack of difference between the water and seawater calibration of methylene chloride is a further indication of the absence of significant matrix effects. Similar results showing the lack of matrix effects and linear analyte responses over several orders of magnitude were obtained for the other VOCs, and are listed in Table 1.

An attempt was made to characterize and compare the performance of microporous and silicone membranes for a number of analytes. The applicability of FIA-MIMS to a variety of VOCs is evident from Table 1, which lists a few compounds studied, together with rise times and detection limits both in water and seawater using silicone and microporous membranes. It is observed that highly polar compounds give longer response times compared to less polar compounds with silicone membranes. Silicone membranes are hydrophobic and are best suited to the analysis of non-polar compounds, whereas mi-

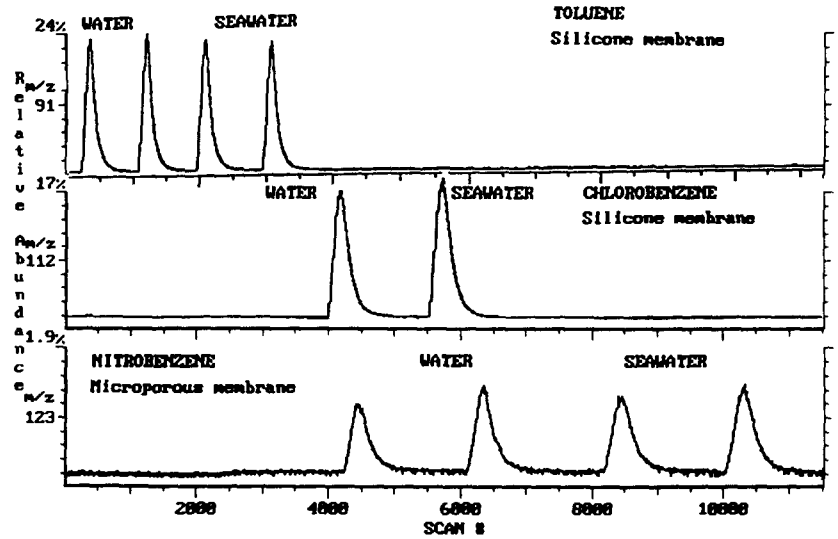


Fig. 4. Responses due to three diffrent analytes (toluene, chlorobenzene, nitrobenzene) in experiments using two types of membrane (silicone and microporous). Plugs of 250 μl injections were made for toluene (500 ppb, $m/z$ 91), chlorobenzene (500 ppb, $m/z$ 112) and nitrobenzene (3 ppm, $m/z$ 123) respectively. The first two peaks for toluene (silicone membrane) and nitrobenzene (microporous membrane) represent the signal for the analyte in water, and the last two represent that in seawater respectively. Only two injections were made for chlorobenzene, one representing the analyte in water and the other in seawater (silicone membrane).

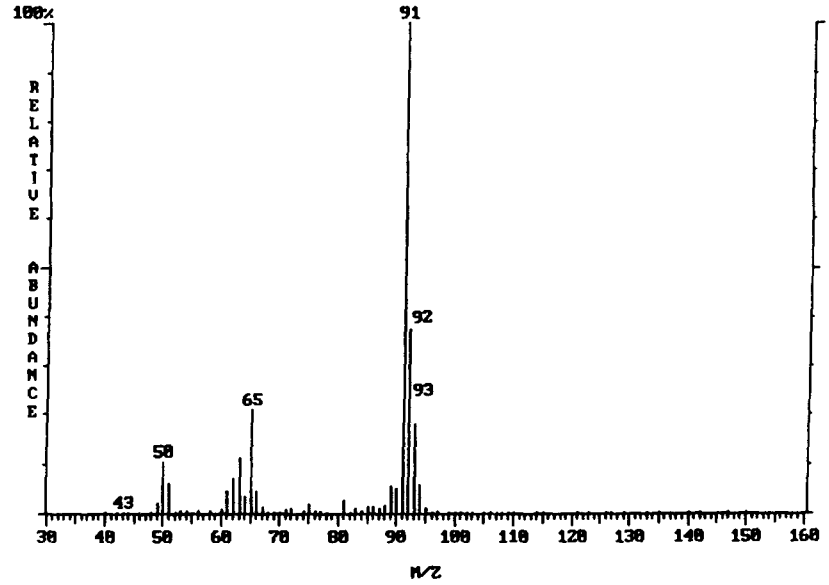


Fig. 5. Background subtracted mass spectrum of 300 ppb toluene ($m/z$ 91) in water using a silicone membrane.

croporous membranes are non-selective and are better suited to the analysis of more polar compounds. As is evident from the detection limit data (based on three times the standard deviation of the blank), non-polar compounds give similar or slightly lower detection limits (1–1.5 times) when using microporous membranes compared to silicone, whereas with polar compounds the microporous membrane yields far lower detection limits (4–5 times) than silicone. The improved detection limits achieved using microporous membranes for polar compounds is a result of poor transmission by silicone membranes, rather than any selectivity for polar compounds by microporous membranes. A universal aspect of microporous membranes is their speed of analyte transfer. Another important aspect of microporous membranes is their ability to pass sufficient amounts of water to facilitate the use of water as the CI gas [23].

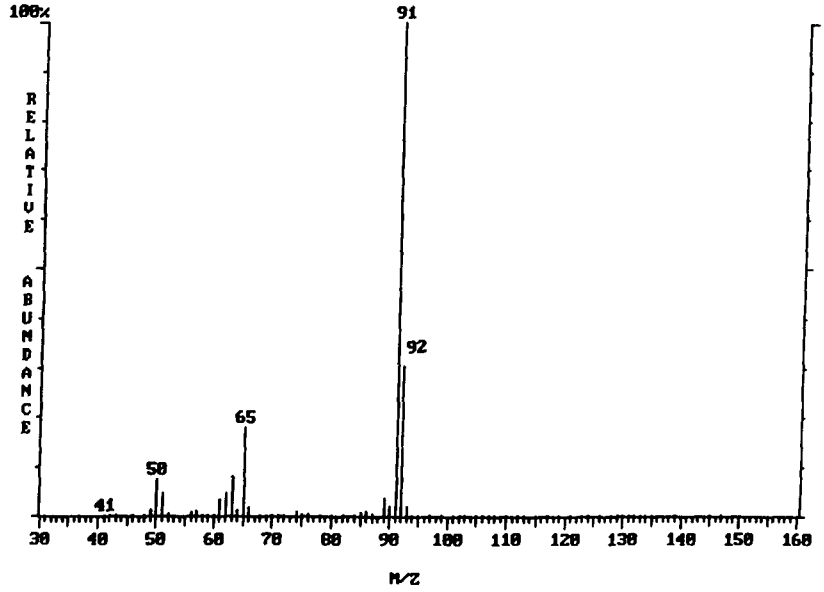


Fig. 6. Background subtracted mass spectrum of 300 ppb toluene ($m/z$ 91) in seawater using a silicone membrane.

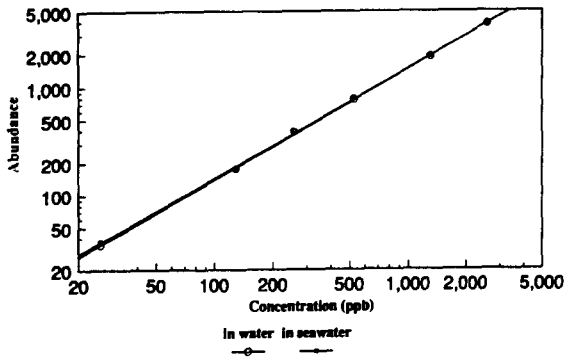


Fig. 7. Log–log plot of ion abundance ($m/z$ 49) vs. concentration for methylene chloride in water (○) and in seawater (■) using a microporous membrane.

Ion chromatograms obtained with a carefully chosen mixture containing seven volatile organic compounds are illustrated for silicone (Fig. 8) and microporous (Fig. 9) membranes. Since the detection limits of methylene chloride, *trans*-1,2-dichloroethylene, benzene, toluene, chloro-benzene, carbon tetrachloride, and 1,1,2-tri-chloroethene are all around 1 ppb, a mixture with concentrations close to the limit of quantification (10 ppb) was prepared in water and seawater. The mixture was chosen so as to contain both polar and non-polar compounds, and experiments with silicone and microporous membranes were carried out under identical conditions on the same day. To further facilitate the comparison, the acquisition scan rate and the mass scan range were held constant. Since the custom-built FIA unit has an RSD of 5–8% and the temperature of the membrane assembly varies by at least $\pm 3$ °C, any small variations in analyte signal intensities can be neglected. The different analyte responses are due to their varying membrane

Table 1
Comparison of detection limits and rise times for amorphous silicone and microporous membranes. Rise times are calculated based on 10–90% of the peak height

| Compound | Silicone membrane | | | | Microporous membrane | | | |
|---|---|---|---|---|---|---|---|---|
| | Detection limit | | Rise time | | Detection limit | | Rise time | |
| | Water | Seawater | Water | Seawater | Water | Seawater | Water | Seawater |
| | (ppb) | | (s) | | (ppb) | | (s) | |
| Toluene | 0.9 | 0.9 | 64 | 65 | 0.6 | 0.6 | 40 | 39 |
| Benzene | 0.5 | 0.5 | 31 | 29 | 0.3 | 0.3 | 18 | 19 |
| *trans*-1,2 Dichloroethene | 0.4 | 0.4 | 26 | 24 | 0.2 | 0.2 | 16 | 17 |
| Carbon tetrachloride | 1.2 | 1.0 | 38 | 38 | 0.7 | 0.7 | 16 | 16 |
| Chlorobenzene | 1.0 | 1.1 | 105 | 102 | 0.3 | 0.3 | 15 | 17 |

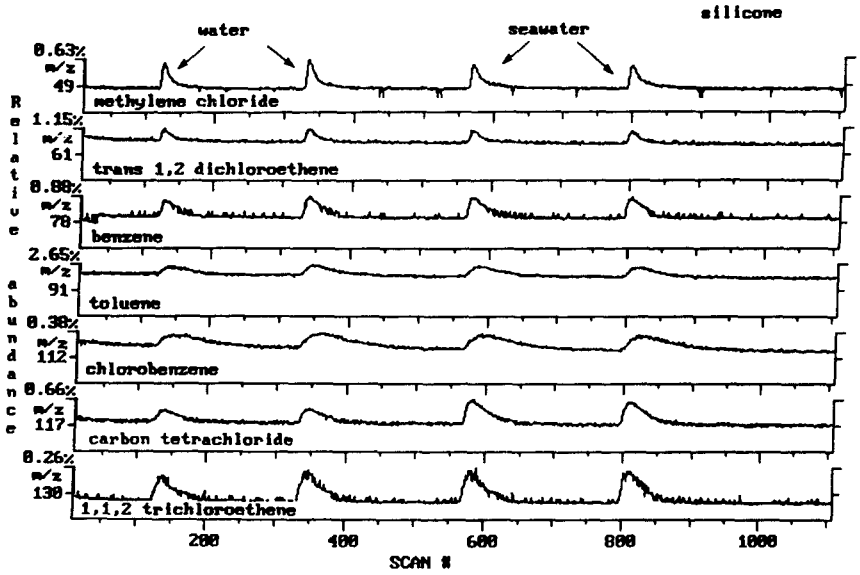


Fig. 8. Ion chromatograms recorded for a seven-component mixture (methylene chloride, *trans*-1,2-dichloroethylene, benzene, toluene, chlorobenzene, carbon tetrachloride and 1,1,2-trichloroethene) at 10 ppb, each using a silicone membrane and 1 ml sample volume. The arrows mark the introductions of the water and seawater samples.

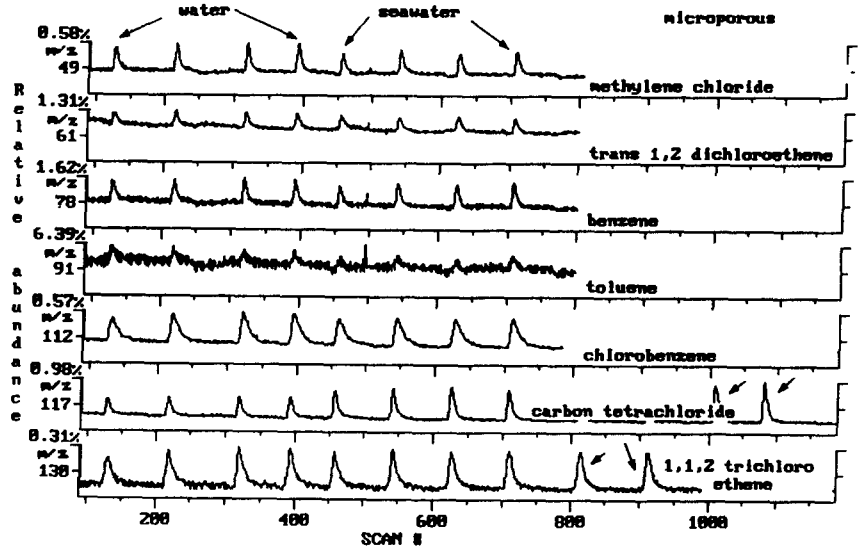


Fig. 9. Ion chromatograms recorded for a seven-component mixture (methylene chloride, *trans*-1,2-dichloroethylene, benzene, toluene, chlorobenzene, carbon tetrachloride and 1,1,2-trichloroethene) at 10 ppb, each using a microporous membrane and 1 ml sample volume. The arrows indicate the injections of water and seawater samples. The last four arrows, two for 1,1,2-trichloroethene and two for carbon tetrachloride, represent each analyte prepared in water in the absence of the other six components.

permeabilities and not due to differences in ionization cross sections. The non-polar compounds methylene chloride, *trans*-1,2-dichloroethene, benzene, toluene, and carbon tetrachloride respond much faster than the relatively polar compounds chlorobenzene and 1,1,2-trichloro-ethene when using the silicone membrane. Thus, the more polar the compound, the slower the response for the silicone membrane. The ion chromatogram for the same mixture recorded using a microporous membrane shows a reduced analysis time and this allowed 12 sample injections in the time requested for four injections with the silicone membrane.

Another possible matrix effect studied was that of one organic analyte on the signal of another. Previously, such analyte matrix effects were observed in the study of binary and ternary solutions performed with a direct inser-

tion probe using a TSQ 4500 mass spectrometer [23]. Under EI conditions, hardly any matrix effect occurred, but using CI a small matrix effect was observed, especially if the proton affinities of the analytes varied significantly. To confirm the lack of mutual matrix effects among the analytes, standards of carbon tetrachloride and 1,1,2-trichloroethylene were prepared in deionized water. Carbon tetrachloride and 1,1,2-trichloroethylene were chosen to represent a non-polar compound and a relatively polar compound respectively. Two injections of each standard were made, as shown in Fig. 9 (the last two peaks of carbon tetrachloride and 1,1,2-trichloroethylene). The signal intensities obtained are identical to that of the mixture, indicating no mutual matrix effects among the analytes for these compounds.

## 4. Conclusion

For the range of analytes and concentrations examined, no preconcentration or sample work up is required for seawater analysis by MIMS. The present results are consistent with and extend the seawater studies of Bauer and Solyom [15]. An attractive feature of the present FIA-MIMS is the simplicity of the experimental set up. The membrane accessibility, availability of various types of membranes, extended operation without membrane clogging, and detection limits in the ppb–ppt range pave the way for the in situ analysis of VOCs in seawater samples. Microporous membranes offer lower detection limits and give faster response times than silicone membranes. By increasing the sample volume, using microporous membranes, and optimizing membrane length, temperature and flow rate, one can achieve detection of specific analytes in the lower ppt range. If FIA-MIMS is combined with SWIFT in addition to the extremely low LODs ($pg\,l^{-1}$), one should be able to perform MS/MS to confirm the identity of minor components in seawater. In addition, the methods used here may prove useful for monitoring of VOCs in real environmental samples and industrial effluents of high ionic strengths.

## Acknowledgment

This work was supported by the Office of Naval Research.

## References

[1] Lawrence A. Baker, Environmental Chemistry of Lakes and Reservoirs, Advances in Chemistry Series 237, Washington, DC, 1994, Chapter 17–19.
[2] M.E. McNally and R.L. Grob, Am. Lab., 17 (1985) 20–63.
[3] E. Fogelqvist, B. Josefsson and C. Roos, Environ. Sci. Tech., 16 (1982) 479–482.
[4] K. Abrahamsson and S. Klick, Chemosphere, 18 (1989) 2247–2256.
[5] T. Kotiaho, F.R. Lauritsen, T.K. Choudhury and R.G. Cooks, Anal. Chem., 63 (1991) 857–883A.
[6] R.G. Cooks and T. Kotiaho, ACS Symp. Ser., Vol. 508, Washington, DC, 1992, Chapter 12.
[7] N. Srinivasan, N. Kasthurikrishnan, R.G. Cooks, M. Krishnan and G. Tsao, Anal. Chim. Acta, in press.
[8] S.J. Bauer and R.G. Cooks, Am. Lab., October (1993) 36–51.
[9] J.S. Patrick, P. Wong, C. Xu, M. Soni, N. Kasthurikrishnan, N. Srinivasan and R.G. Cooks, Process Control Qual., submitted for publication.
[10] P. Wong, R.G. Cooks, M.E. Cisper and P.H. Hemberger, Environ. Sci. Tech., 29 (1995) 215A.
[11] F.R. Lauritsen and S. Gylling, Anal. Chem., submitted for publication.
[12] P.H. Hemberger, Anal. Chem., submitted for publication.
[13] T. Kotiaho, Anal. Chem., submitted for publication.
[14] M. Soni, S. Bauer, J.W. Amy, P. Wong and R.G. Cooks, Anal. Chem., 67 (1995) 1409.
[15] S. Bauer and D. Solyom, Anal. Chem., 66 (1994) 4422–4431.
[16] J. Brodbelt and R.G. Cooks, Anal. Chem., 57 (1985) 1153–1155.
[17] M. Bier and R.G. Cooks, Anal. Chem., 59 (1987) 597–601.
[18] L.E. Dejarme, S.J. Bauer and R.G. Cooks, Rapid Commun. Mass Spectrom., Vol. 7, 1993, pp. 935–942.
[19] L.E. Slivon, M.R. Bauer, J.S. Ho and W.L. Budde, Anal. Chem., 63 (1991) 1335.
[20] M.A. LaPack, J.C. Tou and C.G. Enke, Anal. Chem., 62 (1990) 1265–1271.
[21] P. Wong and R.G. Cooks, Anal. Chim. Acta, in press.
[22] M.J. Hayward, T. Kotiaho, A.K. Lister, R.G. Cooks, G.D. Austin and G. Tsao, Anal. Chem., 62 (1990) 1798.
[23] F.R. Lauritsen, T.K. Choudhury, L.E. Dejarme and R.G. Cooks, Anal. Chim. Acta, 266 (1992) 1–12.
[24] C. Horvath and W. Melander, J. Chromatogr. Sci., 15 (1977) 393.
[25] M.E. Bier, T. Kotiaho and R.G. Cooks, Anal. Chim. Acta, 231 (1990) 175–190.

ELSEVIER

Talanta 42 (1995) 1337–1344

Talanta

# Development of an optical fibre Al(III) sensor based on immobilised chrome azurol S

Musa Ahmad [a,*], Ramaier Narayanaswamy [b]

[a] *Chemistry Department, Faculty of Physical and Applied Science, Universiti Kebangsaan Malaysia, 43600 Bangi, Selangor, D.E., Malaysia*

[b] *Department of Instrumentation and Analytical Science, UMIST, P.O. Box 88, Sacville Street, Manchester M60 1QD, UK*

Received 12 December 1994; revised 20 December 1994; accepted 9 March 1995

**Abstract**

Chrome azurol S immobilised on XAD-2 has been used in this study as a reagent phase for the development of an optical fibre Al(III) sensor. Using a kinetic approach, this sensor was able to give a linear response in the Al(III) concentration range of $1.3 \times 10^{-5}$–$2.0 \times 10^{-4}$ M with a limit of detection of $1.0 \times 10^{-4}$ M. The optimum responses were obtained at pH 6.0 and when the solution was stirred. The sensor response was found to have a repeatability and reproducibility of 1.6% and 5.8%, respectively. The results obtained for Al(III) determination in aqueous sample were in good agreement with those obtained using graphite furnace-atomic absorption spectrometry.

## 1. Introduction

In the past, immobilised reagents have been widely used as preconcentrating agents in analytical detection schemes where the analytes were generally eluted prior to the quantitation step [1]. With a growing interest in the area of chemical sensing using optical fibre, immobilised reagents are now used as a reagent phase in the development of such sensors. The reagents are normally adsorbed onto, chemically bonded to, physically entrapped in or electrostatically attracted to the support. The immobilised reagent is then coupled to the distal end of the fibre.

The performance of the immobilised eriochrome cyanine R on XAD-2 when used as a reagent phase in the development of a flow-cell type optosensor [2] and a probe type sensor [3] has been previously described. In this paper, we report the potential of immobilised chrome azurol S (CAS) as a reagent phase in the development of a probe type sensor.

## 2. Experimental

### 2.1. Reagent

An ammonia acetic buffer of pH 6.0 was prepared as follows. About 50 ml of glacial acetic acid (AR) was mixed with approximately 500 ml of distilled deionised water. Sufficient ammonia solution (s.g. 0.88, AR) was then added to adjust the pH to 6.0 (approximately about 50 ml required), and the mixture was diluted to 1 l with distilled deionised water.

An aluminium standard solution of $4.0 \times 10^{-4}$ M was prepared by dissolving the required amount of aluminium potassium sulphate, $Al_2(SO_4)_3K_2SO_4 \cdot 24H_2O$ in deionised water and then diluting the solution with deionised water to 250 ml. 0.019 g of cetylpyridinium chloride (CP) was dissolved in deionised water and the solution made up to 250 ml volume with deionised water to give a

* Corresponding author.


*SSDI* 0039-9140(95)01591-4

CP standard solution of $2.0 \times 10^{-4}$ M. A solution of CAS (Fluka) was prepared daily in the buffer.

### 2.2. Instrumentation

An aluminium probe incorporated in an optical fibre reflectance measurement rig was used in this study to measure the reflectance of the probe before and after reaction with aluminium. The design of the probe used in this study was the same as described previously [3].

Graphite furnace-atomic absorption spectrometry (GF-AAS) was performed on a Perkin-Elmer 3100 model for atomic absorption measurement of the aluminium samples. The wavelength was set at 309.3 nm. Pyrolytic graphite coated graphite tubes were employed and a hollow aluminium cathode lamp was used as a light source.

### 2.3. Procedure

Adsorption was used in this study to immobilise the reagents onto a solid support. This technique is the most convenient method of immobilisation, since it is exceedingly easy to perform, merely requiring stirring of the reagent and the support. Weak forces such as van der Waals forces and hydrogen bonding may act to immobilise the dye onto a substrate.

The absorbent materials used in this work include the Amberlite XAD series of porous polymers (XAD-2, XAD-4, XAD-7 and XAD-8) and anion exchange resins (Dowex 1-X8 (Cl), IRA-400(Cl), IR-45(OH)). All the solid supports used were supplied by BDH.

Prior to use, the XAD resins had to undergo a pretreatment process, since they were supplied impregnated with ammonium chloride to prevent the formation of mould during storage. The XAD resins were washed thoroughly with distilled water, soaked in acetone and finally thoroughly washed in distilled water again. The ion exchange resins were first washed using acetone and then thoroughly washed with distilled water. All the solid supports were used as supplied without further grinding.

The adsorption of the reagents onto the solid supports was investigated qualitatively using an aqueous CAS solution of $2.0 \times 10^{-4}$ M. The reagent was immobilised alone in the presence of CP and as its aluminium ternary complexes. In the former, 10 ml of distilled water, 30 ml of CP and 30 ml of CAS solution were added to approximatley 1 g of solid support and stirred for about 5 h at room temperature. In the latter, the same procedure was repeated, but instead of distilled water, 10 ml of $2.0 \times 10^{-4}$ M aluminium solution was added. A sample of the solid support with immobilised reagent was then removed from the supernatant liquid, washed with deionised water and left to dry in a desiccator. The solid support, which bound the reagent firmly and at the same time retained the properties of the reagent as in its solution form, was considered the best.

The reflectance measurement was carried out by the use of a kinetic approach where the signal was measured 3 min after placement of the probe in the aluminium solution. The measurements were expressed as a reflectance difference, which is defined as the difference between the reflectance of the aluminium complex and that of the immobilised reagent alone (in the presence of CP), both recorded at the same measurement wavelength (635 nm).

The use of repeatability and reproducibility terms to express variations in probe response has been suggested by Alabbas et al. [4]. The sensor repeatability refers to the successive runs made using a single sensor to evaluate discrepancies in its response. The sensor reproducibility refers to the discrepancies in response between individual members of a batch of similarly constructed sensors. The repeatability and reproducibility of optical fibre sensors are two of its important characteristic features and were studied in this work at an aluminium concentration of $2.0 \times 10^{-4}$ M.

The response of the probe was optimised by studying the effects of pH, stirring of the solution and reagent concentration. The influence of stirring was studied by comparing the response of the probe towards the same concentration of aluminium when the solution was stirred and unstirred. The effect of reagent loading on the probe response was studied using immobilised reagents prepared from different reagent concentrations. The time of immobilisation (5 h) and stirring speed were maintained constant.

The effect of foreign ions was studied by introducing different amounts (moles) of interfering ions to the sensing probe. The degree of interference of these ions was evaluated with reflectance measurements, recorded in the presence and absence of the interfering ion in the determination of a given concentration ($2.0 \times 10^{-4}$ M) of aluminium.

For determination with GF-AAS, three different samples of known concentration (Table 2) were prepared in the laboratory. These samples were diluted 100 times, and 20 μl of the diluted sample was injected into the graphite furnace. The reading (peak height) was recorded at a wavelength of 309.3 nm. The calibration graph was prepared in a similar way using a standard aluminium solution ranging from $1.3 \times 10^{-5}$ to $8.0 \times 10^{-4}$ M.

## 3. Results and discussion

The Amberlite XAD series of porous polymers gave better results than ion exchange resins, since they could make available the reagent functional groups to form a complex with aluminium ion. The colour change of the immobilised reagents after reaction with aluminium was noted to be similar to that in solution (from red to blue). The reagent could also be successfully immobilised on the anionic exchange resin, but the changes in the reflectance signals in presence of aluminium were noticed to be very small. Among the XAD series, the highest reflectance change between the immobilised reagents and its complexes was observed for XAD-2. Therefore, XAD-2 was chosen for further study as a solid support for the immobilisation of CAS.

XAD-2 is an aromatic hydrophobic absorbent which has a styrene–divinylbenzene cross-linked structure [5]. In an adsorption process, XAD-2 will selectively adsorb water soluble organic substances. The hydrophobic portion of the organic substance is preferentially adsorbed while the hydrophilic portion of the molecule will remain oriented in the aqueous phase. The interaction between XAD-2 and CAS may involve the interaction depicted in Fig. 1, since colour changes were observed to be similar to that in solution. Further, as shown in Fig. 2, the optimum pH

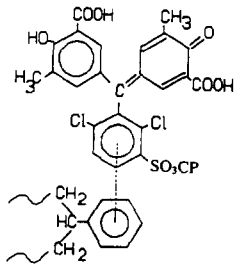


Fig. 1. The possible interaction of XAD-2 with CAS.

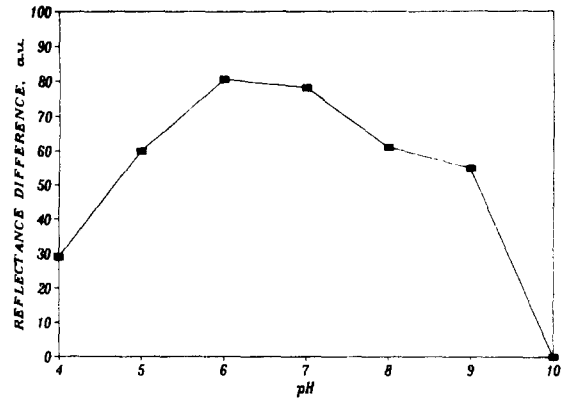


Fig. 2. The effect of pH on the ternary complex formation of aluminium with immobilised CAS in the presence of cationic surfactant.

value for complex formation was found to be identical to that in the solution. Quinolin-8-*o*-sulphonate was found to behave in the same manner when electrostatically immobilised on Amberlite CG-400 resin [6]. From this observation, it can be stated that the interaction between the immobilised reagent and XAD-2 had no effect on the functional groups of the reagent which was used in the formation of complexes with aluminium. Because of competition between hydrogen and aluminium ions for the organic ligands at low pH values and competition between hydroxyl and organic ligand ions for aluminium ions at high pH values, Driscoll and Schecher [7] reported that aluminium–organic complexation is generally at a maximum in the acidic to neutral pH range.

Fig. 3 shows the reflectance spectra of the reagents immobilised alone in the presence of CP and as their aluminium ternary complexes. The decrease in reflectance at all wavelengths in the range 520–720 nm is due to the forma-

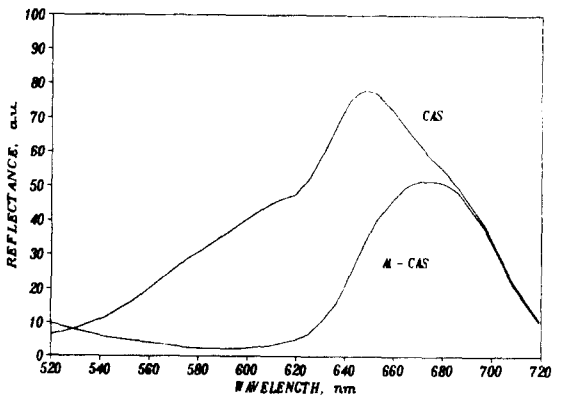


Fig. 3. Reflectance spectra of the reagent CAS immobilised alone in the presence of CP and as its ternary complex with aluminium.

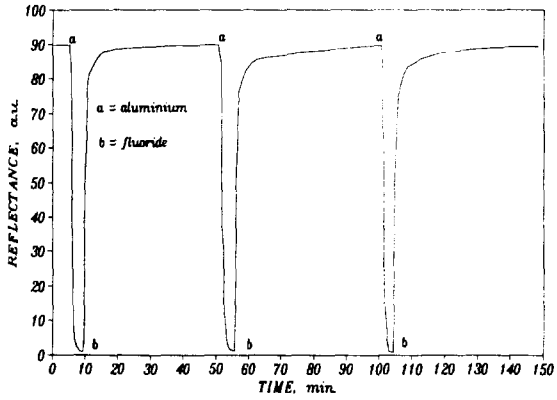


Fig. 4. The alternate reaction of immobilised CAS with aluminium and fluoride solution (regenerating solution).

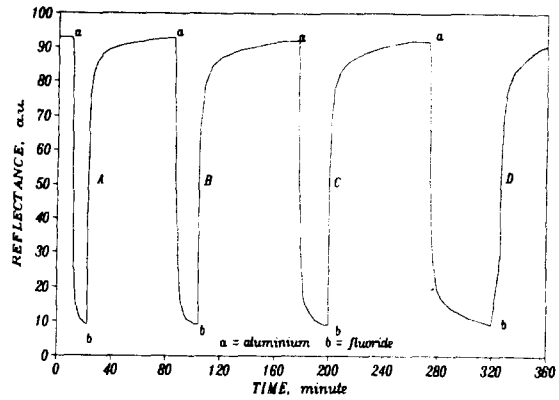


Fig. 5. The response of immobilised CAS to four different concentrations of aluminium, i.e. $6.4 \times 10^{-3}$ M (A), $3.2 \times 10^{-3}$ M (B), $1.6 \times 10^{-4}$ M (C) and $7.8 \times 10^{-4}$ M(D).

tion of a coloured aluminium complex which strongly absorbs the incident light and thus attenuates the intensity of the reflected light. Reflectance measurements were made at a chosen wavelength at which a large change in reflectance signal with aluminium concentration was observed. Therefore, a wavelength of 635 nm was used for measuring reflectance signal from the immobilised CAS.

Fig. 4 shows the reflectance response (measured at a single wavelength of 635 nm) of the immobilised CAS after reaction with aluminium solution and generation with fluoride solution. As can be discerned, regeneration of the reagent was time-consuming. The long regeneration time for CAS can be explained by the fact that it has a bulk chemical structure, since it contains two chlorine atoms. As fluoride has the same ionic charge as chlorine, repulsive forces due to chlorine will be experienced by the fluoride ions approaching the complex to react with aluminium. This repulsion will slow down the regeneration process of the reagent and a longer time is required for regeneration. Eriochrome cyanine R, which has exactly the same structure as CAS except for the two chlorine atoms, was found to be easily regenerated in a shorter time when the same regenerating solution was used [2].

The response of immobilised CAS towards different aluminium concentrations is shown in Fig. 5. As for immobilised eriochrome cyanine R [2], the response was independent of the aluminium concentration used since different concentrations of aluminium were found to give the same final response. The time taken to reach the steady state response, however, depended on the concentration of aluminium. A kinetic approach, whereby the reflectance difference of the system is measured at a fixed time, was therefore used in further studies to characterise this reagent. Fig. 6 shows the responses of immobilised CAS towards different concentrations of aluminium at different reaction times. Reaction times greater than 3–4 min would limit the determination to within a very narrow range.

Stirring the aluminium solution has a significant effect on the response of the probe. As shown in Fig. 7, the rate of increase of the reflectance difference is much higher when the aluminium solution is stirred compared to that without stirring. Stirring the aluminium solution could facilitate the diffusion of aluminium ions across the nylon mesh to the reagent, and therefore speed up the reaction between the reagent and the aluminium. Without stirring, however, the diffusion depended solely on the concentration gradient across the membrane.

The effect of the reagent concentration on the probe response was studied using different concentrations of the reagent during its immobilisation. These immobilised reagents were

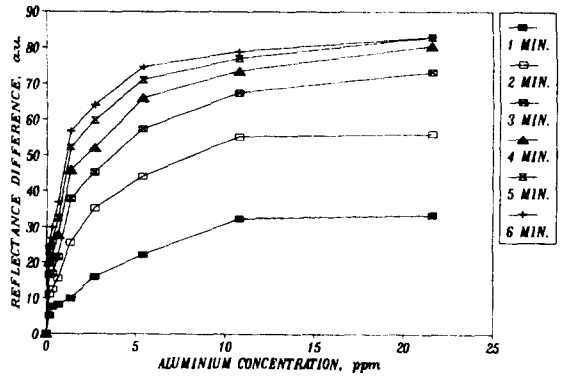


Fig. 6. The response of immobilised CAS to different aluminium concentrations at different reaction times.

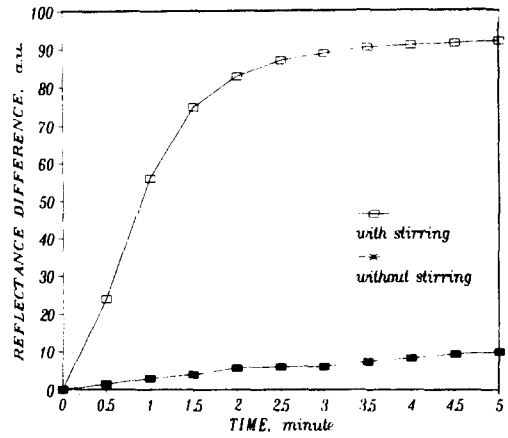


Fig. 7. The effect of stirring on the probe response based on immobilised CAS.

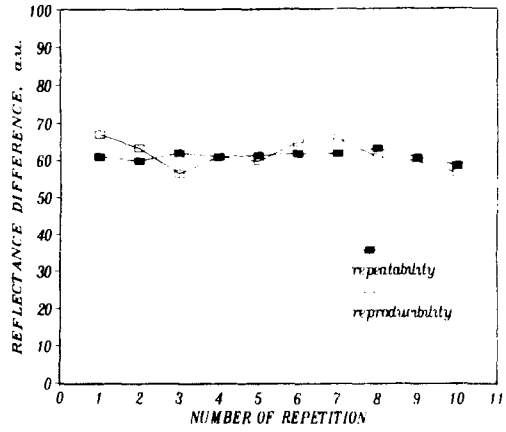


Fig. 9. Reproducibility and repeatability of the aluminium probes based on immobilised CAS.

used for reaction with aluminium of $6.4 \times 10^{-3}$ and $2.0 \times 10^{-4}$ M concentrations. The results, shown in Fig. 8, indicate that the higher the reagent concentration used for immobilisation, the higher the reflectance signal obtained for the same concentration of aluminium. A similar observation was made for blood pH sensor based on compound 5-91 immobilised on cellophane [8]. As indicated in Fig. 8, the amount of reagent in the matrix can be controlled by choosing the appropriate concentration of reagent during immobilisation. No reagent concentration higher than 0.01 M was studied, since at room temperature a saturated solution is produced. Higher solution of concentrations of reagent allowed more of it to be immobilised, resulting in the reaction of more aluminium ions to produce a higher reflectance signal. Although it seems desirable to immobilise as much indicator as possible in order to obtain an intense signal, it is advisable to immobilise just enough indicator to obtain a reasonable signal. For a pH sensor, for example, too heavy a loading of the matrix with the reagent was found to result in lower $pK_a$ values, worse reproducibility of the response and a strong background whose intensity did not vary with pH [9].

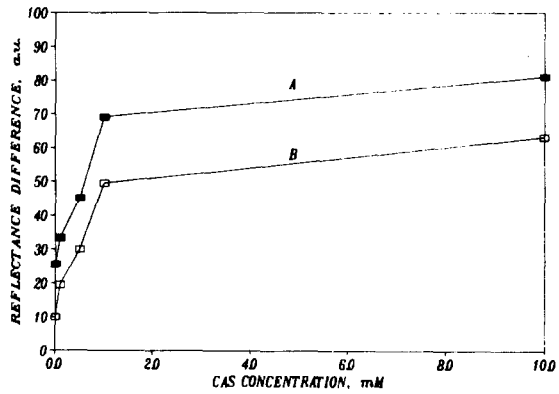


Fig. 8. The effect of concentration of the reagent used for immobilisation on the probe response based on immobilised CAS, at two different aluminium concentrations, i.e. $6.4 \times 10^{-3}$ M (A) and $2.0 \times 10^{-4}$ M (B).

Fig. 9 shows that the repeatability of the probe was always better than its reproducibility. The repeatability of the probe was found to be 1.6% whereas the reproducibility was found to be 5.8%. In the literautre, there is hardly any comment on the effect of variation in construction parameters of the sensor, e.g. the indicator concentration for immobilisation, the amount of polymeric support matrix and the particle size of the matrix. According to Alabbas et al. [4], the variation in the response of an optical fibre sensor has been noted to arise from two main sources, i.e. construction variation and operational variation. The former includes the variation caused by the quantity of matrix, concentration of reagent, particle size and shape of the probe, while the latter is due to variations in analyte concentration. They concluded that the major source of non-uniformity of response lay in the sensor construction (6.5–9.5%) rather than sensor operation (2.6%).

Table 1 shows the results obtained for anion and cation interference studies during aluminium determination. Generally, negative interference was observed for anions whereas cations showed positive interference. Negative interference can result from the reaction of the interferent with the analyte being determined, leading to an incomplete reaction [10]. The most common type of such an interference is the complexing of the analyte by the interfer-

Table 1
Degree of interference of some anions and cations of aluminium using a probe based on immobilised CAS

| $X^{n-}$ | $Al^{3+}:X^{n-}$ | Ref. diff. (a.u.) | % Error | $M^{n-}$ | $Al^{3+}:M^{n+}$ | Ref. diff. (a.u.) | % Error |
|---|---|---|---|---|---|---|---|
| $F^-$ | 1:1 | 49.7 | −12.9 | $Be^{2+}$ | 1:1 | 75.5 | +29.1 |
| | 1:3 | 35.3 | −38.2 | | 1:10 | 79.0 | +35.0 |
| | 1:5 | 14.0 | −75.5 | | 1:100 | 79.8 | +36.4 |
| EDTA | 1:1 | 37.8 | −33.8 | $Fe^{3+}$ | 1:1 | 59.7 | n |
| | 1:3 | 5.6 | −90.2 | | 1:10 | 72.0 | +23.1 |
| | 1:5 | 1.0 | −98.3 | | 1:100 | 77.0 | +31.6 |
| $C_2O_4^{2-}$ | 1:1 | 55.7 | −2.4 | $Cu^{2+}$ | 1:1 | 67.0 | +14.5 |
| oxalate | 1:3 | 40.6 | −28.9 | | 1:10 | 74.0 | +26.5 |
| | 1:5 | 16.6 | −70.9 | | 1:100 | 79.0 | +35.0 |
| $C_4H_5O_7^{2-}$ | 1:1 | 17.0 | −31.7 | $Ga^{3+}$ | 1:1 | 60.0 | n |
| citrate | 1:3 | 3.3 | −88.3 | | 1:10 | 60.0 | n |
| | 1:5 | 0.5 | −93.5 | | 1:100 | 52.5 | −10.3 |
| $C_4O_6H_4^{2-}$ | 1:1 | 82.5 | −6.3 | $Zn^{2+}$ | 1:1 | 60.0 | n |
| tartrate | 1:3 | 62.0 | −24.6 | | 1:10 | 60.0 | n |
| | 1:5 | 48.0 | −45.5 | | 1:100 | 63.0 | +7.7 |
| $PO_4^{2-}$ | 1:1 | 39.6 | −30.7 | $In^{3+}$ | 1:1 | 59.0 | n |
| | 1:3 | 22.7 | −60.3 | | 1:10 | 58.5 | n |
| | 1:5 | 12.3 | −78.4 | | 1:100 | 56.0 | n |

n = no interference; a.u. = arbitrary units.

ent. Since most of the anions used in this study have a tendency to react with aluminium ions to form a colourless complex, a negative type of interference is expected. Positive interferents normally react directly with the reagent along with the analyte and produce coloured species, so that high absorbance is obtained.

Interference from anions such as fluoride, oxalate, EDTA and tartrate is expected, since they form a stable complex with aluminium [11]. As the stability constant (in logarithms) for EDTA, citrate and oxalate complexes with aluminium was reported to be 16.5, 8.1 and 6.1, respectively [12], the degree of anion interferent is expected to vary in the order EDTA > citrate > oxalate. No interferent from hydroxide ions was observed even if its concentration was 100 times higher than of aluminium. This indicates that, at least at the pH used in this study, the tendency of the aluminium to hydrolyse is very small in the presence of the ligands. As well as anions, interference from iron and beryllium ions is also expected, since the ionic radius of the former is similar to that of the aluminium ion [13]. The use of eriochrome cyanine R (which has a similar structure as CAS) solution for the determination of beryllium has been reported in the literature [14].

EDTA showed the highest interference effect, clearly because it has six potential sites for binding with the aluminium ion (the four carboxyl groups and the two amino groups, each of the amino nitrogens with four unshared electrons). The complex formed between EDTA and aluminium is sufficiently stable, which undoubtedly results from the multiple complexing sites within the molecule by which an aluminium ion is effectively surrounded and isolated from the solvent molecules [15].

It should be noted that although a reasonable number of ions in this study were found to interfere with the aluminium determination, not all of these are expected to be present in real water samples. Of these, fluoride and iron ions are normally present in water samples with aluminium. Fluoride ions originate from the salt used to treat the water, whereas iron is present in the sample because of its natural occurrence. One should remember, however, that aluminium is the third most common constituent of the Earth's crust after silicon and oxygen. Thus, the possibility of having a very high concentration of these interfering ions compared to that of aluminium in the water samples is less. At a 1:1 ratio of these interfering ions to aluminium, the interference was shown to be slight and can be overcome by the use of conventional methods, such as applica-

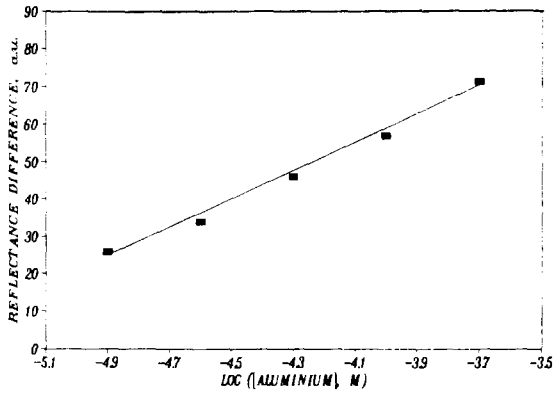


Fig. 10. The dynamic range of aluminium concentration determined by a probe based on immobilised CAS. The reflectance difference was measured 3 min after placement of the probe in the aluminium solution.

tion of a masking agent, or more practical methods, such as synchronous derivative spectrometry. Capitan and co-workers [16,17] have demonstrated the use of the latter type of methods as providing a means for the simultaneous determination of many metal ions.

Fig. 10 shows that the aluminium probe based on immobilised CAS produced a linear relationship between the reflectance difference and the logarithm of aluminium concentration in the range of $1.3 \times 10^{-5} - 2.0 \times 10^{-4}$ M.

An attempt was also made to study the reliability of the results obtained using these probes by comparison with well-established methods such as GF-AAS. The results obtained are shown in Table 2. Although the standard deviation of the reflectance method is found to be slightly greater than that of GF-AAS, the results obtained show very good agreement with the aluminium concentration determined in the sample using the optical sensor.

The limit of detection, defined as the concentration of sample that yields a detector response equal to three times the detector noise, was found to be $1.0 \times 10^{-5}$ M.

Table 2
Determination of aluminium in aqueous sample using both GF-AAS and optical fibre aluminium sensors based on immobilised CAS. With the latter, the reflectance difference was measured 3 min after placement of the probe in aluminium solution

| Concentration | $[Al^{3+}]$ determined by GF-AAS (M) | $[Al^{3+}]$ determined using the CAS probe (M) |
|---|---|---|
| $3.0 \times 10^{-4}$ | $3.0(\pm 0.2) \times 10^{-4}$ | $3.3(\pm 0.3) \times 10^{-4}$ |
| $8.0 \times 10^{-5}$ | $8.0(\pm 0.2) \times 10^{-5}$ | $7.8(\pm 0.4) \times 10^{-5}$ |
| $2.0 \times 10^{-5}$ | $2.0(\pm 0.1) \times 10^{-5}$ | $2.2(\pm 0.4) \times 10^{-5}$ |

## 4. Conclusion

Immobilised CAS on XAD 2 provides good reagent phases for the development of an optical aluminium sensor. The sensor based on this reagent showed optimum response at pH 6.0. The amount of reagent loaded into the matrix was also found to have a significant effect on the response of the probe. The probe appears to be ideal for measurement of the aluminium content in a dynamic system, since it produced a very high reflectance signal when the solution was stirred.

The same steady state response was produced by the probe irrespective of the aluminium concentration used. The time taken to achieve this response is, however, dependent on the aluminium concentration, leading to the use of the kinetic method for quantification of the measurements. This study has also shown that on reaction with aluminium, the reagent produced a reproducible signal especially when the same probe was used in the measurement. Major interferences were observed from fluoride, EDTA, oxalate, citrate, tartrate, $Be^{2+}$, $Cu^{2+}$ and $Fe^{3+}$.

A linear relationship was obtained between the log of the aluminium concentration and the reflectance signal at aluminium concentrations in the range of $1.3 \times 10^{-5}$–$2.0 \times 10^{-4}$ M, with a limit of detection of $1.0 \times 10^{-5}$ M. The results obtained for aluminium determination in unknown samples using the reflectance method were in good agreement with those obtained using the GF-AAS technique.

## Acknowledgements

One of the authors (M. Ahmad) would like to acknowledge the financial support from the Association of Commonwealth Universities and Universiti Kebangsaan Malaysia.

## References

[1] M.A. Ditzler, H. Pierre-Jacques and S.A. Harrington, Anal. Chem., 58 (1986) 195.
[2] M. Ahmad and R. Narayanaswamy, J. Sci. Total Environ., 163 (1995) 221.
[3] M. Ahmad and R. Narayanaswamy, Anal. Chim. Acta, 291 (1994) 255.

[4] S.H. Alabbas, D.C. Ashworth and R. Narayanaswamy, Anal. Proc., 26 (1989) 373.
[5] Summary Bulletin, Amberlite Polymeric Adsorbents, Rohm and Haas Co., Philadelphia, PA, 1978.
[6] Z. Zhujun and W.R. Seitz, Anal. Chim. Acta, 171 (1985) 251.
[7] C.T. Driscoll and W.D. Schechler, in H. Sigel and A. Sigel, Metal Ions in Biological Systems: Aluminium and its Role in Biology, Vol. 24, Marcel Dekker, New York, 1988.
[8] R. Wolthuis, D. McCrae, E. Saaski, J. Hartl and G. Mitchell, IEEE Trans. Biomed. Eng., 39(3) (1992) 531.
[9] H. Offenbacher, O.S. Wolfbeis and E. Furlinger, Sensors Actuators, 9 (1989) 73.
[10] E.B. Sandell and H. Onishi, Photometric Determination of Trace Metals: General Aspects, Wiley, New York, 1978.
[11] Z. Marczenko, Separation and Spectrophotometric Determination of Elements, Wiley, New York, 1986.
[12] A.E. Martell and R.M. Smith, Critical Stability Constant, Vols. 1–5, Plenum, New York, 1974–1982.
[13] J.D. Birchall and J.S. Chappel, in Aluminium in Food and Environment, The Royal Society of Chemistry, London, 1989.
[14] S. Umemoto, Bull. Chem. Soc. Jpn., 29(7) (1956) 845.
[15] D.A. Skoog, D.M. West and F.J. Holler, Fundamental of Analytical Chemistry, Saunders College Publishing, New York, 1988.
[16] F. Capitan, G. Sanchez-Palencia, A. Navalon, L.F. Capitan-Valley and J.L. Vilchez, Anal. Chim. Acta, 259 (1992) 345.
[17] F. Capitan, E. Manzano, A. Navalon, J.L. Vilchez and L.F. Capitan-Valley, Talanta, 39(1) (1992) 21.

ELSEVIER

Talanta 42 (1995) 1345

Talanta

Corrigendum

# Corrigendum to "Direct determination of traces of Ag, Cd, Pb, Bi, Cr, Mn, Co, Ni, Li, Be, Cu and Sb in environmental waters and geological materials by simultaneous multi-element graphite furnace atomic absorption spectrometry with Zeeman-effect background correction" [Talanta 42(1995) 269–281]☆

J.G. Sen Gupta, J.L. Bouvier

The following text was inadvertently omitted from the footnotes of Table 11 (p. 277):

Mixed synthetic standard solutions used for preparation of calibration curves contained the same amount of reagents as the sample and taken through the microwave oven digestion procedure before making up the final volume to 50 ml.

☆SSDI of original article: 0039-9140(94)00256-8.

*SSDI* 0039-9140(95)01652-X

ELSEVIER

Talanta 42 (1995) 1347

Talanta

Erratum

# Erratum to "Mechanistic studies of metal ion binding to water-soluble polymers using potentiometry" [Talanta 42(1995) 219–226]☆

Neil V. Jarvis, Judith M. Wagener

Owing to a printing error, the Publisher regrets that Figs. 9 and 10 were poorly reproduced. They should have appeared as shown below.

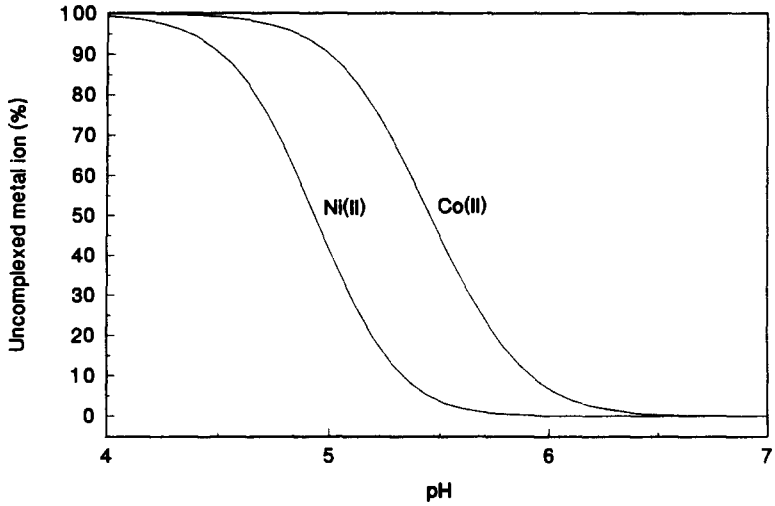


Fig. 9. Species distribution curves for the complexation of Co(II) and Ni(II) at 25°C and 1.0 M $NaNO_3$ (titration 3), as calculated from the apparent formation constants in Table 2. Only the uncomplexed metal ion plots are shown.

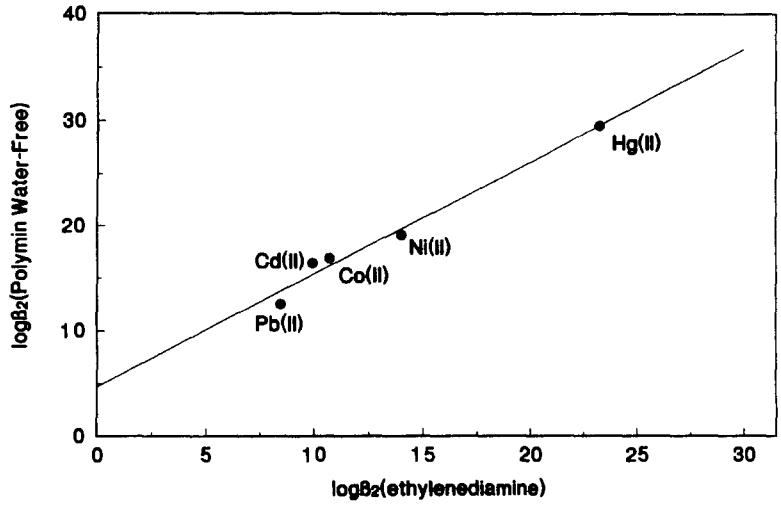


Fig. 10. Plot of log$\beta_2$ (Polymin Water-Free) vs. log$\beta_2$ (ethylenediamine) for the metal ions studied in this paper.

☆SSDI of original article: 0039-9140(94)00231-2.

*SSDI* 0039-9140(95)01655-4

ELSEVIER

Talanta 42 (1995) 1349–1354

Talanta

# Extraction spectrophotometric determination of mercury(II) using thiacrown ethers and Bromocresol Green

Bahruddin Saad [1], Salah M. Sultan *

*Department of Chemistry, KFUPM Box 2026, King Fahd University of Petroleum and Minerals, Dhahran 31261, Saudi Arabia*

Received 19 September 1994; revised 27 December 1994; accepted 5 January 1995

**Abstract**

A reasonably sensitive and highly selective spectrophotometric method for the determination of mercury(II) is proposed. The method is based on the extraction of the ion-associate formed by a mercury(II) thiacrown ether cationic complex with Bromocresol Green as the anionic counter-ion using chloroform as the extracting solvent. The effect of thiacrown ethers of different cavity sizes, namely 1,4,7,10,13-pentathiacyclopentadecane (PTP) and 1,4,7,10,13,16-hexathiacyclooctadecane (HTO), the thiacrown ether concentration, the extracting solvent, the bromocresol green concentration and the aqueous phase pH on the extraction were investigated. Measurement of the absorbance at the $\lambda_{max}$ (420 nm) of the extracted ion-associate reveals that Beer's law is obeyed over 0.5–12.0 ppm mercury(II) for both ligands. Slight interference from copper(II) and cadmium(II) is exhibited by the PTP ligand, while HTO is negligibly affected by these metal ions. Strong interference from silver(I) is evident for both ligands while alkali, alkaline earth and other transition metals tested posed negligible interference. Analysis of mercury in synthetic complex mixtures was satisfactory

## 1. Introduction

The toxicity of mercury compounds have caused widespread public concern as a result of several widely publicized disasters, beginning with the Minamata, Japan incident in 1950 where 111 people were poisoned after eating seafood containing high levels of methyl mercury (27–102 ppm dry wt) [1–3]. This incident and others [2,3] took place in limited areas where there had been heavy localized pollution with mercurial compounds.

Several analytical methods have been developed for the determination of mercury. Currently the most frequently used method for ultra-trace mercury analysis in environmental samples is flameless atomic absorption spectrophotometry [2,4,5]. Other analytical methods reported include spectrophotometry [2,5–8], fluorimetry [2,9] titrimetry [10], neutron activation analysis [11], optical [12] and electrochemical [2,13] methods. These methods, with the exception of neutron activation analysis, are generally suitable for the determination of trace levels of mercury. The spectrophotometric methods reported are mainly based on ion-associates of mercury(II) complexes, using reagents such as Bindschedler's Green [7], tetraphenylpyridine [6], Crystal Violet [5] and triazenes [8]. Although these methods are generally sensitive, they lack selectivity, making them only suitable for the analysis of simple samples.

Our strategy to minimize the interference problem is to exploit the complexing- and ion-

* Corresponding author. Fax: (966)3-860-4277.

[1] Permanent address: School of Chemical Sciences, Universiti Sains Malaysia, 11800 Penang, Malaysia.


*SSDI* 0039-9140(95)01514-0

discriminating ability of thiacrown ethers, which is a class of crown ethers where the donor oxygen atoms on the macrocycle ring have been replaced either partially or totally with sulfur atoms. Since sulfur atoms are soft Lewis bases, thiacrowns are expected to have strong affinity for soft Lewis acids such as mercury(II) [14–18]. Furthermore, thiacrown ethers can form stable cationic complexes with class b metal ions as classified by Ahrland et al. [14], which in turn can be reacted with an appropriate anion to form an ion-associate. Upon extraction with suitable solvents, a spectrophotometric procedure for mercury(II) may be viable. Although some mercury(II) complexes of thia ethers have been isolated and characterized [15,16], there are only a few studies concerning their analytical applications. In this paper we report the investigation of using a five- (**I**) and six- (**II**) membered ring sulfur macrocycle for the extractive spectrophotometric determination of mercury(II), using Bromocresol Green as the counter-ion.

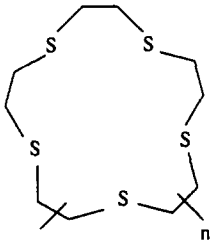


(I) n = 1, PTP
(II) n = 2, HTO

## 2. Experimental

### 2.1. Apparatus

Absorbance measurements were made with a Perkin-Elmer Lambda 5 UV/VIS spectrophotometer in conjunction with a quartz cuvette of 10 mm path length. pH measurements of the aqueous phase were performed with a Corning combination glass electrode (Catalog no. 476530) connected to a Corning pH meter Model 21. Unless otherwise stated, all data are the average of two determinations mainly carried out on different days.

### 2.2. Reagents and chemicals

All inorganic chemicals used were of analytical reagent grade. Sulfates of chromium(III), copper(II), manganese(II), iron(II), zinc(II), cadmium(II), nitrates of nickel(II), lead(II), silver(I) and chloride of cobalt(II) were used. Chloroform stabilized with ethanol of purity at least 99.9% was supplied by Fluka, while Bromocresol Green, sodium salt was purchased from Allied Chemical. The thiacrown ethers **I** and **II** were obtained from Aldrich. Deionized, distilled water was used throughout.

### 2.3. Stock solutions

Mercury(II) standard solution (0.01 M) was prepared by dissolving 0.340 g mercury(II) nitrate (BDH) in 2.0 ml of 2 M nitric acid and diluting to 100 ml with water. The solution was standardized as suggested by Vogel [19].

Bromocresol Green stock solution (0.010 M) was prepared by dissolving 0.360 g of the sodium salt in water and dilution to 50 ml with water.

Thiacrown ether stock solution (0.010 M) were prepared by dissolving 0.1503 and 0.1804 g PTP (**I**) and HTO (**II**), respectively, in chloroform and diluting to 50 ml. Ligand solutions were diluted from the stock solution daily. Macrocyclic sulfur ligands are highly toxic and should be handled with care.

Buffer solution pH (3.5) was prepared by dissolving 100.0 g ammonium acetate in water and adjusting the pH to 3.5 with 7 M hydrochloric acid followed by dilution to 200 ml with water.

### 2.4. Recommended procedure

Aliquots of mercury(II) standard solutions (0.10 or 1.0 mM) were transferred into a series of 125-ml separatory funnels, and 1.00 ml buffer solution (pH 3.5) and 1.00 ml Bromocresol Green solution (1.0 mM). The total volume of the aqueous phase was adjusted to 5.00 ml by addition of distilled water. Finally, 5.00 ml of 0.10 mM thiacrown ether in chloroform was added to each separatory funnel and the contents were shaken for 60 s. The organic phase was allowed to separate from the aqueous phase for at least 120 s and the absorbance of the separated chloroform layer was measured at 420 nm against a reagent blank. Blank solutions were treated in the same manner, except that no mercury(II) was added.

## 3. Results and discussion

### 3.1. Absorption spectra

The absorption spectra of the extracted ion-associates are shown in Fig. 1. Maximum absorption occurred at 420 nm for both ligands and all measurements were made at this wavelength.

### 3.2. Effect of pH

The influence of pH on the extraction was evaluated by measuring the absorbance of 40 ppm of mercury over the pH range 2–6, while keeping the Bromocresol Green and thiacrown ethers solutions constant at 1.0 mM. The pH was adjusted by addition of 1.0 M hydrochloric acid and/or 1 M ammonium hydroxide. Maximum absorbance was obtained for extraction at about pH 3–4.5 for both ligands (Fig. 2). Throughout the studies, an acetate buffer of pH 3.5 was used.

### 3.3. Thiacrown ether concentration

The influence of the ligand concentration on the absorbance signal of the extracted ion-associate was studied with a fixed amount of mercury(II) (2 ppm) and variation of the ligand concentration from 0.050 to 2.0 mM. The results show that the absorbance becomes constant at ligand concentrations of 0.10 mM and above (Fig. 3). To conserve the ligands, studies were conducted with 0.10 mM concentrations for both ligands.

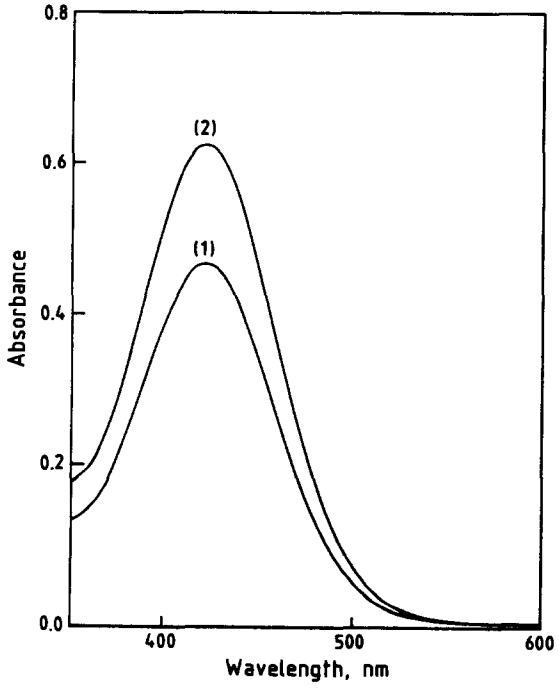


Fig. 1. Absorption spectra of chloroform extracts of thiacrown ether mercury(II)-Bromocresol Green complex. (1) PTP, [mercury(II) = 2.5 ppm]; (2) HTO, [mercury(II) = 4.0 ppm]. Reference: respective blanks.

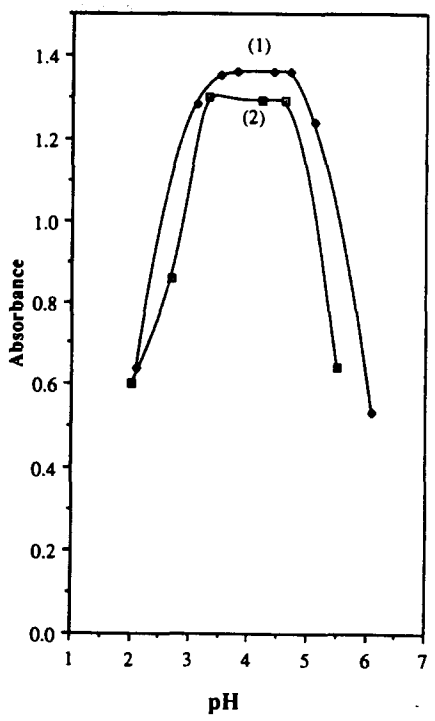


Fig. 2. Effect of pH on the chloroform extracts of thiacrown ether mercury(II)–Bromocresol Green complex, (1) PTP; (2) HTO. Conditions: mercury(II), 40.0 ppm; Bromocresol Green, 1.0 mM; ligand concentration, 1.0 mM.

### 3.4. Bromocresol Green concentration

The superiority of Bromocresol green as a counter-ion for ion-association extraction systems has been demonstrated previously [20,21]. Therefore, the use of other counter-ions was not investigated in this study. The influence of the Bromocresol Green concentration on the absorbance is shown in Fig. 4. For both ligands, the absorbance was constant for counter-ion concentrations of 1.0 mM and above.

### 3.5. Effect of shaking time

Mercury(II) was extracted with shaking times ranging from 30 to 300 s. The absorbance was found to be constant over this time period. A shaking time of 60 s was adopted.

### 3.6. Choice of extracting solvent

Mercury(II) was extracted at pH 3.5 with 1.0 mM Bromocresol Green and 1.0 mM ligand in chloroform, dichloromethane or toluene. The use of a low dielectric constant solvent such as toluene ($\varepsilon = 2.30$) [22], not only resulted in extraction with poor efficiency but also has poor phase separation. The use of chloroform ($\varepsilon = 4.8$) and dichloromethane ($\varepsilon = 9.08$) was satisfactory, probably owing to their higher dielectric constant, which favours extensive ion-pair formation [22]. Chloroform was selected because of its lower volatility.

### 3.7. Precision

The procedure was applied to the repetitive determination of 2.0 ppm of mercury(II) over a period of several days. The relative standard deviation for four determinations was found to be 1.04 and 1.08 for chloroform extractions based on HTO and PTP, respectively.

### 3.8. Calibration graph

The most suitable extraction conditions finally adopted is as follows: ligand concentration (0.10 mM), buffer pH 3.5, Bromocresol Green concentration (1.0 mM), shaking time (60 s), and chloroform as extracting solvent. The results for the extractions based on PTP and HTO are summarized in Table 1. The detection limit, calculated as described earlier [20,23] was found to be similar to that of flame atomic absorption spectrometry (0.14 ppm) [4]. Generally, the analytical characteristics of extractions based on the two ligands are similar.

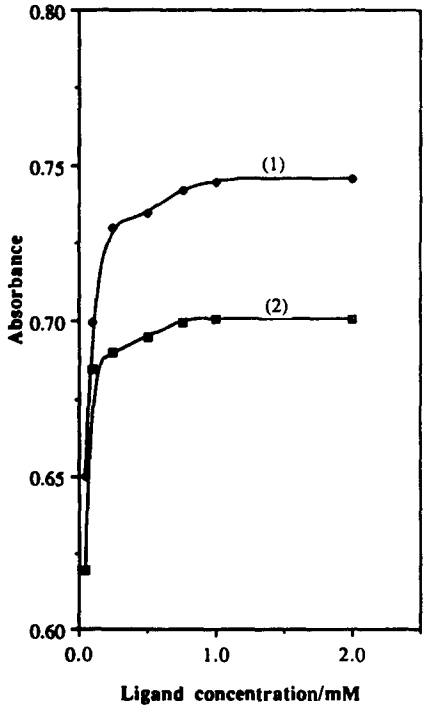


Fig. 3. Effect of ligand concentration on the chloroform extracts of thiacrown ether mercury(II)-Bromocresol Green complex. (1) PTP; (2) HTO. Conditions: mercury(II), 4.0 ppm; pH 3.5; Bromocresol Green, 1.0 mM.

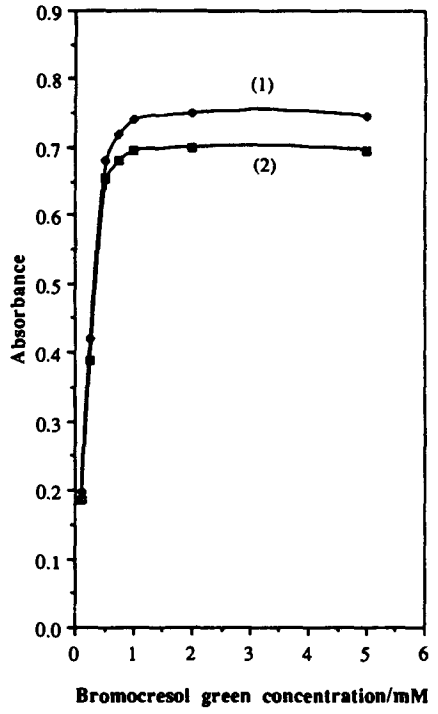


Fig. 4. Effect of Bromocresol Green concentration on the chloroform extracts of thiacrown ether mercury(II)–bromocresol green complex (1) PTP; (2) HTO. Conditions: mercury(II), 4.0 ppm; ligand concentration, 1.0 mM; pH 3.5.

Table 1
Analytical characteristics of mercury(II) thiacrown ether–Bromocresol Green complexes

| Characteristics | Thiacrown | |
|---|---|---|
| | PTP | HTO |
| $\lambda_{max}$ (nm) | 420 | 420 |
| Detection limit (ppm) | 0.15 | 0.14 |
| Dynamic linear concentration range (ppm) | 0.5–13.0 | 0.5–12.0 |
| Calibration graph | | |
| Slope | 0.1306 | 0.1353 |
| Intercept | 0.017 | 0.0857 |
| Correlation coefficient | 0.998 | 0.996 |

Table 2
Effect of other metal cations on the determination of 2.0 ppm of mercury(II)

| Cation | Molar ratio (M:Hg(II)) | Recovery (%) | |
|---|---|---|---|
| | | PTP | HTO |
| $Li^+$ | 1000 | 100.2 | 101.2 |
| $Na^+$ | 1000 | 100.2 | 100.6 |
| $K^+$ | 1000 | 98.6 | 100.4 |
| $Mg^{2+}$ | 1000 | 99.4 | 100.4 |
| $Ca^{2+}$ | 1000 | 102.2 | 99.8 |
| $Co^{2+}$ | 1000 | 101.8 | 99.6 |
| $Cr^{3+}$ | 1000 | 100.4 | 99.7 |
| $Fe^{2+}$ | 1000 | 98.4 | 99.0 |
| $Zn^{2+}$ | 1000 | 103.0 | 104.1 |
| $Pb^{2+}$ | 1000 | 95.2 | 104.3 |
| $Mn^{2+}$ | 1000 | 102.7 | 96.6 |
| $Ni^{2+}$ | 1000 | 102.8 | 98.0 |
| $Cu^{2+}$ | 500 | 120.3 | 104.2 |
| | 1000 | 149.0 | 110.8 |
| $Cd^{2+}$ | 500 | 122.5 | 96.4 |
| | 1000 | 150.0 | 110.0 |
| $Ag^+$ | 10 | 305.1 | 220.0 |
| | 1000 | 850.0 | 410.5 |
| Mixture A [a] | | | 103.2 |
| Mixture B [b] | | | 104.0 |

[a] Contains 100 molar each of $Zn^{2+}$, $Pb^{2+}$, $Ni^{2+}$, $Cu^{2+}$ and $Cd^{2+}$.
[b] Contains 500 molar each of $Zn^{2+}$, $Pb^{2+}$, $Ni^{2+}$, $Cu^{2+}$ and $Cd^{2+}$.

### 3.9. *Effect of foreign metal ions*

Thiacrown ethers generally exhibit high extractability for mercury(II) and silver ions [13–18,22]. The effect of some alkali, alkaline earth and transition metals on the determination of 2.0 ppm of mercury(II) was examined. Initially, solutions were prepared containing 1000 molar excess of the foreign ions relative to mercury(II). For metal ions that were found to cause interference, a lower concentration of the foreign ion was then prepared. The results are shown in Table 2. The data indicate that neither ligand exhibits interference by alkali and alkaline earth metal ions even though they are present in 1000 molar excess to that of mercury(II). Of the transition metal ions tested, only slight interference from copper(II) and cadmium(II) was observed for 1000 molar excesses of the foreign ions for both ligands. Interference with 500 molar excesses of these two metal ions continue to persist for the PTP ligand, while for HTO, the interference is negligible at this level. Based on the cavity size-ionic diameter considerations alone, copper(II) (ionic diameter 1.44 Å) [22] and Cd(II) (ionic diameter 1.94 Å) [22] would be expected to form stronger complexes with the smaller cavity size ligand PTP than HTO. This is probably reflected in the stronger interference of these metal ions by PTP. However, it must be pointed out that selectivity depends not only on the stability of the metal–ligand complex, but also on the nature of the extracting system [17,18].

Silver ion has a disastrous effect on all mercury(II) determinations. Probably the affinity of the thiacrown ether for silver(I) is as great, if not greater, than that for mercury(II). The cavity of the HTO macrocycle seems to be large enough to accommodate mercury(II) (ionic diameter 2.20 Å) and silver (ionic diameter 2.52 Å) ions [15]. The greater affinity of silver ions towards thiacrowns is well known and several analytical applications making use of this phenomenon have been reported. [13,17,18,24,25]. Thallium ion is also known to have high affinity to sulfur-containing ligands and, therefore, expected to exhibit high interference by using thiacrown in the present spectrophotometric method. Nevertheless, the proposed method is generally superior in terms of selectivity to the other spectrophotometric [5–8] and fluorimetric [9] methods reported earlier. However, the proposed method is considered more sensitive than the cold vapor atomic absorption method with lower detection limits. Moreover, the atomic absorption method suffers interferences from all metallic ions reduced together with the mercury especially if they amalgamate or form stable compounds with mercury, thus rendering our present method more selective. A quantitative comparison of the selectivity is difficult to make due to differences in the methods used for their assessment. Strong interference from cadmium(II), silver(I), iron(II) and copper(II) is evident for the use of crystal violet [5] while the use of tetraphenylpyridine [6] as a spectrophotometric reagent exhibits strong interference from cadmium(II) and silver(I). The use of a triazene reagent for mercury(II) determination, while exhibiting good sensitivity, suffer from interference by from these metal ions and others [8]. Interference from silver(I), lead(II) and manganese(II) is exhibited by the fluorimetric procedure [9].

The good recoveries obtained with the HTO ligand in the determination of mercury(II) in complex mixtures containing 100 (Mixture A) and 500 (Mixture B) molar excess each of

zinc(II), lead(II), nickel(II), copper(II) and cadmium(II) are further testimonials of the good selectivity characteristics of the proposed method (Table 2).

It has been reported that silver(I) picrate forms various complexes with HTO such as Ag(HTO)Pic and $Ag_2$(HTO)$Pic_2$ (Pic = picrate ion) [15]. In contrast, it has been established that mercury only forms a 1:1 mercury–thiacrown complex of the type Hg(HTO) $Pic_2$ [15]. Based on this consideration, the nature of the extracted species in this study is believed to be Hg(PTP)$(BCG)_2$ and Hg(HTO)$(BCG)_2$ (BCG = Bromocresol Green anion).

## 4. Conclusion

A sensitive and highly selective spectrophotometric procedure for the determination of mercury(II) which utilizes thiacrown ethers is demonstrated. The use of PTP and HTO thiacrown ethers yields system with identical sensitivity, but HTO is better in terms of overall selectivity. The proposed method has detection limits comparable to that of flame atomic absorption sepectrometry [4] and selectivity characteristics superior to the reported spectrophotometric [5–8] and spectrofluorimetric [9] procedures for mercury(II) determination. Under the conditions examined, the procedure exhibits serious interference only by silverI) and this method could be applied to mercury(II) determinations in complex silver-free samples, such as industrial effluents.

## Acknowledgements

One of us (B. Saad) is indebted to the King Fahd University of Petroleum and Minerals for a post-doctoral fellowship and to the Universiti Sains Malaysia, Penang for granting leave of absence.

## References

[1] L. Kurland, World Neurol., 1 (1960) 370.
[2] J.G. Saha and K.S. McKinlay, in R.W. Frei (Ed.), Analytical Aspects of Mercury and Other Metals in the Environment, Gordon and Breach, London, 1975, p. 2.
[3] P.A. Ditri and F.M. Ditri, Mercury Contamination: a Human Tragedy, John Wiley, New York, 1977.
[4] T.R. Crompton, Analytical Instrumentation for the Water Industry, Butterworth, Oxford, 1991.
[5] M.H. Cordoba, P.N. Navarro and I.L. Garcia, Int. J. Environ. Anal. Chem., 32 (1988) 97.
[6] T.P. Ruiz, J.A. Ortuno and M.C. Torrecillas, Anal. Chim. Acta, 165 (1984) 275.
[7] M. Tsubouchi, Anal. Chem., 42 (1970) 1087.
[8] C. Shiti and L. Xu, Talanta, 39 (1992) 1395.
[9] T.P. Ruiz, J.A. Ortuno and C.S. Pedreno, Analyst, 109 (1984) 1581.
[10] M. Nabrzyski, Anal. Chem., 45 (1973) 2438.
[11] K. Ishida, S. Kawamura and M. Izawa, Anal. Chim. Acta, 50 (1970) 351.
[12] M. Lerchi, E. Reitter, W. Simon, E. Pretsch, D.A. Chowdhury and S. Kamata, Anal. Chem., 66 (1994) 1713.
[13] M.T. Lai and J.S. Shih, Analyst, 111 (1986) 891.
[14] S. Ahrland, J. Chatt and N.R. Davies, Q. Rev., 12 (1958) 265.
[15] D. Sevdic, L. Fekete and H. Meider, J. Inorg. Nucl. Chem., 42 (1980) 885.
[16] D. Sevdic and H. Meider, J. Inorg. Nucl. Chem., 39 (1977) 1409.
[17] K. Saito, Y. Masuda and E. Sekido, Anal. Chim. Acta, 151 (1983) 447.
[18] K. Chayama and E. Sekido, Anal. Sci., 3 (1987) 535.
[19] Vogel's Textbook of Quantitative Inorganic analysis, 4th edn., Longman, London, 1978, p. 346.
[20] B. Saad, S.M. Sultan and F.O. Suliman, Analyst, Submitted for publication.
[21] K. Saito, Y. Masuda and E. Sekido, Bull. Chem. Soc. Jpn, 57 (1984) 189.
[22] M. Hiraoka, Crown Compounds, their Characteristics and Applications, Elsevier, Tokyo, 1982.
[23] C.M. Legua, P.C. Falco and A.S. Cabeza, Anal. Chim. Acta, 283 (1993) 635.
[24] M. Oue, K. Kimura and T. Shono, Anal. Chim. Acta, 194 (1987) 293.
[25] M. Oue, K. Kimura and T. Shono, Analyst, 113 (1988) 551.

ELSEVIER

Talanta 42 (1995) 1355–1360

Talanta

# A microwave digestion-based determination of low molecular weight organic acids in Bayer process liquor

A.R. Baker, A.M. Greenaway *, C.W. Ingram [1]

*Chemistry Department, University of the West Indies, Mona, Kingston 7, Jamaica*

Received 2 May 1994; revised 28 December 1994; accepted 5 January 1995

**Abstract**

A new technique for the determination of low molecular weight organic acids in Bayer process liquors is reported. The acids are partitioned from acidified liquor into butanol, followed by butylation using microwave heating. This method is both rapid (sample preparation time < 15 min) and capable of detecting acids larger than previously reported in the low molecular weight fraction (up to RMM 176). A standard solution containing 15 acids was used to calibrate the technique and 13 of these acids were detected and quantified in a Bayer liquor sample.

## 1. Introduction

Bauxites which are used in the production of alumina through the Bayer process commonly contain between 0.1 and 0.3% organic carbon [1,2]. Much of this carbon is in the form of structurally complex humic materials. Humic concentrations in the Bayer liquor are considerably higher than those of bauxite owing to the cyclical nature of the process [3]. The continual input of organic matter with the bauxite is counterbalanced by degradation of the humics as a result of the harsh process conditions (140–240 °C, 15 atm, 3.5 M NaOH). Eventually both the humics and their degradation products (polycarboxylic benzoic and phenolic acids, aliphatic acids, oxalate and carbonate) reach equilibrium levels in the liquor.

Detrimental effects on plant efficiency and alumina product quality have been attributed to organic matter in general [4–6] and to some low molecular weight acids in particular [1,2,4,7]. These considerations have lead to attempts to characterize the organic components of Bayer liquor [1,2,7], and to efforts to remove organic matter from the process [4,8,9].

Two methods for the determination of low molecular weight acids in Bayer liquors have been reported. Lever [1] used a complicated procedure for the removal of inorganic components from the liquor, prior to butylation of the acids at 110 °C in a sealed vial for 40 min. A much simpler determination was reported by Guthrie and co-workers, [2], in which acidified liquor was heated with butanol (70 °C, 1 h) in a sealed vial to accomplish butylation.

The butyl esters of acids from formic acid up to succinic acid (RMM 118) were detected by these two methods [1,2], and concentrations were calculated using an internal standard (nonanoic acid) by reference to a standard solution [1]. Good recoveries ( ~ 85%) have been reported for the method of Lever [7], despite the analysis involving evaporation of the liquor to dryness several times and the potential loss of the more volatile acids on each occasion. However, in this later work a more vigorous butylation procedure was used (110 °C, 4 h, pressure bomb) and higher molecular weight acids ($M \leqslant 166$) were detected [7].

* Corresponding author.

[1] Present address: Department of Chemistry, Clark Atlanta University, 223 James P Brawley Drive S.W., Atlanta, GA 30014, USA.


*SSDI* 0039-9140(95)01515-9

In this paper we report an improved procedure for the determination of low molecular weight ($M_r \leqslant 176$) organic acids, based on microwave heating of the butylation mixture, which offers advantages in both reduced analysis time and a greater range of organic acids detected over previous methods.

## 2. Experimental

### 2.1. Apparatus

Microwave digestions were carried out in an unmodified Panasonic domestic microwave oven (Model no. NN-7500), containing a sealed 500 ml vessel filled with water to prevent damage to the magnetron. Reactants were contained in Teflon digestion vessels (Savillex Corp., Minnesota). Butylated fractions were analysed by splitless injection on a Varian 3700 gas chromatograph, fitted with a flame ionization detector. The stationary phase was SPB-1 supported on a 30 m capillary column (i.d. 0.75 mm, film thickness 1 μm), with nitrogen (30 ml/min) as a carrier gas. The injector and detector temperatures were 250 and 270 °C, respectively, while the column was initially held at 50 °C for 4 min and then programmed to 250 °C at 10 °C/min and maintained at 250 °C for a further 7 min. Peak areas were determined by a Hewlett Packard HP3396A computing integrator.

### 2.2. Reagents

Extractions were carried out using very high purity butanol (99.4%). Analar grade HCl and Na $HCO_3$ were used for acidification of the process liquors and neutralisation of the butylated products. Low molecular weight acids used in the calibration of the procedure were of the highest grade available (AnalaR or Reagent). Nonanoic acid internal standard was of 90.0% minimum purity (Sigma Chemical Co).

### 2.3. Procedure

A 5 ml aliquot of an acidic (pH 1) solution containing low molecular weight acids (standard mixtures or acidified Bayer liquor) was shaken with 2 ml of an internal standard solution (1 g/l nonanic acid in butanol) for 5 min. After settling, the butanol phase was transferred to a 120 ml. Teflon microwave digestion vessel with 3 drops of 6 M HCl. The vessel was sealed and butylation of the acids was accomplished by heating the sample in a microwave oven (high setting, power output 1.2 kW). After cooling in an ice bath, the butanol layer was removed and neutralized with $NaHCO_3$. The concentrations of organic acids present were then determined by injection of 1 μl of the butanol fraction into the GC and determination of peak areas.

Apparent extraction efficiencies ($E$) for each component (x) of the standard solution were calculated according to eq. (1).

$$E = \frac{A_x V_{Bu} C_{NA}}{A_{NA} V_{aq} C_x} \quad (1)$$

where $A$ is the peak area of the component or the nonanoic acid, $V$ is the volume of the aqueous or butanol phases and $C$ is the concentration of the component or nonanoic acid. The values of $E$ obtained cannot be considered absolute since the flame ionization detector does not respond equally to each of the components of the mixture. However, this difference in flame response is implicitly corrected for in the calibration procedure enabling component concentrations to be determined quantitatively.

## 3. Results and discussion

### 3.1. Solubility of butanol and nonanoic acid

The loss of the internal standard (nonanoic acid) into the aqueous phase during extraction was examined by butylation of the internal standard solution before and after equilibrium with acidified deionized water. While the slight solubility of butanol in water leads to an increase in absolute peak intensity after equilibration, the integrated peak area per original unit volume of internal standard solution was found to be constant (area/ml before equilibration 5.28%, area/ml after equilibration 5.24%).

The concentration effect on component peak areas resulting from dissolution of butanol has been accounted for explicitly in this work. In all cases the relative properties of butanol and water have been kept constant and it is assumed that the fraction of butanol dissolving is also constant.

### 3.2. Calibration

Solutions containing two or three of the low molecular weight organic acids previously reported to be present in Bayer liquors (Table 1) were used to identify GC retention times for each component and to optimize microwave extraction conditions.

Digestion sequences based on numerous short pulses of microwave energy (10 × or 20 × 20 second bursts at 1 min intervals) and on one prolonged irradiation (3–8 min) were examined. Extraction efficiencies for the test solution components were found to be very similar for the short and long pulse regimes. The shorter extraction time and greater simplicity of the long pulse digestion was, therefore, preferred. Increasing digestion time was found to decrease the apparent extraction efficiencies of the lowest molecular acids (particularly formic and acetic acids) while increasing the yields for the larger acids (pentanoic, glutaric and phthalic) (see Fig. 1). A digestion time of 5 min was found to give the highest average extraction efficiencies over all the components.

Once optimum extraction conditions had been identified, a standard solution containing a number of acids of interest was prepared. The major Bayer liquor acids (formic, acetic and succinic) were initially present at concentrations of ca. 1.2 g/l, while the concentrations of the remaining components were ca. 0.6 g/l. The solution was sequentially diluted to one tenth of its original concentration, with three aliquots being removed for butylation at each dilution.

Table 1
Concentrations of low molecular weight organic acids reported in Bayer process liquors

| Acid | Concentration (g/l) | | |
|---|---|---|---|
| | Ref. [1] | Ref. [2] | Ref. [7] |
| Formic | 2.3 | 3.4, 5.9 | 3.0 |
| Acetic | 4.4 | 6.1, 11.0 | 4.6 |
| Propanoic | | – [a] | 0.1 |
| Butanoic | | – [a] | 0.2 |
| Pentanoic | | | 0.6 |
| Lactic | 0.2 | – [a] | 0.1 |
| Oxalic | 2.5 | – [a] | |
| Malonic | | – [a] | |
| Succinic | 1.4 | – [a] | 9.8 |
| Methylsuccinic | | – [a] | 0.4 |
| Hydroxysuccinic | | – [a] | |
| Glutaric | | – [a] | 0.9 |
| Tricarballylic | | – [a] | |

[a] Reported but not quantified.

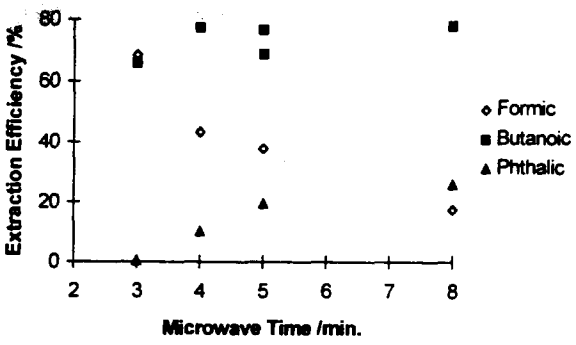


Fig. 1. Variation in extraction efficiency with microwave heating time for formic, butanoic and phthalic acids.

It was noted from preliminary experiments that under some conditions malonic acid underwent decarboxylation during butylation, producing acetic acid. Malonic acid was therefore not included in the standard solution, but was added to an aliquot of it (@0.6 g/l). Dilution of this solution allowed the effect of malonic acid decarboxylation on the apparent acetic acid concentration to be quantified.

The change in component peak area with concentration was quantified by linear regression of the ratio of the component area to that of the internal standard ($R_x$, dependent variable) against concentration ($C_x$, independent variable) (eq. (2)). The results of this regression analysis and the mean and standard deviation extraction efficiencies for each component are shown in Table 2.

$$R_x = m_x \cdot C_x + a_x \quad (2)$$

### 3.3. Calibration results

The extraction efficiencies listed in Table 2 vary between 6.5 and 92.8%, with four compounds having extraction efficiencies below 20%. Of these, the low $E$ value for formic acid is a result of the butylation conditions used (see section 3.2.). It is interesting to note that there is a roughly linear increase in $E$ with carbon number for the $n$-monocarboxylic acids. There is a similar trend for the dicarboxylic acids (malonic, succinic, glutaric), so that the low $E$ value of malonic acid is also probably a consequence of the microwave conditions used. The hydroxycarboxylic acids (lactic and hydroxysuccinic) have the lowest $E$ values (11.8 and 6.5%), as well as high relative standard devia-

Table 2
Results of linear regression analysis on standard solution dilution experiments and component extraction efficiencies.

| Acid | Slope ($m_x$) | Intercept ($a_x$) | $R^2$ | $n$ | Efficiency [$E$ (%)] |
|---|---|---|---|---|---|
| Formic | 0.472 ± 0.016 | −0.023 ± 0.011 | 0.979 | 20 | 16.3 ± 2.3 |
| Acetic | 0.738 ± 0.019 | 0.003 ± 0.013 | 0.992 | 15 | 30.0 ± 1.2 |
| Acetic [a] | 0.719 ± 0.014 | 0.015 ± 0.010 | 0.999 | 5 | 30.1 ± 0.9 |
| Propanoic | 1.322 ± 0.018 | 0.014 ± 0.006 | 0.997 | 20 | 56.3 ± 2.7 |
| Butanoic | 1.868 ± 0.015 | 0.010 ± 0.005 | 0.999 | 19 | 77.0 ± 2.0 |
| 3-Methylbutanoic | 2.266 ± 0.020 | 0.010 ± 0.007 | 0.999 | 20 | 92.8 ± 2.1 |
| Pentanoic | 2.273 ± 0.011 | 0.002 ± 0.004 | 0.999(6) | 19 | 91.5 ± 1.5 |
| Benzoic | 1.662 ± 0.089 | 0.021 ± 0.031 | 0.951 | 20 | 71.9 ± 9.4 |
| Lactic | 0.382 ± 0.017 | −0.025 ± 0.008 | 0.972 | 18 | 11.8 ± 1.9 |
| Malonic | 0.419 ± 0.011 | −0.003 ± 0.004 | 0.998 | 5 | 16.3 ± 0.9 |
| Succinic | 0.617 ± 0.004 | 0.002 ± 0.003 | 0.999 | 19 | 25.0 ± 0.5 |
| Methylsuccinic | 1.176 ± 0.009 | 0.003 ± 0.003 | 0.999 | 19 | 45.0 ± 1.5 |
| Hydroxysuccinic | 0.199 ± 0.006 | −0.009 ± 0.002 | 0.987 | 16 | 6.5 ± 1.3 |
| Glutaric | 0.896 ± 0.007 | 0.006 ± 0.002 | 0.999 | 19 | 37.2 ± 1.1 |
| Tricarballylic | 0.447 ± 0.031 | 0.023 ± 0.011 | 0.921 | 19 | 22.7 ± 4.1 |
| Phathalic | 0.426 ± 0.051 | 0.025 ± 0.018 | 0.796 | 20 | 22.5 ± 6.5 |

$n$ is the number of data points used for regression.
[a] Dilution series carried out in the presence of malonic acid.

tions (16 and 20%, respectively), and it is apparent that these species are not well butylated under the conditions used here.

There is no difference, within experimental error, between the extraction efficiency values determined for acetic acid in the absence and presence of malonic acid (30.0 ± 1.2% absent, 30.1 ± 0.9% present).

Relative standard deviations of the extraction efficiencies are below 5% for most of the components. They are higher for formic acid, lactic and hydroxysuccinic acids and benzoic, pathalic and tricarballylic (1,2,3-propanetricarboxylic) acids. Formic acid elutes on the shoulder of the solvent peak (Fig. 2) and this may account for the variability in its data. Benzoic acid is not completely butylated under the microwave conditions used, and two peaks (one being the unbutylated acid) are seen in the chromatogram (Fig. 2). By using the sum of these two peaks in the calibration the standard deviation is considerably reduced ($E = 95.3 \pm 5.9\%$). However, at low concentrations the smaller, unbutylated acid peak is very difficult to detect and the butylated species only has been used for regression analysis. Incomplete butylation may also be the source of the variability in the phthalic and tricarballylic acid data, although only one peak each was detected for these compounds.

Linear regressions ($R_x$ on $C_x$) of the dilution series data for each acid generally gave $R$-squared values of better than 0.99, with lower values being found for the acids identified above as having high standard deviation extraction efficiencies.

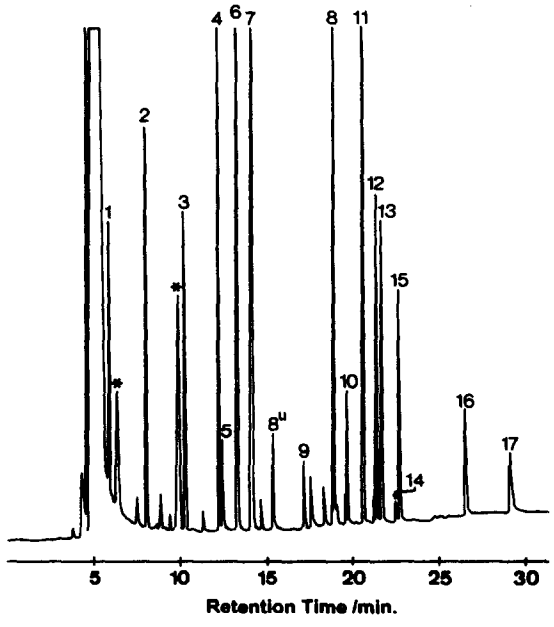


Fig. 2. Chromatogram obtained for the most concentrated standard solution. Peak identities are as follows: 1, formic; 2, acetic; 3, propanoic; 4, butanoic; 5, lactic; 6,3-methylbutanoic; 7, pentanoic; 8, benzoic, 9, 1,1 dibutoxybutane; 10, malonic; 11, nonanoic (internal standard); 12, succinic; 13, methylsuccinic; 14, hydroxysuccinic; 15, glutaric; 16, phthalic; 17, tricarballylic. Peaks marked with an asterisk are solvent impurities, the superscript u indicates that the peak is an unbutylated acid, rather than a butyl ester.

Table 3
Concentrations of organic acids determined in a spent Bayer liquor sample.

| Acid | Concentration (mg/l) | | |
|---|---|---|---|
| | BA1 | BA2 | BA3 |
| Formic | 2830 ± 130 | 2570 ± 130 | 2690 ± 130 |
| Acetic | 2920 ± 90 | 3000 ± 90 | 2950 ± 90 |
| Acetic[a] | 3010 ± 40 | 3090 ± 40 | 3040 ± 40 |
| Propanoic | 66 ± 23 | 61 ± 23 | 62 ± 23 |
| Butanoic | 24 ± 13 | 41 ± 13 | 31 ± 13 |
| 3-Methylbutanoic | 29 ± 17 | 42 ± 17 | 16 ± 17 |
| Pentanoic | 10 ± 8 | | |
| Benzoic | 10 ± 97 | 3 ± 97 | 19 ± 97 |
| Lactic | 290 ± 80 | 350 ± 80 | 270 ± 80 |
| Malonic | 756 ± 26 | 840 ± 26 | 832 ± 26 |
| Succinic | 1100 ± 20 | 1140 ± 20 | 1180 ± 20 |
| Methylsuccinic | 138 ± 12 | 147 ± 12 | 147 ± 12 |
| Glutaric | < 105 | < 99 | < 94 |
| Tricarballylic | 1180 ± 130 | 270 ± 120 | 420 ± 120 |

Triplicate analysis.
[a] Calculated using the results of the dilution series carried out in the presence of malonic acid

### 3.4. Analysis of Bayer liquors

A small aliquot (2.5 ml) of Bayer liquor was transferred to a 25 ml beaker and carefully acidified to pH 1 with 6 M HCl. Equilibration and butylation of the sample was then carried out as for the standard solutions and a portion of the butanol fraction was injected into the GC column.

The concentration of each component in the butanol fraction was calculated from the regression data and its concentration in the Bayer liquor was then determined by correcting for the dilution of the liquor upon acidification (eq. (3)). The uncertainty in the concentration measurement was estimated from the standard errors of the regression.

$$C_x^{BL} = \frac{V_2(R_x - a_x)}{V_1 m_x} \quad (3)$$

where $V_1$ is the original volume of Bayer liquor used, $V_2$ is the total volume of acidified Bayer liquor.

The results of the analysis (in triplicate) of a spent Bayer liquor sample are shown in Table 3. In general, the agreement between the measured concentrations of each of the acids in the three samples is very good. The results for tricarballylic acid are an exception to this, with the first sample giving a much higher concentration than the other (1180, 270 and 420 mg/l). The reason for this discrepancy is unclear, although tricarballylic acid did show a relatively high level of variability in the calibration experiment.

The concentrations of formic and acetic acids determined for this sample (mean values 2.70 and 2.96 (3.05*) g/l, respectively) are comparable to those reported for other Bayer liquors (Table 1). The two concentrations calculated for acetic are the same within experimental error, indicating that the malonic acid present in the Bayer liquor has not undergone a significant amount of decarboxylation. The succinic acid concentration of this sample (mean value 1.14 g/l) is very much lower than that reported by Brown, but is similar to that of another liquor (Table 1). These values probably reflect the natural variability of organic acid concentrations in Bayer liquor, which are affected by the quantity and nature of the incoming organic matter as well as plant operating conditions.

Propanoic, butanoic, 3-methylbutanoic, pentanoic and benzoic acids are all present in the sample studied at concentrations lower than 100 mg/l. The latter four acids are all close to their detection limits, with pentanoic acid detected in only one of the three replicates. Estimated detection limits ($C_d$, eq. (4)) for these acids are 58, 46, 64, 28 and 250 mg/l respectively, these values being greater than the measured concentrations for all but propanoic acid. ($a_x$ approximates the blank reading for each acid and $s_{y/x}$ is an estimate of the error in the blank reading and is obtained from the linear regression.)

$$C_d = a_x + 3s_{y/x} \quad (4)$$

Glutaric acid co-elutes with an unknown Bayer liquor component, so that the concentrations listed in Table 3 are maximum values only. Hydroxysuccinic and phthalic acids were not detected in this sample.

## 4. Conclusions

The procedure set out above offers several advantages over previously reported methods for determining concentrations of low molecular weight organic acids in Bayer liquors. The use of a microwave oven for heating the butylation mixture both significantly reduces the analysis time and increases the number of liquor components which can be quantified. Selection of microwave conditions which are more sensitive to the larger (and less abundant) acids than the more abundant formic and acetic acids can also increase the range of compounds analysed. More vigorous conventional heating techniques may be used to extend the range of components analysed [7], but there is a corresponding increase in analysis time.

## Acknowledgements

We would like to express our thanks to Alcan (Jamaica) Ltd. for supplying a sample of Bayer liquor for analysis and to Mr Gregory Simpson of Chemistry Department, UWI, for assistance with GC instrumentation.

## References

[1] G. Lever, Light Met., (1978) 71.
[2] J.D. Guthrie, P.J. The and W.D. Imbrogno, Light Met., (1984) 127.
[3] L.K. Hudson, Alumina production, in A.R. Burkin (Ed.), Production of Aluminium and Alumina, Critical Report on Applied Chemistry, Vol. 20, J. Wiley & Sons, 1987, p. 11.
[4] H.H. Pohland and A.J. Tielens, Light Met., (1983) 211.
[5] M. Susic and L.G. Armstrong, J. Chromatog., 502 (1990) 443.
[6] O.F. Safonova and L.G. Kulina, Obogashch. Rud (Leningrad), 3 (1986) 26.
[7] E.R. Brown, Ph.D. Thesis, University of the West Indies, Mona, 1991.
[8] W. Arnswald, H.G. Kaltenberg, and E. Guhl, Light Met., (1991) 23.
[9] A.D. Stewart and T. Tran, Light Met., (1988) 887.

ELSEVIER

Talanta 42 (1995) 1361–1371

Talanta

# Evolving projection analysis of multicomponent mixtures

Stephen G. Hughes, Peter D. Wentzell *

*Trace Analysis Research Centre, Department of Chemistry, Dalhousie University, Halifax, NS B3H 4J3, Canada*

Received 10 October 1994; accepted 28 December 1994

**Abstract**

The application of evolving projection analysis (EPA) to second-order bilinear data sets consisting of more than two components is described. EPA is a method for rank analysis of ordered data matrices where the components appear sequentially as a function of time or some other ordinal variable. It was found that extension of the method to mixtures of more than two components was best accomplished using principal components analysis to preprocess the data. The algorithm is demonstrated using simulated four-component chromatographic data, and experimental data from liquid chromatography (three- and four-component mixtures) and a spectrophotometric titration (four components), both employing UV-visible diode array detection.

## 1. Introduction

The determination of the number, identity and concentration of chemical components in a mixture is a difficult and pervasive problem in analytical chemistry. Quite often a physical separation of the components in a mixture can be accomplished through chromatography or other means, but this is not always possible. In some cases, mixture components may be incompletely resolved by the chromatography. In other cases, such as the study of solution equilibria or chemical kinetics, it may not be possible to remove a representative sample for physical separation. In these cases, a mathematical separation of the components may be possible even if the identities or characteristics of the components are unknown. For this to be accomplished, three criteria have to be met. First, measurements must be made with a first-order detector, that is, one with multiple sensor elements, such as a spectrometer. Second, a series of mixtures must be available in which the component concentrations vary independently. It is not necessary to know the precise nature of how the concentrations change, and many situations exist in chemistry where such variations occur naturally. These include partially overlapped peaks in chromatography, reacting mixtures, and equilibria perturbed by some external factor (e.g. temperature, pH). The third requirement is that each of the components present exhibits a unique response pattern (e.g. spectrum) at the detector. The response is also required to change linearly with concentration for most methods.

When the above conditions are met, an $m \times n$, data matrix, **D**, is produced, where $m$ is the number of mixtures and $n$ is the number of sensor elements in the detector. A mathematical rank analysis of **D** can yield information about the number of observable components present in the mixture. In chemistry, the most common approach to this problem has been principal components analysis (PCA) [1]. This method, and others like it, take advantage of the fact that components with different response and concentration profiles (i.e. observable components) will increase the rank of **D** so that it is equal to the number of observable components. In practice, the determination of the number of components (chemical rank) is

* Corresponding author. Fax: (902)494-1310.


*SSDI* 0039-9140(95)01522-1

complicated by the fact that the mathematical rank is not usually equal to the chemical rank. There are three main reasons for this. First, experimental noise tends to inflate the mathematical rank to its maximum possible value (i.e. the smaller of the number of rows or number of columns in **D**). Various methods have been devised to account for the problem of residual measurement errors, with varying degrees of success. A second complication is the problem of observability. Taking chromatography as an example, if two components have concentration or spectral profiles with identical shapes, it is impossible to distinguish them on a purely mathematical basis. Obviously, the degree of similarity in each of these domains relative to the level of measurement noise is an important factor in the rank estimation process. Finally, the validity of the model is an important consideration. PCA and related methods assume a linear model of the form:

$$\mathbf{D} = \mathbf{CK} + \mathbf{E}$$

where **C** is the $m \times p$ matrix of component concentrations ($p$ components), **K** is the $p \times n$ matrix of detector response factors, and **E** is the $m \times n$ matrix of residual errors. Deviations from this model, particularly in the form of nonlinear response characteristics, can artificially inflate the rank.

PCA has been successfully used for rank analysis in a wide variety of chemical applications for many years. More recently, a number of PCA-based methods designed to examine local rank have become popular [2–12]. These methods seek to determine the number of components in substructures of the full matrix, **D**, and exploit the fact that data sets such as those already mentioned are ordered; that is, the rank changes systematically with some ordinal variable such as time. One advantage of these methods is that they provide a relative measure of changes in rank, making it easier to distinguish the appearance of additional components in the mixture from measurement noise. A second advantage is that these techniques indicate regions in the data set where a smaller number of components may be represented, making the mathematical extraction of concentrations and spectral profiles easier.

One method which has been quite successful for the analysis of ordered data sets is called evolving projection analysis (EPA) [13–15]. Formerly referred to as evolving principal components innovation analysis (EPCIA), this technique is normally implemented through the use of parallel Kalman filter networks, although this is not essential. EPA has several advantages over similar techniques and can be adapted to deal with such practical problems as nonlinear responses and non-uniform measurement noise [15]. So far, applications of this method have focused mainly on peak purity determination in chromatography and have been limited to two-component mixtures. In this paper, the extension of the EPA algorithm to mixtures of more than two components is investigated. Experimental and simulated data sets are used, and examples are drawn from chromatography and spectrophotometric titrations.

## 2. Background

The theoretical basis of EPA has been covered in detail elsewhere, so only a brief summary of the method is given here to accentuate the modifications to the algorithm necessary for multicomponent mixtures. If **D** is an $m \times n$ matrix of $n$ responses for $m$ mixtures, each of the $m$ mixtures can be plotted in an $n$-dimensional response space. In the case of liquid chromatography with diode array detection (LC-DAD), one of the most common examples, each of the $m$ mixtures corresponds to a different elution time for the fused peak. The coordinates of the point for each of these mixtures in the $n$-dimensional absorbance space ($A^n$ space) would correspond to the absorbance values at the wavelength used, i.e. the spectrum of each mixture. Assuming a bilinear matrix in the absence of random and systematic errors, and assuming that the components in the mixture are not completely overlapped and exhibit adequate spectral differences, these points will define a space whose dimensionality is equal to the chemical rank of the mixture under study; i.e. the number of independently observable components. Therefore, if there is a single component present, all the points will lie on a straight line. If there are two components present, the points should define a two-dimensional plane in $A^n$ space; three components will define a three-dimensional hyperplane; and so on. Therefore, if one could determine the dimensionality of this subspace, the chemical rank of the mixture could be found. PCA has long been used for this purpose, although experimental errors often make it difficult

to clearly confirm the presence of minor components.

The principle behind EPA is to first project the $m$ points in the $n$-dimensional space onto $n-1$ two-dimensional subspaces. If there is only one component present, then all of the points should project onto straight lines. Therefore, linear models in all of the subspaces, obtained by regression, should adequately model the data within experimental error. If any of these models fails to represent the corresponding projection, a rank greater than one is indicated. Likewise, the points can be projected into $n-2$ three-dimensional subspaces and modeled with planar equations, or $n-3$ four-dimensional subspaces and modeled with three-dimensional hyperplanar equations, and so on. This process is continued until the dimensionality of the model is sufficient to describe the data within experimental error. This is taken as the chemical rank of the data set. Models of higher order will also adequately model the data (e.g. data that fall on a line will also lie on a plane), but overestimate the rank.

The 'evolving' part of this projection analysis comes in the analysis of ordered data sets, such as spectrochromatograms. In these instances, response vectors (e.g. spectra) are added to the data matrix in a sequence determined by the ordinal variable (e.g. time). The data matrix is analyzed by the projection procedure described above after each new addition. To evaluate the validity of each model, the residual for the *newest* point is calculated. Unlike the usual regression analysis (where errors are assumed to be only on one axis) the residual is not calculated in the vertical direction but rather in a direction orthogonal to the model. This avoids excessively large residuals if the projection happens to be aligned close to the vertical axis. This orthogonal residual will be referred to as the *fit error*, FE. The original implementation of EPA employed a prediction error instead [13], but it has since been found that the fit error is somewhat more well behaved in certain circumstances [15].

The fit error is calculated for each projection with each iteration of the cycle; that is, as each new response vector (e.g. spectrum) is added to the data matrix. As long as the model being used is valid, the sequence of fit errors should exhibit the characteristics of the measurement noise. When model errors occur owing to an increase in rank beyond the dimensionality of the current model, the sequence of fit errors will exhibit a systematic variation. This is illustrated in Fig. 1 with a typical projection into a two-dimensional response space. Initially, the projections fall on a straight line and the fit errors follow the expected distribution. As the rank of the matrix increases, however, the model no longer holds and the fit error sequence begins to show systematic deviations. It is this deviation that signals the presence of a new component.

Of course, not all projections for a given dimensionality may show systematic deviations in the fit errors. Depending on the system under study, the variations could be confined largely to one projection or distributed evenly over all projections. For this reason, the root mean square of the fit error (RMS(FE)) is calculated for all projections of a given dimensionality. In the absence of systematic deviations, this quantity should reflect the magnitude of experimental noise. When systematic deviations appear, there should be an increase in RMS(FE).

The EPA algorithm is normally implemented through the use of Kalman filter networks which have been described elsewhere [13]. The recursive nature of the Kalman filter makes it ideal for this purpose. The details of this implementation will not be discussed here.

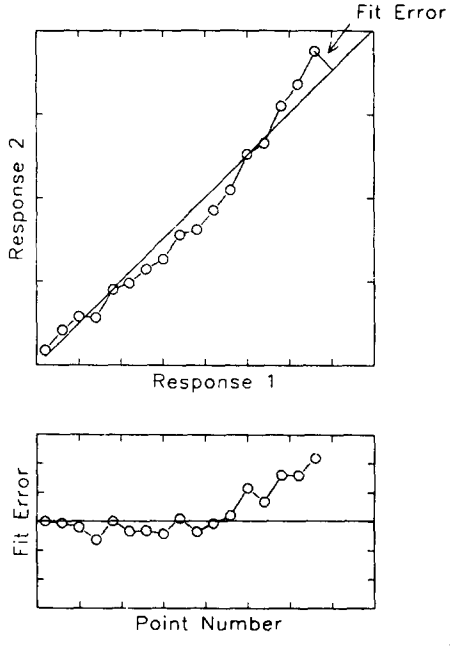


Fig. 1. Typical projection of ordered data into a two-dimensional response space and the evolution of fit errors for a one-component model. Systematic deviations of the fit error (orthogonal residual for the most recent point) indicate the appearance of a second component.

The usual procedure with EPA is to apply several models of increasing dimensionality to an ordered data set. Failure of a model with a given dimensionality signals an increase in rank beyond that value and the appearance of a new component. For example, in the analysis of a spectrochromatogram containing three overlapping components, one would expect to see failure of the one-component model when the second component appears, and failure of the two-component model when the third component appears. The fit error traces for the three-component model (and models of higher dimensionality) should remain flat throughout the chromatogram since it has sufficient dimensionality to model the entire data set.

One aspect of EPA that needs to be addressed when moving to higher dimensions is the selection of wavelengths to be used for the projections. Consider, for example, the equation for one projection of UV-visible absorbance values onto a four-dimensional space:

$$A_i = \alpha_i A_p + \beta_i A_q + \gamma_i A_r \quad (i \neq p, q, r) \tag{1}$$

The indices of the wavelengths corresponding to the independent axes in the model have been designated as $p$, $q$, and $r$. These will be the same for all $n-3$ models. The index $i$ corresponds to the wavelength being modeled for this particular projection and will vary for the $n-3$ models, as will the coefficients of the regression, $\alpha$, $\beta$, and $\gamma$. The selection of $p$, $q$, and $r$ is important. For numerical stability, absorbances at these wavelengths should exceed baseline values and should not exhibit a high degree of collinearity. Also, they should be selected to optimally distinguish among the components. In peak purity applications, the selection of the wavelength to act as an independent variable is not critical since the problem of collinearity does not arise for a one-component model. For multicomponent analysis, however, the selection is important for determining the success of the algorithm.

Several approaches to the problem of wavelength selection were tried. In one approach, a wavelength for the one-component model was first selected and that model was applied to the data set. When the one-component model failed, the wavelength showing the greatest deviation was then selected as the second independent axis, and the two-component model was applied. This procedure was repeated until the dimensionality of the model satisfied the data set. Unfortunately, the success of this approach was found to be very dependent on the nature of the data set. For example, the second wavelength selected, while effective for distinguishing between the first two components, may not be as effective for components two and three.

A successful alternative approach was found to be pretreatment of the data with PCA. The first $k$ principal components were then used to represent the data; i.e. the scores on the first $k$ eigenvectors were used instead of the absorbances at $n$ wavelengths. Typically $k$ was chosen to be large enough to ensure that it exceeded the rank of the data set, yet small enough so some of the noise was excluded. A value of $k = 10$ was found to be satisfactory for this work. Since the eigenvectors are ordered according to the proportion of variance they encompass, and since they are by definition orthogonal, the independent axes were simply selected as the first $j$ eigenvectors, where $j$ is the dimensionality of the model. Therefore, the three-component model is defined in a manner analogous to Eq. (1):

$$T_i = \alpha_i T_1 + \beta_i T_2 + \gamma_i T_3 \quad (i \neq 1, 2, 3) \tag{2}$$

where $T_i$ represents the score on principal component $i$. Using this data pretreatment step had several advantages. First, it provided a reliable method of variable selection that resulted in consistent performance of the algorithm. Second, it increased sensitivity to model deviations by reducing the contribution of wavelengths containing little or no information. Finally, because the algorithm only needed to deal with $k$ variables rather than $n$ wavelengths, computation time was reduced. For all of the results presented here, preprocessing via PCA was used and the first 10 principal components were retained.

## 3. Experimental

### 3.1. Chromatography

Chromatographic data obtained from simulations and from real three- and four-component mixtures were used to evaluate the EPA algorithm. The three-component mixture consisted of toluene (11.48 mM), naphthalene (0.42 mM) and *m*-xylene (8.12 mM) in a 7:1 (v:v) methanol: water solvent (analytes are given in the order of elution). The effective

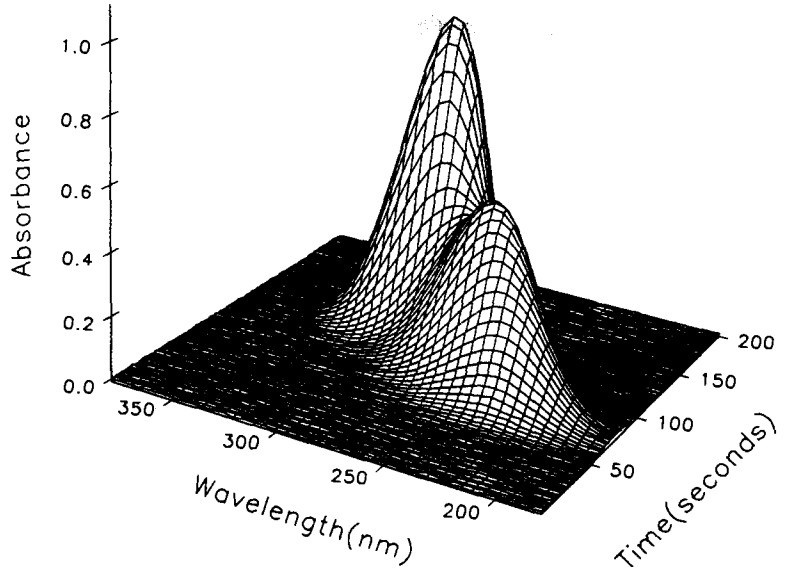


Fig. 2. Typical spectrochromatogram for a simulated four-component mixture.

concentration ratio of the analytes (i.e. compensating for the maximum molar absorptivity of each compound) is ca. 1.3:1:1.1. The four-component mixture consisted of toluene (11.54 mM), napththalene (0.42 mM), *m*-xylene (7.97 mM) and biphenyl (0.22 mM), with an effective concentration ratio of 1.3:1:1.1:2. These mixtures were analyzed on a chromatographic system consisting of a Shimadzu LC-6A pump (Shimadzu, Columbia, MD), a 50 µl injection valve (Rheodyne model 5020, Cotati, CA), a Partisphere $C_8$ column (12.5 cm × 4.6 mm with 5 µm packing) (Whatman, Hillsboro, OR), and an HP 8452A diode array spectrometer (Hewlett-Packard, Palo Alto, CA) with 30 µl flow cell (Hellma Cells, Jamaica, NY). Isocratic elution was used with 7:1 methanol:water as the mobile phase. These conditions ensured sufficiently poor resolution to test the algorithm. Spectra were obtained at 0.5 s intervals with an integration time of 0.4 s. Data were acquired between 61 and 169 s after injection for the three-component mixture, and up to 183.5 s for the four-component mixture.

### 3.2. Spectrophotometric titration

The spectrophotometric titration of pyrocatechol violet (Aldrich, Milwaukee, WI) was carried out by first placing 100 ml of a 0.01 M solution in a beaker and adding dilute hydrochloric acid to adjust the pH to 3.00. Spectra were obtained on an HP 8452A diode array spectrometer between pH 3.00 and 12.00 at intervals of 0.25 pH units by adding small amounts of dilute sodium hydroxide. Spectra were obtained between 266 and 818 nm at 4 nm intervals with an integration time of 1 s.

### 3.3. Computational aspects

All calculations were carried out on a 33-MHz 80486-based computer using Matlab 4.0 (Mathworks, Natick, MA) for Windows (Microsoft, Redmond, WA).

## 4. Results and discussion

### 4.1. Chromatography

Initial investigations into the application of EPA to multicomponent chromatographic systems were carried out using simulations. This permitted an examination of the algorithm in the absence of certain experimental artifacts that can complicate real chromatograms, such as scan time effects, baseline variations, detector nonlinearity and heteroscendastic noise. It also allowed a direct comparison to be made between the times at which components begin to elute and the fit error traces for EPA. A typical simulated spectrochromatogram for a four-component mixture are shown in Fig. 2. In this case, Gaussian profiles were used in both the spectral and chromatographic domains. The spectrum and elution profile of each component was shifted by one standard deviation from the preceding one. The effective concentration ratio (components 1–4) was

1:2:1:4. The maximum absorbance was set to unity and Gaussian noise was added at a level of 0.1% of the maximum.

The noise free chromatographic elution profiles for the four components in the mixture are shown in Fig. 3a, and the fit error traces after processing the data with the EPA algorithm in the forward and reverse directions, respectively, are shown in Fig. 3b and c. Focusing first on Fig. 3b, it can be seen that the fit error trace for the one-component model shows deviations from the baseline shortly after the appearance of the second component. Likewise, the two- and three-component models fail with the elution of the third and fourth components. As expected, the RMS(FE) for the four-component model remains flat throughout the chromatogram. Figure 3c, which is obtained by presenting the chromatographic data to the algorithm in the reverse order, provides complementary information to that in Fig. 3b. The results confirm the presence of four components and indicate where the elution of each component is complete. A knowledge of the regions where each component elutes can be useful in curve resolution for the individual components.

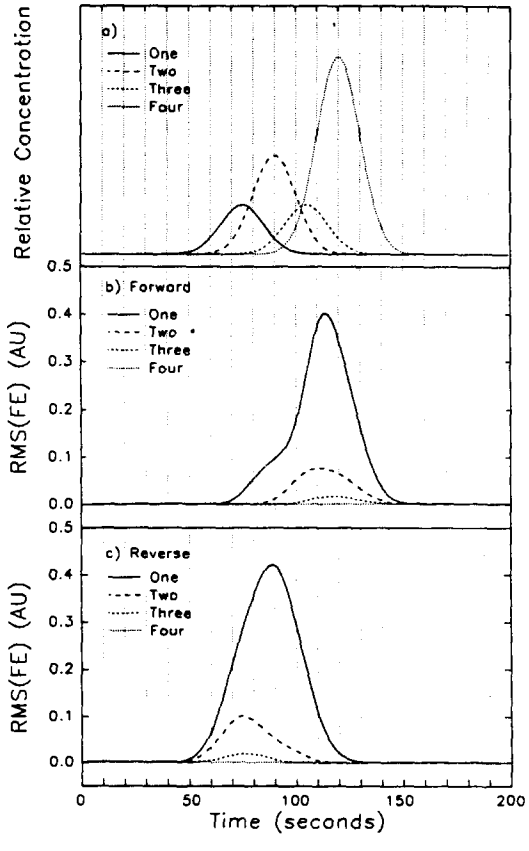


Fig. 3. Evolving projection analysis of the data in Fig. 2: (a) chromatographic elution profiles for the individual components; (b) fit error traces obtained from processing the data with the EPA algorithm in the forward direction (increasing time); and (c) fit error traces obtained by processing the data in the reverse direction (decreasing time).

In earlier work with two-component mixtures, it was demonstrated that the error traces for the one-component model closely matched the chromatographic elution profile of the second component [14]. With more than two components, the shape of the fit error trace to the elution profiles is more complex, arising from a combination of elution profiles for multiple components. The precise shape of the trace, including the position of the maximum, will depend on a number of factors, including the order of the model, the number of components present, spectral and chromatographic resolution, and relative concentration ratios. However, it appears that the trace for the final component (i.e. the $(n-1)$th order model for an $n$-component mixture) matches the elution profile for that component well. Therefore, it is possible to obtain an indication of the elution profiles for the first and last components with this approach.

Another feature of the RMS(FE) traces is that they tend to decrease in maximum amplitude as the order of the model increases. This is expected, since deviations from high-order models will be smaller than for the low-order models, which are less capable of describing the multicomponent mixture. Again, absolute magnitudes will depend on chromatographic resolution and spectral correlation of the overlapped components, as well as their concentrations and elution order. These factors, along with the level of measurement noise, will ultimately determine the sensitivity of this method to minor components in the mixture. While the sensitivity of this method has been studied for two-component mixtures [14], the case of multicomponent mixtures is more difficult because of the large number of factors influencing performance. Nevertheless, a simple study to test the limitations of the method was undertaken. In this study, a four-component mixture with Gaussian spectral and chromatographic profiles was simulated, with equal peak separation in the chromatographic and spectral domains. The first three components had a maximum absorbance of 0.25, while the fourth component was varied from 0 to 0.025. The maximum amplitude of RMS(FE) was then

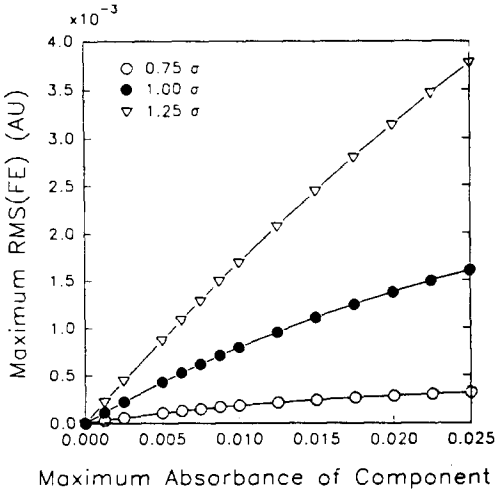


Fig. 4. Maximum fit error obtained for the three-component model applied to a simulated four-component mixture as a function the maximum absorbance of the fourth component. Three cases of chromatographic/spectral resolution are shown. The maximum absorbance of each of the other three components was set to 0.25.

measured for the three-component model running in the forward direction. This should represent a 'worst-case' scenario, since the last component will produce the smallest trace. Results from this study are plotted in Fig. 4 for peak separations of 0.75, 1, and 1.25 standard deviations. As expected, larger model deviations are observed as the relative concentration and resolution (spectral and chromatographic) of the fourth component increase. As was found to be the case for peak purity detection [14], the detectability of the fourth component will depend on the level of experimental noise. For example, if noise at a level of $1 \pm 10^{-3}$ A.U. were added to the simulated data sets, the fourth component will not be detectable when its effective concentration falls below 0.3 and 0.7% of the total for chromatographic/spectral separations of 1.25 and $1\sigma$, respectively.

The analysis of real chromatographic mixtures is more problematic. A number of non-idealities, such as baseline drift, refractive index effects, detector scan time effects, heteroscedastic noise, and detector nonlinearity, are well known to cause problems in the rank analysis of real chromatographic data [14–18]. The spectrochromatograms for the three- and four-component mixtures used in this study are shown in Fig. 5. Spectra for the four components used are shown in Fig. 6 and are presented in the order of elution. The forward and reverse rms fit error sequences for the three-component study are shown in Fig. 7. As expected, the traces in the forward direction indicate the presence of the second and third components with the successive failure of the one- and two-component models, but the traces are somewhat different from the simulation results in several ways. First, the shape is different, but this is expected since the non-ideal chromatographic conditions promote non-Gaussian peaks. Second, it is clear that the fit error traces for the three- and four-component models do not remain completely flat, making it difficult to detect the presence of additional minor components. It is expected that this is due to baseline variations and/or non-ideal detector behavior. Finally, small perturbations in the fit error traces are often observed coincident with the appearance of new components in the mixture. These perturbations, appearing as small 'bumps', precede the true failure of the model when it occurs. This behavior is routinely observed for real chromatographic data and arises from the fact that the baseline noise has some non-random structure. In the case of the one-component model, for example, this structure will be fit to the model. When the first component does appear, a couple of iterations are necessary for the model to lock onto the true structure of the data, and it is during this transition that increased errors are observed. Similar effects are observed for the higher order models. Nevertheless, the forward fit error traces clearly indicate the presence of at least three components.

The reverse traces (Fig. 7b) complement the information in the forward traces. Again, the presence of three components is indicated by the failure of the one- and two-component models, and again the traces are not completely flat for the three- and four-component models. The error traces have a somewhat different shape in this case, since the chromatographic profiles are not symmetric under these conditions. Also, there is a shift towards earlier times for the peaks in the reverse trace as the order of the components being modeled has changed. By combining the two traces, information such as the region occupied by component 2 can be extracted.

The forward and reverse fit error traces for the four-component mixture are shown in Fig. 8. The comments made for the three-component case are also valid here, except for the additional component. The deviations for the

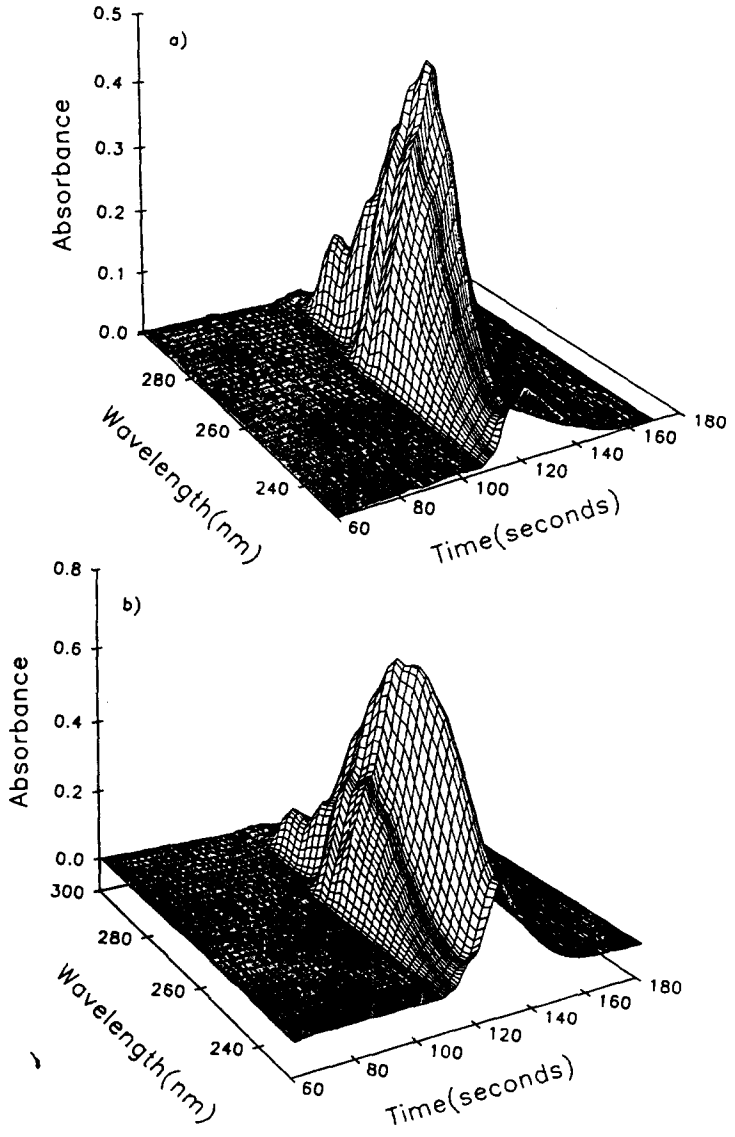


Fig. 5. Experimental spectrochromatograms for (a) three-component and (b) four-component mixtures.

three-component model are smaller than for models of lower order, as expected from the simulation studies, and begin to approach levels that make them difficult to discern from the artifacts already noted. The presence of a fourth component is still clearly indicated in this case, however.

### 4.2. *Spectrophotometric titration*

The spectrophotometric titration of pyrocatechol violet was employed as an alternative example of an ordered data set. Although this is not an exceptionally challenging case for rank analysis since the spectral profiles of the four species are reasonably well separated, it serves to illustrate the principles of the method. The data from the spectrophotometric titration are shown in Fig. 9 and the expected distributions of species calculated using reported equilibrium constants in Fig. 10 [19]. The fit error traces in the forward and reverse directions are shown in Fig. 10b and c, respectively. The traces are not as smooth as for the chromatography example, since the points are sampled less frequently, but clearly indicate the presence of four components. The successive failure of the models in the forward direction approximately matches the expected distribution, although deviations for the two- and three-component models seem to lag the appearance of the third and fourth components slightly. There is also an unexpected perturbation of the four-component model at the very

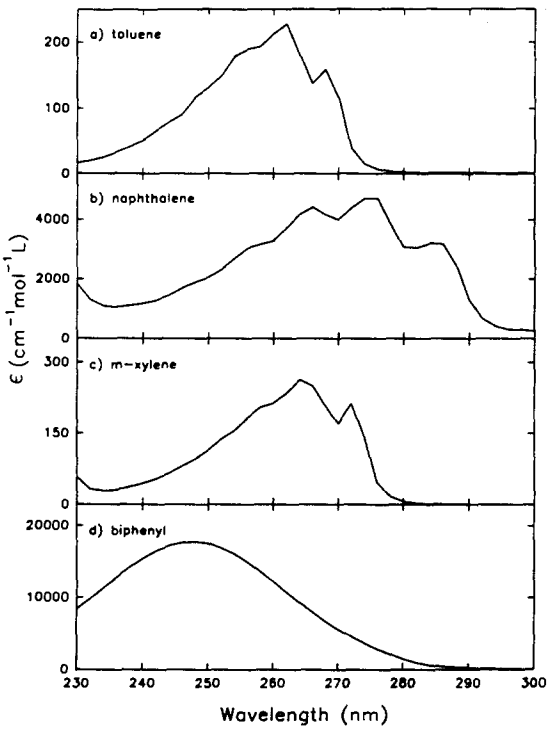


Fig. 6. Spectra for the four components employed in the chromatography experiments.

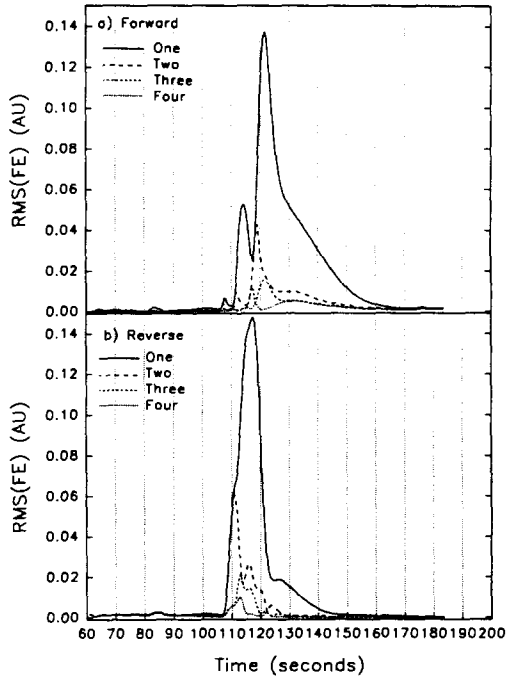


Fig. 8. Results of evolving projection analysis of the four-component data in Fig. 5b in (a) the forward and (b) the reverse directions.

end, but the number of points is insufficient to support the presence of a fifth species. The fit error trace in the reverse direction (Fig. 10c) is less well-behaved because there is no initial one-component region for the models to stabilize. Nevertheless, the trace for the four-component model remains flat while the others show obvious deviations, clearly signaling the presence of three components. In this case, the initial point of model failure for the two- and three-component models seems to be displaced to higher pH. This, coupled with the observations for the forward traces, suggests that perhaps there are some deviations from the reported values for the equilibrium constants.

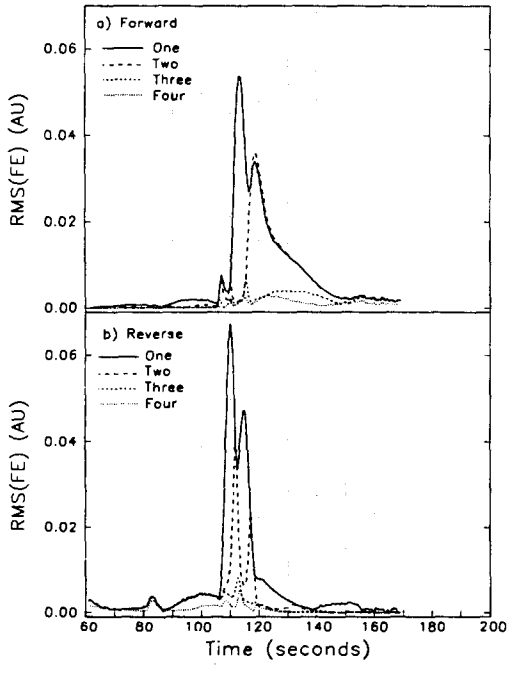


Fig. 7. Results of evolving projection analysis of the three-component data in Fig. 5a in (a) the forward and (b) the reverse directions.

## 5. Conclusions

The results presented here demonstrate the EPA is a useful technique for the rank analysis of ordered data sets consisting of more than two components. Best results were obtained when the original data were preprocessed with PCA and the scores were used in place of the original data. EPA has the advantage of providing relative measures of changes in rank and indicates where new components appear in the data set. No prior information needs to be presented to the algorithm. In the case of chromatographic data, simulations have shown that, in the ideal situation, minor components

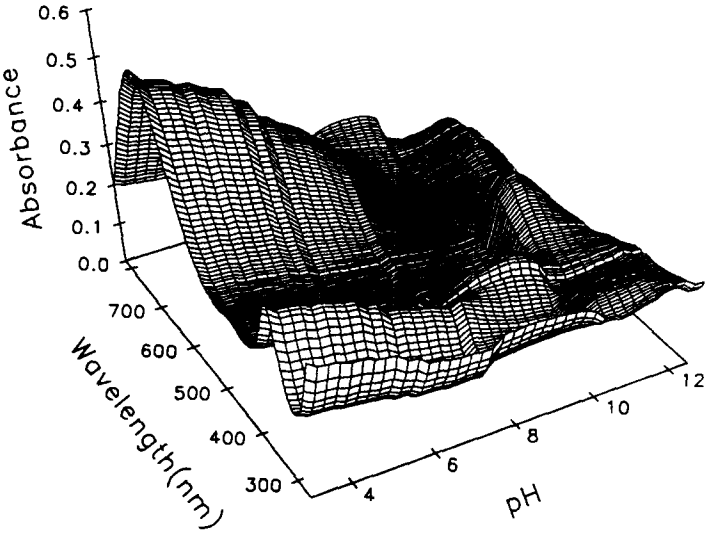


Fig. 9. Data from the spectrophotometric titration of pyrocatechol violet.

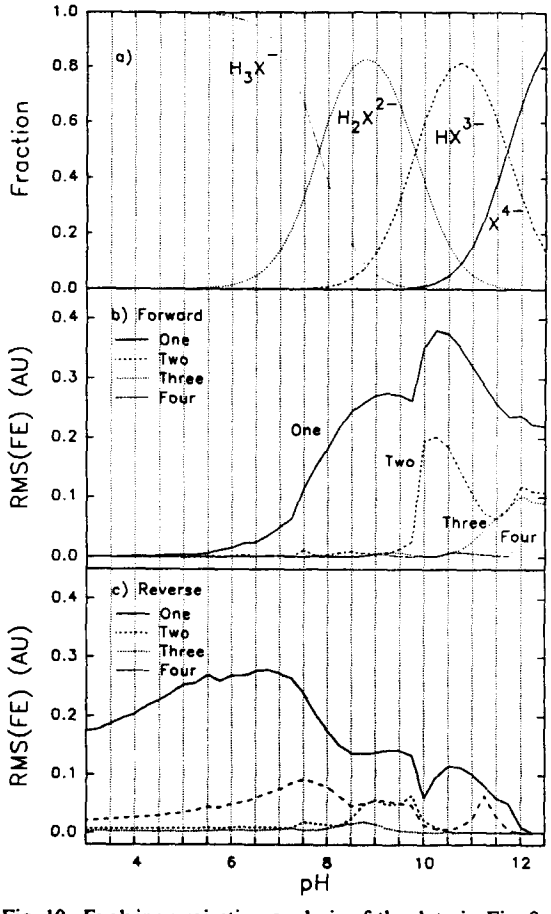


Fig. 10. Evolving projection analysis of the data in Fig. 9: (a) distribution of four forms of pyrocatechol violet as calculated from equilibrium constants; (b) results of EPA in the forward direction (increasing pH); and (c) results of EPA in the reverse direction (decreasing pH).

can be detected at relatively low concentrations. In practice, artifacts such as baseline drift and non-ideal detector characteristics are likely to limit the method before baseline noise. This is expected to be a problem for all evolving rank analysis methods, however, and clearly is a problem which deserves more attention.

## Acknowledgments

The authors gratefully acknowledge assistance provided by Prof. R.D. Guy in the course of this work. This work was supported by the Natural Sciences and Engineering Research Council (NSERC) of Canada. SGH acknowledges support through NSERC and Sumner Fellowships.

## References

[1] E.R. Malinowski, Factor Analysis in Chemistry, 2nd edn., Wiley, New York, 1991.
[2] H. Gampp, M. Maeder, C.J. Meyer and A.D. Zuberbühler, Talanta, 32 (1985) 1133.
[3] M. Maeder, Anal. Chem., 59 (1987) 527.
[4] P. Geladi and S. Wold, Chemom. Intell. Lab. Syst., 2 (1987) 273.
[5] P.J. Gemperline and J.C. Hamilton, J. Chemom., 3 (1989) 455.
[6] J. Kankare, J. Lukkari, T. Pajunen, J. Ahonen and C. Visy, J. Electroanal. Chem., 294 (1992) 59.
[7] H.R. Keller and D.L. Massart, Anal. Chim. Acta, 246 (1991) 379.

[8] H.R. Keller, D.L. Massart and J.O. De Beer, Anal. Chem., 65 (1993) 471.
[9] J. Toft and O.M. Kvalheim, Chemom. Intell. Lab. Syst., 19 (1993) 65.
[10] M.K. Alam and J.B. Callis, Anal. Chem., 66 (1994) 2293.
[11] S.P. Gurden, R.G. Brereton and J.A. Groves, Chemom. Intell. Lab. Syst., 23 (1994) 123.
[12] C.S.P.C.O. Silva, J.C.G. Esteves de Silva and A.A.S.C. Machado, Appl. Spectrosc., 48 (1994) 363.
[13] S.J. Vanslyke and P.D. Wentzell, Anal. Chem., 63 (1991) 2512.
[14] S.J. Vanslyke and P.D. Wentzell, Chemom. Intell. Lab. Syst., 20 (1993) 183.
[15] P.D. Wentzell, S.G. Hughes and S.J. Vanslyke, Anal. Chim. Acta, 307 (1995) 459.
[16] H.R. Keller, D.L. Massart, P. Kiechle and F. Erni, Anal. Chim. Acta, 256 (1992) 125.
[17] H.R. Keller and D.L. Massart, Anal. Chim. Acta, 263 (1992) 21.
[18] H.R. Keller, D.L. Massart, Y.Z. Liang and O.M. Kvalheim, Anal. Chim. Acta, 263 (1992) 29.
[19] J.H. Kennedy, Analytical Chemistry: Principles, 2nd edn., Saunders, New York, 1990, p. 309.

ELSEVIER

Talanta 42 (1995) 1373–1378

Talanta

# A modified program for computation of formation constants of synergetic extraction complexes with two-phase titrations by using the Marquardt–Fletcher algorithm

Cai Qingyan, Peng Yan, Nie Lihua, Yao Shouzho *

*Chemistry and Chemical Engineering Department, Hunan University, Changsha, Hunan 410082, People's Republic of China*

Received 19 August 1994; revised 6 December 1994; accepted 27 December 1994

**Abstract**

A modified computer program SCTPT for the computation of formation constants of extraction complexes with two-phase pH titration data by using the Marquardt–Fletcher algorithm is described. It can be used to deal with extraction systems which consist of a metal, an acidic extractant and a neutral synergistic reagent with no need of new subroutine. It has been applied successfully to the Pb–PMBP(1-phenyl-3-methyl-4-benzoyl-pyrazolone-5)–TBP (tributyl phosphate) system. The results obtained are in agreement with those published in the literature.

## 1. Introduction

PH titrations have been widely used in the study of stability of metal complexes with acidic ligands [1]. There are, however, few reports for this method being used in the study of the extraction equilibrium [2–5]. The main difficulty is the treatment of the experimental data. Compared with partition methods by which both pH and metal concentration in aqueous phase or organic phase are to be determined, the two-phase titration method is a simple and time-saving experimental method since only the determination of pH in the aqueous phase is required. All the quantitative information needed from the system studied can be obtained if the experiment is designed step by step. By this method, the chelate and synergistic extraction mechanism of metal ions can be studied with a pH electrode only. The method was first proposed by Dyrssen [6] to determine dissociation constants of weak acid (HA) in water and the partition constants between two phase solutions, and was then used by Jensen [2] to determine formation constants of extraction complexes. In recent years, the method has been applied to chelate and synergistic extraction systems [3–5]. However, graphical methods were used in the treatment of the data and complicated mathematical calculations and a number of mathematical approximations were involved in their procedure [2–4,6], which made it impossible to apply the method to complicated systems (e.g. more than three unknown species present). In order to obtain reliable results and simplify the complicated calculation, it is necessary to design a powerful program for data treatment.

Many computer programs for the computation of formation constants of metal complexes in aqueous solution equilibrium have been described [7] but programs for the evaluation of two-phase pH titrations have not been seen so far except one that we reported previously [5]. The most used programs are SCOGS [8] and MINIQUAD [9] which are both based on the Newton–Gauss algorithm. In these programs, good estimates of the initial parameters are usually important. However, Marquardt's

* Corresponding author.


*SSDI* 0039-9140(95)01523-X

method [10], which combines the steepest descent and Newton–Gauss algorithm in a powerful way, has no strict demands of the initial estimates and has been introduced in some programs [11,12]. The Marquardt–Fletcher algorithm, i.e. Marquardt's method modified by Fletcher [13], is more effective on the convergence efficiency. We have compared the Marquardt–Fletcher algorithm [13] with MINIQUAD, the result shows that there is no difference between them for general nonlinear refinement problems such as $y = f(x,t)$ (where $y$ and $x$ are the observation points, and $t$, the parameters to be refined); but for two-phase systems in which the parameters to be resolved are formation constants and free concentrations effected by formation constants, the Marquardt–Fletcher algorithm is more stable. However, as it is easy for the unknown parameters to be near to linear correlation in a two-phase system, the Marquardt–Fletcher algorithm should be used cautiously. When the initial estimates are far from the truth, it often gives an erroneous descent direction in the first iterations. If it is limited so that the sum of the squares of the residuals should be reduced in each iteration according to the Marquardt-Fletcher algorithm, the refinement will diverge or pace up and down on a saddle point, so the control of the shifts is important, especially in the first iterations. Sometimes when an iteration cannot give a smaller sum of squares and the Marquardt's parameter is very large, it is allowable that the iteration ends without decrease of the sum of squares in order to skip over the saddle point.

We have previously reported a FORTRAN program SCTPT [5] (Stability Constants for Two-Phase Titrations) for the computation of pH titrations in an extraction system with an acidic extractant. In this paper, a new version of the SCTPT is described. It can be used to deal with extraction system with an acidic extractant and a neutral synergetic reagent. Owing to the use of analytical derivatives combined with the Marquardt–Fletcher technique, the program SCTPT can converge to a stable minimum with no need of a good estimate of the initial parameters. The work of the program will be illustrated by using data for the lead – 1 - phenyl - 3 - methyl - 4 - benzoyl - pyrazolone-5–tributyl phosphate (Pb–PMBP-TBP) extraction system.

## 2. Mathematical background

For a system which consists of a metal M, an acidic extractant $H_nA$ and a neutral synergistic reagent B, the equations related to the equilibrium and formation constants $\beta$ are:

$$lM + mA + nB_o + hH = M_lA_mB_nH_{ho} \quad (1)$$

$$\beta_{lmnh} = [M_lA_mB_nH_h]_o/[M]^l[A]^m[B]^n_o[H]^h \quad (2)$$

$$lM + mA + hH = M_lA_mH_h \quad (3)$$

$$\beta_{lmh} = [M_lA_mH_h]/[M]^l[A]^m[H]^h \quad (4)$$

The total concentration of metal ion M can be expressed as follows:

$$V_{aq} \cdot T_M = V_{aq} \cdot [M] + V_{aq} \sum l[M_lA_mH_h] + V_0 \sum l[M_lA_mB_nH_h]_o \quad (5)$$

$$T_M = [M] + \sum l[M_lA_mH_h] + V_0/V_{aq} \sum l[M_lA_mB_nH_h]_o \quad (6)$$

where $V_{aq}$ is the total aqueous volume and $V_0$ the total organic volume. Let $R = V_0/V_{aq}$ and $R = 1$ for aqueous species and omit the subscript 0, Eqs. (7) and (8) can be obtained.

$$T_M = [M] + R \cdot \sum l[M_lA_mB_nH_h] \quad (7)$$

$$E = T_M^{calc} - T_M^{exp} = [M] + R \cdot \sum l[M_lA_mB_nH_h] - C_M V_M/V_{aq} \quad (8)$$

For A, B and H, their residual function can be obtained in the same way:

$$F = T_A^{calc} - T_A^{exp} = [A] + R \cdot \sum m[M_lA_mB_nH_h] - C_{H_nA} \cdot V_{H_nA}/V_{aq} \quad (9)$$

$$G = T_B^{calc} - T_B^{exp} = R \cdot [B]_o + R \cdot \sum n[M_lA_mB_nH_h] - C_B \cdot V_B/V_{aq} \quad (10)$$

$$H = T_H^{calc} - T_H^{exp} = [H] - [OH] + R \cdot \sum h[M_lA_mB_nH_h] - (C_H \cdot V_H + N \cdot C_{H_nA} \cdot V_{H_nA} - C_{OH} \cdot V_{OH})/V_{aq}, \quad (11)$$

where $C_M$, $C_{H_nA}$, $C_B$, $C_H$ and $C_{OH}$ represent, respectively, the initial concentration of M, $H_nA$, B, inorganic strong acid and base; $V_M$, $V_{H_nA}$, $V_B$, and $V_H$ are their added volume correspondingly, and $V_{OH}$ is the titrated volume. From the above equations we can see that the form of the mass balance equations for the two-phase system is the same as that for aqueous solution except that the species in the organic phase are multiplied by the phase ratio $V_0/V_{aq}$. From Eqs. (8)–(10) the three unknown concentrations [M], [A] and [B] represented by $M$, $A$ and $B$ can be calculated by the Newton–Raphson [8] method in which the functions $E$, $F$, and $G$ are expanded as a Taylor series truncated at the first-order term (Eqs. (12)–(14)):

$$0 = E = E^\circ + \partial E/\partial M \cdot \Delta M + \partial E/\partial A \cdot \Delta A + \partial E/\partial B \cdot \Delta B \quad (12)$$

$$0 = F = F^\circ + \partial F/\partial M \cdot \Delta M + \partial F/\partial A \cdot \Delta A + \partial F/\partial B \cdot \Delta B \quad (13)$$

$$0 = G = G^\circ + \partial G/\partial M \cdot \Delta M + \partial G/\partial A \cdot \Delta A + \partial G/\partial B \cdot \Delta B \quad (14)$$

With the shift $\Delta M$, $\Delta A$ and $\Delta B$, the solutions are obtained by iteration at a set of given parameters. At this point the concentrations of all species $M_lA_mB_nH_h$ are also known and hence the function $H$ to be fitted (Eq. (11)) and the residuals square sum (Eq. (15)) can be obtained.

$$U = \sum_{\text{points}} (T_H^{\text{calc}} - T_H^{\text{exp}})^2 = \sum_{\text{points}} H^2 \quad (15)$$

To obtain the best parameters the minimum of $U$ must be found and according to the standard least-squares expression (Eq. (16)) the parameters $\beta_{lmnh}$ represented by $\beta_l$ can be obtained by iteration (Eq. (17)).

$$(J^TJ + P \cdot I)S = J^TH \quad (16)$$

$$\beta_j^{k+1} = \beta_j^k + \beta_j^k \cdot S, \quad (17)$$

where $P$ is the Marquardt parameter, $I$ the unit matrix, and J the Jacobian matrix given by $J_{ij} = \partial H_i/\partial \log \beta_j$ ($i$, the experimental points). As discussed by Nagypal et al. [14], $J_{ij}$ is determined in Eq. (18):

$$\partial H_i/\partial \log \beta_j = R \cdot h \cdot [M_lA_mB_nH_h]_j + \frac{\partial H_i}{\partial M}\frac{\partial M}{\partial \log \beta_j} + \frac{\partial H_i}{\partial A}\frac{\partial A}{\partial \log \beta_j} + \frac{\partial H_i}{\partial B}\frac{\partial B}{\partial \log \beta_j} \quad (18)$$

$\partial H/\partial M$, $\partial H/\partial A$ and $\partial H/\partial B$ can be calculated from Eq. (11), whereas $\partial M/\partial \log\beta_j$, $\partial A/\partial \log \beta_j$ and $\partial B/\partial \log \beta_j$ are determined from the three linear equations shown below:

$$0 = \partial E/\partial \log \beta_j = R \cdot l \cdot [M_lA_mB_nH_h]_j + \frac{\partial E}{\partial M}\frac{\partial M}{\partial \log \beta_j} + \frac{\partial E}{\partial A}\frac{\partial A}{\partial \log \beta_j} + \frac{\partial E}{\partial B}\frac{\partial B}{\partial \log \beta_j} \quad (19)$$

$$0 = \partial F/\partial \log \beta_j = R \cdot m \cdot [M_lA_mB_nH_h]_j + \frac{\partial F}{\partial M}\frac{\partial M}{\partial \log \beta_j} + \frac{\partial F}{\partial A}\frac{\partial A}{\partial \log \beta_j} + \frac{\partial F}{\partial B}\frac{\partial B}{\partial \log \beta_j} \quad (20)$$

$$0 = \partial G/\partial \log \beta_j = R \cdot n \cdot [M_lA_mB_nH_h]_j + \frac{\partial G}{\partial M}\frac{\partial M}{\partial \log \beta_j} + \frac{\partial G}{\partial A}\frac{\partial A}{\partial \log \beta_j} + \frac{\partial G}{\partial B}\frac{\partial B}{\partial \log \beta_j} \quad (21)$$

where $\partial E/\partial M$, $\partial E/\partial A$, $\partial E/\partial B$, $\partial F/\partial M$, $\partial F/\partial A$, $\partial F/\partial B$, $\partial G/\partial M$, $\partial G/\partial A$ and $\partial G/\partial B$ are already known from the Newton–Raphson solution for the concentrations.

In order to ensure that $\beta$ is positive in each iteration, $s'$, the smallest shift of $S$, should be greater than $-0.99$, otherwise, let $S = S \cdot (-0.99/s')$. On this occasion, it is unreasonable to adjust the Marquardt's paramater $P$ according to the Marquardt–Fletcher algorithm. So the following is done: in the case of convergence, set $P$ constant; in the case of divergence, $P$ is increased by multiplying it by 5 until convergence. When $P$ is much greater (greater than a predetermined value $P_m$) and no smaller $U$ can be obtained, this iteration is ended too and $P$ is set to a smaller value $P_c$, which is calculated according to Marquardt–Fletcher algorithm or is assigned by experience. The refinement may be terminated when both the relative shifts and the relative variation of the residual square sum are less than a predetermined tolerance (e.g. $10^{-4}$, or $10^{-5}$).

## 3. Program

The program SCTPT is written in FORTRAN77 and has been compiled and run on a

desk-top computer, PC/XT 386. It contains a main program which reads the experimetal data, the parameters describing the model and the initial estimates of the formation constants either through the keyboard or through a data file by using the DOS pipe command. The $\beta$ values may be held to be constant (KEY = 0) or varied (KEY = 1) at will. After subroutine MINI is called to refine parameter $\beta$, it then prints out the results and calls subroutine PLOT to plot the concentration distribution diagram and the fitting titration curves at will (LPT = 0 or 1). The dimension statement in the program is such that a total number of 300 titration points (points per curve times number of curves) and up to 10 complex species can be used. For a single curve, up to 60 points can be used. This program can perform different tasks by changing the value of the parameters ML and MLB:

ML = −1 Only water solution system, no B presents

0 Two-phase system containing no metal

1 Two phases system containing metal

The synergetic reagent B is present or not if MLB = 1 or 0 for a two-phase system. If strong acid is added as titrant, its concentration should be given a negative sign and the pre-added strong base, if present, should be given a negative sign also.

CAFUN: to calculate the free concentrations, the squares sum $U$ and to set up matrix $J^TJ$ or not by setting NXC = 1 or 0 point by point.

CHOL: a general purpose symmetric linear equations solver based on Choleski factorization.

PLOT: a plot sub. It can also be designed as a program so that it can be run on another computer with strong plot function. To run this program, the β values are input.

MINI: a main minimization sub. Its flow diagram is following:

(1) Call CAFUN to calculate $U^k$, matrix $J^TJ$ and vector $J^TH$

(2) Call CHOL to solve equations $(J^TJ + P \cdot I) \cdot S = -J^TH$

(3) If $s'$, the smallest shift of $S$, is greater than $-0.99$, goto (7), otherwise goto (4)

(4) Set $S = S \cdot (-0.99/s')$, Call CAFUN to calculate $U^{k+1}$

(5) If $U^{k+1} < U^k$ goto (8); otherwise goto (6)

(6) $P = P \times 5$, if $P < P_m$ ($P_m$ is set by experience) goto (2), otherwise set $P = P_c$, goto (8)

(7) Adjust $P$ according to Marquardt–Fletcher method

(8) Set $\beta^{k+1} = \beta^k + \beta^k \cdot S$, $k = k + 1$

(9) If the termination tolerance is achieved or the number of iterations is greater than the predetermined number, go out, otherwise goto (1).

## 4. Experimental

The Pb–PMBP(1-phenyl-3-methyl-4-benzoyl-pyrazolone-5)-TBP(tributyl phosphate) system was chosen for use as a model system to test the program.

### 4.1. Chemicals and solutions

All chemicals were analytical-grade. Solvent benzene was pre-saturated with 0.1 M $KNO_3$ and the solvent water was pre-saturated with benzene also. TBP and PMBP were purified according to the literature [3]. Their solutions were prepared with benzene in different concentrations. Other chemicals were used without further purification. All solutions were prepared with doubly distilled water. The ionic strength was kept at 0.1 M with $KNO_3$ and the temperature was kept constant at 25.0 ± 0.2 °C.

### 4.2. Operation

A 10 ml $Pb^{2+}$ solution, 10 ml PMBP–benzene solution, 2 ml TBP–benzene solution and a certain quantity of strong acid ($HNO_3$) were taken into a double walled cell. Under the protection of $N_2$, a certain quantity of potassium hydroxide was added and the solution was stirred until the equilibrium was achieved. Then the pH value in the aqueous phase was determined.

The experiment was divided into several parts. Firstly, the two-phase solution involving PMBP and TBP was titrated. The result shows that no synergistic compounds (such as $H_nA \cdot nB$) were present. Then the solution containing PMBP and $Pb^{2+}$ was titrated at two different concentrations of PMBP. Finally the titrations with $Pb^{2+}$, PMBP and TBP were run at three different concentrations of TBP. In this way, the number of unknown parameters de-

Table 1
Acid dissociation constants of PMBP and computed values of formation constants of Pb–PMBP–TBP together with those published in the literature, [3], the complex species are defined as $[M_lA_mB_nH_h]$

| Species $l, m, n, h$ | Log $\beta_{lmnh}$ ($\sigma_{\log \beta_{lmnh}}$) computed | Log $\beta_{lmnh}$ literature [3] |
|---|---|---|
| 0, 1, 0, $1_o$ | 7.53 [a] | 7.55 |
| 0, 1, 0, $1_{aq}$ | 4.1 [a] | 4.1 |
| 1, 2, 0, $0_o$ | 11.93 (0.029) | 12.08 |
| 1, 2, 1, $0_o$ | 12.90 (0.018) | 13.00 |

[a] Value is taken from the literature [5].

creases gradually and linear correlation between the parameters is prevented. For each curve, at least 30 points were titrated.

## 5. Results

The computed values of formation constants, together with those published in the literature [3] are given in Table 1. The effect of initial estimates on formation constants is given in Table 2. The concentration distribution and the fitting curves are given in Figs 1 and 2. The values found are in agreement with those already published in the literature [3]. The main complexes are $Pb(PMBP)_2$ and $Pb(PMBP)_2 \cdot TBP$ in the Pb–PMBP–TBP system. We also postulated the presence of $PbA_2 \cdot HA$ (HA represents PMBP). The $\beta_{1310}$ varied with its initial estimate and the sum of squares was unchanged, indicating that the species must be rejected.

## 6. Discussion

The program SCTPT possesses the following advantages over other programs for formation-constant calculation. (i) The refinement was

Table 2
Effect of initial estimates on formation constants

| Species $l, m, n, h$ | Log $\beta_{lmnh}$ (initial estimates) | Log $\beta_{lmnh}$ (computed value) | Number of iterations |
|---|---|---|---|
| 1, 2, 0, $0_o$ | 2.0 | 11.93 | 13 |
| | 18.0 | 11.93 | 7 |
| | 24.0 | 11.93 | 10 |
| 1, 2, 1, $0_o$ | 6.0 | 12.90 | 6 |
| | 13.0 | 12.90 | 4 |
| | 23.0 | 12.90 | 9 |

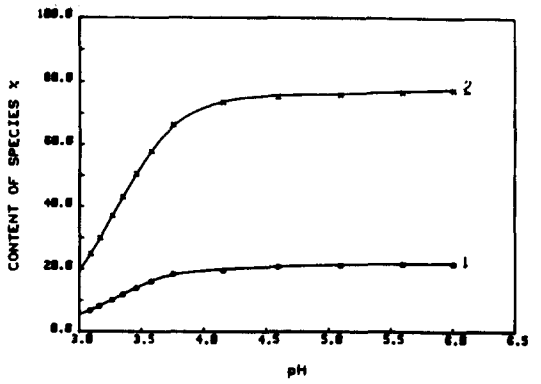


Fig. 1. The concentration distribution of the complex species. (1) $Pb(PMBP)_{2o}$; (2) $Pb(PMBP)_2(TBP)_o$.

done with the Marquardt–Fletcher algorithm [13] in which the Marquardt parameter $P$ was adjusted according to the ratio of the practical decrease of the sum of squares $U$ to the expected decrease in the sum of the squares. Thus, it possesses a more effective convergence than the Marquardt method. (ii) The use of the analytical derivatives eliminates the errors inevitably introduced during numerical differentiation. Consequently the initial estimates of the parameters need not be accurate and can be varied in a large range (about $\pm 10^5$). (iii) The formation constants are stored in mantissa and exponent form $(a, b)$, i.e. $\beta = a \cdot 10^b$ and the refinement is made to refer to the mantissa of the formation constants only, the exponent remaining unchanged. So that the partial products are not fortuitously larger or smaller than can be held in the computer's store. (iv) When a synergetic extraction system is too complicated and weak species are present (e.g. more than three species unknown present), the following method may be taken: at first compute

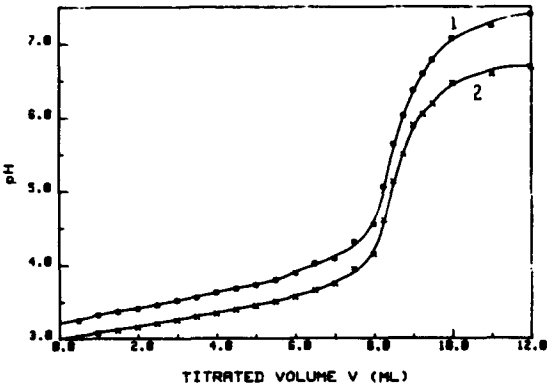


Fig. 2. The fitting titration curve. ○ and × are the experimental points. (1) $C_{PMBP} = 0.0212$ M, $C_{TBP} = 0.0220$ M; (2) $C_{PMBP} = 0.0212$ M, $C_{TBP} = 0.0110$ M.

$\beta$ of the main species and neglect the weak species, since their presence has little effect on $\beta$ of the main species; then compute $\beta$ of the weak species by setting $\beta$ of the main species constant (KEY = 0); finally all the parameters $\beta$ are computed with above calculated value as initial estimates which should be close to the true value.

The running time of the Program SCTPT on the model is less than 2 min on a PC/XT 386 computer.

## References

[1] F.C. Rossotti and H.S. Rossotti, The Determination of Stability Constants, McGraw-Hill, New York, 1961.
[2] B.S. Jensen, Acta Chem. Scand., 18 (1964) 739.
[3] Li Lemin and Xsu Kwang-hsie. Chem. J. Chin. Univ., 2(5) (1981) 256.
[4] Wang Wenqing and Mou Xiru, Chem. J. Chin. Univ., 2(3) (1981) 275.
[5] Zhang Kaichen and Cai Qingyun, Chem. J. Chin. Univ., 10(2) (1989) 135.
[6] D. Dyrssen, Suensk Kem. Tidskr., 64 (1952) 213.
[7] F. Gaizer, Coord. Chem. Rev., 27 (1979) 195.
[8] I.G. Sayce, Talanta, 15 (1968) 1397.
[9] A. Sabatini, A. Vacca and P. Gans, Talanta, 21 (1974) 53.
[10] D.W. Marquardt, J. Soc. Ind. Appl. Math., 11 (1963) 431.
[11] R.M. Alcock, F.R. Hartley and D.E. Rogers, J. Chem. Soc., Dalton Trans., 115 (1978).
[12] A.D. Zurberbuhler and Th. A. Kaden, Talanta, 29 (1982) 201.
[13] R. Fletcher, AERE, Harwell, Report No. R6799, 1971.
[14] I. Nagypal, I. Paka and L. Zekani, Talanta, 25 (1978) 549.

ELSEVIER

Talanta 42 (1995) 1379–1383

Talanta

# Sample illumination configurations for spatially resolved Raman spectrometry using a charge-coupled device detector

L.M. Cabalín, J.J. Laserna *

*Department of Analytical Chemistry, Faculty of Sciences, University of Málaga, E-29071 Málaga, Spain*

Received 19 October 1994; revised 16 January 1995; accepted 16 January 1995

**Abstract**

In this paper two simple configurations for sample illumination using a charge-coupled device (CCD) detector have been shown. The choice of an appropriate sample illumination can be crucial to obtain spatial and spectral information of complex samples. It is demonstrated that simultaneous Raman spectra of a heterogeneous sample of three compounds can be obtained using a vertical sample illumination. Spatially resolved resonant Raman and surface-enhanced resonant Raman spectra of a complex (Ni-PAPH) have been observed with a low integration time. Dividing the CCD in two regions and with horizontal multiline sample illumination (argon–ion laser at 488 nm and He–Ne laser at 632.8 nm) spatially resolved fluorescence spectra of a homogeneous mixture of dyes have been obtained. The total image was acquired in only 1 s.

## 1. Introduction

Owing to the modern analytical technique requirement for detectors with high sensitivity and low noise, charge-coupled device (CCD) detectors have recently been introduced in analytical spectroscopy as an alternative to photomultiplier tubes (PMT) and photodiode arrays (PD). A description of the devices, their characteristics and spectroscopic applications was first reported by Denton and co-workers [1–7].

The characteristics of CCDs of high quantum efficiency, high sensitivity from the soft *X*-ray to the near-IR regions, minimum dark current, large dynamic range, low read noise and the ability to integrate for long periods of time make them ideal tools for a wide variety of analytical applications [8–16]. However, CCDs are usually preferred for low-light-levels spectroscopies such as Raman [17] and luminescence. As CCDs have few restrictions on the choice of laser wavelength for Raman excitation, researchers have addressed their investigation in all spectral regions. Pemberton et al. have reported the combination of a CCD detector and He–Ne laser for Raman spectroscopy [16]. Wang and McCreery [18] have demonstrated that NIR-Raman spectroscopy with a CCD detector may offer superior sensitivity to Nd:YAG excited FT-Raman, while avoiding fluorescence excitation in most molecules. The coupling of CCD/diode laser system to fiber optic was also reported [19]. Other researchers have exploited a variety of novel readout techniques directed at improving the capabilities of the CCD, including binning [20,21] fast spectral framing and time-delayed-and-integration (TDI) mode imaging.

The main characteristics of CCDs derive from their bidimensional configuration, which permits the spatial information imaged on the spectrograph entrance slit to be readily investigated [22–25]. Imaging spectrographs com-

* Corresponding author.


*SSDI* 0039-9140(95)01528-0

bined with CCD detectors have been applied to simultaneous acquisition of multiple spectral inputs from several optical fibers [26]. In a recent work, we reported the spatially resolved SER spectrometry on silver-coated filter paper substrate of 9-aminoacridine using simple excitation–collection optics [27]. In this work the performance of a CCD detector for spatially resolved Raman and fluorescence techniques is demonstrated. Two different sample illumination modes have been employed whose configurations are simple and inexpensive compared with the other CCD methods reported in the literature and do not require the use of the optical fiber or cylindrical lens.

## 2. Experimental

### 2.1. Instrumentation

A schematic diagram of two illumination configurations employed is shown in Fig. 1. In the first configuration (Fig. 1A), the sample was excited by the 488-nm line of an argon-ion laser (Coherent, model Innova 70-5) and was vertically illuminated. In the second configuration (Fig. 1B) the sample along the vertical axis was excited by two different wavelengths, an argon–ion laser turned at 488 and 632.8 nm line of a He–Ne laser (Siemens, model LGK 7626S) were used. Two laser beams were horizontally focused on the glass cuvette. The separation between two laser beams was 0.7 cm.

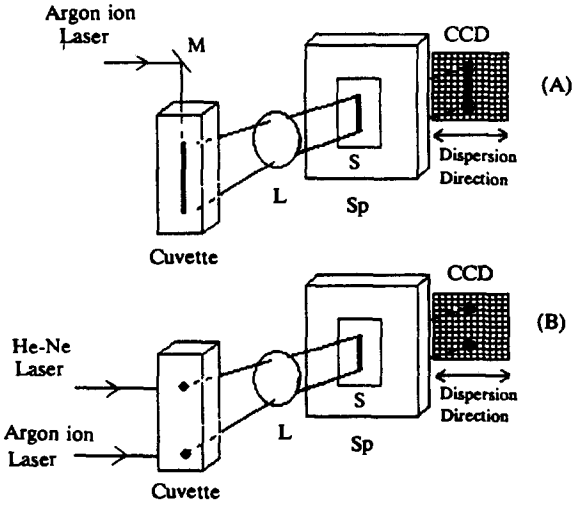


Fig. 1. Configurations for vertical (A) and horizontal (B) sample illumination of the CCD detector. L = Lens; M = mirror; S = spectrograph entrance slit; Sp = spectrograph.

In both systems, the laser beams were focused into the cuvette with a plano convex glass lens with a focal length of 25 cm and f-number of 4. Collection was performed with a glass biconvex lens with focal length of 25.4 mm and f-number of 1. The cuvette was placed approximately 11.5 cm from the collection lens, with the distance from the entrance slit to the lens being 5 cm. Thus the optical magnification was ca. 0.5. The scattered light was collected onto the entrance slit of a triple indexable granting spectrograph (Acton Research Corporation, SpectraPro 275, Czeny-turner; with F number of 3.8; fitted with three gratings of 300, 600 and 1800 grooves/mm). The spectral coverage and resolution varied gradually with spectral region and grating employed. The reciprocal linear dispersion of the spectrometer are 12 and 1.5 nm/mm with the 300 and 1800 grooves/mm gratings, respectively.

A solid-state two-dimensional charge coupled device (CCD) (EG&G Princeton Applied Research, Thomson CSF, THX-31159A) was used as detector. The CCD consists of $512 \times 512$ elements each being $19 \times 19$ μm. The active area $9.7 \times 9.7$ mm overall. This system has a quantum efficiency of 32% at 550 nm. The CCD was cooled to $-70$ °C by a Peltier system. When cooled to $-70$ °C, this detector exhibits a dark current of 10 photoelectrons pixel$^{-1}$ s$^{-1}$ and a readout noise of 4–5 electrons per scan. The calibration of the detector system was conducted with a mercury pen lamp. Operation of the detector was controlled by a personal computer (486 computer at 66 MHz, equipped with 8 Mbytes of extended memory and math coprocessor) with OMA Spec 4000 software. The spectrometer was connected to the controlling PC by a conventional IEEE-488 general-purpose interface bus (GPIB).

### 2.2. Chemicals and procedure

Analytical-reagent grade chemicals and distilled, deionized water were used throughout. Cresyl Violet 670, rhodamine 6G and 2-pyridinecarboxyaldehyde 2-pyridylhydrazone (PAPH) were purchased from Merck and used as methanolic solutions. Silver colloids were prepared at room temperature by adding 1 ml of $1 \times 10^{-3}$ M silver nitrate to 3 ml of $2 \times 10^{-3}$ M sodium tetrahydroborate. After mixing, 0.1 ml of 100 μg/ml analyte solution was added. Ni–PAPH complexes were prepared at room temperature by adding the

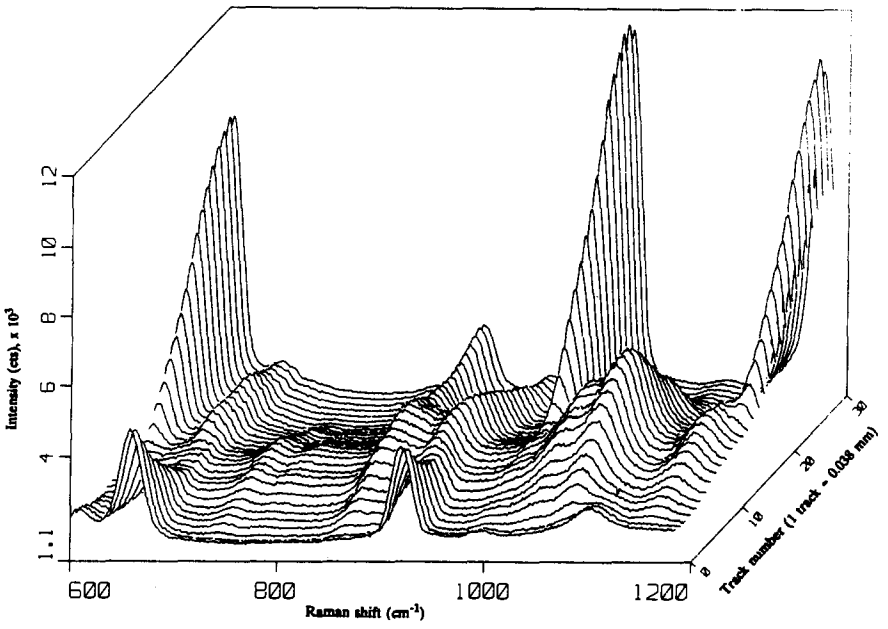


Fig. 2. Space-resolved Raman spectra of nitromethane (bottom), triethanolamine (middle) and benzene (top). Binning was 10-fold in the slit dimension. Acquisition time was 120 s and laser power 40 mW (Argon ion laser was tuned at 488 nm).

volume ratio (1:1 v/v) of 100 μg/ml PAPH (in aqueous or chloroform solutions) to 25 μg/ml of nickel(II) nitrate prepared in water.

## 3. Results and discussion

One of the main goals of the introduction of charge-coupled devices (CCD) as detectors in analytical chemistry was to exploit their two-dimensional nature. This feature permits to obtain simultaneous spectral and spatial information of the analyzed sample. The acquisition of high-quality space-resolved spectra requires an appropriate sample illumination and collection of scattered light by the spectrograph/detector system. In this work, two sample illumination configurations have been evaluated for improving device performance and operation of Raman analysis of liquid samples (Fig. 1). Figure 1A shows a configuration involving vertical illumination of sample. Since the dispersion direction of the spectrograph used was horizontal, the vertical direction in the CCD is available for spatially resolved spectrometry. To create a spatially heterogeneous sample, three immiscible solvents: nitromethane, triethanolamine and benzene were located in a glass cuvette. The separation of the compounds of the sample was determined by the different densities of the solvents (1.14, 1.12 and 0.88 g/ml for nitromethane, triethanolamine and benzene, respectively). The spatially resolved Raman spectra of this immiscible sample are shown in Fig. 2. The height dimension in the figure represents the tracks number (each track was made up of 10 rows of pixel) in the CCD detector. Since the pixel height is 19 μm and the optical magnification of the collection optics is about 0.5, each track represents 0.038 mm in the cuvette height. This means that only 1.5 cm of cuvette height is observed by the small area of the CCD detector. In this case the image was binned 10-fold in the slit dimension and the resulting 31 spectra were acquired. The power at the laser head was 300 mW of which 40 mW reached the sample. The Raman bands corresponding to nitromethane (up to 10 track), triethanolamine (from 10 to 20 track) and benzene (from 20 to 30 track) are well resolved (Fig. 2). It should be noted that the acquisition time of this image was only 120 s. The less intense zones in the figure result from the interphases nitromethane–triethanolamine and triethanolamine–benzene.

The simultaneous acqusition of the resonant Raman (RR) spectrum and the surface-enhanced resonant Raman (SERR) spectrum of the complex of nickel with 2-pyridinecarboxyaldehyde 2-pyridylhydrazone (PAPH) is shown in Fig. 3, using the vertical approach described in the Experimental section (Fig. 1A). The sample was placed into a glass cuvette, with the Ni–PAPH complex dissolved in

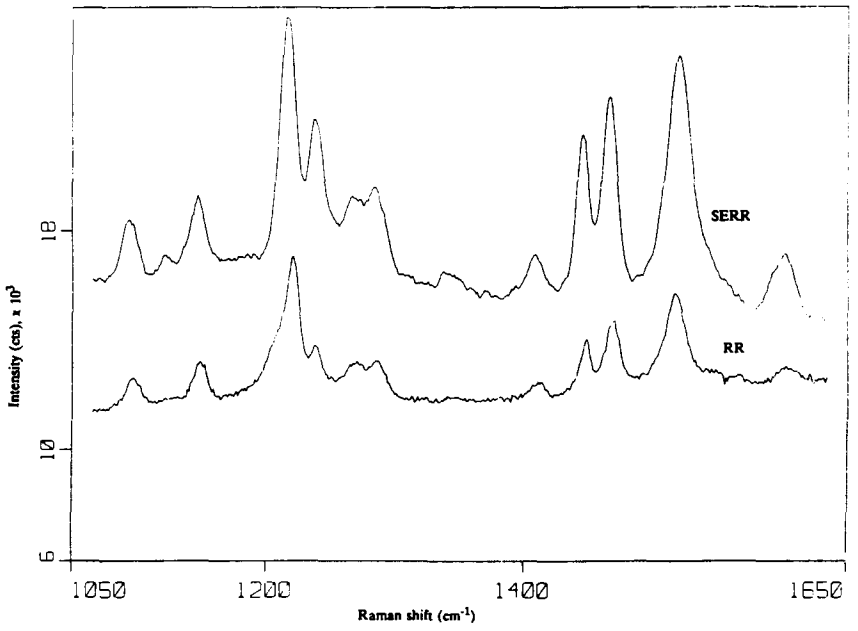


Fig. 3. Simultaneous acquisition of resonant Raman (bottom) and SERR (top) spectra of Ni–PAPH complex. Binning were 200-fold and 20-fold in the slit dimension for RR and SERR spectra, respectively. Acquisition time was 180 s. The 488-nm line of the argon ion laser (25 mW) was used.

chloroform at the bottom and the aqueous Ni–PAPH complex adsorbed on silver hydrosol at the top, so RR and SERR spectra were obtained, respectively. As shown, the line positions and relative intensities in the RR and SERR spectra correlate quite well. What is of interest for the present is that, as expected, the SERR bands are more intense than the corresponding RR bands. The flexibility of the CCD system permits comparable intensities in both spectra to be obtained by using different binning in the two spatial regions. Binning was 200-fold in the slit dimension for the RR spectrum and 20-fold for the SERR spectrum. This difference in the binning was also due to the attenuation of the laser power by the aggregated colloidal silver, thus more binning was needed for RR spectrum. The image was acquired in 180 s with a laser power of 25 mW.

The sensitivity and imaging performance of the instrument for analytical purposes was also tested with a homogeneous mixture of Cresyl Violet 670 and rhodamine 6G. The spatially resolved fluorescence spectra of the mixture are shown in Fig. 4. An argon ion laser tuned at 488 nm (2 mW) and a He–Ne laser at 632.8 nm (12 mW) were aligned horizontally so that two regions of the sample along the vertical axis were excited by the two beams (see Fig. 1B). The emitted light from the sample was then imaged onto the entrance slit of the spectrograph, dispersed and detected by the CCD detector. As each vertical region was excited by a wavelength (488 or 632.8 nm as excitation source) different fluorescence spectra are observed. In this figure, the first region (bottom) was excited by the 488 nm line and only the spatially resolved fluorescence spectrum of rhodamine 6G was observed. In the second region (top) the excitation wavelength was 632.8 nm and only Cresyl Violet was detected. The fluorescence maxima of rhodamine 6G and Cresyl Violet are at 550 and 621 nm, respectively. The large peak observed at 632.8 nm corresponds to the He–Ne laser line. The CCD was binned 10-fold in the spatial dimension, and the resulting 32 spectra are stored. The total image was acquired in only 1 s.

To conclude, the combination of imaging spectrographs and CCD detectors have revolutionized the field of spectroscopic investigation and have helped to interpret the results. Space resolved spectra of complex samples can be acquired simultaneously in a fraction of the time previously required by conventional detectors. To fully exploit CCD performance, an adequate and simple configuration is needed to illuminate the sample and to collect the scattered light in the small area of CCD detectors.

Depending on the illumination mode, components in heterogeneous or homogeneous samples can be studied in situ with satisfactory

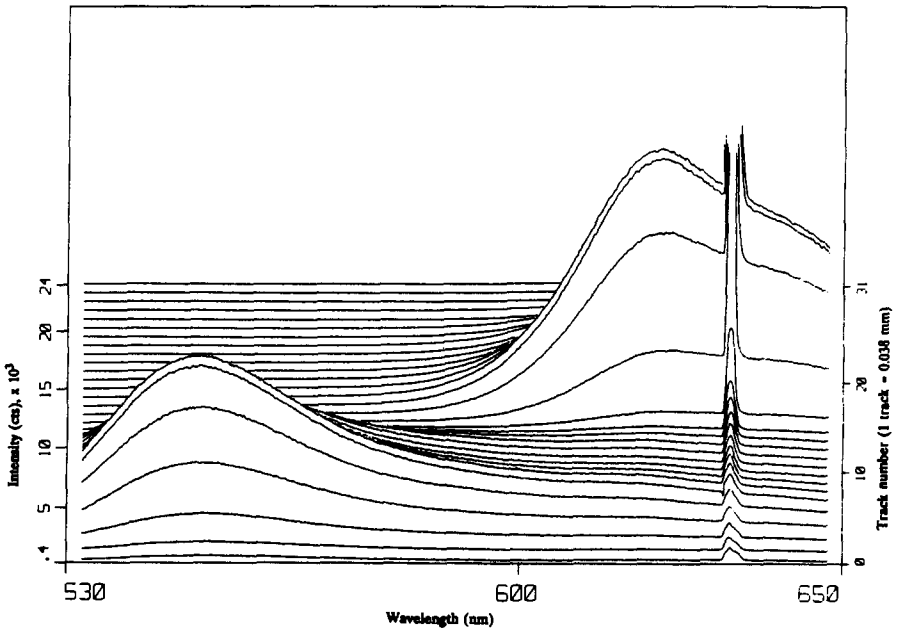


Fig. 4. Space-resolved fluorescence spectra of a mixture of rhodamine 6G ($10^{-6}$ M) and Cresyl Violet ($10^{-5}$ M) excited by the 488 nm line of the argon ion laser (2 mW) and the 632.8 nm line of the He–Ne laser (12 mW). Binning was 10-fold in the slit dimension. Acquisition time 1 s.

spatial and spectral resolution and low integration time.

## Acknowledgement

Research was supported by Dirección General de Investigación Científica y Técnica (Ministerio de Educación y Ciencia, Madrid, PB90-0814) and Dirección General de Universidades e Investigación (Junta de Andalucía, Sevilla), Spain.

## References

[1] R.B. Bilhorn, J.V. Sweedler, P.M. Epperson and M.B. Denton, Appl. Spectrosc., 41 (1987) 1114.
[2] R.B. Bilhorn, J.V. Sweedler, P.M. Epperson and M.B. Denton, Appl. Spectrosc., 41 (1987) 1125.
[3] J.V. Sweedler, R.D. Jalkien and M.B. Denton, Appl. Spectrosc., 43 (1989) 953.
[4] J.V. Sweedler, R.B. Bilhorn, P.M, Epperson, G.R. Sims and M.B. Denton, Anal. Chem., 60 (1988) 282A.
[5] P.M, Epperson, J.V. Sweedler, R.B. Bilhorn, G.R. Sims and M.B. Denton, Anal. Chem., 60 (1988) 327A.
[6] C.W. Earle, M.E. Baker, M.B. Denton and R.S. Pomeroy, Trends Anal. Chem, 12 (1993) 395.
[7] J.V. Sweedler, K.L. Ratzlaff and M.B. Denton, in Y. Talmi (Ed.), Charge Transfer Devices in Spectroscopy, VCH, Weinhein, 1994 p. 5.
[8] R.D. Jalkian and M.B. Denton, Appl. Spectrosc., 42 (1988) 1194.
[9] C. Hsiech, S. Petrovic and H.L. Pardue, Anal. Chem., 62 (1990) 1983.
[10] J.V. Sweedler, J.B. Shear, H.A. Fishman, R.N. Zare and R.H. Scheller, Anal. Chem., 63 (1991) 496.
[11] Y.F. Cheng, R.D. Piccard and T. Vo-Dinh, Appl. Spectrosc., 44 (1990) 755.
[12] D.S. Mantus, G.A. Valaskovic and G.H. Morrison, Anal. Chem., 63 (1991) 788.
[13] T.W. Barnard, M.J. Crockett, J.C. Ivaldi, P.L. Lundberg, D.A. Yates, P.A. Levine, and D.J. Sauer, Anal. Chem., 65 (1993) 1231.
[14] C.A. Murray and S.B. Dierker, J. Opt. Soc. Am., 3 (1987) 2151.
[15] S.B. Dierker, C.A. Murray, J.D. LeGrange and N.E. Schlotter, Chem. Phys. Lett., 137 (1987) 453.
[16] J.E. Pemberton and R.L. Sobocinski, J. Am. Chem. Soc., 111 (1989) 432.
[17] N.J. Pothier and R.K. Forcé, Appl. Spectrosc., 46 (1992) 147.
[18] Y. Wang and R.L. McCreery, Anal. Chem., 61 (1989) 2647.
[19] C.D. Allred and R.L. McCreery, Appl. Spectrosc., 44 (1990) 1229.
[20] P.M. Epperson and M.B. Denton, Anal. Chem., 61 (1989), 1513.
[21] L.M. Cabalín and J.J. Laserna, Quim. Anal., 12 (1993) 209.
[22] H. Knobloch and W. Knoll, J. Chem. Phys., 94 (1991) 835.
[23] M. Bowden, P. Donaldson, D.J. Gardiner, J. Birnie and D.L. Gerrard, Anal. Chem., 63 (1991) 2915.
[24] J.J. Laserna, N. Calvo, L.M. Cabalín, Anal. Chim. Acta, 289 (1993) 113.
[25] L.M. Cabalín, N. Calvo, L. Ayala and J.J. Laserna, Quim. Anal., 12 (1993) 96.
[26] F. Purcell, Laser Focus World, 29 (1993) 93.
[27] L.M. Cabalín and J.J. Laserna, Anal. Chim Acta, in press.

ELSEVIER

Talanta 42 (1995) 1385–1388

Talanta

# Application of the Folin–Ciocalteau reagent to the determination of salbutamol in pharmaceutical preparations

Novelette P. Sadler *, Helen Jacobs

*Department of Chemistry, University of the West Indies, Mona, Kingston 7, Jamaica*

Received 27 July 1994; revised 23 January 1995; accepted 24 January 1995

**Abstract**

A method for the determination of salbutamol in both tablets and syrups is described. It utilizes the reduction of the Folin–Ciocalteau reagent by the phenolic group, monitoring the absorbance of the resulting complex at 760 nm. Results obtained are linear over the range 0–6 μg $ml^{-1}$ salbutamol. Coloring material was removed by anionexchange chromatography prior to analysis and there was no interference from sucrose, neutral flavorings or the common preservative sodium benzoate. This method appears suitable as a general assay for salbutamol.

## 1. Introduction

Salbutamol, 1, α-[(*tert*-butylamino)methyl]-4-hydroxy-*m*-xylene-α,α′-diol, the structure of which is shown in Fig. 1, is a sympathomimetic amine containing a phenolic group. Salbutamol sulfate in various forms — aerosol spray, tablets, syrups, injection — is extensively used in the treatment of asthma.

The recent expiration of the proprietary rights of the original patent holders has led to the widespread utilization of the generic substance in formulations for oral dosage, many of which are flavored and colored to appeal to specific local tastes.

The most recent official B.P. [1] and U.S.P. [2] assays for salbutamol (as the sulfate) in formulation are based on HPLC and non-aqueous titration, and are described specifically for tablets, injection solutions and aerosol sprays. Although the non-aqueous titration method is straightforward, it is inapplicable to syrups and solutions, while the other methods are unsuitable for the technologically less well-developed settings in which it is often necessary to quantify salbutamol in formulations. An earlier B.P. method [3] is based on anion-exchange chromatography and the UV absorption at 276 nm of the salbutamol cation in acid. Although suitable to relatively low-technology environments and, in principle, applicable to a number of formulations, this method is described specifically for tablets only; it is subject to interference from neutral and cationic excipients, and additives, several of which absorb in the same mid-UV region as salbutamol.

Recently published salbutamol assays include a microtitrimetric method [4], described in application for tablets only, and a number of others which entail the formation of highly unstable derivatives with various chromogenic agents [5–16].

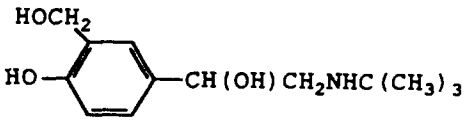


Fig. 1. Structure of salbutamol.

* Corresponding author. Fax: (809)927-1640.

*SSDI* 0039-9140(95)01534-5

The phenolic group in salbutamol makes it a reductant for the Folin–Ciocalteu reagent, a chromogenic agent which has been widely applied to the determination of a number of compounds with reducing properties [17], and has been successfully used to quantify phenol morphine in the presence of its methyl ether codeine [18].

## 2. Experimental

### 2.1. Apparatus

A Phillips single beam P48670 visible/near-IR spectrophotometer was used for the absorbance measurements at 760 nm. For the B.P. method [3] and the measurement of spectra of neutral solutions obtained by ion-exchange chromatography of syrups, UV absorbances were determined on a Hewlett-Packard 8452 diode array spectrophotometer. A 1 cm quartz cell was used in both cases. An Orion model EA 920 pH meter was used for pH measurements.

### 2.2. Materials

Pure drug samples were obtained from P.A. Benjamin Manufacturing Co. Ltd., Kingston, Jamaica. Dosage forms were acquired from local and overseas sources, and the following formulations were used.

(A) Ventasol syrup, salbutamol sulfate equivalent to 2 mg salbutamol per 5 ml syrup, no color or flavor. (P.A. Benjamin Manufacturing Co. Ltd., Kingston, Jamaica).

(B) Fedbutamol syrup, salbutamol sulfate equivalent to 2 mg salbutamol per 5 ml syrup, colored and flavored. (Federated Pharmaceutical Co. Ltd., Kingston, Jamaica).

(C) Ventolin tablets, salbutamol sulfate equivalent to 2 mg salbutamol per tablet, colored. (Glaxo Operations UK Ltd., Greenford, UK).

(D) Ventolin syrup, salbutamol sulfate equivalent to 2 mg salbutamol per 5 ml syrup, no color or flavor. (Glaxo Operations UK Ltd., Greenford, UK).

(E) Albuterol syrup, salbutamol sulfate equivalent to 2 mg salbutamol per 5 ml syrup, colored and flavored. (Allen & Manbury's (Division of Glaxo), Research Triangle, NC 27709, USA).

### 2.3. Reagents

Distilled deionized water was used throughout. Folin–Cioicalteu reagent was prepared according to a published procedure [18]. The reagent was used as soon as possible after preparation, although colorimetric solutions prepared from reagent that was 54 h old gave results indistinguishable from those obtained with freshly prepared reagent.

Ion-exchange chromatography utilized the commercially available chloride form of a strongly basic ion-exchange resin (usually Dowex 1-X2, 50–100 mesh) which, prior to use, was stirred briefly with 0.1 M NaCl or 0.1 M HCl and washed free of chloride ions.

Saturated $Na_2CO_3$ solutions were cooled and filtered before use.

### 2.4. Standard drug solutions

A solution of salbutamol sulfate in water of concentration equivalent to 50 $\mu g\,ml^{-1}$ salbutamol was made up, and appropriate aliquots taken for preparation of colorimetric solutions used to generate the standard curve.

### 2.5. Analytical samples from pharmaceutical preparations

Anion-exchange chromatography was carried out to remove coloring materials where present, as most common food dyes are anionic and non-phenolic. This procedure also removed benzoate.

*Tablets*

Ten tablets were weighed and powdered, and a quantity of powder containing the equivalent of 5 mg salbutamol suspended in 30 ml water. The suspension was filtered, the filtrate passed through 10–15 ml of the chloride ion-exchange resin contained in a 50 ml burette, and the resin washed with water until the volume of eluant was 100 ml.

*Syrups*

For syrups with and without color, a volume of syrup containing the equivalent of 5 mg salbutamol was diluted with an equal volume of water, the solution passed through 10–15 ml of the chloride resin, and 100 ml eluant collected. Solutions of syrups without color were also prepared by dilution to 100 ml of a volume of syrup containing the equivalent of 5 mg salbutamol.

Table 1
Limits, optical characteristics, accuracy

| | |
|---|---|
| Beer's law limits ($\mu g\ ml^{-1}$) | 0–6 |
| Molar absorptivity ($l\ mol^{-1}\ cm^{-1}$) | 15240 |
| Regression equation [a] | |
| Slope ($m$) | $15240 \pm 99$ |
| Intercept ($n$) | $0.005 \pm 0.001$ |
| Correlation coefficient ($r$) | 0.998 |
| $R$-squared [b] | 99.7% |

[a] $y = n + mc$, where $c$ is the concentration in $\mu g\ ml^{-1}$.
[b] Six replicate samples of each concentration.

### 2.6. Preparation of colorimetric solutions

Aliquots of standard or sample solutions containing the equivalent of 5, 10, 20, 30, 40, 50, 100, 200, 400, 600 and 800 μg salbutamol were placed in 100 ml volumetric flasks. To each flask was added 2 ml of Folin–Ciocalteu reagent and 3 ml of saturated $Na_2CO_3$ solution, and the volume made up to the mark with water. Five hours were allowed for development of the maximum blue color, after which the absorbance could be measured within 18 h.

## 3. Results and discussion

### 3.1. Effect of concentration

Plots of optical density versus concentration were made over the range 0–8 $\mu g\ ml^{-1}$ using salbutamol standards. Excellent linear correlation was obtained up to 6 $\mu g\ ml^{-1}$, and the slope of the plot over this range was used to calculate the molar absorptivity at 760 nm by Beer's law. The results of linear regressional analysis of the data are shown in Table 1. The salbutamol concentration in each pharmaceutical preparation was again determined using Beer's equation, making substitutions for the above-determined molar absorptivity and for the measured absorbance. Several concentrations of each preparation were used and the average calculated, along with its standard deviation. Table 2 summarizes the results obtained.

### 3.2. Effect of flavoring and benzoate

The flavorings and benzoate present in the syrups did not interfere with the determination of salbutamol using the colorimetric method. The results obtained using syrup solutions prepared via ion-exchange chromatography were identical to those for solutions made up by simple dilution of syrups. UV analysis (monitoring 278 nm) of neutral solutions obtained from the ion-exchange chromatography of colorless syrups in some cases revealed severe interference by cationic or neutral species present as flavoring.

In all the cases studied, the salbutamol concentrations obtained by this method were in agreement with those stated by the manufacturers of the formulations, which were given to one significant figure.

The reaction between salbutamol and the Folin–Ciocalteau reagent results in the formation of an intensely blue complex ($\lambda_{max} = 760$ nm), which is probably a reduced heteropolyanion of molybdenum and tungsten [19]. Isopoly- and heteropolyanions of molybdenum and tungsten have been extensively studied, and their structures are fairly well understood. They can be reversibly reduced by the addition of one to six electrons per anion to give the "heteropoly blues", a generic name derived from their intense coloration. These "blues" can be classified as mixed-valence complexes containing Mo(V) and Mo(VI), or W(V) and W(VI). It is likely that the phenolic group of salbutamol reduces the Mo(VI) and W(VI) centers to produce these relatively stable mixed-valence complexes. The intense, fairly broad band observed at 760 nm in the visible/near IR is typical of these complexes, and has been attributed to intervalence charge-transfer bands between Mo(V) and Mo(VI) via an oxo bridge, or to d–d bands for Mo(V) [20]. The large value of $\varepsilon$ obtained in this study is consistent with those usually observed for d–d transitions [19,20].

Table 2
Salbutamol determination in formulations

| Formulation | Nominal amount (mg per tablet or mg per 5 ml syrup) | Found [a] | Official method [3] |
|---|---|---|---|
| *Tablets* | | | |
| Ventolin | 2 | $2.05 \pm 0.13$ | $1.96 \pm 0.06$ |
| *Syrups* | | | |
| Ventolin | 2 | $2.10 \pm 0.11$ | |
| Fedbutamol | 2 | $2.02 \pm 0.17$ | |
| Albuterol | 2 | $2.16 \pm 0.05$ | |
| Ventasol | 2 | $1.93 \pm 0.02$ | |

[a] Average $\pm 2 \times$ standard deviation of six determinations.

## Acknowledgment

The authors thank P.A. Benjamin Co. Ltd., Kingston, Jamaica, for providing samples of Ventasol and some funding for this research.

## References

[1] British Pharmacopeia, Vol II, Her Majesty's Stationery Office, London, 1993, p. 1090.
[2] United States Pharmacopoeia, 23rd edn., Mack Publishing Co., Easton, PA, 1995.
[3] British Pharmacopoeia, Vol. II, Her Majesty's Stationery Office, London, 1988, p. 1001.
[4] N. Geeta and T.R. Baggi, Mikrochim. Acta, 1 (1990) 95.
[5] B. Pathak and M. Basu, Indian Drugs, 28 (1990) 109.
[6] N. Geeta and T.R. Baggi, Microchem. J., 39 (1989) 137.
[7] D.G. Sankar, C.S.P. Sastry, M.N. Reddy and N.R.P. Singh, Microchem. J., 24 (1987) 410.
[8] R.B. Patel, A.A. Patel and U. Pattani, Microchem. J., 24 (1987) 298.
[9] D.M. Shingbal and R.R. Naik, Microchem. J., 22 (1985) 273.
[10] P.K. Chatterjee, C.L. Jain and P.D. Sethi, Microchem. J., 23 (1986) 635.
[11] D.M. Shingbal and S.V. Joshi, Microchem. J., 21 (1984) 398.
[12] R.T. Sane, C.H. Thombare, A.B. Ambardekar and A.Y. Sathe, Microchem. J., 19 (1982) 195.
[13] R.T. Sane, V.G. Nayak and V.B. Malkar, Talanta, 32 (1985) 31.
[14] D.M. Shingbal and S.D. Naik, Can. J. Pharm. Sci., 16 (1981) 6515.
[15] S. Delgado and G. Gonzalez, Rev. Cubana Farm., 13 (1979) 141.
[16] A. Wahbi, H. Abdine, M. Korany and M. Abdel-Hay, J. Assoc. Off. Anal. Chem., 61 (1978) 1113.
[17] C.S.P. Sastry, A. Sailaja, T.T. Rao and D.M. Krishna, Talanta, 39 (1992) 709.
[18] F.C. Klee and E.R. Kirsch, J. Am. Pharm. Assoc., 42 (1953) 146.
[19] R.I. Buckley and R.J.H. Clark, Coord. Chem. Rev., 65 (1985) 167.
[20] C. Sanchez, L. Livage, J.P. Launay, M. Fourneir and Y. Jeannin, J. Am. Chem. Soc., 104 (1982) 3194.

ELSEVIER

Talanta 42 (1995) 1389–1394

Talanta

# Indirect measurement of brucine by adsorptive stripping voltammetry at mercury electrode

Meixian Li, Naifei Hu*, Shuchang Lin

*Department of Chemistry, Beijing Normal University, Beijing 100875, People's Republic of China*

Received 26 October 1994; revised 3 February 1995; accepted 17 February 1995

**Abstract**

After reaction with nitric acid, brucine can be transformed into cacotheline, and then measured indirectly by adsorptive stripping voltammetry. This method is based on the adsorptive accumulation of cacotheline at a hanging mercury drop electrode, followed by cathodic linear sweep voltammetry. The cathodic peak potential is about −0.35 V (vs. saturated Ag/AgCl). The detection limit of $2.0 \times 10^{-9}$ M is obtained under optimized conditions. The electrochemical behaviour of cacotheline and the mechanism of the electrode reactions are discussed.

## 1. Introduction

Brucine is an alkaloid, and exists mainly in the seeds of *Strychnos nux-vomica*. Its structure is shown in Fig. 1a. The seeds of *Strychnos nux-vomica* have been used in traditional Chinese medicine with a long history. Its main efficacy includes pain relief, reduction of swelling and promotion of circulation [1,2]. Several well-known traditional Chinese medicines have the seeds as one of their main ingredients. As a drug, brucine itself is known as a central nervous system stimulant. It can be adsorbed by the human body and enters into the bloodstream. Generally, the concentration of brucine in urine and blood is low after metabolization. Thus, the establishment of highly sensitive methods for the determination of brucine is of pharmacological importance. Brucine is also known as a drug with great toxicity. The determination of trace amounts of brucine is thus not only of toxicological, but also of forensic significance. Various chromatographic and other procedures have been employed for this purpose [3–6]. For example, Dadisch [7] established a chromatographic method for the detection of brucie in urine. Korany and Seif El-Din [8] developed a spectrophotometric method to determine brucine in *nux vomica* liquid extract. The limit of detection was about $8 \times 10^{-6}$ M. Nyasulu [9] studied the electrochemical oxidation of brucine at a carbon paste electrode. However, brucine has no electroactivity of reduction at a mercury electrode [10].

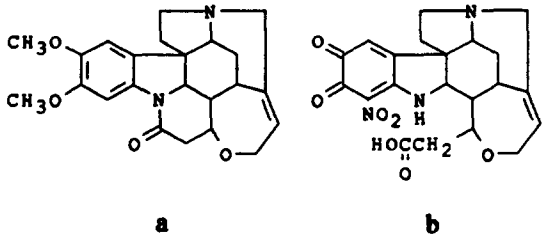


Fig. 1. Structure of (a) brucine and (b) cacotheline.

Cacotheline (CAC), as a nitration product of brucine, is an analytical reagent used in the detection and determination of various metal

* Corresponding author.


*SSDI* 0039-9140(95)01563-9

ions and organic compounds [11–13]. Its structure is shown in Fig. 1b. Vijayalakshmi and Saraswathi [14] studied the polarographic and cyclic voltammetric behaviour of cacotheline at a mercury electrode. They found there were two cathodic polarographic waves between pH 2.0 and 12.0. The first wave involved two electrons for the reversible reduction of the *o*-quinone group to hydroquinone, while the second underwent a four-electron irreversible reduction of the nitro group to hydroxylamine. However, they did not mention the adsorptive properties of cacotheline at a mercury electrode, and the detection limit of determination of cacotheline was only about $1 \times 10^{-4}$ M.

This paper studied the electrochemical properties of cacotheline, especially its adsorptive characteristics at a mercury electrode. On the basis of this, a new electroanalytical method for the indirect measurement of brucine was established. After reaction with nitric acid, brucine was transformed into cacotheline, which was then determined by adsorptive stripping voltammetry at a mercury electrode. Adsorptive stripping voltammetry (AdSV) has been used for trace measurements of numerous compounds of pharmaceutical significance [15]. As illustrated in this paper, by this method a detection limit of $2 \times 10^{-9}$ M was achieved for the determination of cacotheline or brucine.

## 2. Experimental

### 2.1. Apparatus

A model 370 electrochemical system (EG&G Princeton Applied Research, U.S.A.) was used for cyclic voltammetry, adsorptive stripping voltammetry and phase-selective a.c. voltammetry. The working electrode was a model 303 static dropping mercury electrode (SDME). A medium-sized drop (surface area, 0.0171 $cm^2$) was employed. The counter electrode was a platinum wire and the reference electrode was a saturated Ag/AgCl electrode.

### 2.2. Chemicals

Brucine was obtained from Heidelberg (U.S.A.). A stock standard solution of brucine ($1.00 \times 10^{-3}$ M) in 5% ethanol–95% water (v/v) was prepared and stored in the dark; working standard solutions ($1.00 \times 10^{-4}$, $1.00 \times 10^{-5}$ and $1.00 \times 10^{-6}$ M) were prepared by dilution with water. Cacotheline was obtained from Drs. Fraenkel and Landau (Germany). A stock standard solution of cacotheline ($1.00 \times 10^{-3}$ M) in water was prepared and stored in the dark; working standard solutions ($1.00 \times 10^{-4}$ M and less) were prepared by dilution with water. All other chemicals were of analytical reagent grade. Triply distilled water was used throughout.

### 2.3. Procedure

*Measurement of cacotheline by AdSV*

A 10-ml volume of 0.02 M acetic acid–sodium acetate (HOAc–NaOAc) buffer solution (pH 4.0) containing a specific amount of cacotheline sample solution was added to the cell, which was purged with purified nitrogen for at least 4 min to remove oxygen. The SDME was set to the hanging mercury electrode mode. The preconcentration potential (−0.1 V) was then applied to a new mercury drop for a selected time while the solution was stirred at 400 rev $min^{-1}$. The stirring was then stopped, and after 15 s the voltamperogram was recorded by applying a linear sweep scan. The scan was terminated at −0.5 V.

*Nitration of brucine*

A certain amount of brucine (about 0.05 g) was placed in a flask and 1 ml of 3.5 M nitric acid was added. The flask was then heated on a water bath and kept at 60–70 °C while stirring the solution inside. After 2 h of reaction, brucine was believed to be completely transformed into cacotheline. All the products and the solution were thoroughly transferred into a beaker. With water added, the beaker was heated until all the solid product was dissolved. After cooling down, the solution was transferred to a 100 ml volumetric flask and diluted with water to the mark. This solution or its diluted version could be used as sample solutions. After measuring cacotheline in this solution by adsorptive stripping voltammetry, the amount of brucine could be determined indirectly.

## 3. Results and discussion

### 3.1. Nitration of brucine

Brucine is electroinactive at a mercury electrode. For example, in buffer solution of

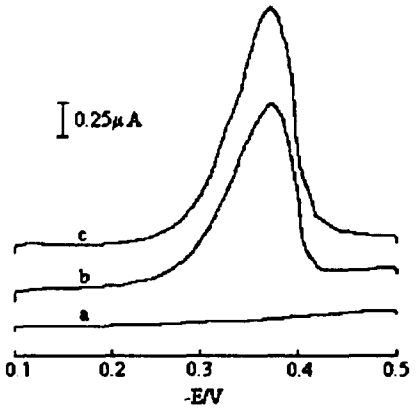


Fig. 2. Cathodic sweep voltamperograms for (curve a) $3 \times 10^{-5}$ M brucine, (curve b) $3 \times 10^{-5}$ M cacotheline and (curve c) nitration product of $3.45 \times 10^{-5}$ M brucine. (Electrolyte, 0.02 M HOAc–NaOAc, pH 4.0; scan rate, 100 mV s; initial potential, −0.10 V.).

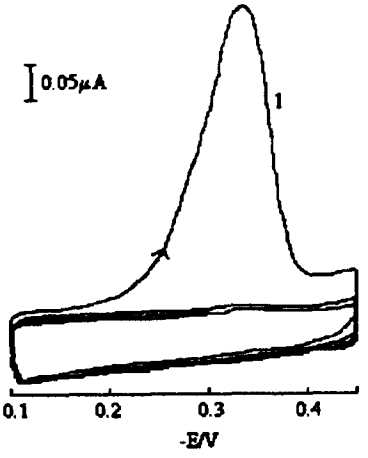


Fig. 3. Repetitive cyclic voltamperograms for $1 \times 10^{-6}$ M cacotheline after 30 s accumulation at −0.1 V. Four cycles; other conditions as for Fig. 2.

HOAc–NaOAc (pH 4.0), brucine does not show any reduction peak over the potential range −0.10– −0.50 V (Fig. 2, curve a). Thus, there is no way of determining brucine by voltammetry at the mercury electrode. However, in the same electrolyte, cacotheline shows a well-defined reduction peak at about −0.37 V (Fig. 2, curve b). This prompted us to use a nitration method to transform brucine into cacotheline first, and then determine cacotheline by voltammetry. Brucine can thus be measured indirectly. The procedure of nitration of brucine was described in detail in the experimental section. The voltamperogram of the nitration product is shown in Fig. 2, curve c. Compared with Fig. 2, curve b, this product has the same cathodic peak potential as cacotheline, which indicates that the nitration product of brucine obtained by this procedure is indeed cacotheline.

### 3.2. Adsorptive properties of cacotheline

Fig. 3 is a repetitive cyclic voltamperogram for $1 \times 10^{-6}$ M cacotheline, recorded after preconcentration at −0.1 V for 30 s. A large and well-defined cathodic peak is observed at the first scan (designated as 1) at −0.32 V. Subsequent scans exhibit a dramatic decrease of the peak to a stable value representing the response of the solution species. This is an obvious indication that cacotheline has adsorptive characteristics at a mercury electrode. No peaks are observed in the anodic branch, illustrating that the reduction of cacotheline at a mercury electrode is irreversible.

Fig. 4 shows plots of cathodic peak current ($i_{pc}$) of linear sweep voltammetry vs. preconcentration time ($t$) for different concentrations of cacotheline. At first, $i_{pc}$ increased linearly with $t$ at all four levels, indicating that before adsorptive equilibrium is reached, the longer the preconcentration time, the more cacotheline was adsorbed and the larger the peak current. However, after a specific period of accumulation time, the peak current at different concentration levels invariably tended to level off, showing that the adsorptive equilibrium of cacotheline on the mercury electrode surface was achieved.

The adsorption of cacotheline can be used as an effective preconcentration step before the voltammetric measurements. In this way, highly sensitive adsorptive stripping voltammetric measurements of cacotheline can be achieved.

### 3.3. Selection of experimental conditions

Various supporting electrolytes, such as HCl, HOAc–NaOAc, $NH_3$–$NH_4Cl$, $KH_2PO_4$–$K_2HPO_4$, NaOH, KCl, $Na_2B_4O_7 \cdot 10H_2O$ and Britton-Robinson buffer solution, were tested by AdSV and HOAc–NaOAc was found to be the best because of the well-defined voltamperogram and reasonably high sensitivity. The experiments revealed that the conditions of a total concentration of HOAc–NaOAc between 0.002 and 0.18 M, and pH value between 3.7 and 5.0 offered the best responses. Thus 0.02 M HOAc–NaOAc and pH 4.0 was chosen in all experiments. The experiments of the effect of preconcentration

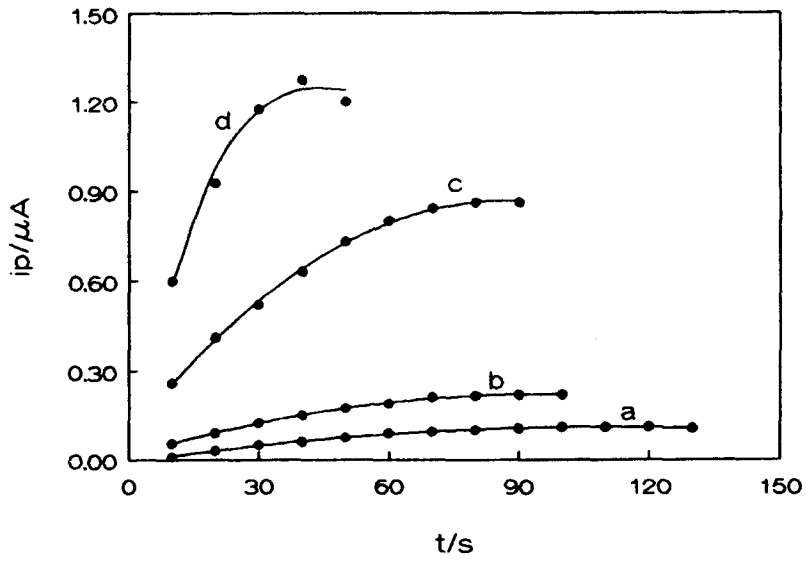


Fig. 4. Effect of preconcentration time on the cathodic voltammetric peak current for (curve a) $5 \times 10^{-8}$ M, (curve b) $1 \times 10^{-7}$ M, (curve c) $5 \times 10^{-7}$ M and (curve d) $1 \times 10^{-6}$ M cacotheline. Other conditions as for Fig. 2.

potential showed that over the range 0– $-0.15$ V, $i_{pc}$ remained almost constant at a high level, but beyond this range it decreased. Thus $-0.10$ V was chosen as the best preconcentration potential.

The adsorptive stripping voltammetric response of cacotheline was further characterized concerning concentration ($c_{CAC}$) dependence, detection limit and reproducibility. Under the optimized conditions with a 100 mV $s^{-1}$ scan rate, the peak current had a linear relationship with $c_{CAC}$ over the range from $2.0 \times 10^{-8}$ to $1.0 \times 10^{-6}$ M when the accumulation time was 30 s (correlation coefficient, 0.9991). The detection limit achieved was $2.0 \times 10^{-9}$ M when the preconcentration time was set to 3 min ($S/N = 3$). The precision was estimated by nine successive measurements of $5 \times 10^{-7}$ M cacotheline under the same conditions as above with a 30 s accumulation. The average peak current was 0.46 μA, range 0.43–0.52 μA, and relative standard deviation 2.7%.

Table 1
Results of indirect measurement of brucine

| No. | Amount of brucine added (g) | Amount of brucine measured[a] (g) | Recovery rate (%) | Standard deviation (%) |
|---|---|---|---|---|
| 1 | 0.0559 | 0.0538 | 96.2 | 2.4 |
| 2 | 0.0473 | 0.0453 | 95.8 | 1.3 |

[a] $n = 5$.

As described above, brucine can be transformed into cacotheline by nitration and then determined by AdSV. Under the optimized conditions mentioned above, brucine was measured indirectly by the standard additions method. Certain results are listed in Table 1. The transformation rate of above 95% indicated that brucine was almost completely transformed into cacotheline. This result illustrated again that the method of first nitrating and then determining by AdSV was feasible for the indirect measurement of brucine.

### 3.4. System weakly adsorbed reactant

The effect of the square root of the scan rate ($v^{1/2}$) on $i_{pc}$ of cacotheline at different preconcentration times was examined. When $t = 0$, $i_{pc}$ had a linear relationship with $v^{1/2}$, illustrating that the reduction of cacotheline was diffusion-controlled. When $t = 10$ s, the $i_{pc}$ vs. $v^{1/2}$ curve showed upward bending, indicating that the system began to show some adsorptive characteristics. When $t = 60$ s, as more cacotheline was adsorbed, upward turning of the $i_{pc}$–$v^{1/2}$ curve became more pronounced.

The effect of the concentration of cacotheline on $i_{pc}$ is shown in Fig. 5. When $t = 0$, the relative peak current expressed as the ratio of $i_{pc}/c_{CAC}$ was small and remained nearly constant on increasing the concentration of cacotheline (curve a). This indicated that the reduction of cacotheline at the mercury electrode was almost totally diffusion-controlled.

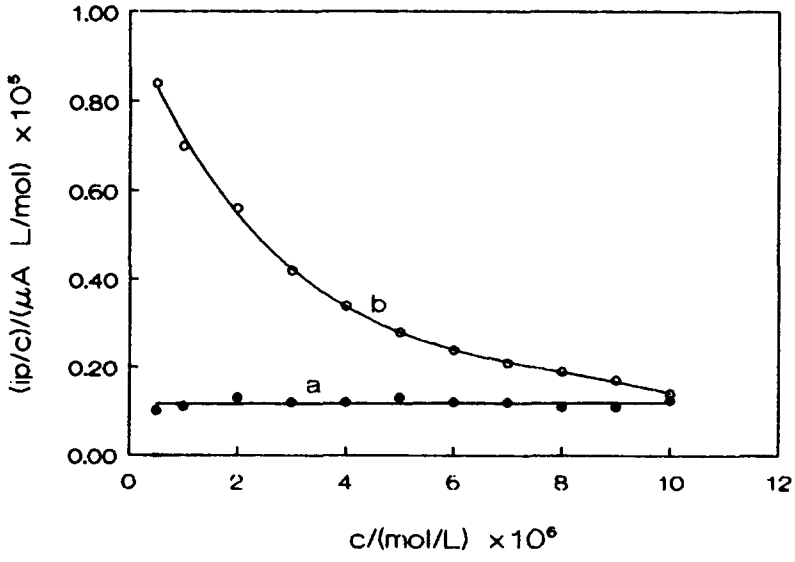


Fig. 5. Effect of concentration of cacotheline on the relative peak current as the ratio of the cathodic peak current to the cacotheline concentration. Preconcentration period: (curve a) 0 s; (curve b) 30 s. Other conditions as for Fig. 2.

However, when $t = 30$ s, because more cacotheline was adsorbed on the mercury surface, the values of $i_{pc}/c_{CAC}$ were much larger than those of curve a at lower $c_{CAC}$. At higher $c_{CAC}$, however, the adsorption of cacotheline reached saturation and its contribution to the peak current did not increase any more. The ratio then declined very rapidly with increasing concentration of cacotheline, and eventually tended toward the constant value of curve a (curve b). All of these suggest a gradual transformation of the system from adsorption-controlled to diffusion-controlled when the concentration of cacotheline increases. This is also a characteristic of the system involving a reactant that is weakly adsorbed [16].

### 3.5. Mechanism of reduction of cacotheline at mercury electrode

Over the potential range from 0.20 to −0.50 V, cacotheline has a pair of reversible peaks at about 0.03 V and an irreversible peak at −0.40 V. Electrolysis experiments with a

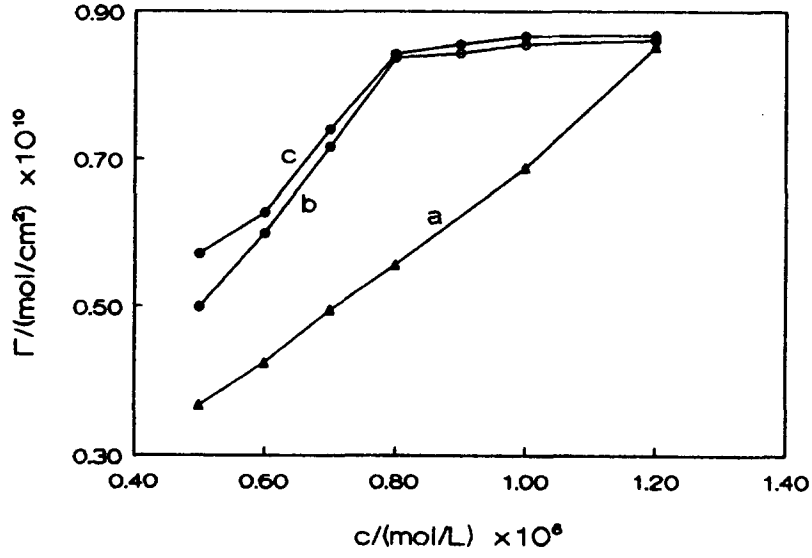


Fig. 6. Influence of cacotheline concentration on the amount of cacotheline adsorbed on the mercury electrode surface. Preconcentration time: (curve a) 30 s; (curve b) 60 s; (curve c) 90 s. Other conditions as for Fig. 2.

large area of the mercury cathode at the potential of −0.2 V showed that the number of electrons transferred for the first cathodic peak ($n_1$) was 2. Electrolysis at −0.50 V revealed that the number of electrons transferred for both cathodic peaks was 6. Thus, the number of electrons for the second irreversible reduction peak ($n_2$) should be equal to 4. This result is in good agreement with that of Vijayalakshmi and Saraswathi [14]. The mechanism of electrode reduction of cacotheline at the mercury electrode involves two processes. The first cathodic peak is most probably due to the reversible reduction of the *o*-quinone group to hydroquinone involving two-electron transfer. The second is possibly the irreversible reduction of the nitro group to hydroxylamine with four-electron transfer. It is the second peak, showing adsorptive characteristics, that we are interested in.

### *3.6. Measurement of the amount of cacotheline adsorbed*

As mentioned above, under the conditions of low $c_{CAC}$, long $t$ and fast $v$, the reduction of cacotheline can be considered to be totally controlled by the adsorption of cacotheline. In this case, the cathodic peak current almost decays to its baseline with little diffusion tail (see Fig. 3). Integration of this peak gives a charge $Q_a$, which represents the reduced charge of the surface species of cacotheline adsorbed at the mercury electrode. According to the equation

$$\Gamma = Q_a/(nFA)$$

the surface coverage $\Gamma$ (mol cm$^{-2}$) can then be calculated, where $A$ is the area of electrode (0.0171 cm$^2$), $n$ is the number of electrons transferred (4) and $F$ is the Faraday constant.

Fig. 6 illustrates the relationship between $\Gamma$ and $c_{CAC}$ at three different accumulation times. When the concentration of cacotheline was small, the surface coverage increased linearly with $c_{CAC}$. However, at higher concentrations of cacotheline, the curves tended to level off. The surface coverage $\Gamma$ at three different levels tended to reach the same constant value, which represented a full surface coverage of $8.60 \times 10^{-11}$ mol cm$^{-2}$. Each cacotheline molecule adsorbed thus occupied an area of 1.93 nm$^2$, if the adsorption of cacotheline was as a monolayer.

## Acknowledgement

The financial support of the National Natural Science Foundation of China is gratefully acknowledged.

## References

[1] Beijing Medical College and Beijing Traditional Chinese Medical College (Eds.), Zhongchaoyao Chengfen Huaxue (Component Chemistry of Traditional Chinese Medicine), People's Health Press, Beijing, 1980, p. 139.
[2] Institute of Materia Medica, Chinese Academy of Medical Sciences (Ed.), Zhongyaozhi (The Dictionary of Traditional Chinese Medicine), 2nd edn., People's Health Press, Beijing, 1984, p. 181.
[3] A.A.M. Wahbi, M.A. Abonnassif and E.R.A. Gad-Kariem, Arch. Pharm. Chem., Sci. Ed., 15 (1987) 87.
[4] D.W. Hill and K.J. Langner, J. Liq. Chromatogr., 10 (1987) 377.
[5] M. Abdel-Salam, M.S. Mahrous and A.S. Issa, J. Pharm. Belg., 41 (1986) 226.
[6] E.A. Julian and E.M. Plein, J. Forensic Sci., 28 (1983) 992.
[7] G.L. Dadisch, W. Vycudilik and G. Machata, Forensic Sci., 10 (1977) 205.
[8] M.A. Korany and A.A. Seif El-Din, J. Assoc. Off. Anal. Chem., 67 (1984) 138.
[9] F.W. Nyasulu, Electroanalysis, 2 (1990) 327.
[10] G.C.F. Clark, G.J. Moody and J.D.R. Thomas, Anal. Chim. Acta, 98 (1978) 215.
[11] K. Kodama, Methods of Quantitative Inorganic Analysis, Interscience–Wiley, New York, 1963.
[12] N.K. Murthy, Y.P. Rao and V. Satyanaranyana, Fresenius' Z. Anal. Chem., 272 (1974) 367.
[13] N. Gallo, Ann. Chim. (Rome), 57 (1967) 54.
[14] I. Vijayalakshmi and K. Saraswathi, Anal. Chim. Acta, 196 (1987) 213.
[15] J. Wang, in A.J. Bard (Ed.), Electroanalytical Chemistry, Vol. 16, Dekker, New York, 1989, pp. 1–89.
[16] R.H. Wopschall and I. Shain, Anal. Chem., 39 (1967) 1514.

ELSEVIER

Talanta 42 (1995) 1395–1409

Talanta

# Evaluation of metal fractions in river sediments and waters: application of chelation chromatography-differential pulse anodic stripping voltammetry

S. Sundd, B.B. Prasad *

*Analytical Division, Chemistry Department, Faculty of Science, Banaras Hindu University, Varanasi-221 005, India*

Received 1 August 1994; revised 6 December 1994; accepted 28 February 1995

**Abstract**

The ability of chelation chromatography in combination with differential pulse anodic stripping voltammetry (DPASV) to provide a simple, fast and reliable way of dealing with interionic interferences, competitive complexations, re-adsorption of released metal ions and sorption of spiking metal ions by organic/inorganic materials in the complex matrixes of real natural samples has been critically examined. The technique is based on the selective complexation of target metal fractions on some novel sorbents which are polymeric chelating resins doped on stationary supports (Whatman No. 1 paper and silica gel). The usual complications of leaching of the resin and/or the chelating ligand and colloid retention on the sorption bed at any stage of separation were largely obviated with these sorbents under the operational conditions of metal sorption. A detailed study on the application of such sorbents to the differentiation of ionic (free), labile (ionic plus weakly complexed) and bound (strongly complexed) metal fractions present in local river-sediment and water samples was carried out. Chelating resin-impregnated paper (CRIP) and chelating resin-immobilized silica gel column (CRISC) methods of chromatographic separation of analyte trace metals in combination with the follow-up 'standard addition' procedure of the DPASV technique were employed. A modest attempt has been made to formulate a speciation (fractionation) scheme for metal contents present in river-sediments and waters on the basis of selective retention of ionic and labile fractions on complexing resins.

## 1. Introduction

Selective separation of trace metals from aquatic complex matrixes and their fractionations in different forms is considered an arduous task, owing to the severe interferences caused by the high levels of cations, anions, organic colloids and particulates present in the natural sample [1–6]. Of several chromatographic techniques widely used to isolate trace metals, the applications of chelating resins are found to be potentially more selective than those of ordinary cation-exchange resins. However, it may be recalled that the retention of total metal species by a chelating resin (Chelex-100) column was found to be quantitative using synthetic solutions, but later was found prone to error using natural waters and seawater. The reason is that the heavy metals in natural samples may not exist entirely in the free (ionic) form, but may be present partly as the colloidal and/or complexed form, which will not equilibrate with the added ionic spike during the time of the separation experiments [7,8]. Also, the natural samples may contain a large fraction of the trace metals in a form which is not retained by the resin, and the anodic stripping voltammetry (ASV) method used to determine labile metal content may not respond to this inactive fraction [7]. In another technique where ion-exchangers were used to collect only labile forms, anodic ASV was

* Corresponding author.


*SSDI* 0039-9140(95)01573-6

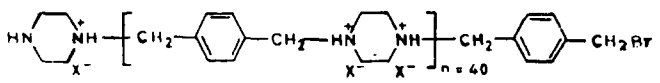

( $X^-$ = IHQS$^-$ )

PXPi ( IHQS )$_2$ [ Mol. wt. 36310 ]

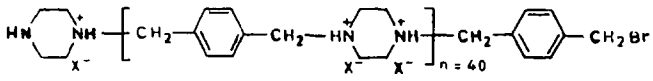

( $X^-$ = SSA$^-$ )

PXPi ( SSA )$_2$ [ Mol.wt. 25680 ]

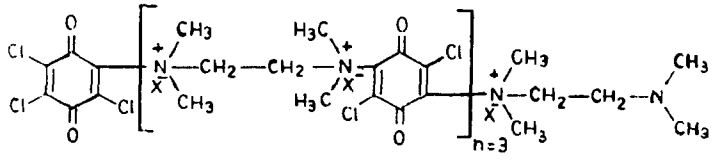

( $X^-$ = SSA$^-$ )

PCED ( SSA )$_2$ [ Mol. wt. 2979 ]

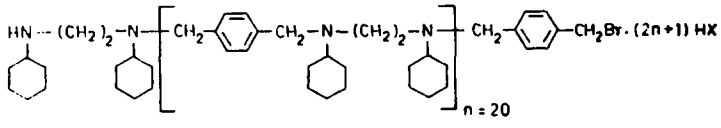

( $X^-$ = IHQS$^-$ )

$C_2EX$ ( IHQS )$_2$ [ Mol. wt. 21364 ]

Fig. 1. Structure of chelating polyelectrolytes.

aided by cation-exchanger [9,10] retention. This was found useful to some extent in combating the general problems of trace metal analysis, such as ASV peak distortion [3–6], peak resolution owing to competing complexations (metal-supporting electrolyte complexation [11], chlorocomplexation [12], metal-humate complexation [6]), re-adsorption of labile metals onto particulates [9], adsorption of suspended matter onto an electrode [5,6,13], and sorption of metal ions used in peak spiking by colloidal hydrous oxides or humic acid components of sediments [14]. Nevertheless, all these procedures have limitations in overcoming other major complications, i.e. interionic interferences due to diverse metal ions, intermetallic formation [15,16] and the dissociation of sparingly soluble salts along with surface-held ions [9]. Moreover, the retention of metal-rich colloidal particles in the larger pores of resins may cause spurious results on acid digestion/elution.

In the quest for a fool-proof solution to various problems as stated above and to procure chelating functionalities immobilized on polymeric substrates which are effective for the quantitative retention of trace metal ions with desired selectivity, some novel chelating polyelectrolytes (Fig. 1) doped on stationary supports (Whatman No. 1 paper strip and silica gel), in accordance with Grahame's modification of Stern–Gouy–Chapmans' electrical double layer theory [17], appeared quite promising. The application of these sorbents in the chelating resin-impregnated paper (CRIP) and chelating resin-immobilized silica gel column (CRISC) method of chromatographic separation has already been established with synthetic water samples [18–21]. In the present investigation, a total speciation (fractionation) scheme of metals was formulated employing these methods for river-sediments, on the basis of selective chemical extraction followed by selective retention of the metal fraction of de-

sired 'lability' on complexing sorbents. An attempt has also been made to employ the CRIP method for metal fractionations in river water samples.

## 2. Experimental

### 2.1. Sediment samples

Sediment sampling from a local river (Ganges) was carried out separately for two types of samples. The first type is the natural sediments which were collected from the middle current of Nagwa Ghat (NG), Shivala Ghat (SG) and Raj Ghat (RG). Samples of the other type were drawn from the section of the river in the vicinity of the outfalls of sewage and waste-water drains through Nagwa nullah (NN) and City nullah (CN). The sampling was conducted by a USBM-54 bed material sampler which scoops bed samples from about 6–9 inches depth in the river bed. The samples were dried in air under atmospheric conditions, packed in polyethylene bags, properly labelled and brought to the laboratory for analysis. The water samples tested were drawn from two local ghats (Harishchandra Ghat (HCG) and Rajendra Prasad Ghat (RPG)) with the help of a dissolved oxygen water sampler. The collection points at these centres were adjoining nullah, mixing point of nullah and river (each at a depth of 1 m from the top), and the middle current of the river (0.6 m of the total depth from the top of the river).

### 2.2. Chemical extractant solutions

A small amount of sediment (400 mg) was placed in a vial with 30 ml of extracting solution and then sealed. This was equilibrated overnight by mixing with the help of an end-over-end mixing unit and allowed to settle for several hours; only supernated suspension was taken as test aliquot. The extractants used were: 0.02 M $HNO_3$ (pH 1.8–2.3), 4 M $CH_3COOH$/0.4 M $NH_2OH$–HCl, 0.13 M $CH_3COOH$/0.4 M $CH_3COONa_3$ (pH 5) and 0.05 M $CaCl_2$. These four base solutions cover the entire range of labile metal contents, e.g. 0.02 M nitric acid, low-pH labile; hydroxylamine hydrochloride in acetic acid, metals in reducing conditions; acetic acid/acetate buffer, weakly sorbed and carbonate bound; 0.05 M calcium chloride, exchangeable fraction at neutral system pH.

### 2.3. Selective retention of labile metal species by chelation chromatography

The use of two different modes (CRIP and CRISC) of chromatographic separation lead to the detection of primarily two different categories of biologically available metal ions, namely (a) ionic form by CRIP and (b) ionic plus weakly bound metal ions by CRISC (if the CRIP and CRISC methods give identical results, this indicates the presence of the ionic form only in the sample). The following chelating resins, which were originally reported [18–21] from our laboratory, were used in the chromatographic separations (structures are shown in Fig. 1):

(i) poly[*N*-*p*-xylylene piperazinium-di-iodohydroxyquinoline sulfonate] (PXPi(IHQS)$_2$) (MW 36 310);
(ii) poly[*N*-*p*-xylene piperazinium-di-sulfosalicylate] (PXPi(SSA)$_2$) (MW 25 680);
(iii) poly[*N* - chloranil - *N*,*N*,*N*′,*N*′ - tetramethyle -thylenediammonium-di-sulfosalicylate] (PCED(SSA)$_2$) (MW 2979);
(iv) poly[*N*-*p*-xylylene-*N*,*N*′-dicyclohexylethyl-enediammonium-di-iodo-hydroxyquinoline sulfonate] ($C_2$EX-[IHQS)$_2$) (MW 21 364).

The CRIP chromatographic method was executed on Whatman No. 1 paper strips (25 × 1.5 cm$^2$) which were impregnated with finely powdered chelating resins, PXPi(IHQS)$_2$ and PXPi(SSA)$_2$, in the manner described elsewhere [18,19]. Sediment extract was placed as a single spot (0.2 ml) on the bottom of the paper with the help of a microsyringe pipette for ascending chromatographic separations based on differential migration of heavy metals in suitable solvents (water; PXPi(IHQS)$_2$ strip and acetone–water (97:3, v/v); PXPi(SSA)$_2$ strip) based on the differences in their solubility product equilibria [22]. The lower portion of the paper fixes the target metal at the starting point through complexation, whereas in the upper portion, all the mobile ions were found together as stable complexes in an 'elliptical zone' with PXPi(IHQS)$_2$-impregnated strip [18] and in a 'narrow band' with PXPi(SSA)$_2$-impregnated strip [19]. The preferential order of selectivity for cations is $Fe^{3+} > Cu^{2+} > Cd^{2+}$, $Pb^{2+}$, $Zn^{2+}$. The chelation of $Cu^{2+}$ at the starting point was only feasible in the absence of $Fe^{3+}$; other diverse metal ions $Cd^{2+}$, $Pb^{2+}$ and $Zn^{2+}$ moved with the solvent and had an affinity for the functional groups of the sorbent

in the upper zone. The fine particles of metal-rich colloids/clays introduced at the starting point by microsyringe, although negligible, were dispersed around the middle of the paper by ascending carrier solvent; the upward moving metal ions with the solvent front have apparently higher $R_f$ values required for separation from strongly bound metals, if any, on colloids/clays. Both upper and lower parts were perfectly digested in 2 ml of concentrated $HNO_3$ (Suprapur ExcelaR), diluted to 25 ml and finally subjected to DPASV measurements.

CRISC chromatography was performed with two sorbents, silica gel–PCED(SSA)$_2$ and silica gel–$C_2$EX(IHQS)$_2$, and their column performance with a synthetic water sample containing different heavy metals has been reported elsewhere [20,21]. Column operations were employed in the usual manner with 1.5 g chelating sorbent (≈20–60 mesh) loosely packed (1 cm height) in a glass column (13 × 1.4 cm) under optimized conditions: pH 3.0 ($Fe^{3+}$), 4.0 ($Pb^{2+}$), 5.0 ($Cu^{2+}$) with flow rate 5 ml min$^{-1}$ for silica gel–$C_2$EX(IHQS)$_2$ sorbent; pH 5.0 ($Fe^{3+}$), 3.2 ($Cd^{2+}$), 4.5 ($Cu^{2+}$) with flow rate 5 ml min$^{-1}$ for silica gel–PCED(SSA)$_2$ sorbent. In all cases, 1 ml of the extract was diluted to 50 ml at the optimized pH and then passed through the column at a specified flow rate of analyte metal ions. This was followed by double or triple washings of bed materials with water to remove impurities due to fine particles or metal-rich colloids, if any, introduced during the loading step of the test aliquot. It may be pointed out that both sorbents have fast sorption kinetics suitable for column operation [23] with a $t_{1/2}$ (time required to reach half of the maximum sorption) value of 2 min and a $P_{2\,min}$ (the percentage attainment of equilibrium in 2 min) value of 50% metal sorption [20,21]. Moreover, with the thin bed of chelating resin and the flow rate of 5 ml min$^{-1}$, the contact time (10 min) of soluble complexes with the resin phase is apparently sufficient for the dissociation of labile metal fractions from weakly complexed metal-humate and fulvate or colloid species. Metal ions sorbed onto the column were finally eluted by 10 ml of Suprapur ExcelaR grade 0.1 M HCl (silica gel–$C_2$EX(IHQS)$_2$ column) and 1 M $HNO_3$ (silica gel–PCED(SSA)$_2$ column), diluted to 50 ml and finally subjected to DPASV (standard addition) monitoring.

### 2.4. Differential pulse anodic stripping voltammetry (DPASV) operating conditions

Differential pulse anodic stripping voltamperograms were obtained at ≈25 °C in the conventional manner with an EG and G Princeton Applied Research model 264A polarographic analyzer in conjunction with a model 303A static mercury drop electrode (SMDE) stand and an Omnigraphic $X$–$Y$ recorder. The mercury drop was renewed after de-aeration of the cell contents for each run. The DPASV peaks were spiked by the corresponding standard metal ion solution to evaluate the metal contents of the various solutions following the 'standard addition method' of quantitative analysis. The spiked standard peaks were relatively sharper than test ASV peaks, giving a better comparison of their respective peak heights.

In each run, 1 ml of digested/eluted test aliquot was added to 10 ml of buffer containing background electrolytes[1], sodium tartrate buffer ($\mu = 0.001$ M, pH = 11) for $Fe^{3+}$ and ammonium citrate buffer ($\mu = 0.2$ M, pH = 3) for $Cu^{2+}$, $Cd^{2+}$, $Zn^{2+}$, $Pb^{2+}$. The representative curves obtained under optimized conditions (see Figure captions) of voltammetric operation after CRIP and CRISC separation methods are shown in Figs. 2 and 3.

Direct and simultaneous analyses of the sediment extracts [13] were also undertaken by introducing 10 ml of extract directly into the voltammetric cell. Typical runs are depicted in Fig. 4. Suitable voltammetric operational parameters, such as deposition potential, scan rate and pulse height, were examined for all the sample extracts, as exhibited in Fig. 5. The optimum DPASV parameters — deposition time, 240 s; deposition potential vs. Ag/AgCl, −1.2 V; pulse height, 25 mV; scan rate, 5 mV s$^{-1}$ — were exercised for all sediment extracts. Prior to each deposition step, the test sample was purged with nitrogen for 4 min. In the reproducible repeat analysis, the cell contents had to be mechanically mixed between each deposition step. For both standard solution and suspension, the relative standard deviation of repeated scans was ±8% or better, and the replicate precision was of the same order. The peak potentials for different metal ions in sediments in direct and simultaneous

[1] Purified buffers were obtained following the CRISC method, as reported in Ref. [21].

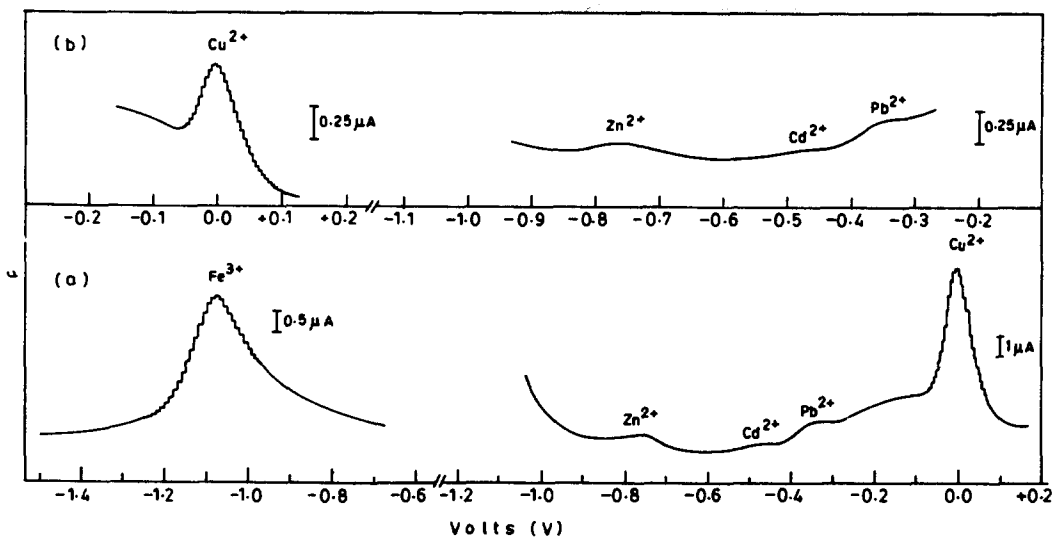


Fig. 2. Differential pulse stripping voltammograms of metals in Nagwa nullah sediment preconcentrated by the CRIP method. (a) $PXPi(IHQS)_2$ impregnated strip (0.02 M $NHO_3$ sediment extract), ($Fe^{3+}$, 0.001 M sodium tartrate buffer, pH 11; $Zn^{2+}$, $Pb^{2+}$, $Cu^{2+}$, 0.2 M ammonium citrate buffer pH 3). (b) $PXPi(SSA)_2$ impregnated strip (sodium acetate sediment extract) ($Cu^{2+}$, 0.2 M ammonium citrate buffer, pH 3; $Zn^{2+}$, $Cd^{2+}$, $Pb^{2+}$, 0.2 M ammonium citrate buffer, pH 3). (DPASV operational conditions: deposition time = 60 s, scan rate = 10 mV $s^{-1}$, pulse height = 25 mV, deposition potential (vs. Ag/AgCl) = −1.5 V ($Fe^{3+}$), −1.2 V ($Zn^{2+}$, $Cd^{2+}$, $Pb^{2+}$), −0.6 V ($Cu^{2+}$).)

DPASV analysis when varied with base electrolyte solution are portrayed in Table 1.

The residual metal impurities introduced during various stages of separation, digestion or elution in the present work were always subjected to the necessary corrections. The blank runs in DPASV determination of residual metal ions were made with 1 ml of digested (25 ml)/eluted (50 ml) solution (without any sediment extract or water samples) in 10 ml of an appropriate buffer of known pH, and corresponding amounts were calculated for subtraction from the final results. In direct and simultaneous analysis, the metal impurities present in extractants were determined by separate DPASV runs, prior to extract analysis for blank corrections.

### 2.5. Total metal contents

The total metal contents were determined by DPASV after sample digestion using a $KNO_3$–

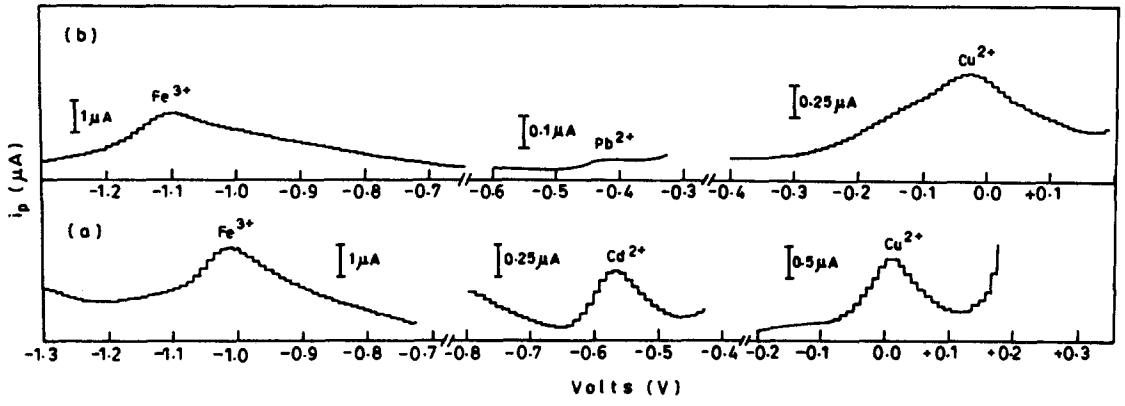


Fig. 3. Differential pulse stripping voltammograms of metals in Nagwa Ghat sediment preconcentrated by the CRISC method. (a) Silica gel–$PCED(SSA)_2$ column (0.02 M $HNO_3$ sediment extract) ($Fe^{3+}$, 0.001 M sodium tartrate buffer, pH 11; $Cd^{2+}$, $Cu^{2+}$, 0.2 M ammonium citrate buffer, pH 3). (b) Silica gel–$C_2EX(IHQS)_2$ column (0.02 M $HNO_3$ sediment extract) ($Fe^{3+}$, 0.001 M sodium tartrate buffer, pH 11; $Cu^{2+}$, $Pb^{2+}$, 0.2 M ammonium citrate buffer, pH 3). (DSPASV operational conditions: deposition time = 60 s, scan rate = 10 mV $s^{+1}$, pulse height = 25 mV, deposition potential (vs. Ag/AgCl) = 1.5 V ($Fe^{3+}$), −1.2 V ($Zn^{2+}$, $Cd^{2+}$, $Pb^{2+}$), −0.6 V ($Cu^{2+}$).)

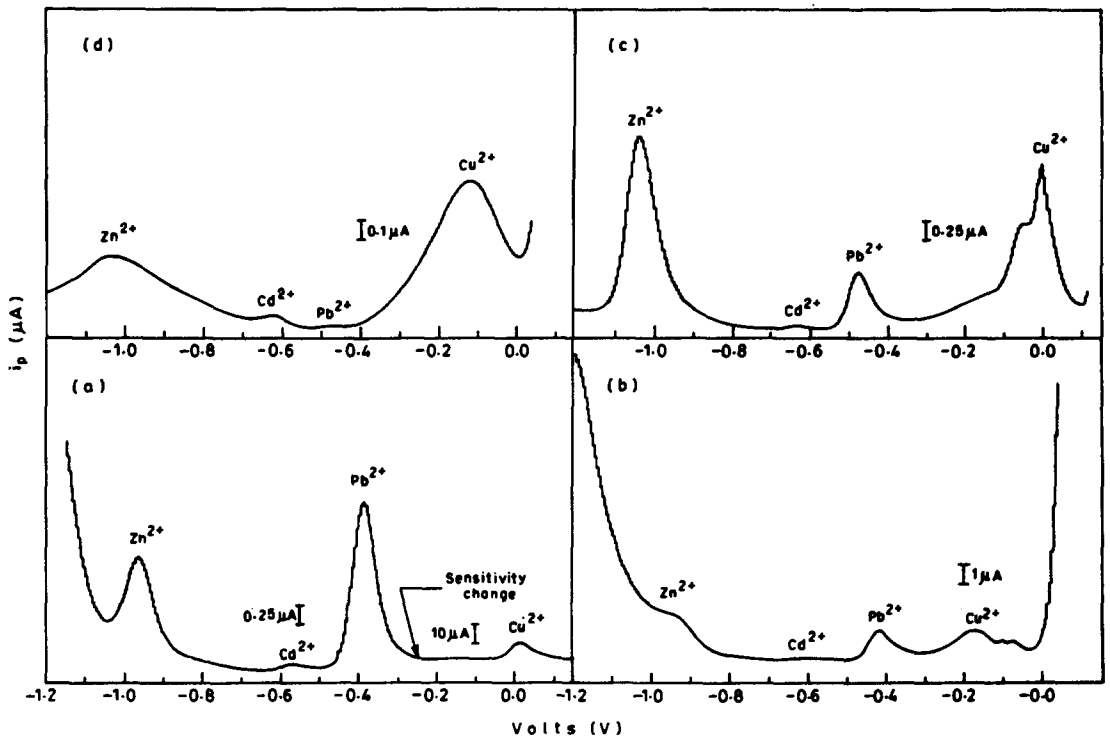


Fig. 4. Typical voltammograms of direct and simultaneous analysis of metals in Raj Ghat sediment in different extracts: (a) 0.02 M $HNO_3$, (b) 0.4 M $NM_2OH \cdot HCl$/4 M $CH_3COOH$, (c) 0.13 M $CH_3COOH$/0.4 M $CH_3COONa$ (pH 5) and (d) 0.05 M $CaCl_2$ extract.

$NaNO_3$ fusion technique [24] in which 2.0 g sediment sample was predigested in 5 ml concentrated $HNO_3$ at low heat. This was subsequently treated with $KNO_3$–$NaNO_3$ melts at 400 °C. The follow-up involved adding 10.0 ml aqueous acid, $NH_4OH$ neutralization and ammonium citrate buffer maintaining pH 3.0. Comparison was also made here between the direct simultaneous analysis of extracts and the amounts obtained after chromatographic separations (Table 2).

## 3. Results and discussions

The four major extractants (acidic, reducing, metal complex and neutral salt) used for the extraction of metal ions from sediments have distinctive characteristics in metal speciation [13]. The trace analyses with the CRIP and CRISC techniques are found to be equally efficacious for real as well as synthetic samples, insofar as evaluation of free and labile fractions is concerned. The ligand anions exposed outwardly as gegenions of polyelectrolyte coated on the stationary support are found to be readily available for strong chelation of even trace levels of labile metal species with a higher degree of selectivity and sensitivity. Hence, no spiking of sediment extracts is required, e.g. with chelex-100 resin [7], in the present study. Despite the fact that the CRIP and CRISC techniques are likely to give an estimation of only ionic (free) and labile (ionic plus weakly-complexed) metal fractions, respectively, strongly bound metals (and unreactive labile fractions if any) are not extracted at all. The instability problem of chelating resins caused by their bleeding, preswelling and cracking under the influences of medium effects and elution processes is found to be completely obviated in the present instance. Further, the sorbents studied here only take less than 4 min for 100% metal sorption [18–21]. A very small amount of colloids or fine particles in test aliquots of sediment extracts would not vitiate the sorption kinetics and also could not be retained with polymer coated resins of negligible pore size, during the extract loading.

The retention of heavy metals from local river (Ganges) sediments and waters on CRIP and/or CRISC supports was studied by analysing the original natural sample and the paper or column effluent, using DPASV moni-

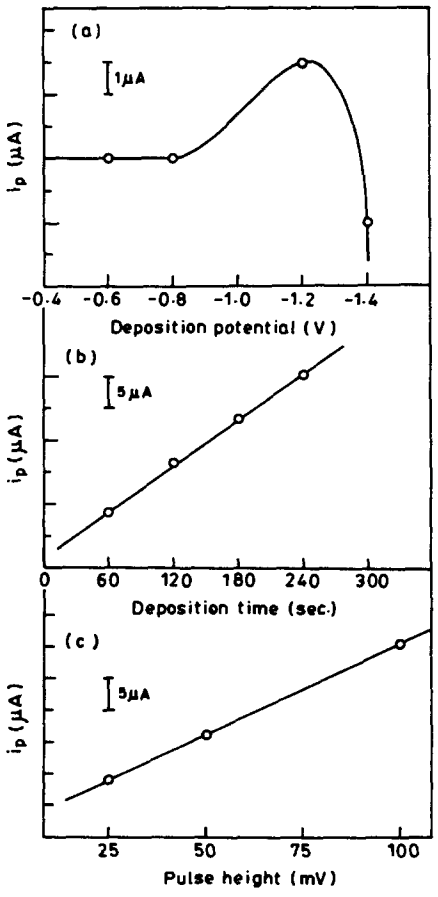


Fig. 5. Effect of operational parameters on copper peak current. (a) Deposition potential, −0.4 V to 1.4 V vs. Ag/AgCl; deposition time 60 s; pulse height, 25 mV. (b) Deposition potential, −1.2 V vs. Ag/AgCl; deposition time, 60–240 s; pulse height, 25 mV. (c) Deposition potential, −1.2 V vs. Ag/AgCl; deposition time, 60 s; pulse height, 25–100 mV.

toring. Retention of the total metal, naturally present, was not quantitative since only ionic and labile fractions were retained by chelating sorbents in the present study. The direct DPASV analysis of the original sample suffers the serious set-back of readsorption effect(s) in contrast with the earlier works [7,13]. As a matter of fact, the substantial shift in $E_p$ values (Table 1) of metal ions in sediment extracts studied can be considered as an indication of difficult oxidation due to the heavy sorption of diverse materials during both the deposition and stripping steps. However, the combination of chelation chromatography with DPASV appears to be an advantageous approach to the alleviation of serious problems of ASV peak resolution, owing to the competitive role of calcium ions [10] released through particle dissolution of sediment component, interionic interferences [14], intermetallic formation [15,16] and also to the readsorption effect in cells by diverse metal ions, surfactants and organic colloids present in the complex matrixes of real natural samples.

### 3.1. Low-pH labile contents

Dilute nitric acid (0.02 M) treatment of sediments releases metal ions associated with acid soluble matrix components (e.g. carbonates and amorphous hydroxides) and also displaces metals from organic acid colloids and surface sites [13]. The direct and simultaneous DPASV of $Cu^{2+}$, $Cd^{2+}$, and $Pb^{2+}$ gave flat baselines, where as a sloping baseline was obtained for $Zn^{2+}$ (Fig. 4(a)).

The increase in peak height was accompanied by an increase in pulse height and deposition time (Fig. 5). However, in all cases, a pulse height of 25 mV was used for DPASV runs, which provided a current well within the range of the recorder. In fact, a deposition time of a few seconds should have been adequate to avoid colloid effects for sediment extracts containing high levels of metal ions. However, the weakly-complexed colloid surface-held trace metal ions (ASV labile fraction) might not be easily retrieved and migrate to the mercury drop cathode under the influence of the applied potential, in such short time of deposition. As a matter of fact, a relatively large peak current was observed in the present study, when a higher negative potential of −1.2 V vs. Ag/AgCl and sufficient time of 240 s were employed (Fig. 5(b)) for ASV deposition for extracts containing large amounts of insoluble colloids/clay particles in direct DPASV analysis. The effects of variation of pulse height, deposition time and deposition potential are almost similar in all extracts for each metal studied.

It has been observed that direct DPASV through the standard addition method for $Fe^{3+}$ in nitric acid extract has never been possible, as the current for a sample consisting of free or weakly- bound iron metal is drastically reduced on spiking (Fig. 6). This reflects a favoured complexation equilibrium upon addition of spiking metal solution and consequent electrode adsorption perturbation. The problem is successfully solved by the application of CRIP/CRISC methods of isolation of iron from the extract. This step is also advantageous in combating the iron interferences [14] in the

DPASV measurement of multi-element samples. Both PXPi(IHQS)$_2$ and PXPi(SSA)$_2$ resins were found to be equally suitable for $Fe^{3+}$ retention by the CRIP method (Table 3) within the limit of errors incurred during the separation and monitoring steps. In contrast, sorbent silica gel–PCED(SSA)$_2$ is selective for $Cu^{2+}$, $Cd^{2+}$, $Fe^{3+}$, whereas silica gel–$C_2$EX(IHQS)$_2$ is selective for $Cu^{2+}$, $Pb^{2+}$ and $Fe^{3+}$ under the specified conditions of pH and flow rate. The selective retention of $Zn^{2+}$ was not possible by the CRISC method. A very low or almost negligible value for $Cu^{2+}$, $Cd^{2+}$, $Zn^{2+}$ and $Pb^{2+}$ in real samples is obtained by direct DPASV as compared to those obtained after chromatographic separations by both techniques. This indicates the drastic reduction of metal ion concentrations in direct DPASV analysis of sediment extract, presumably due to the re-adsorption of ionic and ASV labile loosely bound ions by colloidal particles along with the massive $Fe^{3+}$ interferences; this questions the validity of the data and tenuous nature of the direct method of sample monitoring with sediment samples.

Table 3 shows 'low-pH labile' metal content data, after chromatographic separation, in various sediments by the CRIP method to estimate only the ionic form, and the CRISC method to estimate ionic plus weakly-complexed (or loosely sorbed ions on particles in the extract) fractions as total biologically available 'low-pH labile' metals. The larger values of labile metal contents obtained by the CRISC method can be rationalized from the fact that the solution is passed slowly in this method, allowing enough equilibration time to extract metal easily from weakly complexed materials in addition to the free metal ions (stability constants [25] (log $K$) of complexes $Cu^{2+}$–SSA (9.5) and $Cu^{2+}$–I HQS (11.8) are larger than those for $Cu^{2+}$–humic acid (6, 8)/$Cu^{2+}$–fulvic acid (7.8, 8.5) complexes [26]). On the basis of a comparative study of 'low-pH labile' metal contents where the CRISC method gave higher results than the CRIP method, it may be concluded that there were weakly-bound metal fractions of $Cu^{2+}$ in Nagwa nullah, City nullah, Shivala Ghat, and $Pb^{2+}$ in all four samples barring City nullah. The metals $Cd^{2+}$ and $Fe^{3+}$ were always present as free ionic fraction ($Zn^{2+}$ could be only estimated as the free form by the CRIP method, as the CRISC method was not feasible).

### 3.2. Low-pH labile reducing conditions

The major fraction of total metal contents in soils and sediments is associated with hydrous oxides of iron, manganese and aluminium, and can be extracted with the help of reducing agents e.g. hydroxyl amine hydrochloride in 25% acetic acid [13].

A typical direct DPASV voltammogram in $NH_2OH \cdot HCl$/25% acetic acid medium is shown in Fig. 4(b). A system peak appears at $-0.75$ V at lower pulse height ($<100$ mV) as a consequence of the absorption of colloidal matter on the baseline slope of $Cu^{2+}$ [13]. As usual, the drastic iron interferences as well as the presence of organic particulates and $Cl^-$ ions impart a negligibly small amount of metal ions ($Cu^{2+}$, $Cd^{2+}$, $Zn^{2+}$, $Pb^{2+}$) by direct and simultaneous DPASV measurements. It is interesting to note that direct iron analysis in $NH_2OH \cdot HCl$/acetic acid did not pose any

Table 1
Peak positions of different metals in sediment sample extractants in direct DPASV measurements

| Extractant solution | Peak position (V) vs. Ag/AgCl [a] | | | |
|---|---|---|---|---|
| | $Zn^{2+}$ | $Cd^{2+}$ | $Pb^{2+}$ | $Cu^{2+}$ |
| 0.02 M $HNO_3$ | −0.975 (−1.150) | −0.525 (−0.725) | −0.375 (−0.510) | +0.250 (−0.080) |
| 0.4 M $MH_2OH \cdot HCl$/4 M $CH_3COOH$ | −0.925 (−0.995) | −0.600 (−0.685) | −0.425 (−0.480) | −0.175 (−0.255) |
| 0.13 M $CH_3COOH$/0.4 M $CH_3COONa$ (pH 5) | −1.25 (−1.150) | −0.625 (−0.740) | −0.475 (−0.480) | −0.125 (−0.235) |
| 0.05 M $CaCl_2$ | −1.500 (−1.165) | −0.625 (−0.750) | −0.475 (−0.560) | −0.050 (−0.135) |

[a] Values in parentheses denote peak potentials ($E_p$) for pure elements in different chemical extractants.

Table 2
Total metal contents in various sediments ($\mu g\ g^{-1}$)

| Metal ions | NN | | CN | | NG | | SG | | RG | |
|---|---|---|---|---|---|---|---|---|---|---|
| | Direct method | CRIP method | Direct method | CRIP method | Direct method | CRIP method | Direct method | CRIP method | Direct method | CRIP method |
| $Cu^{2+}$ | 2482 | 5613 | 2002 | 6680 | 849 | – | 1679 | 7305 | 973 | 11464 |
| $Cd^{2+}$ | 16805 | 16805 | 6397 | 6397 | 718 | 7298 | 5951 | 26212 | 406 | 1409 |
| $Zn^{2+}$ | 68689 | 2433 | 12539 | 12539 | 10783 | 5617 | 3949 | 11469 | 2272 | 1711 |
| $PB^{2+}$ | 2836 | 7131 | 1844 | 2892 | 392 | 13976 | 1515 | 2020 | 395 | 4132 |
| $Fe^{3+}$ | 22154 | 96030 | 82571 | 97761 | 45055 | 48108 | 59539 | 63120 | 79646 | 81517 |

NN = Nagwa nullah, CN = City nullah, NG = Nagwa Ghat, SG = Shivala Ghat, RG = Raj Ghat; Error $\leq \pm 8\%$.

problem in spiking, unlike in the nitric acid extract. It is noted that the results by direct analysis of iron are practically consistent with those obtained (excluding Nagwa Ghat sample) after chromatographic separations within the error limit ($\pm 8\%$). The reason may be that $NH_2OH \cdot HCl$ extract leaves very few active sites for reabsorption of iron by completely dissolving the organic colloidal particles. The exception with the Nagwa Ghat sample may be attributed to the presence of favoured adsorption by inorganic particulates in direct analysis. In the case of other metals, direct analysis data (Table 4) are always spurious owing to severe adsorption by undissolved residues other than hydrous oxides.

Chromatographic separations (Table 4) reveal that the zinc and copper contents are higher in Nagwa Ghat but lower in Raj Ghat. A small amount of $Cd^{2+}$ ions are found in Raj Ghat, and a higher amount in Nagwa nullah. The tributary Nagwa nullah has a lower $Pb^{2+}$ content, although Nagwa Ghat showed a relatively high $Pb^{2+}$ deposit in the river bed. The $Fe^{3+}$ contents were found to be relatively lower in Shivala Ghat as compared to Nagwa nullah.

The comparison of the CRIP and CRISC methods in $NH_2OH \cdot HCl$/acetic acid extract revealed that $Cu^{2+}$, $Cd^{2+}$ and $Fe^{3+}$ were present only in the free (ionic) form in all ghats, as the CRIP and CRISC values are in agreement with each other without showing a significant contribution from weakly labile complexed metal. Both weakly bound and free $Pb^{2+}$ were found in Nagwa nullah, City nullah, Nagwa Ghat, Raj Ghat and Shivala Ghat, as the CRISC method resulted in larger values than the CRIP method.

### 3.3. Weak acid (pH 5) labile

The sodium acetate buffer releases metal bound to ion-exchange sites or carbonate minerals through acetato complexation, rendering minimized pH effects on peak size [13]. Table 5 revealed that $Cu^{2+}$ is present in negligible amounts in all the sediments studied. The reason may be that the acetato complex is inefficient in destroying the weak bonding of metal ions and, further, hydrous oxides associated with large amounts of other metal ions are readily dissolved. In the direct analysis of the acetate buffer extract of Raj Ghat and Shivala Ghat, $Cu^{2+}$ peak splitting (Fig. 4(c)) was observed, probably owing to metal-humate complex formation. However, the emergence of a second copper wave can also be assigned to the formation of copper(I) hydroxy species or adsorption of Cu(II) hydroxy species in moderately acidic medium (pH > 5) [27].

The chromatographic separation results (Table 5) show that all samples are relatively

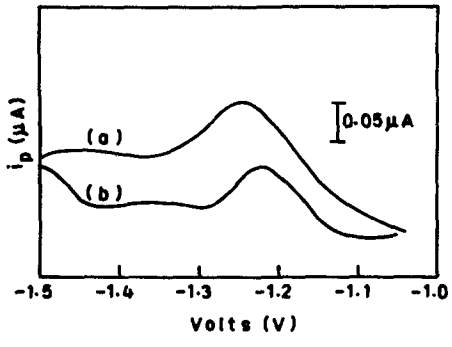


Fig. 6. Effect of metal spiking for $Fe^{3+}$ in 0.02 M $HNO_3$ extract of Raj Ghat sediment: (a) sample peak, (b) spiked peak.

Table 3
'Low-pH labile' metal contents of sediments in 0.02 M $HNO_3$ extract ($\mu g\ g^{-1}$)

| Metal | Sample | Direct method | CRIP method [a] $PXPi(IHQS)_2$ | CRISC method | |
|---|---|---|---|---|---|
| | | | | Silica gel–$PCED(SSA)_2$ | Silica gel–$C_2EX(IHQS)_2$ |
| $Cu^{2+}$ | NN | 31 | 491 | 712 | 713 |
| | CN | 180 | 1316 | 1745 | 1728 |
| | NG | 2 | 8319 | 8334 | 8333 |
| | SG | 5 | 1096 | 1396 | 1384 |
| | RG | 3 | 826 | 843 | 833 |
| $Cd^{2+}$ | NN | 0 | 1184 | 1248 | ns |
| | CN | 5 | 1247 | 1267 | ns |
| | NG | nd | 1128 | 1286 | ns |
| | SG | nd | 3617 | 3891 | ns |
| | RG | nd | nd | nd | ns |
| $Pb^{2+}$ | NN | 1 | 3536 | ns | 4125 |
| | CN | 3 | 500 | ns | 543 |
| | NG | 1 | 832 | ns | 896 |
| | SG | 3 | 597 | ns | 1278 |
| | RG | nd | 61 | ns | 437 |
| $Zn^{2+}$ | NN | 52 | 269 | ns | ns |
| | CN | 10 | 6561 | ns | ns |
| | NG | 1 | 12789 | ns | ns |
| | SG | nd | 7098 | ns | ns |
| | RG | 11 | 10753 | ns | ns |
| $Fe^{3+}$ | NN | $ND^+$ | 44262 | 46172 | 48006 |
| | CN | $ND^+$ | 46469 | 46582 | 55817 |
| | NG | $ND^+$ | 3869 | 3914 | 4236 |
| | SG | $ND^+$ | 42816 | 46011 | 48745 |
| | RG | $ND^+$ | 30744 ($PXPi(IHQS)_2$)<br>30478 ($PXPi(SSA)_2$) | 31864 | 33962 |

Error $\leq \pm 8\%$; nd = not detected; ns = not selective; $ND^+$ = on spiking $Fe^{3+}$; peak drastically reduced and standard addition method fails; NN = Nagwa nullah; CN = City nullah; NG = Nagwa Ghat; SG = Shivala Ghat; RG = Raj Ghat.
[a] Upper part of strip (except $Fe^{3+}$, which was preconcentrated in the lower part).

free from copper. Raj Ghat contains virtually no $Zn^{2+}$, $Pb^{2+}$ and $Cd^{2+}$. On moving from Raj Ghat to Nagwa Ghat, it is observed that the $Zn^{2+}$ contents in the free ionic form are increasingly higher compared to other metal ions. Although the $Cd^{2+}$ ion content is negligible in Nagwa nullah, it is substantial in Nagwa Ghat sediment.

On comparison of the CRIP and CRISC methods, Table 5 showes that $Cu^{2+}$ and $Cd^{2+}$ are present in trace amounts only in the free (uncomplexed) form in all samples studied. Some of the bound $Pb^{2+}$ contents are also present in Nagwa nullah, City nullah and Shivale Ghat, along with the free species.

### 3.4. Sediment pH (6–8) labile

Insofar as the extractions of metal ions held by electrostatic forces (i.e. occupying ion-exchange sites) are concerned, neutral salt solutions have been recommended [13]. For instance, 0.05 M $CaCl_2$ has been considered as a suitable medium for the selective extraction of copper in direct analysis.

A typical direct DPASV voltammogram in $CACl_2$ medium is shown in Fig. 4(d), where the broadening of the $Cu^{2+}$ peak is attributed to the presence of $Cl^-$ ions [9]. The low values of $Cu^{2+}$ (Table 6) found by both the CRIP and CRISC techniques reveal that abundances of electrosticted $Cu^{2+}$ are apparently less in all sediments, although the total $Cu^{2+}$ content is estimated to be considerably large (Table 2). The much smaller $Cu^{2+}$ ion content in the sediments from the middle of river current is probably due to the severe deterioration of the ion-exchange structure of sediments by the changing kinetics of water flow in adjacent layers. Nevertheless, the chromatographic sepa-

Table 4
'Low-pH labile' (reducing conditions) metal contents in $NH_2OH \cdot HCl/25\%$ acetic acid extract of sediment ($\mu g\, g^{-1}$)

| Metal | Sample | Direct method | CRIP method [a] $PXPi(1HQS)_2$ | CRISC method | |
|---|---|---|---|---|---|
| | | | | Silica gel–$PCED(SSA)_2$ | Silica gel–$C_2EX(IHQS)_2$ |
| $Cu^{2+}$ | NN | 3 | 584 | 566 | 583 |
| | CN | 122 | 1137 | 1216 | 1205 |
| | NG | nd | 8297 | 8420 | 8418 |
| | SG | 44 | 1531 | 1534 | 1534 |
| | RG | 1 | 348 | 351 | 344 |
| $Cd^{2+}$ | NN | 1 | 8841 | 8865 | nd |
| | CN | 105 | 1203 | 1225 | ns |
| | NG | nd | 2298 | 2325 | ns |
| | SG | nd | 1785 | 1801 | ns |
| | RG | nd | 45 | 45 | ns |
| $Pb^{2+}$ | NN | 4 | 68 | ns | 82 |
| | CN | 47 | 392 | ns | 616 |
| | NG | 2 | 1267 | ns | 2118 |
| | SG | 1 | 776 | ns | 944 |
| | RG | 1 | 89 | ns | 322 |
| $Zn^{2+}$ | NN | 22 | 2872 | ns | ns |
| | CN | 102 | 8684 | ns | ns |
| | NG | 1 | 14719 | ns | ns |
| | SG | nd | 2477 | ns | ns |
| | RG | 3 | 541 | ns | ns |
| $Fe^{3+}$ | NN | 34268 | 36366 | 38614 | 39505 |
| | CN | 28801 | 31011 | 31392 | 34987 |
| | NG | 3184 | 25871 | 26019 | 26486 |
| | SG | 7013 | 7781 | 7827 | 7946 |
| | RG | 24249 | 23723 ($PXPi(1HQS)_2$)<br>24285 ($PXPi(SSA)_2$) | | 29646 |

Error $\leq \pm 8\%$; nd = not detected; ns = not selective; NN = Nagwa nullah; CN = City nullah; NG = Nagwa Ghat; SG = Shivala Ghat; RG = Raj Ghat.
[a] Upper part of strip (except $Fe^{3+}$ which was preconcentrated in the lower part of the paper strip).

rations (CRIP and CRISC) gave enhanced $Cu^{2+}$, particularly in City nullah and Nagwa nullah sediments as compared with direct techniques, whereas in the middle river-sediments $Cu^{2+}$ remained unaltered irrespective of the techniques employed (Table 6). The negligible value of $Cu^{2+}$ obtained from direct analysis may be taken as suggestive of exclusive adsorption onto the complexed matrices in $CaCl_2$ extract or drastic deterioration of the sediment network as suggested above, for any of the samples studied. The almost equal value of $Cu^{2+}$ from CRIP and CRISC strongly supports that all river sediments studied have an exclusively free form of copper in trace levels in their respective $CaCl_2$ extracts.

### *3.5. A general survey of the metal contents in sediment samples*

The chemical speciation procedure in the present instance is limited to only fractionation of metal contents of sediments. In spite of the ambiguous links between extraction category and 'biological availability', the selective chemical extraction by four major extractants covers almost all metal fractions present in sediment samples. If $M_1$ is taken as the total sum of all free (ionic) metals determined by the CRIP method and $M_2$ is the total sum of labile (ionic + weakly complexed) metals determined by the CRISC method available in all four extracts, the weakly complexed fraction could be obtained as $(M_2 - M_1)$. The

Table 5
'Weak acid (pH 5) labile' metal content in sodium acetate/acetic acid extract of sediment ($\mu g\ g^{-1}$)

| Metal | Sediment | Direct method | CRIP method [a] $PXPi(SSA)_2$ | CRISC method | |
|---|---|---|---|---|---|
| | | | | Silica gel–$PCED(SSA)_2$ | Silica gel–$C_2EX(1HQS)_2$ |
| $Cu^{2+}$ | NN | 1 | 22 | 24 | 24 |
| | CN | 9 | 9 | 9 | 9 |
| | NG | 1 | 1 | 5 | 5 |
| | SG | 44 | 53 | 59 | 57 |
| | RG | 4 | 4 | 5 | 5 |
| $Cd^{2+}$ | NN | nd | nd | 26 | ns |
| | CN | 11 | 1200 | 1314 | ns |
| | NG | nd | 3122 | 3265 | ns |
| | SG | nd | 4062 | 4104 | ns |
| | RG | nd | – | 87 | ns |
| $Pb^{2+}$ | NN | 1 | 100 | ns | 207 |
| | CN | 3 | 302 | ns | 395 |
| | NG | nd | – | ns | 2 |
| | SG | 2 | 218 | ns | 404 |
| | RG | nd | – | ns | 1 |
| $Zn^{2+}$ | NN | 21 | 3741 | ns | ns |
| | CN | 102 | 1282 | ns | ns |
| | NG | 18 | 1398 | ns | ns |
| | SG | nd | 605 | ns | ns |
| | RG | nd | – | ns | ns |

Error $\leqslant 8\%$; nd = not detected; ns = not selective; NN = Nagwa nullah; CN = City nullah; NG = Nagwa Ghat; SG = Shivala Ghat; RG = Raj Ghat.
[a] Upper part of the strip (except $Cu^{2+}$ which was preconcentrated in the lower part of the strip).

strongly complexed (bound) fraction is also estimated by subtraction of $M_2$ from the total metal contents obtained by the CRIP method from Table 2 (total metal contents obtained by the direct method are not acceptable owing to readsorption and matrix complications). $Zn^{2+}$ was obtained only in the ionic form by the CRIP method; other fractions could not be estimated. The results obtained on the basis of the above-formulated speciation (fractionation) scheme for metal contents of different sediments are portrayed in Table 7.

A decreasing trend of 'biologically available' metal contents ($Cu^{2+}$, $Ca^{2+}$, $Pb^{2+}$) ($M_2$) is observed on moving from Nagwa Ghat (upstream) to Raj Ghat (downstream) in sediments. This can only happen if the waste-water from the city chemically interacts with river-water to release the metal contents of sediments from solute phase to solution phase. In other words, city-waste disposal into the river through nullah introduces sufficient chelator/ligands for retrieval of metals from the sediment-bed, and subsequently pushes away these metals with the flowing water layers causing a drastic reduction in the metal contents of the sediments.

An entirely opposite trend of $Fe^{3+}$ contents, i.e. an increasing trend proceeding from Nagwa Ghat downwards, to Raj Ghat, can be attributed to the following possibilities: large contents of $Fe^{3+}$ being introduced into the river via Nagwa nullah which slowly settle on the river bed as ferrous hydroxides during the course of its flow downstream (Raj Ghat). Further substantial addition of City nullah enhances $Fe^{3+}$ as a free and weakly complexed form to a greater extent. Also, the $Fe^{3+}$ ions released by chelator/ligand tend to resettle on the river bed as ferrous hydroxide layers during the course of the downstream flow of the river.

### 3.6. Evaluation of copper in water samples

A modest attempt is made to analyse Ganges water samples in Varanasi, which were collected from two different stations, i.e. Rajendra Prasad Ghat (RPG) and Harischandra Ghat (HCG). The complexing ability of $Cu^{2+}$ has been determined for different samples by the

Table 6
'Sediment pH (6–8) labile' metal content in 0.05 M $CaCl_2$ extract of sediments ($\mu g\ g^{-1}$)

| Metal | Sediment | Direct method | CRIP method [a] PXPi(SSA)$_2$ | CRISC method | |
|---|---|---|---|---|---|
| | | | | Silica gel–PCED(SSA)$_2$ | Silica gel–$C_2$EX(IHQS)$_2$ |
| $Cu^{2+}$ | NN | 1 | 103 | 110 | 105 |
| | CN | 2 | 43 | 44 | 41 |
| | NG | 2 | 5 | 11 | 11 |
| | SG | 1 | 1 | 9 | 1 |
| | RG | 5 | 5 | 1 | 8 |
| $Cd^{2+}$ | NN | 1 | – | 13 | ns |
| | CN | 40 | – | 75 | ns |
| | NG | nd | – | 257 | ns |
| | SG | nd | – | 41 | ns |
| | RG | nd | nd | 2 | ns |
| $Pb^{2+}$ | NN | nd | – | ns | 40 |
| | CN | nd | – | ns | 8 |
| | NG | nd | – | ns | 1 |
| | SG | nd | nd | ns | nd |
| | RG | nd | – | ns | nd |
| $Zn^{2+}$ | NN | nd | nd | ns | ns |
| | CN | nd | 304 | ns | ns |
| | NG | nd | nd | ns | ns |
| | SG | nd | nd | ns | ns |
| | RG | nd | nd | ns | ns |

Error ≤ 8%; nd = not detected; ns = not selective; NN = Nagwa nullah, CN = City nullah; Ng = Nagwa Ghat; SG = Shivala Ghat; RG = Raj Ghat.
[a] Upper part of strip (except $Cu^{2+}$ which is preconcentrated in the lower part of the strip).

method of ASV titrations [26]. A combination of chromatography and direct DPASV analysis led to the fractionation of copper; the other metals present as labile fractions could not be detected. In addition, the laboratory tap-water was also analysed. The problem of re-adsorption was immaterial in water samples, in contrast to the sediment analysis; therefore, the direct and simultaneous analysis yielded ASV labile metal fractions (ionic plus weakly complexed) of copper. To obtain the total $Cu^{2+}$, 10 ml water sample was digested in the voltammetric cell with 2 ml of concentrated nitric acid without boiling, and eventually evaporated to dryness. The direct and simultaneous analysis of the residue was then carried out in 0.2 M ammonium citrate buffer (pH 3) by DPASV.

As is evident from Table 8, both the CRIP and direct DPASV methods gave similar results for Rajendra Prasad nullah. Hence, it is obvious that this sample does not particularly contain weakly complexed species except the ionic form of free $Cu^{2+}$ ion. On the contrary, the mixing points of nullah and river at Rajendra Prasad and Harish Ghandra Ghat containing the purely weakly complexed form of $Cu^{2+}$ ion, obtainable in the direct method of simultaneous analysis as the CRIP method, fails to detect any free metal ions. The non-detectable ionic fraction of $Cu^{2+}$ ions in the CRIP method at the mixing points of nullah and river at these stations strongly reveals the presence of chelating matters like humic and fulvic acids or any other organic substances which complex $Cu^{2+}$ ions very effectively. The middle streams of Rajendra Prasad Ghat and Harishchandra nullah were devoid of both ionic and weakly complexed forms of copper. Here, it could be surmised that the higher complexing ability of these samples may be the governing factor restricting 'ASV labile' fraction in direct and/or CRIP analysis. The tap-water sample had only the ionic form of $Cu^{2+}$ available for CRIP analysis, while the weakly labile form could not be detected through direct analysis.

The very low values of total $Cu^{2+}$ contents are surprisingly unrealistic, and this could be only rationalized if one assumes that there is a strong possibility of the formation of intermetallic compounds on the surface of SMDE, which might result in illusive and frivolous values.

Table 7
Metal fractions in sediments ($\mu g\ g^{-1}$)

| Metal | Sample | Ionic ($M_1$) | Labile (ionic + weakly complexed) ($M_2$) | Weakly complexed ($M_2 - M_1$) | Strongly complexed complexed (Total $- M_2$) |
|---|---|---|---|---|---|
| $Cu^{2+}$ | NN | 1200 | 1435 | 235 | 4178 |
| | CN | 2507 | 3012 | 509 | 4668 |
| | NG | 16622 | 16770 | 148 | nd |
| | SG | 2680 | 2988 | 308 | 4317 |
| | RG | 1183 | 1193 | 10 | 10271 |
| $Cd^{2+}$ | NN | 10023 | 10152 | 129 | 6653 |
| | CN | 3650 | 3879 | 229 | 2518 |
| | NG | 6540 | 7277 | 737 | 21 |
| | SG | 9463 | 9795 | 372 | 16349 |
| | RG | 44 | 133 | 89 | 1276 |
| $Pb^{2+}$ | NN | 3703 | 4473 | 770 | 2668 |
| | CN | 550 | 1562 | 1012 | 1230 |
| | NG | 2401 | 3015 | 614 | 2601 |
| | SG | 1591 | 2626 | 1035 | nd |
| | RG | 149 | 759 | 610 | 4373 |
| $Fe^{3+}$ | NN | 80628 | 84786 | 4158 | 11244 |
| | CN | 75270 | 77974 | 2704 | 19787 |
| | NG | 29739 | 29933 | 194 | 18175 |
| | SG | 50597 | 53838 | 3421 | 9182 |
| | RG | 55029 | 57158 | 2129 | 24359 |

NN = Nagwa nullah; CN = City nullah; NG = Nagwa Ghat; SG = Shivala Ghat; RG = Raj Ghat; $M_1$ = total sum of ionic fractions present in all extracts studied; $M_2$ = total sum of labile (ionic + weakly complex) fractions present in all extracts studied; error limit $\leq 8\%$.

Table 8
Analysis of $Cu^{2+}$ in Ganges waters

| Sample | pH | BOD (ppm) | $Cu^{2+}$ complexing ability ($\times 10^{-8}$ M) | Direct method ($\mu g\ l^{-1}$) | CRIP method $PXPi(SSA)_2$ strip ($\mu g\ l^{-1}$) | Total ($\mu g\ l^{-1}$) |
|---|---|---|---|---|---|---|
| HCG nullah | 6.8 | 120.1 | 20.0 | nd | nd | 5 |
| HCG mixing pt. | 8.05 | 1.28 | 2.3 | 6875 | nd | nd |
| RPG nullah | 6.5 | 172.1 | 2.0 | 24750 | 24750 | 1 |
| RPG mixing pt. | 8.13 | 2.3 | 1.7 | 11000 | nd | 28 |
| RPG mid. stream | 8.2 | 0.85 | 1.2 | nd | nd | 64 |
| Tap water | 7.1 | – | 1.7 | nd | 19626 | 15 |

HCG = Harishchandra Ghat, RPG = Rajendra Prasad Ghat; nd = not detected, error $\leq \pm 8\%$; temperature = 26 °C.

## 4. Conclusion

A major objective in this investigation was to evaluate the feasibility of a chelation-chromatographic approach to the differentiation of ionic and labile metal fractions in river/water samples. It has been concluded that the direct and simultaneous analysis of metals in sediment undoubtedly has drastic re-adsorption/competitive effects from a complex matrix of sediment extract. The introduction of a filtering step before analysis is not advisable, as some fractions loosely bound with the suspension are likely to be lost. However, the application of the CRIP and CRISC methods to the selective retention of heavy metals has proven to be an advantageous step to remove the possible complications of re-adsorption, intermetallic formation, separation of exchanger from sediment, competitive effect of multi-elemental matrix, and electrode perturbation, etc. The CRIP method measures only ionic (free) met-

als, whereas the CRISC method gives an estimation of the labile (ionic plus weakly complexed) fraction of the metals. Further, the validity of the standard addition method, which has been reported to be unsuccessful in direct analysis, could be restored by chelation-chromatographic analysis. The pH effect of the base extractants on peak height is also eliminated, since analyte metal ions are essentially isolated prior to analysis and monitored by DPASV in the suitable buffers at optimized pH. Further, the proposed CRIP-DPASV technique is found to be very simple and an efficient alternative to avoid peak distortion and iron interferences in the direct analysis of heavy metals at trace levels in water.

Although we cannot fully account for the wide spectrum of results at different intervals of time (or season) in different sections of the river, the present work, within a limited framework, merits special significance to establish an analytical scheme for the classification of various types of metal fractions present in real natural samples.

## References


[1] W.F. Pickering, C.R.C. Crit. Rev. Anal. Chem., 12 (1981) 233.
[2] W.F. Pickering, Ore Geol. Rev., 1 (1986) 83.
[3] T.U. Auliitia and W.F. Pickering, Talanta, 34 (1987) 231.
[4] T.U. Auliitia and W.F. Pickering, Water, Air, Soil Pollut., 35 (1987) 171.
[5] T.U. Auliitia and W.F. Pickering, Water Res., 20 (1986) 1397.
[6] T. Ugapo and W.F. Pickering, Talanta, 32 (1985) 131.
[7] T.M. Florence and G.E. Batley, Talanta, 23 (1976) 179.
[8] J.P. Riley and D. Taylor, Anal. Chim. Acta, 40 (1968) 479.
[9] A. Beveridge, P. Waller and W.F. Pickering, Talanta, 36 (1989) 535.
[10] A. Beveridge, P. Waller and W.F. Pickering, Talanta, 36 (1989) 1217.
[11] E.A. Schonberger and W.F. Pickering, Talanta, 27 (1980) 11.
[12] M. Pinchin and J. Newham, Anal. Chim. Acta, 90 (1977) 91.
[13] P.A. Waller and W.F. Pickering, Talanta, 37 (1990) 981.
[14] Kh.Z. Brainina, Stripping Voltammetry in Chemical Analysis, Wiley, New York, 1974, pp. 64, 65.
[15] J.A. Wise, D.A. Roston and W.R. Henman, Anal. Chim. Acta, 154 (1983) 95.
[16] H. Bloom, B.N. Noller and D. Richardson, Anal. Chim. Acta, 109 (1979) 157.
[17] D.C. Grahame, Chem. Rev., 41 (1947) 441.
[18] S. Sundd, S.K. Prasad, A. Kumar and B.B. Prasad, Talanta (in press).
[19] B.B. Prasad and S. Sundd, Chromatographia (in press).
[20] B.B. Prasad, A. Kumar and S. Sundd, React. Polym., 23 (1994) 229.
[21] B.B. Prasad and S. Sundd, Bull. Chem. Soc. Jpn. (in press).
[22] A.M. Liimata and J.D. Spain, Anal. Chem., 35 (1963) 1898.
[23] P.M.M. Jonas, D.J. Eve and J.R. Parrish, Talanta, 36 (1989) 1021.
[24] W. Holak, J.A.O.A.C., 58(4) (1975) 777.
[25] K.S. Lee, W. Lee and D.W. Lee, Anal. Chem., 50 (1978) 256.
[26] Van Liv and J.D. Ingle, Talanta, 36 (1989) 185.
[27] E.A. Schonberger and W.F. Pickering, Talanta, 27 (1980) 11.

ELSEVIER

Talanta 42 (1995) 1411–1418

Talanta

# The separation of platinum, palladium and gold from silicate rocks by the anion exchange separation of chloro complexes after a sodium peroxide fusion: an investigation of low recoveries

Jacinta Enzweiler [1], Philip J. Potts *

*Department of Earch Sciences, The Open University, Walton Hall, Milton Keynes, MK7 6AA, UK*

Received 8 December 1994; revised 1 March 1995; accepted 2 March 1995

**Abstract**

A series of experiments was undertaken to measure the recovery efficiency of platinum, palladium and gold from silicate rocks using a sodium peroxide fusion followed by anion exchange separation of the analytes as chloro complexes. Results obtained by graphite furnace atomic absorption spectrometric analysis of standard solutions prepared in dilute HCl or HCl-acidified sodium peroxide solution showed that recoveries were near quantitative. However, when standard solutions were added to an alkaline sodium peroxide solution, which was then acidified, low results were obtained for platinum and gold (46% and 76% respectively). Low and variable results were also obtained when standard solutions were added to a peridotite sample that had been dissolved by the state procedure, and in the analysis of the South African Bureau of Standards certified reference material, SARM 7. Various experiments were undertaken to investigate these low recoveries, but the reason proposed here is the formation of hydroxychloro compounds in alkaline solution which are not, on acidification with HCl, converted quantitatively to the chloro complex necessary for quantitative anion exchange separation. It is concluded that a sodium peroxide fusion followed by an anion-exchange separation does not appear to form the basis of a successful technique for the determination of platinum, palladium and gold in silicate rocks.

*Keywords:* Anion exchange separation; Chloro complexes; Gold; Palladium; Platinum; Sodium peroxide fusion

## 1. Introduction

In the absence of "definitive methods" for the determination of the platinum group elements (Pt, Pd, Rh, Ru, Os, Ir) in geological samples, there is continuing interest in the development of new and more effective analytical procedures. These elements present a significant analytical challenge since the concentration in many geological samples is in the nanograms per gram or even the sub-nanograms per gram range. Even when using the most sensitive analytical techniques, it is necessary to separate the platinum group elements (PGEs) from matrix elements and concentrate them before analysis.

One of the most widely used separation techniques is based on fire assay using nickel sulphide [1,2], or for a more limited selection of elements, lead-based fluxes [3,4]. These preconcentration procedures are considered by the geological community to be some of the most reliable and offer the advantage of accepting

* Corresponding author.

[1] On leave from: Universidade Estadual de Campinas, Instituto de Geociências, Cidade Universitária, 'Zeferino Vaz', Campinas, SP, PO Box 6152, CEP 13081, Brazil.


*SSDI* 0039-9140(95)01577-9

relatively large sample masses (normally up to 10–50 g). However, the fire assay procedure is not without some difficulties, notably the requirement to adjust flux composition according to sample matrix composition and the relatively large quantities of reagents required with the potential consequential increase in blank levels. Furthermore, some reports have suggested that the nickel sulphide fire assay procedure does not always yield quantitative recoveries of Au and the PGEs [5] and that without care, losses can also occur in the subsequent dissolution of the nickel sulphide button prior to analysis [6].

For these reasons, there is considerable contemporary interest in developing alternative analytical procedures which offer advantages over established techniques. Of the alternative procedures, ion exchange separations offer considerable potential. In particular, Alimarin et al. [6a] have shown that high performance liquid chromatography is capable of separating the PGEs as 8-hydroxyquinolinates, and they recommended their procedure for the analysis of "technological solutions, concentrates, alloys and catalysts". For the analysis of geological samples, our particular interest was in a review of published distribution coefficients [7], which indicated that conventional anion exchange resins have, in theory, several advantages. Not only are the PGEs and Au chloro complexes strongly adsorbed by anion exchange resins from dilute hydrochloric acid solutions, but few other elements that are found at significant concentrations in silicate rocks form anionic species under these conditions (Table 1). More specifically, according to Korkisch [7], only the following restricted range of elements is also adsorbed by anion exchange resins from 0.5 M HCl solutions: Ag, Cu(I), Re(VII), Tc(VII), Zn, Cd, Hg, Tl(III), Sn, Pb, Sb(III), Bi, Te(IV). Chromium, which may be present at substantial concentrations in silicate rocks, is also strongly adsorbed as Cr(VI), but if it is reduced to Cr(III), no adsorption occurs. Consequently, solutions resulting from anion exchange separation are likely to be free of high dissolved salt contents as well as species that could cause interferences in high sensitivity techniques such as graphite furnace atomic absorption spectrophotometry (GF-AAS) or inductively coupled plasma-mass spectrometry (ICP-MS).

An anion exchange separation was used by Branch and Hutchinson [8] to preconcentrate Pt and Pd after an aqua regia attack of the sample, with determinations made by GF-AAS. Their results were near quantitative, but alternative work [9] has shown that aqua regia is not capable of dissolving the more refractory PGE minerals, so this procedure is not appropriate for all silicate rock samples. An alternative, and potentially more effective dissolution procedure is one based on a sodium peroxide fusion (or sinter) [10]. Such procedures have been used extensively and successfully in radiochemical separations [11–14], particularly for the determination of the rare earth elements, but not so commonly with other analytical procedures. However, sodium peroxide fusion offers the advantage that sulphide and refractory minerals are effectively attacked and the released PGEs are uniformly converted to a high oxidation state. An anion exchange separation procedure has then the potential to separate selectively the PGEs and Au from the large concentrations of flux and matrix elements. To accommodate the relatively large volume of solution which results from dissolution of the peroxide cake, the anion exchange can be carried out in batch rather than column mode, a procedure that has been shown to offer quantitative recoveries for species with high distribution coefficients such as the PGE and Au chloro complexes [8,15]. However, despite these favourable characteristics, a review of the scientific literature did not reveal any methods in which anion exchange chromatography had been used following a sodium peroxide fusion of geological samples for the determination of the PGEs and Au at the nanograms per gram level — hence the justification for the present work.

In this paper, the results of a preliminary investigation are presented into the development of a method for the determination of platinum, palladium and gold in silicate rock samples based on sodium peroxide sample fusion, followed by anion exchange separation in the column or batch mode. Unexpected difficulties attributable to low recoveries of these analytes are described and discussed.

Table 1
Approximate distribution coefficients of Pt, Pd and Au in 0.5 M hydrochloric acid solution onto strongly basic resin [7]

| Pt(IV) | Pd(II) | Au(III) |
|---|---|---|
| $10^4$ | $10^3$ | $10^6$ |

## 2. Experimental

### 2.1. Reagents

Stock standard solutions of platinum and palladium were prepared by dissolving $(NH_4)_2PdCl_4$ and $(NH_4)_2PtCl_6$ (Johnson Matthey Chemicals Ltd.) in 1 M HCl. For gold, an atomic absorption solution (100 μg $ml^{-1}$) (Aldrich) was used. Quartz-distilled HCl, subboiling distilled nitric acid and deionised water were used in the analytical procedures. All other chemicals were analytical reagent grade. PTFE apparatus and glassware were cleaned by soaking in aqua regia overnight and then by repeatedly soaking and rinsing with deionised water. Between fusions, the zirconium crucible was cleaned by soaking in hot concentrated HCl and then rinsing with deionised water.

### 2.2. Sample dissolution

Samples were digested by either sintering or fusing with sodium peroxide in zirconium crucibles, using the following procedure. About 2 g of sodium peroxide were weighed into the crucible and 0.5 g of sample (which had been dried at 105 °C) was added. After thorough mixing, more sodium peroxide was added (0.5 g for sinter or 1 g for fusion) and mixed with the contents of the crucible. The crucible was then covered with a lid and placed in a cold furnace.

For the sintering procedure, the temperature was raised to about 200 °C and maintained for 15 min. The temperature was then raised to 480 °C and held for about 90 min. The crucible was removed from the furnace and allowed to cool for 2 min before transferring to a 600 ml beaker, adding 60 ml of warm water and covering with a watch glass. After the reaction had subsided, the crucible was rinsed with water, 6 M HCl (2 ml) and then water again and these rinses were added to the sample solution. The precipitate was dissolved by adding 25 ml of 6 M HCl, stirring the solution whilst the acid was added.

For the fusion procedure, the temperature of the furnace was raised to 550 °C and maintained for about 20 min. The crucible was swirled to ensure mixing and then placed back in the furnace, and the temperature was raised to 575 °C and maintained for a further 20 min. The crucible was swirled again and the temperature was raised to 600 °C for 20 more min. The crucible was removed from the furnace and allowed to cool for some minutes before being transferred to a beaker, to which 20 ml of cold water were added. The beaker was covered with a watch glass to allow the cake to dissolve. After completion of the reaction, the same procedure as described above was followed. Both the crucible and the lid were rinsed with small amounts of 6 M HCl, which were added to the main solution.

In each case, the volume of solution was adjusted to approximately 150 ml. Hydrogen peroxide (1 ml) was then added and the solution was boiled for some minutes to reduce chromium(VI), which otherwise would be strongly retained by the anion exchange resin. The solution was cooled to room temperature and the pH was adjusted to 0.3.

### 2.3. Anion exchange

A strongly basic anion exchange resin (Bio-Rad AG1-8X; 100–200 mesh) was used in this work. In the majority of the experiments a batch procedure was employed, but the cleaning and conditioning of the resin was always undertaken in PTFE columns 0.5 cm in diameter with a 30 ml bulb and a polypropylene frit to retain the resin. Resin (1 g) was transferred to the column in the form of a slurry. The resin was cleaned and conditioned following the procedure of Colodner et al. [16], using hot 12 M nitric acid (10 ml), followed by 8 M nitric acid (10 ml), water (20 ml), 6 M HCl (10 ml) and finally 0.5 M HCl (20 ml).

For a batch separation, the resin was added to the sample solution and stirred for 1 h using a magnetic stirrer. Experiments on the kinetics of absorption confirmed that this time was sufficient for the quantitative recovery of the elements of interest. After this time the resin slurry was quantitatively transferred to the column and washed with 0.5 M HCl (20 ml) and water (20 ml). The column was eluted with hot (approximately 90 °C) 12 M $HNO_3$ (30 ml), added 1 ml at a time. The eluate was collected in a 40 ml PTFE beaker. The solution was evaporated down to a volume of approximately 0.5 ml under an infrared lamp. It was then transferred to a 5 ml volumetric flask and the volume made up with 0.5 M HCl. The elements Pt, Pd and Au were determined using a Perkin–Elmer Zeeman 3030 graphite furnace atomic absorption spectrophotometer, employing the conditions listed in Table 2.

Table 2
Graphite furnace atomic absorption spectrophotometry operating parameters for the determination of Pt, Pd and Au [25]

| Operating parameters | | Pt | Pd | Au |
|---|---|---|---|---|
| Wavelangth (nm) | | 265.6 | 247.6 | 242.8 |
| Furnace programme: | | | | |
| Drying 1 | Temperature (°C) | 90 | 90 | 90 |
| | Ramp time (s) | 1 | 1 | 1 |
| | Hold time (s) | 9 | 9 | 9 |
| Drying 2 | Temperature (°C) | 130 | 130 | 130 |
| | Ramp time (s) | 10 | 10 | 10 |
| | Hold time (s) | 15 | 15 | 15 |
| Char | Temperature (°C) | 500 | 500 | 500 |
| | Ramp time (s) | 10 | 10 | 10 |
| | Hold time (s) | 15 | 10 | 15 |
| Ash | Temperature (°C) | 1300 | 800 | 1000 |
| | Ramp time (s) | 10 | 10 | 10 |
| | Hold time (s) | 15 | 25 | 15 |
| Atomisation | Temperature (°C) | 2650 | 2650 | 2000 |
| | Ramp time (s) | 0 | 0 | 0 |
| No gas flow | Hold time (s) | 3 | 3 | 3 |
| Clean out | Temperature (°C) | 2650 | 2650 | 2650 |
| | Ramp time (s) | 1 | 1 | 1 |
| | Hold time (s) | 4 | 4 | 4 |

In some experiments, the separation was undertaken by passing the solution through the column instead of using a batch separation procedure. As well as separations involving dissolved silicate rock samples, experiments were also performed with standard elemental solutions, to evaluate the behaviour and recovery of the PGE chloro complexes.

## 3. Results and discussion

Preliminary results on applying the proposed scheme to the analysis of the certified reference material SARM-7 gave low and sometimes variable recoveries of the elements of interest when analysed values were compared with certified values. To evaluate the effectiveness of the anion exchange procedure, therefore, a series of experiments was carried out using standard solutions of Pt, Pd and Au. The concentrations of Pt, Pd and Au, and where appropriate, sodium peroxide and hydrochloric acid, were selected to match those found in sample solutions prepared from SARM-7 by the procedure summarised above. The results of these experiments showing the percentage recoveries of the elements of interest are listed in Table 3. The interesting and unexpected differences may be summarised as follows.

### 3.1. Standard solution experiments

When Pt, Pd and Au were added to a simple solution of 0.5 M HCl (experiment (a) in Table 3) or to an acidified solution of sodium peroxide (experiment (b)), the recoveries of Pt, Pd and Au after anion exchange were near quantitative (within experimental error), having mean values in the range 92–98%. These results indicate that the anion exchange procedure summarised above is effective, as expected from the favourable distribution coefficients for chloro complexes of PGEs. The large excess of sodium ions in acidified solutions does not appear to interfere significantly with the batch separation.

However, when the standard solutions were added to an alkaline solution of sodium peroxide, which was then acidified with HCl, as would be required in the full procedure for silicate rocks summarised above, recoveries were more variable, ranging from 46% (Pt) to 76% (Au) to 96% (Pd) (experiment (c) in Table 3). Thus, the palladium recovery was still near quantitative, but less than 50% of the platinum was detected after anion exchange separation, and the gold recovery was also low and variable.

These data suggested that on acidifying the alkaline solution, complete conversion of the Pt and probably the Au species to anionic chloro

Table 3
Results obtained for Pt, Pd and Au recoveries using an anion exchange resin

| Experiment [a] | Recovery (%) [b] | | |
|---|---|---|---|
| | Pt | Pd | Au |
| (a) Std. soln. in 0.5 M HCl ($n = 6$) | 97 ± 6 | 98 ± 5 | 92 ± 6 |
| (b) Std. soln. added to a acidified soln. of $Na_2O_2$ ($n = 5$) | 98 ± 5 | 96 ± 9 | 96 ± 7 |
| (c) Std. soln. added to a $Na_2O_2$ soln. and then acidified ($n = 3$) | 46 ± 6 | 96 ± 4 | 76 ± 12 |
| (d) Std. soln. added to a $Na_2O_2$ soln., acidified and chlorinated | 83 | 96 | 55 |
| (e) Std. added to a peridotite sample and fusion | 15 | 74 | 65 |
| (f) Peridotite fusion, dissolution, acidification, then std. addition | 84 | 75 | 80 |
| (g) SARM-7 sintering or fusion ($n = 10$) | 34 ± 17 | 78 ± 9 | 84 ± 19 |
| (h) SARM-7, fusion chlorination | 30 | 78 | 68 |
| (i) SARM-7, fusion in Ni crucible | 33 | 79 | 125 |
| (j) SARM-7, fusion after HF treatment | 38 | 64 | 86 |
| (k) SARM-7, HF, aqua regia attack ($n = 2$) | 99 ± 4 | 80 ± 2 | 98 ± 8 |
| (l) SARM-7, fusion, Te coprecipitation | 99 | 91 | 107 |

[a] When not stated, $n = 1$.
[b] ±, One standard deviation.

complexes was not occurring. A further experiment was, therefore, carried out in which chlorine gas was bubbled through the acidified sodium peroxide solution to promote the formation of anionic chloro complexes (experiment (d) in Table 3). In these circumstances, the recovery of platinum was increased to 83% with the palladium recoveries remaining near quantitative, but the recovery of Au was reduced to 55%, for reasons which are not clear.

Two further experiments were undertaken in which standard solutions were added to a peridotite sample which had been dissolved following the procedure listed above. In the first case, the standard solution was added to the peridotite sample before fusion with peroxide, dissolution to form an alkaline solution, acidification and anion exchange separation (experiment (e) in Table 3). Following the trend observed in experiment (c), low recoveries were observed for all elements as follows: Pt (15%), Pd (74%) and Au (65%). In the second experiment ((f) in Table 3), the standard solution was added after acidification of the solution derived by fusion of the peridotite sample (i.e. just before anion exchange). Although near-quantitative recoveries might be expected by analogy with experiment (b), in fact recoveries were 12–23% lower, as follows: Pt (84%), Pd (75%), Au (80%). This result indicated that the presence of the peridotite sample or some aspect of the fusion procedure had interfered with the anion separation procedure.

### 3.2. Experiments using certified reference material, SARM 7

A series of experiments was then carried out using the certified reference material SARM-7 (platinum ore) distributed by the South African Bureau of Standards. This silicate sample has relatively high abundances of Pt, Pd and Au (3.74 $\mu g\,g^{-1}$, 1.53 $\mu g\,g^{-1}$ and 0.31 $\mu g\,g^{-1}$, respectively) compared with "typical" silicate rocks. However, it offers the advantage in testing the procedure that determinations made by GF-AAS are well above the detection limit of the technique and so results would not be affected seriously by poor analytical precision.

In the first series of experiments, the sample was attacked using the sintering procedure. These data were compared with results using the full fusion procedure. No significant difference was detected between the respective ranges of measurements, and the average of all 10 determinations are listed as experiment (g) in Table 3. The measured recoveries were Pt (34%), Pd (78%) and Au (84%).

To evaluate further these discrepancies, additional experiments were undertaken as follows: fusion of SARM-7 followed by chlorination of the acidified solution before anion exchange (experiment (h)); substitution of nickel for zirconium crucibles in the standard procedure in case the presence of small amounts of Zr dissolved from the crucible interfered with the separation procedure (experiment (i)); and treatment of SARM-7 with HF prior to fusion to remove Si in case the presence of silica

interfered with the separation (experiment (j)). Low recoveries were observed in all these experiments, with values ranging as follows: Pt (30–38%), Pd (64–79%) and Au (68%–125%).

The final two experiments with SARM-7 (experiments (k) and (l) in Table 3) employed an alternative sample dissolution or preconcentration procedure as follows. In experiment (k), SARM 7 was dissolved by an HF-aqua regia attack using a pressure bomb. The sample (1.0 g), HF (11 ml) and aqua regia (4 ml) were mixed in a PTFE bomb and sealed with a PTFE gasket in a stainless steel jacket, which was left in an oven at 180 °C overnight. After evaporation of the resultant solution and conversion of the residue to chlorides, the solution was filtered, the pH of the filtrate adjusted to 0.3 and the solution was passed through an anion-exchange column. Pt and Au recoveries were near quantitative (99% and 98% respectively, Pd being lower at 80%. In experiment (l), SARM-7 was attacked using the peroxide fusion procedure but a Te coprecipitation was carried out on the resultant solution using established procedures [14]. The Te precipitate was filtered using a Millipore type HA 0.45 mm filter disk which was then removed from the PTFE holder and the precipitate quantitatively washed into a PTFE beaker using concentrated nitric acid. The same was done with any precipitate adhering to the holder. The solution was evaporated, and the residue dissolved in 0.5 ml of aqua regia, and was transferred to a 5 ml vessel, which was made up to volume with 0.5 M HCl and the analytes determined by GF-AAS. Recoveries for Pt were again near-quantitative (99%) with high recoveries for Pd (91%) and Au (107%).

### 3.3. PGE chemistry

All these results show that the separation of the PGEs by anion-exchange as the chloro complexes is not as simple as might be expected from the favourable distribution coefficient data. However, some conclusions can be made from these experiments in relation to potential difficulties previously reported in the literature.

#### 3.3.1. Formation of hydroxy complexes

The first problem concerns the formation of PGE and Au hydroxy and hydroxychloro species in the alkaline solution during dissolution of the sodium peroxide cake, species which may not easily be converted to chloro complexes on acidification with HCl. In a paper dealing with the speciation of gold(III) chloride complexes in aqueous systems, Peck et al. [17] showed that with increasing pH, measurements by UV-vis and Raman spectroscopy were consistent with the successive replacement of chloride by hydroxide ligands with $[AuCl(OH)_3]^-$ and $[Au(OH)_4]^-$ being formed at high pH. The results of Peck et al. also showed that these hydroxychloro complexes were more stable than predicted on the basis of theoretically estimated stability constants. Hartley [18] reported that hydroxy complexes of Pt(IV) are obtained when a chloroplatinum(IV) complex is treated with sodium hydroxide. If this effect influenced the procedure used in the present work, it would be expected that by bubbling chlorine for several minutes through the acidified solution obtained after dissolving the peroxide cake, the recovery of Pt would be increased. An increase in recovery was in fact observed when a standard solution was used (experiment (d)) but not with SARM-7 (experiment (h)), and no improvement was observed when the peroxide cake was dissolved directly in 6 M HCl instead of first leaching in water (the resultant silica precipitate had to be separated by filtration before anion exchange).

Davidson and Jameson [19] measured the equilibrium constant of the reaction

$$[PtCl_6]^{2-} + H_2O = [PtCl_5(H_2O)]^- + Cl^-$$

as $3.25 \times 10^{-2}$ at 50 °C. From these data, it would then be expected that more than 90% of the platinum present in 0.5 M HCl solutions should be in the form of the hexachloro complex. This statement agrees with the results obtained from standard solutions added to HCl solutions or to already acidified solutions of sodium peroxide (experiments (a) and (b)). However, when Pt was added to the basic solution and then acidified (experiment (c)), the results are not satisfactory. Chugaev and Klopin [20] obtained ammonium dihydroxyplatinate from the reaction between diammonium tetrachloroplatinate and hydrogen peroxide in acidic medium. The same workers reported that in alkaline medium, the reactions are complex and that all chlorine atoms are substituted by $OH^-$ ligands. This substitution reaction cannot be reversed except by heating with HCl at 150 °C. These conditions could not be applied in the current scheme of analysis as $SiO_2$ would dehydrate and precipitate. Colod-

ner et al. [16], using the anion-exchange procedure to preconcentrate Pt from seawater and sediments, reported recoveries above 80%, but obtained systematically lower results when their work was compared with other published data. They attributed this discrepancy to the fairly unreactive nature of Pt in sea water and the slow kinetics of Pt–ligand exchange reactions (as previously reported by Elding [21]), both of which could affect the spike equilibration of their isotope dilution technique.

Although this effect (the presence of PGE/Au hydroxychloro complexes) appears to us to be the most likely cause of the discrepancies described here, other sources were evaluated.

*3.3.2. Interference from Zr*

Zirconium from the crucible oxidises to zirconium dioxide during heating and it has been shown [22] that hydrated zirconium dioxide can be used to concentrate trace amounts of chlorocomplexes of the Pt group elements, an effect that could lead to low recoveries. However, substitution of a nickel crucible did not significantly improve recoveries (experiment (i)).

*3.3.3. Coprecipitation with silica*

The presence of any silica in solution could interfere either by coprecipitating the noble metals and/or affecting the anion exchange procedure. However, when one sample was treated with HF, which was then removed together with silica by evaporation with $HNO_3$ and HCl (experiment (j)) and the residue fused (minus silica) with peroxide, the Pt recovery was only 38%.

From all these results, it is inferred that in alkaline solution, platinum forms hydroxychlorocomplexes and that the substitution of chloro ligands for hydroxy ligands is not quantitative when the solution is then acidified with HCl. Any alternative explanation involving the precipitation of significant amounts of Pt as an insoluble residue during dissolution of the sodium peroxide cake is not supported by results presented here. The selectivity of the anion exchange resin is much higher towards the choro rather than the hydroxy complexes [23]. For this reason, if hydroxychloro complexes are present in solution, then the recovery efficiency is likely to be much lower and it is this that is inferred as the limiting factor from the Pt data reported in Table 3. Although direct measurements have not been carried out to confirm this hypothesis, it is possible that future experiments involving the application of high-performance liquid chromatography (e.g. Alimarin et al. [6a]) might permit identification of the hydroxychloro Pt species present.

Palladium and Au showed a more consistent behaviour in experiments using both standard solutions and the reference sample SARM-7. However, the results obtained for Pd for sample SARM-7 are systematically low for all the procedures used (experiments (g)–(k)). This observation was not the case in the experiments using standard solutions where results were quantitative. One possibility, which could explain incomplete recoveries of Pd, is that after dissolution of the sodium peroxide cake, Pd may be present as $Pd(OH)_2$, a proportion of which may be reduced to metallic Pd by hydrogen peroxide [18] in alkaline medium. However, this explanation does not fit in with the low results obtained when an acid attack was used (experiment (k)) or with the quantitative results obtained in experiment (c). Nevertheless, this possibility cannot be rejected completely and it must be considered for Pt and Au as well, since the hydroxy species of these metals can also be reduced by hydrogen peroxide in alkaline medium.

Attempts were not made to determine the other Pt group elements for the following reasons: Os forms the volatile tetroxide in acidic medium and so would be lost from sample solutions. Ruthenium(IV) is strongly absorbed from 1 M HCl solutions, but in more dilute HCl medium [24], it forms species like $Ru(OH)_2Cl_2$ which is not retained by the resin. Rhodium(III) forms $RhCl_2^+$ in 0.1–0.5 M HCl solutions and is not absorbed by anion exchange resins, while Rh(IV) is very strongly absorbed, but oxidation of rhodium in solution to form the tetravalent state is not possible with common oxidising agents. Iridium is strongly adsorbed by the resin when oxidised and complexed as $IrCl_6^{2-}$, but this species is easily reduced to the trivalent complex, which is not retained by the resin.

## 4. Conclusions

The results obtained in this work show that the solution chemistry of Pt, Pd and Au is more complicated than expected when investigating a method for determining these elements in silicate rocks by peroxide fusion, followed

by an anion ion exchange separation. Although both Pt and Pd chloro complexes have favourable distribution coefficients towards anion exchange separation, and the separation procedure is potentially highly selective towards these elements (the dichromate ions of Cr being the only other species likely to interfere), the advantage of these favourable characteristics cannot readily be taken in the analysis of silicate rocks. It is suggested that hydroxy- and/or hydroxychloro- Pt complexes formed in alkaline sodium peroxide solutions do not react quantitatively to form the equivalent chloro complexes when these solutions are acidified with HCl, even when a chlorination procedure is used. Equivalent reactions may affect Pd and Au, although apparently to a lesser extent. Alternative procedures must be investigated in order to develop a successful analytical technique, examples of which are given by Van Loon and Barefoot [26].

## Acknowledgements

The authors acknowledge valued discussions with Graham Pearson. J.E. acknowledges financial support from the Brazilian agency FAPESP.

## References

[1] R.V.D. Robért, E. Van Wyk and R. Palmer, Nat. Inst. Metall. Repub. S. Afr. Rep., 1371 (1971).
[2] E.L. Hoffman, A.J. Naldrett, J.C. Van Loon, R.G.V. Hancock and A. Manson, Anal. Chim. Acta, 102 (1978) 157.
[3] D.C. Bowditch, Aust. Min. Dev. Lab. Bull. (AMDEL), 15 (1973).
[4] G.E.M. Hall and G.F. Bonham-Carter, J. Geochem. Explor., 30 (1988) 255.
[5] R. Palmer and J.I.W. Waterson, Nat. Inst. Metall. Repub. S. Afr. Rep., (1971) 1185.
[6] S.E. Jackson, B.J. Fryer, W. Gosse, D.C. Healey, H.P. Longerich and D.F. Strong, Chem. Geol., 83 (1990) 119.
[6a] I.P. Alimarin, E.M. Basova, A.Yu. Malykhin and T.A. Bol'shova, Talanta, 17 (1990) 485–489.
[7] J. Korkisch, Handbook of Ion Exchange Resins: Their Application to Inorganic Analytical Chemistry, Vol. 3, CRC Press, Boca Raton, FL, 1989, pp. 3–65.
[8] C.H. Branch and D. Hutchinson, J. Anal. At. Spectrom., 1 (1986) 433.
[9] C.J.B. Gowing and P.J. Potts, Analyst, 116 (1991) 773.
[10] Z. Sulceck, P. Povondra and J. Dolezal, CRC Crit. Rev. Anal. Chem., 6 (1977) 255.
[11] R.A. Nadkarni and G.H. Morrison, J. Radioanal. Chem., 38 (1977) 435.
[12] S.J. Parry, Analyst, 105 (1980) 1157.
[13] M. Oddone, S. Meloni and R. Vannucci, J. Radioanal. Nucl. Chem., 142 (1990) 489.
[14] W.E. Stone and J.H. Crocket, Chem. Geol., 106 (1993) 219.
[15] J.B. McHugh, Talanta, 33 (1986) 349.
[16] D.C. Colodner, E.A. Boyle and J.M. Edmond, Anal. Chem., 65 (1993) 1419.
[17] J.A. Peck, C.D. Tait, B.I. Swanson and G.E. Brown, Geochim. Cosmochim. Acta, 55 (1991) 671–676.
[18] F.R. Hartley, The Chemistry of Platinum and Palladium, Applied Science Publishers Ltd., London, 1973.
[19] C.M. Davidson and R.F. Jameson, Trans. Faraday Soc., 61 (1965) 2462.
[20] L. Chugaev and V. Klopin, Chem. Abstr., 20 (1926) 1765.
[21] L.I. Elding, Inorg. Chim. Acta, 28 (1978) 255.
[22] S.A. Simanova, E.S. Boichinova, L.V. Nikol'skaya, G.S. Krylova and G.V. Kuznetsova, Zh. Prikl. Khim., 65 (1992) 1659.
[23] Ion Exchange Manual, Code 88/0590, Bio-Rad, U.K., p. 16.
[24] Y. Marcus, Coord. Chem. Rev., 2 (1967) 257.
[25] C.J.B. Gowing, Ph.D. Thesis, The Open University, U.K., 1993.
[26] J.C. Van Loon and R.R. Barefoot, Determination of the Precious Metals, Wiley, Chichester, 1991, p. 276.

ELSEVIER

Talanta 42 (1995) 1419–1423

Talanta

# Direct determination of boron in a cobalt-based alloy by graphite furnace-atomic absorption spectrometry

Benling Gong *, Yongming Liu, Yuli Xu, Zhuanhe Li, Tiezheng Lin

*Dalian Institute of Chemistry Physics, Academia Sinica, 161 Zhongshan Road, Dalian, People's Republic of China*

Received 10 November 1994; revised 28 February 1995; accepted 10 March 1995

**Abstract**

A matrix modifier composed of nickel and zirconium, and a graphite tube treated with zirconium solution were proposed for the determination of boron in cobalt-based alloys by graphite furnace-atomic absorption spectrometry. The effects of this matrix modifier and the treated graphite tube were studied, and the combination of 60 μg of nickel and 20 μg of zirconium as matrix modifier, and a graphite tube soaked with 10 g $l^{-1}$ of zirconium solution were found to give the highest analytical sensitivity. The interference effects of major components (cobalt) and eight minor components (chromium, nickel, tungsten, iron, tantalum, molybdenum, titanium, aluminium and manganese) were studied. Boron in four cobalt-based alloys was determined by graphite furnace-atomic absorption spectrometry employing the proposed matrix modifier and the treated graphite tube, without the preseparation of matrix. The relative standard deviation was 3.3% for 0.048% of boron. A characteristic mass was 500 pg.

## 1. Introduction

The addition of appropriate amounts of some elements improves the performance of steels and alloys appreciably. A microamount of boron increases the degree of quenching and the strength and toughness of steels and alloys. However, excess amounts of boron may cause their performance to deteriorate. Therefore the exact determination of boron in steels and alloys is required for metallurgical applications.

Cobalt-based alloys contain many components (chromium, nickel, tungsten, aluminium, tantalum, iron, manganese, silicon, carbon, etc.), as well as its main component (cobalt) and boron. Such a complex composition causes severe spectral and chemical interferences in the determination of boron by atomic spectroscopy. Although separation of the matrix from the sample solution before the measurements are performed and overcome these interferences, this requires a tedious treatment, easily resulting in either contamination or loss. Therefore it is preferable to determine boron in such alloys by direct measurements without the preseparation of the matrix from the sample solution.

Inductively coupled plasma-atomic emission spectrometry has been widely used for the determination of microamounts of boron [1–11], but this method is unsuitable for direct determinations because it necessitates preseparating the matrix from the sample solution in order to remove spectral interferences.

Graphite furnace-atomic absorption spectrometry, another sensitive method, also suffers severely from matrix interferences. Moreover, boron combines very easily with the carbon of the graphite tube, resulting in low analytical results and severe memory effects. Nevertheless, the selective application of a suitable matrix modifier and the pretreatment of the graphite tube could resolve the above problems. To date, some matrix modifiers such as

* Corresponding author. Fax: (86)411-363-2426.


*SSDI* 0039-9140(95)01585-X

Table 1
Instrumental parameters and operating conditions

| Parameter/conditions | Value |
|---|---|
| Wavelength (nm) | 249.7 |
| Slit width (nm) | 0.7 |
| Lamp current (mA) | 15 |
| Integration time (s) | 6 |
| Mode | Peak height |
| Injected sample volume (μl) | 20 |

Heating programme

| Parameter/conditions | Step | | | | | |
|---|---|---|---|---|---|---|
| | 1 | 2 | 3 | 4 | 5 | 6 |
| Temperature (°C) | 120 | 1200 | 2700 | 20 | 2650 | 20 |
| Ramp time (s) | 10 | 10 | 1 | 1 | 1 | 1 |
| Hold time (s) | 20 | 20 | 3 | 3 | 3 | 3 |
| Read time (s) | – | – | 0 | – | – | – |
| Internal gas flow rate (ml $min^{-1}$) | 300 | 300 | 50 | 300 | 300 | 300 |

calcium [12,13], strontium [14], magnesium [13,14], nickel [15] and some pretreatment methods for the graphite tube have already been proposed.

In this work, a mixture of nickel and zirconium as a matrix modifier, and the coating of the graphite tube with zirconium solution are proposed, because zirconium was often used for coating the graphite tube to protect against the formation of carbide during the analyses of elements that easily form carbides, and nickel was one of the commonly used matrix modifiers. It was found that this combination of a mixed matrix modifier and a zirconium-coated graphite tube resulted in excellent performance, increasing the analytical sensitivity and suppressing the memory effect for the determination of boron. With the application of this mixed matrix modifier and a zirconium-coated graphite tube, satisfactory results for the determination of boron in cobalt-based alloys by graphite furnace-atomic absorption spectrometry without the preseparation of the matrix were obtained.

## 2. Experimental

### 2.1. Apparatus

A Perkin-Elmer model 5000 atomic absorption spectrometer equipped with a model HGA 500 graphite furnace, a Data Station 10 and a PR 100 printer was used. An Eppendorf micropipette was used for injecting the sample solution into the graphite furnace.

A pyrolytic graphite tube was soaked in a 10 g $l^{-1}$ solution of zirconium for 2 days, then dried at 120 °C for 2 h and stored in a desiccator. Such a tube can be used for 200–300 firings. Alternatively, the pyrolytic graphite tube was placed in the graphite furnace, 20 μl of 10 g $l^{-1}$ zirconium solution were injected and one heat cycle of the heating programme was performed. This operation was repeated five times. The life of the tube treated using the latter method was shorter than that of the tube treated using the soaking method.

Instrumental parameters and operating conditions were optimized by means of experiments, and are shown in Table 1.

### 2.2. Reagents

All chemicals used were of analytical grade, and distilled, deionized water was used throughout.

A stock standard solution of boron (1000 mg $l^{-1}$) was prepared by dissolving boric acid in water, and was stored in a polyethylene bottle. The working standard solution (10 mg $l^{-1}$) was prepared by dilution of the stock standard solution with 0.2% nitric acid solution.

A 20 g $l^{-1}$ solution of nickel was prepared by dissolving 9.90 g of $Ni(NO_3)_2 \cdot 2H_2O$ in 100 ml of water.

A 20 g $l^{-1}$ solution of zirconium was prepared by dissolving 7.06 g of $ZrOCl_2 \cdot 8H_2O$ in 100 ml of water.

A 20 g $l^{-1}$ solution of iron was prepared by dissolving 9.68 g of $FeCl_3 \cdot 6H_2O$ and diluting to 100 ml with 0.2% nitric acid.

A 10 g $l^{-1}$ solution of chromium was prepared by dissolving 1.00 g of metallic chromium in a minimum volume of concentrated hydrochioric acid and diluting to 100 ml with water.

A 10 g $l^{-1}$ solution of cobalt was prepared by dissolving 4.94 g of $Co(NO_3)_2 \cdot 6H_2O$ and diluting to 100 ml with 0.2% nitric acid.

A 10 g $l^{-1}$ solution of tungsten was prepared by dissolving 17.95 g of $Na_2WO_4 \cdot 2H_2O$ in about 200 ml of water, 100 ml of 10% NaOH solution were added, and the solution was diluted to 1 l with water and stored in a polyethylene bottle.

A 5 g $l^{-1}$ solution of aluminium was prepared by dissolving 0.50 g of aluminium foil in 10 ml of hydrochloric acid, adding several drops of nitric acid, and diluting to 100 ml with water.

A 5 g $l^{-1}$ solution of titanium was prepared by dissolving 1.61 g of $TiCl_3$ in 20 ml of hydrochloric acid and diluting to 100 ml with water.

A 2 g $l^{-1}$ solution of manganese was prepared by dissolving 2.00 g of manganese metal in a minimum volume of (1:1) $HNO_3$ and diluting to 1 l with 0.2% $HNO_3$.

A 2 g $l^{-1}$ solution of tantalum was prepared by dissolving 3.96 g of $TaCl_5$ in 1 l of water.

A 1 g $l^{-1}$ solution of molybdenum was prepared by dissolving 1.00 g of metallic molybdenum in 25 ml of nitric acid and diluting to 1 l with water.

To construct the calibration graphs, 0, 0.5, 1, 1.5 and 2 ml of a 5 mg $l^{-1}$ working solution of boron were placed in 10 ml volumetric flasks, 1.5 ml of a 20 g $l^{-1}$ solution of nickel were added to each flask, and the solutions were diluted to the mark with water. The pH values of the final solutions were 5–7.

### 2.3. Procedure

About 30 mg of finely granulated sample was weighed exactly in a quartz beaker, 2.5–3.0 ml of aqua regia were added, and the solution was allowed to stand for at least 1 h at room temperature. The beaker was then heated in a water bath at about 70 °C to decompose the sample completely until some carbon particles only remained in the sample solution. After cooling, the sample solution was transferred to a 20 ml graduated test tube with the minimum volume of 0.2% nitric acid solution. A yellow precipitate of tungstic acid may stick on the beaker bottom, but this did not affect the analytical results. The sample solution was neutralized to pH 5–7 carefully with concentrated ammonia solution, and was diluted to the mark with water. After shaking, a 5 ml aliquot of this solution was pipetted into a 10 ml graduated test tube containing 1.5 ml of a 20 g $l^{-1}$ nickel solution, and the solution was diluted to the mark with water. After shaking well, a 20 µl aliquot of this final sample solution and 10 µl of a 2000 mg $l^{-1}$ solution of zirconium were injected into the graphite furnace, and the peak height was measured.

## 3. Results and discussion

### 3.1. Neutralization of the sample solution to be measured

After the decomposition, the sample solution must be carefully neutralized with ammonia solution to pH 5–7 to match the pH of the standard solution used for preparing the calibration graph. At this time, a pink precipitate of cobalt hydroxide may appear. The acidity of the injected sample solution affects the analytical sensitivity considerably, i.e. the sensitivity decreases with increase of acidity.

### 3.2. Effect of coating the graphite tube

The effect of coating the pyrolytic graphite tube was studied for the determination of 500 µg $l^{-1}$ of boron with 60 µg of nickel and 20 µg of zirconium as matrix modifier, using a zirconium-coated and an uncoated pyrolytic graphite tube. The results, shown in Table 2, indicated that coating with zirconium enhanced the sensitivity approximately two fold.

Table 2
Effect of coating the graphite tube on the sensitivity [a]

| Type of tube | Absorbance, $A$ |
|---|---|
| Coated | 0.090 |
| Uncoated | 0.048 |

[a] For 500 µg $l^{-1}$ boron, 60 µg of nickel/20 µg of zirconium modifier.

Table 3
Effects of nickel, zirconium and nickel–zirconium as matrix modifiers on the sensitivity [a]

| Amount of Ni (μg) | Amount of Zr (μg) | Absorbance, A | Factor |
|---|---|---|---|
| 0 | 0 | 0.015 | 1 |
| 0 | 20 | 0.024 | 1.6 |
| 60 | 0 | 0.036 | 2.4 |
| 60 | 20 | 0.090 | 6 |

[a] For 500 μg $l^{-1}$ of boron.

Table 5
Effect of different amounts of zirconium with a constant amount (60 μg) of nickel on sensitivity [a]

| Amount of Zr (μg) | Absorbance, A |
|---|---|
| 0 | 0.036 |
| 20 | 0.090 |
| 40 | 0.000 |

[a] For 500 μg $l^{-1}$ of boron.

### 3.3. Effect of matrix modifier

The bond strength of Zr–C ($134 \pm 6$ kcal $mol^{-1}$) is larger than that of B–C ($107 \pm 7$ kcal $mol^{-1}$) [16], so when boron and zirconium are atomized simultaneously, zirconium may combine predominantly with carbon in the graphite tube. This results in the retarding of the combination of boron with carbon. Hence it makes the sensitivity increase, and at the same time causes the memory effect to be suppressed. Nickel was known to be useful as a matrix modifier for many elements, and was found by us to be able to increase the ashing temperature for the analysis of steels and alloys up to 1200 °C. This is undoubtedly useful for decreasing the matrix effect.

The effect was studied of a matrix modifier composed of nickel and zirconium on the determination of 500 μg $l^{-1}$ of boron with a zirconium-coated pyrolytic graphite tube. The results obtained are shown in Tables 3, 4 and 5.

In Table 3 it is worth noticing that although both nickel and zirconium have some enhancing effects on the analytical sensitivity, the combination of these two elements shows a multiple enhancing effect, i.e. a matrix modifier composed of nickel and zirconium increases the analytical sensitivity six times, which is higher than the sum (4 times) of the enhancing factor of nickel (2.4 times) and that of zirconium (1.6 times).

In Tables 4 and 5 it is seen that nickel and zirconium both have an optimal quantity for achieving the best sensitivity, i.e. a larger or smaller quantity than the optimal one causes the sensitivity to decrease. Combination of these elements leads to the same situation, i.e. the combination of 60 μg of nickel and 20 μg of zirconium gives the highest analytical sensibility. Moreover, the above experiments also show that the memory effect decreases rapidly with increasing amount of zirconium.

Table 4
Effect of different amounts of nickel with a constant amount (20 μg) of zirconium on the sensitivity [a]

| Amount of Ni (μg) | Absorbance, A |
|---|---|
| 20 | 0.075 |
| 60 | 0.090 |
| 100 | 0.042 |
| 200 | 0.043 |

[a] For 500 μg $l^{-1}$ of boron.

### 3.4. Interferences of coexisting elements

The investigated cobalt-based alloys contain 53–57% of cobalt, 25% of chromium, 10–14% of nickel, 7–7.5% of tungsten, 0.8% of aluminium, 0.15–0.35% of zirconium, 0.25% of tantalum, 0.16% of iron, 0.15% of titanium, 0.07% of silicon, 0.03% of manganese and 0.48–0.8% of carbon, as well as 0.027–0.05% of boron.

The interference effects from the above elements except nickel, zirconium, silicon and carbon were studied with use of a matrix modifier composed of 60 μg of nickel and 20 μg of zirconium, and a zirconium-coated tube. The results are shown in Table 6. It is seen that among these coexisting elements, chromium shows the most severe interference effects relatively, but the use of a matrix modifier composed of nickel and zirconium and a zirconium-coated graphite tube could avoid the interferences from all coexisting elements including chromium, provided the amount of sample does not exceed 35 mg.

Table 6
Permissible amounts of coexisting elements [a]

| Element | Maximum content in sample (%) | Maximum amount [b] calculated ($mg\,l^{-1}$) | Permissible amount obtained ($mg\,l^{-1}$) |
|---|---|---|---|
| Co | 57 | 427 | 1375 |
| Cr | 25 | 187.5 | 225 |
| W | 7.5 | 56.25 | 375 |
| Al | 0.8 | 6 | 125 |
| Ta | 0.25 | 1.875 | 110 |
| Fe | 0.16 | 1.2 | 3000 |
| Ti | 0.15 | 1.125 | 200 |
| Mn | 0.03 | 0.225 | 250 |

[a] For 500 $\mu g\,l^{-1}$ of boron.
[b] The amount contained in 10 ml of final sample solution prepared from a 30 mg sample.

Table 7
Determination of boron in cobalt-based alloys by use of nickel–zirconium as the matrix modifier and a zirconium-coated graphite tube

| Sample number | Certified value (%) | Obtained value (%) | Difference (%) | Permissible difference [a] (%) |
|---|---|---|---|---|
| Co-68 | 0.027 | $0.026_9$ [b] | 0.0001 | 0.005 |
| Co-35 | 0.048 | $0.048_4$ [c] | 0.0004 | 0.005 |
| Co-70 | 0.049 | $0.049_0$ [b] | 0.0000 | 0.005 |
| Co-21 | 0.050 | $0.050_7$ [b] | 0.0007 | 0.005 |

[a] Based on the Chinese national standard for the determination of boron in steels and alloys, GB223.6-81, the permissible difference is 0.005% for the content of 0.026–0.050% of boron.
[b] Mean of four determinations.
[c] Mean of ten determinations.

### *3.5. Determination of boron in cobalt-based alloys*

The proposed method was applied to the determination of boron in four cobalt-based alloys. The results are shown in Table 7. It is seen that the differences between the values obtained and the certified values are all smaller than the permissible differences.

The relative standard deviation was 3.3% for 0.0480% boron ($n = 10$; the values were 0.0475, 0.0472, 0.0463, 0.0493, 0.0507, 0.0487, 0.0508, 0.0465, 0.0480 and 0.0489; with a mean of 0.0480).

A characteristic mass was 500 pg.

## References

[1] G. Mezger, E. Grallath, U. Stix and G. Tolg, Fresenius' Z. Anal. Chem., 317 (1984) 765.
[2] V.K. Pin, Anal. Chim. Acta, 159 (1984) 387.
[3] J.N. Walsh, Analyst, 110 (1985) 959.
[4] K. Fujimoto, T. Okano, Y. Matumura and S. Harima, Bunseki Kagaku, 35 (1986) 651.
[5] Y. Takahashi, Bunseki Kagaku, 36 (1987) 693.
[6] G. Bauer, I. Rehana, W. Wegscheider and H.M. Ortner, Spectrochim. Acta, part B, 43 (1988) 971.
[7] G. Zeibig, Mikrochim. Acta, 1989III, 389.
[8] I. Hlavacek, Mikrochim. Acta, 1989III, 309.
[9] Hu Bin, Fresenius' Z. Anal. Chem., 340 (1991) 435.
[10] J. Ciba and B. Smolec, Fresenius' Z. Anal. Chem., 348 (1994) 215.
[11] T. Miyatani, H. Suzuki and O. Yosimoto, Bunseki Kagaku, 43 (1994) 475.
[12] Operational Manual, Perkin-Elmer model HGA-500.
[13] Yongqing Jiang, Jinyu Yao and Benli Huang, Fenxi Huaxue, 17 (1989) 456.
[14] Yongqing Jiang, Jinyu Yao and Benli Huang, Fenxi Shiyanshi, 7 (1988) 21.
[15] M. Luguera, Y. Madrid and C. Camera, J. Anal. At. Spectrom., 6 (1991) 669.
[16] R.C. Weast (Ed.), CRC Handbook of Chemistry and Physics, 70th edn., CRC Press Inc., Boca Raton, FL, 1990, F197–198.

ELSEVIER

Talanta 42 (1995) 1425–1432

Talanta

# Colorimetric determination of macrolide antibiotics using ferric ion

Patricia A. Gallagher, Neil D. Danielson *

*Department of Chemistry, Miami University, Oxford, OH 45056, USA*

Received 8 December 1994; revised 13 March 1995; accepted 14 March 1995

**Abstract**

Macrolide antibiotics such as erythromycin, oleandomycin, spiromycin, and tylosin are found to react with $Fe^{3+}$ in the presence of an acetic acid–sulfuric acid mixture to form a colored product having a useful absorption band at 592 nm. Troleandomycin forms only a weakly colored product upon reaction. The molar absorptivity is about 2900 l mol$^{-1}$ cm$^{-1}$ for erythromycin and the detection limit is 5 μg ml$^{-1}$. This colorimetric method permits the analysis of fermentation broths containing either erythromycin or tylosin without a separation step.

## 1. Introduction

Macrolide antibiotics, all composed of either a 14-membered or a 16-membered oxygenated ring with several sugars attached, have proved to be effective antibacterial agents for many years. The structures of five common macrolide antibiotics are shown in Fig. 1. Erythromycin is certainly the most well-known compound of this class; however troleandomycin is also available as a pharmaceutical product and tylosin is used widely by veterinarians [1].

At least six colorimetric methods have previously been developed for several of these macrolide antibiotics. Hydrolysis of the sugar groups of erythromycin [2] or oleandomycin [3] in concentrated sulfuric acid produced a yellow product measurable at 470 nm. This reaction has recently been extended to the other three macrolide antibiotics shown in Fig. 1 with a comparison of linearity and detection limits [1]. Tetrazolium blue can react generally with reducing agents such as erythromycin to form a dark blue solution [4]. Complex formation with Bromcresol Purple has been applied to the colorimetric determination of erythromycin [5]. A variety of other dyes which undergo ion pair formation with erythromycin in chlorinated solvents can be utilized [6]. Erythromycin and tylosin have been determined at 842 nm using tetracyanoquinodimethane [7]. A colorimetric method at 532 nm for oleandomycin using diazotized sulphanilic acid is known [8]. However, all of these methods are nonspecific or require a nonaqueous solvent and would be difficult to use for the determination of macrolide antibiotics in aqueous complicated matrices such as fermentation broths without a prior separation step. The reaction of *cis*-aconitic anhydride with a tertiary amine such as a macrolide antibiotic permits the formation of a colored product detectable at 525 nm. Although this reaction has been applied to the determination of tylosin in fermentation broths, extraction of the broth with sufficient isopropyl acetate to give a residue that could be reconstituted to attain a 1 mM concentration level is required [9].

We report here a colorimetric method for macrolide antibiotics which involves the

* Corresponding author.


*SSDI* 0039-9140(95)01587-6

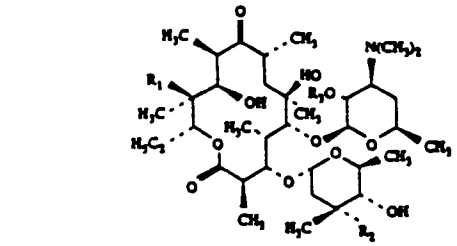

ERYTHROMYCIN A

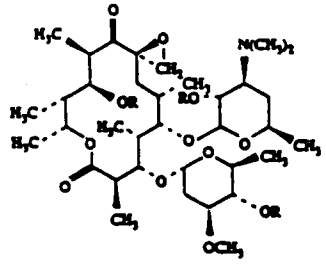

OLEANDOMYCIN R = H
TROLEANDOMYCIN R = —COCH$_3$

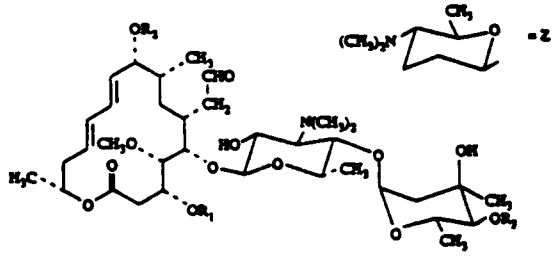

SPIRAMYCIN

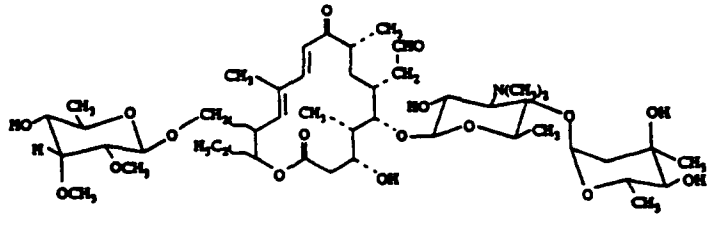

TYLOSIN

Fig. 1. Structures of macrolide antibiotics.

macrolide ring and not the sugar or tertiary nitrogen moiety. After dehydration of the macrolide antibiotic in concentrated acetic acid, the addition of $Fe^{3+}$ will generate a coloured product measurable at 592 nm. The determination of erythromycin or tylosin in fermentation broths is possible without sample pretreatment.

## 2. Experimental

### 2.1. Chemicals

The macrolide antibiotics (Fig. 1) were purchased from Sigma Chemical Co. (St. Louis, MO, USA). The erythromycin ethylsuccinate and sulfisoxazole acetyl oral suspension was

obtained from Abbott Laboratories (North Chicago, IL, USA). There were two different fermentation broths used for this research. One was a dehydrated Antibiotic Medium 3 purchased from Difco Laboratories (Detroit, MI, USA) and the second, donated by Eli Lilly (Indianapolis, IN, USA) was a dehydrated fermentation broth used for tylosin production. The Difco product was composed of beef extract, yeast extract, peptone, dextrose, sodium chloride, dipotassium phosphate, and monopotassium phosphate. The Eli Lilly sample was made up of yellow corn meal, fish meal, corn gluten meal, sodium chloride, ammonium phosphate, calcium carbonate, crude soybean oil, and cane molasses. The ferric chloride was purchased from MCB Manufacturing Chemists, Inc. (Cincinnati, OH, USA). The sulfuric acid and acetic acid were both purchased from Fisher Scientific (Cincinnati, OH, USA) and the triply distilled water obtained from a Barnstead Nanopure distillation unit (Sybron/Barnstead, Dubuque, IA, USA).

### 2.2. Equipment

The spectrophotometry was conducted either on a Varian (Humboldt, CA, USA) DMS 90 UV-ViS spectrophotometer or a Hewlett-Packard (Palo Alto, CA, USA) model 8452A diode-array instrument. The sample compartment was heated to 50°C using a Fisher Scientific (Cincinnati, OH, USA) model 900 isotemp refrigerated circulator water bath.

### 2.3. Procedure

A 500 $\mu g\ ml^{-1}$ erythromycin stock solution prepared in glacial acetic acid was allowed to react at 45°C for at least 30 min (often 2 h) before use. A ferric ion stock solution was prepared by weighing 0.080 g of ferric chloride, pipeting 2 ml concentrated sulfuric acid and 2 ml of triply distilled water into the 100 ml volumetric flask, and diluting to the mark with concentrated glacial acetic acid. Erythromycin–ferric ion standards generally ranging from 10–250 $ug\ ml^{-1}$ were prepared by pipeting 5 ml of ferric ion stock solution and the appropriate amount of erythromycin stock solution before dilution to a 10 ml volume with glacial acetic acid. The fermentation broths were prepared by adding either 17.5 g of dehydrated Antibiotic Medium 3 or the entire Eli Lilly sample to a 1000 ml volumetric flask and filling to the mark with triply distilled water. A 5 ml aliquot of the spiked fermentation broth sample was placed in a 50 ml volumetric flask and filled to the mark with concentrated glacial acetic acid. The blank was prepared in exactly the same way as the sample except that the fermentation broth was not spiked with the macrolide antibiotic. All fermentation samples and blanks were heated in the 45°C water bath. The standards for this part were prepared exactly the same as for the sample except triply distilled water was used instead of the fermentation broth. The pharmaceutical sample was prepared by measuring out in a volumetric test tube 1 ml of the erythromycin ethylsuccinate–sulfisoxazole acetyl oral suspension and quantitatively transfering it to a 100 ml volumetric flask before filling to the mark with concentrated glacial acetic acid. This was heated in the 45°C water bath. The above procedure for preparing the erythromycin–ferric ion standards was carried out for all the samples. All standards, samples and blanks, after mixing with ferric ion, were allowed to react in the heated (50°C) curvette holder for 15 min before the absorbance measurement was taken.

## 3. Results and discussion

### 3.1. Proposed reaction mechanism

Previously, it had been proposed [10] that the reaction of cholesterol in an acetic acid–sulfuric acid mixture with $Fe^{3+}$ will lead to the formation of trienylic and tetraenylic cations detectable at about 480 nm and 560 nm, respectively (Fig. 2). The wavelength maxima are dependent on the sulfuric acid concentration in the $Fe^{3+}$ stock solution. It is also known [11] that erythromycin in the presence of concentrated acetic acid can undergo dehydration, forming the 8,9-anhydroerythromycin-6,9-hemiketal (Fig. 3). The hydroxy group beta to the double bond in this hemiketal product is a remarkably similar key functional group to that in cholesterol. Using LC–MS, we confirmed the formation of this hemiketal product as evidenced by the disappearance of the $M^+$,$MH^+$ ion peak pair at $M/z = 734$, 735 and the formation of the ion peak at $M/z = 716$. No peak for the diene carbonium ion was evident. A peak at $M/z = 558$ present in both the erythromycin and hemiketal spectra represents the fragment ion of erythromycin minus a

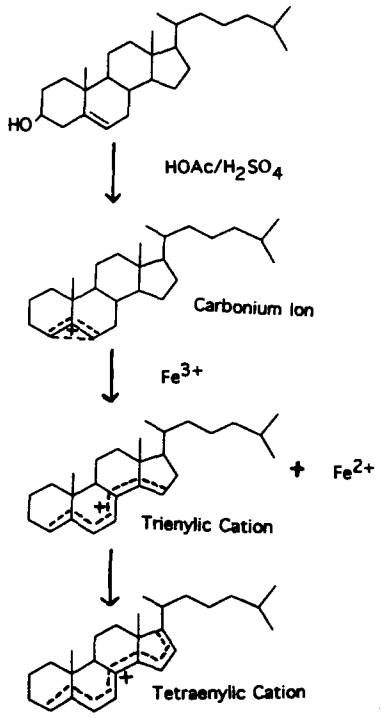


Fig. 2. Proposed mechanism of the cholesterol–$Fe^{3+}$ reaction (from Ref. [10]).

sugar group. An absorption spectrum of the hemiketal product after reaction with $Fe^{3+}$ using the optimum conditions shows two strong peaks at 484 and 592 nm (Fig. 4). A spectrum of the cholesterol reaction run using an 80% acetic acid–20% sulfuric acid $Fe^{3+}$ solution showed three peaks with wavelength maxima at 620, 453, and 412 nm. A spectrum of the hemiketal product run using the same 80% acetic acid–20% sulfuric acid $Fe^{3+}$ solution also showed three peaks with wavelength maxima of 596, 486, and 412 nm. A glucose stock solution gave no reaction with $Fe^{3+}$, providing furthur evidence that the likely source of the colored product was from the macrolide ring and not the sugar groups attached to the macrolide ring. Although LC–MS could not provide a clear mass spectrum for the formation of trienylic or tetraenylic cations for the $Fe^{3+}$–erthyromycin reaction, we feel this is the likely type of colored product.

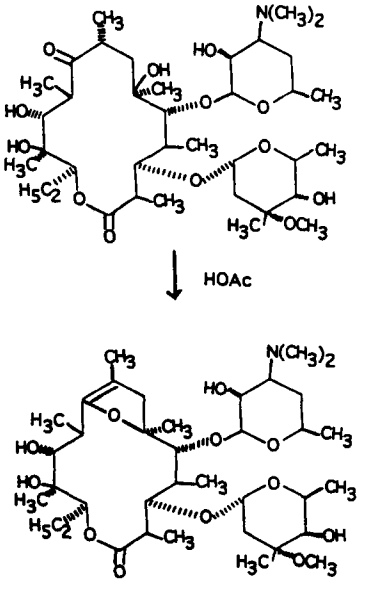


Fig. 3. Acetic acid degradation of erythromycin A to form the hemiketal product.

### 3.2. Optimization of colorimetric response

A time study of the dehydration reaction in concentrated acetic acid at 45°C for all five compounds shown in Fig. 1 was carried out (Fig. 5). All the macrolide antibiotics except troleandomycin seemed to undergo significant dehydration to form a product that would react with $Fe^{3+}$ ion. Because troleandomycin has an ester group instead of the hydroxyl group as in oleandomycin, this difference in reactivity is not surprising. Both spiramycin and tylosin already have some conjugation in their structures which is apparently expanded after reaction with $Fe^{3+}$. The spectra of the $Fe^{3+}$–antibiotic products for oleandomycin, spiromycin, and tylosin were similar to that of erythromycin. The following optimum heating times for the macrolide antibiotic stock solutions were 120 min for erythromycin, 90 min for oleanomycin, 60 min for spiromycin and 0 min for tylosin. Although the optimum heating times were quite varied, in general a reaction time of only 30 min would be sufficient for good dehydration to the $Fe^{3+}$ reactive product.

The effect of water in the erythromycin stock solution on the colorimetric reaction was studied (Fig. 6). It appears that 20% water can lower the absorbance to zero; only 5% water in the acetic acid solution caused a 50% decrease in the absorbance of the $Fe^{3+}$–hemiketal product. Therefore, it was decided that for best detectability the macrolide antibiotic stock solution in acetic acid should be a prepared if possible from a solid instead of an aqueous sample.

The proper amount of sulfuric acid needed to be added to the ferric chloride stock solution prepared in glacial acetic acid to give maxi-

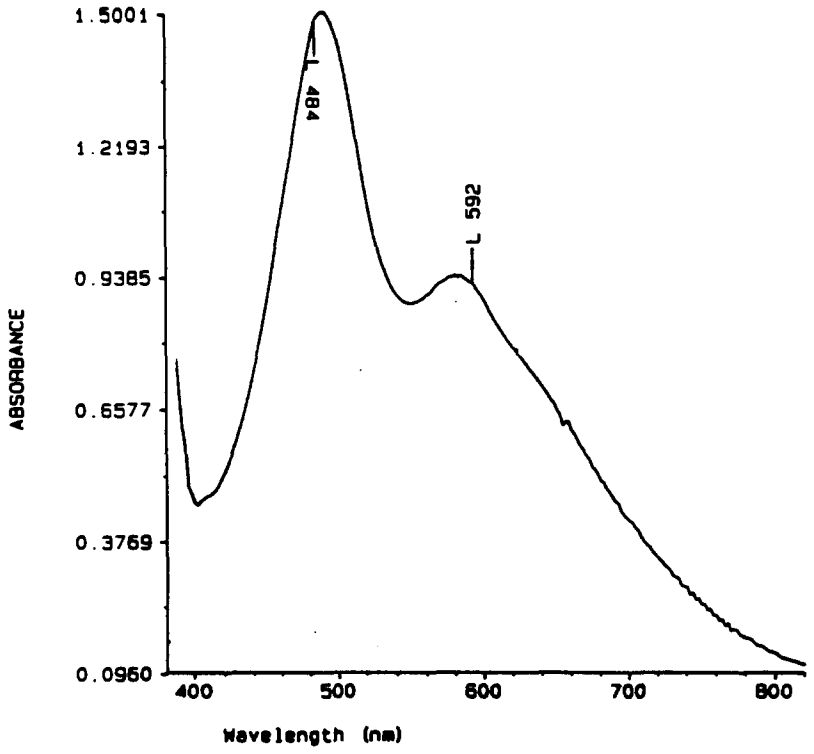


Fig. 4. Absorbance spectrum of the $Fe^{3+}$–hemiketal reaction product of erythromycin (250 μg $ml^{-1}$).

mum absorbance was determined. Ferric chloride solutions containing 1, 2 and 4 ml of sulfuric acid were prepared and time studies were completed (Fig. 7). In comparison, the cholesterol–$Fe^{3+}$ reaction would not work using such low concentrations of sulfuric acid. The absorbance profiles for the 2 and 4 ml solutions were almost exactly the same. There were some reproducibility problems; the inconsistency in the results were believed to be caused by the sulfuric acid absorbing water. To alleviate this problem, small amounts of water were added to the ferric chloride stock solution (Table 1). Therefore, it was determined that 2 ml of water as well as 2 ml of sulfuric acid should be added to 100 ml of ferric chloride solution to obtain the optimum absorbance and reproducibility.

At room temperature, the $Fe^{3+}$–anhydrohemiketal macrolide reaction rate is very slow; therefore, the solution was heated at 40, 50 and 60°C (Fig. 8). At 50°C, the data obtained produced a reproducible plateau from approximately 10 to 30 min. Some loss in signal was observed after 10 min using a 60°C reaction temperature. Therefore reaction con-

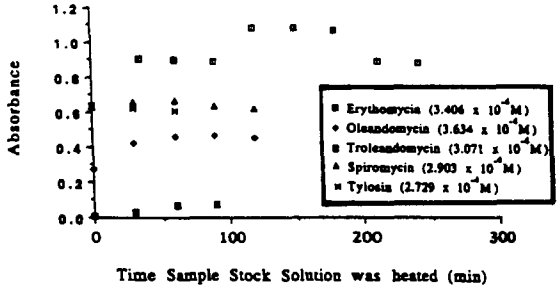


Fig. 5. Reaction of macrolide antibiotics with acetic acid at 45°C as a function of time. The reaction was followed at 592 nm using $Fe^{3+}$.

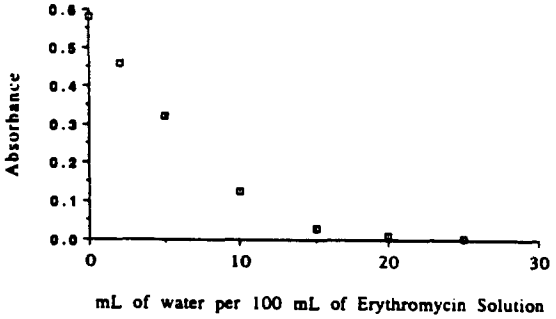


Fig. 6. Effect of water in the erythromycin stock solution on the absorbance. The reaction was followed at 592 nm using $Fe^{3+}$.

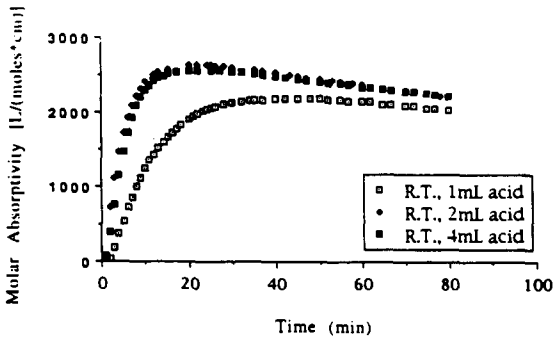


Fig. 7. Optimization of the molar absorptivity as a function of sulfuric acid volume in the $Fe^{3+}$–acetic acid solution. The reaction was followed at room temperature (RT) at 592 nm using $Fe^{3+}$.

ditions of 15 min at 50°C were used for all analytical work.

A detailed linearity and reproducibility study of this colorimetric reaction was completed (Table 2). It was determined that the detection limit was 5 ppm erythromycin at the 592 nm wavelength. At 10 ppm the average absorbance was 0.025 with a relative standard deviation (RSD) of 16%; at 100 ppm the average absorbance was 0.369 with a RSD of 1.7%; at 250 ppm the average absorbance was 0.938 with a RSD of 1%. The RSD of the slope at 592 nm was 1%. The detection limit was determined to be 2.5 ppm of erythromycin at a wavelength of 484 nm; however, the linearity at 484 nm was not as good as at the 592 nm. The RSD of the slope at 484 nm was 2.5%.

### 3.3. Real sample analysis

Because of the better selectivity at 592 nm, all real samples were analyzed at this wavelength despite the sacrifice in sensitivity. The real life samples chosen to be tested were spiked fermentation broths and an erythromycin oral suspension (Table 3). The determination of erythromycin in the oral suspension, a white sample matrix containing suspended solids, gave mixed results. It is believed that the error fluctuation was due to the difficulty in measuring the 1 ml aliquot of the oral suspension or the inhomogeneity of the sample. More work is necessary to decide if pharmaceutical samples can be assayed in this way. The fermentation broths represented a more challenging matrix due to their dark brown color as well as suspended solids. The assay of fermentation broths is commercially important in order to determine which microorganisms are effective in producing antibiotics in high yield. The expected range for macrolide antibiotics in fermentation broths is from about 1 to 10 ppt (mg $ml^{-1}$). Therefore,

Table 1
Effect of water in the ferric ion solution on the absorbance of the $Fe^{3+}$–erythromycin product at 592 nm

| Amount of water added to 100ml of ferric chloride solution (ml) | Average absorbance ($n = 3$) | Standard deviation | Relative standard deviation |
|---|---|---|---|
| 5 | 0.317 | 0.00289 | 0.00912 |
| 2 | 1.141 | 0.00785 | 0.00688 |
| 1 | 0.741 | 0.0197 | 0.0265 |
| 0.5 | 0.750 | 0.0497 | 0.0663 |

Table 2
Spectrophotometric linearity of the erythromycin–ferric ion complex

| Wavelength (nm) | Data points | Linear range (mg $l^{-1}$) | Least squares [a] | Correlation coefficient |
|---|---|---|---|---|
| 592 | 29 | 5–250 | $m = 3.9 \times 10^{-3} \pm 3.9 \times 10^{-5}$<br>$b = -9.2 \times 10^{-3} \pm 5.1 \times 10^{-3}$ | 0.9997 |
| 484 | 16 | 2.5–250 | $m = 5.92 \times 10^{-3} \pm 1.5 \times 10^{-4}$<br>$b = 2.90 \times 10^{-2} \pm 1.8 \pm 10^{-2}$ | 0.9979 |

[a] Equations $Y = mx + b$.

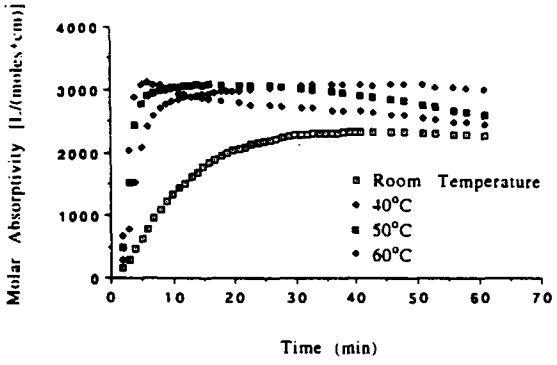


Fig. 8. Optimization of the molar absorptivity as a function of temperature for the $Fe^{3+}$–hemiketal reaction.

three samples of Difco broth were spiked with erythromycin from 0.8–5 ppt. The recoveries at 2 and 5 ppt averaged 103% while that at 0.8 ppt was 94%. The lower recovery at 0.8 ppt may be because the actual erythromycin determined was at the low end of the linear range, 25 μg $ml^{-1}$. The recovery of tylosin at 10 ppt from the Eli Lilly broth was good. The results from these spiked samples imply that this technique could easily and accurately determine the macrolide antibiotic concentration in actual incubating fermentation broths.

## 4. Conclusion

It was determined that erythromycin will react with ferric ion in the presence of an acetic acid–sulfuric acid mixture to form a colored product likely due to a tetraenylic cation in the macrolide ring. The erythromycin molar absorptivities are about 2900 l $mol^{-1}$ $cm^{-1}$ at 592 nm and 4400 l $mol^{-1}$ $cm^{-1}$ at 484 nm. This colorimetric reaction is general for similar macrolide antibiotics except troleandomycin. Because this method requires two 15–30 min heated reaction steps, automation by flow injection would likely be difficult. Although dilution of aqueous samples in concentrated acetic acid is required, this simple inexpensive colorimetric method can be used on fermentation broth samples with an average recovery of 99%.

## Acknowledgments

Summer support was provided by an NSF Undergraduate Research grant. We thank A. Tietz of Eli Lily for on of the fermentation broths and T. Pekol for assistance with the LC–MS study.

Table 3
Percent recovery of erythromycin and tylosin from various sample matrices

| | Concentration of antibiotic | | Recovery |
|---|---|---|---|
| Sample | Added | Found | (%) |
| Difco fermentation broth | Erythromycin | | |
| # 1 | 2.01 mg $ml^{-1}$ | 2.07 mg $ml^{-1}$ | 103 |
| # 2 | 2.01 mg $ml^{-1}$ | 2.19 mg $ml^{-1}$ | 108 |
| # 3 | 5.01 mg $ml^{-1}$ | 5.12 mg $ml^{-1}$ | 102 |
| # 4 | 5.01 mg $ml^{-1}$ | 4.96 mg $ml^{-1}$ | 99.0 |
| # 5 | 810 μg $ml^{-1}$ | 720 μg $ml^{-1}$ | 88.9 |
| # 6 | 810 μg $ml^{-1}$ | 820 μg $ml^{-1}$ | 101 |
| # 7 | 810 μg $ml^{-1}$ | 760 μg $ml^{-1}$ | 93.8 |
| # 8 | 810 μg $ml^{-1}$ | 760 μg $ml^{-1}$ | 93.8 |
| Eli Lily fermentation broth | Tylosin | | |
| # 1 | 10.0 mg $ml^{-1}$ | 9.96 mg $ml^{-1}$ | 99.6 |
| Oral suspension | Erythromycin | | |
| # 1 | 400 μg $ml^{-1}$ | 424 μg $ml^{-1}$ | 106 |
| # 2 | 400 μg $ml^{-1}$ | 417 μg $ml^{-1}$ | 104 |
| # 3 | 400 μg $ml^{-1}$ | 329 μg $ml^{-1}$ | 82.3 |
| # 4 | 400 μg $ml^{-1}$ | 299 μg $ml^{-1}$ | 74.8 |

## References

[1] N.D. Danielson, J.A. Holeman, D.C. Bristol and D.H. Kirzner, J. Pharm. Biomed. Anal., 11 (1993) 121.
[2] J.H. Ford, G.C. Prescott, J.W. Hinman and E.L. Caron, Anal. Chem., 25 (1953) 1195.
[3] V.B. Korchangin, K.I. Surkove, N.V. Stepushkina and N.A. Vokulenko, Antibiotiki, 7 (1962) 962.
[4] P.E. Manni and J.E. Sinesheimer, Anal. Chem., 33 (1961) 1900.
[5] D. Dabrowska, A. Regosz, L. Tamkun and E. Kaminska, Sci. Pharm., 52 (1984) 220.
[6] D. Dabrowska, A. Regosz, R. Piekos, M. Mierzwa and B. Paruch, Microchem. J., 41 (1990) 210.
[7] A.S. Issa, M.A. Abdel Salam, H.M.G. Daabees and N.S. Boni, Alexandria J. Pharm. Sci., 4 (1990) 7.
[8] M. Tsuneko, J. Pharm. Soc. Jpn., 79 (1959) 29.
[9] F.L. Neely, Anal. Chim. Acta, 281 (1993) 243.
[10] R.W. Burke, B.I. Diamondstone, R.A. Velpoldi and O. Menis, Clin. Chem., 20 (1974) 794.
[11] P. Kurath, P.H. Jones, R.S. Egan and T.J. Perun, Experientia, 27 (1970) 362.

ELSEVIER

Talanta 42 (1995) 1433–1445

Talanta

# Potentiometric characterization of weak acids by multiple sample addition
# II. The effect of chemical interferences and the practical performance of linearization methods

Carlo Maccà *, Arben Merkoci [1], G. Giorgio Bombi

*Department of Inorganic and Analytical Chemistry, University of Padua, Via Marzolo 1, I-35131 Padova, Italy*

Received 28 October 1994; revised 1 March 1995; accepted 1 March 1995

**Abstract**

Potentiometric multiple addition of a sample containing a pure weak acid to a solution of supporting electrolyte has been previously shown [C. Maccà and A. Merkoci, Talanta, 41 (1994) 2033] to be formally suitable for the determination of the dissociation constant and concentration of the sample acid. Linear equations have been developed for the treatment of experimental data to yield, simultaneously or separately, the chemical parameters of the acid solution. These equations are now tested on real samples together with analogous equations for titrations, and the results are compared with those obtained with rigorous statistical methods. For the determination of the acidity constant with samples of known concentration, multiple samples addition is comparable with titration. When the sample concentration is unknown and must be determined simultaneously to the acidity constant, the results obtained by linearized multiple sample addition can be seriously affected by impurities present, even at low level, either in the sample or in the supporting solution. Linear equations accounting for the effects of basic or acidic impurities in the sample or in the supporting solution are developed.

Sample addition is confirmed to be a useful complement to pH-metric titration for the determination of acidity constants of moderately weak acids by non-linear regression; linearization of data is a convenient technique for screening purposes and a powerful means of detecting and correcting some common pitfalls, interferences and contaminations, whose effects are enhanced in linearized sample addition.

## 1. Introduction

It has been shown [1] that the multiple sample addition technique is suitable for characterization of weak acid in pure solution. The basic equation relating the experimental variables (added sample volume and hydronium ion concentration) to the analytical parameters of the sample solution, i.e. the acidity constant and the sample concentration, has been rearranged in different forms for the convenience of applications. For this purpose, pairs of auxiliary variables have been defined, by which the experimental data are transformed to fit linear equations. Thereby, both the analytical parameters of the sample (Table 1 of Ref. [1], Eqs. (8)–(13)), or one of them if the other is known (Eqs. (6) and (2) of Ref. [1]) can be calculated from the parameters of a linear equation or of the corresponding plot. The effect of systematic and random errors of measurement has been discussed, in order to evaluate the intrinsic performance of the method in its different applications, with particular concern for the determination of the acidity constant [1].

* Corresponding author.

[1] Permanent address: Department of Analytical Chemistry, University of Tirana, Albania.


*SSDI* 0039-9140(95)01592-2

In this paper, the results of some of the experimental tests to which the method has been subjected for validation are reported and interpreted by considering the different causes of error that can occur in practice, particularly those of chemical origin.

Solutes with acidic or basic properties other than the sample acid cause the hydronium ion concentration in the measured solution to be different from that of the pure sample acid at the given concentration. As a consequence, the plots of the auxiliary variables of the equations for pure acid (Eqs. (2), (6), (8)–(13) of Ref. [1]) are expected to deviate from the theoretical behaviour to some extent, causing errors in the analytical parameters thereby calculated. Interfering substances are here assumed to be present only at the level of impurities. Equations suitable for forecasting the deviations due to impurities and, at least in principle, for evaluating the amount of impurities and to correct for their presence are developed in the Theory section. The theoretical deviations from linear behaviour caused by impurities are examined in the Discussion section.

The experimental results of linearized sample addition are compared with those of titration and are also checked by a least-squares treatment of the original variables.

## 2. Experimental

### 2.1. Apparatus

The measured solution, contained in a jacketed cell, was flushed with purified nitrogen and stirred with a PTFE-coated magnetic bar and a magnetic stirrer. Motor-driven microburettes (MicroBUR 2030 Crison, Barcelona) equipped with 1, 2.5 or 10 ml Hamilton syringes (0.4, 1 and 4 µl resolution, respectively; standard deviation better than resolution) were used for the additions of standard, sample and titrant solutions. The additions were managed with a potentiometric titrator MicroTT 2050 Crison. The e.m.f. of a combination glass electrode with encapsulated Ag/AgCl reference electrode in 3 M KCl and sleeve junction (Ingold type 405.60.88.E) was measured with 0.1 mV resolution (instrumental standard deviation better than resoluton) during the additions. For each part of an experiment, a data file was created by the titrator on a PC.

### 2.2. Reagents

Analytical or higher grade reagents (e.g. recrystallized NaCl or Merck Suprapur KCl, as the supporting electrolyte) were dissolved in freshly prepared ultrapure water (MilliQ-Plus grade). HCl solutions for electrode calibration were prepared from primary standard acid obtained by azeotropic distillation of an analytical reagent grade product.

### 2.3. Procedure

A typical experiment began with electrode calibration by multiple addition ($5 \times 8.0$ µl + $24 \times 40.0$ µl) of 0.1 M primary standard hydrochloric acid to 25 ml of 0.1 M supporting electrolyte (sodium of potassium chloride or nitrate). The smaller initial additions allowed the presence of basic impurities in the supporting solution to be detected (see Calculations section). Calibration was completed by titration through multiple constant addition ($20 \times 100.0$ µl) of 0.1 M sodium hydroxide. After careful washing, the cell was again filled with supporting electrolyte and multiple addition (typically, 20 additions of 50 or 125 µl) of the sample acid at suitable concentration (1–0.003 M) was performed; thereafter, the acid was titrated by multiple constant addition of sodium hydroxide. After three to five complete experiments of sample addition and titration, a second calibration by strong acid addition and titration with sodium hydroxide was performed.

### 2.2. Calculations

Calibration by multiple (hydrochloric) acid addition at practically constant ionic strength allowed the hydronium ion concentration $[H^+]$ to be measured in the pH range of interest. The data of hydrochloric acid multiple addition were beforehand linearized by least-squares fitting with the Gran function [2] using the theoretical electrode slope (Nernst factor); a statistically significant, although small, positive value of volume at the intercept was taken as an indication of the presence of basic impurity in the supporting electrolyte solution. The same data, after correction for impurity, were used for calculation of the electrode calibration parameters.

The sample addition data were linearized using the linear functions introduced in Ref. [1]

and in the following Theory section. The data of the subsequent titration were used to obtain reference values of the sample analytical parameters, as described in the Results section. All the experimental data were also treated with the generalized (non-linear) least-squares program based on a modification of the pit-mapping method [3].

## 3. Theory

Impurities can be present either in the original sample or in the supporting solution (water + supporting electrolyte) to which the sample is added. In the first case, the concentration ratio (interfering substance)/(analyte) in the measured solution is constant throughout each experiment; in the second case, this ratio decreases with the progress of addition. Impurities whose presence is hardly avoidable are volatile substances easily dissolved or absorbed by chemicals from the laboratory atmosphere, such as the acid carbon dioxide or the base ammonia. Reasonably, under the conditions of measurement, all the bases present at the impurity level behave as strong bases. Indeed, a weak base originally present in the sample as a very small fraction of the acid reacts completely with it, notwithstanding the dilution undergone by both reactants in the measured solution. When present in the supporting solution, weak bases can be assumed to react completely if their concentration ratio to the acid added with the sample is small after the first addition. The interference by weak acids present at the level of impurities is moderate, particularly for acids weaker than the analyte. Therefore, only strongly basic impurities and, to a lesser detail, strongly acid contaminants will be considered in the following.

### 3.1. Basic impurities in the sample

A sample containing a weak acid contaminated by a strong base can be treated as being composed either of the acid with a strong base or of the acid with its salt. The second assumption yields slightly simpler equations which, moreover, are more suitable for comparison between the experimental results of multiple addition and of titration. Therefore, it is assumed here that the sample contains the weak acid HA at concentration $C$ and the conjugated weak base, i.e. the salt NaA, at concentration $C_i$. The presence of the base modifies the mass balances from which the basic equation relating the measured variable (the hydronium ion concentration $[H^+]$) with the controlled variable (the added volume $V$) is obtained (see Eq. (2) of Ref. [1]). The relevant mass balances express the total amount of the solute system (acid + salt) after each sample addition:

$$(C + C_i)V = (V^\circ + V)([HA] + [A^-]) \quad (1)$$

the amount of counter-ion of the salt:

$$C_i V = (V^\circ + V)[Na^+] \quad (2)$$

and the electroneutrality condition:

$$[H^+] + [Na^+] = [OH^-] + [A^-] \quad (3)$$

Substitution for the equilibrium concentrations in Eq. (1) using Eqs. (2) and (3) together with the expression of the acid dissociation constant, $K_a = [H^+][A^-]/[HA]$, and the expression for $K_w$ yields

$$\begin{aligned} CV &= (V^\circ + V)([H^+] - K_w/[H^+])(1 + [H^+]/K_a) \\ &\quad + C_i V[H^+]/K_a \\ &= H(1 + [H^+]/K_a) + C_i V[H^+]/K_a \end{aligned} \quad (4)$$

where [1]

$$H = (V^\circ + V)([H^+] - K_w/[H^+]) \quad (5)$$

(in acidic solution, $H \approx (V^\circ + V)[H^+]$).

Eq. (4) must be compared with the 'rigorous Gran function' $F$ for the determination of $C$ by addition of pure weak acid sample (see Eqs. (2) and (4) of Ref. [1]):

$$F = H(1 + [H^+]/K_a) = CV \quad (6)$$

The function $F$ can be calculated from the experimental data when the acidity constant is known; the concentration of acid in the sample, $C$, is obtained as the slope of the linear plot $F$ against $V$ [1]. However, when $C_i$ has a non-zero value, the value of $F$ calculated as above corresponds to

$$F = CV - C_i V[H^+]/K_a \quad (7)$$

instead of $CV$; therefore, deviation of the plot of $F$ against $V$ from linearity and of its (mean) slope from $C$ must be expected.

Eq. (4) can be rearranged to give the equation

$$H(1 + [H^+]/K_a)/V = C - C_i[H^+]/K_a \quad (8)$$

which is transformed into a linear equation, $Y = a + bX$, by introducing the auxiliary variables $X = [H^+]/K_a$ and $Y = F/V = H(1 + [H^+]/$

Table 1
Linear equations for the determination of the acidity constant $K_a$ and of the content of basic impurities $C_i$ of a weak monoprotic acid by multiple sample addition ($H$, Eq. 5)

| $X$ | $Y$ | $C_i$ | $K_a$ | Equation $Y = a + bX$ | |
|---|---|---|---|---|---|
| $\frac{CV-H}{V[H^+]}$ | $\frac{H}{V}$ | $-a$ | $b$ | $\frac{H}{V} = -C_i + K_a\frac{CV-H}{V[H^+]}$ | (9) |
| $\frac{V}{H}$ | $\frac{CV-H}{H[H^+]}$ | $\frac{b}{a}$ | $\frac{1}{a}$ | $\frac{CV-H}{H[H^+]} = \frac{1}{K_a} + \frac{C_i}{K_a}\frac{V}{H}$ | (10) |
| $\frac{V[H^+]}{CV-H}$ | $\frac{H[H^+]}{CV-H}$ | $-b$ | $a$ | $\frac{H[H^+]}{CV-H} = K_a - C_i\frac{V[H^+]}{CV-H}$ | (11) |

$K_a)/V$, which can be calculated from the experimental data, and the values of the known parameters $V°$, $K_a$ and $K_w$. Accordingly, $C$ can be obtained together with $C_i$ from the parameters of the transformed Eq. (8) from the intercept $Y(X=0)$ and from the slope, respectively, by least-squares or graphical interpolation. However, it must be expected that the results are strongly affected by the imprecision of $[H^+]$ and by the inaccuracy of $K_a$ [1].

The determination of $K_a$ using a sample with known $C$ is a more suitable application of the sample addition method [1]. For this purpose, Eq. (4) is rearranged to give Eqs. (9)–(11) of Table 1; $K_a$ is obtained together with $C_i$ by calculating the parameters of a linear equation using any pair of auxiliary variables $X$ and $Y$ defined in the Table.

Other possible cases can be solved, at least in principle, with different linear transformations of Eq. (4). When both $C$ and $C_i$ are known, according to

$$[H^+](H + C_iV) = K_a(CV - H) \quad (12)$$

the acidity constant can be obtained from the slope of a straight line with the auxiliary variables $X = CV - H$ and $Y = [H^+](H + C_iV)$. When only $C_i$ is known, equations of forms corresponding to those of the Eqs. (8)–(13) of Ref. [1] are obtained. For brevity, only the Hofstee-type [1,4,5] equation (Eq. 13), giving $C$ as the intercept and $K_a$ as the negative reciprocal of the slope, is reported here:

$$H/V = C - [H^+](H + C_iV)/VK_a \quad (13)$$

Eqs. (12) and (13) (and the other analogous equations) are of little interest for the present purpose; however, they could be useful for the determination of the acidity constant by multiple addition of a buffer with known composition or with known content of base, respectively.

When both $C$ and $K_a$ are unknown and evidence is found of a finite but unknown concentration of basic impurity in the sample, for the determination of all the three parameters $C$, $C_i$ and $K_a$ it is necessary to resort to a numerical optimization method, employing either Eq. (4) or directly the system of simultaneous equations used for its derivation.

In practice, impurities of the sample undergo a large dilution in the measured solution and, therefore, are possibly of lesser concern than impurities present in the supporting solution, at least when their original concentration level is similar.

### 3.2. Basic impurities in the supporting solution

Basic impurities present in the supporting solution before the beginning of additions are most probably weak bases, such as ammonia dissolved in the water from the atmosphere or carbonate originating from the supporting electrolyte. It is reasonably assumed that the initial concentration, $C_j$, of any basic impurity in the measured solution is small enough for it to behave like a strong base and react quantitatively with the sample weak acid, this being present in excess after the first addition. By substituting the equilibrium concentration in the relevant mass balance of the sample acid:

$$CV = (V° + V)([HA] + [A^-]) \quad (14)$$

and using the mass balance of the contaminant, for instance ammonia,

$$C_jV° = (V° + V)([NH_3] + [NH_4^+]) \approx (V° + V)[NH_4^+] \quad (15)$$

the electroneutrality condition,

$$[H^+] + [NH_4^+] = [OH^-] + [A^-] \quad (16)$$

Table 2
Linear equations for the determination of the acidity constant $K_a$ and of the concentration $C$ of weak monoprotic acid by multiple addition to a solution of strong base at known concentration $C_j$ ($H$, Eq. 5)

| Named after [1] | $X$ | $Y$ | $C$ | $K_a$ | Equation $Y = a + bX$ | |
|---|---|---|---|---|---|---|
| Hofstee | $\frac{(H + C_jV^\circ)[H^+]}{V}$ | $\frac{H + C_jV^\circ}{V}$ | $a$ | $-\frac{1}{b}$ | $\frac{H + C_jV^\circ}{V} = C - \frac{(H + C_jV^\circ)[H^+]}{K_aV}$ | (21) |
| Lineweaver and Burk | $[H^+]$ | $\frac{V}{H + C_jV^\circ}$ | $\frac{1}{a}$ | $\frac{a}{b}$ | $\frac{V}{H + C_jV^\circ} = \frac{1}{C} + \frac{1}{CK_a}[H^+]$ | (22) |
| Scott | $\frac{1}{[H^+]}$ | $\frac{V}{(H + C_jV^\circ)[H^+]}$ | $\frac{1}{b}$ | $\frac{b}{a}$ | $\frac{V}{(H + C_jV^\circ)[H^+]} = \frac{1}{CK_a} + \frac{1}{C[H^+]}$ | (23) |

and the expressions for $K_a$ and $K_w$, Eq. (17) is obtained:

$$CV = (V^\circ + V)([H^+] - K_w/[H^+])(1 + [H^+]/K_a) + C_jV^\circ(1 + [H^+]/K_a) = (H + C_jV^\circ)(1 + [H^+]/K_a) \quad (17)$$

The Gran function $F$ for weak acid addition, Eq. (6), calculated from the experimental data is thereafter affected by the presence of a base with a non-zero value of $C_j$, corresponding in this instance to

$$F = CV - C_jV^\circ(1 + [H^+]/K_a) \quad (18)$$

instead of $CV$. However, according to

$$H(1 + [H^+]/K_a)/V = C - C_jV^\circ(1 + [H^+]/K_a)/V \quad (19)$$

obtained by rearrangement of Eq. (17), both $C$ and $C_j$ can be obtained, when $K_a$ is known, by linearizing the experimental data with the use of the auxiliary variables $X = F/V = H(1 + [H^+]/K_a)/V$ and $Y = (1 + [H^+]/K_a)/V$. The least-squares intercept $Y(X = 0)$ of the transformed linear equation $Y = a + bX$ yields the sample concentration $C$, while the slope factor, on division by $V^\circ$ (the initial volume of supporting solution), yields the original concentration of basic contaminant. It must be expected, however, that the results are very sensitive to the inaccuracy of $K_a$ [1].

Unfortunately, it is impossible to linearize Eq. (19) in the more interesting case when $C$ is known and $K_a$ and $C_j$ are unknown, i.e. for the determination of the acidity constant by addition of sample at known concentration in the presence of unknown background basic impurities. A solution of this problem (as in the case when $C$ is also unknown) can only be sought by treatment of the experimental data of sample addition with a numerical optimization method.

If both $C$ and $C_j$ are known, the acidity constant can be obtained from the slope of the plot of $Y = (C_jV^\circ + H)[H^+]$ against $X = (CV - C''V^\circ + H)$, according to

$$(C''V^\circ + H)[H^+] = K_a(CV - C_jV^\circ - H) \quad (20)$$

If only $C_j$ is known, it is possible to determine $C$ together with $K_a$ by means of the linear Eqs. (21)–(23) in Table 2. The relationships between the quantities $C$ and $K_a$ and the parameters $a$ and $b$ of Eqs. (21), (22) and (23) are the same as for Eqs. (8), (10) and (12), of Ref. [1], respectively (the correspondence is made clear by putting $C_j = 0$); equations related to Eqs. (9), (11) and (13) of Ref. [1] can be obtained by interchanging the auxiliary variables (for convenience, each one of these new equations could be termed according to the name [4–7] assigned to the corresponding equation of Ref. [1]).

It is interesting to note that, as a consequence of the approximation made by assuming a quantitative reaction of the weak base (see Eq. 15), Eqs. (17)–(23) are the same as the titration of a strong base at concentration $C_j$ with weak acid at concentration $C$. However, the use of Eqs. (17)–(23) with titration data is out of the scope of the present work.

### 3.3. Strongly acidic impurities

For completeness, the effect of the presence of strong acids either in the sample or in the supporting solution is also shortly considered.

A strong acid contamination in the sample solution can arise, for instance, from the synthesis or purification of the substance investigated. By combining the mass balance of the contaminant, for instance hydrochloric acid, present in the added sample solution at concentration $C_h$:

$$C_h V = (V^\circ + V)[Cl^-] \quad (24)$$

with the mass balance (Eq. 14), the electroneutrality condition:

$$[H^+] = [OH^-] + [A^-] + [Cl^-] \quad (25)$$

and the expressions of the equilibrium constants, the following equations are obtained:

$$CV = (H - C_h V)(1 + [H^+]/K_a) \quad (26)$$

as the Gran-type equation for the determination of $C$ at known $K_a$ and $C_h$;

$$H(1 + [H^+]K_a)/V = C + C_h(1 + [H^+]/K_a) \quad (27)$$

for the determination of $C$ and $C_h$ at known $K_a$; and

$$(H - C_h V)/V = C - [H^+](H - C_h V)/VK_a \quad (28)$$

as the Hofstee-type equation for the simultaneous determination of $K_a$ and $C$ at known $C_h$ (even in this instance, five more equations can be formulated for the same purpose). Linearization is not possible when only $C$ is known.

The salts of analytical purity employed as the supporting electrolyte are more frequently contaminated by traces of strong acids than commonly believed (however, a prolonged heating of sodium or potassium chloride at 120°C has been found to be effective for a practically complete elimination of hydrochloric acid traces). By combining the mass balance of the contaminant, for instance hydrochloric acid, at concentration $C_k$ in the initial solution:

$$C_k V^\circ = (V^\circ + V)[Cl^-] \quad (29)$$

with the mass balance (Eq. 14), the electroneutrality condition (Eq. 25) and the expressions of the equilibrium constants, the following equations are obtained:

$$CV = (H - C_k V^\circ)(1 + [H^+]/K_a) \quad (30)$$

as the Gran-type equation for the determination of $C$ at known $K_a$ and $C_k$;

$$H(1 + [H^+]/K_a)/V = C + C_k V^\circ(1 + [H^+]/K_a)/V \quad (31)$$

for the determination of $C$ and $C_k$ at known $K_a$; and

$$(H - C_k V^\circ)/V = C - [H^+](H - C_k V^\circ)/VK_a \quad (32)$$

as the Hofstee-type equation for the simultaneous determination of $K_a$ and $C$ at known $C_k$ (as before, five other equations can be formulated for the same purpose). Linearization is not possible when only $C$ is known.

The above equations, particularly those including the contaminant concentration as one of the parameters to be determined, are reasonably suspected to be strongly affected by the uncertainty in the measured variable. In the present work, they have been used only to evaluate the reliability of the results obtainable with the equations [1] valid for pure solutions, and to investigate qualitatively the causes of the experimental deviations from the anticipated linear behaviour.

## 4. Discussion

Linear methods of data treatment are specially suited for obtaining preliminary data of acidity constants and for general use in laboratories that are not particularly equipped to deal with sophisticated experimental apparatus and computer programming. Therefore, the present experimental work was more aimed at testing the robustness of the proposed method when subjected to the disturbances most commonly encountered in practice, than confirming with ideally behaving model systems the theoretical expectations of the equations proposed.

Preliminarily, the way in which the different causes of deviation affect the results of the linear equations has been investigated by determining the extent of their theoretical effect. For brevity, discussion is restricted here to those deviations of chemical origin that, by comparison with experimental results, seemed the most important ones in practice. The attention is focused on the linear equation for determination of the acidity constant by addition of pure acid at known concentration:

$$H[H^+] = K_a(CV - H) \quad (33)$$

(Eq. (6) of Ref. [1]), on the linear equations for the simultaneous determination of $K_a$ and $C$ (Eqs. (8)–(13) of Ref. [1]), taking as an example the Hofstee-type function:

$$\frac{H}{V} = C - \frac{H[H^+]}{K_a V} \quad (34)$$

and on some of the equations that take into account the presence of an impurity in the supporting solution.

### 4.1. The effect of basic impurities in the supporting solution

For the evaluation of the effect of basic contaminants present in the supporting solution on the results obained using the linear equations for pure solutions, the auxiliary variables of the various linear equations have been calculated using theoretical values [8] of hydronium ion concentration, $[H^+]$, for series of additions at different values of the parameters $K_a$, $C$ and $C_j$. These synthetic data were interpolated by linear least-squares fitting to recalculate the desired parameters of the sample acid.

According to the results thus obtained, the determination of $K_a$ using Eq. (33) is only moderately impaired by the presence of basic impurities in the supporting solution, if the ratio of the concentration of acid made up in the measured solution:

$$C_{HA} = CV/(V^\circ + V) \quad (35)$$

to the concentration of contaminant base, $C_j$, is large enough. As a rough indication, the ratio $C_{HA}/C_j$ must be larger than 10 after the first sample addition; however, the weaker the sample acid, the more adverse the effect of a given concentration of contaminant and the larger the ratio $C_{HA}/C_j$. Therefore, basic impurities can limit the application of Eq. (33) towards small acidity constants. It must be remembered that, in contrast, the condition $C_{HA}/K_a > 1$ required [1] for minimizing the effect of systematic and random e.m.f. measurement errors on the results of Eq. (33) is more easily satisfed with weaker acids. Both these contrasting requirements must be considered in planning the experimental use of Eq. (33) for determination of $K_a$.

Plots of Eq. (33) are shown in Fig. 1 for three synthetic experiments, differing only by the impurity level. These plots show that the presence of basic impurities in the supporting solution may cause barely appreciable deviations from linearity, even when it causes errors in $K_a$ (indeed, simulated experiments give apparently curved plots only at $C_{HA}/C_j < 10$). Therefore, apparent linearity does not give safe evidence of the acceptability of experimental $K_a$ values. A significant negative value of the intercept $Y(X = 0)$ (see Fig. 1) has been found to be a more suitable indicator of unacceptably large (negative) errors in $K_a$ due to basic contaminants in the supporting solution. (However, a negative volume error of the first addition, due, for instance, to an air bubble in the tip of the dispensing capillary, which can be significant if the added volume aliquots are very small, can have a similar effect [1] on the intercept, without altering the slope with respect to the theoretical value.)

The same synthetic data as above have been used to calculate the auxiliary variables $Y = H/V$ and $X = H[H^+]/V$ of the Hofstee-type function, Eq. (34). Data from a few simulated experiments are plotted in Figs. 2 and 3; for easier comparison, auxiliary variables have been normalized to the form $Y' = 1 + X'$ by putting $Y' = Y/C$ and $X' = XCK_a$. It is seen that simultaneous determination of $K_a$ and $C$ is very badly affected by basic impurities in the supporting solution, even at a low contamination level. The error in $K_a$ is positive (in contrast with the negative error caused by basic contaminants when Eq. (33) is used); the error in $C$ is negative, and relatively smaller. Acceptable errors are obtained only with stronger acids at higher $C_{HA}/C_j$ ratios. Even with these equations, the deviations due to basic impurities in the supporting solution are in the same direction as those due to constant negative error in the added volume (see Fig. 8 of Ref. [1]).

It has been shown [1] that the effect of random errors of $[H^+]$ measurement on the

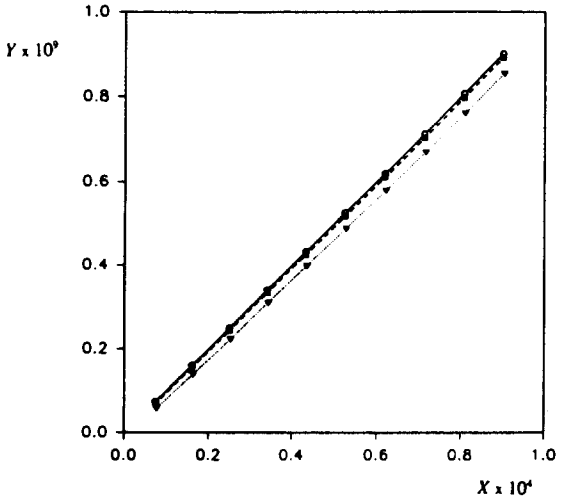


Fig. 1. Plot of Eq. (33) with synthetic data including the effect of basic impurities in the supporting electrolyte solution. Auxiliary variables $X = CV - H$, $Y = H[H^+]$ ($H$, see Eq. 5) calculated for 10 additions of weak acid sample with $pK_a = 5$, $C = 0.01$ M, $V^\circ = 100$ ml, $V = i$ ml, $i = 1$–10. ○ ——, concentration of basic impurities $C_j = 0$; □ – – –, $C_j = 1.0 \times 10^{-6}$ M; ▽ · · ·, $C_j = 5.0 \times 10^{-6}$ M.

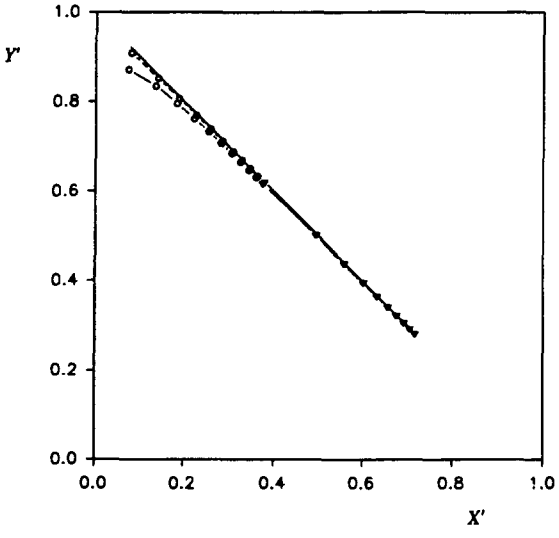


Fig. 2. Plot of Hofstee-type function, Eq. (34), with normalized auxiliary variables $X' = X/CK_a$ and $Y' = Y/C$ calculated from synthetic values of $[H^+]$ for multiple addition of an acid with $pK_a = 3$ over different $C_{HA}/K_a$ ranges in the presence of basic contaminant in the supporting solution at initial concentration $C_j$. $V^\circ = 100$ ml, $V = i$ ml, $i = 1-10$. ○, $C = 0.001$ M, $C_{HA}/K_a \approx 0.1-1$; ▽, $C = 0.01$ M, $C_{HA}/K_a \approx 1-10$. ——, $C_j = 0$; – – –, $C_j = 1.0 \times 10^{-6}$; · · ·, $C_j = 5.0 \times 10^{-6}$. $X'$ increases and $Y'$ decreases with the progress of sample addition.

precision of values of $K_a$ and $C$ obtained with Eq. (34) and the other equations of Ref. [1] (Table 1) depends strongly on the ratio $C_{HA}/K_a$ of the actual weak acid concentration in the measured solution, $C_{HA} = CV/(V^\circ + V)$, to the acidity constant. For optimal precision, each experiment should cover at least a decade of $C_{HA}/K_a$ ratios, for instance 0.1–1, 1–10, or, less preferably, $10-10^2$; the effect of measurement errors is amplified both at smaller and larger ratios. When $K_a$ is small, attainment of this optimal concentration range requires a small acid concentration; as a consequence, the concentration of impurities in the supporting solution becomes important. This makes Eq. (34) and similar equations practically unsuitable for the simultaneous determination of acidity constant and sample concentration of acids with a $pK_a$ larger than 4 or 5, unless special precautions are taken against the uptake of base by the measured solution.

A better insight can be gained by inspection of Table 3, in which representative results obtained with Eqs. (33) and (34) (including Figs. 1–3) are summarized. For each simulated experiment, the parameters (column 1–6) were arranged so as to operate over one decade of values of the $C_{HA}/K_a$ ratio (column 4) within or near to the optimal range [1]. The values in columns 7–10 are calculated by linear least-squares fitting; the standard deviations due to variations from linearity are seen to be, in many instances, sufficiently small to be concealed in practice by random measurement errors. The normalization of the intercept $Y(X = 0)$ of Eq. (33) as the ratio to $Y_{max}$ calculated for the last addition (column 7) allows direct comparison between different experiments.

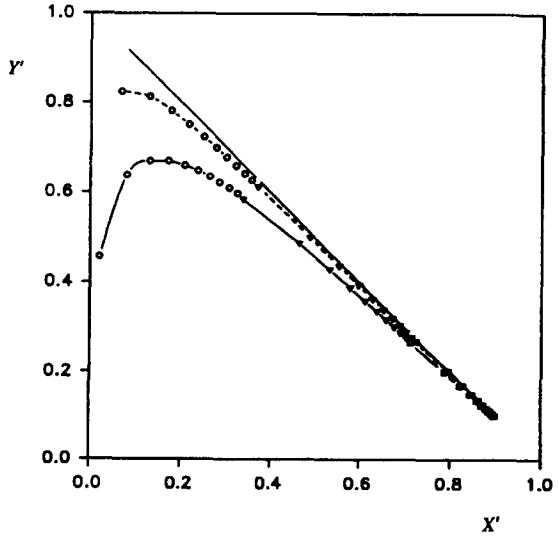


Fig. 3. Plot of Eq. (34) for an acid with $pK_a = 4$. □, $C = 0.1$ M; $C_{HA}/K_a \approx 10-10^2$; other symbols and parameters as in Fig. 2.

### 4.2. Other types of impurities

Basic impurities in the sample cause the plots to deviate towards the same side as do basic impurities in the supporting solution. However, the deviation increases with addition by effect of the increase in contaminant concentration in the measured solution, proportional to the increasing acid concentration, so affecting the calculated parameters with errors in the opposite direction to those for bases in the supporting electrolyte. This effect is shown in Fig. 4 (to be compared with Fig. 3) for the Hofstee-type function, Eq. (34), where the deviation causes a negative error in $K_a$ and a positive error in $C$.

Strong acid impurities, either in the sample or in the supporting solution, cause deviations qualitatively symmetrical with those due to strong basic contaminants, as shown in Fig. 4 (where, in order to make deviations clearly detectable, the assumed level of contaminants in the sample is much higher than reasonably

Table 3
Effect of basic impurities at concentration $C_j$ in the supporting solution on the values of $K_a$ and $C$ determined in simulated experiments (concentrations in mol $l^{-1}$)

| Parameters | | | | | | Results | | | |
|---|---|---|---|---|---|---|---|---|---|
| $pK_a$ | $C$ | $C_{HA}$ | $C_{HA}/K_a$ | $C_j \times 10^6$ | $\frac{C_{HA}}{C_j}$ | Eq. (33) | | Eq. (34) | |
| | | | | | | $\frac{-Y(X=0)}{Y_{max}}$ | $\frac{(K_a \pm \sigma)_{calc}}{(K_a)_{true}}$ | $\frac{(C \pm \sigma)_{calc}}{C_{true}}$ | $\frac{(K_a \pm \sigma)_{calc}}{(K_a)_{true}}$ |
| 3.00 | 0.1 | $10^{-3}$–$10^{-2}$ | 1–10 | 1 | $10^3$–$10^4$ | 0.000 | $1.000 \pm 0.000$ | $0.997 \pm 0.000$ | $1.003 \pm 0.000$ |
| | | | | 5 | $2 \times 10^2$–$2 \times 10^3$ | 0.001 | $0.999 \pm 0.000$ | $0.986 \pm 0.001$ | $1.018 \pm 0.001$ |
| | 0.01 | $10^{-4}$–$10^{-3}$ | 0.1–1 | 1 | $10^2$–$10^3$ | 0.003 | $0.999 \pm 0.000$ | $0.989 \pm 0.001$ | $1.029 \pm 0.004$ |
| | | | | 5 | 20–200 | 0.016 | $0.994 \pm 0.001$ | $0.947 \pm 0.006$ | $1.16 \pm 0.02$ |
| 4.00 | 0.1 | $10^{-3}$–$10^{-2}$ | 10–100 | 1 | $10^3$–$10^4$ | 0.006 | $0.999 \pm 0.000$ | $0.985 \pm 0.000$ | $1.016 \pm 0.001$ |
| | | | | 5 | $2 \times 10^2$–$2 \times 10^3$ | 0.002 | $0.996 \pm 0.000$ | $0.931 \pm 0.001$ | $1.077 \pm 0.001$ |
| | 0.01 | $10^{-4}$–$10^{-3}$ | 1–10 | 1 | $10^2$–$10^3$ | 0.002 | $0.997 \pm 0.000$ | $0.972 \pm 0.001$ | $1.036 \pm 0.002$ |
| | | | | 5 | 20–200 | 0.012 | $0.986 \pm 0.001$ | $0.873 \pm 0.007$ | $1.19 \pm 0.01$ |
| | 0.001 | $10^{-5}$–$10^{-4}$ | 0.1–1 | 1 | 10–$10^2$ | 0.032 | $0.987 \pm 0.001$ | $0.90 \pm 0.01$ | $1.37 \pm 0.06$ |
| | | | | 5 | 2–20 | 0.16 | $0.933 \pm 0.006$ | Strong curvature | Strong curvature |
| 5.00 | 0.1 | $10^{-3}$–$10^{-2}$ | $10^3$–$10^2$ | 1 | $10^3$–$10^4$ | 0.001 | $0.998 \pm 0.000$ | $0.895 \pm 0.001$ | $1.118 \pm 0.001$ |
| | | | | 5 | $2 \times 10^2$–$2 \times 10^3$ | 0.005 | $0.989 \pm 0.001$ | $0.632 \pm 0.007$ | $1.588 \pm 0.001$ |
| | 0.01 | $10^{-4}$–$10^{-3}$ | 10–100 | 1 | $10^2$–$10^3$ | 0.004 | $0.993 \pm 0.000$ | $0.871 \pm 0.003$ | $1.167 \pm 0.003$ |
| | | | | 5 | 20–200 | 0.021 | $0.963 \pm 0.002$ | Strong curvature | Strong curvature |
| | 0.001 | $10^{-5}$–$10^{-4}$ | 1–10 | 1 | 10–$10^2$ | 0.024 | $0.973 \pm 0.002$ | $0.77 \pm 0.03$ | $1.40 \pm 0.03$ |
| | | | | 5 | 2–20 | 0.12 | $0.86 \pm 0.01$ | Strong curvature | Strong curvature |

expected in practice). In the case of strong acid impurities in the sample, it is easy to understand why deviations caused by contaminants in the sample increase with the progress of addition; indeed, the dissociation degree of the sample weak acid decreases with increasing concentration and, therefore, the ratio between strong and weak acid being constant, the relative contribution of the contaminant to the measured $[H^+]$ becomes more and more important. The opposite decrease in the deviations caused by contaminants in the supporting solution, whose concentration remains practically constant with the progress of addition, is quite trivial.

## 5. Results

Many series of experiments were performed with sample acids of different strength and concentration. Only a limited selection, most suitable for emphasizing the performance differences and the advantages or pitfalls of the various applications of the linearized sample addition method, is reported here.

Most experiments of sample addition were followed by titration of the final solution with strong base. Thereby, the mean values of sample concentration determined by titration were taken as the reference values. Titration data were also used to calculate the acidity constant. The sample concentration was first determined from the equivalence volume of the titration, obtained by linearization of the part of the titration preceding the equivalence point with the appropriate Gran function [2,4]:

$$G = V_t \times 10^{E/S} \tag{36}$$

where $V_t$ is the added titrant volume, $E$ is the measured electromotive force, and $S$ is the electrode slope factor (the theoretical Nernst value was taken, being generally within the uncertainty of the experimental slope). Only titration points lying in the theoretical linearity range of the approximate Gran function [9,10] were considered. Using this value of $C$, the value of the acidity constant was calculated as the least-squares slope of the auxiliary variable $Y = W[H^+]$ against $X = (CV_s - W_s)$, according to the equation

$$W[H^+] = K_a(CV_s - W) \tag{37}$$

where $W$ is given by

$$W = C_b V + (V^\circ + V_s + V_t)([H^+] - K_w/[H^+]) \quad (38)$$

$V_s$ is the total sample volume added stepwise before titration, $C_b$ is the concentration of the titrant base, and the other symbols have the customary meanings (see Theory section; Eq. (37) is easily obtained by rearrangement of the basic equation [4] for the titration of a weak acid with a strong base).

The values of the chemical parameters $C$ and $K_a$ determined by titration were also used when the equation employed for treatment of experimental multiple samples addition data required one of them to be known.

It was deemed interesting to compare the performance of linearized titration [4] and of linearized multiple sample addition for the simultaneous determination of the weak acid concentration and of its acidity constant. For this purpose, the titration data were treated using the three types of relevant linear equations (Hofstee, Lineweaver–Burk and Scott) [4] corresponding to those used for multiple addition.

The auxiliary variables of practically all of the linearized equations are not independent of each other, as they contain both the experiment variables. As a consequence, the linearized equations do not fulfil important requirements for treatment by simple least-squares fitting. However, this treatment was chosen to preserve a moderate level of sophistication (indeed, if a rigorous statistical evaluation of results is required, we presume that a treatment of direct experimental variables with one of the existing generalized least-squares computer programs is to be chosen, rather than treatment of transformed variables with any of the modified linear least-squares programs proposed for similar purposes). When the uncertainty of the measured variable $[H^+]$ was found to affect the auxiliary variable defined as the $X$ of a transformed equation to a greater extent than the corresponding $Y$ [1], the auxiliary variables were inverted [1,4] in the least-squares treatment of data.

Generally, when $K_a$ was calculated with Eqs. (33) and (37), respectively, at a given sample concentration, the results of multiple sample addition were found to be in very good agreement with the results of titration, and both were in satisfactory agreement with literature data.

For the simultaneous determination of $K_a$ and $C$, linearized titrations generally yielded good results. On the contrary, the results obtained from sample addition data with Eq. (34) and the other equations of Table 1, Ref. [1], were generally poorer. The deviations found in each series of experiments had a systematic component definitely depending on the batch of supporting electrolyte used. Most frequently, the direction of deviations was in agreement with the presence of a base in the supporting solution. When this kind of deviation occurred, the presence of a base in the supporting electrolyte was also suggested by the trend of data of the electrode calibration, performed by multiple strong acid addition to an identical portion of supporting electrolyte solution (see Experimental section); indeed, Gran linearization [2] yielded a positive intercept with abscissa (that is, a positive equivalence volume, corresponding to the titration of a base), although most freqently at the limits of statistical significance. When the supporting electrolyte was directly dissolved (at 0.1 mol $l^{-1}$) in the measuring vessel, the concentration level of contaminant base was never much higher than $10^{-6}$ M, corresponding to a reasonable contamination level of $10^{-5}$ mol of base per 1 mol of electrolyte salt; larger amounts, indicating a stronger contamination by absorption of volatile bases from the atmosphere, were found when a batch of supporting solution prepared a long time beforehand was repeatedly used. In some instances, however, deviations occurred in the opposite direction, leading to a suspected contamination of the supporting electrolyte by traces of (strong) acid.

Moreover, the deviations found showed a dependence on both the strength and the concentration of the sample acid, i.e. on the ratio $C_{HA}/K_a$, in qualitative agreement with the theoretical expectations [1].

The results of a series of experiments representative of the adverse effects of impurities on measurements of two acids of different strength, formic acid and acetic acid, are summarized in Table 4. 2.5 ml of approximately 0.3 M formic acid (literature value $pK_a = 3.55 \pm 0.01$ at 25°C and 0.1 M ionic strength) [11] were added stepwise (in 20 aliquots) to 0.1 M potassium chloride, and were subsequently titrated with standard sodium hydroxide (0.1 M, in order to produce negligible variation of ionic strength). Using the value of

Table 4
Results of calculation of $K_a$ and $C$ from titrations and multiple sample additions of formic acid and acetic acid at 24.9°C (concentrations in mol $l^{-1}$; uncertainties as standard deviations)

| Method | Quantity calculated | Formic acid, $K_a \times 10^4$ | | Acetic acid, $K_a \times 10^5$ | |
|---|---|---|---|---|---|
| | | Titration ($n = 3$) | Sample addition ($n = 4$) | Titration ($n = 5$) | Sample addition ($n = 5$) |
| Gran | $C$ | $0.2952 \pm 0.007$ | n.c. | $0.3015 \pm 0.0006$ | n.c. |
| Eqs. (37), (33) | $K_a$ | $3.018 \pm 0.017$ | $3.016 \pm 0.017$ | $2.836 \pm 0.019$ | $2.846 \pm 0.025$ |
| Hofstee | $C$ | $0.2935 \pm 0.0010$ | $0.267 \pm 0.009$ | $0.3000 \pm 0.0008$ | $0.222 \pm 0.035$ |
| | $K_a$ | $3.018 \pm 0.013$ | $3.33 \pm 0.20$ | $2.836 \pm 0.019$ | $3.98 \pm 0.72$ |
| Lineweaver–Burk | $C$ | $0.2912 \pm 0.0010$ | $0.268 \pm 0.013$ | $0.2972 \pm 0.0023$ | $0.215 \pm 0.034$ |
| | $K_a$ | $3.058 \pm 0.016$ | $3.36 \pm 0.20$ | $2.877 \pm 0.046$ | $4.13 \pm 0.73$ |
| Scott | $C$ | $0.2951 \pm 0.0007$ | $0.270 \pm 0.014$ | $0.3018 \pm 0.0002$ | $0.223 \pm 0.035$ |
| | $K_a$ | $2.962 \pm 0.009$ | $3.32 \pm 0.21$ | $2.792 \pm 0.013$ | $3.97 \pm 0.71$ |
| GLS[a] | $K_a$ | $2.976 \pm 0.027$ | $2.984 \pm 0.008$ | $2.799 \pm 0.018$ | $2.809 \pm 0.032$ |
| GLS[b] | $C$ | $0.2945 \pm 0.0011$ | $0.2930 \pm 0.0007$ | $0.3012 \pm 0.0001$ | $0.3011 \pm 0.0002$ |
| | $K^a$ | $2.977 \pm 0.081$ | $2.889 \pm 0.005$ | $2.791 \pm 0.021$ | $2.717 \pm 0.080$ |

GLS = generalized least squares.
[a] One adjustable parameter.
[b] Two adjustable parameters.

the sample concentration obtained from Gran titration, $pK_a = 3.520 \pm 0.002$ was obtained from the titration data with Eq. (37) and $pK_a = 3.521 \pm 0.003$ from the sample addition data with Eq. (33), with excellent agreement between the two sets.

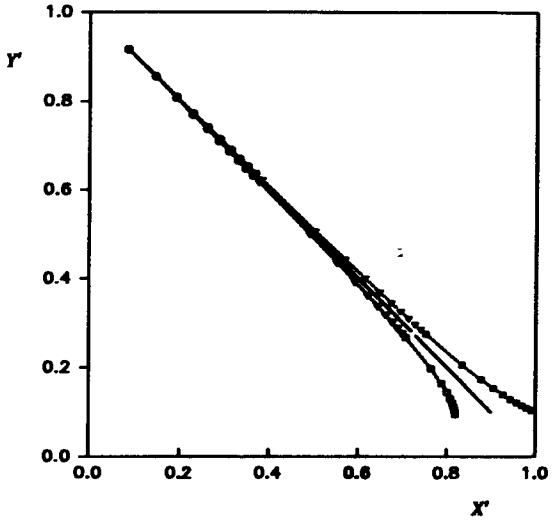


Fig. 4. Plot of Hofstee-type function, Eq. (34), with normalized auxiliary variables $X' = X/CK_a$ and $Y' = Y/C$ calculated from synthetic values of $[H^+]$ for multiple addition of an acid with $pK_a = 4$ over different $C_{HA}/K_a$ ranges in the presence of contaminant in the samples. $V^\circ = 100$ ml, $V = i$ ml, $i = 1-10$. ——, $C_j = 0$. Basic impurity (conjugated base) at 1% concentration ratio: ○, $C = 0.001$ M, $C_{HA}/K_a \approx 0.1-1$; ▽, $C = 0.01$ M, $C_{HA}/K_a \approx 1-10$; □, $C = 0.1$ M, $C_{HA}/K_a \approx 10-10^2$. Strong acid impurity at 1% concentration ratio represented by full symbols; other parameters as above.

The results of the simultaneous determination of $K_a$ and $C$ from the linearized titration data are also good, although they show some dependence upon the linear equation used. In contrast, the corresponding experimental plots of the sample addition data (see Eq. (34) and Table 1 of Ref. [1]) deviate from the theoretical plots calculated with the above values of the chemical parameters in the direction corresponding to the presence of a base in the supporting electrolyte, in qualitative accordance with Figs. 2 and 3. As a consequence, the calculated value of the acidity constant is affected by a positive error and that of the sample concentraton by a negative error. In spite of the appreciable shifting, any deviation from linearity, being small in the experimental concentration range (see Discussion section), is practically masked by the dispersion of the points (although small).

As expected (see Discussion section, Figs. 2 and 3), larger shifts in the experimental plots and, therefore, larger errors in the simultaneous determination of $K_a$ and $C$, were found with the weaker acetic acid in the same concentration range ($pK_a = 4.50 \pm 0.03$ at 25°C) [11] with supporting electrolyte taken from the same batch. Larger deviations also occurred with more dilute solutions of the same acids. In contrast, the determination of the acidity constant with Eq. (33) using an independently determined value of sample concentration yielded good results over a much larger range of experimental conditions.

The results of linearized titration and sample addition were also evaluated by comparison with generalized least-squares treatment of the original experimental variables. The results obtained with the data from the same experiments are shown in Table 4. Data treatment with the acidity constant as the only adjustable parameter shows very good agreement with linearization for both titration and sample addition. When both acidity constant and sample concentration are adjusted, generalized least-squares results of titration and of sample addition agree very well each other, and with those obtained from titration by linear equations. When the concentration of impurities in the supporting solution is also taken as an adjustable parameter, the value of sample concentration does not change and that of the acidity constant only changes a little; however, for several experiments, an unreasonably high concentration of basic impurities was calculated, apparently due to high correlation between this quantity and the acidity constant.

## 6. Conclusions

The theoretical investigation of the effect of basic and acid impurities and the experimental results have confirmed that multiple sample addition of weak acid is very suitable for the determination of the acidity constant by multiple sample addition, particularly when a standard solution is used, i.e. when the sample concentration is accurately known. The accuracy and precision of $K_a$ are comparable with those attained by titration. Multiple sample addition is then a convenient substitute for titration, removing the problems inherent in the use of a strong base as the titrant (for instance, the massive absorption of carbon dioxide by the titrant solution). More generally, multiple sample addition can offer a valid complement to titration, particularly when a very limited amount of the substance to be investigated is available; indeed, potentiometric measurements during the stepwise addition of the sample to be subsequently titrated, in accordance with the procedure herein followed, make it possible to double the number of experimental data using the same amount of sample (the effect is much more significant than that of intensifying the titration points). For simultaneous determination of acidity constant and sample concentration by multiple sample addition, a more scrupulous control of contaminants is necessary, with additional limitations on the strength and concentration of the acid.

Rigorous mathematical solution requires application of non-linear regression. Linearized multiple addition, besides not being a statistically sound method of data treatment, is more affected than non-linear regression (to a greater extent than linearized titrations) by pitfalls, interferences and contaminations common in pH-metric measurements. However, by addition of standard solution, good or acceptable values of the acidity constant are easily obtained. In contrast, the adverse effects are particularly enhanced when the acidity constant and sample concentration are simultaneously determined. In this instance, data linearization is only suitable for a rough preliminary evaluation of the desired quantities.

Notwithstanding the above limitations, linearized multiple sample addition has a place in analytical research. According to our experience, a great benefit can be gained from the preliminary use of this method just because of such amplified deviations from the linear models. A comparison of the shape of deviations of the linearly transformed data with the behaviour anticipated by the theoretical treatment (which, for this reason, is rather detailed in this and in the previous paper [1]) is frequently highly diagnostic of the nature of the contaminants and, in general, of the pitfalls of the analytical environment; it also helps to detect and to eliminate, correct or counteract some important sources of error, perhaps to greater effect than the distribution of residuals in non-linear regression.

## Acknowledgements

The work was supported by C.N.R. cont. No. 91.03156.CT03. A.M. acknowledges a research grant from Università di Padova. The skillful technical assistance provided by Lidia Soldà is gratefully acknowledged.

## References

[1] C. Maccà and A. Merkoci, Talanta, 41 (1994) 2033.
[2] G. Gran, Analyst, 77 (1952) 661.
[3] L.G. Sillén, Acta Chem. Scand., 16 (1962) 159; 18 (1964) 1083.
[4] C. Maccà, Fresenius' J. Anal. Chem., 336 (1990) 29.

[5] B.H. Hofstee, Science, 31 (1960) 39.
[6] R.L. Scott, Recl. Trav. Chim., 75 (1956) 787.
[7] H. Lineweaver and D. Burk, J. Am. Chem. Soc., 56 (1934) 658.
[8] K. Ebert, H. Ederer and T.L. Isenhour, Computer Applications in Chemistry, VCH, Weinheim, 1989.
[9] C. Maccà and G.G. Bombi, Analyst, 114 (1989) 463.
[10] C. Maccà, Analyst, 114 (1989) 689.
[11] A.E. Martell and R.M. Smith, Critical Stability Constants, Vol. 3: Other Organic Ligands, Plenum, New York, 1977.

ELSEVIER

Talanta 42 (1995) 1447–1455

Talanta

# Experimental and computational study of species formed during electrochemical stripping oxidation of copper in chloride media Determination of copper(II) in the ng $l^{-1}$ range by stripping potentiometry

D. Jagner *, E. Sahlin, L. Renman

*Department of Analytical and Marine Chemistry, University of Göteborg and Chalmers University of Technology, S-412 96 Göteborg, Sweden*

Received 5 January 1995; revised 28 February 1995; accepted 14 March 1995

**Abstract**

A novel glassy carbon electrode design, permitting medium exchange in batch mode without loss of electrode potential control, has been used for the study of copper(I) and copper(II) species formed during constant current stripping oxidation of copper in chloride media. It was found that copper(II) species dominated at chloride concentrations below about 1 mM and that soluble copper(I) species dominated at chloride concentrations above about 100 mM. In the concentration range 1–100 mM, soluble copper(I) and copper(II) species are formed as well as solid copper(I) chloride, the latter giving rise to a split peak as it is further oxidised to copper(II). The experimental results agreed satisfactorily with computer calculated equilibria data using the HALTAFALL program. The medium exchange procedure has, furthermore, been used for the determination of copper(II) in seawater reference samples, 7.5 M ammonium acetate/2.5 M acetic acid being used as stripping medium. The detection limit, after 15 min of electrolysis, was found to be 6 ng $l^{-1}$ (0.10 nM) and the relative precision 6–10%.

## 1. Introduction

Although copper is one of the elements most frequently studied electroanalytically, the stripping analysis for copper(II) is far from straightforward in practical work. Batley [1] has summarised five main problems in the study of copper(II) in natural waters using stripping analysis as (i) the ability of copper(II) to bind strongly to organic and inorganic ligands, (ii) its existence in two oxidation states, (iii) the occurrence of the copper stripping peak at potentials at which many organic species are adsorbed onto mercury electrodes, (iv) the low solubility of copper in mercury and (v) the irreversibility of the copper reduction. Nelson [2,3] and Nelson and Mantoura [4–6] have extensively studied the reduction of copper in natural waters containing, in addition to chloride, other complexing agents, e.g. glycine, as well as surfactants such as gelatine. Recently, Boussemart et al. [7], in a study involving chromatographic fractions of commercial humic substances, explained the split peaks, frequently observed during oxidative stripping of copper, by the oxidation of organic copper(I) species adsorbed onto the mercury electrode surface.

In all the studies referred to above, the electrochemical reduction (electrolysis) of

* Corresponding author.


*SSDI* 0039-9140(95)01593-0

copper(II) and the subsequent electrochemical oxidation (stripping) was performed in the same solution. This means that effects from various complexing agents and surfactants on the reduction process could not be distinguished from the effects of these substances on the oxidation process. For this reason, the interpretation of the results is complicated and sometimes speculative. The introduction of a novel "three-in-one" electrode design, permitting medium exchange under a controlled electrode potential in batch mode [8], considerably simplifies the separate study of the reduction and the oxidation reactions. In addition, the electrode design makes it possible to perform stripping in a medium of optimum composition, with respect to e.g. selectivity, linear range and sensitivity, irrespective of sample composition.

In this article, the novel electrode design has been used to study the effect of the chloride concentration on the reduction of copper(II) and the subsequent rapid oxidation of copper. Stripping potentiometry has been chosen for the experiments, since this is the electroanalytical stripping technique best suited to the study of rapid electrode reactions. The experimental results have been interpreted using computer calculations based on known thermodynamical data. Further, a method for the determination of copper(II) in the $ng\,l^{-1}$ range, involving medium exchange, is presented as well as results from the analysis of reference seawater samples.

## 2. Experimental

### 2.1. Instrumentation, software and electrodes

All experiments were performed using a stripping potentiometry analyser (Tracelab™, PSU 22) in combination with a sample changer (SAC 80), both controlled by the TAP2 Trace Talk Method Builder and Commander through a personal computer. The software and all equipment, except the computer, were produced by Radiometer Analytical S.A., Lyon, France.

Two different commercial three-in-one electrodes (gCC 540, Radiometer Analytical S.A., Lyon), based on the principles described by Jagner et al. [8], were used for the measurements. The Ag/AgCl reference and counter electrodes inside the electrodes were immersed in 3 M hydrochloric acid, which also provided the electrical connection to the outside 3 mm diameter glassy carbon disk working electrode through a ceramic plug. When lifted out of a solution, a droplet always remained under the electrode, i.e. under the glassy carbon disk and the ceramic plug surrounding it. In this way the electrical conductance between the three electrodes, and thus the working electrode potential, could be preserved when the sample changer moved the electrode from one solution to the next. Unless otherwise stated, all potentials given below are vs. Ag/AgCl (3 M HCl).

### 2.2. Transformation of experimental potential values to the standard hydrogen electrode potential scale

In order to be able to compare the experimentally determined electrode potentials, $E_{exp}$, obtained from the Ag/AgCl (3 M HCl) reference electrode with the standard hydrogen electrode potential, $E_{SHE}$, used in the thermodynamic calculations, the experimental values must be transformed to the latter potential scale. This was achieved by measuring the potential difference between the Ag/AgCl (3 M HCl) electrode and a saturated calomel electrode, SCE, in 0.001, 0.01, 0.1, and 1 M hydrochloric acid, i.e. in the media used in the computer calculations. Measurement was also made in 3 M hydrochloric acid in which the liquid junction potential in the Ag/AgCl (3 M HCl) is equal to zero. A potential value of 0.248 V was used for SCE vs. SHE and the liquid junction potentials of the calomel electrode, at different acid concentrations, were taken from Linnet [9]. The electrical resistance in the ceramic plug separating the Ag/AgCl (3 M HCl) electrode from the sample solution was found to be approximately 0.7 kΩ, i.e. the iR potential drop due to the stripping current of 10 μA was equal to 7 mV and this value was corrected for in the transformation between the two potential scales.

### 2.3. Chemical and cleaning of sample vessels

All chemicals were of analytical grade except the hydrochloric acid which was freshly distilled. Millipore water was used for the preparation of all solutions which were handled in a laminar flow cabinet except during analysis. Prior to use, the 45 ml volume polyethylene sample vessels were soaked in 4 M hydrochlo-

ric acid for at least one week and then carefully rinsed with Millipore water.

### 2.4. Solutions and seawater reference samples

The mercury plating solution was prepared by adding concentrated hydrochloric acid and a stock solution of 20 g $l^{-1}$ of mercury(II), prepared by dissolving high purity liquid mercury in concentrated nitric acid and subsequent dilution with 1 M hydrochloric acid, to Millipore water to yield total concentrations equal to 0.10 M and 200 mg $l^{-1}$, respectively. The blank solution referred to below contained 0.025 M hydrochloric acid, 5 μg $l^{-1}$ of lead(II) and 10 mg $l^{-1}$ of mercury(II). The calibration sample used for the determination of copper(II) in seawater was prepared by adding 1 μg $l^{-1}$ of copper(II) to the blank solution. The stripping solution used for the determination of copper(II) in seawater was prepared by mixing acetic acid and ammonia to give an ammonium acetate concentration equal to 7.5 M and an acetic acid concentration equal to 2.5 M (pH = 5, $\eta$ = 0.01 Pa s at 25°C).

The reference seawater samples were obtained from the National Research Council of Canada, apart from the preliminary European Commission Reference Sample BCR 505. The samples had been acidified to pH = 1.6 with nitric acid on sampling, and 10 mg $l^{-1}$ of mercury(II) and 5 μg $l^{-1}$ of lead(II) (internal standard) were added to the samples prior to analysis. All certified lead(II) values were below 50 ng $l^{-1}$, i.e. negligible in comparison with the lead(II) concentration added as internal standard.

### 2.5. Electrode pretreatment

Prior to first use, the electrodes were polished with diamond paste with a diameter of 1 μm and then carefully rinsed ultrasonically in 50% v/v ethanol–water containing 0.10 M hydrochloric acid. Once polished, the electrodes were never repolished. The inner electrode solution of 3 M hydrochloric acid was changed monthly. On storage in 0.1 M hydrochloric acid, the glassy carbon electrode surface of one of the two electrodes used slowly deteriorated, and this gave rise to ghost stripping peaks close to that of copper. This interference, which was of minor concern when the copper(II) concentration exceeded 1 μg $l^{-1}$, was eliminated by a daily electrochemical cleaning procedure involving electrolysis in the plating solution for 4 min at a potential of −2.00 V. The second electrode never gave rise to any ghost peaks.

### 2.6. Electroanalytical procedure

All electroanalytical measurements were composed of three steps: deposition of a fresh mercury film in the mercury plating solution, electrolysis in the samples and, finally, oxidation of the element(s) in the stripping solutions. The electrode was automatically moved from one solution to the next by the sample changer. Prior to each experiment, the electrode was rinsed with Millipore water and ethanol and finally cleaned with a tissue whereby the used mercury film was removed. All solution volumes were 20 ml.

In all experiments, a fresh mercury film was obtained by electrolysis for 30 s at a potential of −1.00 V in the mercury plating solution, the rotation rate of the propeller stirrer being 1500 rpm. The potential was then increased to −0.05 V for 1 s in order to oxidise copper emanating from possible trace impurities of copper(II) in the plating solution. After that, the potential was decreased to −0.15 V, the stirrer stopped, and the electrode transferred to the sample solution. Deposition of copper was performed for 5–15 min, depending on the copper(II) concentration in the sample, at a potential of −0.80 V and a stirring rate of 1500 rpm. During deposition, the electrolysis potential was decreased to −2.00 V for 0.2 s at intervals of 30 s in order to remove trace organic impurities which might have adsorbed onto the electrode surface [10]. Subsequent to copper deposition, the stirrer was stopped and the electrode was transferred to the stripping solution at a controlled potential of −0.80 V. After 30 s at this potential, with a stirring rate of 1500 rpm, the stirrer was stopped and 5 s later the electrode was lifted out of the stripping solution. Another 10 s later stripping was initiated, under quiescent conditions in the stripping solution drop hanging under the electrode employing oxidative currents in the range 1–12 μA. Finally, the electrode was again immersed in the stripping solution and stirring at 1500 rpm was started in order to remove copper(II) ions close to the electrode surface. After this, the measurement cycle in the stripping medium described above was repeated, the first stripping curve registered being denoted as the analytical stripping curve, and the second as the background stripping curve.

Table 1
Stability and solubility constants used in computer calculations

| Metal ion | Ligand | Species formed | Logarithm of equilibrium constant | Ref. |
|---|---|---|---|---|
| $Cu^+$ | $Cl^-$ | CuCl | 2.70 | [14] |
| $Cu^+$ | $Cl^-$ | $CuCl_2^-$ | 5.48 | [15] |
| $Cu^+$ | $Cl^-$ | $CuCl_3^{2-}$ | 4.81 | [15] |
| $Cu^+$ | $Cl^-$ | $Cu_2Cl_4^{2-}$ | 10.32 | [15] |
| $Cu^+$ | $Cl^-$ | CuCl(s) | −6.70 | [15] |
| $Cu^+$ | $e^-$ | Cu(s) | −8.99 | [16] |
| $Cu^+$ | $-e^-$ | $Cu^{2+}$ | −2.63 | [16] |

## 3. Computational

### 3.1. Software and equilibrium constants

All calculations were performed with the HALTAFALL program [11] using a Turbo Pascal version modified for use by personal computers and running under Microsoft DOS [12]. The stability, solubility and redox constants used in the calculations are specified in Table 1 according to the nomenclature used in Ref. [13]. In spite of the fact that the ionic strength varied greatly between the different media investigated, the same constants were used for all calculations, i.e. no activity factor corrections were made. Owing to the considerable controversy [14,15,17–20] among different authors on the stability and solubility constants in the copper(I) chloride system in aqueous solution, corrections of the constants in Table 1, due to different ionic strengths, were not considered meaningful.

### 3.2. Electron activity and total concentrations

The aim of the computer calculations was to simulate the chemical reactions taking place at the interface between an electrode surface and solutions containing different chloride concentrations, as the electrode potential was made increasingly oxidative and copper consequently oxidised to different copper(I) and copper(II) species. In the calculations, four different chloride concentrations, 0.001, 0.01, 0.10 and 1.0 M, were investigated, and the electrode potential was varied between −0.200 and 0.500 V vs. SHE in steps of 0.020 V. The electron activity, $\{e^-\}$ values used in the computer calculations [12,13] were obtained from the $E$ vs. SHE values as

$$\{e^-\} = \exp(-EF/RT) \quad (1)$$

where $R$, $T$ and $F$ have their usual meanings. All computer calculations were carried out with a relative accuracy equal to $10^{-6}$% of the total concentrations [12,13].

The total concentration of oxidised copper species at the electrode surface, $C_{x=0}$, during constant current oxidation of copper was approximated according to Buffle [21] as

$$C_{x=0} = C_{x=\infty} + (\delta/D) i_{ox}/nFA \quad (2)$$

where $i_{ox}$ denotes the stripping current, $\delta$ is the diffusion layer thickness during stripping, $C_{x=\infty}$ is the stripping medium concentration of analyte, $D$ is the diffusion coefficient of the oxidised copper species, $n$ is the number of electrons involved in the oxidation, and $A$ is the electrode surface area. In the experiments described below, the applied oxidative current was equal to 10 μA and the chemical contribution (see below) to the oxidation equal to approximately 3 μA. By comparing the diffusion current obtained during stirring with that obtained under quiescent conditions in the hanging stripping medium drop and by assuming a $\delta$ value equal to 30 μm under stirring conditions, the diffusion layer thickness in the hanging drop was estimated to be 460 μm. Using a $D$ value of $10^{-5}$ cm$^2$ s$^{-1}$ and an $n$ value equal to unity, the surface concentration of copper was estimated to be 8.8 mM at the 3 mm diameter disk electrode, $C_{x=\infty}$ being, of course, equal to zero after medium exchange. This concentration was used in all computer simulations below.

## 4. Results

### 4.1. Effect of chloride concentration on the reduction rate of copper(II)

The effect of chloride ion concentration on

the reduction of copper(II) was investigated by electrolysis for 5 min in samples containing 5 μg $l^{-1}$ of copper(II) and lead(II), and hydrochloric acid at concentrations varying between 0.001 and 1.00 M. Stripping was performed in 7.5 M ammonium acetate–2.5 M acetic acid with an oxidative current of 1 μA. The dependence of the copper and lead signals on the chloride concentration is shown in Fig. 1. From this, it is obvious that the rate of copper(II) reduction is independent of the chloride concentration, which is also found, as expected, for lead(II). In addition, it can be seen that the reproducibility of the copper signal (RSD = 4.8%; $n = 13$) is lower than that for lead (RSD = 3.6%; $n = 13$). The relative standard deviation of the ratio between the two signals, 4.9%, indicates a modest co-variation between the two signals (Fig. 1).

### 4.2. *Effect of chloride concentration on the oxidation of copper*

On electrochemical oxidation of copper, either copper(I) or copper(II) species are formed initially. In order to elucidate the effect of the chloride concentration on the oxidation state, electrolysis was performed for 5 min in samples containing 50 μg $l^{-1}$ of copper(II) and lead(II) prior to stripping in solutions containing 0.0005, 0.001, 0.002, 0.005, 0.01, 0.10, 1.00 and 3.00 M hydrochloric acid. Perchloric acid, at a total concentration of 0.025 M, was used as an inert electrolyte. Six different stripping currents, 2, 4, 6, 8, 10 and 12 μA, were used at each chloride concentration. The experiment was also performed using 7.5 M ammonium acetate–2.5 M acetic acid as stripping medium. During constant current oxidation of elements, electrons are removed by two sources [22]: one is the applied oxidative current, $i_{ox}$, and the other is the flow of oxidants, present in the stripping solution, to the electrode surface. In non-deaerated solutions, dissolved oxygen is normally the main oxidant to be considered. The chemical contribution to the oxidation of an element can be expressed as a chemical current, $i_{chem}$. By plotting the inverse of the stripping signal, $t_s^{-1}$, vs. the applied oxidative currents, a linear relationship is obtained from which the chemical current, at each chloride concentration and for each element studied, can be obtained as the negative intercept on the current axis when $t_s^{-1}$ is extrapolated to zero [22].

The total charge, $Q_M$, used for the oxidation of an element, M, can thus be calculated as

$$Q_M = t_s(i_{chem} + i_{ox}) \quad (3)$$

Assuming that lead is oxidised to lead(II), irrespective of chloride concentration, and, by plotting $R = Q_{Cu}/Q_{Pb}$ vs. the chloride concentration in the stripping medium normalised with the value for this ratio, obtained at a chloride concentration equal to 0.5 mM, it was found that copper(II) species dominated at chloride concentrations below approximately 0.002 M (Fig. 2). Copper(I) species were found to dominate at chloride concentrations above approximately 0.05 M, the normalised value for $R$ being equal to 0.50 within experimental errors. At intermediate chloride concentrations, both copper(II) and copper(I) species were formed (Fig. 2). It was also found that only copper(I) species were formed in 7.5 M ammonium acetate–2.5 M acetic acid medium. Owing to the high viscosity of this medium, the copper(I) species formed diffused very slowly away from the electrode surface and, as the electrode potential was made increasingly oxidative, a second stripping peak, due to the oxidation of copper(I) to copper(II), was sometimes observed, particularly at copper(II) concentrations above 5 μg $l^{-1}$.

Species formed during oxidation of copper were further investigated by comparison with computer calculations as shown in Figs. 3(a)–

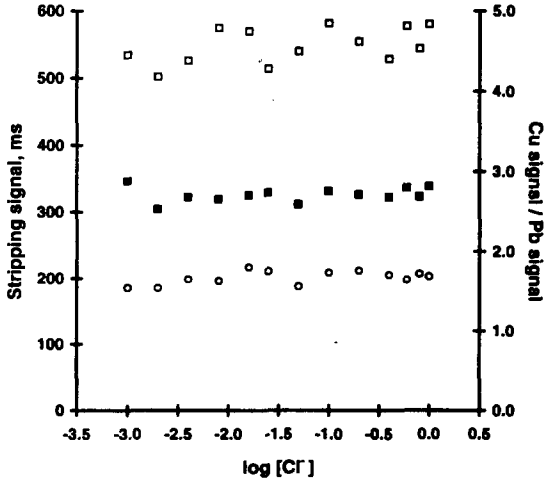


Fig. 1. Dependence of copper and lead stripping signals on sample chloride concentration. Electrolysis for 5 min in samples containing 5 μg $l^{-1}$ of copper(II) and lead(II), and chloride concentrations varying between 0.001 and 1.00 M. ■ = Pb, □ = Cu, ○ = Cu/Pb (right-hand scale).

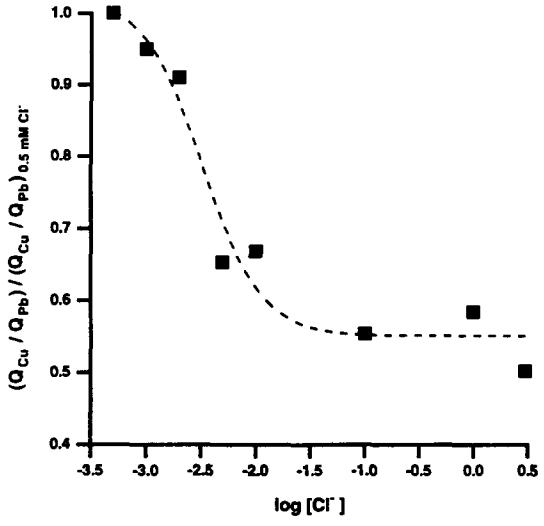


Fig. 2. Dependence of copper oxidation state on stripping medium chloride concentration. Electrolysis for 5 min in samples containing 50 μg $l^{-1}$ of copper(II) and lead(II), and subsequent oxidation in 0.0005, 0.001, 0.002, 0.005, 0.01, 0.10, 1.00 and 3.00 M hydrochloric acid. The total charge needed for the oxidation of copper, $Q_{Cu}$, was divided by the total charge needed for the oxidation of lead, $Q_{Pb}$, and normalised with the value for this ratio at a hydrochloric acid concentration of 0.0005 M.

3(d). In these, calculated molar fractions, $X$, have been plotted against electrode potentials, on the SHE potential scale, for four different hydrochloric acid concentrations, 0.001, 0.01, 0.1 and 1 M (Figs. 3(a)–3(d), respectively). Experimental stripping curves, obtained after electrolysis for 5 min in a solution containing 0.025 M hydrochloric acid, 50 μg $l^{-1}$ copper(II) and 10 mg $l^{-1}$ mercury(II) prior to stripping in 0.001, 0.01, 0.10 and 1.0 M hydrochloric acid containing 0.025 M perchloric acid with an oxidative current equal to 10 μA, are also shown, on the SHE potential scale, in Figs. 3(a)–3(d). Experimental curves (3) show the background strips, curves (2) the analytical strips and curves (1) the background corrected strips.

The calculated molar fraction diagrams in Fig. 3(a) indicate that only copper(II) species are formed during copper oxidation in 0.001 M hydrochloric acid. This is also shown by the experimental stripping curves, the experimental stripping peak potential being close to the calculated potential. At a chloride concentration equal to 0.01 M, the computer calculations (Fig. 3(b)) indicate that copper(II) is formed simultaneously with solid copper(I) chloride. On increasing oxidative potentials, the latter compound is oxidised to copper(II) giving rise to the split stripping peak in the experimental stripping curves in Fig. 3(b). On increasing the chloride concentration to 0.10 M, only copper(I) species are formed according to the calculated molar fraction diagrams in Fig. 3(c). This is also indicated by the disappearance of the split peak in the experimental curves. The computer calculations show that both soluble and insoluble copper(I) species are formed in 0.10 M chloride. They also show that not all the solid copper(I) chloride had been oxidised to copper(II) at the oxidation potential at which the experimental oxidation was stopped in order to avoid mercury oxidation (0.30 V vs. SHE). The remaining solid copper(I) chloride, adhering to the electrode surface, is reduced to copper as the electrode potential is made negative, prior to the registration of the background strip, and gives rise to a stripping peak in the background strip as seen in Fig. 3(c). Finally, the molar fraction diagram in Fig. 3(d) indicates that at a chloride concentration equal to

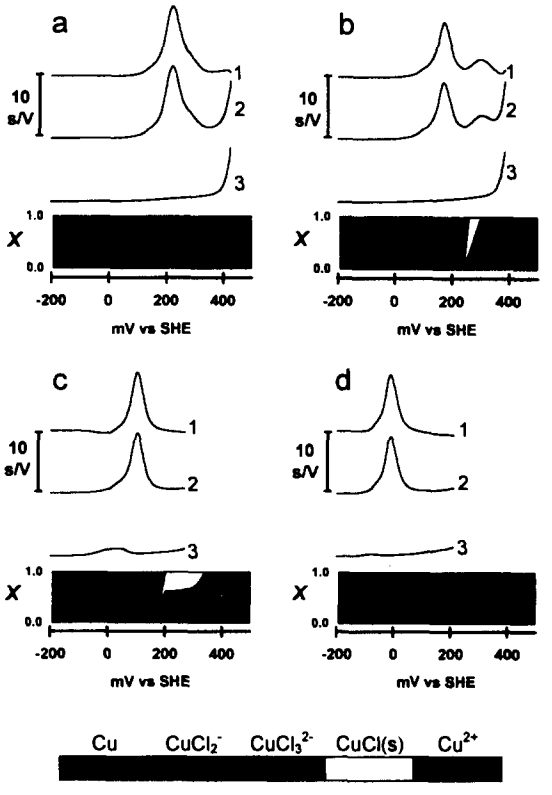


Fig. 3. Computer calculated molar fraction diagrams for the electrochemical oxidation of copper in (a) 0.001 (b) 0.01 (c) 0.10 and (d) 1.00 M hydrochloric acid. Comparison with experimental results obtained after electrolysis for 5 min in samples containing 50 μg $l^{-1}$ of copper(II) and subsequent stripping in (a) 0.001 (b) 0.01 (c) 0.10 and (d) 1.00 M hydrochloric acid. (1) Background corrected stripping curves, (2) analytical curves and (3) background curves.

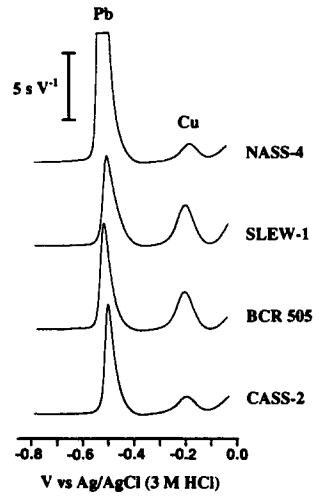


Fig. 4. Stripping potentiometry curves obtained in the determination of copper(II) in four different reference seawater samples to which 5 μg $l^{-1}$ of lead(II) had been added as internal standard. Electrolysis for 5 min (NASS-4, 15 min) was carried out prior to stripping in 7.5 M ammonium acetate–2.5 M acetic acid (see Table 2).

1.00 M, only soluble copper(I) species are formed, $CuCl_2^-$ being the predominant one.

### 4.3. Determination of copper(II) in seawater reference samples

The three-in-one electrode design used in this investigation makes it possible to choose the stripping medium composition independent of the sample composition. A stripping medium to be used for the determination of copper(II) in the ng $l^{-1}$ range must, of course, be extremely pure with respect to copper(II). Further, the stripping medium should, preferably, be a concentrated electrolyte so that the dissolved oxygen concentration is low and the viscosity high, both properties decreasing the chemical oxidation rate [23]. The ammonium acetate–acetic acid medium used in this investigation fulfils these requirements.

Fig. 4 shows the background corrected stripping curves, obtained after electrolysis for 5 min (15 min for NASS-4) in four different seawater reference samples, with a certified copper(II) concentration ranging between 0.23 and 1.7 μg $l^{-1}$, and subsequent stripping in ammonium acetate–acetic acid solution with a constant current equal to 1 μA. Prior to analysis, 5 μg $l^{-1}$ of lead(II) had been added to the samples as internal standard. The copper(II) concentrations in the reference samples were evaluated subsequent to calibration in a sample containing 1 μg $l^{-1}$ of copper(II) and 5 μg $l^{-1}$ lead(II) in 0.025 M hydrochloric acid. The results, evaluated with and without internal standard, are shown in Table 2. The reference value given for BCR 505 in Table 2 was obtained employing the solvent extraction/graphite furnace method described by Danielsson et al. [24].

As can be seen from Table 2, the results obtained by the proposed method agree satisfactorily with the certified values for the seawater reference samples. The value obtained for the deep ocean sample NASS-4 is, for unknown reasons, significantly below the certified range. As is also seen from Table 2, the relative standard deviation of the proposed method is in the range 6–10%, both with and without internal standard.

### 4.4. Detection limit, sensitivity and linear range

The detection limit of the proposed method was studied by adding known copper(II) concentrations to the blank solution. Fig. 5 shows the background corrected stripping curves obtained after the addition of 0, 10, 20, 40, 60, 80 and 100 ng $l^{-1}$ of copper(II) and electrolysis for 15 min prior to stripping in the ammonium acetate–acetic acid medium with a constant current of 1 μA. Also shown in Fig. 5 is the calibration plot, the correlation coefficient being equal to 0.9958, the intercept on the concentration axis equal to −0.90 ng $l^{-1}$ and the slope 0.35 ms l $ng^{-1}$.

The minimum detectable signal when using a 90 kHz potentiometric stripping analyser is normally 0.2–0.3 ms, corresponding to approximately 20–30 real time measurements. Since, however, the copper stripping peak is close to the commencement of mercury oxidation, the background is higher than it is for e.g. lead and cadmium [25], which makes the background correction difficult. A detection limit of 2 ms, corresponding to a copper(II) concentration of approximately 6 ng $l^{-1}$ (0.10 nM) after 15 min of electrolysis, is thus a more realistic value for the detection limit (see Fig. 5).

The linear range was investigated by analysing blank solutions to which 0, 1, 2, 3, 4 and 5 μg $l^{-1}$ of copper(II) had been added, the time for electrolysis being 15 min and the stripping current 1 μA. The correlation coefficient of the calibration plot was 0.9999 ($n = 6$), the intercept on the concentration axis −0.025 μg $l^{-1}$ and the sensitivity 0.28 ms l $ng^{-1}$. The last number indicates that the sensitivity decreases

Table 2
Copper(II) determination in seawater reference samples. The reference value for BCR 505 was obtained according to the method of Danielsson et al. [24]

| Reference sample | Electrolysis time (min) | Certified range ($\mu g\,l^{-1}$) | $[Cu]_{found} \pm \sigma$ ($\mu g\,l^{-1}$)($n = 6$) | |
|---|---|---|---|---|
| | | | With internal standard | Without internal standard |
| SLEW-1 | 5 | 1.67–1.85 | $1.66 \pm 0.10$ | $1.55 \pm 0.09$ |
| BCR 505 | 5 | (1.65) | $1.63 \pm 0.07$ | $1.59 \pm 0.06$ |
| CASS-2 | 5 | 0.636–0.714 | $0.682 \pm 0.062$ | $0.652 \pm 0.062$ |
| NASS-4 | 15 | 0.217–0.239 | $0.186 \pm 0.009$ | $0.176 \pm 0.010$ |

slightly as the sample concentration of the analyte is increased, as is frequently the case in electroanalytical stripping techniques.

## 5. Discussion and conclusions

The experimental results and the computer calculations clearly show that the reactions taking place on the electrochemical stripping oxidation of copper are highly dependent on the chloride concentration in the oxidation medium. Copper(II) species only dominate at chloride concentrations below about 1 mM, i.e. at concentrations considerably lower than in most real samples. In the concentration range 1–100 mM, both copper(I) and copper(II) species are formed. The interpretation of the stripping data in this concentration range is further complicated by the fact that copper(I) species initially formed, and remaining in the vicinity of the electrode surface, can be further oxidised giving rise to an overlapping peak. Since, furthermore, the fraction of copper(I) species oxidised to copper(II) is highly dependent on the hydrodynamic conditions at the electrode surface, the second stripping peak is frequently very irreproducible. A further complication is that solid copper(I) chloride can be formed. This adheres to the electrode surface and is only partly oxidised to soluble copper(II) species. It is, however, easily reduced on an electrode surface. Consequently, if the same mercury film is used for consecutive analysis, as is frequently the case, copper(I) chloride will be carried from one sample to the next yielding an overly high copper stripping signal in this sample. Medium exchange, as used here, is obviously one way of circumventing the problem arising from varying chloride concentrations in real samples. If this possibility is not available, an alternative way of solving the problem would be the addition of excess chloride, e.g. 1 M hydrochloric acid, to each sample prior to analysis. In this way, formation of solid copper(I) chloride is prevented and, moreover, hydrochloric acid is normally free from copper(II) impurities.

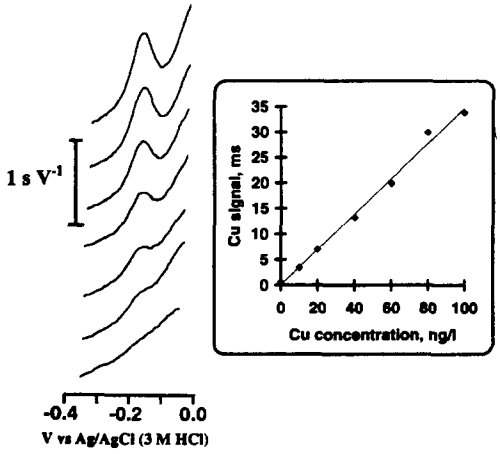


Fig. 5. Stripping potentiometry curves (left) and calibration plot (right) obtained after 15 min of electrolysis in samples containing (from the bottom) 0, 10, 20, 40, 60, 80 and 100 $ng\,l^{-1}$ of copper(II) and subsequent stripping in 7.5 M ammonium acetate–2.5 M acetic acid.

A medium exchange procedure, similar to that described in this article, has previously been applied to the determination of cadmium(II) and lead(II) in seawater [25]. In this investigation a detection limit equal to 0.2 $ng\,l^{-1}$ was obtained for cadmium(II) by exploiting a multiple stripping procedure. On a molar scale, this is approximately 50 times lower than that obtained for copper(II) in this investigation. The main reason for this is that multiple stripping cannot be used for the determination of copper owing to the high background close to the commencement of mercury oxidation, which makes the re-reduction efficiency very low [25]. Another reason for the difference in detection limit is, of course, that oxidation of copper in the stripping medium involves only one electron while lead and cad-

mium are always oxidised to their divalent oxidation states.

Although not demonstrated here, the proposed medium exchange procedure would, undoubtedly, be suitable for the study of copper(II) speciation and copper(II) complexing capacity [26–30] in natural waters. Specific advantages would be that mercury(II) ions do not have to be used, the addition of which to the natural water might alter the equilibria. Further, oxidation of copper would always take place under uniform conditions making the interpretation of the results considerably simpler. From a practical point of view, the investigations could, moreover, be made fully automatic taking advantage of the sample changer and flexible software of the stripping analyser.

## Acknowledgements

The authors acknowledge the support of this work by the Swedish Natural Science Research Council.

## References

[1] G.E. Batley, Anal. Chim. Acta, 189 (1986) 371.
[2] A. Nelson, Anal. Chim. Acta, 169 (1985) 273.
[3] A. Nelson, Anal. Chim. Acta, 169 (1985) 287.
[4] A. Nelson and R.F.C. Mantoura, J. Electroanal. Chem., 164 (1984) 237.
[5] A. Nelson and R.F.C. Mantoura, J. Electroanal. Chem., 164 (1984) 253.
[6] A. Nelson and R.F.C. Mantoura, J. Electroanal. Chem., 164 (1984) 265.
[7] M. Boussemart, L. Menargues and J.Y. Benaim, Electroanalysis, 5 (1993) 125.
[8] D. Jagner, L. Renman and Y. Wang, Electroanalysis, 4 (1992) 267.
[9] N. Linnet, pH Measurement in Theory and Practice, 1st edn., Radiometer A/S, Copenhagen, 1970, p. 168.
[10] L. Almestrand, M. Betti, C. Hua, D. Jagner and L. Renman, Anal. Chim. Acta, 209 (1988) 399.
[11] N. Ingri, W. Kakolowicz, L.G. Sillén and B. Warnqvist, Talanta, 14 (1967) 1261.
[12] L. Renman, unpublished work, 1995.
[13] L.G. Sillén and E. Martell, Stability Constants of Metal Ion Complexes, Special Publication No. 17, The Chemical Society, London, 1964.
[14] S. Ahrland and J. Rawsthorne, Acta Chem. Scand., 24 (1970) 157.
[15] J.J. Fritz, J. Phys. Chem., 84 (1980) 2241.
[16] CRC Handbook of Chemistry and Physics, 65th edn., CRC Press, Boca Raton, FL, 1984–1985, p. D-156.
[17] T.G. Sukhova, O.N. Temkin, R.M. Flid and T.K. Kaliya, Russ. J. Inorg. Chem., 13 (1968) 1072.
[18] H. Hikita, H. Ishikawa and N. Esaka, Nippon Kagaku Kaishi, 1 (1973) 13.
[19] T.G. Sukhova, N.Ya. Borshch, O.N. Temkin and R.M. Flid, Russ. J. Inorg. Chem., 14 (1969) 362.
[20] T. Hurlen, Acta Chem. Scand., 15 (1961) 1231.
[21] J. Buffle, J. Electroanal. Chem., 125 (1981) 273.
[22] D. Jagner and Y. Wang, Electroanalysis, 7 (1995) 614.
[23] D. Dyrssen, H. Eskilsson and C. Haraldsson, J. Electroanal. Chem., 262 (1989) 161.
[24] L.G. Danielsson, B. Magnusson and S. Westerlund, Anal. Chim. Acta, 98 (1978) 47.
[25] D. Jagner, E. Sahlin and L. Renman, Talanta, 41 (1994) 515.
[26] R. Pardo, E. Barrado, M. Vega, L. Deban and M.L. Tascon, Water Res., 28 (1994) 2139.
[27] J. Labuda, M. Vanickova, E. Uhlemann and W. Mickler, Anal. Chim. Acta, 284 (1994) 517.
[28] V.N. Iyer and R. Sarin, Anal. Lett., 25 (1992) 1915.
[29] T. Miwa, A. Mizuike and M. Murakami, Anal. Chim. Acta, 219 (1989) 1.
[30] H.M.V.M. Soares and M.T.S.D. Vasconcelos, Anal. Chim. Acta, 293 (1994) 261.

ELSEVIER

Talanta 42 (1995) 1457–1463

Talanta

# Determination of carbaryl as its primary metabolite, 1-naphthol, by reversed-phase high-performance liquid chromatography with fluorometric detection

Kurt A. Massey [a], Debra L. Van Engelen [a,*], Isiah M. Warner [b]

[a] *Department of Chemistry, University of North Carolina at Asheville, Asheville, NC 28804, USA*
[b] *Department of Chemistry, Louisiana State University, Baton Rouge, LA 70803, USA*

Received 6 January 1995; revised 22 March 1995; accepted 23 March 1995

**Abstract**

Carbaryl and its hydrolysis product, 1-naphthol, are determined simultaneously, and in a mixture of other pesticides, by reversed-phase high-performance liquid chromatography (HPLC). Fluorometric detection affords a higher degree of selectivity than absorbance detection, while providing detection limits of 1.0 ng $ml^{-1}$ and 1.4 mg $ml^{-1}$ for 1-naphthol and carbaryl, respectively. The described method requires no enrichment of samples and includes a simple hydrolysis step. Additionally, enhancement of fluorescence detection signal intensity is explored through HPLC solvent composition effects as well as through formation of cyclodextrin inclusion complexes. The method described in this report is a selective and fast alternative to the currently accepted U.S. Environmental Protection Agency (EPA) method of detection carbaryl in ground water.

## 1. Introduction

Carbaryl ($C_{12}H_{11}NO_2$), a member of the carbamate class of nitrogen-containing organic pesticides, is a broad spectrum pesticide, and is extensively used owing to its effectiveness and relatively low acute mammalian toxicology (560 mg $kg^{-1}$) [1]. Carbaryl is an inhibitor of acetylcholinesterase and is degraded very rapidly compared to other classes of pesticides, such as the organophosphorus esters [2]. Unfortunately, the primary metabolite of carbaryl, 1-naphthol, is as toxic to many marine invertebrates as the parent pesticide. Owing to the widespread use of carbaryl, as well as the toxicity of its hydrolysis product, a rapid, selective, economical and sensitive method is needed to monitor both compounds in enviromental water samples.

The carbamate class of pesticides is characterized by susceptibility to thermal degradation, which complicates determination by gas chromatography or any other method involving temperatures significantly above ambient [3]. Therefore, methods used to determine carbaryl content implement primarily high-performance liquid chromatography (HPLC) with either UV/vis absorbance or fluorescence detection, owing to the non-thermal properties of this method [4–6]. Derivatization, followed by fluorometric measurement, is another useful means of detection [7]. Carbaryl can also be hydrolyzed and reacted with diazotized sulfanillic acid, and the carbaryl content subsequently determined with a spectrophotometer [8]. Enviromental Protection Agency (EPA) Method 531.1 prescribes hydrolysis of carbaryl and then derivatization, followed by fluorometric detection. The retention time of carbaryl for the EPA method is approximately 20.29 min and the estimated detection limit is 2.0 ng $ml^{-1}$.

* Corresponding author. Fax: (704) 251-6002.


*SSDI* 0039-9140(95)01595-7

Although both carbaryl and 1-naphthol (as the 1-naphtholate ion) fluoresce, 1-naphtholate is more sensitive to fluorescence detection over the experimental range of $1.0-10^3$ ng ml$^{-1}$. Given the greater relative fluroescence intensity of 1-naphtholate than that observed for carbaryl, a reversed-phase HPLC method was devised to detect 1-naphthol as the hydrolysis product of carbaryl. Detection of carbaryl by this coupled assay provides a lower detection limit for the pesticide, because 1-naphthol can be determined in lower quantities than can carbaryl by direct analysis.

Cyclodextrin inclusion complexes and variations in HPLC solvent composition were also studied with regards to their effect upon the fluorescence spectra of carbaryl and 1-naphthol. The modifications in the mobile-phase matrix could be implemented to improve the detection limits of carbaryl or 1-naphthol in solution where fluorometric detection is employed.

Carbaryl, as well as its hydrolysis product 1-naphthol, forms inclusion complexes with certain cyclodextrins (CDs). CDs are cyclic oligosaccharides composed of six or more glucopyranose units bonded via 1–4 ether linkages [9]. The inclusion complex is characterized by a guest molecule physically moving into the hydrophobic inner cavity of the CD. The pesticide/CD complex is dependent upon the spatial qualities of the pesticide relative to those of the internal cavity of the CD ring, as well as the polarity of the pesticide. Three native varieties of CDs are available: alpha ($\alpha$), beta ($\beta$) and gamma ($\gamma$), with internal cavity diameters of 0.57, 0.78 and 0.98 nm respectively. Complexation alters physical and chemical properties of the guest molecule, such as availability of substituents for reactions and interaction with the stationary phase in HPLC.

Cyclodextrin complexation has been shown to increase luminescence efficiency with certain compounds versus that observed in a bulk solution of water. The factors responsible for this increase in luminescence efficiency are: (1) shielding of the analyte molecule from quenching due to water molecules or water-borne quenchers, (2) decrease in oxygen quenching, and (3) the analyte experiencing a less polar and more rigid local microenviroment [10]. Far fewer compounds fluoresce than absorb strongly, so fluorescence is a more selective method of detection than absorbance. If the fluorophor exhibits increased emission intensity due to CD complexation, it can be determined at a lower detection limit.

The described HPLC procedure to detect 1-naphthol as the hydrolysis product of carbaryl is fast, highly selective, sensitive, accurate, economical and little sample preparation is required. Other benefits are few possible interferents and the lack of necessity for a complex derivatization procedure. This procedure is effective for the simultaneous determination of carbaryl and 1-naphthol, and could prove environmentally useful in the monitoring of agricultural drainage as well as water supplies. Economy is another asset over EPA Method 531.1, as no post-column reaction equipment is required. Also, CD inclusion studies provide information which may be used to improve the fluorometric analysis of carbaryl or its hydrolysis product.

## 2. Experimental

### 2.1. Reagents

All reagents were used without further purification, with the exception of 1-naphthol. Water, methanol and acetonitrile were HPLC grade and purchased from Mallinkrodt. The NaOH was 99% pure from Fisher and the HCl was obtained from EM Science. A borax/NaOH buffer was prepared with pH $\approx$ 10 from 99% pure reagents from Fisher.

The carbaryl was 99+% pure from Reagents, Inc. and the 1-naphthol was Sigma Grade 3 obtained from Aldrich. Recrystallization of 1-naphthol was performed in chloroform. Stock solutions were prepared for carbaryl and 1-naphthol by dissolving an appropriate quantity of the compound in HPLC-grade methanol to give a final concentration of 0.2 ng ml$^{-1}$. The carbaryl and 1-naphthol were stored with refrigeration and prepared every two weeks. Serial dilutions were made from these stock solutions in order to obtain experimental concentrations. Methanolic NaOH (5%) was prepared with HPLC-grade water, HPLC-grade methanol and 99% pure Fisher NaOH pellets.

CDs and CD derivatives were provided by Amaizo and also purchased from Aldrich. All CDs were used without further purification; however, a method of purification has recently been developed should impurities in the CD present a problem [11].

### 2.2. Apparatus

Steady-state fluorescence measurements were taken using a Spex Industries Model 1680 Fluorometer with accompanying fluroescence management software, also by Spex.

A Bronson 3200 Sonic Bath was used for preparation of experimental solutions to expedite dissolution.

HPLC experiments were performed on a Bio Rad series 800 HRLC system. The solvent delivery system was Bio Rad model 2700 and the fluroescence detector was Fluor LC model 304 by Linear. An automated sampling system was employed. The HPLC reversed-phase column was a Zorbax $C_8$.

### 2.3. Procedure

All fluorometric determinations were performed at ambient temperature. Excitation wavelengths used were 282 nm and 330 nm for carbaryl and 1-naphthol, respectively. Maximum emission occurs around 333 nm for carbaryl and 472 nm for 1-naphthol, which is actually the 1-naphtholate ion and not the molecular form in this method. Incident radiation and emission bandwidths were both 5 nm for steady-state fluorometric determinations, and 5 nm for the HPLC detector. The integration time constant was 0.5 s with a wavelength resolution of 1 nm. Each experiment was performed three times to ensure reproducibility. All solutions were sonicated for 30 min and allowed to cool to room temperature before fluorometric determination of HPLC analysis of the sample. A water bath was not employed, as no experimental variation was noted with minor fluctuations in column temperature.

All experimental solutions were prepared by dilution of the stock methanol solution containing the 1-naphthol or carbaryl in an appropriate volume of the aqueous experimental solution for steady-state fluorometric analysis, or methanol for HPLC analysis of the sample. A borax/NaOH buffer with a pH of $\approx 10$ was prepared with HPLC-grade water and used as the aqueous portion for each experimental solution requiring water, unless otherwise specified.

Preliminary experiments involved the determination of relative fluorescence intensities for carbaryl versus 1-naphthol. Relative sensitivities were then calculated for both compounds over a range of $1.0–2.0 \times 10^3$ ng ml$^{-1}$.

Solvent composition was varied in order to optimize the mobile-phase composition, providing maximum fluorescence enhancement. The mobile phase was a standard aqueous/organic composition. Methanol and acetonitrile were compared as organic components of the mobile phase.

Once fluorescence enhancement data had been acquired, the method for hydrolyzing carbaryl to 1-naphthol was developed. The rate of hydrolysis of carbaryl is a function of pH and solvent used [12]. The method of hydrolysis used in this report is similar to one defined in previous literature regarding the kinetic determination of carbaryl and its hydrolysis product, 1-naphthol [1]. An appropriate quantity of the stock methanolic solution of carbaryl, to provide the desired final concentration, was spiked into a 10 ml volumetric flask. One ml of 5% methanolic 2 M sodium hydroxide was then added, and the mixture allowed to stand in the dark for 15 min to allow complete hydrolysis. One ml of 2 M hydrochloric acid was then added to neutralize the base and terminate the hydrolysis reaction. The final step was dilution to the mark with methanol for HPLC experiments, or the appropriate buffer or solution for steady-state fluorescence measurements.

The optimized experimental conditions for the described procedure are as follows. A mobile-phase matrix of 45:55 acetonitrile/water was utilized. The fluorescence detector was adjusted to $\lambda_{ex} = 330$ nm and $\lambda_{em} = 472$ nm, which are the relative maxima of the 1-naphtholate anion. A buffer of pH 10 was used as the aqueous portion of the mobile phase, as fluorescence of 1-naphtholate is considerably greater than that of the molecular form and significantly larger than cation fluorescence. It should be noted that the described procedure actually only detects the 1-naphtholate ion. Although the molecular form does fluoresce, the observed emission wavelength is around 345 nm. To avoid confusion over which ionic/molecular form of this compound is being assayed, the molecular form is not measured and any appearance of 1-naphthol in the discussion should be considered to refer to the anionic form.

Although the final procedure does not include a CD-modified mobile phase, additional observations regarding this topic are included owing to possible application in future methods. Adequate details involving CD-modified

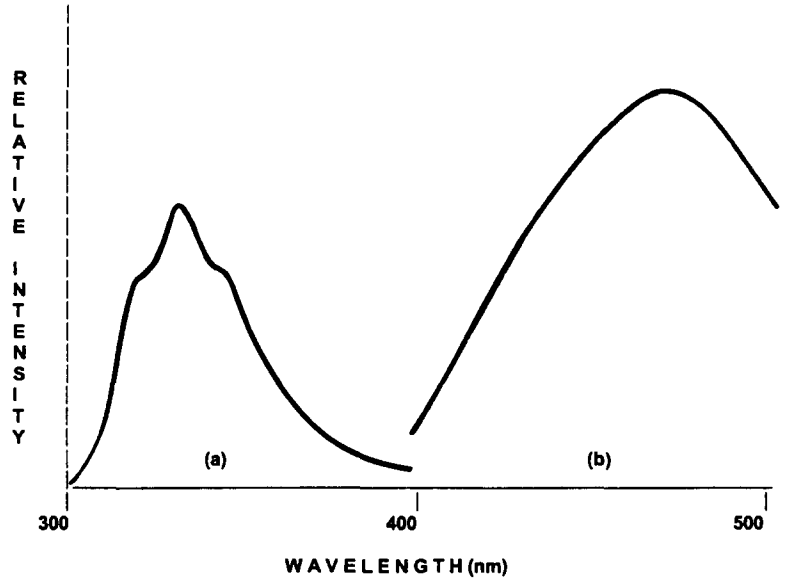


Fig. 1. Relative fluorescence intensity of 1-naphtholate (b), which is greater than that of an equimolar quantity of carbaryl (a) in aqueous solution.

mobile-phase compositions are provided to incorporate such improvements into this or similar procedures, where fluorescence enhancement and/or retention time decreases would be beneficial.

The final experiments prove the selectivity of this method for determining the concentration of carbaryl via its hydrolysis product in a mixture of four other commonly used pesticides and herbicides which could act as possible interferents. Additionally, carbaryl and 1-naphthol were simultaneously assayed in a mixture of the two, without other pesticides present. For the simultaneous determination of carbaryl and 1-naphthol, each analyte was present at similar concentrations.

The four pesticides combined with carbaryl were: azinphos-methyl, methomyl, chlorimuron ethyl and aldicarb. These pesticides (possible interferents) were spiked into the sample in identical (ng $ml^{-1}$) concentrations to that of the carbaryl. These experiments indicate the value of this method for the determination of carbaryl in a mixture of other pesticides, or in a solution with 1-naphtho initially present before hydrolysis.

## 3. Results and discussion

Results of the relative fluorescence emission intensity studies indicate that 1-naphtholate displays greater relative intensity than an equimolar concentration of carbaryl (see Fig. 1). The relative fluorescence intensity of $4.97 \pm 10^{-6}$ molar 1-naphthol (as the 1-naphtholate ion) was a factor of 1.33 greater than $4.97 \pm 10^{-6}$ molar carbaryl.

Likewise, carbaryl had a lower relative sensitivity than 1-naphthol, where relative sensitivity is a measure of signal change versus change in concentration. Given that 1-naphthol is more sensitive to fluorescence detection and is also characterized by greater relative fluorescence intensity, it is beneficial to perform trace-analysis of carbaryl via the determination of its hydrolysis product.

Fluorescence emission of 1-naphthol is also a function of the pH of the solution. The HPLC mobile phase was buffered at a pH of approximately 10.0, which was observed to be the pH of greatest luminescent efficiency for 1-naphthol. The hydrolysis of carbaryl takes place instantaneously in 2 M NaOH, which allowed for quick sample preparation. EPA Method 531.1 uses a post-column hydrolysis chamber as well as a derivitization reaction chamber. This requires additional reagent preparation and apparatus set-up, which is absent in the method presented here.

Control of pH was an important factor owing to the fact that high hydronium ion concentrations are known to quench fluorescence for 1-naphthol [13]. 1-Naphthol can experience efficient excited state ionization in solution. Since the anionic form is the one actually de-

termined by this method, the buffered mobile phase keeps the pH at an optimum level for ionization to occur, producing the highly fluorescent anion. It is possible to have both the molecular and anionic forms present in some binary aqueous–organic solvents. At low pH values, molecular 1-naphthol and ionic 1-naphtholate are converted to the 1-naphtholonium ion, which does not fluoresce. The use of a buffer should compensate for any pH changes due to volumetric errors that may occur when hydrolyzing carbaryl with sodium hydroxide and then adding an equimolar concentration of hydrochloric acid. A small pH variance in the experimental solutions used for HPLC determinations is not important, since the mobile phase is buffered and an isocratic solvent composition is used in this method.

The experimental yield of hydrolysis for the method described in the procedure section was confirmed to be 100% as follows. A solution of carbaryl was hydrolyzed as described above and the intensity of the fluorescence spectrum was compared to that of a known equimolar solution of 1-naphthol. Within experimental error, the results were identical in terms of fluorescence intensities for both the hydrolyzed sample and the prepared sample.

Once fluorescence data had been acquired in aqueous solution, different solvent compositions were studied fluorometrically in conjunction with carbaryl and 1-naphthol, in an attempt to develop an optimum mobile-phase composition which would provide maximum fluorescence enhancement. Methanol/water and acetonitrile/water solutions were investigated in order to maximize their effect on the fluorescence emission of 1-naphthol and carbaryl.

Solvent effects were an important factor in optimizing emission intensity. Methanol is not a suitable organic solvent for 1-naphthol owing to fluorescence quenching. A trend was noted in which increasingly concentrated methanol solutions quenched the observed fluorescence in proportion to the percentage of methanol by volume.

Acetonitrile was determined to be the most desirable organic solvent for use in the HPLC mobile phase. A concentration of 55% water and 45% acetonitrile, without CD, enhanced the relative fluorescence of 1-naphthol by a factor of 1.86 above that observed in an aqueous solution (see Table 1). The retention time for the hydrolyzed carbaryl on the $C_8$ column with a mobile phase of 55% water, 45% acetonitrile and pH 10 was approximately 3.3 min, which allows for rapid analysis. The $R_t$ for carbaryl was 5.2 min.

A calibration graph for 1-naphthol, and an estimate of the detection limit and the relative sensitivity over the range of $1.0–10^3$ ng ml$^{-1}$ was obtained experimentally by the use of HPLC. A line or fit to the calibration data with a correlation coefficient ($R$ value) of 0.997 was obtained. The calibration curve was linear over the experimental range of $1.0–10^3$ ng ml$^{-1}$ for 1-naphthol, allowing reasonably accurate extrapolation of data to determine experimental 1-naphthol concentrations.

Having verified the accuracy of 1-naphthol detection at low concentrations, a method was developed for the simultaneous determination of carbaryl and 1-naphthol by HPLC. Carbaryl and 1-naphthol can be assayed simultaneously be determining the 1-naphthol present before and after the sample has been hydrolyzed. The difference in 1-naphthol concentrations can be correlated with the molar quantity of carbaryl initially present. A series of experiments were designed to explore this possibility.

The selectivity available by this method should be noted. EPA Method 531.1 tests for approximately 10 of the *N*-methylcarbamoyloximes and *N*-methycarbamates. The presented method only tests for carbaryl and its primary metabolite, 1-naphthol. However, possibilities of peak overlap and interference are eliminated, as no compounds aside from the two analytes are detected in this procedure. This quality could prove an asset in a situation where only carbaryl and/or 1-naphthol are assayed.

Compared to EPA Method 531.1, with a carbaryl $R_t$ of over 20 min, the given procedure is much more conducive for rapid analysis as the actual analysis time is greatly reduced. Multiple sample assays should be less time-consuming as a result. Additionally, gradient elu-

Table 1
Simultaneous determination of carbaryl and its primary metabolite in the same sample via hydrolysis[a]

| Carbaryl spiked | 1-Naphthol spiked | Carbaryl determined | 1-Naphthol determined |
|---|---|---|---|
| 0.020 ppm | 0.015 ppm | 0.018 ppm | 0.014 ppm |

[a] HPLC mobile phase: 55% water, 45% acetonitrile, pH 10. $\lambda_{ex} = 330$ nm, $\lambda_{em} = 472$ nm. ($S$) = standard deviation of three replicate samples. ($S$) carbaryl = 0.000 071. ($S$) 1-naphthol = 0.0047.

Table 2
Determination of carbaryl in a mixture of other pesticides via hydrolysis (carbaryl + aldicarb, azinphos-methyl, chlorimuron ethyl and methomyl)[a]

| Carbaryl spiked | Others spiked | Carbaryl determined | (S) carbaryl |
|---|---|---|---|
| 0.020 ppm | 0.020 ppm | 0.017 ppm | 0.007 |
| 0.112 ppm | 0.100 ppm | 0.106 ppm | 0.003 |
| 0.700 ppm | 0.700 ppm | 0.690 ppm | 0.007 |

[a] HPLC mobile phase: 55% water, 45% acetonitrile, pH 10. $\lambda_{ex} = 330$ nm, $\lambda_{em} = 472$ nm. (S) = standard deviation of three replicate samples.

tion techniques are not utilized, which translates to fewer equipment requirements. A single eluent suffices here, because essentially one compound is being assayed and separations are rendered unnecessary owing to the selective nature of this scheme.

Table 1 provides results for the simultaneous determination of carbaryl and 1-naphthol in the same solution, which were the only compounds present. This experiment involved the determination of 1-naphthol initially present followed by a hydrolysis step. After hydrolysis, the 1-naphthol was determined again and the difference in 1-naphthol concentrations represented the molar quantity of carbaryl initially present. Standard deviations were within accepted ranges given the concentrations of the analytes.

Table 2 represents data from a series of experiments designed to determine carbaryl at varying concentrations in the presence of other pesticides and herbicides, which could possibly be found along with carbaryl in environmental samples. For each solution, the four additional compounds were present at approximately the same concentration as carbaryl. None of the additional pesticides were detected in this scheme and there was no interferents in the detection of the hydrolysis product of carbaryl. Sample solutions were prepared in methanol with carbaryl and a combination of four other pesticides and herbicides (see Table 2). Each experiment was repeated three times and the standard deviations (S) estimated. The experiments involving hydrolysis of a mixture of pesticides, including carbaryl, gave highly reproducible results.

Experiments were also performed with varying mobile-phase media to possibly improve upon the coupled assay described in this report. When a suitable organic mobile-phase component had been identified, the effects of native CDs as well as β-CD derivatives were investigated fluorometrically to determine if the fluorescence intensity of 1-naphthol could be further increased. The derivatized CDs examined were: hydroxypropyl-β-CD, hydroxyethyl-β-CD, heptakis (tri-o-methyl)-β-CD and heptakis(2,6-di-o-methyl)-β-CD. Previous literature suggests the possible advantages of these derivatives over the native CDs [9]. The solubilities of the CD derivatives are usually much greater in water-based solutions than those of the native CDs.

Table 3 summarizes a series of experiments designed to determine the effects of various solvent compositions and CD inclusions on the fluorescence emission intensities of 1-naphthol and carbaryl.

The greatest fluorescence enhancement for carbaryl occurred in a 50/50 aqueous/methanol solution with β-CD. Steady-state fluorescence enhancement was increased by a factor of 1.77 above that observed for native carbaryl in a bulk aqueous solution. The CD derivative, hydroxypropyl-β-CD, had the greatest fluorescence enhancement factor for 1-naphthol in a pure aqueous solution.

Native β-CD had a greater enhancement factor for 1-naphthol than heptakis(2,6-di-o-methyl)-β-CD, heptakis(tri-o-CD and hydroxyethyl-β-CD. Urea-solubilized β-CD solutions were also tried with limited success. Although native β-CD is only soluble to approximately 14 mM in water, it performed significantly bet-

Table 3
Solvent and cyclodextrin effects on fluorescence intensity of 1-naphthol

| 0.72 ppm 1-naphthol + | Fluorescence enhancement factor |
|---|---|
| water | 1.00 |
| methanol | 0.58 |
| aq. 2 mM β-CD | 1.55 |
| aq. 6 mM β-CD | 1.57 |
| aq. 10 mM β-CD | 1.60 |
| aq. 14 mM β-CD | 1.50 |
| aq. 8.5 M urea/0.2 M β-CD | 1.22 |
| aq. 0.2 M hydroxypropyl β-CD | 1.94 |
| aq. 0.2 M heptakis(D-o-M)-β-CD | 0.80 |
| aq. 0.2 M heptakis(T-o-M)-β-CD | 0.80 |
| aq. 0.2 M hydroxyethyl-β-CD | 1.56 |
| aq. 2 mM α-CD | 1.05 |
| aq. 2 mM γ-CD | 1.05 |
| 55% water/45% acetontrile | 1.86 |

ter than the two other commonly used native CDs, i.e. alpha ($\alpha$) and gamma ($\gamma$). Both $\alpha$-CD and $\gamma$-CD enhanced the fluorescence of 1-naphthol by factors of 1.05, while $\beta$-CD gave an enhancement factor of 1.60 for 1-naphthol in aqueous solution.

CD complexes coupled with mobile-phase solvent conditions provided greater emission intensity than the solvent effect alone, for both carbaryl and 1-naphthol. CDs should be considered as a component of the mobile phase for future fluorometric analysis of carbaryl and 1-naphthol.

The CD-modified acetonitrile/water mobile phase did not enhance the fluorescence intensity of 1-naphthol over that of the same mobile phase without the presence of the CD. The relative emission intensity was independent of the presence of CD. The relative emission intensity was independent of the presence of CD. However, when the CD was present, a 10% decrease in retention time for 1-naphthol was observed. The pesticide/CD complex might not be expected to occur in a acetonitrile mobile phase owing to competition from the acetontrile to occupy the hydrophobic cavity of the CD. Although 1-naphthol fluorescence intensity is unaltered in the CD/acetonitrile/water matrix, the shortened retention time would indicate increased interaction with the mobile phase when CD is present. Whether a complex is actually forming or some other mechanism exists to decrease the retention time will be explored in the future.

This HPLC method exhibited sensitivity, speed and high selectivity with good precision. The greatest potential for an interferent would be another compound which hydrolyzes to 1-naphthol, which is unlikely. The limits of detection were 1.0 ng $ml^{-1}$ and 1.4 ng $ml^{-1}$ for 1-naphthol and carbaryl, respectively. These detection limits are comparable to those of other methods [14–16]. The detection limit obtained here for carbaryl is certainly comparable to that of the EPA method, which is 2 ng $ml^{-1}$. No complex derivatizations were necessary as in other commonly used procedures [17,18], which makes this method an attractive alternative to determine carbaryl or its metabolite in a variety of water sources.

## Acknowledgments

I.M. Warner acknowledges the support of NSF (CHE-9001412). Funding for this research was also provided in part by supplementary grants from The National Science Foundation, Research Experience for Undergraduates Award and a Research Opportunity Award. We wish to thank George Reed of American Maize for providing some of the cyclodextrins used for this study.

## References

[1] M.C. Quintero, M. Silva and D. Perez-Bendito, Talanta, 35 (1988) 943.
[2] J.R. Straight, G.C. Thronwall and M. Ehrich, J. Agric. Food Chem., 39 (1991) 710.
[3] R.J. Bushway, J. Chromatogr., 457 (1988) 437.
[4] P. Bottomley and P.G. Baker, Analyst, 109 (1984) 85.
[5] C.H. Marvin, I.D. Brindle, C.D. Hall and M. Chiba, J. Chromatogr., 503 (1990) 167.
[6] Sm M. Lee, M.L. Papthakis, H.C. Feng, G.F. Hunter and J.E. Carr, Fresnius' J. Anal. Chem., 339 (1991) 376.
[7] T. Yoshida, H. Taniguchi, S. Otuka and S. Nakano, Chem. Pharm. Bull., 37 (1989) 1823.
[8] K.M. Appaioch, U.C. Nag, O.P. Kopur and K.V. Nagahara, J. Food Sci. Technol., 20 (1983) 252.
[9] R.P. Frankewich, K.N. Thimmaiah and W.L. Hinze, Anal. Chem., 63 (1991) 2924.
[10] W.L. Hinze, N. Srinvasan, T.K. Smith, S. Igarashi and H. Hoshino, in I.M. Warner and L.B. McGown (Eds.), Advances in Multidimensional Luminescence, Vol. 1, JAI Press, Greenwich, 1991, Chapter 8, pp. 149–206.
[11] A. Sophianopoulus and I.M. Warner, Anal. Chem., 64 (1992) 2652.
[12] J.J. Aaron and N. Some, Analusis, 10 (1982) 481.
[13] R.A. Agbaria, B. Uzan and D. Gill, J. Phys. Chem., 93 (1989) 3856.
[14] C.J. Miles and H.A. Moye, Chromatographia, 24 (1987) 628.
[15] F.G. Sanchez and C.C. Blanco, Talanta, 37 (1990) 573.
[16] J. Sanceón, J.L. Carrión and M. De La Guardia, Talanta, 36 (1989) 1165.
[17] M.T. Tena, M.D. Luque de Castro and M. Valcarcel, J. Chromatrgr. Sci., 30 (1982) 276.
[18] C.J. Miles, J. Chromatrogr., 592 (1992) 283.

ELSEVIER

Talanta 42 (1995) 1465–1469

Talanta

# Determination of hydrazine derivatives by flow-injection analysis with spectrophotometric detection

M.I. Evgen'yev [a,*], S.Y. Garmonov [a], I.I. Evgen'yeva [a], H.C. Budnikov [b]

[a] *Department of Analytical Chemistry, Faculty of Oil, Kazan State Technological University, 420015, Kazan, Russia*
[b] *Department of Analytical Chemistry, Faculty of Chemistry, Kazan State University, 420008 Kazan, Russia*

Received 18 August 1994; accepted in final form 21 March 1995

**Abstract**

Flow-injection analysis for the determination of hydrazine derivatives based on their nucleophilic substitution reaction with 4-chloro-5,7-dinitrobenzofurazan in aqueous medium, and spectrophotometric detection has been described. The calibration graphs were linear in the range from 0.15 to 4.0 μg $ml^{-1}$ of hydrazine derivatives, with sampling rates of up to 28–32 samples $h^{-1}$. Interferences from amino compounds, benzoic acids, aliphatic amines and ammonia have been evaluated. The procedure has been applied to the determination of hydrazine derivatives in serum, urine, apressin drugs and artificial mixtures.

## 1. Introduction

Hydrazine derivatives (hydrazides and N-substituted hydrazines) are very important groups of organic compounds, having various applications in analytical chemistry [1]. Many of these substances are physiologically active and are used as a remedy against tuberculosis, leprosy, mental disorder and hypotension. Various analytical techniques have been applied for their determination in biological fluids, drugs and other substances. Among the assay procedures listed in official compendia [2], titrimetric methods for the determination of pure drugs are most widely used. Other methods described in the literature are based on high-performance liquid chromatography [3–5], gas chromatography [6], fluorimetry [7], colorimetry and specrophotometry [8–10]. In these cases, the preliminary derivatization of the compounds under determination by various reagents (4-dimethylaminobenzaldehyde, 2,4-pentadione, 3-salicyclic aldehyde, 4-trinitrobenzenesulfonic acid and others) is needed. However, these reactions are rather slow and often demand high temperatures [11]. That is why their applications in a flow-injection analysis (FIA) system for the determination of hydrazine derivatives is undesirable. Besides, the spectral characteristics of the reaction products formed from the substituted hydrazines and other amino compounds (alkylamines, amino acids, etc.) are similar. Therefore, the utilization of these reactions in the FIA of compounds of complicated composition with spectrophotometric detection is restricted. At the same time, there is a necessary to use FIA for the determination of substituted hydrazines in various substances.

The application of 4-chloro-5,7-dinitrobenzofurazan (DNBF) in selective spectrophotometric determinations of hydrazine, hydrazides acids and arylamines in complicated mixtures containing alkylamines, phenols, amino acids and other organic and inorganic substances has been described in previous papers [12–15]. It was stated that DNBF exhibited high reactivity in modification reactions with amino compounds. The colored products have high molar

* Corresponding author.


*SSDI* 0039-9140(95)01596-5

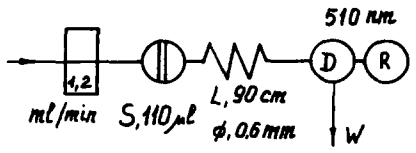


Fig. 1. Manifold used for the determination of hydrazine derivatives.

absorptivity. The application of DNBF in FIA determinations of the substituted hydrazines in pure forms of drugs, tablets and biological matrix is of great interest.

## 2. Experimental

### 2.1. Apparatus

The Carl Zeiss Jena M-40 (Germany) and LOMO SF-26 (Russia) spectrophotometers with 10 mm pathlength glass cells were applied for spectral recording and absorbance measurements, and a Pracitronic MV-87S pH-meter was used for pH measurements. The home-made flow-injection system (see Fig. 1) consisted of a Zalimp 304 peristaltic pump (Poland), Mikrotechna six-way injection valve and SPECOL-210 (Carl Zeiss Jena) spectrophotometer, with a 5 mm pathlength glass microcell as a detector. The connecting tubes were 0.6 mm bore PTFE, and end fittings and connectors (Microtechna) were applied. The output of the detector was monitored by a Carl Zeiss Iena K-100 chart recorder.

Sendimentation of proteins from biological liquids was performed using a centrifuge K-23 (Janetzki).

### 2.2. Reagents

All inorganic chemicals were of analytical-reagent grade and were used without further purification. Doubly-distilled water was used throughout.

DNBF was prepared as previously described [14]. A 0.02 M solution of DNBF was prepared by dissolution in pure acetonitrile.

$10^{-3}$ M stock solutions of isonicotinic (isoniazide, INH), diphenylphosphinylacetic (phosphabenzide, DPPAH), salicylic (SH) and benzoic (BH) hydrazides, and 1-hydrazinophthalazine hydrochloride (apressin, hydralazine, HPH) were made from commercial compounds by dissolution in water. Since the DNBF derivative of INH is only slightly soluble in water, a $10^{-3}$ M stock solution of isoniazide was prepared by dissolution in a mixture of water and dimethylsulfoxide (70:30, v/v). Working solutions were prepared from this stock solution by dilution with water or water–dimethylsulfoxide (70:30, v/v). Freshly prepared solutions were used.

An acetate buffer solution (analytical grade, pH 5.5) was used for determination of hydrazine derivatives in biological samples.

Liophilized human albumin and standard amino acid solutions were of analytical grade.

The solution of trichloracetic acid (analytical grade) was prepared by dissolving 30 g of this chemical in 100 ml of water.

### 2.3 Procedure

Fig. 1 shows the manifolds used for the determination of hydrazine derivatives by FIA and the experimental conditions. The 0.02 M reagent solution of DNBF was injected directly into a carrier solution of the hydrazine derivatives (concentration range 0.15–4.0 μg $ml^{-1}$) and the peak height at 510 nm was measured. For the determination of HPH in apressin drug, 20 tablets were weighed and powdered. An accurately weighed amount of powder equivalent to 10 mg of the drug was transferred into a 100 ml standard flask and diluted to the mark with distilled water. The mixture was shaken vigorously and filtered through dry paper, discarding the first portion of filtrate. A 5 ml portion was then diluted with the distilled water to obtain a final solution containing 1 μg of the drug per ml.

For the determination of chemicals in a complex biological matrix (plasma, urine and albumin) the proteins were eliminated by addition of 1 ml of solution of trichloroacetic acid to 4 ml of a sample followed by centrifugation at 6000 r.p.m.

The supernatant was neutralized by addition of 0.5 ml of pH 5.5 buffer solution. When analyzing plasma and urine, blank samples were prepared by precipitation and centrifugation as above, and the supernatant was destroyed by addition of 0.1 ml of 30% hydrogen peroxide solution. The amount of DPPAH in blood and urine was calculated by extrapolaction.

## 3. Results and discussion

Hydrazine derivatives react rapidly in organic and mixed solutions with DNBF, form-

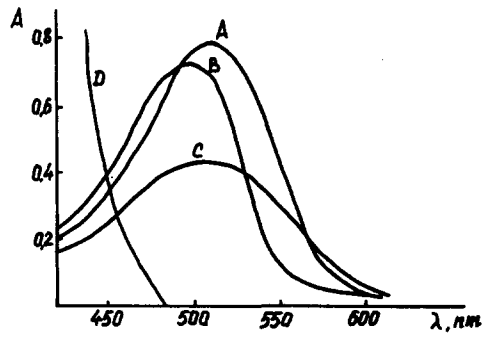


Fig. 2. Absorption spectra of DNBF derivatives ($2 \times 10^{-5}$ mol $l^{-1}$) of: (A) INH; (B) DPPAH; (C) HPH in dimethylsulfoxide. (D) Reagent blank.

ing intensively colored red products of nucleophilic substitution:

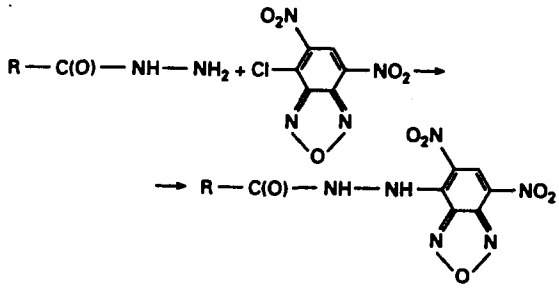


These products were isolated [15], and found to have a maximum absorption at 500–515 nm (see Fig. 2). The molar absorptivity of these compounds is $2.2 \times 10^4$–$3.9 \times 10^4$ l mol$^{-1}$ cm$^{-1}$ in water–dimethylsulfoxide (90:10, v/v). Absorbance measurements were performed in the 500–520 nm range where the reagent blank had negligible absorbance against the pure solvent. Quantitative determination showed the reaction to be completed immediately after the reagent was mixed with the compounds at temperatures of 15–30 °C, owing to high DNBF reactivity. The reaction products were stable for several days. In accordance with the high reactivity of DNBF in water and aqueous organic mixtures, it is hydrolyzed forming on inactive hydroxy derivative (4-hydroxy-5,7-dinitrobenzofurazan). The reaction is rapidly completed even in the presence of a small amount of water in non-aqueous solvents (such as alcohols, dimethylsulfoxide and dimethylformamide). However, solutions of DNBF are stable in acetonitrile even in the presence of high amounts of water (up to 5%, v/v). For this reason, acetonitrile was used as a solvent for preparing DNBF solutions. At the same time, completion of the raction between DNBF and the substituted hydrazines in aqueous–organic mixtures is not influenced by the water content, because of differences in nucleophilic properties of analytes and solvent. Therefore, an acetonitrile solution of the reagent is preferable in the converted variant of FIA for which the reagent is injected into the analyte stream. Our approach is guided by the restricted solubility of the determined substraces and the products of their reactions with DNBF in acetonitrile. Moreover, this restricted solubility can lead to a change in the baseline with time in the FIA system.

The optimum pH was found by use of universal buffer solutions in the pH range 2–8. Absorbance measurements of the products and the reagent blank showed that the color system was not influenced by pH in the range 4–7.

The Beer's law plots were linear over the whole concentration range of $2 \times 10^{-6}$–$10^{-4}$ mol $l^{-1}$ for all hydrazine derivatives under the conditions described for acetonitrile, dimethylsulfoxide, methanol, ethanol and their water mixtures. Since the absorbance for the blank at 510 nm was negligible and the reaction was fast, the formation of derivatives with DNBF was suitable for the routine determination of substituted hydrazines.

The flow-rate of the carrier was varied between 0.8 and 2.5 ml min$^{-1}$. A value of 1.2 ml min$^{-1}$ was chosen as a good compromise between residence time and sampling frequency.

A reactor length ($L$) of less than 90 cm had no influence on peak height, and $L = 90$ cm and an inner diameter of 0.6 mm were chosen as a compromise between maximum peak height and sampling frequency. The optimum volume of injected DNBF solutions was found to be 110 μl.

The influence of DNBF concentrations on the peak heights was studied in the range $5 \times 10^{-3}$–$4 \times 10^{-2}$ M. The highest peaks were obtained with $1 \times 10^{-2}$ M DNBF, and the peak height was unaffected by higher concentrations.

Analytical characteristics of FIA are summarized in Table 1. With the manifold described, peak height without correction for the blank vs. concentration of hydrazine derivatives in the sample was linear in the range 0.15–4.0 μg ml, a small intercept being on the ordinate. During the determination of hydrazine derivatives in serum and urine, the peak

Table 1
Analytical characteristics of FIA methods for hydrazine derivatives

| Chemical [a] | Calibration equation ($\mu g\ ml^{-1}$) | Linear range ($\mu g\ ml^{-1}$) | Correlation coefficient | Sampling frequency ($h^{-1}$) |
|---|---|---|---|---|
| INH | $H$ (mm) = 73.7 [INH] − 0.7 | 0.15–2.5 | 0.9986 | 32 |
| DPPAH | $H$ (mm) = 28.5 [DPPAH] − 0.7 | 0.25–3.5 | 0.9993 | 28 |
| SH | $H$ (mm) = 35.6 [SH] − 0.8 | 0.35–4.0 | 0.9992 | 28 |
| BH | $H$ (mm) = 41.2 [BH] + 0.5 | 0.2–2.5 | 0.9987 | 30 |
| HPH | $H$ (mm) = 58.2 [HPH] − 0.8 | 0.15–2.5 | 0.9991 | 30 |

[a] INH = isonicotinic hydrazide; DPPAH = diphenylphosphinylacetic hydrazide; SH = salicylic hydrazide; BH = benzoic hydrazide; HPH = 1-hydrazinophthalazine hydrochloride.

heights were corrected with respect to the pretreatment of biological solutions (see Section 2.3). If blank samples are not used, the biological matrix components cause an error of 6% in DPPAH determination at a concentration of 1 $\mu g\ ml^{-1}$ in urine and plasma.

A systematic study of potential interferences in the proposed method was carried out. Amino acids, ammonia, and methyl- and dimethylamine also react with 4-chloro-5,7-dinitrobenzofurazan, yielding yellow DNBF derivatives [16]. The absorption spectra of the products obtained under these conditions and used for hydrazine derivative determination have bands with maximum absorption between 430 and 450 nm. The low absorbance of these products at 510 nm leads to an increase in hydrazine derivative signal and to positive errors in the determination when their concentration exceeds the concentration of hydrazine 25 times (see Table 2). The high content of benzoic and salicylic acids, and inorganic salts does not influence the peak height. To investigate the application of FIA, the hydrazine derivative content in apressin drug, serum, urine and in model samples was determined using recovery tests. The results are summarized in Table 3. The accuracy of HPH determination in drugs was estimated by comparison with data obtained by an official compendia method, based on iodine titration [2].

Table 2
Interferences of other compounds in the determination of hydrazine derivatives ($n = 7$, $P = 0.95$)

| Hydrazine derivative (added 1 $\mu g\ ml^{-1}$) | Species | | Hydrazine derivative found ($\mu g\ ml^{-1}$) [a] | $S_r$ [b] |
|---|---|---|---|---|
| | Compounds | Amount added ($mg\ ml^{-1}$) | | |
| BH | Benzoic acid | 0.122 | 1.02 ± 0.03 | 0.04 |
| | Sodium chloride | 5.9 | | |
| | Potassium chloride | 8.5 | | |
| | Sodium phosphate | 13.1 | | |
| BH | Methylamine | 0.093 | 1.03 ± 0.04 | 0.05 |
| BH | Ammonia | 0.051 | 1.02 ± 0.03 | 0.04 |
| INH | Standard amino acid | 6.11 | 1.04 ± 0.04 | 0.05 |
| DPPAH | Standard amino acid | 6.11 | 1.04 ± 0.04 | 0.05 |
| SH | Salicylic acid | 0.1 | 1.03 ± 0.04 | 0.05 |
| | Methylamine | 0.05 | | |
| | Dimethylamine | 0.05 | | |
| | Ammonia | 0.02 | | |

[a] Mean ± confidence limit.
[b] Standard deviation.

Table 3
Determination of hydrazine derivatives in a biological matrix and in commercial preparations ($n = 5$, $P = 0.95$)

| Sample | Chemical | Added [b] ($\mu g\ ml^{-1}$ or mg per tablet) | Found [b] ($\mu g$ ml or mg per tablet) |
|---|---|---|---|
| Serum | DPPAH | 1.10 | $0.98 \pm 0.06$ |
| Urine | DPPAH | 2.19 | $2.1 \pm 0.1$ |
| Appressin tablets | HPH | $10.1 \pm 0.2$ [a] | $9.8 \pm 0.2$ |

[a] Ref. [2].
[b] Mean ± confidence limit.

## 4. Conclusion

Hydrazine derivatives can be determined as pharmaceuticals in a biological matrix in the presence of various biogenic amines using spectral characteristics of their derivatives with DNBF. Since the entire analytical cycle can be accomplished within 2 min, the FIA approach seems to be of interest and relevance. We also believe that our technique has significant potential for the assay of pharmaceutical hydrazine derivatives in serum samples.

## References

[1] A.P. Grekov and G.V. Otroshko, Hydrazinometrija, Naukova Dumka, Kiev, 1981 (in Russian).
[2] Pharmacopoeja USSR, Meditsina, Moscow, 1987.
[3] Ken-ichi Mawatari, F. Iinuma and M. Watanabe, Anal. Sci., 6 (1990) 515.
[4] Ch. Gaitonde and P.V. Pathak, J. Chromatogr. Biomed. Appl., 532 (1990) 418.
[5] K. Wong, Th. Joyce and H. Morrow, J. Chromatogr., 385 (1987) 261.
[6] F. Matsui, D.L. Robertson and F.G. Lovering, J. Pharmacol. Sci., 72 (1983) 948.
[7] P.C. Ioannou, Talanta, 34 (1987) 857.
[8] J. Joda, K. Mayashi and M. Umemoto, Bunseki Kagaku, 28 (1989) 26.
[9] T. Ono, J. Taniguchi, H. Mitsumaki, F. Takahata, A. Shibuya, Y. Kasakara and F. Koshimizu, Clin. Chem., 34 (1988) 552.
[10] E.W. Schmidt, Hydrazine and its derivatives: preparation, properties and applications, Wiley, New York, 1984.
[11] L. Mazor. Methods of organic analysis, Mir, Moscow, 1986 (in Russian).
[12] M.I. Evgen'yev, F.S. Levinson, I.I. Evgen'yeva, N.A. Moskva and R.I. Tarasova, USSR Patent No. 1 642 372, 1992.
[13] M.I. Evgen'yev, I.I. Evgen'yeva, N.G. Nikolaeva, N.A. Moskva, F.S. Levinson and B.I Demchenko, Khim.-Farm. Zh., 25 (1991) 80.
[14] M.I. Evgen'yev, N.G. Nikolaeva, I.I. Evgen'yeva, F.S. Levinson and H.C. Budnikov, Zh. Anal. Khim., 47 (1992) 1123.
[15] M.I. Evgen'yev, I.I. Evgen'yeva, N.A. Moskva, N.G. Nikolaeva, I.A. Geltukhin and H.C. Budnikov, Zh. Anal. Khim., 48 (1993) 1226.
[16] N.G. Nikolaeva, Dissertation, Kazan University, 1994.

ELSEVIER

Talanta 42 (1995) 1471–1478

Talanta

# The retention behaviour and separation of some water-soluble organophosphorus insecticides on polyester-based polyurethane foams

M.S. El-Shahawi [a,*], A.M. Kiwan [a], S.M. Al-Daheri [a], M.H. Saleh [b]

[a] *Department of Chemistry, Faculty of Science, UAE University, Al-Ain, P.O. Box: 17551, United Arab Emirates*
[b] *Ministry of Health, Abu Dhabi, P.O. Box: 848, United Arab Emirates*

Received 28 October 1994; revised 16 March 1995; accepted 20 March 1995

**Abstract**

This paper reports the concentration of some dissolved organic phosphorus insecticides in water by open-cell polyurethane foam. The results of preliminary screening tests on the retention of the tested insecticides (Diazinon, Malathion and Chloropyrifos) by polyester foams indicated that a very high percent removal of the insecticides was obtained. The retention rate was fast and reaches equilibrium in a few minutes. The various parameters affecting the preconcentration of the tested insecticides by unloaded foam, e.g. pH, extraction media, shaking time, salt effect, flow rate, temperature and sample volumes have been optimized via the static mode of separation. The unloaded foams were employed in columns for the retention and recovery of the tested species. The sorption efficiency and the recovery of the tested compounds by the unloaded foam column were found to be up to 95.5%. The equivalent to a theoretical plate by the unloaded foam was found in the range $1.12-1.32 \pm 0.2$ mm. The sorption mechanism of the tested species by the foam is discussed. The separation of some of the tested species in a mixture was achieved. The foam membrane offers unique advantages over conventional bulk-type granular sorbents and solvent extraction in offering high flow rates, rapid, versatile, effective separation and preconcentration of different species from aqueous samples. The foam provides the advantages of being, insoluble, easily separable and non-polluting, as well as inexpensive.

## 1. Introduction

The classes of compounds responsible for the pollution of potable water resources include polyaromatic hydrocarbons, detergents, phenols, polychlorinated biphenyls and pesticides [1]. The pesticides are not toxic agents and are widely and regularly applied over large areas accessible to the public [2]. The compounds can enter water systems from various sources, e.g. run-off from agricultural land, direct entry from crop spraying, industrials and sewage effluent, cattle spraying, dust and rainfall [3,4]. These species are deliberately directed against living organisms and applications almost occur without control [5].

The removal or reduction of these water pollutants to an acceptable concentration by extraction with cellulose triacetate membrane filters, steam distillation, oxidation reactions, reversed liquid–liquid partition filter chromatography and adsorption on active carbon has been reported [6–9]. Such preconcentration methods are often slow or cumbersome and are too expensive for routine analysis where large volume samples are concentrated on-site prior to quantitative analysis [8,9].

The use of unloaded polyurethane foams (PuF) in separation and preconcentration pro-

* Corresponding author. Permanent address: Chemistry Department, Faculty of Science at Damiatta, Mansoura University, Mansoura, Egypt.


*SSDI* 0039-9140(95)01597-3

cesses led to the revealing of the potential of their spherical geometric form: a spherical membrane-shaped geometry and the proposal of their general use in column operations as a substitute for the traditional granular supports in extraction chromatography [10]. Thus, in recent years considerable progress has been made in the use of polyurethane foam as an inexpensive solid extractor and effective sorbent for the removal of water pollutants [11–23]. The membrane-like structure of the foams together with efficient sorption and mass-transfer properties offer a higher concentrating ability and flow rate compared with other solid supports. The solid foam concentrates various species in solution by a phase distribution mechanism rather than adsorption.

The object of the work described herein was to evaluate the applicability of polyurethane foam for the extraction and separation of some insecticides from large volume samples of aqueous media. Conclusions concerning the most probable sorption mechanism by the foam have also been drawn.

## 2. Experimental

### 2.1. Reagents and materials

All reagents and chemicals used were of analytical reagent grade. Universal Britton-Robinson (B-R) buffer solutions containing a mixture of equal amounts (0.04 mol $l^{-1}$) of phosphoric acid, boric acid and acetic acid with sodium hydroxide (0.01 mol $l^{-1}$ were used to provide different pH ranges. Polyurethane foam, an open-cell polyester-type (bulk density, 30 kg $m^{-1}$) was supplied by Greiner K.G. Schaum (Stoffwerk, Kremsmunster, Austria). Foam cubes of volume approximately 1 $cm^3$ were cut from polyurethane foam sheet. These foam cubes were soaked in 1 M hydrochloric acid for 10 h with occasional squeezing to remove any possible inorganic species, and were washed with water until they were acid-free. They were then washed with acetone in a Soxhlet extractor for 24 h to remove organic contaminants and finally dried as previously reported [18].

The insecticides tested were Chloropyrifos, *o,o*-diethyl-*o*-(3,5,6-trichloro-2-pyridyl)phosphorothioate; Malathion; diethyl [(dimethoxyphosphinothioyl)thio]butanedioate and Diazinon, *o,o*-diethyl-*o*-(3-isopropyl-6-methyl-pyrimidine)phosphorothioate. Stock solutions (200 μg $cm^{-3}$) of each compound were prepared in 10 $cm^3$ ethanol and were diluted with distilled water. A series of standard solutions of these compounds was prepared by diluting their stock solutions with distilled water. The solutions were stored in polyethylene bottles.

### 2.2. Apparatus

A Pye–Unicam double-beam UV-Visible spectrophotometer model Sp 8-400 with 10 mm quartz cells was used for all the absorbance measurements. An Orion pH meter, a mechanical shaker type G10 Gyrotary (New Brunswick, Scientific Co.) and glass columns (15 cm × 1.5 cm i.d.) were also employed.

### 2.3. General procedures

*Batch experiments*

To investigate the effect of shaking time on the sorption of the tested insecticides on polyurethane foam, the foam cubes (0.2 g) were equilibrated with 100 $cm^3$ of each compound (100 μg $cm^{-3}$) in separate polyethylene bottles, and were shaken for time intervals up to 2 h. The foam cubes were then separated by decantation. The amount of compound remaining in the solution was measured spectrophotometrically at the wavelength of maximum absorption. The sorption behaviour of the compounds as evaluated from the degree of sorption ($E$) and the distribution ratio ($D$)

$$E = \frac{[C]_i - [C]_f}{[C]_i} 100 \quad (1)$$

$$D = \frac{[C]_i - [C]_f}{[C]_f} \frac{V}{W} \quad (2)$$

where $[C]_i$, and $[C]_f$ are the initial and final insecticide concentrations, respectively, in the solution, $V$ is the volume of the solution ($cm^3$) and W is the weight of dry foam (g). Following these procedures, the effects of solution pH employing Britton-Robinson buffer, acidity, temperature, compound concentration, extraction medium and increasing salt concentration ($\leqslant$0.1 M) of different alkali metal ($Li^+$, $Na^+$, $K^+$, $NH_4^+$) chlorides on the sorption efficiency of the tested species by the polyester-based polyurethane foam were critically examined.

Table 1
The logarithm distribution coefficient ($D$) data for the sorption of the tested insecticides by unloaded foams in the presence of different univalent cations [a]

| Cation concentration (M) | Logarithm distribution coefficient, $D$ | | |
|---|---|---|---|
| | Chloropyrifos | Malathion | Diazinon |
| LiCl | | | |
| 0.01 | 3.8 ± 0.1 | 2.9 ± 0.2 | 2.3 ± 0.2 |
| 0.05 | 3.8 ± 0.1 | 3.2 ± 0.1 | 2.50 ± 0.07 |
| 0.1 | 3.70 ± 0.09 | 3.6 ± 0.1 | 2.8 ± 0.1 |
| NaCl | | | |
| 0.01 | 4.1 ± 0.1 | 1.70 ± 0.05 | 1.9 ± 0.1 |
| 0.05 | 4.1 ± 0.1 | 1.8 ± 0.1 | 1.6 ± 0.1 |
| 0.1 | 4.0 ± 0.1 | 1.9 ± 0.1 | 0.40 ± 0.07 |
| KCl | | | |
| 0.01 | 4.3 ± 0.1 | 1.5 ± 0.1 | 1.75 ± 0.07 |
| 0.05 | 4.4 ± 0.1 | 1.6 ± 0.1 | 1.55 ± 0.09 |
| 0.1 | 4.5 ± 0.1 | 1.5 ± 0.1 | 0.90 ± 0.05 |
| $NH_4Cl$ | | | |
| 0.01 | 4.3 ± 0.1 | 1.3 ± 0.1 | 1.50 ± 0.08 |
| 0.05 | 4.3 ± 0.1 | 1.4 ± 0.1 | 1.28 ± 0.07 |
| 0.1 | 4.2 ± 0.1 | 1.3 ± 0.1 | 0.76 ± 0.09 |

[a] Extraction from aqueous solution (100 $cm^3$) at the pH of maximum extractibility of each insecticide (80 $\mu g\ cm^{-3}$). Average of five measurements ± standard deviation (S.D.) at room temperature.

*Flow experiments*

In the column experiments, 3 g of dry foam were homogeneously packed into the column using the vacuum method of foam column packing [12]. Tap or distilled water (0.1–5 $dm^3$) samples containing 0.1 mg of the insecticide tested were passed through the foam column at 10–15 $cm^3\ min^{-1}$. After squeezing water from the foam, the compound was then recovered quantitatively from the foam with 200 $cm^3$ of acetone in a Soxhlet extractor for 8 h. The analyte was determined by measuring the absorbance of the solution against a reagent blank after being concentrated to a volume of 25 $cm^3$ with a rotary evaporator. The effect of sample volume, flow rate and column foam bed on the extraction efficiency of the compounds by the foam were also determined. The chromatographic separation of Malathion and Chloropyrifos were carried out employing the foam packed column procedures.

## 3. Results and discussion

Preliminary experiments using unloaded polyester-type-based polyurethane foam have shown that the extraction of the investigated compounds (I, II, III in Fig. 1) is rapid and equilibrium is reached in less than 50 min, followed by a plateau. The results obtained are summarized in Fig. 2. (Each point in the figure represents an average of five measurements ($n = 5$) with relative standard deviations in the range 1.8–2.1%.) Rapid preconcentration and good extraction efficiency of the tested compounds from aqueous media were obtained. The average values of the half-life ($t_{1/2}$) of equilibrium sorption calculated from Fig. 2 are in the range 2–3 min.

### 3.1. Extraction isotherm

The uptake of the tested compounds from aqueous solution by the unloaded foam was dependent on the initial concentration. There-

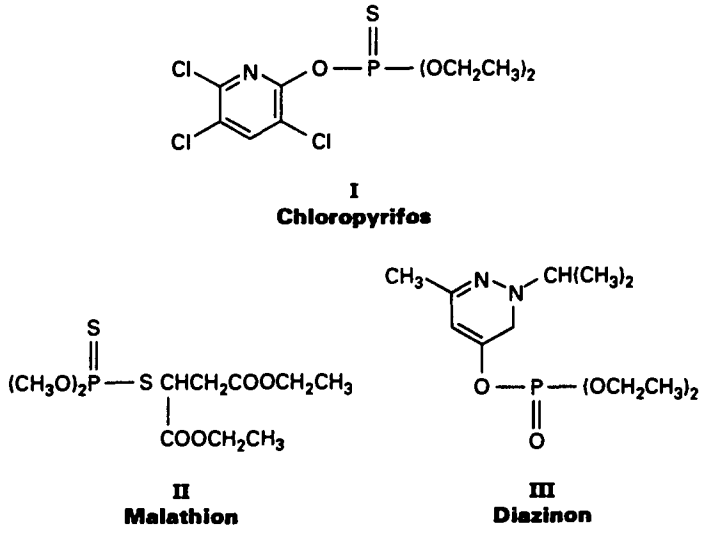


Fig. 1. Structure of the tested insecticides.

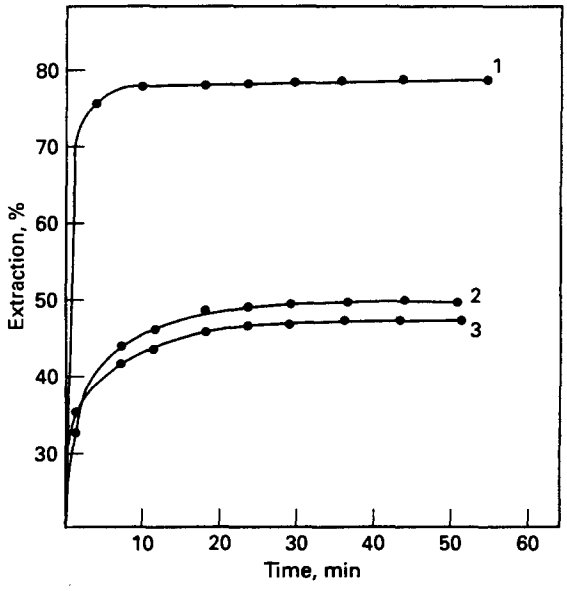


Fig. 2. Effect of shaking time on the sorption profiles of (curve 1) Chloropyrifos, (curve 2) Malathion, and (curve 3) Diazinon at 100 μg cm$^{-3}$ in aqueous solution (100 cm$^3$) at pH 5–6 and 20 ± 0.1°C by unloaded foams (0.3 g).

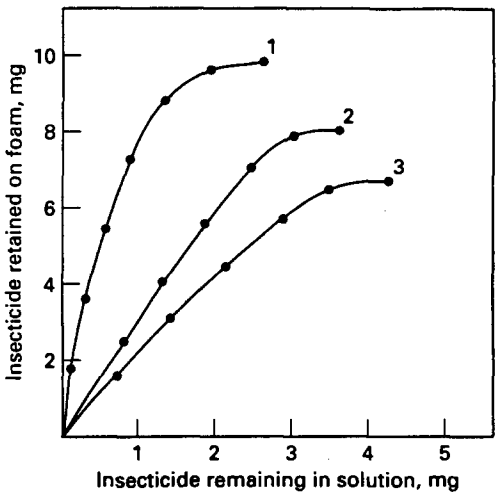


Fig. 3. Extraction isotherms of (curve 1) Chloropyrifos, (curve 2) Malathion and, (curve 3) Diazinon at concentrations 10–200 μg cm$^{-3}$ by unloaded foams from a 100 cm$^3$ aqueous solution sample at pH 5–6 and 20.0 ± 0.1°C and 1 h extraction time.

fore, the sorption isotherms were determined over a wide range of equilibrium concentrations (10–200 μg cm$^{-3}$) for each insecticide at 20°C. The pH values of the aqueous media in these experiments were adjusted with Britton-Robinson buffer to pH 5–6, so that the compounds were predominantly in the undissociated form. At low concentration of the compounds, the sorption isotherms exhibited first-order behaviour and tended to plateau at higher bulk solution concentration as shown in Fig. 3. The sorption of the different species by the unloaded foam increases in the order

Chloropyrifos > Malathion > Diazinon

Similar trends for the sorption of the tested compounds were obtained with diethyl ether and for other similar species retained on polyurethane foams [14,15]. Therefore solvent extraction is the most probable mechanism for the sorption of the tested species by the polyester foam from aqueous media at the tested pH [15]. However, it is worth noting that the molecular weight ($Mw$) of Chloropyrifos ($Mw = 345.5$), Diazinon ($Mw = 268$) and Malathion ($Mw = 330.5$) are also participating factors in the extraction step by the polyester foam. These data are consistent with the general understanding that the higher the molecular weight of the sorbate, the larger the amount of the tested insecticides retained on the foam when the substances concerned are similar in nature [24,25].

The influence of the pH of the aqueous solution on the sorption profile of the compounds at concentration 100 μg cm$^{-3}$ by the unloaded foams was determined over a pH range of 1–12 employing 0.1 mol l$^{-1}$ hydrochloric acid solution and Britton-Robinson buffer. The sorption profiles of the compounds by the unloaded foams are summarized in Fig.

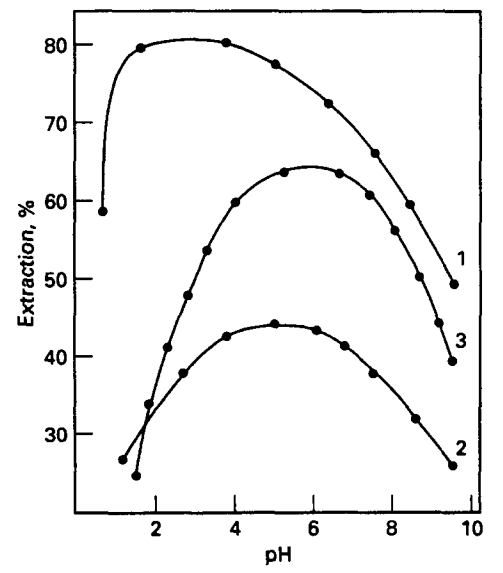


Fig. 4. Effect of pH on the extraction percentage of (curve 1) Chloropyrifos, (curve 2) Malathion and, (curve 3) Diazinon by unloaded foam (0.3 g) from a 100 cm$^3$ aqueous sample (80 μg cm$^{-3}$). Other conditions in Fig. 2.

4. The extraction percentage of Chloropyrifos reached a maximum in the pH range 2–4 and decreased at moderate and higher pH. Diazinon and Malathion display maximum retention at pH 6–8, at which the compounds exist in the neutral form. Thus the sorption mechanism involves neutral species and this is consistent with a solvent-extraction mechanism as previously reported [14,20].

The effect of different concentrations of alkali metal chlorides, e.g. LiCl, NaCl, KCl and $NH_4Cl$, at concentrations $\leq 0.1$ M on the sorption profiles of the tested compounds (80 μg $cm^{-3}$) was investigated. The results obtained are summarized in Table 1. A significant increase in the sorption profiles of Diazinon and Malathion by the polyester foam was observed in the presence of the salts LiCl, NaCl, KCl and $NH_4Cl$ at concentrations $\leq 0.1$ M and the order of sorption $Li^+ > Na^+ > K^+ > NH_4^+$ was observed for Diazinon and Malathion (Table 1). The distribution ratio of Malathion increased with the amount of salt added from $\log D = 2.9$ and 1.7 to $\log D = 3.6$ and 1.9 (Table 1) while for Diazinon it changed from $\log D = 2.3$ and 1.9 to $\log D = 2.8$ and 0.4 for $Li^+$ and $Na^+$ ions at 0.01 M and 0.1 M, respectively. The added salts ($Li+$, $Na^+$) increased the sorption profiles of the Diazinon and Malathion into the foams by reducing the number of water molecules available to solvate the sorbed species which would therefore be forced out of the solvent phase into the foam, since some amount of "free" water molecules are preferentially used to solvate the ions added [17,18]. Hence the influence of these salts can be explained by the salting out effect and "solvent extraction" is the most probable mechanism [21,26].

The sorption profiles of Chloropyrifos by the foam increased in the presence of the alkali salts in the following order of cations: $K^+ > NH_4^+ > Na^+ > Li^+$ (Table 1). Therefore, the ion–dipole interactions of $NH_4^+$ ions with oxygen atom sites of the polyurethane foam are possibly highly predominating in the sorption of Chloropyrifos. According to the "cation-chelation mechanism", the presence of $K^+$ ions should facilitate the extraction of the Chloropyrifos by the foam more than the other alkali metal ions ($NH_4^+$, $Na^+$ or $Li^+$) because of the better fit of this ion into the central cavity of the oxygen-rich helix in the polyurethane foam. Therefore, the obtainable results of the sorption profiles of Chloropyrifos are in good agreement with the data recently reported by Palagyi et al. [26,27]. Therefore the "cation-chelation mechanism" is the most probable mechanism for the sorption of Chloropyrifos. In accordance with this mechanism, the polyalkenoxy chains of the PuF sorbent form a helical structure [28]. This helical structure of the polyurethane foam sorbent forms a clathrate with suitable simple cations.

To confirm the salting out of the salts added on the sorption profiles of Diazinon and Malathion by the foams, an extraction of 200 $cm^3$ of the former compound at 80 μg $cm^{-3}$ was investigated at pH 4 and 9 after shaking for 30 min. The added $Li^+$ ions (0.01 M) to the sorption media enhanced the distribution ratio of Diazinon more in a solution of pH 4 ($\log D = 3.6$) than at pH 9 ($\log D = 2.4$). This behaviour is possibly attributed to the increased amount of neutral species at pH 4 as compared to pH 9 and the compound is highly extractable in the neutral form. Thus a "solvent-extraction mechanism" with the salts acting as salting out agents is the most probable mechanism for the preconcentration of Diazinon and Malathion by the polyurethane foam [14].

The influence of temperatures of 35, 45 and 55°C on the sorption profiles of the tested species by the foam were determined at the pH of maximum extraction of each insecticide. Similar trends to that obtained at 20°C were found and the percentage retention increases slightly with increasing temperature. Assuming no precipitation or chelation and that the extracted compounds exist as neutral species, then the equilibrium constant $K$ for the equation

$$\text{Compound}_{aq} \rightleftharpoons \text{Compound}_{org} \quad (3)$$

is equivalent to the partition ratio, $D$. Employing the equation

$$\ln K = -\Delta H^\circ/RT + \Delta S^\circ/R \quad (4)$$

the values of the standard entropy change, $\Delta S^\circ$ for the sorption of the Diazinon and Malathion by the unloaded foams were found to be in the range $-32 - -36 \pm 2$ J $mol^{-1}$ $deg^{-1}$. The value of $\Delta S^\circ$ for the sorption of Chloropyrifos by the foam was found to be $-19 \pm 2$ J $mol^{-1}$ $deg^{-1}$. The low values of the entropy change for Diazinon and Malathion are possibly attributed to the decrease in the freedom of movement of the organic compound in the polyurethane foam as previously

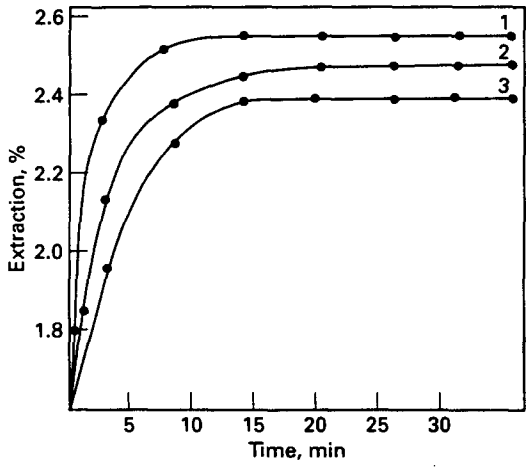


Fig. 5. Effect of extraction media on the sorption profile of Malathion by unloaded foam at pH 6–7 and a 1 h extraction time. Ethanol additions: curve 1, 0%; curve 2, 10%; curve 3, 15%. Other conditions as in Fig. 2.

reported [14]. These results are consistent with the solvent-extraction mechanism. The values of the standard enthalpy change, $\Delta H°$ were found to be in the range $26 \pm 4$ kJ mol$^{-1}$. Raising the temperature may facilitate the partition of the tested species through the polyurethane foam via the urethane linkage and/or ester oxygen atoms.

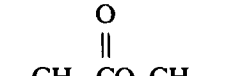

or

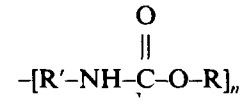

The influence of the extraction media on the sorption percentage of the tested species by the polyurethane foam was examined by the addition of ethanol (0–15%). The sorption profiles of Diazinon and malathion by the unloaded foams decreased on the addition of ethanol to the aqueous media up to 15%. Representative results are summarized in Fig. 5. This behaviour is possibly due to the formation of a lipophilic association in the aqueous solution [29]. Water is a solvent with a high dielectric constant; therefore, ions in the aqueous solution are well solvated and so it is difficult for these species to form ion pairs in the aqueous solution. These data are consistent with the fact that with a compound of low dielectric constant and another which has a high dielectric constant, the retention percentage should increase with increase in the solvent polarity of the polar phase. These results are also consistent with the solvent-extraction mechanism in the sorption of these species by the unloaded foam. The nature of the media has therefore a marked effect on the sorption characteristics of the compounds.

### 3.2. Flow experiments

The sorption behaviour of the tested compounds from aqueous solution with the unloaded polyurethane foam suggests a possible application of the foam in the column extraction mode for the quantitative collection and recovery of the tested compounds from aqueous media at the pH of maximum extractability for each compound. Distilled or tap water samples (0.1–5 dm$^3$) containing 0.1 mg of each compound were percolated separately through the foam columns at a flow rate of 10–15 cm$^3$ min$^{-1}$. Complete retention of the tested compounds was achieved by the foam column. After squeezing water from the foam the compounds were then recovered from the foam with acetone in a Soxhlet extractor. Satisfactory recovery percentages (91.5–95.5%) of the tested compounds from the aqueous media by the proposed foam column method are obtained (Table 2). The effects of flow rate and sample volume on the retention of the compounds by the unloaded foams were also examined by percolating aqueous sample volumes (0.1–5 dm$^3$) of Diazinon (0.1 mg) through the column at various flow rates between 5 and 25 cm$^3$ min$^{-1}$. Complete retention of the compound was obtained from 5 dm$^3$ of aqueous

Table 2
Extraction and recovery of the tested insecticides (0.1 mg) from 3 dm$^3$ of aqueous solution at a 10 cm$^3$ min$^{-1}$ flow rate by the proposed unloaded foam column [a]

| Compound | Recovery % | | Wavelength [b] (nm) | p*Ka* |
|---|---|---|---|---|
| | (a) | (b) | | |
| Chloropyrifos | 93 ± 2 | 95 ± 2 | 206 (4.4) | 4.55 |
| Malathion | 92 ± 1 | 93 ± 3 | 280 (3.13) | 5.21 |
| Diazinon | 95 ± 2 | 96 ± 2 | 290 (2.94) | 4.97 |

[a] Conditions: Extraction from aqueous solution (200 cm$^3$) at the pH of maximum sorption of each insecticide. Average of five measurements from (a) distilled water and (b) tap water ± SD at room temperature.
[b] The logarithm of the extinction coefficient ($\epsilon$, 1 mol$^{-1}$ cm$^{-1}$) of the tested insecticides is given in parentheses.

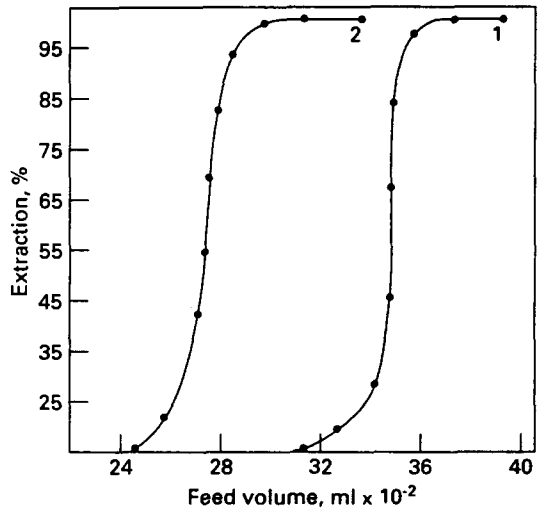


Fig. 6. Break through capacity curves of the sorption profiles of Diazinon by unloaded foam at flow rates of (curve 1) 15 $cm^3 min^{-1}$ and (curve 2) 25 $cm^3 min^{-1}$ by unloaded foam column.

solution and the extraction efficiency decreased significantly to 76% at 25 $cm^3 min^{-1}$ from a 5 $dm^3$ aqueous volume. To determine the performance of the foam column by the chromatogram method, quantitative retention of Diazinon (0.01 mg) followed by elution with 200 $cm^3$ of acetone–HCl (3:1 (v/v)) through the foam column at a 5 $cm^3 min^{-1}$ flow rate was carried out. The height equivalent to a theoretical plate (*HETP*) was obtained from the elution curves using the equation [11]

$$N = \frac{8V_{max}^2}{W_e} = \frac{L}{HETP}$$

where $N$ is the number of theoretical plates, $V_{max}$ is the volume of eluate at the peak maximum, $W$ is the width of the peak at 1/e the maximum solute concentration and $L$ is the length of the column foam bed. The *HETP* values were found to be equal to 1.1 ± 0.2 mm and 1.3 ± 0.2 mm at flow rates of 15 $cm^3 min^{-1}$ and 20 $cm^3 min^{-1}$, respectively.

The *HETP* value for the unloaded foam column was also calculated from the breakthrough capacity curve (Fig. 6) of Diazinon at 15 $cm^3 min^{-1}$ and 25 $cm^3 min^{-1}$ employing the equation [11]

$$N = \frac{V\bar{V}}{(V\bar{V})^2} = \frac{L}{HETP}$$

where $V$ is the volume of effluent at the center of the S-shaped section of the breakthrough capacity curve where the concentration is one-half of the initial concentration, and $\bar{V}$ is the volume at which the effluent has a concentration of 0.1578 of the initial concentration. The value of the *HETP* obtained by this method was 1.2 ± 0.2 mm, confirming the values obtained from the elution curves.

The separation of Malathion (0.1 mg) from Chloropyrifos (0.05 mg) in aqueous solution at pH 2 and in the presence of sodium chloride (0.1 M) for Chloropyrifos has been successfully carried out on the polyurethane foam. The solution mixture was percolated through the foam column at 15 $cm^3 min^{-1}$. The sorption of Chloropyrifos took place while Malathion was not retained on the foam column and collected quantitatively in the effluent. Chloropyrifos was then recovered from the foam with 100 $cm^3$ of acetone at 2–3 $cm^3 min^{-1}$ and was determined spectrophotometrically at 206 nm.

## 4. Conclusion

Unloaded foams in the batch and the column modes can be applied to trap trace amounts of insecticides from water, and the retained species can be recovered with an appropriate eluent. The separation of the tested species can be achieved provided that there is a sufficiently large difference in the optimum condition of extraction of each compound. A study of the rested compounds shows that the insecticides are extracted in their neutral form by a simple solvent-extraction mechanism. This conclusion is supported by the short time required for extraction equilibrium and the slating out phenomenon. The nature of the sorption media has a marked effect on the extraction performance of the tested species by the foam. Moreover, the foam offers a wider range of modifications than normal granular solids. The good hydrodynamic properties of the foam sorbent give the unique advantage of rapid, and versatile preconcentration of the tested compounds.

## Acknowledgment

The authors wish to thank Professor Salah Elnahwy, Dean of the Faculty of Science for his excellent support and help during this work.

## References


[1] J.R.H. Malissa, Egypt J. Anal. Chem., 1 (1990) 49.

[2] A.S.Y. Chau, B.K. Afghan and J.W. Robinson, Analysis of Pesticides in Water, Significance, Principles, Techniques and Chemistry of Pesticides, Vol. 1, *CRC Press, Boca Raton*, FL, 1982.

[3] C.A. Edward, Persistent Pesticides in the Environment, 2nd edn., CRC Press, Boca Raton, FL, 1973.

[4] C.A. Edward, Environmental Pollution by Pesticides, Plenum Press, New York, 1981, p. 409.

[5] L.T. Kurkland, S. Shibko, A. Kolbye and R. Shapiro, Environ. Res., 4 (1971) 9.

[6] A.H. Romano and R.S. Safferman, J. Am. Water Works Assoc., 55 (1963) 169.

[7] J.F. Uthe, J. Reinke and H.D. Gesser, Environ. Lett., 3 (1972) 117.

[8] B. Ahling and S. Jensen, Anal. Chem., 36 (1964) 134.

[9] H. Oda and C. Yokokawa, Carbon, 21 (1983) 483. H. Oda, M. Kishida and C. Yokokawa, Carbon, 19 (1981) 243.

[10] T. Brawn, J.D. Navratil and A.B. Farag, Polyurethane Foam Sorbents in Separation Science, CRC Press, Boca Raton, FL, 1985.

[11] S. Palagyi and T. Brawn, Separation and Preconcentration of Trace Elements and Inorganic Species on Solid Polyurethane Foam Sorbents, in Z.B. Alfassi and C.M. Wai (Eds.), Preconcentration Technique for Trace Elements, CRC Press, Boca Raton, FL, 1992.

[12] A.B. Farag, A.M. El-Wakil, M.S. El-Shahawi and M. Mashaly, Anal. Sci. (Jpn.), 5 (1989) 415.

[13] A.B. Farag and M.S. El-Shahawi, J. Chromatogr., 552 (1991) 371.

[14] M.S. El-Shahawi, Talanta, 41 (1994) 1481.

[15] M.S. El-Shahawi, A.B. Farag and M.R. Mostafa, Sep. Sci. Technol, 29 (1994) 289.

[16] A.B. Farag, A.M. El-Wakil and M.S. El-Shahawi, Fresenius' Z. Anal. Chem., 324 (1986) 59.

[17] P. Fong and A. Chow, Talanta, 39 (1992) 497–825.

[18] I.I. Stewart and A. Chow, Talanta, 40 (1993) 1345.

[19] L. Schumack and A. Chow, Talanta, 34 (1987) 957.

[20] T. Braun, Fresenius, Z. Anal. Chem., 333 (1989) 785.

[21] B.K. Afghan, R.J. Wilinson, A. Chow, T.W. Findley, H.S. Gesser and K.I. Srikameswaran, Water Res., 18 (1984) 9.

[22] T. Braun and A.B. Farag, Anal. Chim. Acta, 99 (1978) 1.

[23] G.J. Moody and J.D.R. Thomas, Chromatographic Separation with Foamed Plastics and Rubbers, Dekker, New York, 1982.

[24] K.G. Kirkwood, J. Chem. Phys., 2 (1934) 351.

[25] A.W. Adamson, Physical Chemistry of Surfaces, 2nd edn., Academic Press, New York, 1967.

[26] S. Palagyi and T. Braun, J. Raidonal. Nucl. Chem., 163 (1992) 69 and references therein.

[27] S. Palagyi and T. Braun, Z. Homonnay and A. Vertes, Analyst, 117 (1992) 1537 and references therein.

[28] A. Roychaudhuri, S.K. Roy and A.K. Chakraburty, Talanta, 39 (1992) 1377.

[29] R.C. West, Handbook of Chemistry and Physics, 54th edn., CRC Press, Boca Raton, FL, 1973.

ELSEVIER

Talanta 42 (1995) 1479–1485

Talanta

# Spectrophotometric methods for the determination of tamoxifen citrate

Chilukuri S.P. Sastry *, J.S.V.M. Lingeswara Rao, Kolli Rama Rao

*Foods and Drugs Laboratories, School of Chemistry, Andhra University, Visakhapatnam 530 003, India*

Received 4 November 1994; revised 29 February 1995; accepted 28 March 1995

**Abstract**

Three simple and sensitive spectrophotometric methods for the determination of tamoxifen citrate have been developed. They are based on the formation of an ion-association complex between the drug and a dye, Erioglaucine A, which is extractable into chloroform and has an absorption maximum at 625 nm (method A), oxidation with excess potassium permanganate and the determination of unconsumed permanganate using Fast Green FCF (method B), or by the formation of a coloured cobalt thiocyante coordination complex which is extracted into benzene and measured at 635 nm (method C). Beer's law limits for methods A, B, and C are 0.5–3.0 μg $ml^{-1}$, 1.0–6.0 μg $ml^{-1}$ and 100–500 μg $ml^{-1}$, respectively. No interference was observed from tableting additives and the applicability of the methods was examined by analysing tablets containing tamoxifen. The quantities determined were 99.0–100.03% of the exptected values.

## 1. Introduction

Tamoxifen (molecular formula $C_{26}H_{29}NO$; molecular weight, 371.48 g) is chemically known as [Z]-2-[4-(1,2-diphenyl-l-butenyl)-phenoxy]-*N*,*N*-dimethylethanamine. It is an antineoplastic agent used as its citrate in the treatment of breast cancer. The drug is official in the British Pharmacopoeia [1] and the United States Pharmacopoeia [2]. A survey of the literature revealed that only a single ultraviolet and two visisble spectrophotometric methods have been reported [3]. The latter two methods are based on the formation of an ion-association complex between tamoxifen and Methyl Orange and the reaction of tamoxifen citrate with a citric acid–acetic anhydride reagent [3]. Other methods include polarography [4], thin layer chromatography [5], gas chromatography [6–10], and high-performance liquid chromatography [11–13]. The reported spectrophotometric methods possess deficienceis such as a low $\lambda_{max}$ value or lower sensitivity. It is, therefore, of interest to develop simple and sensitive procedures with higher $\lambda_{max}$ values for the determination of tamoxifen citrate in pharmaceutical formulations. This paper describes three visible spectrophotometric methods for the determination of tamoxifen citrate, exploiting its basic nature, unsaturation, and the presence of an aliphatic tertiary amine group.

Acidic dyes have been utilised for the determination of compounds exhibiting basic properties [14]. In method A, the acidic dye, Erioglaucine A (EG-A) (C.I. no. 42 090), was choosen for the direct determination of tamoxifen citrate. Gordon reported few indirect colorimetric procedures for the determination of some organic compounds possessing double bonds by oxidimetry [15]. Cobalt thiocyanate (CTC) has been used as a reagent for the determination of compounds containing a tertiary amino group [16,17]. We have applied these reagents to the determination of tamoxifen citrate in bluk form and in pharmaceutical formulations. Method A describes the spectrophotometric determination of an ion-associ-

* Corresponding author.

*SSDI* 0039-9140(95)01598-1

ation complex formed between the drug and EG-A which is extracted into chloroform. In method B, the drug was treated with standard $KMnO_4$ in excess. The consumed $KMnO_4$ corresponding to tamoxifen citrate was obtained by determining unconsumed $KMnO_4$ spectrophotometrically with Fast Green (FG)-FCF based on a report that the decolorisation of FG-FCF by $KMnO_4$ is quantitative [15]. Method C involves the formation of a coloured CTC coordination complex of the drug, which is benzene extractable.

## 2. Experimental

### 2.1. Apparatus

A Systronics model 106 spectrophotometer with 1 cm matched glass cells and a Milton Roy spectronic 1201 spectrophotometer with 1 cm matched quartz cells were used for absorbance measurements in the visible and ultraviolet regions respectively. An Elico-digital model LI-120 pH meter was used for the pH measurements.

### 2.2. Materials and reagents

All reagents were analytical grade, and all solutions were prepared with double-distilled water. Freshly prepared solutions were always used.

Aqueous solutions of sodium sulphate (BDH; 1.0 M), potassium permanganate (BDH; $2.0 \times 10^{-3}$ M) in 2.0 M $H_2SO_4$, and FG-FCF (Chroma; $1.23 \times 10^{-5}$ M) in 1.0 M $H_2SO_4$ were prepared with double-distilled water.

EG-A (Chroma; $2.53 \times 10^{-5}$ M) was prepared in aqueous medium and washed with chloroform prior to use. A buffer solution (pH 1.2) was obtained by mixing 146 ml of 0.1 M glycine solution (0.1 M, 7.507 g of glycine + 5.85 g of NaCl dissolved in 1 l of distilled water) to 854 ml of 0.1 M HCl and adjusting the pH of the solution to 1.2.

CTC ($2.5 \times 10^{-1}$ M) was prepared by dissolving 7.25 g of cobaltous nitrate and 3.8 g of ammonium thiocyanate in 100 ml of distilled water. A buffer solution (pH 2.0) was prepared by mixing 306 ml of trisodium citrate (0.1 M), 694 ml of HCl (0.1 M), and adjusting the pH of the solution to 2.0.

### 2.3. Preparation of standard drug solutions

#### 2.3.1. Preparation of tamoxifen standard for method A

An accurately massed amount of tamoxifen citrate equivalent to 100 mg of tamoxifen was transferred to a 125 ml separatory funnel containing 10 ml of aqueous 1.0 M sodium hydroxide and the free base was extracted with chloroform (4 × 15 ml). The combined chloroform extracts were diluted to 100 ml to obtain a stock solution of 1 mg $ml^{-1}$. Diluted standard solutions were prepared by dilution of the stock solution with chloroform.

#### 2.3.2. Preparation of tamoxifen citrate for methods B and C

A 1 mg $ml^{-1}$ standard solution of tamoxifen citrate prepared in a DMF: $H_2O$ (1:5) mixture by warming was used as such for method C. The solution was further diluted with distilled water to obtain a concentration of 50 μg $ml^{-1}$ for method B.

### 2.4. Optimisation experiments for the methods

The optimum conditions for the development of methods A–C were established by varying the parameters one at a time, keeping the others fixed, and observing the effect produced on the absorbance of these solutions.

In order to establish the optimum pH range for method A, the drug was allowed to react with EG-A in aqueous solution bufferred to pH 1.0–3.0, and the complex formed was extracted with chloroform for measurement. Constant absorbances were obtained over the pH range 1.1–1.4. Hence a pH of 1.2 was chosen. A 10 ml portion of EG-A solution was found to be optimal. Shaking times of 1–3 min produced a constant absorbance; hence a shaking time of 2 min was selected. A ratio of 2:1 aqueous to non-aqueous phases was required for the efficient extraction of the coloured species. A series of experiments with other organic solvents such as $CCl_4$, $CH_2Cl_2$, and *n*-butanol showed that chloroform was the best choice. The absorption spectrum of the coloured species is shown in Fig. 1.

In order to establish the experimental conditions for method B, the strength and the volume of $KMnO_4$ was studied. The use of 0.5 ml of $KMnO_4$ in 2.0 M $H_2SO_4$ was found to give constant and reproducible absorbance values. The strength of the acid in the preparation of

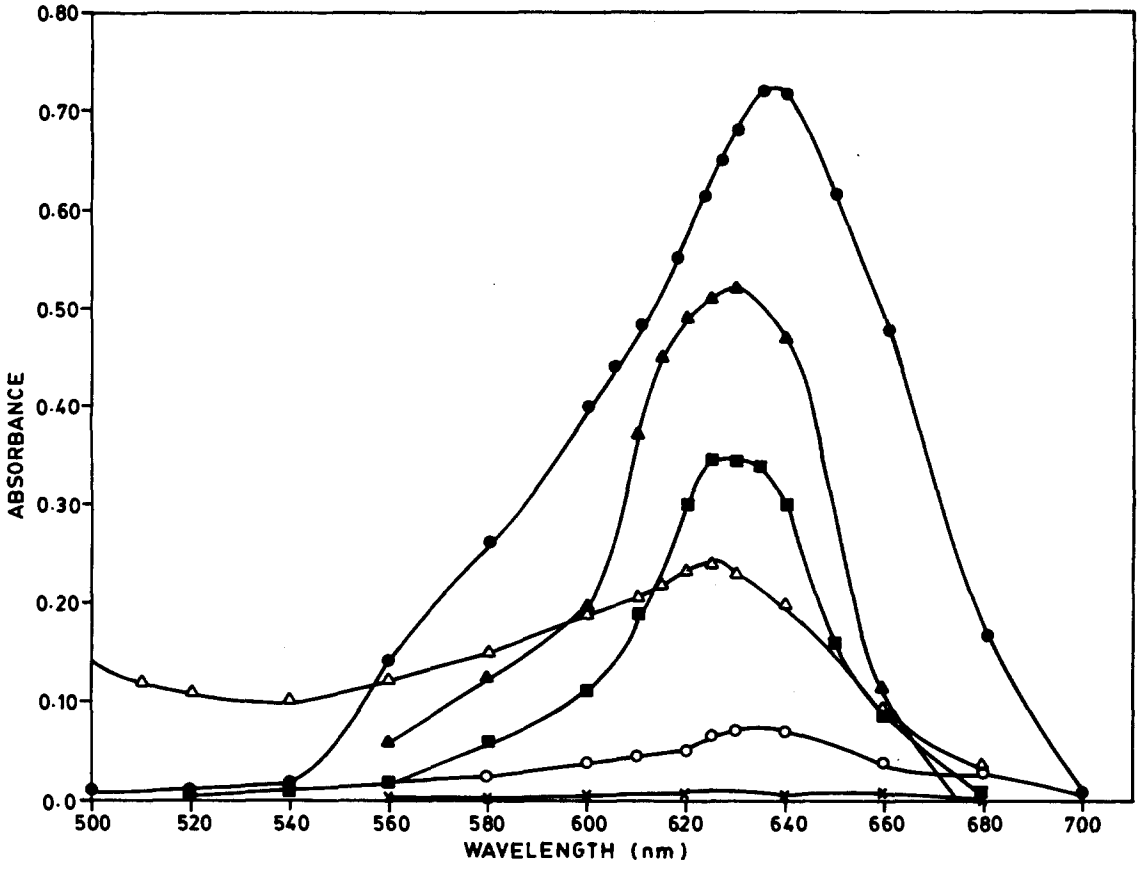


Fig. 1. Absorption spectra of the tamoxifen–EG-A system (tamoxifen concentration $1.07 \times 10^{-5}$ M; EG-A concentration $2.53 \times 10^{-3}$ M) the tamoxifen citrate–FG-FCF/$KMnO_4$ system (tamoxifen citrate concentration $7.09 \times 10^{-6}$ M; FG-FCF concentration $4.94 \times 10^{-5}$ M; $KMnO_4$ concentration $4.0 \times 10^{-5}$ M) and the tamoxifen citrate–CTC system (tamoxifen citrate concentration $8.87 \times 10^{-4}$ M; CTC concentration $1.25 \times 10^{-1}$ M). The three spectra are blank-corrected. ●, CTC; ▲, $KMnO_4$–FG-FCF; ■, EG-A; ○, EG-A BLK; ×, CTC BLK; △, $KMnO_4$–FG-FCF BLK.

$KMnO_4$ was found to have a significant effect on the absorbance. The oxidation time was established by increasing it in increments of 5 min. The absorbance values (after colour development) were found to increase to a maximum up to an oxidation time of 15 min and remained constant for 15 min. Hence, an oxidation time of 15 min at room temperature ($28 \pm 5$°C) was chosen. Increasing the temperature produced no additional increase in absorbance. The addition of 0.4 ml of FG-FCF and 4.0 ml of sodium sulphate were found to be optimal. The spectrum obtained for these solutions produced by the suggested procedure is shown to have maximum absorbance at 630 nm, as shown in Fig. 1.

To establish the experimental conditions for method C, the drug was allowed to react with CTC in aqueous solution buffered from pH 1.1 to 3.0 and the complex was extracted with benzene. Constant absorbances were obtained over the pH range 1.8–2.4; hence a pH of 2.0 was used. It has been found that 2.0 ml of buffer are necessary to maintain the pH of the aqueous phase. From 4 to 7.0 ml of CTC were found to give a constant absorbance value; hence a 5.0 ml portion of CTC was used. Benzene was used for the selective extraction of the coordination complex formed between the drug and CTC. A ratio of 1.2:1.0 aqueous to organic phases was required for efficient extraction of the coloured species. Constant absorbance was obtained for shaking periods between 1 and 4 min; hence a shaking time of 2.0 min was chosen for use.

### *2.5. Procedures*

#### *2.5.1. Method A*

Aliquots of the tamoxifen standard solution (1.0–6.0 ml; 5 μg $ml^{-1}$) were placed in a series of 125 ml separatory funnels, and 10.0 ml of buffer (pH 1.2) and 10.0 ml of EG-A solution were added to each. The total volume of the

Table 1
Optical characteristics, precision and accuracy

| Parameter | Method | | |
|---|---|---|---|
| | A | B | C |
| Beer's law limits ($\mu g\ ml^{-1}$) | 0.5–3.0 | 1.0–6.0 | 100–500 |
| Detection limits ($\mu g\ ml^{-1}$) | 0.036 | 0.134 | 1.32 |
| Molar absorptivity ($l\ mol^{-1}\ cm^{-1}$) | $(6.15 \times 10^4)$ $\pm 258.2$ | $(7.23 \times 10^4)$ $\pm 303.7$ | $(7.6 \times 10^2)$ $\pm 12.2$ |
| Sandell's sensitivity ($\mu g\ cm^{-2}$ per 0.001 absorbance unit) | $(6.038 \times 10^{-3})$ $\pm(2.85 \times 10^{-5})$ | $(7.79 \times 10^{-3})$ $\pm(3.14 \times 10^{-5})$ | $(7.35 \times 10^{-1})$ $\pm(1.22 \times 10^{-2})$ |
| Relative standard deviation (%) [a] | 0.52 | 0.27 | 0.41 |
| Range of error [a] (95% confidence limit) | 0.55 | 0.28 | 0.43 |

[a] Six replicate samples.

chloroform layer in each separating funnel was adjusted to 10.0 ml. The contents were shaken for 2 min and absorbance of the separated chloroform layer was measured at 625 nm against a reagent blank within 30 min. The amount of drug was computed from a Beer–Lambert plot.

*2.5.2. Method B*

To a series of 25 ml calibrated tubes containing aliquots (0.5–6.0 ml) of tamoxifen citrate ($50\ \mu g\ ml^{-1}$), 0.5 ml of $KMnO_4$ solution was added to each and the total volumes were adjusted to 10.0 ml with distilled water. After allowing to stand for 15 min at room temperature, 0.4 ml of FG-FCF solution and 4.0 ml of sodium sulphate solution were added successively. After 10 min, the volume was increased to 25 ml with distilled water. The absorbances were measured against a reagent blank at 630 nm within 3 h. The amount of drug were computed from a Beer–Lambert plot.

*2.5.3. Method C*

Aliquots of drug standard solution (1.0–5.0 ml, $1\ mg\ ml^{-1}$) were transferred to a series of 125 ml separatory funnels, and 2.0 ml of buffer (pH 2.0) and 5.0 ml of CTC solution were added to each. The total volume of the aqueous phase in each separatory funnel was adjusted to 12.0 ml with distilled water. After the addition of 10 ml of benzene the contents were shaken for 2 min. The two phases were allowed to separate and the absorbances of the benzene layers were measured at 635 nm against a reagent blank. The amount of drug was computed from the Beer–Lambert plot.

*2.5.4. Pharmaceutical formulations*

Twenty tablets were massed and powdered. The powder equivalent to 100 mg of tamoxifen was treated with chloroform in the presence of alkali (for method A) or a DMF:$H_2O$ (1:5) mixture (for methods B and C) as under the standard drug solution preparation (Section 2.3). The insoluble residue was filtered to obtain the solution of concentration $1\ mg\ ml^{-1}$. Stock solutions were further diluted to the requisite concentration and analysed using the procedure for the bulk drug.

*2.5.5. British Pharmacopoeia reference method [1]*

Twenty tablets were massed and powdered. To a quantity of the powder containing the equivalent of 25 mg of tamoxifen, 100 ml of methanol were added. The mixture was shaken for 15 min, and the volume was adjusted 250 ml with methanol. After filtration, 10 ml of the filtrate were diluted to 100 ml with methanol, and the absorbance of the resulting solution was measured against a methanol blank at 275 nm. The content of the drug was computed from its Beer–Lambert plot.

*2.6. Analytical data*

The Beer's law limits, molar absorptivity, Sandell's sensitivity, detection limits [20], regression equation, and correlation coefficient obtained by a least-squares treatment of the results are given in Tables 1 and 2. The precision of each method was tested by analysing six replicate samples containing $2.0\ \mu g\ ml^{-1}$, $4.0\ \mu g\ ml^{-1}$ or $350\ \mu g\ ml^{-1}$ of the bulk drug for methods A, B or C, respectively. The per cent standard deviation and the per cent range

Table 2
Regression characteristics for the calibration of methods

| Parameter [a] | Methods | | |
|---|---|---|---|
| | A | B | C |
| Slope, $m$ | 0.165 | 0.127 | 0.00136 |
| Intercept, $b$ | $1.1 \times 10^{-3}$ | $0.6 \times 10^{-3}$ | $-7.4 \times 10^{-3}$ |
| Correlation coefficient, $r$ | 0.9999 | 0.9999 | 0.9997 |
| Standard error, $S_e$ | $1.12 \times 10^{-3}$ | $2.0 \times 10^{-4}$ | $6.78 \times 10^{-3}$ |
| Standard deviation on slope, $S_m$ | $5.34 \times 10^{-4}$ | $4.78 \times 10^{-4}$ | $2.02 \times 10^{-5}$ |
| Standard deviation on intercept, $S_b$ | $1.04 \times 10^{-3}$ | $1.86 \times 10^{-3}$ | $6.7 \times 10^{-3}$ |

[a] With respect to $Y = mC + b$ where $C$ is the concentration ($\mu g\ ml^{-1}$) and $Y$ is absorbance units.

of error at a 95% confidence level of the method are given in Table 1.

Values obtained by these methods and the British Pharmacopoeia reference method for pharmaceutical formulations are incorporated into Table 3. They are in good agreement. As an additional demonstration of accuracy, recovery experiments were performed by adding a fixed amount of the drug to the preanalysed formulations. These results are summarised in Table 3.

### 2.7. Chemistry of the coloured species

Tamoxifen, being basic in nature, forms an ion-association complex with the acidic dye EG-A in method A which is extractable into chloroform from the aqueous phase. The stoichiometric ratio of the drug to the dye was determined with use of the slope-ratio method [18,19], and was found to be 3:1 (scheme 1).

Method B involves two steps. In the first step, tamoxifen citrate was treated with excess $KMnO_4$ of known concentration; 7 mol of potassium permanganate are required to oxidise 1 mol of tamoxifen citrate. The oxidation of citric acid under similar conditions shows that each mole of citric acid consumes 4 mol of potassium permanganate. From this study it is clear that each mole of tamoxifen (free base) consumes 3 mol of potassium permangante. Attempts to estimate tamoxifen directly with permangante have failed due the insoluble nature of the free base in a water: DMF mixture. In the second step, unreacted $KMnO_4$ was determined by using the dye FG-FCF. Approximately 1.8 $KMnO_4$ molecules are reduced to Mn(II) by 1 dye molecule (a $9e^-$ reaction). The consumed $KMnO_4$ corresponds to the concentration of the drug.

The coloured species formed in method C can be regarded as a coordinate complex of the drug (electron donor) and the central metal atom of cobalt thiocyanate (electron acceptor) based on an analogy in previous work [16,17]. The composition of the coloured complex in benzene was studied by re-extraction into the aqueous phase with 3 x 20 ml portions of distilled water, and cobalt was determined with 0.01 M EDTA solution using Xylenol Orange as the indicator. The thiocyanate concentration was determined by Volhard's method. It was observed that the drug, cobalt, and thiocyanate were in the ratio of 2:1:4 in complex, as indicated in Scheme 2.

## 3. Conclusion

The order of $\lambda_{max}$ values among the proposed methods and a reference method (R) in the determination of tamoxifen is $C > B > A > R$. The higher $\lambda_{max}$ of the proposed methods is a decisive advantage since the interference from the associated ingredient should be far less at higher wavelengths than at lower wavelengths. The senstivity order of the methods is $R > B > A > C$.

Method A has the advantage that it can be applied to the determination of individual components in a multicomponent mixture. This aspect of spectrophotometric analysis is of major interest in pharmaceutical analysis, since it offers distinct possibilities in the assay of a particular component in a complex dosage formulation. Although method B is an indirect one, it is more sensitive. Method C is selective for the estimation of compounds containing an aliphatic tertiary amino group.

Table 3
Analysis of pharmaceutical preparations by proposed and reference methods

| Pharmaceutical preparation (tablets) | Nominal amount (mg) | Found [a] (mg) | | | Reference [b] method | Recovery (%) [c] | | |
|---|---|---|---|---|---|---|---|---|
| | | Method A | Method B | Method C | | Method A | Method B | Method C |
| I | 10 | 9.87 ±0.079 | 9.92 ±0.081 | 9.94 ±0.087 | 9.89 ±0.087 | 99.6 ±0.82 | 99.9 ±1.04 | 100.03 ±1.0 |
| II | 20 | 19.98 ±0.075 | 19.95 ±0.075 | 19.89 ±0.063 | 19.90 ±0.062 | 99.4 ±0.4 | 99.7 ±0.96 | 99.90 ±0.69 |

[a] Average of three determinations.
[b] B.P. reference method (average of three determinations).
[c] Recovery of 10 mg added to the pharmaceutical preparations (average of three determinations).

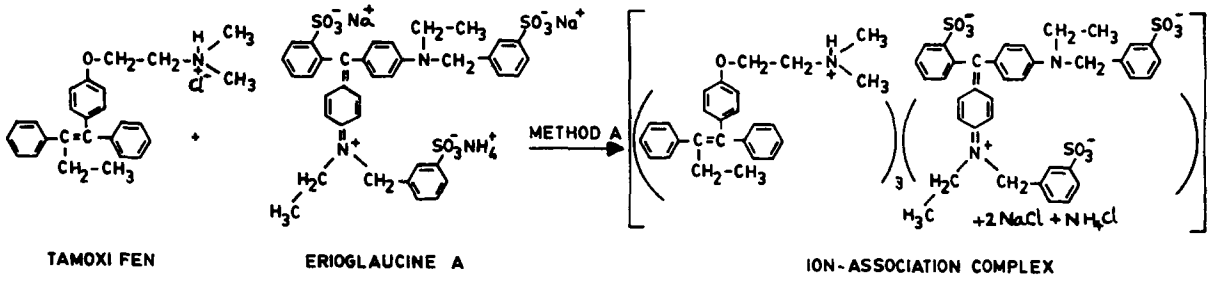


TAMOXI FEN ERIOGLAUCINE A ION-ASSOCIATION COMPLEX

Scheme 1.

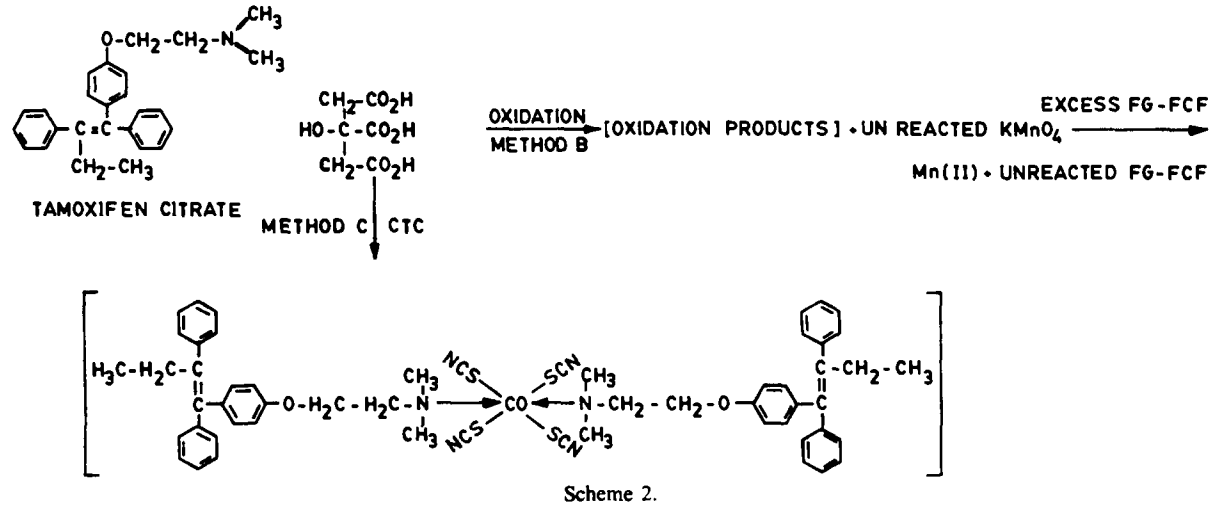


TAMOXIFEN CITRATE

Scheme 2.

Thus the proposed methods are simple, selective and sensitive for the determination of tamoxifen citrate, and provide a wide choice depending upon the needs of the specific situation.

## Acknowledgements

The quality control managers of Torrent Pharmaceuticals Ltd. and Lyka Labs Ltd. were duly acknowledged for providing gift samples of tamoxifen citrate.

## References

[1] British Pharmacopoeia, Vols. I, II, HMSO, London, 1988, p. 364, 1008.
[2] United States Pharmacopoeia, Vol. 22, U.S.P. Convention, Rockville, 1990, p. 1310.
[3] I.I. Hewala, Anal. Lett., 26 (1993) 625.
[4] Z. Fijalek, J. Chodkowski and M. Warowna, Acta Pol. Pharm., 45 (1988) 245.
[5] H.K. Adam, M.A. Gay and R.H. Moore, J. Endocrinol., 84 (1980) 35.
[6] N.M. Sanghavi and M.A. Fruitwala, Indian Drugs, 29 (1992) 694.
[7] C.P. Daniel, S.J. Gaskell, G. Bishop and R.I. Nicholson, J. Endorcrinol., 83 (1979) 401.

[8] S.J. Gaskell, C.P. Daniel and R.I. Nicholson J. Endocrinol., 78 (1974) 293.
[9] C. Murphy, T. Fotsis, P. Pantzar, H. Adlercreutz and F. Martin, J. Steroid. Biochem., 26 (1987) 547.
[10] R.T. Sane, S.V. Desai, K.K. Sonawane and V.G. Nayak J. Chromatogr., 331 (1985) 432.
[11] P.J. Weir, D.S. Ireland and A. Moledina J. Pharm. Biomed. Anal., 7 (1989) 393.
[12] H.G. Jalonen, J. Pharm. Sci., 77 (1988) 810.
[13] R.T. Sane, K.K. Sonawane, M.L. Kubal and V.G. Nayak Indian Drugs, 24 (1986) 154.
[14] C.S.P. Sastry, T. Thirupathi Rao, A. Sailaja and T.A.S.R. Prasad, Indian J. Pharm. Sci., 54 (1992) 125.
[15] H.T. Gordon, Anal. Chem., 23 (1951) 1853.
[16] S.S. Zarapaker, R.V. Rele and V.J. Doshi, Indian Drugs, 24 (1987) 560.
[17] R.G. Bhatkar and D.C. Madkaiker, Indian J. Pharm. Sci., 42 (1980) 145.
[18] H. Irving, F.J.C. Rossotti and R.J.P. Williams, J. Chem. Soc., 1 (1995) 1906.
[19] J. Ryoberg and B. Ryoberg, Ark. Kemi., 9 (1956) 81.
[20] IUPAC, Spectrochim. Acta, 33B, (1978) 242.

ELSEVIER

Talanta 42 (1995) 1487–1491

Talanta

# Simultaneous determination of Ru(III) and Rh(III) using octadecyldithiocarbamate by first-derivative spectrophotometry

K. Malathi, M. Subbaiyan *

*Department of Analytical Chemistry, University of Madras, Guindy Campus, Madras-600 025, India*

Received 10 November 1994; revised 22 March 1995; accepted 28 March 1995

**Abstract**

A first-derivative spectrophotometric method is described for the simultaneous determination of Ru(III) and Rh(III) using octadecyl dithiocarbamate. The complexes are insoluble in water, but easily extractable into chloroform. Quantitative determination of Ru(III) and Rh(III) is possible in the ranges 0.5–6.0 μg $ml^{-1}$ and 1.0–10.0 μg $ml^{-1}$ respectively, with a standard deviation of ±0.10. A statistical evaluation of the experimental results is reported.

## 1. Introduction

Derivative spectrophotometry has been used to increase the selectivity and sensitivity of the determination of various substances whose absorption spectra overlap. The selectivity of the determination can be improved using the zero-crossing method, as described by many workers [1,2]. In this method, the derivative amplitude is measured at the wavelength at which the interfering derivative band crosses the zero line, thus yielding a suitable measurement for the analyte of interest.

Interest in the analytical applications of derivative spectrometry has been on the increase for the past few decades, owing to the introduction of commercial spectrometers capable of operating in the derivative mode. Notable reports are the determination of beryllium and magnesium with 1-hydroxy-2-carboxyanthraquinone [2], ruthenium and palladium with 2-thiobarbituric acid [3], iron and copper with 2-thiobarbituric acid [4] and uranium and thorium with arsenazo III [5].

Dithiocarbamates of lower series have been used in inorganic analysis, in the colorimetric estimation of many metal ions [6]. Dithiocarbamates derived from higher homologues of hydrocarbon series offer scavenging capacity for metal ions and easy extractability over the lower series. The present work describes the application of first-derivative spectrophotometry to the simultaneous determination of ruthenium and rhodium using octadecyldithiocarbamate.

## 2. Experimental

### 2.1. Apparatus

A DMS varian-80 double beam spectrophotometer was used for recording the normal and first-derivative spectra of the complexes.

An AR3410 ICP-atomic emission spectrometer was used for the estimation of the metal ions.

* Corresponding author.


*SSDI* 0039-9140(95)01599-X

### 2.2. Reagents

Analytical reagent-grade chemicals and doubly-distilled water were used throughout the estimations.

The ammonium salt of octadecyldithiocarbamate (ODDTC) was prepared from octadecylamine (Fluka) according to the method of Srinivasan [7]. Ethanolic ODDTC solutions (0.2% (m/v)) were employed.

Rhodium(III) and ruthenium(III) stock solutions (1 mg ml$^{-1}$) were prepared from $RhCl_3$ and $RuCl_3$ (CDH) respectively. The exact metal content was determined by ICP-AES.

### 2.3. Procedure

The absorption spectra (normal and first-derivative) of the following solutions were recorded against the reagent blank in order to determine the characteristics of absorption of the metal–reagent complexes and their mixture.

(1) An aliquot of the sample (1 ml) containing 2–20 μg of ruthenium was placed in a 25 ml separating funnel. To this were added 2 ml of acetate buffer solution (pH 5), 2 ml of 0.2% (m/v) ODDTC in ethanol and 5 ml of water. The above solution was extracted with 5 ml of chloroform.

(2) An aliquot (1 ml) of the sample containing 2–20 μg of rhodium was placed in a separating funnel and processed as in (1).

(3) An aliquot of the sample (1 ml) containing 2–20 μg of ruthenium and 2–20 μg of rhodium was placed in a separating funnel. To this were added 2 ml of acetate buffer (pH 5), 4 ml of 0.2% (m/v) ODDTC in ethanol and 3 ml of water. Extraction was carried out with 5 ml of chloroform.

## 3. Results and discussion

Octadecyldithiocarbamate forms green and greenish-yellow coloured complexes with ruthenium and rhodium respectively in slightly acidic media (pH 5–6), which are easily extractable into chloroform. Maximum absorbances of both the complexes were observed when 2 ml of 0.2% (m/v) ODDTC in ethanol was used. The composition of both the complexes was found to be 1:3 (M:L) by Job's continuous variation method. The complex formation was found to be instantaneous and the absorbance was found to remain stable for more than 24 h. Quantitative extraction was observed for single equilibration. Alcohol, used to form a solution of ODDTC, remained in the aqueous phase and was not extracted into $CHCl_3$ under the experimental conditions.

### 3.1. Spectral characteristics

The absorption spectra of the solution of Ru complex, Rh complex and a mixture of Ru and Rh complexes in chloroform exhibited $\lambda_{max}$ values at 420 nm, 430 nm and 430 nm respectively (Fig. 1). The reagent did not show any significant absorbance in this region. Among the various solvents tried, chloroform, benzene and dichloromethane were found to be more potent in extracting the complexes. Of the three solvents, the complexes evinced maximum molar absorptivity and higher solubility in chloroform. Hence, $CHCl_3$ was chosen as the suitable solvent.

Since there is a large overlap between the spectra of the individual elements in the normal mode, spectrophotometric determination of these ions when present in the same sample becomes difficult. To overcome this, derivative spectrophotometry, which involves the differentiation of a normal spectra with respect of wavelength, was used.

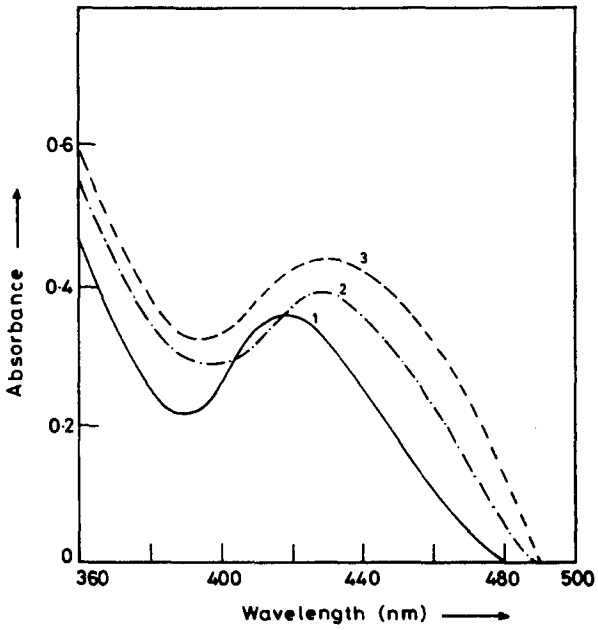


Fig. 1. Absorption spectra of (1) Ru–ODDTC complex, (2) Rh–ODDTC complex and (3) mixture of Ru–ODDTC and Rh–ODDTC complexes. Ru(III) = 2.00 μg ml$^{-1}$; Rh(III) = 3.38 μg ml$^{-1}$.

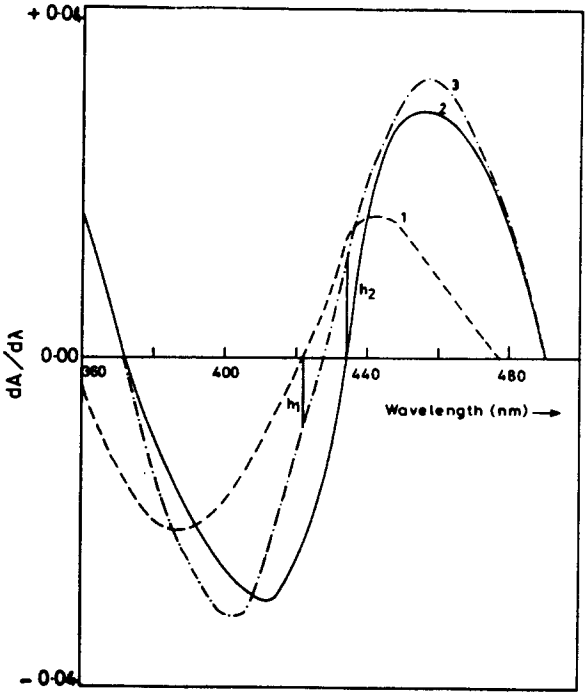


Fig. 2. First-derivative spectra of (1) Ru–ODDTC complex, (2) Rh–ODDTC complex and (3) mixture of Ru–ODDTC and Rh–ODDTC complexes.

Fig. 2 shows the first-derivative spectra of Ru complex, Rh complex and a mixture of Ru and Rh complexes in chloroform. The two most commonly used techniques in derivative spectrophotometry [8] are the "graphical method", which involves graphical constructions on a chart recording of the spectrum, and the "zero-crossing method", which involves measurement of the absolute values of the total derivative spectrum at a wavelength corresponding to the zero-crossing point of the derivative spectrum of the interfering component. In this case, the graphical method cannot be used, because of the closeness of the overlapping spectra which results in poor resolution of the spectrum of the mixture. Hence, the zero-crossing method was used in this work. The heights $h_1$ and $h_2$ in the first-derivative spectrum of the mixture corresponding to the values taken at 423 nm and 435 nm are proportional to the Rh(III) and Ru(III) concentrations respectively.

A sensitivity of 0.007–0.010 unit is lost for both the elements on going from absorbance to first-derivative spectra. In the normal mode, since they have closer $\lambda_{max}$ values, they interfere with each other in their estimations if present in the same sample. Therefore, it is necessary to mask one element, which can be avoided when first-order spectra (zero-crossing method) are recorded.

Fe, Cu, Ni, Bi, Pd and Pt interfere strongly in the determination (tolerance limit ≈ 1 ppm), and they should be removed prior to the estimation of the metal ions. Anions like $Cl^-$, $Br^-$, $OAc^-$, $SO_4^{2-}$ and $PO_4^{3-}$ can be tolerated up to 10 000 ppm. The tolerance limit for EDTA is 0.05 M. The ODDTC complexes of the base metals like Fe, Cu, Ni etc., are soluble in $CCl_4$ while those of Ru and Rh are insoluble in the pH range 3–5. Hence, such interferences can be avoided by carrying out a preliminary extraction with $CCl_4$ or chloroform extraction in the presence of 0.01 M EDTA.

The instrumental parameters such as wavelength scan rate and slit width which affect the shape of the derivative spectra are to be optimised to give good selectivity and sensitivity in the determination. An optimised scan rate of 100 nm $min^{-1}$ and a slit width of 1 nm were used throughout the investigation.

### *3.2. Statistical analysis of the determination of ruthenium and rhodium in mixtures*

The following experiments were performed to test the non-interference of the analytical signals of Ru(III) and Rh(III).

Two calibration graphs were constructed from first-derivative signals for standards containing between 0.5 and 10 μg $ml^{-1}$ of ruthenium in the presence of 2.0 and 4.0 μg $ml^{-1}$ of rhodium. Similarly, two calibration graphs were prepared for standards containing between 0.5 and 10 μg $ml^{-1}$ of rhodium in the presence of 2.1 and 4.0 μg $ml^{-1}$ of ruthenium.

A critical evaluation of the proposed method was performed by assessing the results of the statistical analysis of the experimental data [9]. The slope, intercept, correlation coefficient and standard deviation are shown in Table 1. The linearity of the calibration graphs and adherence of the systems to Beer's law are validated by the high value for the correlation coefficient of the regression equation and by the intercept value on the $y$-axis, which is close to zero. Ten calibration points were generated to obtain the above correlation.

From Table 1 it can be seen that the slope of the calibration graphs for ruthenium is independent of the rhodium concentration. Similarly, the slope of the calibration graph for rhodium is independent of ruthenium concentration. Therefore, it can be inferred that the amplitude of the derivative signal of the mixture, measured at the zero-crossing point of the

Table 1
Statistical analysis of the determination of ruthenium and rhodium in mixtures by first-derivative spectrophotometry

| Element detd. | Other element | | Slope | Intercept | Correlation coefficient | Standard deviation ($\mu g\ ml^{-1}$) |
|---|---|---|---|---|---|---|
| | Element | Conc. ($\mu g\ ml^{-1}$) | | | | |
| Ru(III) | Rh(III) | 4.0 | 1.977 | $5.37 \times 10^{-2}$ | 0.999 | 0.110 |
| | | 2.0 | 1.968 | $5.26 \times 10^{-2}$ | 0.999 | 0.059 |
| Rh(III) | Ru(III) | 4.0 | 0.9924 | $7.60 \times 10^{-3}$ | 0.999 | 0.079 |
| | | 2.1 | 0.9965 | $2.30 \times 10^{-3}$ | 0.999 | 0.048 |

derivative spectrum of one of the two components, is a function of the concentration of the component under consideration in accordance with theoretical predictions.

Statistical analysis of the experimental results permits the calculation of the error $S_c$ in the determination of a given concentration, $c$, of a component, and is calculated using the equation

$$S_c = \frac{S_0}{b}\left[1 + \frac{1}{n} + \frac{(D-\bar{D})^2}{b^2(\Sigma\, c^2 - n\bar{c}^2)}\right]^{1/2}$$

where $S_0 = [\Sigma\,(D-D')^2/n-2]$; $D$ = experimental value of the first derivative; $D'$ = first-derivative value calculated from the regression equation; $b$ = angular coefficient of the regression line; $\bar{c}$ and $\bar{D}$ are the average concentration and first-derivative value, respectively, for '$n$' standard specimens. Graphs of $S_c$ versus rhodium and ruthenium concentration are shown in Figs. 3 and 4, respectively, as histograms.

The quantity $S_c$ allows the calculation of confidence limits at the selected level of significance for the determination of unknown concentrations. The results are shown in Fig. 5 in the form of percentage uncertainty in the concentration ($t_p S_c/c$) for all the calibration graphs, where $t_p$ is the value of the Student's quantity at a 0.05 level of significance (95% probability) for $n-2$ degrees of freedom.

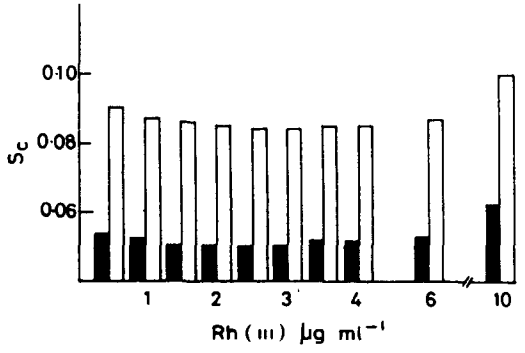


Fig. 3. Histograms of the error in the determination of Rh(III) concentration. Shaded area, in the presence of 2.1 $\mu g\ ml^{-1}$ of Ru(III); unshaded area, in the presence of 4.0 $\mu g\ ml^{-1}$ of Ru(III).

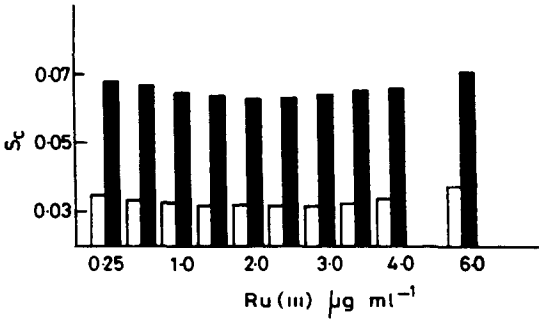


Fig. 4. Histograms of the error in the determination of Ru(III) concentration. Shaded area, in the presence of 4.0 $\mu g\ ml^{-1}$ of Rh(III); unshaded area, in the presence of 2.0 $\mu g\ ml^{-1}$ of Rh(III).

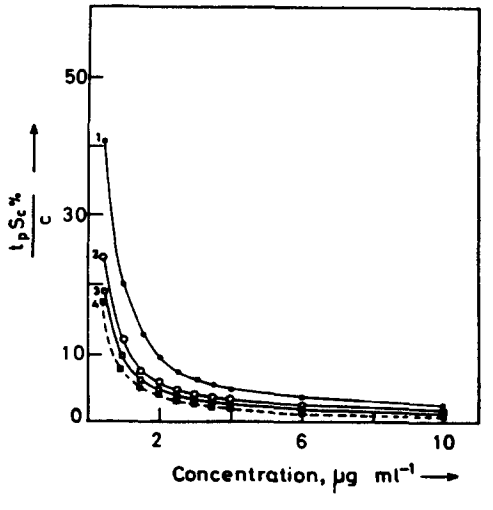


Fig. 5. Variation of the confidence limit at a level of significance of $p = 0.05$ (95% probability) in the form of percentage uncertainty in the concentration of Ru(III) and Rh(III). (1) Ru(III) = 4.0 $\mu g\ ml^{-1}$; (2) Ru(III) = 2.1 $\mu g\ ml^{-1}$; (3) Rh(III) = 4.0 $\mu g\ ml^{-1}$; (4) Rh(III) = 2.0 $\mu g\ ml^{-1}$.

Table 2
Results of the quantitative determination of ruthenium and rhodium by first-derivative spectrophotometry

| Amount taken ($\mu g\ ml^{-1}$) | | Amount found ($\mu g\ ml^{-1}$) | | Relative error (%) | |
|---|---|---|---|---|---|
| Ru | Rh | Ru | Rh | Ru | Rh |
| 1.20 | 1.20 | 1.25 | 1.20 | 4.16 | 0.00 |
| 2.00 | 1.20 | 2.00 | 1.20 | 0.00 | 0.00 |
| 4.00 | 6.00 | 4.00 | 6.10 | 0.00 | 1.66 |
| 6.00 | 4.80 | 5.90 | 4.65 | −1.66 | −3.12 |

The method was applied to the determination of Rh(III) and Ru(III) in binary mixtures, and the results are presented in Table 2. The method can successfully be applied to determination of the title metal ions when present above 0.1 $\mu g\ ml^{-1}$ in ores and minerals.

## 4. Conclusions

A general procedure for the determination of ruthenium and rhodium in mixtures by first-derivative spectrophotometry using ODDTC as a reagent is proposed, and the usefulness of derivative spectrophotometry is discussed. The proposed method permits the simultaneous determination of ruthenium and rhodium in mixtures in the range 0.5–6.0 $\mu g\ ml^{-1}$ for Ru(III) and 1.0–10.0 $\mu g\ ml^{-1}$ for Rh(III), without a prior separation procedure. The method based on "zero-crossing measurement" gives satisfactory levels of precision and accuracy, and can be used for the simultaneous determination of Ru and Rh in ore samples.

## References

[1] S. Kus and Z. Marczenko, Analyst, 114 (1989) 207.
[2] F. Salinas, A. Munoz dela Pena and J.A. Murillo, Analyst, 112 (1987) 1391, and references cited therein.
[3] B. Morelli, Analyst, 108 (1983) 1506.
[4] B. Morelli, Analyst, 108 (1983) 870.
[5] R. Kuroda, M. Kurosaki, Y. Hayashibe and S. Ishimaru, Talanta, 37 (1990) 619.
[6] J. Stary, The Solvent Extraction of Metal Chelates, Pergamon Press, Oxford, 1964.
[7] V. Srinivasan, Ph.D. thesis, University of Madras, 1988.
[8] T.C. O'Haver and G.L. Green, Anal. Chem., 48 (1976) 312.
[9] V.V. Nallimov, The Application of Mathematical Statistics to Chemical Analysis, Pergamon Press, Oxford, 1963.

ELSEVIER

Talanta 42 (1995) 1493–1496

Talanta

# Solvent extraction separation of cobalt(II) with hexaacetatocalix(6)arene

Anita Gupta, S.M. Khopkar *

*Department of Chemical Technology, University of Bombay, Matunga, Bombay 400 019, India*

Received 3 November 1994; revised 7 March 1995; accepted 28 March 1995

**Abstract**

A new method is proposed for the solvent extraction separation of cobalt(II) with hexaacetatocalix(6)arene in toluene. Cobalt(II) was extracted at pH 7.4 with $10 \times 10^{-4}$ M hexaacetocalix(6)arene, stripped with 2 M nitric acid, and determined spectrophotometrically at 500 nm as its complex with nitroso-*R*-salt. Cobalt was separated from any associated elements. The method was extended to the analysis of cobalt(II) in real samples such as vitamin B-12.

## 1. Introduction

The calixarenes constitute a new class of supramolecular compounds with a variety of cavity sizes [1,2]. The annular space in calixarene compounds provide a unique basket-like structure which is useful for trapping metal ions in their three-dimensional network [3]. Many oxygenated solvent and chelating extractants have been found to be ineffective for extraction of cobalt [4]. When crown ethers were used from perchlorate media, 18-crown-6 was found to be most effective [5]. Crown ethers with 4 acylpyrazol-5-ols could be used to extract [6] cobalt at pH 3.5. Tetraazacrown ether has also been used for the extraction of cobalt at pH 1.0–7.0 with metanil yellow, facilitating separation of cobalt from manganese, bismuth, aluminium and iron [7]. The extraction chromatographic separation of cobalt [8] with DB18-crown-6 as the stationary phase is also effective. The complexation behaviour of calixarene [9] was recently discovered. Calix(4)-arene and calix(6)arene proved to be versatile extractants [10] for transition metals, while derivatives of *p-tert*-butylcalixarenes in carboxylic acid [11] were useful for the extraction of inner transition metals.

This paper describes the synthesis and application of hexaacetatocalix(6)arenes for extraction of cobalt(II). The proposed method was tested for the analysis of cobalt in vitamin B-12. Although atomic absorption or emission spectoscopic methods are good for the determination involving no separation, the proposed method is useful when it is necessary to separate cobalt from interfering ions before subsequent analysis by a suitable method other than AAS.

## 2. Experimental

### 2.1. Apparatus and reagents

A UV visible spectrophotometer (Model Lamda 3B) with 10 mm matched quartz cells was used.

A stock solution of cobalt(II) was prepared by dissolving 0.403 g of cobalt chloride hexahydrate (BDH, Anal R) in 1 l of distilled water containing 5 ml of concentrated hydrochloric acid. The solution was standardized complexometrically [12] and was found to contain

* Corresponding author, Professor Emeritus, Indian Institute of Technology, Bombay -400 076, India.


*SSDI* 0039-9140(95)01600-7

100 μg ml$^{-1}$ of cobalt(II). A diluted solution containing 10 μg ml$^{-1}$ of cobalt(II) was prepared by tenfold dilution of the stock solution.

Hexaacetatocalix(6)arene was synthesized [3] by the following procedure.

5, 11, 17, 23, 29, 35-Hexatertbutyl-37, 38, 39, 40, 41, 42-hexahydroxycalix(6)arene was prepared by dissolving about 10 g (0.666 mol) of *p-tert*-butyphenol in 6 ml of 5 M potassium hydroxide and 9.70 g of 37% formaldehyde solution. The mixture was heated at 110–120°C for 2 h to give a light yellow taffy-like precursor. This precursor was mixed with 10 ml of xylene and heated to 210–220°C for 3 h in an atmosphere of nitrogen with a Dean and Stark collector. The cooled reaction mixture was filtered and then suspended in 300 ml of chloroform, and was shaken with 100 ml of 1 M hydrochloric acid. The organic layer was separated, washed with water, dried over anhydrous sodium sulphate and concentrated to 100 ml. The addition of methanol caused precipitation of a solid which was removed by filtration to give the colourless product. Recrystallization was carried out from chloroform and methanol. The product had a melting point of 380–388°C and a yield of 80%. The spectral characteristics were as follows. IR (KBr): 3400, 3150 cm$^{-1}$ (OH stretching). $^1$H NMR ($CDCl_3$): $\delta$ 10.2 (s, 1, ArOH), $\delta$ 7.10 (s, 2, ArH), $\delta$ 3.88 (s, 2, $CH_2$), $\delta$ 1.25 (s, 9, $C(CH)_3)_3$. $^{13}$C NMR ($CDCl_3$): $\delta$ 147.2 (15% Ar), $\delta$ 144.2 (15% Ar), $\delta$ 126.1 (65% Ar), $\delta$ 34.0 (17% $ArCH_2Ar$), $\delta$ 33.1 (25% $C(CH_3)_3$).

Synthesis of hexaacetatocalix(6)arene derivative was carried out as follows. About 2.0 g of *tert*-butylcalix(6)arene was treated with 50 ml of acetic anhydride as well as two drops of concentrated sulphuric acid. The mixture was heated and refluxed for 2 h. The crude product on recrystallization from chloroform/methanol gave white platelets with an m.p. of 360–362°C and a yield of 84%. The spectral characteristics of the derivative were as follows. IR (KBr): 1760 cm$^{-1}$ (>C=O stretching). $^1$H NMR ($CDCl_3$): $\delta$ 6.9 (s, ArH), $\delta$ 3.6 (br, CH), $\delta$ 1.9 (s, $OCOCH_3$), 1.2 (s, $C(CH_3)_3$).

### 2.2. Procedure

An aliquot of a solution containing cobalt(II) was taken. Its pH was adjusted to 7.4 with hydrochloric acid or tetramethyl ammonium hydroxide. The solution was then transferred to a separating funnel. The total volume was made up of 10 ml. 10 ml of a $10.0 \times 10^{-4}$ M solution of hexaacetatocalix(6)arene in toluene was added. The solution was shaken for 5 min. The two phases were allowed to settle and separate. Colbalt from the organic phase was stripped with 10 ml of 2 M nitric acid, and was determined spectrophotometrically as its complex with nitroso-*R*-salt [13] at 500 nm against the reagent blank. It is possible to carry out extractions with a large volume of the aqueous phase. For the purpose of simplicity, in calculations the volumes of the aqueous and organic phases were maintained the same at 10 ml.

## 3. Results and discussion

### 3.1. Extraction as a function of pH

When cobalt(II) was extracted in the pH range of 1.0–10.0 with $10.0 \times 10^{-4}$ M hexaacetatocalix(6)arene in toluene, the extraction was quantitative between pH 7.0 and 7.6 (Table 1). Therefore, all extractions were carried out at pH 7.4. The results represent figures for triplicate determinations, and are reproducible and precise.

### 3.2. Extraction as a function of extractant concentration

Cobalt(II) was extracted with varying amounts of hexaacetatocalix(6)arene. The concentration was varied from $0.1 \times 10^{-4}$ to $25.0 \times 10^{-4}$ M (Table 2). The extraction was quantitative with $10.0 \times 10^{-4}$ M of hexaaceta-

Table 1
Extraction of cobalt(II) as a function of pH

| pH | $E^a$ (%) |
|---|---|
| 1.0 | 55.2 |
| 2.0 | 56.8 |
| 3.0 | 58.4 |
| 4.0 | 60.8 |
| 5.0 | 64.8 |
| 6.0 | 72.0 |
| 7.0 | 99.2 |
| 7.2 | 99.9 |
| 7.4 | 99.9 |
| 7.6 | 99.9 |
| 7.8 | 97.6 |
| 8.0 | 80.8 |
| 9.0 | 60.0 |
| 10.0 | 51.2 |

[a] *E*, percentage extraction.

Table 2
Effect of calixarene concentration on extraction of cobalt-(II)

| Calixarene concentration ($1 \times 10^{-4}$ M) | $E$ (%) |
|---|---|
| 0.10 | 2.0 |
| 0.25 | 18.0 |
| 0.50 | 30.0 |
| 0.75 | 37.8 |
| 1.00 | 47.6 |
| 2.50 | 78.5 |
| 5.00 | 92.0 |
| 7.50 | 96.5 |
| 10.0–25.0 | 99.9 |

tocalix(6)arene; hence, this concentration was utilized for routine work. The extractant itself was stable for a number of days in the solvent.

### 3.3. Extraction with various diluents

Cobalt(II) was extracted with $10.0 \times 10^{-4}$ M of hexaacetatocalix(6)arene in different diluents. The percentage extraction was as shown in brackets: carbon tetrachloride (73%), cyclohexane (62%), benzene (48.2%), toluene (99.9%), xylene (60%), chloroform (62.9%), dichloromethane (89%), 1,2-dichloroethane (84%), chlorobenzene (56%) and nitrobenzene (54.6%). Thus, the extraction was quantitative only with toluene as diluent, while with other solvents the extraction was incomplete. Hence, toluene was perferred as the diluent.

### 3.4. Effect of various stripping agents

After extraction, cobalt(II) was stripped with various stripping agents (Table 3). It was noted that cobalt was backwashed completely with 1.5–4 M nitric acid, while with other acids stripping was incomplete. Therefore, 2 M nitric acid was generally used as the stripping agent.

Table 3
Effect of various stripping agents

| Stripping acid | Extraction (%) | | | | |
|---|---|---|---|---|---|
| | 0.5 M | 1 M | 1.5 M | 2 M | 4 M |
| HCl | 74.9 | 80.5 | 83.3 | 86.9 | 91.6 |
| $HClO_4$ | 87.6 | 90.8 | 91.4 | 91.6 | 92.5 |
| $HNO_3$ | 74.1 | 87.6 | 99.9 | 99.9 | 99.9 |
| $H_2SO_4$ | 55.8 | 65.7 | 68.4 | 71.1 | 75.8 |

Table 4
Effect of diverse ions (cobalt taken = 10 μg)

| Diverse ions | Ratio | Amount tolerated (μg) |
|---|---|---|
| $Li^+$, $Na^+$, $K^+$, $Cs^+$, $Mg^{2+}$ $Ca^{2+}$, $Sr^{2+}$, $Ba^{2+}$, $Mn^{2+}$, $Sn^{4+}$, $Bi^{3+}$, $Cl^-$, $Br^-$, $I^-$, $NO_3^-$, $SO_4^{2-}$, $SO_3^{2-}$ | 1:100 | 10000 |
| $Al^{3+}$, $In^{3+}$, $Se^{4+}$, $Te^{4+}$ | 1:50 | 500 |
| $Y^{3+}$, $Zn^{2+}$, $Cd^{2+}$, $Ce^{3+}$ | 1:25 | 250 |
| $Mo^{6+}$, $V^{+5}$, $W^{6+}$, $Pb^{2+}$, $Th^{4+}$ | 1:5 | 50 |
| $Cr^{3+}$, $Fe^{3+}$, $UO_2^{+2}$ | 1:1 | 10 |
| $Ni^{2+}$, $Cu^{2+}$, $Ag^+$, $Pd^{2+}$ | 0 | Interfere |

### 3.5. Period of equilibriation

The extraction of cobalt(II) was carried out with varying periods of shaking. The optimum period of shaking was 5 min. A 5 min equilibration period was therefore employed throughout the investigation.

### 3.6. Nature of extracted species

Calix($n$)arene is a three-dimensional network with annular space with a basket-like structure where the metal is trapped. There is no true covalent bond formation in these supramolecular compounds, but a kind of ionic attraction; hence, the chloride ion is not involved in complexation. Further, no kind of aggregate formation is usually encountered. The trapping of cobalt is favoured in alkaline media promoting higher extraction due to increasing electrostatic attraction.

Plots of log $D$ versus log[hexaacetatocalix(6)-arene] at a fixed pH of 7.4 had a slope of 2.91. Therefore the probable composition of the extracted species is 1:3 (Co:hexaacetato-calix(6)-arene). Of course, these findings need additional support with X-ray diffraction studies [14].

### 3.7. Effect of diverse ions

Cobalt(II) was extracted in the presence of a large number of diverse ions (Table 4). It was possible to carry out actual separations. The tolerance limit was set as the amount of foreign ion causing an error of ±2.0% in the recovery of cobalt(II). The s-block metals and p-block metals, such as arsenic, tin and bismuth, were tolerated in ratios of 1:100. Aluminium, in-

Table 5
Analysis of cobalt(II) from real sample

| No. | Co Concentration | | Recovery (%) | Error |
|---|---|---|---|---|
| | Taken (μg) | Found (μg) | | |
| 1 | 5.22 | 5.30 | 101.53 | +1.53 |
| 2 | 7.83 | 7.60 | 97.06 | −2.94 |
| 3 | 10.44 | 10.30 | 98.66 | −1.34 |

dium, selenium and tellurium were tolerated in ratios of 1:50. Yttrium, zinc, cadmium and cerium were tolerated in ratios of 1:25. Molybdenum, vanadium, tungsten, mercury, lead and thorium were tolerated in ratios of 1:5. Chromium, iron and uranium were tolerated in the lower ratio of 1:1. Nickel, copper, silver and palladium showed strong interference. Most of the anions were tolerated in ratios exceeding 1:1. It is thus observed that, amongst various derivatives of calix(6)arene, the acetate derivative gives the best results [15].

### *3.8. Application to analysis of cobalt in vitamin B-12*

Vitamin B-12 (IP, 1000 mcq, Anglo French Company) from an ampoule of 1 ml was used for the preparation of stock solution. It was diluted to 25 ml with deionized water. An aliquot containing vitamin B-12 was taken and its pH was adjusted to 7.4 as usual. It was then extracted by the procedure described earlier. The experimental results showed good agreement with certified values (Table 5).

## Acknowledgement

Thanks are due to Science and Engineering Research Council of Department of Science and Technology, New Delhi, for sponsoring this project.

## References

[1] M.N. Gandhi and S.M. Khopkar, Bull. Indian Assoc. Nucl. Chem. Allied Sci., 10 (1994) 20.
[2] M.N. Gandhi and S.M. Khopkar, J. Sci. Ind. Res., 53 (1994) 630.
[3] C.D. Gutsche, "Calixarene", Monograph in Supramolecular Chemistry, Royal Society of Chemistry, London, 1989.
[4] M.N. Gandhi, S.M. Khopkar and N.V. Deorkar, Talanta, 40 (1993) 1535.
[5] S.M. Khalifa and H.F. Aly, Talanta, 36 (1989) 406.
[6] B. Rusoliarso, A. Messaondi and J.P. Brunette, Talanta, 40 (1993) 805.
[7] A. Yu Nazarenko and T.A. Bykh, Zh. Anal. Khim., 38 (1983) 1946.
[8] Yi.Yu. Vin and S.M. Khopkar, Ind. J. Chem., 27 (1988) 458.
[9] R.M. Izatt, J.D. Lamb, R.M. Hawkins, P.R. Brown, S.R. Izatt and J.J. Christensen, J. Am. Chem. Soc., 105 (1983) 1782.
[10] R. Ludvig, K. Inoue and T. Yamato, Solvent Exch. Ion Exch., 11 (1993) 311.
[11] R. Ludvig, K. Inoue, S. Shinkai and K.S. Gloe, Int. Solvent Extraction Conference York University, UK, 15 September 1993, Vol. I, Royal Society of Chemistry, London, 1993, p. 273.
[12] A.I. Vogel, Quantitative Inorganic Analysis, 3rd edn., Wiley, New York, 1962, pp. 443 and 688.
[13] F.D. Snell, Photometric and Fluorometirc Methods of Analysis, Wiley, New York, 1978.
[14] M.A. Mckervey, E.M. Seward, G. Ferguson, B. Ruhl and S.J. Harris, J. Am. Chem. Soc., Chem. Commun., 388 (1985).
[15] S. Shinkai, H. Koveshi, K. Ueda, T. Arimura and O. Manobe, J. Chem. Soc., 109 (1987) 6371.

ELSEVIER

Talanta 42 (1995) 1497–1503

Talanta

# The application of trimesic acid to the determination of terbium by spectrofluorimetry☆

Jinzhang Gao *, Guohu Zhao, Jingwan Kang

*Institute of Chemistry, Northwest Normal University, Lanzhou 730070, People's Republic of China*

Received 19 December 1994; revised 30 March 1995; accepted 3 April 1995

**Abstract**

A sensitive, direct spectrofluorimetric method for the trace determination of terbium with use of trimesic acid (TMA) has been developed. The reaction conditions for the fluorescence system of terbium with TMA were studied. The terbium ion can form a stable binary chelate with TMA, having a ratio of 1:1 in the pH range 3.5–6.5. The maximum excitation and emission wavelengths are 260 nm and 545 nm for the terbium chelate, respectively. The reaction is instantaneous and the fluorescence intensity of the terbium chelate remains stable from 0.25 to 4 h. Under the optimal experimental conditions the fluorescence intensity is a linear function of concentration in the range 0.0248–6.35 $\mu g\,ml^{-1}$ of terbium. The relative standard deviation is still within $\pm 4\%$ in the presence of one-thousandfold amounts of the other lanthanide ions, and common foreign ions hardly interfere in the determination. The method can be employed for the determination of trace amounts of terbium in rare earth ores or oxides because of its high sensitivity and selectivity with good reproducibility and accuracy.

## 1. Introduction

The fluorescence method for the determination of rare earth element has long been recognized [1], especially for the analytical determination of samarium, europium and terbium. The derivative spectrofluorimetric method has received much attention and has been an important subject of our studies in recent years [2–7]. The analytical method involving derivative fluorescence spectra shows a higher sensitivity and selectivity than the method utilizing normal fluorescence spectra. When it is employed for the simultaneous determination of trace amounts of samarium, europium and terbium, this method shows good reproducibility and accuracy. As part of this study, we have recently made a systematic investigation of the new fluorescence system of terbium with trimesic acid (benzene-1,3,5-tricarboxylic acid (TMA)). TMA has already been used extensively as a catalytic agent for chemical reactions and as an additive etc. [8,9], as well as compounds similar to TMA; benzene-1,2-dicarboxylic acid, benzene-1,2,4,5-tetracarboxylic acid, pyridine-2-carboxylic acid, pyridine-3-carboxylic acid and pyridine-2,6-dicarboxylic acid etc. have been employed as complexing agents or chelating agents for studying the fluorescent properties of a solid chelate with terbium [10], the crystal structure of complexes with Eu and Er [11,12] and the intermolecular interaction energy between lanthanide complexes in solution [13]. However, up to now it has not been applied as a fluorescence reagent. In this work we report a new fluorescence reagent and the development of a fluorimetric method for the determination of terbium.

☆ Project supported by the Gansu Province Natural Science Foundation, People's Republic of China.

* Corresponding author.



*SSDI* 0039-9140(95)01601-5

## 2. Experimental

### 2.1. Apparatus

Fluorescence measurements were made with a Shimadzu RF-540 spectrofluorimeter (Japan) equipped with a xenon light source, and the excitation and emission slits used were both 5 nm. The pH measurements were obtained with use of an SPM-10 pH meter (Shanghai, China).

### 2.2. Reagents

All the chemicals used in this paper were of analytical reagent grade or the highest purity available, and distilled, deionized water was employed throughout the study.

A stock solution of lanthanide ions (0.0200 mol $l^{-1}$) was prepared by dissolving requisite amounts of the corresponding oxides (purity, 99.99%): $La_2O_3$, $Pr_6O_{11}$, $Nd_2O_3$, $Sm_2O_3$, $Eu_2O_3$, $Gd_2O_3$, $Tb_4O_7$, $Dy_2O_3$, $Ho_2O_3$, $Er_2O_3$, $Tm_2O_3$, $Yb_2O_3$, $Lu_2O_3$ and $Y_2O_3$, in concentrated HCl and evaporating the solution to a syrup and diluting with distilled deionized water to the desired volume. A stock solution of cerium (0.0200 mol $l^{-1}$) was obtained by dissolving cerium oxide (purity, 99.99%; $CeO_2$) in a mixture of sulphuric acid and ammonium sulphite followed by the addition of $H_2O_2$ to the solution, converting $Ce^{4+}$ to $Ce^{3+}$. All the stock solutions were standarized with EDTA, using Xylenol Orange as indicator. Working solutions of lanthanide ions (0.0010 mol $l^{-1}$) were obtained by diluting corresponding stock solutions of lanthanide ions with distilled, deionized water. An HAc–NaAc buffer solution (pH 5.5) was obtained by adjusting the pH of a saturated sodium acetate solution to 5.5 with concentrated acetic acid. A solution of the chelating agent, TMA, (0.0100 mol $l^{-1}$) was prepared by dissolving 0.5250 g of TMA in 200 ml of distilled, deionized water with heating, and then diluting the solution to 250 ml with distilled, deionized water. Solutions of a large number of inorganic ions were prepared from their water-soluble salts (or oxides and carbonates in hydrochloric acid).

### 2.3. Procedure

A standard solution of terbium or the sample solution was placed in a calibrated tube with 3 ml of TMA solution (0.0100 mol $l^{-1}$) and 5 ml of acetic acid–sodium acetate buffer solution, pH 5.5. The final volume was made up to 25 ml with distilled, deionized water. The relative fluorescence intensity of the chelate was measured within 0.25–4 h at an emission wavelength of 545 nm in a 1 cm quartz cell, keeping the excitation wavelength maximum at 260 nm.

## 3. Results and discussion

### 3.1. Fluorescence spectra

The excitation and emission spectra of the system Tb + TMA at pH 5.5 were recorded with use of the spectrofluorimeter. The maximum wavelengths of excitation and emission were found to occur at 260 nm and 545 nm, respectively. The excitation spectrum is shown in Fig. 1a. In aqueous media at room temperature, a $4 \times 10^{-5}$ mol $l^{-1}$ solution of $Tb^{3+}$ only gives a very weakly measurable emission and a $8 \times 10^{-4}$ mol $l^{-1}$ solution of TMA does not give measurable emission upon excitation at 260 nm. The addition of a more than twentyfold excess of TMA to the $Tb^{3+}$ solution does not induce any emission changes, but results in greatly enhanced $Tb^{3+}$ emission. For $Tb^{3+}$ four distinct emission bands are

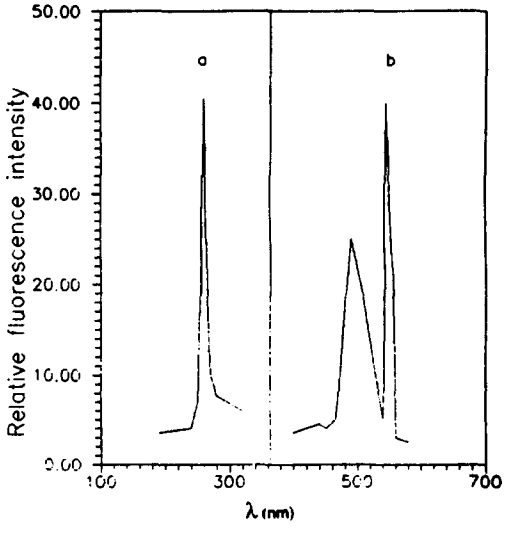


Fig. 1. (a) Excitation spectrum of the chelate of terbium with TMA. (b) Emission spectrum of the chelate of terbium with TMA. (Conditions: Tb, 1.589 μg $ml^{-1}$; TMA, $1.2 \times 10^{-3}$ mol $l^{-1}$; pH 5.5; excitation slit, 5 nm; emission slit, 5 nm.)

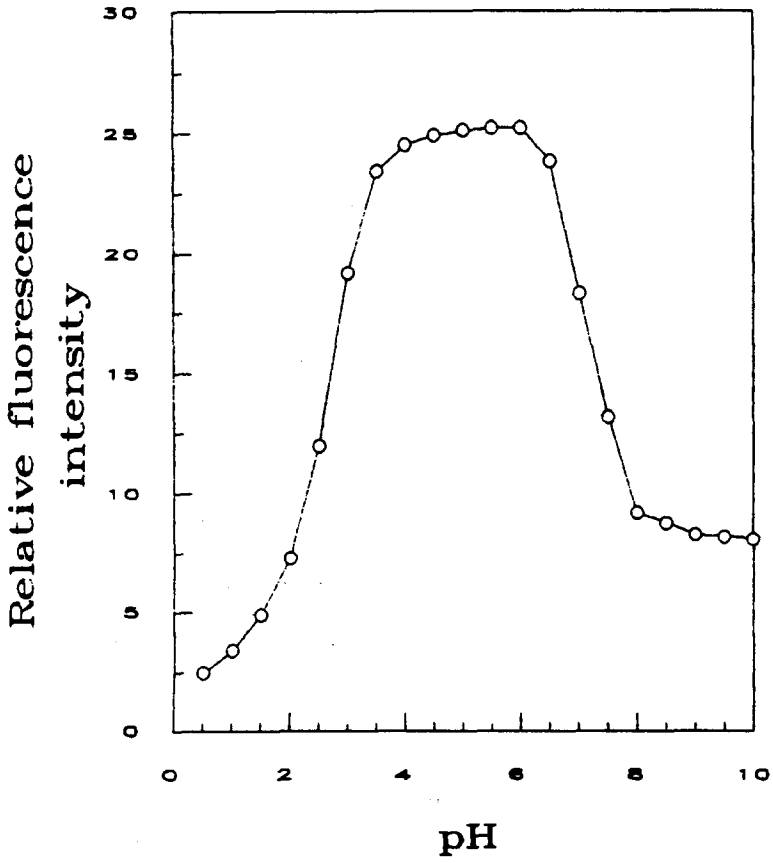


Fig. 2. Effect of pH on the fluorescence intensity of the terbium chelate. The pH values of the solution systems were adjusted with standard 0.1000 mol $l^{-1}$ KOH or HCl solutions. (Terbium, 1.589 μg $ml^{-1}$; TMA, $1.2 \times 10^{-3}$ mol $l^{-1}$.)

observed and these are found at 491 nm, 545 nm, 585 nm and 621 nm, respectively, corresponding to the $^5D_4 \rightarrow {}^7F_6$, $^5D_4 \rightarrow {}^7F_5$, $^5D_4 \rightarrow {}^7F_4$ and $^5D_4 \rightarrow {}^7F_3$ transitions [14,15]. Only the $^5D_4 \rightarrow {}^7F_6$ and $^5D_4 \rightarrow {}^7F_5$ transitions have appreciable intensity, with the transition to the $^7F_5$ level being the most intense. All the above are represented in Fig. 1b. Thus we can speculate that the mechanism for obtaining the luminescence spectra is an A–LMET–E process [16,17], i.e. the triplet level of the chelating agent, TMA, lies just above that of the terbium ion, so TMA absorbs ultraviolet light and transfers energy to the central terbium ion (namely the Antenna effect) [18–21], and then the terbium ion produces the characteristic sensitive metal-centred (MC) fluorescence spectrum.

### 3.2. *Effect of the acidity of the solution*

The variation in the fluorescence intensity at 545 nm for the terbium chelate was investigated as a function of pH. Maximum constant fluorescence intensity was obtained when the pH of the fluorescent chelate solution was maintained between 3.5 and 6.5 by the addition of dilute HCl or KOH. When the pH was adjusted using a buffer solution containing sodium acetate and acetic acid (pH 5.5) instead of HCl and KOH, it caused no change in the emission wavelength and only a slight change in the emission intensity. In this paper, a buffer solution containing sodium acetate and acetic acid (pH 5.5) was selected to maintain the solution acidity.

Fig. 2 shows that the fluorescence intensity of the terbium chelate becomes weaker at pH < 2.5 and pH > 8. The reason for this is that the protonation of three carboxyl groups of the chelating agent at pH < 2.5 and the intensive hydrolysis of the trivalent terbium ion at pH > 8 both result in a decrease in the concentration of the chelate of terbium with TMA, causing a decrease in the fluorescence intensity of the terbium chelate with TMA.

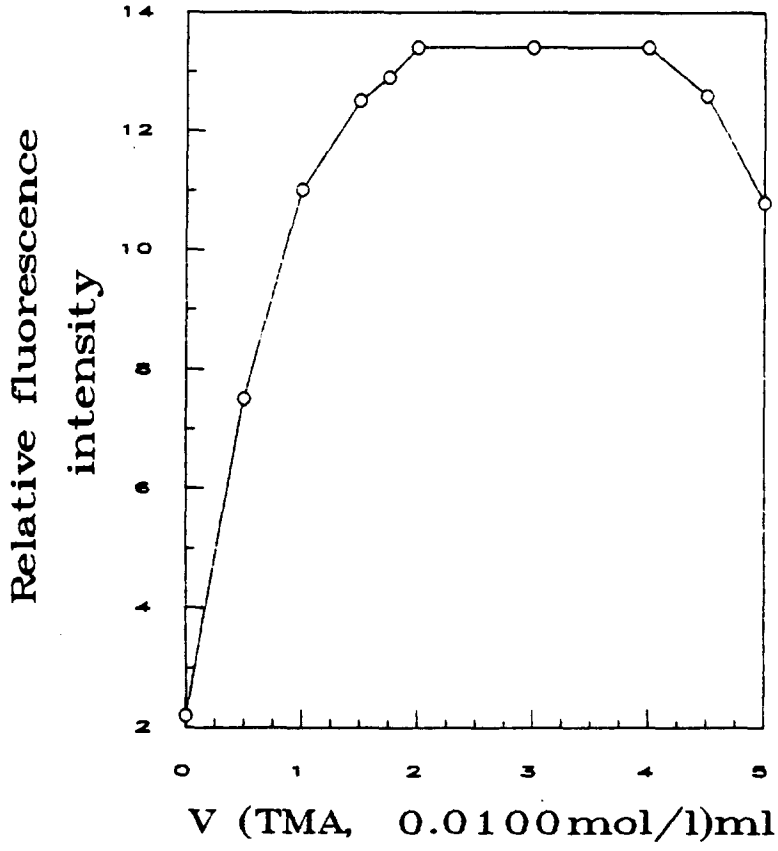


Fig. 3. Effect of the volume of 0.0100 mol $l^{-1}$ TMA on the fluorescence intensity of the terbium chelate with TMA. (Terbium, 1.589 μg $ml^{-1}$; pH 5.5.)

### 3.3. *Effect of the concentration of the chelating agent TMA*

Fig. 3 shows the variation in fluorescence intensity with the variation in volume of 0.0100 mol $l^{-1}$ TMA. The variation in fluorescence intensity was examined as a function of the volume of 0.0100 mol $l^{-1}$ TMA.

A set of solutions, each of volume 25 ml, was prepared by mixing a fixed amount of terbium ($4 \times 10^{-5}$ mol $l^{-1}$), different amounts of the reagent and a fixed volume of the sodium acetate–acetic acid buffer solution (5.00 ml). It was found that the fluorescence intensity of the chelate was most intense and constant over the volume range 2–4 ml for a 0.0100 mol $l^{-1}$ TMA solution.

### 3.4. *Effect of time*

The fluorescence intensity remained at its maximum from 15 min to 4 h, and then started to alter, with the relative standard deviation going beyond ±4%.

### 3.5. *Composition of the terbium chelate*

The Job's method of continuous variation was applied to determine the stoichiometric composition of the binary fluorescent chelate of terbium with TMA. Fig. 4 shows the curve of the relative fluorescence intensity as a function of the mole fraction of terbium. The branch point of two tangent lines indicates a composition ratio of 1:1 of terbium to TMA in water. TMA is a neutral electron donor and its chelate with terbium exists in the form of a positively charged ion. Therefore, the general formula of the chelate is $[Tb(TMA)]Cl_3$ in water.

### 3.6. *Calibration curve*

Fig. 5 shows the calibration curve for the determination of terbium. Using the experi-

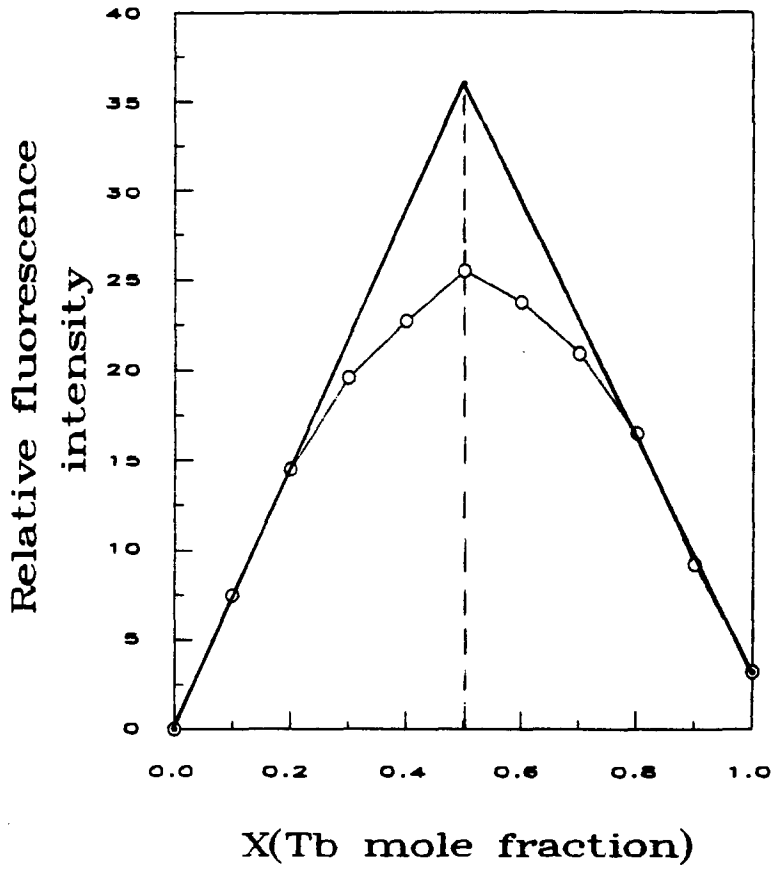


Fig. 4. Plot of the fluorescence intensity versus mole fraction of terbium. (pH 5.5.)

mental method described above, the relative fluorescence intensity is a linear function of concentration in the range 0.0248–6.356 μg ml$^{-1}$ of terbium. The linear equation is $F = 1.155 + 11.036C$ (where $F$ is the relative fluorescence intensity and $C$ is the concentration of terbium), and the linear correlation coefficient $R = 0.9996$.

### 3.7. Determination of the recovery

A standard sample of biyttrium trioxide (99.988%) as the matrix was obtained from the Rare Earth Company of Gansu, Gansu, P.R. China. It is actually a mixture of oxides and its composition is as follows: $La_2O_3$ (0.0040%), $Ce_2O_3$ (0.0002%), $Pr_6O_{11}$ (0.0005%), $Nd_2O_3$ (0.0005%), $Sm_2O_3$ (0.0005%), $Eu_2O_3$ (0.00015%), $Gd_2O_3$ (0.0004%), $Tb_4O_7$ (0.0005%), $Dy_2O_3$ (0.0005%), $Ho_2O_3$ (0.0004%), $Er_2O_3$ (0.0004%), $Tm_2O_3$ (0.0004%), $Yb_2O_3$ (0.0004%), $Lu_2O_3$ (0.0002%), $Y_2O_3$ (99.988%), and trace amounts of $Fe^{3+}$, $SiO_3^{2-}$, etc. Obviously, if a good recovery is obtained with a matrix of this type of $Y_2O_3$, the results will show that the determination of terbium using the Tb–TMA fluorescence system has good repeatability.

The synthesized samples 1 and 2 have molar ratios of 100:1 and 25:1 for Y:Tb, respectively.

The requisite amount of sample was dissolved in hot, concentrated HCl, and the solution was evaporated to a syrup then diluted with distilled, deionized water to the desired volume. The determination was performed according to the experimental method given above.

The analytical results are listed in Table 1.

### 3.8. Interferences of foreign ions

In the fluorescence determination of rare earth ions, interference occurs between these ions themselves, which is especially serious for $Sm^{3+}$, $Eu^{3+}$, $Tb^{3+}$ and $Dy^{3+}$ (with ethanol or DMF as solvents, the interference is even more serious). We were surprised to find that $Eu^{3+}$, $Sm^{3+}$ and $Dy^{3+}$ ions give rise to few interfer-

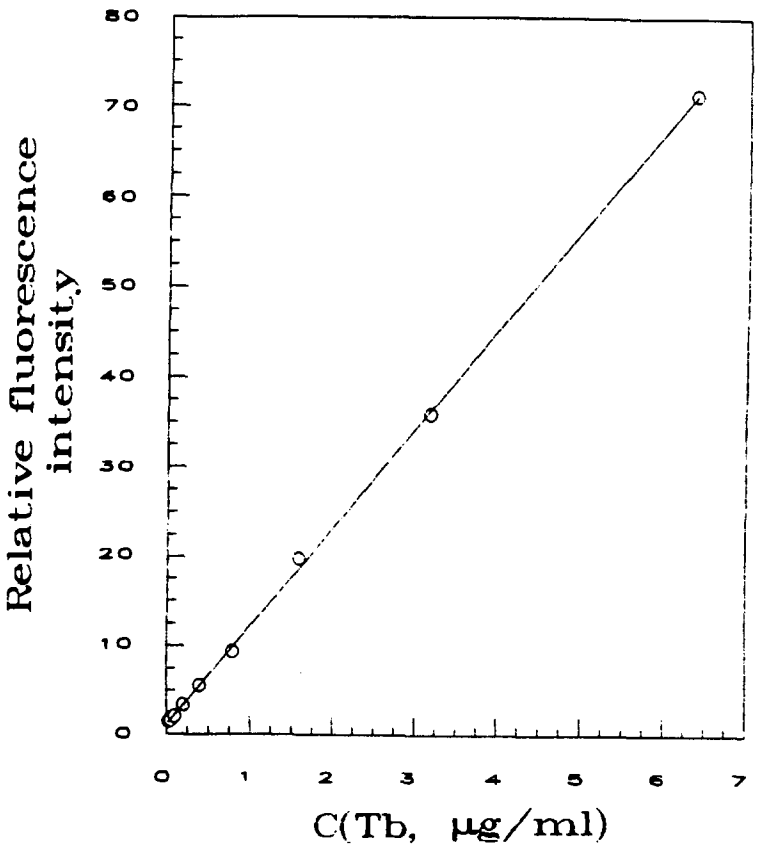


Fig. 5. Calibration curve. ($C_{Tb}$ = 0.0246–6.35 μg ml$^{-1}$; TMA, 1.2 × 10$^{-3}$ mol l$^{-1}$; pH 5.5.)

ences in the determination of terbium with the TMA–Tb system; perhaps $H_2O$ can extinguish the fluorescences of $Eu^{3+}$, $Sm^{3+}$ and $Dy^{3+}$.

When the concentration of terbium was maintained at 1.589 μg ml$^{-1}$, the interferences of 39 ions were examined by measuring the fluorescence intensity under the same experimental conditions. In this work, as the relative standard deviation was kept within ±4%, it was confirmed that 800 μg ml$^{-1}$ of $NH_4^+$, $K^+$, $Na^+$, $Ca^{2+}$, $Mg^{2+}$, $F^-$, $Cl^-$, $Br^-$, $Ac^-$, $SO_4^{2-}$, $NO_3^-$, $PO_4^{3-}$ and $SiO_3^{2-}$ ions; 220 μg ml$^{-1}$ of $Ba^{2+}$ ions; 40 μg ml$^{-1}$ of $Nd^{3+}$ ions; 16 μg ml$^{-1}$ of $Ti^{4+}$ and $Ag^+$ ions; 12 μg ml$^{-1}$ of $Co^{2+}$ ions; 10 μg ml$^{-1}$ of $Cr^{3+}$ ions; 6 μg ml$^{-1}$ of $Ta^{4+}$, $Th^{2+}$ and $Mn^{2+}$ ions; 4 μg ml$^{-1}$ of $Fe^{2+}$ ions; 2 μg ml$^{-1}$ of $Fe^{3+}$ and $Cu^{2+}$ ions; 158.9 μg ml$^{-1}$ of $Ce^{3+}$, $Pr^{3+}$, $Nb^{3+}$ ions; 320 μg ml$^{-1}$ of $Sm^{3+}$, $Eu^{3+}$, $Gd^{3+}$, $Dy^{3+}$, $Ho^{3+}$, $Er^{3+}$, $Tm^{3+}$, $Tm^{3+}$, $Yb^{3+}$, $Lu^{3+}$ and $Y^{3+}$ ions; and 3.2 μg ml$^{-1}$ of $La^{3+}$ ions did not interfere with the determination.

### *3.9. Analyses of artificially mixed ore samples and a standard ore sample*

Following Ref. [22] and taking into account the interferences listed above, two kinds of ore samples, Cainosite ($Y_2Ca_2[Si_4O_{12}]CO_3 \cdot H_2O$) and Fergusonite ($YNbO_4$), were synthesized artificially. Solutions of artificially mixed ore samples and a standard ore sample were obtained according to the method for producing working solutions of lanthanide ions. Under the experimental conditions given in section 2, the relative fluorescence intensity was determined and the results are shown in Table 2.

From the above, it can be concluded that the method can be used to determine trace amounts of terbium with the new fluorescence agent TMA because of the predominant advantages of high sensitivity, high selectivity, high accuracy and high reproducibility.

Table 1
Analytical results for terbium contained in biyttrium trioxide[a]

| Sample | Known value ($\mu g\ ml^{-1}$) | Determination result ($\mu g\ ml^{-1}$) | Average value ($\mu g\ ml^{-1}$) | Recovery (%) | RSD[b] (%) |
|---|---|---|---|---|---|
| 1 | 1.00 | 1.03, 1.00 0.97, 1.03 1.02 | 1.01 | 101 | 2.34 |
| 2 | 4.00 | 4.07, 4.17 4.09, 4.12 4.08 | 4.10 | 102 | 3.94 |

[a] $n = 5$.
[b] Relative standard deviation.

Table 2
Results of the determination of terbium in ore samples

| Ore sample | Known value ($\mu g\ ml^{-1}$) | Determination result ($\mu g\ ml^{-1}$) | Average value ($\mu g\ ml^{-1}$) | RSD (%) |
|---|---|---|---|---|
| Fergusonite, $YNbO_4$[a] | 0.500 | 0.510, 0.512 0.521, 0.493 0.503 | 0.508 | 1.05 |
| Cainosite, $Y_2Ca_2[Si_4O_{12}]\,CO_3 \cdot H_2O$[b] | 0.500 | 0.521, 0.530 0.512, 0.521 0.503 | 0.517 | 1.03 |
| Standard sample[c] | 0.300 | 0.289, 0.290 0.295, 0.311 0.297 | 0.296 | 0.89 |

[a] The amount of component ions per 100 μg of the synthetic sample of Fergusonite are Ca, 25.74; Mg, 0.288; Mn, 0.03; Pb, 0.138; Fe(II), 0.114; Fe(III), 0.354; Al, 1.176; U, 2.376; Th, 0.613; $SiO_3^{2-}$, 0.078; Ti, 0.906; Nb, 0.27; Ta, 1.5; Eu, 0.2; Gd, 1.8; Tb, 0.48; Dy, 4.48; Ho, 1.36; Er, 2.76; Tm, 0.52; Yb, 2.96; Lu, 0.744; Y, 22.48.
[b] The amount of component ions per 100 μg of the synthetic sample of Cainosite are $SiO_3^{2-}$, 21.11; $CO_3^{2-}$, 3.44; Ca, 9.98; Mg, 0.025; Na, 0.24; La, 0.228; Ce, 0.532; Pr, 0.342; Nd, 0.292; Sm, 2.28; Eu, 0.342; Gd, 4.56; Tb, 0.684; Dy, 3.8; Ho, 2.8; Er, 1.976; Tm, 0.304; Yb, 0.99; Lu, 0.76; Y, 19.
[c] The standard sample is produced by the Rare Earth Institute of Baotou, Baotou, P.R. China. Its composition is as follows: $La_2O_3$, 0.09%; $Ce_2O_3$, 0.27%; $Pr_6O_{11}$, 5.18%; $Nd_2O_3$, 16.75%; $Sm_2O_3$, 1.295%; $Eu_2O_3$, 0.23%; $Gd_2O_3$, 0.40%; $Tb_4O_7$, 0.39%; $Dy_2O_3$, 7.11%; $Ho_2O_3$, 20.04%; $Er_2O_3$, 0.027%; $Tm_2O_3$, 0.0085%; $Yb_2O_3$, 0.013%; $Lu_2O_3$, 0.003%; $Y_2O_3$, 49.21%.

## References


[1] E.C. Stanley, B.I. Kinneberger and L.P. Varga, Anal. Chem., 38 (1966) 1362.
[2] J. Gao, J. He, X. Wang, Z. Wang and G. Bai, Analyst, 112 (1987) 1081.
[3] J. Gao, J. He, X. Wang and G. Bai, Inorg. Chim. Acta, 140 (1987) 273.
[4] X. Du, J. Gao, J. Kang and G. Bai, Chin. Chem. Lett., 3 (1992) 821.
[5] X. Du, J. Gao, J. Kang and G. Bai, Chin. Chem. Lett., 3 (1992) 825.
[6] X. Du, J. Gao, Q. Xie and J. Kang, Chin. Chem. Lett., 4 (1993) 989.
[7] X. Du, J. Gao, Q. Xie and J. Kang, Talanta, 41 (1994) 201.
[8] V.G. Pastushenko and S.S. Krivolapov, Zh. Anal. Khim, 44(3) (1989) 536 (in Russian).
[9] S.S. Yoon and W. Clark Still, J. Am. Chem. Soc., 115 (1993) 823.
[10] J. Sheng, D. Zhou and C. Huang, Zhongguo Xitu Xuebao, 12(1) (1994) 85.
[11] L. Li, D. Chen, X. Chen, B. Kang and L. Jin, Wuji Huaxue Xuebao, 9(4) (1993) 418.
[12] Y. Xin, Z. Jing, Z. Duan and J. Li, Acta Chim. Sinica, 45 (1987) 1044.
[13] H.G. Brittain. Inorg. Chem., 17(10) (1978) 2762.
[14] N. Filipescu, W.F. Sager and F.A. Serafin, J. Phys. Chem., 68 (1964) 3324.
[15] J.J. Freeman and G.A. Crosby, J. Phys. Chem., 67 (1963) 2717.
[16] M.L. Bhaumik, J. Chem. Phys., 40 (1964) 3711.
[17] M.L. Bhaumik and M.A. El-Sayed, J. Chem. Phys., 42 (1965) 787.
[18] G.A. Crosby, R.E. Whan and J.J. Freeman, J. Phys. Chem., 66 (1962) 2493.
[19] G.A. Crosby and R.E. Whan, J. Chem. Phys., 32 (1960) 614.
[20] G.A. Crosby and R.E. Whan, J. Chem. Phys., 36 (1962) 863.
[21] R.E. Whan and G.A. Crosby, J. Mol. Spectrosc., 8 (1962) 315.
[22] Inst. Globe-Chemistry of Guiyang of the Acad. Sci. China, Xitu Kuangwu Ceding Shouce, 1977, pp. 318–359.

ELSEVIER

Talanta 42 (1995) 1505–1512

Talanta

# Solid-surface room-temperature phosphorescence detection of serotonin, tryptamine, and gramine enhanced by inorganic salts and sodium dodecyl sulfate

José de Ribamar F. Júnior, A.D. Campiglia *

*Departamento de Química, Universidade de Brasília, Brasília, DF, CEP 70910-900, Brazil*

Received 5 October 1994; revised 27 March 1995; accepted 3 April 1995

**Abstract**

Room-temperature phosphorescence characteristics of serotonin (5-hydroxytryptamine), typtamine, and gramine ([3-(dimethylaminomethyl)indole]) were studied on low-background paper substrates. Several experimental parameters were optimized for maximum signal intensity. Sodium iodide, thallium(I) nitrate, silver(I) nitrate, and lead(II) nitrate were tested as phosphorescence enhancers. The effect of sodium dodecyl sulfate on the enhancement efficiency of these inorganic salts was also studied. The pH values of the solutions were adjusted to optimize the interaction between analyte molecules and solid substrates. Under the experimental conditions for maximum phosphorescence intensity, working curves ranging from two (gramine) to four (typtamine) orders of magnitude were obtained. Limits of detection at the nanogram level were estimated for the three compounds, showing the potential of solid-surface room-temperature phosphorimetry as a detection technique for biogenic amines.

## 1. Introduction

The role played by indole alkylamines in the central nervous system (CNS) has been a subject of interest in the area of clinical chemistry [1–3]. Serotonin (5-hydroxytryptamine) and tryptamine, which are naturally present in the CNS as a result of tryptophan biotransformation [4,5], are two important indole alkylamines acting as neurotransmitters. Incorrect concentrations of these compounds in physiological fluids and body tissues have been related to several pathological conditions [6–8]. Their determination has been performed by analytical methods involving HPLC [5,9–11], fluorimetry [12,13], radioimmunological assays [14,15], and enzymatic techniques [16].

In this article, we will report on a sensitive method of detection of serotonin and tryptamine based on solid-surface room-temperature phosphorimetry (SSRTP) [17,18]. Our studies have also been extended to gramine ([3-(dimethylaminomethyl)indole]), which is another biogenic amine present in the CNS, resulting from tryptophan biotransformation [19].

Although tryptophan phosphorescence emission has been extensively studied at 77 K [20,21] and at room temperature [22–24], this is the first time—to the best of our knowledge—that the room-temperature phosphorescence (RTP) characteristics of these indole alkylamines are reported.

Several experimental parameters that usually affect phosphorescence emission were optimized for maximum signal intensity. Chromatography paper previously treated for paper background reduction [25] was employed as the solid substrate. KI, $AgNO_3$, $TlNO_3$, and $Pb(NO_3)_2$ were tested as phosphorescence enhancers [26,27].

* Corresponding author. Present address: 8647 Eagle Point Drive, Knoxville, TN 37931, USA.


*SSDI* 0039-9140(95)01602-3

The effect of sodium dodecyl sulfate, which is a surfactant commonly employed to increase heavy atom enhancement efficiency [28–30], was also studied. Finally, the interactions responsible for RTP emission between analyte molecules and a solid substrate were optimized by adjusting the pH of the solutions [31–33].

Under experimental conditions for a maximum RTP signal, calibration curves with linear dynamic ranges varying from two to four orders of magnitude, and limits of detection in the nanogram range were estimated. The analytical figures of merit, associated with the practical advantages of SSRTP [17,18], show the potential of the technique for the detection of biogenic amines.

## 2. Experimental

### 2.1. Instrumentation

The treatment for paper background reduction was performed in a Rayonet photochemical reactor using five lamps with maximum wavelengths ($\lambda_{max}$) of emission at 250 nm, and seven with $\lambda_{max}$ at 300 nm.

The absorption spectra of the studied compounds were monitored with use of a single-beam spectrophotometer (model DU-650, Beckman Instruments, Fullerton, CA) equipped with deuterium and tungsten lamps, a concave holographic grating, and a silicon photodiode detector.

All RTP spectra and intensity measurements were collected with an Aminco–Bowman spectrofluorimeter (SLM Instruments, Urbana, II) equipped with a 150 W xenon arc lamp (Conrad-Hanovia, Newark, NJ) as an excitation source. The optical transducer was a potted IP21 photomultiplier (Hamamatsu Corp.) with an S4 spectral response. The signal from the detector was amplified by means of an SLM–Aminco microphotometer and fed to a Hewlett-Packard $X-Y$ recorder (model 7010 B). Short-lived scattering and possible fluorescence signals were minimized with an Aminco–Keirs rotating-can phosphoroscope attachment. A laboratory-constructed sample holder [34] was employed to introduce solid substrates into the spectrofluorimeter.

### 2.2. Reagents

All the chemicals were analytical-reagent grade and were used without further purification. Whatman no. 1 chromatography paper (USA) and tridistilled (in glass) water were used throughout.

Gramine (Gra), typtamine (Try), and serotonin (50HTry) were acquired from Sigma (USA). Ethanol, hydrochloric acid, sodium hydroxide, and silver(I) ntirate were purchased from Merck (Brazil). Sodium dodecyl sulfate (specically purified for biomedical work), lead(II) nitrate, and potassium iodide were from BDH Chemicals Ltd, UK. Thallium(I) nitrate was obtained from Fluka (Switzerland).

### 2.3. Procedures

*Paper treatment*

The treatment for paper background reduction has been described in detail elsewhere [25]. It basically consisted of a combination of water extraction and ultraviolet irradiation. The strips of chromatography paper were water-extracted in a Soxhlet apparatus for 8 h, dried under a stream of hot air, and exposed to ultraviolet irradiation for the same period of time. To fit in the sample holder [34], the paper strips were cut in appropriate sizes ($20 \times 10\ mm^2$). The solid supports were then stored in a dessicator to be used during the analysis.

*Solution preparation*

Stock solutions of gramine, tryptamine and serotonin (each $10^{-2}$ M) were prepared in ethanol/water (50:50 (v/v)). Working solutions were obtained by appropriate dilution of the stock solutions with an ethanol/water (50:50 (v/v)) solution.

The 1 M KI, 0.5 M $AgNO_3$, 0.5 M $Pb(NO_3)_2$, and 0.1 M $TlNO_3$ solutions were made up in water. The KI and $TlNO_3$ solutions employed in the optimization of heavy atom concentrations were prepared, respectively, by serial dilution of a 5 M and a 0.25 M solution. Serial dilution was also used to prepare the sodium dodecyl sulfate solutions. A 0.5 M stock solution (in water) was prepared. Lower surfactant concentrations were obtained by appropriate dilution of the stock solution.

The analyte solutions for the pH studies were made up by adding concentrated HCl or NaOH to volumetric flasks with the compounds dissolved in ethanol/water (50:50 (v/v))

The standard solutions for the calibration curves were prepared in ethanol/water (50:50 (v/v)) (5-OHTry) and at basic pH (Gra and

Table 1
Room temperature phosphorescence characteristics of Gra, Try, and 5-OHTry on low-background paper substrates. Effects of heavy atom [a] and sodium dodecly sulfate [b] as phosphorescence enhancers

| Compound [c] | Net RTP signals [d,e] | | | | |
|---|---|---|---|---|---|
| | No NaDS | | NaDS | | |
| | No HA salt | 1 MKI | 1 M KI | 0.1 M $TlNO_3$ | 0.5 M $AgNO_3$ |
| Gra | – | 248.6 (274/438) | 280.3 (275/436) | 379.5 (274/436) | 110.7 (280/448) |
| Try | 6.1 (284/453) | 621.1 (276/442) | 688.47 (276/443) | 210.0 (276/446) | 18.4 (286/461) |
| 5-OHTry | – | 259.0 (292/442) | 219.4 (290/447) | 45.0 (289/452) | 4.2 (294/490) |

[a] Heavy atom (HA) salt solutions were prepared in water.
[b] A 2% solution in water was employed.
[c] Analyte solutions ($10^{-4}$ M) prepared in ethanol/water (50:50 (v/v)) were employed.
[d] Net RTP signals were obtained by subtracting the blank signals from the analyte + blank signals. In each case, six determinations were employed in order to calculate the average values. The precision of the measurements was within 10–15%.
[e] The $\lambda_{exc}/\lambda_{em}$ ratios are given in parentheses, where $\lambda_{exc}$ and $\lambda_{em}$ are the excitation and emission wavelength maxima in nanometers. The variation in wavelength for instrumental response was $\pm 2$ nm.

Try). Basic solutions were made up using appropriate volumes of concentrated NaOH. Tryptamine and gramine standard solutions were, respectively, 1 M and 0.1 M in NaOH.

*General Procedure*

Analyte solutions were spotted on solid substrates with a microliter pipette. The heavy atom and surfactant solutions were added with a microliter syringe. In all cases, a volume of 5 μl was employed. The spotted substrates were vacuum-dried at room temperature for 1 h and were then placed in a desiccator with silica until the measurements were carried out. The desiccator was covered with aluminium foil to avoid possible light effects. Prior to the measurements, a flow of dry nitrogen was directed towards the surface of the paper substrate for 5 min. All RTP measurements were performed under this gas to avoid possible quenching effects from oxygen and moisture [17,18]. A silica gel bed was used to remove water vapour traces from the drying flow.

## 3. Results and discussion

### 3.1. RTP characteristics of Gra, Try, and 5-OHTry on low background paper

*Heavy atom and sodium dodecyl sulfate effect*

The deposition of $10^{-4}$ M solutions of Gra, Try, and 5-OHTry on chromatography paper substrates were an inefficient attempt to observe their phosphorescence emission. The analyte-to-background signals ratios were close to unity, showing a lower capacity of the indole alkylamines for emitting RTP. Since the broad, featureless bands of the excitation and background emission of cellulose substrates usually overlap the analyte spectra [25,35–37], we applied a background reduction treatment to the paper substrate [25].

Table 1 presents the RTP characteristics of the three compounds on low-background paper substrates. Try was the only one to show phosphorescence emission in the absence of RTP enhancers. Surprisingly, the hydroxyl group of 5-OHTry, which is capable of increasing the analyte rigidity by establishing hydrogen bonding with the solid substrate, did not favor phosphorescence emission from the compound. Usually, substituent groups with a hydrogen bonding capacity enhance the RTP signal of the indole moiety [30].

The external heavy atom (HA) effect was tested by taking five inorganic salts with general phosphorescence enhancers [26,27]. Before analyte deposition, 1 M KI, 0.1 M $TlNO_3$, 0.5 M $AgNO_3$, 0.5 M $Pb(NO_3)_2$, and 0.25 M $HgCl_2$ were deposited on low-background paper substrates. In the presence of Tl(I), Ag(I), Pb(II), and Hg(II) ions, none of the studied compounds showed RTP enhancement. On the other hand, 1 M KI increased the phosphorescence emission of the three compounds. The

Table 2
Room temperature phosphorescence characteristics of Gra, Try, and 5-OHTry at several pH values

| Compound [a] | Net RTP signal [b,c] | | | | | | |
|---|---|---|---|---|---|---|---|
| | $EtOH/H_2O$ (50:50 (v/v)) | HCl | | | NaOH | | |
| | | 0.01 M | 0.1 M | 1 M | 0.01 M | 0.1 M | 1 M |
| Gra | 100 (275/444) | 54.7 (276/444) | 17.3 (274/446) | – | 177.3 (220, 278/444) | 177.1 (222, 278/444) | 111.7 230, 284/444) |
| Try | 100 (220, 278/445) | 78.8 (225, 280/443) | 15.4 (279/447) | 3.9 (285/472) | 91.6 (225, 280/448) | 174.6 (225, 281/447) | 194.4 (284/448) |
| 5-OHTry | 100 (294/454) | 93.2 (293/454) | 33.5 (290/456) | – | 83.1 (298/461) | 62.4 (300/459) | – |

[a] Analyte solutions of concentration $10^{-3}$ M were employed. Acid and basic soltuions were prepared in ethanol/water (50:50 (v/v)).

[b] Net RTP signals were obtained by subtracting the blank signals from the analyte + blank signals. In each case, six determinations were employed to calculate the average values. All RTP signals were normalized to the net analyte signals in neutral media.

[c] The $\lambda_{exc}/\lambda_{em}$ ratios are given in parentheses. When necessary, the maximum excitation peak is underlined.

net analyte signals in the presence of 1 M are presented in Table 1.

The addition of sodium dodecyl sulfate (NaDS) to the solid substrate usually increases the HA efficiency and enhances the phosphorescence emission [28–30]. Apparently, the long hydrocarbon chains of the surfactant promote the necessary interaction between analyte molecules and HA ions, thus improving RTP enhancement [28]. We tested, therefore, the effect of NaDS on the RTP signals of Gra, Try, and 5-OHTry.

The presence of the surfactant increased the $TlNO_3$ efficiency for the three indole alkylamines. The net RTP signals in the presence of Tl(I) and Ag(I) are presented in Table 1. The $Pb(NO_3)_2$ and $HgCl_2$ efficiencies, on the other hand, were not increased by NaDS. Probably, these two HA salts do not favor the singlet–triplet intersystem crossing rates of the studied indoles [17,18]. Finally, the surfactant improved iodiode efficiency for Gra and Try. The 5-OHTry signal, however, was higher in the absence of NaDS (see Table 1). This signal reduction could have been caused by the use of an incorrect concentration of sufactant. In previous studies [38,39], Aucélio and Campiglia have shown that, depending on the compound and HA ion, there is an optimum concentration of NaDS for improvements in HA efficiency to be observed.

*pH effect*

The RTP characteristics of Gra, Try, and 5-OHTry were studied at several pH values (see Table 2) employing $10^{-3}$ M analyte solutions which guaranteed (in a neutral medium) analyte-to-background signal ratios higher than 4.

All solutions were monitored by absorption spectrometry in the ultraviolet and visible regions. A pH variation did not cause significant modifications in the absorption spectra of Gra and Try. However, the 5-OHTry spectrum was drastically altered in alkaline medium. Neutral solutions of 5-OHTry (ethanol/water (v/v)) gave three peaks with absorption maxima at 219, 262, and 279 nm. In 0.01 M NaOH solution the 5-OHTry spectrum showed four peaks (241, 269, 279, and 309 nm), and in 1 M NaOH solutions, showed six peaks (228, 252, 269, 281, 317, and 324 nm). In addition, after 2 h of solution preparation, a change in color was observed. The neutral solutions were colorless, while the 0.01 M NaOH and 1 M NaOH solutions were pink and purple, respectively. These observations strongly suggest that 5-OHTry decomposed in basic medium.

The pH variation caused minor shifts in the maximum RTP excitation and emission wavelengths of the studied compounds. Gra showed an additional excitation peak in basic medium, of which the maximum wavelength depended upon the NaOH concentration (see Table 2).

The intensities of the RTP signals, on the other hand, were drastically affected by the pH values of the solutions. The phosphorescence signals were quenched in acidic medium. The degree of quenching increased with acid concentration, obviously along with the degree of protonation of indole alkylamines [19]. The

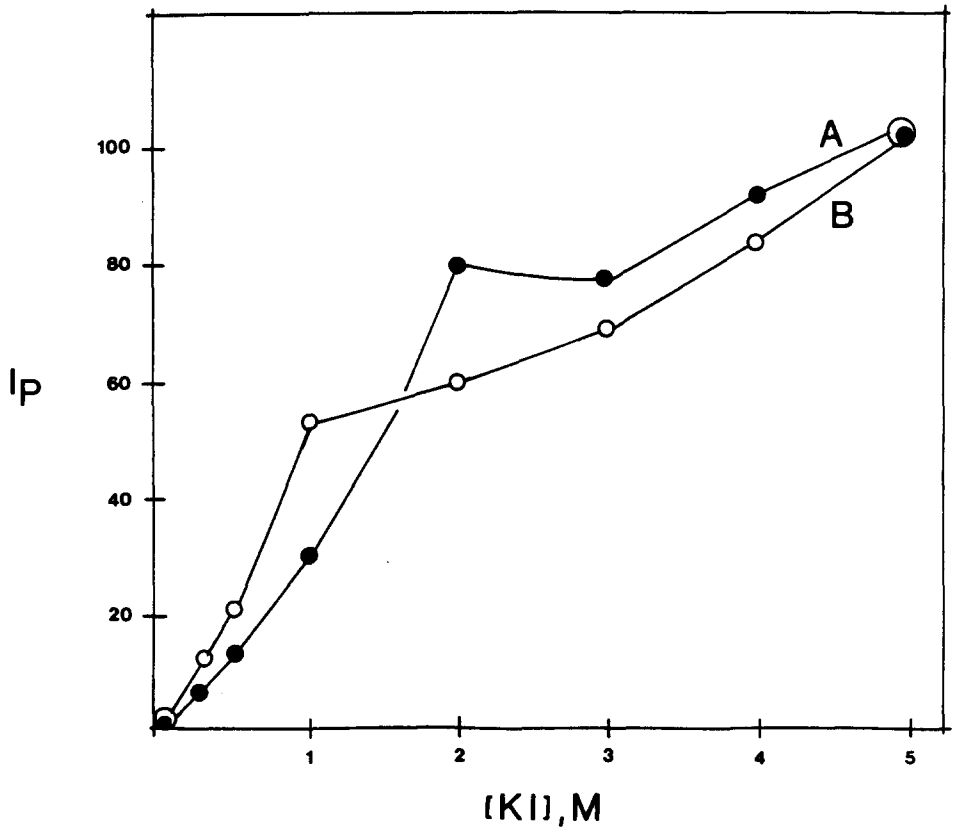


Fig. 1. Net phosphorescence intensity ($I_p$) of (curve A) 5-OHTry and (curve B) Try as a function of molar concentration of potassium iodide. Analyte solutions of concentration $10^{-4}$ M were employed. The 5-OHTry was dissolved in ethanol/water (50:50 (v/v)), and Try was dissolved in 1 M NaOH (ethanol/water (50:50 (v/v)). Net analyte signals were normalized to the maximum intensity observed.

acid quenching could result from a lower capacity of the protonated species for forming hydrogen bonds with the solid substrate. In addition, the excess of $H_3O^+$ ions in acid solutions, which increases competition for the OH groups of the solid substrate and inhibits hydrogen bonding with the analyte molecules, could also contribute to reduce the RTP signals.

These assumptions are also supported by the fact that Gra and Try showed their highest signals in basic media. In NaOH solutions, the dissociation equilibrium of these indoles is inhibited, the $H_3O^+$ ion concentration is at a minimum, the unprotonated species are predominant. On the other hand, 5-OHTry showed the highest RTP signal in neutral medium. As previously mentioned, however, this compound might have undergone degradation in basic medium. Its degradation product obviously does not have characteristics needed for RTP emission.

*Analytical figures of merit*

The analytical figures of merit (AFOM) were obtained under the experimental conditions for maximum RTP emission. The HA salt and NaDS concentrations were optimized for each compound. Based on the results shown in Table 1, $TlNO_3$ was used to enhance the Gra RTP signal, and KI was employed to obtain the AFOM for Try and 5-OHTry. The pH values of the solutions were chosen in agreement with the data presented in Table 2. Gra solutions were prepared in 0.1 M NaOH, Try solutions in 1 M NaOH, and 5-OHTry solutions in ethanol/water (50/50 (v/v)).

Fig. 1 shows the phosphorescence intensity of Try and 5-OHTry as a function of KI molar concentration. In both cases, the maximum phosphorescence intensity was obtained with a 5 M KI solution. Higher concentrations were not tested due to KI solubility limitations. Fig. 2 shows the RTP signal of Gra as a function of $TlNO_3$ molar concentration. The highest emission was observed with a 0.025 M $TlNO_3$ solution. More concentrated solutions than 0.025 M reduced the analyte signal. Probably, the excess of $TlNO_3$ caused a matrix prefilter

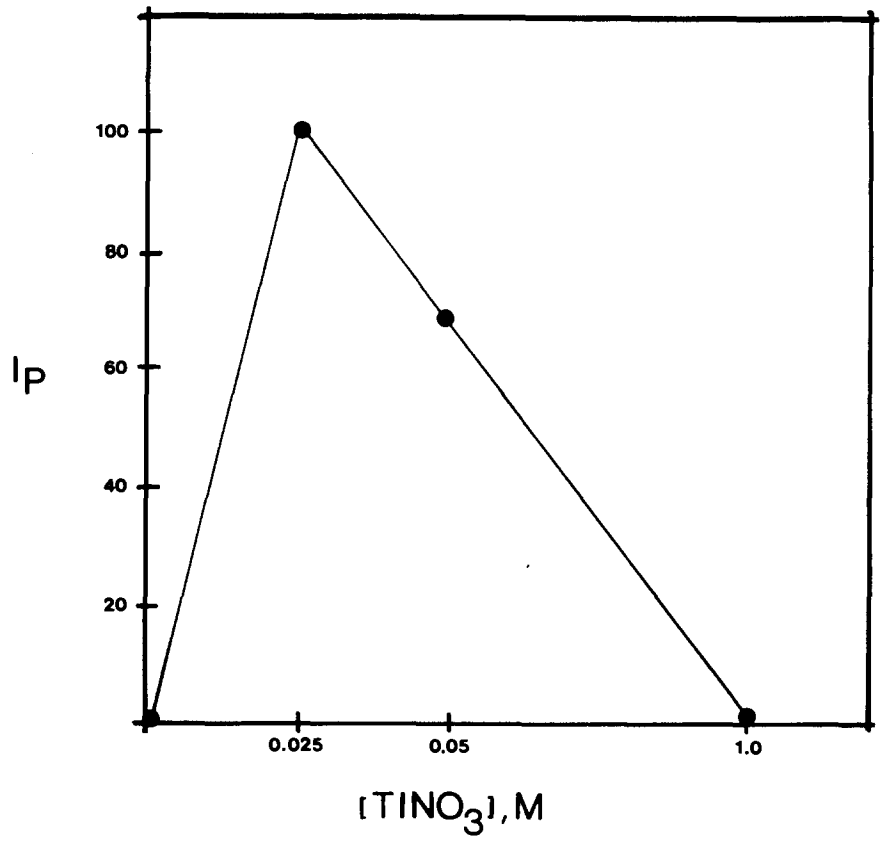


Fig. 2. Net phosphorescence intensity ($I_p$) of Gra as a function of molar concentration of thallium(I) nitrate. A $10^{-4}$ M Gra solution prepared in 0.1 M NaOH (ethanol/water (50:50 (v/v)) was used. Net Gra signals were normalized to the maximum intensity observed.

effect and reduced the excitation energy reaching the analyte molecules [25].

The NaDS concentration was optimized in the presence of the HA salts. A 5 M KI solution was employed for Try and 5-OHTry, and 0.025 M $TlNO_3$ was used for Gra. In all cases, the surfactant concentration varied from 0.01 to 0.5 M. The optimum value depended on the compound. Gra and 5-OHTry showed the highest RTP signals with a 0.2 M NaDS solution, while Try showed its maximum signal with a 0.1 M surfactant solution.

Table 3 summarizes the AFOM at optimum pH, and HA and NaDS concentrations. Try showed a calibration curve with the linear dynamic range (LDR) extended over four orders of magnitude ($4.8 \times 10^{-7}$–$5 \times 10^{-3}$ M) while the 5-OHTry and Gra LDRs extended, respectively, over three ($3.2 \times 10^{-7}$–$2 \times 10^{-4}$ M) and two ($6.4 \times 10^{-6}$–$5 \times 10^{-4}$ M) orders of magnitude. The slopes of the log–log plots showed a linear relationship between phosphorescence intensity and analyte concentration. For Try and 5-OHTry, the correlation coefficients of the calibration curves were close to unity, showing a good precision of the measurements. The relative standard deviations (within the LDR) varied form 10 to 15%. For Gra, however, a poorer precision was obtained (20%). Apparently, the presence of $TlNO_3$ in the solid substrate caused the observed variation. The standard deviation for 16 blank repetitions with this salt was considerably higher than that obtained with KI. The limits of detection (LOD) were estimated from the equation $C_L = Ks_b/m$, where the standard deviation ($s_b$) from 16 blank determinations, the slope of the calibration curve ($m$), and $K = 3$ were employed [40]. The absolute LOD, for a sample volume of 5 μl, were in the nanogram level.

## 4. Conclusions

In this article, we have reported the RTP characteristics of Gra, Try, and 5-OHTry on low-background paper substrates. Several experimental parameters that usually affect the

Table 3
Analytical figures of merit for Gra, Try, and 5-OHTry obtained under experimental conditions for maximum RTP emission

| Compound | Solvent [a] | [HA] [b] | [NaDS] [c] (M) | $\lambda_{exc}/\lambda_{em}$ | LDR [d] (ng) | Slope, log–log | Correlation coefficient | ALOD [e] (ng) |
|---|---|---|---|---|---|---|---|---|
| Gra | 0.1 M | 0.025 M $TlNO_3$ | 0.2 | 276/442 | 5.6–400 | 0.80 | 0.9814 | 5.6 |
| Try | 1 M NaOH | 5 M KI | 0.1 | 281/446 | 0.4–4000 | 0.90 | 0.9990 | 0.4 |
| 5-OHTry | EtOH/$H_2O$ (50:50 (v/v)) | 5 M KI | 0.2 | 290/450 | 0.3–200 | 0.91 | 0.9988 | 0.3 |

[a] Basic solutions were prepared in ethanol/water (50:50 (v/v)).
[b] Refers to concentration of HA solutions spotted on Whatman no. 1 chromatography paper previously treated for background reduction.
[c] Concentration of surfactant solution spotted on the solid substrate.
[d] Linear dynamic range representing the amount of phosphor deposited on the paper substrate. Sample volume, 5 µl.
[e] Absolute limit of detection; see text for definition. Sample volume, 5 µl.

intensity of phosphorescence emission were studied. KI, $TlNO_3$, $Pb(NO_3)_2$, $HgCl_2$, and $AgNO_3$ were tested as RTP enhancers. With the exception of KI, none of the HA salts increased the phosphorescence signals of the studied compounds. With 1 M KI, the intensities of the net analyte signals varied from 248.6 (Gra) to 621.1 (Try). The addition of NaDS to the paper substrates, however, improved the enhancements efficiency of $TlNO_3$ and $AgNO_3$. With 0.1 M $TlNO_3$, and employing a 2% surfactant solution, the Gra net RTP intensity was 379.5, which was higher than that observed with 1 M KI. In addition, NaDS increased the iodide efficiency, causing the highest enhancements for Try and 5-OHTry net RTP signals, 688.47 and 219.4, respectively.

The effect of the pH was also studied. Gra and Try showed the highest RTP signals in basic medium (in 0.1 M and 1 M NaOH solutions, respectively), while 5-OHTry, which apparently degrades in alkaline solution, emitted the highest signal in neutral solution (ethanol/water (50:50 v/v)).

To obtain the AFOM under the experimental conditions for maximum RTP emission, optimizations of HA and NaDS concentrations were performed. The strongest emissions of Try and 5-OHTry were observed with 5 M KI. The NaDS optimum concentrations were, respectively, 0.1 M and 0.2 M. $TlNO_3$ enhance the Gra signal to its highest intensity at a concentration of 0.025 M, and so did NaDS at a concentration of 0.2 M. Employing these HA and NaDS concentrations, and preparing the analyte solutions at optimum pH, the LDRs of the calibration curves varied from two (Gra) to four (Try) orders of magnitude. The ALOD, for a sample volume of 5 µl, were in the nanogram range.

The sensitivity of SSRTP, therefore, has shown to be adequate for determining biogenic amines at the concentration levels usually required [1–3]. The proximity of the $\lambda_{exc}$ and $\lambda_{em}$ obtained, however, shows a lack of selectivity. The detection of one of these compounds in binary mixtures, for example, will require previous separation steps. HPLC–SSRTP analysis [41,42] will certainly overcome this limitation. The experimental parameters optimized in this study, therefore, could be employed in order to obtain maximum sensitivity.

## Acknowledgements

We wish to thank the Conselho National de Desenvolvimento Cientifico e Tecnologico-CNPq for financial support, and Ms. Martha P. Cloutier Dobal for linguistic advice.

## References

[1] A.P. Grafleo and B.L. Karger, Clin. Chem., 22 (1976) 184.
[2] N.H. Joseph and H.F. Baker, Clin. Chim. Acta, 72 (1976) 125.
[3] N. Seiler, J. Chromatogr., 143 (1977) 221.
[4] W.J. Hurst, J. Liq. Chromatogr., 13 (1990) 1.
[5] M.C. Gennaro and C. Abrigo, Chromatographia, 31 (1991) 381.
[6] D.A. Curran, H. Hinterberger and J.W. Lance, Brain, 88 (1967) 997.
[7] K. Belenduik, W. Belenduik and D.X. Freedman, Arch. Gen. Psychiatry, 37 (1982) 325.
[8] G.B. Baker, J.T.F. Wong, R.T. Curtis and F.M. Pasutto, J. Chromatogr., 392 (1987) 317.
[9] W.H. Lyness, N.M. Friedle and K.E. Moore, Life Sci., 26 (1980) 1109.

[10] P.C. Tagari, D.J. Boulin and C.L. Davies, Clin. Chem., 30 (1984) 131.
[11] M. Picard, D. Olichon and J. Gombert, J. Chromatogr., 341 (1985) 445.
[12] P. Frattini, M.L. Gucchi, G. Santagostino and G.L. Corona, Clin. Chim. Acta, 92 (1979) 353.
[13] G.T. Vatassery, M.A. Sheridan and A.M. Krezowski, Clin. Chem., 27 (1981) 328.
[14] J.M. Kellum and B.M. Jaffe, Gastroenterology, 70 (1976) 516.
[15] F. Engback and B. Voldy, Clin. Chem., 28 (1982) 624.
[16] M.N. Hussain and M.J. Sole, Anal. Biochem., 11 (1981) 105.
[17] T. Vo-Dinh, Room Temperature Phosphorimetry for Chemical Analysis, Wiley, New York, 1984.
[18] R.J. Hurtubise, Phosphorimetry: Theory, Instrumentation and Applications, VCH Publishers Inc., New York, 1990.
[19] R.J. Sundberg, The Chemistry of Indoles, Vol. 16, Academic Press, New York, 1970.
[20] I. Weinryb and R.F. Steiner, Biochemistry, 7 (1968) 2488.
[21] R.M. Purkey and W.C. Galley, Biochemistry, 9 (1970) 3569.
[22] S.L. Wellons, R.A. Paynter and J.D. Winefordner, Spectrochim. Acta, 30A (1974) 3133.
[23] T. Vo-Dinh, E. Lue-Yen and J.D. Winefordner, Anal. Chem., 48 (1976) 1186.
[24] M.L. Meyers and P.G. Seybold, Anal. Chem., 51 (1979) 1609.
[25] A.D. Campiglia and C.G. De Lima, Anal. Chem., 59 (1987) 2822.
[26] I.M. Jakoviljevic, Anal. Chem., 49 (1977) 2048.
[27] T. Vo-Dinh and J.R. Hooyman, Anal. Chem., 51 (1979) 1915.
[28] C.G. De Lima, M.M. Andino and J.D. Winefordner, Anal. Chem., 58 (1986) 2867.
[29] J.J. Aaron, A.D. Campiglia and J.D. Winefordner, Anal. Chim. Acta, 236 (1990) 257.
[30] S.M.C. Gioia and A.D. Campiglia, Anal. Chim. Acta, 287 (1994) 89.
[31] R.M. Ramassamy and R.J. Hurtubise, Anal. Chem., 54 (1982) 1642.
[32] R.J. Hurtubise and G.A. Smith, Anal. Chim. Acta, 139 (1982) 315.
[33] R.J. Hurtubise, Talanta, 28 (1981) 145.
[34] A.D. Campiglia and C.G. De Lima, Anal. Chem., 60 (1988) 2165.
[35] R.P. Bateh and J.D. Winefordner, Talanta, 29 (1982) 713.
[36] S.Y. Su, D.L. Bolton and J.D. Winefordner, Chem. Biomed. Environ. Instrum., 12 (1982) 55.
[37] D.L. McAleese and R.B. Dunlap, Anal. Chem., 56 (1984) 600.
[38] R.Q. Aucélio and A.D. Campiglia, Talanta, 41 (1994) 2131.
[39] R.Q. Aucélio and A.D. Campiglia, Mikrochim. Acta, 117 (1994) 75.
[40] G.L. Long and J.D. Winefordner, Anal. Chem., 55 (1983) 713A.
[41] A.D. Campiglia, A. Berthod and J.D. Winefordner, J. Chromatogr., 508 (1990) 37.
[42] A.D. Campiglia, J.J. Laserna, A. Berthod and J.D. Winefordner, Anal. Chim. Acta, 244 (1991) 215.

ELSEVIER

Talanta 42 (1995) 1513–1517

Talanta

# Spectrophotometric determination of trace amounts of tungsten in geological samples after preconcentration on Amberlite XAD-1180

Mustafa Soylak *, Latif Elçi, Mehmet Doğan

*Erciyes University Fen-Edebiyat Faculty, Department of Chemistry, 38039 Kayseri, Turkey*

Received 30 December 1994; revised 27 March 1995; accepted 3 April 1995

**Abstract**

A method for the preconcentration of trace amounts of tungsten as its thiocyanate complex, using a column filled with Amberlite XAD-1180 resin, is proposed. After elution with a small volume of acetone, the analyte was determined spectrophotometrically with potassium thiocyanate and stannous chloride. The influence of several ions, as interferents, is discussed. The proposed method was applied to the determination of tungsten in geological samples with good analytical results, such as recoveries of 95% or above, relative standard deviations of 6% or below ($n = 10$) and a detection limit of 12 $\mu g\, l^{-1}$.

## 1. Introduction

The direct determination of tungsten in various matrices such as geological samples, steels, natural waters, etc. has presented some problems, due to the low tungsten content and large concentration of accompanying elements. Many preconcentration and separation methods have been used for the determination of tungsten at low concentrations, such as liquid–liquid extraction [1,2], adsorption [3] and ion exchange [4,5].

Up to now, a tin(III) chloride–thiocyanate method has been combined with a preconcentration and separation procedure for the determination of tungsten [6–10]. Columns filled with Amberlite XAD resin have been used for the preconcentration and separation of trace amounts of several metal ions from various matrices [11–13]. However, little work in this field has been done using Amberlite XAD-1180 resin [14,15].

This paper describes a sorbent extraction system for the preconcentration of tungsten based on its solvent extraction as a thiocyanate complex. In this system, the sorption of the W(V)–thiocyanate complex is carried out by using Amberlite XAD-1180 resin. After elution, tungsten is determined spectrophotometrically. The procedure has been applied satisfactorily to the determination of tungsten in geological samples.

## 2. Experimental

### 2.1. Apparatus

A Hitachi 150-20 double-beam spectrophotometer equipped with a pair of 1 cm path length quartz cuvettes was used for the absorbance measurements. The determination of tungsten was performed at 400.0 nm.

* Corresponding author.


*SSDI* 0039-9140(95)01604-X

### 2.2. Reagents and solutions

All the chemicals used were of analytical grade, and aqueous reagents were prepared in doubly distilled, deionized water.

A 1000 μg $ml^{-1}$ stock solution of tungsten was prepared by dissolving an appropriate amount of sodium tungstate dihydrate in water and diluting it to 1000 ml. The stock solution was standardized gravimetrically by the tannic acid–phenazone method [16]. Appropriate standards and solutions of tungsten were prepared daily by dilution with water. $SnCl_2$ solution (20% (w/v)) was prepared in concentrated HCl. KSCN solution (25% (w/v)) was prepared in water.

Amberlite XAD-1180 resin (particle size, 0.1–0.2 mm; Rohm and Haas Co.) was prepared using the reagents and the washing steps as reported previously [17].

### 2.3. Column preparation

An Amberlite XAD-1180 column, 10 cm long and 1 cm in diameter, containing about 400 mg of resin (about a 20 mm bed) was used for the experiments. The column was prepared by aspirating a water slurry of Amberlite XAD-1180 (400 mg) into the glass column. It was equilibrated with 10–15 ml of 3 M HCl solution containing 1.0 ml of 25% KSCN and 1.0 ml of 20% $SnCl_2$, after which the column was used in the preconcentration study.

### 2.4. Column preconcentration

The column method was optimized using 25–100 ml of model solution containing 40 μg of tungsten. Solutions containing 0.2–5 ml of 25% KSCN and 0.2–5 ml of 20% $SnCl_2$ were prepared in 0.5–10 M HCl solution. The resulting solutions were drawn through the column at a flow rate of about 3–5 ml $min^{-1}$ by vacuum. The column was then washed with the blank solution and the retained tungsten was eluted into a 25 ml beaker with 2–10 ml of acetone at a rate of 1–2 ml $min^{-1}$. The eluate was evaporated to 0.5–1 ml on a hot plate, then cooled. The concentrated residue was transferred to a calibrated volumetric flask containing 1.5 ml of 25% KSCN and 1.5 ml of 20% $SnCl_2$, and the solution was made up to 5–10 ml with 3 H HCl solution. The tungsten concentration was determined spectrophotometrically as the thiocyanate complex at 400.0 nm [8].

### 2.5. Determination of tungsten concentration in geological samples

The geological samples were collected from Sorgun Yeni Çeltek Mine Quarry (Yozgat, Turkey). The decomposition procedure described by Welsch [18] was applied to the determination of the tungsten concentration in geological samples. The samples were ground and sieved to 80–100 mesh, 0.1–0.5 g amounts were weighed and transferred to 100 ml Teflon beakers, and 5 ml of concentrated nitric acid and 20 ml of concentrated HF were added to each beaker. The sample mixtures were evaporated to dryness, heated overnight at 125°C in a sand bath, and 2 ml of warm water and 8 ml of concentrated HCl were added to each residue and mixed. The mixtures were filtered through Whatman no. 42 filter paper, and 20 ml of water were added to each filtrate. The resultant solutions were drawn through the column as in the described procedure above.

## 3. Results and discussion

### 3.1. Effects of the reagents and hydrochloric acid concentration on the recovery of tungsten

The effects of the KSCN and $SnCl_2$ amounts on the recovery of tungsten on Amberlite XAD-1180 resin were examined. The recoveries were quantitative (above 95%) in the range 0.5–5 ml of 25% KSCN and in the range 0.2–0.5 ml of 20% $SnCl_2$ (Fig. 1).

The influence of the hydrochloric acid concentration on the retention of tungsten on Amberlite XAD-1180 resin is shown in Fig. 2. The highest sensitivity for tungsten was obtained in the HCl concentration range 2–9 M.

In all subsequent studies, 1.0 ml of 25% KSCN and 1.0 ml of 20% $SnCl_2$, as optimum amounts, were used. The concentration of the medium was made up to 3 M HCl with concentrated HCl.

### 3.2. Influences of eluent type and volume

The effects of the various eluents on the retention of tungsten on XAD-1180 resin was investigated. As can be seen in Table 1, elution with chloroform and diethyl ether was not quantitative. The recoveries of tungsten were quantitative when acetone, methanol, ethanol, *n*-butanol and *n*-propanol were used as eluent.

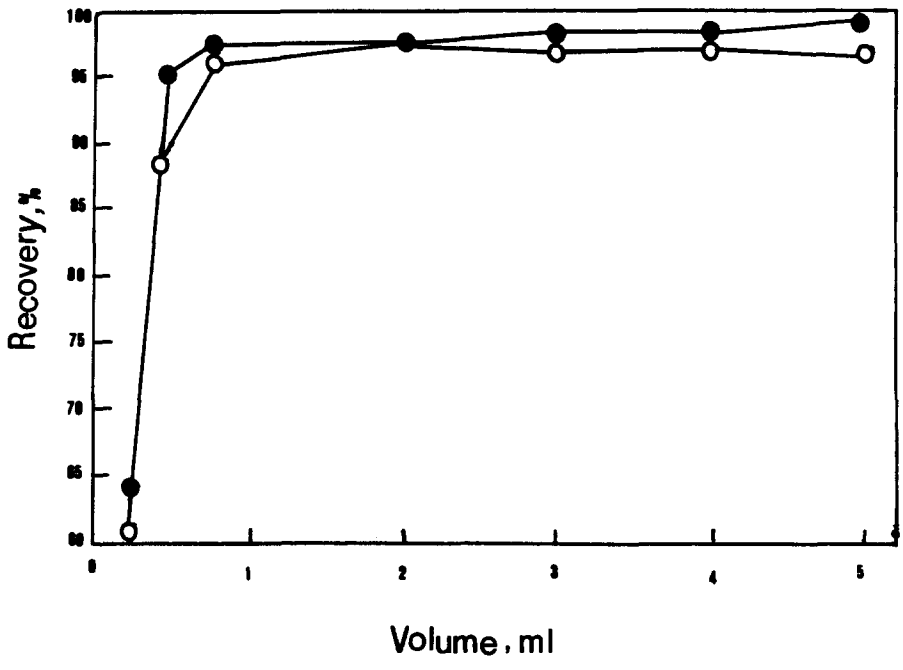


Fig. 1. Effect of the $SnCl_2$ and KSCN amounts on the recovery of tungsten on Amberlite XAD-1180 resin ((●) ml of 20% $SnCl_2$ and (○) ml of 25% KSCN).

However, the evaporation of *n*-propanol and *n*-butanol is slower than that of acetone. The period of elution with methanol and ethanol is longer than that for the other eluents. As a result, acetone was selected as eluent in subsequent work.

The influence of the eluent volume on the recovery of tungsten was studied by using various volumes of acetone varying from 2 to 30 ml. The recoveries were quantitative in the range 2–20 ml. In the subsequent studies, 10 ml of eluent were used.

### 3.3. *Effects of resin amounts and sample volume*

The effect of XAD-1180 resin amounts on the recovery of tungsten was studied by varying the amounts of resin from 200 to 800 mg. Quantitative recoveries were obtained in the range 300–600 mg of the resin; as the optimum, 400 mg of Amberlite XAD-1180 resin were used. The same resin sample was used repeatedly for 300 sample analyses at least without loss of activity.

The effect of sample volume was examined with solutions containing 40 μg of tungsten. Recoveries of the analyte concentrated into 2–10 ml of eluent from 50 to 500 ml sample volumes were found to be 97–100%. In this case, the highest preconcentration factor was found to be 250.

### 3.4. *Calibration graph and detection limit*

The calibration graph for a 100 ml sample was linear up to 200 μg of tungsten. The detection limit, based on three times the standard deviation of the blank, was 12 μg $l^{-1}$ ($n = 21$) and the relative standard deviation was 2% ($n = 10$) at the 40 μg of tungsten per 100 ml level.

### 3.5. *Effects of foreign ions*

The effects of foreign ions on the determination of tungsten were investigated. For these studies, different amounts of the ionic species were added to 40 μg of tungsten determined by the standard procedure. The results are summarized in Table 2. The tolerance limits of the foreign ions were obtained with a relative error not greater than 5%.

The results in Table 3 show that the recoveries were unaffected when the solution contained chloride, sulfate, iodide, fluoride, sodium, magnesium and calcium ions. However, $Cu^{2+}$, $Mo^{6+}$ and $Fe^{3+}$ ions interfere. The interference of copper was prevented by the addition of appropriate amounts of a 10% potassium ferricyanide solution [18]. $Fe^{3+}$ ions in the samples were completely reduced with 3 ml of 20% $SnCl_2$. Therefore, the interference effect of the $Fe^{3+}$ ions was prevented. The concentrations

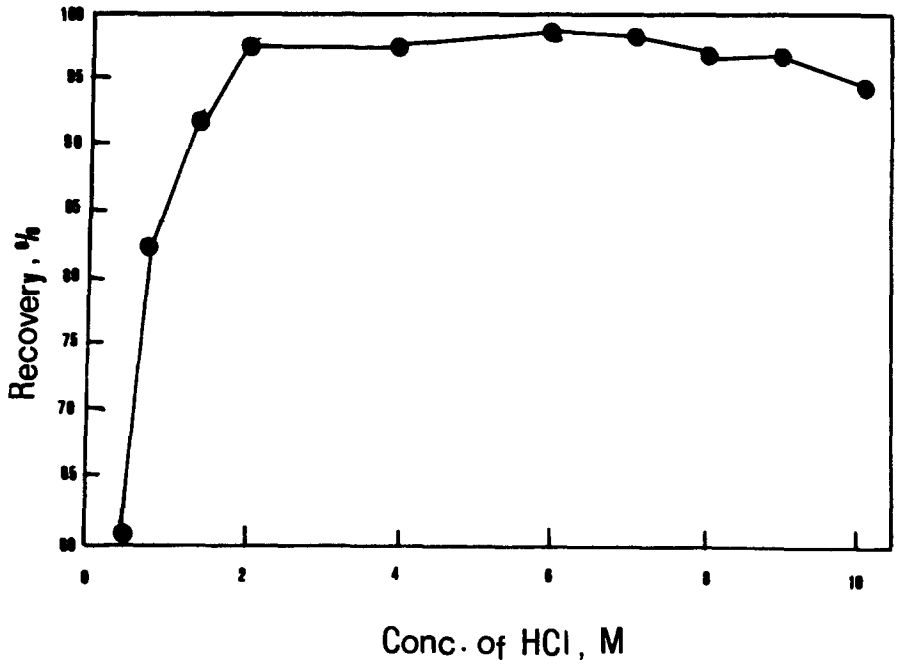


Fig. 2. Effect of the concentration of HCl on the recovery of tungsten on Amberlite XAD-1180 resin.

Table 1
Recoveries[a] of tungsten on Amberlite XAD-1180 with various eluents[b]

| Eluent | Recovery (%) |
|---|---|
| Acetone | 97 ± 1 |
| Methanol | 95 ± 3 |
| Ethanol | 96 ± 1 |
| *n*-Butanol | 96 ± 3 |
| *n*-Propanol | 99 ± 4 |
| Chloroform | <5 |
| Diethyl ether | <5 |

[a] $n = 7$.
[b] Eluent volume, 10 ml.

Table 2
Tolerance limits of foreign ions for the recovery of tungsten on Amberlite XAD-1180[a]

| Ion | Added as | Tolerance limit (μg ml$^{-1}$) |
|---|---|---|
| $Ca^{2+}$ | $CaCl_2$ | 2500 |
| $Na^{+}$ | NaCl | 10000 |
| $Mg^{2+}$ | $MgCl_2$ | 1000 |
| $SO_4^{2-}$ | $Na_2SO_4$ | 1000 |
| $NO_3^{-}$ | $NaNO_3$ | 500 |
| $F^{-}$ | NaF | 250 |
| $Fe^{3+}$ | $FeCl_3$ | 50 |
| $Cu^{2+}$ | $CuCl_2$ | 5 |
| $Mo^{6+}$ | $Na_2MoO_4$ | 5 |
| $Co^{2+}$ | $Co(NO_3)_2$ | 15 |
| $Zn^{2+}$ | $Zn(NO_3)_2$ | 50 |
| $Bi^{3+}$ | $Bi(NO_3)_3$ | 25 |
| $Cd^{2+}$ | $Cd(NO_3)_2$ | 50 |

[a] Sample volume, 250 ml; $n = 4$.

of $Co^{2+}$, $Zn^{2+}$, $Bi^{3+}$, $Cd^{2+}$ and $Mo^{6+}$ ions in the geological samples were found to be within their tolerance limits.

### 3.6. Tungsten content of geological samples

The method was applied to the determination of tungsten in geological samples collected from the Mine Quarry (Yozgat, Turkey). The results are given in Table 3. The determination of the tungsten content in the samples was also performed using a well-known and accepted extraction method [9]. There are no significant differences between the concentration values obtained by both methods at the 95% confidence level. However, better precision is obtained with the column method.

## 4. Conclusion

The Amberlite XAD-1180 column method was applied to the determination of the tungsten concentration in geological samples, and accurate results were obtained. The results obtained using this column method and the extraction method are in agreement. The

Table 3
Concentration of tungsten in geological samples collected from the Sorgun Yeni Çeltek Mine Quarry (Yozgat, Turkey)

| Depth (m) | Concentration of tungsten ($\mu g\ g^{-1}$)[a] | | | |
|---|---|---|---|---|
| | Column | RSD (%) | Extraction | RDS (%) |
| 60 | $195 \pm 10$ | 5.13 | $187 \pm 14$ | 7.51 |
| 100 | $176 \pm 10$ | 5.68 | $162 \pm 12$ | 7.36 |
| 170 | $311 \pm 17$ | 5.51 | $316 \pm 25$ | 7.91 |
| 220 | $224 \pm 13$ | 5.83 | $220 \pm 12$ | 5.45 |
| 220[b] | $218 \pm 5$ | 2.29 | $222 \pm 11$ | 5.01 |
| 360 | $479 \pm 19$ | 4.01 | $489 \pm 36$ | 7.39 |

[a] $n = 7$; $P$: 0.95; $\pm t.s/\sqrt{n}$.
[b] Samples were collected from two different zones at a depth of 220 m.

proposed method can easily be used for the determination of tungsten in industrial samples such as alloys and steel samples, etc.

## Acknowledgement

This work was supported by TÜBITAK (the Scientific and Technical Research Council of Turkey project no. DPT/TBAG-26).

## References

[1] V. Yatirajam and S. Dhamija, Talanta, 24 (1977) 497.
[2] N.K. Roy and A.K Das, Talanta, 33 (1986) 277.
[3] J. Verbeeck, B. Vanderborght and R. Van Grieken, Anal. Chim. Acta, 128 (1981) 207.
[4] J.S. Fritz and J.J. Topping, Talanta, 18 (1982) 865.
[5] S. Greenfield, T.M. Durrani, S. Kaya and J.F. Tyson, Analyst, 115 (1990) 531.
[6] A.T. Gowda and K.S. Rangappa, Anal. Chem., 61 (1989) 149.
[7] C.H. Kim, P.W. Alexander and L.E. Smythe, Talanta, 23 (1976) 573.
[8] Z. Marczenko, Separation and Spectrophotometric Determination of Elements, Wiley, Chichester, 1986.
[9] J. Musil and J. Dolezal, Anal. Chim. Acta, 92 (1977) 301.
[10] M. Soylak, L. Elçi and M. Doğan, EUROANALYSIS VIII, Edinburgh, U.K., Abstr., 1993, p. 27.
[11] M.R. Plantz, J.S. Fritz, F.G. Smith and R.S. Houk, Anal. Chem., 61 (1989) 149.
[12] X.G. Yang and E. Jackwerth, Fresenius' Z. Anal. Chem., 331 (1988) 588.
[13] L. Elçi, M. Soylak and M. Doğan, Fresenius' J. Anal. Chem., 342 (1992) 175.
[14] Ş. Tokalıoğlu, Ş. Kartal and L. Elçi, Anal. Sci., 10 (1994) 779.
[15] M. Soylak, Ph.D. Thesis, Erciyes University, Kayseri, 1993.
[16] A. Vogel, Textbook of Quantitative Inorganic Analysis, 4th edn., Longman, London, 1978.
[17] M. Soylak, L. Elçi and M. Doğan, Anal. Lett., 26 (1993) 1997.
[18] E.P. Welsch, Talanta, 30 (1983) 876.

ELSEVIER

Talanta 42 (1995) 1519–1524

Talanta

# The polarographic and voltammetric behaviour of the copper(II) mitoxantrone complex and its analytical application

Hongfei Wang, Erbing Hua, Pin Yang *

*State Key Laboratory of Coordination Chemistry, Nanjing University, Nanjing, People's Republic of China*

Received 13 December 1994; revised 28 March 1995; accepted 3 April 1995

**Abstract**

The polarographic and voltammetric behaviour of the copper(II)–mitoxantrone complex have been studied. A well-defined linear sweep voltammetric peak was obtained at −0.275 V (vs. Ag/AgCl) or −0.325 V (vs. SCE) in ammonia–ammonium chloride (20 mmol $l^{-1}$, pH 9.0). The characteristics of the peak have been examined in detail. The experimental results show that the reduction of the copper(II) mitoxantrone complex is irreversible and the peak displays adsorption characteristics at the dropping mercury electrode. A mechanism is proposed for the reduction of the complex, comprising one-electron reduction of the copper(II) of the complex, is reduced directly in the complex form. A single-sweep oscillopolarographic method was developed for the determination of copper(II). The peak current is proportional to the concentration over the range $5 \times 10^{-8}$–$2 \times 10^{-5}$ mol $l^{-1}$. The method reported here has the advantage that the interference of many common metal ions is small.

## 1. Introduction

Polarography and voltammetry are very sensitive methods for the determination of many trace metal ions; for example, stripping voltammery is based on concentration by electrolysis. However, the formation of intermetallic compounds with coexisting metal ions at the electrode can cause serious errors [1]. Adsorptive accumulation is useful for concentrating an analyte selectively for voltammetric analysis or for concentrating the metal ions when they are converted into adsorbable complexes by reaction with an organic ligand [2,3]. The voltammetric determination of copper(II) based on the adsorptive accumulation of the Cu(II)-5-Br-PADAP complex on a hanging mercury drop electrode has been reported [4], but the interference of many common metal ions is still obvious.

In this paper, the polarographic and voltammetric behaviour of the Cu(II) complex with mitoxantrone (1,4-dihydroxy-5,8-bis(2-((2-hydroxyethyl)amino)ethylamino)-9,10-anthracenedione; MX) was studied by various electrochemical methods. The structure of mitoxantrone is shown in Scheme 1. The characteristics of the reduction peak and the reduction mechanism have been examined in detail. Furthermore, the conditions of complexation including the coordination group and the

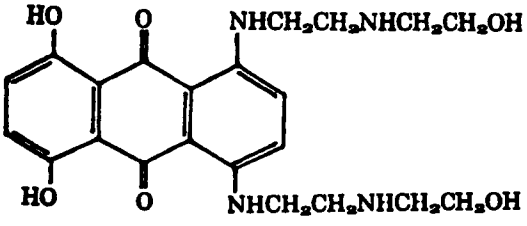


Scheme 1. Structure of mitoxantrone.

* Corresponding author. Present address: Institute of Molecular Science, Shanxi University, Taiyuan 030006, People's Republic of China.


*SSDI* 0039-9140(95)01605-8

coordination configuration were analyzed. The stability constants of the complex were also calculated by pH titration. MX is a ligand more fitted for the voltammetric determination of copper(II); the method described here has the advantage of little interference from many coexisting metal ions. On the basis of the above results, the cause of the small amount of interference of many common metal ions was discussed.

## 2. Experimental

### 2.1. Apparatus

A BAS-100A electrochemical analytical instrument (Bioanalytical System, Inc., USA), with a PAR 303 electrode system (SMDE, DME, HMDE) as the working electrode, a saturated Ag/AgCl reference electrode, and a platinum wire as auxiliary electrode, was used. All figures were drawn on a DMP-40 digital plotter (USA). A JP-2 single-sweep oscillopolarograph (Chengdu Instrument Factory, China) with a saturated calomel electrode (SCE) as the reference electrode was used for the quantitative analysis of the samples. The absorption and fluorescence spectra were measured on a UV-365 spectrophotometer (Shimadzu) and an RF-850 fluorescence spectrophotometer (Hitachi), respectively. The pH was recorded by means of a pHS-2 acidic meter (Shanghai Leici Factory, China).

### 2.2. Reagents

Mitoxantrone (chromatographically pure) was provided by the Zhenan Pharmaceutical Corporation, China. A $2 \times 10^{-4}$ mol $l^{-1}$ stock solution of mitoxantrone was prepared by dissolving an appropriate amount of MX in ammonia–ammonium chloride (20 mmol $l^{-1}$; pH 9.0). A $1 \times 10^{-2}$ mol $l^{-1}$ stock solution of copper(II) was prepared by dissolving copper metal (99.999%) in 5% nitric acid. The stock solutions were transferred and diluted with ammonia–ammonium chloride (20 mmol $l^{-1}$; pH 9.0) to give the working solutions before the measurements. Other chemicals were of analytical reagent grade, and deionized, distilled water was used.

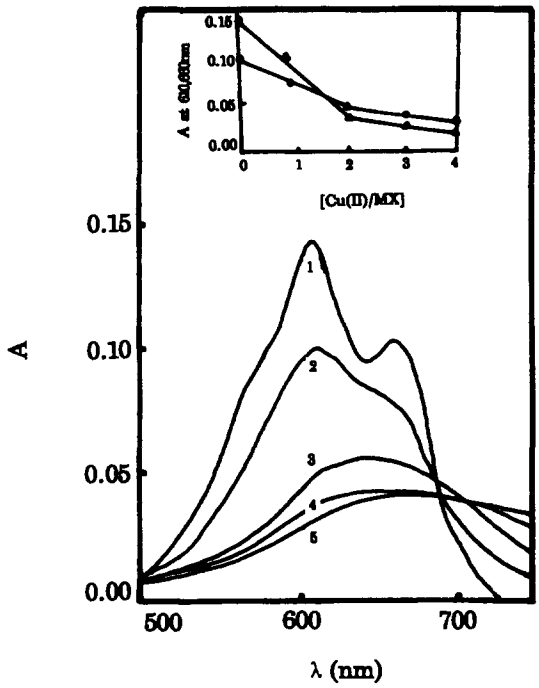


Fig. 1. Absorption spectra for different molar ratios of copper(II)/MX. 1, $1.0 \times 10^{-5}$ mol $l^{-1}$ MX; 2, 1:1; 3, 2:1; 4, 3:1; 5, 4:1.

### 2.3. Procedure

Appropriate amounts of mitoxantrone and the copper(II) solutions were transferred to a 10 ml volumetric flask, then ammonia–ammonium chloride (20 mmol $l^{-1}$; pH 9.0) was added, and the solution was diluted to give the final volume. The solution was deaerated by the passage of pure nitrogen for 5 min. The potentials were scanned in a negative direction over the range $-100$– $-500$ mV; all measurements were carried out at room temperature.

## 3. Results and discussion

### 3.1. Complexation properties

On adding copper(II) to $1 \times 10^{-5}$ mol $l^{-1}$ MX solution, obvious changes in the absorption spectra and fluorescent spectra were observed, as shown in Figs. 1 and 2. When the molar ratio of [Cu(II)]/[MX] was increased to 2:1, the absorption spectra did not obviously change, and the fluorescence emission peak was quenched complemently. On adding copper(II) to the $1 \times 10^{-5}$ mol $l^{-1}$ MX solution, a new reduction peak appeared at $-0.275$ V (vs. Ag/AgCl), as shown in Fig. 3. The peak at

$-0.817$ V (vs. Ag/AgCl) corresponds to the reduction potentials of the 9,10-quinone of MX [5]. Adding MX to $1 \times 10^{-5}$ mol $l^{-1}$ copper(II) solution determined the height of the peak current at $-0.275$ V; when the [MX]/[Cu(II)] ratio was 1:2, the height did not change and then levelled off. This indicated that one molecule of drug can bind with two Cu(II) ions. The height of the peak current at $-0.275$ V increased with added amounts of copper(II) and then levelled off; however the peak potential and peak current at $-0.817$ V changed very little. This showed that the Cu(II) ion complexes with nitrogen atoms of the side-chain of MX, but not with the oxygen atoms of the hydroxyl groups at the 1,4 position and the oxygen atoms of the carbonyl function at C9 and C10. The Pd(II)–MX complex has been studied by analyzing the absorption spectra of MX and ametantron (a drug without the 1,4-hydroxyl group of MX) [6]; the results showed that the Pd(II) ion is only bound to the nitrogen atoms of the side-chain. This study is similar to ours, and supports our points also. The nitrogen atoms of the drug molecules are candidates for the binding to copper(II), taking into account steric hindrance and that Cu(II)–amine complexes are usually tetracoordinated.

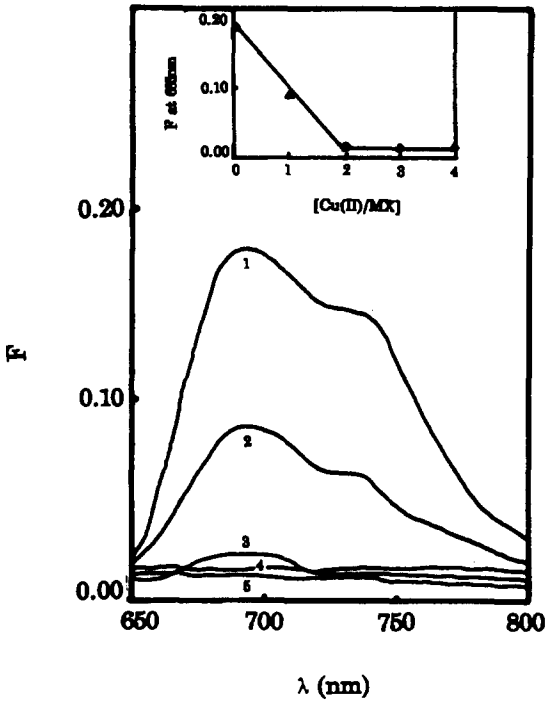


Fig. 2. Fluorescence spectra for different molar ratios of copper(II)/MX. 1, $1.0 \times 10^{-5}$ mol $l^{-1}$ MX; 2, 1:1; 3, 2:1; 4, 3:1; 5, 4:1.

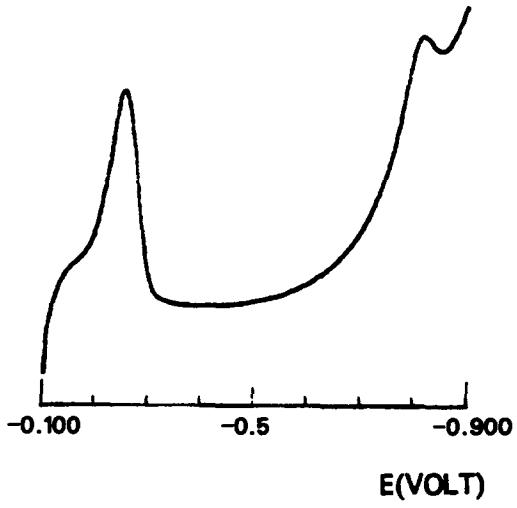


Fig. 3. Linear sweep voltammogram of the copper(II)–MX complex ($1.0 \times 10^{-6}$ mol $l^{-1}$ Cu(II); $1.0 \times 10^{-5}$ mol $l^{-1}$ MX) in ammonia–ammonium chloride (20 mmol $l^{-1}$, pH 9.0) solution. (Scan rate, 250 mV $s^{-1}$; rest time, 10 s.)

We suggest that one Cu(II) ion is bound to the two nitrogen atoms of the side-chain at C5 of the drug molecule, and the second Cu(II) ion to the two nitrogen atoms of the side-chain at C8 of the drug molecule; the other two coordination positions of copper(II) are $NH_3$ or $H_2O$. A tetrahedral coordination geometry is preferable.

The pH titration curves are shown in Fig. 4. These show that the complex formed above

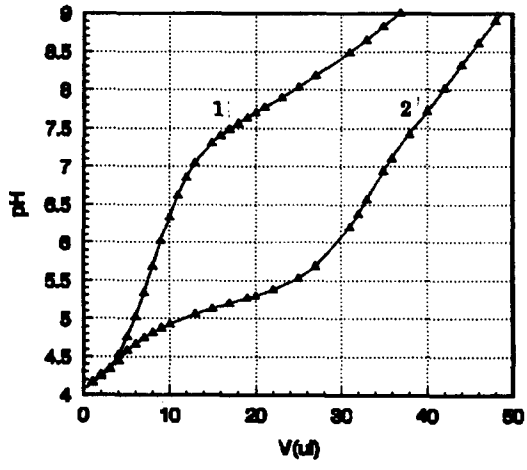


Fig. 4. pH titration curves. 1, MX ($1 \times 10^{-4}$ mol $l^{-1}$). 2, MX + Cu(II) (1:1; $1 \times 10^{-4}$ mol $l^{-1}$) ($I = 0.1$ N $KNO_3$; $T = 25$°C; $N_2$ flow).

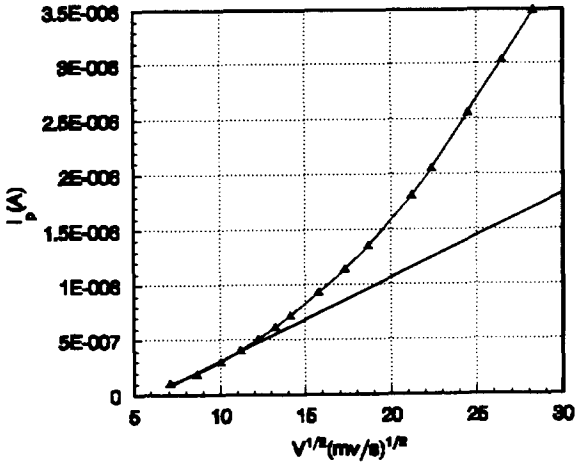


Fig. 5. Variation of $i_p$ with $v^{1/2}$.

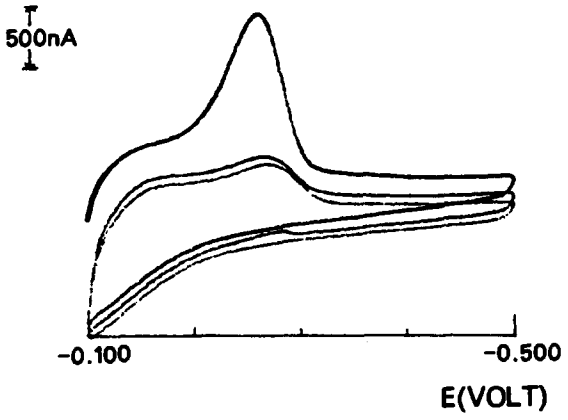


Fig. 6. Repetitive cyclic voltammogram of copper(II)–MX complex ($1.0 \times 10^{-6}$ mol $l^{-1}$ Cu(II); $1.0 \times 10^{-5}$ mol $l^{-1}$ MX) in ammonia–ammonium chloride (20 mmol $l^{-1}$, pH 9.0) solution. (Scan rate, 250 mV $s^{-1}$; rest time, 10 s.)

pH 4.5. From the equation of material equilibrium and the non-linear least-squares method [7], the stability constants of the complex were calculated

$$\log \beta_{CuHL} = 9.9, \log \beta_{CuH_2L} = 6.5$$

where subscript L denotes the ligand.

### 3.2. Adsorption properties

The effects of rest time, starting scan potential and scan rate ($v$) on the peak current were investigated. The results indicated that the peak current increased as the rest time increased, and decreased as the starting potential became more negative. If the rest time and starting scan potential are fixed, plotting $i_p$ against $v^{1/2}$ gave an ascending curve, shown in Fig. 5, according to the Randles–Sevcik equation, in a linear diffusion-controlled process, $i_p \propto v^{1/2}$. This resulted in an upward inclined curve, which indicated the adsorptive nature of the reduction current and that the reductant is adsorbed on the SMDE [8].

The electrocapillary curve showed that the surface tension of the mercury drop decreased in the presence of $1.0 \times 10^{-6}$ mol $l^{-1}$ Cu(II)–MX complex. The peaks decreased with the addition of surfactant (0.01 mol $l^{-1}$ sodium dodecyl sulfonate, 0.002% Triton X-100). The temperature coefficients are 1.97% per °C (5.5–18.0°C), 1.77% per °C (18.0–30.5°C) and 0.61% per °C (30.5–44°C), respectively. These are all the characteristic feature of adsorptive wave.

In order to elucidate further the electrode reaction of the complex, a repetitive cyclic voltammogram (Fig. 6) at the SMDE was recorded. In the cyclic voltammogram, the reduction peak is observed on the cathodic branch; no oxidation peak is observed on the anodic branch. The cathodic peak current decreased in the second and following cycles. This indicated that the electrode reaction is irreversible and that the peak current is influenced by the adsorption of reactant.

The above experimental results indicate that the reduction peak of the complex is an irreversible polarographic wave having adsorption characteristics.

### 3.3. Mechanism of the reduction

The effect of scan rate ($v$) on the peak potential ($E_p$) was determined by linar sweep voltammetry (LSV); the results are shown in Table 1. These indicated that $E_p$ shifts to a more negative direction with increasing scan rate. From the equation [9]

Table 1
The effect of scan rate ($v$) on peak potential ($E_p$)

| $v$ (mV $s^{-1}$) | $E_p$ (mV) | $v$ (mV $s^{-1}$) | $E_p$ (mV) |
|---|---|---|---|
| 50 | −231 | 300 | −275 |
| 75 | −240 | 350 | −281 |
| 100 | −247 | 400 | −284 |
| 125 | −253 | 450 | −288 |
| 150 | −258 | 500 | −290 |
| 175 | −260 | 600 | −292 |
| 200 | −264 | 700 | −297 |
| 250 | −271 | 800 | −301 |

$$E_p = E^\circ + RT/\alpha nF[\ln(k_s/D^{1/2}) - 0.5\ln(\alpha nFv/RT) - 0.78]$$

where $\alpha$ is the transfer coefficient, and $n$ is the number of electrons, a value of $\alpha n$ of 0.499 was calculated from the slope of the line (correlation coefficient, $r = 0.9989$) and $\alpha = 0.5$, so $n = 0.998$, namely, the number of electrons transfered in the reaction was equal to 1. The peak potential of the complex between MX, $\Delta E_p$, is independent of pH and the concentration of Cu(II). Therefore the reduction mechanism of the Cu–MX complex is such that it does not dissociate but is directly reduced in the complex form [9]. According to the above results, the following reduction mechanism can be proposed

$$Cu(II) + 1/2MX \rightleftharpoons [Cu(II)-MX_{1/2}]ads$$

$$[Cu(II)-MX_{1/2}]ads + e \rightleftharpoons Cu(I)-MX_{1/2}$$

### 3.4. Analytical application

The dependence of the derivative peak heights on concentration was investigated by single-sweep oscillopolarography (SSOP). The calibration curve demonstrates good linearity over the range $5 \times 10^{-8}$–$2 \times 10^{-5}$ mol $l^{-1}$, with a correlation coefficient of 0.9985. The limit of detection is $1 \times 10^{-8}$ mol $l^{-1}$. The peak current is stable over the range of continuous measurements for 2 h. The precision of the SSOP determination of copper(II) is excellent; at a concentration of $5 \times 10^{-7}$ mol $l^{-1}$, the relative standard deviation is 2.9% ($n = 5$).

The influence of metal ions was investigated by adding them to a solution containing $1 \times 10^{-6}$ mol $l^{-1}$ Cu(II) and $1 \times 10^{-5}$ mol $l^{-1}$ MX. One-thousandfold amounts of K(I), Na(I), Ca(II), Mg(II) and Mn(II), and ten-to-fiftyfold amounts of Fe(III), Cr(III), Co(II), Cd(II), Ni(II) and Zn(II) did not interfere. The results are very encouraging.

We think that the interference of the co-existing metal ions arises in two ways. First, both the interfering metal ions and the ions to be determined can complex with the same group on the organic ligand; this binding contest has an effect on the normal complexation and reduction of the determined metal ions. Second, the reduction potentials of the interfering and determined metal ions in the same matrix are close to each other; this may have an effect on the normal shape of the reduction peak of the determined ions. In the system described here, for example, Fe(III) can complex with MX, but it complexes with the oxygen atoms of 9,10-quinone, not with the nitrogen atoms of the side-chain, which is the coordination group of the Cu(II) ion. Therefore, it does not influence the complexation of Cu(II) with MX and the reduction of Cu(II). Although Zn(II), Ni(II) and Co(II) in the matrix of the system produce stronger reduction peaks, the reduction potentials are more negative than $-0.6$ V, far from the reduction potential of the Cu(II)–MX complex, so they do not influence the determination of Cu(II) due to a change in the shape of the reduction peak. According to the Irving-Williams rule, complexes of the Cu(II) ion with dozens of ligands have the highest stability among the divalent metal ions of first-row transition elements. The stability constants of the Cu(II) ion with ligands such as $NH_2$–$CH_2$–$CH_2$–$NH_2$, $OH^-$, and $NH_3$, are thousands of times higher than those of Zn(II), Ni(II), Co(II), etc. [11]. Therefore, although Zn(II), Co(II) and Ni(II) may complex with MX, under the condition of sufficient ligand, the effect of the binding contest can be eliminated. From the above study and analysis, we think that selecting the appropriate ligand and increasing the amount of organic ligand are important for improving the analytical selectivity and sensitivity.

The SSOP method described here is sensitive, rapid, reliable, and simple to perform, and the interference of many common metal ions in this system is small; thus it is very suitable for analytical application in practical systems.

## Acknowledgments

We are very grateful for the help of Professor Jinhao Pan, Gerong Zhou and Huizhi Fan. Part of the work was completed in their laboratory.

## References

[1] M.S. Shuman and G.P. Woodwand, Anal. Chem., 48 (1976) 1979.
[2] H. Sawamoto, J. Electroanal. Chem., 147 (1983) 279.
[3] V. Gemme-Colos and R. Neeb, Anal. Chem., 327 (1987) 547.
[4] S. Tanaka, K. Sugawara and M. Taga, Talanta, 37 (1990) 1001.
[5] B. Nguyen and P.L. Gutierrez, Chem. Biol. Interactions, 74 (1990) 139.

[6] P. Kolodziejczyk and A. Garnier-Suillerot, Biochim. Biophys. Acta, 926 (1987) 249.
[7] S.F. Fu and L.M. Li, J. Mol. Sci., 3 (1985) 2.
[8] X.X. Gao and M.P. Zhang, Anal. Chem., 56 (1984) 1912.
[9] F. Anson, Electrochemical and Electroanalytical Chemistry, Beijing University Press, 1983, p. 45.
[10] X.X. Gao, Polarographic Catalysis Wave, Science Press, Beijing, 1991, p. 142.
[11] Y.X. Ci and T.Z. Zhou, Coordination Compound in Analytical Chemistry, Beijing University Press, Beijing, 1986, p. 76.

ELSEVIER

Talanta 42 (1995) 1525–1532

Talanta

# Determination of vanadium by solid-phase spectrophotometry after its preconcentration as an Eriochrome Cyanine R complex on a dextran-type exchanger

S. Boudra, J.M. Bosque-Sendra *, M.C. Valencia

*Department of Analytical Chemistry, Faculty of Sciences, University of Granada, 18071 Granada, Spain*

Received 27 November 1994; revised 31 March 1995; accepted 4 April 1995

**Abstract**

A method is described for the determination by solid phase spectrophotometry (SPS) of trace amounts of vanadium in natural water and crude petroleum samples. The procedure is based on fixation on a dextran-type anion exchanger of the complex V(IV)–Eriochrome Cyanine R. The absorbance of the gel, at 563 and 750 nm, packed in a 1 mm cell, is measured directly. Vanadium can be determined in the 0.6–25.0 $\mu g\, l^{-1}$ range with a relative standard deviation of 2.2%. The comparison of the SPS method and the gallic acid persulphate method shows that the linearity, analytical sensitivity and precision were better for the SPS method, and that the latter method has lower detection and quantification limits than the gallic acid persulphate method.

## 1. Introduction

The toxicity of vanadium and its compounds and the fact that its industrial use produces occupational health problems are well known [1,2]. In addition, crude petroleum and its derivatives produce an environmental problem, due to the presence of vanadium in the form of porphyrin complexes in these products [2]. However, it has been established that there is a relationship between the presence of vanadium at the microgram per litre level in tap water and the prevention of the cardiopathies [3]. Therefore the determination of vanadium in biological and environmental samples is necessary [4,5], requiring sensitive techniques [6,7].

Triphenylmethane reagents have been widely used for the spectrophotometric determination of vanadium(IV), producing a coloured compound [8]. One of these, Eriochrome Cyanine R (ECR), is a good chromogenic reagent for the determination of V(IV), and its ternary complexes with cationic surfactants have been described and used for spectrophotometric analysis in solution [9]. Ascorbic acid can be used as a reducing agent; V(V) is reduced to V(IV) and a complex between ECR and V(IV) is formed [8,10].

Solid phase spectrophotometry (SPS) is a methodology that is based on the production of a chromogenic compound between the analyte and an appropriate reagent, the preconcentration of this compound on a solid matrix, usually an ion exchanger, and the direct measurement of the absorbance in the solid phase. This provides an increase in selectivity and sensitivity for SPS methods with respect to solution methods [11,12].

The fixation of the V(IV)–ECR complex on a dextran-type exchanger is discussed here. The application of SPS methodology has produced a higher sensitivity and a lower detection limit than is given by the solution methods for the determination of vanadium at microgram per litre levels.

* Corresponding author.


*SSDI* 0039-9140(95)01608-2

A comparison was made of the proposed SPS method and the gallic acid persulphate method [13,14]. It was concluded that the linearity, analytical sensitivity and precision were better with the SPS method than with the gallic acid persulphate method, and that the detection and quantification limits were lower for the SPS method.

The proposed method was applied to the determination of vanadium in natural water and crude petroleum samples, and the results were compared with those obtained by the gallic acid persulphate method and the ASTM method [15], respectively. No significant differences were observed.

## 2. Experimental

### 2.1. Reagents

All chemicals used were of analytical grade unless stated otherwise. The water used for the dilution of the reagents and samples was reverse-osmosis quality water. All experiments were carried out at room temperature.

Eriochrome Cyanine R (ECR; Carlo Erba) solutions of various concentrations were prepared by dissolving the necessary amount of dye in reverse-osmosis water and adjusting the final acid concentration to $5 \times 10^{-3}$ M with HCl. The solutions were stored under refrigeration. Under these conditions the solutions are stable for 1 day.

Vanadium(V) stock solution ($1\ g\ l^{-1}$) was prepared by dissolving 0.2297 g of ammonium metavanadate (Merck) in 1 ml of concentrated nitric acid and 75 ml of reverse-osmosis water, and dilution to volume with reverse osmosis water in a 100 ml standard flask. The working standard solution was freshly prepared every day by dilution with reverse-osmosis water.

Ascorbic acid (PanReac) was used in the solid state, due to the instability of ascorbic acid solutions.

As a solid ion exchanger, Sephadex DEAE A-25 anion exchanger (Sigma) was used in the chloride form as received from the supplier and without pretreatment in order to avoid contamination.

Buffer solutions of the required pH were prepared from 2 M sodium acetate solution (Merck) and 2 M acetic acid (Merck).

### 2.2. Apparatus

The apparatus used included a Perkin–Elmer Lambda 2 UV/Vis spectrophotometer equipped with 1 mm cells and connected to a IE 486 computer, an Agitaser model 2000 rotating-bottle agitator, and a Crison Digit-501 pH meter with a combined glass–Calomel electrode.

### 2.3. Absorbance measurements

The absorbance of the reaction product fixed on the exchanger was measured in a 1 mm cell at 563 and 750 nm (the latter is within the range where the exchanger only causes attenuation of light) against a 1 mm cell well-packed with exchanger equilibrated with water. The absorbance of the blank (a 1 mm cell packed with resin equilibrated with blank solution) was measured at the same wavelengths. The blank absorbance results from the Eriochrome Cyanine R fixed on the exchanger.

The net absorbance, $A_{NC}$, for the complex was obtained from [12] $A_{NC} = A_{complex} - A_{blank}$, where $A_{complex} = A_{563} - A_{750}$ (for the sample) and $A_{blank} = A_{563} - A_{750}$ (for the blank).

### 2.4. Standard procedure

The following, in this order, were introduced into a 2000 ml polyethylene bottle: a 1000 ml sample containing 0.6–25.0 $\mu g\ l^{-1}$ of V(V), 5 ml of 2 M buffer solution (pH 5.0), 0.2 g of ascorbic acid, 3 ml of $7.46 \times 10^{-3}$ M ECR solution and 0.080 g of the Sephadex DEAE A-25 anion exchanger. The mixture was shaken mechanically for 45 min. The coloured exchanger beads were then collected by filtration under suction and, with the aid of a pipette, were packed into a 1 mm cell together with a small portion of the filtrate. The cell was centrifuged for 1 min at 25 *g*. A blank solution containing all the reagents was prepared in the same way as described for the sample. The absorbances at 563 and 750 nm for the sample and the blank were measured against a 1 mm reference cell, similarly packed with exchanger equilibrated with water, and the net absorbance, $A_{NC}$, was obtained as described in section 2.3.

For a 250 ml sample system, solutions containing 3.0–130.0 $\mu g\ l^{-1}$ of V(V), 5 ml of 2 M buffer solution (pH 5.0), 0.3 g of ascorbic acid, 1 ml of $7.46 \times 10^{-3}$ M ECR solution and

0.080 g of the Sphadex DEAE A-25 anion exchanger were added. The mixture was shaken mechanically for 15 min. The absorbance of the coloured beads was measured as above.

### 2.5. Treatment of the sample

*Natural water samples*

The water samples were preserved by the addition of nitric acid (2 ml of concentrated nitric acid per litre), and were collected in a polyethylene container that had been carefully cleaned with nitric acid. Prior to the measurements, the water sample was filtered through 0.45 μm pore-size membrane filters (Millipore, type HA).

*Crude petroleum samples*

A suitable quantity of the three different crude petroleum samples (between 7 and 25 g in order to permit also the application of the ASTM method) was treated with concentrated sulphuric acid (1 ml per gram of sample) with continuous agitation to avoid foam formation, followed by combustion of the carbonaceous ash at 525 ± 25°C. The inorganic residues were treated for 10–15 min with 20 ml of hydrochloric acid (1:1). After complete dissolution of the ash and concentration to 3–4 ml of solution 0.2 ml of concentrated nitric acid was added and the solutions were heated gently. The solutions were finally diluted to 50 ml with reverse-osmosis water. The pH of the samples, prior to the determination, was adjusted with 2 M NaOH (0.5–1 ml).

## 3. Results and discussion

### 3.1. Absorption spectra

In solution, ECR reacts with vanadium(IV) at pH 4.9 to form a red complex having a maximum absorbance at 550 nm [9]. In addition, ternary complexes are formed at pH 4.5–5.2 in the presence of cationic surfactants, producing a hyperchromic effect and a bathochromic shift of the absorption maximum (580–620 nm), whereas vanadium(V) does not form ternary complexes with these cationic surfactants [9,10].

Vanadium(V) does not react with ECR in the presence of anion exchanger while the complex obtained from the reaction between vanadium(IV) and ECR at pH 5.0 is fixed on the Sephadex anion exchanger (Fig. 1). The wavelength and the absorbance of the compound formed and fixed on the exchanger vary when the [ECR]/[V] molar ratio is modified. A red colour is obtained with an absorption maximum between 560 and 593 nm and a small increase in the absorbance using the Sephadex DEAE A-25 anion exchanger (Fig. 1, spectra a and b). Furthermore, a significant hyperchromic effect is also observed in relation to the binary complex of vanadium(IV) with ECR in solution at pH 5.0 (Fig. 1 spectrum c). This change is similar to that observed, in solution, between the binary complex (V(IV)–ECR) and the ternary system (V(IV)–ECR–cationic surfactants).

The complex of vanadium(IV) with ECR is anionic in nature due to the fact that it is not fixed on cation exchangers.

### 3.2. Optimization of conditions

*pH dependence*

The optimum pH for the formation and fixation of the complex falls in the range 4.7–5.0 (Fig. 2). At pH values below 4.0 the complex was not fixed on the exchanger and at pH values above 5.1 the net absorbance, at 563 nm, decreased due to two opposing effects: the increase in the absorbance of the blank and

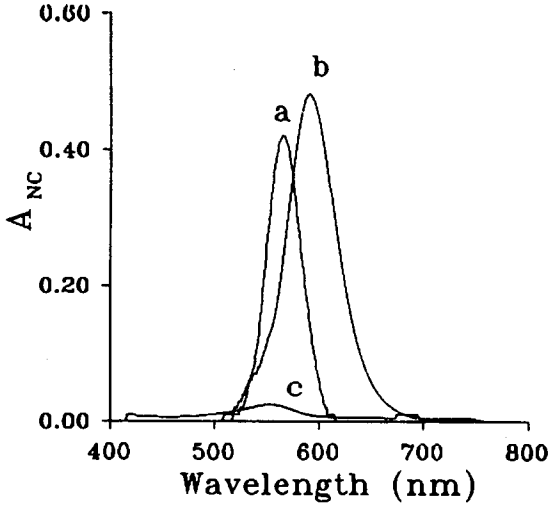


Fig. 1. Net absorption spectra of the Vanadium(IV)–ECR complex at pH 5.0. Spectra a and b, with the ion exchanger: spectrum a, $[ECR] = 2.24 \times 10^{-5}$ M, 0.2 g of ascorbic acid; spectrum b, $[ECR] = 3.73 \times 10^{-5}$ M, 0.2 g of ascorbic acid ($[V] = 1.96 \times 10^{-7}$ M; 80 mg of Sephadex DEAE A-25; sample volume, 1000 ml; stirring time, 45 min; optical path length, 1 mm). Spectrum c, in aqueous solution ($[V] = 1.57 \times 10^{-6}$ M, $[ECR] = 2.24 \times 10^{-5}$ M; 0.2 g of ascorbic acid; optical path length, 10 mm).

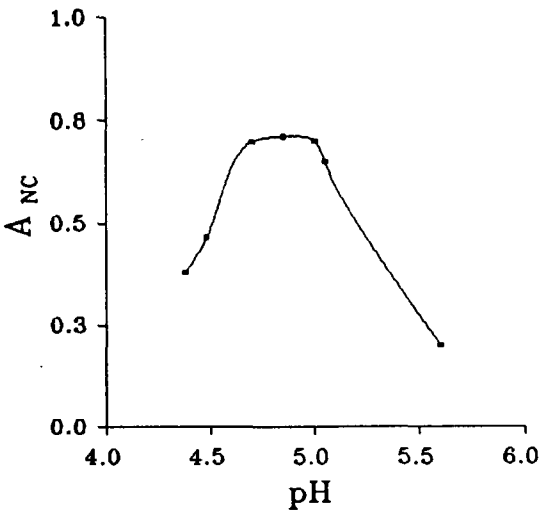


Fig. 2. Influence of pH on the colour development (conditions: 50 μg · l$^{-1}$ of vanadium; 1.87 × 10$^{-5}$ M ECR; 0.3 g of ascorbic acid; 80 mg of Sephadex DEAE A-25; stirring time, 20 min; sample volume, 1000 ml.)

the decrease in the absorbance of the V(IV)–ECR complex. We chose pH 5.0 as the best pH value for the standard procedures. The best of the buffer systems examined was acetic acid–sodium acetate.

*Influence of buffer concentration*

The effect of buffer concentration on the absorbance of the blank and the absorbance of the V(IV)–ECR complex was tested for concentrations in the range 0.01–0.12 M. Within this range, an increased absorbance of the blank and the complex as observed. Between buffer concentrations of 0.01 and 0.04 M the net absorbance was practically constant, due to a similar increase in absorbance both in the blank and in the sample. Meanwhile, in the range 0.04–0.12 M the absorbance of the blank increased to a greater degree than the sample absorbance, and the decrease in the net absorbance in this interval was very nearly 55%. Therefore the use of 5 ml of 2 M acetic acid–sodium acetate buffer was chosen for both the 1000 ml and the 250 ml sample systems, with the aim of maintaining the pH value at 5.0 despite the addition of ascorbic acid.

*Influence of ascorbic acid and ECR concentrations*

A certain amount of ascorbic acid is necessary due to the fact that this is the reducing agent. The absorbance of the complex is constant between molar ratios of 3000 and 9200 (ascorbic acid to vanadium). Molar ratios greater than 9200 produce a larger increase in the absorbance of the blank than the absorbance of the complex. Hence, to propose two methods for different ranges of vanadium concentrations, 0.2 g of ascorbic acid (a molar ratio of about 6000) was selected for the 1000 ml sample system and 0.3 g (a molar ratio of about 8600) for the 250 ml sample system. Furthermore, an optimum range of molar ratios (ascorbic acid to ECR) of between 25 and 250 was obtained for both methods, in which the net absorbance of the complex was practically invariable. Thus, as a consequence of the quantity of ascorbic acid employed in each sample system, a concentration of 2.98 × 10$^{-5}$ M was required for the 250 ml sample system, and for the 1000 ml sample system the necessary reagent concentration was 2.24 × 10$^{-5}$ M.

*Other experimental conditions*

The optimum stirring time was 15 min for the 250 ml sample system and 45 min for the 1000 ml sample system. The fixed compound was stable for at least 50 min after equilibration.

The reproducibility of the method is improved if the cells packed with the solid phase are centrifuged before spectrophotometric measurements are taken [16]. The time of centrifugation used here was 1 min at 2500 rev min$^{-1}$ (25*g*).

The quantity of exchanger must be chosen as being a compromise between obtaining the highest absorbance (minimum quantity of exchanger) and working under adequate operational conditions (between 0.025 and 0.100 g of exchanger). An quantity of 0.08 g of exchanger was chosen as the most suitable for our purpose in this occasion. However, the use of lower quantities, within the preceding range, is possible, and this will permit us to develop methods with different sensitivities.

The order of addition used here was vanadium + buffer + ascorbic acid + ECR + exchanger.

*3.3. Nature of the fixed complex*

The probable nature of the species fixed on Spehadex was established at the working pH of 5.0 using the Yoe–Jones method and a log–log plot. The plot of the logarithm of the distribution ratio versus the logarithm of the ECR

Table 1
Analytical parameters

| Parameter | Sample volume (ml) | |
|---|---|---|
| | 250 | 1000 |
| Intercept | $-6.8 \times 10^{-3}$ | $-9.9 \times 10^{-3}$ |
| Slope (1 $\mu g^{-1}$) | 0.010 | 0.044 |
| Linear dynamic range ($\mu g\,l^{-1}$) | 3.0–130 | 0.6–25 |
| Correlation coefficient | 0.995 | 0.999 |
| RSD (%) | 2.2 | 2.2 |
| Detection limit ($\mu g\,l^{-1}$) | 3.0 | 0.6 |
| Quantification limit ($\mu g\,l^{-1}$) | 10.0 | 2.0 |

concentration gave a slope of 1.1, and using a fixed ECR concentration, the plot of the logarithm of the distribution ratio versus the logarithm of the V(IV) concentration gave a slope of 1.1. Moreover, the Yoe–Jones method showed a ratio [ECR]/[V(IV)] = 1.1. The results show that the stoichiometry of the V(IV)–ECR complex fixed on the anionic exchanger is 1:1.

### 3.4. Analytical data

The calibration graphs are reasonably linear over the concentration ranges 3.0–130.0 $\mu g\,l^{-1}$ of vanadium for the 250 ml sample system and 0.6–25.0 $\mu g\,l^{-1}$ for the 1000 ml sample system using 0.080 g of exchanger. The analytical parameters are shown in Table 1.

The reproducibility was established for a series of nine independent determinations at 52 $\mu g\,l^{-1}$ of vanadium for the 250 ml samples and 10 $\mu g\,l^{-1}$ for 1000 ml samples (Table 1).

The fluctuations in the background absorbance measured for the blank, calculated as the average of ten determinations and expressed as SD units, for the 250 ml and 1000 ml sample systems were 0.010 A and 0.008 A, respectively. The IUPAC detection limit ($K = 3$) [17] and the quantification limit ($K = 10$) [18] were calculated for both sample systems (Table 1). From the data shown in Table 1, it can be seen that the 1000 ml sample system has a lower detection limit (0.6 $\mu g\,l^{-1}$) than obtained by the gallic acid persulphate method (1.92 $\mu g\,l^{-1}$) [3] and an even lower one than than those for some sensitive techniques such as flame atomic absorption spectrometry or atomic emission spectrometry [6].

The sensitivities of the proposed methods, expressed as Sandell's index $S$ (concentration ($\mu g\,ml^{-1}$) of vanadium required to obtain an absorbance of 0.001 in a 1 cm cell), are compared in Table 2 with those of spectrophotometric procedures in published methods. The higher sensitivity of our methods is apparent.

### 3.5. Effects of foreign ions

The effect of foreign ions on the determination of vanadium at the 40 $\mu g\,l^{-1}$ level was studied, following the above procedure, for a 250 ml sample system. Tolerance is defined as the amount of foreign ions which produces an error of $\pm 5\%$ in the determination of the analyte. The results are summarized in Table 3.

In order to apply the method to the determination of vanadium in water and crude petroleum samples, the interferences of those species commonly found in these types of samples was studied. The interference was negative for Pb(II), Cu(II), Mn(II), Zn(II) and $PO_4^{3-}$, and positive for the other ions.

The interference level, however, can be reduced by diluting the samples, taking into account the sensitivity on the sample volume. Furthermore, this is possible without reducing the accuracy and at the same time maintaining the simplicity and the short duration of the analysis (Table 1).

For the purpose of studying the recovery in the 1000 ml sample system, a synthetic water sample was prepared having 10 ppb of V(V) and different concentrations of various metallic ions: Fe(III), 40 ppb; Mn(II), 50 ppb; Cu(II), 15 ppb; Zn(II), 40 ppb; U(VI), 10 ppb; Co(II), 20 ppb; Mo(VI), 40 ppb; Ni(II), 50 ppb; Be(II), 5 ppb and Al(III), 30 ppb. A recovery of 98.4% was obtained as the average of six determinations and with an RSD of 2.3%.

Table 2
Comparison of the sensitivities of some vanadium determination methods

| Method | $10^6 S$ ($\mu g\ ml^{-1}$) | Reference |
|---|---|---|
| ASTM method | 42450 | [15] |
| Eriochrome Cyanine R/CP [a] | 717 | [9] |
| 4,5-Dibromophenylfluorone/CTAB [b] | 509 | [21] |
| 3,5-Dinitrocatechol/Rhodamine B | 242 | [22] |
| Gallic acid/persulphate | 30 | [13] |
| SPS method (250 ml) | 10 | This paper |
| SPS method (1000 ml) | 2.3 | This paper |

[a] Cetylpyridinium chloride.
[b] Cetyltrimethylammonium bromide.

### 3.6. Comparison of SPS and gallic acid persulphate method

As it is difficult to obtain analytical data from the literature in order to compare methods, we developed a comparative study of the SPS method and the standard method for the determination of vanadium at the microgram per litre concentration in water samples [3], i.e. the gallic acid persulphate method. We choose for the study an application of a statistical model for single linear regression on the calibration graphs [19]. This allows a comparative study under similar experimental conditions using a relatively small number of experiments. In addition, this model has the advantage that the errors inherent in the calibration graphs are included.

We performed an analysis in triplicate of five samples with the vanadium concentration ranging from 0.0 to 20.0 $\mu g\ l^{-1}$ by both the SPS method (1000 ml sample system) and the gallic acid persulphate method (final volume, 12 ml). Table 4 shows the quality parameters calculated from the results obtained in the analysis. Examination of these data shows that the SPS method displays better linearity and lower RSD values of the concentration, RSD ($C$)%, than does the gallic acid persulphate method. The lower analytical sensitivity of the SPS method compared to the other method shows that it is possible to discern smaller differences in concentration than in the gallic acid persulphate method. In addition, the quantification limits for the solution method and the SPS method are about 6.6 $\mu g\ l^{-1}$ and 3.6 $\mu g\ l^{-1}$, respectively.

Table 3
Effect of foreign ions on the determination of 40 $\mu g\ l^{-1}$ of vanadium

| Foreign ion | Tolerance level ($\mu g\ l^{-1}$) |
|---|---|
| $NO_3^-$ | 30000 |
| Ca(II) | 28000 |
| $Cl^-$ | 27000 |
| Mg(II) | 9600 |
| $SO_4^{2-}$ | 8000 |
| $S_2O_3^{2-}$ | 5600 |
| $F^-$ | 3000 |
| EGTA [a] | 2500 |
| Ni(II) | 1600 |
| Mn(II) [b] | 940 |
| Mo(VI) [b] | 400 |
| Fe(II,III) [c] | 400 |
| Al(III) [c] | 380 |
| Zn(II) | 200 |
| $PO_4^{3-}$ | 200 |
| Co(II) | 150 |
| $SiO_3^{2-}$ | 150 |
| Pb(II) | 100 |
| U(VI) [c] | 80 |
| Cu(I,II) [d] | 60 |
| Be(II) [c] | 30 |

[a] 3,6-Dioxaoctane-1,8-diamine-$N,N,N',N'$-tetracetic acid.
[b] In a solution containing 2.5 ppm of EGTA.
[c] In a solution containing 3 ppm of $F^-$.
[d] In a solution containing 5 ppm of $S_2O_3^{2-}$.

Table 4
Quality parameters of the SPS and the gallic acid persulphate method [a]

| Parameter | SPS | Gallic acid |
|---|---|---|
| Linearity (%) | 98.2 | 96.8 |
| Analytical sensitivity ($\mu g\ l^{-1}$) | 0.5 | 0.9 |
| Detection limit ($\mu g\ l^{-1}$) | 1.1 | 2.0 |
| Quantification limit ($\mu g\ l^{-1}$) | 3.6 | 6.6 |
| RSD ($c$) (%) | 6.3 [b] | 9.2 [b] |
| | 2.9 [c] | 6.0 [c] |
| | 2.2 [d] | 3.8 [d] |
| | 1.8 [e] | 3.3 [e] |

[a] The statistical model proposed in ref. [19] was used.
[b,c,d,e] At vanadium concentrations of 5.0 $\mu g\ l^{-1}$, 10.0 $\mu g\ l^{-1}$, 15.0 $\mu g\ l^{-1}$ and 20.0 $\mu g\ l^{-1}$, respectively.

Table 5
Analytical applications in water samples

| Method | Sample Volume (ml) | Vanadium concentration ($\mu g\ l^{-1}$) Mean, $n = 3$ | Standard deviation |
|---|---|---|---|
| Gallic acid | 10.0 | 12.7 | 0.46 |
| SPS | 500.0 | 13.2 [a] (1.82) | 0.35 (1.67) |
| | 750.0 | 13.9 (2.92,s) | 0.56 (1.50) |

The experimental $t$ and $F$ values are given in parentheses; $t_{5,0.05} = 2.57$; $t_{4,0.05} = 2.78$; $F_{2,3,0.05} = 19.2$; $F_{2,2,0.05} = 19$; s, significant.
[a] $n = 4$.

Table 6
Analytical applications in petroleum samples

| Sample | Method | Vanadium concentration (mg per 100 g of sample) Mean, $n = 3$ | Standard deviation |
|---|---|---|---|
| Leona | ASTM | 10.49 | 0.08 |
| | SPS | 10.29 (2.56) | 0.02 (10.63) |
| Light Iran | ASTM | 2.75 | 0.08 |
| | SPS | 2.60 (2.42) | 0.07 (1.16) |
| Kirkuk | ASTM | 10.40 | 0.06 |
| | SPS | 10.75 (2.70) | 0.12 (3.56) |

The experimental $t$ and $F$ values are given in parentheses; $t_{4,0.05} = 2.78$; $F_{2,2,0.05} = 19$.

### 3.7. Analytical applications

The SPS methodology allows the creation of made-to-measure methods by selecting the sample volume. In this way it is possible to analyse different samples with great differences in vanadium concentration. Thus the SPS sample systems proposed have been applied to the determination of the vanadium content of natural water and crude petroleum samples.

*Determination, of vanadium in water samples*

The method was applied to the determination of vanadium in natural water samples by the standard additions method. The 1000 ml sample system was used. The constant error was corrected by using the Youden blank [20]. The results obtained by the proposed method were compared with those obtained by the gallic acid persulphate method. Table 5 summarizes the results. According to a $t$-test for the means and $F$-test for the standard deviations, the results show that there is only a significant difference between the mean derived from the SPS method (750 ml) and the mean from the gallic acid persulphate method, while the precision of both methods is the same.

*Determination of vanadium in crude petroleum samples*

The 250 ml sample system was used to analyse crude petroleum samples due to a larger concentration of vanadium in the samples. As a reference method, the ASTM method was used. The ASTM and the proposed method were applied to an aliquot of the solution obtained from three crude petroleum samples of difference composition and density, after the treatment previously described. The results are presented in Table 6. A statistical comparison by the $F$-test and the $t$-test showed no significant difference between the results of both methods. However, it is necessary to point out that due to the higher sensitivity of the SPS methods over the ASTM method (Table 2) it is possible to treat a smaller amount of the crude petroleum sample (between 1.5 and 3 g in our samples, depending on the vandium concentration) with a shorter duration of the analysis and equivalent precision and accuracy.

## Acknowledgement

This research was funded by the Dirección General de Investigación Científica y Técnica (DGICYT) del Ministerio de Educación y Ciencia (Spain) project No. PS88-0101).

## References

[1] M.J.C. Taylor and J.F. van Staden, Analyst, 119 (1994) 1263.
[2] E. Berman, Toxic Metals and their Analysis, Meyden & Son Ltd., London, 1980, Chapter 30 pp. 221–232.
[3] Métodos Normalizados para el Análisis de Aguas Potables y Residuales, American Public Health Association, American Water Works Association, Water Pollution Control Federation, Díaz de Santos, Madrid, 1992 Chapter 3, pp. 3.70–3.81.
[4] T.M. Florence and G.E. Batley, Crit. Rev. Anal. Chem., 9, (1980) 219.
[5] E. Nakayama, Y. Suzuki, K. Fujiwara and Y. Kitano, Anal. Sci., 5 (1989) 129.
[6] K. Heydorn, R. Zeisler and V.P. Guinn (Eds.), in Nuclear Analytical Methods in the Life Sciences Humana Press, Clifton, NJ, 1990, p. 541.
[7] K. Hirayama, S. Kageyama and N. Unohara, Analyst, 117 (1992) 13.
[8] S. Marczenko, Separations and Spectrophotometric Determination of Elements, Ellis Horwood, Chichester, 1986, Chapter 5, pp. 621–635.
[9] M. Jarosz and Z. Marczenko, Analyst, 109 (1984) 35.

[10] K. Kania and F. Buhl, Chem. Anal. (Warsaw), 35 (1990) 775.
[11] K. Yoshimura and H. Waki, Talanta, 32 (1985) 345.
[12] F. Capitán, L.F. Capitán-Vallvey, M.C. Valencia, J.M. Bosque-Sendra, F. Molina and I. de Orbe, Analusis, 19 (1991), 177.
[13] M.J. Fishman and M.V. Skougstad, Anal. Chem., 36 (1964) 1643.
[14] Q. Weiguo, Anal. Chem., 55 (1983) 2043.
[15] American Society for Testing and Materials, 1975 Books of ASTM Standards, Method D, Philadelphia, 1975, pp. 1548–1563.
[16] J.M. Bosque-Sendra, C. Mérida and L.F. Capitán-Vallvey, Analusis, 18 (1990) 531.
[17] IUPAC, Spectrochim. Acta, Part B, 33 (1978) 242.
[18] Analytical Methods Committee, Analyst, 112 (1987) 199.
[19] L. Cuadros Rodríguez, A.M. García Campaña, C. Jiménez Linares and M. Román Ceba, Anal. Lett., 26 (1993) 1243.
[20] M.J. Cardone, Anal. Chem., 58 (1986) 438.
[21] D. Wang, G. Xie, W. Zhang and Q. Pan, Huaxue Shiji, 7 (1985) 33.
[22] R. Lobisky and Z. Marczenko, Anal. Sci., 4 (1988) 629.

ELSEVIER

Talanta 42 (1995) 1533–1544

Talanta

# Determination of $^{34}S$:$^{32}S$ ratios by FTIR spectroscopy

Antonio F. Fuentes[1], Iain L. Marr *

*Chemistry Department, University of Aberdeen, Aberdeen, AB9 2UE, UK*

Received 22 December 1994; revised 24 March 1995; accepted 24 March 1995

**Abstract**

A new method for determining $^{34}S$:$^{32}S$ ratios using Fourier transform infrared spectroscopy has been developed. The four sulphur-containing gases SCO, $H_2S$, $SF_6$ and $SO_2$ are assessed as possible compounds for the spectroscopic measurements, from which, after a consideration of available lines showing a clear isotopic shift and also of possible synthetic routes to the gas starting from a range of natural sample types, $SO_2$ was selected for further development of the instrumental method for the isotopic ratio determination. Sulphur in the samples present as the element, as metal sulphides or as organosulphur compounds, is converted by heating with $V_2O_5$ into gaseous $SO_2$, and a part of the 518 $cm^{-1}$ band is recorded in the absorbance mode. The optimisation of instrumental parameters and of the chemical reaction conditions is described, and the results from the application of the method to the measurement of the level of enrichment of $^{34}S$ in a soil fungus are presented. The agreement between results at the natural abundances of 4.2% was better than 0.04% absolute for a sample size of 1.5 mg of sulphur.

## 1. Introduction

The determination of $^{34}S$:$^{32}S$ ratios, largely used in geochemical studies, has only recently become relevant in other fields such as soil–plant systems [1,2]. The element is an essential nutrient for plants; it is used in the synthesis of amino acids present in proteins and is needed in the synthesis of chlorophyll, even though it does not appear in the final molecule. Attention is now focusing on the availability of soil sulphur, making the use of stable isotopes the obvious choice for understanding chemical reactions and in tracing the path that sulphur follows in different living organisms.

The high natural abundance of the isotope of mass 34 (4.21% on average) should make it rather easy to quantify in a natural sample, but on the other hand it presents the problem that relatively large amounts of the isotope would have to be added (as a tracer) for experiments involving spiking. Isotopic ratio determinations are routinely made by mass spectrometry. Sulphur compounds present in nature must therefore normally be first transformed into suitable sulphides such as those of cadmium, lead or silver which in turn are burned in the inlet system of the mass spectrometer, yielding sulphur dioxide which is allowed to leak into the analyser.

Isotopic sulphur determinations by mass spectrometry do, however, present some difficulties derived from the "stickiness" of sulphur dioxide which makes it slow to leak into the inlet system as well as creating problematic memory effects, and also from the existence in nature of the various oxygen isotopes. The first factor has been found to be dependent on both the length of the inlet system and its temperature, and necessitates the use of correction factors which will be different for different systems [3]. The surface adsorption effects render difficult any comparison of results between laboratories while the existence in nature of

* Corresponding author.

[1] Present address: Facultad de Ciencias, U.A.N.L. Monterrey, Mexico.



*SSDI* 0039-9140(95)01609-0

different stable oxygen isotopes makes it necessary to carry out complex theoretical corrections on the experimental data, since both species used in these determinations, $SO^+$ and $SO_2^+$, involve atoms of oxygen. It is generally accepted that this problem can be overcome if the samples and standards are obtained in the same way and by using the same oxygen source.

Sulphur hexafluoride has also been proposed as a vehicle for sulphur isotopic determinations by mass spectrometry [4]. When using $SF_6$, it is not necessary to make any theoretical correction of the experimental data regarding the presence of different isotopes since fluorine has only one stable isotope, $^{19}F$. However, difficulties in the preparation of $SF_6$ have limited its use.

All these problems, and the success obtained in this Department in determining isotopic ratios for nitrogen [5] and for carbon [6] by FTIR spectroscopy of small molecules in the gas phase, led us to the idea of applying the same technique to sulphur isotopic ratio determinations. The initial problem lay in the choice of a suitable sulphur compound, and the second in optimising the experimental conditions for quantitative measurement.

Since the frequencies of both the vibrational and rotational modes of a molecule depend upon the masses of their constituent atoms, substitution of one isotope for another in a small molecule will produce an infrared spectrum different from that of the normal molecule. The isotopic shift in an infrared band will depend upon the extent to which the atoms exchanged participate in the specific vibration which produces the band, and in particular on the change in the moment of inertia due to the substitution. The magnitude of this change is given by the ratio between the reduced mass ($\mu$) of the normal species and that of the isotopically substituted species:

$$\frac{\nu_i}{\nu} = \sqrt{\frac{\mu}{\mu_i}} = \alpha < 1$$

Thus the heavier isotope will be associated with the lower vibrational frequency.

The aim of this work was to test the applicability of Fourier transform infrared spectrometry (FTIR) as an alternative to mass spectrometry for sulphur isotopic determinations: its characteristics of high resolution, and high spectrometric and photometric accuracy make FTIR a very powerful analytical tool. In addition, as has been shown for the analysis of the nitrogen and carbon isotopes [5,6], adequate resolution for these applications can sometimes be obtained with smaller bench-top instruments. This makes the proposed technique more widely applicable than if it were to demand the use of a high performance research instrument.

The ideal compound for such a determination would have to meet several criteria.

(i) It should be volatile at room temperature, since only in the gas phase is it possible to see the fine rotational structure, necessary if isotopic lines are to be measured.

(ii) It should contain only one atom of sulphur so as to avoid problems derived from the presence in the same molecule of different isotopes of sulphur at the same time.

(iii) The IR spectrum should exhibit at least one intense band which should not be too complicated if the isotopic shifts are to be identified, and which should be in an area of the spectrum free from overlap with bands of common atmospheric molecules such as water and carbon dioxide.

(iv) The isotopic shift in the band should be such that the fingerprint of the different isotopes can be easily identified.

(v) The selected compound should be easy to synthesise from a variety of different chemical forms of the element.

The compounds considered for investigation were carbonyl sulphide, SCO, hydrogen sulphide, $H_2S$, sulphur hexafluoride, $SF_6$, and sulphur dioxide, $SO_2$.

## 2. Experimental

### 2.1. Instrumentation

All the IR spectra were collected on a Nicolet model 7199 FTIR spectrometer, fitted with a liquid-nitrogen-cooled MCT detector. As it is a single-beam device, a background spectrum must be collected before, and preferably also after, each set of sample spectra. The spectra must be displayed in the absorbance mode.

### 2.2. Materials

Isotopes were purchased as elemental sulphur. Pure $^{32}S$ was obtained through Delta Isotopes from the Soviet–Great Britain Joint Venture "ISOFLEX" with a purity of 99.97%. The $^{34}S$ was purchased from MSD Isotopes and came with purity of 91.6 at.% $^{34}S$.

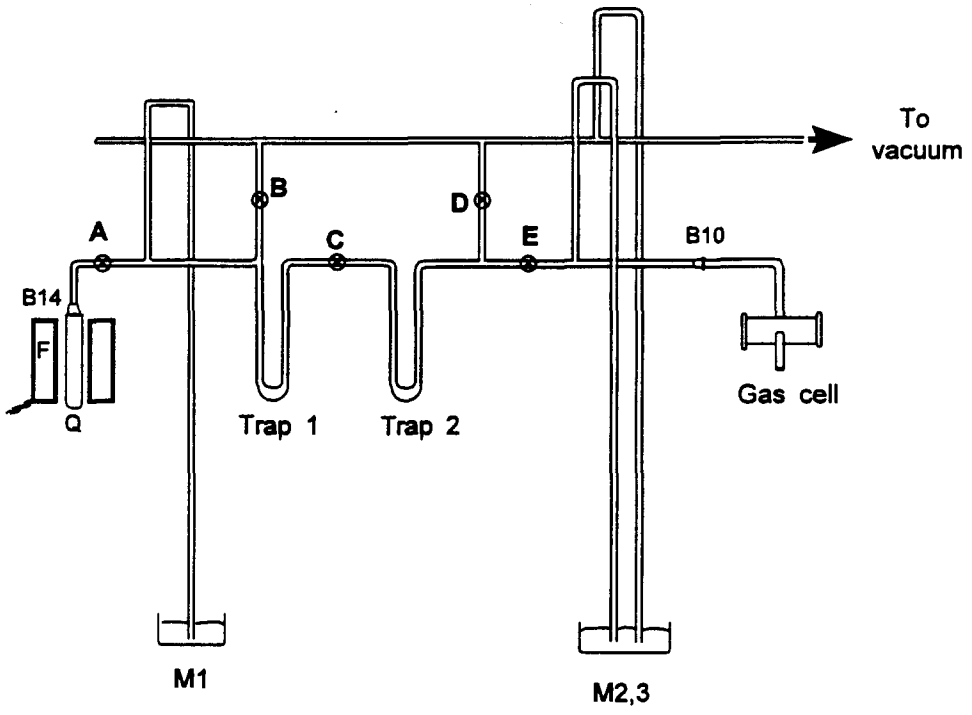


Fig. 1. Schematic diagram of the vacuum line: A, B, C. D and E are Teflon keyed vacuum stopcocks; M 1, M 2 and M 3 are mercury manometers; F is a small furnace, (750 W) surrounding the quartz reaction tube Q.

### 2.3. *Handling $SO_2$ on the vacuum line*

The synthesis was carried out on a vacuum line (shown diagramatically in Fig. 1) which was evacuated by a rotary pump down to 0.1 Torr. Trap 1 was cooled with a liquid nitrogen/carbon tetrachloride mush bath (−23 °C) to remove water, and trap 2 in liquid nitrogen (−196 °C), to collect the sulphur dioxide (m.p., −72.7 °C). Gaseous $SO_2$ could be transferred from the cold trap 2 to an evacuated gas cell for measurement of the spectrum, or to a 30 ml glass storage tube fitted with a Teflon keyed tap.

### 2.4. *Preparation of $SO_2$ from elemental sulphur or from cadmium sulphide*

Weigh out around 10 mg of elemental sulphur (or 30 mg of cadmium sulphide) of natural abundance, or consisting of two separately weighed portions of the isotopically pure $^{34}S$ and $^{32}S$ isotopes, and transfer the sample to a quartz reaction tube 10 mm in external diameter 100 mm long, and fitted with a B-14 cone by which it can be attached to the vacuum line. Add to this about 30 mg of oven-dried vanadium pentoxide and mix well by shaking. Push a wad of glass wool down the tube to a few centimetres above the reaction mixture (a part of the tube which will not reach the maximum temperature of the furnace) and cover the glass wool with a 5 mm layer consisting of pieces of partly oxidised copper wire (as used for the Dumas nitrogen determination). This is to reduce any $SO_3$ which might be formed.

Fit the reaction tube to the vacuum line and evacuate it. Raise the small tube furnace (closed at the lower end) to envelop the reaction tube, start heating, and continue pumping until the furnace temperature reaches 200 °C. At this point, close tap B, leaving the quartz reaction tube connected only to the traps, and place the mush baths in position. Increase the temperature further to 800 °C and collect the evolved $SO_2$ in trap 2 over a period of 20 min. Now close tap C to isolate the product, and remove the liquid nitrogen bath round trap 2. Transfer the gas to either a gas cell or a storage tube, as required, by evacuating the cell or the tube, cooling the cold finger of the gas cell, or the lower part of the storage tube in liquid nitrogen, and opening the connecting tap E. The reaction can be followed by noting the changing height of the mercury manometer M1. Likewise, the pressure in the cell can be measured, in mmHg (Torr), on manometer M2.

### 2.5. Synthesis of $SO_2$ from barium sulphate

Weigh out about 50 mg of barium sulphate, mix well with 300 mg of a 1:1 (m/m) mixture of vanadium pentoxide and ground silica, and take the furnace temperature up to 1000 °C. Follow the remainder of the procedure given above for starting with elemental sulphur.

### 2.6. Preparation of fungus samples for isotopic ratio measurements

Suspensions containing the fungus *Aspergillus flavus* were filtered using Whatman ashless filter paper number 42, and were washed using a solution with the same composition as that of the growing medium, then sucked free of solution. After freeze drying for 24 h, the samples were ground by shaking in a plastic container together with four steel balls. At this stage, they were ready for sulphur analysis.

### 2.7. Recommended FTIR parameters

Fill a Pyrex gas cell, 150 mm long, 15 mm in diameter and fitted with KBr windows (ground to a 1° wedge to avoid interference fringes), with $SO_2$ to a pressure of $30 \pm 3$ Torr. Record the IR spectrum at a resolution of 0.25 $cm^{-1}$ with 100 scans, from 600 to 400 $cm^{-1}$ using the Happ–Genzel apodisation function. Integrate the lines with baseline correction (see below) and calculate the area ratios of the line pairs 548 $cm^{-1}$ (line a) for $^{34}S$ and 588 $cm^{-1}$ (line 6) or 592 $cm^{-1}$ (line 7) for $^{32}S$. Compare the ratios with the two calibration lines to estimate the isotopic composition of the sample.

## 3. Results and discussion

### 3.1. Selection of a gas for the determination of sulphur stable isotope ratios

*Carbonyl sulphide, SCO*

Carbonyl sulphide is an asymmetric linear molecule with the atom of carbon in the centre, and therefore belongs to the symmetry group $C_{\infty v}$. It presents three fundamental vibrations of which, using the notation given by Herzberg [7], $\nu_3$ and $\nu_1$ are the two stretching modes of higher and lower frequency respectively and $\nu_2$ is the bending mode (see Table 1).

Callomon et al. [9] and Allen et al. [10] pointed out the difficulties in assigning the spectrum due to overlapping and coupling between bands. Interactions between pairs of bands are very strong, producing variations in the frequencies of the bands from those predicted theoretically. Additionally, the whole spectrum is complicated by the superposition of bands due to "hot" transitions upon the main absorption bands.

The isotopic analysis of the IR spectrum of carbonyl sulphide is further complicated by the fact that the number of possible combinations of different isotopes within the molecule is large. Oxygen has three stable isotopes, $^{16}O$ (99.76%), $^{17}O$ (0.04%) and $^{18}O$ (0.2%), and carbon another two, $^{12}C$ (98.89%) and $^{13}C$ (1.11%), which, added to the four isotopes of sulphur, $^{32}S$ (95.0%), $^{33}S$ (0.76%), $^{34}S$ (4.2%) and $^{36}S$ (0.014%), makes for 24 possible isotopic combinations. Overlap between the bands of $^{32}S^{12}C^{16}O$ and those of the isotopically substituted species, and the numerous "hot" bands is frequent, making necessary the use of very high resolution if a detailed study of the rotational structure is desired.

The lack of a suitable band in its IR spectrum on which to base our study, together with the difficulty in synthesising it from elemental sulphur, drove us to the conclusion that SCO was not a suitable compound for carrying out sulphur isotopic determinations.

*Hydrogen sulphide, $H_2S$*

The hydrogen sulphide molecule belongs to the symmetry group $C_{2v}$ and presents three fundamental vibrations. Table 2 shows the designation and position of the main bands.

Table 1
Bands seen in a low resolution IR spectrum of carbonyl sulphide, SCO [8]

| Band | Frequency ($cm^{-1}$) |
|---|---|
| $\nu_2$ | 520 |
| $\nu_1$ | 858 |
| $2\nu_2$ | 1047 |
| $2\nu_1$ | 1711 |
| $\nu_1 + 2\nu_2$ | 1892 |
| $\nu_3$ | 2062 |
| $4\nu_2$ | 2104 |
| $\nu_1 + \nu_3$ | 2918 |
| $2\nu_2 + \nu_3$ | 3095 |

Table 2
Bands seen in a low resolution IR spectrum of hydrogen sulphide, $H_2S$ [11,12]

| Band | Frequency ($cm^{-1}$) |
|---|---|
| $\nu_2$ | 1182 |
| $2\nu_2$ | 2353 |
| $\nu_1$ | 2614 |
| $\nu_3$ | 2628 |

This molecule presents a large absorption area between 2200 and 2800 $cm^{-1}$ which can be divided into three parts corresponding to strong, weak and medium absorptions, but any interpretation of this area is complicated by the strong interactions between the three bands. Another inconvenience is the existence in this area of the main absorption band of carbon dioxide which has its centre at 2396 $cm^{-1}$.

The other fundamental vibration $\nu_2$ has the centre of its band at 1182.7 $cm^{-1}$, in a part of the spectrum where water vapour absorbs. Gillis and Edwards [12], using a grating spectrometer with 0.05 $cm^{-1}$ resolution, made a detailed study of the $\nu_2$ band, and were able to assign some lines to the $^{33}S$ and $^{34}S$ isotopes, but the number of lines and quality of the spectrum did not allow them to carry out a complete isotopic analysis.

Though the gas can be prepared readily from metal sulphides, and they in turn can be prepared from elemental sulphur, the complexity of the spectrum, together with the extreme weakness of the absorption bands, forced us to the conclusion that this was not a suitable candidate for the isotopic analysis of sulphur either. However, as the synthesis is straightforward, it could serve as a useful intermediate for the extraction of sulphur from natural samples, before conversion to another, spectroscopically more suitable, compound.

*Sulphur hexafluoride, $SF_6$*

Sulphur hexafluoride has a highly symmetrical structure with the sulphur atom at the centre of a regular octahedron whose corners are occupied by the six fluorine atoms. Thus the molecule belongs to point group $O_h$ and shows six fundamental vibrations of which only two, $\nu_3$ at 947.98 $cm^{-1}$ and $\nu_4$ at 615.02 $cm^{-1}$, are IR active [13,14]. As fluorine is monoisotopic, this molecule does meet one of the important criteria for an FTIR determination of the sulphur isotopic ratio.

However, a large number of combination bands is present in its IR spectrum: 29 bands have been described by McDowell et al. [15], using an FTIR spectrometer at a resolution of 0.05 $cm^{-1}$. The $SF_6$ spectrum is further complicated by the fact that at room temperature, only some 34% of the molecules are present in the vibrational ground state [16], which results in a high probability (and hence intensity) of "hot" bands in the spectrum, and in a considerable susceptibility of the normal band intensities to changes in temperature.

The spectrum shows eight bands — two of them are the fundamental vibrations and the other six are combination bands. The designations of these combination bands as well as their positions in reciprocal centimeters are given in Table 3.

Four of the combination bands have their frequencies in the region 1900–1250 $cm^{-1}$ where the $\nu_2$ band of the water molecule lies. Therefore, in a high resolution spectrum, it is possible to see numerous water absorption lines superimposed on those of sulphur hexafluoride. The isotopic shifts for the combination bands $(\nu_1 + \nu_3)$ and $(\nu_1 + \nu_4)$ have been given by Klimov and Lobikov [17] as 16 $cm^{-1}$ and 2 $cm^{-1}$ respectively. The centre of the combination band $(\nu_2 + \nu_3)$ for the species $^{34}SF_6$ was given by the same authors as 1569 $cm^{-1}$, which gives an isotopic shift of approximately 17 $cm^{-1}$. However, these isotopic shifts are not useful for our purposes since no lines are observed as clean "fingerprints" of the different isotopes.

The other two combination bands, $(\nu_5 + \nu_6)$ and $(\nu_2 + \nu_6)$, do not exhibit any sulphur shifts since the sulphur atom is not involved in the fundamental vibrations which contribute to these combination bands.

The rotational structure of the strongest band in the spectrum, $\nu_3$, is not resolved even

Table 3
Combination bands seen in a low resolution IR spectrum of $SF_6$ [16]

| Band | Frequency ($cm^{-1}$) |
|---|---|
| $(\nu_5 + \nu_6)$ | 870 |
| $(\nu_2 + \nu_6)$ | 991 |
| $(\nu_2 + \nu_4)$ | 1257 |
| $(\nu_1 + \nu_4)$ | 1388 |
| $(\nu_2 + \nu_3)$ | 1587 |
| $(\nu_1 + \nu_3)$ | 1719 |

when using 0.25 $cm^{-1}$ resolution. A maximum spacing of 0.04 $cm^{-1}$ between two successive lines has been calculated by Brunet and Perez [18] — much smaller than the resolution of the spectrometer. The isotopic shift for the $\nu_3$ $^{34}SF_6$ band has been given as 17.4 $cm^{-1}$, based on the assumption that the small peak in the natural $SF_6$ spectrum at 930.50 $cm^{-1}$ is due to the $^{34}S$ isotope [18]. However, because quantitative work for our purposes would require integration of the whole of the $^{32}SF_6$ band at 948 $cm^{-1}$, which is broad and unresolved at 0.25 $cm^{-1}$ resolution, and very susceptible to changes in shape with change in pressure, this compound was ruled out. Synthesis in the laboratory, using elemental fluorine, is in any case difficult and unattractive for routine use.

*Sulphur dioxide, $SO_2$*

The molecule of sulphur dioxide, like that of hydrogen sulphide, belongs to the symmetry group $C_{2v}$ and therefore shows three fundamental vibrations. Two of them ($\nu_1$ and $\nu_2$) are B-type bands and the other one ($\nu_3$) is A-type. In A-type bands the oscillating dipole moment lies along the axis of the least moment of inertia and they are characterised by a strong central Q branch and J subbranches. The rotational structure in this group of bands presents strong irregularities and it is not possible to see individual lines without using a very high resolution.

In B-type bands the oscillating dipole moment lies along the axis of the intermediate moment of inertia and they are represented by Q branches, in this case spaced approximately 3.4 $cm^{-1}$ apart. While in A-type bands a considerable number of Q lines fall near the band centre, for B-type bands no Q line occurs near the centre but instead they overlap the P and R branches. Each Q branch has associated with it a P and an R branch giving rise to numerous weak lines which form the background absorption between Q branches.

The low-resolution IR spectrum of sulphur dioxide is shown in Fig. 2. It was collected using 1 $cm^{-1}$ resolution and 20 Torr of gas in a 10 $cm^{-1}$ gas cell. Along with the fundamental vibrations there is also a combination band ($\nu_1 + \nu_3$) at 2500 $cm^{-1}$ which is strong enough to be seen in a low pressure spectrum. The positions of these bands are listed in Table 4.

The IR spectrum of isotopically substituted sulphur dioxide has been studied by different workers [19–22]. A summary of their findings,

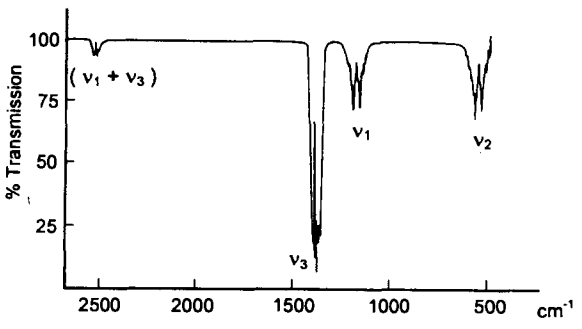


Fig. 2. Low-resolution infrared spectrum of sulphur dioxide, $SO_2$.

in the form of frequencies of the origins of the four main bands for the species $^{32}SO_2$ and $^{34}SO_2$, is shown in Table 4.

Values in Table 4 show a significant isotopic shift for each band ranging from approximately 7 $cm^{-1}$ for $\nu_1$ to 22 $cm^{-1}$ for ($\nu_1 + \nu_3$), which is the largest shift presented by any of the sulphur compounds assessed. However, it is not possible to identify individual peaks corresponding to different isotopes in the A-type bands, ($\nu_1$ and $\nu_2$) which makes than unattractive for isotopic analysis.

It follows then, that only the $\nu_1$ and $\nu_2$ bands can be used if individual lines are going to be integrated. A closer look at $\nu_1$ (Fig. 3) reveals a very complex band without well-defined rotational lines. It was decided not to use this band since a changeable shape was going to make for poor integration reproducibility. Besides, it was not possible to identify any single line in this band as a fingerprint of the $^{34}S$ isotope in sulphur of natural abundance.

The only band left was $\nu_2$ at 512 $cm^{-1}$, which is not exempt from problems either. The fact that it lies close to the end of the working range of both the Hg–Cd–Te detector and the KBr windows (400 $cm^{-1}$) makes its baseline noisier than it should be. It is also affected by the presence in this area of a "hot" band

Table 4
Bands seen in a low resolution IR spectrum of $SO_2$ [20,22,23]

| Band | Frequency ($cm^{-1}$) | |
|---|---|---|
| | $^{32}SO_2$ | $^{34}SO_2$ |
| $\nu_2$ | 517.87 | 512.30 |
| $\nu_1$ | 1155.71 | 1144.48 |
| $\nu_3$ | 1362.06 | 1345.09 |
| ($\nu_1 + \nu_3$) | 2499.87 | 2475.83 |

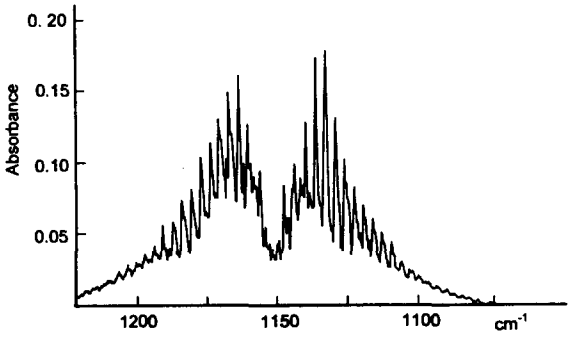


Fig. 3. Fundamental vibration band, $\nu_1$ for $SO_2$ at 1156 $cm^{-1}$.

$(2\nu_2 - \nu_2)$ centred at 517.25 $cm^{-1}$ which gives rise to additional peaks complicating the background absorption [23].

Nevertheless, the high frequency part of the band, around 550–600 $cm^{-1}$, is relatively well defined, and it was decided to investigate this further. Fig. 4 shows the relevant section of the spectra of the natural abundance $SO_2$ and of the isotopically substituted molecules $^{34}SO_2$, from which it can be seen that the isotopic shift is significant, and that there are three lines in the natural abundance spectrum, at 560.39, 552.27 and 548.29 $cm^{-1}$, which are clearly due to the $^{34}S$ isotopically substituted molecule. The final choice for the determination of sulphur isotopic ratios was therefore $SO_2$ as the gas, and the high frequency end of its $\nu_2$ band around 550 $cm^{-1}$ as the region of the spectrum.

### 3.2. Optimisation of experimental parameters

*Synthesis of $SO_2$*

The synthesis of $SO_2$ from elemental sulphur by combustion in oxygen is apparently the simplest route. However, this was tried and discarded since most of the sulphur taken crept up the walls of the silica tube where the reaction was taking place and condensed as a liquid in those parts of the tube close to the upper end of the electric furnace, remaining unavailable for chemical conversion.

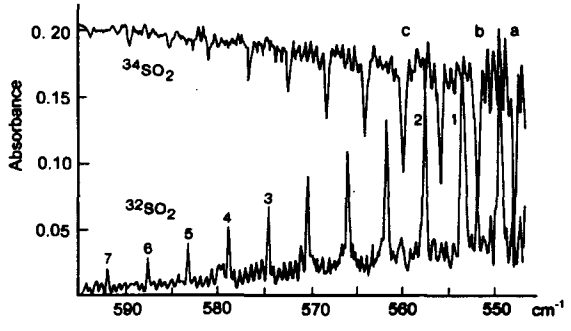


Fig. 4. A section of the 518 $cm^{-1}$ fundamental vibration band $\nu_2$ of $SO_2$ with the natural abundance spectrum recorded in the absorbance mode (bottom) and the $^{34}SO_2$ spectrum in the transmission mode (top).

Solid oxygen donors offer an alternative route to the synthesis. Copper (I) oxide has been suggested as a solid oxygen donor for sulphides [24] but it needs to be prepared shortly before use, to prevent oxidation to the copper (II) oxide and the absorption of other gases. Vanadium pentoxide, which is commercially available and which can be used without needing major purification, has been proposed by Gavelin for producing $SO_2$ from precipitated cadmium sulphide [25]. Yanagisawa and Saka [26] published a variation of this procedure using barium sulphate as the source of the sulphur, in which ground silica was added to the reaction mixtures to moderate the evolution of $SO_2$. It also increased the viscosity of the reaction mixture so that it did not creep up the wall of the reaction tube. Vanadium pentoxide serves in this case as both an acid flux and an oxygen buffer, rather than just as an oxygen donor, and lowers the decomposition temperature of the sulphate to roughtly 1000 °C, which is the reaction temperature employed in the proposed procedure. Ueda and Krouse applied this modified approach to transform sulphide and sulphate minerals into gaseous $SO_2$ for isotopic analysis by mass spectrometry [27]. This approach has been adopted in the present investigation, and has been shown to work well also with elemental sulphur.

*FTIR parameters*

Isotopic analysis by FTIR is affected by the choice of instrumental parameters such as resolution, number of scans, apodisation function and choice of spectral lines, as well as by variables such as the size of the sample (working pressure), the method of peak measurement (area or height) and the reference background. All these variables need to be optimised.

*Choice of spectral lines*

There are three lines in the $\nu_2$ region of the spectrum from natural abundance sulphur dioxide which are due mainly to the $^{34}S$ isotope: these situated at 548.29 $cm^{-1}$, 552.27 $cm^{-1}$ and 560.39 $cm^{-1}$, labelled a, b,

and c respectively in Fig. 4. The band shows an irregular baseline which could not be improved by collecting the spectrum with a higher number of scans, indicating that there is an important contribution from the presence of numerous P and R branches in between the Q branches, and of a "hot" band centred at 517.25 $cm^{-1}$ as suggested by Coudert et al. [23]. It was even possible to see these lines in the spectrum of pure $^{32}SO_2$, proving that they are not entirely due to the presence of $^{34}S$ in the molecule. However, the lack of any other peaks which could be used made these lines the only possible choice. For $^{32}SO_2$, those lines with the best baseline were chosen (line 6 or 7 in Fig. 3) even though they were not the most intense of the band. These circumstances make for a noisier background absorption which is due not to instrumental noise but to the molecular structure itself. In general, lines selected for the $^{34}S$ isotope, which is present at lower concentrations, are more affected than those chosen as "fingerprints" of the major isotope, $^{32}S$.

The intention was to construct a calibration graph for the isotopic composition by plotting the ratio of a pair of lines (one line for each isotope) versus concentration of $^{34}S$. The first point to consider was the choice of spectral resolution.

*Resolution*

In FTIR spectroscopy, resolution is determined by the distance traversed by the moving mirror in the interferometer. The optimum instrumental resolution is that which is equivalent to the natural resolution of the sample spectrum itself. If too low a resolution is used, separated bands will not be resolved and information will be lost, while if the resolution is too high, the spectrum will be noisier and no additional information will be obtained. Additionally, collecting a spectrum at higher resolution is more time consuming. To collect and transform 100 scans at 1 $cm^{-1}$ will take about 4 min, while at 0.25 $cm^{-1}$ it will require over 12 min. It is important to find a compromise between the volume of information required and the time needed for the analysis.

Three resolutions, 0.25, 0.5 and 1 $cm^{-1}$, were investigated. With 1 $cm^{-1}$ resolution it was not possible to pick up any $^{34}S$ isotope line. A resolution of 0.5 $cm^{-1}$ partially resolved the $^{34}S$ lines, but with 0.25 $cm^{-1}$ resolution the lines were well resolved although the baseline became noisier with a large number of extra lines appearing (see Fig. 5). Nevertheless, this was the resolution chosen since it gave the best peak profiles.

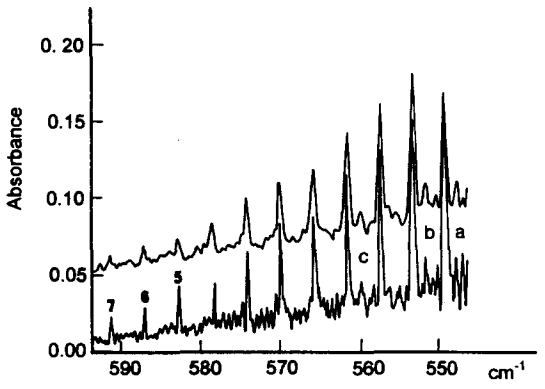


Fig. 5. A section of the $\nu_2$ band of natural abundance $SO_2$ showing the lines selected for measurement of the isotopic ratio, recorded at 0.25 $cm^{-1}$ (lower) and 0.5 $cm^{-1}$ (upper) resolution.

*Peak measurement*

Individual lines can be measured in terms of peak absorbance or integrated area. Both possibilities have been investigated.

*Peak area (A)*

The NICOLET has a routine which allows one to integrate a band/peak between two given limits, with or without baseline correction (Fig. 6). If baseline correction is chosen (AwBLC) the computer draws an imaginary line between the two limits specified by the operator and integrates the area of the peak

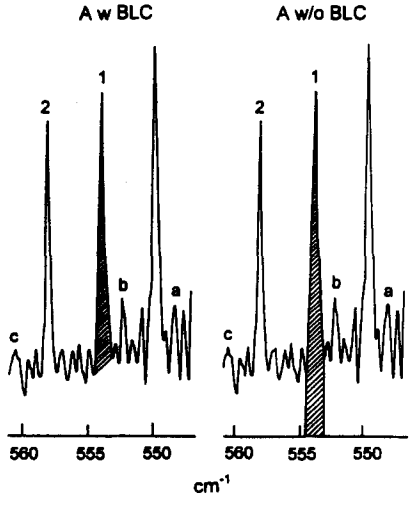


Fig. 6. Measurement of peak areas by integration: (a) AwBLC; (b) Aw/oBLC.

Table 5
Precision of line ratio measurements for selected line pairs

| Line pair | Relative standard deviation of ratio (%) | | |
|---|---|---|---|
| | AwBLC | Aw/oBLC | ABS |
| b/1 | 1.35 | 0.78 | 1.14 |
| b/2 | 1.13 | 0.75 | 0.75 |
| a/1 | 1.65 | 0.51 | 1.13 |
| a/2 | 1.57 | 0.58 | 0.75 |
| c/2 | 1.53 | 0.95 | 1.24 |
| c/3 | 1.62 | 0.45 | 1.04 |

enclosed between this line and the peak contour. This possibility is preferred since it is free from the influence of possible instrumental drift. Integration without baseline correction (Aw/oBLC) measures the area under the peak, but above the line $A = 0$, and may include a large background component.

*Peak absorbance*

The true absorbance of a peak (ABS) can be measured if the spectrum is first drawn using the $X-Y$ plotter, but this is rather time-consuming. Alternatively, it is possible to work directly on-screen using the cursor. The "baseline" absorbance was read at two points, in the valleys on either side of the peak, averaged and the mean subtracted from that at the peak maximum. Such results (*ABS*) were considered to be the "real" absorbances of the lines and were also used for calculating the ratios.

A comparison of these three possible methods of quantitation, given as the precision of five measurements, is shown in Table 5. The resolution used was 0.25 $cm^{-1}$, the number of scans was 100 and the working pressure was 30 Torr in a 15 cm long gas cell.

Table 5 shows that the best precision was obtained when working with areas without baseline correction but this apparently better performance is probably attributable to the rather large, but very constant, area below the base of the peak and above the line of zero absorbance. The precision referred to the area of the peak itself, without the large instrumental artefact, which is here called area with baseline correction (AwBLC), is poorer, but more realistic. Moreover, for the same reason, AwBLC is more sensitive to change in the isotopic ratio so it is more appropriate for this determination.

*Choice of spectral lines*

Several line combinations (e.g. a for $^{34}SO_2$ and 3 for $^{32}SO_2$) were measured and the area ratios were compared. The sensitivity would be poorer if there were a significant peak in the $^{32}SO_2$ spectrum, arising, for example, from a hot band or an overtone, coinciding with the selected line in the $^{34}SO_2$ spectrum. However, as the line pair ratios change by much the same for all combinations (see Table 6), there is no one line which seems to suffer significantly more or less than the others from this problem. The results are summarised in Table 6.

*Running the background*

A background spectrum was run at the beginning of the session and then again immediately after four replications for the sample. This method gave good precision and is also time-saving since the gas cell is filled only once with each sample. Additionally, possible errors derived from adjusting the position of the gas cell in the cell holder or from reading the pressure when filling the cell a few times are avoided. Instrumental drift is also minimised since all the operations are carried out in the smallest interval of time possible.

*Number of scans*

The signal-to-noise ratio depends on the square root of the number of scans. The relative standard deviations of the line ratios were compared for 50, 100 and 200 scans with 30 Torr of $SO_2$. This comparison showed, as predicted, that the performance was best for the highest number of scans, with RSD of 1.25%, 1.03% and 0.63% respectively for the a/3 line-pair combination.

However, it was decided to use only 100 scans as a good compromise between precision and time needed for the analysis. The working

Table 6
Area ratios (AwBLC) for natural abundance $SO_2$ and $^{32}SO_2$

| Ratio | $SO_2$, nat [a] | $^{32}SO_2$ [a] | Difference relative (%) |
|---|---|---|---|
| a/3 | 1.214 (0.70%) | 1.065 (1.03%) | 14 |
| a/5 | 2.003 (1.49%) | 1.734 (0.92%) | 15.5 |
| c/5 | 1.140 (1.12%) | 0.985 (1.31%) | 15.8 |
| b/3 | 0.777 (1.66%) | 0.680 (1.51%) | 14.3 |

The resolution was 0.25 $cm^{-1}$ for a sample pressure of 30 Torr in a 15 cm cell. The number of scans was set at 100.
[a] The RSD is given in parentheses.

Table 7
Effect of sample size on the precision of the line area ratio

| Line pair | Precision RSD (%) [a] | | |
|---|---|---|---|
| | 20 Torr | 30 Torr | 50 Torr |
| a/2 | 1.61 | 1.50 | 1.00 |
| b/1 | 2.51 | 1.35 | 1.29 |
| b/2 | 2.05 | 1.13 | 1.04 |

[a] $n = 5$.

time would be approximately doubled if 200 scans were collected, which means, for five replications plus two background scans, nearly 1 h longer for only a small improvement in the precision of the measurement.

*Sample size*

Increasing the pressure of a gas sample may result in band broadening, which could affect the measured line absorbance ratios. Data obtained for one sample run at 20, 30 and 50 Torr working with AwBLC are shown in Table 7. The improvement in precision on going to 50 Torr was significant but not large, and in the interest of minimising sample size it was decided to use 30 Torr as working pressure (which means about 1.5 mg of $SO_2$ in the cell, and about double this to allow for filling the manometer on the line).

The effect of sample pressure on the ratio itself was then investigated, covering a smaller working range, from 25 to 37.5 Torr. ANOVA showed that the variance of the line ratios between sample pressure was not significantly different from the variance at any one pressure, form which one may conclude that changes in pressure within this range do not have a noticeable influence on the ratios within reasonable margins.

### 3.3. Calibration graphs

Sulphur isotopic standards were prepared form elemental sulphur (using 99.9% $^{32}S$ and 92% $^{34}S$) by combustion on a vacuum line with vanadium pentoxide as solid oxygen donor. These standards covered the range form 3.5 to 10 at.% $^{34}S$. All the spectra were collected on the same day and in the shortest possible interval of time. Lines were integrated between the limits chosen previously (valleys on either side of the line), ratios calculated and the regression lines of the calibrations plotted.

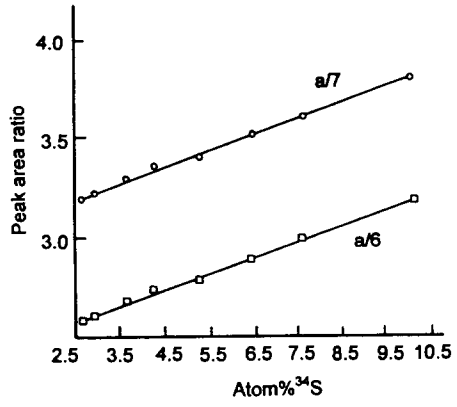


Fig. 7. Calibrations for sulphur isotopic ratio determinations using line pairs a/6 and a/7.

Several possible linear calibrations were obtained using AwBLC. The $^{34}S_2$ line at 560 $cm^{-1}$ (designated as c in Fig. 4) did not give good results in most cases, possibly due to the fact that it is strongly affected by the background absorption of the band. The line designated as b (552 $cm^{-1}$) gave good results in a number of cases, while it was with the one designated as a, located at 548 $cm^{-1}$, that the best calibration lines were obtained. This is the most intense of those $^{34}S_2$ lines which appear reasonably free from intererence, and it is also the most sensitive to changes in the isotopic composition as can be seen from the fact that it gives, in general, the graphs with the largest slopes. Two such calibration lines are shown in Fig. 7.

Parameters of some calibration lines are shown in Table 8. The slopes are small but sufficient for the quantification of modest enrichments of $^{34}S$. Relative standard deviations for the points which make up the calibration graphs were in most cases between 1% and 2%. Taken over the natural abundance of the $^{34}S$ isotope, this precision implies an uncertainty of 0.16% (absolute) when determining isotopic ratios by this method.

The intercepts of these calibration graphs were found to vary with time. Although slopes

Table 8
Parameters of calibrations for sulphur isotopic abundance measurements

| Line pair | Correlation coefficient | Intercept | Slope $(\%\ ^{34}S)^{-1}$ |
|---|---|---|---|
| a/6 | 0.996 | 2.261 | 0.0906 |
| a/7 | $0.997_5$ | 2.874 | 0.0909 |
| a/5 | 0.997 | 1.718 | 0.0719 |

Table 9
Results for the analysis of labelled *Aspergillus flavus*

| Sample | $^{34}S$ in samples (% (m/m)) | | |
|---|---|---|---|
| | Mass spectrometry | FTIR | Difference (% absolute) |
| Natural abundance | 4.224 | 4.190 | 0.034 |
| Enriched in $^{34}S$ | 4.468 | 4.429 | 0.039 |

were constant, the lines moved up and down with respect to each other. A similar situation was noticed by other workers when performing quantitative determinations by FTIR [5,28]. A possible explanation for this change is to be found in the long-term instabilities of the interferometer. This phenomenon was studied by Van Karsten [29] and was thought to be due to slow thermal or material elasticity of the interferometer or non-uniformity in temperature or composition of the purge gas.

### 3.4. Sulphur isotope ratio measurements on a $^{34}S$-labelled soil fungus

To evaluate the proposed method on some real samples, a sulphur isotopic analysis of a labelled fungus was carried out. The species chosen for this project was *Aspergillus flavus* which has a large sulphur requirement. It was provided by Prof. K. Kilham from the Plant and Soil Science Department, University of Aberdeen (UK). Two sets of samples were grown: one in a Czapek–Dox nutrient medium containing natural abundances of each sulphur isotope and the other one in a medium enriched in $^{34}S$. The latter was prepared by combusting some pure $^{34}S$ and absorbing the $SO_2$ in aqueous potassium hydroxide.

Portions of this (neutralised) solution were then used in the preparation of the nutrient medium. Fungal spores were incubated in the nutrient medium for 1 week, on an orbital shaker, then the suspensions were analysed using the procedure given under Section 2. Samples were also analysed by isotopic ratio mass spectrometry with the aim of comparing the results given by both techniques. These results can be seen in Table 9.

It should be pointed out that the results given in Table 9 were obtained using a compromise set of conditions, and that by accumulating 200 scans instead of 100, and by filling the cell to 50 Torr instead of 30, a modest improvement in precision could be attained. This would reduce the estimated uncertainty of 0.16% (absolute) to around 0.1% (absolute) in the measurement of 4% (absolute) $^{34}S$. In the light of these estimates, the agreement between the FTIR values and the IR–MS ratios seen from Table 9 — differences of 0.03–0.04% absolute — is very satisfactory. However, the RSD (%) obtained by the FTIR method is larger than that obtained by mass spectrometry. This fact does confirm that although FTIR cannot compete with IR–MS when determining sulphur isotopic ratios at natural levels, it could be used with a degree of confidence to carry out this kind of analysis when working with isotopically enriched samples.

## Acknowledgements

The authors would like to express their gratitude to the Spanish Ministry of Education and Science for the grant given to Dr. Fuentes which made possible this project. Thanks are also due to the UK SERC for funding for the Nicolet spectrometer. And finally, the authors wish to express their gratitude to Professor D.C. McKean for his continued interest in their work on isotope ratio measurements, and to Prof. Ken Kilham for his assistance with growing the soil fungi.

## References

[1] J.J. Schoenau and J.R. Bettany, Soil Sci. Soc. Am. J., 52 (1988) 297.
[2] J.J. Schoenau and J.R. Bettany, J. Soil Sci., 40 (1989) 397.
[3] C.E. Rees, Geochem. Cosmochim. Acta, 42 (1978) 383.
[4] H. Leskovsek, J. Marsel and J. Slivnik, Isotopenpraxis, 5 (1969) 72.
[5] A. Kindness, I.L. Marr, M.S. Cresser, Analyst, 112 (1987) 1491.
[6] A. Kindness, Ph.D. Thesis, Aberdeen University, 1989.
[7] G. Herzberg, Infrared and Raman Spectra of Polyatomic Molecules, Van Nostrand, New York, 1945.
[8] A.G. Maki, E.K. Plyler, and E.D. Tudwell, J. Res. Natl. Bur. Stand., A66 (1962) 163.
[9] H.J. Callomon, D.C. McKean, and H.W. Thompson, Proc. R. Soc. London, Sec. A, 208 (1951) 341.
[10] H.C. Allen, E.K. Plyler and L.R. Blaine, J. Chem. Phys., 26 (1957) 400.
[11] W.C. Lane, T.H. Edwards, J.R. Gillis, F.S. Bonomo and F.J. Murcray, J. Mol. Spectrosc., 95 (1982) 365.
[12] J.R. Gillis, T.H. Edwards, J. Mol. Spectrosc., 85 (1981) 55.

[13] B. Bobin, C.J. Bordé, J. Bordé and C. Bréant, J. Mol. Spectrosc., 121 (1987) 91.
[14] R.S. McDowell and B.J. Krohn, Spectrochim. Acta, Part A, 42 (1986) 371.
[15] R.S. McDowell, B.J. Krohn, H. Flicker and M.C. Vasquez, Spectrochim. Acta, Part A, 42 (1986) 351.
[16] A. Aboumajd, H. Berger and R. Saint-Loup, J. Mol. spectrosc., 78 (1979) 486.
[17] V.D. Klimov and E.A. Lobikov, Opt. Spectrosc., 30 (1971) 25.
[18] H. Brunet and M. Perez, J. Mol. Spectrosc., 29 (1969) 472.
[19] R.D. Shelton, A.H. Nielsen and W.H. Fletcher, J. Chem. Phys., 21 (1953) 2178.
[20] E.C.M. Grigg and G.R. Johnston, Aust. J. Chem., 19 (1966) 1147.
[21] A. Barbe, C. Secroun, P. Jouve, B. Duterage, N. Monnanteuil and J. Bellet, Mol. Phys., 34 (1977) 127.
[22] G. Guelachvili, O.V. Naumenko and O.N. Ulenikov, J. Mol. Spectrosc., 125 (1987) 128.
[23] L. Coudert, A.G. Maki and W.B. Olson, J. Mol. Spectrosc., 124 (1987) 437.
[24] W. Robinson and M. Kusakabe, Anal. Chem., 47 (1975) 1179.
[25] S. Gavelin, A. Parwell and R. Ryhage, Econ. Geol., 55 (1960) 510.
[26] F. Yanagisawa and H. Sakai, Anal. Chem., 55 (1983) 985.
[27] A. Ueda and H.R. Krouse, Geochem. J., 20 (1986) 209.
[28] J.A. De Haseth, Appl. Spectrosc., 36 (1982) 544.
[29] P.H.G. Van Karsten, in J.R. Durig (ed.), Quantitative Aspects of FTIR in Industrial Applications, Reidel, Dordrecht, 1980.

ELSEVIER

Talanta 42 (1995) 1545–1551

Talanta

# Flow/sequential injection determination of gaseous ammonia with a glass diffusion denuder

Yongyi Luo, Rashed Al-Othman, Gary D. Christian *, Jaromir Ruzicka

*Center for Process Analytical Chemistry, Department of Chemistry, BG-10, University of Washington, Seattle, WA 98195, USA*

Received 17 January 1995; revised 28 March 1995; accepted 28 March 1995

**Abstract**

A new combination of a flow/sequential injection method for the analysis of ammonia has been developed. Gaseous ammonia is selectively absorbed in a phosphoric acid coated glass tube and determined with Berthelot reagents by flow injection. The combination of the gas diffusion denuder sampler with flow injection makes this method very sensitive and selective. The limit of detection of 0.15 μg $NH_3$.

## 1. Introduction

Ambient air continuously receives ammonia through the decomposition of organic material, and human activity. Because ammonia is an important indicator of environmental pollution and a predominant gas-phase atmospheric base, it plays a paramount role in atmospheric chemistry [1]. Traditional colorimetric methods [2], as well as ion-selective electrode [1,3], photothermal beam deflection [4] and fluorometric methods [5] have been used for the determination of ammonia in aqueous solution.

To determine ammonia in air with the methods described above, gaseous ammonia must first be collected by a suitable solid or liquid phase. Among all the sampling methods, the diffusion-based samplers, such as the diffusion denuder tube, have the following advantages: low back pressure, high collection efficiency and enrichment factor, and no interference of particle-borne ammonium [6].

A diffusion denuder is a glass tube whose inner wall has been coated with a suitable sorbent for gaseous analytes. Stevens et al. [7] were the first to describe the use of a phosphorous acid coated tube for the collection of atmospheric ammonia. Oxalic acid [1] and citric acid [8] coated tubes were used for the same purpose. Glass tubes coated with different chemicals have been used to collect other gases, e.g. $HNO_2$ [9], $HNO_3$ [9–12], HCl [13], $SO_2$ [13], and the simultaneous collection of several gases [9,12,13]. Although the diffusion denuders have the above mentioned characteristics, the coating, drying and washing are laborious procedures. Automating this technique will also improve the precision and reduce the risk of contamination. Bos [8] reported an automatic system in which three pumps were used and the washing solution was delivered to the measuring cuvette by gravity.

More recently, much research has been devoted to the theoretical [14] and practical [15] aspects of membrane-based gas diffusion in flow injection analysis (FIA). The theory is based on two flowing streams (donor and acceptor) which are physically separated by a hydrophobic membrane that allows only gases to cross. Thus, reactive gases can be determined by monitoring the gas that crosses the membrane and accumulates on the acceptor side via reaction with the acceptor reagent. A gas-permeable membrane in combination with

* Corresponding author.


*SSDI* 0039-9140(95)01610-4

a pH indicator has been used for determination of ammonia in air [16], water [17,18] and fermentation medium [19]. The actual limit of detection for gaseous ammonia is 200 ppb [16], but acidic gases in sample air, such as $CO_2$, $NO_2$ and $SO_2$, interfere with the determination of low ammonia concentrations. A more complex membrane-based diffusion denuder, called a diffusion scrubber or permeation denuder [20], was introduced by Dasgupta [21] for the continuous collection and analysis of water-soluble gases, such as $NH_3$, $SO_2$, $H_2O_2$ and HCHO. With a fluorescence detection system, the detection limit for gaseous ammonia is estimated to be 0.01 ppbv [22]. Unfortunately, the collection of gases in a diffusion scrubber is not 100% effective, and usually in the range 5–30% [20]. The collection efficiency (fluorescence response) depends on the length of the membrane, atmospheric pressure, temperature and relative humidity [22].

Our research has been focused on the development of a simple injection system which is capable of measuring gases at low concentrations (ppbv) without the influences of varying enviromental parameters and interferences from other gases. Ammonia is taken as a model for its important role in the atmosphere as mentioned above. The present paper is studying the feasibility of coupling a gas diffusion denuder with a flow/sequential injection system for the measurement of ammonia.

## 2. Experimental

### 2.1. Apparatus

Fig. 1 provides a schematic diagram of the injection system used in this study. The flows were driven by an Alitea XV peristalic pump (Alitea USA, Medina, WA) with Masterflex # 13 pump tube (Cole-Parmer Instrument Company, Chicago, IL) and solutions were selected by an eight-port rotary selection valve $V_1$ (Valco Instruments Co. Inc., Houston, TX). Unused ports were plugged with Upchurch fittings (Upchurch, Oak Harbor, WA). Valves $V_2$ and $V_3$ were three-port glass valves with inner diameter (i.d.) of 1.0 mm (Machine Shop of the Chemistry Department, University of Washington), both of which were switched manually. The diffusion denuder sampling tube (ST) was a 20 cm long Pyrex glass tube of 1.0 mm i.d. The holding coil (HC) was 300 cm

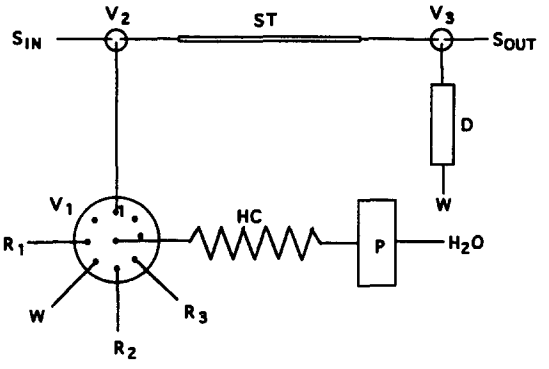


Fig. 1. Schematic diagram of the injection manifold: P, pump; HC, holding coil; $V_1$, $V_2$, $V_3$, valve; $R_1$, coating solution; $R_2$, hypochlorite solution; $R_3$, phenate solution; ST, sampling tube; $S_{IN}$ and $S_{OUT}$, inlet and outlet of gas sample; D, flow through detector; W, waste.

of 0.8 mm i.d. Teflon tubing (Upchurch, Oak Harbor, WA) and was connected to the common port of the selection valve. Teflon tubing (0.8 mm i.d.) and Teflon nuts and ferrules (Upchurch, Oak Harbor, WA) connected valves and the detection cell. The connections of the glass tube and valves were made with Masterflex # 13 pump tube (Cole-Parmer Instrument Company, Chicago, Il) and the section was made as short as possible to reduce the contact of flows with the pump tubing. The detection cell was a sandwich cell made of two pieces of rigid PVC (30 mm × 30 mm × 12 mm) with a 1.0 mm Teflon spacer [23]. A Brinkmann colorimeter (PC-701, Brinkmann Analytical, Wesburg, NY) served as both the light source and the detector. The reflected light was passed through a 610 nm filter and was measured as the absorbance. The pump and valve $V_1$ and the data collection were controlled with Atlantis (Lakeshore Technologies Inc, Chicago, IL) and subsequent data processing was performed with Matlab (The Math Works Inc. Natick, MA).

### 2.2. Chemicals

All chemicals (except household bleach solution) were reagent grade. All solutions were prepared in purified water (NANOpure II, Syborn Barnstead, Dubuque, IA). Calibrated gaseous ammonia standards were obtained from gas permeation tubes, part numbers 111-200-0140 (5730 ng $min^{-1}$ at 30 °C) and 112-010-0140 (288 ng $min^{-1}$ at 30 °C) from VICI Metronics, Inc., Santa Clara, WA.

The coating solution was made by diluting 5.0 ml of phosphoric acid and 5 ml of glycerol with water to 100 ml. An alkaline phenate solu-

tion was made by dissolving 5.0 g of phenol, 12.0 g of sodium hydroxide and 33 ml of ethanol in water and diluting to 100 ml. Alkaline hypochlorite solution was prepared by dissolving 2 g of sodium hydroxide and 2 g of sodium tetraborate decahydrate in 61 ml of household bleach solution (containing 5.25% active chlorine) and diluting to 100 ml.

### 2.3. Procedure

The standard gaseous ammonia used was from a calibrated gas permeation tube. The permeation tube bleeds a certain amount of ammonia per unit time at a specified temperature, given by the calibration equation provided by the manufacturer. Ammonia from a permeation tube was diluted with zero air (house air purified with phosphoric acid impregnated silica gel) in the permeation tube holder (VICI Metronics Inc. Santa Clara, CA) using a gas calibrator (GC Industries, Chatsworth, CA) at a flow rate of 300 ml $min^{-1}$ (unless otherwise specified). Since the amount of ammonia in the gaseous flow is time dependent, accurate amounts of ammonia are acquired by exact timing.

The flow cycle typically followed the following scheme. With valves $V_1$, $V_2$ and $V_3$ open from the pump/holding coil to the detector (position 1), water was driven through valves $V_1$ and $V_2$, the sampling tube, valve $V_3$ and the detection cell to wash all the system for 15 s at a flow rate of 0.6 ml $min^{-1}$. Valve $V_3$ was then changed to position 2, and the pump was reversed to remove water from the sampling tube while leaving water in the detector. When all the wash water was back to the holding coil, valve $V_1$ was switched to port $R_1$, and the coating solution was aspirated into the holding coil for 20 s. Next, the pump was changed back to forward and at the same time valve $V_1$ was switched back to position 1. The coating solution was driven through valves $V_1$ and $V_2$ to the sampling tube, and when the coating solution arrived at valve $V_3$, the pump was reversed to drive the coating solution back to the holding coil. Following that, valve $V_2$ was changed to the sampling position ($S_{in}$) to start the sampling, and the gas sample flowed through the sampling tube and exited at $V_3$ (a real sample can be aspirated through the sampling tube by the connection of an air pump at the outlet of $V_3$). Valve $V_1$ was switched to port W and the pump was changed back to forward to push all the coating solution and wash water in the holding coil to the waste bottle. After a certain sampling time, valve $V_2$ was turned back to position 1 to end the sampling, Valve $V_1$ was switched first to port $R_2$ and then $R_3$ to sequentially aspirate hypochlorite solution and phenate solution for 4 s each, with the pump reversed, then valve $V_1$ was switched back to position 1 and the pump back to forward. The phenate solution and hypochlorite solution were driven through the sampling tube. When the solution arrived at valve $V_3$ (just to the far end of the hole in the valve), the pump was stopped for 45 s, and valve $V_3$ was turned back to position 1. Finally, the pump was started to drive the colored liquid (including the sorbent) through the detection cell, the signals were collected at 2 Hz and the data were saved in Atlantis for further processing, and a response curve (as shown in Fig. 2) was obtained.

## 3. Results and discussion

### 3.1. Colorimetric determination

When the air sample passes through the coated glass diffusion tube, gaseous ammonia diffuses to the wall of the tube and is converted to ammonium phosphate ($NH_4H_2PO_4$). Nessler's reagent and the Berthelot reaction are the most frequently used colorimetric methods for the determination of ammonium and/or ammonia. Both have been utilized in flow injection systems [24–28]. We first attempted to use Nessler's reagent because only one reagent solution is needed. Unfortunately, it forms a precipitate with ammonia and some of the precipitate is adsorbed on the wall of the tube. Neither linear response nor reproducible results were obtained. With the Berthelot reagent, ammonia is oxidized by hypochlorite to form chloramine which then reacts with phenol to generate a blue indophenol dye. In the range 0.15–4.0 μg ammonia, the absorbance of the indiphenol dye at 610 nm is quite linear with the amount of ammonia. In addition, the sensitivity and reproducibility of the Berthelot reaction are much better than with Nessler's reagent. Thus, the Berthelot reaction is chosen for the colorimetric determination of ammonia collected in the tube wall.

The effects of the sequence of the addition of hypochlorite and phenate solutions on the formation and intensity of the color was checked

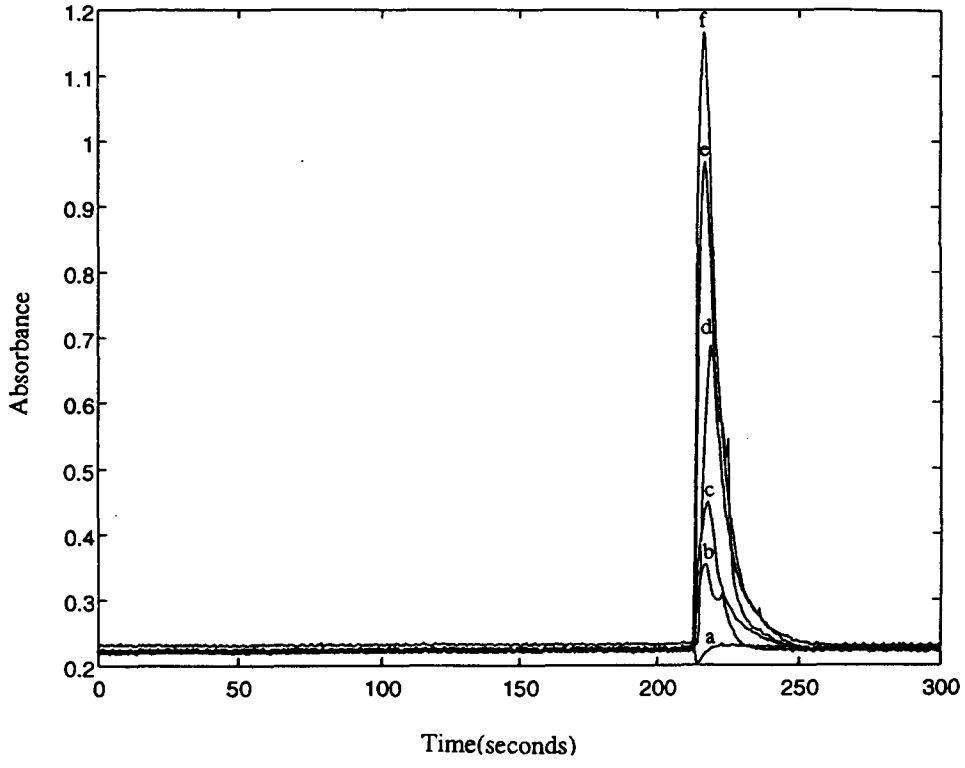


Fig. 2. Response curves for gaseous ammonia standards from a permeation tube: curve a, blank; curve b, 0.5 μg $NH_3$; curve c, 1.0 μg $NH_3$; curve d, 2.0 μg $NH_3$; curve e, 3.0 μg $NH_3$; curve f, 4.0 μg $NH_3$. Conditions: tube length, 20 mm; coating solution, 5% $H_3PO_4$ + 5% glycerol; gas flow rate, 300 ml $min^{-1}$; liquid flow rate, 0.6 ml $min^{-1}$.

by changing the orders in which the reagents were aspirated into the holding coil. The volume and ratio of the reagents, the flow rate of liquid flows and the time for color development were optimized, with the following results.

(i) Reproducible results can be obtained only with the sequence described in the analytical procedure, i.e. the alkaline phenate zone should be the first solution passing through the glass diffusion tube.

(ii) The peak height decreased slowly with increased reagent volumes in the range 20–100 μl. When the volumes of hypochlorite and phenate solution are less than 20 μl, the reproducibility decreases dramatically.

(iii) A ratio 1:1 of the volume of hypochlorite and phenate solutions gave the highest absorbance.

(iv) With fixed volume and ratio of the reagents, the peak height did not change significantly with flow rate of liquid flows in the range 0.4–1.0 ml $min^{-1}$, even though the peak width decreased with the increased flow.

(v) The color intensity of the indophenol dye increased with the time for color development very quickly in the first 20 s, then slowly, and after 40 s, the color development essentially finished and the increase of absorbance was not significant. Instead of a reaction coil between the glass diffusion sampling tube and detection cell, the pump was stopped for 45 s for color development. Thus the dispersion of the colored indophenol dye was reduced.

### 3.2. Sampling tube

The diffusion sampling tube is a glass tube, the inner wall of which has been coated with sorbent. Tubes with 3–5 mm i.d. [1,8] were used for off-line batch analysis, but these tubes are not suitable for flow injection analysis because of their large inner diameter. Glass tubes with 1 mm i.d. were chosen in this study. When an air sample passes through the coated tube, gaseous ammonia diffuses to the tube wall and is absorbed by reaction with the coated sorbent. The following equations have been used to describe the absorption of ammonia in a coated tube [1]:

$$C/C_0 = 0.819\exp(-14.6272\Delta) + 0.0976\exp(-89.22\Delta) + 0.01896\exp(-212\Delta) \quad (1)$$

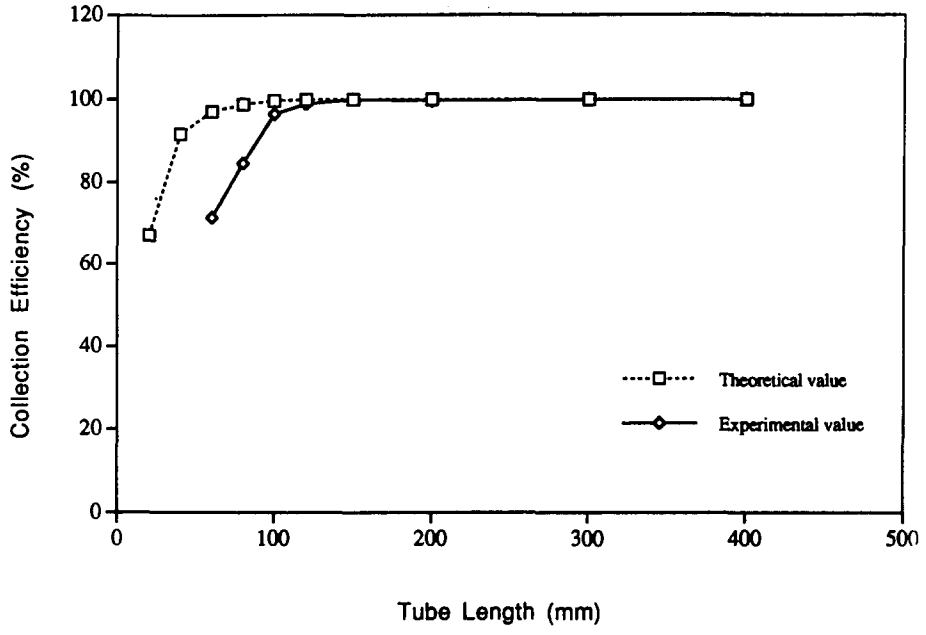


Fig. 3. Effect of tube length on the collection efficiency. Conditions are the same as for Fig. 2 except the tube length.

with a laminar gas flow (Re < 2000).

$$\Delta = \pi DL/4F \quad (2)$$

where $C$ is the mean ammonia concentration in the gas leaving the tube, $C_0$ is the concentration in the incoming gas, $D$ is the diffusion coefficient, $L$ is the length of tube, $F$ is the gas flow rate, and Re is Reynolds number.

It is readily apparent in these equations that the absorption efficiency of a coated tube is a function of the gas flow rate and the tube length. The determination of the collection efficiency of tubes with different lengths was carried out in the following manner. Two glass tubes (1 mm i.d.) were connected in series. The length of the second tube was always 20 cm, but the first one was changed as needed. Both of the tubes were coated with the coating solution, and 4 μg of ammonia from the permeation tube were aspirated through the tubes at a flow rate of 300 ml $min^{-1}$. The ammonia collected in the two tubes was separately determined by the proposed method. Braman et al. [29] pointed out that there is a minimum tube length value after which Eq. (1) is valid. The equation was derived on the assumption that there was an infinite number of chemisorption sites, i.e. the tube is very long. Fig. 3 shows that theoretical calculation and the experimental collection efficiencies of our system. The threshould tube length is about 10 cm, and a 20 cm glass tube was used in the proposed system.

### 3.3. Coating solutions

Two substances have formerly been used as sorbents for ammonia: oxalic acid, $H_2C_2O_4$ [1] and phosphorous acid, $H_3PO_3$ [7]. Although very effective, both of them are reductants and will probably interfere with the color formation and density for the reaction of ammonia with Berthlot reagents [25]. Phosphoric acid was used in the proposed method as absorbent for gaseous ammonia and it was demonstrated to be very effective. The collection capacity of the coated tube (20 cm × 1.0 mm i.d.) increases almost linearly with phosphoric acid concentration in the coating solution (shown in Fig. 4). For constant color development, a corresponding increase in sodium hydroxide concentration is needed as the acid concentration increased. Glycerol was added to the coating solution to increase the viscosity, thus aiding in the coating of the tube wall.

### 3.4. Gas flow rate

Eq. (1) and (2) indicate that the collection efficiency of a coated tube is a function of gas flow rate. The effect of the gas flow rate on the collection efficiency was checked by aspirating

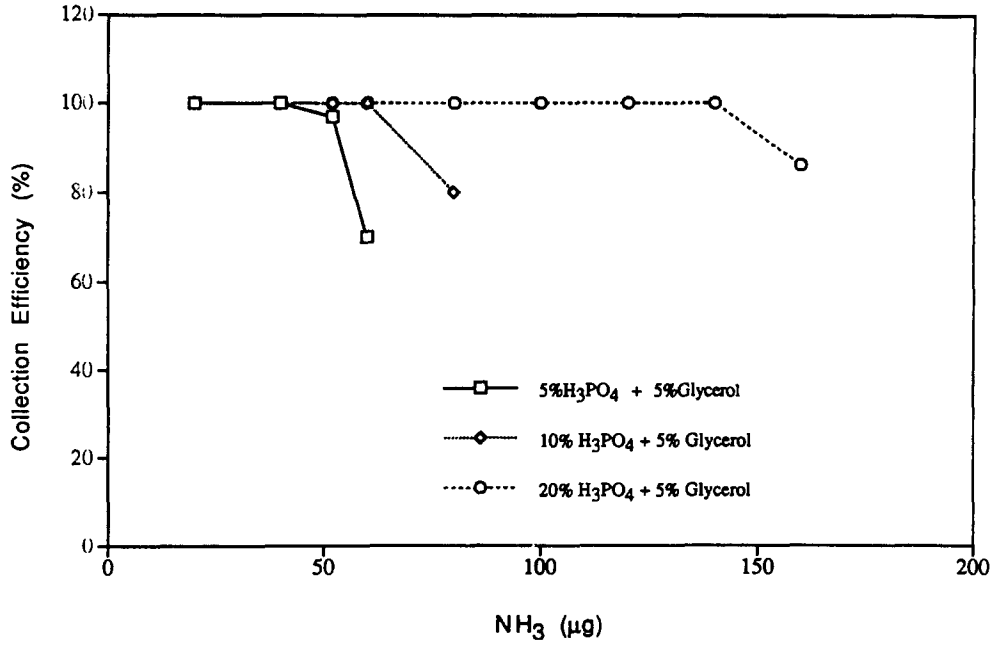


Fig. 4. Effect of coating solutions on the collection efficiency. Conditions are the same as for Fig. 2 except the coating solution.

an accurate amount (4 μg) of ammonia through the coated sampling tube at different flow rates and then determining the ammonia absorbed in the tube. No significant decrease in collection efficiency was observed with the gas flow rate in the range 200–1000 ml $min^{-1}$ (data not shown). Flow rates higher than 1000 ml $min^{-1}$ have not been studied because they are not available with our gas calibrator. It is evident that the collection efficiency will decrease when the gas flow rate exceeds a certain limiting value, because the flow conditions in the sampling tube will not be laminar if the flow rates are larger than 1.45 l $min^{-1}$ [1,8].

### 3.5. Calibration curve and statistics

Fig. 2 shows typical response profiles of ammonia from the permeation tube. The peak height is proportional to the ammonia amount in the range 0.15–4.0 μg. The calibration curve from the data presented in Fig. 2 was

$$Y = (0.243\ \text{AU}\ \mu g^{-1})X - 4.80 \times 10^{-3}\ \text{AU} \qquad (R^2 = 0.997)$$

The negative response of the blank is due to the presence of ethyl alcohol in the phenate solution and its value depends on the mixing process of the reagent with water. We have noted that less than 0.15 μg of ammonia can produce a positive signal, but these levels cannot be discriminated from each other. The actual LOD is 0.15 μg ammonia. The LOD for an air sample depends on the gas flow rate and sampling time. If air sample was collected at 800 ml $min^{-1}$ for 5 min at 25 °C, the LOD for air was 50 ppb. Lower LODs can be achieved by increasing sampling time and/or flow rate. The total time of a single analysis also depends on the sampling resolution. The time of a typical analysis shown in Fig. 2 is 5.0 min. The relative standard deviations for the determination of 1.2 μg ammonia ($n = 7$) and 2.7 μg ammonia ($n = 8$) were 4.4% and 3.25% respectively.

## 4. Conclusion

The combination of a gas diffusion denuder sampler and flow/sequential injection results in a selective and sensitive measurement of gaseous ammonia. The selective absorption of ammonia in the glass sampler eliminates the interference of coexisting acidic gases, such as $SO_2$, $NO_2$ and $CO_2$, which interfere with membrane and pH indicator systems. The high collection efficiency and enrichment factor of the sampler concentrates low levels of ammonia in a large air sample into a very small amount of sorbent. In combination with SIA, only small amounts of reagents are needed, and the developed color is limited to a small zone of the

flow, making this method very sensitive. As an ongoing study, we will investigate the deposition of the particles at the inlet of the sampling tube which will probably happen when real samples are analyzed. Further, the system will be modified so that higher flow rates can be used and the effect of long-term sampling on the reproducibility of the measurements will be studied. This system can be used for both online and offline analysis of ammonia and exploited for the determination of other gaseous analytes, such as $SO_2$, $NO_2$ and $H_2S$.

## Acknowledgments

The authors would like to thank Mr. Oleg Egorov for valuable help in running Atlantis and Dr. David Holman and Ms. Kristina Peterson for their helpful discussion in the preparation of this manuscript. The financial support of the U.S. Environmental Protection Agency is acknowledged.

## References

[1] M. Ferm, Atmos. Environ., 13 (1979) 1385.
[2] Standard Methods for the Determination of Water and Wastewater, American Public Health Association, Washington, DC, 1992.
[3] M.D. Love, H.L. Purdue and G. Pagan, Anal. Chem., 64 (1992) 1269.
[4] E. Strauss, J.-P. Fsbort, D. Bicanic, K.V. Asselt and M. Lubbers, Analyst, 116 (1991) 77.
[5] G. Zhang and P.K. Dasgupta, Anal. Chem., 61 (1989) 408.
[6] G. Zhang, P.K. Dasgupta and D. Sheng, Environ. Sci. Technol., 23 (1989) 1467.
[7] P.K. Stevens, T.G. Dzubay, G. Russworm and D. Rickel, Atmos. Environ., 12 (1978) 55.
[8] R. Bos, J. Air Pollut. Control Assoc., 30 (1980) 1222.
[9] C. Perrino, F. De Santis and A. Febo, Atmos. Environ., 24A (1990) 617.
[10] J. Forest, D.J. Spandau, R.L. Tanner and L. Newman, Atmos. Environ. 16 (1982) 1473.
[11] M. Ferm, Atmos. Environ., 20 (1986) 1193.
[12] G. Lammel, Fresenius' J. Anal. Chem., 340 (1991) 684.
[13] M.P. Reuken, C.A.M. Schoonebeek, A. van Wensveen-Louter and J. Slanina, Atmos. Environ., 22 (1988) 2541.
[14] S.D. Kolev and W.E. van der Linden, Anal. Chim. Acta, 268 (1992) 7.
[15] J.S. Canham, G. Gorden and G.E. Pacey, Anal. Chim. Acta, 209 (1988) 157.
[16] P.J. Baxter, J. Ruzicka and G.D. Christian, Talanta, 41 (1994) 347.
[17] J.R. Clinch and P.J. Worsford, Anal. Chim. Acta, 214 (1988) 401.
[18] K.M. Pederson, M. Kümmel and Søeberg, Anal. Chim. Acta, 238 (1990) 191.
[19] I. Lukkari, J. Ruzicka and G.D. Christian, Fresenius' J. Anal. Chem., 346 (1993) 813.
[20] W. Frenzel, Anal. Chim. Acta, 291 (1994) 305.
[21] P.K. Dasgupta, D. Sheng, H. Hwang, H.C. Yang and G. Zhang, Anal. Chim. Acta, 22 (1988) 949.
[22] L.L. Sørensen, K. Granby, H. Niesen and W.A.H. Asman, Atmos. Environ., 28 (1994) 3637.
[23] J.L.P. Pavon, E.R. Gonzalo, G.D. Christian and J. Ruzicka, Anal. Chem., 64 (1992) 923.
[24] F.J. Krug, J. Ruzicka and E.H. Hansen, Analyst, 104 (1979) 47.
[25] J.W.B. Stewart, J. Ruzicka, H. Bergamin Filho and E.A. Zagatto, Anal. Chim. Acta, 81 (1976) 371.
[26] J.S. Cosano, J.L. Calle, J.L. Pinillos, P. Linares and M.D. Luque de Castro, Anal. Chim. Acta, 221 (1989) 173.
[27] M. del Walle, M. Poch, J. Alonso and J. Bartroli, Anal. Chim. Acta, 241 (1990) 31.
[28] M. Gam, M. Gisin, C. Thommen and P. Cevey, Biotechnol. Bioeng., 43 (1989) 423.
[29] R.S. Braman, T.J. Shelley and W.A. McClenny, Anal. Chem., 54 (1982) 358.

ELSEVIER

Talanta 42 (1995) 1553–1557

Talanta

Short communication

# TLC separation and derivative spectrophotometry of some amino acids

Irena Baranowska *, Małgorzata Kozłowska

*Department of Analytical and General Chemistry, Silesian Technical University, 44-101 Gliwice, Poland*

Received 22 November 1994; revised 23 February 1995; accepted 24 February 1995

**Abstract**

Chromatographic systems for the separation of amino acid mixtures on RP-18 as a stationary phase have been elaborated. The best results were obtained using methanol–water (1:1, v/v; 1:3, v/v; 1:5, v/v) as a mobile phase.

The following amino acids have been examined: asparagine, arginine monohydrochloride, cystine, cysteine chloride, glycine, histidine monohydrochloride, hydroxyproline, isoleucine, leucine, lysine monochloride, methionine, ornithine monohydrochloride, phenylalanine, proline, threonine, tryptophan, tyrosine, serine, valine. Histidine (as monohydrochloride) and methionine were determined by first-, second- and third-derivative spectrophotometry in a mixture of several amino acids.

*Keywords:* Amino acids; Spectrophotometry; TLC

## 1. Introduction

The analysis of amino acids as well as their chromatographic separation is still a current problem, especially in medical analysis. In the literature, several chromatographic systems, based on adsorption TLC, are described for chosen groups of amino acids. Separation has been carried out on silica gel [1–5] and cellulose [6,7]. Bidirectional adsorption chromatography has also been used [8]. Several works are concerned with the method of detection of chromatograms [2–4]; ninhydrin is most often used. In the present work, reversed-phase partition TLC (RP-18) was applied to separation of a chosen group of amino acids. Up to the present time, such separation has not been described.

In addition to these investigations, derivative spectrophotometry was used. Spectrophotometry is also frequently applied to the analysis of amino acids which form coloured compounds with various substances. Cystine and cysteine have been determined spectrophotometrically with Cu(II)–neocuproin reagent [9,10], and also with $OsO_4$ in urine [11]. Amino acids have been analysed as compounds with carbon disulphide [12] and cystein as a compound with OPA [13]. *p*-Benzoquinoline has also been used for the determination of amino acids [14]. The obtained results were not always satisfactory.

The reason for applying derivative spectrophotometry [15] is that it can be more sensitive and selective than zero-order spectrophotometry. A derivative spectrum is a graphical dependence of a value of the differential of absorbance with respect to wavelength on the wavelength. It can be described by the formula

$$\frac{d^n A}{d\lambda^n} = {}^nD_{x,\lambda} = f(\lambda)$$

* Corresponding author.

*SSDI* 0039-9140(95)01569-8

Table 1
$R_f$ values of amino acids on bonded phase RP-18 and colour of spots after ninhydrin detection

| Amino acids | Colour of spot | $R_f$ | | | | | | |
|---|---|---|---|---|---|---|---|---|
| | | Methanol/water | | | | Propanol/water | | |
| | | 3:1 | 1:1 | 1:3 | 1:5 | 3:1 | 1:1 | 1:3 |
| Cysteine chloride | Pink | 0.79 | 0.86 | 0.87 | 0.96 | 0.76 | 0.89 | 0.94 |
| Cystine | Pink | 0.62 | 0.83 | 0.88 | 0.89 | 0.88 | 0.90 | 0.94 |
| Phenylalanine | Violet | 0.68 | 0.53 | **0.48** | 0.48 | 0.84 | 0.74 | 0.63 |
| Glycine | Pink | 0.80 | 0.89 | 0.91 | 0.93 | 0.84 | 0.94 | 0.96 |
| Hydroxyproline | Yellow | 0.85 | 0.9 | **0.90** | 0.93 | 0.86 | 0.95 | 0.95 |
| Isoleucine | Pink | 0.73 | 0.69 | 0.71 | 0.68 | 0.85 | 0.79 | 0.80 |
| Asparagine acid | Pink | 0.81 | 0.9 | **0.94** | 0.97 | 0.85 | 0.92 | 0.97 |
| Leucine | Pink | 0.73 | 0.68 | **0.66** | 0.66 | 0.86 | 0.79 | 0.76 |
| Methionine | Pink | 0.77 | 0.76 | **0.75** | 0.78 | 0.85 | 0.82 | 0.82 |
| Lysine monochloride | Violet | | | | | | | 0.90 |
| Arginine monohydrochloride | Violet | | | | | | | 0.80 |
| Histidine monohydrochloride | Violet | | | | | | | 0.84 |
| Ornithine monohydrochloride | Violet | | | | | | | 0.91 |
| Proline | Yellow | 0.76 | 0.79 | **0.81** | 0.82 | 0.81 | 0.91 | 0.89 |
| Serine | Pink | 0.82 | 0.91 | 0.95 | 0.95 | 0.85 | 0.96 | 0.96 |
| Threonine | Pink | 0.78 | 0.91 | 0.94 | 0.93 | 0.86 | 0.95 | 0.95 |
| Tryptophan | Violet | 0.69 | 0.44 | **0.34** | 0.29 | 0.85 | 0.79 | 0.50 |
| Tyrosine | Pink | 0.82 | 0.74 | 0.72 | 0.69 | 0.88 | 0.89 | 0.77 |
| Valine | Pink | 0.78 | 0.81 | 0.83 | 0.84 | 0.86 | 0.91 | 0.87 |

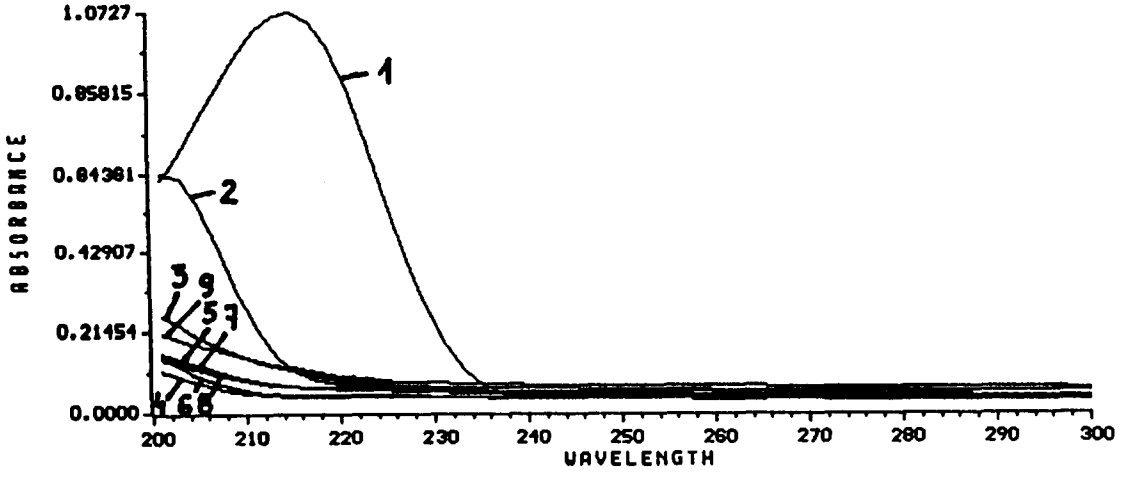


Fig. 1. "Zero-order" spectra of histidine (1), arginine (2), asparagine (3), hydroxyproline (4), isoleucine (5), ornithine (6), proline (7), serine (8) and valine (9).

where $n$ is the derivative order, and ${}^{n}D_{x,\lambda}$ is the value of the $n$th-order derivative of the absorption spectra of a substance x at a certain wavelength $\alpha$.

Derivative spectrophotometry is especially useful in improving selectivity. Tryptophan and tyrosine in synthetic peptides [16], and aromatic amino acids — tryptophan, tyrosine and phenylalanine — in proteins [17], were analysed by the use of second-order derivative spectrophotometry.

In the present paper, the determination of histidine and methionine in the mixtures containing several amino acids was elaborated.

## 2. Experimental

### 2.1. Equipment

TLC separation was done on $10 \times 20\ cm^2$ glass plates covered with a 0.25 mm layer of

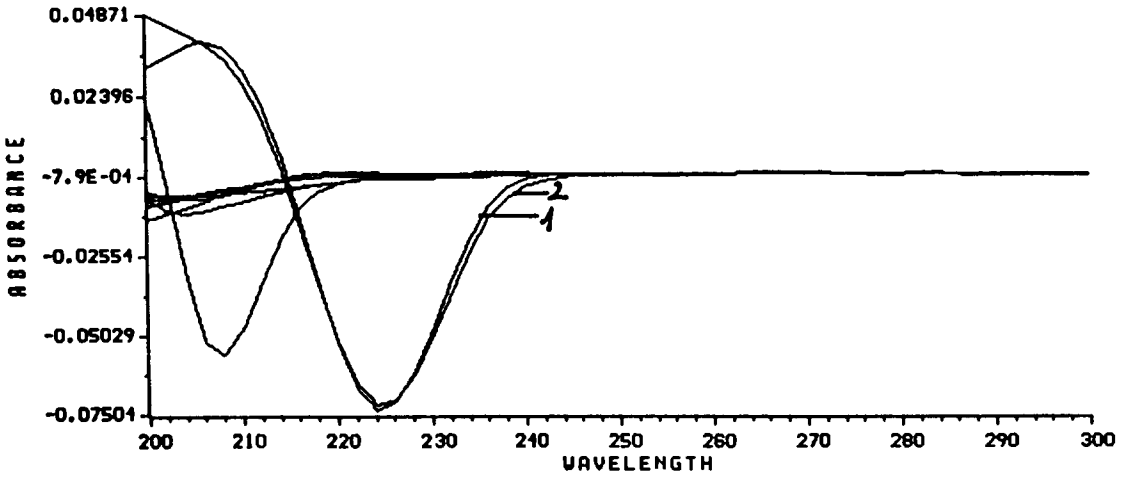


Fig. 2. First-derivative spectra of histidine (1), arginine, ornithine, asparagine, proline, hydroxyproline, isoleucine, serine, valine and mixtures (2).

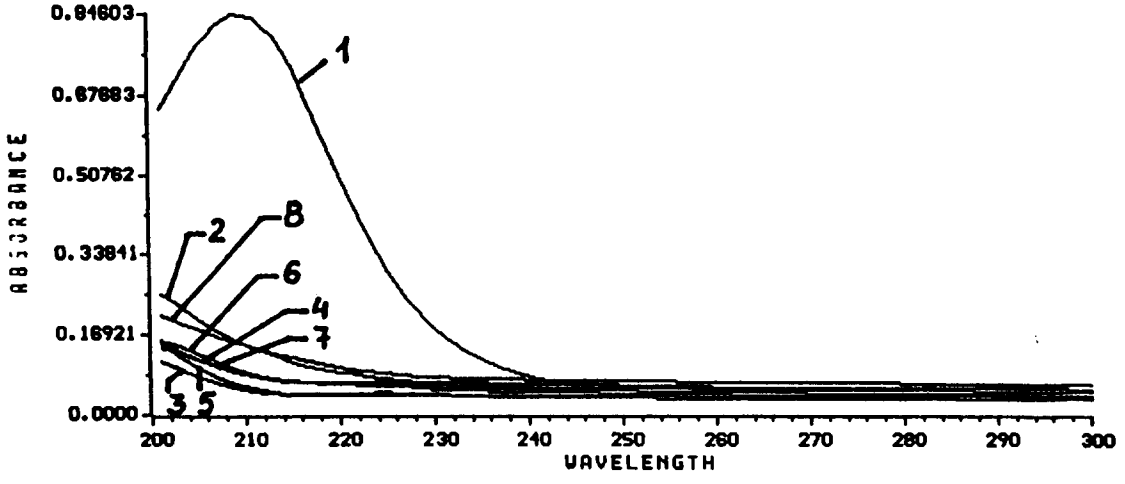


Fig. 3. "Zero-order" spectra of methionine (1), asparagine (2), hydroxyproline (3), isoleucine (4), ornithine (5), proline (6), serine (7) and valine (8).

RP-18 (E. Merck, Darmstadt) in Shandon's containers. The absorption spectra were recorded on a Hewlett Packard HP-8452A UV/vis spectrophotometer with 1 cm cells.

### 2.2. Reagents

All amino acids were produced by E. Merck, Darmstadt. 1 mg $ml^{-1}$ aqueous solutions of amino acids were used, except in the case of cystine (0.1 mg $ml^{-1}$) and tyrosine (0.45 mg $ml^{-1}$), for TLC. Solutions containing 0.1 mg $ml^{-1}$ of amino acids, except for histidine (0.05 mg $ml^{-1}$), were used in derivative spectrophotometry.

### 2.3. Procedure

All chromatograms were developed over a distance of 15 cm in Shandon's containers. The following developing mixtures were applied: methanol–water (3:1, v/v; 1:1, v/v; 1:3, v/v; 1:5, v/v), propanol–water (3:1, v/v; 1:1, v/v; 1:3, v/v) and acetonitrile–water (1:1, v/v). Chromatograms were detected by a 0.25% solution of ninhydrin in acetone. Derivative spectra were calculated by the use of a standard software procedure.

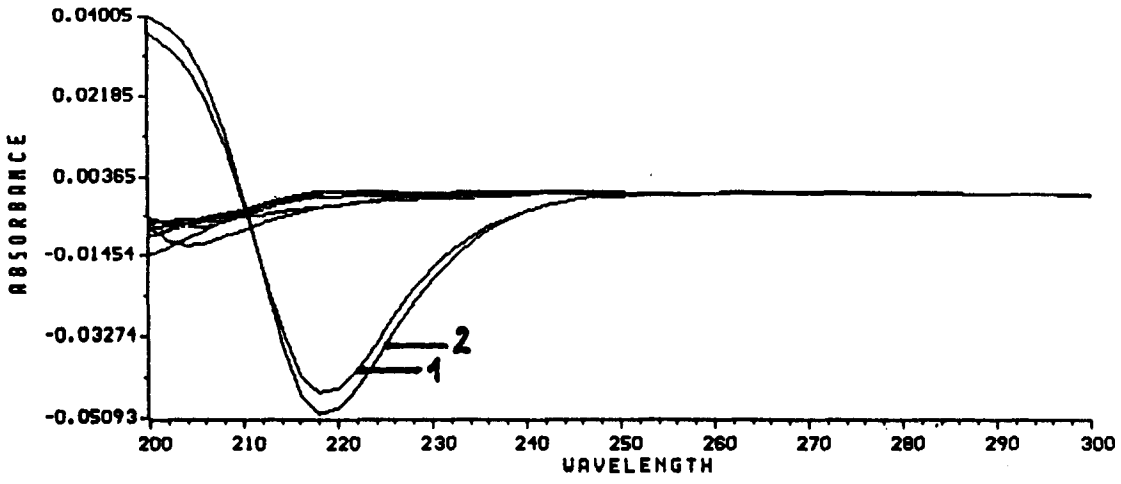


Fig. 4. First-derivative spectra of methionine (1), ornithine, asparagine, proline, isoleucine, hydroxyproline, serine, valine and mixtures (2).

Table 2
Parameters of the straight line dependence and correlation coefficient of histidine and methionine for first-derivative (D), second-derviative ($^2$D) and third-derivative ($^3$D) spectrophotometry

| | Histidine | | | | Methionine | | | |
|---|---|---|---|---|---|---|---|---|
| | $\lambda$ (nm) | $a$ | $b$ | $r$ | $\lambda$ (nm) | $a$ | $b$ | $r$ |
| D | 224.6 | $-1.97 \times 10^{-3}$ | −1.49 | 0.998 | 218.9 | −2.76 | −0.49 | 0.997 |
| $^2$D | 231.8 | $3.51 \times 10^{-5}$ | 0.14 | 0.997 | 224.6 | −2.09 | 0.03 | 0.996 |
| $^3$D | 236.4 | $1.39 \times 10^{-6}$ | −0.02 | 0.996 | 216.3 | −4.89 | 0.01 | 0.997 |

## 3. Results and conclusions

### 3.1. Thin-layer chromatography

Some systems suitable for the separation of amino acids have been found (Table 1). The greatest differences between $R_f$ values of investigated compounds were obtained for the systems containing methanol and water. The six amino acids cysteine chloride, isoleucine, phenylalanine, methionine, serine, tryptophan were separated in the mixture methanol–water (1:1, v/v); phenylalanine, methionine, threonine, tryptophan, tyrosine, valine were separated in the mixture methanol–water (1:5, v/v).

The best results were obtained for the mixture methanol–water (1:3, v/v). Under these conditions, seven amino acids can be separated: asparagine acid, hydroxyproline, phenylalanine, leucine, methionine, proline, and tryptophan.

In spite of the fact that the results obtained in the systems propanol–water are not so good, monohydrochlorides and monochlorides of chosen amino acids can be separated in these circumstances. To the best of our knowledge, such separations are not reported in the literature.

Spots of all amino acids were of good visibility, with sharp edges against the white background of the plates.

### 3.2. Derivative spectrophotometry

Spectrophotometric determination of histidine was carried out by the use of derivative spectrophotometry to complete chromatographic separation and analysis of this amino acid in the mixture. The following amino acids were used in this determination: histidine, arginine, ornithine, asparagine, proline, hydroxyproline, isoleucine, serine, valine (Figs. 1 and 2).

Zero-order spectrophotometry cannot be applied in this case, while first-, second- and third-order derivative spectrophotometry allows histidine to be determined with a good accuracy at a concentration of 8 $\mu g\ ml^{-1}$.

Methionine in a mixture with ornithine, asparagine acid, proline, hydroxyproline, iso-

leucine, serine, valine was analysed in the same way (Figs. 3 and 4). In this case it was also possible to determine a methionine concentration of 10 μg ml$^{-1}$. Straight line dependence was evaluated for amino acids by the use of derivative spectrophotometry. Parameters of the equation

$$''D = ac + b$$

where $''D$ is the value of derivative, $c$ is the concentration, $a$ is the intercept and $b$ is the slope, for a particular order of derivatives and suitable correlation coefficients for histidine and methionine, are gathered in Table 2.

## References


[1] Z. Illes and T. Cserhati, J. Planar Chromatogr., 1 (1988) 231–234.

[2] B. Basak and S. Laskar, Talanta, 37 (1990) 1105–1106.

[3] S. Laskar, U. Bhattacharaya and B. Basak, Analyst, 116 (1991) 625–626.

[4] C.G. De Lima, T.C.M. Pastore, C.A. Schwartz, I.S. Cruz and A. Sebben, Talanta, 38 (1991) 1303–1307.

[5] M. Alaiz, J.L. Navarro, I. Giron and E. Vioque, J. Planar Chromatogr., 5 (1992) 143–146.

[6] L. Sentier, I. Marchal, I. Boudrout and P. Germain, J. Chromatogr., 547 (1991) 531–537.

[7] T.K.X. Huynh, A.O. Kuhh and M. Leder, J. Chromatogr., 626 (1992) 301–304.

[8] B. Borkowski, Chromatografia cienkowarstwowa w analizie farmaceutycznej, PZL, Warszawa, 1973.

[9] E. Tutem and R. Apak, Anal. Chim. Acta, 255 (1991) 121–125.

[10] M.L. Iskander and H.A.A. Medien, Microchem. J., 41 (1990) 172–182.

[11] I. Bertini, C. Mannucci, R. Noferini, A. Perico and P. Rovero, J. Pharm. Sci., 82 (1993) 179–182.

[12] A. Besada, N.B. Tadros and Y.A. Gawargious, Mikrochim. Acta, (1989) 143–146.

[13] I. Chrastil, Analyst, 115 (1990) 1383–1384.

[14] H.J.M. Hernandez, R.M. Camanas and M.C.G. Alvarez-Coque, Microchem. J., 40 (1989) 292–296.

[15] Z. Marczenko, S. Kuś and N. Obarski, Chem. Anal., 36 (1991) 879–890.

[16] A.W.M. Lee, W.H. Chan and M.F. Ho, Anal. Chim. Acta, 246 (1991) 443–445.

[17] Y. Nozaki, Arch. Biochem. Biophys., 277 (1990) 323–333.

ELSEVIER

Talanta 42 (1995) 1561–1566

Talanta

# Studies on urea biosensors based on immobilized corynebacterium glutamicum and their kinetic response processes

Cheng-Hong Lei [a], Ya-Fang Bao [a], Jia-Qi Deng [a,*], Cheng-Xiang Lei [b]

[a] *Department of chemistry, Fudan University, Shanghai 200433, People's Republic of China*
[b] *Institute of Genetics, Fudan University, Shanghai 200433, People's Republic of China*

Received 5 January 1995; accepted 20 March 1995

**Abstract**

Two novel biosensors for urea based on immobilized corynebacterium glutamicum 617 and corynebacterium glutamicum ATCC13032 in calcium alginate gel coupled with an ammonia gas-sensing electrode, were designed and constructed. Calibration plots of measured potential difference (mV) vs. log of urea concentration were linear in the range of $5.6 \times 10^{-5}$–$1.4 \times 10^{-2}$ and $5.6 \times 10^{-5}$–$1.1 \times 10^{-2}$ mol $l^{-1}$, with slopes of 59.2 and 61.3 mV per decade respectively, in pH 8.0, 0.1 mol $l^{-1}$ phosphate buffer solution at 30°C. The relationship between the initial response velocity and the substrate concentration was also discussed. The results indicate that the kinetic response process of the reaction catalyzed by bacteria is similar to that by isolated enzyme. Using an Eadie–Hofstee plot, the apparent Michaelis constant $K_m$ and the maximum initial response velocity $V_m$ for urease in the immobilized bacterial membrane were determined. The two urea biosensors were successfully applied for the actual measurement of urea in urine and were relatively stable for 20 and 40 days respectively.

## 1. Introduction

As the development of enzyme electrodes is limited by the need to purify the required enzyme and the demanding conditions for preserving it, and as the pure enzyme without any cofactors is not efficient enough to catalyze the expected biochemical reactions, a current trend in the development of biosensors is the utilization of novel biological materials as biocatalytic layers. Among these are living microorganisms, animal and plant tissues [1]. The use of living microorganisms such as bacteria, because of their good catalytic behavior, abundant source and lack of seasonal limitations, as possible alternatives to highly expensive isolated enzymes is a rapidly developing method. Divies designed the first amperometric bacterial biosensor [2], and the first potentiometric-based one was later reported by Rechnitz et al. [3]. Bacterial sensors sensitive to L-glutamine [4], L-cysteine [5], glucose [6], methane [7], L-aspartate [8,9], glutamic acid [10], sulfate [11], DL-phenylalanine [12], etc., have successively been reported by many workers.

The determination of urea by means of biosensors is of importance in clinical and other areas. Several urea biosensors based on immobilized isolated urease were constructed by various groups [13–15] in the 1970s. A jack bean meal biosensor for urea was reported by Arnold and Scott [16] in 1984 to be a good alternative to the urease-based ones, but a demand of fresh jack bean must be satisfied. With this in mind, living microorganisms containing abundant urease would be considered. Proteus mirabilis was applied as a paste to the dialysis membrane and coupled with a gas-permeable

* Corresponding author.


*SSDI* 0039-9140(95)01594-9

electrode to constitute the biosensors for urea by Ihn and co-workers [17,18]. In this paper, we found two kinds of corynebacterium glutamicum (617 and ATCC13032) containing abundant urease that can specifically catalyze the decomposition of urea into carbon dioxide and ammonia. These two immobilized bacterial membranes in calcium alginate gel were held on an ammonia electrode to constitute the biosensor for urea. Both resulting biosensors showed a longer lifetime and linear detection range from a lower substrate concentration than that based on Proteus mirabilis. The relationship between the initial response velocity and the substrate concentration was also studied. The results indicate that the kinetic response process of the reaction catalyzed by bacteria is similar to that catalyzed by isolated enzyme [19–21]. The authors think this is just the theoretical basis on which bacteria can be used instead of isolated enzyme. Corynebacterium glutamicum, which can be cultured rapidly and used safely, is usually utilized in the fermentation industry. To our knowledge, the utilization of corynebacterium glutamicum as a biocatalytic material for biosensors has not been previously described.

## 2. Experimental

### 2.1. Apparatus and reagents

A Hitachi 20PR-52D type high speed refrigerator centrifuge was used to treat the cultured bacterium suspension liquid. All potentiometric measurements were made with a model PXS-215 ionic activity recorder (No. 2 Shanghai analytical instrument factory) in conjunction with a YEW type 3086 strip chart recorder. A model 501 ammonia electrode (Jiangsu Electroanalytical Instrument Factory, Taixian, China) was employed and modified as described below. Measurements were carried out in a thermostated stirrer.

Analytical grade reagents were used to prepare all buffers and standard solutions. All solutions were prepared in freshly deionized water. The amino acids were obtained from Shanghai biochemical reagents store. Corynebacterium glutamicum 617 was obtained from the Genetics Institute of Fudan University, and ATCC13032 from American Type Culture Collection.

### 2.2. Procedure

The medium for culturing bacteria was composed of 1.0% peptone, 0.5% yeast powder, 1.0% sodium chloride and 0.004% nalidixic acid. This medium was autoclaved at 121°C, 1.1 kg $cm^{-2}$ for 20 min. The solution was allowed to cool and the corynebacterium glutamicum was aspetically inoculated on this liquid medium. The inoculated medium was kept in a temperature controlled vibratile culture case at 30°C for 20 h. The cells were harvested by centrifuge at 7000$g$ for 6 min at 4°C, washed twice with 0.1 mol $l^{-1}$ phosphate buffer solution and centrifuged. The cells were kept in a refrigerator at 4°C when not in use. 90 mg of the collected cells and 150 mg of 4% sodium alginate were completely mixed and spread on a glass plate to make a $6 \times 1.5$ $cm^2$ membrane. This was immersed in a 4% calcium chloride solution for 1 h to immobilize the cells. A piece (weight 20 mg, thickness 0.2 mm, diameter 10 mm) of such an immobilized bacterial membrane was cut off and washed with water, and then sandwiched between two piece of cellulose acetate dialysis membranes and held on the gas-permeable membrane of an ammonia gas-sensing electrode to construct the biosensor for urea (see Fig. 1). An internal reference solution of 0.1 mol $l^{-1}$ $NH_4Cl$ was used. This prepared biosensor was stored in the 0.1 mol $l^{-1}$ phosphate buffer in a refrigerator when not in use.

Potentiometric measurements of the steady-state response were carried out in the usual manner. An aliquot of the 0.1 mol $l^{-1}$ urea stock solution was pipetted into a 25 ml beaker

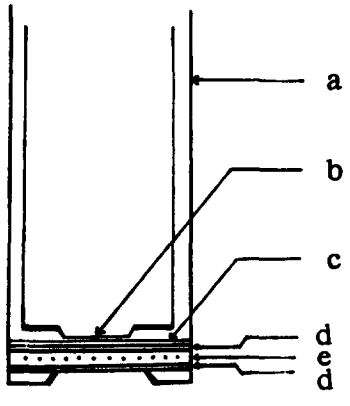


Fig. 1. Schematic diagram of the bacterial biosensor for urea: (a) ammonia-sensing electrode body; (b) pH-sensing glass electrode; (c) ammonia-sensing membrane; (d) cellulose acetate dialysis membrane; (e) bacterial membrane.

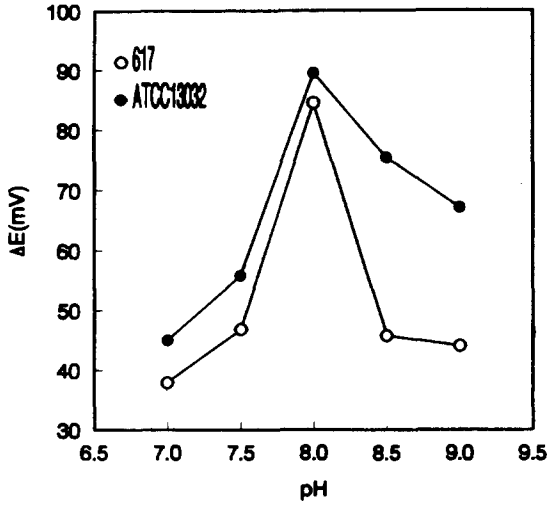


Fig. 2. pH profile for two urea biosensors in 0.1 mol $l^{-1}$ $Na_2HPO_4$–$KH_2PO_4$ buffer solution at 30°C; [urea] = $10^{-3}$ mol $l^{-1}$.

containing 10 ml of 0.1 mol $l^{-1}$ phosphate buffer. The solution was magnetically stirred and the steady-state potential was recorded. After a measurement, the biosensor was washed free of residual urea and ammonia with water until a stable blank potential was obtained.

## 3. Results and discussions

### 3.1. Working conditions

The principal reactions of corynebacterium glutamicum to urea are

$$NH_2CONH_2 + H_2O \xrightarrow{\text{urease}} CO_2 + NH_3$$

$$NH_3 + H_2O \rightarrow NH_4^+ + OH^-$$

The optimal pH value of the urease catalyzed reaction is from 6 to 7. However, the strong pH dependence of the enzymatic activity and the gas-sensing electrode make the solution pH a critical parameter. The effect of pH on the bacterial sensor response was studied at different pH values in 0.1 mol $l^{-1}$ $Na_2HPO_4$–$KH_2PO_4$ buffer. Fig. 2 shows the pH profile for the two biosensors. It can be seen that optimal biosensor responses are obtained at pH 8.0. Borax–potassium dihydrogen phosphate buffer solution was also tried as a working buffer system, but showed very poor response. This result indicates that the buffer system not only controls the pH value of the working solution, but also inhibits or activates the enzymatic activity of bacteria. Hence, the buffer solution of pH 8.0, 0.1 mol $l^{-1}$ $Na_2HPO_4$–$KH_2PO_4$ was used throughout this paper.

The variation in signal was only 5% as the temperature increased from 20 to 40°C. However, at temperatures lower than 20°C, the activity of the enzyme in the cells was rather lower and the response time was relatively longer. At temperatures higher than 35°C, the lifetime of the sensors was shortened. Taking both the lifetime and response time into consideration, 30°C was the selected temperature for this work.

### 3.2. Biosensor response characteristics and lifetime

Typical calibration curves were obtained from two biosensors (Fig. 3). A comparison of the response characteristics of the two urea biosensors is shown in Table 1.

It can be seen that the biosensors based on both corynebacterium glutamicum 617 and ATCC13032 show good Nernstian behavior. The latter can provide a satisfactory reproducible potential even at lower concentrations. Thus, the nonlinear portion of its calibration curve could be used without significant error. Comparing these two sensors, that based on corynebacterium glutamicum ATCC13032 had a narrower linear range, but a lower detection limit, faster response and longer lifetime than the other.

It took 1–5 and 3–7 min to obtain a 98% response for the biosensors based on corynebacteria glutamicum ATCC13032 and 617 within the linear range of the sensors' response. It took

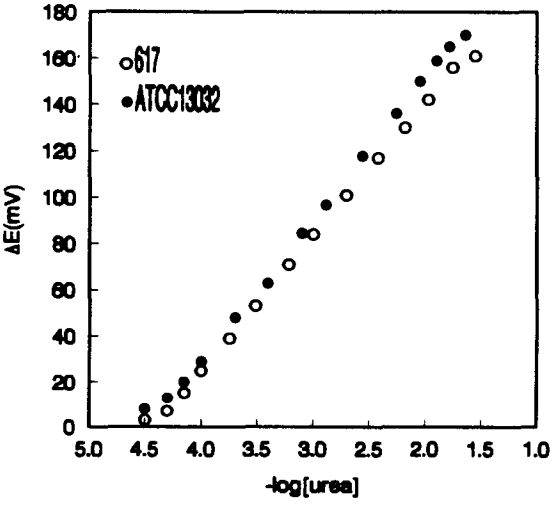


Fig. 3. Typical calibration curve for two urea biosensors.

Table 1
Comparison of the response characteristics of two urea biosensors

| | Bacteria | |
|---|---|---|
| | 617 | ATCC13032 |
| Linear range (mol $l^{-1}$) | $5.6 \times 10^{-5}$–$1.4 \times 10^{-2}$ | $5.6 \times 10^{-5}$–$1.1 \times 10^{-2}$ |
| Slope (mV per decade) | 59.2 | 61.3 |
| Detection limit (mol $l^{-1}$) | $2.0 \times 10^{-5}$ | $1.5 \times 10^{-5}$ |
| Response time (min) | 8–14 | 5–9 |
| Lifetime (days) | at least 20 | at least 40 |

a longer time to obtain the steady-state response (see Table 1).

After 28 days, the ATTCC13032 sensor slope reached a constant value of 58 mV per decade, and showed little change in the response and linear range. It continued to respond in a useful fashion after 40 days. In contrast, the 617 sensor reached a remained constant value of 45 mV per decade, and showed little change in the response and linear range after 12 days; it continued to be usable for up to 20 days (see Table 2).

The biosensors based on both corynebacterium glutamicum 617 and ATTCC13032 showed linear ranges from a lower substrate concentration and a longer lifetime than that based on Proteus mirabilis [17,18].

An isolated enzyme biosensor and a jack bean biosensor that display excellent response characteristics for urea have been reported by Mascini and Guilbault [15] and Arnold and Glazier [16]. However, isolated urease is considerably more expensive and it is not easy to obtain fresh jack bean. Corynebacterium glutamicum that can be cultured at any time at room temperature, which is usually used for producing glutamic acid by employing urea as a nitrogen source, is an effective replacement for pure urease.

### 3.3. Selectivity and recovery

Although urease is highly selective for urea, it is known that microorganisms sometimes contain certain kinds of deaminases for amino acids. Hence, the interference that might be caused by them was investigated (see Table 3). The results indicated only six out of all the usual amino acids were involved in interference for urea. Glucose, saccharose and some inorganic salts also gave rise to a bit of interference. DL-Alanine, L-lysine, L-leucine, DL-threonine, L-proline, glycine, DL-methionine, L-histidine, L-tyrosine, DL-tryptophan, DL-phenylalanine, L-ornithine, L-cystine, L-glutamate, adenine monohydrochloride, $ZnSO_4$, $NaSO_4$, $MgSO_4$, $Cd(NO_3)_2$ and NaAc gave no response. The bacterial urea biosensors based on immobilized corynebacterium glutamicum gave similar results to those from Proteus mirabilis [17,18].

Interference, created in particular by amino acids, is a problem which is hard to avoid owing to living bacteria usually containing more than one kind of enzyme. However, this does not obstruct the successful measurement of some real world samples containing a much higher concentration of urea than its interference substances or no main interference (see Table 4). Further studies are being carried out, employing enzyme inhibitors or HPLC, on the selectivity of bacterial urea biosensors based on immobilized corynebacterium glutamicum at this laboratory.

The recoveries of six urea samples with concentrations of $1.0 \times 10^{-4}$–$1.0 \times 10^{-2}$ mol $l^{-1}$ were determined by a calibration curve method. The average recoveries of the two sensors were in the range 94.0–103%.

### 3.4. Determination of urea in urine

A standard addition method was used for the determination of urea in urine by employing the two urea biosensors (617 and ATCC13032, see Table 4). The procedure was the same as described above. The raw urine samples were measured without any pretreatment by mixing 0.2 ml of urine with 10 ml of 0.1 mol $l^{-1}$ phosphate buffer in the thermostated cell. The potential was recorded under stirring, until a steady-state reading was established. 0.2 ml of 0.1 mol $l^{-1}$ urea standard solution was then added and the new steady-state potential recorded. The urea concentration was determined from the calibration curve. Corresponding experiments were carried out on an

Table 2
Stability of the two urea biosensors

| | Bacteria | | | |
|---|---|---|---|---|
| | 617 | | ATCC13032 | |
| | 20 days | 28 days | 40 days | 60 days |
| Slope (mV per decade) | 43.1 | 39.4 | 56.9 | 55.0 |
| Linear range ($mol\ l^{-1}$) | $1.4 \times 10^{-4}$–$1.0 \times 10^{-2}$ | $3.0 \times 10^{-4}$–$8.0 \times 10^{-3}$ | $1.2 \times 10^{-4}$–$9.6 \times 10^{-3}$ | $3.2 \times 10^{-4}$–$8.1 \times 10^{-3}$ |

Table 3
Selectivity of the two urea biosensors

| | Response ratio [a] | | Response ratio [b] | |
|---|---|---|---|---|
| | 617 | ATCC13032 | 617 | ATCC13032 |
| Urea | 100 | 100 | 100 | 100 |
| L-Glutamine | 13.3 | 11.5 | 20.0 | 13.4 |
| L-Arginine | 6.7 | 14.3 | 10.6 | 17.2 |
| L-Asparagine | 1.2 | 45.1 | 3.8 | 51.0 |
| L-Aspartate | 1.1 | – | 2.7 | – |
| L-Serine | – | 2.0 | – | 6.4 |
| L-Valine | 4.2 | – | 8.8 | – |
| NaCl | 2.4 | 4.3 | 1.7 | 1.3 |
| KBr | 3.1 | 3.2 | 1.1 | 2.2 |
| D-Glucose | −2.4 | −5.5 | −2.1 | −3.7 |
| Saccharose | −3.4 | −4.1 | −1.8 | −2.0 |

[a] [substrate] = $10^{-3}$ mol $l^{-1}$. [b] [substrate] = $10^{-2}$ mol $l^{-1}$.

ASTRA-8 automated stat/routine analyzer (the Auto-Analyzer) by a local hospital, for which the same samples had to be urease-treated and diluted 100-fold throughout.

As shown in Table 4, the analytical results using the bacterial urea biosensors correspond to those using this kind of Auto-Analyzer. However, the method using the urea biosensors described here does not require such sophisticated equipment, or the elimination of proteins and coloration for the conventional spectrophotometric method and any other pretreatment. Therefore, it is an easy, quick and precise means of determining urea.

### 3.5. Kinetic response process

Fig. 4 shows the relationship between the initial response velocities ($V$, $dE/dt$) and the substrate concentration ([S]) for two urea biosensors. It can be seen that when [S] < $6.0 \times 10^{-4}$ mol $l^{-1}$, $V$ increased rapidly and linearly with [S]. However, when [S] was higher than this concentration, $V$ rose more and more slowly towards a maximum, indicating that the urease in the bacterial cells was gradually saturated by the substrate urea. Such a kinetic response process is similar to that of the reaction catalyzed by isolated enzyme [19–21]. This is just

Table 4
The results of urea determinations in urine

| Sample No. | By the biosensor 617 | | By the biosensor ATCC13032 | | By the Auto-Analyzer |
|---|---|---|---|---|---|
| | [urea]* | Recovery (%) | [urea]* | Recovery (%) | [urea]* |
| 1 | $1.19 \times 10^{-1}$ | 95.7 | $1.22 \times 10^{-1}$ | 98.9 | $1.24 \times 10^{-1}$ |
| 2 | $1.75 \times 10^{-1}$ | 94.8 | $1.71 \times 10^{-1}$ | 97.3 | $1.76 \times 10^{-1}$ |
| 3 | $1.59 \times 10^{-1}$ | 96.1 | $1.67 \times 10^{-1}$ | 96.4 | $1.62 \times 10^{-1}$ |
| 4 | $1.34 \times 10^{-1}$ | 96.9 | $1.31 \times 10^{-1}$ | 97.5 | $1.37 \times 10^{-1}$ |

[urea]*: mol $l^{-1}$.

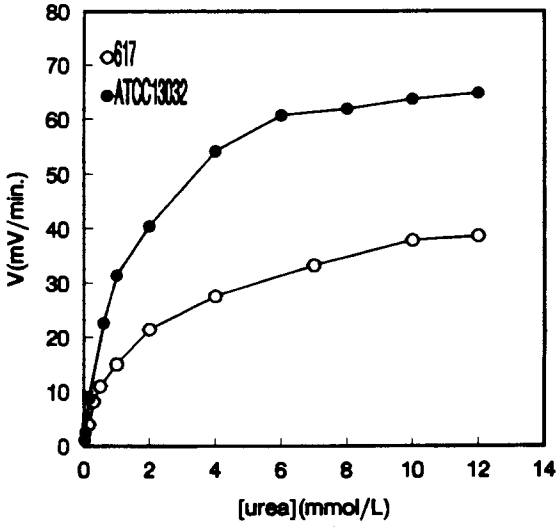


Fig. 4. Relationship between [S] and V for two urea biosensors.

Table 5
The kinetic data for two biosensors

| Bacteria | $K_m$ mol $l^{-1}$ | $V_m$ (mV $min^{-1}$) |
|---|---|---|
| 617 | $2.8 \times 10^{-3}$ | 49.1 |
| ATCC13032 | $1.4 \times 10^{-3}$ | 73.2 |

the theoretical basis on which bacteria can take the place of isolated enzyme as a biocatalyst. This phenomenon shows that the enzyme in the whole bacterial cell could directly catalyze the substrate. It combined with the substrate to give a kind of transient state [19,20]:

First step: $B(E) + S \rightleftharpoons B(E) \cdot S$

Second step: $B(E) \cdot S \rightleftharpoons B(E) + P$

where B(E) represents the enzyme in the whole bacterial cell.

From the Michaelis–Menten equation, $V = (V_m[S])/(K_m + [S])$, using an Eadie–Hofstee plot [19,20], $V = V_m - K_m(V/[S])$, the maximum response velocity $V_m$ ($dE/dt$, mV $min^{-1}$) and the apparent Michaelis constant $K_m$ for urease in the bacterial membrane of sodium alginate were determined. For the same substrate, the higher the rate at which the enzyme catalyzes a given biochemical reaction, the greater the activity of the enzyme. A comparison of the kinetic data of the two urea biosensors is shown in Table 5. The results indicate that the biosensor ATCC13032 had a lower $K_m$ and higher response velocity, i.e. the urease activity within corynebacterium glutamicum ATCC13032 was higher than that within corynebacterium glutamicum 617. Similarly, the biosensor ATCC13032 had a longer lifetime. Under identical experimental conditions, the activity of identical enzymes in different bacteria should be relative to the nature of the bacteria themselves in which the enzyme exists.

## Acknowledgment

This work was supported by the National Natural Science Foundation of China and the National Open Laboratory of the Changchun Institute of Applied Chemistry of Chinese Academia Sinica.

## References

[1] A.P.F. Turner, I. Karube and G.S. Wilson, Biosensors, Oxford University Press, 1987, p. 13.
[2] C. Divies, Ann. Microbiol., 126A (1975) 175.
[3] G.A. Rechnitz, R.K. Kobos, S.J. Riechel and C.R. Gebauer, Anal. Chim. Acta, 94 (1977) 357.
[4] G.A. Rechnitz, T.L. Riechel, R.K. Kobos and M.E. Meyerhoff, Science, 199 (1978) 440.
[5] M.A. Jensen and G.A. Rechnitz, Anal. Chim. Acta, 101 (1978) 125.
[6] I. Karube, S. Mitsuda and S. Suzuki, Eur. J. Appl. Microbiol. Biotechnol., 7 (1979) 343.
[7] T. Okada, I. Karube and S. Suzuki, Eur. J. Appl. Microbiol. Biotechnol., 12 (1981) 97.
[8] R.K. Kobos and G.A. Rechnitz, Anal. Lett., 10 (1978) 751.
[9] Qing Wang and Jiaqi Deng, Chem. J. Chin. Univ., 15(7) (1993) 974–976.
[10] R. Klaus and S. Frieder, Analyst, 112 (1987) 341–342.
[11] R.K. Kobos, Anal. Lett., 19(3/4) (1986) 353–362.
[12] G.S. Ihn and I.T. Kim, Bioelectrochem. Bioenerg., 21 (1989) 223–231.
[13] T. Anfalt, A. Graneli and D. Jagner, Anal. Lett., 6(11) (1973) 969–975.
[14] D.D. Papastathopoulos and G.A. Rechnitz, Anal. Chim. Acta, 79 (1975) 17–26.
[15] M. Mascini and G.G. Guilbault, Anal. Chem., 49(6) (1977) 795–798.
[16] M.A. Arnold and Scott A. Glazier, Biotechnol. Lett., 6(5) (1984) 313–318.
[17] G.S. Ihn, S.T. Woo, M.J. Sohn and R.P. Buck, Anal. Lett., 22(1) (1989) 1–13.
[18] G.S. Ihn, B.W. Kim, M.J. Sohn and I.T. Kim, J. Kor. Chem. Soc., 32(4) (1988) 323.
[19] Tong Shen, Jingyan Wang and Bangti Zhao, Biochemistry, Advanced Education Press, Bejing, 1980, p. 232.
[20] L. Michaelis and M. Menten, Biochem. Z., 49 (1913) 333.
[21] G.G. Guilbault, R.K. Smith and J.G. Montalvo, Jr., Anal. Chem., 41 (1969) 600–605.

ELSEVIER

Talanta 42 (1995) 1567–1574

Talanta

# A β-cyclodextrin based fiber-optic chemical sensor: a fractal analysis

Ajit Sadana [a,b,1], J.P. Alarie [a], T. Vo-Dinh [a,*]

[a] *Health Sciences Research Division, Oak Ridge National Laboratory, Oak Ridge, TN 37831-6101, USA*
[b] *Chemical Engineering Department, University of Mississippi, University, MS 38677-9740, USA*

Received 14 October 1994; revised 27 March 1995; accepted 27 March 1995

**Abstract**

A fractal analysis is presented for the binding of pyrene in solution to β-cyclodextrin attached to a fiber-optic chemical sensor. The specific ($k_1$) and non-specific binding rate coefficients and the fractal dimension ($D_f$) (specific binding case only) both tend to increase as the pyrene concentration in solution increases from 12.4 to 124 ng ml$^{-1}$. Predictive relations for the binding rate coefficient (specific as well as non-specific binding) and for $D_f$ (specific binding case only) as a function of pyrene concentration are provided. These relations fit the calculated $k_1$ and $D_f$ values in the pyrene concentration range reasonably well. Fractal analysis data seem to indicate that an increase in the pyrene concentration in solution increases the "ruggedness" or inhomogeneity on the fiber-optic biosensor surface. The fractal analysis provides novel physical insights into the reactions occuring on the fiber-optic chemical surface and should assist in the design of fiber-optic chemical sensors.

*Keywords:* Binding rate coefficient; Chemical sensor; Fractal dimension

## 1. Introduction

There is an increasing demand for sensitive detection systems which are required to detect analytes in often very dilute and diverse circumstances. Fiber-optic biosensors have recently gained a lot of interest, and different 'schemes" have been proposed and applied to detect a wide variety of analytes [1–16]. Biosensors are finding increasing application nowadays. The antibody–antigen or enzyme–analyte recognition or reaction provides the basis for the sensitivity and/or selectivity of the reaction. The transduction of the biochemical signal to an electrical signal is often a critical step wherein a large fraction of the "signal loss", for example, fluorescence (by quenching) may occur. This leads to deleterious effects on the sensitivity and selectivity of the biosensor, besides decreasing the quality of the reproducibility of the biosensor.

The above "sensing principles" proposed initially for biosensors have recently been extended to a "chemical sensor" [17]. Here the analyte molecule that has to be detected is "sequestered" in β-cyclodextrin molecules immobilized on the distal end of the fiber-optic chemical sensor. Cyclodextrins are sugar molecules that possess the structure of a truncated cone with a hydrophobic cavity (see Fig. 1). It is in this hydrophobic cavity that the analyte is complexed and placed in a hydrophobic environment. This leads to fluorescence quenching protection (for example, from water) that can lead to a fluorescence enhancement effect [18].

The complexation of the analyte by β-cyclodextrin (β-CD) is influenced by the van der Waals interaction, hydrogen bonding, displace-

[1] Visiting Faculty at Oak Ridge National Laboratory.
* Corresponding author.

*SSDI* 0039-9140(95)01607-4

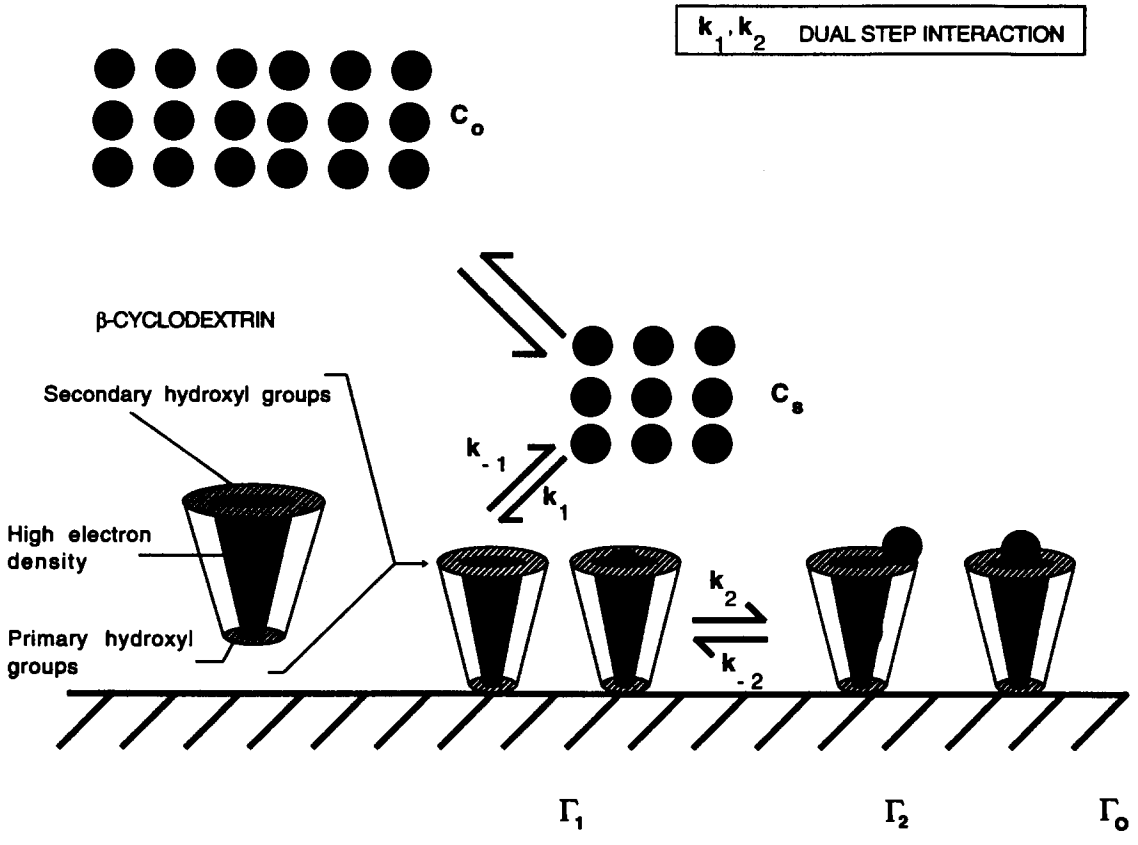


Fig. 1. Elementary steps involved in the binding of the pyrene (analyte) in solution to the $\beta$-cyclodextrin ($\beta$-CD) immobilized to the chemical sensor surface (dual-step binding).

ment of high energy molecules from the cavity, and release of the strain energy of the $\beta$-CD on inclusion of the guest molecule [19,20]. Furthermore, the hydrophobicity of the guest molecule plays a critical role in the stability of the complex. Considering the different factors that are involved in the formation of the complex, it is reasonable to assume that, in the real situation, one obtains a distribution (Gaussian or otherwise) or inhomogeneity of the "sequestered" analyte states in the $\beta$-cyclodextrin cavity. Furthermore, the sequesteration of an analyte molecule may very reasonably influence the complexation of the analyte by nearby $\beta$-cyclodextrin molecules (the "nearest neighbor" effect). Also, it has been emphasized that the extent of complexation, which is directly connected to the sensitivity is strongly dependent on analyte geometry as well as on functional group orientation [16]. It has been indicated [21] that these types of surface irregularities or inhomogeneities may be characterized using Mandelbrot's non-Euclidean fractal geometry [22].

Fractal analysis has provided novel physical insights into the diffusion-limited reactions occurring at the antibody–antigen interface [23,24]. It is worthwhile extending the fractal analysis concept for antibody–antigen systems for biosensor applications to $\beta$-cyclodextrin–analyte systems for chemical sensor applications. More generally, one may extend the analysis to "receptor–analyte" systems. It has been emphasized that when too many parameters are involved in a reaction, the fractal dimension for reactivity may be useful as an "integrated" or "lumped" parameter [25]. There is no reason to believe that the fractal analysis should be restricted only to antibody–antigen reaction systems. The capture of different molecules by $\beta$-cyclodextrins immobilized on a chemical sensor surface may also, as indicated above, in the general sense, be analyzed by the treatment presented below.

Fractals are disordered systems which can be described in terms of non-integral dimensions [26]. The fractal dimension is a global property, and is insensitive to structural or morphologi-

cal details [27]. As long as surface irregularities show scale invariance (that is, dilatation symmetry) they can be characterized by a single number, the fractal dimension, $D_f$ [27].

Antibodies are heterogeneous and their immobilization on a fiber-optic surface, for example, would exhibit a certain degree of heterogeneity. Similarly, the immobilization of $\beta$-cyclodextrins on a silica optical fiber by Armstrong's method [28] would also exhibit some degree of heterogeneity. In this method a silanized silica gel is obtained with thermal epoxy, alkene, or haloalkyl groups by reacting by anhydrous organic solvent containing $C_{2-20}$ silanes with a high purity particulate silica gel. These are good examples of a "disordered" system, and a fractal analysis is appropriate for such systems. In this type of diffusion–reaction system, the diffusion is conventional in the sense that it follows the classical diffusion equation. It is the boundary condition on the fractal surface (chemical sensor surface in our case) that is complicated. The cyclodextrin–analyte reactions on the surface are good examples of a low dimension reaction system in which the distribution tends to be "less random" [29].

In this paper the fractal dimension values for the kinetics of the binding of pyrene molecules (analyte) to immobilized $\beta$-cyclodextrin in a chemical sensor system is presented and analyzed. The influence of a variable (pyrene concentration) on the fractal dimension value is also presented and analyzed.

## 2. Theory

The binding of the antigen in solution to the antibody on the surface has been described previously [30,31]. It is briefly presented here as a model example since no formal presentation of $\beta$-cyclodextrin–analyte binding kinetics presumably is available in the literature. It is anticipated that the general form of the "capture kinetics" of molecules in solution by "receptors" immobilized on a chemical sensor surface would also exhibit similar characteristics (kinetics).

### *2.1. Analyte in solution/receptor on the surface [32]*

*Dual-step binding*

The modeling of binding of an analyte in solution to a "receptor" immobilized on the surface is done in a two-step process. The elementary steps involved in the reaction scheme are shown in Fig. 1. Here $\Gamma_0$ is the total concentration of the receptor sites on the surface, $\Gamma_1$ is the surface concentration of receptors that are bound to a single analyte at any time $t$, $c_S$ is the concentration of the analyte close to the surface, $k_1$ and $k_2$ are the forward reaction rate constants, $k_{-1}$ and $k_{-2}$ are the reverse reaction rate constants, and $\Gamma_2$ is the surface concentration of the receptor which binds two analyte molecules. For initial binding kinetics, it has been shown that the rate of binding can be described by Eq. (1) [31]:

$$d\Gamma_1/dt = k_f c_s^2 \Gamma_0 \tag{1}$$

## 3. Variable rate coefficient

Kopeman [29] has recently indicated that classical reaction kinetics are sometimes unsatisfactory when the reactants are spatially constrained on the microscopic level by either walls, phase boundaries, or force fields. Such heterogeneous reactions, for example bioenzymatic reactions, that occur at interfaces of different phases, exhibit fractal orders for elementary reactions and rate coefficients with temporal memories. In such reactions, the rate coefficient exhibits a form given by

$$k_1 = k' t^{-h} \qquad 0 \leqslant h \leqslant 1 \qquad (t \geqslant 1) \tag{2}$$

In general, $k_1$ depends on time, whereas $k' = k_1(t = 1)$ does not. Kopelman [29] further indicates that in three dimensions (homogeneous space), $h$ equals zero. This is in agreement with the results obtained in classical kinetics. Also, with vigorous stirring, the system is made homogeneous and $h$ again equals zero. However, for diffusion-limited reactions occurring in fractal spaces, $h > 0$; this yields a time-dependent coefficient.

Havlin [33] has briefly reviewed the role of the diffusion of reactants towards fractal surfaces and indicates that the diffusion of a particule (for example, analyte) from the homogeneous solution to a solid surface (the chemical sensor surface) where it reacts to form a product (analyte–"receptor" complex) is given by [34–36]

$$(\text{Analyte–receptor}) \propto \begin{cases} t^{(3-D_f)/2} = t^{h} & t < t_c \\ t^{1/2} & t > t_c \end{cases} \tag{3}$$

Table 1
Experimental and predicted values of the fractal dimension $D_f$ and the integrated binding rate coefficient $k_1$ for a $\beta$-cyclodextrin fiber-optic chemical sensor

| Pyrene concentration (ng ml$^{-1}$) | $k_1$ | | $p$ | $D_f$ | |
|---|---|---|---|---|---|
| | Experimental | Predicted | | Experimental | Predicted |
| (a) | | | | | |
| 12.4 | 207.1 ± 11.04 | 222.9 ± 5.50 | 0.2766 ± 0.029 | 2.4468 ± 0.058 | 2.4433 ± 0.048 |
| 62.0 | 1104 ± 75.23 | 1115 ± 27.50 | 0.2121 ± 0.038 | 2.5758 ± 0.076 | 2.5803 ± 0.0511 |
| 99.8 | 1899 ± 152.2 | 1794 ± 44.27 | 0.1991 ± 0.045 | 2.6018 ± 0.090 | 2.6223 ± 0.0519 |
| 124 | 2152 ± 179.5 | 2229 ± 55.01 | 0.1684 ± 0.047 | 2.6332 ± 0.094 | 2.6417 ± 0.0526 |
| (b) | Non-specific binding studies: no $\beta$-cyclodextrin immobilized | | | | |
| 12.4 | 62.86 ± 21.18 | 54.97 ± 0.0997 | 0.2036 ± 0.206 | 2.5928 ± 0.412 | – [a] |
| 62.0 | 286.9 ± 136.0 | 274.8 ± 4.981 | 0.1484 ± 0.294 | 2.7032 ± 0.588 | – [a] |
| 99.8 | 449.7 ± 206.7 | 438.6 ± 8.018 | 0.1527 ± 0.285 | 2.6946 ± 0.569 | – [a] |
| 124 | 534.0 ± 248 | 549.7 ± 9.962 | 0.1481 ± 0.289 | 2.7038 ± 0.577 | – [a] |

[a] Not predicted.

where $D_f$ is the fractal dimension of the surface and $p$ is a coefficient. Havlin indicates that the cross-over value $t_c$ (where the fractal nature is lost) may be determined by $t_c \approx r_c^2$. Above the characteristic length $r_c$, the self-similarity of the surface is lost and may be considered homogeneous. Note that the product (analyte–receptor) in the reaction, analyte + receptor → (analyte–receptor), on a solid fractal surface scales with $p = (3 - D_f)/2$ at short time scales, and $p = 1/2$ at intermediate time scales. The equation is associated with the short-term properties of a random walk on a fractal surface. Also, note that in perfectly stirred kinetics on a regular surface, $k_1$ is a constant, and is independent of time. The appearance of the exponent $p = -b$ different from $p = 0$ is the consequence of two different phenomena: the heterogeneity (fractality of the surface), and the imperfect mixing (diffusion-limit) condition.

## 4. Experimental

### 4.1. Optical configuration

The optical system configuration has been described previously [17]. Briefly, the 325 nm line of an He–Cd laser was passed through a beam splitter consisting of a mirror with a 2 mm pinhole through its center. The laser beam was then focused into the distal end of the optical fiber. The fluorescence emitted was transmitted back through the fiber, reflected by the mirror and focused into the photomultiplier detector with a 400 ± 10 nm bandpass filter selecting the fluorescence wavelength. The current from the photomultiplier tube was measured with a picoammeter and recorded on a strip chart recorder.

The fibers were derviatized with $\beta$-CD as previously described [17]. In this case, the fibers were pulled to a 25 nm tip using a Sutter Instruments model P-2000 fiber puller prior to derivatization with $\beta$-CD.

### 4.2. Measurements

All measurements were performed as follows. The fiber was placed in distilled $H_2O$ to determine the baseline and background signal. The fiber was then placed in the pyrene solution and the fluorescence signal was monitored periodically over the 10 min incubation period. All curve-fittings procedures were performed using SigmaPlot (Jandal Scientific, San Rafael, CA).

## 5. Results

Alarie and Vo-Dinh [17] have developed a CD-based fiber-optic chemical sensor with $\beta$-CD immobilized at the distal face of an optical fiber. Their process combines the selectivity of the CD along with enhancement of the fluorescence of the complexed molecule, pyrene. Detailed studies of the capture of pyrene present in different initial concentrations in solution by $\beta$-CD immobilized on an optical fiber were performed (Table 1(a)). In this study the influence of non-specific binding (no $\beta$-CD immobilized on the optical fiber) was also analyzed (Table 1(b)).

In the pyrene concentration range studied (12.4–124 ng ml$^{-1}$) an increase in the pyrene concentration in solution increases $D_f$ or the inhomogeneity (disorder) on the surface. Table 1(a) shows the values (along with the error bars) of the fractal dimension $D_f$ and the binding rate coefficient $k_1(t = 1)$. An increase in the pyrene concentration by a factor of 10 from 12.4 to 124 ng ml$^{-1}$ increases the fractal dimension by 7.6% from 2.4468 to 2.6332. The high values of $D_f$ obtained indicate a significant amount of spatial inhomogeneity at the analyte–receptor interface. The fractal dimension $D_f$ may provide a useful integrated parameter for evaluating sensor performance and a predictive equation for $D_f$ was generated in an attempt to understand (a) the nature of $D_f$ and (b) how $D_f$ changes with pyrene concentration. In the pyrene concentration range studied, $D_f$ may be represented by

$$D_f = (2.243 \pm 0.04438)[\text{pyrene}]^{0.03391 \pm 0.0048} \quad (4)$$

Different functional forms were attempted such as the linear form, etc. Eq. (4) accurately predicts within 1% the $D_f$ values obtained in the pyrene concentration range studied. Note the functional form of the slight dependence (of "empirical" power 0.034) of $D_f$ on the pyrene concentration. This non-integer dependence indicates mechanistic complexities at the reaction interface, and also points towards or lends support to the fractal nature of the surface. Further studies are required to delineate the significance of this power dependence, presumably by unraveling the elementary steps involved in the reaction mechanism, and/or by making more quantitative the extent of disorder or inhomogeneity that exists on the surface. It is also of interest to note that an increase in pyrene concentration in solution leads to increases in both the $D_f$ and $k_1$ values. In other words, higher degrees of inhomogeneity on the surface also yield higher binding rate coefficients, in this case. Previous work on antibody–antigen systems also shows this type of behaviour [37]. Further experiment along the theoretical modeling is required to "tie-in" the changes in the fractal dimension with biosensor performance parameters such as sensitivity, stability, response time, and reproducibility.

Fig. 2 shows the fit of Eq. (3) for the amount of pyrene in solution bound to the $\beta$-CD. Once again, the model is able to fit the experimental data with a high degree of accuracy. A model involving a constant binding rate coefficient $k_1$ cannot fit the data (especially the curve nature at later times); thus this is a simple way of justifying (pictorially) why a time-dependent (temporal) coefficient works better than a constant $k_1$. Besides, the fractal and changing nature of the surface warrants the utilization of a temporal binding coefficient vis-a-vis a constant binding coefficient. One notes that an increase in the pyrene concentration in solution increases the $k_1$ value. An increase in the pyrene concentration by a factor of 10 from 12.4 to 124 ng ml$^{-1}$ increases $k_1$ by a factor of 10.38 from 207.1 to 2152. In the pyrene concentration range studied, $k_1$ may be represented by Eq. (5):

$$k_1 = (17.98 \pm 0.4436)[\text{pyrene}] \quad (5)$$

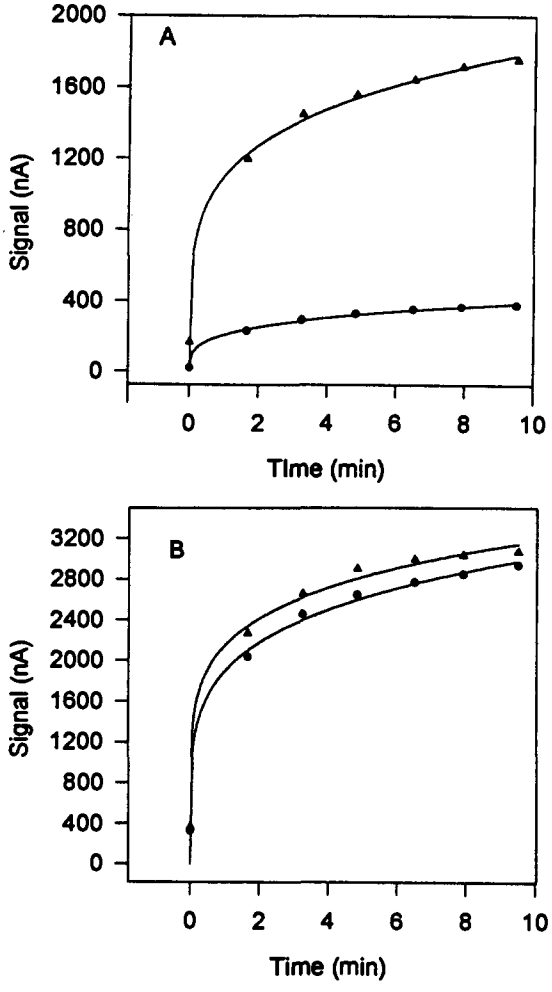


Fig. 2. Fit of the model (Eq. (3)) to the binding of different initial pyrene concentrations in solution to the $\beta$-CD immobilized to the chemical sensor surface: (A) ●, 12.4 ng ml$^{-1}$; ▲, 62 ng ml$^{-1}$. (B) ●, 99.8 ng ml$^{-1}$; ▲, 124 ng ml$^{-1}$.

where [pyrene] is the concentration (ng ml$^{-1}$). The predicted values of $k_1$ (Table 1) obtained from Eq. (5) are within 8% of the experimental $k_1$ values obtained by the curve-fitting procedure. Predictive equations for the binding coefficient would be of considerable assistance in the design of biosensors, besides helping to understand better the reactions and kinetics at the interface.

Non-specific binding can play a significant role in the development of effective fiber-optic biochemical and chemical sensors since it affects the sensitivity, stability, response time, and reproducibility of these sensors. Often, only estimates of the amount of non-specific binding relative to the amount of specific binding are available in the literature.

Table 1(b) shows the values (along with error bars) of the fractal dimension $D_f$ and the binding rate coefficient for non-specific binding, $k_{ns}$. As seen in Table 1, the error bars for $D_f$ are four to six times the change in the $D_f$ values obtained. This makes it impossible to develop accurately a functional form for $D_f$. For all practical purposes, considering the error bars, there is hardly any change in $D_f$ as the pyrene concentration in solution changes by a order of magnitude from 12.4 to 124 ng ml$^{-1}$. Strictly speaking, there is no "chemical" driving force to the chemical sensor surface, i.e. there is no complexation. Apparently, in this case the extent of inhomogeneity or disorder on the surface is "dominated" by the characteristics of the non-specific binding, with "minor" contributions coming in due to increased pyrene concentrations in solution. Note that in this case the pyrene is not "permanently" adsorbed. The removal of the chemical sensor from the pyrene solution and placing it in water yields a very small residual signal. In the $\beta$-CD case, a strong signal remains from the complexed pyrene–$\beta$-CD.

Fig. 3 shows the fit of Eq. (3) for the amount of pyrene in solution "reversibly" adsorbed to the fiber-optic chemical sensor with no $\beta$-CD immobilized to the fiber-optic surface. Once again, Eq. (3) is able to fit the experimental data reasonably well. An increase in the pyrene concentration increases $k_{ns}$ (as also observed for the specific binding rate coefficient $k_1$). An increase in the pyrene concentration by a factor of 10 from 12.4 to 124 ng ml$^{-1}$ increases $k_{ns}$ by a factor of 8.5 from 62.86 to 534. Note the relatively high values of the error bars for $k_{ns}$ values for all of the pyrene concentrations

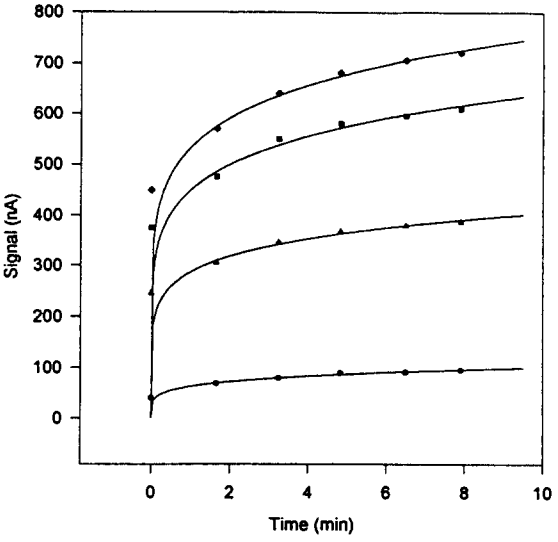


Fig. 3. Fit of the model (Eq. (3)) to the binding of different initial pyrene concentrations in solution directly to the chemical surface (with no $\beta$-CD attached — non-specific binding): ●, 12.4 ng ml$^{-1}$; ▲, 62 ng ml$^{-1}$; ■, 99.8 ng ml$^{-1}$; ◆, 124 ng ml$^{-1}$.

studied. Presumably, this reflects a characteristic (at present, undetermined) of the non-specific binding of the polycyclic aromatic hydrocarbon in solution directly to the fiber-optic surface. In the pyrene concentration range studied, $k_{ns}$ may be represented by Eq. (6):

$$k_{ns} = (4.433 \pm 0.08034)[\text{pyrene}] \quad (6)$$

Eq. (6) fits the $k_{ns}$ values in the pyrene concentration range studied within 13%.

## 6. Conclusion

The fractal analysis of the $\beta$-cyclodextrin–pyrene reaction occurring on the chemical sensor surface provides a semi-quantitative indication of the state of disorder and inhomogeneity of the system at the "receptor–analyte" surface.

The data presented in Table 1(a) and Table 1(b) provide valuable physical insights by providing a "semi-quantitative" measure of the degree of disorder or inhomogeneity that exists on the chemical sensor surface. The influence of the pyrene concentration in solution on the specific $k_1$ and non-specific $k_{ns}$ binding rate coefficients and on the fractal dimension $D_f$ could be correlated. When $\beta$-CD is immobilized on the fiber-optic surface, one notes that an increase in the pyrene concentration in solu-

tion increases both the $k_1$ and $D_f$ values. It is of interest to note that an increase of the spatial inhomogeneity or disorder on the surface (increasing $D_f$ values) with higher pyrene concentrations in solution leads to higher $k_1$ values. "Predictive type" relations suggested for $D_f$ and $k_1$ are of considerable value in helping to design biosensors and in understanding the kinetics. These equations do seem to fit the calculated values of $k_1$ and $D_f$ respectively well.

When no $\beta$-CD is attached to the fiber-optic surface (non-specific binding studies), one notes that an increase in the pyrene concentration in solution increases the non-specific binding rate coefficient $k_{ns}$ values. The high error bars obtained for $k_{ns}$ values indicates presumably a characteristic of non-specific binding, at least for this case. More data of this type and for other chemical sensor systems are required to help further validate and/or modify the above for chemical sensor applications. Further studies on the complexation of pyrene and of other analytes of interest by $\beta$-CD will be undertaken in this laboratory in the near future to delineate further the reaction complexities and the degree of inhomogeneity that exists at the chemical sensor surface.

The fractal analysis of the $\beta$-CD–pyrene chemical sensor application helps provide novel physical insights into the conformational states of the $\beta$-CD–pyrene binding complex on the chemical sensor surface. The analysis of different chemical sensors taken together would help form a framework, wherein the data on different chemical sensors may be compared. The build-up of the database on conformational states should also assist in helping to improve the sensitivity, stability, reproductibility, and reaction time of fiber-optic chemical sensors. Predictive relations for $k_1$, $D_f$ and for other important parameters are particularly appealing, and should be of considerable assistance in the design of chemical sensors. It may be recommended that further similar studies (both theoretical as well as experimental) be carried out to delineate further the conformational states of the "receptor–analyte" on chemical sensor surfaces.

## Acknowledgements

This work was sponsored by the U.S. Department of Energy, Office of Health and Environmental Research under contract DE-AC05-84OR214000 with Martin Marietta Energy Systems and the ORNL Laboratory Directed Research and Development Funds (LDRD-Biosensor Project). This research was supported by the appointment of A. Sadana to the ORISE 1994 Summer Faculty Research Program at ORNL.

## References

[1] T. Vo-Dinh, G.D. Griffin and K.R. Ambrose, Appl. Spectrosc., 40(5) (1986) 696.
[2] T. Vo-Dinh, B.J. Tromberg, G.D. Griffin, K.R. Ambrose, M.J. Sepaniak and E.M. Gardenhire, Appl. Spectrosc., 5 4(5) (1987) 735.
[3] T. Vo-Dinh, T. Nolan, Y.F. Cheng, M.J. Sepaniak and J.P. Alarie, Appl. Spectrosc., 44(1) (1990) 128.
[4] T. Vo-Dinh, M.J. Sepaniak, G.D. Griffin and J.P. Alarie, Immunomethods, 3 (1993) 85.
[5] B.J. Tromberg, M.J. Sepaniak, T. Vo-Dinh and G.D. Griffin, Anal. Chem., 59 (1987) 1226.
[6] B.J. Tromberg, M.J. Sepaniak, J.P. Alarie, T. Vo-Dinh and R.M. Santella, Anal. Chem., 60 (1988) 1901.
[7] J.P. Alarie, M.J. Sepaniak and T. Vo-Dinh, Anal. Chim. Acta, 225 (1990) 169.
[8] B.I. Bluestein, M. Craig, G. Slovacek, L. Stundtner, C. Uricouli, I. Walczak and A. Luderer, Evanescent Wave Immunosensors for Clinical Diagnostic, in D. Wise and I.B. Wingard, Jr. (Eds), biosensors with fiberoptics, The Humana Press, New York, NY, 1991.
[9] E. Eddowes, Biosensors, 3 (1987/1988) 1.
[10] N. Hygren and M. Stenberg, J. Colloid Interface Sci., 107 (1985) 560.
[11] J.F. Place, R.M. Sutherland and C. Dahne, Biosensors 1 (1985) 321.
[12] M.J. Sepaniak, M.J. Tromberg, J.P. Alarie, J.R. Bowyer, A.M. Hoyt and T. Vo-Dinh, Design considerations for antibody-based fiberoptic chemical sensors, in W.R. Heineman, J. Janata and W.R. Seitz (Eds.), chemical sensors and miocroinstrumentation, American Chemical Society, Washington, DC, 1989 Chapter 21, p. 318.
[13] R.M. Sutherland, C. Dahne, J.F. Place and A.S. Ringrose, Clin. Chem. 30(9) (1984) 1533.
[14] M. Stenberg, L. Stiblert and H. Nygren, J. Theor. Biol., 120 (1986) 129.
[15] J.F. Place, R.M. Sutherland, A. Riley and C. Mangan, Immunoassay kinetics at continuous surfaces, in D. Wise and L.B. Wingard, Jr. (Eds.), biosensors with fiberoptics, The Humana Press, New York, NY, 1991.
[16] F.V. Bright, Appl. Spectrosc., 47(8) (1993) 1152.
[17] J.P. Alarie and T. Vo-Dinh, Talanta, 38(5) (1991) 529.
[18] A.M. Alak, E. Heiwel, W.L. Hinze, K. Oh and D.W. Armstrong, J. Liq. Chromatogr., 7 (1984) 1273.
[19] J. Szejtli, cyclodextrins and their inclusion complexes, Akademiai Kiado, Budapest, 1982.
[20] K.S. Litwiler, G.C. Catena and F.V. Bright, Anal. Chim. Acta, 237 (1990) 485.
[21] D. Avnir, D. Farin, and P. Pfeifer, J. Colloid Interface Sci. 103(1) (1985) 112.
[22] B.B. Mandelbrot, the fractal geometry of nature, Freeman, San Francisco, CA, 1982.

[23] A. Sadana and A. Madugula, Biosens. Bioelectron., 9(1) (1994) 45.
[24] A. Sadana and A. Beela Ram, Biotechnol. Prog., 10 (1994) 291.
[25] G. Daccord, Dissolutions, Evaporations, Etchings, in D. Avnir (Ed.), The fractal approach to heterogeneous chemistry: surfaces, colloids, polymers, Wiley, New York, 1989, p. 181.
[26] P. Pfeifer and M. Obert, Fractals: basic concepts and terminology, in D. Avnir (Ed.), The fractal approach to heterogeneous chemistry: surfaces, colloids, polymers, Wiley, New York, 1989 p. 11.
[27] T. Pajkossy and L. Nyikos, Electrochim. Acta 34(2) (1989) 171.
[28] D.W. Armstrong, U.S. Patent 4 539 399, 1985; Chem. Abstr., 103 (1985) 226754f.
[29] R. Kopelman, Science, 241 (1988) 1620.
[30] A. Sadana and D. Sii, J. Colloid Interface Sci., 151(1) (1992) 166.
[31] A. Sadana and D. Sii, Biosens. Bioelectron., 7 (1992) 559.
[32] A. Sadana and A. Madugla, Biotechnol. Prog., 9 (1993) 259.
[33] S. Havlin, Molecular diffusion and reactions, in D. Avnir (Ed.), the fractal approach to heterogeneous chemistry: surfaces colloids, polymers, Wiley, New York, 1989, p. 251.
[34] L. Nyikos and T. Pajkossy, Electrochim. Acta, 31(10) (1986) 1347.
[35] P.G. De Gennes, Radiat. Phys. Chem., 22 (1982) 193.
[36] P. Pfeifer, D. Avnir and J. Farin, J. Colloid Interface Sci., 103(1) (1984) 112.
[37] A. Sadana, J.P. Alarie and T. Vo-Dinh, Sens. Actuators, in press.

ELSEVIER

Talanta 42 (1995) 1575–1579

Talanta

# Fluorimetric determination of hydrogen peroxide in water using acetaminophen

Nianqin Jie [a,*], Jinghe Yang [a], Xirong Huang [a], Rui Zhang [a], Zhongqing Song [b]

[a] *Department of Chemistry, Shandong University, Jinan, China*
[b] *Chemistry Teaching-Research Section, Dalian Maritime University, Dalian, China*

Received 19 January 1995; accepted 3 April 1995

**Abstract**

A fluorimetric procedure for the determination of hydrogen peroxide, based on the oxidation of acetaminophen with hydrogen peroxide in acidic medium, is described. The calibration graph was linear in the range $5.0 \times 10^{-8}$–$2.4 \times 10^{-5}$ M hydrogen peroxide at an emission wavelength of 333 nm with excitation at 298 nm. The method has been applied to the determination of hydrogen peroxide in rain water, and the recoveries in milk samples were good.

## 1. Introduction

Hydrogen peroxide is produced by photochemical reactions in the atmosphere. Acid rain may possibly form when hydrogen peroxide reacts with $SO_2$ [1]. Therefore the chemistry of hydrogen peroxide is very important in the field of environmental science. In addition, its carcinogenicity has raised interest in recent years. A rapid, simple method for its microlevel determination is needed. Fluorimetric methods for the determination of hydrogen peroxide have been reported [2–4]. Some of the methods require very expensive reagents.

The use of acetaminophen as a fluorescent reagent for the determination of Ce(IV) has been developed [5]. In this paper, a new fluorimetric method, based on the oxidation of non-fluorescent acetaminophen to a fluorescent compound by hydrogen peroxide in 0.12 M $H_2SO_4$, is described. The method possesses distinct advantages over other fluorimetric methods with respect to simplicity, expense, and determination range.

* Corresponding author.

## 2. Experimental

### 2.1. Apparatus

An RF-540 spectrofluorimeter (Shimadzu, Kyoto, Japan) was used.

### 2.2. Reagents

Analytical-grade reagents and distilled water were used throughout.

A solution of hydrogen peroxide was prepared by dilution of a 30% solution and was checked by permanganimetry.

Acetaminophen stock solution (0.01 M) was prepared by dissolving 0.3780 g of acetaminophen in warm water, stirring for 10 min and diluting to 250 ml in a calibrated flask after cooling.

Sulphuric acid solution of concentration 2 M was used.

### 2.3. Procedure

To a 25 ml volumetric flask were added 2.5 ml of acetaminophen solution ($1.0 \times 10^{-2}$ M), 1.5 ml of sulphuric acid solution (2 M) and


*SSDI* 0039-9140(95)01603-1

a suitable working solution of hydrogen peroxide. The flask was placed in a boiling-water bath for 40 min, then it was cooled under tap water and diluted to the mark with water. The fluorescence intensity resulting from an excitation wavelength of 298 nm and an emission wavelength of 333 nm was measured against a reagent blank.

## 3. Results and discussion

### 3.1. Fluorescence spectra

The excitation and emission spectra of the system investigated are shown in Fig. 1. The fluorescent species has excitation and emission maxima at 298 nm and 333 nm, respectively.

### 3.2. Effect of acetaminophen concentration

The effect of acetaminophen concentration on the fluorescence intensity of the system was studied. It was found that a maximum and constant fluorescence intensity was obtained for acetaminophen concentrations in the range $8.0 \times 10^{-4}$–$1.1 \times 10^{-3}$ M. An acetaminophen concentration of $1.0 \times 10^{-3}$ M was selected (Fig. 2).

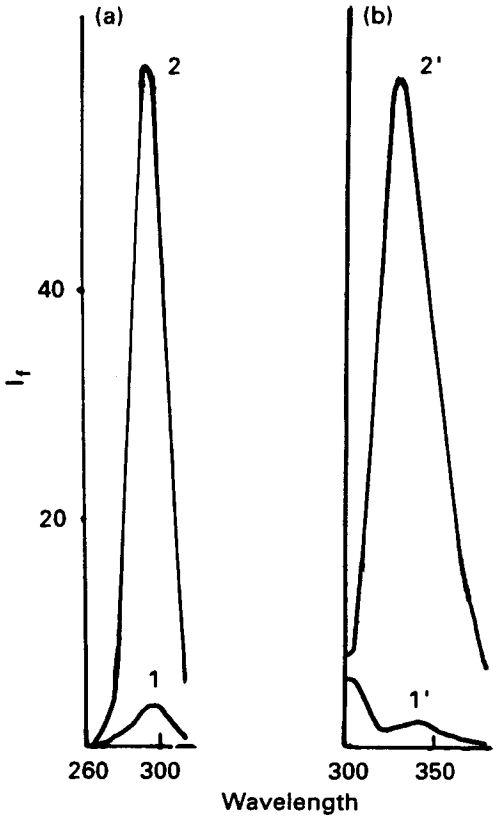


Fig. 1. Fluorescence spectra: (a) excitation, 298 nm; (b) emission, 333 nm. Curves 1 and 1', acetaminophen–$H_2SO_4$ system (reagent blank): curves 2 and 2', acetaminophen–$H_2O_2$–$H_2SO_4$ system. Conditions: $[H_2O_2]$, $4.0 \times 10^{-6}$ M; [acetaminophen], $1.0 \times 10^{-3}$ M; $[H_2SO_4]$, 0.12 M.

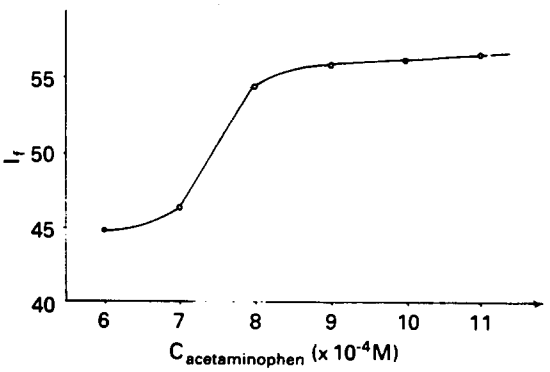


Fig. 2. Effect of acetaminophen concentration. Conditions as in Fig. 1.

### 3.3. Effect of sulphuric acid concentration

The experimental results indicated that when the concentration of sulphuric acid was between 0.08 and 0.16 M, the fluorescence inten-

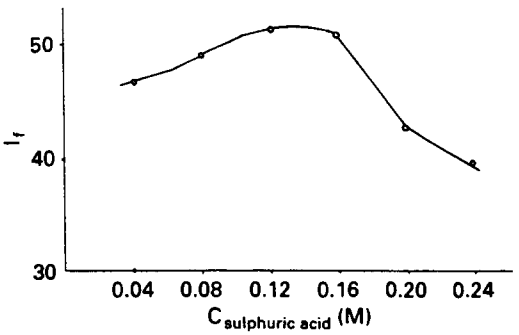


Fig. 3. Effect of sulphuric acid concentration. Conditions as in Fig. 1.

Table 1
Tolerance limits for interfering ions [a]

| Ion | Ratio to $H_2O_2$, (w/w) |
|---|---|
| $F^-$ | 200 |
| $K^+$, Mo(VI) | 150 |
| $Ca^{2+}$, $Sr^{2+}$, $Mg^{2+}$, $Zn^{2+}$ | 100 |
| $Be^{2+}$, $Cd^{2+}$, $C_2O_4^{2-}$ | 50 |
| Sn(IV), $Pb^{2+}$, $I^-$, $Cl^-$ | 30 |
| $Cu^{2+}$, EDTA | 20 |
| Cr(III) | 5, 100 [b] |
| Fe(III) | 3, 50 [b] |
| Hg(II), Cr(VI) | 1, 80 [b] |

[a] $H_2O_2$, 1 μg per 25 ml.
[b] In the presence of 0.02 M EDTA.

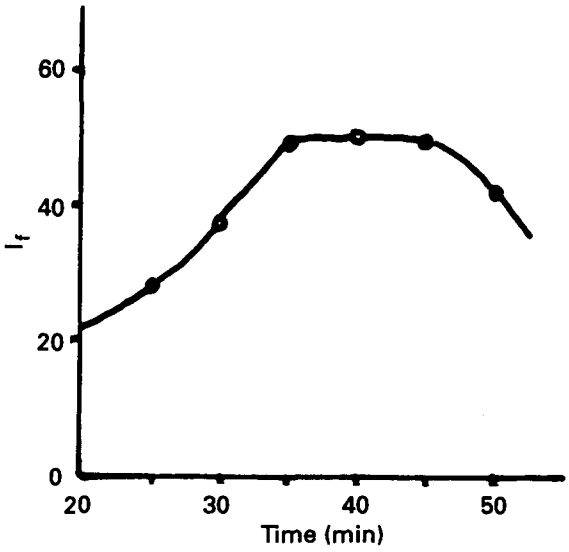


Fig. 4. Effect of heating time. Conditions as in Fig. 1.

sity reached a maximum. A sulphuric acid concentration of 0.12 M was chosen (Fig. 3).

### 3.4. Effect of temperature and time

Optimal reaction conditions of temperature and time were investigated for the assay of hydrogen peroxide, and a standard procedure was established, involving standing for 40 min at 100°C (Fig. 4).

### 3.5. Calibration graph

A linear calibration graph of fluorescence intensity of the system vs. hydrogen peroxide concentration was obtained, covering the ranges $5.0 \times 10^{-8}$–$2.8 \times 10^{-6}$ M and $2.0 \times 10^{-6}$–$2.4 \times 10^{-5}$ M. The detection limit is $1.5 \times 10^{-8}$ M, the blank plus three times the standard deviation of the blank [6].

### 3.6. Effect of diverse ions

The influence of diverse ions on the determination of 1 μg per 25 ml of hydrogen peroxide was examined, and the tolerance limits were taken as the amounts that caused about a ± 5% error in the fluorescence intensity. Table 1 shows that only Fe(III), Hg(II), and Cr(VI) caused severe interference, because of their oxidizing nature. These ions can be masked by adding EDTA.

### 3.7. Application

The proposed method was used to assay hydrogen peroxide in rain water. The samples were collected and filtered before analysis. A suitable volume of rain water was transfered to a 25 ml volumetric flask. The determination was carried out by the procedure described above. The results obtained are presented in Table 2. The recovery of hydrogen peroxide in rain water was 96–102%.

In addition, the recovery of hydrogen peroxide in milk was tested. To 1 ml of pasteurized milk were added 0.1 ml of glacial acid and 2.5 μg, 5.0 μg, or 12.0 μg of hydrogen peroxide. The solution was mixed and centrifuged, and the supernatant was assayed. The recovery was good (95%, 98%, and 102%, respectively).

### 3.8. Luminescence mechanism

Sultan et al. [7] reported that acetaminophen is oxidized by Ce(IV) to form *p*-benzoquinone, which has been used for the spectrophotometric determination of acetaminophen (paracetamol). In this system, acetaminophen might be oxidized to p-benzoquinone. In order to investigate the nature of the reaction product of the system, the ultraviolet and fluorescence spectra of the acetaminophen–$H_2SO_4$–$H_2O_2$ and *p*-benzoquinone–$H_2SO_4$ systems were studied. Fig. 5 shows that *p*-benzoquinone in 0.12 M sulphuric acid solution has excitation and emission maxima at 298 nm and 333 nm, respectively. This is similar to those of the acetaminophen–$H_2SO_4$–$H_2O_2$ system. The ultraviolet spectra show that the absorption bands of the two systems are also very similar (Fig. 6). These results indicate that a product might be *p*-benzoquinone. The reaction between acetaminophen and hydrogen peroxide is as follows:

Table 2
Determination of $H_2O_2$ in rain water

| Sample | $H_2O_2$ found (μg ml$^{-1}$) | |
|---|---|---|
| | Proposed method | Other method [a] |
| 1 | 0.38 | 0.40 |
| 2 | 0.56 | 0.61 |

[a] Using HPMQ (*N*–(4'-hydroxyphenyl)-*N*-(4-methylquinolinyl)-amine) as the fluorescent reagent (Ref. [4]).

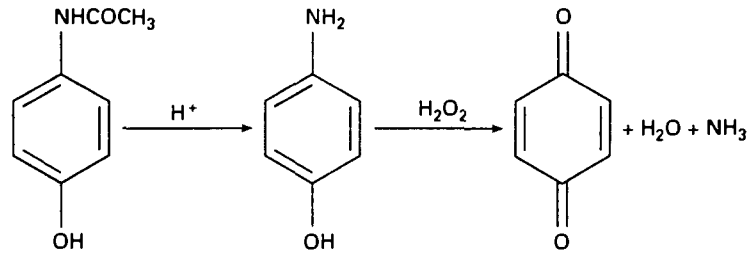


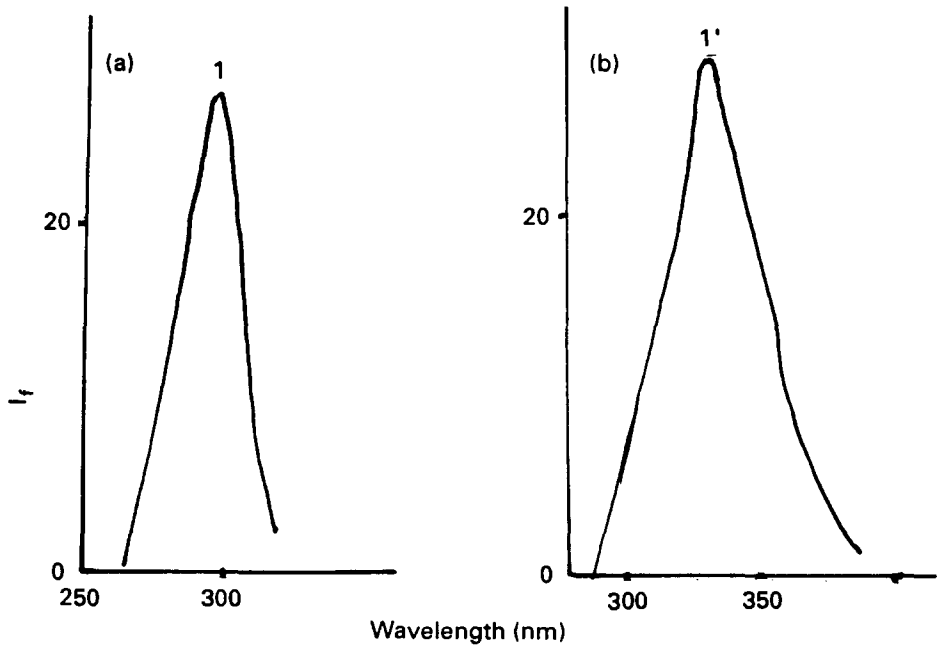


Fig. 5. Fluorescence spectra: (a) excitation, 298 nm; (b) emission, 333 nm. Curves 1 and 1', $p$-benzoquinone–$H_2SO_4$ system. ([$H_2SO_4$], 0.12 M.)

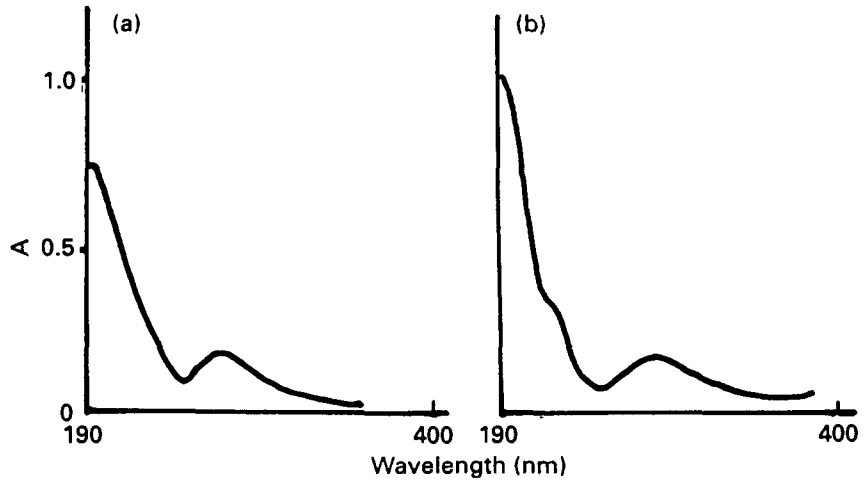


Fig. 6. Ultraviolet spectra: (a) $H_2O_2$ (excess)–acetaminophen–$H_2SO_4$ system; (b) $p$-benzoquinone–$H_2SO_4$ system. ([$H_2SO_4$], 0.12 M).

## 4. Conclusions

In summary, this report presents a new fluorimetric method useful for the determination of hydrogen peroxide in rain water. The method is rapid, simple and inexpensive.

## References

[1] C. Seigneur and P. Saxema, Atmos. Environ., 18 (1989) 2109.
[2] T.R. Holm, G.K. George and M.J. Barcelina, Anal. Chem., 59 (1987) 582.
[3] Y. Ci and F. Wang, Chem. J. Chin. Univ., 10 (1989) 229.
[4] I. Mori, Y. Fujita, M. Toyoda, K. Kato, N. Yoshida and M. Ykagl, Talanta, 38 (1991) 683.
[5] N.Q. Jie, J.H. Yang and T. Liu, Talanta, 41 (1994) 415.
[6] ACS Committee on Environmental Improvement, Anal. Chem., 52 (1980) 2242.
[7] S.M. Sultan, L.Z. Alzamil, A.M. Aziz, S.A. Altamrah and Y. Ashs, Analyst, 111 (1986) 919.

ELSEVIER

Talanta 42 (1995) 1581–1593

Talanta

# Compositions and structures of copper hexacyanoferrates(II) and (III): experimental results

S. Ayrault [a], C. Loos-Neskovic [a,*], M. Fedoroff [b], E. Garnier [c], D.J. Jones [d]

[a] *Laboratoire P. Süe, C. E. N. Saclay, 91 191 Gif-sur-Yvette, France*

[b] *Centre d'Etudes de Chimie Métallurgique, 15, rue Georges Urbain, 94 407 Vitry-sur-Seine, France*

[c] *Laboratoire de Chimie Théorique, Université de Poitiers, 40, Avenue du Recteur Pineau, 86 022 Poitiers, France*

[d] *Laboratoire des Agrégats Moléculaires et Matériaux Inorganiques, Université Montpellier II, Place Eugène Bataillon, 34 095 Montpellier, France*

Received 13 February 1995; revised 4 April 1995; accepted 7 April 1995

**Abstract**

The preparation, composition and structure of copper hexacyanoferrates have been investigated. Three methods were used: precipitation, local growth in an aqueous solution, and growth in a gel. Four compounds were obtained, either in powdered form or as single crystals: $Cu^{II}_2Fe^{II}(CN)_6 \cdot xH_2O$, $Cu^{II}_3[Fe^{III}(CN)_6]_2 \cdot xH_2O$, $Na_2Cu^{II}Fe^{II}(CN)_6 \cdot 10H_2O$ and $K_2Cu^{II}Fe^{II}(CN)_6$. Powders of $Cu^{II}_2Fe^{II}(CN)_6 \cdot xH_2O$ and $Cu^{II}_3[Fe^{III}(CN)_6]_2 \cdot xH_2O$ are easily prepared by precipitation and can also be obtained by local growth. They crystallise generally with cubic symmetry, in space group $Fm\bar{3}m$, and are structurally disordered. The mixed copper hexacyanoferrates of general formulae $M^I_2Cu^{II}Fe^{II}(CN)_6$ or $M^ICu^{II}Fe^{III}(CN)_6$ (here $M^I$ is Na, K) were not obtained by precipitation. The appropriate method was local growth for the preparation of powders of $K_2Cu^{II}Fe^{II}(CN)_6$. Single crystals of $Na_2Cu^{II}Fe^{II}(CN)_6$ were obtained by growth in a gel, and their study using single crystal X-ray diffraction revealed a new monoclinic structure.

## 1. Introduction

Transition metal hexacyanoferrates are well known for their high affinity towards caesium in a wide range of pH [1,2]. They have numerous applications in analytical chemistry for the concentration of radioactive caesium and the measurement of radioactive fall-out in the environment [3–5]. They are primary candidates for caesium removal from radioactive liquid wastes. They are also efficient for the recovery of silver and palladium from dilute solutions [6–8]. The concentration of these elements could be useful for analytical purposes or for recovery from liquid wastes. Hexacyanoferrates(II) and (III) with several different transition metals were studied for the removal of caesium [9–12]. The question concerning the best compound is still pendant. One of the reasons for this uncertainty is that these compounds exhibit a great variety of compositions and structures. Several kinds of compound may be observed with the same transition metal, depending on the preparation method. It is therefore difficult to establish a relationship with the sorption properties. In an effort to clarify this situation, we performed a systematic study of the preparation methods, compositions and structures of zinc and nickel hexacyanoferrates(II) [13,14]. More recently we started with copper hexacyanoferrates(II) and (III). These compounds not only exhibit a strong affinity for caesium [15–17], but they are also of potential interest for the fixation of palladium and other precious metals [7,18]. The applications of such products in analytical chemistry and for industrial separations are strongly connected with obtaining reproducibly

* Corresponding author.


*SSDI* 0039-9140(95)01611-2

defined compounds. Their use would be greatly facilitated if they could be produced under the form of hard granular solids mechanically stable in ion exchange columns.

Before undertaking a systematic study of the exchange properties of these compounds, it was essential to define a few preparative methods which lead to reproducible chemical compositions and structures. Certain general features may be deduced from a review of the literature [19]. Copper hexacyanoferrates(II) exhibit several compositions and structures. They belong to at least two families, having formulae $Cu_2^{II}Fe^{II}(CN)_6$ and $K_2Cu^{II}Fe^{II}(CN)_6$. Methods leading to these compounds have been described [20,21]. Other definite mixed hexacyanoferrates(II) such as $K_2Cu_3^{II}[Fe^{II}(CN)_6]_2$ [22,23], have often been reported but their existence is questionable. Copper hexacyanoferrates(III) have been less studied, and the formula generally presented is $Cu_3[Fe^{III}(CN)_6]_2$ [24–28]. In a few cases, potassium has been found in this compound [25,28,29].

Since the first publication by Keggin and Miles [30], hexacyanoferrates of divalent metals such as Cu, Ni and Co [31–33] have frequently been described as cubic, space group $Fm\bar{3}m$, with $a_0 \approx 10$ Å. This $a_0$ value is equal to twice the length of the Fe–C–N–$M^{II}$ group. These compounds seem to remain isostructural when alkali metal ions are incorporated into them [26,34,35]. One potassium copper hexacyanoferrate(II) departs from this cubic structure [21]. In previous studies, we ascribed several different structures to compounds belonging to the zinc hexacyanoferrate group. $Zn_2Fe^{II}(CN)_6 \cdot 2H_2O$ was found to have a trigonal structure $P\bar{3}m1$, $M_2^{I}Zn_3[Fe^{II}(CN)_6]_2 \cdot xH_2O$ (here $M^{I}$ is Na, K, Cs) has a rhombohedral arrangement $R\bar{3}c$ [36–39] and $Zn_3[Fe^{III}(CN)_6]_2 \cdot xH_2O$ is either cubic $Fm\bar{3}m$ or rhombohedral $R\bar{3}c$ ($x = 2$) [40,41].

However, several questions still remain. Apart from the compounds of end compositions $Cu_2^{II}Fe^{II}(CN)_6$ and $K_2Cu^{II}Fe^{II}(CN)_6$, what are the regions of alkali metal ion content in mixed copper hexacyanoferrates? Do solid solutions really exist? If not, what are the formulae of the other mixed alkali-metal copper compounds of defined composition?

We have tested various methods of preparation and have characterised the products obtained in each case. We report here results concerning the composition, granulometry, yield of various particle sizes, and the structure of four compounds: $Cu_2^{II}Fe^{II}(CN)_6$, $Cu_3^{II}[Fe^{III}(CN)_6]_2$, $K_2Cu^{II}Fe^{II}(CN)_6$ and $Na_2Cu^{II}Fe^{II}(CN)_6$. Single crystals of $Na_2Cu^{II}Fe^{II}(CN)_6$ (main dimension larger than 100 $\mu$m) were prepared for the X-ray diffraction studies.

Practical interest in copper hexacyanoferrates includes the production of sorbents with good mechanical properties for use in columns. One of the aims of this study was to find a preparation process which controls the grain size and produces granular materials suitable for this purpose. We have tested a new process that leads to the formation of beads [42,43].

## 2. Experimental

### 2.1. Reagents

The alkaline hexacyanoferrates $Na_4Fe^{II}(CN)_6 \cdot 10\,H_2O$, $K_4Fe^{II}(CN)_6 \cdot 3\,H_2O$, $K_3Fe^{III}(CN)_6$, mineral acids and copper sulphate were of reagent grade and were supplied by Prolabo (France). Cupric nitrate and granular cuprous chloride ($Cu^{I}Cl$) were obtained from Carlo Erba Farmitalia (Italy), Dowex 50 W-X8 resin and tetramethoxysilane from Fluka (Switzerland), and sodium metasilicate from Baker (Netherlands).

### 2.2. Synthesis

New synthetic procedures were developed and compared with published methods. The three principal preparation modes can be classified as: precipitation, local growth and gel growth.

#### 2.2.1. Precipitation methods

The preparation conditions are described in Tables 1 and 2. For compounds that have been described previously, we quote the main reference for the experimental procedure. $H_4Fe^{II}(CN)_6$ solution was prepared by the ion exchange of $Na_4Fe^{II}(CN)_6$(0.125 M) on Dowex 50 W-X8 resin in the $H^+$ ion form. The solution was used immediately. The solution turns blue on standing.

A solution of $Li_4Fe^{II}(CN)_6$ was prepared from $Na_4Fe^{II}(CN)_6$(0.6 M) using a Dowex 50 W-X8 resin in the $Li^+$ form ($H^+$ form treated with $LiNO_3$(1 M) until no $H^+$ ions were detected in the eluted solution). The concentration of the hexacyanoferrate ions in the solutions prepared was measured by iodometric titration [44], and was then adjusted by dilution.

Table 1
Preparation of copper hexacyanoferrates(II) by precipitation: conditions of synthesis, chemical composition, yield and solid phases identified by X-ray diffraction

| Reference no. | Reagents | Volume (l) | Reagent ratio | Experimental procedure | Chemical composition | Total yield (%) | yield, $>25\ \mu m$ (%) | Preparation mode[a] | Phases detected by powder X-ray diffraction |
|---|---|---|---|---|---|---|---|---|---|
| Cu93-10 | A, 0.125 M $Li_4Fe^{II}(CN)_6$<br>B, 0.375 M $Cu^{II}(NO_3)_2$<br>C, deionised water | A, 0.13<br>B, 0.124<br>C, 2 | Cu/Fe, 2.9<br>Li/Fe, 4<br>Li/Cu, 1.4 | A + B poured in C at 55°C, washing, decantation | $K_{0.03}Na_{0.01}Cu_{1.83}Fe(CN)_6 \cdot 9\ H_2O$ | ~ 100 | ~ 100 | (i) | $Cu_2^{II}Fe^{II}(CN)_6$ |
| Cu93-13 | A, 0.125 M $H_4Fe^{II}(CN)_6$<br>B, 0.125 M $Cu^{II}(NO_3)_2$<br>C, deionised water | A, 0.038<br>B, 0.038<br>C, 1.8 | Cu/Fe, 1<br>H/Fe, 4<br>H/Cu, 4 | A + B poured in C at 25°C, washing, decantation | $Na_{0.01}Cu_{1.60}Fe(CN)_6 \cdot 14\ H_2O$ | 55 | - | (i) | - |
| Cu93-25 | A, 0.125 M $Na_4Fe^{II}(CN)_6$<br>B, 0.0125 M $Cu^{II}(NO_3)_2$<br>C, deionised water | A, 0.273<br>B, 0.273<br>C, 2 | Cu/Fe, 0.1<br>Na/Fe, 4<br>Na/Cu, 40 | A + B poured in C at 30°C | colloidal | < 1 | 0 | (i) | - |
| 90-15 | A, 0.125 M $Na_4Fe^{II}(CN)_6$<br>B, 0.125 M $Cu^{II}(NO_3)_2$<br>C, deionised water | A, 0.16<br>B, 0.16<br>C, 0.25 | Cu/Fe, 1<br>Na/Fe, 4<br>Na/Cu, 4 | A + B poured in C, filtration (0.2 μm) | $Na_{1.01}Cu_{1.93}Fe(CN)_6 \cdot 17\ H_2O$ | < 1 | - | (ii) | $Cu_2^{II}Fe^{II}(CN)_6$ |
| Cu93-2 | A, 0.125 M $Na_4Fe^{II}(CN)_6$<br>B, 0.125 M $Cu^{II}(NO_3)_2$<br>C, 0.1 M $NaNO_3$ | A, 0.2<br>B, 0.2<br>C, 1.65 | Cu/Fe, 1<br>Na/Fe ≥ 10<br>Na/Cu ≥ 10 | A + B poured in C at 60°C, washing, decantation | $Na_{0.08}Cu_{2.02}Fe(CN)_6 \cdot 1\ H_2O$ | 76 | 40 | (i) | $Cu_2^{II}Fe^{II}(CN)_6$ |
| Cu93-3 | A, 0.125 M $Na_4Fe^{II}(CN)_6$<br>B, 0.125 M $Cu^{II}(NO_3)_2$<br>C, deionised water | A, 0.203<br>B, 0.492<br>C, 1.8 | Cu/Fe, 2.4<br>Na/Fe, 4<br>Na/Cu, 1.7 | A + B poured in C at 50°C, washing, decantation according to Ref. [16] | $Na_{0.03}Cu_{2.05}Fe(CN)_6 \cdot 9.6\ H_2O$ | 98 | 30 | (i) | $Cu_2^{II}Fe^{II}(CN)_6$ |
| Cu93-1 | A, 0.125 M $Na_4Fe^{II}(CN)_6$<br>B, 0.125 M $Cu^{II}(NO_3)_2$<br>C, deionised water | A, 0.160<br>B, 0.482<br>C, 2 | Cu/Fe, 3<br>Na/Fe, 4<br>Na/Cu, 1.3 | A + B poured in C at 60°C washing, decantation according to Ref. [16] | $Na_{0.02}Cu_{1.90}Fe(CN)_6 \cdot 9\ H_2O$ | 53 | 47 | (i) | $Cu_2^{II}Fe^{II}(CN)_6$ |
| Cu93-14 | A, 0.125 M $Na_4Fe^{II}(CN)_6$<br>B, 0.125 M $Cu^{II}(NO_3)_2$<br>C, deionised water | A, 0.138<br>B, 0.138<br>C, 2 | Cu/Fe, 3<br>Na/Fe, 4<br>Na/Cu, 1.3 | A + B poured in C at 50°C, Washing, decartation according to Ref. [16] | $K_{0.01}Na_{0.03}Cu_{1.94}Fe(CN)_6 \cdot 16\ H_2O$ | 51 | 50 | (i) | $Cu_2^{II}Fe^{II}(CN)_6$ |
| 90-21 | A, 0.02 M $Na_4Fe^{II}(CN)_6$<br>B, 0.02 M $Cu^{II}(NO_3)_2$<br>C, deionised water | A, 0.16<br>B, 0.48<br>C, 4 | Cu/Fe, 3<br>Na/Fe, 4<br>Na/Cu, 1.3 | A + B poured in C, filtration (0.2 μm) | $Na_{<0.1}Cu_{2.29}Fe(CN)_6$ | 89 | - | (ii) | $Cu_2^{II}Fe^{II}(CN)_6$ |

Table 1. (continued)

| Reference no. | Reagents | Volume (l) | Reagent ratio | Experimental procedure | Chemical composition | Total yield (%) | Yield, >25 μm (%) | Preparation mode[a] | Phases detected by powder X-ray diffraction |
|---|---|---|---|---|---|---|---|---|---|
| 90-25 | A, 0.02 M $K_4Fe^{II}(CN)_6$<br>B, 0.02 M $Cu^{II}(NO_3)_2$<br>C, deionised water | A, 0.125<br>B, 0.125<br>C, 4 | Cu/Fe, 1<br>K/Fe, 4<br>K/Cu, 4 | A and B poured in C, filtration (0.2 μm) according to Ref. [16] | Colloidal | 0 | – | (ii) | – |
| Cu93-6 | A, 0.125 M $K_4Fe^{II}(CN)_6$<br>B, 0.125 M $Cu^{II}(NO_3)_2$<br>C, 0.125 M $KNO_3$ | A, 0.207<br>B, 0.197<br>C, 2 | Cu/Fe, 0.95<br>K/Fe, ≥ 14<br>K/Cu, ≥ 15 | A + B poured in C at 50°C, washing, decantation according to Ref. [30] | $K_{0.53}Cu_{1.69}Fe(CN)_6 \cdot 7\ H_2O$ | 77 | 55 | (i) | – |
| FeCuAR | A, 0.35 M $Cu^{II}SO_4$<br>B, 0.5 M $K_4Fe^{II}(CN)_6$<br>C, 0.01 M $HNO_3$ | – | Cu/Fe, ≥ 1.7<br>K/Fe, 4<br>K/Cu, ≥ 2.4 | B poured in A + C at 30°C, filtration | $K_{1.02}Cu_{1.48}Fe(CN)_6 \cdot 3\ H_2O \cdot 0.5\ K_2SO_4$ | – | – | (iii) | $Cu_2^{II}Fe^{II}(CN)_6$ |
| FeCuI | A, 0.35 M $Cu^{II}SO_4$<br>B, 0.5 M $K_4Fe^{II}(CN)_6$<br>C, 0.01 M $HNO_3$ | – | Cu/Fe, ≥ 1.7<br>K/Fe, 4<br>K/Cu, ≥ 2.4 | B poured in A + C at 30°C, filtration (0.2 μm) | $K_{0.76}Cu_{1.62}Fe(CN)_6 \cdot 7\ H_2O \cdot 0.05\ K_2SO_4 \cdot 0.05\ KNO_3$ | 85 | 82 | (iii) | $Cu_2^{II}Fe^{II}(CN)_6$ |
| 90-16 | A, 0.125 M $Na_4Fe^{II}(CN)_6$<br>B, 0.125 M $Cu^{II}(NO_3)_2$<br>C, 1 M $KNO_3$ | A, 0.16<br>B, 0.16<br>C, 0.16 | Cu/Fe, 1<br>Na/Cu, 4<br>K/Cu, ≥ 8 | A and B poured in C, filtration (0.2 μm) | $K_{1.66}Cu_{1.35}Fe(CN)_6 \cdot 9\ H_2O$ | 87 | – | (ii) | – |

[a] See experimental section.

Table 2
Preparation of copper hexacyanoferrates(III) by precipitation: conditions of synthesis, chemical composition, yield and solid phases identified by X-ray diffraction

| Reference no. | Reagents | Volume (l) | Reagent ratio | Experimental procedure | Chemical composition | Total yield (%) | yield, >25 μm (%) | Preparation mode[a] | Phase detected by powder X-ray diffraction |
|---|---|---|---|---|---|---|---|---|---|
| 90-14 | A, 0.125 M $H_3Fe^{III}(CN)_6$<br>B, 0.125 N $Cu^{II}(NO_3)_2$<br>C, 1 M $HNO_3$ | A, 0.35<br>B, 0.25<br>C, 0.2 | Cu/Fe, 1<br>H/Fe, ≥4<br>H/Cu, ≥4 | A + B poured in C at 20°C<br>filtration (0.2 μm) | $K_{0.14}Cu_{1.20}Fe(CN)_6 \cdot 11\ H_2O$ | 2.5 | – | (ii) | $Cu_3^{II}[Fe^{III}(CN)_6]_2$ |
| 90-24 | A, 0.02 M $H_3Fe^{III}(CN)_6$<br>B, 0.02 M $Cu^{II}(NO_3)_2$<br>C, 0.05 M $HNO_3$ | A, 0.125<br>B, 0.125<br>C, 4.2 | Cu/Fe, 1<br>H/Fe, ≥11<br>H/Cu, ≥11 | A + B poured in C,<br>filtration (0.2 μm) | $Cu_{1.47}Fe(CN)_6 \cdot 17\ H_2O$ | 73 | | (ii) | $Cu_3^{II}[Fe^{III}(CN)_6]_2$ |
| 90-17 | A, 0.1 M $H_3Fe^{III}(CN)_6$<br>B, 0.1 M $Cu^{II}(CH_3COO)_2$<br>C, deionised water | A, 0.16<br>B, 0.48<br>C, 0.25 | Cu/Fe, 3<br>H/Fe, 3<br>H/Cu, 1 | A + B poured in C,<br>filtration (0.2 μm) | $K_{0.03}Cu_{1.43}Fe(CN)_6 \cdot 15\ H_2O$ | 23 | | (ii) | $Cu_3^{II}[Fe^{III}(CN)_6]_2$ |
| 90-12 | A, 0.125 M $K_3Fe^{III}(CN)_6$<br>B, 0.125 M $Cu^{II}(NO_3)_2$<br>C, deionised water | A, 0.16<br>B, 0.16<br>C, 0.25 | Cu/Fe, 1<br>K/Fe, 3<br>K/Cu, 3 | A + B poured in C,<br>filtration (0.2 μm) | $K_{0.53}Cu_{1.28}Fe(CN)_6 \cdot 16\ H_2O$ | – | | (ii) | $Cu_3^{II}[Fe^{III}(CN)_6]_2$ |
| 90-13 | A, 0.125 M $K_3Fe^{III}(CN)_6$<br>B, 0.125 M $Cu^{II}(NO_3)_2$<br>C, deionised water | A, 0.11<br>B, 0.11<br>C, 1 | Cu/Fe, 1<br>K/Fe, 3<br>K/Cu, 3 | A + B poured in C,<br>filtration (0.2 μm) | $K_{0.18}Cu_{1.40}Fe(CN)_6 \cdot 14\ H_2O$ | – | | (ii) | $Cu_3^{II}[Fe^{III}(CN)_6]_2$ |
| Cu93-28 | A, 0.125 M $K_3Fe^{III}(CN_3)_6$<br>B, 0.125 M $Cu^{II}(NO_3)_2$<br>C, deionised water | A, 0.11<br>B, 0.11<br>C, 3 | Cu/Fe, 1<br>K/Fe, 3<br>K/Cu, 3 | A + B poured in C at 30°C,<br>washed by centrifugation | $K_{0.11}Cu_{1.41}Fe(CN)_6 \cdot 5\ H_2O$ | 84 | | (i) | $Cu_3^{II}[Fe^{III}(CN)_6]_2$ |
| 90-20 | A, 0.02 M $K_3Fe^{III}(CN)_6$<br>B, 0.02 M $Cu^{II}(NO_3)_2$<br>C, deionised water | A, 0.16<br>B, 0.48<br>C, 4 | Cu/Fe, 3<br>K/Fe, 3<br>K/Cu, 1 | A + B poured in C,<br>filtration (0.2 μm) | $K_{0.07}Cu_{1.46}Fe(CN)_6 \cdot 9\ H_2O$ | 77 | | (ii) | $Cu_3^{II}[Fe^{III}(CN)_6]_2$ |
| Cu93-29 | A, 0.125 M $K_3Fe^{III}(CN)_6$<br>B, 0.375 M $Cu^{II}(NO_3)_2$<br>C, deionised water | A, 0.148<br>B, 0.148<br>C, 3 | Cu/Fe, 3<br>K/Fe, 3<br>K/Cu, 1 | A + B poured in C at 30°C<br>washed by centrifugation<br>according to Ref. [22] | $K_{0.04}Cu_{1.39}Fe(CN)_6 \cdot 5\ H_2O$ | 93 | – | (i) | $Cu_3^{II}[Fe^{III}(CN)_6]_2$ |

[a] See experimental section.

Three procedures were used: (i) and (ii) are classical laboratory processes, which differed mainly in the washing methods and the reagent addition rates; and (iii) was used for the preparation of larger quantities (up to a few kilograms).

(i) Solutions of the appropriate reagents were mixed in a 6 l round-bottomed flask by slow simultaneous addition at speeds between $0.5 \times 10^{-3}$ and $2.25 \times 10^{-3}$ mol $h^{-1}$, with gentle mechanical stirring. The temperature was maintained constant with a water bath. The slurries were washed with deionised water by decantation at least eight times using a total washing volume of at least 1.7 l. The precipitate was allowed to dry in air and was weighed (giving the total yield) after which 200, 100 and 25 $\mu$m sieves were used to separate the fractions having particles sizes above and below 25 $\mu$m. The fractions were dried in air between 20 and 40°C and were weighed (giving the above 25 $\mu$m yield).

(ii) The rate of addition was varied from $0.15 \times 10^{-3}$ to $2.25 \times 10^{-3}$ mol $h^{-1}$. If not otherwise stated, the slurries were then allowed to stand for 48 h at 70°C, filtered (0.2 $\mu$m) and dried at 40°C in air. The powders were then washed with water, decanted, dried in air at temperatures below 50°C and weighed (giving the global yield).

(iii) One solution was rapidly added to the other with stirring. Small particles ($\phi \leq 100$ $\mu$m) recovered from sieving a previous preparation were added to this solution, which was allowed to stand for 20 h. The slurries were then filtered under pressure for 2 h. They were washed on the filters with 0.006 M nitric acid and filtered before drying on a warm surface (80°C) for 48 h. The product was ground. The particles with dimensions less than 100 $\mu$m were separated and those with dimensions above 500 $\mu$m were ground again.

*2.2.2. Local growth method*

This method was developed with the aim of preparing beads having particles of controlled size [45]. This procedure was used when the above precipitation methods led to colloidal solutions.

The preparation conditions are given in Table 3. Crystals of the corresponding alkali metal hexacyanoferrate were placed in a concentrated solution of copper nitrate or, alternatively, crystals of copper sulphate were placed in a concentrated solution of alkali metal hexacyanoferrate. Under defined conditions of concentration and temperature, a film of insoluble hexacyanoferrate appears around the crystal, the thickness of which increases until the starting solid is completely consumed. This procedure is described more in detail in Ref. [42], while the growth mechanisms are discussed in Ref. [43].

*2.2.3. Growth of single crystals in gels*

The preparation of single crystals is required for a complete structural determination by X-ray diffraction. Single crystals of zinc hexacyanoferrates have previously been obtained by slow diffusion of the reagents [46]. The details of the syntheses are given in Table 4. In order to slow down the speed of diffusion of copper ions, copper tartrate crystals were used, prepared by diffusion of a copper nitrate solution through a tetramethoxysilane gel containing tartaric acid. The copper tartrate crystals were placed at the bottom of a test tube and covered by a metasilicate solution neutralised to various pH values with a 1 M acetic acid solution. After formation of a metasilicate gel, an alkaline hexacyanoferrate solution was introduced and allowed to diffuse slowly (for at least 1 month) [47].

The crystals were individually separated from the gel using a binocular magnifier and glass capillaries and were washed several times in a drop of water.

*2.3. Chemical analysis*

Non-destructive neutron activation analyses were performed for the determination of the concentration of the elements Na, K, Cl, Cu and Fe using the facilities of the Pierre Süe Laboratory. Analyses were performed in duplicate when the discrepancy between the two results was less than 5%, otherwise one more analysis was made. The compositions represent the mean values of the results. The water content was deduced by difference, and considering that one Fe atom is bound to six cyanide groups. For a complete determination of the anions, some products were analysed at the Service Central d'Analyses of the CNRS, Vernaison, France.

Due to the small quantities available, single crystal compositions were determined during observation with a scanning electron microscope by analysis of the secondary X-ray beam. We used a Quantum detector, a Kevex analysis

Table 3
Preparation conditions and chemical compostion of some hexacyanoferrates prepared by local growth

| Reference | Solid | Weight (g) | Salt in solution | Concentration (M) | Volume (ml) | Temp. (°C) | Time (h) | Composition | Yield, > 25 μm % | Phases detected by X-ray diffraction |
|---|---|---|---|---|---|---|---|---|---|---|
| I. Solid sodium hexacyanoferrate(II) + cupric salt solution | | | | | | | | | | |
| Cu90.6 | $Na_4Fe^{II}(CN)_6$ | 10 | $Cu^{II}(NO_3)_2$, $HNO_3$ | 1.6<br>0.1 | 100 | 20 | 15 | $K_{<0.1}Na_{0.04}Cu_{2.09}Fe(CN)_6$ | – | $Cu^{II}_2Fe^{II}(CN)_6$ |
| II. Solid cupric sulphate + potassium hexacyanoferrate(II) solution | | | | | | | | | | |
| Cu89.9 | $Cu^{II}SO_4$ | 1.00 | $K_4Fe^{II}(CN)_6$ | 0.6 | 50 | 20 | 63 | $K_{2.09}Na_{0.01}Cu_{1.08}Fe(CN)_6$ | – | $K_2Cu^{II}Fe^{II}(CN)_6$ |
| Cu93-5 | $Cu^{II}SO_4$ | 1.14 | $K_4Fe^{II}(CN)_6$ | 0.5 | 50 | 20 | | $K_{1.97}Cu_{1.00}FE(CN)_6$ | 42 | $K_2Cu^{II}Fe^{II}(CN)_6$ |
| Cu93-8 | $Cu^{II}SO_4$ | 1.03 | $K_4Fe^{II}(CN)_6$ | 0.7 | 50 | 20 | | $K_{1.77}Cu_{1.17}Fe(CN)_6 \cdot 1.3\,H_2O$ | 100 | $K_2Cu^{II}Fe^{II}(CN)_6$ |
| Cu93-9 | $Cu^{II}SO_4$ | 1.01 | $K_4Fe^{II}(CN)_6$ | 0.8 | 50 | 20 | | $K_{1.93}Cu_{1.10}Fe(CN)_6 \cdot 1.5\,H_2O$ | 66 | $K_2Cu^{II}Fe^{II}(CN)_6$ |
| Cu93-24 | $Cu^{II}SO_4$ | 14 | $K_4Fe(CN)_6$ | 0.6 | 500 | 25 | 24 | $K_{1.91}Cu_{1.05}Fe(CN)_6 \cdot 1.5\,H_2O$ | 41 | $K_2Cu^{II}Fe^{II}(CN)_6$ |
| Cu93-26 | $Cu^{II}SO_4$ | 14 | $K_4Fe^{II}(CN)_6$ | 0.7 | 500 | 25, 35 | 23, 2 | $K_{1.51}Cu_{1.39}Fe(CN)_6 \cdot 4.8\,H_2O$ | 37 | $Cu^{II}_2Fe^{II}(CN)_5$ + $K_2Cu^{II}Fe^{II}(CN)_6$ |
| Cu90.31 | $Cu^{II}SO_4$ | 25 | $K_4Fe^{II}(CN)_6$ | 0.8 | 100 | 40 | 63 | $K_{1.56}Na_{<0.01}Cu_{1.42}Fe(CN)_6$ | – | $Cu^{II}_2Fe^{II}(CN)_6$ + $K_2Cu^{II}Fe^{II}(CN)_6$ |
| III. Solid cuprous chloride + potassium hexacyanoferrate(II) solution | | | | | | | | | | |
| Cu93-19 | $Cu^{I}Cl$ | 1.00 | $K_4Fe^{II}(CN)_6$ | 0.8 | 50 | 25 | 24 | $K_{1.60}Cu_{2.46}Fe(CN)_6 \cdot 0.33\,CuCl \cdot 1.5\,H_2O$ | 70 | – |
| Cu93-20 | $Cu^{I}Cl$ | 1.00 | $K_4Fef^{II}(CN)_6$ | 0.7 | 50 | 25 | 48 | $K_{1.88}Cu_{2.03}Fe(CN)_6 \cdot 0.08\,CuCl \cdot 1.3\,H_2O$ | 64 | – |
| IV. Solid potassium hexacyanoferrate(III) + $Cu^{II}$ salt solution | | | | | | | | | | |
| Cu90.3 | $K_3Fe^{III}(CN)_6$ | 10 | $Cu^{II}(NO_3)_2HCl$ | 1.3, 0.1 | 50 | 20 | 15 | $K_{<0.1}Na_{0.01}Cu_{1.5}Fe(CN)_6$ | – | $Cu^{II}_3[Fe(CN)_6]_2$ |
| Cu89.13 | $K_3Fe^{III}(CN)_6$ | 200 | $Cu^{II}(NO_3)_2$ | 1.4 | 1000 | 45 | 15 | $K_{0.07}Cu_{1.51}Fe(CN)_6$ | – | $Cu^{II}_3[Fe(CN)_6]_2$ |
| V. Solid cupric sulphate + potassium hexacyanoferrate(III) solution | | | | | | | | | | |
| Cu93-30 | $Cu^{II}SO_4$ | 1.00 | $K_3Fe^{III}(CN)_6$ | 0.7 | 50 | 25 | 5 | $K_{0.25}Na_{0.01}Cu_{1.47}Fe(CN)_6 \cdot 8\,H_2O$ | 3 | – |
| Cu93-31 | $Cu^{II}SO_4$ | 1.00 | $K_3Fe^{III}(CN)_6$ | 1 | 50 | 25 | 19 | $K_{0.14}Cu_{1.79}Fe(CN)_6 \cdot 5\,H_2O$ | 8 | – |
| Cu90.34 | $Cu^{II}SO_4$ | 10.00 | $K_3Fe^{III}(CN)_6$ | 1 | 50 | 20 | 15 | $K_{0.30}Na_{0.01}Cu_{1.42}Fe(CN)_6$ | – | – |
| VI. Solid cuprous chloride + potassium hexacyanoferrate(III) solution | | | | | | | | | | |
| Cu90.38 | $Cu^{I}Cl$ | 1.00 | $K_3Fe^{III}(CN)_6$ | 1 | 10 | 20 | 15 | $K_{1.28}Na_{<0.01}Cu_{1.07}Fe(CN)_6$ | – | – |
| Cu90.42 | $Cu^{I}Cl$ | 50 | $K_3Fe^{III}(CN)_6$ | 1 | 500 | 20 | 24 | $K_{1.58}Na_{0.01}Cu_{1.79}Fe(CN)_6$ | – | – |

Table 4
Preparation conditions, morphology and structure type of copper hexacyanoferrate crystals obtained by the gel method

| Reference | Gel | pH | Solution | Crystal | Composition | Structure type |
|---|---|---|---|---|---|---|
| S1 | $Na_2SiO_3$[a] + copper tartrate | 10.5–11 | $Na_4Fe(CN)_6$, 0.125 M | Platelike, red brown, ≥ 100 μm[c] | $Na_{1.90}Cu_{1.00}Fe(CN)_6$[g] $Na_{1.98}Cu_{1.00}Fe(CN)_6$[f] | $Na_2Cu^{II}Fe^{II}(CN)_6$ |
| S3 | $Na_2SiO_3$[a] + copper tartrate | 10.5 | $K_4Fe(CN)_6$, 0.125 M | Aggregates of 20 μm crystals, red[c] | $K_{1.85}Cu_{1.00}Fe(CN)_6$[g] | $K_2Cu^{II}Fe^{II}(CN)_6$ |
| S4 | $Li_2SiO_3$[b] + copper tartrate | 10.6 | $K_4Fe(CN)_6$, 0.125 M | Aggregates of 20 μm crystals, red[c] | $K_{2.05}Cu_{1.00}Fe(CN)_6$[g] | $K_2Cu^{II}Fe^{II}(CN)_6$ |
| A90-25 | $Na_2SiO_3$[a] + $K_3Fe(CN)_6$ | 5 | $Cu(NO_3)_2$ | Cubes, ≤ 2 μm | $Na_{0.14}Cu_{1.57}Fe(CN)_6 \cdot 5\,H_2O$[f] | $Cu^{II}_3[Fe^{III}(CN)_6]_2$ |
| A90-26 | $Na_2SiO_3$[a] + $K_3Fe(CN)_6$ | 6 | $Cu(NO_3)_2$ | Cubes, ≤ 2 μm[e] | $Na_{0.15}Cu_{1.70}Fe(CN)_6 \cdot 9\,H_2O$[f] | $Cu^{II}_3[Fe^{III}(CN)_6]_2$ |

[a] Concentration 10 g per 100 ml.
[b] Concentration 20 g per 100 ml.
[c] Washed with deionised water.
[e] Washed with a 10% HF solution, dried in air at 51°C.
[f] Neutron activation analysis.
[g] Energy dispersed X-ray spectrometry.

system and the XPP software [48] to calculate the relative atomic percentages. The determination of the compositions is semiquantitative because of the uncertainty of the geometry between the surface sample and the detector. To confirm these results, a few milligrams of single crystals were also analysed by neutron activation analysis; some other crystals were analysed by the secondary X-ray beam method. No discrepancies greater than 5% in the Cu/Fe and Na/Fe ratios were found (see S1 in Table 4).

### 2.4. Morphology

Optical microscopy and scanning electron microscopy were used to characterise the morphology.

### 2.5. Yield

The product yield was calculated as the ratio of the quantity of iron or copper in the product obtained to that introduced with the minor reagent. The global yield refers to the quantity of dry product obtained after decantation (precipitation by method (i)) or filtration (precipitation by methods (ii) and (iii)). The yield of the fraction composed of particles whose sizes are above 25 μm is also given when possible.

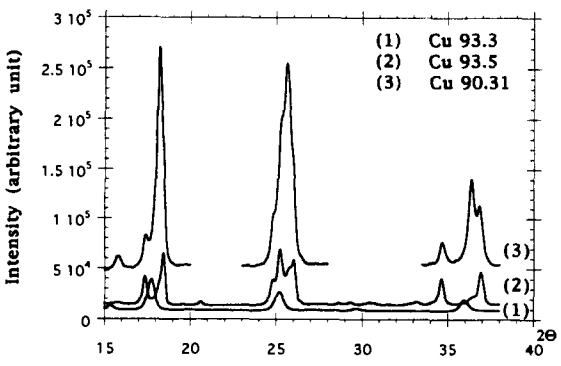


Fig. 1. Superposition of the X-ray powder diffraction patterns of Cu93-3 ($Cu_2Fe(CN)_6$), Cu93-5 ($K_2CuFe(CN)_6$) and Cu90.31, a mixture of the former phases.

### 2.6. X-ray crystallographic analyses

A Siemens diffractometer D500 and an Enraf Nonius CAD4 diffractometer were used for studies on the powders and single crystals, respectively.

The identification of the phases present was made by reference to the ICDD database (release 1993). X-ray powder diffraction was simulated using Cerius$^2$ (release 1.5) software from Molecular Simulations Incorporated.

## 3. Results and discussion

### 3.1. Composition and yield of preparation

We indicate in Tables 1–4 the main experimental conditions, the compositions, as they result from the chemical analyses, the overall yield of each product and the yield for particles of sizes greater than 25 μm. We also give the solid phases detected by X-ray diffraction by reference to the ICDD database.

The water content was deduced from the elemental analysis by difference. An excess of cations with respect to the hexacyanoferrate complex anion was frequently observed; this was particularly noticeable when high concentrations of the starting salts were used and with the local growth method. The presence of other anions resulting from the adsorption of the starting compound (nitrate, sulphate or chlo-

Table 5
Fractional atomic coordinates and site occupancy parameters for $Na_2Cu^{II}Fe^{II}(CN)_6 \cdot 10\,H_2O$, $Cu_3^{II}[Fe^{III}(CN)_6]_2 \cdot xH_2O$ and $Cu_2^{II}Fe^{II}(CN)_6 \cdot xH_2O$

| Atom | Atomic coordinates | | | Site occupancy |
|---|---|---|---|---|
| Part 5a. $Na_2Cu^{II}Fe^{II}(CN)_6 \cdot 10\,H_2O$ [a] | | | | |
| Cu | 0 | 0 | 0 | – |
| Fe | 1/2 | 1/2 | 0 | – |
| Na1 | 1/2 | 0 | 1/2 | – |
| Na2 | 0 | 0 | 1/2 | – |
| C1 | 0.314 | 0.310 | 0.019 | – |
| N1 | 0.199 | 0.197 | 0.030 | – |
| C2 | 0.583 | 1/2 | 0.191 | – |
| N2 | 0.641 | 1/2 | 0.307 | – |
| Part 5b. $Cu_3^{II}[Fe^{III}(CN)_6]_2 \cdot xH_2O$ [b]. | | | | |
| Fe 4(a) | 0 | 0 | 0 | 2/3 |
| Cu 4(b) | 1/2 | 0 | 0 | 1 |
| C 24(c) | 0.186 | 0 | 0 | 2/3 |
| N 24(c) | 0.298 | 0 | 0 | 2/3 |
| Part 5c. $Cu_2^{II}Fe^{II}(CN)_6 \cdot xH_2O$ [c] | | | | |
| Fe 4(a) | 0 | 0 | 0 | 2/3 |
| Cu1 4(b) | 1/2 | 0 | 0 | 1 |
| Cu2 8(c) | 1/4 | 1/4 | 1/4 | 0.1667 |
| C 24(c) | 0.186 | 0 | 0 | 2/3 |
| N 24(c) | 0.298 | 0 | 0 | 2/3 |

[a] P2/m; $a = 6.998$ Å; $b = 7.055$ Å; $C = 9.889$ Å; $\beta = 97.56°$; $z = 1$. [b] $Fm\bar{3}m$; $a \approx 10.10$ Å; $z = 1 + 1/3$. [c] $Fm\bar{3}m$; $a \approx 10.0$ Å; $z = 2 + 2/3$.

ride), as occurs in nickel and zinc hexacyanoferrates [14], was confirmed by chemical analysis. In a few cases, we observed a deficit of cations. $Cu^{II}$ solutions are acidic (pH about 3), and the introduction of protons into the solid compounds could account for this apparent reduction in the copper content.

*3.1.1. Precipitation*

The results obtained by using the precipitation method (i), (ii) and (iii) are given in Table 1. The compounds resulting from the use of lithium, hydrogen, sodium and potassium hexacyanoferrates(II) are presented successively.

A very general feature of our results is that, for lithium and sodium hexacyanoferrate(II) solutions, low concentrations of alkaline metals are incorporated into the precipitate. The only exception to this rule is sample 90–15. However, in this last case, we observe an excess of cations, which may be explained by sorption of sodium salts on a precipitate with very small particles: the washing process used during filtration (ii) seems to be less effective than in the multiple decantation method (i). When potassium hexacyanoferrate(II) solutions are used, a more alkaline element is incorporated into the precipitate (Cu93-6, FeCuAR, FeCul). In the case of $H_4Fe(CN)_6$, it seems that some protons are incorporated into the precipitate (Cu93-13), as a deficit of cations has been measured (Na and Cu).

A general rule is that, in all our experiments, the only crystalline phase detected by X-ray diffraction is the cubic $Cu_2^{II}Fe^{II}(CN)_6$ (ICDD 1.0244), with, however, some discrepancies concerning the positions of the diffraction lines and their intensities.

The highest yield was obtained starting from lithium hexacyanoferrate(II) (Cu93-10). The use of ferrocyanhydric acid leads to an overall yield of 55% (Cu93-13). This precipitate is not stable and turns rapidly to a navy-blue colour.

In the case of sodium hexacyanoferrate(II), the main parameter influencing the yield seems to be the copper-to-iron ratio. For ratios of 1 or less, very small particles are obtained although the yield is close to zero (Cu93-25 and 90-15). The yield can be increased by adding a salt such as $NaNO_3$ to the solution (Cu93-2). For Cu/Fe above 2, a rather good yield is obtained (Cu93-3 to 90-21).

Using potassium hexacyanoferrate(II), a high K/Cu ratio also leads to very small particles and to a low yield (90-25). Higher yields are obtained by using lower K/Cu ratios (FeCu 1) or by adding $KNO_3$ (Cu93-6). By comparison to other alkali metals, a significant

quantity of potassium is incorporated into the solid. The phase detected by X-ray diffraction is $Cu^{II}_2Fe^{II}(CN)_6$ (Cu93-6 to FeCu 1). The presence of another phase containing potassium is not excluded, but this phase is not detected by X-ray diffraction, because of too-small crystallites or amorphous particles.

The poor yield of some preparations may probably be explained by the formation of a copper hexacyanoferrate(II) including alkali metal ions in a colloidal form or in very small particles. The higher the alkaline-metal-to-copper ratio, the higher the proportion of this small particulate hexacyanoferrate(II), and the lower the yield. For potassium, it seems that a non-negligable part of this alkali metal containing hexacyanoferrate(II) is mixed with the separated solid phase (Cu93-6 to FeCu 1), but, nevertheless, in no case is any alkali metal containing hexacyanoferrate(II) detected by X-ray diffraction.

These results may be compared with those of Shabandeh and Streat [49] who reported a $Na_{0.47}Cu_{1.77}Fe(CN)_6$ composition but an X-ray diffraction pattern similar to that of $Cu^{II}{}_2Fe^{II}(CN)_6$. To the best of our knowledge, Gellings [21] described the only case in the literature where a potassium copper hexacyanoferrate(II) phase was detected by X-rays. We could not reproduce this result, probably because our experimental conditions were different. The behaviour of lithium is different from that of the other alkali metals. This element does not seem to incorporate into hexacyanoferrates [50], thus leading to the precipitation of $Cu^{II}_2Fe^{II}(CN)_6$ with a 100% yield.

The solids obtained starting from soluble hexacyanoferrates(III) are given in Table 2. Potassium hexacyanoferrate(III) was the only available salt. Ferricyanhydric acid was prepared from this by ion exchange. In all the solids studied, only cubic $Cu^{II}_3[Fe^{III}(CN)_6]_2$ could be detected (ICDD 13.0214), despite the presence in the solid of varying amounts of potassium. The Cu/Fe ratio is close to 1.5, although generally slightly lower. As for copper hexacyanoferrates(II), it is probable that a phase containing the alkali element is removed with the liquid phase. A small part of this solid phase may also be mixed with $Cu^{II}_3[Fe^{III}(CN)_6]_2$.

### 3.1.2. *Local growth from a solid compound*

In this method of preparation, the choice of reagents, of their state (solid or in aqueous solution) and of the concentration in solution is limited to a narrow range suitable for adequate osmotic pressures and favourable growth conditions [43]. The compositions of the solids obtained are strongly dependent on the experimental conditions (Table 3). Interpretable X-ray diffraction patterns were not always obtained, owing to the small sizes of the crystals, the possible mixture of phases and the lack of reference spectra.

When $Na_4Fe(CN)_6$ is used as the solid reagent, chemical analysis and X-ray diffraction show the presence of $Cu^{II}_2Fe^{II}(CN)_6$ (Cu90.6). If $CuSO_4$ is used as the solid reagent in a solution of $K_4Fe(CN)_6$, much more alkali element is incorporated into the solid (Cu89.9 to Cu90.31). A pure $K_2Cu^{II}Fe^{II}(CN)_6$ phase is detected (ICDD 20.0875) with a chemical composition close to this formula (Cu89.9 to Cu93-24). Such a phase could not be obtained alone by precipitation. In some cases, we also obtained mixtures of $Cu^{II}_2Fe^{II}(CN)_6$ and $K_2Cu^{II}Fe^{II}(CN)_6$, as revealed by X-ray diffraction (Cu93-26 and Cu90.31) (Fig. 1).

Local growth from solid cuprous chloride was also attempted. Copper seems to be partly oxidised in the product obtained, but the composition is close to $K_2Cu^{I}_2Fe^{II}(CN)_6$ (Cu93-19 and Cu93-20).

Using solid potassium hexacyanoferrate(III), a $Cu^{II}_3[Fe^{III}(CN)_6]_2$ phase was detected (Cu90.3 and Cu89.13). Using solid $CuSO_4$ in a solution of $K_3Fe^{III}(CN)_6$, a composition close to $Cu^{II}_3[Fe^{III}(CN)_6]_2$ was obtained, but the yield was low (Cu93-30, Cu93-31, Cu90.34). The use of cuprous chloride led to irreproducible results, probably on account of oxidation (Cu90.38, Cu90.42).

### 3.1.3. *Preparation of single crystals by the gel method*

The results are presented in Table 4. The largest crystals were obtained in a sodium silicate gel containing copper tartrate in contact with a $Na_4Fe(CN)_6$ solution (S1). This produced a compound of composition $Na_2Cu^{II}Fe^{II}(CN)_6 \cdot 10H_2O$ with a novel structure. The yield could be estimated as 20%. A sodium or lithium silicate gel containing copper tartrate in contact with a $K_4Fe(CN)_6$ solution leads to $K_2Cu^{II}Fe^{II}(CN)_6 \cdot x\,H_2O$ (S3, S4). The X-ray powder diffraction patterns of S3 and Cu89.9 to Cu93-24 are similar and do not reveal a tetragonal structure, contrary to Gellings [21]. $Cu^{II}_3[Fe^{III}(CN)_6]_2 \cdot xH_2O$ was ob-

tained in a gel containing sodium silicate and potassium hexacyanoferrate(III) in contact with a cupric nitrate solution (A90-25, A90-26). $Cu_2^{II}Fe^{II}(CN)_6$ was not obtained using this method.

*3.1.4. Reproducibility of the preparations*

In the cases when $Cu_2^{II}Fe^{II}(CN)_6$ or $Cu_3^{II}[Fe^{III}(CN)_6]_2$ were obtained with a good yield, it was easy to repeat the experiments. For example, starting from $Li_4Fe^{II}(CN)_6$, we always obtained $Cu_2^{II}Fe^{II}(CN)_6$ (see Cu93.10); starting from $K_3Fe^{III}(CN)_6$, a composition next to $Cu_3^{II}[Fe^{III}(CN)_6]_2$ was reached (see Cu93.28; Cu90.20; Cu93.29).

Using the local growth method, it was more difficult to prepare a single-phased $K_2Cu^{II}Fe^{II}(CN)_6$ product. In many cases, we could detect a small percentage of the $Cu_2^{II}Fe^{II}(CN)_6$ phase. The factors affecting the results are numerous, such as the quantities of the reactants, the size of the crystals of the starting solid and the volume of water used for washing the precipitates.

*3.2. Morphology*

*3.2.1. Precipitation*

On the laboratory scale (total amount below 100 g), the particles formed have dimensions ranging between 10 μm and 1 mm. For preparations concerning larger quantities (about 20 kg), drying was performed up to 80°C, which causes the particles to agglomerate, and the fraction of particles larger than 1 mm is high. The mechanical strength of these aggregates when they are shaken in solution is questionable. Observations by electron microscopy did not permit the observation of the crystallites in the products obtained by the precipitation. The crystallite sizes have been determined by X-ray diffraction and the Cerius software, the dimensions are between 100 and 200 Å.

*3.2.2. Local growth method*

Particles prepared by growth on solid copper salts or alkaline hexacyanoferrate crystals differ from those obtained for nickel or zinc hexacyanoferrates [42]. The large particles (100 μm or above) are irregular in shape with a rough surface. In the cases of the zinc and nickel salts, spheres of diameters related to the starting crystals sizes were obtained. In Cu90.31, a mixture of $Cu^{II}{}_2Fe^{II}(CN)_6$ and $K_2Cu^{II}Fe^{II}(CN)_6$, the crystallite sizes are 100 Å and 300 Å, respectively.

*3.2.3. Single crystals obtained by the gel method*

The dimensions and main morphological characteristics are indicated in Table 4. Single crystals of $Na_2Cu^{II}Fe^{II}(CN)_6 \cdot 10\,H_2O$ up to 500 μm in size were obtained. An example of the dimensions is $272 \times 273 \times 16\ \mu m^3$. These single crystals are destroyed by dehydration, leading to a stack of thinner plates.

*3.3. Crystal structure determination*

Compounds of composition closest to stoichiometric $Cu_2^{II}Fe^{II}(CN)_6$, $Na_2Cu^{II}Fe^{II}(CN)_6$ and $Cu_3^{II}[Fe^{III}(CN)_6]_2$ were selected for the structure determination. Crystal models were built with the Cerius[2] software and compared to the experimental diffraction patterns.

The powder pattern of $Na_2Cu^{II}Fe^{II}(CN)_6 \cdot 10\,H_2O$ is not reported in the ICDD database, and a complete determination on a single crystal showed the presence of a new structural arrangement [47]. $Na_2Cu^{II}Fe^{II}(CN)_6 \cdot 10\,H_2O$ crystallises in the monoclinic system, with space group P2/m (Table 5, part a). The $Fe(CN)_6$ and $Cu(CN)_4$ units are linked into layers, which lie parallel to the *ab* plane, through bridging cyano groups. Chains of hydrated Na ions $-(H_2O)_2-Na-(H_2O)_2-Na-$ run parallel to the hexacyanoferrate/tetracyanocuprate sheets, and water molecules above and below the plane of these chains serve to complete the coordination spheres both of sodium and copper, and to link the cyanometallate layers together. $Na_2Cu^{II}Fe^{II}(CN)_6 \cdot 10\,H_2O$ dehydrates spontaneously in air with a concomitant loss of single crystal character.

$Cu_3^{II}[Fe^{III}(CN)_6]_2 \cdot x\,H_2O$ is cubic $Fm\bar{3}m$ and with $z = 1 + 1/3$, leading to a disordered structure. $FeC_6$ octahedra and planar $CuN_4$ units are linked by cyanide bridging, leading to the usual parameter of about 10 Å (Table 5, part b).

$Cu_2^{II}Fe^{II}(CN)_6 \cdot x\,H_2O$ is cubic $Fm\bar{3}m$ ($z = 2 + 2/3$) and is also a disordered structure. The distribution of copper in the cell is quite different from that of $Cu_3^{II}[Fe^{III}(CN)_6]_2$ (Table 5, part c).

Determinations of the structure (from a Rietveld refinement of powder X-ray diffraction data) of $Cu_2^{II}Fe^{II}(CN)_6$ and $Cu_3^{II}[Fe^{III}(CN)_6]_2$ are to be published [47]. Powder diffraction patterns correspond to ICDD 1.0244 and ICDD 23.0214 respectively, but with some discrepancies.

In the case of $K_2Cu^{II}Fe^{II}(CN)_6$, the diffraction patterns have only a few lines and hence are difficult to index. Intensities and reflections are somewhat different from those published by Gellings (ICDD 20.0875) and do not correspond to the quadratic structure mentioned [21].

## 4. Conclusion

Three methods were evaluated for the preparation of copper hexacyanoferrates(II) and (III): precipitation, local growth and growth in a gel. The aim of the two former methods was to obtain powders, while the latter was used to produce single crystals for structure determination. A systematic and accurate study by X-ray diffraction has been performed. Four compounds, identified by their chemical analysis and X-ray diffraction patterns were obtained, either in powdered form, or as single crystals: $Cu^{II}_2$-$Fe^{II}(CN)_6$, $Cu^{II}_3[Fe^{III}(CN)_6]_2$, $Na_2Cu^{II}Fe^{II}(CN)_6$ and $K_2Cu^{II}Fe^{II}(CN)_6$. The structure of the last compound remains undetermined as yet because of the lack of single crystals. However, its X-ray powder diffraction pattern does not correspond to the reported cubic [31] or tetragonal structures [21].

$Cu^{II}_2Fe^{II}(CN)_6$ and $Cu^{II}_3[Fe^{III}(CN)_6]_2$ powders are easily prepared by precipitation and by local growth. They are cubic $Fm\bar{3}m$ and present disordered structures. These two compounds differ from each other in the positions of the copper atoms. The distribution of copper could be an important parameter for the fixation of caesium: the sorption of caesium on $Cu^{II}_3[Fe^{III}(CN)_6]_2$ is very low compared to that on $Cu^{II}_2Fe^{II}(CN)_6$.

Although cited in the literature, the mixed copper hexacyanoferrates of general formulae $M^I_2Cu^{II}Fe^{II}(CN)_6$ or $M^ICu^{II}Fe^{III}(CN)_6$ (where $M^I$ is Na, K) could not be synthesised by precipitation as pure phases, in a form easily separated from the solution and detected by X-ray diffraction. However, the presence of such compounds in the form of colloids or very small particles is not excluded, except in the case of lithium. The most appropriate method for the preparation of $K_2Cu^{II}Fe^{II}(CN)_6$ powders was local growth. Single crystals of $Na_2Cu^{II}Fe^{II}(CN)_6 \cdot 10\,H_2O$ were obtained by growth in a gel. The complete X-ray crystallographic characterisation of this compound has shown a new structural arrangement whereby the $Cu(CN)_4$ and $Fe(CN)_6$ groups are linked into layers.

In all cases, X-ray diffraction revealed a limited number of compounds of defined composition. Mixed non-stoichiometric compounds such as $M^I_{2x}Cu^{II}_{2-x}Fe^{II}(CN)_6$ were not observed, and their very existence is questionable.

The aim of our work is the selection of the product presenting the highest affinity for caesium and at the same time stable enough for long term storage. Disordered and layered structures could be involved in quantitative sorption of caesium. The basic data presented here are fundamental for our studies concerning the mechanisms of the fixation of caesium on these compounds and their further analytical and industrial applications.

## Acknowledgements

S. Ayrault thanks the Association pour la Recherche Scientifique (Ministère de l'Enseignement Supérieur et de la Recherche) and the company S.T.M.I. (Société des Techniques en Milieux Ionisants), France, for financial support and for supplying information about the precipitation of FeCuAR and FeCul, prepared on an industrial scale by S.T.M.I..

## References

[1] H. Loewenschuss, Radioactive Waste Management, 2 (1982) 327.
[2] G. B. Barton, J. L. Helpworth, E. D. McClanahan Jr., R.L. Moore and H. H. Van Tuyl, Ind. Eng. Chem., 50 (1958) 212.
[3] M. T. Ganzerli Valentini, R. Stella, L. Maggy and G. Ciceri, J. Radioanal. Nucl. Chem., 114 (1) (1987) 105.
[4] Z. Hölgye, Fresenius J. Anal. Chem., 340 (1991) 59.
[5] C. Y. Huang, J. D. Lee, C. L. Tseng and J. M. Lo, Anal. Chim. Acta, 294 (1994) 221.
[6] M. Fedoroff and C. Loos-Neskovic, Mater. Tech. Fr., (1982) 357.
[7] M. Fedoroff, C. Loos-Neskovic, S. Abousahl, F. Adekola, J. C. Rouchaud, N. Boisseau, E. Garnier, E. Jackwerth, M. Dierkes, U. Rostek and M. Kaeschagen, EUR 13646 EN, (1989) p.145.
[8] C. Loos-Neskovic, M. H. Dierkes, E. Jackwerth and M. Fedoroff, New Developments in Ion Exchange, ICIE'91, Japan, 1991, p.601.
[9] K. H. Oehlmann, Waste Management, Arizona USA, 1987.
[10] E. W. Hooper, IAEA-TecDoc-675, 1992, p.68.
[11] D. O. Campbell, D. D. Lee, T. A. Dillow and J. L. Collins, IAEA-TecDoc-675, 1992, p.85.
[12] J. Lehto, Proc. Ion-Ex'93, 4–7 April 1993, Wrexham, UK.
[13] C. Loos-Neskovic, M. Fedoroff, E. Garnier and P. Gravereau, Talanta 31 (1984) 1133.

[14] C. Loos-Neskovic, M. Fedoroff and E. Garnier, Talanta, 36 (1989) 749.
[15] E. F. T. Lee and M. Streat, J. Chem. Tech. Biotechnol., 33A (1983) 333.
[16] R. Pfrepper, G. Pfrepper and M. Süss, Zfi-Mitteilungen, 116 (1986) 43.
[17] P. Nielsen, B. Dresow and H. C. Heinrich, Z. Naturforsch., 42b (1987) 1451.
[18] C. Loos-Neskovic, M. H. Dierkes, E. Jackwerth, M. Fedoroff and E. Garnier, Hydrometallurgy, 32 (1993) 345.
[19] S. Ayrault, C. Loos-Neskovic, M. Fedoroff and E. Garnier, Talanta, 41 (1994) 1435.
[20] S. Kawamura, H. Kuraku and M. Izawa, Nat. Inst. Radiol. Sci. Ann. Rept., 68 (1967) 11.
[21] P. J. Gellings, Z. Phys. Chem., 54 (1967) 296.
[22] R. Pâris, C. R. Acad. Sci., 199 (1934) 863.
[23] A. Bellomo, Talanta, 17 (1970) 1109.
[24] H. B. Weiser, W. O. Milligan and J. B. Bates, J. Phys. Chem., 46 (1942) 99.
[25] A. Bellomo, A. Casale and D. De Marco, Talanta, 20 (1973) 335.
[26] J. B. Ayers and W. H. Waggoner, J. Inorg. Nucl. Chem., 33 (1971) 721.
[27] A. K. Van Bever, Rec. Trav. Chim., 57 (1938) 1259.
[28] M. T. Ganzerli-Valentini, R. Stella and M. Cola, J. Radioanal. Nucl. Chem., 102 (1986) 99.
[29] A. K. Jain, R. P. Singh and C. Bala, J. Radioanal. Chem., 75 (1982) 85.
[30] J. F. Keggin and F. D. Miles, Nature, 137 (1936) 577.
[31] R. Rigamonti, Gazz. Chim. Ital., 67 (1937) 146.
[32] V. G. Kuznetsov, Z. V. Popova and G. B. Seifer, Zh. Neorg. Khim., 15 (1970) 1860.
[33] T. Ceranic, Z. Naturforsch., 33b (1978) 1484.
[34] V. V. Vol'khin, E. A. Shul'ga and M. V. Zil'berman, Izv. Akad. Nauk. Neorgan. Mater., 7 (1971) 77.
[35] M. V. Zil'berman and V. V. Vol'Khin, Zh. Struk. Khim., 12 (1971) 649.
[36] A. Renaud, P. Cartraud, P. Gravereau and E. Garnier, Thermochim. Acta, 31 (1979) 243.
[37] P. Gravereau, E. Garnier and A. Hardy, Acta Cryst., B35 (1979) 2843.
[38] E. Garnier, P. Gravereau and A. Hardy, Acta Cryst., B38 (1982) 1401.
[39] P. Gravereau and E. Garnier, Rev. Chim. minéral., 20 (1983) 68.
[40] P. Gravereau and E. Garnier, Acta Cryst., C40 (1984) 1306.
[41] E. Garnier, P. Gravereau, K. Ahmadi and A. Hardy, Rev. Chim. minéral., 21 (1984) 144.
[42] C. Loos-Neskovic, S. Abousahl and M. Fedoroff, J. Mater. Sci., 25 (1990) 677.
[43] S. Abousahl, C. Loos-Neskovic and M. Fedoroff, J. Crystal Growth, 137 (1994) 569.
[44] W. John Williams, Handbook of anion determination, Butterworths, London, 1979, P. 93.
[45] M. Fedoroff and C. Loos-Neskovic, French Patent 84-12139, 1984.
[46] E. Garnier, PhD. Thesis, Poitiers, France, 1985.
[47] S. Ayrault, C. Loos-Neskovic, M. Fedorott, E. Garnier, D.J. Jones and J. Rozieres, J. Mater. Chem., to be published.
[48] J. L. Pouchou, F. Pichoir and D. Boivin, Microbeam Analysis, San Francisco Press, 1990, p.120.
[49] M. R. Shabandeh and M. Streat, J. Chem. Tech. Biotechnol., 32 (1982) 580.
[50] N. G. Tchovnik and G. A. Kleibs, Zh. Anal. Khim., 3 (1948) 303.
[51] S. Kawamura, S. Shibata, K. Kurataki and H. Takeshita, Anal. Chim. Acta, 102 (1978) 225.

ELSEVIER

Talanta 42 (1995) 1595–1607

Talanta

# Direct ICP-MS determination of trace and ultratrace elements in geological materials after decomposition in a microwave oven
# I. Quantitation of Y, Th, U and the lanthanides☆

J.G. Sen Gupta *, N.B. Bertrand

*Geological Survey of Canada, Ottawa, Ont. K1A OE8, Canada*

Received 7 October 1994; revised 10 February 1995; accepted 10 April 1995

**Abstract**

A microwave digestion technique using a mixture of $HF + HNO_3 + HCl + H_3BO_3$ was found to be effective for the rapid dissolution of various silicate rock and sediment reference samples. From the solutions thus prepared, it was possible to determine quantitatively trace and ultratrace amounts of yttrium, thorium, uranium and the lanthanides by inductively coupled plasma-mass spectrometry (ICP-MS) without any separation of matrix elements or preconcentration. In the ICP-MS determinations, oxide and non-spectral interferences on individual masses of the rare earth element ions were corrected by the method of algebraic approach of elimination and dilution, respectively, and measurement drift was controlled by ruthenium and rhenium internal standards. The method yielded excellent results comparable with "recommended", "consensus" and "working" values of the literature for the specified elements on various well-known international reference materials such as andesite (AGV-1), basalts (BCR-1, BHVO-1, BIR-1 and BE-N), granites (G-2 and NIM-G), syenite (SY-2), gabbro (MRG-1), diabase (W-2 and DNC-1), marine mud (MAG-1), river sediment (NBS 1645), lake sediments (LKSD-1–LKSD-4) and stream sediment (GSD-1, GSD-5, GSD-6 and STSD-1–STSD-4)). New values for Er, Gd, Ho, Pr and Tm in LKSD-1–LKSD-4 and STSD-1–STSD-4, and Er, Ho, Lu, Nd, Pr, Tb, Tm and Yb in NBS 1645 are first reported in this work.

## 1. Introduction

The rare-earth elements (REEs) play an important role in geochemistry for modelling earth's crustal and mantle evolutionary processes and for dating ages of rocks. Their applications in industry varies from uses in electronics to the manufacture of superconductors, supermagnets and cathode ray tubes. A knowledge of their behaviour and abundances in aqueous environment helps to devise effective ways of disposal of nuclear wastes since they are produced in nuclear generators during the fission of uranium and polonium.

Since Y and the REEs are a group of closely related elements having similar physical and chemical properties, their terrestrial and extraterrestrial abundances being very low, special preconcentration procedures such as solvent extraction [1], co-precipitation [2–5] or ion exchange separation [2,4–11] are needed before their determination by instrumental methods. Some early examples of the utilization of these preconcentrations techniques are found in their determinations by flame and electrothermal atomic absorption spectrometry [2–4], X-ray fluorescence spectrometry [5,6],

☆ Geological Survey of Canada contribution number 40594.

* Corresponding author. Present address: 6074 Meadowglen Drive, Gloucester, Ont., K1C SR6, Canada.


*SSDI* 0039-9140(95)01612-0

neutron activation [7], spark source mass spectrometry [9], isotope dilution mass spectrometry [8–12], inductively coupled plasma-atomic emission spectrometry (ICP-AES) [12,13], direct current plasma-atomic emission spectrometry [14], and inductively coupled plasma-mass spectrometry (ICP-MS) [1,15,16].

Since the use of a preconcentration procedure before determination by an instrumental method is laborious and time-consuming, some workers have used silicate rock sample solutions prepared by acid digestions in open vessels with or without fusion of any insoluble residue for the direct determination of the REEs by ICP-MS [15,17,18], Bailey et al. [19] determined Th and U in basalts by ICP-MS after digestion in an open vessel with acids. Pin et al. [20] used the isotope dilution ICP-MS method to determine Th and U in silicate rocks after decompositions with acids and ion-exchange separation of the matrix elements.

The sample dissolution procedure used in most ICP-MS laboratories involving open vessel digestions with acids, repeated evaporations to expell HF and/or $HClO_4$, dissolution, filtration and subsequent fusion of any insoluble residue is very tedious and slow for the routine analyses of a large number of geological materials in a day, There is, therefore, a need for an alternative technique which is less labour-intensive and faster with respect to the sample dissolution procedure to improve productivity.

A microwave digestion procedure which involved heating the sample with HF + aqua regia + $H_3BO_3$ + EDTA in a Teflon pressure vessel was used by Sen Gupta and Bouvier [21] for the direct determination of some trace and ultratrace elements in geological materials by multielement Zeeman-effect graphite furnace-atomic absorption spectrometry (GF-AAS). The same decomposition procedure found relatively fast and environmentally friendly compared to the conventional open vessel digestion procedures [22] was used in this work for preparation of solutions of some geochemical reference materials. Since the sensitivities of Y, Th, U and most REEs were not sufficient for their direct determination from rock solutions by multielement GFAAS, it was decided to determine these elements by a much more sensitive ICP-MS method. This paper describes the results of such a study.

The accuracy and precision of the proposed microwave digestion and direct ICP-MS determination procedure for the specified elements were evaluated by four to five replicate analyses of United States Geological Survey (USGS) reference rock BCR-1 (basalt) and Canadian Certified Reference Materials Project (CCRMP) reference rocks SY-2 (syenite) and MRG-1 (gabbro). The analytes were also determined from 21 other international geochemical reference materials, mostly in duplicate. The results were then compared with "consensus" [23,24], "working" [25], or "recommended" [26] literature values. In most cases, excellent agreement was found with the "working" values of Govindaraju [25]. In some cases the results of this work were within the statistical range of "consensus" or "recommended" values of Gladney et al. [23,24,26].

## 2. Experimental

### 2.1. Apparatus

A Perkin-Elmer/Sciex model 5000 ICP-mass spectrometer equipped with an AS-91 autosampler and an IBM PS/2 (model 70) computer was used for multielement mass spectral analysis. The mass spectrometer operating conditions and the data acquisition parameters are given in Table 1.

A Milestone microwave oven (model MLS-1200 MEGA) equipped with six 100 ml Milestone pressure decomposition Teflon vessels, a micrwave digestion rotor (model HPR 100016) and a remote control panel was used for the decomposition of the samples.

Table 1
Instrumental operating conditions and data acquisition parameters

| Condition/parameter | Result |
|---|---|
| ICP mass spectrometer | |
| R.f. power (kW) | 1.0 |
| Plasma argon gas flow rate (l $min^{-1}$) | 15 |
| Auxiliary argon gas flow rate (l $min^{-1}$) | 0.9 |
| Nebulizer argon gas flow rate (l $min^{-1}$) | 0.9 |
| Sampler skimmer | Nickel |
| Data acquisition | |
| Dwell time (ms) | 100 |
| Scan mode | Peak hopping |
| Points across peak | 1 |
| Sweeps reading$^{-1}$ | 10 |
| Number of replicates | 2 |

A Hamilton digital diluter was used for diluting all sample solutions.

### 2.2. Reagents and standard solutions

All reagents used were of A.C.S. grade, and ultrapure water (ASTM type 1) prepared by reverse osmosis with a Millipore apparatus was used throughout the procedure.

Synthetic standard solutions were prepared by diluting 10 μg $ml^{-1}$ mixed high purity ICP-MS standard solutions (Delta Scientific Laboratory Products Ltd., Mississauga, Ont.) with 3% (v/v) nitric acid to obtain solutions of elemental concentration range 20–100 ng $ml^{-1}$. Ruthenium and rhenium were added (as internal standards to control drift) to each standard solutions to give a final concentration of 50 ng $ml^{-1}$ of each. Also, 2 drops of concentrated hydrofluoric acid were added to each standard solution before making up the final volume in order to approximately match the concentration of hydrofluoric acid in the microwave-digested sample solution.

To prepare a mixed solution of boric acid (2.2%) and ethylenediaminetetraacetic acid (EDTA; 0.165%); in a 1 l borosilicate beaker, 1.65 g of EDTA were treated with concentrated ammonia solution dropwise with stirring until the solution became clear. To this solution 22 g boric acid were added, the mixture was diluted with water to 500 ml and the beaker was heated on a hot plate with stirring until the solid dissolved. The solution was then diluted with water to 1 l.

All solutions were stored in Nalgene bottles fitted with screw caps.

### 2.3. Procedure

Details of the sample decomposition procedure are given in a previous paper [21]. Briefly, the method involved heating 0.5 g of the finely powdered sample in a Teflon pressure vessel with a mixture of 2.5 ml of 27 M HF, 3 ml of 16 M $HNO_3$ and 3 ml of 12 M HCl in a Milestone microwave oven for 16 min using Program 1 of Table 2. After cooling, 30 ml of the boric acid and EDTA mixture were added, and then the vessel was further heated for 8 min using Program 2 of Table 2. After bringing to room temperature by cooling in a cold water bath, the contents of the vessel were quantitatively transferred to a 50 ml graduated polypropylene tube by rinsing with 2% (v/v) nitric acid and the volume was made up to 50 ml. A clear solution was obtained at this stage for most silicate rocks and sediments. An aliquot of this solution was diluted 10 times in the digital diluter with 3% (v/v) nitric acid containing ruthenium and rhenium internal standards, and the solution was transferred to a 15 ml polypropylene tube equipped with a stopper. The concentration of Ru and Re in the final diluted solution was 50 ng $ml^{-1}$ of each. A reagent blank was run throughout the procedure.

Table 2
Milestone microwave oven operating programmes

| Power (W) | Time (min) | Vent (min) |
|---|---|---|
| Program 1 | | |
| 250 | 2 | |
| 1000 | 2 | |
| 600 | 2 | |
| 250 | 10 | |
| | | 1 |
| Program is ready, power is off | | |
| Program 2 | | |
| 1000 | 3 | |
| 250 | 5 | |
| | | 5 |
| Program is ready, power is off | | |

### 2.4. Multielement ICP-MS determination

The calibration curves were prepared with a blank and three synthetic mixed standard solutions with concentrations as follows.

Standard 1, 20 ng $ml^{-1}$ of each element.
Standard 2, 50 ng $ml^{-1}$ of each element.
Standard 3, 100 ng $ml^{-1}$ of each element.

In constructing these calibration curves, instrumental operating parameters given in Table 1 and isotopic masses listed in Table 3 were used, and corrections for isobaric oxides (Table 4) were made using the method of algebraic approach of elimination [27].

The unknown sample solutions (ten fold diluted solutions of concentration 1 ng $ml^{-1}$ each and containing 50 ng $ml^{-1}$ each of Ru and Re internal standards) were run in a group of six through the automatic sampler. Each group of these six samples was preceded by and followed by the reading of the concentration of a 20 ng $ml^{-1}$ synthetic standard to check the recovery. The accuracy of the re-

Table 3
List of isotopes of yttrium, rare earth elements and thorium together with ruthenium and rhenium employed in this work

| Group 1 | Group 2 |
|---|---|
| $^{89}Y$ | $^{151}Eu$ |
| $^{139}La$ | $^{159}Tb$ |
| $^{140}Ce$ | $^{160}Gd$ |
| $^{141}Pr$ | $^{163}Dy$ |
| $^{143}Nd$ | $^{165}Ho$ |
| $^{147}Sm$ | $^{166}Er$ |
| $^{101}Ru$[a] | $^{169}Tm$ |
| | $^{174}Yb$ |
| | $^{175}Lu$ |
| | $^{232}Th$ |
| | $^{238}U$ |
| | $^{185}Re$[b] |

[a] Used as an internal standard to correct for instrumental drift and matrix effects on Group 1 elements.
[b] Used as an internal standard to correct for instrumental drift and matrix effects on Group 2 elements.

sults was also checked at intervals of six samples and the said synthetic standard by analyzing three USGS geochemical reference rocks (AGV-1, BCR-1 and BHVO-1), solutions of which were prepared identically to the unknown sample solutions. The use of ruthenium and rhenium internal standards automatically corrected for instrumental drift and matrix effects.

The instrument software automatically performed blank subtraction, calibration, oxide correction, drift control, and calculation of elemental concentrations of the synthetic standard, unknown samples and the reference materials. From the print-out of these concentration data, the recovery of the 20 ng ml$^{-1}$ synthetic standard was checked, and, if required, a correction factor was applied to the results for the unknown samples and the reference materials. If the final data of the reference materials thus obtained fell within the range of "consensus values" [23,28], then the data for the unknown samples were considered acceptable for reporting. In actual practice, this procedure worked well since the data for the specified reference materials obtained in this way were always within the range of acceptable literature values.

Table 4
Spectral overlap of barium and rare earth element oxides on rare earth elements Eu–Yb

| Mass | Element | Interferences |
|---|---|---|
| 151 | Eu | $^{135}Ba^{16}O$ |
| 160 | Gd (21.6) | $^{144}Nd^{16}O$ |
| 159 | Tb (100)[a] | $^{143}Nd^{16}O$ |
| 163 | Dy (25.0) | $^{147}Sm^{16}O$ |
| 165 | Ho (100)[a] | $^{149}Sm^{16}O$ |
| 166 | Er (33.4)[a] | $^{150}Nd^{16}O$ |
| 174 | Yb (31.8)[a] | $^{158}Gb^{16}O$ |

[a] Major naturally occurring isotope.

## 3. Results and discussion

The ICP-MS determination limits of this work were Y, Pr, Sm, Eu, Gd, Tb, Dy, Ho, Er, Tm and Lu 0.02 μg g$^{-1}$; La, Ce and Nd, 0.10 μg g$^{-1}$; Yb, 0.05 μg g$^{-1}$.

Interferences in the determination of the REEs by ICP-MS have been discussed by other workers [15,17,27,29]. In the analysis by ICP-MS the analyte ion $M^+$ may also be distributed among several other species such as $MO^+$, $MOH^+$ or $M^{2+}$. This will cause spectral interferences due to mass overlaps or isobaric interferences. For the REEs the spectral interferences are principally due to oxide-forming elements which cause isotopic mass overlaps as shown in Table 4. However, in choosing the isotopic masses of the REEs in this analysis, only those isotopes were selected for which isotopic mass overlaps due to oxide-forming elements were at a minimum. The method for isobaric oxide correction used in this work was mentioned earlier in Section 2.4. The contribution of $MOH^+$ in the REE analysis by ICP-MS, representing about 1/10th of the oxide correction, was negligible. Also, no correction for a doubly charged ion ($M^{2+}$) was required in the lanthanide determination.

Tables 5–7 show the results obtained by the proposed method for some geochemical reference materials of the USGS (AGV-1, BCR-1, BHVO-1, BIR-1, W-2, DNC-1, G-2 and MAG-1), the CCRMP (MRG-1, SY-2, LKSD-1–LKSD-4 and STSD-1–STSD-4), the National Institute of Metallurgy, South Africa (NIM-G), the International Working Group, France (BE-N), the Institute of Geophysical and Geochemical Exploration, China (GSD-1, GSD-5 and GSD-6) and the National Bureau of Standards (NBS 1645). The mean and standard deviations of four replicate determinations of BCR-1 and of five replicate determinations of MRG-1 and SY-2 are given in Tables 5 and 6, respectively. For most other samples the results for two independent

determinations are given (See Tables 5–7). These results are then compared with the "consensus" [23,24,28], "recommended" [26,30], "working" [25] or "provisional" [31] literature values. It should be pointed out here that these "consensus", "recommended", "working" or "provisional" literature values were derived by the respective workers from a compilation of data from many laboratories and then subjecting them to rigorous selections in which very low or high values, called outliers, were rejected and a cluster of values at the median, where the majority of data converged, were accepted for the statistical calculation. Therefore, for any method development work a comparison of the recovery or "accuracy of elemental concentrations" for natural geochemical reference materials cannot be made with "absolute" values. It should be sufficient if the results of the proposed method fall within a "median" statistical range of values. Bearing this in mind, an attempt will be made to discuss the results of this work and a correlation with the literature values.

The data of Tables 5-7 (mean values) are plotted in Figs. 1 and 2 for a quick assessment of the nature of the correlation between the results of this work and the literature values. It is found that excepting two Ce values higher than 150 $\mu g\, g^{-1}$, there is a fairly good correlation between the two sets of values for each element since the 45° line passes through the majority of the points.

The microwave digestion ICP-MS (MDICPMS) data from this work (mean values), normalized to the C1 chondritic abundance data of Sun and McDonough [32] are plotted in Figs 3 and 4. Yttrium was plotted between Dy and Ho because of its similar chemical properties to those of the REEs, its ionic radius (0.0893 nm) being close to those of Dy (0.0908 nm) and Ho (0.0894 nm). Excepting negative anomalies for europium in SY-2, G-2, BCR-1, NIM-G and sediment samples ($Eu^{+2}$) and a few minor anomalies for Ce in some samples, these figures show very smooth patterns for Y and most REEs, fitting the curves, thereby providing support to the accuracy of the MDICPMS data.

A more detailed discussion of the data for individual sample would be pertinent at this point. In Table 5 excellent agreement between the MDICPMS results and the literature range of values is noted for all elements in BCR-1. Satisfactory agreement between the results of this work with the range of other values is also noted for other samples in Table 5. For MRG-1 and SY-2 (see Table 6), although initially the results for some REEs from various laboratories were few and scattered, as found in the compilation of data by Abbey et al. [33], more representative data became available much later through the compilation of Gladney and Roelandts [26]. The MDICPMS replicate data for MRG-1 (see Table 6) agree very well with the "recommended" values [26]. For SY-2, except for somewhat lower mean values for Ce and La, there is very good agreement with the "recommended" values for the other REEs. However, the chondrite-normalized plot for SY-2 in Fig. 3 shows no scatter for Ce and La, thereby supporting the validity of the results.

For lake and stream sediment samples (see Table 6), the MDICPMS data could be compared with the "provisional" values of Lynch [31] only for Ce, Dy, Eu, La, Lu, Nd, Sm, Tb, Th, U, Y and Yb. It is found that the MDICPMS results for these elements are within the range of the literature values. New data for Er, Gd, Ho, Pr and Tm obtained by MDICPMS in this work are given in Table 6. These data fit well in the chondrite-normalized plots (see Fig. 4).

Since for NIM-G, BE-N, GSD-1, GSD-5, GSD-6 and NBS 1645 (Table 7) recommended values are not available in the literature, a comparison of the MDICPMS values is made with the "range of other values" [34] (NIM-G) and/or Govindaraju's "working" [25] values. Except for Ce in BE-N, the MDICPMS data for these samples either fall within the range of other values or agree well with Govindaraju's working values in most cases. However, in the chondrite-normalized plot of BE-N (Fig. 3), MDICPMS data for Ce seem to fit well between La and Pr, supporting its acceptability.

For NBS 1645, new values for Er, Ho, Lu, Nd, Pr, Tb, Tm and Yb are first reported in this paper. The data for these elements give a smooth pattern in the chondrite-normalized plot (see Fig. 4).

From the data of Tables 5–7 it would appear that the "recommended" or "working" values for certain elements (e.g. Pr in AGV-1, W-2 and NIM-G; Gd in NIM-G and BE-N; Er in SY-2, NIM-G and BE-N) may require revision since they are either low or there are significant standard deviations from the mean

Table 5
Determination of Y, Th, U and the lanthanides in some USGS reference rocks and a sediment by ICP-MS after dissolution by microwave digestion ($\mu g\ g^{-1}$)

| Element | AGV-1 (andesite) | | BCR-1 (basalt) | | BHVO-1 (basalt) | | BIR-1 (basalt) | | W-2 (diabase) | | DNC-1 (diabase) | | G-2 (granite) | | MAG-1 (marine mud) | |
|---|---|---|---|---|---|---|---|---|---|---|---|---|---|---|---|---|
| | This work | Literature value[a] | This work[b] | Literature value[a] | This work | Literature value[c] | This work | Literature value[d] | This work | Literature value[d] | This work | Literature value[d] | This work | Literature value[a] | This work | Literature value[e] |
| Ce | 72 | 66 ± 6 | 53.8 ± 2.1 | 53.7 ± 0.8 | 40 | 41 ± 4 | 2.0 | 2.5 ± 1.1 | 23 | 24 ± 2 | 9 | 10.6 ± 2.4 | 154 | 159 ± 11 | 86 | 88 |
| | 69 | 67[e] | | | 38 | 39[e] | 2.3 | 1.95[e] | | 23[e] | | 10.6[e] | | 160[e] | 86 | |
| Dy | 3.9 | 3.8 ± 0.4 | 6.1 ± 0.1 | 6.35 ± 0.12 | 5.5 | 4.8 ± 0.2 | 2.4 | 2.4 ± 0.3 | 3.9 | 3.8 ± 0.4 | 2.7 | 2.7 ± 0.4 | 2.3 | 2.5 ± 0.5 | 5.2 | 5.2 |
| | 4.0 | 3.6[e] | | | 5.2 | 5.2[e] | 2.6 | 2.5[e] | | 3.8[e] | | 2.7[e] | | 2.4[e] | 5.2 | |
| Er | 1.7 | 1.61 ± 0.22 | 3.8 ± 0.1 | 3.61 ± 0.09 | 2.4 | 2.0 ± 0.3 | 1.7 | 1.8 ± 0.3 | 2.4 | 2.5 ± 0.6 | 2.1 | 2.0 ± 0.2 | 1.0 | 1.2 ± 0.3 | 2.7 | 3 |
| | 1.8 | | | | 2.6 | 2.4[e] | 1.8 | 1.7[e] | | | | | | 0.92[e] | 2.8 | |
| Eu | 1.5 | 1.66 ± 0.11 | 1.95 ± 0.06 | 1.96 ± 0.05 | 2.3 | 2.0 ± 0.4 | 0.54 | 0.54 ± 0.04 | 1.2 | 1.10 ± 0.08 | 0.6 | 0.59 ± 0.03 | 1.2 | 1.41 ± 0.12 | 1.4 | 1.55 |
| | 1.6 | | | | 2.1 | 2.06[e] | 0.55 | | | | | | | | 1.4 | |
| Gd | 5.0 | 5.2 ± 0.6 | 6.98 ± 0.25 | 6.68 ± 0.13 | 7.0 | 7 ± 2 | 1.9 | 1.9 ± 0.4 | 3.9 | 3.6 ± 0.5 | 2.2 | 2.0 ± 0.4 | 4.1 | 4.1 ± 0.8 | 5.8 | 5.8 |
| | 5.2 | 5[e] | | | 6.8 | 6.4[e] | 1.9 | 1.85[e] | | | | | | | 6.0 | |
| Ho | 0.7 | 0.73 ± 0.08 | 1.2 ± 0 | 1.25 ± 0.14 | 1.0 | 0.94 | 0.50 | 0.50 ± 0.08 | 0.79 | 0.76 ± 0.09 | 0.62 | 0.62 ± 0.14 | 0.37 | 0.37 ± 0.02 | 1.0 | 1.02 |
| | 0.9 | 0.67[e] | | | 1.0 | 0.99[e] | 0.54 | | | | | | | | 1.0 | |
| La | 39 | 38 ± 3 | 25 ± 0.8 | 25 ± 0.1 | 16.0 | 16.7 ± 0.8 | 0.7 | 0.88 ± 0.33 | 11.1 | 11.4 ± 1.8 | 3.9 | 3.8 ± 0.4 | 85 | 86 ± 5 | 42 | 43 |
| | 40 | | | | 16.5 | | 0.8 | | | | | | | | 43 | |
| Lu | 0.28 | 0.28 ± 0.03 | 0.55 ± 0.02 | 0.51 ± 0.03 | 0.32 | 0.32 | 0.22 | 0.26 ± 0.04 | 0.34 | 0.33 ± 0.07 | 0.30 | 0.32 ± 0.04 | 0.08 | 0.113 ± 0.024 | 0.4 | 0.4 |
| | 0.30 | | | | 0.32 | | 0.26 | | | | | | | | 0.4 | |
| Nd | 32 | 34 ± 5 | 29.3 ± 1 | 28.7 ± 0.6 | 27 | 24 ± 6 | 2.3 | 2.5 ± 0.7 | 14 | 14 ± 5 | 5.0 | 4.9 ± 0.2 | 54 | 53 ± 8 | 38 | 38 |
| | 36 | 33[e] | | | 27 | 25.2[e] | 2.5 | | | 14[e] | | | | | 39 | |
| Pr | 7.9 | 6.5 ± 0.9 | 7.0 ± 0.3 | 6.9 ± 0.6 | 5.6 | 5.6 | 0.40 | 0.5 ± 0.4 | 3.1 | 5.9 ± 5.2 | 1.2 | 1.3 ± 0.6 | 17 | 19 ± 2 | 9.3 | 9.3 |
| | 8.8 | 7.6[e] | | | 5.5 | | 0.43 | 0.38[e] | | | | 1.3[e] | | 18[e] | 9.3 | |
| Sm | 5.7 | 5.9 ± 0.5 | 6.7 ± 0.2 | 6.58 ± 0.17 | 6.5 | 6.1 ± 0.7 | 1.0 | 1.08 ± 0.09 | 3.3 | 3.25 ± 0.23 | 1.4 | 1.38 ± 0.15 | 7.2 | 7.2 ± 0.6 | 7.4 | 7.5 |
| | 6.2 | | | | 6.2 | 6.2[e] | 1.0 | | | | | | | | 7.7 | |
| Tb | 0.70 | 0.71 ± 0.10 | 1.05 ± 0.08 | 1.05 ± 0.09 | 1.0 | 1.0 ± 0.2 | 0.4 | 0.41 ± 0.05 | 0.62 | 0.63 ± 0.12 | 0.4 | 0.41 ± 0.03 | 0.46 | 0.48 ± 0.07 | 0.92 | 0.96 |
| | 0.72 | 0.7[e] | | | 1.0 | | 0.4 | | | | | | | | 0.90 | |
| Th | 6.7 | 6.5 ± 0.37 | 5.7 ± 0.1 | 6.0 ± 0.6 | 1.3 | 1.1 ± 0.2 | 0.04 | 0.03[d] | 2.3 | 2.2 ± 0.4 | 0.25 | 0.20 ± 0.09 | 26 | 24.6 ± 1.5 | 12 | 11.9 |
| | 6.9 | | | | 1.3 | | 0.06 | | | | | | | 24.7[e] | 12 | |
| Tm | 0.30 | 0.32 ± 0.05 | 0.59 ± 0.03 | 0.59 ± 0.04 | 0.36 | 0.31 ± 0.04 | 0.24 | 0.27 ± 0.07 | 0.35 | 0.38 ± 0.07 | 0.31 | 0.33 ± 0.05 | 0.12 | 0.17 ± 0.07 | 0.41 | 0.43 |
| | 0.32 | | | | 0.35 | 0.33[e] | 0.27 | | | | | | | 0.1[e] | 0.42 | |
| U | 2.1 | 1.89 ± 0.25 | 1.7 ± 0.1 | 1.7 ± 0.16 | 0.48 | 0.42 ± 0.06 | < 0.02 | 0.025 | 0.53 | 0.53 ± 0.08 | 0.1 | 0.1 | 2.0 | 2.04 ± 0.17 | 2.9 | 2.7 |
| | | | | | | | | | | | | | | | 2.9 | 2.9[e] |
| Y | 18 | 21 ± 6 | 34 ± 1 | 39 ± 7 | 26 | 28 ± 2 | 15 | 16 ± 2 | 22 | 24 ± 3 | 17 | 18 ± 3 | 10 | 11.4 ± 2.3 | 26 | 28 |
| | 20 | 20[e] | | 38[e] | 26 | 27.6 | 15 | 16[e] | | 24[e] | | | | 11[e] | 27 | |
| Yb | 1.7 | 1.67 ± 0.17 | 3.6 ± 0.1 | 3.4 ± 0.08 | 2.1 | 2.1 ± 0.5 | 1.7 | 1.70 ± 0.19 | 2.2 | 2.05 ± 0.12 | 2.0 | 2.01 ± 0.10 | 0.6 | 0.78 ± 0.14 | 2.4 | 2.6 |
| | 1.8 | 1.7[e] | | | 2.2 | 2.02[e] | 1.5 | 1.65[e] | | | | | | | 2.5 | |

[a] "Consensus value" given in a compilation of data by Gladney et al. [23] unless otherwise indicated.
[b] Mean and standard deviation of four replicate determinations.
[c] Quoted from a compilation of data by Gladney and Goode [28] unless otherwise indicated.
[d] "Consensus value" given in a compilation of data by Gladney and Roelandts [24] unless otherwise indicated.
[e] "Working value" given in a compilation of data by Govindaraju [25] unless otherwise indicated.

Table 6
Determination of Y, Th, U and the lanthanides in the CCRMP reference materials gabbro (MRG-1), syenite (SY-2), lake sediments (LKSD-1–LKSD-4) and stream sediments (STSD-1–STSD-4) by ICP-MS after dissolution by microwave digestion ($\mu g\ g^{-1}$)

| Element | MRG-1 | | SY-2 | | LKSD-1 | | LKSD-2 | | LKSD-3 | | LKSD-4 | | STSD-1 | | STSD-2 | | STSD-3 | | STSD-4 | |
|---|---|---|---|---|---|---|---|---|---|---|---|---|---|---|---|---|---|---|---|---|
| | This work[a] | Literature values[b] | This work[a] | Literature values[b] | This work | Literature values[c] | This work | Literature values[c] | This work | Literature values[c] | This work | Literature values[c] | This work | Literature values[c] | This work | Literature values[c] | This work | Literature values[c] | This work | Literature values[c] |
| Ce | 25 ± 0.7 | 26 ± 4 | 158 ± 6 | 175 ± 35 | 25 | 27 ± 2 | 107 | 108 ± 12 | 87 | 90 ± 7 | 42 | 48 ± 6 | 45 | 51 ± 6 | 90 | 93 ± 10 | 63 | 63 ± 8 | 41 | 44 ± 3 |
| | | | | | 26 | | 104 | | 85 | | 44 | | 45 | | 87 | | 57 | | 39 | |
| Dy | 2.9 ± 0.1 | 2.9 ± 0.9 | 18.6 ± 0.6 | 18 ± 3 | 3.4 | 3.4 ± 0.4 | 7.4 | 7.3 ± 0.7 | 5.0 | 4.9 ± 0.6 | 3.5 | 3.7 ± 0.2 | 5.8 | 5.6 ± 0.9 | 6.1 | 6.5 ± 0.6 | 5.7 | 5.4 ± 0.6 | 3.7 | 3.8 ± 0.5 |
| | | | | | 3.3 | | 7.2 | | 4.9 | | 3.7 | | 5.8 | | 6.2 | | 5.3 | | 3.7 | |
| Er | 1.1 ± 0.1 | 1.1 ± 0.3 | 14 ± 0 | 12.4 ± 1.7 | 2.0 | –[d] | 4.0 | –[d] | 2.8 | –[d] | 2.0 | –[d] | 3.3 | –[d] | 3.2 | –[d] | 3.2 | –[d] | 2.1 | –[d] |
| | | | | | 2.0 | | 4.1 | | 2.7 | | 2.1 | | 3.4 | | 3.2 | | 3.0 | | 2.1 | |
| Eu | 1.5 ± 0.04 | 1.4 ± 0.1 | 2.5 ± 0.1 | 2.4 ± 0.3 | 1.0 | 0.9 ± 0.2 | 1.9 | 1.9 ± 0.2 | 1.5 | 1.5 ± 0.3 | 1.1 | 1.1 ± 0.3 | 1.6 | 1.6 ± 0.4 | 2.0 | 2.0 ± 0.4 | 1.5 | 1.3 ± 0.5 | 1.1 | 1.2 ± 0.5 |
| | | | | | 1.0 | | 1.9 | | 1.4 | | 1.1 | | 1.5 | | 1.9 | | 1.4 | | 1.0 | |
| Gd | 4.3 ± 0.2 | 4.0 ± 0.7 | 17.6 ± 0.6 | 17.0 ± 1.8 | 3.5 | –[d] | 8.9 | –[d] | 6.4 | –[d] | 4.0 | –[d] | 6.5 | –[d] | 7.3 | –[d] | 6.5 | –[d] | 4.2 | –[d] |
| | | | | | 3.4 | | 8.9 | | 6.2 | | 4.3 | | 6.4 | | 7.2 | | 6.0 | | 4.2 | |
| Ho | 0.5 ± 0.02 | 0.5 ± 0.01 | 4.5 ± 0.15 | 3.8 ± 0.6 | 0.70 | –[d] | 1.4 | –[d] | 1.0 | –[d] | 0.70 | –[d] | 1.1 | –[d] | 1.2 | –[d] | 1.2 | –[d] | 0.75 | –[d] |
| | | | | | 0.70 | | 1.4 | | 1.0 | | 0.75 | | 1.2 | | 1.2 | | 1.1 | | 0.75 | |
| La | 9.1 ± 0.1 | 9.8 ± 0.8 | 65 ± 3.5 | 75 ± 9 | 14 | 16 ± 2 | 61 | 68 ± 6 | 46 | 52 ± 3 | 24 | 26 ± 2 | 26 | 30 ± 3 | 52 | 59 ± 6 | 33 | 39 ± 3 | 20 | 24 ± 3 |
| | | | | | 14 | | 63 | | 47 | | 22 | | 26 | | 53 | | 36 | | 21 | |
| Lu | 0.12 ± 0.05 | 0.12 ± 0.04 | 3 ± 0 | 2.7 ± 0.4 | 0.30 | 0.4 ± 0.1 | 0.60 | 0.6 ± 0.1 | 0.40 | 0.4 ± 0.1 | 0.30 | 0.5 ± 0.01 | 0.50 | 0.8 ± 0.1 | 0.50 | 0.7 ± 0.04 | 0.50 | 0.8 ± 0.1 | 0.32 | 0.5 ± 0.1 |
| | | | | | 0.31 | | 0.62 | | 0.41 | | 0.33 | | 0.51 | | 0.44 | | 0.45 | | 0.33 | |
| Nd | 18.4 ± 0.6 | 19.2 ± 2.2 | 77 ± 1 | 73 ± 11 | 16 | 16 ± 1 | 59 | 58 ± 4.6 | 43 | 44 ± 3.6 | 23 | 25 ± 2.4 | 30 | 28 ± 4.2 | 45 | 43 ± 4.4 | 35 | 33 ± 3.5 | 21 | 21 ± 1.7 |
| | | | | | 17 | | 59 | | 43 | | 25 | | 31 | | 44 | | 32 | | 21 | |
| Pr | 3.5 ± 0.1 | 3.4 ± 0.7 | 18.6 ± 0.6 | 18.8 ± 1.8 | 3.7 | –[d] | 15.2 | –[d] | 11.2 | –[d] | 6.0 | –[d] | 7.4 | –[d] | 11.9 | –[d] | 8.9 | –[d] | 5.4 | –[d] |
| | | | | | 3.9 | | 15.2 | | 11.3 | | 6.2 | | 7.4 | | 11.9 | | 8.2 | | 5.3 | |
| Sm | 4.3 ± 0.1 | 4.5 ± 0.5 | 16.4 ± 0.6 | 16.1 ± 1.0 | 3.9 | 4.0 ± 0.5 | 10.7 | 11 ± 1.1 | 7.8 | 8.0 ± 0.6 | 4.6 | 5.0 ± 0.9 | 6.5 | 6.0 ± 0.7 | 8.4 | 8.0 ± 0.8 | 7.0 | 7.0 ± 0.8 | 4.5 | 5.0 ± 0.5 |
| | | | | | 3.8 | | 10.6 | | 7.7 | | 4.8 | | 6.5 | | 8.4 | | 6.5 | | 4.3 | |
| Tb | 0.55 ± 0 | 0.51 ± 0.1 | 3.0 ± 0.1 | 2.5 ± 0.9 | 0.54 | 0.6 ± 0.2 | 1.30 | 1.4 ± 0.2 | 0.9 | 1.0 ± 0.1 | 0.6 | 1.2 ± 0.7 | 1.0 | 1.2 ± 0.3 | 1.1 | 1.3 ± 0.2 | 1.0 | 1.1 ± 0.2 | 0.63 | 0.8 ± 0.2 |
| | | | | | 0.52 | | 1.23 | | 0.9 | | 0.7 | | 1.0 | | 1.1 | | 1.0 | | 0.62 | |
| Th | 1.1 ± 0.2 | 0.9 ± 0.2 | 359 ± 47 | 379 ± 29 | 1.9 | 2.2 ± 0.3 | 12.9 | 13.4 ± 1.0 | 11 | 11.4 ± 0.7 | 4.7 | 5.1 ± 0.7 | 3.4 | 3.7 ± 0.5 | 16 | 17.2 ± 1.3 | 8.2 | 8.5 ± 0.7 | 4.0 | 4.3 ± 0.4 |
| | | | | | 2.0 | | 12.6 | | 11 | | 5.1 | | 3.3 | | 16 | | 8.0 | | 3.4 | |
| Tm | 0.16 ± 0 | 0.11 ± 0.05 | 2.4 ± 0.3 | 2.1 ± 0.2 | 0.31 | –[d] | 0.61 | –[d] | 0.43 | –[d] | 0.30 | –[d] | 0.50 | –[d] | 0.47 | –[d] | 0.47 | –[d] | 0.32 | –[d] |
| | | | | | 0.30 | | 0.60 | | 0.40 | | 0.33 | | 0.51 | | 0.46 | | 0.46 | | 0.33 | |
| U | 0.26 ± 0.03 | 0.24 ± 0.04 | 283 ± 26 | 284 ± 9 | 9.8 | 9.7 ± 1 | 7.6 | 7.6 ± 0.9 | 4.7 | 4.6 ± 0.5 | 29.1 | 31 ± 1.8 | 8.0 | 8.0 ± 0.6 | 18.1 | 18.6 ± 1.0 | 10.6 | 10.5 ± 0.9 | 2.7 | 3.0 ± 0.5 |
| | | | | | 9.8 | | 7.8 | | 4.6 | | 30.0 | | 8.0 | | 18.0 | | 10.0 | | 2.8 | |
| Y | 13 ± 0.5 | 14 ± 5 | 129 ± 2 | 128 ± 17 | 19 | 19 ± 9 | 40 | 44 ± 7 | 27 | 30 ± 10 | 20 | 23 ± 10 | 34 | 42 ± 11 | 33 | 37 ± 6 | 33 | 36 ± 9 | 21 | 24 ± 8 |
| | | | | | 19 | | 40 | | 27 | | 21 | | 35 | | 33 | | 30 | | 21 | |
| Yb | 0.78 ± 0.05 | 0.6 | 17 ± 0 | 17 | 1.9 | 2.0 ± 0.3 | 3.9 | 4.0 ± 0.5 | 2.7 | 2.7 ± 0.4 | 2.0 | 2.0 ± 0.2 | 3.2 | 4.0 ± 0.8 | 3.0 | 3.7 ± 0.6 | 3.1 | 3.4 ± 0.5 | 2.1 | 2.6 ± 0.6 |
| | | | | | 1.9 | | 3.9 | | 2.5 | | 2.1 | | 3.3 | | 3.0 | | 3.0 | | 2.1 | |

[a] Mean and standard deviation of five replicate determinations.
[b] "Recommended values" of Gladney and Roelandts [26].
[c] "Provisional values" given in a compilation of data by Lynch [31].
[d] Data not available in the literature.

Table 7
Determination of Y, Th, U and the lanthanides in some international reference materials by ICP-MS after dissolution by microwave digestion ($\mu g\ g^{-1}$)

| Element | NIM-G (granite) | | BE-N (basalt) | | GSD-1 (stream sediment) | | GSD-5 (stream sediment) | | GSD-6 (stream sediment) | | NBS 1645 (river sediment) | |
|---|---|---|---|---|---|---|---|---|---|---|---|---|
| | This work | Literature value[a] | This work | Literature value[a] | This work | Literature value[a] | This work | Literature value[a] | This work | Literature value[a] | This work | Literature value[a] |
| Ce | 165 | 145–200[b] | 131 | 152 | 85 | 81 | 89 | 89 | 68 | 68 | 24 | 23 |
| | 180 | | 130 | | | | 88 | | 70 | | 23 | |
| Dy | 17 | 17 | 6.5 | 6.4 | 4.4 | 4.4 | 4.3 | 5 | 3.7 | 3.8 | 1.2 | 1 |
| | 18 | | 6.7 | | | | 4.0 | | | 3.8 | 1.3 | |
| Er | 12 | 10.5[c] | 2.7 | 2.5 | 2.7 | 2.3 | 2.3 | 3.1 | 2 | 2.1 | 0.7 | –[d] |
| | 12 | | 2.9 | | | | 2.2 | | 2 | | 0.7 | |
| Eu | 0.4 | 0.35 | 3.9 | 3.6 | 1.4 | 1.4 | 1.3 | 1.4 | 1.4 | 1.5 | 0.4 | 0.32 |
| | 0.4 | | 3.9 | | | | 1.3 | | 1.5 | | 0.6 | 0.5[c] |
| Gd | 15 | 14 | 10.9 | 9 | 6.1 | 6.1 | 5.2 | 6.4 | 4.6 | 5.5 | 1.3 | 1.06 |
| | 15 | | 11.0 | | | | 5.0 | | 4.6 | | 1.3 | 1.1[c] |
| Ho | 3.8 | 3.6[c] | 1.1 | 1.1 | 0.93 | 0.91 | 0.82 | 1.1 | 0.72 | 0.78 | 0.30 | –[d] |
| | 4.1 | | 1.1 | | | | 0.80 | | 0.73 | | 0.25 | |
| La | 104 | 109 | 78 | 82 | 45 | 43 | 41 | 46 | 34 | 39 | 9.6 | 9 |
| | 105 | 100–115[c] | 80 | | | | 41 | | 36 | | 9.6 | |
| Lu | 2.1 | 2 | 0.25 | 0.24 | 0.5 | 0.45 | 0.32 | 0.46 | 0.30 | 0.36 | 0.11 | –[d] |
| | 2.1 | | 0.26 | | | | 0.33 | | 0.30 | | 0.11 | |
| Nd | 72 | 72 | 74 | 70 | 36 | 39 | 34 | 35 | 30 | 33 | 7.6 | –[d] |
| | 76 | | 75 | | | | 34 | | 32 | | 8.2 | |
| Pr | 20 | 19.5[c] | 18 | 17.5 | 10 | 10 | 9.1 | 9.6 | 8.0 | 8.2 | 2.2 | –[d] |
| | 21 | | 18 | | | | 9.0 | | 8.1 | | 2.2 | |
| Sm | 14.2 | 15.8 | 12.7 | 12 | 7 | 7.2 | 6.1 | 6.6 | 5.5 | 5.6 | 1.5 | 1.22 |
| | 16.2 | 14.6–17[b] | 12.7 | | | | 6.2 | | 5.7 | | 1.5 | |
| Tb | 2.7 | 3 | 1.37 | 1.3 | 0.8 | 0.86 | 0.8 | 0.9 | 0.72 | 0.69 | 0.19 | –[d] |
| | 2.9 | | 1.33 | | | | 0.7 | | 0.63 | | 0.21 | |
| Th | 51 | 51 | 11 | 11 | 23 | 28 | 16.2 | 15.2 | 9.0 | 9 | 2.0 | 1.62 |
| | 52 | | 12 | | | | 16.1 | | 9.4 | | 1.9 | |
| Tm | 2 | 2 | 0.36 | 0.36 | 0.41 | 0.42 | 0.36 | 0.48 | 0.30 | 0.38 | 0.11 | –[d] |
| | 2 | | 0.36 | | | | 0.34 | | 0.30 | | 0.11 | |
| U | 18 | 15 | 2.6 | 2.4 | 4.1 | 4.4 | 3.7 | 2.6 | 2.6 | 2.4 | 1.25 | 1.11 |
| | 18 | | 2.5 | | | | 3.0 | | 2.9 | | 1.32 | |
| Y | 110 | 100–145[b] | 29 | 30 | 26 | 22.5 | 22 | 26 | 20 | 20.2 | 7.4 | 6.6 |
| | 111 | | 30 | | | | 20 | | 20 | | 7.3 | 7.2[c] |
| Yb | 14 | 14.2 | 1.8 | 1.8 | 2.6 | 2.36 | 2.3 | 2.9 | 2.0 | 2.1 | 0.70 | –[d] |
| | 15 | | 1.9 | | | | 2.2 | | 2.0 | | 0.84 | |

[a] "Working value" given in a compilation of data by Govindaraju [25] unless otherwise indicated.
[b] Quoted from a compilation of data by Steele et al.[34].
[c] "Recommended value" quoted from a compilation of data by Potts et al. [30].
[d] Data not available in the literature.

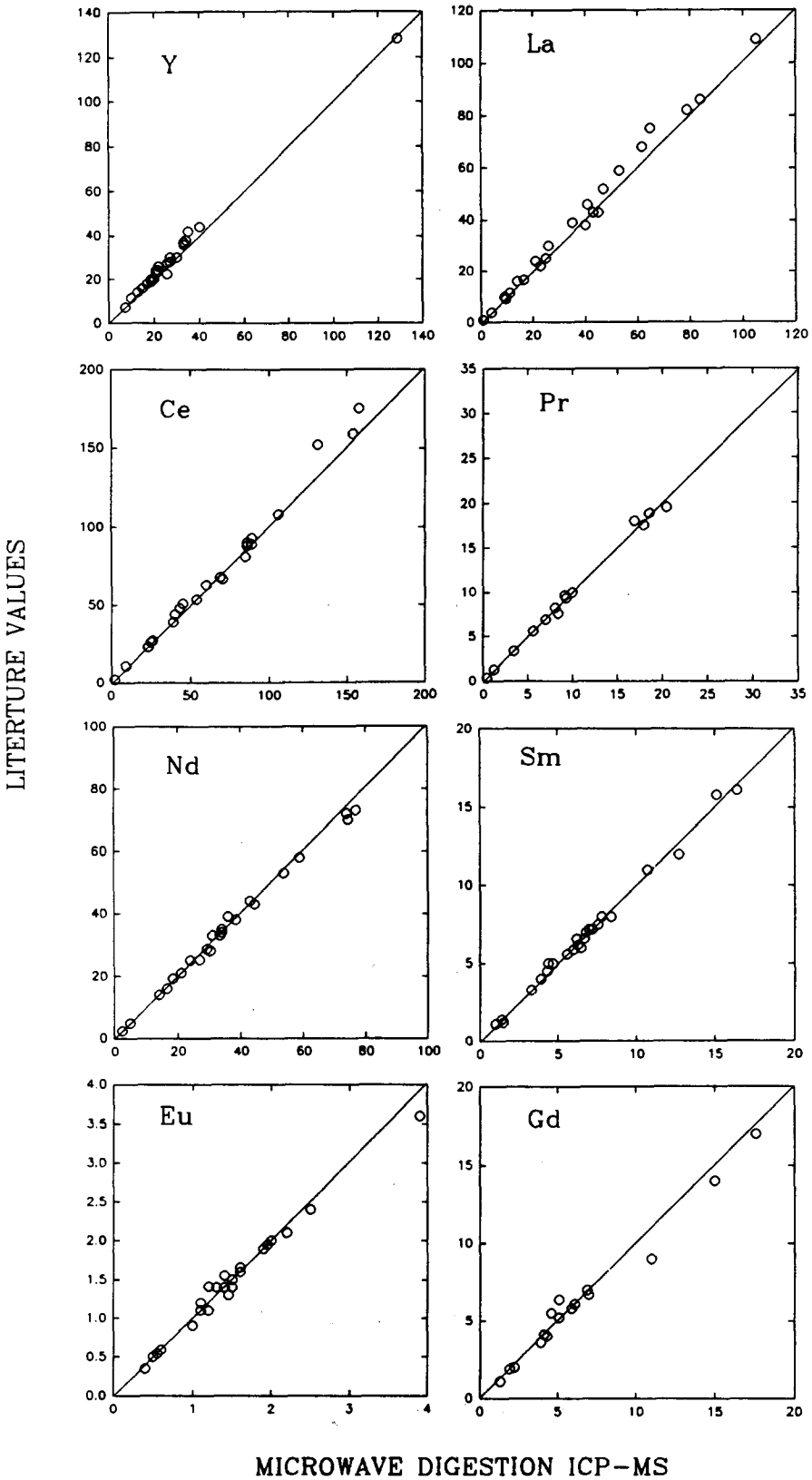


Fig. 1. Correlation plots for the microwave digestion ICP-MS results versus the literature values for Y, La, Ce, Pr, Nd, Sm, Eu and Gd in some international reference samples of rocks and sediments (concentration is given in micrograms per gram).

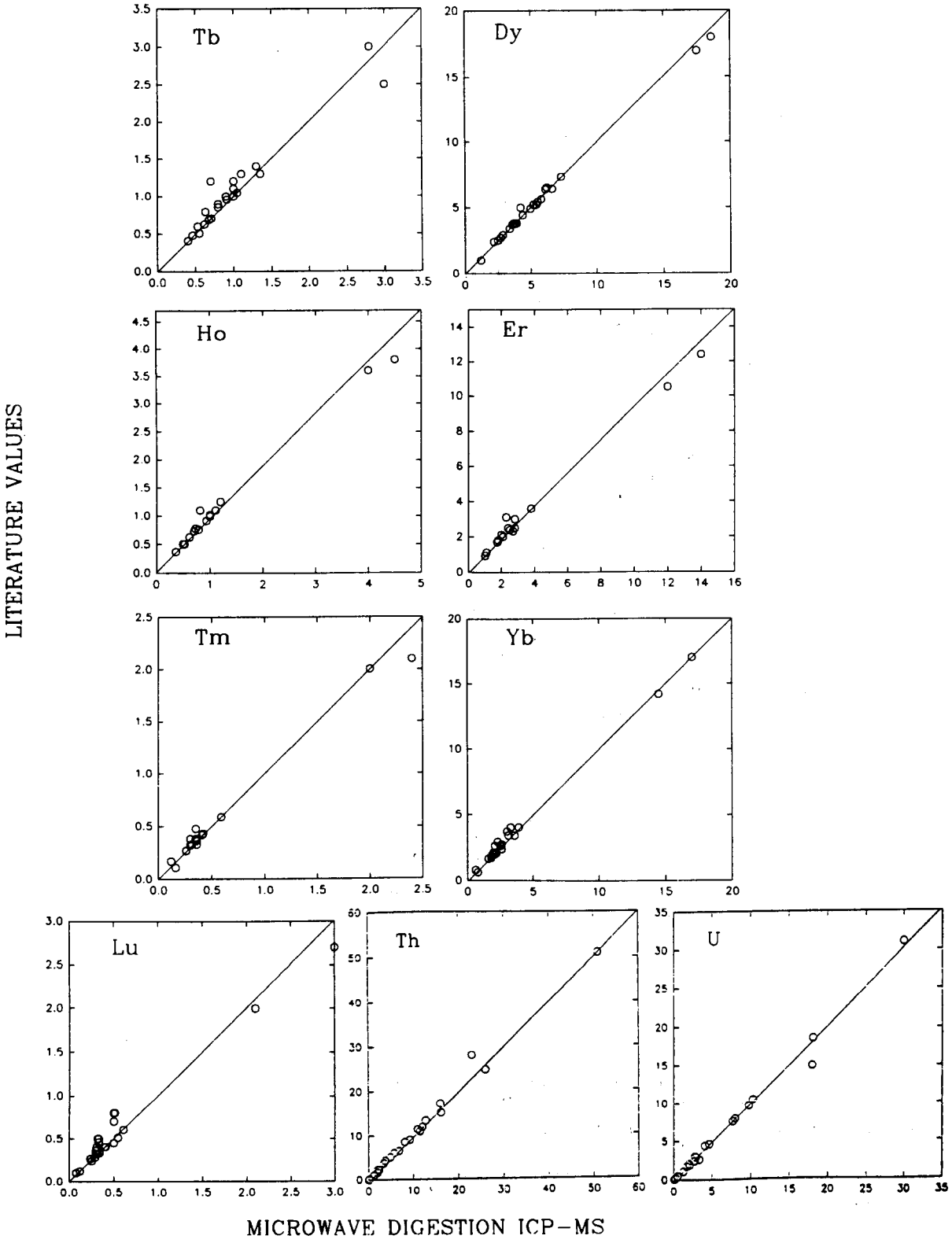


Fig. 2. Correlation plots for the microwave digestion ICP-MS results versus the literature values for Tb, Dy, Ho, Er, Tm, Yb, Lu, Th and U in some international reference samples of rocks and sediments (concentration is given in micrograms per gram).

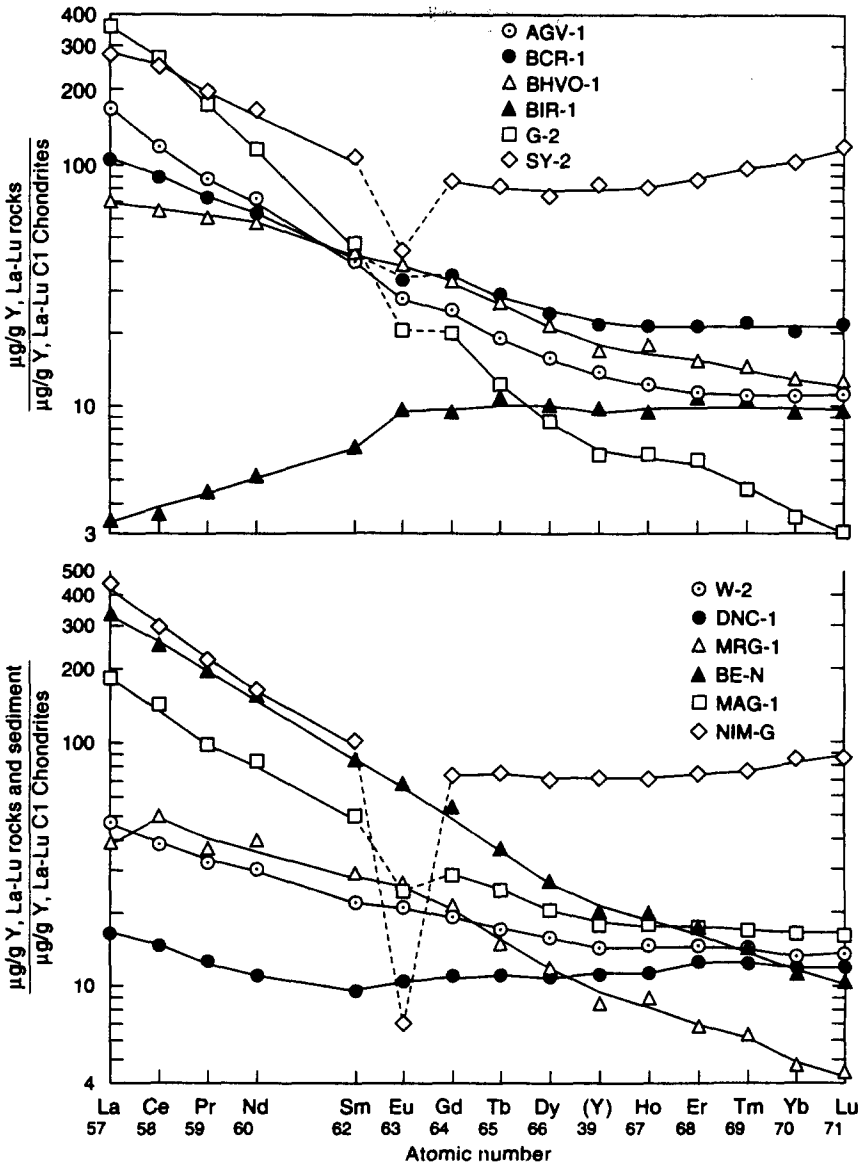


Fig. 3. Chondrite-normalized Y and REE patterns for the international reference rocks AGV-1, BCR-1, BHVO-1, BIR-1, G-2, SY-2, W-2, DNC-1, MRG-1, BE-N and NIM-G, and a marine sediment MAG-1.

values. From the above discussion and the data presented, it may be concluded that direct ICP-MS determination of Th, U, Y and the lanthanides in common rocks and sediments is possible with acceptable accuracy and precision after the decomposition of the samples by microwave digestion with acids and the complexation of excess HF and fluorides with boric acid and EDTA. The method is reasonably fast, less strenuous compared to open vessel digestion and fusion methods, and environmentally friendly since no evaporation of acids is required.

**Acknowledgements**

The authors are indebted to J.L. Bouvier for the decomposition of some of the samples reported in this work, and to K.N. De Silva for critical reading of the manuscript.

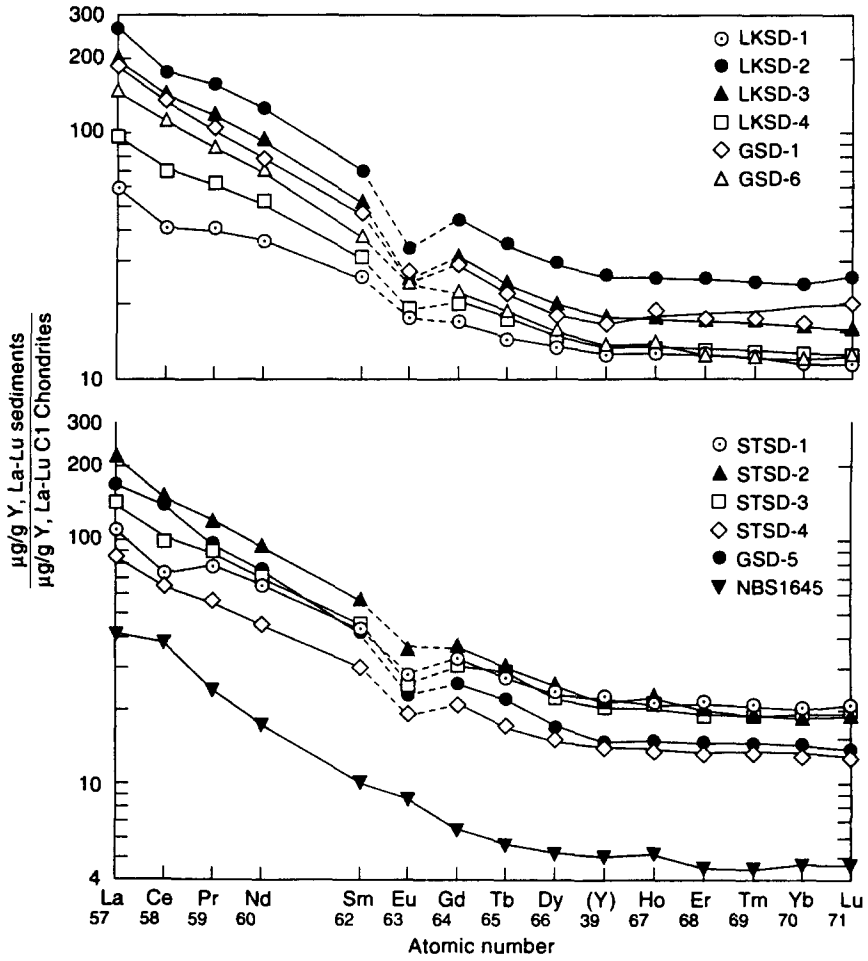


Fig. 4. Chondrite-normalized Y and REE patterns for international reference materials of lake sediments (LKSD-1–LKSD-4), stream sediments (STSD-1–STSD-4, GSD-1, GSD-5 and GSD-6) and a river sediment (NBS 1645).

## References


[1] M.B. Shabani and A. Masuda, Anal. Chem., 63 (1991) 1.
[2] J.G. Sen Gupta, Talanta, 31 (1984) 1045.
[3] J.G. Sen Gupta, Talanta, 32 (1985) 1.
[4] J.G. Sen Gupta, J. Anal. At. Spectrom., 8 (1993) 93.
[5] G.N. Eby, Anal. Chem., 44 (1972) 2137.
[6] P. Robinson, N.C. Higgins and G.A. Jenner, Chem. Geol., 55 (1986) 121.
[7] A.O. Brunfelt, I. Roelandts and E. Steinnes, Analyst, 99 (1974) 277.
[8] M.J. Greaves, H. Elderfield and G.P. Klinkhammer, Anal. Chim. Acta, 218 (1989) 265.
[9] F.W.E. Strelow and P.F.S. Jackson, Anal. Chem., 46 (1974) 1481.
[10] C.C. Schnetzler, H.H. Thomas and J.A. Philpotts, Anal. Chem., 39 (1967) 1888.
[11] P.J. Hooker, R.K. O'nions and R.J. Pankhurst, Chem. Geol., 16 (1975) 189.
[12] J.N. Walsh, F. Buckley and J. Barker, Chem. Geol., 33 (1981) 141.
[13] K. Jarvis and I. Jarvis, Geostand. Newsl., 12 (1988) 1.
[14] M.D. Feigenson and J.C. Michael, Chem. Geol., 51 (1985) 19.
[15] W. Doherty and A. Vander Voet, Can. J. Spectrosc., 30 (1985) 135.
[16] C. Riddle, A. Vander Voet and W. Doherty, Geostand. Newsl., 12 (1988) 203.
[17] A.R. Date and D. Hutchison, J. Anal. At. Spectrom., 2 (1987) 269.
[18] K.E. Jarvis, Chem. Geol., 68 (1988) 31.
[19] E.H. Bailey, A. J. Kemp and K.V. Ragnarsdottir, J. Anal. At. Spectrom., 8 (1993) 551.
[20] C. Pin, S. Lacombe, P. Telouk and J.L. Imbert, Anal. Chim. Acta, 256 (1992) 153.
[21] J.G. Sen Gupta and J.L. Bouvier, Talanta, 42 (1995) 269.
[22] J.G. Sen Gupta, Geostand. Newsl., 18 (1994) 111.
[23] E.S. Gladney, C.E. Burns and I. Rolandts, Geostand. Newsl., 7 (1983) 3.
[24] E.S. Gladney and I. Roelandts, Geostand. Newsl., 12 (1988) 63.
[25] K. Govindaraju, Geostand. Newsl., 18 (1994) 1.
[26] E.S. Gladney and I. Roelandts, Geostand. Newsl., 14 (1990) 373.
[27] M.A. Vaughan and G. Horlick, Appl. Spectrosc., 44 (1990) 587.
[28] E.S. Gladney and W.E. Goode, Geostand. Newsl., 5 (1981) 31.
[29] D.J. Douglas and R.S. Houk, Prog. Anal. At. Spectrosc., 8 (1985) 1.

[30] P.J. Potts, A.G. Tindle and P.C. Webb, in Geochemical Reference Material Compositions, Whittles Publishing, CRC Press, Boca Raton, FL, 1992, pp. 1–313.
[31] J.J. Lynch, Geostand. Newsl., 14 (1990) 153.
[32] S.-S. Sun and W.F. McDonough, in A.D. Saunders and M.J. Norry (Eds.), Magmatism in the Ocean Basins, Special Publication no. 42, Geological Society London (U.K.), 1989, pp. 313–345.
[33] S. Abbey, A.H. Gillieson and G. Perrault, CANMET MSL Technical Report, 1975, MRP/MSL 75–132 (TR); Can. J. Spectrosc., 20 (1975) 113.
[34] T.W. Steele, A. Wilson, R. Goudvis, P.J. Ellis and A.J. Radford, Geostand. Newsl., 2 (1978) 71.

ELSEVIER

Talanta 42 (1995) 1609–1617

Talanta

# On the spectrophotometric flow injection determination of chromium(VI) in natural waters after on-line preconcentration on activated alumina

Mauricio C. Pannain, Ricardo E. Santelli *

*Geochemistry Department of Federal Fluminense University, Niterói-RJ, 24020-007, Brazil*

Received 9 May 1994; revised 3 April 1995; accepted 7 April 1995

**Abstract**

The feasibility of chromium(VI) preconcentration on to activated alumina in a continuous flow system with spectrophotometric detection was investigated. Chemical and flow variables, and the influence of concomitant species were studied both with and without preconcentration systems. The best results were obtained by using a 2.5 cm long, 1.6 mm i.d. alumina minicolumn, and selecting $1 \times 10^{-4}$ M nitric acid as the preconcentrating medium and 0.1 M ammonium hydroxide as the eluent. The eluted chromium(VI) was mixed with diphenylcarbazide in acidic medium and the absorbance of the colored complex was measured at 540 nm. Linear calibrations for 5, 25 and 50 ml sample volumes were established over the concentration ranges 10–50 $\mu g\,l^{-1}$, 2–10 $\mu g\,l^{-1}$ and 1–5 $\mu g\,l^{-1}$ with sensitivity enhancements of 44, 196 and 392 and detection limits ($3\sigma$) of 3.0 $\mu g\,l^{-1}$, 0.3 $\mu g\,l^{-1}$ and 0.2 $\mu g\,l^{-1}$, respectively. The method is relatively fast and cheap. Natural waters were analyzed with use of the developed procedure.

*Keywords:* Activated alumina; Chromium(VI) determination; Chromium(VI) preconcentration; Flow analysis; Spectrophotometry

## 1. Introduction

Chromium(III) is considered an essential micronutrient for humans [1], whereas chromium(VI) is a potential carcinogenic agent [2]. This leads to a great interest in the speciation and determination of chromium in biological and environmental samples, especially chromium(VI), due to its potential toxicity.

Vast quantities of chromite ore are used for the production of stainless steel, chrome-plated metals, pigments and chemicals [3]. The main chromium emissions into surface waters are from metal-finishing processes such as electroplating, pickling and bright dipping. Uncontrolled emissions are potential contaminating sources in fresh waters, especially with regard to the toxic chromium(VI). Other discharges of chromium(VI) are related to additives in circulating cooling waters, laundry chemicals and animal glue manufacture [3].

Several techniques have been utilized for chromium determination, such as inductively coupled plasma-atomic emission spectrometry (ICP-AES), flame atomic absorption spectrometry (FAAS), electrothermal atomic absorption spectrometry (ETAAS), and spectrophotometry, the latter being favored for rapid analysis in view of its ease of automation and simple and low-cost instrumentation. The 1,5-diphenylcarbazide (DPC) method is used worldwide, and is highly sensitive and selective.

Flow injection analysis (FIA) is a very fast, multipurpose analytical technique which reduces the use of volumetric glassware and manual sample manipulation [4,5]. Also, the

* Corresponding author.


*SSDI* 0039-9140(95)01613-9

Table 1
A summary of FIA procedures for the spectrophotometric detection or speciation of chromium

| Analyte | Analytical range ($\mu g\ ml^{-1}$) | Main conditions | Interferents | Applications | Reference |
|---|---|---|---|---|---|
| Cr(VI) | 1–20 | Single line FIA/DPC RSD, 1.3%; 70 $h^{-1}$ | Not related | Soil extracts | [16] |
| Cr(VI) | 0.05–5 | Single line FIA/DPC RSD, 1.2%; 120 $h^{-1}$ | Not related | – | [17] |
| Cr(VI) and total Cr | – | FIA/DPC | Not related | – | [18] |
| Cr(III) | 0–4 | FIA/DPC | $Fe^{3+}$, $Mo^{6+}$, | Synthetic | [19] |
| Cr(VI) | 0–3 | | $Hg^{2+}$, $V^{5+}$, $Cu^{2+}$ | mixtures and effluent waters | |
| Cr(VI) | 0.1–20 | Sequential FIA/DPC | Not related | Synthetic sea water | [20] |
| Total Cr | 1–50 | AAS; 120 $h^{-1}$ | | | |
| Cr(VI) | 0.2–8 | Sequential and | $S^{2-}$, $Hg^{2+}$, $NO_3^-$ | – | [21] |
| Total Cr | – | simmultaneous FIA/DPC RSD, 0.8%; 40 $h^{-1}$ | | | |
| Cr(III) | 0.5–3 | rFIA | Not related | – | [22] |
| Cr(VI) | 0.2–1.3 | | | | |
| Total Cr | 0.5–10 | FIA/DPC RSD, 1%; 40 $h^{-1}$ | Not related | – | [23] |
| Cr(VI) | 0.3–10 | FIA sandwich 60 $h^{-1}$ | Not related | – | [24] |

implementation of separation/preconcentration procedures in a continuous flow mode has gradually superseded their manual batch counterparts [6]. Several solid/liquid interfaces using ion exchange [7], chelating resins [8,9], precipitation/dissolution [10–12], C-18 bonded silica [13], functionalized cellulose [14] and activated carbon [15] have been exploited for the preconcentration of metal species. FIA systems with spectrophotometric detection proposed for chromium determination and/or speciation are summarized in Table 1 [16–24]. Some of them take advantage of the fact that chromium(III), being kinetically inert, is easily oxidized to chromium(VI) in order to determine chromium(VI) and total chromium. The concentration of chromium(III) is then obtained by difference. These procedures have seldom been applied to real samples and the sensitivity is not sufficient for trace concentration determination. For the latter separation/preconcentration steps are needed.

Activated alumina has often been used for chromatographic purposes. The possible mechanisms of the retention of inorganic salts on activated alumina were discussed in early 1949 by Sacconi [25]. Schmitt and Pietrzyk [26] in 1985 pointed to ion exchange as being the major factor contributing to the retention of inorganic ions from aqueous solutions. Activated alumina can then behave as a cation exchanger in basic medium and as an anion exchanger in acidic medium. More recently, Cox et al. established FIA procedures for chromium determination with desirable on-line separation/preconcentration on activated alumina. In the first method [27], 0.01 M nitric acid was used as the carrier and chromium(III) (neutral or cationic) was not retained; chromium (VI) (anionic) was preconcentrated and both ions were detected by ICP-AES. In the second method [28], chromium(III) was preconcentrated on an activated alumina minicolumn in the basic form and detected by ICP-AES. This procedure was successfully applied to human urine. Sperling et al. [29] exploited alumina's amphoteric characteristics to preconcentrate and determine both chromium species with a flow injection system with FAAS detection. Using a 50 µl microcolumn, recoveries of 90–106% (20, 50 and 100 µg of chromium (III) and chromium(VI)) were achieved for spiked natural water samples.

Also, modern automated techniques such as adsorptive cathodic stripping voltammetry (ACSV) [30], high-performance flow atomic spectrometry (HPF-AS) [13], anodic stripping voltammetry (ASV), a flow system interfaced

with inductively coupled plasma-mass spectrometry (ICP-MS) [31] and high-performance liquid chromatography (HPLC) coupled to direct current plasma-atomic emission spectrometry (DCP-AES) [32] have been used for chromium(VI) determinations.

The aim of this work was to study activated alumina as a preconcentrator of the toxic anionic chromium(VI) in natural water analysis in continuous flow. The effect of concomitant species typically found in waters was also studied in depth in order to establish an inexpensive, fast, reproducible and accurate flow system for the determination of toxic chromium(VI), including a minicolumn for on-line preconcentration and spectrophotometric detection.

## 2. Experimental

### 2.1. Reagents and solutions

All solutions were prepared using distilled water and analytical reagent grade chemicals.

Chromium(VI) stock solution, 1000 μg $ml^{-1}$, was prepared by dissolving 2.8287 g of $K_2Cr_2O_7$ in water and diluting to a final volume of 1 l. Working solutions were prepared daily by dilutions of the stock in $1 \times 10^{-4}$ M nitric acid.

The reagent solution, 0.05% (w/v) 1,5-diphenylcarbazide, was prepared by dissolving 0.125 g of 1,5-diphenylcarbazide in 12.5 ml of acetone and diluting to 250 ml with water. This solution was prepared daily.

The eluent solution was 0.1 M ammonium hydroxide, the acidifier solution was 0.7 M nitric acid, and the carrier solution was $1 \times 10^{-4}$ M nitric acid.

Activated alumina, acid form, Brockman grade 1, particle size range 63–100 μm (Merck, Germany), was used as received.

### 2.2. Apparatus

A Desaga PLG peristaltic pump furnished with Tygon and silicone rubber tubes, and a Micronal B 380 spectrophotometer equipped with a Hellma 178.011 flow cell (80 μl inner volume, 10 mm optical path) and connected to a Phillips PM 8251 single pen recorder were used. The manifolds were constructed with 0.8 mm i.d. polypropylene and PTFE tubing and both Tygon and silicone rubber connectors. To commutation, a proportional injector [33], manufactured by Perspex, was used. A minicolumn made of silicone rubber (length, 2.5 cm, 1.6 mm i.d.) was packed with 50 μl of activated alumina.

## 3. Results and discussions

### 3.1. Flow system without preconcentration

With the intention of studying the spectrophotometric 1,5-diphenylcarbazide method, a flow system was built, as can be seen in Fig. 1A. In this system, the sample (S; 90 μl) is introduced into the carrier stream (C, 5.10 ml $min^{-1}$) and merges immediately with the reagent (R; 0.36 ml $min^{-1}$). The color is developed in the 100 cm reaction coil (RC), and the passage of the colored zone through the flow cell results in a transient signal measured at 540 nm. The peak height was used for all calculations.

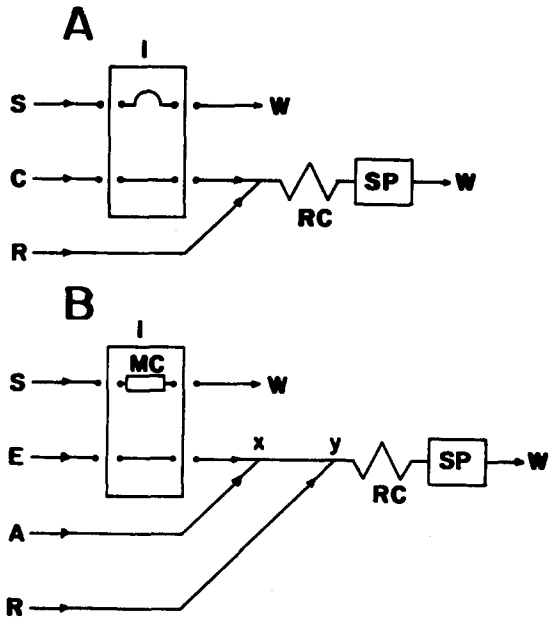


Fig. 1. Flow diagrams. (A) Flow system without preconcentration: S, sample (90 μl); C, carrier solution (0.1 M nitric acid, 5.10 ml $min^{-1}$; R, reagent (0.05% DPC, 0.36 ml $min^{-1}$); RC, reaction coil (100 cm); SP, spectrophotometer; I, proportional injector; W, waste. (B) Flow system with preconcentration: S, sample, (5.10 ml $min^{-1}$); E, eluent solution (ammonium hydroxide, 2.73 ml $min^{-1}$); A, acidifier solution (0.7 M nitric acid, 0.92 ml $min^{-1}$); R, reagent (0.05% DPC, 0.76 ml $min^{-1}$); MC, activated alumina minicolumn; RC, reaction coil (100 cm); SP, spectrophotometer; I, proportional injector; W, waste.

Table 2
Relative signals obtained for chromium(VI) in the presence of interferents using the flow system without preconcentration (Fig. 1A)

| Interferent species | Interferent concentration ($\mu g\ ml^{-1}$) | | | | | |
|---|---|---|---|---|---|---|
| | 100 | 50 | 10 | 5 | 1 | 0,1 |
| $Cl^-$ | 1.02 | – | – | – | – | – |
| $BO_3^{3-}$ | 1.00 | – | – | – | – | – |
| $SiO_4^{4-}$ | 1.02 | – | – | – | – | – |
| $PO_4^{3-}$ | 1.00 | – | – | – | – | – |
| $SO_4^{2-}$ | 1.13 | 1.10 | 1.00 | 1.00 | 1.03 | 1.02 |

Chemical and flow variables were studied in order to obtain the best sensitivity. This study was carried out by the univariate method, a 0.5 $\mu g\ ml^{-1}$ Cr(VI) solution always being introduced into the system in triplicate.

The influence of the pH was studied within the 0–4 range. The best results were obtained at pH 1, which is in agreement with Sandell's [34] description of the batch process but not with the results of other FIA workers [16,17]. Next 0.1 M nitric acid was chosen as the reaction medium and as the carrier stream. The DPC concentration was studied in the range 0.01–0.2% (w/v), and the best sensitivity was obtained with a concentration of 0.05% (w/v), in agreement with literature data [18–23]. The proportion of acetone in the reagent was investigated in the range 5–20% (v/v), and no changes in the analytical signals were observed. A 5% (v/v) concentration was then chosen in order to use less organic solvent in the solution. The influence of the ionic strength was studied by using analytical solutions containing 0.1–3.0 M potassium nitrate, all in 0.1 M nitric acid. No effect due to variations of this parameter was found, so the ionic strength did not need to be regulated.

The reactor coil (RC; Fig. 1A) was place in a thermostated bath at temperatures from 26 to 67°C. The signal increased constantly with the increase in temperature. At 67°C the signals were 30% higher than at 26 °C. However, ambient temperature was used in all measurements in order to simplify the system design.

The reagent flow rate was varied from 0.18 to 1.76 ml $min^{-1}$ keeping the carrier flow rate at 1.76 ml $min^{-1}$. No changes in the absorbance signals were observed and therefore a flow rate of 0.36 ml $min^{-1}$ was chosen, yielding enough reagent for the reaction. The carrier flow rate was studied between 0.76 and 5.85 ml $min^{-1}$. From 0.76 to 5.10 ml $min^{-1}$, the absorbance signals remained constant, but a slight decrease at higher flow rates was observed (at 5.85 ml $min^{-1}$ the decrease in signal was only 10%). Therefore a flow rate of 5.10 ml $min^{-1}$ was chosen because it allowed good sample throughput.

In order to verify the effect of concomitant species, some anions were tested as potential interferents. Solutions containing each interferent alone at a concentration of 100 $\mu g\ ml^{-1}$ were prepared and introduced into the flow system. Also, solutions containing 0.5 $\mu g\ ml^{-1}$ of chromium(VI) and 100 $\mu g\ ml^{-1}$ of each interferent individually, were measured. As a control, chromium(VI) analytical solutions containing 0.5 $\mu g\ ml^{-1}$ were measured also. In this way, the maximum ratio of analyte: interferent tested was 1:200. Phosphate, chloride, silicate, borate and sulphate were investigated. The results are shown in Table 2. Only sulphate displays some interference at concentrations higher than 50 $\mu g\ ml^{-1}$.

This flow system without preconcentration (Fig. 1A) shows such typical calibration equations as $A = -0.002 + 0.1052$ [Cr(VI)] where [Cr(VI)] is in micrograms per milliliter with $r = 0.999$. The relative standard deviation (RSD) when introducing 0.5 $\mu g\ ml^{-1}$ Cr(VI) solutions, was below 1% for triplicate measurements. The flow system dispersion coefficient measured with the aid of a dye was 2.

### 3.2. Flow system with preconcentration

In Fig. 1B a schematic diagram of the manifold with a preconcentration column can be seen. The sample (S, 5.10 ml $min^{-1}$) flows through an activated alumina minicolumn (MC) during the time of preconcentration. By switching the proportional injector (I), the minicolumn with adsorbed chromium is inserted into the eluting stream (E) and chromi-

um(VI) is then displaced by ammonium hydroxide. At the point x this solution coalesces with the acidifier solution (A) for suitable pH adjustment. The sample zone merges with the reagent stream (R), at point y, the color is developed in the reaction coil (RC) and the transient signal is measured at 540 nm.

Both the chemical and flow variables were studied in this flow system in order to improve the preconcentration step. This study was also carried out by using the univariate method employing 50 $\mu g\,l^{-1}$ Cr(VI) solution.

The influence of the sample pH was tested in the range 1–5. The best analytical signals were observed with $1 \times 10^{-4}$ M nitric acid (pH 4). At pH values below and above 4 reductions in the signal were observed, and all subsequent studies were carried out at pH 4. The possibility to using a buffer to keep a constant pH of 4 was investigated using sodium acetate/acetic acid from 0.05 to 0.2 M for both species (pH adjusted to 4 with nitric acid). When this buffer system was used, a considerable drop in sensitivity was noted (at a 0.05 M buffer concentration, a drop in signal of 30% was observed and at 0.2 M this reduction was 50%). This effect probably occurs due to anionic competition between acetate and chromium(VI) ions. Therefore, buffer was not used further. The eluent concentration was investigated by using 0.01–2.0 M ammonium hydroxide streams. Between 0.01 and 0.1 M $NH_4OH$, the signals improved significantly but in the range 0.1–1 M they remained constant. The concentrations higher than 1 M showed a significant decrease in signal; therefore, 0.1 M was chosen as the eluent concentration. Also, higher eluent concentrations should be avoided in order to avoid Schlieren noise. Sodium hydroxide was also tested as eluent at the same concentrations, but the signals were lower and not reproducible, probably due to a modification of the alumina surface by strong alkali. This effect was also observed by Cox et al. [27] when using potassium hydroxide. As the colorimetric reaction takes place in acidic medium and elution requires basic media, the use of an acidifier solution (A, Fig. 1B) became necessary. For this task, nitric acid was tested in the range 0.1–2.0 M. As between 0.6 and 2.0 M the signal variations were insignificant (about 3%), 0.7 M nitric acid was chosen.

The eluent flow rate was studied between 1.76 and 5.10 ml $min^{-1}$. Lower flow rates, below 2.26 ml $min^{-1}$, were not enough to perform effective elution thereby causing smaller signals. From 2.73 to 5.10 ml $min^{-1}$ the peak heights were the same and total elution was obtained, without a memory effect. For that reason, 2.73 ml $min^{-1}$ was chosen as the eluent flow rate. The flow rate of the acidifier solution was changed from 0.28 to 1.76 ml $min^{-1}$. Smaller signals at reduced flow rates (25% at 0.28 ml $min^{-1}$) due to an insufficient acid amount were observed. At flow rates of 0.55 ml $min^{-1}$ upwards, the signals were highest and constant. Thus, a 0.92 ml $min^{-1}$ flow rate was chosen. Analytical solutions in $1 \times 10^{-4}$ M nitric acid at flow rates ranging from 3.8 to 6.0 ml $min^{-1}$ were introduced into the system. No analytical signal variations were observed, and a flow rate of 5.1 ml $min^{-1}$ was then selected. The reagent flow rate was examined within the 0.55–3.80 ml $min^{-1}$ range. The signals were constant up to a flow rate of 1.54 ml $min^{-1}$. At 3.80 ml $min^{-1}$ a decrease in the signal occurred probably due to the increase in dispersion. A 0.76 ml $min^{-1}$ reagent flow rate was chosen. The volume of the reactor coil, needed for the completion of the spectrophotometric reaction, was investigated from 125 to 1350 µl. With volumes from 125 to 400 µl, the signals did not change but with volumes above 400 µl they decreased (a 20% reduction in the signal with an 800 µl reactor coil was observed). A 200 µl reactor was chosen (100 cm, 0.5 mm i.d.). The length of a coil placed immediately after the point of introduction of the acidifier solution (point x, Fig. 1B) was also investigated. The best results were obtained without this coil, although the reactor coil (RC, Fig. 1B) is suitable for all reagent mixtures and reactions.

The length of the activated alumina column was investigated between 2.5 and 10 cm (50–200 µl). In the analytical range of this work, an increase in the activated alumina amount did not improve the preconcentration and recovery of chromium(VI). Both the retention and elution were the same and because of this a minicolumn 2.5 cm long was selected.

### 3.3. Interference studies

When considering the utilization of activated alumina as preconcentrator for chromium(VI) in water analysis, the following potential interferents were examined: chloride, borate, silicate, phosphate, sulphate, fluoride, bicarbonate and iron(III). Solutions containing the interfer-

Table 3
Relative signals obtained for chromium(VI) in the presence of interferents using the flow system with preconcentration (Fig. 1B)

| Interferent species | Interferent concentrations ($\mu g\ ml^{-1}$) | | | | | | |
|---|---|---|---|---|---|---|---|
| | 0.1 | 1.0 | 5.0 | 10 | 25 | 50 | 100 |
| $Cl^-$ | 0.98 | 0.98 | 0.97 | 0.96 | - [a] | 0.95 | - |
| $BO_3^{3-}$ | 1.01 | 1.02 | 1.01 | 1.01 | - | 1.01 | - |
| $SiO_4^{4-}$ | - | 0.99 | 1.02 | 1.01 | 1.04 | 1.05 | 0.25 |
| $PO_4^{3-}$ | 1.01 | 0.97 | 0.89 | 0.91 | - | 0.62 | - |
| $SO_4^{2-}$ | 1.02 | 0.98 | 0.97 | 0.98 | - | 0.90 | - |
| $HCO_3^-$ | 1.00 | 1.02 | 1.01 | 1.03 | - | 1.08 | 1.08 |
| $F^-$ | 1.03 | 1.05 | 1.04 | 1.00 | - | 0.96 | - |
| $Fe^{3+}$ | 0.98 | 0.83 | 0.44 | 0.31 | - | 0.18 | 0.14 |
| $Cl^-$, $BO_3^{3-}$, $SiO_4^{4-}$, $PO_4^{3-}$ $SO_4^{2-}$, $HCO_3^-$ | - | 1.00 | 0.99 | 1.01 | 0.17 | 0.06 | - |

[a] Not tested.

ents individually at several concentrations, and binary solutions of analyte interferent were prepared and introduced into the flow system, always with volumes of 5 ml. Table 3 shows the results. Chloride, borate, silicate, bicarbonate and fluoride did not exhibit any interference at the 50 $\mu g\ ml^{-1}$ level. Sulphate, phosphate and iron(III) showed interferences at the 50 $\mu g\ ml^{-1}$ level. Sulphate concentrations up to 10 $\mu g\ ml^{-1}$ (200 times the analyte concentration) revealed no influence on the signal. Phosphate interference was more severe and a level of 1 $\mu g\ ml^{-1}$ (20 times the analyte concentration) only allowed in the solution. The results of McLeod et al. [35] corroborated this observation that activated alumina has a great affinity for phosphate ions. Sperling et al. [29] also observed hard phosphate interference although they used phosphate buffer for the pH experiments, concluding that the signal disappeared in this medium. These concomitant ion effects could only be explained in terms of ion-exchange competition between the chromium(VI) species ($CrO_4^{2-}$ or other chromium(VI) anionic species) and the concomitants. The most severe interference is due to iron(III). Its presence reduces drastically the absorbance signals. Only concentrations below 0.1 $\mu g\ ml^{-1}$ (twice the analyte concentration) can be present. This fact cannot easily be explained unless by the presence of any anionic species containing iron(III) or as being due to the formation of an anionic complex containing both species. Interferents present individually, even at the highest concentrations, did not give rise to analytical signals. As activated alumina has a distinct affinity for anionic species in acidic medium, the species compete with the anionic chromium(VI), impairing its retention. Analytical solutions with 50 $\mu g\ l^{-1}$ of chromium(VI) and all the interferents with the exception of iron(III) and fluoride present at levels up to 10 $\mu g\ ml^{-1}$ did not show any interference (ratio of analyte:interferent of 1:200). However, from a level of 25 $\mu g\ ml^{-1}$ upwards, a sharp signal reduction, proportional to the interferent concentrations, was observed. Also, an analytical solution containing all these interferents at a level of 50 $\mu g\ ml^{-1}$ without chromium(VI) did not show any analytical signal (Table 3).

It was verified that daily use of the preconcentration system with the activated alumina minicolumn (Fig. 1B) for 6 months, with analytical chromium(VI) solutions as samples, does not change its efficiency. However, when working with more complex matrices than water (geological or biological matrices which contain higher concentrations of iron(III) and anionic interferents), its efficiency gradually diminished, and replacement of the activated alumina was needed. Several analytical curves were constructed for different preconcentration volumes. These analytical characteristics as well as the enrichment factors can be seen in Table 4. Also, in a test involving the introduction of a solution containing 2 $\mu g\ l^{-1}$ Cr(VI) in $1 \times 10^{-4}$ M nitric acid, from 10 to 200 ml sample volumes the analytical curve was linear (Abs = 0.002 + 0.000980 [volume]) where the volume is in milliliters, showing preconcentration is possible even when larger sample volumes are used.

Table 4
Analytical features of the flow system with preconcentration

| Injected volume (ml) | Concentration range ($\mu g\,l^{-1}$) | Equation [a] | RSD (%) | Detection limits ($\mu g\,l^{-1}$) | Enrichment factors [b] | Sampling rate ($h^{-1}$) |
|---|---|---|---|---|---|---|
| 5 | 10–50 | Abs = 0.002 + 0.00338 [Cr(VI)] | 0.6 | 3 | 44 | 40 |
| 25 | 2–10 | Abs = −0.002 + 0.0207 [Cr(VI)] | 2.5 | 0.3 | 196 | 10 |
| 50 | 1–5 | Abs = −0.001 + 0.0412 [Cr(VI)] | 4.7 | 0.2 | 392 | 5 |

[a] Chromium(VI) concentration given in micrograms per liter.
[b] Enrichment factors were calculated by slope relationship compared to the flow system without preconcentration.

### 3.4. Sample pH and preservation

The sample pH and sample preservation are very important in the trace chromium determination. Sperling et al. [36] found an optimum sample pH of 9 for the preconcentration of chromium(VI) on C-18 bonded silica reverse-phase sorbent with ETAAS. According to these workers, the reduction of chromium(VI) to chromium(III) can occur due to the presence of various substances in river water, and it can be eliminated by using pH 9 and also by the addition of 1 drop of 5% (w/v) potassium permanganate to the river water before spiking. These workers also recommend avoiding conventional sample preservation with nitric acid for the speciation of chromium. The same pH 9, but using carbonate buffer and ethylenediaminetetraacetic (EDTA), was found to be optimum for the preservation of chromium(VI) by Pavel et al. [37]. Also, pH 4 was considered safe by Sperling et al. in their work [29], which included preconcentration on alumina. In the present work the water samples were preserved with nitric acid at pH 4 at the time of sampling.

### 3.5. Application to real samples

Water samples were introduced into the flow system with the minicolumn (Fig. 1B) according to the procedure described elsewhere. Analytical solutions, blanks and samples were similarly run. Recovery tests showed that even for samples with relatively simple matrices, the presence of interferents reduced or eliminated the chromium(VI) signals, due to the competition between the anionic species. In order to circumvent this drawback, it was decided to carry out all determinations by using the standard additions method. The results are shown in Table 5. This determination could only be carried out successfully for some water samples, due to low chromium concentrations or interferences. These limitations have been often reported by other workers [29,36,38].

## 4. Conclusions

The flow system with preconcentration studied here is suitable for preconcentrating chromium(VI) from diluted solutions. Depending on the volumes introduced, concentrations as low as 1 $\mu g\,l^{-1}$ can easily be determined, and precise results are obtained (RSD < 4.7% for three measurements). Sample throughput is relatively high and depending on the sample volume, a preconcentration of 5 ml of water takes only 1.5 min until the signal measurement (40 $h^{-1}$). The spectrophotometric method is inexpensive and therefore can be used by any analytical laboratory. The detection limits found with the developed methodology (3–0.2 $\mu g\,l^{-1}$) are very good owing to enhanced sensitivity when using the preconcentration system, and were of the same order of magnitude as those in the literature [14,27,29].

However, an interference study emphasized serious interference effects which reduces the chromium(VI) retention. In this work, the presence of more than 10 $\mu g\,ml^{-1}$ of sulphate or 1 $\mu g\,ml^{-1}$ of phosphate has an effect on the analytical signals. These results agree with the affinity order of sorption of anions on acid alumina [39]. Other "ion exchangers", such as functionalized cellulose, show the same interference effects; the presence of 10 $\mu g\,ml^{-1}$ of sulphate causes a significant decrease of chromium(VI) sorption [14].

In the study of Sperling et al. [29] the tolerance level was 500 $\mu g\,ml^{-1}$ for sulphate and 10 $\mu g\,ml^{-1}$ for phosphate. The effect of phosphate was very drastic when phosphate buffer was used to control the pH. Aspects of this work and the work of Sperling et al. [29] which

Table 5
Results obtained in the determination of chromium(VI) in water

| Sample | Introduced volume (ml) | Cr(VI) found ($\mu g\,l^{-1}$) | Additions curve slopes |
|---|---|---|---|
| Mineral water 1 | 5 | <3 | 0.00501 |
| Mineral water 1 | 25 | 1 | 0.00170 |
| Mineral water 1 | 50 | 1 | 0.0108 |
| Mineral water 2 | 25 | <0.3 | 0.0194 |
| Mineral water 3 | 25 | <0.3 | 0.00297 |
| Mineral water 4 | 25 | 3.4 | 0.00173 |
| Drinking water | 25 | <0.3 | 0.00193 |

differ are probably the sample compositions and the analytical range. In the work of Sperling [29] the analytical range varied from 20 to 100 $\mu g\,l^{-1}$, while in this study the analytical range varied from 2 to 10 $\mu g\,l^{-1}$, i.e. ten times lower. Also, the samples were always spiked with 20 $\mu g\,l^{-1}$ of chromium(VI) before analysis in the work of Sperling et al. [29]. Cox et al. [27] established a similar FIA ICP-AES methodology for preconcentrating and determining chromium(VI), which performed well but was not applied to real sample analysis. Recent work [40] described an interlaboratory comparison for chromium determinations in water samples. The two laboratories that employed alumina as preconcentrator did not obtain good results for the analysis of water samples spiked with 9.3 $\mu g\,l^{-1}$ of chromium(VI) (analytical range similar to that used in this work).

In the flow system studied for chromium(VI) preconcentration and determination, the most relevant problem was iron(III) interference. Its effect on the decreasing chromium(VI) signals could not be easily explained. Atomic absorption tests with the preconcentration system revealed that even at a level of 1000 $\mu g\,ml^{-1}$, iron(III) is not retained on the activated alumina. All the iron(III) passes through the minicolumn in the preconcentration step, because the elution step does not give rise to any signals. Otherwise, AAS recovery tests show that the presence of iron(III) impaired the quantitative recovery of chromium(VI). Any chemical interaction between chromium(VI) and iron(III) could take place in the solution environment, promoting poorer recovery in the flow system.

In the majority of papers, found in the literature concerning activated alumina or other sorption methods, the workers were not able to detect chromium(VI) in natural water samples, either due to the lower concentration or to the interference effects of concomitants [13,14,29,36].

In conclusion, continuous flow methodology using activated alumina could be used in real sample analysis with appropriate care. Also, to minimize interferences, the standard additions method should be utilized. To succeed well with methodologies involving chromium(VI) preconcentration on activated alumina appear to be more difficult, especially when more complex matrices and lower chromium(VI) concentrations are involved. Apparently, this means that better results will be achieved by eliminating or reducing the effects of the main interferents.

## Acknowledgements

The authors are grateful to CNPq and FINEP for partial financial support, to A.M.R. Figueiredo for discussions, and to E.A.G. Zagatto and M. de la Guardia for critical comments.

## References

[1] K.M. Hambidge, in W. Mertz and W.E. Cornatzer, Newer Trace Elements in Nutrition, Marcel Dekker, New York, 1971, p. 169–193.
[2] M. Littig, Priority Toxic Pollutants, Health Impacts and Allowable Limits, Noyes Data Corporation, New Jersey, 1980.
[3] J.W. Moore and S. Ramamoorthy, Heavy Metals in Natural Waters, Applied Monitoring and Impact Assessment, Springer Verlag, New York, 1984, p. 58–76.
[4] M. Valcárcel and M.D. Luque de Castro, Flow Injection Analysis: Principles and Applications, Ellis Horwood, Chichester, 1987.

[5] J. Ruzicka and E.H. Hansen, Flow Injection Analysis, 2nd Edn., Wiley, New York, 1988.
[6] M. Valcárcel and M.D. Luque de Castro, Non-Chromatographic Continuous Separation Techniques, Royal Society of Chemistry, Cambridge, 1991.
[7] J.R. Ferreira, E.A.G. Zagatto, M.A.Z. Arruda and S.M.B. Brienza, Analyst, 115 (1990) 779.
[8] S. Olsen, L.C.R. Pessenda, J. Ruzicka and E.H. Hansen, Analyst, 108 (1983) 905.
[9] E.M. Pedrazzi and R.E. Santelli, Talanta, 40 (1993) 551.
[10] R.E. Santelli, M. Gallego and M. Valcárcel, Anal. Chem., 61 (1989) 1427.
[11] R.E. Santelli, M. Gallego and M. Valcárcel, J. Anal. At. Spectrom., 4 (1989) 547.
[12] Z. Fang, M. Sperling and B. Welz, J. Anal. At. Spectrom., 6 (1991) 301.
[13] J. Posta, H. Berndt, S.K. Luo and G. Schaldach, Anal. Chem., 65 (1993) 2590.
[14] A.M. Naghmush, K. Pyrzyńska and M. Trojanowicz, Anal. Chim. Acta, 288 (1994) 247.
[15] R.E. Santelli, M. Gallego and M. Valcárcel, Talanta, 41 (1994) 817.
[16] S.S. Jorgensen and M.A.B. Regitano, Analyst, 105 (1980) 292.
[17] J.C. de Andrade, J.C. Rocha, C. Pasquini and N. Baccan, Analyst, 108 (1983) 621.
[18] J.C. de Andrade, J.C. Rocha and N. Baccan, Analyst, 109 (1984) 645.
[19] J.C. de Andrade, J.C. Rocha and N. Baccan, Analyst, 110 (1985) 197.
[20] T.P. Linch, N.J. Kernoghan and J.N. Wilson, Analyst, 109 (1984) 839.
[21] J. Ruz, A. Rios, M.D. Luque de Castro and M. Valcárcel, Anal. Chim. Acta, 186 (1986) 139.
[22] J. Ruz, A. Torres, A. Rios, M.D. Luque de Castro and M. Valcárcel, J. Autom. Chem., 8 (1986) 70.
[23] M.J. Whitaker, Anal. Chim. Acta, 174 (1985) 375.
[24] A.N. Araujo, J.L.F.C. Lima, A.O.S.S. Rangel, J. Alonso, J. Bartroli and R. Barber, Analyst, 114 (1989) 1465.
[25] L. Sacconi, Discuss Faraday Soc., 7 (1949) 173.
[26] G.L. Schmitt and D.J. Pietrzyk, Anal. Chem., 57 (1985) 2247.
[27] A.G. Cox, I.G. Cook and C.W. McLeod, Analyst, 110 (1985) 331.
[28] A.G. Cox and C.W. McLeod, Anal. Chim. Acta, 179 (1986) 487.
[29] M. Sperling, S. Xu and B. Welz, Anal. Chem., 64 (1992) 3101.
[30] A.M. Dobney and G.M. Greenway, Analyst, 119 (1994) 293.
[31] J.R. Pretty, E.A. Blubaugh, J.A. Caruso and T.M. Davidson, Anal. Chem., 66 (1994) 1540.
[32] I.S. Krull, K.W. Panaso and L.L. Gersheim, J. Chromatogr. Sci., 21 (1983) 460.
[33] A.O. Jacintho, E.A.G. Zagatto, H. Bergamin F°, F. J. Krug and B.F. Reis, Anal. Chim. Acta, 130 (1981) 243.
[34] E.B. Sandell, Colorimetric Determination of Traces of Metals, 3rd edn., pp. 388–401, Interscience, New York, 1959.
[35] C.W. McLeod, I.G. Cook, P.J. Worsfold, J.E. Davies and J. Queay, Spectrochim. Acta, 40B (1985) 57.
[36] M. Sperling, X. Yin and B. Welz, Analyst, 117 (1992) 629.
[37] J. Pavel, J. Kliment, S. Stoerk and O. Luter, Fresenius' Z. Anal. Chem., 321 (1985) 587.
[38] N.A.R. Pedro, V.P.S. Freitas, M.I.C. Badolato and E. de Oliveira, Quim. Nova, 14 (1991) 108.
[39] J.A. Dean, Anal. Chem., 23 (1951) 1096.
[40] S. Dig, R. Cornelis, B. Griepink, P. Quevanviller and J.M. Christensen, Paper P-IV.23 presented at 12th Int. Symp. on Microchemical Techniques, Córdoba, 1992.

ELSEVIER

Talanta 42 (1995) 1619–1623

Talanta

# Chemiluminescence investigation of $NH_2OH$–fluorescein–$Cu^{2+}$ system and its application to copper analysis in serum

Jinming Lin *, Toshiyuki Hobo

*Department of Industrial Chemistry, Faculty of Technology, Tokyo Metropolitan University, Minami-Oshawal-1, Hachioji, Tokyo 192-03, Japan*

Received 25 January 1995; revised 10 April 1995; accepted 11 April 1995

**Abstract**

A novel chemiluminescent system, fluorescein–$NH_2OH$–$OH^-$, was developed for the determination of copper(II) in serum. A weak light emission arises from hydroxylamine in the presence of the organic reagent fluorescein in basic aqueous solution. Under the conditions of $1.2 \times 10^{-3}$ mol $l^{-1}$ $NH_2OH$ and $5 \times 10^{-3}$ mol $l^{-3}$ fluorescein, the light intensity is linearly dependent upon the concentration of copper(II) within the range 1–20 ppb. The relative standard deviation of the determination of copper(II) is 4.2% ($n = 13$) and the detection limit is 0.5 ppb. The system is highly selective for copper except in the presence of iron(II,III) and cobalt(II). In conjunction with potassium fluoride as masking agent, the method was successfully applied to the determination of microamounts of copper(II) in serum. A mechanistic study of the chemiluminescence reaction is also discussed.

## 1. Introduction

The determination of copper in body fluids such as serum is of increasing clinical importance. A number of investigations regarding the use of chemiluminescence have been proposed [1–3]. Most analytical methods for copper using liquid-phase chemiluminescence are based on the reaction of chemiluminescent reagents (such as luminol, lecigenin, lophine, and oxalate esters) with $H_2O_2$ catalysed by copper, which results in poor selectivity. In our laboratory, we have developed two new systems for copper determination without chemiluminescent reagents [4,5], both of which were used for tap water [4] or sea water [6]. The application of fluorescein as a chemiluminescent reagent has been reported previously [7], and recently it was also used for the determination of ultratrace amounts of copper(II) [8], unfortunately, which were also concerned with luminol or horseradish peroxidase, respectively. In the course of our studies on the application of the chemiluminescence method to the determination of copper, we found that in alkaline aqueous solution, a trace amount of copper can lead to hydroxylamine luminescence, which can be enhanced by adding an appropriate amount of fluorescein solution. Among 20 coexisting ions tested, only iron(II,III) and cobalt(II) showed interferences when their concentrations exceeded by two fold that of copper(II). Based on this finding, we have proposed a highly selective chemiluminescent system for the determination of copper(II). Experimental variations such as pH values, reactant concentrations and the effects of coexisting ions have been studied. The application of this method to the determination of copper in serum gave a good result. A possible mechanism for the chemiluminescence of the $Cu^{2+}$–

* Corresponding author. Fax: (81)426-77-2821; e-mail: A911067 @ ibm 3090.comp.metro-u.ac.jp


*SSDI* 0039-9140(95)01614-7

$NH_2OH$–fluorescein system has been discussed. It was thought that the emission was from the excited molecular oxygen species and the light arose either from the deactivation of the excimer oxygen species or was emitted from the excited organic molecules generated by energy transfer.

## 2. Experimental

### 2.1. Apparatus and reagents

A home-made biochemiluminescence detector was used. Details of the construction and principles of the apparatus have been described elsewhere [9]. A Shimadzu C-E3A Chromatopac instrument (Kyoto, Japan) was used for the measurement of the chemiluminescence signals.

A copper(II) standard solution was prepared by dissolving 0.25 g of analytical-reagent-grade copper chloride in 100 ml of 0.05 mol $l^{-1}$ HCl solution to give a concentration of about 1 mg $ml^{-1}$ of copper. The concentration of copper in the solution was determined by EDTA titration. A working solution was prepared by dilution of the stock solution with water just before use. Fluorescein (FL) was purchased from Merck; a stock solution was prepared by dissolving 0.3323 g of FL in 5 ml of 0.2 mol $l^{-1}$ KOH–50% ethyl alcohol solution, then adding water to 100 ml. Diluted solutions were prepared from the stock solution. Hydroxylamine hydrochloride was prepared by dissolving an appropriate amount of $NH_2OH \cdot HCl$ in water to obtain the requisite concentration before use.

All chemicals were analytical-reagent-grade and were used as received. Redistilled water was used throughout the experiment.

### 2.2. Procedure

To the luminescence cell, 100 µl of 0.01 mol $l^{-1}$ fluorescein solution, 500 µl of 0.10 mol $l^{-1}$ borate buffer solution (pH 12.00) and 170 µl of $1.25 \times 10^{-3}$ mol $l^{-1}$ $NH_2OH$ solution were added by means of micropipettes. The cell compartment was then transferred into the dark room of the chemiluminescence meter and the light gate was opened for passage of light through the cell. Finally, 100 µl of standard copper(II) solution or sample solution are injected into the luminescence cell from the sample injection system. The chemiluminescence signals were then recorded.

## 3. Results and discussion

### 3.1. Primary experiment for chemiluminescence reaction

By using the home-made biochemiluminescence meter, we studied the chemiluminescence behaviour of the reducing agent hydroxylamine hydrochoride, and discovered that in basic aqueous solution, some metal ions such as copper(II), iron(II,III), cobalt(II) and nickel(II) can react with $NH_2OH$, giving a faint light without any oxidation reagent being present. The addition of fluorescein solution to copper(II) can affect the luminescence sensitivity significantly, especially at high pH values, and the peak heights of the chemiluminescence signals show a linear relationship with the concentration of copper(II).

### 3.2. Effect of pH

Although various buffer solutions such as Tris–HCl, carbonate and phosphate were examined for the chemiluminescence reaction, the most promising was $H_3BO_3$–KOH buffer solution. The effect of pH on the chemiluminescence (peak height) is shown in Fig. 1. The peak height increased with the increase in pH to pH 11.7. The most favourable value of the pH was 12.0.

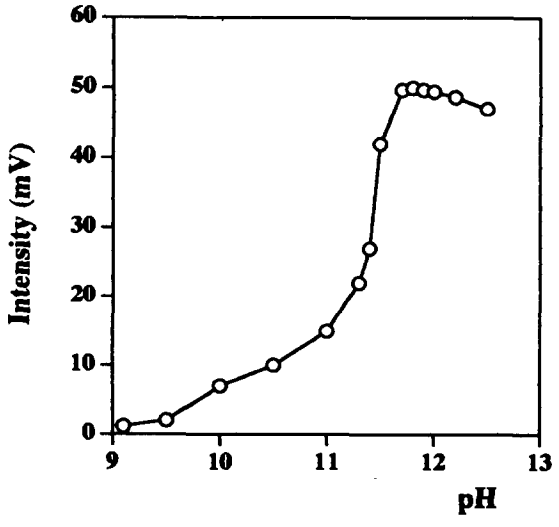


Fig. 1. Effect of pH on the luminescence intensity.

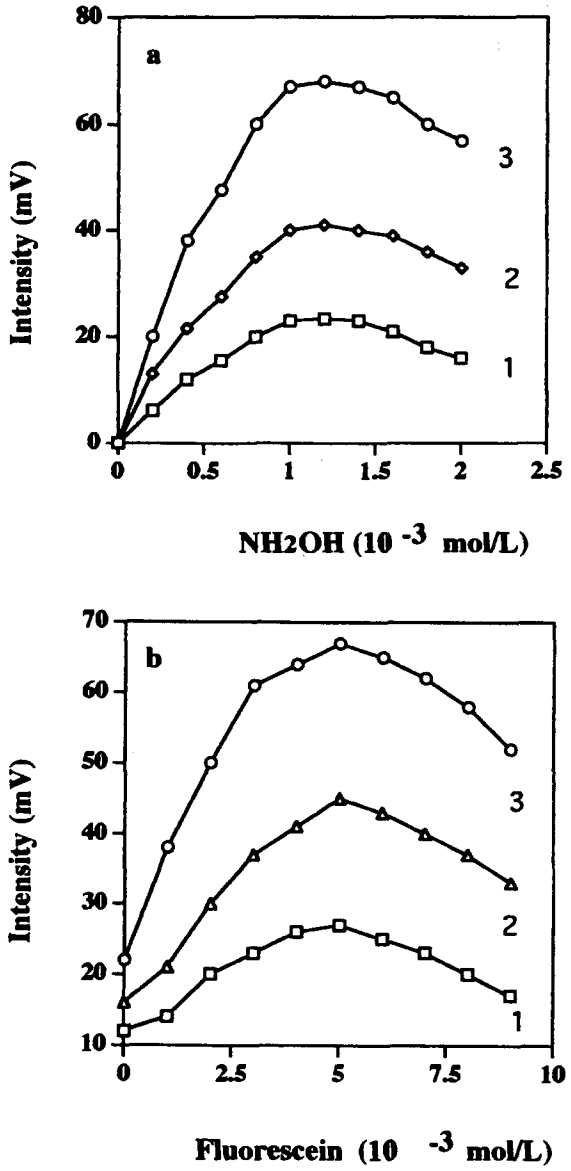


Fig. 2. Effect of concentrations of hydroxylamine and fluorescein on the chemiluminescence intensity. (a) $NH_2OH$; (b) Fluorescein. Curve 1, 5 ppb Cu(II); curve 2, 10 ppb Cu(II); curve 3, 15 ppb Cu(II).

### 3.3. *Effects of the concentrations of hydroxylamine and fluorescein*

The effect of the concentrations of hydroxylamine and fluorescein on light emission are shown in Figs. 2a and 2b, respectively. Almost constant chemiluminescence was observed for hydroxylamine in the range $(1.0–1.5) \times 10^{-3}$ mol $l^{-1}$, and the most suitable concentration was $1.2 \times 10^{-3}$ mol $l^{-1}$. The chemiluminescence intensity increased as the concentration of fluorescein was increased from 0 to $5 \times 10^{-3}$ mol $l^{-1}$. A $5 \times 10^{-3}$ mol $l^{-1}$ fluorescein concentration was chosen for subsequent experiments.

### 3.3. *Calibration graph and detection limit*

Using the optimum conditions described above, a calibration graph was obtained for the determination of copper. The analytical characteristics of the graph are summarised in Table 1. The relative standard deviation for thireen replicate analyses of 1 ppb of copper(II) was 4.2%, which means that this method is satisfactory for the determination of copper.

### 3.4. *Interferences of coexisting ions*

The effects of various inorganic ions on the determination of 5 ppb of copper(II) were examined using the proposed method. The tolerance limit was taken as the amount which caused an error of $\pm 5\%$ in each peak height. The results are summarised in Table 2. Most ions have almost no effect on the copper(II) determination at high concentrations. Only iron(II,III) and cobalt(II) interfered seriously when their concentrations were over two fold higher than that of copper(II). Therefore a 0.01 mol $l^{-1}$ potassium fluoride solution was chosen for masking the iron ions because a low concentration of KF has no effect on the luminescence intensity. The influence of cobalt(II) was not investigated further because the samples to be tested contained very little cobalt.

### 3.5. *Application*

There are many analytical methods available for the determination of copper. One of those most frequently employed for copper determination is atomic absorption spectrometry (AAS) although there are some reproducibility and interference problems [10]. The present method was applied satisfactorily to the determination of copper(II) in serum and was found to be simple, highly sensitivity and displayed excellent selectivity. The samples were pretreated with a mixture of concentrated nitric acid and 30% hydrogen peroxide in a small beaker, carefully heated under a cover on a hot plate until the liquid had almost evaporated, and then treated with concentrated hydrochloric acid and evaporated by dryness. The residue was dissolved in 10 ml of 0.01 mol $l^{-1}$ KF solution. An aliquot of the resulting solution was

Table 1
Analytical characteristics of copper obtained by the present method

| Characteristic | Result | | | | | | | |
|---|---|---|---|---|---|---|---|---|
| Copper (ppb) | 0 | 0.5 | 1 | 4 | 8 | 12 | 16 | 20 |
| Intensity (mV) | 2.5 | 5 | 8 | 19 | 38 | 57 | 73 | 82 |
| Linear range (ppb) | 1 – 20 | | | | | | | |
| Limit of detection [a] (ppb) | 0.5 | | | | | | | |
| RSD for 1 ppb Cu(II) ($n = 13$)(%) | 4.2 | | | | | | | |

[a] Signal-to-noise ratio, 2.

determined by using the standard curve. The results agreed well with those obtained by AAS. The recoveries were good enough for practical use and all the results are listed in Table 3.

### 3.6. Possible mechanism of the present chemiluminescence (CL) reaction

It is well known that light emission is frequently accompanied by an oxidation reaction involving large free energy changes. Most chemiluminescence of organic molecules occurs in the presence of $H_2O_2$ or other oxidising agents. In contrast, the present CL system does not have such reagents added deliberately. This enables us to discuss the possible CL reaction scheme of the hydroxylamine–fluorescein system.

*Chemiluminescence and fluorescence spectra*

The chemiluminescence spectrum of the $NH_2OH$ reaction with copper was detected by means of a series of filters. The results indicated that there were two luminescence peaks at 480 nm and 580 nm, respectively. The CL spectrum of hydroxylamine–fluorescein was similar to the fluorescence spectrum ($\lambda_{max} = 560$ nm) before and after reaction with copper(II). When nitrogen or oxygen was bubbled through the solution the copper(II) peak height decreased with nitrogen and increased with oxygen. The results indicated that the reaction involved dissolved oxygen. Brown [11] and Khan and Kasha [12] reported that the single exited molecular oxygen species ($^1O_2^*$) and the formation of the $(^1O_2^*)_2$ species arose from the emission due to the deactivation of excimer oxygen species; we thought that the luminescence emitted from the $NH_2OH$–Cu(II) system was due to the generation of $O_2(^1\Sigma_g^+)$ and thus a molecular pair, $O_2(^1\Delta_g)O_2(^1\Sigma_g^+)$. In this work, however, no detectable emission was observed during the reaction. Khan and Kasha [12] proposed that in a system generating excited molecular oxygen, luminescence arising from any energetically favourable species can be produced, and observed as the CL reaction direct energy transfer from the excited oxygen molecular pairs. Therefore, there was significant evidence that dissolved oxygen has an important role in the CL reaction. The oxidation mechanism of hydroxylamine has been investigated [13]. Hughes and Nicklin [14] proposed a possible mechanism for hydroxylamine oxidation in basic aqueous solution. They thought that in the presence of alkaline solution, $NH_2OH$ existed in the form of $NH_2O^-$, which can be attacked by the dissolved oxygen

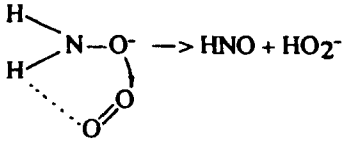

(1)

Table 2
Tolerance limits of foreign ions on the determination of 5 ppb of copper(II)

| Tolerance limit (ppb) | Foreign ion |
|---|---|
| $5 \times 10^3$ | $Cl^-$, $SO_4^{2-}$, $PO_4^{3-}$, $HCO_3^-$, $NO_3^-$, $F^-$, $Na^+$ $K^+$, $Ca^{2+}$, $Mg^{2+}$ |
| $1 \times 10^3$ | $Zn^{2+}$, Al(III), $Cd^{2+}$, Se(IV), Au(III), Bi(III) |
| $1 \times 10^2$ | Ga(III), $Ag^+$, $As^{3+}$, $Au^{3+}$ |
| 50 | Cr(III), $Pb^{2+}$, $Ni^{2+}$, Fe(III) |
| 10 | Fe(II), Co(II) |

The oxidation scheme of metal-ion-catelysed hydroxylamines has been studied by Anderson [15]. It was described as the following

$$2Cu^{2+} + NH_2OH \rightarrow 2Cu^+ + NOH + 2H^+ \quad (2)$$

$$2NOH \rightarrow N_2O + H_2O \quad (3)$$

$$H^+ + 2Cu^+ + O_2 \rightarrow 2Cu^{2+} + HO_2^- \quad (4)$$

Table 3
Determination of copper in serum samples

| Serum | Cu content [a] (ppm) | | Cu added (ppm) | Cu found (ppm) | Recovery (%) |
|---|---|---|---|---|---|
| | This method | AAS method | | | |
| 1 | 1.08 | 0.98 | 1.00 | 0.94 | 94 |
| 2 | 1.04 | 1.00 | 1.00 | 0.97 | 97 |
| 3 | 1.12 | 1.05 | 1.00 | 0.96 | 96 |
| 4 | 0.84 | 0.85 | 1.00 | 0.94 | 94 |
| 5 | 0.89 | 0.91 | 1.00 | 0.96 | 96 |
| 6 | 0.92 | 0.90 | 1.00 | 0.96 | 96 |

[a] $n = 3$.

Stauff [16] reported that $HO_2^-$ free radicals can attack each other, giving a molecular pair $(O_2^*)_2$

$$O_2H^- + O_2H^- \rightarrow (O_2O_2)^* \quad (5)$$

In the present work, the reaction scheme of hydroxylamine may be represented by the following two equilibria

$$O_2H^{-*} + O_2H^{-*} \rightarrow (O_2O_2)^* \quad (6)$$

$$(O_2O_2)^* \rightarrow 2O_2 + h\gamma(\lambda_{max} = 478, 580\ nm) \quad (7)$$

The chemiluminescence of fluorescein used in analytical chemistry has been reported [8,17], and was based on the reaction of fluorescein with $H_2O_2$ and horseradish peroxidase (HRP).

$$FL + H_2O_2 \xrightarrow{HRP} FL^* \rightarrow FL + h\gamma \quad (8)$$

From the above discussion, a possible reaction scheme is proposed for the chemiluminescence of fluorescein–$NH_2OH$ with copper(II). First, an autoxidation reaction to give hydroxylimine took place in the basic aqueous solution with copper(II) ions as catalyst. The emission was thought to be from the excited molecular oxygen species (excimers) which were produced from hydroxylamines reacting with dissolved oxygen, catalysed by copper(II). The excited molecular oxygen species $(^1O_2^*)_2$ then transferred energy to the fluorescein molecule, forming excited organic molecules, and the emission was generated.

$$(^1O_2^*)_2 + FL \rightarrow 2^3O_2 + FL^*$$

$$FL^* \rightarrow FL + h\gamma(light)$$

## 4. Conclusion

A simple and selective chemiluminescence method for the determination of copper in serum has been proposed. The method utilises the autoxidation of hydroxylamine in alkaline solution catalysed by copper(II). The chemiluminescence intensity was enhanced by the addition of fluorescein. The mechanism has also been discussed.

## References

[1] F. Zhang and G.N. Chen, Fenxi Huaxue, 13(10) (1985) 790.
[2] F. Zhang and Y.L. Chen, Fenxi Shyanshi, 6(4) (1987) 44.
[3] K. Robards and P.J. Worsfold, Anal. Chim. Acta, 147 (1992) 266.
[4] X.Z. Wu, M. Yamada, T. Hobo and S. Suzuki, Anal. Chem., 61 (1989) 1505.
[5] M. Yamada and S. Suzuki, Anal. Lett., 17(A4) (1984) 251.
[6] K.H. Coale and K.S. Johnson, Anal. Chim. Acta, 266 (1992) 345.
[7] P-A. Johansson, Bo Karlberg and S. Thelander, Anal. Chem. Acta, 114 (1980) 215.
[8] T. Kamidate, I. Kuniya, T. Segawa and H. Watanabe, Chem. Lett., (1992) 887.
[9] J. Lin and F. Zhang, Fenxi Yiqi, 1 (1992) 26.
[10] J.C. Van Loom, Analytical Atom Absorption Spectroscopy: Selected Methods, Academic Press, New York, 1980.
[11] R.J. Brown, Proc. Chem. Soc., London, (1964) 117.
[12] A.U. Khan and M. Kasha, J. Am. Chem. Soc., 88 (1966) 1574.
[13] B.Q. Sklarz, Rev. Chem. Soc., 21 (1967) 3.
[14] M.N. Hughes and H.G. Nicklin, J. Chem. Soc. A, (1971) 164.
[15] J.H. Anderson, Analyst, 89 (1964) 357.
[16] J. Stauff, Z. Phys. Chem. (Frankfurt am Main), 40 (1964) 64; 49 (1966) 58; 55 (1967) 39.
[17] T. Segawa, T. Kamidate and H. Watanabe, Anal. Sci., 6 (1990) 763.

ELSEVIER

Talanta 42 (1995) 1625–1630

Talanta

# Sorption and preconcentration of metal ions in ethanol solution with a silica gel surface chemically modified with benzimidazole

Newton L. Dias Filho [a,*], Yoshitaka Gushikem [b], Wagner L. Polito [c], José C. Moreira [d], Emmanuel O. Ehirim [e]

[a] *Departamento de Física e Química, UNESP, C.P. 31, 15385-000, Ilha Solteira, SP, Brazil*
[b] *Instituto de Química, UNICAMP, 13081-970, Campinas, SP, Brazil*
[c] *Instituto de Química, USP, 13560-250, São Carlos, CP, Brazil*
[d] *Instituto de Química, UNESP, 14800, Araraquara, SP, Brazil*
[e] *Departamento de Engenharia Química, UFSCar, 13560-905, São Carlos, SP, Brazil*

Received 4 January 1995; revised 18 April 1995; accepted 21 April 1995

**Abstract**

The adsorption isotherms of $MCl_2$ (M = Mn, Ni, Cu, Zn and Cd) and $FeCl_3$ by silica gel chemically modified with benzimidazole molecules ($\equiv Si(CH_2)_3-NC_7H_5N$) were studied in ethanol solution at 298 K. A column made of modified silica was used to adsorb and preconcentrate the above metal ions from ethanol solution. Elution was done with 0.1 M hydrochloric acid in an ethanol/water mixture having a mole fraction of water of 0.8. The material was applied in the preconcentration of metal ions from commercial ethanol normally used as engine fuel.

*Keywords:* Benzimidazole; Preconcentration of heavy metals; Adsorption isotherms; Silica gel functionalized

## 1. Introduction

Surfaces of inorganic solids have been modified with chelating groups in order to adsorb and preconcentrate metal ions from solutions [1–7].

The preparation of a silica chemically modified with benzimidazole molecules ($\equiv Si(CH_2)_3-NC_7H_5N$) and a study of the adsorption of $CuX_2$ (X = Cl, Br, $ClO_4$) from non-aqueous solvents were recently investigated [8–10]. This material, abbreviated here as SiL, can react with copper(II) ions in ethanol solution forming very stable complexes. Considering the potential usefulness in chemical analysis, the SiL can be applied to the preconcentration of metal ions from commercial ethanol (a mixture of ethanol and water).

The development of methods to determine traces of metals has been one aspect of interest in the research on ethanol as a fuel. The presence of some metal ions in ethanol fuel can induce corrosion in the vehicle components in contact with the liquid [11–14].

Since benzimidazole can coordinate with several metals, and considering the growing interest in the modification of surfaces, we report in this work the results of our sorption and preconcentration study of Mn(II), Fe(III), Ni(II), Cu(II), Zn(II) and Cd(II) by SiL in ethanol solution. The coordination complexes that are formed upon adsorption were characterized by infrared spectroscopy. The application of this material to the preconcentration and removal of the above metal ions from commercial ethanol is also described.

* Corresponding author. Fax: (55)187-622-735.


*SSDI* 0039-9140(95)01621-X

## 2. Experimental

### 2.1. Preparations

Silica gel 60 (Merck, Darmstadt, Germany) having a particle size between 0.2 and 0.05 mm was chemically modified with a benzimidazole molecule according to the procedure described earlier [8]. Silica gel (≈50 g) previously activated at 420 K under vacuum ($10^{-3}$ torr, ≈0.133 Pa), was suspended in dry xylene (200 ml), 3-chloropropyltrimethoxysilane (15 ml) was added and the mixture was stirred for 24 h at 380 K in a nitrogen atmosphere. The resulting modified silica, $\equiv Si(CH_2)_3Cl$, was immersed in pure dimethylformamide (150 ml) and benzimidazole (17.5 g, 0.15 mol) was added. The mixture was stirred for 24 h at 380 K under a nitrogen atmosphere. The resulting modified silica was filtered off and washed with dimethylformamide and ethanol. The product was heated for 8 h at 353 K under vacuum ($10^{-3}$ torr).

The amount of benzimidazole attached to the silica surface was determined by nitrogen analysis using the Kjeldahl method. The specific surface area was determined by the Brunauer–Emmett–Teller (BET) method using a Micromeritics Flow Sorb 2300 apparatus of Micromeritics Instrument Corporation (Norcross, USA).

### 2.2. Adsorption isotherms

The adsorption isotherms of metal ions on benzimidazole-modified silica, hereafter denoted as SiL, were determined for $MCl_2$ (M = Mn, Ni, Cu, Zn and Cd) and $FeCl_3$ in dry ethanol solutions. Solutions of the metal ions (concentration between $1 \times 10^{-4}$ and $5 \times 10^{-3}$ M) were shaken with SiL (0.1 g) at $298.0 \pm 0.2$ K for 40 min. The supernatants were decanted and the amount of metal ions was determined by flame atomic absorption spectroscopy (flame AAS).

### 2.3. Preconcentration experiments

For these experiments, a glass column of 20 cm height and 0.8 cm internal diameter was packed with about 2 g of the sorbent to give a bed height of about 10 cm. The material was activated for each run by washing with 5 ml of aqueous solution of 0.1 M hydrochloric acid, treating with 5 ml of 0.5% (w/v) potassium hydroxide in ethanol, and finally washing with 20 ml of ethanol to remove all hydroxide.

Solutions of Mn(II), Fe(III), Ni(II), Cu(II), Zn(II) and Cd(II) ions with concentrations of $5 \times 10^{-3}$ M were prepared in dry ethanol. In each run, 5 ml ($25 \times 10^{-6}$ mol) of metal ion solution was passed through the column with a flow rate between 0.5 and 1.0 ml $min^{-1}$. The adsorbed metal ions were eluted by passing 10 ml of an aqueous ethanolic 0.1 M hydrochloric acid solution in which the ethanol/water ratio was varied. Lower acid concentrations such as 0.075 or 0.05 M were less effective in desorbing the metal. The metals were quantified by flame AAS.

### 2.4. Adsorption and recovery of a mixture of ions

In these studies, solutions of Mn(II), Fe(III), Ni(II), Cu(II), Zn(II) and Cd(II) ions ($0.1 \times 10^{-3}$ M each) were used. Higher concentrations ($5.0 \times 10^{-3}$ or $0.5 \times 10^{-3}$ M) were also tested. For adsorption, 10 ml of solution was percolated through the column. The adsorbed metal ions were eluted by passing 10 ml of 0.1 M HCl in 0.8 mole fraction ethanol/water through the column and collected for analysis by flame AAS.

## 3. Results and discussion

### 3.1. Characteristics of the material

The chemical analysis of SiL showed $0.48 \times 10^{-3}$ mol $g^{-1}$ attached molecules and a specific surface area of 477 $m^2$ $g^{-1}$. The maximum retention capacity for individual ions from ethanol solution was evaluated by adsorption isotherms (see Table 1). This retention

Table 1
Adsorption of $MX_2$ and $FeCl_3$ by SiL from ethanol solution at 298 K

| | $10^{-3}$ $b$ (l $mol^{-1}$) | $10^3$ $N_f^S$ (mol $g^{-1}$) | $r$ |
|---|---|---|---|
| $CuCl_2$ | 3.4 | 0.26 | 0.998 |
| $NiCl_2$ | 1.4 | 0.19 | 0.998 |
| $ZnCl_2$ | 6.4 | 0.28 | 0.999 |
| $CdCl_2$ | 12.3 | 0.30 | 0.999 |
| $FeCl_3$ | 10.5 | 0.43 | 0.999 |
| $MnCl_2$ | 0.8 | 0.14 | 0.995 |

$b$ is a constant given by the ration $b = Keq/a$; $N_f^S$ is a constant representing the maximum sorption capacity.

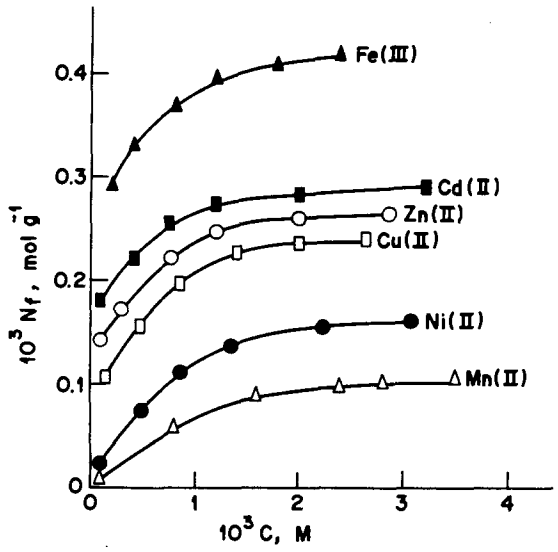


Fig. 1. Adsorption isotherms of metal ions from solution by SiL at 298 K. $N_f$ is the amount of metal ions adsorbed per gram of the solid phase, and $C$ is the residual concentration of metal ions in equilibrium with the solid phase.

capacity was not affected after several retention/elution cycles during 6 months of continuous use. The adsorbent material was resistant to the attack of concentrated acids, but not to the attack of concentrated aqueous alkali solution.

### 3.2. Adsorption isotherms

The results of the adsorption measurements of metal ions, as plots of $N_f$ against $C$, are shown in Fig. 1. Isotherms with similar shapes but different adsorption capacities were observed, Fe(III) being the most adsorbed and Mn(II) the least adsorbed.

The metal ions are adsorbed from solutions by the immobilized benzimidazole molecule, in a process of competition between solute and solvent. The isotherm obtained by these systems can be represented by the Langmuir adsorption model [8]:

$$\frac{C}{N_f} = \frac{1}{bN_f^S} + \frac{C}{N_f^S}$$

In this expression, $C$ is the residual concentration (M) of the metal ion in equilibrium with the solid phase, $N_f$ is the number of moles of the solute adsorbed per gram of solid, $N_f^S$ is a constant which represents the maximum sorption capacity (mol of solute per gram of adsorbent), and $b$ is a constant given by the ration $b = Keq/a$, where $a$ represents the activity of the solvent in solution. The value of $b$ and $N_f^S$ were obtained from the angular and linear coefficients by plotting $C/N_f$ against $C$, and the values are listed in Table 1. The correlation coefficients $r$ of the straight lines were always $>0.99$.

The maximum retention capacity of metal ions on the solid SiL showed the sequence Fe(III) > Cd(II) > Zn(II) > Cu(II) > Ni(II) > Mn(II).

The calculated values of the constant $b$ are very high in every case, suggesting that the sorption of the metal from solution by the solid phase occurs with the metal directly coordinating with the unsubstituted benzimidazole nitrogen.

### 3.3. Infrared spectra

Recently, we reported [8–10] that coordination of copper(II) ion benzimidazole nitrogen shifted the band at 1500 cm$^{-1}$ of SiL infrared spectrum to a higher frequency. This particular band is assigned to the skeleton vibrational mode of the ring which involves coupled vibration ($\nu$CN + $\nu$CC). This is an evidence that the copper(II) ion is coordinated to the benzimidazole free nitrogen and is not only physically sorbed onto the surface. The remaining spectra of the other metals adsorbed onto the modified surface, are very similar to that of SiL $CuX_2$, as shown in Table 2.

### 3.4. Preconcentration and elution of individual metal ions

In every run, the effluent was collected and a quantity of metal ions analyzed. The metals were eluted by passing 10 ml of 0.1 M HCl in ethanol/water through the column. The results are shown in Fig. 2.

It can be observed that, under the experimental conditions used, for Mn(II) and Ni(II) the extents of elution are independent of the ethanol/water ratio. Cu(II), Zn(II) and Cd(II) ions showed nearly similar behaviour and were completely eluted from the column with a mole fraction of water ($\chi_B$) of approximately 0.8, 0.85 and 0.9, respectively. However, the beginning of the elution was different for the three cases: elution of Cu(II) began at $\chi_B \approx 0.2$, Zn at $\chi_B \approx 0.35$ and Cd(II) at $\chi_B \approx 0.65$.

In contrast, Fe(III) was completely eluted at $\chi_B \approx 0.4$, but the elution decreased with an increase in the mole fraction of water in the

Table 2
Infrared bands ($cm^{-1}$) of modified silica [a]

| SiL | $CuCl_2^*$ | $NiCl_2^*$ | $ZnCl_2^*$ | $CdCl_2^*$ | $FeCl_3^*$ | $MnCl_2^*$ | Approximate assignment |
|---|---|---|---|---|---|---|---|
| 1660w | – | – | – | – | – | – | Combination band |
| 1630(br) | 1630(br) | 1630(br) | 1628(br) | 1627(br) | 1629(br) | 1627(br) | $\delta(H_2O)$ |
| 1567m | 1566m | 1568m | 1569m | 1568m | 1568m | 1567m | $\nu(CC) + \delta(CH)$ |
| 1500m | 1520m | 1507m | 1515m | 1509m | 1531m | 1504m | $\nu(CN) + \nu(CC)$ |
| – | 1480vw | 1484vw | 1486w | 1486w | 1487w | 1485w | $\nu(CN) + \delta$(ring) |
| 1458m | 1463m | 1462m | 1464m | 1464m | 1466m | 1465m | |
| 1382w | 1385vw | 1385vw | 1387vw | 1386vw | 1385vw | 1386vw | propyl $\delta(CH_2)$ |
| 1353w | 1352w | 1350w | 1352w | 1352w | 1352w | 1352w | |

[a] Starred metal halides indicate adsorbed metal on the modified silica; v = very; m = medium; w = weak; br = broad.

mixture. Previously, it was reported that in a binary mixture of methanol and water the hydrolysis constant of Fe(III), expressed by $K = [Fe(OH)_2^+][H^+]/[Fe^{3+}]$, increases with the mole fraction of methanol in the mixture [15,16]. If such behaviour can be extended to Fe(III) in a mixture of ethanol and water, it seems likely that the less charged complex ion $Fe(OH)^{2+}$, which is present at higher concentrations for lower $\chi_B$, will be more easily eluted than the $Fe^{3+}$ ion itself. Ni(II) and Mn(II) were eluted from the column in a similar way, whether the silica was modified or not; also, they were not completely retained (Table 1). Presumably, nickel and manganese complexes with benzimidazole groups are very weak.

### 3.5. Adsorption and recovery of a mixture of ions

Adsorption and elution studies of a mixture of metal ions were carried out. In these studies, a series of solutions was prepared in which the metal ion concentrations were fixed at $0.1 \times 10^{-3}$ M, except for one of them which was fixed at $5.0 \times 10^{-3}$ or $0.5 \times 10^{-3}$ M. The results are presented in Table 3.

It can be observed that the recoveries of Mn(II) and Ni(II) were practically complete in the presence of other metal ions at concentrations 5 or 50 times higher. In view of this, the percentage of elution of Mn(II) and Ni(II) was higher than that found for the individual ion experiment. This fact is reasonable, taking into account that there was no loss of Mn(II) and Ni(II) when the mixture was passed through the column, since the concentrations of the metals were 25 times lower than that used for the individual ion experiments.

The recovery of Fe(III) was about the same as in the individual ion experiment, whereas for Cu(II), Zn(II) and Cd(II) the recoveries were lower. Generally, it can be considered that the presence of one of the ions in excess did not significantly affect the recoveries of the others.

### 3.6. Determination of metals in ethanol fuel

Quantitative sorption–desorption of the heavy metals studied serves as a basic for a rapid method for the preconcentration and subsequent determination by flame AAS of these metals in commercial ethanol from five different plants.

In general, Cd(II) does not occur in commercial ethanol, or its content is lower than the contents of the other metals by a factor of 10–100. The content of Fe(III) depends on the degree of corrosion of the distillation equipment [14]. The concentration of Ni(II) normally found in the commercial ethanol is below $50\ \mu g\ l^{-1}$ and Zn(II) is not detected when the conventional preconcentration method is used, in which the first step has been to evaporate the ethanol solution to dryness [14].

Therefore, the contents of the metals studied were determined in commercial ethanol from five different plants using the recommended method by passing, depending on the origin, between 0.2 and $6.5\ l^{-1}$ of the sample through the column. Complete elution of the metals adsorbed was carried out using about 40 ml of an ethanol/water mixture with a mole fraction of water of 0.80. All the experiments were done in triplicate.

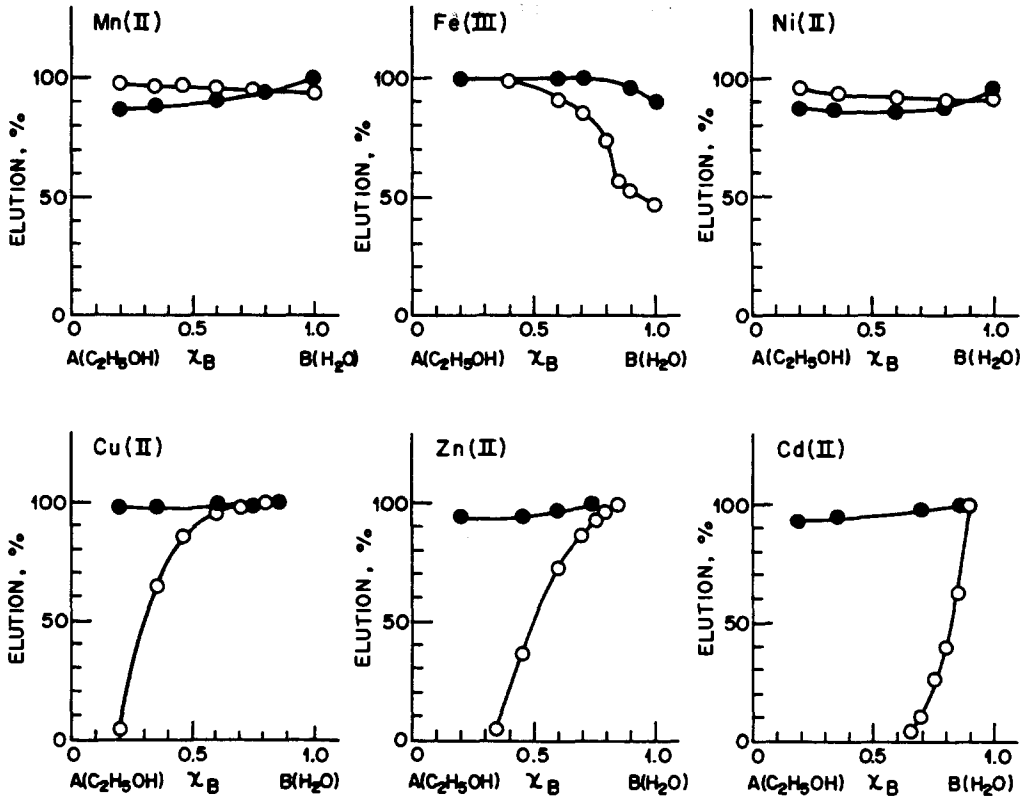


Fig. 2. Elution of the metal ions from different column packings: (○) modified silica; (●) untreated silica.

Table 3
Recovery of metal ions from a mixture

| Ion | Concentration ($10^{-3}$ M) | Recovery (%) [a] | | | | | |
|---|---|---|---|---|---|---|---|
| | | Mn(II) | Fe(III) | Ni(II) | Cu(II) | Zn(II) | Cd(II) |
| Mn(II) | 5.0 | – | 76 | 100 | 79 | 30 | 22 |
| | 0.5 | – | 77 | 100 | 86 | 26 | 26 |
| Fe(III) | 5.0 | 97 | – | 97 | 78 | 32 | 24 |
| | 0.5 | 98 | – | 100 | 71 | 25 | 33 |
| Ni(II) | 5.0 | 100 | 77 | – | 85 | 28 | 19 |
| | 0.5 | 100 | 78 | – | 77 | 25 | 23 |
| Cu(II) | 5.0 | 100 | 76 | 100 | – | 29 | 13 |
| | 0.5 | 100 | 76 | 100 | – | 23 | 19 |
| Zn(II) | 5.0 | 100 | 81 | 100 | 76 | – | 26 |
| | 0.5 | 100 | 84 | 100 | 84 | – | 25 |
| Cd(II) | 5.0 | 98 | 75 | 97 | 86 | 28 | – |
| | 0.5 | 100 | 76 | 98 | 78 | 27 | – |

[a] Concentration of each ion was $0.1 \times 10^{-3}$ M.

The results are shown in Table 4. Cd(II) was not detected in any sample. The accuracy of this method was tested and the results obtained using the recommended method are in good agreement with those obtained by direct determination, without any preconcentration.

**Acknowledgement**

The authors acknowledge the Usinas Pioneiros, Água Limpa, Generalco, Santa Isabel e São José da Estiva, which supplied ethanol for this work.

Table 4
Preconcentration of metal ions in ethanol fuel

| Plant | Vol[a] (l) | Concentration found ($\mu g\ l^{-1}$) | | | | |
|---|---|---|---|---|---|---|
| | | Mn(II) | Fe(III) | Ni(II) | Cu(II) | Zn(II) |
| A | 1–2 | $2.3 \pm 0.4$ | $4 \pm 1$ | $7 \pm 2$ | $180 \pm 30$ | $3.1 \pm 0.3$ |
| B | 4–6 | $2.0 \pm 0.3$ | $9 \pm 2$ | $5 \pm 0.5$ | $10 \pm 3$ | $2.9 \pm 0.2$ |
| C | 0.2–1 | –[b] | –[b] | $29 \pm 5$ | $250 \pm 30$ | $5.2 \pm 0.7$ |
| D | 4–6.5 | $2.5 \pm 0.5$ | $5.5 \pm 0.7$ | $4 \pm 0.3$ | $7 \pm 1$ | $2.0 \pm 0.4$ |
| E | 2–4 | $2.4 \pm 0.4$ | $14 \pm 2$ | $5 \pm 0.5$ | $45 \pm 6$ | $2.6 \pm 0.4$ |

[a] Volume passed through the column containing 2 g of functionalized silica gel.
[b] Not detected.

## References


[1] K. Terada and K. Nakamura, Talanta, 28 (1981) 123.
[2] D.E. Leyden and W. Wegscheider, Anal. Chem., 53 (1981) 1059A.
[3] P. Sutthivaiyakit and A. Kettrup, Anal. Chim. Acta, 169 (1985) 331.
[4] I.P. Alimarin, V.I. Fadeeva, G.V. Kudryavtsev and I.M. Loskutova, Talanta, 34 (1987) 103.
[5] S. Akiyama, Anal. Sci., 10 (1994) 365.
[6] L.T. Kubota, J.C. Moreira and Y. Gushikem, Analyst, 114 (1989) 1383.
[7] N.L. Dias Filho, W.L. Polito and Y. Gushikem, Talanta, 1995, in press.
[8] N.L. Dias Filho, Y. Gushikem, E. Rodrigues, J.C. Moreira and W.L. Polito, J. Chem. Soc., Dalton Trans., (1994) 1493.
[9] N.L. Dias Filho and Y. Gushikem, J. Mol. Struct. (Theochem.), 335 (1995) 175.
[10] N.L. Dias Filho, Y. Gushikem, J.C. Moreira, W.L. Polito and E. Rodrigues, J. Braz. Chem. Soc., 5(1) (1994) 53.
[11] I.M.R.A. Bruning and E.B. Malm, Research and Development Center of Petrobras Company, Rio de Janeiro, 1980, p. 15.
[12] D.K. Tanaka, S. Wolynec, S. Fairbanks and F.B.P. Pinto, Proc. VIIIth National Seminar on Corrosion, Brazilian Corrosion Society, Rio de Janeiro, Brazil, 1981, p. 59.
[13] D.K. Tanaka and S. Wolynec, Proc. of IXth National Seminar on Corrosion, Brazilian Corrosion Society, Rio de Janeiro, Brazil, 1982, p. 166.
[14] I.M.R.A. Bruning and E.B. Malm, Bol. Tec. Petrobras, 25 (1982) 217.
[15] G. Wada and A. Endo, Bull. Chem. Soc. Jpn., 45 (1972) 1073.
[16] G. Wada and Y. Kobayashi, Bull. Chem. Soc. Jpn., 48 (1975) 2451.

ELSEVIER

Talanta 42 (1995) 1631–1640

Talanta

# Third order derivative spectrophotometric determination of ascorbic acid in fruits and vegetables

Mahmure Üstün Özgür *, Sıdıka Sungur

*Yıldız Technical University, Department of Chemistry, Şişli, 80270, Istanbul, Turkey*

Received 2 November 1993; revised 21 September 1994; accepted 11 April 1995

**Abstract**

Ascorbic acid (AA) has been determined in kiwi, parsley and grapefruit by third order derivative spectrophotometry without using any separation or background correction techniques and reagents. The method is based on the measurement of the distances between two extremum values (peak-to-peak amplitudes) in the third order derivative spectra of the extracts. A metaphosphoric acid (3% w/v)–acetic acid (8% v/v) mixture was found to be the most suitable extraction solution. In the third order derivative spectrum, the extrema of 259.4 nm and 276.2 nm were used for the quantitative determination of AA in kiwi, and the extrema of 227 nm and 237 nm were used for the quantitative determination of AA in parsley and grapefruit. Calibration curves were constructed for the 2.0–10.0 μg $ml^{-1}$ concentration range. Relative standard deviations were calculated from the assay results of 14 samples. They were found to be in the ranges of 0.53–2.45% and 0.50–1.41% for the proposed method and the Association of Official Analytical Chemists (AOAC) method, respectively.

The obtained results were statistically compared with those of the official method of AOAC using the *F* test. There was no significant difference between the precisions at a 95% confidence level.

*Keywords:* Ascorbic acid; Fruits; Derivative spectrophotometry

## 1. Introduction

Ascorbic acid (AA) is widely distributed in plant materials, with fruits and vegetables being the major source in most human diets.

The concentration of AA in vegetables and fruits is a maturity index, and the determination of this constituent in such samples is of special interest in quality control.

The need for a fast and selective method is obvious, especially when routine determinations are required. Many analytical methods have been developed for the determination of AA and the quality control of products containing AA. These include titrimetric [1–3], spectrophotometric [4–7], fluorimetric [8], chromatographic [9–11], polarographic [12–14], amperometric [15,16], coulometric [17,18] and enzymatic methods [19–21], as well as combinations of various other techniques [22,23].

The titrimetric AOAC method [24] with 2,6-dichlorophenolidophenol as the titrant is used in many of the determinations. Although this method is rapid, the reagent itself is unstable and must be standardized before use. Moreover, the technique is unsuitable for coloured samples which interfere with the detection of the end point. Titrimetric methods suffer the disadvantage of using a large amount of sample and undergoing interference from many redox reagents with the determination. The fluorimetric method is too time consuming. For the chromatographic methods, the use of expensive equipment and the demand for more operator attention prevent their application in

* Corresponding author.


*SSDI* 0039-9140(95)01622-8

small industrial laboratories where only a few analyses are performed each day. The polarographic method requires long analysis time and suffers interferences from electrochemical impurities present in the food sample, whereas the enzymatic technique is generally considered to be too specialized for ordinary chemical laboratory use.

Spectrophotometry is a fast and simple method for AA determination, but it cannot be used in samples with complex matrices because of background absorption in the UV region. Various background correction techniques have been proposed such as thermal decomposition, direct ultraviolet irradiation, alkaline treatment and an enzymatic method [25,26]. Some visible spectrophotometric methods often require tedious pre-separation techniques to remove possible interferences from coloured materials.

Derivative spectrophotometry is a useful technique for extracting qualitative and quantitative information from spectra composed of unresolved bands [27], and for eliminating the effect of baseline shifts and baseline tilts [28]. Derivative spectrophotometry is now a reasonably priced standard feature of modern microcomputerized UV/vis spectrophotometry.

The purpose of this work is to develop a direct and simple UV-spectrophotometric method for the determination of AA in fruits and vegetables without pre-seperation or background correction procedures.

Among fruits and vegetables, kiwi, parsley and grapefruit were chosen owing to their high AA content. Several kiwi, parsley and grapefruit samples were analyzed for their AA content and the results were compared with those obtained by AOAC [24].

## 2. Experimental

### 2.1. Apparatus

A Philips PU 8700 UV/vis spectrophotometer was used with a cell having a path length of 1 cm and a volume of 3 ml. For the spectrophotometric measurements, suitable settings were chosen: 2 nm slit width, 250 nm $min^{-1}$ scan speed for kiwi samples; 2 nm slit width, 125 nm $min^{-1}$ scan speed for parsley and grapefruit samples; very high smoothing for derivative spectra.

### 2.2. Reagents

All reagents used were of analytical reagent grade. Bidistilled water was used throughout the work.

The extraction solution was 3% (w/v) metaphosphoric acid–8% (v/v) acetic acid. This reagent can be kept for three days in a refrigerator.

The ascorbic acid stock solution (100 μg $ml^{-1}$) was prepared by dissolving 10 mg of AA in 100 ml extraction solution. This solution was freshly prepared and was diluted to obtain standard solutions for the preparation of calibration curves.

### 2.3. Analytical procedures

*Preparation of sample solutions*

Samples were purchased from the local markets for analysis. The edible portions of each sample were analyzed using two methods on the same day of purchase.

In the case of grapefruit, the juice was easily obtained from the fruit with a glass press. A 25 ml aliquot of the juice was homogenized with 75 ml of extraction solution using a mechanical stirrer for about 5 min.

The parsley and kiwi samples (5–10 g) were chopped and then homogenized with 100 ml extraction solution using a mechanical stirrer (with a glass rood) for about 45 min.

After homogenization of the samples, the extracts were clarified by centrifuging at 2000 rpm for 5 min and then filtering through a filter paper (Whatman 541) using a vacuum pump.

The filtrates were then diluted to provide the necessary working concentration (2.0–10.0 μg $ml^{-1}$).

### 2.4. Determination

*Calibration graph*

The third order derivative absorption spectra of AA standard solutions (2.0–10.0 μg $ml^{-1}$) were recorded against extraction solution between 190–300 nm.

In these spectra, the peak-to-peak amplitudes of 227 nm and 237 nm were used for the establishment of the calibration graphs for parsley and grapefruit samples.

For kiwi samples, 259.4 nm and 276.2 nm extrema were used for the same purpose. A regression equation of the calibration graph was calculated by the method of least squares.

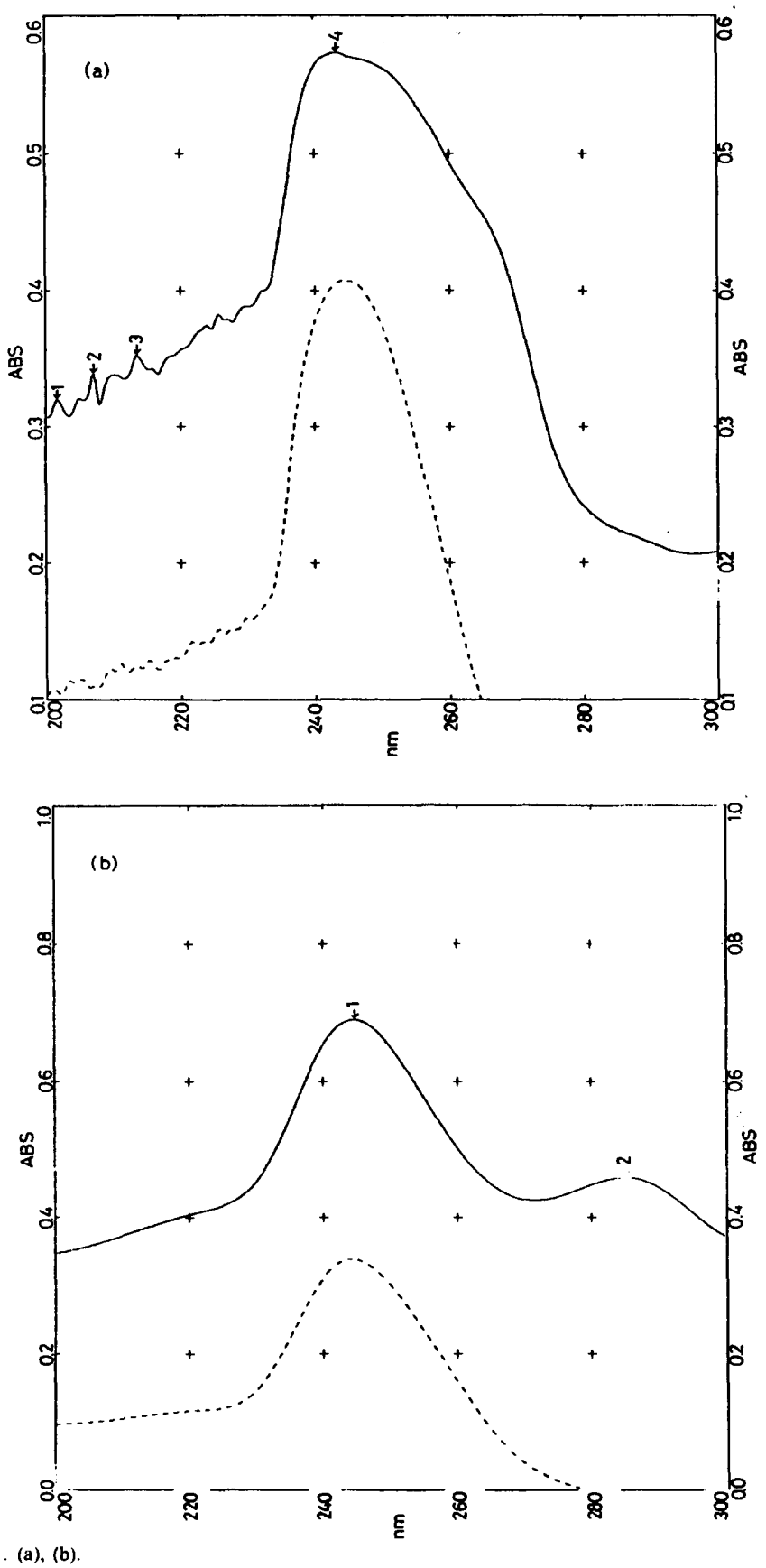


Fig. 1. (a), (b).

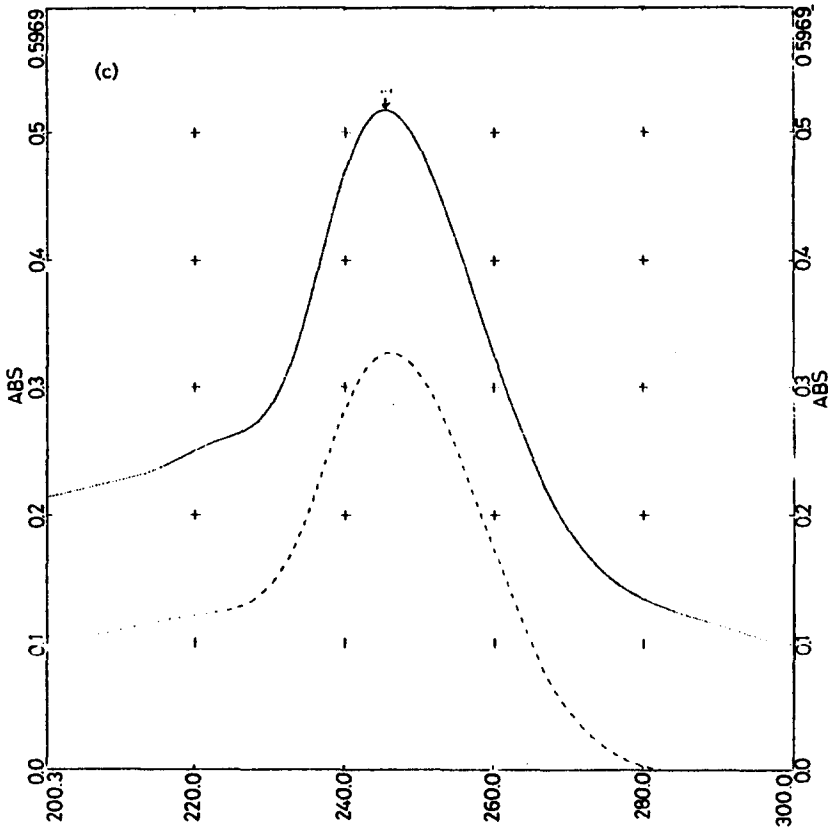


Fig. 1. Absorption spectra of (a) parsley (——); (b) grapefruit (——); (c) kiwi (——); and ascorbic acid (– – –) solutions. Concentration: 6 μg ml$^{-1}$ in extraction solution. Reference: extraction solution.

*Sample analysis*

Third order derivative spectra of sample solutions were recorded against the extraction solution. Peak-to-peak amplitudes of 227–237 nm (for parsley and grapefruit samples) or 259.4–276.4 nm (for kiwi samples) were obtained from these spectra.

The concentration of AA in the sample solutions was deduced by means of the regression equation of the related calibration graph.

## 3. Results and discussion

A UV-spectrophotometric method cannot be used directly for the determination of ascorbic acid in fruits and vegetables owing to the matrix effect of UV-absorbing substances in the sample matrix. This effect is clearly seen in Fig. 1, which shows the absorption spectra of kiwi, parsley and grapefruit extracts, together with the spectra of standard ascorbic acid solutions prepared in the same solvent medium having the same concentration as the sample extract. To overcome this difficulty, some tedious background correction techniques have been used [25,26]. In contrast, the derivatization of the absorption spectrum and measurement of the distance between two neighbouring extremum values allow the elimination of matrix effects, because the variable background absorptions overlapping the analyte peaks are smoother in derivative spectra. Figs. 2, 3 and 4 show first, second and third order derivatives, respectively, of the absorption spectra given in Fig. 1. As seen, the third order spectra of sample and standard solutions completely overlap each other in the regions of 259.4–276.2 nm for kiwi, and 227–237 nm for parsley and grapefruit. This means that matrix effects are eliminated by derivatization of the absorption spectra. The extraction solution of these samples is the mixture metaphosphoric acid (3%)–acetic acid (8%). It was found to be the most suitable extraction medium among the various mixtures tested for the extraction such as oxalic acid (5%), trichloroacetic acid (5%), metaphosphoric acid (6%), acetic acid (8%), citric acid (5%) and metaphosphoric acid–acetic acid (3%–8% and 1.5%–4%).

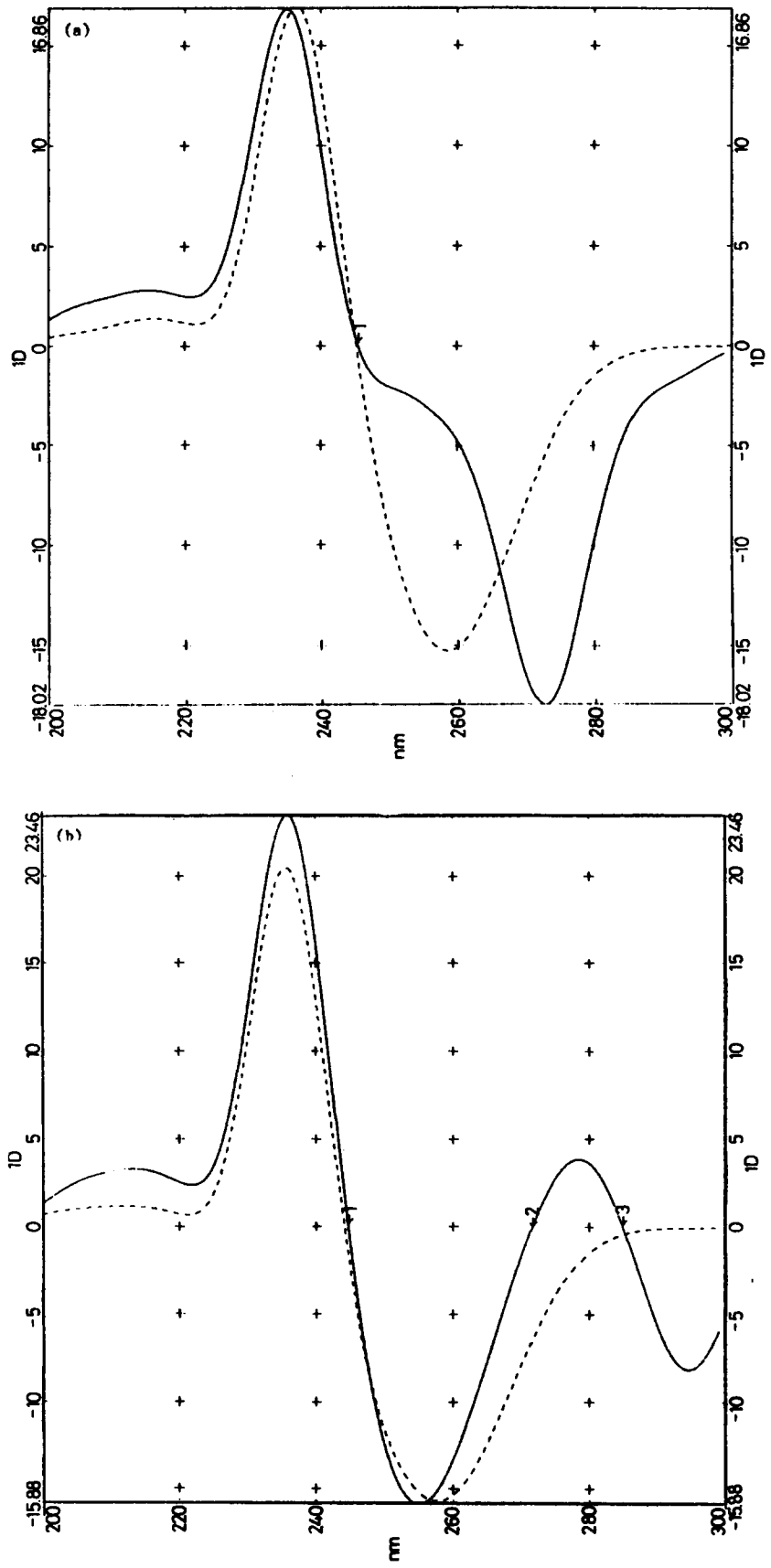
(a)
16.86
10
5
0
-5
-10
-15
-18.02
1D
200
220
240
260
280
300
nm
(b)
23.46
20
15
10
5
0
-5
-10
-15.88
1D
200
220
240
260
280
300
nm
1
2
3

Fig. 2. (a), (b).

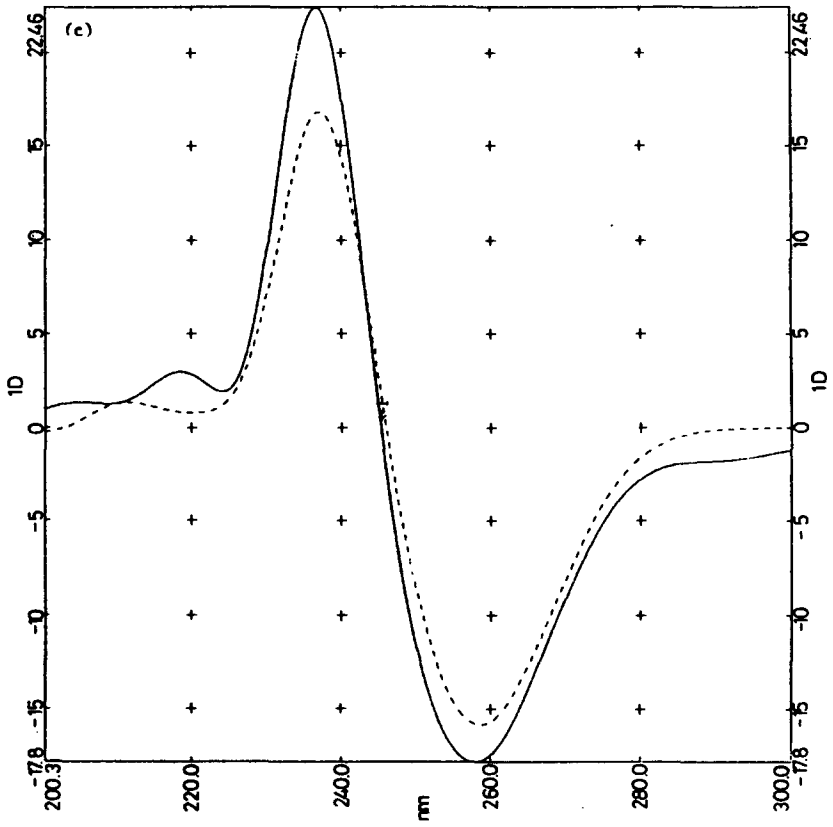


Fig. 2. First order derivative spectra of (a) parsley (——); (b) grapefruit (——); (c) kiwi (——); and ascorbic acid (– – –) solutions. Concentration: 6 μg ml$^{-1}$ in extraction solution. Reference: extraction solution.

Linear relationships were obtained between the AA concentration (2.0–10.0 μg ml$^{-1}$) and peak-to-peak amplitudes ($^3D$) of third order spectra at the wavelengths stated above. The regression equations were as follows:

$$^3D_{259.4-276.2} = 0.0367C + 0.0046$$

(kiwi) ($r = 0.9998$)

$$^2D_{227-237} = 0.1871C - 0.0132$$

(parsley and grapefruit) ($r = 0.9994$)

The contents of AA in five parsleys, five kiwis and four grapefruits were determined by the proposed method. With the purpose of comparison of the results obtained by derivative spectrophotometry, the same extracts were analyzed for AA by the official method recommended in AOAC. The results obtained by the two methods were statistically compared. This statistical comparison is depicted in Table 1. The results obtained by the developed method and by the official method were compared at the 95% confidence level with the aid of an $F$ test for precision.

As can be seen from Table 1, the calculated $F$ values were less than the corresponding ones obtained from the standard table for the selected confidence level and population number.

As a conclusion, the derivative spectrophotometric method is relatively easy, fast and cheap for determination of the ascorbic acid content of kiwi, parsley and grapefruit. Because it does not require expensive solvents and reagents, it may be recommended for the rapid precise and sensitive quantification of ascorbic acid in these products. The major instrument required is a modern, microcomputerized UV/vis spectrophotometer, which can be purchased at a reasonable price. This method also takes less time than the others, and the absorption values of the solutions used are stable for at least 2 h. The method can be extended to ascorbic acid determination in various fruits and vegetables provided that the proper wavelengths for peak-to-peak measurements are accurately selected.

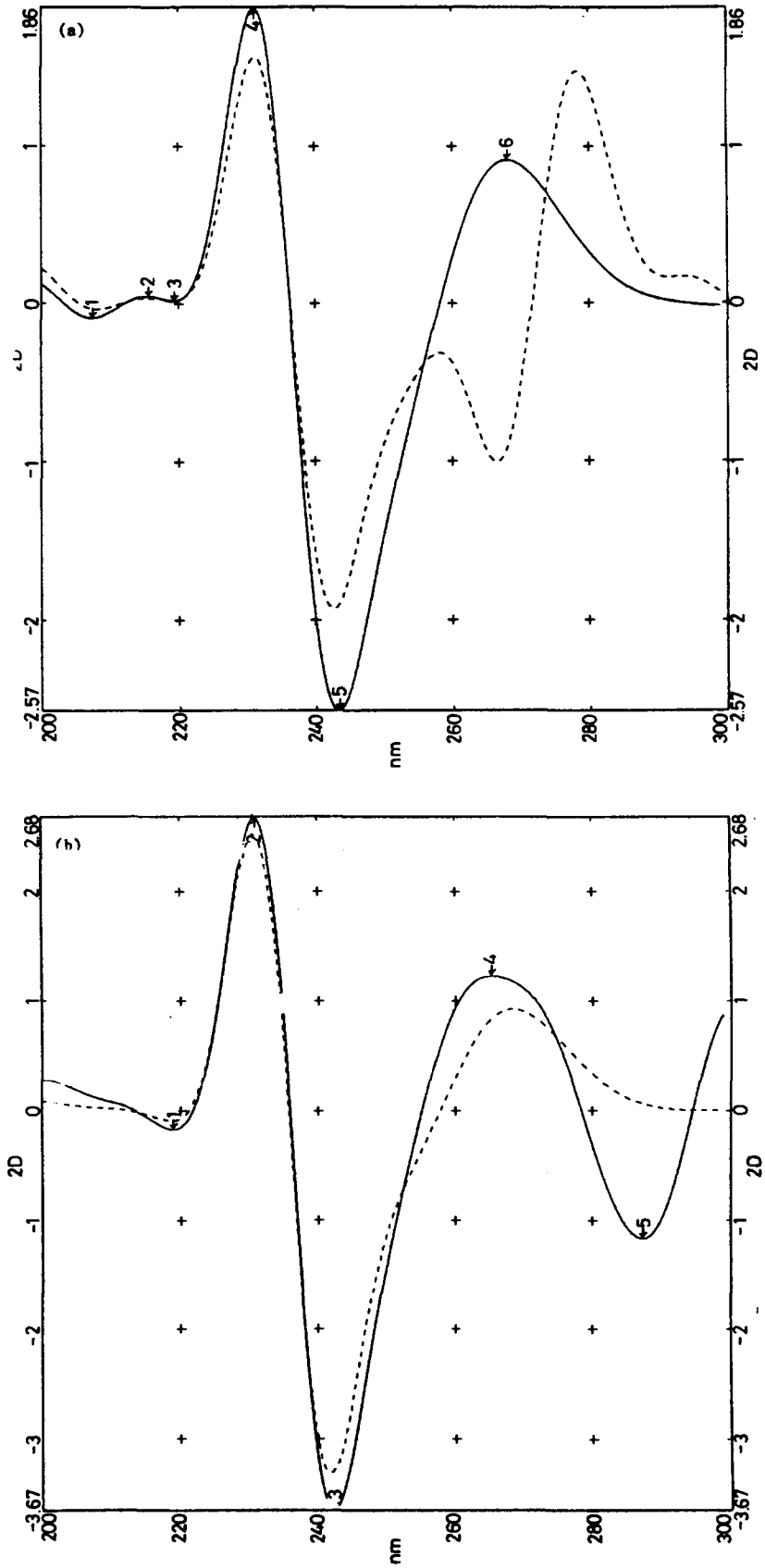
(a)
1.86
1
0
-1
-2
-2.57
2D
200
220
240
260
280
300
nm
(b)
2.68
2
1
0
-1
-2
-3
-3.67
2D
200
220
240
260
280
300
nm

Fig. 3. (a), (b).

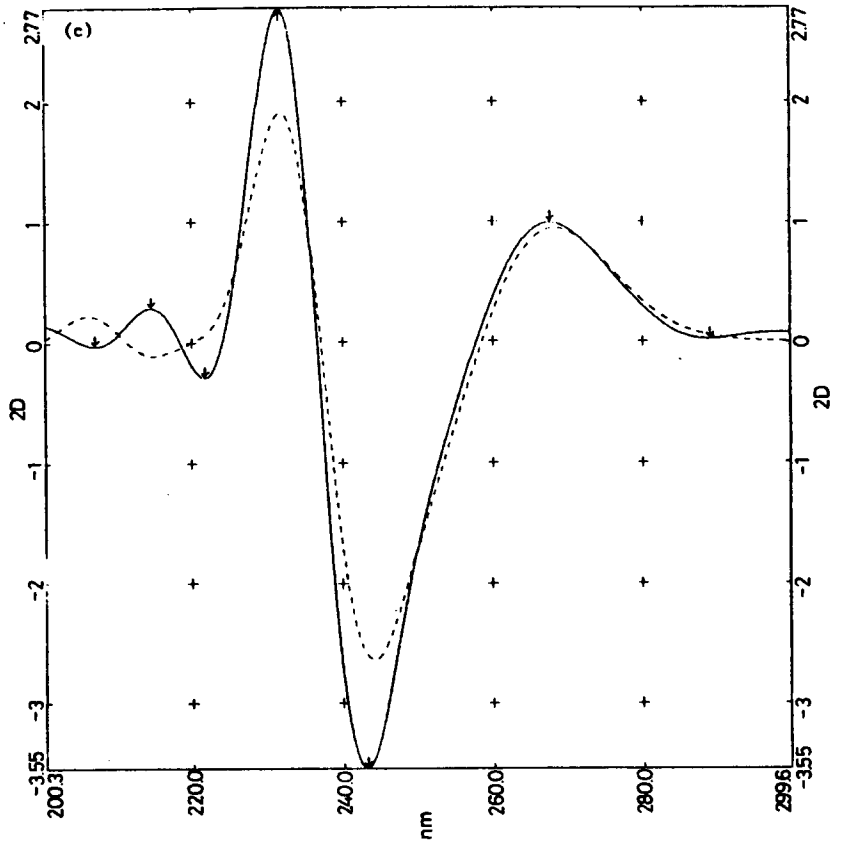


Fig. 3. Second order derivative spectra of (a) parsley (——); (b) grapefruit (——); (c) kiwi (——); and ascorbic acid (– – –) solutions. Concentration: 6 μg ml$^{-1}$ in extraction solution. Reference: extraction solution.

For this selection, the first, second and third order derivative spectra of the sample extract and standard AA solution in the same concentration and solvent medium are plotted on the same graph, and the region in which the two spectra completely overlapped was determined.

Table 1
Comparison of the results for ascorbic acid determination by the proposed method and the AOAC method

| Sample | No. | Value obtained (5%), mg per 100 g [a] | | $F$ calc. [b] |
|---|---|---|---|---|
| | | Proposed method | AOAC method [c] | |
| Parsley | 1 | 172.9 (1.68) | 172.4 (1.37) | 1.50 |
| | 2 | 142.4 (1.58) | 144.0 (0.95) | 2.69 |
| | 3 | 129.7 (1.80) | 131.1 (1.01) | 3.14 |
| | 4 | 149.5 (0.53) | 150.7 (0.62) | 1.40 |
| | 5 | 94.8 (0.97) | 93.2 (0.94) | 1.08 |
| Kiwi | 1 | 74.3 (0.53) | 74.2 (0.50) | 1.12 |
| | 2 | 78.0 (0.76) | 75.9 (0.58) | 1.84 |
| | 3 | 68.9 (0.71) | 72.0 (0.53) | 1.60 |
| | 4 | 44.6 (0.90) | 46.2 (0.82) | 1.07 |
| | 5 | 79.9 (0.74) | 83.0 (0.53) | 1.84 |
| Grapefruit | 1 | 35.5 (2.45) | 32.2 (1.12) | 5.82 |
| | 2 | 41.4 (1.57) | 36.9 (1.41) | 1.56 |
| | 3 | 42.4 (0.80) | 38.7 (1.29) | 2.08 |
| | 4 | 30.8 (1.18) | 33.9 (1.00) | 4.17 |

[a] Titration with 2,6-dichlorophenolindophenol.
[b] $F$ theory = 6.39.
[c] Average of five experiments, with relative standard deviation (%) given in parentheses.

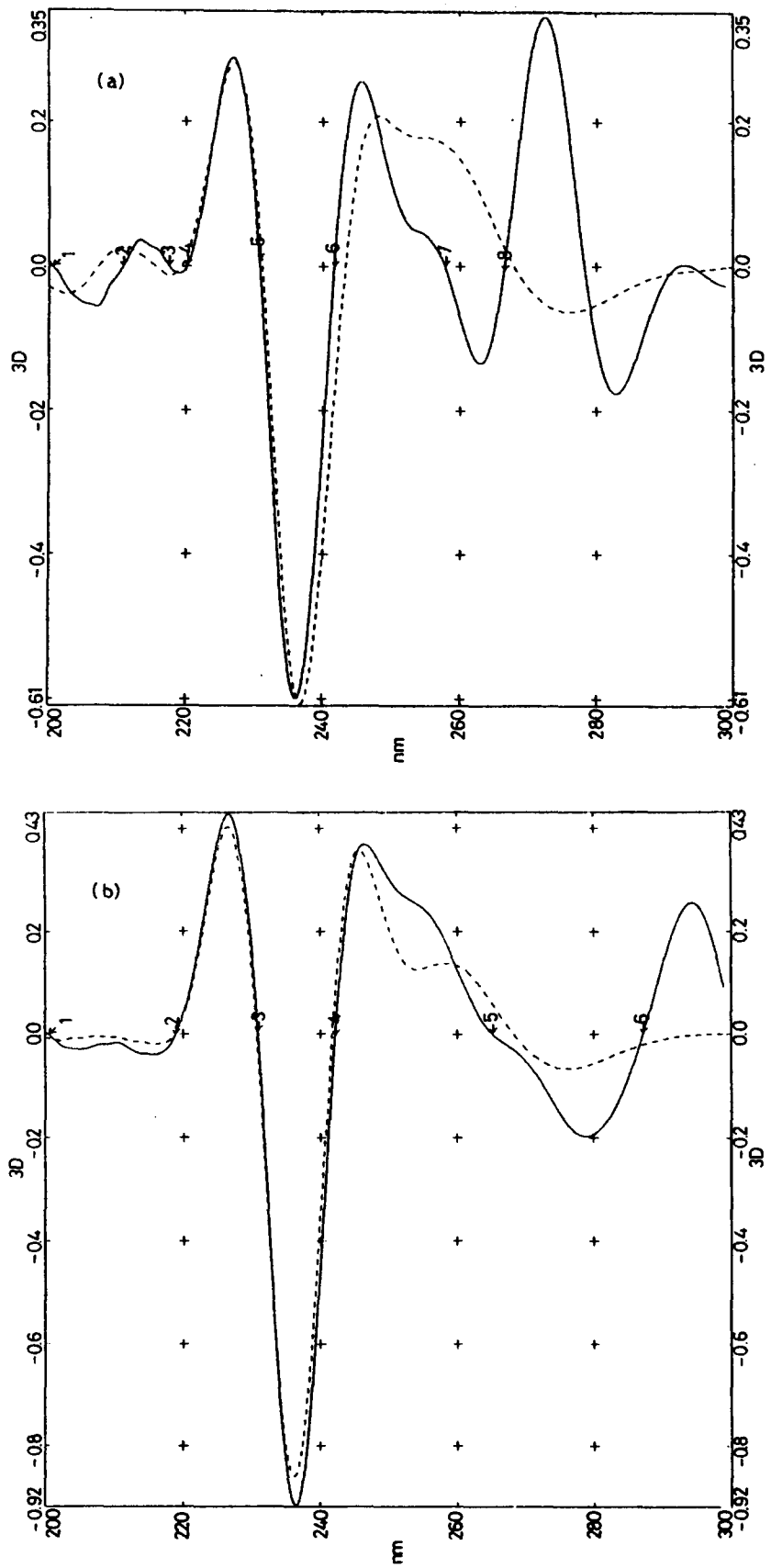


Fig. 4. (a), (b).

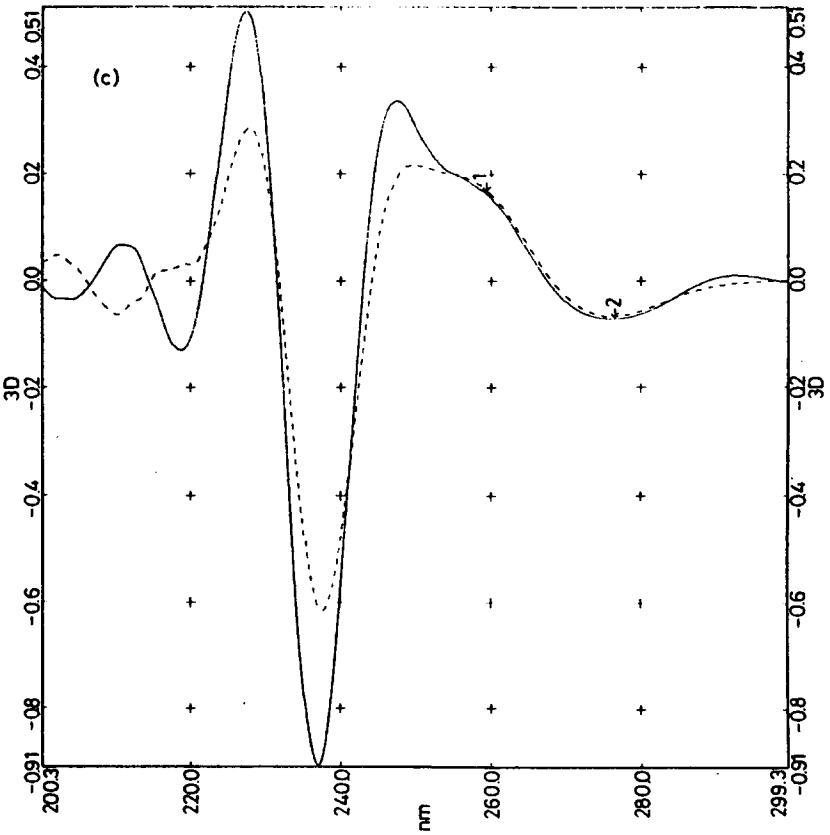


Fig. 4. Third order derivative spectra of (a) parsley (——); (b) grapefruit (——); (c) kiwi (——); and ascorbic acid (– – –) solutions. Concentration: 6 μg $ml^{-1}$ in extraction solution. Reference: extraction solution.

## References


[1] D.E. Hugles, J. Pharm. Sci., 72 (1983) 126.
[2] M.M. Aly, Anal. Chim. Acta, 106 (1979) 379.
[3] J. Rohle and F. Voight, Nahrung, 28(5) (1984) 579.
[4] Y.S. Fung and S.F. Luk, Analyst, 110(2) (1985) 201.
[5] O.W. Lau and S.F. Luk, J. Assoc. Off. Anal. Chem., 70(3) (1987) 518.
[6] F. Buhl and B. Mikula, Chem. Anal., 33(1) (1988) 103.
[7] A.M. Frigola Canoves and F. Basch Serrat, An. Bramatol., 40(1) (1988) 79; Chem. Abstr., 110 (1989) 73 933.
[8] W. Horwitz (Ed.), Official Methods of Analysis of the Association of Official Analytical Chemists, Washington, DC, 1980, p. 43.061.
[9] J. Carnevale, Food Technol. Aust., 32(6) (1980) 302; Chem. Abstr., 93 (1980) 148 240 u.
[10] L.L. Lloyd, F.P. Warner, J.F. Kennedy and C.A. White, J. Chromatogr., 437(2) (1988) 447.
[11] R.J. Bushway, J.M. King and M. Krishnan, J. Liq. Chromatogr., 11(16) (1988) 3415.
[12] J. Lindguist and S.M. Farroha, Analyst, 100 (1975) 377.
[13] O.W. Lau, K.K. Shiu and S.T. Chang, J. Sci. Food Agric., 36(8) (1985) 733.
[14] S. Kozar, A. Bujak, J. Eder-Trifunovic and G. Kniewald, Fresenius' Z. Anal. Chem., 329(7) (1988) 760.
[15] B.B. Prasad and T.B. Singh, Acta Pol. Pharm., 36(6) (1979) 729; Chem. Abstr., 93 (1980) 225 680 s.
[16] U. Shukla and B.B. Prasad, Chem. Anal., 33(4) (1988) 639; Chem. Abstr., 111 (1989) 121 009 d.
[17] L.E. Edholm, Talanta, 23 (1976) 709.
[18] R. Cardova-Drellana and X. Lucena-Conde, Talanta, 24 (1977) 124.
[19] T. Tono and S. Fujita, Agric. Biol. Chem., 45 (1981) 2947.
[20] L. Casella, M. Gullotti, A. Marchesini and M. Petrarulo, J. Food Sci., 54(2) (1989) 374.
[21] U. Morisaka, S. Miyakoshi, Shirazaki, K. Ohkubo, H. Kensho and T. Hasegawa, Hokuriku Koshu Eisei Gakkaishi, 15(2) (1988) 18; Chem. Abstr., 110 (1989) 133 790 u.
[22] J.O. Schenk, E. Miller and R.N. Adams, Anal. Chem., 54 (1982) 1452.
[23] K. Matsumoto, K. Yamada and Y. Osajima, Anal. Chem., 53 (1981) 1974.
[24] W. Horwitz, Official Methods of Analysis, AOAC, Arlington, VA, 1980, Sections 43.056–43.057.
[25] Y.S. Fung and S.F. Luk, Analyst, 110 (1985) 201.
[26] O.W. Lau, S.F. Luk and K.S. Wong, Analyst, III (1986) 665.
[27] E.M. Abdel-Moety, Z. Lebensm-Unters. Forsch, 186 (1988) 412; Anal. Abstr., 50 (1988) 8F51.
[28] P. Deng, H. Li, A. Lu and Y. Dai, Shipin Kexue (Beijing), 98 (1988) 51; Anal. Abstr., 51 (1989) 2F46.

ELSEVIER

Talanta 42 (1995) 1641–1649

Talanta

# Chemical amplification methods for the sequential determination of trace amounts of ruthenium by titrimetric and spectrophotometric procedures

M.S. El-Shahawi [a,*], S.A. Barakat [b]

[a] *Department of Chemistry, Faculty of Science, UAE University, Al-Ain, P.O. Box 17551, United Arab Emirates*
[b] *Department of Chemistry, Jordan University of Science and Technology, Irbid, P.O. Box 3030, Jordan*

Received 13 May 1994; revised 13 March 1995; accepted 19 April 1995

**Abstract**

Two simple, inexpensive and rapid iodometric and spectrophotometric procedures were developed for trace amount determination of ruthenium. The proposed methods were based on the oxidation of ruthenium(II or III) with sodium periodate at pH 2.4–3.6, masking the excess periodate with sodium molybdate. The released iodate was then allowed to react with KI at pH 3, with subsequent determination of the released iodine spectrophotometry as triiodide at 350 nm or iodometry with 0.005 M sodium thiosulphate. This procedure offers an 18- and 15-fold amplification per Ru(II) or Ru(III) ion, respectively. Alternatively, the produced iodine was extracted with $CHCl_3$, shaken with an aqueous solution of sodium sulphite and the produced iodide ion was then allowed to react with bromine (or sodium periodate). The released iodate was subsequently determined by iodometry or spectrophotometry after addition of KI. The bromine and sodium periodate oxidation procedures offered 90- and 360-fold amplification per ruthenium(III) ion, and 108- and 432-fold amplification per ruthenium(II) ion. Ruthenium(IV) content was determined by these procedures after prior reduction to Ru(III) with sulphurous acid. The binary mixtures Ru(II)–Ru(III); Ru(III)–Ru(IV) and Ru(II)–Ru(IV) in aqueous solution at concentration 0.05 $\mu g\ ml^{-1}$ were successfully analyzed by the developed procedures. The utility of the proposed methods for the analysis of ruthenium in its complexes was demonstrated. Natural seawater and seawater spiked with ruthenium were analyzed satisfactorily.

*Keywords:* Ruthenium; Iodometry; Spectrophotometry; Trace analysis; Natural water

## 1. Introduction

Compared to most other elements, ruthenium has a limited influence on the biosphere because only small quantities ever reach living organisms [1]. The amount of ruthenium readily introduced into rivers, lakes and oceans through industrial wastes is minute [1]. Thus, sensitive, reliable and practicable methods are required for the quantitation of ruthenium at trace levels. The most common reported spectrophotometric procedures for ruthenium determination require laborious enrichment steps [2–6], e.g. flotation, precipitation and solvent extraction. However, most of these methods suffer from lack of selectivity and sensitivity [3–5].

Recently, several polarographic and voltammetric methods have been developed for the determination of ruthenium [7–10]. These methods were based on adsorptive collection of ruthenium(III) chelates on HMDE, but neither their sensitivity nor selectivity are very satisfactory and they are not practicable in routine analysis of ruthenium.

* Corresponding author. On leave from the Chemistry Department, Faculty of Science at Damiatta, Mansoura University, Mansoura, Egypt.


*SSDI* 0039-9140(95)01623-6

Recently, the application of the so-called Leipert amplification reaction [11] was reported, in which potassium periodate solution in aqueous acidic media was used for the oxidation of various metal ions [12–15] and the produced iodate was subsequently determined by iodometry. The present paper describes two simple and accurate amplification procedures for the measurement of trace levels of ruthenium in aqueous solution.

## 2. Experimental

### 2.1. Reagents and materials

Unless otherwise specified, all reagents were of analytical reagent grade. All solutions were prepared from doubly-distilled water. Stock solutions (1 mg $ml^{-1}$) of ruthenium(III) (atomic absorption standard, BDH) and 100 mg $ml^{-1}$ of Ru(V) were prepared from ruthenium dioxide [16] and diluted with water for standard addition whenever required. Ruthenium(II) solution (100 μg $ml^{-1}$) was prepared by the reduction of a measured solution of $RuCl_3 \cdot 6H_2O$ (Johnson Mathey, London) in HCl–$H_2O$ (1:20, v/v) as previously reported [17]. Buffer solutions of pH 2.4–4.6 were prepared by mixing about 200 ml of glacial acetic acid with approximately 200 ml of water and the pH adjusted with a saturated solution of sodium acetate. Sodium thiosulphate (0.005–0.01 M) was prepared and standardized against $KIO_3$ (0.01 M) of the same normality. Sodium periodate (0.35% w/v), sodium molybdate (10% w/v) and sodium sulphite (5% w/v) solutions were prepared in doubly-distilled water.

### 2.2. Apparatus

A Pye-Unicam double beam UV/visible spectrometer model Sp-8-400 with 10 mm quartz cells was used for the absorbance measurements. A Philips digital pH-meter (model 9418) with glass and saturated calomel electrodes, and a 250 ml oxygen-flask with fused silica sample holder were used.

### 2.3. Recommended procedure

*I. Determination of ruthenium(II) or (III)*

To a 100 ml conical flask (or 100 ml separating funnel) was transferred 1–5 ml of sample solution containing 5–200 mg of Ru(II) or Ru(III) solution and 10 ml of water. The pH (2.4–3.6) of the solution was adjusted with 10 ml acetate buffer, 5 ml of sodium periodate added and the reaction mixture left for 5 min. $Na_2MoO_4$ (5 ml) was added to mask the unreacted periodate and the solution shaken twice with 10 ml (2 × 5) of $CCl_4$. The aqueous layer was separated and then treated by one of the following procedures.

*(a) 18- or 15-fold amplification.* To the aqueous solution of the produced iodate was added a few crystals of KI at pH ≈ 3, and the released iodine was determined by spectrophotometry as triiodide at 350 nm or by iodometry with 0.005 M $Na_2S_2O_3$. These procedures offer 18- and 15-fold amplification of Ru(II) and Ru(III), respectively. A blank was run for correction.

*(b) 108- or 90-fold amplification.* The aqueous solution of the released iodate was allowed to react with KI (50–70 mg) at pH 3 and the released iodine twice extracted with 10 ml (2 × 5) of $CHCl_3$ in a separating funnel. The chloroform solution was shaken with 25 ml of water containing 2 ml of sodium sulphite to reduce the iodine to iodide. The aqueous (upper) layer was transferred to a 100 ml Erlenmeyer flask, 5 ml of bromine added, and the solution left for 3–5 min. The excess bromine was removed by boiling off the solution or by drop-wise addition of formic acid. Five millilitres of 2N $H_2SO_4$, and three to four crystals of KI were added and the released iodine determined by spectrophotometry or iodometry, as described earlier. A blank was run to correct the reagent error. This procedure offers 108- and 90-fold amplification of Ru(II) and Ru(III), respectively.

*(c) 432- or 360-fold amplification.* To the aqueous solution of the produced iodide was added 5 ml of $NaIO_4$, the flask stoppered, and the reaction mixture allowed to stand for 5 min at room temperature. The flask was placed in a boiling water bath for about 15 min, allowed to cool and then 10 ml of acetate buffer, 5 ml of $Na_2MoO_4$, three to four crystals of KI (≈0.1 g) were added and the released iodine determined by spectrophotometry or by iodometry; a blank was run for correction.

*II. Determination of ruthenium(IV)*

Aliquot portions (1–100 μg) of the ruthenium(IV) element were transferred to a 100 ml conical flask. Five millilitres of $Na_2SO_3$ and 5 ml of HCl (20% w/v) were added and the reaction mixture left to stand for 5 min.

The solution was evaporated gently on a hot plate until the excess $SO_2$ was completely removed, and then 20 ml of $H_2O$ and 0.5 g of $Na_2CO_3$ were added to neutralize the unreacted acid; the produced ruthenium(III) was determined using the recommended procedure I. A blank was run for correction. Quantitative reduction of Ru(IV) to Ru(III) was confirmed by determining the content of the ruthenium(III) produced colorimetrically [18].

*III. Analysis of the binary mixtures ruthenium(II) and (III)*

Aliquots of the mixture were transferred into a 100 ml flask and the recommended procedure I-a followed. Another aliquot of sample mixture was reduced to the divalent ruthenium as previously reported [17] and procedure I-a followed. On the basis of the proposed procedure, if the volume of the sodium thiosulphate consumed in the first solution is $V_1$ ml and for the second solution is $V_2$ ml, the concentration of Ru(II) and Ru(III) can be obtained.

*IV. Analysis of binary mixture ruthenium(III) and (IV)*

Aliquots containing various amounts of ruthenium(III) and (IV) were transferred into a 100 ml conical flask and the described procedure I-a followed. Another aliquot sample was then reduced to the trivalent ruthenium as described in procedure II and the solution determined according to procedure I-a. According to the proposed procedure, if the volume of thiosulphate solution consumed for the first aliquot mixture is $V_1$ ml and that used for titration of the second aliquot mixture is $V_2$ ml, the concentration of Ru(III) and Ru(IV) can be obtained.

*V. Analysis of ruthenium(II) or (III) in their complexes*

The ruthenium complexes used in this work were prepared by the previously reported [19,20] procedures. Exactly 2–3 mg of the organoruthenium complexes was weighted and wrapped as usual by the Schoniger technique [21] in a 250 ml oxygen-flask filled with a fused silica spiral. Ten millilitres of aquaregia was placed in a 250 ml oxygen-flask, the flask filled with oxygen and the sample combusted. When the combustion was complete, the flask was shaken for 2–3 min, opened and the stopper and the sample holder rinsed down with 5 ml of $HNO_3$ (5% v/v). The solution was heated to dryness and 10 ml of $H_2O$, 2 ml of conc. HCl and 10 ml of $Na_2SO_3$ added. The solution was left for 2 min at room temperature. It was then boiled to remove $SO_2$, and reduced with hydroxylamine as previously reported [17], finally the recommended procedure I-a was followed for ruthenium(II) determination. A blank was run for corrections.

## 3. Results and discussion

Amplification reactions proved to be very efficient for the determination of analytes at low levels [12–15]. Thus iodometric amplification procedures with their simplicity and sensitivity are still of special attraction. This motivated us to search for new procedures for the determination and speciation of microamounts of various ruthenium species with the use of iodine–starch end point or spectrophotometry of the released iodine as triiodide at 350 nm.

Amplification procedures based on oxidation with sodium periodate are extendable to any species possessing two oxidation states with sufficiently low standard redox potential. Thus, the proposed procedures for ruthenium(II), (III) or (IV) determination were principally based on oxidation of these ions in acid media to octavalent ruthenium with sodium periodate according to the following equations:

$$Ru^{2+} + 3IO_4^- + 6H^+ \rightarrow Ru^{8+} + 3IO_3^- + 3H_2O \quad (1)$$

$$Ru^{3+} + \tfrac{5}{2}IO_4^- + 5H^+ \rightarrow Ru^{8+} + \tfrac{5}{2}IO_3^- + \tfrac{5}{2}H_2O \quad (2)$$

$$Ru^{4+} + 2IO_4^- + 4H^+ \rightarrow Ru^{8+} + 2IO_3^- + 2H_2O \quad (3)$$

The released iodate and ruthenium(VIII) can oxidize potassium iodide according to the equations

$$IO_3^- + 5H^- + 6H^+ \rightarrow 3I_2 + 3H_2O \quad (4)$$

$$RuO_4 + 5I^- + 8H^+ \rightarrow Ru^{3+} + \tfrac{5}{2}I_2 + 4H_2O \quad (5)$$

Table 1
Determination of various amounts of $Ru^{2+}$ (or $Ru^{3+}$) by iodometry (a) and spectrometry (b) using the 18-fold (or 15-fold) amplification procedures [a]

| Metal ion taken (μg) | Metal ion found (μg) | | Error (%) [b] | |
|---|---|---|---|---|
| | a | b | a | b |
| 5 | 5.2 ± 0.2 | 5.1 ± 0.2 | 4 | 2 |
| 10 | 10.1 ± 0.3 | 10.1 ± 0.3 | 1 | 1 |
| 20 | 20.3 ± 0.3 | 20.2 ± 0.2 | 1.5 | 1 |
| 50 | 51.1 ± 0.3 | 50.3 ± 0.3 | 2.2 | 0.6 |
| 75 | 76.1 ± 0.5 | 75.6 ± 0.3 | 2.1 | 0.8 |
| 100 | 101.4 ± 0.5 | 101 ± 0.3 | 1.5 | 1 |
| 150 | 152 ± 0.3 | 152 ± 0.2 | 1.3 | 1.3 |
| 200 | 203 ± 0.2 | 202 ± 0.3 | 1.5 | 1.0 |

[a] Average ± standard deviation ($n = 5$).
[b] Error % = [(metal taken-metal found) × 100]/(metal taken).

Reactions (1)–(4) proceeded rapidly and quantitatively in acidic media (pH < 4) as can be predicted from the redox potential concerned [15]. Moreover, reaction (5) took place and proceeded forwards in acidic medium, i.e. ruthenium(VIII) liberated iodine from KI. This statement is criticized in this work, where preliminary experiments showed that the Ru(VIII)–I reaction was a function of the solution pH and the reaction was quite negligible in the solution of pH > 2.4, while in 2N $H_2SO_4$ it took place faster and proceeded quantitatively.

Further preliminary experiments showed that the oxidation of ruthenium(II), (III) or (IV) with sodium periodate was pH and reaction time dependent. Therefore, the effects of these factors were studied for a fixed concentration (60 mg) of each of these ions in the pH range 2.4–6. The solutions were then allowed to react with $NaIO_4$ for different time intervals (2–30 min). The pH of the solutions was adjusted to pH ≈ 3 using acetate buffer and the excess unreacted $NaIO_4$ was masked with sodium molybdate at the same pH. The released iodate and ruthenium(VIII) were then allowed to react with KI and the liberated iodine was determined by iodometry (with 0.005 M $Na_2S_2O_3$) and by spectrophotometry of the triiodide species formed at 350 nm against a reagent blank. The results indicated that the optimum pH of the complete oxidation of the ruthenium species was in the range 2.5–4 after 5 min. Under these conditions, each original ruthenium(II), (III) and (IV) released 18, 15 and 12 equivalent iodines, i.e. the proposed method afforded 18-, 15 and 12-fold amplification per ruthenium(II), (III) and (IV) ion, respectively. At pH < 2, reactions from (5)–(9) proceeded rapidly with 23-, 20- and 17-fold amplification of Ru(II), (III) and (IV) respectively, but under these conditions sodium molybdate did not mask the unreacted periodate quantitatively since the molybdate–periodate complex was partially decomposed [22] and also aerial oxidation of iodide could occur. Thus, the percentage recovery of the tested ruthenium ion and blank values were erroneously high owing to reaction of the released periodate with iodide. At pH > 5, reactions (5)–(7) proceeded slowly to form perruthenate ($RuO_4^-$) ions [2] of lower amplification, and the iodide–iodate reaction was slow under these conditions. Fortunately, the pH values suitable for the quantitative oxidation of ruthenium(II), (III) or (IV) ions were quite appropriate for masking the excess unreacted periodate with molybdate. The developed method was employed for the determination of various amounts (5–200 mg) of ruthenium(II) or (III) by iodometry and spectrophotometry. The results are summarized in Table 1. Satisfactory results with standard deviations ($n = 5$) in the range 0.2–0.5 and 0.2–0.3 were obtained employing the iodometry and spectrophotometry procedures for Ru(II) or (III) respectively. It is worth mentioning that before addition of KI it was advisable to shake the solution with 10 ml $CCl_4$ (2 × 5) to remove the produced $RuO_4$ and to prevent any possibility of reaction between $RuO_4$ and KI at the optimum pH.

Moreover, the sensitivity of the proposed method for ruthenium(IV) determination can be increased by prior reduction to Ru(III) using sodium sulphite, hydroxylamine or zinc/HCl followed by determination according to procedure I. Sodium sulphite in acidic media

Table 2
Determination of various amounts of ruthenium(IV) by iodometry (a) and spectrometry (b) using the 15-fold amplification procedure [a]

| Ruthenium(IV) taken (μg) | Ruthenium(IV) found (μg) | | Error (%) | |
|---|---|---|---|---|
| | a | b | a | b |
| 10 | 10.1 ± 0.3 | 10.1 ± 0.2 | 1 | 1 |
| 20 | 20.2 ± 0.4 | 20.2 ± 0.2 | 1 | 1 |
| 50 | 51.3 ± 0.4 | 50.7 ± 0.2 | 2.5 | 1.4 |
| 75 | 76 ± 0.5 | 75.3 ± 0.4 | 1.3 | 0.4 |
| 100 | 103 ± 0.5 | 101.3 ± 0.2 | 3 | 1.3 |

[a] Average ± standard deviation ($n = 5$).

was found to be the most suitable reagent, where the unreacted sulphite ion could be easily removed by boiling off the formed sulphur dioxide. The determination of various amounts (10–100 μg) of ruthenium(IV) in aqueous media by the proposed method is given in Table 2. Satisfactory results were obtained by iodometry and spectrophotometry with relative standard deviations in the range 0.5–2.9 and 0.2–1.9%, respectively.

The proposed method was also employed for the anlysis of the binary mixture Ru(II) and (III) in aqueous media. An aliquot mixture was first allowed to react with sodium periodate employing procedure I-a. Another aliquot mixture was then reduced to ruthenium(II) as previously reported [16], followed by determination of the total Ru(II) by the proposed procedure I-a. On this basis, if $V_1$ and $V_2$ ml were the volumes of the sodium thiosulphate equivalent to the aliquot mixture in the first and second steps, respectively, then we obtain

$$C_1(\mu g) = (6V_1 - 5V_2)M(\text{A.W.})10^3/18 \quad (6)$$

$$C_2(\mu g) = (V_2 - V_1)M(\text{A.W.})10^3/3 \quad (7)$$

where $C_1$ and $C_2$ are the concentrations of Ru(II) and Ru(III), in μg, respectively, A.W. is the atomic weight of ruthenium and $M$ is the molarity of sodium thiosulphate. Satisfactory results were obtained (Table 3) employing iodometric procedures with 18- and 15-fold amplifications. The absolute standard deviation was found in the range 0.3–0.4.

Moreover, the analysis of the binary mixture Ru(II) and (IV) was also employed by the proposed 15- and 12-fold amplification procedure. An aliquot mixture was first reacted with sodium periodate employing procedure I-a. Another aliquot mixture was then reduced with sulphite ions in acidic media to reduce ruthenium(IV) to Ru(III) as described in procedure II, followed by determination of the total Ru(III) by the described procedure I-a. According to these procedures, if $V_1$ and $V_2$ ml were the volumes of the sodium thiosulphate consumed for the first and second aliquot, then we obtain

$$C_1(\mu g) = (5V_1 - 4V_2)M(\text{A.W.})10^3/15 \quad (8)$$

$$C_2(\mu g) = (V_2 - V_1)M(\text{A.W.})10^3/3 \quad (9)$$

where $C_1$ and $C_2$ are the concentration of Ru(II) and Ru(IV), in μg, respectively. The results obtained are summarized in Table 4, with a relative absolute error in the range 0.5–3.4%. In separate experiments, aliquot samples containing various amounts of Ru(III) and (IV) in a concentration range of 0.05–1 μg ml$^{-1}$ ($n = 5$) were analyzed by the developed spectrophotometric procedure. Satisfactory results were obtained with 99 ± 2% recovery and absolute standard deviations in the range 0.12–0.28.

The proposed iodometric procedure for the analysis of various amounts of the binary mixture Ru(II) and Ru(IV) was also carried out. An aliquot mixture was first allowed to react with $NaIO_4$ employing procedure I-a. Another aliquot mixture was reduced with sulphite ions in acidic media from Ru(IV) to Ru(III) and the reaction mixture was then allowed to react with sodium periodate as described in procedure II. On this basis, if $V_1$ and $V_2$ ml were the volumes of the sodium thiosulphate consumed in the first and second aliquot mixture, then we obtain

$$C_1(\mu g) = \frac{(5V_1 - 4V_2)M(\text{A.W.})10^3}{18} \quad (10)$$

$$C_2(\mu g) = \frac{(V_2 - V_1)M(\text{A.W.})10^3}{3} \quad (11)$$

Table 3
Simultaneous determination of various amounts of ruthenium(II) and (III) in their binary mixtures by iodometry employing the 18- and 15-fold amplification procedure [a]

| Metal ion taken (μg) | | Metal ion found (μg) | |
|---|---|---|---|
| $Ru^{2+}$ | $Ru^{3+}$ | $Ru^{2+}$ | $Ru^{3+}$ |
| 20 | 50 | 20.1 ± 0.3 | 51.1 ± 0.3 |
| 40 | 50 | 40.2 ± 0.4 | 51.2 ± 0.4 |
| 100 | 50 | 101.3 ± 0.4 | 51.2 ± 0.4 |
| 150 | 100 | 153.3 ± 0.4 | 101.9 ± 0.5 |
| 200 | 100 | 202 ± 0.3 | 101.6 ± 0.3 |

[a] Average ± standard deviation ($n = 3$).

where $C_1$ and $C_2$ are the concentrations of Ru(II) and Ru(IV), in μg, respectively in the binary mixture. Satisfactory results were obtained with good accuracy and reproducibility in the concentration range 5–100 μg of Ru(II) or Ru(IV) ions.

Moreover, the proposed 18-, 15- and 12-fold amplification procedures of Ru(II), Ru(III) and Ru(IV), respectively could be increased by employing further oxidation by bromine water and sodium periodate [23]. The released iodine from Eqs. (1)–(3) after addition of potassium iodide was quantitatively extracted twice with 10 ml portions (2 × 5) of $CHCl_3$ or $CCl_4$ and shaken with sodium sulphite solution to reduce the iodine to iodide. The released iodide in the aqueous (upper) layer was then allowed to react with bromine as well as with sodium periodate to produce iodate ions. The produced iodate was quantitatively determined iodometrically or spectrophotometrically after adjusting the pH and addition of KI as described earlier. The overall fold amplifications of ruthenium(II) determination were 108- and 432-fold employing oxidation of the produced iodide by bromine and sodium periodate, respectively. Similarly, the overall amplifications of ruthenium(III) determination involving oxidation of the produced 15 $I^-$ by bromine and sodium periodate were 90- and 360-fold, respectively. The two proposed amplification procedures, 90- and 360-fold have been employed iodometrically for the analysis of various amounts (2–50 μg) of ruthenium(III). The results obtained are summarized in Table 5 with an average absolute error of 0.2–2.5%. The blank values taken through the whole procedure using freshly prepared periodate, doubly-distilled water and molybdate solutions ranged between 0.10 and 0.15 ml of 0.005 M $Na_2S_2O_3$. The sensitivity of the proposed procedures could be improved by the addition of traces of ascorbic acid after addition of iodide to prevent the oxidation of iodide by atmospheric oxygen [24].

In addition, the spectrophotometric procedure employing 90-fold amplification of ruthenium(III) determination was carried out. The absorbance–concentration relationship was found to be linear in the concentration range from 0.1 to 5 mg $l^{-1}$ of ruthenium(III). A linear calibration curve was also obtained in the concentration range 0.05–5 mg $l^{-1}$ at 360-fold amplification and $\lambda = 350$ nm for ruthenium(III) determination. Moreover, the sensitivity of these amplification procedures could be extended to lower concentrations (<0.1 mg $l^{-1}$) of ruthenium(III), by extraction of the released iodine in $CHCl_3$–$C_2H_5OH$–KI and measuring the absorbance of the triiodide at 360 nm [24]. The standard deviation ($n = 3$) for a solution of 5 mg $l^{-1}$ Ru(III) was 0.4 and 0.22 at 90- and 360-fold amplification, respectively. The detection limit (3× noise) was 0.03 mg $l^{-1}$. It is worth mentioning that, for a reasonably large amount of ruthenium(II) or (III) (>50 mg) present, it is advisable to dilute the solution of the released iodate from oxidation of iodide ions by bromine or sodium periodate and follow the previously recommended procedure.

### 3.1. Interference studies

The interference of various cations, e.g. $Cd^{2+}$, $Ni^{2+}$, $Sn^{2+}$, $Pd^{2+}$, Ir(III), Os(III), $Au^+$, $Ca^{2+}$, $Mg^{2+}$, $Al^{3+}$, $UO_2^{2+}$, $Pt^{2+}$, $Pt^{4+}$, $Zn^{2+}$, and $Li^+$, at 0.5 mg and pH 3 on the selectivity of the proposed method were examined by the determination of a fixed concentration (30 mg) of ruthenium(II) or (III) in aqueous solution. The percentage recovery of ruthenium(II) or (III) was found to be 100 ± 2.4%. The toler-

Table 4
Simultaneous determination of various amounts of ruthenium(III) and (IV) in their binary mixtures by iodometry employing the 15- and 12-fold amplification procedure [a]

| Metal ion taken (μg) | | Metal ion found (μg) | |
|---|---|---|---|
| $Ru^{3+}$ | $Ru^{4+}$ | $Ru^{3+}$ | $Ru^{4+}$ |
| 20 | 50 | 20.1 ± 0.3 | 51.1 ± 0.2 |
| 40 | 50 | 40.3 ± 0.4 | 51.2 ± 0.3 |
| 100 | 50 | 101.3 ± 0.2 | 51.2 ± 0.2 |
| 150 | 100 | 153.3 ± 0.5 | 101.6 ± 0.5 |
| 200 | 100 | 202 ± 0.3 | 103.4 ± 0.3 |

[a] Average ± standard deviation ($n = 4$).

ance limits of various anions at 30 μg ruthenium(II) or (III) in the presence of a relatively high excess (1 mg) of the anions $AsO_2^-$, $AsO_3^-$, $SbO_2^-$, $SbO_3^-$, $SeO_3^{2-}$, $SeO_4^{2-}$, $TeO_4^{2-}$, $NO_3^-$, $SO_4^{2-}$, $PO_4^{3-}$, $HPO_4^{2-}$, $Cl^-$, $Br^-$, $SCN^-$, formate, $WO_4^{2-}$ and $SiO_3^{2-}$ have been critically investigated. The percentage recovery of ruthenium(III) was 100 ± 2.6% and the standard deviation was found in the range 0.2–0.7. In the presence of some other ions which are commonly found associated with ruthenium, e.g. $V^{5+}$ and $Pb^{2+}$ at 100-fold excess of ruthenium(III) at 30 μg concentration, simple modifications involving addition of 10 ml of NaF (1 M) to the aqueous solution were introduced. The percentage recovery of ruthenium(III) was 100 ± 3%. Interference of cobalt(II), iron(III) and bismuth(III) at 100-fold excess of ruthenium(III) was eliminated by adding 5 ml of EDTA (0.01 M). Bismuth(III) was also eliminated by shaking the aqueous solution at pH 9–10 with 10 ml xylene in the presence of sodium diethyldithiocarbamate (2% v/v). Copper(II) interfered seriously with the proposed procedure.

Under the optimum conditions of the proposed procedures ($2.5 < pH < 3.6$), chromium(VI) did not interfere owing to the reaction

$$Cr_2O_7^{2-} + 6I^- + 14H^+ \rightarrow 2Cr^{3+} + 3I_2 + 7H_2O \quad (12)$$

This reaction was pH dependent and did not occur at $pH > 2.3$. These results are in good agreement with the published work by El-Wakil et al. [13] on chromium(VI) determination.

Chromium(III) interfered seriously with the proposed method, since the reaction

$$2Cr^{3+} + 3IO_4^- + 4H_2O \rightarrow Cr_2O_7^{2-} + 3IO_3^- + 8H^+ \quad (13)$$

proceeded at $pH < 4$. However, this interference from chromium(III) could be removed easily by oxidizing the aliquot solution of chromium(III) with $H_2O_2$ in 2N $H_2SO_4$, and the produced blue perchromic acid extracted quantitatively with diethylether as previously reported [25] according to

$$CrO_4^{2-} + H_2O_2 \rightarrow \underset{\text{deep blue colour}}{CrO_5} + H_2O \quad (14)$$

$$CrO_5 + C_2H_5OC_2H_5 \rightarrow \underset{\text{adduct}}{CrO_5C_2H_5OC_2H_5} \quad (15)$$

Thus, chromium(III) interference could be removed completely. The excess hydrogen period was eliminated by adding tin(II), and the ruthenium species was then determined by the proposed procedure II.

Table 5
Determination of various amounts of ruthenium(III) by iodometry using 90-fold and 360-fold amplification procedures [a]

| Ruthenium(III) taken (μg) | Metal ion found (μg) | |
|---|---|---|
| | 90-fold | 360-fold |
| 2 | 2.05 ± 0.1 | 2.0 ± 0.1 |
| 5 | 5.1 ± 0.1 | 5.1 ± 0.1 |
| 10 | 10.1 ± 0.1 | 10.1 ± 0.1 |
| 20 | 20.2 ± 0.1 | 20.1 ± 0.1 |
| 50 | 50.2 ± 0.1 | 50.1 ± 0.2 |
| 100 | 100.4 ± 0.2 | 100.5 ± 0.3 |

[a] Average ± standard deviation ($n = 3$).

### 3.2. Applications of the proposed methods

#### 3.2.1. Analysis of ruthenium(II) and (III) in their complexes

The proposed procedure I-a for the analysis of ruthenium(II) or (III) in their complexes [19] was carried out successfully after combustion of the sample as described earlier. Ruthenium usually present in the di-, tri- and tetravalent

Table 6
Results of the extractive spectrophotometric determination of Ru in various ruthenium(III) complexes [a]

| Complet | Ru present [b] (%) | Ru found [c] (%) |
|---|---|---|
| $RuCl_2(PPh_3)_2$(Koj) | 24.52 | 24.5 ± 0.2 |
| $RuCl_2(PPh_3)_2$(Malt) | 24.46 | 24.40 ± 0.3 |
| $RuCl_2(PPh_3)_2$(trop) | 24.7 | 24.9 ± 0.3 |
| $RuCl_2(PPh_3)_2$(acac) | 25.32 | 24.9 ± 0.2 |
| Ru(5 Cl-$Sal_2$en)$(PPh_3)_2$ | 10.43 | 10.78 ± 0.3 |

[a] Abbreviations: Kojic acid (Koj); maltol (malt); tropolone (trop); acetylacetone (acac); and *N,N*-ethylenebis(5-chlorosalicylideneiminato)bis(triphenylphosphine(5-Cl-$Sal_2$en)$(PPh_3)_2$.
[b] Certified value.
[c] Average ± standard deviation ($n = 5$).

state was reduced to ruthenium(II) [17], and determined by iodometry and spectrophotometry with the help of the concurrently proposed standard curve under the same experimental conditions as the described procedure I-a. The results are summarized in Table 6 with an average absolute error of 0.2–0.3. The blank values taken throughout the whole procedure using freshly prepared reagents ranged between 0.2 and 0.25 ml of 0.005 M $Na_2S_2O_3$. Evidently, for ruthenium complexes containing a large percentage of ruthenium, it was advisable to dilute the solution of the produced iodate in the first procedure I-a to 25 ml with distilled water and treat 5 ml of this solution as described earlier.

### *3.2.2. Determination of ruthenium in natural waters*

The applicability of the proposed method for the determination of low concentrations of spiked ruthenium(III) ions to tap-, mineral and seawater (0.1–1 l) is possible by the standard addition procedure. In separate experiments, aliquot samples were allowed to react with 5 ml of bromine water for 10 min, and the excess bromine was removed by boiling off the solution. The samples were then spiked with various amounts (5–40 μg) of Ru(III). Filtration of the sample solution through a 0.45 μm membrane was carried out, followed by addition of 10 ml of EDTA (0.001 M) and 10 ml of NaF (1 M); the sample was then analyzed employing procedure II. The concentration of the tested ruthenium species in such water was under the detection limit and recovery of the spiked Ru(III) was achieved. The results of the analysis of various amounts of ruthenium(III) spiked tapwater and seawater are summarized in Table 7. Good reproducibility with relative standard deviations in the range 1–2.9% ($n = 5$) was obtained. The analysis of very low concentrations (less than nanomolar levels) of Ru(III) in water is also possible using the proposed procedure by prior preconcentration of the element from a large sample volume on polyurethane foam column, followed by elution of the extracted Ru(III) species from the foam as reported earlier [26] and subsequent determination of the ruthenium(III) in the effluent according to the described procedure I-a with the help of a concurrently prepared standard curve at the same instrumental setting.

## 4. Conclusion

The present work presents accurate, precise, inexpensive, reliable methods in routine analysis for the trace determination of ruthenium ions in their matrix. Therefore, the method provides an attractive alternative approach to determination of the atomic absorption of ruthenium. The advantages of the method are that it is not only applicable to Ru(II), (III) and (IV) speciation in their solutions, but it can also be used for the analysis of ruthenium in its complexes and natural water samples. The sensitivity and selectivity of the developed methods can be improved by prior preconcentration of the trace amounts of ruthenium species from large sample volumes on polyurethane foam column. Elution of ruthenium from the column is possible with selective eluting agent followed by determination with the proposed procedure. The 15-fold amplification procedure for Ru(III) determination was faster, but the 90- and 360-fold amplification procedures were more sensitive and applicable at very low concentrations of the tested element. The determi-

Table 7
Analysis of various amounts of ruthenium(III) spiked seawater by iodometry (a) and spectrophotometry (b) employing the 90-fold amplification procedure [a]

| ruthenium(III) added (μg) | Ruthenium(III) found (μg) [b] | | Error (%) | |
|---|---|---|---|---|
| | a | b | a | b |
| 5 | 5.1 ± 0.1 | 5.10 ± 0.1 | 2 | 2 |
| 10 | 10.30 ± 0.3 | 10.1 ± 0.2 | 3 | 1 |
| 20 | 20.3 ± 0.3 | 20.2 ± 0.3 | 1.5 | 1 |
| 25 | 25.7 ± 0.4 | 25.2 ± 0.3 | 2.8 | 0.8 |
| 40 | 40.7 ± 0.5 | 40.65 ± 0.4 | 1.8 | 1.25 |

[a] Average ± standard deviation ($n = 5$).
[b] Total volume of aqueous seawater was 0.1 $dm^3$.

nation of Ru(II) besides Ru(III) or Ru(IV) besides Ru(II) is also possible with good accuracy.

## References


[1] E. Merian, Metals and their Compounds in the Environment, Occurrence, Analysis and Biological Relevance, VCH, Weinheim, 1981, p. 1143.
[2] M.S. El-Shahawi, A.Z. Abu Zuhri and S.M. Al-Dhaheri, Fresenius' Z. Anal. Chem., 350 (1994) 874.
[3] R.K. Sharma, Bull. Chem. Soc. Jpn., 66 (1933) 1084, and references cited therein.
[4] Z. Marczenko, Separation and Spectrophotometric Determination of Elements, Ellis Horwood, New York, 1986, p. 492.
[5] A.M. Almuaibed and A. Townshend, Microchem. J., 48 (1933) 21.
[6] M.S. El-Shahawi and M. Al-Mahdy, J. Chromatogr., 697 (1995) 185.
[7] M.S. El-Shahawi, A.Z. Abu Zuhri and M.M. Kamal, Fresenius' Z. Anal. Chem., 348 (1994) 730.
[8] R. Palaniappan and T.A. Kummar, Analyst, 118 (1993) 293.
[9] R. Palaniappan and V. Revathy, Analyst, 114 (1989) 517.
[10] R. Palaniappan, Bull. Electrochem. Soc., India, 39 (1991) 367.
[11] T. Leipert, Mikrochemie, (1992) 226.
[12] A.M. El-Wakil, A.B. Farag and M.S. El-Shahawi, Talanta, 36 (1989) 783.
[13] J.W. Hamaya and A. Townshend, Talanta, 19 (1972) 141.
A.M. El-Wakil, A.B. Farag and M.S. El-Shahawi, Fresenius' Z. Anal. Chem., 337 (1990) 886.
[14] A.M. El-Wakil, A.B. Farag and M.S. El-Nahas, Talanta, 40 (1993) 841.
[15] A.B. Farag, M.S. El-Shahawi and E.M. El-Nemma, Fresenius' Z. Anal. Chem., 346 (1993) 455.
[16] D.R. Lide, Handbook of Chemistry and Physics, 72nd edn., CRC Press, Boca Raton, FL, 1991/1992, p. 493.
[17] G. Ciantelli, P. Legithimo and F. Pantani, Anal. Chim. Acta., 52 (1971) 303.
[18] C.W. McDonald and J.H. Bedenbaugh, Mikrochim Acta (Wien), (1970) 612.
[19] A.M. El-Hindawy and M.S. El-Shahawi, Polyhedron, 118 (1993) 293.
[20] M. Armando, R. Lena, M. Rafael and D.J. Federico, J. Coord. Chem., 29 (1993) 359.
[21] T.S. Ma and R.C. Rinter, Modern Organic Elemental Analysis, Dekker, New York, 1979.
[22] D. Brunel, CR. Acad. Sci., Paris, 261 (1965) 1982.
[23] D. Amin, K.Y. Saleem and W.A. Bashir, Talanta, 29 (1982) 694, and references cited therein.
[24] T.C. Ovenston and W.T. Rees, Anal. Chim. Acta, 5 (1951) 123.
[25] A.M. El-Wakil, M.S. El-Shahawi and A.B. Farag, Anal. Lett., 23 (1990) 103.
[26] S.J. Al-Bazi and A. Chow, Talanta, 31 (1984) 189.

ELSEVIER

Talanta 42 (1995) 1651–1662

Talanta

# Solubility of some calcium–carboxylic ligand complexes in aqueous solution

Alessandro De Robertis [a,*] Antonio Gianguzza [b], Silvio Sammartano [a]

[a] *Dipartimento di Chimica Inorganica, Analitica e Struttura Molecolare, Universitá, Salita Sperone 31, I-98166 S. Agata di Messina, Italy*

[b] *Dipartimento di Chimica Inorganica, Universitá, Via Archirafi 26, I-90123 Palermo, Italy*

Received 12 September 1994; revised 8 December 1994; accepted 19 April 1995

**Abstract**

Insoluble species were identified in the systems $Ca^{2+}$–hemimellitate, $Ca^{2+}$–1,2,3,4-butanetetracarboxylate and $Ca^{2+}$–citrate, and their solubilities were determined in aqueous solution at $T = 25°C$. Values of $pK_{s0}$ were obtained for the species CaLH (L = benzene-1,2,3-tricarboxylate or hemimellitate), $Ca_2L$ (L = 1,2,3,4-butanetetracarboxylate), CaLH and $Ca_3L_2$ (L = citrate), together with their dependence on ionic strength. Solid compounds were also characterized by thermogravimetry. The complex formation in solution for the system $Na^+$– and $Ca^{2+}$–hemimellitate was studied too.

*Keywords:* Calcium–carboxylic ligands; Solubility

## 1. Introduction

In recent years, there has been a upsurge in the study of solution equilibria because of: (a) the interest of these studies in the speciation of natural and biological fluids, such as sea, river, lake, and underground water, urine, blood, etc.; (b) the need to use equilibrium data in modeling multicomponent solutions, i.e. solutions containing a large amount of metal ions and ligands; (c) the availability of excellent calculation programs, and powerful and fast computers.

Compilations in this field report a very large number of papers dealing with thermodynamic formation data, related to ligand protonation, simple and mixed metal–ligand complexation, cation hydrolysis, etc. [1–5].

Notwithstanding this, there remains a series of substantial gaps. (1) Studies on weak interactions between alkali and alkaline-earth cations with low molecular weight ligands are still to be examined closely and to be completed. (2) The dependence of thermodynamic formation parameters on ionic strength has still not been thoroughly investigated. (3) Studies of solution equilibria are generally carried out neglecting both the possibility of the formation of solid and/or gaseous phases, and interaction with other phases. If we consider the last three points together, it is evident that they are very closely linked.

Therefore, we decided to make a systematic further study of a research topic already begun [6] on the stability and solubility of some Ca–polycarboxylate complexes. In this paper, we report the results obtained for the following systems: Ca–(hmt), Ca–(btc) and Ca–(cit) (hmt = benzene-1,2,3-tricarboxylate, or hemimellitate; btc = 1,2,3,4-butanetetracarboxylate; cit = citrate). Moreover, since we use formation constants of the species present in solution for the determination of the solubilities of the salts,

* Corresponding author.


*SSDI* 0039-9140(95)01624-4

potentiometric measurements for the systems $Na^+$– and $Ca^{2+}$–hemimellitate (whose thermodynamic data are not reported in the literature) were performed.

## 2. Experimental

### 2.1. Materials

The solution of NaCl was prepared from C. Erba A.C.S. reagent, previously dried at 110°C. $CaCl_2$ solution was prepared from analytical reagent Fluka and standardized with EDTA [7]. NaOH and HCl solutions were prepared by diluting concentrated ampoules (C. Erba), and standardized against potassium biphthalate or sodium carbonate, respectively. Tetramethylammonium chloride ($(Me_4N)Cl$) and tetraethylammonium iodide ($(Et_4N)I$) (Fluka or C. Erba) were recrystallized from acetone/methanol [8] before use. $Ca_3(cit)_2 \cdot 4H_2O$ (Fluka), was used as purchased. Hemimellitic, 1,2,3,4-butanetetracarboxylic and citric acids were used without further purification, because their purity, checked alkalimetrically, was always >99.6%. All solutions were kept free from $CO_2$ using soda lime traps.

### 2.2. Apparatus

Hydrogen-ion concentration was measured with a Metrohm mod. 654 potentiometer, coupled with a combination pH glass electrode Orion mod. 81-02 (Ross type). The titrant, standard NaOH, was delivered by a motorized burette Metrohm Dosimat mod. 665. Both potentiometer and dispenser were controlled by a personal computer and suitable software was used in order to run automatic titrations and data reading. The glass electrode was standardized by titrating HCl (20–30 mM) with standard NaOH under the same ionic strength conditions as the solutions being investigated, and therefore $E^0$ and the junction potential, $E_j = j_a[H^+]$, were calculated; following this procedure we obtained $pH \equiv \log[H^+]$, i.e. pH in terms of molar concentration. The accuracy of the system was $\pm 0.15$ mV in e.m.f. measurements and $\pm 0.002$ ml in the delivered titrant volume. The measurement cell was thermostatted at $25.0 \pm 0.1$°C and magnetic stirring was employed. All the titrations were carried out by bubbling pre-saturated and purified nitrogen through the solution, in order to exclude $CO_2$ and $O_2$.

The solids were characterized by thermogravimetric analysis using a Perkin Elmer thermobalance TBS-2 equipped with data station, working at a heating rate of 10°C $min^{-1}$, in air.

### 2.3. Potentiometric measurements

Alkalimetric titrations were performed under the following analytical conditions (L = hemimellitic acid): for protonation constants, $C_L$ = 5–7 mM, $C_{(Et_4NI)} = 0.1–0.75$ M (25 titrations); for $Na^+$ complex formation constants, $C_L$ = 5–7 mM, $C_{NaCl} = 0.1–0.75$ M (25 titrations); for $Ca^{2+}$ complex formation constants, $C_L$ = 2–5 mM, $C_{CaCl_2} = 3–20$ mM, $C_{NaCl} = 0–0.7$ M; or $C_{CaCl_2} = 3$ mM, $C_{(Et_4NI)} = 0.2–0.4$ M (31 titrations). For each titration, 40–60 data points were obtained. In several cases, an excess of HCl (20–30 mM) was added to the solutions in order to calculate internal $E^0$, $E^0_{int}$ (i.e. the standard potential obtained from the same solution being investigated); when $|E^0_{int} - E^0| > 1$ mV, the titration was rejected and repeated.

### 2.4. Preparation and analysis of insoluble compounds[1]

Insoluble compounds were prepared in plugged ampoules by mixing suitable quantities of reactants in 100 ml of total volume, as reported in Table 1. The proton concentration was varied by adding NaOH and/or $Ca(OH)_2$, and the ionic strength was adjusted with NaCl and/or $(Me_4N)Cl$. The ampoules were mechan-

Table 1
Analytical concentrations (mM) and details for the preparation of insoluble compounds

| Species | Ligand | | |
|---|---|---|---|
| | $(hmt)^{3-}$ | $(btc)^{4-}$ | $(cit)^{3-}$ |
| L | 22.92 | 10.0–20.0 | 33.34–66.89 |
| $Ca^{2+}$ | 10.07–40.01 | 20.43–61.35 | 50.00–60.42 |
| $H^+$ | 21.75–43.68 | 2.39–60.73 | 0–79.86 |
| NaCl | 0–394 | 0–81 | 0–513 |
| $(Me_4N)Cl$ | – | 0–605 | 0–501 |
| $[H^+]/[Ca^{2+}]$ | 0.54–1.71 | 0.07–2.15 | 0–1.32 |
| Runs | 12 | 20 | 19 |

[1] Supplementary material is reported in Appendix A.

ically shaken in a box thermostated at 25.0 ± 0.1°C, for 24 h; shaking times of up to 72 h gave equal results. The solution was recovered first, by filtration (Schleicher Schnell 589/3) into a 100 ml volumetric flask, in which 10 ml of distilled water had previously been placed, in order to prevent precipitation. Then, the solid was filtered using a Gooch crucible (porosity 10–15 μm), washed with a small quantity of water and vacuum-dried. The solutions were analyzed in order to determine their analytical concentrations in proton and calcium ions, by using standard NaOH and EDTA, respectively. Each titration was repeated at least twice. The ligand concentration was estimated on the basis of mass balance, i.e. solution electroneutrality.

### 2.5. Calculations

The purities of the reagents and the $E^0$ values were calculated by the computer program ESAB2M [9]. Protonation and formation constant values of $H^+$–, $Na^+$–, $Ca^{2+}$–hemimellitate complexes were determined by the non-linear least-squares computer programs STACO [10] and/or BSTAC [10]; both programs can deal with potentiometric data at different ionic strengths, and compute parameters $C$ and $D$ of the dependence of formation constants on ionic strength (see text).

For the calculation of solubilities, free concentrations of proton, calcium and ligands were computed (ES4ECI [10] computer program) from the correspondent analytical concentrations, and from the protonation and formation constants determined here or reported previously [1–5,11–13]. All the calculations were performed by also considering the interactions of the background salt with all the components of the solutions, such as reported in previous investigations [11,13,17].

## 3. Results and discussion

### 3.1. Formation constants of hemimellitate

Table 2 reports the protonation constants of hemimellitate and formation constants with $Na^+$ and $Ca^{2+}$, at infinite dilution and $T$ = 25°C. Values obtained in $(Et_4N)I$ can be considered as "effective" protonation constants, since the interaction of $(Et_4N)^+$ with carboxylic ligands is negligible. The protonation

Table 2
Protonation and formation constants of hemimellitate with $Na^+$ and $Ca^{2+}$ at $T$ = 25°C and $I$ = 0 M, and $C_{exp}$ values of Eq. (2)

| pq | M | $\log \beta^a_{pq} \pm 3s^b$ | $C^c_{exp}$ | $\log K^a_{pq}$ |
|---|---|---|---|---|
| 01 | H | 6.17 ± 0.02 | 1.41 | 6.17 |
| 02 | | 10.41 ± 0.03 | 2.39 | 4.24 |
| 03 | | 13.18 ± 0.03 | 2.93 | 2.77 |
| 10 | Na | 1.53 ± 0.08 | 1.41 | 1.53 |
| 11 | | 7.04 ± 0.07 | 2.39 | 0.87 |
| 12 | | 10.70 ± 0.07 | 2.93 | 0.29 |
| 20 | | 2.45 ± 0.12 | 2.39 | 0.92 |
| 21 | | 7.04 ± 0.18 | 2.93 | 0.00 |
| 10 | Ca | 4.28 ± 0.03 | 3.06 | 4.28 |
| 11 | | 9.35 ± 0.02 | 3.88 | 3.18 |
| 12 | | 13.05 ± 0.02 | 3.52 | 2.64 |
| 20 | | 6.57 ± 0.06 | 3.88 | 2.29 |

[a] Overall formation constants $\beta_{pq}$ refer to the reaction

$$pM^{z+} + L^{3-} + qH^+ = M_pLH_q^{(zp+q-3)}$$

Stepwise formation constants $K_{pq}$ refer to the reaction

$$M^{z+} + M_{p-1}LH_q^{[z(p-1)+q-3]} = M_pLH_q^{(zp+q-3)}$$

[b] $s$ = standard deviation.
[c] Eq. (2).

constants are in agreement (Table 3) with those reported in both Refs. [14] and [15], whilst there is disagreement with $\log K_1$ and $\log K_2$ of Ref. [16]. As regards the Na–L–H system, we found, under our experimental conditions, three mononuclear ($NaLH_2^0$, $NaLH^-$, $NaL^{2-}$) and two binuclear ($Na_2LH^0$, ($Na_2L^-$) species. Comparison with literature findings is not possible, since these are the first available data; nevertheless, we can attempt a comparison (see Table 3) with the Na-complexes of other similar ligands having the same residual charge, i.e. −3: citrate [11], 1,2,3-propanetricarboxylate [17], hydrogen-1,2,3,4-butanetetracarboxylate [13]. As we can see, the values of the constants for the same reaction are fairly similar. Calcualtions (L = 1 mM, NaCl = 0.25 M) of the distribution of the species vs. pH show high formation percentages of $NaL^{2-}$ and $Na_2L^-$ (at pH 7, ≈75% of the ligand). Analysis of the potentiometric data of the Ca–hemimellitate–H system, allowed us to identify four complex species, and the formation constant values are reported in Table 2. Since other literature data are not available at present, we can only compare the thermodynamic values of Ca-complexes of hemimellitate with those of 1,2,3-propanetricarboxylate [17], citrate [12] and hy-

Table 3
Literature comparisons ($T = 25°C$)

*Protonation constants of hemimellitate*

| $i$ | $\log K_i^H$ [a] ($I = 0$ M) | | | $\log K_i^H$ [a,b] ($I = 1$ M) | |
|---|---|---|---|---|---|
| | This work | Ref. [14] | Ref. [16] | This work (NaCl) | Ref. [15] ($NaClO_4$) |
| 1 | 6.17 | 6.27 | 7.13 | 4.82 | 4.96 |
| 2 | 4.24 | 4.33 | 4.75 | 3.58 | 3.69 |
| 3 | 2.77 | 2.85 | 2.88 | 2.48 | 2.51 |

*Formation constants of $Ca^{2+}$ and $Na^+$ complexes for hemimellitate, citrate, 1,2,3-propanetricarboxylate and hydrogen-1,2,3,4-butanetetracarboxylate*

| Ligand | M | $\log K_{pq}$ [c] ($I = 0$ M) | | | | Ref. |
|---|---|---|---|---|---|---|
| | | $pq = 10$ | $pq = 11$ | $pq = 12$ | $pq = 20$ | |
| $(hmt)^{3-}$ | Na | 1.53 | 0.87 | 0.29 | 0.92 | This work |
| $(cit)^{3-}$ | | 1.55 | 0.89 | 0.15 | 0.79 | [11] |
| $(tca)^{3-}$ | | 1.40 | 0.82 | 0.15 | 0.58 | [17] |
| $H(btc)^{3-}$ | | 1.49 | 0.93 | 0.22 | 0.64 | [13] |
| $(hmt)^{3-}$ | Ca | 4.28 | 3.18 | 2.64 | 2.29 | This work |
| $(cit)^{3-}$ | | 4.91 | 2.81 | | | [12] |
| $(tca)^{3-}$ | | 3.28 | 2.18 | 1.04 | 1.18 | [17] |
| $H(btc)^{3-}$ | | 3.37 | 2.79 | 1.91 | 1.11 | [13] |

[a] Stepwise protonation constant: $K_i^H = [H_iL]/([H][H_{i-1}L])$.
[b] Apparent protonation constants (obtained by neglecting $Na^+$ complexes).
[c] Indices refer to the reaction

$$M^{z+} + (M_{p-1}LH_q)^{[z(p-1)+q-3]} = (M_pLH_q)^{(zp+q-3)}$$

drogen-1,2,3,4-butane-tetracarboxylate [13] (see Table 3). Fig. 1 shows the distribution of the species vs. pH, evidencing the preferential formation of $CaLH_2^+$ and $Ca_2L^+$ complexes.

The dependence of thermodynamic parameters on ionic strength was taken into account using a Debye–Hückel type equation [11,14,18, 19] ($I$ = ionic strength, M):

$$\log X = \log {}^TX - z^*\sqrt{I}/(2 + 3\sqrt{I}) + CI + DI^{3/2} \quad (1)$$

with

$X = \beta$ or $K$ or $K_{s0}$; ${}^TX = \beta$ or $K$ or $K_{s0}$ values at $I = 0$;

$C = c_0p^* + c_1z^*$ and $D = dz^*$,

where

$c_0 = 0.1$, $c_1 = 0.23$, $d = -0.1$;

$p^* = \sum (\text{moles})_{\text{reactants}} - \sum (\text{moles})_{\text{products}}$;

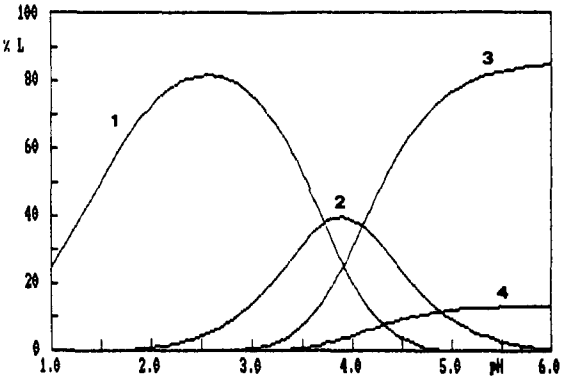


Fig. 1. Distribution diagram of complex species in the Ca–hemimellitate–H system (protonation omitted) versus pH, at $T = 25°C$ and $I = 0.25$ M.
Species: (1) $CaLH_2^+$, (2) $CaLH^0$, (3) $Ca_2L^+$, (4) $CaL^-$.
Concentrations: L = 0.001 M; $CaCl_2$ = 0.09 M.

$z^* = \sum (\text{charges})^2_{\text{reactants}} - \sum (\text{charges})^2_{\text{products}}$.

A simplified equation, used in this work, is

$$\log X = \log {}^TX - z^*g(I) + CI \quad (2)$$

with

$$g(I) = \sqrt{I}/(2 + 3\sqrt{I}) + 0.1I^{3/2}$$

In Table 2, experimental values of $C$ are reported.

### 3.2. Insoluble compounds

*Ca–hemimellitate–H system*

From the differences between the concentrations of $H^+$ and $Ca^{2+}$ reactants and those found by titration of solutions after precipitation, it is possible to compute the quantities of $H^+$ and $Ca^{2+}$ in the solid phase: the ratio (mmol $Ca^{2+}$)/(mol $H^+$) is always close to 1.0 (average of 12 runs = 0.98 ± 0.03) and, therefore, in the precipitate the ratio $Ca^{2+}$:$H^+$:$L^{3-}$ is 1:1:1, i.e. minimum formula CaLH. The thermodynamic value of $pK_{s0} \pm 3s$ together with its dependence on ionic strength ($0.06 \leqslant I \leqslant 0.03$ M), is 12.98 ± 0.05 (Eq. (1), $C = 2.4$, $D = 0$) or (see Eq. (2)) $pK_{s0} = 12.95 \pm 0.05 - 14g(I) + 3.28I$.

*Ca–1,2,3,4-butanetetracarboxylate–H system*

Quantitative analysis of 20 different solutions has shown that the number of mmol of $Ca^{2+}$ recovered was lower than at the start, whereas that of $H^+$ was always the same. This experimental evidence allows us to assert that the insoluble compound formed must contain only $Ca^{2+}$ and $L^{4-}$, with the formula $Ca_2L$.

For the calculation of $Ca_2L$ solubility, the total concentration of $Ca^{2+}$ was directly determined, and that of $L^{4-}$ was estimated as the initial value minus half the amount of $Ca^{2+}$ lost in the precipitation. The thermodynamic value of $pK_{s0}$ ($0.03 \leqslant I \leqslant 0.62$ M) is $14.60 \pm 0.05$ (Eq. (1), $C = 2.8$, $D = 0$) or, using Eq. (2), $pK_{s0} = 14.53 \pm 0.05 - 24g(I) + 4.63I$.

*Ca–citrate–H system*

The saturated solutions were analyzed for their $H^+$ and $Ca^{2+}$ content, whereas the concentration of the ligand was computed on the basis of the electroneutrality of the solutions. The found quantities of $Ca^{2+}$, $H^+$ and $L^{3-}$ are not consistent with the formation of a single compound, except for the trials for which the precipitate, in the absence of protons, kept the formula $Ca_3L_2$. To establish the composition of the species present into the mixed precipitates, we took the following into account: (a) a study on the crystal lattice of $CaLH \cdot 3H_2O$ is reported in the literature [20]; (b) the crystal lattice of $Mg_3L_2 \cdot 10H_2O$ [21] shows an aquate magnesium ion which is like a bridge between two $MgL^-$ units; owing to the strong likeness between $Mg^{2+}$ and $Ca^{2+}$, it is possible to assume similar behavior for the $Ca^{2+}$; (c) in any trial in which acids were present, their initial quantity was always greater than that found after precipitation, i.e. among the precipitates, some are protonated; (d) the charge on $CaL^-$ can be saturated with a proton, to give the neutral species CaLH (see (a)). Therefore, starting from the diminished concentration in solution of the proton, due to the formation of CaLH, we calculate the quantities of two species. We experienced a certain difficulty in obtaining the formation of CaLH, which is always $<50\%$ owing to the many equilibria involving the protonated species of $L^{3-}$ in the interval of pH taken into consideration ($3.76 \leqslant pH \leqslant 5.03$). The precipitation of protonated species is a maximum in the solutions having $pH \approx 4.8$, since at these pH values there is maximum formation $HL^{2-}$ [14], i.e. the optimum acidity conditions required to obtain CaLH. Attempts to obtain quantitative formation of CaLH (trials with increased proton concentration) failed owing to the formation of more protonated citrate soluble species. In the interval $0.2 \leqslant I \leqslant 0.54$ M we calculate, for CaLH and $Ca_3L_2$, $pK_{s0} = 11.39 \pm 0.09$ (Eq. (1), $C = 4.9$, $D = 0$) and $pK_{s0} = 17.03 \pm 0.08$ (Eq. (1), $C = 6.3$, $D = 0$), respectively; using Eq. (2), we obtain $pK_{s0} = 11.35 \pm 0.09 - 14g(I) + 5.95I$ and $pK_{s0} = 16.95 \pm 0.08 - 30g(I) + 8.52I$, respectively.

### 3.3. Thermal analysis[2]

The results concerning the thermoanalytical curves of the insoluble compounds are as follows.

CaLH (L = hemimellitate) is monohydrate, and the water is lost gradually starting from $T = 80$°C up to $T = 200$°C. At $T = 365$°C, the decomposition of the anhydrous compound into $CaCO_3$ begins, and the reaction is complete at $T = 600$°C. At $T = 780$°C the familiar pyrolysis of the carbonate steps in and, under our experimental conditions, the reaction is complete at about $T = 815$°C. We also note an inflexion of the thermogram at $T = 530$°C due to superimposed decomposition of CaLH into benzoic acid and $CaCO_3$. $Ca_2L$ (L = 1,2,3,4-butanetetracarboxylate) is hexahydrate, and the water is lost in two steps: the first dehydration begins at room temperature and continues up to $T = 145$°C, when the second dehydration is superimposed, which proceeds very gradually. At about $T = 400$°C the decomposition of the anhydrous compound starts, to give $CaCO_3$ and then, at $T = 770$°C, the usual formation of CaO takes place. The thermogram of $Ca_3L_2$ (L = citrate) shows a two-stage dehydration reaction: at first one molecule and then, at $T = 135$°C, three molecules. The anhydrous citrate decomposes in three clear transformations: their decomposition ($T = 350$°C) to give $CaCO_3$ and then CaO, and the superimposition of a thermal decomposition at about $T = 480$°C, due to the loss of a molecule of water from a H– and an OH– of the citrate. Thermograms of mixtures of $Ca_3(cit)_2 + Ca(cit)H$ have not supplied clear evidence of the stages of decomposition, but only on the degradation of the solid in $CaCO_3$ and then in CaO.

### 3.4. Solubility and ionic strength

The solubility of the above reported species is fairly low in pure water or in tetraalkylammonium salt solution, whilst it increases appreciably in sodium salt solutions. This is due to the formation of Na–carboxylate and Ca–Cl soluble complexes [22,23]. For example, the

[2] Supplementary material is reported in Appendix B.

solubility of $Ca_2(btc)$ at $I = 0.5$ M in tetraalkylammonium salt solution is $s = 6.6 \times 10^{-5}$ M, whilst in a NaCl solution, at the same ionic strength, it is $s = 1.4 \times 10^{-3}$ M. As regards the dependence on ionic strength, the $C_{exp}$ values (Eq. (2)) obtained for both $pK_{s0}$ and $\beta_{pq}$ are in fairly good agreement with previous findings [11,14,18,19] (see Appendix C).

## 4. Conclusions

A simple laboratory technique allowed us to characterize the formation of insoluble calcium–carboxylic ligand complexes. Quantitative results on solubility, together with the complete speciation of solution, are of great help in modeling the interaction of calcium with natural compounds containing several carboxylic groups. Results relative to the dependence on ionic strength of $pK_{s0}$ are quite useful, since they allow calculation of the solubilities for different natural fluids under different ionic strength conditions. We underline that in the calculation of $pK_{s0}$ values, all the interactions occurring in the solutions are taken into consideration.

## Appendix A — Solubility

*Example of calculation*

Here we report analytical details and calculations referring to the systems Ca–hmt–H (Tables A1–A3), Ca–btc–H (Tables A4–A6) and Ca–cit–H (Tables A7–A9). In particular, we consider here, as an example, the run no. 4 of the Ca–cit–H system.

In 100 ml of total volume we mixed $Ca_3L_2$, NaOH and NaCl in order to obtain the following initial concentrations (mM) before precipitation: $Ca^{2+} = 53.68$, $L^{3-}$ 35.79, $H^+ = 10.86$, NaCl = 102.7 (see Table A7, columns 2,3,4 and 5). After 24 h, we separated the precipitate from the solution, which was analyzed for $Ca^{2+}$ and $H^+$ concentrations (14.04 and 7.19 mM, respectively (see Table A7, columns 7 and 9). The analytical concentration of $L^{3-}$ after precipitation was estimated as the differ-

Table A2
Ca–hemimellitate–H system. Composition of the precipitate [a] (mmol)

| Run | Ca | H | Ca/H |
|---|---|---|---|
| 1 | 1.160 | 1.229 | 0.94 |
| 2 | 1.604 | 1.662 | 0.97 |
| 3 | 1.673 | 1.773 | 0.94 |
| 4 | 1.428 | 1.414 | 1.01 |
| 5 | 0.951 | 0.923 | 1.03 |
| 6 | 1.658 | 1.728 | 0.96 |
| 7 | 1.386 | 1.379 | 1.01 |
| 8 | 0.932 | 0.920 | 1.01 |
| 9 | 1.162 | 1.217 | 0.95 |
| 10 | 1.672 | 1.778 | 0.94 |
| 11 | 0.950 | 0.933 | 1.02 |
| 12 | 1.400 | 1.400 | 1.01 |
| Average | | | $0.98 \pm 0.03$ |

[a] Calculated, for Ca and H, from $[(C_i)_b - (C_i)_a]$ (see Table A1) and by considering the volume (100 ml) of the solution.

Table A1
Ca–hemimellitate–H system. Analytical concentrations (mM) of the solutions

| Run | Before precipitation $(C_i)_b$ | | | | After precipitation $(C_i)_a$ | | |
|---|---|---|---|---|---|---|---|
| | Ca | L | H | NaCl [a] | Ca | L [b] | H |
| 1 | 25.46 | 22.92 | 43.66 | – | 13.86 | 11.32 | 31.37 |
| 2 | 25.04 | 22.92 | 33.70 | – | 9.00 | 6.88 | 17.08 |
| 3 | 40.00 | 22.92 | 33.70 | – | 23.27 | 6.19 | 15.97 |
| 4 | 15.11 | 22.92 | 21.75 | – | 0.83 | 8.64 | 7.61 |
| 5 | 10.07 | 22.92 | 21.75 | – | 0.56 | 13.41 | 12.52 |
| 6 | 40.01 | 22.92 | 33.70 | 78.1 | 23.43 | 6.34 | 16.42 |
| 7 | 15.11 | 22.92 | 21.75 | 320.4 | 1.12 | 9.06 | 7.96 |
| 8 | 10.07 | 22.92 | 21.75 | 394.4 | 0.75 | 13.60 | 12.55 |
| 9 | 25.49 | 22.92 | 43.68 | – | 13.87 | 11.30 | 31.51 |
| 10 | 40.01 | 22.92 | 33.73 | – | 23.29 | 6.20 | 15.95 |
| 11 | 10.08 | 22.92 | 21.76 | – | 0.58 | 13.42 | 12.43 |
| 12 | 15.10 | 22.92 | 21.76 | 320.4 | 1.10 | 8.92 | 7.76 |

[a] NaCl is added for ionic strength adjustment.
[b] Concentrations calculated from $(C_L)_a = (C_L)_b - [C_{Ca}]_b - (C_{Ca})_a]$.

Table A3
Ca–hemimellitate–H system. Free concentrations of species [a], $I$ values [a] and $pK_{s0}$ calculations

| Run | pCa | pL | pH | pCa + pL + pH = $pK_{s0}$ | $I$ (M) |
|---|---|---|---|---|---|
| 1 | 2.059 | 7.601 | 2.344 | 12.004 | 0.060 |
| 2 | 2.240 | 6.920 | 2.710 | 11.870 | 0.057 |
| 3 | 1.757 | 7.526 | 2.557 | 11.840 | 0.064 |
| 4 | 3.824 | 3.110 | 4.936 | 11.870 | 0.043 |
| 5 | 4.106 | 2.947 | 4.845 | 11.898 | 0.057 |
| 6 | 1.780 | 7.392 | 2.549 | 11.721 | 0.120 |
| 7 | 3.298 | 3.653 | 4.555 | 11.506 | 0.276 |
| 8 | 3.590 | 3.623 | 4.456 | 11.669 | 0.325 |
| 9 | 2.054 | 7.602 | 2.339 | 11.996 | 0.059 |
| 10 | 1.748 | 7.518 | 2.547 | 11.813 | 0.062 |
| 11 | 4.110 | 2.954 | 4.851 | 11.915 | 0.064 |
| 12 | 3.301 | 3.650 | 4.560 | 11.511 | 0.273 |

$pK_{s0} = 12.95 - 14g(I) + 3.28I$

[a] ES4ECI calculations, from analytical concentrations of the species, after precipitation (Table A1) and from formation constants of hemimellitate with $H^+$, $Na^+$ and $Ca^{2+}$. The formation of $NaCl^0$ and $CaCl^+$ was also taken into consideration.

Table A5
Ca–1,2,3,4-butanetetracarboxylate–H system. Composition of the precipitate (mmol)

| Run | Ca [a] | L [b] |
|---|---|---|
| 1 | 0.793 | 0.396 |
| 2 | 1.359 | 0.679 |
| 3 | 1.402 | 0.701 |
| 4 | 1.829 | 0.914 |
| 5 | 1.474 | 0.737 |
| 6 | 0.381 | 0.191 |
| 7 | 0.389 | 0.194 |
| 8 | 1.550 | 0.775 |
| 9 | 1.567 | 0.784 |
| 10 | 2.708 | 1.354 |
| 11 | 3.665 | 1.832 |
| 12 | 1.575 | 0.787 |
| 13 | 1.605 | 0.803 |
| 14 | 1.678 | 0.839 |
| 15 | 1.246 | 0.623 |
| 16 | 0.492 | 0.246 |
| 17 | 1.226 | 0.613 |
| 18 | 1.264 | 0.632 |
| 19 | 1.318 | 0.659 |
| 20 | 1.296 | 0.648 |

[a] Calculated from $[(C_{Ca})_b - (C_{Ca})_a]$ (see Table A4) and by considering the volume (100 ml) of the solution.
[b] These quantities are one half of the corresponding values for Ca.

ence between its initial content and that precipitated (8.14 mM (see Table A7, column 8 and footnote b)). Taking into account the differences in the ion concentrations before and after precipitation and the volume of the solution, we can calculate the number of mmol of $Ca^{2+}$, $L^{3-}$ and $H^+$ in the precipitate (3.964, 2.765, 0.367, respectively (see Table A8, columns 2,3 and 4)). By considering that the proton is present in the precipitate as CaLH (see consid-

Table A4
Ca–1,2,3,4-butanetetracarboxylate–H system. Analytical concentrations (mM) of the solutions

| Run | Before precipitation, $(C_i)_b$ | | | | | After precipitation, $(C_i)_a$ | |
|---|---|---|---|---|---|---|---|
| | Ca | L | H | NaCl [a] | $Me_4NCl$ [a] | Ca | L [b] |
| 1 | 40.38 | 10.0 | 20.16 | 19.44 | – | 32.45 | 6.04 |
| 2 | 30.28 | 10.0 | 10.43 | 29.91 | – | 16.69 | 3.21 |
| 3 | 40.38 | 10.0 | 10.19 | 29.91 | – | 26.36 | 2.99 |
| 4 | 21.54 | 10.0 | 2.39 | 37.89 | – | 3.25 | 0.86 |
| 5 | 25.57 | 20.0 | 40.53 | 39.88 | – | 10.83 | 12.63 |
| 6 | 40.38 | 20.0 | 60.31 | 80.76 | – | 36.57 | 18.09 |
| 7 | 50.67 | 20.0 | 60.73 | 19.94 | – | 46.78 | 18.06 |
| 8 | 35.30 | 20.0 | 40.66 | 39.88 | – | 19.70 | 12.25 |
| 9 | 45.06 | 20.0 | 40.82 | 39.88 | – | 29.39 | 12.17 |
| 10 | 45.06 | 20.0 | 20.83 | 59.82 | – | 17.98 | 6.46 |
| 11 | 45.06 | 20.0 | 4.98 | 75.77 | – | 8.41 | 1.68 |
| 12 | 21.04 | 20.0 | 39.44 | – | – | 5.29 | 12.13 |
| 13 | 45.59 | 20.0 | 40.90 | – | – | 29.54 | 11.97 |
| 14 | 61.35 | 20.0 | 40.50 | – | – | 44.57 | 11.61 |
| 15 | 20.35 | 20.0 | 40.96 | – | 390.1 | 7.89 | 13.77 |
| 16 | 51.28 | 20.0 | 60.41 | – | 168.0 | 46.36 | 17.54 |
| 17 | 20.51 | 20.0 | 42.51 | – | 604.6 | 8.25 | 13.87 |
| 18 | 20.43 | 20.0 | 42.69 | – | 302.3 | 7.79 | 13.68 |
| 19 | 20.66 | 20.0 | 42.14 | – | 201.5 | 7.48 | 13.41 |
| 20 | 20.51 | 20.0 | 42.30 | – | 201.5 | 7.55 | 13.52 |

[a] NaCl and $Me_4NCl$ were added for ionic strength adjustment.
[b] Concentrations calculated from: $(C_L)_a = (C_L)_b - [(C_{Ca})_b - (C_{Ca})_a]/2$.

Table A6
Ca–1,2,3,4-butanetetracarboxylate–H system. Free concentrations of species [a], $I$ values [a], and $pK_{s0}$ calculations

| Run | pCa | pL | pH | $(2pCa + pL) = pK_{s0}$ | $I$ (M) |
|---|---|---|---|---|---|
| 1 | 1.566 | 9.682 | 3.12 | 12.814 | 0.049 |
| 2 | 1.842 | 9.303 | 3.33 | 12.987 | 0.038 |
| 3 | 1.642 | 9.774 | 3.18 | 13.058 | 0.049 |
| 4 | 2.539 | 7.940 | 3.97 | 13.018 | 0.031 |
| 5 | 2.113 | 8.471 | 3.36 | 12.697 | 0.048 |
| 6 | 1.566 | 9.445 | 3.05 | 12.577 | 0.050 |
| 7 | 1.451 | 9.660 | 2.97 | 12.562 | 0.061 |
| 8 | 1.826 | 9.166 | 3.17 | 12.818 | 0.045 |
| 9 | 1.642 | 9.450 | 3.08 | 12.734 | 0.056 |
| 10 | 1.843 | 8.955 | 3.29 | 12.641 | 0.058 |
| 11 | 2.147 | 8.312 | 3.67 | 12.606 | 0.060 |
| 12 | 2.452 | 8.703 | 3.43 | 13.607 | 0.012 |
| 13 | 1.615 | 9.554 | 3.02 | 12.784 | 0.072 |
| 14 | 1.017 | 9.997 | 2.98 | 12.031 | 0.093 |
| 15 | 2.404 | 7.132 | 3.66 | 11.940 | 0.406 |
| 16 | 1.495 | 9.451 | 2.93 | 12.441 | 0.260 |
| 17 | 2.487 | 7.031 | 3.75 | 12.005 | 0.617 |
| 18 | 2.382 | 7.082 | 3.65 | 11.846 | 0.319 |
| 19 | 2.362 | 7.147 | 3.62 | 11.871 | 0.219 |
| 20 | 2.361 | 7.111 | 3.63 | 11.833 | 0.217 |

$$pK_{s0} = 14.53 - 24g(I) + 4.63I$$

[a] ES4ECI calculations, from analytical concentrations of the species, after precipitation (Table A4) and from formation constants of 1,2,3,4-butanetetracarboxylate with $H^+$, $Na^+$, $Ca^{2+}$. The formation of $NaCl^0$ and $CaCl^+$ was also taken into consideration.

Table A8
Ca–citrate–H system. Composition of the precipitate [a] (mmol)

| Run | Ca | L | H | CaLH [b] | $Ca_3L_2$ [c] |
|---|---|---|---|---|---|
| 1 | 4.037 | 2.807 | 0.346 | 0.346 | 1.230 |
| 2 | 2.936 | 2.093 | 0.405 | 0.405 | 0.844 |
| 3 | 2.280 | 1.665 | 0.435 | 0.435 | 0.615 |
| 4 | 3.964 | 2.765 | 0.367 | 0.367 | 1.199 |
| 5 | 4.318 | 2.960 | 0.242 | 0.242 | 1.359 |
| 6 | 3.968 | 2.745 | 0.258 | 0.258 | 1.237 |
| 7 | 4.045 | 2.801 | 0.312 | 0.312 | 1.244 |
| 8 | 2.523 | 1.841 | 0.475 | 0.475 | 0.683 |
| 9 | 2.448 | 3.413 | 0.218 | 0.218 | 0.743 |
| 10 | 4.539 | 3.026 | – | – | 1.513 |
| 11 | 4.508 | 3.006 | – | – | 1.503 |
| 12 | 4.534 | 3.022 | – | – | 1.511 |
| 13 | 4.753 | 3.048 | – | – | 1.524 |
| 14 | 4.632 | 3.152 | 0.191 | 0.191 | 1.480 |
| 15 | 3.592 | 2.643 | 0.745 | 0.745 | 0.949 |
| 16 | 4.007 | 2.898 | 0.680 | 0.680 | 1.109 |
| 17 | 4.408 | 3.159 | 0.661 | 0.661 | 1.249 |
| 18 | 4.638 | 3.311 | 0.657 | 0.657 | 1.327 |
| 19 | 4.979 | 3.542 | 0.668 | 0.668 | 1.437 |

[a] Calculated from $[(C_i)_b - (c_i)_a]$ (see Table A7) and by considering the volume (100 ml) of the solution.
[b] All protons are present in the precipitate as CaLH.
[c] Calculated as $[(\text{mmol Ca})_{tot} - (\text{mmol Ca})_{as\ CaLH}]3$.

Table A7
Ca–citrate–H system. Analytical concentrations (mM) of the solutions

| Run | Before precipitation $(C_i)_b$ | | | | | After precipitation $(C_i)_a$ | | |
|---|---|---|---|---|---|---|---|---|
| | Ca | L | H | NaCl [a] | $Me_4NCl$ [a] | Ca | L [b] | H |
| 1 | 52.63 | 35.09 | 10.86 | – | – | 12.26 | 7.02 | 7.40 |
| 2 | 50.00 | 33.34 | 20.73 | – | – | 20.64 | 12.41 | 16.68 |
| 3 | 51.31 | 34.21 | 30.60 | – | – | 28.51 | 17.56 | 26.25 |
| 4 | 53.68 | 35.79 | 10.86 | 102.7 | – | 14.04 | 8.14 | 7.19 |
| 5 | 53.52 | 35.69 | 5.92 | 102.7 | – | 10.34 | 6.09 | 3.50 |
| 6 | 51.38 | 34.39 | 5.92 | 246.3 | – | 11.70 | 6.94 | 3.34 |
| 7 | 53.79 | 35.86 | 5.92 | 513.5 | – | 13.34 | 7.85 | 2.80 |
| 8 | 53.10 | 25.41 | 30.60 | – | – | 27.87 | 17.00 | 25.85 |
| 9 | 52.26 | 34.84 | 30.60 | – | – | 27.78 | 17.79 | 28.42 |
| 10 | 51.31 | 34.21 | – | – | 52.6 | 5.92 | 3.95 | – |
| 11 | 51.38 | 34.39 | – | – | 122.3 | 6.50 | 4.33 | – |
| 12 | 52.21 | 34.80 | – | – | 301.6 | 6.87 | 4.58 | – |
| 13 | 52.58 | 35.05 | – | – | 500.9 | 6.85 | 4.57 | – |
| 14 | 53.05 | 35.37 | 3.95 | – | – | 6.73 | 3.85 | 2.04 |
| 15 | 60.40 | 66.89 | 79.86 | – | – | 24.48 | 40.46 | 72.41 |
| 16 | 60.04 | 60.36 | 61.00 | – | – | 19.97 | 31.38 | 54.20 |
| 17 | 60.31 | 55.23 | 45.08 | – | – | 16.23 | 23.64 | 38.47 |
| 18 | 60.42 | 52.41 | 36.39 | – | – | 14.04 | 19.30 | 29.82 |
| 19 | 60.27 | 48.01 | 23.50 | – | – | 10.48 | 12.59 | 16.82 |

[a] NaCl and $Me_4NCl$ were added for ionic strength adjustment.
[b] Concentrations calculated from

$$(C_L)_a = (C_L)_b - \{[(C_{Ca})_b - (C_{Ca})_a] \times 2 + [(C_H)_b - (C_H)_a]\}/3$$

Table A9
Ca–citrate–H system. Free concentrations of the species [a], $I$ values [a], and $pK_{s0}$ calculations

| Run | pCa | pL | pH | $(pCa + pL + pH) = pK_{s0}$ | $(3pCa + 2pL) = pK_{s0}$ | $I$ (M) |
|---|---|---|---|---|---|---|
| 1 | 2.030 | 4.707 | 4.208 | 10.945 | 15.504 | 0.030 |
| 2 | 1.779 | 4.718 | 3.962 | 10.459 | 14.772 | 0.052 |
| 3 | 1.629 | 4.726 | 3.828 | 10.183 | 14.337 | 0.074 |
| 4 | 2.023 | 4.284 | 4.342 | 10.649 | 14.637 | 0.132 |
| 5 | 2.205 | 4.114 | 4.650 | 10.968 | 14.842 | 0.121 |
| 6 | 2.206 | 3.987 | 4.794 | 10.986 | 14.590 | 0.258 |
| 7 | 2.239 | 4.008 | 5.030 | 11.277 | 14.733 | 0.492 |
| 8 | 1.635 | 4.758 | 3.817 | 10.210 | 14.419 | 0.073 |
| 9 | 1.632 | 4.836 | 3.775 | 10.242 | 14.566 | 0.062 |
| 10 | 2.695 | 3.720 | (8.1) | – | 15.525 | 0.060 |
| 11 | 2.669 | 3.545 | (8.1) | – | 15.097 | 0.131 |
| 12 | 2.707 | 3.438 | (8.2) | – | 14.998 | 0.312 |
| 13 | 2.801 | 3.457 | (8.2) | – | 15.317 | 0.543 |
| 14 | 2.372 | 4.593 | 4.668 | 12.402 | 16.689 | 0.007 |
| 15 | 1.708 | 4.619 | 3.683 | 10.009 | 14.361 | 0.063 |
| 16 | 1.803 | 4.631 | 3.756 | 10.191 | 14.673 | 0.051 |
| 17 | 1.908 | 4.621 | 3.855 | 10.384 | 14.965 | 0.041 |
| 18 | 1.983 | 4.608 | 3.932 | 10.523 | 15.165 | 0.035 |
| 19 | 2.143 | 4.575 | 4.110 | 10.828 | 15.580 | 0.024 |
| | | | | $pK_{s0} = 11.35 - 14g(I) + 5.95I$ | $pK_{s0} = 16.95 - 30g(I) + 8.52I$ | |

[a] ES4ECI calculations, from analytical concentrations of the species, after precipitation (Table A7) and from formation constants of citrate with $H^+$, $Na^+$, $Ca^{2+}$. The formation of $NaCl^0$ and $CaCl^+$ was also taken into consideration.

erations in the text), mmol CaLH = mmol $H^+$ (0.367) and mmol $Ca_3L_2$ is 1/3 of the difference between the total mmol $Ca^{2+}$ in the precipitate minus mmol CaLH (1.199), as reported in Table A8 columns 5 and 6).

Starting from analytical concentrations of $Ca^{2+}$, $L^{3-}$, $Na^+$, $Cl^-$ and $H^+$ in solution, we have calculated the relative free concentrations. We underline that in the input data files to run ES4ECI, the mass balance equations of all the equilibria that taken place into the solution are taken into considerations, i.e. protonation of $L^{3-}$, complex formation between $L^{3-}$, $Na^+$ and $Ca^{2+}$, and formation of $NaCl^0$ and $CaCl^+$. For the considered run, we have obtained the following results: pCa = 2.023, pL = 4.284. pH = 4.342 (see Table A9, columns 2,3 and 4). Taking into consideration the definition of

Table B1
Analytical data and results of the thermogravimetric analysis

| Stage | Theoretical % weight loss | Reactions involved | Ratios of % weight loss | |
|---|---|---|---|---|
| | | | Theor. | Exper. |
| $Ca(hmt)H \cdot H_2O$ | | | | |
| 1 | 100 → 92.0 | $CaLH \cdot H_2O \rightarrow CaLH$ | 1.09 | 1.07 |
| 2 | 92.0 → 36.2 | $CaLH \rightarrow CaCO_3$ | 2.53 | 2.48 |
| 3 | 36.2 → 20.0 | $CaCO_3 \rightarrow CaO$ | 1.81 | 1.78 |
| $Ca_2(btc) \cdot 6H_2O$ | | | | |
| 1 | 100 → 84.0 | $Ca_2L \cdot 6H_2O \rightarrow Ca_2L \cdot 2H_2O$ | 1.19 | 1.21 |
| 2 | 84 → 75 | $Ca_2L \cdot 2H_2O \rightarrow Ca_2L$ | 1.12 | 1.12 |
| 3 | 75 → 47.5 | $Ca_2L \rightarrow 2\,CaCO_3$ | 1.58 | 1.55 |
| 4 | 47.5 → 26.0 | $2CaCO_3 \rightarrow 2CaO$ | 1.83 | 1.78 |
| $Ca_3(cit)_2 \cdot 4H_2O$ | | | | |
| 1 | 100 → 95.5 | $Ca_3L_2 \cdot 4H_2O \rightarrow Ca_3L_2 \cdot 3H_2O$ | 1.05 | 1.03 |
| 2 | 95.5 → 88.0 | $Ca_3L_2 \cdot 3H_2O \rightarrow Ca_3L_2$ | 1.09 | 1.11 |
| 3 | 88.0 → 54.0 | $Ca_3L_2 \rightarrow 3\,CaCO_3$ | 1.63 | 1.66 |
| 4 | 54.0 → 28.7 | $3CaCO_3 \rightarrow 3CaO$ | 1.88 | 1.78 |

$pK_{s0}$, we calculate the $pK_{s0}$ of CaHL (10.649) and of $Ca_3L_2$ (14.637) at $I = 0.132$ (see Table A9, columns 5,6 and 7). Starting from a $pK_{s0}$ value of the same species at different ionic strength values, we calculate the thermodynamic $pK_{s0}$ by fitting Eq. (2) (see text).

## Appendix B — Thermogravimetry

In this section we report full data on the thermal decomposition of the recovered precipitates (Table B1) and, as an example, the thermogravimetric diagram of $Ca_2$(btc) (Fig. B1).

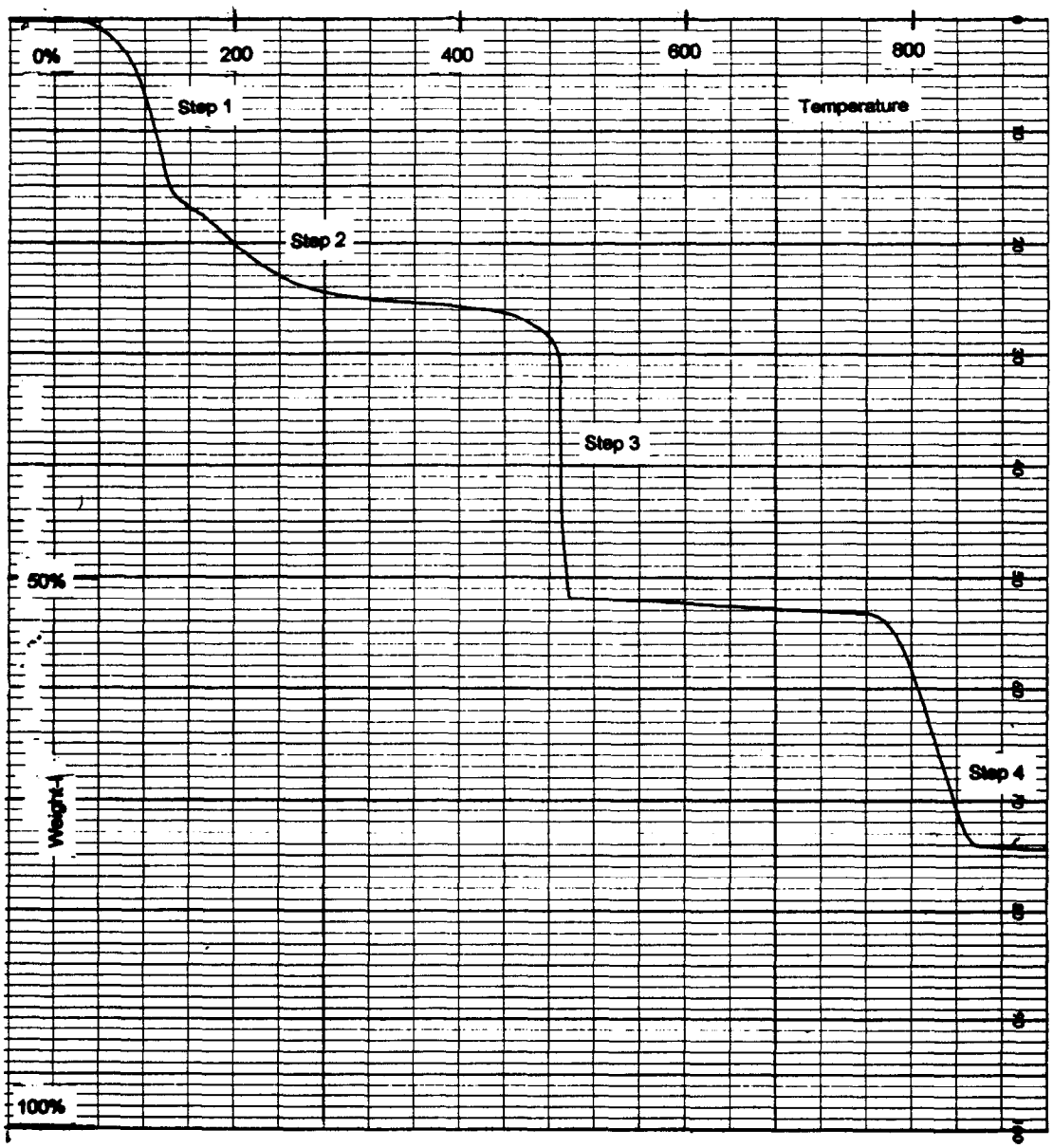


Fig. B1. Thermogravimetric diagram of $Ca_2$(btc).

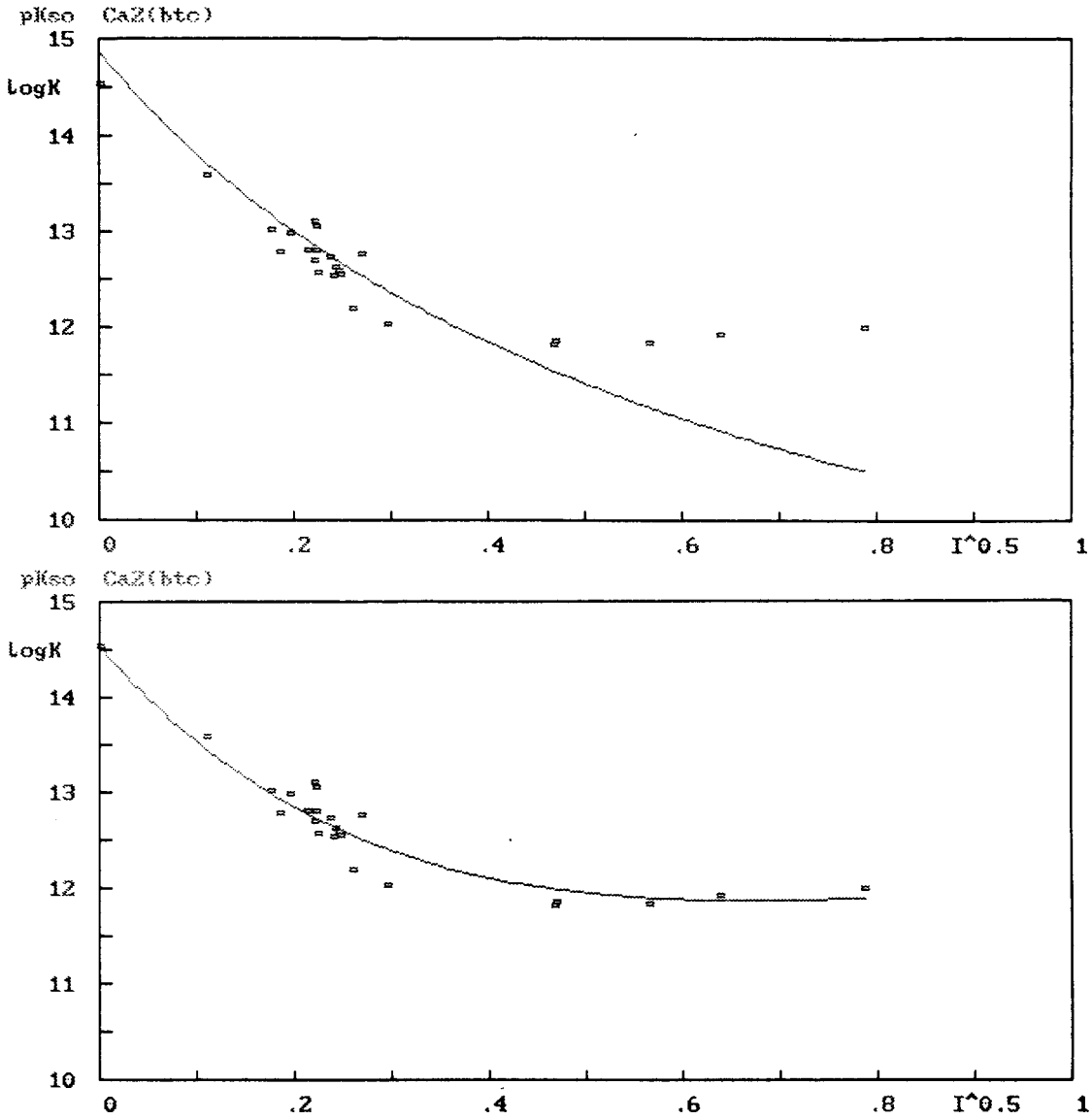


Fig. C1. Comparison of different equations for the dependence on $I$ of $pK_{s0}$ for the complex $Ca_2$(btc.) Top: Eq. (1) without linear term; no adjusted parameter. Bottom: Eq. (2) with C adjusted parameter.

## Appendix C

Here is graphically reported the role of parameter $C$ of the dependence on ionic strength of solubility product (Fig. C1).

## References

[1] L.G. Sillen and A.E. Martell, Stability Constants, Chem. Soc. Spec. Publ., no. 17, The Chemical Society, London, 1964; no. 25, 1971.

[2] D.D. Perrin, Stability Constants, Part B: Organic Ligands, Pergamon, Oxford, 1979.

[3] J.J. Christensen, L.D. Hansen, and R.M. Izatt, Handbook of Proton Ionization Heats, Wiley, New York, 1976.

[4] J.J. Christensen and R.M. Izatt, Handbook of Metal Ligand Heats, Dekker, New York, 1983.

[5] A.E. Martell and R.M. Smith, Critical Stability Constants, Plenum, New York, Vol. 1, 1974; Vol. 3, 1977; First Supplement, Vol. 5, 1982.

[6] R. Curini, G. D'Ascenzo, A. De Robertis, A. Casale and S. Sammartano, Thermochim. Acta, 173 (1990) 25.

[7] H.A. Flaschaka, EDTA Titrations, Pergamon, London, 1959.

[8] D.D. Perrin, W.L.F. Armorego and D.R. Perrin, Purification of Laboratory Chemicals, Pergamon, Oxford, 1966.

[9] C. De Stefano, P. Princi, C. Rigano and S. Sammartano, Ann. Chim. (Rome), 77 (1987) 643.

[10] C. De Stefano, P. Mineo, C. Rigano and S. Sammartano, Ann. Chim. (Rome), 83 (1993) 243; idem, unpublished results.

[11] P.G. Daniele, A. De Robertis, C. De Stefano, A. Gianguzza and S. Sammartano, J. Chem. Res., (1990) (S) 300 (M) 2316.
[12] P. Amico, P.G. Daniele, C. Rigano and S. Sammartano, Ann. Chim. (Rome), 72 (1982) 1.
[13] A. De Robertis, C. Foti and A. Gianguzza, Ann. Chim. (Rome), 83 (1993) 485.
[14] A. De Robertis, C. De Stefano, C. Rigano and S. Sammartano, J. Solution Chem., 19 (1990) 569.
[15] S.O. Ajayi, A. Olin and P. Svanstrom, Acta Chem. Scand., Ser. A, 33 (1979) 97.
[16] N. Purdie, M.B. Tomson and N. Riemann, J. Solution Chem., 1 (1972) 465.
[17] C. De Stefano, C. Foti and A. Gianguzza, Talanta, 41 (1994) 1715.
[18] P.G. Daniele, A. De Robertis, C. De Stefano, S. Sammartano and C. Rigano, J. Chem. Soc., Dalton Trans., (1985) 2353.
[19] P.G. Daniele, A. De Robertis, C. De Stefano and S. Sammartano, in S. Alegret et al. (Eds.), Miscellany of Scientific Papers Offered to Eric Casassas, Barcelona, Spain, 1991, p. 121.
[20] B. Sheldrick, Acta Crystallogr., Sect. B, 30 (1974) 2056.
[21] C.K. Johnson, Acta Crystallogr., Sect. B, 18 (1965) 1004.
[22] A. De Robertis, C. Rigano, S. Sammartano and O. Zerbinati, Thermochim. Acta, 115 (1987) 241.
[23] A. De Robertis, C. De Stefano, S. Sammartano and A. Gianguzza, Chem. Speciation Bioav., 6 (1994) 65.

ELSEVIER

Talanta 42 (1995) 1663–1673

Talanta

# Cyclic voltammetric analysis of pH-dependent complex formation equilibria in anion coordination chemistry

Antonio Doménech *, Enrique García-España, Jose Antonio Ramírez

*Department of Inorganic Chemistry, University of Valencia, c/Dr. Moliner 50, 46100 Burjassot, Valencia, Spain*

Received 5 January 1995; revised 29 March 1995; accepted 18 April 1995

**Abstract**

A procedure to analyze pH-dependent complex formation equilibria from cyclic voltammetry is described. Application to adduct formation equilibria between $[Fe(CN)_6]^{4-}$ and $[Fe(CN)_6]^{3-}$ with different polyammonium receptors is discussed. Extension to the interaction of substrates such as ATP, $NAD^+$, $NADP^+$, and carboxylate ions with these receptors by means of competitive interaction with hexacyanoferrate(II) ion is presented.

*Keywords:* Anion coordination chemistry; Cyclic voltammetry

## 1. Introduction

Anion coordination chemistry has been extensively studied over the last two decades [1–7]. A representative part of the research in this field is focused on the coordination of $[Fe(CN)_6]^{4-}$, $[Co(CN)_6]^{3-}$, carboxylates, ATP, ADP, and polyphosphates by polyammonium macrocycles and linear polyamines [8,9]. These compounds behave as anionic receptors because of their ability to form charged species in aqueous solution even at neutral pH and because of their capability to form multisite hydrogen-bond networks. These reagents are useful for analytical purposes; for instance, double armed crown ethers and armed macrocycles can be used as metal-selective reagents [10] and polyammonium macrocycles are useful for selective recognition of carboxylate ions [11].

The formation equilibria of anion-receptor adduct species can be represented as (charges omitted for brevity)

$$rX + sL + wH \rightleftharpoons X_r L_s H_w \quad (1)$$

In this kind of system, different receptor-substrate species differing only in their number of protons, $r$, are formed in a stepwise manner. Formation equilibria take place simultaneously with the protonation equilibria of the ligand, L, and, eventually, of the anionic substrate, X:

$$X + tH \rightleftharpoons XH_t \quad (2)$$

$$L + jH \rightleftharpoons LH_j \quad (3)$$

Since multiple protonation and complex formation equilibria are involved, computer-assisted analysis of potentiometric data has been extensively used to determine the stoichiometry and stability constants of the complex species [12].

Although potentiometry has surely been revealed as the most accurate technique to analyze multiple anion coordination equilibria [1–9], it is advisable to develop complementary techniques allowing for an independent quantitative study.

In some favourable cases there is a reduced number of complex species predominating in solution over a well-defined pH range. It is then possible to determine their stoichiometry

* Corresponding author.


*SSDI* 0039-9140(95)01625-2

and conditional formation constant by applying the classical stoichiometric methods to other techniques, such as spectrophotometry or polarimetry. In particular, the generalized Molar-Ratio method [13] can be applied to cyclic voltammetric and chronoamperometric techniques, yielding satisfactory results including, as already reported [14], the analysis of non-electroactive species from competitive complexation equilibria by electroactive agents.

In the present article, a method involving cyclic voltammetry is described as a generalization of the classical Viossat method [15–17]. The current method provides direct estimates of the degree of condensation, stoichiometry and number of protons in the complex species. This is based on estimations of the molar fraction of complexed substrate at different pH values by cyclic voltammetric and, eventually, chronoamperometric measurements. In spite of the fact that a variety of electrochemical techniques can be used, the simplicity of the treatment presented here together with the simplicity and versatility of cyclic voltammetric and chronoamperometric techniques makes this procedure a potentially interesting way of rapidly analyzing the data. The main points are: (i) the method can be applied to a variety of systems for which spectrophotometric techniques are unavailable; (ii) complex formation in two different oxidation states can be simultaneously investigated; (iii) the method can be applied to non-electroactive species by introducing any competing electroactive agent.

## 2. Cyclic voltammetric analysis of complex formation equilibria

Polarographic methods have long been found useful for studying complex formation equilibria. From the seminal work of DeFord and Hume [18], different methods have been developed for analyzing single and multiple complex formation equilibria, including, among others [19], multiple ligand systems [20] and investigation of non-electroactive species by means of the competitive complexation forming electroactive species [21,22].

The extension to cyclic voltammetry of classical polarographic techniques to study single and multiple metal–ligand equilibria has recently been described [23,24]. In addition, general simulation procedures for linear scan or cyclic voltammetric curves have been described for the characterization of complexes at small and large excess of ligand, and in pH-dependent complex equilibria [25–28]. Despite their usefulness, the extension of simulation procedures to complicated systems requires an accurate fit of a number of parameters, namely the diffusion coefficients of all the electroactive species and their electron transfer coefficients in the case of completely irreversible electrode processes. Further, deviations from reversibility in almost reversible systems or uncompensated ohmic losses in the cell can significantly distort the voltammetric curves [29], therefore increasing the difficulty of simulating the $i-E$ curves. The present method is based on the analysis of the currents for diffusion-controlled processes, as used in polarography for single [30–32] and competitive systems [21,22]. The application of competitive electrochemical studies in anion coordination chemistry was suggested in 1981 [33]. We consider here the general case in which both the uncomplexed anionic substrates and their complex ions are reversibly reduced (or oxidized) from a higher to a lower valency state, as occurs for the coordination of the $[Fe(CN)_6]^{4-}$ ion by polyammonium receptors.

Aqueous solutions of $[Fe(CN)_6]^{4-}$ exhibit a well-known reversible or quasi-reversible one-electron cyclic voltammetric couple which can be represented as

$$[Fe^{II}(CN)_6]^{4-} \rightleftharpoons [Fe^{III}(CN)_6]^{3-} + e^- \quad (4)$$

As shown in Fig. 1, upon addition of increasing amounts of a macrocyclic receptor at constant pH, an anodic shift of the peak potentials accompanied by a significant decrease of the peak current is observed. For receptor/$[Fe(CN)_6]^{4-}$ molar ratios $>1$, the cyclic voltammetric pattern remains unchanged [34,35]. The dependence of potentials and peak currents on the receptor/$[Fe(CN)_6]^{4-}$ molar ratio ($c_L/c_M$), plotted in Fig. 2 (curves A), clearly suggests that 1:1 electroactive complex species are formed.

In an excess of receptor, the observed dependence of the peak current and the peak potentials with the sweep rate corresponds to that expected for a one-electron process without kinetic or chemical complications [36]. Thus, one can conclude that electroactive $[Fe(CN)_6]^{4-}$-receptor species are oxidized reversibly:

$$[Fe^{II}(CN)_6LH_q]^{(4-q)-} \rightleftharpoons [Fe^{III}(CN)_6LH_q]^{(3-q)-} + e^- \quad (5)$$

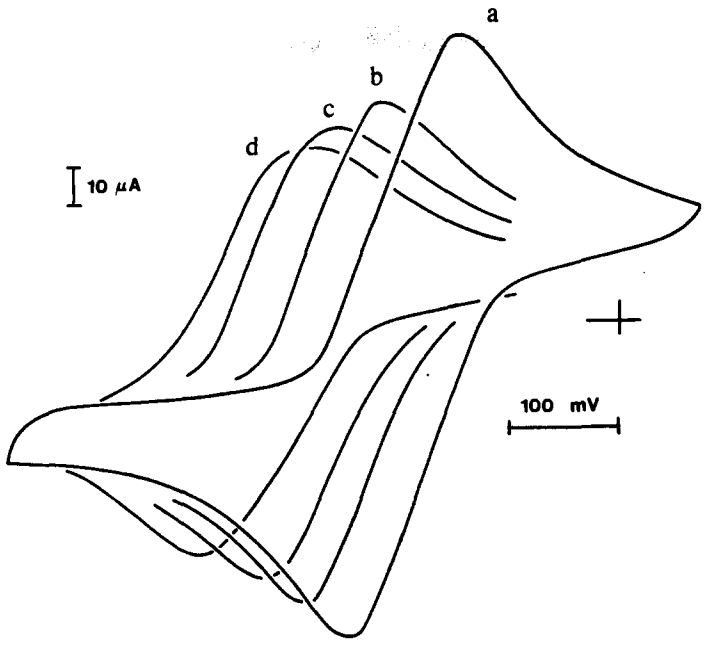


Fig. 1. pH-dependence of the cyclic voltammogram of a solution containing $[Fe(CN)_6]^{4-}$ (2.0 mM) and [21]aneN$_7$ (2.5 mM). Platinum electrode, $v = 0.10$ V s$^{-1}$. pH values: (a) 10.0; (b) 9.0; (c) 8.0; (d) 7.0.

As shown in Fig. 3, the formal potential of this couple becomes more positive when the pH decreases. In fact, at acidic pH values and for receptor/$[Fe(CN)_6]^{4-}$ molar ratios between 0 and 1, the difference in the formal potentials of free and coordinated $[Fe(CN)_6]^{4-}$ is sufficiently large to produce cyclic voltammetric curves which appear to be the superposition of two waves.

The observed cyclic voltammetric pattern must be described in terms of oxidation of two electroactive species in chemical equilibrium. This problem, subject to recent studies [37,38], is complicated by the fact that the electroactive species exhibit different diffusion coefficients and formal potentials.

For receptor/$[Fe(CN)_6]^{4-}$ molar ratios less than unity, no single correlations between the $i-E$ curves and the solution composition are available in the pre-peak region of potentials. Therefore, peak potentials and peak currents are not strictly suitable for measuring the composition of the solution.

The simplified treatment adopted here is based on the assumption that for potentials sufficiently past the electrode potential of all the electroactive species, the total current is governed by the diffusion of uncomplexed $[Fe(CN)_6]^{4-}$ and its adduct species. Thus, for potentials less than the voltammetric peaks, the current is controlled by Nernstian behaviour, while for potentials sufficiently past both the anodic and cathodic peaks, the current becomes purely diffusion-controlled in such a way that it can be described in terms of the $i-E$ form of the Cottrell equation [39–41]:

$$i = \frac{nFAcD^{1/2}v^{1/2}}{\pi^{1/2}(E - E^*)} \tag{6}$$

where $E^*$ represents the convergence potential at which the linear sweep voltammetric current becomes equal to the chronoamperometric current, and the other symbols have their usual significance. Since $E^*$ is, a priori, not known, it is convenient to rearrange this equation to give

$$\frac{1}{i^2} = \frac{\pi}{n^2F^2A^2c^2Dv}E - \frac{\pi E^*}{n^2F^2A^2c^2Dv} \tag{7}$$

For pure diffusion control, a plot of $1/i^2$ versus $E$ should give a straight line whose slope allows a direct estimate to be made of the diffusion coefficient $D$ for a defined composition of the solution. For a system in which both the metal and its complexes are electroactive, Eq. (7) can be applied inserting a mean diffusion coefficient, $D$, which can be defined as in polarography [19] verifying

$$D = \frac{\sum D_q\beta_q[L][H]^q}{\sum \beta_q[L][H]^q} \tag{8}$$

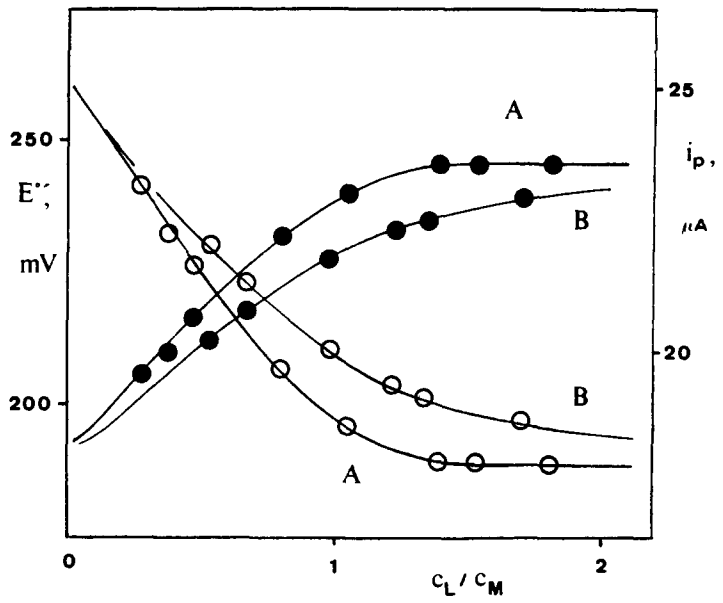


Fig. 2. Plots of the peak potential (●) and the peak current (○) as a function of the $c_L/c_M$ ratio for the $[Fe(CN)_6]^{4-}$–[18]aneN$_6$ (a) and $[Fe(CN)_6]^{4-}$–[18]aneN$_6$–ATP (B) systems at pH 7.50. All concentrations were 1.50 mM. CV at the GCE, scan rate 0.13 V s$^{-1}$.

Therefore, the molar fraction of complexed metal, defined as $\alpha_M = \Sigma [ML_nH_q]/c_M$, can be calculated at a given pH by

$$\alpha_M = (D - D_M)/(D_{ML} - D_M)$$
$$= (D/D_M - 1)/(D_{ML}/D_M - 1) \quad (9)$$

where $D_M$ denotes the diffusion coefficient of the $[Fe(CN)_6]^{4-}$ ion. $D_{ML}$ is the value for the diffusion coefficient of the complex species, which can be obtained as the limiting $D$ value in solutions containing a sufficiently large excess of receptor. As depicted in Fig. 4, the mean diffusion coefficient changes drastically with pH in the presence of receptor species, and the $D_{ML}$ values can be assigned to the plateau values in the $D = f(\text{pH})$ curve.

A direct estimate of these coefficients can be obtained from chronoamperograms at a potential sufficiently large to ensure diffusion-limited current for all species [39–41]. Alternatively, the diffusion coefficients can be directly calculated from the chronoamperometric analysis of the diffusive portion of the cyclic voltammograms. Independent $\alpha_M$ values for the Fe(II) and Fe(III) systems can then be calculated by studying separately the anodic and cathodic portions of the cyclic voltammograms. Providing a sufficiently large switching potential is attained, it is convenient to use a strip-chart recorder for satisfactorily defining the base line for current measurements [42].

If the total concentration of ligand reaches a sufficient excess, the plateaus in the $E^{\circ\prime} = f(\text{pH})$ curve can be associated with a sequence of different complex species quantitatively formed. The cyclic voltammograms thus obtained allow direct estimates of the formal potential and the diffusion coefficient of such complex species. The formal potential determined at the selected pH values as the half-sum of the peak potentials is given by

$$E^{\circ\prime}(M^{III}L/M^{II}L) = E^{\circ\prime}(M^{III}/M^{II}) + \frac{59}{n} \log \frac{\beta_{II}}{\beta_{III}} \quad (10)$$

Where $\beta_{II}$ and $\beta_{III}$ are, respectively, the stability constants of the $Fe^{II}$ and $Fe^{III}$ complexes. This equation can be applied to calculate the $\beta_{III}$ constants provided the $\beta_{II}$ constants are known.

For intermediate pH values, the apparent formal potential of the $Fe^{III}/Fe^{II}$ couple may be approached as [19]

$$E^{\circ\prime} = E^{\circ\prime}(M^{III}/M^{II}) + \frac{59}{n} \log \frac{\sum \beta_{II}[L][H]^p}{\sum \beta_{III}[L][H]^q} \quad (11)$$

On the assumptions that (a) all species exhibit nernstian behaviour, (b) total equilibrium is rapidly reached near the electrode surface, and (c) the pH of the solution does not change during the potential scan, not even near the electrode surface, Eq. (11) becomes

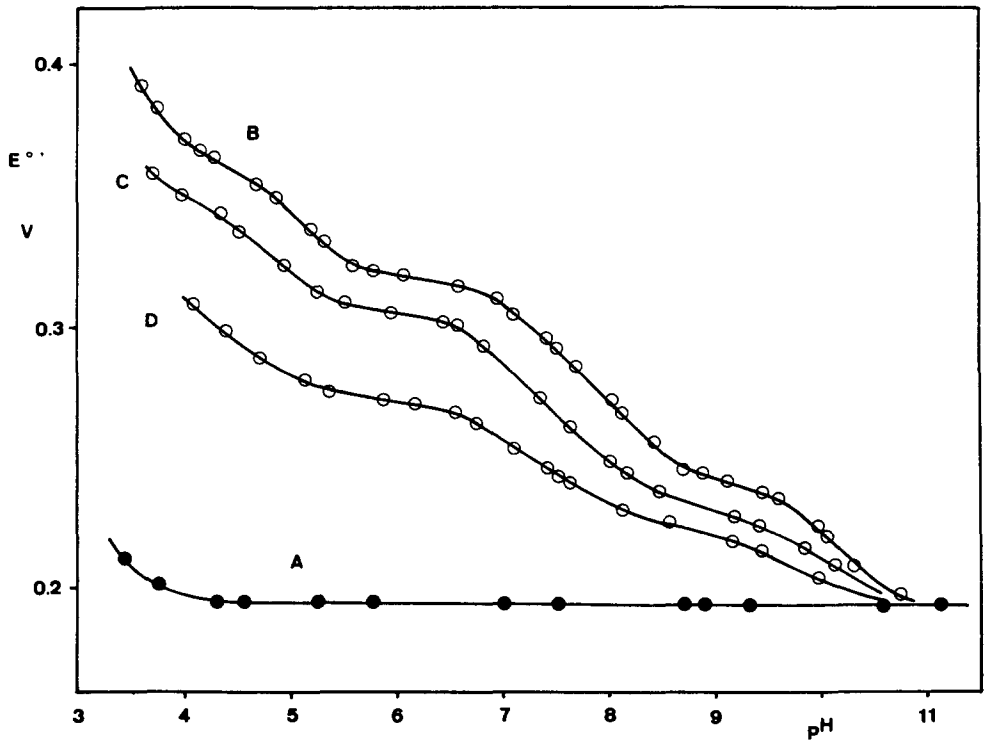


Fig. 3. Dependence of the formal potential on the pH for solutions containing: (A) $[Fe(CN)_6]^{4-}$; (B) $[Fe(CN)_6]^{4-}$ and [21]aneN$_7$; (C) as B in the presence of $NAD^+$; (D) as B in the presence of $NADP^+$. In all cases, from CV at the Pt electrode at $v = 0.10\ V\ s^{-1}$. All concentrations were 2.0 mM.

$$E^{\circ\prime} = E^{\circ\prime}(M^{III}/M^{II}) + \frac{59}{n} \log \frac{\sum \beta^{II}(c_L - n\alpha^{II}_M c_M)[H]^p}{\sum \beta^{III}(c_L - \alpha^{III}_M c_M)[H]^q} \quad (12)$$

where $c_L$, $c_M$ represent, respectively, the total concentrations of ligand and metal. The case $p = q$ must correspond to the plateau regions in the $E^{\circ\prime} = f(pH)$ curve.

Once the stability constants and the molar fractions have been calculated, the experimental values of $E^{\circ\prime}$ can be compared with those determined inserting into Eq. (12) different sequences of protonation numbers.

The above procedure can be extended to study the complexation of non-electroactive anions using the $[Fe(CN)_6]^{4-}$ ion as a competing substrate. Thus, upon addition of increasing amounts of ATP, $NAD^+$, $NADP^+$ and carboxylate anions to a equimolar solution of $[Fe(CN)_6]^{4-}$ and a macrocyclic ligand, the cyclic voltammogram exhibits intermediate parameters between that of free $[Fe(CN)_6]^{4-}$ and the limiting voltammogram in the presence of receptor as can be seen in curves B in Fig. 2.

In the used potential window (from +0.6 to −0.2 V versus SCE) no electrode processes affecting competitive $NAD^+$, $NADP^+$ substrates were detected, in agreement with data in the literature [43]. No adsorption complications were detected in ternary systems, and cyclic voltammograms exhibited identical parameters to those of the $[Fe(CN)_6]^{4-}$–receptor systems. Under these conditions, the evaluations of the molar fraction of complexed $[Fe(CN)_6]^{4-}$ allows for a direct estimate of the competitive effect of the non-electroactive anion.

## 3. Determination of the metal:ligand:proton stoichiometry

### 3.1. Single systems

To confirm the stoichiometry of the adduct species as well as the number of protons involved in the first formation step, a modified version of the Viossat method may be applied [15]. This requires that each one of the complex species predominates in a well-defined pH range. Thus, if the formation equilibrium of an $m$-nuclear complex is represented as,

$$mM + nL + qH = M_m L_n H_q \quad (13)$$

for given $c_L$, $c_M$, and pH values, $[M_m L_n H_q] =$

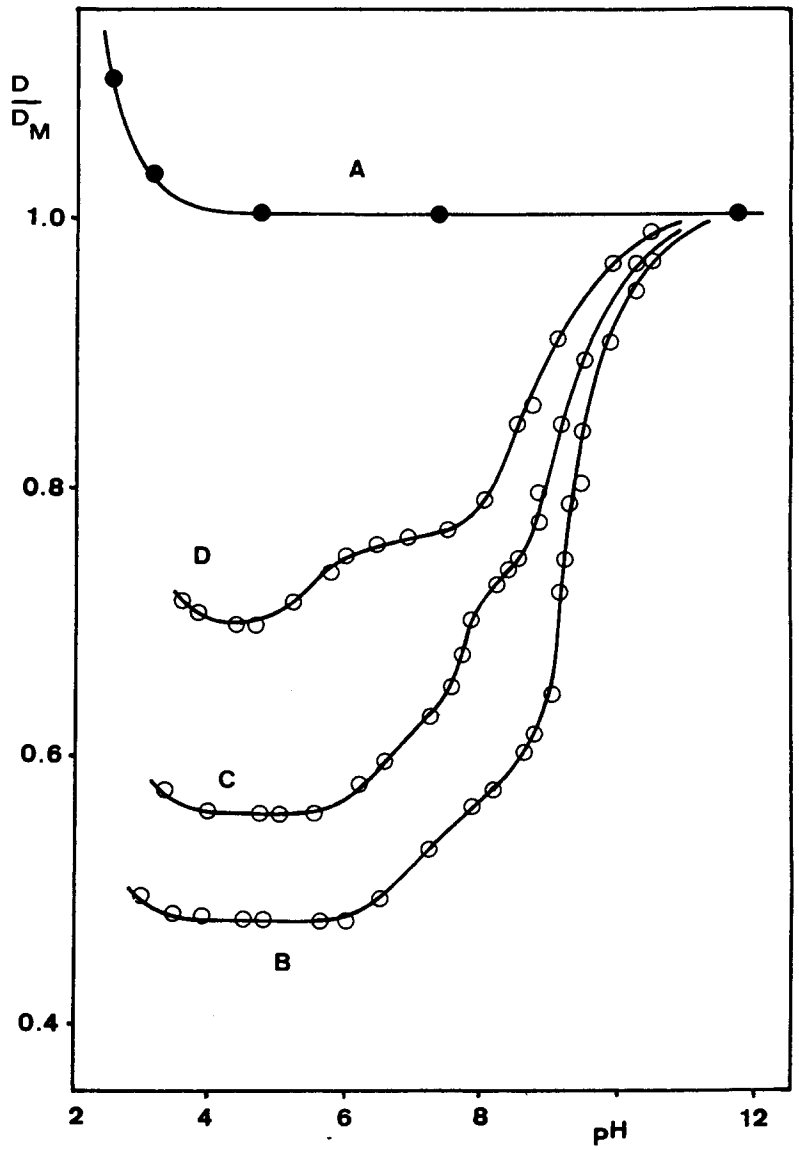


Fig. 4. Plots of $D/D_M$ versus pH for 2.0 mM solutions of potassium hexacyanoferrate(II); (A) alone; (B) with 2.0 mM [24]aneN$_8$; (C) as B with 2.0 mM $NAD^+$; (D) as B with 2.0 mM $NADP^+$.

$\alpha_M c_M/m$, $[M] = (1-\alpha_M)c_M$, and $[L] = (c_L - n\alpha_M c_M/m)/(1+\Sigma\beta_j[H]^j)$, $\beta_j$ being the protonation constant of the ligand. The equation for the equilibrium constant then reduces to

$$\beta_q = \frac{\alpha_M c_M^{1-m}(1+\Sigma\beta_j[H]^j)^n}{m(1-\alpha_M)^m(c_L - n\alpha_M c_M/m)^n[H]^q} \quad (14)$$

This equation can be rewritten as

$$f(\alpha, H) = \log \frac{\alpha_M^{1/n}(1+\Sigma\beta_j[H]^j)}{m^{1/n}(1-\alpha_M)^{m/n}(c_L - n\alpha_M c_M/m)^n}$$
$$= (1/n)\log\beta_q + [(m-1)/n]\log c_M + (q/n)\text{pH} \quad (15)$$

Providing the cumulative protonation constants of the ligand are known, this equation predicts a linear variation of $f(\alpha_M, H)$ with pH only for adequate values of the stoichiometric coefficients, $m$ and $n$. The number of protons, $q$, involved in the first complexation step is directly given by the slope of the $f(\alpha_M, H) = f(\text{pH})$ representation. The method can be easily extended to determine the number of protons involved in each intermediate complex formation step and must apply to both the $M^{II}$ and $M^{III}$ oxidation states.

### 3.2. Competitive systems

If the stoichiometry and stability constants of the adducts $M_m L_n H_q$ are known, the de-

scribed method can be extended to elucidate the number of protons of the complexes formed by the ligand with a non-electroactive substrate X (Eq. 1).

For a solution containing the electroactive species M, the substrate X, and the receptor, L, and assuming that only one M–L and one X–L complex species exist in the investigated pH range, the total concentration of ligand is

$$c_L = [L](1 + \Sigma \beta_j[H]^j) + n[M_m L_n H_q] + s[X_r L_s H_w] \quad (16)$$

If one calculates the concentration of uncomplexed ligand from the molar fraction of coordinated M (estimated from cyclic voltammetric data)

$$[L] = \frac{\alpha_M}{(1-\alpha_M)\beta_q[H]^q} \quad (17)$$

The molar fraction of complexed substrate, $\alpha_X$, can be calculated as

$$\alpha_X = \frac{c_L - (n/m)\alpha_M c_M - [L](1 + \Sigma \beta_j[H]^j)}{(s/r)c_X} \quad (18)$$

where $c_X$ is the total concentration of X. The $\alpha_M$ and $\alpha_X$ values must verify

$$g(\alpha_M, \alpha_X) = \log\left[\frac{m^{1/n}\alpha_X^{1/s}(1-\alpha_M)^{m/n}}{r^{1/s}\alpha_M^{1/n}(1-\alpha_X)^{r/s}}\right] = \log\frac{\beta_w^{1/s}}{\beta_q^{1/n}} + \log\frac{c_X^{(1-r)/s}}{c_M^{(1-m)/n}} + \left(\frac{w}{s} - \frac{q}{n}\right)\text{pH} \quad (19)$$

enabling us to evaluate the stoichiometry and number of protons involved in the complexation of the substrate X.

## 4. Experimental

A series of samples containing a constant amount of potassium hexacyanoferrate(II), ligand, and, eventually, competitive product, with a constant excess of ligand were prepared at different pH values in the range from pH 2.0 to 10.0. The supporting electrolyte was 0.15 M $NaClO_4$, the pH being adjusted to the required value by adding the appropriate amounts of $HClO_4$ and/or NaOH.

Cyclic voltammograms were obtained using a conventional device with a potentiostat (AR 100), a signal generator (Newtronic 200P), an $x$–$y$ recorder (Riken-Denshi F35) and a $y$–$t$ recorder (JJ CR550). A standard three-electrode cell was used with platinum ($A = 0.11$ cm$^2$), gold ($A = 0.018$ cm$^2$) and glassy carbon ($A = 0.071$ cm$^2$) working electrodes, a saturated calomel reference electrode (SCE) and a platinum-wire auxiliary electrode. No adsorption processes were detected and all working electrodes provided comparable results. To compensate for eventual differences in the effective area of the electrodes, $[Fe(CN)_6]^{4-}$ solutions were used as standard for each one of the series of experiments. The ratio $D/D_M$ was then tabulated for calculations.

All experiments were carried out under an argon atmosphere in a cell thermostatted at 298.15 K. Prior to a series of runs the working electrodes were cleaned, polished and activated [42].

The diffusion coefficients were also determined from the experimental $i$–$t$ chronoamperometric curves by applying the Cottrell equation, ($i = nFAcD^{1/2}/(\pi t)^{1/2}$) from the slope of the $i$ versus $t^{-1/2}$ plot. Since a recent report has stated that chronoamperometric data obtained at short times (< 1 s) are often unreliable and seems to imply that such data cannot be used to accurately determine diffusion coefficients [44], conventional long-time experiments were used. In all experiments, linear relationships between the observed anodic current and $t^{-1/2}$ were observed for times up to 3 s after the potential step.

For the cyclic voltammetric data, linear relationships between $1/i^2$ and $E$ were found in all cases for the +0.40 to 0.60 V potential range, corresponding to the diffusive region of the anodic cyclic voltammetric curve. The $D$ values calculated from the slope of these representations agreed with those calculated from chronoamperometric data.

Potentiometric measurements were carried out in aqueous solution at 298.1 K in the same medium by using equipment already described [8,9]. The program SUPERQUAD [45] was used to calculate the stability and protonation constants. The titration curves for each system were treated as a single set or separately without significant variations in the values of the constants.

## 5. Results and discussion

Different polyazaalkane–$[Fe(CN)_6]^{4-}$ systems have been examined to compare theoreti-

cal and experimental data. Prior potentiometric studies were carried out for each one of these systems. Several complexes with 1:1 receptor:$[Fe(CN)_6]^{4-}$ stoichiometry and different numbers of protons are formed in a stepwise manner. The stability constants of the hexacyanoferrate(II)–receptor species and protonation constants of ligand and, eventually, competitive agent were obtained.

CV-pH titrations confirm the stepwise pH-dependent formation of different complex species. Fig. 3 shows the pH-dependence of the formal potential for the system $[Fe(CN)_6]^{4-}$–[21]aneN$_7$ ([21]aneN$_7$ = 1,4,7,10,13,16,19-heptaazacyclohenicosane). Curve A corresponds to hexacyanoferrate(II) solutions and curve B corresponds to samples with a $[Fe(CN)_6]^{4-}$/ligand ratio of 1.50. The pH-dependence of the formal potential exhibits in all cases a close agreement with the distribution diagram calculated from potentiometric data.

Direct estimates of the percentages of complexed $[Fe(CN)_6]^{4-}$ calculated from the cyclic voltammetric diffusion coefficients (Eq. 7) are in close accordance with those independently obtained from the potentiometric data. Insertion of the $\beta_{II}$ and $\beta_{III}$ values calculated from anodic and cathodic currents into Eq. (12) provides $E^{\circ\prime}$ values close to that determined as the half-sum of the determined peak potential in all the studied cases.

The anion coordination equilibria between polyammonium receptors and non-electroactive monohydrogen carboxylate and dihydrogencarboxylate anions [8,9], ATP [46], and other anions has been studied by cyclic voltammetry and chronoamperometry on the basis of the competitive effect with the $[Fe(CN)_6]^{4-}$ ions. The addition of competitive anions to a solution containing $[Fe(CN)_6]^{4-}$ and a receptor causes a displacement of the cyclic voltammetric parameters towards those corresponding to the uncomplexed hexacyanoferrate(II). This can be seen in curves B of Fig. 2, and curves C and D of Fig. 3. As expected, increasing the amounts of substrate X leads to curves which increasingly differ from the limiting curves in the absence of competitive agent and approach those of uncomplexed hexacyanoferrate(II) solutions. Fig. 4 presents the pH dependence of the $D/D_M$ ratio for solutions of$[Fe(CN)_6]^{4-}$, [24]aneN$_8$ ([24]aneN$_8$ = 1,4,7,10,13,16,19,22-octaazacyclotetracosane) and $NAD^+$ or $NADP^+$ as a competitive agent. The diffusion coefficient of uncomplexed $[Fe(CN)_6]^{4-}$ at pH > 4 was taken as a reference ($D_M$). Below pH 4, this diffusion coefficient increases as the pH decreases; this fact is attributable to the protonation of the hexacyanoferrate(II) ion [47,48]. From these data, direct estimates of the molar fraction complexed $[Fe(CN)_6]^{4-}$ can be made quantifying

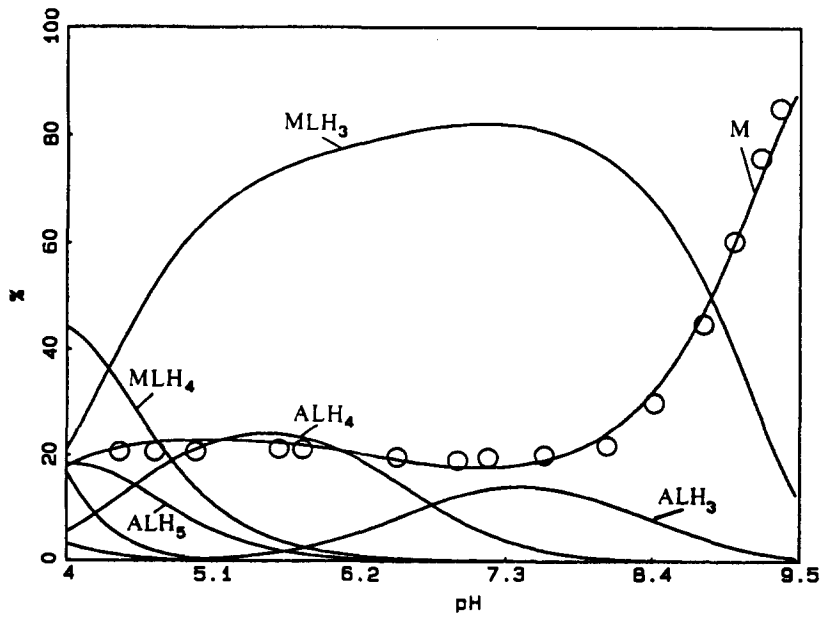


Fig. 5. Distribution diagram for a solution of $[Fe(CN)_6]^{4-}$ (1.36 mM), Me$_4$[18]aneN$_6$ (1.44 mM) and ATP (1.25 mM) calculated from potentiometric data. Circles represent the values of the molar fraction of uncomplexed $[Fe(CN)_6]^{4-}$ calculated from CV data.

the ability of $NAD^+$ and $NADP^+$ to link with the anionic receptor.

The $\alpha_M$ values calculated from CV and CA measurements can be compared with those estimated from the numerical analysis of potentiometric data. Fig. 5 plots the distribution diagram for the mixed system $[Fe(CN)_6]^{4-}$–$Me_4[18]aneN_6$–ATP($Me_4[18]aneN_6$ = 1,4,7,10,13,16-hexaazacyclooctadecane) in which the values of the molar fraction of uncomplexed $[Fe(CN)_6]^{4-}$ calculated from CV data have been represented as individual data points. This procedure allows a way of evaluating the selectivity in the different anion–receptor systems by measuring the differences in the molar fraction of complexed competitive agent [34].

However, the stoichiometry of the complex and the number of protons involved in the first complexation stage were calculated from the $D = f(pH)$ curves. As depicted in Fig. 6, corresponding to the $[Fe(CN)_6]^{4-}$–bmaph (bmaph = 1,17-bis(methylamino)-3,6,9,12,15-pentaazaheptadecane) system, a linear relationship between $f(\alpha_M, H)$ and pH is obtained only for the correct stoichiometric coefficients, $m = 1$ and $n = 1$. The slope of such a representation was $q = 4$, in accordance with potentiometric data. From Eq. (15) one obtains $\log \beta_q = 39.8(4)$ in excellent agreement with the potentiometric value, $\log \beta_q = 40.40(1)$.

Competitive experiments also provide satisfactory results. For instance, Table 1 shows the $g(\alpha_M, \alpha_X)$ values in the pH range from 8.4 to 9.6 for the competing complexation of [21]$aneN_7$ with hexacyanoferrate(II) and 1,3-BDC. A complex species with 1:1 sustrate:receptor stoichiometry was found, the first protonation step involving three protons: $q = w = 3$. For these cases, Eq. (20) reduces to $g(\alpha_M, \alpha_X) = \log(\beta_w/\beta_q)$, predicting the pH-independence of the $g(\alpha_M, \alpha_X)$ values. As can be seen in Table 1, for other $r$, $s$ values, the $g(\alpha_M, \alpha_X)$ function monotonically increases or decreases. Finally, the value of $\log(\beta_w/\beta_q)$ ($-0.31(5)$) is in good agreement with those calculated from potentiometric data ($\log \beta_q = 31.03(4)$, $\log \beta_w = 30.66(4)$). Table 2 summarizes the results for the competitive

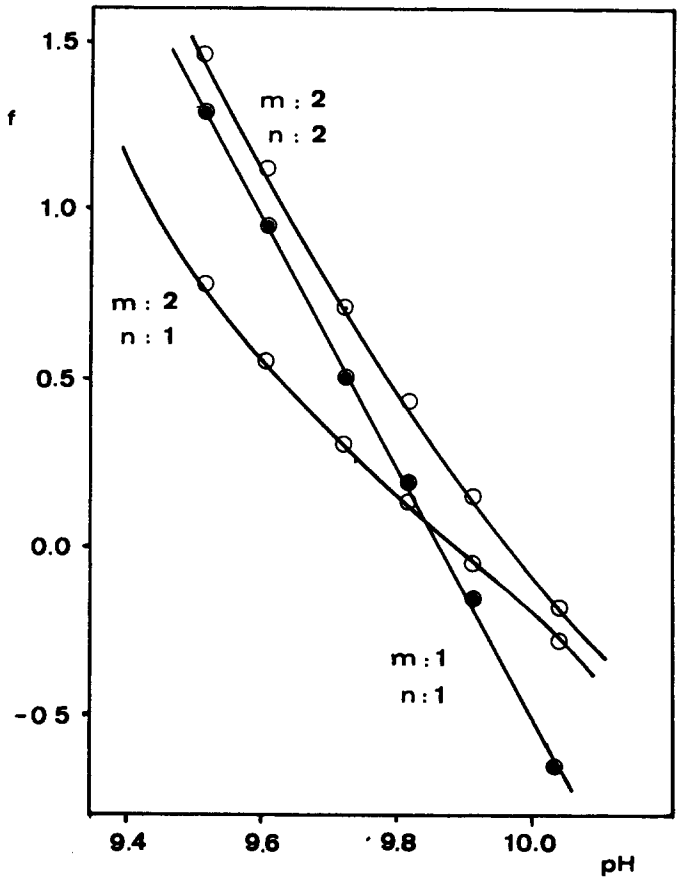


Fig. 6. Representation of $f(\alpha_M, H)$ versus pH for the $[Fe(CN)_6]^{4-}$–bmaph system for several $m$, $n$ coefficients.

Table 1
Analysis of the competitive complexation in the $[Fe(CN)_6]^{4-}$–[21]aneN$_7$–1,3-BDC system. All reagents in conc. 2.00 mM. Diffusion coefficients determined from the GCE cyclic voltammograms at 0.10 V s$^{-1}$. $D_{ML}/D_M = 0.450$. $g(\alpha_M, \alpha_X, H)$ values calculated from Eq. (19) assuming $m = n = 1$

| pH | $D/D_M$ | $\alpha_M$ | $s\alpha_X$ | $g(\alpha_M, \alpha_X, H)$ | | | |
|---|---|---|---|---|---|---|---|
| | | | | 1:1 | 2:2 | 1:2 | 2:1 |
| 9.60 | 0.953 | 0.085 | 0.037 | −0.38 | 0.18 | 0.16 | −0.33 |
| 9.50 | 0.934 | 0.120 | 0.062 | −0.31 | 0.14 | 0.12 | −0.23 |
| 9.40 | 0.912 | 0.161 | 0.083 | −0.33 | 0.06 | 0.04 | −0.21 |
| 9.20 | 0.865 | 0.246 | 0.138 | −0.31 | −0.03 | −0.08 | −0.09 |
| 9.00 | 0.824 | 0.320 | 0.188 | −0.31 | −0.10 | −0.16 | 0.01 |
| 8.80 | 0.793 | 0.377 | 0.223 | −0.32 | −0.15 | −0.23 | 0.08 |
| 8.60 | 0.770 | 0.418 | 0.245 | −0.34 | −0.19 | −0.28 | 0.12 |
| 8.40 | 0.760 | 0.436 | 0.280 | −0.30 | −0.17 | −0.28 | 0.27 |

Table 2
Comparison of potentiometric and cyclic voltammetric data for competitive systems. M = $[Fe(CN)_6]^{4-}$, L = [21]aneN$_7$. X = *c,c*-TMCTC (*cis,cis*-1,3,5-trimethyl-1,3,5-cyclohexanetricarboxylic), *c,t*-TMCTC (*cis,trans*-1,3,5-trimethyl-1,3,5-cyclohexanetricarboxylic), 1,2-BDC (1,2-benzenedicarboxylic), 1,3-BDC (1,3-benzenedicarboxylic), $NAD^+$ and $NADP^+$. In all cases, 1:1:3 stoichiometry was found. $\log \beta_M = 31.03(4)$

| Substrate | $\log \beta_X$ [a] | $\log(\beta_X/\beta_M)$ [a] | $\log(\beta_X/\beta_M)$ [b] |
|---|---|---|---|
| *c,c*-TMCTC | 31.05(7) | 0.0(1) | −0.05(8) |
| *c,t*-TMCTC | 30.23(4) | −0.80(8) | −0.70(8) |
| 1,2-BDC | 30.85(2) | −0.18(6) | −0.10(7) |
| 1,3-BDC | 30.66(4) | −0.37(8) | −0.31(5) |
| $NAD^+$ | 30.82(4) | −0.21(8) | −0.2(1) |
| $NADP^+$ | 31.05(5) | 0.02(9) | 0.1(1) |

[a] From potentiometric data. [b] From cyclic voltammetric data.

complexation of [21]aneN$_7$ by $[Fe(CN)_6]^{4-}$ and $NAD^+$, $NADP^+$ and different carboxylates.

To summarize, cyclic voltammetric data can be used in suitable cases to quantitatively study complex formation equilibria allowing direct estimates of the stoichiometry and the number of protons involved. A reasonable combination of potentiometric and voltammetric techniques is potentially interesting for analyzing complex formation in unstable oxidation states. Finally, cyclic voltammetric monitoring of competitive complexation can be used to establish the selective character of complexing agents.

## References


[1] F. Vötgle, H. Sieger and W.H. Müller, Top. Curr. Chem., 98 (1982) 197.
[2] E. Kimura, Top Curr. Chem., 128 (1985) 113.
[3] H.M. Colquhoun, J.F. Stoddart and D.J. Williams, Angew. Chem. Int., 25 (1986) 487.
[4] F.P. Schmidtchen, A. Gleich and A. Schimmer, Pure Appl. Chem., 61 (1989) 1535.
[5] B. Dietrich, M.W. Hosseini and J.M. Lehn, J. Am. Chem., 109 (1981) 1282.
[6] M.W. Hosseini, J.M. Lehn, L. Maggiora, K.B. Mertes and M.P. Mertes, J. Am. Chem. Soc., 109 (1987) 537.
[7] J.F. Marecek, C.P.A. Fisher and J. Burrows, Tetrahedron Lett., 29 (1988) 6231.
[8] E. García-España, M. Micheloni, P. Paoletti and A. Bianchi, Inorg. Chim. Acta, 102 (1985) L9–L11.
[9] A. Bencini, A. Bianchi, P. Dapporto, E. García-España, M. Micheloni and P. Paoletti, Inorg. Chem., 28 (1989) 1188–1191.
[10] H. Tsukube, Talanta, 40 (1993) 1313.
[11] A. Bencini, A. Bianchi, M.I. Burgueté, P. Dapporto, A. Doménech, E. García-España, S.V. Luis, P. Paoli and J.A. Ramírez, J. Chem. Soc., Perkin Trans., (1994) 569.
[12] F. Gaizer and I.I. Kiss, Talanta, 41 (1994) 419.
[13] A. Beltrán, D. Beltrán, A. Cervilla and J.A. Ramírez, Talanta, 30 (1983) 124.
[14] A. Bianchi, A. Doménech, E. García-España and S.V. Luis, Anal. Chem., 65 (1993) 3137.
[15] B. Viossat, Rev. Chim. Miner, 9 (1972) 737.
[16] A. Cervilla, J.A. Ramírez and E. Llopis, Can. J. Chem., 63 (1985) 1041.
[17] A. Doménech, E. Llopis, E. García-España and A. Cervilla, Trans. Met. Chem., 15 (1990) 425.
[18] D.D. DeFord and D.N. Hume, J. Am. Chem. Soc., 73 (1951) 5321.
[19] D.R. Crow, Polarography of Metal Compexes, Academic Press, London, 1970.
[20] W.B. Schaap and D.L. McMasters, J. Am. Chem. Soc., 83 (1961) 4699.
[21] G. Schwarzenbach, R. Gut and G. Anderegg, Helv. Chim. Acta, 37 (1954) 937.
[22] G. Schwarzenbach and H. Ackerman, Helv. Chim. Acta, 35 (1952) 485.
[23] H.M. Killa, J. Chem. Soc., Faraday Trans. 1, 81 (1985) 2659.
[24] H.M. Killa, Polyhedron, 8 (1989) 2299.
[25] G. Gampp, Anal. Chem., 59 (1987) 2456.
[26] J.E. Spell and R.H. Philp, J. Electroanal. Chem., 112 (1980) 281.

ELSEVIER

Talanta 42 (1995) 1675–1683

Talanta

# Palladium complexes in concentrated nitrate and acid solutions

E. Camacho Frias [1], H. Pitsch K. *[,2], J. Ly [2], C. Poitrenaud

*CEA-SACLAY, INSTN/SECh, 91191 Gif sur Yvette, France*

Received 25 January; revised 10 April 1995; accepted 11 April 1995

**Abstract**

A spectrophotometric study of palladium complexation in concentrated nitrate and acid solutions is presented. The water activity of the solutions was fixed to control activity coefficients. The existence of the species $PdNO_3^+$, $Pd(NO_3)_2$ and $PdOHNO_3$ has been evidenced and their stability was evaluated. An activity diagram for the predominance of soluble palladium species is presented and the precipitation limit is drawn.

*Keywords:* Palladium complexes; Concentrated solutions; Spectrophotometry

## 1. Introduction

Palladium is one of the most abundant transition metals among the fission products in nuclear spent fuel. Highly hydrolysable, it induces disturbances in the reprocessing operations: it interferes in the acidity monitoring of aqueous layers and complicates the separation of the phases in the liquid–liquid extraction operations by the formation of insoluble compounds. Within the programs devoted to control this type of problem in order to improve the Purex process, the purpose of the present work is to provide an accurate description of the chemical behaviour of palladium in acid solutions containing high concentrations of nitrate.

In aqueous solutions, the prevailing oxidation state of palladium is II, except for very strong complexes of Pd(IV) [1]. Shmidt et al. [2] confirmed this statement for nitric media when they reprecipitated $Pd(NO_3)_2$ from solutions obtained by dissolution of metallic palladium in 12 M nitric acid. Neither paratoluenesulphonate nor perchlorate forms complexes with palladium [3]. Jørgensen et al. [4] demonstrated that in concentrated perchloric acid, $Pd^{2+}$ is the unique species up to 0.01 M total metal; its absorption spectrum shows a large band with a maximum at 380 nm and a second one at 170 nm.

Hydrolysis of $Pd^{2+}$ is easily performed: in very dilute solutions, the formation of the complexes $PdOH^+$ and $Pd(OH)_2$ starts at pH $\approx$ 1 and insoluble $Pd(OH)_2$ precipitates from fairly acid solutions. Above pH 2, when the total concentration of palladium is higher than $10^{-5}$ M, polynuclear forms have been identified and their evolution into red-brownish polycondensated products has also been described [5–7]. Complexation with chloride ions has been studied spectrophotometrically [8,9], and it is known that palladium forms stable complexes or insoluble species with numerous organic molecules [3]. As far as nitrate is concerned, the complexes are certainly much less stable than those with chloride, but evolution of the absorption spectrum with the concentration of

* Corresponding author.

[1] Present address: Laboratoire de biochimie et bioorganique, ENSCP, 11 rue Pierre et Marie Curie, 75005 Paris, France.

[2] Present address: CEA, DCC/DESD/SESD/SGC, BP No 6, 92265 Fontenay aux Roses, France.



*SSDI* 0039-9140(95)01626-0

ELSEVIER

Talanta 42 (1995) 1675–1683

Talanta

# Palladium complexes in concentrated nitrate and acid solutions

E. Camacho Frias [1], H. Pitsch K. *,[2], J. Ly [2], C. Poitrenaud

*CEA-SACLAY, INSTN/SECh, 91191 Gif sur Yvette, France*

Received 25 January; revised 10 April 1995; accepted 11 April 1995

**Abstract**

A spectrophotometric study of palladium complexation in concentrated nitrate and acid solutions is presented. The water activity of the solutions was fixed to control activity coefficients. The existence of the species $PdNO_3^+$, $Pd(NO_3)_2$ and $PdOHNO_3$ has been evidenced and their stability was evaluated. An activity diagram for the predominance of soluble palladium species is presented and the precipitation limit is drawn.

*Keywords:* Palladium complexes; Concentrated solutions; Spectrophotometry

## 1. Introduction

Palladium is one of the most abundant transition metals among the fission products in nuclear spent fuel. Highly hydrolysable, it induces disturbances in the reprocessing operations: it interferes in the acidity monitoring of aqueous layers and complicates the separation of the phases in the liquid–liquid extraction operations by the formation of insoluble compounds. Within the programs devoted to control this type of problem in order to improve the Purex process, the purpose of the present work is to provide an accurate description of the chemical behaviour of palladium in acid solutions containing high concentrations of nitrate.

In aqueous solutions, the prevailing oxidation state of palladium is II, except for very strong complexes of Pd(IV) [1]. Shmidt et al. [2] confirmed this statement for nitric media when they reprecipitated $Pd(NO_3)_2$ from solutions obtained by dissolution of metallic palladium in 12 M nitric acid. Neither paratoluenesulphonate nor perchlorate forms complexes with palladium [3]. Jørgensen et al. [4] demonstrated that in concentrated perchloric acid, $Pd^{2+}$ is the unique species up to 0.01 M total metal; its absorption spectrum shows a large band with a maximum at 380 nm and a second one at 170 nm.

Hydrolysis of $Pd^{2+}$ is easily performed: in very dilute solutions, the formation of the complexes $PdOH^+$ and $Pd(OH)_2$ starts at $pH \approx 1$ and insoluble $Pd(OH)_2$ precipitates from fairly acid solutions. Above pH 2, when the total concentration of palladium is higher than $10^{-5}$ M, polynuclear forms have been identified and their evolution into red-brownish polycondensated products has also been described [5–7]. Complexation with chloride ions has been studied spectrophotometrically [8,9], and it is known that palladium forms stable complexes or insoluble species with numerous organic molecules [3]. As far as nitrate is concerned, the complexes are certainly much less stable than those with chloride, but evolution of the absorption spectrum with the concentration of

* Corresponding author.

[1] Present address: Laboratoire de biochimie et bioorganique, ENSCP, 11 rue Pierre et Marie Curie, 75005 Paris, France.

[2] Present address: CEA, DCC/DESD/SESD/SGC, BP No 6, 92265 Fontenay aux Roses, France.



*SSDI* 0039-9140(95)01626-0

nitrate shows evidence of complexation: the stability constant $\beta_1 = 1.2 \pm 0.4$ has been evaluated in nearly 2 M mixtures of $HNO_3$, $HClO_4$ and $NaClO_4$ at pH $\approx 0$ [4]. Mixed complexes with nitrate ions and organic ligands have also been reported [10]. Considering the strong hydrolysability of palladium, mixed species such as $PdOHNO_3$ are to be expected.

From the reviewed literature, several conclusions may be drawn. In the first place, perchloric acid is a good non-complexing reference medium for the purpose of this work. Secondly, spectrophotometry is an adequate method for characterising soluble nitric species of palladium. Considering the known stability data, large variations in the concentration of nitrate are necessary for an accurate determination of the thermodynamic constants; this implies that a strict control of medium effects is necessary. Finally, special care has to be taken at each step to avoid rapid or even slow precipitation of hydroxide.

## 2. Model for the non-ideality

The determination of low stability constants requires discrimination between chemical and medium effects, i.e. to strictly control the activity coefficients when the concentration of the ligand is varied over a large interval. This problem has been discussed elsewhere [11–13] and only the conclusions will be recalled here. For *simple systems*, i.e. solutions that obey Zdanovskii's law of water activity conservation through mixing [14], the activity coefficient of any species in the solution depends only on $a_w$, the water activity of the solution, and $\sigma$, the total concentration of dissolved species [15]:

$$y_k = f_k(a_w)/\sigma$$

where $f_k$ is a characteristic function of species k.

The activity of species k may be written as

$$a_k = (k) = [k] \cdot y_k = f_k(a_w) \cdot [k]/\sigma$$

where [k] is the concentration of k.

Hence, it appears that, at constant water activity, the activity of k is proportional to the ratio of its concentration to the total concentration of dissolved species. Consequently, we will from now on refer to this ratio as *the relative activity of k at the considered water activity*.

A further consequence is that any equilibrium may be described by a characteristic function of the water activity, say $G(a_w)$; for example, if $\beta_i^\circ$ is the thermodynamic constant of the following equilibrium:

$$M + iL \rightleftharpoons ML_i$$

$$\beta_i^\circ = [ML_i]/([L]^i[M])$$

$$= [[ML_i]/([L]^i[M])][f_{ML_i}/(f_L^i f_M)]\sigma^i$$

$$G_i(a_w) = \beta_i^\circ[(f_L^i f_M)/f_{ML_i}]$$

$G_i(a_w)$ depends only on the temperature and the water activity. When its value has been experimentally determined, the previous equations show that the concentration constant in any specific medium of known $a_w$ and $\sigma$ can be calculated in a simple way:

$$\beta_i = [ML_i]/([L]^i[M]) = G_i(a_w)/\sigma^i \quad (1)$$

The expression of the classical complexation coefficient [16,17] is

$$\alpha_{M(L)} = \sum [G_i(a_w)([L]/\sigma)^i]$$

Its value depends only on the temperature, on the activity of water and on the relative activity of the ligand at this value of $a_w$.

An important consequence is that a strict control of medium effects is obtained if the water activity in the system is fixed. Practically, this may be obtained in a relatively simple way using solutions with the same water activity. According to Zdanovskii's law, all their mixtures will have the same water activity. As far as data processing is concerned, the significant variable will be the above-mentioned ratio [k]/$\sigma$.

## 3. Experimental

### 3.1. General conditions

The fixed value of the activity of water ($0.750 \pm 0.002$) was chosen according to the conditions of the Purex process ($0.7 < a_w < 0.85$), the necessity to obtain the highest possible concentration of nitrates and the restrictions due to the limited solubility of the pure background salts that had to be used. Mixtures of nitrates, alkaline perchlorates and their corresponding acids follow Zdanovskii's rule over a large range of concentrations [18]. This oriented the choice of the electrolytes, as the

Table 1
Mother solutions

| Electrolyte | Concentration (mol $l^{-1}$) | Density (25°C) |
|---|---|---|
| $HNO_3$ | $5.180_1$ | 1.1632 |
| $HClO_4$ | $3.788_2$ | 1.2118 |
| $NaNO_3$ | $7.562_2$ | 1.3784 |
| $NaClO_4$ | $5.402_1$ | 1.4010 |

former model of non-ideality effects applies to these systems.

A highly acid medium was necessary to avoid precipitation risks and to limit hydrolysis in order to characterise pure nitrate complexes. Therefore, perchloric and nitric acid, diluted in order to reach $a_w = 0.75$, were used as the non-complexing and the most complexing medium, respectively, at the highest acidity level. To be able to explore the domain of hydroxylated or mixed complexes, sodium perchlorate and nitrate were chosen because of their high solubility, good hygroscopy and available purity; owing to the high concentration of the electrolytes (see Table 1), it is of course very important to use very pure products in order not to introduce any strong complexing agent which may interfere. All the media described in this paper were obtained by mixing these "pure poles"; Fig. 1 shows the corresponding points on the relative activity diagram. To avoid precipitation of palladium hydroxide, mother solutions of palladium could only be prepared in the pure acids. Therefore, the experimentally accessible activity domain is limited in the less acidic region. The lower limit in nitrate activity is due to the nitrates from the palladium salt which was dissolved to obtain the perchloric mother solution. The limits of the experimental domain are not straight lines because of the variation of $\sigma$ throughout the diagram and because of the formation of molecular nitric acid at high concentrations of nitrate [19].

### 3.2. Preparation of solutions

Vials, flasks, funnels and other glassware were rinsed with deionised water (MilliQ sys-

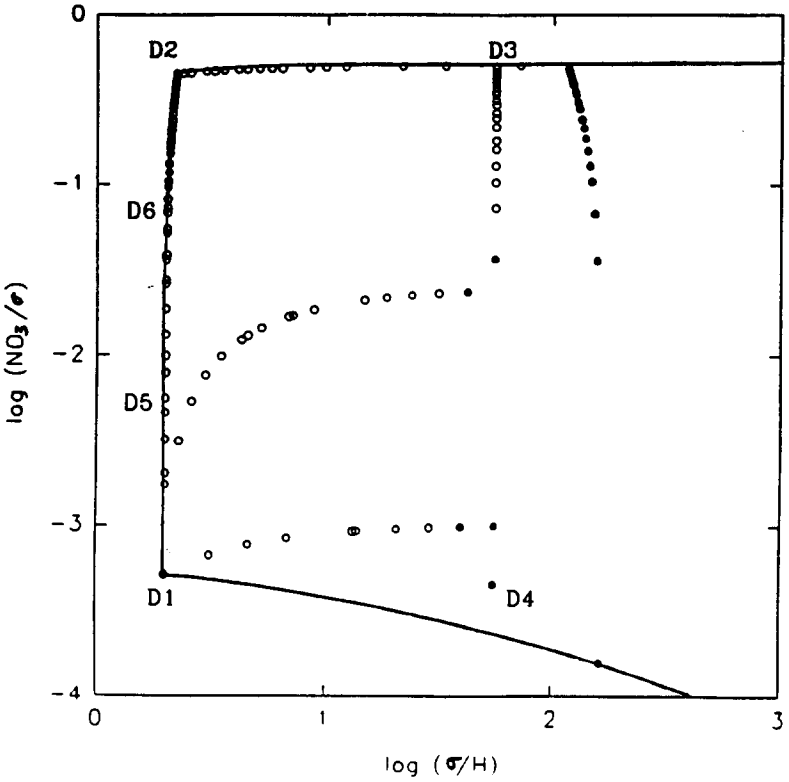


Fig. 1. Relative activity domain accessible at $a_w = 0.75$. Upper limits are imposed by the background electrolytes. The lower limit in the nitrate activity is set by the nitrates of the dissolved palladium salt. The experimental points used for the interpretation of solution equilibria are indicated by circles. Filled symbols denote solutions where slow precipitation was observed. Daughter solutions: D1, $HClO_4$; D2, $HNO_3$; D3, $HNO_3 + NaNO_3$; D4, $HClO_4 + NaClO_4$; D5 and D6, $HClO_4 + HNO_3$.

tem from Millipore), cleaned with 0.1 M perchloric acid and rinsed with water again. All reagents were of analytical grade (Merck, Prolabo and Strem Chemicals).

All primary solutions were prepared by weighing on a AE 260 Delta range balance from Mettler. They were filtered on Millipore HA (nitrates) or PTHK (perchlorates) filters; the porosity was 0.45 μm for "pure poles" and 0.22 μm for palladium solutions. Concentrations of background electrolytes were checked by densitometry at 25°C with a PAAR DMA 55 densitometer and adjusted to the exact value. Absence of precipitation was assumed if no diffusion of the light beam of a helium–neon laser was observed. Mixtures of solutions were also prepared by weighing, equilibrated at 25°C and checked for the absence of precipitation. Their density was measured and used to calculate the exact molar concentrations of the components. The error in the concentrations is estimated to be less than 0.1%.

Palladium nitrate was used to prepare the mother solutions in spite of its hygroscopy. Indeed, Pd is only soluble in concentrated nitric acid and its dissolution is difficult to control in terms of by-products, PdO is insoluble even in hot acids and $PdCl_2$ could not be used because of the complexing effect of the chloride. Two mother solutions were prepared by carefully adding the concentrated acid at $a_w = 0.75$ to the weighed salt and shaking on a Certomat HK thermoregulated bench for several hours. After filtering at 0.22 μm, the concentration was checked by the classical gravimetric method with dimethylglyoxime [20]; both solutions contained $(4.82 \pm 0.05) \times 10^{-2}$ mol $l^{-1}$ of palladium, in $HClO_4$ (solution M1) or $HNO_3$ (solution M2).

### 3.3. Spectrophotometry

Except when otherwise mentioned, absorptiometry in the region 350–800 nm was carried out on solutions containing a total palladium concentration of $2.41 \times 10^{-3}$ mol $l^{-1}$; this was chosen to be high enough to give a signal measurable with good accuracy and precision ($\pm 0.002$ uA) and sufficiently low to avoid precipitation. Neither the salt nor the acids used here absorb in this region, the only absorbing species being palladium components. The strong bands of the nitrate (maximum at 303 nm and 250 nm) do not allow work at shorter wavelengths. A model 634 UV/vis double-beam spectrophotometer from Varian and a Servotrace registrator were used for spectra scanning and absorption measurements. All experiments were carried out on solutions equilibrated at 25°C. In order to compensate for slight fluctuations in the temperature or instabilities of the instrument during the measurements, the actual analysed signal was the difference between the absorption at the desired wavelength and the absorption at 800 nm, where no significant signal is observed.

Table 2
Molar absorptivity coefficients (l $mol^{-1}$ $cm^{-1}$) of $Pd^{2+}$ in 3.788 M $HClO_4$

| Wavelength (nm) | This work | Literature | Ref. |
|---|---|---|---|
| 380 | $88.9 \pm 0.7$ | 86 | [4] |
| 392 | $91.1 \pm 0.7$ | | |
| 400 | $84.6 \pm 0.6$ | $85.0 \pm 0.5$ | [21] |
| 415 | $72.3 \pm 0.5$ | | |

## 4. Results and discussion

### 4.1. Absorbance of palladium solutions

In agreement with previous observations [3,4,21], it was assumed that, in the absence of chemical effects, the absorption spectrum of a given species in the visible region does not depend on the medium. This is likely to be true in our experimental conditions, inasmuch as the activity of water is maintained constant. Consequently, the changes in the spectrum of palladium solutions have been interpreted as the effect of complexing reactions.

The first question was then to define the reference point, i.e. to check that the free cation is the actual species in perchloric acid. This was done by measuring the variation in the absorbance at different wavelengths with the concentration of palladium nitrate dissolved in 3.788 M $HClO_4$. A straight line is obtained, showing that $Pd^{2+}$ is the unique species; the formation of a complex would have induced a non-linear dependency. At 415 nm, the regression equation on ten experimental points is $A = (72.3 \pm 0.5)C - (0.0006 \pm 0.0010)$, with $r^2 = 0.9999$. Similar results were obtained at other wavelengths, and the absorptivity coefficients of $Pd^{2+}$ are in good agreement with previous results (Table 2).

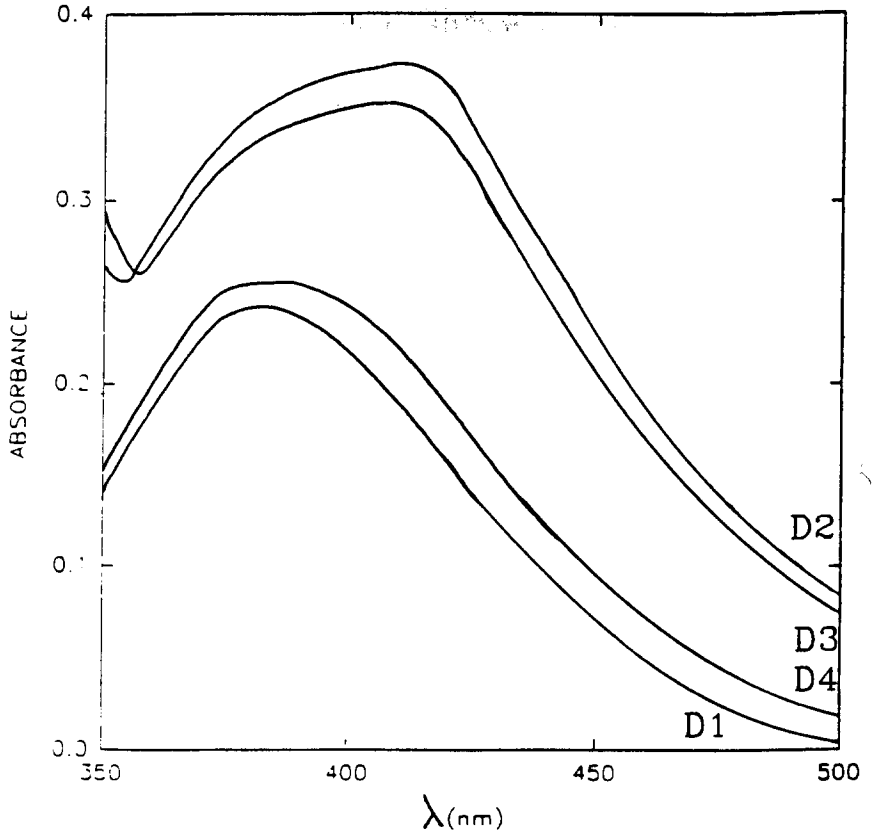


Fig. 2. Spectra of solutions of $2.41 \times 10^{-3}$ M palladium at the extremities of the explored domain. D1, $HClO_4$; D2, $HNO_3$; D3, $HNO_3 + NaNO_3$; D4, $HClO_4 + NaClO_4$.

Four daughter solutions containing $2.41 \times 10^{-3}$ M of total palladium were prepared by dilution of M1 with $HClO_4$ (solution D1) or $NaClO_4$ (D4), and of M2 with $HNO_3$ (D2) or $NaNO_3$ (D3), respectively. The absorption spectra of these solutions, which represent the extreme points of the accessible domain (Fig. 1) are shown in Fig. 2. It can be observed that, with respect to the perchloric acid solution (D1), the presence of nitrate greatly increases the absorbance (D2) whereas a decrease in the acidity has a much lesser, but not negligible, influence in a nitric (D3) as well as in a perchloric medium (D4). It can be concluded that complexation occurs with both nitrate and hydroxyl, and that a mixed complex cannot be discarded in the region of concentrated nitrate and low acidity (D3).

Complementary experiments have shown that in more concentrated nitric acid, up to 11.7 M, the large absorption band spreads onto two bands, indicating the presence of at least two nitric complexes. However, $2.41 \times 10^{-3}$ M palladium precipitates at pH 1 from dilute media without forming intermediate soluble complexes with $OH^-$ [6]. At $a_w = 0.75$, we observed that solutions of low acidity, denoted by filled symbols in Fig. 1, showed a relative instability; a colloidal precipitate formed after several weeks, while the other solutions remained stable for four months at least. It is possible that hydroxylated species like $Pd(OH)_x$ or $Pd_x(OH)_y$ could form as intermediates in a slow precipitation process and account for the differences between the spectra of D1 and D4. As this does not correspond to a thermodynamical equilibrium situation, the corresponding points were discarded from the selected set for the quantitative interpretation. As a reasonable hypothesis for the remaining domain, the following species were presumed: $Pd^{2+}$, $PdNO_3^+$, $Pd(NO_3)_2$ and $PdOHNO_3$.

### 4.2. Basic equations

For the considered species, according to the model chosen for non-ideality, the basic complexation equations and their characteristic water activity functions are

$$Pd^{2+} + iNO_3^- \rightleftharpoons Pd(NO_3)_i^{2-i}$$

$$G_{i0} = \frac{[Pd(NO_3)_i^{2-i}]}{[Pd^{2+}]([NO_3^-]/\sigma)^i}$$

$$Pd^{2+} + NO_3^- + H_2O \rightleftharpoons PdOHNO_3 + H^+$$

$$G_{11} = \frac{[PdOHNO_3]}{[Pd^{2+}]([NO_3^-]/\sigma)(\sigma/[H^+])}$$

The total concentration of palladium in any solution containing nitrates is

$$C_T = [Pd^{2+}] + [PdNO_3^+] + [Pd(NO_3)_2] + [PdOHNO_3]$$

and its complexation coefficient can be written as

$$\alpha_{Pd(NO_3,OH)} = C_T/[Pd^{2+}] = 1 + G_{10}[NO_3^-]/\sigma + G_{20}([NO_3^-]/\sigma)^2 + G_{11}([NO_3^-]/\sigma)(\sigma/[H^+])$$

The absorbance of this solution is

$$A = \varepsilon_{00}[Pd^{2+}] + \varepsilon_{10}[PdNO_3^+] + \varepsilon_{20}[Pd(NO_3)_2] + \varepsilon_{11}[PdOHNO_3]$$

where $\varepsilon_{ij}$ is the molar absorptivity coefficient of the species $Pd(NO_3)_i(OH)_j$.

Dividing $A$ by $C_T$ and rearranging the equation by introducing the formation functions, yields the following expression:

$$A = C_T \frac{\varepsilon_{00} + \varepsilon_{10}G_{10}[NO_3^-]/\sigma + \varepsilon_{20}G_{20}([NO_3^-]/\sigma)^2 + \varepsilon_{11}G_{11}([NO_3^-]/\sigma)(\sigma/[H^+])}{1 + G_{10}[NO_3^-]/\sigma + G_{20}([NO_3^-]/\sigma)^2 + G_{11}([NO_3^-]/\sigma)(\sigma/[H^+])} \quad (2)$$

It is then possible to calculate the complexation functions $G_{ij}$ and the absorptivity coefficients $\varepsilon_{ij}$ by fitting this function of the two variables $\sigma/[H^+]$ and $[NO_3^-]/\sigma$ to the measured values of the absorbance. $C_T$ is known, and $\varepsilon_{00}$ has been determined separately, as has been stated above. To calculate the values of the variables from the total acid and salt concentrations introduced in each solution, the formation equilibrium of nitric acid, which is the only weak background electrolyte, had to be taken into account:

$$H^+ + NO_3^- \rightleftharpoons HNO_3 \qquad G_H = \frac{[HNO_3]\sigma}{[NO_3^-][H^+]}$$

The value of $G_H$ can be calculated from published data of the dissociation coefficient of pure nitric acid in water [22]; at $a_w = 0.75$ it is 2.0212.

### 4.3. Determination of the complexation functions and the absorptivity coefficients

Different series of 10–25 solutions have each been prepared by mixing different proportions of two of the daughter solutions D1, D2, D3, D4 and two additional ones: D6 (M1 diluted with $HNO_3$) and D5 (M2 diluted with $HClO_4$). All these solutions contained the same concentration of palladium ($2.41 \times 10^{-3}$ M) and, according to Zdanovskii's law, had the same water activity (0.75). Their absorption at 415, 392 and 380 nm was measured after equilibration at 25°C. As the major absorbance difference in the spectra is observed at 415 nm, this wavelength has been chosen for the determination of the complexation functions. The results were interpreted for four series independently, after discarding those solutions where diffusion of the light beam of a laser showed initiating precipitation:

- — high acidity, large variation of $[NO_3/\sigma]$; mixture of D1 with D6 and D2 with D5;
- — low acidity, large variation of $[NO_3/\sigma]$; mixture of D3 with D4;
- — concentrated nitrates, variation of the acidity; mixture of D2 with D3.

Fig. 1 shows the representative points of all the examined solutions in the relative activity diagram.

As an example, the results for the first series are represented in Fig. 3: in these very acidic media, only $PdNO_3^+$ and $Pd(NO_3)_2$ are present and the expression of the absorbance reduces to

$$A = C_T \frac{\varepsilon_{00} + \varepsilon_{10}G_{10}[NO_3^-]/\sigma + \varepsilon_{20}G_{20}([NO_3^-]/\sigma)^2}{1 + G_{10}[NO_3^-]/\sigma + G_{20}([NO_3^-]/\sigma)^2}$$

The results for the four series provided compatible values of the absorptivity coefficients and the complexation functions which were used as initial values for a refined fitting over the whole set of data, numbering 97 altogether, using a Marquardt–Levenberg algorithm (Sigmaplot software, Jandel). The residuals of the fitting appear in Fig. 4; the mean relative absolute difference between measured and calculated values is 1.2%, and the relative standard deviation is 1.6%. The complexation functions are reported in Table 3, as well as the stability constants that can be deduced for a pure nitric acid medium at $a_w = 0.75$, using Eq. (1). The value obtained for $\beta_1$ is not significantly different from the estimate given by Jørgensen et al. [4], who did not strictly control

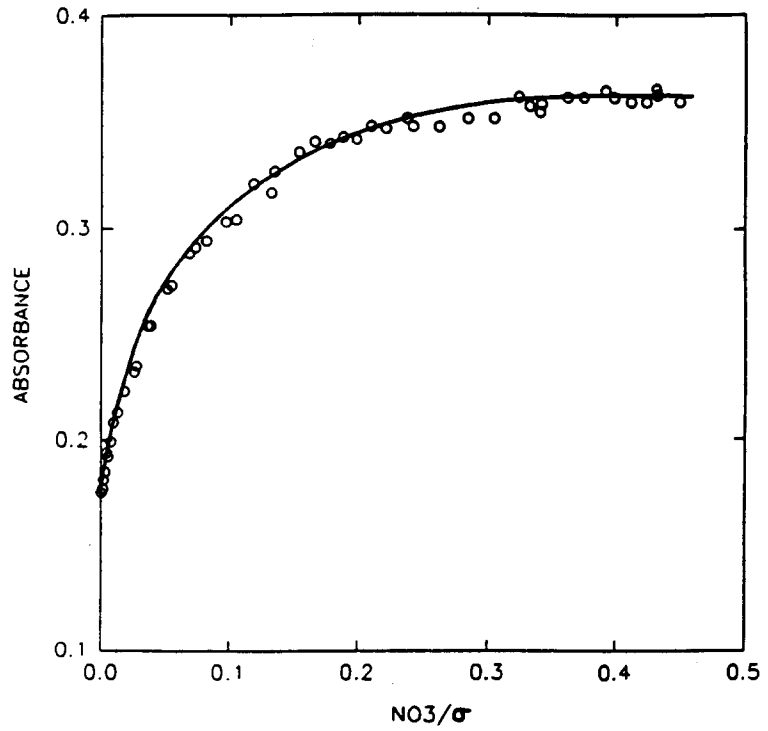


Fig. 3. Experimental absorbance values at $\lambda = 415$ nm in the very acidic region and fitted curve, considering only complexation with nitrate ions.

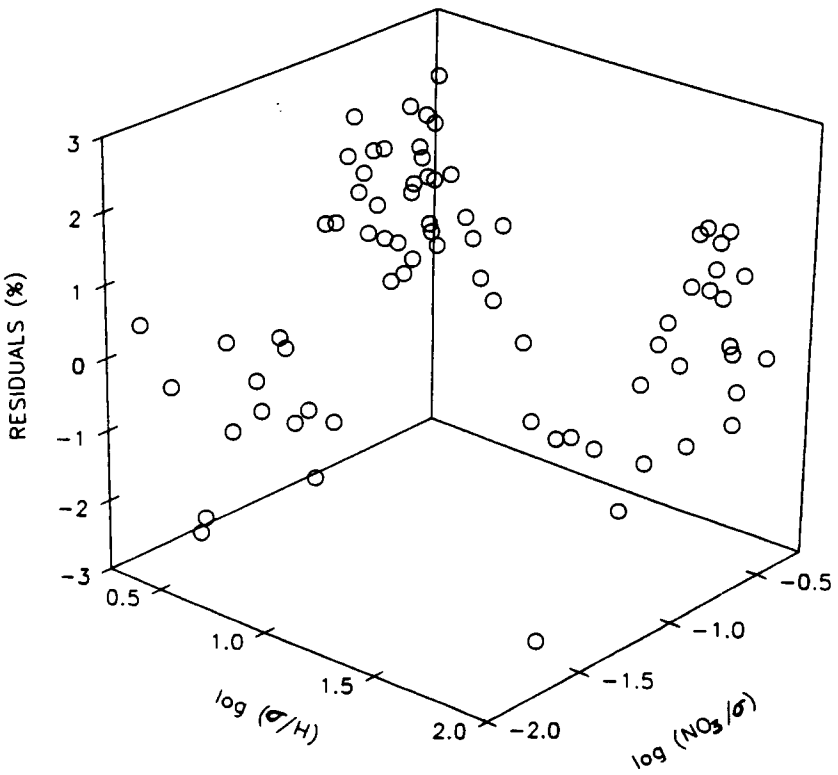


Fig. 4. Residuals of the final fitting to absorbance data at 415 nm.

Table 3
Complexation functions at $a_w = 0.75$ and deduced stability constants in 5.18 M nitric acid

| Species | $G_{ij}$ | $\beta_{ij}$ |
|---|---|---|
| $PdNO_3^+$ | 15.5 ± 0.8 | 1.47 ± 0.08 |
| $Pd(NO_3)_2$ | 19.2 ± 1.7 | 0.173 ± 0.015 |
| $PdOHNO_3$ | 0.224 ± 0.018 | 0.224 ± 0.018 |

Table 4
Molar absorptivity coefficients ($l\,mol^{-1}\,cm^{-1}$) of palladium complexes at different wavelengths

| Species | 415 nm | 392 nm | 380 nm |
|---|---|---|---|
| $PdNO_3^+$ | 163 ± 3 | 123 ± 5 | 116 ± 6 |
| $Pd(NO_3)_2$ | 147 ± 8 | 118 ± 16 | 112 ± 13 |
| $PdOHNO_3$ | 133 ± 5 | 104 ± 9 | 102 ± 6 |

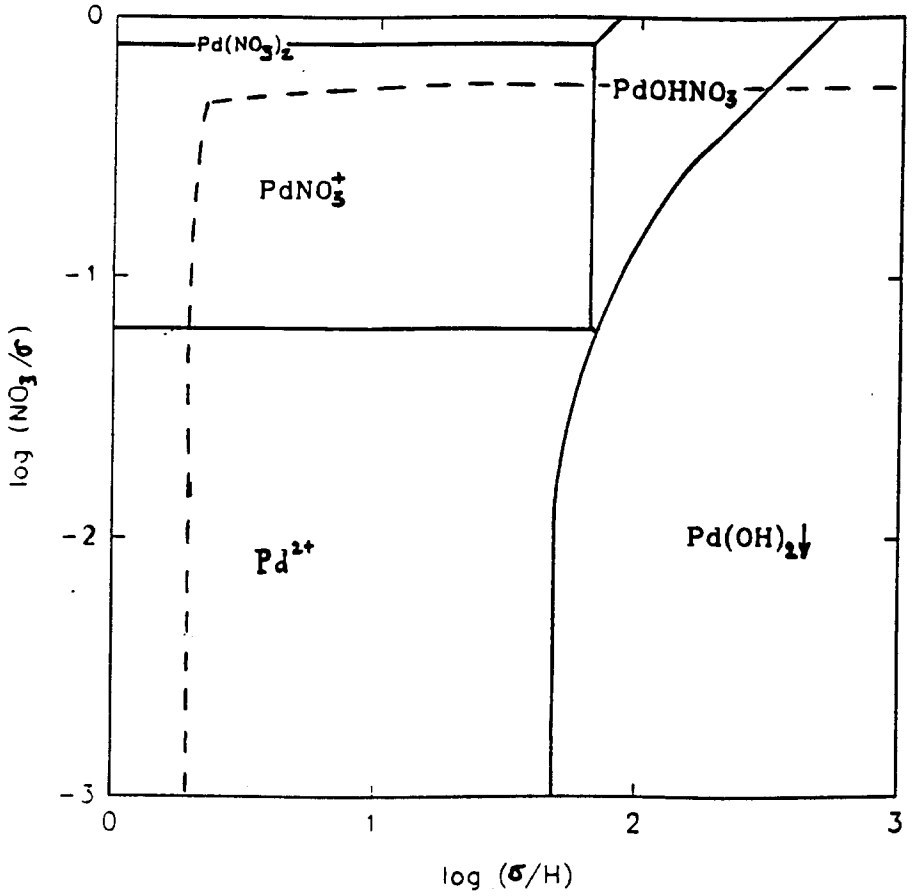


Fig. 5. Predominance zones for palladium species at $a_w = 0.75$, as a function of the relative activities of nitrate and proton. The limit of precipitation is indicated for a relative activity of palladium of $10^{-4}$.

the medium effects: in their experiments, $\sigma$ was 2.05 ± 0.05 M and $a_w$ varied between 0.91 and 0.93. This shows a weak influence of the medium effects on stability, at least for this first complex.

The molar absorptivity coefficients of the complex species at the other wavelengths were then calculated, by fitting function (2) to the absorbances at 380 and 392 nm respectively keeping the complexation functions constant. The final results appear in Table 4 and show sufficient regularity to affirm robustness of the model.

Finally, the complexation functions were used to calculate the borders of the predominance zones in the relative activity diagram presented in Fig. 5. It appears that the most important complexes at $a_w = 0.75$ are $PdNO_3^+$ and $PdOHNO_3$. The zone where $Pd(NO_3)_2$ predominates is clearly out of the accessible domain: at the most, this species can represent 40% of the total dissolved palladium.

### 4.4. Precipitation limit

As was stated before, precipitation occurred in the solutions denoted in Fig. 1 by a filled symbol. This provides an experimental limit for

the solubility in each series. As at each of these points the complexation coefficient of the palladium is easily obtained using the previously determined complexation functions, it is possible to estimate the value of the precipitation function corresponding to the equilibrium

$$Pd^{2+} + 2H_2O \rightleftharpoons Pd(OH)_2 \downarrow + 2H^+$$

$$G_s = \frac{[H^+]^2}{[Pd^{2+}]\sigma} = \frac{\sigma\alpha_{Pd(NO_3,OH)}}{C_T(\sigma/[H^+])^2}$$

$$G_s \approx 4$$

From this value, the precipitation limit can be calculated over all the activity diagram for any activity of palladium. This was done for a relative activity of palladium of $10^{-4}$, which corresponds approximately to a concentration of $10^{-3}$ M. The precipitation line is indicated in the predominance diagram of Fig. 5.

## 5. Conclusion

The model for non-ideality used here allowed us to draw the speciation diagram in terms of relative activities of the ligands; hence, the medium effects are included in the predictive capacity of the representation. For any solution of water activity equal to 0.75, whatever its composition may be, the concentrations of palladium complexes with $NO_3^-$ and $OH^-$ can be calculated from the presented characteristic functions, provided these are the only ligands or the stability of other complexes is also known.

Further developments should include the variation of the water activity to extend the domain of applicability. Taking into account the experimental difficulties in obtaining palladium solutions of precisely known composition, a serious improvement would be to perform whole spectrum analysis and hence to process simultaneously a much larger set of data, with the help of appropriate software. This would suppose, of course, numerical acquisition of the spectra, which was unfortunately not available for the present work.

## References


[1] P. Pascal, Nouveau traité de chimie minérale, Tome XIV, Masson, Paris, 1958.

[2] V.S. Shmidt, N.A. Shrokhov, A.A. Vashman and V.E. Samsonov, Zh. Neorg. Khim., 27 (1982) 1254–1256.

[3] Gmelin handbook of Inorganic Chemistry, Vol. B2, Palladium main, 1986, pp. 18–99.

[4] C.K. Jørgensen and V. Parthasarathy, Acta Chim. Scand., A32(10) (1978) 957–962.

[5] R.M. Izatt, D. Eatough and J.J. Christensen, J. Chem. Soc. (A), (1967) 1301–1304.

[6] J. Kragten, Atlas of metal–ligand equilibria in aqueous solutions, Wiley, New York, 1978, pp. 576–577.

[7] B.I. Nabivanets and L.V. Kalabina, Russian J. Inorg. Chem., 15 (1970) 812–821.

[8] C.D. Tait, D.R. Janecky and P.S.Z. Rogers, Geochim. Cosmochim. Acta, 55 (1991) 1253–1264.

[9] E. Blasius, W. Preetz and R. Schmitt, J. Inorg. Nucl. Chem., 19 (1961) 115–232.

[10] P.B. Critchlow and S.D. Robinson, Coord. Chem. Rev., 25 (1978) 69–101.

[11] J. Ly and C. Poitrenaud, Analusis, 14(4) (1986) 192.

[12] H. Pitsch K. and C. Poitrenaud, Rev. Soc. Quim. México, 30(4) (1986) 152–157.

[13] H. Pitsch K. and C. Poitrenaud, Rev. Soc. Quim. México, 33(3) (1989) 86–92.

[14] A.B. Zdanovskii, Trudy Solyanoi Laboratorii Akad. Nauk. SSSR, 6 (1936) 1.

[15] V.M. Vdovenko and M.A. Ryazanov, Zh. Fiz. Khim., 42 (1968) 1936.

[16] G. Schwarzenbach, Complexometric Titrations, Interscience, New York, 1957.

[17] A. Ringbom, Les complexes en chimie analytique, Dunod, Paris, 1967.

[18] H. Chen, J. Sangster, T.T. Teng and F. Lenzi, Can. J. Chem. Eng., 51 (1973) 234.

[19] W. Davis, Jr. and H.J. Bruin, J. Inorg. Nucl. Chem., 25 (1964) 1069.

[20] A.I. Vogel, Quantitative Inorganic Analysis, Longmans, London, 1961, p. 511.

[21] J. Ly, Thèse de doctorat en sciences physiques, Université Paris 6, 1984.

[22] R. Haas, K.H. Ducker and H.A. Kuppers, Ber. Bunenges Phys. Chem., 69 (1965) 97.

ELSEVIER

Talanta 42 (1995) 1685–1690

Talanta

# Improvement of the silver/silver chloride reference electrode and its application to pH measurement

Satoshi Ito[a,b,*], Hiromitu Hachiya[a], Keiko Baba[a], Yasukazu Asano[a], Hiroko Wada[b]

[a]*Research Center, DKK Corp., 4-13-14, Kichijoji Kitamachi, Musashino, Tokyo 180, Japan*
[b]*Department of Applied Chemistry, Nagoya Institute of Technology, Gokiso, Showa, Nagoya 466, Japan*

Received 16 December 1994; revised 24 April 1995; accepted 24 April 1995

**Abstract**

When a silver/silver chloride (Ag/AgCl) reference electrode was used continuously in a low conductivity solution or reductive solution, it was often observed that stability of the liquid junction potential was lost. This phenomenon was remarkable with a Ag/AgCl reference electrode compared to a calomel reference electrode. We found that 340 mg $l^{-1}$ of silver was dissolved in 3 M potassium chloride (KCl) internal solution as silver complex ions ($AgCl_x^{-(x-1)}$) for $x = 2$ or 3. However, only 1.93 mg $l^{-1}$ of silver chloride (AgCl) can theoretically be dissolved in water. The complex ion that effused into the sample solution through the liquid junction clogged the liquid junction (e.g. porous ceramic) as AgCl, or as metallic silver (Ag) in reducing solution. Therefore, the constant effusion of KCl internal solution was inhibited, and the liquid junction potential became unstable or fluctuating. A new reference electrode was developed, which can eliminate $AgCl_x^{-(x-1)}$ in 3 M KCl internal solution by the use of chelating resins. A combination of this reference electrode with a pH electrode made long-term stable pH measurements possible.

*Keywords:* pH measurement; silver/silver chloride reference electrode

## 1. Introduction

The stability of a reference electrode in potentiometry is very important for the reliability and accuracy of the obtained data because a potential error of 1 mV causes about 0.02 pH error in pH measurement and also an approximate 4 or 8% concentration error, respectively, for mono- and divalent ion measurements using ion-selective electrodes.

The calomel electrode introduced by Ostwald in 1890 has been used as a reference electrode for glass pH electrode measurements, since their inception [1]. These days, because of the toxicity and environmental concern of mercury, the Ag/AgCl reference electrode has been used instead of the calomel reference electrode. An agar–agar salt bridge is generally not used as a laboratory or industrial reference electrode because of its high maintenance and stability, but alternative ion transfer vehicles such as exudation of KCl have been used [2]. In reference electrodes with ion transfer such as KCl exudation, continuous exudation of KCl is one of the most important parameters for reliable performance [3]. Sometimes, the KCl internal solution is pressurized by compressed air to stabilize the rate of KCl exudation. Thus, 0.1 to several ml per day of KCl internal solution exudes constantly through the liquid junction of the reference electrode. If the exudation of

*Corresponding author. Present address: Research Center, DKK Corp., 4-13-14, Kichijoji Kitamachi, Musashino, Tokyo 180, Japan. Fax: (81)422-52-2042.


*SSDI* 0039-9140(95)01628-7

KCl internal solution from the inside of the breference electrode to the outside (into sample solution) is stopped, the KCl solution on the surface of the liquid junction becomes dilute. The reference electrode loses its normal efficiency and gives a different liquid junction potential, and the liquid junction potential becomes unstable or fluctuating. However, this restriction of exudation of KCl solution is considered to be caused by particles of dirt and soil in the sample solution. Even when no dirt or soil was present in the sample solution, we occasionally found that plugging of the liquid junction occurred. In an Ag/AgCl reference electrode, clogging of its liquid junction is thought to be the essential problem. To maintain the initial stable condition in the reference electrode, it is important that the mechanism of plugging be made clear. Nevell and Walsh [2] noticed that silver effused through the liquid junction from a Ag/AgCl reference electrode, and mercury effused from a calomel reference electrode. They stated only that the toxicity of Ag or Hg might adversely influence some substances in the sample solution. Brezinski pointed out that AgCl clogged the liquid junction in a Ag/AgCl reference electrode [4]. We found that chelating resins could eliminate Ag ions existing in the KCl inner solution, and developed a long-term stable reference electrode with a liquid junction that could be kept clean using chelating resins.

## 2. Experimental

### 2.1. Reagents

All chemicals used were of analytical reagent grade. Potassium chloride (KCl) and silver chloride (AgCl) were obtained from Wako Chemicals (Osaka, Japan). Pure water was used throughout the work. Cation chelating resin Model CR-10 was purchased from Mitsubisi kasei (Tokyo, Japan). Chelating resin Model MX-8, Z-7 and S-1 were purchased from Miyosi Oil & Fat (Tokyo, Japan). The functional groups of each chelating resin of Model CR-10, Model MX-8, Model Z-7 and Model S-1 are $-N(CH_2COOH)_2$, $>N-CH_2-CH_2-COOH$, $>N-CS_2H-SH$ and $-SH$, respectively.

### 2.2. Apparatus

A Hitachi Model 208 atomic absorption spectroscopy (air–acetylene flame) was used for the determination of silver in 3 M KCl solution. A DKK Model COM-20 potentiometer, a DKK Model EL7100 silver ion electrode, a DKK Model EL7020 chloride ion electrode and a DKK Model EL4083 reference electrode were used for silver ion measurements. A DKK Model EL6156 glass electrode was used for pH adjustment throughout this work.

### 2.3. Measurement of silver in 3 M KCl solution

In water, the solubility of AgCl is 0.7 mg $l^{-1}$ at 0°C, 1.93 mg $l^{-1}$ at 25°C, 5.4 mg $l^{-1}$ at 50°C and 21 mg $l^{-1}$ at 100°C [5]. However, in high concentrations of KCl solution such as 3 M KCl, the solubility of Ag is not found in the literature. Therefore, we measured the total silver concentration for saturated AgCl in 3 M KCl solution at 25°C and at 80°C.

To keep silver ions in the complex state, sample solutions were prepared in 3 M KCl solution. Two 3 M KCl solutions containing 1% (supersaturated) AgCl were prepared. These were allowed to stand overnight in a water bath at 25°C and 80°C, respectively. Sample solutions were prepared by accurately diluting ten-fold each supernatant solution containing 3 M KCl solution. The sample solution was analyzed at 25°C.

Table 1 shows the result of measurements by atomic absorption spectroscopy. At 25°C, the solubility of AgCl in 3 M KCl solution is 340 mg $l^{-1}$, although it is 1.93 mg $l^{-1}$ in water. At 80°C, it is 700 mg $l^{-1}$ in 3 M KCl solution, and is approximately 13 mg $l^{-1}$ in water. With an increase in the concentration of KCl, the colour of the flame changed to purple owing to the potassium and the flame was not stable. Although the values of measurements by atomic absorption spectroscopy were not pre-

Table 1
Concentrated of total silver in 3 M KCl solution

| Condition | | Concentration of silver |
|---|---|---|
| Temperature (°C) | Chelate resin [a] | |
| 25 | None | 340 mg $l^{-1}$ |
| 80 | None | 700 mg $l^{-1}$ |
| 25 | Added | ND (less than 0.2 mg $l^{-1}$) |
| 80 | Added | ND (less than 0.2 mg $l^{-1}$) |

[a] Model S-1 and Model Z-7 were used effectively.

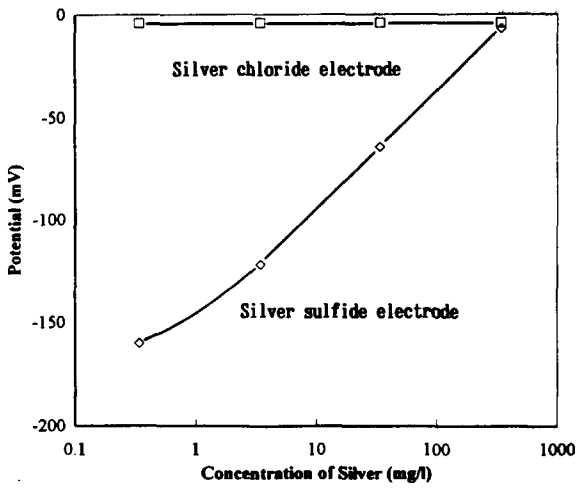


Fig. 1. Relationship between electrode potential and silver ion concentration.

cise, we could estimate the concentration of silver in 3 M KCl solution. The data obtained were sufficiently accurate for the purpose of this experiment.

### 2.4. Elimination of silver in 3 M KCl solution

Silver in 3 M KCl solution exists as $AgCl_x^{-(x-1)}$ complex ions. We tried to use cation ion exchange resin for the adsorption of $Ag^+$ ions, in equilibrium with the chloro-complex. A preliminary simple experiment was tried using several types of ion exchange resin. According to a study on adsorption properties towards heavy metal ions [6], we found that chelating resins were effective at eliminating $Ag^+$ ions in the presence of high concentrations of $K^+$ ions.

### 2.5. Potentiometric measurements of silver in the presence of chelating resin

Silver standard solutions were prepared as follows. Saturated AgCl in 3 M KCl solution at 25°C was used as 340 mg $l^{-1}$ silver standard solution. By ten-fold dilution of this 340 mg $l^{-1}$ silver standard solution with 3 M KCl solution, 34 mg $l^{-1}$ silver standard solution was prepared. In a similar manner, 3.4 mg $l^{-1}$ and 0.34 mg $l^{-1}$ silver standard solutions were prepared. The relationship between potential and silver concentration is shown in Fig. 1. Chloride ion electrodes with AgCl membrane (□) do not respond to silver ion concentration. Silver ion electrodes with $Ag_2S$ membrane (◇) show good Nernstian response. Silver ions in 3 M KCl solution could be measured with a silver ion electrode, but not with a chloride ion electrode.

Chelating resin (10 g was a sufficient amount for eliminating Ag) was added to 100 ml of 3 M KCl solution, the pH of which was adjusted to about 7 with hydrochloric acid or potassium hydroxide. The silver ion electrode potential was initially measured in 100 ml of saturated AgCl in 3 M KCl solution at 25°C. After adding 10 g chelating resin to this solution, the potential was measured periodically every 10 min for 12 h.

### 2.6. Improvement of the structure of the reference electrode

We developed a double junction reference electrode as shown in Fig. 2. The inner chamber is a conventional Ag/AgCl reference electrode, in 3 M KCl solution. The outer chamber is filled with some chelating resin and 3 M KCl solution. The inner chamber is closed, but the outer chamber and the inner chamber are connected through an inner chamber ceramic junction. The 3 M KCl solution in the outer chamber serves to keep the junction more stable. There is a hole in the outer chamber for pressure balance, and to supply 3 M KCl solution. The small amount of silver ions in the 3 M KCl solution that diffuses through the inner chamber ceramic junction is adsorbed by chelating resin. The 3 M KCl solution effusing through the outer chamber ceramic junction does not contain any appreciable amount of dissolved silver.

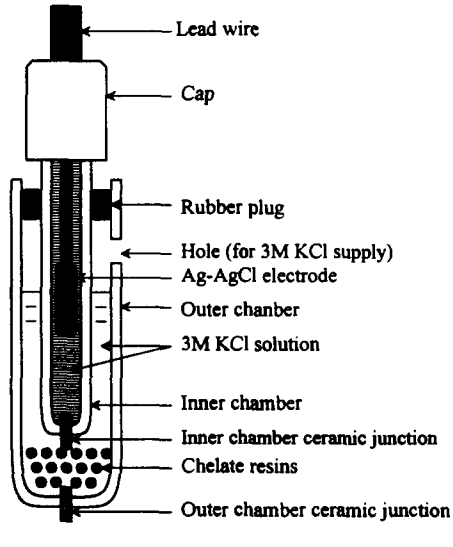


Fig. 2. Structure of long-term stable double junction reference electrode.

## 3. Results and discussion

Two kinds of double junction reference electrodes were prepared. One was placed in a water bath at 25°C, and the other in a water bath at 80°C. As the inner solution of the outer chamber was gradually reduced, 3 M KCl solution was supplied to the initial level periodically. Water in the water bath was often exchanged to maintain low conductivity. Once a month, the silver concentration of the inner solution in the outer chamber was measured by atomic absorption spectroscopy. The measurement was continued for 6 months.

### *3.1. Change in silver concentration of the outer chamber solution*

Depending upon the chelating resin, different results were obtained. In Model CR-10, the silver concentration in the outer chamber solution gradually rose to 10 mg $l^{-1}$ at 25°C and to 50 mg $l^{-1}$ at 80°C over 6 months. In Model MX-8, it was below the detection limits (less than 0.2 mg $l^{-1}$) at 25°C, but gradually rose to 10 mg $l0^{-1}$ at 80°C. In Model Z-7 and Model S-1, it was not detected (less than 0.2 mg $l^{-1}$) at 25°C or 80°C. After 6 months, the rate of effusion of the outer inner solution was measured. In the test reference electrode, in which was observed the existence of dissolved silver in the outer chamber, i.e. in Model CR-10 at 25°C and 80°C and in Model MX-8 at 80°C, the rate of effusion was reduced to one-half or one-quarter of its initial value, and the appearance of the outer chamber ceramic junction changed to brown owing to AgCl. Table 1 shows the concentration of silver in 3 M KCl solution after 6 months measured by atomic absorption spectroscopy. In the case of addition of Model S-1 chelate resin or Model Z-7 chelate resin, silver was not detected. The addition of these chelate resins was very useful for the elimination of silver in the KCl solution.

### *3.2. Eliminating ability with chelating resins*

Fig. 3 shows the eliminating ability of the chelating resins. The silver ion electrode potential decreased gradually with addition of chelating resins, and became constant after 12 h. Final potentials showed 187, 30, 2.4, 0.3 mg $l^{-1}$ $Ag^+$ concentration, respectively, against each chelating resin of Model CR-10, Model MX-8, Model S-1 and Model Z-7. The adsorption ability of chelating resins for $Ag^+$ changed in the order Model Z-7 > Model S-1 > Model MX-8 > Model CR-10. Model Z-7 had the best adsorption power among them.

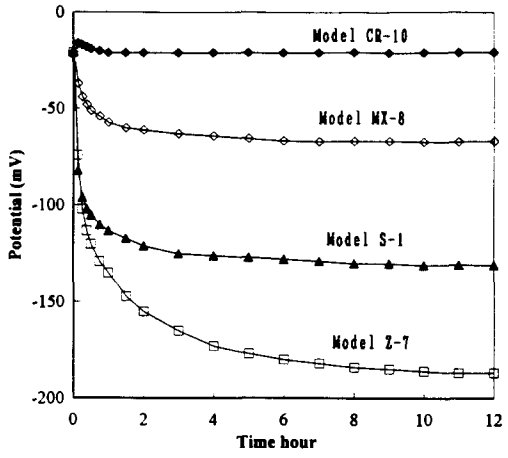


Fig. 3. Eliminating ability of chelate resins.

### *3.3. Application to pH combination electrode*

In Fig. 4, a conventional-type electrode is shown which is the most popular model of a combination pH electrode. It consists of a glass electrode, reference electrode and temperature sensor. To compensate for temperature effects, the glass electrode and reference electrode have similar structures. In addition, an inner junction tube of porous polypropylene resin for improved-type electrodes was added to the inner chamber of the pH and reference electrodes for prevention of diffusion of $Ag^+$ or $AgCl_x^{-(x-1)}$ ions.

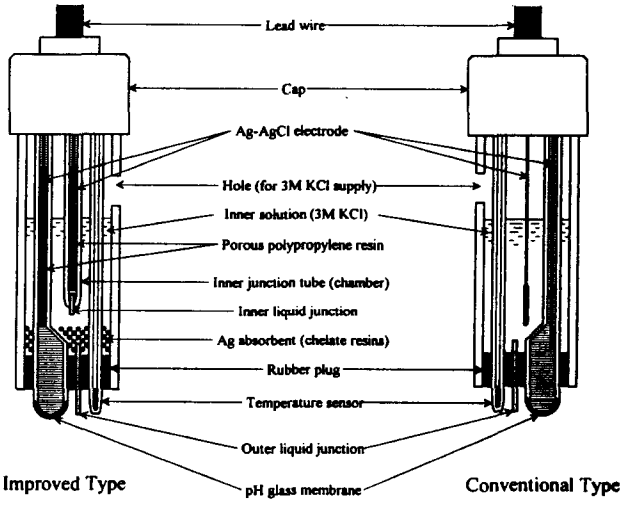


Fig. 4. Comparison of pH electrode structure in improved-type and conventional-type combination electrodes.

Based on the results mentioned above, we improved our conventional-type combination pH electrode as shown in Fig. 4. A double junction-type reference electrode was fabricated. The Ag/AgCl electrode was enclosed in the plastic junction tube, i.e. the inner chamber. The Ag/AgCl electrode was made shorter than in the conventional-type electrode, and was put in the upper part of the improved-type electrode. The distance between the Ag/AgCl electrode and the inner ceramic junction was longer than in the conventional-type electrode. Further, porous polypropylene resin was packed between them. Using this idea, the rate of diffusion of Ag complex ions became slow. As a result, the activation rate of the junction based on Ag was minimized. The silver absorbent, i.e. the chelating resin, was placed in the outer chamber of the reference electrode. Owing to the presence of this chelating resin, silver complex ions were no longer exuded from the outer ceramic junction to the sample solution, and the junction potential became very stable for long periods of time.

### 3.4. Effect of improved pH combination electrode in field test

When a pH electrode is used in a low conductivity solution (less than 0.1 mS $cm^{-2}$), abnormal phenomena in pH measurements, such as errors and fluctuation of pH values, sometimes occur. These phenomena are accelerated when the sample temperature becomes high. Fig. 5 shows an example of measurements in low conductivity solution. There is a remarkable difference between the improved-type pH electrode and the conventional-type pH electrode. The data of continuous pH measurement using the improved-type pH electrode were in fairly good agreement with the pH from the batch sampling method, within $\pm 0.05$ pH units.

When the pH electrode was used in boiler water containing a reductant such as hydrazine in a power plant, some abnormal phenomena in pH measurements occurred, which are shown in Fig. 6. The data of continuous pH measurement using the improved-type pH electrode were again in fairly good agreement with the pH from the batch sampling method, within $\pm 0.02$ pH units. In the case of the conventional-type pH electrode, the observed pH values are generally lower than normal. This error often reaches pH $-0.3$ to $-0.7$.

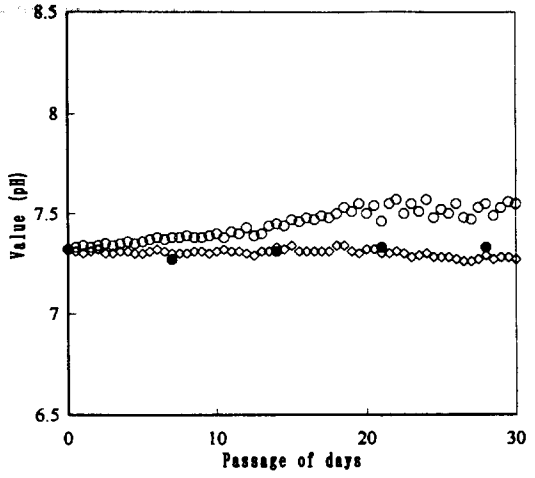


Fig. 5. Example of measurements in a low conductivity solution. The sample is an industrial supply of water (underground water), the electric conductivity of which is about 0.05 mS $cm^{-2}$. Data from the conventional-type pH electrode (○) and improved-type pH electrode (◇) are shown, as well as data from a laboratory pH electrode by the batch sampling method (●). ○ and ◇ are from continuous measurement data, and ● are manual analysis data taken once a week.

### 3.5. Mechanism of deterioration in the Ag/AgCl reference electrode

Although silver chloride is only slightly soluble in water, AgCl is more soluble in concentrated KCl solution than in water. We measured the concentration of silver in 3 M

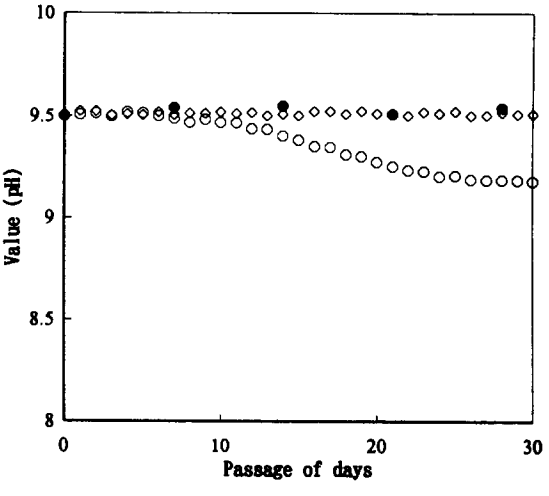


Fig. 6. Example of measurements in boiler water containing several mg $l^{-1}$ hydrazine. The electric conductivity is about 0.01 mS $cm^{-2}$. Data from the conventional-type pH electrode (○) and improved-type pH electrode (◇) are given, as well as data from a laboratory pH electrode by the batch sampling method (●). ○ and ◇ are from continuous measurement data, and ● are manual analysis data taken once a week.

KCl solution, and showed that the solubility was larger by about two orders of magnitude than in water. In 3 M KCl solution, Ag seems to exist as $AgCl_x^{-(x-1)}$ for $x=2$ or 3. The inner solution containing $AgCl_x^{-(x-1)}$ in the reference electrode effuses to the sample solution through the liquid junction. At the surface of the liquid junction, the effused solution is then diluted by the sample solution, and the concentration of KCl becomes lower. Therefore, $AgCl_x^{-(x-1)}$ ions that were soluble in the inner solution revert to AgCl, and AgCl is deposited on the surface of the liquid junction. Silver chloride adheres gradually on the material comprising the liquid junction such as porous ceramic or a glass sleeve. Further, when reductant was present in the sample solution, AgCl was reduced and changed to metallic Ag. The form of silver under some conditions is shown as follows:

$$\underset{\text{(in concentrated KCl solution)}}{AgCl_x^{-(x-1)}} \longrightarrow \underset{\text{(in water)}}{AgCl} \longrightarrow \underset{\text{(after reduction)}}{Ag}$$

The potential of a liquid junction covered with AgCl will be influenced by the $Cl^-$ ion concentration or activity; further, one covered with Ag will be influenced by the redox potential, because the functioning of the reference electrode deteriorates on adhesion of AgCl or Ag at the liquid junction. Some examples of this are as shown in Figs. 5 and 6.

We believe there are various mechanisms by which the inner solution containing $AgCl_x^{-(x-1)}$ is prevented from effusing through the liquid junction. One is that gelation of the inner solution prevents its diffusion or convection, and slows down the movement of $AgCl_x^{-(x-1)}$ from the Ag/AgCl electrode to the sample solution; another is that diffusion is slowed down by a sufficiently long distance between the Ag/AgCl electrode and the liquid junction. Although Brezinski reported a method for eliminating AgCl by mechanical barriers such as cation-selective membrane [4], it is not desirable to create membrane potentials between the Ag/AgCl electrode and the liquid junction in a reference electrode. The use of mechanical barriers seems to provide incomplete elimination of AgCl, resulting in an unnecessary potential or high electrical resistance. We conclude that this method with chelating resins is one of the most practical, because the operational characteristics of the reference electrode are kept stable for long periods of time.

## References

[1] A.S. Brown, J. Am. Chem. Soc., 56 (1934) 646.
[2] T.G. Nevell and F.C. Walsh, Trans. Inst. Metal Finish, 70 (1992) 144.
[3] A.K. Covington and P.D. Whalley, Anal. Chim. Acta, 169 (1985) 221.
[4] D.P. Brezinski, Anal. Chim. Acta, 134 (1982) 247.
[5] W.F. Linke, Solubilities: Inorganic and Metal–Organic Compounds, Vol. 1, 4th edn., American Chemical Society, Washington, DC, 1958, p. 59.
[6] A. Lezzi, S. Cobianco and A. Roggero, J. Polym. Sci., Part A: Polym. Chem., 32 (1994) 1877.

ELSEVIER

Talanta 42 (1995) 1691–1700

Talanta

# Interfacial reaction in the synergistic extraction rate of Ni(II) with dithizone and 1,10-phenanthroline

Hitoshi Watarai *, Katumi Sasaki, Ken Takahashi, Junko Murakami

*Department of Chemistry, Faculty of Education, Akita University, Akita 010, Japan*

Received 30 March 1995; accepted 28 April 1995

**Abstract**

The kinetic synergistic effect of 1,10-phenanthroline (phen) on the extraction rate of Ni(II) with dithizone (HDz) into chloroform was studied by means of a high-speed stirring method combined with photodiode-array spectrophotometry. The initial extraction rate of the adduct complex $NiDz_2phen$ depended upon the concentrations of both HDz and phen, suggesting the formation of $NiDzphen^+$ as the rate-controlling step. When [HDz] < [phen], the initial extraction of $NiDz_2phen$ competed with the formation of an intermediate complex, which was adsorbed at the interface and assigned most probably to $NiDzphen_2^+$. The intermediate complex was gradually converted to $NiDz_2phen$ at a later stage of the extraction. The rate constants for the formation and consumption of the intermediate were determined, and the kinetic mechanism in the synergistic extraction was discussed.

## 1. Introduction

The kinetics of the solvent extraction of metal complexes has been extensively studied, but further efforts are still required to clarify the dynamics of chemical and physical processes taking place at an interface as well as in bulk phases. Our previous studies employing the high-speed stirring method demonstrated the important role of the liquid–liquid interface in the kinetic mechanisms of chelate extraction and ion-pair extraction [1]. The high-speed stirring method made the best use of stirring a two-phase system by achieving a larger specific interfacial area, as high as 400 $cm^{-1}$, and by promoting mass transfer between the two phases. It was shown in the chelate extraction of Ni(II) and Cu(II) with hydrophobic 2-hydroxyoximes that the interfacial adsorption of the extractants and the formation of a 1:1 complex at the interface were the principal factors determining the kinetic extraction mechanism [2,3]. In the ion-association extraction of Fe(II) with 1,10-phenanthrolines, the interfacial adsorptivity of the Fe(II)–1,10-phenanthroline complexes as well as that of the extractants affected the extraction rates [4].

Our current interest is in the role of the interface in synergistic extraction systems which could be thought of as combinations of the chelate and ion-association extraction systems. Freiser and Freiser reported the synergistic effect of 1,10-phenanthroline (phen) on both the equilibrium and kinetics of the extraction of nickel(II) with dithizone (HDz) [5]. They determined the extraction constants as $\log K_{ex} = -0.7$ and $\log K'_{ex} = 5.3$ for the following extraction reactions respectively:

$$Ni^{2+} + 2HDz_o = NiDz_{2,o} + 2H^+ \quad K_{ex} \qquad (1)$$

$$Ni^{2+} + 2HDz_o + phen = NiDz_2phen_o + 2H^+ \quad K'_{ex} \qquad (2)$$

* Corresponding author. Present address: Department of Chemistry, Faculty of Science, Osaka University, Osaka 560, Japan. Fax: (81)6-850-5411.


*SSDI* 0039-9140(95)01630-9

This synergistic system is advantageous for the photometric determination of Ni(II), because the absorption spectrum of the adduct complex in the organic phase (a maximum at 520 nm) can readily be distinguished from that of HDz (a maximum at 605 nm). Akaiwa et al. reported the accelerating effect of phen on the rate of extraction of Ni(II) with thenoyltrifluoroacetone [6]. However, nothing has been reported on the role of the interface in these synergistic systems.

In the present study, we will assess the role of the interface in the kinetics of extraction of Ni(II) with HDz and phen by means of the high-speed stirring method, which made it possible to monitor the spectral change in the organic phase with the aid of photodiode-array spectrophotometry.

## 2. Experimental

### 2.1. Chemicals

Dithizone, Wako G.R., was purified by a back extraction from its chloroform solution into aqueous ammonia and by subsequent neutralization with sulfuric acid of the aqueous phase. 1,10-Phenanthroline, Wako G.R., was used as purchased. The stock solution of $1.0 \times 10^{-3}$ M nickel(II) was prepared by dissolving nickel(II) sulfate hexahydrate in distilled and deionized water. The pH of the aqueous phase used in the kinetic studies was controlled by 0.006 M acetate buffer and the ionic strength was maintained at 0.1 by sodium sulfate. Chloroform, Wako G.R., was triply washed with an equal volume of water prior to use.

### 2.2. High-speed stirring measurements

The extraction rate of Ni(II) with HDz in the presence or absence of phen was measured by means of the high-speed stirring apparatus. Absorption spectra of the organic phase during the extraction were measured at an acquisition rate of 0.64 or 1.28 s per spectrum in the range of 380–670 nm using a photodiode-array UV/vis detector Shimazu SPD-M6A interfaced with a NEC PC9801 microcomputer.

A typical procedure for the extraction rate measurement was as follows: 45 ml of aqueous buffer solution, and 50 ml of HDz and phen in chloroform were agitated at a stirring rate of 4700 rpm in the glass stir cell. The stirring rate was controllable over the range 200–4700 rpm. The organic phase was continuously separated from the agitated mixture by means of a Teflon phase separator and circulated through a flow cell at a flow rate of 13–16 ml $min^{-1}$ by the Flumax Junior pump. 5 ml of Ni(II) stock solution was injected into the mixture and the extraction of Ni(II) was initiated.

For the measurement of the extraction rate of the pre-formed Ni(II)–phen complex in aqueous phase with HDz, the aqueous phase (50 ml) containing $Ni^{2+}$ and phen was left for 1 h to equilibrate in the stir cell. Chloroform (45 ml) was added and the two phases were stirred for 1 min, and then 5 ml of HDz in chloroform was injected into the mixture to start the extraction.

The rate of reaction between Ni(II) and phen in the aqueous phase was also measured by the high-speed stirring apparatus, making use of the unextractability of the Ni(II)–phen complex ion. A chloroform solution of phen (50 ml) and an aqueous buffer (45 ml) were stirred, and 5 ml of Ni(II) solution was then injected. The decrease in the absorbance of phen in the chloroform phase was recorded as a function of time at the absorption maximum (280 nm).

### 2.3. Stopped-flow measurement

The rate of adduct formation, i.e. the reaction between $NiDz_2$ and phen in chloroform, was measured by the use of the stopped flow spectrophotometer RA-401 (Photal, Japan). The $NiDz_2$ solution, prepared by the extraction of Ni(II) with HDz in chloroform in the presence of excess nickel ion, and the chloroform solution of phen was mixed within 5 ms in a mixing cell. The formation rate of the adduct was measured at 520 nm as a function of time. By the use of Guggenheim analysis, the apparent first-order rate constants for the adduct formation were calculated.

All the kinetic measurements were carried out at $25.0 \pm 0.1$°C.

## 3. Results

### 3.1. Photodiode-array measurements of extraction rates

The extraction rate of Ni(II) with dithizone alone was rather slow, even under the neutral

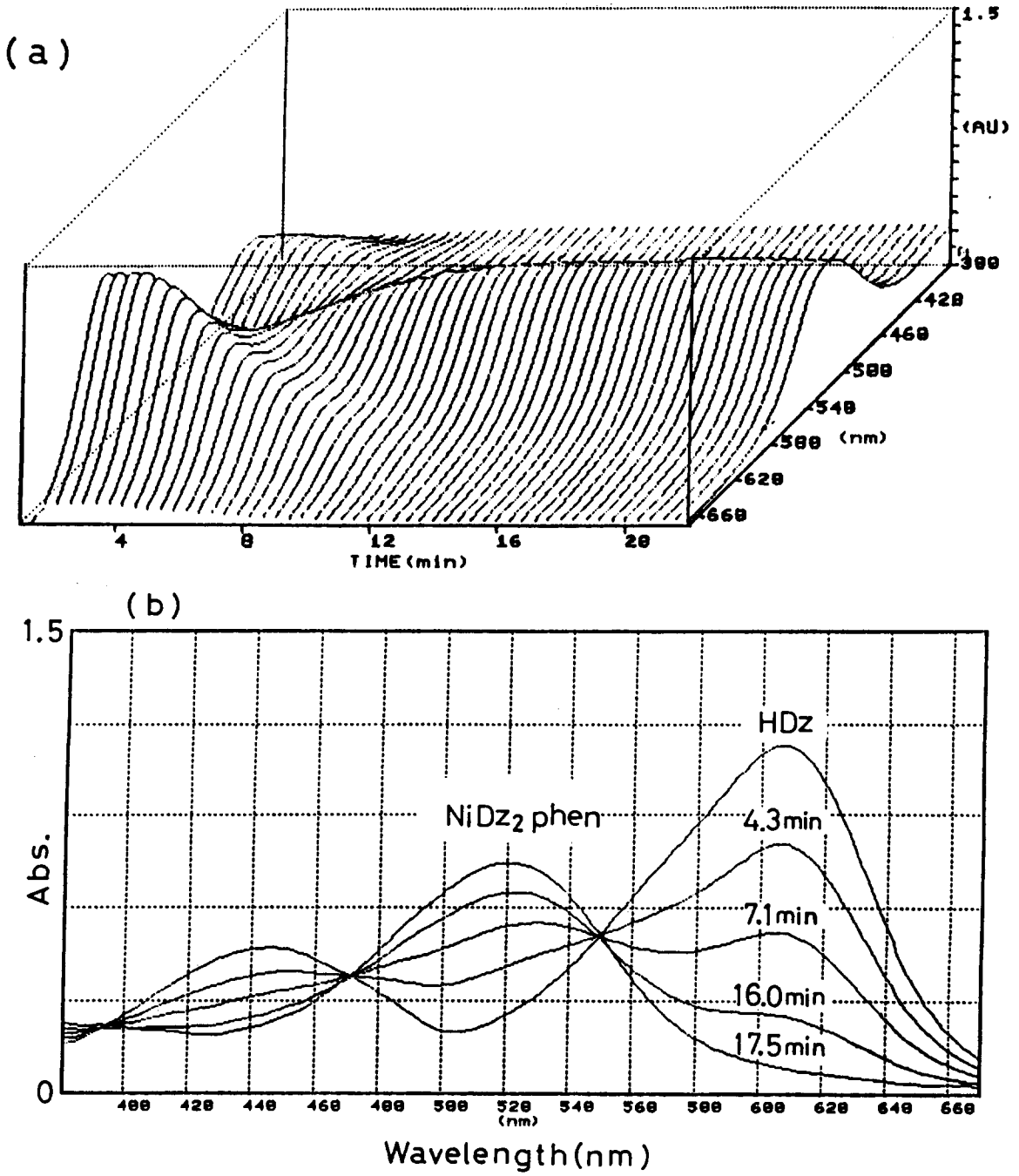


Fig. 1. (a) Three-dimensional representation of the absorbance change in the chloroform phase on the course of the Ni(II) extraction and (b) the spectral change showing isosbestic points; $[Ni^{2+}] = 1.0 \times 10^{-3}$ M, [HDz] = $2.99 \times 10^{-5}$ M and [phen] = $4.0 \times 10^{-5}$ M.

conditions (pH = 6–7) and high nickel concentration ($10^{-3}$ M), because of the large distribution constant of HDz, $K_D = 10^{6.4}$ [7], which resulted in an extremely low aqueous HDz concentration. In the presence of phen, the extraction rate of Ni(II) was significantly accelerated, yielding the adduct complex $NiDz_2phen$ in the organic phase. Fig. 1(a) represents the three-dimensional spectral change in the organic phase during the extraction. Soon after the injection of Ni(II) solution, the absorbance of HDz at 605 nm decreases and simultaneously that of the adduct complex at 520 nm increases. When the concentration of phen was

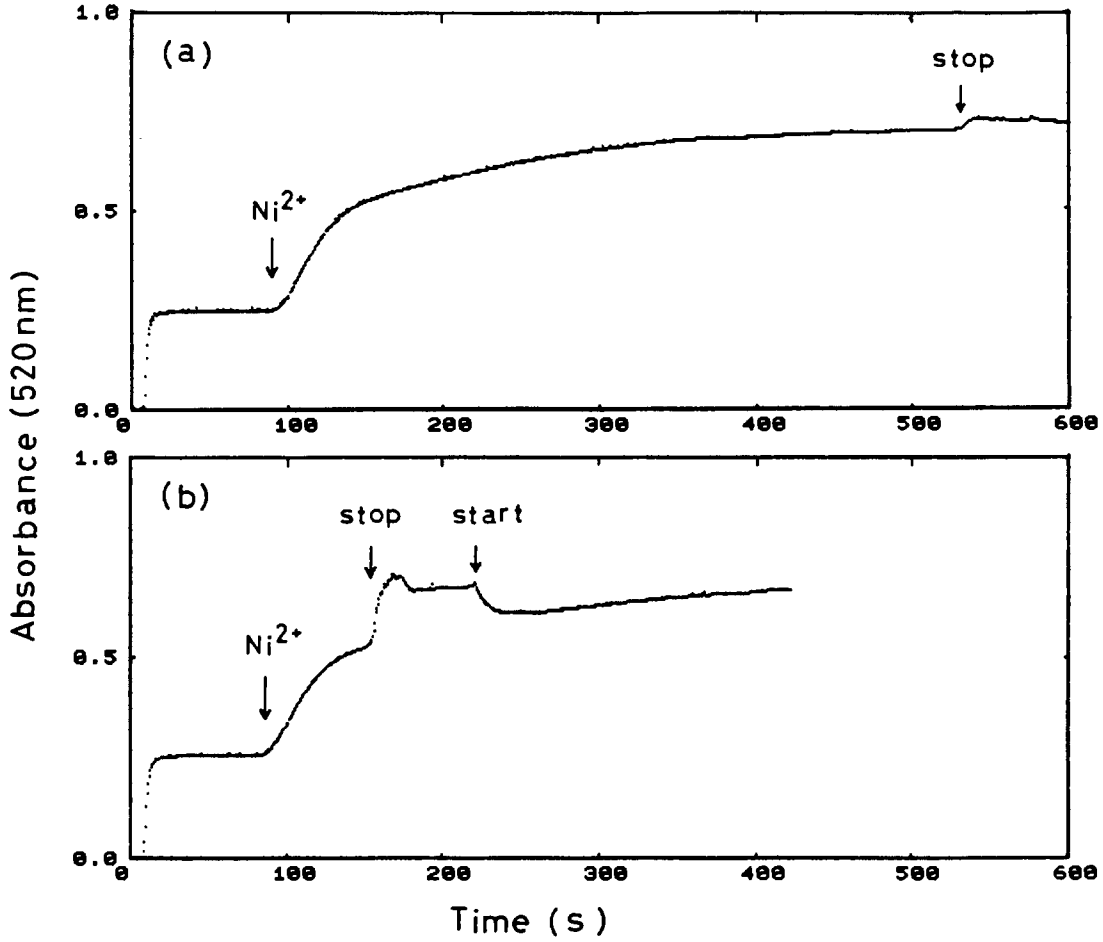


Fig. 2. Profile of the synergistic extraction of Ni(II), in which the stirring (4700 rpm) was stopped (a) at the final stage of the extraction and (b) at the initial stage where an abrupt increase in the absorbance was noticed; $[Ni^{2+}] = 1.0 \times 10^{-3}$ M, $[HDz] = 2.99 \times 10^{-5}$ M and $[phen] = 1.0 \times 10^{-3}$ M.

lower than that of HDz, the time-resolved spectra exhibited distinct isosbestic points as shown in Fig. 1(b). The absorbance at 520 nm was monotonously increased, and the rate of increase of the adduct was exactly one-half of rate of decrease of HDz, corresponding to the stoichiometry shown in Eq. (2). In contrast, at a higher concentration of phen than that of HDz, the extraction profile apparently showed two steps, the faster step in the earlier stage and the slower step in the later stage, as seen in Fig. 2(a). In this case, there were no distinct isosbestic points in the time-resolved spectra. Stopping the stirring during the extraction caused an abrupt increase in the organic phase absorbance, and restarting the stirring lowered the abosrbance, as shown in Fig. 2(b). These stirring effects suggested the existence of some Ni(II) complex adsorbing at the liquid–liquid interface.

### 3.2. Initial extraction rates

The extraction rate of Ni(II) with HDz alone was observed at 490 nm, an absorption maximum wavelength of $NiDz_2$ in the chloroform phase. The absorbance of the organic phase at a given wavelength $\lambda$ can be written as

$$A(\lambda) = \varepsilon_\lambda [HDz]_o + \varepsilon'_\lambda [NiDz_2]_o \quad (3)$$

where $\varepsilon_\lambda$ and $\varepsilon'_\lambda$ are the molar absorptivities of HDz and $NiDz_2$ in chloroform respectively, and the subscript "o" refers to the concentration in the organic phase. Hence, the rate of change of absorbance can be written as

$$dA(\lambda)/dt = \varepsilon_\lambda d[HDz]_o/dt + \varepsilon'_\lambda d[NiDz_2]_o/dt \quad (4)$$

Thus, the initial extraction rate of $NiDz_2$ defined by $(d[NiDz_2]_o/dt)_{t=0}$ was obtained by the next equation, taking into account the spectral overlap of $NiDz_2$ and HDz:

$$\begin{vmatrix}(dA(490)/dt)_{t=0}\\(dA(605)/dt)_{t=0}\end{vmatrix} = \begin{vmatrix}\varepsilon_{490} & \varepsilon'_{490}\\ \varepsilon_{605} & \varepsilon'_{605}\end{vmatrix} \times \begin{vmatrix}(d[NiDz_2]_o/dt)_{t=0}\\(d[HDz]_o/dt)_{t=0}\end{vmatrix} \quad (5)$$

where $(dA(490)/d)_{t=0}$ and $(dA(605)/dt)_{t=0}$ are the initial rates in the absorbance changes at 490 nm and 605 nm respectively, and the molar absorptivities in chloroform are $\varepsilon_{490} = 2.8 \times 10^4$ and $\varepsilon_{605} = 7.8 \times 10^3$ for $NiDz_2$, and $\varepsilon'_{490} = 1.8 \times 10^4$ and $\varepsilon'_{605} = 3.6 \times 10^4$ for HDz. The rate-determining step in the extraction of $NiDz_2$ has been reported as the formation of $NiDz^+$ in the aqueous phase [7,8]:

$$Ni^{2+} + Dz^- \rightarrow NiDz^+ \qquad k_0 \quad (6)$$

In the aqueous reaction regime, the initial extraction rate can be represented by

$$(d[NiDz_2]_o/dt)_{t=0} = k_0 K_a [Ni^{2+}][HDz]_o / K_D[H^+] \quad (7)$$

where $k_0$ and $K_a$ refer to the formation rate constant of $NiDz^+$ in the aqueous phase and the dissociation constant of HDz respectively. Hence, the value $(d[NiDz_2]_o/dt)_{t=0} = 6.00 \times 10^{-8}\ M^{-1}\ s^{-1}$ obtained in the present study, under the conditions $[HDz] = 3.6 \times 10^{-5}$ M, $[Ni^{2+}] = 1.0 \times 10^{-3}$ M and pH 7.1–7.6, gave the value of $k_0 = 5.97 \times 10^3\ M^{-1}\ s^{-1}$ using $K_a/K_D = 10^{-10.21}$ [7].

The initial extraction rate of $NiDz_2phen$ can also be represented by an equation analogous to Eq. (5):

$$\begin{vmatrix}(dA(520)/dt)_{t=0}\\(dA(605)/dt)_{t=0}\end{vmatrix} = \begin{vmatrix}\varepsilon_{520} & \varepsilon''_{520}\\ \varepsilon_{605} & \varepsilon''_{605}\end{vmatrix} \begin{vmatrix}(d[NiDz_2phen]_o/dt)_{t=0}\\(d[HDz]_o/dt)_{t=0}\end{vmatrix} \quad (8)$$

where $\varepsilon''$ denotes the molar absorptivity of $NiDz_2phen_o$ in the chloroform phase. From Eq. (8), the initial extraction rate $r^0$ was derived as

$$r^0 = (d[NiDz_2phen]_o/dt)_{t=0} = 2.06 \times 10^{-5}\{[dA(520)/dt]_{t=0} - 0.224[dA(605)/dt]_{t=0}\} \quad (9)$$

where the numerical coefficients were calculated from the molar absorptivities at 520 nm and 605 nm for each of HDz and $NiDz_2phen$. The values of $r^0$ thus obtained depended on the concentrations of HDz, phen and pH, as shown in Figs. 3–5 respectively. The stirring speed was also one of the factors governing the initial extraction rate. For example, the observed initial rate, $r^0_{obs}(520) = (dA(520)/dt)_{t=0}$, increased with the stirring speed in the region 1000–3000 rpm, and reached a constant value in the region 4000–5000 rpm; thus, 4700 rpm was adopted for the kinetic measurements.

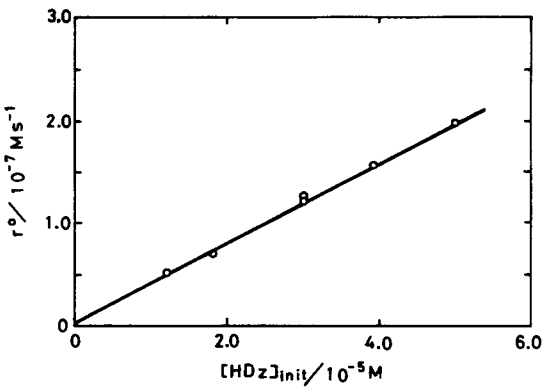


Fig. 3. Dependence of the initial extraction rate on HDz concentration; $[Ni^{2+}] = 1.0 \times 10^{-3}$ M, [phen] = $1.0 \times 10^{-4}$ M, pH = 6.7.

When the aqueous phase containing both Ni(II) and phen was mixed with the chloroform solution of HDz, the initial extraction rate of the adduct complex was remarkably increased even at a phen concentration lower than $10^{-4}$ M, as shown in Fig. 6. At a phen concentration higher than $2 \times 10^{-4}$ M, it was reduced to a constant value independent of the phen concentration.

### 3.3. Formation rate of the Ni(II)–phen complex

The rate of consumption of phen in the chloroform phase with Ni(II) in the aqueous phase was measured at 280 nm by means of the

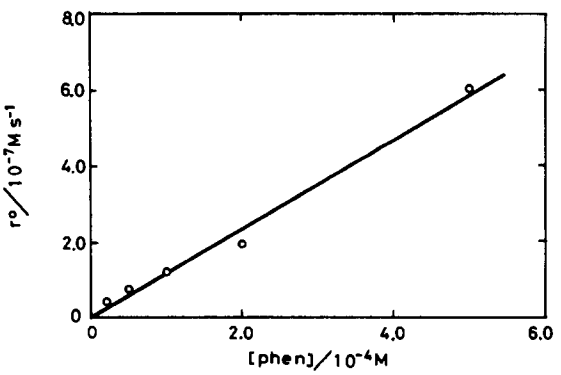


Fig. 4. Dependence of the initial extraction rate on phen concentration; $[Ni^{2+}] = 1.0 \times 10^{-3}$ M, [HDz] = $5.88 \times 10^{-5}$ M, pH 6.4.

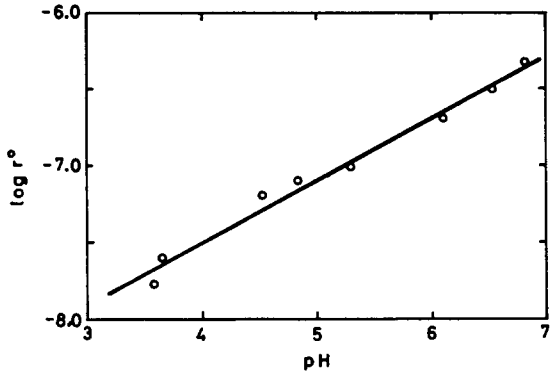


Fig. 5. pH dependence of the initial extraction rate; $[Ni^{2+}] = 1.0 \times 10^{-3}$ M, $[HDz] = 3.00 \times 10^{-5}$ M and $[phen] = 1.0 \times 10^{-3}$ M.

high-speed stirring method, in order to obtain the rate constant between Ni(II) and phen in the aqueous phase. The observed initial consumption rate of phen, $r^0_{obs}$, was linearly proportional to the total phen concentration $[phen]_T$, as shown by

$$r^0_{obs} = 4.21[phen]_T + 3.06 \times 10^{-5}$$
$$\text{(correlation coefficient} = 0.998) \qquad (10)$$

### 3.4. Adduct formation rate in chloroform

The observed formation rate constants of the adduct in chloroform were linearly proportional to each concentration of $NiDz_2$ and phen, as expected from the equation

$$NiDz_{2,o} + phen_o \rightarrow NiDz_2phen_o \qquad (11)$$

From the observed first-order rate constants at 520 nm, the rate constant for reaction (11) was determined as $(1.74 \pm 0.05) \times 10^5$ $M^{-1}$ $s^{-1}$, as given in Table 1.

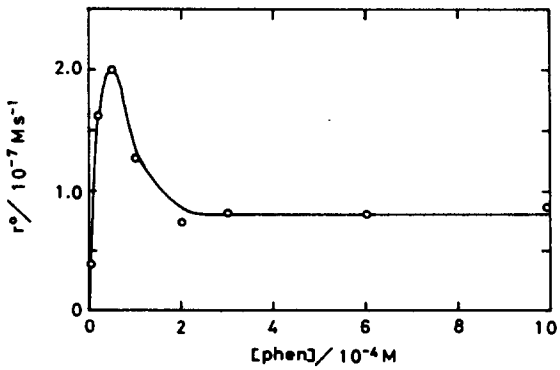


Fig. 6. Initial extraction rates of Ni(II) from the aqueous phase including pre-equilibrated $Ni^{2+}$–phen complexes; $[Ni^{2+}] = 1.0 \times 10^{-3}$ M, $[HDz] = 3.00 \times 10^{-5}$ M, pH 6.50 and 4700 rpm.

## 4. Discussion

### 4.1. Reaction between Ni(II) and phen in the aqueous phase

The linear relationship of Eq. (10) can be interpreted by the following reactions:

$$phen \rightleftharpoons phen_o \qquad K_{DL} \qquad (12)$$

$$Ni^{2+} + phen \rightarrow Niphen^{2+} \qquad k_1 \qquad (13)$$

The observed initial rate can then be represented by

$$r^0_{obs} = \frac{\varepsilon_L l k_1}{1 + K_{DL}} [Ni^{2+}]_{init}[phen]_T \qquad (14)$$

where $\varepsilon_L$, $l$, $k_1$ and $K_{DL}$ refer to the molar absorbtivity of phen in the organic phase, the optical length of the flow cell, the formation rate constant of $Niphen^{2+}$ and the distribution constant of phen respectively, and $[Ni^{2+}]_{init}$ is the initial concentration of free $Ni^{2+}$ in the aqueous phase. Therefore, the coefficient 4.21 in Eq. (10) corresponds to $\varepsilon_L k_1 [Ni^{2+}]_{init}/(1 + K_{DL})$. The values of $\varepsilon_L$ and $K_{DL}$ were previously determined as $3.49 \times 10^3$ and 723 [9], and the value of $[Ni^{2+}]_{init}$ was calculated as $1.29 \times 10^{-4}$ M from the total $Ni^{2+}$ concentration of $1.0 \times 10^{-3}$ M and the total $SO_4^{2-}$ concentration of 0.033 M, taking into account the formation constant of 209 [10] for the following reaction:

$$Ni^{2+} + SO_4^{2-} \rightleftharpoons NiSO_4 \qquad (15)$$

Finally, the value of $k_1$ was calculated as $6.79 \times 10^3$ $M^{-1}$ $s^{-1}$, which is fairly comparable with the values available in the literature, $1.4 \times 10^4$ $M^{-1}$ $s^{-1}$ [11] and $3.9 \times 10^3$ $M^{-1}$ $s^{-1}$ [12].

### 4.2. Formation of an intermediate complex at the interface

Under the condition $[HDz] < [phen]$, the decreasing rate of $[HDz]_o$ became larger than twice the increasing rate of $[NiDz_2phen]_o$. This implies that the total concentration of HDz in the organic phase, $[HDz]_o + 2[NiDz_2phen]_o$, is less than the initial concentration of HDz in the organic phase before contact with the aqueous phase. When the stirring was stopped during the extraction, an abrupt increase in the organic phase concentration of the adduct complex was observed. These facts suggest the existence of some interfacially adsorbed Ni(II) species which includes at least one molecule of

Table 1
The reaction rate constant between $NiDz_2$ and phen in chloroform at 25°C [a]

| No. | Concentration | | $k_{obs}$ ($s^{-1}$) | $k$($M^{-1}$ $s^{-1}$) |
|---|---|---|---|---|
| | $NiDz_2$ (M) | phen (M) | | |
| 1 | $6.58 \times 10^{-6}$ | $5.0 \times 10^{-5}$ | 8.15 | $1.63 \times 10^5$ |
| 2 | $6.58 \times 10^{-6}$ | $5.0 \times 10^{-4}$ | 85.4 | $1.71 \times 10^5$ |
| 3 | $3.32 \times 10^{-6}$ | $2.5 \times 10^{-4}$ | 41.9 | $1.68 \times 10^5$ |
| 4 | $3.32 \times 10^{-6}$ | $5.0 \times 10^{-5}$ | 9.33 | $1.87 \times 10^5$ |
| 5 | $1.33 \times 10^{-6}$ | $5.0 \times 10^{-6}$ | 0.909 | $1.82 \times 10^5$ |
| Average | | | | $(1.74 \pm 0.05) \times 10^5$ |

[a] Measured by the stopped-flow method.

dithizone. According to this assumption, the total concentration of HDz in the two-phase system can be represented by

$$[HDz]_T = [HDz]_o + 2[NiDz_2phen]_o + [INT]A_i/V_o \quad (16)$$

where [INT], $A_i$ and $V_o$ stand for the interfacial concentration of the adsorbed complex (mol $cm^{-2}$), the total interfacial area ($cm^2$) and the volume of the organic phase (l) respectively. The absorbance changes at 605 nm and 520 nm allowed calculation of the concentration of each species on the right hand side of Eq. (16) as a function of time. Fig. 7 shows typical examples of the calculated concentration changes of the three species at lower and higher concentrations of phen than that of HDz. At a higher concentration of phen, the formation of the interfacial complex and its slow conversion to the adduct complex $NiDz_2phen$ are clearly demonstrated.

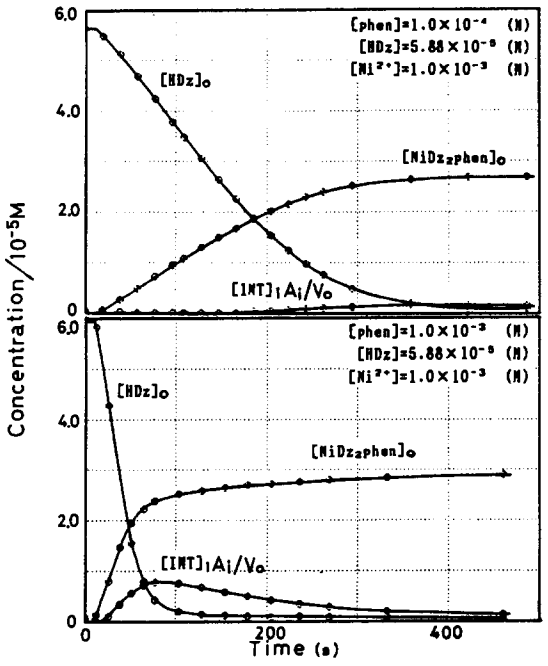


Fig. 7. Calculated changes in $[HDz]_o$, $[NiDz_2phen]_o$ and $[INT]_iA_i/V_o$ during the course of the extraction.

The change in the interfacial complex concentration calculated by Eq. (16) has been analyzed by a non-linear least-squares procedure based on the Marquardt method [13]:

$$[INT]A_i/V_o = c_1k_1'(k_2' - k_1')^{-1} \times \{\exp[-k_1'(t + c_2)] - \exp[-k_2'(t + c_2)]\} \quad (17)$$

where $c_1$ and $c_2$ are constants, and $k_1'$ and $k_2'$ refer to the apparent rate constants for the increase and decrease of the interfacial complex respectively. The four parameters, $c_1$, $c_2$, $k_1'$ and $k_2'$, were optimized until the sum of the squared difference between the calculated and observed values for $[INT]A_i/V_o$ could be minimized.

Fig. 8 shows a typical fitting curve for the concentration change of the interfacial complex. The differentiation of Eq. (17) with respect to $t$ at $t = -c_2$ gave an expression for the initial formation rate of the interfacial complex, $r^{0'}$:

$$r^{0'} = \left(\frac{d[INT]A_i/V_o}{dt}\right)_{t=0} = c_1k_1' \quad (18)$$

The values of $r^{0'}$ depended linearly on the HDz concentration, while those of $k_2'$ were independent of HDz concentration, as shown in Fig. 9. An average value of $k_2'$ of $3.1 \times 10^{-3}$ $s^{-1}$ was obtained. These results suggest that $r^{0'}$ most probably reflects the interfacial complexation:

$$Niphen_2^{2+} + Dz^- \rightarrow NiDzphen_2^+ \quad (19)$$

because the predominant species in the aqueous phase is $Niphen_2^{2+}$, as described be-

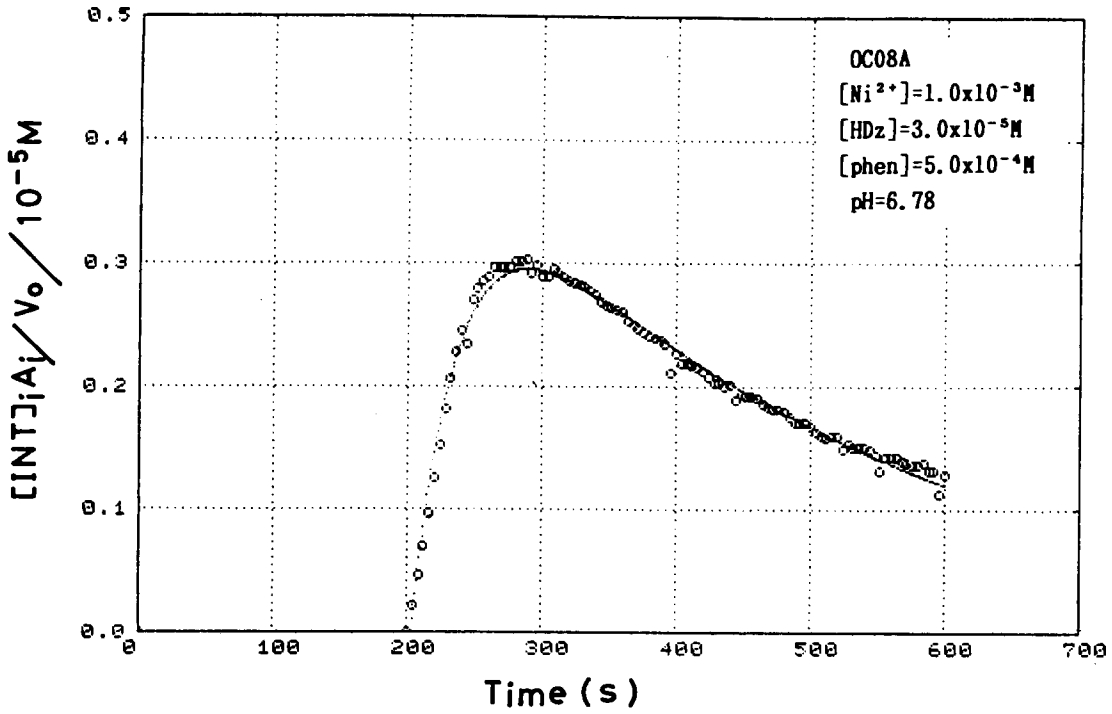


Fig. 8. Non-linear regression analysis of the concentration change of the interfacial complex; $[Ni^{2+}] = 1.0 \times 10^{-3}$ M, $[HDz] = 3.00 \times 10^{-5}$ M, [phen] = $5.0 \times 10^{-4}$ M, pH 6.78.

low. $k'_2$ is ascribable to the first-order dissociation reaction of the interfacial complex:

$$NiDzphen_2^+ \rightarrow NiDzphen^+ + phen \quad (20)$$

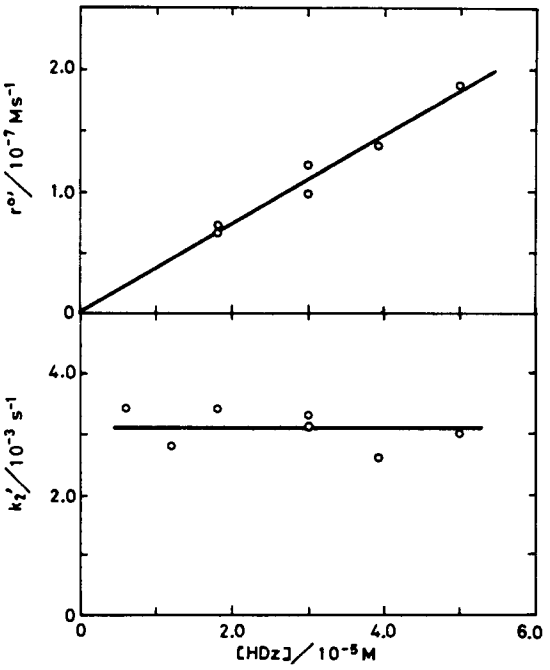


Fig. 9. Dependences of $r^0$ and $k'_2$ on HDz concentration; $[Ni^{2+}] = 1.0 \times 10^{-3}$ M, [phen] = $5.0 \times 10^{-4}$ M, pH 6.52–6.78.

which leads to the formation of $NiDz_2phen$. The overall conversion of $NiDzphen_2^+$ to $NiDz_2phen$ is represented by a disproportionation reaction:

$$2\ NiDzphen_2^{2+} \rightarrow NiDz_2phen + Niphen_3^{2+} \quad (21)$$

The extraction rate of $NiDz_2phen$ from the aqueous solution containing Ni(II)–phen complexes with the chloroform solution of HDz gave further insight into the composition of the interfacial species. As noticed in Fig. 6, there was no phen concentration dependence on the initial extraction rate in the higher concentration range of [phen] > $2 \times 10^{-4}$ M, showing the constant value of $r^0 = 7.7 \times 10^{-8}\ M^{-1}\ s^{-1}$. The calculation of each concentration of $Niphen^{2+}$, $Niphen_2^{2+}$ and $Niphen_3^{2+}$ in the aqueous phase using the corresponding formation constants [14] revealed that the concentrations of $Niphen^{2+}$ and $Niphen_2^{2+}$ are comparable when [phen] > $2 \times 10^{-4}$ M, while at phen concentrations below $2 \times 10^{-4}$ M, $Niphen^{2+}$ is the predominant species. Thus, it can be reasonably expected that when [phen] = $2 \times 10^{-4}$–$1 \times 10^{-3}$ M, the adsorbed complex $NiDzphen_2^+$ is rapidly formed through Eq. (19) and converts slowly to $NiDz_2phen_o$. The constant value of the initial extraction rate shown in Fig. 6 can therefore be related to $k'_2$ by the equation $r^0 = k'_2[INT]A_i/V_0$. Thus, $k'_2 = 3.5 \times 10^{-3}\ s^{-1}$

was determined from the values of $r^0 = 7.7 \times 10^{-8}\ M^{-1}\ s^{-1}$ and $[INT]A_i/V_0 = 2.2 \times 10^{-5}$ M calculated from Eq. (16). The value $3.5 \times 10^{-3}\ s^{-1}$ is in good agreement with $3.1 \times 10^{-3}\ s^{-1}$ obtained from the decreasing rate of $[INT]A_i/V_0$. These results strongly support the mechanism proposed herein.

### 4.3. Kinetic scheme of the synergic extraction

The first step of the extraction should be the reaction of $Ni^{2+}$ with $Dz^-$ and/or phen in the aqueous phase, i.e. Eqs. (6) and (13). The rate constants for the two processes in the aqueous phase are comparable: $k_0 = 5.97 \times 10^3\ M^{-1}\ s^{-1}$ for Eq. (6) and $k_1 = 6.79 \times 10^3\ M^{-1}\ s^{-1}$ for Eq. (13). Therefore, the relative significance of the two processes will be determined by the initial aqueous phase concentrations of $Dz^-$ and phen. The calculated concentrations using the values of $K_{DL}$ and $K_a/K_D$ are $[Dz] = 2.0 \times 10^{-8}$ M and $[phen] = 1.4 \times 10^{-7}$ M, provided that the initial concentrations for $[HDz]_o$ and $[phen]_o$ are $1.0 \times 10^{-4}$ M at pH 6.5. In this situation, reaction (13) will proceed in preference to reaction (6) by a factor of 70.

$Niphen^{2+}$ will further react with $Dz^-$ and phen according to the following competitive reactions:

$$Niphen^{2+} + Dz^- \rightarrow NiDzphen^+ \quad k_2 \qquad (22)$$

$$Niphen^{2+} + phen \rightarrow Niphen_2^{2+} \quad k_3 \qquad (23)$$

Reaction (22) may be responsible for the formation of the adduct complex to be extracted, while reaction (23) can become significant when [HDz] < [phen], leading to the formation of the interfacial complexes, $NiDzphen_2^+$ and $Niphen_3^{2+}$ [9]:

$$Niphen_2^{2+} + Dz^- \rightarrow NiDzphen_2^+ \quad k_4 \qquad (24)$$

$$Niphen_2^{2+} + phen \rightarrow Niphen_3^{2+} \qquad (25)$$

According to Eqs. (6), (13) and (22)–(24), the initial extraction rate of $NiDz_2phen$ and the initial formation rate of the interfacial complex are respectively represented by

$$r^0 = \left(\frac{d[NiDz_2phen]_o}{dt}\right)_{t=0} = \frac{k_1 k_2 [Ni^{2+}][phen][Dz^-]}{k_{-1} + k_2[Dz^-] + k_3[phen] - \alpha} \qquad (26)$$

and

$$r^{0'} = \left(\frac{d[INT]A_i/V_o}{dt}\right)_{t=0} = \frac{k_1 k_3 k_4 [Ni^{2+}][phen][Dz^-]}{(k_{-1} + k_2[Dz^-] + k_3[phen] - \alpha)(k_{-3} + k_4[Dz^-])} \qquad (27)$$

where $k_{-1}$ and $k_{-3}$ are the rate constants for the reverse reactions of Eqs. (13) and (23) respectively, $\alpha = k_3 k_{-3}[phen]/(k_{-3} + k_4[Dz^-])$, $[Dz^-] = K_a[HDz]_T/K_D[H^+]$ and $[phen] = [phen]_T/723$. The plots of Fig. 3 confirmed the linear correlation between $r^0$ and $[Dz^-]$, which was predicted from Eq. (26) under the condition $k_{-1} + k_2[Dz^-] - \alpha \ll k_3[phen]$ and gave the value $k_2 = 1.1 \times 10^5\ M^{-1}\ s^{-1}$ by introducing $k_1 = 6.79 \times 10^3\ M^{-1}\ s^{-1}$ and $k_3 = 7.4 \times 10^3\ M^{-1}\ s^{-1}$ [11]. When $k_{-1} + k_3[phen] - \alpha \ll k_2[Dz^-]$, Eq. (26) can be approximated by $r^0 = k_1[Ni^{2+}][phen]$. Fig. 4 confirmed the linear relation between $r^0$ and [phen], and gave a value of $k_1 = 6.57 \times 10^3\ M^{-1}\ s^{-1}$, which was fairly close to $k_1 = 6.79 \times 10^3\ M^{-1}\ s^{-1}$ determined by the separate experiment. The pH dependence of $r^0$, giving a slope of 0.40 as shown in Fig. 5, was different from the inverse first-order behavior expected from Eq. (26). This may be ascribable to the difference between the pH near the interface and the bulk pH [15]. Eq. (27) predicts that the initial formation rate of the interfacial complex is proportional to [phen], provided $k_2[Dz^-] \ll k_3[phen]$. Experimental results indeed supported the linear relationship, suggesting $k_1$ to be in the order of $10^3\ M^{-1}\ s^{-1}$.

In conclusion, the existence of the intermediate complex formed at the liquid–liquid interface was proved in the present study and the kinetic features of the interfacial complex were revealed. It was also shown by this study that even thermodynamically unfavorable complexes in homogeneous solutions could be formed in appreciable amounts at the liquid–liquid interface. The formation of charged complexes such as $NiDzphen_2^+$ at the interface may be of relevance to the response mechanism in the liquid–membrane ion-selective electrodes [16]. Further studies on the kinetics and equilibria in the interfacial complex formation with other extractants are in progress.

**Acknowledgments**

This work was supported by Grant-in-Aids for General Scientific Research from the Ministry of Education, Science and Culture, Japan (No. 05453066).

## References

[1] H. Watarai, Trends Anal. Chem., 12 (1993) 313.
[2] H. Watarai, M. Takahashi and K. Shibata, Bull. Chem. Soc. Jpn., 59 (1986) 3469.
[3] H. Watarai and M. Endoh, Anal. Sci., 7 (1991) 137.
[4] H. Watarai, K. Sasaki and N. Sasaki, Bull. Chem. Soc. Jpn., 63 (1990) 2797.
[5] B.S. Freiser and H. Freiser, Talanta, 17 (1970) 540.
[6] H. Akaiwa, H. Kawamoto and Y. Ueda, Proc. Symp. Solv. Extr., December 1988, Tokyo, Japan, p. 115.
[7] K. Ohashi and H. Freiser, Anal. Chem., 52 (1980) 767.
[8] B. E. MaClellan and H. Freiser, Anal. Chem., 36 (1964) 2262.
[9] H. Watarai, Y. Horii and M. Fujishima, Bull. Chem. Soc. Jpn., 61 (1988) 1159.
[10] H.C. Helgeso, J. Phys. Chem., 71 (1967) 819.
[11] G. Colovos, A. Yokoyama and H. Freiser, Anal. Chem., 47 (1975) 2441.
[12] R.H. Holyer, C.D. Hubbard, S.F.A. Kettle and R.G. Wilkins, Inorg. Chem., 4 (1965) 929.
[13] R.H. Bisby and E.W. Thomas, J. Chem. Educ., 63 (1986) 990.
[14] J.P. Sharff and M.R. Paris, Bull. Soc. Chim. Fr., (1967) 1782.
[15] X. Zhao, S. Ong, H. Wang and K.B. Eisenthal, Chem. Phys. Lett., 214 (1993) 203.
[16] Y. Itoh, H. Akaiwa, M. Sugawara and Y. Umezawa, Anal. Sci., 7 (1991) 947.

ELSEVIER

Talanta 42 (1995) 1701–1705

Talanta

# Polarographic investigation of Cu(II) complexes with *N,N,N′,N′*-tetrakis-(2-hydroxypropyl)-ethylenediamine

Eugenijus Norkus, Algirdas Vaškelis*, Irena Žakaitė, Jonas Reklaitis

*Institute of Chemistry, A. Goštauto 9, 2600, Vilnius, Lithuania*

Received 25 October 1994; revised 13 February 1995, accepted 5 May 1995

**Abstract**

During investigation of the formation of $Cu^{2+}$ ion complexes with *N,N,N′,N′*-tetrakis-(2-hydroxypropyl)-ethylenediamine (Quadrol-Q) by means of constant current polarography (20°C, ionic strength $J = 3$ mol $l^{-1}$), the possibility of the formation of two complex compounds; $CuQ^{2+}$ and $CuQ_2^{2+}$, was shown within the pH range from 6 to 8. The logarithms of the stability constants for these compounds are $10.6 \pm 0.3$ and $14.6 \pm 0.4$ respectively. Cu(II) complexation increases sharply when the pH increases from 8 to 10. It was shown that the data at a pH of greater than 10 are in accordance with the existence of the hydroxy complexes $CuQ(OH)_2$ and $CuQ_2(OH)_2$, the logarithms of the stability constants being $26.9 \pm 0.5$ and $29.1 \pm 0.3$.

*Keywords:* Copper; Complexation; Polarography

## 1. Introduction

*N,N,N′,N′*-tetrakis-(2-hydroxypropyl)-ethylenediamine, which is also known as Quadrol, is widely used as a ligand in solutions of electroless copper plating [1,2]. There is little information about Cu(II) complexes with Quadrol in the literature. The authors of Ref. [3] have investigated the formation of the above complex by means of spectrophotometric, conductometric and pH-metric titration methods. They have determined that Quadrol forms complexes with Cu(II) ions in the ratio 1:1 and the stability constant logarithm is approximately 9. The authors of Ref. [4] identified the same complex with a stability constant logarithm of 8.45 (25°C, $J = 0.1$) when the pH-metric titration method was used. Only the authors of Ref. [5] detected the presence of $CuQ_2^{2+}$ complex ($\log \beta = 13.6$, 25°C, $J = 0.5$) besides the $CuQ^{2+}$ complex ($\log \beta = 9.80$). As can be seen from the literature, it is not quite clear whether the diligand complex $CuQ_2^{2+}$ really exists. Further, based on the data of the stability of the known complexes, it is not at all clear how the alkaline solutions of electroless copper plating can exist when Quadrol is used as a ligand for Cu(II) ions. The calculations show that $Cu(OH)_2$ should precipitate in solutions with a pH value exceeding 8–9. Apparently, Quadrol forms more stable complexes with Cu(II) in alkaline solutions.

Therefore, this work describes the investigation of Cu(II) complex formation with Quadrol by means of the DC-polarographic method which has not been used for this system before.

## 2. Experimental

$NaNO_3$ and NaOH were used to keep the ionic strength of the solutions constant, and the pH of the solutions was controlled using aqueous

* Corresponding author.


*SSDI* 0039-9140(95)01635-X

NaOH and $HNO_3$. Analytical grade chemicals were used, and Quadrol was of a practical grade (over 98%) from Fluka.

The polarographic curves were recorded by a PU-1 polarograph (Belorusia) using a dropping mercury electrode in a thermostatted three-electrode cell at $20 \pm 0.1$°C. The potential scanning rate was 100 mV $min^{-1}$, and the capillary characteristics were $m = 2.95$ mg $s^{-1}$, $t = 3.73$ s. The reference electrode was a silver–silver chloride electrode with saturated KCl solution. The total concentration of Cu(II) ions was $5 \times 10^{-4}$ mol $l^{-1}$.

The slope of the dependence $\log(\bar{i}/\bar{i}_{lim} - \bar{i}) - E$ for Cu(II) polarographic waves is equal to 35–38 mV, i.e. the waves are quasireversible. The values of the reversible half-wave potential $E^r_{1/2}$ were determined within $\pm 1$ mV from the plots of $\log(\bar{i}/\bar{i}_{lim} - \bar{i}) - E$ using the method of quasireversible polarographic waves of Matsuda and Ayabe [6].

The values of the reversible half-wave potential were used for calculations of parameters of copper complexes by equations from Ref. [7]. On the grounds of experimental dependencies of $E^r_{1/2}$ on pH and total Quadrol concentration, we assumed that the complexes $CuQ_n(OH)_m^{2-m}$, where $n = 1,2$ and $m = 0–4$, could be formed in the solution under investigation. The possibility of complex formation with protonated Quadrol $HQ^+$ — $Cu(HQ)^{3+}$, $CuQ(HQ)^{3+}$, $Cu(QH)_2^{4+}$ — was also considered. The stability constants of copper complexes were obtained during iterative approximation by minimizing the least squares functional, obtained from equations published in Ref. [7]. To estimate the accuracy of the stability constants we made an assumption that the determination of the reversible half-wave potential was within $\pm 2$ mV. If in the next iteration the accuracy of any stability constant diverges to infinity, then deletion of such a complex from the functional has no influence on the least-squares sum. In this case we assume that such a complex does not exist under these conditions.

## 3. Results and discussion

### 3.1. Quadrol protonation

Usually, unprotonated Quadrol molecules form complexes with $Cu^{2+}$ [3–5]. Since we found no information about Quadrol protonation constants under the conditions of our work at 20°C when $J = 3$ mol $l^{-1}$, we carried out a series of pH-metric titrations of Quadrol solutions at different ionic strengths. The first and the second protonation constants were calculated according to Ref. [8] (Fig. 1). The values $\log K_1 = 9.5 \pm 0.1$ and $\log K_2 = 5.0 \pm 0.1$ were used for further treatment of the polarographic data obtained at $J = 3$.

### 3.2. Solutions at pH < 8

We carried out several series of experiments with different concentrations of Quadrol and at different pH values in solutions of pH = 5–8, which had been investigated earlier by other authors. As can be seen from the results obtained (Fig. 2(a)), with an increase in the pH of the solutions and an increase in the total Quadrol concentration, $E^r_{1/2}$ is shifted to more negative potential values. $\Delta E_{1/2}$ changes by 30–45 mV on a 10-fold increase of the total Quadrol concentration at constant pH. This shows that one or two Quadrol molecules can participate in the complex formation when a one-step two-electron discharge of copper ions occurs. When the total Quadrol concentration is constant, an increase in the pH of the solution by one unit shifts $\Delta E^r_{1/2}$ to more negative values by 45–50 mV. This also confirms that one or two Quadrol molecules take part in the complex formation, since the equilibrium concentration of unprotonated Quadrol increases 10-fold with one pH unit in this region.

When minimising the least-squares functional, it was shown that the data are in accor-

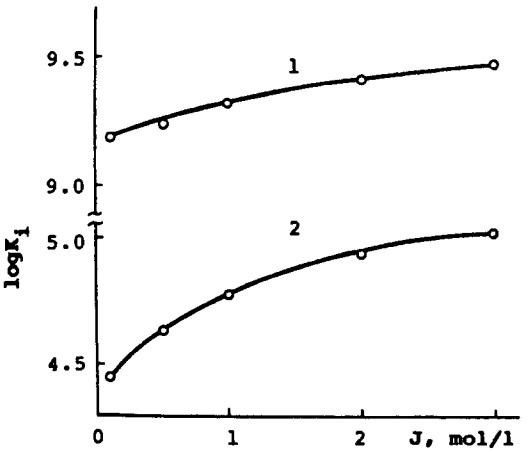


Fig. 1. Dependence of the first (curve 1) and second (curve 2) Quadrol protonation constants on the solution ionic strength.

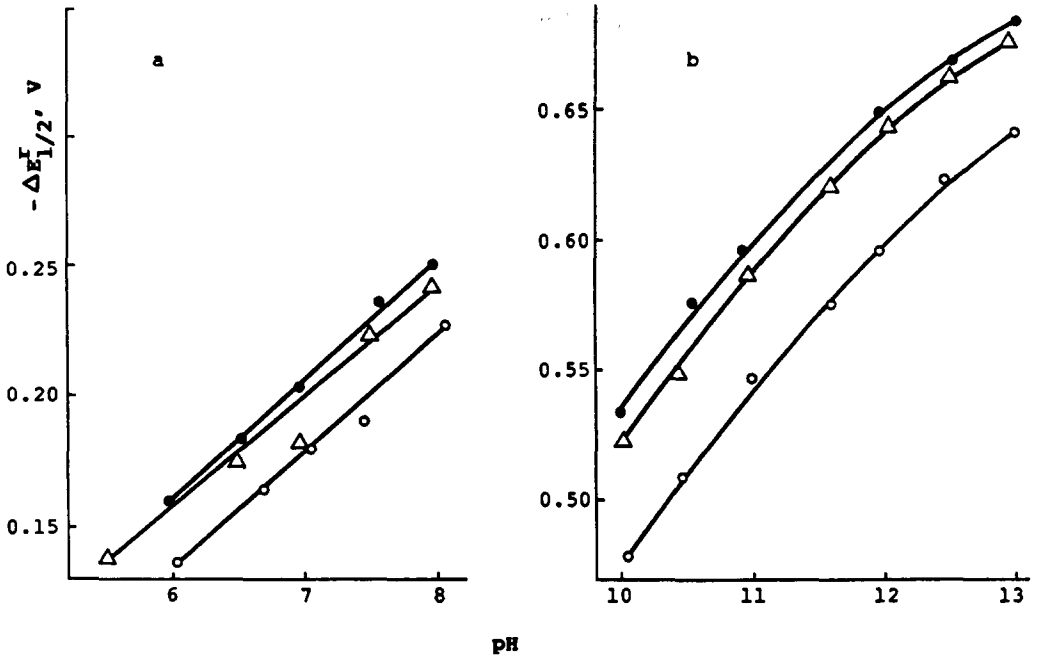


Fig. 2. Dependence of the reversible half-wave potential shift ($\Delta E^r_{1/2}$) on pH. The total Cu(II) concentration is $5 \times 10^{-4}$ mol $l^{-1}$, and the total Quadrol concentrations are $5 \times 10^{-3}$ (○), $2.5 \times 10^{-2}$ (△) and $5 \times 10^{-2}$ (●) mol $l^{-1}$.

dance with the existence of the complexes $CuQ^{2+}$ and $CuQ_2^{2+}$, the stability constant logarithms being $10.6 \pm 0.3$ and $14.6 \pm 0.4$. These values are slightly higher than the literature data, which may be explained by the influence of high ionic strength.

The characteristics of Cu(II) complexes obtained from the polarographic data were in agreement with the general behaviour of these Cu(II) solutions. The solutions become turbid and $Cu(OH)_2$ precipitates as the pH increases to over 5.9, the Cu(II) and Quadrol concentration being $5 \times 10^{-3}$ mol $l^{-1}$. The calculations using Cu(II)–Q complex stability constants showed that the concentration of free copper ions at pH 5.9 indeed exceeds the value allowed by the $Cu(OH)_2$ solubility product.

### 3.3. Solutions at pH > 8

A sharp increase in Cu(II) complexation was observed at pH > 8, i.e. when increasing the pH of the solutions from 8 to 10 the $E^r_{1/2}$ became more negative by approximately 300 mV. This means that the concentration of free Cu(II) ions reduces by approximately 10 orders of magnitude (Fig. 3). A sharp increase in the Cu(II)–Quadrol complex stability at pH > 8 may be related to the substantial changes in the structure of the complexes. The available experimental data are not sufficient for adequate estimation of Cu(II) complex species in the pH region 8–10.

With a further increase in solution alkalinity (pH > 10), $\Delta E^r_{1/2}$ shifts to more negative values (Fig. 2(b)), although the equilibrium unprotonated Quadrol concentration is actually constant in these solutions. This fact could be accounted for by participation of a new ligand

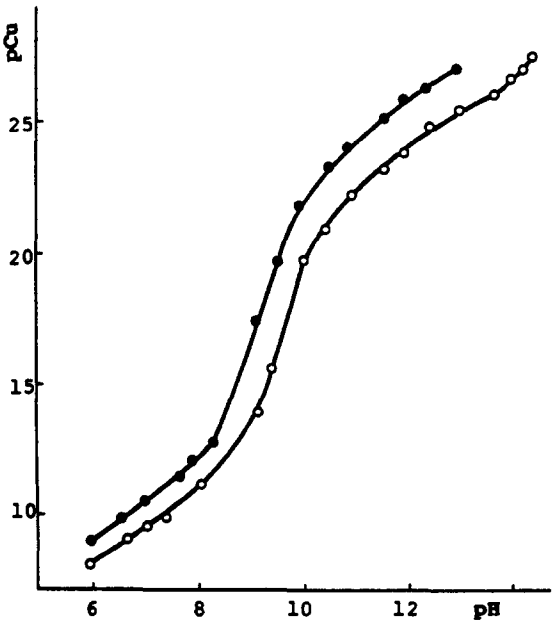


Fig. 3. Dependence of pCu on pH. Cu(II) concentration is $5 \times 10^{-4}$ mol $l^{-1}$, Quadrol concentrations are $5 \times 10^{-3}$ (○) and $5 \times 10^{-2}$ (●) mol $l^{-1}$

(namely, $OH^-$ ions) in the complex formation. Analysis of the data obtained shows that copper hydroxy complexes with two $OH^-$ groups (with increase in pH of one unit the $\Delta E^r_{1/2}$ becomes more negative by 58 mV) and one or two Quadrol molecules (at the same pH of the solution and a 10-fold higher Quadrol concentration, $\Delta E^r_{1/2}$ becomes more negative by about 50 mV) may be formed in this system.

The calculations using the LS technique indicated the presence of two kinds of hydroxy complexes in the system, namely $CuQ(OH)_2$ and $CuQ_2(OH)_2$. Their stability constant logarithms are $26.9 \pm 0.5$ and $29.1 \pm 0.3$ respectively.

Polarographic data in solutions at pH > 13 (up to 3 mol $l^{-1}$ NaOH) showed that the complex $CuQ_2(OH)_2$ dominated (at a total concentration of Quadrol of over 0.01 mol $l^{-1}$) under these conditions. In such highly alkaline solutions, Cu(II) complexes with Quadrol do not transform to tetrahydroxycuprate(II) $Cu(OH)_4^{2-}$ as occurs for Cu(II) complexes with EDTA, tartrate and NTA. This is in agreement with the value of the stability constant of $Cu(OH)_4^{2-}$: $\log \beta = 15.5$ [9].

### 3.4. Distribution of Cu(II) complexes

As follows from the analysis of polarographic data, we were not able to describe Cu(II) complex formation with Quadrol by one set of complex species over the range of solution pH values investigated. Therefore, we can only discuss the complex distribution in two separate pH regions: at pH = 5–8 and at pH > 10.

The calculations of copper ion distribution among the complexes showed that at pH 5–6 the $CuQ^{2+}$ complex predominates. With rising pH it converts to $CuQ_2^{2+}$, which predominates at pH 7–8. In alkaline solutions at pH > 10, a dihydroxy complex $CuQ_2(OH)_2$ is found to predominate, and at a total Quadrol concentration higher than 0.01 mol $l^{-1}$ (Fig. 4). The complex $CuQ(OH)_2$ predominates in solution only at low Quadrol concentrations.

It should be noted that according to our polarographic data the hydroxy Cu(II) complexes with Quadrol of high stability do not exist at pH < 8, although the formal calculation would show the presence of $CuQ(OH)_2$ at pH values as low as 7. The abrupt increase in Cu(II) complexation at pH > 8 (Fig. 3) indicates some changes not only in Cu(II) complex structure, but apparently also in ligand molecule structure, and new complex formation equilibria appear at pH > 8.

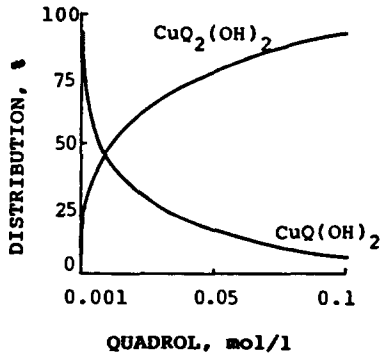


Fig. 4. Distribution of copper(II)–Quadrol complexes at different Quadrol concentrations. The total Cu(II) concentration is $0.5 \times 10^{-4}$ mol $l^{-1}$, at pH 12.0.

A similar situation is observed in the copper(II)–tartrate system: according to complex stability data [10,11], the hydroxy complex $CuTart_2(OH)_2^{4-}$ should predominate at a wide range of pH values (7–14), but it was detected by EPR techniques only in alkaline solutions at pH > 11 [12].

The newly obtained data on copper(II) and Quadrol complexes in alkaline solutions show that they are among the most stable Cu(II) complexes under these conditions. The pCu values are much higher than 20 at pH > 10 (Fig. 3), and this not only prevents the formation of $Cu(OH)_2$, but also enables the existence of rather concentrated alkaline Cu(II) solutions in the presence of Quadrol. Therefore, the use of Quadrol in electroless copper plating solutions is quite natural. The better technological parameters of these solutions compared with other practically used electroless plating solutions containing tartrate or EDTA are apparently related to the higher stability of Cu(II) complexes with Quadrol.

## References

[1] M. Paunovic, J. Electrochem. Soc., 124 (1977) 349.
[2] F.M. Donahue, D.J. Sajkowski, A.C. Bosio and L.L. Schafer, J. Electrochem. Soc., 129 (1982) 717.
[3] J.L. Hall, F.R. Jones, C.E. Delchamps and C.W. Williams, J. Am. Chem. Soc., 79 (1957) 3361.
[4] I.J. Israely, J. Inorg. Nucl. Chem., 27 (1965) 2271.
[5] M. Orama, H. Saarinen and L. Kaila, Finn. Chem. Lett., 2 (1979) 182.
[6] H. Matsuda and Y. Ayabe, Z. Elektrochem., 63 (1959) 1164.

[7] J. Heyrovsky and J. Kuta, Principles of Polarography, Academic Press, New York, 1966.
[8] J. Inczedy, Analytical Applications of Complex Equilibria, Akademiai Kiado, Budapest, 1976.
[9] E. Norkus and A. Vaškelis, Polyhedron, 13 (1994) 3041.
[10] D.D. Perrin (Ed.), Stability Constants of Metal–Ion Complexes, Part B: Organic Ligands, Pergamon Press, Oxford, 1979.
[11] M.M. Petit-Ramel and C.M. Blanc, J. Inorg. Nucl. Chem., 34 (1972) 1241.
[12] L.N. Schoenberg, J. Electrochem. Soc., 118 (1971) 1571.

ELSEVIER

Talanta 42 (1995) 1707–1710

Talanta

# Dissolved oxygen removal from aqueous media by the chromatomembrane method

L.N. Moskvin *, O.V. Rodinkov, A.N. Katruzov, G.L. Grigor'ev, S.N. Khromov-Borisov

*Department of Chemistry, St. Petersburg State University, Petrodvorets, Universitesky pr. 2, 198804 St. Petersburg, Russia*

Received 11 November 1994; revised 3 May 1995; accepted 5 May 1995

**Abstract**

The possibilities of the new chromatomembrane method in the removal of oxygen dissolved in water are studied. The scheme of the water deoxygenation process is determined. The new reagent-free method allows production of water with oxygen content at the level of a few ppb.

*Keywords:* Oxygen removal; Chromatomembrane

## 1. Introduction

The elaboration of efficient methods for the removal of dissolved oxygen from aqueous solutions is one of the preparative problems in chemistry [1]. Chemical deoxygenation methods are based upon the introduction of strong reducing agents into aqueous medium to fix the amount of dissolved oxygen. These methods are of limited use and they cannot satisfy strict requirements as to the purity of the water obtained. The possibilities of membrane methods for mass-exchange processes in the liquid–gas system are limited by the slow rates of membrane diffusion. The most common methods for removal of dissolved gases (boiling, purging with inert gas) are based upon the redistribution of gaseous components in the liquid–gas system. Their efficiency is also insufficient in many cases. With optimal design of the corresponding equipment, the residual oxygen content in water is 900 ppb for boiling and 200 ppb for bubbling [1].

The conceptually new chromatomembrane principle for the realization of mass-exchange processes in liquid–liquid and liquid–gas systems [2,3] opens up new possibilities in the removal of dissolved gases from aqueous solutions.

The chromatomembrane method of interphase exchange is based upon capillary effects that occur within a porous hydrophobic matrix [2]. It is possible to pass flows of two phases simultaneously through the porous medium when there are two types of pores that substantially differ in size. The aqueous solution, which does not wet the surface of the hydrophobic material, fills the macropores of the biporous matrix and moves within them. The gas phase moves within the micropores, which are inaccessible to the aqueous phase because of capillary forces. In order to avoid entry of the gas phase into the macropores, the aqueous phase pressure is maintained higher than the pressure of the gas phase throughout the mass-exchange space. To provide a separate inlet and outlet for flows of both phases, the gas phase enters the mass-exchange space through microporous hydrophobic membranes. The membranes are nonpermeable to the aqueous phase, which goes immediately into the

* Corresponding author.

*SSDI* 0039-9140(95)01636-8

biporous medium. So, the chromatomembrane method provides continuous isolation of volatile admixtures from aqueous solutions while combining the main advantages of chromatographic (high efficiency of the mass-exchange process) and membrane (continuous regime) separation methods.

The scope of the present work was to develop a chromatomembrane method for the deoxygenation of aqueous solutions and to estimate its prospects for the production of water with low oxygen content.

## 2. Experimental

A scheme of the experimental device is shown in Fig. 1. The aqueous sample of known oxygen content is passed with a certain flow rate through the regulatory valve (1) and manifold (2) into the mass-exchange layer (3) of the chromatomembrane cell (4), and then to waste. Simultaneously, the extracting gas of known oxygen content is passed by regulatory valve (5) and manifold (2) with a certain flow rate through the microporous membranes (6) and mass-exchange layer (3). To determine the depth of deoxygenation, the oxygen content in aqueous solution at the outlet of the chromatomembrane cell was monitored by means of gas chromatography with a common thermal conductivity detector and preconcentration stage. The dissolved oxygen was preconcentrated and extracted into a gas phase by means of liquid–gas chromatography [4]. This method allows detection of the dissolved oxygen to within 10–10 000 ppb, with a relative error of less than 20%.

The experimental chromatomembrane cells were made of polytetrafluoroethylene (PTFE). The cells had membranes of 0.8 mm thickness with an average pore size of about 1 μm. The

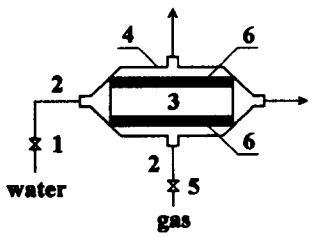


Fig. 1. Scheme of the experimental device: (1) regulatory valve for aqueous sample supply; (2) manifold; (3) mass-exchange layer; (4) case of the chromatomembrane cell; (5) gas regulatory valve; (6) microporous membrane.

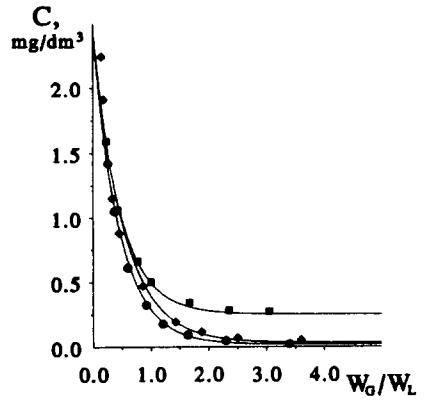


Fig. 2. Relationship between $O_2$ content in the outlet aqueous solution ($C$) and the ratio of volume rates ($W_G/W_L$). Aqueous sample flow rate $W_L = 20\ cm^3\ min^{-1}$. The mass-exchange layer dimensions of the cell are 5 × 4 × 1 cm. Initial oxygen content in the extracting gas: (■) 8.7 mg $dm^{-3}$; (◆) 0.85 mg $dm^{-3}$; (●) <0.05 mg $dm^{-3}$.

micropores within the mass-exchange layer are of the same size. The average radius of the macropores is 0.5–3.0 mm. The dimensions of the mass-exchange layer are presented hereafter in the form "length × width × height". The length is measured along the aqueous phase flow, the height being measured in the direction of the gas passage. The mass-exchange units have a hermetic case of PTFE (about 1 cm thickness) that prevents oxygen diffusion from ambient air. The cells in this study allow variation of the aqueous phase flow within the 0–350 $cm^3\ min^{-1}$ range and of the extracting gas flow within the 0–800 $cm^3\ min^{-1}$ range.

## 3. Results and discussion

Two main factors determine the degree of the chromatomembrane deoxygenation: the ratio of the volume rates of gas $W_G$ and aqueous solution $W_L$ flowing through the chromatomembrane cell, and the oxygen content in the extracting gas $C_G$ (Fig. 2). In the case of low $W_G/W_L$ values, the oxygen content in the outlet aqueous solution $C$ is virtually independent of the oxygen content in the extracting gas. The former will decrease exponentially with an increase in the $W_G/W_L$ ratio. In the limiting case, with a sufficiently high value of $W_G/W_L$, the oxygen content in the outlet aqueous solution is related to its content in the extracting gas flow simply by

$$C = C_G/K \quad (1)$$

where $K$ is the distribution coefficient of the component for the liquid–gas system, i.e. the ratio of the oxygen equilibrium concentrations in the gas and in the liquid.

The latter gives evidence of the high efficiency of mass exchange within the chromatomembrane cells. This is sufficient to obtain the ultimate possible purification of water from oxygen with its given content in the extracting gas.

To predict the degree of removal of dissolved gases by means of the chromatomembrane method, one can proceed from common features of the chromatomembrane process and continuous gas extraction (stripping). The same process of distribution of volatile components within a liquid–gas system forms the basis for both techniques. Various models of stripping and their mathematical description are discussed in detail by Vitenberg and Ioffe [5]. The high efficiency of mass exchange inherent in the chromatomembrane process allows us to assume an instant equilibration between the total volume of the liquid phase and the total volume of the gas phase in the system. Hence, we chose the model of stripping that assumes thermodynamic equilibrium between the liquid phase and gas bubbles passing through it, and also between the liquid phase and the gas phase above the solution. The process in this case is described with the equation proposed by Wahlroos [6,7] for the measurement of liquid–gas partition coefficients:

$$C_G^V = C_G^0 \exp\left(\frac{-V}{V_L/K + V_G}\right) \quad (2)$$

where $C_G^V$ is the component concentration in the gas phase after passing a gas volume $V$ through the liquid, $C_G^0$ is the initial component concentration in the gas phase, and $V_G$ and $V_L$ are the geometric volumes of the gas and liquid phases within the chromatomembrane cell respectively. It is important to note that we use in this article the distribution coefficient that is characteristic of extraction systems, whereas the reciprocal coefficient is more common in the description of head-space analysis.

Under the equilibrium conditions, the component concentration in the liquid is related to its concentration in the gas phase by the ratio $C = C_G/K$. Hence, we may transform Eq. (2) to

$$C = C^0 \exp\left(\frac{-V}{V_L/K + V_G}\right) \quad (3)$$

where $C^0$ is the component concentration in the liquid before passing the gas through.

A certain portion of the component will pass immediately into the gas phase present in the system before the stripping starts. From the equation of material balance

$$C_L V_L = C^0 V_L + K C^0 V_G \quad (4)$$

we obtain

$$C^0 = \frac{C_L}{1 + K V_G/V_L} \quad (5)$$

where $C_L$ is the initial concentration of the component in the liquid sample before contact with the gas phase. Combining Eqs. (5) and (3) we obtain, after simple transformations,

$$C = \frac{C_L}{1 + K V_G/V_L} \exp\left[\frac{-V}{V_L(1 + K V_G/V_L)}\right] \quad (6)$$

In the chromatomembrane process, the ratio of purging gas volume $V$ to the volume of liquid $V_L$ is equivalent to the ratio of the volume rates of liquid and gas phase flows through the chromatomembrane cell $W_G/W_L$. Hence, we can modify Eq. (6) to the form

$$C = \frac{C_L}{1 + K V_G/V_L} \exp\left[\frac{-W_G}{W_L(1 + K V_G/V_L)}\right] \quad (7)$$

where $C$ and $C_L$ are the component concentrations in the liquid phase at the outlet and at the inlet of the chromatomembrane cell respectively.

When the concentration of the component to be removed is not zero in the purging gas, one should take into account its contribution by means of Eq. (1). Finally, we derive an equation that allows us to predict the depth of removal of dissolved gases by the chromatomembrane method:

$$C = \frac{C_L}{1 + K V_G/V_L} \exp\left[\frac{-W_G}{W_L(1 + K V_G/V_L)}\right] + \frac{C_G}{K} \quad (8)$$

When the $V_G/V_L$ ratio is in the 0.3–1.0 range, deoxygenation of water from saturation to the 50–60 $\mu g\, dm^{-1}$ level is reached with a $W_G/W_L$ ratio of 2:1 or more. This is evident from Eq. (8) and is proved by the experimental data (see Fig. 2 and Table 1).

Comparison of the deoxygenation efficiency at chromatomembrane cells with different geometric parameters and for various rates of phase flows (Table 1) gives evidence that the degree of oxygen removal depends weakly on

Table 1
Effect of volume rates of aqueous ($W_L$) and gas ($W_G$) flows on the efficiency of chromatomembrane deoxygenation for distilled water and pure nitrogen. The water is saturated with atmospheric oxygen. The residual oxygen content in reagent-grade nitrogen is below 20 μg dm$^{-3}$. The mass-exchange layer dimensions of the three cells are: (A) 5 × 20 × 1 cm; (B) 5 × 5 × 4 cm; (C) 1 × 2 × 3 cm.

| $W_G$ (cm$^3$ min$^{-1}$) | $W_L$ (cm$^3$ min$^{-1}$) | $W_G/W_L$ | $O_2$ content in water at the outlet of the cell (μg dm$^{-3}$) | | |
|---|---|---|---|---|---|
| | | | A | B | C |
| 15 | 30 | 0.5 | 305 | 326 | 320 |
| 30 | 30 | 1.0 | 148 | 153 | 151 |
| 45 | 30 | 1.5 | 85 | 90 | 83 |
| 60 | 30 | 2.0 | 62 | 68 | 60 |
| 60 | 120 | 0.5 | 194 | 235 | 217 |
| 120 | 120 | 1.0 | 63 | 68 | 59 |
| 180 | 120 | 1.5 | 32 | 35 | 34 |
| 240 | 120 | 2.0 | 22 | 24 | 27 |
| 150 | 300 | 0.5 | 41 | 47 | - |
| 300 | 300 | 1.0 | 25 | 24 | - |
| 600 | 300 | 2.0 | 19 | 18 | - |

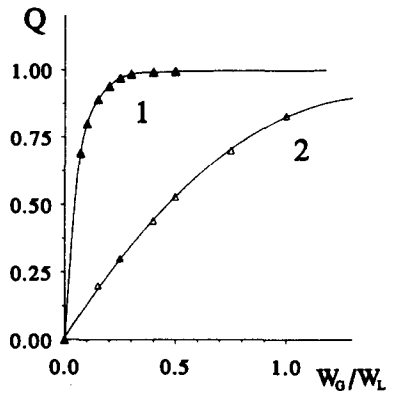


Fig. 3. Relationship between the degree of extraction of dissolved oxygen ($Q$) and the ratio of volume rates ($W_G/W_L$) of extracting gas and aqueous sample flows. (1) Chromatomembrane method. (2) Countercurrent gas extraction. Aqueous sample flow rate 10 cm$^3$ min$^{-1}$. The inner dimensions of the mass-exchange cell and extractor are 5 × 4 × 1 cm. The extracting gas is of the same purity.

the absolute rates, but is determined by their ratio to a crucial extent. When raising both phase flows, even a marked increase in the degree of deoxygenation takes place at the expense of a decrease in the $V_G/V_L$ value (see expression 8). It can be deduced from this that when using the chromatomembrane method, equilibrium between the phases is reached so rapidly that this is not the factor limiting the process efficiency.

The latter is one of the main advantages of the chromatomembrane method. In the common bubbling technique, the efficiency of removal of volatile components depends on the purge rate and, starting from rather low extracting gas rates, this efficiency decreases with an increase in rate. The performance of the chromatomembrane method is much higher for high rates of flow. This is obvious from the comparative results of dissolved gas extraction in the chromatomembrane cell and in a countercurrent gas extractor of equal dimensions (Fig. 3). We can estimate the performance of the method with the value of 10 dm$^3$ min$^{-1}$ per 1 dm$^3$ of mass-exchange cell volume with an extracting gas consumption of 2–3 dm$^3$ per 1 dm$^3$ of purified water while producing water with an oxygen content below 20 ppb.

The values obtained in the present work of residual oxygen content in purified water at the 20 ppb level are not the limiting ones. The pattern of relationships between the degree of deoxygenation and the process parameters proves unambiguously that this level can be lowered when using sufficiently pure extracting gas.

## References

[1] I.B. Butler, M.A.A. Schoonen and D.T. Rickard, Talanta, 41 (1994) 211.
[2] L.N. Moskvin, J. Chromatogr., 669 (1994) 81.
[3] L.N. Moskvin, Dokl. Akad. Nauk, 334 (1994), 599.
[4] L.N. Moskvin and O. V. Rodinkov, Crit. Rev. Anal. Chem., 24 (1994) 317.
[5] A.G. Vitenberg and B.V. Ioffe, J. Chromatogr., 471 (1989) 55.
[6] O. Wahlroos, Acta Chem. Scand., 15 (1961) 2053.
[7] O. Wahlroos, Acta Chem. Scand., 20 (1966) 197.

ELSEVIER

Talanta 42 (1995) 1711–1717

Talanta

# pH-metric studies on ternary metal complexes of some amino acids and benzimidazole

M.T. El-Haty *, A.H. Amrallah, R.A. Mahmoud, A.A. Ibrahim

*Chemistry Department, Faculty of Science, Aswan, Egypt*

Received 22 November 1994; revised 28 February 1995; accepted 8 May 1995

**Abstract**

The stability constants of binary and ternary complexes of copper(II) and nickel(II) with some amino acids (D-histidine, DL-serine, lysine) as primary ligands and benzimidazole as a secondary ligand were determined pH-metrically. The study was conducted in 10% (v/v) ethanol–$H_2O$ medium and at an ionic strength of 0.1 mol $dm^{-3}$ $NaNO_3$ at $20 \pm 1$°C. Values of $\Delta \log K$ were discussed on the basis of statistical considerations and the nature of the species formed. The stability of the binary and mixed ligand complexes are discussed in terms of the molecular structure of benzimidazole and the amino acids as well as the nature of the metal ion.

*Keywords:* Amino acids; Benzimidazole; pH-metric study; Ternary metal complexes

## 1. Introduction

Metal complexes with imidazole compounds are of great interest with respect to their biological applications as imidazole occurs in purine and the amino-acid histidine [1]. The study of mixed ligand complexes has been receiving considerable attention recently. Although several studies have been made on the use of amino acids in ternary complex formation [2–4], results on ternary complexes containing amino acids and benzimidazole are still scarce.

In the present paper, a systematic study on complex formation between the metal ions Cu(II) and Ni(II), and benzimidazole and some amino acids namely D-histidine, DL-serine and lysine, has been carried out using the potentiometric titration technique. This study is concerned with the formation and stability of the ternary complexes in relation to those of the binary complexes.

* Corresponding author.

## 2. Experimental

### 2.1. Materials and solutions

Analytical grade metal salts $Cu(NO_3)_2 \cdot 3H_2O$ and $NiCl_2 \cdot 6H_2O$ were used. The benzimidazole as well as the amino acids (D-histidine, DL-serine and lysine) used were A.R. grade, BDH products. Standard solutions (0.01 mol $dm^{-3}$) of benzimidazole (B) and the metal salts were prepared by dissolving the quantity required in absolute ethanol. Amino acid (A) NaOH, $NaNO_3$ and $HNO_3$ solutions were dissolved in $CO_2$-free bidistilled water.

### 2.2. Potentiometric titrations

Numerous titrations with a relatively highly concentrated standard, carbonate-free sodium hydroxide solution of the parent ($M^{2+}$–A) and/or the B mixture in a 1:5:5 molar ratio ($1 \times 10^{-3}$ mol $dm^{-3}$ of each) were carried out at $20.0 \pm 0.5$°C and in 10% (v/v) ethanol–$H_2O$ media in order to overcome the weak solubility


*SSDI* 0039-9140(95)01641-4

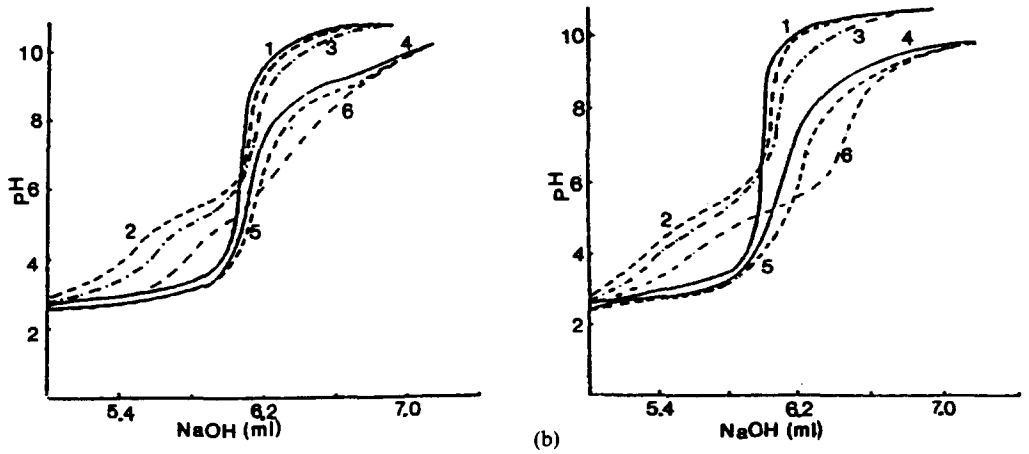


Fig. 1. Titration curves for the ternary complexes (1:1:1) at 20 °C and at $I = 0.1$ mol dm$^{-3}$ $NaNO_3$ ([NaOH] = 0.08 mol dm$^{-3}$). (a) Serine–benzimidazole–Ni(II); (b) lysine–benzimidazole–Cu(II). Curve 1, 0.01 mol dm$^{-3}$ $HNO_3$ + 0.1 mol dm$^{-3}$ $NaNO_3$, curve 2, solution (1) + $1.0 \pm 10^{-3}$ mol dm$^{-3}$ benzimidazole; curve 3, solution (2) + $2.0 \times 10^{-4}$ mol dm$^{-3}$ metal ion; curve 4, solution (1) + $1.0 \pm 10^{-3}$ mol dm$^{-3}$ amino acid; curve 5, solution (4) + $2.0 \times 10^{-4}$ mol dm$^{-3}$ metal ion; curve 6, solution (5) + $1.0 \times 10^{-3}$ mol dm$^{-3}$ benzimidazole.

of the studied systems in pure aqueous medium. The ionic strength and the total volume were kept constant at 0.1 mol dm$^{-3}$ $NaNO_3$ and 50 ml, respectively. Purified nitrogen gas was passed into the solutions before and during the titrations. Multiple titrations were carried out for each system. pH-metric measurement were performed using an Orion 601 Digital Research pH-meter with a glass calomel electrode assembly, accurate to 0.005 unit. The solutions were titrated according to the following scheme: 1, $HNO_3$; 2, $HNO_3 + B$; 3, $HNO_3 + B + M^{2+}$; 4, $HNO_3 + A$; 5,$HNO_3 + A + M^{2+}$; 6, $HNO_3 + B + A + M^{2+}$.

The pH-meter readings were corrected according to the Douheret procedure [5]. The pH-meter reading in the 10% (v/v) ethanol–$H_2O$ mixture, pH($R$), differs by an amount $\delta$ from the corrected reading in aqueous medium, pH*, according to the equation $pH^* = pH(R) - \delta$. The $\delta$ value in 10% (v/v) ethanol–$H_2O$ as reported to be 0.02 [5]. Accordingly the presence of 10% ethanol–$H_2O$ has a minor influence on the protonation or complex stability constants obtained.

## 3. Results and discussion

### *3.1. Stability constants of the binary metal complexes*

Fig. (1) represents a set of constructed titration curves for the free and complexed ligands according to the sequence described in the experimental section. In all the ternary systems, the amino acids are regarded as primary ligands and benzimidazole (B) as secondary ligand. The protonation constants have been determined under our experimental conditions using the Irving–Rossotti method [6]. The values obtained (Table 1) are more or less in good agreement with those reported earlier [7–13]. Examination of the titration curves in the presence of the metal ions Cu(II) and Ni(II) indicates that the addition of the metal ion to the ligand solutions causes a decrease in the pH value. This shows that the complexation reaction proceeds by the replacement of protons from such ligands. Generally, complex formation starts in the pH range 3.5–6.5 in the $M^{2+}$–A binary system and 3.7–5.3 in the $M^{2+}$–B binary system. It is worth mentioning that there is no precipitation during the titrations, ruling out the possibility of hydrolysis of the studied metal ions in the presence of excess ligand. The pH-metric titration curve for histidine in the presence of the metal ions exhibits two inflections corresponding to the consumption of 2 mol of NaOH. This is indicative of the liberation of two protons from the histidine molecule on complexation. In the case of serine and lysine, the complex titration curve (Figs. 1a and 1b, curve 5) shows one inflection at $a = 2$, due to the liberation of two protons corresponding to the simultaneous formation of 1:1 and 1:2 complex species (where $a$ is the number of moles of alkali added per mole of amino acid). This is clearly due to coordination

Table 1
Equilibrium constant values of the free ligands

| Ligand | Calculated [a] | | Reported [b,c] | |
|---|---|---|---|---|
| | Log $\beta_1$ | Log $\beta_2$ | Log $\beta_1$ | Log $\beta_2$ |
| Benzimidazole | 5.34 ± 0.03 | – | 4.98 | – |
| L-Histidine | 9.08 ± 0.02 | 15.08 ± 0.04 | 9.18 | 15.14 |
| DL-Serine | 9.16 ± 0.01 | – | 9.21 | – |
| Lysine | 9.24 ± 0.03 | – | 9.47 | – |

[a] The value determined at 20 °C.
[b] The value determined at 25 °C.
[c] Refs. [7–13].

of the carboxylate group and the α-nitrogen atom of the amino acid to the metal ion leading to the formation of a five-membered chelate ring of 1:1 and a two-mentioned chelated ring of the 1:1 and the 1:2 metal–amino acid chelates, respectively.

The complex formation of benzimidazole, B, with the metal ions proceeds via the replacement of a proton of the protonated pyridyl nitrogen atom of the benzimidazole moity. Thus, the inflection observed in the benzimidazole–metal ion titration curve is interpreted on the basis of competing reactions of the metal ions and protons with benzimidazole. Hence, metal complex formation is favoured instead of the protonation reaction. The liberation of a proton from the reaction of the metal ions with $^{+}$HB consumes 1 mol of NaOH.

These equilibria can be represented as follows:

$$M + {}^{+}HB \rightleftarrows MB + H^{+} \quad K^{M}_{MB} = [MB]/[M][B] \tag{1}$$

$$\log K^{M}_{MB} = \log [MB] - (\log [M] + \log [B]) \tag{2}$$

$$MB + {}^{+}HB \rightleftarrows MB_2 + H^{+} \tag{3}$$

$$K^{MB}_{HB_2} = [MB_2]/[MB][B]$$

$$\log K^{MB}_{MB_2} = \log [MB_2] - (\log [MB] + \log [B]) \tag{4}$$

Similarly, for amino acids

$$\log K^{M}_{MA} = \log [MA] - (\log [M] + \log [A]) \tag{5}$$

$$\log K^{MA}_{MA_2} = \log [MA_2] - (\log [MA] + \log [A]) \tag{6}$$

The overall equilibrium constants for the binary complexes formed ($\log \beta = \log K^{M}_{MB} + \log K^{MB}_{MB_2}$) are calculated by using standard procedures based on the calculation of the average number of ligands bound per metal ion, $\bar{n}$, and the free ligand exponent, pL. From the titration curves 2,3 and 4,5 in Figs. 1a and 1b using the Irving and Rossotti method [6], the formation constant values for different binary chelates were obtained (Table 2).

By applying the equation $\bar{n}/\{(1-\bar{n})[L]\} = \beta_1 + 2 - \bar{n}/(1-\bar{n})\beta_2[L]$ for the subject binary systems, the best linear fit for the chelates are obtained.

### 3.2. Stability constants of the ternary metal chelates

Fig. 1 (as representative) shows typical pH-metric titration curves for the different $M^{2+}$–A–B ternary complexes studied at 20°C and at an ionic strength of 0.1 mol dm$^{-3}$. It is worth mentioning that the different ternary metal chelates show no precipitation; thus they do not undergo hydrolysis under the experimental conditions, even in the high pH region. This behaviour may be explained on the basis that the electron density of the metal–ligand bonds in ternary chelates is redistributed in such a way that the ternary chelates are more polar than the binary chelates and hence are not easily hydrolyzed in the high pH region.

Examination of the curves obtained for the ternary systems reveals that these curves overlap the binary $M^{2+}$–amino acid complex solution curves (curve 6 in Fig. 1) at low pH values. This indicates that the benzimidazole does not participate in ternary complex formation at lower pH values. At higher pH values (5.5–7.1 in the case of the $M^{2+}$–histidine–B systems, 5.7–6.5 in the case of the $M^{2+}$–serine–B systems and 5.9–7.5 in the case of the $M^{2+}$–lysine–B system, the involvement of benzimidazole in the $M^{2+}$ –A–B ternary complex formation begins. This is indicated by the presence of a second buffer region in the ternary titration curves which is below the

Table 2
Formation constants for the metal–ligand binary complexes in 10% (v/v) ethanol–water [a]

| | Benzimidazole | Histidine | Serine | Lysine |
|---|---|---|---|---|
| Cu(II) | | | | |
| Log $\beta_1$ | 4.10 ± 0.03 | 10.62 ± 0.05 | 8.10 ± 0.07 | 7.36 ± 0.02 |
| Log $\beta_2$ | 7.71 ± 0.08 | 20.23 ± 0.03 | 15.25 ± 0.01 | 13.75 ± 0.02 |
| Ni(II) | | | | |
| Log $\beta_1$ | 3.88 ± 0.07 | 10.10 ± 0.08 | 7.32 ± 0.02 | 7.02 ± 0.03 |
| Log $\beta_2$ | 7.15 ± 0.01 | 18.85 ± 0.03 | 13.24 ± 0.03 | 12.84 ± 0.01 |

[a] At 20°C and at $I = 0.1$ mol dm$^{-3}$ $NaNO_3$.

buffer region in which the binary complexes are formed.

Further evidence for the formation of mixed ligand complexes (MAB) from the corresponding binary MA and MB complexes was provided by comparing the mixed ligand titration curves with a composite curve drawn theoretically by adding the horizontal distance of the MA curve to the titration of the free ligand B. A deviation of the composite curve from the mixed-ligand titration curve is observed in each case studied. This observation provides evidence for the formation of mixed ligand complexes.

Generally, the shape of the complex titration curves suggest the formation of a 1:1 MA complex at lower pH values than for a 1:1 MB complex, and the MA species do not hydrolyze even at higher pH values. This indicates that the amino acids may be considered as primary ligands, and benzimidazole as a secondary ligand.

Further, the titration curves of the ternary complexes (curve 6 in Figs. 1a and 1b) exhibit two inflections at $m = 1$ before the acid curve and at $m = 1$ after the acid curve (where $m$ is the number of moles of alkali added per mole of metal ion), and then are superimposed over the MA binary complex titration curves at higher pH values. This indicates that only 1:1:1 mixed ligand complex species are formed in all the systems studied. Also, the titration curves for the 1:1:1 ternary complexes are slightly above the $M^{2+}$–amino acid titration curves at lower pH values, then are superimposed and are consequently moved below them. This indicates the formation of some 1:1:1 MAB complexes after completing the formation of the 1:1 MA complex. Such an observation has not been noted by Gergely et al. [14], for the ternary complexes of amino acids.

The stepwise complex formation in the ternary complex reaction can be represented by the following equilibria

$$M + xA \rightleftarrows MA_x \quad (7)$$

$$MA_x + yB \rightleftarrows MA_xB_y \quad (8)$$

(The charges are omitted for the sake of simplicity.).

The stability constants of the ternary metal ion complex systems can be represented by the following possible complexation equilibria

$$M + A + B \rightleftarrows MAB \quad (9)$$

$$\beta^{M}_{MAB} = [MAB]/[M][A][B]$$

$$\log \beta^{M}_{MAB} = \log [MAB] - (\log [M] + \log [A] + \log [B]) \quad (10)$$

Since

$$\log [M] + \log [A] = \log [MA] + \log K^{M}_{MA} \quad (11)$$

by

$$\beta^{M}_{MAB} = \log [MAB] - \log [MA] + \log K^{M}_{MA} - \log [B] \quad (12)$$

$$MB + A \rightleftarrows MBA \quad (13)$$

$$K^{MB}_{MBA} = [MBA]/[MB][A] \quad (14)$$

$$\log K^{MB}_{MBA} = \log [MBA] - (\log [MB] + \log [A]) \quad (15)$$

Similarly

$$MA + B \rightleftarrows MAB \quad K = [MAB]/[MA][B] \quad (16)$$

$$\log K^{MA}_{MAB} = \log [MAB] - (\log [MA] + \log [B]) \quad (17)$$

The overall stability constant $\beta^{M}_{MAB}$, which is experimentally determined, is connected with $K^{MA}_{MAB}$ and $K^{MB}_{MBA}$ by the equations

$$\log \beta^{M}_{MAB} - \log K^{M}_{MA} = \log K^{MA}_{MAB} \quad (18)$$

and

$$\log \beta^{M}_{MBA} - \log K^{M}_{MB} = \log K^{MB}_{MBA} \quad (19)$$

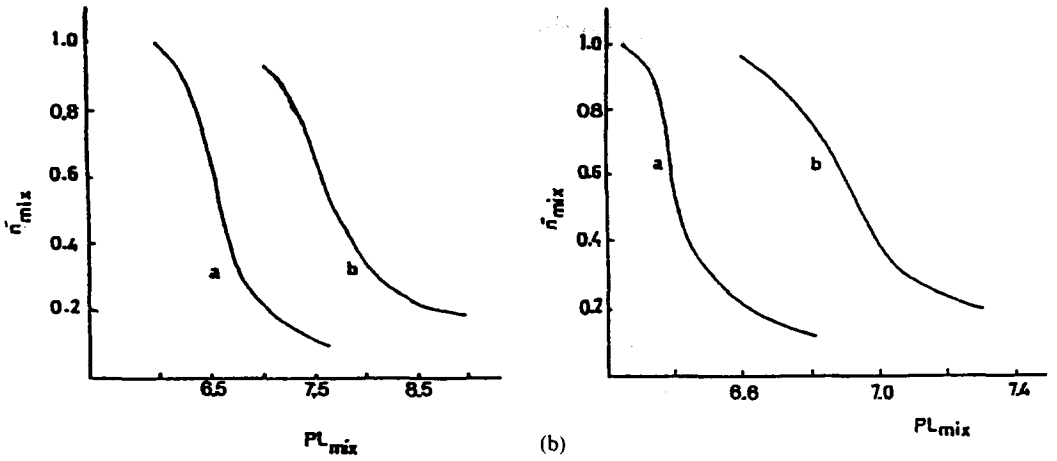


Fig. 2. $\bar{n}_{mix}$–$pL_{mix}$ relationships for the metal ion–A–B ternary complexes. (a) Serine–benzimidazole–metal ion; (b) lysine–benzimidazole–metal ion. Curve a, Ni(II); b, Cu(II).

The formation constants of the ternary complexes were calculated using a modified Irving–Rossotti titration technique [15]. The experimental $\bar{n}_{mix}$–$pL_{mix}$ curves (Fig. 2 is representative) are used to evaluate the stability constant of the ternary system.

Examination of the stability constant values given in Table 3, indicates that Eq. (18) is favoured instead of Eq. (19). This confirms the assumption that the amino acids under study act as primary ligands in these systems.

The stability of mixed ligand complexes is conveniently characterized by comparing the differences in stabilities ($\Delta \log K$) of the binary and ternary complexes. The values of $\Delta \log K$ can be calculated for the reaction of the secondary ligand (B) either with the metal ion–primary complex ($MA + B \rightleftarrows MAB$) or with the free metal ion ($M + B \rightleftarrows MB$); hence, $\Delta \log K = \log K^{MA}_{MAB} - \log K^{M}_{MB}$. The two equilibria above represent the overall equilibrium $MA + MB \rightleftarrows MAB + M$, and hence

$$\Delta \log K = \log \beta_{MBA} - (\log K_{MA} + \log K_{MB}) \quad (20)$$

Generally, the results indicate that $K_1 > K_2$. This is due to the hydrated metal ion being available for binding the first ligand to the metal ion, rather than the second. The addition of ligand B to MA should also display the same trend, i.e. $\Delta \log K$ would be negative generally between $-0.5$ and $-2.0$ [16–18] depending on the geometry of the complex. A positive value of $\Delta \log K$ suggests a significant stabilization of the ternary complex.

The other approach commonly used to quantify the apparent stabilization of ternary complexes is based on the disproportionation constant, $X$, [19,20] as defined by the equation $MA_2 + MB_2 \rightleftarrows 2\,MAB$; hence

$$X = [MAB]^2/[MA_2]\,(MB_2] \quad (21)$$

by

$$X = 2 \log \beta^{M}_{MAB} - (\log \beta^{M}_{MA} + \log \beta^{M}_{MB}) \quad (22)$$

$$\log X = (\log K^{MA}_{MAB} - \log K^{MB}_{MB_2}) + (\log K^{MB}_{MBA} - \log K^{MA}_{MA_2}) \quad (23)$$

For statistical reasons, the expected value for $\log X$ for all geometries is $-0.6$ [18,20].

Table 3
Formation constants of the ternary complexes [a]

| | | |
|---|---|---|
| $\log \beta^{M}_{MAB}$ | $14.22 \pm 0.18$ Cu (II) | $13.27 \pm 0.14$ Ni(II) |
| Metal ion–Histidine–Benzimidazole | | |
| $\log \beta^{M}_{MAB}$ | $14.22 \pm 0.18$ | $13.27 \pm 0.14$ |
| $\log K^{MA}_{MAB}$ | $3.6 \pm 0.12$ | $3.17 \pm 0.09$ |
| $\log K^{Mb}_{MBA}$ | $10.12 \pm 0.08$ | $9.39 \pm 0.06$ |
| $\Delta \log K$ | $-0.5$ | $-0.71$ |
| $\log X$ | $+0.6$ | $+0.54$ |
| *Metal ion–serine–benzimidazole* | | |
| $\log \beta_{MAB}$ | $11.79 \pm 0.11$ | $10.49 \pm 0.08$ |
| $\log K^{MA}_{MAB}$ | $3.69 \pm 0.07$ | $3.14 \pm 0.04$ |
| $\log K^{MB}_{MBA}$ | $7.69 \pm 0.08$ | $6.58 \pm 0.06$ |
| $\Delta \log K$ | $-0.41$ | $-0.74$ |
| $\log X$ | $+0.62$ | $+0.53$ |
| *Metal ion–lysine–benzimidazole* | | |
| $\log \beta^{M}_{MAB}$ | $11.03 \pm 0.04$ | $10.28 \pm 0.03$ |
| $\log K^{MA}_{MAB}$ | $3.67 \pm 0.02$ | $3.26 \pm 0.02$ |
| $\log K^{MB}_{MBA}$ | $7.93 \pm 0.01$ | $6.40 \pm 0.02$ |
| $\Delta \log K$ | $-0.43$ | $-0.62$ |
| $\log X$ | $+0.6$ | $+0.57$ |

[a] At 20 °C, $I = 0.1$ mol dm$^{-3}$, and in 10% (v/v) ethanol–water medium.

The values of $\Delta \log K$ and $\log X$ were calculated and they are presented in Table 3. Based on the above binary and ternary complex stability constant values, the following conclusions could be drawn.

(a) The overall stability constant values of the same metal ion binary or ternary complexes decrease according to the following order: M–histidine > M–serine > M–lysine; M–histidine–B > M–serine–B M–lysine–B. (The charges are omitted.) This behaviour can mainly be explained in terms of the decrease in basicity of the amino acid in the same direction.

The high stability of the histidine complexes indicates that it acts as a tridentate ligand, coordinated through the carboxylic oxygen, amino nitrogen and imino nitrogen atoms of the imidazole ring [21]. For serine, the position of the three donor groups renders them sterically unfavourable for effective tridentate coordination. This is in agreement with the lower stability of its complex than that of histidine–metal complexes.

Lysine behaves as a bidentate ligand and coordinates through adjacent carboxylic and amino groups, thus forming a five-membered chelate ring. The coordination of the second amino group is excluded, due to steric hindrance caused by the lysine chain length.

(b) A comparison of $\log K^{MA}_{MAB}$ and $\log K^{MB}_{MBA}$ for all the studied systems with those of the 1:1 and 1:2 binary complexes of the secondary ligand reveals that the stability constants of the ternary chelates are greater than those of the 1:1 but less than those of the 1:2 binary systems. This means that the ligands under study prefer to form the ternary complexes MAB rather than the binary complexes MA or MB. These observations can be interpreted by assuming the existence of $M \rightarrow L\pi$ bonding due to back donation of electrons from the metal $\pi$ orbitals. This behaviour may reduce the charge and electronegativity of the metal ions used in this species as compared to that of the hydrated metal ions [15].

(c) For all the systems under study, the $\Delta \log K$ values are generally negative in accordance with statistical expectations [22], where the statistical, steric and electrostatic factors resulted in lower stability constants for the ternary complexes as compared with the corresponding binary systems. The negative $\Delta \log K$ values confirm the formation of ternary complexes. This also demonstrates that the ternary chelates show significant instability. The absence of stabilization is compatible with the explanations given by Sigel et al. [23–25] for the possible stabilization of ternary complexes. Based on the fact that $\Delta \log K$ values depend on the coordination number of the metal ion and the ligands [26,27], the change in the $\Delta \log K$ values obtained may be attributed to the change in the geometry of the metal complex. For square planar complexes with bidentate ligands, the $\Delta \log K$ value is $-0.6$ units. For a regular and distorted octahedral geometry, $\Delta \log K$ values are $-0.4$ and $-0.9$ units, respectively [17].

(d) The $\log X$ values obtained for the ternary chelates are, in general, found to be in the range of the statistically expected $\log X$ values (0.6) [18,20]. A critical study of $\log X$ values reveals that for the Ni(II) chelates, the $\log X$ values are smaller than 0.6, indicating that the binary chelates are favoured over the corresponding ternary chelates.

(e) The stability constants of both Cu(II) binary and ternary chelates are higher than those of the Ni(II) complexes; this is due to the smaller size of Cu(II). This behaviour is in line with the stability order of Irving and Williams [28].

## References

[1] I.L. Finar, Organic Chemistry, Vol. 2, 4th edn., Longman, London, 1970, p. 532.
[2] Z. Khatoon and Kabir-ud-din, Polyhedron, 9 (1990) 2437.
[3] J.D. Joshi, J. Indian Chem. Soc., 65 (1988) 590.
[4] A.M. Shaker, M.M.A. Hamed, N.M. Ismail and M.R. Mahmoud, Bull. Fac. Sci., Assiut Uni., 22 (1 – B), (1993) 139–141.
[5] G. Douheret, Bull. Soc. Chim. Fr., (1967) 1412; (1968) 3122.
[6] H. Irving and H.S. Rossotti, J. Chem. Soc., (1954) 2904.
[7] I. Uruska, and H. Karaczewska, J. Solution Chem., 8 (1979) 105.
[8] B.L. Marwein, M.P. Mahajam and S.N. Bhat, Indian. J. Chem., 22A (1983) 1012.
[9] J.V. Metzgerin; in K.T. Potts (Ed.), Comperhensive Heterocyclic Chemistry, Vol. 6, Pergamon Press, Oxford, New York, 1984, p. 252.
[10] R.A. Abramovitch, in A.R. Katritzky (Ed.), Advances in Heterocyclic Chemistry, Vol. 23, Acadaemic Press, New York, London, 1978 p. 204.
[11] N.K. Wilson, J. Phys. Chem., 83 (1979) 2649.
[12] R.A. Mahmoud, A.A. El-Samahy and M.M. Rabia, J. Solution Chem., 13 (1984) 517.
[13] D.D. Perrin and B. Dempsey, Buffers for pH and Metal Ion Control, Vol. 92, Chapman and Hall, 1974, p. 80.

[14] A. Gergely, I. Sovago, I. Nagypal and R. Kiraly, Inorg. Chim. Acta, 6 (1972) 435.
[15] M.V. Chidambaram and P.K. Bhattacharga, J. Inorg. Chem., 32, (1970) 3271.
[16] B.E. Fischer and H. Sigel, Inorg. Chem., 18(2) (1979) 425.
[17] H. Sigel, Metal ions in Biological System, Marcel Dekker, New York, 1973, p. 65.
[18] S. Kida, Bull. Chem. Soc. Jpn, 29 (1956) 805.
[19] R.B. Martin and P. Pradas, J. Inorg. Nucl. Chem., 36 (1974) 1665.
[20] R. Dewitt and J.I. Watters, J. Am. Chem. Soc., 76 (1954) 3810.
[21] M.S. El-Ezaby and F.M. Al-Sogair, Polyhedron, 1(11) (1982) 791.
[22] H. Sigel, in D. Banerjea (Ed.), Coordination Chemistry, Vol. 20, Pergamon Press, Oxford, 1980.
[23] H. Sigel, Chimica, 21 (1967) 489.
[24] H. Sigel, B.E. Fischer and B. Pijs, J. Am. Chem. Soc., 99 (1977) 4489.
[25] H. Sigel and C.F. Naumann, J. Am. Chem. Soc., 98 (1976) 730.
[26] B. Sen, Anal. Chim. Acta, 27 (1962) 515.
[27] V.S. Sharma and T.J. Schubert, J. Chem. Educ., 46 (1969) 506.
[28] H. Irving and R.J.P. williams, J. Chem. Soc., (1953) 3192.

ELSEVIER

Talanta 42 (1995) 1719–1723

Talanta

# Determination of fosinopril in pharmaceutical formulations containing hydrochlorothiazide by multiwavelength UV spectrophotometry

Antonio L. Magri' [a,*], Fabrizio Balestrieri [b], Andrea D. Magri' [a], Domenico Marini [c]

[a] *Dipartimento di Chimica, Universita' "La Sapienza", Roma, Italy*
[b] *Istituto di Merceologia, Universita' di Perugia, Perugia, Italy*
[c] *Laboratorio Chimico delle Dogane e II.II., Roma, Italy*

Received 24 November 1994; revised 27 February 1995; accepted 8 May 1995

**Abstract**

A sensitive, simple, rapid and precise method for the simultaneous determination of fosinopril (FOS) and hydrochlorothiazide (HCT) in pharmaceutical formulations is presented. These active ingredients are extracted in aqueous solution and measured by multiwavelength UV spectrophotometry using the program QUEST. HCT acts as an internal standard to verify the accuracy of the analysis. Some aspects of the chemical, spectroscopic and thermoanalytical behaviour of FOS are also reported.

*Keywords:* Fosinopril; Hydrochlorothiazide; UV-spectrophotometry

## 1. Introduction

Fosinopril (FOS), (4s)-4-cyclohexyl-1-[[[(*RS*)-2-methyl-1-(propionyloxy)propoxy](4-phenylbutyl)phosphinyl]acetyl]-L-proline, sodium salt (SQ28555), is the first member of a new chemical class of angiotensin converting enzyme (ACE) inhibitors [1,2], which is equipotent to captopril as an inhibitor of pressor response, but it has a longer effect [3,4]. During or following absorption, FOS, a prodrug, is hydrolyzed [5] to the active diacid (SQ27519), (see Form 1).

In tablet formulations, FOS is usually combined with a diuretic agent [6], such as hydrochlorothiazide (HCT).

In the literature, a high-performance liquid chromatographic (HPLC) method is described to evaluate the purity of FOS [7], but no methods are reported for its determination in pharmaceutical formulations when other ingredients are present.

UV-visible spectrophotometry is an instrumental technique suitable for multicomponent analysis, because generally the procedures involve neither complicated and time-consuming sample treatments nor the need for special reagents. Only processing of the spectrophotometric data for the mixture solution by means of an adequate software package is required. However, it should be emphasized that the accurate resolution of a mixture with multiwavelength computational programs requires the prior knowledge of the components actually present and of their contribution to the mixture absorbance. In fact, the occurrence of a component scarcely contributing to the overall absorbance may result in significant deviations, and very good fits between experimental and calculated spectra do not necessarily reflect

* Corresponding author.


*SSDI* 0039-9140(95)01642-2

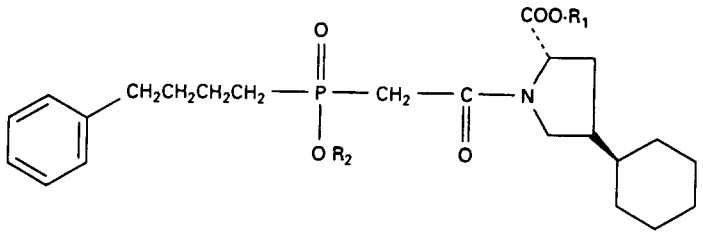

| COMPOUND | $R_1$ | $R_2$ |
|---|---|---|
| SQ 28.555 | Na | $(CH_3)_2-CH-CH-O-C(=O)-C_2H_5$ |
| SQ 27.519 | H | H |

Form 1.

the accurate resolution of the mixture. For this reason, it is essential to check if a mixture may be analyzed by this method, find the best experimental conditions, and provide for a final verification of the results.

The aim of our studies was to solve these problems for FOS and HCT mixtures and to propose a simple and rapid method for their simultaneous determination in pharmaceutical formulations.

## 2. Experimental

### 2.1. Instruments

The thermal measurements were carried out using a Perkin-Elmer TGS-2 thermal analyzer and a DSC-4 differential scanning calorimeter connected to a model 3700 Data Station equipped with a software package. Thermogravimetry (TG) and differential scanning calorimetry (DSC) runs were made on samples of about 1 mg, in a stream of nitrogen or oxygen (flow rate, 50 ml $min^{-1}$). The heating rate was 10°C $min^{-1}$.

IR spectra were recorded using a Perkin-Elmer 1760 FT-IR spectrometer.

UV spectra were acquired on a Perkin-Elmer 320 UV-vis spectrophotometer furnished with 1 cm quartz cells and connected to the Data Station equipped with software packages "CDS-13", for the mathematical treatment of the spectra, and "QUEST" which performs a least-squares best fit for multicomponent analysis of the mixture spectrum.

Millipore filtering apparatus fitted with 0.45 μm membrane disks (HAWPO2500) and class A glass apparatus as used.

### 2.2. Materials

Distilled, deionized water was used throughout.

Tablets: each tablet contains 20.32 mg of FOS sodium salt, and 12.27 mg of HCT, and tablet excipients are lactose, polyvinylpyrrolidone, sodium stearylfumarate, sodium croscaramellose and a dye mixture. All were a gift from Bristol-Myers Squibb (Anagni, Italy).

### 2.3. Analytical techniques

#### 2.3.1. Preparation of normalized standard curves

A standard aqueous solution of FOS was prepared by weighing, and working solutions were prepared by appropriate dilution in water to obtain final concentrations of this component giving absorbance readings in the range 0.5–1.5 [8]. Because the reliability of the mixture resolution depends primarily on the accuracy of the spectral data of the pure components used as a reference in resolving the mixture, a standard spectrum of FOS was obtained by recording the spectra of five different working solutions, normalizing them at a concentration of 10 mg $l^{-1}$ and then averaging the obtained spectra to give a single spectrum.

This procedure was used also for HCT. The spectra of the excipients were obtained more simply by scanning the aqueous solutions pre-

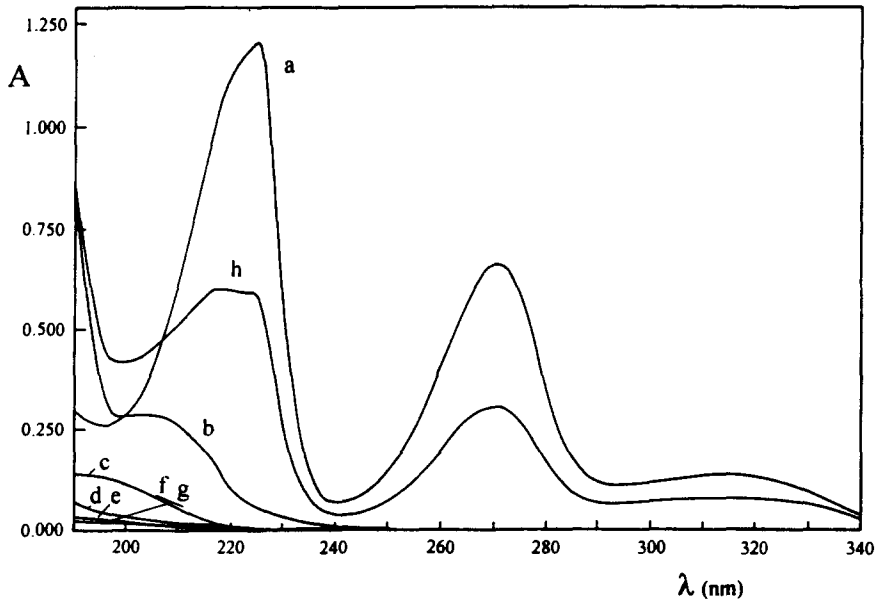


Fig. 1. Curve a, UV absorption spectra of hydrochlorothiazide; curve b, fosinopril sodium; curve c, PVP; curve d, lactose; curve e, dye mixture; curve f, sodium stearylfumarate; curve g, sodium croscaramellose; curve h, tablet aqueous solutions.

pared by dissolving an appropriate quantity of each component, and filtering when necessary.

*2.3.2. Simultaneous determination of FOS and HCT in tablets*

The average weight of a tablet was determined by weighing at least 10 tablets.

One or more tablets were finely powdered, and a portion of about 0.3 g of the powder was weighed accurately and 25 ml of water were added. The mixture was stirred gently for about 15 min at room temperature and then filtered on a 0.45 μm membrane filtering disk, collecting the solution in a dry Erlenmeyer flask.

Of this solution, 1 ml was diluted with water to 10 ml. This sample solution was analyzed by UV spectrophotometry. The mixture spectra were resolved using a computational program (QUEST).

The content (in milligrams per tablet) of FOS and HCT may be calculated by use of the following formula

$$\text{Content in milligrams} = \frac{amf}{c}$$

where $a$ is the concentration (mg $l^{-1}$) of the analyte in the final solution; $m$ is the weight (mg) of a tablet; $f$ is the dilution factor (25/100); and $c$ is the weight (mg) of the assay portion.

## 3. Results and discussion

### *3.1. Analytical behaviour of HCT and FOS*

The chemical and spectroscopic behaviours of HCT are common knowledge, so our study was limited to verify its solubility in water and the UV absorbance spectrum of its aqueous solution. As is shown in Fig. 1, curve a, there are three absorption bands with maxima at 315 nm ($\varepsilon = (3.10 \pm 0.03)\ 10^3\ l\ mol^{-1}\ cm^{-1}$), 271 nm ($\varepsilon = (1.91 \pm 0.02)\ 10^4\ l\ mol^{-1}\ cm^{-1}$) and 226 nm ($\varepsilon = (3.60 \pm 0.02)\ 10^4\ l\ mol^{-1}\ cm^{-1}$).

FOS sodium salt has been less studied as an analytical species, and we thought it convenient to investigate its chemical, spectroscopic and thermoanalytical behaviour.

FOS sodium salt is a white powder fairly soluble in methanol and water. Its aqueous solution is stable for several hours, but, on adding sodium hydroxide, FOS is hydrolyzed to the corresponding diacid. However, FOS precipitates as the protonated form on adding hydrochloric acid.

The UV spectrum of the aqueous solution (Fig. 1, curve b) shows only one absorption band with the maximum at 206 nm ($\varepsilon = (1.67 \pm 0.02)\ 10^4\ l\ mol^{-1}\ cm^{-1}$).

The IR spectrum (KBr disc) is presented in Fig. 2, showing the characteristic function of grouping of FOS.

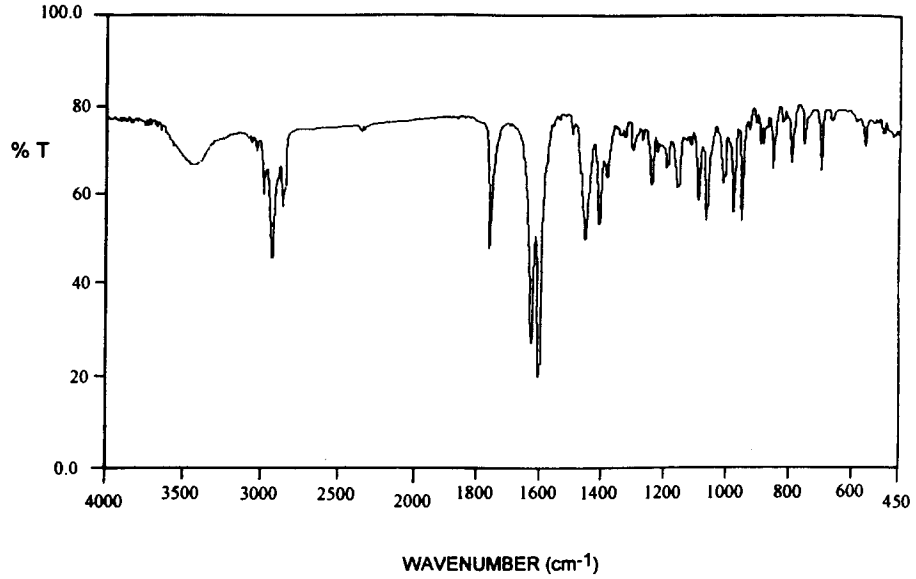


Fig. 2. IR spectrum (KBr disc) of fosinopril sodium.

TG analysis in a dynamic nitrogen atmosphere shows that FOS is stable up to about 200°C and then it decomposes in at least three steps giving a constant final residue at 550°C that consists mainly of $(NaPO_3)_x$ (calculated 17.41%; found, 16.1%).

The DSC curve shows two overlapping peaks in the temperature range 190–202°C; the first, endothermic peak, is connected with the melting of the compound, and the second, exothermic peak, with its first decomposition step. In an oxygen atmosphere the thermal decomposition takes place in an almost identical temperature range.

### *3.2. Content determination of FOS and HCT simultaneously in their tablets*

From the spectra of the aqueous solutions of the components of each tablet (Fig. 1, curve h), the optimum wavelength range for the analysis (240–210 nm) was established and justified away from the interfering species. Satisfactory results were obtained using standard solution spectra of FOS and HCT and only two blank solution spectra (lactose and PVP). The other excipients do not interfere because they are almost insoluble in water, and the small amount of absorption in the measurement range is compensated by the other blank solutions.

The results of eight replicate determinations of FOS and HCT in tablets demonstrate that the method is quite precise (relative standard deviations were 0.01 and 0.03 for FOS and HCT, respectively).

To test the quantitative recovery of both active ingredients, the technique of spiked samples was applied: known amounts of FOS and HCT were added to a powdered tablet and the mixtures were analyzed following the procedure described. The overall results are collected in Table 1.

## 4. Conclusions

The proposed spectrophotometric method for the simultaneous determination of FOS and HCT in tablets is easily carried out and rapid, requiring only few minutes to prepare the samples and to measure the absorbances. In spite of this, the method is sensitive, accurate and precise. However, to avoid unexpected interferences, it might be convenient to add an internal standard to the analyzed mixture. Comparing the amount found with the added amount of standard species, it is possible to verify the accuracy of the analysis. In the proposed method, HCT acts as an internal standard because it may be determined by measuring the mixture absorbance at a fixed wavelength. In fact, at 271 nm only HCT absorbs (Fig. 1, curve a) and these results should be in agreement with those found by multiwavelength analysis.

Table 1
Determination of FOS and HCT in tablets and in spiked samples [a]

| Sample [b] | FOS found [c] (mg per tablet) | | | | | | HCT found [c] (mg per tablet) | | | | | | | |
|---|---|---|---|---|---|---|---|---|---|---|---|---|---|---|
| | a | Recovery (%) | b | Recovery (%) | c | Recovery (%) | a | Recovery (%) | b | Recovery (%) | c | Recovery (%) | d | Recovery (%) |
| 1 | 25.6 | 126.0 | 20.2 | 99.4 | 20.3 | 99.9 | 11.4 | 92.9 | 11.9 | 97.0 | 11.8 | 96.2 | 12.0 | 97.8 |
| 2 | 41.7 | 116.9 | 35.4 | 99.2 | 35.5 | 99.5 | 11.5 | 93.7 | 11.8 | 96.2 | 11.9 | 97.0 | 12.0 | 97.8 |
| 3 | 26.2 | 128.9 | 20.1 | 98.9 | 20.2 | 99.4 | 20.7 | 92.6 | 21.7 | 97.1 | 21.7 | 97.1 | 21.9 | 98.0 |
| 4 | 38.3 | 117.1 | 32.5 | 99.3 | 32.5 | 99.3 | 19.9 | 94.2 | 20.5 | 97.1 | 20.5 | 97.1 | 20.8 | 98.5 |

[a] Each result is the average of at least three independent assays. Relative standard deviations, in any case, were less than 0.02 and 0.03 for FOS and HCT, respectively.
[b] (1) Tablet (certified contents: FOS, 20.32 mg per tablet; HCT, 12.27 mg per tablet). (2) Sample spiked with FOS (FOS, 35.67 mg per tablet; HCT, 12.27 mg per tablet). (3) Sample spiked with HCT (FOS, 20.32 mg per tablet; HCT, 22.35 mg per tablet). (4) Sample spiked with FOS and HCT (FOS, 32.72 mg per tablet; HCT, 21.12 mg per tablet).
[c] (a) Analysis performed by QUEST without blank solution spectra. (b) Analysis performed by QUEST with lactose and PVP blank solution spectra. (c) Analysis performed by QUEST with all excipients blank solution spectra. (d) Analysis performed by referring to a calibration curve prepared at 271 nm.

## References

[1] K.L. Duchin, J.A. Manning, D.N. McKinstry and D.A. Willard, J. Clin Pharmacol., 24 (1984) 422.
[2] J.M. De Forrest, T.L. Waldron, C. Harvey, B. Scalese, B. Rubin, J.R. Powell, E.W. Petrillo and D.W. Cushman, J. Cardiovasc. Pharmacol., 14 (1989) 730.
[3] M.A. Ondetti, B. Rubin and D.W. Cushman, Science, 196 (1977) 441.
[4] D.W. Cushman, H.S. Cheung, E.F. Sabo and M.A. Ondetti, Biochemistry, 16 (1977) 5484.
[5] J.I. Tu, J. Brennan, B. Stouffer and W.C. Eckelman, Ther. Drug Monit., 12 (1990) 404.
[6] R.L. Jerzewski, T.M. Wong, L.J. Gryziewcz, N.B. Jain and A.B. Thakur, Eur. Pat. EP 408 273 (Cl. A61k31/675), 16 January 1991.
[7] J. Kirschbaum, J. Noroski, A. Cosey, D. Mayo and J. Adamovics, J. Chromatogr., 507 (1990) 165.
[8] I.M. Kolthoff, E.B. Sandell, E.J. Meehan and S. Bruckenstein, Quantitative Chemical Analysis, 4th ed., The Macmillan Company, Collier-Macmillan Ltd., 1969, p. 978.

ELSEVIER

Talanta 42 (1995) 1725–1729

Talanta

# An electrochemical method for the determination of residual styrene in polystyrene

M.D. Geraldo [a], M.I. Montenegro [a,*], D. Pletcher[b,*]

[a] *Departamento de Química, Universidade do Minho, Largo do Paço, 4719 Braga, Portugal*
[b] *Department of Chemistry, The University, Southampton SO17 1BJ, UK*

Received 13 February 1995; revised 12 May 1995; accepted 12 May 1995

**Abstract**

A rapid electroanalytical method for the determination of residual styrene in polystyrene is described. The sample of polymer was dissolved in toluene and, following the addition of 10% DMF and electrolyte, a square-wave voltammogram was recorded at a gold microdisc electrode (radius, 6 μm). A standard addition technique was used to relate the peak current to the styrene concentration in solution and, hence, the styrene content of the polymer. The method gave results which are similar to those of the accepted standard procedure. It does not, however, require the precipitation of the polymer and hence is quicker and more convenient.

## 1. Introduction

The determination of residual monomer in polymers used for food packaging is a routine test since leaching of the monomer into the foodstuff is known to degrade the taste and is a potential toxic hazard. This paper describes a rapid procedure for the determination of styrene in polystyrene; in contrast to the standard procedure [1], where it is necessary to precipitate the polystyrene before the determination of the styrene in solution by gas chromatography, no treatment of the solution is necessary before the analytical determination. The method is based on the measurement of the electrochemical response for styrene [2]. In the development of the method, it was necessary to define a medium (a) in which polystrene is readily soluble, and (b) where good quality electrochemical responses could be obtained. In fact, polystyrene is insoluble in most of the solvents generally used for electrochemistry. The medium selected, 90% toluene/10% *N,N*-dimethylformamide (DMF) would normally be considered a very poor one for electrochemistry and the procedure is entirely dependent on the use of an ultramicroelectrode, which, in this work, is a gold microdisc of radius 6 μm. It is only during the past decade that the properties and advantages of ultramicroelectrodes have been widely recognized [3]. Here, the key property is the ability to obtain high quality responses in a medium of high resistance. The analytical measurement used square-wave voltammetry which led to a well-defined and easily measured peaked response.

## 2. Experimental

Both the linear potential sweep and square-wave voltammetry experiments were carried out using a potentiostat/galvanostat EG&G PAR 273. The data acquisition and treatment was performed using a LVM 486, 33 MHz computer, using the PAR software M270, version 3.00. The voltammograms were plotted on a Roland plotter, type DXY-980A.

* Corresponding authors.


*SSDI* 0039-9140(95)01643-0

All experiments were carried out in a two-electrode cell. The working electrode was a gold microdisc with a radius of 6 μm. The radius was checked by measuring the steady-state diffusion-controlled current for a known concentration of ferrocene in acetonitrile containing $Bu_4NClO_4$ [4]. The electrode was first polished with fine emery paper and then on a polishing cloth with 0.3 and 0.05 μm alumina (Buehler) with a polishing machine (Buehler, Ecomet 3); afterwards, it was washed with water and dried before use. Prior to each experiment, the electrode was polished with 0.3 μm alumina, rinsed with water, wiped on a clean, wet polishing cloth, rinsed again and dried. The reference/counter electrode was a Radiometer, model 401, saturated calomel electrode (SCE) and all potentials are quoted versus the SCE.

All solutions were prepared with the highest grade chemicals available in high purity toluene/DMF mixtures, previously dried with Prolabo alumina, size 2–5 mm. The supporting electrolytes used were $Bu_4NClO_4$ and $Bu_4NBF_4$. The first was available in high purity and the second was prepared by mixing aqueous solutions of $NaBF_4$ and $Bu_4NHSO_4$.The product in each case was recrystallized in methanol/water and dried under vacuum.

Experiments were conducted at room temperature, and all solutions were degassed with a fast stream of argon prior to the experiments.

## 3. Results

### 3.1. The selection of the medium

Polystyrene is most readily soluble in aromatic hydrocarbon solvents such as toluene and ethylbenzene. Hence, the objective was to use a medium with a high content of one of these solvents. Peña et al. [5] have studied a model electrode reaction, the oxidation of ferrocene in toluene/acetonitrile solutions using ultramicroelectrodes; they reported that the addition of a small percentage of the aprotic solvent to toluene led to a large improvement in the quality of the electrochemical responses. They also concluded that the addition of an electrolyte, e.g. 0.1 mol $dm^{-3}$ $Bu_4NBF_4$, was essential in media with a high percentage of toluene. We have carried out a wide range of experiments with styrene in toluene/DMF mixtures which will be reported elsewhere [6] but, in general, our conclusions are the same.

Fig. 1 shows current vs. potential curves for the reduction of styrene in different concentrations at a gold microdisc electrode (radius, 6 μm) in 90% toluene/10% DMF containing 0.1 mol $dm^{-3}$ $Bu_4NBF_4$ and deoxygenated with a fast stream of dry argon. It can be seen for each concentration that well-formed reduction waves are observed with $E_{1/2} \approx -2.51$ V vs. SCE; the waves are steep with $E_{3/4} - E_{1/4} \approx -110$ mV. Most importantly for analysis, there is a good plateau current extending over a potential range of a few hundred millivolts before reduction of the solvent/electrolyte commences (in fact, dissolved polystrene showed slightly more complex behaviour, see below). The height of the waves are proportional to the styrene concentration. In fact, the limiting current, $I_L$, at a microdisc electrode is given by the equation

$$I_L = 4nFDcr$$

where $n$ is the number of electrons involved in the reduction, $F$ is the Faraday constant, $D$ is the diffusion coefficient of styrene, $c$ is the concentration of styrene and $r$ is the radius of the microdisc. The $I_L$(A) vs. $c$ (mol $cm^{-3}$) plot is linear and is represented by the equation (correlation coefficient, 0.997)

$$I_L = 7.67 \times 10^{-6} c + 0.91 \times 10^{-10}$$

whose slope leads to a value of $4.0 \times 10^{-5}$ $cm^2$ $s^{-1}$ for $nD$, consistent with $n = 2$ [2] and $D = 2.0 \times 10^{-5}$ $cm^2$ $s^{-1}$.

The voltammograms for the dissolved polystyrene were not always the same quality as those for styrene. The plateaux were often slop-

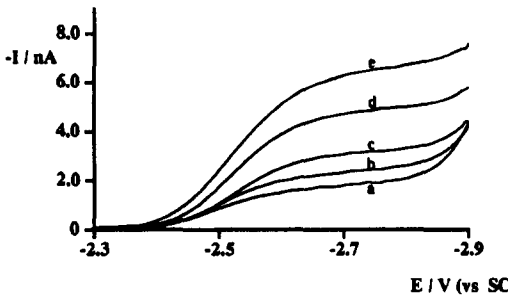


Fig. 1. Current–potential curves for the reduction of styrene in different concentrations at a gold microdisc electrode (radius 6 μm) in 90% toluene/10% DMF, containing 0.1 mol $dm^{-3}$ $Bu_4NBF_4$. Curve a, $2.0 \times 10^{-4}$ mol $dm^{-3}$; curve b, $3.0 \times 10^{-4}$ mol $dm^{-3}$; curve c, $4.0 \times 10^{-4}$ mol $dm^{-3}$; curve d, $6.0 \times 10^{-4}$ mol $dm^{-3}$; curve e, $8.0 \times 10^{-4}$ mol $dm^{-3}$.

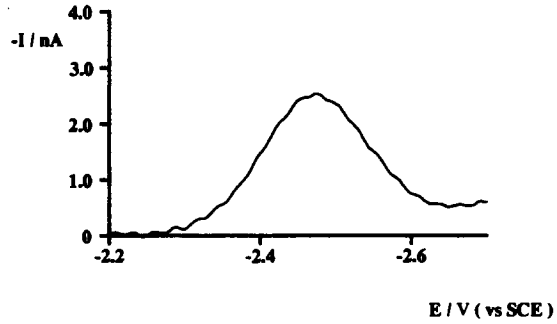


Fig. 2. Square-wave voltammogram of styrene ($3.0 \times 10^{-4}$ mol dm$^{-3}$) in 90% toluene/10% DMF, containing 0.1 mol dm$^{-3}$ $Bu_4NBF_4$ at a gold microdisc (radius, 6μm). (Square-wave amplitude, 2 mV; step height, 60 mV; frequency, 100 Hz.)

ing and sometimes the slow scan voltammetry showed a drawn out wave perhaps arising from a second overlapping reduction wave at slightly more negative potentials. This suggests that polystyrene may contain species other than styrene reducible at very negative potentials. The specificity essential for the determination of styrene in polystyrene could, however, readily be obtained by using square-wave voltammetry. Square-wave voltammetry is recognised to give much better resolution between overlapping reduction processes and converts the wave response into a peak [7]. The theory of square-wave voltammetry has been applied to ultramicroelectrodes by Osteryoung and O'Dea [8] and it has been shown that the peak current is given by

$$I_p = nFAc(D/\pi t_p)^{1/2}\Psi_p$$

where $t_p = \tau/2$ is the pulse width, $\tau$ being the period of the square wave, and $\Psi_p$ is the dimensionless current given by

$$\Psi_p = 0.846/\lambda + 0.750 + 0.177\exp(-1.13/\lambda)$$

where $\lambda = r/2(Dt_p)^{1/2}$

Fig. 2 shows a square-wave voltammogram of styrene ($3.0 \times 10^{-4}$ mol dm$^{-3}$) in 90% toluene/10% DMF containing 0.1 mol dm$^{-3}$ $Bu_4NBF_4$, at a gold microdisc electrode. A well-defined peak is observed at a potential of −2.49 V vs. SCE. A range of square-wave voltammograms was recorded for concentrations of styrene between 2.0 and $8.0 \times 10^{-4}$ mol dm$^{-3}$ and, as expected, a good linear relationship was found between the peak current and the concentration, given by the equation coefficient, 0.994)

$$I_p = 4.70 \times 10^{-6}c + 6.93 \times 10^{-10}$$

where $I_p$ is amps and $c$ is in mol dm$^{-3}$.

### 3.2. Analytical procedure

The sample of polystyrene (approximately 2 g) was dissolved in about 20 cm$^3$ of toluene using an ultrasonic bath. After complete dissolution (1 h), $Bu_4NBF_4$ (approximately 0.8 g) was added as a solid together with 2.5 cm$^3$ of DMF. When the electrolyte was fully dissolved, the solution was made up to 25 cm$^3$ with toluene in a volumetric flask. A 5 cm$^3$ portion of this solution was transferred to a simple electrochemical cell equipped with the polished gold microdisc electrode and a saturated calomel counter/reference electrode. Alumina was added to adsorb any water present and the oxygen was removed from the solution in a fast stream of argon. A square-wave voltammogram of the unstirred solution was then recorded at room temperature. A standard addition technique was employed to establish the relationship between the peak current and the styrene concentration in solution because it was considered likely that the presence of polymer in solution would cause a change in the viscosity and therefore in the diffusion coefficient of styrene. Several 3 μl additions of a solution containing styrene (0.30 mol dm$^{-3}$) in 90% toluene/10% DMF containing 0.1 mol dm$^{-3}$ $Bu_4NBF_4$ were made, and a square-wave voltammogram was recorded after each addition. Fig. 3 presents the voltammograms, not corrected for the background current, obtained for a sample of polystyrene BP(HIPS), and Fig. 4 shows the corresponding

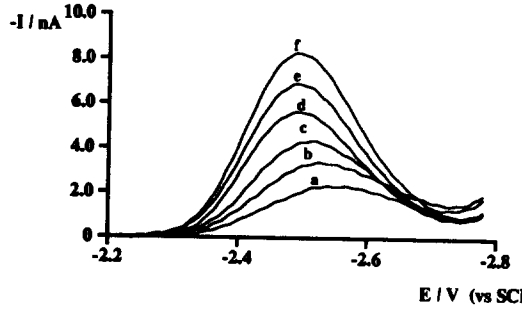


Fig. 3. Square-wave voltammograms of styrene in polystyrene BP(HIPS), (2.02 g in 25 cm$^3$) in 90% toluene/10% DMF, containing 0.1 mol dm$^{-3}$ $Bu_4NBF_4$ at a gold microdisc (radius 6 μm). (Square-wave amplitude 2 mV; step height, 60 mV; frequency, 100 Hz.) Addition to 5 cm$^3$ of sample solution were (a) 0 mol, (b) 0.9 μmol, (c) 1.8 μmol, (d) 2.7 μmol, (e) 3.6 μmol, (f) 4.5 μmol.

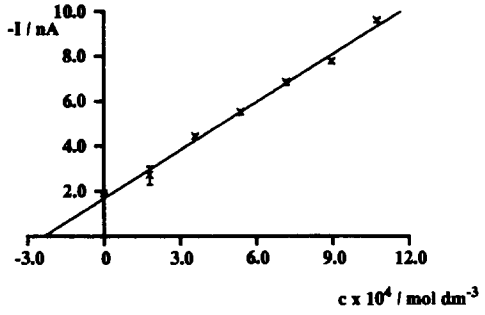


Fig. 4. Plot of square-wave peak current vs. concentration in the standard addition method for the sample of polystyrene BP(HIPS) in 90% toluene/10% DMF, containing 0.1 mol $dm^{-3}$ $Bu_4NBF_4$, as presented in Fig. 3. Each error bar represent twice the standard deviation of six determinations.

$I_p$ vs $c$ plot. A "tangent subtraction" on the computer was used to correct for background currents which were found to be more significant for dissolved samples of polystyrene than for solutions of pure styrene in the medium. In this subtraction method, a baseline was drawn between the response at the start of the peak and the minimum in the response negative to the peak; this peak height was then measured subtracting the baseline response at the peak potential. Using this measurement procedure, it can be seen that there is a good linear relationship (with a correlation coefficient of 0.998) between peak height and styrene concentration. The error bars on the figure are twice the standard deviation of six determinations. Another effect of the increased background current in the sample solution is the shift in peak potential to more positive potentials with increasing styrene concentration. This shift is not seen with solutions prepared from styrene. The origin of this background current is not clear and certainly no peaks could be defined in the square-wave voltammetry. They could arise from trace amounts of electroactive plasticizers, stabilizers, antioxidants or other additives in the polymer. It will be seen below that they are not a problem when the analysis was done by square-wave voltammetry. The errors were more significant when the analysis was based on the limiting current from steady-state voltammetry. The preference for square-wave voltammetry is not surprising since it is well known that techniques which give a "differential" response improve selectivity significantly [9].

### *3.3. Typical analyses*

The procedure described above has been used to determine the residual styrene content of four samples of polystyrene; three were commercial samples and the other a pot manufactured for Portuguese yogurt. The analyses for all four samples were straightforward and no interferences or complications were observed. The results from these analyses are reported in Table 1 along with analyses carried out by two commercial laboratories using the standard gas chomatographic method.

It can be seen that the results compared well especially since results from the standard procedure are normally only quoted to one significant figure. It should also be noted that the specification for polystyrene used in food packaging requires the residual styrene to be below 0.1%.

## 4. Discussion

The analytical procedure described in this paper has been shown to lead to estimates for the residual styrene content of polystyrene which compare well with the accepted standard procedure based on gas chromatography. It is, however, more rapid since it is not necessary to precipitate the polymer from solution before the analytical determination and it is much quicker to record the square-wave voltammogram than a chromatogram. It should be emplasized that the electroanalytical approach is only feasible because of the use of an ultramicroelectrode. It would not be possible to employ a traditionally sized electrode in a medium compatible with facile dissolution of the polymer. The application of ultramicroelectrodes in analysis has, in recent years, proved a fruitful innovation and they have been applied in several diverse analytical procedures [9]. The application of square-wave voltammetry was also found to improve the analytical procedure significantly. For a routine method, the equipment could be simplified substantially. The cell could be an enclosed beaker and the counter/reference electrode could be copper, aluminium or another metal (although there would, of course, be a shift in the peak potential). It would also be possible to write simple software for a microcomputer which controls the experiment, applies the potential/time function and analyzes the response to give the styrene content of polystyrene.

Table 1
Comparison of the results for the analyses of residual styrene in polystyrene by the new electroanalytical method and the standard procedure

| Sample | % Styrene by electrochemical method | % Styrene by gas chromatography [a] |
|---|---|---|
| BP | 0.031 ± 0.002 | 0.024 |
| BASF | 0.026 ± 0.004 | 0.032 |
| HCC | 0.021 ± 0.002 | 0.028 |
| Yogurt pot | 0.026 ± 0.004 | 0.024 |

[a] Each analysis was carried out by the Instituto Nacional de Engenharia e Tecnologia Industrial and Centro Nacional de Embalagem. Errors vary between 0.001 and 0.004%.

## Acknowledgement

This work has been supported by the Human Capital and Mobility Programme (Network ERBCHRXCT 920073).

## References

[1] Portuguese Standard Procedure NP 3993 or ISO 2561.
[2] B.L. Funt and D.G. Gray, J. Electrochem. Soc., 117 (1970) 1020.
[3] M.I. Montenegro, M.A. Queirós and J.L. Daschbach (Eds.), Microelectrodes: Theory and Applications, NATO ASI Series, Ser. E, Vol. 197, Kluwer, Dordrecht, 1991.
[4] J.E. Baur and R.M. Wightman, J. Electroanal. Chem., 305 (1991) 73.
[5] M.J. Peña, M. Fleischmann and N. Garrard, J. Electroanal. Chem., 220 (1987) 31.
[6] M.D. Geraldo, M.I. Montenegro and D. Pletcher, in preparation.
[7] J. Osteryoung and J.J. O'Dea, Square Wave Voltammetry, in A. Bord (Ed.), Electroanalytical Chemistry, Vol. 14, Marcel Dekker, New York, 1987.
[8] D. Whelan, J.J. O'Dea, J. Osteryoung and K. Aoki, J. Electroanal. Chem., 202 (1986).
[9] C.M. Delerue-Matos and M.I. Montenegro, Port. Electrochim. Acta, 8 (1990) 115.

ELSEVIER

Talanta 42 (1995) 1731–1744

Talanta

# Determination of cadmium in biological and environmental samples by slurry electrothermal atomic absorption spectrometry

L.C. Robles, A.J. Aller *

*Department of Biochemistry and Molecular Biology, University of León, E-24071 León, Spain*

Received 29 November 1994; revised 22 February 1995; re-revised 15 May 1995; accepted 17 May 1995

**Abstract**

The retention of cadmium by the bacteria *Escherichia coli* and *Pseudomonas putida* was optimized in order to develop a rapid and selective preconcentration method for cadmium from biological and environmental samples prior to determination by electrothermal atomic absorption spectrometry. Living and lyophilized cells for both bacteria were used, but the method using dead cells shows better analytical capabilities. Cadmium from aqueous solutions is easily retained on the outer membrane of both bacteria in the pH range 4–10, although the selected working pHs for *E. coli* and *P. putida* were 5 and 9, respectively. Cadmium retained by the bacteria was dispersed in 3.5 M nitric acid and the slurry was introduced directly into the graphite tube. The best sensitivity and detection limit were obtained for *E. coli* (0.03 ng $ml^{-1}$ and 0.04 ng $ml^{-1}$ respectively, in the absence of any chemical modifier). A strong spectral interference from nickel chloride was found and methods to overcome it were developed. The proposed extraction procedure was tested by the determination of cadmium in different standard biological and environmental samples.

*Keywords:* Cadmium determination; Slurry electrothermal atomization atomic absorption spectrometry; Bacteria; Microorganisms

## 1. Introduction

At present, there is great interest in clarifying the role of toxic elements in the development and evolution of certain illnesses. This interest is an obvious result of the improved prevention of acute poisoning. In addition, an increased awareness concerning chronic exposure is absolutely essential because such exposure may play a role in the causation of diseases with a multifactorial etiology.

Cadmium is one of the most toxic elements for animals and man. It is a ubiquitous and biologically non-essential element, being also classified as a class B and borderline element. Industrial exposure to cadmium can be the origin of acute and chronic toxicity in man. Low-level long-term exposure to cadmium seems to be associated with abnormally high hypertension, being related to renal sodium retention or to a direct effect on vascular smooth muscle [1]. The way of entry into the organisms can be by either inhalation or ingestion. Ingestion is related to severe gastroenteritis and inhalation to fatal pulmonary edema. The assimilation route of this element is similar to that of copper, zinc and manganese, being stored in the protein metallo-thionein [2]. An additional problem of cadmium toxicity is its accumulative character because about 30 mg can be accumulated during a lifetime. The main sources of cadmium are the food chain and the environment. From the analytical point of view, a problem emerges because con-

* Corresponding author


*SSDI* 0039-9140(95)01648-1

centrations of this element in biological and environmental samples are usually below the detection limits of the most sensitive techniques.

Cadmium has been successfully determined by different techniques: neutron activation analysis [3], atomic fluorescence spectrometry [4], flame atomic absorption spectrometry [5] and inductively coupled plasma-atomic emission spectrometry [6]. However, one of the most sensitive techniques for the determination of cadmium is electrothermal atomization atomic absorption spectrometry (ETAAS). Although some methods have been developed for the determination of cadmium either directly or with minimum sample manipulation in complex matrices (urine [7,8], seminal fluid [9], cigarettes [10]), many problems arising in the determination of cadmium by ETAAS have derived both from losses by vaporization prior to atomization and matrix interferences [11]. To solve these problems, different chemical modifiers [12–15] are currently used, in combination with metallic or metal-impregnated graphite platforms or tubes as atomizers [16–19]. However, different separation/preconcentration procedures have also been used to isolate cadmium from interferent matrices [11].

Some recently developed procedures for the identification and determination of cadmium use different biological systems. Thus, the crayfish, *Cambarus bartoni (Fab.) (Decapoda, Crustacea)* has been used as a reliable indicator of the presence of cadmium in the fresh water ecosystem [20]. The yeast *Saccharomyces cerevisiae* was immobilized on controlled pore glass and used in flow injection-atomic absorption spectrometry for the preconcentration of cadmium and other metals [21]. However, the most commonly used microoganisms in these tasks are algae. Cadmium ions have been preconcentrated from dilute solutions and marine reference samples by using different algae strains, *Stichococcus bacillaris* [22–24], *Chlorella pyrenoidsa* [24], *Chlamydomonas reinhart* [24,25], and *Selenestrum capricornutum* [26,27]. On the other hand, the outer membrane of bacteria displays many functional groups that can be used to retain some toxicological or precious metals. Analytical capabilities of the bacteria *Escherichia coli* (K-235) and *Pseudomonas putida* have been tested recently for gold [28] and beryllium [29]. In this paper, we will use these bacterial cells, *E. coli* and *P. putida*, to develop a preconcentration procedure for cadmium from biological and environmental samples prior to determination by slurry ETAAS.

## 2. Experimental

### 2.1. Apparatus and measurements

The experiments were carried out using a Thermo Jarrel Ash atomic absorption spectrophotometer SH 11 equipped with a heated graphite atomizer, model CTF-188, and the Smith–Hieftje background correction system. The operating parameters used were as follows: wavelength, 228.8 nm; a cadmium hollow cathode lamp, Visimax II, was used under the recommended conditions; slitwidth, 1 nm. Standard, uncoated, rectangular graphite tubes and standard pyrolytic graphite-coated platforms were used for platform atomization. An Epson 118 recorder was used. Solutions were injected into the graphite atomizer by means of the Fastac automatic aerosol deposition system, and argon (99.995% purity) served as the purge gas. The temperature programme used is shown in Table 1. The solution (10 μl) was injected into the atomizer at 150°C. Three replicate determinations based on both integrated absorbances (PA) and peak height (PH) were used for each measurement.

A Mettler AE 240 semimicro analytical balance (sensitivity, ±0.01 mg) was used for weighing the samples. The slurry was maintained during sample introduction into the atomizer using a Brasonic sonicator (model B-5). A pH meter (Crison model Digit 505) was used to measure the acidity of the aqueous phase. Potentiometric measurements were made with a radiometer automatic titrator (Mettler DL 25) (accuracy, ±0.1 mV) equipped with a combined platinum ring electrode (Mettler DM 140).

### 2.2. Reagents, preparation of cells and procedures

Cadmium stock solution (1000 μg $ml^{-1}$ Cd) was prepared by dissolving a suitable amount of cadmium oxide of the highest quality (Suprapur, Merck) in the smallest quantity of nitric acid then adding the appropriate volume of demineralized water. The test solutions were prepared by appropriate dilution of the stock solution immediately prior to their use. The

Table 1
Graphite furnace programme

| Parameter | Drying | Pyrolysis 1 | Pyrolysis 2 | Atomization | Cleaning |
|---|---|---|---|---|---|
| Temperature (°C) | 150 | 200, ⩾1400 [a] | 250 | 1400, 2200 [a] | 2200, 2400 [a] |
| Ramp time (s) | 2 | 10(3) [a] | 10 | 0 | – |
| Hold time (s) | 0 | 0 | 0 | 4 | 3 |
| Purge, position | 1 | 2 | 1 | 0 | 3 |
| Read on (s) | – | – | – | 5 | – |

The sampling time was 10 s, and the sampling volume was 10 µl.
[a] Values used to remove the interference from the nickel chloride.

inorganic acids and other chemicals used in this study were of the highest quality (Suprapur, Merck). Distilled, deionized water was used for the preparation of samples and standards. The TSA medium was obtained from Merck and the TSB from Biolife.

The preparation of the bacterial cells is a key stage in the retention procedure of metals, because the membrane composition changes with modification of those variables, affecting the cultivation process. Thus, the amount and type of fatty acids and phospholipids vary with temperature, growing medium, cultivation time [30–32], etc. Therefore, strict control in all stages of the preparation of the cells is needed. Cells were prepared as described elsewhere [28,29]. The retention efficiency was measured directly on the biomass. Glass (Pyrex) beakers were used in all measurements.

### 2.3. Procedure for the separation of cadmium

A 25 mg amount of biomass was added to 25 ml of cadmium solution at the corresponding pH. After 20 min stirring time, the biomass was separated by centrifugation (12 400*g*). The Cd–biomass pellet was treated with a 4 ml volume of 3.5 M nitric acid solution in order to prepare the slurry. The slurry was ultrasonically destabilized during sampling. The amount of cadmium sorbed by the biomass was deduced by determining the content of cadmium in either the slurry introduced into the graphite tube or in the supernatant solution after separation of the biomass. The solution pH was adjusted by using $HNO_3$ and NaOH solutions as necessary.

### 2.4. Sample treatment

National Institute of Standards and Technology (NIST) standard reference materials SRM 1577b bovine liver, SRM 1567a wheat flour and SRM 1568a rice flour were digested in triplicate with nitric acid. The digests were obtained by decomposing 0.2 g of bovine liver, and 4 g each of the dry powder sample materials wheat flour and rice flour with 10.0 ml of 1:1 (v/v) nitric acid. The solutions were evaporated to near dryness at 155 °C and the volumes made up to 25 ml with 0.05 mol $l^{-1}$ nitric acid. Prior to the determination of cadmium, the digests of bovine liver and wheat flour were diluted to 100 ml with 0.01 mol $l^{-1}$ nitric acid.

Air-dried coal fly ash SRM 1633a was ground to pass through a number 60 (250 µm) sieve and then ashed at 750°C to remove carbonaceous material. A 0.5 g sample of coal fly ash was digested in triplicate with 10 ml of hydrochloric acid ($d = 1.19$; 37.9% (w/w)) and 20 ml of nitric acid ($d = 1.42$, 69.8% (w/w)) to near dryness. A 20 ml amount of perchloric acid ($d = 1.53$; 60% (w/w)) was then added, and the sample was allowed to evaporate to dryness. A mixture of 10 ml of hydrofluoric acid ($d = 1.13$; 40% (w/w)) and 1 ml of sulfuric acid ($d = 1.84$, 96% (w/w)) was then added and the sample was again heated to dryness. The residue was dissolved in water and transferred quantitatively to a 100 ml volumetric flask.

## 3. Results and discussion

### 3.1. Sorption of cadmium

The best retention for cadmium (1 ng $ml^{-1}$) was obtained in the pH range 4.0–10.0 for both *E. coli* and *P. putida* (Fig. 1). However, the retention capacity (defined as the amount of cadmium retained on a percentage basis of the total cadmium in the original solution) for *P. putida* is nearly constant over the whole optimum pH interval, while for *E. coli* the

maximum retention occurs at a pH of 5.0. The selected working pHs for the following experiments were 5.0 and 9.0 for *E. coli* and *P. putida*, respectively. This versatility in the retention pH of cadmium using dead cells shows an advantage with respect to living cells because the latter can only work at a fixed pH (the pH of the culture medium). An advantage of the lyophilized bacterial cells is based on the fact that the useful retention pH is extended to acidic pH (3.5) and basic pH (11) compared with other extractants, such as algae (immobilized *Selenestrum capricornutum*: pH 9 and retention decreases strongly at higher and lower pH values [27] yeast immobilized *Saccharomyces cerevisiae*: pH above 6.5 [21], resins (7-dodecenyl-8-quinolinol: pH above 6) [33], and cyanobacteria (immobilized *spirulina platensis*: pH above 6.5 [34].

Two types of functional groups (Lewis bases (>CO, –COOH, –OH, etc.) at low pH and Lewis acids ($-NH_2$) at basic pH seems to be involved in the binding of cadmium, mainly for the bacterium *E. coli*, as a result of the data shown in Fig. 1, because the maximum retention capacity differs with the pH of the medium. At very strong acid (below 4–5) or basic (above 9–10) pHs, cadmium is not retained by the membrane wall because acidic functional groups are strongly protonated or cadmium in solution is bound to hydroxyl groups, respectively. It is also possible to conclude that these bacterial surfaces have a number of basic functional groups smaller (*E. coli*) or larger (*P. putida*) than the corresponding ones for the acidic functional groups, or alternatively, basic functional groups would have an affinity for cadmium smaller or larger than that of the corresponding acidic groups.

At the selected retention pH, the binding process shows typical two-phase kinetics (Fig. 2) where an initial period of rapid uptake occurs within minutes, followed by a period of slow, constant uptake over many minutes. This process seems to be much more true for *P. putida* than for *E. coli* and it can be explained by the cadmium ions binding first to the functional groups with the highest affinity (or accessibility) and subsequently to groups with lower affinity (or accessibility).

The maximum uptake was achieved in 20 min for *E. coli*, but the retention of cadmium by the bacterium *P. putida* went on for longer periods of time (Fig. 2). When a steady state is obtained (after 25 min), the percentage of cadmium retained is about 80.0% for both bacteria. However, for shorter periods of time, cadmium is retained more quickly by the bacterium *P. putida* than by *E. coli*, while for longer periods of time (60 min) the retention capacity for *P. putida* increases slowly (85.85%) and for *E. coli* decreases (77.24%). In conclusion, the bacterium *E. coli* has a slightly lower retention capacity for the cadmium ion compared with that obtained for the *P. putida*. The percentage of metal adsorbed by these bacteria is higher than that shown by the algae at pHs buffered at 5.5–6.5: *Stichococcus bacillaris* (35–53% depending on cadmium concentration, 0.1–4 mg $l^{-1}$), *Chlorella pyrenoidsa* (20–60%), and *Chlamydomonas reinharti* (20–35%) [24]. However, using the algae *Stichococcus bacillaris* (200 mg $l^{-1}$) and a higher cadmium concentration (144 mg $l^{-1}$), the cadmium recovery increases to 100% at neutral pH [23].

Using living cells, the removal of the cadmium ions from the solutions depends not only on the uptake rate, but also on the growth rate of the bacterial cells, because the number of cells increases during cultivation. Therefore we found only the maximum retention of cadmium. However, the retention of cadmium by living cells is always lower than when using lyophilized cells, probably due to some resistance mechanisms developed by the cells during their growth [35]. This represents a second advantage of the use of the lyophilized cells and, consequently, these cells will be the main tools used in the following experiments.

The retained cadmium increases with sample volume for a constant concentration of cadmium (0.1 ng $ml^{-1}$), but to a lesser extent than expected because the slope of the straight line

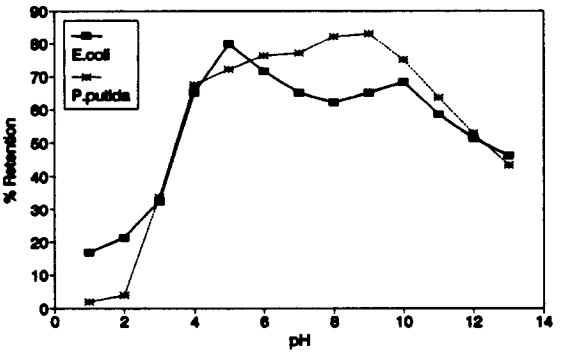


Fig. 1. Effect of pH on the retention of cadmium (1 ng $ml^{-1}$) by the lyophilized bacterias (25 mg) in 25 ml of solution (integrated absorbances by slurry platform atomization).

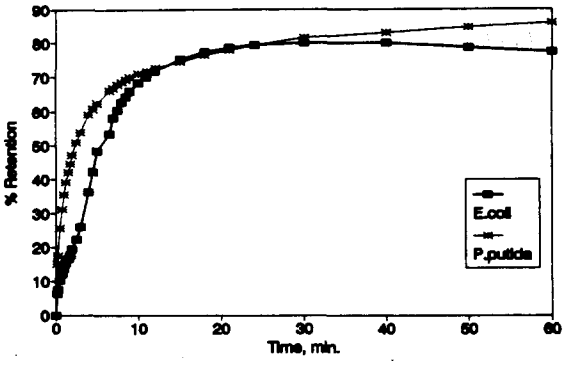


Fig. 2. Kinetics of cadmium (1 ng ml$^{-1}$) uptake by the outer membrane of lyophilized *E. coli* and *P. putida* (50 mg of cells in 50 ml of solution).

obtained by plotting absorbance versus sample volume is below unity. This suggests that in order to obtain the best uptake capacity of cadmium for increasing sample volume, it is necessary to use larger retention (stirring) times. On the other hand, no increase is obtained when the total amount of cadmium is maintained constant.

### *3.2. Mechanism of cadmium adsorption at the selected pHs*

The adsorption isotherms for cadmium show Langmuir shapes mainly for *E. coli* (Fig. 3), suggesting that the earlier retained cadmium ions do not affect the sorption of the neighbouring binding sites and the following cadmium-adsorbed species (Table 2). However, an anti-Langmuirian profile might exist at higher concentrations for *P. putida*, suggesting that the species adsorbed are favoured by those previously retained. This last result agrees well with the adsorption studies obtained using algae as extractants, where isotherms for cadmium have always shown general anti-Langmuirian shapes [24].

Adsorption studies [36] can usually be described by either the Freundlich isotherm ($s = K_F c^{1/n}$) or the Langmuir isotherm ($1/a = (1/a_m K_L)(1/c) + 1/a_m$). Both adsorption isotherms establish a relationship between the amount of metal adsorbed ($s$ is in nanograms per gram, $a$ is in milligrams per gram) by the bacteria and the concentration of metal in solution ($c$ is in nanograms per millilitre for the Freundlich isotherm and milligrams per litre for the Langmuir isotherm). The high values of the constants $K_F$ and $1/n$ show a high adsorption ability, while the parameters $a_m$ and $K_L$ represent the amount (mg) of metal adsorbed at saturation and the equilibrium constant of the adsorption process, respectively. The values of these parameters in Table 2 show a quite high ability of these bacterial cells to be used for preconcentration of cadmium. The Langmuir plot ($1/a$ vs. $1/c$) for both bacteria shows a straight line which represents the existence of only one functional group responsible for the retention of cadmium at the selected working pH. These results permit us to use a unique formation constant to describe the Cd–membrane bond in the concentration range studied (0.1–100 ng ml$^{-1}$ Cd). In contrast, results from the paper by Holcombe and co-workers [24] show two slopes in the Langmuir plot, although for a different concentration range (0.1–4 mg l$^{-1}$ Cd).

The mechanism of cadmium adsorption at the best retention pH for each bacterial membrane can be explained, as for other elements, on the basis of the chemical bond. In order to obtain an explanation of this adsorption mechanism, different experiments were carried out in which variations in the pH of a solution were recorded for the experimental cases shown in Table 3. Firstly, by adding lyophilized bacteria (50 mg) to water (50 ml) at the corresponding pH (case (i) in Table 3) we can deduce the amount of protons retained or liberated by the cells; secondly, if bacterial cells (50 mg) are added to a cadmium (1 ng ml$^{-1}$) solution (50 ml) (case (ii) in Table 3), the pH variation is also due to the influence of cadmium on the retention process; and thirdly, when a cadmium solution (10 ml) is added to an aqueous solution of cells (50 mg bacteria per 40 ml of solution) at the corresponding pH (cases (iii) in Table 3), the variations of pH are due to the retention of cadmium.

From the results of the first case (case (i) in Table 3), we can deduce that the bacterium *E. coli* in contact with water at pH 5.0 retains protons in an amount similar to that at which the *P. putida* at pH 9.0 retains hydroxyl groups. As a result of this, we can assume that the retention mechanism of protons by *E. coli* and of hydroxyl groups by *P. putida* seems to be similar. Therefore the charge of the overall membrane will be positive for *E. coli* (at pH 5.0) and negative for *P. putida* (at pH 9.0). For the second case, Fig. 4 shows the variation of solution pH during the retention process for cadmium by the bacteria. Data in Table 3 (case (ii)) were derived from Fig. 4 for a time interval

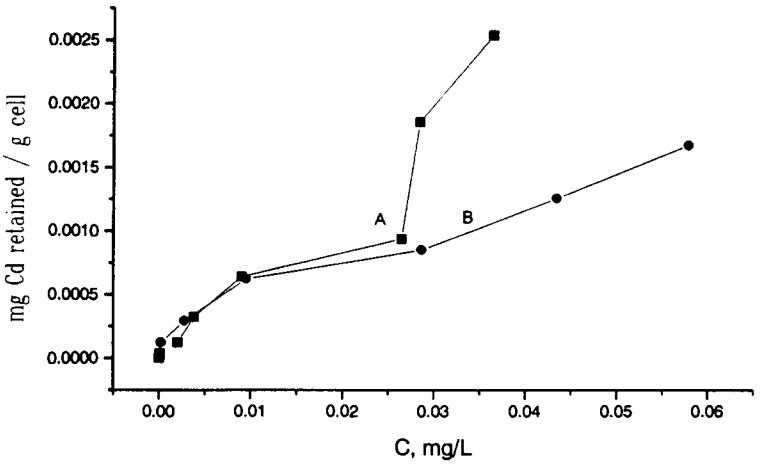


Fig. 3. Adsorption isotherm of cadmium for *P. putida* (curve A) and *E. coli* (curve B). Data shown were obtained by measuring the amount of cadmium in the supernatant solution and represent the average of three experiments with a repeatability of 3.5%.

of 20 min. The opposite trend in the variation of pH with both bacteria means that different types of ions are released from the bacterial membrane during the retention of cadmium. From Fig. 4 it is logical to think that hydroxyl groups should be released (directly or indirectly through the retention of protons) to the solution from the *E. coli* wall (at the retention pH of 5.0), while protons seems to be the most plausible ions liberated (directly or indirectly through the retention of hydroxyls groups) from the *P. putida* membrane (at pH 9.0). For this second case, the variation of pH (ΔpH) for *E. coli* ($\Delta pH_{E.\ coli} = 1.6$) is larger than that obtained for *P. putida* ($\Delta pH_{P.\ putida} = 1.1$; (Fig. 4); case (ii) in Table 3), while in the third case, the addition of cadmium to the bacterial suspension shows a smaller variation of pH of the medium (cases (iii) in Table 3).

These differences suggest that the retention mechanism of cadmium ions differs for each bacterium, being also in agreement with the results obtained for the retention rates (Fig. 2). The pH variations suggest that a proton (or hydroxyl group)–cadmium interchange process can occur, but this mechanism must not necessarily be the only process present because an alternative explanation based on conformational changes of the outer membrane components can also be assumed. In this case, any change in the structural conformation of the outer membrane components causes inner functional groups to be displayed to the aqueous environment, so retaining additional protons from solution.

Changes in the structural conformation of the membrane are suggested because it is possible to derive from Table 3 that the number of protons (or hydroxyl groups) liberated per cadmium ion retained is very high. Differences in these values for both bacteria suggest that different conformational changes occur in both bacterial membranes at the appropriate pH. It is reasonable to think that bacterial membranes in contact with the solution display their negative groups to the surrounding environment at low pH (5.0) and positive functional groups at basic pH (9.0). Cadmium ions would be bound to the negative charges of the membrane, changing their structural conformation in a different way depending on the solution pH.

### *3.3. Determination of Cd by slurry ETAAS*

The retention process was adapted to develop a procedure for the determination of cadmium by ETAAS. In this stage, those factors affecting the atomic absorption signal of cadmium were evaluated. These are the slurry characteristics (the washing acid concentration and slurry concentration), interferences from other elements and some instrumental parameters.

*Slurry characteristics*

Although the Cd–biomass pellet is introduced into the graphite tube as a slurry, we have found better atomic absorption signals for cadmium when the Cd–biomass slurry is treated with nitric acid solution. Therefore we use different concentrations of nitric acid in

order to obtain the best atomic absorption signal. Different concentrations of nitric acid could be used successfully (Fig. 5) at each retention pH, but the best results were obtained using a 3.5 M nitric acid solution at the selected retention pH. The 3.5 M nitric acid acts as a digestion agent, breaking or destroying organic compounds of the biomass, releasing in part the Cd ions under ultrasonic agitation. This total or partial release of cadmium from the biomass would also explain high cadmium values for the slurry in comparison to the supernatant solution. However, another role can also be attributed to $HNO_3$ in the slurry sample. Nitric acid acts also as a modifier because the sensitivity of the determination of cadmium is higher when the slurry is prepared with 3.5 M nitric acid than with the water-prepared slurry. The nitric acid-prepared slurry shows a sensitivity 1.22 (PH) and 1.18 (PA) times better for *E. coli* and 1.12 (PH) and 1.07 (PA) times better for *P. putida* than the water-prepared slurry. These results suggest that the 3.5 M nitric acid favours mainly the atomization rate of the cadmium. This nitric acid concentration was used in all experiments, even when working with living cells.

The washing time over intervals up to 38 h (using 4 ml of 3.5 M nitric acid every time) does not show a strong effect on the atomic absorption signal of cadmium (0.1 ng $ml^{-1}$) by ETAAS. Hence, a time interval of 20 min was selected in all experiments. We have also explored the possibility of determining cadmium in either the biomass pellet by the slurry sampling or in the supernatant after separation by centrifugation. However, higher absorbances for cadmium were obtained using the slurry sampling, suggesting the participation of the biomass on the atomization of cadmium. It is possible that, like other elements, organic matter acts as a chemical modifier. When cadmium was determined in the supernatant, a different behaviour for *E. coli* and for *P. putida* was noted, although results from the pellets were similar. Results from the analysis of supernatant show that for the *P. putida*, cadmium seems to be liberated for short time intervals, but it seems to be again retained for larger washing times. This can be due to the destruction (denaturation) of the macromolecular assembly of the cell walls for long washing times, providing soluble organic molecules with a high complexation capacity for cadmium. The behaviour of *E. coli* seems to be a little more irregular.

Table 2
Parameters of the adsorption isotherms

| Parameter | Bacteria | |
|---|---|---|
| | *E. coli* | *P. putida* |
| Freundlich's isotherm | | |
| $K_F$ (ng $g^{-1}$) | 101.95 | 108.09 |
| $1/n$ | 0.71 | 0.80 |
| Correlation coefficient | 0.97769 | 0.98474 |
| Langmuir's isotherm | | |
| $K_L$ | 678.68 | 737.22 |
| $a_m$ (mg $g^{-1}$) | $5.7 \times 10^{-4}$ | $5.1 \times 10^{-4}$ |
| Correlation coefficient | 0.98985 | 0.99712 |

The retention of cadmium can increase with bacterial mass. However, this behaviour might not necessarily be observed in the atomic absorption signal of cadmium. This is because cadmium is introduced into the graphite tube as a slurry, and biomass affects the atomization path of cadmium as was noted before, or it can even alter the sample introduction stage because the concentration of cells in the slurry sample increases with the amount of cells, making difficult the aspiration of the slurry by clogging the aspiration capillary. The cadmium absorbances increase gradually with the bacterial mass used in the retention process. This effect is mainly due to a clogging of the aspiration capillary of the Fastac sample introduction system, which occurs using amounts of *E. coli* above 20 mg (Fig. 6). From this figure we can conclude that the bacterial mass favours the atomization of cadmium. As a result of this, we can deduce that the maximum *effective* uptake capacity, defined as the amount of cadmium retained by a mass unit of the bacterial cells corresponding to the maximum atomic absorption signal of cadmium when it is introduced as slurry, was about 0.1 ng of cadmium per milligram of bacteria for both bacteria. As it is logical, this value represents an amount of cadmium a little lower than that derived from the Langmuir isotherm for the amount adsorbed at saturation ($a_m$) (Table 2).

*Effect of other elements*

Different elements could compete with cadmium during the retention process at the wall sites, showing interference effects on the final stage of the determination of cadmium by ETAAS. Thus, a ten-thousandfold concentration (1 μg $ml^{-1}$) of the following ions: Ag(I), Al(III), Au(III), Be(II), Bi(III), Ca(II), Ce(IV),

Table 3
Variation of pH ($\Delta pH = pH_{initial} - pH_{final}$) during the retention process for a time interval of 20 min

| System | *E. coli* | | | *P. putida* | | |
|---|---|---|---|---|---|---|
| | $pH_{initial}$ | $pH_{final}$ | ΔpH | $pH_{initial}$ | $pH_{final}$ | ΔpH |
| (i) $H_2O \leftarrow$ Bacteria | 5.10 | 6.50 | −1.40 | 9.00 | 7.56 | 1.44 |
| (ii) $H_2O$ + Cd [a] ← Bacteria | 5.10 | 6.70 | −1.60 | 8.75 | 7.65 | 1.10 |
| (iii) $H_2O$ + Bacteria ← Cd [a] | 5.05 | 5.14 | −0.09 | 9.03 | 8.76 | 0.27 |
| (iii) $H_2O$ + Bacteria ← Cd [b] | 5.05 | 5.23 | −0.18 | 9.02 | 8.85 | 0.17 |

[a] For cadmium solutions of concentration 1 ng $ml^{-1}$.
[b] For cadmium solutions of concentration 50 ng $ml^{-1}$ in the final volume.

Co(II), Cr(VI), Cu(II), Fe(III), Hg(II), K(I), Mn(VII), Na(I), Nb(IV), Pd(II), Se(IV), Sr(II), Te(IV), Th(IV), Ti(III), Tl(I), V(V), Zn(II) and Zr(IV) do not interfere (below 5%) in the cadmium ETAAS determination using either *E. coli* or *P. putida* for preconcentration (Fig. 7). Only La(III) and Ni(II) using *E. coli* and Ni(II), and to a lesser extent, Mg(II), using *P. putida* increase the atomic absorption of cadmium. However, increased interferences are obtained for Ni(II), Pd(II) and Zr(IV) using *E. coli*, and Ni(II), Co(II), Pd(II), Sr(II) and Zr(IV) using *P. putida* at higher concentrations (100 μg $m^{-1}$) of these elements.

The interference effects depend on the selected parameter (integrated absorbances or peak heights) used for the measurements, the bacterial cells, the concentration level of interfering elements and the counterion present. Therefore, using peak height measurements, interferences are qualitatively and quantitatively different to those obtained using integrated absorbances for both bacteria. Thus, some elements (Cr) affect only the peak heights, but others (Co, Ni, Pd, Zr) affect both peak heights and integrated absorbances. This suggests that metal concomitants are retained

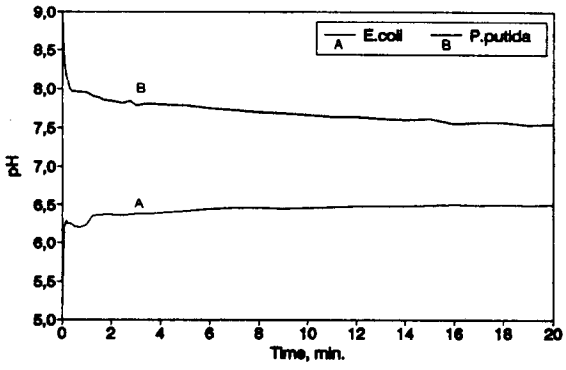


Fig. 4. Variation of pH during the retention of cadmium (lyophilized cells). These results were obtained on a continuous basis using potentiometric measurements.

together with cadmium and affect the atomization or the atomization rate of cadmium. In the same way, Ti and Cr, and, to a less extent Zr (at a 1 μg $ml^{-1}$ concentration) do not affect the integrated absorbances of cadmium but they increase the peak height of the atomic absorbance of cadmium using *E. coli*. This reflects a positive contribution of these elements upon the atomization rate of cadmium. This effect seems not to be dependent on the counterion because Cr was prepared in the absence of chlorides, while Ti was dissolved from titanium trichloride. However, using *P. putida*, this effect is mainly observed for Cr and Zr. This is probably due to the fact that the retention of Ti ions by the bacterium *P. putida* takes place to a lesser extent.

Interferences from the same concomitant differs with the bacterial cell used (La, Mg, Ti), suggesting a different participation (as an organic chemical modifier?) of the biomass in the atomization mechanism of cadmium or alternatively a different behaviour during the retention process. Interferences also vary with the concentration of the concomitant metals, and similar results to those obtained above were also found for both bacteria working at a higher concentration of the concomitant elements (100 μg $ml^{-1}$). A few elements interfere more at lower concentrations than at higher concentrations (La for *E. coli* and Mg for *P. putida*). This reflects either the existence of an antagonistic/synergistic effect with the retention of cadmium, or the presence of concomitant metals in the graphite tube, modifying the atomization path of cadmium.

The strongest interference effect arises from the presence of nickel at concentrations above 100 ng $ml^{-1}$. The interference of nickel shows a particular behaviour because its interference effect is only present when the original sample solution contains nickel as chloride but not as

nitrate. Using nickel chloride as interferent, the peak height of the atomic absorption signal of cadmium grows with the $NiCl_2$ concentration in the original sample solution, but the integrated absorbance increases much more. The interference of this element was studied to a greater extent, assuming that the enhanced interference effect can be explained on the basis of the following factors: (i) a synergistic effect on the retention of cadmium by the bacterial wall; (ii) a positive effect on the atomization of cadmium; or (iii) spectral interference.

In order to understand the positive interference of nickel, cadmium solutions without biomass were introduced into the graphite tube together with either nickel chloride or nickel nitrate, and solutions containing increased amounts of these salts were vaporized separately. The following considerations can be outlined concerning the interference of nickel: (i) the atomic absorption signal of cadmium increases with concentration of nickel chloride; (ii) no interference effect on the atomic absorption signal of cadmium in the presence of increased concentrations of the nickel nitrate exists; (iii) similar positve peaks to those reported in the presence of cadmium were obtained with increasing concentrations of the nickel chloride alone; (iv) a flat signal was obtained with increasing concentration of the nickel nitrate alone; (v) positive interferences appear again if nickel nitrate solutions (alone or together with cadmium) are vaporized in the presence of HCl. This indicates that the positive influence of nickel is due to the simultaneous presence of both the chloride and the concomitant metal. This also suggests that $Cl^-$ ions are retained together with the Ni and Cd ions by the cells used as sorbents. This interference effect appears even when the metal–biomass pellet is washed with nitric acid solution before introduction into the atomizer.

We explored different ways of overcoming this interference by using palladium and magnesium salts as chemical modifiers, by employing living cells as an extractant for cadmium, and by varying the temperature programme. The interference of Ni ($10\ \mu g\ ml^{-1}$) on the atomic absorption of cadmium ($26\ ng\ ml^{-1}$) was not completely overcome by adding Pd-based or Mg-based chemical modifiers at concentrations between 20 and $1000\ \mu g\ ml^{-1}$. We also explored the possibility of using living cells to separate cadmium from the nickel chloride solution. Therefore two sets of experiments were developed using bacterial cells grown together with, and in the absence of, cadmium with increasing concentrations of nickel as the chloride or the nitrate. Stronger interferences were also obtained as the nickel chloride concentrations increased. However, for nickel concentrations of $100\ \mu g\ ml^{-1}$ and above, the bacterial cells did not grow. The retention of the nickel and chloride ions by bacterial cells was clearly demonstrated, because these microorganisms, cultured in the presence of nickel chloride but without cadmium, also show a strong positive peak which increases as the nickel chloride concentration increases. A very small positive peak was also obtained when the cells were grown in a nickel nitrite solution, probably due to the presence in the culture medium of small amounts of chlorides. For the third approach, however, the interference of nickel was avoided using a higher temperature programme (Table 1). There is a relationship between interference and temperature, suggesting that the interfering species were simple molecules, probably NiCl or $NiCl_2$ molecules. The production of the nickel chloride molecules in the gas phase has been previously reported [38,39]. On the other hand, theoretical support for this assumption was also obtained [40]; it was shown [40] that the nickel chloride is stable in an argon atmosphere on the graphite surface to 630°C.

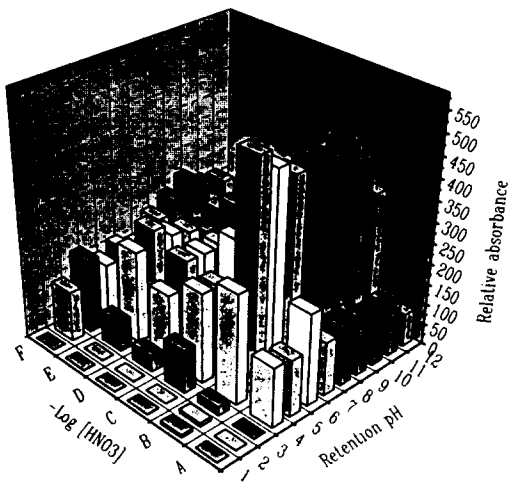


Fig. 5. Simultaneous effect of the retention pH and the washing nitric acid concentration ($mol\ l^{-1}$) on the atomic absorption signal of cadmium for *E. coli* ($-\log [HNO_3] = -0.86$ (A); $-0.56$ (B); 0.0 (C); 1.0 (D); 2.0 (E); 3.0 (F)). (integrated absorbances). Similar results were obtained for *P. putida*. The relative absorbance is the integrated absorbance multiplied by a factor of 1000.

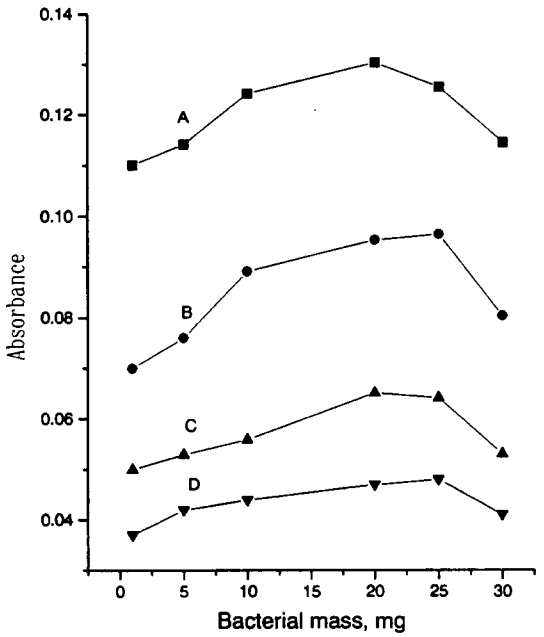


Fig. 6. Effect of biomass on the atomic absorption signal of cadmium (curves A, B) without and (curves C, D) with the extraction stage (nitric acid treatment). A and C, Cd–*E. coli* slurry; B and D, Cd–*P. putida* slurry.

In conclusion, the cause of this interference would be spectral, where a strong absorption from nickel chloride exists. These nickel species would exhibit a strong molecular absorption at the cadmium wavelength during the low-current pulse of the hollow cathode lamp used for the Smith–Heeftje background correction system of the spectrophotometer. However, the $NiCl_2$ could also show a small positive contribution in the atomization of cadmium owing to a partial hydrolysis of the nickel chloride [37] during the pyrolysis stage, seemingly a nickel chemical modifier. As a general rule, main interferences resulted from those concomitants used as chlorides, except Sr(II) and Cr(VI) which were prepared from the nitrate and potassium dichromate, respectively.

*Effect of some instrumental parameters on the atomization of cadmium*

The effect of some instrumental parameters (platform atomization, gas flow) upon the atomization of cadmium were studied for both bacteria.

*Platform atomization*

The rectangular graphite tubes described in the experimental section can be used in a vertical or horizontal manner. The two modes of the platform atomization differ in the orientation of the platform relative to the sample introduction jet. In addition, different heating rates can be experienced by the platform for the two modes. The atomic absorption signals of cadmium are very similar in each case, although showing some peculiarities (Fig. 8). Using horizontal platform atomization, atomic absorption peaks of cadmium appear at later times, showing also wider peaks. On the other hand, a second peak at the appearance time of 0.2 s appears in the atomic absorption peak profile of cadmium for concentrations of 1 ng $ml^{-1}$ (vertical platform) and 10 ng $ml^{-1}$ (horizontal platform) in the original aqueous solution. These results suggest that cadmium species are simultaneously vaporized from both the tube wall and the platform surface. Vaporization from the tube wall is more pronounced when using the platform in a vertical manner, probably due to the fact that the aerosol sample introduced into a graphite tube is deposited to a large extent on the tube wall. This does not happen using aqueous solutions because the atomic absorption signal of cadmium appears earlier, overlapping the first peak.

*Gas flow*

The influence of the purge gas flow during atomization was also studied using the *E. coli* slurry (Fig. 8) and the results can be summarized as follows. When the gas flow is "off" (i) the appearance time of the cadmium atoms is always 1 s; (ii) an increased peak width is obtained, (iii) the declining part of the peak continues on for longer times; and (iv) the appearance of a second peak is observed at 0.2 s for 10 ng $ml^{-1}$ Cd (in the original sample solution). When the gas flow is "on'," (i) the appearance time of the cadmium atoms is always 0.8 s; (ii) a smaller peak width is obtained; (iii) symmetrical peaks occur; and (iv) a smaller integrated absorbance is seen (Fig. 8B). From these results we can conclude that the presence of the purge gas flow during the atomization stage contributes to the desorption of cadmium species from the graphite surface as well as to the expulsion of cadmium atoms outside the tube. Cadmium is also vaporized as free atoms at low temperatures. Interactions between cadmium and graphite occur more strongly and the sensitivity is increased if the gas flow is "off". The results obtained from aqueous solutions show only one peak in the absorbance–time profile of cadmium at 0.2 s, and the sensitivity is a little lower than that obtained

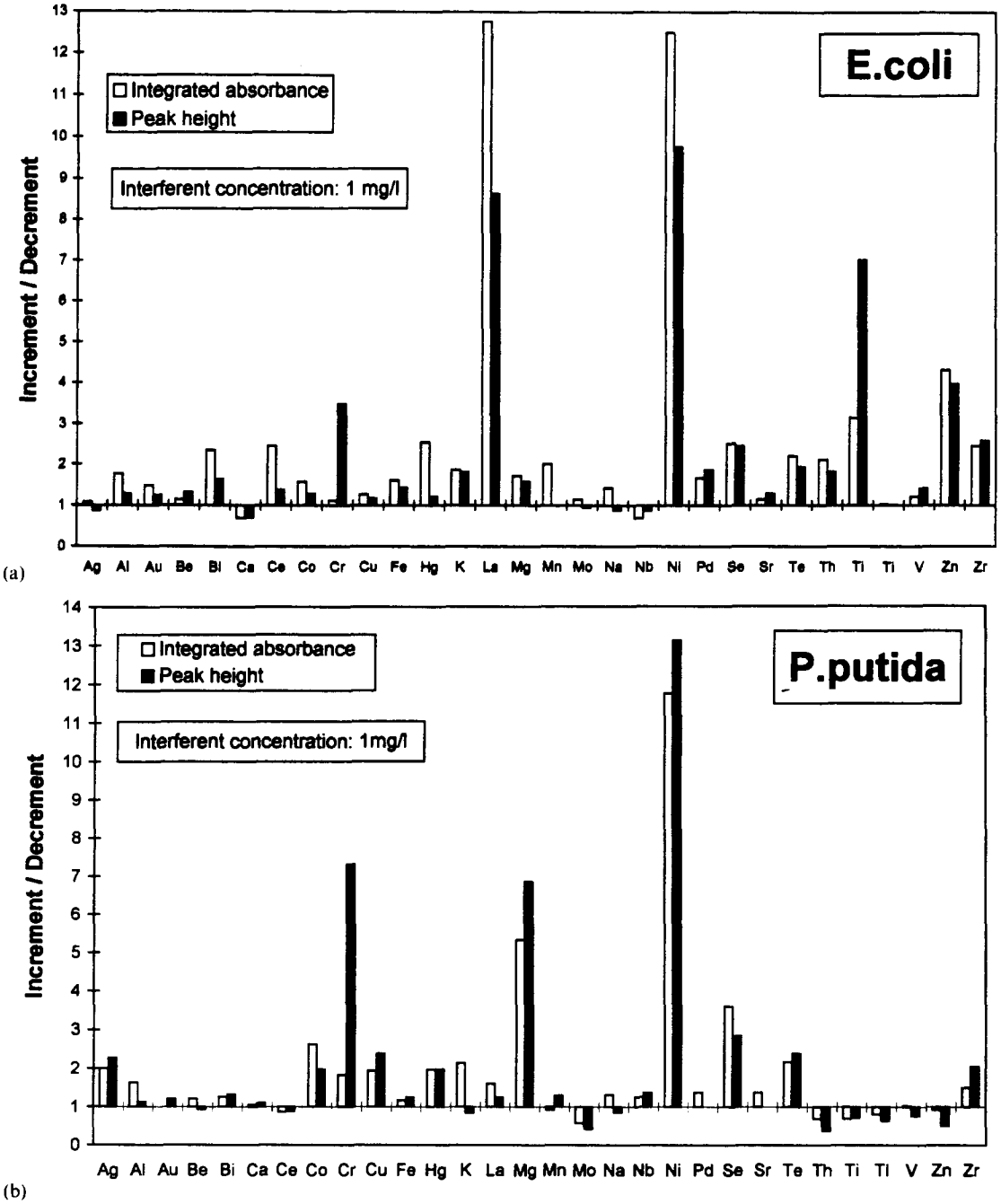


Fig. 7. Interferences of different elements (1 μg $ml^{-1}$) on the retention/determination of 0.1 ng $ml^{-1}$ Cd in the original sample for (a) *E. coli* and (b) *P. putida*.

from slurry atomization. This suggests that bacterial cells delay, simultaneously favouring, the atomization process of cadmium.

*Figures of merit*

The analytical characteristics (Table 4) show both that these bacterial cells were effective at preconcentrating small amounts of cadmium and that it is possible to determine cadmium by slurry ETAAS in the presence of an organic matrix. Beneficial effects were derived by using bacterial cells not only in the extraction step but also in the atomization process, because the introduction of cadmium together with the biomass into the graphite tube favours its atomization.

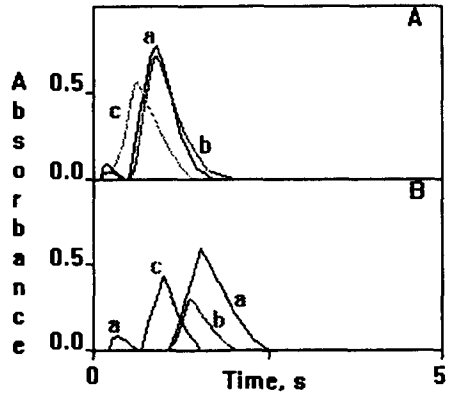


Fig. 8. Atomic absorption peak profile of cadmium (0.625 ng) for (A) vertical and (B) horizontal platform atomization. (A) curve a, *E. coli*; curve b, *P. putida*; curve c, aqueous solution. (B) curve a, *E. coli*; curve b, *P. putida*; curve c, the same as for curve a but with the gas flow "on". The gas flow was "off" always except in B, curve c.

The blank level of cadmium from the biomass against water was 0.005 AU and it was compensated for in the determination of the samples by setting the "zero" of the instrument for a biomasss slurry without cadmium. Calibration graphs were constructed by treating cadmium standards in the same way as the sample according to the procedures described in the experimental section. The sensitivity represents the slope of the analytical calibration graph of absorbance versus concentration (ng $ml^{-1}$) obtained by linear regression. Limits of detection found in this paper (Table 4) are similar to (0.05 ng $ml^{-1}$ [27], 0.06 ng $ml^{-1}$ [33]) or even better than (0.2 ng $ml^{-1}$ [21], 0.4 ng $ml^{-1}$ [34], 0.6 ng $ml^{-1}$ [41]) those reported in other work for different extractants.

The preconcentration factor was defined as the ratio between the volume of the initial sample and the final volume obtained after the extraction step. As the first aim of this paper was not to find a high preconcentration factor, a comparison with the very high concentration factors found in other work [33,42] using immobilized resins is unreliable. The AAS signal obtained on the direct injection of an aqueous cadmium solution compared with the obtained on the injection of a cadmium–pellet slurry of the same cadmium concentration (1 ng $ml^{-1}$) was termed the atomization factor. The atomization factor is the result of the simultaneous positive contribution of $HNO_3$ and the biomass to the atomization of cadmium. As the positive contribution factor ($f_a$) of $HNO_3$ was derived previously (see the section on slurry characteristics (3.3)) from the values of the atomization factors ($F_A$) shown in Table 4, we can derive the positive contribution factor of the biomass ($f_b$), because $F_A = f_a f_b$. From the results found for $f_b$, 1.81 (PA) and 2.38 (PH) for *E. coli* and 2.52 (PA) and 1.43 (PH) for *P. putida*, we can conclude that the biomass shows a positive effect larger than does the nitric acid. The enhancement factor of Table 4 was derived by comparing the AAS signal obtained on direct injection with that obtained after preconcentration and treatment with the appropriate volume and concentration of the nitric acid solution. The enhancement factors obtained were good for both bacteria.

The repeatability varies from 2.45 to 4.50% for cadmium concentrations between 0.5 and 12.5 ng $ml^{-1}$, but the best relative standard

Table 4
Figures of merit

| Parameter | Aqueous solution, PA(PH) | Lyophilized bacteria | | Living cells |
|---|---|---|---|---|
| | | *E. coli*, PA(PH) | *P. putida*, PA(PH) | *E. coli* (*P. putida*), PA [a] |
| Linear range [b] (ng $ml^{-1}$) | 0.3–25(0.2–10.0) | 0.1–5.0(0.1–4.0) | 0.1–12.0(0.1–10.0) | 0.1–25 |
| Sensitivity (ng $ml^{-1}$) | 0.16(0.09) | 0.07(0.03) | 0.09(0.05) | 0.31(0.22) |
| Limit of detection [c] (ng $ml^{-1}$) | 0.20(0.10) | 0.05(0.04) | 0.08(0.05) | 0.1 |
| Characteristic mass (pg) | 1.57(0.94) | 0.73(0.30) | 0.88(0.55) | 3.14(2.2) |
| Preconcentration factor | 1 | 6.25 | 6.25 | 25 |
| Atomization factor | 1 | 2.14(2.9) | 2.7(1.6) | 0.28 [d](0.2) [d] |
| Enhancement factor | 1 | 13.4(18.1) | 16.9(10) | 7.0(5.0) |
| RSD [e] $_{(1\ ng\ ml^{-1})}$(%) | – | 2.45 | 2.74 | 7.25(7.56) |

[a] Similar results were obtained from peak height measurements.
[b] The optimum linear range was established over which the measured and predicted absorbances differed by less than 5%.
[c] Three values of nine consecutive measurements of the signal from a blank.
[d] These values have been obtained against the absorbance of an aqueous solution.
[e] Relative standard deviation ($n = 9$).

Table 5
Accuracy of the developed method using lyophilized bacteria ($n = 3$)

| NIST sample | Cd certified [a] ($\mu g\ g^{-1}$) | Cd found [a] ($\mu g\ g^{-1}$) | |
|---|---|---|---|
| | | *E. coli* | *P. putida* |
| Bovine liver SRM 1577b | $0.500 \pm 0.003$ | $0.497 \pm 0.003$ | $0.502 \pm 0.005$ |
| Wheat flour SRM 1567a | $0.026 \pm 0.002$ | $0.027 \pm 0.002$ | $0.028 \pm 0.002$ |
| Rice flour SRM 1568a | $0.022 \pm 0.002$ | $0.021 \pm 0.002$ | $0.023 \pm 0.002$ |
| Coal fly ash SRM 1633a | $1.00 \pm 0.15$ | $0.988 \pm 0.030$ | $1.005 \pm 0.033$ |

[a] The errors represent two standard deviations.

deviation was obtained for a cadmium concentration of 1 ng $ml^{-1}$ for both bacteria (Table 4). The accuracy of this procedure was tested by replicate determinations of cadmium in different standard samples, and the measured cadmium concentrations compared well with the certified values (Table 5). The blank levels of the NIST standard reference samples were estimated by parallel experiments applying the same separation procedure to 100 ml of Milli-Q water with the same amount of cadmium. These values represent 0.005 AU for the digestion procedure for the biological samples and 0.010 AU for the digestion procedure for the coal fly ash sample.

## 4. Conclusions

From this study we can conclude that the bacteria *E. coli* and *P. putida* show similar analytical possibilities when they are used to separate and preconcentrate cadmium from complex biological and environmental samples. The retention process for both bacteria shows higher efficiency over a wide pH interval, and the procedure for the retention/determination of cadmium exhibits good analytical sensitivity and excellent specificity.

## Acknowledgement

We gratefully acknowledge the "Ramón Areces" Foundation for funding this research programme.

## References

[1] L. Caprino, G. Togna and A.R. Togna, Pharmacol. Res. Commun., 11 (1979) 731.
[2] J. Overnell, Comp. Biochem. Physiol. B, 73 (1982) 555.
[3] S. Landsberger, S. Larson and D. Wu, Anal. Chem., 65 (1993) 1506.
[4] L. Ebdon, P. Goodall, S.J. Hill, P.B. Stockwell and K.C. Thompson, J. Anal. At. Spectrom., 8 (1993) 723.
[5] I. Kojima and S. Kondo, J. Anal. At. Spectrom., 8 (1993) 115.
[6] M.C. Valdés-Hevia y Temprano, M.R. Fernández de la Campa and A. Sanz-Medel, J. Anal. At. Spectrom., 9 (1994) 231.
[7] S.-M. Lin, Anal. Sci., 7 (1991) 155.
[8] R. Fernando, B.T. Jones and F.K. Ennever, Appl. Spectrosc., 47 (1993) 1696.
[9] J. Jurasovic and S. Telisman, J. Anal. At. Spectrom., 8 (1993) 419.
[10] J. Alvarado and A.R. Cristiano, J. Anal. At. Spectrom., 8 (1993) 253.
[11] A. Mazzucotelli, F. Soggia and B. Cosma, Appl. Spectrosc., 45 (1991) 504.
[12] E. Pruszkowska, G.R. Garnrick and W. Slavin, Anal. Chem., 55 (1983) 182.
[13] K.S. Subramanian, J.-C. Meranger and J.E. MacKeen, Anal. Chem., 55 (1983) 1064.
[14] K.G. Feitsma, J.P. Franke and R.A. de Zeeuw, Analyst, 109 (1984) 789.
[15] C. Eloi, J.D. Robertson and V. Majidi, J. Anal. At. Spectrom., 8 (1993) 217.
[16] Z. Benzo, C. Cecarelli, N. Carrion, M.A. Alvarez, C. Rojas and M. Rosso, J. Anal. At. Spectrom., 7 (1992) 1273.
[17] M. Yizai, B. Jian, W. Jiazhen, L. Zhikun, Z. Lei, L. Yongquan, Z. Hui and L. Bingwei, J. Anal. At. Spectrom., 7 (1992) 425.
[18] E. Tserovsky, S. Arpadjan and I. Karadjova, J. Anal. At. Spectrom., 8 (1993) 85.
[19] M.F. Giné, F.J. Krug, V.A. Sass, B.F. Reis, J.A. Nóbrega and H. Berndt, J. Anal. At. Spectrom., 8 (1993) 243.
[20] M.A. Alikhan, G. Bagatto and S. Zia, Water Res., 24 (1990) 1069.
[21] A. Maquieria, H.A.M. Elmahadi and R. Puchades, Anal. Chem., 66 (1994) 1462.
[22] V. Majidi and J.A. Holcombe, Spectrochim. Acta, 43B (1988) 1423.
[23] V. Majidi and J.A. Holcombe, J. Anal. At. Spectrom., 4 (1989) 439.
[24] C.A. Mahan, V. Majidi and J.A. Holcombe, Anal. Chem., 61 (1989) 624.
[25] H.-B. Xue, W. Stuum and L. Sigg, Water Res., 22 (1988) 917.

[26] M.L.S.S. Gonçalves, M.F.C. Vilhena and M.A. Sampayo, Water Res., 22 (1988) 1429.
[27] H.A.M. Elmahadi and G.M. Greenway, J. Anal. At. Spectrom., 6 (1991) 643.
[28] L.C. Robles, C. García-Olalla and A.J. Aller, J. Anal. At. Spectrom., 8 (1993) 1015.
[29] L.C. Robles and A.J. Aller, J. Anal. At. Spectrom., 9 (1994) 871.
[30] A.G. Marr and J.L. Ingraham, J. Bacteriol., 84 (1962) 1260.
[31] J.E. Cronan, Jr., J. Bacteriol., 95 (1968) 2054.
[32] M. Ishinaga, R. Kanamoto and M. Kito, J. Biochem., 86 (1979) 161.
[33] K. Isshiki, F. Tsuji, T. Kuwamoto and E. Nakayama, Anal. Chem., 59 (1987) 2491.
[34] A. Maquieria, H.A.M. Elmahadi and R. Puchades: Anal. Chem., 66 (1994) 3632.
[35] B. Poolman, D. Molenaar and W.N. Konings, in M. Shinitsky (Ed.), Biomembranes, Vol. 2. Structural and Functional Aspects, VCH, Weinheim, 1994, pp. 329–379.
[36] A.W. Adamson Physical Chemistry of Surfaces, 4th edn., John Wiley, New York, 1982, pp. 521–523.
[37] M.M. Chaudhry, D. Mouillere, B.J. Ottaway and D. Littlejohn, J. Anal. At. Spectrom., 7 (1992) 701.
[38] S. Yasuda and H. Kakiyama, *Anal. Chim. Acta*, 84 (1976) 291.
[39] X.P. Shan, Z.-N. Yuan and Z.-M. Ni, Anal. Chem., 57 (1985) 857.
[40] J. Dèdina, W. Frech, A. Cedergren, I. Lindberg and E. Lundberg, J. Anal. At. Spectrom., 2 (1987) 435.
[41] S. Devi, K. A.J. Habib and A. Townshend, Quim. Anal. (Barcelona), 8 (1989) 159.
[42] R.E. Sturgeon, S.S. Berman, S.N. Willie and J.A.H. Desaulniers, Anal. Chem., 53 (1981) 2337.

ELSEVIER

Talanta 42 (1995) 1745–1749

Talanta

# Preparative supercritical fluid extraction of pyrethrin I and II from pyrethrum flower

Wynn H.T. Pan [a], Cheng-Chin Chang [b], Tien-Tsu Su [b], Fong Lee[b], Ming-Ren Steve Fuh [c,*]

[a] *Institute of Pharmacology, National Yang-Ming University, Shih-Pai, Taipei, Taiwan, ROC*
[b] *R&D Division, Taiwan Fertilizer Company, Ltd., Taipei, Taiwan, ROC*
[c] *Department of Chemistry, Soochow University, Shih-Lin, Taipei, Taiwan, ROC*

Received 14 March 1995; revised 30 May 1995; accepted 31 May 1995

**Abstract**

A preparative supercritical fluid extraction system is described and was used with supercritical carbon dioxide to extract the active insecticide components pyrethrin I (PI) and pyrethrin II (PII) successfully from pyrethrum flower. A high-performance liquid chromatography method was developed and was used to separate and analyze the supercritical carbon dioxide extracts. Extraction efficiencies under several different extraction conditions were examined. Under the conditions examined, the most effective extractions of PI and PII ($140 \pm 18$ mg and $55 \pm 9$ mg per 100 g of dry pyrethrum flower powder) were performed at 40°C and 1200 psi. The results showed that extraction efficiencies of supercritical carbon dioxide are much better than those of *n*-hexane for pyrethrins I and II. During the extraction process, the most efficient extraction period was the first 3 h of the experiment.

*Keywords:* High-performance liquid chromatography; Insecticides; Preparative supercritical fluid extraction; Pyrethrin I; Pyrethrin II; Pyrethrum flower

## 1. Introduction

Natural pyrethrum insecticides that contain six similar pyrethrins have been prepared from the organic solvent extracts of pyrethrum flowers [1,2]. Pyrethrins have been used for the control of insects on animals in the house and on plants in agriculture for many years [3,4]. They possess exceptionally high selectivity ratios (mammalian oral $LD_{50}$/insect topical $LD_{50}$) compared to other classes of insecticides. Selectivity ratios for pyrethrins are generally greater than 1000, whereas those for members of other insecticide classes, e.g. organochlorines, organophosphorus, and carbamate, are typically less than 100 [5,6]. Therefore, the use of natural pyrethrum insecticides has increased tremendously [7]. In recent years, since people are now more concerned about environmental contamination and vertebrate toxicity, scientists are searching for new extraction techniques for pyrethrins to replace conventional solvent extraction.

Supercritical fluid extraction (SFE) has proved to be an effective technique for the extraction of flavors and active ingredients from plant materials [8–10], polyaromatic hydrocarbons from contaminated soil [11,12], and pyrethrins from pyrethrum flowers [13]. Supercritical carbon dioxide has been used as primary solvent for SFE, because it has no toxicity and a relative low critical temperature (31°C) and pressure (1070 psi). Supercritical carbon dioxide is an excellent solvent for non-

* Corresponding author.


*SSDI* 0039-9140(95)01657-0

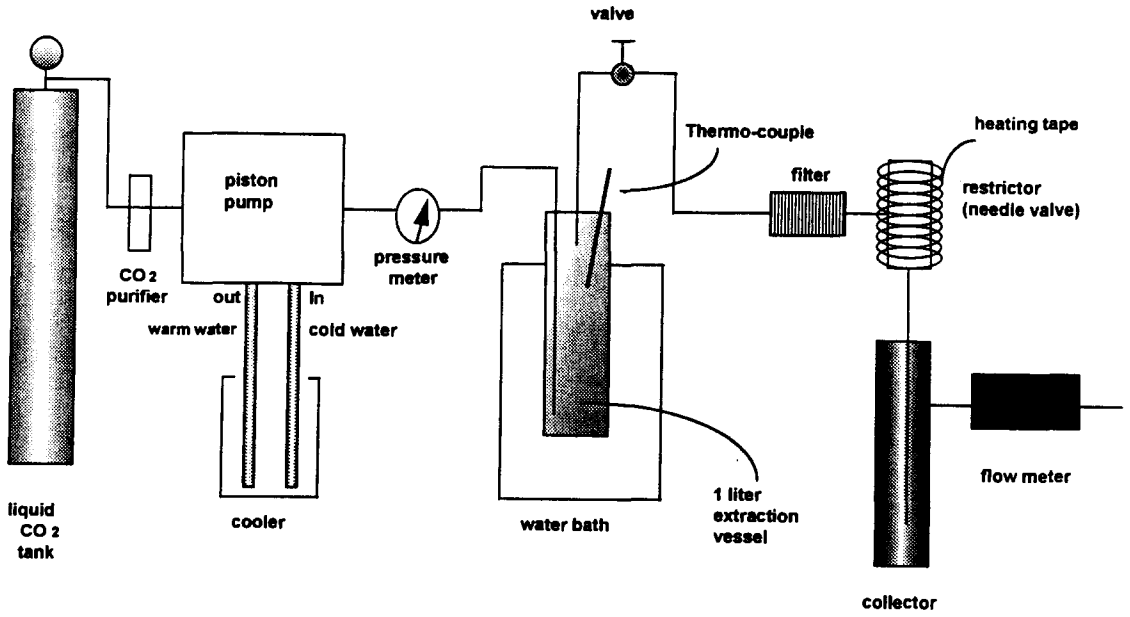


Fig. 1. The configuration of the SFE system used in this study.

polar organics because its solvating power and polarity can be controlled and adjusted by changing the temperature and pressure and by adding organic modifiers [14,15].

Dried pyrethrum flowers contain about 1–2% of natural pyrethrins by weight. Natural pyrethrins include pyrethrin I (PI), pyrethrin II (PII), jasmolin I (JI), jasmolin II (JII), cinerin I (CI), and cinerin II (CII) [12]. Among these six active ingredients, PI and PII are the major components and PI is the most potent one [7,16]. Therefore, the purpose of this investigation was to examine the usefulness of SFE for the extraction of PI and PII from pyrethrum flower powder; moreover, for comparison purposes, organic solvent extraction was performed and evaluated. In addition, an HPLC method was developed to determine the amount of PI and PII in the exctracts.

## 2. Experimental

### 2.1. Reagents

Carbon dioxide was purchased from Chin-Fong Hong (99.999%; Taipei, Taiwan, ROC). Dry pyrethrum flower was purchased from S.A. Pyrethrum Company, Ltd. (Landsberg, South Africa). HPLC-grade *n*-hexane was obtained from J.T. Baker Inc. (New Jersey, USA). Deionized water was collected from a Milli-Q water purification system (Millipore Corp., Massachusetts, USA). HPLC-grade anhydrous dichloromethane was purchased from Mallinckrodt Chrom AR (Germany). Saturated dichloromethane was prepared by shaking dichloromethane with Milli-Q water (80:20, v/v) for 15 min, letting the mixture stand for 10 min, and then discarding the aqueous portion. Pyrethrin standard was obtained from Riedel-deHaën AG (Germany). The composition of this standard is 26.8% of PI, 19.9% of PII, 1.4% of JI, 1.1% of JII, and a trace amount of CII. The standard (250 mg) was dissolved in 50 ml of *n*-hexane then dispensed into five 10 ml light-shield bottles and stored in a refrigerator.

### 2.2. Supercritical fluid extraction

A supercritical extraction system with a 1 l extraction vessel was self-assembled as shown in Fig. 1. A $CO_2$ purifier from J&W (model 300 – 1, California, USA) was used. A dual piston pump was used to increase the pressure in the system (LCD Corp., model 2396-89, Florida, USA), a 1 l extraction vessel was purchased from Zaar Tech. Inc. (Chicago, IL, USA), and a water bath was used to maintain the extraction temperature. A strainless steel in-line filter (part no. 2F-F4L, Parker-Hannifin Corp., Alabama, USA) was used to prevent clogging of the restrictor. A needle valve

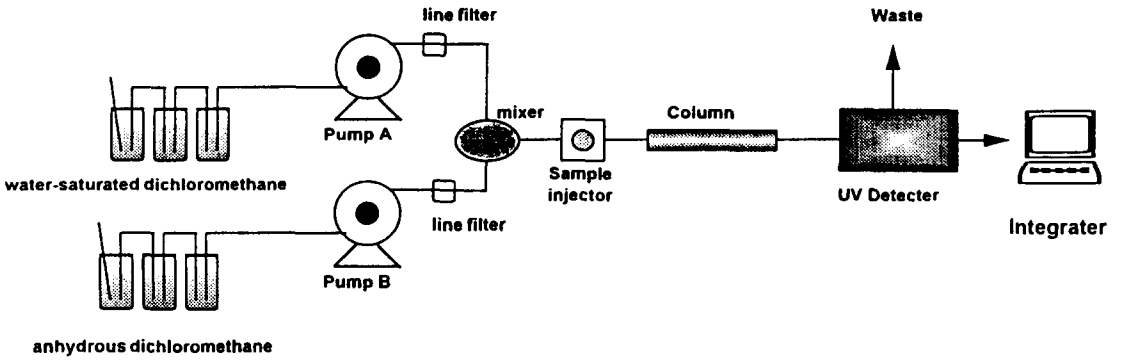


Fig. 2. Schematic of the semi-closed solvent delivery system and HPLC apparatus used in this study.

(Micrometering valve, part no. 30048-12, Autoclave Engineering Corp., Pennsylvania, USA) wrapped with a heating tape was used as a restrictor.

It has been demonstrated that the thermolabile PI and PII could be extracted without decomposition in the temperature range from 20 to 40°C [9]. Since the critical temperature of $CO_2$ is 31°C, the extraction temperature was fixed at 40°C in order to prevent PI and PII decomposition and to keep $CO_2$ in the supercritical phase. Four different extraction pressures were used: 1200, 2000, 2800 and 3600 psi. Each pressure was repeated at least three times. The outlet flow rate of atmospheric $CO_2$ during extraction was set at 3 l $min^{-1}$. About 200 g of dry ground pyrethrum flower powder were used in each SFE extraction. The extraction outlet was inserted into a flask containing 100 ml of *n*-hexane for trapping the crude extracted materials. Since some *n*-hexane evaporates during the collection period, additional *n*-hexane was added to maintain an adequate amount of the trapping solvent. After each extraction, *n*-hexane was added to the extraction flask to a total of 100 ml.

### 2.3. Organic solvent extraction

A 50 g portion of dry ground pyrethrum flower powder and 200 ml of *n*-hexane were placed in a flask wrapped with aluminum foil. After 5 h of continuous stirring at room temperature with a magnetic stirrer, the flask was refrigerated overnight, and the solution was then filtered. The filtered solution was stored in a light-shield bottle which was kept in a refrigerator. A 50 µl portion of the *n*-hexane extract was injected for HPLC analysis. All the above procedures were repeated three times on different days.

### 2.4. Chromatographic analysis

A Dionex 4000i chromatography system with a UV detector (California, USA) was used for HPLC analysis. The analytical separation was achieved on a 300 mm × 3.9 mm i.d. µ-Porasil column (Waters Association, Massachusetts, USA) with a mixture of 40% water-saturated dichloromethane and 60% anhydrous dichloromethane (v/v) as mobile phase. A Spectra-Physics (model 4400) data jet integrator (California, USA) was used for data acquisition and recording. The HPLC flow rate was 0.8 ml $min^{-1}$. A 2 ml portion of the SFE extract was combined with *n*-hexane to give a 100 ml solution, and 50 µl aliquots were then injected into the HPLC system for quantitative analysis.

A semi-closed solvent delivery system (shown in Fig. 2) was used to minimize the evaporation of the mobile phase during analysis. This system consisted of three identical solvent reservoirs placed in series, with only the reservoir furthest from the pump vented to the air, while the others were totally closed. Details of the chromatography data will be discussed in the following section.

## 3. Results and discussion

The relatively long analysis time required by published HPLC methods for the analysis of pyrethrins makes them less desirable [17,18]. We developed a rapid and reliable method. An evaluation of the effect of different mobile phase compositions on the retention times of PI and PII is summarized in Table 1. Results

Table 1
Retention times of PI and PII for different mobile phase compositions

| Water-saturated dichloromethane (%, v/v) | Anhydrous dichloromethane (%, v/v) | Retention time (min) | |
|---|---|---|---|
| | | PI | PII |
| 0 | 100 | 53.66 | 71.50 |
| 25 | 75 | 15.18 | 78.08 |
| 40 | 60 | 9.00 | 16.64 |
| 50 | 50 | 7.08 | 10.3 |
| 75 | 25 | 6.09 | 9.41 |

show that the retention times of PI and PII decreased as the amount of water-saturated dichloromethane increased. Adequate separation of each component was achieved by using a mixture of 40% water-saturated dichloromethane and 60% anhydrous dichloromethane (v/v) as mobile phase. The chromatogram is shown in Fig. 3, and the retention times of PI and PII with this mobile phase composition were approximately 9.0 min and 16.5 min, respectively. Furthermore, good linearity ranges were observed from 0.7 to 214 mg $L^{-1}$ for PI ($r^2 = 0.999$) and from 0.9 to 151 mg $L^{-1}$ for PII ($r^2 = 0.999$), respectively.

The total amounts of PI and PII extracted at various pressures by SFE are shown in Fig. 4. The extracted amount described in this figure has been normalized to 100 g of dry pyrethrum flower powder. At 40°C, the best extraction efficiencies for PI and PII were observed at

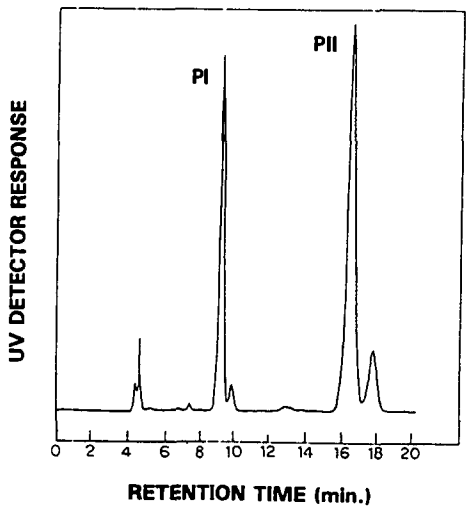


Fig. 3. Chromatogram of a standard. (Mobile phase flow rate; 0.8 ml $min^{-1}$; injection volume 50 µl. The UV detector was set at 254 nm.) PI is pyrethrin I and PII is pyrethrin II.

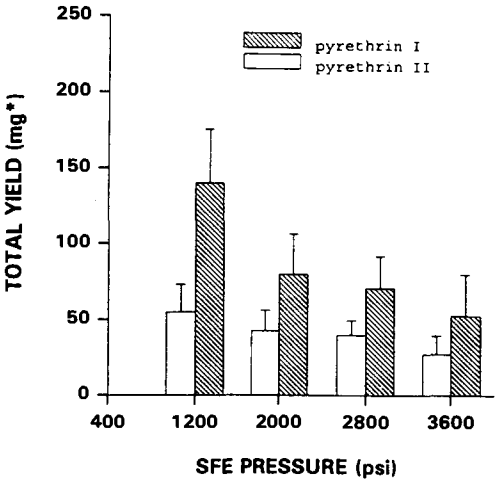


Fig. 4. Effect of SFE extraction pressure on the total yields of PI and PII. The values are the mean ± the standard error of the mean (SEM). The asterisk denotes milligrams of extract per 100 g of dry pyrethrum flower powder.

1200 psi (140 ± 18 mg and 55 ± 9 mg per 100 g of sample). This might be attributed to a low density and a high diffusivity of supercritical carbon dioxide at low pressure. As the extraction pressure increases from 1200 to 2000 psi, the density of supercritical carbon dioxide increases from 0.337 to 0.768 g $ml^{-1}$. As a result, the SFE extraction efficiencies for PI and PII decrease significantly. However, there is much less change in the extraction efficiency when the pressure is increased from 2000 to 3600 psi since the density of supercritical carbon dioxide increase to a lesser extent (0.768–0.885 g $ml^{-1}$) from 2000 to 3600 psi.

For comparison purposes, *n*-hexane extraction was performed and the total amounts of PI and PII extracted were 70 ± 8 mg and 39 ± 7 mg per 100 g of pyrethrum flower powder, respectively. This study demonstrated that SFE has a much better extraction efficiency than of *n*-hexane extraction, with 100% and 41% enhancement for PI and PII, respectively.

Fig. 5 shows SFE extraction kinetics of PI and PII from pyrethrum flower powder samples at 40°C and 1200 psi. The results indicate that the extraction of PI and PII from pyrethrum flower powder is most effective during the first 3 h; the extraction rate decreased significantly after 3 h.

## 4. Conclusion

Supercritical carbon dioxide extraction has been shown to be an effective technique for the

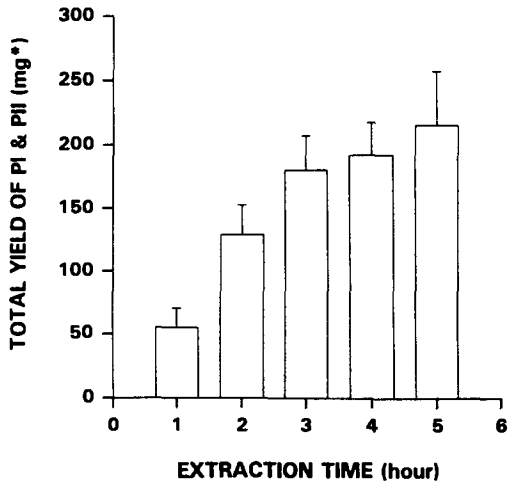


Fig. 5. Detection of the total yield of PI and PII in the SFE collector vs. extraction time. Values are the mean ± SEM. The asterisk denotes milligrams of extract per 100 g of dry pyrethrum flower powder.

extraction of pyrethrins from pyrethrum flower powder. For the temperature and pressure range examined, the most effective extraction conditions are 40°C and 1200 psi. Compared with the *n*-hexane extraction method, there is significant enhancement in extraction efficiencies for PI and PII by using SFE.

An HPLC method was developed and has been used successfully to separate the extracts. A semi-closed solvent delivery system was used to eliminate the mobile phase evaporation problem. Adequate separation of each component was achieved by using a mixture of 40% water-saturated dichloromethane and 60% anhydrous dichloromethane (v/v) as mobile phase. In addition, excellent linearity ranges for PI and PII were achieved.

We are currently studying the effectiveness of SFE extracts as insecticides. The initial test data indicate that the extract obtained by the SFE method is as effective as that obtained using the *n*-hexane extraction method.

## Acknowledgments

This work was supported by research grants from the Taiwan Fertilizer Company, Ltd. to Wynn Pan (grant no. 750) and from the National Science Council to Steve Fuh (NSC-83-0208-M-031-012).

## References

[1] M. Matsumoto, Jpn Patent 119,682, 1974.
[2] L.W. Levy, Br. Patent 870,459, 1961.
[3] G. Forget, J. Toxicol. Environ. Health, 32 (1991) 11.
[4] V.M. Valentine, Veterinary Clinics of North America-Small Animal Practice, 20 (1990) 375.
[5] J.E. Casida, D.W. Gammon and A.H. Glickman, Annu. Rev. Pharmacol. Toxicol., 23 (1983) 413.
[6] A.H. Glickman and J.E. Casida, Neurobeha Toxicol Teratol. 4 (1982) 793.
[7] E. Stahl, K.-W. Quirin and D. Gerard, Dense Gases for Extraction and Refining, Springer-Verlag, Berlin, 1998.
[8] M. Verschuere, P. Sandra and F. David, J. Chromatogr. Sci., 30 (1992) 388.
[9] W.H.T. Pan, C.-K. Liu, L.-Y. Chou and M.-H. Lee, J. Chin. Med., 5 (1994) 71.
[10] J.W. King, J. Chromatogr. Sci., 28 (1990) 9.
[11] J.J. Langenfeld, S.B. Hawthorne, D.J. Miller and Pawliszyn, J. Anal. Chem., 65 (1993) 338.
[12] S.B. Hawthorne, Anal. Chem., 62 (1990) 633A.
[13] E. Stahl, E. Schütz, Planta Med., 40 (1980) 12.
[14] J.J. Pawliszyn, Chromatogr. Sci., 31 (1993) 31.
[15] J.J. Langenfeld, S.B. Hawthorne, D.J. Miller and Pawliszyn, J. Anal. Chem., 66 (1994) 909.
[16] J.E. Casida, Environ. Health Perspect, 34 (1980) 189.
[17] D.A. Otieno, I.J. Jondiko, P.G. McDowell and F.J.J. Kezdy, Chromatogr. Sci., 20 (1982) 566.
[18] A.M. McEldoweny and R.C. Menary, J. Chromatogr., 447 (1988) 239.

ELSEVIER

Talanta 42 (1995) 1751–1755

Talanta

# Chemiluminometric flow-injection method for determination of free L-malate in wine with co-immobilized malate dehydrogenase/NADH oxidase

Nobutoshi Kiba *, Junko Inagaki, Motohisa Furusawa

*Department of Applied Chemistry and Biotechnology, Faculty of Engineering, Yamanashi University, Kofu 400, Japan*

Received 21 March 1995; revised 2 June 1995; accepted 2 June 1995

**Abstract**

A flow-injection system with a co-immobilized malate dehydrogenase/reduced nicotineamide adenine dinucleotide (NADH) oxidase reactor and a chemiluminometer is described for the determination of free L-malate in wine. Malate dehydrogenase and NADH oxidase were co-immobilized on poly(vinyl alcohol) beads and packed into a stainless-steel column (5 cm × 4 mm i.d.). The hydrogen peroxide produced was detected chemiluminometrically via a luminol–hexacyanoferrate(III) reaction. The calibration graph was linear from $3 \times 10^{-7}$ M to $2.5 \times 10^{-4}$ M (the linear correlation coefficient was 0.9998); the detection limit (signal-to-noise ratio, 3) was $8 \times 10^{-8}$ M. The sample throughput was 30 $h^{-1}$ without carryover. The reactor was renewed every 2 weeks.

*Keywords:* Chemiluminescence; Flow injection; Co-immobilized enzyme reactor; Malic acid; Wine

## 1. Introduction

L-Malic acid affects the sensory characteristics of wines and its content is associated with microbial changes during aging and handling.

Enzymatic flow-injection (FI) methods for the specific determination of L-malate in wine have been developed using L-malate dehydrogenase (EC 1.1.1.37; MDH) [1–6]. Since the equilibrium constant [7] for the reaction catalyzed by MDH [L-malate + nicotineamide adenine dinucleotide ($NAD^+$) = oxaloacetate + reduced nicotineamide adenine dinucleotide (NADH) + $H^+$] is $6 \times 10^{-13}$, hydrazine is added to the carrier at a relatively high concentration to shift the reaction equilibrium toward oxaloacetate production through hydrazone formation [4]. However, hydrazine, which is carcinogenic [8], is not suitable for use in routine assays. Almuiabed et al. [6] developed a hydrazine-independent assay for malate, in which a higher pH (11.0) and a higher concentration of $NAD^+$ (3.6 mM) are used to shift the enzymatic reaction in the direction of oxaloacetate. The method is unsuitable for use in routine analysis because controlled-pore glass, which was used as a support for the covalent attachment of MDH, is unstable in alkaline solution [9]. Aspartate aminotransferase (EC 2.6.1.1; AAT) [10] and oxaloacetate decarboxylase (EC 4.1.1.3; OXD) [11] were used as trapping enzymes to shift the equilibrium of the MDH reaction in the direction of oxaloacetate.

In this work, NADH oxidase (NAOD) was used as a trapping enzyme, which catalyzes the oxidation of NADH with the production of hydrogen peroxide in the presence of molecular oxygen as an electron acceptor (NADH + $O_2$ +

* Corresponding author. Fax: (81) 552-20-8568.


*SSDI* 0039-9140(95)01660-0

$H^+ = NAD^+ + H_2O_2$]. The NAOD was co-immobilized with MDH onto poly(vinyl alcohol) beads. The NADH produced by the MDH reaction is removed by the NAOD reaction with concomitant formation of hydrogen peroxide.

FI systems with immobilized oxidase reactors and the chemiluminometric detection of $H_2O_2$ with luminol were used for rapid and sensitive determination of the substrates [12–15]. Unfortunately, the high pH (pH 10–11) required for efficient light production is not compatible with most oxidase reactions. A problem with such enzyme-coupled chemiluminometric FI systems is that a two-storage buffer sequence must be employed. A simple chemiluminometric FI system for the determination of substrates for dehydrogenases can be achieved by coupling a co-immobilized dehydrogenase/NAOD reactor with luminol chemiluminescent detection of $H_2O_2$.

In the present investigation we have developed a FI system for the chemiluminometric determination of L-malate with a co-immobilized MDH/NAOD reactor, in which enzymatic reactions and the luminol reaction were performed in the same buffer system (0.3 M carbonate buffer (pH 10.0)); in this system the pH mismatch problem previously encountered in coupled enzymatic luminol chemiluminometric detection systems can be eliminated. The method was adapted to the assay of wines.

## 2. Experimental

### 2.1. Chemicals and reagents

MDH (from *Thermus* sp., type III, 120 U $mg^{-1}$) and NAOD (EC number not assigned, from *Bacillus megaterium*, 50 U $mg^{-1}$) were obtained from the Amano Pharmaceutical Co. (Nagoya) and Asahi Kasei (Tokyo), respectively. The activity for MDH was evaluated from the increase in absorbance at 340 nm with L-malic acid and $NAD^+$ at pH 9.0 at 40°C. For NAOD it was estimated from the decrease in absorbance at 340 nm with NADH as substrate at pH 9.0 at 40°C. $NAD^+$ (free acid; 96%) and NADH (98%) were from Khojin (Tokyo). Poly(vinyl alcohol) beads (GS-520, 13 μm) and nylon beads (A-1030, 100–150 mesh) were purchased from Showa Denko (Tokyo) and Unitika (Osaka), respectively. The purity of L-malic acid, which was obtained from Sigma, was tested by the enzymatic method [16]. All other chemicals were of analytical-reagent grade.

A carbonate buffer (pH 10.0) consisting of 0.3 M sodium carbonate–0.3 M sodium hydrogen carbonate was used. A potassium hexacyanoferrate stock solution (150 mM) was prepared and diluted fivefold with water before use. $NAD^+$ solution (1.5 mM $NAD^+$ in 0.01 M phosphate buffer (pH 7.0)) was prepared daily. Luminol solution (3.0 mM luminol in 0.3 M carbonate buffer (pH 10.0)) was prepared and stored for 3 days in a refrigerator before use [12,17]. By means of the incubation, the background chemiluminescence emitted on admixing with the luminol solution and potassium hexacyanoferrate solution reduced to about one-half of its initial value, for unknown reasons.

Nylon beads were packed into a stainless-steel column (2 cm × 4 mm i.d.) having a needle for injection, with use of the dry-packing method (nylon cartridge). The cartridge was used for filtration and removal of polyphenols and dyes.

### 2.2. Preparation of the co-immobilized enzyme reactor

MDH and NAOD were immobilized simultaneously onto the poly(vinyl alcohol) beads. The beads were aminated with epichlorohydrine and ammonia water; the procedure was similar to that described previously [18]. The aminated beads were packed into a stainless-steel column (5 cm × 4 mm i.d.) and activated with 2.5% glutaraldehyde in 0.1 M phosphate buffer (pH 7.0). Enzyme solution (5 mg MDH (600 U) and 5 mg NAOD (250 U) in 10 ml of 0.1 M phosphate buffer (pH 7.0)) was circulated through the column for 6 h at a flow rate of 0.2 ml $min^{-1}$. The time course of the immobilization process for NAOD was monitored by use of a spectrophotometer (Jasco Uvidec-100-VI) equipped with a flow-through cell at 380 nm. The NAOD was immobilized with a 82% yield. The reactor was washed with the NAD solution and stored in a refrigerator when not in use.

### 2.3. FI system and procedure

A schematic diagram of the system is shown in Fig. 1 The system consisted of four piston pumps (Hitachi L-6000), an injection valve

(Sanuki SVI-6M2) equipped with a 50 µl loop, a reactor, a luminometer (Soma S-3400) with a flow-through cell (100 µl) connected to a signal cleaner (SIC SC77) and a recorder (TOA FBR-251A). The reactor was maintained at 40°C.

Wine (about 3 ml) was placed in a glass syringe. A nylon cartridge was fitted at the tip of the syringe, and the first 1 ml was discarded, after which 500 µl of filtrate were diluted two-hundredfold with water. An aliquot (50 µl) was injected into a carrier stream. The cartridge was renewed for each sample.

The results obtained by the present method were compared with those obtained by use of an F-kit (Boehringer Mannheim) with soluble MDH and AAT.

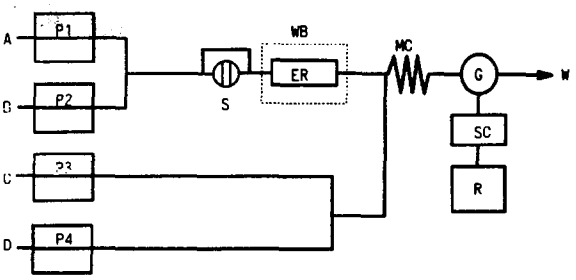


Fig. 2. Flow-injection manifold for the enzyme activity measurements. A, $NAD^+$ solution (0.3 ml $min^{-1}$); B, carbonate buffer (0.3 ml $min^{-1}$); C, 30 mM potassium hexacyanoferrate solution (0.3 ml $min^{-1}$); D, 1.5 mM luminol in 0.3 M carbonate buffer (pH 10.0) (0.3 ml $min^{-1}$); P1, P2, P3 and P4 pumps; S, injector with a 50 µl loop; ER, co-immobilized enzyme reactor; WB, water bath; MC, mixing coil; G, luminometer with flow-through cell (100 µl); SC, signal cleaner; R, recorder; W, waste.

## 3. Results and discussion

### *3.1. Properties of co-immobilized MDH/NAOD*

In order to determine the optimum operating parameters for chemiluminometric FI determination of L-malate using a co-immobilized MDH/NAOD reactor, the system shown in Fig. 2 was used and a series of investigations was first conducted in order to determine the influence of pH, temperature and $NAD^+$.

The effect of pH on the activity of the reactor was studied in the pH range 9.0–10.5 by injecting 10 µM L-malate (50 µl). The optimum pH for the reactor was about 10.0, as shown as Fig. 3. The activity of the reactor at different temperatures was examined over the range 40–50°C. The reactor exhibited maximum activity at 50°C, as shown in Fig. 3. The water bath was thermostated at 40°C to prolong the lifetime of the reactor. The effect of $NAD^+$ concentration on peak height was examined over the range 0.2–6 mM at an L-malate concentration of 500 µM. The optimum $NAD^+$ concentration was about 1.0 mM; for the MDH reaction lower $NAD^+$ concentrations are undesirable for the formation of NADH, and at higher concentrations the equilibrium of the reaction is shifted to the right. However, for the NAOD reaction, higher $NAD^+$ concentrations are undesirable for the production of

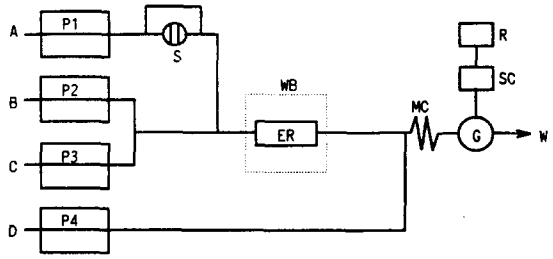


Fig. 1. Schematic diagram of chemiluminometric flow-injection system for the determination of L-malate with a co-immobilized malate dehydrogenase/NADH oxidase reactor. A, $H_2O$ (0.3 ml $min^{-1}$); B, 1.5 mM $NAD^+$ in 0.01 M phosphate buffer (pH 7.0) (0.3 ml $min^{-1}$); C, 3.0 mM luminol in 0.3 M carbonate buffer (pH 10) (0.3 ml $min^{-1}$); D, 30 mM potassium hexacyanoferrate solution (0.3 ml $min^{-1}$); $P_1$, $P_2$, $P_3$ and $P_4$, pumps; S, injector with a 50 µl loop; ER, co-immobilized enzyme reactor (5 cm × 4 mm i.d.); WB, water bath thermostatted at 40°C; MC, mixing coil (100 cm × 0.5 mm i.d.); G, luminometer with a flow-through cell (100 µl); SC, signal cleaner; R, recorder; W, waste. All connecting tubing (0.5 mm i.d.) was of Teflon.

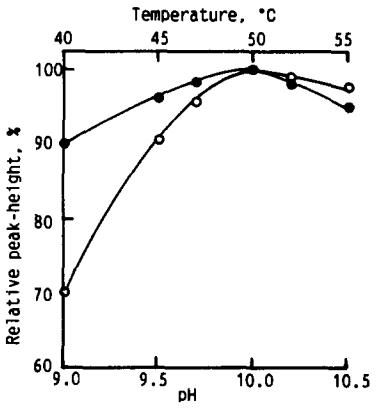


Fig. 3. Effects of pH and temperature on the response. ○, Effect of pH on the enzyme reactions; ●, effect of temperature on the enzyme reactions. The FI system shown in Fig. 2 was used. The concentrations of $NAD^+$, luminol and potassium hexacyanoferrate were 1 mM, 1.5 mM and 30 mM, respectively. All values were within 0.6% of the relative standard deviation ($n = 6$).

$H_2O_2$. A $NAD^+$ solution of 1.5 mM was used in this system; as shown in Fig, 1, since the solution is diluted threefold with the luminol solution and carrier stream, the $NAD^+$ concentration in the reactor is 0.5 mM.

The influence of luminol concentration on the peak height was studied from 0.3 to 12 mM, using the system shown in Fig. 1. The reactor exhibited a maximum response at 9 mM, but the inactivation of the reactor commenced at above 4.5 mM. The response for $H_2O_2$ increased linearly with increase in luminol concentration when the reactor was omitted. A luminol solution of 3 mM was used in this system; the luminol concentration in the reactor is 1 mM.

The operational stability of the reactor was evaluated over a period of 6 weeks. The reactor was used for 4 h per day (120 injections of 300 μM L-malate solution containing 15 mM ethanol) and then washed with the $NAD^+$ solution and stored in a refrigerator when not in use. The activity decreased slowly to 82% of the initial value after 6 weeks (5000 injections). When the daily washing procedure was eliminated, the activity decreased rapidly to 32% of the initial value after 5 days.

The chemiluminescence intensity–time variation was measured by changing the flow rates of the reactor eluent and the potassium hexacyanoferrate solution, using the smaples containing only $H_2O_2$. During the experiments the flow rate ratio of the eluent and the solution was kept at 3:1. Maximum response was obtained about 10 s after the mixing of the solutions. The peak height was measured by changing the flow rates of the $NAD^+$ solution, the luminol solution and the carrier stream, keeping the flow rate ratio of the solutions at 1.0. The peak height decreased linearly from 0.3 to 1.2 ml $min^{-1}$ for the total flow rate. The peak height at 0.3 ml $min^{-1}$ was about 1.6 times that at 1.2 ml $min^{-1}$ and the half peak width for the former was 1.9 times that of the latter. A total flow rate of 0.9 ml $min^{-1}$ (0.3 ml $min^{-1}$ each) was selected, as a compromise between sensitivity (peak height) and sample throughput; at this flow rate, the sample throughput was 30 $h^{-1}$. On the basis of these results, the flow rate of the potassium hexacyanoferrate solution selected was 0.3 ml $min^{-1}$; since the total flow rate was 1.2 ml $min^{-1}$ at the flow through cell, a mixing coil of 100 cm × 0.5 mm i.d. was used.

The influence of reducing substances on the peak height for malate (50 μM) was measured over the range 5–50 μM. The presence of equimolar amounts of sodium ascorbate and sodium sulfite depressed the peak height to 97% and 96%, respectively. Under the same conditions, the peak height did not change with the presence of 1 mM concentrations of carboxylates such as tartrate, citrate, lactate, succinate and acetate, and of ethanol up to 30 mM. The relative activities for L-malate and D-malate were 100 and 2, respectively.

### 3.2. Calibration

Under the conditions shown in Fig. 1, the plot of peak height against malate concentration was linear from 0.3 to 250 μM. The least-squares calibration equation for malate was $Y = 0.7085x + 5.6464$, where $Y$ is log(peak height (cm)) and $x$ is log(malate concentration (M)), with a linear correlation coefficient of $r = 0.9998$ (15 data points). In the reactor malate reacted in 48% yield. Below a concentration of 0.3 μM a concave graph was obtained, and above a concentration of 300 μM the graph was convex. The relative standard deviation (R.S.D.) for seven replicate injections of 100 μM malate was 0.54%. The R.S.D. ($n = 7$) for 100 μM malate in the system shown in Fig. 2 was 1.4% because of incomplete mixing of the luminol solution with the reactor eluent.

The lower limit of detection (signal-to-noise ratio = 3) was $8 \times 10^{-8}$ M (0.5 ng in a 50-μl injection).

### 3.3. Application

The method was applied to the determination of the free L-malate content in wines.

### 3.4. Recovery

First, a recovery test was performed by using a red wine sample which was supplemented with L-malate to give a final concentration of 45.5 mM. The results that had poor recoveries were obtained by subjecting wine samples that were merely diluted, without filtration through the nylon cartridge. These results are probably due to the presence of sulfites which are attached to dyes and polyphenols in wine; they react with the $H_2O_2$ produced in the reactor. Good results were obtained after removal of

Table 1
Recovery of L-malate added to red wine using the present method [a]

| Added (mM) | Recovered [b] (mM) | Recovery (%) |
|---|---|---|
| 5.00 | 4.92 ± 0.03 | 98 |
| 10.0 | 9.90 ± 0.06 | 99 |
| 15.0 | 15.2 ± 0.1 | 101 |
| 20.0 | 20.1 ± 0.1 | 101 |
| 25.0 | 25.0 ± 0.1 | 100 |
| 25.0 [c] | 18.5 ± 0.4 | 74 |

[a] Values corrected for L-malate (16.5 mM) already present in wine.
[b] Mean ± standard deviation. The values are the means of nine determinations.
[c] sample without filtration through nylon cartridge.

the compounds with the nylon cartridge (Table 1). The recovery was in the range 98–101%.

### 3.5. Precision and reproducibility

Red wine was repeatedly analyzed over a period of 3 weeks with use of the reactor. The reactor was used for the analysis of 90 samples per day and standards were measured at 30-sample intervals, in order to correct the variation of conversion efficiency. The reactor was renewed every 2 weeks. This method gave precise and reproducible results; for red wine containing 6.72 mM, the within-day R.S.D. was 0.51% and the day-to-day R.S.D. was 0.97%.

### 3.6. Comparison with a reference method

The results ($n = 23$: 12 red wines, from 3.71 to 41.8 mM; 11 white wines, from 15.6 to 45.2 mM) were compared with those obtained by use of an F-kit (Boehringer Mannheim) with soluble MDH and AAT. The results are summarized in Fig. 4. The calculated linear regression and correlation coefficient were $y = 0.9993 - 0.0029$ and $r = 0.9999$, respectively.

## 4. Conclusion

The flow-injection system with a co-immobilized MDH/NAOD reactor and chemiluminometic detection is useful for the sensitive and reliable measurement of L-malate in wine. Compared with fluorimetric FI methods utilizing co-immobilized MDH/AAT [9] and MDH/OXD [10], the $NAD^+$ concentration is about half and the sensitivity is two-times higher. The high sensitivity of luminescence allows the drawback of rather low conversion efficiency to be overcome. The co-immobilized MDH/NAOD reactor is stable enough to permit the measurement of more than 1000 samples.

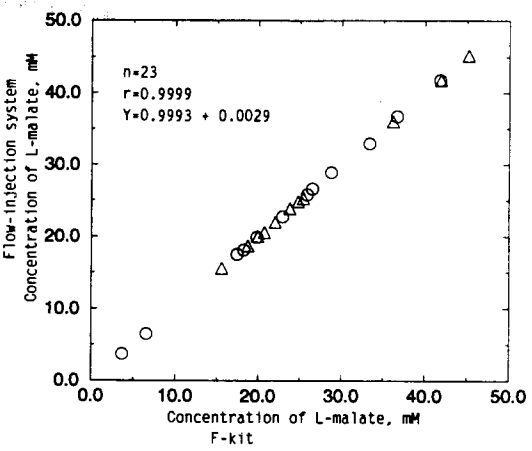


Fig. 4. Comparison of L-malate concentration in wines determined by the flow-injection method and by use of the F-kit (Boehringer Mannheim). ○, red wines; △, white wines.

## References

[1] J.L.F.C. Lima and A.O.S.S. Rangel, Am. J. Enol. Vitic, 43 (1992) 58.
[2] S. Yashioka, H. Ukeda, K. Matsumoto and Y. Osajima, Electroanalysis, 4 (1992) 545.
[3] R. Puchades, M.A. Herrero, A. Maquieira and J. Atienza, Food Chem., 42 (1991) 167.
[4] C. Garcia De Maria, T.M. Munoz, A.A. Mateos and L. Garcia De Maria, Anal. Chim. Acta, 247 (1991) 61.
[5] H. Ukeda, Y. Nakada, K. Matsumoto and Y. Osajima, Bunseki Kagaku, 39 (1990) 723 (in Japanese).
[6] A. Almuiabed and A. Townshend, Anal. Chim. Acta, 221 (1989) 337.
[7] A. Yoshida, J. Biol. Chem., 240 (1965) 1118.
[8] B. Toth, Cancer, 35 (1975) 3693.
[9] E.P. Plueddemann, Silane Coupling Agents, Plenum, New York, 1982, p. 227.
[10] G.C. Chemnitius and R.D. Schmid, Anal. Lett., 22 (1989) 2897.
[11] N. Kiba, M. Oguchi and M. Furusawa, Talanta, 40 (1993) 1163.
[12] M. Tabata, C. Fukunaga, M. Ohyabu and T. Murachi, J. Appl. Biochem., 6 (1984) 251.
[13] E.H. Hansen, L. Nørgaard and M. Pedersen, Talanta, 38 (1991) 275.
[14] N. Kiba, F. Ueda, M. Furusawa and T. Yamane, Anal. Chim. Acta, 269 (1992) 187.
[15] K. Robards and P.J. Worsfold, Anal. Chim. Acta, 266 (1992) 147.
[16] H.O. Beutler and B. Wurst, Dtsche. Lebensm. Rundsch., 86 (1990) 341.
[17] C.A. Koerner and T.A. Nieman, Anal. Chem., 58 (1986) 116.
[18] N. Kiba, Y. Oyama and M. Furusawa, Talanta, 42 (1995) 449.

ELSEVIER

Talanta 42 (1995) 1757–1759

Talanta

# Short communication

# Uses of antimony pentachloride for thermometric determination of urea in acetic anhydride

Turgut Gündüz*, Esma Kılıç, Orhan Çakırer

*Department of Chemistry, Faculty of Science, University of Ankara, Ankara, Turkey*

Received 19 January 1995; revised 3 May 1995; rerevised 31 May 1995; accepted 1 June 1995

*Keywords:* Antimony pentachloride; Thermometric analysis; Urea

## 1. Introduction

Recently we have reported a potentiometric method for the titration of urea with perchloric acid in acetic anhydride as solvent [1]. Subsequent to this report, we also have titrated urea thermometrically with antimony pentachloride in the same solvent and have obtained very identical results to those obtained in the previous work.

## 2. Experimental, results and discussion

The antimony pentachloride used in this titration was purchased from Merck (99% purity) in small ampules and was used without further purification. In order to prepare a solution of this compound, an ampule was cooled to approximately 4°C [2,3]. The ampule was then opened and its contents were decanted immediately into a 50.0 ml volumetric flask containing about 25 ml of purified 1,2-dichloroethane [2]. The volumetric flask was then weighed accurately. Since the flask together with its contents had been weighed before the antimony pentachloride was decanted into the flask, the difference between the weights was taken to be the mass of the antimony pentachloride. The flask containing the antimony pentachloride solution was shaken vigorously and then left for 2 h to attain thermal equilibrium. Subsequent to this process the flask was filled to the red line and was then stoppered. The solution prepared in this way was stored as stock solution. By taking the required amount of solution from this stock solution, a 0.2 M antimony pentachloride solution was prepared and standardized against 1,3-diphenylguanidine.

The 1,3-diphenylguanidine was purchased from Fluka (99.5% purity) and was recrystallized twice from pure dry toluene, then dried at 100°C for 2 h (m.p., 148°C). A compound dried in this way is one of the best primary standards for non-aqueous-medium acids [4].

Urea was purchased from Fisher Scientific (99.5% purity) and was recrystallized three times from absolute ethanol. In addition, the compound was analyzed five times by the Kjeldahl method in order to determine its percentage purity; this was found to be 99.3%. This latter was accepted to be the true value. A 0.0200 M stock solution was prepared from this compound in acetic anhydride and was used in the titrations.

Acetic anhydride was purchased from Merck (99.8% purity) and was used without further purification.

Titrations were carried out in a fume cupboard made heat-proof with blown polystyrene sheeting. Its small window was left unisolated in order to view the whole titration assembly and to operate it properly, (see Fig. 1). The

* Corresponding author.


*SSDI* 0039-9140(95)01661-9

assembly was simple and consisted of (i) a small Dewar flask with a capacity of 30 ml; (ii) a tin-tipped semi-microburette with a reservoir; (iii) a Beckmann and two good-quality thermometers; and (iv) a good-quality magnetic stirrer. The Dewar flask was placed in a beaker with a capacity of 250 ml, and the walls of the Dewar flask were insulated from the walls of the beaker with blown polystyrene sheeting. The beaker was also insulated from the magnetic stirrer with blown polystyrene sheeting.

The Dewar flask was covered with a blown polystyrene lid suitably pierced to hold the Beckmann thermometer and the tin-tipped semi-microburette with a reservoir holding the titrant. On top of the reservoir was placed U-tubing filled with anhydrous calcium chloride in order to prevent moisture entering. The Beckmann thermometer was immersed in the urea solution to a definite depth in each titration, and enabled temperature changes to be read to within 0.001°C. The tin-tipped semi-microburette enabled the volume of the titrant solution to be read to within 0.01 ml. Except for the graduated parts and the tap, the semi-microburette was also insulated with blown polystyrene sheeting in order to prevent heat exchange with the operator during the titration (see Fig. 1). Two thermometers were used to measure the ambient temperature of the whole assembly and to measure the temperature of the titrant in the reservoir. Both thermometers were able to read the temperature to within 0.01°C.

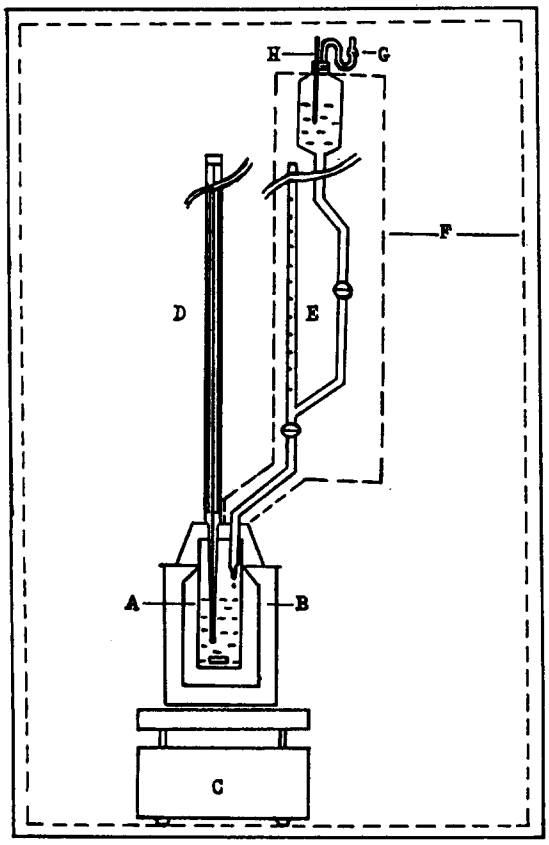


Fig. 1. Thermometric titration assembly: A, Dewar flask; B, blown polystyrene insulation layer; C, magnetic stirrer; D, Beckmann thermometer; E, microburnette and its reservoir; F, blown polystyrene insulation layer; G, tubing filled with dry calcium chloride to keep the titrant dry; H, a sensitive thermometer to read the temperature of the titrant.

Stock 0.0200 M urea solution was kept in the insulated fume cupboard to keep it in thermal equilibrium with the titrant. The sample volumes of the urea solution placed in the Dewar flask are 15.0 ml and the solutions were magnetically stirred during the addition of titrant. Addition of the titrant was performed discontinuously, and the amount of the solution added at a time was 0.25 ml. After each addition of titrant, the solution was allowed to attain thermal equilibrium for at least 1 min and then the corresponding temperature increase was determined by use of the Beckmann thermometer. Each temperature reading was repeated three times and the mean of these was taken as the temperature increase for each addition. The temperature increases were rather large to be monitored accurately by the Beckmann thermometer. One titration run was completed in about 25 min. A titration curve for each urea sample was drawn and the endpoint of titration was then fixed. One of the titration curves is presented in Fig. 2 as an example.

Five accurately weighed 1,3-diphenylguanidine samples, each dissolved in 10 ml of acetic anhydride, were titrated with approximately 0.2 M antimony pentachloride solution, and the true concentration of the antimony pentachloride was then calculated and was found to be 0.2070 M. Seven urea samples from the 0.0200 M solution were then taken and titrated with 0.2070 M antimony pentachloride solution. The mean value of the recovery of urea was 99.8% and the relative standard deviation was 0.2%. This result clearly shows that the thermometric method proposed is very suitable for the titration of urea.

In addition, we also have titrated eleven aliphatic and aromatic amines including tri-*n*-

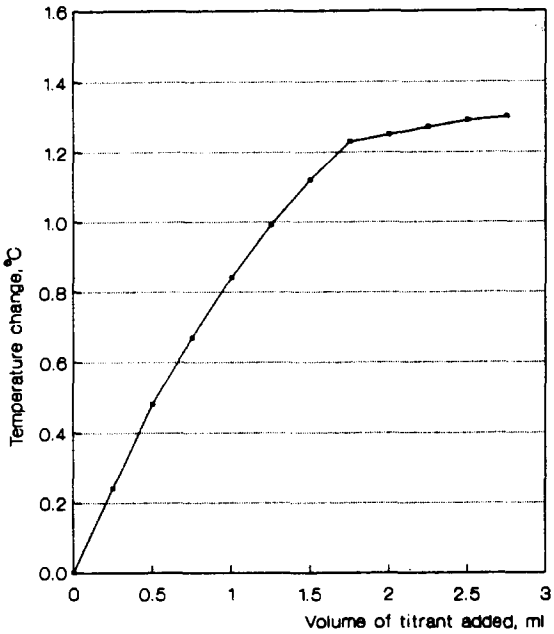


Fig. 2. Thermometric titration curve of a urea sample with antimony pentachloride in acetic anhydride, at 20 ± 1°C.

butylamine, piperidine and aniline with antimony pentachloride in 1,2-dichloroethane as solvent, and have obtained recoveries for tri-*n*-butylamine of 98.2%, for piperidine of 97.5% and for aniline of 98.5%. The relative standard deviations of these are, respectively, 0.2%, 0.4% and 0.2% [5]. The concentrations of the amines were approximately 0.02 M and the concentration of the titrant was 0.2070 M. The changes in temperature during the titrations of these compounds were 0.85–1.10°C. This obviously shows that antimony pentachloride, as a Lewis acid, has no steric hindrance in an appreciable amount. Therefore the use of antimony pentachloride as a Lewis acid titrant can be extended further to the thermometric titration of other compounds containing a basic side or sides.

We believe that the coordinate covalent bond is formed between antimony pentachloride and urea as follows

$$Cl_5Sb \leftarrow OC(NH_2)_2$$

As is well known, antimony pentachloride forms a strong coordinate covalent bond with oxygen [6,7].

## References

[1] T. Gündüz and S. Yılmaz, Talanta, 41 (1994) 1471.
[2] D.D. Perrin, W.L.F. Armarego and R.D. Perrin, Purification of Laboratory Chemicals, Pergamon Press, Oxford, 1966.
[3] A.V. Naidu, C.V. Rajeswari and P.R. Naidu, Indian J. Chem., A23 (5) (1984) 448.
[4] J.S. Fritz, Acid–Base Titrations in Nonaqueous Solvents, Allyn and Bacon, Boston, 1973.
[5] T. Gündüz, E. Kılıç and O. Çakırer, unpublished results, 1995.
[6] V. Gutmann, Coord. Chem. Rev., 15 (1975) 207.
[7] V. Gutmann, Electrochim. Acta., 21 (1976) 661.

ELSEVIER

Talanta 42 (1995) 1763–1773

Talanta

Review

# Enzyme catalysis in organic solvents: a promising field for optical biosensing

M.E. Díaz-García *, M.J. Valencia-González

*Department of Physical and Analytical Chemistry, University of Oviedo, c/ Julián Clavería 8, E-33006 Oviedo, Spain*

Received 14 November 1994; revised 28 March 1995; accepted 28 March 1995

**Abstract**

The ability of enzymes to work in non-aqueous media offers new and almost unexploited possibilities for the development of new optical biosensors. The advantages of performing biocatalytic reactions in non-aqueous media are discussed in relation to their possible application in optical biosensor design. Attention is focused on the factors that influence enzymatic catalysis in organic solvents, including the role of enzyme-associated water, criteria for solvent selection and the alteration of enzyme specificity. Recent examples of relevant applications and future prospects of organic-phase optical biosensing are discussed.

*Keywords:* Optical biosensing; Organic phase enzymatic catalysis

## 1. Introduction

A biochemical sensor is an analytical device comprising a biological recognition element (enzyme, receptor, antibody or microbe) in intimate contact with a physicochemical transducer (electrochemical, optical, mass, thermal) which is capable of converting the particular biochemical event into a continuous signal which is proportional to the concentration of a specific chemical or group of chemicals.

Enzymes were the first biological components employed in optical biosensors [1] and remain by far the most commonly used elements. Enzymes possess extremely high catalytic activity and unique substrate specificity. It is these merits that make the application of enzymes in optical sensing devices extremely promising. Conventional enzymatic methods have been conducted in aqueous solutions mainly due to the preconceived idea that an aqueous environment is optimal to maintain the native, catalytically active enzyme conformation for binding and catalysis. This notion is not completely true. Many enzymes (or multienzyme complexes) such as lipases, estearases, dehydrogenases and those responsible for xenobiotic metabolism, function in natural hydrophobic environments, usually in the presence of or immobilized to a membrane [2]. The water concentration in the proximity of these enzymes is significantly less than 55.5 M, the bulk water concentration in aqueous environments.

The activation of enzymes in organic solvents is a noteworthy achievement in the fields of enzymology and organic chemistry. Many enzymes were shown to be catalytically active in a wide variety of different organic solvents [3–7], their catalytic efficiency in organic media being comparable to that in water. From an analytical viewpoint there are numerous potential advantages in carrying out enzymatic reactions in organic media as opposed to aqueous solutions: (i) efficient catalysis may be achieved with substrates poorly soluble in water; (ii) undersirable side reactions in organic media as well as substrate and product inhibition may be

* Corresponding author.


*SSDI* 0039-9140(95)01606-6

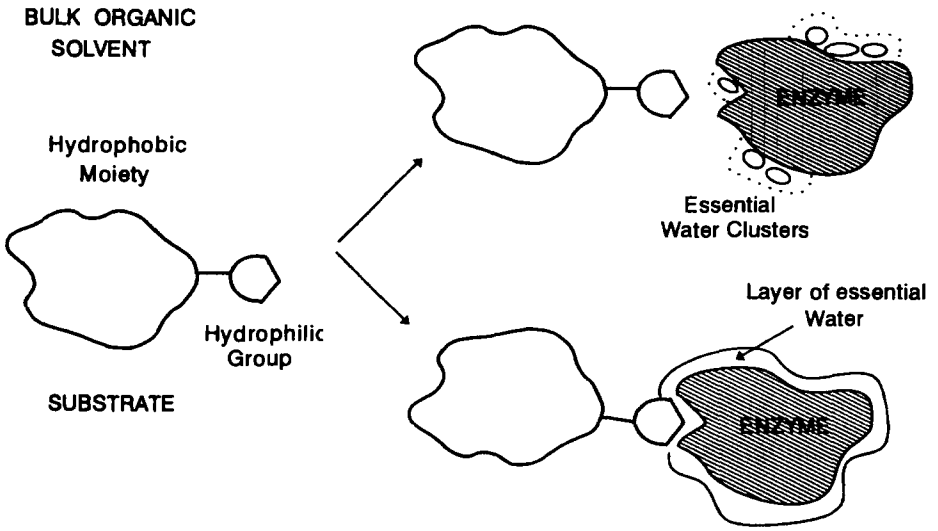


Fig. 1. Grossly simplified representation of enzymatic catalysis in organic solvents.

reduced; (iii) thermal stability of the enzymes is enhanced; (iv) immobilization is often unnecessary as enzymes are insoluble in organic solvents; (v) if immobilization is desired, adsorption onto non-porous surfaces is satisfactory as enzymes are unable to desorb from these surfaces in non-aqueous media; (vi) microbial contamination is eliminated; and (vii) recovery and reuse of the enzyme is easier.

At present, various organic-phase enzymatic electrodes have been developed for monitoring some water-insoluble substrates [8–11]. However, little or no attention has been paid to the development of optical sensing schemes based on biocatalysis in organic media despite the variety of optical transduction methods suitable for sensing applications. This article is intended to bring this methodology to the attention of analytical chemists by discussing the basic principles of organic-phase enzymology and giving specific examples of optical biosensing in organic solvents that open up promising analytical prospects in the field.

## 2. Role of water

In an aqueous environment, the folding of an enzyme is driven by the tendency of hydrophobic amino acid residues to be excluded from water and confined to the interior of the protein molecule. In turn, the charged and hydrophilic residues are exposed to the aqueous solvent. When water is replaced by an organic solvent, not only the tertiary structure but also the secondary structure such as the alpha helix and the beta structure may be distorted.

In order to ensure a catalytically active enzyme conformation in organic media the enzyme molecule must have a definite hydration shell [12,13] to separate the solvent from contact with the protein surface. Water is essential for enzyme catalysis because of its contribution to all non-covalent bonding and to the hydrogen bonds of the protein structure: however, the appropriate amount of water necessary for enzyme activity in organic media has been the subject of numerous discussions and papers [14–16]. Zaks and Klibanov [15] examined three model enzymes, polyphenol oxidase, alcohol dehydrogenase and alcohol oxidase, in solvents of different hydrophobicities and water contents. They showed that the enzyme activity was related to the amount of water bound to the protein and not to the concentration of water in the organic solvents. Water bound to those enzymes in organic solvents could not form a true water layer coverage but rather a few clusters probably around charged and polar regions on the ezyme surface. Taking into account that water is required absolutely for the catalytic function of enzymes in organic solvents, that "wet" immediate microenvironment of the enzyme could be considered as the region through which the enzymatic reaction should proceed. The situation is schematically presented in Fig. 1.

Although the presence of essential bound water remains a necessary condition for the retention of enzyme catalytic activity and stability in non-aqueous solvents, there have been

studies [17–20] in which some enzymes, such as erythrocuprein, porcine pancreatic lipase, subtilisin or xanthine oxidase, have been shown to retain catalytic activity in truly anhydrous organic solvents (dimethyl sulphoxide, formamide, pyridine or dimethylformamide). The molecular mechanisms protecting the enzyme conformation and catalytic properties in these dry organic solvents still remain unclear.

## 3. Criteria for solvent selection

The selection of a suitable solvent is crucial because it may affect enzymatic catalysis in different ways. Firstly, the solvent can inactivate the enzyme by directly interacting with it: the solvent may alter the native conformation of the enzyme by penetrating into the hydrophobic core of protein thus disrupting hydrogen bonding and hydrophobic interactions and leading to reduced activity and stability [21]. This situation is particularly important with soluble enzymes in biphasic systems (water/water-immisicible organic solvent) and aqueous systems with low concentrations of water-miscible organic solvents. In contrast, the insolubility of enzymes in monophasic organic solvents prevents the enzyme from severe distortion of its conformational stability. In fact, many enzymes in monophasic organic media are known to retain their native conformation even after vigorous vortexing [14]. An additional stabilization of the enzyme could also be due to a "cage effect": enzyme molecules inside the protein particle would be tightly squeezed from all sides by surrounding molecules, resembling an immobilized state that should favour increased conformational stabilities [22].

Another way in which solvents affect enzymatic activity is by interacting directly with the essential water around the enzyme molecule [23]. Although this interaction may not affect the enzyme itself, it does have implications for catalysis. Highly polar solvents are capable of thirstily absorbing water and stripping the hydration shell from the enzyme, entailing the loss of catalytic properties. Conversely, hydrophobic solvents are less able to pull away or distort the hydration shell and hence are less likely to affect catalytic activity.

It is important to note that although this solvent effect holds true for most enzymes, there are some notable exceptions, as we have seen before. Xanthine oxidase [18], porcine pancreatic lipase [19] and subtilisin [20] still function when suspended in some water-miscible solvents. One possible explanation of this fact is that these enzymes are capable of retaining their hydration shell so tightly that even hydrophilic solvents cannot usurp the water [19]. Such enzymes are active in both hydrophobic and hydrophilic solvents. Although our understanding of the effects of organic solvents on enzyme activity and stability is growing, the choice of the suitable solvent is not straight forward and, recently, some general empirical rules have been formulated for the optimization of biocatalytic activity in different organic solvents [15]. The parameter $P$ (the partition coefficient of the solvent between octanol and water) was introduced as a quantitative measure of solvent polarity [24,25]. Generally, the enzymatic activity is low in polar solvents having $\log P < 2$, is moderate in solvents having $\log P = 2–4$ and is high in apolar solvents having $\log P > 4$ (see Table 1).

Another consideration for solvent selection is the solubility of substrate and product in the media [26]. For example, sugars are soluble only in hydrophilic water-miscible solvents such as pyridine or dimethylformamide. The use of water-immiscible solvents is impractical for enzyme-catalysed sugar oxidation as there would be no interaction between the insoluble sugar and insoluble enzyme. In a similar way, compatibility of the enzymatic reaction products with the solvent is crucial. Polar products tend to remain in the water shell surrounding the enzyme and this could cause inhibition or undergo undesirable side reactions. This situation was found in the catalysis of phenols by

Table 1
Log $P$ values of some organic solvents [a]

| Solvent | Log $P$ | Solvent | Log $P$ |
|---|---|---|---|
| Dimethyl sulphoxide | −1.30 | Dipropyl ether | 1.90 |
| Dioxane | −1.10 | Chloroform | 2.00 |
| Methanol | −0.76 | Heptanol | 2.40 |
| Acetonitrile | −0.33 | Toluene | 2.50 |
| Ethanol | −0.24 | Xylene | 3.10 |
| Propanol | 0.28 | Hexane | 3.50 |
| Tetrahydrofuran | 0.49 | Decanol | 4.00 |
| Butanol | 0.80 | Heptane | 4.00 |
| Cyclohexanone | 0.96 | Octane | 4.50 |
| Hexanone | 1.30 | Dodecanol | 5.00 |
| Phenol | 1.50 | Dibutylphthalate | 5.00 |
| Cyclohexanol | 1.50 | Undecane | 6.10 |
| Hexanol | 1.80 | Tetradecane | 7.60 |
| Benzoic acid | 1.90 | Butyl oleate | 9.80 |

[a] Data taken from Ref. [25].

polyphenol oxidase in hexane [5], the polar quinone products are insoluble in hexane and rapidly polymerize in the water environment around the enzyme, giving rise to its incativation. In the more polar chloroform, products (quinone, catechol) favourably partition into the bulk solvent and do not inactivate the enzyme [5,27].

This is not the only example. A similar situation was observed in the oxidation of benzyl alcohol by alcohol oxidase in non-aqueous solvents [28]. Benzaldehyde, the reaction product, partitions differently between the water bound to the enzyme and the organic medium depending on the solvent chosen. For example, using hexane benzaldehyde was favourably partitioned into the aqueous enzyme environment giving rise to alcohol oxidase inhibition. However, using toluene the product was efficiently solubilized in the organic phase, so minimizing benzaldehyde inhibition of alcohol oxidase.

Another interesting practical problem concerns the effect of the reaction pH. All enzymatic reactions in water are strongly pH dependent. In organic solvents, a difficulty stems from the fact that one cannot reliably use a glass electrode; even if this could be done in the vicinity of the enzyme, no reliable value could be obtained because for this "special" aqueous environment no pH calibration is available. Quoting Klibanov [19], an enzyme "remembers" the pH of the aqueous solution from which it was last recovered. In an aqueous buffer solution the enzyme's ionogenic groups acquire the corresponding ionization state, which then remains unchanged in organic solvents as well as in the solid state. Moreover, the buffering capacity of the aqueous microenvironment can be controlled by the enzyme itself. Therefore, it is often worthwhile to employ enzymes that have been lyophilized or precipitated from an appropriate pH (and buffer) before use [29].

Other criteria that should be taken into account in the selection of organic solvents for developing optical biosensors include compatibility with the optical transducer, toxicity flammability, waste disposal and cost.

## 4. Enhancement of thermal stability

In aqueous media at high temperatures, enzymes inactivate due to both alterations in the primary structure of the molecule and unfolding of the enzyme molecule [30,31]. The chemical and structural changes that result in irreversible thermal inactivation all require water. Therefore, if enzymes are placed in an essentially water-free solvent, it should be possible to enhance the thermostability. In fact, it has been confirmed by Zaks and Klibanov [32] who showed that porcine pancreatic lipase in aqueous solutions at 100°C was completely inactivated within seconds. Conversely, in a dry tributyrin–heptanol mixture the lipase had a half-life at 100°C of 12 h. Furthermore, at this temperature the enzyme is 10 times more active than at 20°C. Reslow et al. [33] ($\alpha$-chymotrypsin dried onto glass beads) and Zaks and Klibanov [15,32] (crude lipase powder, lyophilized pure $\alpha$-chymotrypsin and subtilisin) agree that thermal stability increases with solvent hydrophobicity. However, for any given solvent, adding water (less than 1%) reduces enzyme half-life. This result has been interpreted as an increased enzyme flexibility due to the higher water content [34].

Biosensors, in general are operated at optimum temperatures for the biocatalytic reaction to proceed rapidly and sensitively, although such a condition could not be optimum for wide applicability. The enhanced thermal stability of enzymes in non-aqueous media is an important advantage from an analytical point of view because it extends the temperature range in which a given optical biosensing device is analytically useful.

## 5. Alteration of enzyme specificity

There exists the possibility that enzyme specificity may be altered by the presence of an organic solvent by modifying the active site conformation. Elimination of bulk water results in conformational rigidity [22] and the inability to accommodate a given substrate. For example, "wet" porcine pancreatic lipase can accept a broad range of substrates of varying sizes, which suggests that the protein backbone of lipase is flexible and can adopt a variety of conformations to accommodate substrate molecules. However, the "dry" enzyme does not react with bulky substrates, presumably due to its now rigid active site not being able to open up to accommodate them [4].

Also, organic solvents may affect the binding of substrates to the active site by altering the apparent $K_m$ values. For instance, in aqueous

solutions chymotrypsin hydrolyses non-polar amino acid substrates. The driving forces of enzyme–substrate binding are the hydrophobic interactions operative in aqueous media; hydrophobic substrates are "expelled" from water into the enzymatic active centre [14]. In non-polar organic media, this partitioning is reduced and the apparent $K_m$ increases [35]. Therefore, in water the catalytic efficiency ($k_{cat}/K_m$) of *N*-acetyl-L-phenylalanine ethyl ester hydrolysis is nearly 100 times higher than with the ethyl ester of *N*-acetyl-L-histidine because of the lipophilicity of the former substrate. In octane the substrate specificity is reversed and the histidine derivative becomes a markedly better substrate than phenylalanine.

Such specificity shifts could have significant implications on the development of optical biosensing devices for compounds for which enzyme-catalysed reactions are not feasible in water. For example, lipase — the most studied enzyme in organic media — can catalyse, in organic media of lower water concentrations with low water activities, a variety of reactions including transesterification, esterification, aminolysis, thiotransesterification oximolysis and acyl exchange [6,36]. In water, these reactions are almost completely suppressed by hydrolytic processes.

Some enzymes in non-aqueous media exhibit very high stereospecificity. The preferred interaction of the enzyme with one of the two enantiomers is due to several geometric factors and differences in the binding energy [37] and this fact could be used in the development of optical biosensors to recognize optical isomers.

## 6. Enzyme immobilization

In order to develop an efficient and effective optical biosensor it is required that the enzyme is in close proximity with the optical transducer. On the other hand, to preserve the integrity and activity of enzymes in organic solvents it is necessary to fix the conformation of the catalytically active enzyme to the increase rigidity.

Enzyme immobilization has proved to be an extremely powerful approach to fulfill the above requirements. Various methods are available to immobilize enzymes: entrapment within a support (membrane, gel, microcapsule), physical adsorption, cross-linking between molecules and covalent binding [38].

Due to the insolubility of the enzymes in organic solvents, simple adsorption on a solid support is often sufficient. Adsorption is used here in its broadest sense to cover all the processes by which enzymes are held at the phase boundary by non-covalent forces. The adsorption of enzymes onto solid phases can be achieved by using finely divided particles or macroporous structures with large surface areas [5]. There is easy availability of good, ready-made support materials, such as ion exchangers [39], alumina [8], polymeric gels [40] and, especially, glass porous beads [41]. The bound enzyme will have no propensity to desorb from the surface and facile immobilization is feasible by impregnation of the support with an aqueous solution of enzyme, without the cumbersome covalent cross-linking or entrapment procedures required in conventional aqueous-based systems. Moreover, organic solvents may attack the covalent binding of enzymes to the support.

The support was regarded as inert and without influence on the kinetic behaviour of the enzyme. However, an important aspect of immobilized enzymes in organic solvents is the possibility of the support to alter the microenvironment close to the enzyme [42,43]. Hydrophilic supports such as calcium alginate are compatible with enzymes and can be used to increase the level of enzyme hydration, avoiding the formation of a separate aqueous phase in the organic solvent. On the other hand, extremely polar supports may limit the rate of mass transfer of hydrophobic substrates to the enzyme layer. This fact should cause apparent $K_m$ values to increase and the enzyme catalytic efficiency to decrease. Hydrophobic supports such as polyurethanes [44] overcome the latter problem but are less compatible with hydrophilic enzymes. An elegant solution to obtain optimal hydrophilicity/hydrophobicity matching between reagents and the support matrix has been devised by the use of gels based on photopolymerizable resins and urethane macromonomers by varying the ratio between hydrophilic and hydrophobic moieties in the monomer molecules [45].

In order to quantify the support influence and to derive general rules to predict the performance of the enzyme in organic solvents using specific supports, the concept of aquaphilicity has been introduced [46]. Aquaphilicity is a measure of how the water in a volume of water-saturated diisopropyl ether is parti-

Table 2
Examples of recent applications of organic-phase enzyme electrodes

| Enzyme | Solvent | Analyte | Detector | Detection limit (mM) | Ref. |
|---|---|---|---|---|---|
| Horseradish peroxidase | Dioxane | Hydrogen peroxide | Carbon electrode | 10 | [47] |
| | Ethanol | Organic peroxides | Carbon microelectrode | 1 | [48] |
| | Acetonitrile | Hydrogen peroxide | Carbon electrode[a] | 0.0003 | [49] |
| Tyrosinase | Ethanol | Phenols | Carbon microelectrode | 0.7 | [48] |
| | Acetonitrile | Phenols | Carbon electrode[a] | 0.0001 | [49] |
| | Various | Phenols | Oxygen electrode | 0.0002 | [50,51] |
| | Acetonitrile | Moisture | Carbon electrode | 0.072% (v/v) | [52] |
| Vegetal tissues | Choloroform | Phenols | Graphite electrode | 0.03 | [53] |
| Cholesterol oxidase | Hexane/chloroform | Cholesterol | Oxygen electrode | – | [8] |
| Laccase | Alcohols | Hydroquinone | Glassy carbon electrode | 0.0006 | [10] |
| Glucose oxidase | Acetonitrile/water | Glucose | Glassy carbon electrode | – | [54] |

[a] Enzyme entrapment into polyester sulphonic membranes.

tioned between the ether phase and a fixed amount of dry support. The higher the aquaphilicity of the support, the greater its tendency to sequester water from the ether phase, thus leaving less for enzyme hydration and thereby decreasing its activity.

## 7. Current and potential analytical applications

The analytical applications of enzymes in organic solvents centre around the development or organic-phase enzyme electrodes. Table 2 summarizes some of the recently reported examples of applications. Apart from isolated enzymes, whole cell preparations from plant sources have been proposed as biocatalytic materials for the construction of biosensors. Plant-tissue-based biosensors are constructed by physically retaining a thin slice of the tissue at the surface of a detection element using a porous membrane. An example is the phenol sensor [53] when a thin slice of mushroom or banana is held at the surface of a graphite disc electrode (see Table 2).

Flow measurements of enzyme inhibitors and trace water in non-aqueous media represent attractive and novel applications of organic-phase enzyme electrodes. Inhibition of tyrosinase and horseradish peroxidase (HRP) in acetonitrile by thiourea, benzoic acid and other poorly water-soluble inhibitors can be indirectly monitored from the decrease of the flow-injection peak of the phenol substrate, used as the maximum reference signal [55]. A wide variety of inhibitors with poor water solubility (pesticides, PAHs, drugs) could be measured based on inhibitor biosensors in organic media. Also, a tryosinase electrode has been used to measure water in an organic solvent [56]. Here, the influence of low levels of water on the rate of the biocatalysed phenol oxidation can be related to the water concentration. This indirect biosensing approach, pioneered by Wang and Reviejo [56], is an attractive alternative to the Karl-Fisher titration method.

While most of the recent advances in organic-phase enzyme biosensors have been made using electrochemical detection techniques, there have been very scarce efforts to use optical sensing approaches. A number of optical transducing mechanisms and sensing designs are potentially available for application in organic-phase biosensing. Parameters such as oxygen, $CO_2$, hydrogen peroxide or pH are commonly detected in biocatalytic reactions and, for them, a wide choice of spectrophotometric methods and/or sensors (absorbance, reflectance, fluorescence, room-temperature phosphorescence and chemi/bioluminescence) are feasible. However, most, if not all, have yet to realize their full potential for developing optical organic-phase biosensing approaches.

Up to now, the physical combination of immobilized enzymes and optical transducers to form selective detection devices in the organic phase has followed three main approaches (see Fig. 2):

(i) Enzyme reactor–optical detection systems, where the biochemical event produced in an enzymatic reactor in a flow system is followed by directly monitoring either production or consumption of a chromophore. Braco et al. [57] reported the first example of this type of biosensing in organic media for cholesterol analysis. The system, previously studied by Ka-

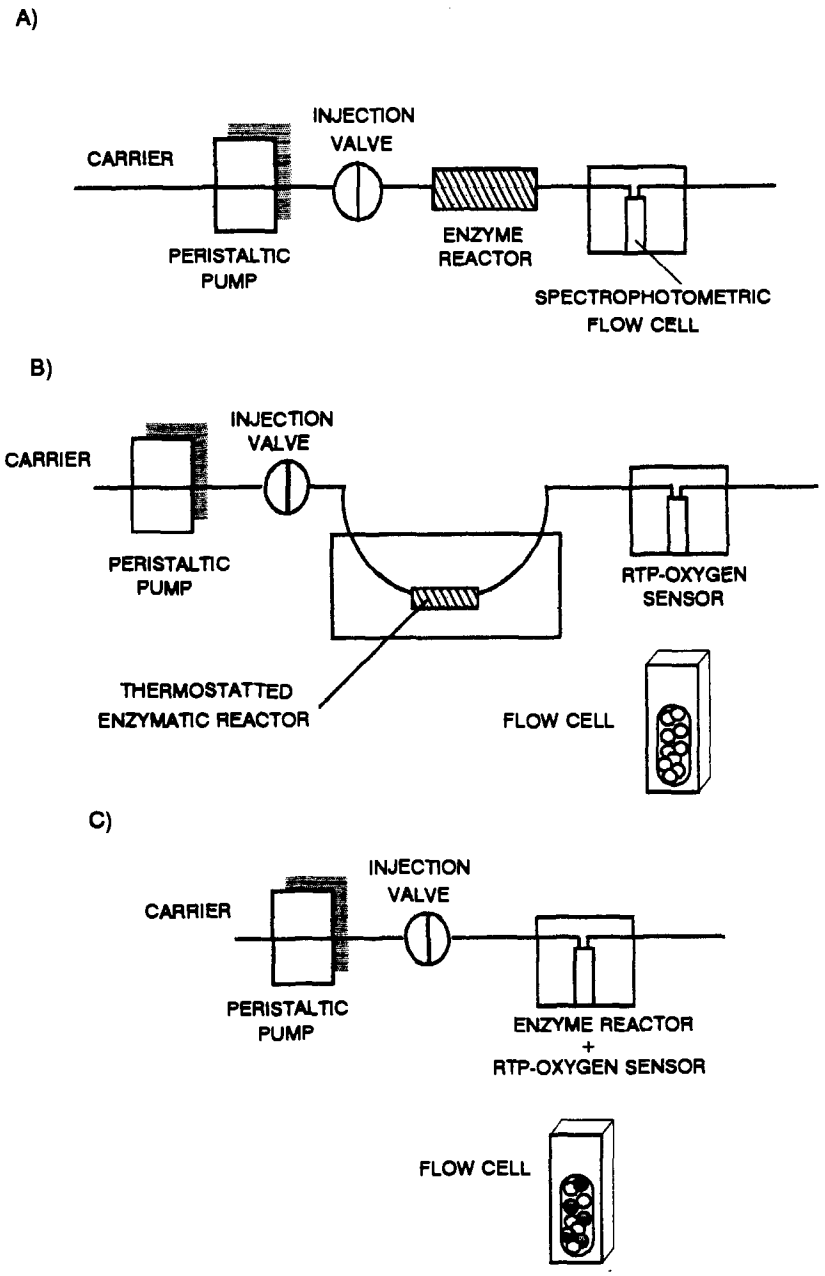


Fig. 2. Different approaches for organic-phase optical biosensing. (A) Enzyme reactor–optical detection system. (B) Enzyme reactor–optical sensor system. (C) Flow-through enzyme optosensing.

zandjian et al. [14] using a batch approach, used a non-covalently immobilized cholesterol oxidase (COD) and HRP reactor operating in toluene. Cholesterol is first oxidized by molecular oxygen in a COD-catalysed reaction, releasing stoichiometrically equivalent hydrogen peroxide, which is, in turn, converted to water by HRP in oxidizing *p*-anisidine (chromogenic indicator substrate) yielding a coloured product which was monitored at 458 nm by means of a flow-cell UV–vis detector. The strategy developed combines the remarkable benefits offered by enzymology in organic solvents and the advantages inherent to flow injection methods.

(ii) Enzyme reactor–optical sensor systems, where the enzyme is immobilized in a reactor preceding an optical sensor in a flow system. A COD reactor–room-temperature phosphorimetric sensor system, operating in a chloroform–hexane mixture for use in a flow-injection system has been developed [58]. Oxygen consumption during the enzymatic choles-

Table 3
Comparative analytical performance characteristics for optical biosensing of cholesterol in organic media

| Conditions/ performance characteristics | Enzyme reactor–optical detection | Enzyme reactor–RTP sensor | | Flow-through enzyme optosensing |
|---|---|---|---|---|
| Temperature (°C) | 25 | 35 | 25 | 25 |
| Detection limit (M) | $10^{-6}$ | $5 \times 10^{-5}$ | $1.4 \times 10^{-4}$ | $3 \times 10^{-4}$ |
| Linear range (M) | Up to $2 \times 10^{-4}$ | Up to $4 \times 10^{-3}$ | More than $10^{-2}$ | Up to $10^{-2}$ |
| RSD (%) | – | 2.5 | 2 | 3 |
| Response time (min) | – | 2 | 2 | 1.5 |
| Solvent | Toluene | Chloroform–hexane | Chloroform–hexane | Chloroform–hexane |

terol oxidation was followed via the changes in the room-temperature phosphorescence (RTP) of an oxygen-sensitive metal chelate immobilized on an anion exchange resin packed into a conventional flow-through cell [59,60]. This work has opened the door for similar analytical sensor devices to measure other poorly water-soluble analytes such as bilirubin, fatty and other carboxylic acids, aldehydes, etc. for which suitable oxidases are available.

(iii) Flow-through enzyme optosensing, where the immobilized enzyme is in close proximity to the optical sensing phase in a flow configuration. A flow-through cholesterol RTP biosensing device using the optical sensing basis mentioned above illustrated this latter point [58]. The immobilized COD glass beads and the RTP sensing beads were mixed and packed into the small space of a flow-through cell. Although the detection limit for cholesterol working at room temperature was twice higher than that obtained with the reactor–room-temperature phosphorimetric sensor approach, a strict comparison among the systems cannot be made because reactors are generally designed with an excess of reagent (large reactor volume), whereas the flow-through approach offers a limited surface for the enzyme reaction to take place.

The immobilized COD glass beads and the RTP sensing beads mixture could be placed on the common end of the bifurcated optical fibre in order to develop an organic-phase optrode. Work in this direction using fluorescence and RTP sensing materials for oxygen is currently in progress in our laboratory.

Some important analytical features of these systems are listed in Table 3.

While the concept of organic-phase optical biosensing (OPOB) is presented here within the framework of on-line cholesterol analysis, the approach may have a bright future in several fields, due not only to the several important advantages accrued from enzymology in organic media but also from the use of fibre-optic chemical sensors [61]. On the other hand, sample pretreatment can be eliminated or minimized, which is extremely attractive in some instances for continuous monitoring purposes. For example, a field in which OPOB could find important applications is food technology and food testing, with its many challenging water-insoluble samples. Frequently performed analyses are of aldehydes or phenol in fats and oils, cholesterol or lactose in butter and margarines, quality of edible oils monitoring, etc. Temperature abuse detection is another area in which OPOB may find an application. The monitoring of temperature maintenance is important in the transport of chilled or frozen foods and pharmaceuticals and other heat-sensitive materials. A prototype of a device was developed which relies on the low catalytic activity of peroxidase in a solid solvent (hexadecane at 4 °C) to reliably, accurately and irreversibly detect temperature abuse [62]. Once the temperature rises above the melting point of the solvent, the peroxidase quickly catalyses the oxidation of *p*-anisidine and colour is produced. Adequate mixing of various hydrocarbons allows the melting point of the solvents to be varied.

Another area in which OPOBs could be used is clinical diagnostics. Poorly water-soluble analytes such as cholesterol or bilirubin are amenable to detection using the approach. An area of growing importance is the monitoring of the quality of water and effluents. The determination of water contaminants such as fat-soluble biodegradable pesticides, phenol and other organic contaminants may be made possible by the implementation of OPOBs. In most cases, an organic extraction will be necessary in order to preconcentrate the organic contaminant.

The pharmaceutical industry is another area in which OPOBs could make a significant contribution as many pharmaceutical products are not readily dissolved in aqueous media. For example, of interest are steroids and steroid-based drugs production or peroxide bleaching agents in cosmetic products. One of the most valuable features of some enzymes in non-aqueous media is their ability to discriminate between enantiomers of racemic substrates and, therefore, could be used to determine optically active (chiral) products in pharmaceuticals.

Other opportunities come from the petrochemical industry, where many analytes such as alcohols, aldehydes and esters could be analysed in an organic phase using suitable enzymes. However, in this industry, environmental conditions are generally too harsh (high temperature and/or pressure) for the immobilized biocatalyst and/or the optical transducer to work effectively. The operation may be limited to an automated off-line arrangement.

Future research is likely to solve the critical issues of optical sensor stability in organic solvents, ease of fabrication and calibration. Although the basic technology is straightforward, each application requires customized engineering to produce optical biosensing devices with the expected capabilities.

Enzymatic catalysis has recently been extended to the gas phase and some enzyme-based sensors for use in the gase phase are at present under development. For example, an alcohol-oxidase-based sensor for the analysis of ethanol in air has been developed [63] and is attractive for breathalyser analysis. Alcohol oxidase and catalase (to prevent $H_2O_2$-based inactivation of the alcohol oxidase) were codeposited onto cellulose particles and the reaction was followed in situ by oxidation of a chromogen. In another approach, Barzana et al. [63] also described a method for detecting harmful organic vapours using solid state enzymes. The fact that enzymes retain their catalytic activity in an almost dry state has interesting implications for the development of fibre-optic-mediated biosensors. Fiber optic chemical sensors for the measurement of oxygen, ammonia or carbon dioxide could be coupled with solid state enzymes in the gaseous phase to produce a biosensor. We have begun to explore the suitability of this new optical biosensor scheme for alcohols using an RTP sensor based on a xanthene dye.

Enzymatic catalysis in organic media is an exciting field capable of revolutionizing analytical technology in disciplines as diverse as veterinary medicine, agriculture, bioprocessing, clinical biochemistry and defence. The use of new biocatalysts in organic media — either through protein and antibody engineering or recent isolation — could also open up new areas of research. Future prospects and opportunities of organic-phase biosensing (in the context of electrochemical and other transducers) have recently been discussed by Saini et al. [9] and Wang et al. [11].

## 8. Conclusions

The development of organic-phase optical biosensing is still very much at the basic research stage. From a practical standpoint the ability to easily immobilize and retain the activity of enzymes within an organic solvent should find many applications in optical biosensor technology, e.g. via the use of sensitive optical detection techniques and/or via the use of multienzyme systems. On the other hand, the possibility of finding or inducing new biocatalysts (enzymes or antibodies) tailored to a particular analytical need could also open up new areas of research and application. From a basic point of view several fundamental issues remain unresolved: the parameters that govern enzymatic activity in non-aqueous media must be addressed, the role of water and the nature of the organic solvent on the biocatalyst must be fully understood, a mechanistic and kinetic description of enzymatic catalysis in organic solvents is needed, etc. Biocatalysts in non-aqueous media thus open up another promising horizon for basic study and the application of biochemical analysis. We hope this overview stimulates fresh ideas and new approaches that will aid progress in this exciting field.

## Acknowledgements

Financial support from the Fondo de Investigaciones Sanitarias de la Seguridad Social (FISss, Proj. 93/0469) and the Fundación para el Fomento en Asturias de la Investigación Cientifica, Aplicada y la Tecnologia (FICYT) is gratefully acknowledged.

## References


[1] L.C. Clark and C. Lyons, Ann. N.Y. Acad. Sci., 102 (1962) 29.
[2] B. Borgstrom and H.L. Brockman (Eds.), Lipases, Elsevier, Amsterdam, 1984.
[3] C. Laane, J. Tramper and M.D. Lilly (Eds.), Biocatalysis in Organic Media, Elsevier, Amsterdam, 1987.
[4] A. Zaks and A.M. Klibanov, Science, 224 (1984) 49.
[5] R.Z. Kazandjian and A.M. Klibanov, J. Am. Chem. Soc., 107 (1985) 5448.
[6] J. Grunwald, A.M. Klibanov, M.P. Scollar and B. Wirz, J. Am. Chem. Soc., 108 (1986) 6732.
[7] L. Kvittingen, Tetrahedron, 50 (1994) 8253.
[8] G. Hall and A.P.F. Turner, Anal. Lett., 24 (1991) 1375.
[9] S. Saini, G.F. Hall, M.E.A. Downs and A.P.F. Turner, Anal. Chim. Acta, 249 (1991) 1.
[10] J. Wang, Y. Lin, A. Eremenko, A. Ghindilis and I. Kurochkin, Anal. Lett., 26 (1993) 197.
[11] J. Wang, Talanta, 40 (1993) 1905.
[12] I.D. Kuntz and W. Kauzmann, Adv. Protein Chem., 28 (1974) 239.
[13] J.A. Rupley, E. Gratton and G. Careri, Trends Biochem. Sci., 8 (1983) 18.
[14] R.Z. Kazandjian, J.S. Dordick and A.M. Klibanov, Biotechnol. Bioeng., 28 (1986) 417.
[15] A. Zaks and A.M. Klibanov, J. Biol. Chem., 263 (1988) 3194.
[16] N.W. Ross and H. Schneider, Enzyme Microb. Technol., 13 (1991) 370.
[17] M.A. Simonyan and R.M. Naibandyan, Biochim. Biophys. Acta, 446 (1976) 432.
[18] F.R. Dastoli and S. Price, Arch. Biochem. Biophys., 118 (1967) 163.
[19] A. Zaks and A.M. Klibanov, Proc. Natl. Acad. Sci. U.S.A., 82 (1985) 3192.
[20] S. Riva, J. Chopineau, A.P.G. Kieboom and A.M. Klibanov, J. Am. Chem. Soc., 110 (1988) 584.
[21] A.C. Williams, J.M. Woodley, P.A. Ellis and M.D. Lilly, Denaturation and Inhibition Studies in a Two-Liquid Phase Biocatalytic Reaction. The Hydrolysis of methyl actetate by pig liver esterase, in C. Laane, J. Tramper and M.D. Lilly (Eds.), Biocatalysis in Organic Media, Elsevier, Amsterdam, 1987, pp. 399–404.
[22] Y.L. Khmelnitsky, A.V. Levashow, N.M.L. Klyachko and K. Martinek, Enzyme Microb. Technol., 10 (1988) 710.
[23] L.A.S. Gorman and J.S. Dordick, Biotechnol. Bioeng., 39 (1992) 392.
[24] A. Leo, C. Hansch and D. Elkins, Chem. Rev., 71 (1971) 525.
[25] C. Laane, S. Boeren, R. Hihorst and C. Veerger, Optimization of Biocatalysis in Organic Media, in C. Laane, J. Tramper and M.D. Lilly (Eds.), Biocatalysis in Organic Media, Elsevier, Amsterdam, 1987, pp. 65–84.
[26] K. Martinek, I.V. Berezin and A.N. Semenov, Biochim. Biophys. Acta, 658 (1981) 76.
[27] S.G. Burton, J.R. Duncan, P.T. Kaye and P.D. Rose, Biotechnol. Bioeng., 42 (1993) 938.
[28] S.J.B. Duff and W.D. Murray, Biotechnol. Bioeng., 34 (1989) 153.
[29] K.R. Natarajan, J. Chem. Educ., 68 (1991) 13.
[30] R.E. Feeny, in J.R. Whitaker and M. Fujimaki (Eds.), Chemical Deterioration of Proteins, American Chemical Society, Washington, 1980, p. 1.
[31] T.J. Ahern and A.M. Klibanov, Science, 228 (1985) 1280.
[32] A. Zaks and A.M. Klibanov, Science, 224 (1984) 1249.
[33] M. Reslow, P. Adlercreutz and B. Mattiasson, Appl. Microbiol. Biotechnol., 26 (1987) 1.
[34] J.A. Rupley and G. Careri, Adv. Protein Chem., 41 (1991) 37.
[35] A. Zaks and A.M. Klibanov, J. Am. Chem. Soc., 108 (1986) 2767.
[36] E. Santaniello, P. Ferraboschi and P. Grisenti, Enzyme Microb. Technol., 15 (1993) 367.
[37] C.S. Chen and C.J. Sih, Angew Chem. Int. Ed. Engl., 28 (1989) 695.
[38] M.N. Gupta and B. Mattiasson, Unique Applications of Immobilized Proteins in Bioanalytical Systems, in C.H. Suelter and L. Kricka (Eds.), Bioanalytical Applications of Enzymes. Methods of Biochemical Analysis, Vol. 36, Wiley, Chichester, 1992, pp. 1–34.
[39] D.S. Yang and J.S. Rhee, Biotechnol. Bioeng., 40 (1992) 748.
[40] J. Wang, Y. Lin and Q. Chen, Analyst, 118 (1993) 277.
[41] P. Estrada, W. Baroto, M.P. Castillón, C. Acebal and R. Arche, J. Chem. Tech. Biotechnol., 56 (1993) 59.
[42] J. Tramper, Trends Biotechnol., 3 (1985) 45.
[43] T. Yamane, H. Nakatani, E. Sada, T. Omata, A. Tanaka and S. Fukui, Biotechnol. Bioeng., 21 (1979) 2133.
[44] K. Yokozeki, S. Fukui, Y. Hirose, K. Sonomoto, K. Takinami, A. Tanaka, T. Utagawa and T. Yamanaka, Appl. Microbiol. Biotechnol., 14 (1982) 225.
[45] A. Tanaka and S. Fukui, in A. I. Laskin (Ed.), Enzymes and Immobilized Cells in Biotechnology, Benjamin/Cummings, London, 1985, pp. 149–176.
[46] B. Mattiasson and P. Adlercreutz, Tibtech, 9 (1991) 394.
[47] F. Schubert, S. Saini and A.P.F. Turner, Anal. Chim. Acta, 245 (1991) 133.
[48] J. Wang, L.H. Wu and L. Angnes, Anal. Chem., 63 (1991) 2993.
[49] J. Wang, L. Lin and Q. Chen, Electroanalysis, 5 (1993) 23.
[50] L. Campanella, G. Favero, M. Sammartino and M. Tommasetti, Talanta, 41 (1994) 1015.
[51] L. Campanella, A. Fortuney, M. Sammartino and M. Tommasetti, Talanta, 41 (1994) 1397.
[52] E.I. Iwuoha and M.R. Smyth, Analyst, 119 (1994) 265.
[53] J. Wang, N. Naser, H.S. Kwon and M.Y. Cho, Anal. Chim. Acta, 264 (1992) 7.
[54] S. Mannino, M.S. Cosio and J. Wang, Analyst, 119 (1994) 2001.
[55] J. Wang, E. Dampsey, A. Eremenko and M.R. Smith, Anal. Chim. Acta, 279 (1993) 203.
[56] J. Wang and A.J. Reviejo, Anal. Chem., 65 (1993) 845.
[57] L. Braco, J.A. Darós and M. De la Guardia, Anal. Chem., 64 (1992) 129.
[58] M.E. Díaz-García and M.J. Valencia-González, Anal. Chem., 66 (1994) 2726.
[59] R. Pereiro-García, Y.M. Liu, M.E. Díaz-García and A. Sanz-Medel, Anal. Chem., 63 (1991) 1759.
[60] Y.M. Liu, R. Pereiro-García, M.J. Valencia-González, M.E. Díaz-García and A. Sanz-Medel, Anal. Chem., 66 (1994) 836.

[61] O.S. Wolfbeis, Fiber Optical Fluoresensors in Analytical and Clinical Chemistry, in J.G. Schulman (Ed.), Molecular Luminescence Spectroscopy. Methods and Applications. Part 2, Wiley, New York, 1988, pp. 129–281.

[62] C.G. Boeriu, J.S. Dordick and A.M. Klibanov, Biotechnology, 4 (1986) 997.

[63] E. Barzana, A.M. Klibanov and M. Karel, Appl. Biochem. Biotechnol., 15 (1986) 25.

ELSEVIER

Talanta 42 (1995) 1775–1781

Talanta

# Salicylate-selective electrode based on lipophilic tin(IV)phthalocyanine

Jun-Zhong Li, Xin-Yu Pang, De Gao, Ru-Qin Yu *

*Department of Chemistry and Chemical Engineering, Hunan University, Changsha, 410082, People's Republic of China*

Received 22 July 1994; revised 6 September 1994; accepted 8 May 1995

**Abstract**

A new PVC membrane electrode based on lipophilic (2,9,16,23-tetra-*tert*-butylphthalocyanine)tin(IV) dichloride which demonstrates excellent selectivity and fast response toward the salicylate ion is described. The membrane electrode displayed a linear response for salicylate in the concentration range $10^{-5}$–0.1 M and exhibited an antiHofmeister pattern, with high selectivity for salicylate compared with lipophilic inorganic and biologically important organic anions. The electrode was successfully applied to the determination of salicylate in pharmaceutical preparations and biological samples.

## 1. Introduction

The conventional anion-selective electrodes based on quaternary ammonium or phosphonium salts are essentially non-selective because the selectivity is determined by the hydration energy and the relative solubility of the individual anions in the solvent mediator, i.e. the electrodes always display the so-called Hofmeister sequence [1,2]. Recently, electrodes using plasticized poly(vinyl chloride) (PVC) membranes incorporating derivatives of vitamin $B_{12}$ [3], the porphyrin complexes of Co(III) [4], Sn(IV) [5], In(III) [6], Mn(III) [7], organometallic compounds such as organotin [8] or organomercury [9] compounds as well as Schiff's base complexes have been reported. Many of them showed potentiometric anion-selectivity sequences which were derived from the Hofmeister pattern. The mechanism for the selectivity obtained is believed to be based on the coordination of the analyte ions with the respective metal atoms involved in the carrier molecules. The work reported here extends this concept with the development of a new salicylate-selective membrane electrode based on the tin(IV)–phthalocyanine complex, $TTBPcSnCl_2$.

Salicylate and its analogues such as acetylsalicylate (aspirin) are commonly used as effective analgesics. Despite their utility as pain relievers and antipyretics, salicylate derivatives can be quite toxic if taken in large doses. The most widely used spectrophotometric method [10] for determining "total" salicylate is rather tedious and exhibits poor selectivity. With the wide use of aspirin, there is an increasing need for measurement of "free" salicylate in biological samples such as urine and serum. Polymeric membrane electrodes for salicylate measurements have been proposed previously [11]. Since these earlier probes were based on dissociated ion exchangers such as quaternary ammonium or phosphonium salts, they lacked adequate selectivity for salicylate over a number of phisiologically important anions such as chloride and lactate. A salicylate-selective electrode useful in the analysis of biological samples were reported by Meyerhoff and co-workers [5] using tetraphenylporphyrin-tin(IV) dichloride as the carrier. The electrode, unfortunately, possessed a relatively long response time (2–10 min to reach 90% of equi-

* Corresponding author.


*SSDI* 0039-9140(95)01639-2

librium). This drawback prompted us to develop a new salicylate-selective electrode with a rapid response as well as a high selectivity. The metal phthalocyanines, with a structure similar to the metal porphyrins, neverthlesss exhibit properties different from the latter, probably owing to the difference in, say, the "hole" size [12]. In addition, the metal phthalocyanines are more easily obtained and chemically stable than the metal porphyrins. This paper describes a new lipophilic phthalocyaninetin(IV) based salicylate sensor with a relatively high selectivity over common inorganic and organic anions, rapid response time, and wide linear range. The proposed membrane electrode provides an alternative useful device for measuring salicylate in pharmaceutical preparations and physiological samples.

## 2. Experimental

### 2.1. Reagents and chemicals

All potentiometric measurements were carried out in phosphate buffer solutions. Aqueous solutions were prepared with doubly distilled water. Tetrahydrofuran (THF), high molecularweight poly(vinylchloride) (PVC), potassium tetraphenylborate (KTPB), dinonyl sebacate (DNS), and *n*-dibutyl phthalate (DBP) were obtained from Shanghai Chemicals Co. Chemicals used for the synthesis were of reagent grade quality and were used without further purification.

### 2.2. Preparation of (2,9,16,23-tetra-tert-butylphthalocyanine)tin(IV) dichloride (TTBPcSn(IV), Fig. 1)

The synthesis based on the literature [13] was modified as follows. A finely powdered mixture of 2.9 g (48.5 mmol) of urea (water-free), 235 mg (4.5 mmol) of ammonium chloride, 575 mg (2.5 mmol) of stannous chloride and 34 mg (0.03 mmol) of ammonium molybdate was mixed thoroughly with 1.8 g (8.1 mmol) of 4-*tert*-butylphthalic acid prepared according to Hanack et al. [14]. The mixture was heated at 180 °C and kept at this temperature for 30 min. The temperature was then increased to 200 °C and maintained for 4 h. The crude product was boiled for 1 h in 1 mol $l^{-1}$ HCl, filtered, and washed with water until the filtrate was neutral. The product obtained was further purified by dissolving in $CHCl_3$ and the resulting solution was chromatographed using a silica gel column with elution with a mixture of $CHCl_3$ and $CH_3OH$ (8:1 v/v). The eluted solution was evaporated under reduced pressure, and a blue solid was obtained. Analysis: calculated for $C_{48}H_{48}N_8SnCl_2$(Mr., 926.62); C, (62.16%) H (5.18%); N (12.08%); found: C (62.61%); H (5.47%); N (11.95%).

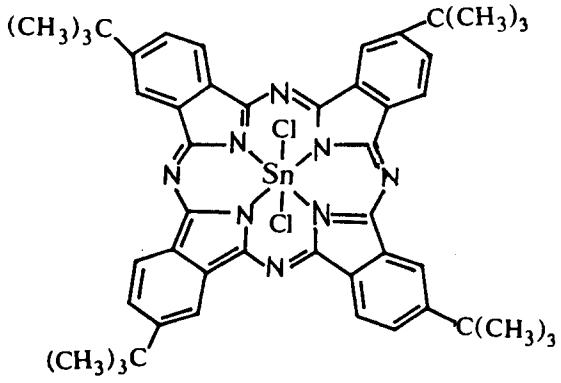


Fig. 1. Structure of the carrier studied.

### 2.3. Apparatus

Potentiometric and pH measurements were made with use of a model PHS-10A digital Ionnalyzer (Xiaoshan). The cells used for millivolt measurements were of the following type: $Hg/Hg_2Cl_2$(s), KCl(saturated)|sample solution‖PVC membrane‖NaSal(0.001 M), KCl(0.1 M), AgCl/Ag. The cell potentials were measured at room temperature (10 °C). The solutions were buffered with 0.05 mol $l^{-1}$ phosphate and adjusted to the required pH with KOH.

### 2.4. Electrode preparation and handling

The PVC membrane electrodes were fabricated from various carriers and assembled according to Thomas and co-workers [15,16]. The membrane composition was 2 wt.% TTBPcSn(IV), 31 wt.% PVC and 67 wt.% DNS. The Aliquat-336 membranes were prepared with 7 wt.% Aliquat, 30 wt.% PVC and 63 wt.% DBP. Before use, the electrodes were conditioned in 0.01 mol $l^{-1}$ NaSal solutions for 2 h. When not in use, the electrodes were stored in $10^{-4}$ mol $l^{-1}$ NaSal solutions at room temperature and protected from the ambient light to prevent any possible photodecomposition of the ionophores as a precautionary measure, although during a period of at least 1 month

there was no detectable change of the electrode characteristics.

### 2.5. Determination of EMF response and selectivity of the membranes

Anion selectivity coefficients, $\log K^{pot}_{Sal,anion}$, were determined in 0.1 M solutions of the corresponding sodium salts by the separate solution method [17]. The solutions were buffered with 0.05 M phosphate adjusted with KOH to pH 5.5. Concentrations were used rather than activities due to uncertainties in estimating the ionic strengths of zwitterion background electrolytes. The concentration of the dissociated anions of weak acids in the test solutions was calculated using the Henderson–Hasselbalch equation. The pH response curve of the salicylate-membrane electrode was obtained by titrating 0.05 M phosphoric acid with small aliquots of KOH, while simultaneously monitoring the pH of the sample solution with a combination glass pH electrode.

### 2.6. A.c. impedance experiments

The a.c. impedance spectra of the electrode membrane containing TTBPcSn(IV) were recorded with use of a PAR M368-2 system (EG & G Princeton Applied Research, USA) in 0.05 mol $l^{-1}$ phosphate at pH 5.5. The frequency range used was $10^5$–0.01 Hz (at 10 °C). The a.c. amplitude was 5 mV.

### 2.7. UV-Vis absorption spectra

Spectra of the chloroform phase obtained by shaking a solution of the TTBPcSn(IV) complex in $CHCl_3$ with water (pH 5.5) or with 0.1 mol $l^{-1}$ NaSal for 30 min were recorded on a PE Lamada 17 spectrophotometer (Perkin-Elmer).

### 2.8. Determination of salicylate in aspirin tablets and urine

Tablets of aspirin (Central South Pharmaceutical Co., Hunan) were finely powdered and treated according to the procedure described by Choi and Fung [11]. A standard additions method was employed to evaluate the concentration of salicylate. A standard procedure for the assay of soluble aspirin tablets [18] was used as the reference method.

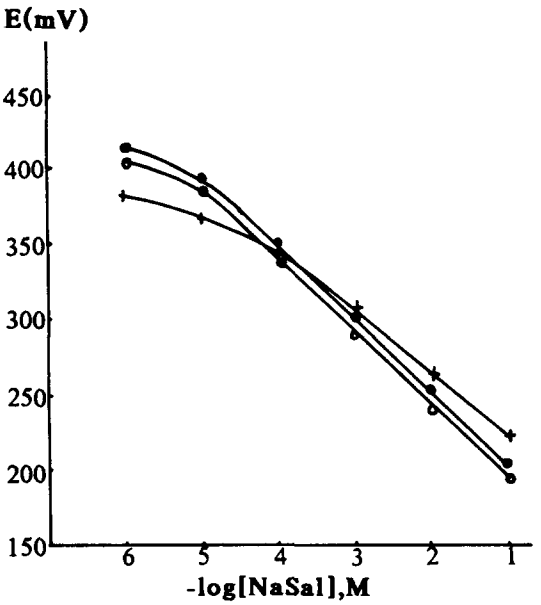


Fig. 2. Potentiometric response curves of the electrode at various pH values in 0.05 mol $l^{-1}$ phosphate buffer. ●, pH 5.5; ○, pH 6.2; +, pH 7.2.

Recovery experiments were undertaken on urine samples drawn from healthy persons not taking aspirin. Urine samples (5 ml) were diluted with 0.05 mol $l^{-1}$ phosphate buffer (pH 5.5) to the appropriate volume and the standard additions method was used to obtain the salicylate concentration which was compared with the results obtained by the conventional colorimetric method [10].

## 3. Results and discussion

### 3.1. Potentiometric response

The calibration curves of the electrode incorporating TTBPcSn(IV) are shown in Fig. 2. The electrode showed a linear potentiometric response over a wide concentration range of $1 \times 10^{-5}$–0.1 mol $l^{-1}$ salicylate (with a slope of −50– −54 mV per decade at room temperature, 10 °C) in 0.05 mol $l^{-1}$ phosphate buffer solution, pH 5.5. The limit of detection was determined to be $7 \times 10^{-6}$ mol $l^{-1}$ salicylate. The standard deviation of the potential readings was 0.8 mV when the electrode pair was dipped alternately into $10^{-3}$ and $10^{-2}$ M NaSal solutions.

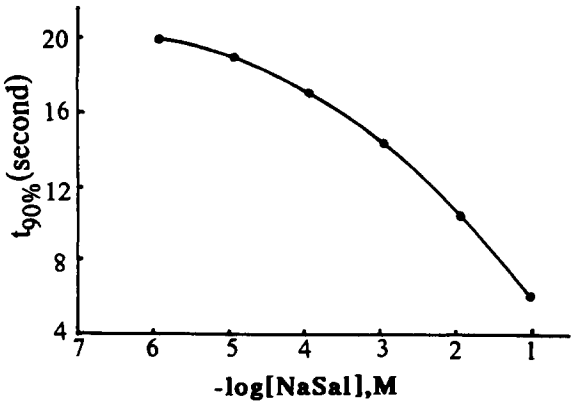


Fig. 3. The $t_{90\%}$ response time of the electrode as a function of sample salicylate concentration in phosphate buffer, pH 5.5.

### 3.2. Response time

For analytical applications, the response time of a sensor is an important factor. With a salicylate-selective electrode based on tetraphenylporphyrintin(IV), $t_{90\%}$ values of 2–10 min have been reported, depending on the concentration of salicylate tested, and the relatively long response time was ascribed to the exchange between salicylate and the axial coordination anions. For the membrane electrode containing TTBPcSn(IV), the $t_{90\%}$ was determined to be 20–6 s from lower to higher salicylate concentrations, which is similar to those observed with classical ion-exchange membrane electrodes (see Fig. 3). It seems that the compound $TTBPcSnCl_2$ could act as a charge carrier in the membrane after exposure to the test solutions. In fact, in UV-Vis spectroscopic experiments as described in the experimental section 2.7, the TTBPcSn(IV) complex in $CHCl_3$, after shaking with a phosphate buffer, showed a change in the absorption spectra (see Fig. 4). This spectral change is thought to have originated from the axial coordination of either $H_2O$ or $OH^-$ ions at the fifth and/or sixth coordination positions, that is to say, the substitution of $H_2O$ or $OH^-$ ions with salicylate ions. It was noticed that the equilibration time in such spectroscopic experiments was relatively fast compared with the time observed in a similar spectroscopic experiment for tetraphenylporphyrintin(IV) (3–4 days) [19]. It seems that the kinetic rate for axial ligand-exchange on TTBPcSn(IV) is faster than that of tetraphenylporphyrintin(IV); this may be associated with the relatively short response time of the TTBPcSn(IV)-based electrode compared with the tetraphenylporphyrintin(IV)-based electrode.

### 3.3. Effect of pH

The pH response profiles for TTBPcSn(IV) were examined by titrating 0.05 mol $l^{-1}$ phosphoric acid with KOH (Fig. 5). Similar to the electrodes based on metal porphyrins and other organometallic compounds, the TTBPcSn(IV)-based membrane also exhibits pH sensitivity, possibly as a consequence of the tendency of the central metal atom to form oxides and, or hydroxides at moderate or high pH values. For metal-phthalocyanine based membrane electrodes, this might be explained by the coordination of water molecules or hydroxyl groups as axial ligands to the central metal atoms. The calibration curves for the TTBPcSn(IV)-based

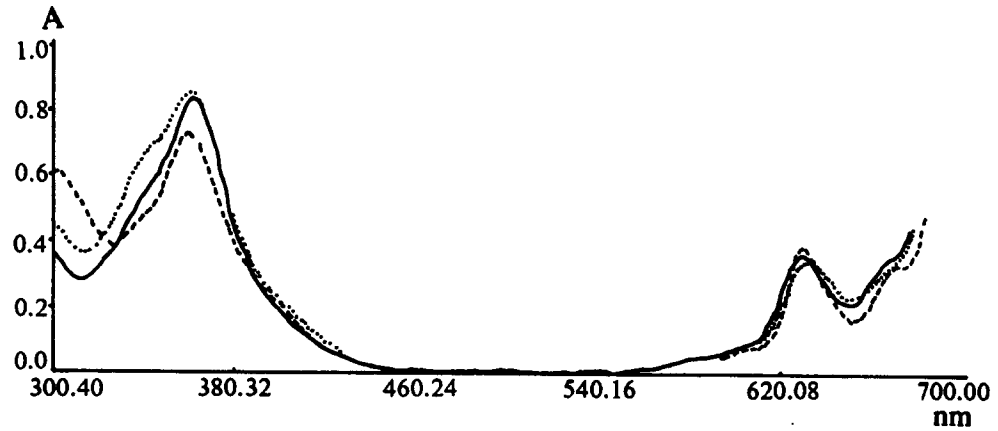


Fig. 4. UV-Vis absorption spectra of the TTBPcSn(IV) complex: ——, spectrum of $CHCl_3$ solutions of TTBPcSn(IV); . . . . . ., spectrum of the above solution after extraction with phosphate buffer for 30 min; ------, spectrum after extraction with 0.1 mol $l^{-1}$ aqueous NaSal for 30 min.

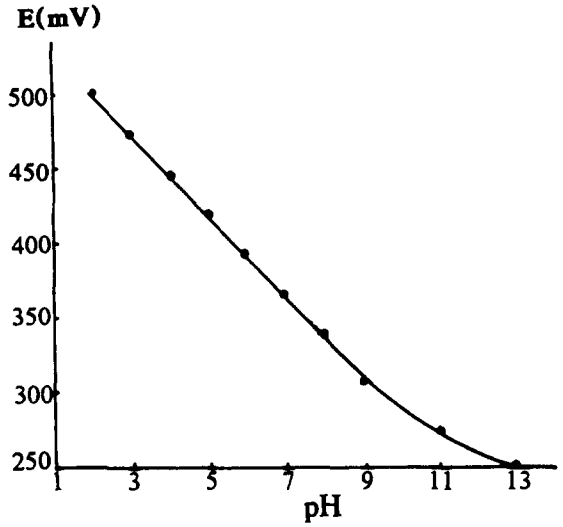


Fig. 5. pH response of the TTBPcSn(IV)-based membrane electrode.

Table 1
Potentiometric selectivity coefficients, $\log K^{pot}_{sal/x}$ of salicylate electrodes prepared with different carriers

| Anion | TTBPcSn(IV) | TTBPcSn(IV) [a] | Aliquat 336–sal |
|---|---|---|---|
| Salicylate | 0 | 0 | 0 |
| Chloride | −4.78 | −4.80 | −1.96 |
| Bromide | −3.95 | −4.20 | −1.31 |
| Nitrate | −3.60 | −4.00 | −1.05 |
| Nitrite | −2.89 | −3.40 | −1.86 |
| Perchlorate | −1.78 | −3.33 | 2.10 |
| Thiocyanate | −1.65 | −2.91 | 0.90 |
| Iodide | −2.58 | −3.58 | 0.14 |
| Citrate | −3.36 | −3.48 | −1.61 |
| Acetate | −3.31 | −3.42 | −2.31 |
| Lactate | −1.29 | −1.64 | −2.01 |
| Benzoate | −0.76 | −1.12 | −1.11 |

[a] The membrane composition is the same as that described in the experimental section with the addition of about 0.1 wt.% KTPB.

electrode at different pH values are shown in Fig. 2. There is no obvious difference between the calibration curves for the electrode at pH 5.5 and pH 6.2 due to the relatively weak pH response of the TTBPcSn(IV)-based electrode. (At pH values below 5.5 a significant fraction of salicylate changes to the protonated form which is not detected by the electrode.) At pH 7.2, on the other hand, owing to the increased interference of the hydroxide ions, the detection limit of the electrode for salicylate deteriorates.

### 3.4. Selectivity of the electrode

The potentiometric selectivity coefficients for membranes containing different carriers are shown in Table 1. For comparison, the selectivity data for a conventional salicylate electrode based on Aliquat-336s are also presented. The TTBPcSn(IV)-based membrane displayed substantially improved selectivity for salicylate over common inorganic and biologically important organic anions. Most of these ions would be expected to interfere seriously with classical anion-exchanger-type membrane sensors. It is evident that the binding constant between tin and the salicylate anion is much higher than those for most other anions; the relatively high electron density around the central tin atom of TTBPcSn(IV) would weaken the coordinating ability of this atom. The selective bonding of the salicylate ion is thought to be the origin of the high selectivity of the

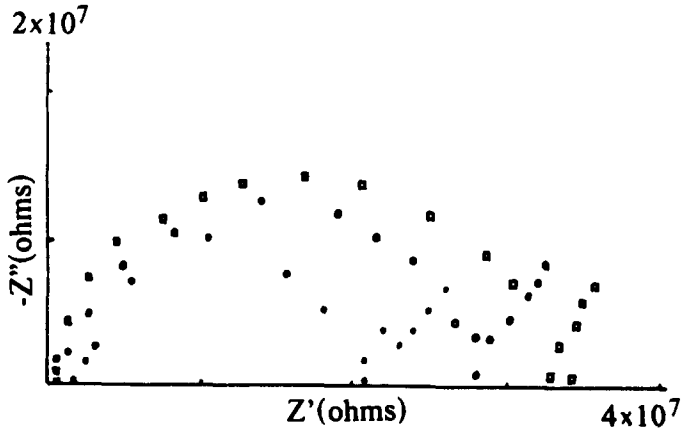


Fig. 6. The a.c. impedance of the membrane incorporating TTBPcSn(IV) after conditioning for 2 h in (●) $10^{-1}$ mol $l^{-1}$ NaSal solution, (○) $10^{-3}$ mol $l^{-1}$ NaSal solution, and (□) $10^{-5}$ mol $l^{-1}$.

Table 2
Recovery of salicylate added to human urine

| Sample | Salicylate added (mmol $l^{-1}$) | Salicylate found (mmol $l^{-1}$) | | Average recovery (electrode) (%) |
|---|---|---|---|---|
| | | Electrode method [a] | Colorimetric method [b] | |
| 1 | 0.00 | 0.86 ± 0.02 | 0.84 | |
| | 1.89 | 2.83 ± 0.01 | | 104 |
| 2 | 0.00 | 0.61 ± 0.01 | 0.69 | |
| | 0.95 | 1.52 ± 0.04 | | 94.7 |
| 3 | 0.00 | 1.16 ± 0.03 | 1.20 | |
| | 0.49 | 1.66 ± 0.07 | | 102 |

[a] average of three determination ± standard deviation.
[b] Single measurement.

TTBPcSn(IV)-based electrode of salicylate over other anions. It is of particular significance that the electrode displayed a very high selectivity over chloride, making possible the use of the electrode for the determination of salicylate in biological samples. The selectivity of this salicylate-sensitive TTBPcSn(IV)-based electrode relative to perchlorate and thiocyanate is somewhat worse than that of the Sn(IV)–porphyrin system, as reported by Meyerhoff and coworker [9].

Recently, Schaller et al,[20] and Bakker et al, [21] have demonstrated independently that for anion ionophores which operate via a charged carrier mechanism, the addition of small amounts of negative sites in the membranes will benefit the selectivity of electrodes. To check whether it is possible to further improve the selectivity of the TTBPcSn(IV)-based electrode, a small amount of potassium tetraphenylborate (KTPB) was added to the membrane. The selectivity coefficients of such a membrane incorporating KTPB are also shown in Table 1. The selectivity of the resulting electrode over other anions, especially perchlorate and thiocyanate, is really slightly improved. On the other hand, according to the theoretical models that predict the effects of lipophilic anion sites on the selectivity of membranes [20–21], it also demonstrates that the membrane incorporating TTBPcSn(IV) is operating via a charged carrier mechanism.

### 3.5. A.c. impedance spectra

The a.c. impedance spectra of the membrane incorporating TTBPcSn(IV) were recorded after conditioning in salicylate solutions for 2 h. Well-defined semicircles at high frequency and Warburg impedance at low frequency intervals were observed (see Fig. 6). The bulk resistance increased with the decrease in the concentration of aqueous salicylate solutions, indicating that the transfer process of salicylate across the solvent polymeric membrane was controlled by the diffusion process. It is interesting to notice that according to the cyclic voltammetric experiments of Nakamura et al. [22], a phthalocyaninecobalt-immobilized polymer membrane also showed facilitated transfer of some anion species.

### 3.6. Analytical applications

The high selectivity for salicylate over common inorganic and organic anions as well as the lower detection limit of the TTBPcSn(IV)-based electrode made it possible to determine salicylate in pharmaceutical preparations and biological samples. The electrode was employed for the assay of aspirin. The salicylic acid produced by the hydrolysis of acetylsalicylic acid was determined as described in the experimental section. The result obtained was 44.80 ± 0.34% (by weight, $n = 5$), which was in fair agreement with that of the pharmacopoeia method (44.67 ± 0.29%; $n = 5$).

A more detailed evaluation of the electrode method for determining salicylate in urine was carried out. Recovery studies with salicylate-spiked urine yielded recoveries ranging from 95 to 104% as shown in Table 2. The results obtained by the electrode method were in agreement with those of the colorimetric procedure. The new TTBPcSn(IV)-based electrode seemed to provide a nice alternative device for the direct determination of salicylate in biological samples.

## Acknowledgements

This work was supported by the National Science Foundation of China and partially by the Laboratory of Electronanlalytical Chemistry, Changchun Institute of Applied Chemistry, Academy of Science.

## References

[1] M.A. Arnold and R.L. Arnold, Anal. Chem., 58 (1986) 84R–101R.
[2] R.Q. Yu, Ion-Sel. Electrode Rev., 3 (1986) 153.
[3] P. Schulthess, D. Amman, B. Krautler, C. Caderas, R. Stepanek and W. Simon, Anal. Chem., 57 (1985) 1397.
[4] R. Stepanek, B. Krautler, P. Schulthess, B. Lindemman, D. Amman and W. Simon, Anal. Chim. Acta., 182 (1986) 83.
[5] N.A. Chaniotakis, S.B. Park and M.E. Meyerhoff, Anal. Chem., 61 (1989) 566.
[6] S.B. Park, W. Matuszewski, M.E. Meyerhoff and Y.H. Liu, Electroanalysis, 3 (1991) 309.
[7] S.C. Ma, N.A. Chaniotakis and M.E. Meyerhoff, Anal. Chem., 60 (1988) 2293.
[8] U.Wuthier, H.V. Pham, R. Zünd, D. Welti, R.J.J. Funck, A. Bezegh, D. Amman, E. Pretsch and W. Simon, Anal. Chem., 56 (1984) 535.
[9] D.M. Praniti and M.E. Meyerhoff, Anal. Chim. Acta, 217 (1989) 123.
[10] P. Trinder, Biochem. J., 57 (1954) 301.
[11] K.K. Choi and K.W. Fung, Anal. Chim. Acta, 138 (1982) 385.
[12] A.M. Schaffer, M. Goutermann and E.R. Davidson, Theor. Chim. Acta, 9 (1973) 30.
[13] W.J. Kroenke and M.E. Kenney, Inorg. Chem., 3 (1964) 251.
[14] M. Hanack, J. Metz and G. Pawlowski, Chem. Ber., 115 (1982) 2836.
[15] G.J. Moody, R.B. Oke and J.D.R. Thomas, Analyst., 95 (1970) 910.
[16] A. Graggs, G.J. Moody and J.D.R. Thomas, J. Chem. Educ., 51 (1974) 541.
[17] G.G. Guilbault, R.A. Durst, M.S. Rant, K. Freiser, E.H. Hansen, T.S. Light, E. Pungor, G. Rechnitz, N.M. Rice, T.J. Rohm, W. Simon and J.D.R. Thomas, Pure Appl. Chem., 48 (1976) 127.
[18] Pharmacopoeia of the People's Republic of China, Chemical Industry Press Peoples Healthy Press, Beijing, 1985, p. 4.
[19] C.E. Kibbey, S.B. Park, G. Deadwylder and M.E. Meyerhoff, J. Electroanal. Chem., 335 (1992) 135.
[20] U. Schaller, E. Bakker, U.E. Spichiger and E. Pretsch, Anal. Chem., 66 (1994) 391.
[21] E. Bakker, E. Malinowska, R.D. Schiller and M.E. Meyerhoff, Talanta, 41 (1994) 881.
[22] T. Nakamura, C. Hayashi, K. Matsuda and K. Isutsu., Rev. Polarogr., 37 (1991) 17.

ELSEVIER

Talanta 42 (1995) 1783–1789

Talanta

# Preparation and characterization of a new enzyme electrode based on solid paraffin and activated graphite particles

C. Petit, A. Gonzalez-Cortes, J-M. Kauffmann *

*Free University of Brussels, Institute of Pharmacy, Bd. Triomphe, Campus Plaine, CP 205/06, 1050 Brussels, Belgium*

Received 28 March 1995; accepted 15 May 1995

**Abstract**

A new electrochemical biosensor was developed by incorporating an enzyme into a solid-paraffin–graphite-particle matrix. Tyrosinase served as model enzyme and the biosensor response was characterized with respect to its response to dopamine. The influence of different experimental parameters (tyrosinase loading, flow rate, oxygen dependence, pH, etc.) was investigated in order to optimize the biosensor performance. The electrode response was fast, reversible and linear in a large concentration domain (0.1 μM–1 mM). The enzyme–solid paraffin carbon paste electrode (CPE) showed markedly improved stability in flow injection analysis compared to the classical liquid paraffin–graphite-based biosensors. The biosensor allowed a sampling rate of 79 samples per hour, the repeatability of the injections was improved with respect to the classical CPE with a relative standard deviation of 2.2% ($N = 63$), and the detection limit for dopamine was 50 nM. The biosensor response to some phenol and catechol derivatives was also investigated.

## 1. Introduction

Amperometric biosensors are increasingly of considerable interest for monitoring analytes in flowing streams in pharmaceutical and environmental analysis [1–5]. The immobilization of a biological component in a water-insoluble matrix such as carbon paste (graphite + liquid paraffin) is currently extensively used for the development of amperometric biosensors [3–6]. Interestingly, the carbon paste electrode (CPE) exhibits a low background current compared to other solid electrodes [7], and enzyme-modified CPEs show fast responses due to the proximity of the biocatalyst–graphite particles. The electrode may be additionally mixed with a catalyst (redox mediator [8–12], metal particles [13–16]) and the biocatalyst is protected by the hydrophobic matrix of the electrode [17]. The enzyme loading may be important, allowing high rates of substrate conversion. However, applications under hydrodynamic conditions are limited by the instability of such biosensors [3,8], due in part to the poor mechanical strength of the paste [18] giving rise to enzyme leakage along with progressive erosion of the electrode surface [8,19]. Several interesting strategies have been considered for improving these so-called bulk-modified enzyme electrodes by using carbon composite matrixes such as epoxy [20–22], Kel-F [23], silicone grease [2], PVC [24], or Teflon [25] as binders, by stretching a dialysis membrane over the electrode [13,17,26], by chemically modifying the enzyme [27], or by chemically attaching the enzyme to the graphite particles [28]. In our

* Corresponding author.


*SSDI* 0039-9140(95)01645-7

preliminary work, we described the preparation of a new solid paraffin-based carbon paste electrode (SCPE) for the development of an enzyme-immobilized electrode [29]. By studying the latter under hydrodynamic conditions (how injection analysis (FIA)), it appeared that the solid paraffin improved remarkably the mechanical stability of the biosensor, and the reproducibility and repeatability of the results compared to a liquid paraffin-based biosensor. We report here the characterization and properties of a tyrosinase-immobilized solid CPE (SCPE) by studying phenol and catechol derivatives and dopamine as model compounds in FIA and batch experiments. Tyrosinase (polyphenoloxidase) has already been used extensively for biosensor preparation [2,9,22,26, 28,30–34]. The enzyme is known to catalyze the oxidation of phenolic compounds via hydroxylation in the presence of molecular oxygen to catechol and finally to the corresponding *o*-quinone. The latter can be monitored amperometrically at −0.2 V vs. a saturated calomel electrode (SCE) and quantitatively related to the concentration of phenol or catechol derivatives [30–32]. A tyrosinase-immobilized CPE has been extensively studied by Ortega et al. [28,32] and the results have shown the high instability of the paste under hydrodynamic conditions, e.g. in HPLC [32]. Here, the electrochemical detection of quinones occurs at low potentials; this reduces the magnitude of the background current and minimizes the risks of interferences by uric acid, ascorbic acid and acetaminophen [33,35].

## 2. Experimental

### 2.1. Apparatus

*FIA experiments*

The experimental set-up consisted of an analytical pump (Perkin-Elmer, series 10, liquid chromatograph) with a sample injector of volume 20 µl, connected to the detector by a conduit of 40 cm length (Peek tubing, 0.03 cm i.d.).

The wall-jet configuration consisted of a large volume cell [36] containing the reference electrode (SCE); the enzyme electrode and a stainless-steel chromatographic tube as auxiliary electrode completed the cell. An applied potential of −0.2 V was maintained with a Bruker E 230 LC potentiostatic detector. The surface of the biosensor was positioned at a distance of 1 mm in front of the impinging jet.

A flow-through cell of thin layer design was also employed to check for the oxygen dependence of the biosensor. It was positioned within the FIA experimental set-up outlined above. The detection cell (BAS) housed the enzyme electrode (dual electrode, 3 mm in diameter), an Ag/AgCl (3 M NaCl) reference electrode (BAS) and a stainless-steel block as auxiliary electrode. The potential was controlled by a BAS LC 4B amperometric detector. The current output was displayed on a Kipp and Zonen $Y-t$ recorder.

Samples for injection were prepared using the carrier solution.

*Batch experiments*

Amperometric measurements were performed with use of a 20 ml cell containing the working electrode, an SCE as reference electrode and a glassy carbon electrode as the auxiliary electrode. The applied potential was maintained with a Bruker E 230 LC potentiostatic detector. A magnetic stirrer and a stirring bar provided convection. The current output was displayed on a Kipp and Zonen recorder.

Voltammetric measurements were performed with use of a Bioanalytical system (BAS) model CV 27 voltammetric analyzer connected to a 7090A Hewlett Packard printer.

All measurements were made at room temperature (22 ± 1°C).

### 2.2. Reagents

All chemicals were of analytical grade (Merck or Sigma) and were used as received. Stock solution of dopamine, catechol and phenol derivatives were prepared in nitrogen-deaerated phosphate buffer solutions. The latter were prepared from sodium dihydrogen phosphate and the pH was adjusted to the desired value by $H_3PO_4$ or NaOH. Deionized water was used for preparing the solutions. Graphite particles (diameters 10–100 µm) were cleaned by lixiviation with acetone, then activated with aqua regia and thoroughly rinsed with water to neutral pH and finally dried at 400°C for 4 h. The carbon paste electrode (CPE) was prepared by using commercial carbon pastes from Metrohm (E.A.207c), namely type A, consisting of 76% graphite and 24% liquid paraffin, and type B having 66% graphite and 34% liquid paraffin. Tyrosinase EC 1.14.18.1 (tyrosinase activity, 3900 U $mg^{-1}$ solid; polyphenol oxidase activity, 84 000 U $mg^{-1}$ solid; catechol oxidase ac-

tivity, 400 000 U $mg^{-1}$ solid) was purchased from Sigma as a lyophilized powder.

### 2.3. Electrode preparation

The solid carbon paste electrode (SCPE) was prepared by melting paraffin wax for 15 min in a mortar thermostated in a water bath, at a temperature close to its melting point (46–48°C) in the presence of graphite particles in the ratio 34:66 (m/m). The mortar was removed from the water bath and the paste was thoroughly mixed and crushed with a pestle.

For the enzyme-immobilized paste preparation, and in order to achieve optimum responses and reproducibility between pastes the dry enzyme powder was added by direct admixing with the carbon paste [32].

*Metrohm carbon paste electrode (EMCPE) types A and B*

The enzyme tyrosinase was mixed homogeneously with the Metrohm carbon paste (MCPE) in a mortar (5% (m/m)) at room temperature.

*New solid carbon "paste" electrode (ESCPE)*

The paraffin wax was melted in a mortar thermostated in a water bath at a temperature close to its melting point (46–48°C). The mortar was then removed from the bath and the lyophilized tyrosinase was added and thoroughly mixed. Subsequently, the graphite particles were added and mixed with a glassy spatula to obtain a prehomogeneous paste. The final "solid paste" was obtained by crushing with a pestle in the mortar. A portion of this mixture was packed into the Teflon body of the electrode (1 mm i.d.). Before the measurements, the new enzyme electrode was smoothed to a mirror finish using a clean paper card.

## 3. Results and discussion

The hardness of the ESCPE greatly minimized the leakage of the enzyme into the solution compared with a tyrosinase–MCPE. This was confirmed in batch conditions by dipping the enzyme-modified electrode (5% (m/m)) into a 20 ml cell containing 0.1 M phosphate buffer (pH 7.0) during 22 h under mild stirring. The presence of solubilized tyrosinase was demonstrated by the addition of catechol ($10^{-4}$ M) to the solution and monitoring the *o*-quinone produced by amperometric reduction using an MCPE. No reduction current was observed in the solution which contained the ESCPE, in contrast to the result obtained with the solution which contained the EMCPE type A.

### 3.1. Influence of flow rate

The dependence of the peak height upon the flow rate of the carrier (0.1 M phosphate buffer (pH 7.0)) was investigated in the range 0.3–2 ml $min^{-1}$ using the ESCPE by injecting a 34 μM dopamine solution into the FIA wall-jet system. A nearly exponential decrease of the signal was observed on increasing the flow rate in accordance with literature data [28, 32] which showed that the enzymatic conversion is limiting the response. It should be noted that at a flow rate of 1.0 ml $min^{-1}$, the response obtained represented approximately 55% of the response achieved at 0.3 ml $min^{-1}$. The latter flow rate was used for further experiments.

### 3.2. Influence of pH

The optimum pH for the ESCPE was determined in 0.1 M phosphate buffer in the pH range 5–9 using a 12 μM solution of dopamine. Experiments were carried out with the FIA system (wall-jet configuration) and the batch set-up (100% steady state). As shown in Fig. 1, curves A and B, similar behaviour was observed, with a maximum response at pH 7.0 in accordance with literature data on tyrosinase immobilized in a polypyrrole matrix [34], in a CPE [28,32], and in a graphite–epoxy composite electrode [23].

### 3.3. Influence of buffer concentration

The ESCPE response was investigated in the FIA system (wall-jet configuration) by varying the phosphate buffer concentration between 0.01 and 0.2 M at pH 7.0. The response decreased by approximately 50% from 0.01 to 0.1 M, then it stabilized to reach a plateau at 0.1 M. The response was quasi-independent of buffer concentration between 0.1 and 0.2 M. Further experiments were performed using a 0.1 M pH 7.0 buffer concentration.

### 3.4. Influence of temperature and enzyme loading

In order to check for the risk of enzyme degradation by heat, the influence of the tem-

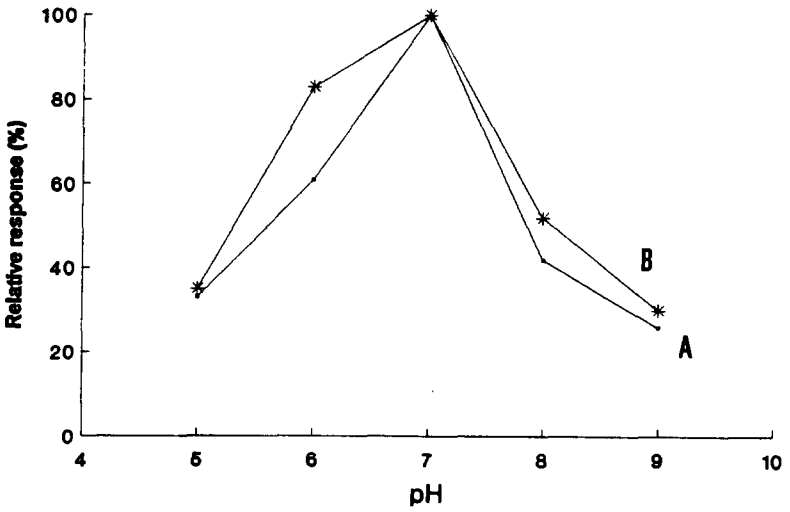


Fig. 1. Relative response of the ESCPE as a function of pH. Experimental conditions were optimized (see details in text). Curve A, FIA systems; curve B, Batch set-up.

perature during the paste preparation was investigated at 48, 58, and 68°C. No significant difference in the responses was observed (within experimental error) in this temperature range. The response of the biosensor (5.4 μM dopamine injection) increased non-linearly by raising the enzyme loading, e.g. 0.31 nA, 0.95 nA, and 2.2 nA at 2%, 5% and 8% (m/m), respectively. The second paste composition was selected in this study as it showed a better background current stability than the 8%, (m/m) loading. Using the latter, the background current was stable for 2 h then it started to increase gradually. This may be related to a higher hydrophilicity (inferred from an initially higher background) of the electrode surface, dissolution of the enzyme and progressive erosion of the electrode surface.

### 3.5. ESCPE stability in FIA

The operational stability of the ESCPE (5% (m/m)) and the tyrosinase–MCPE types A and B (5% (m/m)) were compared by repetitive injections of a 9.2 μM dopamine solution. As shown in Figs. 2A and 2B, a progressive increase of the background current and a peak current decrease with time were observed for the tyrosinase–MCPE types A and B compared to the ESCPE. As expected, the enzyme electrode with a higher graphite loading i.e. EMCPE type A (Fig. 2A), showed dramatic behaviour under hydrodynamic conditions due to its lower mechanical strength. For identical electrode compositions with respect to the binder:graphite:enzyme ratio, the ESCPE showed a markedly improved behaviour compared with the EMCPE type B (Figs. 2C and 2B, respectively). Note also that the initial response at the EMCPE were four times higher than at the ESCPE. This suggested that a larger amount of tyrosinase was spread over the tyrosinase–MCPE surface than over the ESCPE, but progressive dissolution of the enzyme (peak decrease) and gradual erosion (background increase) of the EMCPE types A and B limited their applicability. The ESCPE maintained 100% and 90% of its initial FIA response after 12 h and 24 h of continuous use, respectively. The long-term storage stability of the solid paste at 5°C was determined by studying the response of the ESCPE (injection of 12 μM dopamine in FIA). The ESCPE showed 69% of its initial response using a 65-days-stored solid paste.

The background current at the ESCPE was stabilized within 30 min following the application of the potential under the FIA optimal conditions.

### 3.6. Influence of oxygen

In the wall-jet configuration, the ESCPE response was not significantly affected when the carrier was permanently deaerated by nitrogen. This might be explained by the presence of traces of oxygen absorbed and entrapped in the ESCPE [19]. The oxygen non-dependence was also observed when using the FIA thin-layer configuration. The presence of entrapped oxy-

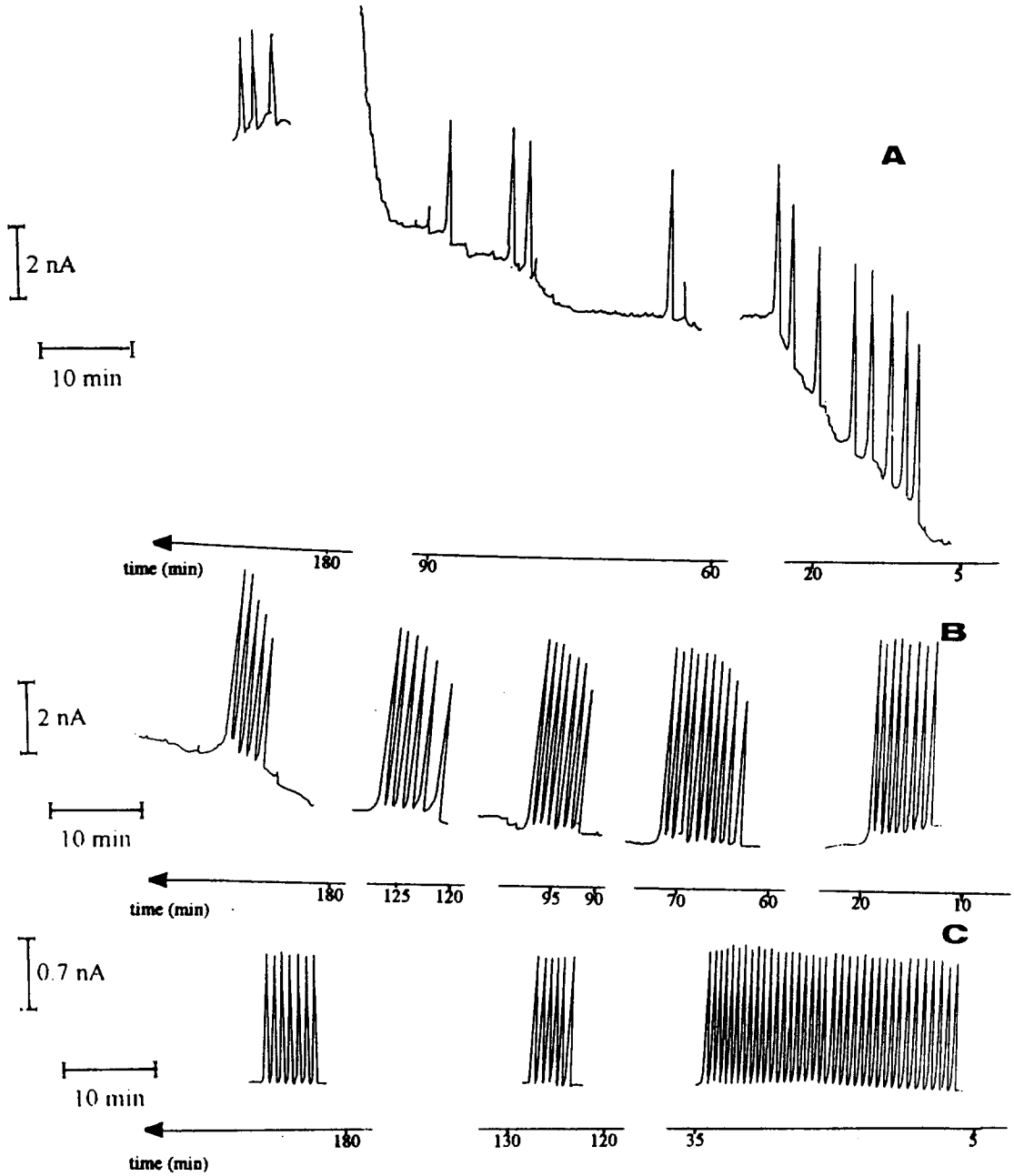


Fig. 2. Typical amperometric recordings in FIA. (Dopamine concentration, 9.2 μM; injection loop, 20 μl; 0.1 M phosphate buffer (pH 7.0); flow rate, 0.3 ml $min^{-1}$, $E_{app} = -0.2$ V vs. SCE.) (A) Metrohm CPE (type A)–tyrosinase 5% (m/m); (B) Metrohm CPE (type B)–tyrosinase 5% (m/m); (C) solid CPE–tyrosinase 5% (m/m).

gen was inferred from the broad reduction peak observed (in the negative potential range below −0.34 V) in the cyclic voltammetric curves recorded in nitrogen-degassed 0.1 M phosphate buffer (pH 7.0) at MCPE types A, B and the SCPE (figures not shown).

In FIA, using the wall-jet configuration under optimum conditions (flow rate, 0.3 ml $min^{-1}$; 0.1 M in phosphate buffer (pH 7.0)) the reproducibility (calculated by studying dopamine injections at two different concentrations, 3.6 μM and 5.4 μM) for different electrode surfaces ($N = 5$) was 5.1%. The ES-CPE showed a linear response (FIA wall-jet system) in the concentration range 0.1 μM–1 mM; $Y = 0.151x - 0.617$ where $Y$ is in

nanoamps and $x$ is in micromoles; and with a linear correlation coefficient of $r = 0.997$ (eight data points). The detection limit (signal-to-noise ratio, 3) was 50 nM. The calculated repeatability of several injections ($N = 63$) corresponded to a relative standard deviation (RSD) of 2.2%. The electrode response was fast, with a half-peak value of 23 s corresponding to a sampling frequency of 79 injections per hour.

It was of interest to compare the sensitivity for dopamine of the new biosensor with the results obtained by the direct oxidation of dopamine at the SCPE at a potention of +0.6 V vs. SCE. At the latter potential, the linear domain range was from 0.2 μm to 1 mM and the detection limit was 40 nM, but the responses were less reproducible (RSD, approximately 5%) and less selective due to the relatively high applied potential.

Trends in sensitivity taking into consideration other related molecules were established by studying the relative response for four phenol and catechol derivatives (taking the dopamine sensitivity as 100%). A calibration graph was obtained for each molecule investigated in the FIA system (wall-jet), using a flow rate of 1 ml $min^{-1}$. The results reported in Table 1 are in accordance with those reported by Ortega et al. for a tyrosinase–CPE [28]. The high response towards catechol may be attributed to the high catechol oxidase activity of the enzyme (see reagents). Differences in sensitivity among the catechols (catechol > dopamine > noradrenaline) are likely to be due to differences in the $K_m$ values of the catechol oxidase [37].

With respect to the possible use of the electrode in liquid chromatography, the ESCPE behaviour was tested in aqueous hydro organic media (methanol–buffer or acetonitrile–buffer) in the FIA system. On repetitive injections ($N = 23$) of a $6.5 \times 10^{-4}$ M dopamine solution, the response decrease slightly but continuously, using both the acetonitrile (10% (v/v)-containing and methanol (10% (v/v)))-containing carriers. The initial response was reduced by approximately 12% after 23 injections. A slightly more rapid decrease in response was observed in the acetonitrile-containing carrier. By raising the acetonitrile content to 40%, the intensity of the current dropped by 75% of its initial value within 2 h of use. Using a 40:60 (v/v) methanol–0.1 M phosphate buffer (pH 7.0), the intensity of the response (intermittent injections) was stable for 8 h. Further studies were carried out using 10:90 (v/v) methanol–buffer. Reproducible results (RSD, 1.8%; $N = 14$) were observed by allowing a waiting time of 5 min between each injection. A calibration graph was obtained in the concentration range 2.5 μM–1.8 mM; $Y = 0.026x + 0.232$, where $Y$ is in nanoamps and $x$ is in micromoles; $r = 0.9992$; with a detection limit of 1 μM.

Despite its gradual loss in sensitivity, the biosensor response was regenerated to 85% of its initial value by allowing a phosphate buffer carrier to flush over the biosensor for 1 h.

Table 1
Relative responses (slopes of the calibration curves) in the FIA wall-jet system of the tyrosinase–solid carbon paste electrode towards various substrates

| Compound | Slope (%) |
|---|---|
| Dopamine | 100 |
| Catechol | 680 |
| Phenol | 380 |
| L-Tyrosine | 51 |
| Noradrenaline | 23 |

## 4. Conclusion

The immobilization of an enzyme such as tyrosinase in solid paraffin in the presence of graphite particles appeared to be a judicious way of preparing electrochemical (micro) biosensors showing high stability and rapid response rates suitable for hydrodynamic applications. The detection limits were as good as those obtained at the enzyme-carbon paste electrode i.e. 40 nM, but the reproducibility of the response and the stability of the probe in aqueous organic media were considerably improved. Possible application of this new "robust" enzyme electrode may be considered in on-line phenol (and derivatives) monitoring, in "in vivo" sensing or as a detector in HPLC analysis.

## Acknowledgement

Thanks are expressed to Bioanalytical System Inc., for instrumentation support.

## References


[1] J. Wang, Talanta, 40 (12), (1993) 1905.
[2] M.P. Connor, J. Sanchez, J. Wang, M.R. Smyth and S. Mannino, Analyst, 114 (1989) 1427.
[3] J. Wang and N. Naser, Electroanal., 6 (1994) 571.
[4] K. Kalcher, J. Wang, J.-M. Kauffmann, I. Svancara, K. Vytras, C. Neuhold and Y. Zhongping, Electroanal., 7 (1995) 5.
[5] L. Gorton, Electroanal., 7 (1995) 23.
[6] J. Kulys and H.E. Hansen, Biosensors Bioelec., 9 (1994) 491.
[7] M.E. Rice, Z. Galus and R.N. Adams, J. Electroanal. Chem., 143 (1983) 89.
[8] N. Motta and A. Guadalupe, Anal. Chem., 64 (1994) 566.
[9] M. Bonakdar, J.L. Vilchez and H.A. Mottola, J. Electroanal. Chem., 266 (1989) 47.
[10] A. Amine, J.-M. Kauffmann, G.G. Guilbault and S. Bacha, Anal. Lett., 26(7) (1993) 1281.
[11] J. Kulys, H.E. Hansen, T. Buch-Rasmussen, J. Wang and M. Ozsoz, Anal. Chim. Acta, 288 (1994) 193.
[12] P.C. Pandey, V. Pandey and S. Mehta, Biosensors Bioelec., 9 (1994) 365.
[13] T. Katsu, X. Yang and G.A. Rechnitz, Anal. Lett., 27(7) (1994) 1215.
[14] J. Wang, J. Liu, L. Chen and F. Lu, Anal. Chem., 66 (1994) 3600.
[15] J. Wang, F. Lu and D. Lopez, Biosensors Bioelec., 9 (1994) 9.
[16] F. Cespedes, E. Martinez-Fabregas and S. Alegret, Anal. Chim. Acta, 284 (1993) 21.
[17] A. Amine and J-M. Kauffmann, Bioelectrochem. Bioenerg., 28 (1992) 117.
[18] K. Stulick, V. Pacakova and B. Starkova, J. Chromatogr., 213 (1981) 41.
[19] A. Amine, J. Deni and J.-M. Kauffmann, Bioelectrochem. Bioenerg., 34 (1994) 123.
[20] J. Wang and K. Varughese, Anal. Chem., 62 (1990) 318.
[21] J. Wang, E. Gonzalez-Romero and M. Ozsoz, Electroanal., 4 (1992) 539.
[22] J. Wang, L. Fang and D. Lopez, Analyst, 119 (1994) 455.
[23] J. Wangsa and N.D. Danielson, J. Chromatogr., 514 (1990) 171.
[24] S. Sakura and R.P. Buck, Bioelectrochem. Bioenerg., 28 (1992) 387.
[25] J. Wang, A.J. Reviejo and L. Angnes, Electroanal., 5 (1993) 575.
[26] P. Skladal, Collect. Czech. Chem. Commun., 61 (1991) 1427.
[27] S. Yabuki, F. Mizutani and T. Katsura, Biosensors Bioelec., 7 (1992) 695.
[28] F. Ortega and E. Dominguez, G. Jönsson-Pettersson and L. Gorton, J. Biotechnol., 31 (1993) 289.
[29] C. Petit and J.-M. Kauffmann, Anal. Proc., 32 (1995) 11.
[30] F.A. McArdle and K.C. Persaud, Analyst, 118 (1993) 419.
[31] S. Uchiyama, Y. Hasebe, H. Shimizu and H. Ishihara, Anal. Chim. Acta, 276 (1993) 341.
[32] F. Ortega, E. Dominguez, E. Burestedt, J. Emneus, L. Gorton and G. Marko-Varga, J. Chromatogr. A, 675 (1994) 65.
[33] J. Wang, N. Naser and U. Wollenberger, Anal. Chim. Acta, 281 (1993) 19.
[34] S. Cosnier and C. Innocent, Bioelectrochem. Bioenerg., 31 (1993) 147.
[35] M. Moutet, R. Vallot and R. Buvet, Bioelectrochem. Bioenerg., 18 (1987) 137.
[36] L.J. Nagels, J.-M. Kaufffmann, C. Dewaele and F. Parmentier, Anal. Chim. Acta, 234 (1989) 75.
[37] A. Navaratne, M. Shan Lin and G.A. Rechnitz, Anal. Chim. Acta, 237 (1990) 107.

ELSEVIER

Talanta 42 (1995) 1791–1798

Talanta

# Thick film voltammetric sensors for trace copper based on a cation-exchanger-modified surface

Christian G. Neuhold [a], Joseph Wang [a,*], Valberes B. do Nascimento [a], Kurt Kalcher [b]

[a] *Department of Chemistry and Biochemistry, New Mexico State University, Las Cruces, NM 88003, USA*
[b] *Institut fuer Analytische Chemie, Karl-Franzens Universitaet Graz, Universitaetsplatz 1, 8010 Graz, Austria*

Received 28 March 1995; revised 5 May 1995; accepted 15 May 1995

**Abstract**

Strip-type, preconcentrating/voltammetric sensors, prepared by incorporating a cation-exchange resin within screen-printed carbon inks, are described. Such single-use strips combine the efficient electrostatic accumulation of heavy metals with the use of "mercury-free" surfaces. The uptake of copper(II) from dilute solutions (under open circuit conditions) is followed by voltammetric measurements in a separate blank solution. Various experimental variables have been optimized to yield low detection limits (e.g. 0.5 $\mu g\,l^{-1}$ with 10 min accumulation) and good reproducibility (relative standard deviation, 2%). The applicability to assays of drinking water is demonstrated.

*Keywords:* Cation-exchanger-modified surface; Trace copper; Voltammetric sensors

## 1. Introduction

There is a growing need for decentralized testing of trace metals in connection with environmental field screening or near-patient clinical diagnosis [1]. The remarkable sensitivity of electroanalytical procedures, coupled with their compact instrumentation and low-power requirements, make them very attractive for the task of on-site metal analysis. Particularly useful are single-use sensor strips based on screen-printing technology. Such thin film microfabrication capability allows the mass production of highly reproducible, and yet extremely inexpensive disposable electrode strips [1–3]. Useful metal sensors have thus been developed based on the coupling of screen-printed electrodes with highly sensitive electrochemical stripping procedures [1,4]. Voltammetric and potentiometric stripping operations of these disposable electrodes offer reliable and yet convenient quantitation of heavy metals down to the nanomolar concentration level. One concern related to the field application and disposal of stripping-based screen-printed electrodes is their reliance on mercury-coated surfaces. The development of "mercury-free" metal sensors thus represents a challenging and important task.

This paper describes the performance of a cation-exchanger-based single-use sensor for heavy metals. While chemically modified screen-printed electrodes have been reported previously in connection with electrocatalytic modifiers [2,5], no reports are available on analogous tailoring of screen-printed electrodes with preconcentrating agents. The preconcentration/voltammetric strategy enjoys remarkable sensitivity [6], and its coupling to screen-printing technology holds great promise

* Corresponding author.


*SSDI* 0039-9140(95)01647-3

for on-site metal analysis. Preconcentrating modified electrodes also allow the use of medium-exchange procedures, i.e. the removal of the sensor from the sample matrix and potential interferences. In the present study, a cation-exchanger resin, Dowex 50W-X8, was dispersed within a commercial carbon ink prior to the screen-printing process. The ability of this cation exchanger to rapidly collect metal ions from dilute solutions was demonstrated earlier in connection with modified carbon paste electrodes [7–9]. Similarly, as will be illustrated in the following sections, this resin modifier retains its attractive electrostatic accumulation behavior upon incorporation within printing carbon inks, and the resulting screen-printed preconcentrating electrode offers convenient quantitations of trace copper, lead and cadmium.

## 2. Experimental

### 2.1. Apparatus

All voltammetric experiments were carried out using an EG&G PAR Model 264A voltammetric analyzer, in connection with an EG&G PAR Model 0073 $X-Y$ recorder. Measurements were performed in a 10 ml electrochemical cell (BAS, Model VC-2). The working electrode strip, reference electrode (Ag/AgCl, Model RE-1, BAS) and platinum wire auxiliary electrode joined the cell through holes in the Teflon cover.

pH measurements were carried out using a Beckman Φ12 pH/ISE meter, in combination with a Beckman combined pH electrode (No. 39 831).

### 2.2. Screen-printing fabrication

A semiautomatic screen printer (Model TF-100, MPM Inc., Franklin, MA) was used for fabricating the working electrode strips. The modified inks were prepared by thoroughly mixing the appropriate amounts of commercial carbon ink (product no. G-488 [1], Ercon, Waltham, Ma) with the solid cation exchanger Dowex 50W-X8 ($H^+$ form, 20–50 mesh (Fluka)) in a porcelain mortar. Prior to mixing, the cation exchanger was ground in a mortar to a very fine powder. A group of ten electrodes was printed onto the alumina ceramic plate (1.33 in × 4.00 in) through a pattern stencil. Each electrode consisted of a $1.5 \times 30\ mm^2$ area. After letting the electrodes dry at room temperature, a layer of insulator was placed onto part of the printed ink, leaving a defined $1.5 \times 5\ mm^2$ working-electrode area.

### 2.3. Reagents

All solutions were prepared with deionized or nanopure water (for experiments using very low concentrations of copper). The disodium salt of ethylenediaminetetraacetic acid (EDTA) and dipotassium hydrogen phosphate were received from Fisher, while potassium dihydrogen phosphate was obtained from Aldrich. Chemicals were used as received. Standard solutions of copper, antimony, bismuth, cadmium, iron, mercury, lead, silver and zinc ($1000\ mg\ l^{-1}$) were purchased as standards for atomic absorption from Aldrich, and were diluted with nanopure water prior to use. The ground water sample was collected at Hanford site (Richland, WA), while the drinking water was sampled at the NMSU laboratory (Las Cruces). Both samples could be used after adjustment of the pH with nitric acid (Fisher) without further treatment.

### 2.4. Procedure

Both unmodified and modified screen-printed electrodes were used without further pretreatment.

*Preconcentration*

For the accumulation of copper, the electrode was exposed to the stirred sample solution (10 ml of double-distilled water, pH 5.7) containing copper(II) for the required time. After the preconcentration period, the electrode was removed, rinsed with water, placed into the voltammetric cell and connected to the polarograph.

*Voltammetry*

The supporting electrolyte for the voltammetric measurements was phosphate buffer (0.005 M; pH 5.7). Cyclic voltammograms (CV) were recorded with a scan rate of $50\ mV\ s^{-1}$; the scan was initiated at +0.6 V and then switched in direction at −0.6 V. All quantitative measurements were performed in the differential pulse mode (DPV). The initial potential was −0.4 V; the final potential was +0.3 V. An equilibration time of 15 s with the

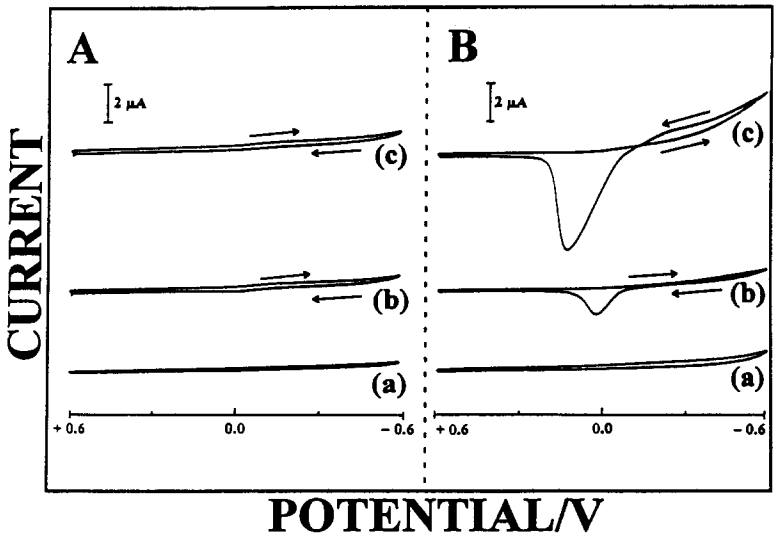


Fig. 1. Cyclic voltammograms for copper, preconcentrated at (A) plain and (B) modified screen-printed electrodes: (curves a) 0 ppm, (curves b) 1 ppm and (curves c) 4 ppm of copper in the sample solution, respectively. (Scan rate, 50 mV $s^{-1}$; supporting electrolyte, 0.005 M phosphate buffer, (pH 5.7). Medium exchange technique: accumulation time, 1 min; pH of the sample solution, 5.7. Modifier (Dowex 50W-X8) loading (B), 5% (w/w).)

initial potential applied was required to obtain complete reduction of copper(II) to copper(0). The pulse height was 50 mV and the scan rate was 20 mV $s^{-1}$ with an increment of 4 mV per data point. The current range was set according to the concentration of copper.

*Regeneration*

Following the voltammetric quantitation, the strip was immersed in a well-stirred aqueous solution of EDTA (0.1 M) for 15 s. After careful rinsing with water, the blank voltammogram was recorded.

## 3. Results and discussion

Solid cation exchangers have not been employed for the modification of screen-printed electrodes. The finely ground Dowex 50W-X8 particles, admixed thoroughly within the carbon ink, retain their attractive uptake properties following the screen-printing process. Fig. 1 compares the voltammetric response of the (A) plain and (B) modified screen-printed strips, following accumulation from copper solutions and transfer to a blank solution. As can be clearly seen, accumulation of copper takes place only when modified screen-printed electrodes are used, resulting in a rather small and broad cathodic wave corresponding to the reduction of copper(II) to copper(0) at a potential of about −0.1 V (vs. Ag/AgCl), and in a very sharp and well-defined reoxidation (stripping) signal at +0.1 V; the anodic peak shifts to more positive potentials with increasing copper concentration. No distinctive copper peaks are observed with unmodified screen-printed electrodes.

The irreversible character of the reduction of copper(II) is in contrast to its behavior at Dowex-50W-X8-modified carbon paste electrodes [8]. In this latter case the reduction of copper(II) yielded a sharp signal, which was exploited for DPV quantitation. As only the copper reoxidation yielded a defined response at the modified screen-printed electrodes, this signal was exploited for all further investigations. For quantitation purposes, the accumulated copper is first reduced to the metallic state during the equilibration step (at the initial potential of −0.4 V), and then reoxidized upon scanning in the anodic direction. An equilibration time of 15 s was found to be sufficient to ensure complete reduction of the accumulated copper prior to measurement. The ion-exchange accumulation and measurement processes may be described by the following equations

Accumulation:

$$2[RSO_3^- H^+]_{surf} + [Cu^{2+}]_{sol} \leftrightarrow [(RSO_3^-)_2 Cu^{2+}]_{surf} + 2H^+_{sol} \quad (1)$$

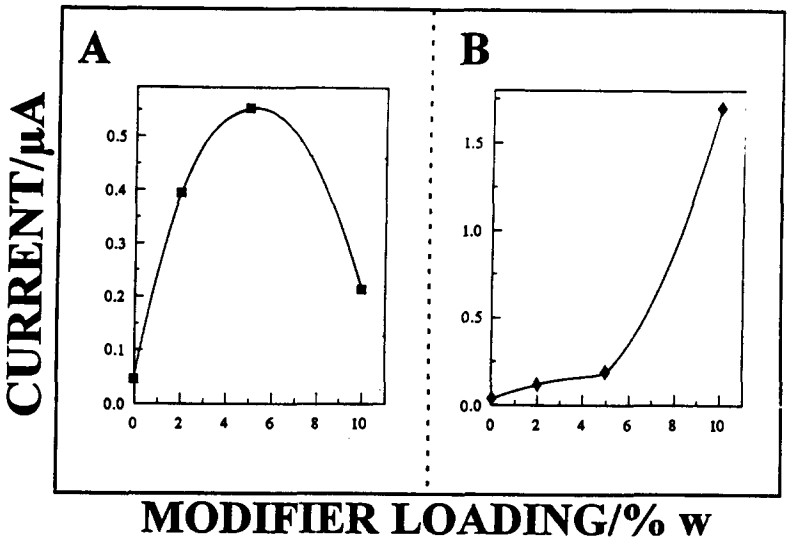


Fig. 2. Effect of modifier loading on the (A) peak and (B) background current. (Differential pulse voltammetry: potential, −0.4–+0.3; scan rate, 20 mV $s^{-1}$. Medium exchange technique: 100 ppb copper; 1 min accumulation time. Other conditions as in Fig. 1).

Equilibration (−0.4 V)

$$[(RSO_3^-)_2Cu^{2+}]_{surf} + 2H^+_{sol} + 2e^- \leftrightarrow 2[RSO_3^-H^+]_{surf} + [Cu^0]_{surf} \quad (2)$$

Measurement (−0.4– + 0.3 V)

$$[Cu^0]_{surf} \leftrightarrow [Cu^{2+}]_{sol} + 2e^- \quad (3)$$

The removal of accumulated copper residues after the voltammetric measurement is essential for the repeated use of the electrode strips. Such cleaning is possible by exposure of the electrode to solutions of EDTA or KCN. As screen-printed electrodes are aimed mainly for on-site environmental applications, the use of KCN as the regeneration agent was considered to be less favorable. A 15 s immersion of the electrode in a 0.1 M EDTA solution was sufficient for complete regeneration of the surface, without loss of analytical performance. Reproducible repetitive runs require recording of the blank voltammogram after each regeneration procedure, probably to remove complexed copper from the electrode surface, and to return the cation exchanger to its "active" form. Careful rinsing of the electrode after exposure to the regeneration solution was found to be extremely important in order to avoid contamination of the sample or measurement solutions with EDTA.

The loading of the resin modifier within the ink has a profound effect on the performance of the modified screen-printed electrode strips. Higher surface loadings normally result in a higher accumulation capacity, but also in larger background currents. In order to optimize the composition of the modified electrodes, strips were prepared with various loadings of the resin modifier. Similar to the trend obtained with Dowex-40W-X8-modified carbon paste electrodes [8] it was found that the exchange capacity increased up to a modifier loading of 5% (w/w), but decreased with higher modifier loadings accompanied by a drastic increase of the background current for loadings greater than 5% (Fig. 2). Screen-printed electrodes with a modifier loading of 5% (w/w) were thus found to yield the optimum signal-to-background ratio.

While screen-printed electrodes are mainly designed for "one-shot" applications, the Dowex-modified strips are also found to yield high stability and reproducibility after regeneration. They can be used throughout several days, without deterioration of the analytical performance. No special pretreatment is necessary when using freshly prepared strips, and the copper signals attain a constant height after two preliminary accumulation/measurement/regeneration cycles, yielding a relative standard deviation of less than 2% for 10 consecutive measurements. The variability between different electrodes is also good. A relative standard deviation of 5% was calculated for the response of 100 μg $l^{-1}$ Cu at five different electrodes (accumulation time of 1 min).

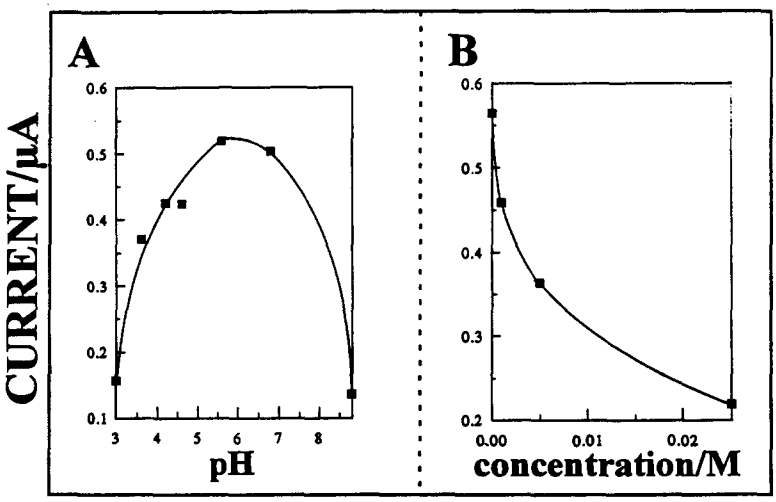


Fig. 3. Effect of (A) pH and (B) ionic strength on the peak current (5% (w/w) modified screen-printed electrode; (B) pH 5.7; other conditions as in Fig. 2).

Experiments were performed to explore the optimum conditions for the accumulation/measurement procedure. When varying the differential pulse scan rate between 10 and 100 mV $s^{-1}$, it was found that a scan rate of 20 mV $s^{-1}$ provided the optimum ratio between peak height and peak shape. Lower scan rates resulted in much smaller peak currents, whereas with higher rates, broadening of the peaks took place, without any gain in peak height.

Parameters which influence the analytical performance of preconcentration strip electrodes to a great extent are the composition and pH of the measurement and sample solutions. As for the supporting electrolyte (for the measurement solution), it was found in preliminary investigations that both non-complexing potassium nitrate and phosphate buffer are suitable electrolytes for the modified screen-printed electrodes. Similar results were obtained when modified carbon paste electrodes were used [8]. However, as the pH of the measurement solution had a great influence on the peak current of the copper reoxidation signal in the range between 6 and 8, and to ensure constant pH, phosphate buffer was chosen as the supporting electrolyte. The optimum pH for the measurement step was found to be 5.7, in conjunction with a phosphate buffer concentration of 0.005 M. The influence of dissolved oxygen was investigated with respect to the applicability of the Dowex-modified electrodes in field analysis. It was found that removal of oxygen by purging nitrogen through the solution results in slightly higher peak currents (approximately 5%), but did not alter or improve the general voltammetric behavior. Therefore, this procedure is not necessary for improving the results.

Even more important than the measurement solution are the composition and pH of the sample solution as they directly effect the accumulation step. Fig. 3A displays the dependence of the peak current on the pH of the sample solution. As can be seen, the pH has a great influence on the accumulation behavior. At high concentrations of hydronium ions, the equilibrium of Eq. (1) is shifted to the left-hand side, in favor of the binding of hydronium ions to the sulfonic acid groups of the cation exchanger. On the other hand, the presence of high levels of hydroxide ions may lead to ion pairs with copper, which is no longer acessible for accumulation. Additionally, it is possible that the pH influences the accumulation capacity of the cation exchanger itself. A pH of 5.7 thus offers an optimum accumulation of copper. The pH had to be kept constant throughout a whole series of measurements, and was monitored periodically (after five consecutive accumulation/measurement cycles).

As can be seen from Fig. 3B, an increase of the ionic strength of the sample solution leads to a rapid decrease of the peak current, due to competition by coexisting cations of the electrolyte solution for the surface cation-exchanger sites.

As expected for preconcentration electrodes, the response of the sensor strip is strongly dependent upon the accumulation time. Fig. 4 shows the dependence of the peak current on

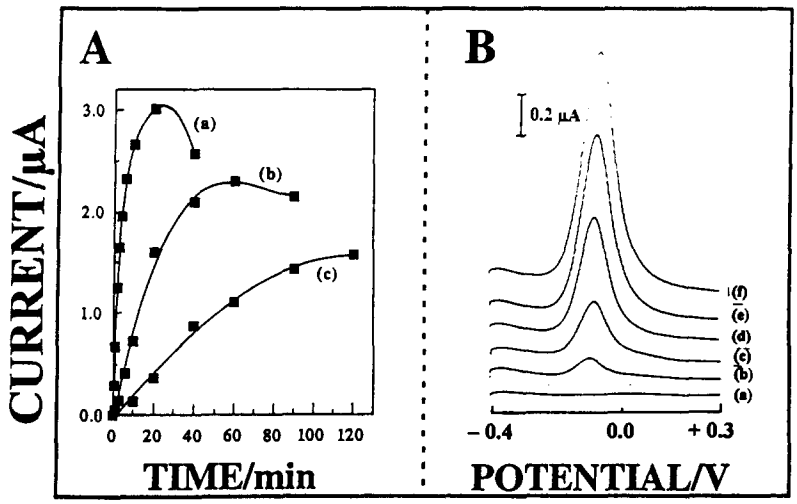


Fig. 4. (A) Dependence of the peak current on the accumulation time; (B) the resulting differential pulse voltammograms. (A) Copper concentrations: (curve a) 100 ppb; (curve b) 10 ppb; (curve c) 1 ppb. (B) Copper concentration, 10 ppb; accumulation times: (curve a) 0 min; (curve b) 3 min; (curve c) 5 min; (curve d) 8 min; (curve e) 12 min; (curve f) 15 min. Other conditions as in Fig. 3.

the preconcentration time for three different copper concentrations (Fig. 4A), as well as the corresponding differential pulse voltammograms for 10 ppb of copper with increasing times. The curves for 100 and 10 ppb of copper in Fig. 4A display an initial linear increase of the peak current with increasing preconcentration times, followed by a leveling off, indicating saturation of the modifier functionalities with copper ions; a slight decrease is observed at very long accumulation times. The corresponding curve for the 1 ppb copper level exhibits a linear increase of up to 60 min preconcentration time, followed again by a horizontal region. There is no deterioration of the peak shape with very long accumulation times, as can be seen from the response of Fig. 4B. Notice also the well-defined response for 10 ppb copper (even at short times of 3–5 min curves b, and c), and the low background current. As expected, the linear range is wider when lower copper concentrations are used, as saturation effects occur only with longer preconcentration periods. The results obtained in this study indicate that the exchange between the copper and the hydronium ions bound to the surface of the modified screen-printed electrode takes place rather slowly.

The lowest achievable limit of detection depends on the preconcentration time used. For a preconcentration period of 10 min, copper levels as low as 0.5 ppb can be determined with high precision (relative standard deviation (RSD), 2%). The detection limit could be even further reduced with longer preconcentration times (although such periods are not practical).

An additional study was carried out to assess the accumulation behavior in quiescent (unstirred) solutions, with the prospect of placing sample drops on these modified screen-printed electrode strips, as is common for stripping assays of lead in urine and drinking water [4]. Experiments showed that the resulting peak currents were approximately five times lower without stirring than with stirring, but that the peak shape was not altered at all. Due to the overall remarkable sensitivity, low parts-per-billion concentrations can be measured for quiescent solutions. The dependence on the preconcentration time without stirring displayed a wider linearity than with stirring, as saturation can be obtained only for very long preconcentrations periods.

As expected for ion-exchange equilibria, the amount of collected ions is related to their solution concentration (as long as saturation effects are not observed). Fig. 5 shows the dependence of the peak current on the concentration of copper in the sample solution, for a 2 min accumulation time. The peak current increases linearly with increasing copper concentration of up to 110 ppb, and then starts to level off, reaching a constant value at 400 ppb, indicating saturation of surface functionalities.

Several other metal ions were examined with respect to their influence on the copper response (50 ppb; 1 min accumulation time). Due to the nature of the electrostatic accumulation

process, interferences from these cations, present in the sample soluution, are expected. However, it was found that at the same concentration level (50 ppb) only Pb(II) interfered strongly, leading to a decrease of the copper signal by 40%; in contrast, Sb(III), Zn(II), Bi(III), Cd(II), Ag(I), Hg(II) and Fe(III) had no or very little effect (less than 10%). A less than 10% change in peak height was observed in the presence of a tenfold excess of Sb(III), Zn(II), Bi(III), Cd(II) and Fe(III). A tenfold excess of Pb(II) and Ag(I) decreased the peak height by 50%, the latter yielding a second peak at about +0.2 V, and an increased background current at the beginning (around −0.4 V). Strong interference was found only for a tenfold excess of mercury.

To investigate the practical applicability, the new strips were employed for the determination of copper in drinking and ground water samples. Fig. 6 displays the results for the drinking water sample. An accumulation time of 2 min was sufficient to yield a defined copper signal for the sample (curve a), as well as for successive standard additions of 10 ppb (curves b–e). A copper value of 12 ppb was estimated based on the resulting standard addition plot. It can clearly be seen that the presence of coexisting inorganic or organic compounds does not affect the shape of the copper signal, and no overlap with other peaks occurs. The

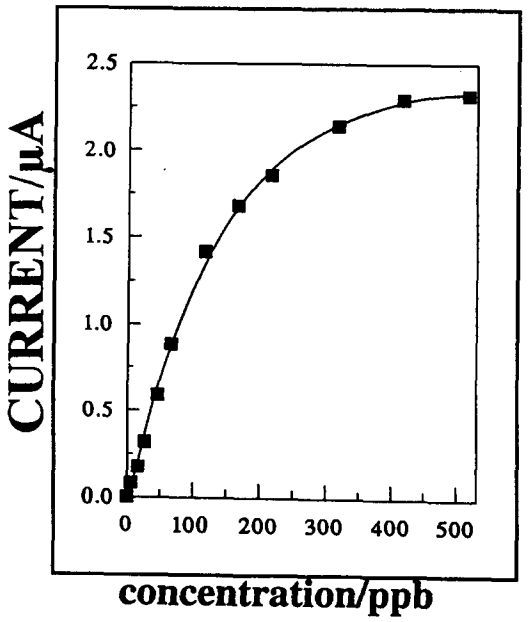


Fig. 5. Dependence of the peak current on the concentration of copper in the sample solution. Accumulation time, 2 min; other conditions as in Fig. 3.

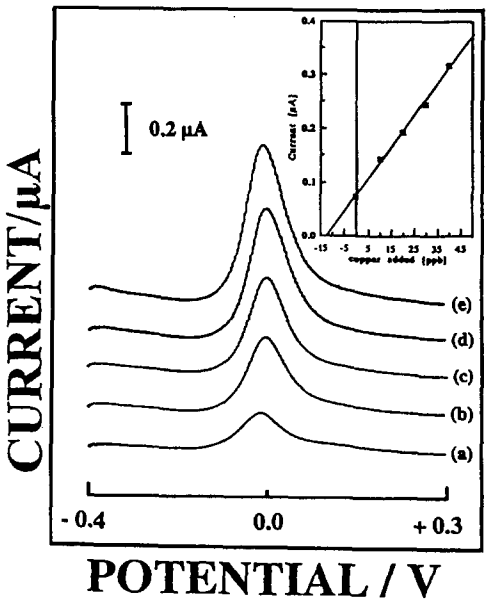


Fig. 6. Assay of drinking water sample. Response for the sample (curve a), as well as for subsequent additions of (curve b) 10 ppb, (curve c) 20 ppb, (curve d) 30 ppb, (curve e) 40 ppb copper (accumulation time, 2 min; other conditions as in Fig. 3). Also shown (inset) is the resulting standard addition plot.

absolute peak currents are slightly lower than those in pure sample solutions, but the precision of the determination is quite high.

In the case of groundwater, a 5 min preconcentration time had to be employed, as the amount of copper was very low (1 ppb). Due to a higher content of interfering substances in the ground water samples, additional peaks, as well as higher background currents, were observed. However, as these additional peaks did not overlap with the copper reoxidation signal, quantitation was possible.

Finally, attempts were made to employ the Dowex-modified screen-printed electrodes in the simultaneous analysis of several metal ions. Fig. 7 displays differential pulse voltammograms for subsequent additions of cadmium, lead and copper to the sample solution, using 2 min preconcentration. Although the conditions had been optimized only for the accumulation of copper, defined oxidation signals are observed for cadmium (at a potential of −0.9 V) and lead (−0.6 V). These peaks increase linearly upon increasing concentration of these metal ions. The peaks are well-separated, with no obvious interference.

In conclusion, the results presented above demonstrate that modified screen-printed electrodes, prepared by direct admixing of the

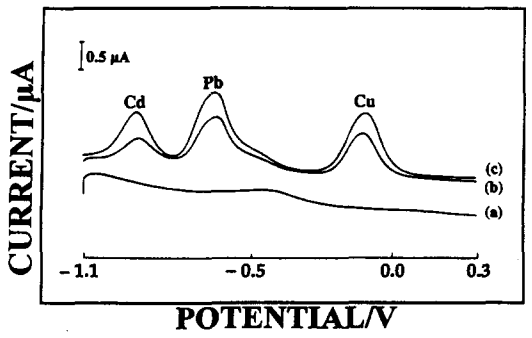


Fig. 7. Simultaneous differential pulse voltammograms for cadmium, lead and copper. Potential, −1.1–+0.3 V; 2 min accumulation time; curve (a) blank; (curve b) 50 ppb Cu, 100 ppb Cd and 100 ppb Pb; (curve c) 100 ppb Cu, 200 ppb Cd and 200 ppb Pb. Other conditions as in Fig. 3.

cation exchanger to the carbon ink prior to the screen-printing process, allows efficient preconcentration of copper(II) ions before voltammetric measurement. High precision and very low detection limits in the nanomolar region can be obtained with short preconcentration times. The modified screen-printed electrode strips provide a useful tool for multielement analysis of metal ions analogous to stripping-based sensors (but without a mercury coating). Future attention will be given to adopting these screen-printed strips for the on-site field screening of environmentally important trace metals. Even though the concept is presented in the context of the Dowex cation exchanger, a number of other sensors based on non-electrolytic preconcentration schemes can be visualized. For example, a new "one-shot" sensor for nitrite was recently developed in our laboratory based on admixing a liquid anion exchanger with carbon inks [10].

## Acknowledgments

Financial support from the Centers for Disease Control and Dow USA is gratefully acknowledged. C. Neuhold wishes to acknowledge fellowships from the Exportakademie der Bundeswirtschaftskammer Oesterreich, as well as from the Oesterreichischen Forschungsgemeinschaft. V.B. Nascimento acknowledges a fellowship from CNPq-Conselho Nacional de Desenvolvimento Cientifico e Tecnologico (Brazil).

## References

[1] J. Wang, Analyst, 119 (1993) 763.
[2] J.P. Hart and S.A. Wring, Electroanalysis, 6 (1994) 617.
[3] M. Alvarez-Icaza and U. Bilitewski, Anal. Chem., 65 (1993) 450R.
[4] J. Wang and B. Tian, Anal. Chem., 64 (1992) 1706.
[5] S. Wring and J.P. Hart, Analyst, 117 (1992) 1281.
[6] D.W. Arrigan, Analyst, 119 (1993) 1953.
[7] J. Wang, B. Green and C. Morgan, Anal. Chim. Acta, 158 (1984) 15.
[8] L. Hernandez, P. Hernandez, M.H. Blanco and M. Sanchez, Analyst, 113 (1988) 41.
[9] L. Hernandez, J.M. Melguizo, M.H. Blanco and P. Hernandez, Analyst, 114 (1989) 397.
[10] C.G. Neuhold, J. Wang, X. Cai and K. Kalcher, Analyst, in press.

ELSEVIER

Talanta 42 (1995) 1799–1802

Talanta

# Book reviews

***Encapsulation and Controlled Release***, edited by D.R. Karsa and R.A. Stephenson, The Royal Society of Chemistry, Cambridge, 1993, viii + 178 pp., £37.50. ISBN 0-85186-615-8.

This book is based on a symposium organised by the North West Region of the Industrial Division of the Royal Society of Chemistry and the Water Soluble Polymers Sector Group of the British Association for Chemical Specialities at UMIST, Manchester, UK on 14–15 October 1992. It is classified as specialist publication No. 138 by the RSC.

The contents consist of 15 papers by industrial and academic researchers from not only the UK but also from Germany, Italy, Denmark, Belgium, the Netherlands and USA. As expected, the majority of topics are related to drug delivery but there are also papers on pesticides, flavours and fragrances, inorganic pigments ($TiO_2$) and enzyme encapsulation.

The multi-disciplinary approach required for this subject area is apparent in this publication but, as it is aimed at chemists, the biological aspects related to release of drugs are kept somewhat in the background. It is mainly the technology of producing microspheres, microparticles and nanoparticles and the use of biodegradable/non-biodegradable polymers that is covered here. Of course, much information in this field is commercially sensitive as teaching old drugs new tricks can be very profitable. This is borne out in the text where most papers are clear and complete whilst a few leave you feeling that some details are missing, perhaps requiring a visit to the patent literature. The paper on the infusion of drugs into polymers, for example, is intriguing but is one of only two presentations which lacks references.

Most of the papers are general rather than specific and are therefore very useful introductions to this area. For example, Industrial Microencapsulation—Polymers for Microcapsule Walls by C.A. Finch, Encapsulation and Controlled Release of Flavours and Fragrances by H.C. Greenblatt et al., and Biodegradable Microspheres for Controlled Drug Release by T.L. Whateley (who is, incidentally, the editor of the Journal of Microencapsulation) are excellent summaries of methods and materials. I also enjoyed reading—and benefited from—the papers on Nanoparticles by J. Kreuter and Softgels by K. Hutchinson.

A useful subject index is provided and the various fonts and print sizes do not detract from the quality of the contributions. Indeed all the papers should be of interest to those involved in the expanding field of controlled release technology and this is certainly a book that I recommend to those working in this area.

P.J. Cox

***Flame Spectrometry in Environmental Chemical Analysis—A Practical Guide***, by M.S. Cresser, The Royal Society of Chemistry, Cambridge, 1994, x + 108 pp., £29.50. ISBN 0-85186-734-0.

Every once in a while being asked to review a book can be a real pleasure and for me this was the case on this occasion. All too often authors are tempted to over-play their pet topics, resulting in the omissions in other often relevant areas, and a resultant imbalance in the final text. Thus such books tend to miss the mark with respect to their target audience. This book however is exactly what its title implies—a practical guide to flame spectrometry and its use in environmental analysis. It is written in a style ideally suited to students and non-specialists who want a no-frills approach, but at the same time want to fully understand what they are doing and what is happening when they use the instrumentation. Thus this book addresses the essential components of flame AAS, AES and AFS instruments, instrumental optimisation and useful techniques to aid analysis such as hydride generation and the use of discrete

ELSEVIER

Talanta 42 (1995) 1799–1802

Talanta

# Book reviews

***Encapsulation and Controlled Release***, edited by D.R. Karsa and R.A. Stephenson, The Royal Society of Chemistry, Cambridge, 1993, viii + 178 pp., £37.50. ISBN 0-85186-615-8.

This book is based on a symposium organised by the North West Region of the Industrial Division of the Royal Society of Chemistry and the Water Soluble Polymers Sector Group of the British Association for Chemical Specialities at UMIST, Manchester, UK on 14–15 October 1992. It is classified as specialist publication No. 138 by the RSC.

The contents consist of 15 papers by industrial and academic researchers from not only the UK but also from Germany, Italy, Denmark, Belgium, the Netherlands and USA. As expected, the majority of topics are related to drug delivery but there are also papers on pesticides, flavours and fragrances, inorganic pigments ($TiO_2$) and enzyme encapsulation.

The multi-disciplinary approach required for this subject area is apparent in this publication but, as it is aimed at chemists, the biological aspects related to release of drugs are kept somewhat in the background. It is mainly the technology of producing microspheres, microparticles and nanoparticles and the use of biodegradable/non-biodegradable polymers that is covered here. Of course, much information in this field is commercially sensitive as teaching old drugs new tricks can be very profitable. This is borne out in the text where most papers are clear and complete whilst a few leave you feeling that some details are missing, perhaps requiring a visit to the patent literature. The paper on the infusion of drugs into polymers, for example, is intriguing but is one of only two presentations which lacks references.

Most of the papers are general rather than specific and are therefore very useful introductions to this area. For example, Industrial Microencapsulation—Polymers for Microcapsule Walls by C.A. Finch, Encapsulation and Controlled Release of Flavours and Fragrances by H.C. Greenblatt et al., and Biodegradable Microspheres for Controlled Drug Release by T.L. Whateley (who is, incidentally, the editor of the Journal of Microencapsulation) are excellent summaries of methods and materials. I also enjoyed reading—and benefited from—the papers on Nanoparticles by J. Kreuter and Softgels by K. Hutchinson.

A useful subject index is provided and the various fonts and print sizes do not detract from the quality of the contributions. Indeed all the papers should be of interest to those involved in the expanding field of controlled release technology and this is certainly a book that I recommend to those working in this area.

P.J. Cox

***Flame Spectrometry in Environmental Chemical Analysis—A Practical Guide***, by M.S. Cresser, The Royal Society of Chemistry, Cambridge, 1994, x + 108 pp., £29.50. ISBN 0-85186-734-0.

Every once in a while being asked to review a book can be a real pleasure and for me this was the case on this occasion. All too often authors are tempted to over-play their pet topics, resulting in the omissions in other often relevant areas, and a resultant imbalance in the final text. Thus such books tend to miss the mark with respect to their target audience. This book however is exactly what its title implies—a practical guide to flame spectrometry and its use in environmental analysis. It is written in a style ideally suited to students and non-specialists who want a no-frills approach, but at the same time want to fully understand what they are doing and what is happening when they use the instrumentation. Thus this book addresses the essential components of flame AAS, AES and AFS instruments, instrumental optimisation and useful techniques to aid analysis such as hydride generation and the use of discrete

sampling devices, all from a user standpoint. The author deliberately avoids specialist theory but uses the first chapter to provide an overview of the subject area to underpin the rest of the book.

Having described the instrumentation the remaining five chapters in the book are devoted to practical analysis. There is a useful chapter on sample preparation and a chapter on interferences and how to overcome them, including a section on background correction in AAS. There is also a chapter which looks at the practical problems of determining individual elements. This chapter has 28 elements listed in turn and a small section on speciation and hybrid techniques. The last two chapters in the book discuss quality control, error detection, the use of reference materials and safety.

The style of this book makes it easy and indeed enjoyable to read, and the 101 pages of text are full of advice and guidance. Clearly some areas are not covered in minute detail—that is not the aim of the book. However there are references throughout, conveniently located at the foot of the page, to aid access to further reading if required. I would warmly recommend this book, although disappointingly it is only available in hardback at the present time and thus possibly beyond the pockets of those who would benefit most from owning a personal copy.

S. Hill

***Undergraduate Instrumental Analysis***, 5th edn., by J.W. Robinson, Dekker, New York, 1994, xxiii + 858 pp., US$65.00. ISBN 0-8247-9215-7.

This is an extensive book (over 800 pages) which has been revised and expanded for the fifth edition. The layout is good and the majority of the diagrams are clearly drawn. At the end of each chapter there are up-to-date references and further readings, some suggested experiments and, as would be expected in an American book, plenty of problems to test the students' understanding. An introductory chapter on 'The Concepts of Analytical Chemistry' is followed by eleven chapters on the various spectrometric techniques plus chapters on chromatography, thermal analysis, surface analysis and electrochemistry. The emphasis is on spectrometry (over 70 percent of the book) so that the whole of chromatography is covered in only 80 pages whereas the infrared and mass spectrometry chapters are both longer. Consequently, the very important techniques of gas and high performance liquid chromatography (particularly the latter) receive insufficient coverage in depth, and high performance capillary electrophoresis, a technique of rapidly-growing importance, is not mentioned at all.

The balance of the material between theory, instrumentation and applications within each chapter is generally good but the treatment of some important topics is too superficial, e.g. the very brief section on the statistical assessment of quantitative data, the causes of curvature in Beer's Law plots, chemical shift, spin–spin splitting and 2-D techniques in nuclear magnetic resonance spectrometry, and the whole of high performance liquid chromatography. In the section of potentiometry, the fluoride ion-selective electrode, one of the best and most widely-used, is dismissed in two lines and gas-sensing electrodes are omitted altogether.

As the book is written for American undergraduates, much of the material is rather basic and possibly more appropriate for first and perhaps second year students taking degree courses in the UK and Europe. The content is variable in quality and although it contains many useful tables of comparative data, particularly on the sensitivities of various analytical techniques, it is most unfortunate that in 1995 'cps' is used instead of Hertz, 'Gauss' instead of Tesla and 'micrometer' in preference to wavenumbers in discussing infrared spectra. Whilst I cannot wholeheartedly recommend this book for the reasons outlined above, there is much useful material in it that is suitable for introductory courses in analytical chemistry.

D. Kealey

***Interfacial Design and Chemical Sensing***, T.E. Mallouk and D.J. Harrison, ACS Symposium Series 561, American Chemical Society, Washington, DC, 1994, xi + 338 pp. ISBN 0-8412-2931-7.

Interfacial Design and Chemical Sensing contains 27 papers from a symposium at the August 1993 American Chemical Society meeting. The papers are organized into three separate categories: New Materials, Structurally Tailored Interfaces and Chemical Sensor Designs.

sampling devices, all from a user standpoint. The author deliberately avoids specialist theory but uses the first chapter to provide an overview of the subject area to underpin the rest of the book.

Having described the instrumentation the remaining five chapters in the book are devoted to practical analysis. There is a useful chapter on sample preparation and a chapter on interferences and how to overcome them, including a section on background correction in AAS. There is also a chapter which looks at the practical problems of determining individual elements. This chapter has 28 elements listed in turn and a small section on speciation and hybrid techniques. The last two chapters in the book discuss quality control, error detection, the use of reference materials and safety.

The style of this book makes it easy and indeed enjoyable to read, and the 101 pages of text are full of advice and guidance. Clearly some areas are not covered in minute detail—that is not the aim of the book. However there are references throughout, conveniently located at the foot of the page, to aid access to further reading if required. I would warmly recommend this book, although disappointingly it is only available in hardback at the present time and thus possibly beyond the pockets of those who would benefit most from owning a personal copy.

S. Hill

***Undergraduate Instrumental Analysis***, 5th edn., by J.W. Robinson, Dekker, New York, 1994, xxiii + 858 pp., US$65.00. ISBN 0-8247-9215-7.

This is an extensive book (over 800 pages) which has been revised and expanded for the fifth edition. The layout is good and the majority of the diagrams are clearly drawn. At the end of each chapter there are up-to-date references and further readings, some suggested experiments and, as would be expected in an American book, plenty of problems to test the students' understanding. An introductory chapter on 'The Concepts of Analytical Chemistry' is followed by eleven chapters on the various spectrometric techniques plus chapters on chromatography, thermal analysis, surface analysis and electrochemistry. The emphasis is on spectrometry (over 70 percent of the book) so that the whole of chromatography is covered in only 80 pages whereas the infrared and mass spectrometry chapters are both longer. Consequently, the very important techniques of gas and high performance liquid chromatography (particularly the latter) receive insufficient coverage in depth, and high performance capillary electrophoresis, a technique of rapidly-growing importance, is not mentioned at all.

The balance of the material between theory, instrumentation and applications within each chapter is generally good but the treatment of some important topics is too superficial, e.g. the very brief section on the statistical assessment of quantitative data, the causes of curvature in Beer's Law plots, chemical shift, spin–spin splitting and 2-D techniques in nuclear magnetic resonance spectrometry, and the whole of high performance liquid chromatography. In the section of potentiometry, the fluoride ion-selective electrode, one of the best and most widely-used, is dismissed in two lines and gas-sensing electrodes are omitted altogether.

As the book is written for American undergraduates, much of the material is rather basic and possibly more appropriate for first and perhaps second year students taking degree courses in the UK and Europe. The content is variable in quality and although it contains many useful tables of comparative data, particularly on the sensitivities of various analytical techniques, it is most unfortunate that in 1995 'cps' is used instead of Hertz, 'Gauss' instead of Tesla and 'micrometer' in preference to wavenumbers in discussing infrared spectra. Whilst I cannot wholeheartedly recommend this book for the reasons outlined above, there is much useful material in it that is suitable for introductory courses in analytical chemistry.

D. Kealey

***Interfacial Design and Chemical Sensing***, T.E. Mallouk and D.J. Harrison, ACS Symposium Series 561, American Chemical Society, Washington, DC, 1994, xi + 338 pp. ISBN 0-8412-2931-7.

Interfacial Design and Chemical Sensing contains 27 papers from a symposium at the August 1993 American Chemical Society meeting. The papers are organized into three separate categories: New Materials, Structurally Tailored Interfaces and Chemical Sensor Designs.

sampling devices, all from a user standpoint. The author deliberately avoids specialist theory but uses the first chapter to provide an overview of the subject area to underpin the rest of the book.

Having described the instrumentation the remaining five chapters in the book are devoted to practical analysis. There is a useful chapter on sample preparation and a chapter on interferences and how to overcome them, including a section on background correction in AAS. There is also a chapter which looks at the practical problems of determining individual elements. This chapter has 28 elements listed in turn and a small section on speciation and hybrid techniques. The last two chapters in the book discuss quality control, error detection, the use of reference materials and safety.

The style of this book makes it easy and indeed enjoyable to read, and the 101 pages of text are full of advice and guidance. Clearly some areas are not covered in minute detail—that is not the aim of the book. However there are references throughout, conveniently located at the foot of the page, to aid access to further reading if required. I would warmly recommend this book, although disappointingly it is only available in hardback at the present time and thus possibly beyond the pockets of those who would benefit most from owning a personal copy.

S. Hill

***Undergraduate Instrumental Analysis***, 5th edn., by J.W. Robinson, Dekker, New York, 1994, xxiii + 858 pp., US$65.00. ISBN 0-8247-9215-7.

This is an extensive book (over 800 pages) which has been revised and expanded for the fifth edition. The layout is good and the majority of the diagrams are clearly drawn. At the end of each chapter there are up-to-date references and further readings, some suggested experiments and, as would be expected in an American book, plenty of problems to test the students' understanding. An introductory chapter on 'The Concepts of Analytical Chemistry' is followed by eleven chapters on the various spectrometric techniques plus chapters on chromatography, thermal analysis, surface analysis and electrochemistry. The emphasis is on spectrometry (over 70 percent of the book) so that the whole of chromatography is covered in only 80 pages whereas the infrared and mass spectrometry chapters are both longer. Consequently, the very important techniques of gas and high performance liquid chromatography (particularly the latter) receive insufficient coverage in depth, and high performance capillary electrophoresis, a technique of rapidly-growing importance, is not mentioned at all.

The balance of the material between theory, instrumentation and applications within each chapter is generally good but the treatment of some important topics is too superficial, e.g. the very brief section on the statistical assessment of quantitative data, the causes of curvature in Beer's Law plots, chemical shift, spin–spin splitting and 2-D techniques in nuclear magnetic resonance spectrometry, and the whole of high performance liquid chromatography. In the section of potentiometry, the fluoride ion-selective electrode, one of the best and most widely-used, is dismissed in two lines and gas-sensing electrodes are omitted altogether.

As the book is written for American undergraduates, much of the material is rather basic and possibly more appropriate for first and perhaps second year students taking degree courses in the UK and Europe. The content is variable in quality and although it contains many useful tables of comparative data, particularly on the sensitivities of various analytical techniques, it is most unfortunate that in 1995 'cps' is used instead of Hertz, 'Gauss' instead of Tesla and 'micrometer' in preference to wavenumbers in discussing infrared spectra. Whilst I cannot wholeheartedly recommend this book for the reasons outlined above, there is much useful material in it that is suitable for introductory courses in analytical chemistry.

D. Kealey

***Interfacial Design and Chemical Sensing***, T.E. Mallouk and D.J. Harrison, ACS Symposium Series 561, American Chemical Society, Washington, DC, 1994, xi + 338 pp. ISBN 0-8412-2931-7.

Interfacial Design and Chemical Sensing contains 27 papers from a symposium at the August 1993 American Chemical Society meeting. The papers are organized into three separate categories: New Materials, Structurally Tailored Interfaces and Chemical Sensor Designs.

The New Materials category includes papers on subjects from zeolite synthesis to devices in which dye absorption and polymer oxidation are observed through their effect on high temperature superconductors. Some of the new materials are designed to offer new approaches to selectivity, e.g. synthetic zeolites and metal phosphonate thin films with molecular voids of known dimensions. Other goals are to increase the effective surface area of sensors and to prepare membranes with photogated ion channels.

The papers in the Structurally Tailored Interfaces are more focused towards a particular goal. Several papers involve systems in which a host–guest binding event modifies the permeability of a thin layer on the surface of an electrode. Other topics range from a study of nucleation and growth of molecular crystals on molecular interfaces to the preparation of ordered monolayers by molecular beam epitaxy.

The papers in the Chemical Sensor Designs section described the actual preparation of sensor systems. It includes papers on the use of chemical modified electrodes, interfaces for acoustic wave devices and micromachined chemical systems. Even in this section the emphasis is on illustrating sensor concepts rather than on solving particular problems.

Despite the diversity of topics, it is possible to make several generalizations about this book. Throughout, the quality of the science is high. There is a strong emphasis on preparing thin films of known structure and then characterizing the properties of these films. While many different types of films are described, self-assembled monolayers and Langmuir–Blodgett films are common to many of the papers in the first two sections. The most common characterization methods are electrochemistry and atomic force microscopy. Interestingly, the emphasis shifts to polymer films in the Chemical Sensor Design section, an indicator perhaps that polymer films remain the most practical for actual sensors at this point in time.

The emphasis throughout is on new materials and concepts.

W.R. Seitz

***Medicinal Chemistry—Principles and Practice***, edited by F.D. King, The Royal Society of Chemistry, Cambridge, 1994, xxiv + 314 pp., £39.50, Softback. ISBN 0-85186-494-5.

As a member of a pharmaceutical department I was particularly interested in reviewing this book as many of the topics covered are of direct relevance to activities in the pharmaceutical industries. Indeed much of the content is provided by UK authors from Zeneca, SmithKline Beecham, Glaxo, Fisons, etc. and is directed at graduate chemists—primarily synthetic chemists who have just started their careers in industry. The book represents the lectures delivered at the 7th RSC Medicinal Chemistry School held in 1993 at the University of Kent, Canterbury, UK.

There are 19 chapters in the book and each one is written by a different author. There is no stated intention to group these chapters into sections but the editor has, I believe, arranged them in a logical order which takes the reader through some of the basic concepts and ends with several examples of case histories.

The first 6 chapters concentrate on biochemical aspects: drug-receptor interactions, signal transduction and second messengers, enzyme inhibitors, biological evaluation, pharmacokinetics, and drug metabolism. These subjects should have been previously covered by biochemists, pharmacologists and pharmacists but perhaps not by graduate chemists. Bibliographies and details of further reading related to these chapters also help the chemist come to grips with these topics.

Hopefully, the chemist will feel more at home with the next three chapters: physiochemical properties and drug design, quantitative structure-activity relationships, and use of computational chemistry techniques. Again, space permits only an overview of these subjects.

The next chapter on patent medicine is excellent and is complimented by the ingredient most welcomed by students young and old—humour. The following chapter on molecular biology, which gives a brief overview of gene cloning, is most appropriate to any modern text on medicinal chemistry.

Finding a starting point is the basis of the next three chapters which are entitled: devising a research strategy, past approaches to discovering new drugs, and bioisosteres, conformational restriction and pro-drugs. Chapters on specific case histories follow and conclude with a chapter on drug development. There are various appendices and a subject index.

The New Materials category includes papers on subjects from zeolite synthesis to devices in which dye absorption and polymer oxidation are observed through their effect on high temperature superconductors. Some of the new materials are designed to offer new approaches to selectivity, e.g. synthetic zeolites and metal phosphonate thin films with molecular voids of known dimensions. Other goals are to increase the effective surface area of sensors and to prepare membranes with photogated ion channels.

The papers in the Structurally Tailored Interfaces are more focused towards a particular goal. Several papers involve systems in which a host–guest binding event modifies the permeability of a thin layer on the surface of an electrode. Other topics range from a study of nucleation and growth of molecular crystals on molecular interfaces to the preparation of ordered monolayers by molecular beam epitaxy.

The papers in the Chemical Sensor Designs section described the actual preparation of sensor systems. It includes papers on the use of chemical modified electrodes, interfaces for acoustic wave devices and micromachined chemical systems. Even in this section the emphasis is on illustrating sensor concepts rather than on solving particular problems.

Despite the diversity of topics, it is possible to make several generalizations about this book. Throughout, the quality of the science is high. There is a strong emphasis on preparing thin films of known structure and then characterizing the properties of these films. While many different types of films are described, self-assembled monolayers and Langmuir–Blodgett films are common to many of the papers in the first two sections. The most common characterization methods are electrochemistry and atomic force microscopy. Interestingly, the emphasis shifts to polymer films in the Chemical Sensor Design section, an indicator perhaps that polymer films remain the most practical for actual sensors at this point in time.

The emphasis throughout is on new materials and concepts.

W.R. Seitz

***Medicinal Chemistry—Principles and Practice***, edited by F.D. King, The Royal Society of Chemistry, Cambridge, 1994, xxiv + 314 pp., £39.50, Softback. ISBN 0-85186-494-5.

As a member of a pharmaceutical department I was particularly interested in reviewing this book as many of the topics covered are of direct relevance to activities in the pharmaceutical industries. Indeed much of the content is provided by UK authors from Zeneca, SmithKline Beecham, Glaxo, Fisons, etc. and is directed at graduate chemists—primarily synthetic chemists who have just started their careers in industry. The book represents the lectures delivered at the 7th RSC Medicinal Chemistry School held in 1993 at the University of Kent, Canterbury, UK.

There are 19 chapters in the book and each one is written by a different author. There is no stated intention to group these chapters into sections but the editor has, I believe, arranged them in a logical order which takes the reader through some of the basic concepts and ends with several examples of case histories.

The first 6 chapters concentrate on biochemical aspects: drug-receptor interactions, signal transduction and second messengers, enzyme inhibitors, biological evaluation, pharmacokinetics, and drug metabolism. These subjects should have been previously covered by biochemists, pharmacologists and pharmacists but perhaps not by graduate chemists. Bibliographies and details of further reading related to these chapters also help the chemist come to grips with these topics.

Hopefully, the chemist will feel more at home with the next three chapters: physiochemical properties and drug design, quantitative structure-activity relationships, and use of computational chemistry techniques. Again, space permits only an overview of these subjects.

The next chapter on patent medicine is excellent and is complimented by the ingredient most welcomed by students young and old—humour. The following chapter on molecular biology, which gives a brief overview of gene cloning, is most appropriate to any modern text on medicinal chemistry.

Finding a starting point is the basis of the next three chapters which are entitled: devising a research strategy, past approaches to discovering new drugs, and bioisosteres, conformational restriction and pro-drugs. Chapters on specific case histories follow and conclude with a chapter on drug development. There are various appendices and a subject index.

Overall an excellent book for those making a move into pharmaceutical/medicinal chemistry research and for those who wish to broaden their knowledge of all the disciplines involved in this area.

P.J. Cox

***A spreadsheet workbook for quantitative chemical analysis***, By R. de Levie, McGraw-Hill, New York, 1992, approx. 170 pp., spiral bound. ISBN 0-07-016274-3.

This workbook begins with a brief introduction to the use of a spreadsheet, in this case Quattro Pro. In the rest of the book, instructions are given for entering chemical calculations into the spreadsheet; at first, in some detail, but later, just in outline, as the student is assumed to be become more familiar with the software. The topics covered include acid–base equilibria (simple and more complicated), acid–base titrations, logarithmic concentration diagrams for calculation of pH, complexation equilibria, extraction equilibria, precipitation equilibria, electrochemical equilibria, redox titrations, activity effects, curve-fitting, differentiation, integration, and finding roots.

Much of the treatment is rather detailed, and in the UK would probably be considered suitable for use in postgraduate rather than undergraduate courses, because it would be difficult to provide enough computer time for an undergraduate class to work through all the material. It will be a valuable resource for postgraduate students–I would have found it invaluable for my own Ph.D. work, in which I made use of the textbooks referred to by this author.

It is a problem of books that utilize computer packages that they very quickly become dated. This book is no exception, particularly because the past two years have seen *Windows* applications virtually take over the DOS ones. Students find the new *Windows* spreadsheets (such as *QP for Windows*) to be very much easier to use than their DOS predecessors, so Chapter 1 will soon be seen as out-of-date. However, since much of the rest of this book consists of chemistry and chemical equations, it should remain of value for use with other spreadsheet packages.

M. Masson

Overall an excellent book for those making a move into pharmaceutical/medicinal chemistry research and for those who wish to broaden their knowledge of all the disciplines involved in this area.

P.J. Cox

***A spreadsheet workbook for quantitative chemical analysis***, By R. de Levie, McGraw-Hill, New York, 1992, approx. 170 pp., spiral bound. ISBN 0-07-016274-3.

This workbook begins with a brief introduction to the use of a spreadsheet, in this case Quattro Pro. In the rest of the book, instructions are given for entering chemical calculations into the spreadsheet; at first, in some detail, but later, just in outline, as the student is assumed to be become more familiar with the software. The topics covered include acid–base equilibria (simple and more complicated), acid–base titrations, logarithmic concentration diagrams for calculation of pH, complexation equilibria, extraction equilibria, precipitation equilibria, electrochemical equilibria, redox titrations, activity effects, curve-fitting, differentiation, integration, and finding roots.

Much of the treatment is rather detailed, and in the UK would probably be considered suitable for use in postgraduate rather than undergraduate courses, because it would be difficult to provide enough computer time for an undergraduate class to work through all the material. It will be a valuable resource for postgraduate students–I would have found it invaluable for my own Ph.D. work, in which I made use of the textbooks referred to by this author.

It is a problem of books that utilize computer packages that they very quickly become dated. This book is no exception, particularly because the past two years have seen *Windows* applications virtually take over the DOS ones. Students find the new *Windows* spreadsheets (such as *QP for Windows*) to be very much easier to use than their DOS predecessors, so Chapter 1 will soon be seen as out-of-date. However, since much of the rest of this book consists of chemistry and chemical equations, it should remain of value for use with other spreadsheet packages.

M. Masson

ELSEVIER

Talanta 42 (1995) 1803–1810

Talanta

# Binding of cadmium to Laurentide fulvic acid. Justification of the functionalities assigned to the predominant acidic moieties in the fulvic acid molecule

Andrew S. Mathuthu [a], James H. Ephraim [b,*]

[a] *Department of Chemistry, University of Zimbabwe, P.O. Box MP 167, Mount Pleasant, Harare, Zimbabwe*
[b] *Department of Water and Environmental Studies, Linköping University, S-581 83, Linköping, Sweden*

Received 26 January 1995; revised 10 April 1995; accepted 11 April 1995

**Abstract**

The binding of cadmium to a fulvic acid (FA) extracted from peat was studied as a function of pH (4–8), ionic strength (0.01 and 0.10 M $NaNO_3$) and ratio of fulvic acid to metal ion concentrations (FA/Cd = 8, 4, and 2). An overall complex formation function of approximately $10^{3.14}$ was determined to enable comparison with previous studies. Additionally, literature values of complex formation constants were employed to describe the interaction between Cd(II) and the individual acidic sites. A good prediction of the experimental results is considered as a justification of the functionalities assigned to the predominant acidic sites in the fulvic acid molecule.

*Keywords:* Cadmium; Fulvic acid; Functionalities

## 1. Introduction

The importance of humic substances in terrestrial and aquatic environments is measured by the role they play in the mobility and distribution of metal ions and low-molecular weight organics. Even though many papers have been published on the binding of metal ions by humic substances, there is still a lack of complete understanding of the metal–humate equilibrium, primarily because of inadequate characterization of the humic substance molecule as a ligand. Earlier studies involving humic substances were carried out by agronomists and soil scientists, but recently the solution chemistry of these natural organic acids has aroused the interest of researchers from different disciplines [1–9]. The complicating factors influencing the solution chemistry of these natural organic acids have been hypothesized to be the functional group heterogeneity and the heterogeneity in the molecular size and shape leading to ionic strength effects [1,2,5–8]. Our earlier adaptation of the Gibbs–Donnan-based model to humic substances has prompted research into the identification of acidic functionalities in the fulvic acids, e.g. moieties with $pK_a \leqslant 3$ [9].

Despite the consensus among researchers that natural organic acids (humic substances) are heterogeneous with respect to both molecular weight and functional group, descriptions of metal interactions with these substances have failed to take such characteristics into consideration. Some recent metal–humate interaction papers have considered the functional group heterogeneity using the discrete ligand model and the continuous distribution model [2–8]. In an earlier paper [10], the dissociation properties of Laurentide fulvic acid have been described following the Gibbs–Donnan-based approach [1] and identifying the predominant

* Corresponding author.


*SSDI* 0039-9140(95)01627-9

acidic sites. Such a consideration draws criticism from various schools which believe that a continuous distribution approach must be employed. However, we are guided by the philosophy that in the formation of a stable compound, a limited number of vectors converge to form the product; thus, the overall properties may be described by considering the most predominant components of the material. In this paper, the binding of Cadmium by a well-characterized soil fulvic acid is described by employing the functional groups identified in an earlier acid–base analysis, and the stability constants reported in the literature for the complex formation between Cd(II) and the monomeric acid envisaged to resemble the functional group in the fulvic acid molecule. In order to facilitate a comparison of our results with earlier work, an overall complex formation function had additionally been computed for the Cd–fulvate systems studied.

## 2. Experimental

### 2.1. Chemicals and materials

Analytical grade chemicals, $Cd(NO_3)_2$, $HNO_3$, $NaNO_3$, were employed for the preparation of all reagents. The fulvic acid, extracted from peat, was obtained from the Department of Chemistry, Concordia University at Montreal, Canada [11]. Potentiometric titrations of the fulvic acid have been performed and the predominant sites responsible for the observed acidic behaviour have been proposed [12]. The analytical concentrates used to prepare NaOH, which was employed to obtain a range of pH values, and $NaNO_3$, which was used to alter bulk electrolyte concentrations, were purchased from J.T. Baker Chemicals.

### 2.2. Methods

Two approaches were used in the ion-selective electrode technique employed in the study. In the first approach, starting with an initial ratio of fulvic acid (FA) to metal ion, the proton and metal ion concentrations were determined after each addition of NaOH. The concentration of fulvic acid employed in the studies was fixed at 100 ppm ($7.6 \times 10^{-3}$ M), while a range of metal ion concentrations ($9.8 \times 10^{-5}$–$4.0 \times 10^{-4}$ M) was used. In the second approach, the initial degree of dissociation of the FA was fixed, and the ratio of metal to FA was changed by stepwise addition of metal ion. The equilibrium concentrations of both proton and metal ions were measured with the appropriate electrode at each addition of metal ion. Details of the experimental procedure are described elsewhere [13,14].

## 3. Heterogeneity considerations

A heterogeneous ligand like fulvic or humic acid could potentially bind metal ions both with and without the release of protons. The extent of proton release is a direct function of the $pK_a$ of the acid and the free energy of complex formation, $\Delta G$. The overall equilibrium may, however, be described by considering each acid site to be involved in a one-to-one complexation mode with the metal as follows:

$$S_i + M \rightleftharpoons S_iM \tag{1}$$

This representation implies that at equilibrium, each active site, $S_i$, reacts with the metal ion, M, to yield a complex, $S_iM$. All species are in equilibrium with each other, their relative concentrations determined by their respective free energy of formation, $\Delta G_{SiM}$. It is necessary to note that in such a consideration, site-to-site interactions have not been incorporated because there is no available method for their determination.

For a given initial concentration of metal ions, $M_T$, the fraction of metal bound, $\theta_M$, is given by

$$\theta_M = \frac{\sum M_{b_i}}{M_T} = \frac{\sum \beta_i A_i}{1 + \sum \beta_i A_i} \tag{2}$$

where $\beta_i$ is the complex formation constant (equivalent $l^{-1}$) for each site and $A_i$ is the concentration (equivalent $l^{-1}$) of the ionised form of each acid site. At each experimental pH, if the metal ion content is determined simultaneously, $\theta_M$, may be calculated and $A_i$ for the individual site may also be estimated via the application of the unified physicochemical approach [1,15], where four to five predominant acid sites are conceptualized. In the presence of metal ions, material balance considerations allow the following to be written for each site:

$$Ha_{i,T} = A_{i,f} + HA_i + A_{i,b} \tag{3}$$

Table 1
Site characterization of Laurentide fulvic acid and stability constants employed to predict Cd(II) binding to the envisaged sites (see Ref. [12])

| Site | $pK_a$ | Abundance | Functionality | Stability constant |
|---|---|---|---|---|
| I | 1.7 | 0.320 | -COOH | 25 |
| II | 3.0 | 0.210 | -COOH | 25 |
| III | 4.0 | 0.204 | -COOH | 25 |
| IV | 5.1 | 0.140 | -OH | $10^{3.83}$ |
| V | 6.5 | 0.126 | -OH | $10^{5}$ |

where $HA_{i,T}$ and $HA_i$ are the respective concentrations (equivalent $l^{-1}$) of the total titratable and the protonated form of the acid site at equilibrium, $A_{i,f}$ is the ionised form of the acid at equilibrium and $A_{i,b}$ is the bound form of the acid site. Rearrangement of Eq. (3) yields

$$A_{i,f} = \left( \frac{HA_{i,T}}{1 + \frac{H}{K_i} + \beta_i M_f} \right) \quad (4)$$

where $K_i$ is the dissociation constant of the acid site, $\beta_i$ is the complex formation constant for reaction in Eq. (1), $M_f$ is the free metal ion concentration and $H$ is the proton concentration. Incorporation of Eq. (4) into Eq. (2) yields Eq. (5), where $f_i$ is the fraction of the $i$th site and $HA_T$ is the total concentration of titratable acid in the system:

$$\left[ \frac{\theta_M}{(1-\theta_M)} \right] \frac{1}{HA_T} = \sum_{i=1}^{n} \left( \frac{\beta_i f_i}{1 + \frac{H}{K_i} + \beta_i M_f} \right) \quad (5)$$

Note that $HA_{i,T}$ and $HA_T$ are related as follows:

$$HA_{i,T} = f_i HA_T \quad (6)$$

The left-hand-side (LHS) of Eq. (5) is obtainable from experimental values and thus designated as experimental, while the right-hand-side (RHS) of the equation is obtained using literature values of $\beta_i$ [16] and $f_i$ obtained from fitting potentiometric titrations (see Table 1). The complexation constant for the interaction between Cu(II) and monomeric acids is directly related to the $pK_a$ of the acid [16,17]. The absence of such a linear relationship has motivated the use of a single complex formation constant of 25 for the interaction between Cd(II) and the -COOH moieties. The acid site IV is considered to mimic an enolic -OH which, via tautomerism, resembles an acetylacetone. The value of $10^{3.83}$ reported for $Cd^{2+}$–acetylacetone complexation constant has been employed. Acid site V has been envisaged to resemble a kojic acid arrangement, i.e. an -OH group in an ortho position to a carbonyl group. The complex formation constant of $10^{5.0}$ has thus been employed in this exercise.

## 4. Results

In the first experimental approach, where standard alkali was added to an initial ratio of fulvic acid to metal ion, the binding of Cd(II) by Laurentide fulvic acid, presented in Fig. 1, followed the pattern which may be summarized as follows. The fraction of metal ion bound generally:

(1) increased with an increase in pH for all FA/Cd(II) ratios;

(2) increased with a decrease in ionic strength for the same FA/Cd(II) ratio;

(3) increased with an increase in FA/Cd(II) ratio at the same ionic strength.

The increase in the fraction of metal bound with an increase in pH for all systems has been attributed to an increase in ionization of the fulvic acid molecule. Such an ionized species, $A^-$, is considered to be involved in binding with the $Cd^{2+}$ ion. It must be noted, however, that the fraction of Cd(II) bound in the pH range of 4–8 reaches a maximum of 0.7, as compared to the case of Cu(II) binding which reaches a maximum of 1 at pH values as low as 5 [17].

The increase in fraction of Cd(II) bound with a decrease in ionic strength for the same FA/Cd(II) ratio may be explained by the electrolyte screening effect being minimal at lower ionic strength and increasing with an increase in ionic strength. Such an increase in screening leads to the effect of low binding at higher ionic strength. In Fig. 1, using the same FA/Cd(II) ratio of 4, a decrease in ionic strength from 0.100 M $NaNO_3$ to 0.010 M yielded a

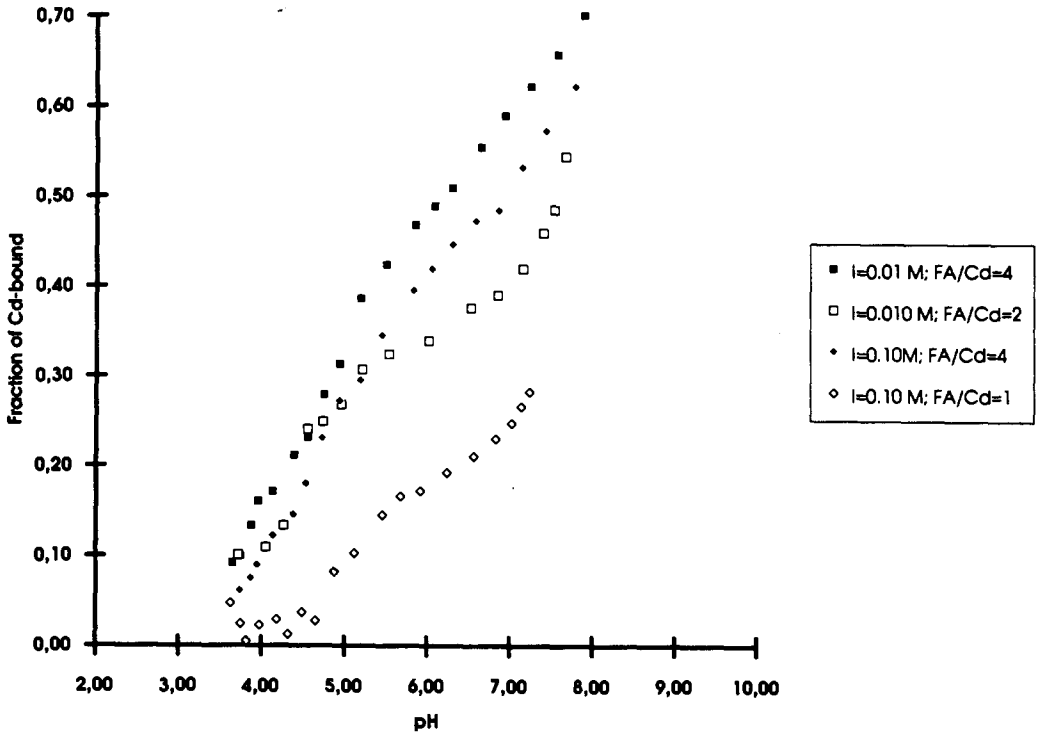


Fig. 1. The fraction of Cd(II) bound as a function of pH, ionic strength and the initial ratio of FA/Cd(II) for the system where aliquots of standard base were added to an initial fixed ratio of FA/Cd(II).

pH-insensitive increase of approximately 0.07 in the fraction of Cd(II).

The increase in the fraction of Cd(II) bound with an increase in FA/Cd(II) ratio is explicable by the argument that more ligands are available to effect more binding. However, a decrease in FA/Cd(II) ratio (especially with Cd(II) concentrations approaching that of fulvic acid) may induce considerable aggregation in the fulvic acid molecule [18]. That this may be the situation can be inferred from the characteristically different shape of the plots in Fig. 1 in cases where the amount of Cd(II) is increased. At an ionic strength of 0.01 M $NaNO_3$, an increase in the FA/Cd(II) ratio from 2 to 4 yielded a pH-dependent increase in the fraction of Cd(II) bound which ranged from 0.06 to 0.20 in the pH range of 4–7 (Fig. 1). At an ionic strength of 0.10 M $NaNO_3$, an increase in the FA/Cd(II) ratio from 1 to 4 yielded a similar pH-dependent increase in the fraction of Cd(II) bound, which ranged from 0.08 to 0.29 in the pH range of 4–7. The results of the second experimental approach (addition of metal ion to FA at a defined initial degree of ionization) showed similar effects of ionic strength and ratio of FA/Cd(II) on the binding pattern (Fig. 2). The fraction of metal bound decreased with an increase in the total amount of cadmium. For the same amount of cadmium added, the higher the pH, the higher the fraction of metal bound. The inverse relationship between ionic strength and the fraction of metal bound is additionally illustrated.

The results of Cd(II) binding to Laurentide fulvic acid obtained as a function of pH have been analyzed via the resolution of an overall complex formation function (Table 2) to allow comparison with previous results [19–24]. The overall complex formation function, $\beta_{ov}$, was estimated by the following equation:

$$\beta_{ov} = \frac{\sum M_b}{M_f \gamma_{M^{z+}} \sum A^-} \quad (7)$$

where $\Sigma M_b$ is the total amount of metal bound, $M_f$ is the free metal ion concentration, $\gamma_M$ is the activity coefficient of the metal ion, and $\Sigma A^-$ is the total amount of the ionized form of the fulvic acid. The activity coefficients yielded $\log \beta_{ov}$ values (3.3–3.2) essentially equivalent for the system at 0.01 and 0.10 M $NaNO_3$ bulk electrolyte concentrations. The only deviation was the lower value (2.69) obtained at an ionic strength of 0.10 M $NaNO_3$ when the Cd(II) concentration was slightly higher than the fulvic acid concentration. These values reported in Table 2 are significantly lower than earlier reported constants for

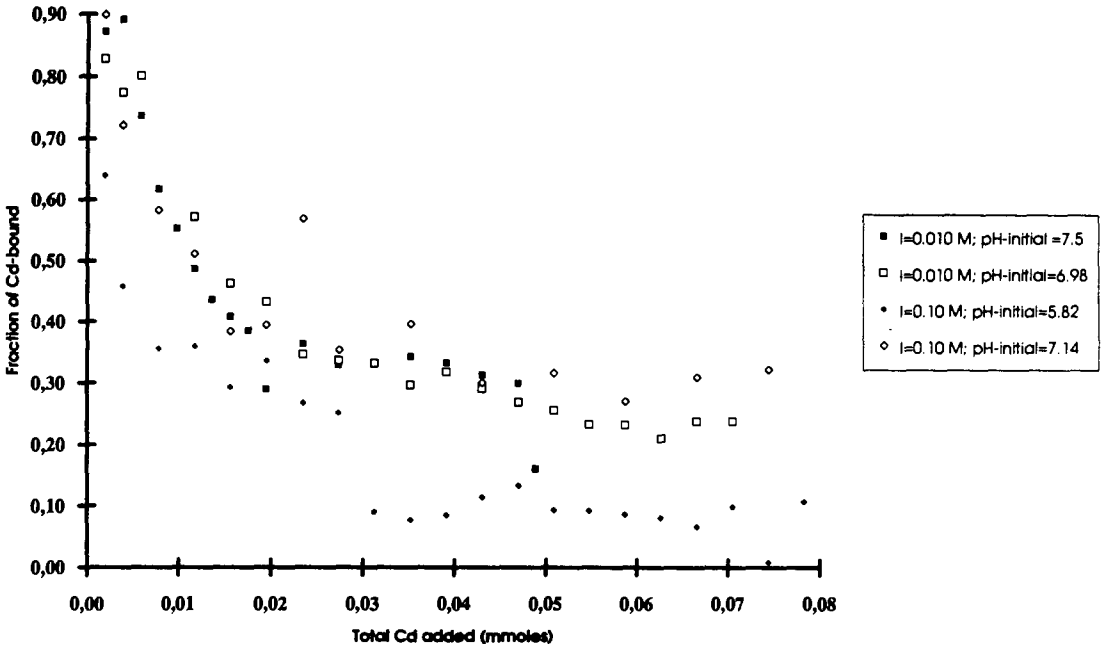


Fig. 2. The fraction of Cd(II) bound as a function of total Cd(II) added, pH and ionic strength for the system where Cd(II) was added to a fixed initial degree of neutralization (pH) of the fulvic acid.

Cd(II) binding [19,21], but are in good agreement with others [20,22].

### 4.1. Heterogeneity considerations

The use of stability constants to describe the complex formation between Cd(II) and the proposed functional group in the fulvic acid molecule (Table 1) has allowed a comparison of the RHS of Eq. (5) (model computed) to the LHS of the equation (experimental). The results of such an exercise are shown in Figs. 3 and 4. It should be noted that the object of the exercise has not been to fit the LHS with the RHS by adjusting parameters. Rather, it has been the goal to describe how best the experimental data are described using literature values of stability constants considered to mimic the interaction of Cd(II) with the acidic moieties postulated to be present in the fulvic acid molecule.

The results shown in Figs. 3 and 4 give testimony that the envisaged functionality given to the predominant acidic sites in the fulvic acid molecule is reasonable. In Fig. 3(a), the binding of cadmium to Laurentide FA in 0.010 M $NaNO_3$ at two different ratios of FA/Cd is reasonably predicted by the use of the literature values of complex formation constants. In Fig. 3(b), the model computed parameters appear larger than the experimental values for the Cd(II)–FA system at an ionic strength of 0.100 M $NaClO_4$. However, the pattern of the experimental values as a function of pH is closely followed by the model computed values. In Figs. 4(a) and 4(b), the results of the model computed comparison with the experiment for the system where Cd(II) was added to fulvic acid at a defined initial degree of neutralization are shown. At both ionic strengths and for all the different initial pH values, the model computed values (RHS of

Table 2
Resolved overall complex formation function for the interaction between Laurentide fulvic acid and cadmium

| No. | FA (mmol $ml^{-1}$) | Cd (mmol $ml^{-1}$) | $I(NaNO_3)$ | pH range | $\log \beta_{ov}(M^{-1})$ |
|---|---|---|---|---|---|
| 1 | $7.69 \times 10^{-4}$ | $1.96 \times 10^{-4}$ | 0.010 M | 3.6–7.9 | $3.28 \pm 0.30$ |
| 2 | $7.69 \times 10^{-4}$ | $3.92 \times 10^{-4}$ | 0.010 M | 3.7–7.7 | $3.24 \pm 0.20$ |
| 3 | $7.69 \times 10^{-4}$ | $1.96 \times 10^{-4}$ | 0.100 M | 3.7–7.8 | $3.36 \pm 0.33$ |
| 4 | $7.69 \times 10^{-4}$ | $7.83 \times 10^{-4}$ | 0.100 M | 3.6–7.2 | $2.69 \pm 0.50$ |

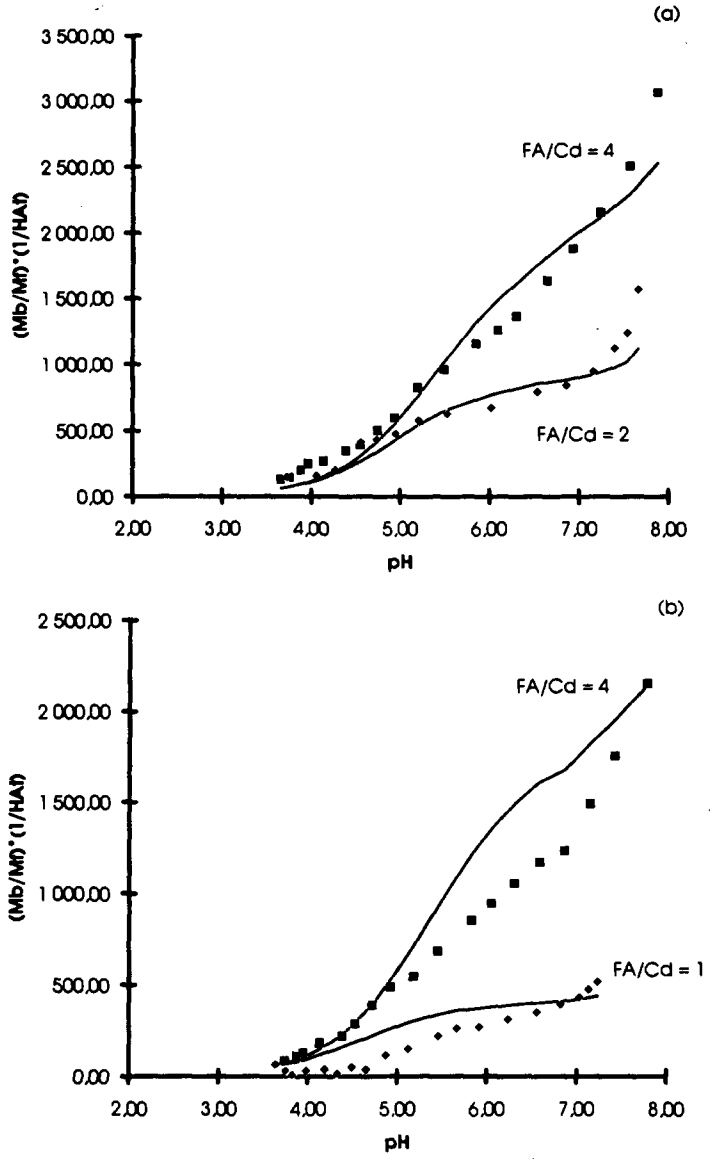


Fig. 3. Comparison of model predicted (RHS of Eq. 5) and experimental (LHS of Eq. 5) values for the Cd(II)–fulvate system where aliquots of base were added to an initial fixed ratio of FA/Cd(II). The model predicted values are designated by the continuous line. (a) $I = 0.010$ M $NaClO_4$; (b) $I = 0.100$ M $NaClO_4$. The ratios of FA/Cd(II) are the same as in Fig. 1.

Eq. 5) compare reasonably well with the experimental values (LHS of Eq. 5). It should be noted that it has not been the objective to fit the experimental values, otherwise the stability constants in Table 1 would have been changed until a perfect fit was obtained between the model computed and the experimental values.

## 5. Discussions and conclusions

The binding of Cd(II) to Laurentide fulvic acid has been described by considering the most predominant oxygen-containing functional groups postulated to be present in the fulvic acid molecule [10]. The description of metal–humate interactions by estimating the binding due to the most predominant functional groups existent in the humic substance molecule is considered to be a better treatment of the system than considering the humic substance as a "black-box" ligand with some average affinity. The complex formation constant reported for the binding of Cd(II) to the monomeric oxygen-containing functional group has thus been utilized to describe the

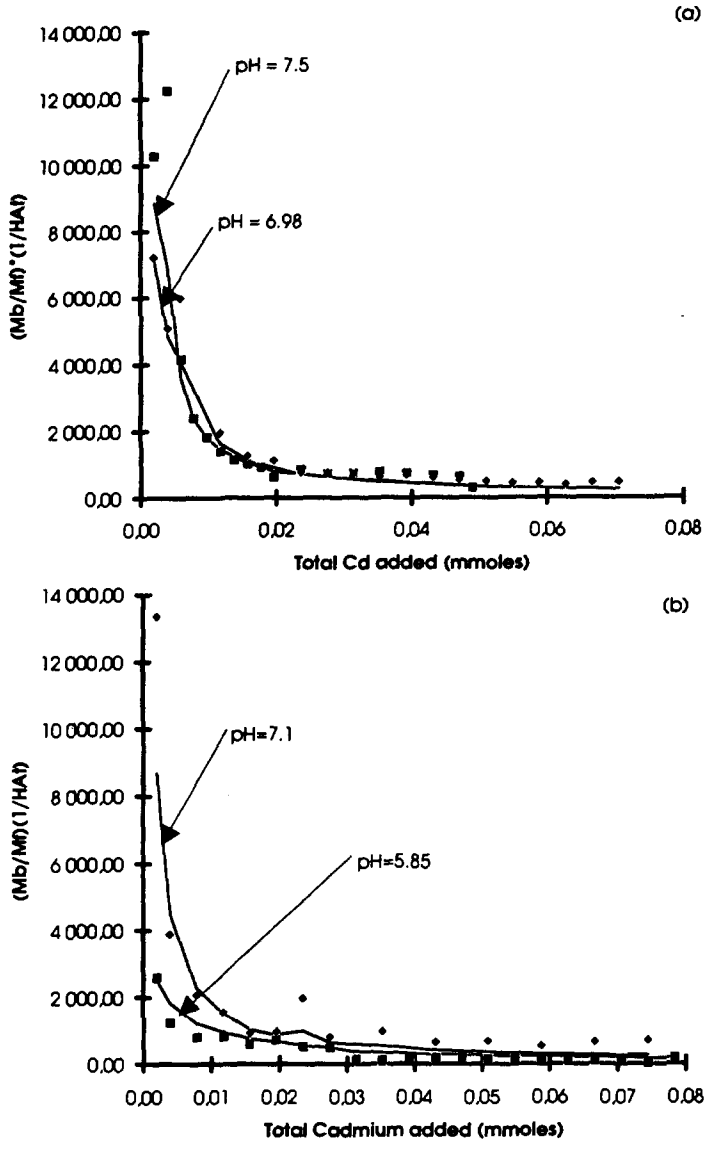


Fig. 4. Comparison of model predicted (RHS of Eq. 5) and experimental (LHS of Eq. 5) values for the Cd(II)–fulvate system where aliquots of standard Cd(II) were added to a fulvic acid solution at an initial fixed pH. The model predicted parameter is designated by the continuous line. (a) $I = 0.010$ M $NaClO_4$; (b) $I = 0.100$ M $NaClO_4$. The initial pH values are the same as in Fig. 2.

experimentally observed complexation. The good prediction of the experiment by the model is considered to justify the hypothesized functionality in the fulvic acid molecule. The novelty of the approach is the possibility it provides for the design of experimental techniques towards the identification of the total functional group heterogeneity in the humic substances [9,25]. It should be noted that the approach does not rely on the luxury of just fitting experimental data, but rather places emphasis on chemical-based verification of the proposed functional group. With this philosophy, it may be stated that the proposed functional groups in the Laurentide fulvic acid are reasonable (Figs. 3 and 4).

## Acknowledgements

The authors are grateful to the Swedish Natural Science Research Council and the Swedish Agency for Research Cooperation with Developing Countries for financial support.

## References


[1] J. Ephraim, S. Alegret, A. Mathuthu, M. Bicking, R.L. Malcolm and J.A. Marinsky, Environ. Sci. Technol., 20 (1986) 357.

[2] E. Tipping and M.A. Hurley, Geochim. Cosmochim. Acta, 56 (1992) 3627.

[3] D.S. Gamble, A.W. Underdown and C.H. Langford, Anal. Chem., 52 (1980) 1901–1908.

[4] J.D. Allison and E.M. Perdue, in N. Senesi and T. Miano (Eds.), Humic Substances in the Global Environment and Implications on Health., Elsevier, Amsterdam, 1994, p. 927.

[5] J.C.M. De Wit, W.H. Van Riemsdijk and L.K. Koopal, Environ, Sci. Technol., 27 (1993) 2005–2014.

[6] B.M. Bartschat, S.E. Cabaniss and F.M.M. Morel, Environ. Sci. Technol., 26 (1992) 284.

[7] J.A. Marinsky, in J.A. Marinsky and Y. Marcus (Eds.), Ion Exchange and Solvent Extraction, Vol. 11, Marcel Dekker, New York, 1993, pp. 237–334.

[8] M.F. Benedetti, C.J. Milne, D.G. Kinniburgh, W.H. van Riemsdijk and L.K. Koopal, Environ. Sci. Technol., 29 (1995) 446–457.

[9] N. Paxeus and M. Wedborg, Anal. Chim. Acta, 169 (1985) 87–98.

[10] J.A. Leenheer, R.L. Wershaw and M.M. Reddy, Environ. Sci. Technol, 29 (1995) 393.

[11] D.S. Gamble, C.H. Langford and J.P.K. Tong, Can. J. Chem., 54 (1976) 1239.

[12] A.S. Mathuthu, J.A. Marinsky and J.H. Ephraim, Talanta, 42 (1995) 441.

[13] A.S. Mathuthu and J.H. Ephraim, Talanta, 40 (1993) 521.

[14] J.H. Ephraim and J.A. Marinsky, Anal. Chim. Acta, 232 (1990) 171.

[15] J.H. Ephraim, M.M. Reddy and J.A. Marinsky, in B. Allard, H. Borén and A. Grimvall (Eds.), Lecture Notes in Earth Sciences, Vol. 33, Springer-Verlag, Berlin, 1991, p. 263.

[16] A.E. Martel and R.M. Smith, Critical Stability Constants, Vol. 3, Other organic ligands, Plenum, New York, 1977.

[17] J.H. Ephraim and B. Allard, Environ. Int., 20 (1994) 89.

[18] D.S. Gamble, C.H. Langford and A.W. Underdown, Org. Geochem., 8 (1985) 35.

[19] R.A. Saar and J.H. Weber, Can. J. Chem., 57 (1979) 1263.

[20] J.H. Ephraim and H. Xu, Sci. Total Environ., 81/82 (1989) 625.

[21] B. Chakravartia, S.K. Saha and S.K. Chakravarti, Indian Chem. Soc., 61 (1984) 297.

[22] S.K. Saha, S.L. Dutta and S.K. Chakravarti, Indian Chem. Soc., 56 (1979) 1129.

[23] G.A. Bhat and J.H. Weber, Anal. Chim. Acta, 141 (1982) 95–103.

[24] R.A. Saar and J.H. Weber, Geochim. Cosmochim. Acta, 44 (1980) 1381–1384.

[25] I. Arsenie, H. Borén and B. Allard, Sci. Total Environ., 116 (1992) 213–220.

ELSEVIER

Talanta 42 (1995) 1811–1815

Talanta

# Magnetic field effects-polarization-resonant synchronous fluorescence spectrometry for simultaneous analysis of polynuclear aromatic hydrocarbons in mixtures

Yong Zhang [a,*], Yaxian Zhu [b], XiongZhi Xue [a], Xianzhi Huang [b]

[a] *Environmental Sciences Research Center, Xiamen University, Xiamen, 361005, People's Republic of China*
[b] *Department of Chemistry, Xiamen University, Xiamen, 361005, People's Republic of China*

Received 27 December 1994; revised 24 April 1995; accepted 26 April 1995

**Abstract**

The level and undulation of scattered light can be effectively suppressed by magnetic field effects-polarization-resonant synchronous fluorescence spectrometry. The established technique was used for simultaneous determination of a sample mixture containing fluorene, acenaphthene, anthracene, benzo-[a]-pyrene (B-[a]-P) and perylene. The detection limits were 0.23, 7.90, 0.13, 1.10, 0.0083 ng $ml^{-1}$ for fluorene, acenaphthene, anthracene, B-[a]-P and perylene, respectively. The relative standard deviations were less than 5%.

## 1. Introduction

Polynuclear aromatic hydrocarbons (PAHs) are widespread in the atmosphere, water, the earth, plants, as well as animals and their products. Because this class of compounds contributes to carcinogenicity [1], chemists and environmental researchers have been searching for effective techniques to control and monitor them. PAHs have been extensively studied by luminescence spectrometry. Synchronous fluorescence spectrometry (SFS), introduced by Lloyd [2], has been applied to the multicomponent analysis of PAHs [3–5]. Constant-energy synchronous fluorescence spectrometry (CESFS) was first described by Inman and Winefordner [6,7], and has also been applied to PAH analysis [8–11].

Derivative fluorescence spectrometry was first reported by Green and O'Haver and has since been developed [12–14]. However, the application of this technique to constant-wavelength synchronous fluorescence spectrometry (CWSFS) was still in its developing stage [15–20]. As a successful example, derivative techniques have been combined with CWSFS to analyze PAH mixtures by Vo-Dinh [21] and Romanovskaya and Chibisov [22]. A combination of the derivative technique and CESFS for the further elimination of Raman scattering interference was suggested [23], and was used to analyze multicomponent mixtures by Li et al. [24,25]. This combination technique was adopted by variable-angle synchronous fluorescence spectrometry and applied to binary mixture analysis [26].

Successful research projects in CWSFS have used an organized medium (such as micellar solution) for multicomponent analysis of PAHs [27–31]. However, the established methods were used for simultaneous analysis of not more than four components, and focussed only on the sensitivity. It has been reported that every component would give a very narrow peak for resonant synchronous fluorescence spectra (RSFS) in supersonic jet resonant synchronous fluorometry. This implies that a good selectivity would be achieved with $\Delta\lambda = 0$ [32]; however, this sensitivity would be greatly decreased by the scattered light interference.

* Corresponding author.


*SSDI* 0039-9140(95)01629-5

In this study, fluorene, acenaphthaene, anthracene, benzo-[a]-pyrene (B-[a]-P) and perylene were selected as model compounds for the evaluation of the recently established technique magnetic field effects-polarization-resonant synchronous fluorescence spectrometry (MFEPRSFS); the proposed technique can be conveniently used to effectively suppress the scattered light interference, while simultaneously analyzing the model compounds.

## 2. Experimental

### 2.1. Reagents

Fluorene, acenaphthene, anthracene, B-[a]-P and perylene were products of Aldrich. Stock standard solutions were prepared by dissolving them in distilled ethanol.

### 2.2. Apparatus

All spectra were obtained on a Hitachi 650-10S spectrofluorometer equipped with a polarization device, and including a home-made cell holder and a 1 cm quartz cell; a $CT_7$ Teslarmeter was purchased from The Fourth Electrometer Factory of Shanghai. The magnetic field was generated by two sets of magnets. The experimental devices are shown in Fig. 1. Fig. 1(a) shows the device for normal fluorescence determination; Fig. 1(b) shows the device combining polarization and normal fluorescence (the excitation polarizer and emission polarizer were oriented vertically); Fig. 1(c) illustrates the magnetic field applied with the device in Fig. 1(b), the magnetic field strength on the light path being about 70 mT.

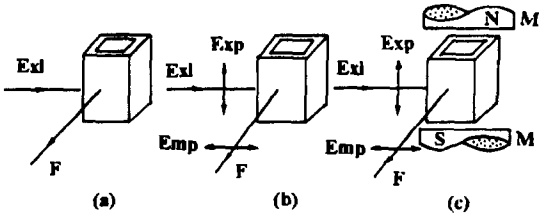


Fig. 1. Schematic diagram of the sample cell setup used for: (a) general fluorometry; (b) polarization fluorometry; (c) MFEs-polarization fluorometry. Exl, Exp, Emp, F and M are abbreviations for excitation light, excitation polarizer, emission polarizer, fluorescence and magnets, respectively.

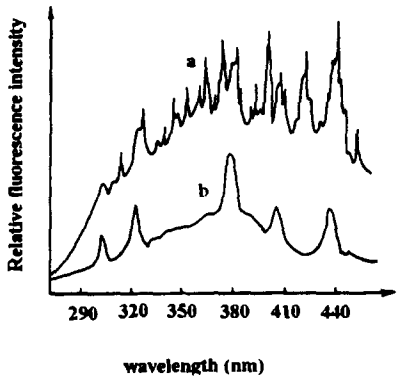


Fig. 2. (a) Resonant synchronous fluorescence spectra of the mixture solution; (b) MFEs-polarization-resonant synchronous fluorescence spectra of the mixture solution. The concentrations of fluorene, acenaphthene, anthracene, B-[a]-P and perylene were 10.0, 100.0, 10.0, 10.0 and 1.0 ng $ml^{-1}$, respectively.

### 2.3. Procedures

The prepared mixtures of fluorene, acenaphthene, anthracene, B-[a]-P and perylene were transferred into the 1 cm quartz cell. The cell was covered and then inserted into the cell holder. Both the excitation and emission slits were set at 5 nm. The "sensitivity" switch was set at a suitable position. The interval between emission wavelength and excitation wavelength was kept at zero ($\Delta\lambda = 0$). After applying external magnetic field effects (MFEs) to the sample cell for 10 min, resonant synchronous scanning within the spectral region of interest was carried out while the excitation polarizer and emission polarizer were vertically orientated, and MFEs were presented. The MFEPRSFS spectra of the PAHs being tested were recorded as illustrated in Fig. 2(b).

Ten mixed samples, as listed in Table 1, were prepared for the calibration measurements. In order to keep the light intensity of MFEPRSFS and RSFS at about the same level, all the MFEPRSFS spectra were obtained with an instrumental sensitivity set at a higher scale than that for RSFS. For MFEPRSFS spectra, the analytes were quantified by peak height after correcting for the background.

## 3. Results and discussions

### 3.1. RSFS and MFEPRSFS of fluorene, acenaphthene, anthracene, B-[a]-P and perylene

The standard solutions of fluorene, acenaphthene, anthracene, B-[a]-P and perylene in

Table 1
Preparation of mixtures for calibration measurements

| No. | Concentration (ng ml$^{-1}$) | | | | |
|---|---|---|---|---|---|
| | Fluorene | Acenaphthene | Anthracene | B-[a]-P | Perylene |
| 1 | 2.0 | 20.0 | 2.0 | 1.5 | 0.15 |
| 2 | 4.0 | 40.0 | 4.0 | 3.0 | 0.30 |
| 3 | 6.0 | 60.0 | 6.0 | 4.5 | 0.45 |
| 4 | 8.0 | 80.0 | 8.0 | 6.0 | 0.60 |
| 5 | 10.0 | 100.0 | 10.0 | 7.5 | 0.75 |
| 6 | 12.0 | 120.0 | 12.0 | 9.0 | 0.90 |
| 7 | 14.0 | 140.0 | 14.0 | 10.5 | 1.05 |
| 8 | 16.0 | 160.0 | 16.0 | 12.0 | 1.20 |
| 9 | 18.0 | 180.0 | 18.0 | 13.5 | 1.35 |
| 10 | 20.0 | 200.0 | 20.0 | 15.0 | 1.50 |

ethanol were analyzed and their RSFS recorded. The results demonstrate that RSFS fluorescence peaks for the five components were located at 305, 325, 380, 407 and 438 nm, respectively, whether the MFEs were applied or not.

In the previous study, it was found that the undulation of scattered light interference caused by solvent ethanol in resonant synchronous spectrofluorometry could be suppressed by MFEs [33]. It was also reported by our research group recently that the total level of scattered light could be restricted by the polarization technique [34]. In this study, a combination of the above two techniques with RSFS was used to improve the detection limits of the PAHs being tested.

In the proposed MFEPRSFS technique, the magnetized time for suppressing the undulation of scattered light interference should be optimized. Magnetized times from 0 to 15 min were investigated; it was found that for most of the test pure hydrophilic solvents, 5 min was sufficient when the magnetic field strength was about 70 mT [33]. The magnetized time selected in this study was 10 min.

A polarizer was placed in each of the excitation and the emission light paths. The observing polarizer was orientated perpendicular to the direction of the excitation polarizer. Polarized light was produced when the exciting light passed through the excitation polarizer. The sample molecules were excited by polarized light to produce a weakly polarized fluorescence signal. In contrast, the scattered light was totally depolarized. When all emissions reached the emission polarizer, only the fluorescence signal and a small portion of scattered light with the same orientation as that of the fluorescence were allowed to pass through the emission polarizer and reach the detector. The total level of scattered light interference could thus be suppressed by 95–98%.

It is well known that taking advantage of band-narrowing effects can improve the selectivity in synchronous spectrofluorometry for analyzing PAHs [35,36]. However, if the selected $\Delta\lambda$ value is not large enough, the scattered light interference can be serious. It is difficult to obtain high sensitivity and good selectivity at the same time with CWSFS alone. Excellent sensitivity and selectivity can be achieved with the proposed MFEPRSFS technique which combines polarization, MFEs, and CWSFS. The total level and undulation of scattered light interference was effectively restricted owing to the utilization of the polarization, MFEs with CWSFS together.

Fig. 2 shows the RSFS and MFEPRSFS spectra for the mixture of fluorene, acenaphthene, anthracene, B-[a]-P and perylene. Curve (a) is the normal RSFS spectra. It was difficult to distinguish the fluorescence signal from the noise in curve (a). Curve (b) was obtained with the proposed MFEPRSFS technique. The scattered light interference caused by the solvent was eliminated, resulting in an effectively reduced fluorescence background and a greatly enhanced signal-to-noise ratio. Each fluorescence signal of the five components appeared to be smooth and clear. The detection limits for fluorene, acenaphthene, anthracene, B-[a]-P and perylene were improved. The reported results for fluorene, acenaphthene, anthracene and perylene in Ref. [34] were 1.1, 10.0, 1.8 and 0.26 ng ml$^{-1}$ respectively, with the polarization technique only. The experimental results obtained by MFEPRSFS were 0.23, 7.9, 0.13 and

Table 2
Data of analytical merit

| PAH | Calibration [a] $I = aC + b$ | $r$ | Blank signal [b] | | Detection limit (ng ml$^{-1}$) | RSD (%) [c] ($n = 11$) |
|---|---|---|---|---|---|---|
| | | | Mean | SD | | |
| Fluorene | $I = 1.32C$-0.15 | 0.995 | 0.1 | 0.10 | 0.23 | 4.5 |
| Acenaphthene | $I = 0.14C$-0.90 | 0.998 | 0.3 | 0.37 | 7.90 | 4.9 |
| Anthracene | $I = 2.38C$-0.73 | 0.997 | 0.2 | 0.13 | 0.13 | 4.4 |
| B-[a]-P | $I = 0.77C$-1.05 | 0.997 | 0.2 | 0.28 | 1.10 | 1.5 |
| Perylene | $I = 39.73C$-1.61 | 0.997 | 0.2 | 0.12 | 0.0083 | 4.7 |

[a] $I$ = relative fluorescence intensity; $C$ = concentration in ng ml$^{-1}$; $a$ and $b$ are constants.
[b] The instrument sensitivity scale was set at the same as that in the blank measurement. SD represents the standard deviation blank measurement.
[c] Relative standard deviation for the mixtures containing 10.0 ng ml$^{-1}$ fluorene, 80.0 ng ml$^{-1}$ acenaphthene, 10.0 ng ml$^{-1}$ anthracene, 10.0 ng ml$^{-1}$ B-[a]-P and 0.5 ng ml$^{-1}$ perylene.

Table 3
Results of recovery experiments

| PAH | Known (ng ml$^{-1}$) | Added (ng ml$^{-1}$) | | Found (ng ml$^{-1}$) | | Recovery (%) | |
|---|---|---|---|---|---|---|---|
| | | A | B | A | B | A | B |
| Fluorene | 7.9 | 5.0 | 10.0 | 12.6 | 18.0 | 97.9 | 100.6 |
| Acenaphthene | 82.2 | 50.0 | 100.0 | 129.3 | 176.5 | 97.9 | 86.8 |
| Anthracene | 10.1 | 5.0 | 10.0 | 15.1 | 20.7 | 100.0 | 103.1 |
| B-[a]-P | 9.0 | 3.0 | 6.0 | 12.2 | 14.9 | 101.4 | 99.3 |
| Perylene | 0.50 | 0.30 | 0.50 | 0.76 | 1.0 | 95.2 | 101.0 |

0.0083 ng ml$^{-1}$, respectively. For perylene, the detection limit was about 30 times lower than that reported in Ref. [34]. In this work, however, the detection limit of B-[a]-P was somewhat higher than that reported in Ref. [31]. This was due to $\Delta\lambda = 0$ selected in MFEPRSFS scanning; the obtained synchronous fluorescence intensity corresponded only to the 0–0 band transition. The 0–0 band transition for B-[a]-P, however, is not the strongest transition band. Therefore, with $\Delta\lambda = 0$, the selectivity was enhanced but the sensitivity was reduced. In Ref. [31], the $\Delta\lambda$ value selected by the author was 42 nm. This value was nearly equal to the difference between the maximum emission and the maximum excitation of B-[a]-P in conventional fluorescence spectra. Under that condition, the sensitivity was higher but the selectivity was rather poor.

### 3.2. Data of analytical merit

With MFEPRSFS, one fluorescence peak corresponded to one component in the mixture and the peak height was measured for quantitative analysis. The analytical data are summarized in Table 2. Comparing the results listed in Table 2 with those in Ref. [34], the detection limit of each component was improved to a different degree based on the spectral properties of the different compounds and the instrumental parameters.

### 3.3. Recovery experiment

Standard solutions of the five test PAHs were mixed to prepare the mixture sample. The recovery experiment was carried out and the results are listed in Table 3.

The study demonstrated that the proposed technique has the advantages of being simple, easy, selective, sensitive and almost free of interference from the scattered light. The proposed technique can be used for simultaneous PAH analysis and other multicomponent analysis.

**Acknowledgements**

The authors wish to acknowledge financial support provided by the National Natural Science Foundation of China. The authors also express their gratitude to Professor G.Z. Chen

and D.X. Yuan for helpful discussion and encouragement.

## References

[1] G. Grimmer, Toxicol. Environ. Chem., 10 (1985) 171.
[2] J.B.F. Lloyd, Nature, 231 (1971) 64.
[3] J.E. Thompson and H.L. Pardue, Anal. Chim. Acta, 152 (1983) 73.
[4] M. Furusawa, M. Tachibana and Y. Hayashi, Bunseki Kagaku, 31 (1982) 229.
[5] T. Kazuyoshi and S. Masashi, Analyst, 113 (1988) 509.
[6] E.L. Inman, Jr., and J.D. Winefordner, Anal. Chim. Acta, 138 (1982) 245.
[7] E.L. Inman, Jr., and J.D. Winefordner, Anal. Chem., 54 (1982) 2018.
[8] M.J. Kerkhoff, T.M. Lee, E.R. Allen, D.A. Lundgreb and J.D. Winefordner, Environ. Sci. Technol., 19 (1985) 695.
[9] M.J. Kerkhoff and J.D. Winefordner, Anal. Chim. Acta, 175 (1985) 257.
[10] L.A. Files, B.T. Jones, S. Hanamura and J.D. Winefordner, Anal. Chem., 58 (1986) 1440.
[11] Y.Q. Li and X.Z. Huang, Fenxi Huaxue (China), 18 (1990) 827.
[12] G.L. Green and T.C. O'Haver, Anal. Chem., 46 (1974) 2191.
[13] J.C. Garcia Borron, J. Escribano, N. Jimenez and J.D. Iborra, Anal. Biochem., 125 (1982) 277.
[14] H.C. Robert and C.D. McGiothlin, Anal. Chem., 54 (1982) 2015.
[15] F. Garica Sanchez, C. Cruoes and A.L. Ramos Rubio, J. Mol. Struct., 143 (1986) 473.
[16] F.V. Bright and L.B. McGoown, Analyst, 111 (1986) 205.
[17] M.W. Kabbani, S. Rubio-Borros and L.M. Pole-Dicz, Anal. Chim. Acta, 218 (1989) 167.
[18] F. Salinas, A. Muñz de la Peña, C.F. Capitan-Vallvey and A. Navalon, Analyst, 114 (1989) 1297.
[19] G.F. Sanchez and C.C. Blanco, Talanta, 37 (1990) 573.
[20] G.F. Sanchez, A.L.R. Rubio and C.C. Blanco, Talanta, 37 (1990) 579.
[21] T. Vo-Dinh, Appl. Spectrosc., 36 (1982) 576.
[22] G.I. Romanovskaya and A.K. Chibisov, Zh. Anal. Khim., 43 (1988) 1120.
[23] Y.Q. Li, X.Z. Huang, J.G. Xu and G.Z. Chen, Chin. Sci. Bull., 36 (1991) 1312.
[24] Y.Q. Li, X.Z. Huang, J.G. Xu and G.Z. Chen, Chin. Chem. Lett., 2 (1991) 23.
[25] Y.Q. Li, X.Z. Huang, J.G. Xu and G.Z. Chen, Anal. Chim. Acta., 256 (1992) 285.
[26] B.J. Clark, A.F. Fell, K.T. Milen, D.M.G. Pattio and H. Williams, Anal. Chim. Acta., 170 (1985) 35.
[27] J.J. Santana Rodriguez, Z. Sosa Ferrea, A. Afonso Perera and V. Gonzalez Diaz, Anal. Chim. Acta, 225 (1991) 107.
[28] A. Bermjo Martin-Lãzaro, J. Hernãndez Garcia and J.J. Santana Rodriguez, Fresenius' J. Anal. Chem., 343 (1992) 509.
[29] J.J. Santana Rodriguez and Z. Sosa Ferrea, Talanta, 39 (1992) 1611.
[30] L.F. Capitãn-Vallvey, M. del Olmo Iruela, R. Avidad Castañeda and J.L. Vilchez Quero, Anal. Lett., 26 (1993) 2443.
[31] J.J. Santana Rodriguez, J. Hernãndez Garcia, M.M. Bernal Suãrez and A. Bermjo Martin-Lãzaro, Analyst, 118 (1993) 917.
[32] Gouzhen Chen, Xianzhi Huang and Jinguo Xu, Yingguangfenxijinzhan (China), Xiamen, Xiamendaxuechubanshe, 1992, p. 53.
[33] Y. Zhang, X.Z. Huang, J.G. Xu and G.Z. Chen, Chin. Sci. Bull., 39 (1994) 1439.
[34] L.Z. Gu, Y.B. Wong, X.Z. Huang, J.G. Xu and G.Z. Chen, Chem. J. Chin. Univ., 31 (1992) 1214.
[35] L.Z. Gu, Y.B. Wong, X.Z. Huang, J.G. Xu and G.Z. Chen, Guangpuxue Yu Guangpufenxi, 13 (1993) 87.
[36] G.Z. Chen, X.Z. Huang, Z.Z. Zheng, J.G. Xu and Z.B. Wang, Yingguangfenxifa, Kexuechubanshe, Dierban, Beijing, 1992, p. 469.

ELSEVIER

Talanta 42 (1995) 1817–1825

Talanta

# Evaluation of a magnetically coupled microcavity hollow cathode discharge for atomic emission spectroscopy

A.R. Raghani, M.A. Bolshov[1], B.W. Smith, J.D. Winefordner*

*Department of Chemistry, University of Florida, Gainesville, Florida 32611, USA*

Received 27 March 1995; revised 28 April 1995; accepted 29 April 1995

**Abstract**

A magnetically coupled microcavity hollow cathode discharge device was evaluated for its analytical potential as a boosted atomic emission source. A magnetic field using an electromagnet was applied perpendicular to the axis of the microcavity hollow cathode. The intensity of the atomic emission of copper, aluminum and the ionic emission of magnesium increased with increasing magnetic field until it reached a maximum. A further increase in the field strength did not lead to an enhancement of these emissions. The attainment of the maxima was attributed to the increase in the electron temperature and radial diffusion of the electrons from the center of the microcavity axis. Electron temperatures in the presence of the magnetic field calculated based on the semicorona model were shown to be proportional to the square of the reduced field strength. Further, these maxima were correlated to the energies of the upper levels of the transition studied.

*Keywords*: Atomic emission spectroscopy; Electron temperature; Magnetic field effects; Microcavity hollow cathode

## 1. Introduction

Hollow cathode discharge devices (HCDs) have been employed for many years as a source in atomic absorption, fluorescence and emission spectroscopy. In atomic emission spectroscopy, they have found applications where a solid sample is used as a cathode or a liquid sample is deposited on the cathode and its residue is analyzed. However, the output of the emission intensity is lower than in most of the other atomic emission techniques. There are various ways by which enhancement of the emission intensity is possible, including the application of external fields such as microwaves [1,2], radiofrequency [3,4] magnetic field [5,6] or by pulsing the discharge [7] or using an auxiliary discharge [8]. Another mode of boosting the emission intensity is by modifying the geometry of the hollow cathode. Examples of this include the conical-bottom hollow cathode [9] or the microcavity hollow cathode [10]. Microcavity hollow cathodes typically have a diameter less than 2 mm and a depth less than 10 mm.

Microcavity hollow cathodes have been applied in the trace analysis of subnanoliter volume liquid samples for the determination of elements of physiological importance [11,12]. Recently, in our laboratory we have successfully demonstrated the analytical potential of a microcavity HCD for the analysis of microliter volumes of liquid samples by constructing a

*Corresponding author.

[1]Present address: Institute of Spectroscopy, Russian Academy of Sciences, 142092 Troitzk, Moscow Region, Russia.


*SSDI* 0039-9140(95)01633-3

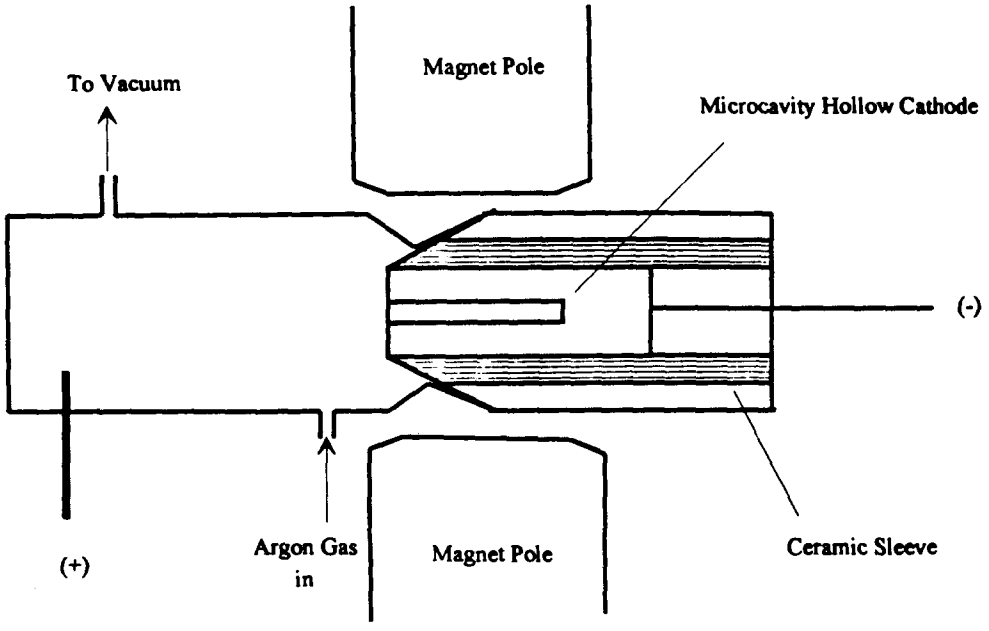


Fig. 1. Experimental arrangement of a microcavity HCD with respect to the magnetic field.

miniature quartz glow discharge chamber with a volume less than 100 ml [13]. Excellent detection limits for lead and copper ( 210 fg and 10 pg, respectively) were obtained.

There have been numerous reports on the study of the influence of a magnetic field on the HCD using conventional-diameter hollow cathodes. Rudnevsky and Maksimov [14] arranged the magnetic field parallel and perpendicular to the cathode axis and obtained an about an order of magnitude improvement in the detection limit. In order to further improve upon the sensitivity of this device, we have investigated the influence of a magnetic field on the microcavity hollow cathode discharge, which is the basis of this report.

## 2. Experimental

The experimental set-up for atomic emission is given in detail elsewhere [13]. The set-up was modified for this study and only a brief account is presented here. Microcavity hollow cathodes 1.5 mm in diameter and 6 mm in depth were machined from high purity metals. For the magnesium studies, NIST standard reference material 124b was used, which contains 4.54% magnesium in aluminum alloy. The cathodes were then secured using epoxy adhesive in a quartz inner tapered joint. A glow discharge chamber was made from a quartz outer tapered joint with an optical quality window fused at one end of the joint. A stainless steel anode wire, 2 mm in diameter, was sealed inside this chamber. The outer tapered joint contained an inlet and an outlet for the flow of the fill gas and a vacuum connection. The inner joint with the electrode and the outer joint formed a demountable assembly which held the tight vacuum necessary for low pressure discharges. Argon gas was used as the fill gas and its pressure inside the chamber was maintained at 1 Torr. An electromagnet (Anac, model 3470) was used for the application of the magnetic field and the field strength was varied by changing the coil current of the magnet. Magnetic field measurements were carried out using a gaussmeter probe (Bell, Inc., model 640). The microcavity HCD was placed between the two poles of the magnet, and the field was applied perpendicular to the axis of the microcavity (see Fig. 1). The poles were brought as close as possible to the chamber in order to obtain maximum interaction of the magnetic field with the discharge.

The emission from the microcavity was focused on the entrance slit (slit width, 10 $\mu$m; slit height, 4 mm) of a 1 m focal length grating spectrometer (reciprocal linear dispersion of 0.02 nm $mm^{-1}$) equipped with a photodiode-array detector with a spectral range of 20 nm. The diode-array pixel height was 3 mm. Therefore each observed spectral line intensity repre-

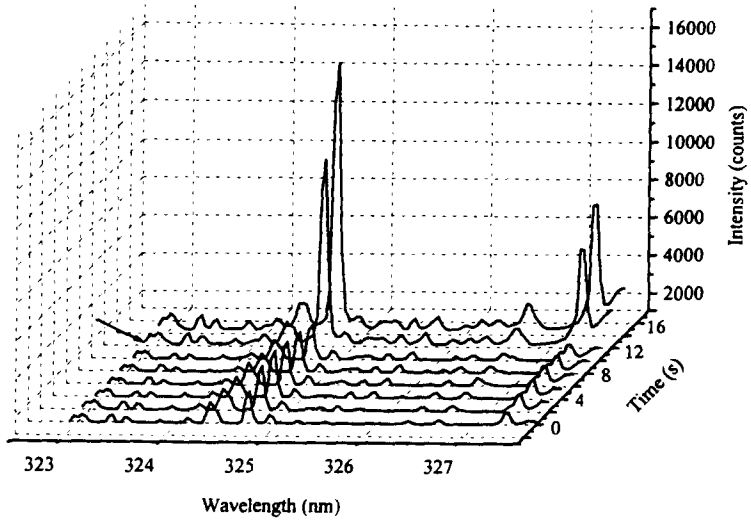


Fig. 2. Temporally resolved emission spectra of a solution containing 100 ng of copper residue in the aluminum microcavity hollow cathode (arrow indicates the point at which the magnetic field was turned on).

sents an average intensity over a thin vertical slice of the discharge. The horizontal spatial resolution is about 50 $\mu$m which was chosen as the measurement increment. Data were acquired with a personal computer and data acquisition software (OSMA I-120, Princeton Instruments, Inc., Trenton, NJ, USA).

Radial profiles of the atomic emission from the microcavity were obtained by moving the lens at 50 $\mu$m increments across the diameter of the microcavity using an $x$–$y$ translator and focusing the image on the slit of the monochromator.

## 3. Results and discussion

Application of the magnetic field resulted in a very intense positive column and the negative glow was seen to further penetrate inside the microcavity. The emission from the inside of the microcavity was brighter in the presence of the magnetic field. Fig. 2 shows the temporally resolved emission spectra of a solution containing 100 ng of copper deposited in an aluminum microcavity. The discharge current was 38 mA at an argon pressure of 1 Torr. Since we used a photodiode- array detector with a 20 nm spectral window, we could simultaneously observe the two resonance lines of copper at 324.75 and 327.40 nm. At the beginning of the discharge (0 s in Fig. 2), no magnetic field was applied, and the line at 324.75 nm had a good signal-to-background (S/B) ratio whereas the line at 327.40 nm had a poor S/B ratio. As soon as the field was turned on (as shown by the arrow in Fig. 2), the intensity of the line at 324.75 nm increased by up to four times and the emission line at 327.40 nm began to appear well above the background. Similar results were reported by Rudnevsky and Maksimov [14] for the magnetically boosted HCD of conventional dimensions. The precision of our measurements was, however, about 30% for solution analysis. In order to optimize experimental conditions such as magnetic field strength, current and pressure, we studied the effect of the magnetic field on solid samples before further evaluation of solution sample residues.

Fig. 3 shows the enhancement of the atomic emission of copper from the copper microcavity for the two lines at 324.75 and 327.40 nm with increasing magnetic field strength. The emission intensity increased by a factor of about two up to a magnetic field of 2500 G, and further increase in the magnetic field resulted in a decrease in the emission intensity. The background emission was unaffected by the magnetic field. The precision (percentage relative standard deviation) for these measurements was less than 2%. A possible mechanism involved the negative glow inside the microcavity being pushed towards the inside walls of the microcavity as the magnetic field is increased further, as reported by Pavlovic and Dobrosavljevic [15]. As a consequence, there would be a reduction in the intensity at the center of the microcavity at higher field strengths. However, this possibility was ruled out by measuring the radial profiles of the

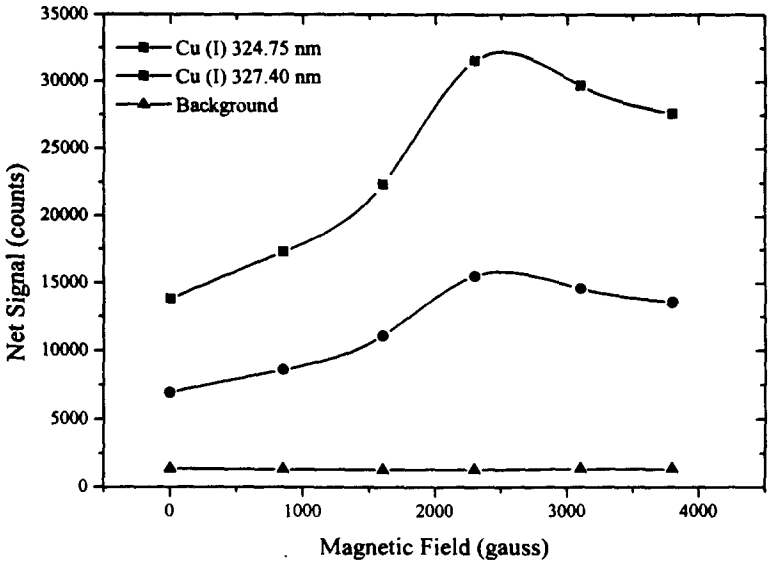


Fig. 3. Effect of magnetic field on copper emission at 324.75 and 324.40 nm from a copper microcavity hollow cathode.

copper microcavity emission at 324.75 nm at different field strengths. The results are shown in Fig. 4. The intensity of the emission is maximum at the center of the microcavity at all magnetic field values, indicating that there is no localization of the negative glow near the inside walls of the microcavity. Atomic emission from an aluminum microcavity hollow cathode was also observed under identical discharge conditions to those used for the copper emission study; the results are shown in Fig. 5. Once again, as with the copper emission, there was an increase and then a decrease in the atomic emission intensity of the aluminum lines at 394.15 and 396.40 nm as the magnetic field was increased. The background was again constant over the range of magnetic field strengths. A similar study was conducted for magnesium ion lines by observing the emission from the microcavity hollow cathode made from an NIST sample of aluminum containing 4.54% magnesium. The results for magnesium ion emission for the lines at 279.55 and 280.27 nm, shown in Fig. 6, exhibit the same trends as for copper and aluminum. Somersan and Popovici [16] studied the effect of a magnetic field on the atomic emission of lead at 405.78 nm using different fill gases; the emission intensities did not change much after reaching a maximum. However, no theoretical explanation was given. Rudnevsky et al. [17] have studied residues of the alkali metals deposited in an HCD in a magnetic field; they also observed a similar pattern. A reduction in the molecular emission background of CN was observed with increasing magnetic field strength. However, in our case, the background was fairly constant near the emission lines of all the three elements.

Hollow cathode discharges are known to show self-absorption, and the decrease in the emission intensity for the analytes studied here may be due to an increased sputtering rate with increasing magnetic field. However, on studying the effect of magnetic field strength on argon ion emission at 404.29 nm (see Fig. 7), a steady decrease in the emission intensity with magnetic field strength was observed. This implies that there is no increase in the ionization of the argon gas with increasing magnetic field. In other words, it is possible that there is no increase in the sputtering rates with increasing magnetic field strengths at an argon pressure of 1 Torr.

Sen et al. [18] observed the variation of the spectral emission intensities of helium, hydrogen and mercury as fill gases in glow discharges as a function of magnetic field strength, and they reported similar variations in emission with increasing magnetic field for the atomic lines of the fill gases used. The attainment in the emission maxima was attributed to two discharge-related factors that are simultaneously influenced by the applied magnetic field; these factors are electron temperature and the electron number density along the axis of the discharge [18]. It was assumed in their studies that the excitation mechanism was mostly by electron impact [19]. The electron

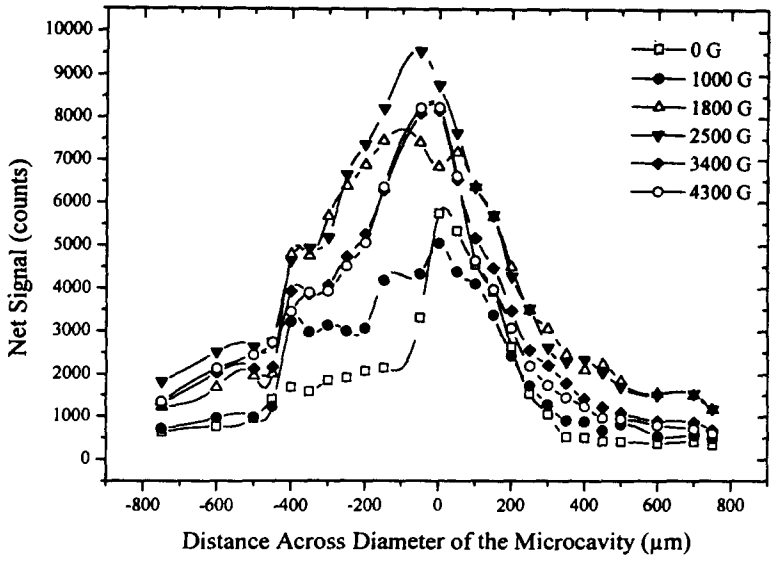


Fig. 4. Radial profiles of atomic emission from a copper microcavity at different magnetic field strengths.

temperature increases with magnetic field, whereas there is a radial diffusion of electrons from the axis of the discharge with increasing magnetic field. In order to confirm that a similar argument can be used to justify the trend observed in our case for the sputtered materials, the following mechanism is speculated.

The electron temperature in a magnetic field, $T_{eB}$, is related to the electron temperature without a magnetic field, $T_e$ as follows [18]

$$T_{eB} = T_e\left(1 + C_1\frac{B^2}{P^2}\right)^{1/2} \quad (1)$$

where $B$ is the magnetic field strength (G), $P$ is the pressure (Torr) and $C_1$ is a constant (Torr$^2$ G$^{-2}$) dependent on the fill gas which is given by

$$C_1 = \left(\frac{eL}{mv_r}\right)^2 \quad (2)$$

where $e$ is the electronic charge (C), $L$ is the electron mean free path (m) at a pressure of 1 Torr, and $v_r$ is the random velocity of the electron (m s$^{-1}$).

The electron number density, $n_{eB}$ (cm$^{-3}$) along the axis of the microcavity HCD in the presence of the magnetic field is given as [20]

$$n_{eB} = n_e\exp\left(-\frac{eEC_1^{1/2}rB}{2kT_eP}\right) \quad (3)$$

where $n_e$ is the electron density (cm$^{-3}$) in the absence of a magnetic field and $E$ is the axial electric field per centimeter (V cm$^{-1}$). This equation implies that there is a reduction in the electron number density at a distance $r$ from the axis due to the presence of the magnetic field.

The intensity of the emission arising from a transition $j \rightarrow i$, for an optically thin semicorona plasma, in the absence of magnetic field, is given by [20]

$$I_{ji} = n_e n_a\left(\frac{hlv_{ji}}{4\pi}\right)\chi_{gj}\left(\frac{A_{ji}}{\sum_{m<j} A_{jm}}\right)\exp\left(-\frac{U_j}{kT_e}\right) \quad (4)$$

where $h$ is Planck's constant (J s), $l$ is the path length (cm), $n_a$ is the number density of the analyte atoms or ions in the ground state (cm$^{-3}$), $A_{ji}$ is the Einstein coefficient of transition probability (s$^{-1}$), $\Sigma_{m<j} A_{jm}$ is the summation of all the transition probabilities between the upper and the lower levels, $\chi_{gj}$ is the collisional excitation rate coefficient from the ground state $g$ to the excited state $j$ (cm$^{-3}$ s$^{-1}$), $U_j$ is the energy of the upper level (eV), and $v_{ji}$ is the frequency of the emitted radiation (s$^{-1}$).

In the presence of a magnetic field, $I_{ij}$ is given by [20]

$$(I_{ji})_B = n_e n_a\left(\frac{hlv_{ji}}{4\pi}\right)\chi_{gi} \times \exp\left(-\frac{eEC_1^{1/2}rB}{2kT_eP}\right)\left(\frac{A_{ji}}{\sum_{m<j} A_{jm}}\right)_B \times \exp\left(-\frac{U_j}{kT_{eB}}\right) \quad (5)$$

Taking the ratio of Eqs. (4) and (5) and substitution for $T_{eB}$ from Eq. (1) and maximizing the result with respect to $B$ gives

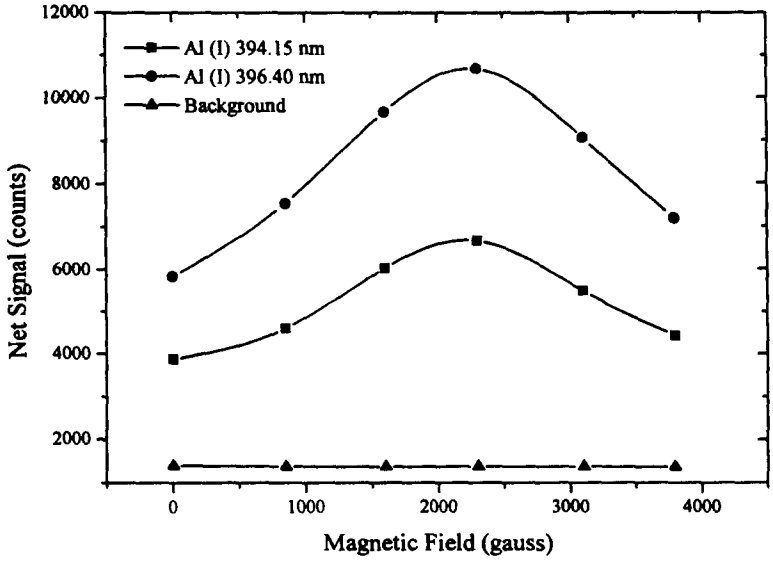


Fig. 5. Effect of magnetic field on aluminum emission at 394.15 and 396.40 nm from an aluminum microcavity hollow cathode.

$$e^2E^2r^2 = 4C_1B_{max}^2U_j^2\left[P^2\left(1 + C_1\frac{B_{max}^2}{P^2}\right)^{-1}\right] \quad (6)$$

For a particular gas, we deduce that $B_{max}U_j(1 + C_1B_{max}^2/P^2)^{-1/2}$ is almost a constant. There is some degree of uncertainty involved in the theoretical calculation of the value for $B_{max}$ using Eq. (6) since the values of $E$ and $r$ are not precisely known. Therefore, it will suffice to prove that for a given set of emission lines for a particular element

$$B_{max}U_j(1 + C_1B_{max}^2/P^2)^{-1/2} = C_2 \quad (7)$$

where $C_2$ is a constant. In order to calculate $C_1$ from Eq. (2), one has to know the collision cross-section of electrons and fill gas atoms to calculate the mean free path. Since the collision cross-section depends on the energy of the electron and that of the gas atoms, its precise determination is difficult. Sadhya and Sen [20] proposed a method for calculating the value of $C_1$ from Eq. (1 by plotting the electron temperature in a magnetic field at various field strengths, the slope of which gives $C_1$. Further-

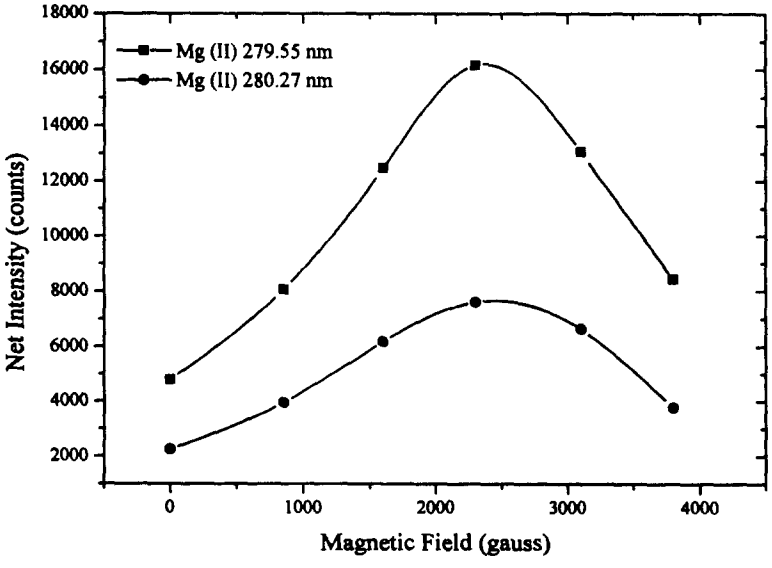


Fig 6. Effect of magnetic field on magnesium ion emission at 279.55 and 280.27 nm from an NIST standard aluminum alloy microcavity hollow cathode. (This standard contains 4.54% magnesium).

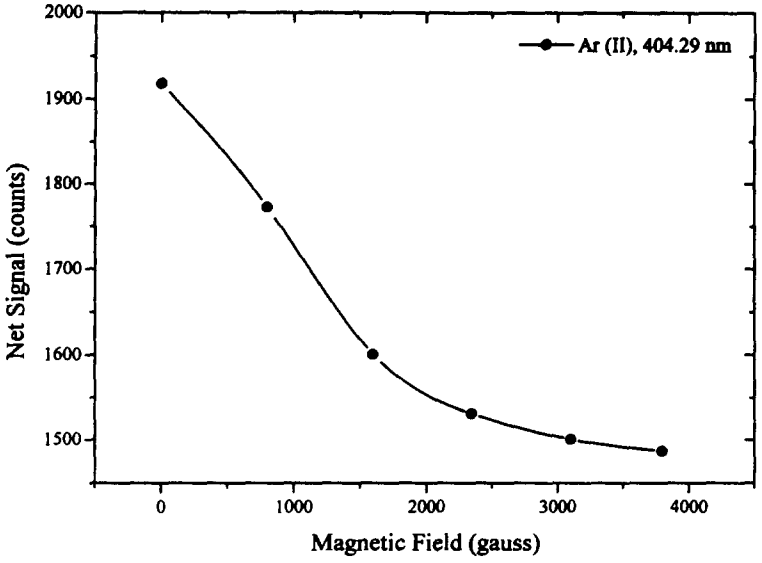


Fig. 7. Effect of magnetic field on argon ion emission at 404.29 nm.

more, the electron temperature $T_e$ without the magnetic field was calculated from the intensity ratio of two lines assuming the gas was in local thermodynamic equilibrium (LTE). Since a low pressure discharge is not in LTE, a semicoronal equilibrium was assumed to prevail inside the discharge [19].

Assuming another transition $k \rightarrow i$ and taking the ratio of the intensity of the two lines gives

$$kT_e = (U_k - U_j)/\ln\left(\frac{I_{ji}\lambda_{ji}{}^3 f_{ik}}{I_{ki}\lambda_{ki}{}^3 f_{ij}}\right) \quad (8)$$

assuming the excitation rate coefficients $\chi_{gj}$ and $\chi_{gk}$ are the same due to the similarity of excited states $g$ and $j$. When the magnetic field is applied

$$\frac{1}{T_e} - \frac{1}{T_{eB}} = \frac{k}{(U_k - U_j)} \ln\left[\frac{(I_{ki})_B (I_{ji})}{(I_{ji})_B (I_{ki})}\right] \quad (9)$$

where $f_{ij}$ and $f_{ik}$ are the oscillator strengths (dimensionless) of the respective transitions and $T_{eB}$ is the electron temperature in the presence of the magnetic field. It is important to note that this equation is valid only for those emission lines which have the same

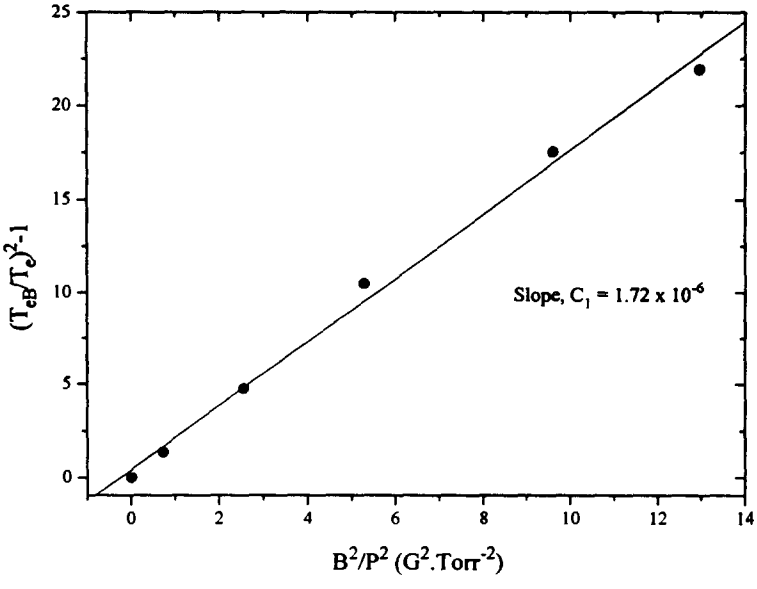


Fig. 8. Effect of magnetic field on the electron temperature.

ground states because the statistical weights of the ground state are also affected by the applied magnetic field as a result of Zeeman splitting. The ratio of the statistical weights in the presence of the magnetic field is unity if the two ground levels are the same. We selected two resonance lines of copper (324.70 and 327.40 nm) for the calculation of electron temperatures both with and without the magnetic field using Eqs. (8) and (9). A plot of $(T_{eB}/T_e^2) - 1$ versus $B^2/P^2$ (where $B/P$ is known as the reduced magnetic field) is shown in Fig. 8. It is evident from this plot that the electron temperature is constantly increasing with applied magnetic field strength (where pressure is kept constant). The value of the slope of this plot, which corresponds to $C_1$, gives $1.72 \times 10^{-6}$ for argon which is in the same range calculated for helium by Sadhya and Sen [20]. Table 1 lists the values of the constant in Eq. (7). As can be seen from Table 1, for a particular element, the value of $C_2$ is almost constant. Therefore, the closer the energies of the upper levels of the lines of a particular element, the closer are the maxima of the emission intensities that occur when the field strength is increased as seen in Figs. 3, 4 and 6. For all three elements chosen in this study, $B_{max}$ values are nearly the same for a given element. For example, aluminum has the same energy of the upper levels for both lines at 394.40 and 396.15 nm and shows maxima for these lines at 2300 G.

## 4. Conclusions

It can be concluded that the two-field dependent factors, electron temperature and radial diffusion of the electron, are both acted upon simultaneously and opposite to each other by the applied magnetic field. The electron temperature increases with magnetic field, whereas there is an increase in radial diffusion of the electron with increasing magnetic field. Therefore, a maximum in emission intensity does occur at a certain field strength and this maximum is dependent upon the energy of the upper state of the analytical line. Since there is no substantial advantage of using a very high magnetic field strength, it might be appropriate to use permanent magnets which tend to have sufficient field to produce the positive effect of magnetic field on atomic emission intensity [21]. Use of a permanent magnet will facilitate a compact discharge design. We are currently developing a compact magnetically boosted glow discharge device using permanent magnets for the analysis of residues of microliter volume liquid samples.

Table 1
Relationship between intensity maxima and energy of upper level

| Analyte | Wavelength (nm) | Energy of the upper level (eV) | $B_{max}$ [a] (G) | $C$ (G eV) |
|---|---|---|---|---|
| Cu(I) | 324.75 | 3.817 | 2500 | 2784 |
| Cu(I) | 327.40 | 3.786 | 2500 | 2761 |
| Mg(II) | 279.55 | 4.434 | 2400 | 3222 |
| Mg(II) | 280.27 | 4.422 | 2500 | 3225 |
| Al(I) | 394.40 | 3.143 | 2300 | 2275 |
| Al(I) | 396.15 | 3.143 | 2300 | 2275 |

[a] The $B_{max}$ values correspond to magnetic field strengths giving the maximum signals in Figs. 3, 5 and 6.

## References


[1] S. Caroli, A. Alimoti and F. Petrucci, Anal. Chim. Acta, 136 (1982) 269.
[2] S. Caroli, A. Alimonti and F. Petrucci, Trends Anal. Chem., 1 (1982) 368.
[3] T. Araki, J.P. Walters and S. Minami, Appl. Spectrosc., 34 (1980) 33.
[4] P.B. Farnsworth and J.B. Walters, Anal. Chem., 54 (1982) 885.
[5] R.A. Kruger, R.M. Bombella and K. Lagua, Spectrochim. Acta, Part B, 35 (1980) 589.
[6] S. Brewer, T. Holbrook, Z. Shi, K. Trivedi and R. Sacks, Appl. Spectrosc., 45 (1991) 1327.
[7] J.B. Dowson and D.J. Ellis, Spectrochim. Acta, Part A, 23 (1967) 565.
[8] Zs. Szilvássy, in S. Caroli (Ed.), Improved Hollow Cathode Lamps for Atomic Spectroscopy, Ellis Horwood Ltd., UK, 1985, p. 178.
[9] D. Zhachev, in S. Caroli (Ed.), Improved Hollow Cathode Lamps for Atomic Spectroscopy, Ellis Horwood Ltd., UK, 1985, p. 203.
[10] J. Czakow, in S. Caroli (Ed.), Improved Hollow Cathode Lamps for Atomic Spectroscopy, Ellis Horwood Ltd., UK, 1985, p. 35.
[11] J.L. Tseng, J.C. William, R.B. Bartlow, S.T. Griffin and J.C. Williams, Jr., Anal. Chem., 63 (1991) 1933.
[12] J.L. Tseng, J.Y. Kung, J.C. Williams and S.T. Griffin, Anal. Chem., 64 (1992) 1931.
[13] C.A. Morgan, C.L. Davis, B.W. Smith and J.D. Winefordner, Appl. Spectrosc., 48 (1994) 261.
[14] N.K. Rudnevsky and D.E. Maksimov, in S. Caroli (Ed.), Improved Hollow Cathode Lamps for Atomic Spectroscopy, Ellis Harwood Ltd., UK, 1985, p. 148.
[15] B.V. Pavlovic and J.S. Dobrosavljevic, Spectrochim. Acta, Part B, 44 (1989) 1191.
[16] M. Somersan and C. Popovici, Appl. Phys. Lett., 9 (1966) 65.

[17] N.K. Rudnevsky, D.E. Maksimov and L.P. Lazareva, Zh. Anal. Khim., 39 (1972) 1422.
[18] S.N. Sen, P.R. Das and R.N. Gupta, J. Phys. D, 5 (1972) 1260.
[19] R. Mewe, Br. J. Appl. Phys., 71 (1966) 1239.
[20] S.K. Sadhya and S.N. Sen, Phys. Lett., 79A (1980) 162.
[21] K. Trivedi, S. Brewer, L. McCaig, N. Sesi and R. Sacks, Spectrochim. Acta, Part B, 46 (1991) 229.

ELSEVIER

Talanta 42 (1995) 1827–1831

Talanta

# Determination of calcium, magnesium and zinc in unused lubricating oils by atomic absorption spectroscopy

A.P. Udoh

*Department of Chemistry and Biochemistry, University of Uyo, Uyo, Akwa Ibom State, Nigeria*

Received 20 June 1994; revised 3 May 1995; accepted 5 May 1995

**Abstract**

Varying concentrations of lanthanum and strontium were added to solutions of ashed unused lubricating oils for the determination of calcium, magnesium and zinc content using flame atomic absorption spectrophotometry. At least 3000 $\mu g\ g^{-1}$ of lanthanum or strontium was required to completely overcome the interference of the phosphate ion, $PO_4^{3-}$, and give peak values for calcium. The presence of lanthanum or strontium did not cause an appreciable increase in the amount of magnesium and zinc obtained from the analyses. The method is fast and reproducible, and the coefficients of variation calculated for the elements using one of the samples were 1.6% for calcium, 3.5% for magnesium and 0.2% for zinc. Results obtained by this method were better than those obtained by other methods for the same samples.

*Keywords:* Calcium; Magnesium; Zinc; Lubricating oils; Atomic absorption spectroscopy

## 1. Introduction

Lubricating oils are employed to separate metallic surfaces in mechanical systems. The performance characteristics of these oils are usually improved by the incorporation of additives which contain one or more of the following elements — phosphorus, barium, calcium, magnesium, zinc, antimony, nickel, boron, cadmium, chromium, mercury, molybdenum, selenium and tin [1–3]. A rapid and accurate analytical procedure is needed for routine analysis of these elements in order to provide proper control of plant blending operations. The American Society for Testing and Materials [4] recommended ashing at 650–700°C. The institute of Petroleum [5–7] also recommended ashing at 550°C until the ash is free of all visible traces of carbon. Udoh et al. [8] observed that with lubricating oils marketed in Nigeria, complete oxidation of carbon was not possible at any of these standard temperatures. This could perhaps account for the need to filter the solution in the above cases. Suspecting that incomplete oxidation of carbon may lead to lower values for the added elements, Udoh et al. [8] designed a series of experiments that led to the recommendation of an ashing temperature of $900 \pm 50$°C.

There are a number of methods which can be used to determine the above elements in solubilised ash. These include titrimetry, emission spectroscopy [1,9] and chemical analysis [4–7]. Such methods are laborious and impractical, especially when large numbers of samples are involved. The Institute of Petroleum [10] recommended an atomic absorption spectrometric analysis of the unused oil for barium, calcium, magnesium and zinc after dilution with white spirit, but this method is not suitable for lubricating oils that contain viscosity index improvers. Other organic solvents can be used, but they pose a lot of difficulties [11] and the


*SSDI* 0039-9140(95)01634-1

results obtained depend on the type of organometallic compound used for calibration [12]. Such difficulties were believed to be overcome by the use of oxygenated solvents and mixed solvent systems, but flame problems are still common even though they allow for the application of aqueous inorganic salt standards which make the analyses cheaper.

Surprisingly, with the ready availability of flame atomic absorption spectrophotometers (using an air–acetylene flame), no method has been described to apply this facility using aqueous standard and the inorganic ash, perhaps owing to the common interference of phosphorus in the determination of the alkaline earth metals by flame absorption. This interference by phosphorus in inorganic systems is usually overcome by the addition of lanthanum or strontium solution. Varying concentrations of lanthanum in the final solution have been recommended when analysing different classes of materials [13–16]. To my knowledge, none has yet been recommended as being adequate for the determination of these elements in the ashed lubricating oils. If the interference due to phosphorus in the ashed oil is overcome, its incorporation into the above-mentioned procedure [8] can provide a rapid method for routine analysis, perhaps with more quantitative results than from direct dilution with organic solvents or chemical analysis.
This paper describes how the interference from phosphorus is overcome, and recommends a cheaper and reliable procedure for routine analysis of unused lubricating oils.

## 2. Experimental

### 2.1. Reagents and apparatus

All the reagents were of analytical grade. Doubly-distilled water was used to prepare all the solutions. Stock (1000 $\mu g\ g^{-1}$) Ca, Mg and Zn was prepared from carbonate (Ca), sulphate (Mg) and oxide (Zn), stored in polythene bottles and diluted appropriately to obtain working solutions. 10 000 $\mu g\ g^{-1}$ of lanthanum (as nitrate) and strontium (as chloride) was added to the sample solutions as buffer to overcome the interference of the phosphate ion.

A Gallenkamp muffle furnace with a temperature range of 0–1000°C was used for ashing. A Unicam AA919 atomic absorption/flame emission spectrophotometer equipped with a premix chamber and a 10 cm single element hollow cathode lamps as sources was used for the analysis.

### 2.2. Lubricating oil samples

The samples analysed were purchased from producing companies as sold at their appropriate stations in Nigeria. All samples were stored in polythene bottles and were assigned numbers to differentiate between them in this work. Both premium quality SAE 20/50 and medium quality SAE 40 were used. A detailed list is presented in Table 1. All the samples are highly viscous and amber coloured, except sample 9 which is reddish.

### 2.3. Effects of varying the concentrations of lanthanum and strontium on the recovery of calcium and magnesium

10.0 g of sample 2 was weighed into different porcelain evaporating dishes, ashed, solubilised and concentrated as described below. Varying concentrations of lanthanum and strontium solution were added to the resulting solutions, and the volumes made up to 20.0 $cm^3$. The amounts of calcium and magnesium in each case were determined. The results of duplicate determinations are presented in Table 2.

### 2.4. Recommended procedure

10.0 g [4] of the lubricating oil was weighed into a 100 $cm^3$ capacity evaporating dish and heated gently with a bunsen flame until it ignited. The flame was removed and the oil allowed to burn until a coke residue was

Table 1
Lubricating oil samples analysed

| Sample No. | Grade of oil | Producer |
|---|---|---|
| 1 | SAE 20W/50 | Total |
| 2 | SAE 20W/50 | Mobil |
| 3 | SAE20W/50 | Unipetrol |
| 4 | SAE 40 | National |
| 5 | SAE 40 | Agip |
| 6 | SAE 40 | Texaco |
| 7 | SAE 20W/50 | Rotella |
| 8 | SAE 20W/50 | Texaco |
| 9 | SAE 20W/50 | Whiz |
| 10 | SAE 20W/50 | Agip |
| 11 | SAE 20W/50 | National |
| 12 | SAE 40 | Unipetrol |
| 13 | SAE 40 | African petroleum |

Table 2
Effect of increasing concentrations of lanthanum and strontium on the determination of calcium and magnesium using sample 2

| Concentration of La or Sr ($\mu g\ g^{-1}$) | Concentration of calcium ($\mu g\ g^{-1}$) | | Concentration of magnesium ($\mu g\ g^{-1}$) | |
|---|---|---|---|---|
| | with La | with Sr | with La | with Sr |
| 0 | 308.0 | 308.0 | 2020.0 | 2020.0 |
| 250 | 539.0 | 501.0 | 2100.0 | 2140.0 |
| 750 | 769.0 | 769.0 | 2100.0 | 2140.0 |
| 1000 | 999.0 | 1075.0 | 2110.0 | 2200.0 |
| 2000 | 1152.0 | 1225.0 | 2130.0 | 2220.0 |
| 2500 | 1539.0 | 1564.0 | 2120.0 | 2220.0 |
| 3000 | 1632.0 | 1608.0 | 2151.0 | 2200.0 |
| 4000 | 1628.0 | 1608.0 | 2120.0 | 2119.0 |
| 5000 | 1633.0 | 1608.0 | 2120.0 | 2129.0 |

formed. Heating with the flame was recommenced until all volatile matter had been driven off. The evaporating dish was then transferred to a muffle furnace set at $900 \pm 50$ °C [8] and heated until the ash was free from all visible traces of carbon. This occurred about 3 h after the attainment of the above temperature. The evaporating dish was removed from the furnace and allowed to cool. The residue was treated with 20.0 $cm^3$ of 6 M hydrochloric acid and the solution concentrated on a steam bath to about 5.0 $cm^3$. The solution was transferred quantitatively to a 20.0 $cm^3$ volumetric flask. 6.0 $cm^3$ of 10 000 $\mu g\ g^{-1}$ lanthanum or strontium solution was added and the solution diluted to the mark with water.

The resulting solution was used for the determination of the elements using atomic absorption. A blank solution was also prepared.

### 2.5. *Evaluation of the procedure*

The reproducibility of the procedure was established by applying the proposed procedure six times in turn to sample 1 and determining the elements of interest. The reproducibility in the determination of the various determinant elements is appropriately discussed.

In a comparison of methods, some samples were prepared in duplicate and analysed for calcium, magnesium and zinc using other approaches (precipitation as oxalate followed by titration with $KMnO_4$ solution for Ca, precipitation as 8-hydroxyquinaldinate for Mg, and titration with EDTA for Zn) and the results compared with those obtained for the same samples using the recommended procedure. The data are presented in Table 3.

## 3. Results and discussion

The concentrations of calcium obtained continued to increase with the concentration of either lanthanum or strontium until a peak concentration was obtained, at a lanthanum or strontium concentration of 3 000 $\mu g\ g^{-1}$. Once reached, the peak value remained virtually constant when higher concentrations of lanthanum or strontium were applied. Plotted against increasing concentration of lanthanum or strontium, the concentration of calcium increased linearly to the peak value and thereafter mainted a plateau up to a lanthanum or strontium concentration of 5000 $\mu g\ g^{-1}$. Although the results of Table 2 relate to sample 2, the same trend was observed for the other samples. Table 2 also shows that an increase in the concentration of lanthanum or strontium did not give a corresponding increase in the concentration of magnesium and that all the magnesium was recovered with or without the addition of lanthanum or strontium. Generally, magnesium is not known to be affected by interference due to the phosphate ion, $PO_4^{3-}$.

The recommended procedure gives highly reproducible analysis for unused lubricating oils. Replicate analysis of sample 1 gives the following results — calcium $1648 \pm 26$, magnesium $1620 \pm 57$ and zinc $1160 \pm 2\ \mu g\ g^{-1}$. Table 2 also shows that the results obtained from the procedure are more enhanced for calcium than those obtained from gravimetry, and also that the same sample solution gives comparatively good results for magnesium and zinc. Statistical analysis shows that the new AAS method is free from determinate error at 95% probability. The differences in results between the new AAS

Table 3
Sample results and comparison of methods

| Element | Sample number | Concentration ($\mu g\ g^{-1}$) | |
|---|---|---|---|
| | | Recommended procedure [a] | Other approaches [a] |
| Calcium | 1 | 1648.0 | 1387.0 |
| | 2 | 1631.0 | 1442.0 |
| | 3 | 753.0 | 498.0 |
| | 4 | 268.0 | 169.0 |
| | 5 | 833.0 | 650.0 |
| | 6 | 1295.0 | 1120.0 |
| | 7 | 11.0 | N.D. |
| | 8 | 779.0 | N.D. |
| | 9 | 8.0 | N.D. |
| | 10 | 610.0 | N.D. |
| | 11 | 840.0 | N.D. |
| | 12 | 20.0 | N.D. |
| | 13 | 738.0 | N.D. |
| Magnesium | 1 | 1620.0 | 1347.0 |
| | 2 | 2120.0 | 2418.0 |
| | 3 | 2940.0 | 2993.0 |
| | 4 | 13.0 | 10.0 |
| | 5 | 8.0 | 5.0 |
| | 6 | 19.0 | 19.0 |
| | 7 | 710.0 | N.D. |
| | 8 | 10.0 | N.D. |
| | 9 | 4.0 | N.D. |
| | 10 | 706.0 | N.D. |
| | 11 | 480.0 | N.D. |
| | 12 | 980.0 | N.D. |
| | 13 | 1319.0 | N.D. |
| Zinc | 1 | 1160.0 | 1095.0 |
| | 2 | 1091.0 | 1105.0 |
| | 3 | 1600.0 | 1455.0 |
| | 4 | 133.0 | 147.0 |
| | 5 | 451.0 | 474.0 |
| | 6 | 920.0 | 964.0 |
| | 7 | 916.0 | N.D. |
| | 8 | 1554.0 | N.D. |
| | 9 | 218.0 | N.D. |
| | 10 | 960.0 | N.D. |
| | 11 | 1207.0 | N.D. |
| | 12 | 422.0 | N.D. |
| | 13 | 1453.0 | N.D. |

N.D. = not determined.
[a] Average of duplicate determinations.

method and other conventional approaches could be attributed to the reduced sensitivity of the other methods for calcium and magnesium. Comparable results are obtained for zinc in most of the samples. It must be noted that the sample solution is a complex matrix and the effects of the presence of many other unknown ions interfere with the sensitivity of the conventional methods, leading to a positive or negative influence on the values obtained. Although comparable results are obtained for zinc from titration and the new method, this element alone cannot be determined by titration and the others by AAS when all of them can be determined very fast by AAS.

The procedure presented in this article offers many advantages over other approaches hitherto described. It reduces the analysis time, and the same sample solution can be used to determine all the additive elements included in this work instead of preparing the sample separately for the determination of each element as in the Institute of Petroleum Methods. It overcomes all the problems posed by the use of organic solvents for direct dilution. The procedure employs the use of aqueous inorganic salt standards, thereby freeing the results form dependence on the type of organometallic salt used for calibration. Also, a larger number of samples can be handled simultaneously.

## 4. Conclusion

Additive elements in lubricating oils have hiterto been determined by atomic absorption spectrophotometry after dilution with organic solvents or by chemical analysis of the solubilised ash. This article has demonstrated that the problems encountered in other approaches are easily overcome by the procedure described herein. The method is accurate and fast, and particularly suitable for progressive monitoring of plant blending operations.

## Acknowledgement

I am grateful to the University of Uyo Research Committee for funding this research. I am also grateful to Roberta Mbale Eta and Mfon Johnson Atang for helping to carry out the analysis.

## References

[1] J.P. Pagliassotti and F.W. Porsche, Anal. Chem., 23 (1951) 1820.
[2] T.F. Yen (Ed.), The pole of Trace Metals in Petroleum, Ann Arbor Science Publishers Inc. Ann. Arbor, MI, 1975, p. 123.
[3] L.F. Hatch and S. Matar, From Hydrocarbons to Petrochemicals, Gulf Publishing Company, Book Division, Houston, TX, 1981.
[4] American Society for Testing and Materials, Method DS 11–82, Annual Book of ASTM Standards, Petroleum Products, Lubricants and Fossil Fuel, Section 5, Vol. 5.01, 1984, pp. 341.

[5] Institute of Petroleum, Method IP 110/82, IP Standards for Petroleum and its Products, Part 1: Methods for Analysis and Testing, Vol. 1, 45th edn., Institute of Petroleum, London, 1985, p. 1104.
[6] Institute of Petroleum, Method IP 111/82, IP Standards for Petroleum and its Products, Part 1: Methods for Analysis and testing, Vol. 1, 45th edn., Institute of Petroleum, London, 1985, p. 111.1.
[7] Institute of Petroleum, Method IP 117/82, IP Standard for Petroleum and its Products, Part 1: Methods for Analysis and Testing, Vol. 1, 45th edn., Institute of Petroleum, London, 1985, p. 117.1.
[8] A.P. Udoh, S.A. Thomas and E.J. Ekanem, Af. J. Sci. Tech., Ser. B, 5 (1991) 8.
[9] Institute of Petroleum, Method IP 87/66 (81), IP Standards for Petroleum and its Products, Part 1: Methods for Analysis and Testing, Vol. 1, 45th edn. Institute of Petroleum, London, 1985, p. 187.1.
[10] Institute of Petroleum, Method IP 308/85, IP Standards for Petroleum and Its Products, Part 1; Methods for Analysis and Testing, Vol. 2, 45th edn., Institute of Petroleum, London, 1985, p. 308.1.
[11] S.T. Holding and J.W. Noah, Analyst (London), 95 (1970) 1041.
[12] G. Sebor, I. Lang, D. Kolihova and O. Weisser, Analyst (London), 107 (1982) 1350.
[13] S.E. Allen (Ed.), Chemical Analysis of Ecological Materials, Blackwell Scientific, Oxford, 1974.
[14] American Public Health Association — American Water Association, Standard Methods for the Examination of Water and Wastewater, 14th edn., American Public Health Association, Washington DC., 1975, p. 150.
[15] W. Horwitz (Ed.), Official Methods of Analysis of the Association of Official Analytical Chemists, 13th edn., Association of Official Analytical Chemists, Washington, DC, 1980, p. 31.
[16] S.K. Rajhan and G. Krishna, Laboratory Manual for Nutrition, Vikas, PVT Ltd., 5 Ansari Road, New Delhi, 1980, p. 83.

ELSEVIER

Talanta 42 (1995) 1833–1838

Talanta

# Luminescence determination of europium microquantities after its preconcentration on polyurethane foam

S. Beltyukova *, G. Balamtsarashvili

*A.V. Bogatsky Physico-Chemical Institute of the National Academy of Sciences of Ukraine, 86 Chernomorskaya Doroga, 270 080, Odessa, Ukraine*

Received 12 December 1994; revised 4 April 1995; accepted 24 April 1995

**Abstract**

Sorption of the mixed-ligand complexes of europium(III) with thenoyltrifluoroacetone (TTA) and 1,10-phenanthroline (Phen) on polyurethane foam (PUF) has been studied by a luminescence method. The optimum conditions of sorption have been found. The sorbate composition on PUF has been determined (the Eu:TTA:Phen ratio was 1:3:1). Luminescence spectra of the europium complexes in solution and on PUF at 77 K have been investigated. It was concluded that the character of the $Eu^{3+}$ coordination both in solution and on the sorbent is the same. Stability constants for the complexes in solution ($\lg K = 8.4$) and on the sorbent ($\lg K = 5.5$) have been calculated. The decrease of the stability of the complex on PUF is explained by the deformation of the complex molecule in the sorbent phase. Sorption coefficients for europium (245) and scandium (2.35) and the coefficient of selectivity for europium in $Sc_2O_3$ (102.3) have been determined. A method for the sorption–luminescence determination of europium in $Sc_2O_3$ with a lower limit of contents determined of $1 \times 10^{-6}$% has been developed.

*Keywords:* Europium; Polyurethane foam; Luminescence determination; Preconcentration

## 1. Introduction

Over the past years, polyurethane foam (PUF) has been used successfully in analytical chemistry for the determination of different elements. The sorption of a large quantity of transition, rare earth and toxic elements on PUFs with the aim of their further determination in the eluate or directly on the sorbent by one of the spectroscopic methods, has been reported [1–3].

Only the selective separation of cerium(III) on PUF modified with tri-*n*-butyl phosphate and thenoyltrifluoroacetone [4] or di(2-ethylhexyl) phosphoric acid [5], as well as the luminescence determination of yttrium immobilized on PUF as complexes with quinosol [6] have been described.

In this paper, the sorption of europium from a solution of its mixed-ligand complex with thenoyltrifluoroacetone (TTA) and 1,10-phenanthroline (Phen) on solid PUF has been studied, and the possibility of application of the luminescence properties of the sorbate to the determination of europium in scandium oxide has been demonstrated. Use of the sorption of europium allowed us to carry out its preconcentration as well as to eliminate factors which cause the non-radiative loss of excitation energy (to increase the rigidity of the system, to decrease the thermal motion of molecules, and to decrease the free rotation of ligand fragments).

* Corresponding author.


*SSDI* 0039-9140(95)01637-6

## 2. Experimental

### 2.1. Reagents

Solutions of lanthanide chlorides (0.1 mol $l^{-1}$ and 1 mg $ml^{-1}$) were prepared by dissolution of the corresponding oxides in HCl. The solutions were then evaporated to the wet salts, which were then diluted with water.

The concentration was determined by complexometric titration with Arsenazo I [7]. Solutions of mixed-ligand complexes were prepared according to a literature procedure [8]. Industrial PUF, mechanically pounded to a grain size of 1 mm, was used as the sorbent. The pounded sorbent was treated with 1 M HCl and ethanol and was dried in air.

### 2.2. Apparatus

The pH values of the solution were measured using a pH-meter pH-340. The luminescence spectra of europium were recorded in the region of the $^5D_0 \rightarrow {}^2F_2$ transition (520–630 nm) using an СДЛ-2 spectrometer. The excitation source was a ДКсЭл-1000-5 ultrahigh pressure xenon discharge lamp (power, 1000 V; luminour flux, 32 klm).

### 2.3. Procedure

Sorption was studied under static conditions. The sorbent weight was equilibrated by shaking with 10 ml of a solution of known composition. Equilibrium was controlled by the luminescence of the equilibrium solution.

## 3. Results and discussion

### 3.1. Optimum conditions for sorption

As can be seen in Fig. 1, complete sorption of europium from a solution of the thenoyltrifluoroacetone and 1,10-phenanthroline complex is observed in 10 min. The decrease in luminescence intensity ($I_{lum}$) of the europium sorbate after sorption (10 min) could be connected with the fact that on increase in the sorption time, the sorption of unbound ligands (TTA and Phen) increases and this could lead to a concentration quenching of europium luminescence in the sorbate. Sorption of the europium mixed-ligand complex on PUF is observed over the pH range 7–9, i.e. in the region of existence

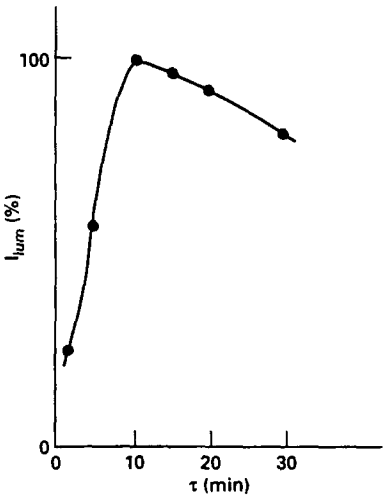


Fig. 1. Dependence of $I_{lum}$ of europium on the sorbent on sorption time ($C_{Eu} = 1 \times 10^{-6}$ mol $l^{-1}$).

of the complex in solution. The highest luminescence intensity of europium on PUF is observed at pH 8 (Fig. 2). The required value of the pH in solution was obtained with urotropine (0.5 ml of a 40% solution) as buffer.

A study of the dependence of the sorption of europium on the amount of complexing substance in solution has shown that a one-hundred to two-hundred fold excess of the reagents (TTA and Phen) is necessary for obtaining the maximum $I_{lum}$ value (Fig. 3). The large excess of the reagents might be due to the additional sorption of unbound ligands on PUF. The choice of the optimum amount of PUF shows that the highest $I_{lum}$ of europium is observed with a sorbent addition of 40 mg (at $C_{Eu} = 1 \times 10^{-5}$ mol $l^{-1}$) (Fig. 4).

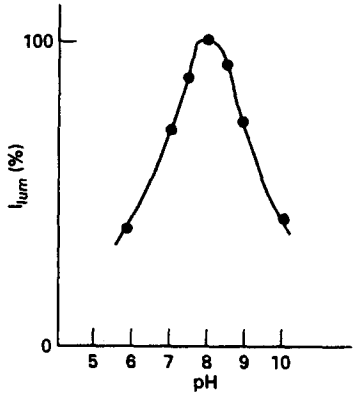


Fig. 2. Dependence of $I_{lum}$ of the europium sorbate on the pH of the solution ($C_{Eu} = 1 \times 10^{-6}$ mol $l^{-1}$).

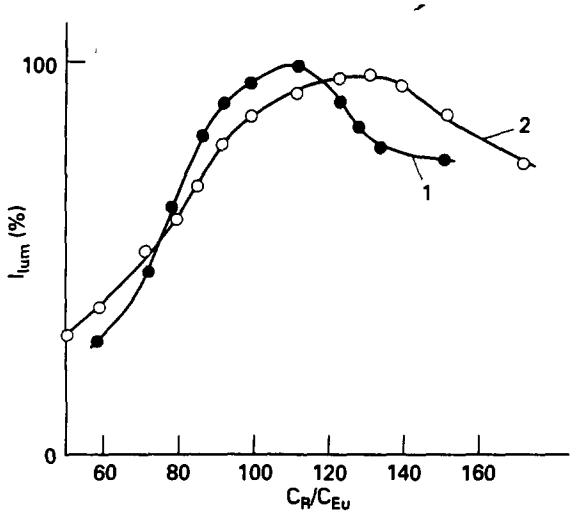


Fig. 3. Dependence of $I_{lum}$ of the europium sorbate on the amount of TTA (curve 1) and Phen (curve 2) in solution ($C_{Eu} = 1 \times 10^{-5}$ mol $l^{-1}$).

### 3.2. Influence of solvent

Values of $I_{lum}$ of the europium complex on PUF in the presence of series of solvents (20% vol.) with different donor–acceptor properties are summarized in Table 1.

As can be seen in the table, the highest $I_{lum}$ value of europium is observed with dimethylformamide and increases threefold. The influence of the electric field of the solvent on the 4f shell of the lanthanide ion has previously been reported [9,10] for the solutions of some complexes of europium and terbium and is exhibited in the dependence of the $I_{lum}$ of these ions on the permittivity of the solvent. However this influence is not observed for sorbates. A dependence of the $I_{lum}$ of europium on the sorbent on the different parameters characterizing the solvent donor–acceptor ability, such as the solvation energy, the acceptor ability, the relative coordination force, and the general base is also not observed.

The influence of the character of the solvent on the $I_{lum}$ of europium in solution and on the sorbent is different. If the $I_{lum}$ in the solution is maximal for water–alcohol solutions, then the $I_{lum}$ on PUF in the presence of these solvents is low. It could be supposed that, in this instance, the solvent influences the sorption ability of the complex. However, the $I_{lum}$ of europium in solution after sorption is low; for example, sorption in the presence of dimethylformamide is 100% and in the presence of ethanol is 87%. On the one hand, it is evident that solvation of the complex molecules by alcohols reduces the total energy of the solvate–sorbate interaction; on the other hand, the sorbating molecules of the solvent definitely influence the processes of non-radiative energy transfer of the electron excitation of the complexes on the sorbates.

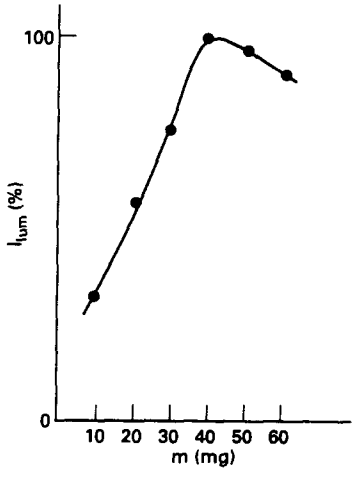


Fig. 4. Dependence of $I_{lum}$ of the europium sorbate on the amount of sorbent ($C_{Eu} = 1 \times 10^{-5}$ mol $l^{-1}$).

### 3.3. Influence of surfactants

The influence of surfactants on the $I_{lum}$ of europium in the mixed-ligand complexes with TTA and Phen (or TOPO) has been reported by many authors [11]. The use of micellar media allows the detection limit of europium to be significantly decreased. Hence, it was interesting to follow the influence of the surfactants on the $I_{lum}$ of sorbed europium on the solid matrix. The sorption of europium was carried out from solutions of mixed-ligand complexes into which different surfactants were introduced. The results obtained are summarized in Table 2. As can be seen, the highest $I_{lum}$ of europium on PUF is observed for the sorption in the absence of surfactants. The introduction of surfactants decreases in either degree the luminescence intensity on the sorbent. Hence, it can be supposed that, in any given instance, a decrease in the degree of sorption and the decrease in the $I_{lum}$ on the sorbent results from solubilization of the complex in solution. The luminescence intensity of the solutions in the presence of surfactants remains fairly high after sorption. This fact testifies in favour of the above supposition.

Table 1
The dependence of the $I_{lum}$ of europium sorbates and solutions of europium and TTA and Phen complexes on the nature of the solvent

| Solvent | $\varepsilon_{Dp}$ | $I_{lum}$ europium (%) | |
|---|---|---|---|
| | | Sorbent | Solution |
| Water | 80.31 | 29 | 100 |
| Dimethylsulfoxide | 48.9 | 75 | 83 |
| Dimethylformamide | 37.6 | 100 | 59 |
| Methanol | 33.6 | 35 | 148 |
| Ethanol | 24.5 | 46 | 162 |
| Propanol | 20.75 | 15 | 135 |

### *3.4. Determination of the degree of sorption and the sorbate composition*

The degree of sorption of europium on PUF was determined by carrying out the sorption under the optimum conditions. The sorbent was dried, burnt in a muffle furnace, the residual ashes were dissolved, and the europium content was determined with Arsenazo III as previously described [7]. The degree of europium sorption in the presence of cetyltrimethylammonium bromide, OC-20 and Triton X-100 were 60%, 20% and 16.6%, respectively, i.e. a significantly higher solubilization of the europium complex in non-ionic surfactants (OC-20, Triton X-100) led to a lower degree of sorption in their presence. Europium forms a complex with TTA and Phen in water–organic media and extracts. The ratio of the components (Eu:TTA:Phen) is 1:3:1. The application of the method of limited logarithms has shown that the sorbate composition corresponds to the composition of the complex in solution.

Europium sorbates exhibit an intensive luminescence which exceeds by two orders the $I_{lum}$ of europium in solutions of the same complex. The distribution of radiation energy on the $^5D_0 \rightarrow {}^7F_j$ (where $j = 1, 2$) transitions and on the separate lines within the transition is approximately equal for the sorbate and a solution of the complex at 77 K (Fig. 5). The major part of the radiative energy in the sorbate is on the line of the $^5D_0 \rightarrow {}^7F_2$ electric-dipole transition. It is known that the intensity of the lines corresponding to the $^5D_0 \rightarrow {}^7F_1$ magnetic-dipole transition is lower than the intensity of the line of the $^5D_0 \rightarrow {}^7F_2$ electric-dipole transition by one order of magnitude. The $\Delta F_{1,2}$ magnitudes, which are recorded in the low temperature luminescence spectra, are sensitive indicators of the $Eu^{3+}$–coordinated ligands interaction. The splitting of the Stark components $^7F_j$ for sorbates and complexes in solution are similar; this could testify to the identical character of the coordination of the europium ion in solution and on the sorbent.

Table 2
The dependence of the $I_{lum}$ of europium in solution of complexes with TTA and Phen in the sorbates on the nature of the surfactants

| Surfactant | $I_{lum}$ of europium in solution before sorption (%) | $I_{lum}$ of europium on PUF (%) |
|---|---|---|
| None | 32 | 100 |
| Cetyltrimethylammonium | 52 | 42 |
| Cetylpyridinium bromide | 21 | 38 |
| Aethonium | 34 | 11 |
| OC-20 | 53 | 51 |
| Triton X-100 | 63 | 45 |
| Tetramethylammonium bromide | 21 | 39 |
| Tetrabutylammonium bromide | 20 | 37 |
| Lauryl sulphate | 30 | 12 |

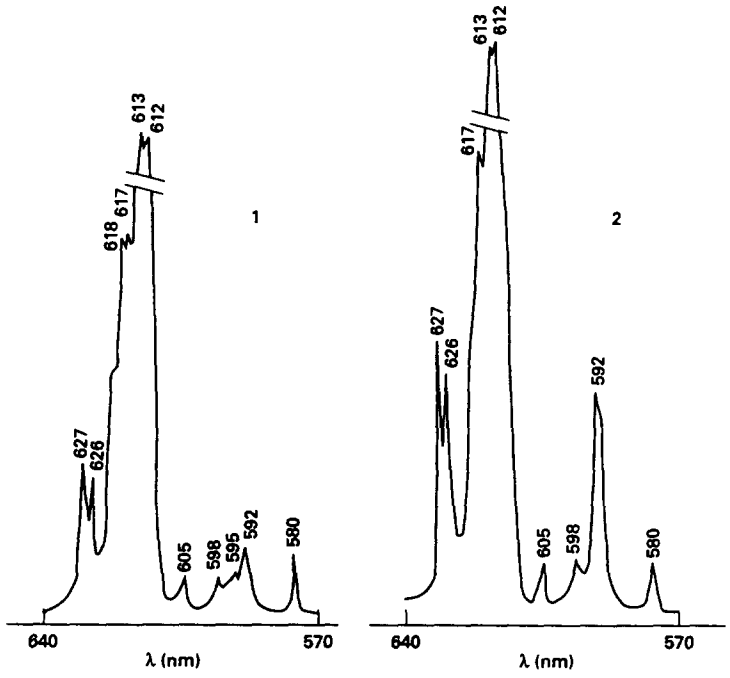


Fig. 5. Luminescence spectra of a mixed-ligand complex of europium with TTA and Phen (spectrum 1) in solution and (spectrum 2) on the sorbent at 77 K.

### 3.5. Stability of the complexes in the sorbates

A mathematical model describing similar systems [12] has been applied to the stability evaluation of the obtained complexes on polyurethane foam. According to this model, the inverse magnitude of the metal concentration on the sorbent ($Y$) and the inverse magnitude of its equilibrium concentration ($X$) in solution are bound by the rectilinear dependence

$$I/Y = A_1(I/X) + A_0$$

where $A_1$ and $A_0$ are coefficients of this equation. The stability constant of the europium complex on the sorbent, $K_{stab} = A_0/A_1$.

Stability constants of the complex in solution were calculated for comparison purposes. The least-squares method has been applied in the calculations in both instances. Correlation coefficients of the linear equations are within the limits 0.95–0.98. The obtained results show that the stability of the complexes on the sorbent (lg $K = 5.5$) is lower than that in solution by several orders (lg $K = 8.4$). This could be connected with the fact that the fixed on matrix ligands take place in complexing in the sorbate instance. If all the ligands can take the necessary geometric configuration in solution, then this is connected with the additional energy expenditure in the sorbent layer. This energy is needed for the taking up of the necessary geometric position by the attached ligand groups, i.e. to deform the natural position of the attached ligands as well as the matrix itself [14]. Deformed complex, which is attached to the matrix, has a lower stability.

### 3.6. Possibility of analytical application of the sorbate

The high luminescence intensity of sorbates of europium phenanthrolinethenoyltrifluoro-acetonate may be used to develop methods for the determination of europium in lanthanide oxides with much lower detection limits, i.e. of the order of $n.10^{-6}$–$n.10^{-7}$%. At present, the analysis of lanthanide oxides as well as scandium oxide is very actual. It is known that differences between the formation conditions and the stability of the europium and scandium complexes with TTA are applied in the separation by extraction of these elements. Thus, scandium is extracted by benzole from more acidic solutions ($pH_{1/2(Sc)}$ 0.5) than europium ($pH_{1/2(Eu)}$ 2.9). The extraction constants of these elements (lg $K(Sc) = -0.77$, lg $K(Eu) = -7.9$ [13]) are also different. It could be supposed that, by analogy

with the extraction processes, the differences in the properties of the complexes are intensified on sorption. Hence, the determination of europium in the presence of large amounts of scandium will be possible. It has been established that the degree of sorption of scandium from solutions in the presence of both TTA and Phen under optimum conditions for the sorption of europium on PUF is 50%.

Sorption coefficients for europium and scandium are 245 and 2.35, respectively. The selectivity coefficient for europium in scandium oxide is 102.3. hence, it may be concluded that application of PUF allows the detection limit of europium in scandium oxide to be reduced.

### *3.7. Method of determination*

The scandium oxide to be analyzed is dissolved in HCl, the solution is evaporated to the wet salts, and the residue is dissolved in distilled water. Samples of the solution to be analyzed are placed in three beakers; the solution contains 50–100 μg of scandium oxide. Different amounts of a solution of europium chloride are added to two of the beakers. To each beaker are then added 0.5 ml of 0.5% TTA, 0.15 ml of 3% Phen, 2 ml of dimethylformamide, and 0.5 ml of 40% urotropine. The solution is diluted to 10 ml with water, 40–50 mg of PUF are added, and sorption is carried out for 10 min. The sorbent is filtered, washed with distilled water and dried in air. Luminescence spectra are recorded using the СДЛ-2 spectrometer (or any other spectrometer) at $\lambda = 612$ nm. The europium content of the sample solution and of the sample with additions is calculated using the additions method in accordance with the size of the luminescence peak. The accuracy of the analysis has been tested by the additions method and by varying the sample additions. The europium content in the samples of scandium oxide to be analyzed according to the certified data is below $1 \times 10^{-4}$%. Additions of europium (0.002 and 0.005 μg) to aliquots of $Sc_2O_3$, carried out for all analyses, are 0.0019 μg and 0.0051 μg at $n = 5$, $P = 0.95$ and $S_r = 0.06$ and 0.05, respectively.

As the data show, the developed methods allow europium to be determined in scandium oxide with satisfactory accuracy and reproducibility.

The detection limit of europium, i.e. $1 \times 10^{-6}$%, was calculated according to the $3\sigma$-criterion.

## References

[1] T. Braun and A.B. Farag, Anal. Chim. Acta, 99 (1978) 1.
[2] R.F. Hamon, A.S. Khan and A. Chow, Talanta, 29 (1982) 313.
[3] S. Palaqyi, T. Braun, J. Radioanal. Nucl. Chem., 163 (1992) 69.
[4] A. Raychandhuri, I. Somlai, J. Radioanal. Nucl. Chem., Lett., 166 (1992) 153.
[5] M. Aziz, S.C. Beneiz, K. Shakiz, J. Radioanal. Nucl. Chem., 157 (1992) 105.
[6] N.A. Nazarenko, Zh.I. Grabovskaya, S.V. Cygankova, S.V. Beltyukova, Zh. Anal. Khim., 48 (1993) 61.
[7] S.B. Savvin, Organic Reagents of Arsenazo II Group, Atomizdat, Moscow, 1971.
[8] N.S. Poluektov, L.I. Kononenko, N.P. Efryushina and S.V. Beltyukova, Spectrophotometric and Luminescent Methods for the Determination of the Lanthanides, Naukova Dumka, Kiev, 1989.
[9] L.I. Kononenko, S.V. Beltyukova, S.B. Meshkova, V.N. Drobiazko, N.S. Poluektov, Dokl. Akad. Nauk. Ukr. SSR, Ser. B (1975) 816.
[10] L.I. Kononenko, S.V. Beltyukova, S.B. Meshkova, T.B. Kravchenko, N.S. Poluektov, Zh. Prikl, Spektrosk., 28 (1978) 1009.
[11] S.B. Savvin, R.K. Chernova and S.N. Shtykov, Surfactants, Nauka, Moscow, 1991.
[12] A.P. Filippov, Teor. Eksp. Khim., 19 (1983) 463.
[13] I.S. Stary, Extraction of Chelates, Mir, Moscow, 1966.
[14] R. Hering, Chelate forming ion-exchangers, Mir, Moscow, 1971.

ELSEVIER

Talanta 42 (1995) 1839–1848

Talanta

# Catalytic oxidation of ascorbic acid by some ferrocene derivative mediators at the glassy carbon electrode. Application to the voltammetric resolution of ascorbic acid and dopamine in the same sample

M.H. Pournaghi-Azar*, R. Ojani

*Electroanalytical Chemistry Laboratory, Faculty of Chemistry, University of Tabriz, Tabriz, Iran*

Received 5 January 1995; revised 21 February 1995; re-revised 19 April 1995; accepted 19 April 1995

**Abstract**

Direct-current cyclic voltammetry is used to investigate the suitability of some ferrocene derivatives such as ferrocenecarboxylic acid, ferroceneacetic acid and ferrocenemethanol as mediators for ascorbic acid oxidation in aqueous solutions with low pH. The ascorbic acid coupled catalytically to three ferrocene derivatives exhibiting homogeneous second-order rate constants $k_s$, in the range $7.36 \times 10^5$–$1.23 \times 10^7$. The catalytic oxidation peak current was linearly dependent on the ascorbic acid concentration and the linearity range obtained in the presence of ferrocenecarboxilic acid, having the largest second-order rate constant, was $5 \times 10^{-5}$–$1.5 \times 10^{-3}$ M. The catalytic effect of the ferrocene derivatives on the electrochemical oxidation of ascorbic acid reduced the oxidation potential of ascorbic acid, resulting in the separation of the overlapping voltammograms of ascorbic acid and dopamine at the glassy carbon electrode in a mixture. This allowed the determination of ascorbic acid in the presence of dopamine. The calibration graph obtained by linear sweep voltammetry for ascorbic acid in the presence of dopamine of fixed concentration is linear in the range $5 \times 10^{-5}$–$1.5 \times 10^{-3}$ M. In a similar manner, dopamine is determined in the presence of a high concentration of ascorbic acid, up to 100 times that of dopamine, using ferroceneacetic acid as the most suitable mediator for this purpose.

*Keywords:* Ascorbic acid; Dopamine; Ferrocene mediators; Glassy carbon electrode; Voltammetry

## 1. Introduction

Ascorbic acid (vitamin C) is a hexuronic acid with $pK_a$ values of 4.17 and 11.5. In biological solutions at neutral pH it exists primarily as the monohydrogen ascorbate anion. Ascorbic acid/ascorbate is a vital component in the diet of humans. Ascorbate is the agent which prevents scurvy and is known to take part in several biological reactions. Ascorbate is possibly the primary antioxidant in human blood plasma and is present in mammalian brain in the presence of several neurotransmitter amines including dopamine, epinephrine and norepinephrine. In addition, ascorbic acid is found in high concentration in some fruits and foods together with vasoactive amines such as dopamine.

Many of the fundamental studies on ascorbic acid oxidation have examined the reaction at metal electrodes. It is now established that the oxidation of ascorbic acid (1) at low pH proceeds via two consecutive one-electron pro-

* Corresponding author.


*SSDI* 0039-9140(95)01638-4

TAL 42-12-0

cesses involving the participation of a radical anion intermediate (2) (the latter being confirmed from electron paramagnetic resonance spectroscopy [1], to form dehydro-L-ascorbic acid (3). The latter species subsequently undergoes a hydration reaction characteristic of carbonyl groups to form the final electroinactive product (4). Consequently the overall reaction can be classified as an EC process:

$$AH_2 - 2e \rightarrow A + 2H^+ \quad E \quad (1)$$

$$A + H_2O \rightarrow B \quad C \quad (2)$$

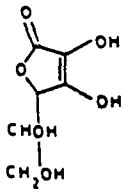

$AH_2$
(1)

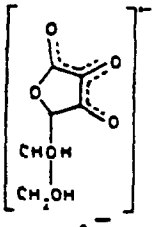

A
(2)

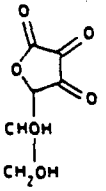

A
(3)

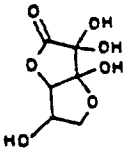

B
(4)

Note also that at pHs between the first and second $pK_A$ values ($4.17 < pH < 11.5$), the oxidation process will only involve the loss of a single proton owing to the fact that ascorbic acid will be of the form $AH^-$.

The selective amperometric determination of ascorbic acid is of much current interest. In samples with low pH, it is almost too difficult to determine this compound electrochemically by direct oxidation on a conventional electrode because of fouling by the oxidation products. A carbon electrode, when subjected to an appropriate pretreatment procedure, exhibits minimal propensity for surface fouling. However, the kinetics of electron transfer are quite sluggish. This last characteristic of electrochemical irreversibility means that ascorbic acid will be oxidized only at potentials considerably removed from its standard redox potential. It has been demonstrated [2] that ascorbic acid can undergo mediated oxidation via a homogeneous process by electrogenerated hexacyanoferrate (III). In addition, some chemically modified electrodes with various active mediators immobilized at the electrode surface for the mediated oxidation of ascorbic acid in acidic solution have been used [3–7].

This paper describes the suitability of some ferrocene derivatives as mediators for the mediated oxidation and determination of ascorbic acid in aqueous solutions with relatively low pH values. The homogeneous second-order rate constants ($k_s$) for the interaction between ascorbic acid and electrogenerated ferricinium derivatives are determined by cyclic voltammetry. In view of the fact that normally it is difficult to obtain separate voltammetric waves for ascorbic acid and dopamine in the presence of each other, mainly when ascorbic acid is present at high concentration [8,9] the ability of the mediators to promote the voltammetric resolution of ascorbic acid and dopamine is investigated.

## 2. Experimental

### 2.1. Reagents and chemicals

The solvent used for the electrochemical studies was doubly distilled water. Lithium perchlorate from Fluka was used as supporting electrolyte. The ferrocene derivatives were from Janssen and were used without further purification. All other reagents were of analytical grade. The solutions were bubbled with nitrogen gas (99.99%) and were kept under a nitrogen atmosphere during the electrochemical experiments.

### 2.2. Instrumentation

The electrochemical experiments were carried out using the EG&G potentiostat/galvanostat model 273 coupled with an IBM personal computer connected to an Epson model FX-850 printer. A conventional three-electrode cell with a calomel electrode as the reference electrode, a platinum wire as the auxiliary electrode and a glassy carbon disk as the working electrode ($A = 0.126\ cm^2$; obtained from EG&G) as used. A pH-meter, model 654 (from Metrohm), was also used.

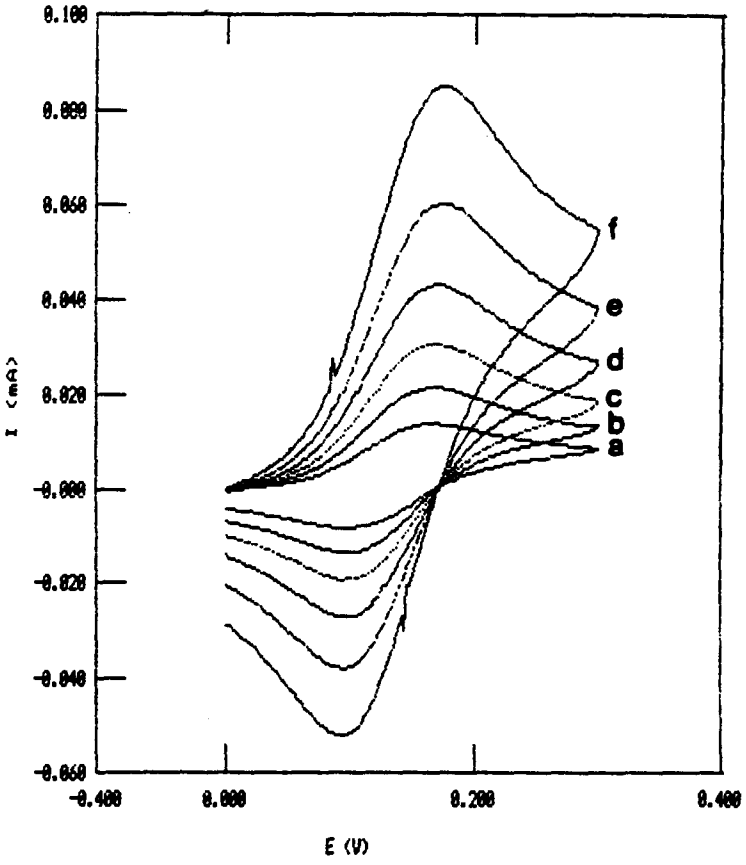


Fig. 1. Cyclic voltammograms of 2 mM ferroceneacetic acid in 0.5 M acetic buffer + 0.1 M $LiClO_4$ at pH 5, using a glassy carbon working electrode, at scan rates of (curve a) 20 mV $s^{-1}$, (curve b) 50 mV $s^{-1}$, (curve c) 100 mV $s^{-1}$, (curve d) 200 mV $s^{-1}$, (curve e) 400 mV $s^{-1}$, and (curve f) 800 mV $s^{-1}$.

## 3. Results and discussion

### 3.1. Electrochemistry of mediators

It has been demonstrated that the optimum characteristics for mediators that can be used in the catalytic electrochemical reaction of substrate include reversible electrochemistry at the electrode surface and rapid reaction with the substrate. The reversibility of ferrocene/ferricinium derivative systems used as mediators in this study was examined by cyclic voltammetry. Cyclic voltammograms for ferroceneacetic acid are shown as examples in Fig. 1 and a summary of electrochemical data for the mediators obtained at the glassy carbon electrode is presented in Table 1. As can be seen in the table, the peak separation potentials $\Delta E_p$ are consistent with an almost reversible oxidation process for the mediators.

### 3.2. Mediated oxidation of ascorbic acid

Previously, $Fe(CN)_6^{4-}$ was shown to be able to electrocatalyze the oxidation of ascorbic acid via a homogeneous process when the ferrocyanide is present in the dissolved form

Table 1
Heterogeneous rate constants for ferrocene derivatives at the glassy carbon electrode

| Ferrocene derivative | $E^a_{1/2}$ (mV) | $\Delta E^b_p$ (mV) | $k^c_0$ (cm $s^{-1}$) |
|---|---|---|---|
| Carboxylic acid | 300 | 74 | $1.6 \times 10^{-2}$ |
| Acetic acid | 139 | 64 | $7.4 \times 10^{-2}$ |
| Methanol | 180 | 70 | $2.0 \times 10^{-2}$ |

[a] Half-wave potential vs. SCE.
[b] Peak separation, at a scan rate $v = 50$ mV $s^{-1}$.
[c] Approximate heterogeneous rate constant calculated according to Ref. [11].

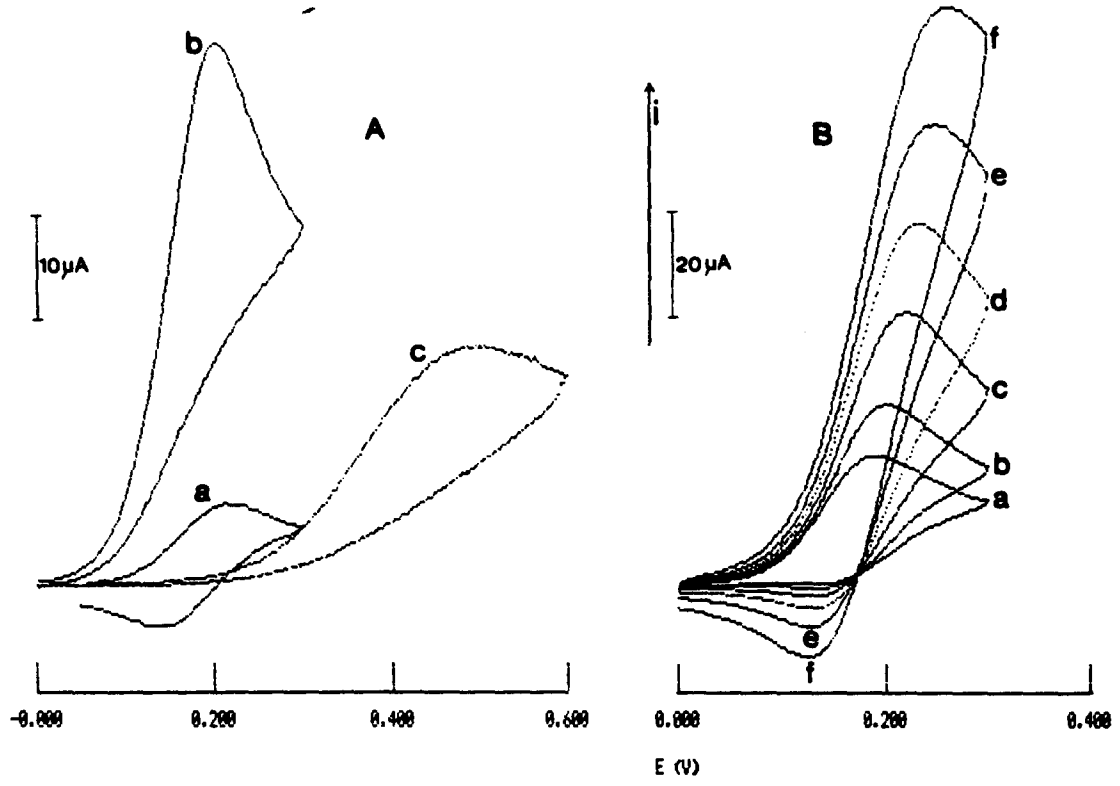


Fig. 2. (A) Cyclic voltammograms of (curve a) saturated ferrocenemethanol in 0.5 M glycine buffer + 0.1 M $LiClO_4$ at pH 4, (curve b) a + 5 mM ascorbic acid, and (curve c) 5 mM ascorbic acid in a buffer solution of pH 4; scan rate, 5 mV $s^{-1}$. (B) catalytic oxidation of 1 mM ascorbic acid at scan rates of (curve a) 10 mV $s^{-1}$; (curve b) 20 mV $s^{-1}$; (curve c) 50 mV $s^{-1}$; (curve d) 100 mV $s^{-1}$; (curve e) 200 mV $s^{-1}$ and (curve f) 400 mV $s^{-1}$. Solution conditions as in (A).

[2]. Accordingly, we decided to examine the ability of ferrocene derivative mediators compared with ferrocyanide to catalyze the ascorbic acid oxidation.

Typical examples of cyclic voltammograms obtained for a saturated ferrocenemethanol solution and for $5 \times 10^{-3}$ M ascorbic acid solutions in the presence and absence of ferrocenemethanol at pH 4 are shown in Fig. 2A. As can be seen in this figure (curve c), the oxidation of ascorbic acid in the absence of mediator occurred irreversibly with a peak potential of almost 0.5 V vs. SCE, while in the presence of ferrocenemethanol as the mediator, its oxidation appeared at the potential of the mediator (curve b); the anodic peak current of the mediator was greatly increased over that normally observed just for the mediator redox couple, while the corresponding cathodic wave was substantially depressed on the reverse voltage scan (curve b). This behaviour is typical of that expected for mediated oxidation. The cyclic voltammograms shown in Fig. 2B for the ascorbic acid–ferrocenemethanol couple at various potential scan rates reveal that the catalytic effect of the mediator appeared even at high scan rates of up to 100 mV $s^{-1}$ (curves a–d), due to a considerable catalytic reaction rate. The other ascorbic acid–ferrocene derivative couples showed a similar behaviour at the appropriate solution pH.

### 3.3. Optimization of the solution pH

Cyclic voltammograms obtained for the solutions containing ascorbic acid and the ferrocene derivative mediators in strongly acidic media showed that ascorbic acid did not couple catalytically with the ferrocenes. Therefore, optimization of the solution pH for each ferrocene–ascorbic acid couple was necessary in order to obtain the catalytic couple. The study of the pH effect was carried out with the aid of two different buffers and the cyclic voltammograms are shown in Fig. 3. The optimum pH values obtained for the carboxylic acid, methanol and acetic acid ferrocene derivatives were 4, 4 (0.5 M glycine buffer) and 5 (0.5 M acetic buffer), respectively.

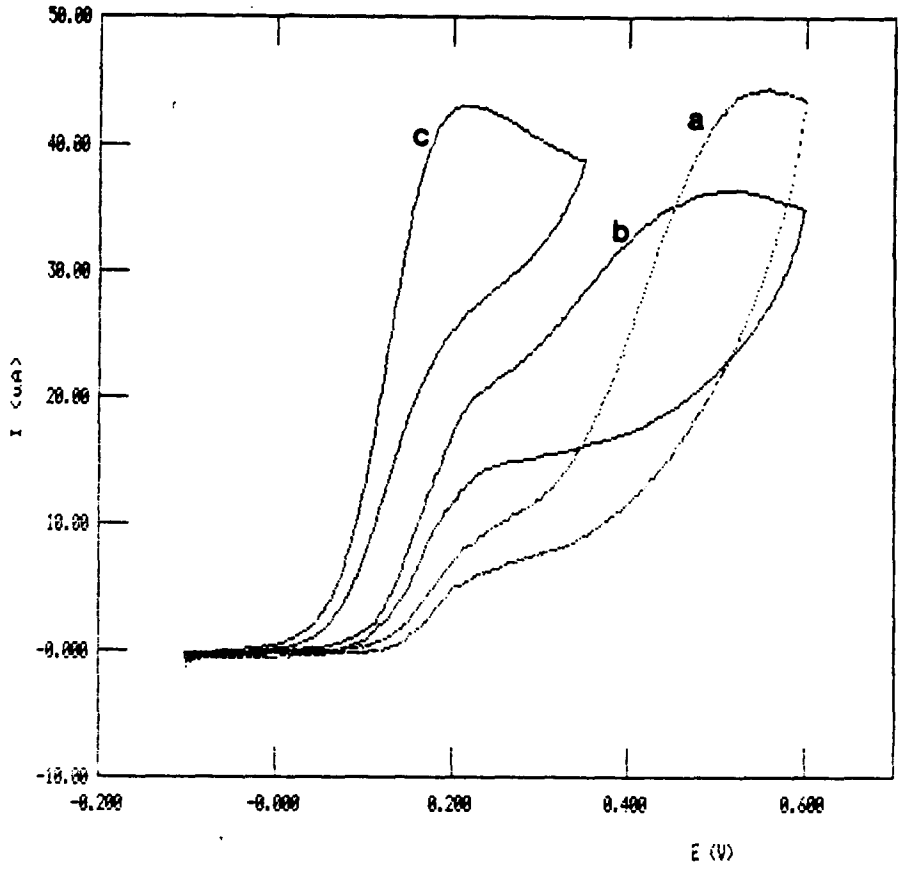


Fig. 3. Cyclic voltammograms of 10 mM ascorbic acid in the presence of 1 mM ferroceneacetic acid at (curve a) pH 2 (0.5 M glycine buffer) (curve b) pH 3 (0.5 M glycine buffer) and (curve c) pH 5 (0.5 M acetic buffer). In all cases 0.1 M $LiClO_4$, was used as the supporting electrolyte. The scan rate was 5 mV $s^{-1}$.

### 3.4. Evaluation of catalytically coupled reaction rates

The theory of stationary electrode voltammetry developed by Nicholson and Shain [10] can be used to analyze a catalytically coupled reaction. The reaction scheme can be described as

$$R - e^- \rightleftharpoons O \qquad Z + O \xrightarrow{k_f} R$$

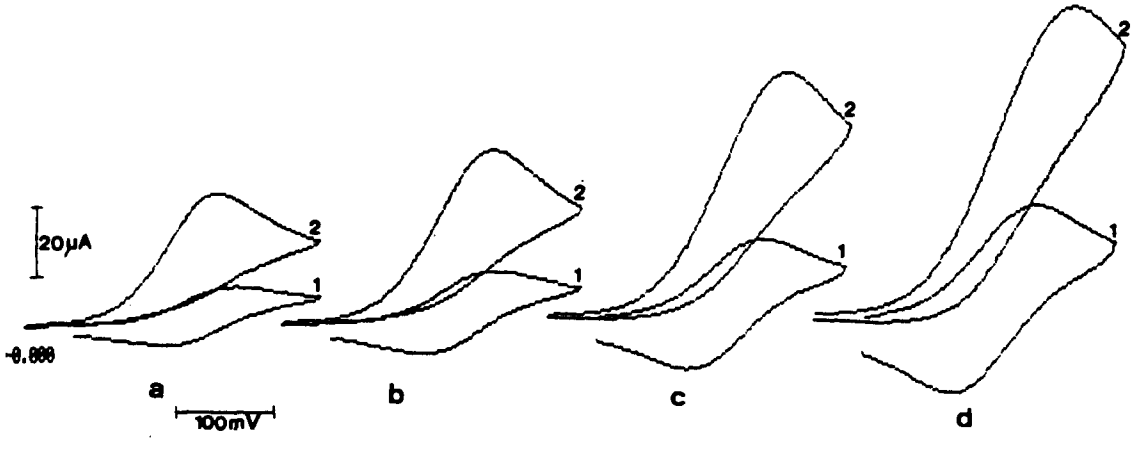


Fig. 4. Cyclic voltammograms of saturated ferrocenemethanol in 0.5 M glycine buffer + 0.1 M LiClO at pH 4 (curves 1; $i_p = i_D$) and 1 + 2 mM ascorbic acid (curves 2; $i_p = i_K$) at a scan rate of (a) 10 mV $s^{-1}$, (b) 20 mV $s^{-1}$, (c) 50 mV $s^{-1}$ and (d) 100 mV $s^{-1}$.

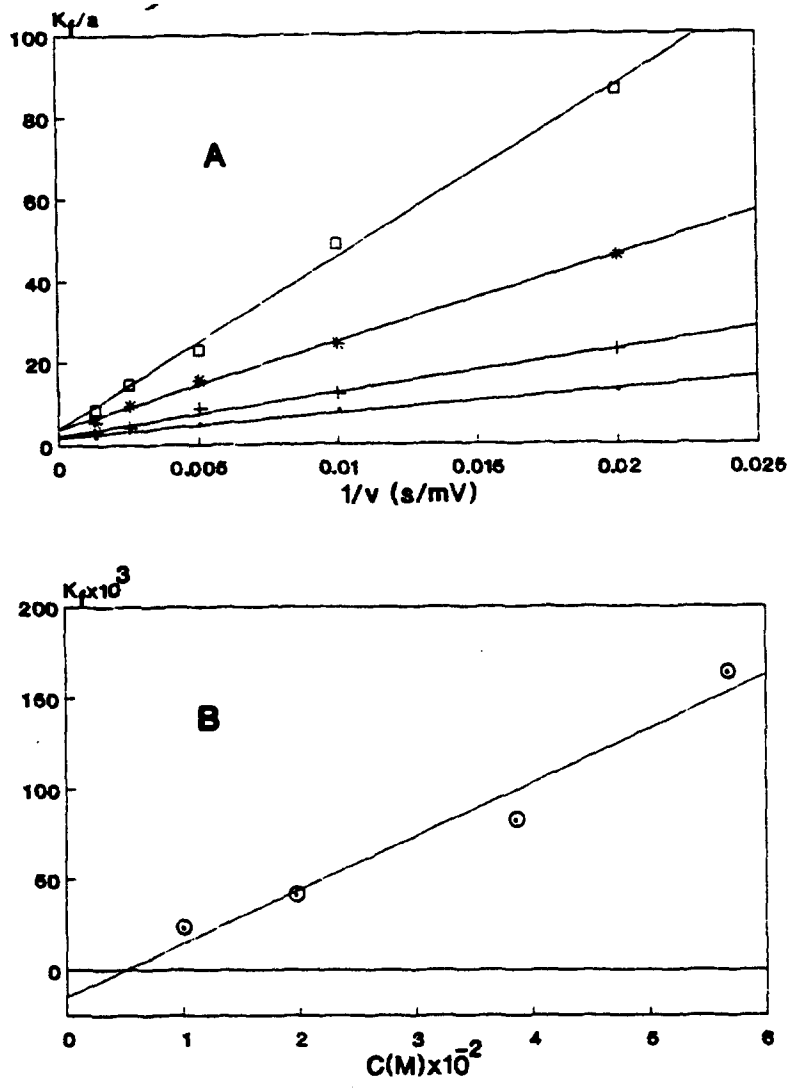


Fig. 5. (A) Kinetic parameter $k_f/a$ as a function of $1/v$ for the interaction between 2 mM ferroceneacetic acid and (●) 9.9 mM, (+) 19.6 mM, (•) 38.5 mM, or (□) 56.6 mM ascorbic acid in acetic buffer (pH 5) at 25 °C. (B) Pseudofirst-order rate constant $k_f$ (calculated from (A)) as a function of the ascorbic acid concentration.

where R and O represent the respective reduced and oxidized forms of the mediators, Z represents ascorbic acid, and $k_f(=k[Z])$ is the pseudofirst-order rate constant. Using experimental values of $i_K/i_D$, the ratio of the kinetically controlled current (in the presence of ferrocene) to the diffusion-controlled current (in the absence of ferrocene) (Fig. 4), a value of $k_f/a$ for each ascorbic acid–ferrocene couple can be derived from the working [10] curve ($i_K/i_D$ vs. $(k_f/a)^{1/2}$, where $a = nFv/RT$, $v$ being the scan rate (V s$^{-1}$). A plot of $k_f/a$ vs. $1/v$ at each ascorbic acid concentration under pseudofirst-order conditions should be linear, with a slope of $RTk_f/nf$ (Fig. 5A). This procedure allows the pseudofirst-order rate constant to be obtained independently of the scan rate. A plot of $k_f$ vs. ascorbic acid concentration is also linear with a slope equal to the second-order homogeneous rate constant $k_s$ for the reaction between the ferricinium derivatives and ascorbic acid (Fig. 5B). The rate constants for the mediators used in this study were determined by the method mentioned above with the ascorbic acid concentration expressed in moles per litre (Table 2).

## 4. Analytical aspects

### 4.1. Determination of ascorbic acid

Linear sweep voltammetry (LSV) of ascorbic acid at a glassy carbon electrode, using fer-

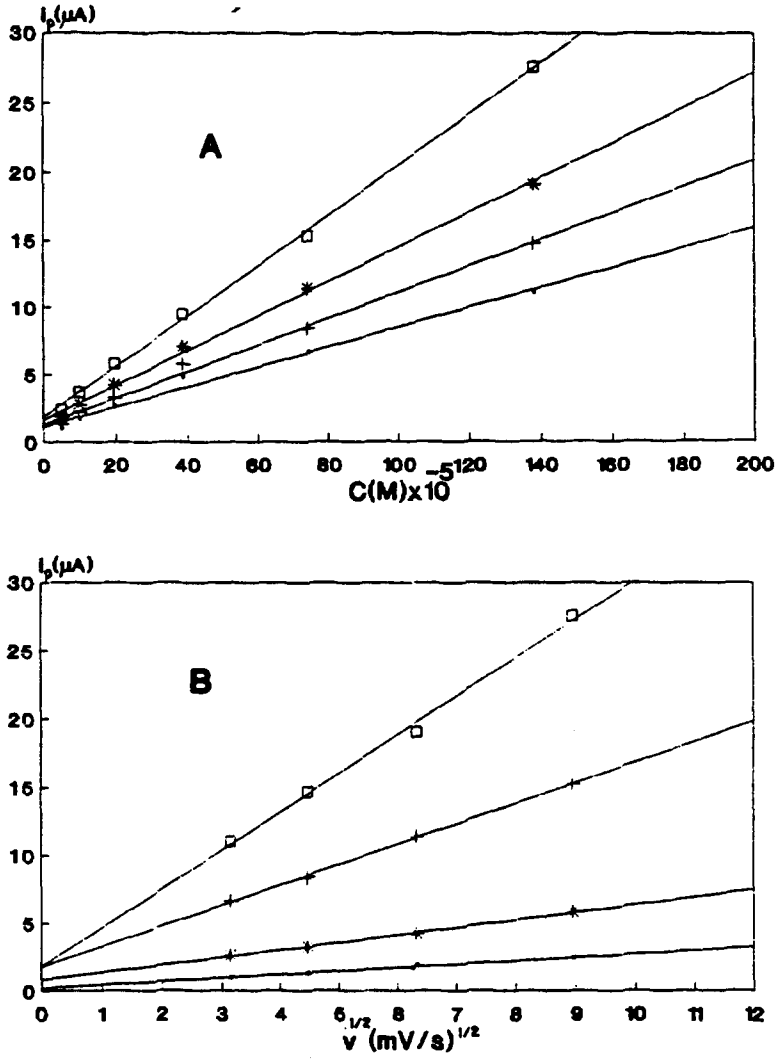


Fig. 6. (A) Dependence of the peak current on the concentration of ascorbic acid at pH 4 for different scan rates: (●) 10 mV s$^{-1}$; (+) 20 mV s$^{-1}$; (*) 40 mV s$^{-1}$; (□) 80 mV s$^{-1}$. The mediator was 0.1 mM ferrocenecarboxylic acid; (B) Dependence of the peak current on the square root of the scan rate for different ascorbic acid concentrations: (●) 4.98 × 10$^{-5}$ M; (*) 1.96 × 10$^{-4}$ M; (+) 7.41 × 10$^{-4}$ M; (□) 1.38 × 10$^{-3}$ M. Solution conditions as in (A)

rocenecarboxylic acid as a convenient mediator, showed that the mediated oxidation current was linearly dependent on the substrate concentration and the square root of the applied potential scan rate (Figs. 6A and 6B). Fig. 6B indicates that the current is diffusion-controlled and the effect of slow charge-transfer kinetics is not apparent. The calibration graph was linear in the range $5 \times 10^{-5}$–$10^{-3}$ M with a correlation coefficient of 0.999. The detection limit, taken as the concentration that gave a signal equal to three times the standard deviation of the blank signal, calculated from the calibration graph, was $2 \times 10^{-5}$ M. Thus the catalytic oxidation of ascorbic acid can readily be applied to the determination of ascorbic acid.

Table 2
Homogeneous second-order rate constant ($k_s$) for the interaction between ascorbic acid and the ferrocene derivatives, determined by cyclic voltammetry

| Ferrocene derivative | $k_s$ (l mol$^{-1}$ s$^{-1}$) | $t$ (°C) | pH |
|---|---|---|---|
| Carboxylic acid | $1.23 \times 10^7$ | 25 | 4.0 |
| Acetic acid | $2.96 \times 10^6$ | 25 | 5.0 |
| Methanol | $7.36 \times 10^5$ | 25 | 4.0 |

### 4.2. Determination of ascorbic acid in the presence of dopamine

Fig. 7, curve a shows that the differential pulse voltammograms of ascorbic acid and dopamine of equal concentration were overlap-

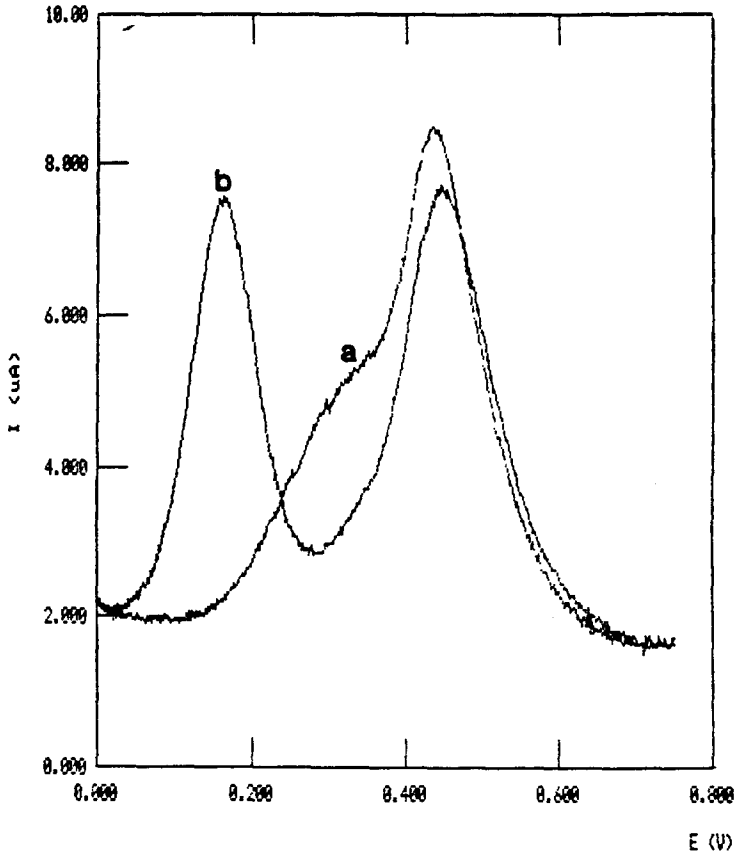


Fig. 7. Differential pulse voltammograms of 0.5 mM ascorbic acid and 0.5 mM dopamine obtained in 0.5 M glycine buffer + 0.1 M $LiClO_4$ at pH 4 in (curve a) the absence and (b) the presence of ferrocenemethanol. Scan rate, 5 mV $s^{-1}$; pulse amplitude, 50 mV; pulse time, 25 ms.

ping, while two distinct differential pulse voltammograms were obtained in the presence of the ferrocene derivative mediators (Fig. 7, curve b) due to the mediated oxidation of ascorbic acid at a sufficiently negative potential. The separation between the two peak potentials for these compounds was the largest in the presence of ferrocenemethanol, and is large enough (about 300 mV) to allow the determination of ascorbic acid in a mixture. However the calibration graph obtained by differential pulse voltammetry was not linear in the concentration range below $5 \times 10^{-4}$ M ascorbic acid. As seen in Fig. 8A, a relatively large separation between the two peaks was observed by linear sweep voltammetry at a stationary glassy carbon electrode under the same solution conditions; therefore the identification and determination of ascorbic acid in the presence of dopamine is feasible. Linear sweep voltammetric peak currents were found to vary linearly with the concentration of ascorbic acid between $5 \times 10^{-5}$ and $1.4 \times 10^{-3}$ M, with a correlation coefficient of 0.996 (inset Fig. 8B).

### *4.3. Determination of dopamine in the presence of a high concentration of ascorbic acid*

One factor that is of importance when applying ascorbic acid catalytically coupled mediators is the ability to separate or resolve voltammetric waves of ascorbic acid and dopamine in a mixture, because it is normally difficult to obtain separate voltammetric waves for these compounds in the presence of each other, largely when ascorbic acid is present at high concentration [8,9].

The voltammetric response of dopamine is hindered by electroactive species, mostly ascorbic acid, which are present at a substantially higher concentration than dopamine. In order to resolve this problem, i.e. to introduce specificity, we have carried out the catalytic oxidation of ascorbic acid using a high concentration of mediator. This may be achieved by the use of ferroceneacetic acid "having both the desired solubility and the catalytic ability" as the most suitable mediator for the mediated oxidation of ascorbic acid at high concentration, at a suffi-

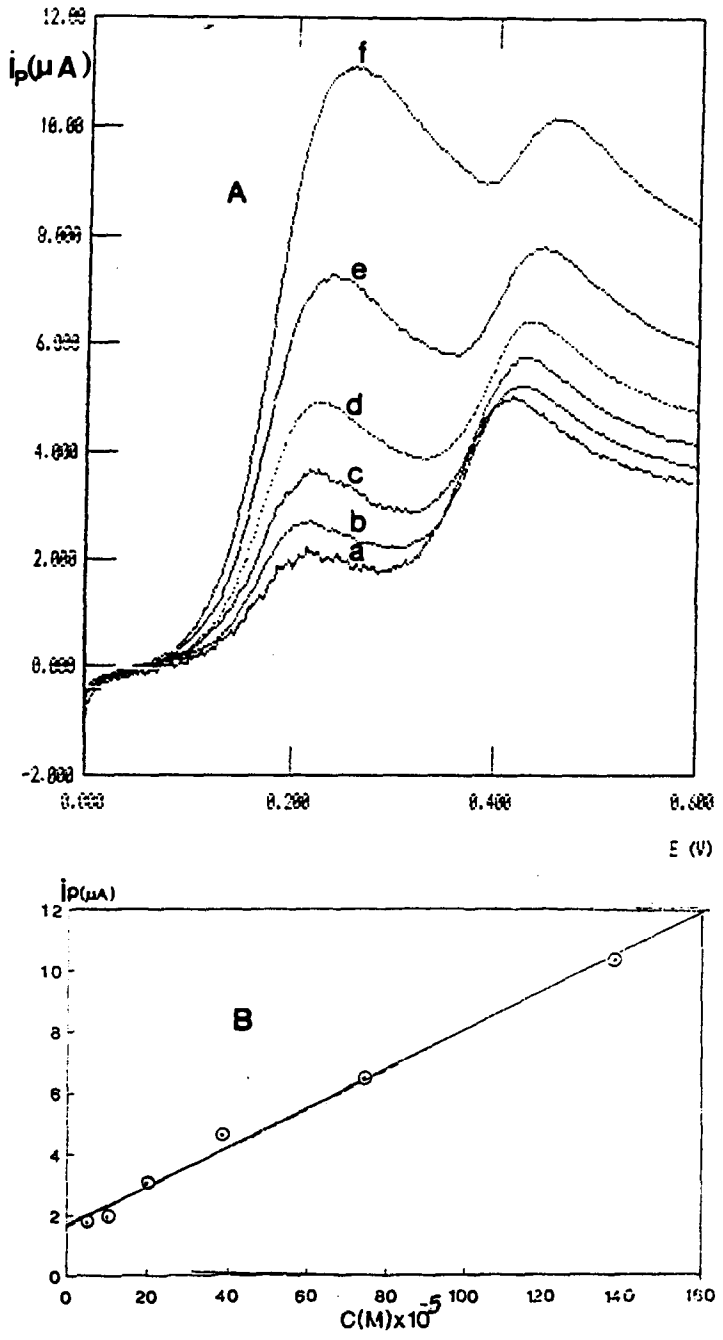


Fig. 8. (A) Linear sweep voltammograms of ascorbic acid of various concentrations: (curve a) $4.98 \times 10^{-5}$ M; (curve b) $9.9 \times 10^{-5}$ M; (curve c) $1.96 \times 10^{-4}$ M; (curve d) $3.85 \times 10^{-4}$ M; (curve e) $7.4 \times 10^{-4}$ M; (curve f) $1.38 \times 10^{-3}$ M; in the presence of dopamine with a fixed concentration of $5 \times 10^{-4}$ M. (B) Plot of linear sweep voltammetric peak current (shown in (A)) vs. the ascorbic acid concentration. Solution conditions: pH 4 (0.5 M glycine buffer), 0.1 M $LiClO_4$, ferrocenemethanol (saturated). Scan rate, 5 mV $s^{-1}$.

ciently lower positive potential compared with that of dopamine oxidation (Fig. 9A). The figure shows that in spite of the fact that the concentration of ascorbic acid is 100 times higher than that of dopamine, a distinct anodic wave associated with the oxidation of dopamine is observed at 0.45 V. As seen in Fig. 9B, differential pulse voltammetric peak currents for dopamine in the presence of ascorbic acid of a fixed concentration vary linearly with concentration (the correlation coefficient was 0.998) between $2 \times 10^{-4}$ and $1.4 \times 10^{-3}$ M. The LSV technique was less sensitive.

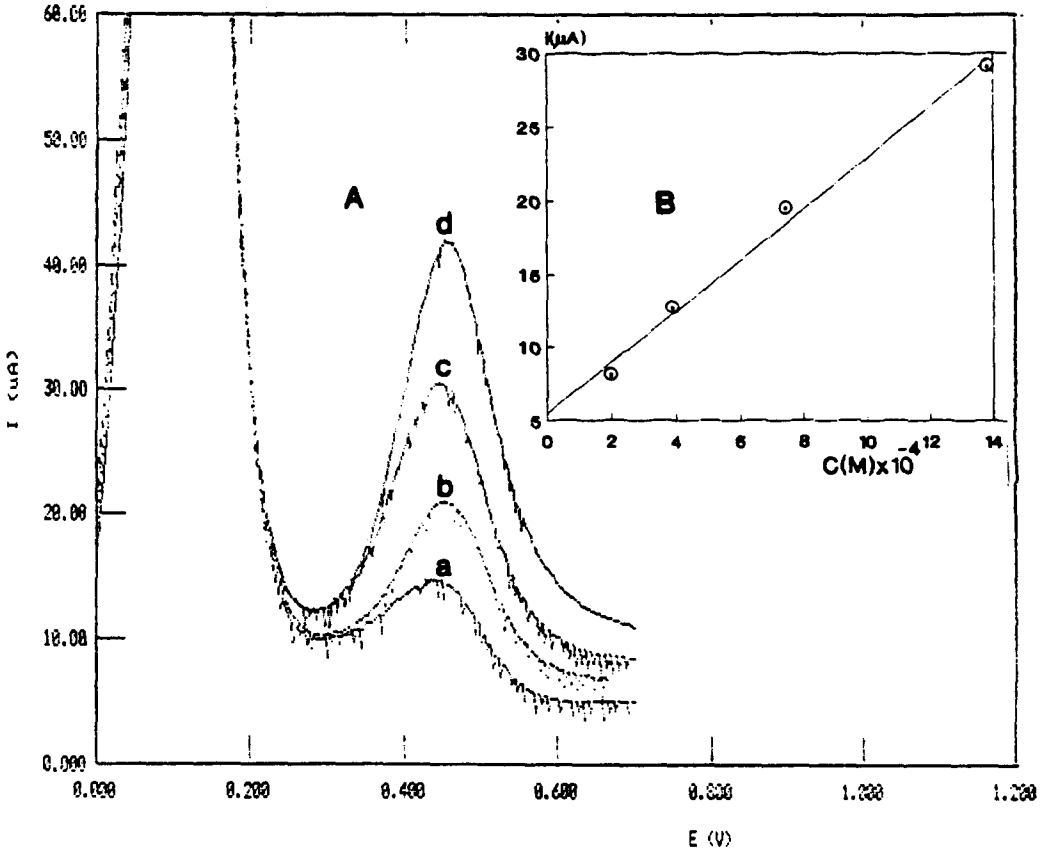


Fig. 9. (A) Differential pulse voltammograms of dopamine of various concentrations: (curve a) $1.96 \times 10^{-4}$ M; (curve b) $3.85 \times 10^{-4}$ M; (curve c) $7.41 \times 10^{-4}$ M; (curve d) $1.38 \times 10^{-3}$ M; in the presence of ascorbic acid with a fixed concentration of $2 \times 10^{-2}$ M. Solution conditions: $5 \times 10^{-3}$ M ferroceneacetic acid, 0.1 M $LiClO_4$ and pH 5 (0.5 M acetate buffer). Scan rate, 10 mV $s^{-1}$; pulse amplitude, 50 mV; pulse time, 25 ms. (B) Plot of differential pulse voltammogram peak current shown in (A) vs. the dopamine concentration.

## 5. Conclusion

Some ferrocene derivatives, soluble in acidic aqueous solutions, exhibit reversible electrochemistry at the glassy carbon electrode. Carboxylic, acetic and methanol ferrocene derivatives can act as mediators in the electrocatalytic oxidation of ascorbic acid. The analysis of catalytically coupled reactions between electrogenerated ferricinium derivatives and ascorbic acid reveals that the highest second-order rate constant ($k_s$) belongs to ferrocene monocarboxylic acid. In the presence of the ferrocene mediators, the catalytic peak currents are linearly dependent on the ascorbic acid concentration for various potential scan rates. The mediated oxidation of ascorbic acid in the presence of ferrocenemethanol as the most convenient mediator occurred at a sufficiently less positive potential than for dopamine oxidation and allowed the determination of ascorbic acid in a mixture. Dopamine can be determined in the presence of ascorbic acid of a fixed concentration 100 times higher than that of dopamine, using ferroceneacetic acid as a suitable mediator for this purpose.

## References

[1] A. Aldaz and A.M. Aquie, J. Electroanal. Chem., 47 (1973) 532.
[2] N. Winograd, H.N. Blount and T. Kuwana, J. Phys. Chem., 73 (1969) 3456.
[3] P.W. Geno, K. Ravichandran and R.P. Baldwin, J. Electroanal. Chem, 183 (1985) 155.
[4] M. Petersson, Anal. Chem. Acta, 187 (1986) 333.
[5] M.H. Pournaghi-Azar and R. Ojani, Submitted to Talanta.
[6] J. Facci and R.W. Murray, Anal. Chem., 54 (1982), 772.
[7] M.F. Dautartas and J.F. Evans, J. Electroanal. Chem., 109 (1980), 301.
[8] R.A. Saraceno, J.G. Pack and A.G. Eving, J. Electroanal. Chem., 197 (1986) 265.
[9] F. Malem and D. Mandler, Anal. Chem., 65 (1993) 37.
[10] R.S. Nicholson and I. Shain, Anal. Chem., 36 (1964) 706.
[11] R.S. Nicholson, Anal. Chem., 37 (1965) 1351.

ELSEVIER

Talanta 42 (1995) 1849–1856

Talanta

# Fluorimetric determination of aminoglycoside antibiotics using lanthanide probe ion spectroscopy

M. Rizk [a], Y. El-Shabrawy [a,*], N.A. Zakhari [a], S.S. Toubar [a], L.A. Carreira [b]

[a] *Anal. Chem. Dept., Faculty of Pharmacy, Mansoura University, Mansoura, 35516, Egypt*
[b] *Chemistry Dept., University of Georgia, Athens, GA, 30602, USA*

Received 20 January 1995; revised 10 May 1995; accepted 12 May 1995

**Abstract**

The application of probe ion fluorimetry has succeeded in the microdetermination of six aminoglycoside antibiotics: neomycin, streptomycin, gentamicin, tobramycin, amikacin and kanamycin as sulfate salts in pure form and in some pharmaceutical preparations. The method is based on the reaction of $Eu^{3+}$ ions with aminoglycosides through amino and hydroxy groups. Such interactions enhance the intensity of the 616 nm fluorescence emission of the $Eu^{3+}$ ion. The fluorescence at 592 nm comes from a non-hypersensitive transition and is not affected by the ligand which is bound to the probe ions. The intensity ratio $R$, defined as $I_{592}/I_{616}$ was used to determine the amount of free and bound europium ions. A linear relationship between bound europium ions and aminoglycoside was found within the concentration ranges 20–100 ppm for neomycin, 5–60 ppm for streptomycin, and 10–70 ppm for gentamicin, tobramycin, amikacin, and kanamycin as sulfate salts. The percentage recoveries ranged from 99.22 to 101.07, with standard deviations ranging from $\pm 1.5$ to $\pm 4.38$. The relative stability constants ranged from $5 \times 10^3$ to $2 \times 10^4$. The optimum reaction conditions were studied and the results obtained compared favourably with the fluorimetric method using fluorescmine reagent.

*Keywords:* Probe ion fluorimetry; Aminoglycoside antibiotics; Europium ions, Pharmaceutical analysis

## 1. Introduction

Numerous procedures are available for the determination of aminoglycoside antibiotics such as spectrophotometry [1–4], densitometry [5], fluorimetry [6,7], polarography [8], gas chromatography [9], radioimmunoassay [10], HPLC [11,12], MS [13], and NMR [14]. Many of these methods have been reviewed [15–19]. The official methods usually involve microbiological procedures [20–22].

Lanthanide ion probe spectrofluorometry (LIPS) was introduced in 1979 by Horrocks and Sundnick [23]. This technique employs two emission lines of $Eu^{3+}$ located at 592 nm and 616 nm. The 616 nm emission line is produced by a hypersensitive transition [24], $^5D_0 \rightarrow {}^7F_2$, which is normally a forbidden transition, but interaction with ligands makes the transition allowed and enhances the intensity of its emission. The fluorescence at 592 nm comes from a non-hypersensitive transition and is not affected by the ligand which is bound to the probe ion [25]. Thus, the ratio of these intensities can be used to determine free and ligated $Eu^{3+}$.

The applications of probe ion spectroscopy in pharmaceutical analysis are limited in spite

* Corresponding author. Present address: Chemistry Dept., University of Georgia, Athens, Georgia, 30602, USA. Fax: (706) 542-9454; e-mail: yaser@sunchem.chem.uga.edu.


*SSDI* 0039-9140(95)01640-6

of the availability of the method for the determination of many pharmaceutical compounds. Europium ions have been used for the fluorimetric determination of tetracycline [26,27], diclofanec sodium [28] and theophylline [29] in blood serum and in pharmaceutical preparations. In this article, we describe a spectroscopic method for the determination of aminoglycoside antibiotics in pure form and in pharmaceutical formulations using the LIPS spectrofluorometric technique.

## 2. Experimental

### 2.1. Apparatus

A Lambda Physic EMG 102 XeCl excimer laser and a FL 3002 tunable dye laser were used in tandem to supply a high intensity tunable source. The average output of the XeCl excimer was 1.6 W (10 Hz repetition rate) at 308 nm. A tunable ultraviolet emitting dye laser was used to provide an excitation source of 394.3 nm, which corresponds to a resonant absorption transition of the Eu metal ions. The Eu fluorescence was collected and frequency analyzed with a Spex 1877 triple monochromator. The fluorescence was detected by a charge coupled detector (ccd 9000 Photometric Ltd.). The recorded curves were fitted with Lab Calc (Galactic Software) using a gaussian model. The areas under the two peaks at 592 nm and 616 nm were integrated and the ratio of the two peaks was taken as the $R$ value of the sample.

### 2.2. Materials

Neomycin sulfate, streptomycin sulfate, gentamicin sulfate, tobramycin sulfate, amikacin sulfate and kanamycin sulfate were obtained from Sigma and the various dosage forms from commercial sources. Europium(III) chloride was from Aldrich. Hydrochloric acid, chloroform and ammonia solutions were Baker analyzed reagents.

### 2.3. Reagents

All chemicals were analytical reagent grade. The following reagents were used:

(1) Stock solutions of aminogycosides were freshly prepared as 0.5 mg $ml^{-1}$ in deionized water.

(2) $1E^{-4}$ M, $1E^{-5}$ M and $2.5E^{-5}$ M $Eu^{3+}$ ion solutions were prepared by dissolving an appropriate amount of europium chloride hexahydrate in 1 l of deionized water, and adjusting to pH 5.5 using hydrochloric acid solution.

(3) Aqueous solutions of pH 2, 5.5, 8, and 10 were prepared by serial dilution of hydrochloric acid and sodium hydroxide with deiionized water, and pH adjustment hydrochloric acid solution or sodium hydroxide solution using a Fisher pH meter.

### 2.4. Procedure

*A. Calibration lines*

An aliquot volume of standard aminoglycoside antibiotic solution equivalent to 0.2–1.0 mg neomycin sulfate, 0.05–0.6 mg streptomycin sulfate, and 0.1–0.7 mg gentamicin sulfate, tobramycin sulfate, amikacin sulfate and kanamycin sulfate was transferred into a 10 ml calibrated flask. 1 ml of $2.5E^{-5}$ M $Eu^{3+}$ solution was added to the neomycin sulfate and streptomycin sulfate, 1 ml of $1E^{-4}$ M $Eu^{3+}$ solution was added to the gentamicin sulfate and tobramycin sulfate, and 1 ml of $1E^{-5}$ M $Eu^{3+}$ solution was added to the amikacin sulfate and kanamycin sulfate. 2 ml of a hydrochloric acid solution of pH 5.5 was added and brought to volume with deionized water. The fluorescence was measured from 576 to 633 nm (excitation at 394.3 nm). The curves were integrated using a gaussian model and the area under the two peaks at 592 nm and 616 nm was taken as the $R$ value of the sample.

*B. For injections*

An accurate volume of the mixed contents of three vials, equivalent to 10 mg of drug, was transferred into a CM (carboxylic acid) ion exchange resin column [10,31] loaded with water–hydrochloric acid solution pH 2, and then eluted with 25 ml of water–hydrochloric acid solution pH 2. The column was washed with 25 ml of pH 7 deionized water. The elution and washing water were discarded. Aminoglycoside was eluted using 30 ml of aqueous pH 11 solution and 10 ml of deionized water into a 50 ml calibrated flask. The solution was mixed well and its pH adjusted to about 5.5 using hydrochloric acid solution; it was brought to volume with deionized water. 2 ml of this solution was assayed as described in the previous section.

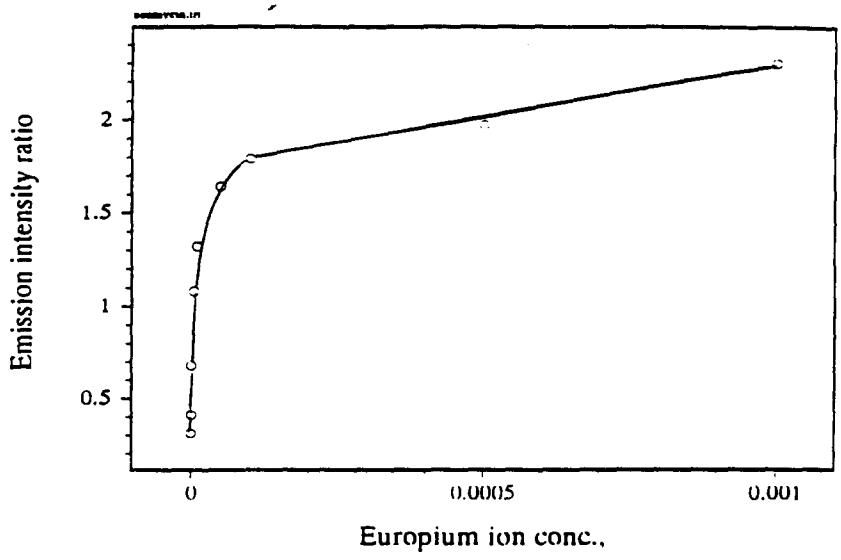


Fig. 1. Effect of $Eu^{3+}$ ions on the emission ratio of $1 \times 10^{-4}$ M neomycin sulfate.

*C. For tablets*

Twenty tablets were weighed and powdered. To the quantity of powder equivalent to 500 mg was added 10 ml of deionized water, and the mixture sonicated for 20 min. It was then filtered into a 100 ml calibrated flask, the powder washed three times each with 5 ml water, and the combined filtrate mixed well and brought to volume with deionized water. 2 ml of the filtrate was transferred into a CM ion exchange column and the procedure was completed as described in the previous section.

*D. For ointment*

The contents of two bottles of ointment were weighed and mixed. A quantity of ointment equivalent to 20 mg of drug was transferred into a separating funnel, and 50 ml of ether was added. Gentamicin was extracted three times with pH 8 water. The pH of the extract was adjusted to pH 5.5 using hydrochloric acid solution and brought to volume (100 ml) with deionized water. 2 ml of this solution was assayed as described in Section 2.4 A.

## 3. Results and discussion

### *3.1. Lanthanide ion probe*

In a study of any probe, the most fundamental and necessary characteristic is the ability to determine quantitatively the concentration of the free and bound metal ions simultaneously.

The use of lanthanide ions as fluorescent probes has been well documented [32]. The europium metal ion has been the lanthanide of choice in most applications and its spectral features are widely documented [33]. This speciation information is uniquely encoded in the experimental $Eu^{3+}$ profile. Fig. 1 shows a typical spectral titration plot of $Eu^{3+}$ using $1E^{-4}$ M aminoglycoside (neomycin sulfate). In the early stages of the titration process there is only a small amount of fluorescent metal probe ion compared to the available binding sites, and hence the majority of metal ions are bound to the ligand. Consequently, the hypersensitive emission band at 616 nm is larger than the non-hypersensitive band at 592 nm, and the intensity ratio $R$ is small and close to the lower limit value, $L_S$. As the titration progresses the relative amount of total bound species gradually increases. Consequently, the intensity ratio, $R$, gradually increases as more metal ions are added to the system. At the end of titration the ratio $R$ is close to its upper limit value, $L_B$, and the concentration of $Eu^{3+}$ is much greater than the concentration of ligand. The optimum concentration of $Eu^{3+}$ ions in a such study is that required to produce a ratio value $R$ between $L_S$ and $L_B$. A ratio value of around unity has been shown to be the most sensitive for this type of measurement [25,34]. All the aminoglycoside antibiotics behave similarly to neomycin sulfate, except in the amount of $Eu^{3+}$ ions added which is due to the differences in the molecular weights.

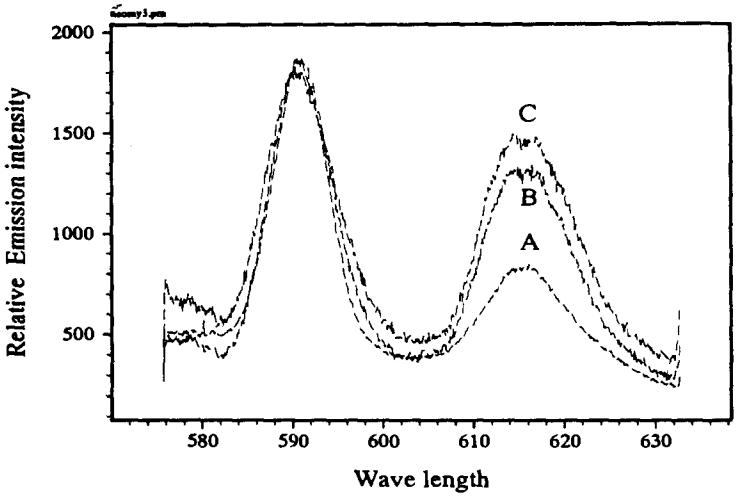


Fig. 2. Emission spectra of 1 ml of $2.5E^{-5}$ M of europium ions: (A) without neomycin sulfate; (B) in the presence of 600 μg neomycin sulfate; and (C) in the presence of 900 μg neomycin sulfate, in a total volume of 10 ml.

Suitable $Eu^{3+}$ ion concentrations for such a study were found to be $2.5E^{-5}$ M Eu(III) ions for the determination of neomycin sulfate and streptomycin sulfate, $1E^{-5}$ M $Eu^{3+}$ for the determination of gentamicin sulfate and tobramycin sulfate, and $1E^{-4}$ M $Eu^{3+}$ for the determination of amikacin sulfate and kanamycin sulfate. Fig. 2 shows emission spectra of $Eu^{3+}$ ions in the presence and absence of neomycin sulfate.

### 3.2. *Effect of buffer and pH*

Fig. 3 shows that the complexes formed were pH dependent and must be controlled between pH 5 and 6. Acidic buffers such as acetate, phosphate, MOPS, MES and THAM buffer systems were not suitable in such a study owing to the formation of europium salts or complexes which interfered with the measurement; such observations have been made in our laboratory [25]. At a pH below 5, the competition between the proton and $Eu^{3+}$ will decrease the formation of Eu–aminoglycoside complex, and in neutral solution $Eu(OH)^{2+}$ is formed which interferes with the measurement. Adjusting the initial pH of the $Eu^{3+}$ solution to pH 5.5 and using 2 ml of aqueous hydrochloric acid solution at pH 5.5 kept the pH of the mixtures between 5 and 6.

### 3.3. *Molar ratio*

Eu is bound with aminoglycoside in a 1:1 molar ratio. Fig. 4 shows the spectroscopic titration of 1 ml of $1 \times 10^{-4}$ M neomycin sulfate with $1 \times 10^{-4}$ M $Eu^{3+}$ ions.

### 3.4. *Effect of time and temperature*

The complex formation between $Eu^{3+}$ ions and aminoglycoside was almost instantaneous, as a stable ratio was produced within 5 min and the complexes were stable for at least 24 h. Temperature had little effect on the complex formation and its stability, so the reaction was carried out at ambient temperature.

### 3.5. *Effect of ionic strength*

Ionic strength is a factor that sometimes cannot be neglected. The effect of ionic strength on the spectral titration plot was studied by varying the concentration of the background electrolyte, sodium chloride. The choice of sodium chloride was based on the fact that the $Na^+$ ion is very weakly bound, if at all, to the aminoglycoside binding sites, and $Cl^{-1}$ is already in the system as a counter ion that comes from dissolving $EuCl_3$. Three titration plots correspond to 0.0, 0.01 and 0.1 M sodium chloride added as background electrolyte. The addition of background electrolyte will decrease the total concentration of bound species of the probe ion. It should be emphasized here that this decrease is not due to the competition effect of sodium ion (similar to proton competition) to occupy the same set of aminoglycoside sites, but purely due to electrostatic forces as previously reported with humic acid substances [34].

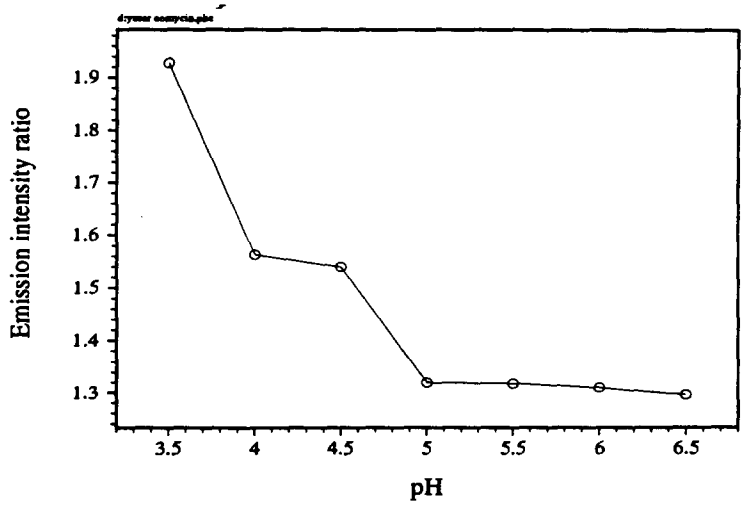


Fig. 3. Effect of pH on emission ratio of 50 μg ml$^{-1}$ neomycin sulfate and 1.00 ml of 2.5E$^{-5}$ M $Eu^{3+}$ ions.

## 4. Performance characteristics

The investigated aminoglycosides possess amino and hydroxy groups which can form complexes with metal ions. Evangelista and Schapoval [1] have determined these compounds by spectrophotometric determination of their blue complexes with copper ions at 634 nm.

Aminoglycoside antibiotics complex $Eu^{3+}$ ions, and such ligation leads to a hypersensitive transition of $Eu^{3+}$ ions, and such ligation leads to a hypersenstive transition of $Eu^{3+}$ ions, $^5D_0 \rightarrow {}^7F_2$ (616 nm). These hypersensitive transitions are specific absorption or emission transitions of lanthanide ions that are extremely sensitive to ligation. The intensity of a hypersensitive transition is enhanced in the metal–ligand complex relative to that transition in aquo ions. Experimentally, this is observed by making the concentration of $Eu^{3+}$ ions small relative to the aminoglycoside concentration, so that the majority of the metal ions are complexed with aminoglycosides. Such effects are most obvious from the observation of several emissions of $Eu^{3+}$ ions with neomycin sulfate concentrations (Fig. 2). The absolute emission intensity is not important here as we are concerned only with the change in the integrated emission ratio $R$ ($I_{592}/I_{616}$) due to the aminoglycoside antibiotics. These $R$ values decrease upon the addition of antibiotics owing to the enhanced emission at 616 nm relative to the emission at 592 nm. The 592 nm emission is not effected by ligation.

Susetyo and co-workers [25,35] have developed a statistical model for the distribution of binding sites in humic acid. This model was applied to study the spectral titration plot generated by lanthanide ion probe spectroscopy. They expressed the free and bound $Eu^{3+}$ ions as a function of experimental parameters. The free $Eu^{3+}$ ions could be expressed as

$$M = \frac{C_M L_B (R - L_S)}{R(L_B - L_S)} \quad (1)$$

where $M$ is the concentration of free metal ions, $C_M$ is the total concentration of metal added, $L_B$ is the ratio of the two Eu peaks at 592 nm and 616 nm when the concentration of $Eu^{3+}$ was very large with respect to ligand concentration, and $L_S$ is the ratio when the $Eu^{3+}$ concentration was very small with respect to the ligand concentration. Table 1 shows $L_B$ and $L_S$ for each aminoglycoside. $R$ is the ratio $I_{592}/I_{616}$ of the free and bound metal species which was quantitatively determined from the experimentally observed parameters.

The bound $Eu^{3+}$ ion concentration could be expressed as

$$ML = C_M - M \quad (2)$$

Calibration lines were calculated by plotting $ML$ against the concentration of aminoglycoside. It was found that there was a linear relation between the concentration of aminoglycoside and the concentration of bound $Eu^{3+}$ ions within the ranges shown in Table 1, with standard deviations from 4.338 to 1.50 ppm.

Table 1 also shows regression equations and correlation coefficients of aminoglycosides us-

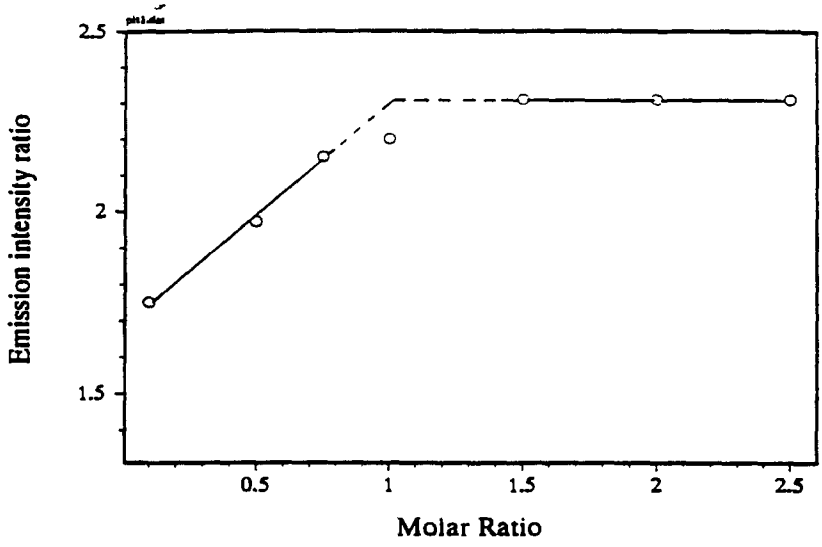


Fig. 4. Spectroscopic titration of 1 ml of $1 \times 10^{-4}$ M neomycin sulfate with $1 \times 10^{-4}$ M $Eu^{3+}$ ions.

ing the proposed method. This has proved to be an accurate method for the determination of aminoglycosides. As compared with conventional organic fluorescent probes [6,7], fluorescent lanthanide chelates can offer several advantages. They have narrow-banded emission lines well distinguished from any disturbing background. Chelates have exceptionally wide Stokes' shifts, over 200 nm, while with fluorescamine it is only 50–70 nm. In addition to spectral resolution, their emission can be distinguished from any organic background interference owing to the very long fluorescence decay time ($\sim 110$ μs) associated with $Eu^{3+}$ fluorescence which makes them an ideal choice for a fluorimetric system [36].

Table 2 shows the assay results of aminoglycosides by the proposed method and fluorescamine fluorimetric methods [6]. The proposed method, when compared to the official microbial assays, offers advantages with regards to rapidity, simplicity and precision, so we compared these results to the fluorimetric method using fluorescamine. The calculated student's $t$ and variance ratio $F$ tests were less than the respective tabulated one at $P = 0.05$, so the results obtained by the proposed method have proved to be in good agreement with those obtained by the reference fluorimetric method.

Results of the determination of aminoglycosides in different dosage forms by the probe

Table 1
Regression data, correlation coefficients, stability constants of Eu–aminoglycoside complexes, concentrations of Eu used for calibration, and concentration ranges of aminoglycoside antibiotics determined by the proposed spectroscopic probe ion method

| Aminoglycoside sulfate salt | Regression data [a] | | | | | Conc. [b] range | $L_B$ | $L_S$ |
|---|---|---|---|---|---|---|---|---|
| | $C_0$ | $C_1$ | $r$ | $k$ | $C_M$ | | | |
| Neomycin | $3.59E^{-8}$ | $4.77E^{-9}$ | 0.99681 | $2.1E^{4}$ | $2.5E^{-5}$ | 20–100 | 2.30 | 0.31 |
| Streptomycin | $1.08E^{-9}$ | $1.91E^{-8}$ | 0.99983 | $1.3E^{4}$ | $2.5E^{-5}$ | 5–60 | 2.30 | 0.31 |
| Gentamicin | $4.78E^{-7}$ | $2.82E^{q-8}$ | 0.99086 | $3.1E^{3}$ | $1.0E^{-4}$ | 10–70 | 2.55 | 0.61 |
| Tobramycin | $7.12E^{-7}$ | $4.29E^{-8}$ | 0.99892 | $2.5E^{3}$ | $1.0E^{-4}$ | 10–70 | 2.55 | 0.61 |
| Amikacin | $1.13E^{-7}$ | $2.48E^{-9}$ | 0.99857 | $3.5E^{3}$ | $1.0E^{-5}$ | 10–70 | 2.17 | 0.47 |
| Kanamycin | $1.11E^{-7}$ | $3.52E^{-9}$ | 0.99935 | $5.7E^{3}$ | $1.0E^{-5}$ | 10–70 | 2.17 | 0.47 |

$C_0$ is the intercept, $c_1$ is the slope, $r$ is the correlation coefficient, $K$ is the stability constant of the Eu–aminoglycoside complex, $C_M$ is the molar concentration of $Eu^{3+}$ ions used for calibration, $L_B$ is taken to be the ratio of the two $Eu^{3+}$ peaks in the absence of aminoglycoside, $L_S$ is taken to be the ratio when the $Eu^{3+}$ concentration was very small with respect to a large ligand concentration.

[a] Average of at least seven triplicate determinations within the concentration range.

[b] Concentration ranges were calculated in ppm.

Table 2
Assay results of aminoglycoside antibiotics in bulk using the proposed method and the reference method [6]

| Aminoglycoside sulfate salt | % Recovery [a], ±SD | |
|---|---|---|
| | Proposed method | Reference method [b] |
| Neomycin | 100.16 ± 1.05<br>$t$ = 0.175 (2.179) [c] | 100.04 ± 1.48<br>$F$ = 1.987 (4.28) [c] |
| Streptomycin | 98.61 ± 3.57<br>$t$ = 0.421 (2.179) [c] | 99.25 ± 1.86<br>$F$ = 3.684 (4.28) [c] |
| Gentamicin | 100.82 ± 2.30<br>$t$ = 1.660 (2.179) [c] | 99.00 ± 1.82<br>$F$ = 1.689 (4.28) [c] |
| Tobramycin | 100.26 ± 2.23<br>$t$ = 0.481 (2.179) [c] | 99.68 ± 2.28<br>$F$ = 1.045 (4.28) [c] |
| Amikacin | 98.81 ± 4.52<br>$t$ = 0.500 (2.179) [c] | 97.82 ± 2.66<br>$F$ = 2.875 (4.28) [c] |
| Kanamycin | 100.19 ± 1.50<br>$t$ = 0.956 (2.179) [c] | 99.14 ± 2.49<br>$F$ = 2.756 (4.28) [c] |

[a] Average of at least seven triplicate determinations.
[b] Fluorometric determination of antibiotics using fluorescamine [6].
[c] Values in parentheses are theoretical values at $P = 0.05$.

ion method and the fluorescamine fluorimetric method are presented in Table 3. The proposed procedure was selectivity enhanced by an ion exchange resin resolution of the interferences, since it is well known that $Eu^{3+}$ ions are strongly bound by charged oxygen donor atoms such as carboxylic or phenolic groups [29]. Ingredients other than aminoglycosides, such as additives, stabilizers and antioxidants of tablets, ampoules and ointments, are removed by this procedure and do not interfere with the recommended method. They were separated from aminoglycosides in an ion exchange resin (carboxylic acid resin) by aqueous buffer at pH 2 [30,31]. The proposed procedure is as sensitive as the fluorescamine fluorimetric method [6], and gives good agreement with it. The proposed method is simpler and more rapid, and the reaction products are more stable than for conventional fluorometric methods. Moreover, the determination bound $Eu^{3+}$ using the relative intensity ratio $R$ as a function of the concentration of aminoglycoside antibiotics is more reliable, and has less experimental error (about ±5%), than that using the absolute emission intensity in conventional organic fluorescent methods. In conventional organic fluorometric methods the absolute emission value is strongly effected by many systemic errors due to blank and analyte interferences. Moreover, the absolute emission intensity is highly dependent on the intensity of the excitation source, the quantum yield of the complexes which is low compared to the $Eu^{3+}$-complex (≈0.18) [37], and the detector used for the measurement rather than the fluorescence of the analyte [30]. Thus, the proposed procedure can be used for routine analysis and quality control of aminoglycosides in pharmaceutical preparations.

Table 3
Assay results of aminoglycoside antibiotics in some pharmaceutical preparations by the proposed method and the reference method

| Drug | % Recovery, ±SD [a] | |
|---|---|---|
| | Proposed method | Reference method [b] |
| Neomycin Tablets 500 mg (Memphis Co., Egypt) | 100.99 ± 0.36 | 98.98 ± 2.16 |
| Gentamicin Oint., 0.1% (Memphis Co., Egypt) | 104.74 ± 1.6 | 97.54 ± 1.98 |
| Gentamicin Amp. 20 mg (Memphis Co., Egypt) | 101.22 ± 2.39 | 98.23 ± 1.71 |
| Gentamicin Amp. 80 mg (Memphis Co., Egypt) | 102.53 ± 1.03 | 98.93 ± 1.98 |
| Nebcin Amp. 20 mg Tobramycin (Lily France S.A. France) | 103.49 ± 0.64 | 99.68 ± 2.28 |
| Amikin Amp. 1 g Amikacin (Briston Co., USA) | 101.20 ± 1.66 | 99.68 ± 0.87 |
| Kanamycin vial, 1 g per vial | 99.27 ± 0.41 | 99.52 ± 1.62 |

[a] Average of at least three triplicate determinations, calculated relative to nominal content.
[b] Fluorometric determination of aminoglycoside antibiotics using fluorescamine [6].

## 5. Conclusion

From the foregoing discussion, the $Eu^{3+}$ probe ion fluorimetric technique has been applied to the determination of six aminoglycosides in pure form and in pharmaceutical preparations. Ion exchange was carried out for resolution of aminoglycoside antibiotics from other additives such as EDTA, sodium citrate, phenol, and other injection and tablet additives.

## References


[1] R.C. Evangelista and E.E.S. Schapoval, Rev. Cienc. Farm., 5 (1983) 21–27.
[2] P.R. Bontchev, P. Papzova, M. Confino and D. Dimova, Mikrochim. Acta, 111 (1984) 459–465.
[3] N.M. Alykov, Zh. Anal. Khim., 39 (1984) 1425–1427.
[4] Nashaat A. Zakhari, Anal. Lett., 23 (1990) 1843–1865.
[5] M. Breilnger, H. Paulus and W. Weigrebe, Dtsch. Apoth. Zth., 120 (1980) 1699.
[6] J. Kusnir and K. Barna, Z. Anal. Chem., 271 (1974) 288.
[7] N.M. Alyokov, Zh. Anal. Khim., 36 (1982) 1387.
[8] M.M. Ayad and M. Yousef, Analyst, 110 (1985) 963.
[9] K. Tsuiji and J.H. Robertson, Anal. Chem., 42 (1970) 1661.
[10] S.G. Thompson and J.F. Burd, Antimicrob. Agents Chemother., 18 (1980) 264.
[11] D.M. Barends, J.S. Van der Sandt and A. Hulshoff, J. Chromatogr. Biomed. Appl., 8 (1980) 201.
[12] P. Gambardella, R. Punziano, M. Gionti, C. Guadalupi, G. Mancini and A. Mangia, J. Chromatogr., 348 (1985) 229–240.
[13] B.V. Rozynov, Yu.V. Zhdanovich, A.D. Kuzovkov, R.N. Elizabeth and A.S. Tikhonova, Antibiotiki, 25 (1980) 652.
[14] N.P. Reuter, A.C. Hawke, E. Lewis, T.G. Alexander, E. Mazzola and A. Aszalos, J. Assoc. Off. Anal. Chem., 65 (1882) 1413.
[15] K. Florrey, Analytical Profiles of Drug Substances, Academic Press, London, Vol. 6, 1977, p. 259.
[16] K. Florrey, Analytical Profiles of Drug Substances, Academic Press, London, Vol. 8, 1979, p. 399.
[17] K. Florrey, Analytical Profiles of Drug Substances, Academic Press, London, Vol. 9, 1980, p. 295.
[18] K. Florrey, Analytical Profiles of Drug Substances, Academic Press, London, Vol. 12, 1983, p. 37.
[19] K. Florrey, Analytical Profiles of Drug Substances, Academic Press, London, Vol. 16, 1987, p. 505.
[20] The United State Pharmacopeia XXII — National Formulary XVII, Rockville, MD, 1990.
[21] British Pharmacopeia, Her Majesty's Stationary Office, London 1993.
[22] European Pharmacopeia, Maisonneuve, S., 57 Sainte-Ruffin, France, 1975.
[23] W. Dew, Horrocks and D.R. Sundnick, J. Am. Soc., 101, (1979) 334–340.
[24] W.T.T. Carnall, J.V. Beitz, H. Crosswhite, K. Rajank and J. B. Mann, In S.P. Sinha (Ed), Systematic and Properties of the Lanthanides, D. Reidal, Boston, MA, 1983, pp. 389.
[25] W. Susetyo, J.C. Dobbs, L.A. Carreira, L.A. Azarraga and D.M. Grimm, Anal. Chem., 62 (1990) 1251–1221.
[26] L.M. Hirschy, E.V. Dose and J.D. Winefordner, Anal. Chem. Acta, 147 (1983) 311–316.
[27] L.A. Files, L. Hirschy and J.D. Winefordner, J. Pharm.-Biomed. Anal., 3 (1985) 95–100.
[28] L.A. Carreira, M. Rizk, N.A. Zakhari, S.S. Toubar and Y. El-Shabrawy, in press.
[29] L.M. Perry and J.D. Winefordner, Talanta, 37 (1990) 965–969.
[30] G.H. Ford, M.E. Bergy, A.A. Brooks, E.R. Garrett, J. Alberti, J.R. Dyer and H.E. Carter, J. Am. Chem. Soc., 77 (1955) 5311.
[31] H. Galina and B.N. Kolarz, J. Chromatogr., 179 (1979) 173–175.
[32] W. Dew, Horrocks and D.R. Sundnick, Acc. Chem. Res., 14 (1981) 384.
[33] J.C. Dobbs, W. Susetyo, F.E. Knight, M.A. Castles, L.A. Carreira and L.V. Azarraga, Intern. J. Environ. Anal. Chem., 37 (1989) 1.
[34] W. Susetyo, L.A. Carreira, L.A. Azarraga and D.M. Grimm, Fresenius' Anal. Chem., 339 (1991) 624–635.
[35] J.C. Dobbs, W. Susetyo, F.E. Knight, M.A. Castles, L.A. Carreira and L.V. Azarraga, Anal. Chem., 61 (1989) 483–488.
[36] I. Hemmila, Scand J. Clin. Invest., 48 (1988) 389–400.
[37] E. Soini and T. Lougren, CRC Crit. Rev. Anal. Chem., 18 (1987) 105.
[38] J.E. Ingle and S.R. Crouch, Spectrochemical Analysis, Prentice-Hall, Englewood Cliffs, New Jersey, 1988.

ELSEVIER

Talanta 42 (1995) 1857–1865

Talanta

# Lead determination at the ppb level using stopped-flow FIA

Mingshu Li, G.E. Pacey *

*Department of Chemistry, Oxford, OH 45056, USA*

Received 16 January 1995; revised 12 May 1995; accepted 12 May 1995

**Abstract**

A flow-injection-based kinetic method for the determination of lead ions was developed. In this method, resazurin was reduced to resorufin by sulfide and lead ions. The method has a detection limit of 1 ppb with a relative standard deviation of 5.2% at the 20 ppb level. Interferences can be removed by prior extraction.

*Keywords:* Flow injection analysis; Kinetic methods; Lead determination; Resazurin; Water analysis

## 1. Introduction

Adverse health effects from exposure to lead are now recognized to be among industrialized society's most significant health problems [1]. Drinking water is the major source of lead exposure for the general population. Lead seldom occurs naturally at a level higher than 5 $\mu g\,l^{-1}$ in surface water supplies such as rivers and lakes [2]. Lead enters drinking water primarily as a result of the corrosion, or wearing away, of materials containing lead in the water distribution system and household plumbing [3]. USEPA has set strict regulations on lead concentrations in drinking water. Effective from December 1992, the maximum permissible concentration of lead in drinking water is 50 $\mu g\,l^{-1}$ [3]. EPA requires "lead action" if the concentration of the lead exceeds 15 $\mu g\,l^{-1}$ in more than 10% of tap water samples collected during any monitoring period [3]. Improved, more-cost-effective automated methods for lead determinations are needed.

Current lead determinations at the ppb–ppm levels [4–10] are performed using preconcentration techniques followed by atomic absorption spectrophotometry (AAS) with reported detection limits from 0.08 [11] to 1 $\mu g\,l^{-1}$. Unfortunately, these methods are problematic when a large number of samples have to be determined, since the preconcentration step is usually too labor- and time-consuming.

Other techniques used for lead determinations include isotope dilution GC–MS [12], flow-injection Donnan dialysis–inductively coupled plasma-atomic emission spectrometry [13,14], anodic stripping voltammetry [15–17], potentiometry [18], laser atomic fluorescence spectrometry [19,20], the flow injection analysis (FIA)-based crown ether dicyclohexyl-18-crown-6 extraction method [21], the FIA-based 4-(2-pyridylazo)resorcinol (PAR) complex method [22], and the FIA-based 5,10,15,20-tetra(4-*n*-sulfoethylpyridinium)porphyrin (T(4-sp)p method [23]. Kinetic methods include catalytic persulfate oxidation of hematoxylin [24] and reduction of resazurin by sodium sulfide [25].

Given the variety of techniques and methods that exists, there is not much point in develop-

* Corresponding author. Fax: (513)529-7284.


*SSDI* 0039-9140(95)01644-9

ing another method unless it can yield a significantly higher sampling frequency, lower detection limit, and easier operation without preconcentration. An FIA-spectrophotometric-based method is suggested. Therefore, the objective of this research was to develop a simple, reliable FIA method for lead ion determination in water without preconcentration with a detection limit of 1 ppb and a relative standard deviation of less than 10% at the 20 ppb level. Resazurin chemistry with sufilde using lead ions as the catalyst was investigated for this work [25].

## 2. Experimental

### 2.1. Reagents

All reagents were reagent grade and the water was deionized triply distilled with 18 megohm–cm resistance.

A resazurin stock solution was prepared by dissolving 0.1000 g of resazurin (Aldrich Chemical Company, Inc.) into 100 ml of water. The working resazurin solutions were made by appropriate dilution of the stock solution, which was stable for several months.

The sodium sulfide stock solution was made by dissolving 20 g of sodium sulfide (Fisher Scientific) in 100 ml of water. This solution had to be freshly prepared daily. The working sodium sulfide solutions were made by diluting the stock solution appropriately.

The stock sodium hydroxide solution was prepared by dissolving 200 g of sodium hydroxide in 1000 ml of water.

All three reagent solutions were heated in a hot-water bath for 30 min and were cooled to room temperature before use.

A 1% nitric acid solution was prepared by diluting 10 ml of high-purity (low metal content) nitric acid to 1 l with water.

Phosphate buffer solution was prepared by dissolving 3.4 g of monobasic potassium phosphate in 100 ml of water and adjusting the solution pH to 7 by adding sodium hydroxide.

Dimethylglyoxime solution was prepared by dissolving 0.1000 g of dimethylglyoxime (Fisher Scientific) in 100 ml of absolute ethanol.

A quinolin-8-ol–chloroform extraction solution was prepared by dissolving 14.5 g of quinolin-8-ol in 1 l of chloroform.

An aqueous lead standard stock solution was prepared by dissolving 1.5985 g of lead nitrate (Fisher Scientific) with 20 ml of concentrated nitric acid and diluting to 1 l. Working solutions were prepared by appropriate dilution of the stock solution.

### 2.2. Equipment

The manifold used for lead determination is shown in Fig. 1. All tubing was 0.5 mm i.d. Teflon and all pumping tubes were Tygon. A Tecator model 5020 flow injection analyzer was used throughout the investigation.

The detector was a Waters 991 M photodiode-array spectrophotometer controlled by a Millennium 2010 chromatography manager computer software system. The detecting system was able to scan the spectra between 200 and 800 nm and measure the absorbance at the desired wavelength and time. For a specific peak, it was able to provide peak height or area.

### 2.3. Glassware

All the glassware was cleaned with detergent, rinsed with tap water followed by distilled water, soaked overnight in a nitric acid (1:2, v/v) bath, carefully rinsed with a small amount of Norchromix (15% in concentrated sulfuric acid), then rinsed with distilled water and finally with triply distilled deionized water.

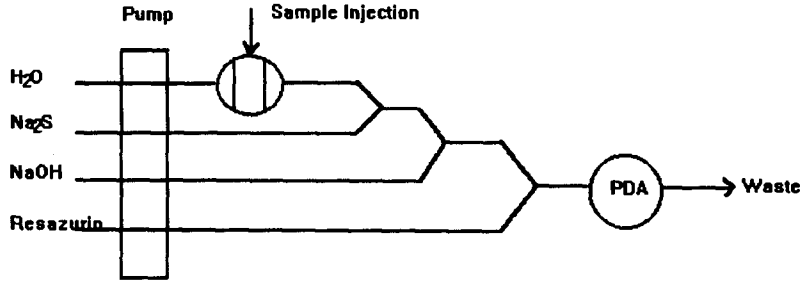


Fig. 1. Diagram of flow injection manifold used in this investigation.

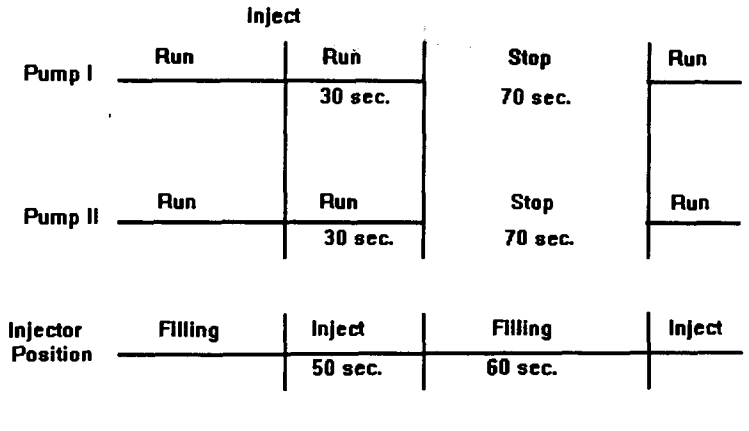


Fig. 2. Timing of cycles in the lead method.

### 2.4. Procedures

For samples that do not contain interferents, the sample is injected directly into the FIA manifold. If interferences are anticipated, a 50 ml sample is added to a 250 ml Erlenmeyer flask which contained 2 ml of pH 7 phosphate buffer solution. To this mixture are added the appropriate reagents for removing the interferences.

Before pumping reagents, the FIA system was cleaned by pumping 1:4 hydrochloric acid solution through the FIA manifold for about 5 min and then deionized distilled water for another 5 min. The run-stop times for pump I and pump II were set as indicated in Fig. 2(a) and sample loading and injecting times for the valve were as indicated in Fig. 2(b).

The FIA system pumped the reagents through the manifold shown in Fig. 1 and the computer started collecting data before the reagents reached the detector in order to obtain the baseline absorbance. The sample solutions were injected when the resazurin absorbance was at a maximum and stable, usually between 2.500 and 3.000 au. The absorbance changed observed for a 100 ppb lead sample was about 2.000–2.500 au using a stopped-flow period of 70 s. At least three injections were made for every sample solution. The decrease (negative peak) in the absorbance at 608.2 nm was monitored and the peak area measured. The peak area was converted to the lead ion concentration using a calibration curve.

A calibration curve was obtained by injecting 0, 10, 20, 40, 60, and 100 ppb lead standard solutions. These standard solutions were prepared in 50 ml volummetric flasks, adding 5 ml of 1% nitric acid to each, then 0.0, 0.5, 1.0, 2.0, 3.0, and 5.0 ml of the lead working solution (1 ppm), and diluting to the mark with water. At least three injections were also made of the standard solutions. The average values of the peak areas were used for the calibration.

For interferents that can be eliminated by the dimethylglyoxime procedure, 2 ml of dimethylglyoxime–alcohol solution and 15 ml of chloroform were added to the buffered sample. After extraction, the chloroform phase was separated and the aqueous phase was injected into the FIA manifold. For the interferents removed by quinolin-8-ol, 15 ml of quinolin-8-ol–chloroform solution were added to the buffered sample. After extraction, the chloroform phase was separated and the aqueous phase was injected into the FIA manifold. In extreme cases, both procedures may be needed. If the aqueous phase formed precipitates, they were filtered (Whatman; qualitative; #1) and then used for the determination. Although this part of the procedure was not automated, FIA-based extractions have been demonstrated.

A comparison of this new method with the standard dithizone method was performed. All

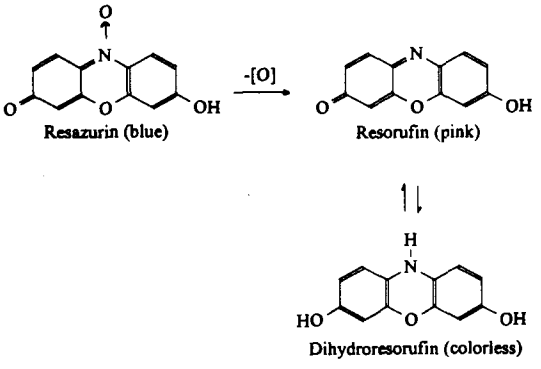


Fig. 3. The resazurin reduction reaction.

reagents and procedures for the lead ion determination with the dithizone standard method were prepared and followed as described elsewhere [2].

Sampling procedures for tap water comprised allowing the water to run for 15 min at the maximum flow rate before collecting a sample. A 1 l polypropylene bottle was rinsed with three 20 ml portions of sample before collecting the final sample. The collected sample has 1 ml of high-purity concentrated nitric acid added before mixing thoroughly.

## 3. Results and discussion

Resazurin is reduced by sulfide in alkaline solution to resorufin, Fig. 3. The first step is irreversible and proceeds very slowly without catalyst, but the second step is reversible and is reported to be fast [25]. In the presence of trace amount of lead, the reduction rate of the first step increases significantly. This catalytic effect is the bases for this work.

The absorption spectra of resazurin and resorufin exhibit a decrease in the absorbance at 608 nm (decrease in concentration of resazurin). In order to find the optimum conditions, the concentration of all reagents, the temperature and the basicity on the reaction rate was optimized.

The rate of the reaction is related to the sulfide concentration. However, since the sulfide concentration is kept constant in every determination and only a reduction of the resazurin concentration is observed, the effect of the sulfide concentration on the detected absorbance can be treated as a constant; therefore

$$dx/dt = \chi C_k^0 \pi_c$$

is a generalized equation for the rate of catalytic reactions, where $\chi$ is catalytic coefficient and $\pi_c$ is the combined concentrations of all reagents and $C_k^0$ is the lead concentration. To derive the integrated form of this equation, the approximate order of the reaction needs to be determined. Three possible orders, zero order, first order and second order were tested using the FIT program.

$$x = k_1[Pb^{2+}]t \quad \text{(zero order)}$$

$$\ln[\alpha/(\alpha - x)] = k_2[Pb^{2+}]t \quad \text{(first order)}$$

$$1/\alpha - 1/(\alpha - x) = k_3[Pb^{2+}]t \quad \text{(second order)}$$

where $\alpha$ is initial concentration of resazurin, and $x$ is the concentration of resazurin at time $t$.

The line equations and the correlation coefficients for the fitted data for the zero-

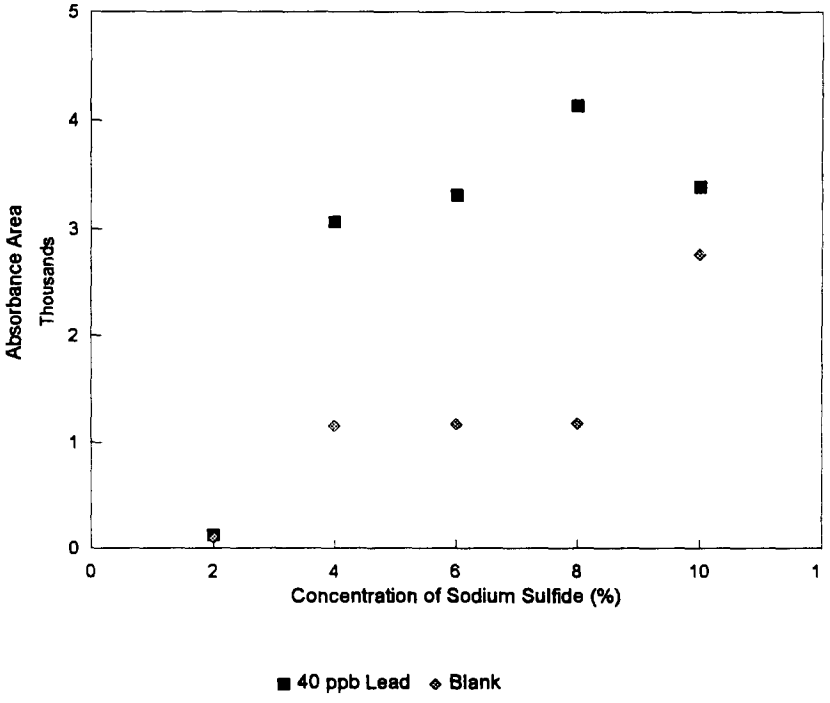


Fig. 4. Absorption spectra of resazurin and resorufin.

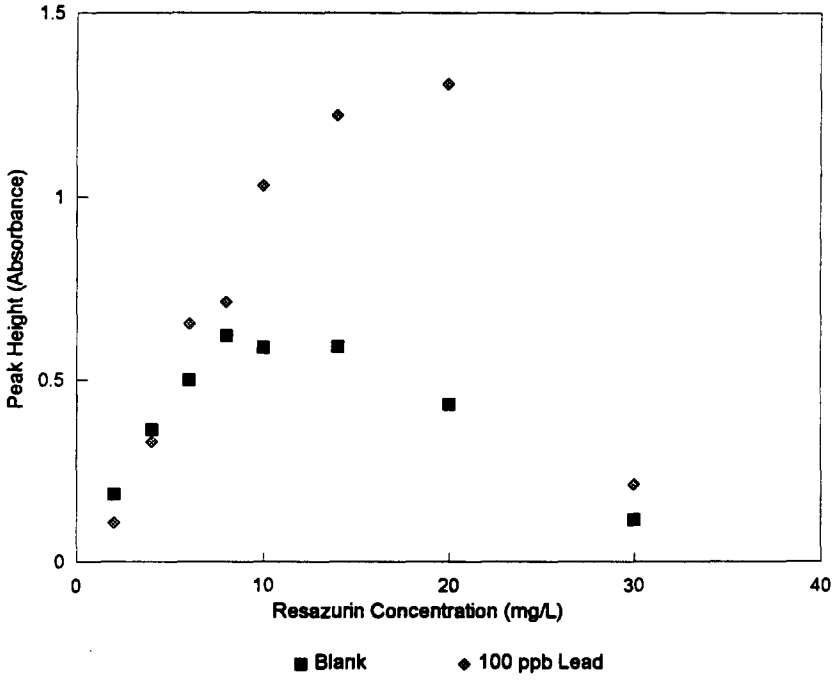


Fig. 5. Optimization of the resazurin concentration.

order, first-order and second-order reactions are: area = 2725 + 51020[$Pb^{2+}$], $r^2 = 0.9988$; area = 8.0787 + 7.4466[$Pb^{2+}$], $r^2 = 0.9805$; and area = $2.9474 \times 10^{-4} - 1.2747 \times 10^{-3}$ [$Pb^{2+}$], $r^2 = 0.9108$, respectively. Although the data are insufficient to draw a definitive conclusion, it is clear that the reaction is not second order [26]. With a correlation coefficient of 0.9988, the results suggest that the reaction may be zero order. The first-order equation also demonstrated a good fit. However, for the determination of low lead levels, the assumption that the reaction rate is zero order is acceptable. The high intercept for zero order is indicative of the presence of some uncatalyzed reaction [27].

The effect of temperature on the reaction rate was studied at 22 °C (room temperature) and at 55 °C. With an increase in temperature, the reaction rate for both catalyzed and uncatalyzed reactions (zero lead concentration) increased. The increase in reaction rate is higher for the uncatalyzed reaction than for the catalyzed reaction. This is a major disadvantage for trace ion analysis. Therefore, a temperature higher than room temperature is not recommended unless there is a way to suppress the reaction rate for the uncatalyzed reaction.

One interesting and unexplained observation is that when the reagents were heated for 30 min in a hot-water bath, then cooled and used, the amount of uncatalyzed reaction was reduced by a factor of 10. Similar results were found by Safavi et al. [28] in their research on selenium determination based on the reduction of resazurin by sulfide. They claimed that heating the mixture of reagents and cooling them down to room temperature increased the catalyzed reaction and stabilized the uncatalyzed reaction. The detection limit was reduced by one order of magnitude in their work. This is not just a degassing step, since purging the reagents with helium or nitrogen did not produce the same results.

The concentration of sulfide ions had a very close relationship with the rate of reaction. Fig. 4 shows this relationship. When the concentration of sodium sulfide increased from 2 to 4%, the integrated absorbance area jumped from $1.194 \times 10^6$ to $30.288 \times 10^6$ for the catalyzed reaction, while the increase for the uncatalyzed reaction was from $0.876 \times 10^6$ to $1.420 \times 10^6$. For a concentration increase from 4% to 10%, the increase in absorbance area for both the catalyzed and the uncatalyzed reactions was not as significant. At higher sulfide concentrations, the rate of the uncatalyzed reaction still increased while the rate of the catalyzed reaction was relatively stable. Therefore, 4% sodium sulfide solution was selected for its high sensitivity and relatively low blank absorbance.

The sodium sulfide solution was unstable overnight. On standing in contact with air, the

sulfide ion in solution was oxidized. Therefore, the reagent needed to be kept in a refrigerator and filtration was needed when the solution was not clear.

It was reported that the concentration of resazurin had no effect on the reaction rate of both catalyzed and uncatalyzed reactions in the range 12–60 mg $l^{-1}$ [25]. It was found in this research that there were maximum rates for both catalyzed and uncatalyzed reactions as the concentration of resazurin changed from 2 to 30 mg $l^{-1}$. Fig. 5 shows the influence of the resazurin concentration on the rate of reaction. The reaction rate of uncatalyzed reaction was stable when the concentration of resazurin was in the range 8–14 mg $l^{-1}$ while the rate of the catalyzed reaction reached a maximum at a resazurin concentration of 10 mg $l^{-1}$. Therefore, 10 mg $l^{-1}$ was chosen for the resazurin concentration which would produce a baseline absorbance ($A_0$) of about 2.50 and $A_0 - A$ of about 1.50 for a 100 ppb lead standard solution.

Because of the instability of sodium sulfide in acidic media and its adverse effect on the stability of the blank, the effect of acidity on the catalysis mechanism was not studied. Only the effect of base was investigated. Fig. 6 shows the results of this investigation. It was observed that with an increase of sodium hydroxide concentration from 0.1 to 8 M, the reaction rates of both catalyzed and uncatalyzed reactions were increased. However, when the concentration of sodium hydroxide was 4–6 M, the area difference for the blank and at the 200 ppb level reached a maximum and remained constant. With a sodium hydroxide concentration higher than 6 M, the system was not stable and the reproducibility was poor. Therefore, a sodium hydroxide concentration of 5 M was selected.

The reason for operating a FIA system in the stopped-flow mode is to increase the measurement sensitivity by increasing the residence time, and therefore the conversion of the measured species. The rate of the resazurin–sulfide reaction under investigation was relatively slow. It was impossible to detect the catalytic effect of trace levels of lead with continuous-flow FIA. Stopping the flow to ensure sufficient time for the reaction was necessary. Fig. 7 shows the relationship between stopping time and sensitivity. It was found that with longer stopping times, the sensitivity increases and the linear range decreases. For lead concentrations higher than 100 ppb, stopping for 15 s provided sufficient sensitivity, with straight-line correlations between 1 and 1000 ppb tested. For the samples with lead concentrations below 100 pbb, which is the case for drinking water, longer stopping times were needed. A

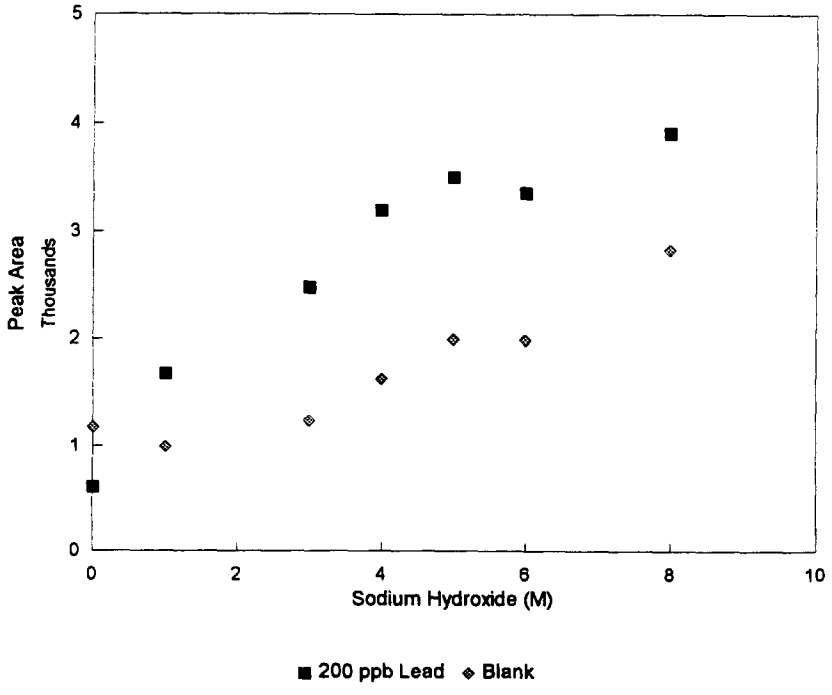


Fig. 6. Optimization of the pH.

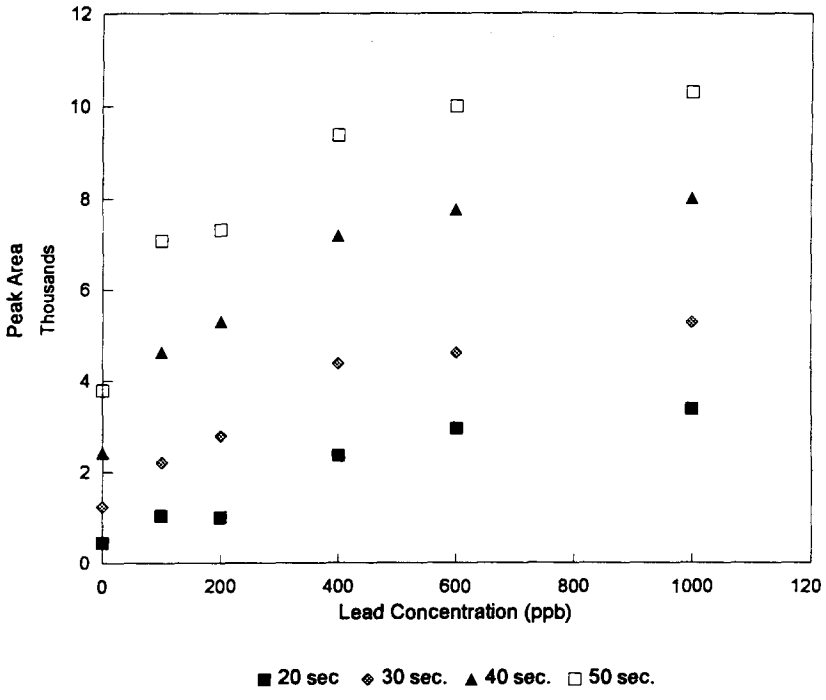


Fig. 7. Optimization of the time.

stopping time of 70 s was selected since it provided high sensitivity and a good linear range.

Since the determination of 1 ppb of lead was the objective of this work, a very small amount of sample dispersion is desired. However the peak must reach a wide enough plateau to allow for a reproducible stopping point. In order to have the smallest dispersion possible, the following experiment was conducted. With the manifold in fig. 1, the ideal dispersion coefficinet would be 3.10, that is, when the sample is used as the carrier stream and there is only dilution from mixing with reagents. A small sample volume would produce too large a dispersion coefficient, e.g. a 9.80 µl sample injection volume gave a dispersion coefficient as large as 5.14 and a large sample volume would reduce the sample throughput. Small sample volumes produce narrow peaks. On increasing the injection volume to 100 µl, the dispersion coefficient was reduced to 3.72 and the peak had a 26.4 s plateau. The peak started at 10.2 s after injection, after 22 s the peak platform formed and lasted for 26.4 s, and the peak returned to baseline in 30 s. Therefore, a volume of 100 µl was selected and run–stop modes for pump I and pump II, and injection and filling times for the injector were established. The sample throughput of the system was 30 injections per hour.

The computer system employed in this work was able to provide information concerning the peak height, area, and its slope. Both height and area were proportional to the lead concentration, but the linear range and precision were different. The peak height was a good representation of the lead concentration for a short stopping time (such as 7 s) for concentrations higher than 100 ppb. With a longer stopping time, the linear range was limited and the precision was poor. Area measurement gave better precision and the calibration lines were linear up to 1000 ppb for all the stopping times. Therefore, area measurements were used for this method.

In order to demonstrate the selectivity of the method, 36 anions and metal ions were tested, as listed in Table 1. The tolerance limit of each foreign ion was taken as the amount of added ion causing less than a $\pm 3\%$ error in the measured parameter for 10 ppb of lead. As can be seen from Table 1, most of the ions tested did not interfere, even when present in 200–2000-fold excess over the lead concentration.

The most severe interferents, copper(II) and cadmium(II), exhibited a positive interfering effect at concentrations higher than 0.25 ppm. Cobalt(II), vanadium(V), bismuth(III), and tin(II) showed a positive interfering effect at concentrations above 1 ppm. Zinc(II) at the 2 ppm level showed a negative effect. Nickel(II) at the 5 ppm level and 10 ppm of iron(III) gave

Table 1
Interfering ion tolerance limits

| Ions tested | Tolerance limit ($mg\,l^{-1}$) | Tolerance limit after removal ($mg\,l^{-1}$) |
|---|---|---|
| $Cu^{2+}$, $Cd^{2+}$ | 0.25 | 10 |
| $PO_4^{3+}$, $SO_3^{2+}$, | $8.0 \times 10^3$ | – |
| $Co_3^{2-}$, $F^-$, $Cl^-$, $I^-$ | $5.0 \times 10^3$ | – |
| $Br^-$ | $1.6 \times 10^3$ | – |
| $SO_4^{2-}$ | $3.8 \times 10^3$ | – |
| $SCN^-$ | 1000 | – |
| EDTA, $La^{3+}$, $Mg^{2+}$, $CrO_4^{2-}$ | 50 | – |
| $Ca^{2+}$ | 400 | – |
| $Ba^{2+}$ | 200 | – |
| $Hg^{2+}$, $Al^{3+}$, $Hg^+$, $Te^{4+}$ | 100 | – |
| $Zn^{2+}$, $Pd^{2+}$ | 2 | 20 |
| $Fe^{3+}$, $Fe^{2+}$ | 10 | 200 |
| $Cr^{3+}$, $Sb^{3+}$ | 10 | – |
| $As^{3+}$, $Tl^+$ | 20 | – |
| $Se^{4+}$, $Ag^+$ | 3 | – |
| $Co^{2+}$, $V^{6+}$, $Sn^{2+}$, $Bi^{3+}$ | 1 | 20 |
| $Ni^{2+}$ | 5 | 100 |

a positive interference. The interfering effects of $Cu^{2+}$, $Ni^{2+}$, $Zn^{2+}$ and $Co^{2+}$ ions were removed by extracting their complexes with dimethylglyoxime into chloroform at pH 7. The addition of 0.1 M quinolin-8-ol to the test solution and extraction with chloroform successfully removed the interferences of $Bi^{3+}$, $cd^{2+}$, $Fe^{3+}$, and $V^{5+}$ ions. Adding 0.01 M ammonium thiocyanate to the sodium hydroxide solution also prevented the interference of $Fe^{3+}$ ions. The tolerance limits of these interfering ions after their removal are also listed in Table 1. A calibration curve of 1–100 ppb lead was determined from the mean of three measurements at each point. The correlation coefficient of the regression line was 0.9992 and the fitted linear equation of the curve was

$$\text{Area} = 1552.8 + 88.54\,[Pb^{2+}]$$

The standard deviation of the blank measurement of peak area ($n = 15$) was 29.35 and the limit of detection at the 99% confidence level ($3\sigma$) was 0.994 ppb. The limit of quantification with $10\sigma$ was 3.6 ppb. The relative standard deviation (RSD) at the 20 ppb level (the area was measured and the stopping time was 70 s) was 5.2% and at the 200 ppb lead level (the peak height was measured and the stopping time was 12 s) was 3.37% ($n = 15$).

Samples were collected and both this method and the standard dithizone method were used to determine lead concentrations. The results in Table 2 are in good agreement with each other. Additions of 20, 40 and 60 ppb lead were made to sample A and the total lead was determined. The recoveries ranged from 98.1 to 103.5%.

## 4. Conclusions

The results of the sample analyses were in good agreement with those of the standard dithizone method. The resazurin method provided a simple and reliable determination of lead in tap water without preconcentration. Minimal interferences were removed by a simple solvent extraction procedure. The method meets the need for a detection limit of 1 ppb and a relative standard deviation of 5.2% at the 20 ppb lead level. The developed method has the potential to be applied to the determination of trace amount of lead in drinking water for regular lead monitoring.

## References

[1] Measuring Lead Exposure in Infants, Children, and Other Sensitive Populations, Committee On Measuring Lead in Critical Populations, Board on Environmental Studies and Toxicology, Commission on Life Sciences, National Academy Press, Washington, DC, 1993, p. 14.

Table 2
Comparison of methods and recoveries

| Sample name | Lead added (ppb) | Total lead (ppb) | | Recovery (%) |
|---|---|---|---|---|
| | | Dithizone method | Resazurin method | |
| A (Oxford OH) | – | 9.98 | 9.55 | – |
| B (Cincinnati OH) | – | 9.6 | 10.1 | – |
| C (Oxford OH) | – | 6.1 | 6.5 | – |
| A (Oxford OH) | 20 | – | 30.59 | 103.5 |
| A (Oxford OH) | 40 | – | 48.61 | 98.1 |
| A (Oxford OH) | 60 | – | 68.88 | 99.0 |

[2] Standard Methods for the Examination of Water and Wastewater, 17th edn., American Public Health Association, American Water Works Association, Water Pollution Control Federation, 1989.
[3] Federal Register, 40 (100–149) 708.
[4] Methods for Chemical Analysis of Water and Wastes, EPA Environmental Monitoring and Support Laboratory, Cincinnati, Ohio (EPA-600/4-79-020), revised March 1983, p. 293.
[5] Z. Fang, T. Guo and B. Welz, Talanta, 38(6) (1991) 613.
[6] K. Brajter and K. Slonawska, Water Resour., 22(11) (1988) 1413.
[7] P.A. Reimer and A. Miyazaki, Anal. Chem., 7 (1992) 1238.
[8] Y. Zhang, P. Riby, A.G. Cox and C.W. Mcleod, Analyst, 113 (1988) 125.
[9] S. Olsen, L.C.R. Pessenda, J. Ruzicka and E.H. Hansen, Analyst, 108 (1983) 95.
[10] Z. Fang, J. Ruzicka and E.H. Hansen, Anal. Chim. Acta, 164 (1984) 23.
[11] I.J. Fletcher, Anal. Chim. Acta, 154 (1983) 235.
[12] R. Lobinski, W.M.R. Dirkx, J. Szpunar-Lobinska and F.C. Adams, Anal. Chim. Acta, 286 (1984) 381.
[13] Methods of the Determination of Metals in Environmental Samples, Office of Research and Development, Washington, DC, EPA/600/4-91/010, June 1991, 200.8.
[14] N. Kasthurikrishnan and J.A. Koropchak, Anal. Chem., 65 (1993) 857–862.
[15] S. Dong, and Y. Wang, Talanta, 35 (1989) 819.
[16] K.G. Heumann, Anal. Chim. Acta, 283 (1993) 230.
[17] O. Klinghoffer, J. Ruzicka and E.H. Hansen, Talanta, 27 (1980) 169.
[18] T. Gangaiah, P. Ramadevi, K. Seshaiah, and G.R.K. Naidu, Acta Chim. Acad. Sci Hung., 125 (1988) 177.
[19] C.F. Boutron, M.A. Bolshov, V.G. Koloshnikov, C.C. Patterson and N.I. Barkov, Atmos. Environ., 24(7) (1990) 1797.
[20] M.A. Bolshov, C.F. Boutron and A.V. Zybin, Anal. Chem., 61 (1989) 1758.
[21] E.A. Novikov, L.K. Shpigun and Y.A. Zolotov, Anal. Chim. Acta, 230 (1990) 157.
[22] V. Kuban and R. Bulawa, Col. Czech. Chem. Commun., 54 (1989) 2673.
[23] J.A. Schneider and J.F. Hornig, Analyst, 118 (1993) 933.
[24] Z. Gu and Y. Zhang, Tongji Daue Xuebao, 18 (1990) 389.
[25] A. Afkhami, A. Safavi and A. Massoumi, Anal. Lett., 24 (1991) 1643.
[26] G. Gordon, Note in Chemical Kinetics-CHM 674, Miami University, 1993, p. 300.
[27] H.B. Mark and G.A. Rechnitz, Kinetics in Analytical Chemistry, Interscience, 1968, p. 27.
[28] A. Safavi, A. Afkhami and A. Massoumi, Anal. Chim. Acta, 232 (1990) 351.

ELSEVIER

Talanta 42 (1995) 1867–1874

Talanta

# Equilibrium reactions network for the *cis*- or *trans*-bis(pyrazine)tetraammineruthenium(II/III) and ruthenium(II/III)–EDTA complexes

Henrique E. Toma *, Rosana L. Sernaglia

*Instituto de Química, Universidade de São Paulo, Caixa Postal 26077, CEP 05599-970 São Paulo, SP, Brazil*

Received 8 February 1995; revised 16 May 1995; accepted 17 May 1995

**Abstract**

The elecrochemical and spectroelectrochemical behavior of the binuclear and trinuclear complexes generated from the association of *cis*- or *trans*-$[Ru(NH_3)_4(pz)_2]^{3+/2+}$ (where pz represents pyrazine) and $[RuEDTA(H_2O)]^{2-/-}$ complexes has been investigated in aqueous solution. Based on two sets of spectrophotometrically determined equilibrium constants and on the formal redox potentials, the complex network of equilibrium reactions involving mixed valence species has been elucidated.

*Keywords:* Bis(pyrazine)tetraammineruthenium(III) complexes; Electrochemical behavior; Equilibrium constants; Equilibrium reactions; Redox potentials; Ruthenium(II/III)–EDTA complexes; Spectrochemical behavior

## 1. Introduction

Polymetallic complexes exhibiting redox active groups are particularly interesting as electron-transfer mediators in molecular devices and in multielectron transfer catalysis [1–8]. A typical compound displaying a strong electrocatalytic response in the reduction of molecular oxygen has been obtained by the association of four $[Ru^{III/II}EDTA]^{-/2-}$ complexes to the *meso*-tetrapyridylporphyriniron(II) species [2]. The binding of the $[Ru^{III}EDTA]^-$ complex to multibridged species is a rather simple way of obtaining polymetallic systems; however, in the absence of a large excess of the ruthenium complex a complicated network of equilibrium reactions can result. An interesting case, involving a double bridging $[Ru(NH_3)_4(pz)_2]^{2+}$ where pz represents pyrazine in the presence of $[Ru^{III}EDTA]$ ions, is reported here. This work deals with the determination of equilibrium and electrochemical parameters, providing a good example of the elucidation of a complex network of equilibrium reactions.

## 2. Experimental

The $[Ru(HEDTA)(H_2O)]$ and *cis*-, *trans*-$[Ru(NH_3)_4(pz)_2](PTS)_2$ complexes (where PTS represents the *p*-toluenesulfonate ion) were prepared and characterized as previously reported in the literature [9–12]. The binuclear and trinuclear mixed complexes were studied in aqueous solution, under an argon atmosphere, at pH 4.7, in 0.10 M acetate buffer. The cis and trans trinuclear compounds have also been isolated and characterized in the solid form, for comparison purposes. The procedure consisted

* Corresponding author. Fax: (55)11-815-5579; E-mail: HENETOMA@QUIM.IQ.USP.BR


*SSDI* 0039-9140(95)01646-5

of mixing stoichiometric amounts of the complexes in aqueous solution, and precipitating with acetone. The solids precipitated were collected on a filter, washed with acetone and dried under vacuum. Elemental analyses were carried out by the Microanalytical Laboratory of the University of São Paulo. Calculated for *cis*-$[Ru(NH_4)_4\{pzRuEDTA\}_2] \cdot 12H_2O$: C, 25.4; N, 12.8; H, 5.3. Found: C, 25.4; N, 12.7; H, 4.1. Calculated for *trans*-$[Ru(NH_3)_4\{pzRuEDTA\}_2] \cdot 5H_2O$: C, 28.0; N, 14.0; H, 4.7. Found: C, 28.0; N, 14.1; H, 4.4.

Cyclic voltammetry was carried out using a Princeton Applied Research Corp. model 173 potentiostat and model 175 universal programmer. A glassy carbon working electrode and a platinum wire auxiliary electrode were employed for the measurements versus an Ag/AgCl (1 M KCl) reference electrode ($E^0 = 0.222$ V versus SHE) [13]. When mentioned in the text, reversible behavior of the voltammetric waves has been proposed, considering, simultaneously, (a) the separation of the anodic and cathodic peaks, typically in the 60–70 mV range; (b) their similar intensities; and (c) the linear response of the peak currents versus the square root of the scan rates.

The electronic spectra were recorded on a Hewlett-Packard model 8452-A diode-array spectrophotometer, or on a Guided-Wave model 260 fiber-optics instrument. Spectrophotometric titrations of the cis and trans complexes, $3.9 \times 10^{-5}$ M and $2.6 \times 10^{-5}$ M, respectively, with 0.42 M $[Ru^{III}EDTA(H_2O)]^-$ were carried out using a quartz cuvette (1 cm pathlength) attached to a cylindrical reservoir. An ultraprecision Gilmont micrometer syringe ($\pm 0.0001$ ml) was employed in the experiments. Spectroelectrochemical measurements were carried out using the potentiostat in parallel with the diode-array spectrophotometer. A three-electrode system was designed for a quartz cell of 0.025 cm internal optical pathlength. A gold minigrid was used as a transparent working electrode, in the presence of a small Ag/AgCl (1 M KCl) reference electrode and a platinum auxiliary electrode. Because of the semi-infinite diffusion conditions employed, the measurements were carried out after the decay of the Faradaic currents and the stabilization of the spectra (about 3 min). The reversibility of the spectroelectrochemical behavior was evaluated based on the regeneration of the initial spectra after returning the applied potential to the starting point, and on the analysis of the Nernst plots.

## 3. Results and discussion

### 3.1. Spectrophotometric titrations

The $[Ru^{III}EDTA(H_2O)]^-$ complex is the major species [11] generated from the dissolution of $[Ru^{III}HEDTA(H_2O)]$ in aqueous solution in the pH range 3.0–6.5. This ion undergoes a rapid substitution of the labile water molecule in the presence of *N*-heterocyclic ligands, such as pyrazine, pyridine and related species [11,14] yielding the corresponding substituted complexes. The products containing *N*-heterocyclic ligands display weak absorption bands in the visible region and, in general, are not suitable for spectrophotometric studies. In the case of the *cis*- and *trans*-$[Ru(NH_3)_4(pz)_2]^{2+}$ complexes, the binding of $[Ru^{III}EDTA]^-$ groups at the pyrazine bridging ligands can easily be monitored, since it leads to pronounced changes in the ruthenium(II)-to-pyrazine charge transfer (MLCT) bands, as illustrated in Figs 1A and 2A. The $Ru^{III}$ ions are expected to act as electron withdrawing groups at the pyrazine ring, lowering the energies of the $\pi^*$ orbitals and shifting the MLCT bands from 398 nm ($\log \varepsilon = 4.08$), and 474 nm ($\log \varepsilon = 3.94$) (cis) and 486 nm ($\log \varepsilon = 4.34$) (trans) in the starting complexes to 424 nm ($\log \varepsilon = 4.08$), 537 nm ($\log \varepsilon = 4.28$) (cis) and 558 nm ($\log \varepsilon = 4.59$) (trans) in the trinuclear species. The absorption band at 424 nm in the cis trinuclear complex is masked by absorption of the excess $[Ru^{III}HEDTA(H_2O)]^-$ in Fig. 1A; however, it can be detected spectroelectrochemically (see Fig. 4A) or in the absorption spectrum of the solid complex.

Typical spectrophotometric titration plots for the cis and trans isomers can be seen in Figs. 1B and 2B, respectively. The lack of inflection in the spectrophotometric plots indicates the existence of overlapping equilibrium reactions. Two successive reactions (1) and (2) have been considered in this work

$$Ru^{III} + LRu^{II}L \overset{K_{32}}{\rightleftharpoons} Ru^{III}LRu^{II}L \quad (1)$$

$$Ru^{III}LRu^{II}L + Ru^{III} \overset{K_{323}}{\rightleftharpoons} Ru^{III}LRu^{II}LRu^{III} \quad (2)$$

where $Ru^{III}$ refers to $[Ru^{III}EDTA(H_2O)]^-$, $LRu^{II}L$ refers to $[Ru^{II}(NH_3)_4(pz)_2]^{2+}$, and the subscripts in $K_{32}$ and $K_{323}$ represent the oxidation states of the ruthenium ions as they appear in the formulas.

The calculation of the equilibrium constants $K_{32}$ and $K_{232}$ from the spectrophotometric data

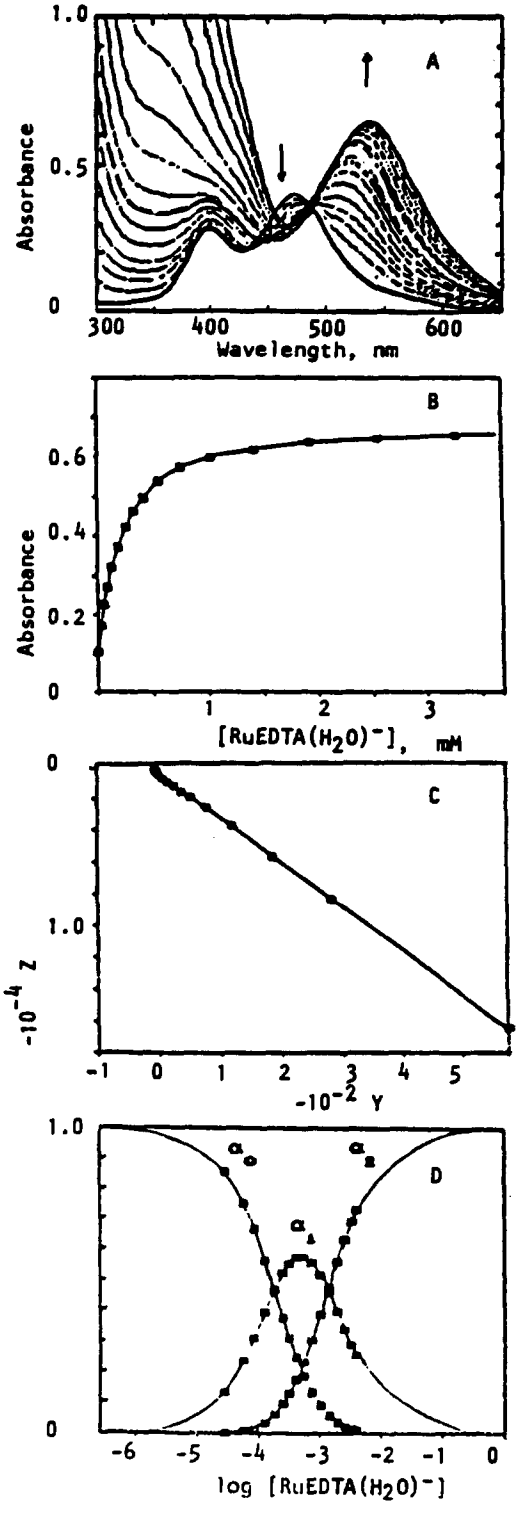


Fig. 1. (A) Spctrophotometric titration of *cis*-$[Ru(NH_3)_4(pz)_2]^{2+}$ ($3.9 \times 10^{-5}$ M) with $[Ru^{III}EDTA(H_2O)]^-$, at pH 4.7, in 0.10 M acetate buffer; (B) absorbance plot ($\lambda = 537$ nm); (C) linear regression analysis of $Z$ versus $Y$ (see text); (D) plots of the distribution functions for the starting complex ($\alpha_0$) and the binuclear ($\alpha_1$) and trinculear ($\alpha_2$) species (solid line represents the theoretical curves).

can be carried out using the general method proposed by Yatsimirskii [15] based on a successive extrapolation procedure. An alternative method has been proposed by Toma and Morino [16] and is based on the linearization of the general Eq. (3) for $\varepsilon_i = A/[Ru_T]$, where $A$ is the measured absorbance, and $[Ru_T]$ is the total Ru(III)–EDTA concentration. Under the conditions of this work, $[Ru^{III}]$ is in large excess over $[LRu^{II}L]$, and is practically equivalent to $[Ru_T]$.

$$\varepsilon_i = \frac{\varepsilon_{LRuL} + \varepsilon_{32}K_{32}[Ru^{III}] + \varepsilon_{323}K_{323}[Ru^{III}]^2}{1 + K_{32}[Ru^{III}] + K_{32}K_{323}[Ru^{III}]^2} \quad (3)$$

This equation can be rearranged as

$$\frac{(\varepsilon_i - \varepsilon_{LRuL})}{(\varepsilon_i - \varepsilon_{323})}[Ru^{III}]^2 = -K_{32}K_{323} - K_{32}\frac{(\varepsilon_i - \varepsilon_{32})}{(\varepsilon_i - \varepsilon_{323})}[Ru^{III}] \quad (4)$$

or

$$Z = -K_{32}K_{323} - K_{32}Y \quad (5)$$

In this method, $\varepsilon_i$ is calculated for each $[Ru^{III}]$ concentration and the extinction coefficients for the starting and final species, $\varepsilon_{LRuL}$ and $\varepsilon_{323}$, are previously known. By means of an iterative least-squares analysis, it is possible to find values of the extinction coefficients for the binuclear complex ($\varepsilon_{32}$) which give the best fit for the linear Eqs. (4) or (5), and simultaneously determine the equilibrium constants $K_{32}$ and $K_{323}$. The best values for $\varepsilon_{32}$ were $13.9 \times 10^3$ $m^{-1}\,cm^{-1}$ (537 nm) and $28.0 \times 10^3$ $M^{-1}\,cm^{-1}$ (558 nm) for the cis and trans isomers, respectively, leading to the linear plots shown in Figs. 1C and 2C. The corresponding equilibrium constants, $K_{32}$ and $K_{323}$, for the cis and trans complexes were $(5.6 \pm 0.1) \times 10^3$ $M^{-1}$ and $(7.3 \pm 0.9) \times 10^2$, and $(5.2 \pm 0.1) \times 10^3$ $M^{-1}$, and $(1.5 \pm 0.2) \times 10^3$ $M^{-1}$, respectively. Similar results were obtained by means of the Yatsimirskii method, e.g. $(5 \pm 1) \times 10^3$ $M^{-1}$ and $(6 \pm 1) \times 10^2$ $M^{-1}$, and $(5 \pm 1) \times 10^3$ $M^{-1}$ and $(1.3 \pm 0.6) \pm 10^3$ $M^{-1}$, respectively; however, the precision was much smaller because of the many successive non-linear extrapolations involved.

### 3.2. Cyclic voltammetry

Typical cyclic voltammograms for the cis and trans isomers in the presence of $[Ru^{III}EDTA(H_2O)]^-$ ions are shown in Figs. 3A and

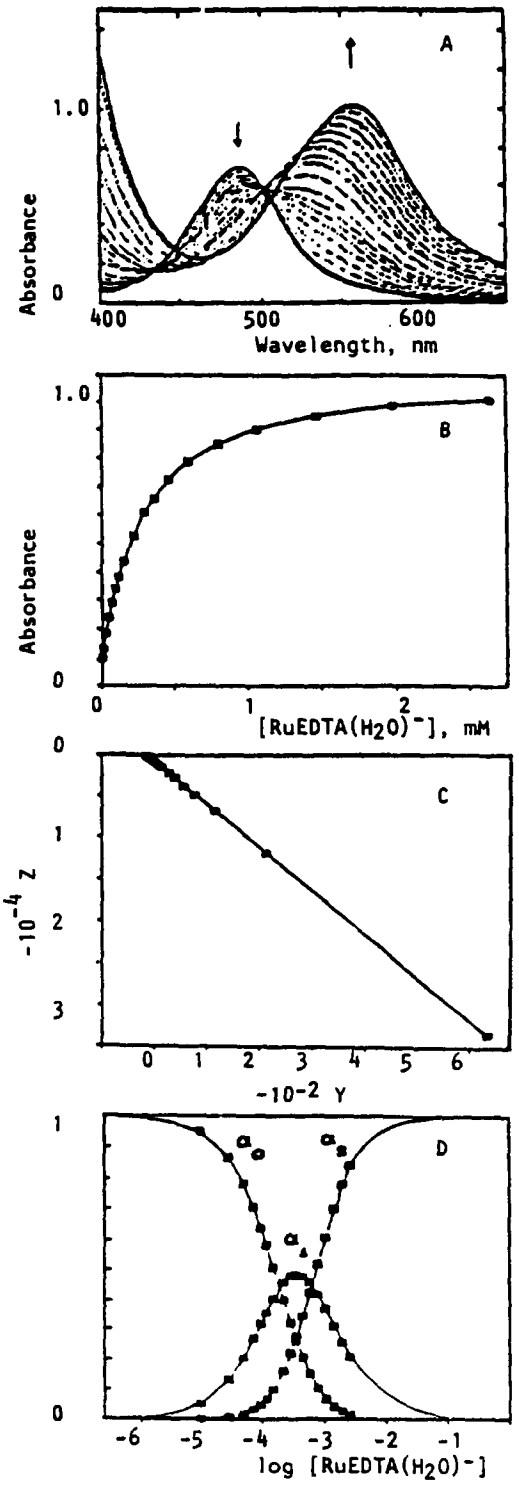


Fig. 2. (A) Spectrophotometric titration of *trans*-$[Ru(NH_3)_4(pz)_2]^{2+}$ ($2.6 \times 10^{-5}$ M) with $[Ru^{III}EDTA(H_2O)]^-$, at pH 4.7, in 0.10 M acetate buffer; (B) absorbance plot ($\lambda = 558$ nm); (C) linear regression analysis of $Z$ versus $Y$ (see text); (D) distribution plots for the starting complex ($\alpha_0$) and the binuclear ($\alpha_1$) and trinuclear ($\alpha_2$) species (solid line represents the theoretical curves).

3B, respectively. The starting *cis*- and *trans*-$[Ru^{II}(NH_3)_4(pz)_2]^{2+}$ complexes exhibit a reversible wave at $E^{0'} = 0.88$ V and 0.81 V, associated with the $Ru^{III/II}$ redox couples (25 °C; 0.10 M KCl). Under the same experimental conditions, the $[Ru^{III}EDTA(H_2O)]^-$ complex exhibits $E^{0'} = -0.01$ V. The binding of the $[Ru^{III}EDTA]^-$ ion to the *cis*- and *trans*-$[Ru^{II}(NH_3)_4(pz)_2]^{2+}$ complexes gives rise to a new, reversible wave at 0.27 V, ascribed to the $[Ru^{III/II}EDTA(pz)]^{-/2-}$ moieties, and is accompanied by an increase, up to 100 mV, in the $E^{0'}$ values for the $[Ru^{III/II}(NH_3)_4(pz)_2]^{3+/2+}$ group. These results reflect the influence of $\pi$-backbonding effects through the $Ru^{II}$–pz bonding, induced by the attached $[Ru^{III}EDTA]^-$ groups. The $E^{0'}$ values are shown in Table 1.

The corresponding $E^{0'}$ values for the cis and trans trinuclear complexes, e.g. 0.98 V and 0.91 V, were evaluated from measurements obtained in the presence of a large excess of $[Ru^{III/II}EDTA(H_2O)]^{-/2-}$ species (above 6 mM) to ensure that the formation of products is more than 90% complete. In this case, the voltammograms obtained starting from a cathodic scan were practically identical to those obtained by scanning the potentials in the opposite direction. Unfortunately, under such conditions, the background currents increase very rapidly near the positive limit of the aqueous solvent, and the voltammograms become distorted above 0.9 V, as one can see in Fig. 3. On the other hand, in the negative region, there is a very strong peak associated with the excess of $[Ru^{III/II}EDTA(H_2O)]^{-/2-}$ species (not shown in Fig. 4).

The $E^{0'}$ values for the cis and trans binuclear complexes, i.e. 0.94 V and 0.87 V, were estimated from the measurements carried out using a 1:1.1 molar ratio, coinciding with the maximum in the distribution curves of Figs. 1D and 2D. The peak positions were not sensitive to the initial scan direction. Because of the presence of 25% of the mononuclear and trinuclear species, the voltammograms were slightly broader than for a single species; however the peak positions should reflect the major contribution of the binuclear complexes as the main species in solution. This conclusion is supported by simulation or deconvolution analysis, considering three reversible, monoelectronic waves, exhibiting 1:2:1 intensities, separated by 50 mV. On the other hand, it should be noted that measured $E^{0'}$ values coincide with the estimated values, based on the arithmetic average of the

Table 1
Equilibrium constants and formal redox potentials for the $[RuEDTA]^{-\,2-}$ and $[Ru(NH_3)_4(pz)_2]^{2+\,3+}$ systems

| Redox potentials/ equilibrium constants[a] | *cis*-$[Ru(NH_3)_4(pz)_2]$ +[RuEDTA] | *trans*-$[Ru(NH_3)_4(pz)_2]$ +[RuEDTA] |
|---|---|---|
| $E^{0'}_{3,2}$ (V) | −0.01 | −0.01 |
| $E^{0'}_{32,22}$ (V) | 0.27 | 0.27 |
| $E^{0'}_{223,222}$ (V) | 0.27 | 0.28 |
| $E^{0'}_{323,223}$ (V) | 0.28 | 0.30 |
| $E^{0'}_{33,32}$ (V) | 0.94 | 0.87 |
| $E^{0'}_{333,323}$ (V) | 0.98 | 0.91 |
| $E^{0''}_{3,2}$ (V) | 0.88 | 0.81 |
| $K_{22}$ ($M^{-1}$) | $3.1 \times 10^8$ | $2.8 \times 10^8$ |
| $K_{222}$ ($M^{-1}$) | $6.0 \times 10^7$ | $3.8 \times 10^8$ |
| $K_{223}$ ($M^{-1}$) | $1.1 \times 10^3$ | $4.8 \times 10^3$ |
| $K_{32}$ ($M^{-1}$) | $5.6 \times 10^3$ | $5.2 \times 10^3$ |
| $K_{323}$ ($M^{-1}$) | $7.3 \times 10^2$ | $1.5 \times 10^3$ |
| $K_{33}$ ($M^{-1}$) | $5.4 \times 10^2$ | $5.0 \times 10^2$ |
| $K_{333}$ ($M^{-1}$) | $1.5 \times 10^2$ | $3.1 \times 10^2$ |

[a] The subscript refers to the oxidation states of the ruthenium ions, as described in the text.

formal redox potentials for the mononuclear and trinuclear complexes.

### 3.3. Spectroelectrochemistry

Spectroelectrochemical measurements for the cis and trans trinuclear complexes are shown in Figs. 4 and 5. The totally reduced species, $Ru^{II}LRu^{II}LRu^{II}$, exhibit very strong absorption bands in the visible region, which can be deconvoluted in its three bands at 420 nm (3.70), 490 nm (4.36) and 590 nm (4.54) for the cis isomer, and into two bands at 530 nm (4.43) and 600 nm (4.81), for the trans species. The high energy bands correlate with the MLCT bands observed for the *cis*- and *trans*-$[Ru^{II}(NH_3)_4(pz)_2]^{2+}$ complex. The low energy bands can be ascribed to Ru-to-pyrazine charge-transfer transitions in the energy bands can be ascribed to Ru-to-pyrazine charge-transfer transitions in the $[Ru^{II}EDTA$–pyrazine$]^{2-}$ moiety, since their intensities depend on the number of [$Ru^{II}$EDTA] groups and undergo complete decay after their oxidation at 0.4 V. The spectroelectrochemical measurements were also extended to the near-infrared region (2200 nm), with no evidence of intervalence transfer bands with $\varepsilon > 100\ M^{-1}\,cm^{-1}$.

The [$Ru^{III\,II}$EDTA] moieties display a typically reversible response, allowing very accurate spectroscopic measurements as a function of the applied potentials. The corresponding Nernst plots exhibit a small inflection, with two parallel lines displaying a slope of 0.059. These results can be interpreted in terms of two successive, reversible, monoelectronic processes exhibiting very close $E^0$ values, here denoted $E^0_{323,223}$ and $E^0_{223,222}$ (Table 1).

$$Ru^{III}LRu^{II}LRu^{III} \underset{E^0_{323,223}}{\overset{+e}{\rightleftharpoons}} Ru^{II}LRu^{II}LRu^{III} \underset{E^0_{223,222}}{\overset{+e}{\rightleftharpoons}} Ru^{II}LRu^{II}LRu^{II} \quad (6)$$

The difference in the successive $E^{0'}$ values is smaller than 30 mV, indicating a negligible interaction between the peripheral $[Ru^{II}EDTA]^{2-}$ and $[Ru^{III}EDTA]^-$ groups in the mixed valence $[Ru^{II}LRu^{II}LRu^{III}]$ complex.

In contrast to the $[Ru^{II}EDTA]^{2-}$ groups, the electrochemical oxidation of the $[Ru^{II}(NH_3)_4(pz)_2]^{2+}$ center proceeded in an irreversible way in the time scale of the spectroelectrochemical measurements. The measurements varied systematically as a function of time, and the starting spectrum was not completely recovered after returning the potential to the initial value. In this case, the $E^0$ values were obtained from the cyclic voltammograms.

### 3.4. Thermodynamic network

Based on the equilibrium constants and $E^{0'}$ values determined in this work, the following thermodynamic scheme can be elaborated and solved

$$\begin{array}{ccccc} Ru^{II} + LRu^{II}L & \overset{K_{22}}{\rightleftharpoons} & Ru^{II}LRu^{II}L(+Ru^{II}) & \overset{K_{222}}{\rightleftharpoons} & Ru^{II}LRu^{II}LRu^{II} \\ & & \downarrow E^0_{3/2} & & \downarrow E^0_{223/222} \\ \downarrow E^0_{3/2} & & Ru^{II}LRu^{II}L\ (+Ru^{III}) & \overset{K_{223}}{\rightleftharpoons} & Ru^{II}LRu^{II}LRu^{II}LRu^{III} \\ & & \downarrow E^0_{32/22} & & \downarrow E^0_{323/223} \\ Ru^{III} + LRu^{II}L & \overset{K_{32}}{\rightleftharpoons} & Ru^{III}LRu^{II}L(+Ru^{III}) & \overset{K_{323}}{\rightleftharpoons} & Ru^{III}LRu^{II}LRu^{III} \\ \downarrow E^{0'}_{3/2} & & \downarrow E^0_{33/32} & & \downarrow E^0_{333/323} \\ Ru^{III} + LRu^{III}L & \overset{K_{33}}{\rightleftharpoons} & Ru^{III}LRu^{III}L(+Ru^{III}) & \overset{K_{333}}{\rightleftharpoons} & Ru^{III}LRu^{III}LRu^{III} \end{array} \quad (7)$$

For each square cycle, the equilibrium constants $K_i$ and $K_j$ are related to $E^0_i$ and $E^0_j$ by the free energy relationship

$$nFE^0_i + RT \ln K_i = +nFE^0_j + RT \ln K_j \quad (8)$$

$$\frac{K_j}{K_i} = 10^{(E_i - E_j)/0.0591} \quad (9)$$

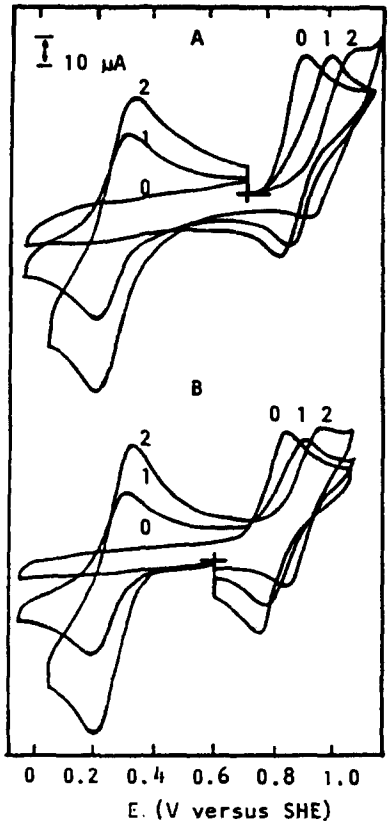


Fig. 3. Cyclic voltammograms of the (A) *cis*- and (B) *trans*-$[Ru(NH_3)_4(pz)_2]^{2+}$ complexes (1.0 mM) (voltammogram 0), and of the binuclear (voltammogram 1) and trinuclear (voltammogram 2) species, generated in the presence of 1.1 μm and 6.0 mM $[Ru^{III}EDTA(H_2O)]^-$, respectively (0.10 M KCl; glassy carbon disc electrode (0.20 $cm^2$); 100 mV $s^{-1}$; 25 °C.

where $n$, $F$, $R$ and $T$ have the conventional meaning. This equation is extremely useful since, from the known values of $K_i$, $E^0_i$ and $E^0_j$, one can readily calculate $K_j$ [17]. The thermodynamic cycle requires that the redox potentials correspond to those of the initial and final states. Therefore, in the measurements of $E^0_j$ it is important to ensure that the formation of the products in the square cycle is complete, as we have pursued in this work. This means that $K_i[\text{complex}_i] \gg 1$ and $K_j[\text{complex}_i] \gg 1$; otherwise a concentration-dependent equation should be employed, e.g.

$$E^{0'}_j = E^0_i + (RT/F) \ln\{(K_i[\text{complex}_i] + 1) / (K_j[\text{complex}_i] + 1)\}$$

In our case, the thermodynamic constants and $E^0$ values were replaced by the conditional equilibrium constants and formal redox potentials, $E^{0'}$. This procedure is normally adopted, since the electrochemical measurements require the use of supporting electrolytes, and the activity coefficients for the oxidized and reduced species are not expected to differ appreciably at high, constnat, ionic strengths.

Starting from the spectrophotometrically determined $K_{32}$ and $K_{323}$ constants, it is possible to solve four associated free energy cycles, i.e.

$$\log(K_{33}/K_{32}) = (E^{0''}_{3/2} - E^{0'}_{33/32})/0.0591 \quad (10)$$

$$\log(K_{333}/K_{323}) = (E^{0'}_{33/32} - E^{0'}_{333/323})/0.0591 \quad (11)$$

$$\log(K_{22}/K_{32}) = E^{0'}_{32/22} - E^{0'}_{3/2})/0.0591 \quad (12)$$

$$\log(K_{223}/K_{323}) = (E^{0'}_{323/223} - E^{0'}_{32/22})/0.0591 \quad (13)$$

Based on the calculated $K_{223}$ values, another cycle can be solved

$$\log(K_{222}/K_{223}) = (E^{0'}_{223/222} - E^{0'}_{3/2})/0.0591 \quad (14)$$

The complete set of equilibrium constants calculated in this way can be seen in Table 1,

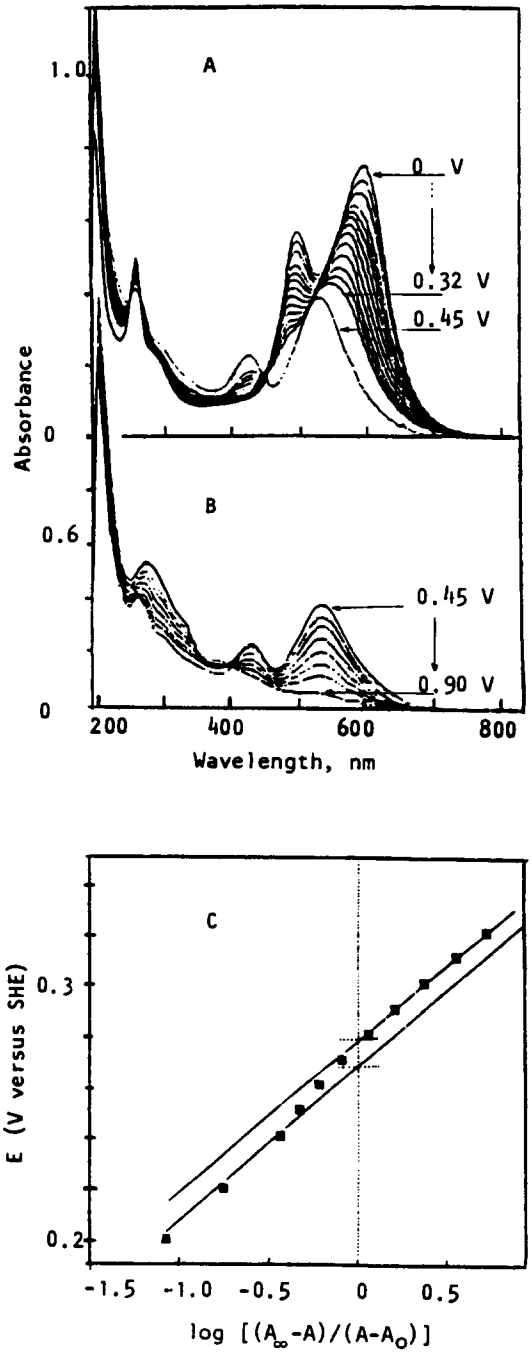


Fig. 4. Spectroelectrochemical behavior of the trinuclear complex, *cis*-$[Ru(NH_4)_4\{(pz)RuEDTA\}_2]$, 1.0 mM in the presence of 6.0 mM $[Ru^{III}EDTA(H_2O)]^-$, and 0.1 M KCl, showing the oxidation of (A), the $[Ru^{II}EDTA(pz))]^{2-}$ moiety (A) and (B) the $[Ru^{II}(NH_3)_4(pz)_2]^{2+}$ moiety, and (C) the Nernst plot employed for the evaluation of $E^0_{223,222}$ and $E^0_{323,223}$.

along with the corresponding $E^{0'}$ values. Because of the errors involved in the $E^{0'}$ measurements and of the small variation in the activity coefficients, the results should be regarded as good estimated values of the equilibrium constants, in the absence of thermodynamic data extrapolated to infinite dilution.

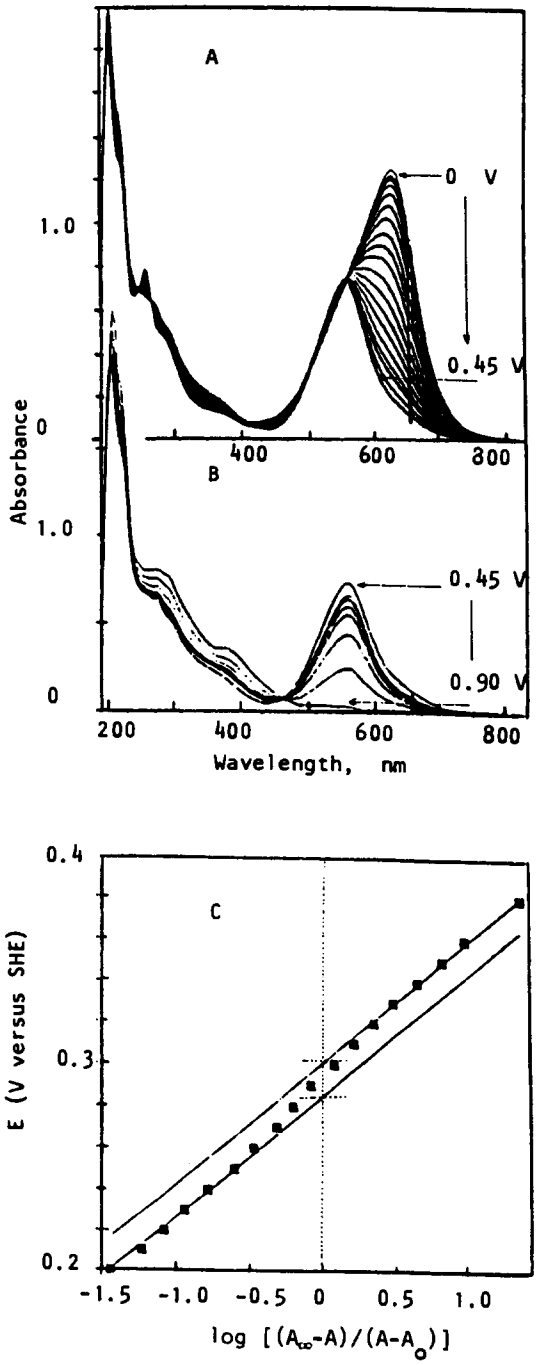


Fig. 5. Spectroelectrochemical behavior of the trinuclear complex, *trans*-$[Ru(NH_4)_4\{(pz)RuEDTA\}_2]$, 1.0 mM, in the presence of 6.0 mM $[Ru^{III}EDTA(H_2O)]^-$, 0.1 M KCl, showing the oxidation of moiety (A) the $[Ru^{II}EDTA(pz)]^2$ and (B) the $[Ru^{II}(NH_3)_4(pz)_2]^{2+}$ moiety, and (C) the Nernst plot employed for the evaluation of $E^0_{223/222}$ and $E^0_{323/223}$.

## 4. Conclusion

This work has shown that based on the determination of the redox potentials and of two successive equilibrium constants, the complete network of association reactions for the *cis*- and *trans*-$[Ru(NH_3)_4(pz)_2]^{3+/2+}$ + $[RuEDTA(H_2O)]^{-/2-}$ complexes can be elucidated.

From the data in Table 1, one can see that the $[Ru^{II}EDTA]^{2-}$ ion exhibits a remarkable affinity for the pyrazine bridging ligands, leading to the formation of very stable binuclear and trinuclear species. In comparison with the corresponding $[Ru^{III}EDTA]^{-}$ complexes, the difference of six orders of magnitude in the stability constants is consistent with strong backbonding interactions in the [$Ru^{II}$EDTA–pyrazine] moiety.

Except for the *trans*-$[Ru^{II}LRu^{II}LRu^{II}]$ complex, successive equilibrium constants decrease systematically according to statistical behaviour, for instance $K_{32} > K_{323}$ and $K_{33} > K_{333}$. In the case of the *trans*-$[Ru^{II}LRu^{II}LRu^{II}]$ complex, $K_{22} < K_{222}$ indicates a cooperative effect associated with the backbonding interactions in the complex. This is not observed in the cis isomer, presumably because of its greater susceptibility to steric hindrance effects.

## Acknowledgments

The support from FAPESP, CAPES, CNPq and PADCT is gratefully acknowledged.

## References

[1] H.E. Toma and K. Araki, J. Chem. Res., (1990) 82.
[2] K. Araki and H.E. Toma, J. Electroanal. Chem., 297 (1991) 301.
[3] K. Araki and H.E. Toma, Inorg. Chim. Acta, 179 (1991) 293.
[4] C. Shi and F.C. Anson, J. Am. Chem. Soc., 113 (1991) 9564.
[5] B. Steiger, C. Shi and F.C. Anson, Inorg. Chem., 32 (1993) 2107.
[6] K. Araki and H.E. Toma, J. Chem. Res., S (1994) 290; M (1994) 1501.
[7] K. Araki and H.E. Toma, J. Photochem. Photobiol. A, 83 (1994) 245.
[8] C. Hidalgo-Luangdilok and A.B. Bocarsly, Inorg. Chem., 29 (1990) 2894.
[9] Y. Yoshino, T. Uehiro and M. Saito, Bull. Chem. Soc. Jpn., 52 (1979) 160.
[10] M. Mukaida, H. Okuno and T. Ishimori, Nippon Kagaku Sasshi, 86 (1965) 589 (in Japanese).
[11] T. Matsubara and C. Creutz, Inorg. Chem., 18 (1979) 1956.
[12] H.S. Lim, D.J. Barclay and F.C. Anson, Inorg. Chem., 11 (1972) 1460.
[13] R.G. Bates and V.E. Bower, J. Res. Natl. Bur. Std., 53 (1954) 283.
[14] H.E. Toma and R.L. Sernaglia, Talanta, 40 (1993) 515.
[15] K.B. Yatsimirskii, Zh. Neor. Khim., 1 (1956) 2306.
[16] H.E. Toma and L.A. Morino, Talanta, 31 (1984) 224.
[17] D.A. Buckingham and A.M. Sargeson, in F.P. Dwyer and D.P. Mellow (Eds.), Chelating Agents and Metal Chelates, Academic Press, New York, 1964, Chapter 6.

ELSEVIER

Talanta 42 (1995) 1875–1882

Talanta

# Protonation constants of some substituted 2-hydroxy-1-naphthalideneanilines in dioxan–water mixtures

Fitnat Köseoğlu [a,*], Esma Kiliç [b], Dilek Uysal [a]

[a] *Department of Sciences, Faculty of Gazi Education, University of Gazi, Ankara, Turkey*
[b] *Department of Chemistry, Faculty of Science, University of Ankara, Ankara, Turkey*

Received 3 October 1994; revised 10 January 1995; accepted 18 May 1995

**Abstract**

The protonation constants of ten Schiff's bases synthesized by the condensation of 2-hydroxy-1-naphthaldehyde with aniline and *o*-, *m*-, and *p*-substituted methylanilines, ethylanilines and methoxyanilines in various dioxan–water mixtures have been determined potentiometrically using an electrode system calibrated in concentration units of the hydrogen ion. The influence of substituents in the molecular structure on the protonation constants is discussed. The log $K_2$ values relating to the protonation of imine nitrogen atoms are in accordance with the Hammett relationship for all solvent compositions. A reverse relationship is observed between log $K_2$ for all Schiff's bases and the mole fraction of dioxan. However, the log $K_1$ values corresponding to the protonation of naphtholate O-ions have been found to increase with the increase in concentration of dioxan. Both electrostatic and non-electrostatic contributions influencing these constants are briefly discussed.

*Keywords:* Dioxan–water mixture; 2-Hydroxy-1-naphthalideneanilines; Potentiometry; Protonation constants; Schiff's bases; Solvent effect; Substituent effect; Titrimetry

## 1. Introduction

Among different physicochemical properties of organic compounds, protonation constants determined in mixed solvents provide an important basis for speculation about whether solvent and substituent effects influence their acidity or basicity. Knowledge of equilibrium data also facilitates the design of new separation and analytical procedures such as acid–base titration, complex formation and solvent extraction. In a continuation of our previous work [1–3] on various protonation equilibria in water–organic solvent mixtures, the present work reports the protonation constants of substituted 2-hydroxy-1-naphthalideneanilines (I) in different water–dioxan mixtures. There have been a number of publications on the protonation constants of 2-hydroxy-1-naphthalideneanilines in mixed solvents but no systematic reports dealing with these Schiff's bases in dioxan–water mixtures have appeared so far [4–10].

In addition, the results obtained in the present paper have been compared with those for salicylideneanilines in dioxan–water mixtures in order to gain a better understanding of solute–solvent interactions and structural variations. Such studies are now being conducted in our laboratories and will be reported later.

* Corresponding author.

*SSDI* 0039-9140(95)01649-X

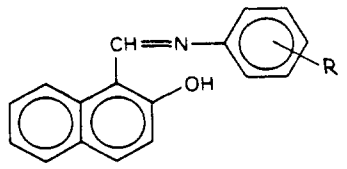


I

where R is H (2-hydroxy-1-naphthalideneaniline; used as a reference), 2-$CH_3$ (2-hydroxy-1-naphthalidene-2-methylaniline), 3-$CH_3$ (2-hydroxy-1-naphthalidene-3-methylaniline), 4-$CH_3$ (2-hydroxy-1-naphthalidene-4-methylaniline), 2-$C_2H_5$ (2-hydroxy-1-naphthalidene-2-ethylaniline), 3-$C_2H_5$ (2-hydroxy-1-naphthalidene-3-ethylaniline), 4-$C_2H_5$ (2-hydroxy-1-naphthalidene-4-ethylaniline), 2-$OCH_3$ (2-hydroxy-1-naphthalidene-2-methoxyaniline), 3-$OCH_3$ (2-hydroxy-1-naphthalidene-3-methoxyaniline), 4-$OCH_3$ (2-hydroxy-1-naphthalidene-4-methoxyaniline).

## 2. Experimental

### 2.1. Materials

The 2-hydroxy-1-napthalideneanilines were prepared by the condensation of 2-hydroxy-1-naphthaldehyde with aniline and 2-methylaniline, 3-methylaniline, 4-methylaniline, 2-ethylaniline, 3-ethylaniline, 4-ethylaniline, 2-methoxyaniline, 3-methoxyaniline and 4-methoxyaniline. The purity of these compounds was confirmed by a non-aqueous titrimetric method. Stock solutions of Schiff's bases were prepared in dioxan purified by the method given in Ref. [11]. 2-Hydroxy-1-naphthaldehyde and all anilines were purchased from Merck. The water used was deionized water redistilled twice, once over alkaline $KMnO_4$ and then in an all-glass still, and was stored under nitrogen. Standard solutions of perchloric acid and sodium hydroxide were prepared as described elsewhere [1].

### 2.2. Procedure

The study was performed by potentiometric measurement of the hydrogen ion concentration at $25.0 \pm 0.1$°C and under a nitrogen atmosphere in water–dioxan mixtures containing 30, 40, 50, 60 and 70% dioxan (v/v). Ionic strengths of the media were maintained at 0.1 M using sodium perchlorate (Merck).

For each solvent mixture, the pH-ionmeter (Orion 940), fitted with a combined pH electrode (Ingold) containing a filling solution of 0.01 M NaCl–0.09 M $NaClO_4$ as calibrated in concentration units of the hydrogen ion as described previously, using a standard solution of sodium hydroxide as the titrant prepared in the corresponding solvent mixture [1]. The preparation of the test solutions for the potentiometric measurements and the procedure employed for the estimation of new protonation constants have been described in Ref. [1]. All test solutions were freshly prepared before taking the measurements. Computations were carried out with the software termed pKAS, which handles protonation constants with a high degree of efficiency [12,13].

## 3. Results and discussion

The stoichiometric protonation constants of Schiff's bases derived from 2-hydroxy-1-naphthaldehyde and substituted anilines in dioxan–water mixtures at 25°C are tabulated in Table 1.

The log $K_1$ values correspond to the protonation equilibrium of naphtholate O-ions and log $K_2$ to the imine nitrogen atom. These equilibria are $L^- + H^+ \leftrightarrow HL$ and $L + H^+ \leftrightarrow H_2L^+$, respectively. The magnitudes of the differences between log $K_1$ and log $K_2$ values for all Schiff's bases show that the protonation nitrogen atom and naphtholic hydrogen atom are completely dissociable in separate steps.

It is interesting to compare the protonation constants of 2-hydroxy-1-naphthalideneanilines with those of salicylideneanilines reported in our previous paper [1]. It is seen that both the log $K_1$ and the log $K_2$ values of naphthalideneanilines (NA) studied are lower than those of the corresponding salicylideanilines (SA) for each dioxan–water mixture. This result can be attributed to the fact that the electron densities of nitrogen atoms and $O^-$ ions in the case of naphthalideneanilines are smaller because of the higher electron withdrawing tendency of the naphthaline ring compared with the benzene ring. One can think that these values obtained for the protonation constants of the NA and SA can also be explained by comparing the conformational structures of these compounds. Both SA and NA can exist in two planar conformations, one of which has an intramolecular hydrogen bond. The hydrogen-

Table 1
The protonation constants of substituted 2-hydroxy-1-naphthalideneanilines at 25.0 ± 0.1°C for different dioxan–water mixtures (μ = 0.1 M $NaClO_4$) [a] and the Hammett constants (σ) [14]

| R | σ | 30% dioxan, $x = 0.08$ [b] | | | 40% dioxan, $x = 0.12$ [b] | | | 50% dioxan, $x = 0.17$ [b] | | | 60% dioxan, $x = 0.24$ [b] | | | 70% dioxan, $x = 0.33$ [b] | | |
|---|---|---|---|---|---|---|---|---|---|---|---|---|---|---|---|---|
| | | $\log K_1$ | $\log K_2$ | $\Delta \log k$ [c] | $\log K_1$ | $\log K_2$ | $\Delta \log k$ [c] | $\log K_1$ | $\log K_2$ | $\Delta \log k$ [c] | $\log K_1$ | $\log K_2$ | $\Delta \log k$ [c] | $\log K_1$ | $\log K_2$ | $\Delta \log k$ [c] |
| H | – | 8.24 | 4.05 | – | 8.45 | 3.88 | – | 8.60 | 3.72 | – | 8.78 | 3.54 | – | 9.40 | 3.42 | – |
| 2-$CH_3$ | – | 8.25 | 3.80 | – | 8.56 | 3.66 | – | 8.69 | 3.52 | – | 8.85 | 3.29 | – | 9.25 | 3.20 | – |
| 3-$CH_3$ | −0.07 | 8.29 | 4.10 | 0.05 | 8.49 | 3.96 | 0.08 | 8.66 | 5.81 | 0.09 | 8.84 | 3.68 | 0.14 | 9.37 | 3.55 | 0.13 |
| 4-$CH_3$ | −0.17 | 8.27 | 4.45 | 0.40 | 8.53 | 4.30 | 0.42 | 8.65 | 4.19 | 0.47 | 8.76 | 4.04 | 0.50 | 9.35 | 3.95 | 0.53 |
| 2-$C_2H_5$ | – | 8.32 | 3.75 | – | 8.48 | 3.58 | – | 8.57 | 3.45 | – | 8.73 | 3.25 | – | 9.27 | 3.15 | – |
| 3-$C_2H_5$ | −0.04 | 8.28 | 4.09 | 0.04 | 8.50 | 3.95 | 0.07 | 8.60 | 3.78 | 0.06 | 8.75 | 3.60 | 0.06 | 9.25 | 3.45 | 0.03 |
| 4-$C_2H_5$ | −0.15 | 8.25 | 4.45 | 0.40 | 8.51 | 4.27 | 0.39 | 8.58 | 4.13 | 0.41 | 8.72 | 4.00 | 0.46 | 9.38 | 3.88 | 0.46 |
| 2-$OCH_3$ | – | 8.18 | 4.00 | – | 8.43 | 3.85 | – | 8.63 | 3.65 | – | 8.75 | 3.53 | – | 9.30 | 3.38 | – |
| 3-$OCH_3$ | 0.12 | 8.26 | 3.78 | −0.27 | 8.41 | 3.62 | −0.26 | 8.52 | 3.50 | −0.22 | 8.80 | 3.43 | −0.11 | 9.30 | 3.30 | −0.12 |
| 4-$OCH_3$ | −0.27 | 8.27 | 4.50 | 0.45 | 8.50 | 4.40 | 0.52 | 8.65 | 4.30 | 0.58 | 8.86 | 4.20 | 0.66 | 9.32 | 4.10 | 0.68 |

[a] All errors are 0.05 or lower.
[b] $x$ = The mole fraction of dioxan.
[c] $\Delta \log k = \log K_2 - \log K_{2(\mathrm{Ref.})}$.

bonded conformation will be more probable for the NA due to the steric effect of the C8 atom and its attached hydrogen atom. Thus, in the case of NA, the electron density of the hydrogen acceptor imine nitrogen atom decreases and the observation of lower $\log K_2$ values for the NA derivatives compared with those of the corresponding SA derivatives can be explained in terms of their stereochemistry. However, when it comes to $\log K_1$ values, in NA, where an intramolecular hydrogen bonded structures formed by the protonation $O^-$ ion is more probable, one would have expected that the $\log K_1$ values should have been higher than those of SA, contrary to experimental findings. However, the fact that the differences between the $\log K_2$ values of naphthalideneanilines and the corresponding salicylideneanilines decrease with the increasing mole fraction of dioxan suggests that solute–solvent interactions as well as inductive effects are also of importance in the determination of the numerical values of the protonation constants of Schiff's bases.

The protonation constants given in Table 1 are considered in more detail in order to gain more information about the specific effects of the substituents and the effect of the solvent composition on the basicities of the Schiff's bases.

### 3.1. Substituent effect

The variation of the $\log K_2$ values of naphthalideneanilines shows that substitution on the aniline component influences the electron density at the imine nitrogen atom. When the basicities of alkyl derivatives with differing substitution patterns are compared, the order 2-R < reference < 3-R < 4-R (where R is $CH_3$ and $-C_2H_5$) is found in all solvent mixtures. This order can be used as an indication of the extent of the contributions of the alkyl groups to the basicity of the azomethine nitrogen atom. Furthermore, electronic and steric effects of the alkyl groups can also be inferred. Methyl and ethyl groups are capable of releasing electrons by a resonance mechanism and are best able to stabilize a positive center when positioned ortho or para to it. This effect is known as hyperconjugation [14]. If the hyperconjugation was only the effect on the basicity of the azomethine nitrogen atom, the 2-R derivatives would also be more basic than the reference. The fact that the reference is more basic than the 2-R derivatives indicates that the steric effect is dominant over the resonance effect in the case of ortho substitution. The 4-R derivative is more basic than the 3-R derivative. This is in agreement with the prediction that the *p*-alkyl group will contribute more to the electron density of the azomethine group than the *m*-alkyl group.

Considering the reported values of $\log K_2$ of the methyl- and ethylnaphthalideneanilines with the same pattern of substitution, it is observed that the value for each ethyl derivative is slightly smaller than those for the methyl analogs regardless of the medium. In addition, it is found that the orders obtained for the alkyl derivatives of naphthalideneanilines are similar to those of salicylideneanilines in all dioxan–water mixtures [1]. However, as regards the order of the basicities for the methoxy derivatives of naphthalideneanilines, we have found different orders from those obtained for the methoxy derivatives of salicylideneanilines in all the media investigated [1,2]

For naphthalideneanilines

$$3\text{-}OCH_3 < 2\text{-}OCH_3 \leq \text{Reference} < 4\text{-}OCH_3$$

For salicylideneanilines

$$3\text{-}OCH_3 < \text{Reference} < 2\text{-}OCH_3 < 4\text{-}OCH_3$$

The fact that the 2-methoxy derivatives of naphthalideneanilines, in contrast to salicylideneanilines, are slightly less basic than the reference reveals that the steric effect of the methoxy group is more pronounced in the case of the naphthalideneanilines compared to the salicylideneanilines.

In agreement with the observations obtained in our previous work on salicylideneanilines [1,2], any regularity between the $\log K_1$ values and the type and position of the substituents was also not found for naphthalideneanilines in the present study. This lack of regularity is further evidence supporting the lack of significance of electronic effects of the substituents located far from the reaction sites.

Although almost every kind of organic reaction has been treated via the Hammett equation or its extended form in various water–organic solvent mixtures [15–19], any study related to the protonation of Schiff's bases in dioxan–water mixtures is yet to appear in the literature. It is of interest to examine the question whether the Hammett equation can be used to predict the effect of substituents on the basicity of 2-hydroxy-1-naphthalideneaniline in dioxan–water mix-

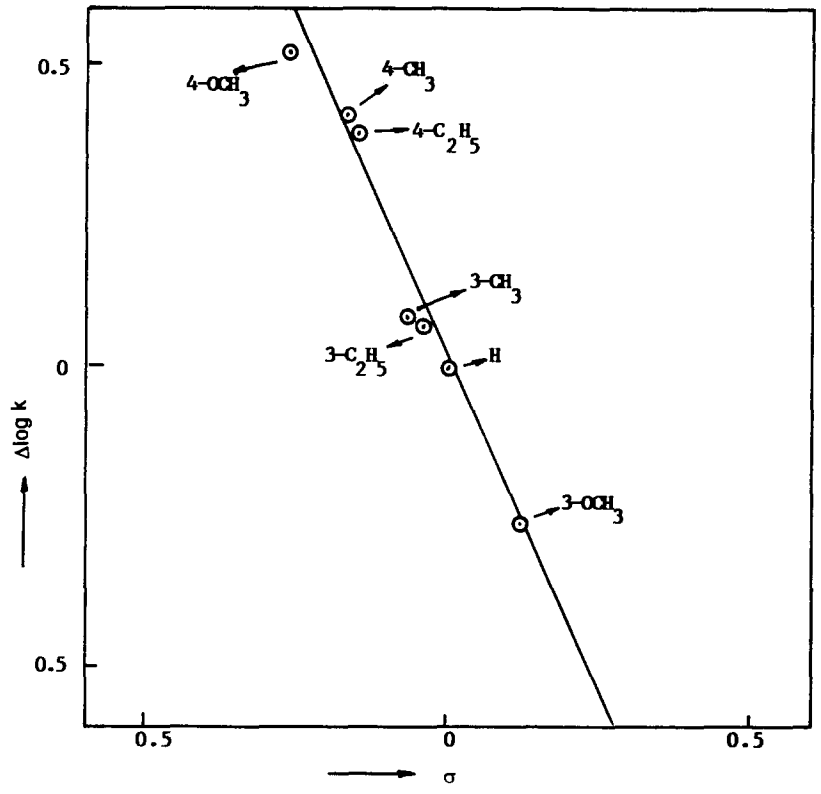


Fig. 1. Plot of $\Delta \log k$ of substituted 2-hydroxy-1-naphthalideneanilines against the Hammett substituent constants ($\sigma$) in 40% dioxan–60% water.

tures. The plots of the $\Delta \log k$ values, i.e. $\log K_2 - \log K_{2(\text{Ref.})}$ for the substituted naphthalideneanilines against the Hammett substituent constants ($\sigma$) are obtained for each dioxan–water mixture studied and the plot for 40% dioxan–60% water is given in Fig. 1 as an example. The equations of the best straight lines through the points are given in Table 2 together with their regression coefficients. From these results, it can be concluded that the Hammett equation, to a reasonable approximation, represents the effects of substituents on the protonation reaction of the imine nitrogen atoms 2-hydroxy-1-naphthalideneanilines in dioxan–water mixtures. Although one can claim that it may not be proper to make any conclusive remarks about the applicability of the Hammett equation, considering that the range of substituent types investigated in this study was not too large and all the substituents were electron donors in nature, a similar observation made in our previous study [2], in which the effect of seven electron donor and acceptor substituents upon salicylideneanilines having similar structures to naphthalideneanilines was investigated, supports our above conclusion regarding the applicability of the Hammett equation to naphthalideneanilines.

Table 2
Linear relationships between $\Delta \log k$ of 2-hydroxy-1-naphthalideneanilines and the Hammett constants ($\sigma$) in various dioxan–water mixtures at 25.0 ± 0.1°C

| Dioxan (%) | Equation | $r$ [a] | $s$ [b] |
|---|---|---|---|
| 30 | $\Delta \log k = -2.059\sigma - 0.021$ | −0.962 | 0.072 |
| 40 | $\Delta \log k = -2.154\sigma - 0.005$ | −0.981 | 0.051 |
| 50 | $\Delta \log k = -0.230\sigma + 0.056$ | −0.975 | 0.074 |
| 60 | $\Delta \log k = -2.184\sigma + 0.084$ | −0.964 | 0.080 |
| 70 | $\Delta \log k = -0.267\sigma + 0.066$ | −0.958 | 0.087 |

[a] Regression coefficient.
[b] Standard deviation of the regression line.

Furthermore, we attempted to examine the question whether the extended Hammett equation proposed by Hoefnagel and Webster [16] for use in water–organic solvent mixtures covers the experimental data better. We observed that this equation could no longer give any improvement for the substituted naphthalideneanilines in dioxan–water mixtures.

### 3.2. Solvent effect

The numerical $\log K_2$ values for ten naphthalideneanilines determined in dioxan–water

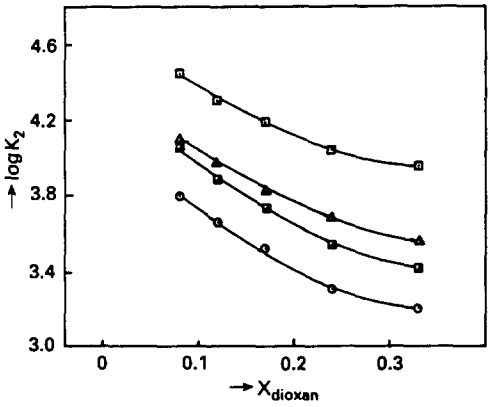


Fig. 2. Variations of $\log K_2$ values of methyl-substituted Schiff's bases with the mole fraction of dioxan ($x_{dioxan}$). ◪, Reference; ⊙, 2-$CH_3$; △, 3-$CH_3$; ⊡, 4-$CH_3$.

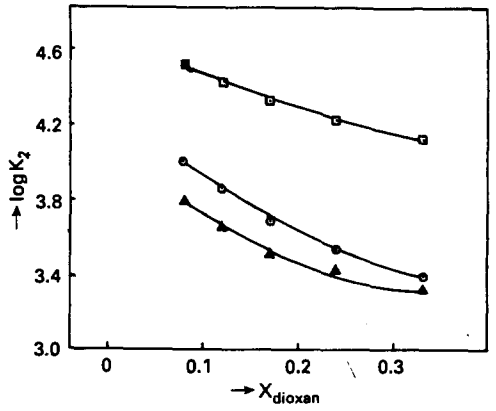


Fig. 4. Variations of $\log K_2$ values of methoxy-substituted Schiff's bases with the mole fraction of dioxan ($x_{dioxan}$). ⊙, 2-$OCH_3$; △, 3-$OCH_3$; ⊡, 4-$OCH_3$.

mixtures decrease with increasing dioxan content in the solvent mixture as shown in Figs. 2–4. For all Schiff's bases studied, it is observed that the relationships are linear over the range of dioxan mole fractions from 0.08 to 0.24. However, $\log K_2$ values at a mole fractionof dioxan of 0.33 are slightly higher than those expected from the linear trend. The linear equations and the related regression coefficients are listed in Table 3. This linear variation is very similar to that found for salicylideneanilines in the same media [1]. This observation is not surprising as the molecular species HL would be solvated better than the ionic species $H_2L^+$ in the solvent mixture rich in dioxan. The fact that an increase in $\log K_2$ values appeared at $x_{dioxan} = 0.33$ suggests that these values may pass through a minimum as the water content becomes low. Such deviations of linearity are characteristic of the dissociation of the charged acids in a number of mixed solvent media and can satisfactorily be explained by differences in solvent stabilization of the species $H^+$ and $H_2L^+$, resulting from the marked preference of the proton for water [20,21]. It may also be caused by ignoring the variation of the dielectric constant of the solvent molecules in the vicinity of an ion that can arise from preferential solvation of the solute by water or an organic component of the solvent mixture [14,22,23]. We have also observed similar behaviors for both salicylideneanilines and pyridines in aqueous ethanol [2,3]. It can thus be said that the nature of the solvent effects on the protonation of the imine nitrogen atoms of Schiff's bases is as expected from that of the uncharged bases in mixed solvent media.

When the variation of $\log K_1$ values of the phenolic moiety of Schiff's bases with solvent composition is examined, it is found that the

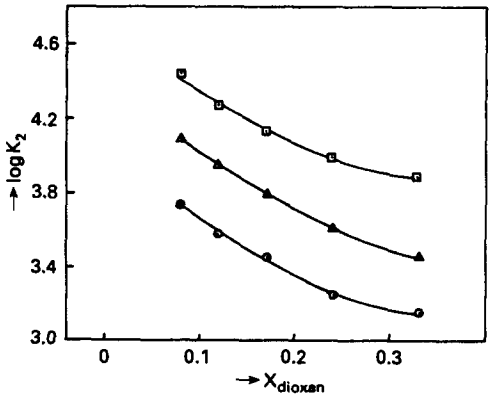


Fig. 3. Variations of $\log K_2$ values of ethyl-substituted Schiff's bases with the mole fraction of dioxan ($x_{dioxan}$). ⊙, 2-$C_2H_5$; △, 3-$C_2H_5$; ⊡, 4-$C_2H_5$.

Table 3
Linear relationships between the $\log K_2$ values of substituted 2-hydroxy-1-naphthalideneanilines and the mole fraction of dioxan (from 0.08 to 0.24)

| R | Equation | $r$ [a] | $s$ [b] |
|---|---|---|---|
| H | $\log K_2 = 4.277 - 3.144x$ | −0.994 | 0.025 |
| 2-$CH_3$ | $\log K_2 = 4.048 - 3.151x$ | −0.999 | 0.008 |
| 3-$CH_3$ | $\log K_2 = 4.298 - 2.657x$ | −0.991 | 0.028 |
| 4-$CH_3$ | $\log K_2 = 4.625 - 2.490x$ | −0.991 | 0.031 |
| 2-$C_2H_5$ | $\log K_2 = 3.972 - 3.046x$ | −0.995 | 0.093 |
| 3-$C_2H_5$ | $\log K_2 = 4.322 - 3.065x$ | −0.997 | 0.017 |
| 4-$C_2H_5$ | $\log K_2 = 4.630 - 2.741x$ | −0.980 | 0.038 |
| 2-$OCH_3$ | $\log K_2 = 4.210 - 2.968x$ | −0.981 | 0.040 |
| 3-$OCH_3$ | $\log K_2 = 3.906 - 2.124x$ | −0.956 | 0.045 |
| 4-$OCH_3$ | $\log K_2 = 4.633 - 1.856x$ | −0.992 | 0.016 |

[a] Regression coefficient.
[b] Standard deviation of the regression line.

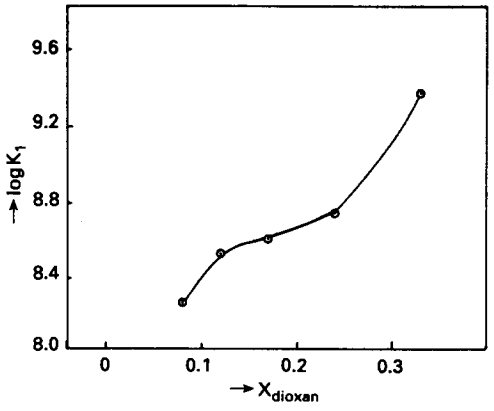


Fig. 5. Variations of $\log K_1$ values of 2-hydroxy-1-naphthalidene-4-ethylaniline with the mole fraction of dioxan ($x_{dioxan}$).

general trends of the curves obtained are qualitatively similar. All the curves increase as the mole fraction of dioxan increases up to 0.24, above which they rise rapidly, as seen in the example given in Fig. 5 for 2-hydroxy-1-naphthalidene-4-ethylaniline. In an attempt to assess more clearly the electrostatic contributions to the solvent effect on protonation, $\log K_1$ values are plotted as a function of the reciprocal of the dielectric constants ($1/\varepsilon$) of the mixed solvent. Fig. 6 shows such a plot. It is evident that a straight line is not obtained, as would be expected if the simple Born's model were an adequate representation of solvent effects on the protonation constants of uncharged acids such as phenols [21,24,25]. This observation may be explained by the existence of a non-electrostatic contribution to the variation in $\log K_1$ with increasing dioxan content which is a result of selective interactions between the molecular or anionic form of the Schiff's base and the preferred species of solvent molecules. In the related equilibrium, the HL species

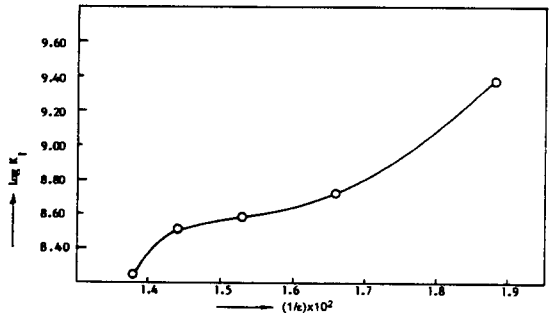


Fig. 6. Variations of $\log K_1$ values of 2-hydroxy-1-naphthalidene-4-ethylaniline the reciprocal of dielectric constants ($1/\varepsilon$) of dioxan–water mixtures.

would be solvated better than the $L^-$ species in solvents containing a higher concentration of dioxan, whereas the opposite would be true for a solvent rich in water, and thus the $\log K_1$ values would be expected to increase as observed with increase of dioxan concentration. The steep increase of the $\log K_1$ values at $x_{dioxan} = 0.33$ may be connected at least partially with a change in the effective dielectrc constant in the cibotactic region [14]. Thus, our results for Schiff's bases in the present and previous work [1,2] support the hypothesis that solute–solvent interactions of a non-electrostatic nature play an important role in controlling acid–base processes in the mixed solvents.

## Acknowledgment

We gratefully acknowledge the financial support of Gazi University Research Fund (project no. GEF. 04/93-2).

## References

[1] T. Gündüz, E. Kiliç, F. Köseoğlu and E. Canel, Anal. Chim. Acta, 282 (1993) 489.
[2] F. Köseoğlu, E. Kiliç, E. Canel and N. Yilmaz, Anal. Chim. Acta, 293 (1994) 87.
[3] E. Kiliç, F. Köseoğlu and Ö. Başgut, Anal. Chim. Acta, 294 (1994) 215.
[4] M.S. Mayadeo, A.P. Rao and M.B. Kabadi, J. Indian Chem. Soc., 53 (1976) 1071.
[5] M.S. Mayadeo and S.H. Hussain, J. Indian Chem. Soc., 56 (1979) 143.
[6] M.S. Mayadeo and A.M. Chaubal, J. Indian Chem. Soc., 56 (1979) 922.
[7] M.S. Mayadeo and A.M. Chaubal, J. Indian Chem. Soc., 56 (1979) 142.
[8] M.S. Mayadeo and S.S. Purohit, J. Indian Chem. Soc., 57 (1980) 265.
[9] M.S. Mayadeo and V.P. Dhakappa, J. Indian Chem. Soc., 57 (1980) 580.
[10] M.S. Mayadeo and S. Bhattacharjee, J. Indian Chem. Soc., 60 (1983) 606.
[11] D.D. Perrin and W.L.F. Armarego, Purification of Laboratory Chemicals, Pergamon, 1992.
[12] A.E. Martell and R.J. Motekaitis, The Determination and Use of Stability Constants, VCH, 1988.
[13] R.J. Motekaitis and A.E. Martell, Can. J. Chem., 60 (1982) 168.
[14] N.S. Isaacs, Physical Organic Chemistry, Longman Scientific and Technical, New York, 1986.
[15] C. Hansch, A. Leo and R.W. Taft, Chem. Rev., 91 (1991) 165.
[16] A.J. Hoefnagel and B.M. Webster, J. Chem. Soc. Perkin Trans 2, (1989) 977.
[17] M. Charton, J. Org. Chem., 30 (1965) 3341.

[18] H.H. Jaffe, Chem. Rev., 53 (1953) 191.
[19] A.J. Hoefnagel, M.A. Hoefnagel and B.M. Webster, J. Org. Chem., 43 (1978) 4720.
[20] R.G. Bates, J. Electroanal. Chem., 29 (1971) 1.
[21] R.G. Bates, Determination of pH, Theory and Practice, 2nd edn., John Wiley, New York, 1973.
[22] M. Paobo, R.G. Bates and R.A. Robinson, J. Phys. Chem., 70 (1966) 247.
[23] J. Juillard and N. Simonet, Bull. Soc. Chim. Fr., (1968) 1883.
[24] G.H. Parsons and C.H. Rochester, J. Chem. Soc. Faraday 1, 71 (1975) 1058.
[25] K.S. Siow and K.P. Ang, J. Solution Chem., 18 (1989) 937.

ELSEVIER

Talanta 42 (1995) 1883–1890

Talanta

# Inorganic tin(II) determination by FIA with amperometric detection of its oxinate complex

K. Boutakhrit, Z.P. Yang, J.-M. Kauffmann *

*Institute of Pharmacy, Free University of Brussels, Campus Plaine CP 205/6, 1050 Brussels, Belgium*

Received 6 March 1995; revised 18 May 1995; accepted 19 May 1995

**Abstract**

A highly selective, rapid and direct amperometric method, based on the formation of a complex between tin(II) and 8-hydroxyquinoline (oxine), has been developed for the determination of trace levels of tin(II) using flow injection analysis. Tin(II) electro-oxidation was catalyzed by oxine; its oxidation peak occurred at +0.05 V vs. Ag/AgCl at a glassy carbon electrode in 0.1 mol $l^{-1}$ acetate buffer (pH 6). A linear relationship was obtained between the peak current and the tin(II) concentration in the range 0.25–20 μmol $l^{-1}$. The detection limit was 0.1 μmol $l^{-1}$ and the relative standard deviation calculated by the injection of a 10 μmol $l^{-1}$ tin(II) solution was 5% ($n = 20$). Optimization of several experimental parameters has been carried out and the influence of numerous cations and possible interfering molecules encountered in radiopharmaceuticals and in dental gels has been investigated. The method was applied to the determination of tin(II) in dental gels.

*Keywords:* Amperometric detection; Dental gel; Flow injection analysis; 8-Hydroxyquinoline; Tin(II) determination

## 1. Introduction

Tin occurs in trace amounts in most foods and in larger amounts in canned foods [1]. A rapid, selective and quantitative assay for inorganic tin(II) used as a reducing agent for radioactive $^{99m}$Tc(VII) would be very desirable in the quality assurance control of radiopharmaceutical "kits". Tin (II) fluoride is used in gel formulations for the treatment of dental surfaces. However, on standing, tin(II) is oxidized and the gel loses its activity. Actually, the determination of tin(II) in the presence of tin(IV) is of considerable interest.

Many techniques have been described for the determination of total tin after conversion to tin(II) or tin(IV), such as atomic absorption spectrometry [2–6], fluorimetry [7], spectrophotometry [8–14], polarography [15–19] and anodic stripping voltammetry [20–25]. Tin, when present in appreciable amounts, can be determined by gravimetry or oxidative volumetry with potentiometric detection [26–29] or by complexometry [27]. Few methods allow the determination of tin(II) in the presence of tin(IV); they are generally complex, insensitive, and time-consuming. Tin(II) is the least favourable cation for analytical investigations; it is not only readily oxidized by air [30] ($E_0$(Sn(II)/Sn(IV) ≈ +0.15 V vs. NHE), but it also precipitates and forms basic oxides above pH 2 [31].

The compound 8-Hydroxyquinoline (oxine; 8-quinolinol) is a well-characterized reagent

* Corresponding author.


*SSDI* 0039-9140(95)01650-3

that reacts with more than 60 metal ions to form complexes whose aqueous phase formation constants range from about $10^4$ ($Ba^{2+}$) to $10^{38}$ ($Fe^{3+}$) [32]. It is a useful reagent for the extraction, separation and spectrophotometric detection of metal ions [33]. Oxine (HOx) has been extensively applied to the polarographic [34–37] and adsorptive stripping voltammetric [38–41] determination of trace metals using mercury electrodes. The latter, however, are quite unstable under hydrodynamic conditions. Recently, Cai and Khoo [42] determined aluminium(III) at trace levels in water samples by differential pulse adsorptive stripping voltammetry based on the oxidation of the aluminium(III)–HOx complex at a glassy carbon electrode at +0.88 V vs. $Ag/Ag^+$. The complexation kinetics were fast; however, numerous other metals interfere since they show, once complexed by oxine, an oxidation peak close to the aluminium(III)–oxine oxidation peak [42]. In a project devoted to tin(II) analysis, we discovered that the oxidation of tin(II) at solid electrodes was catalyzed thanks to its complexation by oxine and occurred at a potential close to +0 V vs. $Ag/Ag^+$ [43]. In the present work, flow injection analysis (FIA) with amperometric detection was used for the rapid and selective determination of tin(II). A study of the possible interferences present in radiopharmaceutical kits and its application to tin(II) analysis in a dental gel formulation is illustrated.

## 2. Experimental

### 2.1. Apparatus

Voltammetric measurements were made with a BAS CV 27 electrochemical analyzer and a three-electrode cell coupled to a HP 7090A recorder. A 3 mm diameter glassy carbon electrode (BAS), a platinum wire and an Ag/AgCl (3 M NaCl) electrode (BAS), served as working, auxiliary and reference electrodes, respectively. The other working electrodes used were a dual carbon paste electrode (BAS; diameter, 3 mm) prepared from standard paste (Metrohm Ea 207c) and a carbon paste electrode bulk modified by 8-hydroxyquinoline (5% (m/m)). The flow system consisted of a pump (Hiload™ pump P-50) used to deliver the carrier, and a rotary valve with a 20 µl loop for sample injection. The reaction coil was 50 cm × 0.02 cm i.d. Peek tubing connected to a thin-layer electrochemical cell (BAS; LC-CC5 dual glassy carbon working electrode 2 × 3 mm in diameter). The electrode potential was adjusted by means of a potentiostat (BAS; LC-4B). Amperometric currents were recorded using a $Y-t$ recorder (Kipp & Zonen, type BD 41). The pH measurements were made with a Tacussel Mini 80 pH meter.

### 2.2. Reagents

All chemicals were of analytical grade. Tin(II) chloride dihydrate was from Merck. Oxine (HOx), 8-hydroxyquinoline-5-sulfonic acid hydrate, 8-hydroxyquinoline-7-iodo-5-sulfonic acid, and 8-hydroxyquinoline-*N*-oxide were obtained from Aldrich. Methylene diphosphonic acid (medronic acid), (α, D)-glucoheptonic acid and gentisic acid were from Sigma, pentetic acid (Schuchardt München), dimercaptosuccinic acid (DMSA) and 4-aminobenzoic acid were from Aldrich. A standard solution of tin(II), prepared in nitrogen-deaerated HCl, was titrated iodometrically [44,45]. A fresh solution (0.01 mol $l^{-1}$) was prepared daily and kept in the dark before use. Tin(IV) and other metal ion solutions were prepared by dissolution of the corresponding salts in 0.1 mol $l^{-1}$ HCl. A stock solution (0.01 mol $l^{-1}$) of oxine was prepared in methanol and protected from light by storage in a dark glass bottle. A 0.1 mol $l^{-1}$ acetate buffer (pH 6) served as the carrier and for solution dilution. It was prepared by sodium acetate trihydrate dissolution in demineralized double-distilled water and the pH was adjusted to 6 with 0.1 mol $l^{-1}$ HCl solution.

### 2.3. Analytical procedure

The amperometric signal was obtained by holding the electrode at +0.15 V vs. Ag/AgCl. The carrier flow rate was 1 ml $min^{-1}$. Several media were tested for the tin(II) stock solution preparation, namely acetonitrile [46], DMSO [47], DMF [48], glycerol and polyalcohols [48–50], but better repeatability of the tin(II)–oxine response was obtained using 1 mol $l^{-1}$ HCl. The tin(II)–oxine complex was prepared by adding aliquots (less than 100 µl) of the deaerated tin(II) stock solution to 10 ml of 0.1 mol $l^{-1}$ acetate buffer (pH 6) containing 0.25 mmol $l^{-1}$ oxine (the latter was the blank). After standing for 1 min, the tin(II)–oxine solution was injected into the FIA system. It

should be mentioned that the pH of the injected solution was lower than the carrier pH, at worst by approximately 0.3 pH units. The blank response was low, and its magnitude, i.e. 2 nA, was subtracted from the tin(II)–oxine response. The tin(II)–oxine solutions were prepared just before injection. Before each set of experiments (i.e. daily), the glassy carbon working electrode (GCE) was polished with 0.01 μm alumina slurry on a polishing cloth (BAS).

## 3. Results and discussion

### 3.1. Linear scan voltammetry

A linear scan voltammogram (LSV) of 0.1 mmol $l^{-1}$ tin(II) (Fig. 1, curve a) in 0.1 mol $l^{-1}$ acetate buffer (pH 6) showed an oxidation process starting at +0.15 V and spread over a large potential range (from +0.15 to +0.6 V). The broad shape of the curve was not very useful from an analytical point of view (in terms of sensitivity and selectivity). The linear scan voltammogram of 0.2 mmol $l^{-1}$ oxine in 0.1 mol $l^{-1}$ acetate buffer (pH 6) showed one well-defined oxidation peak (P1) at +0.58 V (Fig. 1, curve b). On the addition of tin(II) (0.05 mmol $l^{-1}$), P1 decreased and two new oxidation peaks appeared, one (P2) located at a less positive potential (+0.05 V) and the other (P3) at a more positive potential than P1 (+1.13 V) as shown in Fig. 1, curve c. Subsequent additions of tin(II) lead to an increase in the peaks P2 and P3 and a decrease in peak P1. On the addition of tin(IV), P1 decreased and the oxidation peak P3 increased (not shown). As reported previously [43], peak P2 corresponded to the oxidation of tin(II) catalyzed by oxine and P3 corresponded to the oxidation of the oxinate complexed to tin(IV). At this point in the work, it is interesting to note that an electrode held at +0.15 V will not sense oxine or tin(II), but will sense the tin(II)–oxine complex.

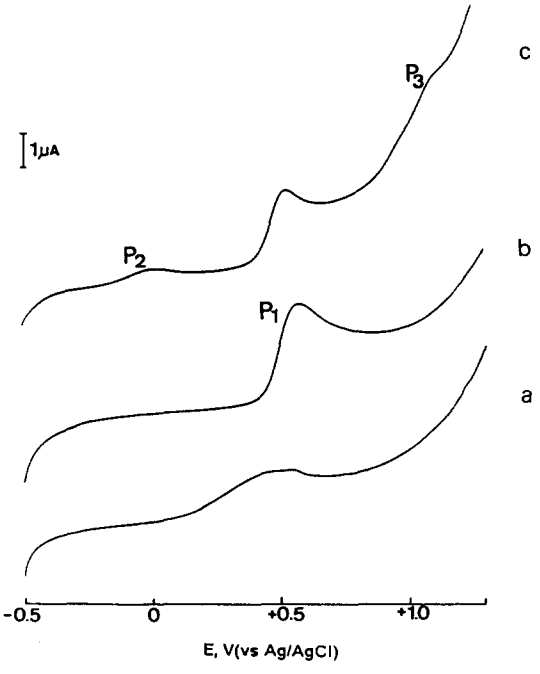


Fig. 1. Linear-scan voltammograms at the glassy carbon electrode in 0.1 mol $l^{-1}$ acetate buffer (pH 6). (Curve a) buffer + 0.1 mmol $l^{-1}$ tin(II); (curve b) buffer + 0.2 mmol $l^{-1}$ HOx, P1 is at +0.58 V; (curve c) buffer + 0.2 mmol $l^{-1}$ HOx + 25 μmol $l^{-1}$ tin(II), P2 is at +0.05 V, P3 is at +1.13 V. (Scan rate, 20 mV $s^{-1}$.)

Several molecules structurally related to oxine have also been investigated as possible complexing agents for tin(II) catalytic oxidation (see experimental section), but oxine was found to give the best signal in terms of peak shape and ease of oxidation [43].

### 3.2. Optimization of Sn(II)–HOx formation

*Effect of HOx concentration*

The intensity of the tin(II)–HOx peak (P2) was measured by LSV in acetate buffer (pH 6) as a function of the HOx concentration in the presence of 50 μmol $l^{-1}$ tin(II) (Fig. 2). The peak height increased linearly on raising the HOx concentration from 20 to 50 μmol $l^{-1}$ (slope 1) and from 50 to 80 μmol $l^{-1}$ (slope 2); it remained constant beyond 80 μmol $l^{-1}$ oxine (i.e. the complete complexation of tin(II)–HOx was attained). From the structure of the isolated and spectroscopically characterized (NMR, Mössbauer, IR) tin(II)–oxine, and in accordance with the UV-vis spectroscopic data [51], our results suggested that complexes with stoichiometries of 1:1 tin(II)/HOx (slope 1) and 1:2 tin(II)/HOx (slope 2) were formed, respectively.

*Influence of pH*

The solution pH may influence the distribution both of tin(II) [31] and of the HOx species ($pKa_1 = 4.9$; $pKa_2 = 9.8$) [52]. In the pH range 5–9, HOx existed mainly in its neutral form. At pH values above 8.8 and below 5.9, HOx was converted to the phenolate $C_9H_6NO^-$ ion

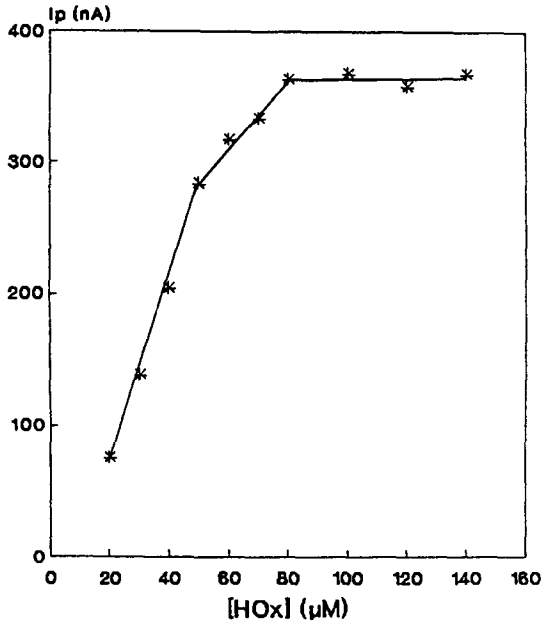


Fig. 2. Peak current (LSV) of tin(II)–HOx as a function of the HOx concentration. ($C_{Sn(II)} = 50$ μmol $l^{-1}$; 0.1 mol $l^{-1}$ acetate buffer (pH 6).)

and the oxinium $C_9H_6N^+OH$ cation, respectively. The peak height of the tin(II)–HOx complex, studied by LSV, was constant in the pH range 5–7, whereas at lower or higher pH values it diminished (Fig. 3). This indicated that the complexation was complete in the pH

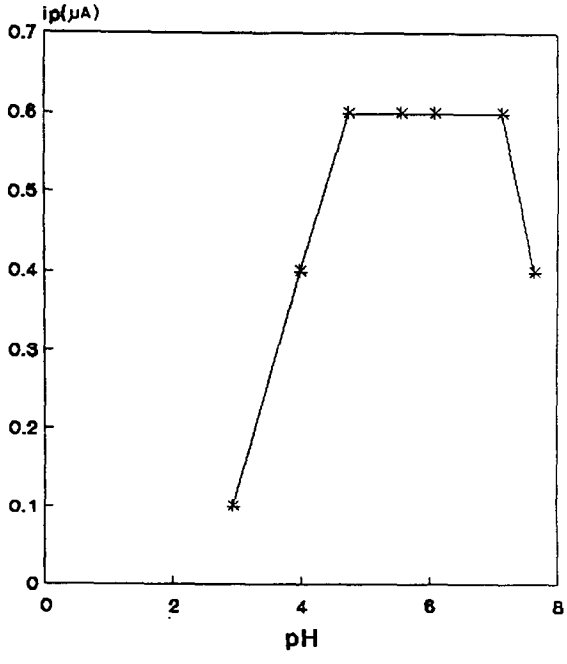


Fig. 3. Peak current (LSV) of tin(II)–HOx as a function of pH (acetate adjusted with HCl or NaOH). ($C_{Sn(II)} = 50$ μmol $l^{-1}$; $C_{HOx} = 0.1$ mmol $l^{-1}$. Scan rate, 20 mV $s^{-1}$.)

range 5–7 i.e. where oxine existed in its neutral form. Below pH 5, the protonation of oxine inhibited tin(II)–HOx formation and above pH 7, formation of the complex $Sn(OH)_3^-$ may occur [31,51]. We note also that the tin(II)–HOx peak (P2) shifted to less positive values by raising the pH from 2 to 5 and it became pH independent in the range 5–8. Several electrolytes have been tested, namely NaOAc–HCl, $NH_4OAc$, $NH_4Cl$–$NH_3$, $NaH_2PO_4$–$Na_2HPO_4$ and $H_4Cit$–$Na_3HCit$ (all at a concentration of 0.1 mol $l^{-1}$ and at pH 6). The oxidation peak shape (intensity and potential) of the tin(II)–HOx complex was found to differ significantly depending on the electrolyte used. In phosphate buffer, a 40% peak decrease was observed compared with the peak obtained in acetate buffer, a phenomenon likely to be due to competition between phosphate and oxine for tin(II) complexation. In subsequent work, a pH 6 NaOAc–HCl buffer was selected because of a better peak sensitivity and buffering capacity (acetate is also a weak competitor for tin(II) complexation).

### 3.3. Flow injection analysis of tin(II)

*Stability of the tin(II)–HOx complex*

Solutions of tin(II) (10 μmol $l^{-1}$) in the presence of 0.2 mmol $l^{-1}$ oxine at pH 6 were injected into the FIA set-up, the electrode being held at +0.15 V (see experimental section). Experiments were performed in the presence and in the absence of dissolved oxygen in the sample and the carrier. The FIA response was reproducible for the first 10 min following the preparation of the complex, then a gradual current decrease was observed with a loss of 25% of the peak height after 20 min of standing. Since no significant difference was observed in the presence or absence of dissolved oxygen, the decline in the response may most likely be attributed to the poor solubility of the metal–oxinate complex (between 1 nmol $l^{-1}$ and 1 μmol $l^{-1}$) [53]. From these results we may infer that the linear scan voltammetric determination of tin(II)–oxine, using the standard additions method, would be inappropriate due to the length of the procedure. With use of FIA, the total analysis time was reduced to 3 min per sample.

*Choice of the working electrode*

In LSV, the GCE needed resurfacing by manual polishing after each scan in order to

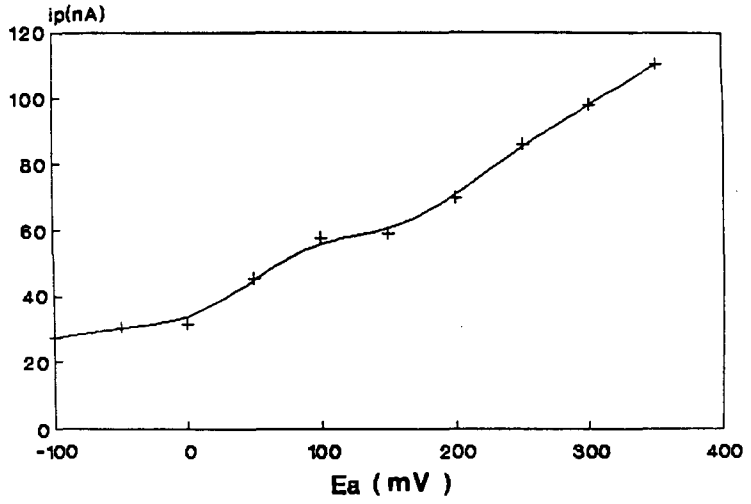


Fig. 4. Hydrodynamic voltammogram of 50 μmol $l^{-1}$ tin(II) (carrier, 0.1 mol $l^{-1}$ acetate buffer (pH 6); flow rate, 1 ml $min^{-1}$).

remove adsorbed products due to tin(II)–HOx oxidation. In FIA, the electrode was renewed daily since fouling was minimized due to reduced contact time and thanks to the washing out effect exerted by the carrier flow. A comparative study of several working electrodes has been carried out. The slope of the calibration graph obtained in FIA at the GCE was seven and three times higher than at the carbon paste electrode (CPE) and oxine-modified CPE, respectively.

*Effect of the applied potential and flow rate*

As reported in Fig. 4, the hydrodynamic voltammogram (HDV) of the tin(II)–HOx complex (10 μmol $l^{-1}$) at the GCE showed an almost sigmoidal curve, indicating a diffusion-controlled process. In order to achieve good signal stability and sensitivity, an applied potential of +0.15 V was selected. The FIA response of the injected tin(II)–HOx complex (10 μmol $l^{-1}$) increased linearly upon raising the flow rate to 0.7 ml $min^{-1}$; it remained constant beyond this value. A flow rate of 1 ml $min^{-1}$ was selected for further studies.

*Analytical characteristics*

Actually, the FIA experiments may be performed as described above (see experimental section) or by using a carrier containing the complexing agent, provided that the complexation is fast. The latter procedure consisted of using a 0.1 mol $l^{-1}$ acetate buffer carrier at pH 6 containing oxine (0.25 mmol $l^{-1}$) and injecting the tin(II) sample just after its preparation in the acetate buffer. Both procedures have been shown to be suitable for tin(II) determination, with no significant differences in terms of sensitivity. A linear relationship was observed between the amperometric signal and tin(II) concentrations between 0.25 and 20 μmol $l^{-1}$; $Ip$ (nA) = 10.1 × [$Sn^{2+}$] (μmol $l^{-1}$) + 2.98 ($r$ = 0.998). Typical FIA responses as a function of tin(II) concentration are shown in Fig. 5. The repeatability was studied by serial injections of a 10 μmol $l^{-1}$ tin(II)–HOx solution and the relative standard deviation was 5% ($n$ = 20). The detection limit (three times the standard deviation of the blank) was 0.1 μmol $l^{-1}$ by FIA and 10 μmol $l^{-1}$ (signal-to-noise ratio, 3) by LSV.

*Interferences*

In the amperometric tin(II)–HOx determina-

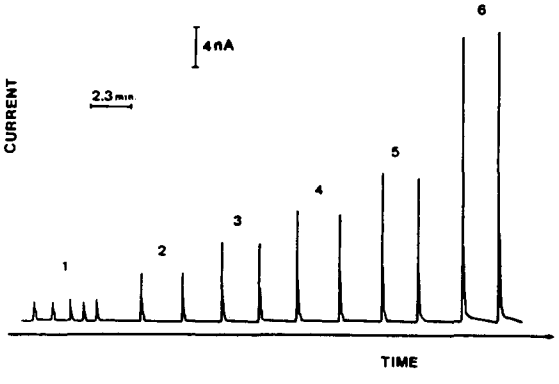


Fig. 5. Calibration peak signals for tin(II) determination by FIA. ($E_a$ = +0.15 V; flow rate, 1 ml $min^{-1}$; tin(II) concentration: peaks 1, blank (buffer + 0.2 mmol $l^{-1}$ HOx); peaks 2, 0.25 μM; peaks 3, 0.5 μM; peaks 4, 0.75 μM; peaks 5, 1 μM; peaks 6, 2 μM.

Table 1
Oxidation peak potential of metal–HOx complexes at the glassy carbon electrode [a]

| Metal ion | P2 | P3 (V vs. $Ag/Ag^+$) |
|---|---|---|
| Al(III) | | 0.94 |
| Ca(II) | | – |
| Cd(II) | | – |
| Co(II) | | 0.86 |
| Cr(III) | | – |
| Cu(II) | | 0.84 |
| Fe(II) | | 0.89 |
| Fe(III) | | 0.89 |
| Mg(II) | | – |
| Mn(II) | | 1.10 |
| Ni(II) | | 0.83 |
| Pb(II) | | – |
| Sn(IV) | | 1.13 |
| Sn(II) | 0.05 | 1.13 |
| Zn(II) | | – |

[a] In 0.1 mol $l^{-1}$ acetate buffer (pH 6; $C_{HOx} = 50$ μmol $l^{-1}$; $C_{Metal} = 10$ μmol $l^{-1}$.

tion, provided that there was an excess of oxine, the cations investigated did not interfere at the applied potential because, once complexed by oxine, they showed no response (Ca, Cd, Cr, Mg, Pb, Zn) or an oxidation peak P3 at a high positive potential (Al, Co, Cu, Fe, Mn, Ni, Sn(IV)) (Table 1) [41]. The influence of different molecules which may be present in radiopharmaceutical kits along with tin(II) has been studied. As shown in Table 2, except for DMSA and ascorbic acid (AA), the molecules were not electroactive at +0.15 V. The effect of these molecules on the tin(II)–HOx peak is also shown in Table 2. It appeared that in addition to AA and DMSA interference, radiopharmaceutical kits containing molecules which form strong complexes with tin(II), such as medronic acid, 4-aminobenzoic acid and pentetic acid gave rise to a decrease in the tin(II)–HOx peak. The interference of AA, however, could be avoided by injecting the sample in the absence (AA response) and in the presence of oxine (AA + tin(II)–HOx response) and subtracting the signals.

*Application*

The method was applied to the determination of tin(II) by analyzing two lots of dental gel formulation (gel composition: sorbitol, water, hydrated silica, PEG-32, sodium lauryl sulfate, xanthum gum, stannous pyrophosphate, flavour, titanium dioxide, zinc citrate, sodium fluoride, sodium saccharin). The sample was dissolved in 1 mol $l^{-1}$ deaerated HCl and sonicated for 5 min. Samples were clarified by standing and the supernatant was injected after passage through a 0.45 μm filter. Two samples have been analyzed (5 assays per sample, 5 injections per assay). The tin(II) results were obtained by reference to the calibration curve and were in good agreement with results obtained by iodatometry [44,45] (Table 3). The calculated $t$ and $F$ values did not exceed the theoretical values (Table 4). From the obtained data, it

Table 2
Electroactivity and effect of interferents on tin(II)–HOx oxidation, in FIA [a]

| Interferent | Concentration (mol $l^{-1}$) | Electroactivity [b] | Tin(II)–HOx peak [c] | Peak change (%) |
|---|---|---|---|---|
| Inositol | $10^{-2}$ | – | – | 0 |
| Sodium chloride | $10^{-3}$ | – | – | 0 |
| Dimercaptosuccinic acid | $10^{-4}$ | + | + | +17 |
| Sodium tartrate | $10^{-2}$ | – | – | 0 |
| Pentetic acid | $10^{-2}$ | – | + | −49 |
| Albumin | 0.025% (m/v) | – | – | 0 |
| Ascorbic acid | $10^{-4}$ | + | + | +34 |
| Lactose | $10^{-2}$ | – | – | 0 |
| Succinic acid | $10^{-2}$ | – | – | 0 |
| Gentisic acid | $10^{-4}$ | – | – | 0 |
| Sodium (α, D)-glucoheptonate | $10^{-4}$ | – | – | 0 |
| Medronic acid | $10^{-4}$ | – | + | −56 |
| 4-Aminobenzoic acid | $10^{-4}$ | – | + | −17 |
| Sodium laurylsulfate | $10^{-4}$ | – | – | 0 |

[a] $E_a = +0.15$ V; flow rate, 1 ml $min^{-1}$.
[b] –, No electroactivity.
[c] –, No effect.

Table 3
Determination of tin(II) and total tin in dental gel ($n = 5$)

| Sample | Volumetric methods | | Proposed method (amperometry) |
|---|---|---|---|
| | Tin(II) [a] (%) | Total tin [b] (%) | Tin(II) (%) |
| I | $0.19 \pm 0.01$ | $0.77 \pm 0.01$ | $0.18 \pm 0.01$ |
| II | $0.11 \pm 0.01$ | $0.75 \pm 0.03$ | $0.10 \pm 0.01$ |

[a] Determined by iodatometry.
[b] Determined by complexometry [27,54] and corrected from the Zn content (0.12% by ICP–AES).

Table 4
Statistical data concerning the results in Table 3

| Analyte | $t_{calculated}$ | $t_{theoretical}$ | $F_{calculated}$ | $F_{theoretical}$ |
|---|---|---|---|---|
| Tin(II) | 1.414 | 2.776 | 1 | 6.39 |
| Total tin | 0.16 | 2.90 | 196 | 225 |

appeared that the gels have a quite low tin(II) content with respect to total tin and that the tin(II) content was lower in the aged sample II.

## Acknowledgements

Thanks are expressed to Bioanalytical Systems, Inc., (BAS-USA) for providing instrumentation support. Thanks are also expressed to O. Dufour for ICP-AES analysis of zinc.

## References

[1] G. Weber, Fresenius Z. Anal. Chem., 321 (1985) 217.
[2] K.C. Thompson and D.R. Thomerson, Analyst, 99 (1974) 595.
[3] R. Pinel, I.G. Gandjar, M.Z. Benabdallah, A. Astruc and M. Astruc, Analusis, 12 (1984) 404.
[4] R.V.C. Peddy, G. Kalpana and V. Koshy, Analyst, 117 (1992) 27.
[5] Z. Fang and L. Sun, Talanta, 39 (1992) 383.
[6] B. Welz, M. Schubert-Jacobs and T. Guo, Talanta, 39 (1992) 1097.
[7] S. Rubio, A. Gomez-Hens and M. Valcarcel, Analyst, 110 (1985) 43.
[8] D.-J. Wang, Z.-H. Xie, Q.-L. Wu, Y.-J. Song and S.-Y. Jin, Analyst, 116 (1991) 1189.
[9] M. Omar and H.J.M. Bowen, Analyst, 107 (1982) 654.
[10] V.H. Kulkarni and M.L. Good, Anal. Chem., 50 (1978) 973.
[11] R. Pyare and P. Nath, Analyst, 110 (1985) 1321.
[12] S. Bajic and B. Jaselskis, Analyst, 116 (1991) 1059.
[13] Y.K. Agrawal and V.J. Bhatt, Analyst, 110 (1985) 1325.
[14] L.F. Capitán-Vallvey, M.C. Valencia and G. Mirón, Anal. Chim. Acta, 289 (1994) 365.
[15] G. Weber, Anal. Chim. Acta, 186 (1986) 49.
[16] S.K. Bhowal and F. Umland, Z. Anal. Chem., 285 (1977) 226.
[17] M.D. McBride, R. George, W. Kessler and S. Shaw, J. Pharm. Sci., 66 (1977) 870.
[18] J. Guiñón and J. García-Antón, Anal. Chim. Acta, 177 (1985) 225.
[19] G. Somer and A. Arslantas, Analyst, 119 (1994) 1257.
[20] P. Debacker, J.L. Vandenbalck, G.J. Patriarche and G.D. Christian, Microchem. J., 26 (1981) 192.
[21] T.V. Nghi and F. Vydra, J. Electroanal. Chem., 71 (1976) 333.
[22] E. Desimoni, F. Palmisano and L. Sabbatini, Anal. Chem., 52 (1980) 1889.
[23] S. Dogan, G. Nembrini and W. Haerdi, Anal. Chim. Acta, 130 (1981) 385.
[24] P. Kiekens, H. Verplaetse, L. De Cock and E. Temmerman, Analyst, 106 (1981) 305.
[25] J. Wang, P. Tuzhi, R. Li and J. Zadeii, Anal. Lett., 22 (1989) 719.
[26] W. Malik and M. Ajmal, J. Electronanal. Chem., 6 (1963) 450.
[27] M.A. Marcilio de Almeida and C.P. Gonaçalves Da Silva, J. Radioanal. Nucl. Chem., 176 (1993) 225.
[28] S.N. Muddukrishna, A. Chen, T.R. Sykes and A.A. Noujaim, Appl. Radiat. Isot., 45 (1994) 293.
[29] L.R. Chervu, B. Vallabhajosyula, J. Mani, S.B. Chung and M.D. Blaufox, Eur. J. Nucl. Med., 7 (1982) 291.
[30] S. Glodowski and Z. Kublik, Anal. Chim. Acta, 130 (1981) 133.
[31] M. Pettine, F. Millero and G. Macchi, Anal. Chem., 53 (1981) 1039.
[32] R.E. Sturgeon, S.S. Berman, S.N. Willie and J.A.H. Desaulniers, Anal. Chem., 53 (1983) 2337.
[33] C. Baiocchi, G. Saini, P. Bertolo, G.P. Cartoni and G. Pettiti, Analyst, 113 (1988) 805.
[34] B. Magyar and P. Richner, Mikrochim. Acta (Wien), II, (1987) 121.
[35] R.M. Dagnall and S.K. Hasanaddin, Talanta, 15 (1968) 1025.
[36] P. Bosserman, D.T. Sawyer and A. Page, Anal. Chem., 50 (1978) 1300.
[37] Y. Nagaosa and K. Kobayashi, Talanta, 31 (1984) 593.
[38] C.M.G. Van den Berg, J. Electroanal. Chem., 215 (1986) 111.
[39] C.M.G. Van den Berg, Analyst, 114 (1989) 1527.
[40] C. Sun, J. Wang, W. Hu, X. Mao and W. Jin, J. Electroanal. Chem., 306 (1991) 252.
[41] J. Wang and J. Lu, Talanta, 39 (1992) 801.
[42] Q. Cai and S.B. Khoo, Anal. Chim. Acta, 276 (1993) 99.
[43] Z.P. Yang, J. Arcos, M. Alafandy, K. Boutakhrit and J.M. Kauffmann, Electroanalysis, in press.
[44] J. Hefferren, J. Pharm. Sci., 52 (1963) 1090.
[45] N.H. Furman, Standard Methods of Chemical Analysis, 6th edn., Vol. 1, Robert E. Krieger, 1975, p. 1079.
[46] L.A. Avaca, E.R. Gonzalez and N.R. Stradiotto, J. Electroanal. Chem., 130 (1981) 255.
[47] S.M.A. Jorge and N.R. Stradiotto, Anal. Lett., 22 (1989) 1709.

[48] M. Manzini and L.O. de S. Bulhóes, Anal. Lett., 24 (1991) 287.
[49] S. Arribas, R. Rincón, R. Moro and M.L. Alvarez, Anal. Chim. Acta, 33 (1965) 205.
[50] M.A. Sienra-Alvarez, A. Costa-Garcia, P. Tuñon-Blanco and S. Arribas-Jimeno, J. Electroanal. Chem., 179 (1984) 201.
[51] M. Alafandy, Ph.D. Thesis, Free University of Brussels, 1995.
[52] H.A. Mottola and H. Freiser, Talanta, 13 (1966) 55.
[53] B.M. Vanderborght and R.E. Van Grieken, Anal. Chem., 49 (1977) 311.
[54] M. Goldstein and G. Kober, Z. Anal. Chem., 279 (1976) 1287.

ELSEVIER

Talanta 42 (1995) 1891–1895

Talanta

# Indirect thermo-optical detection for capillary electrophoresis

Jicun Ren [a,1], Bincheng Li [a], Yanzhuo Deng [b,*], Jieke Cheng [a]

[a] *Department of Chemistry, Wuhan University, Wuhan 430072, People's Republic of China*
[b] *Department of Analysis and Testing Science, Wuhan University, Wuhan 430072, People's Republic of China*

Received 28 October 1994; revised 16 May 1995; accepted 23 May 1995

**Abstract**

Indirect thermo-optical detection for capillary electrophoresis is described first. A 20 mW helium–neon laser (632.8 nm) was used to provide the pumping beam and a 2 mW helium–neon laser (632.8 nm) supplied as the probe beam; Methylene Blue dye was used as a background absorber. The addition of ethanol to the background electrolyte solution can be performed to reduce adsorption of Methylene Blue onto the capillary wall. The detection method was applied to the detection of amino acids separated by capillary electrophoresis. The detection limit for lysine was $5 \times 10^{-6}$ mol $l^{-1}$ (signal-to-noise ratio, 2).

*Keywords:* Amino acids; Capillary electrophoresis; Indirect-optical detection; Methylene Blue

## 1. Introduction

Capillary electrophoresis (CE) is a highly efficient microvolume separation technique that can be applied to the separation of a variety of compounds, including proteins, peptides, DNA fragments, pharmaceuticals, inorganic ions and organic compounds [1]. The detection methods used in CE mainly include UV absorbance detection [2], fluorescence detection [3], electrochemical detection [4], laser interference refractive index detection [5], thermo-optical detection [6], etc. However, many compounds do not inherently possess the necessary characteristics for sensitive detection, indirect detection can be used as a more universal method for non-absorbing analytes (non-fluorescent and electrochemically inactive analytes) after CE separation. The possibilities for indirect laser-induced fluorescence detection have been studied by Yeung [7]. He used the latter detection method in the separations of amino acids, nucleotides, proteins, sugars and inorganic ions. Olefirowicz and Ewing [8] first demonstrated the use of indirect amperometric detection with CE and reported the successful separation of amino acids and dipeptides. Indirect UV absorbance detection has been used extensively to detect inorganic ions, organic acids, amino acids, etc. [9]. However, the detection limit for indirect UV absorbance detection is limited by a short light path in the UV absorbance detector.

Crossed-beam thermo-optical detection provides very small volumes, typically on the order of a few picoliters. The sensitivity of this method is almost unrelated to the light path. The thermal lensing and the thermo-optical interference approach were used in the crossed-beam thermo-optical method. Since the internal diameter of the capillary is small, the thermal lensing approach is difficult to use in CE. The interference detection technique has been widely employed in the crossed-beam thermo-optical detection method for CE. In thermo-optical detection, the two laser beams

* Corresponding author.
[1] Present address: Department of Chemistry, Hunan Normal University, Changsha, 410081, China.


*SSDI* 0039-9140(95)01653-8

are located perpendicular to each other and in a plane orthogonal to the capillary tube. When the analyte passes through the detection window, absorbance by the analyte will generate a temperature rise in the buffer. Since the refractive index of almost every substance changes with temperature, absorbance of the pumping beam results in a refractive index change within the buffer that can be detected as a change in the intensity of the probe beam. Yu and Dovichi [10,11] exploited the high intensity and focusing ability of a laser to construct a thermo-optical detection system, which was used to detect derived amino acids after CE separation. The detection limit for glycine was 42 attomol. But thermo-optical detection is relative to the molar absorption coefficient of the analytes, the detector cannot be used directly to detect non-absorbing analytes.

In this paper, an indirect thermo-optical detection method for detecting native amino acids after CE separation is first described. In the CE detector, Methylene Blue was used as a background absorber, and the addition of ethanol to the background electrolyte solution (BGES) can reduce the adsorption of Methylene Blue onto the capillary wall and enhance the detector signal.

## 2. Experimental

### 2.1. Instrumentation

The capillary electrophoresis system was constructed in the laboratory [5], and was similar to that described previously by Jorgenson and Lukacs [12]. A high-voltage d.c. power supply (0–30 kV; made in Shanghai, China) was employed to provide a high voltage. The capillary used was of uncoated fused-silica, 75 μm in i.d. (Yongnian Optical Fiber Factory), and 59 cm in length (48 cm to the detector). A 1 cm length of the polymer coating was carefully scraped; this was used as the window of the detector. The indirect thermo-optical detection system is shown in Fig. 1, and is similar to that described by Yu and Dovichi [10]. A 20 mW helium–neon laser (M1000 mode; made at the Shanghai Institute of Laser Technology) provided the pumping beam, and a 2 mW helium–neon laser (TEMOO mode; made at the Shanghai Institute of Laser Technology), provided the probe beam. Other detector components included a lock-in amplifier (ND240 mode; Nanjin University Instrument Factory), a chopper (194A mode, EG&G, USA), a photodiode (Wuhan University semiconductor factory), and lens (3) and lens (6) ($f = 9$ mm). A recorder (Dahua instrument factory; Shanghai) was used to record the electropherograms of the analytes.

### 2.2. Chemicals

Lysine, alanine and isoleucine were purchased from Sigma Co. Other chemicals were of analytical reagent grade (Shanghai Chemical Co.). Water was double-distilled. Samples were dissolved in the BGES.

### 2.3. Experimental procedure

Alignment of the optical system was performed by filling the capillary with BGES containing Methylene Blue. The positions of the two lenses were adjusted so that the beams were both focused onto the capillary, this required an iterative process to ensure maximum overlap between the pumping and probe laser beams. The probe beam was aligned first. The position of the focused lens was adjusted carefully to obtain a high-contrast interference pattern in the forward direction of the probe beam. Subsequently, the pumping beam was focused onto the capillary until maximum overlap between the pumping and probe beams and minimum light scattering of the pumping beam at the point of detection were achieved; this generated the maximum signal. Once this

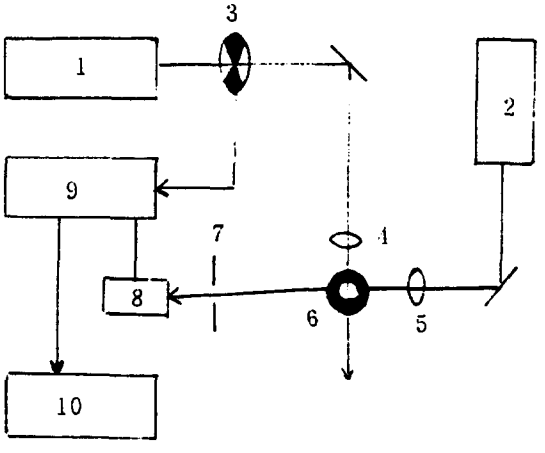


Fig. 1. Schematic diagram of the detection system. 1 and 2, helium–neon laser; 3, chopper; 4 and 5, lenses; 6, capillary; 7, aperture; 8, photodiode; 9, lock-in amplifier; 10, recorder.

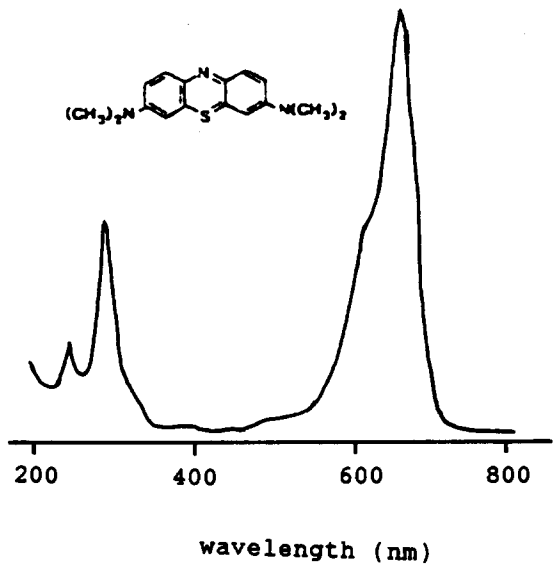


Fig. 2. The structure and spectrum of Methylene Blue. (Buffer, $2.5 \times 10^{-3}$ mol $l^{-1}$ $H_3PO_4$ + 20% ethanol; concentration of Methylene Blue, $10^{-5}$ mol $l^{-1}$).

was achieved, all optical components were fixed. In indirect detection, the power of the pump laser beam was 20 mW and its modulated frequency was 12 Hz. CE was performed as below.

A new capillary was rinsed with 0.1 mol $l^{-1}$ sodium hydroxide, double-distilled water and BGES, in the appropriate order. The capillary was filled with BGES by the hydrostatic method. The high-voltage output and the ground were connected to platinum electrodes, which were placed in 6 ml electrolyte reservoirs. The ends of the fused silica capillary were dipped in both reservoirs, completing the circuit. The sample solution was introduced by siphoning at a given height. The electrophoresis was performed at constant voltage. A recorder was used to record the electropherograms of the analytes.

## 3. Results and discussion

### 3.1. Choice of background absorber

In indirect thermo-optical detection, a helium–neon laser (632.8 nm) was used to provide a pumping beam. Experiments showed that the absorption wavelength of Methylene Blue can match that of the helium–neon laser beam. The structure and spectrum of Methylene Blue are shown in Fig. 2. The molar absorption coefficient of the absorber at 633 nm is about $5 \times 10^4$ l mol$^{-1}$ cm$^{-1}$.

In acidic buffer, adsorption of Methylene Blue onto the capillary surface was noted by Higashijima et al. [13]. In the experiments, we found that the addition of ethanol to BGES can reduce the adsorption of the capillary surface. The results are shown in Fig. 3. The increase in the concentration of ethanol was beneficial, leading to an improvement in the peak shape of Methylene Blue. This phenomenon can be attributed to the fact that ethanol can limit the dissociation of silanol on the capillary surface and the adsorption of Methylene Blue. Meanwhile, ethanol also enhanced the Methylene Blue detection signal, because $dn/dT$ of ethanolic solutions is larger than that of water solutions; this was beneficial for the improvement of sensitivity in indirect thermo-optical detection.

### 3.2. Indirect detection

The indirect thermo-optical detection of amino acids was accomplished by the addition of cationic absorber, Methylene Blue, to the BGES. When the capillary was filled with BGES containing Methylene Blue, a constant background thermo-optical signal was produced in the detection system. Due to the need to maintain charge neutrality of the sample zone in CE, Methylene Blue in BGES was displaced by cationic analytes when they passed by the detection window. The displacement lead to a decrease in the background signal. As a result, negative peaks were expected in the electropherogram. Fig. 4 shows an electropherogram of amino acids in a phosphoric

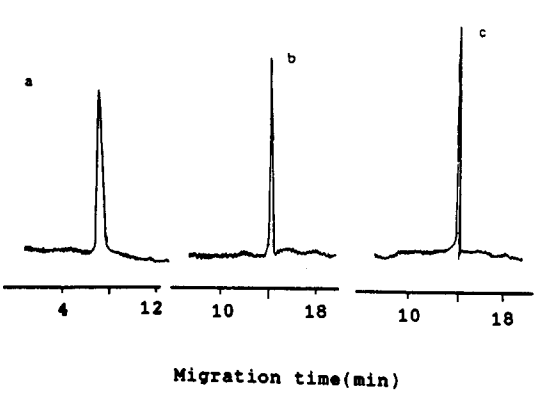


Fig. 3. Electropherogram of Methylene Blue. Buffer a, $2.5 \times 10^{-3}$ mol $l^{-1}$ $H_3PO_4$; buffer b, $2.5 \times 10^{-3}$ mol $l^{-1}$ $H_3PO_4$ + 20% ethanol; buffer c, $5 \times 10^{-3}$ mol $l^{-1}$ $NaH_2PO_4$ + 40% ethanol, 19 kV; sample, $10^{-4}$ mol $l^{-1}$ Methylene Blue.

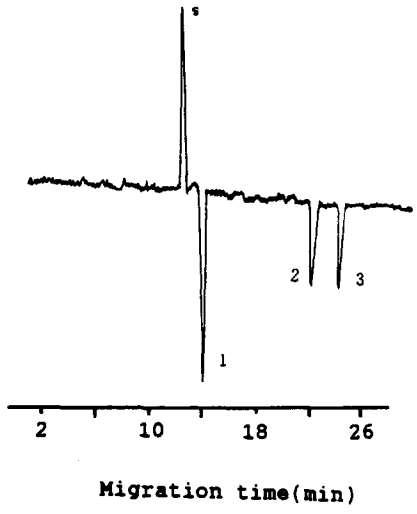


Fig. 4. An electropherogram of amino acids. Electrophoretic conditions: buffer, $2.5 \times 10^{-3}$ mol $l^{-1}$ $H_3PO_4$ + 20% ethanol + $10^{-4}$ mol $l^{-1}$ Methylene Blue; 19 kV. s, System peak; 1, lysine ($5 \times 10^{-5}$ mol $l^{-1}$); 2, alanine ($10^{-4}$ mol $l^{-1}$); 3, isoleucine ($10^{-4}$ mol $l^{-1}$).

acid–ethanol–Methylene Blue buffer. In this buffer, both the amino acids and the Methylene Blue possessed positive charges; the amino acids were detected by the indirect thermo-optical method. The migration time of the first peak(s) in the electropherogram corresponded with that of Methylene Blue. Of three amino acids, the peak height of lysine was the largest since its mobility was nearest to that of Methylene Blue and it had the highest displacement ratio.

### 3.3. Linearity and detection

In CE analyses, the reproducibility depends on factors such as sampling, temperature, voltage, and position of the probe aperture in the thermo-optical detector. The effects of the above-mentioned factors can be reduced by using the internal standard method [14]. Fig. 5 shows an electropherogram of tetrabutylammonium bromide and lysine. In phosphate–ethanol–Methylene Blue buffer, the two compounds exhibited good peak shapes. Fig. 6 illustrates the relationship between relative peak height and the concentration of lysine using tetrabutylammonium bromide as internal standard. When the concentration of lysine was below $10^{-4}$ mol $l^{-1}$, the equation for the calibration curve was $h = 1.04 \times 10^{-4} C - 3.85 \times 10^{-6}$ (where $h$ is the relative peak height and $C$ is the concentration of lysine; $r = 0.9994$). The detection limit for lysine was $5 \times 10^{-6}$ mol $l^{-1}$ (signal-to-noise ratio, 2).

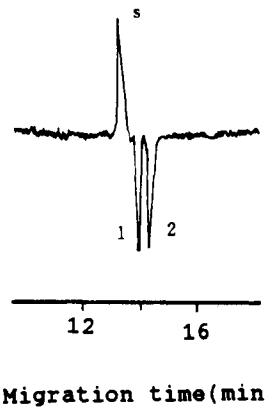


Fig. 5. An electropherogram of lysine and tetrabutylammonium bromide. Electrophoretic conditions: buffer, $56 \times 10^{-3}$ mol $l^{-1}$ $NaH_2PO_4$ + 40% ethanol + $10^{-4}$ mol $l^{-1}$ Methylene Blue; 19 kV. s, System peak; 1, lysine ($2.5 \times 10^{-3}$ mol $l^{-1}$); 2, tetrabutylammonium ($2.5 \times 10^{-5}$ mol $l^{-1}$).

## 4. Conclusions

In the present work, we have demonstrated indirect thermo-optical detection for CE. With Methylene Blue added to BGES as an absorber, three amino acids were separated on a home-made CE system with indirect thermo-optical detection. Since the conditions in our laboratory were limited, in indirect thermo-optical detection, helium–neon lasers (632.8 nm) were used to provide both the probe beam and the pumping beam. If the probe beam is supplied by another laser, such as an argon ion laser, the detection limit in indirect thermo-optical detection can be further improved due to

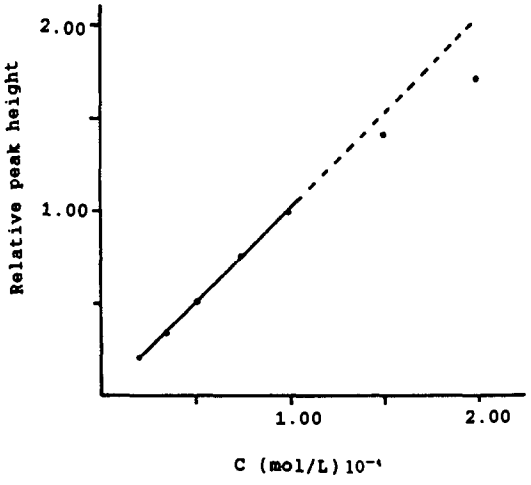


Fig. 6. Calibration curve of lysine. Conditions as in Fig. 5. Internal standard, tetrabutylammonium bromide ($10^{-4}$ mol $l^{-1}$).

a decrease in the effects of light scattering from the probe beam. Future work will investigate possible improvements to the detection sensitivity including the use of highly stable lasers, and the improvement of the optical configuration in the indirect thermo-optical detector to decrease the detector noise, leading to an enhancement of the signal-to-noise ratio.

## Acknowledgment

This work was supported by the National Natural Science Foundation of China.

## References

[1] C.A. Moning and R.T. Kennedy, Anal. Chem., 66 (1994) 280R.
[2] R.M. McCormick and R.T. Zagursky, Anal. Chem., 63 (1991) 750.
[3] M. Albin, R. Weinberger, E. Sapp and S. Moring, Anal. Chem., 63 (1991) 417.
[4] P.D.J. Curry, S.C.E. Engstrom and A.G. Ewing, Electroanalysis, 3 (1991) 587.
[5] J.C. Ren, Y.Z. Deng and J.K. Cheng, Chem. J. Chin. Univ. 14 (1993) 1661.
[6] M. Yu and N.J. Dovichi, Anal. Chem., 61 (1989) 2226.
[7] E.S. Yeung, Acc. Chem. Res., 22 (1989) 125.
[8] T.M. Olefirowicz and A.W. Ewing, J. Chromatogr., 499 (1990) 713.
[9] F. Foret, S. Fanali, L. Ossicini and P. Bocek, J. Chromatogr., 470 (1989) 299.
[10] M. Yu and N.J. Dovichi, Appl. Spectrosc., 43 (1989) 196.
[11] M. Yu and N.J. Dovichi, Mikrochim. Acta, 2 (1988) 27.
[12] J.W. Jorgenson and K.D. Lukacs, Anal. Chem., 53 (1981) 1298.
[13] T. Higashijima, T. Fuchigami, T. Imasaka and N. Ishibashi, Anal. Chem., 64 (1992) 711.
[14] E.V. Dose and G.A. Guiochon, Anal. Chem., 63 (1991) 1154.

ELSEVIER

Talanta 42 (1995) 1897–1903

Talanta

# Studies on $\beta$-type reaction and kinetics of lanthanides with *p*-bromochloroarsenazo

Jinzhang Gao *, Fei Zha, Hui Chen, Jingwan Kang

*Institute of Chemistry, Northwest Normal University, Lanzhou 730070, China*

Received 16 January 1995; revised 15 May 1995; accepted 23 May 1995

**Abstract**

The reaction behaviour of the $\beta$-type chelates of lanthanide ions ($Ln^{3+}$) with *p*-bromochloroarsenazo (4-CAsA-pB) in 0.01 mol $l^{-1}$ $HClO_4$ solution has been studied systematically by a spectrophotometric method. All the lanthanide ions can form $\beta$-type chelates with *p*-bromochloroarsenazo. The maximum absorption wavelength is in the range 727–731 nm, the molar absorptivities are about $6.0 \times 10^4$–$9.0 \times 10^4$ $cm^2$ $mol^{-1}$, the composition ratio of $Ln^{3+}$ ions with 4-CAsA-pB is 1:2 and the actual combining ratio is 2:4. The optimum acidity range ($\Delta$pH value) of the formation of $\beta$-type chelates has been obtained. Kinetic parameters, such as the reaction order and rate constants, have also been studied and a formation mechanism for the $\beta$-type chelates has been proposed.

*Keywords:* Absorption spectra; $\beta$-Type chelates; *p*-Bromochloroarsenazo; Kinetic parameters; Lanthanides

## 1. Introduction

The interaction between lanthanide ions and some 2,7-bis(arylazo) derivatives of chromotropic acid, which form chelates that have high molar absorptivities in the 700–800 nm region, has been for a long time, of interest to analysts [1,2]. Many authors [3–7] have reported that these reactions can be used for the determination of trace amounts of light lanthanide elements in the presence of heavy lanthanide elements. Some authors [7,8] have presented the kinetics and mechanisms of the formation of $\beta$-type chelates. However, information concerning the reaction behavior of arsenazo-type reagents which contain an axochromic group in the benzyl ring linked to the analytic group is still sparse.

Therefore, as part of a systematic study, in this paper we describe the $\beta$-type chelates of lanthanide ions with *p*-bromochloroarsenazo (a new non-symmetric azo-type reagent; see Scheme 1). We determine the composition ratio and the actual combining ratio, investigate the optimum acidity range ($\Delta$pH value) of the formation of $\beta$-type chelates, the reaction order and the rate constants, and propose a process for the formation of the $\beta$-type chelates.

Scheme 1. The structure of 4-CAsA-pB

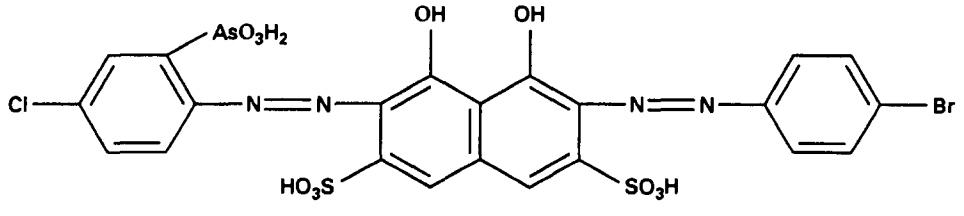


* Corresponding author. Fax: (86) 931-766-8159.


*SSDI* 0039-9140(95)01654-6

Table 1
The optimum acidity range (ΔpH value) for the formation of β-type chelates for the system $Ln^{3+}$ with 4-CAsA-pB

| pH parameter | $Ln^{3+}$ ion | | | | | | | | | | | | | |
|---|---|---|---|---|---|---|---|---|---|---|---|---|---|---|
| | La | Ce | Pr | Nd | Sm | Eu | Gd | Tb | Dy | Ho | Er | Tm | Yb | Lu |
| $pH_1$ | 3.64 | 3.48 | 3.24 | 3.06 | 3.24 | 3.05 | 2.70 | 2.38 | 2.56 | 2.69 | 2.62 | 2.96 | 2.98 | 3.08 |
| $pH_2$ | 4.19 | 4.06 | 3.86 | 3.70 | 3.92 | 3.76 | 3.72 | 3.48 | 3.60 | 3.76 | 3.74 | 6.08 | 6.25 | 6.46 |
| ΔpH | 0.55 | 0.58 | 0.62 | 0.64 | 0.68 | 0.71 | 1.02 | 1.10 | 1.04 | 1.08 | 1.12 | 3.12 | 3.27 | 3.38 |

$T = 288$ K.

## 2. Experimental

### 2.1. Apparatus

The absorption is measured by means of a U-3400 spectrophotometer (Hitachi, Japan) at a constant temperature controlled by a model 501 Super Thomostat (Shengzhen, China). The acidity is determined by means of a model pHS-3C meter (Zhejiang, China).

### 2.2. Reagents

Standard solutions of the lanthanide(III) ions were prepared by dissolving their corresponding oxides, which were of spectral purity, in hot perchloric acid (adding hydrogen peroxide when dissolving $CeO_2$), then evaporating the excess acid and diluting with redistilled, deionized water to a given volume. The *p*-bromochloroarsenazo was provided as a gift by Professor Bincai Wu, Department of Chemistry, East China Normal University, and was used without further purification (more than 94% pure). The other reagents were all analytical grade, and all solutions were prepared with redistilled, deionized water.

### 2.3. Procedure

(1) Preparation of the complex solution involved adding 3.0 ml of $1.0 \times 10^{-4}$ mol $l^{-1}$ *p*-bromochloroarsenazo (4-CAsA-pB) to a 25 ml calibrated flask which contained 1.0 ml of a $1.0 \times 10^{-4}$ mol $l^{-1}$ solution of the lanthanide ion and requisite amounts of 0.01 mol $l^{-1}$ $HClO_4$ solution or 0.02 mol $l^{-1}$ NaOH solution (the resultant pH of the final solution is shown in Table 1), diluting to the mark with water and allowing to stand overnight. The absorption was then measured in a 1.0 cm cell against a reagent or water blank.

(2) Determination of the rate constants for the formation of the β-type chelates involved adding 2.0 ml of $1.0 \times 10^{-4}$ mol $l^{-1}$ 4-CAsA-pB to a 25 ml calibrated flask which contained 1.0 ml of a $1.0 \times 10^{-4}$ mol $l^{-1}$ solution of the lanthanide ion and 2.0 ml of 0.01 mol $l^{-1}$ $HClO_4$ at a constant temperature, diluting to the mark with water, mixing well rapidly, then immediately measuring the variation of absorption with the time in the kinetic system, with use of the U-3400 spectrophotometer.

## 3. Results and discussion

### 3.1. Absorption spectra

The β-type reactions of 14 lanthanides with 4-CAsA-pB in 0.01 mol $l^{-1}$ $HClO_4$ solution (pH 3.40–3.70) were studied and the results are given in Fig. 1. All the lanthanide ions form

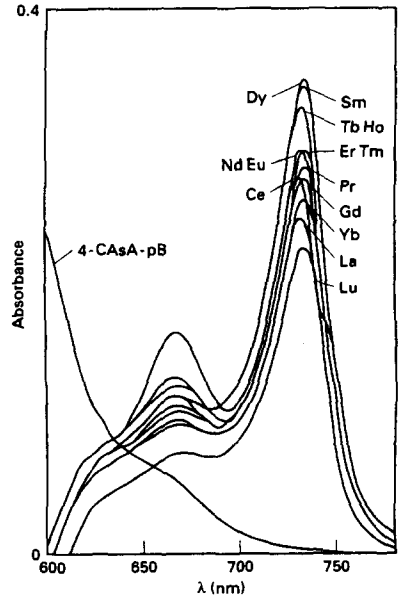


Fig. 1. The absorption spectra of β-type chelates of $Ln^{3+}$ ions with 4-CAsA-pB. ($C_{Ln^{3+}} = 4.0 \times 10^{-6}$ mol $l^{-1}$; $C_{4\text{-CAsA-pB}} = 1.2 \times 10^{-5}$ mol $l^{-1}$; pH 3.40–3.70; $HClO_4$; $T = 296 \pm 0.3$ K; against reagents.)

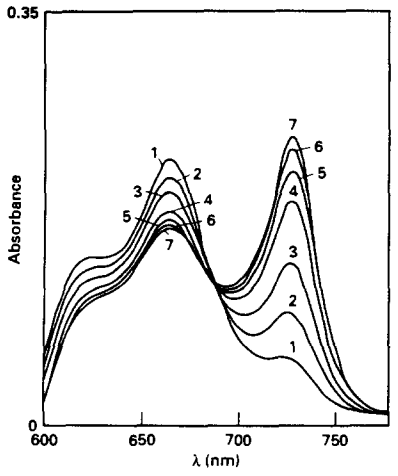


Fig. 2. Absorption scans of $\beta$-type chelates with respect to time for the system $Eu^{3+}$ with 4-CAsA-pB. ($C_{Eu} = 4.0 \times 10^{-6}$ mol $l^{-1}$; $C_{4\text{-CAsA-pB}} = 1.2 \times 10^{-5}$ mol $l^{-1}$; pH $3.40 \pm 0.1$; $T = 296 \pm 0.3$ K). Curve 1, 2.0 min; curve 2, 5.0 min; curve 3, 10.0 min; curve 4, 20.0 min; curve 5, 30.0 min; curve 6, 40.0 min; curve 7, 50.0 min.

homonuclear $\beta$-type chelates with 4-CAsA-pB, the maximum absorption peaks of which shift from 727 nm to 731 nm with increasing atomic number of the lanthanides, and the absorptivities correspondingly vary from $6.0 \times 10^4$ to $9.0 \times 10^4$ $cm^2$ $mol^{-1}$.

Results from continuous scanning of the absorption with respect to time show that there is a transformation from $\alpha$-type to $\beta$-type chelates (see Fig. 2 for the system of $Eu^{3+}$ ions with 4-CAsA-pB. A similar transformation was observed for the other lanthanides). During the transformation process, the absorption of the $\alpha$-type chelates decreased while the absorption of the $\beta$-type chelates increased. The $\beta$-type chelates were stable for at least 12 h after the transition of the $\alpha$-type chelates to the $\beta$-type had reached equilibrium (for each lanthanide system, the time of equilibrium was different). However, on standing for more than 48 h, the absorbance decreased and a blue precipitate appeared.

### *3.2. Determination of the optimum acidity range (ΔpH value) of the formation of the β-type chelates*

As is known, the acidity of the solution plays an important role in the formation of the $\beta$-type chelates. We systematically determined the optimum acidity range (ΔpH value) for the formation of the $\beta$-type chelates of the lanthanide ions with 4-CAsA-pB. The results are listed in Table 1. The determination showed that the optimum acidity range is different for each of the lanthanide systems; the ΔpH value is extended with increasing atomic number of the lanthanides and these changes can be divided into three groups: for La to Eu, the ΔpH value is about 0.5–0.7, for Ga to Er, the ΔpH value is about 1.0–1.1, and for Tm, Yb, Lu, the ΔpH values are about 3.1, 3.3 and 3.4, respectively. The conclusions are similar for the system of lanthanides with *p*-bromochlorophosphonazo [9].

It is worth noticing that there is some definite relationship between the optimum acidity range for the formation of $\beta$-type chelates and the deprotonation constants of the analytic functional group $-AsO_3H_2$. The minimum and maximum pH values ($pH_1$, $pH_2$) are almost approximately $pk_3$, $pk_4$ if we consider the influence of some lanthanide characteristics (i.e. the atomic number, the ionic radius, etc.). That is to say, the optimum acidity range is influenced by the deprotonation constants of the $-AsO_3H_2$ group and some lanthanide characteristics.

### *3.3. Investigation of the composition ratio and the actual combining ratio of the β-type chelates*

Using the continuous variation method [10] and the equilibrium shift method [11], we investigated the composition ratio of the $\beta$-type chelates of lanthanide ions with 4-CAsA-pB

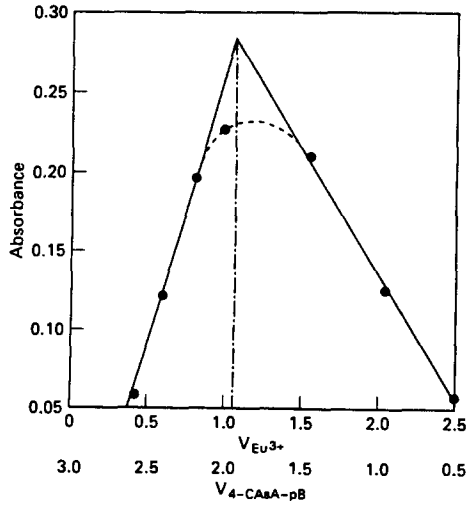


Fig. 3. Investigation of the composition of $\beta$-type chelates by the continuous variation method. (Eu; wavelength $\lambda = 728.5$ nm; pH 3.20–3.40; $T = 296 \pm 0.3$ K.)

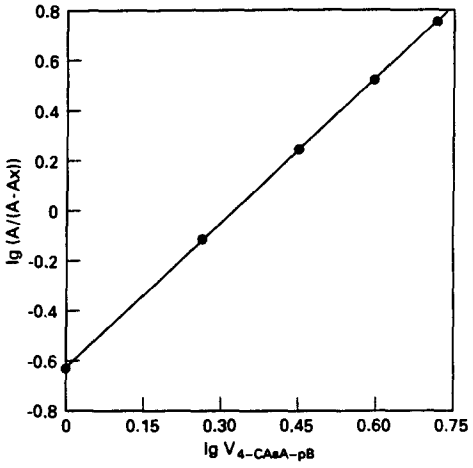


Fig. 4. Investigation of the composition of $\beta$-type chelates by the equilibrium shift method. (Eu; $\lambda = 728.5$ nm; pH 3.20–3.40; $T = 296 \pm 0.3$ K.)

(see Figs. 3 and 4 for Eu; similar results are obtained for other lanthanide systems). The composition ratio, $Ln^{3+}$:4-CAsA-pB was found to be 1:2. Furthermore, the actual combining ratio of the $\beta$-type chelates is insured to be 2:4 by a graphical method involving the dilution effect model [12,13] (see Figs. 5 and 6 for Ce; similar results are obtained for the other lanthanide systems). These investigations show that the $\beta$-type chelates of lanthanides with 4-CAsA-pB are polymers.

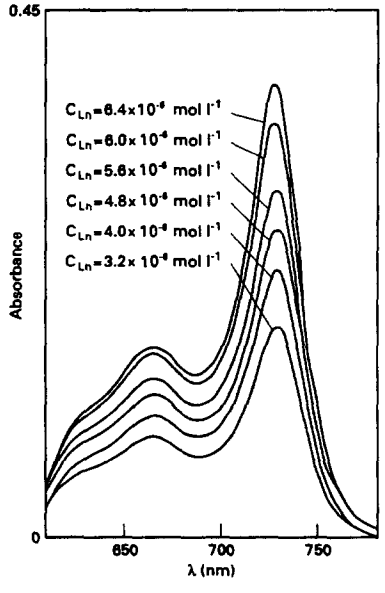


Fig. 5. Dilution absorption spectra of $\beta$-type chelates in the system $Ln^{3+}$ with 4-CAsA-pB. (Ce; the Ln: 4-CAsA-pB ratio is 1:2; $T = 296 \pm 0.3$ K.)

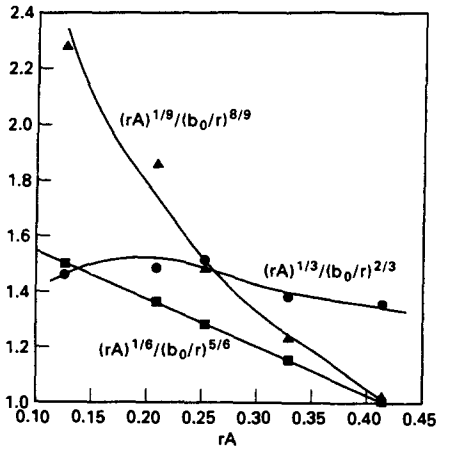


Fig. 6. Actual combining ratio of $\beta$-type chelates. (Ce; $\lambda = 727.8$ nm; $T = 296 \pm 0.3$ K.)

### 3.4. The kinetics of $\beta$-type chelates

From the absorption spectra of $Ln^{3+}$ with 4-CAsA-pB (see Fig. 1) we know that $\lambda_\beta = 727–731$ nm, $\lambda_\alpha = 662–665$ nm, $\lambda_{4\text{-CAsA-pB}} = 572$ nm, $\Delta\lambda_\alpha = 90–92$ nm, $\Delta\lambda_\beta = 155–159$ nm and $\Delta\lambda_{\alpha,\beta} = 65–67$ nm, so there is no influence on the scan of the absorption of the $\alpha$-type chelate and the $\beta$-type chelate with respect to time. Fig. 2 shows the conversion of $\alpha$-type chelates to $\beta$-type chelates, and the reaction order determination is shown in Fig. 7. It is concluded that the conversion from $\alpha$-type chelates to $\beta$-type chelates in 0.01 mol $l^{-1}$ $HClO_4$ is a second-order reaction. Using the same graphical method, we investigated the rate constants for the $\beta$-type conver-

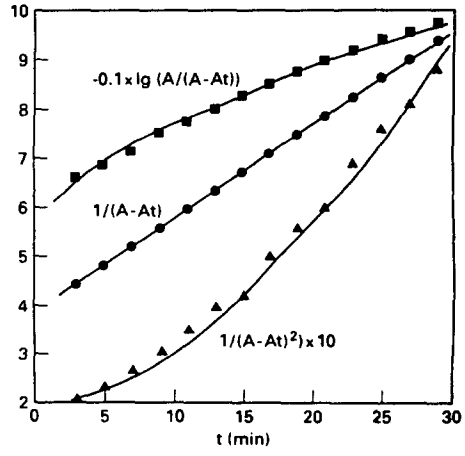


Fig. 7. The reaction order of $\alpha$-type chelates conversion to $\beta$-type chelates. ($C_{Eu^{3+}} = 4.0 \times 10^{-6}$ mol $l^{-1}$; $C_{4\text{-CAsA-pB}} = 8.0 \times 10^{-6}$ mol $l^{-1}$; $\lambda = 728.5$ nm; $T = 296 \pm 0.3$ K; pH $3.40 \pm 0.1$.)

Table 2
Rate constants for the $\alpha$-type to $\beta$-type conversion reaction for the system $Ln^{3+}$ with 4-CAsA-pB

| Reaction rate | $Ln^{3+}$ ion | | | | | | | | | | | | | |
|---|---|---|---|---|---|---|---|---|---|---|---|---|---|---|
| | La | Ce | Pr | Nd | Sm | Eu | Gd | Tb | Dy | Ho | Er | Tm | Yb | Lu |
| $k$ ($m^3 mol^{-1} s^{-1}$) | 0.31 | 0.33 | 0.69 | 1.02 | 21.2 | 23.0 | 20.8 | 25.9 | 28.0 | 30.1 | 31.2 | 14.0 | 46.4 | 21.9 |

$T = 296 \pm 0.3$ K; pH $3.56 \pm 0.2$.

Table 3
The influence of acidity on the reaction rate of $\beta$-type chelates in the system $Eu^{3+}$ with 4-CAsA-pB

| Reaction rate | pH | | | | | |
|---|---|---|---|---|---|---|
| | 3.03 | 3.07 | 3.14 | 3.28 | 3.56 | 4.23 |
| $k$ ($m^{-3} mol^{-1} s^{-1}$) | 19.56 | 19.79 | 32.48 | 25.78 | 23.84 | 16.81 |

$T = 298 \pm 0.3$ K.

sion from the $\alpha$-type reaction in the system of lanthanide ions with 4-CAsA-pB at $T = 296 \pm 0.3$ K and pH $3.56 \pm 0.2$. The results listed in Table 2 show that the rate constants increased with increasing atomic number of the lanthanides and that the rate constants for light rare earth elements and heavy rare earth elements are very different.

We also studied the influence of acidity and temperature on the reaction rate in the system $Eu^{3+}$ with 4-CAsA-pB. The results are listed in Tables 3 and 4. The reaction rate increased with increasing acidity at $298 \pm 0.3$ K. However, if the pH is below 3.07, the reaction rate decreased. It also increased with increasing temperature at pH $3.60 \pm 0.2$ when the temperature is below 303 K. Otherwise, it decreased.

### *3.5. Proposed mechanism of the formation of $\beta$-type chelates*

The conclusion of the transformation from $\alpha$-type chelates to $\beta$-type chelates has been reported as a deprotonation process, in which the ligand loses one proton and forms a "Z"-type chelate in the system of heavy rare earth elements [8]. As the structure of 4-CAsA-pB and its reaction behaviour with lanthanide ions is different, we have suggested another mechanism for the formation of $\beta$-type chelates for the system 4-CAsA-pB with lanthanide ions. Usually, the structure of 4-CAsA-pB in acidic solution is as presented in Scheme 2 [14]. The hydrogen bond makes the –N=N– group more stable and it also decreases the deprotonating ability of the –OH group linked to the naphthyl ring. The dissociation pathway of azo-type reagents also shows that the deprotonating ability of –OH groups linked to the naphthyl ring in acidic solution is very weak [14]. In contrast, the deprotonating ability of the $-AsO_3H_2$ group is increased on decreasing the electronic clouds around the oxygen atom in the $-AsO_3H_2$ group by adding a strong electronic acceptor (–Cl) onto the benzyl ring linked to the $-AsO_3H_2$ group. Therefore, in highly acidic solution, the coordinating ability of the $-AsO_3H_2$ group is greater than that of the –N=N– group and the –OH group linked to the naphthyl ring. The probable coordination pattern may be lanthanide ions combining with oxygen atoms in the $-AsO_3H_2$ group and forming a bridging bond between the lanthanide atoms and the oxygen atoms (see Scheme 3 for its structure).

## 4. Conclusion

According to the above results, the following conclusions may be drawn. The 4-CAsA-pB reagent forms sensitive $\beta$-type chelates with all the lanthanide ions. The optimum acidity range of the formation of the $\beta$-type chelates ($\Delta$pH value) is extended with increasing atomic number of the lanthanides. There is a definite relationship between the optimum acidity and the deprotonation constants of the $-AsO_3H_2$ groups.

Table 4
The influence of temperature on the reaction rate of $\beta$-type chelates in the system $Eu^{3+}$ with 4-CAsA-pB

| Reaction rate | Temperature (K) | | | | | |
|---|---|---|---|---|---|---|
| | 286 | 291 | 296 | 299 | 303 | 306 |
| $k$ ($mmol^{-1}\,s^{-1}$) | 11.24 | 16.45 | 18.90 | 20.24 | 15.74 | 13.51 |

pH $3.60 \pm 0.2$.

Scheme 2. The structure of 4-CAsA-pB in the acidic solution

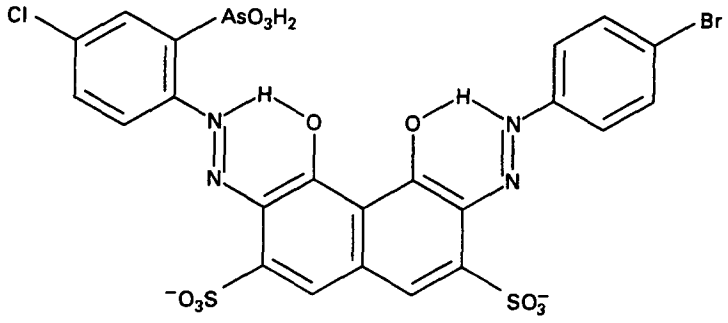


Scheme 3. The structure of the β-type chelates of $Ln^{3+}$ with 4-CAsA-pB

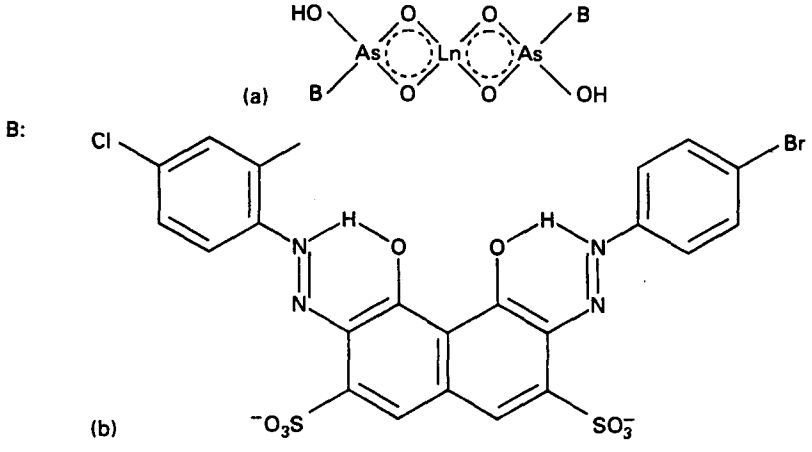


The $\beta$-type chelates are polymers formed from $\alpha$-type chelates. The formation procedure is a second-order reaction and the reaction rate increases with increasing atomic number of the lanthanides. The influence of acidity and temperature on the reaction rate is such that, over a defined range, the reaction rate is increased with increasing temperature and acidity.

## Acknowledgement

This work was supported by the Gansu Province Nature Foundation and the Gansu Province Education Commission, China.

## References

[1] H.C. Liu, Y.X. Qiu, B.C. Wu and J.B. Lin, Li Hua Jian Yan (Hua Xue Fen Ce), 20 (1984) 57; 20 (1984) 59; 20 (1984) 56.
[2] C. Wu and Q. Yin, Fen Xi Hua Xue, 15 (1987) 175.
[3] J.Z. Gao, X.M. Zhu, J.W. Kang and G.B. Bai, Anal. Lett., 18(A12) (1985) 1507.
[4] J.Z. Gao, R.Y. Chen, J.G. Hou and G.B. Bai, Analyst, 112 (1987) 1177.
[5] J.Z. Gao, H. Chen and G.B. Bai, Inorg. Chim. Acta, 140 (1987) 271.
[6] J.G. Hou, J.W. Kang and J.Z. Gao, Talanta, 41 (1994) 15.
[7] J.Z. Gao, J.W. Kang, J.G. Hou, Y.S. Wang and G.B. Bai, Rare Earth (JPN.), 16 (1990) 142.
[8] Z.X. Ling and Y.E. Zen, Gao Deng Xue Xiao Hua Xue Xue Bao, 3 (1982) 243.

[9] Z.M. Xu, L. Yuan, Z.Z. Shen and L.M. Gao, Xi Bei Shi Fan Da Xue Xue Bao (Zi Ran Ke Xue Ban), 26 (1990) 26.
[10] P. Job, Ann. Chim., 9 (1928) 113.
[11] H.E. Bent, J. Am. Chem. Soc., 63 (1941) 568.
[12] D.V. Gonzdez Darcia, A. Arrebola Ramirez, M. Roman Ceba, Talanta, 26 (1979) 215.
[13] T.R. Galan, A.A. Ramirez and M.R. Ceba, Talanta, 27 (1980) 545.
[14] W.R. Chen, W.L. Zhou, J.M. Pan, Z.G. Xu and S.S. Ge, Fen Xi Hua Xue, 17 (1989) 30.

ELSEVIER

Talanta 42 (1995) 1905–1911

Talanta

# Spectrophotometric determination of scandium based on the cocoloration effect in scandium–cerium–*p*-acetylchlorophosphonazo (CPApA) system

Chung-Gin Hsu*, Shuang-Cheng Liu, Jiao-Mai Pan

*Department of Chemistry, East China Normal University, 3663 Zhong Shan Road(N), Shanghai 200062, People's Republic of China*

Received 27 March 1995; revised 30 May 1995; accepted 31 May 1995

**Abstract**

Scandium in the presence of cerium(III) forms, with *p*-acetylchlorophosphonazo (CPApA), a heteropolynuclei ternary $\beta$-complex of scandium–cerium–CPApA. The complex gives a very sensitive reaction for scandium with a molar absorptivity of $\varepsilon_{Sc} = 2.29 \times 10^5\,l\,mol^{-1}\,cm^{-1}$ due to the cocoloration effect. Most foreign ions can be tolerated in considerable amounts. The optimum conditions and the mechanism of the complex formation reaction are discussed. A simple method is proposed for the determination of scandium in alloys, with satisfactory results.

*Keywords:* Cocoloration effect; Scandium–cerium–*p*-acetylchlorophosphonazo complex; Spectrophotometry

## 1. Introduction

$\beta$-type complex formation reactions [1,2] of rare earths with asymmetric derivatives of chromotropic acid containing the *o*-phosphono-*o'*-hydroxyazo functional group have been widely used for the determination of rare earth elements [3,4].

*p*-Acetylchlorophosphonazo [5] (CPApA; I), one of the reagents synthesized in our laboratory, has been employed to determine total rare earths [5] and cerium subgroup rare earths [6].

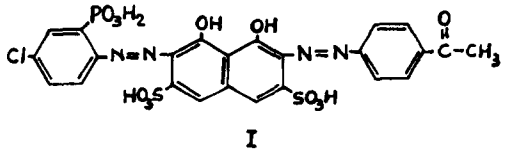


I

Usually, the $\beta$-complex reaction is accompanied by a cocoloration effect [7–9]. It was found that CPApA gave a sensitive $\beta$-reaction with scandium in acidic medium, and the sensitivity of the reaction would be greatly enhanced in the presence of rare earth elements. In this paper, we studied the spectrophotometric characteristics and the mechanism of the cocoloration effect of the scandium–cerium–CPApA system. From the results, a sensitive method has been developed for the determination of scandium in alloys.

## 2. Experimental

### 2.1. Reagents

A standard stock solution of scandium was prepared by dissolving scandium oxide (Spec-

* Corresponding author.

*SSDI* 0039-9140(95)01658-9

pure; Johnson Matthey) in hydrochloric acid (1 + 1), evaporating the excess acid and diluting with hydrochloric acid (1 + 100) to a given volume. The solution was standardized by EDTA titration with Xylenol Orange as indicator. The working standard solution was prepared by diluting as required with hydrochloric acid (1 + 100).

A standard solution of cerium(III) was prepared as described previously [10].

*p*-Acetylchlorophosphonazo (CPApA) solution (0.04%) was prepared by dissolving 0.04 g of CPApA in 100 ml of water. CPApA was synthesized as described in the previous work [11].

Other reagents were of analytical-reagent grade.

### 2.2. Apparatus

Absorption spectra and absorbances were recorded and measured with use of a Beckman DU-7HS spectrophotometer and a model 752 spectrophotometer (Shanghai Analytical Instruments). A constant temperature was maintained by using a model CS-501 ultrathermostat.

### 2.3. Procedures

*(A) General procedure*

To 2–8 μg of scandium in a 25 ml calibrated flask, add 25 μg of cerium(III), 1 ml of 3 M hydrochloric acid, and adjust the volume to about 10 ml with water. Add 3.5 ml of 0.04% CPApA and mix well. After allowing to stand for 30 min, dilute to the mark with water. Measure the absorbance at 722 nm in a 1.0 cm cell against a reagent blank.

*(B) Procedure for kinetic study*

Under a constant temperature in a 25 ml calibrated flask, add 5 μg of scandium, 1 ml of 3 M hydrochloric acid, and adjust the volume to about 20 ml with water, add 1.5 ml of 0.04% CPApA, dilute to the mark with water and measure the absorbance at 722 nm in a 1.0 cm cell against a reagent blank without standing.

*(C) Procedure for the determination of scandium in alloys*

To 1.5 g of the sample, add 10 ml of aqua regia (1 + 1), heat to decompose the sample and evaporate almost to dryness. After cooling to room temperature, dissolve the residue in water, transfer the solution into a 100 ml calibrated flask, and dilute to the mark with water. Place 1.0 ml (or another appropriate aliquot) of the resultant solution in a 25 ml calibrated flask, then add 2.0 μg of scandium, and follow the general procedure for the determination of scandium.

## 3. Results and discussion

### 3.1. Absorption spectra

As shown in Fig. 1, the $\alpha$-complex of cerium–CPApA exhibits an absorption peak at 678 nm (curve 2), whereas the $\beta$-complex of scandium–CPApA gives a maximum absorption at 722 nm (curve 3). However, in the presence of cerium(III), a hetero-polynuclei ternary complex of scandium–cerium–CPApA is formed, which greatly enhances the absorption at 722 nm (curve 4) due to the cocoloration effect [7–9,12–14].

### 3.2. Optimum conditions for complex formation

CPApA forms a ternary complex with the mixture of scandium and cerium(III) in acidic medium. In 0.08–0.24 M hydrochloric acid (Fig. 2) and $1.3–1.8 \times 10^{-5}$ M CPApA, the complex gives the highest and a constant absorbance. The temperature at 10–30 °C does not influence the color development.

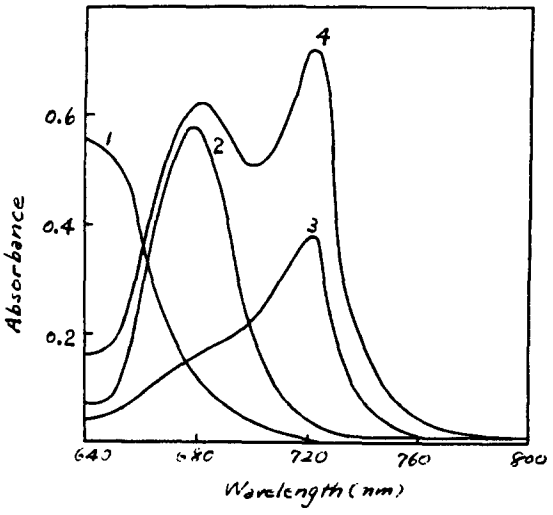


Fig. 1. Absorption spectra of CPApA and its complexes. Curve 1, CPApA vs. water; curve 2, cerium–CPApA; curve 3, scandium–CPApA; curve 4, scandium–cerium–CPApA vs. reagent blank (scandium, 5 μg; cerium, 25 μg; CPApA, $1.55 \times 10^{-5}$ M; HCl, 0.12 M).

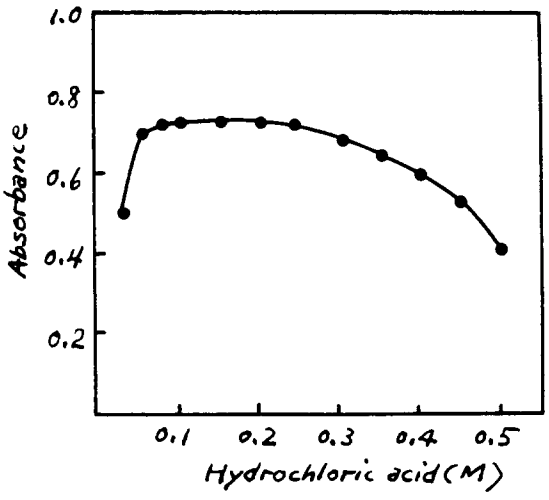


Fig. 2. Effect of acid concentration on the scandium–cerium–CPApA complex (wavelength $\lambda = 722$ cm; other conditions as for Fig. 1).

The reaction rate of $\beta$-complex formation in the scandium–cerium–CPApA systems is slow: maximum absorbance will be obtained after 3 h; however the reaction can be completed within 30 min if a smaller volume (10–15 ml) is used owing to the higher concentrations of the reactants; the solution is then diluted to 25 ml with water in the calibrated flask. The complex once formed will be stable for at least 3 h.

### 3.3. Analytical characteristics of the reaction

The calibration graph prepared by plotting absorbance vs. concentration of scandium was linear over the range 2–8 μg of scandium in 25 ml of solution. For convenience and for the determination of less than 2.0 μg of scandium, a standard addition–deduction method [3,15] was used; i.e. 2.0 μg of scandium were added to each of the standard solutions to construct a calibration graph (starting from 0 μg on the abscissa). For sample analysis, 2.0 μg of scandium were also added to each of the sample solutions; the scandium contents could then be determined directly from the calibration graph.

The straight-line equation obtained by a least-squares treatment ($n = 7$) was $A = 0.204C - 0.286$ ($r = 0.9980$), where $A$ is the absorbance recorded, $C$ is the concentration (number of micrograms of scandium in 25 ml of solution), and $r$ is the correlation coefficient. The apparent molar absorptivity for scandium was found to be $2.29 \times 10^5$ l mol$^{-1}$ cm$^{-1}$. Ten replicate analyses of a test solution containing 5 μg of scandium gave a coefficient of variation of 0.73%.

### 3.4. Effect of foreign ions

A solution containing 3 μg of scandium and various amounts of 37 possible accompanying ions were prepared, and procedure A was followed for the determination of scandium. As shown in Table 1, most of the ions do not interfere with the determination (maximum 5% error); 1.5- to 3-fold amounts of rare earths, uranium(VI), iron(III), titanium and zirconium are tolerated, as well as more than 10 mg magnesium, iron(II), copper and zinc. This property can be utilized to create a satisfactory method for the determination of scandium in these metals and their alloys without separation.

### 3.5. Composition of the complex

The molar composition of the scandium–cerium–CPApA complex was determined by the mole ratio method [16]. According to the conditions described in procedure A, the molar ratios of scandium to cerium(III) in a series of solutions were varied while CPApA was present in excess. An intersection point occurred when

Table 1
Tolerance limits (maximum 5% error) for foreign ions in the determination of 3 μg of scandium

| Foreign ion | Tolerance limit (μg) |
|---|---|
| Cu(II) | 60 000 |
| Zn(II) | 50 000 |
| $NH_4$(I) | 20 000 |
| Fe(III)[a] | 10 000 |
| Mg(II) | 10 000 |
| Mn(II) | 5000 |
| Sb(III) | 2000 |
| Ca(II) | 1500 |
| Ba(II), Cd(II), Ni(II), Co(II) | 1000 |
| Al(III), Sr(II) | 500 |
| V(V) | 200 |
| Cr(VI), Mo(VI), W(VI), Pb(II), Sb(V) | 100 |
| Pd(II) | 80 |
| Bi(III) | 50 |
| Ti(IV), Zr (IV) | 10 |
| La(III), Y(III), Ce(IV), U(VI), Fe(III) | 5 |
| Phosphate | 150 000 |
| Sulphate, ascorbate | 50 000 |
| Citrate | 40 000 |
| Nitrate, tartrate | 20 000 |
| Oxalate | 5000 |
| EDTA | 1500 |

[a] In the presence of 50 mg of ascorbic acid.

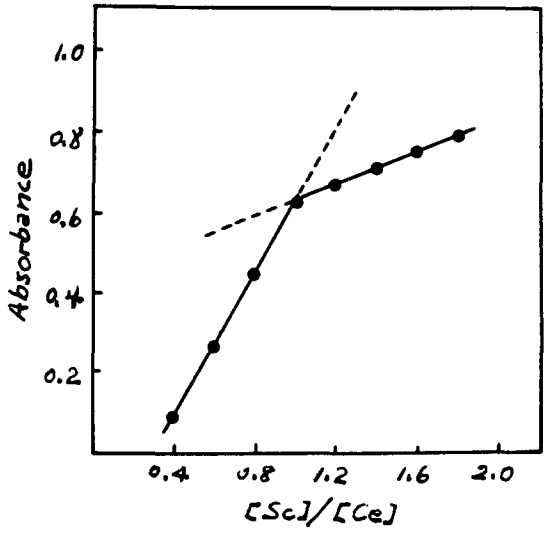


Fig. 3. Molar ratio of scandium to cerium in the ternary complex ($\lambda = 722$ nm; cerium, $4.4 \times 10^{-6}$ M; CPApA, $1.55 \times 10^{-5}$ M; HCl, 0.12 M).

[Sc]/[Ce] = 1 (Fig. 3). Similarly, the concentrations of CPApA were varied; when the mole ratio of scandium to cerium was fixed at 1, the intersection point was at [CPApA]:[Sc] = 2:1 (Fig. 4). Thus, the molar composition of the polynuclei ternary complex was estimated to be scandium:cerium:CPApA = 1:1:2.

### 3.6. Kinetic study and the mechanism of the complex formation

The formation of a hetero-polynuclei complex is often based on the formation of a homo-polynuclei complex [8,9]. In order to

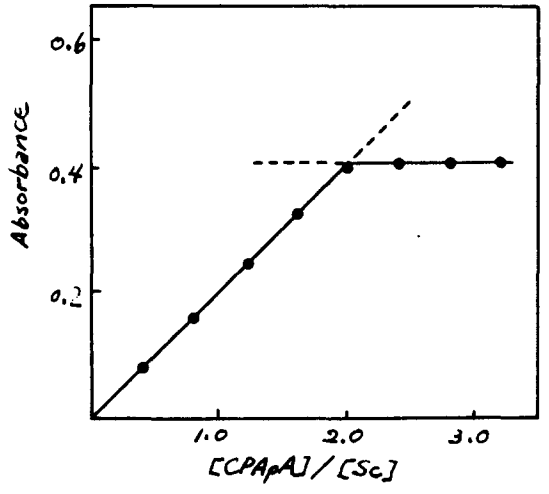


Fig. 4. Molar ratio of CPApA to scandium in the ternary complex (scandium, cerium, $2.70 \times 10^{-6}$ M; other conditions as for Fig. 3).

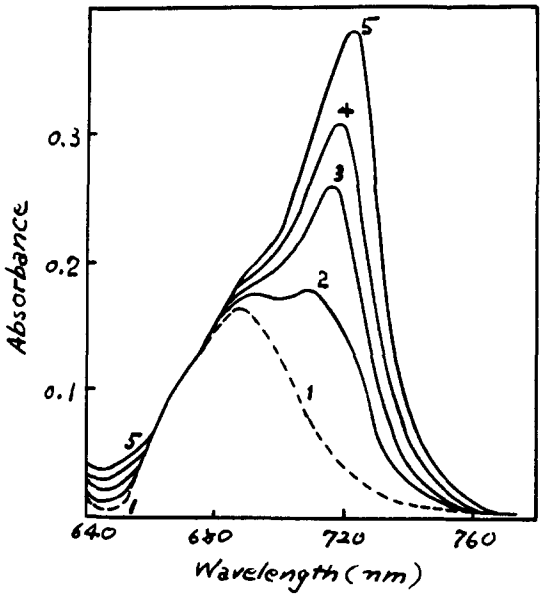


Fig. 5. Absorption spectra of the scandium–CPApA complex at (curve 1) 0 min; (curve 2) 5 min; (curve 3) 10 min; (curve 4) 20 min; (curve 5) 30 min (scandium, $4.44 \times 10^{-6}$ M; CPApA, $6.64 \times 10^{-6}$ M; HCl, 0.12 M; $T = 288$ K).

study the mechanism of the formation of the scandium–cerium–CPApA ternary complex, it is required that the nature of the scandium–CPApA binary complex be understood.

The absorption spectra of the scandium–CPApA complex are shown in Fig. 5. At the beginning of the reaction, an $\alpha$-type complex of scandium–CPApA is formed, with maximum absorption at 687 nm. After standing, the absorption peak will be gradually shifted to a longer wavelength (722 nm) and a $\beta$-type complex is then formed.

Under the conditions described in procedure B, $\log(A_{max} - A_t)$, $1/(A_{max} - A_t)$ and $1/(A_{max} - A_t)^2$ were plotted respectively versus $t$, where $A_{max}$ is the maximum absorbance and $A_t$ is the absorbance at the denoted time. As shown in Fig. 6, the linear relationship between $1/(A_{max} - A_t)$ and $t$ indicates that the transformation reaction of the $\alpha$-complex to the $\beta$-complex is a second-order reaction. The rate constant $K$ obtained from slope of the straight line is $1.72 \times 10^{-1}$ mol$^{-1}$ l min$^{-1}$.

Both the molar compositions of the $\alpha$-complex and the $\beta$-complex of scandium–CPApA were ascertained by the Asmus method [17], and the mole ratio and slope ratio [18] methods. All three methods indicated that the metal-to-ligand ratios of these two complexes were all 1:1. In considering the order of the

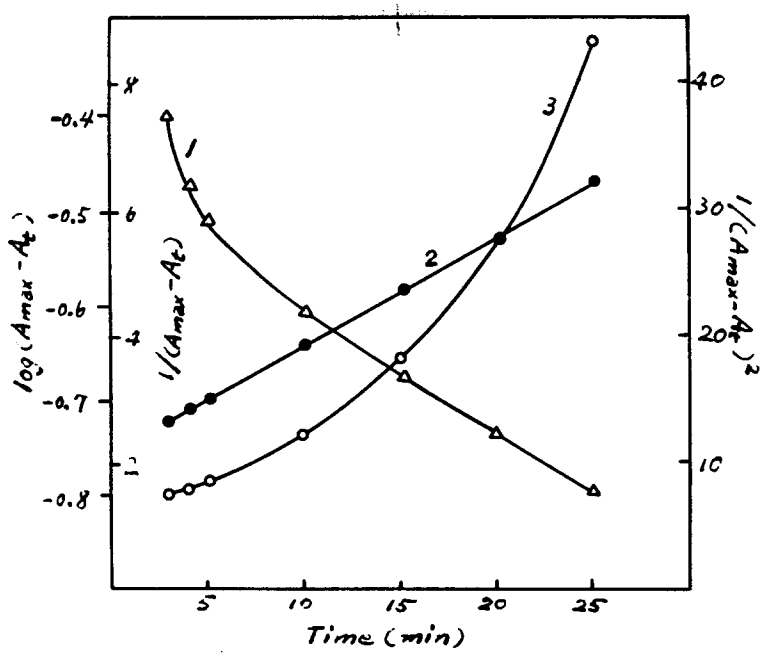


Fig. 6. Determination of the reaction order of the formation of the $\beta$-complex of scandium–CPApA ($\lambda = 722$ nm; other conditions as for Fig. 5). Curve 1, $\log(A_{max} - A_t)$ vs. $t$; curve 2, $1/(A_{max} - A_t)$ vs. $t$; curve 3, $1/(A_{max} - A_t)^2$ vs. $t$.

reaction, the $\beta$-complex of scandium–CPApA will be a dimer, i.e. $Sc_2(CPApA)_2$.

According to the experimental results, the complex formation reaction proceeded as follows.

(a) The $\alpha$-complexes of CPApA with scandium and cerium(III) are formed instantly at first (Eqs. (1) and (2)) (the charges on the ions are omitted for convenience).

$$Sc + CPApA \rightarrow Sc(CPApA) \quad (1)$$

$$Ce + 4CPApA \rightarrow Ce(CPApA)_4[6] \quad (2)$$

(b) Two molecules of the $\alpha$-complex of scandium–CPApA combine together to form one molecule of the $\beta$complex (Eq. (3)).

$$2Sc(CPApA) \rightarrow Sc_2(CPApA)_2 \quad (3)$$

Table 2
Results for the determination of scandium in alloys

| Sample | Scandium ($10^{-3}$%) | | | Relative standard deviation (%) | Recovery (%) |
|---|---|---|---|---|---|
| | Content | Found | Mean | | |
| Brass, BY 1901-2 | 4.6 | 4.70 4.68<br>4.58 4.72<br>4.71 | 4.68 | 1.21 | 102 |
| Aluminium–brass, BY 1912-1 | 9.0 | 9.02 9.04<br>8.88 8.99<br>9.15 | 9.02 | 1.08 | 100 |
| Manganese–brass, BY 1914-1 | 8.8 | 8.76 8.89<br>8.96 8.92<br>8.88 | 8.88 | 0.84 | 101 |
| Zinc alloy, 47# | 9.7 | 10.0 9.88<br>9.98 9.95<br>9.96 | 9.95 | 0.46 | 103 |
| Magnesium alloy, $ZM_5$ | 29.2 | 29.0 29.2<br>29.4 28.9<br>28.8 | 29.1 | 0.83 | 99.5 |

Table 3
Comparison of the sensitivities of methods for the spectrophotometric determination of scandium

| Reagent or system | pH | $\lambda_{max}$ (nm) | $10^{-4}\varepsilon$ ($l\ mol^{-1}\ cm^{-1}$) | Reference |
|---|---|---|---|---|
| Arsenazo I | 6.1 | 570 | 1.7 | [20] |
| Arsenazo III | 1.8 | 675 | 1.9 | [21] |
| Xylenol Orange | 0.01 M $HClO_4$ | 553 | 2.4 | [22] |
| Chlorophosphonazo(III) | 2.5 | 690 | 1.25 | [23] |
| Chlorophosphonazo-*p*-Cl | 2 [a] | 762 | 15.4 | [24] |
| 4-(2'-Thiazolylazo)resorcinol | 8.1 | 540 | 5.06 | [25] |
| Scandium–calcium–Alizarin Red | 3.5 | 528 | 6.6 | [26] |
| Scandium–bismuth–tribromoarsenazo | 0.48 M HCl | 635 | 7.1 | [27] |
| Scandium–lanthanum–*p*-fluorochlorophosphonazo | 0.48 M HCl | 730 | 8.6 | [28] |
| Scandium–Chrome Azurol S–N-dodecyldimethyl-aminoacetic acid | 7.0–7.8 | 620 | 30.0 | [29] |
| Scandium–cerium–*p*-acetylchlorophosphonazo | 0.12 M | 722 | 22.9 | Present method |

[a] Approximate.

(c) Finally, the $\beta$-complex of scandium–cerium–CPApA is formed by the reaction between the $\beta$-complex of scandium–CPApA and the $\alpha$-complex of cerium–CPApA (Eq. (4))

$$Sc_2(CPApA)_2 + 2Ce(CPApA)_4 \rightarrow 2Sc\text{–}Ce\text{–}(CPApA)_2 + 6CPApA \quad (4)$$

in which cerium(III) replaces one atom of the scandium in $Sc_2(CPApA)_2$, with the formation of two molecules of Sc–Ce–$(CPApA)_2$, and the absorbance of the ternary complex will be increased markedly.

### 3.7. Determination of scandium in alloys

Synthetic samples were prepared by introducing known amounts of scandium to standard samples of copper, zinc, and magnesium alloys [19], and the scandium contents were determined by using procedure c. The results obtained (Table 2) indicate that the method is reliable and accurate.

## 4. Conclusions

The present method, based on the formation of the scandium–cerium–*p*-acetylchlorophosphonazo(CPApA) complex, for the spectrophotometric determination of scandium in alloys is simple, accurate and reliable.

Compared with the spectrophotometric methods conventionally used for determination (Table 3), in terms of sensitivity, the described method is superior to the other methods except for that utilizing the scandium–Chrome Azurol S–*N*-dodecyldimethylaminoacetic acid systems. However, the latter suffers serious interferences from iron and aluminium.

Under the experimental conditions employed, 10 mg or more of magnesium, iron, copper and zinc do not interfere, and 0.5 mg of aluminum are tolerated. This gives the described method an advantage over the other methods.

## References

[1] T. Taketatsu and N. Kono, Chem. Lett., (1974) 989.
[2] T. Taketatsu, Bull. Chem. Soc. Jpn., 50 (1977) 1758.
[3] C.G. Hsu and J.M. Pan, Analyst, 110 (1985) 1245.
[4] W, R, Chen, J, M, Pan and W. Zheng, Huaxue Shiji, 8 (1986) 238.
[5] J, M, Pan, R. Yang and Z, J, Xu (C.G. Hsu), Fenxi Huaxue, 18 (1990) 1083.
[6] C, G, Hsu, H. Li and J.M. Pan, Talanta, 41 (1994) 1357.
[7] H.X. Shen and K.H. Xu, Fenxi Huaxue, 9 (1981) 17.
[8] H.X. Shen and L.Wu, Trace Anal., 5 (1989) 39.
[9] H.X. Shen and Z.N. Liu, Huaxue Xuebao, 41 (1983) 144.
[10] C.G. Hsu, X.M. Liao and J.M. Pan, Talanta, 38 (1991) 1051.
[11] J.M. Pan, R. Yang and C.G. Hsu, Anal. Chim. Acta, 257 (1992) 117.
[12] Z.J. Xu (C.G. Hsu), L. Zhang and J.M. Pan, Chin. J. Chem., 10 (1992) 424.
[13] J.Z. Gao, X.M. Zhu, J.W. Kang and G.B. Bai, Anal. Lett., 18(A12) (1985) 1507.
[14] J.Z. Gao, H. Chen and G.B. Bai, Inorg. Chim. Acta, 140 (1987) 271.
[15] C.G. Hsu, X.D. Wang, W.R. Chen and J.M. Pan, Microchem. J., 40 (1989) 175.
[16] H.X. Shen, Z.N. Liu, Fenxi Huaxue, 10 (1982) 399.

[17] E. Asmus, U. Hinz, K. Ohls and W. Richly, Fresenius' Z. Anal. Chem., 178 (1960) 104.
[18] A.E. Harvey and D.L. Manning, J. Am. Chem. Soc., 72 (1950) 4488.
[19] L.Z. Gu, D.H. Wu, Q.F. Ma and Z.M. Zhou, Fenxi Huaxue, 17 (1989) 658.
[20] H. Onishi and C.V. Banks, Anal. Chim. Acta, 29 (1963) 240.
[21] O. Kammori, I. Taguchi and K. Yoshikawa, Bunseki Kagaku, 15 (1966) 458.
[22] S.S. Berman, G.R. Duval and D.S. Russell, Anal. Chem., 35 (1963) 1392.
[23] V.I. Fadeeva and I.P. Alimarin, Zh. Anal. Khim., 17 (1962) 1020.
[24] W.R. Chen, J.M. Pan, C.G. Hsu and S.S. Ge, Mikrochim. Acta, III (1985) 417.
[25] T. Shimizu and E. Momo, Anal. Chim. Acta, 52 (1970) 146.
[26] M.X. Sun and J.C. Zhang, Fenxi Huaxue, 19 (1991) 70.
[27] H.S. Li and Q.Y. Luo, Fenxi Huaxue, 21 (1993) 908.
[28] J.M. Cao, H.S. Li and Z.Y. Hou, Fenxi Huaxue, 21 (1993) 1306.
[29] H.M. Shi and G.Z. Zhang, Fenxi Huaxue, 10 (1982) 716.

ELSEVIER

Talanta 42 (1995) 1913–1918

Talanta

# Spectrophotometric study of coproporphyrin-I complexes of copper(II) and cobalt(II)

Rita Giovannetti [a,*], Vito Bartocci [b], Stefano Ferraro [b], Maura Gusteri [b], Paolo Passamonti [b]

[a] *Centro Interdip. Grandi Apparecchiature, P. le G. da Varano, Università degli Studi di Camerino, 62032 Camerino, Italy*

[b] *Dipartimento di Scienze Chimiche, Via S. Agostino 1, Università degli Studi di Camerino, 62032 Camerino, Italy*

Received 15 February 1995; revised 27 April 1995; re-revised 23 May 1995; accepted 8 June 1995

**Abstract**

The reagent 3,8,13,18-tetramethyl-21*H*,23*H*-porphine-2,7,12,17-tetrapropionic acid or coproporphyrin-I (CPI) was used for the spectrophotometric determination of copper(II) and cobalt(II) in the presence of pyridine and imidazole catalysts. Optimum conditions were investigated and the methods were applied to the determination of parts per billion levels of copper(II) and cobalt(II). The Sandell sensitivities of the recommended procedures were 0.568 μm $cm^{-2}$ and 0.464 μg $cm^{-2}$ (for $A = 0.001$) for copper and cobalt, respectively. The relative standard deviations were 2.0% for copper and 1.0% for cobalt. The kinetics of the reaction of CPI with copper(II) and cobalt(II) in the presence of the catalysts and the influence of the temperature were studied, and their kinetic constants determined.

The influence of light on the photodecomposition of CPI was also studied.

*Keywords:* Copper(II); Cobalt(II); Spectrophotometry; Coproporphyrin-I

## 1. Introduction

Porphyrins have been extensively studied because of their biological importance and analytical applications. Particular attention has been given to the analytical use of porphyrins for spectrophotometric determinations of several metal ions, because they form very stable complexes with very high molar absorptivity (on the order of several hundred-thousands in a 400–500 nm field, the so-called Soret band). However, porphyrins have the disadvantage that the incorporation reaction of the metal ion into the porphyrin ring is generally very slow and must be accelerated by using several catalysts [1], or by metal exchange reactions [2,3]. In many cases, porphyrins have found analytical applications for the determination of several metal ions at the parts per million level [1,4–8].

It has been also observed that porphyrins undergo photoreduction reactions with the formation of stable photoproducts [9,10] that may play an important role in cancer therapy [11].

In this paper, a series of spectrophotometric studies on coproporphyrin-I (CPI) is described in order to verify its possible use for the determination of metal ions. The influence of light on CPI and on CPI complexes and the equilibria between CPI and copper(II) or cobalt(II), and the influence of several catalysts on the reaction rate are studied. A simple method for the spectrophotometric determination of copper(II) and cobalt(II) at the parts per billion level is developed.

* Corresponding author.


*SSDI* 0039-9140(95)01662-7

## 2. Experimental

### 2.1. Reagents

All reagents were of analytical grade and were used without further purification. All the solutions were prepared with distilled, demineralized water.

#### 2.1.1. CPI solution

A $2.8 \times 10^{-4}$ M stock solution was prepared by dissolving 102.1 mg of CPI dihydrochloride in 500 ml of 7.2 mM sodium hydroxide solution, and diluting with water.

#### 2.1.2. Standard copper(II) and cobalt(II) solutions

Stock aqueous solutions containing about 0.4 mmol of $CuCl_2$ or $CoCl_2 \cdot 6H_2O$ per litre, and sufficient acid to prevent precipitation, were prepared. The stock solutions were standardized by inductively coupled plasma (ICP) determinations.

### 2.2. Apparatus

A Hewlett-Packard 8452 A diode-array spectrophotometer with a 1 cm quartz cell connected to a Lauda K2R thermostat was used for the absorbance measurements.

A Metrohm 655 pH meter was used for pH measurement.

An inductively coupled plasma Jobin Yvon JY 24R instrument was used for the metal solution standardization.

A 150 W Osram xenon lamp was used for the photochemical reaction study.

### 2.3. Recommended procedures

#### 2.3.1. Photometric measurements

Ten sample solutions containing from $3 \times 10^{-6}$ M to $2 \times 10^{-5}$ M of CPI at pH ranging from 1 to 13, previously degassed with a nitrogen flow, were illuminated with UV-Vis radiation by use of a xenon lamp with interference filters. An infrared absorbing glass and a water cell were placed in the light path and the absorbance was measured every 5 min in the range from 200 to 800 nm in a 10 mm cell, against a blank.

#### 2.3.2. Kinetic measurements

In 10 ml volumetric flasks were placed from 0.1 to 0.6 ml of the standard solution of CPI, and from 0 to 5 ml of the stock solution of the metals, followed by over 2.5 ml of 4 M imidazole or pyridine solution. The pH of these solutions was adjusted to 8 by the addition of perchloric acid, and the solutions were brought to volume with water. The ionic strength was maintained constant at 0.2 M with sodium perchlorate. The absorbance–time curves of the solutions were obtained by measuring the absorbance every 2 min at 414 nm for the cobalt complex, and at 380 nm for the copper complex in a 10 mm cell against a blank, at temperatures ranging from 20 to 40 °C.

#### 2.3.3. Spectrophotometric titration

Ten samples, containing about 0.1 μg $ml^{-1}$ of cobalt(II) or copper(II), and sufficient $NaClO_4$ and $HClO_4$ to adjust the ionic strength to 0.2 M and the pH to 8, were titrated with a $2.8 \times 10^{-4}$ M CPI solution. After each addition, the solutions were heated in a water bath at 80 °C (with catalysts) or at 90 °C (without catalysts), for 10 min. They were then cooled in cold water, and the absorbances were measured at 414 nm or 380 nm, respectively, in a 10 mm cell thermostatted at 20 °C, against a blank.

#### 2.3.4. Calibration curve method

Calibration curves were obtained by mixing increasing quantities of cobalt(II) or copper(II) (from 35 to 128 ppb) with a slight excess of CPI at pH 8 and ionic strength 0.2 M. Each solution was heated in a water bath at 90 °C for 10 min. After cooling in cold water, the absorbance was measured at 414 nm or 380 nm, respectively, in a 10 mm cell thermostatted at 20 °C, against a blank.

## 3. Results and discussion

### 3.1. Photometric measurements

An aqueous solution of CPI with pH 8 and ionic strength 0.2 mol $l^{-1}$ was deep pink and displayed absorption maxima at 372 nm (Soret band; $\varepsilon = (1.16 \pm 0.02) \times 10^5$ and at 500, 538 and 558 nm, and a shoulder at about 606 nm. The illumination with light of degassed solutions of CPI at pH 5–13 caused the formation of a stable and colourless photoproduct. In Fig. 1 are presented (curves (a)) spectra of CPI, showing an absorbance decrease as a function of time due to exposure to light. The spectrum of the photoproducts has absorption maxima

at 220 and 264 nm, and a shoulder at around 380 nm (see Fig. 1, curve (b)). The photoreaction may be represented by the equation

$$CPI + h\nu \rightarrow \text{photoproduct}$$

the corresponding kinetic equation of which was

$$-\frac{d[CPI]}{dt} = k[CPI] \quad (1)$$

where $k_1$ is the first-order rate constant.

The plots of ln(1/[CPI]) versus the exposure time, measured at two different wavelengths, give good straight lines, the slopes of which represent the first-order rate constant. The two values obtained are in good agreement: $k_{372} = (4.39 \pm 0.01) \times 10^{-6}\ s^{-1}$; $k_{388} = (4.50 \pm 0.02) \times 10^{-6}\ s^{-1}$.

No photoreaction has been observed, either in acidic solution or in the presence of metal ions.

### 3.2. Absorption spectra of the complex

In the presence of an excess of metal, the absorption spectra of metal–CPI complexes gave absorption maxima at 414 nm (Soret band; $\varepsilon = (1.01 \pm 0.05) \times 10^5$ with pyridine and $\varepsilon = (1.95 \pm 0.03) \times 10^5$ with imidazole) for cobalt (Fig. 2, curve (a)) and at 380 nm (Soret band; $\varepsilon = (1.12 \pm 0.01) \times 10^5$ with pyridine and $\varepsilon = (2.03 \pm 0.02) \times 10^5$ with imidazole) for copper (Fig. 2, curve (b)).

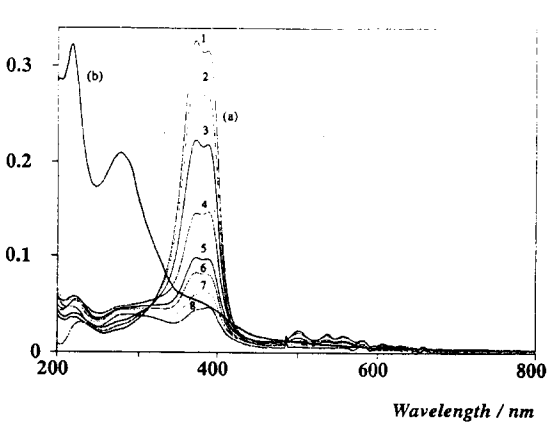


Fig. 1. Curves (a), absorption spectra of CPI ($2.2 \times 10^{-6}$ M; pH 8; ionic strength, 0.2 M) after: (spectrum 1) 0 min; (spectrum 2) 5 min; (spectrum 3) 10 min; (spectrum 4) 15 min; (spectrum 5) 20 min; (spectrum 6) 35 min, (spectrum 7) 40 min, (spectrum 8) and 45 min of light exposure. Curve (b), spectrum of the photoproducts obtained after the light exposure of CPI (absorbance × 5).

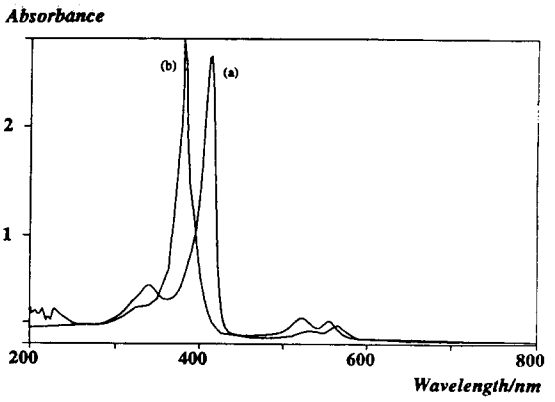


Fig. 2. The absorption spectra of (curve (a)) the cobalt–CPI ($1.34 \times 10^{-5}$ M) complex and (curve (b)) the copper–CPI ($1.38 \times 10^{-5}$ M) complex at pH 8, an ionic strength of 0.2 M, and with imidazole as catalyst.

### 3.3. Composition of the complex

The stoichiometry of the reactions in the copper–CPI and cobalt–CPI systems has been determined by applying the mole ratio method; the ratio was 1:1 in both cases (Fig. 3).

### 3.4. Reaction rate for the formation of the complex

The rate of formation of CPI complexes with metal ions was generally very slow. In order to increase the reaction rate, we carried out measurements in the presence of a catalyst at 20 °C or at higher temperatures in the absence of catalyst. By using pyridine or imidazole as catalysts, an increase in the reaction rate of about 10 times with respect to the uncatalyzed reaction was observed. The reaction rates depended on the pH, and a maximum value was reached at about pH 8. Measurements carried

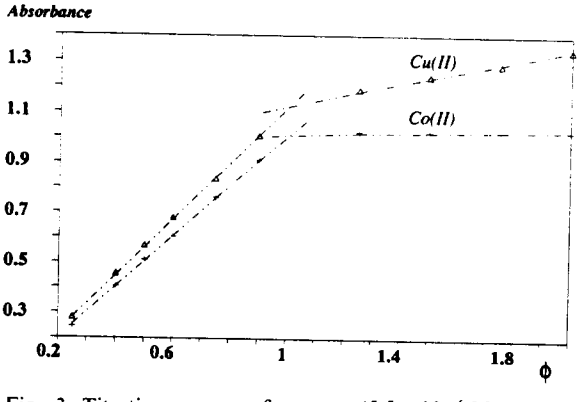


Fig. 3. Titration curves of copper ($5.5 \times 10^{-6}$ M) and cobalt ($5.1 \times 10^{-6}$ M) by CPI at pH 8, ionic strength 0.2 M, with imidazole as catalyst ($\phi$ indicates the CPI: metal ion ratio).

Table 1
First- and second-order kinetic constants for copper and cobalt complexes with different catalysts at 20°C

| Catalyst | Cu(II) | | Co(II) | |
|---|---|---|---|---|
| | $k_1$ ($s^{-1}$) | $k_2$ ($l\ mol^{-1}\ s^{-1}$) | $k_1$ ($s^{-1}$) | $k_2$ ($l\ mol^{-1}\ s^{-1}$) |
| Pyridine | $(5.05 \pm 0.02) \times 10^{-2}$ | $26.85 \pm 1.01$ | $(5.14 \pm 0.03) \times 10^{-2}$ | $23.81 \pm 3.12$ |
| Imidazole | $(4.69 \pm 0.01) \times 10^{-2}$ | $24.88 \pm 0.94$ | $(1.45 \pm 0.02) \times 10^{-2}$ | $18.22 \pm 2.93$ |

Copper(II) and cobalt(II), $4 \times 10^{-6}$–$2 \times 10^{-4}$ M; CPI, $2.8 \times 10^{-6}$–$1.68 \times 10^{-5}$ M; pyridine and imidazole, 1 M; ionic strength, 0.2 M ($NaClO_4$).

out in the presence of a large excess of metal (1:100 relative to CPI) at pH 8 and in the presence of a catalyst at 20 °C have shown that the reactions were completed within 30 min, and followed first-order kinetics, the rates of which may be represented by the equation

$$-\frac{d[CPI]}{dt} = k_1[CPI] \quad (2)$$

where $k_1$ is the conditional rate constant, involving the concentration of hydrogen ions, cobalt or copper.

The plots of $(1/C_L) \ln[(A_0 - A_\infty)/(A_t - A_\infty)]$ versus $t$ (where $A_0$, $A_t$ and $A_\infty$ denote the absorbances of the system at times 0, $t$, and infinity, respectively) give good straight lines, the slopes of which represent the conditional rate constants. Measurements carried out under the same conditions as described above, but in the presence of a small excess of metal (1:5 relative to CPI), showed second-order kinetics, corresponding to the equation

$$-\frac{d[CPI]}{dt} = k_2[M][L] \quad (3)$$

where $k_2$ is the second-order rate constant, involving only the hydrogen ion concentration.

The plot of $[1/(C_M - C_L)] \ln([M]/[L])$ versus $t$ (where $C_M$ and $C_L$ denote the metal and ligand concentration, respectively $[M] = C_M - C_L[(A_0 - A_t)/(A_t - A_\infty)]$ and $[L] = C_L[(A_t - A_\infty)/(A_0 - A_\infty)]$) gave a straight line, the slope of which provided the value of $k_2$. All the results are summarized in Table 1.

Measurements performed under the same conditions but without a catalyst, at temperatures ranging from 20 to 40 °C, showed an increase in the reaction rate of about 0.2 times per degree. At 20 °C, the catalyzed reaction rate is about half that of the uncatalyzed reaction at 40 °C. Plots of $\ln k_1$ against $1/T$ at different wavelengths allowed the determination of the activation energy according to the relationship $\ln k = \ln A - E_a/RT$. The mean value for the cobalt complex was $(4.9 \pm 0.1) \times 10^4\ J\ mol^{-1}$.

### 3.5. Spectrophotometric titration

These titrations have given well-defined curves. A typical plot is shown in Fig. 3. The equivalence point is in accordance with the formation of a 1:1 complex. Using this method, amounts of copper and cobalt in the range $10^{-7}$–$10^{-5}$ M can be determined with relative standard deviations of 2.0% and 1.0%, respectively.

### 3.6. Calibration curve method

Calibration curves obtained according to the procedure described give good straight lines, the equations of which were

$$\text{Amount of Cu} = 0.568(A_0 - A)$$

$$\text{Amount of Co} = 0.464(A_0 - A)$$

where copper and cobalt are in units of micrograms per millilitre, and $A_0$ and $A$ are the absorbances of the reagent blank and the sample, respectively. Minimum detectable amounts in the copper and cobalt determinations were on the order of parts per billion, with a sensitivity for the 0.001 absorbance (Sandell index [7]) of 0.568 $\mu g\ cm^{-2}$ for copper(II) and 0.464 $\mu g\ cm^{-2}$ for cobalt(II). The sensitivity for the copper(II) determination is eight times greater than the sensitivities of the bathocuproine, cuprizon, sodium diethyl dithiocarbamidate methods, and is comparable with that of the diphenylcarbazide method [12–16]. For the cobalt(II) determination, the sensitivity is ten times greater than those obtained using a nitroso-R salt and 2-nitroso-1-naphthol, is four times greater than when using 1-nitroso-2-naphthol, and is twofold greater

than that obtained for the 1-(2-pyridylazo)resorcinol methods [12,15].

### 3.7. Effect of foreign ions

Solutions containing 0.1 mg $l^{-1}$ of copper(II) or cobalt(II) and varying concentrations of several ions metals were analyzed in order to ascertain whether they interfered with the determinations. Mn(II), Zn(II), Ni(II), Pb(II), Cr(II), Fe(III), Mg(II), Ca(II), Sr(II) and Ba(II) did not interfere up to 100 mg (about a one-thousandfold excess). Pd(II), Fe(II) and Hg(II) interfered in the determination. The interference of Pd(II) was removed by the addition of 0.01 M potassium iodide solution, while the interference of Fe(II) was removed by preliminary oxidation to Fe(III). Hg(II) reacted quickly with the CPI and its interference was avoided by the addition of hydroxylamine.

## 4. Conclusions

The illumination of CPI using a UV-Vis light source caused the formation of stable and colourless photoproducts with absorption bands at 220 and 264 nm at pH above 6. In contrast in acidic solutions, and in the presence of metal ions, CPI did not photodecompose. This fact suggests that the photoreaction begins inside the CPI ring in the absence of crowding. The porphyrin ring can be reduced by photochemical or chemical action, giving phlorin, displaying absorption maxima at 400 and 735 nm, porphomethene (500 nm) and porphyrinogen (about 200 nm). The photoreduction proceeds through distinct stages; the third stage (porphyrinogen) is a completely colourless compound that could be reached only with several reducing agents [18]. The photoreduction can concern the $2\beta$ bonds of the pyrroles (absorption maxima at about 650 nm) [19] with the formation of chlorine. The product obtained on irradiation of CPI exhibited the characteristic band of porphyrinogens, therefore this product is the most favourable in this phototransformation. The phototransformation rate was very slow with respect to the complexation reaction rate, in such a way that it did not influence the determination of the kinetic complexation constants and the metal ions.

The Soret bands of CPI and its metal complexes at pH 8 were located at 372 and 414 nm (Co(II)) and 380 nm (Cu(II)). In the analytical determination of cobalt(II), the distance of the complex from the CPI band was sufficient for an easy determination of the absorbance peak, while in the Cu(II) determination, a gaussian decomposition of the peaks was necessary. The application of these direct reactions was impractical because of their small reaction rates even in the presence of catalysts. Actually, after each addition of titrant (CPI), it was necessary to wait at least 10 min for completion of the reactions. Because of the very large absorptivities of CPI and its complexes, after the equivalence point the measured absorbances were proportional to the difference between the absorptivities of CPI and the metal complexes. This influence on the titration curves was more evident for copper than for cobalt (due to the smaller distance between CPI and the peaks of the complex); however, this fact does not influence the titration end point (Fig. 3). This method presents several advantages compared with common titrants, because it forms extremely stable metal complexes with a molar ratio of 1:1 and with a very large molar absorptivity, as well as, high sensitivities, greater than or comparable with those obtained with other ligands.

The calibration curve method was more practical than the titration method because although it was an equally sensitive technique, it was less time consuming. In conclusion, CPI may be considered as a suitable titrant for the determination of several metals despite the low reaction rate observed. Trace amounts of copper or cobalt ions may be directly determined by spectrophotometry with sensitivities of $0.568 \times 10^{-3}$ μg $cm^{-2}$ and $0.464 \times 10^{-3}$ μg $cm^{-2}$ for copper and cobalt, respectively.

## References

[1] M. Tabata and M. Tanaka, Trends Anal. Chem., 10 (1991) 128.
[2] C. Grant and P. Hambright, J. Am. Chem. Soc., 91 (1969) 4195.
[3] K. Kavamura, S. Igarashi and T. Yotsuyanagi, Anal. Sci., 4 (1988) 175.
[4] J.I. Itoh, T. Yotsujanagi and K. Aomura, Anal. Chim. Acta, 74 (1975) 53.
[5] H. Ishii and H. Koh, Talanta, 24 (1977) 417.
[6] M. Tabata, Analyst, 112 (1987) 141.
[7] M. Tabata and N. Kajihara, Anal. Sci., 5 (1989) 719.
[8] M. Tabata and K. Taneko, Analyst, 116 (1991) 1185.
[9] D. Mauzerall, J. Am. Chem. Soc., 84 (1962) 2437.

[10] M. Rougee, T. Ebbesen, F. Ghetti and R.V. Bensasson, J. Phys. Chem., 86 (1982) 4404.
[11] R. Rotomskis, V. Vaicaitis and A. Piskarkas, Chem. Phys. Lett., 202 (1993) 233.
[12] Z. Marczenko, Spectrophotometric Determination of Elements, Wiley, New York, London, Sidney, Toronto, 1976.
[13] J. Friesu and H. Getrost, Organishe Reagenzien fur die Spurenanalyzse, Merck, Darmstadt, 1975.
[14] A.I. Busey and V.M. Ivanov, Z. Anal. Chem., 18 (1963) 208.
[15] W.J. Geary, G. Nickless and F.H. Pollard, Anal. Chim. Acta, 26 (1962) 575.
[16] R.E. Stoner and W. Dasier, Anal. Chem., 32 (1960) 1207.
[18] D. Mauzerall, J. Am. Chem. Soc., 84 (1962) 2437.
[19] H. Alsoph Corvin and O.D. Collins, J. Am. Chem. Soc., 27 (1962) 3060.

ELSEVIER

Talanta 42 (1995) 1919–1923

Talanta

# Conductimetric analysis of the ion binding properties of three leaf extracts of chestnut (*Castanea sativa*), Eucalyptus (*Eucalyptus globulus*) and oak (*Quercus robur*)

F. Rey[a,*], M. Pérez-Asenjo[a], A.A.S.C. Machado[b], P. Facal[a], M.A. Ferreira[a], A. Toja[a]

[a] *Area de Química Física, Universidad de Vigo, Torrecedeira 86, Vigo, Spain*
[b] *LAQUIPAI, Departamento de Química, Faculdade de Ciencias, P-4050 Porto, Portugal*

Received 10 March 1995; revised 23 May 1995; accepted 8 June 1995

**Abstract**

Humic materials extracted from tree leaves of chestnut (*Castanea sativa*), eucalyptus (*Eucalyptus globulus*) and oak (*Quercus robur*) were analyzed by performing conductimetric titrations. Values between about 84 and 236 $\mu S\,cm^{-1}$ for the molar conductivity and between 0.42 and 0.74 for the charge distribution parameter were obtained when the concentrations of the extract are increased from 40 to 100 $mg\,l^{-1}$. These variations were explained by using the counterion condensation theory, and the distance between the charged groups of the polyions, the volume of the counterion condensation and the Debye–Hückel potential were also calculated.

*Keywords:* Conductimetry; Humic acids; Leaf extract

## 1. Introduction

The organic matter of soils is constituted mainly from humic materials (humic acids (HA) and fulvic acids (FA)), polyelectrolyte compounds which play an important role in the behaviour of metals in soils and aquatic environments, due to their ability to complex metal ions. On the other hand, these humic materials are formed by microbial degradation and percolation of water through leaves and other organic litter, so a knowledge of the behaviour and structural properties of leaf extracts in solution may be of interest in understanding the chemical behaviour of humic materials.

In order to study these polyelectrolyte materials in solution, many different techniques (i.e. potentiometry, dialysis, fluorescence spectroscopy, etc.) have been used. Conductimetric titrations are an important tool in the study of these types of compounds, because they provide information on association phenomena and on the nature and behaviour of charged groups [1–11]. However, interpretation of the experimental results has been difficult. The development of the condensation theory [12] was an important advance in the explanation of the polyelectrolyte properties of solutions [13–16], and recently van Leeuwen et al. [17] summarised existing theories of association phenomena and reviewed the literature relating to conductimetric analysis of polyelectrolyte systems. These authors stressed the difficulty of understanding the concentration dependence of the conductivity of polyelectrolyte solutions.

* Corresponding author.


*SSDI* 0039-9140(95)01663-5
TAL 42:12-H

In the present work, the influence of concentration on the conductimetric analysis of the extracts obtained from leaves of three types of trees common in the forests of the Galician country (N.W. Spain), i.e. oak, eucalyptus and chestnut, when titrated with alkali metal hydroxides, is reported. The parameters relating to the "condensation" of counterions (i.e. the line charge density, $\xi$, and the Debye–Hückel potential, $\psi(a)$) and the volume of the zone of the counterion condensation, $V_p$, are calculated.

## 2. Experimental

All reagents were p.a. or similar, and were used without further purification. Carbon-dioxide-free deionised water with resistivity 20 MΩ cm or above was used.

The solutions of the metal ions ($Li^+$, $Na^+$ and $K^+$) were prepared by dilution of stock solutions of their respective hydroxides. Their concentrations were determined by titration with standardised HCl.

The extracts of oak, chestnut and eucalyptus were obtained from leaves collected in different forests of Galicia, and were extracted by using the standard procedure recommended by the IHSS for FA [18,19]. For this purpose, the leaves were dried in air, shaken with 2 M hydrochloric acid solution diluted with water to pH approximately 2, concentrated on Amberlite XAD-8 resin, transformed to their acidic form using cation-exchange resin (Merck ion exchanger I) and freeze-dried. The yield of the process was about 0.3% (w/w).

A CRISON microCM 2101 conductimeter, equipped with a platinum cell (nominal constant 1) and calibrated with a 0.01000 M KCl solution, was used to obtain the conductance of the FA solutions.

In the experiments, 50 ml of diluted salt-free solutions of the extracts (concentrations, 40, 60, 80 and 100 $mg^{-1}$, except for oak because its 100 $mg\,l^{-1}$ solutions were unstable), were introduced into a thermostatted cell (298.0 ± 0.1 K) until thermal equilibrium was reached, and were titrated with metal hydroxide (approximately 0.018 M, in steps of 25 μl) with a CRISON μBUR 2031 burette. Prior and during the titrations the samples were purged and stirred with $CO_2$-free dry air. The conductance values were recorded after stabilisation (conductance variations of 0.1 μS cm or less per 2 min) and average values of three repeated experiments (the differences were less than 0.2 μS cm) were used in the calculations.

## 3. Calculations

The interpretation of the conductimetric behaviour of polyelectrolyte systems is not easy and different theories attemtping to explain it have been published [17]. Of these, the line charge model seems the most interesting, because of the good correlation of predictions with the experimental results and the relatively large number of parameters which can be calculated from the experimental data.

The basic starting point for understanding the conductimetric curves of polyelectrolyte systems is the expression for the molar conductivity (Λ) of a solution which contains only polyions p and their respective counterions

$$K = f(\lambda_c + \lambda_p)C_p$$

$$\Lambda = f(\lambda_c + \lambda_p) \quad (1)$$

where $K$ is the conductance of the solution, $C_p$ is the molar concentration of deprotonated groups of the polyion, Λ is the molar conductivity ( $= K/C_p$ [17]), $\lambda_c$ is the conductivity of the counterions, $\lambda_p$ is the conductivity of the polyion and $f$ ($= 1 - \theta$, where $\theta$ is the fraction of countercharges bounded to the polyion) is a charge distribution parameter which can be related to the fraction of free counterions. The molar conductivity is calculated from the experimental plots of the conductance of the polyelectrolyte solutions vs. the amount of metal hydroxide added in the zone where the concentrations of $H^+$ and $OH^-$ are not great [20]. This equation can be modified [21] to consider $\lambda_c^0$ (the conductivity of the counterions in pure solvent, available from the literature), instead of $\lambda_c$

$$\Lambda = f(\lambda_c^0 + \lambda_p) \quad (2)$$

Eq. (2) expresses the fact that Λ is proportional to $\lambda_c^0$ and, if linear plots are obtained [22], the slope and intercept of the plot of Λ vs. $\lambda_c^0$ for different monovalent cations allows the calculation of $f$ and $\lambda_p$ [23].

On the other hand if it is assumed that the polyion can be considered as a long cylinder with a sufficiently high charge density (due to the presence of a large amount of deprotonated groups in different sites), Manning [13,21] found the following relationships between $f$

and a dimensionless line charge density $\xi$ ($\lambda_p$-dependent; see also Eqs. (7) and (9))

$$f = 0.866|z|^{-1}\xi^{-1} \quad (\xi \geqslant |z|^{-1}) \tag{3}$$

$$f = 1 - \frac{0.55\xi^2}{\pi + \xi} \quad (\xi \leqslant |z|^{-1}) \tag{4}$$

where $z$ is the charge of the cation (Eq. (4) holds for $|z| = 1$ only). On the other hand, $\xi$ is related to the average spacing between charged sites of the polyion, $l$

$$\xi = \frac{l_B}{l} \tag{5}$$

where $l_B$ is the Bjerrum length, defined as

$$l_B = \frac{e^2}{4\pi\varepsilon\varepsilon_0 kT} \tag{6}$$

where $\varepsilon\varepsilon_0$ is the permitivity of the solution. From Eqs. (3)–(6), $\xi$ and $l$ values can be estimated from $f$.

Moreover, if the relaxation effect is considered [21], the following relationship between $\lambda_p$, $\lambda_c^o$, the radius of the cylinder, $a$, and a reciprocal screening length, $\kappa_D$, can be obtained

$$\lambda_p = \frac{0.866H\lambda_c^0 \ln|\kappa_D a|}{|z|\lambda_c^0 + 0.134H \ln|\kappa_D a|} \tag{7}$$

In this expression, $H$ is a standard electrophoretic mobility factor defined by

$$H = \frac{4\varepsilon\varepsilon_0}{3\eta} RT \tag{8}$$

$\eta$ is the viscosity of the polyelectrolyte solution, and $\kappa_D$ can be calculated from

$$\kappa_D^2 = \frac{F^2 C_p}{\varepsilon\varepsilon_0 RT\xi} \tag{9}$$

In the same way, a relationship can be obtained for the electrostatic potential at the surface of the cylinder of radius $a$ ($\Psi(a)$), due to the presence of the counterions ($|z| = 1$ only)

$$\psi(a) = \frac{2kT \ln|\kappa_D a|}{e} \tag{10}$$

Finally, when $\xi$ exceeds unity, the volume of the zone of counterion condensation, $V_p$, (in cubic centimetres per mole if $l$ is expressed in Angströms) can be related to $\xi$ by the equation [24]

$$V_p = 41.1(\xi - 1)l^3 \tag{11}$$

## 4. Results and discussion

The titration curves of polyelectrolyte solutions with metal hydroxides show three different regions (in Fig. 1 a set of typical experimental titration curves at different extract concentrations is presented as an example): (a) the initial part of the curve, where the conductivity decreases down to a minimum, which can be attributed to the neutralisation of free $H^+$ ions by added metal hydroxide; (b) the region after the minimum, where the conductivity increases slowly due to an increase in both negatively charged groups on the polyelectrolyte molecules and the concentration of free metal ions; and (c) the final part, where a larger slope is obtained due to an increase in the concentration of free metal hydroxide.

Of these three regions, the second (where the concentrations of $H^+$ and $OH^-$ ions are low) is the most important for performing the calculations of the conductimetric parameters of polyelectrolytes, because the conductivity depends only on the fraction of free counterions, and on the molar conductivities of the counterion in the pure solvent and the polyion. Therefore, application of Eqs. (1) or (2) allows the calculation of $f$ and $\lambda_p$. These equations predict that the plots of $K$ vs. $C_p$ have an intercept equal to zero; if this is not the case, the $K$ values must be corrected by subtracting the value of $K$ obtained by extrapolation of $OH^-_{added}$ to zero. Values for $\lambda_p$ and $f$ in that region of the curves for the three extracts analysed, obtained by using Eq. (2), are sum-

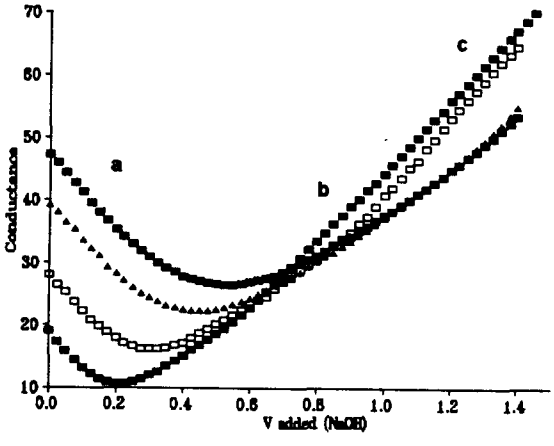


Fig. 1. Variation of the conductance ($\mu S\ cm^{-1}$) of eucalyptus extract solutions (of concentrations (■) 40 mg $l^{-1}$, (□) 60 mg $l^{-1}$, (▲) 80 mg $l^{-1}$ and (⊠) 100 mg $l^{-1}$) when titrated with NaOH. For an explanation of the a, b and c regions, see the text.

Table 1
Parameters obtained from the conductimetric titration of eucalyptus, chestnut and oak

| Parameter | Extract concentration ($mg\,l^{-1}$) | | | |
|---|---|---|---|---|
| | 40 | 60 | 80 | 100 |
| Eucalyptus | | | | |
| $f$ | 0.43 | 0.58 | 0.78 | 0.74 |
| $\lambda_p$ | 199.9 | 146.8 | 84.2 | 98.1 |
| $\xi$ | 2.01 | 1.49 | 1.11 | 1.17 |
| $l$ (Å) | 3.6 | 4.8 | 6.4 | 6.1 |
| $V_p$ | 1937 | 2227 | 1185 | 1586 |
| $\psi(a)$Li (V) | 2.1 | 0.74 | 0.27 | 0.34 |
| $\psi(a)$Na (V) | 1.1 | 0.56 | 0.24 | 0.29 |
| $\psi(a)$K (V) | 0.72 | 0.44 | 0.21 | 0.26 |
| Chestnut | | | | |
| $f$ | 0.42 | 0.53 | 0.55 | 0.44 |
| $\lambda_p$ | 235.8 | 169.2 | 154.2 | 197.4 |
| $\xi$ | 2.06 | 1.65 | 1.58 | 1.97 |
| $l$ (Å) | 3.4 | 4.3 | 4.5 | 3.6 |
| $V_p$ | 1712 | 2124 | 2172 | 1726 |
| $\psi(a)$Li (V) | 9.7 | 1.1 | 0.85 | 2.0 |
| $\psi(a)$Na (V) | 1.8 | 0.74 | 0.62 | 1.1 |
| $\psi(a)$K (V) | 0.98 | 0.55 | 0.48 | 0.71 |
| Oak | | | | |
| $f$ | 0.47 | 0.69 | 0.51 | –[a] |
| $\lambda_p$ | 226.8 | 131.2 | 185.7 | –[a] |
| $\xi$ | 1.84 | 1.25 | 1.69 | –[a] |
| $l$ (Å) | 3.9 | 5.7 | 4.2 | –[a] |
| $V_p$ | 2048 | 1903 | 2101 | –[a] |
| $\psi(a)$Li (V) | 5.4 | 0.58 | 1.54 | –[a] |
| $\psi(a)$Na (V) | 1.6 | 0.46 | 0.91 | –[a] |
| $\psi(a)$K (V) | 0.90 | 0.38 | 0.64 | –[a] |

[a] Values not available (see text).

marised in Table 1 (statistical treatment of the plots showed that the above-mentioned corrections were not required).

The results show that an initial decrease of $\lambda_p$ occurs when the concentration of the extract rises until a minimum is reached (at about 60–80 $mg\,l^{-1}$, depending on the extract). The eventual increase in $\lambda_p$ (and related variables) can be attributed to changes in the conformational structures of the polyelectrolyte molecules. These results are in agreement with the theoretical decrease of $\lambda_p$ when the number of deprotonated groups of polyelectrolyte increases [17], due to an increment in the polyion radius and a consequent decrease in $\xi$. As $f$ and $\xi$ are inversely related (Eqs. (3) and (4)), a parallel increase in the fraction of conductimetrically free counter ions is also observed.

From the calculated $f$ values, the line charge density, $\xi$, and the distances between charged groups ($l$) were estimated using Eqs. (3)-(6). The values obtained (also listed in Table 1) fall in the range 3.4–6.4 Å, and are similar to published values for similar systems [24,25], which confirms the polyelectrolyte nature of the extracts. As for $f$, an increment in the $l$ values is observed when the concentration increases, in agreement with an increase in the viscosity values (obtained in salt-free solutions of the extracts) with concentration (the viscosity increases up to 60–80 $mg\,l^{-1}$, but a marked decrease is observed at the highest concentration [25] and this suggests an unscrolling of polyelectrolyte molecules in the concentration range from 40 to 60–80 $mg\,l^{-1}$ and a later scrolling due to changes in their conformation.

From $\lambda_p$ and $\eta$, values of $\psi(a)$ and $V_p$ were estimated using Eqs. (10) and (11). An initial decrease in the Debye–Hückel potential when the concentration increases is obtained; this can be attributed to the enlargement of the extract molecules, in good agreement with the $l$ and $f$ variations calculated before, and with others reported for FA [26]. On the other hand, no definite trend was found for the $V_p$ values, due to the small influence of the counterions on the size of the condensation volume.

When the parameters calculated for the three different extracts are compared, significant differences appear for the eucalyptus at the higher concentrations analyzed. The $f$ and $l$ values are higher than for the other two extracts, showing that the distance between groups is larger and a higher number of counterions are conductimetrically free. This behaviour is in agreement with the less acidic nature of the eucalyptus extract, determined previously [27].

## Acknowledgment

The authors acknowledge the concession of an Acción Integrada Hispano–Portuguesa for the development of this work to the Ministerio de Asuntos Exteriores of Spain and the Conselho de Reitores das Universidades Portuguesas of Portugal.

## References

[1] S. Odén, Ber. Dtsch. Chem. Ges., 35 (1912) 651.
[2] M. Schnitzer and S.I.M. Skinner, Soil Sci., 96 (1963) 86.
[3] D.S. Gamble, Can. J. Chem., 48 (1970) 2662.
[4] W. Flaig, Beutelspacher and E. Rietz, in J.E. Giesseking (Ed.), Soil Components, Vol. 1, Springer, Berlin, 1975.

[5] S.K. Benerjee, S.C. Das and B. Das, J. Indian Chem. Soc., 53 (1976) 186.
[6] S. Arai and K. Kumada, Geoderma, 19 (1977) 21.
[7] N.C. Lockhart, Clays Clay Miner., 29 (1981) 413.
[8] N. Ram and K.V. Ram, Pedologie, 33 (1983) 137.
[9] S.O. Johnson and W.S. Hnojewyj, Proc. N.D. Acad. Sci., 20 (1986) 180.
[10] J. Buffle, Complexation Reactions in Aquatic Systems, Ellis Horwood, 1988.
[11] M. Fukushima, S. Tanaka and M. Taga, J. Chem. Soc. Jpn, 556 (1991).
[12] G.S. Manning, Biopolymers, 9 (1970) 1543.
[13] G.S. Manning, J. Phys. Chem., 79 (1975) 262.
[14] G.S. Manning, J. Phys. Chem., 85 (1981) 1506.
[15] B.M. Bartschat, S.E. Cabaniss and F.M. Morel, Environ. Sci. Technol., 26 (1992) 284.
[16] G. Brun, D.R. Sayag and L. André, The Potentiometric and Conductimetric Characterization of the Complexing Power of Humic Substances, in N. Senesi and T.M. Miano, (Eds.), Humic Substances in the Global Environment and Implications on Human Health, Elsevier, 1994, p. 193.
[17] H.P. van Leeuwen, R.F.M.J. Clevan and P. Valenta, Pure Appl. Chem., 63 (1991) 1251.
[18] International Humic Substances Society (IHSS), Outline of Extraction Procedures, 1981.
[19] S. Kuwatsuka, A. Watanabe, K. Itoh and S. Arai, Soil Sci. Plant Nutr., 38 (1992) 23.
[20] M.A.G.T. van den Hoop, H.P. van Leeuwen and R.F.M.J. Cleven, Anal. Chim. Acta, 232 (1990) 141.
[21] G.S. Manning, J. Chem. Phys., 51 (1969) 924.
[22] H.G. de Jong, J. Lyklema and H.P. van Leeuwen, Biophys. Chem., 27 (1987) 173.
[23] J.T.G. Overbeek, Pure Appl. Chem., 46 (1976) 91.
[24] G.S. Manning, Quart. Rev. Biophys., 11 (1978) 179.
[25] A.A.S.C. Machado and F. Rey, unpublished results, 1994.
[26] F. Rey, A.A.S.C. Machado, F. Arce, M.A. Ferreira and A. Toja, Anal. Chim. Acta, 304 (1995) 375.
[27] F. Rey, A.A.S.C. Machado, M.A. Ferreira and A. Toja, II Reunión Ibérica de Electroquímica, Valencia, Spain, 1993.

ELSEVIER

Talanta 42 (1995) 1925–1929

Talanta

# High-performance liquid chromatographic determination of uranium using solvent extraction and bis(salicylaldehyde) tetramethylethylenediimine as complexing reagent

M.Y. Khuhawar*, S.N. Lanjwani

*Institute of Chemistry, University of Sindh, Jamshoro, Sindh, Pakistan*

Received 23 January 1995; revised 22 May 1995; accepted 12 June 1995

**Abstract**

The reagent bis(salicylaldehyde)tetramethylethylenediimine has been used for the determination of dioxouranium(VI), based on complexation in aqueous solution at pH 6, followed by extraction in chloroform and HPLC determination on a Hypersil ODS (3 μm) column. The complex was eluted with the ternary mixture methanol–acetonitrile–water (40:30:30, v/v/v), with UV detection at 260 nm. Oxovanadium(IV), iron(III), copper(II), cobalt(II), nickel(II) and palladium(II) were completely separated and did not interfere in the determination of uranium. The linear calibration range and detection limits have been obtained. The method has been applied to the determination of uranium together with copper, iron and nickel in mineral ore samples.

*Keywords:* Bis(salicylaldehyde)tetramethylethylenediimine; Complexation; Dioxouranium(VI); HPLC; Solvent extraction; Uranium determination

## 1. Introduction

A number of analytical methods are reported for the determination of uranium, including spectrophotometry, spectrofluorimetry and inductively coupled plasma-atomic emission spectrometry. The methods generally involved prior separation using ion exchange or solvent extraction techniques [1–3]. High-performance liquid chromatography (HPLC) methods for the determination of uranium have also been reported, based on ion exchange, ion pair or ion chromatography and post column derivatization using Arsenazo III or 4(2′-pyridylazo)resorcinol [4–11]. Casoli et al. [12] have used 2,6-diacetylpyridine-bis-(benzoylhydrazone) for solvent extraction, and reversed phase HPLC for the determination of uranium. Main and Fritz [13], after complexing uranium with the bis(quaternary ammonium hydrazones) of 2,6-diacetylpyridine, have determined the uranium complexes chromatographically. Fuping et al. [14] have studied the retention behaviour of α-hydroxyisobutyric acid complexes of thorium and uranium by reversed-phase (RP) HPLC.

The reagent bis(salicylaldehyde)tetramethylethylenediimine ($H_2SA_2Ten$) has been used for the determination of copper and nickel in metal alloys using gas chromatography and normal phase HPLC [15], oxovanadium(IV) in crude petroleum oils using normal phase HPLC [16], and cobalt and iron in pharmaceutical preparations using RP HPLC [17]. In the present work, the selective reaction of $H_2SA_2Ten$

* Corresponding author.


*SSDI* 0039-9140(95)01664-3

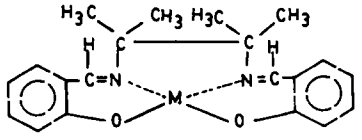


Fig. 1. Structural diagram of the metal–$H_2SA_2Ten$ complex.

(Fig. 1) with a limited number of metal ions (copper(II), nickel(II), cobalt(II), cobalt(III), iron(II), iron(III), palladium(II), platinum(II), manganese(II), oxovanadium(IV) (VO(II)) and dioxouranium(VI) ($UO_2$(II)) [15–19]) combined with simple isocratic RP-HPLC has been used for the determination of uranium.

## 2. Experimental

The reagent $H_2SA_2Ten$ and its copper(II), nickel(II), palladium(II), iron(III), oxovanadium(IV) and dioxouranium(VI) complexes were prepared as reported earlier [15–18].

### *2.1. Solvent extraction of dioxouranium(VI)*

An aliquot of a solution (1–10 ml) containing uranium (0–200 μg) was transferred to a well-stoppered test tube. Sodium acetate–acetic acid buffer (pH 6; 2 ml) and reagent solution (1.5 ml; 1% (w/v) in ethanol) were added. The mixture was warmed on a water bath for 10 min, and after cooling, chloroform (2 ml) was added. The layers were mixed well and 1 ml of the extract was transferred to a sample vial. The solvent was removed and the complex was redissolved in 1 ml of methanol. Portions of the solution (1–5 μl) were injected on to a column (150 mm × 4.6 mm) of Hypersil ODS (3 μm) and the complex was eluted with a ternary mixture of methanol–acetonitrile–water (40:30:30, v/v/v) with a flow rate of 0.5 ml $min^{-1}$. Detection (UV) was performed at 260 nm.

### *2.2. Analysis of uranium in mineral ore samples*

Samples (1) 38834 (0.5 g), (2) 38842 (0.5 g), (3) 38835 (0.2 g), (4) 388496 (0.2 g) and (5) 38850 (0.2 g) were transferred to beakers and hydrochloric acid (60 ml; 37%) and nitric acid (20 ml; 65%) were added. The contents of the beaker were heated gently on a hot plate and when most of the acids had evaporated, nitric acid (20 ml; 65%) was added. The beaker contents were again heated to near dryness and the residues were dissolved in nitric acid (0.1 N). The solutions were filtered and the volumes was adjusted to 25 ml. The solution (10 ml) resulting from sample 1 or those (5 ml) resulting from samples 2, 3, 4 and 5 were transferred to well-stoppered test tubes and the pHs were adjusted to 5–6. The procedure described in section 2.1 was then followed.

### *2.3. Analysis of uranium using standard addition technique*

To sample 38842 (0.2 g) were added 40, 80, 120, 160 and 200 μg of uranium, and the procedure described in section 2.2 was then followed.

### *2.4. Simultaneous extraction of copper(II), nickel(II), iron(II) and dioxouranium(VI)*

To a solution (5 ml) containing (0–200 μg) of copper, nickel, iron and uranium were added the reagents, and that procedure described in section 2.1. was followed. The aqueous phase was transferred to a volumetric flask (10 ml), and the volume was adjusted to 10 ml. The amount of copper, nickel and iron remaining in the aqueous phase was determined using atomic absorption spectrophotometry.

### *2.5. Simultaneous extraction and determination of copper(II), nickel(II), iron(II) and dioxouranium(VI) in mineral ore samples*

The mineral ore samples (1 g) were transferred to beakers and the analytical procedure described in section 2.2 was followed. The final volume was adjusted to 50 ml. An aliquot of the solution (0.1–25 ml) was taken and the volume was adjusted to 10 ml. The procedure described in section 2.1 was then followed.

The mineral samples (sandstone house reference standards) were obtained from the Atomic Energy Minerals Centre, Lahore, and uranyl nitrate (BDH Chemicals Ltd.) was used for the preparation of a uranium standard solution (1 mg $ml^{-1}$).

HPLC studies were carried out with use of a Hitachi 655A liquid chromatograph connected

to a variable wavelength UV monitor, a Rheodyne 7125 injector and a Hitachi Chromato integrator D-2500.

A column (150 mm × 4.6 mm i.d.) of Hypersil ODS (3 μm) (Shandon, USA) was used throughout the study. Spectrophotometric studies were carried out with use of a Hitachi 220 spectrophotometer. A Varian Spectr AA 20 atomic absorption spectrophotometer with an air–acetylene nebulizer was used.

## 3. Results and discussion

The reagent $H_2SA_2Ten$ forms a neutral complex with dioxouranium(VI), which is easily extractable into chloroform ethyl acetate and methyl isobutyl ketone (MIBK). The absorbtion maximum for the complex is at 470 nm and Beer's law is obeyed at a final concentration of 2–20 μg $ml^{-1}$ in chloroform. The effect of pH on the extraction of dioxouranium(VI) was investigated spectrophotometrically. It was observed that dioxouranium(VI) is extracted in the pH range 3–9, but optimal extraction was observed at pH 6.

The uranyl complex was easily eluted from the Hypersil ODS column, but optimal separation from an excess of the reagent occurred when elution was effected with a ternary mixture of methanol–acetonitrile–water (40:30:30, v/v/v) (Fig. 2). Copper(II), cobalt(II), nickel(II), iron(III), palladium(II) and oxovanadium(IV) complexes of $H_2SA_2Ten$, when present together, eluted separately from the uranyl complex and did not interfere in the uranium determination. However complete separation between dioxouranium(VI), oxovanadium(IV), palladium(II), nickel(II), cobalt(II), iron(II) and copper(II) was observed when isocratic elution was performed with methanol–acetonitrile–water (70:10:20, v/v/v) (Fig. 3).

Linear calibration of uranium was obtained with 0–100 μg $ml^{-1}$ of the extract by plotting the average peak height ($n = 3$) versus concentration. The coefficient of correlation ($r$) was 0.998. The detection limit measured at least three times the background noise was 2.5 μg $ml^{-1}$, corresponding to 12.5 ng per injection. The test solutions were analyzed for content of uranium, and a relative percentage error within 0–4.2% was found. The effects of aluminium(III), chromium(VI), manganese(II) and zinc(II) on the extraction of uranium were examined. Aluminium(III), manganese(II) and zinc(II) decreased the percentage extraction of uranium. Aluminium was masked with ammo-

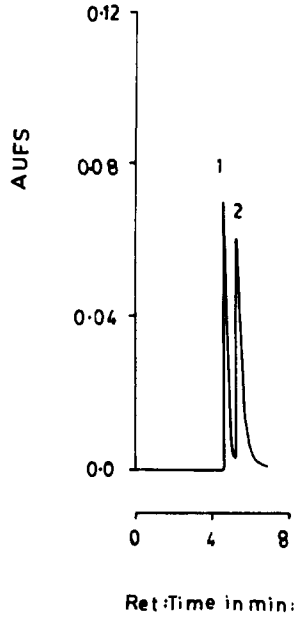


Fig. 2. HPLC separation of (peak 1) the reagent, and (peak 2) the dioxouranium complex, on a column (150 mm × 4.6 mm i.d.) of Hypersil ODS (3 μm), with elution with methanol–acetonitrile–water (40:30:30, v/v/v) at a flow rate of 0.5 ml $min^{-1}$, and with UV detection at 260 nm.

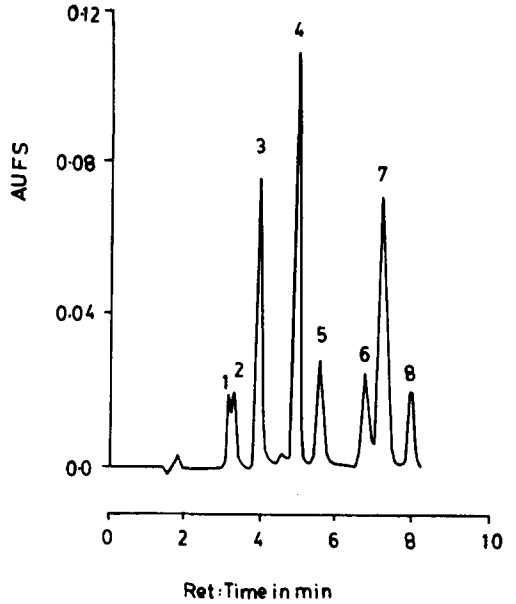


Fig. 3. HPLC separation of chelates of (peak 1) $H_2SA_2Ten$, (peak 2) cobalt, (peak 3) oxovanadium, (peak 4) dioxouranium, (peak 5) iron, (peak 6) palladium, (peak 7) nickel, (peak 8) copper, on a column (150 mm × 4.6 mm i.d.) of Hypersil ODS (3 μm), with elution with methanol–acetonitrile–water (70:10:20, v/v/v) at a flow rate of 0.8 ml $min^{-1}$ and with detection at 260 nm.

Table 1
Analyses of uranium in mineral samples

| Sample no. | Sample | Amount of uranium reported ($\mu g\ g^{-1}$) | Amount of uranium found[a] ($\mu g\ g^{-1}$) |
|---|---|---|---|
| 1 | 38834 | 106.0 | 98.5(2.7) |
| 2 | 38842 | 423.0 | 392.0(4.5) |
| 3 | 38835 | 626.6 | 586.0(2.8) |
| 4 | 38849 | 1273.7 | 1210.0(3.8) |
| 5 | 38850 | 1718.0 | 1620.0(4.6) |

[a] Coefficients of variation (%) are given in parentheses.

nium fluoride (1 ml; 1% (w/v)) and manganese(II) and zinc(II) could be tolerated at a concentration similar to that of uranium. The mineral samples were analyzed for content of uranium (Table 1), and the values obtained showed coefficients of variation (C.V) within 2.7–4.6%, which is 5.0–7.3% lower than the expected values. Sample 2 (38842) was also analyzed by the standard addition method and the results obtained (395 $\mu g\ g^{-1}$ with a C.V. of 3.5%) was close to the previously obtained value. It may be suggested that the complexation extraction and HPLC determination are quantitative, but slightly low results (5–7.3%) could be attributed to a low dissolution efficiency of uranium in hydrochloric acid–nitric acid from sandstone.

Finally, it was observed that the mineral samples contained copper, iron and nickel,

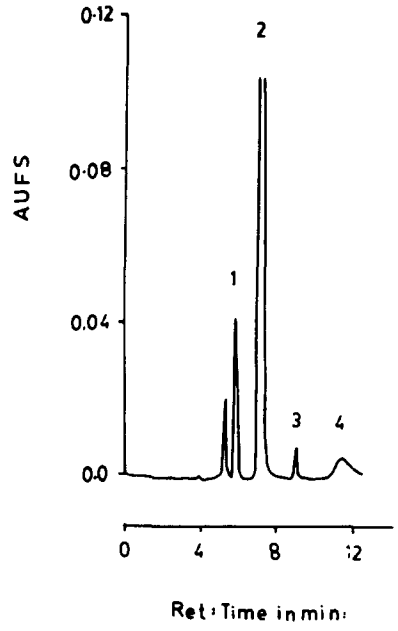


Fig. 4. Simultaneous HPLC determination of chelates of (peak 1) dioxouranium(VI) (peak 2) iron(III), (peak 3) nickel(II), (peak 4) copper(II) in sample no. 38842,on a column (150 mm × 4.6 mm i.d.) of Hypersil ODS (3 μm), with elution with methanol–acetonitrile–water (40:40:20, v/v/v) at a flow rate of 0.8 ml $min^{-1}$ and with detection at 260 nm.

which were simultaneously extracted with uranium. The transfer of metals from the aqueous to the organic phase was examined. The metal ions remaining in the aqueous phase were determined using atomic absorption spectrophotometry. It was observed that 92%, 93% and

Table 2
Analyses of copper, iron and nickel in mineral samples

| Sample no. | Sample | Metal ion | Amount found by HPLC[a] ($\mu g\ g^{-1}$) | Amount found by atomic absorption spectrophotometry[a] ($\mu g\ g^{-1}$) |
|---|---|---|---|---|
| 1 | 38834 | Ni | 37(5.1) | 40(5.0) |
| | | Cu | 38(5.0) | 35(2.2) |
| | | Fe | 10400(3.8) | 10600(1.1) |
| 2 | 38842 | Ni | 48(5.0) | 45(4.5) |
| | | Cu | 47(4.5) | 45(2.1) |
| | | Fe | 60000(4.9) | 60600(0.8) |
| 3 | 38835 | Ni | 52(6.10) | 50(3.9) |
| | | Cu | 23(6.6) | 20(2.3) |
| | | Fe | 16500(2.8) | 16900(2.1) |
| 4 | 38849 | Ni | 42(4.5) | 40(4.5) |
| | | Cu | 32(4.7) | 30(2.1) |
| | | Fe | 18400(1.3) | 18100(1.4) |
| 5 | 38850 | Ni | 44(5.5) | 45(3.9) |
| | | Cu | 22(4.8) | 20(1.8) |
| | | Fe | 49000(2.0) | 49400(0.5) |

[a] Coefficients of variation (%) are given in parentheses.

94% of copper, nickel and iron were transferred with C.V.s of 1.54%, 2.86% and 0.86%, respectively, using a single extraction. Thus an attempt was made to determine copper, iron and nickel together with uranium using HPLC (Fig. 4). The same extraction procedure was used as for uranium. The results in Table 2 indicate a close correlation between the amounts obtained by HPLC and atomic absorption spectrophotometry. Coefficients of variation obtained by HPLC were 2.0–6.6%, compared to 0.5–5.0% by atomic absorption spectrophotometry.

## 4. Conclusions

A simple HPLC method has been used for the determination of uranyl, based on pre-column derivatization and using $H_2SA_2Ten$ as complexing reagent. The method has been used for the determination of uranium together with copper, iron and nickel in mineral samples after acid dissolution.

## Acknowledgements

Dr. Fazal-Ur-Rehman, CSO, and the Director, Atomic Energy Mineral Centre, Lahore are acknowledged for providing us with five house reference standards for use in the development of the HPLC method.

## References

[1] S.D. Hartensten, Anal. Chim. Acta, 228 (1990) 2793.
[2] F.A. Centanni, A.M. Ross and M.A. Desera, Anal. Chem., 28 (1956) 651.
[3] A.S. Al-Ammar, H.A. Hamid, B.H. Rashid and H.M. Basheer, J. Chromatogr., 537 (1991) 287.
[4] A. Kerr, W. Kupfer Schmidt and M. Attas, Anal. Chem., 60 (1988) 2729.
[5] I. Jancaroua, H. Krizova and V. Kuban, Talanta, 38 (1991) 1093.
[6] D.J. Barkley, M. Blanchettes, R.M. Casidy and S. Elchek, Anal. Chem., 58 (1986) 2222.
[7] C.H. Knight, R.M. Cassidy, B.M. Recoskie and L.W. Green, Anal. Chem., 56 (1984) 474.
[8] J.P. Muller, J. Cojean and A. Deloge, Analusis, 15 (1987) 209.
[9] M. Riaz, S.B. Butt and Ehan-ul-Hag, J. Liq. Chromatogr., 16 (1993) 1589.
[10] M.P. Harrold, A. Siriraks and J.M. Riviello, J. Chromatogr., 602 (1992) 19.
[11] C.A. Lucy, L. Gureli, S. Elchuk, Anal. Chem., 65 (1993) 3320.
[12] A. Casoli, A. Mangia and G. Predieri, Anal. Chem., 57 (1985) 561.
[13] M.V. Main and J.S. Fritz, Anal. Chem., 16 (1989) 1272.
[14] H. Fuping, P.R. Haddard, P.E. Jackson and J. Carnevale, J. Chromatogr., 640 (1993) 187.
[15] M.Y. Khuhawar and G.Q. Khaskheli, J. Chem. Soc. Pak., 13 (1991) 10.
[16] M.Y. Khuhawar, S.N. Lanjwani and G.Q. Khaskheli, J. Chromatogr., 689 (1955) 39–43.
[17] M.Y. Khuhawar and S.N. Lanjwani, J. Chromatogr. A, 695 (1995) 132.
[18] D.F. Averill and R.E. Borman, Inorg. Chem., 17 (1978) 338.
[19] C.J. Borcham and B. Chiswell, Inorg. Chim. Acta., 24 (1977) 77.

ELSEVIER

Talanta 42 (1995) 1931-1935

Talanta

# Electrochemical approach to monitoring metal exchange reaction of acetylacetonate complexes with cadmium, copper and zinc ions

Ryoko Fujiyoshi *, Meiseki Katayama

*Faculty of Engineering, Hokkaido University, Sapporo 060, Japan*

Received 14 April 1995; revised 8 June 1995; accepted 13 June 1995

**Abstract**

Metal exchange reactions of acetylacetonate complexes with Cd(II), Cu(II) and Zn(II) ions were investigated by using cadmium and copper ion selective electrodes. Changes in the electrode potential and pH of the solutions were monitored upon adding the pertinent metal Zn(II) of the acetylacetonate (AA) complexes. In the reverse system in which a stable Cu–AA complex exists in the solution prior to adding a secondary metal ion (Cd(II) or Zn(II)), no Cu(II) was replaced by either ion. In the systems containing Cd(II) and Zn(II) as a complexed form with AA or as free ions, the exchange reactions were not explained by considering the equilibrium stability constants of the Cd–AA and Zn–AA complexes.

*Keywords:* Acetylacetonate complexes; Cadmium(II) ions; Copper(II) ions; Electrochemistry; Ion selective electrodes; Metal exchange reactions; Zinc(II) ions

## 1. Introduction

Speciation studies of trace elements in the natural environment have been carried out extensively to elucidate the fates and bioavailability of toxic pollutants [1–3]. Several methods are used for these purposes, which can be classified into three categories: thermodynamic (and kinetic) calculations, direct analysis of environmental samples (including in situ analysis), and model experiments (experimental simulations in the laboratory). The individual methods and their appliations strongly depend on the nature of the medium to be analyzed, and on the different physicochemical forms to be determined. The electrochemical approach is one of the promising methods for this purpose [4]. The accuracy and sensitivity are sometimes not sufficient to deal with most natural water systems. The solution pH may be another limiting factor for ion selective electrode (ISE) measurements. However, in some cases, in which the concentration of the element of interest is rather high, e.m.f. measurement can be applied to environmental monitoring.

The purpose of the present study is to elucidate the possibility of evaluating exchange reactions of metal complexes by using ion selective electrodes. As a preliminary example, metal exchange reactions of well-known acetylacetonate (AA) complexes have been investigated using cadmium and copper electrodes. The authors try to find unknown exchange reactions in the natural environment through certain metal complexes with known stability constants.

* Corresponding author.


*SSDI* 0039-9140(95)01665-1

## 2. Experimental

### 2.1. Reagents and solutions

All chemicals used in this study were purchased from Wako Pure Chemical Industries and were of analytical reagent grade.

Standard solutions of Cd(II), Cu(II) and Zn(II) were prepared by dissolving the pertinent metals (99.9% purity) in a small amount of concentrated $HNO_3$. An aqueous solution of acetylacetone was prepared from direct dilution of the reagent.

### 2.2. Procedure

The free ion concentration of Cd(II) or Cu(II) in the solution was measured by using an ion analyzer (Orion Model EA940) with a cadmium ion selective electrode (Orion Model 9448BN) or a copper ion selective electrode (Orion Model 9429BN), an Ag/AgCl double-junction reference electrode (Orion 900200) and an automatic temperature compensation probe (Orion 917001). The solution pH was also monitored with a pH meter (Horiba D12).

Calibration was carried out within the linear working range ($10^{-7}$–$10^{-5}$ M) for individual metal ions (Cd(II) or Cu(II)) to obtain a characteristic slope in the pertinent e.m.f. measurement. Factors affecting the electrode potential are temperature, pH, ionic strength and also ionic and/or non-ionic species coexisting in the solution. The experimental conditions in this study were set as follows: temperature, $20 \pm 0.1$°C; pH 4–5; $I = 0.01$ M (with $NaNO_3$). The linearity of the electrode potential for both the cadmium and the copper electrodes was examined in the concentration range from $10^{-7}$ to $10^{-5}$ M. The reproducibility of the calibration curve was carefully checked before and after the experiment. The effects of coexisting ions on the electrode potential were evaluated by changing the amount of pertinent salts added to the solution of constant ionic strength.

## 3. Results and discussion

In order to elucidate the ISE response to the acetylacetonate complexation of Cd(II) and Cu(II), titration curves of these ions were obtained by using cadmium and copper electrodes. Figs. 1 and 2, respectively, show the

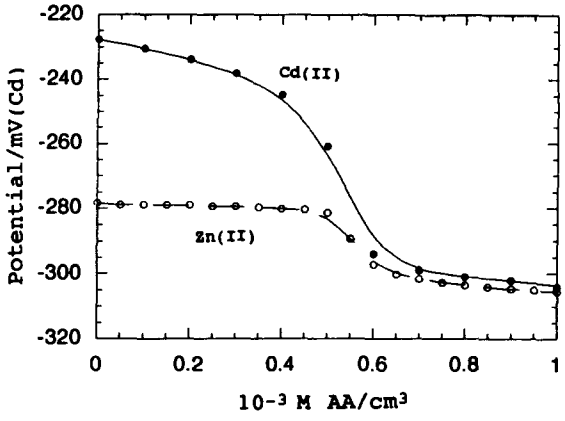


Fig. 1. Titration curves of Cd(II) and Zn(II) solutions with $10^{-3}$ M AA aqueous solution monitored with a cadmium selective electrode. ●, $5.0 \times 10^{-6}$ M Cd(II); ○, $5.0 \times 10^{-6}$ M Zn(II).

results for Cd–AA and Cu–AA systems, in which the concentration of each metal ion was adjusted to $5 \times 10^{-6}$ M at pH 5 and $I = 0.01$ M initially. An aqueous solution of AA ($10^{-3}$ M) was used as a titrant. Considering the acid dissociation constants of acetylacetone ($pK_a = 8.9$), [5] virtually all AA in aqueous solution is in the neutral form, i.e. AAH at pH 5. The suitable pH range for ISE measurement is restricted by hydroxide formation for both Cu(II) and Cd(II), which is not detected by an ISE. Under the experimental conditions specified in this study, the complexation at pH 5 is fast enough to monitor a change in the e.m.f. of the solution electrochemically. Proton exchange is supposed to occur simultaneously in the AA complexation at pH 5.

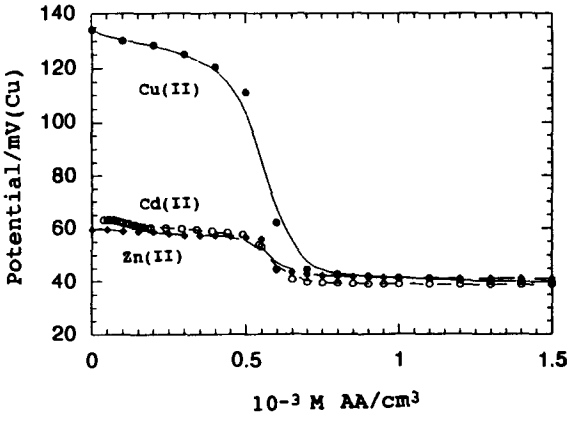


Fig. 2. Titration curves of Cd(II), Cu(II) and Zn(II) solutions with $10^{-3}$ M AA aqueous solution monitored with a copper selective electrode. ○, $5.0 \times 10^{-6}$ M Cd(II); ●, $5.0 \times 10^{-6}$ M Cu(II); ◆, $5.0 \times 10^{-6}$ M Zn(II).

Table 1
Electrode response to the ion (M') present in the solution at 20°C, pH 5 and $I = 0.01$

| Electrode | Ion (M') | Selectivity coefficient[a] | Concentration ($\times 10^{-7}$ M) |
|---|---|---|---|
| Cadmium | Cu(II) | $10 \sim 35$[b] | 1–10 |
| | Zn(II) | $10^{-2}$ | 1–50 |
| Copper | Cd(II) | $10^{-2}$ | 1–50 |
| | Zn(II) | $10^{-2}$ | 1–50 |

[a] The selectivity coefficient was obtained by the mixed solution method with both fixed primary ion and fixed interference.

[b] The value was not constant but increased with increasing amount of Cu(II) ion present in the solution.

The absolute value of the e.m.f. after the endpoint of a titration is known to be dependent on the type of complexing agent in the solution, its concentration and pH [6]. The endpoints obtained in both systems correspond to the formation of a stoichiometric 1:1 complex of metal-acetylacetonate. Figs. 1 and 2 also show the results of the titration of Zn(II) with AA using a cadmium electrode and also of Zn(II) and Cd(II) using a copper electrode, respectively. The endpoints on the curves also suggest the formation of a 1:1 complex of the metal-acetylacetonates. Any metal species other than free ions are not detected by the ISE measurements. The acetylacetonates of Cd(II), Cu(II) and Zn(II) are supposed to be 1:2 (metal:AA) with respect to chemical composition under the present experimental conditions.

The effects of Zn(II) ions on the ISE potential of the cadmium electrode, and Zn(II) or Cd(II) ions on that of the copper electrode were investigated separately by using the mixed solution method with both a fixed primary ion and fixed interference [7].

Table 1 lists the response of both cadmium and copper electrodes to the ions (M') present in the solutions. The presence of Zn(II) ions and also Zn(II) and Cd(II) ions ($5 \times 10^{-6}$ M or lower) did not affect the electrode potential significantly on using the cadmium electrode and copper electrode, respectively [8]. Cd(II) ions in the solution do not interfere in the ISE measurement of Cu(II) ions with the copper electrode. The most striking effect appeared to be on the e.m.f. measurement of the Cd(II) ions in the solution containig cupric ions. The selectivity coefficients of the cadmium electrode was not constant but increased with increasing amount of Cu(II) ions in the solution ($10^{-7}$ M < Cu(II) < $5 \times 10^{-6}$ M).

The metal exchange reaction was then investigated by titrating a solution containing a known amount of primary metal–AA complex ($5.0 \times 10^{-6}$ M) with a standard solution of a secondary metal ion ($10^{-4}$ M). The following systems were examined

(a) $CdAA_2$ + Cu(II) (Cu)
(b) $ZnAA_2$ + Cu(II) (Cu)
(c) $CdAA_2$ + Zn(II) (Cd)
(d) $ZnAA_2$ + Cd(II) (Cd)
(e) $CuAA_2$ + Cd(II) (Cd)
(f) $CuAA_2$ + Zn(II) (Cu)

where the element in parenthesis refers to the ISE used in the system.

Fig. 3 shows the results of two typical examples, systems (b) and (e), where the ISE potential (mV) of the copper electrode is plotted against the logarithmic concentration (M) of Cu(II) ions added to the solution. The calibration curve for Cu(II) is shown together with the titration curves. As shown in the figure, metal exchange is clearly observed between Zn(II) of the Zn–AA complex and the added Cu(II) ions (System (b)). In contrast, the Cd(II) ion does not replace the Cu(II) of the $CuAA_2$ complex appreciably (System (e)).

From a set of data for e.m.f. measurements from the metal exchange reactions, the per cent exchange of a primary metal ion bound by AA was calculated as a function of the secondary metal concentration in the systems listed above. Figs. 4 and 5 give the results. As shown in Fig. 4, Cd(II) and Zn(II) bound with AA are easily replaced with Cu(II) ions under the experimental conditions specified in this study.

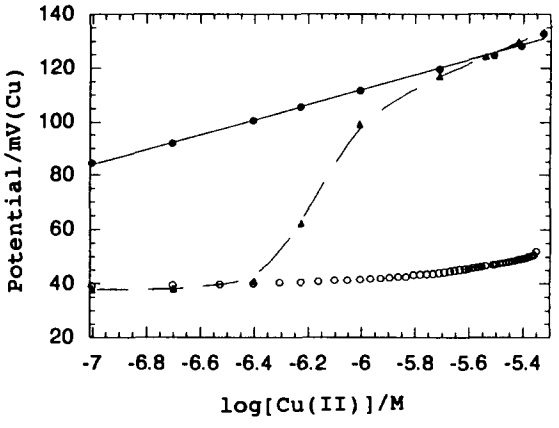


Fig. 3. Change in ISE potential as a function of Cu(II) concentration monitored with a copper selective electrode. ●, Calibration curve; ▲, system (b) ($ZnAA_2$ + Cu(II)); ○, system (e) ($CuAA_2$ + Cd(II)). The initial concentrations of $ZnAA_2$ and $CuAA_2$ in the solution were adjusted to be $5 \times 10^{-7}$ M and $5 \times 10^{-6}$ M, respectively.

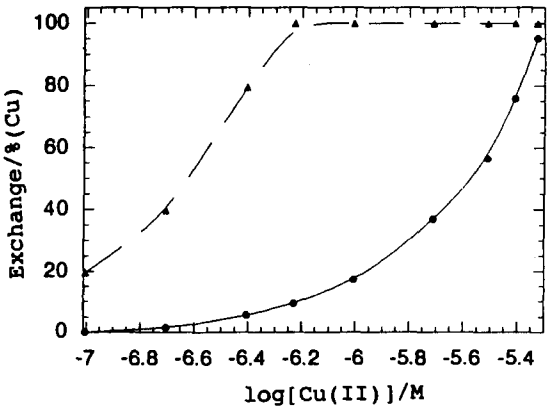


Fig. 4. Per cent exchange of metal–acetylacetonate as a function of Cu(II) concentration in the solution. ●, System (a) ($CdAA_2$ + Cu(II)); ▲, system (b) ($ZnAA_2$ + Cu(II)). The initial concentrations of $CdAA_2$ and $ZnAA_2$ in the solution were adjusted to be $5 \times 10^{-6}$ M and $5 \times 10^{-7}$ M, respectively.

The behavior of Cu(II) in the metal exchange reaction of the AA complex may be explained by considering the large stability constant (log $\beta = 23.7$) of $CuAA_2$. The stability constants (log $\beta$) of $ZnAA_2$ and $CdAA_2$ are reported to be 17.6 and 14.5, respectively at 25°C [9]. It is thus supposed that metal exchange will easily proceed in the system (c). However, as shown in Fig. 5, no exchange occurs before the point on the curve at which an equal concentration of Zn(II) ions to the Cd(II) are added to the $CdAA_2$ solution. After this point, Zn(II) ions begin to replace Cd(II) of $CdAA_2$ to form the Zn–AA complex.

Fig. 5 also shows the result in system (d).

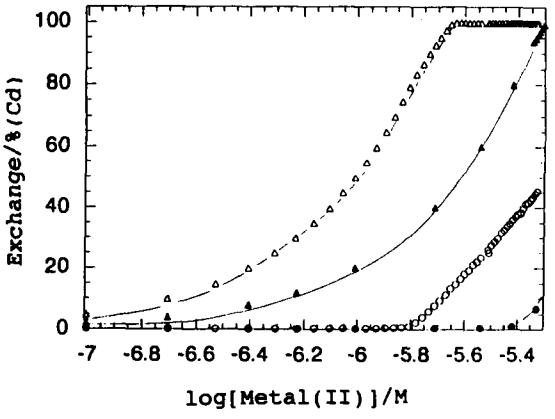


Fig. 5. Per cent exchange of metal–acetylacetonate as a function of titrant (AA complex) concentration in the solution. System (c) ($CdAA_2$ + Zn(II)): ○, $2.0 \times 10^{-6}$ M; ●, $5.0 \times 10^{-6}$ M. System (d) ($ZnAA_2$ + Cd(II)): △, $2.0 \times 10^{-6}$ M; ▲, $5.0 \times 10^{-6}$ M. The initial concentrations of both $CdAA_2$ and $ZnAA_2$ in the solution were adjusted to be $2 \times 10^{-6}$ and $5 \times 10^{-6}$ M.

Table 2
Per cent exchange of $M-AA_2$ in the mixed solutions (equilibrium experiments)

| System | Concentration ($\times 10^{-6}$ M) | | Exchange (%) |
|---|---|---|---|
| | $M-AA_2$ | M′ | |
| (c) | 2.0 | 2.0 | 13.0 |
| | | 5.0 | 45.3 |
| | | 10.0 | 100 |
| (d) | 2.0 | 2.0 | 90.2 |
| | | 5.0 | 100 |
| | | 10.0 | 100 |

The exchange is unlikely to occur appreciably in this system because of a three orders-of-magnitude difference between the overall stability constants of $ZnAA_2$ and $CdAA_2$. However, as shown in the figure, the per cent exchange of $ZnAA_2$ increases with increasing amount of Cd(II) ions added to the solution. All the Zn(II) bound with AA has been replaced by Cd(II) ions at a point on the curve in which the concentration of Cd(II) ions equals that of Zn(II).

In order to check that the equilibrium consideration is applicable to the results from the titration experiments in systems (c) and (d), the potential of the cadmium electrode was measured in the mixed solutions with known amounts of $CdAA_2$ (or $ZnAA_2$) and Zn(II) ions (or Cd(II) ions) at 20°C. Table 2 shows the per cent exchange of $MAA_2$ obtained from serveral solutions for each system. The results are in agreement with those of the titration experiments.

These facts suggest that the metal exchange in the AA complex does not always proceed according to the stability constants of the pertinent acetylacetonates. This seems particularly to be the case when the difference in the stability constants between primary and secondary metal complexes is not large.

The present authors have studied metal and/or ligand exchange reactions of several metal complexes including porphyrins by using the radiotracer technique [10,11]. The degree of exchange in any of the systems studied previously could be evaluated from the stability constants of each complex.

The applicability of various exchange reactions to natural systems should be further investigated not only by the radiotracer technique, but by another technique, such as ISE measurements.

## 4. Conclusion

Cadmium and copper ion selective electrodes were used to monitor free ion concentrations of Cd(II) and Cu(II) in the metal exchange reaction of acetylacetonate complexes with Cd(II), Cu(II) and Zn(II) ions at 20°C, pH 4–5 and $I = 0.01$ M. In some cases in which Cu(II) is included in the system, the exchange reaction proceeds according to the differences in the stability constants of the metal acetylacetonates. However, in the systems in which Zn(II) and Cd(II) are held in the complex form with AA or as added free ion, respectively, the Zn–AA complex with the higher stability constant releases Zn(II) ions to be Cd–AA complex through titrating Cd(II) ions to the solution.

Further studies on metal exchange reactions are now being undertaken using a radiotracer technique.

## References

[1] M. Bernhard, F.E. Brinckman and P.J. Sadler (Eds.), The Importance of Chemical 'Speciation' in Environmental Processes, Springer-Verlag, Berlin, 1986.
[2] G.E. Batley (Ed.), Trace Element Speciation: Analytical Methods and Problems, CRC Press, Boca Raton, FL, 1989, p. 43.
[3] P. Benes and E. Steinnes, Trace Elements in Natural Water, (B. Salbu and E. Steinnes , (Eds.), CRC Press, Boca Raton, FL, 1993.
[4] K. Hiraki and Y. Nakaguchi, Bunseki, 12 (1994) 1020.
[5] J. Stary, The Solvent Extraction of Metal Chelates, Pergamon Press, Oxford, 1964, p. 51.
[6] G. Nakagawa, H. Wada and T. Hayakawa, Bull. Chem. Soc. Jpn., 48(2) (1975) 424.
[7] Y. Umezawa (Ed.), CRC Handbook of Ion-Selective Electrodes; Selectivity Coefficients, CRC Press, Boca Raton, FL, 1990, p. 285.
[8] W.J. Blaedel and D.E. Dinwiddie, Anal. Chem., 46(7) (1974) 873.
[9] A.E. Martell and R.M. Smith (Eds.), Critical Stability Constants, Vol. 4, Plenum Press, 1976.
[10] R. Fujiyoshi, A. Aono and M. Katayama, J. Radioanal. Nucl. Chem. Lett., 164(3) (1992) 193.
[11] R. Fujiyoshi, T. Arai and M. Katayama, J. Radioanal. Nucl. Chem., Articles, 185(1) (1994) 133.

ELSEVIER

Talanta 42 (1995) 1937–1942

Talanta

# ICP-AES determination of silver after chemical separation from uranium matrix

A.A. Argekar *, M.J. Kulkarni, J.N. Mathur, A.G. Page, R.H. Iyer

*Radiochemistry Division, Bhabha Atomic Research Centre, Trombay, Bombay-400 085, India*

Received 11 January 1995; revised 13 June 1995; accepted 16 June 1995

**Abstract**

The separation of silver from a uranium matrix has been carried out using Cyanex-471X (triisobutylphosphine sulphide) in xylene. The effects of various parameters such as the Cyanex-471X concentration, the nitric acid molarity, the contact time and the nitrate ion concentration on the extraction of silver have been studied. The silver metal ion species extracted into the organic phase was found to be $Ag(NO_3)\cdot 2S$ (where S is Cyanex-471X). The stripping of silver into an aqueous medium was carried out with 5% $NaHSO_3$, followed by its determination using ICP-AES.

*Keywords:* Chemical separation; Cyanex-471X; Extraction; ICP-AES; Silver determination; Silver nitrate; Triisobutylphosphine sulphide; Uranium matrix

## 1. Introduction

In view of the significantly high value of the thermal neutron absorption cross-section for silver, it is considered to be one of the metallic elements to be specially monitored in the chemical quality control of nuclear fuel materials. Inductively coupled argon plasma-atomic emision spectrometry (ICP-AES) has less tolerance for dissolved solids and can generate spectral interferences from uranium/plutonium in the determination of analytes. In order to improve the overall analytical performance, it is, therefore, essential to chemically separate the major matrix from the analytes or to separate the analyte metal ion selectively before ICP/AES determination. A highly selective solvent extraction technique has been developed for the separation of silver from uranium/plutonium.

Metal ions such as gold, silver, mercury, copper and palladium (all classified as "soft acids") are selectively extracted by reagents containing sulphur and phosphorus ("soft bases") as donor atoms [1–5]. Cyanex-471X (triisobutylphosphine sulphide) developed by the American Cynamid Co., has been used successfully [6–10] in the extraction of palladium, mercury, rhodium, gold and silver.

This paper describes the extraction of silver from a uranium matrix using 0.1% Cyanex-471X in xylene, from $HNO_3$ medium. The effect of various parameters on the extraction of silver has also been studied.

## 2. Experimental

### 2.1. Apparatus

A Jarrell-Ash 0.75 M (Mark III: Atomcomp 1100 series) direct reading spectrometer equipped with d.c. arc and ICP excitation sources was used. The spectrometer consists of 48 analytical channels covering 33 elements and a monochromator as a variable wavelength channel. The data acquisition and processing are carried out with an IBM-compatible computer. A high-purity germanium (HPGe) detec-

* Corresponding author.


*SSDI* 0039-9140(95)01666-X

Table 1
Variation in the parameters for the extraction of silver

| Experiment no. | Aqueous phase | | | Organic phase: Cyanex-471X in xylene |
|---|---|---|---|---|
| | Ag carrier ($\mu g\ ml^{-1}$) | $HNO_3$ (M) | $NO_3^-$ (M) | |
| I | – | 2.5 | – | $10^{-5}$–$10^{-2}$ M |
| II | – | 0.01–5.0 | – | 0.1% |
| III | – | 2.5 | 0.1–0.5 | 0.005% |
| IV | 1–100 | 2.5 | – | 0.05–0.01% |

Conditions: aqueous and organic phase volumes, 1.0 ml; radioactive tracer, $^{110m}Ag$; time of equilibration, 15 min; temperature, 25 ± 0.1°C.

tor with a multichannel analyser was used for checking the purity of the $^{110m}Ag$ tracer by recording its gamma energy spectrum. Gross gamma counting of $^{110m}Ag$ was carried out with a gamma scintillation counter using a NaI(Tl) detector (Harshaw, UK, 3 × 3 well-type, type no. 12 SW 12-W 3).

### 2.2. Preparation of standards and samples

All the reagents ($HNO_3$, xylene, $NaNO_3$, $NaHSO_3$) were A.R. grade. Preanalysed high-purity $U_3O_8$ was used for the preparation of the synthetic samples. A radioactive tracer of $^{110m}Ag$ ($\beta$-active; Board of Radiation and Isotope Technology (BRIT), Department of Atomic Energy (India)) was used to monitor the extraction of silver radiometrically. Cyanex-471X was used directly to extract silver in nitric acid medium. Stripping of silver into the aqueous phase was carried out with $NaHSO_3$ solution.

Spec-pure $AgNO_3$ (Johnson Matthey, UK) was dissolved in 0.3 M $HNO_3$ to prepare a stock solution of concentration 1 $mg\ ml^{-1}$. A soluiton of 100 $\mu g\ ml^{-1}$ was prepared in order to optimize the experimental parameters for silver (328.1 nm). A 20 $\mu g\ ml^{-1}$ solution and the reagent blank were used as high-concentration and low-concentration standards for two-point standardisation. The $U_3O_8$ matrix was dissolved in $HNO_3$ in order to prepare a 1 $mg\ ml^{-1}$ uranium stock solution. A 100 $\mu g\ ml^{-1}$ uranium solution was used for the optimisation of the analytical signal for uranium at the 409.01 nm line. The reagent blank and a 10 $\mu g\ ml^{-1}$ uranium solution served as low- and high-concentration standards in a two-point standardisation programme for the monitoring of uranium in the chemically separated silver solution.

### 2.3. Procedure

*Kinetics of silver extraction*

The extraction kinetics of $^{110m}Ag$ were studied by mixing 1.0 ml of 2.5 M $HNO_3$ containing silver tracer with an equal volume of 0.1% Cyanex-471X in xylene and equilibrating by slow rotation (40 rev $min^{-1}$) in a water bath at 25 ± 0.1°C for 0.5–60 min. The solutions were centrifuged and the organic and aqueous phases were separated for radioassay.

*Extraction of $^{110m}Ag$ by Cyanex-471X*

Initial experiments on silver extraction were carried out in aqueous medium without any uranium. Different sets of experiments were performed by varying the Cyanex-471X, $HNO_3$, $NO_3^-$ ion and carrier $Ag^+$ concentrations.

The range of variation for each of the above parameters is given in Table 1. After equilibration, the phases were centrifuged, separated and radioassayed.

*Silver removal from the loaded organic phase*

Silver was extracted by 0.1% Cyanex-471X solution from 2.5 M $HNO_3$ (containing $^{110m}Ag$) and the organic phase was separated. To 1 ml of the loaded organic phase, equal volumes of 1–5% $NaHSO_3$ solution was added. After shaking and centrifuging, the phases were separated and assayed for the $^{110m}Ag$ activity.

Once the experimental parameters were optimised, silver was separated from the uranium matrix. $U_3O_8$ (100 mg) was dissolved in 2.5 M $HNO_3$ to which a known amount of $^{110m}Ag$ tracer was added. The solution was extracted using 0.1% Cyanex-471X in xylene. Both the organic and aqueous phases were separated and assayed for the $^{110m}Ag$ activity to assess the efficiency of extraction.

Two synthetic samples were also prepared by adding known amounts of silver to uranium. Silver was extracted with 0.1% Cyanex-471X in xylene with a 1 min contact time. Silver was removed from the organic phase uisng a 5% $NaHSO_3$ solution.

The ICP-AES method was standardised for the determination of silver stripped into the $NaHSO_3$ solution. Initially, the experimental parameters (argon gas flow rates, signal integration time, viewing positions) were optimised using 100 μg ml$^{-1}$ silver solution. The optimised parameters were then used to carry out a two-point standardisation with 0.3 M nitric acid as the low-concentration standard and 20 μg ml$^{-1}$ solution as the high-concentration standard. Since uranium is not covered by the 48 analytical channels available from the polychromator, the U 409.01 nm line was monitored on the variable wavelength channel. The experimental parameters were optimised using 100 μg ml$^{-1}$ uranium solution. A two-point standardisation was carried using 0.3 M nitric acid as the low-concentration standard and 20 μg ml$^{-1}$ solution as the high-concentration standard. The synthetic samples from which silver was separated were analysed for silver and traces of uranium.

## 3. Results and discussion

The kinetics of extraction of $^{110m}Ag$ by Cyanex-471X has shown that the equilibrium is attained in about 1 min (Fig. 1). The extraction dependence of silver on the Cyanex-471X concentration is shown in Table 2. At 0.1% or above, the extraction is quantitative. The equilibrium for the extraction of silver in the organic phase is

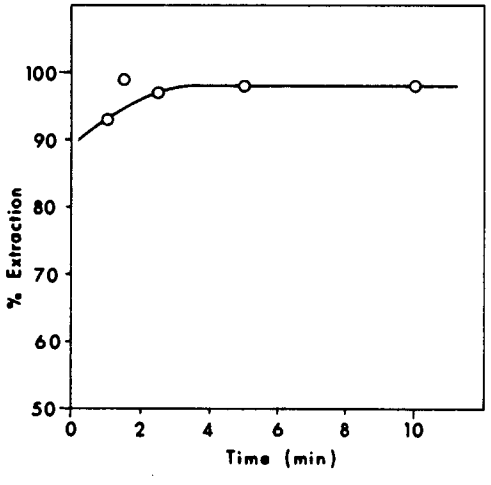


Fig. 1. Plot of percentage extraction vs. time for Ag(I) in 2.5 M $HNO_3$ at a 0.1% Cyanex concentration.

Table 2
Effect of Cyanex-471X concentration on the extraction of silver

| Cyanex concentration (%) | Cyanex concentration (M) | Distribution ratio, $D$ | Extraction (%) |
|---|---|---|---|
| 0.001 | $4.2 \times 10^{-5}$ | 0.043 | 4.4 |
| 0.002 | $8.4 \times 10^{-5}$ | 0.17 | 14.3 |
| 0.003 | $1.26 \times 10^{-4}$ | 0.32 | 24.5 |
| 0.004 | $1.68 \times 10^{-4}$ | 0.59 | 37.3 |
| 0.005 | $2.1 \times 10^{-4}$ | 0.87 | 46.5 |
| 0.008 | $3.4 \times 10^{-4}$ | 2.1 | 68.0 |
| 0.01 | $4.2 \times 10^{-4}$ | 3.3 | 77.0 |
| 0.05 | $2.1 \times 10^{-3}$ | 39.0 | 97.5 |
| 0.10 | $4.2 \times 10^{-3}$ | 99.0 | 99.0 |
| 0.20 | $8.4 \times 10^{-3}$ | 61.5 | 98.4 |
| 0.50 | $2.1 \times 10^{-2}$ | 65.6 | 98.5 |

$$Ag_a^+ + NO_3^- + mS_o \overset{K}{\rightleftharpoons} (AgNO_3 \cdot mS)_o$$

where subscripts a and o represent the aqueous phase and organic phase, respectively, and S signifies Cyanex-471X.

$$K = \frac{[AgNO_3 \cdot mS]_o}{[Ag^+]_a [NO_3^-]_a [S]_o}$$

The distribution ratio ($D$) can be represented by

$$D = \frac{[Ag]_o}{[Ag]_a} = \frac{[AgNO_3 \cdot mS]_o}{[Ag^+]_a}$$

$$K = \frac{D}{[NO_3^-]_a [S]^m}$$

$$\log K = \log D - \log[NO_3^-]_a - m \log[S]_0$$

$$\log D = \log K + \log[NO_3^-]_a + m \log[S]_o$$

Log $D$ was plotted against the logarithm of the Cyanex-471X and the nitrate ion concentrations. Fig. 2 shows a plot of log $D$ vs. log [Cyanex-471X] in 2.5 M nitric acid. The slope is $1.9 \pm 0.1$ suggesting that two molecules of Cyanex-471X are attached to the silver atom. Fig. 3 shows a plot of log $D$ vs. log [$NO_3^-$]; a straight line with a slope of 1.2 suggests that the complex species extracted is $AgNO_3 \cdot 2S$. The free $NO_3^-$ ion concentration was calculated by applying a correction for the dissociation of $HNO_3$.

Table 3 shows the effect of nitric acid molarity on the extraction of silver using 0.1%

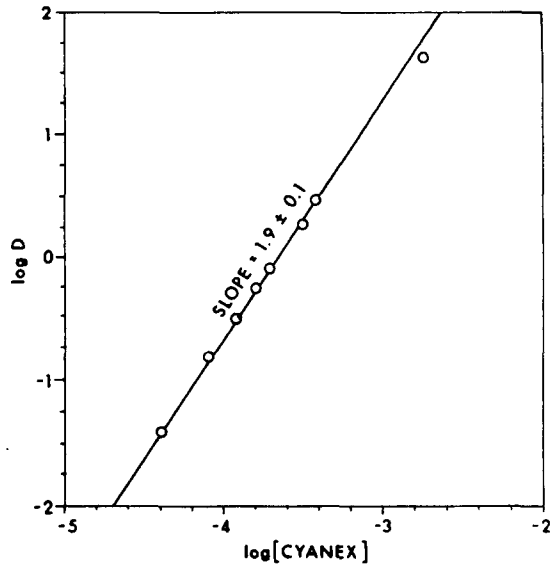


Fig. 2. Plot of log $D$ vs. log[Cyanex] for Ag(I) in 2.5 M $HNO_3$.

Cyanex-471X. With an increase in nitric acid concentration, the extraction of silver increases and becomes almost constant above 4 M.

The loading effect of silver was studied by adding increasing amounts of silver carrier ranging from 1 to 20 μg $ml^{-1}$. Extractions were carried out from 2.5 M $HNO_3$ using 0.05% Cyanex-471X in xylene. Up to 20 μg $ml^{-1}$ silver, the extraction is found to decrease. However, with increased concentration of Cyanex-471X (0.1%) a quantiative extraction of silver up to 50 μg $ml^{-1}$ can be achieved (Table 4).

Table 5 shows the effect of $NaHSO_3$ concentration on the stripping of silver from the organic to the aqueous medium. Silver could

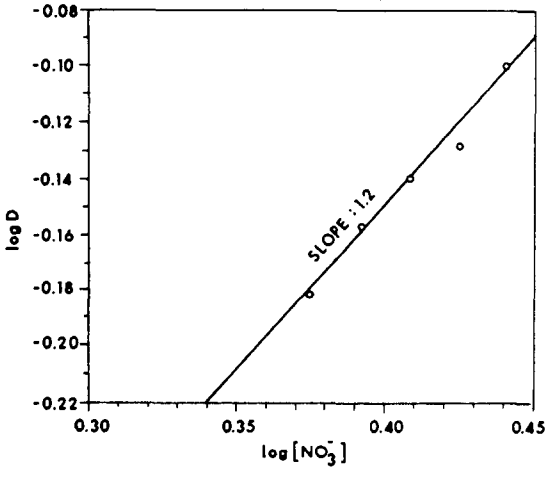


Fig. 3. Plot of log $D$ vs. log[$NO_3^-$] for Ag(I) at a concentration of 0.005% Cyanex in xylene.

Table 3
Effect of acid concentration on silver extraction using 0.1% Cyanex-471X extractant (in xylene)

| $HNO_3$ concentration (M) | Extraction (%) |
|---|---|
| 0.01 | 84.0 |
| 0.05 | 92.0 |
| 1.0 | 93.5 |
| 2.0 | 96.5 |
| 3.0 | 97.8 |
| 4.0 | 98.8 |
| 5.0 | 99.0 |

be stripped to the extent of about 94% into the aqueous medium in a single contact with about a 5% solution of $NaHSO_3$. Since a high concentration of $NaHSO_3$ is used for the stripping of silver which is then determined by ICP-AES, the interference of sodium ions on the determination of silver has also been studied. A $NaHSO_3$ solution at a 5% concentration was nebulised in the ICP and the analytical signal was monitored on the silver channel. The concentration of silver recorded was of the order of the blank. Thus the $NaHSO_3$ concentration was optimised at 5%.

The uranium spectrum gives rise to spectral interference for most analyte elements in ICP-AES. Therefore, the presence of uranium in the silver solution after its chemical separation using Cyanex-471X as extractant was monitored. Uranium up to 10 μg $ml^{-1}$ did not interfere in the determination of silver; however, the coextracted amount of uranium in the present work was found to be below 0.5 μg $ml^{-1}$ in all the samples.

Optimised ICP-AES experimental parameters are tabulated in Table 6. The detection limit for silver is 0.2 ppm and it is based on the

Table 4
Effect of silver ion concentration on loading of Cyanex-471X

| Ag concentration (μg $ml^{-1}$) | % Extraction[a] | % Extraction[b] |
|---|---|---|
| 1 | 98 | – |
| 2 | 98 | – |
| 5 | 99 | – |
| 10 | 97 | – |
| 20 | 96 | 98 |
| 50 | 86 | 98 |
| 100 | 58 | 91 |

[a] 0.05% Cyanex.
[b] 0.1% Cyanex.

Table 5
Effect of $NaHSO_3$ concentration on stripping of silver

| $NaHSO_3$ concentration (%) | Extraction (%) |
|---|---|
| 1 | 53.0 |
| 2 | 74.0 |
| 3 | 88.7 |
| 4 | 93.7 |
| 5 | 94.3 |
| 6 | 94.0 |

Table 6
Experimental parameters for the ICP-AES determination of silver

| | |
|---|---|
| Argon gas flow rates | |
| Outer flow | 20 l $min^{-1}$ |
| Intermediate flow | 1.0 l $min^{-1}$ |
| Sample flow | 0.6 l $min^{-1}$ |
| Nebulizer | Adjustable cross-flow pneumatic type |
| R.F. power | |
| Forward | 1.25 kW |
| Reflected | < 20 W |
| Signal integration time | 10 s |
| Viewing position | |
| Axial | 15 mm above the load coil |
| Radial | Centrally symmetric |
| Slit width | 25 μm |
| Slit height | 3 mm |
| Magnification of image | 1 |

$\bar{X}+3\sigma$ concept ($\bar{X}$ being the average blank signal). The detection is limit calculated by repetitive analyses of the blank. The precision of the determinations is based on ten replicate analyses of synthetic samples. The amounts of silver determined in the synthetic samples were in good agreement with the added amounts. The analytical data obtained are given in Table 7.

Due to the non-availability of suitable reference standards/samples, two uranium samples were prepared synthetically by the addition of silver at the 0.5 and 2.5 ppm levels. These samples, after chemical separation, were analysed by electrothermal atomisation—atomic absorption spectrometry (ETA-AAS) in order to provide an independent check on the recovery of silver. Further, these samples were also analysed by the ICP-AES technique using the optimised procedure. The results of these analyses are included in Table 8, and show good agreement for the estimates of silver in the two samples obtained by these methods and also with their added contents.

Table 7
Results for ICP-AES determination of silver in synthetic samples

| Amount added (ppm) | Amount determined (ppm) | Precision, % RSD ($N = 10$) |
|---|---|---|
| 5 | 5.2 | 2 |
| 10 | 11.3 | 1 |

Concentration corresponding to signal equal to $\bar{X}+3\sigma$.

In conclusion, silver can be separated selectively and quantitatively at trace level concentrations from a uranium matrix using Cyanex-471X extractant in xylene. Silver can then be back-extracted with a 5% $NaHSO_3$ solution. The detection limit for silver in the ICP-AES determination is 20 μg $g^{-1}$ based on a 100 mg uranium sample aliquot. The developed method is suitable for the analysis of nuclear fuel samples.

## Acknowledgements

The authors would like to thank Dr. M.D. Sastry, Head, Spectroscopy Section, Radiochemistry Division, for his close involvement in the progress of this work. The authors are also grateful to Cyanamid International, USA for sending a gift sample of Cyanex-471X.

Table 8
Analytical data on the recovery of silver

| Amount added (ppm) | Amount recovered (ppm) | | Precision, % RSD | |
|---|---|---|---|---|
| | ETA-AAS | ICP-AES | ETA-AAS | ICP-AES |
| 0.5 | 0.4 | 0.52 | 8 | 2 |
| 2.5 | 2.0 | 2.3 | 6 | 1 |

## References

[1] T.H. Handely and J.A. Dean, Anal. Chem., 35 (1962) 1312.
[2] R.H. Zucal, J.A. Dean and T.H. Handely, Anal. Chem., 35 (1963) 988.
[3] T.H. Handely, Nucl. Sci. Eng., 16 (1963) 440.
[4] R. Titonssi, S. Lours and C. Musikas, European Patent 8 014 238, 26 June 1980.
[5] R.W. Cattrall, A.A. Martin and S. Tribuzio, J. Inorg. Nucl. Chem., 40 (1978) 687.
[6] K. Inoue and Y. Baba, Preprints, ISEC 86, Munich, 1986.
[7] Y. Baba, Y. Umezaki, T. Ueda and K. Inoue, Bull. Chem. Soc. Jpn., 59 (1986) 3835.
[8] I. Longden, N.M. Patel and J.R. Thornback, Solvent Extr. Ion Exch., 4(3) (1986) 421.
[9] V. Salvado, M. Hidalgo, A. Masana, M. Munoz, M. Valiente and M. Muhammed, Solvent Extr. Ion Exch., 8(3) (1990) 491.
[10] Y. Abe and D.S. Flett, in T. Sekine (Ed.), Solvent Extraction, Part B, 1990, pp. 1127.

ELSEVIER

Talanta 42 (1995) 1943-1946

Talanta

# Use of cerium oxide ($CeO_2$) as a packing material for the chromatographic separation of $C_{60}$ and $C_{70}$ fullerenes

Yoshifumi Akama

*Department of Chemistry, Faculty of Science and Engineering, Meisei University, Hodokubo, Hino, Tokyo 191, Japan*

Received 4 March 1995; revised 13 June 1995; accepted 16 June 1995

**Abstract**

Cerium oxide ($CeO_2$) was tested as a packing material in liquid chromatography for the separation of $C_{60}$ and $C_{70}$ fullerenes. The separation of $C_{60}$ and $C_{70}$ fullerenes could be achieved within 20 min by using pure *n*-hexane as the mobile phase. Furthermore, some higher fullerenes could also be separated in less than 40 min. The peak area was reproducible to a large extent. The separation of fullerenes by liquid chromatography on $CeO_2$ is shown to be an effective method for their isolation in large amounts. The column efficiency of the $CeO_2$ column was compared with commercial silica gel and ODS columns. The main advantage of the $CeO_2$ column is its ability to separate large amounts of fullerenes ($C_{60}$ and $C_{70}$) in toluene.

*Keywords:* $C_{60}/C_{70}$ fullerene mixtures; Cerium oxide; Column packing material; Fullerenes; High performance liquid chromatography

## 1. Introduction

The physical and chemical characterization of fullerenes have been actively investigated by NMR, IR, mass spectrometry and other spectroscopic techniques.

The purification of the spherical carbon clusters termed fullerenes is an area of increasing importance in chemical and physical testing. However, it is difficult to produce sufficient quantities of high-purity fullerenes to evaluate the possible applications due to their limited solubility in organic solvents. Therefore, there is a need for the development of an efficient separation technique for fullerenes. Until now, many attempts have been made to develop a technique for the separation of fullerenes and their derivatives by column chromatography, e.g. $C_{18}$ reversed-phase [1], silica-gel [2], alumina [3], Pirkle [4], CPS [5], graphite [6], PYE silica [7], multilegged phenyl group bonded silica [8]. Some techniques [9,10] have also been developed for the large-scale purification of fullerenes. While most separation techniques so far utilized are straightforward at the analytical level, they are not suitable for the large-scale purification of fullerenes.

We have recently demonstrated that the polycyclic aromatic hydrocarbons can be effectively separated on a $CeO_2$ stationary phase using *n*-hexane as the mobile phase. As an extension of this work, we have proposed the use of a $CeO_2$ column for the separation of $C_{60}$ and $C_{70}$ fullerenes. For the large-scale separation of $C_{60}$ and $C_{70}$ fullerenes, the $CeO_2$ column was clearly effective compared with the commercial silica gel and ODS columns.

## 2. Experimental

Commercial $CeO_2$ (about 10 g), which was purchased from Soekawa Chemical Co. Ltd., was pretreated before use as a column packing


*SSDI* 0039-9140(95)01667-8

material by suspension in ethanol with mixing for 1 min, then allowed to stand for 10 min. The supernatant was discarded in order to remove any small particles. This procedure was repeated in five times. The pretreated $CeO_2$ with a mean particle size of 5 μm was slurried in 15 ml of ethylene glycol. This mixture was forced into a stainless steel tube (4.6 mm × 135 mm) over a period of 60 min using pure ethanol as the packing solvent, at a constant pressure of 550 kg $cm^{-2}$. However, optimization of the packing is difficult because no satisfactory slurrying solvent has been found. The column was then used as a normal phase support using *n*-hexane as the mobile phase. The stock solutions of $C_{60}$ and $C_{70}$ fullerene standards are prepared by dissolution in toluene due to the higher solubility of the fullerenes. The working standards were prepared by appropriate dilution with toluene or *n*-hexane from the stock solution. The analytical HPCL system consisted of an 880-PU pump, and an 875-UV spectrophotometric detector (both from JASCO, Tokyo), a Rheodyne model 7125 injector with a 20 μl injection loop and a Shimadzu model CR4A Chromatopac integrator. A Personal Pump NP-AX-15 (Nippon Seimitsu Kagaku Co. Ltd., Tokyo) was used for the packing of $CeO_2$ into the stainless steel tube. The mobile phase was 100% *n*-hexane and the flow rate was 1.0 ml $min^{-1}$. The detector was operated at 350 nm and the injection volume was 20 μl. Quantitation was carried out by determination of the peak area.

## 3. Results and discussion

Fig. 1 shows the grain distribution of $CeO_2$ which was untreated (Fig. 1(a)) and pretreated (Fig. 1(b)) with ethanol prior to packing in the column as mentioned in the experimental section. The mean grain size of $CeO_2$ was reduced to approximately 5 μm by the ethanol treatment. The variation in the grain size after the treatment is due to the disentanglement of the ground $CeO_2$ by mixing with ethanol. Further, ethanol washing leads to a narrowed distribution of $CeO_2$ particle sizes, as shown in Fig. 1(b). This result is also clear by a comparison of the scanning electron microscope pictures of treated and untreated $CeO_2$.

The preparative $CeO_2$ column was applied to the fullerenes ($C_{60}$ and $C_{70}$) to evaluate their chromatographic separation. Typical chromatograms of the fullerenes obtained using $CeO_2$, ODS and silica gel columns are illustrated in Fig. 2. It appears that good resolution of $C_{60}$ and $C_{70}$ fullerenes can be achieved in a short time by using the $CeO_2$ column and pure *n*-hexane as the elution solvent. We also found that $C_{60}$ and $C_{70}$ fullerenes can be widely separated; the smaller $C_{60}$ fullerene is eluted before the $C_{70}$, followed by the higher fullerenes. No other solvents examined (methanol, ethanol, ethyl acetate and toluene) effected separations as efficiently as pure *n*-hexane. The use of these solvents as mobile phases results in virtually no retention of $C_{60}$ and $C_{70}$ fullerenes on $CeO_2$. The $CeO_2$ is stable over a wide pH range; however, water or water/organic solvent mixtures cannot be used as the mobile phase.

Surprisingly, effective separation of the fullerenes has been obtained when about 30 ml of $CHCl_3$ or $CCl_4$ are passed through the column at a flow rate of 1.0 ml $min^{-1}$ prior to the use of *n*-hexane as the mobile phase. A similar separation effectiveness has also been observed for polycyclic aromatic hydrocarbons (PAHs) [11]. Thus, the decline in efficiency of the separation due to repetitive use is improved by passing these solvents through the column.

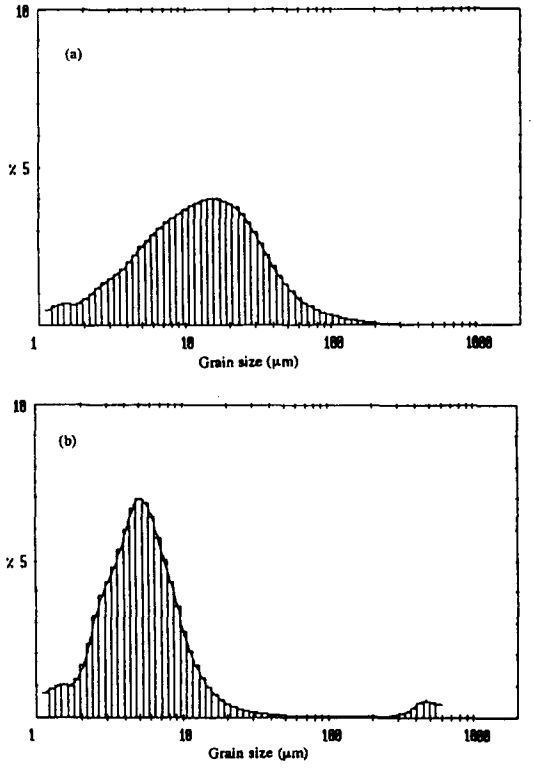


Fig. 1. The distribution curves of grain size of $CeO_2$ used in this experiment. (a) Treated with ethanol; (b) untreated.

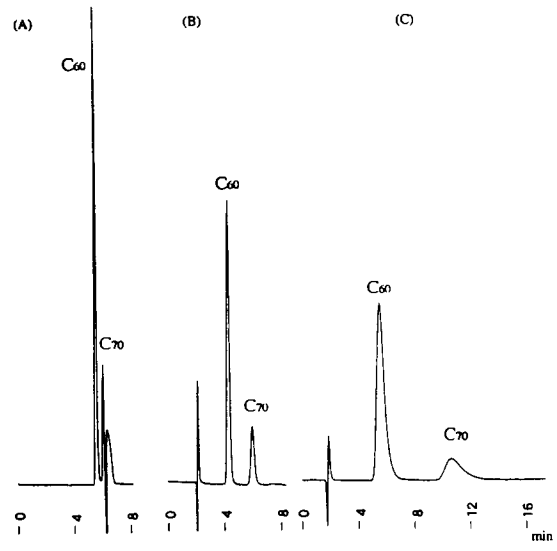


Fig. 2. Separation of fullerenes on a $CeO_2$ column. Chromatographic conditions: mobile phase, *n*-hexane; sample, 8 μg ml$^{-1}$ $C_{70}$; column, (A) Finepak SIL (4.6 mm × 250 mm), (B) Chemcosob 5-ODS-UH (4.6 mm × 150 mm), (C) cerium oxide (4.6 mm × 125 mm); injection volume, 20 μl; flow rate, 1.0 ml min$^{-1}$; detection, UV at 350 nm; attenuation, 4.

This result indicates that the surface of $CeO_2$ may be activated by these solvents; however, further work may be required to understand the origin of these solvent effects.

The retention mechanism of the fullerenes on the $CeO_2$ phase is due to the adsorption contribution, similar to the mechanism of PAH retention on alumina. The fullerenes, which have many π-electrons, strongly interacted with the cerium atom on the surface of the adsorbent. It is expected that a difference in the number of π-electrons will lead to different interactions with $CeO_2$; thus the $C_{60}$ and $C_{70}$ compounds can be separated on this basis. A similar retention mechanism may be applied to the other rare earth oxides when separating the fullerenes or PHAs. However, the separation of the fullerenes could not be performed using $La_2O_3$, $Gd_2O_3$ and $CeO_2$, which have particle sizes below about 1 μm. These results were mainly due to packing difficulties or ease of water adsorption caused by fines. In this study, $CeO_2$ (about 5 μm) was used as a packing material because of its excellent separation capability, and the cost of $CeO_2$ is lower than that of the other rare earth oxides. The column efficiencies for the fullerenes were approximately 500 theoretical plates for the 5 μm $CeO_2$ employed. In general, large-scale purifications of fullerenes are difficult due to their insolubility [12] in organic solvents.

In this study, about 7 mg of a 8:2 $C_{60}/C_{70}$ mixture in 2 ml of toluene solution can be successfully separated, per 20 μl injection, on the preparative $CeO_2$ column, as shown in Fig. 3. Further, it was found that some higher fullerenes could be separated in less than 40 min. Separations of fullerene solutions of concentration 1 and 0.1 mg ml$^{-1}$ are also illustrated in Fig. 4. Fig. 3 shows that the $CeO_2$ column is superior to the silica gel or ODS columns for the resolution of a high concentration of fullerenes. This discrepancy is likely to be associated with many adsorption sites on the surface of a $CeO_2$ particle; this allows a strong interaction between the fullerenes and the Ce(IV) atoms. Consequently we infer that the loading capacity for this material is much greater than that of ODS or silica gel. The loading capacity and column efficiency are very important for both analytical and preparative-scale chromatography, since it is desirable to have a large capacity and a good separation.

The economics of this large-scale chromatographic process for the purification of fullerenes are worth noting. The enhancement of the productivity of fullerenes will be dramatically improved by using a column with a large inner diameter and a longer length. The $CeO_2$ column was found to be quite stable under the conditions used in this study. The reproducibilities of the peak areas were tested by repeated injections (20 replicate injections) of the fullerene standard solution ($C_{60}$, 40 μg ml$^{-1}$; $C_{70}$, 10 μg ml$^{-1}$). The relative standard deviations were 1.4% and 7.7% for the $C_{60}$ and the $C_{70}$, respectively. However, the $CeO_2$ column possesses weakness, in the lack of peak retention reproducibility.

In conclusion, a $CeO_2$ column with high separation efficiency has been developed. The fullerenes ($C_{60}$ and $C_{70}$) could be satisfactorily separated in less than 20 min. The separation of large amounts of $C_{60}$ and $C_{70}$ fullerenes using the $CeO_2$ column was more efficient than with silica gel or ODS columns. The best separation was obtained when $CHCl_3$ or $CCl_4$ was passed through the column prior to use. The retention is probably related to the interaction between the $CeO_2$ and the π-electrons of the fullerene. The main potential use of the $CeO_2$ column is for the separation of fullerenes in large-scale purification. If a large column had been used for the separation, a large amount of fullerenes would be obtained.

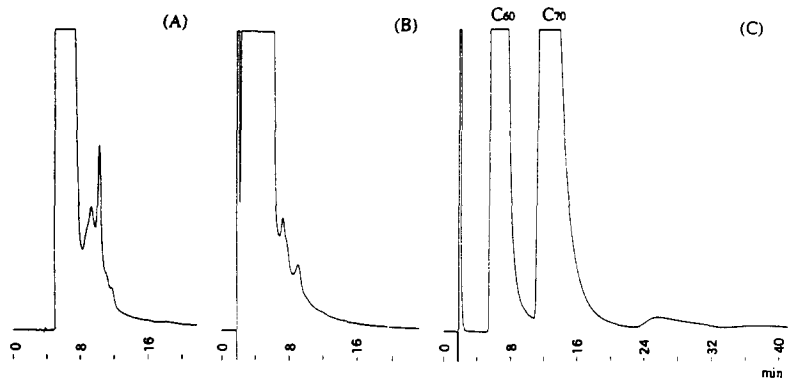


Fig. 3. Separation of fullerenes on a $CeO_2$ column. Chromatographic conditions: sample, 7 mg fullerene in 2 ml toluene (about 80% $C_{60}$, 20% $C_{70}$ and a trace amount of higher fullerenes); column, (A) Finepak SIL (4.6 mm × 250 mm), (B) Chemcosob 5-ODS-UH (4.6 mm × 150 mm), (C) cerium oxide (4.6 mm × 125 mm); attenuation, 5. The other experimental conditions are as in Fig. 2.

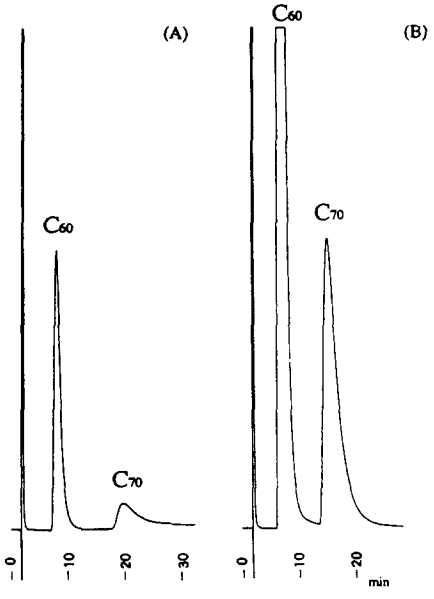


Fig. 4. Separation of $C_{60}$ and $C_{70}$ fullerenes on a cerium oxide column. (A) 0.1 mg $ml^{-1}$ solution of fullerenes ($C_{60}$, 0.08 mg $ml^{-1}$; $C_{70}$, 0.02 mg $ml^{-1}$) in toluene. (B) 1.0 mg $ml^{-1}$ solution of fullerenes ($C_{60}$, 0.8 mg $ml^{-1}$; $C_{70}$, 0.2 mg $ml^{-1}$) in toluene; attenuation, 5. The other experimental conditions are as in Fig. 2.

## Acknowledgment

This present work was partially supported by a Grant-in-Aid for Scientific Research on Priority Areas, New Development of Rare Earth Complexes, no. 06241110 from the Ministry of Education, Science and Culture.

## References

[1] J.F. Anacleto and M.A. Quilliam, Anal. Chem., 65 (1993) 2236.
[2] H. Ajie, M.M. Alvarez, S.J. Anz, R.D. Beck, F. Diederich, K. Fostiropoulos, D.R. Huffman, W. Kratschmer, Y. Rubin, K.F. Schriver, D. Sensharma and R.L. Whetten, J. Phys. Chem., 94 (1990) 8630.
[3] R. Taylor, J.P. Haare, A.K. Abdul-Sada and H.W. Kroto, J. Chem. Soc., Chem. Commun., (1990) 1423.
[4] J.M. Hawkins, T.A. Lewis, S.D. Loren, A. Meyer, J.R. Heath, Y. Shibato and R.J. Saykally, J. Org. Chem., 55 (1990) 6250.
[5] W.H. Pirkle and C.J. Welch, J. Org. Chem., 56 (1991) 6973.
[6] A.M. Vassallo, A.J. Palmisano, L.S.K. Pang and M.A. Wilson, J. Chem. Soc., Chem. Commun., (1992) 60.
[7] K. Kimata, K. Hosoya, T. Araki and N. Tanaka, J. Org. Chem., 58 (1993) 282.
[8] K. Jinno, K. Yamamoto, T. Ueda, H. Nagashima and K. Itoh, J. Chromatogr., 594 (1992) 105.
[9] K. Kikuchi, N. Nakahara, M. Honda, S. Suzuki, K. Saito, H. Shiromaru, K. Yamauchi, I. Ikemoto, T. Kuramochi, S. Hino and Y. Achiba, Chem. Lett., (1991) 1607.
[10] A. Gugel and K. Mulen, J. Chromatogr., 628 (1993) 23.
[11] Y. Akama and H. Kanno, Anal. Chim. Acta, 309 (1955) 153
[12] N. Sivaraman, R. Dhamodaran, I. Kaliappan, T.G. Srinivasan, P.R.V. Rao and C.K. Mathews, J. Org. Chem., 57 (1992) 6077.

ELSEVIER

Talanta 42 (1995) 1947–1957

Talanta

# Direct ICP-MS determination of trace and ultratrace elements in geological materials after decomposition in a microwave oven. Part II. Quantitation of Ba, Cs, Ga, Hf, In, Mo, Nb, Pb, Rb, Sn, Sr, Ta and Tl☆

J.G. Sen Gupta*, N.B. Bertrand

*Geological Survey of Canada, Ottawa, Ont. K1A OE8, Canada*

Received 24 February 1995; revised 16 June 1995; accepted 16 June 1995

**Abstract**

A new method has been developed for the rapid determination of traces of Ba, Cs, Ga, Hf, In, Mo, Nb, Pb, Rb, Sn, Sr, Ta and Tl in silicate rocks and lake, stream and river sediments. The method involved dissolution of samples in a microwave oven by heating in a pressure decomposition Teflon vessel with a mixture of $HF + HNO_3 + HCl + H_3BO_3 + EDTA$ followed by direct multielement determination using inductively coupled plasma-mass spectrometry (ICP/MS). The method is faster than conventional dissolution of samples by open vessel acid digestion and fusion and determination by instrumental methods. The accuracy and precision of the developed method were tested by replicate analyses of a number of international geochemical reference samples of established trace element contents. Satisfactory correlation with the "recommended" or "consensus" values was found and recoveries were in most cases 95–100%. New values for Ga, In, Nb and Tl in several international geochemical reference materials are first reported in this paper.

*Keywords:* Geological materials; ICP-MS; Microwave decomposition; Multielement determination

## 1. Introduction

The determination of trace and ultratrace elements in the Analytical Chemistry Section of the Geological Survey of Canada (GSC) is part of an ongoing task to establish compositions of various geological materials collected by GSC scientists for their petrological, geochemical and mineralogical studies. In the past, this task was performed by colorimetry [1,2], titrimetry, fluorimetry, atomic absorption spectrometry and optical emission spectrometry [2,3]. With the necessity of producing more data on a significantly large number of samples at lower levels, it became increasingly important to switch to modern instrumental techniques such as inductively coupled plasma-atomic emission spectrometry (ICP-AES) and ICP-MS. However, since the detection limits of ICP-MS are much superior to those of ICP-AES, the former technique gained preference in the GSC for the determination of trace and ultratrace elements in geological and environmental materials.

Details of the application of ICP-MS to geoanalysis are found in the reviews by Riddle et al. [4], Hall [5] and Falkner et al. [6]. Prior to

 Geological Survey of Canada contribution number, 61994.

* Corresponding author. Present address: 6074 Meadowglen Drive, Gloucester, Ontario, K1C 5R6, Canada.

*SSDI* 0039-9140(95)01673-2

the ICP-MS determination of trace elements in geological materials, sample solution preparation involved techniques such as (1) open vessel acid attack [7,8]; (2) fusion with sodium peroxide [9] or lithium metaborate [10,11]; (3) decomposition in a screw-top Teflon bomb with $HF + HNO_3 + HClO_4$ followed by evaporation of the excess HF with $HNO_3$ or $HClO_4$ [12,13]. These procedures are generally slow for modern ICP-MS automated instruments which can analyze samples much faster than the time needed to prepare sample solutions. There is, therefore, a need to decrease the solution preparation time in order to increase productivity.

In recent years, the microwave digestion technique for the dissolution of solid samples has gained increasing attention, as was emphasized in a review by Matusiewicz and Sturgeon [14]. Applications are also found in dissolving rocks [15] and catalysts [16].

In part I of this series, the authors [17] described a method for the direct determination of traces of Th, U and the lanthanides in geological materials by ICP-MS after the dissolution of samples by microwave digestion in a Teflon vessel using a mixture of $HF + HNO_3 + HCl + H_3BO_3$ + EDTA. The purpose of this paper is to demonstrate the effectiveness of the sample preparation procedure followed by direct ICP-MS determination for other trace elements also, such as Ba, Cs, Ga, In, Mo, Nb, Pb, Rb, Sn, Sr, Ta and Tl in rocks and sediments.

The accuracy and precision of the developed method was tested by five replicate analyses of international geochemical reference samples SY-2, MRG-1, BCR-1 and MAG-1. Several other international geochemical reference rocks and sediments were also analyzed, in triplicate or duplicate, to ascertain the accuracy. Excellent agreement with the "recommended" values was found for the majority of these samples. The developed method is fast for routine analysis, economical since it involves less chemicals and equipment for sample decomposition, and environmentally friendly because no evaporation of acids is required.

## 2. Experimental

### 2.1. Apparatus

A Perkin-Elmer/Sciex Elan model 5000 ICP-mass spectrometer equipped with an IBM PS/2 computer (model 70) and an AS-91 autosampler was used for mass spectral analysis. A Milestone microwave oven (model MLS 1200 MEGA) equipped with six 100-ml Teflon pressure decomposition vessels, a microwave digestion rotor (model HPR 10016) and a remote control panel was used for the decomposition of the samples.

### 2.2. Reagents and standard solutions

Synthetic standard solutions of elemental concentrations ranging from 20 to 100 ng $ml^{-1}$ were prepared by diluting 10 μg $ml^{-1}$ mixed high purity ICP-MS standard solutions from Delta Scientific Laboratory Products Ltd. (Mississauga, Ontario) with 3% (v/v) nitric acid. Each standard solution also contained 50 ng $ml^{-1}$ each of ruthenium and rhenium in the final volume (these acted as internal standards for ICP-MS drift control) and two drops of concentrated hydrofluoric acid (to stabilize the tantalum in solution).

A mixed solution of 0.165% ethylenediaminetetraacetic acid (EDTA) and 2% boric acid was prepared by dissolving 1.65 g of EDTA in dilute ammonia solution followed by the addition of 22 g of boric acid, heating to dissolve, mixing and diluting to 1 l with water. Deionized water prepared by reverse osmosis and ACS grade reagents were used throughout, and all solutions were stored in stoppered nalgene bottles.

### 2.3. Procedure

The sample decomposition procedure was described in detail elsewhere [17,18]. Briefly, it

Table 1
Instrumental operating conditions and data acquisition parameters

| Condition/parameter | Value etc. |
|---|---|
| ICP mass spectrometer | |
| R.f. power (kW) | 1.0 |
| Plasma argon gas flow rate (l $min^{-1}$) | 15 |
| Auxiliary argon gas flow rate (l $min^{-1}$) | 0.9 |
| Nebulizer argon gas flow rate (l $min^{-1}$) | 0.9 |
| Sampler skimmer | Nickel |
| Data acquisition | |
| Dwell time (ms) | 100 |
| Scan mode | Peak hopping |
| Points across peak | 1 |
| Sweeps reading, reciprocal of | 10 |
| Number of replicates | 2 |

Table 2
List of isotopes of trace elements together with ruthenium and rhenium employed in this work

| Group 1 | Group 2 |
|---|---|
| $^{71}Ga$ | $^{178}Hf$ |
| $^{85}Rb$ | $^{181}Ta$ |
| $^{88}Sr$ | $^{205}Tl$ |
| $^{93}Nb$ | $^{207}Pb$ |
| $^{97}Mo$ | $^{185}Re$[a] |
| $^{115}In$ | |
| $^{118}Sn$ | |
| $^{133}Cs$ | |
| $^{138}Ba$ | |
| $^{101}Ru$[b] | |

[a] Used as an internal standard to correct for instrumental drift and matrix effects on Group 2 elements.
[b] Used as an internal standard to correct for instrumental drift and matrix effects on Group 1 elements.

involved heating a group of six samples in pressurized Teflon vessels, each containing 0.5 g of up to 200 mesh sample and a mixture of 2.5 ml of 27 M HF, 3 ml of 16 M $HNO_3$ and 3 ml of 12 M HCl, in a microwave oven for a total period of 16 min (the power ranged from 250–1000 W). After cooling to room temperature in a water bath, each solution was mixed with 30 ml of the boric acid and EDTA mixture, and the assembled vessels were heated in the microwave oven for an additional 8 min (power ranged from 250–1000 W). The contents of the vessel were then transferred to a polypropylene tube by rinsing with 2% (v/v) nitric acid, and the volume was made up to 50 ml. For ICP-MS determination of the specified elements, an aliquot was diluted 10 times with 3% (v/v) nitric acid containing ruthenium and rhenium internal standards. The final concentrations of ruthenium and rhenium were 20 ng $ml^{-1}$ each in the diluted sample solution; these two elements corrected for matrix effects and controlled instrumental drifts during the ICP-MS measurements. A reagent blank was taken through the procedure. However, multiple blank values for the analytes were found to be negligible.

### 2.4. Multielement ICP-MS determination

Using the instrumental operating parameters of Table 1 and isotopic masses of Table 2, calibration curves were obtained with a blank and three synthetic mixed standard solutions of concentrations 20, 50 and 100 ng $ml^{-1}$ of each element. The 20 ng $ml^{-1}$ synthetic standard solution, six unknown sample solutions (each having a 1 mg $ml^{-1}$ sample concentration and ruthenium and rhenium internal standards) were then run through the autosampler. This

Table 3
Comparison of microwave digestion ICP-MS (MD-ICP-MS) results (in μg $g^{-1}$) for trace elements in CCRMP reference rocks SY-2 and MRG-1 and USGS reference rocks BCR-1 and MAG-1 with the literature values[a]

| Element | SY-2 | | MRG-1 | | BCR-1 | | MAG-1 | |
|---|---|---|---|---|---|---|---|---|
| | MD-ICP-MS, this work | Literature values[b] | MD-ICP-MS, this work | Literature values[b] | MD-ICP-MS, this work | Literature values[c] | MD-ICP-MS, this work | Literature values[d] |
| Ba | 464 ± 58 | 460 ± 50 | 54 ± 9 | 61 ± 23 | 740 | 678 ± 16 | 498 ± 52 | 490 ± 35 |
| Cs | 2.7 ± 0.1 | 2.4 ± 0.3 | 0.6 ± 0.2 | 0.57 ± 0.16 | 0.94 ± 0.04 | 0.97 ± 0.13 | 8.5 ± 0.2 | 8.3 ± 0.5 |
| Ga | 28 ± 1 | 29 ± 3 | 17 ± 1 | 17 ± 4 | 21 ± 0 | 22 ± 2 | 23.0 ± 1.2 | 21.4 ± 0.4 |
| Hf | 8.6 ± 0.16 | 7.7 ± 1.0 | 3.4 ± 0.3 | 3.76 ± 0.22 | 4.8 ± 0.11 | 4.9 ± 0.3 | 3.6 ± 0.7 | 3.6 ± 0.7 |
| In | 0.07 ± 0.004 | < 0.5 | 0.09 ± 0.01 | < 0.5 | 0.09 ± 0.01 | 0.09 ± 0.01 | 0.10 ± 0 | 0.18[e] |
| Mo | 0.3 ± 0.1 | 1.8 ± 1.6? | 0.84 ± 0.15 | 0.87 ± 0.18 | 1.2 ± 0.16 | 1.5[f] | 1.2 ± 0.2 | 1.6[g] |
| Nb | 32 ± 1 | 29 ± 6 | 21 ± 1 | 20 ± 4 | 13 ± 1 | 14 ± 3 | 18 ± 1 | 12[g] |
| Pb | 63 ± 5 | 85 ± 8 | 10 ± 4 | 10 ± 4 | 14.4 ± 0.6 | 13.6 | 28 ± 2 | 25 ± 4 |
| Rb | 210 ± 12 | 217 ± 15 | 7 ± 2 | 8.5 ± 2.4 | 4.6 ± 1.5 | 47 ± 0.6 | 124 ± 6 | 152 ± 3 |
| Sn | 5.6 ± 1 | 5.7 | 3.4 ± 0.4 | 3.6 | < 2 | 2.1 ± 0.6 | 4.6 ± 0.6 | 5.0 |
| Sr | 280 ± 12 | 271 ± 14 | 272 ± 16 | 266 ± 13 | 360 | 330 ± 5 | 167 ± 12 | 156 ± 19 |
| Ta | 2.0 ± 0.1 | 2.0 ± 0.2 | 0.84 ± 0.04 | 0.80 ± 0.05 | 0.64 ± 0.04 | 0.79 ± 0.03 | 1.2 ± 0.2 | 1.0 ± 0.2 |
| Tl | 1.75 ± 0.08 | 1.5 ± 0.3 | 0.06 ± 0.02 | 0.06 ± 0.02 | 0.31 ± 0.02 | 0.30 ± 0.03 | 0.77 ± 0.03 | 0.79 |

[a] Values given represent the mean and standard deviation of five replicate determinations unless otherwise indicated.
[b] "Recommended values" quoted from a compilation of data by Gladney and Roelandts [22].
[c] "Consensus values" quoted from a compilation of data by Gladney et al. [19].
[d] Quoted from a compilation of data by Gladney and Goode [23] unless otherwise indicated.
[e] Quoted from a compilation of data by Potts et al. [24].
[f] "Usable value" quoted from a compilation of data by Abbey [25].
[g] "Working value" quoted from a compilation of data by Govindaraju [20].

Table 4
Direct determination of trace elements (μg $g^{-1}$) in international reference samples of rocks and sediments by ICP-MS after dissolution by microwave oven digestion

| Source | Sample | Ba | | Cs | | Ga | | Hf | |
|---|---|---|---|---|---|---|---|---|---|
| | | This work | Other values | This work | Other values | This work | Other values | This work | Other values |
| USGS | AGV-1 | 1400 | 1221 ± 16[a] | 1.30 ± 0.2 | 1.26 ± 0.12[a] | 20.7 ± 1.2 | 20 ± 3[a] | 5.1 ± 0.1 | 5.1 ± 0.4[a] |
| USGS | BHVO-1 | – | – | 0.06 | 0.086[b] | 21 | 22 ± 3[b] | 4.4 | 4.2 ± 0.2[b] |
| | | | | 0.06 | | 21 | | 4.5 | |
| USGS | BIR-1 | 7 | 7.7 ± 2.2[c] | <0.02 | 0.06[c] | 14 | 16 ± 2[c] | 0.51 | 0.58 ± 0.06[c] |
| | | 10 | | <0.02 | | 13 | | 0.51 | |
| USGS | DNC-1 | 120 | 120 ± 15[a] | 0.3 | 0.4 (1)[a] | 14 | 7 (1)[a] | 1.0 | 1.02 ± 0.07[a] |
| USGS | DTS-1 | 2 | 2.35[a] | <0.02 | 0.058[d] | 1.0 | 1?[b] | 0.02 | 0.015[d] |
| | | 3 | | 0.13 | | 1.2 | | 0.03 | |
| USGS | G-2 | 2200 | 1880 ± 20[a] | 1.3 ± 0 | 1.33 ± 0.14[a] | 22.7 ± 0.6 | 22 ± 2[a] | 2 | 7.9 ± 0.7[a] |
| USGS | W-2 | 190 | 200 ± 40[a] | 0.90 | 1.0 (2)[a] | 18 | 8.3 (1)[a] | 2.4 | 2.58 ± 0.11[a] |
| CCRMP | LKSD-1 | 440 | 430 ± 40[e] | 1.0 | 1.5 ± 1.2[e] | 8.8 | – | 2.0 | 3.6 ± 0.5[e] |
| | | 470 | | 1.0 | | 8.4 | | 2.0 | |
| CCRMP | LKSD-2 | 840 | 780 ± 75[e] | 2.8 | 3.0 ± 0.6[e] | 15 | – | 5 | 7 ± 1[e] |
| | | | | 2.7 | | 14 | | 4 | |
| CCRMP | LKSD-3 | 740 | 680 ± 55[e] | 2.3 | 2.3 ± 0.3[E] | 15 | – | 4 | 4.8 ± 0.7[e] |
| | | 730 | | 2.2 | | 14 | | 3 | |
| CCRMP | LKSD-4 | 320 | 330 ± 55[e] | 1.3 | 1.7 ± 0.6[e] | 7.1 | – | 2 | 2.8 ± 0.5[e] |
| | | 340 | | 1.4 | | 7.1 | | 2 | |

[a] "Consensus value" quoted from a compilation of data by Gladney et al. [19].
[b] Quoted from a compilation of data by Gladney and Goode [23].
[c] Quoted from a compilation of data by Gladney and Roelandts [28].
[d] "Working value" quoted from a compilation of data by Govindaraju [20].
[e] "Provisional value" quoted from a compilation of data by Lynch [27].

Table 5
Direct determination of trace elements (μg $g^{-1}$) in international reference samples of rocks and sediments by ICP-MS after dissolution by microwave oven digestion

| Source | Sample | Ba | | Cs | | Ga | | Hf | |
|---|---|---|---|---|---|---|---|---|---|
| | | This work | Other values | This work | Other values | This work | Other values | This work | Other values |
| CCRMP | STSD-1 | 660 | 630 ± 51[a] | 1.7 | 1.8 ± 3[a] | 11 | – | 3 | 6.1 ± 0.9[a] |
| | | 690 | | 1.6 | | 11 | | 3 | |
| CCRMP | STSD-2 | 590 | 540 ± 43[a] | 11 | 12 ± 1.4[a] | 21 | – | 2 | 5 ± 0.8[a] |
| | | 560 | | 11 | | 20 | | 2 | |
| CCRMP | STSD-3 | 1600 | 1490 ± 120[a] | 5.5 | 5.2 ± 0.8[a] | 15 | – | 3.1 | 5.1 ± 1.2[a] |
| | | 1600 | | 5.0 | | 14 | | 2.4 | |
| CCRMP | STSD-4 | 2000 | 2000 ± 222[a] | 1.5 | 1.9 ± 0.6[a] | 14 | – | 2 | 5.5 ± 1.0[a] |
| | | 2100 | | 1.6 | | 13 | | 2 | |
| NIM | NIM-G | 97 | 120[b] | 0.9 ± 0.1 | 1[b] | 29 ± 2.9 | 27[b] | 12.5 ± 1.3 | 12[b] |
| | | 120 | | | | | | | |
| IWG | BE-N | 1000 | 1025[b] | 0.7 ± 0.1 | 0.8[b] | 17 ± 1.7 | 17[b] | 5.45 ± 0.62 | 5.4[b] |
| | | 1000 | | | | | | | |
| IGGE | GSD-1 | 930 | 950 | 5.0 | 5.1[c] | 17 | 23 | 9.9 | 9.3[c] |
| | | 940 | | 4.8 | | 17 | | | |
| IGGE | GSD-5 | 530 | 440[b] | 9.2 | 9.4[b] | 20 | 20.3[b] | 4 | 6.5[c] |
| | | 490 | | 9.0 | | 19 | | 4 | |
| IGGE | GSD-6 | 350 | 330[b] | 9.0 | 9.1[b] | 15 | 16.7[b] | 3 | 4.7[c] |
| | | 360 | | 9.0 | | 15 | | 3 | |
| NBS | 1645 | 390 | 374[b] | 2.4 | 2.8[b] | – | – | 1.1 | 1.4[c] |
| | | | | 2.4 | | | | 1.1 | |

[a] "Provisional value" quoted from a compilation of data by Lynch [27].
[b] "Working value" quoted from a compilation of data by Govindaraju [20].
[c] Quoted from a compilation of data by Potts et al. [24].

| In | | Mo | | Nb | | Pb | |
|---|---|---|---|---|---|---|---|
| This work | other values | This work | other values | This work | other values | This work | other values |
| 0.05 | 0.04 ± 0.01[a] | 2 | 3 ± 1[a] | 15 ± 0 | 15 ± 3[a] | 37 ± 1.7 | 36 ± 5[a] |
| 0.08 | <4.6[b] | – | – | 19 | 19 ± 2 | 2.7 | 4 ± 2[b] |
| 0.08 | | | | 19 | | 2.6 | |
| 0.06 | – | <0.2 | 0.05[a] | 1 | 2.0 ± 0.05[c] | 3.3 | 3.2 ± 0.8[c] |
| 0.05 | | <0.2 | | 1 | | 3.3 | |
| 0.04 | – | <0.2 | – | 2 | 2.2 (2)[a] | 7.6 | 6.3 ± 1[c] |
| <0.02 | 0.0024[a] | <0.2 | 0.14 ± 0.09[a] | 0.10 | 0.14 ± 0.09[a] | 9 | 12 ± 3[a] |
| <0.02 | | <0.2 | | 0.11 | | 9 | |
| 0.03 | 0.03[a] | <0.2 | 1.0 ± 0.6[a] | 13 ± 0 | 13 ± 4[a] | 32 ± 1 | 31 ± 4[a] |
| 0.05 | – | 0.48 | 0.42 (1)[a] | 7.8 | 8 (2)[a] | 9.7 | 9.3 ± 3.1[c] |
| 0.54 | – | 12 | 12 ± 2[e] | 4.3 | 7 ± 8[e] | 94 | 82 ± 5[e] |
| 0.46 | | 13 | | 4.2 | | 81 | |
| 0.08 | – | 1.0 | 2 ± 0.7[e] | 10 | 8 ± 1[e] | 52 | 44 ± 4[e] |
| 0.07 | | | | 10 | | 52 | |
| 0.05 | – | 1.2 | 2 ± 0.9[e] | 9.5 | 8 ± 1[e] | 37 | 29 ± 3[e] |
| 0.06 | | 1.0 | | 9.2 | | 35 | |
| 0.05 | – | 1.9 | 2 ± 0.6[e] | 4.5 | 9 ± 7[e] | 92 | 91 ± 6[e] |
| 0.06 | | 1.3 | | 4.4 | | 98 | |

| In | | Mo | | Nb | | Pb | |
|---|---|---|---|---|---|---|---|
| This work | Other values | This work | Other values | This work | Other values | This work | Other values |
| 0.06 | – | 1.3 | 2 ± 0.5[a] | 5.8 | 5 ± 3[a] | 41 | 35 ± 3[a] |
| 0.06 | | 1.0 | | 6.8 | | 43 | |
| 0.13 | – | 14.0 | 13 ± 2[a] | 20 | 20 ± 3[a] | 79 | 66 ± 4[a] |
| 0.12 | | 12.0 | | 20 | | 79 | |
| 0.08 | – | 7.2 | 6 ± 2[a] | 13 | 12 ± 4[a] | 52 | 40 ± 3[a] |
| 0.07 | | 5.8 | | 12 | | 50 | |
| 0.11 | – | 1.5 | <5[a] | 7.4 | 9 ± 5[a] | 20 | 16 ± 3[a] |
| 0.10 | | 1.0 | | 7.3 | | 22 | |
| 0.05 | – | 3.0 | 3[b] | 56 ± 2 | 53[b] | 37 ± 1 | 40[b] |
| 0.04 | | 3.2 | | | | | |
| 0.078 ± 0.004 | – | 2.9 | 2.5[b] | 110 ± 0 | 100[b] | 4.4 ± 0.3 | 4[b] |
| | | 3.0 | | | | | |
| 0.06 | – | 1.0 | 0.74[b] | 18 | 35[c] | – | – |
| 0.07 | | 1.9 | | 19 | | | |
| 0.11 | 0.13[b] | 1.0 | 1.2[b] | 19 | 19[b] | 130 | 112[b] |
| 0.10 | | 1.0 | | 18 | | 130 | |
| 0.14 | 0.14[b] | 7.8 | 7.7[b] | 10 | 12[b] | 31 | 27[b] |
| 0.15 | | 7.9 | | 11 | | 32 | |
| 0.24 | – | 14 | 34[b] | 3.3 | – | 670 | 714[b] |
| 0.20 | | 15 | | 3.0 | | 680 | |

Table 6
Direct determination of trace elements ($\mu g\, g^{-1}$) in international reference samples of rocks and sediments by ICP-MS after dissolution by microwave digestion

| Source | Samples | Rb | | Sn | | Sr | | Ta | | Tl | |
|---|---|---|---|---|---|---|---|---|---|---|---|
| | | This work | Other values | This work | Other values | This work | Other valus | This work | Other values | This work | Other values |
| USGS | AGV-1 | 67 | 67 ± 1[a] | 3.4 | 4.2 ± 1.1[a] | 850 | 662 ± 9[a] | 0.96 ± 0.04 | 0.92 ± 0.12[a] | 0.33 ± 0.02 | 0.7 ± 0.5[a] |
| USGS | BHVO-1 | 9.2 | – | – | – | – | – | 1.3 | – | 0.04 | – |
| | | 9.0 | | | | | | 1.3 | | 0.05 | |
| USGS | BIR-1 | 0.9 | 1 ± 0.9[b] | <2.0 | 0.69[b] | 100 | 108 ± 14† | 0.08 | 0.06 ± 0.04[b] | 0.02 | 0.01[b] |
| | | 0.4 | | <2.0 | | 120 | | 0.10 | | <0.02 | |
| USGS | DNC-1 | 3.9 | 1.9–9 (3)[a] | <2.0 | – | 170 | 140–470 (3)[a] 145[c] | 0.18 | 0.11 (1)[a] | 0.03 | – |
| USGS | DTS-1 | 0.3 | 0.1[c] | <2.0 | 0.55[c] | 1.0 | 0.32[c] | 0.05 | 0.04[c] | <0.02 | 0.002[c] |
| | | 0.5 | | <2.0 | | 0.8 | | 0.1 | | <0.02 | |
| USGS | G-2 | 160 | 171 ± 10[a] | <2.0 | 1.6 ± 0.5[a] | 560 | 470 ± 30[a] | 0.83 ± 0.1 | 0.88 ± 0.12[a] | 0.92 ± 0.05 | 1.02 ± 0.08[a] |
| USGS | W-2 | 21 | 23 ± 2 (3)[a] | <2.0 | – | 220 | 150–350 (3)[a] 194[c] | 0.56 | 0.46 (2)[a] | 0.09 | – |
| CCRMP | LKSD-1 | 22 | 24 ± 7[d] | – | – | 260 | 250 ± 53[d] | 0.28 | 0.13 ± 0.03[d] | 0.35 | – |
| | | 23 | | | | 300 | | 0.28 | | 0.34 | |
| CCRMP | LKSD-2 | 78 | 85 ± 10[d] | <2.0 | 5 ± 2[d] | 280 | 220 ± 41[d] | 0.91 | 0.8 ± 0.1[d] | 0.61 | – |
| | | 75 | | | | | | 0.71 | | 0.60 | |
| CCRMP | LKSD-3 | 74 | 78 ± 10[d] | <2.0 | 3 ± 2[d] | 290 | 240 ± 42[d] | 0.3 | 0.7 ± 0.1[d] | 0.57 | – |
| | | | 72 | | <2.0 | | 280[c] | | | 0.55 | |
| CCRMP | LKSD-4 | 23 | 28 ± 10[d] | 3.0 | 5 ± 1[d] | 130 | 110 ± 38[d] | 0.4 | 0.4 ± 0.04[d] | 0.56 | – |
| | | 24 | | 3.0 | | 130 | | | | 0.57 | |

[a] "Consensus value" quoted from a compilation of data by Gladney et al. [19].
[b] "Recommended value" quoted from a compilation of data by Gladney and Roelandts [26].
[c] "Working value" quoted from a compilation of data by Govindaraju [20].
[d] "Provisional value" quoted from a compilation of data by Lynch [27].

Table 7
Direct determination of trace elements ($\mu g\ g^{-1}$) in international reference samples of rocks and sediments by ICP-MS after dissolution by microwave digestion

| Source | Sample | Rb | | Sn | | Sr | | Ta | | Tl | |
|---|---|---|---|---|---|---|---|---|---|---|---|
| | | This work | Other values | This work | Other values | This work | Other values | This work | Other values | This work | Other values |
| CCRMP | STSD-1 | 29 | 30 ± 7[a] | <2.0 | 4 ± 1[a] | 220 | 170 ± 42[a] | 0.40 | 0.40 ± 0.12[a] | 0.47 | – |
| | | 29 | | | | 210 | | 0.40 | | 0.43 | |
| CCRMP | STSD-2 | 99 | 104 ± 10[a] | 3.2 | 5 ± 1[a] | 500 | 400 ± 65[a] | – | – | 0.66 | – |
| | | 95 | | 3.4 | | 460 | | | | 0.61 | |
| CCRMP | STSD-3 | 68 | 68 ± 11[a] | 2.2 | 4 ± 2[a] | 300 | 230 ± 52[a] | 0.9 | 0.9 ± 0.1[a] | 0.69 | – |
| | | 61 | | <2.0 | | 260 | | 0.8 | | 0.60 | |
| CCRMP | STSD-4 | 36 | 39 ± 6[a] | <2.0 | 2 ± 1[a] | 400 | 350 ± 60[a] | 0.52 | 0.6 ± 0.2[a] | 0.33 | – |
| | | 35 | | <2.0 | | 400 | | | | 0.32 | |
| NIM | NIM-G | 277 ± 6 | 320[b] | 3.9 | 4[b] | 9 | 10[b] | 4.7 ± 0.4 | 4.5[b] | 0.97 ± 0.03 | 0.93[c] |
| | | | | 3.8 | | 10 | | | | | |
| IWG | BE-N | 48 ± 1 | 47[b] | <2.0 | 2.4[c] | 1400 | 920–1610[d] | 5.8 ± 0.3 | 5.5[b] | 0.04 ± 0 | 0.05[d] |
| | | | | <2.0 | | 1400 | 1370[b] | | | | |
| IGGE | GSD-1 | 150 | 116[b] | – | – | – | – | 5 | 3.7[b] | 0.65 | 0.61[b] |
| | | 150 | | | | | | 2 | | 0.80 | |
| IGGE | GSD-5 | 120 | 118[b] | 5.0 | 4.6[b] | 230 | 204[b] | 1.6 | 1.4[b] | 1.2 | 1.16[b] |
| | | 120 | | | | 250 | | 1.4 | | 1.2 | |
| IGGE | GSD-6 | 100 | 107[b] | 5.0 | 2.8[b] | 310 | 266[b] | 0.71 | 0.72[b] | 1.0 | 1.08[b] |
| | | 110 | | 6.4 | | 320 | | 0.71 | | 1.0 | |
| NBS | 1645 | 42 | 41[b] | 420 | 360[b] | 1000 | 880[b] | 0.39 | – | 1.4 | 1.44[b] |
| | | 42 | | 400 | | | | 0.18 | | 1.4 | |

[a] "Provisional value" quoted from a compilation of data by Lynch [27].
[b] "Working value" quoted from a compilation of data by Govindaraju [20].
[c] "Recommended value" quoted from a compilation of data by Potts et al. [24].
[d] Quoted from a compilation of data by Govindaraju [28].

was followed by a repeat determination of a 20 ng ml$^{-1}$ synthetic standard solution and the determination of the concentrations of trace elements for three geochemical reference materials (AGV-1, BCR-1 and BHVO-1), the solutions of which were prepared identically to the unknown sample solutions.

The instrument software automatically performed blank subtraction, calibration, drift control and calculation of the concentrations of the elements in the standard (20 ng ml$^{-1}$), unknown sample solutions and the reference materials used as a control, and printed out the data. From the print-out of the data sheet, the

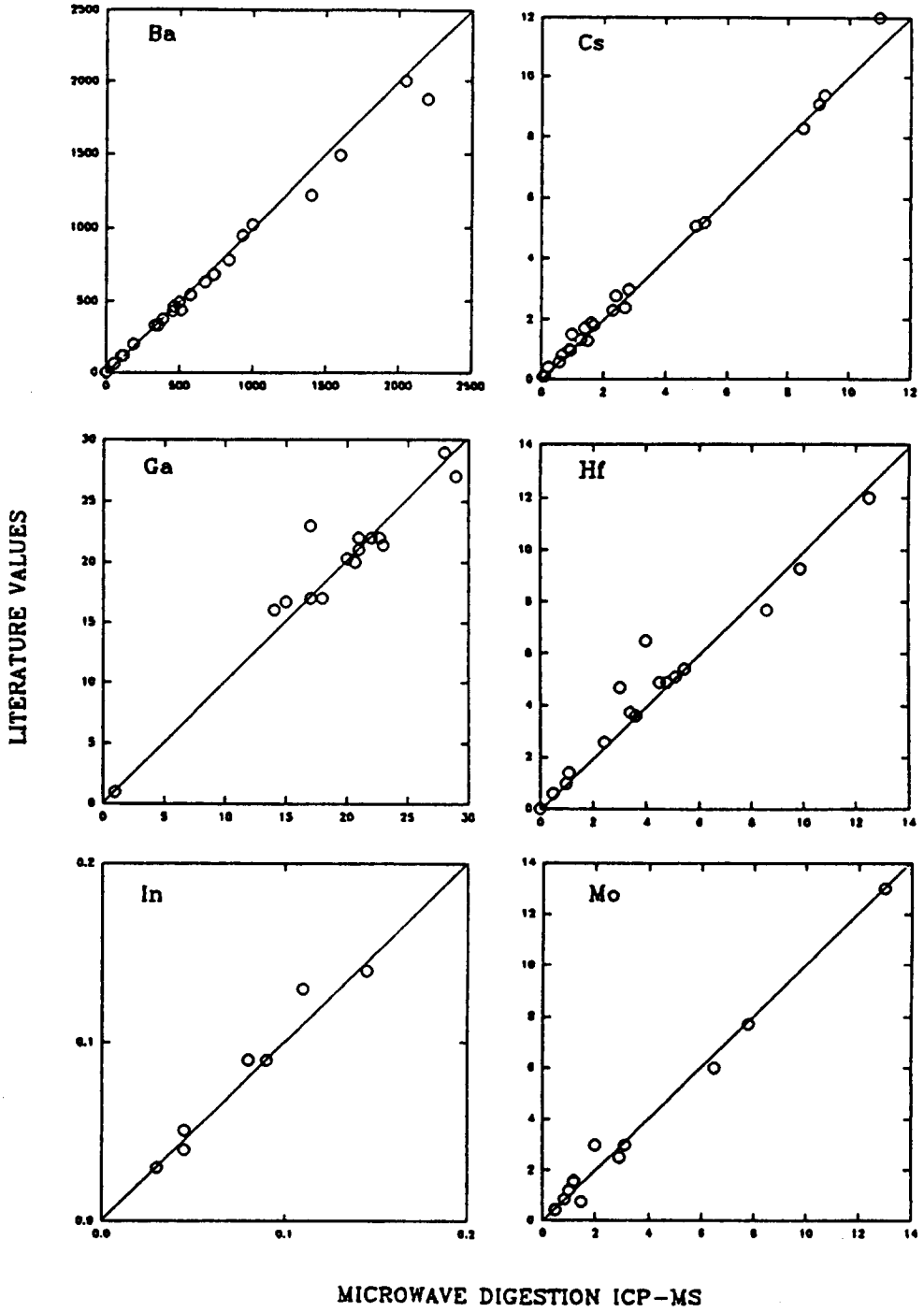


Fig. 1. (Part 1).

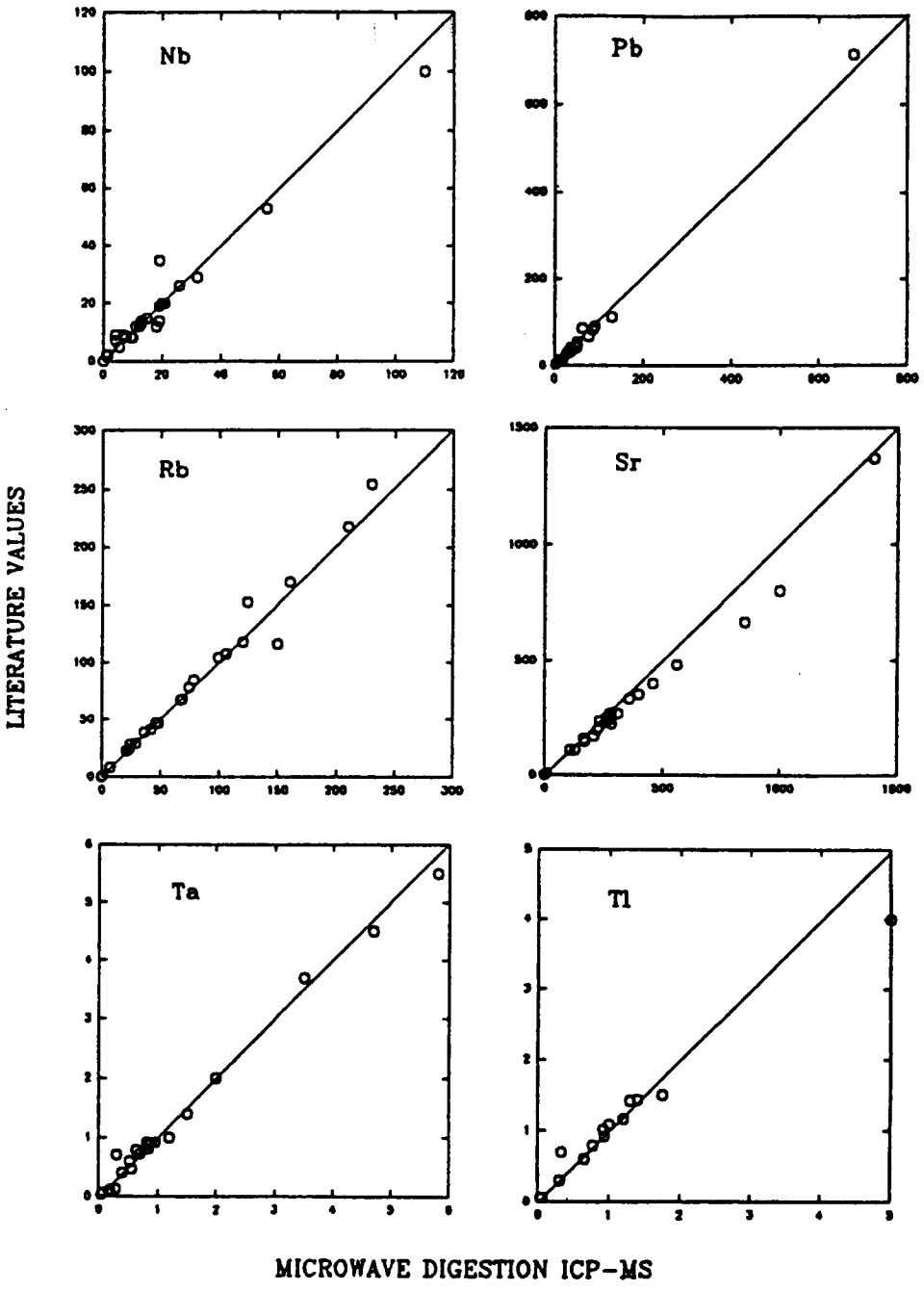


Fig. 1 (continued). Correlation plots for microwave digestion ICP-MS versus the literature values for Ba, Cs, Ga, Hf, In, Mo, Nb, Pb, Rb, Sr, Ta and Tl in some international reference samples of rocks and sediments (concentrations are given in units of micrograms per gram).

recovery of the 20 ng $ml^{-1}$ synthetic standard was checked, and if required, a correction factor (about $1 \pm 0.03$) was applied to the results for the unknown and reference materials. The results for the reference materials were first checked for their accuracy with reference to the "consensus" or "recommended" statistical ranges of literature values [19,20]. If the values for the reference materials fell within acceptable ranges, the results for the unknown samples were presumed correct for reporting purposes. In actual practice, this procedure worked well for the reference materials as well as for the unknown samples.

## 3. Results and discussion

The ICP-MS determination limits (micrograms per gram in the original rock) of this work for 13 trace elements were as follows: Cs, Hf, In, Rb, Tl (0.02); Ga, Nb, (0.10); Mo, Pb, Ta (0.20); Ba (0.5); Sn, Sr (2).

Except for strontium, ICP-MS determination limits of this work for the other elements are superior to those of ICP-AES [7,21]. Isotopic masses of the trace elements analyzed in this work were chosen in such a manner as to possess minimum isobaric interferences. In the case of $^{115}$In, the isobaric contribution of $^{115}$Sn was automatically corrected by the instrument.

Table 3 shows the accuracy and precision of the results for five replicate analyses of Canadian Certified Reference Materials Project (CCRMP) reference rocks SY-2 (syenite) and MRG-1 (gabbro), and USGS reference materials BCR-1 (basalt) and MAG-1 (marine mud), and a comparison with the literature recommended values [19,20,22–25]. For SY-2 and MRG-1 (except for somewhat lower values for lead in SY-2), agreement of the results for the other elements with the recommended values is of the order of 96–100%. However, a large standard deviation in the literature values for Mo in Sy-2 makes them uncertain compared to microwave digestion-ICP-MS (MD-ICP-MS) data. For BCR-1, there is excellent agreement of MD-ICP-MS values with the literature values [19]. For MAG-1, the MD-ICP-MS data compare well with the recommended values in the majority of cases except for niobium, where a significantly higher value was obtained in this work (compare Table 3). In Tables 4–7, MD-ICP-MS results for the specified elements for some international reference materials are given and compared with the literature values [19,20,24,26–28]. These are the USGS reference rocks andesite (AGV-1), basalt (BIR-1), diabase (DNC-1 and W-2), dunite (DTS-1), granite (G-2) and granodiorite (GSP-1), CCRMP lake sediments (LKSD-1 to 4) and stream sediments (STSD-1 to 4), National Institute of Metallurgy (South Africa) granite (NIM-G), International Working Group (France) basalt (BE-N), Institute of Geophysical and Geochemical Exploration (China) stream sediments (GSD-1, GSD-5 and GSD-6) and National Bureau of Standards river sediment (NBS 1645).

MD-ICP-MS results for AGV-1, G-2, NIM-G and BE-N represent mean and standard deviations of three or more determinations. Good agreement between MD-ICP-MS values and the literature values is found in the majority of cases (see Tables 4–7).

New values for gallium in LKSD-1 to 4 and STSD-1 to 4, for indium in BIR-1, DNC-1, W-2, LKSD-1 to 4, STSD-1 to 4, NIM-G, BE-N, GSD-1 and NBS 1645, for niobium in NBS 1645, and for thallium in W-2, LKSD-1 to 4 and STSD-1 to 4 are given in Tables 4–7. It should be pointed out that the literature values for CCRMP lake and stream sediment samples (LKSD-1 to 4 and STSD-1 to 4) are only "provisional", not certified. Therefore, more other values in these samples are needed to make a valid comparison with the results obtained in this work by MD-ICP-MS.

Where possible, the results of this work are also compared graphically with other recommended values (without the standard deviations) in Fig. 1. Most points fall on or near the 45° line supporting the accuracy of the proposed method.

From the data of Tables 4–7 and the above discussion, it can be concluded that for most common types of silicate rocks such as syenites, gabbro, granites, basalts, diabase, etc. and various water sediment samples, the MD-ICP-MS procedure would give results equally as good as those of the open vessel digestion ICP-MS method. But the advantage of the microwave digestion method lies not only in the rapidity of the sample dissolution procedure but also in the economy of reagents and equipment and the smaller amount of environmental pollution since no evaporation of excess acids is required. Approximately 30 sample solutions can be prepared by one operator in one working day by the microwave digestion method.

## Acknowldgements

The authors are indebted to J.L. Bouvier for decomposing some samples, and to K.N. De-Silva for critical reading of the manuscript.

## References

[1] E.B. Sandell, Colorimetric Determination of Traces of Metals, 3rd edn., Interscience Publishers, New York, 1959, pp. 1–1032.

[2] J.A. Maxwell, Rock and Mineral Analysis, Interscience Publishers, New York, 1968, pp. 1–584.

[3] W.M. Johnson and J.A. Maxwell, Rock and Mineral Analysis, John Wiley, New York, 1981, pp. 1–489.
[4] C. Riddle, A. Vander Voet and W. Doherty, Geostds. Newsl., 12 (1988) 203.
[5] G.E.M. Hall, J. Geochem. Explor., 44 (1992) 201.
[6] K.K. Falkner, G.P. Klinkhammer, C.A. Ungerer and D.M. Christie, Annu. Rev. Earth Sci., 23 (1995) 409.
[7] A.R. Date and A.L. Gray, Spectrochim. Acta, Part B, 40 (1985) 115.
[8] F. Poitrasson, C. Pin, P. Telouk and J.L. Imbert, Geostds. Newsl., 17 (1993) 209.
[9] S.E. Jackson, Chem. Geol., 83 (1990) 105.
[10] G.E.M. Hall and J.C. Pelchat, J. Anal. At. Spectrom., 5 (1990) 339.
[11] Y.Q. Tang, K.E. Jarvis and J.G. Williams, Geostds. Newsl., 16 (1992) 61.
[12] G.A. Jenner, H.P. Longerich, S.E. Jackson and B.J. Fryer, Chem. Geol., 83 (1990)133.
[13] A.R. Date and D. Hutchison, Spectrochim. Acta, Part B, 41 (1986) 175.
[14] H. Matusiewicz and R.E. Sturgeon, Prog. Anal. Spectrosc., 12 (1989) 21.
[15] T. Suzuki and M. Sensui, Anal. Chim. Acta, 245 (1991) 43.
[16] O. Platteau and D. Casabiell, Analyst, 119 (1994) 1705.
[17] J.G. Sen Gupta and N.B. Bertrand, Talanta, 42 (1995) 1595.
[18] J.G. Sen Gupta and J.L. Bouvier, Talanta, 42 (1995) 269.
[19] E.S. Gladney, C.E. Burns and I. Roelandts, Geostds. Newsl., 7 (1983) 3.
[20] K. Govindaraju, Geostds. Newsl., 18 (1994) 1.
[21] C.J. Pickford and R.M. Brown, Spectrochim. Acta, Part B, 41 (1986) 183.
[22] E.S. Gladney and I. Roelandts, Geostds. Newsl., 14 (1990) 373.
[23] E.S. Gladney and W.E. Goode, Geostds. Newsl., 5 (1981) 31.
[24] P.J. Potts, A.G. Tindle and P.C. Webb, in Geochemical reference material compositions, Whittles Publishing, CRC Press, Boca Raton, FL, 1992, pp. 1–313.
[25] S. Abbey, Geol. Surv. Can., Pap. 83–15 (1983).
[26] E.S. Gladney and I. Roelandts, Geostds. Newsl., 12 (1988) 63.
[27] J.J. Lynch, Geostds. Newsl., 14 (1990) 153.
[28] K. Govindaraju, Geostds. Newsl., 4 (1980) 49.

ELSEVIER

Talanta 42 (1995) 1959–1963

Talanta

# Determination of impurities in highly pure platinum by inductively coupled plasma-atomic emission spectrometry

Xinhua Zhang*, Huifen Li, Yufang Yang

*Institute of Precious Metals, Kunming, 650221, People's Republic of China*

Received 7 November 1995; revised 9 June 1995; accepted 19 June 1995

**Abstract**

In this work, a cyclone spray chamber system is used in conjunction with an inductively coupled plasma-atomic emission spectrometer instead of the conventional Scott-type chamber system to reduce the lower limit of detection achieved by the instrument, and an internal standard element (Y) is introduced to eliminate the effects caused by the drift in the plasma background level. An ICP-AES method for the determination of 13 impurity elements in a highly pure platinum sample has been developed. In this method, it is not necessary either to add a platinum matrix to the calibration standard or to separate and concentrate the elements to be determined in the samples. The effect of the platinum matrix on the elements to be analyzed is corrected for by a background equivalent concentration subtraction method. The determination ranges of the method are as follows: 0.00010–0.0050% for Mg, Mn, Cu, Ag, Fe and Zn; 0.00030–0.015% for Au, Ir, Ni and Pb; 0.00050–0.025% for Rh and Al; and 0.00080–0.040% for Pd. The method is simple, rapid and accurate, and can be applied to the analysis of 99.9–99.995% pure platinum.

*Keywords:* Cyclone spray chamber; ICP-AES; Impurity elements; Multielement analysis; Platinum

## 1. Introduction

In a previous paper [1], we reported the determination of 13 impurities in 99.99% pure platinum with the ICPQ-1015 direct spectrometer. When there is a demand for the analysis of samples of this metal having a higher purity, the instrument cannot meet the required lower limit of detection of impurity elements. As Browner and Boorn [2] pointed out, the sample introduction system does not always share the excellent properties of the optical and electronic components found in most modern atomic spectrometers. For this reason we introduced a cyclone spray chamber system (CSCS) [3] into the original instrument, and compared the analytical characteristics of the CSCS with those of the conventional Scott-type chamber system (STCS). Under the same operating conditions, the detection limits of the elements to be determined were reduced two- to threefold when the CSCS was used. This means that the lower limit of detection and the amount of sample used can be reduced by use of the CSCS technique. An internal standard element (Y) was introduced to eliminate the effects caused by the drift in the plasma background level [4]. Efforts were made to develop a method for the determination of 13 impurities in 99.9–99.995% pure platinum.

* Corresponding author.

*SSDI* 0039-9140(95)01675-9

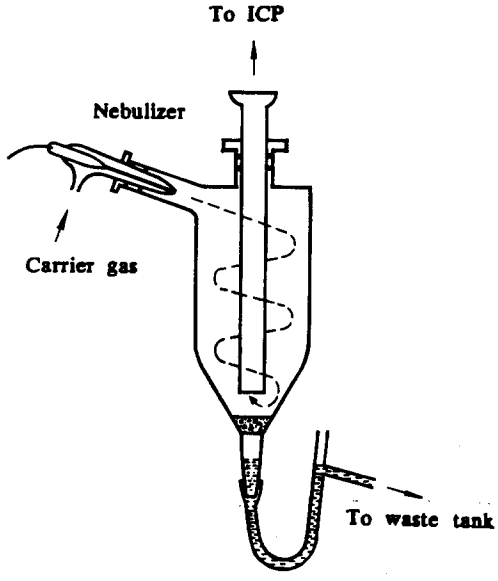


Fig. 1. Diagram of the CSCS.

## 2. Experimental

### 2.1. Apparatus

The determinations were carried out with an ICPQ-1015 direct spectrometer, a CTM-50 monochromator, and an automatic background correction unit. A diagram of the CSCS is shown in Fig. 1. The working conditions given in Table 1 were used throughout the investigation.

### 2.2. Reagents

Hydrochloric acid and nitric acid (suprapure grade), platinum metal (purity, 99.99938%), $Y_2O_3$ (purity, 99.99%), impurity elements (purity more than 99.9%), and doubly distilled water were used.

Table 2
Wavelength of analytical lines

| Element | Wavelength (nm) | Element | Wavelength (nm) |
|---|---|---|---|
| Pd | 363.469 | Cu | 324.754 |
| Rh | 343.489 | Al | 396.152 |
| Ir | 224.268 | Mg | 279.553 |
| Au | 267.594 | Mn | 257.610 |
| Ag | 328.068 | Zn | 202.548 |
| Fe | 259.940 | Pb | 220.353 |
| Ni | 231.604 | Y | 371.030 |

### 2.3. Preparation of solutions

*Calibration standard solutions*

According to the determination ranges, a set of at least three calibration standard solutions were prepared. These solutions contained 10% (v/v) hydrochloric acid, 2 μg $ml^{-1}$ of the internal standard element (Y), and different concentrations of the impurity elements to be determined, but they did not contain a platinum matrix.

*Matrix solution*

A matrix solution containing 20 mg $ml^{-1}$ of platinum was prepared; the solution also contained the same amount of hydrochloric acid and internal standard element as the calibration standard solutions.

*Sample solutions*

The platinum sample was dissolved in aqua regia and was converted to its chloro complex by repeated evaporation with hydrochloric acid. The residue was dissolved in 2 ml of 1:1 hydrochloric acid and the solution was diluted to 10 ml.

Table 1
Working conditions

| Component/parameter | Description/value |
|---|---|
| Torch | A set of three concentric quartz tubes |
| Nebulizer | Concentric |
| Forward r.f. power (kW) | 1.0 |
| Reflected power (W) | <5 |
| Argon coolant flow rate (l $min^{-1}$) | 12 |
| Argon plasma flow rate (l $min^{-1}$) | 1.0 |
| Argon carrier gas flow rate (l $min^{-1}$) | 0.85 |
| Height of observation above load coil (mm) | 15 |
| Integration time (s) | 20 |

Table 3
Comparison of the characteristics of the two systems

| Element | STCS | | | | CSCS | | | |
|---|---|---|---|---|---|---|---|---|
| | $I_b$ | $I_a$ | BEC ($\mu g\ ml^{-1}$) | DL ($\mu g\ ml^{-1}$) | $I_b$ | $I_a$ | BEC ($\mu g\ ml^{-1}$) | DL ($\mu g\ ml^{-1}$) |
| Pt | 0.97 | 5.68 | 2.01 | 0.051 | 0.72 | 10.75 | 0.72 | 0.020 |
| Pd | 3.22 | 15.20 | 2.70 | 0.064 | 1.94 | 29.19 | 0.71 | 0.020 |
| Rh | 4.78 | 25.44 | 2.39 | 0.056 | 3.50 | 51.63 | 0.73 | 0.020 |
| Ir | 4.72 | 74.80 | 0.63 | 0.019 | 1.53 | 59.54 | 0.26 | 0.0077 |
| Ag | 1.49 | 66.04 | 0.23 | 0.0068 | 0.48 | 66.52 | 0.077 | 0.0022 |
| Au | 0.69 | 16.54 | 0.43 | 0.012 | 0.51 | 35.94 | 0.14 | 0.0042 |
| Cu | 1.14 | 56.34 | 0.22 | 0.0061 | 0.39 | 60.14 | 0.066 | 0.0019 |
| Ni | 2.23 | 51.78 | 0.45 | 0.013 | 1.15 | 60.83 | 0.19 | 0.0057 |
| Zn | 1.36 | 96.73 | 0.14 | 0.0042 | 0.43 | 54.39 | 0.079 | 0.0024 |
| Pb | 5.41 | 27.97 | 2.40 | 0.058 | 4.36 | 45.01 | 1.07 | 0.029 |
| Fe | 0.90 | 72.21 | 0.13 | 0.0037 | 0.32 | 59.89 | 0.054 | 0.0016 |
| Y | 0.26 | 61.33 | 0.043 | 0.0013 | 0.084 | 60.44 | 0.014 | 0.00042 |

### 2.4. Analytical procedures

The wavelengths of the analytical lines used are shown in Table 2.

Firstly, the optical system of the instrument was calibrated by using a solution of any single element of a suitable concentration, and the gain (voltage) of the spectrometer photomultipliers were adjusted by using a standard solution of high concentration. Secondly, the spectral intensities of the analytes in the calibration standards were determined. Calibration curves were prepared from the spectral intensities of these analytes, and the concentrations of analytes in the sample were determined. Finally, the background equivalent concentration (BEC) at the wavelength of the analytical line for the analytes were determined with the platinum matrix solution. The above operations were controlled by a computer program, and printed results were provided automatically.

## 3. Results and discussion

### 3.1. Main characteristics of CSCS

The analytical characteristics of the CSCS and the STCS were determined and compared by using a solution containing 19 $\mu g\ ml^{-1}$ of each analyte and a blank solution, under the same conditions. The results are summarized in Table 3. In this table, $I_a$ represents the intensity of the analytical line for analyte A in a solution with concentration $C_a$, $I_b$ represents the intensity of the blank at the same wavelength as for analyte A, BEC (equal to $KI_b$), and DL (equal to $0.03C_a/I_a/I_b$) is the detection limit of the analyte A.

The ICPQ-1015 direct spectrometer is equipped with photomultipliers the gain (voltage) of which can be adjusted automatically. When the concentrations of the analyte and the operating conditions are kept constant, the gain with the CSCS is reduced by 80–100 V relative to that with the conventional STCS. This means that the CSCS works better in the target ranges of the instrument than the STCS. In other words, there are wider dynamic ranges with the CSCS than with the STCS. More aerosols, and smaller and more evenly distributed droplets are introduced from the central tube at the bottom of the chamber into the torch after the solutions are aspirated into the chamber and moved along a spiral path, which provides more opportunities for collision with the wall of the chamber, as shown in Fig. 1. Thus, the noise which originates from the fluctuation of the aerosols is also reduced, and a more stable signal is obtained. From the results obtained in Table 3, it is obvious that, when the CSCS is used, $I_a$ for a specified element is increased while the corresponding $I_b$ and BEC are decreased, and hence $I_a/I_b$ is also increased. The detection limits obtained with the CSCS are reduced two-to-threefold compared with those obtained with the STCS. In other words, the sensitivity obtained with the CSCS is increased two-to-threefold compared with those obtained with the STCS. This means that the lower limits of detection of the instrument and the amount of sample used can be reduced by

Table 4
Influence of platinum matrix on the intensity of analytical lines

| Element | Platinum concentration (mg ml$^{-1}$) | | | | | | | |
|---|---|---|---|---|---|---|---|---|
| | 0 | | 10 | | 15 | | 20 | |
| | $I_{an}$ | $I_{no}$ | $I_{an}$ | $I_{no}$ | $I_{an}$ | $I_{no}$ | $I_{an}$ | $I_{no}$ |
| Mg | 66.2 | 100 | 68.2 | 103 | 69.1 | 104 | 71.1 | 107 |
| Mn | 69.5 | 100 | 72.0 | 104 | 73.2 | 105 | 75.7 | 109 |
| Cu | 39.7 | 100 | 40.6 | 102 | 41.0 | 103 | 41.8 | 105 |
| Ag | 44.0 | 100 | 44.6 | 101 | 45.0 | 102 | 45.8 | 104 |
| Fe | 24.6 | 100 | 28.6 | 116 | 30.7 | 125 | 33.0 | 134 |
| Ni | 17.8 | 100 | 19.2 | 108 | 20.0 | 112 | 21.1 | 118 |
| Al | 32.2 | 100 | 31.7 | 99 | 31.8 | 99 | 32.2 | 100 |
| Zn | 57.5 | 100 | 72.2 | 126 | 79.4 | 138 | 88.6 | 154 |
| Pd | 29.8 | 100 | 30.1 | 101 | 30.3 | 102 | 30.9 | 104 |
| Rh | 37.4 | 100 | 37.9 | 101 | 38.1 | 102 | 38.8 | 104 |
| Ir | 34.8 | 100 | 40.2 | 116 | 43.0 | 124 | 46.4 | 133 |
| Pb | 22.2 | 100 | 24.3 | 110 | 25.3 | 114 | 26.8 | 121 |
| Au | 8.1 | 100 | 71.5 | 879 | 101 | 1243 | –[b] | – |
| Au[a] | 2.5 | 100 | 2.6 | 104 | 2.7 | 108 | 2.8 | 112 |

$I_{an}$, Intensity measured; $I_{no}$, intensity normalized to 100%.
[a] Determined by use of the CTM-50 monochromator.
[b] The intensity measured is beyond the range of determination.

use of the CSCS technique. On the basis of the results obtained, a method has been developed for the determination of 13 impurities in 99.9–99.9955% pure platinum with the use of 20 mg ml$^{-1}$ sample solutions.

### 3.2. *Effect of platinum matrix and correction of spectral interferences*

Spectral interference is one of the most important interferences in ICP-AES. The background caused by the intense emission of the platinum matrix is the main source of interference and must be corrected for before any element can be determined.

The influence of the platinum matrix on the intensity of the analytical lines is shown in Table 4. The investigation was carried out with a solution containing 1 μg ml$^{-1}$ of each of the analytes, and 0, 10, 15, or 20 mg ml$^{-1}$ of platinum. The interference of the matrix platinum on the analyte determination was also observed by using the automatic background correction unit, with solutions containing 10 μg ml$^{-1}$ of analyte and a solution containing 20 mg ml$^{-1}$ of platinum.

From the experimental results, no spectral interferences are found among the platinum group elements. This is in agreement with the results obtained by Kibright and Tinsley [5]. Because the analytical line from the gold channel, Au 242.795 nm, suffers serious interference due to the platinum spectral line (Pt 242.804 nm), gold was determined with use of another line, Au 267.595 nm, by using the CTM-50 Monchromator. The analytical line, Ir 224.268 nm, suffers a slight interference from the spectral line of copper (Cu 224.261 nm), but can be neglected in the present work. The analytical lines of Zn, Fe, Pb and Ni suffer slight interferences from the spectral wings of the platinum lines. Because the values of these spectral wings are small and constant at a fixed concentration of platinum, they are also treated as a background. Almost no spectral lines of other analytes are influenced by the platinum matrix. It was found previously [6] that the Pb 220.350 nm spectral line suffers interference from the Pd 220.349 nm spectral line when a large amount of palladium is present, but no such interference was found with a trace amount of palladium. The analytical line, Pd 363.470 nm, suffers interference from the Ar 363.446 nm spectral line, and thus the sensitivity of palladium is reduced.

The effect of platinum on the analytes was corrected for by a BEC subtraction method. It can be formulated briefly as follows: $C_{tr} = C_{ap} - C_{eq}$, where $C_{ap}$, $V_{eq}$, and $C_{tr}$ are the apparent concentration, background equivalent concentration and true concentrations of the

Table 5
Results of the synthetic samples

| Element | CAL.-A | | | | | | CAL.-B | | | | |
|---|---|---|---|---|---|---|---|---|---|---|---|
| | $C_{eq}$ ($\mu g\ ml^{-1}$) | $C_{ap}$ ($\mu g\ ml^{-1}$) | $C_{ad}$[a] ($\mu g\ ml^{-1}$) | $C_{tr}$ ($\mu g\ ml^{-1}$) | Recovery (%) | RSD (%) | $C_{ap}$ ($\mu g\ ml^{-1}$) | $C_{ad}$[a] ($\mu g\ ml^{-1}$) | $C_{tr}$ ($\mu g\ ml^{-1}$) | Recovery (%) | RSD (%) |
| Mg | 0.034 | 0.148 | 0.10 | 0.11 | 110 | 0.2 | 0.436 | 0.40 | 0.40 | 100 | 0.8 |
| Mn | 0.014 | 0.114 | 0.10 | 0.10 | 100 | 1.6 | 0.433 | 0.40 | 0.42 | 105 | 0.6 |
| Cu | 0.029 | 0.127 | 0.10 | 0.10 | 100 | 0.2 | 0.419 | 0.40 | 0.39 | 98 | 0.7 |
| Ag | 0.034 | 0.128 | 0.10 | 0.09 | 90 | 0.2 | 0.414 | 0.40 | 0.38 | 95 | 0.5 |
| Fe | 0.514 | 0.611 | 0.10 | 0.10 | 100 | 0.9 | 0.909 | 0.40 | 0.40 | 100 | 2.3 |
| Zn | 0.513 | 0.611 | 0.10 | 0.10 | 100 | 0.6 | 0.899 | 0.40 | 0.39 | 98 | 1.8 |
| Au | 0.539 | 0.924 | 0.40 | 0.38 | 95 | 2.1 | 2.093 | 1.60 | 1.55 | 97 | 1.4 |
| Ir | 0.659 | 1.502 | 0.40 | 0.39 | 92 | 1.2 | 2.218 | 1.60 | 1.56 | 98 | 4.4 |
| Ni | 0.188 | 0.575 | 0.40 | 0.39 | 98 | 0.7 | 1.737 | 1.60 | 1.55 | 97 | 3.0 |
| Pb | 0.702 | 1.088 | 0.40 | 0.39 | 98 | 1.4 | 2.240 | 1.60 | 1.54 | 96 | 3.0 |
| Rh | 0.177 | 0.774 | 0.60 | 0.60 | 100 | 0.7 | 2.594 | 2.40 | 2.42 | 96 | 2.9 |
| Al | 0.104 | 0.715 | 0.60 | 0.61 | 102 | 3.1 | 2.531 | 2.40 | 2.43 | 101 | 0.6 |
| Pd | 0.0 | 0.947 | 1.0 | 0.95 | 95 | 1.9 | 3.909 | 4.00 | 3.91 | 98 | 5.2 |

[a] $C^{ad}$, concentration added.

analyte, respectively. Here, $C_{eq}$ practically includes the background, the spectral wing and even the very weak spectral line of the platinum matrix. The purity of the platinum matrix, from which the BEC values of the analyte are determined, is directly related to the reliability of the correction. The platinum matrix used in our research is a special product of our Institute, the purity of which is 99.99938%. The BEC of the matrix is almost constant; it is not necessary to determine the BEC value each time of analysis with the same batch of matrix if the analytical conditions are controlled strictly.

### *3.3. Determination ranges and results for synthetic samples*

The determination ranges are as follows: 0.00010–0.0050% for Mg, Mn, Cu, Ag, Fe and Zn; 0.00030–0.015% for Au, Ir, Ni and Pb; 0.00050–0.025% for Rh and Al; and 0.00080–0.040% for Pd.

The results for two synthetic samples are summarized in Table 5, in which the RSD (relative standard deviation) values for each sample were obtained statistically from 12 replicate determinations in four experiments during a period of 2 months.

## Acknowledgment

The authors thank Professor Yibin Qu for her help in preparing this manuscript.

## References

[1] X. Zhang, H. Li and Y. Yan, Fenxi Huaxue (Analytical chemistry), 19(10) (1991) 1199–1201.
[2] R.F. Browner and A.W. Boorn, Anal. Chem., 56 (1984) 786A.
[3] Z. He, D. Wang and H. Ye, Guangpuxue Guangpufenxi (Spectrosc. Spectr. Anal.), 7(1) (1987) 43–49.
[4] S.A. Myers and D.H. Tracy, Spectrochim. Acta, Part B, 38(9) (1983) 1227–1253.
[5] G.F. Kilbright and H.M. Tinsley, Talanta, 26(1) (1979) 41–45.
[6] X. Zhang, H. Li and Y. Yang, Fenxi Shiyanshi (Anal. Lab.), 10(3) (1991) 70–71.

ELSEVIER

Talanta 42 (1995) 1965–1971

Talanta

# Direct flame atomic absorption spectrophotometric determination of alkalis in geochemical samples

Partha Chattopadhyay

*Regional Research Laboratory, Council of Scientific and Industrial Research, Bhubaneswar-751013, India*

Received 5 January 1995; revised 17 May 1995; accepted 21 June 1995

**Abstract**

Flame atomic absorption spectrometry has been used for the estimation of the alkali metal content (as $Na_2O$ and $K_2O$) in 95 reference materials with diverse matrices (including recently introduced Polish and Chinese standard samples awaiting certification through collaborative studies) using 1000 μg $ml^{-1}$ of lanthanum and 2000 μg $ml^{-1}$ of rubidium as matrix buffers for sodium and potassium, respectively. The $\pm t$ (Student's values for the samples with known recommended values (degree of freedom $n - 1 = 9$), at the 95% and 99% confidence levels) indicate that within the confidence levels 95–99% there is no statistical difference between the data presented and the reference data for most of the samples. The agreement between the reported data and the results obtained are generally good.

*Keywords:* Alkali metals; Flame atomic absorption spectrometry; Geochemicals; Potassium oxide; Sodium oxide

## 1. Introduction

Silicate rocks and minerals contain both sodium and potassium in amounts varying from less than 100 μg $g^{-1}$ in some ultrabasic rocks such as dunite and peridotite, to as much as 10% $K_2O$ or 15% $Na_2O$ in feldspar minerals. Both elements occur as major constituents of many rock-forming minerals, particularly the alkali feldspar group, and are always determined when a complete chemical analysis of a silicate rock or mineral is required. Also, very accurate data for alkali metals are required for limestone and related materials before their end use in ferrous metallurgy. Calibration of spectrochemical methods, including emission and X-ray fluorescence (XRF) spectrometry, requires the use of reference materials (RMs) that are well characterized with respect to the analytes of interest. The accuracy of the measurements is directly related to the quality of the selected RM. The quality control of products has always been a great challenge for analytical chemists. Suitable certified RMs covering a wide range of concentrations must be simultaneously processed with the unknown samples to monitor the analytical accuracy and assure the quality of the data. When the matrix of the incoming sample is not known, then the XRF method is never the preferred method. Flame atomic emission/absorption spectrometry is the most preferred technique for the measurement of the alkali metals [1–5]. One particular characteristic of metals is their low ionization potential. Indeed, the thermal energy of the flame is sufficient to cause a significant degree of ionization of alkali metals. In consequence, a reduction in the atomic absorption signal is observed, since ions exhibit a quite different spectrum from atoms. Caesium has been considered to be the favoured ionization suppressant for the determination of Na and K

*SSDI* 0039-9140(95)01676-7

[6]. Other alkali metals such as lithium and rubidium, are also used for a similar purpose. Hitherto, it was not known which of the alkali metals should be used, and to what extent (in terms of concentration) for the accurate estimation of alkali flame atomic absorption spectrometry metals (FAAS). Comparative studies on probable suppressants revealed that lanthanum and rubidium are the most effective matrix buffers for sodium and potassium respectively, in their FAAS determination [7]. The present author has shown recently that the alkali metals themselves (i.e., potassium for $Na_2O$ determination and sodium for $K_2O$ determination) are also very effective ionization buffers for alkali metal determinations in some Japanese reference materials [5]. The objective of this investigation, therefore, is to develop a standard method for the accurate determination of alkali metals in cases when reference materials have to be analyzed for certification purposes, and simultaneously, to identify a method that could offer increased reliability and wider applicability as far as the accurate estimation of the $Na_2O$ and $K_2O$ content in different geological reference samples with diverse matrices is concerned. A further aim is to contribute data on some samples which are at present either candidates for certification through a collaborative study or have "information values" only. Alkalis are better determined by flame rather than by plasma atomic emission spectrometry (AES) due to reduced sensitivities and stabilities in the much hotter plasma souce.

## 2. Analytical methods

### 2.1. Apparatus and reagents

A Varian Techtron (AA 1475) atomic absorption spectrophotometer with a deuterium arc background correction system coupled with an Epson LX-800 printer and a Varian DS-15 data station were used for the absorbance measurements. Most sensitive resonance lines for sodium (589 nm) and potassium (767.5) were chosen and an air–acetylene flame was used. Other instrumental parameters, e.g. slit width, lamp current, integration time, and burner height were as specified in the manufacturer's instructions.

To prepare a stock sodium solution of concentration 1000 μg $ml^{-1}$, dissolve 2.542 g of NaCl (GR grade; E-Merck) in water and dilute to 1 l with 1% HCl (v/v) solution. To prepare a potassium solution of concentration 1000 μg $ml^{-1}$, dissolve 1.907 g of KCl (GR grade; E-Merck) in 1% HCl solution. A lanthanum (1%) solution was prepared by dissolving 58.7 g of lanthanum oxide (Fluka) in HCl (100, 6.8 M), and making up the volume to 500 ml with distilled water. The resulting solution was diluted ten times with water only. A rubidium solution was prepared by dissolving RbCl (99.7%; Aldrich, USA) in 1% HCl solution.

### 2.2. Reference samples

Information relating to the standard reference materials (USGS; Geological Survey Suriname; Analytisk Sporelement Komite (ASK), Norway; University of Liege, Belgium; and Zentrale Geologisches Institute (ZGI), Germany) is available elsewhere [8]. For CANMET, Geological Survey of Japan (GSJ), British Geological Survey, Chinese and Polish samples, information is available in Refs. [9], [5,10], and [12], [13], [14] and [15], respectively.

### 2.3. Procedure

Weigh accurately 0.1–2.00 g samples in a platinum crucible. Moisten with about 5 ml of distilled water. Add 5–10 ml of $HClO_4$ (70%) drop wise and cover the crucible with a lid. After some time, rinse the lid into the crucible with distilled water. Evaporate the crucible contents to complete dryness on a hot plate. Cool, add 10 ml of HCl (11 M) of HF (48%) and 5 ml of $H_2SO_4$ (1:1). Heat the solution slowly on a hot plate and reduce in volume to approximately 5 ml. Add another 5 ml portion of HF (48%) and HCl (11 M). Evaporate the solution to complete dryness, until no more fumes of $SO_3$ are visible. Finally, heat the crucible strongly with a full flame until all fuming ceases. Cool, and add about 10 ml of HCl (11 M) and an equal volume of water. Evaporate to dryness on a low heat. Add 5 ml each of HCl (11 M) and $H_2SO_4$ (1:1) and 25 ml of water. Digest on a hot plate for about 15 min. Filter into a 100 ml volumetric flask (plastic; Torson, India) using Whatman no. 40 filter paper. Wash the residue with hot water (five times will suffice). Dilution, if any, should be performed using dilute acid solution (5 ml HCl (11 M) + 5 ml $H_2SO_4$ (1:1) + 90 ml distilled

Table 1
Sodium and potassium values ($Na_2O$ and $K_2O$) in 95 reference samples

| Sample | %$Na_2O$ | | | | | %$K_2O$ | | | | |
|---|---|---|---|---|---|---|---|---|---|---|
| | $\bar{x}$ | s.d. | %RSD | %Dev. | Literature value | $\bar{x}$ | s.d. | %RSD | %Dev. | Literature value |
| US Geological Survey[a] | | | | | | | | | | |
| Basalt BCR-1 | 3.28 | 0.07 | 2.13 | 0.30 | 3.27[b] | 1.70 | 0.05 | 2.94 | 0.59 | 1.69[b] |
| Andesite AGV-1 | 4.31 | 0.04 | 0.93 | 1.17 | 4.26[b] | 2.93 | 0.04 | 1.36 | 0.69 | 2.91[b] |
| Dunite DTS-1 | 157.0[c] | 5.34 | 3.40 | 4.67 | 0.015[b] | 13.0[d] | 1.97 | 15.15 | 3.00 | 0.001[b] |
| Granite G2 | 4.09 | 0.30 | 0.73 | 0.24 | 4.08[b] | 4.44 | 0.06 | 1.35 | 0.22 | 4.45[b] |
| | 4.05 | 0.08 | 1.97 | 0.73 | | 4.46 | 0.06 | 1.34 | 0.22 | |
| Granodiroite, GSP-1 | 2.78 | 0.06 | 2.16 | 0.71 | 2.8 | 5.56 | 0.06 | 1.08 | 0.91 | 5.51[b] |
| Peridotite POC-1 | 286.0[c] | 7.68 | 2.68 | 5.92 | 0.027 | 72.0[c] | 3.0 | 4.17 | 2.86 | 0.007[b] |
| Basalt BHVO-1 | 2.28 | 0.02 | 0.88 | 0.88 | 2.26[b] | 0.521 | 0.01 | 1.73 | 0.19 | 0.52[b] |
| | 2.28 | 0.06 | 2.63 | 0.88 | | 0.53 | 0.03 | 5.66 | 1.92 | |
| Marinemud MAG-1 | 3.90 | 0.04 | 1.02 | 1.83 | 3.83[b] | 3.60 | 0.03 | 0.83 | 1.41 | 3.55[b] |
| Quartz latite QLO-1 | 4.11 | 0.05 | 1.22 | 2.14 | 4.20[b] | 3.74 | 0.07 | 1.87 | 3.89 | 3.60[b] |
| Rhyolite RGM-1 | 4.18 | 0.06 | 1.43 | 2.70 | 4.07[b] | 4.34 | 0.02 | 0.46 | 0.93 | 4.30[b] |
| Cody Shale SCO-1 | 0.89 | 0.02 | 2.25 | 1.11 | 0.90[b] | 2.77 | 0.03 | 1.08 | 0.00 | 2.77[b] |
| Micaschist SDC-1 | 2.07 | 0.03 | 1.45 | 0.97 | 2.05[b] | 3.33 | 0.04 | 1.20 | 1.52 | 3.28[b] |
| Shale SGR-1 | 2.98 | 0.05 | 1.68 | 0.33 | 2.99[b] | 1.63 | 0.04 | 2.45 | 1.81 | 1.66[b] |
| Syenite STM-1 | 8.84 | 0.05 | 0.56 | 1.12 | 8.94[b] | 4.33 | 0.05 | 1.15 | 1.17 | 4.28[b] |
| Basalt BIR-1 | 1.72 | 0.02 | 1.16 | 1.71 | 1.75[b] | 287.0[c] | 3.83 | 1.33 | 6.30 | 0.027 |
| | 1.73 | 0.03 | 1.73 | 1.14 | | 274.0[c] | 9.49 | 3.46 | 1.48 | |
| Diabase DNC-1 | 1.83 | 0.02 | 1.09 | 2.13 | 1.87[b] | 0.229 | 0.01 | 0.52 | 0.00 | 0.229[b] |
| Diabase W-2 | 2.12 | 0.06 | 2.83 | 0.93 | 2.14[b] | 0.629 | 0.01 | 0.17 | 0.32 | 0.627[b] |
| Ohio Shale SDO-1 | 0.384 | 0.001 | 0.26 | 1.05 | 0.38[b] | 3.41 | 0.07 | 2.05 | 1.79 | 3.35[b] |
| Mn-Nodule NOD-1 | 1.06 | 0.05 | 4.72 | 1.92 | 1.04 | 6106.0[c] | 50.32 | 0.82 | 1.77 | 0.6 |
| Mn-Nodule-P-1 | 2.24 | 0.08 | 3.57 | 1.36 | 2.21 | 1.26 | 0.04 | 3.17 | 4.13 | 1.21 |
| Jasperoid GXR-1 | 750.0[c] | 31.88 | 4.25 | 7.14 | 0.07 | 631.5[c] | 19.44 | 3.08 | 5.16 | 0.06 |
| Soil GXR-2 | 7591.0[c] | 49.54 | 0.65 | 1.21 | 0.75 | 1.56 | 0.05 | 3.20 | 5.45 | 1.65 |
| Deposit GXR-3 | 1.07 | 0.03 | 2.80 | 5.31 | 1.13 | 0.89 | 55.0 | 0.62 | 1.06 | 0.88 |
| Cu mill head GXR-4 | 0.773 | 62.40 | 0.81 | 1.64 | 0.76 | 4.72 | 0.08 | 1.69 | 2.27 | 4.83 |
| Soil GXR-5 | 1.04 | 0.04 | 3.85 | 0.95 | 1.05 | 1.10 | 0.05 | 4.54 | 3.77 | 1.06 |
| Soil GXR-6 | 0.16 | 0.072 | 4.58 | 11.71 | 0.14 | 2.36 | 0.07 | 2.97 | 4.89 | 2.25 |
| Geological Survey of Japan[e] | | | | | | | | | | |
| Granite JG2 | 3.59 | 0.03 | 0.83 | 1.13 | 3.55 | 4.72 | 0.03 | 0.63 | 0.00 | 4.72 |
| | 3.50 | 0.08 | 2.28 | 1.41 | | 4.65 | 0.09 | 1.93 | 1.47 | |
| Granodiorite JG3 | 4.04 | 0.03 | 0.74 | 0.25 | 4.03 | 2.64 | 0.03 | 1.14 | 0.38 | 2.63 |
| | 3.98 | 0.06 | 1.51 | 1.24 | | 2.58 | 0.06 | 2.32 | 1.88 | |
| Granodiorite JG1a | 3.45 | 0.02 | 0.58 | 1.17 | 3.41 | 4.08 | 0.02 | 0.50 | 1.73 | 4.01 |
| | 3.36 | 0.04 | 0.19 | 1.47 | | 3.96 | 0.09 | 2.27 | 1.24 | |
| Rhyolite JR-1 | 4.17 | 0.04 | 0.96 | 1.71 | 4.1 | 4.57 | 0.03 | 0.66 | 3.60 | 4.41 |
| | 4.03 | 0.04 | 0.99 | 1.70 | | 4.51 | 0.11 | 2.44 | 2.25 | |
| Rhyolite JR-2 | 4.13 | 0.02 | 0.48 | 2.48 | 4.03 | 4.60 | 0.04 | 0.87 | 3.34 | 4.45 |
| | 3.97 | 0.08 | 2.01 | 1.49 | | 4.51 | 0.08 | 1.77 | 1.34 | |
| Basalt JB1a | 2.77 | 0.02 | 0.72 | 1.09 | 2.74 | 1.48 | 2 | 1.35 | 4.19 | 1.42 |
| | 2.65 | 0.05 | 1.89 | 3.28 | | 1.43 | 0.06 | 4.19 | 0.70 | |
| Basalt JB2 | 2.09 | 0.02 | 0.96 | 2.95 | 2.03 | 0.441 | 0.01 | 1.66 | 4.89 | 0.42 |
| | 1.98 | 0.05 | 2.52 | 2.46 | | 0.43 | 0.03 | 5.66 | 2.36 | |
| Basalt JB3 | 2.87 | 0.05 | 1.74 | 1.77 | 2.82 | 0.81 | 0.004 | 0.49 | 3.81 | 0.78 |
| | 2.66 | 0.04 | 1.50 | 5.67 | | 0.79 | 0.05 | 6.33 | 1.27 | |
| Gabbro JGb-1 | 1.22 | 0.02 | 1.64 | 0.81 | 1.23 | 0.248 | 0.004 | 1.69 | 3.22 | 0.24 |
| | 1.22 | 0.03 | 2.46 | 0.81 | | 0.23 | 0.01 | 4.35 | 4.13 | |
| Andesite JA-1 | 3.89 | 0.02 | 0.51 | 0.77 | 3.86 | 0.79 | 0.01 | 8.86 | 1.27 | 0.78 |
| | 3.75 | 0.06 | 1.60 | 2.85 | | 0.80 | 0.06 | 7.50 | 2.54 | |
| Andesite JA-2 | 3.11 | 0.02 | 0.64 | 0.97 | 3.08 | 1.91 | 0.01 | 0.52 | 6.06 | 1.8 |
| | 3.01 | 0.05 | 1.66 | 2.25 | | 1.87 | 0.06 | 3.21 | 3.85 | |
| Andesite JA-3 | 3.20 | 0.01 | 0.31 | 0.94 | 3.17 | 1.43 | 0.02 | 1.40 | 1.41 | 1.41 |
| | 3.14 | 0.06 | 1.91 | 0.94 | | 1.46 | 0.05 | 3.42 | 3.51 | |

Table 1 (contd.)

| Sample | %$Na_2O$ | | | | | %$K_2O$ | | | | |
|---|---|---|---|---|---|---|---|---|---|---|
| | $\bar{x}$ | s.d. | %RSD | %Dev. | Literature value | $\bar{x}$ | s.d. | %RSD | %Dev. | Literature value |
| Feldspar JF-1 | 3.50 | 0.06 | 1.71 | 1.12 | 3.54 | 10.15 | 0.04 | 0.40 | 0.79 | 10.07 |
| Feldspar JF-2 | 2.39 | 0.04 | 1.67 | 2.82 | 2.46 | 13.36 | 0.15 | 1.12 | 1.89 | 13.11 |
| Peridotite JP-1 | 225.0[c] | 8.82 | 3.92 | 7.14 | 0.021 | 39.7[c] | 0.43 | 8.64 | 20.14 | 0.0033 |
| Chert JCh-1 | 328.0[c] | 9.77 | 2.98 | 5.80 | 0.031[b] | 2269.0[c] | 18.38 | 0.81 | 1.28 | 0.2240[b] |
| Dolomite JDo-1 | 111.8[c] | 2.74 | 2.45 | – | 90.0[c] | 87.75[c] | 2.29 | 2.61 | – | 20.0[c] |
| Lake Sediment JLk-1 | 1.19 | 0.08 | 6.78 | 13.22 | 1.05[b] | 2.89 | 0.10 | 3.46 | 4.30 | 2.77[b] |
| Stream Sediment JSd-1 | 2.81 | 0.06 | 2.13 | 2.91 | 2.73[b] | 2.32 | 0.09 | 3.88 | 5.88 | 2.19[b] |
| Stream Sediment JSd-2 | 2.59 | 0.06 | 2.07 | 4.40 | 2.48[b] | 1.23 | 0.05 | 4.06 | 6.90 | 1.15[b] |
| Stream Sediment JSD-3 | 0.45 | 0.02 | 0.49 | 1.42 | 0.44[b] | 2.11 | 0.06 | 2.84 | 4.93 | 2.01[b] |
| Limestone JLS-1 | 25.5[c] | 1.25 | 4.90 | – | 0.002 | 34.35[c] | 1.60 | 4.66 | – | 0.003 |
| Slate JS1-1 | 2.36 | 0.11 | 4.66 | 7.21 | 2.20[b] | 3.00 | 0.09 | 3.00 | 5.26 | 2.85[b] |
| Slate JS1-2 | 1.52 | 0.07 | 4.60 | 9.35 | 1.39[b] | 3.02 | 0.07 | 2.32 | 3.07 | 2.93[b] |
| Analytisk Sporelement Komite (ASK)[a] | | | | | | | | | | |
| Larvikite ASK-1 | 6.43 | 0.12 | 1.87 | 1.07 | 6.5[d] | 4.40 | 0.13 | 2.95 | 4.76 | 4.2[d] |
| Schist ASK-2 | 0.81 | 0.09 | 11.11 | 1.24 | 0.8[d] | 5.12 | 0.10 | 1.95 | 3.37 | 5.3[d] |
| Sulphide ore ASK-3 | 139.3[c] | 5.10 | 3.66 | 7.15 | 0.013[b] | 726.0[c] | 13.29 | 1.83 | 3.68 | 0.07[b] |
| Zentrale Geologisches Institut (ZGI) | | | | | | | | | | |
| Anhydrite AN | 323.5[c] | 3.63 | 1.12 | 1.08 | 0.032[b] | 130.2[c] | 3.76 | 2.89 | 0.00 | 0.013[b] |
| Basalt BM | 4.57 | 0.09 | 1.97 | 1.71 | 4.65[b] | 2055.0[c] | 33.87 | 1.65 | 2.75 | 0.20[b] |
| Granite GM | 3.82 | 0.09 | 2.36 | 1.05 | 3.78[b] | 4.78 | 0.07 | 1.46 | 0.42 | 4.76[b] |
| Greisen Gn A | 809.5[c] | 15.17 | 1.87 | 1.18 | 0.08[b] | 2.62 | 0.07 | 2.67 | 0.38 | 2.63[b] |
| Limestone KH | 0.104 | 0.01 | 0.59 | – | – | 0.411 | 0.01 | 0.26 | 0.14 | 0.41[b] |
| Limestone KH-2 | 1112.0[c] | 31.20 | 2.80 | 1.08 | 0.11[b] | 4397.0[c] | 56.28 | 1.28 | 0.07 | 0.44[b] |
| Limestone KH-3 | 1003.0[c] | 8.88 | 0.88 | 0.30 | 0.10[b] | 4302.5[c] | 7.91 | 0.18 | 0.06 | 0.43[b] |
| Feldspathicsand FK | 2496.5[c] | 30.28 | 1.21 | 0.16 | 0.25[b] | 4.18 | 0.08 | 1.91 | 1.18 | 4.23[b] |
| Serpentinite SW | 135.4[c] | 8.10 | 5.98 | 4.15 | 0.013[b] | 102.0[c] | 5.60 | 5.49 | – | – |
| Black shale TS | 786.5[c] | 15.46 | 1.96 | 0.83 | 0.078[b] | 4.83 | 0.07 | 1.45 | 0.61 | 4.86[b] |
| University of Liege, Belguim[a] | | | | | | | | | | |
| Shale AWI-1 | 7794.0[c] | 92.76 | 1.19 | 5.28 | 0.74[b] | 3.02 | 0.03 | 0.99 | 1.30 | 3.06[b] |
| Schist SBO-1 | 6510.0[c] | 134.25 | 2.06 | 1.35 | 0.66[b] | 3.53 | 0.03 | 0.85 | 0.56 | 3.55[b] |
| Psammite PRI-1 | 1.71 | 0.03 | 1.75 | 0.00 | 1.71[b] | 3.76 | 0.04 | 1.06 | 0.79 | 3.79[b] |
| Limestone CCH-1 | 497.3[c] | 11.52 | 2.32 | 3.57 | 0.048[c] | 789.9[c] | 6.85 | 0.87 | 3.67 | 0.082[b] |
| Dolomite DWA-1 | 404.5[c] | 25.32 | 6.26 | 3.66 | 0.042[b] | 105.2[c] | 4.76 | 4.52 | 5.16 | 0.01[b] |
| Canmet[g] | | | | | | | | | | |
| Lake Sediment (LKSD-1) | 2.16 | 0.09 | 4.17 | 8.00 | 2.0[b] | 1.29 | 0.04 | 3.10 | 13.15 | 1.14[b] |
| Lake Sediment (LKSD-2) | 1.89 | 0.03 | 1.59 | 2.07 | 1.93[b] | 2.49 | 0.04 | 1.61 | 5.68 | 2.64[b] |
| Lake Sediment (LKSF-2) | 2.46 | 0.04 | 1.63 | 6.03 | 2.32[b] | 2.15 | 0.04 | 1.86 | 3.15 | 2.22[b] |
| Lake Sediment (LKSD-4) | 0.80 | 0.01 | 1.25 | 9.59 | 0.73 | 0.84 | 0.01 | 1.19 | 2.44 | 0.82[b] |
| Stream Sediment (STSD-1) | 1.96 | 0.03 | 1.53 | 11.90 | 1.75[b] | 1.31 | 0.02 | 1.53 | 4.76 | 1.25[b] |
| Stream Sediment (STSD-2) | 1.92 | 0.03 | 1.56 | 9.63 | 1.75[b] | 2.26 | 0.03 | 1.33 | 6.55 | 2.12[b] |
| Stream Sediment (STSD-3) | 1.63 | 0.02 | 1.23 | 6.48 | 1.53[b] | 1.95 | 0.03 | 1.54 | 8.33 | 1.80[b] |
| Stream Sediment (STSD-4) | 2.96 | 0.05 | 1.69 | 9.55 | 2.7[b] | 1.63 | 0.02 | 1.23 | 1.86 | 1.60[b] |
| Soil (Till 1) | 2.50 | 0.04 | 1.60 | 3.81 | 2.6 | 2.36 | 0.05 | 2.12 | 2.59 | 2.3 |
| Soil (Till 2) | 2.06 | 0.04 | 1.96 | 1.89 | 2.1 | 3.23 | 0.08 | 2.48 | 4.19 | 3.1 |
| Soil (Till 3) | 2.74 | 0.05 | 1.82 | 5.34 | 2.6 | 2.53 | 0.02 | 0.73 | 5.41 | 2.4 |
| Soil (Till 4) | 2.54 | 0.05 | 1.97 | 5.78 | 2.4 | 3.44 | 0.05 | 1.45 | 4.32 | 3.3 |
| British Geological Survey | | | | | | | | | | |
| Bastansite Ore (IGS-40)[h] | 1201.0[c] | 36.12 | 3.01 | 0.08 | 0.12 | 1.27 | 0.02 | 1.57 | 0.79 | 1.28 |
| Geologcal Survey Suriname[a] | | | | | | | | | | |
| Tropical Soil (K-3) | 993.0 | 46.0 | 4.63 | 0.69 | 0.1 | 330.0[c] | 16.0 | 4.85 | 10.0 | 0.03 |
| Tropical Soil (CS-1) | 1095.0[c] | 28.0 | 2.56 | 9.50 | 0.1 | 5155.0[c] | 107.0[c] | 2.07 | 3.15 | 0.5 |
| Tropical Soil (SAu-1) | 434.0[c] | 23.0 | 5.30 | 8.50 | 0.04 | 545.0[c] | 29.0 | 5.23 | 9.16 | 0.05 |
| Tropical Soil (SUR-1) | 103.0[c] | 9.0 | 8.74 | 3.05 | 0.01 | 1170.0[c] | 39.0 | 3.33 | 6.48 | 0.11 |

Table 1 (contd.)

| Sample | $\%Na_2O$ | | | | | $\%K_2O$ | | | | |
|---|---|---|---|---|---|---|---|---|---|---|
| | $\bar{x}$ | s.d. | %RSD | %Dev. | Literature value | $\bar{x}$ | s.d. | %RSD | %Dev. | Literature value |
| Lateritic Bauxite (BAX-1) | 1046.0[c] | 28.0 | 2.68 | 4.68 | 0.01 | 201.0[c] | 9.00 | 4.48 | 0.50 | 0.02 |
| Chinese Academy of Geological Sciences[i] | | | | | | | | | | |
| Marine Sediment (GSMS-2) | 3.75 | 0.14 | 3.73 | 6.25 | 4.00 | 2.11 | 0.11 | 5.21 | 8.26 | 2.30 |
| Marine Sediment (GSMS-3) | 4.20 | 0.10 | 2.38 | 5.00 | 4.00 | 1.70 | 0.07 | 4.12 | 6.25 | 1.60 |
| Mn-Nodule (GSPN-2) | 2.44 | 0.08 | 3.28 | 6.15 | 2.60 | 1.06 | 0.03 | 2.83 | 6.00 | 1.00 |
| Mn-Nodule (GSPN-3) | 2.82 | 0.10 | 3.55 | 2.08 | 2.88 | 0.96 | 0.01 | 1.04 | 4.00 | 1.00 |
| Glowny Urzard Miar, Poland[j] | | | | | | | | | | |
| Loess (PL-1) | 1.19 | 0.05 | 4.20 | – | 0.81 | 1.66 | 0.05 | 3.01 | – | 1.80 |
| Sandy Loam Soil(BPGM-1) | 0.96 | 0.02 | 2.08 | – | 0.54 | 1.50 | 0.03 | 2.00 | – | 1.56 |
| Soil Control Sample (RAM) | 1.65 | 0.04 | 2.42 | 1.88 | 1.62 | 2.03 | 0.04 | 1.97 | 15.41 | 2.40 |
| Soil Control Sample (RMB) | 1.52 | 0.04 | 2.63 | 2.70 | 1.48 | 2.45 | 0.05 | 2.04 | 2.08 | 2.40 |
| Soil Control Sample (RMC) | 1.65 | 0.03 | 1.82 | 11.49 | 1.48 | 2.47 | 0.03 | 1.21 | 17.98 | 3.00 |

[a] See Ref. [8].
[b] Recommended value.
[c] Results are expressed in micrograms per gram (ppm).
[d] Information value.
[e] See Refs. [10–12].
[f] ASK-3 was ingnited at 700°C for 1 h before acid treatment.
[g] See Ref. [9].
[h] See Ref. [13].
[i] See Ref. [9].
[j] See Ref. [14].
The values given are proposed values unless indicated otherwise. Where two values are given, the first (upper) value was obtained by the recommended procedure and the second (lower) value is taken from Ref. [5].

water). The solution for final aspiration to the air-acetylene flame should contain 1000 μg La $ml^{-1}$ and 2000 μg Rb $ml^{-1}$ for sodium and potassium, respectively.

## 3. Results and discussion

Table 1 shows the mean ($\bar{x}$) of ten replicate analyses with the deviations ($s$), per cent relative standard deviations (%RSD) and the per cent average deviations (%Dev.) using mean and true values available in the literature. The $Na_2O$ and $K_2O$ values for limestone KH and serpentinite, respectively, are not available in the literature [8], and hence could not be compared. The potassium value for JDO-1 was consistently higher than the reported value [12]. Provisional values for the CANMET, Polish and Chinese samples are also quite good. Indeed, there are deviations for those samples along with some cases where only the "information values" are available indicating that more data are still required in order to upgrade the status of some samples from the provisional/conditional level to the certified level. For Japanese samples (JG2, JG3, JG1a, JR-1, JR-2, JB-1a, JB-2, JB-3, JGb-1, JA-1, JA-2 and JA-3) and USGS samples (G2, BIR-1 and BHVO-1) data from the present study along with recently published data [5] are presented for comparison. The recommended procedure is equally effective in both normal rock samples and in highly calcium-rich materials, in which as the previous procedure always yields high values of alkali metals in limestone and related materials, it hence cannot be adapted for certification purposes.

### 3.1. Test on reliability of statistical data

In order to test whether one set of data (with a mean $\bar{x}$) belongs to another population (with a mean $\mu$) to within a specified confidence limit, the value of Student's $t$ has been calculated from the equation $\pm t = (\bar{x} - \mu)\sqrt{n}/s$.

Table 2
The $\pm t$ values and population mean ($\mu$) at the 95% confidence level for well-characterized samples

| Sample | $Na_2O$ | | | $K_2O$ | | |
|---|---|---|---|---|---|---|
| | $\pm t$ | $\mu$ | Lit. (%$Na_2O$) | $\pm t$ | $\mu$ | Lit. (%$K_2O$) |
| BCR-1 | 0.45 | 3.28 ± 0.05 | 3.27 | 0.63 | 1.70 ± 0.03 | 1.69 |
| AGV-1 | 3.95 | 4.31 ± 0.03 | 4.26 | 1.58 | 2.93 ± 0.03 | 2.91 |
| DTS-1 | 4.14 | 157.0 ± 3.82 | 150[a] | 4.81 | 13.0 ± 1.41[a] | 10[a] |
| G2 | 1.04 | 4.09 ± 0.02 | 4.08 | 0.53 | 4.44 ± 0.04 | 4.45 |
| | 1.18 | 4.05 ± 0.06 | – | 0.53 | 4.46 ± 0.04 | |
| GSP-1 | – | – | – | 2.63 | 5.56 ± 0.04 | 5.51 |
| PCC-1 | – | – | – | 2.11 | 72.0 ± 2.15[a] | 0.007 |
| BHVO-1 | 3.16 | 2.81 ± 0.01 | 2.26 | 0.35 | 0.521 ± 0.001 | 0.52 |
| | 1.05 | 2.28 ± 0.004 | – | 1.05 | 0.531 ± 0.02 | |
| MAG-1 | 5.53 | 3.90 ± 0.03 | 3.83 | 5.27 | 3.60 ± 0.002 | 3.55 |
| QLO-1 | 5.69 | 4.11 ± 0.03 | 4.20 | 6.32 | 3.74 ± 0.05 | 3.60 |
| RGM-1 | 5.80 | 4.18 ± 0.04 | 4.07 | 6.32 | 4.34 ± 0.01 | 4.34 |
| SCO-1 | 1.58 | 0.89 ± 0.01 | 0.90 | 0.00 | 2.77 ± 0.02 | 2.77 |
| SDC-1 | 2.11 | 2.07 ± 0.02 | 2.05 | 3.95 | 3.33 ± 0.03 | 3.28 |
| SGR-1 | 0.63 | 2.98 ± 0.03 | 2.99 | 2.37 | 1.63 ± 0.03 | 1.66 |
| STM-1 | 6.32 | 8.84 ± 0.03 | 8.84 | 3.16 | 4.33 ± 0.03 | 4.28 |
| BIR-1 | 4.74 | 1.72 ± 0.01 | 1.75 | – | – | – |
| | 2.11 | 1.73 ± 0.02 | | | | |
| DNC-1 | 6.32 | 1.83 ± 0.01 | 1.87 | 0.00 | 0.229 ± 0.01 | 0.229 |
| W2 | 1.05 | 2.12 ± 0.04 | 2.14 | 5.79 | 0.629 ± 0.01 | 0.627 |
| SDO-1 | 1.49 | 0.384 ± 0.001 | 0.380 | 2.71 | 3.41 ± 0.05 | 3.35 |
| ASK-3 | 5.77 | 139.3 ± 3.65[a] | 0.013 | 6.19 | 726.0 ± 9.51[a] | 0.07 |
| AN | 3.05 | 323.0 ± 2.60[a] | 0.032 | 0.17 | 130.0 ± 2.69[a] | 0.13 |
| BM | 2.81 | 4.57 ± 0.06 | 4.65 | 5.13 | 2055.0 ± 24.24[a] | 0.02 |
| GM | 1.40 | 3.82 ± 0.06 | 3.78 | 0.09 | 4.78 ± 0.05 | 4.76 |
| GnA | 1.98 | 809.5 ± 10.86[a] | 0.08 | 0.45 | 2.62 ± 0.05 | 2.63 |
| KH | – | – | – | 1.90 | 4106.5 ± 7.74[a] | 0.41 |
| KH-2 | 1.22 | 112.0 ± 22.33[a] | 0.11 | 0.17 | 4397.0 ± 40.29[a] | 0.44 |
| KH-3 | 1.07 | 1003.0 ± 4.36[a] | 0.01 | 0.80 | 4302.0 ± 5.66[a] | 0.43 |
| FK | 0.36 | 2496.5 ± 21.65[a] | 0.25 | 1.98 | 4.18 ± 0.06 | 4.23 |
| SW | 2.11 | 135.4 ± 5.60[a] | 0.013 | – | – | – |
| TS | 1.33 | 786.5 ± 11.07[a] | 0.078 | 1.35 | 4.83 ± 0.05 | 4.86 |
| IGS-40 | 0.14 | 1201 ± 25.85[a] | 0.12 | 1.58 | 1.27 ± 0.01 | 1.28 |
| JLk-1 | 5.53 | 1.19 ± 0.06 | 1.05 | 3.79 | 2.89 ± 0.07 | 2.77 |
| JSd-1 | 4.22 | 2.81 ± 0.04 | 2.73 | 4.57 | 2.32 ± 0.06 | 2.19 |
| JSd-2 | 5.80 | 2.59 ± 0.04 | 2.48 | 5.06 | 1.23 ± 0.03 | 1.15 |
| JSd-3 | 9.05 | 4463.0 ± 15.75[a] | 0.44 | 4.74 | 2.11 ± 0.04 | 2.01 |
| JCh-1 | 5.83 | 328.0 ± 6.99[a] | 0.031 | 4.99 | 2269.0 ± 13.15 | 0.224 |
| JS1-1 | 4.60 | 2.38 ± 0.08 | 2.20 | 5.27 | 3.00 ± 0.06 | 2.85 |
| JS1-2 | 5.87 | 1.52 ± 0.05 | 1.39 | 4.06 | 3.02 ± 0.05 | 2.93 |
| AW-1 | 13.43 | 7794 ± 66[a] | 0.74 | 4.22 | 3.02 ± 0.02 | 3.06 |
| SBO-1 | 0.90 | 6510 ± 96[a] | 0.66 | 2.11 | 3.53 ± 0.02 | 3.55 |
| PRI-1 | 0 | 1.71 ± 0.02 | 1.71 | 2.37 | 3.76 ± 0.03 | 3.79 |
| CCH-1 | 4.75 | 497.3 ± 8.25[a] | 0.048 | 4.66 | 789.9 ± 4.90[a] | 0.082 |
| DWA-1 | 1.93 | 404.5 ± 18.12[a] | 0.042 | 3.45 | 105.2 ± 3.41[a] | 0.01 |
| LKSD-1 | 5.62 | 2.16 ± 0.06 | 2.0 | 11.86 | 1.29 ± 0.03 | 1.14 |
| LKSD-2 | 4.22 | 1.89 ± 0.02 | 1.93 | 11.86 | 2.49 ± 0.03 | 2.64 |
| LKSD-3 | 11.07 | 2.46 ± 0.03 | 2.32 | 5.53 | 2.15 ± 0.03 | 2.22 |
| LKSD-4 | 22.13 | 0.80 ± 0.01 | 0.73 | 6.32 | 0.85 ± 0.01 | 0.82 |
| STSD-1 | 22.13 | 1.96 ± 0.02 | 1.75 | 9.49 | 1.31 ± 0.01 | 1.25 |
| STSD-2 | 17.92 | 1.92 ± 0.02 | 1.75 | 14.75 | 2.26 ± 0.02 | 2.12 |
| STSD-3 | 15.81 | 1.63 ± 0.02 | 1.53 | 11.59 | 1.95 ± 0.02 | 1.80 |
| STSD-4 | 16.44 | 2.96 ± 0.03 | 2.70 | 4.74 | 1.63 ± 0.01 | 1.60 |

[a] Value is expressed in micrograms per gram.
Where two values are given, the first (upper) value was obtained from the present work, and the second (lower) value was obtained from previous work [5].

For a population, whose mean has a value of $\bar{x}$, to have a high probability of belonging to the population with a mean value of $\mu$, the $t$-value calculated according to the above equation must be smaller than the appropriate value listed in the Student's $t$-distribution table [16]. The $\pm t$ values for $Na_2O$ and $K_2O$ of well-characterized samples [8] are shown in Table 2. When the $\pm t$ value of less than 2.262 and 3.250 (at a degree of freedom of 9) at a confidence level of 95% or 99%, respectively, there is no statistical difference between the current result ($\bar{x}$) and the reference material data mean ($\mu$).

On rearrangement, the previous equation is expressed as $\mu = \bar{x} + tsn^{1/2}$. The population means at a 95% confidence level (although of course, the $t$-test is not restricted to 95% or any other confidence limits; the 95% limits are most commonly used) for a degree of freedom of 9 are calculated from this equation and are shown in Table 2 for comparison with the true values. This is done just to calculate the error limits about a data set mean ($\bar{x}$) within which the population mean ($\mu$) must lie for a given confidence level.

The present set of data on reference samples (which are useful because they provide a mechanism for assessing the accuracy of a technique and for reaching the goal of better analyses of real samples) of varied composition involving two-step decomposition and a matrix buffer can be applied successfully to the accurate estimation of alkali metals for certification purpose and in quality control assessment.

## Acknowledgements

The Director, Regional Laboratory, Bhubaneswar, is thanked for granting permission to publish this work. Special thanks are to the authorities of the Chinese Academy of Geological Sciences and Glowny Urzard Miar, Poland for the reference samples and associated documents. Mr P.N. Sethi is thanked for excellent secretarial assistance.

## References

[1] R.M. O'Leary and A.L. Meier, U.S. Geol. Surv. Circ., 948 (1984) 26–36.
[2] M.J. Cremer, P.R. Klock, S.T. Neil and J.M. Riviello, U.S. Geol. Surv. Open-File Rep., 84–565 (1984) 139–142.
[3] L.L. Jackson, F.W. Brown and S.T. Neil, U.S. Geol. Surv. Bull., 1770 (1987) G10–G12.
[4] Staff of Geoscience Laboratories, Ontario Geological Survey, The Analysis of Geological Materials, Vol. 2, A manual of Methods, Ontario Geol. Surv. Misc. Pap. 149, 1990, EA 11–EA 11-5.
[5] P. Chattopadhyay and M. Mistry, Microchem. J. 50 (1994) 78.
[6] P.J. Potts, A Hand Book of Silicate Rock Analysis, Blackie, Glasgow, 1992, p. 118.
[7] P. Chattopadhyay, Chem. Anal. (Warsaw), in press.
[8] K. Govindaraju, Geostand. Newl., 18 (1994).
[9] J. Lynch, Geostand. Newl., 14, (1990) 153.
[10] A. Ando, N. Mita and S. Terashima, Geostand. Newl., 11 (1987) 159.
[11] A. Ando, H. Kamioka, S. Terashima and S. Itoh, Geochem. J., 23 (1988) 143.
[12] S. Terashima, A. Ando, T. Okai, Y. Kanai, M. Taniguchi, F. Tkaizawa and S. Itoh, Geostand. Newl., 14 (1990) 1.
[13] Geochemistry Directorate, British Geological Survey, Analysed samples, IGS 40, Bastansite ore.
[14] Polski Komitet Normalizacji, Provisional Values for Polish Samples (RMA, RMB, PL-1 and BPGM-1), Miar, 1993.
[15] Institute of Rock and Mineral Analysis, Chinese Academy of Geological Sciences, Approximate composition of GSPN-2, GSPN-3, GSMS-2 and GSMS-3, 1994.
[16] A.H.M. Vander Voet and C. Riddie, The Analysis of Geological Materials, Vol. 1, A Practical Guide, Ontario Geol. Surv., Paper 149, 1993, p. 14.

ELSEVIER

Talanta 42 (1995) 1973–1978

Talanta

# Spectrophotometric determination of tin in copper-based alloys using Pyrocatechol Violet

A.C. Spinola Costa*, Leonardo S.G. Teixeira, Sérgio L.C. Ferreira

*Universidade Federal da Bahia, Instituto de Química, Salvador, Bahia 40170-290, Brazil*

Received 30 May 1995; accepted 21 June 1995

**Abstract**

In the present paper, a new procedure using Pyrocatechol Violet (PCV) for the determination of tin in copper-based alloys is proposed. The use of HEDTA as masking agent allowed tin to be determined in the presence of large amounts of copper, without any separation procedure. The method is more selective than previous methods. Cetyltrimethylammonium bromide (CTAB) and Tween-20 are used to increase the stability of the system.

The method can be applied directly to an acidic solution of Sn(IV) in the range 2.0–60.0 μg with a final volume of 50 ml. The pH is adjusted to $2.0 \pm 0.2$ with glycine buffer and, after 30 min, the absorbance is measured at 660 nm. Al(III), Cd(II), Co(II), Mg(II), Ca(II), Mn(II), Ni(II) and Pb(II) do not interfere at the 500 mg level; 20 000 μg of Cu(II) and 400 μg of NaCl can be present. The interference at 100 μg of Fe(III) can be masked with ascorbic acid. Bi(III), Sb(V), Ti(IV), Mo(VI), EDTA, tartrate, citrate and iodide interfere. The proposed method was used for tin determination in several copper-based alloys and a comparison of the analytical results with certified values indicates that the procedure provides accurate and precise results.

*Keywords:* Copper-based alloys; Pyrocatechol Violet; Spectrophotometric analysis; Tin determination

## 1. Introduction

Tin is an element frequently present in copper-based alloys. However, the spectrophotometric determination of this element in these matrices is problematic because many of the reagents used also react with the copper and other elements present. Numerous procedures have been published for this determination, and normally these methods are not simple and usually require extensive and laborious steps for the separation of tin from the matrices, using procedures that involve operations such as extraction [1,2], ionic exchange [3,4], precipitation of tin as metastannic acid [5], coprecipitation of tin using copper sulfide [6], manganese dioxide [7], or beryllium hydroxide [8] and until distillation [9], the tin being separated as stannic bromide. Table 1 describes the application of some of the reagents during tin determination in copper matrices.

Pyrocatechol Violet (PCV) [10] is one of the main reagents used in the spectrophotometric determination of tin. Some procedures [11] were proposed that used gelatin to stabilize the color; however, the addition of gelatin causes the absorption band of the Pyrocatechol Violet–tin(IV) complex to become broadened and to extend to longer wavelengths. Therefore, the absorbance measurements must be made at 619 nm, and a loss of sensitivity is observed.

* Corresponding author.


*SSDI* 0039-9140(95)01677-5

Table 1
Reagents used for tin determination in copper and its matrices

| Reagent | Method of separation of tin | Applications | Reference |
|---|---|---|---|
| 8-Hydroxyquinoline | Extraction | Copper and zinc-based alloys | [1] |
| Propylfluorone | Extraction | Bronzes | [2] |
| PCV | Ion exchange | Bronze | [3] |
| Phenylfluorone | Ion exchange | Copper-based alloys | [4] |
| Rhodamine 6Zh | Tin precipitation as metastannic acid | Brass | [5] |
| Gallein | Tin coprecipitation with copper sulfide | Copper metal and brasses | [6] |
| Hematein | Tin coprecipitation with manganese dioxide | Copper-based alloys | [7] |
| Gallein | Tin coprecipitation with berylium hydroxide | Copper | [8] |
| Silicomolybdotungstate | Distillation | Brass | [9] |
| Quercetin[a] | – | Brass and bronze | [8] |
| PCV[b] | – | Brasses and bronzes | This work |

[a] With copper masking with use of thiourea.
[b] With masking using HEDTA.

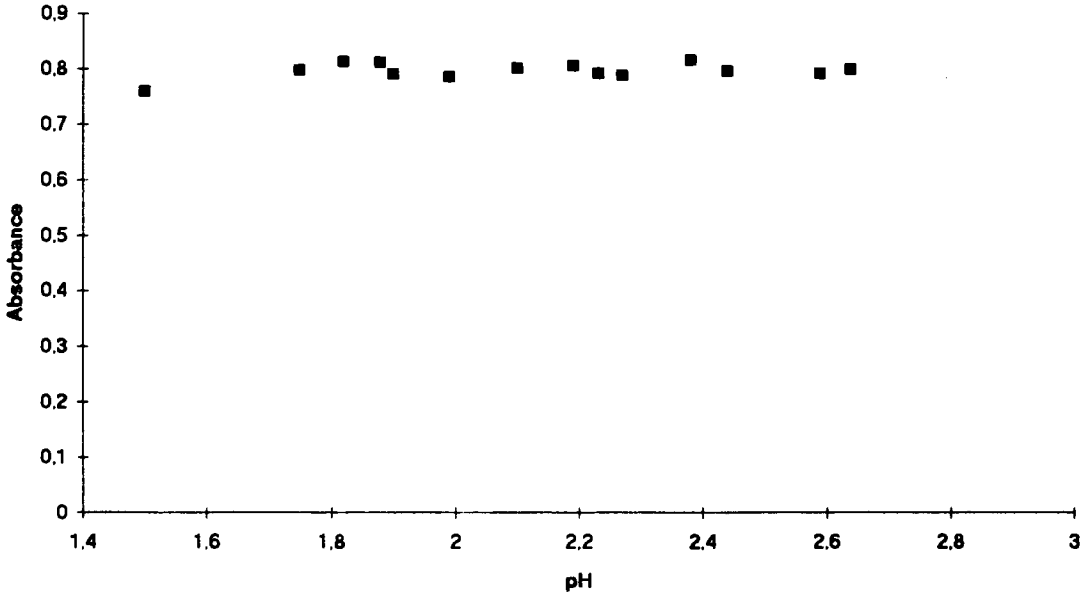


Fig. 1. Effect of the pH on the Sn(IV)–PCV system. [Sn(IV)], 50.00 μg per 50 ml; PCV amount, 1 ml; PCV solution, 0.1%.

Dagnall et al. [12], studied the effect of several surfactants in relation to an increase in stability of the Pyrocatechol Violet–tin(IV) system and found that cetyltrimethylammonium bromide (CTAB) is the most satisfactory. However, the use of this surfactant is not possible in the extraction step, because tetraalkylammonium iodide was precipitated. Pyrocatechol Violet was proposed for tin determination in bronze by Karnaukhova [3], the procedure is based on tin separation on an anionic resin in the chloride form.

In the present paper, we propose a procedure that uses PCV for tin determination in brasses and bronzes, using HEDTA as masking agent for several ions, allowing tin determination without separation. The proposed method is simple, highly selective and reproducible. A mixture of two surfactants, cetyltrimethylammonium bromide and Tween-20, increases the system stability.

## 2. Experimental

### 2.1. Reagents

All reagents were analytical grade unless otherwise stated. The tin solution (100.0 μg $ml^{-1}$) was prepared by dissolving 0.1 g of granulated tin metal (Baker) in 20 ml of concentrated sulfuric acid with heating, and dilution to 1 l with

60 ml of concentrated sulfuric acid and demineralized water. The PCV solution (0.1%) was prepared by dissolving 0.1 g in demineralized water to 100 ml. Tween-20 (1%) was prepared by dissolving 1.0 g in demineralized water to 100 ml. Glycine buffer solution (pH 2.0) was prepared with glycine solution (1.0 M) and the pH was adjusted to 2.0 with hydrochloric acid and/or sodium hydroxide solution. HEDTA solution (0.10%) was prepared by dissolving 0.10 g of *N*-(carboxymethyl)-*N'*-(2-hydroxyethyl)-*N*,*N'*-ethylenediglycine in demineralized water to 100 ml.

### 2.2. Apparatus

The absorption spectra were recorded and measured with a Varian DMS-80 spectrophotometer and an Intralab recorder using 1.0 cm cells. A 300 Analyser pH meter was used to measure the pH values.

### 2.3. General procedure

*Spectrophotometric determination of tin*

Transfer to a 50 ml volumetric flask 1.0 ml of the PCV solution, 2.0 ml of the Tween-20 solution and 2.0 ml of the CTAB solution. Mix and add a portion of tin(IV) solution containing 10–60 μg of tin, 10.0 ml of glycine buffer and 5.0 ml of HEDTA solution. Mix, and after 30 min, dilute to the mark with water and measure the absorbance at 660 nm in a 1 cm cell, using water as a blank.

Table 2
Effect of the amount of glycine buffer solution

| (M) Concentration | Absorbance |
|---|---|
| 0.04 | 0.787 |
| 0.14 | 0.786 |
| 0.20 | 0.795 |
| 0.30 | 0.796 |
| 0.40 | 0.796 |
| 0.50 | 0.797 |

## 3. Results and discussion

### 3.1. Characteristics of the reagent and the complex

The reaction of PCV with the tin(IV) cation in the presence of CTAB and Tween-20 results in a green complex with an absorption maximum at 660 nm. The PCV reagent has an absorption maximum at 441 nm. The complex without surfactants is red, with a maximum absorption at 555 nm.

### 3.2. Effect of the pH

The effect of pH on the tin(IV)–PCV system was studied and the results demonstrated that the absorbance signal is at a maximum and constant in the pH range 1.60–2.7 as can be seen in Fig. 1.

In the described procedure the use of glycine buffer at pH 2 is recommended because at this pH, the selectivity is higher. A glycine buffer

Table 3
Effect of the order of addition of reagents

| Order of addition | Absorbance |
|---|---|
| PCV + Tween-20 + CTAB + Sn(IV) + buffer + HEDTA | 0.802 |
| PCV + CTAB + Tween-20 + Sn(IV) + buffer + HEDTA | 0.796 |
| PCV + Tween-20 + CTAB + Sn(IV) + HEDTA + buffer | 0.790 |
| PCV + Tween-20 + CTAB + buffer + Sn(IV) + HEDTA | 0.720 |
| PCV + Tween-20 + CTAB + HEDTA + Sn(IV) + buffer | 0.021 |
| Tween-20 + CTAB + PCV + Sn(IV) + buffer + HEDTA | 0.803 |
| Tween-20 + CTAB + Sn(IV) + PCV + buffer + HEDTA | 0.789 |
| Buffer + HEDTA + PCV + Tween-20 + CTAB + Sn(IV) | 0.082 |
| Sn(IV) + Tween-20 + CTAB + PCV + buffer + HEDTA | 0.640 |
| Sn(IV) + PCV + Tween-20 + CTAB + HEDTA + buffer | 0.606 |
| Sn(IV) + buffer + PCV + Tween-20 + CTAB + HEDTA | 0.376 |
| Sn(IV) + HEDTA + buffer + Tween-20 + CTAB + PCV | 0.019 |
| Sn(IV) + PCV + HEDTA + Tween-20 + CTAB + buffer | 0.015 |
| Sn(IV) + PCV + HEDTA + buffer + Tween-20 + CTAB | 0.011 |
| Sn(IV) + HEDTA + PCV + Tween-20 + CTAB + buffer | 0.011 |

Table 4
Effect of the amount of HEDTA on the tin(IV)–PCV system

| ($10^{-4}$ M) Concentration | Absorbance |
|---|---|
| 3.6 | 0.805 |
| 7.2 | 0.801 |
| 10.8 | 0.799 |
| 14.4 | 0.795 |

Table 5
Analytical characteristics of the procedures

| Characteristic | Value |
|---|---|
| Molar absorptivity ($l\,mol^{-1}\,cm^{-1}$) | $1.03 \times 10^5$ |
| Calibration sensitivity ($ml\,\mu g^{-1}$) | 0.867 |
| Analytical sensitivity ($ml\,\mu g^{-1}$) | 86.73 |
| Limit of detection, $C_L$; $3\sigma$ ($ng\,ml^{-1}$) | 7 |
| Limit of quantitation, $C_Q$; $10\sigma$ ($ng\,ml^{-1}$) | 25 |
| Linear dynamic range ($\mu g\,ml^{-1}$) | 0.02–1.20 |
| Coefficient of variation (%) | 1.25 |

concentration in the range 0.04–0.50 M does not affect the absorbance signal of the tin(IV)–PCV system (Table 2).

### 3.3. Effect of the order of addition of the reagents on complex formation

The order of reagent addition was studied. This is a critical stage in the reaction. The results demonstrated that the order strongly affects the complex formation, as can be seen in Table 3. The reagent and surfactants must be added before the tin(IV) or sample solution, and only after this can the pH be adjusted.

### 3.4. Effect of the HEDTA amount on the tin(IV)–PCV complex

PCV is not a selective reagent for tin determination. However, the use of HEDTA as masking agent solves this problem. The effect of the HEDTA amount on tin(IV)–PCV complex formation was studied, and the results show that it does not affect the complex formation when present at the least in the range $3.6 \times 10^{-4}$–$14.4 \times 10^{-4}$ M (Table 4). The HEDTA must be added after the formation of the complex.

### 3.5. Analytical characteristics of the method

A calibration curve was prepared according to the general procedure described in the experimental section 2.3, using water as the blank.

Beer's law was obeyed in the concentration range 0–1.20 $\mu g\,ml^{-1}$ of tin and the curve does not pass through the origin. The molar absorptivity was $1.03 \times 10^5\,l\,mol^{-1}\,cm^{-1}$ at 660 nm.

The analytical sensitivity [13], the calibration sensitivity [13], the limit of detection and the limit of quantitation [14] as well as other analytical characteristics are summarized in Table 5.

### 3.6. Effect of interfering ions

Solutions containing 50.00 μg of tin(IV) and various proportions of several cations and anions were prepared, and the general procedure was followed.

Table 6 shows interference levels during tin determination in the absence and presence of HEDTA. The main interferences are vanadium(V), molybdenum(VI), titanium(IV) and iron(III).

Iron(III) interference can be eliminated by reduction to iron(II) with ascorbic acid; 50 mg

Table 6
Tin determination with PCV in the presence and absence of HEDTA

| Cation Amount (μg) | Interference level | |
|---|---|---|
| | Without HEDTA | With HEDTA |
| Ag(I) 500 | +7.03 | −0.38% |
| Ca(II) 500 | −1.35% | – |
| Mg(II) 500 | −0.90% | −0.62% |
| Ba(II) 500 | −0.54% | – |
| Sr(II) 500 | −1.35% | – |
| Th(IV) 500 | −1.50% | – |
| Al(III) 500 | +5.75% | −0.87 |
| Mn(II) 500 | +21.43% | −1.12% |
| Bi(III) 500 | −13.15% | −4.17% |
| Cd(II) 500 | +1.99% | −0.13% |
| Pb(II) 500 | +0.57% | +0.63% |
| Sb(V) 500 | +7.03% | −1.77% |
| Zn(II) 500 | +2.00% | −1.62% |
| Ni(II) 500 | +23.43% | −1.37% |
| Ti(IV) 500 | +209.32% | +9.11% |
| Hg(II) 500 | +5.41% | +2.02% |
| Co(II) 500 | +4.86% | −0.25% |
| Fe(III) 500 | −60.54% | −73.28% |
| Mo(VI) 500 | +319.2% | +63.72% |
| V(V) 500 | −48.50% | −32.49% |
| Cu(II) 20000 | – | +2.92% |
| Cu(II) 5000 | – | +2.54% |
| Cu(II) 500 | +3.93% | +0.12% |

Conditions: [Sn(IV)], 50.00 μg per 50 ml; [HEDTA], $7 \times 10^{-4}$ M; pH 2.00.

Table 7
Tin determination in copper-based alloys (standards)

| Standard | Certified value (%) | Value found[a] (%) |
|---|---|---|
| Brass NIST 62d | 0.38 | 0.38 ± 0.01 (5) |
| Brass NIST 164 | 0.63 | 0.64 ± 0.01 (5) |
| Brass CEPED 486 | 2.81 | 2.82 ± 0.03 (5) |
| Brass NIST 52c | 7.85 | 7.82 ± 0.02 (5) |

[a] At the 95% confidence level.

Table 8
Tin determination in copper-based alloys (samples)

| Sample | ICP method (%) | PCV method[a] (%) |
|---|---|---|
| Brass 40 | 0.14 | 0.13 ± 0.01 (5) |
| Brass 37 | 0.90 | 0.91 ± 0.02 (5) |
| Brass 10 | 4.36 | 4.38 ± 0.02 (5) |
| Brass 1 | 5.50 | 5.50 ± 0.02 (5) |

[a] At the 95% confidence level.

of ascorbic acid are sufficient for masking 1000 μg of iron(III) during the determination of 50.0 μg of tin(IV).

The effect of the ionic strength on the system is negligible up to a sodium chloride concentration of 0.1 M.

### 3.7. Application

*Tin determination in copper-based alloys*

The proposed procedure was applied to tin determinations in several standards and samples of copper-based alloys.

The sample solutions were prepared using nitric and hydrochloric acids. The results are described in Tables 7 and 8, and the matrix compositions are shown in Table 9.

The results shown in Table 7 demonstrate that there is no significant difference between the certified value and the value obtained with PCV at the 95% confidence level for four different alloys.

Application of the paired $t$ test [15] in the results obtained by the PCV procedure and the ICP method (Table 8) showed that there is no significant difference between the two methods at the 95% confidence level.

## 4. Conclusions

The spectrophotometric determination of tin using Pyrocatechol Violet can be improved with the use of HEDTA as masking agent, and Tween-20 and cetyltrimethylammonium bromide as sensitizing and stabilizing agents.

This new proposed method can be used for the spectrophotometric determination of tin in copper-based alloys without carrying out a separation procedure.

## Acknowledgments

The authors acknowledge the financial support of the CNPq, FINEP and CAPES.

## References

[1] A.E. Eberle and M.W. Lerner, Anal. Chem., 34 (1962) 627.
[2] N.L. Olenovich and G.I. Savenko, Zavod. Lab., 41 (1975) 658; Anal. Abstr., 30 (1976) 1B33.
[3] N.N. Karnaukhova, Zavod. Lab., 36 (1970) 1047; Anal. Abstr., 21 (1971) 63.

Table 9
Compositions of the standards and samples analyzed

| Standard/sample | Sn (%) | Cu (%) | Ni (%) | Pb (%) | Zn (%) | Fe (%) |
|---|---|---|---|---|---|---|
| Brass NIST[a] 62d | 0.38 | 59.07 | 0.28 | 0.25 | 37.14 | 0.86 |
| Brass NIST[a] 164 | 0.63 | 63.76 | 0.046 | 0.22 | 21.89 | 2.52 |
| Brass CEPED[b] 486 | 2.81 | 85.86 | 0.29 | 5.32 | 2.87 | 0.21 |
| Brass NIST[a] 52c | 7.85 | 89.25 | 0.76 | 0.011 | 2.12 | 0.004 |
| Brass 40 | 0.14 | 58.10 | 0.001 | 2.45 | 39.10 | 0.007 |
| Brass 37 | 0.90 | 70.78 | 0.58 | 0.94 | 26.65 | 0.076 |
| Brass 10 | 4.36 | 85.13 | 0.33 | 4.72 | 4.71 | 0.211 |
| Brass 1 | 5.50 | 86.75 | 0.50 | 1.97 | 4.80 | – |

[a] National Institute of Standards and Technology, USA.
[b] Centro de Pesquisa e Desenvolvimento da Bahia, Brasil.

[4] V.I. Kurbatova and V.V. Stepin, Tr. Vses. Nauchn.-Issled. Inst. Stand. Obraztsov. Spektr. Etalonov., 1 (1964) 14; Anal. Abstr., 13 (1966) 6802.
[5] N.L. Shestidesyatna, N.M. Milyaeva and L.I. Kotelyankaya, Zavod. Lab., 41 (1975) 653.
[6] S. Ambujavalli and N. Premavathi, Anal. Chem., 48 (1976) 2152.
[7] R. Tanaka, Jpn. Anal., 10 (1961) 336; Anal. Abstr., 10 (1963) 2161.
[8] F.D. Snell, Photometric and Fluorimetric Methods of Analysis, Wiley–Interscience, New York, 1978.
[9] E.F. Tkach, Uch. Zap. Kishinev. Gos. Univ., 68 (1963) 61; Anal. Abstr., 12 (1965) 5662.
[10] Z. Marczenko, Spectrophotometric Determination of Elements, Wiley, New York, 1973.
[11] A. Ashton, A.G. Fogg and D.T. Burns, Z. Anal. Chem., 264 (1973) 133.
[12] R.M. Dagnall, T.S. West and P. Young, Analyst, 92 (1967) 27.
[13] D.A. Skoog and J.J. Leary, Principles of Instrumental Analysis, Saunders College Publishing, Florida, 1992.
[14] F.A. Medinilla and F.G. Sanchez, Talanta, 33 (1986) 329.
[15] G. Chirstian, Anal. Chem., Wiley, New York, 1980, p. 75.

ELSEVIER

Talanta 42 (1995) 1979–1987

Talanta

# Rapid one-step derivatization of Se(VI) to a piazselenol for the spectrofluorimetric determination of selenium in biological material

Karin Johansson *, Xiaoguang Luo, Åke Olin

*Department of Analytical Chemistry, University of Uppsala, P.O. Box 531, S-751 21 Uppsala, Sweden*

Received 4 April 1995; revised 15 June 1995; accepted 15 June 1995

**Abstract**

A spectrofluorimetric method for the determination of total selenium in biological samples has been developed. After oxidative destruction, the sample is reacted with a mixture of bromide and 2,3-diamino-1,4-dibromonaphthalene ($Br_2$-DAN) without pH adjustment. Selenium(VI) is rapidly reduced by bromide to Se(IV) which then forms 4,7-dibromo-5,6-benzopiazselenol ($Br_2$-DAN-Se). The conversion of Se(VI) to $Br_2$-DAN-Se is completed in 6 min at 100°C. The piazselenol is extracted to cyclohexane and the fluorescence measured at 577 nm with excitation at 518 nm. The procedure has been validated by determinations on reference materials with selenium concentrations ranging from 4 to 1460 ng $g^{-1}$. The advantages of the method are the fast reduction of Se(VI) by hydrobromic acid and the properties of $Br_2$-DAN, which permit the piazselenol formation to be carried out in a strongly acidic medium and at high temperature. The limit of detection is 0.6 ng $g^{-1}$ as estimated by three times the standard deviation of the blank determination ($n = 7$).

The rate of reduction of Se(VI) to Se(IV) in hydrobromic acid was investigated as a function of concentration and temperature. The new kinetic data together with previous kinetic and equilibrium data for the piazselenol formation were used to model and optimize the simultaneous reduction–derivatization procedure.

*Keywords:* Selenium; Spectrofluorimetry; Biological material

## 1. Introduction

Several methods for the determination of selenium are available and those most commonly used are molecular fluorescence spectrometry (MFS) [1–6], gas chromatography with electron capture detection (GC-ECD) [7–10], atomic absorption spectrometry after hydride generation (HG-AAS) [11,12] and electro-thermal atomic absorption spectrometry (ETAAS) [13]. These methods, except ETAAS, respond only to selenium in the tetravalent state. Thus, all other forms of selenium have to be converted into Se(IV).

In the determination of total selenium in biological samples destruction of the organic material has to be accomplished in most cases. This is usually performed by treatment of the sample with strong oxidizing acids. Most commonly employed is a mixture of nitric, perchloric and sulfuric acids. Another digestion method, which avoids the hazards connected with the use of perchloric acid, is the combined wet-dry ashing procedure described by Hansson et al. [14]. After the digestion, Se(VI) is reduced to Se(IV), normally with 4–6 M hydrochloric acid [15]. If HG-AAS is used, the sample is ready for analysis. With GC-ECD or

* Corresponding author.


*SSDI* 0039-9140(95)01678-3

MFS, Se(IV) is reacted with an aromatic *o*-diamine in excess to form a piazselenol that is extracted to an organic solvent before the instrumental finish. The extraction step can provide an enrichment of the analyte by up to 500 times [16].

In MFS the most commonly used reagent is 2,3-diaminonaphthalene (DAN) introduced by Parker and Harvey in 1962 [1]. However, the properties of this reagent make the analysis somewhat complicated [17]. The piazselenol formation occurs in a reaction between selenous acid and monoprotonated *o*-diamine and the reaction conditions must therefore be selected so that these species predominate in order to arrive at reasonable derivatization times [4,18]. For a biological sample, which has been digested and then reduced by hydrochloric acid, this implies that considerable pH adjustment is necessary when the DAN reagent is employed. Recently, the use of 2,3-diamino-1,4-dibromonaphthalene ($Br_2$-DAN) as a new spectrofluorimetric reagent was reported [19]. The values of acidity constants of $Br_2$-DAN make this reagent compatible with a strongly acidic medium and hence the pH adjustment is obviated. However, when the piazselenol formation is performed in a medium of hydrochloric acid, an exchange may occur of bromine with chlorine in the reagent and the piazselenol. The chlorinated piazselenol, 4,7-dichloro-5,6-benzopiazselenol ($Cl_2$-DAN-Se), has a lower fluorescence intensity than the corresponding brominated piazselenol, 4,7-dibromo-5,6-benzopiazselenol ($Br_2$-DAN-Se). Therefore, irreproducible results will be obtained when the temperature and concentration of hydrochloric acid are high, conditions that speed up the rates of the reduction and derivatization reactions to expedient values.

Hydrobromic acid has been found to be a suitable alternative to hydrochloric acid, both as a reaction medium for the derivatization with $Br_2$-DAN and as a reducing agent [19]. Few articles have reported on the use of hydrobromic acid for the reduction of Se(VI) [20,21]. This paper delineates the influence of concentration and temperature on the rate of reduction of Se(VI) with hydrobromic acid. The rapid reduction which can be achieved and the thermal stability of $Br_2$-DAN and $Br_2$-DAN-Se suggested that the usual two-step reduction–derivatization sequence could be replaced by a combined reduction–derivatization step. This simplification of the fluorimetric selenium determination has been studied and resulted in a procedure in which Se(VI) is converted to $Br_2$-DAN-Se in about 6 min.

## 2. Experimental

### 2.1. Apparatus and reagents

All fluorescence recordings were made on an Aminco SPF-500 Corrected Spectra Fluorometer as described earlier [19]. Most experiments were performed in 8 ml Pyrex glass tubes equipped with PTFE-faced screw-caps in a laboratory-built aluminum block (150 × 150 $mm^2$) with a capacity of 25 samples and placed on a 2000 W hot-plate. The temperature was regulated by an Eurotherm 904 temperature regulator (Eurotherm International, Strängnäs, Sweden).

All chemicals were of analytical grade from Merck unless otherwise stated. Milli-Q-filtrated (MQ) water (Millipore™) was used throughout. All glassware was cleaned in 7 M nitric acid and rinsed with MQ water. The standard solutions of Se(IV) and Se(VI) were prepared and analysed as described before [10,14]. The three acid mixture was composed of 65% nitric acid, 70–72% perchloric acid and 95–97% sulfuric acid in the proportions 20:5:2. $Br_2$-DAN was synthesized as described before [19]. A 2.05 mM working solution of $Br_2$-DAN was prepared by dissolving 16.2 mg of the chemical in 25 ml of methanol. The solution was stored at room temperature in the dark. It was stable for at least one week.

The reference materials were MA-B-3/TM fish tissue (IAEA, Monaco), SRM 1567 wheat flour, SRM 1577a bovine liver, RM 8433 corn bran, RM 8412 corn stalk, RM 8413 corn kernel (NIST, Gaithersburg, MD) and Seronorm 105 human serum (Nycomed AS, Oslo, Norway).

### 2.2. Kinetic experiments

*Reduction of Se(VI) by hydrobromic acid*

A solution of 1.5, 2.0 or 2.5 M hydrobromic acid (200 ml) was heated in a glass beaker on a hot plate with magnetic stirring facilities and the temperature was regulated by a sensor placed in the solution (Heidolph, Kelheim, Germany). When the desired temperature had been reached and stabilized, a small volume of a standard solution of Se(VI) was added. The

reaction was followed by measurement of the Se(IV) concentration. Part of the reaction mixture was continuously withdrawn from the beaker through Teflon tubing (0.7 mm i.d.) by pumping. The sample stream was immediately cooled and then passed through the sample loop of an injection valve before going to waste. The value was activated at regular intervals by a timer and injected the sample into a HG-AAS instrument [22] for determination of Se(IV). Concentrations were evaluated from a calibration curve determined with matrix-matched standards.

*Simultaneous reduction of Se(VI) and piazselenol formation*

To a set of 12 Pyrex test tubes a 0.95 ml portion of a solution containing 1.6, 2.1 or 2.6 M hydrobromic acid and 53 or 105 μM $Br_2$-DAN was added. The tubes were closed and placed in a thermostatted aluminum block. When the desired temperature had been reached, 50 μl of 200 ng $l^{-1}$ of Se(VI) was added. At predetermined times, a tube was withdrawn from the heating block and the reaction stopped by changing the pH to 5 by addition of a concentrated sodium phosphate solution. The tube was then stored in an ice bath. The extraction of the piazselenol was performed at room temperature with 3 ml of cyclohexane.

### 2.3. Analytical procedures

*Digestion with the three acid mixture*

Weigh 0.5–1 g of sample into a 100 ml Kjeldahl flask. Add 20 ml of the three acid mixture and a few boiling stones and place the flask in the heating stand. Boil the mixture until the sulfuric acid begins to distil. After cooling add 10 ml of 5 M sodium bromide and dilute to 25 ml with water. Transfer 2 ml of this solution to a 8 ml test tube and add 100 μl of 2.05 mM $Br_2$-DAN. Close the tube and place it in the aluminum block for 6 min at 100°C. Cool to room temperature and extract with 3 ml of cyclohexane. Rapid phase separation is obtained by spinning the test tubes.

Measure the fluorescence of the piazselenol extract at an excitation wavelength of 518 nm and emission wavelength of 577 nm.

*Digestion with magnesium nitrate–nitric acid*

Weigh about 0.1 g of dry homogeneous sample into a 8 ml Pyrex test tube. Add 0.3 g of magnesium nitrate hexahydrate, 1 ml of 14 M nitric acid and 50 μl of 12 M hydrochloric acid. Place the tube in the aluminum block and apply the following temperature programme: [(°C)/ramp time (min)/dwell time (min): 50/20/60, 85/20/100, 105/20/100, 125/20/100, 175/120/30, 225/40/30, 500/180/120]. Include an end step that allows the temperature to decrease to 100°C. Withdraw the tube from the block and add 1 ml of a solution containing 3 M perchloric acid and 0.05 M sulfamic acid. When the digestion residue has dissolved, add 1 ml of a solution containing 4 M hydrobromic acid and 2 mM hydroxylammonium sulfate and finally 100 μl of 2.05 mM $Br_2$-DAN. Close the tube and place it in the aluminum block at 100°C for 6 min. The extraction and fluorimetric measurement are then performed as described above.

## 3. Results and discussion

### 3.1. Reduction of Se(VI) in hydrobromic acid

The aim here was to find conditions for rapid reduction of Se(VI) to Se(IV) and only restricted ranges of temperature and hydrobromic acid concentration were therefore studied. For acid concentrations below about 1.5 M the reaction becomes unattractively slow even at high temperature. Concentrations (M) here and elsewhere refer to the value at room temperature for practical reasons and pH will be used freely to denote $-\log[H^+]$. The upper concentration limit was set by the proportionally large volume of hydrobromic acid (8.7 M) which had to be added. Furthermore, one of the batches of hydrobromic acid used contained an unidentified reducing agent, which lead to selenium losses at high temperatures and concentrations of the acid. Hence an upper limit of 2.5 M was chosen as a precaution against selenium losses, but a new batch of hydrobromic acid should always be tested for excessive reducing power before use. The reducing agent might have been iodide, which fairly rapidly reduces Se(VI) to Se(0) even at micromolar concentrations [23]. Losses of selenium can be avoided by the addition of small amounts of bromate. Since bromine interferes in the piazselenol reaction, free bromine must be removed after the reduction if a spectrofluorimetric finish is used.

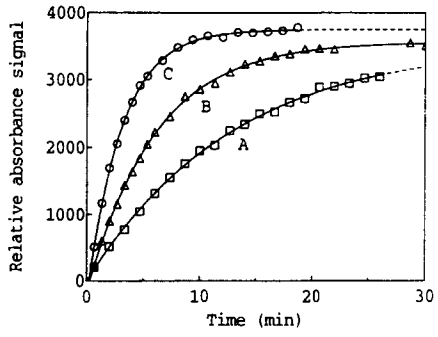


Fig. 1. Dependence of the rate of reduction of Se(VI) to Se(IV) on the concentration of hydrobromic acid at 75°C. The Se(IV) concentration is represented by the relative absorbance signal. A, 1.5; B, 2.0; and C, 2.5 M hydrobromic acid.

Representative formation curves of Se(IV) generated by reduction of Se(VI) with hydrobromic acid are shown in Figs. 1 and 2. The rate constant, $k_r$, was determined by fitting the function [15]

$$y = A - B\,e^{-k_r t} \quad (1)$$

to the data ($t$, [Se(IV)]) by non-linear regression. Experiments with different initial Se(VI) concentrations confirmed that the reaction was of first order with respect to Se(VI). The values of $k_r$ so obtained can be reproduced by

$$k_r = 2.01 \times 10^{12}[HBr]^{2.57}\,e^{-1.11 \times 10^4/T} \quad (2)$$

with $k_r$ in $min^{-1}$. Note the high power in [HBr] which leads to a rapid increase in the reduction rate with acid concentration. A strong rate dependence on concentration has been found for hydrochloric acid also [15].

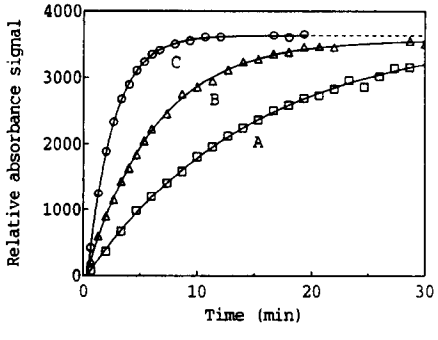


Fig. 2. Dependence of the rate of reduction of Se(VI) to Se(IV) on temperature in 2 M hydrobromic acid. The Se(IV) concentration is represented by the relative absorbance signal. A, 65; B, 75; and C, 85°C.

### 3.2. Simultaneous reduction of Se(VI) and formation of 4,7-dibromo-5,6-benzopiazselenol

The purpose of a simultaneous reduction of Se(VI) and derivatization of the Se(IV) formed to a piazselenol is to simplify the analytical procedure and diminish the analysis time. Therefore, the conditions for fast reduction and derivatization must be considered at the same time and balanced. The rate of the reduction of Se(VI) increases both with temperature and hydrobromic acid concentration as discussed in the previous paragraph and results in a complete conversion to Se(IV). The optimal conditions for the piazselenol reaction will be discussed with reference to the kinetic and equilibrium studies made previously [19]. Data needed for the calculations made in the following paragraphs were taken from this reference.

*Equilibrium considerations*

The formation of $Br_2$-DAN-Se occurs in a reaction between undissociated selenous acid and monoprotonated $Br_2$-DAN. The reaction can be represented by

$$H_2SeO_3 + Br_2\text{-}DANH^+ \underset{k_b}{\overset{k_f}{\rightleftharpoons}} Br_2\text{-}DAN\text{-}Se + H^+$$

where $k_f$ and $k_b$ are the rate constants of the forward and reverse reactions respectively. It was found that the reaction moved towards an equilibrium with incomplete conversion to the piazselenol although the ligand was in great stoichiometric excess. For biological samples the total selenium concentration seldom exceeds 1 μM, whereas the normal ligand concentration is in the range 50–100 μM, thus in a hundred fold excess. The equilibrium constant of the reaction, $\beta$, is given by

$$\beta = \frac{[Br_2\text{-}DAN\text{-}Se]_{eq}[H^+]_{eq}}{[H_2SeO_3]_{eq}[Br_2\text{-}DANH^+]_{eq}} = \frac{k_f}{k_b} \quad (3)$$

The numerical value of $\beta$ is $3 \times 10^5$ at 70°C. The $\beta$ value previously reported was $3.4 \times 10^5$, but an extended analysis of the data has resulted in the new value. The degree of conversion to the piazselenol at equilibrium, defined as $[Br_2\text{-}DAN\text{-}Se]_{eq}/[Se]_{tot}$, can be found from Eq. (3).

Fig. 3 shows the pH dependence of the degree of conversion at two ligand concentrations. As seen directly from Eq. (3) the piazselenol concentration decreases with acidity in strongly acid medium, in which $H_2SeO_3$ and $Br_2$-$DANH^+$ constitute large fractions of the total concentrations of Se(IV) and $Br_2$-DAN respectively. In less acid solution, $Br_2$-DAN is the dominating ligand species and the degree of

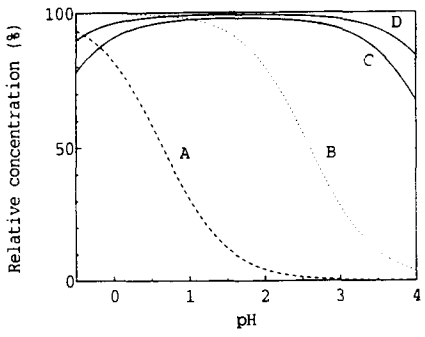


Fig. 3. Distribution diagram for Se(IV) and $Br_2$-DAN, and the calculated pH dependence of the degree of conversion of Se(IV) to the piazselenol at equilibrium for two ligand concentrations. A, fraction of the free ligand as $Br_2$-DANH$^+$; B, fraction of Se(IV) as $H_2SeO_3$; C and D, degree of conversion for 40 and 100 μM ligand respectively.

conversion is almost independent of pH until $H_2SeO_3$ starts to deprotonate. Then the equilibrium shifts to the left. Hence equilibrium considerations indicate that a reaction medium with a pH between 1 and 3 would be optimal. Note, however, that the decrease of the equilibrium concentration of the piazselenol with acidity can be counteracted by an increase of the ligand concentration. The drop in the degree of conversion with acidity is moderate at a ligand concentration of 100 μM.

*Rate considerations*

When the piazselenol reaction is run at a constant pH and a large excess of the ligand, the reaction rate follows

$$r = \frac{d[Br_2\text{-DAN-Se}]}{dt} = k_f[H_2SeO_3][Br_2\text{-DANH}^+] - k_b[Br_2\text{-DAN-Se}][H^+] \quad (4)$$

with the solution

$$[Br_2\text{-DAN-Se}] = [Br_2\text{-DAN-Se}]_{eq}(1 - e^{-kt}) \quad (5)$$

$k$ is a conditional first order rate constant defined by

$$k = k_b[H^+] + \frac{k_f[Br_2\text{-DAN}]_{tot}}{f_1 \cdot f_2} \quad (6)$$

$f_1^{-1}$ denotes the fraction of the ligand present as $Br_2$-DANH$^+$ and $f_2^{-1}$ the fraction of Se(IV) present as $H_2SeO_3$. Fig. 4 shows the variation of the rate constant with pH at 70°C and a ligand concentration of 100 μM. Clearly, the reaction rate drops rapidly with increasing pH. Hence, rapid derivatization is favoured by an increase in acidity, which, however, decreases the degree of conversion to the piazselenol.

The temperature dependence of $k$ was determined previously in 2 M hydrobromic acid and a ligand concentration of 50 μM. From these data the temperature dependence of $k_f(M^{-1}\,min^{-1})$ can be calculated as

$$\ln k_f = 23.2 - \frac{4820}{T} \quad (7)$$

This equation indicates a rapid increase in reaction rate with temperature. Thus, in order to speed up the chemical reactions the temperature should be as high as possible and a high concentration of hydrobromic acid should be used. The influence of temperature on the equilibrium constant of the piazselenol reaction has not been determined, but previous measurements indicate that equilibrium concentrations are only moderately affected by temperature, at least for high ligand concentrations.

*Computer simulations*

As guidance in the choice of proper derivatization conditions, computer simulations were performed. The three simultaneous rate equations for the reaction sequence

$$Se^{VI} \xrightarrow[(HBr)]{k_r} Se^{IV} \underset{(H^+)}{\overset{(Br_2\text{-DAN})}{\overset{k_f}{\underset{k_b}{\rightleftharpoons}}}} Br_2\text{-DAN-Se}$$

were solved subject to the condition of constant acidity and a large excess of ligand and used to study the progress of the reaction sequence for different combinations of temperature, hydrobromic acid and ligand concentrations. The pseudo first order rate constants were calculated from Eqs. (2), (3) and (6). No attempts were made to include temperature or medium corrections in the equilibrium constants.

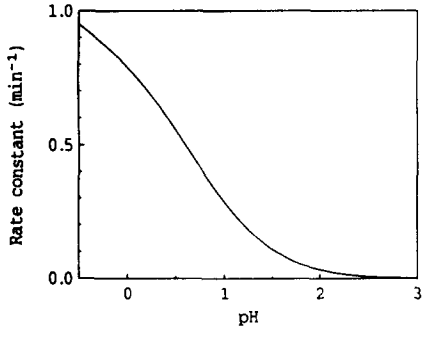


Fig. 4. The rate constant of the piazselenol formation, Eq. (6), as a function of pH at a ligand concentration of 100 μM and 70°C.

Table 1
Computer simulated reaction times for the conversion of Se(VI) to $Br_2$-DAN-Se by simultaneous reduction and derivatization as a function of temperature and the concentrations of hydrobromic acid and $Br_2$-DAN. Relative yield is the degree of conversion to the piazselenol at equilibrium and $t$ is the time needed to reach 98% of the equilibrium concentration

| [HBr] (M) | Temp. (°C) | 50 μM $Br_2$-DAN | | 100 μM $Br_2$-DAN | |
|---|---|---|---|---|---|
| | | Relative yield (%) | $t$ (min) | Relative yield (%) | $t$ (min) |
| 1.5 | 80 | 91 | 31 | 95 | 30 |
| | 90 | | 14 | | 13 |
| | 100 | | 6.3 | | 5.9 |
| 2.0 | 80 | 88 | 16 | 94 | 15 |
| | 90 | | 7.4 | | 6.5 |
| | 100 | | 3.9 | | 3.1 |
| 2.5 | 80 | 86 | 11 | 93 | 8.8 |
| | 90 | | 5.4 | | 4.1 |
| | 100 | | 3.2 | | 2.1 |

The results of the simulations are presented in Table 1, which contains the reaction time needed to reach 98% of the equilibrium concentration of $Br_2$-DAN-Se and the degree of conversion at equilibrium. The figures in the Table demonstrate the great influence of temperature and the hydrobromic acid concentration on the rate of the piazselenol formation. It can also be noted that the ligand concentration has little effect on the rate of formation of the piazselenol, which is largely governed by the rate of reduction of Se(VI). Fig. 5 shows an example of the changes in the concentrations during the progress of the reactions. Since the piazselenol formation cannot proceed faster than the reduction of Se(VI), a high temperature and concentration of hydrobromic acid should be chosen. High acid concentrations will also increase the rate of the piazselenol reaction but the equilibrium concentration of the piazselenol will decrease. However, the shift of the equilibrium position with the concentration of hydrobromic acid will not be pronounced at higher concentrations of $Br_2$-DAN. The degree of conversion, however, is limited by the solubility of the ligand, which is about 100 μM.

*Experimental tests of the computer simulations*

The computer simulations delineated appropriate conditions for fast simultaneous reduction and derivatization. These conditions were tested experimentally on standard solutions of Se(VI). Results from these tests are presented in Figs. 6 and 7 and the agreement is good between the simulated reaction times in Table 1 and the experimental findings. There was some

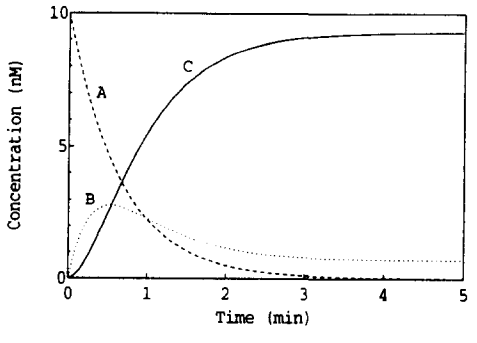


Fig. 5. Calculated concentrations during the formation of $Br_2$-DAN-Se by simultaneous reduction and derivatization at 100°C. Initial Se(VI) concentration 10 nM, ligand concentration 100 μM and hydrobromic acid concentration 2 M. A, Se(VI); B, Se(IV); C, $Br_2$-DAN-Se.

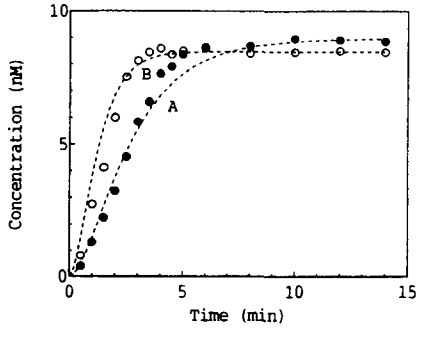


Fig. 6. Simultaneous reduction of Se(VI) and formation of $Br_2$-DAN-Se at 95°C (aluminum block 100°C) for different concentration of hydrobromic acid. Experimental results. Ligand concentration 50 μM. A, 1.5; and B, 2.5 M hydrobromic acid. Drawn curves are calculated formation curves for $Br_2$-DAN-Se.

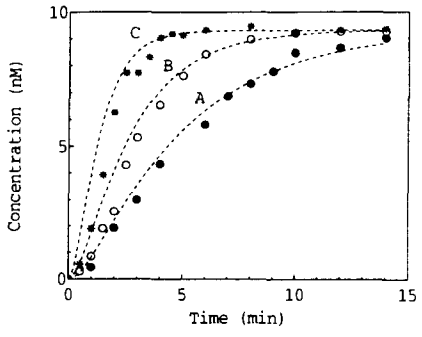


Fig. 7. Temperature dependence of the simultaneous reduction of Se(VI) and formation of $Br_2$-DAN-Se in 2 M hydrobromic acid and 100 μM $Br_2$-DAN. Experimental results. A, 77.5; B, 85; and C, 95°C (aluminum block 80, 90, 100°C). Drawn curves are calculated formation curves for $Br_2$-DAN-Se.

disagreement between the shape of the experimental formation curve and the curve calculated for the temperature of the aluminum block. The differences are caused by difficulties with the timing in the initial part of the experiments and the rather crude temperature control. The actual temperature of the reaction mixture was lower than the set temperature by 2.5–5°C. From the results of the experiments and simulations it was decided to perform the combined reduction and derivatization in 2 M hydrobromic acid and 100 μM $Br_2$-DAN at 100°C in the applications to real samples.

### *3.3. Determination of selenium in biological materials*

*Destruction by a three acid mixture*

We have previously preferred the combined wet/dry ashing method described by Hansson et al. [24] since it does not involve the use of perchloric acid. When hydrobromic acid was added to samples digested with this method, the solutions became colored yellow by bromine which was most likely generated in a redox reaction between added bromide and nitrite formed during the digestion. Bromine is beneficial in the reduction step since the $Br_2/Br^-$ redox couple stabilizes the tetravalent oxidation state of selenium, but it severely interferes in the piazselenol formation step. To avoid bromine formation, the samples were instead digested with a three acid mixture of nitric, perchloric and sulfuric acids. With this destruction method, no appearance of bromine was observed.

The selenium is present in a matrix of concentrated sulfuric acid after destruction by the three acid mixture. A study of the rate of the simultaneous reduction and derivatization at different concentrations of sulfuric acid and 2 M bromide revealed that the piazselenol formation was completed within 6 min in 1 M sulfuric acid at 100°C. It was also observed that the fluorescence signal was somewhat lower in sulfuric acid than in hydrobromic acid of the same concentration. Hence, it was decided to dilute the digested sample to 25 ml, i.e. approximately to 1 M sulfuric acid. Sodium bromide was added to a concentration of 2 M. A 2 ml portion of the diluted sample was used for the spectrofluorimetric finish. The calibration curve was established by addition of Se(VI) standards to a blank solution.

The procedure was evaluated by determinations on the following reference materials; MA-B-3/TM fish tissue (1460 μg $kg^{-1}$, 1350–1770 μg $kg^{-1}$), SRM 1567 wheat flour (1100 ± 200 μg $kg^{-1}$), SRM 1577a bovine liver (710 ± 70 μg $kg^{-1}$), Seronorm 105 human serum (90 ± 6 μg $l^{-1}$), RM 8433 corn bran (45 ± 8 μg $kg^{-1}$), RM 8412 corn stalk (16 ± 8 μg $kg^{-1}$) and RM 8413 corn kernel (4 ± 2 μg $kg^{-1}$). The results are presented in Table 2. The concentrations obtained fall within the specified concentration limits of the reference materials except for SRM 1567 and RM 8413. Low and high results respectively, for these materials have been obtained earlier [14,19,24]. Therefore, it is believed that the results are not caused by the new derivatization method.

*Destruction by wet/dry ashing*

Since access to a digestion method which does not include perchloric acid was considered of value, the previously discussed bromine problem associated with the wet/dry ashing procedure with magnesium nitrate–nitric acid was also addressed. The reaction of nitrous acid with primary amines in acidic solution can be used for the removal of nitrite. Sulfamic acid was used here, since it yields sulfuric acid and nitrogen as reaction products and no interference in the fluorescence measurement was noted. Its performance in conjunction with the present conditions was tested as follows. The reagent was added together with the perchloric acid used for the dissolution of the magnesium oxide and sample residues left after the dry ashing. Hydrobromic acid was then added and the sample was heated at 100°C for about 10 min. The presence of sulfamic acid substan-

Table 2
Selenium concentrations (dry mass) found in seven reference materials. Method A, digestion of 0.5–1.0 g sample with the three acid mixture; method B, digestion of 0.1 g sample with the combined wet/dry ashing method

| Reference material | Method A | | Method B | | Specified concentration ($\mu g\ kg^{-1}$) |
|---|---|---|---|---|---|
| | Mean $\pm$ $s$ ($\mu g\ kg^{-1}$) | $n$ | Mean $\pm$ $s$ ($mg\ kg^{-1}$) | $n$ | |
| MA-B-3/TM, fish tissue | 1410 $\pm$ 33 | 4 | 1393 $\pm$ 28 | 5 | 1350 – 1700[a] |
| SRM 1567, wheat flour | 895 $\pm$ 15 | 4 | 889 $\pm$ 22 | 5 | 1100 $\pm$ 200 |
| SRM 1577a, bovine liver | 703 $\pm$ 15 | 4 | 650 $\pm$ 24 | 5 | 710 $\pm$ 70 |
| Seronorm 105, human serum | 89 $\pm$ 1[b] | 4 | 88 $\pm$ 1[b] | 5 | 90 $\pm$ 6[b] |
| RM 8433, corn bran | 43 $\pm$ 1 | 4 | 45 $\pm$ 2 | 12 | 45 $\pm$ 8 |
| RM 8412, corn stalk | 17 $\pm$ 1 | 2 | 16 $\pm$ 1 | 5 | 16 $\pm$ 8 |
| RM 8413, corn kernel | 8 $\pm$ 1 | 4 | 6.3 $\pm$ 0.3 | 5 | 4 $\pm$ 2 |

[a] 95% non-parametric interval based on the median.
[b] $\mu g\ l^{-1}$.

tially decreased the formation of bromine. However, the bromine formation was not completely suppressed and it was observed that the concentration of bromine increased slowly with time. An increase of the concentration of sulfamic acid did not diminish the slow bromine formation. We believe that nitrite is removed by the addition of sulfamic acid and that the observed slow bromine formation is due to trace amounts of other, unidentified, species present in the digestion residue. It was also observed that the rate of the slow bromine formation, measured by spectrophotometry, was greatly dependent on the volume after dissolution of the sample. If the total volume was increased from 1 (normal volume) to 2 ml at a constant concentration of hydrobromic acid and a constant amount of sulfamic acid, the amount of bromine formed was small enough to be completely removed by the addition of 1 mM hydroxylammonium sulfate. This concentration causes insignificant reduction of Se(IV) to Se(0) at 100°C during 10 min. These findings have been exploited in the proposed analytical procedure, which was applied for the analysis of the reference materials mentioned above. The results are presented in Table 2. The agreement between the results obtained with the two digestion methods is good. As usual [19], a low result was obtained for SRM 1577a after digestion with the small scale version of the wet/dry digestion method.

The detection limit of the spectrofluorimetric method for both digestion techniques is 0.6 $ng\ g^{-1}$, as estimated by three times the standard deviation of the blank determinations ($n = 7$).

## 4. Conclusion

The simultaneous reduction and derivatization of Se(VI) using hydrobromic acid and 2,3-diamino-1,4-dibromonaphthalene as reagents simplifies the spectrofluorimetric method for the determination of selenium in biological samples. It is suitable for samples digested with the three acid method or the magnesium nitrate–nitric acid wet/dry ashing method provided that the necessary precautions against bromine formation are taken in the latter case. It is difficult to recommend one of the procedures in favour of the other as they both have their pros and cons. For laboratories with facilities that allow work with perchloric acid, the three acid procedure is probably the best choice. A scaled-down version of the present method would make it even more attractive. Finally, the short reaction times should make the combined reduction–derivatization approach well suited as part of an automated system for selenium determinations.

## References


[1] C.A. Parker and L.G. Harvey, Analyst, 87 (1962) 558.
[2] P.F. Lott, P. Cukor, G. Moriber and J. Solga, Anal. Chem., 35 (1963) 1159.
[3] W.H. Allaway and E.E. Cary, Anal. Chem., 36 (1964) 1359.
[4] P. Cukor and P.F. Lott, J. Phys. Chem., 69 (1965) 3232.
[5] J.H. Watkinson, Anal. Chem., 38 (1966) 92.
[6] A.B. Grant, N.Z.J. Sci., 24 (1981) 65.
[7] Y. Shimoishi and K. Tôei, Anal. Chim. Acta, 100 (1978) 65.
[8] S. Dilli and I. Sutikno, J. Chromatogr., 298 (1984) 21.
[9] A.F. Al-Attar and G. Nickless, J. Chromatogr., 440 (1988) 333.
[10] K. Johansson and Å. Olin, J. Chromatogr., 598 (1992) 105.
[11] C.A. Cutter, Anal. Chim. Acta, 98 (1978) 59.
[12] J. Piwonka, G. Kaiser and G. Tölg, Fresenius' Z. Anal. Chem., 321 (1985) 225.
[13] I. Harrison, D. Littlejohn and G.S. Fell, J. Anal. At. Spectrom., 10 (1995) 215.
[14] L. Hansson, J. Pettersson and Å. Olin, Talanta, 34 (1987) 829.
[15] J. Pettersson and Å. Olin, Talanta, 38 (1991) 413.
[16] H. Uchida, Y. Shimoishi and K. Tôei, Environ. Sci. Technol., 14 (1980) 541.
[17] Analytical Methods Committee, Analyst, 104 (1979) 778.
[18] J. Nève, M. Hanocq and L. Molle, Mikrochim. Acta, (1980) 41.
[19] K. Johansson, Ö. Andersson and Å. Olin, Analyst, 120 (1995) 423.
[20] Y. Shibata, M. Morita and K. Fuwa, Analyst, 110 (1985) 1269.
[21] A. D'Ulivo, J. Anal. At. Spectrom., 4 (1989) 67.
[22] J. Pettersson, L. Hansson and Å. Olin, Talanta, 33 (1986) 249.
[23] C. Ericzon, J. Pettersson and Å. Olin, Talanta, 37 (1990) 725.
[24] L. Hansson, K. Johansson, Å. Olin and G. Simán, Acta Agric. Scand., Sect. B, 44 (1994) 193.

ELSEVIER

Talanta 42 (1995) 1989–1997

Talanta

# Interaction of 5,7-dichloro-2-methyl-8-hydroxyquinoline with ionic micelles

J.L. Beltrán *, M.D. Prat, R. Codony

*Departament de Química Analítica, Universitat de Barcelona, Av. Diagonal, 647, 08028 Barcelona, Spain*

Received 25 January 1995; revised 21 June 1995; accepted 23 June 1995

**Abstract**

The changes in the apparent acid–base equilibria of 5,7-dichloro-2-methyl-8-hydroxyquinoline (HQ), in solutions of ionic surfactants (sodium lauryl sulphate, SLS; and cetyltrimethylammonium bromide, CTAB) were studied spectrophotometrically in 0.1 M NaCl medium at 25°C. The partition model, in which the different species involved in the equilibria ($H_2Q^+$, HQ and $Q^-$) can distribute betweeen aqueous and micellar pseudophases, was applied to account for the shifts in the apparent acidity constants. A factor analysis procedure was applied to the spectrophotometric data in order to determine the number of species in equilibrium.

The distribution constants for the different species were calculated with the SPDIS program. The proposed models for SLS and CTAB solutions were applied to simulate the apparent $pK_a$ values in these media; the satisfactory agreement between experimental and calculated values indicates that this model provides a good description of the effect of ionic surfactants on the acid–base equilibria of HQ.

*Keywords:* Chlorquinaldol; Surfactants; Distribution constants; Acid–base equilibria

## 1. Introduction

The solute–micelle interactions and the distribution of solutes between aqueous and micellar pseudophases have been studied extensively in order to explain the properties of aqueous micellar systems [1–5]. These media are used in different areas of analytical chemistry, such as the development of fluorimetric methods in order to increase their sensitivity [6,7], or in separation methods, such as micellar liquid chromatography and micellar electrokinetic capillary chromatography [8,9]. Moreover, there are separation methods based on the cloud-point of micellar solutions [10,11]. In most cases, the use of surfactant solutions is due to the ability of micelles to solubilize species, such as organic compounds and metal chelates, which are sparingly soluble in water.

The interaction of solutes with micelles leads to apparent changes in their chemical properties, such as shifts in their absorption spectra and in acid–base equilibria [12–15]. There are different models that explain these changes, such as the binding equilibria [5,16] between solute and micelle aggregates, the partition equilibria [4,16,17] of solutes between aqueous and micellar pseudophases, and the ion-exchange equilibria [18–20]. However, these different models are applied depending on the kind of micelles: the ion-exchange model is applied to explain the behaviour of charged species in solutions of ionic surfactants, whereas the partition equilibria model is applied mainly for non-ionic surfactants; the binding model can be applied for both types of surfactant.

* Corresponding author.

*SSDI* 0039-9140(95)01679-1

In a previous work [21], a program (SPDIS) for the determination of distribution constants according to the partition model was developed and successfully applied to non-ionic micellar solutions. In this paper, we show that the partition model can also be used in solutions of ionic surfactants, provided that the surfactant concentration is above its critical micelle concentration, and that the concentration of background electrolyte is much higher than those of the solutes.

Here, the model was applied to the distribution equilibria of 5,7-dichloro-2-methyl-8-hydroxyquinoline (chlorquinaldol) in solutions of sodium lauryl sulphate (SLS, anionic surfactant) and cetyltrimethylammonium bromide (CTAB, cationic surfactant). The results obtained by the application of the partition model are in accordance with the observed shifts of the dissociation constants of chlorquinaldol in these media. Additionally, we determined the critical micelle concentration of CTAB in 0.1 M NaCl medium, as there are some discrepancies between the values reported in the literature.

Interest in chlorquinaldol is related to its chelating ability towards metal ions and to the analytical applications based on the micelle-enhanced fluorescence of its metal chelates [7,22,23]. Previous studies on the fluorescence properties of metal–chlorquinaldol complexes [24] showed that non-ionic and cationic micelles led to important enhancement in fluorescence, relative to hydro-organic media, whereas the effect of anionic micelles depended on the nature of the metal ion. Studies on the partition equilibria of ligand and metal chelates (now in progress) in different micellar media will provide useful information to understand the mechanism of the micellar fluorescence enhancement.

## 2. Experimental

### 2.1. Apparatus

The absorption spectra were recorded on a Beckman DU-7 single-beam spectrophotometer, using a 1.00 cm quartz cuvette. The spectrophotometer was connected to an IBM-PC via a serial interface, and the absorbance data were acquired by using the DUMOD program [25].

The measurements of surface tension were carried out on a Krüss K-12 tensiometer, equipped with a platinum–iridium plate.

The pCH values were measured with a Radiometer PHM 84 pH meter, equipped with an Orion 81-02 combined glass electrode. Calibration of the electrode was performed according to the Gran method [26].

All spectrophotometric, potentiometric and surface tension measurements were made at 25°C (±0.2°C).

### 2.2. Reagents

5,7-Dichloro-2-methyl-8-hydroxyquinoline (chlorquinaldol, Supro, Troponwerke) was recrystallized twice from ethanol solution. Fresh 0.001 M solutions were prepared daily by dissolving the reagent in 0.02 M hydrochloric acid. SLS and CTAB (both from Merck) were used without further purification, although in some experiments SLS was recrystallized from ethanol. All other chemicals were of analytical grade. Buffer solutions were prepared according to Perrin and Dempsey [27] from hydrochloric acid, formic acid, acetic acid, boric acid, sodium dihydrogenphosphate, tris(hydroxy-methyl)aminomethane and sodium hydroxide. Double distilled water was used throughout.

### 2.3. Procedures

The apparent dissociation and distribution consistants of chlorquinaldol were obtained from spectrophotometric data. Aqueous solutions, containing chlorquinaldol ($2 \times 10^{-5}$ M), surfactant and sodium chloride to adjust the ionic strength to 0.1 M were prepared. The pCH was varied by the addition of hydrochloric acid, sodium hydroxide and/or small amounts (0.002 M) of buffer solutions. The solutions were thermostated in a waterbath at 25°C; after this, the absorption spectra of the solutions were recorded over the spectral range from 220 to 450 nm, at 5 nm intervals, and the $[H^+]$ values were measured.

The critical micelle concentration (cmc) of CTAB was determined from surface tension measurements, according to the Wilhelmy method [28]. Several solutions were prepared by adding variable amounts of CTAB to volumetric flasks containing the buffer, ionic medium and chlorquinaldol (when necessary). The surface tension of the thermostated solu-

tions (25°C) was measured and the cmc obtained by plotting the surface tension versus the logarithm of CTAB concentrations.

## 3. Solute–micelle interactions

The interaction between solutes and micelles can be explained by different models: partition equilibria of species between aqueous and micellar phases, binding equilibria between solutes and micellar aggregates, or by the ion-exchange equilibria.

The interaction between the neutral species HQ and the micellar aggregates (SLS and CTAB) can be described in terms of binding or partition equilibria. The binding equilibria is defined by

$$HQ + C \rightleftharpoons HQC \quad (1)$$

where $C$ means the concentration of surfactant in micellar form: $C = C_T - \text{cmc} - [HQC]$ ($C_T$ is the total concentration of surfactant and cmc its critical micelle concentration), and HQC indicates the chlorquinaldol bound to micelles. The binding constant $K_b$ is equal to

$$K_b = [HQC]/([HQ][C]) \quad (2)$$

where the concentrations of each species are referred to the total volume of the solution.

Alternatively, the partition of the species HQ between aqueous phase and micellar pseudophase can be defined by

$$HQ_{(w)} \rightleftharpoons HQ_{(m)} \quad (3)$$

$K_D$ is the partition constant:

$$K_D = [HQ]_{(m)}/[HQ]_{(w)} \quad (4)$$

Note that in this case the subscript (w) or (m) indicates the concentration of the species in aqueous or micellar phase.

For a given system, the binding and partition constants are related to the partial molar volume of the surfactant in micellar phase ($V_\phi$):

$$K_b = K_D \cdot V_\phi \quad (\text{if } C_T \gg [HQC]) \quad (5)$$

The interaction between charged species ($Q^-$ and $H_2Q^+$) and ionic surfactants is explained in two different ways, depending on the charges of surfactant and solutes. For species with the same charge as the surfactant ($Q^-$ in SLS, or $H_2Q^+$ in CTAB), the equilibria can be described in a similar way to the distribution of neutral species, taking into account that the ionic species can be extracted as the neutral ion associates with counter ions (mainly from the background electrolyte):

$$H_2Q^+_{(w)} + Cl^-_{(w)} \rightleftharpoons H_2Q^+ \cdot Cl^-_{(m)} \quad \text{(in CTAB solutions)} \quad (6)$$

$$Q^-_{(w)} + Na^+_{(w)} \rightleftharpoons Q^- \cdot Na^+_{(m)} \quad \text{(in SLS solutions)} \quad (7)$$

In this case, we can define the extraction constant as

$$K_{EX(H_2Q^+)} = [H_2Q^+ \cdot Cl^-]_{(m)}/([H_2Q^+]_{(w)} \cdot [Cl^-]_{(w)}) \quad (8)$$

$$K_{EX(Q^-)} = [Q^- \cdot Na^+]_{(m)}/([Q^-]_{(w)} \cdot [Na^+]_{(w)}) \quad (9)$$

In the presence of a large excess of background electrolyte with respect to the solute ($C_{NaCl} = 0.1$ M, and $C_{HQ}$ about $2 \times 10^{-5}$ M in our conditions), the free concentration of sodium and chloride ions can be considered as constants. By substituting $[Q^-]_{(m)} = [Q^- \cdot Na^+]_{(m)}$ and $[H_2Q^+]_{(m)} = [H_2Q^+ \cdot Cl^-]_{(m)}$ we can obtain the conditional partition constants for these species:

$$K'_{D(H_2Q^+)} = [H_2Q^+]_{(m)}/[H_2Q^+]_{(w)} = K_{EX(H_2Q^+)} \cdot C_{NaCl} \quad (10)$$

$$K'_{D(Q^-)} = [Q^-]_{(m)}/[Q^-]_{(w)} = K_{EX(Q^-)} \cdot C_{NaCl} \quad (11)$$

For species with opposite charges to surfactant, the interaction cannot be explained by a single partition equilibria; in these cases, the systems are described by the ion-exchange model, taking into account the different ions involved in the equilibrium. To simplify, the interaction of buffer species with the surfactants will be omitted because their concentrations (about 0.002 M) are negligible compared with the background electrolyte.

As an example, the ion-exchange equilibria of $H_2Q^+$ in SLS solutions can be described as

$$H_2Q^+_{(w)} + Na^+_{(m)} \rightleftharpoons H_2Q^+_{(m)} + Na^+_{(w)} \quad (12)$$

The equilibrium constant is defined, in this case, as the selectivity coefficient:

$$K_{H_2Q^+/Na^+} = [H_2Q^+]_{(m)} \cdot [Na^+]_{(w)}/[H_2Q^+]_{(w)} \cdot [Na^+]_{(m)} \quad (13)$$

We must take into account the exchange of hydrogen ion into micellar phase as

$$H^+_{(w)} + Na^+_{(m)} \rightleftharpoons H^+_{(m)} + Na^+_{(w)} \quad (14)$$

The concentrations of $Na^+$ in aqueous and micellar phases are obtained from the mass balance of sodium ion. Let $n_{Na}$ be the total number of moles of $Na^+$ in solution, $V_w$ and $V_m$ the volumes of aqueous and micellar phases, and $V$ the total volume of the solution ($V = V_w + V_m$). The volume of the micellar pseudophase is given by $V_m = C \cdot V \cdot V_\phi$. In practice, it can be assumed that $V_m \ll V_w$, and $V \approx V_w$. Under these conditions, we can write:

$$\begin{aligned} n_{Na} &= (C_T + C_{NaCl}) \cdot V \\ &= [Na^+]_{(w)} \cdot V_w + [Na^+]_{(m)} \cdot V_m \\ &= n_{Na,w} + n_{Na,m} \end{aligned} \quad (15)$$

$$\begin{aligned} n_{Na,w} = C_{NaCl} \cdot V + \alpha \cdot C \cdot V + \text{cmc} \cdot V \\ + [H_2Q^+]_{(m)} \cdot V_m + [H^+]_{(m)} \cdot V_m \end{aligned} \quad (16)$$

$$\begin{aligned} n_{Na,m} &= n_{Na} - n_{Na,w} \\ &= C \cdot V \cdot (1 - \alpha) - [H_2Q^+]_{(m)} \cdot V_m \\ &\quad - [H^+]_{(m)} \cdot V_m \end{aligned} \quad (17)$$

where $\alpha$ is the ionization degree of the micelles, which can be considered constant for surfactant concentrations well above the cmc (typical values range between 0.15 and 0.25). By defining $R$ as the ratio of micellar volume to the total volume ($R = V_m \cdot V^{-1} = C \cdot V_\phi$), the concentration of sodium ion in aqueous and micellar phases is given by

$$\begin{aligned} [Na^+]_{(w)} = C_{NaCl} + \alpha \cdot C + \text{cmc} \\ + [H_2Q^+]_{(m)} \cdot R + [H^+]_{(m)} \cdot R \end{aligned} \quad (18)$$

$$\begin{aligned} [Na^+]_{(m)} &= (1 - \alpha) \cdot C \cdot R^{-1} \\ &\quad - [H_2Q^+]_{(m)} - [H^+]_{(m)} \\ &= (1 - \alpha) \cdot V_\phi^{-1} - [H_2Q^+]_{(m)} - [H^+]_{(m)} \end{aligned} \quad (19)$$

Under our working conditions, $C_{NaCl} \gg (\alpha \cdot C + \text{cmc} + [H_2Q^+]_{(m)} \cdot R + [H^+]_{(m)} \cdot R)$, so we can consider that the concentration of sodium ion in the aqueous phase is nearly constant, and equal to $C_{NaCl}$. Moreover, in Eq. (19), the concentrations of $H_2Q^+$ and $H^+$ in the micellar phase are negligible compared to $(1 - \alpha) \cdot V_\phi^{-1}$, and we can consider that the concentration of sodium in micellar phase is also constant. In this case the selectivity coefficient is given as

$$\begin{aligned} K_{H_2Q^+/Na^+} = [H_2Q^+]_{(m)} \cdot C_{NaCl} \cdot V_\phi / \\ \{[H_2Q^+]_{(w)} \cdot (1 - \alpha)\} \end{aligned} \quad (20)$$

Taking into account that, under our experimental conditions, the concentration of sodium chloride is constant, and that the $V_\phi$ and $\alpha$ values corresponding to surfactant micelles can also be considered constant, we can define a conditional distribution constant for the $H_2Q^+$ species in this medium, which can be related to the selectivity coefficient as

$$\begin{aligned} K'_{D(H_2Q^+)} &= [H_2Q^+]_{(m)}/[H_2Q^+]_{(w)} \\ &= K_{H_2Q^+/Na^+} \cdot (1 - \alpha)/\{C_{NaCl} \cdot V_\phi\} \end{aligned} \quad (21)$$

This treatment can also be applied to the exchange of $Q^-$ species in CTAB micellar solutions, which gives a similar definition for their conditional distribution constant.

Eqs. (13–21) show that by the simplification of the ion-exchange model (in a large excess of background electrolyte at constant concentration and surfactant concentrations above the cmc), the definitions of the equilibrium constants are very similar to those obtained by the partition model. The advantage of this model is that it can be applied to the different species in the SLS or CTAB micellar media, regardless of the kind of solute/micelle interaction or the charge of the individual species. Moreover, the partition model is easier to define, and the results obtained for a given species in different surfactants can be readily compared.

## 4. Data treatment

As noted previously, the partition of one or more species in the micelar phase leads to changes in the apparent dissociation constants of chlorquinaldol. These constants were determined by the application of the STAR program [29] to the spectrophotometric data, at the different surfactant concentrations.

For the determination of the partition equilibria of the different species we have applied a modified version of the SPDIS program [21]. This is a non-linear least-squares program, in which the equilibrium constants are refined by using the Gauss–Newton iterative algorithm, in order to minimize the sum of squared residuals ($U$) in absorbance measurements, defined as

$$U = \sum_{i=1}^{ns} \sum_{j=1}^{nw} (A_{i,j,exp} - A_{i,j,calc})^2 \quad (22)$$

where ns and nw indicate the number of spectra and the number of wavelengths respectively. $A_{i,j,exp}$ is the measured absorbance, and $A_{i,j,calc}$ the calculated absorbance, on the basis of the proposed model. The program also calculates the molar absorptivities of the guessed species at the working wavelengths. In the present version, this program can deal with up to 150 spectra, measured at 50 wavelengths.

Fig. 1 shows the different possibilities for the partition equilibria between aqueous and micellar phases. According to this model, three species could be extracted in micellar media (the neutral form, HQ, and the charged species $H_2Q^+$ and $Q^-$). In order to ascertain the "real" number of extracted species, we determined the number of species in solution by factor analysis of the absorbance data matrix, following the procedure described by Kankare [30]: by plotting the standard deviation of residuals ($S_{k(A)}$) versus the number of species (factors), and by comparing these values with the instrumental error, the number of species can be inferred. The results obtained using this procedure are compared with those obtained by the application of the SPDIS program, based on the partition model.

## 5. Results and discussion

### 5.1. Apparent $pK_a$ micellar media ($pK_a^*$)

To study the effect of SLS and CTAB in apparent acid–base equilibria of chlorquinaldol, the absorption spectra of several series of aqueous micellar solutions were recorded. In each series the surfactant concentration was kept constant, and the pCH was varied from 2 to 11. The results obtained by the application of the STAR program are summarized in Tables 1 and 2. These $pK_a^*$ values clearly show the different behaviour of chlorquinaldol in these different charge-type micellar systems. Thus, the apparent $pK_{a2}$, which involves the uncharged acid HQ and the anionic base $Q^-$, decreases by the addition of CTAB from 7.84 to 6.76, and increases to 9.28 when SLS is added. In contrast, the apparent $pK_{a1}$, which involves the equilibrium between the cationic species $H_2Q^+$ and the neutral form HQ, drastically decreases by the addition of cationic surfactant CTAB (from 3.44 to 1.32), but it increases slightly on addition of anionic surfactant SLS (to 3.93).

The $pK_a^*$ values obtained are displayed in Figs. 2a and 2b, together with those previously reported in Brij-35 micellar media. For comparative purposes, the $pK_a^*$ values are plotted against $R$ (the ratio of micellar volume to the total volume) instead of the surfactant concentration. From these figures, it can be seen that

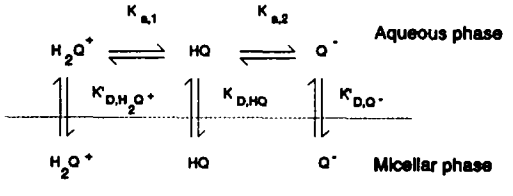


Fig. 1. Partition diagram for the different species of chlorquinaldol.

Table 1
Apparent dissociation constants of chlorquinaldol at different concentrations of sodium lauryl sulphate (in 0.1 M NaCl at 25°C)

| $C_{SLS}$(M) | $pK_{a1}^*$ [a] | $pK_{a2}^*$ [a] | $S_{(A)}$ [b] |
|---|---|---|---|
| – | 3.44(0.02) | 7.84(0.01) | 0.0047 |
| $7.01 \times 10^{-4}$ | 3.42(0.01) | 7.86(0.02) | 0.0031 |
| $1.10 \times 10^{-3}$ | 3.45(0.01) | 7.88(0.02) | 0.0026 |
| $2.10 \times 10^{-3}$ | 3.78(0.01) | 8.14(0.01) | 0.0023 |
| $4.10 \times 10^{-3}$ | 3.90(0.01) | 8.55(0.01) | 0.0019 |
| $6.10 \times 10^{-3}$ | 3.94(0.01) | 8.77(0.02) | 0.0034 |
| $8.10 \times 10^{-3}$ | 3.91(0.01) | 8.89(0.01) | 0.0022 |
| $9.12 \times 10^{-3}$ | 3.94(0.01) | 8.94(0.01) | 0.0028 |
| $1.00 \times 10^{-2}$ | 3.95(0.01) | 8.95(0.01) | 0.0021 |
| $2.00 \times 10^{-2}$ | 3.94(0.01) | 9.15(0.01) | 0.0029 |
| $3.00 \times 10^{-2}$ | 3.93(0.01) | 9.28(0.01) | 0.0022 |

[a] The values given in parentheses correspond to three times the standard deviation of constants (given by the STAR program).
[b] Standard deviation of residuals, in absorbance units.

Table 2
Apparent dissociation constants of chlorquinaldol at different concentrations of cetyltrimethylammonium bromide (in 0.1 M NaCl, at 25°C)

| $C_{CTAB}$(M) | $pK_{a1}^*$ | $pK_{a2}^*$ | $S_{(A)}$ |
|---|---|---|---|
| – | 3.44(0.02) | 7.84(0.01) | 0.0047 |
| $7.56 \times 10^{-5}$ | 3.41(0.02) | 7.40(0.02) | 0.0033 |
| $1.21 \times 10^{-4}$ | 3.29(0.01) | 7.16(0.03) | 0.0022 |
| $3.24 \times 10^{-4}$ | 2.98(0.01) | 6.86(0.01) | 0.0016 |
| $5.22 \times 10^{-4}$ | 2.82(0.01) | 6.76(0.02) | 0.0022 |
| $7.24 \times 10^{-4}$ | 2.69(0.01) | 6.74(0.02) | 0.0024 |
| $1.84 \times 10^{-3}$ | 2.29(0.01) | 6.70(0.01) | 0.0017 |
| $3.68 \times 10^{-3}$ | 1.99(0.01) | 6.71(0.01) | 0.0026 |
| $5.50 \times 10^{-3}$ | 1.82(0.01) | 6.74(0.01) | 0.0020 |
| $9.22 \times 10^{-3}$ | 1.61(0.01) | 6.72(0.01) | 0.0025 |
| $1.38 \times 10^{-2}$ | 1.42(0.01) | 6.74(0.01) | 0.0024 |
| $1.81 \times 10^{-2}$ | 1.32(0.02) | 6.76(0.01) | 0.0032 |

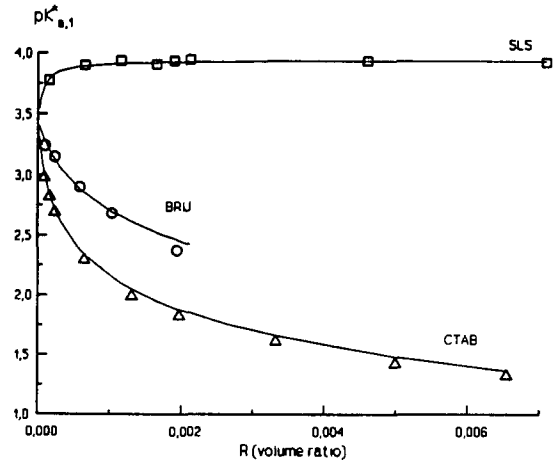


(a)

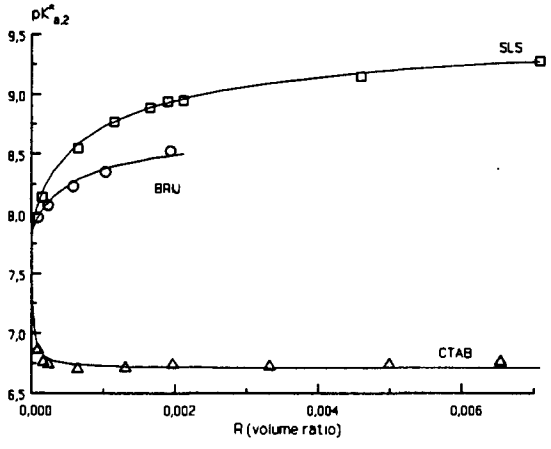


(b)

Fig. 2. Apparent dissociation constants of chlorquinaldol in micellar media. Solid lines indicate the $pK_a^*$ values calculated from the distribution constants. (Data for Brij solutions taken from Ref. [21].)

the trends observed for $pK_{a1}^*$ in CTAB solutions are similar to that observed in Brij-35 solutions, while the $pK_{a2}^*$ variation in Brij-35 is like that observed in SLS.

It should be noted that SLS or Brij-35 surfactants, at concentrations below the cmc, have no significant effect on chlorquinaldol solutions, whereas in CTAB there are marked changes in the absorption spectra and in $pK_a^*$ values, at surfactant concentrations below the cmc reported values [31] (in 0.1 M NaCl ionic medium, these values range from $2 \times 10^{-4}$ to $7.5 \times 10^{-4}$ M). Fig. 3 shows the apparent absorption spectra of the uncharged species HQ in CTAB at low surfactant concentrations (from $0.76 \times 10^{-4}$ to about $7 \times 10^{-4}$ M). Because of these apparently anomalous results, and the poor agreement between the values

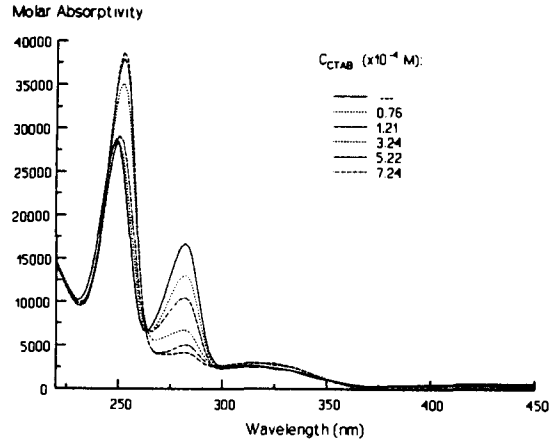


Fig. 3. Apparent absorption spectra of the neutral species HQ at different concentrations of CTAB.

reported by different authors, the cmc of CTAB was determined. The value obtained (see next section) was far below those previously reported, and in accordance with the observed effects on $pK_a^*$ values and on absorbance spectra.

### 5.2. Determination of the cmc of CTAB

The cmc of CTAB was obtained from plots of the surface tension of aqueous solutions of CTAB against the logarithm of their bulk concentration in 0.1 M NaCl solutions. The results obtained show that the presence of NaCl drastically decreases the cmc value, from $9.2 \times 10^{-4}$ M in pure water [6] to $7 \times 10^{-5}$ M (Fig. 4).

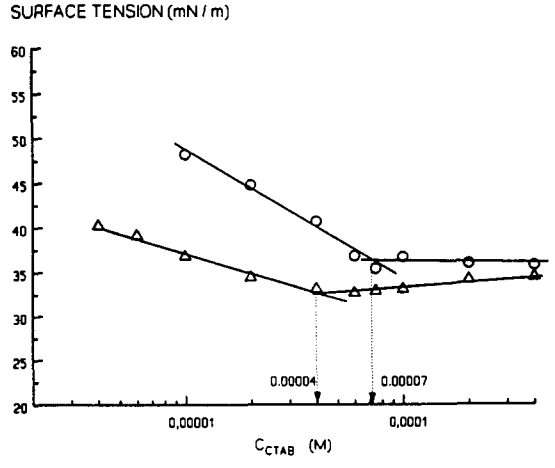


Fig. 4. Determination of the critical micelle concentration of CTAB in ○, 0.1 M NaCl medium; △, 0.1 M NaCl, with $2 \times 10^{-5}$ M chlorquinaldol in alkaline medium.

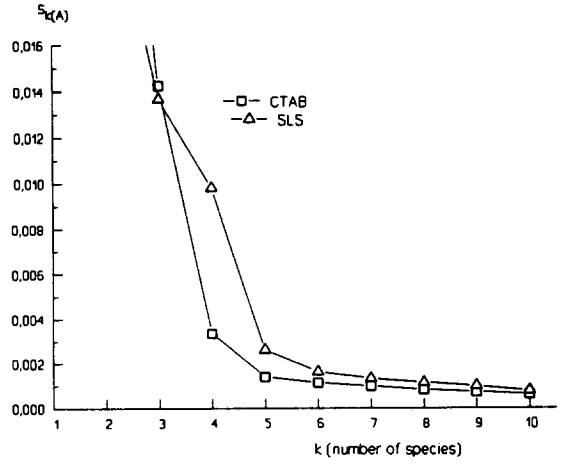


Fig. 5. Determination of the number of species in solution by factor analysis.

Because the addition of solutes can modify the cmc values, the effect of chlorquinaldol on CTAB solutions was also studied. The results indicate that there is no significant difference in the cmc of CTAB in acid and neutral solutions, whereas in alkaline medium it decreases to $4 \times 10^{-5}$ M (see Fig. 4). However, this difference has little relevance in the study of partition equilibria, as the data taken for the calculations correspond to CTAB concentrations well above the cmc.

### 5.3. Partition equilibria

For the distribution equilibria in CTAB solutions, the calculations were carried out over 140 spectra, at CTAB concentrations ranging from $3.2 \times 10^{-4}$ to $1.8 \times 10^{-2}$ M. In the case of SLS micellar media, the concentrations ranged between $6.1 \times 10^{-3}$ and $3 \times 10^{-2}$ M (100 spectra were taken). In both systems, the determination of partition constants was carried out in the spectral range between 240 and 295 nm, corresponding to the absorption maxima of the species involved.

The determination of the number of species by factor analysis of the absorbance data is displayed in Fig. 5. The comparison of the standard deviation of residuals ($S_{k(A)}$) with the instrumental error (about 0.0022 absorbance units in our experimental conditions) indicates that five and six species are needed, in CTAB and SLS solutions respectively, to obtain a standard deviation of residuals lower than the instrumental error. Taking into account that there are three species of chlorquinaldol in aqueous phase ($H_2Q^+$, HQ and $Q^-$), we conclude that there are two partition equilibria in CTAB solutions, and three in SLS solutions.

The distribution equilibria of chlorquinaldol in CTAB and SLS micellar media were studied by using the SPDIS program, according to the partition model.

The first model proposed for both surfactants included, as known parameters, the dissociation constants in water, the absorption spectra of the pure species $H_2Q^+$, HQ and $Q^-$, and the surfactant partial volume and its cmc [32,33] (0.249 l mol$^{-1}$ and $1.46 \times 10^{-3}$ M for SLS, and 0.361 l mol$^{-1}$ and $7.0 \times 10^{-5}$ M for CTAB). The model also contained the partition constants for the three species of chlorquinaldol. This assumption should be valid in the case of SLS solutions, as the results obtained by factor analysis suggested this model. In the case of CTAB solutions, only two species should be extracted according to the factor analysis results; however, this method does not indicate which species are extracted. For this reason, we included all the possibilities in the first model.

The treatment of data corresponding to SLS solutions by the program SPDIS indicates the extraction of the three chlorquinaldol species, in accordance with the model proposed. By applying the same model to CTAB solutions, it was found that the partition constant corresponding to $H_2Q^+$ species was ill-defined, giving a calculated concentration for this species less than 5% of the total chlorquinaldol in solution. Further, taking into account also the results obtained by factor analysis, this species, ($H_2Q^+_{(m)}$), was rejected from the equilibrium model.

The final results obtained by SPDIS are given in Table 3, where the partition constants are also compared with those previously obtained in Brij-35 micellar solutions. These results show that the solubilization of the neutral

Table 3
Partition constants of chlorquinaldol in different surfactants (in 0.1 M NaCl, at 25°C)

| Surfactant | log $K'_{D(H_2Q^+)}$ [a] | log $K_{D(HQ)}$ [a] | log $K_{D(Q^-)}$ [a] |
|---|---|---|---|
| Brij-35 [b] | – | 3.64(0.01) | 2.77(0.05) |
| SLS | 4.40(0.02) | 3.89(0.02) | 2.19(0.04) |
| CTAB | – | 4.25(0.02) | 5.39(0.01) |

[a] The values given in parentheses correspond to three times the standard deviation of the constants (given by the SPDIS program).

[b] After Ref. [21].

species HQ is similar for neutral and ionic surfactants (about 0.6 logarithm units as maximum difference). Otherwise, as may be expected, the extraction of ionic species is clearly favoured when a surfactant of opposite charge is used; thus, the maximum value for the partition constant corresponds to the interaction between the species $Q^-$ and CTAB micelles, followed by the $H_2Q^+$–SLS interaction.

The solubilization ability of SLS anionic micelles should be noted, as in this media the three species of chlorquinaldol can be extracted, despite the charge of the species.

With the set of partition constants given in Table 3, we calculated the theoretical apparent dissociation constants of chlorquinaldol against the volume ratio $R$, in order to evaluate the prediction ability of the partition model in the acid–base equilibria [21]. The results of this evaluation are shown in Figs. 2a and 2b (for the variation of $pK^*_{a1}$ and $pK^*_{a2}$ respectively), where the predicted apparent constants are indicated by the continuous line. The good fit obtained between the predicted and experimental values indicates that the application of the partition equilibria model provides a satisfactory description for the acid–base equilibria in micellar solutions of ionic and non-ionic surfactants.

The approaches described in this work provide several tools for the study of the micelle–solute interactions: first of all, they can be applied to ionic and non-ionic surfactants, regardless of the specific solute–micelle interactions. So the comparison of the equilibrium constants for a given system in different surfactant solutions yields a direct comparison in terms of the extent of "solute–micelle interaction" for the different species or the "ability of solubilization" of the surfactants studied. Moreover, the method is not restricted to acid–base equilibria, and it can be applied to other systems, such as the partition of single species, or metal–ligand complex formation and partition of the species formed. It should also be noted that the equilibrium constants are calculated directly from the experimental absorbance data (at different pCH and surfactant concentrations, in the full range of spectra); this feature is an important advantage over the previous methods established, in which the solute–micelle interactions are determined from the variation in the apparent $pK_a$ of the solutes. In fact, in this work, this variation is applied only for the model validation, and it is unnecessary for the calculation of the partition constants.

Furthermore, this full-spectrum approach allows the determination of the number of significant species in solution by means of factor analysis procedures. This is a useful feature for the data interpretation, as it indicates the number of equilibria to be considered in the chemical model.

## References


[1] T. Saitoh, H. Hoshino and T. Yotsuyanagi, J. Chem. Soc., Faraday Trans., 90 (1994) 479.
[2] A. Berthod and O. Saliba, Talanta, 39 (1992) 371.
[3] P. Mukerjee and J.S. Ko, J. Phys. Chem., 96 (1992) 6090.
[4] H. Watanabe, T. Saitoh, T. Kamidate and K. Haraguchi, Mikrochim. Acta, 106 (1992) 83.
[5] R.K. Dutta and S.N. Bhat, Can. J. Chem., 71 (1993) 1785.
[6] W.L. Hinze, H.N. Singh, Y. Baba and N.G. Harvey, Trends Anal. Chem., 3 (1984) 193.
[7] R. Compaño, A. Grima, A. Izquierdo and M.D. Prat, Anal. Chim. Acta, 227 (1989) 219.
[8] J. Miura, M. Yoshitome, I. Goto, Y. Nakamura and H. Watanabe, Anal. Sci., 9 (1993) 255.
[9] T. Saitoh, N. Ojima, H. Hoshino and T. Yotsuyamagi, Mikrochim. Acta, 106 (1992) 91.
[10] C.G. Pinto, J.L.P. Pavon and B.M. Cordero, Anal. Chem., 66 (1994) 874.
[11] A. Bockelen and R. Niessner, Fresenius' J. Anal. Chem., 346 (1993) 435.
[12] J. Rosendorfova and L. Cermakova, Talanta, 27 (1980) 705.
[13] V. Kuban, I. Jankarova, J. Hedbavny and M. Vrchlabsky, Collect. Czech. Chem. Commun., 54 (1989) 70.
[14] J. Jirasova, J. Bily and L. Cermakova, Collect. Czech. Chem. Commun., 55 (1990) 1491.
[15] A.L. Underwood, Anal. Chim. Acta, 140 (1982) 89.
[16] E. Blatt, R.C. Chatelier and W.H. Sawyer, Chem. Phys. Lett., 108 (1984) 397.
[17] T. Saitoh, Y. Kimura, T. Kamidate, H. Watanabe and K. Haraguchi, Anal. Sci., 5 (1989) 577.
[18] F.H. Quina and H. Chaimovich, J. Phys. Chem., 83 (1979) 1844.
[19] H. Chaimovich, J.B.S. Bonilha, M.J. Politi and F.H. Quina, J. Phys. Chem., 83 (1979) 1851.
[20] C.A. Bunton, L.S. Romsted and L. Sepulveda, J. Phys. Chem., 84 (1980) 2611.
[21] J.L. Beltrán, R. Codony, M. Granados, A. Izquierdo and M.D. Prat, Talanta, 40 (1993) 157.
[22] R. Compañó, A. Izquierdo and M.D. Prat, Quim. Anal., 10 (1991) 27.
[23] R. Compañó, A. Grima, A. Izquierdo and M.D. Prat, Appl. Fluorescence Technol., 3 (1990) 17.
[24] M.D. Prat, R. Compañó, J.L. Beltrán and R. Codony, J. Fluorescence, 4 (1994) 279.
[25] J.L. Beltrán, G. Centeno, A. Izquierdo and M.D. Prat, Talanta, 39 (1992) 981.
[26] G. Gran, Analyst, 77 (1952) 661.
[27] D.D. Perrin and B. Dempsey, Buffers for pH and Metal Ion Control, Chapman and Hall, London, 1974.

[28] N.K. Reddy, A. Foster, M.G. Styring and C. Booth, J. Colloid Interface Sci., 136 (1990) 588.
[29] J.L. Beltrán, R. Codony and M.D. Prat, Anal. Chim. Acta, 276 (1993) 441.
[30] J.J. Kankare, Anal. Chem., 42 (1970) 1322.
[31] C. Samsonoff, J. Daily, R. Almog and D.S. Berns, J. Colloid Interface Sci., 109 (1986) 325.
[32] S. Bouguerra, H. Bahri and P. Letellier, Can. J. Chem., 63 (1985) 2476.
[33] R.J. Williams, J.N. Phillips and K.J. Mysels, Trans. Faraday Soc., 51 (1955) 728.

ELSEVIER

Talanta 42 (1995) 1999-2006

Talanta

# Application of microwave heating to the determination of free, combined and total sulphur in rubber

Wojciech Puacz *, Wiesław Szahun, Mariusz Kopras

*Institute of Chemistry and Technical Electrochemistry, Poznań University of Technology, ul. Piotrowo 3, 60-965 Poznań, Poland*

Received 1 March 1995; revised 24 May 1995; accepted 30 June 1995

**Abstract**

An atomic absorption spectrometry (AAS) method for the determination of total and combined sulphur in rubber and a catalytic method for the determination of free sulphur in rubber are described. The catalytic method is based on the iodine–azide reaction and is followed by an extraction of free sulphur with benzene, toluene or acetone. The catalytic determination, with the aid of gas chromatography, was performed in *N,N*-dimethylformamide after expelling the more volatile solvents used in the extraction. The calibration is linear over the range $2 \times 10^{-6}$–$3 \times 10^{-4}$ M. Before the determination of total and combined sulphur, the rubber samples were decomposed by microwave assisted heating (5 min, 110 W) in a Teflon closed vessel. After microwave heating the solution was clear and homogenous and all sulphur compounds contained in the rubber were quantitatively oxidized to sulphate. The sulphates were then precipitated as $BaSO_4$ and an excess of barium was determined by AAS. From the difference in the results of the determinations of total and free sulphur the amount of combined sulphur can be calculated, and from the difference in the determinations of total and combined sulphur the amount of free sulphur can be calculated. In the latter case the catalytic analysis is not needed.

*Keywords:* Sulphur; Rubber; Microwave heating; Atomic absorption spectrometry

## 1. Introduction

Sulphur is one of the most frequently used vulcanizing agents in natural rubber, synthetic rubber and mixed vulcanizates. Sulphur is used together with vulcanizing accelerators, usually containing sulphur, which, apart from their basic function (accelerating vulcanization) vulcanize themselves. Thus cross-linkings in rubber are formed by elemental sulphur as well as by sulphur from accelerators. Chemical, mechanical and elastic properties of rubber and its ageing resistance depend on the number of cross-linkings and on the amount of sulphur left after vulcanization—so-called free sulphur. In a complicated system such as rubber (containing not only sulphur and accelerators but also extenders, softeners, antioxidizers, etc.), in addition to correct proportioning of its components, a quantitative control of concentrations of different forms of sulphur in the final product is very important.

Among direct methods for sulphur determination only neutron activation and X-ray fluorescence spectrometry allow determinations at parts per billion concentration levels. Both of these methods are very complicated and the instruments are expensive. Radiometric methods, atomic and molecular emission spectrometry and atomic absorption analysis allow direct determination of sulphur and compounds of sulphur in different oxidation states but they are limited by difficulties with atomization of

* Corresponding author.


*SSDI* 0039-9140(95)01680-5

sulphur, are complicated and scarcely given reproducible results. For these reasons indirect methods for determination of sulphur and its compounds are the most frequently presented in the literature.

Vulcanized rubber contains up to 3.5% of sulphur of which free sulphur usually does not exceed 0.15%. Total sulphur in rubber is determined after burning the sample in a pipe furnace [1,2], after melting it with sodium peroxide [3], after wet mineralization [4,5], by the Schöniger method after burning the sample in oxygen [6] or with the use of analyzers based on coulometric, potentiometric, conductometric or spectrophotometric techniques. Free sulphur in rubber is usually determined chromatographically [7,8]. There are also methods based on thiosulphate [9] or thiocyanate [10] formation or iodine–azide catalysis [11].

In this paper microwave energy is used for rubber mineralization and an indirect AAS method is used for total sulphur and combined sulphur determination. Rubber samples are mineralized in Teflon vessels using a high efficiency microwave digestion unit. Sulphates formed during mineralization are precipitated ($BaSO_4$) and the excess of barium is determined by atomic absorption spectrometry (AAS). Free sulphur is extracted from rubber with benzene, toluene or acetone and, after cleavage of S–S bonds in the $S_8$-ring using microwave energy, it is determined by a chromatographic method based on iodine–azide catalysis (i–a). In both cases the use of microwave energy allowed shortening and simplification of analysis and it is as a result of microwave heating that rubber mineralization (determination of total sulphur and combined sulphur) and S–S bond cleavage in the $S_8$-ring (free sulphur determination) reach 100% yields. Quantitative bond cleavage was confirmed by UV spectra before and after microwaving. To check the accuracy of the proposed method the gravimetric method for the determination of combined and total sulphur in rubber following the combustion of the sample by the Schöniger method [12] was used.

## 2. Experimental

### 2.1. Apparatus

A Varian 3700 gas chromatograph, a Beckman 1233 atomic absorption spectrophotometer, a Beckman DU 7500 single beam spectrophotometer with 10 mm quartz cells, a high efficiency microwave digestion unit (Plazmatronika Ltd, Wrocław, Poland) and a Heraeus Mikro K Oxidizer were used.

### 2.2. Reagents

All chemicals used were of analytical-reagent grade and were used without further purification. Organic solvents were taken from the same batch. Standard solutions of sulphur, 10 $\mu g\ cm^{-3}$, in benzene, toluene and acetone were prepared. The precipitating solution (barium, 500 $\mu g\ cm^{-3}$) was made by dissolving 0.8892 g of $BaCl_2 \cdot 2H_2O$ and 13.0 g of NaCl in 50 $cm^3$ of doubly distilled water, adding 500 $cm^3$ of methanol, mixing well and diluting to volume in a 1 l standard flask with water.

## 3. Procedure

### 3.1. Determination of free sulphur in rubber

Finely cut rubber (50–100 mg) was placed in a 100 $cm^3$ conical flask and 50 $cm^3$ of one of the solvents (benzene, toluene or acetone) was added. Flasks were protected from the light with aluminium foil and the solution was purged with nitrogen for 10 min directly before extraction to avoid oxidative or photolytic damage of the network structure. Free sulphur was extracted at 20°C for 18 h (benzene), 22 h (toluene) or 26 h (acetone). The solution was then decanted and the rubber was washed with two 10 $cm^3$ portions of the same solvent that was used for extraction. Combined solutions (50 $cm^3$ + 20 $cm^3$) were placed in a 200 $cm^3$ round-bottomed flask. *N,N*-Dimethylformamide (DMF) (10 $cm^3$) was added and, taking advantage of a big difference in the boiling points of DMF (153.0°C) and the solvents (benzene, 80.1 °C; toluene, 110.6°C, acetone, 56.2°C), the solvent was stripped. $NaN_3$ (3 $cm^3$, 0.20 mg $cm^{-3}$) solution in DMF was added and after making up the solution to 15 $cm^3$ with DMF the sample was microwaved in order to cleave the S–S bonds of the $S_8$-ring. The cleavage of sulphur bonds took place inside the sealed Teflon vessel of 30 $cm^3$ volume with the aid of the high efficiency microwave digestion unit for 4 min at 110 W. The vessel was then cooled (about 15 min) in a water bath

and the solution (15 $cm^3$) was divided into 2 portions: 5 $cm^3$ and 10 $cm^3$. The first one was diluted with 40 $cm^3$ ethanol and then a UV spectrum was recorded using DMF:ethanol 1:8 (v/v) as the reference solution. The spectra give information about the extent of the bond cleavage (under optimum conditions 100% cleavage was reached) and semiquantitative information about the sulphur concentration. Cleaved divalent sulphur was determined in the second part of the sample (10 $cm^3$) by a method based on i–a catalysis using gas chromatography—the nitrogen producted in the catalyzed i–a reaction was in an amount directly proportional to the divalent sulphur catalyst concentration. An analytical column with molecular sieve 5 Å and thermal conductivity detector was used. For quantitative estimation of nitrogen the peak height as well as the peak area were used [13].

### 3.2. Determination of total sulphur in rubber

Finely cut rubber (20–40 mg) was placed in a 30 $cm^3$ Teflon vessel and 5 $cm^3$ of concentrated $HNO_3$ and 0.5 $cm^3$ of 30% $H_2O_2$ were added. The closed vessel was placed in a stainless-steel jacket [14] of the apparatus for the pressure mineralization of rubber with the use of microwave energy. The exposure time was 5 min (determined experimentally) and the microwave heating power was 110 W. The vessel was then cooled (about 15 min) in a water bath and after careful opening of the vessel the sample was transferred into a 50 $cm^3$ beaker. Concentrated HCl (1 $cm^3$) was added and the beaker was heated slightly to expel the residue of $HNO_3$ left after mineralization. The sample was then transferred into a 250 $cm^3$ volumetric flask and made up to the mark with water. The solution after mineralization was homogenous, yellowish and completely clear. All forms of sulphur in the rubber were oxidized into sulphates that were determined by the indirect AAS method. In order to precipitate sulphates 3 $cm^3$ of a precipitating solution of $BaCl_2$ was added to the sample. After vigorous shaking the solution was allowed to stand for at least 8 h (usually overnight). The excess of barium was then determined, without filtration, by AAS with a nitrous oxide–acetylene flame. During aspiration of the samples into the flame it is important not to shake the samples (which would disturb the precipitate, and vitiate the determination). Sodium chloride was added to the precipitating solution to suppress ionization of barium in the nitrous oxide–acetylene flame. The measurements were carried out at $\lambda = 553.6$ nm, using band width 0.41 nm, lamp current 18 mA and nitrous oxide pressure 40 kPa, acetylene 150 kPa.

### 3.3. Determination of combined sulphur in rubber

Rubber (20–40 mg) after extraction of free sulphur was washed twice with acetone and dried in a stream of air for 90 min at 40°C. The sample was placed in a Teflon vessel and mineralized using microwaves. Sulphates formed during mineralization were determined by the AAS method given in the procedure for total sulphur determination.

### 3.4. Calculating the amount of combined sulphur in rubber

The amount of combined sulphur forming cross-linkings was calculated from the difference between the amounts of total and free sulphur.

### 3.5. Calculating the amount of free sulphur in rubber

The amount of free sulphur was calculated from the difference between the amounts of total and combined sulphur. In this case the catalytic analysis based on the i–a reaction need not be performed at all.

## 4. Results and discussion

Almost 20 h of extraction with benzene or toluene or an even longer extraction with acetone is the main drawback of free sulphur determination in rubber. Such long times are necessary for rubber swelling, solvent penetration and extraction of free sulphur. All methods of free sulphur determination known from the literature contain this long extraction step.

We tried to extract sulphur with several portions of solvent and then to determine sulphur in combined solutions. This did not allow us to shorten the extraction time because extraction of sulphur takes place after rubber swelling which is the longest step. In another attempt rubber was frozen in liquid nitrogen and then crushed. In this case we always extracted more free sulphur, probably as a result of cleavage of

sulphur bridges. Our results of free sulphur determination after extraction at boiling points of solvents performed in a flask with reflux condenser or Soxhlet apparatus also did not reflect the actual free sulphur concentration in different samples of rubber. This was because the extraction at the boiling points of the solvents used caused further vulcanization of rubber.

The completeness of the extraction of free sulphur (18, 22 and 26 h for benzene, toluene and acetone respectively) was checked by an extraction of the rubber sample with a new portion of the solvent.

Free sulphur extracted from rubber remains in DMF (after solvent stripping) as elemental, crystalline sulphur, which forms very stable ring cyclo-octasulphur $S_8$. An "opening" of the $S_8$-ring through the cleavage of the sulphur bonds makes the sulphur more reactive. Elemental sulphur, as a Lewis acid, reacts first of all as an electrophilic agent and becomes very flexible to nucleophilic attack via an $S_N2$ mechanism. Activation of sulphur by cleavage of the S–S bonds of the $S_8$-ring may be achieved only in polar solvents.

In order to achieve bond cleavage in the $S_8$-ring several nucleophilic or reducing agents (nitrite [15], azide [16], sulphite [17], cyanide [18], borohydride [19,20], triphenylphosphine [21] and others) were applied. The methods cited above have some drawbacks, such as a yield lower than 100%, long reduction time and limitation on the choice of solvent. The application of microwave heating coupled with the nucleophilic action of $N_3^-$ in DMF on the reduction of the S–S bonds in the $S_8$-ring significantly improves the cleavage procedure.

Effectiveness of microwave heating is connected with absorption of microwave energy by the compound and depends strongly on the polarity of the compound and the solvent. For this reason non-polar solvents (benzene, toluene or acetone) used for sulphur extraction from rubber were stripped. DMF, having a dielectric constant of 36.7, is a good medium for S–S bond cleavage. Due to the application of microwave heating the time needed for cleavage was reduced from hours, in the papers cited [15–21], to a few minutes in the present method. Without a minimum amount of the azide ion in the solution however, the cleavage of the sulphur bonds in the $S_8$-ring did not take place at all, even at very long times and with the highest microwave heating power. The process did not take place either when azide ion in the DMF solution was substituted by any non-nucleophilic anion, e.g. $Cl^-$, $SO_4^{2-}$, $NO_3^-$, etc.

It is very important to achieve quantitative bond cleavage because only solutions with quantitatively cleaved sulphur do not form sols when water is added. Sol formation during sulphur determination, which at low concentrations is practically invisible, always results in errors of determination. In order to control this process UV spectra of sulphur were recorded before and after microwaving. Solutions of sulphur in DMF were diluted with ethanol (DMF:ethanol 1:8, v/v) because DMF spectra cannot be analyzed in the range below 250 nm due to very high solvent absorption.

Fig. 1(a) shows spectra of elemental sulphur at different concentrations (before microwaving). Fig. 1(b) shows spectra of "cleaved sulphur" at different concentrations (after microwaving). The curves give information about the completeness of bond cleavage (i.e. whether microwaving parameters, exposure time and

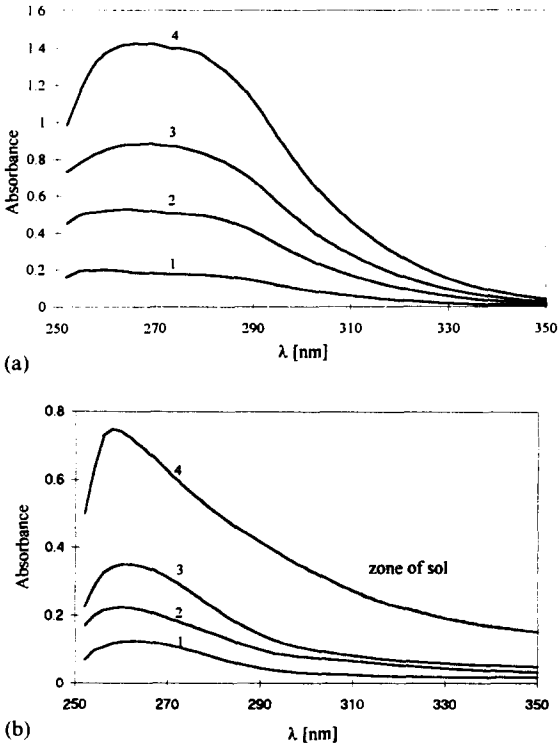


Fig. 1. (a) UV spectra of sulphur in DMF:ethanol (1:8, v/v). Curves 1, 2, 3 and 4 correspond to concentrations of sulphur of 4.0, 8.0, 12.0 and 20.0 μg cm$^{-3}$ respectively. (b) UV spectra of sulphur in DMF:ethanol (1:8, v/v) after microwave assisted heating, concentrations of sulphur (curves 1, 2, 3 and 4) as in Fig. 1(a). Sol of sulphur is formed up to 0.15 of absorbance and at $\lambda > 300$ nm, see zone of sol.

power were chosen properly) and semiquantitative information about sulphur concentration. This latter information is useful when choosing optimum concentrations of components in the i–a catalytic reaction. In Fig. 1(b) curves 1, 2 and 3 show quantitative (100%) bond cleavage. Curve 4 shows partial cleavage—it passes through the "zone of sol". As these data allow us to predict whether sulphur sol will be formed in water or not it is possible to perform microwave heating again under modified conditions (increased exposure time, increased power or both) and to not destroy the sample. $SN_3^-$ is the product of $S_8$ cleavage during microwaving with $N_3^-$.

The i–a reaction is catalyzed by divalent sulphur compounds such as sulphides, thiosulphates, thiocyanates and other R–S and R–S–H compounds. The course of the i–a reaction can be followed by a volumetric [22,23] or gas chromatographic [24,25] determination of the liberated nitrogen, by the determination of the excess iodine using amperometric [26,27] or titrimetric methods [28,29] and by thermometric [30] or enthalpimetric detection [31–34] (the i–a reaction is exothermic).

When a small amount of sulphur (−II) catalyst is added to a solution containing iodine and azide ions, a definite amount of azide is converted into nitrogen and the catalyst is destroyed and removed from the catalytic cycle, being oxidized to a higher oxidation state of sulphur, usually ultimately to sulphate or sulphonic acid:

$$I_2 + 2N_3^- \xrightarrow{S^{2-}} 2I^- + 3N_2$$

Catalytic properties of sulphur (−II) catalysts were determined by a catalytic coefficient expressed by the equation:

$$\text{catalytic coeff.} = \frac{\text{mass } N_2\text{(mg) in i–a reaction}}{\text{mass S(mg)} \times 0.436}$$

The slope of the calibration curve is a measure of the catalytic activity of sulphur (−II) compounds. The value 0.436 is the ratio of moles of nitrogen to sulphur.

In order to determine the "cleaved sulphur" calibration must be performed. Fig. 2 illustrates the calibration curve prepared according to the procedure within a range of $2 \times 10^{-6}$–$3 \times 10^{-4}$ M. As was shown $SN_3^-$ was the final product of the cleavage of S–S bonds in the $S_8$-ring, $ISN_3$ was the catalyst of the i–a reaction and sulphates are the final form of deactivated sulphur. As free sulphur extraction is

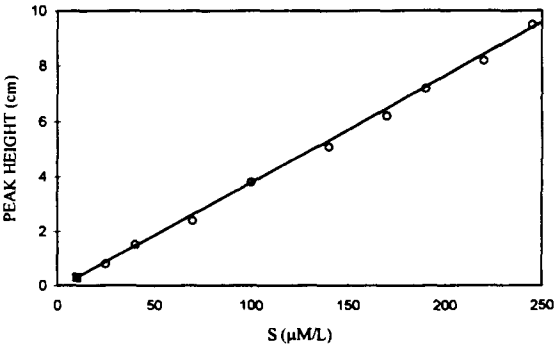


Fig. 2. Calibration graph for sulphur. ■, Reagent blank.

quantitative the precision of the catalytic method given in the Procedure section can be found for known concentrations of sulphur. Results are given in Table 1.

Sulphur was determined in rubber samples manufactured by STOMIL Poznań. Characteristics of rubber samples are given in Table 2 and results of the determinations of free sulphur as given in Table 3.

In the case of sample C, where only 0.4% of elemental sulphur was used for vulcanization, we expected that sulphur bridges would be formed quantitatively. The results do not confirm this prediction. Even in this sample small amounts of free sulphur were found. Our investigations confirm that solubility of sulphur in rubber increases with increasing temperature and, probably, in this state there is no free sulphur—the whole amount is combined. When cooling down the vulcanizate the solubility of sulphur decreases and part of the sulphur may crystallize again in the bulk of the rubber as elemental sulphur. After heating the rubber again new sulphur bridges may be formed from this sulphur. There is a dynamic equilibrium between free and combined sulphur and temperature is the most important parameter for this equilibrium.

Table 1
Results of the determination of elemental sulphur of known amount by the catalytic method

| Taken (μg) | Recovery (%) | Relative standard deviation (%) |
|---|---|---|
| 10 | 98.9 | 1.8 |
| 15 | 101.4 | 1.7 |
| 20 | 101.9 | 1.9 |
| 25 | 102.3 | 2.1 |
| 50 | 102.2 | 2.0 |

All values are means of six determinations.

Table 2
Characteristics of rubbers

| Designation in analysis | Factory marking | Elemental sulphur (%) | Rubber accelerator (%) | | Application of rubber |
|---|---|---|---|---|---|
| A | GM20 | 1.5 | CBS [a] | 0.45 | Coating of wire in tyre |
| | | | MBT [b] | 0.10 | |
| B | CB01 | 1.1 | CBS | 0.45 | Tyre tread |
| C | BGC08 | 0.4 | CBS | 1.9 | Tyre tread |

[a] *N*-cyclohexyl-2-benzothiazolilsulphenamide.
[b] 2-Mercaptobenzothiazole.

Table 3
Result of the determination of free sulphur in rubber samples (A, B and C) by the catalytic method

| Rubber | Sample taken (mg) | Free sulphur found | |
|---|---|---|---|
| | | (mg) | (%) |
| A | 49.85 | 0.048 | 0.096 |
| | 100.60 | 0.093 | 0.092 |
| B | 49.91 | 0.032 | 0.064 |
| | 99.40 | 0.066 | 0.060 |
| C | 50.30 | 0.005 | 0.011 |
| | 101.10 | 0.009 | 0.009 |

Determination of total sulphur in rubber is always preceded by mineralization of rubber. Rubber is one of the least mineralizable materials. All known methods of mineralization (1–6) are technically difficult to reproduce, time-consuming and require complex and expensive equipment. Judging by our experience we can say that application of microwave energy allows fast and quantitative mineralization of different kinds of rubber in a wide range of amounts (0.2–0.8 g). Although mineralization of rubber can be performed in a domestic microwave oven the microwave digestion unit used by us proved to be especially effective. Therefore good efficiency of mineralization of rubber using this apparatus is achieved due to a very high concentration of microwave energy in the sample and application of a self-focusing antenna arrangement which allows direct coupling of microwave energy into the pressure vessel.

Total sulphur in rubber samples A, B and C was determined by an indirect AAS method with a barium lamp and the results are given in Table 4. Earlier we used this technique to determine di-, tri- and tetrasulphides [35].

Combined sulphur in rubber, after free sulphur extraction, was determined in the same way as total sulphur and the results for rubber samples A, B and C are given in Table 5.

Because a "dynamic equilibrium" occurs in rubber between the amount of various sulphur compounds and elemental sulphur the real certified reference materials are not available. The results of the determination of total sulphur (Table 4) and combined sulphur (Table 5) obtained by the proposed AAS method are compared with a gravimetric method, which is a standard one for determining sulphate and is most frequently used to check the accuracy of

Table 4
Results of the determination of total sulphur in rubber samples (A, B and C) by gravimetry and AAS

| Rubber | Sample taken | | Total sulphur found | | | |
|---|---|---|---|---|---|---|
| | Gravimetry (mg) | AAS (mg) | Gravimetry | | AAS | |
| | | | (mg) | (%) | (mg) | (%) |
| A | 80.24 | 20.03 | 1.03 | 1.28 | 0.27 | 1.35 |
| | 160.05 | 39.64 | 1.98 | 1.24 | 0.52 | 1.31 |
| B | 98.60 | 19.68 | 0.89 | 0.90 | 0.18 | 0.92 |
| | 201.92 | 43.36 | 1.68 | 0.83 | 0.37 | 0.87 |
| C | 120.74 | 19.57 | 0.47 | 0.39 | 0.07 | 0.36 |
| | 237.65 | 40.28 | 1.02 | 0.43 | 0.16 | 0.39 |

Table 5
Results of the determination of combined sulphur in rubber samples (A, B and C) by gravimetry and AAS

| Rubber | Sample taken | | Combined sulphur found | | | |
|---|---|---|---|---|---|---|
| | Gravimetry (mg) | AAS (mg) | Gravimetry | | AAS | |
| | | | (mg) | (%) | (mg) | (%) |
| A | 82.08 | 20.40 | 0.95 | 1.16 | 0.24 | 1.18 |
| | 159.26 | 39.84 | 2.07 | 1.30 | 0.50 | 1.25 |
| B | 101.80 | 19.92 | 0.90 | 0.88 | 0.16 | 0.83 |
| | 203.04 | 40.24 | 1.54 | 0.76 | 0.32 | 0.80 |
| C | 120.87 | 20.08 | 0.45 | 0.37 | 0.07 | 0.34 |
| | 239.08 | 39.92 | 0.88 | 0.37 | 0.15 | 0.38 |

the newly developed method. We used a gravimetric method after combustion of rubber samples in oxygen by the well-known Schöniger technique.

The method proposed is simple and, as shown in Tables 4 and 5, the results are similar to those obtained by the gravimetric method. Its only drawback is the long time for $BaSO_4$ crystallization (up to 8 h), but it does not hinder serial analysis.

Results given in Tables 3–5 show that the calculated amounts of free and combined sulphur do not differ from the results of determinations by more than 6%. Therefore in determination of free, combined and total sulphur in rubber it is possible to perform only AAS determination of combined and total sulphur. In the case when only the free sulphur in rubber is determined, the catalytic method is chosen in our laboratory because it is very simple, and as accurate as AAS but less time-consuming.

## 5. Conclusions

Concentrations of free, combined and total sulphur in rubber should be controlled because mechanical and chemical properties of rubber depend strongly on these concentrations and their proportions. Application of microwave energy for mineralization of rubber and cleavage of sulphur bonds in the $S_8$-ring shortens these steps down to several minutes, simplifies the process and gives a yield of 100%. Analytical methods for determination of free (i–a catalysis with gas chromatography), total and combined sulphur (AAS) are simple, precise and inexpensive. The main drawback to this and all other free sulphur determination methods known from the literature is the long time necessary for extraction of sulphur from rubber.

## Acknowledgements

Financial support by the State Committee for Scientific Research (KBN), Poland, Grant No. PB618/P3/92/02 "Application of Microwave Techniques to Analytical Chemistry", is gratefully acknowledged.

## References

[1] B.B. Bauminger, Analyst, 81 (1956) 12.
[2] K. Hummel and M.H. Bertram, Kautsch. Gummi, Kunstst., 13 (1960) 132.
[3] S. Hirano, M. Kurobe and F. Ito, Jpn. Analyst, 4 (1955) 565.
[4] K.E. Kress, Anal. Chem., 26 (1954) 1602.
[5] F. Fujita, H. Matsushita and H. Omori, J. Soc. Rubber Ind. (Japan), 32 (1959) 260.
[6] K. Hozumi and K. Umemoto, Microchem. J., 12 (1967) 46.
[7] J.R. Davies and S.T. Thuraisinham, J. Chromatogr., 35 (1968) 515.
[8] S. Banaszkiewicz and M. Śliwiok, Chem. Anal., 18 (1973) 5.
[9] V. Bolotnikov and V.I. Gurnova, J. Rubber Ind. (Russia), 10 (1933) 214.
[10] J.K. Bartlett and D.A. Skoog, Anal. Chem., 26 (1954) 152.
[11] Z. Kurzawa and W. Puacz, Chem. Anal., 23 (1978) 389.
[12] W. Schöniger, Mikrochim. Acta, (1956) 869.
[13] W. Puacz, Fresenius Z. Anal. Chem., 329 (1987) 43.
[14] H. Matusiewicz, Anal. Chem., 66 (1994) 751.
[15] W. Puacz and J. Puacz, Zesz. Nauk. Polit. Pozn., 16 (1978) 69.
[16] Z. Kurzawa and W. Puacz, Chem. Anal., 22 (1977) 833.
[17] H. Böhme and H. Zinner, Ann. Chem., 585 (1954) 150.

[18] F. Ferér and G. Winkhaus, Z. Anorg. Allg. Chem., 288 (1956) 12.
[19] W. Puacz, Mikrochim. Acta, Part I, (1982) 271.
[20] W. Puacz and J. Puacz, Mikrochim. Acta, Part II, (1983) 271.
[21] H. Brintzinger and M. Langheck, Chem. Ber., 86 (1963) 557.
[22] F. Feigl and E. Chargraff, Z. Anal. Chem., 74 (1928) 376.
[23] W. Puacz, Mikrochim. Acta, Part II, (1981) 155.
[24] L.P. Atkinson and J.G. Natoli, Anal. Chem., 46 (1974) 1316.
[25] W. Puacz, Chem. Anal., 34 (1989) 519.
[26] H.L. Pardue and S. Shepard, Anal. Chem., 35 (1963) 21.
[27] J. Kurzawa and Z. Kurzawa, Chem. Anal., 31 (1986) 45.
[28] W. Puacz and Z. Kurzawa, Mikrochim. Acta, Part II, (1978) 263.
[29] N. Kiba and M. Furusava, Talanta, 28 (1981) 601.
[30] H. Weisz, W. Meiners and G. Fritz, Anal. Chim. Acta, 107 (1979) 301.
[31] N. Kiba, M. Nishima and M. Furusava, Talanta, 27 (1980) 1090.
[32] N. Kiba, T. Suto and M. Furusava, Talanta, 28 (1981) 115.
[33] W. Puacz, Chem. Anal., 33 (1988) 557.
[34] W. Puacz, Mikrochim. Acta, Part III, (1986) 141.
[35] W. Puacz, Chem. Anal., 34 (1989) 79.

ELSEVIER

Talanta 42 (1995) 2007–2015

Talanta

# Comparison of two infrared spectroscopic methods for cheese analysis

Douglas H. McQueen [a,*], Reginald Wilson [b], Arvo Kinnunen [c], Ejner Paaske Jensen [d]

[a] *Chalmers Innovation Center, Chalmers University of Technology, 412 96 Göteborg, Sweden*
[b] *Institute of Food Research, Norwich Laboratory, Colney Lane, Norwich NR4 7UA, UK*
[c] *Technical Research Center (VTT), Food Research Laboratory, P.O. Box 203, 02151 Espoo, Finland*
[d] *Biotechnological Institute, Agro-Industrial Technology Section, P.O. Box 818, 6000 Kolding, Denmark*

Received 13 January 1995; revised 6 July 1995; accepted 11 July 1995

**Abstract**

Two infrared spectroscopic methods, optothermal near infrared (NIR) spectroscopy and Fourier transform mid-infrared–attenuated total reflection (FTIR–ATR) spectroscopy, were applied to 24 cheese samples in order to obtain protein, fat and moisture contents. Reference values of the protein, fat and moisture contents in weight percent were obtained using standard wet chemistry analysis. Prediction correlation coefficients between 0.93 and 0.96 and standard errors of prediction between 2% and 5% were obtained using optothermal spectroscopy while the corresponding values for FTIR–ATR were 0.81–0.92 and 4–9%. Inhomogeneities in the cheeses, primarily due to the fat droplets, are probably the main reason for the differences in the error sizes. The superior results for optothermal spectroscopy are the more attractive because the instrument is easier to use than the FTIR–ATR instrument, it provides results more quickly with simpler statistical analysis and it is more compact and robust.

*Keywords:* NIR spectroscopy; Protein; Fat; Moisture; Dairy products; Cheese

## 1. Introduction

Near infrared spectroscopy has been used more and more in the agricultural and food industries in recent decades. An excellent summary of the field is given by Williams and Norris [1]. In recent years it has become increasingly clear that the application of spectroscopic methods to food analysis can alleviate important problems in the processing and distribution of food and food products [2–4]. More recently the mid-infrared region has attracted considerable interest [5]. It is especially clear that quick, inexpensive, objective methods that do not require special skills on the part of the users are of greatest interest. The ideal case would be that small and medium-sized organizations could handle the spectroscopic instruments in direct connection with their food handling systems, obtaining measurement results in seconds or minutes so that processes could be adjusted and decisions taken quickly. Such smaller production units are not expected to have easy access to highly trained laboratory personnel or to be able to afford expensive and/or sophisticated equipment. Alternatively, quick methods can be used to screen large numbers of samples prior to more detailed analysis of specific samples when and where necessary. The optothermal near infrared (NIR) spectroscopic technique described here can be an appropriate method in some cases while for other applications the repeatability of the measurement results must be improved.

* Corresponding author.


*SSDI* 0039-9140(95)01685-6

An example of an industry in which there is a large number of small medium-sized units processing food products is the cheese industry. There are several steps in the cheese-making process that can directly affect the amounts of fat, protein and moisture in the final products, for instance the step or steps in which the curds are separated from the whey. Further, it is known that because of its texture cheese is difficult to analyze spectroscopically using traditional methods. Fourier transform mid-infrared–attenuated total reflection FTIR–ATR and NIR optothermal analysis are two possible methods for determining fat, protein and moisture contents quickly and accurately as well as at reasonable expense to the cheese producer. Here these two methods are evaluated and the results discussed in terms of the morphology of the cheese samples.

It is known that cheeses (and other similar products) are not spatially homogeneous. For instance, the fat content in one part of a large cheese can be of the order of one percent different from that in another part of the same cheese. On another level, the cheese is very inhomogeneous on a submillimeter scale because of the relatively large fat globules. These conditions have to be taken into account in interpreting measurements of fat, protein and moisture contents of cheeses.

Fat globules in milk have diameters of the order of several microns, with wide variations [6]. The casein micelles are much smaller, of the order of 100 nm, and globular proteins are even smaller.

While there is a great deal of detailed information about the morphology of milk fat and other milk components, the situation is quite different concerning cheese, for which vanishingly little published data is available. However, it is felt that during coagulation there is no reason to expect changes in the sizes of fat globules, even if there can be damage to and surface modifications of the fat globule membrane during pasteurization before the cheese-making process. The fat globule membrane can be altered due to the acidity of the cheese starter or due to physical processing such as centrifugation or membrane processing. None of these factors is expected to reduce the sizes of the fat globules significantly. During ripening the activities of the lipases produced by the microorganisms of the starter modify the fat globule structure, increasingly changing the typical round shape of the globules. In some sufficiently aged cheeses the fat globules disappear to be replaced by aggregates of lipolized fat [7, 8]. Thus it appears that the extent of lypolysis is a prime determinant of the morphology of cheeses at the micron level. The morphologies of fresh cheeses are thus expected to be quite similar to that of the milk from which they were produced, while the aged cheeses may be somewhat less inhomogeneous on the micron scale.

## 2. The cheese samples

Twenty-four cheese samples were studied. Six samples each were obtained from sources in Portugal, UK, Denmark and Finland. They included six fresh cheeses, nine soft cheeses and nine hard cheeses. The widest possible range of cheese types was sought in order that fat, protein and moisture contents show the widest variations possible and so that cheese characteristics affecting the measurement techniques, for instance rheological and mechanical characteristics as well as morphology, be as clearly expressed as possible. However, no separate rheological, mechanical or morphological studies of the cheese samples were carried out.

## 3. Methods

### *3.1. Wet chemistry*

The wet chemistry analysis of the 24 cheese samples was carried out using standardized methods according to the Nordic Committee on Food Analysis. For each component and each cheese at least two samples were analyzed.

The protein contents were determined using the Kjeldahl method in which "The sample is digested with concentrated sulphuric acid, with the addition of potassium sulphate and copper(II) sulphate. The ammonia formed is distilled off with sodium hydroxide solution and collected in boric acid. The nitrogen content of the sample is then determined by titration with hydrochloric acid".

The fat content was determined according to the Schmid–Bondzynski–Ratslaff method in which "The sample is treated with 8 M hydrochloric acid and after addition of ethanol the liberated fat is extracted with a mixture of diethyl ether and petroleum ether. The solvent is then evaporated and the fat is weighed".

The moisture content was measured by drying the sample at 102–105°C for 16–18 h.

It is not possible to assess the accuracy and repeatability of the wet chemistry measurement results in detail. However, for six of the cheeses there are two independent evaluations of the fat contents. In each of the six cases the fat contents according to the two evaluations are different, for instance 31.4% fat and 32.5% fat for one cheese. The average absolute difference between six such pairs of samples is just over 1%. This number can be taken as an estimate of the probable repeatability of the wet chemistry measurements of protein and moisture as well as of fat.

The amount of effort required to analyze all 24 samples for protein, fat and moisture contents in this way was about 2 man weeks including all overheads and incidental costs.

### 3.2. Optothermal spectroscopy

Optothermal spectroscopy is a variation of photoacoustic spectroscopy, which has been described in the literature many times (see for instance Ref. [9]). The optothermal method itself has been described in published reports several times [10–12]. In principle the heat generated when light is absorbed by a sample is measured as a temperature change. The incident light, of the desired wavelength, is chopped at an appropriate frequency (here at 2 Hz) so that the measured temperature changes vary synchronously with the light intensity. This makes sensitive phase-locked detection possible. The wavelengths used are defined by broad bandpass filters, in this case at 1740 nm (bandwidth 75 nm), 1935 nm (bandwidth 110 nm) and 2180 nm (bandwidth 100 nm).

The sapphire surface on which the sample is placed is mounted on the top of the small self-contained optothermal instrument (external dimensions 300 mm × 260 mm × 115 mm). After selection of the appropriate filter the instrument is activated and the sample illuminated with 2 Hz chopped light for about 20 s. The average signal strength and phase are calculated for the last 15 s and the result is presented on a digital display. It is important that good thermal contact is made between the cheese sample and the sapphire as the temperature measurement is dependent on diffusion of the heat generated in the cheese sample to the thin sapphire disc. In practice sufficiently good contact is easily achieved.

The present experiments were carried out as follows. On day one a small piece (about 0.25 $cm^3$) of each cheese sample was applied to (pressed or smeared onto) the sapphire. Each piece was measured three times, first using the 1740 nm filter, then the 1935 nm filter and finally the 2180 nm filter, 20 being taken to complete a single measurement. It took less than 10 min to complete the measurements, change the filters and record the results on each piece of cheese. Application of a new piece of cheese took about 1 or 2 min. In all it took about 4 h to analyze the 24 cheese samples. The averages of the three measurements at each wavelength were then calculated. In general the standard deviation of the individual measurements was under 2% of the measured value. The procedure was repeated on day three and day five using different small pieces from the cheese samples. In the end this produced 3 × 72 data points for the 24 cheeses (one for each of the three wavelengths and each of the three days), each data point being the average of three measurements.

A separate experiment was carried out to assess the effect of poorly applied samples, that is, what the result of poor thermal contact between the cheese sample and the sapphire surface might be. As expected, poor thermal contact results in reduced signal strengths at each of the three wavelengths used. Somewhat contrary to expectations, for this poor thermal contact to become evident the cheese samples had to be very badly applied to the sapphire surface. This may be because of the low chopping frequency used, 2 Hz, for which the thermal diffusion length is more than a tenth of a millimeter in water and in excess of a millimeter in air.

### 3.3. FTIR–ATR spectroscopy

The 24 samples were also analyzed using FTIR–ATR spectroscopy. All spectra were acquired on a Spectra-Tech MONITIR system equipped with a horizontal ATR accessory with 45° zinc selenide element. The wavenumber region used was 5000–400 $cm^{-1}$, corresponding to wavelengths between 2 μm and 25 μm. To obtain the spectra 256 interferograms were added together before Fourier transformation, this process requiring about 3 min. Triangular apodization was used and the resolution was 8 $cm^{-1}$.

The ATR method is an established technique and has been described in the literature many times (see for instance Ref. [9]). It depends on the fact that even when light is totally internally reflected there is some non-radiative penetration of the electromagnetic field into the low refractive index medium, that is, the sample. Since the sample is optically absorbing the reflected light is correspondingly weaker. In the case of zinc selenide and 45° incidence the penetration depth of the light is somewhat more then a tenth of a wavelength (as measured in air) and only weakly dependent on the optical absorption. In the present case the penetration depth is between about 0.2 μm and 5 μm. A recent investigation of this technique applied to dairy cream is given by Kemsley et al. [3].

In the experiments each cheese was carefully cut open and a sample taken from the center. The sample was applied to the ATR element and spread across the entire surface using a soft spatula. The cheese was worked gently with the spatula to ensure complete coverage, the hard cheeses requiring somewhat more physical pressure than the soft ones to insure good contact with the crystal. After spectral acquisition the ATR element was cleaned with tissue followed by water, 0.2% Triton X100 and water before drying. A new single beam reference was collected before each sample was measured. The time required from completion of a measurement on a given sample to completion of the corresponding measurement on the next samle was about 10–12 min. In total the measurements on all 24 samples required about 8 h work including start up time, instrument adjustments and cleaning.

## 4. Results

The measurement results were analyzed statistically using principal component analysis and multicomponent regression techniques. The work was carried out using Unscrambler software from Camo AS, Norway. Initially the wet chemistry results (protein, fat and moisture contents) were taken as the reference data. The spectroscopic data were regressed against the wet chemistry data and calibration formulae were developed. These calibration formulae were then applied to the original spectroscopic data to produce "calculated" protein, fat and moisture contents for the cheese samples. These calculated protein, fat and moisture contents were then plotted against the corresponding wet chemistry values.

Cross validation was used to test the reliability of the calibration formulae because on considering the wide range of properties and the variations in morphological structure 24 samples is too small to be divided into calibration and prediction sets. During the cross validation procedure each sample in turn was deleted from the sample set and predicted using the calibration formula extracted from the rest of the sample set.

### 4.1. Optothermal measurements

In the case of the optothermal measurements there are three data points per sample per day, which should be enough to determine the fat, protein and moisture contents of each cheese sample. In fact, as the sum of the protein, fat and moisture contents must be near 95 wt.%, the system is slightly over-determined.

Inspection of the raw data revealed that data for one cheese sample, # 19, on day three were unusual and inconsistent with the measurement results for day one and day five. Therefore sample # 19 was deleted from the analysis.

First, a straightforward multicomponent regression using the least-squares method of optimization was applied to the data. This produced calibration formulae which were then used to calculate protein, fat and moisture contents for each cheese. The results were regressed against the wet chemistry data using simple linear regression formulae. As would be expected, the correlation coefficients, $r$, obtained in this way were rather low, around 0.85. Our conclusion is that such a straightforward least-squares approach is inappropriate in this case.

Next, more sophisticated statistical methods using Unscrambler software (mainly partial least squares, PLS1) were applied to the data, and new calibration formulae were developed. These were used to produce new calculated protein, fat and moisture contents, which were again regressed against the wet chemistry data. The results are much better than those obtained using the simple least-squares criterion. When 24 data points (less the outlier # 19) are used correlation coefficients of 0.93–0.97 are obtained.

For protein the variable protein content ranged from 6% to almost 30%, as shown in

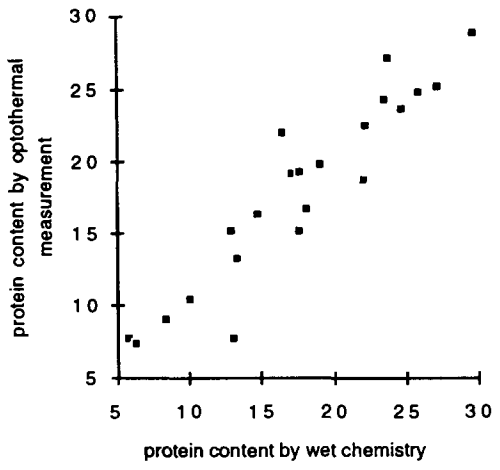


Fig. 1. Protein content (weight percent) of cheeses (sample 19 excluded) according to the optothermal method versus wet chemistry. Correlation coefficient 0.94 and standard error of prediction 2.4. The typical repeatability of the optothermal results is ±1.5 units.

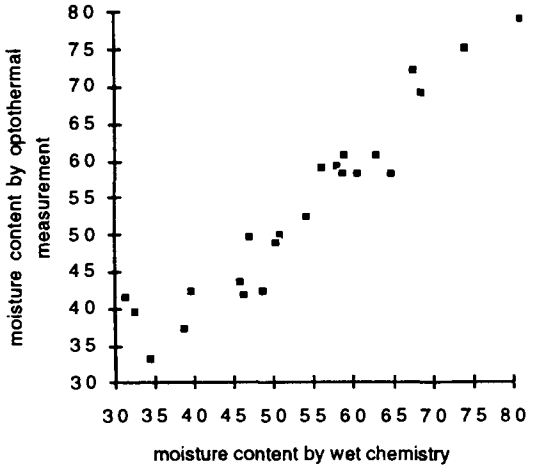


Fig. 3. Moisture content (weight percent) of cheeses (sample 19 excluded) according to the optothermal method versus wet chemistry. Correlation coefficient 0.96 and standard error of prediction 3.9. The typical repeatability of the optothermal results is ±2.5 units.

Fig. 1. Of course this is a much wider range of protein contents (and cheese types) than any ordinary producer of cheese is likely to have to deal with in a single plant. The same is true for the fat contents plotted in Fig. 2, which ranged from zero to 41%, and for the moisture contents shown in Fig. 3 which varied from just over 30% to in excess of 80%. It is entirely possible that regressions limited to certain types of cheese can produce results with less data scatter, but such sample sets were not available for this study. The repeatabilities given in the figure captions are based on comparisons between regression results for day one, day three and day five and correspond to roughly one standard deviation.

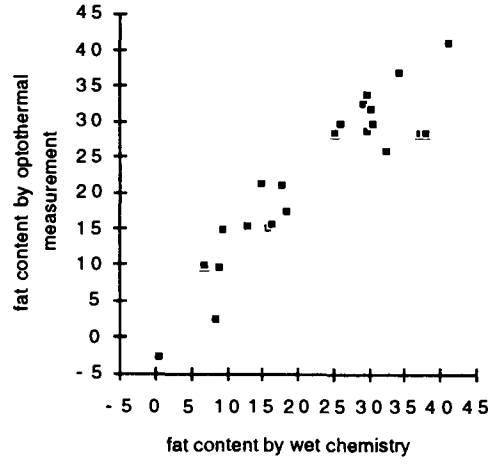


Fig. 2. Fat content (weight percent) of cheeses (sample 19 excluded) according to the optothermal method versus wet chemistry. Correlation coefficient 0.93 and standard error of prediction 4.4. The typical repeatability of the optothermal results is ±2.5 units.

Table 1 summarizes the statistical analysis results (24 cheeses in all) for both the model and the predictions. Comparison of the two indicates that the calibration formulae are quite stable. The reasons for the scatter in the data are several, of course. Among them are the following.

*4.1.1. Limited instrument reproducibility*

This is mainly due to electrical noise in the signal that the instrument analyses. The observed reproducibility of the instrument's response to a given constant input in this type of application is about 1.5% of the signal strength as estimated from over 200 groups of three measurements each on these samples. A more modern version of the instrument has better signal reproducibility.

*4.1.2. Sample application*

As noted above, variations in the thermal contact between the sample and the sapphire affect the signal strengths. For a given sample a reduction of signal strength due to a slight gap between the sample and the sapphire should affect all measurements proportionately. Typically this variation from piece to piece of the same cheese sample is about ±10% or less of the measured signal strength. The regression analysis minimizes this effect by mainly making use of the relative strengths of the signals at the different wavelengths. The effect is not com-

Table 1
Summary of statistical analysis results for optothermal data on 24 cheeses

| | Correlation of the calibration | Standard error of calibration | Correlation of the prediction | Standard error of prediction | Outliers deleted |
|---|---|---|---|---|---|
| Protein | 0.96 | 2.1 | 0.94 | 2.4 | #19 |
| Fat | 0.95 | 3.7 | 0.93 | 4.4 | #19 |
| Moisture | 0.97 | 3.4 | 0.96 | 3.4 | #19 |

pletely eliminated, however, and it is more evident with the hard cheeses than with the soft ones.

*4.1.3. Temperature variations*

The temperatures of the cheese samples on the sapphire can vary and affect the measurement results because the different absorption lines change differently with temperature. In the instrument used in this investigation this effect cannot be compensated for.

*4.1.4. Sample inhomogeneity*

Cheese samples are not perfectly homogeneous on the scale of these measurements. For wet chemistry analysis a piece of cheese of the order of 1 g is used (about 5 g for moisture, 2 g for fat and 1 g for protein), while in the optothermal analysis the sample interrogated corresponds to about 1 mg. Clearly, to obtain appropriate averages using the optothermal method several pieces from each cheese sample should be analyzed and the results averaged. The statistical data analysis above shows that this averaging procedure produces more representative values than do single measurements.

*4.1.5. Errors in wet chemistry values*

However carefully the wet chemistry measurements are carried out, there are residual errors in the results. These errors contribute to the reported data scatter when the optothermal results are plotted against the wet chemistry values.

*4.1.6. Nonlinearities*

Because of the relatively wide range of protein, fat and moisture values nonlinearities in the relationships between the optothermal measurement results and the wet chemistry data are to be expected. However, the calibration and analysis procedures are based on linear relationships only. This simplification is expected to lead to less than perfect fitting of the data.

*4.2. FTIR–ATR*

Because the diameters of the fat globules are of the same order of magnitude as the penetration depth of the light in ATR measurements relatively large variations in signal strengths from measurement are expected, the sample being inhomogeneous at this level and the total measurement volume being small.

The data were analyzed in the wavelength interval 3760–1520 $cm^{-1}$ (corresponding to 2.6–6.6 μm). First a multiplicative scatter correction (Unscrambler software) was applied to the data. Thereafter ten point averages were formed to reduce noise and the complexity of the calculations. Thus each spectrum contained 224 data points.

Application of the Unscrambler software (PLS2) produced regression formulae and predicted protein, fat and moisture contents corresponding to those for the optothermal results. For protein the result was a correlation coefficient of 0.82 and a standard error of prediction of 3.7 using six principal components. The corresponding numbers for fat and moisture are 0.78 and 0.93 for the correlations and 6.6 and 4.5 for the standard errors of prediction using eight and six principal components respectively. At this point the outliers (as "proposed" by the Unscrambler software) were deleted (for protein sample #1, for fat samples #1, #4, #9, #13, #15, #16, #21 and #22 and for moisture samples #1 and #17). The fresh cheeses are over-represented among the deleted outliers. Table 2 summarizes the statistical results where PLS2 was used for protein and moisture and PLS1 was used for fat since the number of samples was only 16. Comparison of the model and prediction results shows that the calibration formulae are unstable. Somewhat surprisingly, for this FTIR–ATR data elimination of the outliers produced somewhat lower correlation coefficients and larger standard errors of prediction. In the case of the

Table 2
Summary of statistical analysis results for FTIR–ATR data on 24 cheeses

| | Correlation of the calibration | Standard error of calibration | Correlation of the prediction | Standard error of prediction | Principal components | Outliers deleted |
|---|---|---|---|---|---|---|
| Protein | 0.97 | 1.9 | 0.81 | 4.4 | 6 | 1 |
| Fat | 0.99 | 1.4 | 0.64 | 9.1 | 8 | 8 |
| Moisture | 0.99 | 2.2 | 0.92 | 5.4 | 6 | 2 |

fat content, where eight samples were deleted, this is because the deleted samples had either very low or very high fat contents. Thus the range of fat contents was reduced by elimination of the outliers.

In both the optothermal results and the FTIR–ATR results the largest standard error of prediction is for fat and the smallest is for protein. Furthermore, for all three components the standard errors of prediction are much larger for the FTIR–ATIR results than for the optothermal results. This supports the proposition that the greatest inhomogeneities on the micron level are for the fat contents, rather than for the moisture contents or the protein contents.

Another reason for scatter in the data could be the fact that fat can preferentially adsorb to the ZnSe ATR crystal. Depending on the nature of the cheese sample this effect can be larger or smaller for different cheeses, thus introducing errors in the measurements. In contrast, there is no evidence for such preferential adsorption onto sapphire.

Other sources of error can be limited instrument reproducibility, temperature variations and errors in wet chemistry values, as discussed above in connection with the wet chemistry results.

## 5. Discussion and conclusions

The above results and analysis indicate clearly that the optothermal method is superior to the FTIR–ATR method for determining the fat, protein and moisture contents of cheeses for several reasons. For prediction the correlation coefficients are significantly higher and the standard errors much smaller for the optothermal results than for the FTIR–ATR results (before and after deletion of the FTIR–ATR outliers). It is quite possible that even better prediction accuracy would have been achieved for optothermal data had the morphological structures of the cheeses not varied so much. The measurements can be made more quickly on the optothermal instrument than on the FTIR–ATR instrument and the data analysis is far less complicated, resulting in a simple regression formula for interpreting the measurement results. Finally, we showed that the quality of sample application to the measurement surface is not as critical for the optothermal method as it is for the FTIR–ATR method. Table 3 summarizes some of the more important characteristics of the three analysis methods used in this investigation.

We found that in the statistical analysis of the optothermal data the Unscrambler software produced much more satisfactory results than did simple least-squares regressions using three variables. However, the limited number of cheese samples precluded more detailed analysis of, for instance, soft cheeses as opposed to hard cheeses or cheeses with low moisture contents as opposed to those with high moisture contents. Further, the limited repeatabilities of the measurement methods make more sophisticated statistical analysis of the present data inappropriate.

Sample homogeneity is already known to be critical for satisfactory performance of both the FTIR–ATR method and the optothermal method. To make progress in understanding the effects of sample inhomogeneity on the measurement results one has to describe the scale of the inhomogeneity in question. In the case of cheese, inhomogeneities on a micron scale are expected primarily because of the fat globules. This is the same scale as the penetration depth of the light into samples in the case of FTIR–ATR, while it is one to two orders of magnitude smaller than the penetration depth in optothermal spectroscopy at a chopping frequency of 2 Hz.

Sample inhomogeneity can also occur on large scales, of course, and it is known that the

Table 3
Summary of several important characteristics of the different analysis methods

| Characteristic | FTIR–ATR | Optothermal method | Wet chemistry |
|---|---|---|---|
| Total time to collect data on 24 cheese samples | 8 h | 4 h | 60–80 h |
| Time to complete measurement on a sample | 10–12 min | 10 min | One method per component with various calibrations and references required |
| Time to obtain a spectrum | 3 min | 3 × 20 s | |
| Calibrations, references | Clean element, remount, collect new reference | Absolute calibration against black stable over long time | Various chemicals required |
| Wavelengths/numbers resolution | 5000 $cm^{-1}$ to 400 $cm^{-1}$ at 8 $cm^{-1}$ resolution | 3 wide band filters (ca. 100 nm) at 1740, 1935 and 2180 nm | |
| Data analysis method | Unscrambler PLS2 | Unscrambler PLS1 | Component by component analysis |
| Data interpretation | Regression formulae with six to eight principal components | Regression formulae with three components | |
| Size of instrument | 60 × 45 × 25 cm ca. 30 kg | 30 × 26 × 12 cm ca. 5 kg | Chemical laboratory required |

fat content of a large cheese can vary by several percent depending on where the sample is extracted from the cheese. The only way to form an appropriate average here is to take samples from different parts of the cheese and combine the results, perhaps using appropriate weighting factors. Since wet chemistry analysis typically makes use of samples weighing of the order of grams only, the large scale inhomogeneity of cheeses has roughly the same effect on wet chemistry results as it does on the spectroscopy results.

Since the optothermal technique is easy to handle and provides results so quickly it could be used to study the fat, protein and moisture contents of cheeses before and during their ripening in cheese factories, making it possible to steer the ripening process toward desired results. Alternatively, the optothermal method can be appropriately applied when reasonably fast screening of large numbers of samples is necessary before possible detailed analysis of suspect samples by wet chemistry, for instance. In either case it is desirable that the repeatability of the measurement results be improved. Instrumental improvements have been made subsequent to the measurements reported here and improved repeatability is expected (although it has not yet been demonstrated).

One could consider homogenizing cheese samples prior to analysis in FTIR–ATR instruments in order to get around the problem of the large fat globules, but this is not easily done for cheese and it would complicate the analysis procedure. In contrast, milk, cream and related products can be homogenized relatively easily and can thus be prepared for analysis by FTIR–ATR instruments. This is not necessary when using the optothermal method. It is expected that the optothermal method could be used to determine fat, protein and moisture contents for a large variety of milk products without pretreatment. Examples include milk, cream, sour cream, butter, mayonnaise, yoghurt and quark.

Finally, we should like to point out that wet chemistry analysis automatically means that the used chemicals must be disposed of in an environmentally acceptable manner, not always a simple matter. Spectroscopic methods

do not produce environmentally unacceptable waste.

## Acknowledgement

This work benefitted from support by the FLAIR Concerted Action No 1 funded by the Commission of the European Communities (CEC) under the DG XII FLAIR AGRO-INDUSTRIAL Research programme.

## References

[1] Near-infrared Technology in the Agricultural and Food Industries, P. Williams and K. Norris (Eds.), American Association of Cereal Chemists, Inc., St Paul, MN, 1987.
[2] C.N.G. Scotter, M.N. Hall and A. Robertson, in A. Turner (Ed.), Food Technology International Europe, Sterling Publications Ltd., London, 1989, p. 313.
[3] A. Robertson, M. Hall and C. Scotter, Food Sci. Tech. Today, 3 (1989) 102.
[4] C. Scotter, Food Control, (1990) 142.
[5] R.H. Wilson, Trends Anal. Chem., 9(4) (1990) 127.
[6] H. Mulder and P. Walstra, The Milk Fat Globule, Centre for Agricultural Publishing and Documentation (Pudoc), Wageningen, The Netherlands, 1974.
[7] R. Giangiacomo, Istituto Sperimentale Lattiero-Caseario, 20075 Lodi, Italy, personnel communication, 1994.
[8] P. Resmini, G. Ottogalli, G. Volonterio, Industria del Latte, 11(2) (1975) 27.
[9] G.W. Chantry, Long-wave Optics, Academic Press, London, 1984.
[10] D.H. McQueen, Int. Lab., 20 (1990) 16.
[11] L. Fondberg and D.H. McQueen, Clin. Phys. Physiol. Meas., 5 (1984) 87.
[12] P. Helander, J. Photoacoustics, 1 (1982) 103.
[13] E.K. Kemsley, G.P. Appleton and R.H. Wilson, Spectrochim. Acta, 50A (1994) 1235.

ELSEVIER

Talanta 42 (1995) 2017–2020

Talanta

# Determination of antimony in lead–zinc concentrates and other smelter products by atomic absorption spectrometry after extraction with di-isopropyl ether and reductive stripping

R. Ravichandra Babu [a], S.C.S. Rajan [a,*], L.S.A. Dikshitulu [b]

[a] *Process Laboratory, Hindustan Zinc Ltd, Visakhapatnam 530 015, A.P., India*

[b] *Department of Inorganic & Analytical Chemistry, Andhra University, Visakhapatnam 530 003, A.P., India*

Received 15 May 1995; accepted 10 July 1995

**Abstract**

Several papers have appeared in the literature describing the determination of antimony, where antimony(V) is extracted into the organic phase and the organic solutions directly analyzed by atomic absorption spectrometry (AAS). This paper describes a procedure where antimony from the organic solution is reductively stripped into an aqueous phase and analyzed for antimony by AAS. The advantage of the method for a routine process control laboratory is highlighted.

*Keywords:* Antimony; Lead–zinc concentrates; Smelter products; Atomic absorption spectrometry

## 1. Introduction

Determination of antimony by atomic absorption spectrometry (AAS) has been fairly comprehensively covered in the literature [1–6]. Donaldson [1] developed several methods for the determination of small amounts of antimony in copper, nickel, lead, zinc and molybdenum concentrates and related materials. These methods involve preliminary separation of antimony(III) from the matrix element by co-precipitation with hydrous ferric and lanthanum oxides. The precipitate is dissolved in dilute hydrochloric acid and the antimony determined either by AAS or, if the sample contains $<100\ \mu g\ g^{-1}$ of antimony, by the spectrophotometric iodide method after further separation from iron, lead and other coextracted elements by chloroform extraction as antimony xanthate. Although these methods yield accurate results for antimony, they are time-consuming, particularly the spectrophotometric method, and the AAS method is not applicable to samples with high lead and iron contents.

Methods have also been employed by several workers in which antimony is extracted by organic solvents from hydrochloric acid solutions and the antimony content determined by aspirating the organic phase into the flame [3–6].

Although analyzing the organic solutions helps to achieve increased sensitivity leading to determination of smaller quantities [2], a few problems ae faced in using this technique. The liquid trap should be drained of the water, and filled with organic solvent. While feeding the organic solution, the fuel content has to be kept low to avoid a sooty flame and the flame tends to flare violently unless the fuel and air are tightly controlled. This leads to unstable conditions and fluctuating results. Especially in

* Corresponding author.

*SSDI* 0039-9140(95)01687-2

a process control laboratory, the analyst would feel more comfortable feeding aqueous solutions for quick analysis. Recently a paper [7] was published from our laboratories wherein thallium was determined in our process solutions and in zinc and cadmium metals by first extracting thallium into isopropyl ether and then stripping back to the aqueous phase using a sodium sulphite solution.

We have now also worked out a procedure for the determination of antimony on similar lines and applied it to lead and zinc smelter products. The procedure involves suitable decomposition of the sample and taking up the salts in 7.5 M hydrochloric acid. Sodium nitrite is added to oxidise antimony(III). The chloro-complex of antimony(V) is extracted with isopropyl ether, antimony is stripped from the organic phase to the aqueous phase with sodium sulphite solution and the stripped solution is analyzed for antimony.

## 2. Experimental

### 2.1. Apparatus

An Electronic Corporation of India model 4103-B atomic absorption spectrometer is used under the following conditions: wavelength, 217.6 nm; spectral band width, 0.2 nm; current, 10 μA; flame, air–acetylene.

### 2.2. Reagents

All chemicals used were of analytical grade.

#### 2.2.1. Standard antimony solution

Pure antimony metal (1 g) is heated with 10 ml of concentrated sulphuric acid in a 250 ml beaker until dense white fumes are evolved. Hydrazine sulphate (1 g) is added after cooling and the solution heated again until dense white fumes are evolved. The beaker is then cooled in ice water. 100 ml of 2 M hydrochloric acid is added and the mixture allowed to attain room temperature. The contents of the beaker are transferred to a 1 l standard flask and made up to the mark with 2 M hydrochloric acid. The solution contains 1 mg $ml^{-1}$ of antimony and is suitably diluted with 7.5 M hydrochloric acid to obtain a 100 μg $ml^{-1}$ solution.

#### 2.2.2. Sodium sulphite solution (0.5% w/v)

Anhydrous sodium sulphite (0.5 g) is dissolved in 100 ml of water.

#### 2.2.3. Sodium nitrite solution (25% w/v)

Sodium nitrite (25 g) is dissolved in 100 ml of water.

### 2.3. Procedures

#### 2.3.1. Calibration

To 30 ml of 7.5 M hydrochloric acid in each of six 125 ml separating funnels 0.0, 1.0, 2.0, 3.0, 4.0 and 5.0 ml of antimony working standard (0–500 μg) solutions are added from a semimicroburette. Sodium nitrite (1 ml) followed immediately by 20 ml of isopropyl ether are added to each separating funnel. The separating funnels are shaken gently for 1 min and the layers are allowed to separate. The lower aqueous layers are transferred to another set of separating funnels containing 10 ml of isopropyl ether and once again shaken for 1 min. The lower aqueous layers are discarded and the organic layers added to the first set of separating funnels.

Sodium sulphite (20 ml) is added to each separating funnel containing isopropyl ether and shaken for 3 min. The layers are allowed to separate.

The aqueous layers are collected in 50 ml volumetric flasks. The organic layers are further shaken with a small portion (10 ml) of sodium sulphite solution and the aqueous portions collected in the same volumetric flasks. The solutions are made up by the addition of the required quantity of water. The aqueous solutions are then analyzed by AAS for antimony. The absorbance of the blank (zero added antimony), if any, is deducted from the absorbance values of the standards.

### 2.4. Sample treatment

Depending upon the antimony content, 0.5–1.0 g of sample is placed in a 250 ml beaker. Potassium bisulphate (1 g) and concentrated sulphuric acid (10 ml) are added and the beaker is heated until dense fumes are evolved (1 h). The beaker is cooled and the walls are washed down with a small quantity of water (10 ml). Hydrazine sulphate (1 g) is added and the beaker is heated again until dense white fumes are evolved. The beaker is cooled in the water, 20 ml of 7.5 M hydrochloric acid is

Table 1
Analytical results obtained for lead–zinc concentrates and other related products

| Sample | Antimony [a] found % (present method) | Standard deviation | Certified antimony value and range, % | Antimony found by AAS method [1] % |
|---|---|---|---|---|
| Zinc concentrate CZN-1 | 0.052 | 0.0005 | 0.052 (0.052–0.054) | 0.053 |
| Zinc concentrate (Zawar mines) | 0.0084 | 0.0010 | – | – |
| Zinc concentrate (Agucha mines) | 0.0100 | 0.0004 | – | 0.0105 |
| Lead concentrate (Agnigundala Mines) | 0.0058 | 0.0005 | – | – |
| Lead concentrate (Sargepalli mines) | 0.1150 | 0.002 | – | 0.1156 |
| Sludge (Zinc Oxide Plant) | 0.0430 | 0.002 | – | – |
| Moore Cake | 0.0380 | 0.0007 | – | – |

[a] Average of five results.

added and the beaker warmed just enough for the salts to dissolve and then cooled. The contents of the beaker are transferred directly to a 125 ml separating funnel. The sides of the beaker are washed with small portions (5 ml at a time) of 7.5 M hydrochloric acid and the washings transferred to a separating funnel. The solution is processed as described under *Calibration* starting from the addition of sodium nitrite. Antimony in the sample is determined in the aqueous phase by comparing with processed standards.

Note: For samples containing more than 600 $\mu g\ g^{-1}$ of antimony, 1.0 g of the sample is processed and the contents are transferred to a 100 ml standard flask and made up to the mark with 7.5 M hydrochloric acid. A suitable aliquot is taken and processed as described above.

## 3. Results and discussion

Table 1 gives the results obtained for antimony in lead–zinc concentrates and other related products. The values for CANMET CZN-1 (zinc concentrate) are comparable with certified values. The values were checked by Donaldson's iron–lanthanum collection/AAS method for zinc concentrate (Agucha mines) and lead concentrate (Sargepalli mines).

The results show that the recommended method can be conveniently applied for the determination of antimony in lead and zinc concentrates and its related products. The values were found to be stable over a period of one week. An analyst can comfortably complete the analysis of 6–8 samples by this method in less than 8 h (one shift).

### 3.1. Selection of organic solvent

Methyl isobutyl ketone (MIBK), *n*-butyl acetate and isopropyl ether are the most common solvents employed in the estimation of antimony. While the extraction of antimony from hydrochloric acid solution into these solvents is quantitative, it was observed that stripping of antimony with sodium sulphite from these solvents did not yield quantitative recoveries. From MIBK, antimony could not be stripped at all, while with *n*-butyl acetate small losses were suspected. Recoveries obtained were about 95% only. With isopropyl ether, the stripping was quantitative and moreover the phase separation was much better than with *n*-butyl acetate. Hence isopropyl ether was preferred in the present work.

## References

[1] E.M. Donaldson, Talanta, 26 (1979) 999.
[2] J.C. Chambers and B.E. McClellan, Anal. Chem., 48 (1976) 2061.
[3] C.R. Walker, O.A. Vita and R.W. Sparks, Anal. Chim. Acta, 47 (1969) 1.
[4] M. Yanagisawa, M. Suzuki and T. Takeuchi, Anal. Chim. Acta, 47 (1969) 121.
[5] P. Hannaker and T.C. Hughes, Anal. Chem., 49 (1977) 1485.
[6] S.S. Murthi and S.C.S. Rajan, Talanta, 35 (1988) 443.
[7] S.S. Murthi, I.V. Sambasiva Rao and S.C.S. Rajan, Talanta, 5 (1989) 601.

ELSEVIER

Talanta 42 (1995) 2021–2026

Talanta

# Correction of iron interface in the spectrophotometric flow injection catalytic determination of molybdenum in plants

Elma Neide Vasconcelos Martins Carrilho, Francisco José Krug *, Elias Ayres Guidetti Zagatto

*Centro de Energia Nuclear na Agricultura, Universidade de São Paulo, P.O. Box 96, 13400-970 Piracicaba, São Paulo, Brazil*

Received 12 April 1995; revised 5 July 1995; accepted 7 July 1995

**Abstract**

Iron interference in the spectrophotometric catalytic determination of molybdenum based on the iodide–hydrogen peroxide reaction can be corrected by using sulphosalicylic acid as masking and color-forming reagent. The catalytic influence of iron ions is circumvented to the extent of about 90% and correction of any remaining iron ions is possible by monitoring the colored iron(III)–salicylate complex at 490 nm. In this way, iron is also determined. With the proposed system, molybdenum can be determined in plant and food digests within the 0–100 μg Mo $l^{-1}$ range in the presence of up to 25 mg Fe $l^{-1}$, at a sampling rate of about 50 determinations $h^{-1}$. The relative standard deviation of 10 consecutive measurements was estimated as < 2%. Results for samples were comparable with those obtained by graphite furnace atomic absorption spectrometry. In addition, recoveries within the range 94–100% were calculated.

*Keywords:* Iron interference; Molybdenum determination; Sulphosalicylic acid; Flow injection; Plants

## 1. Introduction

Molybdenum is an essential nutrient for animals and plants and its determination in plant, soil and food materials is of utmost importance. Nevertheless, only a few well-equipped laboratories accomplish molybdenum determination on a routine basis. In general, molybdenum occurs in low concentrations in plant [1,2] (0.5–3.0 mg $kg^{-1}$) and food materials, which makes the direct determination in the sample digest by simple techniques such as classical spectrophotometry and flame atomic absorption spectrometry difficult. Although an automated spectrophotometric flow injection procedure based on the thiocyanate method with solvent extraction was developed in this laboratory [3], alternative methods exploiting kinetic catalysis have also been investigated [4–6].

The spectrophotometric method based on the catalytic effect of Mo(VI) ions in the oxidation of iodide by hydrogen peroxide [4] has been suggested to be very promising for the determination of molybdenum in biological materials [5–7]. The produced triiodide ion is spectrophotometrically monitored under the same conditions for the catalytic (presence of molybdenum) and non-catalytic (blank) reactions, and the difference between the absorbance signals is proportional to the molybdenum content in the sample. However, selectivity appears to be the main limitation, as other ions have similar catalytic properties. Svehla and Erdey [8] pointed out that interferences of several chemical species in the iodide–

* Corresponding author.

*SSDI* 0039-9140(95)01688-0

hydrogen peroxide reaction were mainly due to the different reaction rates for triiodide formation in the presence and absence of molybdenum.

This indicator reaction has been used in continuous flow systems for molybdenum determination in plant digest by different procedures, but prior iron separation by precipitation as hydroxide [5], on-line iron separation with ion exchange resin [6], or solvent extraction [9] have been needed. Masking agents for iron, such as fluoride in air-segmented flow systems [10], and sulphosalicylic acid in flow injection amperometry [11], have also been recommended.

The aim of the present paper is to describe an alternative procedure for the spectrophotometric catalytic determination of molybdenum by using a flow injection system that does not require previous iron separation or on-line molybdenum concentration. Amongst the several reagents evaluated in the present work, sulphosalicylic acid proved to be suitable for the determination of molybdenum in the presence of iron.

## 2. Experimental

### 2.1. Apparatus

The equipment consisted of a model 432 Femto spectrophotometer (São Paulo, Brazil) furnished with a tubular flow cell (12 mm optical path, 70 µl inner volume) from the same manufacturer and coupled to a REC 61 Radiometer recorder, an Ismatec mp13R peristaltic pump with Tygon tubes, and other accessories.

A manual sliding bar injector with two commutation sections [12], 0.5 mm i.d. Tygon microbore tubing (Norton Performance Plastics), and y-connections made from perspex were used to build the manifold.

### 2.2. Reagents, standards and samples

All chemicals were of analytical-grade quality and freshly distilled–deionized water was used throughout.

A 1000 mg $l^{-1}$ molybdenum stock solution was prepared by dissolving 0.9201 g of $(NH_4)_6Mo_7O_{24} \cdot 4H_2O$ in 500 ml of 1% v/v HCl.

Working standard solutions (0.0–100.0 ng Mo $ml^{-1}$) were prepared in 0.1% v/v nitric acid by appropriate dilutions of the stock solution. For selectivity evaluation, solutions with 5.0–50.0 mg Fe $l^{-1}$ ($Fe_2O_3$), 1.0 mg V $l^{-1}$ ($NH_4VO_3$), 10.0 mg Cr $l^{-1}$ ($K_2CrO_4$), 500 mg Mg $l^{-1}$ ($MgSO_4 \cdot 7H_2O$), 500 mg Al $l^{-1}$ ($AlCl_3 \cdot 6H_2O$), 500 mg P $l^{-1}$ ($Na_2HPO_4$) or 1000 mg Ca $l^{-1}$ ($CaCO_3$) were also prepared in 0.1% v/v nitric acid.

Potassium iodide solution 2.0% w/v ($R_1$, Fig. 1) was prepared by dissolving 2.5 g KI in 100 ml of water and hydrogen peroxide solution 0.025% v/v ($R_2$, Fig. 1) was prepared daily from a 30% $H_2O_2$ solution. The sample carrier stream (C, Fig. 1) was a 0.1% v/v nitric acid solution.

A 0.1 M sulphosalicyclic acid solution (M, Fig. 1) was prepared by dissolving 2.54 g $C_7H_6O_6S \cdot 2H_2O$ in 100 ml of water.

Biological samples were dry ashed according to the following procedure. 2.000 g of ground (60 mesh) and oven-dried (60°C to constant weight) samples was ashed in a porcelain crucible for 4 h at 550°C. The ash was moistened with a few drops of water and 10 ml of 4 M nitric acid was added; the mixture was then dried at 60°C. The residue was taken up with successive portions of 10–15 ml of 0.1 M nitric acid solution, filtered through Whatman filter paper into a 100 ml volumetric flask, and made up to volume with the same acid. Before using, the solution was left to stand for about 12 h.

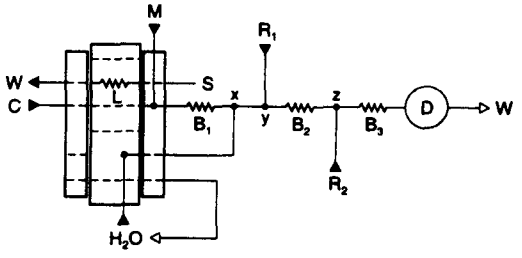


Fig. 1. Diagram of the flow set-up for molybdenum (and iron) determination. $B_1$, $B_2$ and $B_3$ = 10, 20 and 250 cm reaction coils; D = spectrophotometer at 350 nm for molybdenum and/or 490 nm for iron; S = sample, aspirated at 2.6 ml $min^{-1}$; L = sampling loop (200 µl); $R_1$ = 0.025% v/v hydrogen peroxide solution at 0.4 ml $min^{-1}$; $R_2$ = 2.5% w/v potassium iodide solution at 0.8 ml $min^{-1}$; M = 0.1 M sulphosalicylic acid flowing at 0.3 ml $min^{-1}$; W = waste; x, y and z = confluence points; C = sample carrier stream (0.1% v/v $HNO_3$) at 1.6 ml $min^{-1}$; $H_2O$ = water at 2.6 ml $min^{-1}$.

### 2.3. The flow injection system

With the system in the situation depicted in Fig. 1, the sample is continuously aspirated to fill the sampling loop, and the sample carrier stream and reagents are continuously flowing towards detection. Water flows to improve system washing by dissolving any triiodide adsorbed in the inner walls of the analytical path. After introducing the selected sample volume into the sample carrier stream, the water stream recycles in its reservoir. The masking agent is added via a confluence point located in the commutator at a suitable flow rate to avoid excessive dispersion-dilution of the sample zone in the $B_1$ reactor where the masking reaction takes place. The same criterion was used for predefining $R_1$ and $R_2$ flow rates and to provide suitable mixing conditions inside the $B_2$ and $B_3$ helical coils. Thereafter, the sample zone passes through the detector where the absorbance at 350 nm is measured for molybdenum (plus unmasked iron) and at 490 nm for the iron–salicylate complex. The system was dimensioned to provide the best figures of merit for molybdenum. For iron determination at 490 nm, further system optimization was not carried out because the sensitivity was already suitable.

### 2.4. Figures of merit

The detection limits for molybdenum and iron were determined after 20 consecutive measurements of the blank solution (0.1% v/v nitric acid) according to IUPAC [13]. The accuracy for molybdenum determination was assessed by analyzing the same digestes by graphite furnace atomic absorption spectrometry in a Varian SpectrAA40 coupled with a GTA-96 furnace with pyrolytically coated graphite tubes and controlled by a DS-15 Date Station from the same manufacturer. The heating programme was adjusted accordingly. Accuracy assessment for iron determination was made with flame atomic absorption spectrometry with an air–acetylene flame.

## 3. Results and discussion

Concentrations of hydrogen peroxide (0.025% v/v) and potassium iodide (2.5% w/v) and the final pH of the reaction medium were selected by taking into account the ratio between catalytic and non-catalytic signlas and the detection limit. Although the catalytic reaction rate increased with the concentrations of either hydrogen peroxide or potassium iodide, the non-catalytic signal (baseline) also increased. Similar behavior was observed earlier [5].

The pH of the reaction mainly affects the non-catalyzed reaction, i.e. it does not limit sensitivity for reaction pH values lower than two, and the lower the pH value the lower the baseline signal. Therefore, during sample pretreatment it was decided that the final acidity of the digest should be 0.1% v/v nitric acid. To avoid pH gradients along the sample zone, the same acid solution was used as carrier stream. In doing this, the pH of the solution leaving the flow cell was about 1.6.

Preliminary experiments were carried out with several masking agents for iron. Tartrate, citrate, triethanolamine, pyrophosphate and oxalic acid minimized or even suppressed the interference of up to 15 mg $Fe\,l^{-1}$ in the determination of 100 μg $Mo\,l^{-1}$, but they also affected the catalytic reaction. Similar behaviour was observed with a 0.05% w/v sodium fluoride solution which caused a 90% decrease in iron interference and also affected the catalytic reaction rate leading to a 40% lowering in sensitivity. Higher fluoride concentrations did not improve the masking efficiency significantly, but decreased the reaction rate more than proportionally.

Sulphosalicylic acid provided 85% masking efficiency, but with two advantages when compoared with fluoride and other iron-forming complexes. It did not change the catalytic reaction rate due to molybdenum, and iron could be determined as the iron(III)–sulphosalicylate complex [14] at 490 nm by using the same flow injection manifold. The system could also be used for the simultaneous determination of iron and molybdenum with a diode array detector, or sequentially with two spectrophotometers.

The slope and linearity of the analytical calibration curves were not affected by the presence of up to 25 mg $l^{-1}$ iron when sulphosalicylic acid was used (Fig. 2). As a consequence, it was possible to infer that molybdenum could be determined in the presence of iron, because absorbances were additive. By knowing the iron content in the original sample, the absorbance due to molybdenum measured at 350 nm was corrected according to the following equations:

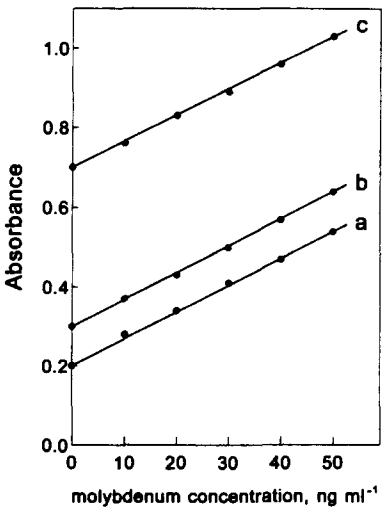


Fig. 2. Molybdenum calibration curves with and without iron in the presence of 0.1 M sulphosalicylic acid (total absorbance values recorded at 350 nm): (a) molybdenum alone ($r = 0.9998$); (b) molybdenum + 5 mg Fe $l^{-1}$ ($r = 0.9997$); (c) molybdenum + 25 mg Fe $l^{-1}$ ($r = 0.9998$).

$$A_{Mo} = A_{Mo+Fe} - a_{Fe}C_{Fe}$$

$$CA_{Mo} = A_{Mo}/a_{Mo}$$

where $A_{Mo}$ = absorbance at 350 nm due to molybdenum, $A_{Mo+Fe}$ = absorbance at 350 nm due to molybdenum plus iron, $a_{Fe}$ and $a_{Mo}$ = iron and molybdenum absorptivities at 350 nm, $C_{Fe}$ = iron concentration determined at 490 nm, and $C_{Mo}$ = corrected molybdenum concentration.

The influence of other elements on molybdenum determination (based on a mass/volume ratio of 1 g per 50 ml of the biological digest) at the 50 μg Mo $l^{-1}$ level was also investigated in the presence of sulphosalicylic acid at 350 and 490 nm. as much as 1000 mg Ca $l^{-1}$, 500 mg Mg $l^{-1}$, 500 mg Al $l^{-1}$ and 500 mg P $l^{-1}$ did not interfere with iron determination at 490 nm. As expected, interferences were observed for high concentrations of chromium (5 mg $l^{-1}$) and vanadium (0.5 mg $l^{-1}$) only at 350 nm with signal enhancements not exceeding 20%. The influences of chromium(VI) and vanadium(V) are well-known since both elements catalyze the iodide oxidation by hydrogen peroxide [15]. Hopefully, chromium and vanadium do not occur at these levels in the digests, taking into account their maximum reported concentrations in dry plant tissues and food materials: i.e. 5 μg Cr $g^{-1}$ and 10 μg V $g^{-1}$ [16–18]. The expected interference of phosphorus due to molybdophosphoric acid formation, also observed in earlier work [6], was only noticed for concentrations of phosphorus 10 times higher than its normal level in the digests, a 15% suppression in the molybdenum absorbance signal being observed in the presence of 250 mg P $l^{-1}$.

Regarding tungsten(VI) and titanium(VI), which also catalyze the indicator reaction, parallel experiments revealed that the system could tolerate their presence up to the maximum repored levels in biological materials [16]. Tungsten and titanium did not interfere at concentrations lower than 0.2 mg $l^{-1}$ and 1 mg $l^{-1}$ respectively. These interferences are also discussed elsewhere [9,19].

There is good agreement between molybdenum concentration values obtained with the proposed flow injection catalytic method and graphite furnace atomic absorption spectrometry (Table 1). In addition, Table 2 shows recoveries of about 100% for the same sample digests referred to in Table 1, which is also a good indication of the accuracy of the proposed method. The relative standard deviation of measurements ($n = 5$) for digests containing molybdenum within the range 10–50 ng $ml^{-1}$ did not exceed 2%. The detection limit was 0.6 ng Mo $ml^{-1}$ for a 200 μl sample volume, and a throughput of 100 determinations per hour (50 per hour for molybdenum and 50 per hour for iron) was typically obtained. The flow system proved to be quite stable, simple and

Table 1
Comparison of procedures for the determination of molybdenum in plant and food digests. Data are averages of three replicates

| Sample | mg Mo $kg^{-1}$ (dry matter basis) | | mg Fe $kg^{-1}$ FIA |
|---|---|---|---|
| | FIA | GFAAS | |
| Coffee leaves | 0.249 ± 0.001 | 0.287 ± 0.020 | 425 ± 4.5 |
| Soya flour | 0.761 ± 0.007 | 0.809 ± 0.036 | < 100 |
| Soybean leaves | 0.368 ± 0.003 | 0.402 ± 0.027 | 225 ± 3.2 |
| Rice leaves | 0.282 ± 0.002 | 0.297 ± 0.022 | 221 ± 2.9 |

Table 2
Molybdenum recoveries from biological digests. Data are averages of three replicates

| Sample | Original concentration (ng Mo $ml^{-1}$) | After addition (ng Mo $ml^{-1}$) | Recovery (%) | % r.s.d. ($n = 5$) |
|---|---|---|---|---|
| Coffee leaves | 5.0 | 15.0 | 100.0 | 1.7 |
| | 5.0 | 25.0 | 100.0 | 0.0 |
| Soya flour | 15.2 | 25.2 | 96.2 | 0.0 |
| | 15.2 | 35.2 | 94.4 | 2.9 |
| Soybean leaves | 7.4 | 17.4 | 101.3 | 1.7 |
| | 7.4 | 27.4 | 103.3 | 0.0 |
| Rice leaves | 5.6 | 15.6 | 103.9 | 0.0 |
| | 5.6 | 25.6 | 101.0 | 2.0 |

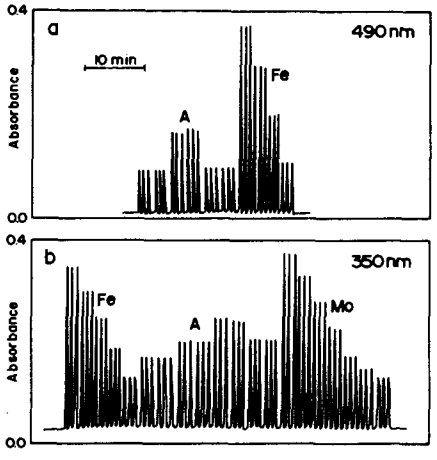


Fig. 3. Recorder tracing of a routine run. All measurements in triplicate. (a) Recording at 490 nm. From right to left, four iron standard solutions (5.0, 10.0, 15.0 and 20.0 mg $l^{-1}$), and eight samples (the last two with iron contents lower than the detection limit). (b) Recording at 350 nm. From right to left, seven molybdenum standard solutions (0.0, 10.0, 20.0, 40.0, 60.0, 80.0 and 100.0 μg $l^{-1}$) eight samples, and five iron standard solutions (0.0, 5.0, 10.0, 15.0 and 20.0 mg $l^{-1}$).

reasonably robust, and can be used for most plant tissues, food and other biological products, where iron content in the digest does not exceed 25 mg $l^{-1}$ (1200 mg Fe $g^{-1}$ dry matter). The calculated detection limit for iron was 0.2 mg $l^{-1}$ at 490 nm. Samples with higher iron contents are not common and were not found for validation but limitations due to the linearity of the analytical calibration curves are expected. In this situation, the injected volume could be reduced accordingly for iron on-line dilution, with a proportional lack of molybdenum sensitivity. A typical recorder tracing relating to molybdenum and iron determination in plant digests is shown in Fig. 3.

## Acknowledgments

The authors are grateful to FINEP (Financiadora de Estudos e Projetos-PADCT II, processo 65.91.0324.00) for financial support, and to CNPq (Conselho Nacional de Desenvolvimento Científico e Technológico) for grants to E.N.V.M.C., F.J.K and E.A.G.Z. Thanks are also due to M.M. Silva for helping with the GFAAS measurements. At the time of this work, E.N.V.M.C. was a graduate student at the Institute de Química de São Carlos, Universidade de São Paulo, São Carlos-SP, Brazil.

## References

[1] D.R. Hoagland, Soil Sci., 60 (1945) 119.
[2] V. Sauchelli, Trace Elements in Agriculture, Van Nostrand, New York, 1969.
[3] H. Bergamin Filho, J.X. Medeiros, B.F. Reis and E.A.G. Zagatto, Anal. Chim. Acta, 101 (1978) 9.
[4] K.B. Yatsimirskii and L.P. Afana's Eva, Zh. Anal. Khim., 11 (1956) 319.
[5] F. Zhao-Lun and X. Shu-Kun, Anal. Chim. Acta, 145 (1983) 143.
[6] L.C.R. Pessenda, A.O. Jacintho and E.A.G. Zhatto, Anal. Chim. Acta, 214 (1988) 239.
[7] J.C. Andrade, S.P. Eiras and R.E. Bruns, Anal. Chim. Acta, 225 (1991) 149.
[8] G. Svehla and L.Erdey, Microchim. J., 7 (1963) 206.
[9] J.C. Andrade, R.E. Bruns and S.P. Eiras, Analyst, 118 (1993) 213.
[10] M.H. Mahr and E. Pungor, Kem.-Kemi, 10 (1980) 585.
[11] M. Trojanowicz, A. Hulanicki, W. Matuszewski, M. Palys, A. Fuksiewicz, T. Hulanicka-Michalak, S. Raszewski, J. Szyller and W. Augustyniak, Anal. Chim. Acta, 188 (1986) 165.
[12] F.J. Krug, H. Bergamin Fo and E.A.G. Zagatto, Anal. Chim. Acta, 179 (1986) 103.
[13] Commission on Spectrochemical and other Optical Procedures for Analysis. Nomenclature, symbols, units and their usage in spectrochemical analysis—II, Spectrochim. Acta, 33 (1978) 241.

[14] Z. Marczenko, Separation and Spectrophotometric Determination of Elements, Ellis Horwood, Chichester, 1986.
[15] F. Eivazi, J.L. Sims and J. Crutchfield, Comm. Soil Sci., Plant Anal., 13 (1982) 135.
[16] H.J.M. Bowen, Trace Elements in Biochemistry, Academic Press, London, 1966, pp. 61–84.
[17] J. Laporte, G. Kovacsik and J. Bellanger, Vegetable Matter, in M. Pinta (Ed.), Atomic Absorption Spectrometry, Adam Hilger, London, 1975, pp. 240–275.
[18] Committee on Biological Effects of Atmospheric Pollutants, Chromium, National Academy of Sciences, Washington D.C., 1974.
[19] B.F. Quin and P.H. Woods, Analyst, 104 (1979) 552.

ELSEVIER

Talanta 42 (1995) 2027–2032

Talanta

# New aspects of the reaction of silver(I) cations with the ethylenediaminetetraacetate ion

Luciana Saran, Eder Cavalheiro, Eduardo Almeida Neves *

*Departamento de Quimica, Universidade Federal de São Carlos, Cx. Post. 676, CEP 13.565-905, São Carlos, Brazil*

Received 3 April 1995; revised 17 July 1995; accepted 17 July 1995

**Abstract**

The highly neutralized ethylenediaminetetraacetate (EDTA) titrant (95–99% as $Y^{4-}$ anion) precipitates with $Ag^+$ cations to form the $Ag_4Y$ species, in aqueous medium, which is well characterized from conductometric titration, thermal analysis and potentiometric titration of the silver content of the solid. The precipitate dissolves in excess $Y^{4-}$ to form a complex, $AgY^{3-}$. Equilibrium studies at 25°C and ionic strength 0.50 M ($NaNO_3$) have shown from solubility and potentiometric measurements that the formation constant (95% confidence level) $\beta_1 = (1.93 \pm 0.07) \times 10^5\ M^{-1}$ and the solubility products are $K_{S0} = [Ag+]^4[Y^{4-}] = (9.0 \pm 0.4) \times 10^{-18}\ M^5$ and $K_{S1} = [Ag+]^3[AgY^{3-}] = (1.74 \pm 0.08) \times 10^{-12}\ M^4$. The presence of $Na^+$, rather than ionic strength, markedly affects the equilibrium; the data at ionic strength 0.10 M are: $\beta_1 = (1.19 \pm 0.03) \times 10^6\ M^{-1}$, $K_{S0} = (1.6 \pm 0.4) \times 10^{-19}\ M^5$ and $K_{S1} = (1.9 \pm 0.5) \times 10^{-13}\ M^4$; at ionic strength tending to zero; $\beta_1 = (1.82 \pm 0.05) \times 10^7\ M^{-1}$, $K_{S0} = (2.6 \pm 0.8) \times 10^{-22}\ M^5$ and $K_{S1} = (5 \pm 1) \times 10^{-15}\ M^4$. The intrinsic solubility is 2.03 mM silver (I) in 0.50 M $NaNO_3$. Well-defined potentiometric titration curves can be taken in the range 1–2 mM with the Ag indicator electrode. Thermal analysis revealed from differential scanning calorimetry a sharp exothermic peak at 142°C; thermal gravimetry/differential thermal gravimetry has shown mass loss due to silver formation and a brown residue, a water-soluble polymeric acid (decomposition range 135–157°C), tending to pure silver at 600°C, consistent with the original $Ag_4Y$ salt.

*Keywords:* Silver(I); EDTA; Differential thermal analysis; Differential scanning calorimetry

## 1. Introduction

Ethylenediaminetetraacetate (EDTA) ($H_4Y$ and $Y^{4-}$ ion), ethylenediaminetetraacetic acid and related compounds (complexones) constitute a class of polycoordinate ligands which have important analytical uses [1–3] due to their formation of strong complexes with a 1:1 ratio of ligand:metal cation in complexometric titrations.

Direct titration of $Ag^+$ with EDTA using a conventional buffer and a colorimetric indicator has never been considered due to a relatively low $\beta_1$ formation constant, as determined by Schwarzenbach [4] to be of the order of $10^7\ M^{-1}$ [1–5], a value that decreases to a smaller conditional constant $\beta'_1$ in a buffered medium. One indirect titration has been proposed through reaction of $Ag^+$ or AgCl with the $[Ni(CN)_4]^{2-}$ anion to form $[Ag(CN)_2]^-$ and release of an equivalent $Ni^{2+}$, able to be titrated with EDTA [6,7].

In a recent article [8] new possibilities for complexometric titrations were proposed on the basis of using complexones at high $\alpha_0$ conditions, i.e. at a highly neutralized species with the active form $Y^{4-}$ which guarantees a full complexing power for the complexone. The titration of $Mg^{2+}$ and other divalent cations with EDTA can be followed potentiometrically

* Corresponding author. Fax: (55) 74-8350.

*SSDI* 0039-9140(95)01692-9

with the glass electrode or the end point found by phenolphthalein, due to a pH jump caused by the hydrolysis of the $Y^{4-}$ anion [8].

Because of the full complexing power of EDTA under this high $\alpha_0$ condition [8] the EDTA/$Ag^+$ reaction deserves to be better studied. As part of this subject equilibrium aspects of this reaction and thermoanalytical data are herein described.

## 2. Experimental

### 2.1. Chemicals and solutions

All chemicals (mostly Merck) were of A.R. specification.

A standard 0.05 M EDTA solution expressed in active [$Y^{4-}$] titre (99% neutralized) was prepared from reaction of NaOH solution with the $Na_2H_2Y \cdot 2H_2O$ salt, as formerly described [8]. This EDTA salt was properly neutralized with standard NaOH to prepare buffers with the desired [$HY^{3-}$]/[$Y^{4-}$] ratio.

Standard NaCl solution was used to standardize 0.1 M $AgNO_3$ potentiometrically. Other solutions containing $NaNO_3$ for ionic strength adjustments and KI for $Ag^+$ titration at the millimeter level were prepared by weighing the dry solid directly without further standardization.

The $Ag_4Y$ solid phase was prepared by reaction of at least 50 ml of the 0.05 M EDTA, $Y^{4-}$, with a volume of 0.1 M $AgNO_3$ in slight excess with regard to the sroichiometric amount (4.01:1) added rapidly at room temperature and in diffuse light. After 10 min the suspension was filtered, washed with small volumes of cold water and finally with ethanol. The solid was then vacuum dried and kept in darkness.

### 2.2. Thermal analysis

Thermogravimetry (TG) analysis and differential thermogravimetry (DTG) analysis were performed with a DuPont TA-951 module joined to a DuPont 9900 thermoanalyzer system. The calorimetric analysis (differential scanning calorimetry, DSC) was performed with a DuPont DSC-910 module. All techniques were computer controlled.

Weighed samples (5–7 mg) were placed in a platinum crucible (for TG) or in an aluminum crucible with a cover (for DSC) under pure dinitrogen at 100 ml $min^{-1}$.

### 2.3. Equilibria and electrochemical measurements

All equilibrium data were obtained at $25 \pm 0.1$°C.

Potentiometric measurements with scale resolution $\pm 0.1$ mV were performed with a Micronal B 375 pH meter. A borax buffer (pH 9.18) was used to calibrate the glass electrode for measurements in alkaline EDTA buffers for p$K'$ determination.

A 1 cm silver wire was used in the potentiometric titrations and other potentiometric measurements in a cell with silver chloride reference electrode (see Results and discussion section). The 0.50 M $NaNO_3$ salt bridge was a gel with 3% agar–agar. All working solutions were previously bubbled with dinitrogen.

The conductometric titration was performed with a Micronal B330 instrument in the region of 2000 μS, with about 0.2% resolution. The cell with two platinized electrodes contained 10.30 ml of 0.1004 M silver nitrate solution which was titrated with 0.04894 M EDTA ($Y^{4-}$) at 25°C. Volume corrections were applied to the measured conductometric data.

In order to characterize the composition of the silver editate at least three dried samples of about 0.3 g were titrated potentiometrically with standard 0.1 M NaCl in the presence of 2–3 ml of 10% nitric acid in order to avoid interference of the ligand.

Saturated solutions of $Ag_4Y$ were obtained by treating about 0.1 g of the solid with volumes of the electrolyte (40 ml) with efficient magnetic stirring for at least 12 min. Saturation occurs in 5–10 min but long contact with aqueous medium causes slow hydrolysis of the precipitate within hours. The excess of solid of the recently saturated solution was separated by filtration and an aliquot of 20.00 ml was treated with 1 ml 10% nitric acid and titrated with 2.00 mM KI, potentiometrically, in order to determine the total silver(I) from the intrinsic solubility. The measured pH of the recently saturated solutions was close to seven.

Data treatment was computer assisted through QuickBASIC programs and the ORGIN graphic system (Microsoft™). All deviations attributed to experimental data were taken at 95% confidence level (Student $t$ test).

## 3. Results and discussion

### 3.1. Formation of $Ag_4Y$

Fig. 1 shows the titration of $Ag^+$ with EDTA (99% as $Y^{4-}$) followed potentiometrically with a silver wire as indicator electrode. The potentiometric curve is assymetrical and distorted due to formation of a white precipitate which dissolves during the course of the titration towards a not well-defined end point but close to a 1:1 ratio of $[Y^{4-}]/[Ag^+]$.

A reverse titration of 2.0 mM EDTA with a 0.1 M $Ag^+$ showed in the initial part a sharp potential jump consistent with a 1:1 ratio of the reactants (Fig. 2), followed by a discontinuity in the upper region of the curve, exactly at the point where precipitation takes place. After this point the $AgY^{3-}$ species is being converted to the $Ag_4Y$ precipitate and a second less well-defined potentiometric jump is attained. This second inflection point is close to a 4:1 ratio of $[Ag^+]/[Y^{4-}]$, as inferred from a derivative curve taken in this second region.

The conductometric titration of $Ag^+$ with EDTA ($Y^{4-}$) has shown a well-defined first step consistent with the precipitation of $Ag_4Y$ (Fig. 3). Conductance increases with the dissolution of the precipitate in the titrant EDTA to form only $AgY^{3-}$, as inferred from a second stoichiometric point, although less well-defined.

Preparation of the solid phase was performed only in cold solutions (see Experimental section). Attempts to use hot solutions or homogeneous precipitation always lead to hydrolysis of $Ag^+$ and parallel reduction to produce a metal mirror. Potentiometric titrations of a dry sample with standard chloride solution to precipitate AgCl, in acidic medium to protonate the ligand, confirmed the composition of the precipitate to be $Ag_4Y$, within 99.9%.

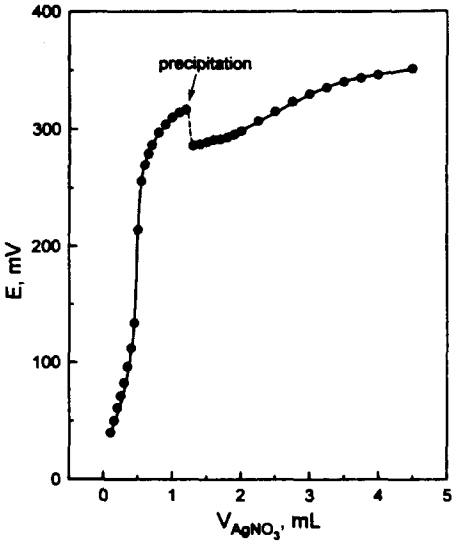


Fig. 2. Potentiometric titration curve of 25.00 ml of 2.000 mM free EDTA (99% neutralized) with 0.1000 M $AgNO_3$ with a silver indicator electrode. First stoichiometric point consistent with $AgY^{3-}$ formation.

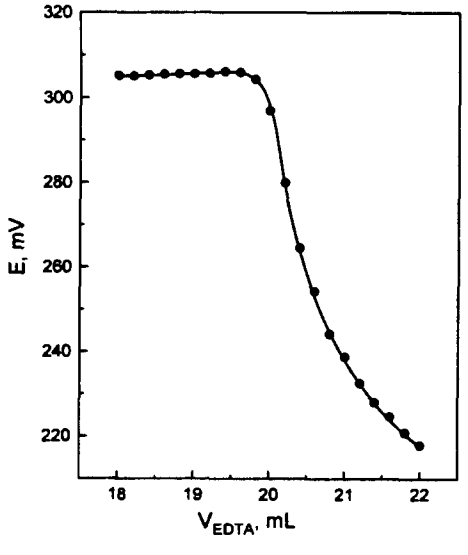


Fig. 1. Potentiometric titration curve of 10.03 ml of 0.1010 M $AgNO_3$ with 0.05010 M free EDTA (99% neutralized) with a silver indicator electrode.

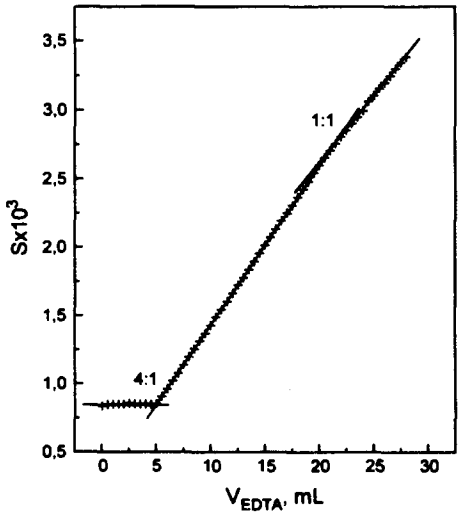


Fig. 3. Conductometric titration of 10.03 ml of 0.1004 M $AgNO_3$ with 0.05010 M free EDTA (99% neutralized) indicating the formation of a $Ag_4Y$ precipitate (first stoichiometric point) and $AgY^{3-}$ complex (second stoichiometric point).

Table 1
Data from homogeneous and heterogeneous equilibrium studies at 25°C

| $I$ (M) | $C_{Ag}$ (M) | $\beta_{AgY^{3-}}$ ($M^{-1}$) | $K_{S0}$ ($M^5$) | $K_{S1}$ ($M^4$) |
|---|---|---|---|---|
| $5.0 \times 10^{-4}$ | $(4.60 \pm 0.14) \times 10^{-4}$ | $(1.82 \pm 0.05) \times 10^{7}$ | $(2.6 \pm 0.8) \times 10^{-22}$ | $(5 \pm 1) \times 10^{-15}$ |
| $1.0 \times 10^{-1}$ | $(1.16 \pm 0.03) \times 10^{-3}$ | $(1.19 \pm 0.03) \times 10^{6}$ | $(1.6 \pm 0.4) \times 10^{-19}$ | $(1.9 \pm 0.5) \times 10^{-13}$ |
| $5.0 \times 10^{-1}$ | $(2.03 \pm 0.02) \times 10^{-3}$ | $(1.93 \pm 0.07) \times 10^{5}$ | $(9.0 \pm 0.4) \times 10^{-18}$ | $(1.74 \pm 0.08) \times 10^{-12}$ |

$C_{Ag}$ is the silver(I) concentration in the saturated solution of $Ag_4Y$.

### 3.2. Equilibrium studies in homogeneous solutions

Potentiometric titration of the 2 mM $Ag^+$ cations with EDTA was initially performed in 0.50 M $NaNO_3$ medium, defining the following cell, virtually free from junction potentials:

Ag|AgCl, 0.10 M NaCl, 0.40 M $NaNO_3$:0.50 M $NaNO_3$: $[Ag^+] = 2.00$ mM, 0.50 M $NaNO_3$|Ag
(Reference electrode) (Salt bridge) (Working solution, 20.00 ml)

This cell presents the following Nernst equation at $25.0 \pm 0.1$°C in non-complexing medium, for a conditional potential $E_S^{0\prime} = 0.4721$ V:

$$E_S = 0.4721 + 0.05916 \log[Ag^+] \quad (1)$$

The EDTA solution used to titrate the working solution had the following composition: $[Y^{4-}] = 0.1250$ M, $[HY^{3-}] = 1.25 \times 10^{-3}$ M and $[Na^+] = 0.50$ M. This solution has an ionic strength greater than 0.5 M, due to the presence of a quadruply-charged anion. However, this parameter was revealed to be not so important as the sodium concentration, which remains constant in the titration.

By addition of the titrant solution to the $[Ag+]/Ag$ compartment the initial potential changes from $E_S$ in non-complexing medium to a lower $E_x$ value in complexing medium, defining a potentiometric curve. Volume corrections were considered and variable $E_x^{0\prime}$ data were calculated from the corresponding $E_x$ value and total silver(I) concentration value, $C_{Ag}$, beyond the stoichiometric point in order to calculate the $[Ag^+]$ value at equilibrium from the Nernst equation (1) above. The free ligand concentration $[Y^{4-}]$ was calculated by discounting the silver(I) concentration used to form $AgY^{3-}$ and also correcting the small decrease caused by ligand hydrolysis. The ratio of $[AgY^{3-}]/[Ag^+][Y^{4-}]$ gives the $\beta_1$ formation constant. Seven values were obtained, and the average $\beta_1$ was $(1.93 \pm 0.07) \times 10^5$ $M^{-1}$. Table 1 shows the results obtained at three ionic strengths together with data obtained for the heterogeneous equilibrium (see next topic). A marked increase in $\beta_1$ is observed at lower ionic strength (about 0.0005 M), tending to the old value referred to in the literature [1–5]. The sodium cation has a marked effect on the equilibria, rather than the ionic strength, due to a non-negligible interaction of $Na^+$ with the highly charged $Y^{4-}$ anion. The titration performed at lower ionic strength could not be performed at constant $[Na^+]$ and the formation constant changes with the volume of the titrant, 0.125 M in $[Y^{4-}]$, requiring extrapolation procedures to the initial condition.

The ligand hydrolysis

$$Y^{4-} + H_2O \rightarrow HY^{3-} + OH^-$$

was used to make small corrections to $Y^{4-}$ concentrations during the titration of the working solutions, by using a conditional $pK'$ (mixed ionization constant of concentrations ratio and $a_{H+}$) value calculated from the buffer equation

$$pK'_4 = pH + \log([HY^{3-}]/[Y^{4-}]) \quad (2)$$

The concentration of both forms was 5.00 mM at two electrolyte concentrations: $NaNO_3$ 0.50 M and $NaNO_3$ 0.10 M; EDTA buffer only at 0.005 M and 0.00050 M. The $pK'_4$ values are respectively 9.04, 9.58, 10.11 and 10.84; the $pK'_b$ values referred to the conjugated basis, used to calculate the hydrolysis, are respectively 4.96, 4.42, 3.89 and 3.16.

### 3.3. Heterogeneous equilibria

More information was obtained for the intrinsic solubility of the solid phase $Ag_4Y$ from 0.50 M $NaNO_3$ in distilled water. The low solubility of silver iodide (solubility product $10^{-17}$ $M^2$) was adequate for the precise deter-

mination of the total silver(I) molar concentration, $C_{Ag}$, in the saturated solutions, as very sharp potentiometric titration curves with iodide solution were obtained at the millimolar concentration level. Some dilute nitric acid is added to protonate the ligand and avoid any interference during the titration.

On the basis of the composition of the solid phase and the high tendency to form the 1:1 complex the following mass balances can be applied for the saturated solution, analyzed for the total silver content $C_{Ag}$, and its relation with the total EDTA, $C_Y$ and ionic species:

$$C_{Ag} = 4C_Y \therefore C_Y = C_{Ag}/4 \quad (3)$$

$$C_Y = [Y^{4-}] + [AgY^{3-}] \cong [AgY^{3-}]$$
$$\text{as } [Y^{4-}] \ll [AgY^{3-}] \quad (4)$$

$$C_{Ag} = [Ag+] + [AgY^{3-}]$$
$$\therefore [Ag+] = [C_{Ag} - [AgY^{3-}] = C_{Ag} - C_Y \quad (5)$$

The $[Ag^+]$ and $[AgY^{3-}]$ values can be calculated from the mass balance and the smaller $[Y^{4-}]$ concentration can be obtained as follows:

$$[Y^{4-}] = [AgY^{3-}]/[\beta_1[Ag^+] \quad (6)$$

This $[Y^{4-}]$ data completes the concentration values necessary to calculate the two solubility products:

$$Ag_4Y \Rightarrow 4Ag^+ + Y^{4-} \qquad K_{S0} = [Ag^+]^4[Y^{4-}] \quad (7)$$

$$Ag_4Y \Rightarrow 3Ag^+ + AgY^{3-} \qquad K_{S1} = [Ag^+]^3[AgY^{3-}] \quad (8)$$

Table 1 also shows the results of these two heterogeneous equilibrium at three experimental conditions. The intrinsic solubility of the solid phase as well as the solubility products suffer marked change with the presence of the electrolyte.

All data in Table 1 show deviations at a 95% confidence level, from application of the Student $t$ test.

The reaction of EDTA anions with $Ag^+$ followed a different behaviour with regard to a large number of studied cations, as precipitation takes place. This became evident during the particular condition of using the tetra-neutralized ligand with predominance of the $Y^{4-}$ anion.

The stability constant ($\beta_1$, at very low ionic strength) for the normal 1:1 complex was found to be higher than that of the $Ag^+$ cation with ethylenediamine [9] which is of the order of $10^6\ M^{-1}$. The affinity with the carboxylic group, as shown in acetate complex [10], is very small in comparison with the amine one. However, some increase in affinity of EDTA with $Ag^+$, in aqueous medium, with regard to the ethylenediamine complex, can be attributed to another five-membered ring formation of one of the three acetate groups with the $Ag^+$ bound to the bicoordinative amine site, neutralizing one positive charge. On this basis only one $Ag^+$ is effectively coordinated to three ligands of EDTA in solution. In the solid phase the three other cations should probably neutralize the negative charge of the $AgY^{3-}$ anion in the crystal lattice.

The $Na^+$ cation is known to interact to some extent with EDTA to form a complex or ion pair for which $\beta_1$ is $4.6 \times 10^1\ M^{-1}$ [11]. This can explain the marked effect on the magnitude of the conditional stability constants of the silver(I)/EDTA system (homogeneous and heterogeneous equilibrium) in the presence of the background electrolyte, $NaNO_3$, rather than being attributed to the increase in ionic strength. This means that the presence of $Na^+$ cations decreases the complexing power of EDTA.

The analytical possibilities of the reaction are limited by the formation of the $Ag_4Y$ precipitate. However, concentrations below the intrinsic solubility provide well-defined potentiometric curves for silver(I) concentrations in the range 1–2 mM by titrating with the highly neutralized EDTA.

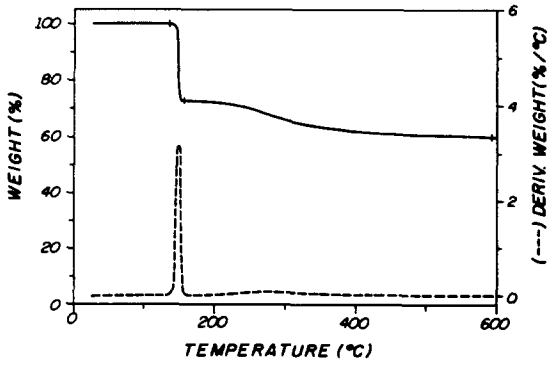


Fig. 4. TG and DTG thermodiagrams with 7.00 mg of $Ag_4Y$, indicating a decomposition range of 135–157°C. Final mass loss of 40.15% at 600°C is consistent with a pure silver residue.

### 3.4. Thermoanalytical data

Fig. 4 shows a thermogravimetric diagram taken with a 6.921 mg sample. It shows a sudden mass loss of 27.2% at 157°C. After 185°C the mass loss continues slowly towards 600°C. The final residue of 4.143 mg is 59.86% of the initial mass and is consistent with the pure silver residue from the thermal decomposition of $Ag_4Y$ (the theoretical value is 59.95%).

A thermal decomposition of about 1 g of the $Ag_4Y$ solid was performed at 162°C under nitrogen in order to obtain some data about the nature of the calcinated residue at this intermediate temperature. The aqueous extract revealed partial solubility of the residue giving a brown acidic solution. This solution does not precipitate with chloride ions, which excludes the presence of $Ag^+$ cations. The extract with diluted nitric acid (0.1 M) presented the same brown color and no precipitation with chloride ions; this excludes the presence of basic species of silver such as $Ag_2O$ or $Ag_2CO_3$ in the calcinated solid. The residue from the aqueous extract dissolves in concentrated nitric acid with nitrous oxide evolution; its diluted solution gave extensive precipitation with chloride ions showing that the calcinated residue contains metallic silver.

Another sample of the calcinated residue (0.0593 g) was suspended in 25 ml of distilled water and gave a pH of 3.74. The potentiometric titration of the suspension with 0.01 M NaOH showed a well-defined potentiometric curve with only one equivalent point of pH 7.49. Calculations from the titration data showed that the soluble brown fraction (possibly a polymeric product) contains an acid group with $pK = 3.9$ and $1.9 \times 10^{-4}$ equivalents of $H^+$ per gram of the solid residue from calcination at 162°C.

Fig. 5 shows an interesting result obtained from the DSC diagram, as a very sharp exothermic peak was found at 141.9°C either in nitrogen or air atmosphere. No endothermic peak characteristic of dehydration or fusion was evident. The peak integration leads to a value of $-115.5\ J\ g^{-1}$, a result that shows a sudden decomposition of $Ag_4Y$, without fusion. A DSC diagram for the acid form $H_4Y$ also gave a sharp but endothermic peak, at 255.9°C, corresponding to $+594.7\ J\ g^{-1}$. It should be mentioned that some differential thermal analysis diagrams for the EDTA chelates of lanthanides [12] and some divalent metal cations [13] show less sharp decomposition peaks, some of them exothermic.

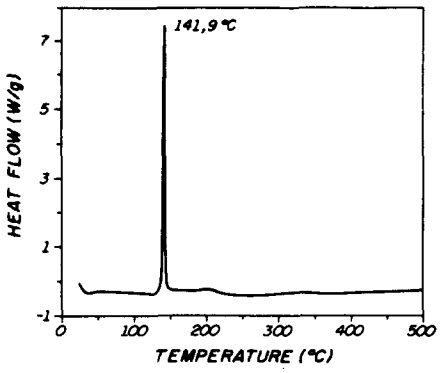


Fig. 5. DSC thermodiagram with 4.80 mg of $Ag_4Y$, showing a sharp exothermic peak at 142°C. Integration leads to $-\Delta H = -115.5\ J\ g^{-1}$.

## Acknowledgments

The authors are greatly indebted to Conselho Nacional de Pesquisa (CNPq), a Brazilian agency, for support.

## References

[1] G. Schwarzenbach and H. Flascka, Complexometric titrations, 2nd edn., Methuen, London, 1969.
[2] H.A. Flascka, EDTA Titrations, 2nd edn., Pergamon Press, London, 1964.
[3] R. Pribil, Applied Complexometry, Pergamon Press, Oxford, 1982.
[4] G. Schwarzenbach, unpublished results; see also Ref. [2].
[5] L.G. Sillen and A.E. Martell, Stability Constants of Metal Ion Complexes, Section I: Inorganic Ligands, The Chemical Society, London, 1960.
[6] H. Flascka and F. Huditz, Fresenius' Z. Anal. Chem., 137 (1952) 104.
[7] P. Klein and V. Skrivánek, Chem. Prum., 12 (1962) 359.
[8] M.V. Rossi, E.F.A. Neves and M.E.V. Suárez-Iha, Analyst, 119 (1994) 1633.
[9] J. Bjerrum, Chem. Rev., 46 (1950) 381.
[10] F.H. MacDougall and S. Peterson, J. Phys. Colloid Chem., 51 (1947) 1346.
[11] G. Schwarzenbach and H. Ackerman, Helv. Chim. Acta, 80 (1947) 1798.
[12] A. Mercadante, M Ionashiro, L.C.S. De Oliveira, C.A. Ribeiro and L. Moscardini D'Assunção, Thermochim. Acta, 216 (1993) 267.
[13] M. Spirandeli Crespi, C.A Ribeiro and M. Ionashiro, Thermochim. Acta, 221 (1993) 63.

ELSEVIER

Talanta 42 (1995) 2033–2038

Talanta

# Two trends of sample dispersion variation with carrier flow rate in a single flow-injection manifold

Yonghung Li, Huichang Ma *

*Research Center for Eco-Environmental Sciences, Academia Sinica, P.O. Box 2871, Beijing 100085, China*

Received 3 January 1995; revised 7 July 1995; accepted 17 July 1995

**Abstract**

Two trends of sample dispersion variation with carrier flow rate in a single flow-injection manifold are completely revealed for the first time and an inflection point in the dispersion coefficient ($D$) vs. flow rate ($q$) curve is discovered. With the increase of the flow rate, the value of $D$ increases before the inflection point but decreases after the inflection point. The value of the carrier flow rate at the inflection point ($q_m$) is independent of the sample injection volume, the tube length, the tube coil radius and the tube inner diameter. It is only affected by the substance diffusion coefficient ($D_m$) of the analysis. The value of $q_m$ decreases as $D_m$ increases. Therefore, the value of $D_m$ for a sample can be estimated according to the $D_m$ vs. $q_m$ curve.

*Keywords:* Sample dispersion variation; Carrier flow rate; Flow-injection manifold

## 1. Introduction

In the flow injection analysis (FIA), the dispersion coefficient ($D$) is defined as $D = C^0/C$, i.e. as the ratio of the concentrations before and after the dispersion process has taken place in the individual elements of fluid. If a readout is taken of $C = C^{max}$, i.e. the element corresponding to the maximum on the output curves, then $D = C^0/C^{max}$. Since the dispersion coefficient represents the degree of dilution of the sample, the value of $D$ directly affects the sensitivity of any flow injection assay. Therefore, the study of the sample dispersion coefficient is very important in basic FIA research.

It is well known in FIA that the factors predominantly affecting the sample dispersion are the sample injection volume ($V_{inj}$), the tube length ($L$) and inner diameter ($d$), the tube coil radius ($R_c$), the carrier flow rate ($q$), the diffusion coefficient of the analyte ($D_m$) and temperature. The originators of FIA, Ruzicka and Hansen [1], determined that the value of $D$ decreases with decreasing flow rate in a single flow injection manifold. However, Li and Narusawa [2] demonstrated in their experiments that the value of $D$ gradually increases with a decrease in flow rate. Gomez-Nieto et al. [3] gave an empirical formula, $D = 2.342L^{0.167}q^{-0.206}d^{0.495}$, which indicates that $D$ is inversely proportional to the flow rate. Thus, there are two completely different opinions. Up until now, no satisfactory explanation has been given for this.

Since flow rate is an important factor which affects the dispersion coefficient, this paper will investigate and experimentally test these two opinions and try to offer a reasonable explanation, which it is hoped will be instructive to experimentalists who wish to design flow injection systems.

* Corresponding author.

*SSDI* 0039-9140(95)01693-7

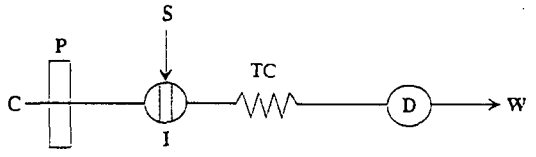


Fig. 1. Manifold for the single flow injection system: P, peristaltic pump; I, injection value; TC, tube coil (made of PTFE); D, detector (with a flow cell of 18 μl and 10 mm pathlength); S, sample; C, carrier; W, waste.

## 2. Experimental

### 2.1. Reagents

Aqueous solutions of $1.59 \times 10^{-2}$ M $Cu(NH_3)_4^{2+}$ in 1.0 M ammonia and 1.0 M ammonia were mainly used as sample and carrier respectively. The sample solution was prepared by dissolving 0.400 g $CuSO_4 \cdot 5H_2O$ in 100 ml of 1.0 M ammonia. Other colored inorganic chemicals such as $K_3Fe(CN)_6$ and $K_2Cr_2O_7$ were also used as samples.

All reagents used were of analytical reagent grade and were obtained from Peking Chemical Works, Peking, China. All solutions were prepared with distilled water.

### 2.2. Apparatus

An FIA-91 flow injection analyzer (made in Shanghai No. 3 Analytical Instrument Factory) was used. This is an integrated instrument which consists of two four-channel peristaltic pumps, a 16-port valve, a grating spectrophotometric detector, a Laser PP40 X–Y printer plotter and a microcomputer system. Program control and data processing are conducted automatically by the microcomputer system.

### 2.3. Procedure

The manifold of the single channel FIA system used is shown in Fig. 1. As can be seen from Fig. 1, after the sample is injected it is forwarded by the carrier to pass through a certain length of coiled tube and eventually to the spectrophotometric detector. For different values of $V_{inj}$, $L$, $R_c$, $d$ and $D_m$, the effect of flow rate on sample dispersion is observed.

## 3. Results and discussion

### 3.1. Effect of flow rate on dispersion coefficient with different injection volumes

In these experiments, an aqueous solution of $1.59 \times 10^{-2}$ M $Cu(NH_3)_4^{2+}$ in 1.0 M ammonia as spiked sample and an aqueous solution of 1.0 M ammonia as carrier were used. Selected results are listed in Table 1 and a group of $D$ vs. $q$ curves are shown in Fig. 2. The correlations between residence time ($T_r$) and flow rate are listed in Table 2. From Table 1 it can be seen that the residence time increases with increasing injection volume ($V_{inj}$) while the dispersion coefficient decreases. For identical values of $V_{inj}$, $T_r$ decreases with increasing flow rate.

From Fig. 2 it is obvious that there is an inflection point (where $dD/dq = 0$) in the $D$ vs. $q$ curve. With increasing flow rate the value of $D$ increases before this point but decreases after this point. The value of $q$ at the inflection point ($q_m$) is independent of the injection volume.

In a single FIA system, $T_r$ decreases as $q$ increases. Ruzicka and Hansen [4] have given a theoretical formula, $D = 2qT_r^{1/2}t_i^{1/2}/W_0\pi(d/2)^2$, where $t_i$ is the mean residence time and $W_0$ is

Table 1
Experimental data obtained for the determination of $Cu(NH_3)_4^{2+}$ dispersion

| $q$ (ml min$^{-1}$) | $V_{inj}$ (μl) | | | | | | | | | |
|---|---|---|---|---|---|---|---|---|---|---|
| | 40 | | 80 | | 120 | | 160 | | 180 | |
| | $T_r$ (s) | $D$ | $T_r$ (s) | $D$ | $T_r$ (s) | $D$ | $T_r$ (s) | $D$ | $T_r$ (s) | $D$ |
| 1.22 | 41.44 | 4.02 | 42.38 | 2.36 | 44.06 | 1.79 | 45.50 | 1.53 | 47.02 | 1.38 |
| 1.53 | 33.62 | 4.14 | 34.37 | 2.43 | 35.71 | 1.83 | 36.89 | 1.55 | 37.91 | 1.39 |
| 2.48 | 21.72 | 4.67 | 22.22 | 2.64 | 23.00 | 1.93 | 23.60 | 1.62 | 24.40 | 1.43 |
| 3.23 | 17.60 | 5.23 | 18.06 | 2.94 | 18.50 | 2.13 | 19.28 | 1.76 | 20.28 | 1.56 |
| 4.29 | 12.66 | 4.89 | 13.20 | 2.82 | 13.62 | 2.00 | 14.02 | 1.70 | 14.10 | 1.48 |
| 5.45 | 10.16 | 4.20 | 10.43 | 2.53 | 10.86 | 1.89 | 11.16 | 1.57 | 11.48 | 1.40 |
| 7.14 | 7.56 | 3.71 | 7.86 | 2.26 | 8.19 | 1.78 | 8.34 | 1.57 | 8.38 | 1.40 |

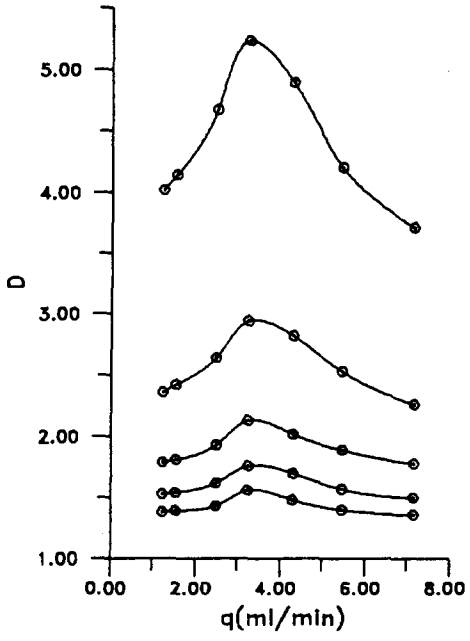


Fig. 2. The $D$ vs. $q$ curves with various injection volumes (tube: $L = 233$ cm; $d = 0.5$ mm; $R_c = 1.0$ cm).

Table 2
The equations of $\lg T_r = a \lg q + b$ ($r$ = correlation coefficient)

| $V_{inj}$ (μl) | Before inflection point | | After inflection point | |
|---|---|---|---|---|
| | $a$ | $r$ | $a$ | $r$ |
| 40 | −0.886 | −0.9996 | −1.052 | −0.9978 |
| 80 | −0.884 | −0.9995 | −1.042 | −0.9940 |
| 120 | −0.896 | −0.9998 | −1.021 | −0.9993 |
| 160 | −0.891 | −0.9993 | −1.047 | −0.9989 |
| 200 | −0.879 | −0.9985 | −1.091 | −0.9941 |

independent of $q$ and $t$. It is known that $t_i = kL/q$ ($k$ = constant). Thus, $D + f(qT_r)^{1/2}$ ($f$ = constant). If $T_r = fq^{-1}$ ($f$ = constant), the two effects, with the inverse changes of $T_r$ and $q$ on the dispersion coefficient, can offset each other. However, Table 2 shows that $T_r = fq^{-0.886}$ ($f$ = constant, $a_{mean} = -0.886$) before the inflection point. This means that $T_r$ decreases more slowly with increasing flow rate than is to be expected. The relative longer $T_r$ time makes $D$ increase with the increase in flow rate. However, after the inflection point, $T_r = fq^{-1.051}$ ($f$ = constant, $a_{mean} = -1.051$) which means that $T_r$ decreases more quickly with increasing flow rate than expected. The relative shorter $T_r$ time makes $D$ decrease with the increase in flow rate. Treating the data in the paper of Li and Narusawa [2] statistically, we obtained $T_r = fq^{-1.018}$ ($f$ = constant, $r = -0.9991$). From Gomez-Nieto et al. [3] we can show that the relationship between $T_r$ and $q$ is $T_r = fq^{-1.022}$ ($f$ = constant, $r = -0.9993$) when $d = 0.35$ mm and $L = 104$ cm or when $d = 0.5$ mm and $L = 154$ cm. The indices of $q$ are both smaller than $-1.0$ while these two papers have the same conclusion, i.e. that $D$ gradually decreases as $q$ increases.

Thus, it is clear that the view of Ruzicka and Hansen [4] coincides with the part before the inflection point while of view of Li and Narusawa [2] coincides with the part after the inflection point in this experiment. Therefore, this experiment has clearly revealed the two trends of sample dispersion variation with flow rate.

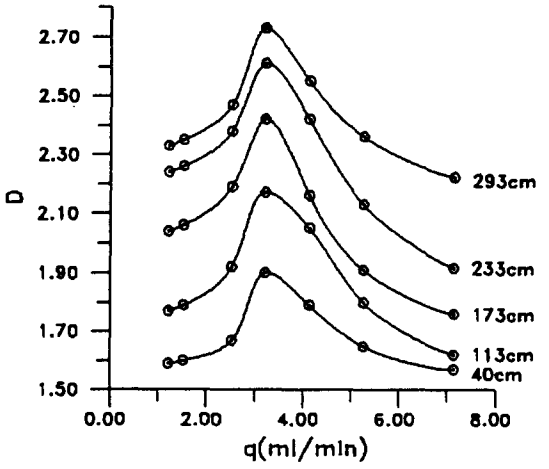


Fig. 3. The $D$ vs. $q$ curves with various tube lengths ($V_{inj} = 80$ μl; tube: $d = 0.5$ mm; $R_c = 1.0$ cm).

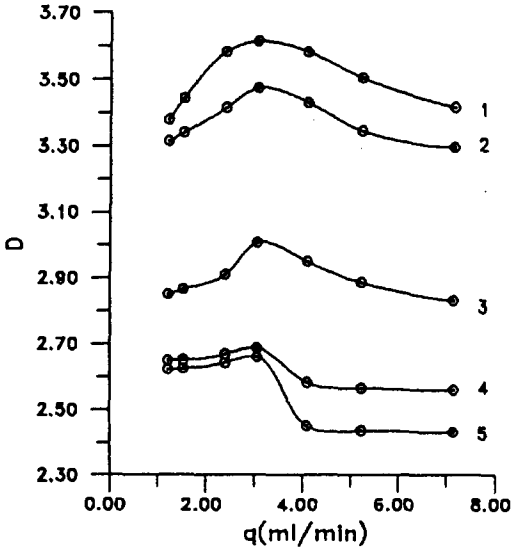


Fig. 4. The $D$ vs. $q$ curves with various tube coil radii ($V_{inj} = 80$ μl, tube: $L = 233$ cm; $d = 0.5$ mm). $R_c$ (cm): (1), 0.5; (2), 1.0; (3), 1.5; (4), 2.0; (5), 2.5.

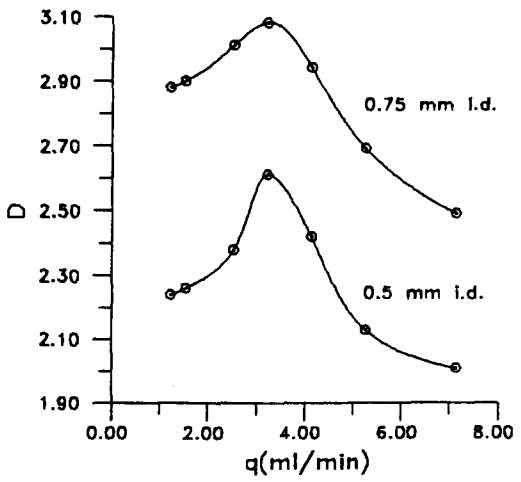


Fig. 5. The $D$ vs. $q$ curves with various tube inner diameters ($V_{inj} = 80$ µl, tube: $L = 233$ cm; $R_c = 1.0$ cm).

### 3.2. *Effect of tube length ($L$) on the D vs. q curve*

The effect of tube length on the correlation between $D$ and $q$ was examined in the range 40–293 cm. Using the same sample and carrier as before, the injection volume was fixed at $V_{inj} = 80$ µl. The results obtained are shown in Fig. 3 which indicates that the value of $D$ increases as $L$ increases at the same flow rate. This is because of longer dispersion times caused by longer tube lengths. According to Fig. 3, it is evident that there is an inflection point in the $D$ vs. $q$ curve at different tube lengths and the value of $q_m$ is constant even as the tube length changes.

### 3.3. *Effect of tube coil radius on the D vs. q curve*

To test the effect of tube coil radius ($R_c$), tube coils of various radii were used. Using the same sample and carrier as before, the FIA system was fixed at $V_{inj} = 80$ µl, tube length $L = 233$ cm. From the results shown in Fig. 4, it is obvious that the value of $D$ increases as the tube coil radius decreases. The results also indicated that there is a inflection point and that the value of $q_m$ remains the same as the tube coil radius varies.

### 3.4. *Effect of tube inner diameter on the D vs. q curve*

The effect of tube inner diameter was investigated by using different inner diameter tubes. The same sample and carrier as before were used and the injection volume was fixed at $V_{inj} = 80$ µl while the tube length was $L = 233$ cm. From the results shown in Fig. 5 it can be seen that $D$ increases as $d$ increases which is identical to former conclusions. The value of $q_m$ remains the same as $d$ varies.

### 3.5. *Effect of the analyte coefficient on the D vs. q curve*

To test the effect of $D_m$, various samples and their corresponding carriers as listed in Table 3 were used. The flow injection manifold was fixed at $V_{inj} = 80$ µl, $L = 233$ cm and $d = 0.5$ mm. The experimental temperature was about 25 °C. The results are shown in Fig. 6.

From Fig. 6 it is obvious that the value of $q_m$ decreases while $D_m$ increases and that $D$ increases with increasing $D_m$ while the flow rate is constant.

It is well known that in a single channel FIA system, the sample dispersion during the flow towards the detector is composed of two parts: one is the convection dispersion which is caused by the flow of the carrier and is directly proportional to the value of the flow rate; the other is the diffusion dispersion which is caused by the diffusion of the analyte and is directly proportional to the diffusion coefficient of the analyte. When $V_{inj}$, $L$, $R_c$, $d$ and $q$ are kept constant, the convection dispersion part remains constant. Therefore, higher dispersion can be obtained because of increased diffusion dispersion of the analyte, i.e. the value of $D$ increases.

It has been shown that before the inflection point, the dispersion increases because of the increase in $q$ and the relatively slower decrease of $T_r$. However, the diffusion dispersion part decreases more quickly for the larger $D_m$ value of the analyte as $T_r$ decreases. Therefore, the value of $q_m$ is smaller when the $D_m$ value of the analyte is larger (Fig. 7).

## 4. Conclusions

The experiments in this paper revealed the law of the variation of sample dispersion coefficient with carrier flow rate in single coiled

Table 3
Samples and carriers used to test the effect of analyte diffusion coefficient on the $D$ vs. $q$ curve (temperature = 25 °C)

| Sample | Carrier | Diffusion coefficient ($\times 10^{-5}$ cm$^2$ s$^{-1}$) |
|---|---|---|
| $4.56 \times 10^{-3}$ M $K_3Fe(CN)_6$ in 1.0 M NaOH[a] | 1.0 M NaOH | 0.45 |
| $2.47 \times 10^{-2}$ M $CuSO_4$ in 0.2 M $H_2SO_4$[b] | 0.2 M $H_2SO_4$ | 0.57 |
| $4.56 \times 10^{-3}$ M $K_3Fe(CN)_6$ in 1.0 M KCl[a] | 1.0 M KCl | 0.76 |
| $4.56 \times 10^{-3}$ M $K_3Fe(CN)_6$[c] | $H_2O$ | 0.96 |
| $6.80 \times 10^{-4}$ M $K_2Cr_2O_7$[c] | $H_2O$ | 1.24 |

[a] Ref. [5]. [b] Ref. [6]. [c] Ref. [7].

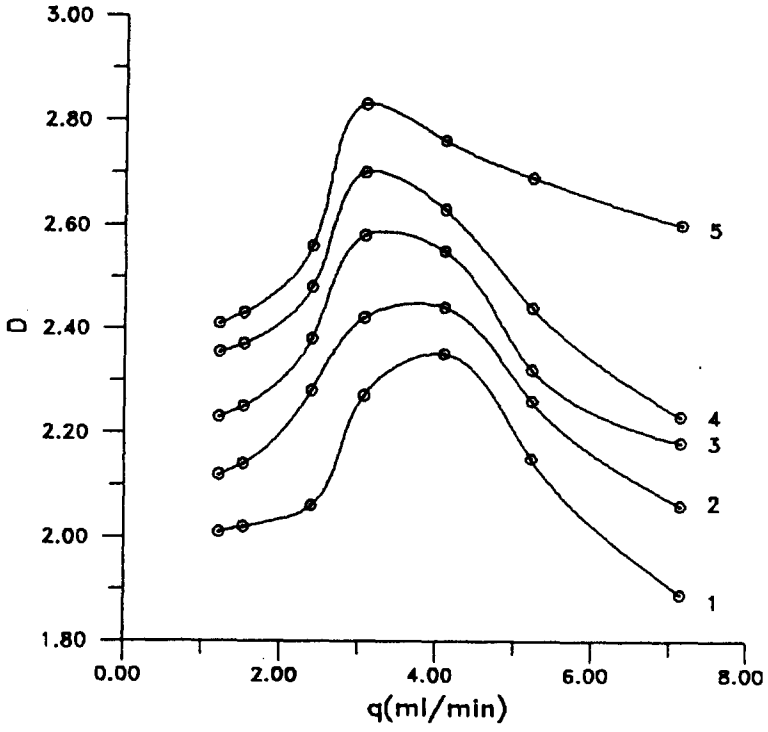


Fig. 6. The $D$ vs. $q$ curves with various analyte diffusion coefficients ($V_{inj} = 80$ μl, tube: $L \approx 233$ cm; $d = 0.5$ mm; $R_c = 1.0$ cm). $D_m$ ($\times 10^{-5}$ cm$^2$ s$^{-1}$: (1), 0.45; (2), 0.57; (3), 0.76; (4), 0.96; (5), 1.24.

tube channel FIA systems and yield the following guidelines which should be useful to experimentalists who wish to design FIA systems.

(1) There is an inflection point (where $dD/dq = 0$) in the $D$ vs. $q$ curve.

(2) With the increase in the flow rate, the value of $D$ increases before the inflection point and decreases after this point.

(3) The value of $q$ at the inflection point is independent of the sample injection volume, the tube length, the tube coil radius and the inner diameter of the tube. It is only affected by the diffusion coefficient of the analyte.

(4) The value of $q_m$ decreases while $D_m$ increases. According to the $q_m$ vs. $D_m$ curve, the $D_m$ value of an unknown analyte can be roughly estimated. Further work on the determination of $D_m$ is now in progress.

## Acknowledgment

The authors gratefully acknowledge Profes-

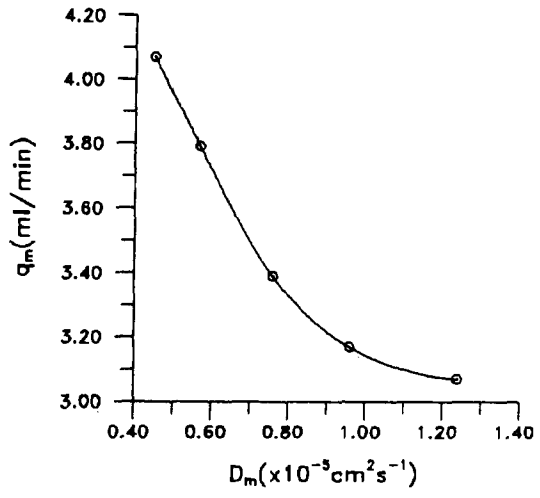


Fig. 7. The effect of $D_m$ on $q_m$ ($V_{inj} = 80$ µl, tube: $L = 233$ cm; $d = 0.5$ mm; $R_c = 1.0$ cm).

sor E. H. Hansen for careful revision of the manuscript.

## References

[1] J. Ruzicka and E.H. Hansen, Flow Injection Analysis, 2nd edn. Wiley, New York, 1988, p. 30.
[2] Y. Li and Y. Narusawa, Anal. Chim. Acta, 289 (1994) 355.
[3] M.A. Gomez-Nieto, M.D. Luque De Castro, A. Martin and M. Valcarcel, Talanta, 32 (1985) 319.
[4] J. Ruzicka and E.H. Hansen, Anal. Chim. Acta, 99 (1978) 37.
[5] G. Gerhardt and R.N. Adams, Anal. Chem., 54 (1982) 2618.
[6] A.J. Bard, Encyclopedia of Electrochemistry of the Elements, Vol. 2, Marcel Dekker, New York, 1974, p. 412.
[7] T. Korenaga, Anal. Chim. Acta, 261 (1992) 539.

ELSEVIER

Talanta 42 (1995) 2039–2042

Talanta

# Selective and efficient uphill transport of Cu(II) through liquid membrane

Afsaneh Safavi *, Saadat Rastegarzadeh

*Department of Chemistry, Shiraz University, Shiraz, Iran*

Received 3 January 1995; revised 29 June 1995; accepted 18 July 1995

**Abstract**

1,2-Bis methyl (2-aminocyclopentene carbodithioate) ethane is an excellent synthetic carrier for efficient and specific transport of Cu(II) ions through a liquid membrane and has the ability to transport Cu(II) ions uphill.

*Keywords:* Liquid membranes; Copper ion transport; Carbodithioate derivatives

## 1. Introduction

The specific transport of metal ions through a membrane is widely known to play an essential role in biological processes [1]. Selective transport of transition metal ions through liquid membranes has become increasingly noteworthy. So far, a number of carriers for heavy metal ions have been reported [2–5], but there are a few which can transport then not only selectively but also efficiently. Different methods for the specific transport of Cu(II) ions across a liquid membrane have the drawbacks of a slow rate of transport or a lack of high selectivity. For example, it has been reported [2] that the urea-containing octameric oligomer $[-CH_2CH_2N(CONHPh)-]_8$ provided the selective passive transport of copper ion through a liquid membrane. However, the flux of transport was small; after 24 h only 37% of total copper ion was transported.

The use of 6-amino-6'-dodecylamino-2,2'-bipyridine [3] as a suitable carrier for the transport of Cu(II) through a liquid membrane showed that after 20 h 50% of the total Cu(II) was transported to the receiving phase.

The transport of Cu(II) ion across a liquid dichloromethane membrane containing a lipophilic dioxycyclam derivative has also been reported [5]. The percentage of Cu(II) transported after 53.5 h was $65 \pm 5\%$.

It was also reported that *N,N'*-bis(8-quinolyl)glutaramide [6] can selectively and effectively transport copper ion (63%) through a chloroform membrane after 2 days. A liquid membrane system with simultaneous proton counter-transport was developed for selective solvent extraction of Cu(II) over Ni(II) and Co(II), using benzoylacetone as a mobile carrier [7], but its selectivity has been questioned [8].

Therefore, the development of effective and specific systems for studying the transport of metal ions, and in particular Cu(II), is still a challenging task from both the practical and theoretical viewpoints.

1,2-Bis methyl (2-aminocyclopentene carbodithioate)ethane (BMACD) (Fig. 1) has been shown to react with Cu(II), and the complex mimics the properties of "blue copper(II)" proteins and oxidases [10,11]. Here, we report that BMACD is an excellent carrier for the specific, rapid and uphill transport of Cu(II) ions through a liquid membrane, which may mimic the characteristics of biological transport.

* Corresponding author.

*SSDI* 0039-9140(95)01694-5

## 2. Experimental

### 2.1. Synthesis of the ligand

The ligand BMACD was synthesized according to the procedure described previously [12].

### 2.2. Transport experiments

All the transport experiments were carried out at ambient temperature (25°C). The cell used for the transport experiments was a cylindrical glass cell (4.0 cm i.d.) holding a glass tube (2.0 cm i.d.) which separated two aqueous phases. The liquid membrane (30 ml of $CH_2Cl_2$ solution of BMACD, $2.7 \times 10^{-3}$ M) was located at the botton of the glass beaker lying below two aqueous phases, and bridging them. The aqueous source phase (2.5 ml) contained one or several kinds of metal ions out of Cu(II), Ni(II), Co(II) and Zn(II) ($10^{-4}$ M) buffered at pH 6.5 with ammonium buffer. The receiving phase (10 ml) contained threonine (0.038 M) at pH 1.8 which acts as a "scavenger" for the transported metal. The cell was covered with aluminum foil to minimize evaporation and light exposure. The organic layer was magnetically stirred by a Teflon-coated bar (27 mm × 5 mm diameter). In the course of the transport experiment, samples of both aqueous phases were analyzed for metal content by atomic absorption spectroscopy (AAS). A similar experiment was carried out in the absence of carrier ligand for reference.

### 2.3. Physical measurements

pH measurements on the aqueous layers were performed by using a combined glass electrode with a Corning pH meter 125. AAS analyses were performed on a Pye Unicam SPQ atomic absorption spectrophotometer.

## 3. Results and discussion

BMACD (Fig. 1) has the desired Cu(II) transport ability which can transport Cu(II) against its concentration gradient. In particular, it is a multidentate ligand which allows the formation of a fairly stable 1:1 complex and also the process of formation of the metal–carrier complex at the aqueous source phase/organic layer membrane interface (as well as the demetalation process at the membrane/receiving phase interface) is sufficiently fast.

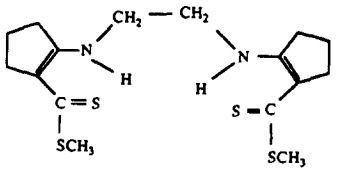


Fig. 1. Molecular structure of BMACD.

It has been reported before [12] that complexation between BMACD and Cu(II) occurs through deprotonation of the ligand. In preliminary experiments, the acidity of the receiving phase was adjusted with different buffers such as citrate, phthalate or sulfuric acid. The results are shown in Table 1. However, later, it was decided to study the effect of the presence of different amino acids in the receiving phase as scavenger for the metal ion (Table 2). The results revealed that although with citrate buffer (pH 3.5) in the receiving phase the transport of Cu(II) ion is possible, the use of amino acids can induce an uphill transport of the cation with a much higher flux and among the different amino acids tried threonine was found to be the most effective metal scavenger.

As expected a minor leaching effect of the ligand into the aqueous phase(s) was observed in the pH range of 1–4. This could be due to the ligand protonation and subsequent stabilization in the aqueous phase(s). Since the leaching only involved charged species, the problem was overcome by introduction of a lipophilic counter ion (such as a fatty acid) in the organic phase which can impart a greater degree of lipophilicity to the charged species.

Table 1
Effect of acidity of the receiving phase adjusted by different compounds on the transport of Cu(II) ion. Experimental conditions: source phase, 2 ml of $1.1 \times 10^{-4}$ M $Cu^{2+}$ ion, pH 7.5; liquid membrane phase, 35 ml of $1.0 \times 10^{-3}$ M BMACD and $1.0 \times 10^{-3}$ M palmitic acid in dichloromethane; receiving phase, 10 ml 0.1 M solution of each compound; rate of stirring = 250 rev $min^{-1}$

| Receiving phase | pH | Time (h) | % Transport to receiving phase |
|---|---|---|---|
| Citrate | 3.5 | 10.15′ | 66.43 |
| | 4.5 | 9.50′ | 0 |
| | 1.75 | 6.15′ | 2.49 |
| Phthalate | 3.16 | 10.15′ | 0 |
| Vitamin C | 3.45 | 7.00′ | 0 |
| $H_2SO_4$ (1 M) | 1 M | 11.40′ | 28.83 |
| Glycine | 3.00 | 10 | 0 |
| | 1.02 | 10 | 42.54 |

Table 2
Effect of receiving phase composition on the transport of Cu(II) ion. Experimental conditions: source phase, 2 ml of $1.1 \times 10^{-4}$ M $Cu^{2+}$ ion, pH 7.5; liquid membrane phase, 35 ml of $10^{-3}$ M BMACD and palmitic acid in dichloromethane; receiving phase, 10 ml 0.1 M solution of each species; pH 1.75; time of transport: 6 h 15′; rate of stirring = 250 rev $min^{-1}$

| Receiving phase | % Transport to receiving phase |
|---|---|
| L-Threonine | 80.2 |
| Arginine | 68.6 |
| Cysteine | 47.4 |
| Glycine | 24.75 |
| Histidine | 17.24 |
| Asparagine | 5.71 |
| Citrate | 2.49 |
| Tryptophan | 0 |

The fatty acid used in this study was palmitic acid, whose concentration was optimized together with other variables in the system via a simplex program. Simplex optimization gave the following conditions as the best for the transport of Cu(II): pH of the source, 6.5; concentration of BMACD, $2.7 \times 10^{-3}$ M; pH of receiving phase, 1.8 adjusted by HCl; volume of source, 2.5 ml; concentration of palmitic acid, $1.9 \times 10^{-3}$ M; volume of receiving phase, 10 ml; concentration of threonine, $3.8 \times 10^{-2}$ M. Using the above optimum conditions, almost all the copper (≈94%) can be transported in less than 3.5 h.

### 3.1. Transport of metal ions

The membrane system operated here is illustrated schematically in Fig. 2. After complexation of a carrier with a metal ion on the left side of the membrane, the complex formed diffuses down its concentration gradient. On the right side of the membrane, the metal ion is released into the receiving phase, probably via a combination of two mechanisms, namely proton exchange [12] and ternary complex formation [13] (ligand–metal–threonine). The released carrier in the neutral form diffuses back

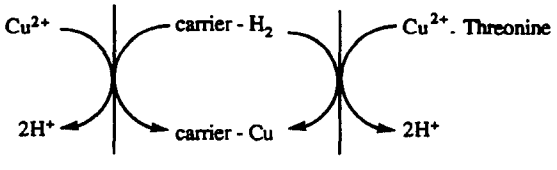


Fig. 2. Liquid membrane system for transport of Cu(II).

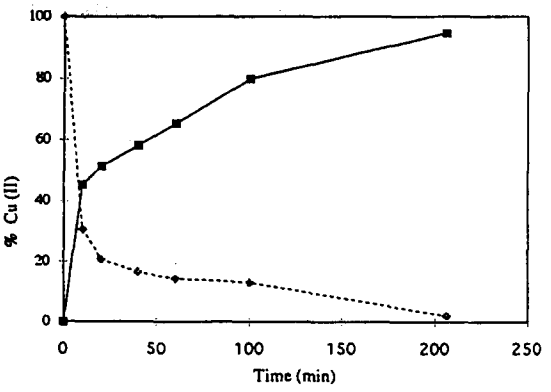


Fig. 3. A plot of Cu(II) ion transport by BMACD vs. time under optimum conditions. (– – –) shows amount of Cu(II) ions in source phase and (—) in receiving phase.

across the membrane. The net result is the transport of metal ion from the source phase, on the left, to the receiving phase, on the right, across the liquid membrane.

Permeability of the membrane system for $Cu^{2+}$ ion also depends largely on the nature of the amino acid in the receiving phase. The presence of a suitable amino acid in the receiving phase is believed to play an essential role in the metal ion releasing process via formation of a ternary complex, carrier–$Cu^{2+}$–amino acid. Such ternary complexes have been recognized as being an important transient species in biological processes [13,14]. Thus, the presence of threonine in the receiving phase and formation of the above-mentioned copper complex reduces the concentration of free Cu(II) ion in the receiving phase and consequently increases the concentration gradient between the two aqueous phases, which in turn results in a higher transport flux. Furthermore, amino acids are hardly soluble in the membrane phase and hence they are found to scarcely move into the aqueous source phase.

It is noteworthy that log $K$ for cation-receiving phase ligand interaction is a very important parameter for determining cation transport selectivity [15], because the larger log $K$, the smaller the concentration of free cation in the receiving phase and the larger the concentration gradient between the aqueous phases. However, towards this end, the importance of the kinetics of liberation of the cation into the receiving phase and its effect on the selectivity of transport should not be ruled out [16].

Additionally the concentration–time profile of Cu(II) transport was studied. Fig. 3 shows a rapid rise in metal concentration in the receiving phase as well as a sharp decrease in Cu(II)

Table 3
Transport of Cu(II) under optimum conditions after 3.5 h in a competitive experiment for an equimolar mixture of Cu(II), Ni(II), Co(II) and Zn(II) in the source phase

| Cation | % Transport to receiving phase | % Remaining in source phase |
|---|---|---|
| $Cu^{2+}$ | 85 | 10 |
| $Ni^{2+}$ | 0 | 100 |
| $Co^{2+}$ | 0 | 100 |
| $Zn^{2+}$ | 0 | 100 |

Table 5
Transport of Cu(II) under optimum conditions after 3.5 h in the presence of equimolar concentrations of Pb(II) and Cd(II)

| Cation | % Transport to receiving phase | % Remaining in source phase |
|---|---|---|
| $Cu^{2+}$ | 94 | 5 |
| $Cd^{2+}$ | – | 100 |
| $Pb^{2+}$ | – | 51 |

concentration of the source phase during the first 20 min of transport.

The selectivity of the above system was studied under the optimum conditions by undertaking competitive transport experiments (starting from an equimolar solution of Cu(II), Ni(II), Co(II) and Zn(II) mixture; the same mixture but with ten times greater concentrations of the interfering ions; and also an equimolar solution of Cu(II), Cd(II) and Pb(II) mixture). The results (Tables 3–5) demonstrate the excellent selectivity of BMACD for transporting Cu(II).

The reproducibility of the transport process was studied by performing the transport experiment several times. The percent relative standard deviation was found to be 2.2%.

## 4. Conclusion

The present study demonstrates that the ligand BMACD is an excellent carrier for selective and efficient transport of Cu(II). The presence of threonine as a "scavenger" in the receiving phase increases the efficiency of transport as well as the speed to a great extent without affecting the selectivity. Uphill transport of Cu(II) against its concentration gradient is easily performed with the above system.

Table 4
Transport of Cu(II) under optimum conditions after 3.5 h in a competitive experiment for a mixture containing Ni(II), Co(II) Zn(II) with concentrations ten times that of Cu(II) in the source phase

| Cation | % Transport to receiving phase | % Remaining in source phase |
|---|---|---|
| $Cu^{2+}$ | 60 | 36.9 |
| $Ni^{2+}$ | – | 85.5 |
| $Co^{2+}$ | – | 89.3 |
| $Zn^{2+}$ | – | 87.5 |

In conclusion, besides the biological importance of the membrane system studies in this work, our experiments demonstrate the potential application for highly selective removal or purification of Cu(II) ion from mixtures with high efficiency, precision and speed.

## Acknowlegment

The authors thank Shiraz University Research Council for support of this work.

## References

[1] Y.A. Ovchinnikov, V.T. Ivanov and A.M. Shkrob, Membrane Active Complexones, Elsevier, Amsterdam, 1974.
[2] K. Maruyama, H. Tsukube and T. Araki, J. Chem. Soc., Dalton Trans., (1981) 1486.
[3] N. Kishii, K. Araki and S. Shiraishi, J. Chem. Soc., Dalton Trans., (1985) 373.
[4] Sh. Dadfarnia and M. Shamsipur, J. Membr. Sci., 75 (1992) 61.
[5] M. Di Casa, L. Fabbrizzi, A. Perotti and P. Tundo, Inorg. Chem., 24 (1985) 1610.
[6] K. Hiratani and K. Taguchi, Chem. Lett., (1990) 725.
[7] D.K. Schiffer, A. Hackhauser, D.F. Euans and E.L. Cassler, Nature, 250 (1974) 484.
[8] K. Maruyama, H. Tsukube and T. Araki, J. Am. Chem. Soc., 102 (1980) 3246.
[9] L.F. Lindoy and D.S. Baldwin, Pure Appl. Chem., 61 (1989) 909.
[10] R.D. Bereman, G.D. Shields, J. Bordner and J.R. Dorfman, Inorg. Chem., 20 (1981) 2165.
[11] R.D. Bereman, M.R. Churchill and G.D. Shields, Inorg. Chem., 18 (1979) 3117.
[12] D.M. Baird, J. Chem. Educ., 62 (1985) 168.
[13] T.P.A. Kruck and B. Sarkar, Inorg. Chem., 14 (1975) 2383.
[14] T. Sakurai and A. Nakahara, Inorg. Chem., 19 (1980) 847.
[15] J.J. Christensen, S.P. Christensen, M.P. Biehi, S.A. Lowe, J.D. Lomb and R.M. Izzatt, Sep. Sci. Technol., 18 (1983) 363.
[16] J. Bolte, C. Demuyunch and G. Jeminet, Can. J. Chem., 63 (1985) 3478.

ELSEVIER

Talanta 42 (1995) 2043–2051

Talanta

# Simultaneous spectrophotometric determination of three food dyes by using the first derivative of ratio spectra

J.J. Berzas Nevado, C. Guiberteau Cabanillas, A.M. Contento Salcedo

*Department of Analytical Chemistry and Foods Technology, University of Castilla-La Mancha 13071, Ciudad Real, Spain*

Received 15 February 1995; revised 13 July 1995; accepted 14 July 1995

**Abstract**

Ternary mixtures of colorants E-123 (Amaranth), E-124 (Ponceau 4R) and E-120 (Carminic acid) are resolved by using the first derivative ratio spectrum–zero crossing method without the need for any separation step. Calibration graphs were linear up to 64 mg $l^{-1}$ of carminic acid, 32 mg $l^{-1}$ of Amaranth and 32 mg $l^{-1}$ of Ponceau 4R. The method was applied to different commercial food products and results concordant with high performance liquid chromatography were obtained.

*Keywords:* Food dyes; First derivative spectrophotometry

## 1. Introduction

Color is the first sensory quality by which foods are judged, and food quality and flavor are closely associated with color. Amaranth and Ponceau 4R are two synthetic azo dyes available as red powders that can be present in common foods, drinks, yoghurts, gelatines, etc. These colorants must be named in the list of ingredients after an extensive study of the genotoxicity of food, drugs, cosmetic color and other azo, tryphenylmethane and xanthrene dyes completed by Combes and Haveland-Smith [1]. If these colorants come into contact with some kinds of drugs (e.g. aspirin, benzoic acid) within the human body they can induce allergic and asthmatic reactions in sensitive people. Carminic acid is another natural colorant which is also present in the same kind of foods as Amaranth and Ponceau 4R. The presence and amounts of these three dyes must be controlled as none of them are totally inoccuous. Taking into account the chromophoric characteristics of the three compounds, visible spectrophotometric methods can be used for their quantitative analysis. However, the absorption spectra of Amaranth, Ponceau 4R and carminic acid are very overlapped and direct measurements of the absorbance are not suitable for resolving mixtures of these colorants without a separation step.

Chromatographic methods have been used for colorant analysis in food [2–4]. These techniques are very suitable when the sample contains several colorants. However taking into account other factors such as economy and rapidity, multicomponent analysis by spectrophotometric methods can be a good choice for resolving the colorants contents in food.

Sasaki and co-workers [5,6], Zhang and Huang [7], Momosaki and Fujimoyo [8] and Zeng and co-workers [9,10], proposed quantitative analysis of food colors and similar dyes by multiwavelength measurements. Sasaki [11,12] determined food colorants by derivative spectrophotometry.

We have developed the "derivative of ratio spectra method" which allows the resolution of


*SSDI* 0039-9140(95)01695-3

binary mixtures [13] of chromophores with overlapped spectra. The method is based on the measurements of signal greatest sensitivity, usually a maximum or a minimum in the derivative ratio spectra. The method was extended to resolving ternary mixtures by the simultaneous use of the zero crossing method and derivative of ratio spectra method [14]. In this case the measurements are made at zero crossing wavelengths.

In previous papers we have used this method for resolving different binary and ternary mixtures of colorants [15–18].

Previously, we have proposed methods to determine Amaranth and Ponceau 4R in a binary mixture [15] using the first derivative of ratio spectra as well as the first derivative of absorption spectra. The method was applied to different commercial products containing these colorants. In this paper we include a third colorant, carminic acid, with the aim of demonstrating the ease with which the derivative methods (ratio spectra) circumvent the problem of overlapping spectral bands, so allowing the simultaneous determination of these three dyes (Amaranth, Ponceau 4R and carminic acid) without prior separation.

The proposed method was applied to different commercial products and the results compared with those obtained with high performance liquid chromatography (HPLC) technique used as reference.

## 2. Experimental

### 2.1. Apparatus

A Beckman Instruments DU-70 Spectrophotometer connected to an EMC fitted with Beckman Data Leader Software [19] and an HP DeskJet 510 Printer were used for all the measurements and treatment of data.

### 2.2. Solutions

All solvents and reagents were of analytical reagent grade. Amaranth and Ponceau 4R aqueous solutions were prepared from Aldrich products and carminic acid aqueous solution from Sigma products. Amaranth, Ponceau 4R and carminic acid stock solutions have a concentration of 200 mg $l^{-1}$. Acetic acid/sodium acetate buffer (0.1 M and pH 4.8) was made from analytical reagent grade materials.

### 2.3. Procedure

Samples were prepared in 25 ml calibrated flasks containing 2–32 mg $l^{-1}$ of Amaranth or 2–32 mg $l^{-1}$ of Ponceau 4R or 8–64 mg $l^{-1}$ of carminic acid or their ternary mixtures and 5 ml of pH 4.8 buffer solution and were diluted with water to the mark. The concentration ratio range of the colorants used in the ternary mixtures was 1:0.7 to 1:4 (determined colorant: total interferent colorants). The absorption spectra of the samples thus prepared were recorded against water at 600 nm $min^{-1}$ and stored in the EMC 486.

The stored spectra of Ponceau 4R, carminic acid and ternary mixtures were divided by a 16 mg $l^{-1}$ standard Amaranth spectrum. The first derivatives of the ratio spectra were obtained with $\Delta\lambda_k$ 8 nm and smoothed with the use of 13 experimental points. By measuring the first derivative ratio spectra at the zero crossing points, we can determine Ponceau 4R at 561 nm ($^1DD_{561}$) (zero crossing point of carminic acid) and carminic acid at 373 nm ($^1DD_{373}$) (zero crossing point of Ponceau 4R).

The concentration of Ponceau 4R is proportional to the amplitude at 561 nm and the concentration of carminic acid is proportional to the amplitude at 373 nm. These wavelengths were used to construct the respective calibration graphs.

In contrast, stored spectra of Amaranth and the ternary mixtures were divided by a standard of carminic acid of 16 mg $l^{-1}$. A $\Delta\lambda$ value of 8 nm was used to obtain the first derivative of ratio spectra which were smoothed with the use of 13 experimental points.

Amaranth is determined by measuring at 549.7 nm in the first derivative of ratio spectra ($^1DD_{549.7}$) (zero crossing point of Ponceau 4R). The signal at this wavelength is proportional to the concentration of Amaranth.

## 3. Results and discussion

### 3.1. Method development

The influence of pH on the absorption spectra of the three aqueous solutions of colorants was studied and it was observed that its influence was negligible between 2–9 (for Amaranth), 1–9 (for Ponceau 4R) and 1–5.5 (for carminic acid). A pH of 4.8 was considered suitable for use throughout. Under these condi-

tions diluted solutions of Amaranth, Ponceau 4R and carminic acid were stable for 15 days at least.

In Fig. 1 the absorption spectra of Amaranth, Ponceau 4R, carminic acid and their mixture recorded between 350 and 650 nm are shown. As can be seen, the absorption spectra of the colorants are very overlapped and because of this the determination of the three colorants is not possible by using direct absorbance measurements. The proposed method can resolve this problem.

The determination of two of the dyes in their ternary mixture can be done by using the spectrum of the third colorant of this mixture as divisor. The ratio spectrum is obtained by dividing the amplitudes of the absorption spectrum of the ternary mixture by a standard spectrum of one of the components. When the first derivative of the ratio spectrum is obtained, we have eliminated the contribution to the signal of the component used as divisor. The other two components can be determined by measurement at the zero crossing points as in derivative spectrophotometry.

Thus, it is possible to determine each colorant by using two divisors, e.g. carminic acid can be determined when Amaranth as well as Ponceau 4R is used as divisor.

In order to obtain good resolution it is necessary to study and to optimize the following parameters: concentration of the standard spectrum used as divisor; $\Delta\lambda$ to obtain the first derivative; smoothing function; and the zero crossing points.

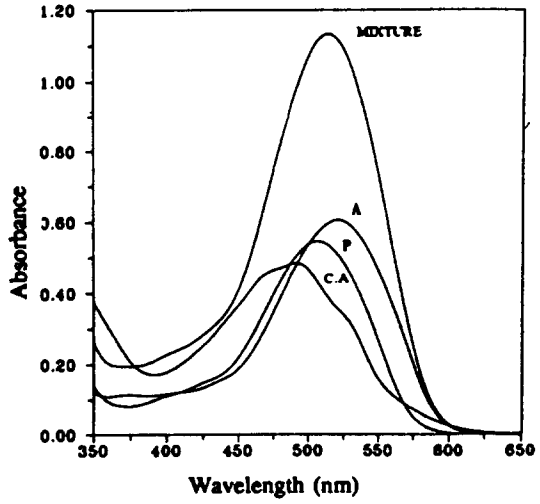


Fig. 1. Absorption spectra of (A) Amaranth (8 mg $l^{-1}$), (P) Ponceau 4R (8 mg $l^{-1}$), (C.A) carminic acid (24 mg $l^{-1}$), and their mixture.

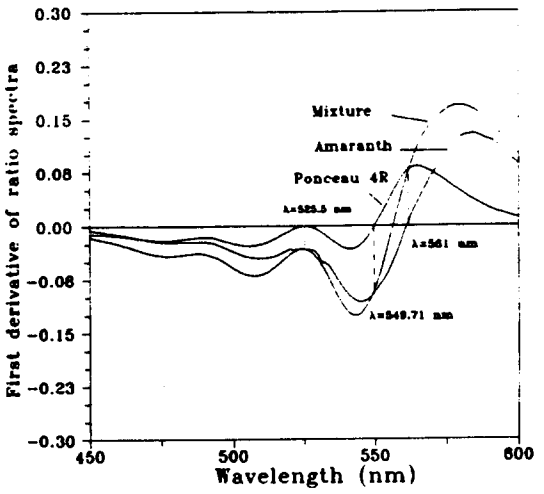


Fig. 2. First derivative of the ratio spectra of Amaranth (8 mg $l^{-1}$), Ponceau 4R (8 mg $l^{-1}$) and ternary mixtures (8 mg $l^{-1}$ of Amaranth, 8 mg $l^{-1}$ of Ponceau 4R and 20 mg $l^{-1}$ of carminic acid) using 32 mg $l^{-1}$ carminic acid spectrum as divisor.

*Determination of Amaranth and Ponceau 4R in the presence of carminic acid*

The influence of the variables mentioned above was studied and the values chosen as optimal were: a standard spectrum of 32 mg $l^{-1}$ of carminic acid to obtain the ratio spectra; a $\Delta\lambda$ value of 8 nm to obtain the first derivative ratio spectra; and 13 experimental points in the smoothing function.

Fig. 2 shows the first derivative ratio spectra of Amaranth, Ponceau 4R and a ternary mixture obtained by using the selected parameter values.

The wavelengths suitable for measuring the signal in the first derivative ratio spectra ($^1DD_\lambda$) were selected taking into account the zero crossing point method. These wavelengths were 561 nm (zero crossing point of the ratio spectrum of Amaranth) to determine Porceau 4R and 549.7 and 525.5 nm (zero crossing point of the ratio spectrum of Ponceau 4R) to determine Amaranth. At these wavelengths the first derivative of ratio spectra of the ternary mixture and standard spectra of Amaranth and Ponceau 4R are coincident, as can be seen in Fig. 2.

The calibration graph of Ponceau 4R was obtained by plotting the $^1DD_{561}$ signal against the concentration and gave a straight line up to 32 mg $l^{-1}$ of Ponceau 4R. For Amaranth, two calibration graphs were obtained at 525.5 nm ($^1DD_{525.5}$) and 549.7 nm ($^1DD_{549.7}$) and gave straight lines up to 32 mg $l^{-1}$ of Amaranth.

*Determination of carminic acid and Ponceau 4R in the presence of Amaranth*

In this case the optimal values established were: a standard spectrum of 16 mg $l^{-1}$ of Amaranth as divisor, a $\Delta\lambda$ value of 8 nm for the derivative ratio spectra, and a smoothing of 13 experimental points. Fig. 3 shows the first derivative ratio spectra of carminic acid and Ponceau 4R. The Ponceau 4R content can be determined by measurement at 561.5, 442.5 and 396.5 nm (zero crossing points for derivative ratio spectra of carminic acid) and carminic acid can be determined by measurement at 459 and 373 nm (zero crossing points for derivative ratio spectra of Ponceau 4R). Calibration graphs were established at wavelengths previously selected and gave straight lines up to 32 mg $l^{-1}$ for Ponceau 4R and 64 mg $l^{-1}$ for carminic acid.

*Determination of carminic acid and Amaranth in the presence of Ponceau 4R*

The values chosen as optimal were: a standard spectrum of 16 mg $l^{-1}$ of Ponceau 4R as divisor, a $\Delta\lambda$ value of 8 nm for first derivative ratio spectra, and a smoothing function of 15 experimental points. Fig. 4 shows the first derivative ratio spectra of carminic acid and Amaranth. As can be seen the carminic acid can be determined by measuring at 460 and 373.5 nm (zero crossing points for derivative ratio spectra of Amaranth) and Amaranth can be determined by measuring at 549.5 and 524 nm (zero crossing points for derivative ratio spectra of carminic acid). Calibration graphs were established at wavelengths selected and gave straight lines up to 32 mg $l^{-1}$ for Amaranth and 64 mg $l^{-1}$ for carminic acid.

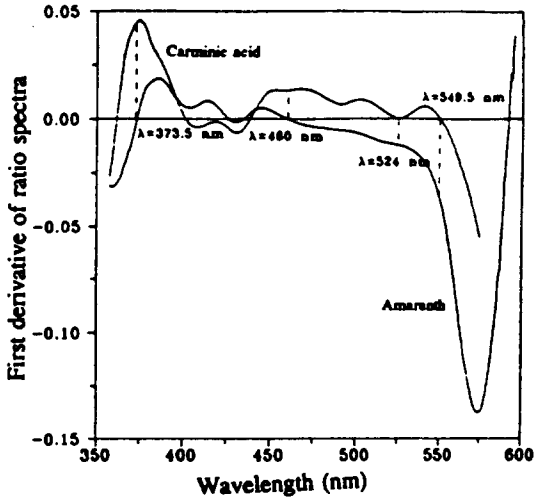


Fig. 4. First derivative of the ratio spectra of carminic acid (32 mg $l^{-1}$) and Amaranth (8 mg $l^{-1}$) using 16 mg $l^{-1}$ Ponceau 4R spectrum as divisor.

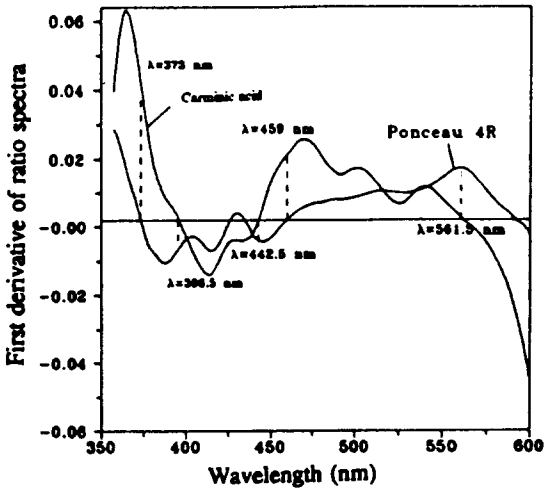


Fig. 3. First derivative of the ratio spectra of carminic acid (32 mg $l^{-1}$) and Ponceau 4R (8 mg $l^{-1}$) using 16 mg $l^{-1}$ Amaranth spectrum as divisor.

### 3.2. Statistical comparative study

Table 1 summarizes the calibration graphs obtained for each dye with each divisor. In all cases good regression coefficients are obtained.

In order to test the precision of the methods replicated samples were measured ($n = 9$) containing Amaranth (8 mg $l^{-1}$), carminic acid (20 mg $l^{-1}$) and Ponceau 4R (8 mg $l^{-1}$) individually (Table 2). The determination limits were calculated for each dye and are shown in the same Table [20,21].

Taking into account the calibration graphs, the reproducibility and the determination limit, we have selected as signals of measurement $^1DD_{549.7}$ and $^1DD_{561}$ to determine Amaranth and Ponceau 4R respectively when carminic acid is used as divisor.

In the case of Amaranth as the divisor, $^1DD_{561.5}$ to determine Ponceau 4R and $^1DD_{373}$ to determine carminic acid were selected. Finally, the determination of Amaranth and carminic acid (when Ponceau 4R is used as divisor) is proposed to be done at $^1DD_{549.5}$ and $^1DD_{524}$ and at $^1DD_{373.5}$ respectively.

Table 1
Calibration graphs ($n = 9$)[a]

| Equation | Regression coefficient | Standard deviation | |
|---|---|---|---|
| | | Slope ($\times 10^6$) | Intercept ($\times 10^4$) |
| Divisor: carminic acid | | | |
| Amaranth (range: 2–32 mg $l^{-1}$): | | | |
| $^1DD_{525.5} = -0.00029 + 0.00163\ C$ | 0.9999 | 0.49 | 0.99 |
| $^1DD_{549.7} = 0.00060 + 0.0058\ C$ | 0.9999 | 1.31 | 2.66 |
| Ponceau 4R (range: 2–32 mg $l^{-1}$): | | | |
| $^1DD_{561} = -0.00068 + 0.0047\ C$ | 0.9999 | 2.16 | 1.02 |
| Divisor: Amaranth | | | |
| Ponceau 4R (range: 2–32 mg $l^{-1}$): | | | |
| $^1DD_{561.5} = -0.00014 + 0.00095\ C$ | 0.9999 | 4.02 | 0.81 |
| $^1DD_{442.5} = 0.000021 + 0.00036\ C$ | 0.9993 | 5.25 | 1.06 |
| $^1DD_{396.5} = -0.00010 + 0.00051\ C$ | 0.9994 | 7.01 | 1.41 |
| Carminic acid (range: 8–64 mg $l^{-1}$): | | | |
| $^1DD_{373} = 0.00086 + 0.00102\ C$ | 0.9997 | 7.15 | 2.89 |
| $^1DD_{459} = 0.000032 + 0.00046\ C$ | 0.9999 | 2.16 | 8.73 |
| Divisor: Ponceau 4R | | | |
| Amaranth (range: 2–32 mg $l^{-1}$): | | | |
| $^1DD_{549.5} = 0.0002 + 0.0022\ C$ | 0.9999 | 5.05 | 1.02 |
| $^1DD_{524} = 0.00015 + 0.00075\ C$ | 0.9999 | 3.38 | 0.68 |
| Carminic acid (range: 8–64 mg $l^{-1}$): | | | |
| $^1DD_{460} = 0.000046 + 0.0004\ C$ | 0.9999 | 1.83 | 0.73 |
| $^1DD_{373.5} = 0.00132 + 0.00136\ C$ | 0.9998 | 9.76 | 3.94 |

[a] Number of points of the calibration graphs.

Table 2
Statistical data

| Signal measured | SD | RSD (%) ($n = 9$) | Determination limit (mg $l^{-1}$)[a] |
|---|---|---|---|
| Divisor: carminic acid | | | |
| Amaranth | | | |
| $^1DD_{525.5}$ | 0.1435 | 1.82 | 0.445 |
| $^1DD_{549.7}$ | 0.2483 | 3.05 | 0.269 |
| Ponceau 4R | | | |
| $^1DD_{561}$ | 0.4747 | 6.24 | 0.001 |
| Divisor: Amaranth | | | |
| Ponceau 4R | | | |
| $^1DD_{561.5}$ | 0.3063 | 3.78 | 0.001 |
| $^1DD_{442.5}$ | 0.2951 | 3.43 | 1.453 |
| $^1DD_{396.5}$ | 0.6327 | 7.47 | 2.202 |
| Carminic acid | | | |
| $^1DD_{373}$ | 0.5753 | 1.86 | 1.892 |
| $^1DD_{459}$ | 1.1887 | 3.72 | 1.523 |
| Divisor: Ponceau 4R | | | |
| Amaranth | | | |
| $^1DD_{549.5}$ | 0.2507 | 3.11 | 0.378 |
| $^1DD_{524}$ | 0.2240 | 2.85 | 0.935 |
| Carminic acid | | | |
| $^1DD_{460}$ | 0.3943 | 1.22 | 2.208 |
| $^1DD_{373.5}$ | 0.7989 | 2.48 | 1.863 |

[a] $C_Q = \frac{10S_B}{m}$ where $C_Q$ = determination limit; $S_B$ = standard deviation of blank; $m$ = slope of calibration.

Table 3
Results obtained for determining Amaranth and Ponceau 4R in synthetic mixtures using carminic acid (32 mg $l^{-1}$) as divisor

| Composition of mixtures (mg $l^{-1}$) | | | % recovery | |
|---|---|---|---|---|
| | | | Amaranth | Ponceau 4R |
| A | P | C.A | $^1DD_{549.7}$[a] | $^1DD_{561}$[a] |
| 12 | 12 | 12 | 101.25 | 93.00 |
| 24 | 12 | 12 | 95.45 | 85.91 |
| 12 | 12 | 24 | 99.25 | 94.37 |
| 12 | 24 | 12 | 92.16 | 93.91 |
| 24 | 24 | 12 | 102.04 | 96.04 |
| 24 | 12 | 24 | 97.50 | 95.00 |
| 12 | 24 | 24 | 102.08 | 95.91 |
| 10 | 10 | 30 | 92.60 | 105.20 |
| 12 | 36 | 12 | 103.25 | 96.25 |
| 36 | 12 | 12 | 102.00 | 104.30 |
| Statistical parameters[b] | | | | |
| $X$ (% means of recovery) | | | 98.76 | 97.11 |
| $S$ | | | 4.12 | 4.46 |
| $S_m$ | | | 1.30 | 1.48 |

[a] Means of three determinations.
[b] Values of recoveries higher than 110% or smaller than 90% have not been considered for calculating these parameters.

Table 4
Results obtained for determining carminic acid and Ponceau 4R in synthetic mixtures using Amaranth (16 mg $l^{-1}$) as divisor

| Composition of mixtures (mg $l^{-1}$) | | | % recovery | |
|---|---|---|---|---|
| | | | Carminic acid | Ponceau 4R |
| A | P | C.A | $^1DD_{373}$[a] | $^1DD_{561.5}$[a] |
| 12 | 12 | 12 | 100.91 | 99.83 |
| 24 | 12 | 12 | 90.73 | 100.75 |
| 12 | 12 | 24 | 98.33 | 97.25 |
| 12 | 24 | 12 | 92.83 | 101.00 |
| 24 | 24 | 12 | 98.02 | 95.75 |
| 24 | 12 | 24 | 95.65 | 99.83 |
| 12 | 24 | 24 | 98.33 | 97.08 |
| 10 | 10 | 30 | 95.87 | 103.33 |
| 12 | 36 | 12 | 96.83 | 97.30 |
| 36 | 12 | 12 | 91.35 | 95.45 |
| Statistical parameters | | | | |
| $X$ (% means of recovery) | | | 95.88 | 98.75 |
| $S$ | | | 3.32 | 2.57 |
| $S_m$ | | | 1.05 | 0.81 |

[a] Means of three determinations.

## 4. Applications

### 4.1. Synthetic mixtures

The proposed method was applied for resolving the determination of Amaranth, Ponceau 4R and carminic acid in synthetic mixtures prepared in different proportions. The results corresponding to these determinations are summarized in Tables 3–5.

Taking into account the recoveries obtained, as well as the calibration graphs and the statis-

Table 5
Results obtained for determining Amaranth and carminic acid in synthetic mixtures using Ponceau 4R (16 mg $l^{-1}$) as divisor

| Composition of mixtures (mg $l^{-1}$) | | | % recovery | | |
|---|---|---|---|---|---|
| | | | Amaranth | | Carminic acid |
| A | P | C.A | $^1DD_{549.5}$[a] | $^1DD_{524}$[a] | $^1DD_{373.5}$[a] |
| 12 | 12 | 12 | 99.86 | 100.70 | 92.62 |
| 24 | 12 | 12 | 95.22 | 97.16 | 82.33 |
| 12 | 12 | 24 | 96.88 | 97.40 | 93.75 |
| 12 | 24 | 12 | 95.05 | 95.20 | 88.00 |
| 24 | 24 | 12 | 98.57 | 99.37 | 79.25 |
| 24 | 12 | 24 | 95.00 | 97.16 | 92.30 |
| 12 | 24 | 24 | 95.35 | 97.40 | 93.00 |
| 10 | 10 | 30 | 88.10 | 94.41 | 89.99 |
| 12 | 36 | 12 | 95.02 | 98.50 | 71.33 |
| 36 | 12 | 12 | 97.54 | 97.35 | 81.05 |
| Statistical parameters[b] | | | | | |
| $X$ (% means of recovery) | | | 96.45 | 97.46 | – |
| $S$ | | | 1.81 | 1.82 | – |
| $S_m$ | | | 0.60 | 0.57 | – |

[a] Means of three determinations.
[b] Values of recoveries higher than 110% or smaller than 90% have not been considered for calculating these parameters.

Table 6
Results obtained for the determination of Amaranth, Ponceau 4R and carminic acid in commercial food products by the method proposed

| Carminic acid (mg $kg^{-1}$ added) | Standard addition | | | Direct preparation | | |
|---|---|---|---|---|---|---|
| | C.A[a] (mg $kg^{-1}$) | A[b] (mg $kg^{-1}$) | P[c] (mg $kg^{-1}$) | C.A[a] (mg $kg^{-1}$) | A[b] (mg $kg^{-1}$) | P[c] (mg $kg^{-1}$) |
| Strawberry gelatin | | | | | | |
| 200 | 230 | 158.23 | 258.00 | 250 | 158.50 | 258.01 |
| 400 | 370 | 159.00 | 273.33 | 410 | 159.00 | 258.35 |
| 800 | 810 | 160.32 | 260.80 | 810 | 161.37 | 260.11 |
| 1600 | 1580 | 159.50 | 257.42 | 1585 | 159.03 | 260.54 |
| HPLC results | – | 151.25 | 273.75 | – | 160.00 | 275.00 |
| Grenadine | | | | | | |
| 40 | 40.21 | 32.02 | 50.32 | 40.23 | 30.25 | 50.12 |
| 32 | 31.53 | 30.65 | 49.83 | 31.59 | 31.25 | 50.66 |
| 24 | 23.74 | 29.78 | 50.12 | 24.58 | 30.83 | 49.53 |
| 16 | 15.00 | 29.34 | 51.03 | 15.11 | 30.58 | 49.23 |
| 8 | 7.12 | 32.03 | 50.70 | 7.00 | 29.85 | 48.75 |
| HPLC results | – | 28.62 | 50.46 | – | 29.50 | 50.86 |

[a] Carminic acid. Measurement at 373 nm (divisor Amaranth).
[b] Amaranth. Measurement at 549.7 nm (divisor carminic acid).
[c] Ponceau 4R. Measurement at 561.5 nm (divisor Amaranth).

tical parameters, we can conclude that the best methods to determine Amaranth is by measurement at 549.7 nm in the first derivative ratio spectrum ($^1DD_{549.7}$) when the divisor used is carminic acid (32 mg $l^{-1}$). The recoveries obtained at the assayed ratios ranged between 92.2 and 102.3%.

In contrast the determination of Ponceau 4R is better when we use as the signal of measurement $^1DD_{561.5}$ (Amaranth as divisor). The recoveries found were between 95.7 and 103.3%.

Finally, the determination of carminic acid is proposed to be done by measurements at 373 nm in the first derivative ratio spectrum ($^1DD_{373}$), when Amaranth is used as divisor. The recoveries found were from 95 to 105%. In conclusion, this method is available for the simultaneous determination of Amaranth, Ponceau 4R and carminic acid.

### 4.2. Commercial products

In a previous paper, we have established methods that permit the determination of Amaranth and Ponceau 4R by using the first derivative absorption spectra and derivative ration spectra [15]. These methods were applied to determine these colorants in commercial food products such as gelatin desserts with strawberry flavor from Royal Brands S.A and beverages such as grenadine from Rives-Pitman S.A.

In order to apply the method proposed to determine Amaranth, Ponceau 4R and carminic acid in food samples, and because we have not found commercial products which contain all three colorants, we have spiked the commercial food products mentioned above with carminic acid: i.e. different amounts of carminic acid were added to 2 g strawberry gelatin and 4 ml grenadine.

The amount of colorant in each sample was calculated by using the established calibration graphs or by using the standard addition method. In both cases the methods described were applied.

The preparation of samples was as follows.

*Strawberry gelatins*

(1) Quantitative determination by direct preparation using the calibration graphs established: 2 g of product was diluted with 10 ml acetic acid/sodium acetate buffer solution (pH 4.8; ionic strength 0.1) and 25 ml distilled water in a beaker over a low heat with gentle swirling until dissolved. The solution was filtered and transferred to a 50 ml flask and diluted with distilled water to the mark. The absorption spectra were recorded with the instrumental conditions previously selected, and the methods described were applied.

(2) Quantitative determination by standard addition: to 2 g product was added different amounts (2, 4, 6, 8 mg $l^{-1}$) of dye to determine and the procedure (1) was followed.

*Grenadine*

(1) Quantitative determination by direct preparation using the calibration graphs established: 4 ml sample was diluted with 5 ml acetic acid/sodium acetate buffer solution (pH 4.8; ionic strength 0.1), transferred to a 25 ml flask and diluted with distilled water to the mark. The absorption spectra were recorded with the instrumental conditions previously selected and the methods described were applied.

(2) Quantitative determination by standard addition: to 4 ml sample were added different amounts (2, 4, 6, 8 mg $l^{-1}$) of dye to determine and the procedure (1) was followed.

We have used an HPLC method to analyze the samples based on the formation of an ion-pair, whose conditions we have previously established [15]. Table 6 shows the results obtained. As can be seen the results obtained by the HPLC method demonstrate that there is good agreement between the methods.

## 5. Conclusion

The methods proposed are suitable to determine synthetic mixtures of carminic acid, Ponceau 4R and Amaranth obtained in the laboratory. It is also possible to determine these colorants in real samples such as gelatin desserts with strawberry flavor and beverages.

## Acknowledgement

The authors gratefully acknowledge financial support from the "Dirección General de Investigación Científica Técnica" (DGICYT) (Projet No. PB 90-0397).

## References

[1] R. Combes and R. Haveland-Smith, Mutat. Res., 98 (1982) 101.
[2] E.F. Lancaster and J.F. Lawrence, J. Assoc. Off. Anal. Chem., 65 (1982) 1305.
[3] J.F. Lawrence, F.E. Lancaster and H.B.S. Conacher, J. Chromatogr., 210 (1981) 168.
[4] M.L. Puttermans, L. Dryon and D.D. Massart, J. Assoc. Off. Anal. Chem., 66 (1983) 4.
[5] H. Sasaki, Shokuhin Eiseigaku Zasshi, 19 (1978) 1.
[6] H. Sasaki, H. Tansei and M. Niwa, Shokuhin Eisegaku Zasshi, 19 (1978) 12.

[7] Z. Zhang and D. Huang, Shadong Daxue Xuebao Ziran Kexueban, 24 (1989) 123.
[8] E. Momosaki and T. Fujimoyo, Fukuoka-shi Eisei shikenshoho, 12 (1987) 53.
[9] H. Zeng, A. Wang, X. Min and C. Fan, Shipin yu Fajiao Gongye, 4 (1983) 20.
[10] H. Zeng and C. Fan, Shipin yu Fajiao Gongye, 2 (1984) 35.
[11] H. Sasaki, Tottori Daigaku Kogakubu Kenyu Hokoku, 9 (1978) 96.
[12] H. Sasaki, Shokuhim Eisegaku Zasshi, 20 (1987) 16.
[13] F. Salinas, J.J. Berzas Nevado and A. Espinosa Mansilla, Talanta, 37 (1990) 347.
[14] F. Salinas, J.J. Berzas Nevado and C. Guiberteau Cabanillas, Talanta, 39 (1992) 547.
[15] J.J. Berzas Nevado, C. Guiberteau Cabanillas and A.M. Contento Salcedo, Analusis, 22 (1994) 5.
[16] J.J. Berzas Nevado, C. Guiberteau Cabanillas and A.M. Contento Salcedo, Fresenius J. Anal. Chem., 350 (1994) 606.
[17] J.J. Berzas Nevado, C. Guiberteau Cabanillas and A.M. Contento Salcedo, Talanta, 41 (1994) 5.
[18] J.J. Berzas Nevado, J. Rodriguez Flores and M.J. Villaseñor Llerena, Bull. Soc. Chim. Belg., 102 (8) (1993).
[19] Beckman Instruments Inc., Spectroscopy, 2 (1987) 16.
[20] IUPAC Nomenclature, Symbols, Units and their Usage in Spectrochemical Analysis, Pure Appl. Chem., 45 (1976) 105.
[21] A.C.S. Committee on Environmental Improvement, Anal. Chem., 52 (1980) 2242.

ELSEVIER

Talanta 42 (1995) 2053–2057

Talanta

# Indirect ultraviolet determination of silver with nickelocyanide ion by flow injection analysis

Amin T. Haj-Hussein

*Chemistry Department, Yarmouk University, Irbid, Jordan*

Received 5 June 1995; revised 20 July 1995; accepted 20 July 1995

**Abstract**

A flow-injection method for the ultraviolet spectrophotometric determination of silver, based on its reaction with nickelocyanide ion, $Ni(CN)_4^{2-}$, in ammoniacal buffer medium (pH 10) and subsequent measurement of the decrease in the absorption of the $Ni(CN)_4^{2-}$ complex at 275 nm is described. The calibration graph is linear in the range 10–400 μm silver. At a sampling rate of about 60 samples $h^{-1}$ with 35 μl sample injections, precision was about 1% relative standard deviation. The proposed method was successfully applied to the determination of silver in some common silver minerals.

*Keywords:* Silver; Nickelocyanide ion; Flow injection analysis

## 1. Introduction

Silver is widely distributed in nature and is a major component of a wide range of minerals. The large number of complex silver compounds which exist yield a correspondingly large number of spectrophotometric, volumetric and gravimetric analysis techniques for silver [1]. Nickelocyanide ion, $Ni(CN)_4^{2-}$, was used as analytical reagent for indirect determination of silver [2]. The analysis is based upon the ionic exchange reaction between $Ni(CN)_4^{2-}$ and $Ag^+$ which proceeds almost completely to the right, with the following stoichiometry in ammoniacal solution:

$$Ni(CN_4^{2-} + 2Ag^+ 2Ag(CN)_2^- + Ni^{2+}$$

The equivalent amount of $Ni^{2+}$ liberated may be titrated with standard EDTA using an appropriate indicator. This reagent, which absorbs in the ultraviolet region, has been used for the spectrophotometric determination of cyanide ion [3].

In an investigation of the reaction between $Ag^+$ and $Ni(CN)_4^{2-}$, in ammoniacal buffer solution, it was found that addition of silver ion decreased the ultraviolet absorbance of the $Ni(CN)_4^{2-}$ reagent. Moreover, the decrease in the ultraviolet absorption is linear with silver concentration up to 400 μM. This property is utilized as the basis for the development of a new ultraviolet–flow injection analysis (UV–FIA) method for the determination of silver.

This work describes improvements in simplicity and speed in the determination of $Ag^+$. A commonly used method is titration of $Ag^+$ with $Ni(CN)_4^{2-}$ followed by a back titration of $Ni^{2+}$ with EDTA and an appropriate indicator. This method can be simplified by eliminating the back titration step because the concentration of $Ni(CN)_4^{2-}$ can be monitored directly by UV absorption. By simplifying the method, the need to titrate to an endpoint is also eliminated. The one-step analysis is more rapid and well suited for the flow injection format which further enhances the speed of analysis.

FIA [4] is now a well-established technique for carrying out automatic wet chemical analy-


*SSDI* 0039-9140(95)01697-X

sis in a rapid and efficient way. It has been successfully applied for direct instrumental analytical methods with various detection techniques [4–9]. Therefore, it is of interest to adapt this silver determination method to a flow injection system for the continuous spectrophotometric determination of silver in silver minerals.

This paper describes a simple, rapid and specific method for the determination of silver, based on the reaction between $Ni(CN)_4^{2-}$ and $Ag^+$ by means of UV–FIA.

## 2. Experimental

### 2.1. Reagents

All chemicals used were analytical reagent grade, unless otherwise specified; all solutions were prepared with deionized water.

#### 2.1.1. Potassium nickelocyanide $K_2[Ni(CN)_4]$

Prepared as described elsewhere [2].

#### 2.1.2. Stock nickelocyanide ion solution, $1.0 \times 10^{-2}$ M

Prepared by dissolving the calculated amount of $K_2[Ni(CN)_4]$ in water.

#### 2.1.3. Stock ammoniacal buffer solutions

These are 1.20 M ammonia/ammonium nitrate buffers at pH 8.5, 9.3, 10.0 and 10.3. The pH values of these buffers were adjusted with ammonia or ammonium nitrate. All pH measurements were made using a Metrohm Herisau (Type E 520) pH meter.

#### 2.1.4. Carrier solutions

The carrier solutions were dilute ammoniacal buffer solutions (10%). Carrier solutions of pH 8.5, 9.3, 10.0 and 10.3 were prepared from the above stock solutions by accurate dilution with water.

#### 2.1.5. Reagent solutions

The reagent solutions, $Ni(CN)_4^{2-}$, were prepared by mixing the calculated amount of stock nickelocyanide ion solution with 10 ml of stock buffer solution of the required pH value, and diluting to 100 ml with water. The reagent solutions prepared are shown in Table 1.

#### 2.1.6. Standard silver solutions

Silver stock solution ($1.0 \times 10^{-2}$ M) was prepared by dissolving the calculated amount of dried $AgNO_3$ in water. The working silver solutions, $0.10–6.0 \times 10^{-4}$ M, were prepared by mixing the calculated amount of the stock silver solution with 10 ml of the stock buffer of the required pH value and diluting to 100 ml with water.

### 2.2. Dissolution of silver minerals

About 100 mg of sample (accurately weighed) was dissolved in 3 ml of 1:1 nitric acid. The solution was boiled until all the oxides of nitrogen were removed. The solution was diluted to about 50 ml and boiled again after addition of 5 ml concentrated ammonia solution. On cooling the insoluble matter was filtered off and made up to 100 ml with water.

Sample solutions of three silver minerals including native silver (Ag), proustite ($Ad_3AsS_3$) and pyrargyrite ($Ag_3SbS_3$) were prepared. Working solutions for the determination of silver were prepared by mixing aliquots of each sample solution (0.5 ml for native silver, 1.0 ml for proustite, and 1.0 ml for pyrargyrite) with 2.5 ml of the stock buffer (pH 10) and diluting to 25 ml with water.

### 2.3. Apparatus

A schematic dagram of the flow injection system is shown in Fig. 1. The system was assembled from 0.51 mm Microline tubing. The manifold consists of two lines, the top one carrying the carrier solution into which the sample is injected and the lower one carrying the reagent solution. Carrier and reagent solutions were delivered by an Ismatic peristaltic pump (Type MINI-S 860) operated with Tygon tubing. Sample solutions were injected manually into the carrier stream using a Reodyne four-way Teflon valve injector (Type 50). A home-made [4] confluence point with mixing point was used to obtain effective mixing without excessive dispersion of the sample solution. A DuPont ultraviolet spectrophotometer, equipped with a 10 mm flow cell, was used

Table 1
Reagent solutions prepared

| Concentration of $Ni(CN)_4^{2-}$ ($10^4$ M) | pH |
|---|---|
| 2.0 | 8.5 |
| 2.0 | 9.3 |
| 0.5, 1.0, 2.0, 3.0, 4.0, 6.0 | 10.0 |
| 2.0 | 10.3 |

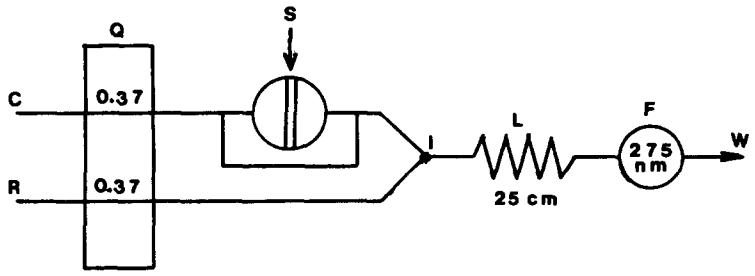


Fig. 1. Two-line manifold for indirect ultraviolet determination of silver. The internal diameter of the Microline tubing was 0.51 mm from the injection valve to the detector. C, carrier stream: R, reagent stream; Q, flow rate (ml $min^{-1}$); S, sample injection; I, confluence point; L, reaction coil; F, flow-through cell; W, waste.

as detector and was connected to a 1 mV Varian recorder (Model 9176).

### 2.4. FIA

The flow system illustrated in Fig. 1 is used. Different volumes in the range 25–200 µl of silver standard solutions were aspirated in the sample loop by means of a syringe. Samples were injected into the carrier stream by pumping at a rate of 0.37 ml $min^{-1}$. The reagent was added at a rate of 0.37 ml $min^{-1}$ in a confluence manner downstream to ensure the rapid and adequate mixing of the sample with the reagent. After an injection, the valve was returned to the load position when the baseline had been reached. The decrease in absorbance was monitored at the wavelength maximum (275 mM) for the $Ni(CN)_4^{2-}$ complex. The output (negative signals) of the ultraviolet spectrophotometer was registered on the chart recorder. When the baseline was reached, another slug of the sample could be injected. The area or the height of the negative absorbance peak can be used for the calibration.

## 3. Results and discussion

Determination of silver by this UV–FIA method is based on the decrease in absorption of nickelocyanide complex ion in ammoniacal buffer solution at 275 nm. The chemical variables and the FIA variables influencing the system were optimized to achieve reproducible results.

### 3.1. Optimization of chemical variables

Absorbance measurements were performed using the manifold shown in Fig. 1. Considering the baseline of the carrier solution (carrier of pH 10 was pumped in both lines of the manifold), the absorbance values at 275 nm of $NI(CN)_4^{2-}$ reagent solutions (pH 10) were measured in the concentration range $0.5 \times 10^{-4}$–$6.0 \times 10^{-4}$ M. Fig. 2 shows that the variation of absorbance with concentration of $Ni(CN)_4^{2-}$ solutions yields a linear relationship up to $2.0 \times 10^{-4}$ M and shows a considerable deviation at higher concentrations.

By injecting standard silver solutions into the carrier stream, using $2.0 \times 10^{-4}$ M $Ni(CN)_4^{2-}$ as reagent, a decrease in the absorbance values was obtained. Fig. 3 shows that the decrease in absorbance values at 275 nm is linear in the silver concentration range 0.10–4.0 $\times 10^{-4}$ M. This permits silver to be determined in quantities up to $4 \times 10^{-4}$ M. Moreover, it indicates that the reaction between $Ni(CN)_4^{2-}$ and $Ag^+$ with a mole ratio of 1:2 proceeds to completion using this FIA system.

The effect of pH on the reaction between silver and $Ni(CN)_4^{2-}$ was studied in ammoniacal ($NH_3/NH_4NO_3$) buffer medium at pH values in the range 8.5–10.3. Fig. 4 shows that no significant changes were observed.

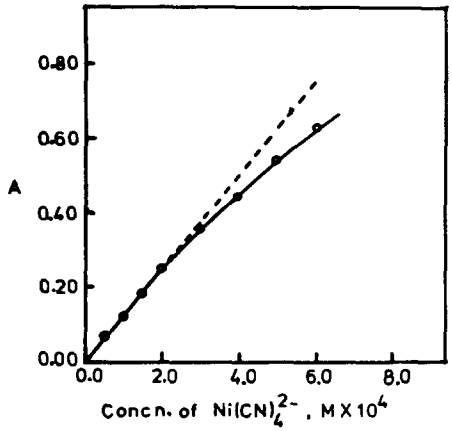


Fig. 2. Plot of absorbance versus concentration of $Ni(CN)_4^{2-}$ reagent solutions at 275 nm. Carrier stream was ammoniacal buffer (pH 10.0).

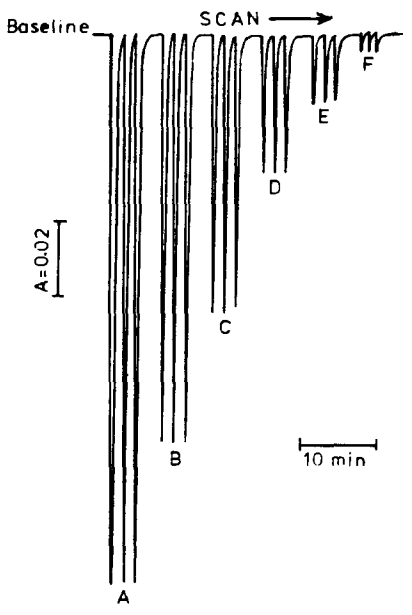


Fig. 3. Flow-injection signals for indirect ultraviolet determination of silver at a rate of approximately 60 samples $h^{-1}$ with the manifold shown in Fig. 1. Silver (μM): A, 400; B, 300; C, 200; D, 100; E, 50; F, 10. Concentration of $Ni(CN)_4^{2-}$ reagent was $2.0 \times 10^{-4}$ M; injection volume, 35 μl; carrier, ammoniacal buffer (pH 10); wavelength, 275 nm.

### 3.2. Optimization of FIA variables

#### 3.2.1. Wavelength selection

Fig. 5 depicts the absorption spectra of $Ni(CN)_4^{2-}$ complex ($2.0 \times 10^{-4}$ M) in ammoniacal buffer solution at pH 10.0. The curve exhibits a band with maximum absorbance at 275 nm which was chosen as the optimum wavelength for studying the factors influencing this FIA system.

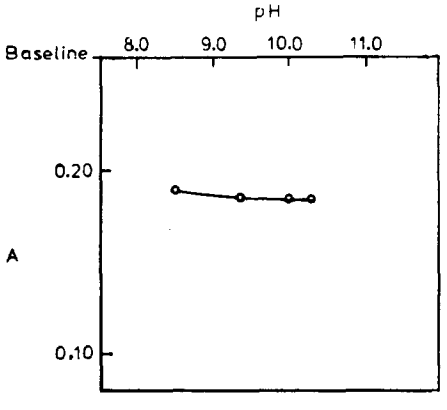


Fig. 4. Effect of pH on the determination of silver. Concentration of silver was $2.0 \times 10^{-4}$ M; other conditions were as given in Fig. 3.

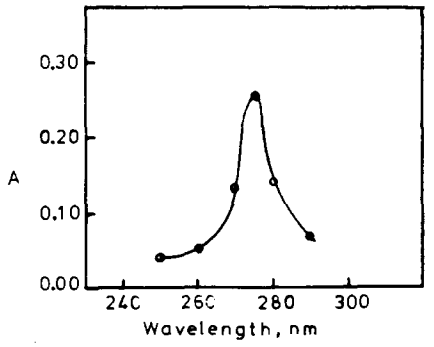


Fig. 5. Absorption spectrum of $Ni(CN)_4^{2-}$ at pH 10 with the manifold shown in Fig. 1. Concentration of $Ni(CN)_4^{2-}$ was $2.0 \times 10^{-4}$ M; carrier, ammoniacal buffer (pH 10.0).

#### 3.2.2. Sample injection volume

The optimum volume of injected sample was found to be 35 μl.

#### 3.2.3. Length of reaction coil

The signal (negative peak) increased linearly with length (15–100 cm) and internal diameter (up to 0.51 mm) of the reactor tube. A reactor length ($L$) of 25 cm and i.d. of 0.51 mm were chosen to give a compromise between maximum peak height and sampling frequency.

#### 3.2.4. Flow rate

The optimum flow rate was found to be 0.7 ml $min^{-1}$. At this flow rate with 35 μl sample injections in this work, the average sampling rate was around 60 samples $h^{-1}$.

### 3.3. System characterization

The flow system in Fig. 1 was used for preparing the calibration graph. The sample solution was injected from a sample loop of 35 μl. Typical signals are shown in Fig. 3. The calibration graph is linear up to $4.0 \times 10^{-4}$ M silver (400 μM). The limit of detection (2 × noise) for silver was 3 μM (0.32 ppm). The percent relative standard deviation for 10 replicate injections was $< 1\%$.

### 3.4. Interference study

A systematic study of potential interferences in the proposed method was made. Copper, nickel, zinc, lead, iron, bismuth and arsenic which may be found in the common silver minerals [10] were studied for their interfering effects. Each metal ion was studied in the range

Table 2
Determination of silver in some silver minerals determined by the proposed FIA method and by AAS

| Sample | Ag content (%) | |
|---|---|---|
| | FIA method | AAS method [a] |
| NS [b] | 96.6 | 97.5 |
| Pr [c] | 25.5 | 25.4 |
| Py [c] | 32.9 | 31.7 |

[a] A Pye Unicam SP9 atomic absorption spectrophotometer equipped with a silver hollow-cathode lamp was used. The wavelength was set at 328.1 nm and the operating conditions were adjusted following standard recommendations.

[b] Provided by the Geology Department, Yarmouk University. NS, native silver (Beaverdall, British Columbia, Canada).

[c] Provided by the Geology Department, University of Jordan. Pr, Prousite; Py, pyrargyrite (Frieberg, Sachsen, Germany).

$4.0 \times 10^{-4}$–$2 \times 10^{-4}$ M silver at pH 10 (ammoniacal buffer solution). No effects were apparent for $Zn^{+}$, $Ni^{2+}$ and $AsO_4^{2-}$ ions over the complete range of concentrations investigated. $Cu^{2+}$ caused decreased peaks when concentration exceeded $4.0 \times 10^{-4}$ M. In contrast, $Pb^{2+}$, $Fe^{2+}$ and $Bi^{3+}$ ions precipitated in the ammoniacal buffer solution. In the determination of silver in silver minerals, however, dissolving these minerals in nitric acid, followed by addition of excess ammonia and filtration would remove all these ions and so prevent interference.

### *3.5. Determination of silver in silver minerals*

The proposed method was applied to the determination of silver in native silver, proustite and pyrargyrite minerals. The results (silver content, %) of the analyses are summarized in Table 2.

A measure of the reliability of the proposed method is given by Table 2 in which the results are compared with those obtained using AAS by complete decomposition with nitric acid [11]. There is general agreement between the results of the methods. It is also apparent that the results for silver were not affected by various elements present in the mineralized samples.

## References

[1] Comprehensive Inorganic Chemistry, Vol. 3, Pergamon Press, Oxford, 1973, p. 125.
[2] A Text-Book of Quantitative Analysis, 3rd edn., Longman, London, 1961, p. 421.
[3] W.J. Williams, Handbook of Anion Determination, Butterworths, London, 1979, p. 79.
[4] J. Ruzicka and E.H. Hansen, Flow Injection Analysis, 2nd edn., Wiley, New York, 1988.
[5] M. Gallego and M. Valcarcel, Anal. Chim. Acta, 169 (1985) 161.
[6] P. Martinez-Jimenez, M. Gallego and M. Valcarcel, Anal. Chim. Acta, 193 (1987) 127.
[7] L. Silva, L.E. Leon and A. Calvo, Anal. Chim. Acta, 192 (1987) 349.
[8] A.G. Fogg, N.K. Bsebsu and M.A. Abdalla, Analyst, 107 (1982) 1462.
[9] A.T. Haj-Hussein, Microchem. J., 39 (1989) 99.
[10] Handbook of Geochemistry, Vol. II-4, Springer-Verlag, Berlin, 1978.
[11] C. Huffman, Jr., J.D. Mensik and L.F. Radar, U.S. Geol. Surv. Prof. Pap., B189 (1966) 550-B.

ELSEVIER

Talanta 42 (1995) 2059–2061

Talanta

Short communication

# Procedure for dissolving wolframite in order to determine trace elements by atomic absorption spectrometry

Silvano Mignardi, Umberto Masi *

*Dipartimento di Scienze della Terra, Università "La Sapienza", P. le A. Moro 5, 00185 Roma, Italy*

Received 25 January 1995; revised 22 June 1995; accepted 30 June 1995

**Abstract**

An analytical procedure for dissolving wolframite in order to determine trace elements by atomic absorption is reported. After decomposition of the mineral by alkaline fusion, the cooled flux is dissolved by heating with aqua regia. The finely crystalline precipitate of tungstite, which forms on standing, is filtered and dissolved by heating with aqua regia. Tungstite forms again in the latter solution and the filtration and solubilization are repeated until the solution contains negligible amounts of trace elements. Following this procedure, trace elements in 35 samples of natural wolframite have been dissolved and the solutions obtained have been analyzed by atomic absorption spectrometry for Fe, Mn, Cu, Zn, Pb, Co, Ni and Cd.

*Keywords:* Wolframite; Trace elements; Atomic absorption spectrometry

## 1. Introduction

Trace element analyses of natural wolframites are very rare. Wolframites are routinely analyzed using an electron microprobe (EM) [1,2], and therefore the results are reliable only for major elements. Trace element concentrations are generally near, or in the range of the analytical error [1,2]. Lack of information about trace element contents of wolframite therefore represents a major handicap in the interpretation of the results of geochemical studies of the origins of ore deposits. For other mineral phases, such as sulfides and oxides for instance, trace element composition is often useful in elucidation of the composition of the parent solutions [3–6].

To fill this gap, this paper describes a procedure for wolframite trace element solubilization, which allows determination of trace element concentrations by atomic absorption spectrometry (AAS). Thirty-five wolframite samples from two major hydrothermal deposits in Portugal have been analyzed. In addition to trace elements, Fe and Mn were also determined in the same solutions by AAS. For these two elements the results were compared with the corresponding concentrations determined by EM analysis with a Jeol JXA 50A with EDS Link system (counting time 100 s, 15 keV and 2 mA) [7].

## 2. Experimental

The procedure presented was derived from the industrial technique of $WO_3$ preparation, namely alkaline fusion of wolframite and subsequent purification of $WO_3$ by repeated acid leaching.

Subsamples of about 200 mg of powdered ($\phi \approx 0.25$ mm) wolframite were mixed with 1 g of $Na_2CO_3$ and 200 mg of $Na_2NO_3$ and the

* Corresponding author.

*SSDI* 0039-9140(95)01681-3

Table 1
Average element concentrations (ppm) determined in the four solutions

| Element | Solution | | | |
|---|---|---|---|---|
| | A | B | C | D |
| Fe | 151536 | 2327 | 231 | 15 |
| Mn | 23201 | 65 | 9 | 5 |
| Cu | 200 | 15 | 10 | – |
| Zn | 210 | 20 | 5 | – |
| Pb | 85 | 10 | – | – |
| Co | 50 | 10 | – | – |
| Ni | 160 | 15 | – | – |
| Cd | 30 | 5 | – | – |

mixture was fused in a platinum crucible at approximately 700°C for 10 min. The fused mass was cooled and dissolved by heating with 10 ml of aqua regia; the solution (solution A) soon became turbid, with a very fine, crystalline (as proved by XRD analyses) precipitate of tungstite ($WO_3 \cdot H_2O$). The precipitate, which still contained some trace elements of wolframite, was filtered off and dissolved by heating with 15 ml of aqua regia in a Teflon crucible. This latter solution (solution B) also soon became turbid because of tungstite precipitation, and it too was filtered. The precipitate was again dissolved in 15 ml of aqua regia in a Teflon crucible and the third solution (solution C) was again filtered.

The three solutions obtained were then analyzed for Fe, Mn, Cu, Zn, Pb, Co, Ni and Cd by AAS using a double-beam Perkin-Elmer Model 460 spectrophotometer and matrix-matched standards.

As expected, solution C for all samples had lower element contents than solution B, which, in turn, was less rich than solution A. However, as solution C did not have negligible trace element concentrations, the tungstite precipitate from this solution was dissolved again in 15 ml of aqua regia, thus giving rise to solution D. After filtration, the latter solution was analyzed by AAS to give, finally, trace element concentrations lower than the analytical error, which thus were negligible.

## 3. Results and discussion

Table 1 shows the results obtained. It is apparent that over 99% of Fe and Mn of wolframite are contained in the two early solutions (solution A and solution B) and trace elements are detectable in all the solutions except solution D. However, the recovery of Pb, Co, Ni and Cd was analytically complete in solutions A and B, whereas that of Cu and Zn was complete only with solution C. This is probably because Cu and Zn are more (2–10 times) abundant than the other trace elements in the samples studied [7].

Table 2 shows major and trace element contents in selected wolframite samples from the Panasqueira mine (Portugal) determined by AAS compared with the data for the same samples analyzed by EM. For Fe and Mn the results obtained by the two techniques show no significant difference as the AAS values fall in the range of EM values at $\pm 1\sigma$; on the contrary, for trace elements the contents determined by EM are indefinite, being all below the analytical error ($\sigma$) and thus no comparison with the AAS data can be drawn.

Table 2
Concentrations of major (mass %) and trace (ppm) elements in selected samples from 35 analyzed wolframites from the Panasqueira deposit (Portugal) determined by AAS and EM. $\sigma$: microprobe analytical error (mass %)

| Element | Sample | | | | | | | | $\sigma$ |
|---|---|---|---|---|---|---|---|---|---|
| | P-501 | | P-511 | | P-512 | | P-525 | | |
| | AAS | EM | AAS | EM | AAS | EM | AAS | EM | |
| Fe | 15.08 | 15.20 | 15.63 | 15.07 | 15.73 | 15.38 | 14.94 | 15.22 | ±0.44 |
| Mn | 2.61 | 3.01 | 2.56 | 2.47 | 2.34 | 2.88 | 2.29 | 2.56 | ±0.52 |
| Cu | 704 | $<\sigma$ | 688 | $<\sigma$ | 70 | $<\sigma$ | 70 | $<\sigma$ | ±0.28 |
| Zn | 457 | $<\sigma$ | 213 | $<\sigma$ | 209 | $<\sigma$ | 219 | $<\sigma$ | ±0.48 |
| Pb | 65 | $<\sigma$ | 35 | $<\sigma$ | 50 | $<\sigma$ | 70 | $<\sigma$ | ±0.18 |
| Co | 70 | $<\sigma$ | 67 | $<\sigma$ | 65 | $<\sigma$ | 50 | $<\sigma$ | ±0.20 |
| Ni | 119 | $<\sigma$ | 148 | $<\sigma$ | 160 | $<\sigma$ | 119 | $<\sigma$ | ±0.23 |
| Cd | 25 | $<\sigma$ | 25 | $<\sigma$ | 30 | $<\sigma$ | 20 | $<\sigma$ | ±0.14 |

## 4. Conclusions

The following procedure is suggested to determine trace element abundance in wolframite. Fuse wolframite with $Na_2CO_3 + Na_2NO_3$ and dissolve the cooled fused mass by heating with aqua regia. Filter the tungstite which precipitates and dissolve the precipitate in aqua regia. Tungstite forms again in the new solution, so filtration and dissolution of the precipitate must be repeated until AAS analyses carried out on the solution give negligible trace element concentrations.

Although the procedure given here is more time-consuming than EM analyses, it is worthwhile as it allows the geochemist to measure trace elements at amounts significantly lower than 1000 ppm, whereas the analytical error of EM is generally larger.

## Acknowledgements

The authors thank Mr. G. Aurisicchio for assistance provided during atomic absorption analyses and Dr. C. Aurisicchio and Dr. M. Rettighieri for help during the microprobe work.

## References

[1] D.A. Polya, Mineral. Mag., 52 (1988) 497.
[2] A. Vilela de Matos, Tesi de Dotourato de Ricerca, Università de Trás-os-Montes e Alto Douro, Vila Real, Portugal, 1991, 312 pp.
[3] I.R. Jonasson and D.F. Sangster, Geol. Surv. Can. Pap., 78-1b (1978) 195.
[4] B.J. Price, M.Sc. thesis, University of British Columbia, Vancouver, B.C., 1972.
[5] G. Udubaşa, in A. Wanschkuhn et al. (Eds.), Syngenesis and epigenesis in the formation of mineral deposits, Springer-Verlag, Berlin, 1984.
[6] Z.U. Bajwah, P.K. Seccombe and R. Offler, Miner. Deposita, 22 (1987) 292.
[7] S. Mignardi, Ph.D. thesis, University "La Sapienza", Rome, Italy, 1992, 201 pp.

ELSEVIER

Talanta 42 (1995) 2065–2072

Talanta

# Simultaneous determination of penicillin and ampicillin by spectral fibre-optical enzyme optodes and multivariate data analysis based on transient signals obtained by flow injection analysis

Jürgen Polster [a,*], Gertraud Prestel [a], Markus Wollenweber [a], Gerolf Kraus [b], Günter Gauglitz [b]

[a] *Lehrstuhl für Allgemeine Chemie und Biochemie, Technical University of Munich, D-85350 Freising-Weihenstephan, Germany*

[b] *Institute for Physical and Theoretical Chemistry, University of Tübingen, Auf der Morgenstelle 8, D-72076 Tübingen, Germany*

Received 4 April 1995; accepted 5 July 1995

**Abstract**

A multicomponent detection system using optical biosensors and flow injection analysis is described. The analysis of mixtures containing penicillin and ampicillin was realised by evaluating dynamic measurements of Phenol Red spectra in penicillinase optodes in combination with a diode array spectrometer. A variety of optodes has been produced by changing the composition of the receptor gel and the working pH. A set of characteristic quantities (describing dynamic and static features) could be obtained for each optode. These were used to compare the predictivity of classical multivariate calibration methods as well as of an artificial neural network. In addition, different algorithms were applied for the evaluation of the spectral data in order to select the most appropriate method for feature extraction. In consequence, the information obtained from the multivariate calibration models was used to set up an optimal sensor array consisting of four optodes with different types of penicillinase at different working pH.

*Keywords:* Penicillin; Ampicillin; Optical biosensors; Flow injection analysis; Multivariate data analysis

## 1. Introduction

Enzyme optodes have become well established as modern tools in certain areas of analytical chemistry during the last 15 years. This type of sensor based on fibre optic techniques has already been described in monographs [1,2]. In spite of this considerably long development time and the efficiency attained in laboratory set-ups the practical application is not established yet. The reasons are: (i) the relatively short lifetime of many optodes and (ii) their lack of signal stability due to interferences in typical analytical matrices. These problems can be overcome by combining optodes with flow injection analysis (FIA) and multivariate data analysis applied to an array of optodes rather than to a single one. Within the multivariate methods, partial least-squares (PLS) [3–7] is applied more and more in optical analysis of chemical systems [8–10].

However, in the area of optical sensing, and especially in the combination of spectral detection methods with an FIA system [11], just a few examples are given in the literature. For example, the determination of pesticides by differential degradation using PLS and spectral data produced in an FIA system is described in

* Corresponding author.


*SSDI* 0039-9140(95)01684-8

Ref. [12]. Using a stopped-flow injection system [13], metal ions can be determined by kinetic analysis of spectra. Finally, mixtures of hydroxybenzaldehydes were analysed by photodiode array detection applying reproducible pH gradients produced by an FIA technique [14].

In this paper, the evaluation of transient signals from penicillinase optodes in an FIA system using multivariate methods is described. Lactam antibiotics, for example penicillin G or V, ampicillin and cephalosporin C, are effective drugs against infectious diseases. Although these drugs have been well studied in the past, new methods are still of interest to determine quickly and safely penicillin derivatives [15,16]. In principle, penicillin compounds can be individually detected by penicillinase optodes [17–19]. However, mixtures of penicillin components have not yet been analysed by enzyme optodes. In the present study, we report results obtained by simultaneous analysis of mixtures of penicillin G and ampicillin by an optode array. We compare several methods for feature extraction and multivariate calibration to select the optimum composition of the optode array.

## 2. Theory

### 2.1. Data evaluation and feature extraction

The data available from the optodes consist of the transient diffuse reflectance spectra in the visible wavelength region obtained at equidistant time intervals after the injection of an analyte into the FIA system. When the analyte reaches the sensor at time $t_0$, the flow is stopped. The change in the reflectance with time may then be described on an empirical basis by the exponential function given in Eq. (1) for each optode $i$:

$$R_i(\lambda, t) = R_i^{\text{stat}}(\lambda)[1 - e^{-k_i(t - t_0)}] \quad (1)$$

Here, $t_0$ corresponds to the time when the optode/analyte interaction starts. $R_i^{\text{stat}}$ comprises the wavelength-dependent maximum change in reflectance for the specific optode $i$ (static information). $k_i$ includes the dynamic behaviour of the optode $i$.

For the sensor evaluation, the dynamic features (i.e. the time dependence of the signal described by $k_i$) and the static features (i.e. the steady state signals described by $R_i^{\text{stat}}$) may be considered. The steady state signals should give information on the total concentration of analytes whereas the dynamic signals should contain analyte-specific information. In this section, we discuss algorithms for the extraction of both dynamic and static information from the spectral data.

The parameters in Eq. (1) may be obtained by non-linear least-squares regression. For online data evaluation, simultaneous application of Eq. (1) to the whole set of wavelengths would be time-consuming and is not necessary. A lot of data reduction techniques exist for removing the wavelength dependency from this equation. Three algorithms are described in the following. Their performance is compared in the results and discussion section.

The simplest algorithm disregards the spectral information measured and concentrates on the most prominent wavelength (i.e. the wavelength of maximum spectral change of the immobilized pH indicator). This algorithm is subsequently called the "monochromatic" algorithm.

More information is retained by using the integral reflectance over the monitored wavelength range. Then $R_i^{\text{stat}}(\lambda)$ is replaced by the integral maximum change in reflectance $R_i^{\text{stat}}$ whereas $k_i$ and $t_0$ should not be affected. This procedure is called the "integrative" algorithm.

The full spectral information is used in the feature extraction step by calculating the first principal component $\boldsymbol{R}_i^{\text{PC}}$ [5] using all reflectance spectra from the current experiment or the previous investigations and by solving the following linear matrix Eq. (2) with respect to the scalar $b_i(t)$ (principal component scores) for each sampling time $t$ (subsequently called the "spectral" algorithm):

$$\begin{aligned} \boldsymbol{R}_i(t) &= \boldsymbol{R}_i^{\text{PC}} \cdot b_i(t) + \boldsymbol{e}(t) \\ b_i(t) &= \frac{(\boldsymbol{R}_i^{\text{PC}})^T}{(\boldsymbol{R}_i^{\text{PC}})^T \cdot \boldsymbol{R}_i^{\text{PC}}} \boldsymbol{R}_i(t) \end{aligned} \quad (2)$$

Here $\boldsymbol{R}_i(t)$ denotes the vector of the spectral reflectance of optode $i$ at time $t$ with the elements $R_i(\lambda, t)$, and $\boldsymbol{R}_i^{\text{PC}}$ denotes the first principal component (PC) of optode $i$ with the elements $R_i^{\text{PC}}(\lambda)$. The stochastical nature of model Eq. (2) is indicated by the residual error term $\boldsymbol{e}(t)$. Eq. (1) is then transformed to

$$b_i(t) = b_i^{\text{stat}}[1 - e^{-k_i(t - t_0)}] \quad (3)$$

As confirmed by our measurements, this spectral algorithm is the most powerful method for several reasons. First, it makes use of the full amount of information obtained by calculation

of the first PC. Second, it offers possibilities to detect time-dependent changes in optode performance by monitoring the change in the first PC with time.

## 3. Experimental

### 3.1. Instrumentation and measurements

The flow injection manifold used is shown in Fig. 1. The following modules were integrated: two peristaltic pumps (MC-MS/CA4/8 and MS-4 Reglo-100) from Ismatec, Wertheim-Mondfeld (Germany); a six-way valve (TMV) from Latek, Eppelheim (Germany); two six-way valves (M-5011) and an injection valve (M-5020) from ERC, Alteglofsheim (Germany). Pumps and valves were interfaced to a PC 486DX by means of a multi input-output card (DCI 385) from Kosiol, Frankfurt am Main (Germany). The reflection/absorption spectra were recorded by a diode array spectrometer (MCS 230) from Carl Zeiss Co., Oberkochen (Germany) employing a bifurcated quartz fibre optic (Y-shape) and a xenon light source (CLX 111) from Zeiss. The biosensors were sequentially placed in an acrylic flow cell made in house [18,19]. All components were connected by Teflon tubes (0.8 mm i.d.) using commercially available connectors.

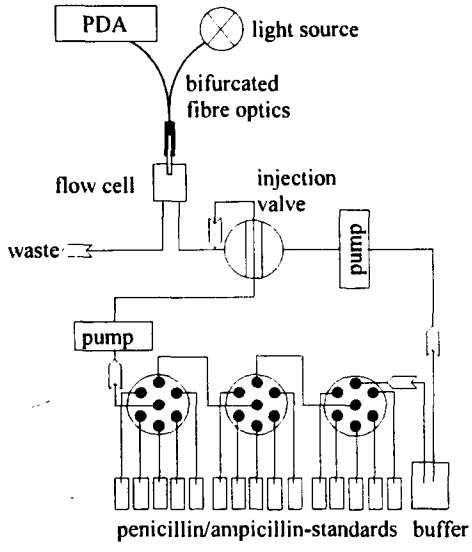


Fig. 1. FIA manifold for enzyme-based detection of time-dependent changes in absorption of a Phenol Red membrane. The spectra are recorded by means of a diode array spectrometer. The different mixtures of penicillin and ampicillin used as calibration and test data sets were stored in an ice-cooled bath during measurements.

During measurements an ice-cooled bath containing all samples retarded premature and non-catalysed hydrolysis of penicillin and ampicillin. The phosphate buffer passed the flow cell for 5 min with a flow rate of about 225 $cm^3 h^{-1}$ removing the previous sample from the sensor layer (thus the time for the regeneration process can be decreased down to 3 min). Simultaneously, the flow system sampling port consisting of three six-way valves was washed for 20 s. Next, the six-way valves were switched to one of the 15 standard solutions to fill the sample loop (250 µl) of the injection valve. When the injected sample volume had passed the sensor layer for 4 s the carrier stream was stopped and the data acquisition started. While penicillin and ampicillin are diffusing into the polyacrylamide gel they are hydrolysed by immobilised preparations of penicillinase causing a local pH shift in the receptor layer. Accordingly, a pH indicator (Phenol Red) changes its colour which is spectrally recorded using time intervals of 10 s for a period of 3 min.

### 3.2. Reagents and samples

Penicillinase ($\beta$-lactamase, EC 3.5.2.6) from *Escherichia coli* and ampicillin (sodium salt, prep. 1) were purchased from Boehringer Mannheim, GmbH (Germany). Penicillinase from *Bacillus cereus*, ampicillin (sodium salt, prep. 2), penicillin G (potassium salt) and Phenol Red (sodium salt) were obtained from Sigma. Phosphate buffer (5 mM) containing 100 mM KCl was prepared from reagents of analytical grade, used without any further purification and dissolved in distilled water. Standard solutions were prepared in phosphate buffer. Their pH was additionally controlled by a pH meter before measuring. The enzymes and the pH indicator Phenol Red were immobilised during the polymerisation of a polyacrylamide layer on a silanized glass substrate (10 mm diameter). The general immobilisation procedure is described in detail in Ref. [18]. The composition of membranes, working pH of the ambient medium, and codes for the investigated optodes are given in Table 1.

### 3.3. Calibration and test data set

Independent data sets were measured for calibration (model building) and testing (validation) of the different methods. The calibra-

Table 1
Sensor composition, pH of ambient medium, and codes for the enzyme optodes utilized in this study (t.i. = time interval for measurements)

| Code | Ambient and optode composition |
|---|---|
| EC7-1 | *E. coli penicillinase* (60 U/optode), Phenol Red, pH 7.0, t.i. 10 s for 180 s |
| BC7-1 | *B. cereus penicillinase* (460 U/optode), Phenol Red, pH 7.0, t.i. 10 s for 180 s |
| EC7.8-1 | *E. coli penicillinase* (60 U/optode), Phenol Red, pH 7.8, t.i. 10 s for 180 s |
| EC7.8-2 | *E. coli penicillinase* (60 U/optode), Phenol Red, pH 7.8, t.i. 5 s for 30 s |
| BC7.8-1 | *B. cereus penicillinase* (930 U/optode), Phenol Red, pH 7.8, t.i. 10 s for 180 s |

tion data set consisted of 11 objects; the test data set consisted of 4 objects. The composition of the binary mixtures is given in Table 2. For each object, the spectral reflectivity in the wavelength range 400–600 nm (100 data points per spectrum) for the five optodes in Table 1 was measured. The mixtures were presented in random sequence. The raw data are available from the authors upon request by electronic mail (gerolf.kraus@ipc.uni-tuebingen.de).

### 3.4. Data pre-processing

The spectral signals were transformed to wavelength-independent variables according to the algorithms described in the theoretical section. The first PC in Eq. (2) was calculated from mean-centered data of the calibration data set and accounted for 99.9% of the total signal variance. The injection time $t_0$ is not considered further. Two variables are thus obtained for each optode $i$ ($k_i$ comprising the dynamic features and $R_i^{stat}$ resp. $b_i^{stat}$ comprising the static features) with different scales. The variables were calculated by nonlinear least-squares regression. The mean relative standard deviation obtained for $b_i^{stat}$ and $k_i$ was 2.0% and 4.5% respectively. In order to weight the two types of variables equally, both scales were confined within the range 0–1 by division by the largest value of all $k_i$ and $R_i^{stat}$, $b_i^{stat}$ respectively. The models established from the calibration data set were used for the validation with the test data set without further alteration.

### 3.5. Characterisation of multivariate methods

For characterisation of the multivariate errors of calibration and prediction, the numbers that are defined by Eqs. (4)–(7) were introduced ($n_C$ and $n_P$ are the number of samples in the calibration and prediction data sets respectively). MSEC and MSEP denote the mean square errors of calibration and prediction, RAEC and RAEP denote the relative absolute errors of calibration and prediction (given in %):

$$\mathrm{MSEC} = \frac{\sum_{\text{calibration data set}} (c_{\text{predicted}} - c_{\text{true}})^2}{n_C} \quad (4)$$

$$\mathrm{MSEP} = \frac{\sum_{\text{prediction data set}} (c_{\text{predicted}} - c_{\text{true}})^2}{n_P} \quad (5)$$

$$\mathrm{RAEC} = \frac{\sum_{\text{calibration data set}} |c_{\text{predicted}} - c_{\text{true}}|/c_{\text{true}}}{n_C} \quad (6)$$

$$\mathrm{RAEP} = \frac{\sum_{\text{prediction data set}} |c_{\text{predicted}} - c_{\text{true}}|/c_{\text{true}}}{n_P} \quad (7)$$

### 3.6. Software

Data acquisition and system control were conducted with FIACRE [20], and MEASURE [21] software running under Windows™. Data evaluation was performed on a PC 80486/33 MHz. Data pre-processing was computed with Microsoft Excel™. Principal component analysis and PLS regression were calculated with Unscrambler 5.0 (CAMO/AS, Trondheim, Norway). The neural network was simulated with our own software running under Windows 3.1. Non-linear least-squares regression was calculated according to the Gauss–Newton–Marquardt algorithm [22] with our own software.

## 4. Results and discussion

An example of the change in spectral reflectivity during one measurement cycle is given in Fig. 2. The diagram demonstrates the reflectivity of a Phenol Red-doped membrane (EC7.8-1; see Table 1) at equidistant time intervals

Table 2
Design of calibration and test data sets

| | Object | | | | | | | | | | |
|---|---|---|---|---|---|---|---|---|---|---|---|
| | 1 | 2 | 3 | 4 | 5 | 6 | 7 | 8 | 9 | 10 | 11 |
| Calibration data set | | | | | | | | | | | |
| $c_{Penicillin}$ (mM) | 2 | 5 | 10 | 0 | 0 | 0 | 2 | 4 | 6 | 10 | 7 |
| $c_{Ampicillin}$ (mM) | 0 | 0 | 0 | 2 | 5 | 10 | 4 | 7 | 10 | 5 | 3 |
| | 1 | 2 | 3 | 4 | | | | | | | |
| Test data set | | | | | | | | | | | |
| $c_{Penicillin}$ (mM) | 8 | 3 | 4 | 5 | | | | | | | |
| $c_{Ampicillin}$ (mM) | 2 | 9 | 4 | 8 | | | | | | | |

between 10 s and 170 s after the analyte peak reaches the sensor and the flow was stopped. The curves show the membrane reflectivity relative to the reflectivity of the optode in a continuous flow of buffer.

### 4.1. Feature extraction

The monochromatic, integrative, and spectral methods described above were applied to the evaluation of the data set and compared with respect to their feature extraction properties. The wavelength at the peak maximum (570 nm) which was used for the monochromatic evaluation is marked by the vertical arrow in Fig. 2. The integrative evaluation was based on the integral absorbance in the range 400–600 nm marked by the horizontal arrows in Fig. 2. In addition, the loadings for the first PC are included in the window in the upper left part of Fig. 2. For the selection of the most appropriate feature extraction method, the whole set of optodes (cf. Table 1) was considered. After pre-processing as described above, the data sets from the different algorithms, each consisting of 10 variables (5 with dynamic features $k_i$, 5 with static features $R_i^{stat}$, $b_i^{stat}$), were subject to PLS2 calibration [7]. The number of primary factors was selected by leave-one-out cross-validation. The resulting models were used to predict the concentrations for the test data. The statistical data and the number of primary factors are summarised in Table 3. The results clearly indicate by the values of MSEP and RAEP that spectral evaluation is the most appropriate method for the extraction of the dynamic and static features. The integrative method which is also based on the spectral data yields slightly worse predictions but behaves better than the monochromatic approach. This demonstrates that spectral detection together with multivariate feature extraction enhances the predictivity and ruggedness of the optode array. The integrative method, although based on the full spectral information, does not make use of the whole information contained in the data set. The characteristic features are optimally extracted by the spectral (multivariate) method which therefore is used throughout the following discussion.

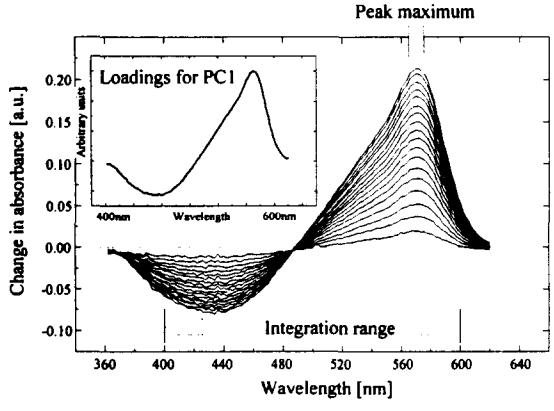


Fig. 2. Change in the spectral reflectivity during a measurement cycle. The peak maximum which was selected for single wavelength (monochromatic) evaluation is marked as well as the range that was selected for integration of the spectrum. The multivariate evaluation procedure was based on the loadings for the first PC (PC1) which are displayed schematically in the upper left part of the diagram. See text for detailed description of the algorithms.

### 4.2. Importance of dynamic and static features

To demonstrate the importance of both the dynamic and static features for solving the problem of multicomponent analysis, we repeated PLS2 calibration with two subsets of the full data set. For each subset 5 variables were selected. The first subset comprised only the static information. The other subset was

Table 3
Statistical data for comparison of different algorithms (monochromatic, integrative, spectral) for feature extraction. The Table includes the MSEC, the RAEC, the MSEP and the RAEP

| Feature extraction | | Calibration | | Prediction | |
|---|---|---|---|---|---|
| Algorithm | Number of primary factors | MSEC ($mM^2$) | RAEC | MSEP ($mM^2$) | RAEP |
| Penicillin | | | | | |
| Monochromatic | 5 | 0.084 | 8.0% | 0.515 | 15.7% |
| Integrative | 5 | 0.125 | 9.8% | 0.326 | 9.5% |
| Spectral | 5 | 0.094 | 5.8% | 0.275 | 7.0% |
| Ampicillin | | | | | |
| Monochromatic | 5 | 0.154 | 7.1% | 1.686 | 26.5% |
| Integrative | 5 | 0.170 | 7.2% | 0.275 | 10.0% |
| Spectral | 5 | 0.156 | 6.1% | 0.093 | 7.1% |

composed of the pure dynamic variables. In both cases, the values for the MSEP increased by a factor of six with respect to the values given in Table 3 for the spectral feature selection algorithm and the full data set. The values for RAEP obtained were greater than 13% (compared to 7% for the full data set). This shows, that neither the dynamic nor the static behaviour alone contains enough information for an optimum prediction.

### 4.3. Comparison of algorithms

Five standard methods for multivariate calibration were compared with respect to their performance for predicting the concentrations of the test samples. Aside from the PLS2 method already discussed, we applied PLS regression for a single compound (PLS1; e.g. Ref. [7]), principal components regression (PCR; e.g. Ref. [6]), multivariate least-squares regression (MLR; e.g. Ref. [5]), and a backpropagation neural network (BPN; e.g. Ref. [23]). The statistical data obtained from these methods are summarised in Table 4. For PCR, the same number of PCs (5) was selected as for PLS2. The backpropagation network was simulated with a partially connected $10{:}2 \cdot (4{:}1)$ architecture (one hidden layer with bipolar transfer functions [24] and sigmoidal transfer functions [23] for the output layer) which was trained with adaptive learning parameters (learning rate 0.01, momentum 0.2) in 1000 epochs. For the training of the artificial neural network, the concentration values of penicillin and ampicillin were scaled to the interval [0..1]. PLS2 results in the best calibration models (cf. MSEC, RAEC in Table 4) for both analytes and predictions (cf. MSEP, RAEP) for ampicillin. The concentration of penicillin is insignificantly better predicted by the PCR method (6.8% RAEC instead of 7.0% RAEC for PLS2). Nevertheless, the PLS2 method is the method of choice for the data considered here. The difficulty with training backpropagation neural networks with a small number of data can be seen from the predictions obtained with BPN. The latter predictions are in fact worse than those obtained by most of the other soft-modelling methods.

### 4.4. Variable selection

All calculations described in the previous sections were based on the full set of 10 variables calculated from the spectral signals of all five optodes (cf. Table 1). As demonstrated above, both dynamic and static features comprise valuable information for the quantification of penicillin and ampicillin. Now, the question arises whether all optodes or variables are necessary to obtain the described performance. The results will be even better if variables with little or no contribution to the calibration problem can be identified and discarded. Selection of the least important variables can be achieved by (i) inspecting the correlation matrix of the sensor signals (pair correlations) or (ii) by inspecting the loadings [7] of the variables for the primary factors. Fig. 3 shows the corresponding loading plot. The correlation matrix reveals two values close to unity for the pair correlations of the dynamic features of EC7.8-2 and BC7.8-1 and the static features of EC7.8-2 and BC7-1. This high correlation with other signals implies that the in-

Table 4
Comparison of the performance of different multivariate methods for correlation of sensor signals with analyte concentrations. The Table includes the statistical data for PLS regression (PLS2 and PLS1 [7]), PCR [6], MLR [5], and BPN [23]. The MSEC and RAEC value for MLR are close to zero because the system of linear equations is only slightly overdetermined (10 variables for 11 objects)

| | Method | | | | |
|---|---|---|---|---|---|
| | PLS2 | PLS1 | PCR | MLR | BPN |
| Penicillin | | | | | |
| MSEC | 0.094 | 0.305 | 0.155 | 0 | 0.326 |
| RAEC | 5.8% | 12.5% | 9.0% | 0% | 11.1% |
| MSEP | 0.275 | 0.456 | 0.273 | 6.242 | 0.598 |
| RAEP | 7.0% | 9.2% | 6.8% | 56% | 11.0% |
| Ampicillin | | | | | |
| MSEC | 0.156 | 0.229 | 0.209 | 0 | 0.214 |
| RAEC | 6.1% | 8.5% | 7.6% | 0% | 7.5% |
| MSEP | 0.093 | 0.115 | 0.294 | 1.226 | 0.273 |
| RAEP | 7.1% | 9.1% | 15.4% | 22.5% | 10.8% |

formation gathered by optode EC7.8-2 is redundant. The loading plot (Fig. 3) shows a weighted picture of the same fact. The loadings of the described pairs of variables look very similar in both cases with the virtual exception of the loadings for the fifth factor with respect to the static features of EC7.8-2 and BC7-1. Since this factor accounts for only 0.1% of the total variance, this difference has in fact no effect on the correlation. This has to be taken into account for the interpretation of the loading plot.

In addition, further information can be obtained from this loading plot. The small loadings of the static features of EC7.8-1 for all five factors show that this variable does not help to solve the calibration problem. In fact, this variable models only the error (as seen by high loadings for the secondary factors which are not presented here). Thus, deleting this variable from the data sets should result in better predictivity of the calibration model. Therefore a new PLS2 model was calculated without this variable and without the redundant optode EC7.8-2. The predictivity of the model increased significantly (MSEP = 0.039, RAEP = 3.9% for penicillin and MSEP = 0.074, RAEP = 5.1% for ampicillin, see Table 4 for comparison). This discussion shows a way to utilise the information from multivariate calibration models to optimise the selection of variables and optodes from an optode array.

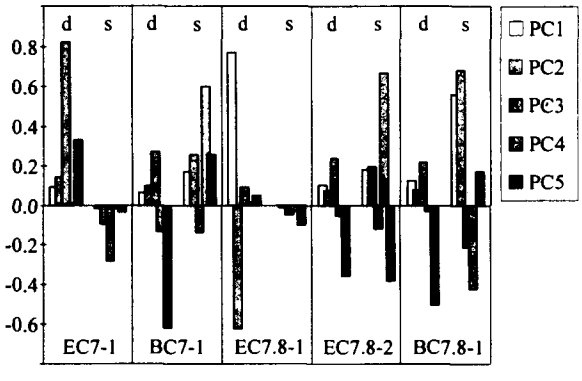


Fig. 3. Diagram of the loadings of the 10 variables for the first five PCs. The corresponding optodes are indicated at the bottom of the picture. The assignment of the variables to dynamic (d) and static (s) features is indicated at the top. See text for a detailed interpretation.

## 5. Conclusion

In the presented study we have shown that simultaneous analysis of penicillin and ampicillin concentrations is feasible with an array of four optodes incorporated in an FIA system. The optodes were based on immobilised penicillinase in the presence of a pH indicator. The concentrations of unknown samples are predictable with a relative absolute error <6%. Detailed analysis of the multivariate data reveals (1) that dynamic together with static features comprise valuable information, (2) feature extraction is best performed by multivariate analysis of the full spectral data, (3) selection of variables and optodes is easily performed on the basis of the loading plots and correlation matrix, and (4) the standard PLS2 method is appropriate for the data analysis. Taking these results into account for future

investigations it should be possible to reduce the calibration set optimising the choice of influencing parameters as the pH, the amounts and types of enzymes or pH indicators. The results clearly demonstrate that multivariate evaluation should be involved in the analysis of optode arrays especially as the presented algorithms are well established and the calculations can be carried out by a personal computer in a matter of seconds.

## Acknowledgements

This project was partially supported by the Deutsche Forschungsgemeinschaft (SFB 145 Biokonversion). We thank Mrs M. Schwenk for "orientating measurements", G.K. and G.G. thank the Fonds der Chemischen Industrie.

## References

[1] E. Wagner, R. Dändliker and K. Spenner (Eds.), Optical Sensors, in W. Göpel, J. Hesse and J.N. Zemel (Eds.), Sensors: A Comprehensive Survey, Vol. 6, VCH, Weinheim, 1992.
[2] O.S. Wolfbeis, Fibre Optic Chemical Sensors and Biosensors, Vols. I and II, CRC Press, Boca Raton, FL, 1991.
[3] H. Wold, in F. David (Ed.), Research Papers in Statistics, Wiley, New York, 1966, pp. 411–444.
[4] S. Wold, H. Martens and H. Wold, The Multivariate Calibration Problem in Chemistry Solved by PLS, in A. Ruhe and B. Kagstrom (Eds.), Matrix Pencils (Lecture Notes in Mathematics), (1994) 286.
[5] D.L. Massart, B.G.M. Vandeginste, S.N. Deming, Y. Michotte and L. Kaufman, Chemometrics: a Textbook, Elsevier, Amsterdam, 1988.
[6] R. Marbach and H.M. Heise, Chemom. Intell. Lab. Syst., 9 (1990) 45.
[7] H. Martens and T. Naes, Multivariate Calibration, Wiley, Chichester, 1989.
[8] J. Havel, F. Jiménez, R.D. Bautista and J.J.A. León, Analyst, 118 (1993) 1355.
[9] E.A. Novikov and L.K. Shpigun, J. Anal. Chem., 48 (1993) 931.
[10] M.S. Peña, A. Muñoz de la Peña, F. Salinas, M.C. Mahedero and J.J. Aaron, Analyst, 119 (1994) 1177.
[11] J. Ruzicka and E.H. Hansen, Flow Injection Analysis, 2nd edn., Wiley, New York, 1988.
[12] A. Espinosa-Mansilla, F. Salinas and A. Zamoro, Analyst, 119 (1994) 1183.
[13] M. Blanco, J. Coello, H. Iturriaga, S. Maspoch and J. Riba, Anal. Chem., 66 (1994) 2905.
[14] L. Nørgaard and C. Ridder, Talanta, 41 (1994) 59.
[15] A.Z.A. Zuhri, A.H. Rady, M.S. El-Shahawi and S.M. Al-Dhaheri, Microchem. J., 50 (1994) 111.
[16] L.H. Christensen, G. Mandrup, J. Nielsen and J. Villadsen, Anal. Chim. Acta, 296 (1994) 51.
[17] T.J. Kulp, J. Camins, S.M. Angel, C. Munkholm and D.R. Walt, Anal. Chem., 59 (1987) 2849.
[18] W. Höbel, A. Papperger and J. Polster, Biosens. Bioelectron., 7 (1992) 549.
[19] M. Busch, W. Höbel and J. Polster, J. Biotechnol., 31 (1993) 327.
[20] M. Busch and J. Polster, Trends Anal. Chem., 11 (1992) 230.
[21] J. Polster, M. Wollenweber, G. Gauglitz and G. Kraus, unpublished work.
[22] P. Valko and S. Vajda, Data Handling in Science and Technology 4: Advanced Scientific Computing in BASIC with Applications in Chemistry, Biology and Pharmacology, Elsevier, Amsterdam, 1989.
[23] B.J. Wythoff, Chemom. Intell. Lab. Syst., 18 (1993) 115.
[24] Z. Li, C. Zhaonian, X. Li and L. Tonghua, Anal. Chem., 65 (1993) 393.

ELSEVIER

Talanta 42 (1995) 2073–2078

Talanta

# Use of poly(ester-sulfonic acid) film-coated electrodes as amperometric detectors in flow injection analysis

T. Gennett *, W.R. Rusin, L.M. Gier

*Chemistry Department, 85 Lomb Memorial Drive, Rochester Institute of Technology, Rochester, NY 14623, USA*

Received 13 June 1994; revised 11 July 1995; accepted 12 July 1995

**Abstract**

Within the past several years significant advances have been made towards the development and incorporation of chemically modified electrodes as selective detectors for high performance liquid chromatography and flow injection analysis. In many cases the chemically modified electrode systems closely approach the "ideal" detector specifications of chemical and mechanical stability along with a significant linear response region. This paper will discuss the characterization and incorporation of ionomeric poly(ester-sulfonic acid) coated electrodes as nonaqueous electrochemical detectors. The orientation of the electrodes in the detector system as well as the increased sensitivity levels to $10^{-10}$ g ml$^{-1}$ for cationic species and $10^{-9}$ g ml$^{-1}$ for neutral species will be presented. Also the applicability of the ionomer coated electrodes as nonelectrolyte detectors achieved a reproducible response with detection limits to $10^{-6}$ g ml$^{-1}$. Overall this system performed as well as, or better than, more specialized and expensive thin layer electrochemical detectors.

*Keywords:* Chemically modified electrodes; Amperometric detectors; Poly(ester-sulfonic acid); Flow injection analysis

## 1. Introduction

The use of ionomer-coated electrodes to enhance electrochemical amperometric signals has been the subject of significant research efforts for the past ten years [1–12]. The incorporation of these modified electrodes into flow analysis systems as ultra-sensitive electrochemical detectors is for use under low and non-electrolyte conditions [12–16].

This paper reports the incorporation of a poly(ester sulfonic acid)-coated dual platinum disc electrode flow cell system as a reduced and non-electrolyte detector for flow injection analysis (FIA). As previously reported, the poly(ester sulfonic acid)-coated electrode systems are stable and exhibit fast partitioning of analyte materials under various nonaqueous conditions [12]. Several different electrochemical flow cell types with modified electrodes have been reported in the literature, however their relatively high cost and degree of specialization have limited their widespread acceptance and use as viable alternatives to spectroscopic detectors [13–16]. The detector system described herein incorporates a chemically modified commercially available thin layer dual electrode cell as the basis for the detector system. The electrode surfaces are coated with a thin film of an ionomeric material via a solution casting process. To accomplish universal flow across the flow cell, the electrode block is oriented such that electrodes

* Corresponding author. Fax: 716-475-5766; e-mail: TXGSCH@RIT.EDU


*SSDI* 0039-9140(95)01689-9

are in series, reference downstream, and the entire cell volume is over the thin film membrane. The resultant thin layer amperometric detector system is stable under flow; has exhibited a reproducible, low detection limit response for both reduced and non-electrolyte experimental conditions; and has shown increased sensitivity for both cationic and neutral analytes as compared to uncoated systems. This electrode/coating system also lowered the capacitive current levels from microamps for uncoated systems to less than 50 ηamps for the coated electrodes. Therefore, while analyte signals did decrease slightly because of diffusion limitations, the S/N ratios were significantly enhanced by approximately two orders of magnitude.

## 2. Experimental

### 2.1. Apparatus

A Bioanalytical System (BAS) Model LC-44 thin layer flow cell was used as the primary detector system. This system consists of a stainless steel mounting block with a removable electrode assembly and Teflon flow spacer. The electrode to be modified was a BAS Model MF-1012 dual 2 mm platinum disk electrode encased in a PEEK block. The Teflon spacers used to define the channel volume of the cell were either 2 or 3 μl. A three electrode configuration was employed with the anionomer coated platinum disk as the working electrode, the stainless steel block as the auxiliary electrode, and the second coated platinum disk as the reference electrode. The poly(ester sulfonic acid)-coated platinum electrode behaved similar to a coated wire electrode with a stable reference potential $225 \pm 5$ mV negative of a Ag/AgCl reference electrode. Therefore all potentials are reported versus the ionomer/platinum reference electrode.

Samples were injected through a Rheodyne Model 7125 injection valve equipped with either a 10 or 20 μl injection loop. The flow of the mobile phase across the FIA cell was maintained with a Hewlett Packard Model 1050 dual piston pump equipped with a pulse damper.

The amperometric signals were measured with an EG&G PAR Model 273 potentiostat/galvanostat. The output was displayed on either a Hewlett Packard Model 7015B time base recorder or a Hewlett Packard Model 3394a integrator. The entire electrochemical flow cell system was encased within a Faraday cage. Voltage regulators were used on all instrumentation to minimize any fluctuations of the 120 V a.c. line.

### 2.2. Reagents

All experiments were performed with Burdick and Jackson HPLC grade acetonitrile which was kept under a continuous helium purge. The electrolyte, tetrabutyl ammonium hexafluorophosphate, was purchased from Aldrich recrystallized thrice from ethanol and dried in vacuo at 100 °C prior to use. The poly(ester sulfonic acid) ionomer, AQ55D, was purchased from Eastman Kodak Co. and filtered through a 0.45 μm Whatman Acrodisk prior to use. $Ru(bpy)_3Cl_2$ and *p*-hydroquinone were purchased from Aldrich and used as received. Ferrocence and $Ru(NH_3)_6Cl_3$ were purchased from Strem Chemical Co. and used as received. Purity of all analytes was confirmed with voltammetric analyses prior to injection into the flowing system.

### 2.3. Procedure

The electrodes were first cleaned and polished with 1.00, 0.30 and 0.05 μm alumina on a Buehler Ecomet II Polisher. The electrodes were than immersed in water and sonicated for 30 min, removed and dried in a 110 °C oven for 1 h, and placed in a vacuum dessicator to cool. AQ-55 films between 4 and 5 μm were solution cast over the entire surface of the flow channel by applying 25 μl of a 2% w/w AQ55 aqueous dispersion. After application of the ionomer solution, the electrodes were placed in an 85 °C oven for 1 h. A detailed description of the AQ55 casting procedures has been summarized in the literature [12,13].

## 3. Results and discussion

This investigation was concerned with the amperometric response of AQ55-coated electrodes to neutral and cationic analytes in FIA. The AQ55 ionomer undergoes minimal swelling, is insoluble, and maintains its structural integrity in acetonitrile under flow conditions of 0.5–2.0 ml $min^{-1}$. Attempts to incorporate AQ55-modified electrodes in non-

buffered aqueous solutions or methanol flowing streams, as has been reported in the literature [13], was unsuccessful because of the unpredictable behavior of the membrane. In most aqueous/methanol experiments the membranes would quickly deteriorate and be completely removed from the electrode surface within seconds. In other experiments, membranes would last for longer periods of time; however, the amperometric signal exhibited a time dependence. With a mobile phase of either acetonitrile, methylene chloride, or tetrahydrofuran the membranes were stable for extended time periods, 24 h or more, and showed no variation in amperometric response. Within this investigation, acetonitrile was the solvent of choice for the low electrolyte and nonelectrolyte FIA investigations because of the known values for membrane diffusion and partitioning rates [12].

Experimental results for the analysis of $Ru(bpy)_3^{2+/3+}$ at a typical coated electrode are summarized in Figs. 1–3. $Ru(bpy)_3^{2+/3+}$ was chosen as the analyte because the $E°$ for the redox couple is at the oxidative extreme of the acetonitrile/platinum potential window; therefore, the amperometric response is in the region where the signal-to-noise ratio would be at a minimum. Experiments were also conducted with hydroquinone to evaluate the response of the coated electrode to an organic molecule with an irreversible oxidation.

Fig. 1 shows representative data for the response of the AQ55-coated detector system under reduced, 0.05 to 0.001 M, electrolyte conditions and an analyte concentration of

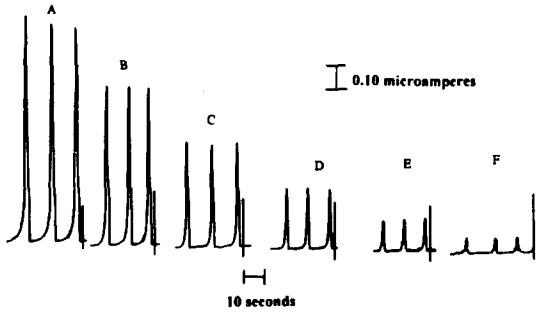


Fig. 1. Repetitive flow injection amperometric response at a dual platinum electrode coated with a 5 Nm AQ55 ionomeric membrane. Experimental conditions: working electrode was a 2 mm platinum disk; a channel volume of 2.9 µl; mobile phase of acetonitrile/0.01 M TBAHP at a flow of 1.0 ml $min^{-1}$; 10 µl injections of $5 \times 10^{-7}$ g $ml^{-1}$ of $Ru(bpy)_3^{2+}$ dissolved in mobile phase. Curves: (A) 0.975 V; (B) 0.950 V; (C) 0.925 V; (D) 0.900 V; (E) 0.875 V; (F) 0.850 V vs. AQ55/platinum reference electrode.

$5.00 \times 10^{-8}$ g $ml^{-1}$. As illustrated, the FIA amperometric signals are extremely reproducible with baseline response times of less than 3 s, an excellent membrane re-equilibrium time. Repetitive injections of the analyte solutions over 8 h showed less than a 1% loss in amperometric response. The hydrodynamic voltammogram generated in Fig. 2 illustrates the exceptional experimental behavior at the membrane-coated detector. The plot of $E$ vs. $\log[(i_{lim} - i)/i]$ was linear with a slope of 64 mV which is in good agreement with the theoretical value of 59 mV. Therefore, it appears that the increased resistance across the ionomeric membrane does not cause an activation overpotential to occur for the described experimental conditions.

In order to determine the detection limits of this membrane-coated, amperometric detector system a series of analyte solutions of various concentrations were evaluated. Fig. 3a illustrates the response of the AQ55-coated detectors down to $10^{-10}$ g $ml^{-1}$. It is apparent that the response of the detector was linear to approximately $10^{-9}$ g $ml^{-1}$ with a lower limit of detection at $10^{-10}$ g $ml^{-1}$. (The log vs. log plot is necessary for clarity, the linear region is similar for the non-logarithm plots.) This detection limit is over 2 orders of magnitude better sensitivity than the response reported at similar uncoated electrodes. Concentrations less than $10^{-10}$ g $ml^{-1}$ were beyond the sensitivity of the potentiostat and therefore not evaluated. Fig. 3b is an example of the response of the detector to the $10^{-10}$ g $ml^{-1}$ solutions. In between each injection of analyte, electrolyte solution was injected to insure that there was no response caused by the injection valve. The piston strokes of the pumping system are the small regular peaks which appear at these current sensitivity settings.

The oxidation of the hydroquinone molecule, under the same electrolyte experimental conditions as $Ru(bpy)_3^{2+/3+}$, was irreversible (as expected) with an $E_{pa} = 0.79$ V vs. coated reference. The hydrodynamic voltammogram and resultant plot of $E$ vs. $\log[(i_{lim} - i)/i]$ showed a linear response with a slope of 180 mV (an irreversible wave) and a detection limit of $10^{-8}$ g $ml^{-1}$.

As mentioned, the 2 mm platinum electrode in a 3 µl flow channel achieved an amperometric current response down to $10^{-10}$ g $ml^{-1}$ for inorganic cationic species. Unexpectedly, the observed detection limits for the oxidation of

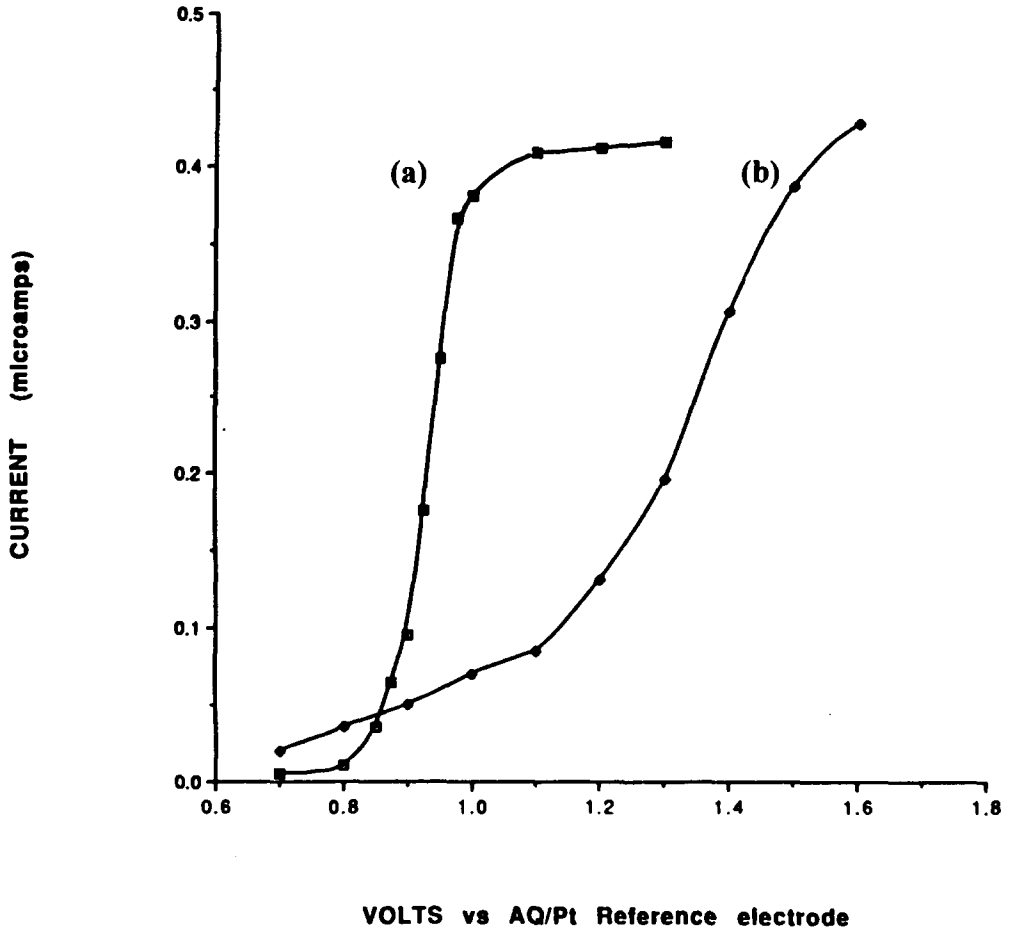


Fig. 2. Hydrodynamic voltammograms for the FIA of $Ru(bpy)_3^{2+}$ in acetonitrile at an AQ55-coated platinum disk electrode: (a) 10 µl injections of $10^{-7}$ g ml$^{-1}$ of $Ru(bpy)_3^{2+}$ in 0.01 M TBAHP; (b) 10 µl injections of $10^{-5}$ g ml$^{-1}$ $Ru(bpy)_3^{2+}$ in acetonitrile with no added electrolyte.

neutral species, $10^{-9}$ g ml$^{-1}$ for ferrocene and $10^{-8}$ g ml$^{-1}$ for hydroquinone, were about 2 orders of magnitude greater than for uncoated electrodes. Fan and Harrison [17] have shown that neutral species can partition into Nafion membranes and have proposed the concept of an effective diffusion coefficient, $D_{eff}$. $D_{eff}$ is equal to the product of the membrane partition coefficient, $K_p$, and the membrane diffusion coefficient, $D_{mem}$, ($D_{eff} = K_p \times D_{mem}$). Partition coefficients of approximately $10^5$ and $10^1$ were observed respectively, for the incorporation of cationic and neutral species from acetonitrile into the AQ55 membranes. However, since the $D_{mem}$ values are $10^{-10}$ and $10^{-5}$ cm s$^{-1}$ for the cationic and neutral species the $D_{eff}$ values for both the cationic and neutral species are of approximately the same magnitude. This equality of $D_{eff}$ contributes to the similar detection limits for the cationic and neutral species.

The evaluation of this detector system under nonelectrolyte conditions is illustrated in the hydrodynamic curve b of Fig. 2. Limited success with the use of the coated design as a nonelectrolyte detector was achieved. Using an acetonitrile mobile phase, ionomer-coated working electrode, and $Ru(bpy)_3^{2+}$ as an analyte, a linear amperometric response to $10^{-6}$ g ml$^{-1}$ was observed. As expected the absence of electrolyte within the mobile phase increased the resistance within the cell, creating a significant activation overpotential. This overpotential is evidenced by the approximately 400 mV positive shift of the $E_{1/2}$ value. Also the increase of the slope to 120 mV is further evidence of the increased resistance across the membrane–electrode interface. Finally, unlike the ionomer-coated electrodes exposed to a mobile phase which maintained a constant electrolyte concentration, the membranes exposed to nonelectrolyte conditions

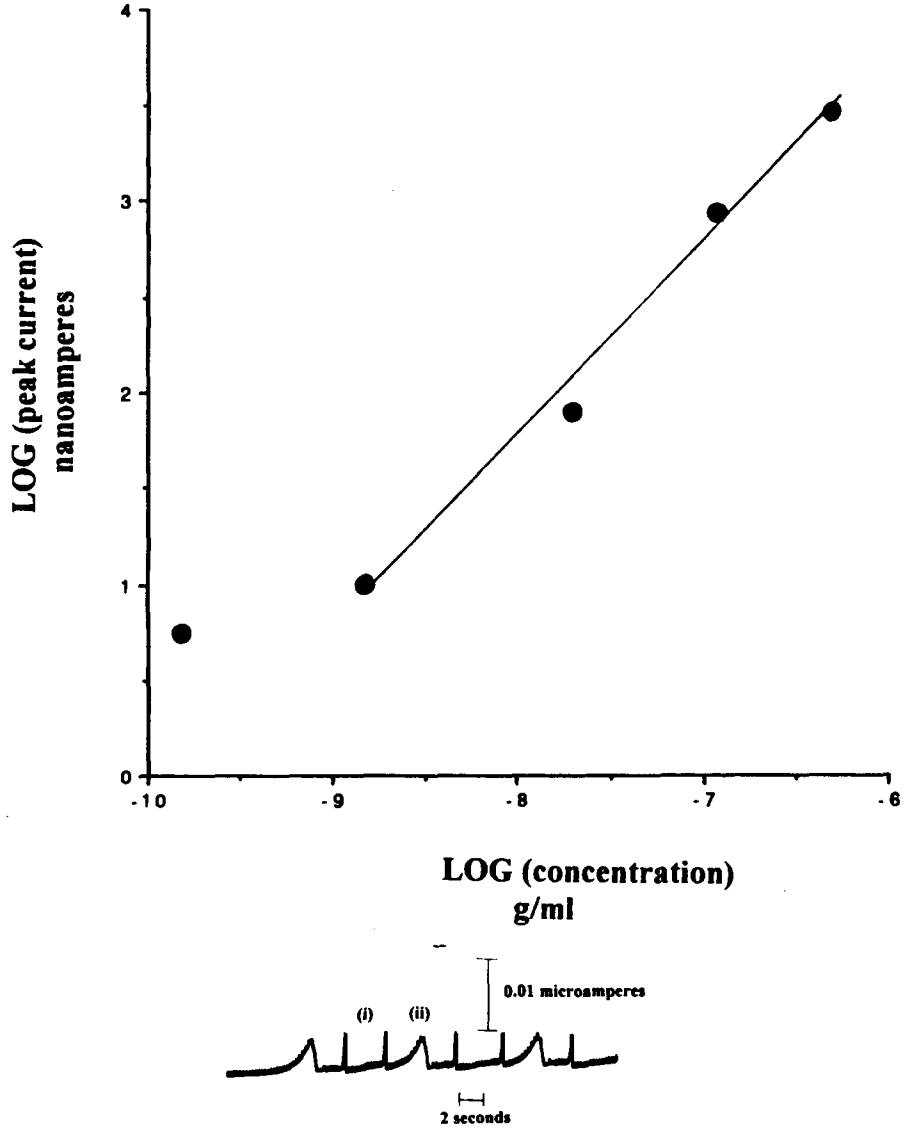


Fig. 3. (a) Detection limits for the amperometric response of $Ru(bpy)_3^{2+}$ at an AQ55-coated platinum electrode in 0.01 M TBAHP/acetonitrile solution at a flow of 1.0 ml $min^{-1}$. (b) Alternate injections of 20 µl of 0.01 M TBAHP solutions, curve (i); and $1.5 \times 10^{-10}$ g $ml^{-1}$ of $Ru(bpy)_3^{2+}$, curve (ii).

were extremely sensitive to the experimental history of the electrode. One explanation for the carryover effects is that $Ru(bpy)_3^{2+/3+}$ incorporates into the membrane and remains as a charge carrier. After repeated experiments the concentration of $Ru(bpy)_3^{3+}$ increases within the membrane causing the decreased signal and lack of reproducibility for the amperometric response. Since under low electrolyte conditions no carryover effects were observed, it is assumed that the electrolyte cations rapidly exchanged with the analyte cations in between injections thereby replenishing the membrane with inert electrolyte ions. Therefore, to eliminate the carryover effects under nonelectrolyte conditions, injections of 0.10 M electrolyte solution were made after every $Ru(bpy)_3^{2+}$ injection. After the injections of 0.10 M electrolyte it is assumed that the membranes absorb a small amount of the electrolyte solution and in essence create an in-situ electrolyte source which maintains a low electrolyte concentration. Under these conditions the amperometric response was not as sensitive as under electrolyte conditions, but did become highly reproducible.

## 4. Conclusion

The high speed and sensitivity of this AQ55 thin layer electrochemical flow cell coupled with its excellent reproducibility, low cost and ease of use make it an attractive alternative to other electrochemical and spectroscopic detector systems. Also, the sensitivity to neutral as well as cationic species, $10^{-9}$ and $10^{-10}$ g ml$^{-1}$ respectively, enhances the applicability well below the detection limits for most flow analysis detectors.

With respect to the nonelectrolyte applications of the AQ55-coated electrode system, while the results with the ionomer coating are promising, much work is still needed to reduce the resistance effects and lower the detection limits. Presently, from preliminary results in our laboratory, the use of cationomeric/anionomeric blends has lowered the resistive effects but the sensitivity levels have not improved. We are continuing our efforts on the incorporation of coated arrays and platinized membranes and hope to construct a viable electrochemical detector for "normal-phase" chromatography.

## Acknowledgments

The authors wish to acknowledge the financial support of the Eastman Kodak Company Outreach Grant; The Research Corporation, Cottrell Grant; and the National Science Foundation, Research Experiences for Undergraduates Program.

## References

[1] M.N. Szentirmay and C.R. Martin, Anal. Chem., 56 (1984) 1989.
[2] M.W. Espenscheid, A.R. Ghatak-Roy, R.B. Moore, R.M. Penner, M.N. Szentirmay and C.R. Martin, J. Chem. Soc., Faraday Trans. 1, 82 (1986) 1051.
[3] L.D. Whitely and C.R. Martin, Anal. Chem., 59 (1987) 1746.
[4] Y. Ikariyama, S. Yamauchi, T. Yukiashi and H. Ushioda, J. Electrochem. Soc., 136 (1989) 702.
[5] J. Wang, L. Wu, Z. Lu, R. Li and J. Sanchez, Anal. Chim. Acta, 228 (1989) 251.
[6] D.J. Harrison, R.F.B. Turner and U.P. Baltes, Anal. Chem., 60 (1988) 2002.
[7] J. Wang and Z. Lu, J. Electroanal. Chem., 266 (1989) 287.
[8] J. Wang, D. Leech, M. Ozsoz, S. Martinez and M.R. Smyth, Anal. Chim. Acta, 245 (1991) 139.
[9] J. Wang and T. Golden, Anal. Chem., 61 (1989) 1397.
[10] M.L. Langmire, M. Watanabe, H. Zhang, T.T. Wooster and R.W. Murray, Anal. Chem., 62 (1990) 747.
[11] H. Van Ryswyk, C.H. Kim and D.S. Solomon, J. Electroanal. Chem., 265 (1989) 317.
[12] T. Gennett and W.C. Purdy, Anal. Chem., 62 (1990) 2155.
[13] J. Wang and L. Chen, Anal. Chem., 63 (1991) 1499.
[14] J.W. Bixler, M. Fifield, J.C. Poler, A.M. Bond and W. Thurmann, Electroanalysis, 1 (1989) 23.
[15] J.W. Bixler and A.M. Bond, Anal. Chem., 58 (1986) 2859.
[16] T. Kaaret and D.H. Evans, Anal. Chem., 60 (1988) 657.
[17] Z. Fan and D.J. Harrison, Anal. Chem., 64 (1992) 1304.

ELSEVIER

Talanta 42 (1995) 2079–2085

Talanta

# Chemically amplified kojic acid responses of tyrosinase-based biosensor, based on inhibitory effect to substrate recycling driven by tyrosinase and L-ascorbic acid

Yasushi Hasebe *, Katsuhiro Oshima, Osamu Takise, Shunichi Uchiyama

*Department of Environmental Engineering, Saitama Institute of Technology, 1690 Fusaiji, Okabe, Saitama 369-02, Japan*

Received 27 April 1995; accepted 24 July 1995

**Abstract**

A tyrosinase-based chemically amplified biosensor, based on the substrate recycling of polyphenols driven by tyrosinase-catalyzed oxidation and chemical reduction by L-ascorbic acid (AsA), has been utilized for the highly sensitive detection of inhibitors of tyrosinase such as kojic acid, benzoic and $SCN^-$ ion. The amplified current response of immobilized tyrosinase-coupling oxygen electrode due to the recycling was suppressed by the addition of inhibitors, and a highly amplified response to kojic acid over other inhibitors was observed in the presence of 5 mM AsA. The amplification factor (AF) of kojic acid is substantially proportional to the AF of substrates, and the AF for $1 \times 10^{-7}$ M kojic acid was increased by up to a factor of 143 when $1 \times 10^{-5}$ M dopamine was used as a competitive substrate in the presence of 5 mM AsA. The amplified calibration curve of kojic acid obtained with 5 mM AsA was shifted towards more than a two decades lower concentration range compared with that of the non-amplified response, and the detection limit of kojic acid was lowered to $7 \times 10^{-8}$ M.

*Keywords:* Biosensors; Tyrosinase; Substrate recycling; L-Ascorbic acid

## 1. Introduction

Tyrosinase (polyphenol oxidase, EC 1.14.18.1) is a copper-containing metallo-enzyme and catalyzes hydroxylation of phenol to catechol and subsequent dehydrogenation to *o*-quinones accompanied by the conversion of molecular oxygen to water, and a number of biosensors using immobilized tyrosinase membrane have been reported [1–5]. However, in order to enhance the sensitivity and decrease the detection limits of enzyme-based biosensors, recycling of substrates and cofactors catalyzed by more than two kinds of enzyme have been utilized for the signal amplification of several biosensor systems [6–11]. In this connection, we have recently proposed the tyrosinase-based chemically amplified biosensing systems for catechol [12] and catecholamines [13,14], in which substrates are recycled between the reduced form (catechol compounds) and the oxidized form (*o*-quinone compounds) by combining tyrosinase-catalyzed oxidation and chemical reduction by L-ascorbic acid (AsA). In these systems, a remarkably amplified signal could be obtained by monitoring the amplified change in the concentration of dissolved oxygen [12,13] and pH [14] during the recycling, and highly sensitive determination of polyphenols (nanomolar to micromolar order) has been achieved.

* Corresponding author.



*SSDI* 0039-9140(95)01698-8

TAL 42:12-5

Kojic acid (5-hydroxy-2-(hydroxymethyl)-4*H*-pyran-4-one) is an antibiotic substance produced in an aerobic process by a variety of micro-organisms from a wide range of carbon sources. The assay of kojic acid is therefore important for monitoring the fermentation process. A convenient and direct biosensor system for kojic acid, however, has not been reported so far to our knowledge. It is known that kojic acid competitively binds to the catalytic site of tyrosinase because of its structural similarity to polyphenols and then inhibits the tyrosinase activity. In practical applications, kojic acid has been used in some cosmetics to prevent serious sun-burning caused by an accumulation of melanin in subcutaneous tissue produced via a tyrosinase-catalyzed metabolic pathway. If the inhibition of kojic acid is reversible and tyrosinase is not inactivated, an effective and highly sensitive determination of kojic acid using chemically amplified polyphenol sensors would be expected because the amplified signal of the sensor is arising from the recycling of trace amounts of substrates that compete with inhibitors. On the bases of a similar analytical concept, the determination of enzymatic inhibitors based on substrate recycling systems using double-enzyme reactions [15] and electroenzyme reactions [16–18] have already been reported by other groups.

In this study, we demonstrate the effectiveness of the chemically amplified recycling biosensor using immobilized tyrosinase and AsA for highly sensitive determination of tyrosinase inhibitors, especially kojic acid, and the amplification characteristics of kojic acid obtained in the presence of AsA are described compared with those of a non-amplified response without AsA.

## 2. Experimental

### 2.1. Materials

Tyrosinase (EC 1.14.18.1, from mushroom, 2400 units $mg^{-1}$ of catechol oxidase activity) was purchased from Sigma, Sodium L-ascorbate (AsA), kojic acid, sodium benzoate, sodium thiocyanate, dopamine nonohydrochloride, catechol, phenol and noradrenaline hydrochloride were of analytical grade and were used without further purification. Acrylamide monomer, *N,N*-methylenebisacrylamide, *β*-dimethyl-aminopropyonitrile, potassium persulfate, potassium dihydrogenphosphate and disodium hydrogenphosphate were of extra pure reagent grade. Deionized water was used for preparing the buffer and sample standard solutions.

### 2.2. Preparation of immobilized-tyrosinase electrode

The enzyme electrode was fabricated by placing a tyrosinase-entrapped polyacrylamide gel ( $\approx 3$ mm diameter, 0.2 mm thickness) on the surface of the gas-permeable membrane of a Clark-type oxygen electrode (Denki Kagaku Keiki Ltd.). The tyrosinase-entrapping gel was prepared as follows: acrylamide monomer (375 mg) and *N,N*-methylenebisacrylamide (20 mg) were dissolved in 2 ml of 0.1 M phosphate buffer (pH 6.5) containing 1–10 mg of tyrosinase, and then poured onto a flat Petri dish (8.5 cm diameter). Next, 5% *β*-dimethylaminopropyonitrile (0.25 ml) and 1% potassium persulfate (0.25 ml) were added, and the solution was polymerized under a nitrogen atmosphere. The tyrosinase membrane thus prepared was cut off with a microtip ($\approx 3$ mm i.d.) for the sensor preparation, and stored in 0.1 M phosphate buffer (pH 6.5) at 4°C in a refrigerator when not in use.

### 2.3. Procedure

Amperometric measurements were conducted using a potentiostat (Nikko Keisoku NPOT-1), one pen recorder (Nippon Denki Kagaku Ltd.) and an immobilized tyrosinase electrode. The enzyme electrode was immersed in 25 ml of 0.1 M phosphate buffer (pH 6.5) containing AsA in a 50 ml beaker and stirred constantly on a thermostated water bath (Eyela, RC-12, Tokyo Rikakikai). A beaker was opened to the atmosphere and the oxygen was supplied continuously from the air. After the steady-state background current baseline had been obtained, 5–50 μl of a standard solution of polyphenols (dopamine, catechol, phenol) was added with a micropipette and the current response based on the consumption of dissolved oxygen was monitored. After the current response to polyphenols reached a steady-state value, standard solutions of tyrosinase inhibitors (kojic acid, benzoic acid, NaSCN) were added, and the decrease in the steady-state current was measured. All measurements were conducted at 35°C and pH 6.5 (optimum

pH for tyrosinase activity; data from Sigma). Standard solutions of substrates and inhibitors were prepared by dissolving the reagents in 0.1 M phosphate buffer (pH 6.5).

## 3. Results and discussion

A cyclic reaction scheme of catechol compounds driven by tyrosinase and L-ascorbate (AsA) for the determination of tyrosinase inhibitors is shown in Fig. 1. Enzymatically oxidised *o*-quinone compounds were chemically reconverted to catechol compounds by L-ascorbate and reoxidized repeatedly. As a result, the current response of immobilized tyrosinase electrode, based on the reduction current of dissolved oxygen, was amplified in the presence of AsA, and permits the highly sensitive determination of catechol compounds (less than micromolar level) [12,13]. It is known that tyrosinase is inhibited by several kinds of compounds (e.g. kojic acid and $SCN^-$ ion) which competitively bind at the recognition site and catalytic site of tyrosinase respectively [16,17]. Consequently these inhibitors hinder the recycling rate and lead to a decrease in the amplified current response of the tyrosinase-modified oxygen electrode.

Fig. 2 illustrates the typical stepwise current response curves of immobilized tyrosinase electrode obtained by successive addition of kojic acid with dopamine as a competitive substrate in the presence and absence of 5 mM AsA. In this system, the concentration of dissolved oxygen in the bulk solution would remain constant throughout the experimental period because the oxygen was constantly supplied from air by constant stirring. The steady-state current (≈400 nA) obtained by the addition of dopamine, where the rate of oxygen consumption in the enzyme layer is equal to the rate of

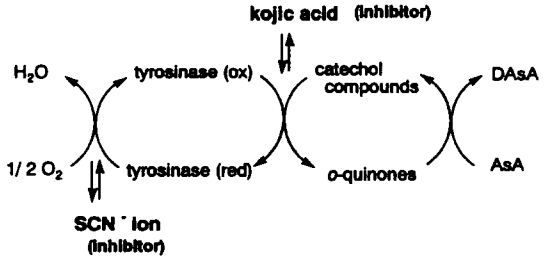


Fig. 1. A redox recycling scheme of polyphenols for the determination of tyrosinase inhibitors, using tyrosinase and L-ascorbic acid (AsA). DAsA: dehydroascorbic acid.

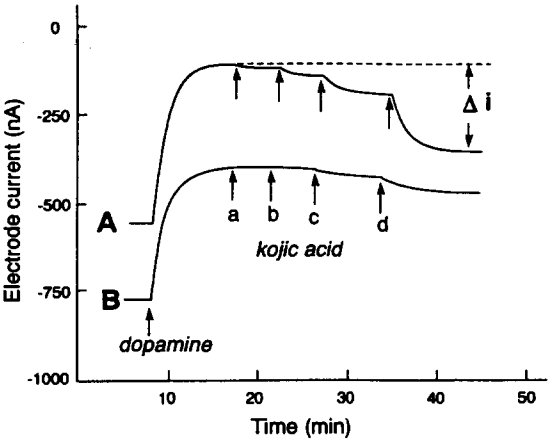


Fig. 2. Typical amplified and non-amplified current response curves of immobilized tyrosinase electrode obtained by successive addition of kojic acid in the presence (A) and absence (B) of 5 mM L-ascorbate in the sample solution with dopamine (A, $1 \times 10^{-5}$ M; B, $2 \times 10^{-4}$ M) as competitive substrate. Kojic acid concentration: a, $1 \times 10^{-6}$ M; b, $3 \times 10^{-6}$ M; c, $1 \times 10^{-5}$ M; d, $1 \times 10^{-4}$ M. 0.1 M phosphate buffer (pH 6.5) was used.

oxygen supply from the bulk solution, was apparently diminished by the addition of kojic acid, and the current reached another steady-state value within ≈4 min. The current difference between the steady-state current before and after kojic acid addition ($\Delta i$) was found to be dependent on the kojic acid added. Furthermore, in the presence of AsA, a lower concentration of kojic acid (micromolar order) induces a current response, whereas no response to kojic acid at less than $1 \times 10^{-5}$ M was observed without AsA. These results indicate that the addition of kojic acid reduces the extent of recycling of dopamine and results in an amplified change in the current response of the tyrosinase electrode. In general, inhibition of enzyme is often irreversible because of the tight binding of non-catalytic inhibitors. In this case, the rinsing of the enzyme membrane by immersing the electrode in phosphate buffer for about 5 min allows the subsequent measurement of dopamine and kojic acid but the current response to dopamine decreases to approximately 92% compared to that of the first response. These results suggest the possibility of highly sensitive detection of kojic acid using a tyrosinase-coupling electrode in the presence of AsA. However, from the practical point of view, the replacement of the enzyme membrane is required after the measurement of a relatively high concentration of kojic acid.

In order to obtain the higher sensitivity, optimal amounts of enzyme should be chosen, so we first investigate the effect of the amount of tyrosinase upon the inhibition current ($\Delta i$) for $1 \times 10^{-4}$ M kojic acid with 5 mM AsA (Fig. 3). The magnitude of $\Delta i$ decreased at higher and lower amounts of tyrosinase, and the largest response was obtained around 5 mg of enzyme. The decrease in the change in current at high enzyme loading may be caused by a shift from enzyme reaction kinetics being rate limiting to a situation where molecular diffusion is rate limiting. In other words, with a large amount of enzyme the kojic acid binds at active sites of the enzyme in the resting state (substrate free) which do not distribute the signal change. Consequently, the remainder of the experiments were carried out using a membrane containing 5 mg of tyrosinase. As reported previously, the sensitivity and amplification factor of the chemically amplified polyphenol sensor were remarkably dependent on AsA concentration, because the reduction rate of *o*-quinones by AsA is directly attributable to the rotation number of substrate per unit time which determines the sensitivity and the magnitude of the amplification factor [12,13]. Fig. 4 shows the effect of AsA concentration on the inhibition current for $1 \times 10^{-4}$ M kojic acid with dopamine as a competitive substrate. This AsA concentration dependency on the inhibition current is essentially similar to that for the amplified response of polyphenols, and maximum response was obtained at an AsA concentration around 5 mM. At a higher concentration of AsA ( > 10 mM), current response is rather decreased, probably because the background concentration of dissolved oxygen to be reacted with the reduced form of enzyme was decreased by the auto-oxidation of AsA by dissolved oxygen.

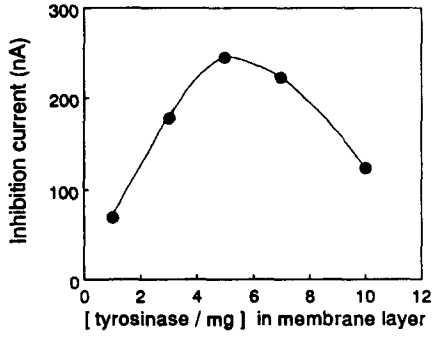


Fig. 3. Effect of the amount of tyrosinase in the membrane layer (in preparation) on the inhibition current to $1 \times 10^{-4}$ M kojic acid in the presence of 5 mM L-ascorbate with $1 \times 10^{-5}$ M dopamine in 0.1 M phosphate buffer (pH 6.5).

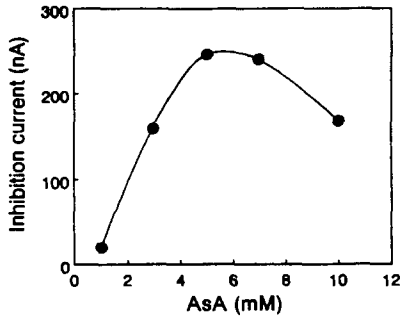


Fig. 4. Effect of AsA concentration on the inhibition current to $1 \times 10^{-4}$ M kojic acid. The amount of enzyme in the membrane layer (in preparation) is 5 mg. Other experimental conditions are the same as in Fig. 3.

Fig. 5 plots the relationship of the amplification factor (AF) between dopamine (substrate) and kojic acid (inhibitor) obtained at each concentration of AsA. AFs of dopamine and kojic acid were calculated by using the following equations and the non-amplified current responses to $2 \times 10^{-4}$ M dopamine (380 nA) and $1 \times 10^{-4}$ M kojic acid (28 nA) obtained without AsA respectively:

$$AF_{dopamine} = [\Delta I_d(nA)/380\ nA] \times [2 \times 10^{-4}\ M/C_d(M)]$$

$$AF_{kojic\ acid} = [\Delta I_k(nA)/28\ nA] \times [1 \times 10^{-4}\ M/C_k(M)]$$

where $\Delta I_d$ and $\Delta I_k$ represent amplified currents for dopamine and kojic acid respectively, and $C_d$ and $C_k$ represent the corresponding concentrations of dopamine and kojic acid respectively. The AF of kojic acid seems to be proportional to the AF of dopamine, suggest-

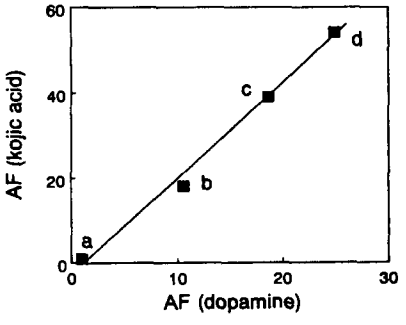


Fig. 5. The relationship of the AF between kojic acid and dopamine obtained at each concentration of L-ascorbate: a, 0 mM; b, 0.5 mM; c, 1 mM; d, 5 mM.

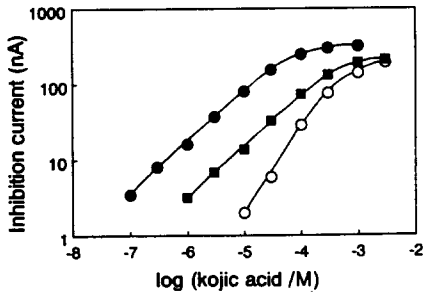


Fig. 6. Amplified and non-amplified calibration curves of kojic acid obtained at (○) 0 mM, (■) 0.5 mM and (●) 5 mM of AsA. The concentrations of dopamine used are $2 \times 10^{-4}$ M, $6 \times 10^{-5}$ M and $1 \times 10^{-5}$ M at 0 mM, 0.5 mM and 5 mM of AsA respectively.

ing that the recycling number of the substrate is substantially in accordance with the sensitivity of kojic acid, probably because the opportunity for the inhibitor to compete with the substrate is increased when the AF (turnover number of the enzyme) is large.

Fig. 6 depicts the amplified and non-amplified calibration graphs of kojic acid, plotting the inhibition current ($\Delta i$) against kojic acid concentration, obtained at each concentration of AsA. Without AsA in the sample solution, no response to kojic acid at less than $1 \times 10^{-5}$ M was observed, and the calibration curve showed a linear response over the concentration range between $1 \times 10^{-5}$ M and $1 \times 10^{-3}$ M. In contrast, the linear portion of the calibration curves apparently shifted towards the lower concentration range with an increase in AsA concentration, and the detection limit of kojic acid was found to be decreased to about $7 \times 10^{-8}$ M ($S/N = 3$, $\approx 3$ nA). In addition, the dynamic range obtained with 5 mM AsA was found to be extended ($1 \times 10^{-7}$–$1 \times 10^{-4}$ M) compared with that of the non-amplified response, indicating that the AF was increased with a decrease in kojic acid concentration. Since the amplified signal arises from the recycling of trace amounts of substrate, signal inhibition is also induced by a lower concentration of competitive inhibitor in the presence of AsA.

As shown in Fig. 1 tyrosinase activity is known to be inhibited not only by polyphenol analogs but also by some anions (i.e. $SCN^-$ ion) which have potential to bind with copper ion at the catalytic site of tyrosinase. Table 1 summarizes the analytical results of several tyrosinase inhibitors (kojic acid, benzoic acid and $SCN^-$ ion) obtained with and without AsA. Highly sensitive responses to kojic acid and benzoic acid over $SCN^-$ ion were observed in the presence of 5 mM AsA, and the AF for $1 \times 10^{-7}$ M kojic acid was increased by more than a factor of 140. These differences in amplified behavior are considered to be explicable in terms of the differences in inhibitory mechanism. Namely, kojic acid and benzoic acid have structural similarity to polyphenols and compete with trace amounts of substrates that are recycled by AsA, and the selectivity of kojic acid over benzoic acid may stem from the structural differences of these inhibitors. In contrast, $SCN^-$ binds with copper ion at the catalytic site of the enzyme and competes with dissolved oxygen. Therefore, the slight amplification of $SCN^-$ ion is due to the differences in background oxygen concentration level (see Fig. 2). The relative standard deviation for five measurements of $2 \times 10^{-6}$ M kojic acid with dopamine and 5 mM AsA was $\approx 5\%$.

In general, tyrosinase has a broad catalytic activity towards a wide variety of mono- and polyphenolic compounds, such as phenol, catechol and catecholamines. Analytical results for kojic acid with several competitive substrates in the presence of 5 mM AsA are summarized in Table 2. The relatively highly sensitive detection of kojic acid was possible when phenol and catechol were used as competitive substrates. Amplification factors of catechol and phenol are higher than those of catecholamines [13,14], so net concentrations of phenol and catechol that compete with kojic acid are lower than those of dopamine and noradrenaline. These results are further evidence that the AF of the substrate determines the sensitivity of kojic acid in this recycling system. The long-term storage stability of the enzyme membrane was also investigated. The tyrosinase membrane used in this study was found to keep its catalytic activity for a period of more than 2 weeks (giving more than 80% current for $1 \times 10^{-5}$ M dopamine; compared to that for the first day) but the current response was decreased to less than 2/3 after 20 days.

The considerable advantages of this method using immobilized tyrosinase and AsA over other recycling systems based on electrochemical enzymatic reactions [16–18] are as follows. (1) A highly amplified signal can be obtained with AsA because the chemical reduction rate of *o*-quinones by AsA occurring in a three-dimensional solution may be larger than the rate of electrochemical reduction occurring at a restricted two-dimensional electrode surface.

Table 1
Analytical results for several inhibitors using a tyrosinase-membrane electrode in the presence of dopamine

| [Inhibitors] (M) | [AsA] (mM) | Kojic acid | | | Benzoic acid | | | $SCN^-$ ion | | |
|---|---|---|---|---|---|---|---|---|---|---|
| | | $\Delta i$ (nA) [a] | AF [b] | D.L. (M) [c] | $\Delta i$ (nA) [a] | AF [b] | D.L. (M) [c] | $\Delta i$ (nA) [a] | AF [b] | D.L. (M) [c] |
| $1 \times 10^{-3}$ | 0 | 152 | 1 | $1 \times 10^{-5}$ | 77 | 1 | $1 \times 10^{-5}$ | 56 | 1 | $8 \times 10^{-5}$ |
| $1 \times 10^{-4}$ | 0 | 28 | 1 | | 21 | 1 | | 17 | 1 | |
| $1 \times 10^{-3}$ | 5 | 312 | 2 | $7 \times 10^{-8}$ | 204 | 3 | $7 \times 10^{-7}$ | 140 | 1.7 | $5 \times 10^{-6}$ |
| $1 \times 10^{-4}$ | 5 | 246 | 9 | | 108 | 5 | | 68 | 1.5 | |
| $1 \times 10^{-5}$ | 5 | 80 | 29 | | 28 | 13 | | 9 | 2 | |
| $1 \times 10^{-6}$ | 5 | 16 | 57 | | 4 | 19 | | n.d. | – | |
| $1 \times 10^{-7}$ | 5 | 4 | 143 | | n.d. [d] | – | | n.d. | – | |

[a] Inhibition currents to each inhibitor in the presence of $2 \times 10^{-4}$ M (non-amplified) and $1 \times 10^{-5}$ M (amplified) of dopamine.
[b] Amplification factors were calculated using non-amplified $\Delta i$ values to $1 \times 10^{-3}$ M and $1 \times 10^{-4}$ M inhibitors.
[c] D.L. = detection limit.
[d] n.d. = none detected.

Table 2
Analytical results of kojic acid using a tyrosinase-membrane electrode in the presence of several competitive substrates and 5 mM AsA

| Substrate | [substrate] [a] (M) | Kojic acid | | |
|---|---|---|---|---|
| | | $\Delta i$ (nA) [b] | Dynamic range (M) | D.L. (M) |
| Dopamine | $1 \times 10^{-5}$ | 80 | $1 \times 10^{-7} \sim$ approx. $1 \times 10^{-4}$ | $7 \times 10^{-8}$ |
| Catechol | $1 \times 10^{-6}$ | 98 | $7 \times 10^{-8} \sim$ approx. $1 \times 10^{-4}$ | $5 \times 10^{-8}$ |
| Phenol | $1 \times 10^{-6}$ | 122 | $7 \times 10^{-8} \sim$ approx. $7 \times 10^{-5}$ | $3 \times 10^{-8}$ |
| Noradrenaline | $2 \times 10^{-5}$ | 55 | $3 \times 10^{-6} \sim$ approx. $1 \times 10^{-3}$ | $1 \times 10^{-6}$ |

[a] The concentration required for the amplified current ( $\approx 350 \sim 400$ nA) in the presence of 5 mM AsA.
[b] Inhibition current to $1 \times 10^{-5}$ M kojic acid.

(2) A relatively wide concentration range and a highly sensitive determination of kojic acid is possible in the presence of AsA. (3) Serious interference by electrochemically active substances is easily avoided by preaddition of AsA to the sample solution. However, at the present stage, the replacement of the enzyme membrane is required after the exposure of the membrane to the solution containing a high concentration of inhibitors (1 mM) because the conplexation of inhibitor with enzyme is not completely reversible. Further, from the point of view of practical applications for the kojic acid sensor, pre-treatments to remove other inhibitors may also be required in advance (i.e. $SCN^-$ ion forms a water-insoluble complex with methylene blue).

In conclusion, a chemically amplified polyphenol sensor using immobilized tyrosinase and AsA is useful for highly sensitive determination not only of substrates but also of enzymatic inhibitors, especially kojic acid, and this analytical concept is expected to be applicable to other enzymatic recycling systems.

## Acknowledgment

The auhtors are grateful to the Ministry of Education, Science and Culture of Japan for partial support of this work through a Grant-in-Aid for Scientific Research (No 06772109).

## References

[1] J.G. Schiller, A.K. Chen and C.C. Liu, Anal. Biochem., 85 (1978) 25.
[2] J. Kulys and R.D. Schmid, Anal. Lett., 23 (1990) 589.
[3] A. Navaratne, M.S. Lin and G.A. Rechnitz, Anal. Chim. Acta, 237 (1990) 107.
[4] J. Wang, L. Fang and D. Lopez, Analyst, 119 (1994) 455.
[5] S. Cosnier and C. Innocent, J. Electroanal. Chem., 328 (1992) 361.
[6] F. Schubert, D. Kirstein, K.L. Schröder and F.W. Scheller, Anal. Chim. Acta, 169 (1985) 391.

[7] F. Mizutani, T. Yamaoka and Y. Tanabe, Anal. Chim. Acta, 177 (1985) 153.
[8] F. Scheller, N. Siegbahn, B. Danielsson and K. Mosbach, Anal. Chem., 57 (1985) 1740.
[9] T. Yao, H. Yamamoto and T. Wasa, Anal. Chim. Acta, 236 (1990) 437.
[10] M.U. Asouzu, W.K. Nonidez and M.H. Ho, Anal. Chem., 62 (1990) 708.
[11] A.W. Wang and M.A. Arnold, Anal. Chem., 64 (1992) 1051.
[12] S. Uchiyama, Y. Hasebe, H. Shimizu and H. Ishihara, Anal. Chim. Acta, 276 (1993) 341.
[13] Y. Hasebe, K. Takamori and S. Uchiyama, Anal. Chim. Acta, 282 (1993) 363.
[14] Y. Hasebe, Y. Tanaka and S. Uchiyama, Anal. Lett., 27 (1994) 41.
[15] P. Seegopaul and G.A. Rechnitz, Anal. Chem., 56 (1984) 852.
[16] M.H. Smit and G.A. Rechnitz, Anal. Chem., 65 (1993) 380.
[17] M.H. Smit and G.A. Rechnitz, Electroanalysis, 5 (1993) 747.
[18] J.L. Besombes, S. Cosnier, P. Labbe and G. Reverdy, Anal. Lett., 28 (1995) 405.

ELSEVIER

Talanta 42 (1995) 2087–2091

Talanta

# Book reviews

***The Kirk-Othmer Encyclopedia of Chemical Technology***, Vol. 7, 4th edn., Composite Materials to Detergency, edited by J.I. Kroschwitz and M. Howe-Grant, Wiley-Interscience, Chichester, 1993, xxviii + 1117 pp., £150.00. ISBN 0-471-52675-4 (v.7).

Reviews of the different volumes of this encyclopedia appear regularly in *Talanta*. Volume 7 covers 37 topics and ranges, alphabetically, from Composite Materials to Detergency. Almost 80 authors, mainly from American academia and industry, have contributed to this volume.

More pages (140) are devoted to technological aspects of copper (Copper, Copper Alloys, Copper Compounds) than any other topic in this current volume. Emphasis here is on copper recovery and processing, wrought and cast alloys are treated separately and the properties and uses of commercially important copper compounds are surveyed.

Composite Materials (108 pages) are presented under the headings: Survey, Polymer-Matrix (e.g. thermoplastics) and Ceramic-Matrix (especially high temperature materials). A combination of mechanical engineering and chemical principles is clearly evident in this treatment. A separate section on Dental Materials (77 pages) covers a wide range of relevant ceramics, cements, plasters, waxes, alloys, etc. and is followed by a small section on Dentifrices.

Other topics in volume 7 which are covered in some depth include Controlled Release Technology (Agricultural and Pharmaceutical—the latter overlapping with the section on Drug Delivery Systems in volume 8), Cosmetics (over 6000 different cosmetics ingredients have been identified) and, Crystallization (kinetics, size distribution, crystallizers). General treatment is given to some computer-related topics—Computer-Aided Design and Manufacturing, Computer-Aided Engineering, Computer Technology and, Databases. The latter contains helpful lists of numerous scientific databases. Some of the minor, but interesting, topics include: Contact Lenses (both rigid and flexible), Contraceptives (including a list of available oral contraceptives), Cryogenics (liquefaction), Cyanides, Desiccants and Design of Experiments.

In common with previous volumes extensive bibliographies are included, the editing is excellent, and every science library should subscribe to this encyclopedia.

P.J. Cox

***Directory of Hyphenated Techniques—TrAC Supplement No. 2***, edited by Z. Deyl, Elsevier, Amsterdam, 1994, 178 pp., US$78.25. ISBN 0-444-82126-0.

The intention of this book is to provide analytical chemists with a world-wide directory of individuals involved in hyphenated techniques. The preface explains that 'every professional repeatedly feels the need for direct communication with other scientists working in the same or in a related field'. To address this problem the book provides an alphabetical list of authors who have made significant contributions to hyphenated techniques. For each author the list gives their full address (including telephone, Fax and E-mail numbers) and a brief curriculum vitae under specific headings (techniques, research topics, applications, most significant publications, etc.). The remainder of the book is devoted to resorting the above information under geographical and technique headings. Finally there is a list of companies with an interest in hyphenated techniques.

Who is this book aimed at? As a researcher with a passing interest in hyphenated techniques I am aware, through literature searches and review articles, who the key players are in GC–MS, LC–MS and CE–MS. With the online data bases and CD/ROM facilities searching through the literature is by no means a tedious task (as the preface to this volume suggests). Indeed before the researcher would wish to contact an acknowledged expert in the

ELSEVIER

Talanta 42 (1995) 2087–2091

Talanta

# Book reviews

***The Kirk-Othmer Encyclopedia of Chemical Technology***, Vol. 7, 4th edn., Composite Materials to Detergency, edited by J.I. Kroschwitz and M. Howe-Grant, Wiley-Interscience, Chichester, 1993, xxviii + 1117 pp., £150.00. ISBN 0-471-52675-4 (v.7).

Reviews of the different volumes of this encyclopedia appear regularly in *Talanta*. Volume 7 covers 37 topics and ranges, alphabetically, from Composite Materials to Detergency. Almost 80 authors, mainly from American academia and industry, have contributed to this volume.

More pages (140) are devoted to technological aspects of copper (Copper, Copper Alloys, Copper Compounds) than any other topic in this current volume. Emphasis here is on copper recovery and processing, wrought and cast alloys are treated separately and the properties and uses of commercially important copper compounds are surveyed.

Composite Materials (108 pages) are presented under the headings: Survey, Polymer-Matrix (e.g. thermoplastics) and Ceramic-Matrix (especially high temperature materials). A combination of mechanical engineering and chemical principles is clearly evident in this treatment. A separate section on Dental Materials (77 pages) covers a wide range of relevant ceramics, cements, plasters, waxes, alloys, etc. and is followed by a small section on Dentifrices.

Other topics in volume 7 which are covered in some depth include Controlled Release Technology (Agricultural and Pharmaceutical—the latter overlapping with the section on Drug Delivery Systems in volume 8), Cosmetics (over 6000 different cosmetics ingredients have been identified) and, Crystallization (kinetics, size distribution, crystallizers). General treatment is given to some computer-related topics—Computer-Aided Design and Manufacturing, Computer-Aided Engineering, Computer Technology and, Databases. The latter contains helpful lists of numerous scientific databases. Some of the minor, but interesting, topics include: Contact Lenses (both rigid and flexible), Contraceptives (including a list of available oral contraceptives), Cryogenics (liquefaction), Cyanides, Desiccants and Design of Experiments.

In common with previous volumes extensive bibliographies are included, the editing is excellent, and every science library should subscribe to this encyclopedia.

P.J. Cox

***Directory of Hyphenated Techniques—TrAC Supplement No. 2***, edited by Z. Deyl, Elsevier, Amsterdam, 1994, 178 pp., US$78.25. ISBN 0-444-82126-0.

The intention of this book is to provide analytical chemists with a world-wide directory of individuals involved in hyphenated techniques. The preface explains that 'every professional repeatedly feels the need for direct communication with other scientists working in the same or in a related field'. To address this problem the book provides an alphabetical list of authors who have made significant contributions to hyphenated techniques. For each author the list gives their full address (including telephone, Fax and E-mail numbers) and a brief curriculum vitae under specific headings (techniques, research topics, applications, most significant publications, etc.). The remainder of the book is devoted to resorting the above information under geographical and technique headings. Finally there is a list of companies with an interest in hyphenated techniques.

Who is this book aimed at? As a researcher with a passing interest in hyphenated techniques I am aware, through literature searches and review articles, who the key players are in GC–MS, LC–MS and CE–MS. With the online data bases and CD/ROM facilities searching through the literature is by no means a tedious task (as the preface to this volume suggests). Indeed before the researcher would wish to contact an acknowledged expert in the

field I would have thought that a literature search would be an essential pre-requisite. The preface goes on to suggest that you can pick up the phone and 'swiftly obtain information one needs regarding experimental set ups, specific consumables, etc.' For those poor souls whose addresses are included in this volume I pass on my sympathy. A suitable quotation to leave on your answer phone comes from a memorable interview between Mohammed Ali and Michael Parkinson... 'read my book'.

There is one very good use for this book that has been considered by the editor. Those who organise international conferences on hyphenated techniques will find the book extremely useful in compiling a list of potential contributors and delegates. If you are in this position the book is a good buy; otherwise I'd be tempted to give this one a miss.

B.A. McGaw

***Inorganic Chemistry***, 2nd edn., by D.F. Schriver, P.W. Atkins and C.H. Langford, Oxford University Press, Oxford, 1994, xviii + 819 pp. + additional information, softback, £19.50. ISBN 0-19-855396-X.

This is the second edition of the textbook published initially in 1990 and which was very successful. The second edition shows considerable modification and reorganization. The book is divided into three parts: Part 1, *Foundations*; Part 2, *Systematic chemistry of the elements* and Part 3, *Advanced topics*. Part 1 (ca. 310 pp.) has chapters on atomic and molecule structure, molecular shape and symmetry, structure of solids, acids and bases, d-metal complexes and oxidation and reduction. After establishing the foundation of the subject the authors, in Part 2 (ca. 170 pp.), provide a systematic comprehensive account of the chemistry of the elements and their compounds. Metals, hydrogen and its compounds, main-group organometallic compounds, boron and carbon groups, nitrogen and oxygen groups and halogens and noble gases are dealt with in six chapters. Part 3 is a very subjective section as the authors had to be very selective in the choice of appropriate topics in order to give the reader a sense of the current frontier research. It contains chapters on electronic spectra of complexes, reaction mechanisms of d-block complexes, d- and f-block organometallic compounds, catalysis, structures and properties of solids and bioinorganic chemistry.

Within each chapter there are worked examples, exercises and problems and short answers are also provided. A set of *Key points* has been introduced at the end of each chapter.

In Part 1, the discussion of molecular shape and symmetry as a separate chapter in this edition is an example of a much improved reorganization of the material. It has also been extended to include topics such as infrared and Raman spectroscopy.

The introduction of the new chapter, *The metals*, is also a necessary improvement from the first edition.

According to the authors, much of the changes were the result of suggestions from readers. As a consequence Part 3 has been augmented, refined and extensively updated.

The shift of topics, for example NMR, to separate sections called *Further information* acknowledges the generality of this material, which in the first edition may have been lost by association with a specific chapter such as hydrogen and its compounds.

A very useful book—highly recommended.

S.M.S.V. Doidge-Harrison

***Chemical Speciation in the Environment***, edited by A.M. Ure and C.M. Davidson, Blackie, London, 1995, xiii + 408 pp., £79.00. ISBN 0-7514-0021-1.

Chemical speciation used to mean the qualitative and quantitative *determination* (expressed as % distribution) of the different chemical forms of a given element. Nowadays it has diverged to embrace the different physical/chemical forms present, not necessarily of a particular element. It can also be interpreted as the description for species composition, i.e. not of analysis. Indeed, these various interpretations have been adopted by contributors of this book.

Physical and/or chemical interactions between different components in an environment give rise to different forms (species) of each element. Thus description of possible interactions is necessary background for speciation. Readers may also expect descriptions on different speciation methods and equally important, the use of speciation results to understand/predict behaviour (e.g. availability and toxicity) in

field I would have thought that a literature search would be an essential pre-requisite. The preface goes on to suggest that you can pick up the phone and 'swiftly obtain information one needs regarding experimental set ups, specific consumables, etc.' For those poor souls whose addresses are included in this volume I pass on my sympathy. A suitable quotation to leave on your answer phone comes from a memorable interview between Mohammed Ali and Michael Parkinson... 'read my book'.

There is one very good use for this book that has been considered by the editor. Those who organise international conferences on hyphenated techniques will find the book extremely useful in compiling a list of potential contributors and delegates. If you are in this position the book is a good buy; otherwise I'd be tempted to give this one a miss.

B.A. McGaw

***Inorganic Chemistry***, 2nd edn., by D.F. Schriver, P.W. Atkins and C.H. Langford, Oxford University Press, Oxford, 1994, xviii + 819 pp. + additional information, softback, £19.50. ISBN 0-19-855396-X.

This is the second edition of the textbook published initially in 1990 and which was very successful. The second edition shows considerable modification and reorganization. The book is divided into three parts: Part 1, *Foundations*; Part 2, *Systematic chemistry of the elements* and Part 3, *Advanced topics*. Part 1 (ca. 310 pp.) has chapters on atomic and molecule structure, molecular shape and symmetry, structure of solids, acids and bases, d-metal complexes and oxidation and reduction. After establishing the foundation of the subject the authors, in Part 2 (ca. 170 pp.), provide a systematic comprehensive account of the chemistry of the elements and their compounds. Metals, hydrogen and its compounds, main-group organometallic compounds, boron and carbon groups, nitrogen and oxygen groups and halogens and noble gases are dealt with in six chapters. Part 3 is a very subjective section as the authors had to be very selective in the choice of appropriate topics in order to give the reader a sense of the current frontier research. It contains chapters on electronic spectra of complexes, reaction mechanisms of d-block complexes, d- and f-block organometallic compounds, catalysis, structures and properties of solids and bioinorganic chemistry.

Within each chapter there are worked examples, exercises and problems and short answers are also provided. A set of *Key points* has been introduced at the end of each chapter.

In Part 1, the discussion of molecular shape and symmetry as a separate chapter in this edition is an example of a much improved reorganization of the material. It has also been extended to include topics such as infrared and Raman spectroscopy.

The introduction of the new chapter, *The metals*, is also a necessary improvement from the first edition.

According to the authors, much of the changes were the result of suggestions from readers. As a consequence Part 3 has been augmented, refined and extensively updated.

The shift of topics, for example NMR, to separate sections called *Further information* acknowledges the generality of this material, which in the first edition may have been lost by association with a specific chapter such as hydrogen and its compounds.

A very useful book—highly recommended.

S.M.S.V. Doidge-Harrison

***Chemical Speciation in the Environment***, edited by A.M. Ure and C.M. Davidson, Blackie, London, 1995, xiii + 408 pp., £79.00. ISBN 0-7514-0021-1.

Chemical speciation used to mean the qualitative and quantitative *determination* (expressed as % distribution) of the different chemical forms of a given element. Nowadays it has diverged to embrace the different physical/chemical forms present, not necessarily of a particular element. It can also be interpreted as the description for species composition, i.e. not of analysis. Indeed, these various interpretations have been adopted by contributors of this book.

Physical and/or chemical interactions between different components in an environment give rise to different forms (species) of each element. Thus description of possible interactions is necessary background for speciation. Readers may also expect descriptions on different speciation methods and equally important, the use of speciation results to understand/predict behaviour (e.g. availability and toxicity) in

field I would have thought that a literature search would be an essential pre-requisite. The preface goes on to suggest that you can pick up the phone and 'swiftly obtain information one needs regarding experimental set ups, specific consumables, etc.' For those poor souls whose addresses are included in this volume I pass on my sympathy. A suitable quotation to leave on your answer phone comes from a memorable interview between Mohammed Ali and Michael Parkinson... 'read my book'.

There is one very good use for this book that has been considered by the editor. Those who organise international conferences on hyphenated techniques will find the book extremely useful in compiling a list of potential contributors and delegates. If you are in this position the book is a good buy; otherwise I'd be tempted to give this one a miss.

B.A. McGaw

***Inorganic Chemistry***, 2nd edn., by D.F. Schriver, P.W. Atkins and C.H. Langford, Oxford University Press, Oxford, 1994, xviii + 819 pp. + additional information, softback, £19.50. ISBN 0-19-855396-X.

This is the second edition of the textbook published initially in 1990 and which was very successful. The second edition shows considerable modification and reorganization. The book is divided into three parts: Part 1, *Foundations*; Part 2, *Systematic chemistry of the elements* and Part 3, *Advanced topics*. Part 1 (ca. 310 pp.) has chapters on atomic and molecule structure, molecular shape and symmetry, structure of solids, acids and bases, d-metal complexes and oxidation and reduction. After establishing the foundation of the subject the authors, in Part 2 (ca. 170 pp.), provide a systematic comprehensive account of the chemistry of the elements and their compounds. Metals, hydrogen and its compounds, main-group organometallic compounds, boron and carbon groups, nitrogen and oxygen groups and halogens and noble gases are dealt with in six chapters. Part 3 is a very subjective section as the authors had to be very selective in the choice of appropriate topics in order to give the reader a sense of the current frontier research. It contains chapters on electronic spectra of complexes, reaction mechanisms of d-block complexes, d- and f-block organometallic compounds, catalysis, structures and properties of solids and bioinorganic chemistry.

Within each chapter there are worked examples, exercises and problems and short answers are also provided. A set of *Key points* has been introduced at the end of each chapter.

In Part 1, the discussion of molecular shape and symmetry as a separate chapter in this edition is an example of a much improved reorganization of the material. It has also been extended to include topics such as infrared and Raman spectroscopy.

The introduction of the new chapter, *The metals*, is also a necessary improvement from the first edition.

According to the authors, much of the changes were the result of suggestions from readers. As a consequence Part 3 has been augmented, refined and extensively updated.

The shift of topics, for example NMR, to separate sections called *Further information* acknowledges the generality of this material, which in the first edition may have been lost by association with a specific chapter such as hydrogen and its compounds.

A very useful book—highly recommended.

S.M.S.V. Doidge-Harrison

***Chemical Speciation in the Environment***, edited by A.M. Ure and C.M. Davidson, Blackie, London, 1995, xiii + 408 pp., £79.00. ISBN 0-7514-0021-1.

Chemical speciation used to mean the qualitative and quantitative *determination* (expressed as % distribution) of the different chemical forms of a given element. Nowadays it has diverged to embrace the different physical/chemical forms present, not necessarily of a particular element. It can also be interpreted as the description for species composition, i.e. not of analysis. Indeed, these various interpretations have been adopted by contributors of this book.

Physical and/or chemical interactions between different components in an environment give rise to different forms (species) of each element. Thus description of possible interactions is necessary background for speciation. Readers may also expect descriptions on different speciation methods and equally important, the use of speciation results to understand/predict behaviour (e.g. availability and toxicity) in

the environment. Of the interactions/background, this book has adequate coverage. Of methods and techniques, there is sufficient coverage for some elements but not for others. Of the implications and applications of speciation, it is generally rather lacking.

The book has 12 chapters. The first is a good overview of the subject and an introduction/summary of the subsequent chapters. Chaper 2 is a comprehensive but brief account of the methodologies used in speciation. Chapter 3 is a useful chapter on techniques of metal speciation, with more details on spectroscopic techniques, particularly on NMR. Chapter 4 is a quite complete but brief account on coupled techniques (e.g. HPLC–MS). Chapter 5 gives a comprehensive background to phase diagrams and computer simulations. A discussion of computer programmes and some examples are given but it would have been helpful to expand this part. Chapter 6 describes the formation mechanisms and interaction mechanisms of metal-containing species in the atmosphere. with examples. This chapter is well-balanced and informative. Chapter 7 gives a brief overview of speciation methodology in fresh waters but the emphasis is on interactions (especially metal complexation) and behaviour of species which is a needed aspect of the book. Chapter 8 describes interactions at surfaces and in solution in the soil environment, with adequate examples. Metal complexation is discussed in greater (and useful) detail. However, the authors used p$K$ for formation of complexes. Formation constants are normally expressed by log $K$ and from their figures and tables, it seems that it is log $K$ that they meant, e.g. a larger p$K$ (log $K$), a stronger complex. Chapter 9 gives a well-balanced account, with adequate examples, of the methodology of metal speciation in sediments and combustion waste. Chapter 10 gives an informative account on the speciation of the important radionuclides. Chapter 11 is a general account on the species of some metals found in micro-organisms, plants and animals. In my opinion, it is very difficult to give a comprehensive account of this subject. Chapter 12 has the title of a concluding chapter (Trends and Development) but is limited to a rather general account on the methodology of speciation, mostly of the metalloids.

Overall the book is very readable, well-presented, up-to-date and reasonably priced for its volume of information. I recommend it to all researchers involved in environmental and analytical studies.

S.C. Tam

***Emerging Technologies in Hazardous Waste Management—IV***, edited by D.W. Tedder and F.G. Pohland, American Chemical Society, Washington, DC, 1994, ix + 317 pp., US$ 89.95. ISBN 0-8412-2857-4.

This volume is a continuation of the symposia on the theme of Emerging Technologies in Hazardous Waste Management organised by the American Chemical Society, and grew out of a selection of 18 papers from the 1992 meeting in Atlanta. The first group deals with aspects of soil remediation, starting with an excellent account of a chemical engineer's approach to modelling a real system from which organics were being removed by vapour extraction. Analysis of the data enabled performance to be measured and predicted, not just from an efficiency point of view but also from an economic one. This is typical of the successful multi-disciplinary approaches to these problems, illustrating how the chemist must broaden his horizons when tackling environmental remediation problems. Electrokinetic remediation—basically large-scale electrophoresis using soil as the bed—is discussed for the removal of anionic pollutants, then a study of the kinetics of the biodegradation of phenols in soils and finally, in this section, the use of bacteria to assist in the mobilisation of heavy metals in soils.

Nine papers deal with minimising the production of waste during the manufacturing stage. Application of artificial intelligence to a programme of waste minimisation presents the general scene for improved process management, and is followed by an account of the removal of mercury from a waste stream by emulsion extraction. The combination of physical adsorption and bacterial degradation is shown to be useful in minimising losses of petrol vapours from air streams, while loss of $SO_2$ from sulphur-rich fuels can be significantly reduced by mixing a scavenger such as lime with the fuel before combustion. Chemically-assisted bacterial degradation of pentachlorophenol (with hydrogen peroxide) and of triazine pesticides (with ozone) has been shown to work significantly faster than microbiological action alone.

the environment. Of the interactions/background, this book has adequate coverage. Of methods and techniques, there is sufficient coverage for some elements but not for others. Of the implications and applications of speciation, it is generally rather lacking.

The book has 12 chapters. The first is a good overview of the subject and an introduction/summary of the subsequent chapters. Chaper 2 is a comprehensive but brief account of the methodologies used in speciation. Chapter 3 is a useful chapter on techniques of metal speciation, with more details on spectroscopic techniques, particularly on NMR. Chapter 4 is a quite complete but brief account on coupled techniques (e.g. HPLC–MS). Chapter 5 gives a comprehensive background to phase diagrams and computer simulations. A discussion of computer programmes and some examples are given but it would have been helpful to expand this part. Chapter 6 describes the formation mechanisms and interaction mechanisms of metal-containing species in the atmosphere. with examples. This chapter is well-balanced and informative. Chapter 7 gives a brief overview of speciation methodology in fresh waters but the emphasis is on interactions (especially metal complexation) and behaviour of species which is a needed aspect of the book. Chapter 8 describes interactions at surfaces and in solution in the soil environment, with adequate examples. Metal complexation is discussed in greater (and useful) detail. However, the authors used p$K$ for formation of complexes. Formation constants are normally expressed by log $K$ and from their figures and tables, it seems that it is log $K$ that they meant, e.g. a larger p$K$ (log $K$), a stronger complex. Chapter 9 gives a well-balanced account, with adequate examples, of the methodology of metal speciation in sediments and combustion waste. Chapter 10 gives an informative account on the speciation of the important radionuclides. Chapter 11 is a general account on the species of some metals found in micro-organisms, plants and animals. In my opinion, it is very difficult to give a comprehensive account of this subject. Chapter 12 has the title of a concluding chapter (Trends and Development) but is limited to a rather general account on the methodology of speciation, mostly of the metalloids.

Overall the book is very readable, well-presented, up-to-date and reasonably priced for its volume of information. I recommend it to all researchers involved in environmental and analytical studies.

S.C. Tam

***Emerging Technologies in Hazardous Waste Management—IV***, edited by D.W. Tedder and F.G. Pohland, American Chemical Society, Washington, DC, 1994, ix + 317 pp., US$ 89.95. ISBN 0-8412-2857-4.

This volume is a continuation of the symposia on the theme of Emerging Technologies in Hazardous Waste Management organised by the American Chemical Society, and grew out of a selection of 18 papers from the 1992 meeting in Atlanta. The first group deals with aspects of soil remediation, starting with an excellent account of a chemical engineer's approach to modelling a real system from which organics were being removed by vapour extraction. Analysis of the data enabled performance to be measured and predicted, not just from an efficiency point of view but also from an economic one. This is typical of the successful multi-disciplinary approaches to these problems, illustrating how the chemist must broaden his horizons when tackling environmental remediation problems. Electrokinetic remediation—basically large-scale electrophoresis using soil as the bed—is discussed for the removal of anionic pollutants, then a study of the kinetics of the biodegradation of phenols in soils and finally, in this section, the use of bacteria to assist in the mobilisation of heavy metals in soils.

Nine papers deal with minimising the production of waste during the manufacturing stage. Application of artificial intelligence to a programme of waste minimisation presents the general scene for improved process management, and is followed by an account of the removal of mercury from a waste stream by emulsion extraction. The combination of physical adsorption and bacterial degradation is shown to be useful in minimising losses of petrol vapours from air streams, while loss of $SO_2$ from sulphur-rich fuels can be significantly reduced by mixing a scavenger such as lime with the fuel before combustion. Chemically-assisted bacterial degradation of pentachlorophenol (with hydrogen peroxide) and of triazine pesticides (with ozone) has been shown to work significantly faster than microbiological action alone.

Finally, a group of papers describes problems of cyclic gas release events in very large tanks storing radio-active waste. Detailed chemical analysis and long-term monitoring have enabled the causes to be elucidated and remedial action to be taken to avoid risk of explosion. Once again, it is the combination of several approaches which is shown to be successful.

There is much fascinating information in this volume, often in considerable detail, which may serve to give pointers to others working in environmental remediation chemistry. This well produced book of carefully selected material is to be recommended.

I.L. Marr

***Determination of Trace Elements***, edited by Z.B. Alfassi, VCH, Weinheim, 1994, xiv + 607 pp., DM 280, £112. ISBN 3-527-28424-9.

What—another book on trace element analysis? This book is certainly large, comprehensive, authoritative and thorough. How does it score otherwise? As it is a multi-author text, the final quality must depend on the work of the editor in helping to structure the individual contributions and then to harmonise them, avoiding overlap of contributions as well as omission of useful material. There are many familar names among the authors. Tölg and Tschöpel give us an updated essay on the sources of systematic errors in trace analysis—always important and therefore essential reading. Kirchmer discusses the concept(s) of limits of detection at some length, and does, I am glad, point out the dangers in using the linear regression of the calibration to estimate the l.d. of a method, an approach which can often give dramatically wrong values, but which is nevertheless often used in commercial software. A chapter on sampling and sample preparation unfortunately repeats too much of Chapter 1 relating to sources of error, but the next, that on separation and preconcentration, gives a good systematic coverage outlining the equilibria involved and giving examples. I think that the chapter on atomic absorption could have been much shorter—there are plenty of texts on this subject, and what is needed here is a survey of the place of AAS in trace and ultra-trace analysis. The balance and the content are much better in the chapter on plasma spectroscopy, which deals with both optical and mass detection systems.

Instrumental neutron activation analysis and radiochemical neutron activation analysis get two separate chapters, in which the author is nearly successful in hiding the distinction between these related topics, but does nevertheless give a lot of detailed information. Polak presents a readable account of surface analytical techniques and shows how they can be used for determination of trace species in solution following adsorption. Wandruszka selects material very carefully for his contribution on electrochemical methods, concentrating on combined preconcentration and stripping methods such as ASV and demonstrating their relevance in speciation at ultra-trace levels.

The combinations of chromatography with atomic spectroscopy, gradually becoming established, especially for determinations of organometallics, strikes a good balance between the overview and the experimental detail, with many helpful examples. The chapter on speciation gives an unusual view in presenting the subject with reference to the use of radio-analytical methods. In the main, this deals with solid phase samples, with speciation in different phases and in depth profiling. The final contribution discusses trace elements in relation to environmental and health sciences, and has much to say on the special considerations which must be given to the history and state of the patient before conclusions can be drawn from the results of chemical analysis. In spite of the tiresome repeated referencing to other writings of the same authors, there is much useful material in this chapter, not so readily available to most analytical chemists.

So, how does it score? The weakness in this volume lies in the editing—several chapters would have benefitted from linguistic assistance, and others could have been shortened without loss to the book as a whole. But there are many well written and informative chapters, contributing to what will certainly prove to be a valuable reference source on the state of trace analysis in the mid 1990s. Many of these chapters could well be useful background reading for postgraduate taught courses. At DM 280 or £112 this is not cheap, but it is certainly worth recommending for the library.

I.L. Marr

Finally, a group of papers describes problems of cyclic gas release events in very large tanks storing radio-active waste. Detailed chemical analysis and long-term monitoring have enabled the causes to be elucidated and remedial action to be taken to avoid risk of explosion. Once again, it is the combination of several approaches which is shown to be successful.

There is much fascinating information in this volume, often in considerable detail, which may serve to give pointers to others working in environmental remediation chemistry. This well produced book of carefully selected material is to be recommended.

I.L. Marr

***Determination of Trace Elements***, edited by Z.B. Alfassi, VCH, Weinheim, 1994, xiv + 607 pp., DM 280, £112. ISBN 3-527-28424-9.

What—another book on trace element analysis? This book is certainly large, comprehensive, authoritative and thorough. How does it score otherwise? As it is a multi-author text, the final quality must depend on the work of the editor in helping to structure the individual contributions and then to harmonise them, avoiding overlap of contributions as well as omission of useful material. There are many familar names among the authors. Tölg and Tschöpel give us an updated essay on the sources of systematic errors in trace analysis—always important and therefore essential reading. Kirchmer discusses the concept(s) of limits of detection at some length, and does, I am glad, point out the dangers in using the linear regression of the calibration to estimate the l.d. of a method, an approach which can often give dramatically wrong values, but which is nevertheless often used in commercial software. A chapter on sampling and sample preparation unfortunately repeats too much of Chapter 1 relating to sources of error, but the next, that on separation and preconcentration, gives a good systematic coverage outlining the equilibria involved and giving examples. I think that the chapter on atomic absorption could have been much shorter—there are plenty of texts on this subject, and what is needed here is a survey of the place of AAS in trace and ultra-trace analysis. The balance and the content are much better in the chapter on plasma spectroscopy, which deals with both optical and mass detection systems.

Instrumental neutron activation analysis and radiochemical neutron activation analysis get two separate chapters, in which the author is nearly successful in hiding the distinction between these related topics, but does nevertheless give a lot of detailed information. Polak presents a readable account of surface analytical techniques and shows how they can be used for determination of trace species in solution following adsorption. Wandruszka selects material very carefully for his contribution on electrochemical methods, concentrating on combined preconcentration and stripping methods such as ASV and demonstrating their relevance in speciation at ultra-trace levels.

The combinations of chromatography with atomic spectroscopy, gradually becoming established, especially for determinations of organometallics, strikes a good balance between the overview and the experimental detail, with many helpful examples. The chapter on speciation gives an unusual view in presenting the subject with reference to the use of radio-analytical methods. In the main, this deals with solid phase samples, with speciation in different phases and in depth profiling. The final contribution discusses trace elements in relation to environmental and health sciences, and has much to say on the special considerations which must be given to the history and state of the patient before conclusions can be drawn from the results of chemical analysis. In spite of the tiresome repeated referencing to other writings of the same authors, there is much useful material in this chapter, not so readily available to most analytical chemists.

So, how does it score? The weakness in this volume lies in the editing—several chapters would have benefitted from linguistic assistance, and others could have been shortened without loss to the book as a whole. But there are many well written and informative chapters, contributing to what will certainly prove to be a valuable reference source on the state of trace analysis in the mid 1990s. Many of these chapters could well be useful background reading for postgraduate taught courses. At DM 280 or £112 this is not cheap, but it is certainly worth recommending for the library.

I.L. Marr

***Laser Spectroscopy—Techniques and Applications***, by E.R. Menzel, Dekker, New York, 1995, xv + 298 pp., US$ 135.00. ISBN 0-8247-9265-3.

This is perhaps the best text that I have read on the techniques and applications of laser spectroscopy. The author makes it clear that the book is intended for the non-specialist and achieves a admirable mixture of the basic essentials (with as little mathematics as possible) and a concise, comprehensive review of applications. Many researchers, especially those in bioscience and medicine to whom a deeper treatment of theoretical aspects is often inappropriate and usually off-putting, will welcome this book as an 'entry level' text. Laser spectroscopy is now a maturing technique that is ripe for exploitation in diverse fields of scientific endeavour.

The book is divided into nine chapters and starts with an overview of the interactions between molecules and light and on the general principles of laser operation. Chapter 2 reviews spectroscopic instrumentation and includes sections on absorption spectrophotometers, spectrofluorometers and synchronous luminescence spectroscopy. Chapters 3–6 are devoted to specific spectroscopic techniques (absorption-based laser spectroscopy, photoluminescence intensity-based and lifetime-based laser spectroscopy, and laser Raman spectroscopy) and give a strong emphasis to recent developments and applications. The book concludes with three chapters on selected applications (including medicine, semiconductors and analytical chemistry), selected spectroscopic techniques (including multidimensional fluorescence, optically detected magnetic resonance, circular dichroism, etc.) and finally a very readable chapter on emerging spectroscopies. The latter covers such exciting techniques as tunable IR lasers, ring lasers and X-ray lasers.

This book will be of great interest to those wanting a 'bird's eye view of laser spectroscopy'. The up-to-date references and comprehensive coverage of applications will be of use to the specialist and non-specialist alike. For those of us teaching applied spectroscopy this book will be an invaluable resource.

B.A. McGaw

# Talanta

The International Journal of Pure and Applied Analytical Chemistry

ELSEVIER

Talanta 42 (1995) i

Talanta

# Announcement

## BIOSENSORS CIRCLES THE GLOBE

Following the tremendous success of the third Biosensors conference held in New Orleans in 1994 involving over 300 submitted abstracts and participants from 30 countries, **The Fourth World Congress on Biosensors** will take place on 29–31 May 1996 in Bangkok, Thailand.

The conference, organised by Elsevier Advanced Technology, returns to the Far East in '96 completing a six year cycle of biannual meetings in strategic sectors of the globe.

**Biosensors '96** is the principal conference in the field. The intense three day event covers every facet of the science, application and commercial exploitation of Biosensors and Bioelectronics and will be attended by all the prime movers in the field.

For the first time in 1996, a symposium on Bioelectronics will be dedicated to the more general exploitation of biochemicals in electronic devices. The plenary sessions in this year's event will emphasise new horizons, with critical appraisals of the opportunities offered by improved understanding of biophysical interactions at the molecular level.

The Biosensors Congress is ***the*** forum for highly original communications and provides a comprehensive picture of recent developments and catalyses interactions that mould the future directions of the area.

### Format of the Congress

The congress will be structured as three symposia:

- Catalytic Biosensors
- Affinity Biosensors
- Bioelectronics

Contributions describing the industrial development of analytical instruments, as well as more fundamental aspects of the technology, will also be encouraged and supplemented by a display of commercial equipment.

### Exhibition

Following the excellent response to the first exhibition held at ***Biosensors '96***, there will be increased space allocated at the '96 event for companies to display their commercial equipment.

### Biosensors and Bioelectronics Award

For the first time the supporting journal for the conference, ***Biosensors and Bioelectronics***, will sponsor an award for the most original oral and poster presentations, to be selected at the conference.

For further information please contact:
Gill Spear, Biosensors '96
Elsevier Science Ltd, Conference Department
The Boulevard, Langford Lane
Kidlington, Oxford OX5 1GB, UK
Fax: +44 (0) 1865 843958 Tel: +44 (0) 1865 843643
e-mail: g. spear@elsevier.co.uk

ELSEVIER

Talanta 42 (1995) i–ii

Talanta

# Announcements

## INTERNATIONAL ION CHROMATOGRAPHY SYMPOSIUM

The International Ion Chromatography Symposium 1995 will be held October 1st–5th at The Grand Kempinski in Dallas, Texas. Program Chairman Donald Pietrzyk heads a scientific committee of internationally renowned ion chromatography experts and an organizing committee of local scientists.

This year's program features six plenary lectures and over 120 technical presentations.

This three-day international meeting provides a unique opportunity for scientists from a variety of disciplines to exchange ideas and results on current methods and procedures in ion chromatography and capillary electrophoresis for the separation and determination of small organic and inorganic ions. Topic areas include:

- Advances in Column Technology and Column Selectivity
- Advances in Detection
- Special Sample Treatment Procedures
- Anion Analysis
- Cation/Transuronic Analysis
- Capillary Wall Modifications
- Environmental Applications
- Pharmaceutical Applications
- Health Science Applications
- Industrial Problem Solving
- On-Line Analysis
- Data Handling

For more information, write to or call:

Century International Inc.
P.O. Box 493
Medfield, MA 02052, USA
Tel: 508/359-8777
Fax: 508/359-8778

---

## XIIITH NATIONAL CONFERENCE ON ANALYTICAL CHEMISTRY

May 23–25, 1996, Craiova, Romania

Organized by the Romanian Society of Analytical Chemistry.

For further information, please contact:

Cristina Matachescu,
Romanian Society of Analytical Chemistry,
13 Blvd. Republicii,
Sector 3, 70346 Bucharest, Romania
Tel/Fax: 40-1-410-2279

---

## INTERNATIONAL CONFERENCE ON ENVIRONMENTAL SCIENCE

January 10–13, 1996, Trivandrum, India

and workshop on

## PRESENT STATUS OF ANALYSIS OF TRACE METALS AND NUTRIENTS IN THE MARINE ENVIRONMENT

January 8–13, 1996, Trivandrum, India

The scientific program of the conference will cover the following topics:

- Multidimensional Techniques for Environmental Monitoring
- Pollutant Sensors
- Speciation
- Quality Assurance for Environmental Data
- Modelling of Environmental Data
- Waste Water and Drinking Water Treatment — Emerging Technologies

The workshop will be devoted to:

- An in-depth discussion on the status of sampling and analysis of sea water, sediments and biota for trace elements; of nutrients in sea water; their distribution in relation to biological, chemical and hydrographic processes
- A review of the data on trace elements in the different oceans
- Guidelines for future research and for interlaboratory collaboration

For further information, please contact:

Dr. C.S.P. Iyer
Convener, ICES-96
Regional Research Laboratory (CSIR)
Trivandrum-695 019, India
Tel: 91-471-77459
Fax: 91-471-75186
Telex: 0435-232

Pergamon

*Talanta*, Vol. 42, No. 2, pp. i–ii, 1995
Elsevier Science Ltd
Printed in Great Britain

# NOTICES

## The James W. Robinson Analytical Chemistry Symposium: Adventures in Analytical Chemistry

3–4 March 1995, Baton Rouge, Louisiana

Contact Isiah M. Warner, Department of Chemistry, Louisiana State University, 232 Choppin Hall, Baton Rouge, LA 70803, U.S.A. Telephone +(504) 388-2829.

If you have any questions or comments, please contact me by e-mail using ISAIAH.WARNER@CHEMGATE.CHEM.LSU.EDU, or by facsimile, +(504) 388-3971.

## SCIENTIFIC CALENDAR ANNOUNCEMENT

The Twenty-second Annual Conference of the Federation of Analytical Chemistry and Spectroscopy Societies (FACSS) will be held in Cincinnati, Ohio, at the Sabin Convention Center during the week of 15–20 October 1995. The deadline for submission of titles and a preliminary 100 word brief is 31 March 1995.

For further information, please contact:

FACSS
198 Thomas Johnson Drive, Suite S-2
Frederick, MD 21702-4317
Tel. +(301) 846-4797

## FIRST ANNOUNCEMENT

### 5th International Congress on Trace Elements in Medicine and Biology

**Therapeutic Uses of Trace Elements**
*Satellite Workshop: Molecular Basis of Copper Metabolic Disorders*

4–7 February 1996, Méribel, France

**MAIN TOPICS:**

- Therapeutic forms of trace elements
- Large epidemiological and intervention studies related to trace elements
- Trace element supplementation of population groups at different periods of age
- Trace elements, bone physiology and bone diseases
- Trace element status and treatment in relation to inflammatory conditions and infections
- Trace elements in digestive diseases and in endocrinology
- Pharmacological applications of trace elements
- Genetic disorders of copper metabolism

**OFFICIAL LANGUAGES:**

French and English (simultaneous translation)

**ORGANIZED BY:**

Société Francophone d'Etude et de Recherche sur les Eléments Trace Essentiels (SFERETE)

For registration and information, please contact:

Arlette Alcaraz
Laboratoire de Biochimie C-CHRUG-B.P. 217
F-38043 Grenoble Cedex 9
France
Tel. +(33) 76 76 54 84
Fax. +(33) 76 76 56 64.

ELSEVIER

Talanta 42 (1995) i–iii

Talanta

# Acknowledgement to referees

The Editors wish to thank the following referees for their services in 1994

Abdel-Moety, E. M.
Ackermann, G.
Akama, Yoshifumi
Akaiwa, Hideo
Alder, J. F.
Anderson, David J.
Armstrong, Daniel W.
Arnold, Mark
Attiyat, A. S.

Baastiaans, Glenn
Bachas, Leonaidas
Bahowlak, Tim
Bailey, Leonard C.
Balcerzak, Maria
Baldwin, Richard P.
Ballentine, Dave
Barnes, Ramon M.
Bartsch, Richard A.
Batley, Graeme
Baxter, Pamela
Beauchemain, D.
Belanger, Daniel
Beltran, J. L.
Benammar, M.
Berg, R.
Bernth, N.
Bersier, P. M.
Berthod, A.
Bild, Richard W.
Blanco, P. Tuñon
Blank, C. LeRoy
Bobbitt, Don R.
Braun, T.
Brayden, Thomas H.
Bright, Frank V.
Britz, D.
Broekaert, J. A. C.
Brooker, M. H.
Brorson, M.
Brown, Steven D.
Bruckner, Carsten
Brunette, J. P.
Buldini, P. L.
Buncel, F.
Bunton, C. A.
Burba, P.
Burgess, Lloyd
Burns, D. T.
Busch Hejlskov, I.
Busch, Kenneth L.
Butler, I. B.
Buttry, Dan
Bye, R.
Byrnard, A.

Calatayud, J. M.
Callis, James B.
Cámara, C.
Campanella, L.
Capitán-Vallvey, L. F.
Carlin, Richard T.
Carnahan, Jon W.
Caroli, S.
Carr, James D.
Caruso, Joseph A.
Castro, L.
Cathum, S. J.
Cattrall, Robert
Cedergren, A.
Chalmers, R.
Charton, M.
Chow, Arthur
Christensen, J. M.
Christofferson, J.
Clark, Gregory D.
Compaño, R.
Cook, Kelsey D.
Cornett, C.
Corsini, Alfio
Cosofret, V. V.
Cosofret, Vasile
Coury, Jr., Louis A.
Covington, A.
Cox, James
Cox, James A.
Crampton, Michael R.
Creager, Stephen E.
Cresser, M.
Crouch, Stanley R.
Cullen, William R.

Dams, R.
Danielsson, L. G.
Dasgupta, Purnendu K.
Deming, Stanley N.
Diaz, A. N.
Doherty, William
D'Orazio, Paul
Dorsey, J.
Doughten, Michael W.
Dovichi, Norman J.
DuVal, Dean

Ebdon, L. C.
Egorov, Oleg
Ehmann, William D.
Eiceman, Gary A.
El-Kommos, M. E.
Elmer, Gary W.
Engels, W.
Ephraim, J. H.
Epstein, Michael
Esbensen, K.
Ettlinger, M.

Falcó, P. Campins
Fang, Z.
Fernando, Quintus
Filby, Roy H.
Flatt, James R.
Fletcher, III, Kenneth S.
Fogg, A. G.
Frech, W.
Freiser, Henry
Frenzel, W.
Fritz, James S.

Gallego, M.
Garcia, L.
Garcia-Vargas, M.
Gonzalez, A. G.
Gonzalo, E. R.
Gorton, L.
Griffiths, Peter R.
Guardia, M. de la
Guidelli, Rolando
Guilbault, G. G.
Gurka, Donald F.

Hage, David S.
Hajós, P.
Haldimann, M.
Hamano, T.
Hammer, Charles F.
Hansen, Elo H.
Hansen, S. H.
Harrison, D. Jed
Hart, John P.
Hartenstein, Steven
Hauugland, Richard
Havel, J.
Havlin, Schlomo
Heineman, William R.
Hendricks, M. M. W. B.
Hernández, L. H.
Hill, Herbert H.
Hinze, Willie L.
Hitchman, Michael
Hladky, Zdenek
Hoenig, Michael
Högfeldt, E.
Holm, Thomas R.
Holman, David
Horvath, Zs.
Houk, R. Sam
Howell, J. A.
Høyer, B.
Huie, Carmen W. K.
Hulanicki, A.
Hungerford, James M.
Hurtubise, Robert J.
Hussey, Charles L.
Huusfeldt-Larsen, E.

Inczédy, János
Ingle, James D.
Ivaska, A.
Izatt, Reed M.
Izutsu, K.

Jackson, G. E.
Jagner, D.
Jensen, O. J.
Jin, Q.
Johansen, K. D.
Johnson, Dennis C.
Johnson, K. S.

Kai, M.
Kalman, David A.
Kalvoda, Robert
Kanetake, Tatsutoshi
Karayannis, M. I.
Karlberg, B.
Kauffmann, J.-M.
Kawaguchi, Horoshi
Kiba, Nobutoshi
Kimura, Keiichi
Kincaid, James R.
Kincaid, W. Frank
Kingston, H. M.
Klinkhammer, Gary P.
Koch, K. H.
Koch, K. R.
Koh, T.
Koirtyohann, S. Roy
Kopelman, Raoul
Korenaga, T.
Kotrlý, Stanislav
Kovacs, Julia A.
Kowalski, Bruce R.
Kragten, J.
Kreutzer, Karen
Kricka, L. J.
Kristiansen, J.
Krohn, Kenneth A.
Kuban, V.
Kubiak, W. W.
Kundu, K. K.
Kuroda, R.

Lacy, Nathan
Lamothe, Paul
Laserna, J. J.
León, J. J. A.
Lewis, R. G.
Lima, Robert
Lin, Zhiaho
Lingeman, H.
Link, Jeanne
Linscheid, M.
Littlejohn, D.
Liu, C. C.
Locascio-Brown, Laurie
Locke, David C.
Logan, Barry
Lohse, C.
López-Cueto, G.
Lopez-Molinero, A.
Lubman, David M.
Lucy, Charles
Lukaszewski, Z.
Lundager Madsen, H. E.
Luong, J. H.
Luque de Castro, M. D.
L'vov, Boris L.

Ma, Shu-Ching
Machado, A.
Maeda, Y.
Mahuzier, G.
Majidi, Vahid
Mark, Harry
Marr, R.
Marshall, William
Martin, C. R.
Mascini, Marco
Maskell, W. C.
Mason, Timothy J.
Matousek, J. P.
Mayes, David
McClelland, J. F.
McDowell, W. J.
McLeod, C. W.
McNally, Mary E.
McNeil, Calum J.
Meloan, Clifton E.
Meloun, M.
Mendez, J. H.
Mentasi, E.
Mentasti, E.
Meyerhoff, Mark
Michelsen, M.
Moody, R. R.
Morelli, B.
Motomizu, S.
Mottola, Horacio A.
Moyer, Bruce
Müller, H.
Munoz, E.

Nagaosa, Yukio
Nagourney, Stuart J.
Nakashima, T.
Ndou, Thilivhila
Nevado, J. J.
Nevissi, Ahmad E.
Nicolaisen, F.
Nielsen, T.
Niessner, R.
Nikolelis, D.
Nørgaard, L.

O'Connell, Kathleen
O'Haver, Thomas C.
Olin, Å.
Olsen, H.
Olson, Donald C.
Olson, Nels
O'Reilly, James E.
Osteryoung, Robert A.
Otto, M.
Ozanich, Richard

Pacey, Gilbert E.
Pagsberg, P
Palágyi, S.
Palleschi, G.
Palmisano, F.
Pardue, Harry
Parthasarathy, N.
Paski, Edgar
Patel, K. S.
Patonay, Gabor
Patterson, H.
Patton, Charles J.
Paulos, C.
Pavón, J. M. C.
Pawliszyn, Janusz B.
Pelizzetti, E.
Pella, Peter A.
Pellerin, F. J.
Peña, A. Muños de la
Peres-Bustamente, J. A.
Pérez-Bendito, D.
Pérez-Ruiz, T.
Perkampus, H. H.
Perone, Sam P.
Pesavento, M.
Pesek, Joseph J.
Peterson, John R.
Peterson, Kristina
Pfeiffer, D.
Pickering, William F.
Piepmeier, Edward H.
Pietrzyk, Donald J.
Pilling, M. J.
Pingarron, Jose M.
Pollema, Cy
Poole, Colin F.
Potter, Noel M.
Poulsen, O. M.
Prat, M. D.
Preston, J. S.
Przeszlakowski, S.
Pungor, E.
Purdy, William C.

Ramis Ramos, G.
Ramos, Scott
Rapsomanikis, S.
Regenstein, W.
Resing, Joseph A.
Ricco, Tony
Ridder, C.
Ríos, A.
Rizvi, G. H.
Robertis, A. De
Robinson, James W.
Rodriguez-Gonzalo, E.
Roelandts, I.
Rojas, Fuensanta S.
Romia, M. Blanco
Røysett, Oddvar
Rubio, Vicente
Rusling, Jim

Sakai, T.
Sammartano, S.
Sánchez-Pedreño, C.
Sanz-Medel, A.
Sastry, C. S. P.
Sawada, K.
Scheper, T.
Schlemmer, G.
Schmidt, H.-L.
Schneider, Jeffery A.
Schultz, Frank A.
Shuttler, I.
Seifert, B.
Seitz, Rudolf
Selkine, Tatsyya
Sepaniak, Michael J.
Sevilla, Michael D.
Shelley, Paul
Shelly, Dennis C.
Shono, T.
Singer, R.
Smith, Dean K.
Smyth, M. R.
Sokolove, P. M.
Solich, P.
Sommer, L.

Sørensen, A. M.
Sørensen, P. E.
Sorenson, John R. S.
Sperling, M.
Stella, R.
Stephens, Roger
Stoecher, Paul
Stojek, Z.
Stulik, K.
Styris, D. L.
Sugii, Atsushi
Sultan, S. M.
Sultan, Saleh M.
Suzuki, K. T.
Suzuki, W.
Svensmark, B.

Takagi, Makoto
Takamatsu, Takejiro
Takeda, Yasuyuki
Tamura, H.
Taylor, Daniel
Terada, K.
Thomas, J. D. R.
Thompson, Michael
Thunus, L.
Tipping, E.
Toei, K.
Tölg, G.
Tosi, G.
Townshend, Alan
Tran, Chieu D.
Trojaniewicz, Marek
Trojanowicz, M.
Turecek, Frantisek
Turner, A. P. F.
Tyson, Julian F.

Uden, Peter C.

Valcárel, M.
van Bennekom, W. P.
van den Berg, C. M. G.
Vanhoe, H.
van Staden, J. F.
Veillon, Claude
Velez, M.
Vessman, J.
Vielstich, W.
Vinther, A.
Voigtman, Jr., Edw. G.
von Wandruszka, Ray
Vytras, K.

Wada, H.
Wade, Adrian P.
Waggoner, Alan
Wai, Chien M.
Wang, Erkang
Wang, Joseph
Wang, Naixing
Ward, Michael
Watanabe, Kunihiro
Weber, Stephen G.
Wegscheider, W.
Wehry, Jr., Earl L.
Welch, Lawrence E.
Welz, B.
Wentzell, Peter D.
West, Steve
Wilson, George S.
Windforder, James D.
Wohltjen, Hank
Wold, Svante
Wolfbeis, O. S.
Worsfold, P. J.
Wrona, P.

Yacynych, Alex
Yamada, M.
Yamane, T.
Yamauchi, O.
Yamazoe, Noburu
Yang, Jia-Zhan
Yao, Toshio

Zagatto, E. A. G.
Zaks, Alek
Zuberbühler, A. D.

Pergamon

*Talanta*, Vol. 42, No. 4, pp. i–iii, 1995
Elsevier Science Ltd
Printed in Great Britain

# NOTICES

## 10TH INTERNATIONAL CONFERENCE ON FOURIER TRANSFORM SPECTROSCOPY

Budapest, August 27–September 1, 1995

**OPENING SPEAKER: R. R. ERNST, NOBEL LAUREATE CHEMISTRY, 1991**

**PLENARY SPEAKERS:**

J. E. BERTIE
J. W. BRAULT
C. CASTIGLIONI
D. B. CHASE
HAI-LUNG DAI
J. P. DEVLIN
C. B. FARMER
J. A. DE HASETH
H. M. HEISE
K. ITOH
J. C. LAVALLEY
J. P. MAILLARD
C. MARCOTT
H. NEUGEBAUER
M. N. POPOVA
E. PRETSCH
F. SIEBERT
W. THEISS
M. WINNEWISSER

**ROUND-TABLE OR PANEL DISCUSSIONS WILL BE ORGANIZED IN THE FOLLOWING TOPICS:**

- Catalysis
- Environmental and life sciences
- Quantitative accuracy of FTIR spectrometry
- Contributed papers as posters: Send your 1-page abstract by March 30, 1995

Special pre-conference event:

**1st EURO-AMERICAN INTENSIVE SHORT COURSE ON ADVANCED INFRARED AND RAMAN SPECTROSCOPY**

Hungarian Academy of Sciences, Veszprém, Hungary, August 23–26, 1995

SPECIAL FOCUS: INDUSTRIAL AND ENVIRONMENTAL ASPECTS

**LECTURERS:**

Prof. D. B. Chase
Prof. J. G. Grasselli-Brown
Prof. P. R. Griffiths
Prof. J. A. de Haseth
Prof. R. Kellner
Prof. J. A. Lercher
Prof. J. Mink
Prof. E. Pretsch
Prof. H. W. Siesler

A special package price is available for both events on request.

For further information please contact:

Prof. János Mink
University of Veszprém, Dept. of Analytical Chemistry,
H-8201 Veszprém, P.O. Box 158, Hungary
Tel: +36-88-421-869; Fax: +36-88-426-016
E-mail: mink@iserv.iki.kfki.hu

## ICFIA '95
## JAFIA

August 13–17, 1995, Seattle, Washington

The seventh International Conference on Flow Injection Analysis **(ICFIA '95)** and the 24th Semi-Annual Meeting of the Japanese Association for Flow Injection Analysis **(JAFIA)** will be held jointly at Meany Tower Hotel in Seattle, Washington.

The meeting will focus on developments in the growing fields of FIA and SIA—methods, applications, software and hardware.

Publishers and producers of instruments, equipment, and software relevant to FIA are invited to exhibit.
Registration fees and deadlines: By May 1, 1995, $225; May 2–July 1, $250; after July 1, $275.
Students: By May 1, $100; after May 1, $125.
Deadline for abstracts: July 1, 1995.

For a registration form or more information, contact

Gary D. Christian
Dept. of Chemistry, BG-10
University of Washington
Seattle, WA 98195
FAX: 206-685-3478
e-mail: christia@chem.washington.edu

---

## 1995 FIRST MEDITERRANEAN BASIN CONFERENCE ON ANALYTICAL CHEMISTRY

Cordoba, Spain, 5–10 November, 1995

In order to promote collaboration among analytical scientists of the whole Mediterranean Basin, the *1995 First Mediterranean Basin Conference on Analytical Chemistry* will provide an adequate forum for reporting and thoroughly discussing the latest research results in basic and instrumental developments in Analytical Chemistry.

Other aims of this Conference are:

- To promote new opportunities for young scientists in the Mediterranean Sea area (particularly for those in the Southern Bank): to attend international meetings in countries of the region, to attend training workshops on new analytical techniques, to attend short courses on new techniques and trends in Analytical Chemistry and to establish new links for research in/or other countries of the region.
- To stimulate the progress of Analytical Chemistry as a whole by solving analytical problems affecting the Mediterranean Area.

The program has been designed to attract participants from industry, universities and research centers. The program will comprise invited plenary and key-note lecturers, contributed oral papers, and posters, distributed in several Symposia covering the following topics: Education of Analytical Chemistry, Environmental Analytical Chemistry, Agriculture and Food Analysis, Geoanalytical Chemistry and Benefitiation of Minerals, Biomedical Analysis, Archeometry and Art Objects Preservation, Quality Assurance and Harmonization of Procedures.

A few Short Courses, Special Sessions on "hot" topics, and an Exhibition of Instrumentation has also been arranged.

Invited lecturers who have already confirmed their contribution include M. Valcárcel, I. B. Brenner, D. Barceló, S. Caroli, A. Laachach, O. X. F. Donnard, M. M. Khater, H. Muntau, J. Albaigés, B. Y. Meklati and P. Quevauviller.

## CALL FOR PAPERS

Titles of submitted oral or poster presentations are solicited with the preliminary registration card by 30 May, 1995. Submission of final Conference Abstracts are requested not later than 30 June, 1995.

## SOCIAL ACTIVITIES

Varied social activities, including a visit to Granada, are being planned.

## FURTHER INFORMATION

For further information and pre-registration forms, please contact:

Prof. Alfredo Sanz-Medel (Chairman)
Department of Physical and Analytical Chemistry
Faculty of Chemistry
University of Oviedo
C/ Julian Claveria, s/n
33006 Oviedo, Spain
Tel: 34-8-5 10 34 80 or 34-8-5 10 34 74
Fax: 34-8-5 10 31 25

---

## Fundamentals of Chromatography Course
## June 12–16, 1995

Kent State University's Department of Chemistry and Varian Associates will co-sponsor a course, "Fundamentals of Chromatographic Analysis", during June 12–16, 1995. This course, which has been well received by the industrial community, has been presented ten previous years.

The course will provide a coherent overview of chemical separations via chromatographic methods. It is unique from most other short courses in that material will be included on gas, liquid and thin-layer methods. It will emphasize the three techniques as complementary rather than competing processes. The course will be a blend of fundamental information on theory and instrumentation with emphasis placed on the latest developments and trends. Additional periods will provide time to discuss practical problems related to HPLC, GC, GC–MS, TLC and CE instrumentation. Some laboratory sessions will be available for the students.

Dr. Roger K. Gilpin, Chairman of Chemistry at Kent State University, and Dr. Neil D. Danielson, Professor at Miami University, will be the principle lecturers. Ronald E. Lewis of Varian will discuss/demonstrate laboratory instrumentation.

Information on this course can be obtained by writing to the Department of Chemistry, Kent State University, Kent, OH 44242, or by calling 216/672-2032.

---

## XIIITH NATIONAL CONFERENCE ON ANALYTICAL CHEMISTRY
May 23–25, 1996, Craiova, Romania

Organized by the Romanian Society of Analytical Chemistry.

For further information, please contact:

Cristina Matachescu,
Romanian Society of Analytical Chemistry,
13 Blvd. Republicii,
Sector 3, 70346 Bucharest, Romania
Tel/Fax: 00 401 631 0060.

Pergamon

*Talanta*, Vol. 42, No. 1, pp. i–iv, 1995
Elsevier Science Ltd
Printed in Great Britain

# NOTICES

## PBA '95 SIXTH INTERNATIONAL SYMPOSIUM ON PHARMACEUTICAL AND BIOMEDICAL ANALYSIS

St Louis, Missouri, U.S.A.
23–26 April 1995

PBA '95 will be held 23–26 April 1995 in the historic Union Station Hyatt Regency Hotel in St Louis. The symposium is organized by the *International Association for Pharmaceutical and Biomedical Analysis*, chaired by Professor John F. Stobaugh, with sponsorship from a wide range of international organizations. It follows highly successful meetings held in Barcelona (1987), York (1990), Boston (1991), Baltimore (1992) and Stockholm (1994). The objectives of the Symposium are to provide a stimulating forum for delegates to meet in the pleasant and sociable surroundings of St Louis, where they can be updated on the latest developments in analytical science and instrumentation, applied across the range of pharmaceutical and clinical sciences. All those involved in the analysis of drugs, related materials, forensic samples and endogenous compounds are cordially invited to attend.

The programme for PBA '95 will start off on 23 April with a series of half-day Workshops on the following topics: Diode-array/Mass Spectrometric Detection in LC; Analysis of Solids and Excipients; Microdialysis Sampling; Laboratory Information Management Systems; Assay Validation; Capillary Electrophoresis; Sample Preparation.

The scientific programme will include invited Keynote Lectures on topical themes, Oral Presentations, Poster Presentations and the ever-popular Poster Discussion Sessions, where authors may summarize their poster in a short Oral Presentation for discussion in smaller groups.

Topics to be covered include:

- Analytical biotechnology
- Bioanalysis in clinical and preclinical drug development
- Sample preparation and derivatization
- Spectroscopic methods (NMR, MS, CD, FT-IT, UV-Vis, CL, FL)
- Advances in separation techniques (LC, CE, GC, SFC)
- Analysis of stereoisomers
- Analytical considerations in drug delivery
- Applications of monoclonal antibodies
- Assay validation and regulatory issues
- Automated methods of analysis
- Drugs of abuse
- Therapeutic drug monitoring, clinical and forensic toxicology
- Pharmaceutical Quality Control—analysis of bulk drugs and formulations

The City of St Louis is an excellent place for meeting colleagues and making new contacts in convivial circumstances designed to maximize the opportunity to obtain the latest information on advances in analysis relevant to pharmaceutical and biomedical analysis. This Symposium will overlap with and be followed by the 6th International Symposium on Chiral Discrimination (ISCD '95) in the same venue, 26–28 April, 1995, giving a unique opportunity to meet delegates and speakers from both fields.

For further information please contact:
Miss Shirley E. Schlessinger, Symposium Manager, PBA '95/ISCD '95
Suite 1015, 400 East Randolph Drive,
Chicago, IL 60601, U.S.A.
Tel: 1-312-527-2011

## ISCD '95: SIXTH INTERNATIONAL SYMPOSIUM ON CHIRAL DISCRIMINATION

St Louis, Missouri, U.S.A.
26–28 April, 1995

ISCD '95 will be held 26–28 April 1995 in the historic Union Station Hyatt Regency Hotel in St Louis. The symposium is chaired by Professor Daniel W. Armstrong, and is sponsored by a number of international organizations. It follows highly successful meetings held in this series in France (1988), Rome (1991), Tübingen (1992), Montreal (1993) and Stockholm (1994).

The objective of ISCD '95 is to provide a stimulating forum for the discussion of recent developments in chiral discrimination, a topic of profound importance in many different scientific fields. This interdisciplinary forum aims to unify and broaden the perspectives of participants through reports and discussions on cutting-edge developments in chiral discrimination and stereochemistry. ISCD '95 will focus on chiral research of specific concern to pharmaceutical and medicinal scientists. All those involved in any aspect of chiral discrimination are cordially invited to attend.

The scientific programme will include invited Keynote Lectures, Oral Presentations, Poster Presentations and Poster Discussion Sessions, where authors will be invited to make a short Oral Presentation for discussion in smaller groups. Topics to be covered include:

- Molecular Recognition
- Racemization
- Chiral Ligand Binding
- Advances in Enantiomeric Separations (LC, CE, GC and SFC)
- Stereochemical Aspects of Pharmacokinetics
- Stereoselective Catalysis
- Catalytic Antibodies
- Regulatory Issues
- Food and Beverage Issues
- Circular Dichroism and Polarimetry
- Chiral NMR Shift Reagents
- Enzymatic Methods
- Stereochemical Aspects of Synthesis
- Large-scale Separation of Enantiomers
- Stereochemical Aspects of Pharmacodynamics
- Stereochemical Theory
- Determination of Absolute Configuration
- Method Validation
- Environmental Issues
- Geochemical Aspects

Delegates will meet in the pleasant and convivial surroundings of St Louis, which is an excellent place for making new contacts and for networking among colleagues to find out the latest information on advances in the field. This Symposium will overlap with and be preceded by the 6th International Symposium on Pharmaceutical and Biomedical Analysis in the same venue, 23–26 April 1995, giving a unique opportunity to meet delegates and speakers from both fields.

For further information please contact:
Miss Shirley E. Schlessinger, Symposium Manager, PBA '95/ISCD '95
Suite 1015, 400 East Randolph Drive,
Chicago, IL 60601, U.S.A.
Tel: 1-312-527-2011

# HPLC '95: 19TH INTERNATIONAL SYMPOSIUM ON COLUMN LIQUID CHROMATOGRAPHY

Innsbruck, Austria
28 May–2 June 1995

HPLC '95 will be held in the Innsbruck Convention Center from 28 May to 2 June 1995. This symposium will be chaired by Professor Wolfgang Lindner and forms the 19th in a distinguished series of meetings, which have been the premier event for the presentation of the latest scientific and instrumental advances in separation science. There will be a strong focus on the most dynamically developing techniques and applications in liquid chromatography, capillary electrophoresis and related methods including hyphenated techniques. All those involved in any area of separation science and its applications are cordially invited to attend.

The format for HPLC '95 will be similar to that for successful meetings held earlier in Europe and the USA, with topical issues in *Oral Sessions*, a strong focus on *Poster Presentations* and special *Poster Discussion Sessions*. A comprehensive *International Technical Exhibition* will be presented as an integral part of the scientific programme. *Workshops* and *Discussion Fora*, also involving the international Exhibitors, will be held on selected topics.
This broad interdisciplinary forum will highlight the following scientific themes:

- Separation methods, including HPLC, SFC, HP-affinity chromatography and related methods
- Capillary electrophoresis and electrokinetic chromatography
- Hyphenated techniques and coupled techniques, including mass spectrometry
- Chiral recognition and separation of stereoisomers
- Separation techniques in biotechnology
- New developments in sorption materials
- Preparative techniques in chromatography
- Selective and sensitive detection systems
- Sample preparation and derivatisation strategies
- Applications in pharmaceutical, clinical, food, environmental and forensic analysis, etc
- Chemometrics in separation science
- Validation and regulatory issues

Delegates will meet in the convivial social surroundings of the Tyrolean city of Innsbruck, where there will be ample time for networking among colleagues and updating on the latest developments in the field.

In view of the rapid developments currently taking place in separation science, the Organizers will be happy to receive **LAST MINUTE CONTRIBUTIONS** as *Poster Presentations*, if an Abstract is submitted by **10 May, 1995**.

For further information please contact:

HPLC '95 Secretariat,
Tyrol Congress,
Marktgraben 2
A-6020 Innsbruck, Austria
Telephone: 43-512-575600
Telefax: 43-512-575607

*or*

Prof. Dr Wolfgang Lindner,
Institute of Pharmaceutical Chemistry
University of Graz,
A-8010 Graz, Austria
Telefax: 43-316-3846324

## INTERNATIONAL MASS SPECTROMETRY SOCIETY

At its meeting in conjunction with the 13th International Mass Spectrometry Conference (IMSC) in Budapest on 31 August, the International Scientific Committee of the International Mass Spectrometry Conference voted to establish an International Mass Spectrometry Society (IMSS). The increasing internationalization of science and the many advantages of formal methods of co-operation across national boundaries prompted this move. To implement this motion, the Committee established a working group to draw up a constitution and policies. This group consists of R. G. Cooks (U.S., Chair), E. Gelpi (Spain), C. Lifshitz (Israel), M. Linscheid (Germany), J. MacLeod (Australia), Y. Nakagawa (Japan), and N. M. M. Nibbering (Netherlands). This group welcomes suggestions from all interested in the future of mass spectrometry. Please contact any of the above individuals with suggestions on objectives, governance, membership, finances and the like.

The committee is also considering the future role of the IMSS in improving communications between mass spectrometry groups and societies, in the organization of the IMSC and the publication of its proceedings, in the preservation of the history of mass spectrometry, in improving the teaching and practice of mass spectrometry in countries in which it is not well-developed, in facilitating acquisition of funding for mass spectrometry from super-governmental bodies and in improving the status of the subject through membership of the IMSS in appropriate international scientific organizations.

# LIST OF CONTENTS

## JANUARY

## FEBRUARY

## MARCH

## APRIL

## MAY

## JUNE



## JULY

## AUGUST

## SEPTEMBER

## OCTOBER

## NOVEMBER

## DECEMBER

# AUTHOR INDEX